

Annual Cumulated Index

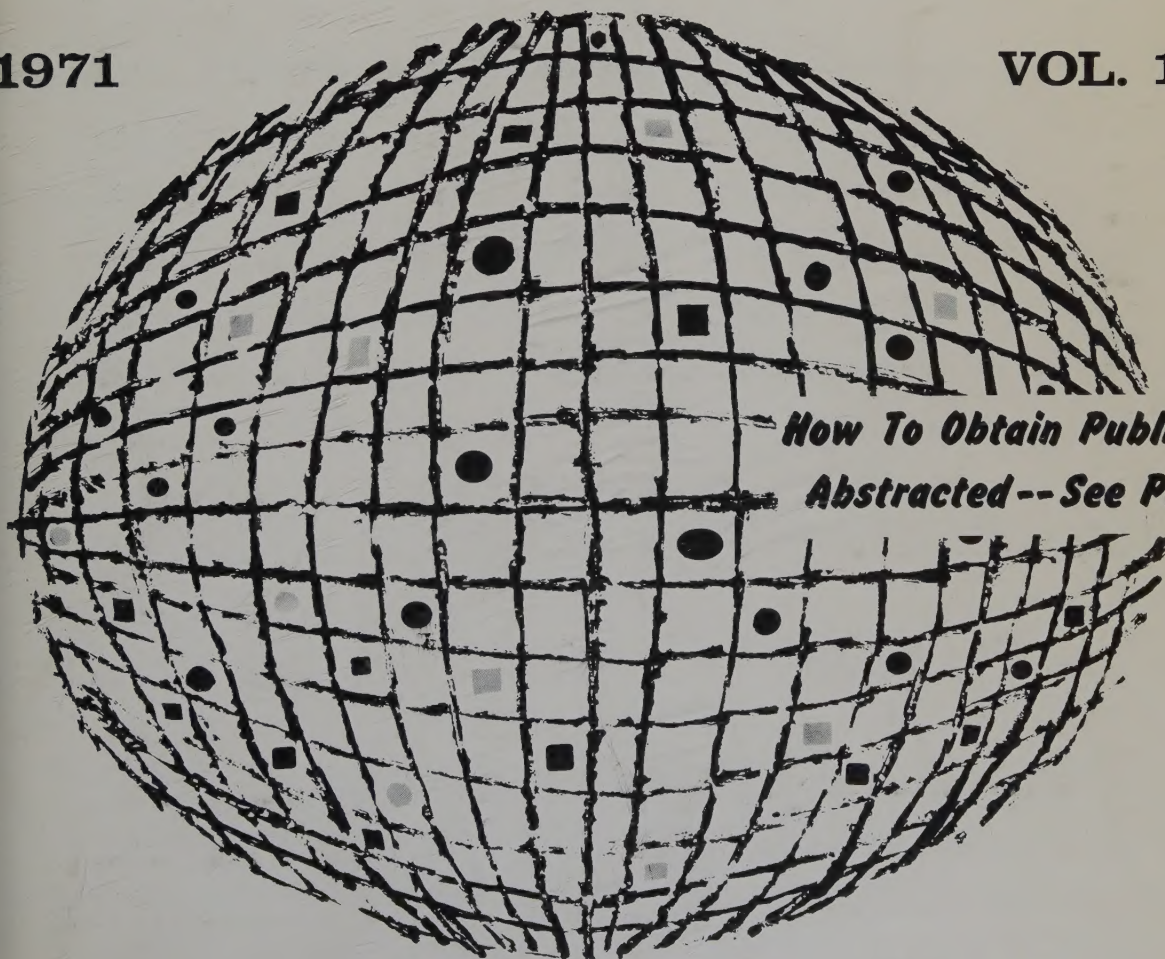
ACCESSION NOS. A71-10001 to A71-45384

INTERNATIONAL AEROSPACE ABSTRACTS

PART 1, PERIODICALS SCANNED, SUBJECT INDEX, A - L

1971

VOL. 11



*How To Obtain Publications
Abstracted -- See Page IV*

PUBLISHED BY THE TECHNICAL INFORMATION SERVICE
AMERICAN INSTITUTE OF AERONAUTICS AND ASTRONAUTICS

INTERNATIONAL AEROSPACE ABSTRACTS

ANNUAL CUMULATED INDEX

PART 1

PERIODICALS SCANNED, SUBJECT INDEX, A – L

VOLUME 11

JANUARY – DECEMBER

1971

ACCESSION NUMBERS A71-10001 to A71-45384

INTERNATIONAL AEROSPACE ABSTRACTS is prepared and published semimonthly (except June and December, which have three issues) by the Technical Information Service, American Institute of Aeronautics and Astronautics, Inc., for the Institute and the National Aeronautics and Space Administration under Contract No. NASW-1949. Editorial and Subscription Offices: 750 Third Avenue, New York, N. Y. 10017. Copyright © 1971 by the American Institute of Aeronautics and Astronautics, Inc. (The indexes, however, may be reproduced for any bibliographic purpose.)

Telephone: 212 TN-7-8300

TWX: 212 867-7265

SUBSCRIPTION INFORMATION. Semimonthly issues: United States and Possessions, 1 year, \$110 postpaid; Foreign Countries, 1 year, \$125 postpaid. Cumulated Index Volumes: United States and Possessions, 1 year, \$75 postpaid; Foreign Countries, 1 year, \$90 postpaid. Second-class postage paid at Phillipsburg, N. J.

CONTENTS

PART 1

INTRODUCTION	iii
HOW TO OBTAIN PUBLICATIONS ABSTRACTED	iv
CROSS REFERENCES	iv
PERIODICALS SCANNED	v - xxvi
SUBJECT INDEX, A - L	A1 - A1047A

PART 2

INTRODUCTION	iv
HOW TO OBTAIN PUBLICATIONS ABSTRACTED	v
CROSS REFERENCES	v
SUBJECT INDEX, M - Z	A1048 - A2106

PART 3

INTRODUCTION	iii
HOW TO OBTAIN PUBLICATIONS ABSTRACTED	iv
PERSONAL AUTHOR INDEX	B1 - B887
CONTRACT NUMBER INDEX	C1 - C33
MEETING PAPER & REPORT NUMBER INDEX	D1 - D13
ACCESSION NUMBER INDEX	E1 - E79

STAFF, AIAA

Administrator—Technical Information Programs, Robert R. Dexter

STAFF, TECHNICAL INFORMATION SERVICE

Director, John J. Glennon

Associate Director—Administrative, Thomas J. Meskel

Associate Director—Technical, Irene W. Bogolubsky

Abstracts Editor, Nanu Davis

Index Editor, Angelica Mihalakos

Chief Librarian, Patricia M. Marshall

INTRODUCTION

INTERNATIONAL AEROSPACE ABSTRACTS (IAA) is an abstracting and indexing service covering the world's published literature in the field of aeronautics and space science and technology. IAA is issued semimonthly, on the 1st and 15th of each month.

Coverage of Published Literature

The following types of publications are covered in IAA:

- Periodicals (including government-sponsored journals) and books.
- Meeting papers and conference proceedings issued by professional societies and academic organizations.
- Translations of journals and journal articles.

Coverage of Reports ("Unpublished" Literature)

Abstracts and indexes of report literature are issued in SCIENTIFIC AND TECHNICAL AEROSPACE REPORTS (STAR), which is published by the Scientific and Technical Information Office, National Aeronautics and Space Administration.

By special arrangement between NASA and the American Institute of Aeronautics and Astronautics, IAA is issued in coordination with the twice-monthly schedule of STAR, which appears on the 8th and 23rd of each month.

IAA and STAR both utilize identical subject categories and indexes, which are described below.

Thus the two services provide comprehensive access to the national and international unclassified report and published literature of current significance to aerospace science and technology.

Arrangement of the Semimonthly Issues

IAA is arranged in two major sections:

- (1) Abstracts Section. This section contains complete bibliographic citations with informative abstracts, arranged by appropriate subject categories to facilitate scanning. The subject categories are numbered from 01 to 34, and the scope of each category is outlined in the Table of Contents and again at the beginning of each category in the Abstracts Section. Each abstract is prefixed by the IAA accession number.
- (2) Index Section. Five indexes are contained in this section: Subject, Personal Author, Contract Number, Meeting Paper and Report Number, and Accession Number. Each index is prefaced by explanatory notes to guide the user to the desired abstract.

Cumulated Indexes

The semi-annual cumulated index is issued promptly at the end of the first six months and the annual cumulated index is issued promptly at the end of the twelve-month period.

Each cumulated index contains the following sections: A—Subject Index, B—Personal Author Index, C—Contract Number Index, D—Meeting Paper and Report Number Index, and E—Accession Number Index.

Indexing Vocabulary

The Preliminary Edition of the NASA THESAURUS (December 1967) (NASA SP-7030) is the authority for the indexing vocabulary that appears in the subject indexes to STAR and IAA. The NASA Thesaurus should be consulted for a total picture of the current indexing vocabulary and associated cross-reference structure. Copies of the NASA Thesaurus may be obtained from the National Technical Information Service or the U.S. Government Printing Office at a price of \$8.50 for the three-volume set.

Information regarding SCIENTIFIC AND TECHNICAL AEROSPACE REPORTS and the availability of INTERNATIONAL AEROSPACE ABSTRACTS to organizations having contractual arrangements with NASA may be obtained from the following address:

National Aeronautics and Space Administration
Scientific and Technical Information Office
Attention: Code KSI
Washington, D. C. 20546

how to obtain publications abstracted

Address all inquiries and requests to:

Technical Information Service
American Institute of Aeronautics
and Astronautics, Inc.
750 Third Avenue, New York, N. Y. 10017

Telephone: 212 TN-7-8300
TWX: 212 867-7265

All documents abstracted are available from the AIAA Technical Information Service as follows:

- Paper copies of accessions announced in IAA and of other published articles in the TIS library are available at \$5.00 per document up to a maximum of 20 pages. The charge for each additional page is \$0.25.
- Paper copies of accessions announced in Scientific and Technical Aerospace Reports (STAR) and of similar unpublished reports in the TIS library are available at the rate of \$0.25 per page, minimum order \$5.00.
- Microfiche of documents announced in IAA are available at the rate of \$1.00 per microfiche on demand. Documents available in this manner are identified by the symbol # following the accession number in the Abstracts Section and in the Meeting Paper and Report Number and the Accession Number Indexes.
- Minimum air-mail postage to foreign countries is \$1.00.
- A number of publications, because of their special characteristics, are available only for reference in the library.

**PLEASE REFER TO THE ACCESSION NUMBER WHEN
REQUESTING PUBLICATIONS**

CROSS REFERENCES

The subject index includes two types of cross references to aid the user of the index in locating the material being sought:

1. "USE" references (U) direct the user to alternate headings under which material on the subject will be found, for example

COLUMBIUM
U NIOBIUM

2. "NARROWER TERM" references (NT) refer the user to more specific headings in the same subject area, for example

LUMINESCENCE
NT ELECTROLUMINESCENCE

The periodicals listed in this section were scanned during the preparation of *International Aerospace Abstracts* for 1971. The periodicals were received regularly in all but a few instances. In the case of titles preceded by an asterisk, only the articles abstracted in *International Aerospace Abstracts* are available. All abstracted articles can be obtained from the AIAA Technical Information Service.

BM — Bimonthly
BW — Biweekly
Irreg. — Irregular
M — Monthly

Q — Quarterly
SA — Semiannual
SM — Semimonthly
W — Weekly

Abastumanskaia Astrofizicheskaia Observatoriia, Biulleten'. Akademiia Nauk Gruzinskoi SSR, Tbilisi. Irreg.

Académie des Sciences (Paris), Comptes Rendus, Série A — Sciences Mathématiques, Série B — Sciences Physiques. Académie des Sciences; Gauthier-Villars, Paris. W

Académie des Sciences (Paris), Comptes Rendus, Série C — Sciences Chimiques. Académie des Sciences; Gauthier-Villars, Paris. W

Académie des Sciences (Paris), Comptes Rendus, Série D — Sciences Naturelles. Académie des Sciences; Gauthier-Villars, Paris. W

Académie Polonaise des Sciences, Bulletin, Série des Sciences Mathématiques, Astronomiques et Physiques. Académie Polonaise des Sciences; Państwowe Wydawnictwo Naukowe, Warsaw. M

Académie Polonaise des Sciences, Bulletin, Série des Sciences Techniques. Académie Polonaise des Sciences; Państwowe Wydawnictwo Naukowe, Warsaw. M

Académie Royale de Belgique, Classe des Sciences, Bulletin. Académie Royale de Belgique; Office International de Librairie, Brussels. M

Académie Serbe des Sciences et des Arts, Bulletin, Classe des Sciences Techniques. Académie Serbe des Sciences et des Arts, Belgrade.

Academy of Sciences, USSR, Bulletin, Physical Series (Akademiia Nauk SSSR, Izvestiia, Serii Fizicheskaia). Columbia Technical Translations, White Plains, N. Y. M

Academy of Sciences, USSR, Izvestiia, Atmospheric and Oceanic Physics (Akademiia Nauk SSSR, Izvestiia, Fizika Atmosfery i Okeana). American Geophysical Union, Washington, D.C. M

Accademia di Scienze e Lettere, Istituto Lombardo, Rendiconti, Serie della Classe di Scienze Matematiche e Naturali, Sezione A — Scienze Matematiche, Fisiche, Chimiche e Geologiche. Istituto Lombardo di Scienze e Lettere, Milan. Irreg.

Accademia Nazionale dei Lincei, Atti, Rendiconti — Classe di Scienze Fisiche, Matematiche e Naturali. Accademia Nazionale dei Lincei, Rome. BM

**Accounts of Chemical Research. American Chemical Society, Washington, D.C. M*

ACM, Communications. Association for Computing Machinery, Baltimore, Md. M

Acoustical Society of America, Journal. Acoustical Society of America; American Institute of Physics, Inc., New York. M

Acta Astronomica. Polska Akademia Nauk; Państwowe Wydawnictwo Naukowe, Warsaw. Q

Acta Biologica et Medica Germanica. Akademie-Verlag GmbH, Berlin. M

Acta Cardiologica. Editions Acta Medica Belgica, Brussels. BM

Acta Científica. CITEFA, Buenos Aires. Q

Acta Electronica. Laboratoires d'Electronique et de Physique Appliquée, Limeil-Brévannes (Val de Marne), France. Q

**Acta Geodaetica, Geophysica et Montanistica. Academiae Scientiarum Hungaricae, Budapest. SA*

Acta Geophysica Polonica. Polska Akademia Nauk; Państwowe Wydawnictwo Naukowe, Warsaw. Q

Acta Mechanica. Springer Verlag, Vienna. 8 issues per year

Acta Metallurgica. Pergamon Press, Inc., Elmsford, N.Y. M

**Acta Oto-Laryngologica. Almqvist & Wiksell Periodical Co., Stockholm. M*

Acta Physica. Aladémiiai Kiadó, Budapest. BM

Acta Physica Austriaca. Österreichische Akademie der Wissenschaften; Springer Verlag, Vienna. Q

Acta Physica Polonica, Seria A. Polska Akademia Nauk, Instytut Fizyki and Polskie Towarzystwo Fizyczne, Warsaw.

**Acta Physiologica Scandinavica. Scandinavian Physiological Society, Stockholm. 3 vols. per year*

Acta Polytechnica Scandinavica, Chemistry Including Metallurgy Series. Scandinavian Council for Applied Research, Stockholm. Irreg.

Acta Polytechnica Scandinavica, Mathematics and Computing Machinery Series. Scandinavian Council for Applied Research, Stockholm. Irreg.

Acta Polytechnica Scandinavica, Mechanical Engineering Series. Scandinavian Council for Applied Research, Stockholm. Irreg.

INTERNATIONAL AEROSPACE ABSTRACTS

- * *Acta Psychologica*. North-Holland Publishing Co., Amsterdam. M
- Acta Technica*. Akadémiai Kiadó, Budapest. 4 vols. per year
- Acta Technica ČSAV*. Československá Akademie Věd, Prague. BM
- Acustica*. S. Hirzel Verlag, KG, Stuttgart, West Germany. Irreg.
- Administrative Science Quarterly*. Cornell University, Graduate School of Business and Public Administration, Ithaca, N.Y. Q
- Advances in Physics*. Taylor & Francis, Ltd., London. BM
- AEG-Telefunken, Technische Mitteilungen*. AEG-Telefunken, Berlin, West Germany. BM
- Aero Medical Society of India, Journal*. Institute of Aviation Medicine, Bangalore.
- Aero-Revue*. Aero-Club der Schweiz and OSTIV; National-Zeitung AG, Basel. M
- Aerodinamika Razrezhennykh Gazov*. Izdatel'stvo Leningradskogo Universiteta, Leningrad. Irreg.
- Aeronautical Journal*. Royal Aeronautical Society, London. M
- Aeronautical Quarterly*. Royal Aeronautical Society, London. Q
- Aeronautical Society of India, Journal*. Aeronautical Society of India, New Delhi. Q
- L'Aéronautique et l'Astronautique*. Association Française des Ingénieurs et Techniciens de l'Aéronautique et de l'Espace and Société Française de l'Astronautique; Editions Air & Cosmos, Paris. M
- Aerospace Management*. General Electric Co., Aerospace Group, Philadelphia, Pa. Q
- Aerospace Medicine*. Aerospace Medical Association, Washington, D.C. M
- L'Aerotecnica — Missili e Spazio*. Associazione Italiana di Aeronautica e Astronautica; Tamburini Editore S.p.A., Milan. BM
- AIAA Journal*. American Institute of Aeronautics and Astronautics, Inc., New York. M
- AIAA Student Journal*. American Institute of Aeronautics and Astronautics, Inc., New York. Q
- AICHE Journal*. American Institute of Chemical Engineers, New York. BM
- Air et Cosmos*. Paris. W
- Air University Review*. Aerospace Studies Institute, Maxwell Air Force Base, Ala. BM
- Aircraft Engineering*. Bunhill Publications, Ltd., London. M
- Airport Forum*. Bauverlag GmbH, Wiesbaden, West Germany. Q
- Akademiia Nauk Armianskoi SSR, Biurakanskaia Observatoriia, Soobshcheniia*. Akademiia Nauk Armianskoi SSR, Yerevan. Irreg.
- Akademiia Nauk Armianskoi SSR, Doklady*. Akademiia Nauk Armianskoi SSR, Yerevan. 10 issues per year
- Akademiia Nauk Armianskoi SSR, Izvestiia, Fizika*. Akademiia Nauk Armianskoi SSR, Yerevan. BM
- Akademiia Nauk Armianskoi SSR, Izvestiia, Mekhanika*. Akademiia Nauk Armianskoi SSR, Yerevan. BM
- Akademiia Nauk Armianskoi SSR, Izvestiia, Seriiia* *Tekhnicheskikh Nauk*. Akademiia Nauk Armianskoi SSR, Yerevan. BM
- Akademiia Nauk Azerbaidzhanskoi SSR, Doklady*. Akademiia Nauk Azerbaidzhanskoi SSR; Izdatel'stvo Elm, Baku. M
- Akademiia Nauk Azerbaidzhanskoi SSR, Izvestiia, Seriiia Fiziko-Tekhnicheskikh i Matematicheskikh Nauk*. Akademiia Nauk Azerbaidzhanskoi SSR; Izdatel'stvo Elm, Baku. BM
- Akademiia Nauk BSSR, Doklady*. Akademiia Nauk Belorusskoi SSR, Minsk. M
- Akademiia Nauk Gruzinskoi SSR, Soobshcheniia*. Akademiia Nauk Gruzinskoi SSR, Tiflis. M
- Akademiia Nauk Kazakhskoi SSR, Izvestiia, Seriiia Fiziko-Matematicheskaiia*. Akademiia Nauk Kazakhskoi SSR, Alma Ata. BM
- Akademiia Nauk Kazakhskoi SSR, Vestnik*. Akademiia Nauk Kazakhskoi SSR; Izdatel'stvo Nauka, Alma Ata. M
- Akademiia Nauk Latviiskoi SSR, Izvestiia, Seriiia Fizicheskikh i Tekhnicheskikh Nauk*. Akademiia Nauk Latviiskoi SSR, Riga. BM
- Akademiia Nauk SSSR, Doklady*. Akademiia Nauk SSSR; Izdatel'stvo Nauka, Moscow. 36 issues per year
- Akademiia Nauk SSSR, Izvestiia, Energetika i Transport*. Akademiia Nauk SSSR; Izdatel'stvo Nauka, Moscow. BM
- Akademiia Nauk SSSR, Izvestiia, Fizika Atmosfery i Okeana*. Akademiia Nauk SSSR; Izdatel'stvo Nauka, Moscow. M
- Akademiia Nauk SSSR, Izvestiia, Mekhanika Tverdogo Tela*. Akademiia Nauk SSSR; Izdatel'stvo Nauka, Moscow. BM
- Akademiia Nauk SSSR, Izvestiia, Mekhanika Zhidkosti i Gaza*. Akademiia Nauk SSSR; Izdatel'stvo Nauka, Moscow. BM
- Akademiia Nauk SSSR, Izvestiia, Metally*. Akademiia Nauk SSSR; Izdatel'stvo Nauka, Moscow. BM
- Akademiia Nauk SSSR, Izvestiia, Neorganicheskii Materialy*. Akademiia Nauk SSSR, Moscow. M
- Akademiia Nauk SSSR, Izvestiia, Seriiia Biologicheskaiia*. Akademiia Nauk SSSR; Izdatel'stvo Nauka, Moscow. BM
- Akademiia Nauk SSSR, Izvestiia, Seriiia Fizicheskaiia*. Akademiia Nauk SSSR; Izdatel'stvo Nauka, Moscow. M
- Akademiia Nauk SSSR, Izvestiia, Seriiia Matematicheskaiia*. Akademiia Nauk SSSR; Izdatel'stvo Nauka, Moscow. BM
- Akademiia Nauk SSSR, Izvestiia, Tekhnicheskaiia Kibernetika*. Akademiia Nauk SSSR; Izdatel'stvo Nauka, Moscow. BM
- Akademiia Nauk SSSR, Sibirskoe Otdelenie, Izvestiia, Seriiia Tekhnicheskikh Nauk*. Akademiia Nauk SSSR, Sibirskoe Otdelenie; Izdatel'stvo Nauka, Novosibirsk. 3 issues per year
- Akademiia Nauk SSSR, Vestnik*. Akademiia Nauk SSSR; Izdatel'stvo Nauka, Moscow. M
- Akademiia Nauk Tadzhikskoi SSR, Doklady*. Akademiia Nauk Tadzhikskoi SSR; Izdatel'stvo Donish, Dushanbe. M

- Akademiia Nauk Turkmenskoi SSR, Izvestiia, Seriiia Fiziko-Tekhnicheskikh, Khimicheskikh i Geologicheskikh Nauk.* Akademiia Nauk Turkmenskoi SSR; Izdatel'stvo Ylym, Ashkhabad. BM
- Akademiia Nauk Ukrains'koi RSR, Dopovidi, Seriiia A — Fiziko-Tekhnichni i Matematichni Nauki.* Akademiia Nauk Ukrains'koi RSR; Izdatel'stvo Naukova Dumka, Kiev. M
- Akademiia Nauk Ukrains'koi RSR, Dopovidi, Seriiia B — Geologiiia, Geofizika, Khimiiia i Biologiiia.* Akademiia Nauk Ukrains'koi RSR; Izdatel'stvo Naukova Dumka, Kiev. M
- Akademiia Nauk Ukrains'koi RSR, Visnik.* Akademiia Nauk Ukrains'koi RSR; Izdatel'stvo Naukova Dumka, Kiev.
- Akademiia Nauk Uzbekskoi SSR, Doklady.* Akademiia Nauk Uzbekskoi SSR, Tashkent. M
- Akademiia Nauk Uzbekskoi SSR, Izvestiia, Seriiia Fiziko-Matematicheskikh Nauk.* Akademiia Nauk Uzbekskoi SSR, Tashkent. BM
- Akademiia Nauk Uzbekskoi SSR, Izvestiia, Seriiia Tekhnicheskikh Nauk.* Akademiia Nauk Uzbekskoi SSR, Tashkent. BM
- Akademiia Navuk BSSR, Vestsi, Seryia Fizika-Tekhnichnykh Navuk.* Akademiia Navuk Belaruskai SSR, Minsk. Q
- Akusticheskii Zhurnal.* Akademiia Nauk SSSR; Izdatel'stvo Nauka, Moscow. Q
- Akustika i Ul'trazvukovaia Tekhnika.* Ministerstvo Vysshego i Srednego Spetsial'nogo Obrazovaniia USSR; Izdatel'stvo Tekhnika, Kiev. Irreg.
- Alata Internazionale.* Etas Kompass, Milan. M
- Alta Frequenza.* Associazione Elettrotecnica ed Elettronica Italiana, Milan. M
- Alta Frequenza (English Edition).* Associazione Elettrotecnica ed Elettronica Italiana, Milan. M
- Alta Frequenza, Supplemento.* Associazione Elettrotecnica ed Elettronica Italiana. Milan.
- Aluminium.* Aluminium-Zentrale, e.V.; Aluminium-Verlag GmbH, Düsseldorf. M
- American Ceramic Society Bulletin.* American Ceramic Society, Inc., Columbus, Ohio. M
- American Ceramic Society, Journal.* American Ceramic Society, Inc., Columbus, Ohio. M
- American Chemical Society, Journal.* American Chemical Society, Washington, D.C. BW
- American Heart Journal.* C. V. Mosby Co., St. Louis, Mo. M
- American Helicopter Society, Journal.* American Helicopter Society, Inc., New York. Q
- American Industrial Hygiene Association Journal.* American Industrial Hygiene Association, Southfield, Mich. BM
- American Journal of Cardiology.* American College of Cardiology; Reuben H. Donnelley Corp., New York. M
- *American Journal of Clinical Nutrition.* American Society of Clinical Nutrition, Inc., Bethesda, Md. M
- *American Journal of Medical Technology.* American Society of Medical Technologists, Houston, Tex. M
- *American Journal of Ophthalmology.* Ophthalmic Publishing Co., Chicago. M
- American Journal of Physics.* American Association of Physics Teachers; American Institute of Physics, Inc., New York. M
- American Journal of Physiology.* American Physiological Society, Bethesda, Md. M
- American Journal of Psychiatry.* American Psychiatric Association, Washington, D.C. M
- *American Journal of Psychology.* University of Illinois Press, Urbana, Ill. Q
- *American Journal of Science.* Yale University, Kline Geology Laboratory, New Haven, Conn. M
- *American Journal of the Medical Sciences.* Ed. Russell S. Weiser, Lea & Febiger, Philadelphia, Pa. M
- American Mathematical Society, Memoirs.* American Mathematical Society, Providence, R. I. Irreg.
- *American Mathematical Society, Proceedings.* American Mathematical Society, Providence, R. I. M
- American Meteorological Society, Bulletin.* American Meteorological Society, Boston. M
- *American Mineralogist.* Mineralogical Society of America, Washington, D.C. BM
- American Society for Information Science, Journal.* American Society for Information Science, Washington, D.C. BM
- American Society of Civil Engineers, Engineering Mechanics Division, Journal.* American Society of Civil Engineers, New York. BM
- American Society of Civil Engineers, Structural Division, Journal.* American Society of Civil Engineers, New York. M
- *Analytical Biochemistry.* Academic Press, Inc., New York. M
- *Analytical Chemistry.* American Chemical Society, Washington, D.C. M
- *Analytical Letters.* Marcel Dekker, Inc., New York. M
- Angewandte Informatik (formerly Elektronische Datenverarbeitung).* Friedr. Vieweg & Sohn GmbH, Braunschweig. M
- *Angewandte Makromolekulare Chemie.* Huethig & Wepf Verlag, Basel. 5 vols. per year
- Annalen der Physik.* Johann Ambrosius Barth Verlag, Leipzig, East Germany. Irreg.
- Annales de Géophysique.* Centre National de la Recherche Scientifique, Paris. Q
- Annales de Physique.* Centre National de la Recherche Scientifique; Masson & Cie., Paris. BM
- Annales des Télécommunications.* Centre National d'Etudes des Télécommunications, Issy-les-Moulineaux (Seine), France. BM
- Annali di Geofisica.* Istituto Nazionale de Geofisica, Rome. Q
- Annals of Physics.* Academic Press, Inc., New York. M
- Antenny.* Nauchno-Tekhnicheskoe Obshchestvo Radiotekhniki i Elektrosviazi imeni A. S. Popova; Izdatel'stvo Sviaz', Moscow. Irreg.
- Aplikace Matematiky.* Československá Akademie Věd, Matematický Ústav, Prague. BM
- APL Technical Digest.* Applied Physics Laboratory, Johns Hopkins University, Silver Spring, Md. BM
- Applicable Analysis.* Gordon & Breach Science Publishers, Ltd., London. Q

INTERNATIONAL AEROSPACE ABSTRACTS

- Applied Electrical Phenomena (Elektronnaia Otrabotka Materialov).* Consultants Bureau, New York. BM
- Applied Mechanics Reviews.* American Society of Mechanical Engineers, New York. M
- Applied Microbiology.* American Society for Microbiology, Bethesda, Md. M
- Applied Optics.* Optical Society of America; American Institute of Physics, Inc., New York. M
- Applied Physics Letters.* American Institute of Physics, Inc., New York. SM
- Applied Scientific Research.* Martinus Nijhoff, The Hague. Irreg.
- Applied Spectroscopy.* Society for Applied Spectroscopy, Boston College, Mass.; American Institute of Physics, Inc., New York. BM
- Archiv der elektrischen Übertragung* (see *Archiv für Elektronik und Übertragungstechnik*).
- Archiv für Elektronik und Übertragungstechnik* (formerly *Archiv der elektrischen Übertragung*). S. Hirzel Verlag, KG, Stuttgart, West Germany. Q
- Archiv für Meteorologie, Geophysik und Bioklimatologie, Serie A — Meteorologie und Geophysik.* Springer Verlag, Vienna. Irreg.
- **Archiv für Mikrobiologie.* Springer Verlag, Berlin, West Germany. 4 vols. per year
- Archiv für technische Messen und industrielle Messtechnik.* Verlag R. Oldenbourg, Munich. M
- Archive for Rational Mechanics and Analysis.* Springer Verlag, Berlin. Irreg.
- Archives of Environmental Health.* American Medical Association, Chicago. M
- Archiwum Automatyki i Telemechaniki.* Polska Akademia Nauk; Państwowe Wydawnictwo Naukowe, Warsaw. Q
- Archiwum Budowy Maszyn.* Polska Akademia Nauk, Komitet Budowy Maszyn; Państwowe Wydawnictwo Naukowe, Warsaw. Q
- Archiwum Elektrotechniki.* Polska Akademia Nauk; Państwowe Wydawnictwo Naukowe, Warsaw. Q
- Archiwum Mechaniki Stosowanej.* Polska Akademia Nauk, Instytut Podstawowych Problemów Techniki; Państwowe Wydawnictwo Naukowe, Warsaw. BM
- Archiwum Procesów Spalania.* Polska Akademia Nauk, Sekcja Spalania; Państwowe Wydawnictwo Naukowe, Warsaw. Q
- Arizona, University, Lunar and Planetary Laboratory, Communications.* University of Arizona, Tucson. Irreg.
- Artificial Satellites.* Polish Academy of Sciences, Warsaw. Q
- ASCE, Transportation Engineering Journal.* American Society of Civil Engineers, New York. Q
- ASLE Transactions.* American Society of Lubrication Engineers; Academic Press, Inc., New York. M
- Aslib Proceedings.* Aslib, London. M
- ASME, Transactions, Series A — Journal of Engineering for Power.* American Society of Mechanical Engineers, New York. Q
- ASME, Transactions, Series B — Journal of Engineering for Industry.* American Society of Mechanical Engineers, New York. Q
- ASME, Transactions, Series C — Journal of Heat Transfer.* American Society of Mechanical Engineers, New York. Q
- ASME, Transactions, Series D — Journal of Basic Engineering.* American Society of Mechanical Engineers, New York. Q
- ASME, Transactions, Series E — Journal of Applied Mechanics.* American Society of Mechanical Engineers, New York. Q
- ASME, Transactions, Series F — Journal of Lubrication Technology.* American Society of Mechanical Engineers, New York. Q
- ASME, Transactions, Series G — Journal of Dynamic Systems, Measurement, and Control.* American Society of Mechanical Engineers, New York. Q
- Association for Computing Machinery, Journal.* Association for Computing Machinery, Inc., New York. Q
- Association Technique Maritime et Aéronautique, Bulletin.* Association Technique Maritime et Aéronautique, Paris. Annual
- Astrofizika.* Akademiia Nauk Armianskoi SSR, Yerevan. Q
- Astronautica Acta.* International Academy of Astronautics; Pergamon Press, Ltd., Oxford. BM
- Astronautical Society of the Republic of China, Transactions.* Astronautical Society of the Republic of China, Taiwan. Annual
- Astronautics and Aeronautics.* American Institute of Aeronautics and Astronautics, Inc., New York. M
- Astronautik.* Hermann Oberth-Gesellschaft, e.V., Hannover, West Germany. Q
- Astronomical Institutes of Czechoslovakia, Bulletin.* Československá Akademie Věd, Prague. BM
- Astronomical Journal.* American Astronomical Society; American Institute of Physics, Inc., New York. 10 issues per year
- Astronomical Society of Australia, Proceedings.* Astronomical Society of Australia; Sydney University Press, Sydney. SA
- Astronomical Society of Japan, Publications.* Astronomical Society of Japan, c/o Tokyo Astronomical Observatory, Mitaka, Tokyo. Q
- Astronomical Society of the Pacific, Publications.* Astronomical Society of the Pacific, San Francisco. BM
- Astronomicheskii Vestnik.* Vsesoiuznoe Astronomo-Geodezicheskoe Obshchestvo; Izdatel'stvo Nauka, Moscow. Q
- Astronomicheskii Zhurnal.* Akademiia Nauk SSSR; Izdatel'stvo Nauka, Moscow. BM
- L'Astronomie.* Société Astronomique de France, Paris. BM
- Astronomie und Raumfahrt.* Deutsche Astronautische Gesellschaft, Berlin, East Germany. BM
- Astronomische Gesellschaft, Mitteilungen.* Astronomische Gesellschaft, Hamburg; G. Braun GmbH, Karlsruhe, West Germany. Irreg.
- Astronomische Nachrichten.* Akademie-Verlag GmbH, Berlin. Irreg.
- Astronomy and Astrophysics.* Springer Verlag, Berlin. M
- Astronomy and Space.* David & Charles, Newton Abbot, Devon, England. M

- Astrophysical Journal*. American Astronomical Society; University of Chicago Press, Chicago. M
- Astrophysical Journal Supplement Series*. American Astronomical Society; University of Chicago Press, Chicago. M
- Astrophysical Letters*. Gordon & Breach Science Publishers, Ltd., London. M
- Astrophysics and Space Science*. D. Reidel Publishing Co., Dordrecht, Netherlands. M
- Atherosclerosis*. Elsevier Publishing Co., Amsterdam. BM
- Atmospheric Environment*. Pergamon Press, Ltd., Oxford. BM
- **Atomic Data*. Academic Press, Inc., New York. Q
- Australian Journal of Physics*. Commonwealth Scientific and Industrial Research Organization, Melbourne. BM
- Australian Journal of Physics, Astrophysical Supplement*. Commonwealth Scientific and Industrial Research Organization, Melbourne. BM
- Australian Meteorological Magazine*. Bureau of Meteorology, Melbourne. Q
- Automatic Monitoring and Measuring (Avtometriia)*. Consultants Bureau, New York. BM
- Automatic Welding (Avtomaticheskaia Svarka)*. The Welding Institute, Cambridge. M
- Automatica*. Pergamon Press, Ltd., Oxford. BM
- Automation and Remote Control (Avtomatika i Telemekhanika)*. Consultants Bureau, New York. M
- Automatizace*. Ministerstvo Průmyslu; Nakladatelství Technické Literatury, Prague. M
- Aviation Review*. Smiths Industries, Ltd., Aviation Div., Wembley, Middx., England. Irreg.
- Aviation Week and Space Technology*. McGraw-Hill, Inc., New York. W
- Aviatsiia i Kosmonavtika*. Voenizdat, Moscow. M
- Aviatsionnaia Tekhnika*. Ministerstvo Vysshego i Srednego Spetsial'nogo Obrazovaniia SSSR; Izdanie Kazanskogo Aviatsionnogo Instituta, Kazan. Q
- Aviazione di Linea — Aeronautica e Spazio*. Publitelco International, Rome. M
- Avtomatika*. Akademiia Nauk Ukrainkoi SSR; Izdatel'stvo Naukova Dumka, Kiev. BM
- Avtomatika i Telemekhanika*. Akademiia Nauk SSSR; Izdatel'stvo Nauka, Moscow. M
- Avtomatika i Vychislitel'naia Tekhnika*. Akademiia Nauk Latvii skoi SSR; Izdatel'stvo Zinatne, Riga. BM
- Avtomatizatsiia Proektirovaniia v Elektronike*. Ministerstvo Vysshego i Srednego Spetsial'nogo Obrazovaniia SSSR; Izdatel'stvo Tekhnika, Kiev. Irreg.
- Babeş-Bolyai, Universitas, Studia, Series Mathematica-Mechanica*. Babeş-Bolyai, Universitas, Cluj, Rumania. SA
- Babeş-Bolyai, Universitas, Studia, Series Physica*. Babeş-Bolyai, Universitas, Cluj, Rumania. SA
- Battelle Research Outlook*. Battelle Memorial Institute, Columbus Laboratories, Columbus, Ohio. Q
- Bayerische Akademie der Wissenschaften, mathematisch-naturwissenschaftliche Klasse, Sitzungsberichte*. Bayerische Akademie der Wissenschaften, Munich. Irreg.
- Beiträge aus der Plasmaphysik*. Akademie-Verlag GmbH, Berlin.
- Beiträge zur Physik der Atmosphäre*. Friedr. Vieweg & Sohn GmbH, Braunschweig. Q
- Beiträge zur Radioastronomie*. Max-Planck-Institut für Radioastronomie; Ferd. Dümmlers Verlag, Bonn. Q
- Bell Laboratories Record*. Bell Telephone Laboratories, Inc., Murray Hill, N. J. M
- Bell System Technical Journal*. American Telephone & Telegraph Co., New York. 10 issues per year
- Bendix Technical Journal*. Bendix Corp., Southfield, Mich. 3 issues per year
- Bildmessung und Luftbildwesen*. Deutsche Gesellschaft für Photogrammetrie; Herbert Wichmann Verlag, Karlsruhe, West Germany. Q
- Biochemical and Biophysical Research Communications*. Academic Press, Inc., New York. SM
- **Biochemical Medicine*. Academic Press, Inc., New York. BM
- **Biochemistry*. American Chemical Society, Washington, D. C. M
- **Biochimica et Biophysica Acta*. Elsevier Publishing Co., Amsterdam. W
- **Biometrics*. North Carolina State University, Institute of Statistics, Raleigh, N. C. Q
- Biophysical Journal*. Biophysical Society; Rockefeller University Press, New York. M
- BioScience*. American Institute of Biological Sciences, Washington, D.C. M
- Biulleten' Eksperimental'noi Biologii i Meditsiny*. Akademiia Meditsinskikh Nauk SSSR; Izdatel'stvo Meditsina, Moscow. M
- B'lgarska Akademiia na Naukite, Fizicheski Institut s ANEB, Izvestiia*. B'lgarska Akademiia na Naukite, Otdelenie za Matematicheski i Fizicheski Nauki, Sofia. Irreg.
- B'lgarska Akademiia na Naukite, Geofizichni Institut, Izvestiia*. B'lgarska Akademiia na Naukite, Sofia. Irreg.
- B'lgarska Akademiia na Naukite, Institut po Khidrologiia i Meteorologiia, Izvestiia*. B'lgarska Akademiia na Naukite, Otdelenie za Matematicheski i Fizicheski Nauki, Sofia. Irreg.
- B'lgarska Akademiia na Naukite, Institut po Tekhnicheska Kibernetika, Izvestiia*. B'lgarska Akademiia na Naukite, Otdelenie za Tekhnicheski Nauki, Sofia. Irreg.
- B'lgarska Akademiia na Naukite, Institut po Tekhnicheska Mekhanika, Izvestiia*. B'lgarska Akademiia na Naukite, Otdelenie za Tekhnicheski Nauki, Sofia. Irreg.
- B'lgarska Akademiia na Naukite, Matematicheski Institut, Izvestiia*. B'lgarska Akademiia na Naukite, Otdelenie za Matematicheski i Fizicheski Nauki, Sofia. Irreg.
- B'lgarska Akademiia na Naukite, Sektsiia po Astronomiia, Izvestiia*. B'lgarska Akademiia na Naukite, Otdelenie za Matematicheski i Fizicheski Nauki, Sofia. Irreg.
- B'lgarska Akademiia na Naukite, Tsentralna Laboratoriia po Geodeziia, Izvestiia*. B'lgarska Akademiia na Naukite, Otdelenie za Matematicheski i Fizicheski Nauki, Sofia. Irreg.

INTERNATIONAL AEROSPACE ABSTRACTS

- Bolgarskaia Akademiia Nauk, Doklady.* B'lgarska Akademiia na Naukite, Sofia. M
- Bollettino di Geofisica Teorica ed Applicata.* Osservatorio Geofisico Sperimentale, Trieste, Italy. Q
- **Botanical Gazette.* University of Chicago Press, Chicago. Q
- Boundary-Layer Meteorology.* D. Reidel Publishing Co., Dordrecht, Netherlands. Q
- Braunschweigische Wissenschaftliche Gesellschaft, Abhandlungen.* Braunschweigische Wissenschaftliche Gesellschaft; Friedr. Vieweg & Sohn GmbH, Braunschweig. Irreg.
- British Astronomical Association, Journal.* British Astronomical Association, Hounslow West, Middx., England. BM
- British Heart Journal.* British Medical Association, London. BM
- British Interplanetary Society, Journal.* British Interplanetary Society, London. M
- Brüel and Kjaer Technical Review.* AS Brüel & Kjaer, Naerum, Denmark. Q
- București, Institutul Politehnic Gheorghe Gheorghiu-Dej, Buletinul.* Institutul Politehnic Gheorghe Gheorghiu-Dej, Bucharest. BM
- **Building Science.* Pergamon Press, Ltd., Oxford. Q
- Bulletin of Mathematical Biophysics.* MIT Press, Cambridge, Mass. Q
- **Bulletins of American Paleontology.* Paleontological Research Institution, Ithaca, N.Y. 2 vols. per year
- Business and Commercial Aviation.* Ziff-Davis Publishing Co., New York. M
- Cambridge Philosophical Society, Proceedings.* Cambridge University Press, London. BM
- Canada, National Research Council, Division of Mechanical Engineering and National Aeronautical Establishment, Quarterly Bulletin.* National Research Council of Canada, Ottawa. Q
- Canadian Aeronautics and Space Journal.* Canadian Aeronautics and Space Institute, Ottawa. M
- Canadian Electronics Engineering.* Maclean-Hunter, Ltd., Toronto. M
- **Canadian Journal of Biochemistry.* National Research Council of Canada, Ottawa. M
- Canadian Journal of Physics.* National Research Council of Canada, Ottawa. SM
- **Canadian Journal of Physiology and Pharmacology.* National Research Council of Canada, Ottawa. M
- **Canadian Journal of Psychology.* Canadian Psychological Association; University of Toronto Press, Toronto. Q
- Canadian Metallurgical Quarterly.* Canadian Institute of Mining and Metallurgy, Metallurgical Society, Ottawa. Q
- Canadian Operational Research Society, Journal.* Canadian Operational Research Society, Ottawa. 3 issues per year
- Cardiology.* S. Karger AG, Basel. BM
- Cardiovascular Research.* British Cardiac Society; British Medical Association, London. Q
- CASI Transactions.* Canadian Aeronautics and Space Institute, Ottawa. SA
- **CATCA Journal.* Canadian Air Traffic Control Association, Inc., Ottawa.
- Celestial Mechanics.* D. Reidel Publishing Co., Dordrecht, Netherlands. Q
- Československý Časopis pro Fysiku, Sekce A.* Československá Akademie Věd, Prague. BM
- Challenge.* Space Division Information Services, Philadelphia, Pa. Q
- Chartered Mechanical Engineer.* Institution of Mechanical Engineers, London. M
- Chem Tech.* American Chemical Society, Washington, D.C. M
- **Chemical Communications.* Chemical Society, London. SM
- Chemical Engineering Progress.* American Institute of Chemical Engineers, New York. M
- Chemical Engineering Progress, Symposium Series.* American Institute of Chemical Engineers, New York. M
- **Chemical Instrumentation.* Marcel Dekker, Inc., New York. Q
- Chemical Physics Letters.* North-Holland Publishing Co., Amsterdam. BW
- **Chemical Reviews.* American Chemical Society, Washington, D.C. BM
- Chubu Institute of Technology, Memoirs.* Chubu Institute of Technology, Nagoya. Irreg.
- Ciel et Terre.* Société Belge d'Astronomie, de Météorologie et de Physique du Globe, Brussels. BM
- Circulation.* American Heart Association, Inc., New York. M
- Circulation Research.* American Heart Association, New York. M
- Cobalt.* Centre d'Information du Cobalt, Brussels. Q
- Columbia Journal of World Business.* Columbia University, Graduate School of Business, New York. BM
- Combustion and Flame.* Combustion Institute; American Elsevier Publishing Co., Inc., New York. BM
- Combustion Science and Technology.* Gordon & Breach Science Publishers, Ltd., London. BM
- Comments on Astrophysics and Space Physics (see Comments on Modern Physics, Part C — Comments on Astrophysics and Space Physics).*
- Comments on Modern Physics, Part C — Comments on Astrophysics and Space Physics.* Gordon & Breach Science Publishers, Inc., New York. BM
- Communications in Behavioral Biology.* Academic Press, Inc., New York. M
- Communications on Pure and Applied Mathematics.* New York University, Courant Institute of Mathematical Sciences; Interscience Publishers, New York. BM
- Composites.* Ilife Science and Technology Publications, Ltd., Guildford, Surrey, England. Q
- Computer Journal.* British Computer Society, London. Q
- **Computers and Biomedical Research.* Academic Press, Inc., New York. Q
- Computers and Structures.* Pergamon Press, Ltd., Oxford. Q
- Computers in Biology and Medicine.* Pergamon Press, Inc., New York. Q

- Computing.* Springer Verlag, Vienna. Q
- Contemporary Physics.* Taylor & Francis, Ltd., London. BM
- **Contributions to Mineralogy and Petrology.* Springer Verlag, Berlin. 3 vols. per year
- Control Engineering.* Reuben H. Donnelley Corp., New York. M
- Coopération Méditerranéenne pour l'Energie Solaire, Bulletin.* Coopération Méditerranéenne pour l'Energie Solaire (COMPLES), Marseilles. SA
- Corrosion.* National Association of Corrosion Engineers, Inc., Houston, Tex. M
- Cosmic Electrodynamics.* D. Reidel Publishing Co., Dordrecht, Netherlands. Q
- Cosmic Research (Kosmicheskie Issledovaniia).* Consultants Bureau, New York. BM
- COSPAR Information Bulletin.* COSPAR Secretariat, Paris. Irreg.
- **Cryobiology.* Society for Cryobiology, Rockville, Md. BM
- Cryogenic Technology.* Cryogenic Society of America; Value Engineering Publications, Inc., Los Angeles. BM
- Cryogenics.* Iliffe Science & Technology Publications, Ltd., London. BM
- Current Science.* Current Science Association, Bangalore. SM
- **Currents in Modern Biology.* North-Holland Publishing Co., Amsterdam. BM
- Czechoslovak Journal of Physics, Section B.* Československá Akademie Věd, Prague. M
- Czechoslovak Mathematical Journal.* Československá Akademie Věd, Prague. Q
- Defence Science Journal.* Indian Ministry of Defence, New Delhi. Q
- Defense Management Journal.* Directorate for Management Improvement Programs, Office of the Assistant Secretary of Defense; Supt. of Documents, Washington, D.C. Q
- Demonstratio Mathematica.* Politechnika Warszawska, Instytut Matematyki, Warsaw.
- DEW-Technische Berichte.* Deutsche Edelstahlwerke Aktiengesellschaft, Krefeld, West Germany. Irreg.
- Deutscher Aerokurier.* Deutscher Aero Club, e.V., Frankfurt/Main. M
- DFVLR-Nachrichten.* Deutsche Forschungs- und Versuchsanstalt für Luft- und Raumfahrt, e.V., Porz-Wahn, West Germany. Irreg.
- Differentsial'nye Uravneniia.* Izdatel'stvo Nauka i Tekhnika, Minsk. M
- Dinamika i Prochnost' Mashin.* Izdatel'stvo Khar'kovskogo Gosudarstvennogo Universiteta, Kharkov. Irreg.
- DISA Information.* DISA Elektronik A/S, Herlev, Denmark. M
- Dornier-Post (English Edition).* Dornier AG, Munich. Q
- Earth and Extraterrestrial Sciences.* Gordon & Breach Science Publishers, Ltd., London. Irreg.
- Earth and Planetary Science Letters.* North-Holland Publishing Co., Amsterdam. M
- L'Echo des Recherches.* Centre National d'Etudes des Télécommunications, Issy-les-Moulineaux, France. Q
- Eesti NSV Teaduste Akadeemia, Toimetised, Füüsika-Matemaatika.* Izdatel'stvo Periodika, Tallin. Q
- Electrical Communication.* International Telephone and Telegraph Corp., New York. Q
- Electrical Communication Laboratory, Review.* Nippon Telegraph & Telephone Public Corp., Tokyo. BM
- Electrical Engineering in Japan (Denki Gakkai Zasshi).* Institute of Electrical Engineers of Japan; Institute of Electrical and Electronics Engineers, Inc., New York. M
- Electrochemical Society, Journal.* Electrochemical Society, Inc., New York. M
- Electroencephalography and Clinical Neurophysiology.* International Federation of Societies for Electroencephalography and Clinical Neurophysiology; Elsevier Publishing Co., Amsterdam. M
- Electron (São Paulo).* Editôra Técnico Gráfica Industrial, Ltda., Sao Paulo, Brazil. BM
- Electron Technology.* Polish Academy of Sciences, Institute of Electron Technology; Państwowe Wydawnictwo Naukowe, Warsaw. Irreg.
- Electronic Design.* Hayden Publishing Co., Inc., New York. BW
- Electronic Engineering.* Morgan-Grampian (Publishers), Ltd., London. M
- Electronics.* McGraw-Hill, Inc., New York. BW
- Electronics and Communications in Japan (Denshi Tsushin Gakkai Ronbunshi).* Institute of Electronics and Communications Engineers of Japan; Institute of Electrical and Electronics Engineers, Inc., New York. M
- Electronics and Power.* Institution of Electrical Engineers, London. M
- Electronics Letters.* Institution of Electrical Engineers, London. BW
- Elektromekhanika.* Ministerstvo Vysshego i Srednego Spetsial'nogo Obrazovaniia SSSR, Novocherkassk. M
- Elektronik.* Franzis-Verlag, Munich. M
- Elektronika.* Wydawnictwa Czasopism Technicznych NOT, Warsaw. M
- Elektronische Datenverarbeitung (see Angewandte Informatik).*
- Elektronische Rechenanlagen.* Verlag R. Oldenbourg, Munich. BM
- Elektrosviaz'.* Ministerstvo Sviazi SSSR and Tekhnicheskoe Obshchestvo Radiotekhniki, Elektroniki i Sviazi; Izdatel'stvo Sviaz', Moscow. M
- Energomashinostroenie.* Ministerstvo Tiazhelogo, Energeticheskogo i Transportnogo Mashinostroeniia SSSR and Nauchno-Tekhnicheskoe Obshchestvo Mashinostroitel'noi Promyshlennosti; Izdatel'stvo Mashinostroenie, Leningrad. M
- Energy Conversion.* Pergamon Press, Ltd., Oxford. Q
- Engineering Bulletin.* Motorola, Inc., Government Electronics Div., Scottsdale, Ariz. Irreg.
- Engineering Cybernetics (Akademiia Nauk SSSR, Izvestiia, Tekhnicheskaiia Kibernetika).* Scripta Publishing Corp., Washington, D.C. BM

INTERNATIONAL AEROSPACE ABSTRACTS

- Engineering Fracture Mechanics.* Pergamon Press, Ltd., Oxford. Q
- Entropie.* Editions Barthélemy & Cie., Paris. BM
- Environmental Engineering.* Society of Environmental Engineers, London; Kenneth Mason, Havant, Hants., England. BM
- Environmental Research.* Academic Press, Inc., New York. BM
- **Enzymologia.* Uitgeverij Dr. W. Junk N.V., The Hague. M
- EOS.* American Geophysical Union, Washington, D.C. M
- **Erdöl und Kohle Erdgas Petrochemie vereinigt mit Brennstoff-Chemie.* German Society for Petroleum Science and Coal Chemistry; Industrieverlag von Hernhaußen, KG, Hamburg, West Germany. M
- Ergonomics.* Ergonomics Research Society, Nederlandse Vereniging voor Ergonomie, International Ergonomics Association; Taylor & Francis, Ltd., London. Q
- ESRO/ELDO Bulletin.* European Space Research Organization and European Space Vehicle Launcher Development Organization, Neuilly-sur-Seine, France. Q
- ESSO Air World.* ESSO International, Inc., New York. BM
- Eurocontrol.* Eurocontrol, Public Relations Div., Brussels. SA
- **European Polymer Journal.* Pergamon Press, Ltd., Oxford. BM
- European Southern Observatory, Bulletin.* Organisation Européenne pour les Recherches Astronomiques dans l'Hémisphère Austral; European Southern Observatory, Hamburg, West Germany.
- Experientia.* Birkhäuser Verlag, Basel. M
- Experimental Brain Research.* Springer Verlag, Berlin. Irreg.
- **Experimental Cell Research.* International Society for Cell Biology; Academic Press, Inc., New York. M
- Experimental Mechanics.* Society for Experimental Stress Analysis, Westport, Conn. M
- Explosifs.* Association des Fabricants Belges d'Explosifs, Liege. Q
- Explosivstoffe.* Erwin Barth Verlag, KG, Mannheim, West Germany. M
- Facilities for Atmospheric Research.* National Center for Atmospheric Research, Boulder, Colo. Q
- **Faraday Society, Transactions.* Aberdeen University Press, Ltd., Aberdeen, Scotland. M
- Finommechanika.* Lapkiadó Vállalat, Budapest. M
- Fizika.* Ministerstvo Vysshogo i Srednego Spetsial'nogo Obrazovaniia SSSR; Izdatel'stvo Tomskogo Universiteta, Tomsk. M
- Fizika Aerodispersnykh Sistem.* Izdatel'stvo Kievskogo Universiteta, Kiev. Irreg.
- Fizika Gorenii i Vzryva.* Akademiia Nauk SSSR, Sibirskoe Otdelenie; Izdatel'stvo Nauka, Novosibirsk. Q
- Fizika i Tekhnika Poluprovodnikov.* Akademiia Nauk SSSR; Izdatel'stvo Nauka, Leningrad. M
- Fizika Metallov i Metallovedenie.* Akademiia Nauk SSSR; Izdatel'stvo Nauka, Sverdlovsk. M
- Fizika Tverdogo Tela.* Akademiia Nauk SSSR; Izdatel'stvo Nauka, Leningrad. M
- Fiziko-Khimicheskaiia Mekhanika Materialov.* Akademiia Nauk Ukrainskoi SSR; Izdatel'stvo Naukova Dumka, Kiev. BM
- Fiziologicheskii Zhurnal SSSR.* Akademiia Nauk SSSR; Izdatel'stvo Nauka, Leningrad. M
- Fiziologichnii Zhurnal.* Akademiia Nauk Ukrainskoi SSR, Institut Fiziologii; Izdatel'stvo Naukova Dumka, Kiev. BM
- Flight International.* Royal Aero Club; IPC Business Press, Ltd., London. W
- Flugrevue/Flugwelt International.* Club der Luftfahrt von Deutschland, e.V., Bonn; Vereinigte Motor-Verlage GmbH, Stuttgart, West Germany. M
- Fluid — Apparechiature Idrauliche e Pneumatiche.* Etas Kompass, Milan. BM
- Fluidics Quarterly.* Ann Arbor, Mich. Q
- FOA Reports.* Försvarets Forskningsanstalt, Stockholm. Irreg.
- **Folia Primatologica.* S. Karger AG, Basel. BM
- Forces Aériennes Françaises.* Comité d'Etudes Aéronautiques Militaires, Paris. M
- Forschung im Ingenieurwesen.* Verein Deutscher Ingenieure; VDI-Verlag GmbH, Düsseldorf. BM
- Franklin Institute, Journal.* Franklin Institute, Philadelphia, Pa.; Pergamon Press, Ltd., Oxford. M
- Frequenz.* Fachverlag Schiele & Schön, Berlin. M
- Fujitsu Scientific and Technical Journal.* Fujitsu, Ltd., Kanagawa, Japan. Q
- Fyzikálny Časopis.* Slovenská Akadémia Vied, Bratislava. Q
- Geliotekhnika.* Akademiia Nauk Uzbekskoi SSR, Tashkent. BM
- Génie Biologique et Médical.* Nancy, France. Q
- Geochimica et Cosmochimica Acta.* Geochemical Society and Meteoritical Society; Pergamon Press, Ltd., Oxford. M
- Geodeziia, Kartografiia i Aerofotos'emka.* Izdatel'stvo L'vovskogo Universiteta, Lvov. Irreg.
- Geodeziia i Aerofotos'emka.* Ministerstvo Vysshogo i Srednego Spetsial'nogo Obrazovaniia SSSR; Izdatel'stvo Moskovskogo Instituta Inzhenerov Geodezii, Aerofotos'emki i Kartografii, Moscow. BM
- Geodeziia i Kartografiia.* Glavnoe Upravlenie Geodezii i Kartografii pri Sovete Ministrov SSSR; Izdatel'stvo Nedra, Moscow. M
- Geodezja i Kartografia.* Polska Akademia Nauk, Komitet Geodezji; Państwowe Wydawnictwo Naukowe, Warsaw. Q
- Geofisica e Meteorologia.* Società Italiana di Geofisica e Meteorologia, Genoa. 3 issues per year
- Geofizicheskii Sbornik.* Akademiia Nauk Ukrainskoi SSR; Izdatel'stvo Naukova Dumka, Kiev. Irreg.
- Geofysikální Sborník.* Československá Akademie Věd, Geofysikální Ústav, Prague.
- **Geological Society of America, Bulletin.* Geological Society of America, Boulder, Colo. M
- Geomagnetism and Aeronomy (Geomagnetizm i Aeronomiia).* American Geophysical Union, Washington, D.C. BM
- Geomagnetizm i Aeronomiia.* Akademiia Nauk SSSR; Izdatel'stvo Nauka, Moscow. BM

- Geomagnitnye Issledovaniia*. Izdatel'stvo Nauka, Moscow. Irreg.
- Geophysical Fluid Dynamics*. Gordon & Breach Science Publishers, Ltd., London. M
- Geophysical Journal*. Royal Astronomical Society; Blackwell Scientific Publications, Ltd., Oxford. M
- Geophysical Magazine*. Japan Meteorological Agency, Tokyo. SA
- **Geophysics*. Society of Exploration Geophysicists, Tulsa, Okla. BM
- Gerlands Beiträge zur Geophysik*. Akademische Verlagsgesellschaft Geest & Portig, KG, Leipzig, East Germany. BM
- Gidromekhanika*. Akademiia Nauk Ukrainskoi SSR; Izdatel'stvo Naukova Dumka, Kiev. Irreg.
- Göttingen, Akademie der Wissenschaften, Nachrichten, Mathematisch-physikalische Klasse*. Vandenhoeck & Ruprecht, Göttingen. Irreg.
- Grumman Horizons*. Grumman Aircraft Engineering Corp., Bethpage, L. I.
- Guadalajara, Universidad, Instituto de Astronomía y Meteorología, Informacion*. Guadalajara, Universidad, Guadalajara, México. M
- Heat Transfer — Soviet Research*. American Society of Mechanical Engineers, New York. BM
- **Helvetica Chimica Acta*. Swiss Chemical Society; Verlag Helvetica Chimica Acta, Basel. 9 issues per year
- High Temperature (Teplofizika Vysokikh Temperatur)*. Consultants Bureau, New York. BM
- **High Temperature Science*. Academic Press, Inc., New York. Q
- High Temperatures — High Pressures*. Pion, Ltd., London. BM
- **Histochemical Journal*. Chapman & Hall, Ltd., London. Q
- Hochfrequenztechnik und Elektroakustik*. Akademische Verlagsgesellschaft Geest & Portig, KG, Leipzig, East Germany. BM
- Hokkaido University, Research Institute of Applied Electricity, Bulletin*. Hokkaido University, Sapporo City, Japan.
- Human Factors*. Human Factors Society, Inc., Santa Monica, Calif.; The Johns Hopkins Press, Baltimore, Md. M
- I & EC — Industrial and Engineering Chemistry, Fundamentals*. American Chemical Society, Washington, D. C. Q
- I & EC — Industrial and Engineering Chemistry, Process Design and Development*. American Chemical Society, Washington, D.C. Q
- I & EC — Industrial and Engineering Chemistry, Product Research and Development*. American Chemical Society, Washington, D.C. Q
- Iași, Institutul Politehnic, Buletinul, Secția I — Matematică, Mecanică Teoretică, Fizică*. Iași, Institutul Politehnic, Iași, Rumania. SA
- Iași, Institutul Politehnic, Buletinul, Secția V — Construcții, Hidrotehnică*. Iași, Institutul Politehnic, Iași, Rumania. SA
- IBM Journal of Research and Development*. International Business Machines Corp., Armonk, N. Y. BM
- IBM Systems Journal*. International Business Machines Corp., Armonk, N.Y. Q
- Icarus*. Academic Press, Inc., New York. BM
- IEEE Reviews*. Institution of Electrical Engineers, London. Annual
- IEEE, Proceedings*. Institute of Electrical and Electronics Engineers, Inc., New York. M
- IEEE Journal of Quantum Electronics*. Institute of Electrical and Electronics Engineers, Inc., New York. M
- IEEE Journal of Solid-State Circuits*. Institute of Electrical and Electronics Engineers, Inc., New York. BM
- IEEE Spectrum*. Institute of Electrical and Electronics Engineers, Inc., New York. M
- IEEE Transactions on Aerospace and Electronic Systems*. Institute of Electrical and Electronics Engineers, Inc., New York. BM
- IEEE Transactions on Antennas and Propagation*. Institute of Electrical and Electronics Engineers, Inc., New York. BM
- IEEE Transactions on Audio and Electroacoustics*. Institute of Electrical and Electronics Engineers, Inc., New York. Q
- IEEE Transactions on Automatic Control*. Institute of Electrical and Electronics Engineers, Inc., New York. BM
- IEEE Transactions on Bio-Medical Engineering*. Institute of Electrical and Electronics Engineers, Inc., New York. Q
- IEEE Transactions on Broadcast and Television Receivers*. Institute of Electrical and Electronics Engineers, Inc., New York. Q
- IEEE Transactions on Circuit Theory*. Institute of Electrical and Electronics Engineers, Inc., New York. Q
- IEEE Transactions on Communication Technology*. Institute of Electrical and Electronics Engineers, Inc., New York. BM
- IEEE Transactions on Computers*. Institute of Electrical and Electronics Engineers, Inc., New York. M
- IEEE Transactions on Electrical Insulation*. Institute of Electrical and Electronics Engineers, Inc., New York. Q
- IEEE Transactions on Electromagnetic Compatibility*. Institute of Electrical and Electronics Engineers, Inc., New York. Q
- IEEE Transactions on Electron Devices*. Institute of Electrical and Electronics Engineers, Inc., New York. M
- IEEE Transactions on Engineering Management*. Institute of Electrical and Electronics Engineers, Inc., New York. Q
- IEEE Transactions on Geoscience Electronics*. Institute of Electrical and Electronics Engineers, Inc., New York. Q
- IEEE Transactions on Industry and General Applications*. Institute of Electrical and Electronics Engineers, Inc., New York. BM
- IEEE Transactions on Information Theory*. Institute of Electrical and Electronics Engineers, Inc., New York. BM

- IEEE Transactions on Instrumentation and Measurement.* Institute of Electrical and Electronics Engineers, Inc., New York. Q
- IEEE Transactions on Magnetics.* Institute of Electrical and Electronics Engineers, Inc., New York. Q
- IEEE Transactions on Man-Machine Systems.* Institute of Electrical and Electronics Engineers, Inc., New York. Q
- IEEE Transactions on Microwave Theory and Techniques.* Institute of Electrical and Electronics Engineers, Inc., New York. M
- IEEE Transactions on Nuclear Science.* Institute of Electrical and Electronics Engineers, Inc., New York. BM
- IEEE Transactions on Parts, Materials and Packaging.* Institute of Electrical and Electronics Engineers, Inc., New York. Q
- IEEE Transactions on Reliability.* Institute of Electrical and Electronics Engineers, Inc., New York. Q
- IEEE Transactions on Sonics and Ultrasonics.* Institute of Electrical and Electronics Engineers, Inc., New York. Q
- IEEE Transactions on Systems, Man, and Cybernetics.* Institute of Electrical and Electronics Engineers, Inc., New York. Q
- IEEE Transactions on Systems Science and Cybernetics.* Institute of Electrical and Electronics Engineers, Inc., New York. Q
- IHI Engineering Review.* Ishikawajima-Harima Heavy Industries Co., Ltd., Tokyo. SA
- *Immunochemistry.* Pergamon Press, Ltd., Oxford. M
- Indian Academy of Sciences, Proceedings, Section A.* Indian Academy of Sciences, Bangalore. M
- Indian Institute of Science, Journal.* Indian Institute of Science, Bangalore. Q
- Indian Journal of Pure and Applied Mathematics.* Indian National Science Academy, New Delhi. Q
- Indian Journal of Pure and Applied Physics.* Council of Scientific and Industrial Research, New Delhi. M
- Indian Journal of Technology.* Council of Scientific and Industrial Research, New Delhi. M
- Indiana University Mathematics Journal.* Indiana University, Dept. of Mathematics, Bloomington, Ind. M
- Industrial Laboratory (Zavodskaya Laboratoriya).* Consultants Bureau, New York. M
- INFOR — Canadian Journal of Operational Research and Information Processing.* INFOR Journal, Ottawa. Q
- Information and Control.* Academic Press, Inc., New York. M
- Information Display.* Society for Information Display; Information Display Publications, Inc., Los Angeles. BM
- Informatsionnye Materialy.* Akademiia Nauk SSSR, Moscow. Irreg.
- Infrared Physics.* Pergamon Press, Ltd., Oxford. Q
- Ingegneria.* Editore Ulrico Hoepli, Milan. M
- Ingegneria Meccanica.* Etas Kompass, Milan. M
- Ingeniería Aeronáutica y Astronáutica.* Asociación de Ingenieros Aeronáuticos, Madrid. BM
- Ingenieur-Archiv.* Springer Verlag, Berlin. BM
- *Inorganic Chemistry.* American Chemical Society, Washington, D.C. M
- Institut Teoreticheskoi Astronomii, Biulleten'.* Akademiia Nauk SSSR, Institut Teoreticheskoi Astronomii; Izdatel'stvo Nauka, Leningrad. Irreg.
- Institute of Mathematics and Its Applications, Journal.* Academic Press, Inc. (London), Ltd., London. Q
- Institute of Navigation, Journal.* Institute of Navigation; John Murray (Publishers), Ltd., London. Q
- Institute of Physical and Chemical Research, Scientific Papers.* Institute of Physical and Chemical Research, Saitama, Japan. Q
- Institution of Electrical Engineers, Proceedings.* Institution of Electrical Engineers, London. M
- Institution of Engineers (India), Journal, Electronics and Telecommunication Engineering Division.* Institution of Engineers, Calcutta. 3 issues per year
- Institution of Engineers (India), Journal, Mechanical Engineering Division.* Institution of Engineers, Calcutta. BM
- Institution of Mechanical Engineers, Proceedings.* Institution of Mechanical Engineers, London. Irreg.
- *Institution of Radio and Electronics Engineers (Australia), Proceedings.* Institution of Radio and Electronics Engineers, Sydney. M
- Institution of Telecommunication Engineers, Journal.* Institution of Telecommunication Engineers, New Delhi. M
- Instruments and Control Systems.* Chilton Co., Philadelphia, Pa. M
- Instytut Lotnictwa, Prace.* Instytut Lotnictwa; Wydawnictwo Naukowo-Techniczne, Warsaw. Irreg.
- Instytut Maszyn Przepływowych, Prace.* Polska Akademia Nauk, Instytut Maszyn Przepływowych, Gdansk; Państwowe Wydawnictwo Naukowe, Warsaw. Irreg.
- Inter-Electronique.* Compagnie Française d'Éditions, Paris. M
- Interavia.* Interavia S.A., Geneva. M
- International Chemical Engineering.* American Institute of Chemical Engineers, New York. Q
- International Journal for Numerical Methods in Engineering.* John Wiley & Sons, Ltd., Chichester, Sussex, England. Q
- International Journal of Biometeorology.* International Society of Biometeorology; Swets & Zeitlinger, Amsterdam. 3 issues per year
- International Journal of Computer Mathematics.* Gordon & Breach Science Publishers, New York. Q
- International Journal of Control, First Series.* Taylor & Francis, Ltd., London. M
- International Journal of Electronics, First Series.* Taylor & Francis, Ltd., London. M
- International Journal of Engineering Science.* Pergamon Press, Ltd., Oxford. M
- International Journal of Fracture Mechanics.* Wolters-Noordhoff Publishing, Groningen, Netherlands. Q

- International Journal of Heat and Mass Transfer.* Pergamon Press, Ltd., Oxford. M
- International Journal of Man-Machine Studies.* Academic Press, Inc. (London), Ltd., London. Q
- International Journal of Mechanical Sciences.* Pergamon Press, Ltd., Oxford. M
- International Journal of Non-Linear Mechanics.* Pergamon Press, Ltd., Oxford. Q
- International Journal of Nondestructive Testing.* Gordon & Breach Science Publishers, London.
- International Journal of Powder Metallurgy.* American Powder Metallurgy Institute, New York. Q
- **International Journal of Quantum Chemistry.* Interscience Scientific Journals, John Wiley & Sons, Inc., New York. BM
- **International Journal of Radiation Biology.* Taylor & Francis, Ltd., London. M
- International Journal of Solids and Structures.* Pergamon Press, Ltd., Oxford. M
- Internationale Elektronische Rundschau.* Verlag für Radio-Foto-Kinotechnik GmbH, Berlin. M
- **Internationale Zeitschrift für angewandte Physiologie einschliesslich Arbeitsphysiologie.* Springer Verlag, Berlin. Q
- Inzhenerno-Fizicheskii Zhurnal.* Akademiia Nauk Belorusskoi SSR; Izdatel'stvo Nauka i Tekhnika, Minsk. M
- Irish Astronomical Journal.* Observatory, Armagh, Northern Ireland. Q
- ISA Transactions.* Instrument Society of America, Pittsburgh, Pa. Q
- Israel Journal of Technology.* Weizmann Science Press of Israel, Jerusalem. BM
- Issledovaniia po Uprugosti i Plastichnosti.* Izdatel'stvo Leningradskogo Universiteta, Leningrad. Irreg.
- İstanbul Teknik Üniversitesi Bülteni.* İstanbul Teknik Üniversitesi, İstanbul. Annual
- İstanbul Üniversitesi, Fen Fakültesi Mecmuası, Seri C — Astronomi-Fizik-Kimya.* İstanbul Üniversitesi, İstanbul. Q
- ITC Publications, Series B.* International Institute for Aerial Survey and Earth Sciences, Delft, Netherlands.
- ITU Telecommunication Journal.* International Telecommunication Union, Geneva. M
- Japan, Defense Academy, Memoirs.* Defense Academy, Yokosuka, Japan. Irreg.
- Japan Air Self Defence Force, Aeromedical Laboratory, Reports.* Aeromedical Laboratory, Tachikawa, Japan. Q
- Japan Institute of Light Metals, Journal.* Japan Institute of Light Metals, Tokyo. BM
- Japan Institute of Metals, Journal (Nippon Kinzoku Gakkai-si).* Japan Institute of Metals, Sendai. M
- Japan Institute of Metals, Transactions.* Japan Institute of Metals, Sendai. BM
- Japan Society for Aeronautical and Space Sciences, Journal.* Japan Society for Aeronautical and Space Sciences, Tokyo. M
- Japan Society for Aeronautical and Space Sciences, Transactions.* Japan Society for Aeronautical and Space Sciences, Tokyo. Irreg.
- Japan Society of Materials Science, Journal.* Society of Materials Science, Kyoto. M
- **Japanese Heart Journal.* Tokyo, University, Faculty of Medicine, Tokyo. BM
- Japanese Journal of Applied Physics.* Physical Society of Japan and Japan Society of Applied Physics, Tokyo. M
- Japanese Journal of Physiology.* Physiological Society of Japan; University of Tokyo Press, Tokyo. BM
- Jemná Mechanika a Optika.* Ministerstvo Průmyslu; Státní Nakladatelství Technické Literatury, Prague. BM
- Jena Review.* VEB Verlag Technik, Berlin. BM
- JETP Letters (ZHETF Pis'ma v Redaktsiiu).* American Institute of Physics, Inc., New York. SM
- Journal de Mécanique.* Gauthier-Villars, Paris. Q
- Journal de Physiologie.* Masson & Cie., Paris. BM
- Journal de Physique.* Société Française de Physique, Paris. M
- **Journal of Agricultural and Food Chemistry.* American Chemical Society, Washington, D.C. BM
- Journal of Air Law and Commerce.* Southern Methodist University, School of Law, Dallas. Q
- Journal of Air Traffic Control.* Air Traffic Control Association, Inc., Washington, D.C. BM
- Journal of Aircraft.* American Institute of Aeronautics and Astronautics, Inc., New York. BM
- Journal of Applied Meteorology.* American Meteorological Society, Boston. BM
- Journal of Applied Physics.* American Institute of Physics, Inc., New York. 13 issues per year
- Journal of Applied Physiology.* American Physiological Society, Washington, D.C. M
- **Journal of Applied Polymer Science.* Interscience Publishers, New York. M
- Journal of Applied Psychology.* American Psychological Association, Washington, D.C. BM
- Journal of Atmospheric and Terrestrial Physics.* Pergamon Press, Ltd., Oxford. M
- Journal of Bacteriology.* American Society for Microbiology, Bethesda, Md. M
- Journal of Biological Chemistry.* American Society of Biological Chemists, Inc., Baltimore, Md. M
- Journal of Biomechanics.* Pergamon Press, Ltd., Oxford. Q
- **Journal of Catalysis.* Academic Press, Inc., New York. BM
- **Journal of Cellular Plastics.* Technomic Publishing Co., Inc., Stamford, Conn. BM
- **Journal of Chemical Engineering of Japan.* Society of Chemical Engineers, Tokyo. SA
- Journal of Chemical Physics.* American Institute of Physics, Inc., New York. SM
- **Journal of Chromatographic Science.* Preston Technical Abstracts Co., Evanston, Ill. M
- **Journal of Chromatography.* Elsevier Publishing Co., Amsterdam. M
- **Journal of Colloid and Interface Science.* Academic Press, Inc., New York. M
- **Journal of Comparative and Physiological Psychology.* American Psychological Association, Inc., Washington, D. C. M
- Journal of Composite Materials.* Technomic Publishing Co., Inc., Stamford, Conn. BM

INTERNATIONAL AEROSPACE ABSTRACTS

- Journal of Computational Physics.* Academic Press, Inc., New York. Q
- Journal of Computer and System Sciences.* Academic Press, Inc., New York. BM
- **Journal of Crystal and Molecular Structure.* Plenum Press, New York. BM
- **Journal of Crystal Growth.* North-Holland Publishing Co., Amsterdam. BM
- Journal of Differential Equations.* Academic Press, Inc., New York. BM
- Journal of Electrocardiology.* Research in Electrocardiology, Inc., Dayton, Ohio. Q
- Journal of Engineering Mathematics.* Wolters-Noordhoff Publishing, Groningen, Netherlands. Q
- Journal of Environmental Sciences.* Institute of Environmental Sciences, Mt. Prospect, Ill. BM
- **Journal of Experimental Psychology.* American Psychological Association, Inc., Washington, D.C. M
- Journal of Fire and Flammability.* Technomic Publishing Co., Inc., Stamford, Conn. Q
- Journal of Fluid Mechanics.* Cambridge University Press, London. 20 issues per year
- **Journal of Geological Education.* National Association of Geology Teachers, c/o Roy L. Ingram, Dept. of Geology, University of North Carolina, Chapel Hill, N. C. 5 issues per year
- Journal of Geomagnetism and Geoelectricity.* Society of Terrestrial Magnetism and Electricity, Kyoto, Japan. Q
- Journal of Geophysical Research.* American Geophysical Union, Washington, D.C. 36 issues per year
- Journal of Hydronautics.* American Institute of Aeronautics and Astronautics, Inc., New York. Q
- Journal of Interdisciplinary Cycle Research.* International Institute for Interdisciplinary Cycle Research, Leiden; Swets & Zeitlinger N. V., Amsterdam. Q
- Journal of Materials.* American Society for Testing and Materials, Philadelphia, Pa. Q
- Journal of Materials Science.* Chapman & Hall, Ltd., London. M
- Journal of Mathematical Analysis and Applications.* Academic Press, Inc., New York. M
- Journal of Mathematical Physics.* American Institute of Physics, Inc., New York. M
- Journal of Mechanical Engineering Science.* Institution of Mechanical Engineers, London. Q
- Journal of Metals.* American Institute of Mining, Metallurgical and Petroleum Engineers, Inc., New York. M
- Journal of Microwave Power.* International Microwave Power Institute, Ltd., Edmonton, Alberta, Canada. Q
- **Journal of Molecular Biology.* Academic Press, Ltd., London. BW
- **Journal of Molecular Spectroscopy.* Academic Press, Inc., New York. M
- **Journal of Molecular Structure.* Elsevier Publishing Co., Amsterdam. BM
- **Journal of Neurochemistry.* Pergamon Press, Ltd., Oxford. M
- **Journal of Neurophysiology.* American Physiological Society, Bethesda, Md. BM
- Journal of Occupational Medicine.* Industrial Medical Association; Charles B. Slack, Inc., Thorofare, N.J. M
- Journal of Optimization Theory and Applications.* Plenum Publishing Corp., New York. M
- **Journal of Organic Chemistry.* American Chemical Society, Washington, D.C. M
- **Journal of Paleontology.* Society of Economic Paleontologists and Mineralogists; Paleontological Society, Tulsa, Okla. Q
- Journal of Photographic Science.* Royal Photographic Society of Great Britain, London. M
- Journal of Physical Chemistry.* American Chemical Society, Washington, D.C. BW
- Journal of Physical Oceanography.* American Meteorological Society, Boston. Q
- Journal of Physics, Part A — General Physics.* Institute of Physics and The Physical Society, London. BM
- Journal of Physics, Part B — Atomic and Molecular Physics.* Institute of Physics and The Physical Society, London. M
- Journal of Physics, Part C — Solid State Physics.* Institute of Physics and The Physical Society, London. M
- Journal of Physics, Part D — Applied Physics.* Institute of Physics and The Physical Society, London. M
- Journal of Physics, Part E — Journal of Scientific Instruments.* Institute of Physics and The Physical Society, London. M
- Journal of Physics, Part F — Metal Physics.* Institute of Physics, London. BM
- **Journal of Physics and Chemistry of Solids.* Pergamon Press, Ltd., Oxford. M
- Journal of Physiology.* Physiological Society; Cambridge University Press, London. M
- Journal of Plasma Physics.* Cambridge University Press, London. Q
- **Journal of Polymer Science, Part A2 — Polymer Physics.* Interscience Publishers, Inc., New York. M
- **Journal of Polymer Science, Part B — Polymer Letters.* Interscience Publishers, Inc., New York. M
- Journal of Quality Technology.* American Society for Quality Control, Inc., Milwaukee, Wis. Q
- Journal of Quantitative Spectroscopy and Radiative Transfer.* Pergamon Press, Ltd., Oxford. M
- **Journal of Radioanalytical Chemistry.* Elsevier Publishing Co., Amsterdam. BM
- Journal of Research, Section A — Physics and Chemistry.* National Bureau of Standards; Supt. of Documents, Washington, D.C. BM
- Journal of Research, Section C — Engineering and Instrumentation.* National Bureau of Standards; Supt. of Documents, Washington, D.C. Q
- Journal of Science and Technology.* The General Electric and English Electric Companies Limited, London. Q
- Journal of Sound and Vibration.* British Acoustical Society; Academic Press, Inc. (London), Ltd., London. BM

- Journal of Spacecraft and Rockets.* American Institute of Aeronautics and Astronautics, Inc., New York. M
- **Journal of Sports Medicine and Physical Fitness.* Fédération Internationale de Médecine Sportive; Edizioni Minerva Medica, Turin. Q
- **Journal of Statistical Physics.* Plenum Publishing Corp., New York.
- Journal of Strain Analysis.* Joint British Committee for Stress Analysis; Institute of Mechanical Engineers, London. Q
- Journal of the Astronautical Sciences.* American Astronautical Society, Inc., Washington, D.C. BM
- Journal of the Atmospheric Sciences.* American Meteorological Society, Boston. BM
- Journal of the Experimental Analysis of Behavior.* Society for the Experimental Analysis of Behavior, Inc., Indiana University, Bloomington, Ind. BM
- Journal of the Less-Common Metals.* Elsevier Sequoia S.A., Lausanne. M
- Journal of the Mechanics and Physics of Solids.* Pergamon Press, Ltd., Oxford. BM
- Journal of Vacuum Science and Technology.* American Vacuum Society; American Institute of Physics, Inc., New York. BM
- JSME, Bulletin.* Japan Society of Mechanical Engineers, Tokyo. BM
- Kakioka Magnetic Observatory, Memoirs.* Kakioka Magnetic Observatory, Kakioka, Japan.
- Kazanskaia Gorodskaiia Astronomicheskaiia Observatoriia, Trudy.* Izdatel'stvo Kazanskogo Universiteta, Kazan. Irreg.
- Kazanskii Aviatsionnyi Institut, Trudy, Serii Aviatsionnaia Tekhnologiia i Organizatsiia Proizvodstva.* Kazanskii Aviatsionnyi Institut, Kazan. Irreg.
- Kazanskii Aviatsionnyi Institut, Trudy, Serii Aviatsionnye Dvigateli.* Kazanskii Aviatsionnyi Institut, Kazan. Irreg.
- Kazanskii Aviatsionnyi Institut, Trudy Serii Aviatsionnye Pribory i Avtomaty.* Kazanskii Aviatsionnyi Institut, Kazan. Irreg.
- Kazanskii Aviatsionnyi Institut, Trudy, Serii Matematika i Mekhanika.* Kazanskii Aviatsionnyi Institut, Kazan. Irreg.
- Kazanskii Aviatsionnyi Institut, Trudy, Serii Radioelekhnika i Elektronika.* Kazanskii Aviatsionnyi Institut, Kazan. Irreg.
- Kazanskii Aviatsionnyi Institut, Trudy, Serii Stroitel'naia Mekhanika.* Kazanskii Aviatsionnyi Institut, Kazan. Irreg.
- Khimiia i Tekhnologiia Topliv i Masel.* Ministerstvo Neftepererabatyvaiushchei i Neftekhimicheskoi Promyshlennosti SSSR, Akademiia Nauk SSSR, and Nauchno-Tekhnicheskoe Obshchestvo Nef-tianoi i Gazovoi Promyshlennosti; Izdatel'stvo Khimiia, Moscow. M
- Koninklijke Nederlandse Akademie van Wetenschappen, Proceedings, Series B — Physical Sciences.* North-Holland Publishing Co., Amsterdam. 5 issues per year
- Kosmicheskaiia Biologiia i Meditsina.* Ministerstvo Zdravookhraneniia SSSR; Izdatel'stvo Meditsina, Moscow. BM
- Kosmicheskie Issledovaniia.* Akademiia Nauk SSSR; Izdatel'stvo Nauka, Moscow. BM
- Kosmicheskie Luchi.* Izdatel'stvo Nauka, Moscow. Irreg.
- Kovové Materiály.* Slovenská Akademia Vied, Bratislava. BM
- Krymskaia Astrofizicheskaiia Observatoriia, Izvestiia.* Akademiia Nauk SSSR; Izdatel'stvo Nauka, Moscow. BM
- **Kunststoffe.* Carl Hanser Verlag, Munich. M
- Kybernetika.* Československá Akademie Věd, Prague. BM
- Kyoto University, Faculty of Engineering, Memoirs.* Kyoto University, Kyoto. Q
- Kyoto University, Faculty of Science, Memoirs, Series — Physics, Astrophysics, Geophysics and Chemistry.* Kyoto University, Kyoto. Irreg.
- Kyushu University, Faculty of Engineering, Memoirs.* Kyushu University, Fukuoka, Japan. Q
- Kyushu University, Research Institute for Applied Mechanics, Reports.* Kyushu University, Fukuoka, Japan. Irreg.
- **Laboratory Animal Science.* American Association for Laboratory Animal Science, Joliet, Ill.
- Laser.* Fachschriftenverlag Aargauer Tagblatt AG, Aarau, Switzerland. Q
- Laser Journal.* Laser Industry Association; A. Z. Publishing Corp., Los Angeles. BM
- **Law Library Journal.* American Association of Law Libraries, Washington State Law Library, Olympia, Wash. Q
- Leningradskii Universitet, Vestnik, Matematika, Mekhanika, Astronomiia.* Izdatel'stvo Leningrad-skogo Universiteta, Leningrad. Q
- Lietuvos Fizikos Rinkiny.* Akademiia Nauk Litovskoi SSR; Izdatel'stvo Mintis, Vilnius. Q
- Lietuvos Matematikos Rinkiny.* Akademiia Nauk Litovskoi SSR; Izdatel'stvo Mintis, Vilnius. Q
- Life Sciences, Part I — Physiology and Pharmacology.* Pergamon Press, Ltd., Oxford. SM
- Life Sciences, Part II — Biochemistry, General and Molecular Biology.* Pergamon Press, Ltd., Oxford. SM
- **Logistics Review.* Technical Economics, Inc., Berkeley, Calif. 5 issues per year
- Logistics Spectrum.* Society of Logistics Engineers, Los Angeles. Q
- Lopatochnye Mashiny i Struinye Apparaty.* Izdatel'stvo Mashinostroenie, Moscow. Irreg.
- Lubrication Engineering.* American Society of Lubrication Engineers, Park Ridge, Ill. M
- Luftfahrttechnik* *Raumfahrttechnik.* Verein Deutscher Ingenieure; VDI-Verlag GmbH, Düsseldorf. M
- Machine Design.* Penton Publishing Co., Cleveland, Ohio. 31 issues per year
- Magnitnaia Gidrodinamika.* Akademiia Nauk Latvii SSR; Izdatel'stvo Zinatne, Riga. Q
- Management Services.* American Institute of Certified Public Accountants, New York. BM

- Manufacturing Engineering and Management.* Society of Manufacturing Engineers, Dearborn, Mich. M
- Marconi Review.* Marconi Co., Ltd., Chelmsford, Essex, England. Q
- Mashinostroenie.* Ministerstvo Vysshego i Srednego Spetsial'nogo Obrazovaniia SSSR; Izdanie Moskovskogo Tekhnicheskogo Uchilishcha imeni N. E. Bauman, Moscow. M
- Matematicheskaiia Fizika.* Akademiia Nauk Ukrainskoi SSR; Izdatel'stvo Naukova Dumka, Kiev. Irreg.
- Matematicheskii Sbornik.* Akademiia Nauk SSSR and Moskovskoe Matematicheskoe Obshchestvo; Izdatel'stvo Nauka, Moscow. M
- Matematichki Vesnik.* Društvo Matematičara, Fizičara i Astronoma SRS and Matematichki Institut, Belgrade. Q
- Matematika.* Ministerstvo Vysshego i Srednego Spetsial'nogo Obrazovaniia SSSR; Izdatel'stvo Kazanskogo Universiteta, Kazan. M
- Materials Evaluation.* American Society for Non-destructive Testing, Inc., Evanston, Ill. M
- Materials Protection and Performance.* National Association of Corrosion Engineers, Houston, Tex. M
- Materials Research and Standards.* American Society for Testing and Materials, Philadelphia, Pa. M
- Materials Science and Engineering.* American Society for Metals, Metals Park, Ohio; Elsevier Sequoia S.A., Lausanne. BM
- **Mathematical Biosciences.* American Elsevier Publishing Co., Inc., New York. Q
- Mathematics of Computation.* American Mathematical Society, Providence, R.I. Q
- Mathematika.* University College, Dept. of Mathematics, London. SA
- Max-Planck-Institut für Aeronomie, Mitteilungen.* Springer Verlag, Berlin, West Germany. Irreg.
- Meccanica.* Italian Association of Theoretical and Applied Mechanics; Tamburini Editore, Milan. Q
- Mechanika Teoretyczna i Stosowana.* Polskie Towarzystwo Mechaniki Teoretycznej i Stosowanej; Państwowe Wydawnictwo Naukowe, Warsaw. Q
- Medical and Biological Engineering.* International Federation for Medical and Biological Engineering; Pergamon Press, Ltd., Oxford. BM
- Medical Research Engineering.* Medical-Research-Technology, Little Falls, N.J. BM
- Mekhanika Polimerov.* Akademiia Nauk Latvinskoi SSR; Izdatel'stvo Zinatne, Riga. BM
- Mekhanika Tverdogo Tela.* Akademiia Nauk SSSR; Izdatel'stvo Nauka, Moscow. Irreg.
- Mémoires Scientifiques de la Revue de Métallurgie.* Paris. M
- Mérés es Automatika.* Lapkiadó Vállalat, Budapest. M
- Messtechnik.* Friedr. Vieweg & Sohn GmbH, Braunschweig. M
- Metal Construction and British Welding Journal.* The Welding Institute, London. M
- Metal Progress.* American Society for Metals, Metals Park, Ohio. M
- Metal Science and Heat Treatment (Metallovedenie i Termicheskaiia Obrabotka Metallov).* Consultants Bureau, New York. BM
- Metal Science Journal.* Institute of Metals and Institution of Metallurgists, London. BM
- **Metall.* Metall-Verlag GmbH, Berlin, West Germany. M
- Metallovedenie i Termicheskaiia Obrabotka Metallov.* Ministerstvo Stankostroitel'noi i Instrumental'noi Promyshlennosti SSSR and Nauchno-Tekhnicheskoe Obshchestvo Mashinostroitel'noi Promyshlennosti; Izdatel'stvo Mashinostroenie, Moscow. M
- Metallurgical Transactions.* Metallurgical Society of the American Institute of Mining, Metallurgical and Petroleum Engineers, Inc., New York; American Society for Metals, Metals Park, Ohio. M
- Metals Engineering Quarterly.* American Society for Metals, Metals Park, Ohio. Q
- Meteor-Forschungsergebnisse, Reihe B — Meteorologie und Aeronomie.* Gebrüder Borntraeger, Berlin. Irreg.
- Meteoritics.* Meteoritical Society and Arizona State University Bureau of Publications, Tempe, Ariz. Q
- Meteoritika.* Akademiia Nauk SSSR; Izdatel'stvo Nauka, Moscow. Irreg.
- Meteornoe Rasprostranenie Radiovoln.* Izdatel'stvo Kazanskogo Universiteta, Kazan. Irreg.
- Meteorological Magazine.* Meteorological Office; Her Majesty's Stationery Office, London. M
- Meteorological Society of Japan, Journal.* Meteorological Society of Japan, c/o Japan Meteorological Agency, Tokyo. BM
- Meteorologiiia i Gidrologiiia.* Glavnoe Upravlenie Gidrometeorologicheskoi Sluzhby SSSR; Gidrometeoizdat, Moscow. M
- Meteorologische Abhandlungen.* Freie Universität Berlin, Institut für Meteorologie und Geophysik; Verlag Dietrich Reimer, Berlin, West Germany. Q
- Meteorologische Rundschau.* Verband Deutscher Meteorologischer Gesellschaften; Springer Verlag, Berlin. BM
- **Metrologia.* Springer Verlag, Berlin, West Germany. Q
- Microelectronics and Reliability.* Pergamon Press, Ltd., Oxford. BM
- Microwave Journal.* Horizon House, Inc., Dedham, Mass. M
- MicroWaves.* Hayden Microwaves Corp., New York. M
- Middle East Technical University Journal of Pure and Applied Sciences.* Middle East Technical University, Ankara. 3 issues per year
- Mikroelektronika.* Izdatel'stvo Sovetskoe Radio, Moscow.
- **Mineralogical Magazine.* Mineralogical Society, London. Q
- Mitsubishi Denki Laboratory Reports.* Mitsubishi Electric Corp., Central Research Laboratory, Amagasaki, Kyogo Prefecture, Japan. Irreg.
- Mitsubishi Heavy Industries Technical Review.* Mitsubishi Heavy Industries, Ltd., Tokyo. BM

- Modern Geology.* Gordon & Breach Science Publishers, Ltd., London. Q
- Molecular Crystals and Liquid Crystals.* Gordon & Breach Science Publishers, Inc., New York. Q
- Molecular Physics.* Taylor & Francis, Ltd., London. M
- Monthly Weather Review.* U. S. Weather Bureau; Supt. of Documents, Washington, D.C. M
- The Moon.* D. Reidel Publishing Co., Dordrecht, Netherlands. Q
- Moskovskii Universitet, Vestnik, Serii I — Matematika, Mekhanika.* Izdatel'stvo Moskovskogo Universiteta, Moscow. BM
- Moskovskii Universitet, Vestnik, Serii III — Fizika, Astronomiia.* Izdatel'stvo Moskovskogo Universiteta, Moscow. BM
- Nachrichtentechnische Zeitschrift.* Nachrichtentechnische Gesellschaft; VDE-Verlag GmbH, Berlin. M
- Nagoya University, Faculty of Engineering, Memoirs.* Nagoya University, Nagoya. Irreg.
- Nagoya University, Research Institute of Atmospherics, Proceedings.* Research Institute of Atmospherics, Toyokawa-Shi, Aichi-Ken, Japan. Irreg.
- National Academy of Sciences, Proceedings.* National Academy of Sciences, Washington, D.C. M
- National Contract Management Journal.* National Contract Management Association, Inglewood, Calif. SA
- Nature.* Macmillan (Journals), Ltd., London. W
- Nature Physical Science.* Macmillan (Journals), Ltd., London. W
- *Naturwissenschaften.* Max-Planck-Gesellschaft zur Förderung der Wissenschaften; Springer Verlag, Berlin. SM
- Naturwissenschaftliche Rundschau.* Wissenschaftliche Verlagsgesellschaft mbH, Stuttgart, West Germany. M
- Nauchno-Issledovatel'skii Institut Gidrometeorologicheskogo Priborostroeniia, Trudy.* Glavnoe Upravlenie Gidrometeorologicheskoi Sluzhby; Gidrometeoizdat, Moscow. Irreg.
- Naval Research Logistics Quarterly.* U. S. Navy, Office of Naval Research; Supt. of Documents, Washington, D. C. Q
- Naval Research Reviews.* U. S. Navy, Office of Naval Research; Supt. of Documents, Washington, D.C. M
- Navigation.* Institute of Navigation, Washington, D.C. Q
- Navigation (Paris).* Institut Français de Navigation, Paris. Q
- NEC Research and Development.* Nippon Electric Ltd., Tokyo. Q
- Nervnaia Sistema.* Izdatel'stvo Leningradskogo Universiteta, Leningrad. Irreg.
- *Neuroendocrinology.* S. Karger AG, Basel. M
- New Scientist (see New Scientist and Science Journal).*
- New Scientist and Science Journal (formerly New Scientist).* New Science Publications; IPC Magazines, Ltd., London. W
- New York Academy of Sciences, Annals.* New York Academy of Sciences, New York. Irreg.
- New York Academy of Sciences, Transactions, Series 2.* New York Academy of Sciences, New York. 8 issues per year
- Nihon University, Research Institute of Science and Technology, Journal.* Nihon University, Tokyo. Irreg.
- Non-Ionizing Radiation.* Iliffe Science & Technology Publications, Ltd., Guildford, Surrey, England. Q
- Nordrhein-Westfalen, Forschungsberichte.* Westdeutscher Verlag, Cologne. Irreg.
- *Northwest Science.* Northwest Scientific Association; Washington State University Press, Pullman, Wash. Q
- Note, Recensioni e Notizie.* Poste e Telecomunicazioni, Istituto Superiore, Rome. BM
- Nouvelle Revue d'Optique Appliquée.* Masson & Cie., Editeurs, Paris. BM
- Nuclear Applications and Technology (see Nuclear Technology).*
- Nuclear Engineering and Design.* North-Holland Publishing Co., Amsterdam. M
- Nuclear Fusion.* International Atomic Energy Agency, Vienna. Q
- *Nuclear Instruments and Methods.* North-Holland Publishing Co., Amsterdam. BW
- *Nuclear Physics.* North-Holland Publishing Co., Amsterdam. W
- Nuclear Science and Engineering.* American Nuclear Society, Inc., Hinsdale, Ill. M
- Nuclear Technology (formerly Nuclear Applications and Technology).* American Nuclear Society, Inc., Hinsdale, Ill. M
- Numerische Mathematik.* Springer Verlag, Berlin. Irreg.
- Nuovo Cimento, Lettere.* Società Italiana di Fisica, Bologna. 36 issues per year.
- Nuovo Cimento, Rivista.* Società Italiana di Fisica; Editrice Compositori, Bologna. Q
- Nuovo Cimento, Rivista, Serie 2.* Società Italiana di Fisica; Editrice Compositori, Bologna.
- Nuovo Cimento, Sezione A.* Società Italiana di Fisica; Editrice Compositori, Bologna. 26 issues per year
- Nuovo Cimento, Sezione B.* Società Italiana di Fisica; Editrice Compositori, Bologna. 26 issues per year
- Observatorio de Madrid, Boletín Astronómico.* Instituto Geográfico y Catastral, Madrid.
- Observatorios de Tonantzintla y Tacubaya, Boletín.* Universidad Nacional Autónoma de México, Observatorio Astronómico, Mexico City. Irreg.
- The Observatory.* Royal Greenwich Observatory, Hailsham, Sussex, England. M
- Obzornik za Matematiko in Fiziko.* Izdaja Društvo Matematikov, Fizikov in Astronomov SR Slovenije, Ljubljana, Yugoslavia. Q
- *Oklahoma Geology Notes.* Oklahoma Geological Survey, University of Oklahoma, Norman, Okla. BM
- *Oncology.* S. Karger AG, Basel. Q
- L'Onde Electrique.* Société Française des Electroniciens et des Radioélectriciens; Editions Chiron S.A., Paris. M

INTERNATIONAL AEROSPACE ABSTRACTS

- ONERA, TP.* Office National d'Etudes et de Recherches Aérospatiales, Chatillon-sous-Bagneux (Seine), France. Irreg.
- Operations Research.* Operations Research Society of America, Baltimore, Md. BM
- Ophthalmic Research.* S. Karger AG, Basel. BM
- Optica Acta.* Taylor & Francis, Ltd., London. M
- Optica Pura y Aplicada.* Sociedad Española de Optica, Madrid. BM
- Optical Sciences Center Newsletter.* University of Arizona, Optical Sciences Center, Tucson, Ariz. Irreg.
- Optical Society of America, Journal.* Optical Society of America, Inc., Washington, D.C.; American Institute of Physics, Inc., New York. M
- Optical Spectra.* Optical Publishing Co., Inc., Pittsfield, Mass. M
- Optics and Laser Technology.* Iliffe Science & Technology Publications, Ltd., Guildford, Surrey, England. Q
- Optics Communications.* North-Holland Publishing Co., Amsterdam. M
- Optika i Spektroskopiia.* Akademiia Nauk SSSR; Izdatel'stvo Nauka, Leningrad. M
- **Opto-Electronics.* Chapman & Hall, London. Q
- **Organic Mass Spectrometry.* Heyden & Son, Ltd., London. BM
- Osaka City University, Faculty of Engineering, Memoirs.* Osaka City University, Osaka, Japan. Annual
- Osaka University, Institute of Scientific and Industrial Research, Memoirs.* Osaka University, Institute of Scientific and Industrial Research, Yamada-Kami, Suita, Osaka, Japan. Irreg.
- Osaka University, Technology Reports.* Osaka University, Osaka, Japan. SA
- Österreichische Akademie der Wissenschaften, Mathematisch-naturwissenschaftliche Klasse, Sitzungsberichte, Abteilung 2.* Österreichische Akademie der Wissenschaften; Springer Verlag, Vienna. Irreg.
- Otbor i Peredacha Informatsii.* Akademiia Nauk Ukrainskoi SSR; Izdatel'stvo Naukova Dumka, Kiev. Irreg.
- Oxidation of Metals.* Plenum Publishing Corp., New York. Q
- **Pacific Science.* University of Hawaii Press, Honolulu, Hawaii. Q
- Papers in Meteorology and Geophysics.* Meteorological Research Institute, Tokyo. Q
- **Perception and Psychophysics.* Psychonomic Journals, Inc., Austin, Tex. M
- Perceptual and Motor Skills.* Missoula, Mont. BM
- Periodica Polytechnica, Electrical Engineering.* Budapest, Technical University, Budapest. Q
- Periodica Polytechnica, Mechanical Engineering.* Budapest, Technical University, Budapest. Q
- Pflügers Archiv.* Springer Verlag, Berlin.
- **Pharmacological Reviews.* American Society for Pharmacology and Experimental Therapeutics, British Pharmacological Society, and Scandinavian Pharmacological Society; Williams & Wilkins Co., Baltimore, Md. Q
- Philips Research Reports.* N. V. Philips' Gloeilampenfabrieken, Research Laboratories, Eindhoven. BM
- Philips Technical Review.* N. V. Philips' Gloeilampenfabrieken, Research Laboratories, Eindhoven. M
- Philosophical Magazine, 8th Series.* Taylor & Francis, Ltd., London. M
- Photogrammetria.* International Society of Photogrammetry; Elsevier Publishing Co., Amsterdam. BM
- Photogrammetric Engineering.* American Society of Photogrammetry, Falls Church, Va. M
- Photographic Applications in Science, Technology and Medicine.* Photographic Applications in Science and Technology, Inc., New York. BM
- Physica.* Physica Foundation; North-Holland Publishing Co., Amsterdam. Irreg.
- **Physica Norvegica.* Norske Videnskaps-Akademie, Oslo.
- Physica Scripta.* Royal Swedish Academy of Sciences; Almqvist & Wiksell Periodical Co., Stockholm. M
- Physica Status Solidi (A) — Applied Research.* Akademie-Verlag GmbH, Berlin; Academic Press, Inc., New York. 3 issues per year
- Physical Review A — General Physics, 3rd Series.* American Physical Society; American Institute of Physics, Inc., New York. M
- Physical Review B — Solid State, 3rd Series.* American Physical Society; American Institute of Physics, Inc., New York. SM
- Physical Review C — Nuclear Physics, 3rd Series.* American Physical Society; American Institute of Physics, Inc., New York. M
- Physical Review D — Particles and Fields, 3rd Series.* American Physical Society; American Institute of Physics, Inc., New York. SM
- Physical Review Letters.* American Physical Society, Inc., New York. W
- Physical Society of Japan, Journal.* Physical Society of Japan, Tokyo. M
- Physics in Medicine and Biology.* Hospital Physicists' Association; Taylor & Francis, Ltd., London. Q
- Physics Letters.* North-Holland Publishing Co., Amsterdam. W
- Physics Letters, Section C — Physics Reports.* North-Holland Publishing Co., Amsterdam. 1 vol. per year
- Physics of Fluids.* American Institute of Physics, Inc., New York. M
- Physics of the Earth and Planetary Interiors.* North-Holland Publishing Co., Amsterdam. BM
- Physics Today.* American Institute of Physics, Inc., New York. M
- **Physikalische Blätter.* Physik Verlag GmbH, Mosbach, West Germany. M
- **Physiology and Behavior.* Pergamon Press, Ltd., Oxford. Q
- **Phytochemistry.* Pergamon Press, Ltd., Oxford. M
- Pisa, Scuola Normale Superiore, Annali, Scienze Fisiche e Matematiche.* Pisa, Scuola Normale Superiore, Pisa. Q
- Planetary and Space Science.* Pergamon Press, Ltd., Oxford. M

- Planseeberichte für Pulvermetallurgie.* Metallwerk Plansee Aktiengesellschaft, Reutte, Austria. 3 issues per year
- **Plant Physiology.* American Society of Plant Physiologists, Washington, D.C. M
- **Planta.* Springer Verlag, Berlin. Q
- Plasma Physics.* Pergamon Press, Ltd., Oxford. M
- PMM — Journal of Applied Mathematics and Mechanics (Prikladnaia Matematika i Mekhanika).* Pergamon Press, Ltd., Oxford. BM
- PMTF — Zhurnal Prikladnoi Mekhaniki i Tekhnicheskoi Fiziki.* Akademiia Nauk SSSR, Sibirskoe Otdelenie; Izdatel'stvo Nauka, Novosibirsk. BM
- Podstawy Sterowania.* Polska Akademia Nauk; Państwowe Wydawnictwo Naukowe, Warsaw. Q
- Point-to-Point Communication.* Marconi Communication Systems, Ltd., Chelmsford, England. 3 issues per year
- Pokroky Matematiky, Fyziky a Astronomie.* Československá Akadémie Věd, Prague. BM
- Polish Medical Journal (Polski Tygodnik Lekarski).* Państwowy Zakład Wydawnictw Lekarskich, Warsaw; National Technical Information Service, Springfield, Va. Irreg.
- Politechnika Warszawska, Prace Naukowe, Mechanika.* Wydawnictwa Politechniki Warszawskiej, Warsaw. Irreg.
- Polska Akademia Nauk, Instytut Automatyki, Prace.* Polska Akademia Nauk, Warsaw. Irreg.
- Poluprovodniki i ikh Primenenie v Elektrotekhnike.* Akademiia Nauk Latviskoi SSR, Fiziko-Energeticheskii Institut; Izdatel'stvo Zinatne, Riga. Irreg.
- Poluprovodnikovaia Tekhnika i Mikroelektronika.* Akademiia Nauk Ukrainskoi SSR; Izdatel'stvo Naukova Dumka, Kiev. Irreg.
- Poluprovodnikovye Pribory i ikh Primenenie.* Izdatel'stvo Sovetskoe Radio, Moscow. Irreg.
- Polymer Engineering and Science.* Society of Plastics Engineers, Inc., Greenwich, Conn. BM
- Pomiary, Automatyka, Kontrola.* Naczelna Organizacja Techniczna, Warsaw. M
- Poroshkovaia Metallurgii.* Akademiia Nauk Ukrainskoi SSR; Izdatel'stvo Naukova Dumka, Kiev. M
- Postępy Astronautyki.* Polskie Towarzystwo Astronautyczne, Lodz. Q
- Postępy Astronomii.* Polskie Towarzystwo Astronomiczne; Państwowe Wydawnictwo Naukowe, Warsaw. Q
- Postępy Fizyki.* Polskie Towarzystwo Fizyczne; Państwowe Wydawnictwo Naukowe, Warsaw. BM
- Priborostroenie.* Ministerstvo Vysshego i Srednego Spetsial'nogo Obrazovaniia SSSR; Izdatel'stvo Leningradskogo Instituta Tochnoi Mekhaniki i Optiki, Leningrad. M
- Pribory i Sistemy Avtomatiki.* Izdatel'stvo Khar'kovskogo Gosudarstvennogo Universiteta, Kharkov. Irreg.
- Pribory i Tekhnika Eksperimenta.* Akademiia Nauk SSSR; Izdatel'stvo Nauka, Moscow. BM
- Prikladnaia Matematika i Mekhanika.* Akademiia Nauk SSSR, Izdatel'stvo Nauka, Moscow. BM
- Prikladnaia Mekhanika.* Akademiia Nauk Ukrainskoi SSR, Otdelenie Matematiki, Mekhaniki i Kibernetiki; Izdatel'stvo Naukova Dumka, Kiev. M
- Priroda.* Akademiia Nauk SSSR; Izdatel'stvo Nauka, Moscow. M
- Problemy Bioniki.* Khar'kovskii Gosudarstvennyi Universitet, Kharkov. Irreg.
- Problemy Difraksii i Rasprostraneniia Voln.* Izdatel'stvo Leningradskogo Universiteta, Leningrad. Irreg.
- Problemy Fiziki Atmosfery.* Izdatel'stvo Leningradskogo Universiteta, Leningrad. Irreg.
- Problemy Kosmicheskoi Fiziki.* Izdatel'stvo Kievskogo Universiteta, Kiev. Irreg.
- Problemy Peredachi Informatsii.* Akademiia Nauk SSSR; Izdatel'stvo Nauka, Moscow. Q
- Problemy Prochnosti.* Akademiia Nauk Ukrainskoi SSR, Institut Problem Prochnosti; Izdatel'stvo Naukova Dumka, Kiev. M
- Problemy Tekhnicheskoi Elektrodinamiki.* Akademiia Nauk Ukrainskoi SSR; Izdatel'stvo Naukova Dumka, Kiev. Irreg.
- Proceedings of Vibration Problems.* Polska Akademia Nauk; Państwowe Wydawnictwo Naukowe, Warsaw. Q
- Progress of Theoretical Physics.* Research Institute for Fundamental Physics and The Physical Society of Japan; Kyoto University, Kyoto. M
- **PSA Journal.* Photographic Society of America, Chicago. M
- Psychological Reports.* Missoula, Mont. BM
- **Psychologische Forschung.* Zeitschrift für Psychologie, Berlin. Irreg.
- Psychonomic Science.* Psychonomic Journals, Inc., Austin, Tex. SM
- **Psychophysiology.* Society for Psychophysiological Research, Detroit, Mich. BM
- Pulkovo, Glavnaia Astronomicheskaiia Observatoriia, Izvestiia.* Izdanie Glavnoi Astronomicheskoi Observatorii, Leningrad. Irreg.
- Pure and Applied Geophysics.* Birkhäuser Verlag, Basel. BM
- Quality Progress.* American Society for Quality Control, Inc., Milwaukee, Wis. M
- Quarterly Journal of Mechanics and Applied Mathematics.* Oxford University Press, London. Q
- Quarterly of Applied Mathematics.* Brown University, Providence, R. I. Q
- **Quarterly Review of Biology.* Ed. H. Bentley Glass, Stony Brook Foundation, Inc., State University of New York, Stony Brook, N.Y. Q
- **Quaternary Research.* Academic Press, Inc., New York. Q
- **Radiation Effects.* Gordon & Breach Science Publishers, Inc., New York. Q
- Radio and Electronic Engineer.* Institution of Electronic and Radio Engineers, London. M
- Radio Engineering and Electronic Physics (Radio-tekhnika i Elektronika).* Scripta Publishing Corp., Washington, D.C. M
- Radio Research Laboratories, Journal.* Ministry of Posts and Telecommunications, Radio Research Laboratories, Tokyo. BM

- Radio Research Laboratories, Review.* Ministry of Posts and Telecommunications, Radio Research Laboratories, Tokyo. Q
- **Radio Rivista.* Associazione Radiotecnica Italiana, Milan. M
- Radio Science.* American Geophysical Union, Washington, D.C. M
- Radiobiologia — Radiotherapia.* VEB Verlag Volk und Gesundheit, Berlin, East Germany. BM
- Radioelektronika.* Ministerstvo Vysshego i Srednego Spetsial'nogo Obrazovaniia SSSR; Izdatel'stvo Kievskogo Politehnicheskogo Instituta, Kiev. M
- Radiofizika.* Ministerstvo Vysshego i Srednego Spetsial'nogo Obrazovaniia SSSR; Izdanie Gor'kovskogo Universiteta, Gorki. M
- Radiotekhnika.* Nauchno-Tekhnicheskoe Obshchestvo Radiotekhniki i Elektrosviazi; Izdatel'stvo Sviaz', Moscow. M
- Radiotekhnika* (Kharkov). Izdatel'stvo Khar'kovskogo Gosudarstvennogo Universiteta, Kharkov. Irreg.
- Radiotekhnika i Elektronika.* Akademiia Nauk SSSR; Izdatel'stvo Nauka, Moscow. M
- Raschety na Prochnost'.* Izdatel'stvo Mashinostroenie, Moscow. Irreg.
- Raumfahrtforschung.* Deutsche Gesellschaft für Luft- und Raumfahrt, e.V., Stuttgart, West Germany. BM
- RCA Review.* RCA Research and Engineering, Princeton, N. J. Q
- La Recherche.* Société d'Editions Scientifiques, Paris. M
- La Recherche Aérospatiale.* Office National d'Etudes et de Recherches Aérospatiales, Chatillon-sous-Bagneux (Seine), France. BM
- La Recherche Spatiale.* Centre National d'Etudes Spatiales; Dunod Editeur, Paris. M
- **Regelungstechnik* (see *Regelungstechnik und Prozess-Datenverarbeitung*).
- **Regelungstechnik und Prozess-Datenverarbeitung* (formerly *Regelungstechnik*). Verlag R. Oldenbourg, Munich. M
- Remote Sensing of Environment.* American Elsevier Publishing Co., Inc., New York. Q
- Report of Ionosphere and Space Research in Japan.* Science Council of Japan, Ionosphere Research Committee, Tokyo. Q
- **Reports of Statistical Application Research (JUSE).* Union of Japanese Scientists and Engineers; Japan Publications Trading Co., Ltd., Tokyo. Q
- Reports on Progress in Physics.* Institute of Physics and The Physical Society, London. BM
- Research/Development.* Technical Publishing Co., Thompson Div., Barrington, Ill. M
- **Research Film.* Institut für den wissenschaftlichen Film, Göttingen, West Germany. SA
- Research Management.* Industrial Research Institute, Inc.; Interscience Publishers, New York. BM
- Respiration Physiology.* North-Holland Publishing Co., Amsterdam. BM
- Review of Scientific Instruments.* American Institute of Physics, Inc., New York. M
- Reviews of Geophysics and Space Physics.* American Geophysical Union, Washington, D.C. Q
- Reviews of Modern Physics.* American Physical Society; American Institute of Physics, Inc., New York. Q
- Reviews on High-Temperature Materials.* Freund Publishing House, Ltd., Scientific Publications Div., Tel Aviv. Q
- Revista de Aeronáutica y Astronáutica.* Ministerio del Aire, Madrid. M
- Revista Transporturilor.* Ministerul Transporturilor; Consiliul National al Inginerilor și Technicienilor, Bucharest. M
- Revue de Médecine Aéronautique et Spatiale.* Société Française de Physiologie et de Médecine Aéronautique et Cosmonautique; Masson & Cie., Paris. Q
- Revue de Métallurgie.* Paris. M
- Revue de Physique Appliquée.* Société Française de Physique, Paris. M
- Revue des Corps de Santé des Armées.* Centre de Recherches du Service de Santé des Armées, Paris. BM
- Revue Française de Droit Aérien.* Société Française de Droit Aérien et Spatial, Paris. Q
- Revue Française de Mécanique.* Société Française des Mécaniciens, Paris. Q
- Revue Générale de l'Air et de l'Espace.* Editions Internationales, Paris. Q
- Revue Générale de Thermique.* Institut Français des Combustibles et de l'Energie; Société Française des Thermiciens, Paris. M
- Revue Internationale des Hautes Températures et des Réfractaires.* Société Nationale Française des Hautes Températures et des Réfractaires; Masson & Cie., Paris. Q
- Revue Roumaine de Mathématiques Pures et Appliquées.* Académie de la République Socialiste Roumaine, Bucharest. 10 issues per year
- Revue Roumaine de Physique.* Académie de la République Socialiste Roumaine, Bucharest. BM
- Revue Roumaine des Sciences Techniques, Série de Mécanique Appliquée.* Académie de la République Socialiste Roumaine, Bucharest. BM
- Revue Scientifique et Technique CECLES/CERS.* Gauthier-Villars, Paris. Q
- Revue Technique Thomson — CSF.* Thomson — CSF, Service de Documentation Technique; Masson & Cie., Paris. Q
- Rheinisch-Westfälische Technische Hochschule, Aerodynamisches Institut, Abhandlungen.* Technische Hochschule, Aachen, West Germany. Irreg.
- Ricerche Astronomiche.* Specola Vaticana, Vatican City. Irreg.
- Rivista Aeronautica.* Rome. M
- Rivista di Medicina Aeronautica e Spaziale.* Servizio Sanitario dell'Aeronautica, Rome. Q
- Rivista di Meteorologia Aeronautica.* Servizio Meteorologico dell'Aeronautica, Rome. Q
- Royal Astronomical Society, Monthly Notices.* Royal Astronomical Society, London; Blackwell Scientific Publications, Oxford. M
- Royal Astronomical Society, Quarterly Journal.* Royal Astronomical Society, London; Blackwell Scientific Publications, Oxford. Q

- Royal Astronomical Society of Canada, Journal.* Royal Astronomical Society of Canada, Toronto. BM
- Royal Institution of Great Britain, Proceedings.* Royal Institution of Great Britain; Elsevier Publishing Co., Barking, Essex, England. 3 issues per year
- Royal Meteorological Society, Quarterly Journal.* Royal Meteorological Society, London. Q
- Royal Society (Edinburgh), Proceedings, Section A.* Royal Society of Edinburgh, Edinburgh. Irreg.
- Royal Society (London), Philosophical Transactions, Series A.* Royal Society, London. Irreg.
- Royal Society (London), Proceedings, Series A.* Royal Society, London. Irreg.
- **Royal Society of New South Wales, Journal and Proceedings.* Royal Society of New South Wales, Sydney. Q
- Rozprawy Inżynierskie.* Polska Akademia Nauk, Instytut Podstawowych Problemów Techniki; Państwowe Wydawnictwo Naukowe, Warsaw. Q
- **Rubber Chemistry and Technology.* American Chemical Society, Akron, Ohio. 5 issues per year
- Ruimtevaart.* Nederlandse Vereniging voor Ruimtevaart, The Hague. Q
- Russian Engineering Journal (Vestnik Mashinostroeniia).* Production Engineering Research Association of Great Britain, Melton Mowbray, Leics., England. M
- SAE Aerospace Information Report.* Society of Automotive Engineers, Inc., New York. Irreg.
- SAE Aerospace Recommended Practice.* Society of Automotive Engineers, Inc., New York. Irreg.
- SAE Aerospace Standards.* Society of Automotive Engineers, Inc., New York. Irreg.
- SAE Journal of Automotive Engineering.* Society of Automotive Engineers, Inc., New York. M
- SAFE Engineering.* Survival and Flight Equipment Association; Value Engineering Publications, Inc., Los Angeles. BM
- SAIT Electronics Review.* SAIT Electronics, Brussels. Q
- Samoletostroenie i Tekhnika Vozdushnogo Flota.* Izдание Khar'kovskogo Gosudarstvennogo Universiteta, Kharkov. Irreg.
- SAMPE Journal.* Society of Aerospace Material and Process Engineers; SAMPE Publications, Inc., Los Angeles. BM
- SAMPE Quarterly.* Society of Aerospace Material and Process Engineers, Azusa, Calif. Q
- SAWE Journal.* Society of Aeronautical Weight Engineers, Inc., Los Angeles. BM
- Schweizer Archiv (see Schweizer Archiv für angewandte Wissenschaft und Technik).*
- Schweizer Archiv für angewandte Wissenschaft und Technik.* Schweizer Verband für die Materialprüfungen und Schweizerische Gesellschaft für Vakuumphysik und Technik; Verlag Vogt-Schild AG, Solothurn, Switzerland. M
- Schweizerische Technische Zeitschrift.* Schweizer Technischer Verband, Zurich. M
- Science.* American Association for the Advancement of Science, Washington, D.C. W
- Science Progrès Découverte.* Société des Ingénieurs Civils de France; Dunod Editeur, Paris. M
- Science Progress.* Blackwell Scientific Publications, Ltd., Oxford. Q
- Sciences (Paris).* Hermann, Paris. BM
- Sciences et Industries Spatiales.* SADESI — Société Anonyme d'Éditions Scientifiques et Industrielles, Geneva. BM
- Scientific American.* Scientific American, Inc., New York. M
- Scripta Metallurgica.* Pergamon Press, Inc., New York. M
- Secrétariat Général à l'Aviation Civile, Revue.* Secrétariat Général à l'Aviation Civile, Paris. Irreg.
- Seismological Society of America, Bulletin.* Seismological Society of America; Waverly Press, Inc., Baltimore, Md. BM
- Seminar po Kraevym Zadacham, Trudy.* Izdatel'stvo Kazanskogo Universiteta, Kazan. Irreg.
- **Separation Science.* Marcel Dekker, Inc., New York. BM
- Shell Aviation News.* Shell Oil Co., London. M
- Shemakhinskaia Astrofizicheskaia Observatoriia, Soobshchenie.* Akademiia Nauk Azerbaidzhanskoi SSR; Izdatel'stvo Elm, Baku. Irreg.
- SIAM Journal on Applied Mathematics.* Society for Industrial and Applied Mathematics, Philadelphia, Pa. 8 issues per year
- SIAM Journal on Control.* Society for Industrial and Applied Mathematics, Philadelphia, Pa. Q
- SIAM Journal on Mathematical Analysis.* Society for Industrial and Applied Mathematics, Philadelphia, Pa. 8 issues per year
- SIAM Journal on Numerical Analysis.* Society for Industrial and Applied Mathematics, Philadelphia, Pa. Q
- SIAM Review.* Society for Industrial and Applied Mathematics, Philadelphia, Pa. Q
- Signal.* Armed Forces Communications and Electronics Association, Washington, D. C. M
- Simulation.* Simulation Councils, Inc., La Jolla, Calif. M
- Sky and Telescope.* Sky Publishing Corp., Cambridge, Mass. M
- Slaboproudý Obzor.* Státní Nakladatelství Technické Literatury, Prague. M
- Sloan Management Review.* Industrial Management Review Association; Massachusetts Institute of Technology, Cambridge, Mass. 3 issues per year
- SMPTE, Journal.* Society of Motion Picture and Television Engineers, Inc., New York. M
- Società Astronomica Italiana, Memorie.* Gia Società degli Spettroscopisti Italiani, Milan. Q
- Società degli Ingegneri e degli Architetti in Torino, Atti e Rassegna Tecnica.* Turin. Irreg.
- Societas Scientiarum Torunensis, Studia, Sectio F — Astronomia.* Societas Scientiarum Torunensis, Torun; Państwowe Wydawnictwo Naukowe, Poznan. Irreg.
- Société Française de Photogrammétrie, Bulletin.* Société Française de Photogrammétrie, Paris. Q
- Société Royale des Sciences de Liège, Bulletin.* Société Royale des Sciences de Liège; Université de Liège, Liège. Irreg.

- Société Royale des Sciences de Liège, Mémoires.* Société Royale des Sciences de Liège; Université de Liège, Liège. Q
- Society for Experimental Biology and Medicine, Proceedings.* Society for Experimental Biology and Medicine, New York. 11 issues per year
- Society for Information Display, Proceedings.* Society for Information Display; Western Periodicals Co., North Hollywood, Calif. Q
- Society of Experimental Test Pilots, Technical Review.* Society of Experimental Test Pilots, Lancaster, Calif. SA
- Society of Instrument and Control Engineers, Transactions.* Society of Instrument and Control Engineers, Tokyo. M
- **Society of Rheology, Transactions.* Interscience Publishers, New York. SA
- Solar Physics.* D. Reidel Publishing Co., Dordrecht, Netherlands. M
- Solar System Research (Astronomicheskii Vestnik).* Consultants Bureau, New York. Q
- **Solid-State Communications.* Pergamon Press, Ltd., Oxford. M
- Solid-State Electronics.* Pergamon Press, Ltd., Oxford. M
- Solid State Technology.* Cowan Publishing Corp., New York. M
- Sound and Vibration.* Acoustical Publications, Inc., Cleveland, Ohio. M
- **South African Mechanical Engineer.* South African Institution of Mechanical Engineers; Kelvin Publications, Ltd., Johannesburg, South Africa. M
- Soviet Astronomy (Astronomicheskii Zhurnal).* American Institute of Physics, Inc., New York. BM
- Soviet Journal of Nondestructive Testing (Defektoskopiia).* Consultants Bureau, New York. BM
- Soviet Journal of Optical Technology (Optiko-Mekhanicheskaya Promyshlennost').* Optical Society of America, Inc., Washington, D.C.; American Institute of Physics, Inc., New York. M
- Soviet Physics — Acoustics (Akusticheskii Zhurnal).* American Institute of Physics, Inc., New York. Q
- Soviet Physics — Doklady (Akademiia Nauk SSSR, Doklady).* American Institute of Physics, Inc., New York. M
- Soviet Physics — JETP (Zhurnal Eksperimental'noi i Teoreticheskoi Fiziki).* American Institute of Physics, Inc., New York. M
- Soviet Physics — Semiconductors (Fizika i Tekhnika Poluprovodnikov).* American Institute of Physics, Inc., New York. M
- Soviet Physics — Technical Physics (Zhurnal Tekhnicheskoi Fiziki).* American Institute of Physics, Inc., New York. M
- Soviet Physics — Uspekhi (Uspekhi Fizicheskikh Nauk).* American Institute of Physics, Inc., New York. BM
- Soviet Plastics (Plasticheskie Massy).* Rubber and Plastics Research Association of Great Britain; Rubber & Technical Press, Ltd., London. M
- Soviet Powder Metallurgy and Metal Ceramics (Poroshkovaia Metallurgiiia).* Consultants Bureau, New York. M
- Space Life Sciences.* D. Reidel Publishing Co., Dordrecht, Netherlands. Q
- Space Science Reviews.* D. Reidel Publishing Co., Dordrecht, Netherlands. 9 issues per year
- Spaceflight.* British Interplanetary Society, London. M
- SPARMO Bulletin.* Solar Particles and Radiation Monitoring Organization, Meudon, France. Irreg.
- Special Steels Review.* British Steel Corporation, Sheffield, Yorks., England. Q
- **Spectrochimica Acta.* Pergamon Press, Ltd., Oxford. M
- SPIE Journal.* Society of Photo-Optical Instrumentation Engineers, Redondo Beach, Calif. BM
- **Der Stahlbau.* Wilhelm Ernst & Sohn, Berlin, West Germany. M
- Sterne und Weltraum.* Verlag Bibliographisches Institut AG, Mannheim, West Germany. M
- Strain.* British Society for Strain Measurement, London. Q
- Strength of Materials (Problemy Prochnosti).* Consultants Bureau, New York. Q
- Studia Geophysica et Geodaetica.* Československá Akademie Věd, Prague. Q
- Studies in Applied Mathematics.* MIT Press, Cambridge, Mass. Q
- Studii și Cercetări de Astronomie.* Academia Republicii Socialiste Romîne, Bucharest. SA
- Studii și Cercetări de Fizică.* Academia Republicii Socialiste Romîne, Bucharest. 10 issues per year
- Studii și Cercetări de Mecanică Aplicată.* Academia Republicii Socialiste Romîne, Bucharest. BM
- Studii și Cercetări Matematice.* Academia Republicii Socialiste Romîne, Bucharest. 10 issues per year
- Sulzer Technical Review.* Sulzer Brothers, Ltd., Winterthur, Switzerland. Irreg.
- Surface Science.* North-Holland Publishing Co., Amsterdam. M
- Systems, Computers, Controls (Denshi Tsushin Gakkai Ronbunshi).* Institute of Electronics and Communication Engineers of Japan; Scripta Publishing Corp., Washington, D.C. BM
- Tech Air.* Society of Licensed Aircraft Engineers and Technologists, Kingston-upon-Thames, England. M
- Technika Lotnicza i Astronautyczna.* Stowarzyszenie Inżynierów i Techników Mechaników Polskich, Sekcja Lotnicza; Naczelna Organizacja Techniczna, Warsaw. M
- Technisch-ökonomische Informationen der zivilen Luftfahrt.* Hauptverwaltung der Zivilen Luftfahrt, Zentralflughafen Berlin-Schönefeld, East Germany. M
- Technische Akademie Wuppertal, Berichte.* Technische Akademie, e.V., Wuppertal; Vulkan-Verlag, Dr. W. Classen Nachf. GmbH, Essen, West Germany. Irreg.
- Technische Mitteilungen Krupp, Forschungsberichte.* Fried. Krupp GmbH, Essen, West Germany.
- Technische Mitteilungen Krupp, Werksberichte.* Fried. Krupp GmbH, Essen, West Germany. Q

- Technology Review*. Massachusetts Institute of Technology, Cambridge, Mass. 9 issues per year
- **Technometrics*. American Statistical Association, Washington, D.C. Q
- Telecommunication Journal of Australia*. Telecommunication Society of Australia, Melbourne. Q
- Telecommunications*. Horizon House, Dedham, Mass. M
- Telecommunications and Radio Engineering. Part I — Telecommunications, Part II — Radio Engineering (Elektrosviaz', Radiotekhnika)*. Scripta Publishing Corp., Washington, D. C. M
- Teledyne Ryan Aeronautical Reporter*. Teledyne Ryan Aeronautical, San Diego, Calif. Q
- Telemetry Journal*. International Foundation for Telemetering; Value Engineering Publications, Inc., Los Angeles. BM
- Tellus*. Svenska Geofysiska Föreningen, Stockholm; Almqvist & Wiksells Boktryckeri AB, Uppsala. BM
- Telonde*. Thomson-CSF, Paris. Q
- Teoreticheskaia i Matematicheskaia Fizika*. Akademiia Nauk SSSR; Izdatel'stvo Nauka, Moscow. M
- Teoriia Funktsii, Funktsional'nyi Analiz i ikh Prilozheniia*. Izdatel'stvo Khar'kovskogo Gosudarstvennogo Universiteta, Kharkov. Irreg.
- Teoriia Veroiatnostei i ee Primneniia*. Akademiia Nauk SSSR; Izdatel'stvo Nauka, Moscow. Q
- Teoriia Veroiatnostei i Matematicheskaia Statistika*. Izdatel'stvo Kievskogo Universiteta, Kiev. Irreg.
- Teplofizika i Teplotekhnika*. Akademiia Nauk Ukrainskoi SSR; Izdatel'stvo Naukova Dumka, Kiev. Irreg.
- Teplofizika Vysokikh Temperatur*. Akademiia Nauk SSSR; Izdatel'stvo Nauka, Moscow. BM
- Teplotyve Napriazheniia v Elementakh Konstruktsii*. Akademiia Nauk Ukrainskoi SSR, Institut Mekhaniki; Izdatel'stvo Naukova Dumka, Kiev. Irreg.
- **Tetrahedron*. Pergamon Press, Ltd., Oxford. SM
- **Textile Research Journal*. Textile Research Institute, Princeton, N.J. M
- Thermochimica Acta*. Elsevier Publishing Co., Amsterdam. BM
- Tohoku University, Institute of High Speed Mechanics, Reports*. Tohoku University, Sendai. Irreg.
- Tohoku University, Research Institute for Strength and Fracture of Materials, Reports*. Tohoku University, Sendai. Irreg.
- Tohoku University, Science Reports, Series 5 — Geophysics*. Tohoku University, Sendai. Irreg.
- Tohoku University, Technology Reports*. Tohoku University, Sendai. Irreg.
- Tokyo, University, Institute of Space and Aeronautical Science, Bulletin*. Tokyo, University, Institute of Space and Aeronautical Science, Tokyo. Q
- Tokyo, University, Institute of Space and Aeronautical Science, Report*. Tokyo, University, Institute of Space and Aeronautical Science, Tokyo. Irreg.
- Tokyo, University, Tokyo Astronomical Observatory, Annals, Second Series*. Tokyo, University, Tokyo. Irreg.
- Tokyo Astronomical Observatory, Tokyo Astronomical Bulletin, Second Series*. Tokyo Astronomical Observatory, Tokyo. Q
- Tokyo Institute of Technology, Bulletin*. Tokyo Institute of Technology, Tokyo. Irreg.
- Torino, Accademia delle Scienze, Classe di Scienze Fisiche, Matematiche e Naturali, Atti*. Torino, Accademia delle Scienze, Turin. Irreg.
- Toshiba Review*. Tokyo Shibaura Electric Co., Ltd., Tokyo. BM
- **Toxicology and Applied Pharmacology*. Academic Press, Inc., New York. BM
- **Transplantation*. Williams & Wilkins Co., Baltimore, Md. M
- Transport Theory and Statistical Physics*. Marcel Dekker, Inc., New York. Q
- Transporturi Auto, Navale si Aeriene*. Ministerul Transporturilor and Consiliul National al Inginerilor si Technicienilor, Bucharest. M
- TsAGI, Uchenye Zapiski*. Tsentral'nyi Aero-Gidrodinamicheskii Institut, Moscow. BM
- Tsvetnaia Metallurgii*. Ministerstvo Vysshogo i Srednego Spetsial'nogo Obrazovaniia SSSR; Izdanie Severokavkazskogo Gornometallurgicheskogo Instituta, Ordzhonikidze. BM
- Twente University of Technology, Physical Communications*. Twente University of Technology, Enschede, Netherlands.
- Ukrains'kii Fizichnii Zhurnal*. Akademiia Nauk Ukrain'skoi RSR, Kiev. M
- Ukrainskii Matematicheskii Zhurnal*. Akademiia Nauk Ukrainskoi SSR; Izdatel'stvo Naukova Dumka, Kiev. BM
- Ultrasonics*. Iliffe Science & Technology Publications, Ltd., Guildford, Surrey, England. Q
- Unione Matematica Italiana, Bollettino*. Nicola Zanichelli Editore, Bologna. BM
- Universitas Comeniana, Acta Facultatis Rerum Naturalium — Mathematica*. Slovenské Pedagogické Nakladateľstvo, Bratislava. Irreg.
- Universität Innsbruck, Veröffentlichungen*. Universität Innsbruck, Innsbruck, Austria. Irreg.
- Uspekhi Fizicheskikh Nauk*. Akademiia Nauk SSSR; Izdatel'stvo Nauka, Moscow. M
- VDI-Forschungsheft*. Verein Deutscher Ingenieure; VDI-Verlag GmbH, Düsseldorf. BM
- VDI-Z*. Verein Deutscher Ingenieure; VDI-Verlag GmbH, Düsseldorf. SM
- VDI-Z Fortschritt-Berichte, Reihe 6 — Energietechnik, Wärmetechnik*. Verein Deutscher Ingenieure; VDI-Verlag GmbH, Düsseldorf. Irreg.
- VertiFlite*. American Helicopter Society, Inc., New York. M
- Vibrotechnika*. Izdatel'stvo Mintis, Vilnius. Irreg.
- Le Vide*. Société Française des Ingénieurs et Techniciens du Vide, Paris. BM
- Vilnius, Astronomijos Observatorijos, Biuletenis*. Vilnius. Irreg.
- Vision Research*. Pergamon Press, Ltd., Oxford. M
- Voenno-Meditsinskii Zhurnal*. Tsentral'noe Voenno-Meditsinskoe Upravlenie Ministerstva Oborony SSSR; Izdatel'stvo Krasnaia Zvezda, Moscow. M

- Voprosy Biokhimii Mozga.* Izdatel'stvo Akademii Nauk Armianskoi SSR, Yerevan. Irreg.
- Voprosy Dinamiki i Prochnosti.* Rizhskii Politekhicheskii Institut; Izdatel'stvo Zinatne, Riga. Irreg.
- Vychislitel'naia i Prikladnaia Matematika.* Izdatel'stvo Kievskogo Universiteta, Kiev. Irreg.
- Vychislitel'naia Tekhnika i Voprosy Kibernetiki.* Leningradskii Gosudarstvennyi Universitet, Vychislitel'nyi Tsentr; Izdatel'stvo Moskovskogo Universiteta, Moscow. Irreg.
- Wärme- und Stoffübertragung.* Springer Verlag, Berlin. Q
- Wear.* Elsevier Sequoia S.A., Lausanne. M
- Wehrmedizinische Monatsschrift.* J. F. Lehmanns Verlag, Munich. M
- Welding Journal.* American Welding Society, New York. M
- Welding Production (Svarochnoe Proizvodstvo).* Welding Institute, Cambridge. M
- Weltraumfahrt Raketentechnik.* Umschau Verlag, Frankfurt/Main. BM
- **Western Pharmacology Society, Proceedings.* Ed. James M. Dille, University of Washington, Seattle.
- Westinghouse Engineer.* Westinghouse Electric Corp., Pittsburgh, Pa. BM
- Wetter und Leben.* Österreichische Gesellschaft für Meteorologie; Verlag Wetter & Leben, Vienna. BM
- Wissenschaftliche Berichte AEG-Telefunken.* AEG-Telefunken, Berlin. Q
- Wissenschaftliche Zeitschrift.* Dresden, Technische Universität, Dresden, East Germany. BM
- WRC Bulletin.* Welding Research Council, New York. 10 issues per year
- Zagadnienia Drgań Nieliniowych.* Polska Akademia Nauk, Instytut Podstawowych Problemów Techniki; Państwowe Wydawnictwo Naukowe, Warsaw. Irreg.
- Zashchitnye Pokrytiia na Metallakh.* Akademiia Nauk Ukrainskoi SSR, Institut Problem Materialovedeniia; Izdatel'stvo Naukova Dumka, Kiev. Irreg.
- Zastosowania Matematyki.* Polska Akademia Nauk, Instytut Matematyczny; Państwowe Wydawnictwo Naukowe, Warsaw. 3 issues per year
- Zeitschrift für angewandte Mathematik und Mechanik.* Akademie-Verlag GmbH, Berlin. M
- Zeitschrift für angewandte Mathematik und Physik.* Birkhäuser Verlag, Basel. BM
- Zeitschrift für angewandte Physik.* Deutsche Physikalische Gesellschaft, e.V.; Springer Verlag, Berlin. M
- Zeitschrift für experimentelle und angewandte Psychologie.* Deutsche Gesellschaft für Psychologie; Verlag für Psychologie, Göttingen. Q
- Zeitschrift für Flugwissenschaften.* Deutsche Gesellschaft für Luft- und Raumfahrt, e.V., and Deutsche Forschungs- und Versuchsanstalt für Luft- und Raumfahrt, e.V.; Friedr. Vieweg & Sohn GmbH, Braunschweig. M
- Zeitschrift für Geophysik.* Deutsche geophysikalische Gesellschaft, Hamburg; Physica-Verlag, Würzburg, West Germany. BM
- Zeitschrift für Luftrecht und Weltraumrechtsfragen.* Köln, Universität, Institut für Luftrecht und Weltraumrechtsfragen; Carl Heymanns Verlag, KG, Cologne. Q
- Zeitschrift für Metallkunde.* Deutsche Gesellschaft für Metallkunde, e.V.; Riederer-Verlag GmbH, Stuttgart, West Germany. M
- Zeitschrift für Meteorologie.* Meteorologische Gesellschaft; Akademie-Verlag GmbH, Berlin. Irreg.
- Zeitschrift für Naturforschung, Teil a.* Verlag der Zeitschrift für Naturforschung, Tübingen. M
- Zeitschrift für Physik.* Deutsche physikalische Gesellschaft; Springer Verlag, Berlin. Irreg.
- Zeitschrift für Vermessungswesen.* Deutscher Verein für Vermessungswesen; Verlag Konrad Wittwer, Stuttgart, West Germany. M
- Zemlia i Vselennaia.* Akademiia Nauk SSSR; Izdatel'stvo Nauka, Moscow. BM
- Zentralblatt für Verkehrs-Medizin, Verkehrs-Psychologie, Luft- und Raumfahrt-Medizin.* Deutsche Gesellschaft für Luft- und Raumfahrt-Medizin and Deutsche Gesellschaft für Verkehrs-Medizin; J. F. Lehmanns Verlag, Munich. Irreg.
- Zhurnal Eksperimental'noi i Teoreticheskoi Fiziki.* Akademiia Nauk SSSR; Izdatel'stvo Nauka, Moscow. M
- **Zhurnal Evoliutsionnoi Biokhimii i Fiziologii.* Akademiia Nauk SSSR; Izdatel'stvo Nauka, Leningrad. BM
- Zhurnal Nauchnoi i Prikladnoi Fotografii i Kinematografii.* Akademiia Nauk SSSR; Izdatel'stvo Nauka, Moscow. M
- Zhurnal Prikladnoi Spektroskopii.* Izdatel'stvo Nauka i Tekhnika, Minsk. M
- Zhurnal Tekhnicheskoi Fiziki.* Akademiia Nauk SSSR; Izdatel'stvo Nauka, Leningrad. M
- Zhurnal Vychislitel'noi Matematiki i Matematicheskoi Fiziki.* Akademiia Nauk SSSR; Izdatel'stvo Nauka, Moscow. BM
- Zhurnal Vysshei Nervnoi Deiatel'nosti.* Akademiia Nauk SSSR; Izdatel'stvo Nauka, Moscow. BM
- Zpráva VZLÚ.* Výzkumný a Zkušební Letecký Ústav, Prague. Irreg.
- Zpravodaj VZLÚ.* Výzkumný a Zkušební Letecký Ústav, Prague. BM

A Notation of Content, rather than the title of the publication, appears under each subject heading; it is listed under several subject headings which provide multiple access to the subject of each accession. The IAA accession number is located under and to the right of the Notation of Content. It is preceded by numbers identifying the issue and page of *International Aerospace Abstracts* where the abstract is located.

To illustrate:

Issue Number	Page Number	Accession Number
05	p795	A71-16573

A

A STARS

Ap-type magnetic stars wavelength dependent polarization, discussing polarimetric observations in different spectrum regions

01 p0153 A71-10355

Hertzsprung-Russell diagram calibration in terms of age and mass for main sequence B and A stars

04 p0646 A71-15234

Magnetic stars, discussing stellar magnetic fields, Ap stars, crossover effect, period line width correlation, overabundances and models

04 p0648 A71-15245

Plutonium in peculiar A stars surfaces as nuclear cosmochronology for determination of r process nuclei age, considering emission line spectra obscurement

05 p0808 A71-16413

High dispersion spectrograms of manganese Ap stars alpha And and pi Boo A, estimating electron concentration

07 p1204 A71-20632

Sr-Cr-Eu class Ap magnetic stars mean surface field estimates, using broadened absorption line measurements

08 p1359 A71-20939

Mn type peculiar A stars relative abundance from curve of growth analysis, discussing isotope shifts, nucleosynthesis, explosion reactions and structure acceleration

09 p1529 A71-23596

Ap and Am stars distribution and ages, considering high proportion in Hyades, Sirius, Praesepe and Coma Berenice clusters

16 p2633 A71-33333

Main sequence A and early F stars with shallow convective envelopes, investigating particle diffusion effects on element abundance data

18 p2960 A71-35939

Eclipsing binaries among Wolf-Rayet AO Cassiopeia and U Geminorum stars from photometric observations

20 p3300 A71-39821

Magnetic A stars accretion model, investigating spectra, abundances, ion capture and braking

21 p3439 A71-40051

Low dispersion luminosity criteria in A and F stars, computing synthetic spectra for atmospheric temperature surface gravity microturbulence and abundance

22 p3601 A71-42166

Rapid neutron capture products evidence on peculiar A star surfaces from observation of promethium and heaviest elements abundance

24 p3865 A71-44567

A-7 AIRCRAFT

A-7 low altitude tactical fighter spin evaluation program, discussing maneuvering capability, external stores and departure mode

07 p1018 A71-19094

A-11 SATELLITE

U ECHO 1 SATELLITE

A-12 SATELLITE

U ECHO 2 SATELLITE

A-300 AIRCRAFT

European air traffic employed in transportation of tourists, considering European Airbus A-300B super twin

19 p3172 A71-37273

ABBREVIATIONS

U SYMBOLS

ABDOMEN

Abdominal pressure decrease resulting in transpulmonary pressure cranio-caudal gradient increase under gravitational effect simulation

13 p2008 A71-28437

Small pressure wave transmission in abdominal venae cavae of dogs in mathematical model development for viscoelastic behavior of large veins

20 p3187 A71-38987

Head and abdomen shielding effects on radiation sickness evolution in dogs under lethal gamma irradiation

22 p3493 A71-42718

Abdomen shielding effects on chromosome aberrations in bone marrow cells of guinea pigs and rats under gamma irradiation

22 p3493 A71-42719

ABEL FUNCTION

Neron-Tate height fine structure of points on Abelian manifolds, considering canonical bounded and diophantine problems

06 p0917 A71-17571

ABERRATION

Aberration analysis for manual retouching of large objective lenses, using unequal arm laser interferometer

04 p0607 A71-14867

Optical systems aberrations, discussing possible deformations transfer from reflecting or refracting elements

05 p0783 A71-17032

Third order aberrations in Cassegrain type telescopes and coma correction in servo-stabilized images

07 p1107 A71-19202

Nonredundant array filtering and postdetection processing for aberration compensation in incoherent imaging

07 p1110 A71-19480

Spherical aberration, limiting magnitude, distortion and coordinate determination accuracy of 20-cm two-camera astrophotograph at Abastumani Astrophysical Observatory

07 p1115 A71-20441

Optical systems with large aberration, deriving merit function expressed as quadratic form of aberration coefficients

08 p1333 A71-21179

Hologram imagery and aberrations computer based analysis, considering hologram geometries and nonchromatic aberrations

08 p1290 A71-21387

Hologram fifth order aberrations, deriving equation and coefficients as functions of hologram construction and reconstruction geometry

08 p1291 A71-21398

Three-beam holographic interferometry featuring sensitivity increase and aberrations compensation

10 p1611 A71-24345

Aberration reduction and optimal in-line and off-axis recording geometry in acoustical holography

12 p1904 A71-26794

Holographic diffraction gratings on plane or concave spherical surface photographic plate, investigating interference fringes and aberration properties

17 p2745 A71-35588

Minimum aberrations in image wave front due to wavelength shift between recording and reconstruction beams in holography, using computer program

18 p2914 A71-35846

Holographic correction of lens aberration in optical system, considering turbulence effect correction

22 p3538 A71-41737

Phase aberrations in Bragg imaging for sound components projecting out of plane normal to light beam

22 p3540 A71-41778

Interference patterns from hologram interferometer related to aberration theory

24 p3826 A71-44980

ABIOTIC GENESIS

Self-sustaining coacervates photochemical formation, discussing enzyme-like properties and abiogenesis

01 p0017 A71-11453

Pentose breakdown photosensitivity from UV irradiation in presence of minerals, considering prebiological period carbohydrates evolution and interaction with purines and pyrimidines

01 p0029 A71-11561

Porphyryns and amino acids chemical bonding under geochemically plausible conditions, considering diagnosis of biogenic compounds and life processes prebiotic chemical evolution

02 p0198 A71-12047

Amino acids synthesis by formaldehyde-ammonia heating and hydrolysis, simulating reactants in weakly reducing atmosphere at volcanic temperatures

03 p0357 A71-13014

Stereoisomeric organic structures in animate nature and life origin on earth

06 p0857 A71-18725

Urea-inorganic phosphate mixtures as prebiotic nucleoside phosphorylating agents

07 p1055 A71-19544

Biophysical model of life origin on earth using primordial gas-small organic molecule-macromolecule-protocell transformations

07 p1043 A71-20125

Extraterrestrial life hypotheses, citing astronomical considerations, inorganic chemical evolution and prebiotic synthesis with emphasis on Mars exploration for microorganisms

07 p1044 A71-20374

Hydrocarbons as foundation for life development universe, discussing chemical composition of galaxy, antimatter existence, interstellar medium and cosmic age factors

13 p2009 A71-28678

Extraterrestrial and earth life genesis, discussing carbon foundation, planetary conditions, water prerequisite and space exploration

13 p2009 A71-28679

Chemical evolution and extraterrestrial life detection, noting cell proliferation methods, automatic biological stations and Mars microorganisms

13 p2009 A71-28680

Hydrocarbons, amino acids and large molecule organic compounds formation in chondrite meteorites by abiogenic reactions

13 p2010 A71-28692

Possible prebiotic synthesis of thymine by heating uracil, paraformaldehyde and hydrazine in ammoniacal solution for three days at 70 C

18 p2855 A71-36231

Cystine synthesis in simulated primitive conditions by UV irradiation of methane, ethane, ammonia, water vapor and hydrogen sulfide in spherical vessel

19 p3014 A71-38678

Abiogenic synthesis of nucleosides, heating adenine and ribose mixture at 170 C in atmosphere of oxygen, nitrogen and carbon dioxide

21 p3346 A71-40576

Methane atmosphere polymerization by solar UV to form primordial oil slick, discussing importance to life development

22 p3535 A71-42074

Organic synthesis in simulated Jovian atmosphere by passing semicorona discharge through methane-ammonia mixture

22 p3602 A71-42180

Polymerized and hydrolyzed polypeptides from condensed amino acid adenylates for prebiological synthesis model

22 p3508 A71-42232

ABLATION

Solar system organic compounds detection and evolution, considering element, isotope and pigment composition, optical activity and polymerization 22 p3496 A71-42824

Prebiotic organic matter in solar system, investigating contamination free amino acid catalytic synthesis from deuterated reactants 23 p3633 A71-43245

ABLATION

Atomic and molecular transport coefficients for various species injected into boundary layer on ablating or transpiration cooled surface 01 p0130 A71-10958

E layer meteor ionization, considering ablation processes effects of meteoroids evaporation and micrometeorites sputtering 03 p0486 A71-13310

Two dimensional incompressible laminar boundary layer flow along ablative blunt body in irradiant environment 04 p0679 A71-15467

Fiberglass-reinforced plastics with and without water content, studying ablation performance 06 p0915 A71-17681

Thoria dispersed Ni-Cr alloy hypersonic entry ablation model, accounting for Cr oxidation [AIAA PAPER 71-34] 06 p1009 A71-18654

Artificial meteors ablation and luminosity measurements, using ballistic range shadowgraph and radiometric equipment for velocity history, shock wave formation and mass loss process 07 p1223 A71-19674

Shock wave interaction with evaporating aerosol for diffusive and ablative models taking into account thermal conductivity 09 p1433 A71-22856

Combustion rate of pure ammonium perchlorate propellants derived from ablation theory 10 p1657 A71-23905

Static aerodynamic characteristics of slender ablating reentry vehicle, discussing coupling between flow field and thermochemical analyses of heat shield materials response [AIAA PAPER 70-826] 11 p1854 A71-25512

Entry vehicle carbon vapor thermochemistry uncertainties effects on nose tip ablation response concerning stagnation point surface recession and temperature levels [AIAA PAPER 71-414] 11 p1857 A71-26207

Reentry spherical vehicles with variable wall thickness, determining heat flux absorption without surface ablation and wake contamination [AIAA PAPER 71-424] 11 p1858 A71-26215

Crosshatched ablation patterns on conical bodies, presenting wind tunnel test results on Mach number, local static pressure and temperature ratio effects 12 p1987 A71-27591

Experimental proof of combustion phenomena in reinforced plastics ablation under simulated atmospheric reentry, using arc plasma jets 12 p1987 A71-27721

NASA-SRI Round Robin Ablation Program summary, discussing dimensional analysis, Teflon, nylon and surface temperature 18 p2985 A71-36279

Heat shields for space applications, reviewing heat sinks, double wall cooling techniques and radiative, transpiration and ablation cooling systems 18 p2848 A71-36433

Carbon difluoride in ablating air-Teflon laminar boundary layers by spectrally and spatially resolved UV thermal radiation measurements 19 p3163 A71-37881

High altitude balloon cosmic dust collection, considering individual particle chemical composition and ablation 20 p3299 A71-39653

Surface patterns of ablating bodies from water jet flow experiment simulation, discussing vortices detection 21 p3317 A71-40019

Monograph on hypersonic low temperature ablation covering cross hatched surface patterns, flow field, turbulent boundary layer, angle of attack, etc [VKI-TN-64] 22 p3621 A71-42031

ABLATIVE MATERIALS

Ablative heat shield char layer, examining reacting nonequilibrium pyrolysis gas flow [AICHE PREPRINT 15B] 01 p0181 A71-11297

Ablative materials performance in high radiative heat flux environments produced by CW carbon dioxide laser [AIAA PAPER 70-864] 03 p0449 A71-14437

Laminar ablating air-Teflon boundary layers with carbon difluoride and atomic fluorine constituents, using UV thermal radiation measurements [AIAA PAPER 71-39] 06 p1008 A71-18500

Cone roll dynamics-ablation patterns coupling in hypersonic wind tunnels 07 p1208 A71-19868

High temperature liquid propellant oxidative-erosion resistant ablative composites containing in situ reaction formed refractory metal carbides for rocket nozzles 08 p1318 A71-20696

Water cooled channel flow test device for arc jet material ablation studies, simulating reentry environment of high energy turbulent boundary layer flow [AIAA PAPER 71-260] 08 p1273 A71-21987

Graphite fiber reinforced ablative composites fabricated into rocket propulsion test units for oxidative liquid high temperature and pressure environments 09 p1459 A71-23685

Thermal conductivity prediction during ablation of phenolic-carbon and phenolic-graphic composites for heating and cooling conditions [AIAA PAPER 71-380] 11 p1783 A71-25304

Ablative plastics - ACS Conference, San Francisco, March-April 1968 11 p1789 A71-26029

Ablative polymers for thermal protection of aerodynamic surfaces, propulsion structures and ground equipment, discussing energy absorption of various polymeric materials 11 p1789 A71-26030

Test streams and chemical composition effects on ablative composites for hypervelocity heat protection of manned atmospheric entry vehicles 11 p1855 A71-26031

Ablative thermal insulation materials testing for naval missile propulsion system application 11 p1789 A71-26032

Epoxy novolac resin-cured alicyclic anhydride amine-catalyzed ablative polymers molecular structure from computer correlation of analytical data 11 p1789 A71-26033

Ablative polymers synthesis from formaldehyde, phenols and ethers reaction products, discussing char yield, thermally stable fillers incorporation and thermogravimetric analysis 11 p1855 A71-26034

Thermosetting polyphenylene resins synthesis and use in reinforced ablative composites, discussing polymerization and curing 11 p1789 A71-26036

Three dimensional reinforced composites for load bearing structural ablator 11 p1789 A71-26037

Epoxy resin heat shield performance prediction based on chemical structure relation to ablative properties, discussing thermal degradation mechanism and char forming reactions 11 p1855 A71-26038

Resin systems for ablative composites, correlating hyperthermal performance characteristics via thermogravimetric, mechanical flexural and ablation tests 11 p1789 A71-26039

Ablation residue, including silicone elastomer foam heat shield material ablative degradation 11 p1855 A71-26040

High performance ablative composites thermal physical characteristics from differential equations, describing thermochemical ablation-in-depth and boundary layer transport processes 11 p1856 A71-26041

High heating rate thermogravimetric analyzer for ablative plastics, predicting response with semiempirical analytical model 11 p1744 A71-26042

Pyrolysis-gas chromatography locating degradation front in phenolic ablative plastics, giving percent phenolic resin vs distance normal to surface 11 p1728 A71-26044

Polymeric ablation materials testing in arc image furnace over various temperatures, pressures and thermal flux 11 p1790 A71-26045

RF transparent ablator of silica filled elastomeric silicone, describing thermal, mechanical and electrical properties at various heating rates 11 p1790 A71-26046

Turbulent submerged wall air jet on ablating graphite surface, examining friction and heat and mass exchange in boundary layer 13 p2160 A71-28569

Multicomponent ionized gas mixtures chemically equilibrated flows over nonporous and ablating surfaces, using Navier-Stokes and Prandtl equations for asymptotically thin boundary layer 13 p2048 A71-28570

Carbon-carbon spacecraft reentry heatshields evaluation and selection by nondestructive and destructive tests on flight cones 14 p2262 A71-29647

Carbon/graphite cloth reinforced aromatic/heterocyclic resins ablative composites pyrolysis kinetics by computer code analysis 14 p2262 A71-29649

Nonequilibrium modeling of pyrolysis gas products flow through char layer of ablative heat shield 14 p2334 A71-29876

Surface temperatures and ablation mechanism of combustion protective plastics reinforced by silica under intense heating measured by IR micropyrometer [ONERA-TP-962] 18 p2984 A71-36028

Jupiter atmosphere entry probes graphite ablative heat shields performance, indicating convective and

radiative blockage and graphite sublimation processes in surface heat balance 19 p3084 A71-37949

Reflecting and ablating Teflon heat shields for radiative environment of outer planets atmosphere [AAS PAPER 71-147] 19 p3084 A71-37950

Carbon-fiber-reinforced carbon composites for high temperature applications, describing filament orientation, matrix composition and heat treatment effects on ablation performance 19 p3085 A71-38350

Elastomeric rocket motor thermal insulants ablation, considering composite properties, heat transfer, compounding and tests 21 p3406 A71-40603

Nonablating inelastic deformable material surface interaction with external supersonic turbulent boundary layer, observing crosshatch patterns 21 p3323 A71-40941

Film ablative cooled gas pressure feed liquid rocket engine unstationary process analysis with digital computer, detailing engine dynamics, heat transfer and temperature profile 22 p3589 A71-42054

ABLATIVE NOSE CONES

Shape and surface roughness effects on turbulent ablation of reentry body nose tip, noting recession rate [AIAA PAPER 69-717] 01 p0071 A71-10934

Three dimensional ablation calculated for reentry sphere-cone taking into account shape changes and internal heat conduction 01 p0180 A71-10952

Axissymmetric ablating graphite nosetip analysis code, demonstrating shape change, heating distribution and internal conduction coupling [AIAA PAPER 71-413] 11 p1856 A71-26206

Graphite heat shield ablation during low velocity low altitude portion of satellite reentry trajectories [AIAA PAPER 71-415] 11 p1857 A71-26208

Graphite ablation under high temperatures for large outer planets entry probes, correlating mass loss rates with surface temperatures and specimen nose cone radii [AIAA PAPER 71-418] 11 p1857 A71-26209

High hyperthermal ablation performance of reinforced carbon-carbon composites for reentry nosetip application [AIAA PAPER 71-416] 12 p1920 A71-26764

Surface roughness effects on heat transfer to ablating cones, using calculation method adaptable to computer routines for smooth wall 15 p2514 A71-32047

Analog analysis of shape history of ablating graphite nose tips of reentry vehicle, eliminating geometrical instabilities 18 p2984 A71-35953

Nonspherical nose bluntness effects on slender vehicle dynamics, considering conical geometry as approximate nose shape after ablation due to turbulent heating [AIAA PAPER 71-931] 19 p3148 A71-37176

Graphitic ablative heat shield fractions and forebody configurations for probe entry into atmospheres of Saturn, Uranus and Neptune [AAS PAPER 71-145] 19 p3141 A71-37948

Conical ablation surface models in hypersonic wind tunnel tests, describing Mach number and nosetip bluntness effects on cross hatching 21 p3476 A71-40965

ABNORMALITIES

NT GEOMAGNETIC HOLLOW

NT MAGNETIC ANOMALIES

NT NEUROSES

NT PSYCHOSES

NT SCHIZOPHRENIA

Ionospheric evening anomaly geographic distribution and relation to neutral winds global pattern 11 p1755 A71-25612

Critical point anomaly in saturation curves of reduced temperature-compressibility planes of pure substances, using metric differential geometry and thermodynamics 18 p2985 A71-36452

Day to day fluctuations of winter anomaly in ionospheric absorption, showing regular and irregular trends 23 p3666 A71-42974

ABORT TRAJECTORIES

Abort and staging separation maneuvers of two equal size reusable lifting entry vehicles in wind tunnel tests [AIAA PAPER 70-260] 01 p0165 A71-11579

ABORTED MISSIONS

Launch facility requirements for liquid fluorine upper stage, considering propellant storage and transfer, vapor disposal, leak detection, spills, aborts and range safety 18 p2898 A71-36457

Apollo lunar explorations, reviewing landing, trajectories, hardware, mission problems and scientific studies 20 p3295 A71-39613

Apollo command module land landing capability in case of abort after liftoff, describing Monte Carlo simulation procedure

22 p3573 A71-42776

ABRASION

Plastic deformation of aluminum oxide by indentation and abrasion at room temperature, using transmission electron microscopy

13 p2093 A71-28989

ABRASION RESISTANCE

Hard metals and WC-Co alloy stress and heat treatment effect on coercive force, crack formation energy and abrasive resistance

06 p0911 A71-17342

Far IR cryogenic black paints absorptive throughout IR with surface stability at liquid He temperature and resistance to abrasion and flaking

08 p1335 A71-21383

Surfacing materials based on transition metal borides with boron carbide additions, testing brittleness, hardness and abrasive wear resistance

15 p2431 A71-32163

Diboride-nitride system dry friction and wear resistance at room temperature

23 p3681 A71-43254

ABRASIVES

NT CARBORUNDUM [TRADEMARK]

Chemical composition effect of low carbon alloys metallic matrix on wear resistance in abrasive medium, showing austenitic manganese alloys superiority to martensitic or ferritic alloys

07 p1136 A71-19630

Brittle materials ultrasonic machining, discussing abrasive particle shape, size, temperature and pressure effects on process accuracy, speed, quality and efficiency

10 p1617 A71-24133

Abrasive capability, shape and strength of refractory powders of fused titanium and niobium carbides and calcium boride compared with synthetic corundum

16 p2592 A71-33574

Chemical composition effect of low carbon alloys metallic matrix on abrasive wear resistance, showing austenitic manganese alloys superiority to martensitic or ferritic alloys

16 p2593 A71-33626

Adhesion effects on interactions between abrasive and metal surfaces in grinding operations as function of grinding speed and contact surfaces properties

24 p3830 A71-44860

ABRIKOSOV THEORY

Abrikosov vortex lattice in superconductors, calculating resonance linewidth and vacancy formation energy

24 p3860 A71-45119

ABSCISSAS

U COORDINATES

ABSOLUTE TEMPERATURE SCALES

U TEMPERATURE SCALES

ABSORPTIONS

Granular lithium hydroxide as carbon dioxide absorbent for closed cycle life support systems, considering porosity, carrier gas and water vapor pressure and bed temperature

22 p3508 A71-41773

ABSORBERS

Acoustic absorbers for combustion instability prevention, discussing design theory and experimental results

[AIAA PAPER 71-699] 14 p2294 A71-30758

ABSORBERS [MATERIALS]

NT NEUTRON ABSORBERS

NT SOLAR ENERGY ABSORBERS

Laser beam self induced thermal distortion in near field absorbing moving medium by theoretical model based on geometrical optics

07 p1128 A71-20389

Carbon dioxide lasers passive Q switching by saturable absorbers, using four state kinetic model

07 p1128 A71-20390

Single longitudinal mode operation and mode locking of pulsed high pressure transversely excited carbon dioxide laser by saturable absorbers

09 p1463 A71-22758

Plane electromagnetic wave scattering, arbitrarily polarized and normally impinging on wedge tapered absorbing structure

09 p1409 A71-23501

German monograph on absorbed anions effect on Ni and Ni-Mo alloys anodic behavior covering temperature dependence, electrons interaction, sulfide ions activation and magnetic properties

10 p1628 A71-24874

Partition walls sound insulation by porous absorbers, discussing differential equations and acoustic properties

12 p1929 A71-27062

Combined conductive and radiative heat transfer in absorbing and scattering materials, using two-flux model for transport and local energy balance equations solution

13 p2164 A71-28983

Absorbent materials for sound attenuation in turbine reactor ducts, examining flow velocity, absorbent structure and cladding effects

14 p2288 A71-30518

Absorbent materials test methods and acoustic data reduction with simulation principle

14 p2275 A71-30525

Lateral spread of nuclear-electromagnetic cascades in iron absorber from three-dimensional Monte Carlo simulation

15 p2452 A71-31810

Repetitive passive Q switching of single frequency carbon dioxide laser with intracavity saturable absorber, developing nonlinear model

15 p2423 A71-32602

Stark effect saturable absorber modulation of passively Q switched carbon dioxide laser, using difluoroethane, difluoroethylene, methyl fluoroform, trichloroethylene and vinyl chloride

16 p2586 A71-33147

Sound absorptive materials selection for jet aircraft noise control

20 p3178 A71-39451

Ellipsometric determination of optical constants for weakly and strongly absorbing specimen

22 p3576 A71-42572

UV absorber dyes in fluorescent tracers, discussing theory of dimensional sensitivity and use in liquid-film developers to quench background fluorescence

23 p3681 A71-43194

ABSORPTANCE

Transparent dielectrics sheet radiation absorptance, emittance and transmittance determination by Monte Carlo method

01 p0183 A71-11591

Semitransparent spherical dielectric shell under diffuse incident radiation, determining absorptance and reflectance by Monte Carlo method

03 p0518 A71-13648

Local radiative heat transfer and equilibrium temperature between identical uniform surface geometry planes, discussing directional dependent emittance and absorptance effects

[AIAA PAPER 71-76] 06 p1008 A71-18533

Venus-Mercury flyby vehicle solar cells, cover glasses, adhesives and Kapton film, investigating space radiation effects on solar absorptance and transmittance

[AIAA PAPER 71-452] 11 p1859 A71-26236

Spacecraft thermal control coatings for long-duration exposure to near-earth orbital conditions, determining optical properties degradation and solar absorptance

[AIAA PAPER 71-454] 11 p1859 A71-26237

Paint absorptance values effect on passive thermal control system primary component, using calibrated computer satellite model

[AIAA PAPER 71-455] 11 p1859 A71-26238

Solar absorptance sensitivity to thermal surface particulate contamination as function of particle composition, quantity, size and linearity with obscured area

[AIAA PAPER 71-473] 11 p1800 A71-26253

Bright comets particles albedo, absorptivity and size observation by combined IR and optical photometry

14 p2314 A71-30649

Absorptance of anisotropically scattering medium compared with measured hemispherical reflectances and transmittances

[ASME PAPER 71-HT-20] 19 p3165 A71-37991

ABSORPTION

Damkohler analysis of nitrogen-silica gel absorption isotherm in multimolecular range, noting vapor phase transport and absorbed phase diffusivities

03 p0517 A71-13175

Continuous deflection strategies in game problems with motion encounters, discussing absorption sets

05 p0782 A71-16978

Nitrogen chemisorption and absorption on polycrystal Ta ribbons, using static method in ultrahigh vacuum

06 p0940 A71-17298

Plastics for long life microcircuit encapsulation, investigating water absorption and resin-to-lead adhesion effects on reliability

07 p1077 A71-19562

Limiting absorption principle and Schrodinger nonelliptic spectral theory for steady state wave propagation in inhomogeneous anisotropic media

12 p1929 A71-26866

Oxidation and nitrogen absorption protection of Cr alloy by Ni alloy claddings applied by gas pressure bonding

13 p2087 A71-29122

Hydrogen absorption by molten aluminum and Al alloys, considering equilibrium delay in metal-gas system

15 p2435 A71-32334

Saturation effects and mode selection for monofrequency He-Ne lasers with nonlinear absorption

17 p2752 A71-34406

Continuous deflection strategies in game problems with motion encounters, discussing absorption sets

18 p2948 A71-36778

ABSORPTION BANDS

U ABSORPTION SPECTRA

ABSORPTION COEFFICIENT

U ABSORPTIVITY

ABSORPTION CROSS SECTIONS

Comparative numerical capture and experimental reaction cross sections for ion-molecule ammonia

01 p0028 A71-10476

Vibrational degrees of freedom effects on capture cross sections and ion-molecule complexes formation in ion-dipole collisions

01 p0130 A71-10477

Cross sections for single-electron capture by C/4 plus/ from He, Ne and Ar target gases

04 p0630 A71-15656

Atmospheric absorption by oxygen, determining metastable molecules absorption cross section at 1095 A

06 p0888 A71-17290

Symmetric excited state electron capture cross sections in ion-atom inelastic scattering, using two state approximation formulas

08 p1338 A71-21235

Spectral distributions of absorption cross sections of IR radiation by quasi-local oscillations

09 p1494 A71-22885

Vibrational effects on capture cross sections and ion-molecule complexes formation based on ion-dipole collisions, noting multiple reflection probabilities and collision lifetimes

09 p1498 A71-23662

Ammonia-parent ion reaction at low energies, comparing numerical and experimental capture cross sections

10 p1573 A71-24416

Oxygen and carbon dioxide continua absorption cross sections in Schumann and far UV regions by photoelectric technique with vacuum monochromator

11 p1801 A71-25364

Pitch angle distribution effects of auroral electrojet on scattering and absorption of fast precipitated electrons in upper atmosphere, using computerized Monte Carlo technique

13 p2119 A71-27794

Astrophysical and aeronomic UV molecular photoabsorption cross sections, discussing experimental techniques and associated systematic and random errors

14 p2190 A71-29905

Electromagnetic absorption cross sections from wave function of free carriers in semiconductors with point defects

16 p2623 A71-34031

Extragalactic background soft X ray diffuse flux consistent with absorption by Small Magellanic Cloud

20 p3278 A71-39108

External and internal absorption spectra of silicon crystal doubly doped with boron and indium acceptors, interpreting line broadening and cross section decrease

21 p3426 A71-40071

Ion-quadrupole effects in ion-molecule collisions by numerical calculations of capture cross sections and computer-plotter studies of ion trajectories

21 p3419 A71-40906

N-type negative resistance, photoconductivity and I-V characteristics of sulfur-doped p-type Si, showing hole capture cross section dependence on electric field

21 p3429 A71-41204

Spectral dependence of photon capture cross section of negative Zn center in Zn-doped n-type silicon during electron excitation to conduction band

21 p3429 A71-41206

Carbon dioxide absorption temperature dependence in 1750-1200 A region, calculating electron densities and transition moments

23 p3641 A71-43326

ABSORPTION SPECTRA

NT FRAUNHOFER LINES

NT HERZBERG BANDS

NT TELLURIC LINES

Carbon disulfide absorption spectrum measurement in far UV region

01 p0129 A71-10251

Rapid internal standard identification method for metals by atomic absorption spectrophotometry, using diluted acid solution of specimen

01 p0028 A71-10257

IR absorption edge measurement in cadmium antimonide crystals grown with various perfection degrees, considering forbidden band and phonon spectrum anisotropy

01 p0138 A71-10432

Short wave reflected radiation fluxes in atmosphere with absorption allowance for water vapor, carbon dioxide and ozone

01 p0144 A71-10538

Carbon dioxide IR absorption bands at elevated pressures, deriving transmission function

01 p0130 A71-11104

Temperature dependence curves and X ray spectrum analyses of different ferrite compositions, indicating absorption band K-edge shift toward shorter wave region

01 p0139 A71-11111

Absorption line formation in scattering planetary atmospheres with cloud particles 01 p0162 A71-11420

Meteoritic iron oxides abundances from recoilless resonance absorption spectra 02 p0306 A71-11993

Mass estimation for quasars and galactic nuclei with absorption line shift into long wave region 02 p0307 A71-12090

Sulfur hexafluoride absorption lines observation by inverted Lamb dip high resolution spectroscopy, using heterodyne methods 02 p0209 A71-12731

Spectrophotometry of methane and ammonia absorption bands indicating decrease toward Jupiter disk edge 03 p0484 A71-13213

Characteristic energy absorption spectra of dielectric solids from direct IR measurements for single crystal and thin film specimens 03 p0385 A71-13645

Solar Lyman alpha emission line absorption by geocoronal atomic hydrogen, comparing observational data with prediction from models 03 p0496 A71-14510

German monograph on molecules in sunspots, discussing molecular absorption lines in umbral spectra recorded in 1969 04 p0643 A71-14974

Phonon-magnon absorption bands temperature dependences in Ni, Co and Li ferrimagnetic spinels, giving graphical data for Curie points 04 p0637 A71-15106

Stellar spectra and spectral types, discussing spectrographs, identification of lines, intensity measurements, absorption lines, Harvard system, etc 04 p0646 A71-15229

High red shift quasars linear polarization, examining absorption lines and depolarization due to Faraday rotation 04 p0649 A71-15272

Multiple absorption red shifts in quasars, discussing measured properties and negative clues 04 p0650 A71-15584

Galactic sources 18 cm OH emission and/or absorption observation 04 p0657 A71-15759

OH absorption line measurements for longitude range near galactic center, suggesting existence of radial velocity gradient 04 p0657 A71-15760

Supernova remnant kinematic distance estimates, using molecular absorption line velocities with Schmidt model 05 p0805 A71-16107

CO laser emission lines and nitrogen oxides absorption lines spectral coincidences observations 05 p0762 A71-16339

IR radiation absorption by water vapor in atmospheric transmittance windows, discussing fine structure of absorption spectrum 05 p0778 A71-16841

Porphyrins optical and semiconductor properties concerning absorption, electrical conductivity and photoconductivity spectra 06 p0941 A71-17526

Solar photosphere macroturbulence effects on Fraunhofer lines and central intensities of various absorption lines 06 p0975 A71-18443

UV absorption line spectra from HI regions, evaluating X ray and photoionization heating models 07 p1190 A71-18853

Liquid water far IR absorption spectrum, presenting transmission coefficients table 07 p1158 A71-18911

Atmospheric oxygen absorption spectra fluctuations related to presence or absence of jet stream 07 p1151 A71-18912

Calculation methods accuracy for spectral absorption of IR radiation by atmospheric gases, analyzing empirical, numerical integration and spectrum model methods 07 p1151 A71-19148

Electron scattering effect on emission and absorption lines in stellar atmosphere, considering primary radiation sources uniform distribution and photosphere radiation transmission through electron atmosphere 07 p1192 A71-19291

Absorption line blanketing, back warming and blocking effects on B and V magnitudes for F-G stars 07 p1193 A71-19295

Optical absorption spectra in Cu-doped p-type GaAs samples 07 p1177 A71-19498

Color changes and absorption line variations in M31, M32 and NGC 4472, attempting synthesis of M31 disk population 07 p1197 A71-19814

Contour maps of antenna temperature in W31 region, discussing H I absorption features 07 p1198 A71-19816

Ionized gas galactic cluster stabilization model construction, considering ionizing radiation enhanced

cosmic flux and quasar PKS 1116 plus 12 absorption spectrum 07 p1198 A71-19830

Erbium ions stimulated emission, spectroscopic properties, pulsed laser action and absorption spectra in yttrium orthoaluminate 07 p1126 A71-20165

Absorption peaks mode numbers and separation using magnetostatic spin waves in axially magnetic YIG rods 07 p1180 A71-20172

Quasars red shift and absorption lines observations, discussing distance measurement, brightness and intergalactic matter 07 p1200 A71-20211

Sunspot boundary displacement toward limb in Fe I, Ti I and H alpha lines in passing from continuum to absorption line observations, discussing Wilson effect 07 p1205 A71-20635

Radiation transport equations for stellar atmosphere model with variable depth magnetic field, considering absorption line formation and polarization characteristics 07 p1205 A71-20637

Electron paramagnetic resonance and optical absorption spectra of transition metal ions in zoisite crystal 08 p1343 A71-20658

Intermediates structure and IR spectrum in OH reaction with CO by vacuum UV photolysis, studying refractive product absorptions and valence force potentials 08 p1336 A71-20661

Carbon dioxide IR absorption bands at elevated pressures, deriving transmission function 08 p1337 A71-20848

Sr-Cr-Eu class Ap magnetic stars mean surface field estimates, using broadened absorption line measurements 08 p1359 A71-20939

Equivalent widths of CO lines in interstellar absorption spectrum of zeta Ophiuchi 08 p1360 A71-20982

Upper atmosphere hydroxyl emission mechanism, discussing absorption band, energy balance, atomic hydrogen and ozone in lower thermosphere and nitrogen oxides 08 p1277 A71-21006

Mass estimation for quasars and galactic nuclei with absorption line shift into long wave region 08 p1362 A71-21140

Organic scintillators as active laser materials, discussing absorption, oscillation and emission spectra and luminescence quantum yield 09 p1461 A71-22386

Energy transmission mechanism in calcium fluoride-europium ion plus holmium ion system, investigating luminescence and absorption spectra 09 p1461 A71-22388

Fluorapatite single crystals absorption spectra and luminescent characteristics under activation by rare earth ions, noting line widening dependence on crystal composition 09 p1507 A71-22390

Atmospheric attenuation in IR windows near sea level from transmittance spectral curves, discussing continuum absorbance 09 p1437 A71-22740

Spectrographic measurements of Jovian Red Spot and Southern Tropical Zone molecular absorption bands related to cloud cover density and depth 09 p1520 A71-22839

Silica minerals in interstellar dust as source of 2200 A interstellar absorption band from comparisons to 2250 A band in Fe or Al bearing quartz spectra 09 p1522 A71-22936

Milky Way northern portion absorption values obtained from star cluster data 09 p1524 A71-23184

Sunspots umbrae spectrum analysis in 4000-8000 A region, identifying molecular absorption lines photoelectrically 10 p1666 A71-23785

NGC 2655 galaxy nucleus emissive gas/absorption line widths and stellar population, using network spectrographs 10 p1667 A71-23827

Spectral transmittance of pressure induced and intrinsic absorption of IR energy by carbon dioxide and water due to Fermi bands and asymmetric molecules 10 p1644 A71-23950

Na I absorption spectrum interpretation between 150 and 900 A in vacuum UV, noting various discrete features 10 p1676 A71-24500

Large Cerenkov detectors in absorption spectrometers during high mountain cosmic ray measurements 10 p1612 A71-24668

Half widths calculation for carbon dioxide broadened water vapor absorption lines in nu sub 2 fundamental, considering dipole-quadrupole interactions 10 p1645 A71-24966

CO absorption spectrum in carbon dioxide atmosphere, comparing self- and nitrogen-broadened half widths 10 p1645 A71-24968

Oxygen and carbon dioxide continua absorption cross sections in Schumann and far UV regions by photoelectric technique with vacuum monochromator 11 p1801 A71-25364

He I absorption line profiles in normal main sequence B star spectra, discussing He abundance and LTE 11 p1821 A71-25536

Venus atmosphere spectra, emphasizing line and continuum absorption coefficients relative to scattering 11 p1823 A71-25697

Martian surface pressure from 1967-1969 apparition observations, discussing micron bands carbon dioxide abundances 11 p1825 A71-25711

Saturn cloud layer molecular absorption from spectral/photographic and photoelectric observations 11 p1827 A71-25730

Interstellar absorption and color excesses in Sco OB-1 from spectral observation and photometry for star cluster and association background 11 p1831 A71-26133

Solar photosphere macroturbulence effects on Fraunhofer lines and central intensities of various absorption lines 12 p1955 A71-26593

Taurus dust cloud magnetic field line of sight component observations and M17 and Cyg A absorption spectra data noting Zeeman splitting at 21 cm H lines 12 p1957 A71-26623

Galactic radio emission, considering continuum radiations, radio polarization, H I regions structure and physics, recombination and absorption lines 12 p1959 A71-26778

Hot water vapor curve of growth, using statistical band model with exponential line intensity distribution yielding spectral absorption coefficients 12 p1904 A71-26793

Refractive index and reflectivity of BiTeBr and BiTeI single crystals from interference measurements in transmission spectra 12 p1944 A71-27545

Gadolinium molybdate neodymium ions stimulated emission, noting luminescence, absorption and spectroscopic properties 13 p2111 A71-28424

Inhomogeneous atmosphere transmission functions, noting Lindholm line shift in O absorption spectra effects 13 p2063 A71-29019

Inverted combination light scattering in liquid and solid crystals, showing polarization effects on absorption coefficient 13 p2101 A71-29020

Crystalline media impurity light absorption spectral band shape, noting laser resonance emission effects 13 p2080 A71-29023

Absorption spectra enhancement by organic dye laser quenching, considering applications for absorbing species spectroscopic detection 13 p2082 A71-29439

Absorbed energy spectra and absorption frequencies from elastic constants of vibrating metals with cubic lattice structure, using cold neutron scattering 14 p2190 A71-30149

Saturn polarimetric observation, noting rings polarization Stokes parameters, methane absorption bands and continuous spectrum 15 p2482 A71-31336

Saturn atmospheric structure and optical properties, investigating methane absorption bands 15 p2483 A71-31337

Arc heated plasma expansion through nozzle, observing population inversion of neutral carbon self-absorption UV atomic line [AIAA PAPER 71-592] 15 p2454 A71-31537

Platinum, palladium and gold detection in silver assay buttons by atomic absorption spectrophotometry 15 p2367 A71-31649

Aircraft noise measurements, noting ground absorption effects 15 p2450 A71-32127

CH free radicals detection in oxyacetylene flame magnetic resonance absorption spectrum by IR water vapor laser 15 p2420 A71-32380

Critique of papers on line formation in magnetic fields, discussing dispersion in absorption matrix 15 p2496 A71-32741

Methane, ammonia and silicate effects on 3.07 micron ice absorption in interstellar grains, using cesium iodide window deposited sample measurements 15 p2498 A71-32774

Group 3A suboxides IR absorption spectra at liquid helium temperatures, measuring bending frequencies and modes 16 p2538 A71-32875

Radiation defects isochronal annealing effects on absorption spectral distribution of gallium arsenide irradiated with fast neutron flux 16 p2620 A71-33184

Molecular oxygen densities at 80-160 km by rocket sounding with absorption of solar Lyman alpha line and C IV doublet at 1550 Å 16 p2574 A71-33966

Energy spectrum parameters from Burstein-Moss effect observation in thin CdO layers, explaining absorption edge shape at various electron concentrations 16 p2622 A71-34029

Black radiation absorption by isothermal gas in entire spectrum, discussing Hottel empirical formula 17 p2836 A71-34214

Quasi-stellar objects, investigating velocity dispersion, column densities and abundance of Mg and Fe in absorbing region by Stromgren method of line pairs 17 p2797 A71-34371

Organic dye laser properties analysis using universal relation between absorption and emission spectra for solvent molecules reorientation after excitation 17 p2752 A71-34388

Frequency selection in He-Ne laser with Ne cell inside resonator effecting nonlinear frequency absorption 17 p2752 A71-34407

Combined differential Faraday and absorption measurements, extracting total electron content, ratio to density squared integral and irregularity sensitive parameter 17 p2698 A71-34428

Vacuum pump fluids spectral absorption coefficient measurement, using variable UV cell 17 p2784 A71-35141

Reflecting layer model for methane band absorption spectrum in Jovian atmosphere 17 p2807 A71-35412

Absorption spectra formation by diffuse reflection from semiinfinite plane parallel scattering planetary atmosphere, using asymptotic expressions for higher order scattering 17 p2736 A71-35568

Excited state absorption in sulfur hexafluoride traversed by carbon dioxide laser beam 18 p2933 A71-37014

Far IR collision induced spectrum in carbon dioxide, observing temperature and pressure dependence in gas phase and absorption in liquid 19 p3106 A71-38051

Formaldehyde absorption and emission lines in Orion IR nebula, indicating pumping suppression by neutral particle collisions 20 p3288 A71-39113

Polycrystalline barium titanates solid solutions with fluorine displacement of oxygen atoms, observing IR absorption spectra 20 p3276 A71-39151

Jovian planets methane and ammonium absorption bands spectrophotometric investigation, noting Saturn spectral variations 20 p3290 A71-39311

SiH molecular ion identification in solar atmosphere by solar absorption spectra 20 p3294 A71-39547

Upper atmosphere hydroxyl emission mechanism, discussing absorption band, energy balance, atomic hydrogen and ozone in lower thermosphere and nitrogen oxides 20 p3218 A71-39586

Millimeter and submillimeter laser action in symmetric tip molecules optically pumped via parallel absorption bands 20 p3246 A71-39759

External and internal absorption spectra of silicon crystal doubly doped with boron and indium acceptors, interpreting line broadening and cross section decrease 21 p3426 A71-40071

Gadolinium molybdate-neodymium ions stimulated emission, noting luminescence, absorption and spectroscopic properties 21 p3427 A71-40082

Spectral analysis of Markarian galaxies, observing emission and absorption lines and hydrogen reversal 21 p3441 A71-40105

Mercury determination in terrestrial and nonterrestrial rock samples by atomic absorption spectroscopy, noting high temperature release patterns 21 p3346 A71-40863

Electroabsorption spectra of cadmium telluride at photon energies smaller than forbidden band width, observing energy levels 21 p3429 A71-41212

Cyclotron absorption and resonance spectra of hot electrons in p-type InSb samples cut from single crystals containing different amounts of impurities 21 p3430 A71-41226

Magneto-optical oscillatory absorption spectrum of tin oxide crystal at 1.3 K observed beyond band-band absorption edge with peaks as function of magnetic field 21 p3431 A71-41235

Cadmium-tin-arsenide conduction and valence band structure parameter refinement from Faraday effect and absorption spectra of single crystals in polarized light 21 p3433 A71-41319

Lead oxide pigment photoconductivity, investigating surface processes effects on spectral sensitivity and absorption spectrum 21 p3434 A71-41329

Quasi-binary InAs-GaP single crystals absorption and diffuse reflection spectra, determining forbidden bandwidth as function of compound composition 21 p3434 A71-41332

Atmospheric molecular absorption spectra in IR region, using 15 meter multiple pass absorption cell 22 p3544 A71-42141

Electronic double differentiator for producing spectroscopic absorption curves second derivatives, considering application to polymers IR examination 22 p3545 A71-42154

Interstellar silicate absorption search using VI Cyg No 12 spectrum observations 22 p3605 A71-42349

Computer controlled image orthicon tube for low light level spectroscopy of metastable excited ions transient absorption spectra 22 p3549 A71-42558

Saturn polarimetric observation, noting rings polarization, Stokes parameters, methane absorption bands and continuous spectrum 22 p3606 A71-42611

Saturn atmospheric structure and optical properties, investigating methane absorption bands 22 p3606 A71-42612

Laboratory analog simulation of absorption line spectra in cloudy planetary atmospheres, comparing with computational model based on plane parallel atmosphere 23 p3700 A71-43075

Single frequency He-Ne laser stabilization by Lorentz absorption contour in external gas cell, obtaining error signal based on absorption line scanning 23 p3683 A71-43396

Mott exciton differential absorption spectrum in parallel and crossed electric and strong magnetic fields 23 p3716 A71-43479

Oxidation state of iron and cation distribution over M1 and M2 sites in clinopyroxenes from Apollo 12 by Mossbauer absorption spectroscopy, noting cooling history 23 p3738 A71-43609

IR vibrational spectroscopic analysis of Apollo 11 and 12 rocks and dust isolated silicate minerals, using LF absorption bands 23 p3759 A71-43766

Apollo 11 and 12 rocks dielectric constants, discussing far IR absorption spectrum of fines 23 p3760 A71-43772

Interferometric measurements of 142 solar absorption lines in light from solar disk center 23 p3767 A71-43835

Mg isotopes in solar atmosphere, analyzing absorption bands in sunspot spectrum 23 p3767 A71-43837

K and M class stars B and V magnitudes in UVB system based on atomic lines and molecular bands spectral absorption 23 p3771 A71-44306

IR spectra temperature dependence of CsI crystals doped with sulfate and carbonate anions and Pb and Cd cations, observing intensive absorption bands 24 p3860 A71-44665

Galactic nucleus X ray source observations by Uhuru satellite, discussing emission and absorption spectra 24 p3866 A71-44915

Galactic neutral hydrogen absorption line spectra at 21 cm wavelength by radio sources interferometric observations, discussing cool gas temperature, ionization rate and Cetus Arc distance 24 p3873 A71-45084

Atomic hydrogen cloud distances determined by interstellar absorption lines of early stars 24 p3874 A71-45145

Absorption spectra of benzene, naphthalene and anthracene crystals, noting resonance coupling type effect on vibrational spectrum 24 p3851 A71-45171

Absorption spectrum of atmospheric gases from laser spectrometer based on tunable ruby laser, measuring water vapor absorption coefficients in multipass cell 24 p3834 A71-45207

HgTe-CdTe thin films structural and optical properties, measuring absorption spectra in UV, IR and visible regions to determine Te contents effect 24 p3862 A71-45251

ABSORPTION SPECTROSCOPY

Absorption intensities of R branch J manifolds of methane band, using half widths and pressure shifts 19 p3106 A71-37410

Apollo 14 lunar soils chemical element concentrations by atomic absorption spectrophotometry and isotope dilution 20 p3292 A71-39381

ABSORPTIVE INDEX

U ABSORPTIVITY

ABSORPTIVITY

Weakly divergent electromagnetic wave beam propagation in optically nonlinear laminarly inhomogeneous medium, considering absorption coefficient and self focusing 01 p0037 A71-11201

Soviet book on optical properties of hot air covering spectral lines, radiative transfer, cross sections, pressure effects and absorptivity 03 p0460 A71-14397

Absorption coefficient of plane wave scattering by thin spherical resistive shell for broadband RF radiation monitoring 04 p0558 A71-15149

Carbon monoxide fundamental band spectral absorptivity distributions at various high temperatures and optical densities 04 p0549 A71-15512

Normal incidence sound absorption coefficient by propagating narrow bandwidth sinusoidal pulse and measuring amplitude before and after reflection 05 p0781 A71-16276

Radiative transfer in nonuniform turbid medium with constant absorption coefficient 05 p0742 A71-16840

Aircraft flyover noise samples, obtaining atmospheric absorption coefficients 08 p1231 A71-21425

Low temperature laboratory measurements of ozone absorption coefficients for atmospheric standards, using Dobson spectrophotometer and quartz iodine source 09 p1438 A71-23026

Umkehr inversion system for vertical ozone distribution observation, calculating error due to ignorance of temperature dependence of ozone absorption 09 p1489 A71-23447

Homogeneous Gaussian beam propagation in inhomogeneous negative absorption media, noting amplification of plane wave 11 p1798 A71-25665

Flash photolysis produced methyl and methylene radical transitions maximum extinction coefficients and oscillator strength in vacuum UV 12 p1876 A71-26788

Optical losses and quantum efficiencies of electron beam pumped CdS lasers, determining extinction coefficient from dependence of threshold current on resonator length 12 p1915 A71-27639

Semiconductor zinc selenide and zinc cadmium selenide crystals two photon absorption coefficients, noting forbidden bandwidth relation 13 p2077 A71-27954

Thermal emissivity and solar absorptivity of Al coated with surface layers of aluminum oxide and silicon oxide, describing fabrication techniques and performance measurements 14 p2335 A71-30128

Continuous nitrogen and oxygen ion spectra due to photoionization and free ion transfers at high temperatures, calculating absorption coefficient 16 p2662 A71-33040

Weakly divergent electromagnetic wave beam propagation in optically nonlinear laminarly inhomogeneous medium, considering absorption coefficient and self focusing 17 p2697 A71-34253

Gray radiative transfer equations, bridging Planck and Rosseland mean absorption coefficients 17 p2839 A71-35557

Spectral composition of emitted radiation, emissivity and absorptivity of Venus atmosphere at high temperatures 19 p3135 A71-37580

Integrated absorption coefficient of pressure induced pure rotational and vibrational transitions in binary collisions of homonuclear diatomic molecules at high temperatures 19 p3108 A71-38719

Pressure induced hydrogen collisions vibrational spectra absorption coefficients at high temperatures and local thermodynamic equilibrium 19 p3108 A71-38720

Atmospheric thermal sounding radiation data interpretation, determining integral Fredholm equation solution, absorption characteristics and temperature profiles 20 p3258 A71-39670

IR spectroscopy of CO using tunable PbS₂ diode laser, measuring Doppler linewidth and room temperature absorption coefficient at line center 20 p3246 A71-39757

Two photon absorption coefficients of ZnSe and zinc cadmium selenide crystals for ruby laser radiation, showing energy gap reduction effect 21 p3395 A71-41340

Pressure dependent absorption of carbon dioxide laser by boron chloride, considering saturation and line overlapping effects 22 p3556 A71-41805

ABUNDANCE

Electromagnetic radiation in stagnation flow region, determining temperature distribution absorption coefficient of carbon dioxide at rest between two parallel plates 22 p3621 A71-42024

UV and IR transmissivity and absorption coefficients of fused quartz between room temperature and 1500 C 22 p3656 A71-42559

Surface energy absorption coefficient determination from decaying sound fields, deriving reverberation time and decay rate equations 23 p3703 A71-43201

Monochromatic absorption coefficients determination for Ar heated in wall-stabilized arc at high temperatures and pressures 23 p3712 A71-43915

Absorption spectrum of atmospheric gases from laser spectrometer based on tunable ruby laser, measuring water vapor absorption coefficients in multipass cell 24 p3834 A71-45207

ABUNDANCE

Nitrous oxide tropospheric abundance from IR solar spectrum altitude variation 01 p0073 A71-10139

Solar Li abundance determined from selected sunspot spectra observations 01 p0161 A71-11382

Solar wind ion abundances from satellite observation, discussing energy spectra, particle distributions, etc 01 p0147 A71-11518

Near earth solar wind Fe, Si and O ions, using electrostatic analyzer on Vela 5A satellite 01 p0148 A71-11520

Meteoritic iron oxides abundances from recoilless resonance absorption spectra 02 p0306 A71-11993

Solar Hg abundance low value by photosphere spectrum absence of Hg I lines, comparing higher content in carbonaceous chondrites 02 p0306 A71-12048

M type supergiants atmospheric metals abundances from high dispersion spectrograms analysis 02 p0308 A71-12095

Elemental abundances of microtektites and tektites, noting differences from Apollo samples 02 p0312 A71-12363

Al and Si abundances of Italian chondrites by instrumental pile neutron activation analysis 02 p0318 A71-12903

Lunar anorthosites from Apollo 11 sample 10085 coarse fines, determining major, minor and rare earth elemental abundances 03 p0482 A71-13012

Apollo 12 lunar rock 12013, discussing major and trace elemental abundances determination by neutron activation analysis 03 p0494 A71-14219

Compton scattering in quasars, discussing gamma rays effects on core chemical abundances 03 p0481 A71-14266

Metal-rich star evolution from main sequence to red giant, examining mass, nuclear reactions and theoretical models 04 p0648 A71-15247

URCA neutrino emission processes explaining anomalous isotopic heavy element abundance in solar system 04 p0651 A71-15660

Solar flare relative abundance and energy spectra of He 3 and He 4, using charged particle telescope on IMP 4 05 p0797 A71-15943

Solar disk computed continuum and estimated line polarizations compared to BCA photosphere values, discussing metal abundances 05 p0803 A71-16019

Small elliptical galaxy associated with radio source 3C 386, noting luminosity, internal velocity dispersion and low metal abundance 05 p0805 A71-16109

Technetium stars characteristics, noting MS, S and N spectral types, a process element enhanced abundances and variability 05 p0806 A71-16206

Quasars primordial He abundance, discussing relation to galactic evolution 05 p0808 A71-16406

Quasars spectrophotometry data, obtaining physical conditions, abundances and electron temperature 05 p0811 A71-16685

Mg 26 isotopic abundance in meteoritic, lunar and terrestrial feldspar by mass spectrometry, suggesting limits on Al 26 in early solar system 06 p0966 A71-17896

K-U abundance systematics in Apollo 11 and 12 lunar rock suites and earth crust 06 p0968 A71-17961

Sunspot lithium abundance observation by high resolution interferometric spectrometer, using line formation theory applicable to medium strength lines 07 p1190 A71-18861

Red giant star s-process and subsequent delayed electron capture, accounting for large Li abundances 07 p1198 A71-19822

M type supergiants atmospheric metals abundances from high dispersion spectrograms analysis 08 p1362 A71-21145

Lower limit helium abundance envelope models of hydrogen deficient stars, using mixing length theory 08 p1364 A71-21418

Chemical elements abundance in ordinary chondrites, terrestrial magma and lunar rocks, considering Alven theory of solar system origin 10 p1665 A71-23741

Primordial Kr and Xe trapping as possible cause of element abundance trend reversal in Apollo 11 and 12 fines 10 p1673 A71-24428

Atomic hydrogen equilibrium abundance in dense dark hydrogen clouds as function of low energy cosmic ray ionization rate 10 p1662 A71-24491

Supernovae detonation model, examining nucleosynthesis for solar system abundances 10 p1675 A71-24492

Critique of paper on earth core-mantle chemical equilibrium, considering upper mantle element abundance, oxidation state and volatiles nature 10 p1607 A71-24987

Mars atmospheric CO abundances and rotational temperature from Voigt line profiles 10 p1646 A71-24993

Binary star 112 Herculis elemental abundances by atmospheric model analysis of spectra 10 p1680 A71-25001

He I absorption line profiles in normal main sequence B star spectra, discussing He abundance and LTE 11 p1821 A71-25536

Martian surface pressure from 1967-1969 apparition observations, discussing micron bands carbon dioxide abundances 11 p1825 A71-25711

Uranus atmospheric molecular hydrogen abundance from pressure induced overtone spectra, using quadrupole moment and polarizability matrix elements theoretical values 11 p1827 A71-25731

FORTAN 4 computer program for gamma ray energy spectra, determining peak locations, peak areas and elemental abundances 11 p1729 A71-26069

Spectral analysis methods for detection of water on celestial bodies, considering possible abundance on planets and stars 12 p1962 A71-26956

Stellar explosive nucleosynthesis and element abundances in galactic chemical evolution 13 p2133 A71-27970

Venus carbon dioxide spectrum, observing spatial and temporal variation in abundance 13 p2134 A71-28287

Photoelectric umbral scans at 6200-6700 A identifying NiH lines, showing equal solar and terrestrial abundance isotopic ratios 13 p2135 A71-28301

K giants, subgiants, M67 and NGC 188 abundances, noting high metallicities 13 p2136 A71-28431

Chemical fractionations in meteorites, considering trace elements abundance in L chondrites and implications for cosmochemistry 13 p2141 A71-29097

Spatial variations in cosmic He abundance attributed to primordial temperature fluctuations at early epochs in Friedmann universe 14 p2303 A71-29587

Water distribution in space, natural satellites and terrestrial planets, discussing Clarke abundance values and hydrochlorosphere concept 15 p2494 A71-32493

Stellar initial metal content effect on nuclear abundance distributions synthesized under explosive carbon, oxygen and silicon burning conditions 16 p2631 A71-33231

IR line radiation from galactic center thermal radio sources, determining element abundances 16 p2633 A71-33336

T Tauri stars Li, Be and B autogenic generation, considering underabundance in surrounding gas 16 p2626 A71-33433

Apollo 11 and 12 lunar soil and rock samples abundance comparison based on Mossbauer spectroscopy 16 p2637 A71-33509

Quasi-stellar objects, investigating velocity dispersion, column densities and abundance of Mg and Fe in absorbing region by Stromgren method of line pairs 17 p2797 A71-34371

Carbon and nitrogen abundances in howardites, enstatite and hypersthene achondrites 17 p2800 A71-34515

Sunspot forbidden Fe I line spectra, showing high solar iron abundance 18 p2961 A71-35944

Solar photosphere iron abundance data from Fraunhofer spectrum and EUV line measurements 19 p3135 A71-37610

Apollo 14 bulk lunar fines sample elemental abundances determination from soils and rocks by activation analysis 20 p3292 A71-39382

Elemental abundance ratio patterns in microscopic spherules collected from atmosphere and polar snows, comparing to terrestrial and lunar rocks 20 p3298 A71-39638

Spiral galaxies N/O abundance gradients across disks from H II regions spectra 21 p3445 A71-40409

Planetary nebulae helium/hydrogen and nitrogen/oxygen abundance ratios from photoelectric observations, taking into account temperature fluctuations and collisional excitation effects 21 p3446 A71-40416

Limiting He 3 abundances in four H II regions 21 p3448 A71-40449

Relative abundances and mass measurements of Li, Be and B isotopes in primary cosmic rays, using balloon flown emulsion stacks 22 p3593 A71-42329

Relative abundances and mass measurements of Li and B isotopes in primary low energy cosmic rays 22 p3593 A71-42339

Beta cephei stars atmospheric He and metal abundances, comparing line spectra data with other early B stars sample 23 p3723 A71-42947

Reduced nebular helium abundances, using capture-cascade and collisional excitation calculations 23 p3733 A71-43081

Rare earth trace elements abundance of Apollo 14 lunar soil samples from Fra Mauro, comparing with chondrites 23 p3735 A71-43248

Apollo 12 specimens elemental abundance from neutron activation analysis, discussing fractional crystallization, partial melting, rare earth abundances and soil mixing model 23 p3747 A71-43674

Spark mass spectrometric analysis of major and trace elements abundance in Apollo 11 and 12 lunar rocks and soil samples, comparing with standard basalt 23 p3749 A71-43686

Apollo 11 and 12 lunar samples elemental composition analysis, using activation and mass spectrometric isotope dilution analysis and emission spectroscopy 23 p3749 A71-43687

Lunar soil samples 10084,141 and 12070,83 and rock fragment 12063,73 multielement analysis using neutron activation and nondispersive X ray fluorescence techniques 23 p3749 A71-43692

Apollo 12 lunar rock rare earth element abundances, comparing to Icelandic basalt flow 23 p3750 A71-43694

Isotopic abundances and composition of U and Th in Apollo 12 soil and breccia samples, using mass spectroscopy 23 p3753 A71-43716

Rare gas concentrations and isotopic abundances in lunar rocks, fines and breccias from Apollo 11 and 12 flights, determining exposure and gas retention ages 23 p3753 A71-43720

Isotopic abundances and concentrations of spallogenic Ne, Kr and Xe in Apollo 12 rock 12002, constructing three stage model of irradiation history 23 p3753 A71-43722

Elemental abundance analysis of Apollo 11 and 12 lunar materials from Auger electron spectroscopy 23 p3759 A71-43762

Cl abundance in sun, discussing low noise photoelectric scan 23 p3767 A71-43833

Solar chromospheric data for 1952, 1958, 1962 and 1966 eclipses, showing helium abundance in prominences 23 p3767 A71-43842

Calcium abundance in solar corona, using measured values for total intensity of continuum and integrated intensities ratio 23 p3768 A71-43845

AC (CURRENT)

U ALTERNATING CURRENT

AC GENERATORS

Thyristor circuitry for AC controllers and single phase frequency converter 01 p0051 A71-10262

High speed homopolar alternators as static frequency converter supplies, optimizing design parameters by computer geometric programming 03 p0352 A71-13052

Nonlinear vector potential analysis of aerospace homopolar inductor alternators, considering fully armature currents 03 p0353 A71-13053

Integrated drive AC generator for aircraft, discussing design improvements in power-weight ratio 07 p1023 A71-19494

- Dual magneto ignition system for business and small military aircraft, describing development, design and test program
[SAE PAPER 710382] 10 p1659 A71-24247
- Steady state and transient performance of Brayton cycle alternator and electronic controls for space power
15 p2355 A71-32215
- Steady state analysis of phase controlled parasitic current, discussing reduction of alternator apparent power requirements and harmonic distortion
15 p2355 A71-32218
- Single phase stable frequency AC current power supplies, using stable master oscillator and asynchronous generator
24 p3793 A71-44717
- C-1 AIRCRAFT**
U DHC 4 AIRCRAFT
ACCELERATED LIFE TESTS
Accelerated creep rupture tests on metals and solder alloys, comparing constant stretch rate and load methods
[SESA PAPER 1672] 03 p0508 A71-13762
- Transistors and Zener diodes temperature dependence and normal and accelerated life tests
05 p0728 A71-16289
- Turboprop aircraft engine service life extension, correcting deficiencies via accelerated tests based on relation between failure rate and usage
09 p1511 A71-22633
- Al alloys HF accelerated fatigue testing, using magnetostrictive transducer excited mechanical resonance and electronic circuitry
09 p1428 A71-22939
- Timesaving reliability tests for Si transistors involving failure mechanism acceleration
09 p1418 A71-23042
- Accelerated testing of jet fuel containment sealant, using reduced pressure and hybrid fluorocarbon silicone
10 p1632 A71-24083
- Organic adhesives performance evaluation based on correlations between accelerated laboratory aging tests and underground exposure in adverse environments
10 p1633 A71-24113
- Al alloys endurance limit determination by accelerated methods, evaluating errors by comparison with conventional tests
12 p1916 A71-26944
- Passenger aircraft structures accelerated testing for safety and fatigue durability under operational conditions, describing tests, planning and evaluation
12 p1974 A71-26946
- Accelerated semiempirical method determining metallurgical processing techniques effects on steel and titanium alloy compressor blades fatigue life, comparing results with experimental data
14 p2252 A71-30269
- Accelerated intergranular corrosion tests under high humidity on Zn-Al alloy with lamellar eutectoid microstructure due to postforming heat treatment
22 p3564 A71-42534
- CECELERATION**
Low cost multichannel peak/average sine vibration control system with acceleration selector and averager
01 p0067 A71-10864
- Gravitational acceleration measurement, using gravimetric recordings on moving base at sea
08 p1294 A71-21787
- Forced dynamic regimes of machines and mechanisms, evaluating role of second order acceleration
13 p2099 A71-27806
- CECELERATION (PHYSICS)**
NT ANGULAR ACCELERATION
NT DECELERATION
NT HIGH ACCELERATION
NT IMPACT ACCELERATION
NT PARTICLE ACCELERATION
NT PLASMA ACCELERATION
NT SPIN REDUCTION
NT TRANSVERSE ACCELERATION
Acceleration waves propagation in elastoplastic materials based on nonlinear thermodynamic theory
01 p0173 A71-10873
- Quartz crystal HF resonator unit for high g environments, discussing tradeoff between stiff support and stress-induced frequency instability
01 p0054 A71-10913
- Rocket probe with constant tangential acceleration in planetary gravitational field, investigating flight direction
03 p0495 A71-14388
- Finite supercavitating wings numerical calculation using acceleration potential method
04 p0526 A71-15210
- Gyroscopic drift tests, using sinusoidal linear VLF acceleration
05 p0750 A71-16312
- Medical transportation by ambulance, helicopter and fixed wing aircraft, considering vibration damping and acceleration
05 p0715 A71-16932
- Aircrew radiological examination of spinal anatomical state, emphasizing traumatism due to vibration, acceleration, ejection and crashes
05 p0715 A71-16936
- Acceleration inequalities of dynamically loaded elastoplastic shells, using permissible stress and displacement velocity fields
06 p0990 A71-17790
- Turbulent boundary layer laminarization prediction in moderate accelerations, using Pathankar-Spalding finite difference formulation and experimental results for shear stress model selection
07 p1085 A71-18767
- Holographic images of moving objects, extending theory to objects moving with constant acceleration
08 p1291 A71-21402
- Optimal acceleration from earth orbit to hyperbolic velocities of low thrust space vehicle, constructing asymptotic expansions near and far from central field
09 p1519 A71-22545
- Astrophysics - Conference, University of Nice, France, April 1969
10 p1670 A71-24186
- Airfoils accelerating near sound velocity, calculating acoustic radiation by linear theory
10 p1553 A71-24816
- F-8D aircraft transonic flight and wing tunnel tests for buffet onset prediction, considering effects of g level and fluctuation amplitude and frequency
[AIAA PAPER 70-341] 10 p1557 A71-24863
- Initially spherical liquid droplet transient response under surface tension accelerated by external gas flow
[AIAA PAPER 71-393] 11 p1749 A71-25355
- Photographic study of burning metallized composite propellant, noting burning rate augmentation by heat transfer from alumina particles retained on propellant surface
[AIAA PAPER 69-173] 11 p1809 A71-25502
- Elemental maximum energy transport formula for wick heat pipe evaporators under artificial gravity and external acceleration, testing by laboratory centrifuge
[AIAA PAPER 71-419] 11 p1857 A71-26210
- Instrument orientation optimization for ballistic missile applications, emphasizing acceleration induced velocity and position errors
11 p1796 A71-26410
- Sound radiation from time varying point force in accelerative motion, applying to fan or helicopter rotor noise at subsonic tip speeds
12 p1867 A71-26702
- Rotation-convection model of solar equatorial acceleration and temperature, assuming inhomogeneous isotropic latitude dependent turbulent energy transport
12 p1968 A71-27644
- Acceleration covariance in turbulent flow of isotropic homogeneous incompressible viscous conducting fluid
13 p2109 A71-29295
- Normal accelerations experienced by transport aircraft fleet from fatigue load meter data analysis, discussing counting rates seasonal variations
14 p2174 A71-29788
- Velocity-aided Kalman filtering for one dimensional motion under random acceleration, obtaining steady state solution and transit time
14 p2197 A71-30793
- Unified raindrop breakup theory, examining spherical liquid drop transient response under surface tension accelerated by uniform external gas flow
16 p2557 A71-32924
- Transient response of water drops to shock wave induced accelerations at near critical Weber numbers
16 p2557 A71-32925
- Critical induced acceleration for shock propagation as function of strain in polymethyl methacrylate
[ASME PAPER 71-APM-14] 16 p2600 A71-33213
- Gravitation phenomena based on uniformly expanding universe cosmological model for acceleration field
16 p2612 A71-33281
- Vertical acceleration effect on gas-hydraulic analogy for turbulent flows with and without jumps with error dependence on Froude number and length to depth ratio
16 p2560 A71-33598
- Pageos spacecraft orbital acceleration prediction by radiation pressure perturbation theory accounting for nonisotropic scattering of solar spectra from rotating ellipsoidal body
16 p2641 A71-33772
- Fluid surface instability under perpendicular acceleration, presenting singular perturbation problem solution by successive approximations method
16 p2561 A71-34160
- Electromagnetic wave propagation in uniform simple medium, demonstrating drag effects relative to inertial and accelerated frame
17 p2699 A71-34431
- Stop test method to study acceleration in movement control processes in man, considering elbow joint movements in normal and pathological tremors in Parkinson disease afflicted subjects
19 p3007 A71-37569
- Rectangular cantilever plate free vibration under in-plane acceleration loads, calculating frequencies and mode shapes by Ritz method and computer technique
19 p3157 A71-37850
- Photographic study of acceleration and pressure effects on Al agglomerates and combustion processes on solid propellant surface, describing pit growth by combustion model
19 p3120 A71-38121
- Burn time and acceleration effects on molten metallic material chemical composition near burning surface of aluminized composite solid propellant
19 p3121 A71-38298
- Radar resolution performance for targets with range acceleration, determining matched filter or correlation radar effects
20 p3195 A71-38868
- Time optimal transfer trajectory in central Newtonian force field between two arbitrary points under jet acceleration
20 p3289 A71-39135
- Missile vibrations during acceleration calculated in matrix form for Saturn 5/Apollo booster configuration
20 p3306 A71-39412
- Plants and animals reactions to environment gravitational component, showing organisms perception of accelerating force
21 p3326 A71-39970
- Radar determination of reference change related to sudden acceleration, deducing Galilean-accelerated reference transition in two dimensional space-time
21 p3415 A71-40513
- Relativistic behavior of uniformly accelerated translational observer motion relative to inertial observer from space-time transformation
21 p3415 A71-40653
- Unsteady boundary layer of viscous incompressible rotating fluid flow due to infinite flat plate accelerated motion, calculating velocity and skin friction
21 p3367 A71-40657
- Acceleration dependent burning rate increases of aluminized composite solid propellants induced by combined erosive and acceleration
21 p3436 A71-40943
- Fluctuating lift and drag forces on accelerating free falling sphere, discussing relation to asymmetrical wake vortex shedding
21 p3324 A71-40970
- Geogravitational acceleration constant determination using two falling interferometer reflectors illuminated by laser light
22 p3574 A71-41650
- Blind goldfish gravity reference response under linear accelerations on motor car and parallel swing from movie camera recording
22 p3487 A71-42228
- Lateral accelerations effect on mice tolerance to toxic doses of aminothiols and indolylalkylamine-series radiation protection drugs
22 p3491 A71-42706
- Artificial satellite lunar orbit calculation, representing unmodeled accelerations by first order Gauss-Markov sequence with time correlated and random components
[AAS PAPER 71-371] 23 p3730 A71-43041
- Gyrocompass with optimal error correction under rapid acceleration change
23 p3675 A71-43297
- Aircraft accelerate-stop factors and regulations, pilot reaction times and accidents during takeoff
23 p3628 A71-43380
- Printed circuit board components and connections survival under severe vibration and G forces, considering resonant frequency, mounting methods and lead wire strain relief
23 p3652 A71-43538
- Flow acceleration coefficient effect at inlet on centrifugal compressor wheel characteristics during axial-radial rotation
23 p3626 A71-43553
- ACCELERATION PROTECTION**
High acceleration resistant electronic trigger fuse for in-flight gun launched projectile payloads ignition and ejection
[AIAA PAPER 70-1389] 03 p0468 A71-13671
- ACCELERATION STRESSES [PHYSIOLOGY]**
NT CENTRIFUGING STRESS
Blood pressure changes in heart cavities and large vessels of dogs exposed to accelerations
01 p0013 A71-11126
- Nystagmus extinction during repeated exposures to angular accelerations in labyrinthectomized guinea pigs
01 p0014 A71-11139
- Proprioception role in perception of arm bending and extension during weightlessness and accelerations in aircraft flight along parabolic trajectory
01 p0014 A71-11143
- Gravitational acceleration effects on hemodynamics, describing mechanocardiographic equipment
02 p0198 A71-11900
- Differential equations for control and adaptation of hand motion in cubital joint under weightlessness and accelerations
03 p0357 A71-12990

ACCELERATION TOLERANCE

Moving cockpit flight simulator design with force and rotational acceleration vectors at pilot head location
[DFVLR-SONDDR-82] 03 p0396 A71-13343

Elasmobranch fish labyrinth electrophysiology, analyzing semicircular canals linear acceleration response
04 p0536 A71-14755

Lower vertebral column forces and moments in seated human under seat-to-head acceleration
04 p0542 A71-14788

Hypokinesia and acceleration effects on plasma proteins displacement and bioelectric activity of striated muscles of rats
06 p0853 A71-17960

Human body thermography for studying physiological changes due to exercise, anoxia or accelerations
06 p0860 A71-18189

Patients transportation pathology, discussing accelerations and vibrations in ambulances, helicopters and fixed wing aircraft
06 p0860 A71-18191

Fluorescein permeability of hemato-ophthalmic barrier of rabbits after acceleration exposure
06 p0854 A71-18364

Sodium bicarbonate intravenous effects on cat and rabbit otolithic reactions to accelerations and motion
06 p0861 A71-18375

Acceleration effects on aortic, coronary and carotid flows in dogs
06 p0855 A71-18380

Manned aerospace vehicular escape systems, discussing human vertebral column structural limits under vertical gravity acceleration
[AIAA PAPER 71-144] 06 p0863 A71-18587

Human biodynamics during deceleration, impact and blast, discussing body positions and protective restraints for crash safety, aircraft ejection, etc
08 p1244 A71-20707

Radial, angular and transverse accelerations physiological effects, discussing physiological acceleration systems, symptoms, human centrifuging, etc
08 p1244 A71-20708

Linear acceleration effects on human otolithic and vestibular apparatus, discussing vestibulovegetative motion sickness syndrome and nystagmus index activation
08 p1242 A71-21956

Centrifugal force effect on pigeon head nystagmus, acting on semicircular canal via otoliths or cupula
09 p1388 A71-22123

Hypothalamus supraoptic nucleus morphological changes in rats under prolonged transverse acceleration
09 p1388 A71-22195

Semicircular canal influence on otolith reactions in pigeons, noting caudal and rostral shifts evoking levator and depressor coccygei contractions during horizontal acceleration
09 p1390 A71-22214

Weightlessness, high acceleration and aerospace vehicle maneuvering effects on cardiovascular and vestibular systems, discussing disorientation, space sicknesses and blood circulation
09 p1398 A71-22357

Mitral valve systolic prolapse aggravation due to G acceleration and aeromedical significance
09 p1395 A71-23246

Book on gravity and acceleration effects on lungs covering breathing mechanics, ventilation distribution, blood flow, gas exchange, arterial oxygen saturation and pulmonary shunting
[AGARDOGRAPH-133] 09 p1402 A71-23620

Positive/latero-lateral accelerations and acute hypoxic hypoxia effects on central visual fields behavior in simulated flight
10 p1571 A71-24978

Alternating acceleration and increased ambient temperatures effects on time interval perception and muscular effort estimation
12 p1874 A71-27164

Visual contrast sensitivity and fundus oculi pattern changes due to accelerations in pelvis-head axis
12 p1870 A71-27165

Somatic and autonomic responses in vestibular tolerance of human subjects, using Coriolis acceleration test
13 p2007 A71-28414

Vertical translational acceleration perception threshold of aircraft pilot seated in upright position
14 p2188 A71-29780

Conditioned auditory reflex behavior in rats under influence of acceleration, noting ontogenetic effects
15 p2356 A71-31249

Inertial properties of segmented cadaver trunk for mathematical model of spinal response to impact in seat ejection acceleration injuries in high speed aircraft
16 p2528 A71-33117

Cardiovascular and respiratory systems, motor and muscular activity, metabolism and body energetics functional changes due to prolonged weightlessness
16 p2531 A71-33676

H reflex changes in spinal marrow of intact and labyrinthectomized rats under radial accelerations
20 p3188 A71-39221

Human retinal blood circulation changes and vision disturbance under transversely directed acceleration, using dark chamber teleophthalmoscopy
20 p3188 A71-39228

Myocardium reactions under 2G acceleration from histological, histochemical and electron microscopic observations on rats, noting dystrophic damage level relationship to duration
20 p3189 A71-39235

Stroke number and vestibular nystagmus duration and frequency under successively increasing angular acceleration from tests on guinea pigs
20 p3189 A71-39238

Radioprotectants effects on mice and guinea pigs physiological reactions to back-to-chest transverse accelerations
21 p3336 A71-41053

Bull frog activity at rest and response to centripetal acceleration by on-board centrifuge in vestibular space experiment OFO-A
22 p3484 A71-41690

Pathomorphological and histochemical changes in rat lungs, liver, heart, diaphragm and adrenal glands from acceleration and cysteamine caused tissue oxygen deficiency
22 p3491 A71-42703

Mice under combined gamma radiation and vibration and acceleration dynamic factors, studying radioresistance recovery rate
22 p3494 A71-42725

Mice acceleration before and after gamma irradiation, determining protective effect of cystamine in adrenaline and amphetamine mixture
22 p3494 A71-42726

Dogs peripheral blood reaction to complex action of transverse accelerations and gamma irradiation
22 p3494 A71-42727

Radioprotective effectiveness of cystamine and S beta-aminoethylisothiouonium in mice under combined gamma irradiation and transverse acceleration loads
22 p3494 A71-42730

Gastrointestinal tract reactions to atropine sulfate, acetylcholine and carbacholine in rats after acceleration exposures, using roentgenograms
22 p3495 A71-42796

Mechanical vibrations effects on mouse embryos growth and development, investigating critical frequencies and accelerations
23 p3637 A71-44246

ACCELERATION TOLERANCE

Guinea pigs vestibular adaptation to repeated angular acceleration dependent on acceleration direction
01 p0012 A71-11056

Aspartic aminotransferase activity relation to clinical and biochemical indices of human tolerance to impact accelerations
01 p0014 A71-11140

Physical exercises to increase cosmonaut space environment tolerance, discussing effects of acceleration, altitude and hypoxia
01 p0027 A71-11556

Computer simulation of human body kinematics under rapid decelerations
04 p0542 A71-14786

Acceleration tolerance improvement in human subjects by gymnastics, games, athletics and aviation pilot training
09 p1399 A71-22920

Space travel genetic effects, discussing radiation, weightlessness, vibration and acceleration
09 p1394 A71-23149

Astronaut selection and training, considering acceleration, hypoxia, weightlessness and temperature variation tolerance
12 p1873 A71-26951

Accelerations effect on receptors in semicircular canals during human movements in rotating environment, using vector analysis
13 p2007 A71-28415

Pilot subjective evaluation of XB-70 aircraft response to atmospheric turbulence in comparison with measured accelerations
14 p2173 A71-29774

Wheat seedling responses to chronic acceleration, considering total height, coleoptile diameter, root length, sensitivity to growth retardation and histological changes
21 p3341 A71-40001

Animals physiological responses to gravity chronic acceleration
21 p3328 A71-40002

Chronic acceleration effects on animals, considering growth rate, food intake, oxygen metabolism and life expectancy
21 p3328 A71-40003

Radioprotectants effect on mice against ionizing radiation and tolerance to back-to-chest accelerations in space flight
21 p3330 A71-40345

Mercaptoalkylamine group radiation protection preparations on resistance of rats and mice to lateral acceleration rate
22 p3491 A71-42700

Beta-aminoethylthiophosphoric acid monosodium salt effect on mice stability to lateral accelerations
22 p3491 A71-42701

Aminothioli group radioprotective drugs effect on guinea pigs cardiac function during lateral acceleration
22 p3491 A71-42702

Acceleration tolerance of gamma irradiated mice with and without radioprotectors
22 p3493 A71-42724

Human orthostatic and vestibular stability responses to weightlessness during extended space flights noting acceleration tolerance, physical efficiency, infection resistance and medication sensitivity
22 p3495 A71-42790

Transverse accelerations effect on human speech features
24 p3795 A71-44471

Transverse acceleration effect on aspartic aminotransferase activity in humans and rats
24 p3795 A71-44528

Correlation coefficients between sensitivity thresholds of cupula-endolymphatic system to angular and Coriolis accelerations with human resistance to motion sickness
24 p3795 A71-44532

Human adaptation to Coriolis and linear accelerations, investigating habituation effect
24 p3795 A71-44533

Coriolis acceleration effect on human organism from optic functions and retinal hemodynamics study
24 p3795 A71-44534

Morphological changes in dogs brain vessels under transverse accelerations
24 p3796 A71-44546

ACCELEROMETERS

Rotating accelerometer with magnetic amplifier for angular acceleration detection, investigating static, dynamic and frequency response characteristics
02 p0252 A71-12421

Frequency response of velocity and acceleration transducers for oscillatory environments instrumentation
11 p1762 A71-25935

ACCELEROMETERS

Accelerometers and dynamic pressure transducers calibration, using laser interferometer system
01 p0082 A71-10862

Random vibrations nonlinear effects on gas bearing pendulous-integrating gyroscopic accelerometer response, using digital simulation
02 p0252 A71-12454

Servoamplifier dynamic response effects on dynamic characteristics of fluid-filled pendulous accelerometers
02 p0252 A71-12455

Accelerometer design for nuclear reactor vibration measurements, considering environmental effects
04 p0587 A71-14824

Fluidic inertial instruments for space sensing, guidance and control including gyroscopes, accelerometers and rate sensors
04 p0535 A71-15322

Precision gyro and accelerometer testing evolution, noting instrument performance and electrical and mechanical equipment
05 p0749 A71-16303

Inertial quality accelerometer tests, including mathematical models and error analysis
[AGARDOGRAPH-128] 05 p0750 A71-16307

Accelerometers linearity variations by centrifuge tests
[AGARDOGRAPH-128] 05 p0750 A71-16313

Gyros and accelerometers with hydrostatic gas bearings, discussing design and adjustments, drift measurement methods and environmental tests
[AGARDOGRAPH-128] 05 p0751 A71-16314

Dry friction autocompensation in inertial navigation accelerometers by forced rotation of platform
05 p0751 A71-16589

Soviet book on inertial navigation systems covering theory, design, construction, coordinate algorithm, linear and angular accelerometers, etc
06 p0897 A71-17434

Null shift errors of compensated electromechanical pendulum accelerometers during random vibration of base
07 p1108 A71-19308

Inertial sensors, considering electromechanical devices, single and two degrees of freedom floated gyros and electromagnetic rebalance pendulous accelerometers
09 p1443 A71-22594

Accelerometer for direct measurements of angular acceleration of rotating shafts, using semiconductor transducers
09 p1443 A71-22706

Piezoelectric accelerometers for high temperature vibration measurements, examining materials critical characteristics, design minimal weights and vibration system test methods
09 p1443 A71-22707

Frequency characteristics determination of fixed piezoaccelerometers, using three mass equivalent system

09 p1450 A71-22797

Amplitude-frequency characteristics of physically similar piezoelectric accelerometric converters

09 p1450 A71-22798

Linear damping in piston type liquid damped accelerometers, using porous glass materials

09 p1451 A71-23173

Piezotron accelerometer for vibration measurement, combining quartz sensing element with subminiature solid state electrostatic amplifier

11 p1767 A71-26442

Modal characteristic pick-up system for vibration tests of rockets or aircraft on ground, using small size accelerometers with individual electronic circuit

12 p1895 A71-27719

Gyroscopic integrating accelerometer dynamics on high frequency angular vibrating base, determining self oscillations and drift motions

13 p2065 A71-27946

Construction, operation and in-flight performance of triaxial bridge accelerometer used in falling sphere experiment for atmospheric density, temperature and pressure determination

13 p2066 A71-28160

Accelerometer precision centrifuge test data reduction by inversion method, extracting odd second order coefficients

13 p2072 A71-29506

French book on optimal inertial navigation and statistical filtering covering Wiener and Kalman filters, gyroscopes, accelerometers, inertial platforms, data processing, computer programming, etc

14 p2271 A71-29940

Transient ground motion velocity measurement system, using piezoresistive acceleration transducers, electronic integrator and digital zeroing circuit

14 p2245 A71-30340

Inertial instruments with outputs indicative of time integral and time double integral of vehicle acceleration for velocity and distance determination

14 p2245 A71-30343

Diffusion electrochemical linear and angular accelerations sensors, noting lack of friction surfaces

15 p2409 A71-32184

Telemetric accelerometer for assessing mental performance under industrial working conditions for work characterized by periodically repeated stereotyped movements

17 p2688 A71-34363

Angular accelerometer with paddle torsion damper, comparing sensitivity with ordinary inertial instrument

17 p2739 A71-34562

Flight test results for CACTUS accelerometer launched by rocket probe at Guiana Space Center, considering atmospheric density profile in 120-150 km altitude zone

18 p2924 A71-36755

Angular acceleration measuring device based on closed loop wide bandwidth sensor, discussing theory of operation, performance and applications [AIAA PAPER 71-909]

19 p2995 A71-37160

Resolution and clutter performance of simultaneous Doppler and acceleration measurement with coherent pulse trains

20 p3195 A71-38855

Transient calibration method for piezoelectric accelerometer in high g-level range [ASME PAPER 71-VIBR-43]

21 p3377 A71-40293

Steady acceleration sensor system with two electrode chambers in closed circuit, producing convective flow by electrolyte density gradients

24 p3828 A71-45099

Experiment dispersion analysis planning, using solution acceptance procedures block diagrams

12 p1988 A71-26711

Diffusion and solubility of thermally induced acceptors in indium antimonide single crystals

04 p0636 A71-15085

Hall effect measurements utilization for simultaneous determination of donors and acceptors concentration in semiconductors, applying to n-type silicon

19 p3118 A71-37487

External and internal absorption spectra of silicon crystal doubly doped with boron and indium acceptors, interpreting line broadening and cross section decrease

21 p3426 A71-40071

Deep level impurity compensation of high resistivity epitaxial films of GaAs by chromium, complex lattice defects and copper acceptors, using cathodoluminescence spectra

21 p3430 A71-41220

Storage arrays of high operational speed with field effect transistors, evaluating contributions to access and cycle times

21 p3354 A71-40734

Fast read only memory design implemented in MOS and bipolar technology, noting low access times

21 p3355 A71-40735

ACCIDENT INVESTIGATION **NT AIRCRAFT ACCIDENT INVESTIGATION** **ACCIDENT PREVENTION**

On-site aviation accidents investigation and prevention, noting National Transportation Safety Board procedures

03 p0522 A71-12963

Aircraft accident hearings for discovering facts, causes and preventive measures

03 p0523 A71-12964

Aircraft flight aerodynamics from accident prevention viewpoint, discussing angle of attack, turbulence effects, weather factors, etc

03 p0346 A71-13017

Aircraft accident trends and preventive practices, considering fatal landing statistics

04 p0529 A71-14995

Military helicopter design and weaknesses correction, considering man/machine combat survivability and operational accidents reduction

04 p0534 A71-15447

Bird strikes incidence and prevention, discussing velocity effects, migration role and uses of distress calls, falconry and radar

06 p0848 A71-18664

Aircraft aquaplaning skidding prevention by runway resurfacing and water depth sensor warning indicators

10 p1609 A71-23946

U.S. General Aviation safety record, discussing National Transportation Safety Board and accident/injury prevention [SAE PAPER 710397]

10 p1557 A71-25132

Tannic acid and water washing effects on prevention of monomethylhydrazine absorption through skin in dogs

16 p2535 A71-33119

Air safety standards and objectives, discussing human factors as accident causes, piloting aids and management

20 p3178 A71-39395

Military pilot handling characteristics, discussing combat operations, accident prevention and blind landing

22 p3504 A71-42239

Cervical vertebral distortion during acrobatic flight, discussing clinical and medico-legal aspects and preventive measures

23 p3632 A71-43219

Aircraft wake turbulence and trailing vortices, investigating physical characteristics, hazard potential and avoidance techniques

23 p3628 A71-43234

ACCIDENTS **NT AIRCRAFT ACCIDENTS** Computerized registry of traumatic injuries with IBM 360/44 system for use in mortality, paired patient and accidental risk factor analyses

16 p2535 A71-33109

ACCLIMATIZATION **NT ALTITUDE ACCLIMATIZATION** **NT COLD ACCLIMATIZATION**

Tolerance time for hot humid conditions, considering acclimatized and unacclimatized men at rest and at work with moderate rate of energy expenditure

05 p0705 A71-16153

Heat acclimatization effects on sweat Na concentration over wide sweat rates range, discussing possible mechanisms

13 p2024 A71-29498

Heat acclimatization by evaporative cooling prevention in men wearing vapor barrier suits, considering body temperature and heart and sweat rates

21 p3331 A71-40355

ACCOMMODATION **NT VISUAL ACCOMMODATION** **ACCOMMODATION COEFFICIENT**

Tangential momentum transfer accommodation coefficient for gas flow based on monocrystalline molecular model of gas-solid interface

01 p0071 A71-10949

Inert gases energy accommodation coefficients dependence on clean metal surface temperature based on lattice theory

21 p3415 A71-40538

Diffusing gas mixtures slipping rate along wall at arbitrary accommodation coefficients, deriving expression based on molecule distribution functions from linearized Boltzmann equations solution

21 p3418 A71-40678

Nitrogen ions surface interactions with Al surfaces at and above earth satellite speeds, measuring normal and tangential momentum accommodation coefficients

22 p3577 A71-41980

Materials thermal accommodation coefficient and emissivity dependence on surface roughness, noting correlation

24 p3888 A71-44934

ACCRETION **U DEPOSITION** **ACCUMULATORS** **NT DUST COLLECTORS**

NT SOLAR REFLECTORS

Thermionic diode with integral guard ring, measuring emitter and collector work functions and heat transfer

02 p0195 A71-12236

Ni-Ti system electrocatalysts for fuel cell and accumulator electrodes

03 p0355 A71-14318

Modified buried collector gauge performance over He pressure range, determining sensitivity dependence on filament geometry

05 p0748 A71-16231

Oleopneumatic accumulators in gearboxes for rationalizing installed power

07 p1023 A71-20004

Thermionic collector work function measurements, considering error sources and I-V characteristics

11 p1711 A71-25881

Klystron power conversion efficiency augmentation by electrostatic depressed collector design, presenting performance prediction calculation method

12 p1889 A71-27734

ACCURACY

Electrochemical machining accuracy, discussing gap geometry, optimal conditions, electrolyte types, etc

[SME PAPER MR-70-205] Aircraft assembly accuracy parameters, using holes as reference points

02 p0257 A71-12564

SAGE/Buic vs Kalman filters for aircraft tracking, determining accuracy by radar model [AIAA PAPER 71-58]

06 p0925 A71-18517

Sun sensor design accuracy and stability parameters for spacecraft ultrafine guidance, comparing bias error with solar simulator measurements

11 p1767 A71-26334

Doppler carrier frequency shift measurement accuracy

20 p3198 A71-39808

ACETATES

Sodium fluoroacetate as radiation protective agent, noting dependence on selective blockade of enzyme anionase

07 p1037 A71-18967

Hypothermia effect on lipid synthesis of hamster tissue following intravenous injection of acetate-C 14

14 p2182 A71-29582

ACETAZOLAMIDE

Acute mountain sickness due to oxygen deficiency, discussing control by acetazolamide, placebo or furosemide pretreatment

06 p0851 A71-17613

ACETIC ACID

NT IODOACETIC ACID
Cytotoxic and radiosensitizing effect of thiol binding agents iodoacetamide [IAA], N-ethylmaleimide [NEM] and iodoacetic acid [IA] on crypt cells of mice duodenum

07 p1038 A71-18975

Hormone movement in geotropism, discussing supraoptimal auxin content and indoleacetic acid in wheat roots

21 p3340 A71-39981

ACETYL COMPOUNDS

Hexosamines biosynthesis control mechanism, considering UDP-N-acetylglucosamine function

05 p0706 A71-16217

Acetylcholine endogenous formation in rabbit myocardium effect on ventricle rhythm guides automatic activity suppression by HF excitations

07 p1040 A71-19281

Template catalysis of acetyl transfer reactions, showing triple helices formation by polyuridylic acid with adenoside derivatives

13 p2026 A71-29479

Acetyl-coenzyme A synthetase in aerobic yeast cells localization in microsomal fraction by density gradients

14 p2187 A71-31003

Gaseous, liquid and polycrystalline biacetyl vibrational spectra and structure, noting mutual exclusion between IR and Raman radiation

16 p2538 A71-32874

Rat brain acetylcholine levels circadian rhythm correlated to spontaneous motor activity and sleep-awake cycle

17 p2684 A71-35326

Activation energy and temperature dependence of radiation induced free radical destruction in N-acetyl-DL-valine, using Arrhenius plots

21 p3345 A71-40203

Cholinesterase activity and acetylcholine level dependence on adrenaline dose injected in heart during rats experimental myocardiodystrophy

24 p3800 A71-44500

ACETYLENE

Detonation waves in gases and two phase systems with nonideal wave front, calculating acetylene explosion parameters for different initial pressures

03 p0520 A71-13991

Acetylene pyrolysis kinetics, considering isothermal vs adiabatic conditions and surface catalyzed vs homogeneous gaseous

[WSS/CI PAPER 70-18] 06 p0943 A71-17660

ACETYSALICYLIC ACID

Excited radical and ion formation in unperturbed acetylene-air and superimposed HF discharge flames, determining activation energy 09 p1402 A71-22379

Critical atomic carbon to oxygen ratio measurement for incipient soot formation in shock heated acetylene, ethylene and ethane/oxygen/argon mixtures 21 p3436 A71-40859

Phenylpropargylene and phenylethynyl nitrene intermediacy, abstracting hydrogen to produce benzylacetylene, phenylallene and 1-methyl-2-phenylacetylene 22 p3508 A71-42886

ACETYSALICYLIC ACID

Acetysalicylic and ascorbic acids effects on mice susceptibility to oxygen toxicity, discussing in vitro sensitivity of red cells to hydrogen peroxide 11 p1721 A71-26126

ACHONDRITES

NT KAPOETA ACHONDRITE

Refractory elements abundances in chondrites, basaltic achondrites and Apollo 11 fines, emphasizing Ca-Al relationship 06 p0966 A71-17894

Rare earth abundance in Apollo 12 basalts and soils and achondritic meteorites, using partial melting model 06 p0966 A71-17899

Chromite and ilmenite analysis in pallasites, mesosiderites, achondrites and meteorites with electron microprobe 14 p2310 A71-30173

Bibliography and review of meteorites not classified as chondrites, considering achondrites, stony irons and iron meteorites 17 p2798 A71-34453

Chondrites bibliography and review, considering classification, metamorphism, ages and thermal history, achondrites and organic compounds 17 p2798 A71-34454

Cosmic radiation and gas retention ages of Chassigny achondrite by measuring Al, K and noble gases contents and production rates in meteorites 17 p2800 A71-34514

Carbon and nitrogen abundances in howardites, enstatite and hypersthene achondrites 17 p2800 A71-34515

Crustal and meteoritic abundances of elements and water, considering chondritic and achondritic composition 19 p3055 A71-38145

ACID BASE EQUILIBRIUM

Middle cerebral artery occlusion effect on cortical blood flow, tissue oxygen pressure and acid base equilibrium in animals under extended ligations 05 p0708 A71-16617

Barometric pressure and exercise effects on erythropoietin titer in normal and hypoxic rat plasma, noting lactic acid concentration and acid base balance changes 08 p1237 A71-20676

Central regulation mechanisms of acidic-alkaline equilibrium in ontogenesis, discussing midbrain intraterine and respiratory postnatal development 08 p1241 A71-21937

Respiratory acid-base disturbances, studying deviations of bicarbonate ion vs pH pathway followed by buffered solution on carbon dioxide titration 13 p2007 A71-28434

Monograph on peripheral chemoreceptors and central chemosensitive area control of ventilation during chronic blood acid base changes and hypoxia in mammals 18 p2852 A71-35869

Respiratory chemoreceptors and acid-base alterations effects on adrenocortical activation during hypoxia in dogs 20 p3187 A71-38986

ACIDITY

Al-Si alloys corrosion resistance in humid atmosphere and acid medium, investigating effects of refining process and hydrogen content 01 p0097 A71-10040

Gas phase acidities of aliphatic alcohols by ion cyclotron resonance spectroscopy 07 p1055 A71-19597

Acidic and alkaline deoxyribonucleases activity by spectrophotometer and horizontal viscosimeter in normal states and pathology 12 p1872 A71-27743

Cement systems based on metal oxides and organic compounds, stressing acidity factor for organic component selection 13 p2090 A71-28007

Aircraft turbine oils acid number potentiometric determination, discussing automatic titration procedure and apparatus and solvents influence on titration curve and inflection point 18 p2940 A71-36680

ACIDOSIS

Chronic hypercapnia oxygen dissociation curves and red cell cation exchange in rats, considering compensated/uncompensated phases of respiratory acidosis 03 p0360 A71-13181

Isocarbic metabolic acidosis effects on blood plasma, electrochemical potential differences and cerebrospinal fluid pH 11 p1722 A71-26361

ACIDS

NT ACETIC ACID
NT ACETYSALICYLIC ACID
NT AMINO ACIDS
NT ASCORBIC ACID
NT ASPARTIC ACID
NT BUTYRIC ACID
NT CARBONIC ACID
NT CARBOXYLIC ACIDS
NT CYSTEINE
NT DEOXYRIBONUCLEIC ACID
NT FATTY ACIDS
NT GLUTAMIC ACID
NT GLUTAMINE
NT GLYCINE
NT HISTIDINE
NT HYDROCHLORIC ACID
NT HYDROFLUORIC ACID
NT IODOACETIC ACID
NT LACTIC ACID
NT METHIONINE
NT NITRIC ACID
NT NUCLEIC ACIDS
NT OXALIC ACID
NT OXIDASE
NT PERCHLORIC ACID
NT PHENYLALANINE
NT PHOSPHORIC ACID
NT PYRIDINE NUCLEOTIDES
NT PYRUVATES
NT RIBONUCLEIC ACIDS
NT SULFURIC ACID
NT THYMINE
NT THYROXINE
NT TRYPTOPHAN
NT URIDYLIC ACID

Benzoylformic and alpha-acetamidoacrylic acid hydrogenation, using modified ion exchange resin-palladium catalysts 03 p0375 A71-13199

Esters synthesis from cyclic trimethylolpropane butyral and monobasic saturated acids mixtures 15 p2438 A71-31679

High purity lithium hexafluoroarsenate preparation methods and hexafluoroarsenic acid properties 23 p3642 A71-43540

ACOUSTIC ATTENUATION

NT SHOCK WAVE ATTENUATION

Acoustic attenuation in condensing vapor, using continuumlike formulation allowing for phase exchange process 01 p0182 A71-11470

Sound wave damping by chemical relaxation, showing dependence on dimensionless reaction heat, equilibrium constant and Damkohler number 05 p0717 A71-16533

Combined continuity and force equations for sound attenuation as function of thermal and viscous losses in liquid gases, taking into account fcc and bcc packing 06 p0927 A71-17569

Plane sound waves incident on flat plate airfoils lattice, obtaining transmitted and reflected pressure amplitudes [AIAA PAPER 71-181] 06 p0885 A71-18620

Turbofan engine noise reduction, using acoustic liners in inlet and exhaust ducts [AIAA PAPER 71-183] 06 p0947 A71-18622

Sound attenuation by warm air fog, using droplet measurements in Wilson cloud chamber 09 p1490 A71-23556

Acoustic beam attenuation through liquid medium under ultrasonically excited cavitation, taking into account bubble configuration 09 p1434 A71-23668

Engine inlet noise prediction from static test and flyover data as function of time at various observer locations, examining suppression effects on total spectra [SAE PAPER 710386] 10 p1659 A71-24250

Nematic liquid crystal ultrasonic measurements at room temperature, showing anisotropic attenuation dependence on magnetic field orientation 11 p1808 A71-26149

Beef liver cell nuclei acoustic absorption at various frequencies, determining relation to protein content 12 p1928 A71-27535

Earmuff hearing protectors evaluation for attenuation of narrow band noise on experienced subjects 14 p2188 A71-30196

Turbulent flow and high sound level effects on acoustic attenuation in narrow rectangular duct 14 p2224 A71-30207

Acoustic wave amplification and attenuation in non-homogeneous steady flows applied to air jet discharging in organ pipe 14 p2224 A71-30208

Absorbent materials for sound attenuation in turbine ducts, examining flow velocity, absorbent structure and cladding effects 14 p2288 A71-30518

Noise attenuation prediction in absorbing ducts adaptable to bypass jet engines, using Morse theory 14 p2288 A71-30522

Acoustic absorbers for combustion instability prevention, discussing design theory and experimental results [AIAA PAPER 71-699] 14 p2294 A71-30758

Acoustic linings for attenuation of fan generated noise in turbofan engines, considering interaction between analytical lining performance prediction and flow duct testing [AIAA PAPER 71-731] 14 p2295 A71-30778

Soundproofing of air inlets and fan exhausts with reference to absorbent systems with resonant cavities, technologies, environmental conditions and materials fatigue 15 p2469 A71-31880

Aircraft noise measurements, noting ground absorption effects 15 p2450 A71-32127

Refraction, terrain, air attenuation, fog and rain, turbulence and shielding effects on acoustic propagation in lower atmosphere 17 p2734 A71-35235

Sound attenuation in lined duct, using Newton-Raphson method for complex roots of equations 18 p2947 A71-36499

Maximum acoustic attenuation in lead-wool-polyurethane and nickel-Cerrobend composites for different compositions, frequencies and pressures 18 p2948 A71-36933

Lithium niobate hypersound attenuation and reflection coefficients frequency dependence determination by scattering laser light at hypersonic oscillations 20 p3244 A71-39162

Sound absorptive materials selection for jet aircraft noise control 20 p3178 A71-39451

Multilayer microwave semiconducting film piezoelectric acoustic transducer loss and frequency response derivation from electromechanical power conversion theory 20 p3240 A71-39764

Lined ducts design for flow with intense sound, discussing analysis methods, testing procedures, liner materials development and acoustic attenuation 21 p3361 A71-40212

Acoustic damping of clamped and hinged rectangular panel at natural frequency, noting dependence on aspect ratio 21 p3416 A71-41200

Review of papers at EUROMECH 23 colloquium on finite amplitude and diffusive effects in acoustics, covering acoustic damping by relaxation, dust and moisture, turbulence effects, etc 23 p3704 A71-43447

Anomalous ultrasonic attenuation in pure superconducting Nb from pulse echo amplitude measurements 24 p3860 A71-44751

Sound field measurement in circular and rectangular air duct with sound-absorbing walls/mufflers, deriving empirical formula for attenuation frequency characteristics 24 p3849 A71-45278

ACOUSTIC COMBUSTION

U COMBUSTION STABILITY

ACOUSTIC DELAY LINES

Elastic wave properties and technological applications, discussing acoustic delay, compression and filtering electric signals 05 p0722 A71-16741

Microwave acoustic delay device incorporated in phase discriminator for AFC, FM noise meters and pseudo-superheterodyne receivers 18 p2893 A71-36599

ACOUSTIC DUCTS

Aircraft engine double-reverberant chamber duct lining test facility, discussing noise fields, air flow layout, performance, insertion and transmission losses, etc 06 p0880 A71-17619

Acoustic duct lining materials, comparing attenuation constants according to Scott theory 08 p1333 A71-20804

Multiple wave propagation in acoustic duct with winds, using perturbation Lagrangian for ideal fluid flow 08 p1276 A71-21652

Acoustical response of closed flow pipe as function of blowing pressure and air jet turbulence level 08 p1276 A71-21760

Eigenvalues of axially uniform fluid waveguide with eccentric annulus cross section and acoustically hard boundaries 12 p1928 A71-26700

Acoustic refraction by two dimensional shear layer in duct, considering sound propagation and initial value problem solution 13 p2051 A71-29240

Boundary layer effect on sound transmission in acoustically treated circular duct with shear flow reducing governing equations to two-point boundary value problem 14 p2224 A71-30198

Turbulent flow and high sound level effects on acoustic attenuation in narrow rectangular duct
14 p2224 A71-30207

Noise attenuation prediction in absorbing ducts adaptable to bypass jet engines, using Morse theory
14 p2288 A71-30522

Acoustic measurement of rotor tones in duct of four blade ventilation fan
19 p3000 A71-38655

Spinning acoustic modes transmission and backscatter in nonuniform long cylindrical ducts with throat
24 p3848 A71-44556

ACOUSTIC EXCITATION

Spherical alcohol droplet vaporization in acoustically disturbed medium, considering convective heat and mass transfer
01 p0179 A71-10798

Closed cylindrical shell response to random sound in contained fluid, investigating cylinder end acoustic boundary conditions with coupled oscillator theory
02 p0239 A71-11998

Discharge current oscillations attributed to acoustic wave excitation by Q switched carbon dioxide laser
02 p0261 A71-12341

Acoustic stimulation effect on electroretinogram of man
03 p0361 A71-13191

Sound field in multiple source enclosures, discussing noise and vibration control, acoustic modes excitation and environment simulation
03 p0511 A71-14142

Interdigital converter for excitation and reception of acoustic surface waves on piezoelectric materials in bandpass filter design
03 p0388 A71-14574

Subphotospheric trapped standing acoustic wave mechanism of 5 minute oscillations on solar surface
05 p0801 A71-15936

Aerodynamic sound generation by turbulent circular free jets, presenting solution to inhomogeneous acoustic wave equation by Lighthill
06 p0881 A71-17421

Rectangular panel acoustic response by variational finite element method, including radiated sound field effects on structural vibration
06 p0984 A71-17622

Thin cylindrical shell in ideal compressible fluid, calculating longitudinal resonance waves for acoustic excitation
06 p0985 A71-17755

Low temperature confined cesium plasma, observing ion-acoustic oscillation excitation effects on transfer process and ionization
07 p1167 A71-19236

Cylindrical shell dynamic response to random acoustic excitation within narrow frequency band of low modal density
09 p1534 A71-22082

Turbulence properties in supersonic flow, considering modes with vorticity, entropy and acoustic aspects
09 p1383 A71-23603

Closed cylindrical shell response to randomly time distributed broadband acoustic excitations, using statistical energy method to compute displacement and interior pressure
11 p1842 A71-25311

Human heart beat phase frequency changes after acoustic stimulation during natural sleep from EEG, EKG, EMG of musculus hypoglossus and eye motions
11 p1721 A71-26292

Apollo spacecraft qualification vibration test program assessment, discussing structural acoustical excitation method
11 p1745 A71-26441

Low temperature confined Ca plasma, observing ion-acoustic oscillation excitation effects on transfer process and ionization
12 p1935 A71-26754

Transverse acoustic wave amplification in solid propellant rocket motor, using discrete mass injection as excitation source
12 p1946 A71-27565

Acoustically induced cylindrical shell vibrations, solving differential equation derived for expression of system axisymmetric forced vibrations
13 p2150 A71-28136

Ultrasonic field distribution patterns from metallic and ceramic concave spherical reflectors under excitation by single or multiple piezoelectric elements
13 p2101 A71-29267

Radiation patterns and scattering cross sections of plane black disks excited by electromagnetic and acoustic waves
14 p2194 A71-30079

Ion-acoustic oscillations excitation in rarefied plasma layers confined by external high frequency TE wave electromagnetic field
14 p2281 A71-30555

Vibratory stresses in heat exchangers due to pressure pulsation induced acoustic resonances, calculating flow pulsations from Karman vortex streets
15 p2513 A71-31635

Structural panel under acoustic loading by supersonic convected turbulence, deriving responses with finite Fourier transforms
15 p2507 A71-32131

Turbulent combustion stability in rocket engine with allowance for walls reflecting acoustic waves excited by flame
16 p2663 A71-33605

Acousto-optical effects, materials and devices of laser beam control using diffraction and refraction by ultrasonic waves
18 p2932 A71-36607

Acoustical oscillations effect on free jet flow stability and structure, using inviscid Orr-Sommerfeld equation for flow disturbances frequency, wavelength and velocity
20 p3175 A71-38806

Sound field excitation by wedge shaped transducer in liquid filled wedge extension region, determining sound field distribution as function of frequency and wedge angle
20 p3268 A71-38812

Shear layers acoustic excitation, considering coupling between sound waves and rotational excited shear waves in flow detachment line
21 p3317 A71-40014

Acoustic pulse excited ionization waves and wakes measurement in glow discharge plasma, giving phenomenological explanation
21 p3421 A71-40089

Transversely vibrating hollow cylindrical beam sound radiation and response to acoustic excitation, predicting resonant frequencies
21 p3461 A71-40320

Heat balance effects of acousto-gravitational waves in upper atmosphere, concerning infrasound from earthquakes, polar auroral arcs and magnetic storms
22 p3533 A71-41656

Coupled plate-cavity acoustic system response at LF and spatially uniform pressure, using plate finite elements and acoustic volume-displacement theory
22 p3617 A71-42540

Traveling ionospheric disturbances excitation in F2 layer by passing acoustic gravity waves
23 p3665 A71-42966

Acoustical harmonic point source in motion relative to surrounding fluid, using Fourier integrals for mathematical representation
24 p3847 A71-44418

Acoustic resonance excitation by vortex shedding from flat plate trailing edge in low speed wind tunnel
24 p3848 A71-44557

Vortex shedding from blunt trailing edge of flat plate spanning wind tunnel under oscillating flap and acoustic resonance excitations
24 p3848 A71-44558

ACOUSTIC FATIGUE

Test facility for acoustic fatigue of materials and structural elements
07 p1083 A71-19167

Stiffened panel acoustically induced stress estimation using experimentally determined random S-N curves with various structural parameters
17 p2826 A71-35033

Test equipment for acoustic fatigue of materials and structural elements
17 p2724 A71-35663

Additive damping control of acoustic resonance fatigue of aerospace structures under severe environments, considering materials, tuned devices and layered techniques
18 p2979 A71-36494

Cavitation erosion of aluminum at high hydrostatic pressure, using chamber focusing acoustic system
18 p2910 A71-36932

Aircraft structures sonic fatigue due to high frequency noise from turbofan engines, discussing case histories, failure diagnosis and precautionary design measures
19 p2997 A71-37843

Flight test measurements of shock cell noise loading of aircraft tail planes, noting alleviation by nozzle and mirror structural modifications
19 p2998 A71-38467

ACOUSTIC GENERATORS

U SOUND GENERATORS

ACOUSTIC IMPEDANCE

Free wave reflection measurements of normal acoustic impedance of ground surfaces in relation to shock waves from large supersonic commercial aircraft
03 p0347 A71-13278

Baffled piston source sound radiation impedance from numerical solution of Fredholm integral equation for vibrating disk in finite rigid concentric baffle
19 p3104 A71-37849

ACOUSTIC INSTABILITY

Acoustic instability of plasma with current under ionizational equilibrium and moderate neutral gas pressures
13 p2105 A71-27878

Cylindrical shaped powder samples vibrational combustion, observing acoustic instability with high speed motion picture photography
17 p2839 A71-35698

Nitroglycerin powder combustion acoustic instability, determining mean pressure and sample and combustion chamber geometry effects
17 p2840 A71-35700

Combustion driven acoustic oscillations in gas fired burner of premixed methane, nitrogen and oxygen, noting mixture ratio and flow rate effects
19 p3123 A71-38098

Long wavelength ion acoustic instability of two temperature collisional fully ionized plasma with heat transfer, noting additional destabilizing currents
21 p3422 A71-40708

Acoustic instability of Joule heated nonisothermal electron plasma
23 p3709 A71-43261

Longitudinal ambipolar sound instability effect on duration of plasma particle motion to wall across magnetic field, using phase method
23 p3709 A71-43263

Nonlinear ion acoustic soliton wave propagation and dissipation in nonhomogeneous nonisothermal weakly absorbing plasma
23 p3714 A71-44333

Injected ion beam interaction with hot plasma in cylindrical magnetic mirror, noting acoustic frequency oscillation heating effect
24 p3854 A71-44514

ACOUSTIC MEASUREMENTS

High resolution automatic measurement of ultrasonic velocity changes using interferometer and FM oscillator
02 p0250 A71-12134

Glow discharge microphone for acoustic pressure detection and measurement at ultrasonic frequencies
02 p0232 A71-12140

Fan/compressor noise research covering vane/blade ratio and geometry effects on transmission through blade rows
03 p0471 A71-14120

Aircraft sound measurement standards, evaluating airport noise control and permissible levels
03 p373 A71-14248

UH-1B helicopter flight test noise measurements data reduction and analysis, presenting sound pressure vs frequency and time plots
04 p0531 A71-15405

Helicopter in-flight noise radiation pattern and spectra measurements for various operating parameters
04 p0531 A71-15406

Prewhitening technique for acoustic turbulent flow data recording and analysis
04 p0600 A71-15598

Acoustic emission monitoring system for real time detection of crack initiation and propagation in complex structure during static and fatigue tests
06 p0906 A71-18461

Monograph on optical imaging of ultrasonic fields by acoustic Bragg diffraction covering heuristic plane wave and ray approach scattered fields
07 p1111 A71-19575

Sound field due to point source inside absorbent lined enclosure for anechoic chamber performance prediction
07 p1160 A71-19587

Acoustic wattmeter with piezometric electric signal sensor and amplifier for measuring elastic wave intensity in liquids
07 p1114 A71-20059

Aircraft flyover noise samples, obtaining atmospheric absorption coefficients
08 p1231 A71-21425

Large space vehicle acoustic environment test facility, investigating combined direct and/or reverberant sound field effects
08 p1272 A71-21430

Lower atmosphere meteorological parameters remote determination by acoustic sounding, discussing range and resolution characteristics
08 p1330 A71-21743

Noise exposure forecasts for cumulative aircraft noise production single number rating as community response indicator
08 p1249 A71-21817

Aircraft noise abatement control on international basis by setting acoustic technological capability compulsory standards of quietness
08 p1379 A71-21826

Cr alloys alloying elements Os, Re, Fe, Co and Mn effect on lattice constant and elastic properties, using acoustic measurements
09 p1473 A71-23229

Vertical velocities in atmosphere measured by acoustic Doppler during diurnal thermal plumes and breaking wave occurrence within nocturnal inversion
10 p1574 A71-23746

Optimum frequency for detection of acoustic sources in upper atmosphere as function of altitude and turbulence
10 p1642 A71-24833

Airport sound prediction using Noise and Number Index deduced from noise logarithmic average and audible aircraft number
11 p1723 A71-25236

Boron and carbon fracture and debonding in epoxy matrix, using acoustic emission analysis
11 p1772 A71-26392

ACOUSTIC PROPAGATION

Nonauditory and auditory physiological effects of noise, discussing hearing conservation, noise measurement and noise hazard

11 p1726 A71-26511

Axial flow fan noise, investigating louvers effects on sound field

12 p1945 A71-26704

Acoustic emission application to nondestructive testing of materials, manufacturing processes and structural components failures

13 p2073 A71-27939

Computer simulation of automatic voice communication link intelligibility measurement, using speech recognition techniques

13 p2032 A71-28872

Fluid velocity measurements by electroacoustic transducers using phase difference relation

13 p2069 A71-28901

Noise exposure index from mean sound intensity measurement, considering harmful effects on humans

13 p2021 A71-29284

Niese procedure for sound intensity determination, considering measurement practice

13 p2101 A71-29285

Point and large sources acoustic free field measurement, predicting reflecting ground surface effects on accuracy

14 p2274 A71-30066

Computer controlled acoustic data acquisition system with real time control of 16 high intensity acoustic generators

14 p2208 A71-30315

Sound fields of flying aircraft from noise measurements, discussing engine operating conditions, speed and attitude

14 p2176 A71-30521

Jet aircraft sound spectrum on ground and in air, comparing calculation with experiment

14 p2289 A71-30524

Absorbent materials test methods and acoustic data reduction with simulation principle

14 p2275 A71-30525

Noise measurement data on various types of blown flap configurations for STOL aircraft, discussing integration effects between jet and flap assembly [AIAA PAPER 71-745]

14 p2171 A71-30785

Atmospheric and man-made noise measurement techniques, using signal generator as reference standard for absolute amplitudes

14 p2204 A71-30978

Acoustic wave after passage through turbulent wake, measuring phase fluctuations

15 p2387 A71-31169

Fan induced low speed jet noise from turbofan engines, discussing results of far field sound measurements for simulated nacelle configurations with and without acoustic liners [AIAA PAPER 71-586]

15 p2467 A71-31533

Aircraft noise reduction criteria, examining noise measurements relation to human behavior and physical measures connection to subjective judgments

15 p2349 A71-31879

Aircraft noise in-flight measurement and analysis, including engine parameters, synchronous recordings, flight paths and coded analog bands

15 p2349 A71-31884

Aircraft engine noise test methods for acoustic certification, investigating jet and compressor silencing, absorbent materials, rotor and propeller noise and psychoacoustic tests

15 p2385 A71-31890

Facility for signal noise measurement in proportional fluidic amplifiers, discussing stored sweep spectra interpretation

15 p2351 A71-32053

Aircraft noise measurements, noting ground absorption effects

15 p2450 A71-32127

Acoustic indicator for remote detection of microcracks in systems with high gas or vapor pressures

15 p2409 A71-32189

Solution concentration, solid content, specific gravity and bulk modulus measurements by sound velocity measurement

15 p2409 A71-32197

Aircraft flyby effective noise duration calculations, examining observation points and analysis methods

15 p2350 A71-32519

Multichannel sound level meter capable of direct and continuous measurement and recording

18 p2897 A71-36221

Helicopter rotor noise due to blade-vortex interaction, using linear gust model

18 p2849 A71-36934

Jet aircraft flyover noise measurement, determining average intrusion level in residential communities under approach and departure corridors

19 p2996 A71-37497

Near field noise measurement on quarter-scale model to estimate fuselage pressure in VTOL aircraft for conventional, short and vertical takeoff configurations

19 p2997 A71-37844

Acoustic measurement of rotor tones in duct of four blade ventilation fan

19 p3000 A71-38655

Acoustic emission technique for nondestructive cracking rate determination in hydrogen embrittled steel, using crack-tip stress intensity factor as critical parameter

20 p3241 A71-38773

Acoustic emission test facility with constant strain rate compressive sample deformation

20 p3208 A71-38823

Sound to light image conversion, emphasizing liquid surface acoustical holography

20 p3238 A71-39343

Micrometeoroid flux acoustic measurements by Cosmos 135 and 163, discussing detection of shower activity

20 p3299 A71-39649

Broadcast sound loudness level monitor as measuring and indicating instrument, discussing technological and psychoacoustical evolution

20 p3271 A71-39763

Noy curves in perceived noise levels, noting relative noisiness dependence on relative intensities

21 p3325 A71-40867

Propeller vortex noise analysis by on-line 1/3 octave band resolution, discussing characteristic results from noise measurements on various propeller configurations

21 p3325 A71-40868

Acoustical holography principles properties and applications, discussing liquid surface levitation, Bragg diffraction and undersea and seismic utilization

21 p3381 A71-40931

Acoustical holographic opaque structures visualization techniques and applications, discussing ultrasound qualities, image converters, detector arrays and medical diagnostic utilization

22 p3540 A71-41752

Optical holographic detection and measurement of ultrasonic waves, providing practical method of investigating LF sound waves

22 p3541 A71-41785

Acoustic noise output from round interfering subsonic jets, considering suppressor nozzle attenuation

24 p3864 A71-44560

ACOUSTIC PROPAGATION

Covering plate steady state response to acoustic vibrations in viscoelastic half space, calculating interface displacement frequency spectra under zero shear stress assumption

03 p0459 A71-13719

Acoustic propagation through variable area duct with steady compressible flow, transforming governing equations into two decoupled linear ordinary differential equations

07 p1160 A71-19952

Cylindrical duct stationary uniform axial flow effects on propagation of acoustic vibration modes of wavelength smaller than damping length [ONERA-TP-969]

12 p1981 A71-27479

Cylindrical lithium niobate single crystal acoustic propagation, determining speed, damping and sound reflection with He-Ne laser light scattering at hypersonic oscillations

13 p2080 A71-29024

Large amplitude ion acoustic wave propagation in streaming ion plasma, noting nonlinear effect in amplitude oscillation observation

14 p2281 A71-30541

Acoustic wave after passage through turbulent wake, measuring phase fluctuations

15 p2387 A71-31169

One dimensional acoustic tunnel effect for incident wave normal to barrier analogous to macroscopic spin waves and quantum mechanics

15 p2449 A71-31703

Sound passage through rigid screen of arbitrary wave thickness with apertures, using linear algebraic equations

15 p2449 A71-31709

Annular ducts finite amplitude spinning acoustic modes propagation and subsonic choking, allowing for nonlinear effects in perturbation procedure

15 p2450 A71-32133

Materials dynamic characteristics determination by acoustic input signal impedance measurement, presenting expressions as functions of reflection factor and signal propagation phase shift

15 p2409 A71-32186

Acoustic propagation in rigid wall rectangular duct with uniform flow, calculating higher mode energy transmission properties

15 p2392 A71-32195

Lunar seismic energy diffusion, calculating transmitted and reflected acoustic wave intensities as time function after explosion

16 p2637 A71-33511

Refraction, terrain, air attenuation, fog and rain, turbulence and shielding effects on acoustic propagation in lower atmosphere

17 p2734 A71-35235

Wave formation during metals explosive welding, indicating process of wave freezing by acoustic equations analysis

17 p2749 A71-33369

Externally excited moving strations measurement in low pressure Ar discharge, comparing with ion acoustic wave propagation derivation from model

18 p2948 A71-33839

Relaxation effects on velocity and temperature of solid particles in gas flows, emphasizing acoustic propagation, compression shock structure and nozzle flows

18 p2909 A71-36441

Seasonal stratospheric wind effects on infrasound propagation to U.S. northeast coast from rocket launched at Cape Kennedy

20 p3306 A71-39762

Acoustic signal pressure mode propagation velocity in infinite rectangular hard-walled duct with steady flow, noting Doppler effect

20 p3271 A71-39765

Handwritten graphical data computer input device with pen position coordinate measurement from acoustic signal propagation delay time in piezoelectric solid plate

21 p3376 A71-40122

Acoustic wave propagation and heating in solar atmosphere, using Harvard Smithsonian reference atmosphere and Stein frequency spectra

22 p3601 A71-42170

Acoustic waves transmitted through solid elastic cylinders, calculating wavefront loci and waves amplitudes

23 p3704 A71-43210

Shear flow effects on sound propagation in rigid rectangular ducts, taking into account boundary layer thickness

23 p3704 A71-43212

Sound transmission through finite closed shells, considering statistical energy analysis, modal coupling and noise reduction

23 p3704 A71-43213

Strong magnetic field effects on acoustic oscillations and instability in stationary inhomogeneous low temperature plasma flow in crossed fields

23 p3712 A71-43917

Sound wave propagation from two dimensional acoustic source in subsonic fluid moving between two reflecting parallel walls

23 p3705 A71-44145

Low speed wind tunnel measurements corrections for acoustic effects due to fan noise propagation

24 p3790 A71-44765

ACOUSTIC PROPERTIES

NT ACOUSTIC IMPEDANCE

NT ACOUSTIC INSTABILITY

NT ACOUSTIC SCATTERING

NT ACOUSTIC VELOCITY

NT REVERBERATION

NT SOUND INTENSITY

Acoustic phenomena accompanying pericardial disease, considering heart valves and chordae tendineae

05 p0711 A71-16959

Supersonic jet noise suppressor with tubes and shrouds, examining flow and acoustic characteristics [AIAA PAPER 71-153]

06 p0884 A71-18594

Short rotor blade span supersonic fan for pressure wave forward propagation elimination, obtaining acoustic and aerodynamic characteristics [AIAA PAPER 71-182]

06 p0885 A71-18621

Shock tube testing of acoustic materials at high sound amplitudes

07 p1083 A71-19588

Aeroacoustic phenomena in free turbulent gas jets: discussing structure, noise-turbulence correlations and acoustic field generation at subsonic/critical velocities

09 p1384 A71-23607

Noise emission and acoustic efficiency in pulsating combustors, considering sound pressure level

13 p2113 A71-28618

Acoustic and gas dynamic characteristics of jet noise muffler, using adapters at outlet section of exhaust nozzle

15 p2469 A71-31710

Helmholtz, half and full mode standing pressure waves for separated flow induced acoustic resonance in open cavities

15 p2391 A71-32106

ACOUSTIC RADIATION

U SOUND WAVES

ACOUSTIC SCATTERING

NT REVERBERATION

Plane acoustic wave diffraction by dense periodic grating, using crimped surface scattering with Neumann and mixed boundary conditions

01 p0128 A71-11120

Acoustic shock wave scattering by cylindrical cavities in inviscid fluid medium, noting shielding effect: peak excitation and inverse logarithmic decay [ASME PAPER 70-WA/APM-57]

03 p0459 A71-14177

Sonic boom and explosion shock wave propagation over long distances through turbulence modeled by

sound speed fluctuation, including acoustic scattering effect
09 p1433 A71-22858

Sound waves propagation and scattering in moving media, deriving wave equation for acoustical pressure by iterative process
11 p1747 A71-25147

Aerodynamic noise scattering near Lighthill multiples, considering intense near-field energy conversion into sound waves
11 p1705 A71-26448

Ray acoustic treatment, estimating diffusion of radiation patterns due to scattering by random inhomogeneities
17 p2783 A71-35036

Spinning acoustic modes transmission and backscatter in nonuniform long cylindrical ducts with throat
24 p3848 A71-44556

ACOUSTIC SIMULATION
Sound field in multiple source enclosures, discussing noise and vibration control, acoustic modes excitation and environment simulation [ASME PAPER 70-WA/DE-8] 03 p0511 A71-14142
Subsonic jet aircraft noise and simulated sonic booms awakening effects on human sleep
11 p1726 A71-26510
Sonic boom wave interaction with topographic models, measuring surface pressure time history [AIAA PAPER 71-619] 15 p2389 A71-31548
Kinematic analysis and simulation of transmission modes of sound energy through middle ear
19 p3002 A71-38062
Optimal design for noise attenuation by diesel engine exhaust mufflers using linearized acoustic models
20 p3268 A71-38961

ACOUSTIC STABILITY
U FREQUENCY STABILITY
ACOUSTIC STREAMING
Unsteady acoustic wind in free sound field from random Reynolds numbers, using stream equation
13 p2101 A71-28847

ACOUSTIC VELOCITY
Ultrasonic sound velocity dispersion in various hydro and gas suspensions, considering viscosity and heat conduction effects
01 p0127 A71-10618
Acoustic turbulence spectrum in compressible fluid with potential motion, using complex traveling wave amplitudes in hydrodynamic equations
02 p0239 A71-11924
Pure shear mode propagation in sapphire, determining acoustic axes velocity
02 p0294 A71-11947
High resolution automatic measurement of ultrasonic velocity changes using interferometer and FM oscillator
02 p0250 A71-12134
Acoustic velocity in water, examining air bubble effects on pressure pulse attenuation
03 p0459 A71-13720
Nozzle throat conditions at sound velocity discontinuity due to transition from one to two condensed phases during expansion
05 p0735 A71-16576
Nonstationary isentropic low density flows with axial or central symmetry, suggesting characteristics with flow rate and sound speed variation as in stationary source flow
07 p1014 A71-19729
Humidity effects on sound velocity in air at constant temperature and normal atmospheric pressure in lower audio frequency range
10 p1642 A71-24815
Airfoils accelerating near sound velocity, calculating acoustic radiation by linear theory
10 p1553 A71-24816
Ion beam deceleration and effective energy transfer to plasma at nonisothermal acoustic velocities in presence of ion acoustic instability
10 p1653 A71-24892
Vapor flow passage wall shear stress effect on sonic velocity limit in Na heat pipes [AIAA PAPER 71-407] 11 p1856 A71-26202
Sound velocity measurements in superheated Cs vapors, using least squares method for analytic relationships on saturation line and isobars
13 p2099 A71-27881
Interplanetary medium characteristics during geomagnetic storms, discussing changes in pressures, energy flux densities, acoustic velocities and static/magnetic pressure ratio
13 p2058 A71-28236
Collisionless heat propagation along plasma magnetic field, showing relation to ion sound velocity
13 p2107 A71-28568
Quasi-unsteady approximation of mutual hydrodynamic drift velocity of aerosol particles in high power sound field
13 p2101 A71-28849
Solution concentration, solid content, specific gravity and bulk modulus measurements by sound velocity measurement
15 p2409 A71-32197

Sound velocity in real gases as function of pressure and temperature, deriving by van Litterbeek result generalization for higher pressures
17 p2783 A71-35038

Transonic nozzle flow with variable stagnation speed of sound across flow, deriving governing equations with stream function as independent variable
21 p3324 A71-40978

Sound wave dispersion in metals in inclined magnetic field, noting sound velocity deviation
21 p3417 A71-41265

Ion beam deceleration and effective energy transfer to plasma at nonisothermal acoustic velocities in presence of ion acoustic instability
21 p3425 A71-41272

Sonic line position measurement in supersonic flow behind detached shock wave preceding axisymmetric or plane blunt bodies
23 p3625 A71-43092

Coherent acoustic wave propagation speed and attenuation coefficient in turbulent flow
23 p3703 A71-43209

Speed of sound measurement in solid and liquid phase suspensions, considering dense phase inertia forces and particles thermal retardation effects
24 p3827 A71-45019

ACOUSTIC VIBRATIONS
U SOUND WAVES
ACOUSTICS
NT MAGNETOACOUSTICS
NT PSYCHOACOUSTICS
NT UNDERWATER ACOUSTICS
Fluidic acoustic signal detector for output determination of HF fluid oscillators, discussing performance, constant loading effect and signal amplitude [ASME PAPER 70-WA/FLCS-7] 03 p0428 A71-14083
Heuristic flow acoustics, discussing noise frequency spectrum in reference to moving singularities
04 p0569 A71-14980
Nonlinear acoustics propagation theoretical solutions by weak shock theory and Burger equation, noting differences in exactness and complexity of methods
05 p0784 A71-17156
Continuity and balance equations of acoustic energy in nonuniform fluid flows
07 p1160 A71-19588
Bessel equation solutions for electromagnetic and acoustic wave equations in form of Hankel functions
08 p1333 A71-20740
Review of September 1970 aerodynamic noise symposium covering jet and helicopter rotor noise, nonlinear acoustics and diffraction theory
19 p2994 A71-38205
HF electric field influence on collisionless electron gas acoustoelectric effect, emphasizing electron scattering mechanism
21 p3431 A71-41232
Acoustical holography - Conference, Newport Beach, California, July 1970, Volume 3
22 p3540 A71-41776
Acoustic holography imaging technology, discussing sound field visualization and applications in nondestructive testing, medical diagnostics, ultrasonic microscopy, seismology and underwater viewing
22 p3546 A71-42478
Elasticity and acoustic theory eigenvalues determination in spherical coordinates using transcendental equation
24 p3882 A71-44836

ACQUISITION
NT DATA ACQUISITION
NT TARGET ACQUISITION
Image quality improvement by successive hologram acquisition process
13 p2070 A71-29026

ACROBATICS
Acrostar acrobatic aircraft design and performance
03 p0346 A71-13016
External oblique inguinal hernia due to acrobatic flying centrifugal accelerations, considering anatomical, clinical and medico-legal aspects
17 p2681 A71-34822
Acrostar Mk II all wood single seat acrobatic light weight aircraft designed for plus/minus 8g and inverted flight
23 p3629 A71-43887

ACRYLATES
Styrene-methyl methacrylate and -acrylonitrile copolymers linear and mass regression rates in hybrid rocket fuels combustion
15 p2464 A71-31640

ACRYLIC RESINS
Thermosetting acryl modified epoxy resin, stressing adhesive bonding strength, workability and curing characteristics
11 p1787 A71-25423

ACRYLONITRILES
High strength flexible carbon fabrics from oxidized polyacrylonitrile yarns for reinforced plastic laminates [PLASTICS INST. PAPER 39] 08 p1319 A71-20900

ACTIVATION [BIOLOGY]
Carbon fibers production by polyacrylonitrile fibers spinning, discussing stretching temperature effects on mechanical properties [PLASTICS INST. PAPER 12] 08 p1320 A71-20909
Pyrolysis products of polyacrylonitrile fibers in low pressure apparatus, using mass spectrometer [PLASTICS INST. PAPER 4] 08 p1250 A71-20926
Graphite fibers mechanical properties based on rayon and polyacrylonitrile, considering tensile, flexural, compressive and shear strength
11 p1784 A71-25398
Fractography of thermoset resins toughened with Hycar carboxyl terminated butadiene acrylonitrile, using electron microscope
11 p1785 A71-25406
Styrene-methyl methacrylate and -acrylonitrile copolymers linear and mass regression rates in hybrid rocket fuels combustion
15 p2464 A71-31640
Polyacrylonitrile and rayon precursor graphite fibers diameter relation to Young modulus and tensile strength
15 p2438 A71-31817

ACTH
U ADRENOCORTICOTROPIN [ACTH]
ACTINIDE SERIES
NT CALIFORNIUM ISOTOPES
NT PLUTONIUM
NT PLUTONIUM 238
NT THORIUM
NT THORIUM ISOTOPES
NT TRANSURANIUM ELEMENTS
NT URANIUM
NT URANIUM ISOTOPES
NT URANIUM 235
Synthetic actinides discovery, characteristics, manufacture and practical applications
02 p0283 A71-12591
Superheavy transactinide isotopes in outer space, discussing single standard composition of cosmos material bulk
08 p1351 A71-20958

ACTINIDE SERIES COMPOUNDS
NT THORIUM COMPOUNDS
NT THORIUM OXIDES
NT URANIUM CARBIDES
NT URANIUM COMPOUNDS
NT URANIUM OXIDES
Physical properties, structure and sintering of refractory oxides of rare earth elements and actinides, including chromia
09 p1478 A71-23399

ACTINOGRAPHS
U ACTINOMETERS
ACTINOMETERS
NT DICKE RADIOMETERS
NT INFRARED DETECTORS
NT INFRARED SCANNERS
NT MICROWAVE RADIOMETERS
NT RADIOMETERS
NT SOLAR SPECTROMETERS
NT SPECTRORADIOMETERS
Actinometric network for monthly sums of overall solar radiation and earth surface radiative balance, estimating random errors mean square values
04 p0621 A71-14640
Soviet papers on actinometry, atmospheric optics and ozonometry, covering atmospheric ozone contents measurement techniques, radiation balance, atmospheric spectral transmissivity, etc
20 p3257 A71-39326
Actinometer thermobatteries surface sensitivity distribution effect on solar radiation flux measurement accuracy
20 p3237 A71-39330
Compensation pyrheliometers and thermoelectric actinometers response lag and irregular operation after instantaneous shadowing, discussing techniques for determining instrument inertial characteristics
20 p3237 A71-39332
Angular distribution of outgoing short wave radiation field intensity as function of sun height on basis of actinometric data from Cosmos 184 satellite
21 p3374 A71-41299

ACTIVATION
Zirconium iodide vapor deposition kinetics, determining activation temperature
15 p2425 A71-31395

ACTIVATION [BIOLOGY]
Stearotherophilus spore germination stimulation, investigating effects of preheating and amino acid and carbohydrate concentration
13 p2010 A71-28695
Rat irradiated spinal cord, detailing orthodromic ventral root and monosynaptic reaction to rhythmic and increasing frequency stimulation
15 p2362 A71-32735
Activation impulse blocking in nerve, using inhomogeneous Lillie electrochemical model
19 p3006 A71-37282
Arousal and activation in nonspecific reticulothalamo-cortical systems due to underlying emotion

ACTIVATION ANALYSIS

- expressed through cortical, visceral and somatomotor channels 21 p3330 A71-40247
- ACTIVATION ANALYSIS**
NT NEUTRON ACTIVATION ANALYSIS
 Apollo 14 bulk lunar fines sample elemental abundances determination from soils and rocks by activation analysis 20 p3292 A71-39382
- ACTIVATION ENERGY**
 Medium alloy structural steels tempering, investigating Mn, Ni, Cr and Mo effect on activation energy of softening 03 p0445 A71-14338
- Secondary recrystallization of Ti, Zr and Nb carbides within homogeneity ranges, determining activation energies as function of carbon deficiency in carbide lattice 04 p0609 A71-14749
- Incomplete energy equilibration in short lived activated complexes, measuring translational energy of unimolecular ion decomposition fragments 05 p0716 A71-15924
- Arrhenius activation energy in relation to excitation functions for various reaction types 05 p0716 A71-15976
- Fe-Ni alloy oxidations parabolic kinetics and activation energies, noting scale development as function of oxidation amount and temperature 05 p0770 A71-17098
- Chromium oxide electric conductivity activation energy and active oxygen, discussing perchloric acid and ammonium perchlorate vapors effect 07 p1182 A71-19247
- Electron trapping in MIS transistor, discussing thermal annealing process activation energy and trap production by radiation 07 p1076 A71-19499
- Co activation rate measurements over temperature range 475-1325 C at various oxygen pressures, determining oxide formation kinetic law and activation energy 07 p1139 A71-20225
- Interstitial impurities effects on relation of activation energy to effective stress in iron, low carbon steel and other bcc metals 08 p1308 A71-21514
- Organic impurities effects on carbon dioxide dissociation activation energy, considering magnitude dependence on experimental conditions and data reduction techniques 08 p1251 A71-21783
- Niobium carbides sintering by hot pressing at various temperatures, discussing kinetics, relative compactness and activation energy 09 p1466 A71-22163
- Excited radical and ion formation in unperturbed acetylene-air and superimposed HF discharge flames, determining activation energy 09 p1402 A71-22379
- Strain rate and temperature effects on flow stress of Ni-Al in polycrystalline and single crystal for activation energies and deformation volumes evaluation 11 p182 A71-26440
- Activation energy anisotropy for Mo and Nb single crystals dislocation relaxation, noting temperature dependence 12 p1917 A71-27300
- Reactive solids ignition by constant energy flux from asymptotic analysis of activation energy limit 14 p2337 A71-30458
- Al and Cu dynamic plastic deformation at elevated temperatures, discussing relationship between strain rate sensitivity and activation energy 15 p2428 A71-31972
- Recrystallization nuclei linear growth rate activation energy relationship to Ni plastic deformation magnitude, temperature and purity 15 p2429 A71-31995
- Compressive creep of aluminum oxide single crystals deformed by dislocation glide and rhombohedral twinning, investigating activation energy and rate controlling mechanism 15 p2439 A71-32439
- Nonpremixed and premixed combustion theory in laminar flows, considering diffusion flame- reaction time ratio and activation energy effects 15 p2515 A71-32564
- Intermetallic formation in Au-Al systems via diffusion couples, determining activation energy, silicon effect and tensile strength 19 p3119 A71-38513
- Creep tests evaluation for stress and temperature effects on apparent activation energy 20 p3250 A71-39018
- Activation energy and temperature dependence of radiation induced free radical destruction in N-acetyl-DL-valine, using Arrhenius plots 21 p3345 A71-40203
- Bronsted relationship between adsorption heat and activation energy in electrocatalysis of purified orthophosphoric acid and phase-oxide-free noble metals 21 p3345 A71-40540

- Temperature dependence of impurity photoluminescence of Cr-doped GaAs single crystals, measuring activation energy 21 p3430 A71-41214
- Transition from metallic to activation conductivity in doped semiconductors, noting activation energy dependence on compensation degree 24 p3860 A71-45121
- ACTIVE SATELLITES**
NT EARLY BIRD SATELLITES
NT SYNCOM SATELLITES
ACTIVITY
 Oxygen solubility and activity in Fe-Al and Fe-Ti melts, using neutron activation analysis 04 p0614 A71-15785
- ACTIVITY [BIOLOGY]**
 Electro-optic monitoring method for single isolated heart cell activity 02 p0202 A71-11672
- Direct continuous radiotelemetry of blood pressure measurements taken from aorta, pulmonary artery and inside heart during normal activity of test subjects 03 p0371 A71-13070
- Physical endurance and muscular activity of man as adaptation process depending on biochemical and functional changes 03 p0361 A71-13192
- Animals tissue activity during winter hibernation under Alaskan environmental conditions, discussing sense of time, anticipation of seasonal changes, etc 07 p1041 A71-19525
- Frog ventricles myocardial fibers spontaneous activity in Ringer solution due to ion conductivity variations 08 p1239 A71-21057
- Unanesthetized rabbits visual cortex cells neuron activity during sound-rhythmic light flashes association 12 p1871 A71-27487
- Marmot ketone bodies concentration during activity, deep hibernation and early arousal, discussing increased oxidative metabolism effects 13 p2014 A71-29125
- Superposition model of spontaneous activity of cerebellar Purkinje cells for spike triggering 13 p2014 A71-29289
- Diurnal variations of mitotic activity in thyroid epithelial cells of different follicle size 15 p2356 A71-31290
- Individual neurons activity during stereotaxic operations on Parkinsonism and hyperkinesia syndromes, describing microelectrodes for extracellular recording 15 p2365 A71-32535
- Neuron response to stimuli compared with background activity on histograms 16 p2532 A71-33898
- Cochlear nucleus and posterior clivus neurons impulse activity due to tonal signals in anesthetized cats auditory system 16 p2532 A71-33899
- Reflexes dominant in organism throughout activity or temporarily dominating reflex system directing work of nervous centers 17 p2685 A71-35363
- Conditioned reflex activity, demonstrating development of individual signals systems interrelation 17 p2685 A71-35365
- Activity correlation of adjacent neurons of cat cerebral cortex somatosensory zone, considering distribution of same direction /cophasic/ and different direction /counterphase/ of background rhythms 19 p3001 A71-37392
- Alpha activity parameters during human performance of motor tasks with open and closed eyes 23 p3631 A71-43108
- Erythropoietic activity dosage in polycythemic mice after intermittent hypobaric hypoxia 23 p3632 A71-43216
- Hypobaric hypoxia effect on polycythemic mice erythropoietic hyperactivity, evaluating iron content in peripheral erythrocytes 23 p3632 A71-43217
- Extrarenal production of erythropoietin in binephrectomized rats after hypobaric hypoxia 23 p3632 A71-43218
- Biological activity in Apollo 11 and 12 core samples searched for after placement in Petri dishes containing media 23 p3757 A71-43747
- Evoked and background activities interaction in computerized self zeroing neuron model 24 p3801 A71-44550
- ACTIVITY CYCLES [BIOLOGY]**
 Light-dark cycle strength as Zeitgeber for circadian rhythms in isolated man 03 p0364 A71-14249
- Cyclic muscular voluntary movements, noting spinal segmental apparatus function 05 p0709 A71-16804
- Biosatellite 3 onboard camera time lapse photography of monkey sleep/wake activity patterns during weightlessness 09 p1394 A71-23240

- Alpha rhythm activity, periodicity and mean frequency in cortex regions of healthy humans based on EEG frequency and correlation analyses 14 p2186 A71-30551
- Interdisciplinary cycle research - Conference, Noordwijk, Netherlands, June 1970 20 p3190 A71-39474
- Biological and biochemical cyclic phenomena, including circadian rhythms 20 p3190 A71-39475
- Chronobiology purposes, techniques and applications, discussing rhythmic or cyclic variation calculation, biological rhythms spectra and classification and time structure alteration of organisms 21 p3329 A71-40149
- Human skin cold receptor diurnal activity rhythm 24 p3795 A71-44499
- ACTUATORS**
 Aircraft flaps and ailerons actuators electronic fly by wire control as alternative to mechanical linkages for maneuverability and reliability in flight 01 p0091 A71-10825
- Aircraft high temperature polyimide hydraulic actuator rod seals, discussing design and performance tests [SAE PAPER 700790] 01 p0091 A71-11543
- Mathematical model and digital simulation for nonlinear characteristics of prototype integrated actuator package for fighter aircraft control 02 p0190 A71-11783
- Pen actuators prototype models for fast response graphic recording instruments, using DC servomotors or galvanometers 09 p1452 A71-23386
- Hydraulic resistance control and actuation switch system designs and classifications, using bridge half components and loop combinations 18 p2850 A71-36203
- Electromagnetic actuator for momentum desaturation of control moment gyros used for attitude stabilization and control of space stations [AIAA PAPER 71-939] 19 p3098 A71-37184
- Power by wire actuators and fly by wire flight controls, discussing systems configuration, reliability, economy and durability 20 p3183 A71-39150
- ACUITY**
NT HYPEROPIA
NT VISUAL ACUITY
 Aircraft noise effects on hearing acuity and perceptual and intellectual judgment tasks 21 p3342 A71-40351
- ADAPTATION**
NT ACCLIMATIZATION
NT ALTITUDE ACCLIMATIZATION
NT COLD ACCLIMATIZATION
NT DARK ADAPTATION
NT LIGHT ADAPTATION
NT RETINAL ADAPTATION
 Physical endurance and muscular activity of man as adaptation process depending on biochemical and functional changes 03 p0361 A71-13192
- Space motion sickness causes and prevention, discussing syndromes, psychophysiological factors, vestibular mechanics and adaptation 04 p0539 A71-15283
- Visceral system regulation processes investigation in human organism during manual labor and environmental adaptation, using multichannel biotelemetry and computer processing 08 p1241 A71-21941
- Carbon dioxide tolerance after hypercarbia adaptation of rhesus monkeys in upright position 09 p1395 A71-23250
- Second order system with structure perturbation affected parameter value, studying identification and autoadaptation by sign functions 10 p1586 A71-24740
- Dynamics of increasing organism resistance to hypoxia, considering reactions occurring in various tissues during adaptation 12 p1869 A71-26653
- Intense muscular work adaptation in rats, reducing biochemical and adaptive changes and enhancing anabolic processes 14 p2186 A71-30552
- Visual field displacement, examining directed attention and maladaptive adaptation 15 p2363 A71-31949
- Adaptive technique feasibility for flight simulator training of pilots 18 p2873 A71-36974
- Astronaut work capacity and adaptation during long term flight of space vehicle Soyuz 9 21 p3342 A71-40259
- Biomedical effects of Apollo 14 space flight, considering weightlessness adaptation 22 p3487 A71-41985
- Human adaptation to Coriolis and linear accelerations, investigating habituation effect 24 p3795 A71-44533

ADAPTERS

Automatic interplanetary station adapter to obtain reflected signals amplitude-altitude-frequency characteristics during ionospheric probes 19 p3058 A71-38392

ADAPTIVE CONTROL

NT LEARNING MACHINES

NT SELF ADAPTIVE CONTROL SYSTEMS

Speech signals digital encoding with adaptive linear predictor for reducing redundancy, discussing digital simulation results and subjective comparison with log-PCM encoder 01 p0030 A71-10472

Adaptive optimal electromagnetic and acoustic detection antenna synthesis, considering signal direction and spatial noise structure 02 p0229 A71-11716

Human operator adaptive response characteristics to step changes in compensatory tracking system dynamics 02 p0207 A71-12349

Adaptation mechanism of human movement control as motor neuron reaction to external stimuli, considering peripheral arch, cerebrosplinal canal and feedback 03 p0356 A71-12986

Controller characteristic adaptive control by disturbance of plant operation under random non-manipulated action, considering cognitive system as Markovian automation-nature game 03 p0389 A71-13516

Optimal adaptive estimation, considering Gaussian process and linear dynamic models and partition theorem for structure and parameter adaptation 03 p0394 A71-14484

CW sounding for HF adaptive control for data transmission with ionospheric phase error 04 p0552 A71-15145

Decision-directed digital adaptive signal equalizer for high speed data transmission, discussing design and advantages 05 p0725 A71-17065

Optimum design of dominant type adaptive control systems with large parameter variations, using fourth order approximation 06 p0878 A71-17449

Adaptive algorithms in particle size and form distribution control, using scanning light beam 06 p0872 A71-18699

Automatic Carrier Landing System with linear adaptive aircraft Navigation Computer, investigating effectiveness in reducing system errors due to nonlinearities and noise effects 07 p1157 A71-20405

Two dimensional adaptive pattern-recognizing model of human operator in visual-manual compensatory tracking task 07 p1053 A71-20406

Digital on-off predictive adaptive control system feasibility analysis 07 p1082 A71-20407

Error analysis of adaptive estimators and gradient following algorithms for engineering regression equations, comparing stochastic approximation 08 p1269 A71-21332

Stability of model tracking adaptive control systems with reduced state feedback and measurement noise 08 p1269 A71-21336

Moving target indicator (MTI) performance improvement in presence of rain, chaff or other broadband clutter disturbances by adaptation for canceler setting optimization 08 p1254 A71-21338

Optimal detector parameters for stochastic signals in noise, discussing analytic and simulation studies of adaptive techniques of pattern recognition 08 p1259 A71-21594

Two-sample nonparametric adaptive detection using computer test statistics selection 08 p1259 A71-21600

Algorithmic threshold directivity pattern for adaptive array processors in quasi-stationary signal and noise fields 08 p1256 A71-21603

Liapunov design technique for model reference adaptive control systems with feedback and prefilter adjustable gains 08 p1270 A71-21669

Adaptive time optimal control for inertial system with air jet attitude control 09 p1423 A71-22611

Adaptive control systems state variables and nonstationary parameters estimation in presence of random disturbance and measurement noise, using nonlinear filtering theory 09 p1423 A71-22612

Soviet book on variable structure system theory covering nonlinear automatic control, stability, optimization, adaptive systems, incomplete information processes, linear filters, etc 10 p1585 A71-24147

Adaptive flight control systems, emphasizing bionics approach to self organizing systems 10 p1682 A71-24227

On-line closed loop adaptive control for tracking filter with several inputs and outputs 10 p1586 A71-24739

Soviet book on optimal, multiply connected and adaptive control systems covering variational methods, dynamic programming, functional analysis and statistical methods 11 p1742 A71-26098

Adaptive systems - Conference, Moscow, March 1970 12 p1926 A71-26714

Flight vehicle adaptive control systems with on-board digital computers, considering control algorithm complexity, processing rates, weight and geometry restrictions, accuracy and adaptability requirements, etc 12 p1883 A71-26715

Adaptive roll control of space vehicle on reentry trajectory, analyzing spacecraft angular motion dynamic equations for optimal conditions determination 12 p1926 A71-26719

Approximate stability criteria-system parameter relationships facilitating higher order adaptive systems synthesis 12 p1890 A71-26722

Equivalent-to-adaptive parametrically invariant automatic control, discussing compensation, variable structure, autoscillator, HF nonlinear, ultracoarse and nonsearching self adjusting systems 12 p1890 A71-26723

Adaptive control systems probability characteristics in presence of random inputs, discussing improvements by coefficients and interpolation methods 12 p1891 A71-26727

Single loop fixed adjustment system with adaptation similar properties, discussing special correcting devices 12 p1891 A71-26733

Adaptive self-organizing and -learning control systems with long and short term memory retention, using logic random searches to find parameter values [ASME PAPER 71-DE-22] 12 p1892 A71-27324

Adaptive array antennas with control loop, deriving noise expression for maximizing signal to noise ratio 12 p1881 A71-27426

Stability of first order gain model reference adaptive control system with sinusoidal input 12 p1973 A71-27580

Adaptive automatic control systems, determining damping coefficient and natural oscillation frequencies with second order differential equations 13 p2041 A71-28639

Adaptive controller consisting of real time identifier and minimum variance regulator approached through stochastic optimal control theory 14 p2219 A71-29696

Unsteady controlled object dynamic characteristics evaluation for search-free self adjusting systems and telemetric information processing improvements 14 p2220 A71-30814

Synthesis algorithms for model reference adaptive control systems using Liapunov second and Popov hyperstability methods 15 p2382 A71-32623

Suboptimization of closed loop adaptive systems by simple dual control method, using dynamic programming 16 p2549 A71-33353

Optimal structure and parameter adaptive estimation for continuous and discrete data Gaussian process models with linear dynamics 17 p2719 A71-34739

Two dimensional adaptive model of human operator control in visual-manual compensatory tracking task using pattern recognition 17 p2691 A71-35046

Adaptive mathematical model of human operator during pursuit tracking, synthesizing brain in accordance with arbitrary reasonability criterion 17 p2692 A71-35169

Error sampled discrete continuous feedback control system performance, comparing adaptive and periodic sampling methods 17 p2722 A71-35184

Optimal state regulator approximate design for nonlinear system with quadratic performance index, determining suboptimal feedback law 17 p2722 A71-35212

French monograph on variable-structure automatic control systems covering algorithms, stability, nonlinear hypersurface slip, minimum time, switching elements, analog simulation, etc 17 p2767 A71-35249

Wide angle microwave antenna radiation beam steering with fixed parabolic reflectors, using adaptive primary feed for intercepted field spatial Fourier transformation 17 p2708 A71-35493

Adaptive frequency selection for reduction of effects of noise differing irregularly from useful pulse signals, estimating error probabilities 18 p2882 A71-36622

Switched mode adaptive terminal control for propulsive landing of nonlifting gravity turn ballistic vehicle under uncertain atmospheric conditions [AIAA PAPER 71-903] 19 p3095 A71-37154

Adaptive algorithm designing minimum expected cost test trees for detection and isolation of single faults in systems 19 p3069 A71-38287

Envelope limiting in control loops of adaptive array antennas, reducing varying noise interference 20 p3195 A71-38863

Rapidly converging second order optimal tracking algorithms for adaptive equalization on basis of estimated bounds for eigenvalues of signal plus noise correlation matrix 20 p3201 A71-38872

Bayesian learning algorithm derivation for statistically optimum adaptive gain control in Rayleigh-distributed signal reception 20 p3206 A71-38874

Hybrid computer control of engine start-up using adaptive logic, adaptive programming and self organizing storage 20 p3208 A71-38998

Adaptive reception of weak repetitive signals on background of intense fluctuating noise, synthesizing adaptive detection system for multipath propagation and small SNR 20 p3199 A71-39809

Computer use in automatic tracking radar systems design, describing adaptive radar hardware 20 p3200 A71-39902

Adaptation algorithm for optimal synthesis of nonlinear radio reception system with additive noise 21 p3361 A71-41143

Radar data video extractor adaptive threshold device synthesis criteria to quantize echoes for ensuring constant false alarm rate and target visibility 22 p3508 A71-41525

Optimal power transfer through atmospheric turbulence by adaptive laser transmitter using beacon waveform to probe channel state 22 p3512 A71-42378

Linear dynamic system sensitivity models simplification conditions application to adaptive nonsearching system synthesis algorithms 22 p3527 A71-42857

Closed loop response speed evaluation for model reference adaptive control system, using sinusoidal test signal 23 p3656 A71-43860

Adaptive random search optimization of optical tracking self organizing feedback control system under inherent coupling signals 23 p3657 A71-43942

Synthesis procedure for feedback parameter adaptive control systems, discussing computer simulation data 23 p3658 A71-44081

Longitudinal adaptive aircraft control through sum of normal acceleration and pitch rate 23 p3629 A71-44093

Adaptive guaranteed cost control for systems with parametric variation, demonstrating system stability and airframe pitch control 23 p3659 A71-44111

German book on adaptive control systems covering flight attitude control, jet engine thrust, marine surface navigation, identification, etc 23 p3660 A71-44187

German book on adaptive control systems covering decision processes and application examples 23 p3660 A71-44188

Minimal partial realizations of linear input/output map, discussing significance in regard to adaptive dynamics identification procedures 23 p3661 A71-44190

ADAPTIVE CONTROL SYSTEMS

U ADAPTIVE CONTROL

ADAPTIVE FILTERS

Doppler pulse radar signal reception, calculating noise signal optimal relationship for comparison with adapted filtration technique 05 p0722 A71-16707

Digital adaptive spectral filtering canceling undesired power spectra based on measured mean square values ratio and stochastic approximation methods 07 p1082 A71-20408

Single and dual channel weak signal adaptive detectors theoretical performance under statistically undefined noise background 08 p1256 A71-21601

Adaptive array processor analysis and optimum design for passive detection of sonar type directional stochastic signals 08 p1256 A71-21602

Liapunov design technique for model reference adaptive control systems with feedback and prefilter adjustable gains 08 p1270 A71-21669

Regular and stochastic algorithms for efficiency estimation of adaptive predicting filters 08 p1260 A71-22021

ADDERS [CIRCUITS]

Quality functional analysis for self adaptive filtration of random signal sequences 13 p2040 A71-28919

Rapidly converging first order training algorithm for adaptive equalizer design in PAM signal reception, using variable step sizes for mean-square error minimization 16 p2545 A71-32821

Recurrent finitely converging algorithms for solving inequalities in automatic control systems involving adaptive filters 22 p3526 A71-41858

ADDERS [CIRCUITS]

U ADDING CIRCUITS

ADDING CIRCUITS

Adder transfer characteristics, demonstrating summation method for signal to noise ratio improvement 09 p1407 A71-23049

Coincidence adders with digit by digit alteration of direct and inverse signals, discussing synthesis and reliability 15 p2376 A71-32183

ADDITION RESINS

NT ACRYLIC RESINS

NT VINYL COPOLYMERS

ADDITION THEOREM

Solid mechanics boundary value problems solution by cylindrical functions addition theorem in polar and curvilinear orthogonal coordinates 07 p1162 A71-20648

Exponential continually discrete analytic functions of complex variable in explicit form, obtaining addition theorem for trigonometric functions 19 p3089 A71-38479

ADDITIONS

NT ANTICING ADDITIVES

NT ANTIOXIDANTS

NT OIL ADDITIVES

NT OPACIFIERS

NT PROPELLANT ADDITIVES

NT PROPELLANT BINDERS

Er lasing efficiency dependence on dopants in Li-Ca-silicate glass host, determining energy transfer rates for optimum concentration 01 p0092 A71-10010

Steels and weld metal alloying for stable austenitic structure under long term cryogenic conditions, investigating optimal Cr, Ni, Mn and nitrogen combinations 01 p0085 A71-10087

Static dissipator additives in aviation fuels for eliminating electrostatic charging hazards 02 p0297 A71-12300

Electron states in highly doped semiconductors, describing energies in conduction and forbidden bands 02 p0297 A71-12616

Doped W wire core porosity and anomalous recrystallization behavior microstructural observation by electron microscopy 02 p0268 A71-12890

Medium alloy structural steels tempering, investigating Mn, Ni, Cr and Mo effect on activation energy of softening 03 p0445 A71-14338

CdS single crystals with Cu and Cl additives, observing optical flash and thermoluminescence in IR band 03 p0468 A71-14385

Sulfide precipitates shape preservation in high strength low alloy hot rolled steel sheets, discussing effects of various additive elements 04 p0614 A71-15782

N-p Si solar cells controlled lifetime doping effects on electrical performance 05 p0700 A71-16063

Si solar cell radiation resistance improvement through Li doping, noting efficiencies in excess of state-of-art N/P cells after exposure to 1 MeV electrons 05 p0703 A71-16088

Li doped Si solar cells recovery after irradiation, examining temperature dependence 05 p0704 A71-16105

Cs plasma thermionic diode, using Penning effect for ionization rate increase via Hg or Cd seeding 05 p0705 A71-16170

Dispersion medium effects on thermal hardening of lubricating oils with Na or Li additives 05 p0772 A71-16385

Doped tungsten high temperature behavior, discussing hypotheses regarding doping agents microstructural effects 05 p0767 A71-16599

Doping effect on positive Faraday rotation in n- and p-type GaAs at different impurity concentrations, noting shift of maximum to lower concentrations in p-type samples 07 p1176 A71-19227

Metastable beta phase Ti-Mo and Ti-V alloys ternary additions effect on decomposition 07 p1138 A71-19982

Additive elements and heat treatment effects on Al-Zn-Mg alloy fracture characteristics, using tensile and stress corrosion tests 07 p1143 A71-20488

Alloying addition effects on wetting of carbon by liquid metals, using sessile drop technique [PLASTICS INST. PAPER 19] 08 p1296 A71-20911

GaAs epitaxial layers inhomogeneous doping in continuous chloride system, discussing electron concentration with respect to gas flow direction 09 p1506 A71-22167

Electron transfer bulk oscillators negative conductivity as function of geometry, field and doping nonuniformities, using computerized simulation for device frequency-voltage characteristics 09 p1417 A71-22689

Photochromic calcium fluoride preparation by rare earth additive coloration techniques 09 p1509 A71-23120

Ni-Cr alloys hardened by Nb and Ta, examining precipitation and plastic deformation mechanisms 09 p1479 A71-23622

Research bibliography on resins and additives covering polyesters, epoxies and new polymers with improved corrosion, fire and heat resistance 11 p1788 A71-25431

Alumina and titania codeposition from acid copper electrolyte as function of oxide crystalline form, discussing addition agents effects 11 p1779 A71-26011

Cr and Zr additives influence on Al-Zn-Mg-Cu alloys quench sensitivity, discussing mechanical properties and electron microscopic investigation of microstructural characteristics 11 p1780 A71-26021

Boron or phosphorus doping of silicon, noting microhardness increase and friction coefficient reduction 12 p1911 A71-26820

Nb and Mo doped Ni-Al alloy with Ni-Nb additions, obtaining diagrams of composition versus heat resistance in high temperature bending tests 12 p1916 A71-26968

Dielectric properties of barium titanate with Nb, noting metal oxide additives effects on conductivity 13 p2092 A71-28661

Al-Zn-Mg alloys, considering Cu and Cr additions effects on nucleation and incoherent precipitates formation 13 p2088 A71-29406

Mo and W single crystals mechanical properties, considering C and iron group additions influence 14 p2255 A71-29516

Net impurity doping profile of double diffused transistors 14 p2210 A71-29792

Transition metals addition effects on cast Zr grain size, microhardness and electrical resistivity, explaining results in terms of solid state electron theory 15 p2424 A71-31239

Molybdenum doped zirconium monocarbide, investigating Hall coefficient, thermal emf and resistivity measurements 15 p2460 A71-31284

Perfluorinated monocarboxylic fatty acids additives for controlling lubricating oils spreading on metals and antifriction properties improvement 15 p2438 A71-31680

Dispersion hardened Co strength and plasticity temperature dependence, determining Ti and Nb carbides additives effects 15 p2434 A71-32237

Coaxial type MHD generator with steady magnetic field and plasma consisting of inert gases and ionizable alkali metal additives, obtaining electrical conductivity 15 p2355 A71-32268

Metal additives catalytic effect on free radicals recombination rates in hydrogen-oxygen-nitrogen flames 15 p2515 A71-32552

Gaseous chromium carbonyl or aqueous chromium salt spray additives behavior photoacoustic investigations in premixed hydrogen-oxygen-nitrogen flames 16 p2540 A71-33374

Steels and weld metal alloying for stable austenitic structure under long term cryogenic conditions, investigating optimal Cr, Ni, Mn and nitrogen combinations 16 p2584 A71-33643

Al-Mg alloy with Ti, Zr, Mo and B additions under tensile and impact loads, investigating mechanical properties, strength and crack formation 16 p2594 A71-33712

Refining and hardening reactive additions effect on slow cooling grain boundary embrittlement response of maraging steel 17 p2756 A71-34490

Overcritically doped Gunn diode I-V characteristics stability under constant voltage, discussing use as subnanosecond switching element 18 p2895 A71-36989

Bubble formation during annealing of W doped with K, Al and Si compounds, using electron microscopy with thin foil and fracture replication techniques 19 p3079 A71-37708

Metal additives catalytic effects on premixed hydrogen-oxygen-nitrogen flames free radical recom-

bination rates, discussing heterogeneous and homogeneous schemes 19 p3012 A71-38082

Deflagration behavior of pure and isomorphously doped ammonium perchlorate, using cinephotomicrography of burning samples and scanning electron microscopy of quenched samples 19 p3120 A71-38118

Heavily Ge doped p-InSb photoelectric and electric properties, showing impurity concentration effects 19 p3120 A71-38526

Mo, W and Al alloying additives effects on mechanical properties and wear resistance of austenitic high Mn electroslag melted steel 21 p3403 A71-41106

Si addition effect on Ni-Cr alloy calorized layer depth, microhardness, phase structure, chemical composition and scaling resistance 21 p3390 A71-41168

High resistance undoped GaAs samples at different temperatures, investigating energy spectra, Hall effect and electron conductivity 21 p3431 A71-41227

High resistivity Fe-doped GaAs, investigating carrier lifetime dependence on Fe atoms concentration 21 p3431 A71-41234

Photoelectric properties of gold doped germanium semiconductor structures, investigating long wavelength background illumination effect on nonequilibrium conductivity 21 p3435 A71-41336

Emitter-base junction degradation by avalanche breakdown in planar transistors with low doped /epitaxial/ base region 22 p3520 A71-41682

Temperature dependent threshold current density and doping gradient at p-n junction in epitaxial GaAs injection laser diodes 22 p3555 A71-41686

Gold doping effect on minority carrier lifetime and other electrical properties of epilayer Si transistors 22 p3520 A71-41702

Radioisotope testing methods for dissolution and mass transfer of alloying additives in Pb-Sb alloys during preparation in electromagnetic pumps 22 p3553 A71-41765

Soot emission suppression from propane diffusion flame by metallic additives 22 p3588 A71-42101

Bulk quantum efficiency in electron beam pumped n-type GaAs lasers at 300 K as function of impurity concentration 22 p3558 A71-42362

Bipolar junction transistor doping effects on bandgap decrease and emitter efficiency, explaining current gain temperature dependence 23 p3648 A71-42911

Lithium additions effect on hydrogen content and mechanical properties of molten aluminum specimens 23 p3691 A71-43522

Germanium extrinsic photoconductive IR detectors with Au, Hg and Cu doping, discussing preparation and electrical and optical characteristics 24 p3860 A71-45070

Cd doped thin polycrystalline CdTe films rectification mechanism and DC conductivity, discussing light, electric field and temperature effects 24 p3861 A71-45248

Jet aircraft fuel additives covering functions and applications 24 p3864 A71-45325

Doping profile effects on performance properties of hypersensitive capacity variation junction diodes, describing basic interrelation between capacity and potential 24 p3812 A71-45351

Alloying elements effects on high-carbon steels phase transformation under shock loading to form martensite-austenitic structure 24 p3840 A71-45376

ADENINES

NT RIBONUCLEIC ACIDS

Abiogenic synthesis of nucleosides, heating adenine and ribose mixture at 170 C in atmosphere of oxygen, nitrogen and carbon dioxide 21 p3346 A71-40576

ADENOSINE DIPHOSPHATE [ADP]

Muscle adenosine triphosphate, creatine phosphate, adenosine diphosphate, glycogen, and lactate concentrations during intermittent exercise 15 p2358 A71-31726

ADENOSINE TRIPHOSPHATE [ATP]

Fatigue factor of lactate, ATP and creatine phosphate /CP/ accumulation in working muscles during short exhaustive exercise in man 02 p0202 A71-11666

Radioprotective mercaptoethylamine /MEA/ effect on aerobic resynthesis of ATP in thymus nuclei and oxidative phosphorylation in rat liver mitochondria 07 p1039 A71-18984

Rats under various exercise programs, determining cardiac ventricle and gastrocnemius muscles calcium activated adenosine triphosphatase activities 09 p1400 A71-23361

Luciferin fermentative oxidation method for adenosine triphosphate determination in extraterrestrial life detection, using extract of firefly luminescent organs
13 p2009 A71-28683

Amytetravite and ATP effect on hemopoiesis of dogs subjected to chronic and repeated gamma irradiation
15 p2357 A71-31312

Muscle adenosine triphosphate, creatine phosphate, adenosine diphosphate, glycogen, and lactate concentrations during intermittent exercise
15 p2358 A71-31726

Adenosine triphosphate addition effects on heat production in intact muscular fibers by calorimetry
17 p2683 A71-35247

Phosphoenolpyruvate as enzyme inhibitor of phosphoribulokinase in *Pseudomonas facilis* with respect to ribulose-5-phosphate and ATP
20 p3185 A71-38820

Extraterrestrial life detection methods, discussing bacterial cultures growth dynamics in nutrient media and iron porphyrin proteins and ATP content increase
21 p3334 A71-40570

ADENOSINES
NT ADENOSINE DIPHOSPHATE [ADP]
NT ADENOSINE TRIPHOSPHATE [ATP]
Coronary blood flow response to acute and chronic hypoxia, observing vascular smooth muscle relaxation relation to released adenosine
14 p2184 A71-30281

Allosteric adenosine monophosphate nucleosidase stabilization by inorganic salts, substrate and essential activator, investigating enzyme inactivation mechanism in low ionic strength environments
23 p3642 A71-44268

ADEQUACY
Excitability, reactivity, adequacy, creativity and guidance at molecular, cellular, systemic and psychic levels in human biophysical neurodynamics, plotting stimulus magnitude vs response duration
21 p3344 A71-41063

ADHEROMETERS
U ADHESION TESTS
ADHESION
Isotactic polypropylene and high pressure polyethylene in contact with steel, examining temperature effect on friction and adhesion
01 p0106 A71-10299

Plastics for long life microcircuit encapsulation, investigating water absorption and resin-to-lead adhesion effects on reliability
07 p1077 A71-19562

Graphite fiber reinforced plastics adhesion and orientation effects on mechanical properties [PLASTICS INST. PAPER 27]
08 p1320 A71-20906

Self adhesion in relay contacts, discussing cold weld conditions and prevention by dry oxygen addition
13 p2074 A71-28835

Adhesive joints bonding strength, discussing relative contribution of interatomic and intermolecular forces and viscoelastic, viscous or plastic deformation effects
14 p2276 A71-29894

Sealing materials adhesion to fiberglass and metals based on rupturing force in loading tests
15 p2414 A71-31655

Chemically activated electroadhesive pads on spacecraft surface, allowing astronauts to maneuver or work in zero gravity environments [AIAA PAPER 71-853]
18 p2872 A71-36645

Adhesion effects on interactions between abrasive and metal surfaces in grinding operations as function of grinding speed and contact surfaces properties
24 p3830 A71-44860

ADHESION TESTS
Ultrasonic methods for evaluating adhesive bond strength in composites, metal to metal laminates and honeycombs
01 p0086 A71-10306

Static metallic adhesion model for sliding friction, using contact resistance measurements
05 p0758 A71-16239

Virgin surfaces adhesion under normal loads, testing Pb, Zn and Cd polycrystal specimens
05 p0759 A71-17167

Measuring instrument for determining shear strength of adhesive bond
09 p1443 A71-22503

Failure/yield points, stiffness and failure energy from adhesive shear stress elongation curves, using computer assisted thick adherend tests
10 p1631 A71-24071

Climbing drum peel adhesion test anomaly in spacecraft adhesive bonded honeycomb structure under lap shear and flatwise tension
10 p1614 A71-24075

Adhesive fracture blister tests, using energy balance for treating stress singularities in brittle elastic materials
10 p1631 A71-24077

Fracture mechanics application to structural adhesives test methods, considering joints crack extension resistance and plane strain fracture toughness
10 p1615 A71-24088

Metallic surfaces adhesive properties and adsorptive capacity from nondestructive testing by peeling
10 p1616 A71-24105

Coupling agents in urethane and epoxy adhesives, discussing lap shear and T-peel tests on mild and stainless steels, Al and glass cloth substrates
10 p1616 A71-24108

Organic adhesives performance evaluation based on correlations between accelerated laboratory aging tests and underground exposure in adverse environments
10 p1633 A71-24113

Weather stress tests for determining optimum adhesive system for bonding reinforced fiberglass panels to Al extrusions held by steel beams
10 p1616 A71-24114

Virgin metal surfaces adhesion under normal loads, testing Pb, Zn and Cd polycrystal specimens
12 p1912 A71-27461

Adhesive strength of metal coatings obtained by simultaneous vacuum condensation of strengthening phase and matrix material vapors
17 p2760 A71-35655

Polyethylene, polypropylene and copolymers sliding friction viscoelastic nature, obtaining relationship between sliding force, adhesional bond shear strength and contact area
19 p3068 A71-37425

Bulk and surface diffusion roles in clean and contaminated Cu-Ni surfaces adhesion
19 p3080 A71-37713

Friction, wear and adhesion of filler and matrix polymer composite bearing materials including glass, carbon, lamellar solids, metal powders, carbons, nylons, PTFE, polyimides, etc
21 p3405 A71-40602

Solid body contact interaction devices at high temperatures in vacuum, gas and air for evaluation of surface coatings, adhesion, diffusion, mechanical properties, etc
21 p3382 A71-41174

Vacuum pumped Apollo 12 lunar soil sample 12001,118 gas exposure effects, interface microanalysis and adhesion measurements in ultrahigh vacuum system
23 p3759 A71-43767

Apollo 12 returned Surveyor 3 surface sampler examination for micrometeorite pits and soil, glassy spheres and other granular materials adhesion to paint
23 p3766 A71-43817

Statistical analysis of spot welded and adhesive joints of high strength Al alloy sheet in aircraft structures
24 p3831 A71-45012

ADHESIVE BONDING
Stress distribution and mechanical properties of adhesive bonded metal and plastic lap joints, using statistical analysis
08 p1372 A71-21711

Adhesive bonding of materials with different coefficients of expansion, discussing strength vs stress relief [SAE PAPER 710108]
08 p1372 A71-21712

Measuring instrument for determining shear strength of adhesive bond
09 p1443 A71-22503

High peel strength epoxy and urethane adhesives for aircraft bonding, discussing high temperature curing and honeycomb panel repair
10 p1630 A71-24064

Polyurethane structural adhesives with excellent tensile shear and T-peel strengths at cryogenic temperatures, long pot lives and good processing characteristics
10 p1630 A71-24068

Surface treatment effects on high shear strength adhesive bonding of fiber reinforced plastics to metal substructures
10 p1630 A71-24069

Low temperature curing nylon epoxy adhesive, discussing high peel strengths
10 p1630 A71-24070

Degradation rate tests on adhesive bonded sandwich panels of temperature resistant composite structural materials at varying atmospheric pressures
10 p1614 A71-24073

Climbing drum peel adhesion test anomaly in spacecraft adhesive bonded honeycomb structure under lap shear and flatwise tension
10 p1614 A71-24075

Cyclic creep test for simulating helicopter rotor blades start-stop cycles effect on adhesive bonded joints, using fixed load-unload cycle
10 p1631 A71-24076

Adhesive fracture blister tests, using energy balance for treating stress singularities in brittle elastic materials
10 p1631 A71-24077

Variable weight composite materials for aircraft optimal adhesive bonding structural designs, discussing C-5A tow weight saving Ti honeycomb applications
10 p1686 A71-24084

Bulk properties effect on adhesive properties of seven epoxy resins, considering stress-strain properties and statistical analysis for tensile shear evaluation
10 p1632 A71-24086

Adhesive bonded joints mechanical behavior relation to materials, processes and experimental techniques, developing statistical analysis and formulas for orthotropic-elastic joints
10 p1614 A71-24087

Fracture mechanics application to structural adhesives test methods, considering joints crack extension resistance and plane strain fracture toughness
10 p1615 A71-24088

Processing variables effects on epoxy adhesive joints fracture toughness and crack extension resistance
10 p1632 A71-24089

Stress corrosion crack extension in adhesive epoxy joints under combined long term static loads and aggressive action of water
10 p1632 A71-24090

Structural bonding with polyurethane adhesives in missile systems
10 p1615 A71-24094

Al alloys and ferrous metals adhesive bonding, discussing surface preparation and surface exposure time influence on bonded joint strength for various epoxy adhesive types
10 p1615 A71-24095

Nondestructive evaluation of ultrasonic wave propagation in adhesively bonded test specimens, using schlieren method
10 p1616 A71-24104

Relativity of nondestructive testing as related to production effort, reviewing structural adhesive bonding in U.S. for past ten years
10 p1616 A71-24106

Silyl peroxides as promotion agents for polymeric materials adhesion to solid substrates and for cross-linking polyethylene to other polymers
10 p1633 A71-24109

Corrosion resistant adhesive bonding tested by exposing sandwich structure to outdoor weathering and salt spray environments
10 p1616 A71-24111

Weather stress tests for determining optimum adhesive system for bonding reinforced fiberglass panels to Al extrusions held by steel beams
10 p1616 A71-24114

Metal-metal adhesive bonds temperature effects, long term static loads, dynamic strength and aging behavior
10 p1618 A71-24684

Structural adhesive bonding of plastics and metals, emphasizing fast curing, high bond strength, environmental resistance and bonding ability
11 p1768 A71-25393

Thermosetting acrylic modified epoxy resin, stressing adhesive bonding strength, workability and curing characteristics
11 p1787 A71-25423

Handbook on adhesive bonding covering adhesive materials, properties selection and compatibility, bonded assembly requirements and joints design, surface preparation, processing, trade sources, etc
11 p1788 A71-25451

Fracture mechanics and time dependent strength of elastic or viscoelastic solids adhesively jointed by soft polymeric bonding layer
11 p1851 A71-26383

Fatigue life, fail-safe capability and corrosion resistance of commercial aircraft structures improved through adhesive metal-metal bonding [ASME PAPER 71-DE-27]
12 p1978 A71-27325

Hand/machine sanded surfaces moderate environment exposure time effects on adhesive bonding of glass fiber reinforced plastic joints
12 p1921 A71-27411

Carbon and boron fiber reinforced plastics adhesive bonded and bolted joints, presenting results of hole deformation tests
13 p2093 A71-29306

Adhesive joints bonding strength, discussing relative contribution of interatomic and intermolecular forces and viscoelastic, viscous or plastic deformation effects
14 p2276 A71-29894

Geometrical parameters and load carrying capacity of fiberglass reinforced plastic composites with elastoplastic adhesive bonding, deriving relations for stress distribution
14 p2264 A71-30270

Automated ultrasonic inspection system for L-1011 adhesive bonded fuselage panels using through transmission technique [SME PAPER IQ-71-746]
15 p2417 A71-32437

Radiation effects on bonding characteristics of epoxy-metal and epoxy-glass adhesive joints
15 p2439 A71-32511

Welded, bearing and interlocking joints and adhesive bonding in carbon fiber reinforced plastics, discussing anisotropy, thermal expansion and electrochemical corrosion problems
17 p2748 A71-34344

ADHESIVES

Tension test for filamentary composites, employing hardened Al alloy wedges adhesive bonded to gripping edges 17 p2739 A71-34818

Composite panel of ten-ply unidirectional boron/epoxy laminate adhesively bonded to Al face sheets, discussing ultrasonic inspection technique 17 p2749 A71-35495

Adhesively bonded structures inspection by laser holography, producing diffraction pattern recording of amplitude and phase shift 18 p2925 A71-37057

Stress distribution in adhesive lapped joints with emphasis on shear stress 21 p3384 A71-40139

Nondestructive testing evaluation of graphite epoxy composites and adhesive bonded Al composite structures using acoustical holography 22 p3554 A71-41781

Corrosive delamination occurrence, reduction and prevention in metal-metal adhesive bonded aircraft structures 22 p3555 A71-42594

Stress concentration factors of bonded single lap joints by finite element method as functions of dimensionless, geometric and material parameters 22 p3619 A71-42835

ADHESIVES

NT GLUES

NT PASTES

Adhesive bonding and detachable joints in multilayered fiber reinforced plastic structures, discussing joint strength test methods, fiber and load force orientation effects, etc 01 p0108 A71-10692

Axially loaded finite stringer bonded to infinite elastic sheet, considering adhesive shear flow 03 p0514 A71-14350

Polybenzothiazole as solid film formulations binder for friction wear improvements, noting thermal and oxidative stability, toughness, adhesive properties and handling ease 05 p0772 A71-16375

Volatile adhesive curing effect on metal-metal bond fatigue strength 05 p0772 A71-16955

Adhesive/metal interface corrosion resistance tests, discussing salt fog chamber for shear, compression buckling and cleavage stresses 05 p0770 A71-17248

High modulus boron-epoxy composite aircraft structures adhesive bonding, discussing mechanical properties, manufacturing techniques and quality control [SAE PAPER 710110] 06 p0904 A71-17624

Adhesive resin metal bond stability, examining surface finish and atmospheric moisture effects at various temperatures on exfoliation 06 p0904 A71-17944

Metal gluing with synthetic polymer based adhesives, discussing history, technology and high temperature resistance 06 p0905 A71-18093

Aerospace adhesives and elastomers - Conference, Dallas, Texas, October 1970, Volume 2 10 p1630 A71-24063

High peel strength epoxy and urethane adhesives for aircraft bonding, discussing high temperature curing and honeycomb panel repair 10 p1630 A71-24064

Powder form structural adhesives for cost reduction and increased productivity 10 p1614 A71-24066

Surface treatment effects on high shear strength adhesive bonding of fiber reinforced plastics to metal substructures 10 p1630 A71-24069

Low temperature curing long open time epoxy adhesives evaluation for 3500 psi shear strength 10 p1631 A71-24072

Structural film adhesives peel-thickness correlation and cure rate study by torsion pendulum 10 p1614 A71-24074

Ultrasonic bonding techniques discussing high frequency activated adhesives, equipment and automated processes 10 p1615 A71-24092

Alloy and heat treatment effect on Ti bondability for adhesive bonded aircraft structure, using annealed and aged Ti-6Al-4V and Ti-6Al-6V-2Sn alloys for testing 10 p1615 A71-24093

Nonflammable self extinguishing nontoxic fluorocarbon elastomers as adhesives and coatings for Apollo program 10 p1632 A71-24097

Fabricated product test program design for meeting customer specifications, outlining routine tests for preimpregnated film adhesive materials 10 p1616 A71-24107

Coupling agents in urethane and epoxy adhesives, discussing lap shear and T-peel tests on mild and stainless steels, Al and glass cloth substrates 10 p1616 A71-24108

Adhesive primers corrosion resistance test methods, noting aircraft design implications 10 p1633 A71-24112

Organic adhesives performance evaluation based on correlations between accelerated laboratory aging tests and underground exposure in adverse environments 10 p1633 A71-24113

Outdoor five year aging tests on polysulfide and silicone adhesive sealants under semiarid, marine and high humidity environments 10 p1634 A71-24119

Microencapsulation of bonded reactive resins in packaging, logistics and adhesive applications at room and elevated temperatures 10 p1634 A71-24120

Handbook on adhesive bonding covering adhesive materials, properties selection and compatibility, bonded assembly requirements and joints design, surface preparation, processing, trade sources, etc 11 p1788 A71-25451

Radiation effects on epoxy adhesive mechanical properties including compressive shear stress, modulus of elasticity and tensile strength 15 p2439 A71-32510

Elastic adhesive interlayer effect on bond fracture strength, considering propellant-liner- steel combination in solid rocket motors 18 p2977 A71-36245

Thermal contact resistance of adhesive joints as function of adhesive solidification pressure and temperature and of joint surface physicochemical and geometrical parameters 24 p3831 A71-45024

ADIABATIC CONDITIONS

Adiabatic temperature gradient requirement for neutral convection mode in general relativity of star in hydrostatic equilibrium 03 p0486 A71-13330

Expanding universe adiabatic density fluctuation evolution, describing photon distribution function collision equation for plasma recombination 05 p0801 A71-15929

Nonadiabatic gas acoustic oscillation instability, examining heat release fluctuations 05 p0838 A71-16777

Acetylene pyrolysis kinetics, considering isothermal vs adiabatic conditions and surface catalyzed vs homogeneous gaseous [WSS/CI PAPER 70-18] 06 p0943 A71-17660

Plasma containment in adiabatic magnetic traps, discussing particles, Coulomb collisions, instabilities, cyclotron resonance masers, Van Allen belts, etc 07 p1166 A71-19097

Ar-oxygen mixture in undiluted nitrogen, discussing relaxation time change during adiabatic excitation and molecule oscillations deactivation 07 p1163 A71-19276

Supersonic air flow pattern over rectangular indentations on plane and axisymmetric surfaces, examining static pressure and adiabatic temperature distributions 07 p1014 A71-19744

Adiabatic and melting point gradients in earth core, discussing temperature distribution inhibition to convection radial components 09 p1436 A71-22642

Latitudinal variations in adiabatic production and destruction of kinetic energy by meridional and zonal motions of atmosphere 09 p1488 A71-23025

Relativistic fluid thermodynamics for compressible fluid reversible adiabatic flow, using variational principle to derive stress-energy tensor 11 p1798 A71-25739

Venus atmosphere adiabatic and isothermal models, investigating water vapor content, pressure and temperature 12 p1964 A71-27085

Supersonic boundary layer transition on adiabatic wall, discussing wind tunnel size, surface roughness and freestream disturbances effects [AIAA PAPER 70-586] 12 p1865 A71-27554

Ar-oxygen mixture in undiluted nitrogen, discussing relaxation time change during adiabatic excitation and molecule oscillations deactivation 14 p2276 A71-30170

Acoustic vibrations generation and transmission in nonadiabatic gas containing heat sources, taking into account conductive and radiative heat transfer and momentum loss 16 p2662 A71-33029

Vortex boundary layer with dissipative viscous wall and isentropic sublayers, calculating adiabatic surface temperature 17 p2669 A71-34217

Venus atmosphere adiabatic and isothermal models, investigating water vapor content, pressure and temperature 19 p3133 A71-37435

Electromagnetic absorption in adiabatically expanding fully ionized cosmic plasma, using Einstein-De Sitter cosmology 21 p3442 A71-40161

Flare induced laminar boundary layer/shock wave interactions on axisymmetric bodies at zero incidence in supersonic flow under adiabatic conditions 24 p3789 A71-44604

Hydrogen and helium thermal dissociation and ionization at Jupiter and Saturn adiabatic atmospheric models conditions 24 p3850 A71-44809

ADIABATIC EQUATIONS

Stress potential for theory of adiabatic reversible processes in nonlinear viscoelastic material undergoing small deformations 01 p0169 A71-10493

Adiabatic invariant of nonlinear periodic wave described by partial differential equations in weakly inhomogeneous medium 05 p0780 A71-16177

ADIABATIC FLOW

Adiabatic compressible turbulent boundary layer equations for two dimensional and axisymmetric flow, discussing methods of solution based on eddy viscosity formulation [AIAA PAPER 69-687] 01 p0071 A71-10933

Approximation of Chaplygin equation for subsonic ideal gas plane adiabatic flow, applying to discharge from flat channel with contraction 07 p1016 A71-20083

Reinforced shells of revolution carrying capacity upper limit subjected to internal adiabatic ideal gas flow 09 p1538 A71-22632

One dimensional plane adiabatic MHD free expansion of relativistic plasma 10 p1676 A71-24495

Reynolds number effects on centrifugal compressor performance characteristics, discussing power losses in compressor, impeller and diffuser stages and compressor adiabatic efficiency [ASME PAPER 71-GT-25] 11 p1703 A71-25967

Adiabatic flow model of noiseless magnetic neutral sheet of finite width, discussing particle trajectory and charge density distribution 13 p2109 A71-29166

Entropy production in adiabatic flow in turbomachines, based on momentum equations for inviscid flow 13 p1994 A71-29446

Recovery factor for highly accelerated adiabatic compressible laminar boundary layer flow 15 p2391 A71-32114

Kinetic and kinematic properties of steady diatomic complex lamellar gas flows 22 p3530 A71-41696

Fundamental derivative γ/ρ and other thermodynamic variables in gas dynamics, considering transonic passage variation, Prandtl-Meyer wave, adiabatic flow and nonlinear wave propagation 22 p3530 A71-41887

Mean void fraction of adiabatic two phase flow by luminescent tracer dispersed in liquid phase 23 p3675 A71-43323

ADIPOSE TISSUES

Prolonged hyperoxia effects on lipid synthesis in rat liver and adipose tissue slices 10 p1559 A71-23969

Mucopolysaccharide content and composition of fatty streaks in young male aortas, discussing atherosclerosis effects 18 p2854 A71-35919

Brown fat thermogenesis regulation, emphasizing adipose tissue and afferent nerves control by experimental system approach, using intact unanesthetized unrestrained animals 18 p2859 A71-36872

Potassium concentrations and osmolality levels changes effects on vascular resistance in subcutaneous adipose tissue blood flow 20 p3189 A71-39379

Stimulatory effects of hypobaric hyperoxia on lipid synthesis in rat liver and adipose tissues under free feeding 22 p3486 A71-41825

Total body adipose tissue mass and composition variations, examining hyperglycemic, obese, exercised and centrifuged animals 23 p3637 A71-44299

ADJOINTS

Two-point boundary value problems for linear differential equation systems, describing adjoints and complementary functions methods 03 p0451 A71-13624

Precommutative bounded and symmetrical unbounded operators extension to commutative bounded and self adjoint operators 04 p0618 A71-14648

Optimization of nonclassical equations of state systems, considering concepts of adjoint and Hamiltonian states 13 p2043 A71-28830

General adjoint relation between linear functional differential equations and Volterra integral equations 13 p2096 A71-29381

Monograph on nonlinear first order differential equations adjunction fields and solutions asymptotic behavior, seeking adjoinable solutions

18 p2940 A71-36098

Frequency response optimization of one dimensional damped linear continuous systems, requiring initial value numerical integration of state and adjoint differential equations

[ASME PAPER 71-VIBR-1] 21 p3456 A71-40265

ADJUSTING

Astatic gyroscope with gimbal system on rocking base, discussing effects of Cardan joint adjustment to insensitivity zone on instrument drift

01 p0080 A71-10631

Pulkovo radio telescope reflector adjustment by phase comparator, using centimeter wave transmitting-receiving antenna for sun, moon and Venus observations

07 p1083 A71-19344

Planimetric aerial photographic block adjustment to ground control

08 p1288 A71-21257

Cam profile selection for altimeters in computing-resolving unit of aneroid sensors of altimeters

13 p2069 A71-28938

Contractor claim of value of delayed payments under government contracts as adjustment for stretch-out, discussing tenability

14 p2341 A71-31131

ADJUSTMENT

U ADJUSTING

ADMINISTRATION

U MANAGEMENT

ADMITTANCE

U ELECTRICAL IMPEDANCE

ADRENAL GLAND

Adrenal gland blood flow and arterial pressure determination under stochastic pulse excitation of anesthetized dogs centripetal and centrifugal nerves, using analog correlator

03 p0357 A71-12994

Hypothalamus and adrenal glands catecholamines relationship for hypophysectomized rats

03 p0362 A71-13293

Stress and behavior regulation, investigating pituitary-adrenal system operation

07 p1043 A71-20213

Adrenocortical function in garden dormouse during autumnal preparation for hibernation, considering environmental temperature factors

13 p2014 A71-29315

Adrenalectomy influence on electrical activity of cortex and subcortical areas in rats under hyperbaric oxygen, using implanted electrode electroencephalographic recordings

16 p2528 A71-33118

ADRENAL METABOLISM

Endocrine and metabolic effects of noise in normal, hypertensive and psychotic subjects, considering increased corticoadrenal and adrenergic activity

03 p0359 A71-13154

Seasonal factors effect on white rat hypophysis-adrenal cortex system functioning by fluorimetric determination of peripheral blood corticosterone content

07 p1041 A71-19282

Control and prolonged exercised rats adrenal and plasma catecholamine, corticosterone and epinephrine level comparisons using fluorimetric analysis

07 p1044 A71-20330

Diurnal rhythm of adrenaline secretion in subjects with different working habits, comparing catecholamine excretion under relaxation conditions

11 p1721 A71-26355

Diurnal variations in catecholamine excretion, alertness and performance of subjects with different working habits

11 p1722 A71-26356

Adrenal medulla biochemistry and morphology, discussing epinephrine synthesis control by glucocorticoid hormones

14 p2187 A71-30809

DC magnetic field effect on organism sympathoadrenal system, noting hypokinesia reduction of noradrenalin in hypothalamus and myocardium

15 p2357 A71-31311

Respiratory chemoreceptors and acid-base alterations effects on adrenocortical activation during hypoxia in dogs

20 p3187 A71-38986

ADRENALINE

U EPINEPHRINE

ADRENERGICS

Circulatory response to beta adrenergic blockade during muscular work, causing reduction in cardiac frequency, exercise tolerance and oxygen consumption

05 p0709 A71-16622

Adrenergic neurons in intramural cardiac ganglia in rabbits, using histochemical luminescent microscopy

09 p1391 A71-22533

Physical exercise oxygen uptake and debt in dogs at ground level and high altitude, investigating beta adrenergic blocking agent effects

16 p2530 A71-33242

M-cholinergic and adrenergic subcortical structures blockage effects on blood flow rate in dog pulmonary circulation system

16 p2534 A71-34113

Alpha adrenergic inhibition of immunoreactive insulin release during deep hypothermia in puppies given glucose infusions

17 p2681 A71-34942

Canine ventricular myocardium as cardiac beta-adrenergic receptor, describing binding of norepinephrine to microsomal particles

19 p3002 A71-37900

Sympathomimetic amines effects on central nervous system reflex activity of irradiated and desympathized animals

22 p3492 A71-42708

Mice acceleration before and after gamma irradiation, determining protective effect of cystamine in adrenaline and amphetamine mixture

22 p3494 A71-42726

ADRENOCORTICOTROPIN [ACTH]

Dog blood leucocyte composition relation to alimentary satiation and adrenocorticotrophic and reticuloendothelial systems, considering effect of ACTH and india ink injections

01 p0008 A71-10092

ADSORBENTS

Cryosorption vacuum pumping, discussing physical and chemical adsorption, adsorbents, surface migration and diffusion, reactivation, deposits, cryopanel adhesion, pump design, etc

20 p3270 A71-39249

ADSORPTION

NT CHEMISORPTION

Langmuir S curves for W /110/-Cs and Mo /100/-Sr adsorption determined by thermionic electron emission microscope, noting minimum work function

02 p0295 A71-12203

Thermionic emitter metal surface adsorption, investigating impurities and additives effects by analytical model

02 p0295 A71-12231

Cesium consumption rates and content in thermionic converter components affecting system performance indicated via integral adsorption reservoir

02 p0195 A71-12245

Desorption and migration of Cs adsorbed on W surface under electric field, using field emission microscope

02 p0296 A71-12340

Interstellar molecular hydrogen formation by physical adsorption on grains, determining H atoms adsorptive potentials on silicates, graphite, solid hydrogen and ice

02 p0287 A71-12582

Adsorption role in empirical ignition laws of various solid nitric acid based hypergolic propellant systems, discussing ignition delay relation to acid concentration

04 p0548 A71-14825

Ultrahigh vacuum deposited Ni, Fe, W and Mo films, determining molecular oxygen adsorption efficiencies

04 p0636 A71-15015

Complex hydrocarbon molecular formation by physical adsorption on interstellar grains in dense clouds

04 p0650 A71-15396

Hydrogen and nitrogen binding states and desorption kinetics on /100/ plane of Mo, using flash mass spectrometry

06 p0865 A71-18302

Adsorbed formaldehyde levels from vaporized paraformaldehyde on various surfaces as function of relative humidity and chemical concentration

07 p1055 A71-19593

Hydrogen adsorption behavior on polycrystalline nickel surfaces, using electron impact desorption flash filament with gas phase and ion spectrometer and vapor deposition

07 p1055 A71-19843

Hydrogen and carbon monoxide coadsorption on platinum single crystal surface, examining interactions and species formation by thermal flash and electron impact techniques in ultrahigh vacuum

07 p1055 A71-19844

Be films evaporated in vacuum on W single crystals, investigating adsorption and electron emission by field emission microscopy

07 p1178 A71-19918

Two phase oxygen adsorption at molybdenum surface, using secondary ion-ion emission measurements

08 p1306 A71-21489

Contact potential measurements of work function dependence on adsorption of alkali metals on Ta/110/ and W/100/ crystals under ultrahigh vacuum

09 p1497 A71-22701

Hydrogen-nickel reaction in presence of CO adsorbed gas, increasing total desorption cross section and eliminating monotonic relation between uptake and H ion current

10 p1573 A71-24540

Equilibrium adsorption isotherms correlation for low temperature cryodeposits, using Dybinn-Raduschevich equilibrium equation to estimate hydrogen capacity of cryosorption pumping system

10 p1643 A71-25011

Mars regolith carbon dioxide, water and Kr adsorption, explaining diurnal brightness phenomena

12 p1961 A71-26875

Surface roughness of 304 stainless steel by Brunauer-Emmett-Teller measurements, using ethylene as adsorbate

14 p2284 A71-30073

Adsorption states of Mo and Re surfaces during oxidation at low oxygen pressures and temperatures up to 2300 K, using noble gas molecular beams

14 p2190 A71-30402

Two phase oxygen adsorption on molybdenum surface from secondary ion-ion emission

14 p2260 A71-30678

Binding states, adsorbate densities and desorption kinetics of hydrogen on crystal planes of tungsten

15 p2367 A71-31676

Oxygen adsorption kinetics at Nb single crystal surface at high temperatures and low pressures

15 p2436 A71-32547

Thermionic emission and adsorption characteristics of Ta single crystal faces in cesium atom streams, using thermoelectronic and surface ionization methods

15 p2453 A71-32643

Carbon fiber surface reactivity from gas chromatographic measurement, discussing adsorption isotherm of various vapors

16 p2541 A71-34049

Ti adsorption on W and Re, measuring field emission average work function at various Ti layer thicknesses

17 p2791 A71-34855

Trace impurities effect on oxygen adsorption by Mo, using low energy electron diffraction, Auger electron spectroscopy and flash desorption mass spectrometry

17 p2694 A71-34856

Oxygen adsorption study on polycrystalline W through work function variation and adhesion coefficient measurements, using mass spectrometry

18 p2874 A71-35974

Adsorption cryopumped He 3 cooled IR detector without encumbrance of external diffusion or mechanical pump

18 p2922 A71-36588

Vacuum deposited thin Cr films on glass substrate, discussing hydrogen adsorption effects

19 p3076 A71-37116

Cryosorption vacuum pumping, discussing physical and chemical adsorption, adsorbents, surface migration and diffusion, reactivation, deposits, cryopanel adhesion, pump design, etc

20 p3270 A71-39249

Heavy rare gases adsorption on terrigenous sediments, comparing earth atmospheric composition with meteoric planetary primordial component

20 p3194 A71-39385

Nitrogen adsorption on single crystal W planes by flash desorption experiment, noting work function change dependence on planes

21 p3345 A71-40539

Bronsted relationship between adsorption heat and activation energy in electrocatalysis of purified orthophosphoric acid and phase-oxide-free noble metals

21 p3345 A71-40540

Apollo 11 lunar fines and ground terrestrial mafic rock powders effective surface areas and heats of adsorption, using Brunauer-Emmett-Teller Kr adsorption method

21 p3450 A71-40648

Field adsorption of inert gas atoms at metal surface from variational calculation

21 p3419 A71-40887

Germanium single crystal surface conductivity, observing carbon monoxide adsorption effects at various pressures

21 p3435 A71-41341

LEED studies of oxygen adsorption on /111/ and /110/ surfaces of Al single crystals

22 p3561 A71-41730

Gas interaction with lunar fines, investigating carbon monoxide, nitrogen, oxygen, argon and water vapor adsorption

23 p3758 A71-43754

Unpaired electrons and oxygen adsorptive capacity of clean lunar rock and soil surfaces, noting decrease of uptake rate at one monolayer coverage

23 p3764 A71-43798

Quartz crystal mass monitor study of monolayer oxygen adsorption on Al films, noting surface roughness variation with deposition temperature

24 p3803 A71-45348

ADSORPTIVITY

Thermoemissive and adsorptive properties of Nb single crystals in Cs atomic beam at various temperatures

01 p0139 A71-11100

Polyatomic organic adsorbates effect on field emission total energy distribution from W and Mo surfaces, discussing electronic and phononic spectra

02 p0297 A71-12733

Metallic surfaces adhesive properties and adsorptive capacity from nondestructive testing by peeling

10 p1616 A71-24105

ADVANCED VIDICON CAMERA SYSTEM [AVCS]

Nimbus AVCS imagery applied to studies of bedrock geology, geomorphology and climate
04 p0597 A71-15309

ADVECTION

Ageostrophic deviations and advection corrections to geostrophic wind velocity and shear stresses above water surface
22 p3570 A71-42849

AERIAL EXPLOSIONS

Finite difference simulation of high energy Mach 120 to 40 air shock experiment
04 p0565 A71-14678

Large scale explosive driven conical shock tube nuclear air blast simulator
04 p0624 A71-14681

Air blast effects on pulmonary ventilation, gas exchange, venous-arterial shunt and blood gas parameters
06 p0851 A71-17601

Critique of paper on explosive hazards of large solid rocket motors, suggesting extrapolation of fractional TNT equivalent
18 p2955 A71-36284

AERIAL PHOTOGRAPHY

Soviet book on gyroscopes in geodesy and aerial photography based on structural analysis for automatic control systems, covering gyro error, theodolites, etc.
01 p0083 A71-11321

Remote sensing systems for vegetation analysis, discussing machine-aided photointerpretation methods for data analysis
01 p0084 A71-11590

[AIAA PAPER 70-308]
Information content and digital storage of aerial photography using assessing entropy of written English text
02 p0248 A71-11953

Aerial photography, discussing optimal exposure selection and control to obtain maximum number of fine details
04 p0585 A71-14642

Aerial photographic film color separation tests
04 p0585 A71-14644

Pseudo radar imagery by high contrast aerial photography at low sun angles for aiding geological analysis
04 p0598 A71-15370

Photogrammetry and aerial photography - Conference, Denver, October 1970
08 p1280 A71-21239

Image specifications and data interpretation techniques for regional resource survey using small scale aerial and space photography
08 p1288 A71-21245

Automatic record of terrain profiles from stereoscopic aerial photographs by intersection of ray traces
08 p1288 A71-21252

Planimetric aerial photographic block adjustment to ground control
08 p1288 A71-21257

Aerial photographic block aerotriangulation error analysis, discussing block configuration, perimeter and vertical controls, premarking, overlapping, etc.
08 p1288 A71-21260

Aerial color negative system for processing Ektachrome aero film type 8442 to obtain negative transparency with fourfold effective film speed increase
08 p1288 A71-21261

Air-photo interpretation to inventory kind of cattle-raising operation practiced on farms of southern Ontario
08 p1282 A71-21437

Optical transfer function measurement and computation test applications to aerial camera wide angle lens standard design, using interlaboratory comparisons
09 p1494 A71-23001

Aerial photographs point marking by Markov instrument, discussing high precision stereophotogrammetric equipment for photogrammetric work and physical marking
09 p1451 A71-23177

Aerial photographs orientation point location, relating measurement weight of transverse parallax
09 p1451 A71-23178

ERTS-A imagery, Apollo 9 and high altitude aircraft photography applications to Land Management Bureau, Indian Affairs and Reclamation
09 p1451 A71-23208

Aerial photography vs orbital acquired imagery resolution for land use data
09 p1439 A71-23212

Aerial photographic measurements of terrain spectral reflectance and analysis of water resource color and quality by scene color standard technique
09 p1439 A71-23218

Side-looking airborne radar (SLAR) for sea ice identification, mapping and ship routing in Northwest Passage
09 p1439 A71-23448

Recording and interpretation of aerial photographs applied to geomorphology
10 p1599 A71-23872

Optimal shapes and sizes of marker signs used in calibrating aerial photographs
12 p1906 A71-26971

Statistical diameter size distribution of random circles on plane or spheres in space from satellite and aircraft measurements for aerial and cloud photography
12 p1929 A71-27100

Flight tests of inertial navigation system in aerial geodetic mapping, achieving automatic side-lap, verticality and line position control
12 p1927 A71-27256

Photography date effects on intensive study sites airphoto interpretations, using color and color-IR films
12 p1907 A71-27258

Black and white television scanning ability of color differentiation and gray tone identification by signal fluctuations in aerial imagery
12 p1907 A71-27261

Vibration effects on image resolution and accuracy of Zeiss RMK AR 15/23 aerial camera, using aircraft vibration simulator for testing
12 p1907 A71-27263

Aerial and block triangulation error analysis accuracy dependence on reference point number, introducing camera internal orientation improvement
13 p0262 A71-28903

Parallax errors in drawing contour lines on universal stereograph due to aerial photographic images brightness difference
13 p0270 A71-29083

Color and color IR films for soil identification, performing optical density measurements on film transparencies with densitometer
13 p0271 A71-29394

Dwelling unit estimation with color IR photos, applying aerial photointerpretation to urban analysis
13 p0264 A71-29396

Land use classification schemes selection with orbital imagery for U.S. thematic mapping
13 p0264 A71-29397

Diseased plants and crop loss per field from aerial IR-color photography
14 p2236 A71-30576

Psychological tests for aerial photograph interpreter selection and performance prediction
16 p2534 A71-32829

Aerial color photography in forestry for species identification, reforestation areas development, watershed studies and land planning
17 p2737 A71-34272

Multispectral color aerial photography for identification of farm crops and tree species, using broadband camera filters
17 p2737 A71-34274

Automatic pattern recognition of urban development changes from aerial photographs, using computer program and nonlinear registration technique for cell pairs partitioning
17 p2711 A71-35043

Remote sensing imaging techniques for oil pollution survey, using airborne UV, IR, color and filtered panchromatic photography
17 p2735 A71-35386

Monograph on satellite-borne orbital photographic imaging techniques application to natural resources survey, discussing remote areas geomorphological and geological reconnaissance maps preparation
18 p2915 A71-35905

Urban environmental quality analysis using color IR aerial photography, considering film sensitivity and haze penetration
18 p2911 A71-36062

Automated pattern recognition for urban texture and land use assessment by aerial photographs, using digitally scanned optical Fourier transforms
18 p2912 A71-36063

Remote subsurface oceanographic imagery from orbital altitudes in blue multispectral region, showing optimum filter passband
18 p2917 A71-36064

Aerial cameras performance prediction by computer simulation technique with random number generation
18 p2917 A71-36069

BTISIM computer simulation technique for application to real time airborne photoreconnaissance imagery data transmission system design and performance analysis
18 p2917 A71-36070

Wideband stabilizer design for high acuity aerial reconnaissance camera to obtain high degree of attenuation to roll and pitch rotational motion inputs
18 p2919 A71-36087

Solid state light emitting diodes in aerial camera data recording system for enhanced spectral matching, increased photo conversion efficiency and lower power drive
18 p2920 A71-36089

Aircraft and satellite remote sensing techniques in geology, soil science, geography and hydrology
18 p2913 A71-36539

Aerospace vehicles high resolution photography, introducing phase rate image tracking sensors for forward motion compensation
18 p2883 A71-36909

Nonlinear compensation for film deformation in aerial photography correcting spatial phototriangulation grids
19 p3063 A71-37270

Environmental water pollution observation by remote sensing, discussing aerial photography
19 p3059 A71-38403

Aerial land rover for special needs of developing countries as passenger and freight aircraft, crop spraying and dusting, aerial survey and fire fighting
21 p3325 A71-40701

Aerial photographic equipment survey, describing topographic cameras, aerial photograph orientation equipment, onboard navigation instruments and mapping survey system
21 p3380 A71-40875

Aircraft heat viewer for underlying surfaces radiation properties, suggesting qualitative survey type thermal aerial photo combination with simultaneous radiometric measurements
21 p3383 A71-41300

Statistical diameter size distribution of random circles on plane or spheres in space from satellite and aircraft measurements for aerial and cloud photography
22 p3537 A71-41655

Earth orbital photography for geologic applications, discussing advantages over aerial photography
22 p3534 A71-41962

IR linescan technique for airborne terrain mapping, discussing choice of waveband, system parameters and display techniques with emphasis on film recording
22 p3546 A71-42425

Atmospheric contrast reduction of aerial images, predicting quality under various target and meteorological conditions
22 p3547 A71-42506

Ocean layer mixing from aerial photographs using dye injections and floating cards under various wind, sea state and thermal profile conditions
22 p3569 A71-42547

Spatial photogrammetric restitution of terrestrial photographs using projective transformations
24 p3825 A71-44756

Arctic ocean pack ice terrain profiling by airborne laser altimeter and coincident photography, analyzing data for ice development stages interpretation
24 p3833 A71-44986

AERIAL RECONNAISSANCE

Side-looking airborne radar (SLAR) imagery and site selection for soil pattern topography
02 p0244 A71-11952

Target detection performance in simulated real time airborne reconnaissance mission, taking into account search time and image type, contrast and rate of motion
08 p1248 A71-21227

Target detection improvement in reconnaissance by black and white TV system, using narrow band filters for conversion to multispectral sensor system
08 p1287 A71-21240

Tethered, ground supplied, rotor-borne, self stabilized surveillance platform (Kiebitz) system, discussing reconnaissance tasks, fire and communication control and data acquisition transmission and evaluation
15 p2347 A71-31212

Optimal sensing recording and signal processing in multispectral photography for aerial reconnaissance capability
15 p2410 A71-32470

Simulation tests of multiagency reconnaissance sensor operations, including multisensor data base, imagery processing laboratory, flight testing and ground truth activities
17 p2775 A71-35764

Real time reconnaissance cockpit display system for airborne sensor systems, providing night combat imagery
17 p2747 A71-35772

Vegetation penetration with K-band side-looking airborne imaging radars, noting multifrequency multipolarization system application for terrain reconnaissance
18 p2875 A71-36365

Aerial and satellite environmental water quality control surveillance, discussing remote sensing techniques and objectives
19 p3059 A71-38402

Latent forest fire detection, describing airborne IR surveillance system
19 p3066 A71-38410

Gaussian and Poisson noise and SNR effects on subjective image quality rating, using transparency aerial scenes
20 p3235 A71-39190

Closed cycle refrigeration system for cryogenic cooling of IR illuminator in helicopter mounted U.S. Army NVASS Night Vision System for night reconnaissance
20 p3184 A71-39275

Earth resources survey satellites, discussing natural sources/radiation, matter-energy interactions and perturbing media, remote sensors, space applications and reconnaissance
21 p3455 A71-40910

Airborne IR linescan equipment for commercial aerial survey, discussing operational principle, temperature sensitivity, data processing and individual system components specifications
22 p3545 A71-42151

AERIAL RUDDERS

Twin turboprop STOL aircraft lateral directional oscillation traced to rudder vibration due to aerodynamic hinge moments interaction with friction
[AIAA PAPER 71-792] 16 p2525 A71-34019

AEROBEE ROCKET VEHICLE

Aerobee 150 sounding rocket cryogenic air sampler, discussing design, operation and air constituents reaction to cooling
01 p0084 A71-11442

Postflight analysis including six degree of freedom trajectory digital simulation of Aerobee 350 sounding rocket behavior under large thrust misalignment
[AIAA PAPER 70-1380] 03 p0498 A71-13663

Earth hydrogen geocorona models comparison with solar Lyman alpha spectrographic data from Aerobee rocket flight measurements
03 p0496 A71-14509

AEROBES

Bacterial spore distribution and dry heat resistance on Mariner-Mars 1969 spacecraft, using randomly selected aerobic mesophilic isolates
19 p3002 A71-37646

Human microflora variation in long term confinement, examining anaerobic and aerobic microorganisms responses
21 p3333 A71-40557

AEROBIOLOGY

Acetyl-coenzyme A synthetase in aerobic yeast cells localization in microsomal fraction by density gradients
14 p2187 A71-31003

AERODYNAMIC AXIS

U AERODYNAMIC BALANCE

Angle of attack amplification due to body trim plane rotation, obtaining pertinent relations by method of stationary phase
[AIAA PAPER 71-48] 06 p0980 A71-18509

Atmospheric reentry dynamics of spinning body with trim angle of attack
07 p1205 A71-18892

Ballistic reentry vehicle roll related to trim angles caused by inertia asymmetries
[AIAA PAPER 70-204] 07 p1208 A71-19867

Probabilistic estimate of aerodynamic imbalance of aircraft gas turbine rotors due to production errors in compressor blade angle
08 p1349 A71-22045

Concorde aircraft fuel system and fuel pumps, considering center of gravity and center of pressure relationship to maintain trim
09 p1512 A71-23581

Transient resonance response of slender entry vehicles in rolling trim at spin-pitch intersection for offset coplanar and orthogonal leading models
11 p1837 A71-25480

Reentry vehicles configuration lift and drag coefficients in hypersonic flow from pressure distribution and balance measurements, comparing with isolated cone data
11 p1702 A71-25487

STAN/MASS system aircraft weight and balance determination, discussing basic concepts, design requirements and applications
[SAWE PAPER 896] 17 p2834 A71-35816

Preflight balance analysis of dual spin satellites, discussing error sources
[SAWE PAPER 882] 17 p2815 A71-35821

Strut pressure and axle strain gage systems testing for balance and weighing onboard De Havilland C-7A aircraft
[SAWE PAPER 881] 17 p2676 A71-35827

Dynamic unbalances effects for axially symmetrical dual spin space station with rigid or low coupling interconnections, considering control moment gyros use
22 p3612 A71-42770

Active flutter mode control system synthesis for flight test, showing mass balancing as possible artificial symmetrical wing destabilization
23 p3629 A71-44106

AERODYNAMIC BRAKES

NT BALLUTES

NT DRAG CHUTES

NT LEADING EDGE SLATS

NT TRAILING-EDGE FLAPS

NT WING FLAPS

Dynamic decelerators using nylon tricot knit fabric and high elongation suspension lines for reduced peak force parachute deployment
[AIAA PAPER 70-1185] 03 p0349 A71-14273

Aerodynamic decelerator technology, emphasizing ribbon parachutes and flexible wings
06 p0846 A71-17692

Low speed wind tunnel stability tests of small guide surface, slotted solid, ring slot, cross and streamer decelerators, considering parachutes and drag measurement
07 p1022 A71-20310

Snatch force during lines-first deployment of aerodynamic decelerator, including effects of canopy skirt acceleration and suspension wave propagation characteristics
[AIAA PAPER 70-1171] 09 p1385 A71-22915

Light aircraft spoilers to minimize landing risk, discussing spoiler/dive brake area effects on glide path angular control
[SAE PAPER 7010387] 10 p1555 A71-24251

Spacecraft capture by ballistic aerobraking during passage through planet atmosphere, proposing analytic models
13 p1233 A71-27987

In-flight deployment balloon launching system with load lowering friction brake, discussing flight test results
14 p2175 A71-30071

AERODYNAMIC BUZZ

U FLUTTER

AERODYNAMIC CENTER

U AERODYNAMIC BALANCE

AERODYNAMIC CHARACTERISTICS

NT AERODYNAMIC BALANCE

NT AERODYNAMIC DRAG

NT AERODYNAMIC STABILITY

NT INTERFERENCE DRAG

NT INTERFERENCE LIFT

NT JET LIFT

NT LIFT

NT ROTOR LIFT

NT STATIC AERODYNAMIC CHARACTERISTICS

NT ZERO LIFT

Statics and aerodynamics of lifting decelerators /parawings and sailwings/ at supersonic and hypersonic speeds
[AIAA PAPER 68-945] 01 p0002 A71-10927

Forward horizontal speed influence on aerodynamic characteristics of air cushion vehicle with circular nozzles and cylindrically or conically shaped curtains
02 p0186 A71-12551

Aerodynamic characteristics of aircraft in steady and unsteady supersonic flow by analog electrical method, including wing-fuselage interactions
03 p0339 A71-13130

Nike-Apache sounding rocket vehicle with canted fins, examining pitch-roll coupling characteristics by equilibrium and dynamic simulation methods
[AIAA PAPER 70-1376] 03 p0497 A71-13659

Sounding rockets nonlinear aerodynamic characteristics from full scale and supersonic wind tunnel free flight data, using wobble analysis
[AIAA PAPER 70-1383] 03 p0498 A71-13666

Sandhawk research sounding rocket performance, aerodynamic and flight characteristics for heavy payload transport to high altitude
[AIAA PAPER 70-1398] 03 p0499 A71-13679

Hypersonic aerodynamic characteristics of flat delta and caret wing models at high incidence angles for space shuttles
03 p0344 A71-14445

Aerodynamic characteristics of low aspect ratio wing in bounded inviscid fluid flow, considering planform relation to lifting force derivative and angle of attack
04 p0525 A71-14589

Linear airfoil theory applicability for wings aerodynamic characteristics, considering high lift, ground effect, angle of attack and aspect ratio
04 p0525 A71-14593

Jet interference effects on rectangular and swept wings, presenting wind tunnel test data for range of jet locations, inclinations and velocity ratios
[DGLR-70-052] 05 p0693 A71-15951

Aerodynamic characteristics of jet engine installation above wing of swept wing aircraft, noting large lift dependent drag
05 p0696 A71-15954

Slender, conical, plane and cambered wing-body combinations with different volume distributions in supersonic flow, comparing experimental with theoretical aerodynamic characteristics
[DFVLR-SONDDR-86] 06 p0841 A71-17418

Finned missiles aerodynamics at high angle of attack, examining body vortex wake region interaction with fins
[AIAA PAPER 71-50] 06 p0980 A71-18511

Sailing aerodynamic characteristics, obtaining aerodynamic loading by two dimensional flexible airfoil and Prandtl lifting line theories
07 p1017 A71-20303

Soviet book on Yak-40 passenger transport aircraft configurational design and aerodynamic characteristics covering stability, controllability and flight under special conditions
08 p1230 A71-20750

Aerodynamic characteristics of conical and pyramidal configurations with various planforms by slender body theory, replacing three dimensional flow by two dimensional flow
08 p1227 A71-20776

Potential flow past cylinder with sources and sinks singularities, deriving formulas for aerodynamic characteristics of infinite span wings with boundary layer control
08 p1227 A71-20777

Large angle cones supersonic aerodynamic and wake characteristics at low Reynolds numbers, including model support interference effects
[AIAA PAPER 71-264] 08 p1228 A71-21990

Elastic swept wing subsonic aerodynamic characteristics, taking into account aerodynamic load redistribution due to aeroelastic deformations
08 p1229 A71-22035

Finned configurations with nonlinear aerodynamic properties, obtaining solutions for angular motion at and near resonance
[AIAA PAPER 70-535] 09 p1532 A71-22909

Supersonic flow separation around cross shaped horizontal tail plane with subsonic leading edge, obtaining pressure distribution and aerodynamic characteristics
09 p1384 A71-23608

Density gradient visualization with schlieren optical system, discussing propeller aerodynamics
10 p1616 A71-24103

Low speed airfoil characteristics calculation by digital computer, using Theodorsen conformal transformation method for potential flow pressure distribution
[SAE PAPER 710389] 10 p1550 A71-24253

Aerodynamic characteristics and flow pattern in wake behind star-shaped body at supersonic speed, determining drag and shock waves location
10 p1551 A71-24371

Inclined engine cold circular jet effects on tail control surfaces aerodynamic characteristics, considering aircraft longitudinal stability
[DFVLR-SONDDR-104] 10 p1552 A71-24593

AERODYNAMIC CHARACTERISTICS

Large angle cones supersonic aerodynamic and wake characteristics at low Reynolds numbers, including model support interference effects
[AIAA PAPER 71-264] 08 p1228 A71-21990

Elastic swept wing subsonic aerodynamic characteristics, taking into account aerodynamic load redistribution due to aeroelastic deformations
08 p1229 A71-22035

Finned configurations with nonlinear aerodynamic properties, obtaining solutions for angular motion at and near resonance
[AIAA PAPER 70-535] 09 p1532 A71-22909

Supersonic flow separation around cross shaped horizontal tail plane with subsonic leading edge, obtaining pressure distribution and aerodynamic characteristics
09 p1384 A71-23608

Density gradient visualization with schlieren optical system, discussing propeller aerodynamics
10 p1616 A71-24103

Low speed airfoil characteristics calculation by digital computer, using Theodorsen conformal transformation method for potential flow pressure distribution
[SAE PAPER 710389] 10 p1550 A71-24253

Aerodynamic characteristics and flow pattern in wake behind star-shaped body at supersonic speed, determining drag and shock waves location
10 p1551 A71-24371

Inclined engine cold circular jet effects on tail control surfaces aerodynamic characteristics, considering aircraft longitudinal stability
[DFVLR-SONDDR-104] 10 p1552 A71-24593

Trisonic wind tunnel calibration tests results including second throat effects, Mach number and static pressure distributions, flow inclination and aerodynamic characteristics
10 p1590 A71-24819

Wind tunnel evaluation of analytical method for predicting longitudinal stability and aerodynamic characteristics of large flexible aircraft applied to supersonic transport configuration
[AIAA PAPER 71-343] 11 p1707 A71-25322

Aerodynamic characteristics of slender body of revolution traveling in long tube with circular cross section, deriving static and dynamic stability derivatives formulas
11 p1702 A71-25477

Static aerodynamic characteristics of slender ablating reentry vehicle, discussing coupling between flow field and thermochemical analyses of heat shield materials response
[AIAA PAPER 70-826] 11 p1854 A71-25512

Asymmetric three dimensional aerodynamic density fields from holographic interferograms, applying to supersonic flow from free jet
11 p1762 A71-25802

Mutual aerodynamic effects of SM-1 helicopters during simultaneous takeoff and landing, determining minimum distances between helicopters
12 p1867 A71-26953

Sounding rockets aerodynamic characteristics, comparing wind tunnel and flight test data
12 p1864 A71-27474

Aerodynamic characteristics similarity and variation in hypersonic flow transition region from free molecular flow to solid medium
13 p1991 A71-29172

Eleons as longitudinal and lateral control elements on low aspect ratio wings, calculating subsonic and supersonic aerodynamic characteristics
13 p1993 A71-29190

Elliptical cones at large angle of attack, calculating three-component real gas properties effects on aerodynamic characteristics
13 p1993 A71-29191

Wing-jet interference effects in cross wind on thrust and aerodynamic characteristics at large distance from and near ground
13 p1993 A71-29207

Wind tunnel simulation of viscous hypersonic flow-laminar boundary layer interactions, presenting similarity parameter effects on aerodynamic characteristics
13 p1994 A71-29224

Longitudinal stability of ground effect airplane, discussing influence on aerodynamic characteristics of height, ground surface roughness and wing aspect ratio
13 p1997 A71-29228

Aerodynamic behavior of bodies in wake of two dimensional bluff bodies, discussing loads
13 p1994 A71-29265

Soviet book on helicopter design covering aerodynamic properties, power plants, control systems, fatigue minimization and strength analysis
14 p1274 A71-29944

Time dependent clearance changes effects on aerodynamic characteristics of sectorially grooved gas bearings, describing lift and drag coefficients calculation
14 p2252 A71-30227

Aerodynamic characteristics of low-aspect-ratio wing mounted on cylindrical body, simulating by system of horseshoe vortices

14 p2170 A71-30264

Multimission strategic aircraft installation effects testing in propulsion and aerodynamic wind tunnels, yielding flowfield definition, inlet internal performance, drag, forebody shape and orientation

[AIAA PAPER 71-759] 14 p2171 A71-30792

L-1011 Tristar antenna arrangement test results, considering weight, aerodynamic and structural design requirements

14 p2218 A71-31060

STOL aerodynamics of leading edge high lift devices on thick profiles, externally blown flaps, boundary layer control and jet flap effect

15 p2343 A71-31214

Computing geometric airplane aerodynamic characteristics during preliminary and detailed design processes

15 p2348 A71-31597

Flat delta and caret wings aerodynamic performance over incidence angle and Mach number range suitable for lifting reentry

16 p2519 A71-32877

Aerodynamic characteristics of arbitrary planform wing moving near screen, ground or water surface, using vortex model

16 p2521 A71-33596

Hypersonic aircraft design usable as transport or space shuttle, determining aerodynamic behavior in viscous flow

18 p2847 A71-36431

Aerodynamic characteristics of space shuttle configurations over entire flight velocity range, stressing coupling effects of control surfaces at large angles of attack

18 p2972 A71-36437

Flight dynamics for aircraft noise reduction, gust effects decrease and dynamic stability of parachute load systems

18 p2850 A71-36752

Digital simulation for predicting static directional aerodynamic forces and moments characteristics of air cushion vehicle configuration through 180 degrees of sideslip

[AIAA PAPER 71-907] 19 p2995 A71-37158

Augmentor wing high-lift aerodynamics, discussing results of wind tunnel tests and simulation studies

[CASI PAPER 72/20] 19 p2993 A71-37606

Spacecraft trajectories for reentry at hyperbolic velocity, examining aerodynamic control loads and characteristics in atmospheric skip

20 p3288 A71-39122

Gas turbine engine adjustable nozzle ring flat arrays aerodynamic characteristics determination from profile loss factor dependence on setting angle

20 p3175 A71-39172

Aerodynamic aspect ratio effects on drag and aircraft performance, noting span loading as major force on wing lifting function

21 p3325 A71-41246

Apollo command module aerodynamic characteristics in hypersonic low density flow, measuring drag, three component force and heat transfer

22 p3480 A71-42027

Minimum drag and lifting line characteristics of large aspect ratio wing in uniform shear flow with velocity variations along span

23 p3625 A71-43312

Flight test measurements for improved estimates of aircraft states and aerodynamic parameters, using relinearized Kalman filter

23 p3629 A71-44089

Slender two dimensional wedge wings aerodynamic characteristics in hypersonic strong interaction flow, determining wall shear stress and lift drag ratio effects

24 p3789 A71-44621

AERODYNAMIC CHORDS

U AIRFOIL PROFILES

U CHORDS [GEOMETRY]

AERODYNAMIC COEFFICIENTS

Nonaffine similarity laws and transformations subject to limitations of Newtonian impact theory for two dimensional bodies, obtaining aerodynamic coefficients

01 p0002 A71-10948

Spheres drag coefficient at hypersonic Mach numbers for near free molecular flow

01 p0002 A71-10969

Critique of Chapman-Kirk iterative method for differential equations yielding aerodynamic coefficients from free flight data

01 p0002 A71-10971

Thin delta wing with leading edge separation, obtaining drag lift and rolling moment coefficients and pressure distribution

02 p0185 A71-12408

Nonlinear aerodynamic moments for arbitrary motions of bodies of revolution in free flight

[AIAA PAPER 70-205] 03 p0341 A71-13435

Ballistic data reduction for drag coefficient of spherical projectiles, using time distance relation for constant coefficient

03 p0341 A71-13467

Lift of slender aircraft with rectangular cross section fuselage and high wing

03 p0342 A71-13737

Slender deformable airfoil in bounded fluid flow, determining lift coefficient by one dimensional integrodifferential equation for elastic large aspect ratio wing

04 p0567 A71-14590

Trailing vortex generation behind jet flapped wing at high wing lift coefficients

04 p0527 A71-15413

Supersonic axisymmetric wake-like and two dimensional shear nonuniform free stream flows effects on inviscid flow fields and aerodynamic coefficients of sharp and spherically blunted cones

[AIAA PAPER 71-51] 06 p0843 A71-18512

Unsteady supersonic aerodynamic coefficients evaluation to desired kinematic consistency level using finite element method

[AIAA PAPER 71-177] 06 p0845 A71-18616

Free flight measurement of aerodynamic coefficients on fixed cruciform fin stabilized bombs, determining aerodynamic forces and moments dependence on angular velocity components

07 p0105 A71-19872

Wing flap slipstream deflection correction method for evaluation of propeller power effect on lift and drag coefficients of Arava twin engine STOL aircraft

11 p1706 A71-25164

Nonlinear aerodynamic stability coefficients from free angular motion of rigid bodies, using three degrees of freedom subsonic wind tunnel tests on Apache model

11 p1837 A71-25515

Two dimensional laminar boundary layer equation local drag coefficient from one and two term Merk expansion in regions upstream of stagnation point

12 p1896 A71-27051

Air flow about low aspect ratio delta wing at large angles of attack, deriving lift coefficient

13 p1990 A71-28282

Supercavitating flow past straight cascade with arbitrary blade shapes, considering lift and drag coefficients, cavitation number, cavity shape and exit flow conditions

[ASME PAPER 71-FE-6] 13 p1995 A71-29448

Hingeless rotor stability characteristics at high advance ratios, examining equations of motion and time variant aerodynamic coefficients

[AIAA PAPER 71-580] 15 p2345 A71-31569

Magnus or Robins effect on rotating spheres, obtaining lift coefficients from conical pendulum periodic time measurements

15 p2346 A71-31927

Slender cone at Mach 10 with underexpanded exhaust plume, determining flow field interactions separation pattern and aerodynamic coefficients

[AIAA PAPER 71-562] 15 p2347 A71-32280

Drag coefficients of bodies of revolution from wind tunnel shock induced steady flow data, considering blast loading experiments in shock tube

16 p2519 A71-32878

Unsteady compressible flow measurement, determining local lift coefficient from pressure distribution along airfoil

16 p2520 A71-33342

Lift and drag coefficients for arbitrary body form in hypersonic flow calculated for cylindrical surface with reference to space shuttle reentry

19 p2992 A71-37320

Atmospheric density variations calculation, using aerodynamic drag coefficient data from gas flow-satellite surface interactions

20 p3223 A71-39706

Direct solution for divergence speed of lifting surface using matrices of structural and static aerodynamic influence coefficients

21 p3456 A71-40171

V shaped notches drag coefficients behavior in transonic regime, observing inviscid-viscid interaction controlling flow separation and reattachment

21 p3323 A71-40954

Magnetosphere aerodynamic parameters, discussing lift and drag coefficient, shape, magnetic field gradients and tail

21 p3374 A71-41353

KC-135 aircraft climb trajectories for optimum constant lift coefficient, range and fuel amount

22 p3481 A71-42834

Performance prediction and evaluation of propulsion-augmented high lift systems for STOL aircraft, considering weight, thrust and wing loading

[AIAA PAPER 71-990] 24 p3791 A71-44585

AERODYNAMIC CONFIGURATIONS

Reentry lifting body hypersonic and subsonic flight enhancement by configuration modifications with compound curvatures minimization, giving wind tunnel model data

02 p0319 A71-11974

Compact aerodynamic reentry vehicle development problems and costs, discussing lifting body vehicle for wind tunnel, ground and flight tests and reentry trajectories

02 p0320 A71-12066

Wing representation by lifting line lattice as computation method for complex configurations unsteady aerodynamic forces, presenting numerical program for wings in two parallel planes

[ONERA-TP-891] 04 p0526 A71-15356

Air flow turbulence effect on heat transfer and boundary layer growth around flat plate, aerodynamic profile and cylinder

04 p0681 A71-15483

Slender, conical, plane and cambered wing-body combinations with different volume distributions in supersonic flow, comparing experimental with theoretical aerodynamic characteristics

[DFVLR-SONDDR-86] 06 p0841 A71-17418

Aerodynamic support interference in wind tunnel testing of configurations involving bulbous base, mass addition, transition near base and hypersonic low density flows

[AIAA PAPER 71-277] 08 p1228 A71-22002

Lifting configurations unsteady air loads prediction, investigating loading singularities in linearized potential theory

22 p3481 A71-42832

AERODYNAMIC DRAG

San Marco satellite attitude determination from on-board aerodynamic drag measurements, using least squares method for three components calculation

01 p0122 A71-10390

Supersonic and transonic flow including effects of pressure oscillations within cavity, predicting rectangular cavities drag from mathematical model

01 p0002 A71-10931

Thrust-minus-drag optimization by base bleed and/or boattailing, using computer program

01 p0004 A71-11589

Spanwise distribution of induced drag in subsonic flow by vortex lattice method, noting applicability to rotary derivatives in stability analysis

02 p0187 A71-12691

Sectional drag relationships in linearized wing theory, examining lifting and thickness problems for various planforms

03 p0344 A71-14240

V/STOL aircraft wing-propeller interaction, using mean flow deflection angle in lift and drag characteristics prediction

04 p0526 A71-14988

Atmospheric density variations determination from Proton 2 braking data for aerodynamic drag coefficient, constructing model for rarefied gas flow-satellite interaction

05 p0804 A71-16043

Approximate bridging relations for heat transfer, surface shear and drag in transitional regime between free molecule and continuous flows

07 p1087 A71-18894

Leading edge suction analogy for predicting low speed lift and drag-due-to-lift characteristics of sharp edge delta and related wing planforms

[AIAA PAPER 69-1133] 10 p1553 A71-24851

Supersonic conical inlet additive drag formula, using flow data in freestream

10 p1553 A71-24866

Reentry vehicles configuration lift and drag coefficients in hypersonic flow from pressure distribution and balance measurements, comparing with isolated cone data

11 p1702 A71-25487

Isolated axisymmetric jet engine exhaust nozzles thrust and drag predictions in sub-, trans- and supersonic flight regimes

[AIAA PAPER 71-719] 14 p2295 A71-30770

Fuselage influence on total aircraft drag in subsonic passenger aircraft, considering high aspect ratio cylindrical fuselages

14 p2177 A71-30821

Separation controlled transonic drag-rise modification for V-shaped notches attributed to inviscid/viscid interaction controlling flow separation and reattachment

[AIAA PAPER 71-568] 15 p2345 A71-31561

Atmospheric density variations determination from Proton 2 braking data for aerodynamic drag coefficient, constructing model for rarefied gas flow-satellite interaction

16 p2635 A71-33447

Axisymmetric inlet design for turbojet powered hypersonic cruise vehicle, examining effects of spillage and cowl drags on air flow characteristics

16 p2521 A71-34149

Sting-free aerodynamic drag measurement on ellipsoidal cylinders in subsonic wind tunnel at transition Reynolds numbers

18 p2843 A71-36037

Lifting entry trajectory control law based on uniform drag, affording heating rate and deceleration control

[AIAA PAPER 71-915] 19 p3096 A71-37165

Critique of paper on spanwise distribution of induced drag in subsonic flow by vortex lattice method, noting infinities in downwash across all vortex lines

19 p2991 A71-37297

Heat transfer and drag during air laminar flow in circular pipe with constant heat flux density at wall

19 p3044 A71-37585

Allen and Vincenti blockage corrections for drag coefficients on circular cylinder in wind tunnel 19 p3041 A71-37888

Momentum transfer between gas and condensed phase in metallized solid propellant rocket motors, measuring noncontinuum and turbulence effects on sphere drag 21 p13437 A71-40861

AERODYNAMIC FORCES

NT AERODYNAMIC DRAG

NT AERODYNAMIC LOADS

NT BLAST LOADS

NT GUST LOADS

NT INTERFERENCE LIFT

NT JET LIFT

NT LIFT

NT ROTOR LIFT

NT WING LOADING

NT ZERO LIFT

Wind tunnel apparatus for reproducing coning and spinning motions of bodies of revolution, using six-component strain gage balance for aerodynamic forces 01 p0002 A71-10930

Turbomachine blades torsional-bending vibrations aerodynamic damping, noting natural frequency shift 03 p0340 A71-13141

Engine turbine blades aerodynamic oscillation damping calculation procedure 03 p0503 A71-13416

Aerodynamic forces on control surfaces in subsonic range, investigating pressure distribution on harmonically oscillating wing 03 p0344 A71-14347

Wind tunnel tests for measuring aerodynamic interaction forces between two tandem lifting surfaces [ONERA-TP-890] 04 p0526 A71-15354

External stores separation induced aerodynamic interactions, using high speed cinematographic recording of drop trajectories and/or store loads weighing in aircraft flow field [ONERA-TP-849] 04 p0527 A71-15357

Slender bodies of revolution with cylindrical afterbodies in subsonic wind tunnel, examining vortex systems and aerodynamic forces 06 p0842 A71-18048

Free flight measurement of aerodynamic coefficients on fixed cruciform fin stabilized bombs, determining aerodynamic forces and moments dependence on angular velocity components 07 p1015 A71-19872

Stochastic Liapunov stability of satellite motion influenced by aerodynamic and gravity gradient torques, considering atmospheric density uncertainty 07 p1208 A71-19883

Elastic, inertial and aerodynamic forces aeroelastic triangle, examining lift changes due to aircraft structure deformation, dynamic flight stability and space shuttle development problems 07 p1215 A71-20063

Aerodynamic forces on harmonically oscillating wing in subsonic flow of ideal gas 09 p1384 A71-23615

Instantaneous aerodynamic force measurements and flow visualization on flapping wing, showing increase of thrust force mean value over maximum steady state value 10 p1550 A71-24362

Aerodynamic forces and hinge moments of delta cruciform control surface in blunt-nosed canard configuration for subsonic, transonic and supersonic flows 11 p1701 A71-25161

Tail flutter analysis, considering dihedral, angle of attack and aerodynamic force effects 11 p1706 A71-25188

Wing-fuselage-tail interacting low speed flutter, considering mechanical tuning and aerodynamic interference couplings [AIAA PAPER 71-326] 11 p1842 A71-25306

Equation error approach to parameter identification in third order pitch plane dynamics for high performance aerodynamically controlled aerospace vehicle 11 p1742 A71-26418

Sailplanes control, deriving incremental aerodynamic load on horizontal tail produced by instantaneous elevator deflection 11 p1708 A71-26487

Computer program for aerodynamic forces on flexible plate undergoing transient motion in shear flow, applying to panel flutter 12 p1866 A71-27559

Photoelectric, bolometric and photographic recording assembly for measurement of light pressure and aerodynamic forces on complex shape body in free molecular flow 13 p2071 A71-29155

Nonlinear mathematical model for dynamical behavior of extensible towing cable subjected to aerodynamic forces generated by uniform flow field, discussing system stability 14 p2171 A71-31026

Side forces on ogive cylinder bodies at large incidence as function of Mach number, nose fineness

and bluntness ratios for laminar and turbulent boundary layers [AIAA PAPER 71-570] 15 p2345 A71-31563

Shearing flows in steady vortex around airfoil in perturbed velocity, considering aerodynamic forces torque 15 p2346 A71-31903

Turbomachinery rotor and stator row aerodynamic interaction, describing discrete tone noise generation from far field measurements 15 p2450 A71-32134

End play influence on dynamic bending vibration stresses induced by aerodynamic forces in axial flow turbine rotor blades in case of resonant vibrations 15 p2508 A71-32298

Oscillating thin wing with control surfaces in two dimensional compressible subsonic flow, calculating aerodynamic forces based on kernel function method [DFVLR-SONDDR-132] 16 p2519 A71-33013

Twin turboprop STOL aircraft lateral directional oscillation traced to rudder vibration due to aerodynamic hinge moments interaction with friction [AIAA PAPER 71-792] 16 p2525 A71-34019

Engine turbine blades aerodynamic vibration damping calculation procedure 17 p2826 A71-35023

Digital simulation for predicting static directional aerodynamic forces and moments characteristics of air cushion vehicle configuration through 180 degrees of sideslip [AIAA PAPER 71-907] 19 p2995 A71-37158

Rocket propulsion system equipped space shuttle dynamics, discussing aerodynamic forces and moments measurement in supersonic wind tunnels 19 p3151 A71-37318

Free flight model accelerations, forces and trajectory measurements in short duration facilities, using optical methods and digital recording 21 p3362 A71-40383

Fluctuating aerodynamic force measurement on stationary circular cylinder spanning wind tunnel, using direct method without support interference 21 p3363 A71-40393

Airloads and moments changes of aircraft flying over trailing vortices, investigating time dependent aerodynamic forces 21 p3321 A71-40508

Time optimal semiactive attitude control for circular orbiting satellite pitch motion, using gravitational and aerodynamic torques 22 p3570 A71-42001

Medium compressibility effect on gas dynamic characteristics and aerodynamic forces and moments in centrifugal compressor end stage blade diffuser 23 p3626 A71-43552

Resultant aerodynamic forces on circular arc profile with normal jet in subsonic steady compressible flow, using Imai-Lamla approximation method 23 p3627 A71-44271

Subsonic force effect calculations on rectangular wings, using downwash velocity potential method 24 p3789 A71-44613

AERODYNAMIC HEAT TRANSFER

NT HYPERSONIC HEAT TRANSFER

NT SUPERSONIC HEAT TRANSFER

Local heat transfer to transverse circular cylinder at low Reynolds numbers, using iterative finite difference approach 04 p0683 A71-15493

Upper air sounding systems problems, discussing aerodynamic heat transfer between temperature sensor and ambient air 08 p1330 A71-21739

Heat transfer to airfoil in oscillating flow at large angles of attack, showing vortex shed reattachment and Nusselt numbers increase 11 p1703 A71-25963

[ASME PAPER 71-GT-18] Aerodynamic nonstationary conjugate heat transfer of thin plate with heat sources in incompressible fluid flow 22 p3622 A71-42684

AERODYNAMIC HEATING

NT SHOCK HEATING

Temperature sensitive paint and thermocouple techniques comparison for boundary layer transition data, considering aerodynamic heating and transition Reynolds numbers 03 p0518 A71-13468

Sounding rockets aerodynamic heating effects approximate prediction methods using computer programs [AIAA PAPER 70-1399] 03 p0518 A71-13680

Optimal weight of aerodynamic heat protection layers of stressed skin and optimal efficiency of cooling system for hypersonic aircraft compartments 08 p1375 A71-20836

Combined radiative-convective heating test facility for atmospheric entry simulation [AIAA PAPER 71-255] 08 p1273 A71-21984

Aerodynamic heating effects on fatigue and creep properties of supersonic aircraft alloys at high temperatures, considering deformation mechanisms interaction 09 p1472 A71-23204

Combustion reactions development with velocity gradient downstream steady shock wave, considering aerodynamic field in supersonic wind tunnel 10 p1694 A71-23813

Aircraft structural elements thermal behavior under aerodynamic heating with linear dependence on initial temperature 12 p1865 A71-27493

Conjugate steady convective aerodynamic heating of plate in longitudinal compressible gas flow, taking into account boundary layer enthalpy distribution 13 p1989 A71-27890

Heat conduction role in leading edge heating of wing in hypersonic flight, using conducting plate theory 13 p2165 A71-29282

Space shuttle vehicle models, calculating surface flow patterns and pressure and aerodynamic heating distributions for comparison with test data [AIAA PAPER 71-594] 15 p2343 A71-31539

Aerodynamic heating of reentry vehicle, suggesting shielding by radiative cooling 18 p2848 A71-36432

Vortex-induced heating alleviation to lee side of slender wings in hypersonic flow by contouring leading edge planform 19 p2993 A71-37892

Hypersonic lee surface vortex heating alleviation on delta wing by apex alignment with free stream 19 p2993 A71-37895

Spacecraft entry into planetary atmosphere, considering heating, deceleration and landing 20 p3305 A71-38814

Aerodynamic heating tests of cone flap reentry vehicle using temperature sensitive paint 20 p3311 A71-39197

Conjugate steady convective aerodynamic heating of plate in longitudinal compressible gas flow, taking into account boundary layer enthalpy distribution 21 p3317 A71-40080

Antenna radome noise temperature under aerodynamic heating as function of losses in material, interface reflection and dielectric surfaces 23 p3647 A71-44324

AERODYNAMIC LIFT

U LIFT

AERODYNAMIC LOADS

NT BLAST LOADS

NT GUST LOADS

NT WING LOADING

LAMS flight demonstration, discussing instrumentation, flutter boundary and dynamic response, aerodynamic testing and structural response to turbulence 02 p0188 A71-11662

Axial flow compressor design emphasizing component efficiency 03 p0470 A71-13825

Rotary inertia effect on critical dynamic pressure parameters and supersonic flutter of in-plane loaded sandwich plates 07 p1213 A71-19887

Elastic swept wing subsonic aerodynamic characteristics, taking into account aerodynamic load redistribution due to aeroelastic deformations 08 p1229 A71-22035

Nonlinear panel flutter analysis and response under random excitation or nonlinear aerodynamic loading, using Rayleigh-Ritz approximation to Hamilton variational principle 09 p1534 A71-22080

Power augmented lift STOL aircraft operating costs reduction by channel wing concept, discussing aerodynamic theory and structural applications to high lift flaps aircraft 09 p1385 A71-22592

Helicopter vibrational behavior prediction in flight with known aerodynamic loads, using branch modes method 09 p1385 A71-23606

Quasi-three dimensional method for radial flow compressor blade loadings computation, presenting combined meridional plane and blade to blade solutions for adaptation to computer 11 p1704 A71-25982

Flutter analysis of clamped thin skew panels with midplane forces in supersonic flow, using Galerkin method 12 p1974 A71-26766

Supersonic flutter analysis of clamped skew panels with in-plane forces by Galerkin method, using two dimensional static approximation for aerodynamic loading 14 p2177 A71-30607

Helicopter rotor blade airload by applying lifting surface solution [AHS PREPRINT 510] 14 p2171 A71-31081

Wake model and computer program to compute geometries, flows and velocity influence coefficients for helicopter blade load calculations [AHS PREPRINT 523] 14 p2172 A71-31089

Large variable sweep wing maneuver load relief system with ailerons reducing resulting bending moment at pivot 15 p2348 A71-31600

AERODYNAMIC MOMENTS

Aerodynamic free vortex loading on two dimensional wing at zero incidence at low speeds in incompressible flow

16 p2521 A71-33420

Large crane heavy lift helicopter stability and controllability, considering effects of slung loads, performance improvement, automatic flight control and physical size

19 p2998 A71-38651

Drooped wing tip effects on trailing vortex sheet structure and position from spanwise load distribution determination by vortex lattice theory

21 p3319 A71-40493

Lifting configurations unsteady air loads prediction, investigating loading singularities in linearized potential theory

22 p3481 A71-42832

AERODYNAMIC MOMENTS U STABILITY DERIVATIVES

AERODYNAMIC NOISE

Turbulent jet noise estimation taking into account retarded time effect on acoustic radiation

01 p0072 A71-11468

Small perturbation subsonic flows aerodynamic noise, using matched asymptotic expansions method

02 p0240 A71-12377

Sound generation by rotor-stator interaction in subsonic axial flow compressors, using acceleration potential and wake technique

03 p0469 A71-13277

Fan/compressor noise research covering vane/blade ratio and geometry effects on transmission through blade rows

[ASME PAPER 70-WA/GT-12] 03 p0471 A71-14120

Control valves aerodynamically generated sound pressure level prediction, using empirical method

[ASME PAPER 70-WA/FE-28] 03 p0403 A71-14136

Exhaust nozzles configurations effect on shear jet noise based on Ribner theoretical model

05 p0735 A71-16278

Aerodynamic noise - Conference, Loughborough, England, September 1970

05 p0783 A71-17152

Aerodynamic sound generation dependence on convective derivative of hydrodynamic pressure within turbulence source region

05 p0784 A71-17154

Rotating blade noise technology, discussing vehicles and components, noise nature, generation, reduction and prediction

05 p0695 A71-17158

Sound radiation by rotor from interaction with nonuniform flow, considering multiple blades

05 p0697 A71-17159

Far field sound radiated from steady loading of isolated subsonic rotor, noting dependence on spatial uniformity of flow entering rotor

05 p0697 A71-17160

Subsonic fan noise, using helicopter rotor noise theory for analysis of phase related and randomly time varying flow distortions

05 p0796 A71-17161

Aerodynamic sound radiation from point force in accelerating circular motion, obtaining closed form for overall far field radiation

05 p0784 A71-17162

Inlet turbulence interaction with rotor potential flow as noise source in axial flow fans, developing expression for sound power radiated

05 p0738 A71-17163

Aerodynamic sound generation by turbulent circular free jets, presenting solution to inhomogeneous acoustic wave equation by Lighthill

[DFVLR-SONDDR-87] 06 p0881 A71-17421

High subsonic jet near-field acoustic energy flux distribution calculation from pressure gradient measurements

[AIAA PAPER 71-155] 06 p0884 A71-18597

Acoustic radiation spectra from turbulent jets, assuming approximate Gaussian statistics and second order velocity correlation space-time characteristics obtainable from frozen flow

07 p1016 A71-19959

Unsteady low Mach number flow calculation by singular perturbation method with matched asymptotic expansions, considering application to aerodynamic noise

10 p1549 A71-23936

Fan noise random propagation and sound power in cylindrical air ducts from modal spectra and pressure measurements

10 p1596 A71-24834

Aerodynamic infrasound, considering atmospheric pressure variations in seconds to minutes period range

10 p1596 A71-24915

Subsonic turbulent boundary layer noise generation and acoustic pressure on aircraft surface, using Lighthill theory

10 p1553 A71-24952

Screech noise generation by supersonic jet impingement on flat plate, discussing jet disintegration mechanism with resultant shock wave oscillations

11 p1751 A71-25521

Sound radiation and wake turbulence spectra from axial compressor single airfoils, including double circular arc profiles

[ASME PAPER 71-GT-4] 11 p1703 A71-25950

Transonic compressor shock wave noise generation and decay rates at multiple tones, using sonic boom analysis

[ASME PAPER 71-GT-7] 11 p1703 A71-25953

Discrete frequency rotor interaction noise from lifting fans, using force harmonics acting on blades

[ASME PAPER 71-GT-12] 11 p1812 A71-25958

Aerodynamic noise scattering near Lighthill multiples, considering intense near-field energy conversion into sound waves

11 p1705 A71-26448

Condenser microphones aerodynamically induced noise, investigating acoustic pressure lower limit dependence on air flow velocity and turbulence

12 p1888 A71-27063

Marginal vortex effects on aerodynamics of helicopter lifting surfaces, considering blade form and noise spectrum tested in hydrodynamic tunnel

12 p1864 A71-27473

Aerodynamic noise produced by supercritical jets, using high speed flash photography for schlieren and shadowgraph studies

13 p2069 A71-28767

Combustion generated aerodynamic noise, considering sound radiation from open turbulent flames, spectral content, power output and origin

[AIAA PAPER 71-735] 14 p2338 A71-30780

Noise measurement data on various types of blown flap configurations for STOL aircraft, discussing integration effects between jet and flap assembly

[AIAA PAPER 71-745] 14 p2171 A71-30785

Jet noise reduction by foam injection, developing mathematical model for foam behavior in sound field

[AIAA PAPER 71-734] 15 p2388 A71-31327

Computational technique for acoustic field of jet aerodynamic noise, using Lighthill theory for spectral calculations

[AIAA PAPER 71-583] 15 p2468 A71-31571

Analytical predictions of supersonic jet noise, considering acoustic intensity, directivity, refraction, convection and peak Strouhal number

[AIAA PAPER 71-584] 15 p2468 A71-31572

Airfoils broadband noise generation mechanism in turbulent flow in anechoic chamber

[AIAA PAPER 71-587] 15 p2468 A71-31573

Aircraft noise in-flight measurement and analysis, including engine parameters, synchronous recordings, flight paths and coded analog bands

15 p2349 A71-31884

Noise research facility for fan and multistage compressor sound radiation, discussing anechoic chamber, power drive, test control, recording and real time analysis system

16 p2553 A71-33418

Subsonic turbulent jets acoustic emission, calculating noise intensity in far field for various Mach numbers

17 p2725 A71-34213

Noise generation due to inlet free stream turbulence incident on isolated stators and rotors, using flat plate cascade blade row model

18 p2956 A71-36498

Fluid mechanics of human whistling as function of resonant cavity and orifice jet velocities, comparing Rayleigh bird call and Pfeifentone

18 p2910 A71-36935

Jet turbulence orderly structure enhancement, control and relation to noise, studying response to periodic surging of frequency and amplitude

19 p3056 A71-38204

Review of September 1970 aerodynamic noise symposium covering jet and helicopter rotor noise, nonlinear acoustics and diffraction theory

19 p2994 A71-38205

Discrete frequency sound radiation from rotating periodic sources covering rotor blade noise in near field and from disk loading asymmetries

19 p2997 A71-38466

Acoustic measurement of rotor tones in duct of four blade ventilation fan

19 p3000 A71-38655

Propeller vortex noise analysis by on-line 1/3 octave band resolution, discussing characteristic results from noise measurements on various propeller configurations

21 p3325 A71-40868

Aerodynamic combustion noise generation from premixed or diffusion open turbulent flames, using fluid mechanics and Lighthill method

23 p3781 A71-43448

AERODYNAMIC STABILITY

Systems analysis application to stability of aerodynamic cross coupling in flight vehicle motions with steady sideslip, using feedback and root locus techniques

02 p0190 A71-12687

Spinning rocket vehicle with aerodynamic asymmetry, deriving equations of motion and steady aerodynamic behavior

[AIAA PAPER 70-1397] 03 p0499 A71-13678

Plane and wedge shaped airfoil profiles of variable thickness, deriving stability in bilateral supersonic air flow

03 p0515 A71-14365

Nonguided finned rocket initial stability problem, evaluating axis and tangent trajectory

05 p0817 A71-16638

Axisymmetric body rapid rotation under center of gravity velocity vector conditions, solving for plane gliding motion stability in air

07 p1159 A71-19354

Nonlinear aerodynamic moment system for nonaxisymmetric bodies free flight motion analysis, taking into account interactions excluded in classical treatment

[AIAA PAPER 71-275] 08 p1228 A71-22006

Vortex breakdown on slender sharp edged and modified delta wings with varying sweep angles investigated in wind tunnel using schlieren system for flow visualization

[AIAA PAPER 69-778] 08 p1229 A71-22028

Spring supported circular cylinder stability in wake flow of similar cylinder at various spacings using quasi-static aerodynamic derivatives and flutter theory

09 p1539 A71-22942

Cylindrical spacecraft reentry body self-sustained pitching oscillations due to separation on downstream portion, examining stability derivatives

09 p1533 A71-23604

Soviet book on aircraft preliminary design specifications as function of performance, aerodynamic and structural parameters, discussing tradeoffs in operational requirements for specific configurations

10 p1554 A71-24012

Stability analysis and design optimization with dynamics and aeroelastic constraints for helicopter rotor blade minimum weight with bending torsion flutter and favorable frequency placements

[AIAA PAPER 71-388] 11 p1846 A71-25352

Nonlinear aerodynamic stability coefficients from free aerodynamic motion of rigid bodies, using three degrees of freedom subsonic wind tunnel tests on Apache model

11 p1837 A71-25515

Hypersonic wakes of two dimensional slender wedges and flat plate, testing stability in transition region in wind tunnel

12 p1866 A71-27561

Army rotorcraft performance data, discussing hovering and forward flight performance out of ground and level flight power requirements and drag and compressibility effects

[AHS PREPRINT 500] 14 p2177 A71-31076

Forward flight performance of coaxial rigid rotor in NASA wind tunnel, comparing to aerodynamic stability with conventional rotors

[AHS PREPRINT 524] 14 p2178 A71-31090

Cylindrical membrane aeroelastic stability and flutter analysis at high supersonic or low hypersonic Mach numbers

15 p2506 A71-32019

Aeroelastic stability of flat plates and shells, considering panel flutter

16 p2648 A71-32987

Space shuttle boost vehicle with various degrees of aerodynamic stability, discussing control laws effects on rigid body bending moment tradeoff

[AIAA PAPER 71-918] 19 p3147 A71-37167

Gravitational and aerodynamic perturbation moment effects on nonsymmetric solid body rotary motion near mass center, using precession model

22 p3612 A71-42870

AERODYNAMIC STALLING

DC-10 flight test program, discussing handling, takeoff and landing, and flutter, stall and stability characteristics

07 p1018 A71-19084

USAF F-4E Stall/Near Stall Investigation, discussing testing requirements, fighter aircraft improvement, spin avoidance and high angle of attack limitations

07 p1019 A71-19095

Rotor blade stall induced helicopter control loads, combining unsteady aerodynamics with aeroelastic rotor analysis

[AHS PREPRINT 513] 14 p2178 A71-31084

Helicopter rotor stall characteristics, investigating blade flexibility, unsteady aerodynamics and variable inflow effects

[AHS PREPRINT 520] 14 p2171 A71-31086

Retreating blade stall experiments on model helicopter rotor, considering series of pressure distribution and boundary layer events

[AHS PREPRINT 521] 14 p2172 A71-31087

Aircraft angle of attack limiter parameters, describing automatic warning system for impending stall

16 p2523 A71-33621

F-4E stall/spin development and flight tests, relating mass distribution and angle of attack aerodynamic design

[AIAA PAPER 71-772] 16 p2524 A71-34000

Unsteady pressure gradient reduction effect on airfoil dynamic stall delay

22 p3481 A71-42844

AERODYNAMIC VEHICLES

U AIRCRAFT

AERODYNAMICS

NT AEROTHERMODYNAMICS

NT HYPERSONICS

NT ROTOR AERODYNAMICS

Unsteady flow theory, describing milestone experiments in aerodynamics

01 p0001 A71-10266

Low altitude slow aerodynamics, discussing earth surface wind modeling, powered-lift flight efficiency and animal flight

01 p0002 A71-10818

Aerodynamic theory of pressure field induced on lifting surface by isotropic atmospheric turbulence, considering transfer function of Concorde aircraft [ICAS PAPER 70-30]

01 p0002 A71-11019

German book on Goettingen Aerodynamic Research Institute /1945-1969/

01 p0068 A71-11406

Space aerodynamics, examining reentry, flow ranges, pressure field visualization and real gas and rarefaction effects

01 p0162 A71-11450

Spacecraft reentry aerodynamics regarding hypersonic high altitude lifting bodies, shock wave and flow field, heat, mass and energy transfer, etc [ICAS PAPER 70-01]

02 p0185 A71-11686

Aircraft flight aerodynamics from accident prevention viewpoint, discussing angle of attack, turbulence effects, weather factors, etc

03 p0346 A71-13017

Internal aerodynamics /turbomachinery/ - Conference, Cambridge University, England, July 1967

03 p0342 A71-13823

Manned space vehicle unsteady aerodynamics, considering flow separation, vortex interference, shock and stall flutter problems in space shuttle design

04 p0526 A71-15337

Aerodynamics of wing immersed in propeller slipstreams, presenting calculation method for lift, drag, pitching moment, normal force distribution and wake characteristics [DGLR-70-057]

05 p0693 A71-15947

ONERA hypersonic wind tunnels used for ballistic and aerodynamic research kinetic heating problems and control surface efficiency

06 p0841 A71-18025

German yearbook on air and space flight covering mechanics, control, aerodynamics and test facilities

06 p0847 A71-18044

Inverse boundary value problems in hydroaeromechanics, involving profile construction from given velocity or pressure distribution and supersonic flow boundaries determination

07 p1091 A71-20078

Water vapor condensation effects on methane-air combustion gases for aerodynamic test medium

08 p1377 A71-21986

Aerodynamic effects of bluntness on slender cones in free flight tests at Mach 17

09 p1381 A71-22090

French book on hypersonic aerodynamics covering aerothermochemistry, flow equations, heat transfer, etc

09 p1382 A71-22278

Symmetrical airfoil in stratified fluid flow determining camber and incidence effects

10 p1552 A71-24589

Cascade and single stage rotating rig data comparison with aerodynamic predictions based on intrablade analysis, including wall boundary layer model [ASME PAPER 71-GT-13]

11 p1703 A71-25959

High temperature aerodynamics with electromagnetic radiation, considering thermally radiating shock layers, electric arc driven wind tunnels and gas dynamic lasers

12 p1940 A71-27277

Three dimensional incompressible flow about slender foil in perfect fluid, stressing vortex field effect

12 p1865 A71-27477

Soviet book on experimental aerodynamics covering wind tunnels, shock tubes, liquid and gas physical properties, flow parameter measurement equipment, etc

14 p2221 A71-29524

Space flight aerodynamic problems and wind tunnel simulation, considering satellites, maneuverability for landing and synergetic orbit rotation, hypersonic problems of reentry, etc

18 p2846 A71-36408

Coriolis coupled bending vibrations of hingeless helicopter rotor blades, noting out-of-plane component contribution to aerodynamic coupling

19 p3154 A71-37294

Aerodynamic testing for space transport vehicle design, discussing experimental gas dynamics role in high stagnation enthalpy systems

19 p3161 A71-37315

Soviet book on practical aerodynamics of aircraft with turboprop engines covering piloting, forces and moments, stability, controllability, takeoff, landing, etc

19 p2994 A71-38534

High speed aerodynamic test facilities development over past 25 years, discussing deficiencies and improvements

22 p3529 A71-41984

Lifting line theory extension to low aspect ratio wings, proposing formulation for Prandtl integral equation

22 p3480 A71-42288

Low speed aerodynamics, detailing relevance tree technological forecasting method of Canadian science council national goals list

22 p3481 A71-42766

V/stol aircraft lift fan aerodynamics, discussing optimum fan pressure ratios, augmentation ratio, noise constraints, wing loading and fan configurations [AIAA PAPER 71-981]

24 p3791 A71-44577

AEROELASTICITY

Dynamic aeroelastic calculations for aircraft, using ground vibration test data

03 p0501 A71-13134

Spinning rocket vehicle with aerodynamic asymmetry, deriving equations of motion and steady aeroelastic behavior

[AIAA PAPER 70-1397]

03 p0499 A71-13678

Sounding rocket vehicle static stability reduction due to aeroelastic bending, using flight characteristics and wind tunnel test data for computerized analysis [AIAA PAPER 70-1400]

03 p0499 A71-13681

Space shuttle vibrational characteristics, investigating dynamic models, aeroelasticity, reentry, wing stall flutter and buffet boundaries

07 p1209 A71-20229

Plane sandwich plates in supersonic gas flow, investigating aeroelastic stability, transverse shear flexibility and axial loads

09 p1543 A71-23609

Nonlinear forced vibrations of aeroelastic plate in two dimensional supersonic flow under harmonic pressure near critical Mach number

10 p1690 A71-24643

Wind tunnel evaluation of analytical method for predicting longitudinal stability and aerodynamic characteristics of large flexible aircraft applied to supersonic transport configuration [AIAA PAPER 71-343]

11 p1707 A71-25322

Separated flow and time lag effects on sinusoidal gust penetration loads and elastic launch vehicle response of Apollo-Saturn class

[AIAA PAPER 71-344]

11 p1836 A71-25323

Stability analysis and design optimization with dynamics and aeroelastic constraints for helicopter rotor blade minimum weight with bending torsion flutter and favorable frequency placements

[AIAA PAPER 71-388]

11 p1846 A71-25352

Aeroelastic aircraft self adjusting automatic control systems, discussing elimination of elastic oscillations caused noise from angular velocity sensing circuits

12 p1926 A71-26718

Mechanical support system role in determination of aeroelastic stability of leeward cylinder immersed in wake using undamped flutter theory

14 p2334 A71-31021

Aeroelastic stability of flat plates and shells, considering panel flutter

16 p2648 A71-32987

Jet engine thrust induced nonconservative effects in aeroelastic analysis of vertical takeoff, using cantilever beam torsion and bending differential equations

16 p2650 A71-33019

Experimental and theoretical aeroelastic analysis of Fokker F-28 T tail, using flutter model and flight flutter tests

17 p2676 A71-35649

AEROEMBOLISM

Decompression sickness physical and physiological aspects, discussing gas transport quantification, inert gas elimination and metabolic gas exchange in recompression therapy, work performance, etc

09 p1394 A71-23236

German monograph on high pressure oxygen toxicity and hyperbaric treatment of gas gangrene

11 p1716 A71-25200

AEROLOGY

Automatic aerological ground station with processing and transmission facilities for radio probe and radar data

01 p0029 A71-10360

Complex monitoring of aerological information on geopotential and temperature of principal isobaric surfaces by static method and optimal interpolation on semiautomatic basis

17 p2769 A71-34299

Synoptic aerological conditions for occurrence of CAT, considering in-flight registrations and observations under jet stream conditions over North Atlantic

19 p3089 A71-37751

Synoptic-aerological conditions of CAT under jet streams, using aircraft measurements

19 p3090 A71-37752

AEROMAGNETISM

U GEOMAGNETISM

AEROMAGNETO FLUTTER

U FLUTTER

AERONAUTICAL ENGINEERING

Aeronautical projects development and planning in European Economic Community, discussing aerospace industry organizational problems and role in economy

02 p0334 A71-11676

Papers on aeronautical sciences, Volume 10, covering thermoelectricity, boundary layers with injection, supersonic wings and aircraft aerodynamics, tunnel ionization in wakes and fluids

03 p0339 A71-13126

Maritime and aeronautical technology - Conference, Paris, May 1970

04 p0571 A71-15204

Ground based flight simulation as engineering aid in aircraft design for evaluation of aircraft dynamics, handling qualities and control system characteristics over entire flight envelope

07 p1084 A71-20309

NASA reliability program provisions for aeronautical and space system contractors, reviewing evolution process

12 p1909 A71-26667

Air transport propulsion systems, discussing aircraft operating economics with reference to weight, size, powerplant efficiency, noise and air pollution

12 p1946 A71-27542

Criteria for converting aeronautical project operational targets into actual requirements and technical specifications, emphasizing cost effectiveness

14 p2177 A71-30824

AERONAUTICS

Papers on aeronautics covering propulsion, power generation, computer utilization, man machine interaction, pilot training, hovercraft, avionics, etc

02 p0189 A71-12609

Earth environment from aviation viewpoint, discussing atmospheric physics and chemistry, flight physiology, radiation, etc

08 p1243 A71-20702

Worldwide aeronautical charts maintenance for weapon systems support, discussing data sources

08 p1281 A71-21254

Aviation and astronautics - Conference, Tel Aviv and Haifa, March 1971

11 p1747 A71-25145

Socioeconomic changes in aeronautics, discussing faster long range aircraft, airport access problems, technological advances, short haul transportation and industry/government relations

12 p1868 A71-27601

Holography applications in aeronautics and astronautics, discussing advantages of three dimensional information in aircraft navigation, space missions and astronomic experiments

15 p2411 A71-32528

Papers on communication satellites for 1970s covering various national domestic systems, aeronautical service, ERTS data transmission and collection problems, etc

21 p3347 A71-40473

CAT energy budget and physical mechanisms in relation to aviation and atmospheric processes incorporating long range numerical prediction model

21 p3411 A71-41178

Aeronautics future, discussing aircraft noise reduction, computer techniques and aircraft design

22 p3482 A71-42237

AERONOMY

D region aeronomy characteristics and ionizing radiation energy spectra during solar flare of 22 October 1969

05 p0799 A71-16818

Quasi-exponential model of electron vertical profile in D region for aeronomic and ionizing radiation characteristics during solar flare of 30 October 1969

07 p1195 A71-19393

Book on aeronomy covering earth upper atmosphere structure, tidal oscillations, gravity waves, aurrow, aurora, ionospheric disturbances, electric currents and turbulence

09 p1437 A71-22778

Upper atmosphere aeronomy historical review, considering meteor trails, radio waves, auroral photography, terrestrial magnetic field and spectroscopy

14 p2229 A71-29704

Astrophysical and aeronomic UV molecular photoabsorption cross sections, discussing experimental techniques and associated systematic and random errors

14 p2190 A71-29905

Scientific goals and mission behavior of Dial aeronomy satellite for spatial distribution determination of atmospheric hydrogen concentration [DGLR-71-004]

15 p2501 A71-32781

Quasi-exponential model of electron vertical profile in D region for aeronomic and ionizing radiation characteristics during solar flare of 30 October 1969

19 p3127 A71-37817

German Aeros satellite for upper atmosphere aeronomy research, describing objectives regarding atmospheric composition and density

22 p3610 A71-42008

AEROPHYSICS

F layer perturbations by intense vertically upward radio waves for aeronomy and plasma control studies 23 p3671 A71-43343

AEROPHYSICS U ATMOSPHERIC PHYSICS AEROS SATELLITE

Aeros satellite active magnetic attitude control system design, operation and testing 15 p2499 A71-31210

German Aeros satellite for upper atmosphere aeronomy research, describing objectives regarding atmospheric composition and density 22 p3610 A71-42008

AEROSOLS NT FOG

Semiautomatic electrophotometer with interference light filters for atmospheric ozone, aerosol and solar radiation recording 01 p0080 A71-10602

Absorption line formation in scattering planetary atmospheres with cloud particles 01 p0162 A71-11420

Self ignition temperature of aerosols of Al-Si powders as function of dispersion and alloy composition 01 p0182 A71-11449

Atmospheric aerosols role in Martian opposition effect, applying Mie theory to integrated scattering intensities calculation for submicron particles 03 p0489 A71-13558

Optical evidence of meteoric aerosols in upper atmosphere at maximum Orionids, showing double red luminosity of sky above Adi Ugr 03 p0489 A71-13750

Aerosol powder suspensions for spectrochemical objectives in plasma jets 03 p0465 A71-13971

Aerosols in stratosphere, describing physical appearance, size distribution and concentration 03 p0418 A71-14206

Visible radiation absorption by aerosol particles, noting gray absorption and imaginary portion of complex index of refraction 04 p0582 A71-15072

Aerosol-induced solar radiation attenuation correlation to humidity in atmospheric boundary layer 04 p0641 A71-15119

Air pollution monitoring instrument for measuring mass concentration of aerosols and particulates in atmosphere 04 p0597 A71-15288

Doubly scattered radiation magnitude as function of heights and aerosol concentrations for bistatic laser radar 04 p0609 A71-15761

Atmospheric aerosol vertical distribution by lidar system, describing ruby Q switched giant pulse laser design and operation 05 p0720 A71-16221

Atmospheric aerosol vertical distribution by lidar system, discussing backscatter function, relative humidity, wind velocity, visibility, etc 05 p0720 A71-16222

Unsteady heat conduction due to radiative energy transfer in dispersed powders, hydrosols and aerosols 06 p1009 A71-18729

Natural aerosols effects on atmospheric electron content, comparing theoretical prediction with experiments on artificial aerosols in D region 07 p1100 A71-19404

Tropospheric temperature and aerosol to molecule ratio measurements by optical radar to determine relative concentrations and scattering cross section contributions 07 p1153 A71-20007

Lidar wavelength optimization for Raman scatter atmospheric studies, taking into account aerosol and weak signal statistical effects 08 p1254 A71-21458

Book on dynamic characteristics of aerosol particles in terms of classical mechanics covering continuum approximation, single particles heat and mass transfer, diffusion, dispersion, etc 09 p1431 A71-22284

Shock wave interaction with evaporating aerosol for diffusive and ablative models taking into account thermal conductivity 09 p1433 A71-22856

Atmospheric Pb 210 /radium D/ aerosols concentration relationship to solar activity from measurement with blue filter 10 p1599 A71-23859

Real and observable radius of roughly dispersed liquid aerosols correlated by electrophotographic method, assessing galactic cosmic rays energy 11 p1815 A71-25582

Atmospheric transmittance vertical structure, using aerosol attenuation and optical densities from aircraft sounding under cloudless conditions 11 p1795 A71-25924

Meteoric aerosols optical manifestation from photometric measurements on stratospheric balloons, demonstrating Orionids effects on twilight sky brightness 12 p1960 A71-26832

Ice forming nuclei in atmosphere during severe convective storms from aged background aerosol and soil particles aerosolized by storm turbulence 12 p1925 A71-27197

Intensity and polarization of diffusively transmitted sunlight, taking into account various aerosols distributions and normal molecular constituents 12 p1902 A71-27198

Quasi-unsteady approximation of mutual hydrodynamic drift velocity of aerosol particles in high power sound field 13 p2101 A71-28849

Aerosol power law distribution exponent and particle limiting radii from turbid atmosphere outgoing visible radiation polarization high altitude measurements 13 p2063 A71-29111

Altitude size distribution of atmospheric aerosol from sky radiance measurements in sun aureole region, calculating sunlight forward single scattering 14 p2310 A71-30125

Signal to noise ratios for coaxial laser radar system heterodyning signal backscattered from atmospheric aerosol 16 p2541 A71-33138

Diffuse skylight measurement for atmospheric dust particle concentration, considering sunlight scattering by air molecules and aerosol layers 16 p2567 A71-33767

Global temperature effects on atmospheric carbon dioxide and aerosols density based on atmospheric model, noting earth surface temperature decrease 16 p2575 A71-34047

Atmospheric short wave radiation angular and vertical distribution relation to aerosol scattering parameters, using transport equation 16 p2605 A71-34104

Time decrease of acoustically irradiated aerosol concentration involving coagulation processes 17 p2784 A71-35347

Backscattered laser radar pulses and downward IR flux enhancements in clear air around small cumulus clouds, discussing hygroscopic aerosols for increased radiance 17 p2707 A71-35381

Direct numerical integration for equation of radiative transfer in turbid atmosphere with allowance for scattering on molecules and aerosols 17 p2736 A71-35564

Spherical microparticles in atmospheric boundary layer and fallout above Pacific Ocean correlated to extraterrestrial origin 17 p2810 A71-35719

Aerosol size distribution from lidar light scattering polarization properties, constructing inversion model 17 p2770 A71-35806

Twilight glow spectrophotometry and visual observations from Soyuz 5 spacecraft, determining atmospheric optics and vertical aerosol profile 18 p2911 A71-36006

Atmospheric radiant heat influx spectral distribution, evaluating vertical profiles of short wave radiation and aerosol effects 19 p3047 A71-37281

Aerosol layers in stratosphere, determining vertical distribution of electrical conductivity 19 p3047 A71-37335

Natural aerosols effects on atmospheric electron content, comparing theoretical prediction with experiments on artificial aerosols in D region 19 p3053 A71-37828

Aerosol scattering coefficient in atmosphere, determining statistical characteristics of vertical and spectral structure 19 p3090 A71-37970

Cloud condensation nuclei supersaturation spectrum and aerosol particle concentration variations with height 19 p3092 A71-38683

Dissolved and mixed water vapor condensation aerosol nuclei thermodynamic properties from aircraft and ground-based cloud measurement data 19 p3092 A71-38686

Rainfall, aerosols and cloud water samples analyzed for chlorides and sulfates content and electrical properties 19 p3092 A71-38687

Ice forming effectiveness and dispersion of reagent particle aerosols through explosion of Elbrus 2 antihail iodide artillery shells in free and clear atmosphere 19 p3094 A71-38697

Chemical composition of atmospheric aerosols from Tokyo region, measuring energy spectrum of neutron irradiated specimens by gamma spectrometer 19 p3094 A71-38698

Water aerosol flux interaction and drop capture with particles of solid reagent, considering agglutiform films and precipitation on thin wires 19 p3094 A71-38699

Stratospheric dust effect on electrical conductivity measurements, noting proportionality to ion concentration 20 p3216 A71-38792

Atmospheric transmittance vertical structure, using aerosol attenuation and optical densities from aircraft sounding under cloudless conditions 20 p3257 A71-39215

Aerosol measurements over Atlantic and Indian Oceans, discussing aerosols optical thickness, effective radii, concentrations, sizes and optical properties variations with latitude and meteorological conditions 20 p3257 A71-39328

Ground based studies of Jupiter at optical frequencies, determining atmospheric chemical composition, temperature and stratification, aerosol layers structure and flyby/penetration experiments results 20 p3297 A71-39633

Altitude variation of atmospheric air scattering coefficient from Soyuz 3 spacecraft measurements considering aerosol stratification 20 p3259 A71-39676

High altitude aerosol layer effects on atmospheric UV albedo, correcting ozone scale height spaceborne measurements 20 p3221 A71-39695

Atmospheric aerosol stratification, turbidity, stratospheric layer and purification zone from optical sounding data 24 p3823 A71-44821

AEROSPACE ENGINEERING NT AERONAUTICAL ENGINEERING

Aerospace engine starting systems military and industry specifications and standards, considering cartridge pneumatic, electric, gas turbine, hydraulic and mechanical types 01 p0067 A71-10103

Grinding characteristics charts of aerospace alloys wheel-workpiece pairs for comparison with single point turning and electrochemical machining [SME PAPER EM-70-100] 01 p0090 A71-11262

Heat pipes structural material and heat carrier for various temperature ranges in satellite technology 02 p0331 A71-12069

High strength polyimide resin composites, discussing commercial and aerospace applications, chemistry, void content, volatiles and moisture absorption 02 p0274 A71-12487

German report on activities of DFVLR covering flow and flight mechanics, navigation, aerospace structures, propulsion systems, space simulation and flight medicine 03 p0394 A71-12975

Space technology and earth problems - AAS Conference, Las Cruces, New Mexico, October 1969 04 p0579 A71-14817

Space technology utilization in weather problems, considering tornado and other meteorological phenomena similarity to swirling vortex formation during missile flight 04 p0621 A71-14818

Analytic functions approximation in complex regions with aid of different systems of functions 07 p1146 A71-19041

Plated wire storage element for military and aerospace scratch pad, main and mass memories of various speeds [IEEE PAPER 7.6] 07 p1077 A71-19608

Emergency backup /secondary pressurization/ devices for aerospace crew and passenger safety and comfort, considering high altitude pressure suits 08 p1244 A71-20716

Aircraft and environment - Conference, New York, February 1971, Part I 08 p1378 A71-21811

Aerospace instrumentation - ISA Conference, Seattle, May 1970, Volume 3 09 p1448 A71-22767

Aerospace adhesives and elastomers - Conference, Dallas, Texas, October 1970, Volume 2 10 p1630 A71-24063

Pulsed laser holographic applications to aerospace components nondestructive testing, inspecting electron beam welds and internal structural flaws [ASME PAPER 71-GT-74] 11 p1770 A71-25988

Ablative polymers for thermal protection of aerodynamic surfaces, propulsion structures and ground equipment, discussing energy absorption of various polymeric materials 11 p1789 A71-26030

Engineering for space environment - ASCE/AIAA Conference, Houston, April 1970 11 p1747 A71-26526

Materials evaluation system for aerospace structural application 12 p1919 A71-27678

Aerospace materials - Conference, Anaheim, California, April 1971 14 p2261 A71-29633

Space systems safety programs, discussing failure mode and single point failure analysis techniques, escape mechanisms and redundancy design 14 p2320 A71-30258

French aerospace research for aircraft, missiles, spacecraft and related power plant developments, discussing optimization methods, materials, reentry phenomena, etc 15 p2500 A71-32699

- European space research center, discussing satellite scientific and engineering data transmission and processing 16 p2553 A71-33422
- Aerospace dynamic balancing machine for measuring unbalance forces of small objects and components, using AI construction to minimize inertial masses [SAWE PAPER 878] 17 p2725 A71-35823
- Aerospace pneumatic and fluidic developments, discussing high speed and response air motors, control functions, thrust reverser actuator and various drive systems 18 p2851 A71-36208
- Diffusion bonding as economical fabrication process for aerospace applications involving Ti alloys, emphasizing mechanical properties and structural reliability improvement [SME PAPER AD-71-245] 18 p2927 A71-36661
- Nickel-zinc batteries for use in hybrid heat engine/electric systems of low pollutant passenger cars, increasing service life by aerospace technology 20 p3181 A71-38936
- Carbon fiber reinforced plastics, considering aerospace and medical applications 21 p3406 A71-40702
- Holographic ultrasonic imaging method for flaw detection in aerospace materials and structures 22 p3554 A71-41782
- Interactive computerized design system for undergraduate aerospace engineering, using remote time sharing computer terminals 22 p3517 A71-41991
- Aerospace industry unemployment and future development prospects, reviewing NASA, DOD, AEC and other aerospace agencies R and D and procurement budgets decline [AIAA PAPER 71-1023] 24 p3892 A71-44601
- ## AEROSPACE ENVIRONMENTS
- NT Cislunar space
- NT Deep space
- NT Interplanetary space
- NT Interstellar space
- Human survivability and work capacity in aerospace environments, discussing sudden unprotected exposure to vacuum 01 p0022 A71-10512
- Low energy particle environment at synchronous altitude during magnetically quiet times from ATS 5 auroral particles experiment 01 p0147 A71-11497
- Manned space station research capabilities in earth orbital environment for agravic force field, hard vacuum, cosmic radiation and spatial disposition [SAE PAPER 700758] 02 p0237 A71-11685
- Materials science and manufacturing in space, discussing potential technologies and laboratory techniques using vacuum, weightlessness, temperature and radiation environment 02 p0255 A71-11973
- Human tolerances to thermal environment extremes in aerospace activities 02 p0207 A71-12388
- Satellite operating conditions effects on INTELSAT IV earth station design, emphasizing communications aspects 02 p0221 A71-12778
- Vestibular function on earth and in space - Conference, Uppsala, May 1968 04 p0536 A71-14751
- Long term human biomedical and behavioral characteristics research, examining enhanced physiological fitness in space 04 p0543 A71-14933
- Orbital environment contamination and effect on optical instruments and astronomical experiments in Skylab Program [AIAA PAPER 71-74] 06 p0902 A71-18531
- Synchronous meteorological satellite mission goals and system design, describing imaging, data collection, facsimile, space environment, trilateration, ranging and transmission 07 p1067 A71-18807
- Space environment and operations from medical viewpoint, discussing gravitation, magnetic fields, particle rays, planetary atmospheres, etc 08 p1357 A71-20703
- Aerospace environments noise effects on human physiology and speech communication 08 p1244 A71-20710
- Book on human factors application in teleoperator design and operation covering aerospace environments, transportation, remote control, sensors and actuator subsystems 09 p1399 A71-22613
- Aerospace research bionics and bioengineering, considering adaptation of man to environment and matching of man and machine 10 p1568 A71-24221
- Luneberg lens antenna theory and gain for communication satellite radio links, discussing shielding from hostile space environment 10 p1583 A71-24450
- Liquid wastes venting into space environment, producing ice particle clouds interference with spacecraft optical instruments 11 p1753 A71-26506
- Space stable thermal control coatings, noting reflectance optical spectroscopy of zinc oxide based paints and zinc orthotitanate 11 p1747 A71-26520
- Engineering for space environment - ASCE/AIAA, Conference, Houston, April 1970 11 p1747 A71-26526
- Space simulation - Conference, Gaithersburg, Maryland, September 1970 13 p2044 A71-28302
- Soviet papers on extraterrestrial life and detection methods covering biological conditions, extremal environmental factors and spacecraft sterilization 13 p2009 A71-28677
- Toxicological evaluation of CO in humans and other mammals, considering pilot performance prediction for aircraft environment 13 p2012 A71-28902
- SAE/DOT conference on aircraft and environments covering noise pollution, airport noise, sonic booms, regulatory/legal aspects and air pollution [AIAA PAPER 71-729] 14 p2295 A71-30776
- Artificial mineralization of water regenerated from human waste products in space flight 15 p2362 A71-31309
- Synchronous meteorological satellite programs, noting earth imaging, data transmission, collection and relay and space environment monitoring 17 p2812 A71-34612
- Atomic clocks on manned space stations, discussing stability in aerospace environment, techniques for earth based time calibration, reference device, maintenance and corrections 17 p2743 A71-35056
- Manned earth-orbital missions performance assessment experiments, studying effects of artificial and zero gravity spacecraft environments on humans [AIAA PAPER 71-891] 18 p2857 A71-36641
- Chemically activated electroadhesive pads on spacecraft surface, allowing astronauts to maneuver or work in zero gravity environments [AIAA PAPER 71-853] 18 p2872 A71-36645
- Space station biological/medical laboratories, discussing physiology, pathology, hematological, static and dynamic equilibrium, neuropsychic, dietetic, radiobiological, hygiene and prophylaxis departments 19 p3006 A71-37308
- Human response to space environment, discussing prolonged weightlessness, extravehicular work and lunar surface activity 19 p3002 A71-37492
- Grand Tour meteoroid environment analysis, considering different asteroid and cometary particle models [AAS PAPER 71-110] 19 p3139 A71-37910
- Ergonomic evaluation of flight crew working conditions from viewpoint of static and dynamic adaptation of aircraft system design to human psychophysical capabilities 19 p3007 A71-38016
- Spherical indium crystal manufacture in space, suspending and positioning weightless containerless melt in air and vacuum by adhesion and cohesion for crystal growth 20 p3247 A71-38767
- Outer space and earth surface galactic cosmic ray intensity data correlation analysis for studying interplanetary magnetic field structure 20 p3278 A71-39129
- Earth-like ecology for habitation in space, considering hollow sunlit rotating space chamber for life cycles in controlled weather environment 21 p3343 A71-40369
- Artificial ecological regenerative life support system design for space environments, discussing biotechnological properties 21 p3343 A71-40563
- Physiological deterioration of monkey onboard Biosatellite 3 and unexpected demise, presenting collected data for response analysis 21 p3333 A71-40564
- Physical and radiobiological studies on earth satellites covering radiation hazards and effects on animals, plants, unicellular organisms and biochemical systems 24 p3798 A71-44886
- ## AEROSPACE INDUSTRY
- NT AIRCRAFT INDUSTRY
- Metal matrix and polymer matrix composite materials in aerospace industry, discussing selection factors for specific applications 01 p0104 A71-11283
- Aeronautical projects development and planning in European Economic Community, discussing aerospace industry organizational problems and role in economy 02 p0334 A71-11676
- Radioisotopes technical applications in industrial and aerospace sciences, discussing radioactive gas penetrants, radiation interaction and geometrical measurements 03 p0455 A71-13533
- Asbestos applications in aerospace technology, considering chemical and molecular structure, heat and radiation resistance, mechanical properties and reinforcement 05 p0772 A71-16465
- Aerospace industry engineering company management and marketing, discussing corporate strategy, production control, market analysis and professionally trained managers 05 p0840 A71-17148
- Nondestructive testing in product cycle in aerospace industry 07 p1118 A71-19949
- Book on configuration management in aerospace industry covering documentation, identification, accounting, etc 09 p1548 A71-22672
- Heat resistant plastics, considering thermal endurance characteristics and use of high strength fillers in aerospace industry 10 p1634 A71-24580
- Spark sintering powder metallurgy using alternating and direct current plus pressure, discussing use in Be components production for aerospace applications 10 p1618 A71-24765
- Refractory metals and alloys products fabrication for aerospace applications, discussing hydrostatic bulge forming and aluminide coating in Nb alloy nozzle extension production 10 p1618 A71-24766
- Instrumentation in aerospace industry - Conference, Las Vegas, May 1971 14 p2243 A71-30309
- Aerospace business future, discussing political, military and social factors effect 17 p2841 A71-34575
- Technical prospects of European aerospace industries participation in post-Apollo program, noting space shuttle development role 19 p3151 A71-37324
- Defense and aerospace industry demand cyclical variations effect on productivity growth and cost 22 p3624 A71-42525
- Commercial air transportation industry trends and optimal planning requirements, discussing airline economic viability, industry regulation, public service and environmental compatibility [AIAA PAPER 71-1022] 24 p3892 A71-44600
- Aerospace industry unemployment and future development prospects, reviewing NASA, DOD, AEC and other aerospace agencies R and D and procurement budgets decline [AIAA PAPER 71-1023] 24 p3892 A71-44601
- Aerospace industry magnetic particle inspection problem identification in complex ferromagnetic structures 24 p3831 A71-45277
- ## AEROSPACE MEDICINE
- Ground based biomedical supervision of crew members during extended space missions, discussing data acquisition and transmission, astronaut medical competence, etc 01 p0027 A71-11451
- Standardized EEG data recordings in Air Force neurological evaluations 02 p0208 A71-12393
- German report on activities of DFVLR covering flow and flight mechanics, navigation, aerospace structures, propulsion systems, space simulation and flight medicine 03 p0394 A71-12975
- Biotelemetry in aviation medicine, discussing telemetric methods and applications for continuous observation of physiological processes under environmental exercise and stress conditions 03 p0370 A71-13063
- Medicophysiological problems in Concorde SST relative to altitude and speed, noting risks of cosmic radiation, ozone in atmosphere, decompression, wing loss and high temperatures 03 p0371 A71-13093
- Soyuz 9 prolonged space flight biomedical effects on human organism, emphasizing weightlessness 03 p0365 A71-14392
- Commercial airline pilots alertness tests, using IR pupillography 04 p0543 A71-15051
- Space base biomedical center based on Integrated Medical and Behavioral Laboratory Measurement System (IMBLMS) concept 04 p0546 A71-15280
- NASA program for aerospace technology application to medicine 04 p0546 A71-15281
- Adverse physiological effects of downwash on man, considering tissue damage, hypothermia, dust and sound pressure effects 04 p0546 A71-15411
- Human factors engineering in man machine systems, evaluating biotechnology and aeronautical medicine relationship 05 p0715 A71-16935
- Soviet book on manned space flight covering spacecraft design, life support systems, mission characteristics, medical considerations, etc 06 p0864 A71-18700

- Papers on aerospace medicine covering earth and space environments, circadian rhythms, hypoxia, barotrauma, decompression sickness, etc
08 p1243 A71-20701
- Space environment and operations from medical viewpoint, discussing gravitation, magnetic fields, particle rays, planetary atmospheres, etc
08 p1357 A71-20703
- Circadian rhythms from aerospace medicine viewpoint, discussing cycle stability and flexibility, air and space travel, etc
08 p1238 A71-20704
- Hypoxia from aerospace medicine viewpoint, discussing respiration physiology, oxygen transport, altitude effects, psychomotor functions, etc
08 p1238 A71-20705
- Barotrauma from aerospace medicine viewpoint, discussing oxygen absorption, barosinusitis, abdominal distention and aerodontalgia
08 p1238 A71-20706
- Labyrinths and proprioceptors from aerospace medicine viewpoint, discussing motion sickness, spatial disorientation, manned space flight and rotation in space
08 p1244 A71-20711
- Aircraft accidents medical aspects, investigating cause, death mode, emergency suddenness, specific injuries and safety equipment evaluation
08 p1244 A71-20713
- Aeromedical requirements, control limitations and hazards of aircraft pressure cabins and rapid decompression
08 p1244 A71-20715
- Aerospace ophthalmology, discussing flying personnel selection, eye anatomy, presbyopia, macular degeneration, cataracts, corneal dystrophy and glaucoma
08 p1238 A71-20721
- Aerospace psychiatry, discussing relationships between personality patterns and environmental factors, adaptability to occupational situations in combat flying and space activities
08 p1238 A71-20722
- Clinical aspects of aerospace neurology, considering central nervous system diseases among flying personnel
08 p1238 A71-20723
- Aerial transportation of patients, potential hazards due to motion sickness, decreased atmospheric pressure and oxygen tension, fatigue, inactivity and dehydration
08 p1245 A71-20726
- Civil aviation medicine practice, discussing airman certification for flight fitness, government legislation, accidents and carrier operations
08 p1245 A71-20728
- Medical flight information on astronauts response to space flight environment in confined and unconfined state and during intra- and extravehicular activities
08 p1246 A71-20731
- Coriolis vestibular reaction testing of pilot trainees, evaluating brief vestibular disorientation test validity and reliability at 10 and 15 rpm test conditions
08 p1247 A71-20823
- Soyuz 9 spacecraft crew medical support and post-flight examination, discussing earth environment readaptation
09 p1397 A71-22197
- Soyuz 9 cosmonauts postflight clinical examination, noting muscle pain, eyelid edema, leg muscle atrophy, etc
09 p1389 A71-22200
- Weightlessness, high acceleration and aerospace vehicle maneuvering effects on cardiovascular and vestibular systems, discussing disorientation, space sicknesses and blood circulation
09 p1398 A71-22357
- Mitral valve systolic prolapse aggravation due to G acceleration and aeromedical significance
09 p1395 A71-23246
- German book on space medicine covering stresses on human organism during ascent into space, weightlessness and radiation effects, spacecraft environment, nutritional problems, etc
10 p1558 A71-23753
- Functions of medical services charged with ensuring flying personnel fitness, stressing aging process
13 p2018 A71-28487
- Functional diagnostics in aerospace medicine for evaluating pilot ability and flight stresses
13 p2018 A71-28488
- Aerospace medicine - Conference, Houston, April 1971
13 p2014 A71-29300
- Possibilities of alcohol detection in blood and other tissue by alcohol examinations using experience from aircraft accidents case histories
13 p2023 A71-29366
- Roentgenological analysis of paranasal sinuses in civil aviators, studying facial cavities infection
13 p2023 A71-29367
- Soviet book on aviation medicine covering human anatomy and physiology, atmospheric physics, flight effects, respiratory systems, crew diets, etc
14 p2188 A71-29943

- Space flight sleep pattern data with EEG, using three descriptors and regression and linear discriminant analysis
16 p2528 A71-33108
- Polish space research covering satellite tracking, solar physics interplanetary gas dynamics, meteorological rockets and aerospace medicine
16 p2666 A71-33856
- Soviet book on space biology and medicine covering cosmonaut selection and training, flight safety, normal life support factors, interplanetary space sojourn, etc
17 p2689 A71-34475
- Space station biological/medical laboratories, discussing physiology, pathology, hematological, static and dynamic equilibrium, neuropsychic, dietetic, radiobiological, hygiene and prophylaxis departments
19 p3006 A71-37308
- USAF aeromedical consultation service experience on vertigo cases covering symptoms and related diseases
21 p3331 A71-40358
- Medical rejection statistics of applicants for BEA/BOAC pilot training, considering ophthalmic, ear, nose, throat and general health condition
22 p3501 A71-41823
- Vertigo due to increased middle ear pressure, discussing etiology from experience of aeromedical consultation service
22 p3502 A71-41833
- Medical preparations use and avoidance by spacecraft and aircraft crew members, discussing after-effects, allergies and health requirements
22 p3491 A71-42705
- Voskhod 2 cosmonauts physiological data, presenting heart beat, respiration rates, oculomotor activity and blood composition
22 p3495 A71-42791
- Book on fatal civil aircraft accidents medical and pathological investigation covering transport, light and glider aircraft case histories and statistics
23 p3638 A71-42910
- Cervical vertebral distortion during acrobatic flight, discussing clinical and medico-legal aspects and preventive measures
23 p3632 A71-43219
- Circadian rhythm relation to aircraft pilot safe performance
23 p3632 A71-43232
- Biorhythms and related physiological and psychic disturbances, stressing importance in aerospace medicine
23 p3637 A71-44245
- Civil aeromedical standards for aerospace transportation vehicles including occupant selection, vehicle design and operational guidelines
23 p3641 A71-44251
- ### AEROSPACE SCIENCES
- Papers on aerospace sciences covering dynamic aeroelasticity, turbulence and shock wave interaction
03 p0346 A71-13133
- Space research on thermosphere H and He properties - COSPAR Conference, Prague, May 1969
03 p0410 A71-14002
- Space research benefits from applications technology satellites and materials utilization, reviewing satellite communication networks, meteorology geodesy, navigation, geology and agriculture
03 p0524 A71-14245
- Space technology and earth problems - AAS Conference, Las Cruces, New Mexico, October 1969
04 p0579 A71-14817
- Papers on aerospace R and D covering wind tunnels, film cooling, blast waves, flow acoustics, fog dissipation, compound ceramics, etc
04 p0568 A71-14976
- Space sciences - Conference, Santa Maria, California, October 1970, Part I
04 p0662 A71-15276
- Aerospace technology application to oceanic instrumentation and communication requirements
04 p0583 A71-15307
- Aerospace technology direct and derived benefits for public, discussing earth resources program, communication satellites and NASA effect on nonaerospace activities and economy
04 p0691 A71-15315
- Space sciences future applications for mankind - Conference, Santa Maria, California, October 1970
04 p0553 A71-15316
- Cooperative international scientific space programs, discussing NASA, ESRO and other foreign space activities
04 p0692 A71-15350
- Aerospace science and agricultural development - Conference, Madison, Wisconsin, November 1969
06 p0895 A71-18405
- Radio amateur satellites contribution to space research and communications
07 p1057 A71-18814
- Aerospace research bionics and bioengineering, considering adaptation of man to environment and matching of man and machine
10 p1568 A71-24221

- Space research utilization in medicine, discussing remote blood pressure measurements, seismocardiography visual analysis, sterilization procedures and equipment for physically handicapped
10 p1571 A71-24754
- Solar system space physics review covering earth atmospheric temperature, density and models, solar wind, auroras, and moon, Venus and Mars data from space missions
13 p2131 A71-27877
- Space research goals emphasizing solar system formation, and plasma physics and chemistry
14 p2310 A71-30197
- Space research impact on general economy and ecology, noting royalty-free licensing to private industry by NASA
14 p2341 A71-30257
- Swiss space research, surveying international cooperative scientific activity relative to upper atmosphere satellite geodesy, solar wind, lunar samples analysis, IR and UV astronomy and celestial mechanics
16 p2665 A71-33852
- Book on high temperature materials covering vacuum or inert gas properties for industrial and aerospace applications
17 p2760 A71-35623
- Book on space science covering celestial coordinates, time and mechanics, planetary atmospheres and interiors, comets, meteors, stellar structure, etc
18 p2963 A71-36246
- Space technology - Conference, Cocoa Beach, Florida, April 1971, Volumes 1 and 2
18 p2972 A71-36442
- Life science and space research - Conference, Leningrad, May 1970
21 p3332 A71-40551
- Book on space technology for developing countries covering economic, social and educational reform, solar system exploration and extraterrestrial civilizations
22 p3623 A71-42066
- Organization problems of research laboratory for space astronomy experiments, delineating roles of chief scientist, project manager and technical services
23 p3785 A71-43456
- Pure and pragmatic science in future NASA programs, discussing interagency cooperation, communications, ATC, education, earth resources, space science, meteorology, budgets and program management
24 p3892 A71-44599
- [AIAA PAPER 71-1021] Space plasma physics, considering solar system origin
24 p3874 A71-45169
- Mullard channel electron multipliers applications to space research, scientific instruments, vacuum devices and mass spectrometers
24 p3811 A71-45332
- ### AEROSPACE SYSTEMS
- Space systems aerospace ground support equipment environmental testing criteria under varying conditions for optimal operation and deterioration reduction in use and storage
01 p0067 A71-10104
- NASA program concerning determination of RF spectrum sharing criteria and automatic data processing in aerospace systems
03 p0381 A71-14588
- Aerospace systems project management using graphic networking critical path method for planning and control
04 p0691 A71-15293
- Aerospace systems instrumentation magnetic tape standardization and testing
04 p0597 A71-15298
- Airborne remote sensing application to agriculture and forestry for crop forecasting, soil mapping, insect infestation detection and range surveys
06 p0896 A71-18406
- Electronics and aerospace systems - IEEE Conference, Washington, D.C., October 1970
07 p1056 A71-18801
- Avionics subsystem design improvements for aeronautical systems, considering standardization, weight impact, environmental control, maintainability, and equipment growth
07 p1069 A71-18829
- Carbon fiber reinforced plastics potential aerospace structural applications, considering weight saving, mechanical properties, thermal expansion, stress concentration, impact resistance, corrosion and lightning problems
08 p1369 A71-20922
- Aerospace instrumentation - Conference, Las Vegas, May 1969, Volume 2
09 p1449 A71-22785
- Model theory identification application to aeronautical systems, discussing transfer function representation, state variable and direct methods
10 p1587 A71-24744
- Analog, digital and special data processing equipment interface for aerospace computer system
11 p1735 A71-25844

- Design analogies of aerospace and commercial systems, describing computerized simulation method for system design evaluation and reliability improvement 12 p1909 A71-26663
- NASA reliability program provisions for aeronautical and space system contractors, reviewing evolution process 12 p1909 A71-26667
- Electromagnetic compatibility program for aerospace systems, considering EM shielding and emission 13 p2001 A71-28866
- Soviet book on space electric rocket engines design and stress analysis covering nuclear reactors, radioactive isotope energy sources and energy converters 13 p2118 A71-29421
- Composite materials fabrication primary and secondary aerospace and aeropropulsion structural components [SME PAPER EM-71-710] 15 p2416 A71-32434
- Aerospace electronics - IEEE Conference, Dayton, Ohio, May 1971 17 p2746 A71-35752
- Weightlessness simulation for aerospace mechanisms, using tower release and gyrometric system for testing stage separation, satellite perturbation, yo-yos, probes and mast development [ONERA-TP-940] 18 p2971 A71-36018
- Aerospace imagery enhancement for visual interpretation, considering ERTS applications 18 p2919 A71-36084
- Additive damping control of acoustic resonance fatigue of aerospace structures under severe environments, considering materials, tuned devices and layered techniques 18 p2979 A71-36494
- Remote sensing aerospace system for agriculture, considering soil mapping, forest fire reconnaissance, productivity evaluation and environmental and ecological conditions assessment 21 p3373 A71-40263
- Cybernetics and automatic control of space systems with pursuit process, using trajectory approximation with mathematical model graphs 21 p3452 A71-40857
- Holographic ultrasonic imaging method for flaw detection in aerospace materials and structures 22 p3554 A71-41782
- NASA NHB reliability engineering provisions for aeronautical and space system contractors, considering criteria for program management, system engineering, manufacturing and facilities 23 p3682 A71-43497
- Aerospace materials and structures shock sensitivity from derivation of dynamic fracture propagation relationship to stress wave 24 p3886 A71-45370
- EROSPACE VEHICLES**
- Spinning aerospace vehicle optimal attitude control system by minimizing reaction fuel, noting application of Pontryagin maximum principle 04 p0623 A71-15143
- Strapdown inertial guidance and software technologies for cosmic speed aerospace vehicles and low speed air, marine and ground transport 04 p0623 A71-15301
- High pressure and temperature seals and sealing in aircraft and spacecraft, including O rings and elastomers use 06 p0905 A71-18056
- Manned aerospace vehicular escape systems, discussing human vertebral column structural limits under vertical gravity acceleration [AIAA PAPER 71-144] 06 p0863 A71-18587
- Lightning stroke probability model for point selection on aerospace vehicles 07 p1020 A71-19928
- Organo-ceramic composites for thermal protection of aerospace vehicles, discussing heat sink property 09 p1483 A71-23206
- Elastomers for aerospace vehicles extreme environments, discussing fuel tank integral high temperature sealants 10 p1631 A71-24078
- Internal structural design loads for aerospace vehicles subjected to random loads, considering shear, moment and torsion as random components of generalized internal load vector 11 p1838 A71-25516
- Equation error approach to parameter identification in third order pitch plane dynamics for high performance aerodynamically controlled aerospace vehicle 11 p1742 A71-26418
- Inertial instruments with outputs indicative of time integral and time double integral of vehicle acceleration for velocity and distance determination 14 p2245 A71-30343
- EROSTATS**
- U AIRSHIPS**
- EROTHERMOCHEMISTRY**
- French book on hypersonic aerodynamics covering aerothermochemistry, flow equations, heat transfer, etc 09 p1382 A71-22278
- Book on homogeneous flows aerothermochemistry covering chemical reactions, heat and mass transfer, entropy production, species continuity, momentum and energy equation 09 p1547 A71-23674
- AEROTHERMODYNAMICS**
- Space shuttle technology, discussing wind tunnel studies, aerothermal and operational flight mechanics, model characteristics, orbiter configurations and booster-orbiter separation 07 p1209 A71-20227
- Space shuttle aerothermodynamics, discussing heat transfer measurements, phase change patterns, electron beam flow visualization and boundary layer transition 18 p2847 A71-36430
- Aerothermodynamics and scale modeling techniques for prediction of plastic burning rates, using Spalding mass transfer theory and dimensional analysis 19 p3171 A71-38250
- AFC [CONTROL]**
- U AUTOMATIC FREQUENCY CONTROL**
- AFCS [CONTROL SYSTEM]**
- U AUTOMATIC FLIGHT CONTROL**
- AFFERENT NERVOUS SYSTEMS**
- Aural and visual limitations effects on athletes rowing rhythms, examining afferent systems interactions 02 p0205 A71-12059
- Data processing analog for human vertical position regulation via afferent nervous system control of skeletal muscles 02 p0206 A71-12064
- Aortic and sinus nerves afferent electric impulse under adrenalin and nicotine, considering age peculiarities 03 p0363 A71-13522
- Cardiovascular and respiratory systems afferent innervation in cats investigating pericardial, expiratory and pneumo-vascular mechanoreceptors 05 p0707 A71-16343
- Ischemic deafferentation of transversostriated muscle quadriceps femoris in cats contributing to hypokinesia and psychophysiological disturbances 06 p0854 A71-18362
- Afferent pulsed activity change in peripheral fibers of severed phrenic nerve during air inhalation and under asphyxia 11 p1719 A71-25671
- Joint action of various afferents in regulation of human posture, considering appropriate differential reactions 13 p2003 A71-27833
- Human odorant evoked response, considering stimulation of olfactory receptors and trigeminal afferences in nose 13 p2012 A71-28891
- Femoral nerve afferent muscle fibers bioelectric activity in anesthetized cats, determining effect of blood circulation level on receptors functional activity 15 p2358 A71-31323
- Lower cardiac nerve unmyelinated afferent fibers detection and functional property characteristics 15 p2362 A71-32736
- Afferent mechanisms of orthostasis in space flight, discussing plasma fluid volume reduction and cardiovascular adjustments on passive tilting 18 p2856 A71-36634
- Afferent nerve impulse traffic from atrial A-type receptor fibers in cats in relation to heart rate control 18 p2857 A71-36688
- Brown fat thermogenesis regulation, emphasizing adipose tissue and afferent nerves control by experimental system approach, using intact unanesthetized unrestrained animals 18 p2859 A71-36872
- Primary biological receptor element analogous electronic model for potential and afferent pulse train responses to stimuli 20 p3191 A71-38894
- Afferent oculomotor pathways to extraocular muscle nuclei, considering discrete unilateral lesion role in head posture disturbance production 22 p3488 A71-42435
- Neural control organization in vestibulo-ocular reflex arc, considering afferent and oculomotor neural signals 22 p3490 A71-42449
- AFRICA**
- Volcanic petrochemical differences of Ethiopian rift and plateaus 09 p1436 A71-22645
- AFTERBODIES**
- Turbulent base pressure on conical afterbodies in supersonic axisymmetric flow, including initial direction effect [AIAA PAPER 70-555] 03 p0344 A71-14450
- Slender bodies of revolution with cylindrical afterbodies in subsonic wind tunnel, examining vortex systems and aerodynamic forces 06 p0842 A71-18048
- Inert and reactive gas injection in near wake behind afterbodies in supersonic flow, considering influence on base pressure and temperature 14 p2336 A71-30213
- Transonic wind tunnel testing of air intake and afterbody of double flux engine nacelle at high subsonic Mach numbers and high Reynolds numbers [ONERA-TP-943] 18 p2956 A71-36021
- AFTERBURNERS**
- U AFTERBURNING**
- AFTERBURNING**
- Concorde aircraft Olympus 593 two-spool turbojet engine, discussing variable nozzle and intake assembly, afterburner and control system 07 p1183 A71-19081
- Afterburning turbofan engine thrust calculation by gas generator method, using F-111A for comparison tests [AIAA PAPER 71-680] 14 p2292 A71-30744
- Optimal gas temperature in bypass and turbojet engines afterburners ensuring minimum fuel flow rate dependence on thrust augmentation 16 p2624 A71-33607
- Performance characteristics of jet engines equipped with afterburner, discussing combustion, flame stabilization, outlet nozzle regulation and operational cost 17 p2793 A71-35439
- Jet engines with afterburners, describing exhaust nozzle control, takeoff and landing advantages and thrust variations 21 p3437 A71-40858
- AFTERGLOWS**
- NT HELIUM AFTERGLOW**
- Active nitrogen afterglow complex spectrum analysis from vacuum UV to IR, proposing energy transfer mechanism 03 p0460 A71-13352
- Thermalization and diffusion of electron cloud injected into afterglow cylindrical plasma, calculating steady state distribution as function of position and velocity 14 p2280 A71-30175
- Afterglow plasma drift-dissipative instability stabilization by RF magnetic and electric fields 14 p2280 A71-30504
- Flame, laser and shock wave plasma generation, considering afterglows, ionized gas flows and high temperature effects 16 p2617 A71-32958
- Electron distributions in afterglow of hot electron mirror contained plasma as function of time, using bremsstrahlung spectra measurement 22 p3582 A71-41903
- Molecular oxygen partial pressure effect on nitrogen afterglow intensity, proposing three-body reaction kinetics 23 p3707 A71-43500
- Microwave upper hybrid resonance absorption, emission and heating of nonuniform axially magnetized afterglow plasma column in waveguide geometry 24 p3851 A71-44430
- AFTERIMAGES**
- Reduction or disappearance of visual aftereffect of movement without patterned surrounding consisting of dots, concentric circles, grid pattern or vertical bars 10 p1558 A71-23744
- Ball lightning as optical illusion resulting from positive afterimages, noting reports of energy release from ball as possible refuting evidence 10 p1599 A71-23751
- Computerized simulation of lateral inhibitory networks for figural aftereffects, discussing light and dark adaptation mechanism 10 p1563 A71-24232
- Human afterimage and pupillary activity in darkness after strong light exposure, noting dependence on stimulus intensity and duration 13 p2018 A71-28463
- Human visual geometrical illusions and figural aftereffects, determining mechanism locations for spatial patterns physical and phenomenal properties 13 p2018 A71-28464
- Visual movement aftereffect storage absence of patterned surround for fixated visible target 15 p2364 A71-31984
- Neurophysiological investigation of visual tilt aftereffect, comparing judgment precision at vertical and horizontal to oblique orientation with/without gravity cue 21 p3335 A71-40671
- Circumscribed eccentric afterimages effect on visual oculomotor control system, examining central transfer functions 23 p3635 A71-43971
- Afterimage induced smooth eye movements despite absence of moving visual stimulus, suggesting retinal image stabilization and saccadic behavior inhibiting processes 24 p3794 A71-44469
- AGC [CONTROL]**
- U AUTOMATIC GAIN CONTROL**
- AGE DETERMINATION**
- U CHRONOLOGY**
- AGE FACTOR**
- Newly formed blood vessels ultrastructure in newborn pups and adult rabbits 01 p0012 A71-11081

Aortic and sinus nerves afferent electric impulsion under adrenalin and nicotine, considering age peculiarities

03 p0363 A71-13522

Spatial field of vision in healthy subjects and glaucoma patients, noting age effect

06 p0853 A71-17950

Age dependent changes in mammalian cells radiosensitivity, emphasizing endogenous nonprotein sulphydryl effects

07 p1034 A71-18945

Arm to tongue blood circulation time for heart disease and failure diagnosis in aged people

07 p1043 A71-20215

Human nervous system stimulus trace retention in various age groups, using skin galvanic reaction

08 p1240 A71-21788

Human crystalline lens protein and lipid discussing cholesterol accumulation with age

09 p1390 A71-22421

Age, obliterating arteriopathy and peripheral arterial sclerosis effects on rheographic wave propagation speed to lower limbs

10 p1566 A71-24976

Age effects on whole blood viscosity with Wells-Brookfield microviscometer, investigating role of hematocrit and plasma protein

11 p1722 A71-26362

Ventricular septal defect, discussing incidence, human physiological responses, morbidity and mortality in various age groups

13 p2004 A71-27862

Near and intermediate vision in civil aircraft crews, presenting statistical evaluation of age factor effect on visual acuity in professional and nonprofessional personnel

13 p2019 A71-28507

Airline flight personnel fitness downgrading, presenting statistical breakdown by age and physiological or psychological causes

13 p2019 A71-28509

Physical fitness relation to flight requirements, pilot performance and age, considering muscular strength, cardio-respiratory capacity, body weight and mental aspects

16 p2528 A71-33114

Epidemiological statistics for age specific incidence rate of serious in-flight pilot failure, considering fatal and nonfatal causes

16 p2535 A71-33121

Lunar vs terrestrial origin of tektites, discussing meteoritic impact craters, age factor and properties

16 p2637 A71-33517

Small lunar maria craters morphological maturity as function of age and dimensions

16 p2638 A71-33670

Factors affecting tissue oxygen supply in old people, showing capillary circulation disturbance role in hypoxia development during aging

17 p2679 A71-34220

Visual evoked potentials and cortical recovery cycle data for normal and psychiatric subjects of various ages

17 p2682 A71-35113

Primary cardiomyopathy, discussing obstructive and nonobstructive cases, myocardial inflammation, chronic alcoholism and age relationships

17 p2682 A71-35120

Aircraft pilot physical examination for regression curves on near vision and eye accommodation, noting age effect

17 p2692 A71-35197

Oxygen intake relation to anaerobic component of work during submaximal exercise on bicycle ergometer by young and older men

17 p2686 A71-35435

Coagulation and fibrinolysis changes after physical exercise in males with atherosclerosis, noting fibrinolytic response differences with age

18 p2853 A71-35918

Collagen and elastin transmedial gradients in human aortas as function of age, discussing relationship to atherogenesis

18 p2858 A71-36751

Intraocular pressure distribution of healthy mental workers in 25-40 years age range, noting symmetry

20 p3189 A71-39234

Age dependent changes in free amino acid content and composition of cerebral and carotid arteries in man and dog

21 p3338 A71-41070

Psychopathological causes for French Air Force flying personnel inaptitude, considering motivational problems and age factor

22 p3500 A71-41575

Physiological relationship of young to old men, considering body composition, aerobic capacity and capillary-muscle fiber ratio

22 p3485 A71-41717

High blood pressure and age effect on human baroreflex arc controlling pulse interval sensitivity, showing systolic pressure response to phenylephrine intravenous injection

24 p3794 A71-44434

Age effects on plasma aldosterone levels, red cell, plasma and total blood volume at sea level and high altitude

24 p3797 A71-44781

AGE HARDENING U PRECIPITATION HARDENING AGENA ROCKET VEHICLES

Ionospheric wake spacecraft potential, electron current and temperature observations, using Agena/Gemini manned two body system sensors

09 p1517 A71-22175

Agena rocket engine pollutants, considering pollution control by scrubbers, engine system modification and micrometeorological data gathering

[AIAA PAPER 71-716] 14 p2294 A71-30768

High density nitric acid oxidizer and unsymmetrical dimethyl hydrazine with silicone fluid additive application to Agena rocket engine for higher performance

[AIAA PAPER 71-736] 14 p2287 A71-30781

AGGLOMERATION

Agglomeration process of dust particles growth in primordial solar nebula, considering early evolutionary phase of nearly free contraction and later phase with nebula flattening into gaseous disk rotating about protosun

09 p1523 A71-23045

Metal particle agglomeration during burning of Al-Mg alloy in ballistic powder, using high speed burning track microphotography

14 p2260 A71-30619

Galactic clusters evolution in universe with zero rest mass particles, showing size dependence on cosmic dust energy density

18 p2969 A71-37040

Supermassive double galaxy spectrographic and photometric data for cluster Abell 1775, showing radial velocity difference, visual magnitude and mass estimates

18 p2969 A71-37041

AGGREGATES

Rock forming monomineralic aggregates thermal conductivity at ordinary temperature and pressure in relation to density, crystal structure and chemical composition

07 p1105 A71-20448

Planetary system formation, examining particulate matter aggregation within dust cloud and gas around sun by computer simulation

11 p1835 A71-26459

Elastically and plastically anisotropic single crystals randomly oriented in polycrystalline aggregate, noting initial yield surface in fcc lattice

13 p2155 A71-29063

AGING

Aging process effects on thermoelectric semiconductors physical stability for cryogenic applications

05 p0793 A71-16799

Low flame temperature propellants, investigating temperature and humidity aging effects on physical and ballistic properties

[AIAA PAPER 71-664] 14 p2286 A71-30732

Omega phase embrittlement in aged Ti-Mo alloy, giving tensile properties and load-elongation diagrams

19 p3082 A71-38176

AGING [BIOLOGY]

Genetics and temporal audiogenic seizures in mice, noting age and exposure effects on susceptibility

03 p0360 A71-13161

Aging effects on blood pressure-flow relations and cardiac output/ventricular end diastolic pressure, discussing pulmonary vascular bed capacity dependence on increasing flow during supine exercise

10 p1561 A71-24128

Age effect on pulmonary circulation in normal subjects, measuring oxygen consumption, cardiac output and pulmonary arterial pressure by floated catheter technique

10 p1561 A71-24129

Age effects on whole blood viscosity with Wells-Brookfield microviscometer, investigating role of hematocrit and plasma protein

11 p1722 A71-26362

Functions of medical services charged with ensuring flying personnel fitness, stressing aging process

13 p2018 A71-28487

Myocardial ischemic lesions age, discussing validity of histopathological criteria and margin of error

15 p2361 A71-32542

Human alveolar wall tissue length-tension characteristics, noting age, sex and expiratory flow relationships

16 p2530 A71-33246

Clock paradox problem resolution in relativity theory, considering space travel effects on time measurement and aging process

20 p3271 A71-39571

AGING [MATERIALS]

NT AGING [METALLURGY]

Elastic characteristics of graphite plastics and graphite materials impregnated with synthetic resins, considering aging effect on elastic modulus

09 p1483 A71-28284

Outdoor five year aging tests on polysulfide and silicone adhesive sealants under semiarid, marine and high humidity environments

10 p1634 A71-24119

Long term oxidative aging effects on interlaminar shear strength retention of low void graphite/ boron reinforced polyimide resin composites

11 p1785 A71-25410

Creep of hereditarily aging body, using Rabotnov fractional exponential function for elastic theory solution

12 p1984 A71-27696

Termination and interface aging resistance of thin film resistors under corrosion, noting Ti-Pd-Au materials

23 p3651 A71-43427

AGING [METALLURGY]

Periodically modulated phase structure transformations in decomposition of Cu-Ti and Cu-Ti-Al alloys during aging at different temperatures

01 p0101 A71-10670

Dislocation pinning by interstitial atoms during Cr and Cr-Ce strain aging, using amplitude dependent internal friction technique

02 p0263 A71-11897

Al-Zn-Mg alloys hardness and conductivity behavior as function of aging time and temperature

04 p0610 A71-14884

Age hardened Ni base material strain-age cracking phenomenon measurements, using constant strain Gleeble technique

04 p0617 A71-15912

Nitrogen-alloyed austenitic steels precipitation hardening, discussing aging and strengthening rates

05 p0767 A71-16767

Al-Zn-Mg alloys low temperature mechanical properties dependence on aging treatment

05 p0767 A71-16769

High strength multiphase Co-Ni-Cr-Mo alloy hardening, noting deformation and aging induced strengthening

06 p0913 A71-18098

Aging effect on tensile mechanical properties and hardness of high purity binary Ni-Cr alloys at 290-530 C

07 p1138 A71-19986

Precracked double cantilever beam specimens, measuring resistance to stress corrosion crack propagation as function of overaging in Al alloys

07 p1142 A71-20363

Low alloy Mo sheet recovery and aging characteristics studied by X ray scattering

08 p1305 A71-21031

Al-Be-Mg alloys under solution treatment, noting aging and prolonged heating effects on mechanical properties from solid solution decomposition diagram

08 p1305 A71-21034

Anomalous dynamic strain aging in supersaturated Al-Cu, Al-Mg and Al-Zn alloy sheet and wire, discussing activation energies and volumes for plastic flow

08 p1310 A71-21534

Mg-Y alloy age hardening due to coherent metastable phase precipitation

08 p1312 A71-21548

Aged Al alloys dislocation substructure effect on mechanical properties at elevated temperatures

08 p1313 A71-21559

Discontinuous decomposition and aging kinetics of supersaturated solid solutions of tungsten in cobalt, comparing to precipitation theories

09 p1469 A71-22848

Impact strength decrease of welded joints in Ti alloys due to air cooling rate after aging

09 p1478 A71-23421

Maraging steel structural analysis under heat treatment, noting age hardening time and temperature

11 p1778 A71-25855

Bi-metallic refractory metal joints electron beam welding and aging for applications to in-pile thermionic converters

11 p1769 A71-25857

Quenched and aged Pt, investigating secondary defects for vacancies clustering modes by transmission electron and field-ion microscopy

11 p1779 A71-26016

Refining process of Fe-NiCu-Mn alloys, discussing aging kinetics, hardening mechanism and strength properties

11 p1781 A71-26159

Plastic deformation and aging effects on fatigue characteristics of steels until rupture under cyclic loads

12 p1916 A71-26945

Ti alloys aging, noting hardness increase and fine structure alpha phase coherent with beta solid solution matrix

12 p1917 A71-27296

Aged beta Ti alloy microstructure and mechanical properties, examining initial dislocation structure and interstitial concentration effects

12 p1917 A71-27297

Long term aged heat resistant Ni base alloys, investigating gamma prime phase chemical composition

12 p1917 A71-27298

Mechanical properties and heat treatment of Ti-V and Ti-V-Al alloys in quenched and quenched-aged states 13 p2083 A71-27872

Grain boundary precipitation in austenitic steels during creep deformation and ordinary aging treatment 13 p2086 A71-28623

Aging behavior of Nb-containing Fe-Ni alloys, considering austenite and martensite in twinned and massive form 13 p2089 A71-29412

Nucleation, growth and spinodal decomposition during aging in Fe-Cr alloys, using Mossbauer spectroscopy 13 p2089 A71-29414

Precipitation kinetics and austenite formation during aging of Fe-Ni-Mo and Fe-Ni-Co-Mo maraging alloys from dilatometry, electrical resistivity measurement and electron microscopy 14 p2257 A71-29838

Al-Zn-Mg-Li solid solutions isothermal phase diagrams, obtaining Al-rich alloys phase compositions for quenching and aging temperatures 15 p2426 A71-31405

High tensile strength maraging steels aging, discussing dispersed precipitates formation by homogeneous nucleation 15 p2427 A71-31525

Aging of cast iron components by thermal shocks, considering heat treatment for machine elements dimensional stabilization 15 p2414 A71-31527

Thermomechanical treatment effect on mechanical properties of high strength Al-Mg-Zn-Cu alloys, considering subsequent aging and state before deformation 15 p2434 A71-32328

Fine structure variations of Al alloy after aging, using harmonic analysis for calculating matrix microdeformation for correlation with mechanical properties 15 p2435 A71-32332

Deformable thermally work hardenable Al-Mg-Li alloy, detailing phase composition changes during aging 16 p2594 A71-33711

Aging theory application to anisotropic strain hardenable metals creep processes description 16 p2659 A71-33984

Storing and plastic deformation effects on artificial aging of Al-Zn-Mg alloy, using thin foil electron microscopy and hardness measurements 17 p2755 A71-34417

Heat treatment effect on fracture behavior of aged Al alloy sheet, investigating toughness dependence on microstructure 17 p2756 A71-34486

Fatigue cracks in tempered and aged Al alloy, using scanning electron microscopy 17 p2760 A71-35474

Ni-Mo single crystals under isothermal aging, observing long range order parameter, domain size and microstrains 19 p3077 A71-37411

Aging conditions effect on stress corrosion resistance in short transverse direction of thick sheet Al alloy, using immersion-emersion tests in air and saline solution 20 p3252 A71-39417

Precipitation hardened Ti-Nb alloy, correlating room temperature tensile properties with microstructure from step aging 21 p3387 A71-40461

Hardness, internal friction, microstress, martensite lattice and density changes during aging of precipitation hardening Fe-Cr-Ni steel, using dilatometric and X ray analysis 21 p3402 A71-41086

Low temperature aging behavior of maraging stainless steels from electrical resistivity measurements 22 p3562 A71-41948

Phase transformations and mechanical properties of heat resistant martensitic stainless steel during precipitation aging at prolonged high temperature exposures 23 p3690 A71-43280

Increased microplastic deformation resistance, relaxation stability and aging of beryllium by cyclic heat treatment 23 p3690 A71-43281

Austenitic Fe-Ni-Ti steel strengthening by precipitation hardening and subsequent aging at 600 C 23 p3690 A71-43282

Age hardenable Mg-Y alloys, investigating impurity phase in solution heat treatment 23 p3696 A71-44292

High temperature aging, structural stability and tensile properties of hot rolled Co-W heat resistant alloy for space applications 24 p3836 A71-44443

AGRICULTURE

Aerospace science and agricultural development - Conference, Madison, Wisconsin, November 1969 06 p0895 A71-18405

Airborne remote sensing application to agriculture and forestry for crop forecasting, soil mapping, insect infestation detection and range surveys 06 p0896 A71-18406

Agronomic research by remote sensing, discussing spatial, spectral and temporal measurements from electromagnetic multispectral response 06 p0896 A71-18407

Agricultural information and advisory service, utilizing remote sensing, computer sciences, research programs, educational involvement, satellites and aircraft 06 p1010 A71-18408

Seasonal and year-to-year crop radar sensing in agriculture for socioeconomic applications 07 p1095 A71-18825

Transavia Airtruk agricultural aircraft, discussing efficiency, work capacity, economics, configuration and performance 08 p1230 A71-21224

Space applications to world needs, emphasizing potential major agricultural production improvements 16 p2665 A71-33589

Remote sensing aerospace system for agriculture, considering soil mapping, forest fire reconnaissance, productivity evaluation and environmental and ecological conditions assessment 21 p3373 A71-40263

ERTS remote sensing techniques, discussing objectives for southeastern U.S. in terms of agriculture, forestry, strip mine land reclamation and thermal pollution 22 p3534 A71-41967

AILERONS

Critical flutter of wing with rigid aileron studied by analog computer modeling 01 p0169 A71-10606

Aircraft flaps and ailerons actuators electronic fly by wire control as alternative to mechanical linkages for maneuverability and reliability in flight 01 p0006 A71-10825

Large variable sweep wing maneuver load relief system with ailerons reducing resulting bending moment at pivot 15 p2348 A71-31600

AIRMP-E

U EXPLORER 35 SATELLITE

AIR

NT ALVEOLAR AIR

NT COMPRESSED AIR

NT EXPIRED AIR

NT HIGH TEMPERATURE AIR

Sulfur hexafluoride effects on equilibrium electron concentrations in air and argon plasmas, discussing earth reentry simulation applications 01 p0133 A71-10957

Atmospheric air breakdown by mode-locked Q switched laser pulse train, investigating threshold electric field dependence on characteristic diffusion length 03 p0440 A71-14178

Burning velocities in 50 percent hydrogen-air mixtures 03 p0376 A71-14282

Initial ionization, relaxation kinetics and nonequilibrium radiation behind strong shock waves in monatomic gases and air 05 p0835 A71-16524

Air and oxygen electron-ion recombination coefficients, considering plasma deionization rate 05 p0756 A71-17208

Oxygen vs air in treatment of divers with decompression sickness 08 p1242 A71-21957

Sound attenuation by warm air fog, using droplet measurements in Wilson cloud chamber 09 p1490 A71-23556

Gasoline-air mixtures normal combustion velocity by photographic observations of flame propagation in transparent tubes 12 p1986 A71-27499

Air and oxygen electron-ion recombination coefficients, considering plasma deionization rate 13 p2067 A71-28263

Mass and mobility measurements for small ions in air by Pu bombardment in closed chamber at low pressure 16 p2614 A71-33380

Free piston shock tube with air driver producing strong waves at speeds corresponding to gas effects 17 p2724 A71-34892

Air and jet fuel-air mixtures, calculating temperature dependent laminar and turbulent heat transfer parameters and transport properties [ASME PAPER 71-HT-41] 19 p3166 A71-38002

Mean charge measurement for heavy ions moving through He and air with aid of gas-filled mass separator, noting anomalies in nuclear charge dependence 21 p3419 A71-41112

Glass fibers durability in air and vacuum conditions, showing stress concentration coefficients at various tensile stresses 23 p3697 A71-44031

AIR BEARINGS

U GAS BEARINGS

AIR BLASTS

U AERIAL EXPLOSIONS

AIR BREATHING ENGINES

NT BRISTOL-SIDDELEY OLYMPUS 593 ENGINE

NT DUCTED FAN ENGINES

NT GAS TURBINE ENGINES

NT J-57 ENGINE

NT J-85 ENGINE

NT JET ENGINES

NT RAMJET ENGINES

NT SUPERSONIC COMBUSTION RAMJET ENGINES

NT TURBOFAN ENGINES

NT TURBOJET ENGINES

NT TURBOPROP ENGINES

NT TURBORAMJET ENGINES

Thrust equation, control volume and propulsive efficiency for rockets and air breathing jets from energy conservation principle 02 p0299 A71-12681

Combustion research for air breathing engines, discussing combustion stability in thrust augmentors, aircraft fire detection, MHD and external burning [AIAA PAPER 71-1] 06 p0946 A71-18476

Composite rocket cum hypersonic airbreathing propulsion reducing space exploration program cost 08 p1348 A71-21301

Stored arc heated air true temperature, flight and altitude simulation facility in Mach number 8 to 10 region for air breathing propulsion research [AIAA PAPER 71-254] 08 p1273 A71-21983

Air breathing nuclear propulsion, considering reactor safety in air cushion vehicles and aircraft 14 p2273 A71-29930

Space shuttle airbreathing propulsion systems requirements and design studies, considering cruise, landing, go-around and ferry capabilities [AIAA PAPER 71-662] 14 p2290 A71-30731

High performance low cost space shuttle propulsion systems airbreathing engines, attitude control thruster and orbital maneuvering [AIAA PAPER 71-656] 15 p2470 A71-32292

Metal particle nonequilibrium effects in mixing and combustion of ducted particle laden flow in air breathing engines 15 p2466 A71-32573

Axisymmetric inlet design for turboramjet powered hypersonic cruise vehicle, examining effects of spillage and cowl drags on air flow characteristics 16 p2521 A71-34149

High temperature gas dynamics, including hypersonic wind tunnel nozzles, air-breathing/ chemical rocket propulsion systems, thermodynamic models and relaxation boundary layers 18 p2846 A71-36425

Space shuttle booster configuration design, comparing stowed, fixed straight and delta wing approaches, discussing air breathing engines, stage mating, fins, etc 18 p2972 A71-36444

AIR CARGO

Air cargo volume development trends, examining worldwide airport terminal capacities and pallet/ containerization systems modular design and operation 10 p1699 A71-24824

C-5A cargo box side wall deformations, examining square plates center deflections with elastic beams 10 p1557 A71-24871

Cargo airship standard atmosphere operation modes, discussing long range gas capacity and short range applications for large compact loads 11 p1708 A71-26309

Frankfurt terminal baggage conveyor system, describing passenger capacity and luggage handling equipment 13 p2045 A71-29312

Aircraft loading system consisting of onboard weight and balance equipment and fully mechanized cargo pallet transfer, using computerized simulation model for parametric evaluation [SAWE PAPER 900] 17 p2676 A71-35811

Exchange regulation of standardized container loading units in air freight transportation 19 p3173 A71-38220

International airport planning, considering runways, hangars, second level loading, cargo handling and safety 20 p3209 A71-39388

International air cargo handling through runways, terminals, parking and maintenance areas, noting facilities planning 20 p3209 A71-39393

Air freight economics and growth forecast, discussing rates, cost and technological aspects 22 p3623 A71-41840

Technology developments in rotor, drive, flight controls and cargo handling systems of heavy lift

AIR CONDITIONING

helicopter system, noting military and commercial applications [AIAA PAPER 71-994] 24 p3792 A71-45296

AIR CONDITIONING

Air conditioning of passenger cabin in SST, noting heat exchanges due to radiation, convection and evaporation 03 p0371 A71-13094

Heat tolerance for resting subjects in event of air conditioning system failure in SST passenger cabin 03 p0371 A71-13095

Ozone atmospheric concentration, dissociation in SST air conditioning systems and biochemical poisoning 03 p0358 A71-13096

Piper Cherokee aircraft air conditioning system, discussing various operating principles, design criteria, power drain, effects on aircraft performance and weight, system serviceability and control [SAE PAPER 710391] 10 p1558 A71-24255

AIR CONDITIONING EQUIPMENT

Aircraft fuel and air conditioning systems vortex valves and diodes, examining flow patterns into and out of chambers 07 p1025 A71-20556

AIR CONDUCTIVITY

Pure tone, air/bone conducting and speech audiometry, considering hearing tests, artificial mastoids, environmental requirements and physical principles 06 p0859 A71-18029

AIR COOLING

Closed system for air cooling of image converter tubes and superorthicons for wear light flux, using refrigerator or dry ice 01 p0080 A71-10622

Closed hermetic air cooling system for high temperature gas turbines 01 p0143 A71-11246

High temperature tests of gas turbine engine with transpiration air cooled blades, discussing blade design, fabrication, ductility and oxidation resistance [ASME PAPER 70-WA/GT-1] 03 p0470 A71-14115

Gas turbine air cooling systems hydraulic characteristics by graph-analytical method 06 p0945 A71-18001

Turbobcharged diesel engine precompressed inlet air cooling by evaporation cooling, considering water injection effects on centrifugal compressor 08 p1347 A71-20781

Injected air cooled turbine blade trailing edges temperature, calculating thermal distribution with differential equations 08 p1348 A71-21265

Impact strength decrease of welded joints in Ti alloys due to air cooling rate after aging 09 p1478 A71-23421

Air cooled turbine blades activated diffusion brazing and gas pressure welding, using composite finned configuration model [ASME PAPER 71-GT-32] 11 p1770 A71-25969

Combustion chamber flame tube cooling by swirling air flow, determining radial and longitudinal temperature distributions for various swirler hub ratios and jet angles 11 p1813 A71-26052

Nozzle vane air cooling system for deflector type gas turbines, estimating profile perimeter average temperature for given coolant air flow rates 11 p1856 A71-26053

Manned space station optimal thermal control design, investigating heat pipe and semipassive/air cooled concepts [AIAA PAPER 71-431] 11 p1838 A71-26220

Cooling air injection effect on turbine efficiency, presenting experimental results for single stage air driven turbine with cylindrical stator and rotor blades 12 p1946 A71-27503

Air cooling methods for aircraft engine turbine rotor blades, considering heat distribution in rotor disk 15 p2467 A71-31461

Transverse flow in cavity ensurance by air exhaust cooling of trailing edges of gas turbine blades with deflector 16 p2624 A71-33544

Fan jet first stage turbine blade air cooling, describing design, heat transfer data, efficiency and temperature distribution 18 p2956 A71-35904

Space station thermal control systems design, discussing pumped loop, air cooled semipassive and heat pipe systems [ASME PAPER 71-AV-36] 18 p2869 A71-36403

Theoretical model for initial stage of cloud condensation developing at constant air cooling rate 19 p3092 A71-38684

Tubular compact air cooled thermoelectric module endurance and performance tests and computer simulation for space reactor power system 20 p3266 A71-38954

Infrared and thermal evaluation of tactical aircraft phased array radar antenna design with cooling air distribution for steady state operating temperature maintenance 21 p3352 A71-40434

Spalding-Patankar numerical integration for heat transfer from air cooled disk rotating near stator, considering frictional heating, disk temperature distribution and nonunity Prandtl numbers 22 p3620 A71-41878

Plane cascades efficiency and exit blade angles dependence on cooling air admitted to air-gas flow area from exhaust nozzle guide vanes 24 p3864 A71-45009

AIR CURRENTS

NT JET STREAMS [METEOROLOGY]

NT MERIDIONAL FLOW

NT VERTICAL AIR CURRENTS

Nighttime airflow deviations over urban areas from radar tracked tetoron flights, discussing effects as function of atmospheric wind and temperature 11 p1793 A71-25377

Solar flares effect on potential gradient and air-earth current characteristics, suggesting solar triggered increase in thunderstorm frequency 13 p2130 A71-29107

Radar returns from convective fields and cells in visually clear atmosphere explained by thermal effects and air motion 19 p3090 A71-37753

Aircraft wing tip vortex air motion measurements, utilizing Doppler radar techniques 21 p3318 A71-40489

AIR CUSHION VEHICLES

U GROUND EFFECT MACHINES

AIR DEFENSE

U.S. tactical missile program evolution since WW II, discussing technology, air defense, assault/antitank weapons, interdiction and battlefield combat support 05 p0818 A71-17149

British Mediator program for joint civil/military ATC system, discussing air defense relationships [CASIPAPER 72/16] 19 p3100 A71-37603

Observer psychological response to air defense oriented visual information displays 23 p3640 A71-43904

AIR DUCTS

Influence coefficients for aircraft engine gas/air ducts parameter deviations, using statistical analysis 03 p0472 A71-14257

Fan noise random propagation and sound power in cylindrical air ducts from modal spectra and pressure measurements 10 p1596 A71-24834

Absorbent materials for sound attenuation in turboreactor ducts, examining flow velocity, absorbent structure and cladding effects 14 p2288 A71-30518

Sound field measurement in circular and rectangular air duct with sound-absorbing walls /mufflers/, deriving empirical formula for attenuation frequency characteristics 24 p3849 A71-45271

AIR FILTERS

VTOL aircraft engine air particle separator development, examining airframe and engine design 04 p0533 A71-15433

AIR FLOW

NT AIR CURRENTS

NT JET STREAMS [METEOROLOGY]

NT MERIDIONAL FLOW

NT VERTICAL AIR CURRENTS

Radar and air flow structure of Alberta hailstorms from radiosonde data, aircraft measured cloud base updrafts and weak echo region concept 01 p0115 A71-10558

Initial surface superheating effects on high temperature oxidation of titanium in oxygen or dynamic air atmosphere 01 p0101 A71-10672

Hydrogen fuel injection into hot oncoming air flow, investigating boundary layer chemical behavior at stagnation point of diffusion flame 02 p0334 A71-12857

Flow separation and reattachment in confined jet mixing of air with secondary flow in duct [ASME PAPER 70-FE-B] 03 p0341 A71-13703

Hypersonic viscous air flow past blunt bodies with radiation, obtaining solution for Navier-Stokes equations by finite difference scheme 03 p0343 A71-14062

Plane and wedge shaped airfoil profiles of variable thickness, deriving stability in bilateral supersonic air flow 03 p0515 A71-14365

Hot-wire anemometer velocity measurement in slow air flow 03 p0430 A71-14374

Nonreflected shock tunnels hypersonic air flow, determining beginning and end times for optimum testing periods 04 p0563 A71-14666

Shock tube run time in acceleration region at turbulent regime for air, using pilot pressure measurements 04 p0563 A71-14668

Flow and radiative properties of air in high explosive shock tube 04 p0586 A71-14700

Flat plate ion density probe with convection and ion production in electric sheath, comparing to shock waves in air 04 p0632 A71-14706

Heat transfer and pressure drop in air flowing in square tube with two dimensional discrete turbulence promoters applied to opposite walls 04 p0675 A71-14781

Soviet monograph on atmospheric boundary layer covering compressible turbulent air flow, diurnal fluctuations, fog, air pollution and lower atmosphere electric field 04 p0621 A71-15399

Wave formation behavior on melting surface of flat plate in heated air stream 04 p0678 A71-15455

Temperature distribution and heat transfer across transitional separated shear layer under subsonic air flow, using interferometric measurements 04 p0679 A71-15470

Film cooling of flat plates by angled cold air injection for turbine blade applications 04 p0639 A71-15472

Wall static pressure and convective heat transfer measurements in subsonic, transonic and supersonic regions in heated air turbulent flow through variable cross section channel 04 p0680 A71-15476

Air flow turbulence effect on heat transfer and boundary layer growth around flat plate, aerodynamic profile and cylinder 04 p0681 A71-15483

Single disk rotating in still air, calculating temperature profiles and local heat transfer coefficients 04 p0683 A71-15494

Air flow turbulence generating grids at nozzle outlet in wind tunnel for measuring turbulence levels 04 p0577 A71-15618

Longitudinal turbulent air flow past plate, applying heat transfer and drag calculations 05 p0838 A71-16784

Pure impulse two stage turbocompressor, preventing surge with automatic adjustment to air flow rate 05 p0796 A71-16798

Heat transfer from rotating disk to parallel nonrotating disk, investigating turbulence effect from air flow pattern observation 06 p1007 A71-18315

Free turbulent mixing of heated high speed central hydrogen jet and cold low speed annular air stream coupled with finite rate chemical reactions [AIAA PAPER 71-5] 06 p0866 A71-18479

Laminar ablating air-Teflon boundary layers with carbon difluoride and atomic fluorine constituents, using UV thermal radiation measurements [AIAA PAPER 71-39] 06 p1008 A71-18500

Large diameter tube high Reynolds number air flow temperature profiles, using chromel-alumel thermocouple 07 p1220 A71-18762

Integral equation solution for air flow over mountain system, considering boundary value problems of Helmholtz equation 07 p1149 A71-18794

Two layer structure of principle air flow over mountain system, noting effect on air waves and rotors formation in leeward region 07 p1149 A71-18795

Blunt cylinder with small throat in anomalous seeded flow in hypersonic wind tunnels, observing separated shock wave distortion 07 p1013 A71-18924

Short term creep effect on high speed air flows, investigating material behavior under vibration loads, corrosion and erosion 07 p1130 A71-19163

Interaction between radiation from shock wave region and oncoming cold air flow in hypersonic flow past blunt body 07 p1014 A71-19730

Supersonic air flow pattern over rectangular indentations on plane and axisymmetric surfaces, examining static pressure and adiabatic temperature distributions 07 p1014 A71-19744

Dissociating airflow over two dimensional blunt body, determining laminar boundary layer chemical reaction suppression effects on heat exchange 07 p1015 A71-19748

Computerized capillary model for fluidic restrictors in multipoint concurrent air flow measurements 07 p1025 A71-20563

Moving part pneumatic logic element static and dynamic characteristics, determining air flow rate and output pressure 07 p1027 A71-20574

Electric breakdown in supersonic Ar or air flow behind shock wave, determining threshold discharge currents 08 p1276 A71-21485

Stationary longitudinal turbulent flow of air with equilibrium ionization and dissociation around plate, calculating heat exchange and frictional drag 08 p1228 A71-21922

- Turbulent air flow in cooled tubes, studying local heat transfer and hydraulic resistance
08 p1377 A71-21924
- Flutter analysis of rotating thin cylindrical shell with outer surface exposed to inviscid helical air flow field
09 p1533 A71-22078
- Turbulent air flow velocity and temperature fluctuations, determining mean fields, Prandtl number distributions and correlation moments and coefficients
09 p1432 A71-22729
- Linear mountain lee wave model with nonlinear lower boundary condition for arbitrary basic flow and two dimensional topography, computing flow field
09 p1487 A71-23024
- Single jet oscillations excitation of two resonant tubes, observing air motion with wool threads and stroboscopic lighting
10 p1591 A71-23823
- Unsteady inward and outward velocities of subsonic radial air flow between two disks, using hot-wire anemometer and cylindrical wave equation
10 p1550 A71-24000
- Air and carbon dioxide intensive injection effect on turbulent boundary layer of subsonic channel air flow
10 p1551 A71-24378
- Turbulent incompressible air flow in-stream static pressure fluctuations measurement, describing bleed type pressure transducer theory, design and operational characteristics
10 p1611 A71-24516
- Coaxial jets development and mixing in axisymmetric twisted turbulent ring air flow injected through inlets
10 p1594 A71-24560
- Finite difference computer algorithm to solve vertical velocity equation of steady air flow about mesoscale obstacle in stably stratified atmosphere
11 p1793 A71-25169
- Forced convection in atmosphere boundary layer, considering nonlinear unsteady vertical airflow velocity increments over temperature spot on earth surface
11 p1793 A71-25170
- Flutter analysis of long thin cylindrical shells rotating in circular helical air flow field
[AIAA PAPER 71-373] 11 p1845 A71-25346
- Water drops deformation and fragmentation due to shock wave impact in high velocity air stream
[AIAA PAPER 71-392] 11 p1749 A71-25354
- Wake flow behind two dimensional perforated plates normal to air stream, measuring drag, shedding, velocity and turbulence at Reynolds number 25,000-90,000
11 p1705 A71-26449
- Errors due to air flow pulsation in orifice meters, discussing various diameter ratios
12 p1906 A71-26872
- Condenser microphones aerodynamically induced noise, investigating acoustic pressure lower limit dependence on air flow velocity and turbulence
12 p1888 A71-27063
- Viscosity effect on initial highly underexpanded jets in Mach 1 to 5.7 nozzles for laminar, turbulent and rarefied air flows
13 p1989 A71-27889
- Air flow about low aspect ratio delta wing at large angles of attack, deriving lift coefficient
13 p1990 A71-28282
- Local and mean heat transfer at initial thermal segment for stabilized turbulent air flow in circular tubes and rectangular channels
13 p2159 A71-28419
- Blowing angle effect on heat protection effectiveness of flat wall in slit injected low speed air flow with turbulent boundary layer in wind tunnel
13 p2159 A71-28420
- Air bypass behind compressor into variable area exhaust nozzle, obtaining energy losses from gas turbine jet engine indices
13 p2115 A71-28586
- Air mass flow rate in can type gas turbine combustion chambers
13 p2117 A71-28747
- Stabilizer structure effect on flame stability of atomized liquid fuel, studying excess air ratio relation to air flow velocity
13 p2163 A71-28963
- Flow direction effect on combined forced and free convective heat transfer from cylinders to air
13 p2164 A71-28985
- Air flow past small aspect ratio thick-section wing at small angles of attack, investigating vortex system effect on flow characteristics in absence of lift
13 p1994 A71-29234
- Separation control of two dimensional air flow with turbulent boundary layer around circular cylindrical wall by jets or suction
13 p2051 A71-29433
- Respiratory air flow optimal regulation hypothesis, testing analytical prediction model results with experiment under stress and rest conditions
13 p2023 A71-29491
- Stratospheric air flow patterns and CAT measurements onboard aircraft over and downwind of Western U.S. mountain terrain
14 p2267 A71-29755
- HF rake probes with high temperature integrated sensor for inflight aircraft engine intake air flow distortion measurements
14 p2243 A71-30321
- Nonsteady air flow direction generation and measurement, comparing three-tube probe with hot-wire anemometer data
14 p2244 A71-30326
- Miniature integrated sensor pressure transducers for inlet air flow distortion and buffet studies of wind tunnel models
14 p2245 A71-30336
- Electrical breakdown of supersonic Ar and air stream behind shock wave, determining threshold discharge currents
14 p2227 A71-30672
- Supersonic hydrogen combustion in vitiated air stream with stepped wall injection, considering temperature, pressure and composition measurements
[AIAA PAPER 71-721] 14 p2286 A71-30772
- Gray air flow in turbulent optically thin boundary layer, determining radiant energy transport by Patankar-Spalding finite difference procedure
14 p2338 A71-30932
- Eddy diffusivity of mass in air measurement discrepancies in circular duct, considering axial concentration and radial distributions
14 p2339 A71-30934
- Arc-heated nonequilibrium air expansion flow mass spectroscopic analysis, noting reservoir entropy effect
[AIAA PAPER 71-621] 15 p2366 A71-31550
- Multicomponent nonequilibrium air flow past axisymmetric blunt body, calculating flow distribution at various attack angles with time dependent technique
[AIAA PAPER 71-595] 15 p2512 A71-31575
- Turbulent mixing between parallel incompressible air streams, using statistical investigation of pressure and velocity fields
15 p2389 A71-31582
- Grid induced turbulence effects on air flow around enclosed diffusion flame
[WSS/CI PAPER 71-14] 15 p2463 A71-31623
- Lee side air flow from cone-cylinder model, determining vortex core regions from subsonic wind tunnel smoke visualization techniques
15 p2346 A71-32117
- Air-water flow pressure loss and phase distribution in tube with wire coil swirl generators
[GESP-449] 15 p2354 A71-32209
- Transverse liquid injection into supersonic airstreams, using photographic techniques to determine jet penetration and spreading for various dynamic pressure and density ratios
[AIAA PAPER 71-724] 15 p2393 A71-32287
- Surface liquid film wave motion effect on air supersonic turbulent boundary layer flow field, discussing film thickness, heat transfer rates and wall temperatures
[AIAA PAPER 71-623] 15 p2515 A71-32544
- Heat transfer and drag calculations in longitudinal turbulent air flow around plate with constant or variable physical properties
16 p2662 A71-33036
- Diaphragm mechanics, discussing thoracic pressure-lung volume and air flow relationships of respiratory system during electrophrenic stimulation in men and cats
16 p2530 A71-33239
- Swirling flow in gas turbine engine combustion chamber forward part, considering air flow characteristics behind blade swirler
16 p2624 A71-33606
- Stationary longitudinal turbulent flow of air with equilibrium ionization and dissociation around plate, calculating heat exchange and frictional drag
17 p2671 A71-35266
- Turbulent air flow in cooled tubes, studying local heat transfer and hydraulic resistance
17 p2838 A71-35268
- Vibration and corrosion-erosion damage effects on material behavior during short term creep in high speed air flows
17 p2760 A71-35659
- Air-methane supersonic diffusion flame in duct, comparing pressure measurement and gas sampling data with two dimensional combustion analysis
[ONERA-TP-961] 18 p2984 A71-36027
- Turbulent flow of air film between rotating circular and stationary plane surfaces, determining pressure distributions, inertial forces effects and velocity profiles
18 p2926 A71-36185
- Air flow in pipe with double screw thread, calculating tangential forces and turbulent viscosity coefficient along isotachs
19 p3043 A71-37266
- Atmospheric total ozone increase during 1960s, investigating possibility due to southward air flow in troposphere and low stratosphere
19 p3047 A71-37298
- Heat transfer and drag during air laminar flow in circular pipe with constant heat flux density at wall
19 p3044 A71-37585
- Two phase flow model of water droplets velocity in air stream, using Fresnel biprism and laser differential scheme
19 p3072 A71-37587
- Free stream turbulence effects on local heat transfer from sphere situated in forced convection air flow
[ASME PAPER 71-HT-8] 19 p3164 A71-37985
- Tollmien-Schlichting waves in flow field of mixed coaxial laminar air diffusion flames, using flow visualization and hot-wire anemometry
19 p3167 A71-38094
- Planetary boundary layer stationary air flow over plane homogeneous surface under geostrophic wind conditions, solving for thermal turbulence field stabilization by iterative method
19 p3091 A71-38468
- Swedish monograph on low air flow velocity measurement with hot-wire anemometer under free and forced convection, using schlieren method
19 p3172 A71-38645
- Transonic and supersonic turbine guide vanes, noting air as flow medium in experiment and steam in actual turbine
20 p3176 A71-39455
- Viscosity effect on initial part of highly underexpanded jets in Mach 1 to 5.7 nozzles for laminar, turbulent and rarefied air flows
21 p3317 A71-40079
- Low speed wind tunnel air velocity measurement with laser velocimeter, using dark background illumination detection of particles scattering across fringe pattern
21 p3378 A71-40398
- Hot split-film anemometer sensors for three dimensional air velocity vector measurement
21 p3378 A71-40487
- Gas exchange between air or gas mixture flows and terrestrial soil in extraterrestrial microorganisms detection, using continuous sampling and gas chromatography
21 p3346 A71-40575
- Heat transfer of short hot wire normal to ambient incompressible air flow, using small perturbation energy equation
21 p3379 A71-40664
- Spectral density functions of velocity pulsations and frequency dependent stability in turbulent plane and axisymmetric channel air flows at different Reynolds numbers
21 p3368 A71-40697
- Jet flame stability characteristics of propane-air mixture ejected into counter air stream by temperature and concentration measurements and visual observation
21 p3475 A71-40758
- Two dimensional supersonic moist air expansion around sharp corner, investigating water vapor condensation by homogeneous nucleation
21 p3369 A71-40952
- Slender body of revolution in supersonic and subsonic air flow, calculating boundary conditions with Lagrange formulation
21 p3323 A71-40963
- Viscous slipstream flow downstream of triple shock wave intersection in supersonic diffuser air flow, using Pitot and static pressure probe measurements
21 p3324 A71-40981
- Convective heat transfer by laminar and turbulent free convection in air on large horizontal and vertical planes
23 p3781 A71-43324
- AIR FREIGHT
U AIR CARGO
AIR INLETS
U AIR INTAKES
AIR INTAKES
NT ENGINE INLETS
NT HYPERSONIC INLETS
NT SUPERSONIC INLETS
Air temperature effects on internal combustion engines intake process, using similarity theory
08 p1347 A71-20782
- Air inlet for simulation of shock wave separated flow in supersonic diffusers, deriving pressure variation profile along free boundary
13 p1992 A71-29175
- Soundproofing of air inlets and fan exhausts with reference to absorbent systems with resonant cavities, technologies, environmental conditions and material fatigue
15 p2469 A71-31880
- Transonic wind tunnel testing of air intake and afterbody of double flux engine nacelle at high subsonic Mach numbers and high Reynolds numbers
[ONERA-TP-943] 18 p2956 A71-36021
- AIR JETS
Air jet mixing with low velocity stream in constant diameter pipe, measuring flow characteristics for non-separating conditions
[ASME PAPER 70-WA/FE-2] 03 p0402 A71-14124

AIR LOCKS

Optical crossed-beam measurements of turbulence intensities in cold subsonic air jet shear layer [AIAA PAPER 71-137] 06 p0902 A71-18580

Twin tube gas heating resonator using bistable air wall attaching supersonic power jet 07 p1028 A71-20582

Low pressure air jet sensing power pneumatic and fluidic circuits and interface valves for low pressure signal stepup to main line pressure, considering circuit design 07 p1030 A71-20597

Volume variations detection by Hartmann air jet fluidic oscillator 07 p1030 A71-20602

Acoustical response of closed flue pipe as function of blowing pressure and air jet turbulence level 08 p1276 A71-21766

Air jet velocity and turbulence measurements by modified Doppler technique, using CW lasers 10 p1609 A71-23874

Velocity distributions in axisymmetric air jets submerged in coaxial oscillating stream measured by hot-wire anemometer 11 p1748 A71-25156

Cross flowing air stream effects on heat transfer characteristics of single lines of air jets impinging on plane surfaces [ASME PAPER 71-GT-1] 11 p1854 A71-25947

Heat transfer coefficients of various jet systems impinging on gas turbine blade inner surfaces, discussing cooling flow rates and solid particles injection into air flow 11 p1811 A71-25955

Noise field from subsonic air jets by velocity dependence and radiation intensity directivity determination 11 p1753 A71-26445

Turbulent submerged wall air jet on ablating graphite surface, examining friction and heat and mass exchange in boundary layer 13 p2160 A71-28569

Air stream injection from circular hole in flat plate into supersonic flow, measuring heat transfer 13 p1992 A71-29184

Average and pulsating velocity distributions during subsonic air jet interaction with plane baffle, describing jet dissipation geometrical pattern 14 p2225 A71-30223

Circular air jet velocity, turbulence intensity and energy spectra distributions, investigating longitudinal acoustic field influence 14 p2225 A71-30226

Reattachment of single two dimensional turbulent air jet, investigating gas flow characteristics in combustion chambers 14 p2170 A71-30419

Liquid phase evaporation rates in free turbulent air-liquid droplet jet, giving droplet dynamic characteristics determination criterion 14 p2227 A71-30613

Sonic boom pressure signature laboratory scale measurement after modification by traveling through air jet turbulence, comparing with statistical prediction [AIAA PAPER 71-618] 15 p2388 A71-31547

Supersonic combustion flowfield transverse hydrogen jet injection into Mach 2.5 airstream, discussing recirculation region upstream [WSS/CI PAPER 71-15] 15 p2463 A71-31624

Submerged free air jet with laminar parabolic profile, investigating pressure recovery characteristics for various tube diameters, spacing and Reynolds number 15 p2389 A71-31683

Aerodynamic flame stabilization by secondary air jets obliquely directed toward combustion chamber main flow, comparing with mechanical devices characteristics [DFVLR-SONDDR-120] 15 p2472 A71-32719

Artificially induced unsteady flows effects on flame stabilization by model opposed jet stabilizer employing premixed propane-air combustible flow and opposed air jet 17 p2840 A71-35706

Theoretical and photographic study of under-expanded air jets ejected simultaneously from several mutually interacting nozzles near origin 18 p2903 A71-36115

Fluid mechanics of human whistling as function of resonant cavity and orifice jet velocities, comparing Rayleigh bird call and Pfeifentone 18 p2910 A71-36935

Convective clouds development stimulation by artificial ascending jets forming above stationary heat and momentum source, discussing propagation in atmosphere 19 p3093 A71-38694

German monograph on flow and combustion changes during hydrogen and methane transverse injection into hot supersonic air jet 21 p3475 A71-40750

Symmetrical and unilateral sticking flow modes of nozzle air jets expelled into plane-parallel and parabolic ducts 22 p3480 A71-42681

AIR LOCKS

Aerodynamic seals theoretical analysis and experimental test results, considering pressure ratios, pressure recovery coefficients and pump efficiency 07 p1117 A71-19422

Long term lunar surface environment, discussing radiation, thermal and meteoroid protection, water budget, carbon dioxide removal and air lock design 11 p1726 A71-26534

AIR MASSES

Isentropic nature of stratospheric air masses motion from balloon measurements of temperature and radiation 23 p3671 A71-43338

AIR NAVIGATION

NT ALL-WEATHER AIR NAVIGATION

Mountain-size atmospheric eddies on leeward slope of Carpathian and Low Tatra mountains, discussing turbulence effects on air navigation 01 p0113 A71-10349

Man role in future navigation from SAC viewpoint, considering relationships to mission and machine 01 p0123 A71-10502

Navigator role in Military Airlift Command /MAC/ as navigator, weather analyst, fuel manager and flight planner 01 p0123 A71-10504

Commercial and military aircraft navigator future role, considering increasing task requirement stringency and growing navigational aids availability 01 p0124 A71-10505

Airborne inertial and area navigation systems performance requirements proposed for U.S. domestic airspace, including projection through 1995 01 p0124 A71-10508

USAF navigator training, discussing operational demands, philosophy, present and future training capabilities, etc 01 p0022 A71-10520

Aircraft navigator training, examining flight and ground trainer balance from cost effectiveness standpoint 01 p0022 A71-10521

Airborne trainer and ground simulator for undergraduate navigator training system 01 p0023 A71-10522

Themis project automatic navigation program, examining optimum stochastic feedback error analysis and sensitivity algorithms 01 p0125 A71-10525

Air navigational training simulators, discussing navigation aids, civilian navigator use, visual simulation and land-mass radar 01 p0125 A71-10526

Time-synchronized approach control combining aircraft precision navigation and guidance with ATC equipment 02 p0280 A71-12894

Area navigation in commuter/air taxi operations concerning airborne equipment, airport utilization and CTOL, STOL and VTOL aircraft 04 p0622 A71-14650

Soviet book on aviation automation covering automatic control systems in piston, turbojet and turboprop engines, navigation, air temperature and pressure 04 p0529 A71-15223

Navigation and traffic control of VTOL commercial transport aircraft, discussing noise, G forces, turbulent wakes, approach profiles and V-ports 04 p0624 A71-15429

Omega for aircraft navigation and traffic control, discussing reliability, resolution and prediction errors 06 p0924 A71-17924

Onboard air navigation computers drift correction by mapping radar, calculating position by region over-flown image/measured geographic features comparison 06 p0925 A71-17952

Communications, navigation and surveillance for aircraft and marine vessels in North Atlantic region, discussing baseline traffic control model 07 p1153 A71-18808

Aircraft final approach and landing aids, describing ILS, VHF omnidirectional radio range, distance measuring equipment and satellite systems for air navigation 07 p1154 A71-19014

Human role in Aerospace Defense Command navigation, discussing Airborne Warning And Control System and navigational aspects of ADC mission 07 p1157 A71-20346

Automatic Carrier Landing System with linear adaptive aircraft Navigation Computer, investigating effectiveness in reducing system errors due to nonlinearities and noise effects 07 p1157 A71-20405

Aircraft radio compass navigation errors due to loop antenna inclinations during maneuvering 08 p1331 A71-20787

VOR/DME ground station oriented aircraft area navigation horizontal guidance capability, discussing digital input/output flight control 08 p1331 A71-21166

Interactive computer graphic system for compiling air navigational data on two dimensional aeronautical charts 08 p1258 A71-21236

Soviet book on navigation and control covering data processing, optimal stochastic self guidance, instrument errors, mean energy consumption and stabilization loop time lag 09 p1491 A71-23163

Commercial V/STOL aircraft area navigation system requirements, discussing airborne computer, flight plan data storage and control subsystems and horizontal orientation display 10 p1639 A71-24150

Area navigation facility, discussing control and display and navigation standards 12 p1927 A71-26879

Airport geodetic control stations, discussing obstruction charting program 12 p1895 A71-27537

Onboard area navigation systems in ATC environment, discussing route structure and flight instruments [SAE PAPER 710453] 13 p2098 A71-28332

Area navigation system based on radio aids by airborne receivers and sensors for aircraft movement improvement, noting advantages of pilot displays [SAE PAPER 710457] 14 p2272 A71-30533

Inertial navigation systems improvements for commercial air transportation, noting digital computer program revision and increased functional capability [SAE PAPER 710458] 14 p2272 A71-30534

Combined inertial and instrument landing aircraft navigation systems with reduced cross runway position and velocity errors, using optimal linear estimation 14 p2272 A71-30606

Air navigation techniques history, considering radio, radar, loran Doppler and inertial navigation 14 p2272 A71-30712

Probabilistic methods for solving ATC and navigation problems, considering stochastic processes theory 15 p2445 A71-31463

Concorde flight simulator at Toulouse, discussing flight control system, air navigation and certification 15 p2384 A71-31881

ESRO preoperational aeronautical satellite system for Atlantic and Pacific coverage, noting position determination for reduced aircraft separation, frequency selection and performance trade-offs 16 p2644 A71-32850

Carousel IV inertial navigation system of Boeing 747 aircraft, discussing informational capabilities, accuracy and reliability 16 p2606 A71-34079

Electronically scanned cruciform slot-array aircraft antenna for satellite controlled navigation aid, discussing circularly polarized wave radiation 16 p2548 A71-34123

Navigation and communication satellites development for civil aviation and shipping, examining technical, organizational, operational and cost problems 17 p2771 A71-34240

ATC system improvement, presenting data acquisition upgrading and ground automation- aircraft navigation systems interface 17 p2771 A71-34614

Precision area navigation system, considering position and velocity continuous measurement in three dimensional space, system components and simulation program 17 p2771 A71-34616

Dioscures communication satellite system for air traffic control and navigation, discussing aircraft antenna beam electronic scanning by computerized control 17 p2714 A71-34681

Air navigation, surveillance and traffic control technology effects on land and airspace uses at airports 17 p2774 A71-35371

ATC system safety problems from user standpoint, considering requirements by pupil, test and airline pilots and light, private, business, taxi and military aircraft 17 p2774 A71-35372

ATC system improvement by area navigation, discussing benefits in services, safety and cost effectiveness 17 p2775 A71-35373

Military and civil aircraft navigation systems development, emphasizing self contained airborne equipment 17 p2775 A71-35374

Airborne communications with AN/ARC-154 transceiver in single radio, discussing extended frequency coverage, multimode operation, navigation and input/output provisions 17 p2775 A71-35758

Doppler satellite/airborne inertial navigation system integration with delayed state Kalman filter 17 p2776 A71-35766

Omega navigation application to general aviation aircraft, presenting diurnal course shift to overcome deficiencies

17 p2776 A71-35767

Integrated airborne Omega/inertial navigation systems performance prediction using statistical models for position fix errors

17 p2776 A71-35769

Air navigation and traffic control systems with application to Western Europe and Atlantic area, noting requirements for ILS successor

18 p2944 A71-35998

Satellite based position fixing data by ranging techniques, discussing application to navigation and ATC

18 p2945 A71-36493

Navigational accuracy improvement by combining VOR/DME information with airspeed and heading data via maximum likelihood filter, using small airborne computer

19 p3097 A71-37174

Radio and radar air navigation for civil aviation, discussing Doppler effect, inertia and satellite systems

19 p3100 A71-37344

Concorde aircraft navigation system comprising triple inertial systems, dual VOR/DME, dual ILS and dual ADF

[CASI PAPER 72/9]

19 p3100 A71-37599

Time and frequency synchronization for EROS airborne collision avoidance system, considering impact on aeronautical communication, navigation and surveillance

[CASI PAPER 72/17]

19 p3100 A71-37604

Aircraft lateral dynamics effect on positioning accuracy along straight flight path, using Loran C data

20 p3261 A71-38864

One man Jaguar aircraft navigation, weapon aiming system and pilot operational tasks, noting inertial platform alignment, displays and target attack modes

20 p3261 A71-39825

Avionics combined display system for area navigation, discussing design, color map projection, overlays, CRT unit and viewability

21 p3413 A71-40137

Satellite navigation system for aviation and marine use, examining operational requirements, economic viability and technical solutions

22 p3570 A71-41509

Navigation role in airways systems development - Conference, Saddle Brook, New Jersey, April 1971

22 p3570 A71-42077

Combined inertial navigation and VOR/DME systems contribution to area navigation accuracy and efficiency

22 p3571 A71-42080

Unaided, integrated and differential OMEGA radio navigation configurations, comparing accuracy and suitability for airways system operations

22 p3571 A71-42082

Analytical model for air navigation and ATC system design, demonstrating system parameters effects on lateral separation standards for parallel flight lanes

22 p3571 A71-42083

Navigation and surveillance interdependence in ATC

22 p3571 A71-42085

ATC integrated communication, navigation and identification system, discussing design, economics, technology and flexibility

22 p3571 A71-42086

VOR/DME air navigation equipment using Kalman-Bucy filter and airborne air data system /ADS/

22 p3573 A71-42289

Book on electronic aids for navigation systems for marine and aerospace transport operation covering measuring and display instruments, radio wave properties, etc

23 p3702 A71-43225

Corporate aircraft operations in Latin America, discussing communication and navigation, fuel, paper work, food, vaccinations and weather

23 p3629 A71-43391

Mobile LF air navigation AN/MRN-13 equipment, operation and maintenance

23 p3702 A71-43878

AIR PIRACY

Airline liability and insurance in relation to aircraft hijacking, sabotage, etc

01 p0183 A71-10359

Hijacking and acts of violence against civil aircraft, concerning draft convention by legal committee of International Civil Aviation Organization

04 p0691 A71-14997

Rumanian air law of 1953 and penal codes of 1969, discussing statutes concerning in flight committed crimes against persons and property or air piracy

06 p1009 A71-17425

Air piracy /hijacking/ bibliography, considering national and international law, extradition, punishment, prevention and safety insurance for passengers and crews

22 p3622 A71-41617

AIR POLLUTION

Gas turbines air pollution control, discussing exhaust composition, combustion chamber design, engine efficiency, etc

01 p0142 A71-10820

High altitude aircraft effects on stratospheric ozone due to added water vapor, discussing effects on solar energy transmission, surface temperature and weather

01 p0120 A71-11341

Satellite sounding of atmospheric pollution by spectral analysis of outgoing thermal radiation

02 p0241 A71-11689

Q switched ruby laser-Raman radar for real time air pollution probe

02 p0213 A71-12014

Atmospheric pollution long term effects measurement and control using spacecraft-mounted instruments

04 p0581 A71-14821

Air pollution monitoring instrument for measuring mass concentration of aerosols and particulates in atmosphere

04 p0597 A71-15288

Soviet monograph on atmospheric boundary layer covering compressible turbulent air flow, diurnal fluctuations, fog, air pollution and lower atmosphere electric field

04 p0621 A71-15399

Thermoconductometric portable hydrogen analyzer for air around industrial centers, using bridge tungsten sensor network

04 p0601 A71-15675

Combustor design for minimum exhaust smoke emission from aircraft gas turbine jet engines, considering air pollution

08 p1347 A71-20867

Commercial supersonic flight, investigating air pollution and alleged climate and weather modification effects due to principal exhaust products

08 p1232 A71-21821

Air pollution emissions at Heathrow Airport, London, from aircraft operations, heating installations and road traffic

08 p1378 A71-21823

Airport pollution dispersion modeling, simulating effect on surrounding areas for abatement strategies calculation

08 p1379 A71-21824

National Air Pollution Control Administration control of aircraft engine pollutant emissions covering measurement, test instrumentation, research, standards and regulations

08 p1379 A71-21831

Aircraft engine smoke emission control, discussing Ringelmann chart assessment for various commercial jet aircraft and airport gaseous pollutants

08 p1380 A71-21832

Aircraft smoke emission control, outlining legal action by New Jersey State Department of Health

08 p1380 A71-21833

Temperature dependent wavelength tuning of Pb-Sn-Te diode lasers, noting air pollution detection use

09 p1463 A71-22764

Air pollution sources testing, discussing gas flow properties, velocity measurement, particulate sampling, continuous monitoring, calibration, etc

09 p1448 A71-22777

Turbulent diffusion in stationary thermally stratified atmospheric boundary layer, considering gravitational sedimentation and impurities lifetime

11 p1795 A71-25585

Air polluting nitric oxide and soot production by jet aircraft, discussing mixing process and atmospheric dispersion

12 p1946 A71-27560

Air pollution study of jet aircraft emissions in airport vicinity, involving exhaust gas testing, ground operations and passenger cabin measurements

13 p2005 A71-28315

Analytical model for performance and pollutant emissions of gas turbine combustors, predicting gas composition and temperature

14 p2294 A71-30765

Modular concept mathematical model for combustion and pollution formation processes in jet engine combustors, including turbulent mixing and reaction kinetics

14 p2294 A71-30766

Agenda rocket engine pollutants, considering pollution control by scrubbers, engine system modification and micrometeorological data gathering

14 p2294 A71-30768

SAE/DOE conference on aircraft and environments covering noise pollution, airport noise, sonic booms, regulatory/legal aspects and air pollution

14 p2295 A71-30776

Radioactive impurities transfer from lower stratosphere into upper troposphere based on vertical air transport data

15 p2400 A71-31970

Aircraft and airports as air pollution sources, stressing industries understanding of applicable control technology

15 p2349 A71-32243

Dispersal of jet aircraft exhaust emissions near airports and of smoke trails in upper atmosphere, assessing pollutant levels near large urban airports

15 p2349 A71-32244

Jet engines nitric oxide air pollutant emission formation, developing gas turbine combustor models

15 p2470 A71-32289

Molecular spectral coincidences of carbon monoxide and carbon dioxide IR lasers for atmospheric pollutant detection by sensing of resonant absorption, thermal emission or fluorescence

16 p2585 A71-33129

Solar radiation field in polluted atmosphere, measuring intensity, polarization and flux due to aerosol scattering for comparison with Mie theory computation

17 p2736 A71-35563

Wideband spectrum utilization above 10 GHz for high rate digital communications and ecology monitoring of sea state, earth surface contour and atmospheric pollutants

19 p3020 A71-38407

Turbine propulsion system smoking and exhaust gas emission, discussing aircraft and automobile pollution emission

20 p3277 A71-39452

Upper temperature inversion as condition producing pollutants turbulent diffusion in atmospheric boundary layer

22 p3568 A71-41648

Global environmental monitoring and remote sensing from satellites, considering thermal, air and water pollution

22 p3534 A71-41961

Atmospheric trace and pollutant molecules global survey, using airborne/spaceborne high resolution Fourier interference IR spectrometer

22 p3542 A71-41963

Physiological effects on mice of air pollution with gaseous toxic substances from urine and feces, noting increased respiration rate and choline esterase activity

22 p3506 A71-42807

Operating variables effect on pollutant exhaust from jet aircraft turbine engines, discussing combustor design techniques for emissions reduction

23 p3718 A71-43600

Resonance scattering laser radar for atmospheric pollution detection, discussing Rayleigh and Mie scattered light suppression

24 p3803 A71-44570

SST operation climatic impact assessment program, considering carbon dioxide, water vapor, contrails, particulates, nitrogen oxides and carbon monoxide

24 p3823 A71-44982

AIR PURIFICATION

Intensive Chlorella cultivation for controlling toxic gaseous contaminants in atmosphere

06 p0861 A71-18357

AIR SAMPLING

Aerohee 150 sounding rocket cryogenic air sampler, discussing design, operation and air constituents reaction to cooling

01 p0084 A71-11442

Upper stratosphere and mesosphere concentrations of Ne, Ar, and Kr from rocket-borne cryogenic air sampler

02 p0246 A71-12701

Air pollution sources testing, discussing gas flow properties, velocity measurement, particulate sampling, continuous monitoring, calibration, etc

09 p1448 A71-22777

AIR SICKNESS

U MOTION SICKNESS

AIR TO AIR MISSILES

Air to air and air to ground missile zinc silver oxide batteries capabilities, including energy density, long storage life and shock and temperature resistance

08 p1236 A71-21104

Air-to-air, air-to-ground and USN surface-to-air guided weapons operational assessment in military environment

09 p1532 A71-22991

AIR TO AIR ROCKETS

U AIR TO AIR MISSILES

AIR TO SURFACE MISSILES

Short range air to ground attack missile system, discussing nuclear warhead, propulsion system, performance characteristics and program cost analysis

10 p1682 A71-24286

Fluidic inertial platform feasibility model for line of sight guidance of air to surface missile

18 p2945 A71-36483

Kalman filter for computerized optimal SRAM air to surface missile alignment, discussing design, digital simulation and flight tests

19 p3098 A71-37189

AIR TRAFFIC

V/STOL services integration into UK air traffic system

03 p0454 A71-13567

Air transport development, examining capital investment, traffic volume and facilities

03 p0524 A71-14246

Large capacity aircraft reception and servicing problems consideration for facilitating traffic 06 p1010 A71-17588

Airport adaptation to large capacity aircraft, considering terminal installations, infrastructures, runways, roads and traffic areas 06 p0879 A71-17589

Urban transit and ATC vehicle identification and position determination system, considering surface and airborne traffic real time information communication 08 p1331 A71-21169

Jurisdiction of air traffic and space law, noting applicability to start and landing phases of spacecraft 09 p1548 A71-23000

Supersonic transport air traffic meteorology, considering high altitude and flight velocities, applications technology satellites for lower stratosphere thunderstorms, clear air turbulence, etc 09 p1488 A71-23070

Motion sequential analysis of airways utilization, using mathematical-statistical methods 12 p1927 A71-27143

Roissy-en-France airport, describing construction, passenger handling, terminal facilities, traffic volume and runway system 13 p2045 A71-29309

Book on air law and civil air policy covering international regulation, air traffic market, passenger and cargo services, etc 14 p2340 A71-29938

Long haul international air transport, analyzing traffic growth rates 14 p2340 A71-30161

Long term prospects of air traffic development in competition with other modes, estimating VTOL service demand 14 p2340 A71-30164

Velocity transposition theory based on velocity perception constancy effects, noting importance for human engineering guidance in sea, land, air and space traffic fields [DFVLR-SONDDR-107] 18 p2863 A71-35829

Finnish air traffic law based on international civil aviation convention, discussing regulations relative to aircraft, personnel and airports 18 p2989 A71-36919

Warsaw air traffic convention agreements as amended at The Hague and Guatemala, presenting air transport regulations in present form 18 p2989 A71-36920

European air traffic employed in transportation of tourists, considering European Airbus A-300B super twin 19 p3172 A71-37273

Air traffic congestion and delay Monte Carlo digital simulation in FORTRAN, exemplifying two-runway airport operation under instrument flight rules 19 p3041 A71-38024

Airport congestion as constraint on air travel, considering runway capacity and adjusted demand 19 p3042 A71-38028

Aircraft anticollision flashing lights, discussing current practices within national and international air traffic regulations regarding flash frequency, color and light sources 22 p3483 A71-41499

Canadian STOL program, discussing Quebec-Windsor corridor passenger traffic [AIAA PAPER 71-982] 24 p3791 A71-44578

STOL aircraft system, discussing ground installations, runways, three dimensional area navigational aids, noise reduction, air traffic and short haul productivity [AIAA PAPER 71-983] 24 p3791 A71-44579

AIR TRAFFIC CONTROL

NT RADAR APPROACH CONTROL

Traffic radar generated weather contours for air traffic controller in helping aircraft avoid thunderstorms 01 p0118 A71-10587

Air traffic control by satellite, discussing CNES-SGAC and ESRO experiments within Dioscures project test program 01 p0125 A71-10748

ATC communication environment simulation via mathematical model based on ATC statistics 01 p0126 A71-10979

ATC automation, using conflict prediction algorithm based on airspace assignment to aircraft entering system 02 p0278 A71-11698

ATC system improvement by procedural changes, applying probability concepts to flight safety 02 p0278 A71-11699

Helicopter operations integration into civil air traffic system, noting special requirements for mixed fixed and rotary wing terminal environments 02 p0279 A71-12892

Maximum throughput-rate capacity for runway and final approach path airspace involving multiple IFR landings 02 p0279 A71-12893

Time-synchronized approach control combining aircraft precision navigation and guidance with ATC equipment 02 p0280 A71-12894

Intercity V/STOL aircraft transport system, solving congestion problems through all weather superiority, low noise level and separate ATC 03 p0347 A71-13571

Short haul STOL concepts including stolport potentials, onboard avionics, vehicle characteristics, tradeoffs and current nonproductive flying due to traffic congestion 03 p0348 A71-13620

Spacecraft and aircraft automatic control man machine interface, bionics and traffic control systems 03 p0455 A71-14393

Statistical connection strategies for automatic multiradar air traffic surveillance using track computer 03 p0380 A71-14395

Navigation and traffic control of VTOL commercial transport aircraft, discussing noise, G forces, turbulent wakes, approach profiles and V-ports 04 p0624 A71-15429

Air traffic control using collision risk equations, noting data handling automation, airborne collision avoidance devices and geostationary satellites 04 p0624 A71-15646

Air traffic control radar separation by pulse repetition frequency discrimination for double and triple stagger configurations 05 p0720 A71-16347

General aviation safety and effectiveness enhancement through electronic technology applications, discussing airspace control system based on beacon transponder, LF-VLF area navigation and vertical radar 05 p0780 A71-17228

Omega for aircraft navigation and traffic control, discussing reliability, resolution and prediction errors 06 p0924 A71-17924

SAGE/Buic vs Kalman filters for aircraft tracking, determining accuracy by radar model 06 p0925 A71-18517

Computer aided automatic fault data logging, classification, analysis and reporting methods in integrated ATC system 07 p1155 A71-19556

System automation evolutionary process in terminal Air Traffic Control environment [AIAA PAPER 71-242] 07 p1155 A71-19717

ATC automated systems, discussing National Airspace System En Route Stage A and Advanced Radar Terminal System [AIAA PAPER 71-244] 07 p1156 A71-19719

National Airspace System air traffic control automation man machine considerations, noting controller productivity increase, input difficulties and symbology clutter 07 p1049 A71-19720

Computer display channel for en route air traffic control flexible real time data processing and display subsystem [AIAA PAPER 71-247] 07 p1156 A71-19721

Associative digital processor with associative memory for high speed ATC data processing, discussing design and operation 07 p1068 A71-19997

U.S. domestic ATC airspace enroute and terminal area navigation system effects on pilot workload, projecting future FAA requirements 07 p1157 A71-20347

Excretion patterns of air traffic controllers for stress appraisal, using urinalysis 08 p1246 A71-20811

Optimal air traffic control coordinating flow and holding patterns of aircraft landing in single runway using linear-quadratic technique 08 p1332 A71-21335

ATC automation program for en route and terminal centers, discussing combined nationwide system features, IFR volume and video digitizer data links 08 p1332 A71-21659

ATC system analysis, discussing airport and airspace utilization, area navigation, midair collisions and traffic mix 09 p1491 A71-22470

Air traffic controllers legal responsibility and disciplinary procedure, considering clearances, flight crew instructions and aircraft accidents 09 p1548 A71-22891

Radar analog simulators for Polish air traffic controllers training, describing optical and electronic equipment 09 p1428 A71-22950

Aircraft industry ATC techniques and equipment contribution to aircraft control and safety 09 p1491 A71-22951

ATC services training and operations methods adopted by International Aeradio Ltd 09 p1491 A71-22952

ATC electronic automation systems development for air safety improvements 09 p1491 A71-22953

Digital simulator for training ATC officers, considering authenticity and working and geographical environments 09 p1428 A71-22954

Secondary surveillance radar in ATC systems, discussing advantages and implications for controllers 09 p1406 A71-22955

Aircraft motion and traffic control at air corridors intersections for minimum flight schedule deviation under random disturbance due to weather, using statistical simulation 10 p1639 A71-24158

ATC station ground to air communication via VHF tropospheric scatter, discussing high power radio transmitters and low noise over the horizon receivers combination 10 p1576 A71-24175

ATC automation system design, considering controllers decision time savings 10 p1640 A71-24271

Digital simulation facility for airborne collision avoidance system effects on ATC terminal automation, discussing operation, hardware and software equipment 10 p1590 A71-24774

ATC regulations considered for Concorde introduction to passenger service, discussing landing and takeoff characteristics 11 p1706 A71-25232

North Atlantic communications, navigation and ATC systems requirements for geostationary satellite operation, considering lifetime rated data and voice channels transmissions volume 11 p1839 A71-26332

Aeronautical satellites, considering air-ground telecommunication, air traffic control and inertial navigation applications 12 p1971 A71-26825

Area navigation facility, discussing control and display and navigation standards 12 p1927 A71-26879

Airport geodetic control stations, discussing obstruction charting program 12 p1895 A71-27537

Midair collisions analysis for civil-military integrated ATC air space, discussing near miss volume, random heading aircraft density and pilots evasive action vs avoidance percentages 12 p1927 A71-27599

Onboard area navigation systems in ATC environment, discussing route structure and flight instruments [SAE PAPER 710455] 13 p2098 A71-28332

Optimum functional integration and performance requirements of navigation aids and ATC in terminal areas [SAE PAPER 710456] 13 p2098 A71-28333

Feasibility of VHF aeronautical satellite system frequency sharing band used by ATC service, employing spatial separation, antenna directivity and frequency offset 13 p2032 A71-28873

En route turbojet aircraft flight speed control, assessing impact on ATC procedures 13 p2098 A71-28884

ATC radar display systems mapping techniques using vectors and optical projections 14 p2271 A71-30014

French ATC, discussing automatic coordinator systems, computer utilization and flight plan data processing 14 p2272 A71-30382

Maastricht Automatic Data Processing and Display ATC system with digital computers for aiding controllers in issuing instructions and making decisions 14 p2272 A71-30383

Aircraft phased arrays for L-band ATC satellite system application, alleviating problems of power budget and vulnerability to multipath and interference 14 p2217 A71-31054

Probabilistic methods for solving ATC and navigation problems, considering stochastic processes theory 15 p2445 A71-31463

Associative processor for ATC with fast arithmetic processing, equality search and input/output operations 15 p2374 A71-31517

Three dimensional ATC radar supporting simultaneous range, azimuth and elevation information for indefinite number of targets by continuous searching 15 p2371 A71-32167

ATC data automation, discussing flight plan processing system /FPPS/, radar data processing system /RDPS/ and signal automatic control system /SATCO/ 15 p2446 A71-32523

ATC satellites providing communications channels between aircraft and ground control stations and aircraft localization 16 p2605 A71-32849

Fatigue and stress measurement on air traffic controllers, using critical fusion frequency methods, tapping tests, self rating and urine catecholamine 17 p2688 A71-34365

ATC system models, covering surface movement, runway utilization, terminal areas and enroute traffic 17 p2771 A71-34523

ATC system improvement, presenting data acquisition upgrading and ground automation- aircraft navigation systems interface 17 p2771 A71-34614

ATC avionics equipment, discussing inertial area navigation, autopilots, airborne data acquisition, altitude reporting, collision avoidance, CAT, satellite communications, etc 17 p2771 A71-34615

Time division multiplexing system for ATS, discussing surveillance geostationary satellite feasibility, delta modulation for data transmission and aircraft equipment 17 p2772 A71-34680

Discusses communication satellite system for air traffic control and navigation, discussing aircraft antenna beam electronic scanning by computerized control 17 p2714 A71-34681

Queueing theory approach to communication satellite network design, applying to ocean air traffic control and worldwide military broadcast systems 17 p2721 A71-35106

Soviet book on air transportation covering ATC, automatic landing and information display systems 17 p2774 A71-35194

Air navigation, surveillance and traffic control technology effects on land and airspace uses at airports 17 p2774 A71-35371

ATC system safety problems from user standpoint, considering requirements by pupil, test and airline pilots and light, private, business, taxi and military aircraft 17 p2774 A71-35372

ATC system improvement by area navigation, discussing benefits in services, safety and cost effectiveness 17 p2775 A71-35373

Aircraft accident litigation related to wake turbulence concerning pilot or air traffic controller faults 17 p2842 A71-35387

Soviet book on radio control of various flight vehicles covering closed loop synthesis, missile guidance, spacecraft trajectory correction and air traffic control 17 p2775 A71-35403

Air navigation and traffic control systems with application to Western Europe and Atlantic area, noting requirements for ILS successor 18 p2944 A71-35998

Satellite based position fixing data by ranging techniques, discussing application to navigation and ATC 18 p2945 A71-36493

ESRO part of joint ATC communication experiment for L band satellite use, giving voice and data transmission and distance measurement techniques tests results 18 p2945 A71-36510

Bit and scanning field synchronizations of time multiplex for air traffic control 18 p2946 A71-36513

Computer-based aircraft tracking with aid of twin radar air traffic control system, discussing components and operation 18 p2883 A71-36993

Computerized automatic estimation techniques application to real time aircraft tracking in ATC system design [AIAA PAPER 71-926] 19 p3096 A71-37172

Aircraft position errors computation for ATC mathematical surveillance models, estimating collision risk [AIAA PAPER 71-927] 19 p3097 A71-37173

Airborne traffic situation display for use with national airspace/automatic radar control terminal system, using computer selected message, map and heading data [AIAA PAPER 71-929] 19 p3097 A71-37175

Airport system utilization, discussing aircraft noise, ATC, STOL development and passenger handling capacity problems [CASI PAPER 72/3] 19 p3041 A71-37594

Automation in third generation ATC requiring distributed management and spacing functions delegation to pilot [CASI PAPER 72/15] 19 p3100 A71-37602

British Mediator program for joint civil/military ATC system, discussing air defense relationships [CASI PAPER 72/16] 19 p3100 A71-37603

Automatic ATC display systems, discussing electronic flight progress strip for telemetry reproduction 19 p3102 A71-38300

Performance prediction model for electromagnetic compatibility of ATC radar beacon system, testing interrogator-transponder links along air route 19 p3102 A71-38435

Time sharing technique application to RF interference with ATC resulting from transmitting and receiving antennas collocation 19 p3102 A71-38436

Convertible rotor transport aircraft, considering ATC, mass transportation systems, safety, noise and socio-economics 20 p3178 A71-39387

Air traffic control delays, airport airspace congestion, flyover noise reduction and performance requirements effect on airline operations economics 20 p3209 A71-39391

Central terminal rapid processing and high speed VTOL aircraft effects on airport design, flight time, cost and ATC 20 p3210 A71-39394

Fast time digital computer simulation model for evaluation of man-machine interface /display/ problem of ATC system including personnel and equipment 21 p3412 A71-40112

Computerized touch display for ATC tasks compared to conventional keyboard tabular display performance 21 p3413 A71-40114

ATC display devices with computer-derived alphanumeric labels on radar screen, examining feasibility and effectiveness 21 p3413 A71-40118

ATC display device man-computer interaction faults and delays effects on operator performance 21 p3413 A71-40119

ATC height and plan position indicator composite picture display system design and operation, combining functions of primary and secondary surveillance radars 21 p3413 A71-40128

UK military and civil ATC coordination, discussing Mediator plan for modernization of communication and navigation equipment and techniques 22 p3570 A71-41519

National Aviation System stage A ATC displaying digitized radar data positions together with automatic track positions 22 p3570 A71-41634

Commercial ATC, considering VFR, flight control and inertial navigation 22 p3570 A71-42078

Analytical model for air navigation and ATC system design, demonstrating system parameters effects on lateral separation standards for parallel flight lanes 22 p3571 A71-42083

U.S. Army ATC cost-effective system developments for high density low altitude helicopter tactical operations to avoid enemy radar under near-all weather conditions 22 p3571 A71-42084

Navigation and surveillance interdependence in ATC 22 p3571 A71-42085

ATC integrated communication, navigation and identification system, discussing design, economics, technology and flexibility 22 p3571 A71-42086

Geostationary satellite oceanic automated ATC center design, estimating cost 22 p3572 A71-42095

Aeronautical satellite systems program planning for improved aircraft communications, ATC and other air traffic services in airspace over oceanic areas 22 p3573 A71-42096

Mathematical models for computerized ATC automatic aircraft flight tracking logics without tracks smoothing 22 p3573 A71-42396

IBM 9020 multiprocessing computer application to ATC, discussing control sectors for inflight control at air route traffic control centers in U.S. 23 p3702 A71-43888

Stochastic optimal control theory application to air-plane rescheduling model, obtaining dynamic programming algorithm for optimal landing and takeoff rules 23 p3702 A71-44104

Computer-aided decision algorithm for ATC problem in near terminal area, emphasizing scheduling and holding strategies 23 p3703 A71-44105

Affect adjective checklist assessment of mood changes as function of stress in air traffic controllers 23 p3640 A71-44240

Supersonic transports and ATC, discussing taxiing, takeoff, landing and terminal area operations 24 p3845 A71-44352

Civil aviation research and development policy review covering aircraft noise, congestion, ATC, runway capacity and airport development problems [AIAA PAPER 71-1024] 24 p3892 A71-44602

AIR TRANSPORTATION

Economic contributions of U.S. domestic airline industry in 1970s regarding air transportation constraints and impact on short haul [AIAA PAPER 70-1309] 01 p0004 A71-10486

Noise reduction relationship to air transportation progress, considering cost/technology balance, quiet engine, research and development programs, etc 01 p0183 A71-10819

Short haul air transportation in U.S., interagency cooperation and federal involvement [AIAA PAPER 70-1286] 01 p0184 A71-10875

Airport system planning from environmental viewpoint, discussing travel market, airport accessibility, airspace utilization and control and land use 02 p0334 A71-11642

Short haul air transportation technological factors for VTOL, STOL, CTOL and light aircraft, considering operating costs, passenger service and environmental impact [AIAA PAPER 70-1287] 02 p0188 A71-11700

Air transportation reliability through turbojet engine performance monitoring 02 p0298 A71-12368

Concorde role in air traffic market, discussing operating costs and profit potential 02 p0190 A71-12746

Intercity V/STOL aircraft transport system, solving congestion problems through all weather superiority, low noise level and separate ATC 03 p0347 A71-13571

VTOL systems for commercial short haul air transportation, discussing large helicopters and compound aircraft applications for system capacity profitability and efficiency increases 03 p0347 A71-13575

V/STOL aircraft in civil air transportation, discussing safety, reliability, maintainability and propulsion system concepts 03 p0348 A71-13576

Short haul STOL aircraft transport system, discussing neighborhood stolport ownership, technical feasibility and economic, emotional, ecological and sociological viability 03 p0523 A71-13618

Compound and VTOL aircraft and prototype compact downtown V-ports for short haul air transportation improvement and expansion 03 p0348 A71-13619

Air transport development, examining capital investment, traffic volume and facilities 03 p0524 A71-14246

Economic trends of international air transport in 1970s 04 p0690 A71-14991

German monograph on socioeconomic evaluation of air transportation systems for developing nations, using cost-benefit analysis 04 p0691 A71-15125

Strapdown inertial guidance and software technologies for cosmic speed aerospace vehicles and low speed air, marine and ground transport 04 p0623 A71-15301

Air transportation systems ride vibration environments in relation to human comfort 04 p0532 A71-15421

Public-use ground level and rooftop helicopter and STOL aircraft landing facilities for city and suburban traffic 04 p0567 A71-15442

Air charter flights legal status, considering public, private and international laws and civil responsibility 06 p1009 A71-17422

Aircraft nationality legal problems concerning regional cooperation and registration 06 p1009 A71-17423

Air transport popularization possibilities, considering group rates and fare adjustments 06 p1009 A71-17586

French statistical system for civil air transport operations from airport viewpoint 06 p1009 A71-17587

Large capacity aircraft reception and servicing problems consideration for facilitating traffic 06 p1010 A71-17588

Patients transportation pathology, discussing accelerations and vibrations in ambulances, helicopters and fixed wing aircraft 06 p0860 A71-18191

Airships and balloons potential commercial use in Canada, discussing cargo, passenger and military applications 07 p1019 A71-19916

Circadian rhythms from aerospace medicine viewpoint, discussing cycle stability and flexibility, air and space travel, etc 08 p1238 A71-20704

Aerial transportation of patients, potential hazards due to motion sickness, decreased atmospheric pressure and oxygen tension, fatigue, inactivity and dehydration 08 p1245 A71-20726

Preventive medicine for air travelers in flight and at route stops, considering disease dissemination and control, international quarantinable diseases, sanitation, etc 08 p1245 A71-20727

Federal assistance to air transportation, considering airport development-environment conflicts 08 p1380 A71-21834

European view on liability and compensation limitation for death and injury in international commercial air transport 09 p1548 A71-22989

U.S. view on legal liability and compensation for death and injury in international air transport
09 p1548 A71-22990

Uncertainty factors in management decisions and operations optimization in international air transportation industry
10 p1698 A71-24265

V/STOL component of unified transportation system, discussing transportation modes, airport locations, noise reduction, cost factors, etc
10 p1556 A71-24274

Hypersonic air transportation future prospects, discussing technical problems and feasibility in view of space shuttle development
10 p1699 A71-24285

U.S. General Aviation safety record, discussing National Transportation Safety Board and accident/injury prevention
[SAE PAPER 710397] 10 p1557 A71-25132

Air and cosmic space common law, discussing boundaries, sovereignty over state territories and jurisprudence related to travel development
11 p1861 A71-26325

European airbus, considering flight trials of first A.300B high capacity transport aircraft
12 p1867 A71-26921

Air transport propulsion systems, discussing aircraft operating economics with reference to weight, size, powerplant efficiency, noise and air pollution
12 p1946 A71-27542

Turbofan STOL transport application to air transportation congestion, discussing conditioning landing field length, navigational/control problems and jet flap concepts
12 p1868 A71-27602

STOL aircraft/engine integrated systems for medium distance air transportation, discussing tradeoff factors involving performance, noise, weight and cost
[SAE PAPER 710469] 13 p2115 A71-28337

SST in relation to U.S. world leadership in air transportation, discussing federal funding needs for technological capability enhancement
13 p1998 A71-29387

Integrated short-haul interurban transportation system, considering combination of conventional jet aircraft, STOL aircraft and high-speed ground transportation
[AIAA PAPER 71-508] 14 p2221 A71-29550

Aviation within total transport system - Conference, London, May 1971
14 p2340 A71-30158

Air transport and travel expansion rate, discussing motivations and cost
14 p2340 A71-30159

Circumstances inducing growth in different air transport sectors, discussing transportation cost, aviation capital requirement and business and leisure air travel
14 p2340 A71-30160

Aviation within total transport system, discussing decision making and management planning
14 p2341 A71-30165

Air transport development trends, considering increased speed and capacity, STOL aircraft, urban service, and European cooperation for manufacturing
14 p2341 A71-30302

STOL vehicle and systems air transportation expansion by reducing trip time, congestion, noise exposures and pollution for DOT, DOD and NASA roles
[SAE PAPER 710464] 14 p2176 A71-30535

French contribution to air transportation, discussing international cooperation on supersonic Concorde, medium range airbus and short range Mercure
15 p2350 A71-32688

Air transport propulsion systems economics, considering first cost, specific weight, fuel consumption and maintenance effect on direct operating cost
16 p2523 A71-33469

Soviet book on air transportation covering ATC, automatic landing and information display systems
17 p2774 A71-35194

Aircraft for international long haul transportation, discussing criteria for selection based on environmental, operational, budgetary and policy considerations
17 p2674 A71-35208

Air transportation safety review covering weather knowledge, aircraft structures, instrumentation, radio aids and power plants
18 p2849 A71-36175

Passenger travel demand model for STOL transportation in underdeveloped areas
18 p2987 A71-36348

Future air transportation concepts, discussing short haul travel market, economic, environmental, safety, convenience and reliability aspects
18 p2989 A71-36671

New IATA passenger and baggage international air transport conditions, discussing passenger/carrier legal relationships, with emphasis on differences between new and old regulations
18 p2989 A71-36918

Hypersonic air transportation based on supersonic combustion ramjet development, discussing economic feasibility
19 p2995 A71-37124

European air traffic employed in transportation of tourists, considering European Airbus A-300B super twin
19 p3172 A71-37273

Costs/benefits strategy for investment in STOL fleets reducing delay and airport congestion, using heuristic computer model
19 p3173 A71-38029

Seasonal distribution of air transportation requirements and utilization rate of transport capacity in passenger traffic
19 p3173 A71-38221

Environmental radiation exposure in air travel, comparing integral radiation dosages for conventional jet transport aircraft and SST
20 p3192 A71-38976

Oxygen supply to air transported patients by chemical compounds, suggesting use of permanganates and chlorates
22 p3500 A71-41571

Sick and injured transportation aboard regular airliners, considering pathological and psychological contraindications
22 p3500 A71-41572

Vibration induced paroxysmal and cardiovascular hazards during patients transport to hospital by air or ambulance, discussing therapeutic and preventive treatments
22 p3500 A71-41573

In-flight study of work/rest cycle effects on double crew performance and fatigue in flying transport missions
22 p3501 A71-41829

Wrongful death liability in aviation and admiralty, considering U.S. Congress refusal to enact legislation
22 p3623 A71-42068

Judicial Panel on Multidistrict Litigation of federal district and court of appeals judges with power to transfer cases to single district
22 p3624 A71-42069

Short haul air transportation, discussing performance requirements, community acceptance and navigation and landing aids
22 p3482 A71-42073

VTOL air system for automobile travel replacement noting noise, cost, pollution and traffic congestion reduction
22 p3624 A71-42527

Future transportation technology impact, considering system design evaluation criteria and civil aviation and urban mass transit systems contributions
[AIAA PAPER 71-1010] 24 p3892 A71-44594

Commercial air transportation industry trends and optimal planning requirements, discussing airline economic viability, industry regulation, public service and environmental compatibility
[AIAA PAPER 71-1022] 24 p3892 A71-44600

Weather interruption effects on air transportation operations and economics, considering fog, snow, freezing rain, thunderstorms, winds, CAT and runway conditions
24 p3845 A71-44983

AIRBORNE EQUIPMENT

NT AIRBORNE/SPACEBORNE COMPUTERS

Airborne trainer and ground simulator for undergraduate navigator training system
01 p0023 A71-10522

CAT radar observation from instrumented and uninstrumented jet fighter flights, analyzing data statistically for spatial correspondence of ground and airborne observations
01 p0116 A71-10566

Aircraft electric systems control by solid state switching, discussing reliability, service life, versatility and compatibility
01 p0007 A71-11627

Reverse flow temperature probe design and calibration for vertical soundings from aircraft, comparing to radiosonde method
02 p0247 A71-11822

Aircraft variable frequency electrical generating systems, discussing weight and size reduction in motors and static inverters by gate controlled switches
02 p0197 A71-12908

Short haul STOL concepts including stolport potentials, onboard avionics, vehicle characteristics, tradeoffs and current nonproductive flying due to traffic congestion
03 p0348 A71-13620

Airborne radar as helicopter approach aid
04 p0624 A71-15425

Airborne radiation thermometry corrections for intervening atmospheric absorption and emission and ocean surface nonblackness
04 p0601 A71-15762

Rocket probe launched by aircraft for measuring pressure, temperature, magnetic field and wind velocity around tornado vortex through radio telemetry
05 p0778 A71-17140

Impulse drive strip-chart recorder with low battery drain for high altitude balloon flights
05 p0755 A71-17143

Atmospheric path effects on spectral radiance intensity in remote airborne multispectral sensors
06 p0898 A71-17559

Side-looking airborne radars ground and slant range imagery mosaic preparation and geoscience interpretation, analyzing terrain geometry, radar shadow and layover
06 p0898 A71-17561

Airborne X band reflect phased array radar antenna design for simultaneous functions including large volume search, target attack with general surveillance and low altitude assist
06 p0876 A71-18096

Aircraft midair collision avoidance, discussing Elimination Range Zero system operation procedures and cost
07 p1154 A71-19079

Airborne surveillance for environmental management, discussing earth resources program, aerial sensors for thermal water pollution, crop disease, salinity and geological structure
07 p1018 A71-19080

Balloon heliophysics, discussing equipment and working program of first Soviet stratospheric solar station
07 p1195 A71-19336

Draw-through cooling of electronic equipment in subsonic and supersonic commercial jet transports, discussing internal circulation system design
[SAE-AIR-64A] 07 p1077 A71-19642

Constant false alarm rate (CFAR) operation of airborne pulse Doppler radar in nonhomogeneous and point clutter, using similar critical region test
07 p1065 A71-20421

Airborne night vision system performance, determining maximum range for ground target acquisition
08 p1286 A71-20692

Horizontally and vertically polarized sferic signals from lightning discharges by airborne instrumentation, using pattern recognition approach
08 p1325 A71-20883

Department of Defense data processing equipment for all weather airborne terrain imaging radar mapping
08 p1288 A71-21250

Side-looking airborne radar and IR line scan systems, discussing instrumental correction of image distortion
09 p1450 A71-22967

Airborne multispectral remote sensing of forests, describing previsual detection of damage from insect infestations, disease organisms and oxidant air pollution
09 p1438 A71-23210

Cartographic characteristics and applications of airborne radar sensors, stressing synthetic aperture radar and electronic techniques and equipment
09 p1452 A71-23219

Airborne electronics reliability testing in temperature controlled chamber
10 p1589 A71-24604

Avionics growth, discussing use of digital computers, solid state transducers, integrated circuits, electronic flight instruments, area navigation and collision avoidance systems
12 p1906 A71-26878

Terrain following radar for airborne guidance of low flying military aircraft
12 p1927 A71-26881

Airborne Doppler radar receiver transmitter failure testing by Versatile Avionics Shop Test computer controlled system
13 p2031 A71-28778

Earth surface temperature measurement by airborne IR radiometers, discussing accuracy provided by narrow and wideband filters
14 p2240 A71-30126

Self contained lightweight airborne data acquisition system for atmospheric and meteorological research, using analog recorder and telemetry system
14 p2243 A71-30311

Integrated flight test data system combining digital airborne data acquisition/recording system with telemetry/microwave link to computerized ground station
14 p2243 A71-30318

Onboard weighing system for gross weight determination and center of gravity location of Alouette helicopter, using load sensors, electrical circuits and visual indicators
14 p2175 A71-30320

Target movement effects on airborne coherent side-looking synthetic aperture imaging radar during scan rate and compression ratio increases
14 p2197 A71-30798

High efficiency autotrack strip-line-fed dipole antenna array for L and S band airborne telemetry
14 p2198 A71-30905

High speed airborne scanning navigational radar antenna with matched patterns, using offset horn feed reflector and polarization modes for improved visual display
14 p2216 A71-31036

- Airborne phased array using computer control for beam steering, investigating row-and-column logic effects on beam shaping and stabilization
14 p2209 A71-31045
- Helicopter aerial design problems, considering antenna multiplicity use of nonmetallic structures and complexity of airborne radio systems
14 p2217 A71-31048
- Collimating optically fed circular antenna array using quadratic phase tapers, emphasizing airborne applications
14 p2206 A71-31064
- Emitter location techniques for airborne passive ECM, discussing accuracies in terms of geometry, sample number, random and bias errors
15 p2375 A71-31205
- Airborne ECM receiver, determining conditions for detecting victim radar signal before signal reflection from aircraft
15 p2368 A71-31207
- Book on fluidic systems design covering analog and digital control, application to aircraft, spacecraft, computers, tracking devices and equivalent circuits
16 p2526 A71-33475
- Category II operations at various airports, considering all-weather landing requirements of airborne equipment, maintenance standards, pilot training, etc [SAE PAPER 710442]
17 p2674 A71-34499
- Airborne display and electric management system, discussing weight reduction, protective function coordination, power quality, onboard maintenance, data processing and reliability
17 p2739 A71-34617
- Comet 4 installation and experimental program, investigating avionics systems integration techniques
17 p2774 A71-35070
- Radio controlled small aircraft as measurement platform for meteorological sensors, discussing development and performance from field tests
17 p2675 A71-35334
- Military and civil aircraft navigation systems development, emphasizing self contained airborne equipment
17 p2775 A71-35374
- Airborne communications with AN/ARC-154 transceiver in single radio, discussing extended frequency coverage, multimode operation, navigation and input/output provisions
17 p2775 A71-35758
- Airborne vidicorder visual communication system for transmitting single frame TV information in digital form from air to ground over narrow and wideband circuits
17 p2709 A71-35760
- Airborne Doppler velocity sensors, considering hydrometeors effects on HF signal attenuation and reflection
17 p2747 A71-35768
- Real time reconnaissance cockpit display system for airborne sensor systems, providing night combat imagery
17 p2747 A71-35772
- Noise equivalent irradiance equation for airborne IR scanner at peak response detector wavelength, involving target scene radiance and hot iridome emittance
18 p2917 A71-36053
- Airborne astrographic camera system for simultaneous determination of multiple object reentry trajectories at Air Force test range
18 p2918 A71-36077
- Operational calibration of airborne IR spectrometer over hydrogeologically significant terrains, obtaining radiance spectra
18 p2920 A71-36363
- Thermal mapping performance of passive airborne IR scanners for remote environmental sensing, estimating SNR and noise equivalent irradiance
18 p2921 A71-36364
- Vegetation penetration with K-band side-looking airborne imaging radars, noting multifrequency multipolarization system application for terrain reconnaissance
18 p2875 A71-36365
- Side-looking airborne radars and image recording scanners design for geoscience applications, discussing gray scale improvement, multispectral sensing, target discrimination, etc
18 p2875 A71-36366
- Aircraft onboard equipment tests in air navigation aid satellite project, estimating tracking random errors
18 p2877 A71-36509
- Emission transistor for Eole balloon transmitter power amplifier, discussing trouble-free emission, high output, wide temperature range, lightweight and reliability features
18 p2891 A71-36563
- Light detection and ranging (LIDAR) system in airborne and ground applications for moving target location and tracking
18 p2882 A71-36615
- Time and frequency synchronization for EROS airborne collision avoidance system, considering impact on aeronautical communication, navigation and surveillance
19 p3100 A71-37604
- Simulator for operating decision rules for control of airborne IR forest fire detection system
19 p3066 A71-38409
- Latent forest fire detection, describing airborne IR surveillance system
19 p3066 A71-38410
- Complex airborne electronic system design for interference minimization, considering electromagnetic compatibility
19 p3033 A71-38464
- Apollo range instrumentation aircraft, describing C-135A modification with airborne lightweight optical tracking systems
19 p3022 A71-38546
- StarLifter borne large aperture astronomical telescope for IR and submillimeter observations, discussing design and operation
20 p3234 A71-39173
- Aircraft sounding of atmospheric microwave radiation transfer compared with IR method, measuring optical Mie characteristics, water vapor content, cloudiness, ice cover, etc
20 p3259 A71-39673
- Auroral conjugacy and time dependent geometry via all sky cameras and image orthicon TV onboard conjugate-flying aircraft
20 p3228 A71-39840
- Aerial photographic equipment survey, describing topographic cameras, aerial photograph orientation equipment, onboard navigation instruments and mapping survey system
21 p3380 A71-40875
- Performance levels prediction for airborne solid state phased array radar transmission sources, considering TRAPATT devices
22 p3509 A71-41630
- Two-axis pneumatic rate gyroscope with externally pressurized gas bearing for airborne vehicle fluidic autostabilizer sensor
22 p3551 A71-41666
- Remote sensing of chlorophyll and temperature in marine and fresh waters by spectroradiometer and differential IR filter radiometers onboard airplane
22 p3534 A71-41986
- Environmental quality indices from spaceborne or airborne remote sensing
22 p3534 A71-41995
- Airborne IR linescan equipment for commercial aerial survey, discussing operational principle, temperature sensitivity, data processing and individual system components specifications
22 p3545 A71-42151
- VOR/DME air navigation equipment using Kalman-Bucy filter and airborne air data system/ADS/
22 p3573 A71-42289
- Electro-optical techniques for particle size measurements from aircraft, noting imaging techniques superiority for nonaerosol and large particles
23 p3677 A71-43514
- Solid state airborne weather radar for civil aviation, discussing design, weight and power requirement reduction
23 p3647 A71-44273
- AIRBORNE INFECTION**
Bacterial contamination in confined sealed space during long term human occupation, observing hemolytic microflora spreading dynamics on bodies, clothes, wall and air
21 p3343 A71-40560
- AIRBORNE RANGE AND ORBIT DETERMINATION**
Radar ranging experiment onboard Jupiter orbiter, concerning perturbations, gravitational harmonics and short arc orbit determination
15 p2487 A71-32041
- AIRBORNE TERRAIN ANALYSIS**
U TERRAIN ANALYSIS
AIRBORNE/SPACEBORNE COMPUTERS
NASA modular aerospace computer for attitude control high speed computation, describing implementation with LSI functional characters
01 p0045 A71-10198
- Airborne military multiprocessor compatible with commercial computers, discussing executive control, input-output interrupts, load balancing, self diagnosis, etc
01 p0046 A71-10206
- On-line software checkout facility for special purpose computers used in developing spaceborne programs
01 p0048 A71-10227
- Space navigator operations, procedures and computer interface and manually aided onboard Apollo cislunar navigation system possible improvement
01 p0124 A71-10510
- Flight test evaluation of onboard automatic computer controlled jet engine monitoring system with reduced fault detection time
03 p0395 A71-13080
- Onboard monitoring sensor trends for airborne computer automatic data systems, noting digital transducers, LSI logic and solid state devices
03 p0395 A71-13081
- Small scientific spacecraft onboard computers, discussing integration into satellite telemetry system and relationship with ground based data processing facilities
03 p0382 A71-13246
- ELDO inertial guidance system digital computer, explaining guidance law subsystem formulation and programming
03 p0454 A71-13247
- Digital computers in aviation electronics, discussing automatic control loop in automatic pilot
03 p0382 A71-13687
- Space launchers flight control and guidance systems technology, emphasizing use of onboard digital computers
05 p0817 A71-16678
- Nimbus 4 satellite telemetry information processor with data sampling and formatting flexibility
05 p0726 A71-17135
- Digital computer techniques for Mars surface imagery systematic video data distortions quantification and correction onboard Mariner 6 and 7
06 p0871 A71-17631
- Kalman filter simulation for estimating aircraft position and velocity from airborne digital computer data in zero-zero landing system
06 p0924 A71-17697
- Onboard air navigation computers drift correction by mapping radar, calculating position by region over flown image/measured geographic features comparison
06 p0925 A71-17952
- Navy avionic modular multiprocessing digital computer operating system reliability, comparing totally software and partly hardware approaches
07 p1067 A71-15833
- Computer requirements of self contained guidance, navigation and control system onboard manned orbital space station
07 p1155 A71-19702
- Passive airborne computer augmented aircraft antenna pointing control system for communication satellites tracking
07 p1077 A71-19710
- Aircraft navigation system requiring computer and display for approach guidance to circular orbit over fixed ground area
07 p1156 A71-20305
- Automatic Carrier Landing System with linear adaptive aircraft Navigation Computer, investigating effectiveness in reducing system errors due to nonlinearities and noise effects
07 p1157 A71-20405
- Flexibly programmable spacecraft data handling system, considering computer aided telemetry system for data acquisition and transmission
08 p1258 A71-21317
- Optimal algorithmic coordination of spacecraft computer-transmitter coupling, using SIMSCRIPT language simulation
08 p1259 A71-21599
- Spacecraft computer centered data systems with standby redundancy, automated flexibility and LSI devices for grand tour mission
08 p1260 A71-21846
- Commercial V/STOL aircraft area navigation system requirements, discussing airborne computer, flight plan data storage and control subsystems and horizontal orientation display
10 p1639 A71-24150
- Flight vehicle adaptive control systems with onboard digital computers, considering control algorithm complexity, processing rates, weight and geometry restrictions, accuracy and adaptability requirements, etc
12 p1883 A71-26715
- Computerized automatic control system for atmospheric reentry, combining computational prediction of motion parameters with closed loop feedback
12 p1926 A71-26720
- Airborne integrated data system capabilities based on flight tests with commercial aircraft
14 p2208 A71-30319
- Onboard computer for aircraft engine testing, monitoring and data reduction, emphasizing automatic in-flight recording for post-flight displays
14 p2290 A71-30727
- Weapons delivery computer for attack helicopters, using planar distributed function generator for general closed form instantaneous solution capability
14 p2209 A71-31092
- European Airbus automatic pilot and flight control system, including computers in electromechanical subassemblies
15 p2446 A71-31914
- On-line real time optimal control computations for aerial combat games between two aircraft, assessing airborne computer requirements
16 p2525 A71-34022
- Discusses communication satellite system for air traffic control and navigation, discussing aircraft antenna beam electronic scanning by computerized control
17 p2714 A71-34681
- Computerized automatic control of aircraft electrical system using remote power controllers and mul-

plexed data bus for wiring reduction and reliability improvement 17 p2677 A71-34700

STOL aircraft guidance capability with onboard digital computer, maintaining time of arrival envelope at way points along complex flight paths [AIAA PAPER 71-770] 17 p2775 A71-35528

Higher order computer language architecture for aerospace software production problems, discussing real time constraints, hardware tradeoffs, memory, computer design and logic circuitry 17 p2712 A71-35777

Hardware executive control with associative memory for avionic digital computer system, comparing computation speed, cost and reliability with software method 17 p2712 A71-35778

Ferrite core memories for information storage of digital computer onboard Eole satellite, discussing design and reliability measures 18 p2891 A71-36560

Low power nonpulsating arithmetic unit of 16 bit integer numbers for spaceborne applications, using module printed circuit cards 18 p2886 A71-36570

BAC 111 autopilot development, discussing computer compatible system for digital representation of airborne flight test data and direct transmission to ground-based computers 18 p2946 A71-36672

Gas controlled variable conductance heat pipe for OAO-C onboard processor temperature stabilization, describing thermal performance tests under simulated flight conditions [AIAA PAPER 71-411] 18 p2975 A71-36775

Navigational accuracy improvement by combining VOR/DME information with airspeed and heading data via maximum likelihood filter, using small airborne computer [AIAA PAPER 71-928] 19 p3097 A71-37174

Airborne traffic situation display for use with national airspace/automatic radar control terminal system, using computer selected message, map and heading data [AIAA PAPER 71-929] 19 p3097 A71-37175

Computerized automatic redundancy management for space shuttle guidance, navigation and control, using fly by wire control technique for in-flight failure detection and correction [AIAA PAPER 71-946] 19 p3098 A71-37187

Kalman filter for computerized optimal SRAM air to surface missile alignment, discussing design, digital simulation and flight tests [AIAA PAPER 71-948] 19 p3098 A71-37189

High reliability computers via multiprocessing for long duration space missions, discarding quad redundant and majority voter approaches [AAS PAPER 71-158] 19 p3152 A71-37927

Europa 3 electrical system as integrated vehicle control system using central processor and data bus 22 p3608 A71-41957

Two stage reusable manned space shuttle computerized onboard data management system hardware and software [IBM-712000405] 22 p3517 A71-41977

Fast spacecraft trajectory computation in n-body inverse square force field, developing closed form recurrence formula for onboard computers [AAS PAPER 71-382] 23 p3731 A71-43052

Landing control algorithm using onboard digital computer for spacecraft hyperbolic velocity reentry, discussing simulation test results 24 p3846 A71-45303

AIRCRAFT

Aerodynamic characteristics of aircraft in steady and unsteady supersonic flow by analog electrical method, including wing-fuselage interactions 03 p0339 A71-13130

Operational preparation and commissioning of IL-62 long distance jet aircraft, considering flight crew and maintenance personnel training at U.S.S.R. plant 11 p1743 A71-25256

Aircraft and airports as air pollution sources, stressing industries understanding of applicable control technology 15 p2349 A71-32243

Aircraft/environment compatibility, emphasizing decision making process for airport planning, site location, development and operation 15 p2516 A71-32248

AIRCRAFT ACCIDENT INVESTIGATION

Aircraft crash investigation, deducing in-flight explosion by failure analysis techniques 01 p0087 A71-10456

Air accident investigation and litigation - Conference, Dallas, March 1970 03 p0522 A71-12961

On-site aviation accidents investigation and prevention, noting National Transportation Safety Board procedures 03 p0522 A71-12963

Aircraft accident hearings for discovering facts, causes and preventive measures 03 p0523 A71-12964

Air carrier accident investigation, noting procedures, individual and group functions, notifications and company field organization 03 p0523 A71-12965

Aviation accident long interrogatories for analyzing man, machine and environmental factors, noting legal aspects and preparation 03 p0523 A71-12967

Aircraft accident reconstruction by lawyers using expert testimony and admissible evidence 03 p0523 A71-12969

Aircraft accident damages recovery trial procedure, discussing pleadings, settlements, depositions and jury summation 03 p0523 A71-12970

Aircraft accidents medical aspects, investigating cause, death mode, emergency suddenness, specific injuries and safety equipment evaluation 08 p1244 A71-20713

Physiological aspects of aircraft accident investigation, considering pilot errors 08 p1247 A71-20825

Materials failure role in Canadian civil aircraft accidents, discussing organized investigation and data flow 08 p1231 A71-21679

Aircraft accidents investigation toxicological aspects, discussing drugs, alcohol and carbon monoxide involvement [SAE PAPER 710395] 10 p1569 A71-24259

General aviation aircraft accidents involving seat belt and shoulder harness restrained occupants, discussing vertical force effects on survivability and injuries in severe crashes [SAE PAPER 710399] 10 p1555 A71-24261

Possibilities of alcohol detection in blood and other tissue by alcohol examinations using experience from aircraft accidents case histories 13 p2023 A71-29366

Computerized simulation techniques for investigating aircraft accidents due to atmospheric turbulence 14 p2221 A71-29779

Air transport accident research in night approach simulators, noting visual information null in descent path and delay in relative motion supplement data 15 p2363 A71-31602

Epidemiology statistics of USAF spatial disorientation aircraft accidents, noting pilot training, flight environment and indoctrination remedy programs 21 p3342 A71-40359

Physiological factors in fatal aircraft accidents, discussing pilot incapacitation and transient functional disturbances 22 p3502 A71-41834

Book on fatal civil aircraft accidents medical and pathological investigation covering transport, light and glider aircraft case histories and statistics 23 p3638 A71-42910

Corporate aircraft 1970 accident statistics analysis stressing pilot selection, training and supervision 23 p3628 A71-43227

Aircraft skidding accidents investigation, comparing airplane stopping distance computations and observations 23 p3628 A71-43228

Continued flight training correlation with general aviation aircraft accident rates reduction 23 p3641 A71-44252

AIRCRAFT ACCIDENTS

Aircraft emergency evacuation illumination standards, considering independent power source, crash survivable installation, operation initiation and exit visibility 01 p0004 A71-10030

ATA Collision Avoidance System based on time and frequency synchronization via ground stations or other aircraft 02 p0280 A71-12895

Aviation accidents liability limitation by treaty and statute for passengers personal injury or death, discussing Warsaw Convention revisions 03 p0523 A71-12966

Air crash litigation liability limitations, noting international inequality 03 p0523 A71-12968

Aircraft flight aerodynamics from accident prevention viewpoint, discussing angle of attack, turbulence effects, weather factors, etc 03 p0346 A71-13017

Civil aircraft accident and maintenance recording regulations and systems, discussing airborne equipment 03 p0348 A71-13735

Aircraft accident trends and preventive practices, considering fatal landing statistics 04 p0529 A71-14995

Air traffic control using collision risk equations, noting data handling automation, airborne collision avoidance devices and geostationary satellites 04 p0624 A71-15646

Corrosion damage relationship to military aircraft accidents, discussing quality control, material selection and manufacturing processes 06 p0911 A71-17415

Human factors in glider accidents, discussing drugs, fatigue, oxygen lack, nervous tension, etc 06 p0860 A71-18196

Aircraft midair collision avoidance, discussing Elimination Range Zero system operation procedures and cost 07 p1154 A71-19079

Aircraft accidents medical aspects, investigating cause, death mode, emergency suddenness, specific injuries and safety equipment evaluation 08 p1244 A71-20713

Civil aviation medicine practice, discussing airman certification for flight fitness, government legislation, accidents and carrier operations 08 p1245 A71-20728

Vision loss from windshield tinting in night visual flying accident 08 p1247 A71-20824

Air traffic controllers legal responsibility and disciplinary procedure, considering clearances, flight crew instructions and aircraft accidents 09 p1548 A71-22891

European view on liability and compensation limitation for death and injury in international commercial air transport 09 p1548 A71-22989

U.S. view on legal liability and compensation for death and injury in international air transport 09 p1548 A71-22990

Aircraft aquaplaning skidding prevention by runway resurfacing and water depth sensor warning indicators 10 p1609 A71-23946

Psychoreactive action caused by flying accident in group, discussing repercussions in civil and military aviation fields 10 p1572 A71-24982

Medical planning and first aid in disasters at airports 11 p1725 A71-26128

Aircraft accident rescue system with helicopters, discussing cooperation between helicopter service and ground personnel 13 p2020 A71-28721

Turbulence-related accidents frequency and severity during past few years from worldwide synopsis 13 p1997 A71-28885

U.S. air carrier accidents due to atmospheric turbulence, considering in-flight weather problems, airborne meteorological radar, CAT detection systems, etc 14 p2172 A71-29770

Aircraft accidents due to engine-out simulation, discussing human factors, minimum control speed certification requirements and pilot flight training procedures [AIAA PAPER 71-793] 16 p2525 A71-34025

Aircraft accident litigation related to wake turbulence concerning pilot or air traffic controller faults 17 p2842 A71-35387

Biomedical requirements and emergency planning for aerodromes, surveying U.S. airports 18 p2864 A71-35999

Air safety standards and objectives, discussing human factors as accident causes, piloting aids and management 20 p3178 A71-39395

Aircraft ditching and flying personnel survival, stressing passenger briefing and crew jacket equipment with VHF transceiver for rescue operations coordination 23 p3628 A71-43229

Aircraft accelerate-stop factors and regulations, pilot reaction times and accidents during takeoff 23 p3628 A71-43380

Barometric altimetry system inadequacies and approach/landing accidents, noting pilot static components blocking hazards 23 p3628 A71-43384

Corporate aircraft pilot ground and flight phase training, errors and accidents 23 p3629 A71-43388

Airport crash fire fighting equipment requirements and rescue operations 23 p3629 A71-43389

Cumulative /chronic/ and acute skill fatigue and physical fitness in aircrews, considering relationship to pilot error accidents 23 p3639 A71-43390

Mortality in survivable or partially survivable U.S. Army aircraft accidents, observing death relationship to aircraft duty and seat location and type 23 p3640 A71-44248

AIRCRAFT ANTENNAS

Passive airborne computer augmented aircraft antenna pointing control system for communications satellites tracking [AIAA PAPER 71-233] 07 p1077 A71-19710

Multiple planar Luneberg lens circular array for airborne electronically scanned X band narrow beam antenna mounted under aircraft nose or fuselage 14 p2216 A71-31038

Structural design, mechanical stability and aircraft compatibility for airborne side-looking radar antennas, using end fed slotted waveguide arrays 14 p2205 A71-31041

Flush mounted aeronautical waveguide antennas with dielectric plug for 5GHz operation

14 p2216 A71-31043

Airborne blade antenna tunable for 26-100 MHz by individual bands, using binary related inductors switched by miniature high vacuum relays

14 p2216 A71-31044

Low carrier power aircraft antenna module for airborne UHF communications system, considering range/field strength measurements

14 p2216 A71-31046

Fincap communication antennas design and environmental tests for vibration, acceleration, waterproofing, salt corrosion, ice formation and compass safe distance

14 p2216 A71-31047

Helicopter aerial design problems, considering antenna multiplicity use of nonmetallic structures and complexity of airborne radio systems

14 p2217 A71-31048

Light aircraft notch antenna for efficient radiation at HF band lower end and minimal interference with aircraft structure

14 p2217 A71-31053

Aircraft phased arrays for L-band ATC satellite system application, alleviating problems of power budget and vulnerability to multipath and interference

14 p2217 A71-31054

High efficiency narrow beam aircraft Cassegrain antenna design for horizon without excessive ground illumination

14 p2217 A71-31056

L band aircraft antenna array consisting of circularly polarized elements and static electronic steering circuits for synchronous satellites radio links

14 p2273 A71-31074

Aerospace antenna design, calculating one-wavelength circular slot aperture radiation from circular cylindrical surface

14 p2206 A71-31075

Electronically scanned cruciform slot-array aircraft antenna for satellite controlled navigation aid, discussing circularly polarized wave radiation

16 p2548 A71-34123

Dioscures communication satellite system for air traffic control and navigation, discussing aircraft antenna beam electronic scanning by computerized control

17 p2714 A71-34681

Meter wave aircraft slot antenna for Concorde air to ground communication via satellite, presenting synthetic radiation patterns

18 p2889 A71-36514

Numerical method for near field antenna coupling over conducting surface of aerospace vehicles applied to L band slot antennas on F-4 Phantom aircraft

19 p3031 A71-38445

Streamer discharges effects on integrated aircraft antenna and associated avionics, emphasizing RF interference and component damage

19 p3033 A71-38462

Beam direction weight center of signal spectrum and effective antenna centers of airborne Doppler velocimeter in horizontal flight

19 p3033 A71-38496

Infrared and thermal evaluation of tactical aircraft phased array radar antenna design with cooling air distribution for steady state operating temperature maintenance

21 p3352 A71-40434

AIRCRAFT APPROACH INSTRUMENTS

U APPROACH INDICATORS

AIRCRAFT APPROACH SPACING

Maximum throughput-rate capacity for runway and final approach path airspace involving multiple lfr landings

02 p0279 A71-12893

Optimal air traffic control coordinating flow and holding patterns of aircraft landing in single runway using linear-quadratic technique

08 p1332 A71-21335

Automation in third generation ATC requiring distributed management and spacing functions delegation to pilot

19 p3100 A71-37602

[CASI PAPER 72/15]

AIRCRAFT BASES

U MILITARY AIR FACILITIES

AIRCRAFT BRAKES

NT LEADING EDGE SLATS

NT TRAILING-EDGE FLAPS

NT WING FLAPS

Snatch force during lines-first deployment of aerodynamic decelerator, including effects of canopy skirt acceleration and suspension wave propagation characteristics

09 p1385 A71-22915

C-5A airplane Be brakes, considering critical design weight environment for optimum load carrying capacity

13 p1996 A71-28313

Concorde lightweight disk brakes, discussing operating costs, weight and volume factors, design philosophy, structural materials, component life, maintenance and reliability

16 p2522 A71-33226

AIRCRAFT BREATHING APPARATUS

U BREATHING APPARATUS

AIRCRAFT CABINS

U AIRCRAFT COMPARTMENTS

AIRCRAFT CARRIERS

Aircraft flying qualities research program, discussing navy test pilot evaluations and longitudinal handling characteristics for simulated carrier landing task

[AIAA PAPER 69-897]

02 p0189 A71-12678

Night carrier landing final approach glide slope altitude, lateral and sink rate pilot errors prediction, using linear regression model

06 p0858 A71-17602

Carrier aircraft inertial navigation system (CAINS)/design, noting thermal modeling, statistically filtered alignment modes and digital data links

22 p3571 A71-42081

AIRCRAFT COMMUNICATION

Communications, navigation and surveillance for aircraft and marine vessels in North Atlantic region, discussing baseline traffic control model

07 p1153 A71-18808

Aeronautical satellites, considering air-ground telecommunication, air traffic control and inertial navigation applications

12 p1971 A71-26825

Airborne radio communication systems, stressing electronic equipment design reliability

12 p1878 A71-26880

Blade antenna linear array design for aircraft-satellite communication, determining mutual influences by array measurements in simulated electrical environment

14 p2206 A71-31062

ATC satellites providing communications channels between aircraft and ground control stations and aircraft localization

16 p2605 A71-32849

Satellite-to-aircraft links propagation characteristics, considering specular reflected signals, diffuse scattering and scattering function

17 p2705 A71-35097

Civil aviation and merchant marine satellites, considering aircraft and surface vessel antenna characteristics and modulation techniques for optimum communication channel frequencies

17 p2775 A71-35582

Satellite to aircraft radio link simulation, evaluating electronic scanning antenna operation, intelligibility, data transmission rate and distance measurement accuracy

18 p2945 A71-36511

Meter wave aircraft slot antenna for Concorde air to ground communication via satellite, presenting synthetic radiation patterns

18 p2889 A71-36514

Frequency memories application to earth-satellite-aircraft UHF communications, repeater apparatus and multiple access transmission of half tone images in worldwide satellite communication

18 p2881 A71-36553

Ground-aircraft link via synchronous communication satellite, discussing transmission frequency selection, ionospheric effect on propagation and satellite antenna

19 p3016 A71-37314

Time and frequency synchronization for EROS airborne collision avoidance system, considering impact on aeronautical communication, navigation and surveillance

[CASI PAPER 72/17]

19 p3100 A71-37604

AN/ARC-144 solid state ultrareliable UHF multimode aircraft transceiver, discussing tuning, frequency synthesis and broadband power amplifier

20 p3196 A71-39209

Aeronautical satellite systems program planning for improved aircraft communications, ATC and other air traffic services in airspace over oceanic areas

22 p3573 A71-42096

Corporate aircraft operations in Latin America, discussing communication and navigation, fuel, paper work, food, vaccinations and weather

23 p3629 A71-43391

AIRCRAFT COMPARTMENTS

Aircraft compartment glare minimization for flight crew visibility conditions and visual performance improvement

01 p0004 A71-10028

Aircraft galley design safety criteria, considering injuries from routine use, normal, crash or ditching conditions component dislodgment, equipment malfunctions and defects

01 p0004 A71-10029

Helicopter design for cabin noise level reduction

04 p0532 A71-15423

Aeromedical requirements, control limitations and hazards of aircraft pressure cabins and rapid decompression

08 p1244 A71-20715

Fluidic cabin pressure automatic control systems for military and civil aircraft, discussing design, operation and performance

14 p2182 A71-30308

AIRCRAFT CONFIGURATIONS

Short haul STOL concepts including stolport potentials, onboard avionics, vehicle characteristics, tradeoffs and current nonproductive flying due to traffic congestion

03 p0348 A71-13620

Reliability and maintenance problems of U.S. Army operational environment, noting inadequate design and test criteria during development

04 p0530 A71-15402

Tilt-rotor VTOL aircraft design, discussing ground proximity effects on blade bending moments and flying qualities

04 p0531 A71-15404

Hypersonic cruise aircraft configuration reliable Reynolds numbers extrapolation from laminar boundary to turbulent layer

[AIAA PAPER 71-132]

06 p0883 A71-18576

Soviet book on Yak-40 passenger transport aircraft configurational design and aerodynamic characteristics covering stability, controllability and flight under special conditions

08 p1230 A71-20750

Transavia Airtuk agricultural aircraft, discussing efficiency, work capacity, economics, configuration and performance

08 p1230 A71-21224

Wind tunnel dynamic stability testing of unconventional aircraft configurations without sting support

[AIAA PAPER 71-276]

08 p1274 A71-22001

Aladin 2 French STOL project, consisting of suitably flapped wings with multiple propulsion units with fishtail exhaust nozzles inside rectangular ejectors

10 p1556 A71-24283

Aircraft continuous elastomechanical system parameters determination by ground vibration tests, using integral equation, phase resonance and separation technique

[DFVLR-SONDDR-103]

10 p1692 A71-24946

Aircraft with T tail configuration, examining dynamic response to lateral gusts

14 p2174 A71-29786

Wind tunnel force test program design for jet aircraft configurations, including propulsion system simulation

14 p2176 A71-30605

Computing geometric airplane aerodynamic characteristics during preliminary and detailed design processes

15 p2348 A71-31597

Optimum vertical surface configuration for STOL transports, considering structural weight and performance requirements

[AIAA PAPER 71-769]

16 p2524 A71-34006

Control configured vehicle design longitudinal requirements due to application of relaxed static stability and maneuver load control

[AIAA PAPER 71-786]

16 p2525 A71-34016

Experimental and theoretical aeroelastic analysis of Fokker F-28 T tail, using flutter model and flight flutter tests

17 p2676 A71-35649

Supersonic aircraft shape for shock waves minimization based on channel configuration with converging inlet and diverging outlet section

24 p3791 A71-44572

Panavia 200 multipurpose military aircraft, describing variable geometry design concept, performance characteristics, engines, armament and electronics

24 p3792 A71-44766

AIRCRAFT CONSTRUCTION

U AIRCRAFT STRUCTURES

AIRCRAFT CONTROL

NT HELICOPTER CONTROL

Aircraft direct lift control based on flight and simulator experiments, discussing effect on design

01 p0005 A71-10754

Aircraft flaps and ailerons actuators electronic fly by wire control as alternative to mechanical linkages for maneuverability and reliability in flight

01 p0006 A71-10825

Mathematical model and digital simulation for nonlinear characteristics of prototype integrated actuator package for fighter aircraft control

02 p0190 A71-11783

Aircraft manual flight control analysis using continuous mathematical pilot model for closed loop digital simulation

02 p0188 A71-11787

Trailing edge flap automatic control for glider performance improvement

03 p0346 A71-13020

Heavy supersonic aircraft controllability, noting irreversible boost control system and stability

03 p0454 A71-13195

Aircraft longitudinal motion decoupling through direct lift control, investigating flight control for landing

03 p0347 A71-13339

Time vector method for aircraft flight test data evaluation, discussing control deflections effects on phugoid motion, lateral stability derivatives and error estimation

03 p0347 A71-13341

AIRCRAFT DESIGN

Spacecraft and aircraft automatic control man machine interface, bionics and traffic control systems
03 p0455 A71-14393

Wing upper surface air suction influence on aircraft longitudinal controllability, considering control stick forces for deflected flaps and angle of attack
04 p0528 A71-14594

Pilot training flight simulators without visual or motion cues, discussing validity for aircraft handling qualities assessment and pilot role in simulation process
[DGLR-70-070] 05 p0733 A71-15968

Aircraft longitudinal control during landing approach, investigating back side operation characteristics by closed loop system analysis regarding pilot and aircraft as elements
05 p0696 A71-16388

Frequency and amplitude during longitudinal control surface pumping by pilots in precise flight path handling for aircraft design
[AIAA PAPER 70-567] 06 p0847 A71-17699

Time vector method extension to equations of motion with real roots, noting applications to aircraft flight control problems
06 p0925 A71-18049

Eigen proportional control method for second order system with time varying parameters, applying to aircraft autopilot systems
06 p0925 A71-18308

F-104D aircraft side stick control system design and function, curriculum maneuvers and component reliability
07 p1018 A71-19092

Design objectives for subsonic, transonic and supersonic civil transport flying characteristics based on MIL-F-8785, considering aircraft control
[SAE-ARP-842B] 07 p1019 A71-19645

Aircraft electronic control systems, considering hydraulic servocontrol, force simulation and reliability models
07 p1156 A71-20064

Airliner acceptance checks characteristics for official licensing prerequisites, investigating takeoff, landing, ascent, stability and control
07 p1022 A71-20065

Two dimensional aircraft automatic landing motions control processes by simulation without use of moving cockpit simulator
07 p1084 A71-20066

Optokinetic and vestibular effects on human operator reliability in aircraft control systems
09 p1399 A71-22681

Aircraft industry ATC techniques and equipment contribution to aircraft control and safety
09 p1491 A71-22951

Soviet book on aircraft flight with incomplete and asymmetrical thrust covering probabilistic characteristics, stability, landing and takeoff with partial engine failures, etc
10 p1554 A71-24013

Automatic control system for fighter aircraft sideslip correction, using rudder position sensor, transverse accelerometer and high pass filter for anticipatory sideslip reduction
10 p1556 A71-24288

Constrained gain problem optimality conditions, presenting algorithm for optimal gains and application to aircraft control problems
10 p1588 A71-24859

Soviet papers on automatic control for flight vehicles, Part 1, covering dynamics of linearized systems, deterministic and random inputs, stability, oscillations, thrust control, etc
10 p1588 A71-24897

Aircraft with automatic thrust controller, calculating transfer functions characterizing speed and attitude control modes
10 p1640 A71-24910

Variable sweep wing aircraft angular motion mathematical model, analyzing inertial moments influence on control dynamics
11 p1708 A71-25661

Sailplanes tail load static derivation for instantaneous unchecked longitudinal maneuver, considering aperiodic response
11 p1708 A71-26486

Sailplanes control, deriving incremental aerodynamic load on horizontal tail produced by instantaneous elevator deflection
11 p1708 A71-26487

Aeroelastic aircraft self adjusting automatic control systems, discussing elimination of elastic oscillations caused noise from angular velocity sensing circuits
12 p1926 A71-26718

Aircraft longitudinal coordinates invariance relative to atmospheric disturbances, giving simultaneous thrust variation, rudder deflection and flap deflection control rules
12 p1867 A71-27339

V/STOL and supersonic commercial aircraft developments, comparing man and machine performance as information processing systems for aircraft control and navigation
13 p2018 A71-28486

V/STOL aircraft instruments, deck display and automatic flight controls for takeoff and landing operation
13 p2098 A71-29132

Quasi-stationary gliding trajectories of aircraft in planetary atmosphere during constant control of attack and bank angles
13 p2143 A71-29185

Elecons as longitudinal and lateral control elements on low aspect ratio wings, calculating subsonic and supersonic aerodynamic characteristics
13 p1993 A71-29190

Jet-supported VTOL aircraft fuel-time-optimal landing control, using mathematical model, Pontryagin maximum principle and analog computer solution
13 p1997 A71-29281

Third Chance flight control system, discussing aircraft control capability with backup hydraulic system after loss of dual main hydraulic systems due to combat damage
13 p1998 A71-29382

Air turbulence primary and secondary effects on aircraft flight and avoidance criteria considerations
14 p2268 A71-29768

V/STOL aircraft flight path and attitude controls in turbulence, discussing design based on state variable methods of control theory
14 p2173 A71-29776

Aircraft gust alleviation, considering movement correction based real time atmospheric turbulence measurement
14 p2174 A71-29785

Soviet book on helicopter design covering aerodynamic properties, power plants, control systems, fatigue minimization and strength analysis
14 p2174 A71-29944

Control, navigation and guidance review, considering application of earth reference coordinates for aircraft, missiles and spacecraft
14 p2272 A71-30710

VTOL aircraft minimum climb-to-cruise time transition optimal open loop and suboptimal closed loop control synthesis
14 p2220 A71-30799

Controlled aircraft motion under strict kinematic constraints in terms of simple subsystems, noting pilots role in Newark theory
14 p2177 A71-31024

Head- or helmet-mounted display/control system in V/STOL aircraft for pilot workload and training reduction
14 p2189 A71-31093

Handling qualities of V/STOL research vehicles during steep terminal area approaches, discussing powered lift fan VTOL aircraft limitations and instrument landing approach
14 p2179 A71-31101

Aircraft integrated command and control system, discussing vertical, aerodynamic and horizontal situations, flight mechanics, power setting, telecommunications, etc
15 p2349 A71-31878

Aircraft optimum control synthesis for powered flight phase, determining angle of attack for transfer to maximum velocity by Cauchy problem
16 p2523 A71-33442

VTOL aircraft gross weight and direct operating costs penalties from additionally installed control power
16 p2524 A71-34005

Soviet book on aircraft automatic control systems covering linear theory, design, autopilot, man machine performance, operation modes, etc
17 p2771 A71-34473

Aircraft pilot learning process with C-8 trainer, determining effective evaluation indexes including error ratio, control numbers, pulse rate and reaction time
17 p2692 A71-35196

Lockheed L-1011 development, discussing flying stabilizer design, direct lift control and autoland system
17 p2675 A71-35532

Random access signaling system application to aircraft control, discussing signal redundancy requirement for access capability optimization based on radio environment model
17 p2747 A71-35783

Discrete time digital flight control systems design resulting in closed loop aircraft response characteristics approximation to prescribed flying quality specifications
19 p3024 A71-37196

Aircraft control design by implicit model-following technique with optimal feedback sampled data and continuous control algorithm, exemplifying STOL aircraft landing approach control
19 p2995 A71-37197

Performance limitation of simplified radio-inertial lateral control guidance system subject to stochastic gusts for automatic landing
19 p3099 A71-37198

Aircraft electronic or fly by wire control systems, discussing aircraft design fuel-structure weight reduc-

tion cycle and control system redundancy requirements
19 p3099 A71-37200

Sight line autopilot /SLAP/ for side-firing aircraft pointing accuracy improvement, using optimal regulator theory to generate control gains
19 p3099 A71-37201

Aerodynamic control surfaces optimal location for flexible aircraft disturbed by random wind gusts, using matrix minimum principle and calculus of variations
19 p2998 A71-38713

Power by wire actuators and fly by wire flight controllers, discussing systems configuration, reliability, economy and durability
20 p3183 A71-39150

Aircraft response to pilot or autopilot command during altitude control maneuver, calculating lag magnitudes
22 p3482 A71-41691

Fluid amplifiers theory and use as temperature and pressure sensors, discussing applications in chemical and ammunition industries and jet aircraft control
23 p3630 A71-42921

SST handling qualities, takeoff speeds and performance evaluation on six degree of freedom flight simulator
23 p3627 A71-42922

Nonreversible hydraulic control design and emergency maintenance for Tu 154 aircraft subsonic cruising at 11 km altitude
23 p3627 A71-42927

Minimum order state vector reconstruction linear filters for constant plants optimal control, applying to aircraft flight multiple control-point problem
23 p3657 A71-44077

Flight test measurements for improved estimates of aircraft states and aerodynamic parameters, using relinearized Kalman filter
23 p3629 A71-44089

Longitudinal adaptive aircraft control through sum of normal acceleration and pitch rate
23 p3629 A71-44093

Integrated system for aircraft control and operation with visualization and manual regulation techniques, emphasizing interconnections with onboard electronic equipment
24 p3791 A71-44353

American development in automatic flight control, noting FAA requirements, pilot involvement and visibility enhancement
24 p3846 A71-44455

STOL aircraft flight control problems, discussing Mach trim, artificial feel, stability, feedback system responses and lateral/directional laws
24 p3792 A71-45297

AIRCRAFT DESIGN
NT HELICOPTER DESIGN

Aladin 2 interurban Stoll transport design with blown wings and jet deflection by wing flaps, emphasizing engine noise reduction
01 p0005 A71-10749

Small gas turbines for aircraft auxiliary power unit, considering compressor and combustor design, noise, fuel consumption and specific weight problems
01 p0006 A71-10751

Aircraft response to atmospheric shock, discussing spectral analysis procedures and calculation results on T-tail aircraft design
01 p0005 A71-10752

Aircraft direct lift control based on flight and simulator experiments, discussing effect on design
01 p0005 A71-10754

F-14A twin engine variable geometry carrier based jet fighter aircraft, discussing design, development program and manufacturing techniques
02 p0188 A71-12050

Subsonic aircraft size effect in conventional design, discussing increased weight increments and economic gain rate
02 p0189 A71-12676

Swept wing fighter aircraft transonic buffet onset lift coefficient from camber and trailing edge deflection, considering design variations
02 p0186 A71-12679

Flight control systems influence on military aircraft design and performance, discussing static stability, ride quality, flutter margin and maneuver load controls
02 p0190 A71-12683

Acrostar acrobatic aircraft design and performance
03 p0346 A71-13016

Environmental effects on VTOL design - Conference, Arlington, Texas, November 1970
04 p0529 A71-15401

Direct lift V/STOL transport aircraft design, discussing environmental factors in relation to noise, air pollution, jet interference and safety
04 p0530 A71-15403

Army rotorcraft hot day standard design hover criterion, developing analytical models for hovering aircraft, cost, climatology and environmental features
04 p0533 A71-15431

Light Sprite aircraft design and construction for building at home by nonprofessionals
04 p0534 A71-15674

- Aerodynamic characteristics of jet engine installation above wing of swept wing aircraft, noting large lift dependent drag 05 p0696 A71-15954
- Airborne flight simulator /helicopter/ as aircraft development aid [DGLR-70-075] 05 p0733 A71-15965
- Elfe S-3 glider flight test, pointing out imperfections in cockpit and wing design 05 p0696 A71-16128
- Light amphibian passenger STOL P-300 Equator aircraft, using single turbosupercharged engine driving two blade propeller at tail assembly 05 p0696 A71-16132
- Universal mini carrier UMC-120 light turboprop STOL transport 05 p0696 A71-16133
- Airborne variable stability helicopter flight simulator for V/STOL aircraft design 05 p0697 A71-16954
- Sensitivity analysis and optimal control theory used to design optimal gust alleviation systems, discussing gain and gear ratios [AIAA PAPER 71-9] 06 p0848 A71-18483
- Naval aircraft testing, discussing weapons systems, funding commitments, outfitting schedules, time frames, contracts and management problems 07 p1018 A71-19077
- ARAVA STOL aircraft, describing payloads, configuration, design flight testing, stability and landing characteristics 07 p1018 A71-19082
- BD-1 Yankee aircraft development, design and construction 07 p1018 A71-19084
- Design objectives for subsonic, transonic and supersonic civil transport flying characteristics based on MIL-F-8785, considering aircraft control [SAE-ARP-842B] 07 p1019 A71-19645
- Aerospace Recommended Practice criteria for flight deck crew escape systems applicable to all commercial aircraft propulsion systems, design speeds and payloads [SAE-ARP-808A] 07 p1019 A71-19646
- Airplane wing high lift and flap designs by interactive computer graphics system [AIAA PAPER 71-227] 07 p1019 A71-19705
- Swept lightning stroke effects on aircraft design involving Ti and Al sheets 07 p1020 A71-19936
- Plastics and metals as construction materials in aircraft, missile and rocket design 07 p1215 A71-20044
- Ground based flight simulation as engineering aid in aircraft design for evaluation of aircraft dynamics, handling qualities and control system characteristics over entire flight envelope 07 p1084 A71-20309
- Toxicology in aerospace vehicles design and operation, discussing occupational exposures, propellant operations, medical aspects, hazards, etc 08 p1244 A71-20712
- Soviet book on Yak-40 passenger transport aircraft configurational design and aerodynamic characteristics covering stability, controllability and flight under special conditions 08 p1230 A71-20750
- Q-Star experimental aircraft design and acoustical characteristics to study Quiet Aircraft Technology 08 p1231 A71-21441
- Motorized glider equipped with Wankel engine for self powered takeoff, describing prototype design and flight test data 08 p1232 A71-21769
- High speed aircraft external store separation testing and prediction techniques, considering flow field survey, dynamically similar drop models and captive trajectory methods [AIAA PAPER 71-294] 08 p1229 A71-22014
- Complex airframe design for economic and safe operation and long life using fatigue and fracture mechanics [AIAA PAPER 70-512] 08 p1374 A71-22025
- Hawker Siddeley Trident 3B flight test program, booster engine, structural features, power plants, systems and landing gear 09 p1385 A71-22890
- Ultrahigh tensile steels for landing gear and other aircraft design applications, discussing composition, mechanical properties, quality requirements, manufacture and testing 09 p1454 A71-22996
- Fluid mechanics of atmospheric environment and flow on swept wings in short and medium range aircraft design, concerning STOL capability in India 09 p1383 A71-23199
- Soviet book on aircraft preliminary design specifications as function of performance, aerodynamic and structural parameters, discussing tradeoffs in operational requirements for specific configurations 10 p1554 A71-24012
- Adhesive primers corrosion resistance test methods, noting aircraft design implications 10 p1633 A71-24112
- FAA flying and handling qualities program, discussing development of optimum and minimum acceptable flight characteristics criteria for new civilian and military aircraft designs [SAE PAPER 710372] 10 p1554 A71-24241
- NASA aerodynamic research applicable to business aircraft concerning wind tunnel and flight tests, STOL performance and high speed cruise technology [SAE PAPER 710378] 10 p1554 A71-24244
- Design optimization of aircraft starting and generating systems, identifying information required and system analysis methods [SAE PAPER 710392] 10 p1558 A71-24256
- Constant attitude light aircraft flight control system, describing design studies for minimum pilot command requirements [SAE PAPER 710393] 10 p1555 A71-24257
- Medium weight NAMC C-1A tactical transport aircraft technical specifications 11 p1706 A71-25231
- Ti intermediate diagonal tension field shear beam analysis and design for Boeing SST, using Rayleigh-Ritz method [AIAA PAPER 71-340] 11 p1843 A71-25319
- Automated optimal weight fully stressed large scale structural design of aircraft, using matrix-mathematical programming technique [AIAA PAPER 71-361] 11 p1844 A71-25340
- Prototype graphite fiber/plastic fuselage component design, test and performance prediction, using structural analysis methods 11 p1787 A71-25428
- Fatigue life, fail-safe capability and corrosion resistance of commercial aircraft structures improved through adhesive metal-metal bonding [ASME PAPER 71-DE-27] 12 p1978 A71-27325
- Automated low cost structural-mechanical design and optimization of wing pivot systems for variable geometry aircraft [AIAA PAPER 71-404] 12 p1980 A71-27410
- Wing design criteria imposed by high speed requirement for short takeoff aircraft, considering thin swept-back wing with small aspect ratio for lateral control 12 p1867 A71-27471
- Ti, B and graphite fiber composites application to aircraft design, discussing mechanical properties and market competition 12 p1918 A71-27676
- Aircraft industry materials development, discussing innovations in governmental programs management, procurement specifications and Department of Defense contracting procedures 12 p1918 A71-27677
- Landing load estimation methods for preliminary design weight prediction for military aircraft 13 p1995 A71-28211
- Economic analysis of subsonic transport airplane design, evaluation and operation [SAE PAPER 710423] 13 p1995 A71-28310
- FAA aircraft design appraisal for maintainability, considering maintenance concepts and adverse airworthiness situations [SAE PAPER 710431] 13 p2073 A71-28316
- Military/commercial STOL transport design, discussing performance, payload and equipment requirements with emphasis on production cost benefits [SAE PAPER 710468] 13 p1996 A71-28336
- STOL aircraft/engine integrated systems for medium distance air transportation, discussing tradeoff factors involving performance, noise, weight and cost [SAE PAPER 710469] 13 p2115 A71-28337
- Structural fatigue in aircraft design, discussing twin engine transport tests, crack propagation rate, residual strength, etc 13 p2158 A71-29434
- Aircraft capabilities in intraurban transportation for Detroit metropolitan area, considering vehicle design, fleet size, cost and terminal location [AIAA PAPER 71-504] 14 p2172 A71-29548
- Materials and structural design development by high velocity impact testing due to transport and subsonic military aircraft susceptibility to bird collision damage 14 p2221 A71-29642
- Atmospheric turbulence statistical models assessment for aircraft design and operation, considering CAT and thunderstorm turbulence data 14 p2266 A71-29751
- V/STOL aircraft flight path and attitude controls in turbulence, discussing design based on state variable methods of control theory 14 p2173 A71-29776
- Jet transport aircraft design for safety under air turbulence conditions, considering cruise altitude limitations and pitch and g excursion reduction by special autopilot mode 14 p2173 A71-29777
- Aircraft structural design requirements based on statistical analysis of air turbulence intensity and gust loads records from large number of research flights 14 p2173 A71-29784
- Aircraft design and fatigue life monitoring, investigating effects of gust velocity frequency distribution in patches of atmospheric turbulence 14 p2174 A71-29789
- Air transport development trends, considering increased speed and capacity, STOL aircraft, urban service, and European cooperation for manufacturing 14 p2341 A71-30302
- Computer aided design program for civil transport aircraft configuration, performance, propulsion, weight and costs to meet given specifications 14 p2175 A71-30398
- Aircraft quantitative maintenance cost requirements translation into design criteria, considering airline operations influence on manufacturer [SAE PAPER 710437] 14 p2341 A71-30529
- Commercial vs military design criteria for STOL transport aircraft, noting landing and takeoff distances and noise levels [SAE PAPER 710465] 14 p2176 A71-30536
- Alpha jet trainer, describing design, configuration, power plants, landing gear maintainability and mission duration 15 p2347 A71-31209
- Computing geometric airplane aerodynamic characteristics during preliminary and detailed design processes 15 p2348 A71-31597
- TU-144-Concorde differences, discussing design philosophy engine mounting and thrust, wing span and profiles, gross weight, fuselage cross sections landing gear, droop nose, etc 15 p2349 A71-31873
- European Airbus automatic pilot and flight control system, including computers in electromechanical subassemblies 15 p2446 A71-31914
- Concorde aircraft automatic landing and flight control system objective, design, reliability and certification tests 15 p2446 A71-31915
- Mechanics of laminated filamentary composite orthotropic material used for cover skin in advanced aircraft component design 15 p2507 A71-32109
- Concorde flight characteristics, discussing performance flight test data relationship to design 15 p2350 A71-32690
- Dynamic characteristics of weakly damped elastic body, considering complex natural modes generation for vibration tests in aircraft design 16 p2657 A71-33403
- Constrained optimization problems solution combining modified pattern search methods and polynomial constraints in aircraft design parameters selection 16 p2603 A71-33721
- Potential benefits accruing to air superiority fighters by integrating automatic feedback control system technology into design, using F-4 as baseline configuration [AIAA PAPER 71-764] 16 p2523 A71-34002
- F-4E stall/spin development and flight tests, relating mass distribution and angle of attack aerodynamic design [AIAA PAPER 71-772] 16 p2524 A71-34008
- Atmospheric turbulence prediction, discussing sensitive aircraft design for structural overload and fatigue failure decreases [AIAA PAPER 71-775] 16 p2524 A71-34011
- Control configured vehicle design longitudinal requirements due to application of relaxed static stability and maneuver load control [AIAA PAPER 71-786] 16 p2525 A71-34016
- Optimization and operational problems of man powered aircraft, noting Kremer Competition design [AIAA PAPER 71-798] 16 p2525 A71-34023
- Future aviation development constraints on manufacturer and purchaser, design, test costs, noise, airport location and multinational operation [AIAA PAPER 71-799] 16 p2667 A71-34024
- Civil V/STOL aircraft projects, discussing design, lift fan engines, weights, flight performance, noise levels, safety and comfort standards 16 p2525 A71-34101
- Axisymmetric inlet design for turbojet powered hypersonic cruise vehicle, examining effects of spillage and cowl drags on air flow characteristics 16 p2521 A71-34149
- Fighter F-14 podded engine high variable sweep wing design including nozzle, nacelle, fuselage shift, aspect ratio and lift control improvements 16 p2526 A71-34152
- VTOL transport optimal airframe/propulsion systems design, discussing thrust requirements, performance, control, cruise functions, fuel consumption and fan characteristics [AIAA PAPER 71-744] 17 p2792 A71-34225
- DC-10 wide body tri-jet aircraft design and development, considering sizing, number of engines and thrust optimization and selection of cruise, approach and stall speeds [AIAA PAPER 71-780] 17 p2674 A71-34525
- Computerized automatic control of aircraft electrical system using remote power controllers and multiplexed data bus for wiring reduction and reliability improvement 17 p2677 A71-34700

DC-10 fuselage pressure shell fail-safe design, presenting analysis methods for residual strength prediction of damaged stiffened panels

17 p2827 A71-35160

Total in-flight simulator (TIFS) in variable stability C-131 aircraft, describing potential as design tool [AIAA PAPER 71-794]

17 p2675 A71-35529

Armored cockpit for attack aircraft combat effectiveness, including mold line tumbling plates, terminal ballistic kinematics and integral structural armor [AIAA PAPER 71-778]

17 p2675 A71-35530

L-1011 flight test program, describing aircraft design and performance

[AIAA PAPER 71-789]

17 p2675 A71-35531

Lockheed L-1011 development, discussing flying stabilizer design, direct lift control and autoland system

[AIAA PAPER 71-782]

17 p2675 A71-35532

Aircraft electric power system design with reliability, simplicity, low cost, weight and size, discussing automatic circuit protection and energy power

[SAWE PAPER 894]

17 p2676 A71-35817

V/STOL aircraft with vectored thrust propulsion systems, noting weight and center of gravity-lift-thrust relationship changes effect on performance

[SAWE PAPER 889]

17 p2835 A71-35825

Wing group weight prediction for subsonic aircraft design, taking into account root bending moments due to lift

18 p2976 A71-35925

Lockheed L-1011 passenger jumbo jet layout, ground handling and servicing

18 p2849 A71-35995

Hybrid V/STOL jet lift aircraft design, examining wing area-lift engine bypass ratios relation [AIAA PAPER 71-767]

18 p2850 A71-36273

Hypersonic aircraft design usable as transport or space shuttle, determining aerodynamic behavior in viscous flow

18 p2847 A71-36431

Strategic bomber B-1A program, discussing airframe and engine contractors, design, characteristics performance, electronic equipment and armament

18 p2850 A71-36757

Aircraft control design by implicit model-following technique with optimal feedback sampled data and continuous control algorithm, exemplifying STOL aircraft landing approach control

[AIAA PAPER 71-956]

19 p2995 A71-37197

Aircraft electronic or fly by wire control systems, discussing aircraft design fuel-structure weight reduction cycle and control system redundancy requirements

[AIAA PAPER 71-959]

19 p3099 A71-37200

Variable geometry B-1A bomber aircraft, discussing size, payloads, speed, altitude range and runway takeoff

19 p2996 A71-37516

Sonic boomless transonic transports design, performance, economics and airline routes at Mach 1.2 and 0.98

[CASI PAPER 72/8]

19 p2996 A71-37598

Aircraft structures sonic fatigue due to high frequency noise from turbofan engines, discussing case histories, failure diagnosis and precautionary design measures

19 p2997 A71-37843

Mercury short range passenger aircraft design conception, analyzing cost

19 p2997 A71-38242

Concorde droop nose for takeoff and landing visibility improvement, describing design and operation

19 p2997 A71-38343

European airbus development, discussing basic, long range and stretched capacity versions and aerodynamic and structural design features

20 p3177 A71-38749

Polycarbonates transparency applications in aircraft windshield design, discussing heat resistance, mechanical, chemical and optical properties

20 p3253 A71-38751

Aircraft fuselage design with marine type bulkhead construction, discussing advantages in cabin decompression and fire hazards reduction

20 p3178 A71-38752

Computer aided aircraft design, analysis and production, discussing Numerical Master Geometry program developed by British Aircraft Corporation

20 p3241 A71-39543

SST sonic boom generation, discussing aircraft design and atmospheric conditions effects and property damage

21 p3325 A71-40705

European airbus design and performance, covering electrical system, air conditioning, engines and flying control circuits

22 p3482 A71-42236

Aeronautics future, discussing aircraft noise reduction, computer techniques and aircraft design

22 p3482 A71-42237

Rotor performance and design for hover and cruise VTOL flights

22 p3482 A71-42238

High lift device application to high performance competition gliders, considering merit of design for conflicting climb/cruise requirements

23 p3627 A71-43089

Acrostar Mk II all wood single seat acrobatic light weight aircraft designed for plus/minus 8g and inverted flight

23 p3629 A71-43887

Sailplane circling cross-country speed increase by variable geometry in high lift flap form for better compromise between cruise and climb performance

23 p3630 A71-44342

AIAA members comments on STOL, VTOL and V/STOL aircraft merits and developments [AIAA PAPER 71-1015]

24 p3791 A71-44596

Panavia 200 multipurpose military aircraft, describing variable geometry design concept, performance characteristics, engines, armament and electronics

24 p3792 A71-44766

AIRCRAFT DETECTION

Ships and aircraft position finding method based on satellite radio signals Doppler measurements, analyzing ionospheric influences

07 p1154 A71-19036

Time-frequency anticollision system for dangerous aircraft detection and avoidance using stable atomic clocks

[ONERA-TP-938]

15 p2445 A71-31875

Radio tracking of aircraft by two geostationary satellites, discussing measurement, navigation and position errors

18 p2945 A71-36508

Aircraft onboard equipment tests in air navigation aid satellite project, estimating tracking random errors

18 p2877 A71-36509

Optical radar aircraft tracking and position system, using IR Q switched flash pumped Nd-YAG laser transmitter and pulse receiver with magnetic tape recorder and real time computer

18 p2900 A71-36905

Computer-based aircraft tracking with aid of twin radar air traffic control system, discussing components and operation

18 p2883 A71-36993

Computerized automatic estimation techniques application to real time aircraft tracking in ATC system design

[AIAA PAPER 71-926]

19 p3096 A71-37172

Aircraft position errors computation for ATC mathematical surveillance models, estimating collision risk

[AIAA PAPER 71-927]

19 p3097 A71-37173

AIRCRAFT ENGINES

Air cooled opposed 4, 6 and 8 cylinder light aircraft engines with or without turbosupercharging, considering horsepower improvement and torsional vibration control

[SAE PAPER 700205]

01 p0142 A71-10129

Aircraft turbine engine development, considering mismatch reduction between engine and airframe in flight tests

01 p0143 A71-11180

Jet engine evolution, considering thrust, combustion chamber, fans, high-pressure-ratio compressors and turbine inlet temperature

01 p0143 A71-11181

Electrochemical machining for aircraft engine metal components, discussing cost, time comparisons, tooling techniques and applications

[SME PAPER MR-70-206]

01 p0089 A71-11252

Electrochemical machining role in jet engine industry, discussing drilling, contouring, electrolyte handling, etc

[SME PAPER MR-70-193]

01 p0089 A71-11253

Electrohydraulic thrust control system for supersonic transport aircraft engines, considering reliability, performance and weight

[SAE PAPER 700819]

01 p0143 A71-11546

Soviet book on aircraft power plant systems and devices covering layout, engine attachment, propellers, control, fuel and oil systems, fire fighting, monitoring, etc

02 p0299 A71-12722

Engine vibration high temperature transducer, discussing piezoelectric materials properties and design considerations relative to temperature, pressure, acoustic noise, humidity environment

02 p0255 A71-12911

Twin jet aircraft engine installation effects and exhaust nozzle integration, noting closely spaced inlet interference

[ICAS PAPER 70-47]

03 p0469 A71-13148

Thrustmeter for direct in-flight measurement of aircraft engine jet thrust

03 p0422 A71-13332

Soviet papers on working processes in aircraft engines covering gas flow, liquid injection, nozzles, gas turbines and supersonic flow

03 p0471 A71-14251

Influence coefficients for aircraft engine gas/air ducts parameter deviations, using statistical analysis

03 p0472 A71-14257

Aircraft propulsion, discussing piston, turbojet, turboprop and turbofan engines in terms of thrust to weight ratio, specific fuel consumption and propulsive efficiency

04 p0638 A71-14977

Soviet book on aviation automation covering automatic control systems in piston, turbojet and turboprop engines, navigation, air temperature and pressure

04 p0529 A71-15223

VTOL aircraft engine air particle separator development, examining airframe and engine design

04 p0533 A71-15433

Soviet book on aircraft gas turbine engine assembly covering organization, specified accuracy, automatic systems, mechanization problems, quality control, etc

04 p0639 A71-15449

Aircraft turbine engines with elevated gas inlet temperatures

04 p0639 A71-15670

Aircraft gas turbine engine components equivalent testing by shortening testing time required to increase service life

05 p0796 A71-16761

Book on fixed and rotary winged aircraft air cooled piston engine design, performance and maintenance in business and military operators manual terminology

05 p0796 A71-17125

Aircraft engine double-reverberant chamber duct lining test facility, discussing noise fields, air flow, layout, performance, insertion and transmission losses, etc

06 p0880 A71-17619

Nuclear powered long distance aircraft engines, discussing high burnup fuel, weight factors and safety problems

06 p0926 A71-17694

Gas turbine aircraft engine compressor blades foreign object ingestion control by inlet vortex flow suppression jets, indicating wind tunnel air intake applications

06 p0945 A71-17696

Small gas turbines for helicopters and fixed wing aircraft, discussing designs, materials, lubrication, etc

06 p0945 A71-18052

Aircraft gas turbine engines nitric oxide emission model, describing flow behavior and chemical processes

[AIAA PAPER 71-123]

06 p0948 A71-18659

High performance fighter aircraft engine pressure ratio and turbine inlet temperature measurement, using fluidic sensors

07 p1028 A71-20586

Fluidic pressure ratio control for vertical takeoff aircraft lift engine fuel system, describing breadboard circuit, test bed and flight standard

07 p1028 A71-20587

Soviet book on aircraft gas turbine and internal combustion engines covering structural design schemes, inlet devices, combustion chambers, materials, compressors, etc

08 p1347 A71-20674

Equivalent test results, studying damaging factors in aircraft engine compared with regular tests

08 p1348 A71-21115

Microelectronic circuits reliability in aircraft engine control applications, discussing testing and selection for severe temperature and vibration environments

[SAE PAPER 700822]

08 p1265 A71-21369

Book on aircraft gas turbine engine technology covering combustion chambers, exhaust systems, lubricating oils, thrust augmentation, inlet ducts and overhaul procedures

08 p1348 A71-21625

Aircraft turbine engines strength and gas dynamic characteristics improved by vibration decrease using elastic elements

08 p1349 A71-21710

National Air Pollution Control Administration control of aircraft engine pollutant emissions covering measurement, test instrumentation, research, standards and regulations

08 p1379 A71-21831

Aircraft engine smoke emission control, discussing Ringelmann chart assessment for various commercial jet aircraft and airport gaseous pollutants

08 p1380 A71-21832

Probabilistic estimate of aerodynamic imbalance of aircraft gas turbine rotors due to production errors in compressor blade angle

08 p1349 A71-22045

Shrouded aircraft engine turbine blades vibration stresses found minimum by setting up paired blades with fixed tension along shroud

09 p1538 A71-22595

Turboprop aircraft engine service life extension, correcting deficiencies via accelerated tests based on relation between failure rate and usage

09 p1511 A71-22633

Cost reduction concepts in gas turbine engine design and fabrication for general aviation aircraft

09 p1511 A71-22811

- Hawker Siddeley Trident 3B flight test program, booster engine, structural features, power plants, systems and landing gear 09 p1385 A71-22890
- D-30 bypass engine hydraulic control system for Tu-134 aircraft, discussing fuel flow regulator assembly and operation 09 p1511 A71-22947
- High thrust aircraft engines test facility design 09 p1428 A71-22956
- Fan propulsion power plants with mechanical and gas dynamical energy distribution systems for commercial VTOL aircraft 09 p1511 A71-22964
- High temperature corrosion in aircraft engine components and gas turbines by sulfur in fuels, vanadium pentoxide and NaCl 09 p1474 A71-23288
- Aircraft engines and stationary gas turbines high precision components, discussing die forging and machining combined with joining processes 09 p1456 A71-23299
- Concorde environmental testing, considering endurance tests, thermal shock rigs and plant for simulating air supply from compressor stages of aircraft gas turbine engines 09 p1430 A71-23583
- Light aircraft standard fuel flight evaluation, discussing compatibility with grades 80/87 and 100/130 certified engines and comparative operational fuel consumption [SAE PAPER 710369] 10 p1657 A71-24239
- Dual magneto ignition system for business and small military aircraft, describing development, design and test program [SAE PAPER 710382] 10 p1659 A71-24247
- Light aircraft engine lubricating oil filter types and model specification, noting dirt holding ratings [SAE PAPER 710383] 10 p1617 A71-24248
- VTOL heat engine and propulsion system design and performance, citing Pegasus jet lift engine as compromise between takeoff and cruise function 10 p1659 A71-24751
- VTOL propulsion systems safety requirements, considering single and double breakdowns 10 p1659 A71-24752
- Boron-glass-epoxy lightweight composite gear case for aircraft engine reduction gearbox, describing design, molding, machining and testing [ASME PAPER 71-GT-85] 11 p1771 A71-25993
- Aircraft gas turbine condition analysis instrumentation used for status diagnosis of naval turbine engines, discussing sensor and electronic data interpretation progress [ASME PAPER 71-GT-86] 11 p1813 A71-25994
- Military aircraft flight test establishments, discussing airframe, engine, flight control and weapons delivery systems tests work flow integration requirements 11 p1708 A71-26315
- Soviet book on theory of aircraft bladed machines covering axial flow, centrifugal and composite turbines and compressors, thermodynamic efficiency, control turbocompressor matching, etc 11 p1814 A71-26401
- Soviet book on aircraft and rocket engines control automation, discussing nuclear power plant/fuel systems design and control simulation methods 11 p1814 A71-26403
- Thrust measurement of aircraft and rocket propulsion systems, comparing cost and characteristics of mechanical, electrical and hydraulic systems 12 p1894 A71-26991
- Air transport propulsion systems, discussing aircraft operating economics with reference to weight, size, powerplant efficiency, noise and air pollution 12 p1946 A71-27542
- Aircraft power plants sealing materials, emphasizing porous cermet seals heat resistance under thermal cyclic loads 12 p1895 A71-27688
- Aircraft piston and turbine engine soot extracts cancerogenic activity in hybrid mice 12 p1872 A71-27724
- VTOL propulsion, discussing gas turbine pressure ratio inlet temperature and lifting and high bypass fans 13 p2114 A71-27838
- Visible exhaust smoke trails from aircraft jet engines, measuring optical density by photographic photometry [SAE PAPER 710428] 13 p2114 A71-28314
- Reduction gearbox reliability problems from development and service experience with PT6A turboprop engine [SAE PAPER 710433] 13 p2073 A71-28318
- Commercial aircraft powerplant development, discussing engine and components test programs and techniques [SAE PAPER 710449] 13 p2114 A71-28327
- Aircraft propulsion system testing, stressing noise reduction and inlet-engine exhaust system compatibility [SAE PAPER 710450] 13 p2114 A71-28328
- Airline engine performance testing from operator perspective, using automated test cell data acquisition system [SAE PAPER 710451] 13 p2044 A71-28329
- High temperature aircraft gas turbine engine design, discussing developments in manufacturing processes, materials, cooling techniques, aerodynamic and mechanical design improvements [SAE PAPER 710462] 13 p2115 A71-28335
- Gas temperature measurement in aircraft combustion chambers, using calorimetric probe 13 p2117 A71-28757
- Aircraft engine production components and alloys mechanical properties evaluation for improved reliability of mass produced products 13 p2075 A71-28944
- Subsonic and supersonic turbojet aircraft engines development, discussing design, operation, reliability, weight, fuel consumption and cost 14 p2287 A71-29811
- Thrust measurement of aircraft propulsion systems, considering hydraulic piston device, edge clearance, oil quantity and calibration 14 p2251 A71-29860
- Concorde power plant fire protection system, describing prototype engine bay overheat detection system and additional UV optical fire detection system 14 p2288 A71-30300
- Aircraft jet engines technological progress review over past 25 years, emphasizing industry economics considerations 14 p2341 A71-30303
- HF rake probes with high temperature integrated sensor for inflight aircraft engine intake air flow distortion measurements 14 p2243 A71-30321
- Low cost go/no-go portable aircraft engine tester connected to engine mounted sensors 14 p2221 A71-30327
- Sound fields of flying aircraft from noise measurements, discussing engine operating conditions, speed and attitude 14 p2176 A71-30521
- Transport aircraft JT9D high bypass ratio engine development, noting maintainability and stability improvements [SAE PAPER 710419] 14 p2289 A71-30527
- Aircraft JT9D engine development for airline operation, discussing construction, condition monitoring, maintenance, noise and smoke reduction [SAE PAPER 710434] 14 p2289 A71-30528
- Design interface requirements for optimal aircraft engine condition monitoring system, using parameter, vibration, oil, borescope and radiography analysis [SAE PAPER 710447] 14 p2289 A71-30531
- VTOL propulsion units lift ratings based on aircraft system requirements [SAE PAPER 710471] 14 p2176 A71-30537
- Onboard computer for aircraft engine testing, monitoring and data reduction, emphasizing automatic in-flight recording for post-flight displays [AIAA PAPER 71-651] 14 p2290 A71-30727
- Engine condition monitoring systems, discussing engineering design requirements with respect to accessibility, accuracy, economics, effectiveness, reliability and maintainability [AIAA PAPER 71-652] 14 p2290 A71-30728
- VTOL turboshaft engine powered propulsion system development, detailing design requirements, program planning, component research and system integration [AHS PREPRINT 562] 14 p2297 A71-31109
- Analytical model of oscillatory combustion in aircraft engine augmentors 15 p2466 A71-31324
- Air cooling methods for aircraft engine turbine rotor blades, considering heat distribution in rotor disk 15 p2467 A71-31461
- Aircraft engine in-flight thrust determination, discussing indirect and direct measurement methods [DFVLR-SONDDER-119] 15 p2350 A71-32720
- Flight mission severity in cumulative damage/low cycle fatigue and creep stress rupture/ not detected by usual nondestructive testing in aircraft gas turbine industry 16 p2624 A71-33298
- Dynamic stress on rotor blades of aircraft engine axial compressor stages with low hub/diameter ratio 16 p2624 A71-33345
- Air transport propulsion systems economics, considering first cost, specific weight, fuel consumption and maintenance effect on direct operating cost 16 p2523 A71-33469
- Soviet book on subsonic gas turbine passenger planes power supply systems covering Boeing 747, short haul aircraft, DC-10, L-1011, etc 17 p2677 A71-34472
- Maximum temperature engine concept, definition and application to future aircraft propulsion system performance [SAE PAPER 710461] 17 p2792 A71-34498
- Linear radial loads effect on stress and strain of hyperboloidal rotor disk applied to aircraft engine compressors with two stream flow of working medium 17 p2822 A71-34597
- Aircraft gas turbine engine components equivalent testing by shortening testing time required to increase service life 17 p2793 A71-35460
- Three micron absolute main oil filter for aircraft gas turbine lubrication system, discussing indicator system and bench and engine tests 17 p2793 A71-35488
- Propulsion systems trends for 1980s, discussing environmental noise levels, stoichiometric gas turbine engines for military aircraft, high bypass ratio engines for V/STOL aircraft, etc 17 p2795 A71-35625
- Integrated drive generator for aircraft electrical power systems, improving weight, life and reliability 17 p2678 A71-35781
- Transonic wind tunnel testing of air intake and afterbody of double flux engine nacelle at high subsonic Mach numbers and high Reynolds numbers [ONERA-TP-943] 18 p2956 A71-36021
- Aircraft jet engine application of electric discharge machining for repetitive continuous production, considering automated closed cycle equipment [SME PAPER MR-71-143] 18 p2927 A71-36658
- Strategic bomber B-1A program, discussing airframe and engine contractors, design, characteristics performance, electronic equipment and armament 18 p2850 A71-36757
- Material, design and operating principles of rotary seals used in gas ducts, bearing elements and fuel systems of aircraft gas turbine engines 19 p3069 A71-38015
- Civil V/STOL aircraft engines requirements, considering noise reduction, thrust, multifunction propulsion/blowing, lift and booster fan engines [CASIPAPER 72/19] 19 p3122 A71-38021
- Multivariable frequency response methods for feedback control design for aircraft gas turbines, involving digital test bed trials 20 p3277 A71-38989
- Aircraft high temperature turbine engine design, reviewing technological advances coupled with laboratory engine and component tests 20 p3277 A71-39399
- Higher pressure ratios trend in aircraft gas turbines leading to higher exit temperatures from compressor, noting real gas effects 21 p3437 A71-40170
- Brazing filler metals as cost effective replacement for Au-Ni in aircraft gas turbine engine component 21 p3387 A71-40621
- Book on aircraft propulsion covering design, dynamics, control, installation, gas turbine, ramjet, rocket and piston engines, compressors, combustion and energy cycles, etc 22 p3589 A71-42427
- In-flight monitoring of aircraft turbine engine reliability 23 p3718 A71-43233
- Operating variables effect on pollutant exhaust from jet aircraft turbine engines, discussing combustor design techniques for emissions reduction 23 p3718 A71-43600
- Digital algorithm for automatic aircraft engine monitoring system, using Boolean algebra and events/states theory 23 p3679 A71-43897
- Nondestructive detection of hot corrosion- sulfidation in U.S. Navy aircraft turbine engines 24 p3865 A71-45280

AIRCRAFT EQUIPMENT

NT AIRCRAFT HYDRAULIC SYSTEMS
NT AIRCRAFT LIGHTS
NT AIRCRAFT TIRES
NT EJECTION SEATS

Aircraft galley design safety criteria, considering injuries from routine use, normal, crash or ditching conditions component dislodgment, equipment malfunctions and defects 01 p0004 A71-10029

Combat aircraft cockpit temperature control system design and operation 01 p0004 A71-10270

Aircraft DC to AC converters frequency stabilization systems, describing circuit diagrams and operation principles 03 p0355 A71-14247

Electrochemical aircrew oxygen breathing systems, considering water electrolysis and oxygen separation and concentration from air 04 p0543 A71-15056

IFR design requirements for STOL navigation equipment from flight tests 04 p0623 A71-15424

Aircraft equipment failures detection and warning systems 04 p0601 A71-15901

Aircraft generator service life improvement and weight minimization by close coupling with drive and

heat producing components cooling with oil spray and mist
06 p0849 A71-18463

Integrated drive AC generator for aircraft, discussing design improvements in power-weight ratio
07 p1023 A71-19494

Military aircraft zinc silver oxide battery service requirements and performance
08 p1236 A71-21103

Soviet book on asynchronous generators for aircraft covering design and operation
09 p1387 A71-23420

Soviet book on airplane and helicopter electrical power supply systems covering storage batteries, DC generators, alternators, voltage regulators, current and frequency control, etc
14 p2180 A71-29525

Soviet handbook of aircraft electrical equipment covering DC and turbine powered generators, lubrication materials, electromagnetic interference countermeasures, etc
14 p2181 A71-29530

Airborne equipment for CAT detection ahead of aircraft, considering pulsed Doppler laser and IR detectors
14 p2268 A71-29765

Naval Air Rework Facility, discussing primary mission, technical disciplines and operational performance feedback
16 p2523 A71-34003 [AIAA PAPER 71-765]

High voltage DC electric power transmission systems with ground return, reducing aircraft wiring weight and energy dissipation
17 p2678 A71-35771

Aircraft permanent magnetic fields strength variation, observing magnetic anomaly detection equipment performance degradation
23 p3674 A71-42923

AIRCRAFT EXHAUST
U EXHAUST GASES
AIRCRAFT FUEL SYSTEMS

Soviet book on aircraft power plant systems and devices covering layout, engine attachment, propellers, control, fuel and oil systems, fire fighting, monitoring, etc
02 p0299 A71-12722

Quick connect/disconnect dry break couplings for aircraft fueling, describing design and operation
06 p0880 A71-18215

Aircraft fuel and air conditioning systems vortex valves and diodes, examining flow patterns into and out of chambers
07 p1025 A71-20556

Concorde aircraft fuel system and fuel pumps, considering center of gravity and center of pressure relationship to maintain trim
09 p1512 A71-23581

Aircraft self sealing fuel tank and fuel cell systems damage control, considering chemical, precompressed foam and swellable elastomer seal concepts
10 p1554 A71-24079

Fluorosilicone sealants for aircraft fuel containment, discussing resistance to heat, jet fuel, moisture and heat aging
10 p1631 A71-24080

Polyurethane foam effects on fuel contamination during installation for fuel system fire and explosion protection
11 p1708 A71-25981 [ASME PAPER 71-GT-54]

Airport jet fuel delivery system salt driers for reducing water content below saturation, lengthening filter life and improving downstream system components performance
13 p2113 A71-28322 [SAE PAPER 710440]

AIRCRAFT FUELS

Soviet book on aircraft fuels, lubrication materials and special fluids covering compositions, physicochemical properties, filtration, etc
01 p0142 A71-11320

Static dissipator additives in aviation fuels for eliminating electrostatic charging hazards
02 p0297 A71-12300

Book on aviation fuels covering gasoline and turbine fuel properties, handling problems and future fuels
03 p0469 A71-14298

Soviet book on automotive and jet aircraft engine fuel chemical stabilizers under storage, transit and operational conditions, examining additives in relation to stability ratings
06 p0942 A71-17433

Light aircraft standard fuel light evaluation, discussing compatibility with grades 80/87 and 100/130 certified engines and comparative operational fuel consumption
10 p1657 A71-24239 [SAE PAPER 710369]

Aircraft fuel tank nitrogen inerting, fire and explosion suppression for foreign particle contamination, sludge and lacquer reduction
11 p1810 A71-25978 [ASME PAPER 71-GT-45]

Kerosene type fuels for aircraft gas turbine engines, discussing combustion problems, smoke emission reduction and bacterial or fungal contamination
13 p2113 A71-28754

Energy state approximation and supersonic aircraft minimum fuel fixed range trajectory optimization, noting not convex velocity set
14 p2177 A71-30609

Aircraft pollutant emission regulation, discussing low smoke combustors and fuel dumping problem
15 p2516 A71-32246

Jet engine advent impact on aviation fuels safety, discussing gasoline hazards in prejet aircraft
23 p3718 A71-43231

Liquid hydrogen as future replacement for hydrocarbon fuels in surface and air transportation, noting advantages in energy per unit weight and pollution-free combustion
24 p3863 A71-44365

Jet aircraft fuel additives covering functions and applications
24 p3864 A71-45325

Aviation fuels lubricating characteristics, discussing refining methods, viscosity, service performance and load testing
24 p3864 A71-45383

AIRCRAFT GUIDANCE

Time-synchronized approach control combining aircraft precision navigation and guidance with ATC equipment
02 p0280 A71-12894

Cockpit simulator motion effects on ILS approach pilot guidance errors, using Erdmann model [DGLR-70-071]
05 p0779 A71-15956

Inertial aircraft lateral guidance system limitations in stochastic gust environment, comparing configurations using aileron or differential spoilers
06 p0925 A71-18489 [AIAA PAPER 71-22]

Aircraft navigation system requiring computer and display for approach guidance to circular orbit over fixed ground area
07 p1156 A71-20305 [AIAA PAPER 69-986]

Optimum automatic flight control techniques in horizontal guidance of aircraft at terminal
07 p1156 A71-20306

VOR/DME ground station oriented aircraft area navigation horizontal guidance capability, discussing digital input/output flight control
08 p1331 A71-21166

Strapdown inertial navigator alignment by digital filtering techniques, discussing application to aircraft and spacecraft
08 p1331 A71-21170

Report on guidance system for approach and landing, discussing airports, aircraft, approach and landing paths, service classes, failure protection and weather penetration
11 p1796 A71-25534

Terrain following radar for airborne guidance of low flying military aircraft
12 p1927 A71-26881

Helicopter automatic flight control equipment, discussing autopilot stabilizer, localization system, ground approach guidance coupler and flight director
15 p2446 A71-31916

ESRO preoperational aeronautical satellite system for Atlantic and Pacific coverage, noting position determination for reduced aircraft separation, frequency selection and performance trade-offs
16 p2644 A71-32850

STOL aircraft guidance capability with onboard digital computer, maintaining time of arrival envelope at way points along complex flight paths
17 p2775 A71-35528 [AIAA PAPER 71-770]

Interceptor aircraft optimal nonlinear command guidance scheme for reduction of airborne computation load with forward prediction of interceptor and target state vectors
19 p3096 A71-37166 [AIAA PAPER 71-916]

All-weather operations, including pilot role, instrument landing systems and guidance aids
19 p3100 A71-37601 [CASI PAPER 72/14]

ATC height and plan position indicator composite picture display system design and operation, combining functions of primary and secondary surveillance radars
21 p3413 A71-40128

Aerospace guidance technology evolution at MIT with emphasis on inertial systems
22 p3570 A71-41993

Modular step scan microwave aircraft landing system /TALAR/ design and operation, noting short takeoff and landing
22 p3572 A71-42088

Doppler scanning landing microwave system for air-derived azimuth and elevation angle aircraft guidance by frequency coding and reference carrier transmission
22 p3572 A71-42089

Scanning microwave landing guidance system coordinates choice, discussing signal format, antennas planar or conical beams and V/STOL application
22 p3572 A71-42090

Microwave scanning beam guidance receiver design for aircraft landing aid, discussing time sharing and flight control
22 p3572 A71-42091

Operational requirements of microwave guidance systems, comparing guidance and position measurement applied to aircraft approach and landing
22 p3572 A71-42092

AIRCRAFT HAZARDS

Aircraft fire hazard reduction, discussing early detection, extinguishing equipment and emergency landing survival
01 p0004 A71-10399

Static dissipator additives in aviation fuels for eliminating electrostatic charging hazards
02 p0297 A71-12300

Medicophysiological problems in Concorde SST relative to altitude and speed, noting risks of cosmic radiation, ozone in atmosphere, decompression, wing loss and high temperatures
03 p0371 A71-13093

Atmospheric turbulence at cruise altitudes of supersonic transport aircraft, considering gusts probability, thunderstorms and mountain waves
03 p0346 A71-13137

Bird strikes incidence and prevention, discussing velocity effects, migration role and uses of distress calls, falconry and radar
06 p0848 A71-18664

Static discharge hazards for aircraft, discussing causes for static charge build-up, dangers and precautionary methods during refueling operations
07 p1019 A71-19424

Statistical information on lightning and static hazards relative to airworthiness
07 p1020 A71-19929

Composite plastic aircraft structures lightning protection, considering hazard to composite materials and use of metal filled or plasma sprayed coatings and metal foil coverings
07 p1021 A71-19943

Aircraft collision avoidance dynamical system, determining barriers between possible capture regions by optimal control problem solution
08 p1331 A71-21322

Commercial supersonic flight, investigating air pollution and alleged climate and weather modification effects due to principal exhaust products
08 p1232 A71-21821

Bird impact hazard to general aircraft, discussing structural damage, flight safety and testing procedures
10 p1557 A71-24997

Aircraft hazards due to frequent low cloud occurrences at Kenya airport, forecasting weather with statistical analysis and radiosounding
13 p2097 A71-29106

Aircraft ice protection problems, considering one dimensional Stefan method for cyclic deicing system
17 p2838 A71-34850

Case histories of aircraft damage due to wind acting on airport surfaces, discussing wind and hail protection
17 p2675 A71-35442

Aircraft wake turbulence (trailing vortex systems/avoidance during flight, describing procedures for pilots and tower operators
19 p2992 A71-37596 [CASI PAPER 72/6]

Aircraft fuselage design with marine type bulkhead construction, discussing advantages in cabin decompression and fire hazards reduction
20 p3178 A71-38752

Flight tests for hazard evaluation to other aircraft from wake turbulence generated by large jet transport airplanes
21 p3321 A71-40506

Simulated airline pilot cerebral incapacitation etiology, incidence and detection, noting unimpaired crew members conduct and reaction times during approach for landing
22 p3501 A71-41824

Aircraft wake turbulence and trailing vortices, investigating physical characteristics, hazard potential and avoidance techniques
23 p3628 A71-43234

Aircraft generated vortex wakes and core air motions hazards for encountering light airplane
23 p3628 A71-43381

AIRCRAFT HYDRAULIC SYSTEMS

Aircraft high temperature polyimide hydraulic actuator rod seals, discussing design and performance tests
01 p0091 A71-11543 [SAE PAPER 700790]

Hydraulic systems in Boeing 747 aircraft, considering piston design
05 p0705 A71-16131

Partial differential equation solution for aircraft hydraulic lines flexural vibration by Bubnov-Galerkin method, reducing to Duffing equation analysis
08 p1286 A71-20783

Analytical nonlinear landing gear model of flexible aircraft and strut lockup-breakout interaction using digital simulation language /DSL/ [SAE PAPER 710401]
10 p1555 A71-24263

Hydraulically powered duplex input servos for flight control system of VFW-Fokker V/STOL fighter aircraft
12 p1867 A71-26884

Optimization of military VTOL aircraft secondary power systems, considering alternate power source for aircraft hydraulics, pneumatic drives, etc [SAE PAPER 710445] 13 p1998 A71-28326
Aerospace fluid power - Conference, Detroit, Michigan, October 1970 20 p3183 A71-39147
Boeing 747 aircraft hydraulic system design, discussing thin wall high pressure tubing, swaged sleeves and welded joints 20 p3183 A71-39148
L-1011 aircraft hydraulic system design modifications and improvements, discussing gas turbine power source, fluids evaluation, filters, welded steel tubing and maintenance procedures 20 p3183 A71-39149
On-condition monitoring of aircraft hydraulic systems for component deterioration, applying to Boeing 747, L-1011 and DC 10 aircraft 22 p3483 A71-42075
Nonreversible hydraulic control design and emergency maintenance for Tu 154 aircraft subsonic cruising at 11 km altitude 23 p3627 A71-42927

AIRCRAFT INDUSTRY
Closed die forgings for aircraft industry, discussing technology, tolerances, materials and costs 07 p1119 A71-20075
Aircraft industry ATC techniques and equipment contribution to aircraft control and safety 09 p1491 A71-22951
Ti alloys in aircraft industry, considering jet engines applications and structural stability improvements related to fracture toughness, fatigue and stress corrosion 09 p1474 A71-23292
British Aircraft Corporation Numerical Master Geometry system using parameter surface mathematics and digital computer 10 p1580 A71-23759
Book on aviation technology and market structure covering technological and scientific effects on industry innovative behavior, R and D programs, operating costs, etc 10 p1698 A71-23982
Aircraft jet engines technological progress review over past 25 years, emphasizing industry economics considerations 14 p2341 A71-30303
Aircraft industrial cleaning agents, processes and techniques applied to components in course of manufacturing and assembly phases, emphasizing emulsion and alkaline methods [ASM PAPER C70-4.3] 16 p2584 A71-33542
French flight test center role in development and certification of Concorde aircraft, considering cooperation with industry [AIAA PAPER 71-784] 17 p2675 A71-35526
Negotiations of BEA/BOAC productivity agreements in aircraft industry 18 p2926 A71-35924
British civil aircraft airworthiness requirements, discussing aircraft industry management philosophy ensuring quality standards in design, development, production, inspection and product support 18 p2989 A71-36673
Civil aircraft market analysis, examining replacement cycle and used aircraft market based on aircraft histories 18 p2989 A71-36676
Aircraft industry license norms and standards, describing indexing procedures, storage techniques and data recovery operations with computer 18 p2886 A71-36810
V/STOL airworthiness certification, considering standards developed by FAA in cooperation with industry [CASI PAPER 72/21] 19 p2997 A71-37607
Soviet aircraft industry R and D organizations and management 23 p3786 A71-44189

AIRCRAFT INSTRUMENTS
NT ALTIMETERS
NT ANEMOMETERS
NT APPROACH INDICATORS
NT ATTITUDE INDICATORS
NT AUTOMATIC PILOTS
NT COMPASSES
NT FLIGHT RECORDERS
NT GYRO HORIZONS
NT GYROCOMPASSES
NT HOT-WIRE ANEMOMETERS
NT MAGNETIC COMPASSES
NT PLAN POSITION INDICATORS
NT POSITION INDICATORS
NT RADIO ALTIMETERS
NT RADIO DIRECTION FINDERS
NT RATE OF CLIMB INDICATORS
NT SOLAR COMPASSES
NT SONIC ANEMOMETERS
NT SPACECRAFT POSITION INDICATORS
NT SPEED INDICATORS
Electronic control indicator for human pilot capability enhancement using color coded cathode ray display, presenting information from seven different instruments 01 p0081 A71-10750
American ATA prototype aircraft collision avoidance equipment and proposed noncooperative system 01 p0125 A71-10753
Aircraft ultrasonic altitude and vertical velocity sensor for low flight, discussing VTOL aircraft automatic hovering control and time lag 01 p0084 A71-11624
B-52 LAMS test vehicle structural modification and instrumentation in flight phase 02 p0188 A71-11661
Vestibular nystagmus and display luminance effects on hand-eye coordination in compensatory tracking of aircraft instrument 02 p0207 A71-12381
Aircraft information display simulation and flight tests of experimental display systems, discussing man machine communication systems development [DFVLR-SONDDR-81] 03 p0396 A71-13344
Clear air turbulence due to large amplitude Kelvin-Helmholtz billows, noting simultaneous measurements by instrumented aircraft and radar 04 p0621 A71-15043
Real time missile radio telemetry data transmission to ground station, using instrumented aircraft 04 p0554 A71-15321
Onboard aircraft refractometer, design, operation principles and effectiveness 05 p0756 A71-17195
Aircraft cockpit instrumentation display media research, discussing brightness and contrast ratio requirements for gray scale displays 07 p1046 A71-18736
Low profile optical system producing annular cone of radiation from point source for high speed aircraft beacon 07 p1107 A71-19203
Terrain-following radar for TSR-2 aircraft, discussing reliability trials and improvement 07 p1062 A71-19557
Aircraft visual warning indicating system, outlining design criteria, color and brightness recommendations [SAE-ARP-1088] 07 p1019 A71-19644
Soviet book on supports and suspensions of aircraft gyroscopic devices covering accuracy, reliability and lifetime factors related to quality and operational conditions 07 p1115 A71-20299
Aircraft radio compass navigation errors due to loop antenna inclinations during maneuvering 08 p1331 A71-20787
Electroluminescent aircraft instrument lighting effects on pilots dark adaptation taking into account color, panel legibility, scotopic sensitivity and acuity 08 p1248 A71-21229
Altitude rate generation for aircraft instruments testing 09 p1448 A71-22770
Aircraft display designs, emphasizing man machine problems 09 p1402 A71-23621
Navy pilots performance improvement through symbolic flight displays 09 p1453 A71-23675
SST problems, including adequate instrumentation and fuel tank immunization to explosion 12 p1867 A71-26883
Onboard aircraft refractometer design, operation and effectiveness 13 p2067 A71-28250
Electrical and physical nature of microbial membranes implicated in aircraft fuel quantity probe malfunction [SAE PAPER 710439] 13 p2113 A71-28321
V/STOL aircraft instruments, deck display and automatic flight controls for takeoff and landing operation 13 p2098 A71-29132
Aircraft personnel radiation hazards from radioactive luminous paint on instrument dials, signs and operational elements 13 p2021 A71-29145
Aircraft instrumentation and data analysis for clear air turbulence, including orthogonal components and temperature and wind distributions 14 p2267 A71-29753
Instrumentation in aerospace industry - Conference, Las Vegas, May 1971 14 p2243 A71-30309
Aircraft barometric altimeter errors caused by atmospheric temperature deviations from International Standard Atmosphere 14 p2244 A71-30323
Holographic techniques, optical data processing and laser properties for aerospace instrumentation 14 p2244 A71-30329
Heavy lift helicopters IFR hover capability with slung load, discussing sensors controls and displays [AHS PREPRINT 540] 14 p2250 A71-31097
Aircraft instrumentation deficiencies from pilot viewpoint, proposing pilot designed display [AIAA PAPER 71-787] 16 p2537 A71-34017

Avionics systems for weapons control in F-14 fighter aircraft, discussing track multiple targets, sighting aids, radar, computer navigation, communications and built-in self testing 16 p2527 A71-34155
Cockpit display, discussing aircraft operators delay in use of head-up displays, area map navigation, CRT and electroluminescent readouts 17 p2691 A71-35110
Radio controlled small aircraft as measurement platform for meteorological sensors, discussing development and performance from field tests 17 p2675 A71-35334
Military and civil aircraft navigation systems development, emphasizing self contained airborne equipment 17 p2775 A71-35374
High aperture wide angle lens design for compact electro-optical systems of airborne moving map projection navigational instruments 18 p2947 A71-36605
Ergonomic evaluation of flight crew working conditions from viewpoint of static and dynamic adaptation of aircraft system design to human psychophysical capabilities 19 p3007 A71-38016
Single seater turbojet aircraft landing via automatic band switch for ARK-5 and ARK-10 radio compass 19 p3101 A71-38017
Simultaneous radar and instrumented aircraft observations in clear air turbulent layer for eddy dissipation rates calculation 20 p3256 A71-39207
Remote image-forming sensors on satellites and aircraft, considering resolving power, contrast rendition, dynamic range, SNR, sensitivity, and reliability as performance measures 20 p3240 A71-39608
Display devices in aircraft cockpit providing pilots with information from various sources, considering head-up display and CRT 21 p3376 A71-40113
Contrast level reading tests of CRT and self luminous display devices with optical filters at high ambient light for cockpit applications 21 p3376 A71-40127
Aircraft head-up display systems for providing pilot information focused at infinity within pilot normal field of view 21 p3413 A71-40131
Canadian Forces experiments on aircraft flashing lights covering warning signals, navigation and anticollision displays and autokinetic phenomenon 22 p3499 A71-41491
Strobe lighting for aircraft midair collision hazard reduction, comparing Collision Avoidance System and Pilot Warning Indicator effectiveness 22 p3499 A71-41493
Angle of attack instrumentation for evaluating aircraft lift performance and phugoid oscillations 23 p3628 A71-43382
Altitude instrumentation for aircraft pilot, discussing three pointer, servo and drum pointer altimeters, digital readout, radar alert and automatic reporting systems 23 p3628 A71-43383
Aircraft pitot static systems design with removable drain plug, noting line installation problems 23 p3675 A71-43387
Astatic gyroscope mounted on aircraft moving arbitrarily near earth surface, obtaining integrals of kinematic equations 24 p3828 A71-45160

AIRCRAFT LANDING
NT CRASH LANDING
NT DITCHING (LANDING)
NT SKID LANDINGS
Steep approach to landing for jet transport aircraft noise abatement, using ground based equipment and onboard TV display 01 p0126 A71-11311
Aircraft all weather automatic landing system, discussing component weights and reliability connected with problem area 02 p0279 A71-12274
All-weather automatic landing electronic technology, describing flight automation landing system for VC 10 BAC 111 and Concorde aircraft 02 p0279 A71-12275
Maximum throughput-rate capacity for runway and final approach path airspace involving multiple IFR landings 02 p0279 A71-12893
Aircraft longitudinal motion decoupling through direct lift control, investigating flight control for landing 03 p0347 A71-13339
V/STOL aircraft operations, considering terminals, landing and approach aids, air traffic, noise and pollution control, performance, airworthiness regulations and licensing 03 p0347 A71-13572
Terminal area operations of V/STOL aircraft, considering approaches, approach speeds, wind and velocity effects and noise 03 p0347 A71-13573

Optimum VTOL aircraft landing maneuverability, using short range three dimensional surveillance system and ground computer

03 p0454 A71-13574

STOL and boundary layer control aircraft takeoff and landing distance, considering jet suction action influence on lift and drag coefficients

04 p0529 A71-14595

Aircraft longitudinal control during landing approach, investigating back side operation characteristics by closed loop system analysis regarding pilot and aircraft as elements

05 p0696 A71-16388

Night carrier landing final approach glide slope altitude, lateral and sink rate pilot errors prediction, using linear regression model

06 p0858 A71-17602

Poor visual flight meteorological conditions, discussing instrumental and visual aids, airport landing and approach, holding patterns and overshoots

06 p0847 A71-17922

All-weather aircraft operations, discussing takeoff, landing, safety and forecasting

06 p0847 A71-17923

Helicopter automatic and manual low visibility landing systems evaluation by hybrid computer simulation

06 p0880 A71-18423

Aircraft automatic landing improvement through use of space diversity ILS receiving system

07 p1153 A71-18830

Structures electromagnetic scattering and multipath transmission effects on aircraft instrument landing system localizer signals, using computer program

07 p1153 A71-18831

Boeing 737 aircraft takeoff and landing performance, emphasizing high lift systems and stopping capability

07 p1018 A71-19083

Airliner acceptance checks characteristics for official licensing prerequisites, investigating takeoff, landing, ascent, stability and control

07 p1022 A71-20065

Two dimensional aircraft automatic landing motions control processes by simulation without use of moving cockpit simulator

07 p1084 A71-20066

Automatic Carrier Landing System with linear adaptive aircraft Navigation Computer, investigating effectiveness in reducing system errors due to nonlinearities and noise effects

07 p1157 A71-20405

Pilot vision during final approach and landing in turbojet transport operations

08 p1247 A71-20826

Soviet book on aircraft flight with incomplete and asymmetrical thrust covering probabilistic characteristics, stability, landing and takeoff with partial engine failures, etc

10 p1554 A71-24013

Light aircraft spoilers to minimize landing risk, discussing spoiler/dive brake area effects on glide path angular control

10 p1555 A71-24251

Wind gradient effect on flight characteristics during aircraft landing approach, particularly path deviation

11 p1706 A71-25194

Aircraft approach and landing under low altitude wind shear conditions, discussing flying hazards and glide path correction procedures

11 p1708 A71-26364

Psychophysical evaluation of glide slope detection accuracy by diamond vs square shape in runway centerline stripping as aircraft landing aid

12 p1875 A71-27252

Transport aircraft all weather automatic landing operation, examining guidance system and independent monitors

13 p2098 A71-28323

Jet-supported VTOL aircraft fuel-time-optimal landing control, using mathematical model, Pontryagin maximum principle and analog computer solution

13 p1997 A71-29281

Automatic aircraft landing system modification for improvement of response to air turbulence effects

14 p2271 A71-29773

Anemometer measurement optimum averaging time of wind speed for conventional aircraft landings

14 p2270 A71-30394

Single anemometer wind measurement required for aircraft landing, comparing data from different sampling periods

14 p2270 A71-30395

Combined inertial and instrument landing aircraft navigation systems with reduced cross runway position and velocity errors, using optimal linear estimation

14 p2272 A71-30606

Caravelle aircraft all-weather Sud Lear automatic landing system operation and performance

15 p2446 A71-31913

Supercooled fog dissipation by liquid propane, determining effectiveness in providing operational support to aircraft landing and takeoff

16 p2604 A71-33536

Lateral-directional handling qualities and roll control power requirements for executive jet and military class II airplanes in landing approach flight phase

[AIAA PAPER 71-771] 16 p2524 A71-34007

Automatic landing systems using inertial navigation derived translational state information, discussing evaluation by simulation of transport aircraft operating with conventional instrument landing system

[AIAA PAPER 71-795] 16 p2605 A71-34020

Trailing wake hazards of large transports in takeoff and landing, examining configuration stability of vortex pair in ground effect

17 p2674 A71-35757

Asphalt pavement design for heavy multiwheel aircraft, using BISTRO computer program

18 p2897 A71-36000

Cost effective high speed projectile trajectory plotting system for gunnery range instrumentation, applying to aircraft path recording during automatic landing control

18 p2924 A71-36613

Pilot workload reduction in steep approach landing of light aircraft from flight test data analysis

[AIAA PAPER 71-904] 19 p3095 A71-37155

Performance monitor for aircraft automatic landing systems safety control

[AIAA PAPER 71-958] 19 p3099 A71-37199

Single seater turbojet aircraft landing via automatic band switch for ARK-5 and ARK-10 radio compass

19 p3101 A71-38017

Jet engines with afterburners, describing exhaust nozzle control, takeoff and landing advantages and thrust variations

21 p3437 A71-40858

Aircraft ILS landing approaches, discussing approach area and surface and obstruction clearance surface and limit

21 p3325 A71-40891

Modular step scan microwave aircraft landing system /TALAR/ design and operation, noting short takeoff and landing

22 p3572 A71-42088

Microwave scanning beam guidance receiver design for aircraft landing aid, discussing time sharing and flight control

22 p3572 A71-42091

Operational requirements of microwave guidance systems, comparing guidance and position measurement applied to aircraft approach and landing

22 p3572 A71-42092

Stereoacuity role in pilot ability to land aircraft at minima, questioning adequacy of Verhoeff depth perception test administration conditions

23 p3637 A71-44244

AIRCRAFT LAUNCHING DEVICES

Attitude and velocity control for VTOL aircraft takeoff and landing operations in hovering flight, discussing simulation devices and testing operations

[DGLR-70-073] 05 p0779 A71-15948

Noise abatement power cutback takeoff procedures, maximum altitude approaches and preferential runway systems for noise relief

08 p1232 A71-21813

AIRCRAFT LIGHTS

Civil aircraft cockpit lighting evaluation guidelines

19 p2999 A71-38241

Aircraft flash light designs, discussing tandem oscillating lights, fixed lamp rotating reflectors and lamps, xenon flashtube, quartz-iodine lamp and flash frequencies

22 p3483 A71-41494

Aircraft anticollision flashing lights, discussing current practices within national and international air traffic regulations regarding flash frequency, color and light sources

22 p3483 A71-41499

AIRCRAFT MAINTENANCE

German monograph on commercial jet aircraft maintenance systems covering changes and adaptations for performance improvement

01 p0004 A71-10114

Commercial transport aircraft maintenance simulation Monte Carlo Modeling techniques, considering application to airline operations

[SAE PAPER 700345] 01 p0067 A71-10128

Digital simulation program in GPSS language for airline operations including aircraft maintenance, flight scheduling, terminal space, equipment, work forces utilization, etc

02 p0227 A71-11809

Nondestructive testing techniques for airline maintenance inspection, describing ultrasonic, eddy current, magnetic particles, and X ray methods

02 p0256 A71-12449

Civil aircraft accident and maintenance recording regulations and systems, discussing airborne equipment

03 p0348 A71-13735

Technical resources pooling among airlines for investment and maintenance cost out of aircraft fleets

04 p0690 A71-14992

Reliability and maintenance problems of U.S. Army operational environment, noting inadequate design and test criteria during development

04 p0530 A71-15402

Helicopter gas turbine engine health indication using instrument panel for correcting gas temperature and producer speed

06 p0945 A71-17690

Civil aviation aircraft mean flight time overhaul schedules, considering statistical evaluation of relationship between operational characteristics and time between overhauls

08 p1230 A71-20797

Light aircraft piston engines design and maintenance, discussing engine design features, materials, lubrication, controlled flight operation and maintenance techniques

[SAE PAPER 710381] 10 p1658 A71-24246

Representative Thornel fiber aircraft fuselage component nondestructive testing and repair, and Thornel fiber, polysulfone and polyamide-imide composites fabrication and evaluation

11 p1787 A71-25427

Jet aircraft airworthiness standards, discussing airline fleet maintenance resources, inspection systems and future requirements

11 p1772 A71-26308

Pan American reliability program effect on airline maintenance, considering cost effectiveness, aircraft performance, data collection and analysis

12 p1910 A71-26671

Methods for engine condition monitoring application to airline operation

13 p2114 A71-28177

MAC malfunction detection, analysis and recording system applications in commercial airlines, emphasizing real time response for maintenance function

[SAE PAPER 710425] 13 p1995 A71-28311

FAA aircraft design appraisal for maintainability, considering maintenance concepts and adverse airworthiness situations

[SAE PAPER 710431] 13 p2073 A71-28316

Airline operator evaluation of maintainability, considering costs and investment return

[SAE PAPER 710432] 13 p2073 A71-28317

Microbiological contamination of jet aircraft fuel tanks in tropical regions, considering maintenance

[SAE PAPER 710438] 13 p1996 A71-28320

Transport aircraft JT9D high bypass ratio engine development, noting maintainability and stability improvements

[SAE PAPER 710419] 14 p2289 A71-30527

Aircraft quantitative maintenance cost requirements translation into design criteria, considering airline operations influence on manufacturer

[SAE PAPER 710437] 14 p2341 A71-30529

Boeing 747 aircraft integrated data system program for reducing engine maintenance and operating costs

[AIAA PAPER 71-648] 14 p2290 A71-30725

Army aircraft automatic inspection and maintenance monitoring system, considering feasibility, technology approach and effectiveness

[AIAA PAPER 71-649] 14 p2177 A71-30726

Onboard computer for aircraft engine testing, monitoring and data reduction, emphasizing automatic inflight recording for post-flight displays

[AIAA PAPER 71-651] 14 p2290 A71-30727

Engine performance monitoring for jet engine troubleshooting, noting analyzable malfunctions

15 p2471 A71-32524

Aircraft reliability and maintenance cost reduction via allocation of effort and money, considering R and M optimization in airline support cycle

16 p2551 A71-33286

Lynx military helicopter design high reliability and low maintenance demands

16 p2523 A71-33457

Air transport propulsion systems economics, considering first cost, specific weight, fuel consumption and maintenance effect on direct operating cost

16 p2523 A71-33469

Integrated logistics support program for F-14 aircraft maximum maintainability, reliability and operational readiness at optimum cost

16 p2553 A71-34154

Category II operations at various airports, considering all-weather landing requirements of airborne equipment, maintenance standards, pilot training, etc

[SAE PAPER 710442] 17 p2674 A71-34499

Aircraft weighing in place during maintenance operations, describing load cell equipped jacks design for time saving weight determination

[SAE PAPER 898] 17 p2724 A71-35814

Lockheed L-1011 passenger jumbo jet layout, ground handling and servicing

18 p2849 A71-35995

Space Shuttle Orbiter Environmental Control and Life Support Systems, discussing maintenance

[ASME PAPER 71-AV-15] 18 p2866 A71-36382

Maintenance control system /MCS/, management information system encompassing subsystems supporting scheduling, forecasting, performance evaluation, modifications and improvement functions

18 p2987 A71-36448

Commercial aircraft reliability and maintainability design philosophy application to reusable space vehicles, considering optimum redundancy, dispatch with component inoperative and fault isolation

18 p2973 A71-36481

- Vacuum brazing for nozzle guide vanes repair in aircraft gas turbine engines, noting economic advantages 19 p3069 A71-38313
- Computer controlled modular automatic test equipment for DC-10 aircraft maintenance, discussing system block diagram 22 p3519 A71-41518
- Nonreversible hydraulic control design and emergency maintenance for Tu 154 aircraft subsonic cruising at 11 km altitude 23 p3627 A71-42927
- Aircraft part repair-throwsaway decisions for minimizing costs over life cycle by economic graphic screening techniques 23 p3661 A71-43197
- Civil transport aircraft and equipment maintenance and reliability problems solutions with best time, cost and weight compromises 24 p3792 A71-44765
- ### AIRCRAFT MODELS
- Aluminum reinforced epoxy model making, testing and stress analysis for aircraft structures, including creep, photoelastic coating and strain gage effects 05 p0821 A71-16346
- Mathematical model of small scale versatile aircraft component production process, developing computer production optimization algorithm 06 p0906 A71-18715
- Integrated project information and simulation system for management of aerospace vehicle development, discussing simulation models application [AIAA PAPER 71-238] 07 p1225 A71-19714
- Ground boundary layer effects of fixed ground plane for powered STOL wind tunnel model, discussing flow breakdown criteria, contraction lag, strut fairing interference, etc [AIAA PAPER 71-266] 08 p1232 A71-21992
- Static aerodynamic data correlation for high subsonic speed transport aircraft model in transonic wind tunnels, including relative buoyancy and turbulence effects [AIAA PAPER 71-291] 09 p1429 A71-23423
- Wing models development by tangent milling on jig-borer, approximating cross section by hand finish smoothed polygon 15 p2413 A71-31439
- Skin friction, trailing edge boundary profiles and tuft flow patterns on model F-4D aircraft in transonic flow [AIAA PAPER 71-762] 16 p2521 A71-34001
- Nonlinear flight dynamic simulation using wind tunnel and aircraft model as analog function generator and computer for motion equation processing and command orientation 21 p3363 A71-40392
- ### AIRCRAFT NOISE
- NT JET AIRCRAFT NOISE
- NT SONIC BOOMS
- Human subjective responses to approaching and receding aircraft sounds during flight over stationary observer 01 p0127 A71-10345
- Noise reduction relationship to air transportation progress, considering cost/technology balance, quiet engine, research and development programs, etc [ASME PAPER 70-WA/DE-9] 03 p0348 A71-14143
- V/STOL aircraft operations, considering terminals, landing and approach aids, air traffic, noise and pollution control, performance, airworthiness regulations and licensing 03 p0347 A71-13572
- Aircraft fuselage internal noise and structural frequency response due to random excitation, using transfer matrix analysis [ASME PAPER 70-WA/DE-9] 03 p0348 A71-14143
- Aircraft sound measurement standards, evaluating airport noise control and permissible levels 03 p0373 A71-14248
- Helicopter in-flight noise radiation pattern and spectra measurements for various operating parameters 04 p0531 A71-15406
- Helicopter wake impulsive noise calculation based on rotor tip vortex interaction 04 p0531 A71-15407
- Helicopter noise minimization by various piloting maneuvers, discussing takeoff and landing, transition to forward flight, route selection, etc 04 p0531 A71-15408
- Helicopter and V/STOL aircraft external noise and downwash measurements during simulated jungle rescue mission 04 p0531 A71-15409
- Helicopter design for cabin noise level reduction 04 p0532 A71-15423
- Lyons-Satolas /France/ International Airport project, discussing layout, facilities and noise control problem 06 p0880 A71-17590
- Noise nuisance value index /noise pollution level/, considering aircraft and motor vehicle noise surveys and tradeoff of intensity against duration 08 p1333 A71-20802
- Helicopter noise minimization by various piloting maneuvers, discussing takeoff and landing, transition to forward flight, route selection, etc 08 p1230 A71-21049
- Sound field interaction with sinusoidally corrugated surface, considering aircraft noise measurement implications 08 p1333 A71-21162
- Aircraft flyover noise samples, obtaining atmospheric absorption coefficients 08 p1231 A71-21425
- Q-Star experimental aircraft design and acoustical characteristics to study Quiet Aircraft Technology 08 p1231 A71-21441
- Aircraft noise as public health problem, discussing effects on physical, mental and social well-being 08 p1249 A71-21816
- Noise exposure forecasts for cumulative aircraft noise production single number rating as community response indicator 08 p1249 A71-21817
- Land use strategies and noise reduction by source control and flight procedures for noise exposed areas minimization 08 p1378 A71-21818
- Community reactions to aircraft noise, discussing short term interim alleviation measures in airport operations and runway usage scheduling 08 p1378 A71-21819
- Noise pollution control and airport noise levels abatement regulation by state government, taking into account economic and technical feasibility 08 p1379 A71-21825
- Aircraft noise abatement control on international basis by setting acoustic technological capability compulsory standards of quietness 08 p1379 A71-21826
- Federal legislation and regulatory activities for control and abatement of aircraft noise 08 p1379 A71-21827
- State, local government and airport proprietor legal role in regulating aircraft noise at airports 08 p1379 A71-21828
- Federal legislation and regulation of aircraft noise, legal rights of airport neighbors and legal aspects of compatible land use, discussing noise control efforts 08 p1379 A71-21829
- Land use control in aircraft noise abatement, considering airport development and community goals 08 p1380 A71-21836
- Land development planning and aircraft noise at Kansas City International Airport 08 p1380 A71-21837
- Human panel comparison of aircraft engine noise tape recordings with synthetic broadband noise approximating pure jet 09 p1398 A71-22255
- Subsonic turbulent boundary layer noise generation and acoustic pressure on aircraft surface, using Lighthill theory 10 p1553 A71-24952
- Two dimensional sound wave equation solution in terms of time retarded arguments, deriving analytical expressions for aircraft noise intensity and power 11 p1797 A71-25144
- Airport sound prediction using Noise and Number Index deduced from noise logarithmic average and audible aircraft number 11 p1723 A71-25236
- Noise disturbance near large airports, considering aircraft noise, public annoyance and socio-psychological conditions 12 p1875 A71-27478
- Temporal and spectral stimuli combinations effects on judged noisiness of aircraft sounds by college students 12 p1868 A71-27531
- Aircraft noise on and near airports and factors affecting its intensity 13 p1997 A71-29304
- Operations research minimum cost model of aircraft noise abatement in airport communities [AIAA PAPER 71-525] 14 p2339 A71-29551
- Sound fields of flying aircraft from noise measurements, discussing engine operating conditions, speed and attitude 14 p2176 A71-30521
- STOL vehicle and systems air transportation expansion by reducing trip time, congestion, noise exposures and pollution for DOT, DOD and NASA roles [SAE PAPER 710464] 14 p2176 A71-30535
- Commercial vs military design criteria for STOL transport aircraft, noting landing and takeoff distances and noise levels 14 p2176 A71-30536
- SAE/DOT conference on aircraft and environments covering noise pollution, airport noise, sonic booms, regulatory/legal aspects and air pollution [AIAA PAPER 71-729] 14 p2295 A71-30776
- Aircraft noise reduction criteria, examining noise measurements relation to human behavior and physical measures connection to subjective judgments 15 p2349 A71-31879
- Aircraft noise in-flight measurement and analysis, including engine parameters, synchronous recordings, flight paths and coded analog bands 15 p2349 A71-31884
- Aircraft noise measurements, noting ground absorption effects 15 p2450 A71-32127
- Aircraft and environment - Conference, Washington, D.C., February 1971, Part 2 15 p2516 A71-32240
- U.S. federal legislation and regulations for aircraft noise and sonic boom 15 p2516 A71-32245
- Aircraft flyby effective noise duration calculations, examining observation points and analysis methods 15 p2350 A71-32519
- Rotorcraft sound characteristics, discussing rotor noise spectrum, directivity, measurement and instrumentation 16 p2523 A71-33417
- Rotorcraft and VTOL aircraft noise characteristics, noting implications of reduction to acceptable levels 16 p2523 A71-33419
- Experimental research at Building Research Station on outdoor sound propagation for building design in relation to aircraft and road traffic noise 17 p2674 A71-35237
- Gulfstream 2 acoustics program for cabin noise level reduction, compliance with FAA takeoff and landing noise certification and structure qualification against sonic fatigue [AIAA PAPER 71-783] 17 p2675 A71-35527
- Flight dynamics for aircraft noise reduction, gust effects decrease and dynamic stability of parachute load systems 18 p2850 A71-36752
- German aircraft noise protection law of 30 March 1971, discussing objectives and applicability 18 p2989 A71-36921
- Helicopter rotor noise due to blade-vortex interaction, using linear gust model 18 p2849 A71-36934
- Airport system utilization, discussing aircraft noise, ATC, STOL development and passenger handling capacity problems [CASI PAPER 72/3] 19 p3041 A71-37594
- Civil aircraft future propulsion requirements, considering larger engine sizes, higher takeoff thrusts and lower noise levels [CASI PAPER 72/10] 19 p3122 A71-37600
- Near field noise measurement on quarter-scale model to estimate fuselage pressure in VTOL aircraft for conventional, short and vertical takeoff configurations 19 p2997 A71-37844
- Super CTOL airport planning, discussing location of runway pairs, aircraft operations, noise reduction, community relations and efficiency 19 p3041 A71-38023
- Aircraft noise effect on hearing impairment of cockpit crews in civil aviation, using audiometric evaluation 19 p3008 A71-38222
- Flight test measurements of shock cell noise loading of aircraft tail planes, noting alleviation by nozzle and mirror structural modifications 19 p2998 A71-38467
- Aircraft noise propagation in city streets due to intertown V/STOL and helicopter ports, using small scale models 20 p3178 A71-39264
- Convertible rotor transport aircraft, considering ATC, mass transportation systems, safety, noise and socio-economics 20 p3178 A71-39387
- Airport operation costs affected by runway utilization, parking bays alignment, baggage handling and aircraft noise 20 p3209 A71-39390
- Air traffic control delays, airport airspace congestion, flyover noise reduction and performance requirements effect on airline operations economics 20 p3209 A71-39391
- Aircraft noise reduction in takeoffs/operational procedures and by land use planning 20 p3209 A71-39392
- Sound absorptive materials selection for jet aircraft noise control 20 p3178 A71-39451
- Speech intelligibility prediction in time varying aircraft noise based on test score relationship to articulation index for steady state noise 20 p3271 A71-39766
- Aircraft noise effects on hearing acuity and perceptual and intellectual judgment tasks 21 p3342 A71-40351
- Time varying aircraft noise effect on speech intelligibility, discussing test for relation to articulation index 21 p3343 A71-40709
- Prediction methods for human aircraft noise perception, assessing weighted sound pressure level or complex loudness-noisiness computation scales 21 p3325 A71-40866

Aeronautics future, discussing aircraft noise reduction, computer techniques and aircraft design 22 p3482 A71-42237

Civil aviation research and development policy review covering aircraft noise, congestion, ATC, runway capacity and airport development problems [AIAA PAPER 71-1024] 24 p3892 A71-44602

Flight dynamics of noise optimal flight profiles for V/STOL aircraft, minimization of gust effects on aircraft and nonlinear dynamic stability of parachute-load systems 24 p3792 A71-44761

Prop rotor and lift fan VTOL aircraft ground noise level reduction, using flight trajectory management [AIAA PAPER 71-991] 24 p3792 A71-45295

AIRCRAFT PARTS

Small gas turbines for aircraft auxiliary power unit, considering compressor and combustor design, noise, fuel consumption and specific weight problems 01 p0006 A71-10751

Peen forming of large complex parts from sheet and plate, illustrating dihedral break in airplane wing skin 01 p0091 A71-11550

Soviet book on bolting and coupling elements threads used in aircraft industry covering configurations selection, cutting, tolerance requirements and quality control 02 p0258 A71-12723

Approximate determination of complex geometry aircraft surfaces in form of discrete points, comparing efficiency to other methods 06 p0848 A71-18714

Mathematical model of small scale versatile aircraft component production process, developing computer production optimization algorithm 06 p0906 A71-18715

VTOL aircraft gear systems, discussing bearings, shaft connection, Ti alloy components, etc 09 p1454 A71-22963

Powder metallurgy parts application in aircraft, illustrating flareless-sleeve coupling nut of pressed and sintered Ti-6Al-4V alloy 10 p1618 A71-24762

Advanced composite vs conventional material components in cost comparison for aircraft parts 14 p2263 A71-29656

Complex structural aircraft components manufacture, using group technology principle based on subdivision of parts classes 14 p2252 A71-30267

Aircraft steering system design, considering oversteering effects in nose wheels, torque for reaction moment balance and tire behavior 16 p2522 A71-33225

Aircraft parts testing by NDT methods, considering ultrasonic system for valve defects and fluorescent particle system for crack detection 18 p2929 A71-37056

Aircraft parts lubrication friction and wear problems, discussing failure modes, solid and liquid lubricants, component damage and lubrication systems 21 p3389 A71-40902

Aircraft parts damage by corrosive friction forces, hot gases and intercrystalline attack, noting worn universal joint and blade grain boundary damage 24 p3836 A71-44574

AIRCRAFT PERFORMANCE

NT HELICOPTER PERFORMANCE

Inertial navigation system augmented by digital distance measuring equipment in FAA flight inspection aircraft for performance evaluation 01 p0124 A71-10507

SST program relation to airline operations, comparing production configuration, performance, economics and operation with subsonics [AIAA PAPER 70-1217] 01 p0005 A71-11248

Flight control systems influence on military aircraft design and performance, discussing static stability, ride quality, flutter margin and maneuver load controls [AIAA PAPER 69-767] 02 p0190 A71-12683

Acrostar acrobatic aircraft design and performance 03 p0346 A71-13016

Standard-Cirrus glider flight test performance, noting cockpit design and instrumentation 03 p0346 A71-13019

Trailing edge flap automatic control for glider performance improvement 03 p0346 A71-13020

STOL future performance and safety level, considering current jet aircraft fatal accident record and proportional perpetuation, airworthiness and operational considerations 03 p0347 A71-13568

DC-10 aircraft test program effectiveness, discussing performance, operational envelope, airworthiness, noise measurements, etc [SAE PAPER 700830] 03 p0348 A71-13726

Ground and airborne aircraft flight simulation methods, discussing simulator layouts and application to Concorde project 04 p0566 A71-15206

VTOL handling qualities criteria for civil IFR qualifications, taking into account pilot abilities 04 p0533 A71-15427

Metro commuter aircraft specifications, performance and CAB certification problems 06 p0846 A71-17573

Kalman filter simulation for estimating aircraft position and velocity from airborne digital computer data in zero-zero landing system [AIAA PAPER 69-944] 06 p0924 A71-17697

F-15 air superiority fighter, describing military requirements, program management and procedures in terms of speed, maneuverability, acceleration and weaponry 07 p1018 A71-19078

Boeing 737 aircraft takeoff and landing performance, emphasizing high lift systems and stopping capability 07 p1018 A71-19083

DC-10 flight test program, discussing handling, takeoff and landing, and flutter, stall and stability characteristics 07 p1018 A71-19085

Alternate reduced order particle dynamics model in aircraft mission analysis featuring instantaneously variable speed by time scale separation 07 p1019 A71-19913

Transavia Airtruk agricultural aircraft, discussing efficiency, work capacity, economics, configuration and performance 08 p1230 A71-21224

Flight time, path and fuel consumption in climb at constant radius turn, variable or constant velocity and constant engine power, deriving approximate simple formulas 08 p1232 A71-22050

Cessna Citation twin turboprop business aircraft design, performance characteristics, communications, navigation and automatic flight control equipment and flight evaluation 09 p1385 A71-22112

Space shuttle flight test instrumentation for launcher, spacecraft and airplane triple operational and maintenance system requirements, discussing digital data bus monitoring concept [AIAA PAPER 71-313] 10 p1609 A71-23974

Soviet book on aircraft preliminary design specifications as function of performance, aerodynamic and structural parameters, discussing tradeoffs in operational requirements for specific configurations 10 p1554 A71-24012

Variable geometry external fuel tanks for high performance aircraft with drag reduction upon fuel transfer [AIAA PAPER 71-395] 11 p1707 A71-25271

Flight test completed on onboard real time engine performance monitoring system, discussing thermodynamic analysis technique [ASME PAPER 71-GT-77] 11 p1813 A71-25991

Aircraft handling rating scales efficiency, noting difficulty in understanding and interpreting pilot opinion 12 p1875 A71-27253

Modal characteristic pick-up system for vibration tests of rockets or aircraft on ground, using small size accelerometers with individual electronic circuit 12 p1895 A71-27719

Supersonic staggered gutter colander combustion system for plenum chamber burning on high bypass Pegasus turbofan engine of Harrier VTOL aircraft, noting performance improvement 13 p2116 A71-28743

German monograph on game theory and planning techniques for aircraft evaluation 13 p1996 A71-28880

Aircraft flight characteristics dependence on angle of attack, roll and pitch 13 p1997 A71-29043

Ejection system performance in relation to aircraft performance dependent extreme flight conditions, examining ejection seat design features and trajectories 13 p1998 A71-29385

Atmospheric turbulence effects on handling qualities and structural loads on aircraft 14 p2174 A71-29787

Aladin II four-jet engine STOL intercity transport aircraft, noting low noise characteristics and passenger capacity 15 p2347 A71-31412

Aircraft-simulating cockpit procedure trainer statistical data and development problems concerning safety, economy and efficiency performance 15 p2384 A71-31883

Concorde flight characteristics, discussing performance flight test data relationship to design 15 p2350 A71-32690

Propeller driven VTOL aircraft performance improvement, comparing variable camber/diameter counterrotating and blowing device equipped propellers [DGLR-71-023] 15 p2350 A71-32786

Aircraft angle of attack limiter parameters, describing automatic warning system for impending stall 16 p2523 A71-33621

Naval Air Rework Facility, discussing primary mission, technical disciplines and operational performance feedback [AIAA PAPER 71-765] 16 p2523 A71-34003

SST stability augmentation system, discussing performance, operational safety and reliability benefits [AIAA PAPER 71-785] 16 p2525 A71-34015

Maximum temperature engine concept, definition and application to future aircraft propulsion system performance [SAE PAPER 710461] 17 p2792 A71-34498

L-1011 flight test program, describing aircraft design and performance [AIAA PAPER 71-789] 17 p2675 A71-35531

V/STOL aircraft with vectored thrust propulsion systems, noting weight and center of gravity-lift-thrust relationship changes effect on performance [SAE PAPER 894] 17 p2676 A71-35817

Composite materials effect on supersonic aircraft weight, design and performance [SAE PAPER 888] 17 p2676 A71-35818

Flight investigation of turbulence effects on aircraft longitudinal flying qualities, evaluating pilot ratings for ILS approach task [AIAA PAPER 71-905] 19 p2995 A71-37156

Variable geometry B-1A bomber aircraft, discussing size, payloads, speed, altitude range and runway takeoff 19 p2996 A71-37516

Aircraft performance and optimal engine flight path control in combat environment 19 p2997 A71-37724

Soviet book on practical aerodynamics of aircraft with turboprop engines covering piloting, forces and moments, stability, controllability, takeoff, landing, etc 19 p2994 A71-38534

Air traffic control delays, airport airspace congestion, flyover noise reduction and performance requirements effect on airline operations economics 20 p3209 A71-39391

Aerodynamic aspect ratio effects on drag and aircraft performance, noting span loading as major force on wing lifting function 21 p3325 A71-41246

Aircraft response to pilot or autopilot command during altitude control maneuver, calculating lag magnitudes 22 p3482 A71-41691

Short haul air transportation, discussing performance requirements, community acceptance and navigation and landing aids 22 p3482 A71-42073

European airbus design and performance, covering electrical system, air conditioning, engines and flying control circuits 22 p3482 A71-42236

Rotor performance and design for hover and cruise VTOL flights 22 p3482 A71-42238

Takeoff and landing performance evaluation for commercial STOL aircraft, noting high bypass ratio turbofans and high lift systems use 22 p3483 A71-42286

SST handling qualities, takeoff speeds and performance evaluation on six degree of freedom flight simulator 23 p3627 A71-42922

High lift device application to high performance competition gliders, considering merit of design for conflicting climb/cruise requirements 23 p3627 A71-43089

Angle of attack instrumentation for evaluating aircraft lift performance and phugoid oscillations 23 p3628 A71-43382

Sailplane circling cross-country speed increase by variable geometry in high lift flap form for better compromise between cruise and climb performance 23 p3630 A71-44342

Performance prediction and evaluation of propulsion-augmented high lift systems for STOL aircraft, considering weight, thrust and wing loading [AIAA PAPER 71-990] 24 p3791 A71-44585

Transient dynamic characteristics of aircraft under unsteady flight, using Laplace-Carson integral transforms 24 p3792 A71-45016

Aircraft fuselage antisymmetric loading strain effects on small aspect delta wing performance 24 p3885 A71-45018

AIRCRAFT PILOTS

NT TEST PILOTS

Helicopter pilot and passengers emergency survival, considering gravitation force, human tolerances, design factors, etc 01 p0026 A71-11376

Coronary artery heart disease detection in aircraft pilots to age 45 during physical examinations 02 p0208 A71-12392

In-flight telemetric ECG recordings of aircraft pilots during normal, abnormal and aerobically flight, analyzing heart rate variations as function of stresses 03 p0370 A71-13064

Superior jet pilots social, military and flying case histories, noting predominance of firstborn children with close father-son relationships 03 p0371 A71-13325

- Commercial airline pilots alertness tests, using IR pupillography 04 p0543 A71-15051
- Early and prognostic signs of arteriosclerosis in aircraft pilots from medical examination records 07 p1045 A71-20541
- F-100 pilots acute HF hearing loss due to noise ground environment and excessive in-flight noise exposure 09 p1400 A71-23249
- Jet pilots training technologies, discussing multimedia instruction, psychological stress reduction, self study, airborne video application and simulation [SAE PAPER 710477] 13 p2017 A71-28342
- Airline pilot training specific behavioral objective concept, noting introduction with Boeing 744 [SAE PAPER 710479] 13 p2017 A71-28344
- Personnel training in airline operations technology at Friedrich List Transportation Institute for aircraft pilots, flight safety engineers and systems engineers 13 p2021 A71-29143
- Vertical translational acceleration perception threshold of aircraft pilot seated in upright position 14 p2188 A71-29780
- Early diagnosis of atherosclerosis in civil aviation pilots by lipid metabolism and electrocardiographic examinations 15 p2357 A71-31318
- Epidemiological statistics for age specific incidence rate of serious in-flight pilot failure, considering fatal and nonfatal causes 16 p2535 A71-31321
- Aircraft pilot learning process with C-8 trainer, determining effective evaluation indexes including error ratio, control numbers, pulse rate and reaction time 17 p2692 A71-35196
- Aircraft pilot physical examination for regression curves on near vision and eye accommodation, noting age effect 17 p2692 A71-35197
- Aircraft pilots anthropometric survey for human factors engineering, discussing measurement techniques and arrangements for training 17 p2692 A71-35198
- Information transfer in all-weather aircraft operation, discussing pilot role in overall reliability based on man machine system information process 17 p2693 A71-35209
- Unconsciousness, confusion, amnesia, syncope and sudden death in flight due to silent ischemic heart diseases 18 p2855 A71-36216
- Spine radiological examination for helicopter pilot fitness determination, discussing spinal weakness symptoms, special exercises, medical examinations and vibration reducing seat construction 22 p3500 A71-41578
- Psychophysiological and conversion mechanisms as unconscious expression of student pilot motivation decrease for further flight training, presenting case histories 22 p3502 A71-41837
- AIRCRAFT POWER SOURCES**
- U AIRCRAFT ENGINES**
- AIRCRAFT PRODUCTION**
- F-14A twin engine variable geometry carrier based jet fighter aircraft, discussing design, development program and manufacturing techniques 02 p0188 A71-12050
- Aircraft assembly accuracy parameters, using holes as reference points 02 p0257 A71-12564
- Surface flaws in metallurgical products for aircraft building, welds and castings, noting material faults-failure relation and acceptance criteria 03 p0431 A71-13251
- Group and form classification of production errors and tolerances in aircraft construction 04 p0602 A71-14610
- Numerical control automation in aircraft bearing production for small batch runs 04 p0603 A71-15672
- Light Sprite aircraft design and construction for building at home by nonprofessionals 04 p0534 A71-15674
- Mathematical model of small scale versatile aircraft component production process, developing computer production optimization algorithm 06 p0906 A71-18715
- Low cost short life gas turbine design based on parametric performance and component selection, outlining turbojet production [ASME PAPER 71-GT-69] 11 p1813 A71-25984
- Traversing Infrared Inspection System for C-5 aircraft fail-safe strap panels of bonded Ti-Al laminates, discussing design and application [ASME PAPER 71-DE-37] 12 p1911 A71-27327
- Aircraft engine production components and alloys mechanical properties evaluation for improved reliability of mass produced products 13 p2075 A71-28944
- Complex structural aircraft components manufacture, using group technology principle based on subdivision of parts classes 14 p2252 A71-30267
- Air transport development trends, considering increased speed and capacity, STOL aircraft, urban service, and European cooperation for manufacturing 14 p2341 A71-30302
- Aircraft manufacturing techniques, discussing structural components fabrication, economics, lightweight, high strength and heat resistance [SME PAPER MR-71-725] 15 p2417 A71-32436
- Multilevel supply system operationally ready aircraft number evaluator based on item stock levels, demand rates and repair/resupply times 15 p2516 A71-32700
- Aircraft industrial cleaning agents, processes and techniques applied to components in course of manufacturing and assembly phases, emphasizing emulsion and alkaline methods [ASM PAPER C70-4.3] 16 p2584 A71-33542
- Future aviation development constraints on manufacturer and purchaser, design, test costs, noise, airport location and multinational operation [ALAA PAPER 71-799] 16 p2667 A71-34024
- Titanium and composite fabrication for F-14 aircraft, discussing hot forming, chemical milling and electron beam welding 16 p2585 A71-34156
- Modular manufacturing for F-14 aircraft at low cost using end product configuration reducing final assembly 16 p2585 A71-34157
- Aircraft jet engine application of electric discharge machining for repetitive continuous production, considering automated closed cycle equipment [SME PAPER MR-71-143] 18 p2927 A71-36658
- AIRCRAFT RELIABILITY**
- Airline experience with dual inertial systems as sole means of navigation, considering equipment reliability, cockpit design, training, etc 01 p0124 A71-10509
- Aviation products liability and warranty law, noting reliability trends and quality control methods 03 p0523 A71-12971
- DC-10 aircraft test program effectiveness, discussing performance, operational envelope, airworthiness, noise measurements, etc [SAE PAPER 700830] 03 p0348 A71-13726
- Airworthiness and Air Registration Board, discussing aims, objectives, technical changes and national and international control 03 p0524 A71-13734
- Reliability and maintenance problems of U.S. Army operational environment, noting inadequate design and test criteria during development 04 p0530 A71-15402
- VTOL aircraft IFR airworthiness, noting necessity of higher safety levels for metropolitan air transit systems 04 p0533 A71-15426
- Concorde progress toward certification, discussing SST airworthiness requirements, flight test program, takeoff and landing operational experience and stability problems at high incidence 05 p0696 A71-16487
- Statistical information on lightning and static hazards relative to airworthiness 07 p1020 A71-19929
- Automatic Carrier Landing System with linear adaptive aircraft Navigation Computer, investigating effectiveness in reducing system errors due to nonlinearities and noise effects 07 p1157 A71-20405
- Concorde airworthiness requirements and Air Registration Board participation in flight test program, considering supersonic flight characteristics 09 p1385 A71-23579
- Costs-reliability relationships in helicopter development testing and demonstration, emphasizing decision making in program management [SAE PAPER 710452] 13 p2167 A71-28330
- Yak 40 aircraft flight test program, discussing airworthiness requirements, static structural, vibration and wind tunnel tests 14 p2174 A71-29911
- Fail-safe helicopter rotor control design, discussing damage tolerant components, redundant system, failure warning and maintenance [AHS PREPRINT 550] 14 p2179 A71-31102
- Aircraft ILS signal reception system, obtaining category III reliability performance by circuit redundancy and automatic incoming information surveillance 15 p2446 A71-31912
- Concorde aircraft automatic landing and flight control system objective, design, reliability and certification tests 15 p2446 A71-31915
- Aircraft reliability and maintenance cost reduction via allocation of effort and money, considering R and M optimization in airline support cycle 16 p2551 A71-33286
- DC-10 design dispatch and component reliability through flight test and follow-up fault isolation programs 16 p2522 A71-33297
- Lynx military helicopter design high reliability and low maintenance demands 16 p2523 A71-33457
- Combat aircraft vulnerability to projectile impact predicted by model giving target penetration, damage size and structural response [AIAA PAPER 71-777] 16 p2660 A71-34013
- Integrated logistics support program for F-14 aircraft maximum maintainability, reliability and operational readiness at optimum cost 16 p2553 A71-34154
- Computerized automatic control of aircraft electrical system using remote power controllers and multiplexed data bus for wiring reduction and reliability improvement 17 p2677 A71-34700
- Information transfer in all-weather aircraft operation, discussing pilot role in overall reliability based on man machine system information process 17 p2693 A71-35209
- Commercial aircraft reliability and maintainability design philosophy application to reusable space vehicles, considering optimum redundancy, dispatch with component inoperative and fault isolation 18 p2973 A71-36481
- British civil aircraft airworthiness requirements, discussing aircraft industry management philosophy ensuring quality standards in design, development, production, inspection and product support 18 p2989 A71-36673
- V/STOL airworthiness certification, considering standards developed by FAA in cooperation with industry [CASI PAPER 72/21] 19 p2997 A71-37607
- Civil transport aircraft and equipment maintenance and reliability problems solutions with best time, cost and weight compromises 24 p3792 A71-44765
- AIRCRAFT SAFETY**
- American ATA prototype aircraft collision avoidance equipment and proposed noncooperative system 01 p0125 A71-10753
- STOL future performance and safety level, considering current jet aircraft fatal accident record and proportional perpetuation, airworthiness and operational considerations 03 p0347 A71-13568
- V/STOL aircraft in civil air transportation, discussing safety, reliability, maintainability and propulsion system concepts 03 p0348 A71-13576
- Civil aviation safety - Conference, Beirut, September-October 1970 04 p0690 A71-14990
- Helicopters safe antitorque control, describing Fenestron ducted fan design 04 p0532 A71-15417
- VTOL aircraft IFR airworthiness, noting necessity of higher safety levels for metropolitan air transit systems 04 p0533 A71-15426
- Aircraft equipment failures detection and warning systems 04 p0601 A71-15901
- All-weather aircraft operations, discussing takeoff, landing, safety and forecasting 06 p0847 A71-17923
- Cargo aircraft crew safety and survival, describing restraint, escape, flight deck interior doors, fire and smoke hazards and personnel environmental protection [SAE-ARP-1139] 07 p1019 A71-19643
- Materials and construction techniques in lightning protection for aircraft and helicopters 07 p1020 A71-19930
- Lightning current transfer tests of p-static discharger for aircraft installations 07 p1020 A71-19935
- Lightning and surge protection devices for survivability of aircraft electrical systems 07 p1021 A71-19941
- Aircraft industry ATC techniques and equipment contribution to aircraft control and safety 09 p1491 A71-22951
- ATC electronic automation systems development for air safety improvements 09 p1491 A71-22953
- Commercial business and utility aircraft chemical oxygen generators to satisfy FAA requirements, discussing weight, size and maintenance savings and increased safety [SAE PAPER 710390] 10 p1558 A71-24254
- Crashworthy personnel restraint systems for general aviation including upper torso restraint [SAE PAPER 710396] 10 p1569 A71-24260
- VTOL propulsion systems safety requirements, considering single and double breakdowns 10 p1659 A71-24752

Bird impact hazard to general aircraft, discussing structural damage, flight safety and testing procedures 10 p1557 A71-24997

U.S. General Aviation safety record, discussing National Transportation Safety Board and accident/injury prevention 10 p1557 A71-25132 [SAE PAPER 710397]

Aircraft wing fatigue test procedures for gust, maneuver, ground-air-ground, taxi and landing impact loads 10 p1694 A71-25133 [SAE PAPER 710403]

Polyurethane foam effects on fuel contamination during installation for fuel system fire and explosion protection 11 p1708 A71-25981 [ASME PAPER 71-GT-54]

SST problems, including adequate instrumentation and fuel tank immunization to explosion 12 p1867 A71-26883

Passenger aircraft structures accelerated testing for safety and fatigue durability under operational conditions, describing tests, planning and evaluation 12 p1974 A71-26946

Weather minimum standards for civil aircraft, considering cloud ceilings, visibility, wind velocity and direction, onboard and ground-based flight control equipment and aircraft characteristics 12 p1924 A71-27141

Airport certification and safety inspection procedures and minimum safety standards 13 p2167 A71-28305 [SAE PAPER 710413]

Plug-in relay hazards and minimization for aircraft flight safety applications 13 p2001 A71-28841

Jet transport aircraft design for safety under air turbulence conditions, considering cruise altitude limitations and pitch and g excursion reduction by special autopilot mode 14 p2173 A71-29777

Aircraft-simulating cockpit procedure trainer statistical data and development problems concerning safety, economy and efficiency performance 15 p2384 A71-31883

Civil aircraft arresting on runway overshoots, describing safe deceleration method by use of soft ground arresters 17 p2674 A71-35210

ATC system safety problems from user standpoint, considering requirements by pupil, test and airline pilots and light, private, business, taxi and military aircraft 17 p2774 A71-35372

ATC system improvement by area navigation, discussing benefits in services, safety and cost effectiveness 17 p2775 A71-35373

Air transportation safety review covering weather knowledge, aircraft structures, instrumentation, radio aids and power plants 18 p2849 A71-36175

International airport planning, considering runways, hangars, second level loading, cargo handling and safety 20 p3209 A71-39388

Air safety standards and objectives, discussing human factors as accident causes, piloting aids and management 20 p3178 A71-39395

Trailing vortex pair behind aircraft, presenting equilibrium characteristics and effects on safety 21 p3321 A71-40504

Aircraft wake turbulence relation to CAT, discussing flight control loss, jumbo jets trailing vortex wakes breakup and detection and safe aircraft spacing 21 p3325 A71-40704

Unassisted aircraft parking system /Accu-Park/, discussing equipment design safety and accuracy 21 p3325 A71-41247

Strobe lighting for aircraft midair collision hazard reduction, comparing Collision Avoidance System and Pilot Warning Indicator effectiveness 22 p3499 A71-41493

Inertial navigation impact on aircraft safety, discussing error sources and midair collision risks 22 p3571 A71-42079

U.S. Army ATC cost-effective system developments for high density low altitude helicopter tactical operations to avoid enemy radar under near-all weather conditions 22 p3571 A71-42084

Corporate aircraft safety - Conference, Washington, D.C. April 1971 23 p3627 A71-43226

Jet engine advent impact on aviation fuels safety, discussing gasoline hazards in prejet aircraft 23 p3718 A71-43231

Circadian rhythm relation to aircraft pilot safe performance 23 p3632 A71-43232

Corporate aircraft safety - Conference, San Antonio, May 1970 23 p3628 A71-43379

AIRCRAFT SPECIFICATIONS

STOL aircraft for tactical support, discussing USAF intertheater requirements 04 p0529 A71-15024

Metro commuter aircraft specifications, performance and CAB certification problems 06 p0846 A71-17573

Cessna Citation twin turbofan business aircraft design, performance characteristics, communications, navigation and automatic flight control equipment and flight evaluation 09 p1385 A71-22112

Soviet book on aircraft preliminary design specifications as function of performance, aerodynamic and structural parameters, discussing tradeoffs in operational requirements for specific configurations 10 p1554 A71-24012

DC 10 specifications for airport planning, including ground clearances, payload-range characteristics and jet engine exhaust velocities 14 p2175 A71-30239

Computer aided design program for civil transport aircraft configuration, performance, propulsion, weight and costs to meet given specifications 14 p2175 A71-30398

Flying qualities military specification, discussing longitudinal static stability, transonic flight relaxation, control forces in maneuvering flight, lateral-directional oscillations, etc [AIAA PAPER 71-766] 16 p2523 A71-34004

AIRCRAFT STABILITY

NT HOVERING STABILITY

Rapid hybrid frequency response method for aircraft flight flutter testing based on hybrid computing system 01 p0049 A71-10228

LAMS flight control systems for gust load alleviation and structural mode stabilization on large flexible aircraft, using aerodynamic surfaces 02 p0188 A71-11659

C-5 military transport stability augmentation for pitch and yaw inertia at low speed, using pilot evaluation on cockpit simulator 02 p0190 A71-12684

Statistical prediction of atmospheric turbulence effects on aeronautical systems 03 p0398 A71-13135

Clear air turbulence effects on flight and structural response of aircraft, using gust loads model [ONERA-TP-867] 03 p0346 A71-13136

Heavy supersonic aircraft controllability, noting irreversible boost control system and stability 03 p0454 A71-13195

Jet interference effects on aircraft static stability with ejector afterbody, noting wind tunnel methods of drag minimization and measurement 05 p0696 A71-15953

Single rotor helicopter directional stability in rectilinear flight with constant angle of side slip 06 p0847 A71-18307

Aft vs canard horizontal tail locations for fighter/attack configuration at sub and supersonic speeds, observing lift coefficient, L/D and longitudinal stability [AIAA PAPER 71-8] 06 p0848 A71-18482

DC-10 flight test program, discussing handling, takeoff and landing, and flutter, stall and stability characteristics 07 p1018 A71-19085

Airliner acceptance checks characteristics for official licensing prerequisites, investigating takeoff, landing, ascent, stability and control 07 p1022 A71-20065

Aircraft elastic mode control for turbulence/gust/alleviation, noting riding quality, structural fatigue life and peak loads 07 p1022 A71-20301

Soviet book on aircraft flight with incomplete and asymmetrical thrust covering probabilistic characteristics, stability, landing and takeoff with partial engine failures, etc 10 p1554 A71-24013

Inclined engine cold circular jet effects on tail control surfaces aerodynamic characteristics, considering aircraft longitudinal stability [DFVLR-SONDDR-104] 10 p1552 A71-24593

Optimal control stabilization under continuous small disturbances applied to aircraft stability in horizontal flight under vertical gust loads 10 p1586 A71-24726

Propulsion system and fuel regulator design effect on thrust change during air ejection for VTOL aircraft stabilization in hovering flight 10 p1659 A71-24753

Nonstationary random analysis of flight vehicle response to atmospheric turbulence, using Priestley evolutionary spectral method 11 p1836 A71-25320 [AIAA PAPER 71-341]

Wind tunnel evaluation of analytical method for predicting longitudinal stability and aerodynamic characteristics of large flexible aircraft applied to supersonic transport configuration 11 p1707 A71-25322 [AIAA PAPER 71-343]

Longitudinal stability of ground effect airplane, discussing influence on aerodynamic characteristics of

height, ground surface roughness and wing aspect ratio 13 p1997 A71-29228

Jet transport aircraft stability and controllability under atmospheric turbulence conditions, discussing longitudinal and lateral-directional characteristics with particular attention to unstable spiral mode 14 p2173 A71-29772

Pilot subjective evaluation of XB-70 aircraft response to atmospheric turbulence in comparison with measured accelerations 14 p2173 A71-29774

Helicopter rotor system vibratory and mechanical stability characteristics, investigating anisotropically mounted flexible swash plate and blade out of track effects [AHS PREPRINT 511] 14 p2178 A71-31082

Hingeless rotor helicopter stability and control characteristics, considering induced flow field, flapwise bending modes and blade-fuselage dynamic coupling [AHS PREPRINT 541] 14 p2179 A71-31098

Stratospheric turbulence induced aircraft buffeting dependence on vertical wind shear, Richardson number and thermal stability change from underlying to overlying layer 15 p2444 A71-31365

Stratospheric turbulence induced aircraft buffeting dependence on horizontal temperature and wind distribution 15 p2444 A71-31366

Aircraft spin tests preparation and evaluation, describing pilot errors 15 p2348 A71-31462

Helicopter stability, using Lockheed rotor system with gyro coupled to cantilevered blades 15 p2348 A71-31599

Aspect ratio influence on instability and non-minimum phase effects of longitudinal motion of aircraft relative to negative lift-drag expression transfer functions [DFVLR-SONDDR-127] 16 p2523 A71-33405

SST stability augmentation system, discussing performance, operational safety and reliability benefits [AIAA PAPER 71-785] 16 p2525 A71-34015

Twin turboprop STOL aircraft lateral directional oscillation traced to rudder vibration due to aerodynamic hinge moments interaction with friction [AIAA PAPER 71-792] 16 p2525 A71-34019

Total in-flight simulator /TIFS/ in variable stability C-131 aircraft, describing potential as design tool [AIAA PAPER 71-794] 17 p2675 A71-35529

STAN/MASS system aircraft weight and balance determination, discussing basic concepts, design requirements and applications [SAWE PAPER 896] 17 p2834 A71-35816

Dynamic positioning stationkeeping and stability criteria for formation flight systems extended to helicopter and V/STOL transports 18 p2849 A71-35923

High speed aircraft maneuvers stability determination by constant angular pitching/rotation velocity, angle of attack and flight speed, using Liapunov method 18 p2849 A71-36176

Soviet book on practical aerodynamics of aircraft with turboprop engines covering piloting, forces and moments, stability, controllability, takeoff, landing, etc 19 p2994 A71-38534

Large crane heavy lift helicopter stability and controllability, considering effects of slung loads, performance improvement, automatic flight control and physical size 19 p2998 A71-38651

Tilt-fold-proprotor VTOL aircraft stability and control, emphasizing pylon tilt and rotor stop-fold effects on flying qualities 19 p2998 A71-38652

Aircraft lateral dynamics effect on positioning accuracy along straight flight path, using Loran C data 20 p3261 A71-38864

Atmospheric and wake turbulence effects on aircraft from discrete gust and spectral interpretations, discussing load production and uncontrollable rolling moments 21 p3321 A71-40507

Parametric and autoparametric instability of aircraft structures 22 p3483 A71-42240

Variable stability aircraft lateral directional flying qualities, investigating turbulence effects 22 p3483 A71-42833

Stability augmentation system for aircraft elastic modes control, discussing active flutter suppression technology 23 p3629 A71-44107

Flexible ram air inflated keel and leading edge parawing design optimization for increased stability and reliability, introducing semirigid member concept [AIAA PAPER 71-986] 24 p3791 A71-44582

STOL aircraft flight control problems, discussing Mach trim, artificial feel, stability, feedback system responses and lateral/directional laws [AIAA PAPER 71-993] 24 p3792 A71-45297

AIRCRAFT STRUCTURES

NT AIRFRAMES
NT FUSELAGES
NT PLASTIC AIRCRAFT STRUCTURES
Aircraft structure fatigue life improvement via material stress coining inside and around holes and slots
01 p0085 A71-10170
Aircraft structures fatigue testing device using programmed control of electrical inputs to electrodynamic vibration stand, noting load cycle effects and damage accumulation
01 p0168 A71-10409
High velocity metal working, discussing airfoil forging, ausforming of bearing case blanks, tooling, etc [SME PAPER MF-70-228]
01 p0090 A71-11267
Composite materials structure cost effectiveness demonstrated in aircraft relief crew compartment panels
01 p0177 A71-11281
Papers on LAMS technology for aircraft structural mode control covering B-52 and C-5A aircraft
02 p0187 A71-11658
LAMS flight control systems for gust load alleviation and structural mode stabilization on large flexible aircraft, using aerodynamic surfaces
02 p0188 A71-11659
B-52 LAMS test vehicle structural modification and instrumentation in flight phase
02 p0188 A71-11661
Sandwich structures applications in aircraft and space vehicles, discussing component characteristics, manufacturing processes and mechanical testing procedures
02 p0324 A71-11959
Aircraft multiwheel undercarriage effect on rigid and flexible pavements, examining failure modes
02 p0189 A71-12164
Dynamic aeroelastic calculations for aircraft, using ground vibration test data
03 p0501 A71-13134
Soviet book on aircraft construction technology covering parts fabrication, protective coatings, production automation, etc
03 p0433 A71-14399
Assembling accuracy of three dimensional joints using assembly holes in aircraft construction
04 p0602 A71-14609
Automatic excitation forces generation for aircraft structural ground vibration tests using digital computer [ONERA-TP-870]
04 p0669 A71-15352
Aluminum reinforced epoxy model making, testing and stress analysis for aircraft structures, including creep, photoelastic coating and strain gage effects
05 p0821 A71-16346
Aircraft light alloys fatigue characteristics for component endurance evaluation
05 p0767 A71-16757
High modulus boron-epoxy composite aircraft structures adhesive bonding, discussing mechanical properties, manufacturing techniques and quality control [SAE PAPER 710110]
06 p0904 A71-17624
Flexible aircraft to atmospheric turbulence transfer functions, discussing in-flight measurements [ONERA-TP-894]
06 p0847 A71-18021
Plane and spatial load transfer and diffusion in linear elastostatics, noting application to aircraft and civil engineering structures and fiber reinforced materials
06 p1001 A71-18222
BD-1 Yankee aircraft development, design and construction
07 p1018 A71-19084
Artificial lightning generation facilities for aircraft component developmental testing by manufacturer
07 p1020 A71-19931
Elastic, inertial and aerodynamic forces aeroelastic triangle, examining lift changes due to aircraft structure deformation, dynamic flight stability and space shuttle development problems
07 p1215 A71-20063
Filament winding manufacturing methods using unidirectional glass reinforcements for design and fabrication of aircraft wing structure [SME PAPER EM-70-406]
07 p1120 A71-20546
Bent structure failure under pulse floor acceleration shocks, concerning aircraft seat damage during crash landing
08 p1367 A71-20747
Aircraft systems assembly methods, discussing rigidity effects on error redistribution in external and internal force field application
08 p1295 A71-20792
Cost aspects of carbon fiber reinforced composites in aircraft structures, suggesting increased aviation market for carbon fiber [PLASTICS INST. PAPER 46]
08 p1378 A71-20929
Strain level counter monitoring aircraft structural fatigue, describing system components consisting of sensors in critical structure areas and indicator unit with visual display
09 p1445 A71-22725

Metallic coating effects on aircraft high strength steel fatigue, considering chromium plating, shot peening and plasma spraying
09 p1469 A71-22889
Hawker Siddeley Trident 3B flight test program, booster engine, structural features, power plants, systems and landing gear
09 p1385 A71-22890
Aircraft wings automated preliminary structural design and weight determination procedures based on external shape, aerodynamic loads and fuel mass interaction
09 p1541 A71-23274
Ti alloys structural high temperature applications in fighter aircraft, considering fabrication and assembly methods
09 p1458 A71-23427
Stress concentration correcting factors for fillets in landed aircraft structures
09 p1542 A71-23539
Corrosion resistance of adhesive bonded airframe structure components under outdoor weather and salt spray conditions, discussing test results with Al alloy specimens
09 p1459 A71-23690
Precision forging and pressing of Al alloy and Ti alloy parts of aircraft structures at cost effective prices
09 p1459 A71-23691
Aircraft structural fatigue life in-flight monitoring, describing sensor installation on aircraft fin structure and measurement results
10 p1685 A71-23938
High peel strength epoxy and urethane adhesives for aircraft bonding, discussing high temperature curing and honeycomb panel repair
10 p1630 A71-24064
Variable weight composite materials for aircraft optimal adhesive bonding structural designs, discussing C-5A tow weight saving Ti honeycomb applications
10 p1686 A71-24084
Alloy and heat treatment effect on Ti bondability for adhesive bonded aircraft structure, using annealed and aged Ti-6Al-4V and Ti-6Al-6V-2Sn alloys for testing
10 p1615 A71-24093
Photochromic paints for nondestructive testing of aerospace materials and structures
10 p1633 A71-24102
Filamentary composites for primary aircraft structural applications, emphasizing boron-epoxy material
10 p1618 A71-24770
C-5A cargo box side wall deformations, examining square plates center deflections with elastic beams
10 p1557 A71-24871
Nonstationary stress modeling in aircraft structures using random pulse generator applied to jet landing gear break strut fatigue test
10 p1692 A71-24954
Glass fiber reinforced plastics aerospace applications covering radomes, dielectric panels, aircraft ducting, secondary structures, furnishings, mouldings and tooling
11 p1788 A71-25652
Passenger aircraft structures accelerated testing for safety and fatigue durability under operational conditions, describing tests, planning and evaluation
12 p1974 A71-26946
Material properties, impregnation, shaping, hardening and structural design in mass production of reinforced laminates for aircraft construction
12 p1920 A71-26954
Flame retardant silicone elastomers for use as aircraft construction materials, describing fabrication techniques, mechanical, aging and weathering properties
12 p1921 A71-27412
Aircraft structural elements thermal behavior under aerodynamic heating with linear dependence on initial temperature
12 p1865 A71-27493
Artificial corrosion pits effect on fatigue durability of smooth samples and aircraft duraluminum skin elements
13 p1995 A71-27819
Filamentary composite reinforced metal aircraft structures, considering boron/epoxy in combination with aluminum
13 p2151 A71-28168
Locating neutral layer and critical curvature radius in aircraft components waffle panels under elastoplastic bending
13 p2074 A71-28940
Structural fatigue in aircraft design, discussing twin engine transport tests, crack propagation rate, residual strength, etc
13 p2158 A71-29434
Soviet book on aircraft materials science and treatment covering steel/cast iron processing, metallography, heat/thermochemical conditioning, surface protection and corrosion prevention
14 p2256 A71-29529
Atmospheric turbulence effects on handling qualities and structural loads on aircraft
14 p2174 A71-29787

Aircraft manufacturing techniques, discussing structural components fabrication, economics, lightweight, high strength and heat resistance [SME PAPER MR-71-725]
13 p2417 A71-32436
Aircraft structures fatigue properties, discussing stresses, life estimates, safety factors and descriptive curves
16 p2656 A71-33343
Airframe structural uses of Al, Ti and Be alloys, discussing need for structural efficiency improvements by proper heat treatment and stress relieving techniques
16 p2594 A71-33875
Advanced composites as future aircraft structural materials, discussing design concepts, service experience, manufacturing methods and quality assurance [AIAA PAPER 71-779]
16 p2660 A71-34014
Fighter F-14 podded engine high variable sweep wing design including nozzle, nacelle, fuselage shift, aspect ratio and lift control improvements
16 p2526 A71-34152
Aircraft structural parameters optimization satisfying flutter velocity constraint and minimum mass, applying to box beam design
17 p2825 A71-34874
Aircraft structures damage tolerance - ASTM Conference, Philadelphia, June 1970
17 p2826 A71-35151
Thickness effect on fracture toughness and crack propagation of Al alloy sheets used for aircraft skins
17 p2758 A71-35153
Damage tolerant aircraft structures material toughness and residual strength, presenting fracture test results on precracked panels reinforced with crack stoppers
17 p2827 A71-35157
Wing structural elements ballistic damage tolerance and residual fracture strength characteristics, discussing projectile velocity, impact angle and target thickness effects
17 p2827 A71-35161
Soviet papers on thin walled aircraft structures strength and stability covering bending theory, circular cylindrical shells, thermal stresses of rectangular plates, etc
17 p2828 A71-35301
Aircraft structural panels under cyclic static loads, examining fatigue life with probability theory, statistics and regression analysis
17 p2829 A71-35312
Light alloys fatigue characteristics for aircraft components endurance evaluation
17 p2759 A71-35456
Weight reduction potential of composite materials in aerospace structures, proposing weight estimation technique [SAE PAPER 887]
17 p2834 A71-35819
Composite structures development, discussing wing, fuselage, aeropropulsion and missile development, weight savings of hardware and fighter empennage applications [AIAA PAPER 71-367]
18 p2979 A71-36275
Feasibility assessment of hypersonic transports with actively cooled airframe structure, considering liquid hydrogen fuel use as coolant
19 p2995 A71-37123
Aircraft structures sonic fatigue due to high frequency noise from turbofan engines, discussing case histories, failure diagnosis and precautionary design measures
19 p2997 A71-37843
Random loading parameters adjustment in fatigue tests of welded aircraft structures
22 p3528 A71-41692
Parametric and autparametric instability of aircraft structures
22 p3483 A71-42240
Corrosive delamination occurrence, reduction and prevention in metal-metal adhesive bonded aircraft structures
22 p3555 A71-42594
Statistical analysis of spot welded and adhesive joints of high strength Al alloy sheet in aircraft structures
24 p3831 A71-45012

AIRCRAFT TIRES
Transport aircraft tire pressure and multiwheeled landing gear limitations regarding pavement design
02 p0189 A71-12163
Aircraft tires mechanical data from small models, discussing mechanical properties, tire stresses and tire temperatures [AIAA PAPER 71-346]
11 p1707 A71-25325
Aircraft steering system design, considering oversteering effects in nose wheels, torque for reaction moment balance and tire behavior
16 p2522 A71-33225
Transfer function system relating cornering force and aligning torque of rolling pneumatic aircraft tire to yaw angle and lateral displacement
21 p3324 A71-40167
Braking performance of runway surfaces and skidding resistance of aircraft tires, considering load

and inflation pressure, tread materials and weather conditions effects 22 p3529 A71-42234

Folding sidewall aircraft tires design, construction and flight tests, noting advantages and disadvantages 24 p3792 A71-44975

AIRCRAFT WAKES

NT HELICOPTER WAKES

NT PROPELLER SLIPSTREAMS

NT SLIPSTREAMS

FAA full scale aircraft vortex wake turbulence flight test programs 06 p0848 A71-18552

In-flight profile drag measurement of gliders with total and static pressure sensors in boundary layer wake, using moments method 09 p1384 A71-23667

Vortex wakes behind STOL operations high lift wings, discussing height above ground and various wind tunnel dimensions effects 13 p1990 A71-28033

Trailing vortices shed by aircraft lifting surfaces, noting wake effects importance at low speeds 13 p1995 A71-28176

Flow field induced by aircraft trailing vortices near ground during takeoff and landing, noting experimental departure from theory 17 p2671 A71-34900

Aircraft vortex wake turbulence including formation, disintegration, hazards reduction, instability and interactions with following vehicles 17 p2673 A71-35753

Jumbo jet trailing vortex mathematical model for studying effect on penetrating aircraft 17 p2673 A71-35754

Large jet transport aircraft trailing vortices, studying velocity fields, core diameters and logarithmic variations of circulation 17 p2674 A71-35755

Trailing wake hazards of large transports in takeoff and landing, examining configuration stability of vortex pair in ground effect 17 p2674 A71-35757

Aircraft wake turbulence /trailing vortex systems/ avoidance during flight, describing procedures for pilots and tower operators [CASI PAPER 72/6] 19 p2992 A71-37596

Aircraft wake turbulence and detection - Conference, Seattle, September 1970 21 p3318 A71-40482

Aircraft wake turbulence, reviewing aerodynamic vortex research as exemplified by Karman vortex street and edgetone phenomenon 21 p3318 A71-40483

Atmospheric stratification effects on downward motion of aircraft vortex wakes, developing approximate model 21 p3318 A71-40486

Subscale modeling of aircraft trailing vortices in controllable laboratory environment 21 p3318 A71-40488

Aircraft wing tip vortex air motion measurements, utilizing Doppler radar techniques 21 p3318 A71-40489

Peak velocity vectors in transverse plane of jet transport aircraft wake, measuring tip vortices core size 21 p3319 A71-40491

Vortex wakes behind straight and swept wings, noting formation of loops and trails close to ground 21 p3319 A71-40494

Spanwise lift distribution over wings and wake formation in thin airfoils of finite aspect ratio in linear subsonic potential flow 21 p3319 A71-40495

Trailing vortices behind wing tip with vortex dissipator, using wind tunnel flow visualization and flight tests 21 p3319 A71-40496

Vortex wake development and aircraft dynamics, using computer graphics and flow visualization techniques 21 p3319 A71-40497

Boeing 747, Lockheed C-5A and other aircraft vortex wake characteristics by tower flyby technique 21 p3320 A71-40498

Vortex wakes transport and decay for various aircraft types, flight modes and meteorological conditions 21 p3320 A71-40499

Aircraft trailing vortex pair linear stability, obtaining flow field near curved vortex filament with swirl and axial velocities 21 p3320 A71-40500

Turbulent shear effect on isolated trailing single vortex decay behind aircraft 21 p3320 A71-40503

Trailing vortex pair behind aircraft, presenting equilibrium characteristics and effects on safety 21 p3321 A71-40504

Flow visualization of aircraft trailing vortex wakes in towing tank with electrochemically activated dye, noting flow instability 21 p3321 A71-40505

Flight tests for hazard evaluation to other aircraft from wake turbulence generated by large jet transport airplanes 21 p3321 A71-40506

Airloads and moments changes of aircraft flying over trailing vortices, investigating time dependent aerodynamic forces 21 p3321 A71-40508

Flight test experiment to evaluate mechanized automatic control system to minimize wake turbulence effects on aircraft 21 p3321 A71-40509

Aircraft wake turbulence relation to CAT, discussing flight control loss, jumbo jets trailing vortex wakes breakup and detection and safe aircraft spacing 21 p3325 A71-40704

Aircraft wake turbulence and trailing vortices, investigating physical characteristics, hazard potential and avoidance techniques 23 p3628 A71-43234

Aircraft generated vortex wakes and core air motions hazards for encountering light airplane 23 p3628 A71-43381

AIRCRAFTS

U FLIGHT CREWS

AIRFIELD SURFACE MOVEMENTS

Taxiing aircraft position and wheel trajectories for specific nose wheel path 02 p0187 A71-11641

Computer generated motion pictures to simulate real events, discussing design problems and airfield simulation with GPSS software package 07 p1111 A71-19511

ATC system models, covering surface movement, runway utilization, terminal areas and enroute traffic 17 p2771 A71-34523

Unassisted aircraft parking system /Accu-Park/, discussing equipment design safety and accuracy 21 p3325 A71-41247

AIRFOIL CHARACTERISTICS

U AIRFOILS

AIRFOIL PROFILES

NT WING PROFILES

NT WING SPAN

Fredholm method for reversible transonic flow in computing aircraft wing and turbomachine or helicopter blade airfoils for compressibility law 01 p0003 A71-11022

Cascade flow test data, considering blade section performance in transonic and supersonic axial flow compressors 03 p0343 A71-13829

Plane and wedge shaped airfoil profiles of variable thickness, deriving stability in bilateral supersonic air flow 03 p0515 A71-14365

Gas flow past straight airfoil, analyzing damped natural oscillations 03 p0345 A71-14561

Symmetric airfoil profiles with sharp and rounded leading edges in inviscid gas unbounded uniform adiabatic transonic flow, solving by nonlinear approximation 04 p0525 A71-14591

Airfoil profiles with flaps at medium Reynolds numbers, determining performance characteristics in wind tunnel tests 04 p0526 A71-15025

Helicopter fuselage design for crashworthiness under specific conditions 04 p0532 A71-15416

Singularity carrier auxiliary curves in airfoil cascade design, formulating and proving existence theorem 05 p0693 A71-16397

Plane steady incompressible MHD flow past slender nonconducting profile, determining magnetic field components boundary conditions 05 p0695 A71-16892

Lateral vibration effects on heaving airfoil blunt trailing edge vortex shedding flows, examining base cavity damping by flow visualization 06 p0984 A71-17621

Transonic supercritical flow past arbitrary airfoils, using integral relations method 06 p0844 A71-18553

Plane sound waves incident on flat plate airfoils lattice, obtaining transmitted and reflected pressure amplitudes [AIAA PAPER 71-181] 06 p0885 A71-18620

Monograph on transonic shock free potential flow around quasi-elliptical airfoil sections, investigating flow stability under unsteady disturbances 07 p1015 A71-19773

Computer calculation of high Reynolds number viscous and inviscid flow over arbitrary shaped two dimensional bodies and airfoils 07 p1017 A71-20313

Hanging shock wave in small supersonic flow past profile with broken generatrix in plane ideal gas 08 p1228 A71-21872

Airfoil profile drag measurements, correlating full scale flight tests and scale model tests in transonic and high Reynolds number wind tunnels [AIAA PAPER 71-289] 08 p1229 A71-22012

Optimization of slot angle, slot positioning and flow quantity affecting boundary layer control in energy transfer over airfoil profiles 09 p1383 A71-23201

Surface roughness ensuring turbulent reattachment at low Reynolds numbers on airfoil sections with separation near leading edge resulting in bubbles [ONERA-TP-923] 10 p1549 A71-23762

Low speed airfoil characteristics calculation by digital computer, using Theodorsen conformal transformation method for potential flow pressure distribution [SAE PAPER 710389] 10 p1550 A71-24253

Airfoils accelerating near sound velocity, calculating acoustic radiation by linear theory 10 p1553 A71-24816

Propeller blade profile thickness distribution for given pressure distribution, deriving integral equation with singular kernel function via source-sink and vorticity distribution linearized theory 10 p1553 A71-24945

Airfoil profiles coupling method for determining complex potential of two dimensional ideal incompressible fluid flow due to arbitrary airfoil section movement near rectilinear wall 10 p1597 A71-25015

Sound radiation and wake turbulence spectra from axial compressor single airfoils, including double circular arc profiles [ASME PAPER 71-GT-4] 11 p1703 A71-25950

Transonic airfoil testing techniques in two dimensional flow, discussing wind tunnel conditions at various Reynolds numbers 12 p1864 A71-27467

Aerofoil cascades with axial velocity change in incompressible flow, determining turbine blade force dependence on circulation 13 p1990 A71-28467

Wind tunnel tests of geometrically compatible airfoils for variable chord sailplane 13 p1994 A71-29257

Two dimensional flow research on high lift airfoils for STOL aircraft, using vorticity distribution and wind tunnel wall blowing techniques 14 p2169 A71-29910

Two dimensional subsonic irrotational isentropic flow around thick profiles, using coordinate perturbation method 15 p2343 A71-31167

Pretwisted cantilever airfoil cross section turbine and compressor blades vibration natural frequencies and mode shapes 17 p2828 A71-35282

Numerical analysis of plane transonic flows past shock free airfoils without boundary layer separation using inverse method of complex characteristics 19 p2994 A71-38307

Resultant aerodynamic forces on circular arc profile with normal jet in subsonic steady compressible flow, using Imai-Lamla approximation method 23 p3627 A71-44271

Transonic airfoil cascade analytical design, determining efficiency from velocity distribution 24 p3791 A71-45381

AIRFOIL SECTIONS

U AIRFOIL PROFILES

AIRFOIL THICKNESS

U AIRFOIL PROFILES

AIRFOILS

NT AERIAL RUDDERS

NT AILERONS

NT CAMBERED WINGS

NT CARET WINGS

NT CRUCIFORM WINGS

NT DELTA WINGS

NT ELEVATORS [CONTROL SURFACES]

NT ELEVONS

NT FIXED WINGS

NT FLAPS [CONTROL SURFACES]

NT FLEXIBLE WINGS

NT HORIZONTAL TAIL SURFACES

NT INFINITE SPAN WINGS

NT JET FLAPS

NT LEADING EDGE SLATS

NT LIFTING ROTORS

NT LOW ASPECT RATIO WINGS

NT PARAWINGS

NT PROPELLER BLADES

NT RECTANGULAR WINGS

NT RIGID ROTORS

NT RIGID WINGS

NT RING WINGS

NT ROTARY WINGS

NT SLENDER WINGS

NT SPOILERS

NT SWEEP WINGS

NT SWEEPBACK WINGS

NT TABS [CONTROL SURFACES]

NT THIN AIRFOILS

NT THIN WINGS

NT TILTING ROTORS

NT TIP DRIVEN ROTORS

NT TRAILING-EDGE FLAPS

NT TWISTED WINGS

NT UNSWEPT WINGS

NT VARIABLE SWEEP WINGS

NT WING FLAPS

NT WINGS

Sound radiation from finite span airfoil in three dimensional turbulent flow, considering lift function effect

03 p0399 A71-13280

Optimal firing temperature schedule during gas turbine loading for minimal thermal fatigue of hot gas path components, considering hollow stationary airfoils

[ASME PAPER 70-WA/GT-2] 03 p0470 A71-14116
Linear airfoil theory applicability for wings aerodynamic characteristics, considering high lift, ground effect, angle of attack and aspect ratio

04 p0525 A71-14593

Shock wave bisector rule improvement, applying to asymptotic behavior of bow shock attached to airfoil in two dimensional supersonic flow

06 p0841 A71-17420

Performance characteristics of horizontal and vertical stabilizers at medium Reynolds number from wind tunnel measurements, considering air foil and flap effects

06 p0842 A71-18249

High lift nose slats generation for arbitrary airfoil, using conformal transformations and computer program

[AIAA PAPER 71-11] 06 p0842 A71-18485
Airfoils in two dimensional nonuniformly sheared slipstreams, predicting pressure distribution from mathematical model for comparison with measurement

[AIAA PAPER 71-94] 06 p0843 A71-18549
Viscous gas flow interaction on delta wing and oblique airfoil at Mach number of infinity

07 p1014 A71-19739

Computerized transonic airfoil design from predetermined supercritical velocity distribution, obtaining equivalent incompressible flow through streamline and potential line network transformation

07 p1017 A71-20304

Two dimensional test facility in blowdown wind tunnel transonic section, discussing porous sidewall boundary layer control effects on airfoils geometric characteristics

[AIAA PAPER 71-293] 09 p1428 A71-22957
Symmetrical airfoil in stratified fluid flow determining camber and incidence effects

10 p1552 A71-24589

Nonuniform transonic shear compressible flow past symmetric airfoil, using linearized small disturbance theory

10 p1552 A71-24761

Plane rigid airfoil with fixed center of gravity, discussing motion in turbulent air and gust loads

10 p1557 A71-24947

Resin matrix composite airfoils in gas turbine engines, considering performance, fabrication and cost

[ASME PAPER 71-GT-47] 11 p1770 A71-25980

Approximation of flow around jet flapped airfoil, discussing ground effect on lift coefficient increments

11 p1705 A71-26314

Hele-Shaw flow viscous tails from airfoil, observing high Reynolds number trailing edge flow for separation and initiation of Kutta condition

11 p1705 A71-26447

Airfoils unsteady stall by testing two dimensional model in harmonic pitching oscillation for helicopter rotor blades characteristics

[ONERA-TP-936] 12 p1866 A71-27609
Compressible transonic flow about two dimensional airfoils, developing inviscid nonlinear potential equations by relaxation procedures

[AIAA PAPER 71-569] 15 p2345 A71-31562
Airfoils broadband noise generation mechanism in turbulent flow in anechoic chamber

[AIAA PAPER 71-587] 15 p2468 A71-31573
Shearing flows in steady vortex around airfoil in perturbed velocity, considering aerodynamic forces torque

15 p2346 A71-31903

Two dimensional wind tunnel tests on airfoil fastened between tunnel walls, investigating variable chord concept applicability in sailplane design

15 p2350 A71-32294

Airfoils with turbulent boundary layers, calculating acoustic radiation from surface distribution of pressure fluctuations

15 p2347 A71-32520

Unsteady compressible flow measurement, determining local lift coefficient from pressure distribution along airfoil

16 p2520 A71-33342

Subcritical nonlinear potential flows over two dimensional subsonic airfoils by multistrip method of integral relations

18 p2845 A71-36330

Unsteady pressure gradient reduction effect on airfoil dynamic stall delay

22 p3481 A71-42841

Transonic flows about two dimensional airfoils, calculating far field boundary conditions with coordinate transformation

24 p3789 A71-44620

AIRFRAME MATERIALS

Fiber reinforced composites application in aerospace and aircraft, discussing boron and graphite and cost effectiveness

01 p0103 A71-11277

Be mechanical and physical properties, corrosion behavior, toxicity, fabrication and application as aircraft and spacecraft structural material

01 p0104 A71-11539

Nonmetallic aircraft construction materials, discussing wood epoxy and polyester resins

02 p0273 A71-12299

Nb alloys in hypersonic glider fabrication, discussing mechanical properties, oxidation resistance and sandwich panel design

02 p0270 A71-12935

Aircraft construction materials for 1990s, discussing need for high temperature resistant materials for supersonic and hypersonic airframe and engine structural components

05 p0839 A71-16141

Structural efficiency improvement by materials selection for airframe structures, discussing Al, Ti-Al-V and steel panels

08 p1299 A71-21685

Airframe structural uses of Al, Ti and Be alloys, discussing need for structural efficiency improvements by proper heat treatment and stress relieving techniques

16 p2594 A71-33875

Advanced composites as future aircraft structural materials, discussing design concepts, service experience, manufacturing methods and quality assurance

[AIAA PAPER 71-779] 16 p2660 A71-34014

Environmental effects on SST structural materials fatigue, discussing Ti alloys studies involving temperature effects, crack propagation and residual strength

17 p2821 A71-34556

Metal embrittlement by gaseous hydrogen, discussing countermeasures against hydrogen metal interaction and cracking

22 p3562 A71-41999

AIRFRAMES

Aircraft turbine engine development, considering mismatch reduction between engine and airframe in flight tests

01 p0143 A71-11180

Concorde airframe structures, discussing numerically controlled machining of aluminum alloy integral units

06 p0904 A71-17954

Complex airframe design for economic and safe operation and long life using fatigue and fracture mechanics

[AIAA PAPER 70-512] 08 p1374 A71-22025

F-111 airframe static test instrumentation, describing computerized processing of simultaneous inputs from 400 channels of tape recorded strain, load and deflection data

09 p1444 A71-22717

Supersonic transport inlet-engine-airframe compatibility programs, noting exhaust nozzle installation effects, distortions and noise

[AIAA PAPER 68-993] 10 p1659 A71-24854

Military aircraft flight test establishments, discussing airframe, engine, flight control and weapons delivery systems tests work flow integration requirements

11 p1708 A71-26315

Strategic bomber B-1A program, discussing airframe and engine contractors, design, characteristics performance, electronic equipment and armament

18 p2850 A71-36757

Automatic flight control accommodation to dynamic characteristics variations of airframe, providing uniform response for all flight conditions

19 p2996 A71-37296

AIRGLOW

NT GEOCORONAL EMISSIONS

NT NIGHTGLOW

NT TWILIGHT GLOW

Lyman alpha and O I 1304 A airglow depressions over poles from OGO 4 satellite observations

01 p0076 A71-11503

Far UV equatorial airglow and aurora intensities and occurrence frequencies from satellite observation

01 p0076 A71-11504

Nocturnal intensity and excitation temperature variation of hydroxyl vibrational rotational band in airglow

04 p0581 A71-15050

Airborne radiation thermometry corrections for intervening atmospheric absorption and emission and ocean surface nonblackness

04 p0601 A71-15762

Vertical NO profile at 100-220 km from 1968 Cosmos 224 measurement of atmospheric glow near horizon

05 p0744 A71-17186

O I 1304-A airglow, observing conjugate excitation with OGO 4 spacecraft

06 p0888 A71-17279

Geomagnetic storm on 24 March 1969, obtaining upper atmosphere emission data in middle latitude zone

06 p0894 A71-17996

Lambda 6300 A /OI/ airglow excitation by soft electron fluxes

07 p1103 A71-20006

Electrophotometric and spectral observations of continuous airglow spectrum

07 p1105 A71-20438

Night airglow measurements over Bulgaria, showing midnight minimum, maximum between 0100 and 0200 hours local time, steady airglow periods and random fluctuations

10 p1599 A71-23877

Rate constant temperature dependence for ozone reaction with oxygen, considering airglow features due to singlet molecular oxygen

11 p1801 A71-25370

UV airglow in 1304 A line of oxygen from Cosmos 215 satellite observation

12 p1899 A71-26638

Dissociative recombination source of atomic oxygen green line excitation in day airglow, considering differential photoelectron flux

13 p2055 A71-27919

Vertical NO profile at 100-220 km from 1968 Cosmos 224 measurement of atmospheric glow near horizon

13 p2059 A71-28243

Equatorial airglow enhancement data, observing 6300 and 5577 A intensity variations

16 p2562 A71-32809

Atomic oxygen 1304-A day airglow observed from OGO-D spacecraft, attributing subsolar emission rates to photoelectron impact excitation

16 p2574 A71-33964

Airglow research review and bibliography covering past four years observations of nightglow, twilight, dayglow and metals in upper atmosphere

17 p2732 A71-34466

Airglow surveys using extended field large aperture interferometer-spectrometer with optical wedge compensators and digital recording

18 p2914 A71-35842

Atomic oxygen concentration from 5577 A green line emission of airglow and chemiluminescence of nitric oxide

20 p3215 A71-38739

Airglow optical emission processes covering resonance scattering, fluorescence, chemical association, ionic reactions and excitation transfer

20 p3226 A71-39827

F 2 and D regions disturbances associated with magnetic storms, emphasizing airglow effects

20 p3227 A71-39836

Height resolved atmospheric turbulence properties from photometric measurements of airglow intensity fluctuations, discussing detection, separation from noise and statistical analysis

20 p3227 A71-39837

IR auroral/airglow study covering hydroxyl emission and dipole moment function determination and atmospheric nitrogen vibrational temperature measurement

20 p3240 A71-39843

Auroral electron and proton precipitation patterns, measuring airglow emissions

20 p3284 A71-39848

Atmospheric neutral and singly ionized He extreme UV emission altitude distribution measurement by sounding rocket-borne thin film photon counters

20 p3231 A71-39891

Day airglow columnar emission rates for Lyman-Birge-Hopfield system of molecular nitrogen as function of solar zenith angle, using OGO 4 observations

20 p3231 A71-39892

Atmospheric atomic hydrogen H alpha emission correlation with hydroxyl vibrational temperature

23 p3665 A71-42961

Photoelectron impact vs dissociative excitation cross sections of atomic oxygen resonance radiation in terrestrial airglow

23 p3669 A71-43171

Night airglow oxygen Herzberg I bands covariation with O I 5577 A line, evaluating NASA 1968 airborne auroral measurements

23 p3670 A71-43186

AIRLINE OPERATIONS

Flight training simulator use in airline operations, discussing economics of various simulator types with projection toward ultimate simulator

01 p0183 A71-10023

Airline liability and insurance in relation to aircraft hijacking, sabotage, etc

01 p0183 A71-10359

Economic contributions of U.S. domestic airline industry in 1970s regarding air transportation constraints and impact on short haul

[AIAA PAPER 70-1309] 01 p0004 A71-10486

Airborne inertial and area navigation systems performance requirements proposed for U.S. domestic airspace, including projection through 1995

01 p0124 A71-10508

Airline experience with dual inertial systems as sole means of navigation, considering equipment reliability, cockpit design, training, etc

01 p0124 A71-10509

SST program relation to airline operations, comparing production configuration, performance, economics and operation with subsonics [AIAA PAPER 70-1217]

01 p0005 A71-11248

Digital simulation program in GPSS language for airline operations including aircraft maintenance, flight scheduling, terminal space, equipment, work forces utilization, etc

02 p0227 A71-11809

Nondestructive testing techniques for airline maintenance inspection, describing ultrasonic, eddy current, magnetic particles, and X ray methods

02 p0256 A71-12449

Collision avoidance system flight test and evaluation program for airline industry CAS specification

02 p0280 A71-12896

Air carrier accident investigation, noting procedures, individual and group functions, notifications and company field organization

03 p0523 A71-12965

V/STOL short haul transport systems, discussing interurban applications, all-weather operation, operating costs, noise and atmospheric pollution

03 p0523 A71-13565

V/STOL services integration into UK air traffic system

03 p0454 A71-13567

V/STOL aircraft operations, considering terminals, landing and approach aids, air traffic, noise and pollution control, performance, airworthiness regulations and licensing

03 p0347 A71-13572

Terminal area operations of V/STOL aircraft, considering approaches, approach speeds, wind and velocity effects and noise

03 p0347 A71-13573

VTOL systems for commercial short haul air transportation, discussing large helicopters and compound aircraft applications for system capacity profitability and efficiency increases

03 p0347 A71-13575

Technical resources pooling among airlines for investment and maintenance cost cut of aircraft fleets

04 p0690 A71-14992

Air transport popularization possibilities, considering group rates and fare adjustments

06 p1009 A71-17586

French statistical system for civil air transport operations from airport viewpoint

06 p1009 A71-17587

Airport adaptation to large capacity aircraft, considering terminal installations, infrastructures, runways, roads and traffic areas

06 p0879 A71-17589

Book on general aviation future and economic impact covering fleet size and distribution, aircraft types, passenger and cargo profiles, etc

06 p1010 A71-17678

Airliner acceptance checks characteristics for official licensing prerequisites, investigating takeoff, landing, ascent, stability and control

07 p1022 A71-20065

Civil aviation aircraft mean flight time overhaul schedules, considering statistical evaluation of relationship between operational characteristics and time between overhauls

08 p1230 A71-20797

Jet aircraft noise over residential areas, discussing actual and permissible noise levels and proposals for remedial action

08 p1230 A71-21163

Airline collision avoidance system test and evaluation program, considering range, rate and altitude accuracy, communications reliability, synchronization and system integration with air traffic control

08 p1331 A71-21167

ATC services training and operations methods adopted by International Aeradio Ltd

09 p1491 A71-22952

Jet aircraft and hygiene, considering communicable diseases spread control measures and sanitation methods by airlines

09 p1400 A71-23071

Operational preparation and commissioning of IL-62 long distance jet aircraft, considering flight crew and maintenance personnel training at U.S.S.R. plant

11 p1743 A71-25256

Tu-154 responsibilities of three-man crews, considering flight plan, refueling, cargo loading and unloading

11 p1744 A71-25258

Flight and operation of IL-62 long distance jet aircraft, considering flight crew composition and training, passenger and cargo handling and refueling

11 p1706 A71-25260

Statistical survey of aeromedical and human aspects of airports, discussing population, facilities, accident treatment, design guide and requirements

11 p1725 A71-26127

Jet aircraft airworthiness standards, discussing airline fleet maintenance resources, inspection systems and future requirements

11 p1772 A71-26308

Pan American reliability program effect on airline maintenance, considering cost effectiveness, aircraft performance, data collection and analysis

12 p1910 A71-26671

Subsonic and supersonic airline operations, restraints, considering noise, air pollution and inadequate airport facilities

12 p1927 A71-26870

Soviet airlines operations planning, discussing principal objectives, methodology and organizational principles

12 p1988 A71-27144

Methods for engine condition monitoring application to airline operation

13 p2114 A71-28177

Airline operator evaluation of maintainability, considering costs and investment return [SAE PAPER 710432]

13 p2073 A71-28317

Airline engine performance testing from operator perspective, using automated test cell data acquisition system [SAE PAPER 710451]

13 p2044 A71-28329

Commercial airlines flight training program, using simulation and improved techniques for safety and economy [SAE PAPER 710475]

13 p2044 A71-28340

Airline flight personnel fitness downgrading, presenting statistical breakdown by age and physiological or psychological causes

13 p2019 A71-28509

Personnel training in airline operations technology at Friedrich List Transportation Institute for aircraft pilots, flight safety engineers and systems engineers

13 p2021 A71-29143

Aircraft noise on and near airports and factors affecting its intensity

13 p1997 A71-29304

Helicopter systems operations in, around and between major metropolitan areas, considering performance of New York Airways [AIAA PAPER 71-507]

14 p2339 A71-29549

Atmospheric turbulence over South America from Lufthansa data, noting occurrence, location, strength and dimensions

14 p2268 A71-29766

Air turbulence primary and secondary effects on aircraft flight and avoidance criteria considerations

14 p2268 A71-29768

U.S. air carrier accidents due to atmospheric turbulence, considering in-flight weather problems, airborne meteorological radar, CAT detection systems, etc

14 p2172 A71-29770

Book on air law and civil air policy covering international regulation, air traffic market, passenger and cargo services, etc

14 p2340 A71-29938

Long haul international air transport, analyzing traffic growth rates

14 p2340 A71-30161

VTOL and STOL aircraft comparative study covering site area, cost and noise and toxic gas production

14 p2175 A71-30163

Aircraft JT9D engine development for airline operation, discussing construction, condition monitoring, maintenance, noise and smoke reduction [SAE PAPER 710434]

14 p2289 A71-30528

Aircraft quantitative maintenance cost requirements translation into design criteria, considering airline operations influence on manufacturer [SAE PAPER 710437]

14 p2341 A71-30529

Civil aircraft antenna design mechanical and environmental aspects and electrical performance, considering serviceability and duplication

14 p2218 A71-31061

Reliability implications of Boeing 747 program, considering problem detection and identification, parts fabrication and installation, airline operating variables, etc

16 p2522 A71-33285

Aircraft reliability and maintenance cost reduction via allocation of effort and money, considering R and M optimization in airline support cycle

16 p2551 A71-33286

Reliability and maintainability as concepts in life cycle costs applied to airline operations

16 p2552 A71-33287

Airline fleet equipment planning, discussing management decision making based on aircraft and ground equipment life cycle costs

16 p2522 A71-33307

Air transport propulsion systems economics, considering first cost, specific weight, fuel consumption and maintenance effect on direct operating cost

16 p2523 A71-33469

Future aviation development constraints on manufacturer and purchaser, design, test costs, noise, airport location and multinational operation [AIAA PAPER 71-799]

16 p2667 A71-34024

German monograph on airport role in national economy and growth and location determination for enterprises maintaining connections with foreign countries

17 p2841 A71-34482

Category II operations at various airports, considering all-weather landing requirements of airborne equipment, maintenance standards, pilot training, etc [SAE PAPER 710442]

17 p2674 A71-34499

Aircraft for international long haul transportation, discussing criteria for selection based on environmental, operational, budgetary and policy considerations

17 p2674 A71-35208

Air transportation safety review covering weather knowledge, aircraft structures, instrumentation, radio aids and power plants

18 p2849 A71-36175

Maintenance control system [MCS], management information system encompassing subsystems supporting scheduling, forecasting, performance evaluation, modifications and improvement functions

18 p2987 A71-36448

Airline operations approach to Cape Kennedy launch processing system for reduced hardware and operational costs of shuttle support

18 p2899 A71-36475

New IATA passenger and baggage international air transport conditions, discussing passenger/carrier legal relationships, with emphasis on differences between new and old regulations

18 p2989 A71-36918

Airport system utilization, discussing aircraft noise, ATC, STOL development and passenger handling capacity problems [CASI PAPER 72/3]

19 p3041 A71-37594

All-weather operations, including pilot role, instrument landing systems and guidance aids [CASI PAPER 72/14]

19 p3100 A71-37601

Airfield surface system digital simulation model application to airport planning for airline operations

19 p3041 A71-38022

Super CTOL airport planning, discussing location of runway pairs, aircraft operations, noise reduction, community relations and efficiency

19 p3041 A71-38023

Air traffic congestion and delay Monte Carlo digital simulation in FORTRAN, exemplifying two-runway airport operation under instrument flight rules

19 p3041 A71-38024

Airport congestion as constraint on air travel, considering runway capacity and adjusted demand

19 p3042 A71-38025

Costs/benefits strategy for investment in STOL fleets reducing delay and airport congestion, using heuristic computer model

19 p3173 A71-38029

Seasonal distribution of air transportation requirements and utilization rate of transport capacity in passenger traffic

19 p3173 A71-38221

Airport operation costs affected by runway utilization, parking bays alignment, baggage handling and aircraft noise

20 p3209 A71-39390

Air traffic control delays, airport airspace congestion, flyover noise reduction and performance requirements effect on airline operations economics

20 p3209 A71-39391

Sick and injured transportation aboard regular airliners, considering pathological and psychological contraindications

22 p3500 A71-41572

Commercial ATC, considering VFR, flight control and inertial navigation

22 p3570 A71-42078

Unaided, integrated and differential OMEGA radio navigation configurations, comparing accuracy and suitability for airways system operations

22 p3571 A71-42082

Analytical model for air navigation and ATC system design, demonstrating system parameters effects on lateral separation standards for parallel flight lanes

22 p3571 A71-42083

Corporate aircraft operations in Latin America, discussing communication and navigation, fuel, power work, food, vaccinations and weather

23 p3629 A71-43391

Commercial air transportation industry trends and optimal planning requirements, discussing airline economic viability, industry regulation, public service and environmental compatibility [AIAA PAPER 71-1022]

24 p3892 A71-44600

Weather interruption effects on air transportation operations and economics, considering fog, snow, freezing rain, thunderstorms, winds, CAT and runway conditions

24 p3845 A71-44983

AIRLINERS

U COMMERCIAL AIRCRAFT

U PASSENGER AIRCRAFT

AIRLOCK MODULES

Skylab program, describing equipment based on Saturn 5 workshop experiments and objectives

07 p1206 A71-19088

On-orbit payload handling for space shuttles, including manipulator arms for drawing docking vehicles together, closed circuit TV and airlocking [AIAA PAPER 71-811] 17 p2814 A71-35427

PLANE PRODUCTION COSTS
Cost reduction concepts in gas turbine engine design and fabrication for general aviation aircraft 09 p1511 A71-22811

AIRPORT LIGHTS
NT RUNWAY LIGHTS
REPORT PLANNING
Airport system planning from environmental viewpoint, discussing travel market, airport accessibility, airspace utilization and control and land use 02 p0334 A71-11642

Aircraft pavement design - Conference, London, November 1970 02 p0237 A71-12162

Transport aircraft tire pressure and multiwheeled landing gear limitations regarding pavement design 02 p0189 A71-12163

Municipal airport rigid pavements design considering supporting effects of soil subgrade, asphaltic concrete subbase and pavement strength 02 p0237 A71-12165

Flexible pavements design for giant transports considering load repetitions, total systems, environmental effects, etc 02 p0238 A71-12166

Runways, aprons and taxiways strengthening to accommodate higher tire pressures and landing speeds, heavier aircraft and surface riding requirements 02 p0238 A71-12169

Aircraft pavements design and construction problems regarding adverse soil conditions 02 p0238 A71-12170

Airport planning by management systems approach, considering airspace, taxiways, runways, terminals, parking lots and roadways 03 p0522 A71-12962

Terminal area operations of V/STOL aircraft, considering approaches, approach speeds, wind and velocity effects and noise 03 p0347 A71-13573

Compound and VTOL aircraft and prototype compact downtown V-ports for short haul air transportation improvement and expansion 03 p0348 A71-13619

Cost efficiency, management and economics of airport operation, considering facilities relationship to airline operations 04 p0690 A71-14993

Airport planning and terminal facilities operation in 1970s, considering impact on developing countries 04 p0566 A71-14994

Helicopters, heliports and helistops, discussing need for public facilities 04 p0692 A71-15440

VTOL and STOL port federal design criteria, outlining planning and construction 04 p0567 A71-15441

Public-use ground level and rooftop helicopter and STOL aircraft landing facilities for city and suburban traffic 04 p0567 A71-15442

Optimum flight paths for V/STOL aircraft operating in short haul transportation near city centers 04 p0624 A71-15443

French statistical system for civil air transport operations from airport viewpoint 06 p1009 A71-17587

Large capacity aircraft reception and servicing problems consideration for facilitating traffic 06 p1010 A71-17588

Airport adaptation to large capacity aircraft, considering terminal installations, infrastructures, runways, roads and traffic areas 06 p0879 A71-17589

Lyons-Satolas /France/ International Airport project, discussing layout, facilities and noise control problem 06 p0880 A71-17590

Airport lighting facilities in Japan, considering fixtures, marker and obstruction lights and apron floodlight 07 p1084 A71-20355

Noise reduction at source, flight methods adjustments and airport compatible land use for jet noise abatement 08 p1378 A71-21815

Airport pollution dispersion modeling, simulating effect on surrounding areas for abatement strategies calculation 08 p1379 A71-21824

Noise pollution control and airport noise levels abatement regulation by state government, taking into account economic and technical feasibility 08 p1379 A71-21825

Federal assistance to air transportation, considering airport development-environment conflicts 08 p1380 A71-21834

Airport system planning for natural and urban environment compatibility 08 p1380 A71-21835

Land use control in aircraft noise abatement, considering airport development and community goals 08 p1380 A71-21836

Land development planning and aircraft noise at Kansas City International Airport 08 p1380 A71-21837

ATC system analysis, discussing airport and airspace utilization, area navigation, midair collisions and traffic mix 09 p1491 A71-22470

Floating airport structural design, using hollow concrete blocks filled with polystyrene foam as runway basic unit 09 p1428 A71-22949

Boeing 747 aircraft passenger handling measures in Frankfurt airport, discussing loading, unloading, baggage claim and customs control 09 p1430 A71-23696

Aircraft aquaplaning skidding prevention by runway resurfacing and water depth sensor warning indicators 10 p1609 A71-23946

Automated fueling for Kennedy jet airport, using computer controlled underground bulk storage- satellite tank pipeline system 10 p1589 A71-24300

Airport sound prediction using Noise and Number Index deduced from noise logarithmic average and audible aircraft number 11 p1723 A71-25236

Statistical survey of aeromedical and human aspects of airports, discussing population, facilities, accident treatment, design guide and requirements 11 p1725 A71-26127

Medical planning and first aid in disasters at airports 11 p1725 A71-26128

Epidemiological aspects of airport medicine in relation to global public health and international cooperation 11 p1725 A71-26129

Noise disturbance near large airports, considering aircraft noise, public annoyance and socio-psychological conditions 12 p1875 A71-27478

Airport certification and safety inspection procedures and minimum safety standards [SAE PAPER 710413] 13 p2167 A71-28305

National Airport Plan changes since 1946, discussing airport management involvement increase [SAE PAPER 710414] 13 p2167 A71-28306

Airport terminal building design and construction, noting economy and expansibility corequirements [SAE PAPER 710418] 13 p2044 A71-28307

Aircraft noise on and near airports and factors affecting its intensity 13 p1997 A71-29304

Airport pavement design principles, considering imposed stresses at flight operation areas, runways, taxiways, apron and waiting position overrun areas, shoulders and strips 13 p2045 A71-29311

Ultra Compact Airport Terminal, describing land-side, terminal and airside elements 13 p2045 A71-29313

Aircraft capabilities in intraurban transportation for Detroit metropolitan area, considering vehicle design, fleet size, cost and terminal location [AIAA PAPER 71-504] 14 p2172 A71-29548

Operations research minimum cost model of aircraft noise abatement in airport communities [AIAA PAPER 71-525] 14 p2339 A71-29551

DC 10 specifications for airport planning, including ground clearances, payload-range characteristics and jet engine exhaust velocities 14 p2175 A71-30239

SAE/DOT conference on aircraft and environments covering noise pollution, airport noise, sonic booms, regulatory/legal aspects and air pollution [AIAA PAPER 71-729] 14 p2295 A71-30776

Airport environmental protection, discussing area-wide agency, FAA planning grant program and legal aspects 15 p2385 A71-32247

Aircraft/environment compatibility, emphasizing decision making process for airport planning, site location, development and operation 15 p2516 A71-32248

Future aviation development constraints on manufacturer and purchaser, design, test costs, noise, airport location and multinational operation [AIAA PAPER 71-799] 16 p2667 A71-34024

German monograph on airport role in national economy and growth and location determination for enterprises maintaining connections with foreign countries 17 p2841 A71-34482

Category II operations at various airports, considering all-weather landing requirements of airborne equipment, maintenance standards, pilot training, etc [SAE PAPER 710442] 17 p2674 A71-34499

Air navigation, surveillance and traffic control technology effects on land and airspace uses at airports 17 p2774 A71-35371

Binational Basle-Mulhouse airport, discussing traffic structure, buildings and runway development 18 p2897 A71-35996

Narita site Tokyo international airport, discussing transportation, runways, ground handling, navigation aids, lighting, etc 18 p2897 A71-35997

Biomedical requirements and emergency planning for aerodromes, surveying U.S. airports 18 p2864 A71-35999

Systems approach to airfield pavement for future aircraft, integrating design, construction, operation and maintenance 18 p2897 A71-36346

Atlanta airport instant runway construction using concrete pavement, compacted subbase and longitudinal/herringbone underdrain 18 p2897 A71-36349

Third London airport planning, discussing site selection, cost analysis and decision making [CASI PAPER 72/1] 19 p3040 A71-37592

Site selection and area planning for major airport, illustrating Montreal and Toronto systems [CASI PAPER 72/2] 19 p3040 A71-37593

Airport system utilization, discussing aircraft noise, ATC, STOL development and passenger handling capacity problems [CASI PAPER 72/3] 19 p3041 A71-37594

Airfield surface system digital simulation model application to airport planning for airline operations 19 p3041 A71-38022

Super CTOL airport planning, discussing location of runway pairs, aircraft operations, noise reduction, community relations and efficiency 19 p3041 A71-38023

Air traffic congestion and delay Monte Carlo digital simulation in FORTRAN, exemplifying two-runway airport operation under instrument flight rules 19 p3041 A71-38024

Baggage handling network, describing automobile luggage check, inbound, connecting, customs claim and recheck systems 19 p3041 A71-38025

Airport facilities operational planning, discussing computer simulation parking systems and arrivals building 19 p3041 A71-38026

Airfield performance evaluation by simulation, providing statistical measures and computer generated motion picture for visual display of simulated future activity 19 p3041 A71-38027

Airport congestion as constraint on air travel, considering runway capacity and adjusted demand 19 p3042 A71-38028

International airport planning, considering runways, hangars, second level loading, cargo handling and safety 20 p3209 A71-39388

Third London airport, discussing interface problems, economic factors, airspace utilization and compatibility with other countries 20 p3209 A71-39389

Airport operation costs affected by runway utilization, parking bays alignment, baggage handling and aircraft noise 20 p3209 A71-39390

International air cargo handling through runways, terminals, parking and maintenance areas, noting facilities planning 20 p3209 A71-39393

Central terminal rapid processing and high speed VTOL aircraft effects on airport design, flight time, cost and ATC 20 p3210 A71-39394

Monograph on satellite airport system modeling for large metropolitan areas covering systems analysis methodology and computer algorithms for optimization [SU-TR-71-1] 21 p3365 A71-40799

Airport design for passenger and baggage handling efficiency, considering choice between continuous and batching type intra-airport transit system 22 p3529 A71-42072

Airports innovations for improved operational efficiency, covering high temperature test trolleys for supersonic flight, underground jet start compressors and air conditioning plant units 22 p3529 A71-42235

Airport crash fire fighting equipment requirements and rescue operations 23 p3629 A71-43389

Civil aviation research and development policy review covering aircraft noise, congestion, ATC, runway capacity and airport development problems [AIAA PAPER 71-1024] 24 p3892 A71-44602

AIRPORTS

NT HELIPORTS
Airport runway mechanical fog dispersal, using trailer mounted rotating wire mesh sieves 04 p0566 A71-14983

Meteorological observations for terminal weather modification in aviation, noting airport fog dispersal 08 p1329 A71-21732

AIRSHIPS

Air pollution emissions at Heathrow Airport, London, from aircraft operations, heating installations and road traffic

08 p1378 A71-21823

Airport runway surface strengthening, discussing overlaying additional rigid or flexible layers, replacing used sections and reinforcement problems

10 p1589 A71-24756

Air cargo volume development trends, examining worldwide airport terminal capacities and pallet/containment systems modular design and operation

10 p1699 A71-24824

Airport geodetic control stations, discussing obstruction charting program

12 p1895 A71-27537

Roissy-en-France airport, describing construction, passenger handling, terminal facilities, traffic volume and runway system

13 p2045 A71-29309

Melbourne/Tullamarine airport, describing facilities, capacity, road system, cargo and passenger handling areas and runway layout

13 p2045 A71-29310

Aircraft and airports as air pollution sources, stressing industries understanding of applicable control technology

15 p2349 A71-32243

Dispersal of jet aircraft exhaust emissions near airports and of smoke trails in upper atmosphere, assessing pollutant levels near large urban airports

15 p2349 A71-32244

Airport noise control regulations enforcement feasibility, noting financial burden

22 p3623 A71-41796

Airports innovations for improved operational efficiency, covering high temperature test trolleys for supersonic flight, underground jet start compressors and air conditioning plant units

22 p3529 A71-42235

Airport certification and safety inspection program mandated by Airport and Airway Development Act of 1971

23 p3661 A71-43235

AIRSHIPS

Airships and balloons potential commercial use in Canada, discussing cargo, passenger and military applications

07 p1019 A71-19916

Cargo airship standard atmosphere operation modes, discussing long range gas capacity and short range applications for large compact loads

11 p1708 A71-26309

AIRSPACE

ATC automation, using conflict prediction algorithm based on airspace assignment to aircraft entering system

02 p0278 A71-11698

International law for states jurisdiction in aerospace, emphasizing airspace lateral to national territories and high seas, vertical to earth surface and outer space

06 p1010 A71-17645

ATC automated systems, discussing National Airspace System En Route Stage A and Advanced Radar Terminal System

[AIAA PAPER 71-244] Motion sequential analysis of airways utilization, using mathematical-statistical methods

12 p1927 A71-27143

Third London airport, discussing interface problems, economic factors, airspace utilization and compatibility with other countries

20 p3209 A71-39389

AIRSPEED

Forward horizontal speed influence on aerodynamic characteristics of air cushion vehicle with circular nozzles and cylindrically or conically shaped curtains

02 p0186 A71-12551

Planetary boundary layer air velocity and temperature measurements from airplane

05 p0777 A71-16666

Altitude-airspeed and Mach number pressure transducer with diaphragm free of temperature and vibration effects

14 p2243 A71-30322

Minimal time climb velocity optimization for stratospheric and tropospheric jet aircraft flights

22 p3482 A71-41972

Pressure altimeter, airspeed and vertical velocity instruments, discussing selection, installation, pilot verification, error identification, repair and use

23 p3675 A71-43385

Sailplane circling cross-country speed increase by variable geometry in high lift flap form for better compromise between cruise and climb performance

23 p3630 A71-44342

AIRWORTHINESS

U AIRCRAFT RELIABILITY

AIRWORTHINESS REQUIREMENTS

U AIRCRAFT RELIABILITY

AIRY FUNCTION

Concentric shield for surface wave propagation loss at bend in open waveguide, using Airy function

09 p1410 A71-23570

Infinite thin plate containing circular holes with elastic inclusions under biaxial tension, calculating maximum stresses on common boundaries based on Airy function

11 p1841 A71-25265

Spherical waveguide eigenvalues calculation from two layer model of earth with radially inhomogeneous atmosphere, using Airy functions

14 p2209 A71-29515

Diffraction limited circular holographic determination of Airy radius by photoelectric scanning of image irradiance

16 p2577 A71-33143

Instrument function for central spot distribution of Fabry-Perot etalon with finite aperture, comparing to Airy formula

21 p3379 A71-40636

ALANINE

Asymmetric synthesis of alanine by hydrogenolytic asymmetric transamination, noting temperature effect

13 p2026 A71-29376

ALARMS

U WARNING SYSTEMS

ALBEDO

NT COSMIC RAY ALBEDO

NT EARTH ALBEDO

Radar observation of planetary surface characteristics, emphasizing albedo, surface roughness and differentiation

02 p0309 A71-12154

Planetary surfaces photometry, discussing parameters, phase laws, albedos, spectral reflectivities, phase function theory and light scattering

02 p0309 A71-12156

Spherical nebula BESM-3M radiation intensity fluxes, calculating optical thickness, particle albedos and light scattering indicatrices

02 p0312 A71-12359

Lunar surface structure, discussing soil grain size-albedo relationship

03 p0492 A71-14054

Age and composition effects on lunar surface processes and optical properties, explaining main albedo, maria, color contrasts and temporal changes

07 p1200 A71-20150

Lunar surface polarimetric properties, discussing grain size effect on normal albedo and polarization maximum degree

10 p1674 A71-24436

Lunar surface optical properties, examining albedo, color, brightness variation and polarization

11 p1822 A71-25688

Mars monochromatic albedos, investigating longitudinal variations and opposition effects

11 p1824 A71-25707

Atmospheric zero light polarization points, examining solar vertical and various almucantars, horizontal and vertical nonuniformities and albedo variations

11 p1795 A71-25925

Lunar soil albedo, discussing radiation darkening, lunar rock particles size and mineral contents effects

11 p1835 A71-26460

Saturn, Titan and ring IR photometric observations, examining brightness temperature albedos, optical thickness and individual particles

13 p2134 A71-28283

Jupiter Galilean satellites narrowband photometric data, observing albedos, spectral reflectivity, rotational phase, and brightness variations

13 p2135 A71-28292

Normal albedo and polarization maximum degree wavelength dependence from terrestrial volcanic pulverized samples

14 p2305 A71-29677

Tables of scattering functions and albedo for semiinfinite atmospheres according to nonconservative Rayleigh phase matrix for diffuse radiation computation

14 p2274 A71-30059

Sky brightness measurements during total solar eclipses, discussing solar elevation, cloud cover and albedo effects

14 p2309 A71-30117

Bright comets particles albedo, absorptivity and size observation by combined IR and optical photometry

14 p2314 A71-30649

Albedo-optical thickness relation in photometry of gas and dust comets

15 p2484 A71-31663

Mars IR spectral geometric albedo of bright and dark regions for surface composition model

15 p2491 A71-32419

Gray tone differences between undisturbed lunar surface and darker ejecta around Surveyor 1 footpads based on footprint photometry and albedo

15 p2493 A71-32482

Mars surface narrow-band spectrophotometric observation, obtaining spectral reflectivities for geometric albedos calculation

18 p2970 A71-37048

Mars IR spectra with Connex-type interferometer, noting atmospheric absorption and albedo drop due to surface water

22 p3602 A71-42176

Saturn disk monochromatic albedos observation by multicolor photoelectric photometry, comparing with Jupiter

22 p3602 A71-42178

Martian polar caps heat balance, noting albedo differences due to irregularities in solid carbon dioxide cover

22 p3603 A71-42190

Jovian geometric albedo at 1800-1950 Å decrease explained as absorption by gaseous and solid ammonia in cubic crystal form

23 p3736 A71-43345

Polarization characteristics, albedos and optical properties of Apollo 11 and 12 rocks, investigating wavelength dependence and proton irradiation effect

23 p3761 A71-43779

Martian surface materials determination by comparing albedo and brightness with spectral and photometric characteristics of crushed reddish volcanic rock and silicate sand mixed with limonite

23 p3770 A71-44052

IR spectral geometric albedos of Jupiter Galilean satellites, noting resemblance to spectra of frosts

24 p3871 A71-44910

ALBUMINS

Myocardial infarction noting serum prealbumins changes

06 p0849 A71-17293

Laser microprobe emission spectroscopy of biological matrix elements, investigating bovine albumine effect on spectrum analysis

07 p1113 A71-19785

Blood serum protein displacement in force direction in albumin injected rats under centrifuging acceleration

09 p1393 A71-22919

Bivalent metal salts effect on blood serum albumin crystallization by isolating pure protein

16 p2531 A71-33468

ALCOHOLS

NT BISPHENOLS

NT ETHYL ALCOHOL

NT GLYCOLS

NT METHYL ALCOHOLS

NT PHENOLS

Spherical alcohol droplet vaporization in acoustically disturbed medium, considering convective heat and mass transfer

01 p0179 A71-10798

Stimulated emission of laser output energy using alcohol rodamin-6G solutions under nonuniform pumping conditions

02 p0260 A71-11939

Gas phase acidities of aliphatic alcohols by ion cyclotron resonance spectroscopy

07 p1055 A71-19597

Phenylalkylcarbinol steric purity determination from asymmetric secondary alcohol derivatives separation by gas chromatographic resolution

09 p1403 A71-22478

Ice, solid carbon dioxide and alcohols oxygen K spectra from long wave X ray spectroscopy

09 p1498 A71-23479

Possibilities of alcohol detection in blood and other tissue by alcohol examinations using experience from aircraft accidents case histories

13 p2023 A71-29366

Alcohol ingestion effects on vertigo and nystagmic vestibular responses to angular acceleration, considering visual fixation and alertness control

22 p3501 A71-41827

Serotonin /5-oxytryptamine/ extraction from rat whole blood in series analysis, using acidic butanol instead of ordinary butanol

24 p3801 A71-44541

ALDEHYDES

NT CHLORAL

NT FORMALDEHYDE

L-erythro-alpha, beta-dihydroxybutyraldehyde radiosensitizing effect on adenocarcinoma Ehrlich ascites tumor cells

07 p1035 A71-18952

Oxidative and hydrolytic enzymes localization in rhesus monkey brain, investigating glutaraldehyde fixation effect with histochemistry

07 p1042 A71-20017

Phenol furfuraldehyde-ammonium perchlorate solid propellant combustion, investigating burning rate

12 p1944 A71-26742

Hypokinesia effect on formation and elimination of ketones, aldehydes, carbon monoxide and ammonia in rats

15 p2356 A71-31305

Solid glyoxal Raman spectrum data, showing operativity of mutual exclusion principle by IR comparison to Raman bands

18 p2873 A71-35830

ALDOSTERONE

Water immersion effect on plasma renin activity, urinary aldosterone excretion and renal sodium and potassium handling in normal man

22 p3485 A71-41720

Age effects on plasma aldosterone levels, red cell, plasma and total blood volume at sea level and high altitude

24 p3797 A71-44781

ALERTNESS

Human vigilance performance in brightness discrimination task under hypoxia, considering reaction time in signal detection

04 p0541 A71-14740

Commercial airline pilots alertness tests, using IR pupillography

04 p0543 A71-15051

Microwave irradiation of animals, noting analeptic effect and increased alertness

11 p1718 A71-25293

Psychological and neurophysiological definitions of vigilance, considering alcohol and tranquilizers effects

16 p2533 A71-34040

ALGAE

Algae physiology, discussing culture techniques, pure species production, past errors and achievements

03 p0365 A71-14332

Unicellular algae photosynthesis measurement by radiometric methods under optimum and equalized conditions of light, temperature and carbon dioxide supply

05 p0714 A71-16815

Algae survival and growth under adverse conditions, considering high and low temperatures, desiccation and halophilism

07 p1048 A71-19522

Optimum mineral medium for algae Chlorella and Scenedesmus cultivation in closed ecological system

09 p1393 A71-22923

Venus life forms, describing algae grown in pure carbon dioxide under pressure in acidic nutrient media at high temperatures

11 p1724 A71-25701

Centrally parietal chromatophore in green coccal algae, noting individual cell division and total number increase throughout ontogeny

16 p2531 A71-33465

Blue-green algae survival or growth ability tests under simulated Precambrian atmospheric conditions

22 p3487 A71-42230

ALGEBRA

ADJOINTS

AUTOMORPHISMS

BANACH SPACE

CANONICAL FORMS

CUBIC EQUATIONS

DETERMINANTS

DIFFERENTIAL EQUATION

EIGENVALUES

EIGENVECTORS

GROUP THEORY

HERMITIAN POLYNOMIAL

HILBERT SPACE

HOMOMORPHISMS

JORDAN FORM

LIE GROUPS

LINEAR EQUATIONS

LINEAR TRANSFORMATIONS

MATRICES [MATHEMATICS]

NONLINEAR EQUATIONS

POLYNOMIALS

QUADRATIC EQUATIONS

SPINOR GROUPS

STATE VECTORS

STRESS TENSORS

SUBGROUPS

TENSORS

VECTOR SPACES

VECTORS [MATHEMATICS]

VORTICITY

LEAF /LISP Extended Algebraic Facility/ as FORTRAN dialect in list structure, extending LISP arithmetic functions to algebraic language level

01 p0045 A71-10192

Algebraic equations system solution by eighth order Runge-Kutta process with eleven function evaluations per step

04 p0619 A71-14812

Algebraic criterion for positive realness of rational functions, using Routh algorithm

09 p1486 A71-23651

Monograph on algebraic theory for ordinary linear time invariant difference systems covering constant shift operators, matrix formalism, operational calculus, etc

16 p2602 A71-33397

Finite Fourier transforms from finite dimensional algebraic viewpoint, deriving fast Fourier transform algorithm via tensor products induced matrix factorization

23 p3698 A71-42920

Relationships among topologies definable on commutative algebraic ring

24 p3843 A71-44798

ALGOL

Algol 60 object time error messages detection with test run in-core load-and-go compiler

13 p2035 A71-29014

Symbolic ALGOL programming of partial differential equations applied to three dimensional MHD runs

21 p3351 A71-40847

ALGORITHMS

Command system and associated algorithm for synthesis of integrated microcircuits composed of components with memories

01 p0051 A71-10090

Computer programs parallel processable tasks recognition techniques survey, discussing algorithms

01 p0043 A71-10177

Complex optimal control problems solution using iterative decomposition algorithms

01 p0111 A71-10319

Electrodynamics boundary value problems numerical solutions, explaining algorithms used

01 p0052 A71-10419

Algorithm for nonstationary thermal regime of electronic equipment using heat balance method for variation in thermal coefficients and source power

01 p0052 A71-10536

Quadratically convergent algorithms for function minimization tested by numerical examples

01 p0112 A71-10847

Algorithm and computer program generating formats and logic equations for addressable remote multiplexed time division telemetry systems

01 p0050 A71-10880

Data acquisition system using associative processor for redundancy removal algorithm

01 p0050 A71-10983

Linear algorithms for determining spacecraft relative orbital state using angle data with digital computer

01 p0163 A71-11588

Nonlinear precision attitude control system stability analysis algorithm based on quadratic Liapunov function

02 p0278 A71-11648

Contour signal characteristics for cloud form recognition by computer using learning algorithm and photographic data

02 p0225 A71-11691

ATC automation, using conflict prediction algorithm based on airspace assignment to aircraft entering system

02 p0278 A71-11698

Thermoplasticity plane problems with complex edge loading, deriving algorithm based on theory of flow with translational hardening

02 p0323 A71-11746

Rigid plane skeletal structures combinatorial properties, considering analytic geometry criteria and graphs from algorithm

02 p0327 A71-12395

Cauchy problem solution for Laplace equation, constructing algorithms based on successive approximations

02 p0276 A71-12538

Matrix algorithm using difference-differential method for thin wall moments of varied thickness anisotropic cylindrical shell

02 p0328 A71-12561

Successive approximation procedure for discrete time nonlinear systems data smoothing, developing Newton method algorithm for two point boundary value problem

02 p0277 A71-12726

Real polynomial quadratic divisors determination with maximum accuracy in floating point arithmetic, using Bairstow method algorithm

03 p0450 A71-13118

Dynamic programming and Bayes algorithm for self organizing and self adjusting Markovian systems

03 p0389 A71-13515

Linear programming functional control solution by generalized searching gradient algorithm at admissible region boundary

03 p0389 A71-13517

Symmetric sparse matrices transformation to triple diagonal form, giving algorithms for nonzero elements growth minimization

03 p0450 A71-13623

Computer algorithm for state variables equations used in linear and nonlinear, active and passive electronic circuits analysis

03 p0389 A71-13807

Boundary motion between media during transport phenomena under Stefan conditions, establishing shock front coordinates by Hadamard algorithm

03 p0520 A71-13951

Algorithm for higher order loops determination in flow graph from subgraphs of linear graph model, considering circuits with ladder/nonladder structures

03 p0382 A71-14310

Thin circular cylindrical plate reinforced by longitudinal rigid stringers, deriving computer algorithm for calculating forced vibration

03 p0515 A71-14367

Sampled data feedback control system analysis and synthesis by state variable method, discussing computer algorithms for optimal pulse control

03 p0392 A71-14409

Nonlinear time optimal off-on feedback control system synthesis, deriving algorithms

03 p0392 A71-14410

On-line parameter tracking algorithm, obtaining parameters in mathematical relation between full wave rectified EMG and human triceps muscle force during isometric task

03 p0374 A71-14423

Linear pattern classifiers design, using error correction and least mean square adaptive algorithms

03 p0383 A71-14480

Pattern classification algorithms using potential functions to construct discriminant functions from sample points set

03 p0383 A71-14481

Successive approximation algorithm for stress concentrations at holes in nonlinear shallow shells, applying to cylindrical and spherical shells with circular and elliptical holes

04 p0664 A71-14602

Maximum likelihood estimation algorithm for arrival direction of narrowband signal under correlated noise

04 p0550 A71-14618

Radar detection problem, using pseudo Bayes techniques to determine likelihood ratio computational algorithms for stochastic process

04 p0551 A71-15007

Algorithms for optimal detection of weak determinate signal on background of Markov process approximated non-Gaussian noises

05 p0719 A71-16009

Satellite flight trajectories construction, proposing algorithms for computer and automatic curve plotter

05 p0779 A71-16040

Nonlinear equation systems solution by epsilon algorithm based second order method

05 p0773 A71-16156

Algorithm for spacecraft rotational maneuver control based on single turn around specific axis, using onboard computer

05 p0816 A71-16176

Matrix algorithms for linear and nonlinear inequalities, discussing rank generation and matrix inversion

05 p0774 A71-16398

Fast transformations algorithm for generalized spectral analysis

05 p0774 A71-16415

Recursive triangular algorithm for Lie transformation from introduction of small parameter into generating function and Hamiltonian

05 p0774 A71-16543

Perturbation theory using Lie transforms, discussing reformulation leading to algorithm

05 p0774 A71-16545

Canonical linear Hamiltonian systems normalization algorithm, applying to restricted three body problem

05 p0810 A71-16547

Finite difference and initial value solutions of nonlinear boundary problems for ordinary differential equations, generating algorithms by quasi-linearization method

05 p0775 A71-16646

Algorithm for stress functions in elastic region, using variational difference method

05 p0827 A71-16759

Random graphs probabilistic characteristics, deriving algorithms for graph connectivity probability estimation

05 p0731 A71-16795

Hierarchical systems effectiveness estimation algorithm, taking into account reliability

05 p0731 A71-16796

Complex configuration solid bodies boundary value problems numerical solution algorithm using R functions

05 p0775 A71-17013

Multicomputer system with preparatory and processing subsystems, discussing algorithm for distributing problems flow among processors

05 p0726 A71-17018

Image recognition process based on binary digit codes descriptions, developing algorithm for minimal system of characteristics

05 p0726 A71-17019

Kalman linear multidimensional filters stability, examining digital computer algorithms

05 p0732 A71-17024

Subsequences of pseudorandom sequences for correlation detection, discussing algorithms for weight distribution moments determination

05 p0724 A71-17062

Constrained function extremization, taking into account modified quasi-linearization algorithm

05 p0776 A71-17088

Optimal control problems for functional extremization, developing modified quasi-linearization algorithm 05 p0776 A71-17089

Large linear systems smallest eigenvalues determination, examining various algorithms 05 p0829 A71-17114

Algorithm for solving parabolic and elliptic partial differential equations with computing time, storage requirement and programming ease advantages 05 p0776 A71-17221

Error estimation for algorithms identifying linear systems described by higher order scalar difference equation 06 p0877 A71-17329

Automatic computer verification of diurnal temperature and geopotential observations on principal isobaric surfaces by statistical data analysis, describing computer algorithm 06 p0922 A71-17504

Computer algorithm for distribution functions of meteorological element on isobaric surface 06 p0922 A71-17506

Analog to digital conversion mathematical model, considering comparators dynamic properties effects on optimal algorithms selection 06 p0871 A71-17523

Analog to digital converter optimal algorithm for detecting and correcting errors caused by pulsed noise at input 06 p0871 A71-17524

State space constrained linear optimal control systems, using cutting plane algorithm for convex programs in Banach spaces 06 p0918 A71-17598

Elastic shell dynamics under initial and boundary conditions, developing variational principle algorithm 06 p0986 A71-17756

Cost-optimal zero moment shell geometry, developing digital computer algorithm with dynamic programming 06 p0992 A71-17804

Reinforced zero moment minimum weight shells strength analysis and optimal design algorithms, using discrete calculation scheme 06 p0998 A71-17854

Nonlinear equations solution, considering Newton method and Henrici algorithm disadvantages and quadratic convergent procedure 06 p0919 A71-18203

Weighted least squares nonlinear estimation problem, presenting partial step algorithm for convergence region enlargement [AIAA PAPER 71-121] 06 p0921 A71-18658

Adaptive algorithms in particle size and form distribution control, using scanning light beam 06 p0872 A71-18699

Kalman-Bucy linear filtering algorithm application to nonlinear estimation of single channel missile attitude control system parameters 07 p1081 A71-18835

Stratified statistical filtering algorithm for numerical simulation of nonlinear systems behavior 07 p1081 A71-18836

Double threshold detection radar performance, defining M out of N algorithm for nonfluctuating target and false alarm cases 07 p1058 A71-18841

Soviet book on gas flow past blunt bodies, Part 1, Flow analysis and calculation methods covering finite difference theory, algorithms, etc 07 p1013 A71-19049

Optimal algorithm for searching minimum of single variable convex function 07 p1146 A71-19177

Rotating asymmetrical disk algorithm using method of local variations in strength and rigidity 07 p1212 A71-19357

Algorithm for simultaneous estimate of spacecraft state and covariance matrix with observation error vector 07 p1148 A71-19882

Computer algorithms for scattering matrix of rectangular waveguide splitters in H plane 07 p1079 A71-20073

Human eye information processing algorithms mathematical model technological materialization 07 p1051 A71-20119

Error correction coding/decoding techniques integration, discussing convolutional and block coding and Viterbi, Sequential and Threshold decoding algorithms 07 p1066 A71-20425

Two body pursuit problem minimax and optimum absorption time control algorithm 07 p1082 A71-20642

Cylindrical shells with arbitrary cross sectional contour, thickness and longitudinal stiffener spacing under tension or compression, presenting computer algorithm for determining stress-strain state 08 p1368 A71-20790

Trajectory measurement program optimization, constructing algorithm for variational problems 08 p1360 A71-21001

Multivibrator frequency stability as function of circuit parameters, using stability/parametric errors sensitivity coefficients for general algorithm 08 p1264 A71-21072

Book on numerical solution of ordinary differential equations covering integration algorithms, Runge-Kutta, single-step, multistep, predictor-corrector and extrapolation methods 08 p1324 A71-21233

Lower triangular matrices and associated foldout algorithm application to network analysis 08 p1268 A71-21271

Two algorithms for decoding beyond Bose-Chaudhuri-Hocquenhem bound 08 p1258 A71-21314

Simple algorithms for accelerating convergence and averting divergence in Kalman filters, using feedback from measurement residuals 08 p1324 A71-21333

Maneuvering vehicles behavior model selection for real time Kalman filter tracking algorithm, based on accuracy predictions and empirical performance 08 p1270 A71-21349

Orthogonal transforms and feature selection using pattern, Harr, Walsh, Fourier and Karhunen-Loeve spaces for providing efficient classification algorithms in pattern recognition 08 p1258 A71-21354

Linear antenna radiation patterns digital computer simulation, applying algorithm based on Kotelnikov to antenna synthesis 08 p1266 A71-21467

Counting rate source encoding algorithm with orthogonal functions in space experiment data processing before telemetering to ground 08 p1259 A71-21592

Algorithmic threshold directivity pattern for adaptive array processors in quasi-stationary signal and noise fields 08 p1256 A71-21603

Adaptation algorithm for real time minimum mean square error array processing, using with multidimensional digital filter 08 p1256 A71-21605

Matrix multiplication algorithm based on degrees of freedom analysis for various transformations and spectral analysis 08 p1260 A71-21662

Algorithms for continuous indirect sequential observations utilization with real time synoptic measurements in objective analysis 08 p1328 A71-21725

Regular and stochastic algorithms for efficiency estimation of adaptive predicting filters 08 p1260 A71-22021

Identification algorithm for estimating parameters in constant coefficient linear system independent of prior estimates [AIAA PAPER 70-34] 09 p1484 A71-22074

Direct search algorithm for automated optimum structural design with spiral stiffened cylindrical shell application 09 p1533 A71-22077

Self adaptive systems with dynamic characteristics stabilization, obtaining algorithm for adaptive loop optimization 09 p1422 A71-22120

Algorithmic analysis of detection characteristics of periodic compensation systems used in moving targets signal detection 09 p1404 A71-22153

Heuristic search algorithm for highest and lowest values of functions, considering Algol program 09 p1485 A71-22313

Fredholm integral equations solutions in atmospheric optics, proposing algorithm for optimal parameter regularization values 09 p1487 A71-22378

Spacecraft autonomous control algorithm to ensure geographically specified landing accuracy, noting atmospheric density 09 p1491 A71-22565

Optimal control theory application to environmental control of confined spaces and life support systems, considering algorithm of Pontryagin principle 09 p1423 A71-22588

Pattern classification as linear programming problem, presenting optimal algorithm 09 p1412 A71-22969

Computer algorithm for optimal linear impulse corrections to satellite orbit under inequality type constraints 09 p1424 A71-23135

Man machine interactive computer graphics for design molding during evolution by computer with nonlinear programming algorithm 09 p1412 A71-23276

Element stiffness matrix generator in terms of material and geometric properties by computer algorithm, using displacement functions, transformation matrices and strain energy expression 09 p1542 A71-23281

Structural design constraints check by computer single program algorithm, resembling similar human activity 09 p1413 A71-23284

Algebraic criterion for positive realness of rational functions, using Routh algorithm 09 p1486 A71-23651

Algorithms for optimal control of nonlinear stochastic systems, minimizing control error variance 09 p1425 A71-23684

Semiimplicit Runge-Kutta schemes absolute stability, using schematization of algorithm 10 p1636 A71-23841

Iterative algorithms for regression function saddle point and applications in reliability and automatic control theories 10 p1585 A71-24156

Continuous identification algorithm for system containing two delays for signal represented by stationary random process with autocorrelation function approximation 10 p1585 A71-24160

Time optimal hierarchical failure-search systems by varying structure for four different search algorithms 10 p1585 A71-24161

Identification algorithm for linear discrete time systems difference equations with input-output measurements coefficients 10 p1586 A71-24737

Optimal nonlinear filtering, deriving algorithm based on statistical approximation of system and observer nonlinearities by second order polynomials 10 p1587 A71-24746

Sensitivity algorithms and application to attitude estimation of rigid body satellite in circular earth orbit 10 p1587 A71-24747

Optimal stochastic orbit transfer strategy solution by dynamic programming algorithm 10 p1678 A71-24844

Algorithm for using presence indicator context and test for target recognition system, discussing simulation technique for use without hardware target recognizer 11 p1734 A71-25143

Hybrid decoding technique for symmetrical binary input channels, using bootstrap algorithm across convolutionally encoded information streams 11 p1730 A71-25375

Algorithms for close earth satellite orbit calculation developed by numerical integration methods, discussing solution efficiency [AIAA PAPER 69-948] 11 p1820 A71-25463

Computer program algorithm for satellite photographic observation data processing based on measurement at one station 11 p1733 A71-25833

Modified Chaplygin algorithm application to bilateral approximate solution of limiting Cauchy problem, discussing convergence and error estimation 11 p1792 A71-26155

Experiment planning, using digital computer in real time with programmed algorithm 12 p1883 A71-26713

Statistical estimation in monitoring and control systems analysis, discussing algorithm construction for computer solution of nonlinear differential equations system 12 p1891 A71-26724

Game theory application to spacecraft reentry problem, obtaining optimal control algorithms 12 p1972 A71-27017

Algorithm for nonparametric estimation of random parameters of general exponential family of unknown density distributions, investigating empirical estimates convergence to Bayes optimal estimates 12 p1892 A71-27022

Variable elasticity algorithm for axial flow turbine disks with allowance for plasticity, creep and loading history 12 p1979 A71-27351

Kalman filtering for complex systems, deriving algorithms for dynamic modeling and bias errors effects in discrete-time state optimum estimation 12 p1893 A71-27435

Minimization algorithms unified derivation, using Hessian matrix inverse 12 p1923 A71-27727

Algorithm for subclass identification in image recognition 13 p2034 A71-27835

Algorithm for numerical analysis of cylindrical shock wave propagation in stationary ideal gas 13 p2046 A71-27903

Explicit recursive algorithms for construction of Lie and von Zeipel transformations 13 p2135 A71-28357

Algorithm for automatic closed form integration of formulas in elliptic motion arising in perturbation theories 13 p2136 A71-28358

Identification by minimization of Gaussian-Markovian representation of stochastic process, considering positive linear systems and algorithm for matrix calculation 13 p2043 A71-28818

- Accelerated gradient projection algorithm for nonlinear constraints, examining terminal phase convergence and compatibility with Davidson process
13 p2043 A71-28821
- Algorithms for constructing minimized abstract automatic subunits and two switch types as basis for arbitrary linear block encoder
13 p2035 A71-28915
- Real time computable partial recursive functions of n variables with expectancy estimate on Minsky machines
13 p2096 A71-28976
- Computer algorithm for liquid sloshing in rotating cavities, using finite difference scheme
13 p2050 A71-29211
- Quantitative performance evaluation of man machine systems in stochastic environments, deriving simulation algorithm
13 p2021 A71-29286
- Heuristic algorithm for computation of failures detection tests in asynchronous sequential logic circuits
14 p2218 A71-29520
- Algorithm determining sequential machine error partition representing inessential errors
14 p2206 A71-29521
- Algorithm for calculating optimal covering of regions in plane, assembling computer program
14 p2264 A71-29552
- Algorithm for minimax and maximin problems in theory of differential games
14 p2265 A71-29555
- Self adaptive systems with dynamic characteristics stabilization, obtaining algorithm for adaptive loop optimization
14 p2220 A71-29998
- Modified steepest descent algorithm for optimum trajectory computation applied to interceptor missile control
14 p2207 A71-30018
- Asymptotically optimal detection/discrimination algorithms for weak signals on correlated noise background
14 p2195 A71-30105
- Stochastic signal optimum linear estimation in multiplicative and measurement noises, deriving algorithms
14 p2197 A71-30794
- Algorithm providing three-gimbal inertial system all-attitude capability by protecting against gimbal lock
14 p2272 A71-30802
- Performance predictions for Viterbi decoding algorithm by simulation on UNIVAC 1108
14 p2200 A71-30922
- One variable unimodal function minimization, describing adaptive algorithm with iterative four point interpolation process
15 p2440 A71-31156
- Ritz-Treffitz algorithm application to optimal state regulator problem computer processing to improve speed of solution and storage requirements
15 p2374 A71-31182
- Statistical method of thunderstorm forecasting, basing algorithm on mathematical techniques
15 p2443 A71-31225
- Time dependent partial differential equations solutions, considering hopscotch class algorithms, Galerkin type methods and finite difference schemes
15 p2441 A71-31352
- Asymptotically optimal rank algorithms for signal resolution at phase and amplitude detectors outputs
15 p2370 A71-31587
- Weak signal detection in additive mixture on non-Gaussian random-correlated noise, deriving algorithms for discrete- and continuous-time and coherent detection problems
15 p2370 A71-31590
- Design algorithms for fluidic combinational and sequential circuits
15 p2352 A71-32068
- Weak harmonic signal detection in narrow band Gaussian noise, using statistical algorithm
15 p2371 A71-32187
- Algorithm convergence for sparse nonlinear equations system solution with Jacobian satisfying Lipschitz condition
15 p2442 A71-32313
- Rapidly converging first order training algorithm for adaptive equalizer design in PAM signal reception, using variable step sizes for mean-square error minimization
16 p2545 A71-32821
- Linear filtering algorithms computational efficiency, deriving formulas for arithmetic operation count and storage requirements
16 p2602 A71-33352
- Computer algorithm for diode detector static and dynamic I-V characteristics calculation by trial and error process with piecewise linear approximation
16 p2546 A71-33399
- Satellite flight trajectories construction, proposing algorithms for computer and automatic curve plotter
16 p2605 A71-33444
- Optimal control algorithm for spacecraft descent in atmosphere at speed near escape velocity, using game theory
16 p2646 A71-33702
- Numerical algorithm for Cauchy problem nonlinear partial differential integral equations solution by invariant imbedding
16 p2604 A71-34082
- Convergence characteristics of sequential and combined conjugate gradient restoration algorithms for mathematical programming, studying constrained function minimization
17 p2764 A71-34520
- Digital generation algorithm for random number sequences with specified autocorrelation and probability density function, illustrating computation accuracy and versatility
17 p2719 A71-34745
- Soviet papers on information systems redundancy using redundant algorithms and structures and redundant coding theory
17 p2720 A71-34951
- Optimum diagnostics algorithm for complex automatic control system state detection based on Bayesian rule successive application for minimum time requirement
17 p2720 A71-34959
- Redundant algorithms and structures, analyzing anisotropic systems described by continuous differentiable functions
17 p2710 A71-34962
- Redundant variables method as solution to problem of functional coding and algorithm synthesis, examining error control and correcting properties
17 p2710 A71-34963
- Decoding at high transmission rates, describing algorithm for mean number of operations and error probabilities
17 p2702 A71-34971
- Algorithms for multiplication and division by different bases in residual class system
17 p2711 A71-34977
- Robots structural description and computer modeling based on various algorithms
17 p2691 A71-35167
- Soviet book on algorithms for electronic circuit analysis covering linear and nonlinear transistor or tube circuits matrix-topological description and frequency-time domain solutions
17 p2717 A71-35219
- French monograph on algorithms for parameters estimation for adaptive identification in real time of linear processes perturbed by related noise
17 p2767 A71-35232
- French monograph on variable-structure automatic control systems covering algorithms, stability, nonlinear hypersurface slip, minimum time, switching elements, analog simulation, etc
17 p2767 A71-35249
- Algorithm for stress functions in elastic region, using variational difference method based on differentiation of strain energy
17 p2832 A71-35458
- Partially liquid filled cylindrical shells with elastically supported end rims, deriving algorithm for nonaxisymmetric natural vibration frequency calculations
17 p2833 A71-35614
- Methods construction for initial value problem solution, using fifth and sixth order algorithms with Adams-Moulton correctors
17 p2768 A71-35686
- Predictor-corrector algorithms with identical regions of absolute or relative stability
17 p2769 A71-35690
- Orthogonal matrix estimate by iterative algorithm with given order of convergence
17 p2769 A71-35692
- Numerically stable algorithm for solving least squares problems with linear equalities and inequalities as additional constraints
17 p2769 A71-35693
- Computer algorithm determining transfer function of linear electronic circuit in autonomous quadrupole form with zero initial conditions
18 p2887 A71-35884
- Computer algorithm for simulating dynamic systems by functional graphs, noting extension to complex systems
18 p2884 A71-35917
- Astronomical data correction for smearing effects applying Fast Fourier Transform algorithm
18 p2960 A71-35933
- Numerical fluid dynamics problems in Hele-Shaw cell secondary flow, blast wave and plane jet electrostatic pinching, presenting algorithms and error estimates
18 p2905 A71-36310
- Numerical solution algorithm for parabolic free boundary problem in statistical decision theory, comparing convergence with asymptotic expansions
18 p2941 A71-36352
- Jacobi algorithm for computation of eigenvalues and eigenvectors of skew symmetric matrix by real arithmetic
18 p2942 A71-36698
- Strassen algorithm as matrix products representation in seven dimensional space
18 p2942 A71-36700
- Syntactical characterization of tautologies for deductive systems and theories based on formalized algorithmic languages
18 p2942 A71-36822
- Serial binary multiplication computation speed, considering recoding algorithm with cellular array multipliers
18 p2894 A71-36829
- Signed binary numbers multiplication algorithm, describing cellular arrays for two-complements multiplication method
18 p2894 A71-36831
- Algorithms and operator matrix language for infinite linear automata analysis, synthesis and identification
19 p3024 A71-37223
- Signal detection on Gaussian noise background, deriving error probabilities and optimal processing algorithms
19 p3015 A71-37224
- MESY systems programming with PL/I, comparing with ALGOL and FORTRAN
19 p3025 A71-37422
- Variable thickness and rigidity cylindrical shells, determining natural frequencies and vibration mode shapes with algorithm based on Ritz method
19 p3155 A71-37531
- Set covering algorithm based on single branch search coupled with linear programming and suboptimization techniques
19 p3025 A71-37546
- Branch-and-bound algorithm for zero-one linear mixed integer programming problems solution
19 p3085 A71-37547
- Linear programs optimality conditions, using differential calculus approach to classical optimization theory in Danzig simplex algorithm development
19 p3086 A71-37548
- Modified linear programming algorithm for columnar methods in mathematical programming applicable to decomposition principle, concave maximization and Lagrange multipliers search
19 p3086 A71-37549
- Game theory application to spacecraft reentry problem, obtaining optimal control algorithms
19 p3152 A71-37687
- Algorithm for nonparametric estimation of random parameters of general exponential family of unknown density distributions, investigating empirical estimates convergence to Bayes optimal estimates
19 p3038 A71-37691
- Stability test for Routh-Hurwitz problem using step by step method based on algorithm
19 p3086 A71-37898
- Adaptive algorithm designing minimum expected cost test trees for detection and isolation of single faults in systems
19 p3069 A71-38287
- Computer algorithm for simulation of one dimensional unsteady compressible fluid flow in presence of area change, wall friction, heat transfer and entropy gradients
19 p3025 A71-38291
- Design algorithm for gyrotropic waveguide consisting of symmetrical rectangular coaxial with magnetized ferrite rods
19 p3019 A71-38333
- Space communications period forecasting algorithm for limited power ground based transmitters and spacecraft in earth orbit
19 p3022 A71-38502
- Feedback system estimation algorithm, comparing performance to algorithm based on stochastic control separation principle
19 p3039 A71-38715
- Modular component computational algorithm for sequential least squares estimation /filtering/ with process noise for straightforward computer code conversion
20 p3201 A71-38757
- Recursive algorithms for detection probabilities of fluctuating targets in Gaussian noise, including cell averaging constant false alarm rate /CFAR/ extension
20 p3195 A71-38860
- Rapidly converging second order optimal tracking algorithms for adaptive equalization on basis of estimated bounds for eigenvalues of signal plus noise correlation matrix
20 p3201 A71-38872
- Bayesian learning algorithm derivation for statistically optimum adaptive gain control in Rayleigh-distributed signal reception
20 p3206 A71-38874
- On-line identification for nonlinear system from noisy measurements, applying stochastic algorithm to hybrid simulation of chemical process models
20 p3207 A71-38974
- Parameter estimation algorithms for state variable models of multivariable linear control systems from noisy input-output records
20 p3208 A71-38999
- Spacecraft interplanetary guidance trajectory correction, deriving algorithm for optimal accuracy and minimum fuel expenditure
20 p3288 A71-39124

Mixed decomposition and convergence of gradient type coordinating algorithm for two-level complex control system using interconnection variables and Lagrange parameters

20 p3208 A71-39472

Algorithm for rational function incomplete decomposition into partial fractions

20 p3255 A71-39490

Trajectory measurement method optimization determined by algorithm, applying to radial velocities of artificial satellite orbit around Mars

20 p3294 A71-39581

Algorithm for linearly elastic structures vibration natural undamped frequency computation, assuming known dynamic stiffness matrix

20 p3311 A71-39964

Third order oscillatory system optimal terminal-state control synthesis by quadratic functional minimization iterative procedure algorithm, using ODDA-1204 computer program

21 p3359 A71-40164

Automatic computational algorithm for parameter identification of nonlinear systems, using deterministic time invariant model with memory and gain functions

21 p3407 A71-40261

Computational algorithms for solving unconstrained and constrained optimization problems

[ASME PAPER 71-VIBR-118] 21 p3407 A71-40337

Direct search penalty function algorithm for treating general mathematical programming form of optimal design problem

[ASME PAPER 71-VIBR-121] 21 p3350 A71-40340

Optimal numerical solutions of linear control systems with quadratic integral form, using dynamic programming, successive optimization and algorithm-aided dynamic programming

21 p3360 A71-40617

Monograph on satellite airport system modeling for large metropolitan areas covering systems analysis methodology and computer algorithms for optimization

[SU-TR-71-1] 21 p3365 A71-40799

Computer algorithms for gamma algebra of electromagnetic form factors in terms of Chebyshev polynomials with photon 4-momentum

21 p3415 A71-40842

Failure diagnosis and localization algorithm for combinational circuits of functional elements, considering arbitrary combinations and essential fault presence

21 p3361 A71-41141

Adaptation algorithm for optimal synthesis of nonlinear radio reception system with additive noise

21 p3361 A71-41143

Algorithms for calculating temperature fields of electronic devices on computers, considering solid body in shape of bounded cylinder

22 p3519 A71-41442

Soviet book on multivariable automatic control system synthesis with adaptation to computer covering methodology, algorithms, transfer function approximation and stability problem

22 p3525 A71-41799

Recurrent finitely converging algorithms for solving inequalities in automatic control systems involving adaptive filters

22 p3526 A71-41858

Computerized system redundancy optimization formulation as zero-one type variables integer programming problem, obtaining algorithmic solution for maximum reliability

22 p3517 A71-42106

Computerized algorithm for redundant configuration system reliability function generation from Boolean algebra transmission function

22 p3517 A71-42107

Cost based algorithm for allocating availability parameters/repair times and failure rates/ to system components

22 p3566 A71-42115

Fast Fourier transform calculating discrete Fourier transform, considering optimized algorithm for digital computers

22 p3566 A71-42249

Maximum likelihood estimation algorithm for arrival direction of narrowband signal under correlated noise

22 p3510 A71-42258

Fano and stack algorithms comparison by computer simulation of two sequential decoding algorithms

22 p3512 A71-42379

Decoding of correlative level coding or partial response signaling systems with ambiguity zone detection, discussing error correction algorithm

22 p3513 A71-42382

Bit synchronization in high SNR digital communication system, using Kalman filtering algorithm

22 p3513 A71-42383

Two spot beam switching without storage at satellite for time division multiple access system in satellite communication, giving switching algorithm

22 p3514 A71-42482

Algorithms for optimal detection of weak determinate signal on background of Markov process approximated non-Gaussian noise

22 p3515 A71-42760

Algorithms for directional antenna boresight orientation estimation errors relative to spacecraft attitude sensor, based on measurement of received signal strength

22 p3525 A71-42775

Linear dynamic system sensitivity models simplification conditions application to adaptive nonsearching system synthesis algorithms

22 p3527 A71-42857

Finite Fourier transforms from finite dimensional algebraic viewpoint, deriving fast Fourier transform algorithm via tensor products induced matrix factorization

23 p3698 A71-42920

Branched trajectory optimization algorithm using steepest descent method applied to space shuttle vehicle mission design

[AAS PAPER 71-326] 23 p3726 A71-43000

Perturbation and projection operator algorithms for Navier-Stokes equations for incompressible flow in rectangular cavities and injection into cylindrical ducts

23 p3662 A71-43238

Signal filtration algorithms and parameter estimation in additive non-Gaussian noise background by conditional Markov process theory

23 p3644 A71-43290

Second order approximation algorithm for nonlinear noisy dynamical system state estimation from noise corrupted observations

23 p3656 A71-43854

Digital algorithm for automatic aircraft engine monitoring system, using Boolean algebra and events/states theory

23 p3679 A71-43897

Exact and approximate algorithms for computation of modeling and bias errors in linear minimum error variance estimation

23 p3656 A71-43940

Smoothed randomized functionals and algorithms in adaptation and learning theory, accounting for constraints by generalized penalty function method

23 p3657 A71-44018

Gradient algorithm for optimal trajectory control with inequality and singular arcs, using nonlinear programming and Euler-Lagrange equations

23 p3658 A71-44085

Stochastic optimal control theory application to airplane rescheduling model, obtaining dynamic programming algorithm for optimal landing and takeoff rules

23 p3702 A71-44104

Computer-aided decision algorithm for ATC problem in near terminal area, emphasizing scheduling and holding strategies

23 p3703 A71-44105

Suboptimal fixed point data smoothing algorithm for parameter and initial state estimation of nonlinear dynamic systems

23 p3659 A71-44113

Suboptimal feedback link estimation algorithms for stochastic control, comparing with separation principle

23 p3660 A71-44118

Sequential zero-pole placement technique for multivariable control systems, developing algorithm for computing closed loop transfer function matrix

23 p3660 A71-44120

Algorithms for discrete message signal reception in background non-Gaussian additive noise with unknown statistical characteristics

23 p3647 A71-44321

Algorithm for dual compromise control problems arising from each subsystem of inner level in multilevel static hierarchical system

24 p3812 A71-44393

Suboptimal control laws calculation, using functional form of variables for algorithm

24 p3813 A71-44615

N-step conjugate gradient minimization algorithm for nonquadratic functions, giving numerical example of application to double precision arithmetic

24 p3842 A71-44623

Stiffness matrix algorithm for triangular plate bending elements using hierarchy of interpolation polynomials

24 p3879 A71-44637

Dual control theory for distributed systems with time lag described by partial differential equations, considering controller and algorithms synthesis

24 p3814 A71-44686

Unsteady random processes structural analysis application to nonlinear dynamic systems, evaluating algorithms effectiveness and improvement by self adaptive operators with finite memory

24 p3815 A71-44705

Algorithm for pure torsion of doubly connected square profile prismatic bars with hole, using R functions and variational technique

24 p3881 A71-44834

Thunderclouds and torrential clouds classification from radar data, developing algorithm model with Bayes method

24 p3845 A71-44884

Algorithm for preparation of nonlinear differential equations for simulation by analog computer in linear form

24 p3807 A71-45156

Position line location determination by discrepancy moduli sum minimization algorithm

24 p3846 A71-45161

Two step spacecraft reentry guidance involving skip trajectory at parabolic speeds, proposing algorithm for running coordinate and speed vector components values

24 p3846 A71-45301

Spacecraft roll stabilization during parabolic earth atmosphere reentry, developing single parameter multistep algorithm

24 p3846 A71-45302

Landing control algorithm using onboard digital computer for spacecraft hyperbolic velocity reentry, discussing simulation test results

24 p3846 A71-45303

Parabolic velocity atmospheric reentry navigation algorithm for spacecraft control, demonstrating guidance accuracy to landing point

24 p3846 A71-45304

Spacecraft motion control algorithm for reentry at escape velocity based on object motion model

24 p3846 A71-45305

Trajectory correction problem optimal measurement set, showing solution by linear programming simplex algorithm method

24 p3846 A71-45306

Extendible, variable profile nozzle for various flow regimes operation, developing numerical design algorithm

24 p3821 A71-45339

Conical and cylindrical shell deformation with nonlinear one dimensional wave processes, describing algorithm for method of characteristics application

24 p3885 A71-45341

ALIGNMENT

NT SELF ALIGNMENT

Galactic interstellar grains alignment by starlight, noting photon intrinsic angular momentum role

01 p0159 A71-10865

Optimal axis alignment for strapdown inertial guidance system, suggesting alternate method of raised mounting pads and cylindrical alignment pins

02 p0279 A71-12456

Visual alignment task performance for marks with vertical separation under various illuminations

04 p0547 A71-15849

True vertical laser application for precision vertical alignment of large structures, using mercury mirror

07 p1122 A71-19206

Strapdown inertial navigator alignment by digital filtering techniques, discussing application to aircraft and spacecraft

08 p1331 A71-21170

Prelaunch automatic azimuth alignment theodolites for Saturn IB and Saturn 5 space vehicles inertial guidance system, discussing return images separation and error signal generation

08 p1289 A71-21375

Nondestructive monitoring calibration and alignment with standard specimens conforming with metrological regulations

08 p1300 A71-21895

Iterative technique using continuous gas laser for alignment of Mach-Zehnder interferometer for monochromatic and white light fringes

09 p1453 A71-23692

Gimballed inertial navigation system, discussing initial alignment by strap-down system at standstill

11 p1796 A71-26416

Preliminary circuit-stage alignment procedures in multistable triggers manufacture with counter input based on tunnel diodes and transistors

14 p2213 A71-30632

Optical coupling between two axes of laser light beam deflector, using reflective relay optical system for loss reduction, cost effectiveness and easy alignment

16 p2585 A71-33139

Hybrid circuit methods for aligning resistors manufactured by different technologies, considering mechanical methods, electric erosion, electron and laser beam alignment, etc

20 p3208 A71-39434

IR ring laser rotation sensor, describing design principles for alignment and eliminating locking phenomenon

22 p3557 A71-42153

ALIPHATIC COMPOUNDS

NT ACETIC ACID

NT ACETYL COMPOUNDS

NT ACETYLENE

NT ACRYLATES

NT ACRYLONITRILES

NT ADENINES

NT ADENOSINE DIPHOSPHATE [ADP]

NT ADENOSINE TRIPHOSPHATE [ATP]

NT ADENOSINES
 NT ALKANES
 NT ALKENES
 NT ALKYL COMPOUNDS
 NT ANTHRACENE
 NT BUTADIENE
 NT BUTENES
 NT CARBON TETRACHLORIDE
 NT CARBON TETRAFLUORIDE
 NT CASTOR OIL
 NT CELLULOSE
 NT CHLORAL
 NT CHLOROETHYLENE
 NT CHLOROFORM
 NT CHOLINE
 NT CYANOGEN
 NT CYCLIC HYDROCARBONS
 NT CYCLOBUTANE
 NT CYCLOPROPANE
 NT CYSTEINE
 NT DIMETHYLHYDRAZINES
 NT ETHANE
 NT ETHYL ALCOHOL
 NT ETHYLENE
 NT FLUOROAMINES
 NT GALACTOSE
 NT GLUCOSE
 NT GLUCOSIDES
 NT GLUTAMATES
 NT GLUTAMIC ACID
 NT GLUTAMINE
 NT GLYCERIDES
 NT GLYCEROLS
 NT GLYCOGENS
 NT GLYCOLS
 NT HEPTANES
 NT HEXOKINASE
 NT HEXOSES
 NT HEXYL COMPOUNDS
 NT HYDRAZIDES
 NT HYDRAZINE NITROFORM
 NT HYDRAZINES
 NT IODOACETIC ACID
 NT ISOPROPYL COMPOUNDS
 NT ISOPROPYL NITRATE
 NT KETONES
 NT LACTATES
 NT LACTIC ACID
 NT METHANE
 NT METHYL ALCOHOLS
 NT METHYL COMPOUNDS
 NT METHYLHYDRAZINE
 NT MONOSACCHARIDES
 NT NAPHTHENES
 NT NITROAMINES
 NT NUCLEOSIDES
 NT OXALIC ACID
 NT OXYACETYLENE
 NT PARAFFINS
 NT PENTOSE
 NT POLYSACCHARIDES
 NT PROPANE
 NT PROPYL COMPOUNDS
 NT PROPYLENE
 NT RIBOSE
 NT SUGARS
 NT THIOLS
 NT TRIMETHYL COMPOUNDS
 NT URETHANES

Gas phase acidities of aliphatic alcohols by ion cyclotron resonance spectroscopy
 07 p1055 A71-19597

Focused ruby laser beam degradation of various gaseous aliphatic and alicyclic hydrocarbons
 07 p1124 A71-19789

Type III carbonaceous chondrite Murchison meteorite, obtaining amino acids, aliphatic and aromatic hydrocarbons from specimen
 09 p1393 A71-22983

ALKALI HALIDES
 NT CESIUM FLUORIDES
 NT CESIUM IODIDES
 NT SODIUM CHLORIDES
 NT SODIUM FLUORIDES
 NT SODIUM IODIDES

Population inversions in shock induced dissociation of alkali halides in 2000 to 7000 K range, considering rate constants and molecular relaxation
 04 p0629 A71-14694

Thermal dissociation rates of alkali chlorides reinterpreted in terms of chloride ion collisional detachment rate
 21 p3346 A71-40889

ALKALI METAL COMPOUNDS
 Crystal lattice energies of solvation of alkali metal perchlorate in water
 22 p3508 A71-42530

ALKALI METALS
 NT CESIUM
 NT CESIUM ISOTOPES
 NT CESIUM VAPOR
 NT CESIUM 133
 NT LIQUID POTASSIUM
 NT LIQUID SODIUM
 NT LITHIUM
 NT LITHIUM ISOTOPES

NT POTASSIUM
 NT POTASSIUM ISOTOPES
 NT RUBIDIUM
 NT RUBIDIUM ISOTOPES
 NT SODIUM
 NT SODIUM VAPOR

Carbon dioxide laser optical pumping by resonant emission from alkali metal lamp
 03 p0434 A71-13290

Apollo 12 lunar rock 12013 rare earth, alkaline and alkali metal and Sr 87/Sr 86 data, discussing light and dark component composition
 03 p0494 A71-14221

Contact potential measurements of work function dependence on adsorption of alkali metals on Ta/110 and W/100/ crystals under ultrahigh vacuum
 09 p1497 A71-22701

Secondary ion component on tungsten target surface during sputtering by alkali metal ions
 09 p1494 A71-22878

Carbon dioxide laser optical pumping by resonant emission from alkali metal lamp
 09 p1464 A71-23266

Infrared laser output from giant pulse laser beam photoexcited alkali metal vapors, assuming buffer gas collisional mechanism
 09 p1464 A71-23380

Electron impact excitation rates of bound electronic states of hydrogen, helium and alkali atoms
 10 p1645 A71-24543

Coaxial type MHD generator with steady magnetic field and plasma consisting of inert gases and ionizable alkali metal additives, obtaining electrical conductivity
 15 p2355 A71-32268

Resonance broadening measurements of alkali metals, giving relation between optically thick and thin full widths for Lorentzian and Gaussian line shapes
 19 p3105 A71-38721

H transition excitation during atomic hydrogen collision with alkali elements and inert gases, discussing inner electron excitation
 23 p3707 A71-43268

Alkali metals vaporization from heated lunar samples, suggesting lunar rock erosion by localized heating due to volcanism or meteorite impact
 23 p3741 A71-43636

Apollo 12 lunar soils, rocks and core samples, determining rare earth, alkali and alkaline earth elements concentrations
 23 p3747 A71-43676

Atmospheric transmission functions for twilight airglow of alkalis Na, Li and K
 23 p3673 A71-43983

Electrode region in plasma with alkali metal admixture, discussing potential drop, thermionic emission, Schottky effect, diffusion, recombination and bulk and surface ionization
 24 p3857 A71-45215

ALKALIES
 NT LITHIUM HYDROXIDES
 NT POTASSIUM HYDROXIDES

Acidic and alkaline deoxyribonucleases activity by spectrophotometer and horizontal viscosimeter in normal states and pathology
 12 p1872 A71-27743

Lost City /Oklahoma/ chondrites, determining alkali, alkaline earth and rare earth element concentrations and Rb-Sr model age
 15 p2489 A71-32355

Peroxide-alkaline polishing solution for GaAs, evaluating optical quality, surface damage, polishing rate and metallic contact resistance
 18 p2955 A71-37004

ALKALINE BATTERIES
 Alkaline fuel cells electrochemical regeneration for controlling carbonate concentration in electrolyte for performance improvement
 03 p0353 A71-13057

Zinc-zinc oxide electrode chemistry, describing interaction with strongly alkaline solution of alkaline battery system
 08 p1233 A71-21078

Zinc morphology electrodeposited from alkaline electrolyte, investigating charging and cell failure
 08 p1233 A71-21081

Silver-silver oxide electrode chemistry in alkaline solutions, describing oxide structure, solubility and stability
 08 p1234 A71-21083

Membrane separate systems ion and water mass transport, noting effect on anolyte concentration and alkaline battery performance
 08 p1234 A71-21092

ALKALINE EARTH COMPOUNDS
 Lost City /Oklahoma/ chondrites, determining alkali, alkaline earth and rare earth element concentrations and Rb-Sr model age
 15 p2489 A71-32355

ALKALINE EARTH METALS
 Rare earth, alkali and alkaline earth elements content of phenocrysts and acidic igneous magma
 23 p3734 A71-43246

Apollo 12 lunar soils, rocks and core samples, determining rare earth, alkali and alkaline earth elements concentrations
 23 p3747 A71-43676

ALKALINE EARTH OXIDES
 NT BARIUM OXIDES
 NT BERYLLIUM OXIDES
 NT CALCIUM OXIDES
 NT MAGNESIUM OXIDES

ALKALOIDS
 NT ATROPINE
 NT NICOTINE
 NT PILOCARPINE

ALKALOSIS
 Alkalosis effect on human maximal performance and lactic acid formation in blood under supramaximal exercise conditions
 20 p3185 A71-38888

ALKANES
 NT ETHANE
 NT HEPTANES
 NT METHANE
 NT PARAFFINS
 NT PROPANE

Ignition delay times behind reflected shock wave of alkanes methane through pentane in stoichiometric argon simulated air mixture
 10 p1657 A71-24047

Long chain alkanes search in Apollo 12 lunar fines, using benzene-methanol extracts
 23 p3756 A71-43745

ALKENES
 NT BUTADIENE
 NT BUTENES
 NT ETHYLENE
 NT PROPYLENE

Frequencies, rotational constants, molecular structure and moments of inertia of five isotopic species of vinylene carbonate from microwave spectrum analysis
 19 p3011 A71-37373

ALKYL COMPOUNDS
 NT HEXYL COMPOUNDS
 NT ISOPROPYL NITRATE
 NT TRIMETHYL COMPOUNDS

Phenylalkylcarbinol steric purity determination from asymmetric secondary alcohol derivatives separation by gas chromatographic resolution
 09 p1403 A71-22478

Mercaptoalkylamine group radiation protection preparations on resistance of rats and mice to lateral acceleration rate
 22 p3491 A71-42700

ALKYNES
 NT ACETYLENE
 NT OXYACETYLENE

ALL SKY PHOTOGRAPHY
 Balloon-measured magnetospheric electric fields comparison with all sky camera pictures of large scale visible auroral form motions, noting relationship
 19 p3047 A71-37363

Auroral luminosity patterns over northern Scandinavia based on ESR0 all-sky camera recordings, noting relationship to electron and proton precipitation
 19 p3060 A71-38573

Auroral conjugacy and time dependent geometry via all sky cameras and image orthicon TV onboard conjugate-flying aircraft
 20 p3228 A71-39840

Magnetotail plasma sheet variations association with auroral display features during substorms from all sky photography
 20 p3230 A71-39880

ALL-WEATHER AIR NAVIGATION
 Man machine considerations in all-weather low level navigation system design, noting off-course error reduction by command information display to pilot
 01 p0125 A71-10515

Aircraft all weather automatic landing system, discussing component weights and reliability connected with problem area
 02 p0279 A71-12274

All-weather automatic landing electronic technology, describing flight automation landing system for YC 10 BAC 111 and Concorde aircraft
 02 p0279 A71-12275

All-weather aircraft operations, discussing takeoff, landing, safety and forecasting
 06 p0847 A71-17923

Man-machine considerations in all-weather low-altitude navigation system design, discussing computer generation of roll command guidance, visual display and pilot modeling
 07 p1157 A71-20344

Technical aspects of tactical all-weather instrument landing system of Swedish STOL aircraft Saab 37 Viggen
 11 p1796 A71-25233

Transport aircraft all weather automatic landing operation, examining guidance system and independent monitors
 13 p2098 A71-28323

[SAE PAPER 710441]
 All-weather landing systems military constraints and requirements, considering ground equipment mobility and insensitivity topographic environments
 15 p2445 A71-31908

Performance category III all-weather capability ILS landing equipment standards, discussing high directivity antennas and transmission and control system redundancy techniques for reliability
 15 p2445 A71-31909

- Caravelle aircraft all-weather Sud Lear automatic landing system operation and performance
15 p2446 A71-31913
- Helicopter radar equipment for obstacle avoidance in all-weather low altitude flight, describing components installation, cockpit display and controls
15 p2446 A71-31919
- Category II operations at various airports, considering all-weather landing requirements of airborne equipment, maintenance standards, pilot training, etc [SAE PAPER 710442]
17 p2674 A71-34499
- Information transfer in all-weather aircraft operation, discussing pilot role in overall reliability based on man machine system information process
17 p2693 A71-35209
- All-weather operations, including pilot role, instrument landing systems and guidance aids
19 p3100 A71-37601
- U.S. Army ATC cost-effective system developments for high density low altitude helicopter tactical operations to avoid enemy radar under near-all weather conditions
22 p3571 A71-42084
- ALLERGIC DISEASES**
- Physiological and biochemical changes arising in allergic reactions and hypothalamic neurohumoral regulation disorders role, comparing with diencephalic syndromes
11 p1718 A71-25667
- Medical preparations use and avoidance by spacecraft and aircraft crew members, discussing aftereffects, allergies and health requirements
22 p3491 A71-42705

ALLOCATIONS

NT RESOURCE ALLOCATION
ALLOYS

- NT ALUMINUM ALLOYS
- NT ANTIMONY ALLOYS
- NT AUSTENITIC STAINLESS STEELS
- NT BAINITIC STEEL
- NT BARIUM ALLOYS
- NT BEARING ALLOYS
- NT BERYLLIUM ALLOYS
- NT BINARY ALLOYS
- NT BISMUTH ALLOYS
- NT BORON ALLOYS
- NT BRASSES
- NT BRONZES
- NT CADMIUM ALLOYS
- NT CARBON STEELS
- NT CESIUM ALLOYS
- NT CHROMIUM ALLOYS
- NT CHROMIUM STEELS
- NT COBALT ALLOYS
- NT COPPER ALLOYS
- NT EUTECTIC ALLOYS
- NT GALLIUM ALLOYS
- NT GERMANIUM ALLOYS
- NT GOLD ALLOYS
- NT HAFNIUM ALLOYS
- NT HASTELLOY [TRADEMARK]
- NT HEAT RESISTANT ALLOYS
- NT HIGH STRENGTH ALLOYS
- NT HIGH STRENGTH STEELS
- NT INCONEL [TRADEMARK]
- NT INDIUM ALLOYS
- NT IRON ALLOYS
- NT LEAD ALLOYS
- NT LITHIUM ALLOYS
- NT MAGNESIUM ALLOYS
- NT MANGANESE ALLOYS
- NT MARAGING STEELS
- NT MARTENSITIC STAINLESS STEELS
- NT MERCURY AMALGAMS
- NT MOLYBDENUM ALLOYS
- NT NEODYMIUM ALLOYS
- NT NICHROME [TRADEMARK]
- NT NICKEL ALLOYS
- NT NICKEL STEELS
- NT NIOBIUM ALLOYS
- NT OSMIUM ALLOYS
- NT PALLADIUM ALLOYS
- NT PERMALLOYS [TRADEMARK]
- NT PLUTONIUM ALLOYS
- NT POTASSIUM ALLOYS
- NT QUATERNARY ALLOYS
- NT RARE EARTH ALLOYS
- NT REFRACTORY METAL ALLOYS
- NT RHENIUM ALLOYS
- NT RHODIUM ALLOYS
- NT RUTHENIUM ALLOYS
- NT SELENIUM ALLOYS
- NT SILICON ALLOYS
- NT SILVER ALLOYS
- NT SODIUM ALLOYS
- NT SOLDERS
- NT STAINLESS STEELS
- NT STEELS
- NT TANTALUM ALLOYS
- NT TELLURIUM ALLOYS
- NT TERNARY ALLOYS
- NT THORIUM ALLOYS
- NT TIN ALLOYS
- NT TITANIUM ALLOYS
- NT TUNGSTEN ALLOYS
- NT UDIMET ALLOYS

- NT VANADIUM ALLOYS
- NT WROUGHT ALLOYS
- NT YTTRIUM ALLOYS
- NT ZINC ALLOYS
- NT ZIRCALOY 2 [TRADEMARK]
- NT ZIRCALOYS [TRADEMARK]
- NT ZIRCONIUM ALLOYS
- High fatigue resistance in metals and alloys - Conference, Atlantic City, July 1969
01 p0098 A71-10161
- Grinding characteristics charts of aerospace alloys wheel-workpiece pairs for comparison with single point turning and electrochemical machining [SME PAPER EM-70-100]
01 p0090 A71-11262
- Strain rate effects on plastic properties of various metals and alloys
02 p0265 A71-12568
- Ultrafine grain alloys ductility from tensile tests, discussing grain size, temperature and strain rate effects
03 p0446 A71-14493
- Superplastic alloys fabrication and applications, discussing grain size and surface area roles
03 p0516 A71-14498
- Aircraft light alloys fatigue characteristics for component endurance evaluation
05 p0767 A71-16757
- Metals and alloys with bcc structure, investigating ductile-to-brittle transition by ultrasonic MHz technique
05 p0770 A71-17251
- Alloys constitution research, discussing experimental methods in phase diagram investigations of multicomponent systems
06 p0910 A71-17340
- Alloy melting technique and heat treatment effects on elastic limit and modulus of elasticity
06 p0912 A71-17947
- Ordered alloys structural applications and physical metallurgy - Conference, Lake George, New York, September 1969
07 p1131 A71-19426
- Intermetallic compounds structural component applications, considering crystal growth, alloy constitution and development, mechanical properties and processing technology
07 p1131 A71-19427
- Alloy matrix short range ordered particle microstructures and properties, correlating electron diffraction and field ion microscopy studies
07 p1132 A71-19439
- Alloy strengthening by ordered precipitates, predicting antiphase boundary energy from flow stress vs particle size plots
07 p1132 A71-19440
- Chemical composition effect of low carbon alloys metallic matrix on wear resistance in abrasive medium, showing austenitic manganese alloys superiority to martensitic or ferritic alloys
07 p1136 A71-19630
- Microporosity morphology relationship to grain size and boundaries in alloys solidification and pores removal kinetics from castings by sintering
07 p1119 A71-19977
- Book on yield point phenomena in metals and alloys covering Fe, Va, Cr, Ni, Mo, Ta, W, Al and alloys, hydrogen in metals and fcc lattices
08 p1304 A71-20999
- Energy dissipation-fatigue strength relationships during vibrations for prestrained metals and alloys
08 p1369 A71-21118
- Multisample test equipment for steels and alloys oxidation resistance at high temperatures in corrosive gaseous atmospheres
08 p1292 A71-21440
- Strength of metals and alloys - Conference, Pacific Grove, California, August-September 1970
08 p1306 A71-21501
- Alloy equivalent susceptibility to damage at intermediary service periods and different stress levels under creep conditions at 750 C
08 p1317 A71-21709
- Harmonic analysis of metals and alloys fine structure X ray photographs via digital computers
08 p1293 A71-21765
- Complex alloying of structural steels, stressing structural changes, electron interactions and phase transition changes
09 p1470 A71-23075
- Soviet book on metal alloys plasticity gaps covering crystallization, thermomechanical treatment, heat induced brittleness zones formation, etc
09 p1472 A71-23161
- Soviet papers on alloys crystal structure and properties covering electron microscopy, X ray analysis, heat treatment and pressure effects on phase transformations
09 p1473 A71-23223
- Solid metals and alloys electron emission, considering applications in surface phenomena observation
09 p1473 A71-23224
- Superconducting alloys order parameter spatial variation and resonance scattering near nonmagnetic impurity at critical temperature, using Heinrich perturbation theory expansion solutions
12 p1942 A71-26744

- Ductility and susceptibility to brittle fracture of alloys under stress at low temperatures
12 p1919 A71-27685
- Semiquantitative X ray nondestructive analysis of metal alloys, noting critical nature of sampling
13 p2074 A71-28438
- Aircraft engine production components and alloys mechanical properties evaluation for improved reliability of mass produced products
13 p2075 A71-28944
- Superplastic metal alloys microstructure, development history and shaping technology, noting Zn-Al alloy for auto bodies fabrication
15 p2429 A71-32004
- Combined mechanical and cyclic thermal stresses effect on plastic deformation buildup in EI435 alloy preceding breakdown
15 p2433 A71-32236
- Steels and alloys structure and properties - Conference, Moscow, May 1968
16 p2596 A71-33914
- Thermal polymorphous metals and alloys crystal structure, discussing plastic deformation due to formation of cubic lattice and metallic bonds
16 p2597 A71-33915
- Structural changes and phases nucleation and growth in metal alloys during prolonged loading at high temperatures, examining steel strengthening precipitates coagulation kinetics
16 p2597 A71-33918
- Light alloys fatigue characteristics for aircraft components endurance evaluation
17 p2759 A71-35456
- Metals and alloys thermal conductivity prediction using Lorentz ratio and electrical resistivity measurements
18 p2938 A71-36991
- AMg6M alloy hot rolling butt joints, showing ductility and strength of welds
19 p3070 A71-38424
- Recovery creep properties and intercrystalline fracture in precipitation hardened alloys heat treated on relative stable conditions
20 p3250 A71-39024
- Diffusion processes electron mechanism in metal-metal and metal-nonmetal systems, using configurational model for valence electrons localization
21 p3403 A71-41159
- Superplasticity and materials forming methods for metal alloys, considering reformation speed increase by finer grained and stable alloys development
22 p3563 A71-42323
- Noble and transition metals dilute alloys electronic structure in hybridized tight binding nearly free electron representation, using Harrison-Kanamori pseudopotential theory
24 p3860 A71-45129
- Noble or transition metals based dilute alloys electronic structure, describing pure metal band structure by interpolation scheme of hybridized tight binding and nearly free electron orbitals
24 p3860 A71-45130
- ALMUCANTAR**
- U ELEVATION ANGLE**
- ALOUETTE HELICOPTERS**
- Onboard weighing system for gross weight determination and center of gravity location of Alouette helicopter, using load sensors, electrical circuits and visual indicators
14 p2175 A71-30320
- French helicopters design and performance, considering Alouette 2 and 3 and military versions
15 p2350 A71-32694
- ALOUETTE SATELLITES**
- NT ALOUETTE 1 SATELLITE
- NT ALOUETTE 2 SATELLITE
- International cooperation in space radio science, considering real time telemetry application via Solrad, Tiros and Alouette satellites
17 p2697 A71-34252
- Stable auroral red arc excitation observations by HF radar scattering, scanning photometers and Alouette 1 satellite, noting local electron concentration increase
19 p3054 A71-38034
- Alouette and Isis satellites flight data comparison with attitude and spin dynamics theory, considering solar radiation pressure and gravitation and magnetic field effects
22 p3609 A71-41997
- ALOUETTE 1 SATELLITE**
- Sunrise behavior of midlatitude topside ionosphere at low sunspot numbers from Alouette 1 electron density and plasma scale height profiles
13 p2055 A71-27920
- ALOUETTE 2 SATELLITE**
- Alouette 2 satellite spin dynamics measurement based on telemetered optical data
03 p0379 A71-14006
- Alouette 2 ionograms frequency interpolation correction allowing measurement accuracy comparable to sounder system resolution
05 p0725 A71-17083
- Alouette 2 satellite housekeeping data processing, obtaining selected satellite temperatures, solar cell

current, geomagnetic field, direction of sun and satellite attitude
12 p1883 A71-26607

Diurnal distribution, latitudinal occurrence and intensity patterns of ELF, VLF and LF whistler-mode noise emissions from Alouette 2 satellite observation
19 p3016 A71-37364

ALPHA PARTICLES

Li quantitative determination in soaps and lubricants by gamma spectroscopy of nuclear reactions with alpha particles from radioactive source
01 p0106 A71-10093

Proton fluxes at 300 keV associated with propagating interplanetary shock waves, noting alpha particle enhancement
01 p0146 A71-11487

Geomagnetically trapped C, N and O nuclei and alpha particles in earth outer radiation zone, noting acceleration and loss mechanisms
01 p0075 A71-11496

Surveyor lunar probes alpha scattering chemical analysis technique tested on rocks of known composition
02 p0305 A71-11984

Black Brant rocket measurement of PCA event at Churchill, Canada on 19 November 1968, discussing electron density and alpha particle and proton flux
03 p0417 A71-14038

Differential energy losses of alpha particles traversing materials in superconducting and normal states
03 p0468 A71-14414

Inelastic alpha particle scattering experiment for studying energy spectrum and angular distribution of Sc-45 excited states
03 p0462 A71-14417

Anomalous low magnetospheric He alpha/proton flux ratio in terms of electrostatic radial diffusion taking into account charge exchange and pitch angle loss processes
06 p0964 A71-17284

Alpha particle abundance in solar wind positive ions observed by ESRO satellite HEOS-1
06 p0950 A71-17919

Low and high linear energy transfer /LET/ cyclotron-accelerated alpha particles effects on *Drosophila melanogaster* longevity
06 p0853 A71-18028

Quiet time fluxes and differential energy spectra of protons and alpha particles at 2-20 MeV measured by cosmic ray detectors on OGO-3
06 p0954 A71-18127

Protons and alpha particles energy spectra during 25 February 1969 solar event from Centaur rocket observations as part of ESRO PCA campaign
06 p0957 A71-18144

Galactic cosmic ray proton and He nuclei spectra measurements aboard Pioneer 8 spacecraft over large energy range, considering solar modulation parameters
08 p1355 A71-21626

Temporal intensity variations of geomagnetically trapped solar alpha particles from Injun 5 observations
08 p1356 A71-21644

Electron radiation bulk damage effects on Si surface barrier detectors, determining reverse leakage current density and alpha particle response changes
08 p1345 A71-21842

Radiation defects distribution in Si irradiated by protons, deuterons and alpha particles
10 p1655 A71-24140

P-n junctions formation in p-silicon irradiated by alpha particles
10 p1656 A71-24145

Alpha particle gas densitometric response to planet atmospheric density profiles in terms of radioactive source energy distribution, considering contoured baffle models
11 p1763 A71-26079

Alpha radiation machmeter with semiconductor pulse detectors, discussing supersonic regime effects on rate variations
12 p1908 A71-27607

Solar cosmic ray acceleration and propagation from time variation and heliocentric distance dependence of relative abundance of protons to helium nuclei
13 p2129 A71-29058

Neutron emission yield during Pu 238 alpha particles interactions with O 18, taking into account recoil Ne isotopes
14 p2276 A71-30177

Statistical measurements of solar protons, alpha particles and heavier nuclei by lunar orbiting Explorer 35
16 p2628 A71-33933

Energetic electrons, protons and alpha particle measurements by Azur satellite over polar cap and in radiation belt during March 1970 solar particle event
19 p3126 A71-37419

Irradiation dose effect on alpha particle irradiated Al foil electrical resistivity recovery, using Wheatstone bridge measurement
23 p3689 A71-42934

Mg 24 photodisintegration rate in stellar silicon burning process, presenting reactions at low alpha particle energies
23 p3723 A71-42952

Inelastic scattering alpha-gamma angular correlations from C 12, Mg 24, Ni 58 and Sn 120 decay measurements
23 p3706 A71-43198

Alpha radioactivity in Surveyor 3 camera visor, calculating upper limit of Po 210 at equilibrium of Oceanus Procellarum
23 p3765 A71-43812

ALPHA RADIATION
U ALPHA PARTICLES

ALPHABETS

Ternary code and three value logic in digital computers, considering economic advantages, signal distinguishability and numerical interpretation of p digit abstract alphabet
22 p3516 A71-41856

ALPHANUMERIC CHARACTERS
NT BINARY DIGITS

Alphanumeric character generation from resistive storage of time derivatives for CRT displays
01 p0047 A71-10216

Alphanumeric display devices with liquid crystal and dynamic light scattering for low voltage, power, cost and fabrication advantages, testing performance
14 p2249 A71-31029

Pattern recognition machine construction for written alphanumeric symbols and human voice identification, providing bibliography
15 p2372 A71-32316

Visual displays preview, noting miniature eight-character alphanumeric, tabular, video, telephone and graphical displays
18 p2924 A71-36619

Data display units as man machine interface elements in data processing operations, discussing combined alphanumeric/graphic CRT units
20 p3202 A71-38885

Monolithic alphanumeric array of planar light-emitting GaAsP diode matrix on common chip for programmed function keyboard use in display devices
21 p3349 A71-40108

Electronic circuit modules effects on alphanumeric display capabilities and costs over wide applications range
21 p3359 A71-40116

ATC display devices with computer-derived alphanumeric labels on radar screen, examining feasibility and effectiveness
21 p3413 A71-40118

Alphanumeric fonts for 5-by-7 matrix display, comparing legibility with USAF font
21 p3350 A71-40121

Readout systems light emitting numerals legibility, determining threshold values from response categorization into correct responses, misreadings and missed signals
21 p3376 A71-40125

Character size, case and symbol generation effects on CRT display search time
22 p3503 A71-42195

ALSEP
U APOLLO LUNAR SURFACE EXPERIMENTS PACKAGE

ALTERNATING CURRENT

Steady high power plasma flows using three phase AC generator
04 p0632 A71-14794

AC signal amplitude measurements, describing circuit design with DC voltage generation proportional to input AC voltage
06 p0899 A71-17926

AC superconducting cables design for utilities underground power transmission lines, discussing superconductor and cryogenic envelope configuration and characteristics
07 p1024 A71-20159

AC power meters using electronic multiplier for overcoming limitations concerning frequency ranges, response times, power factor and distortion
10 p1609 A71-23918

Drift waves dynamic stabilization in collisionless plasma, considering AC electric field effects on low frequency instabilities
12 p1935 A71-26914

Engineering method for synthesizing and calculating AC correcting devices with synchronous switches, deriving equivalent transfer function
13 p2041 A71-27949

AC plasma panel /gas discharge matrix/ display, discussing operation principles, static and switching characteristics and driving circuitry
21 p3352 A71-40120

Highly ionized hot Cs plasma parametric resonance in alternating electric field related to plasma heating
21 p3424 A71-41107

Current harmonics in passively nonlinear resistance subject to simultaneous DC and AC fields
24 p3860 A71-44872

ALTERNATING CURRENT GENERATORS
U AC GENERATORS

ALTITUDE ACCLIMATIZATION

ALTERNATIONS

Operator performance improvement in monitoring automated processes by alternating displays, discussing simulated radar and sonar CRT display laboratory tests
22 p3501 A71-41636

ALTERNATORS (GENERATORS)
U AC GENERATORS

ALTIMETERS
NT LASER ALTIMETERS
NT RADIO ALTIMETERS

Aircraft ultrasonic altitude and vertical velocity sensor for low flight, discussing VTOL aircraft automatic hovering control and time lag
01 p0084 A71-11624

Modulation cancellation altimeter error analysis and performance optimization
12 p1908 A71-27437

Ocean height measurement by orbit determination from satellite altimetry, considering least squares solutions and instrument errors
13 p2066 A71-27983

Cam profile selection for adjustment in computing-resolving unit of aneroid sensors of altimeters
13 p2069 A71-28938

High altitude balloons pressure-altitude transducer assembly, discussing electronic circuitry, calibration and temperature and vibration effects
14 p2240 A71-30070

Altimeter-airspeed and Mach number pressure transducer with diaphragm free of temperature and vibration effects
14 p2243 A71-30322

Aircraft barometric altimeter errors caused by atmospheric temperature deviations from International Standard Atmosphere
14 p2244 A71-30323

Unified error analysis application to altimeter-aided terrestrial inertial navigation systems
19 p3095 A71-37152

Altitude instrumentation for aircraft pilot, discussing three pointer, servo and drum pointer altimeters, digital readout, radar alert and automatic reporting systems
23 p3628 A71-43383

Barometric altimetry system inadequacies and approach/landing accidents, noting pilot static components blocking hazards
23 p3628 A71-43384

Pressure altimeter, airspeed and vertical velocity instruments, discussing selection, installation, pilot verification, error identification, repair and use
23 p3675 A71-43385

General aviation aircraft altimeter errors, tolerances and static system tests
23 p3629 A71-43386

ALTITUDE
NT FLIGHT ALTITUDE
NT HIGH ALTITUDE
NT LOW ALTITUDE

Altitude and azimuth angle values computation using logarithmic and natural haversines table
02 p0280 A71-12899

Density spectrum of cosmic ray showers, discussing altitude effects, structure function and transition
13 p2125 A71-28087

Radaroscope net for target azimuth and distance and for direct altitude readout through beacon numerics
13 p2033 A71-28886

ALTITUDE ACCLIMATIZATION

Physical exercises to increase cosmonaut space environment tolerance, discussing effects of acceleration, altitude and hypoxia
01 p0027 A71-11556

Lower fasting blood glucose levels in high altitude acclimatization
02 p0197 A71-11664

Oxygen tension, blood flow, redox potential and temperature variations in cerebrum and musculus gastrocnemius of rats during high mountain adaptation
03 p0361 A71-13190

Training effect on oxygen tension dynamics in rats brain cortex under progressive high altitude hypoxia conditions, noting adaptation influence on motor activity and survival rate
06 p0850 A71-17394

Oxygen transport and consumption, ventilation and cardiac index in natives and sojourners at high altitudes
06 p0853 A71-18060

Myocardial ventricle contraction in high altitude hypoxia adaptation, using barochamber trained rats
06 p0857 A71-18467

Arterial oxygen, carbon dioxide tension, pH and lactic acid changes during rapid descent from altitude to sea level in deep mine
07 p1052 A71-20334

Myocardial lysosomal enzymes activity in adaptation to high altitude hypoxia and during cardiac diseases, using albino rats
08 p1239 A71-21058

Mitotic activity of kidney undergoing compensatory hypertrophy in high mountain nonadapted rats
08 p1242 A71-21965

ALTITUDE CONTROL

Rat left ventricle isolated papillary muscles contractile force in pressure chamber under high altitude adaptation

09 p1388 A71-22125

Altitude acclimatization of albino rats and guinea pigs, measuring chronic and acute hypoxia effect on oxygen affinity and red cell 2,3 diphosphoglycerate concentration

10 p1558 A71-23894

Renal oxygenation in male Peruvian natives living permanently at high altitudes, determining reduced tubular function cause

12 p1873 A71-27127

Oxygen dissociation curve shift, hemoglobin affinity and diphosphoglycerate concentration in blood of acidotic and normal subjects at altitude

13 p2016 A71-29494

High altitude pulmonary edema in unacclimatized humans, discussing symptoms, etiology incidence and prevention

14 p2183 A71-30277

High altitude acclimatized humans, noting decreased coronary blood flow and increased oxygen extraction

14 p2184 A71-30283

High altitude residents cardiovascular evaluations, showing right ventricular enlargement and reactive pulmonary hypertension

14 p2184 A71-30285

Chronic hypoxia effects on blood oxygen and carbon dioxide tensions and pH changes in unanesthetized chickens at high altitude compared to sea level control

14 p2186 A71-30565

Conditioned reflexes developed by prolonged training in two genetic strains of mice during adaptation to altitude hypoxia

15 p2356 A71-31248

Immunobiological reactivity inhibition in mice under partial adaptation to high altitude hypoxia, observing decreased phagocytic activity, antibody production, hypoplasia and lymph cell number

15 p2356 A71-31289

Cellular respiration and high altitude adaptation effect on cytochrome content and on oxidation and oxidative phosphorylation parameters of brain homogenates in rats

15 p2357 A71-31310

Myocardium ultrastructural and metabolic alterations in altitude acclimated rats, considering heart muscle mitochondria

16 p2529 A71-33193

Trained young runners maximum oxygen consumption rate at sea level and high altitude

16 p2530 A71-33244

High-mountain altitudes inhibition of inflammation and wound healing in rabbits

16 p2531 A71-33522

Ventilatory acclimatization to chronic hypoxia in high altitude natives by cerebrospinal fluid pH decrease

17 p2683 A71-35144

Human adaptation to high altitude, considering effects of physical preconditioning, exercise, high carbohydrate diets and normal food intake maintenance

18 p2859 A71-36867

Physiological responses of burro *Equus asinus* to oxygen lack in mountain altitudes, studying red blood cell and plasma volumes

19 p3005 A71-38560

High altitude exposure effects on concentration and total quantity of electrolytes in human serum and extracellular space

19 p3009 A71-38562

Pigeon acclimatization response to simulated high altitude, determining body weights, hematocrit ratios, hemoglobin concentrations and plasma and blood volumes

19 p3005 A71-38563

Altitude and cold acclimatization effects on human basal heart rate, blood pressure, respiration and breath-holding

21 p3330 A71-40349

Cold pressor response tests under altitude acclimatization and simultaneous hypoxic acclimatization and cold in man

22 p3502 A71-41831

Training cycle in altitude chamber for human adaptation to hypoxia, high temperatures and transverse myogenic loads

22 p3505 A71-42805

Elevated basal metabolism in man under simultaneous altitude hypoxia and cold acclimatization

23 p3636 A71-44239

Ventilatory response to progressively increasing inspired carbon dioxide tensions at ground level and acetazolamide pretreatment before high altitude exposure

23 p3636 A71-44242

Rat thyroid gland changes during acclimatization to simulated high altitude environments, observing high hormone stimulation

23 p3637 A71-44300

Pulmonary carbon monoxide diffusing capacity of sea level and high altitude dwellers at various altitudes, noting early postnatal lung growth effects

24 p3797 A71-44778

Age effects on plasma aldosterone levels, red cell, plasma and total blood volume at sea level and high altitude

24 p3797 A71-44781

ALTITUDE CONTROL

Aircraft response to pilot or autopilot command during altitude control maneuver, calculating lag magnitudes

22 p3482 A71-41691

Altitude dynamics and motion stability analysis of gravity oriented synchronous satellite under perturbation effects of environmental forces due to sun, earth, albedo and cosmic rays

22 p3612 A71-42050

ALTITUDE SICKNESS

Acute mountain sickness due to oxygen deficiency, discussing control by acetazolamide, placebo or furosemide pretreatment

06 p0851 A71-17613

Neurological altitude decompression sickness clinical manifestations, pathophysiology, treatment by compression therapy and subsequent grand mal seizures

06 p0859 A71-17614

Nitrogen, helium, argon and neon containing atmospheres relation to altitude decompression of rats, noting interspecies comparison of metabolic effects

10 p1570 A71-24610

High altitude decompression disorders prevention in humans by increasing pressure level in oxygen equipment assembly

24 p3795 A71-44474

ALTITUDE SIMULATION

Simulated high altitude chronic hypoxia and long term sideropenic anemia adapted animals, investigating acute anoxia tolerance of myocardium

07 p1044 A71-20331

Stored arc heated air true temperature, flight and altitude simulation facility in Mach number 8 to 10 region for air breathing propulsion research

08 p1273 A71-21983

Altitude rate generation for aircraft instruments testing

09 p1448 A71-22770

Simulated altitude test facilities selection for Space Shuttle Orbiter Engine

14 p2292 A71-30743

Pigeon acclimatization response to simulated high altitude, determining body weights, hematocrit ratios, hemoglobin concentrations and plasma and blood volumes

19 p3005 A71-38563

Self regulating steady state cryopump system for simulated altitude testing during rocket engine firings

20 p3184 A71-39198

Visual performance in simulated target acquisition tasks as function of flare-ignition altitude

22 p3503 A71-42196

ALTITUDE TESTS

NT HIGH ALTITUDE TESTS

Altitude engine test stands evolution in Germany, discussing design

04 p0566 A71-14989

Stokes flow parachute extremely lightweight decelerator for increasing altitude and rocket-borne radiosondes atmospheric data sampling quality

11 p1707 A71-25277

Body fat influence with and without denitrogenation on decompression sickness in men exercising after abrupt exposure to altitude

13 p2022 A71-29361

ALTITUDE TOLERANCE

Acute mountain sickness due to oxygen deficiency, discussing control by acetazolamide, placebo or furosemide pretreatment

06 p0851 A71-17613

Physiological characteristics in llamas pulmonary circulation at sea level and changes after 5 and 10 weeks at 3,420 m above sea level, noting arterial hypertension

08 p1237 A71-20678

Chronic hypoxia effects on capillary development during high altitude exposure in decompression chamber and maintenance at sea level

08 p1237 A71-20679

Aircraft crew without pressure suits, noting abrupt ambient pressure drop tolerance in trained and untrained subjects

12 p1876 A71-27659

Polycythemia and altitude hypoxia effects on rats heart and sea level exercise tolerance

20 p3186 A71-38980

Peritoneal macrophagocytic ingestive capacity decrease in mice under hypobaric hypoxia, indicating infection susceptibility in altitude environments

22 p3486 A71-41832

ALU (COMPUTER COMPONENTS)

U ARITHMETIC AND LOGIC UNITS

ALUMINA

U ALUMINUM OXIDES

ALUMINATES

Beta-Li hexafluoroaluminate heat capacity and thermodynamic properties from 15 to 380 K

04 p0674 A71-14727

ALUMINIZING

U ALUMINUM COATINGS

ALUMINUM

NT ALUMINUM ISOTOPES

NT ALUMINUM 26

NT ALUMINUM 27

NT POWDERED ALUMINUM

Mg, Al and Si ions spectral analysis, discussing energy levels and transition lines

01 p0129 A71-10136

High speed light gage Al welding, discussing plasma arc system

01 p0087 A71-10454

Flaw detection system for wide Al sheets, using eddy current equipment with modulation analysis principle

01 p0087 A71-10458

Cu addition effects in solid solution on grain boundary sliding in Al at constant shear stress, considering accompanying crystal dislocations

01 p1012 A71-10739

Secondary fabrication of boron reinforced aluminum matrix composite sheets for aerospace sub-components, detailing joining and autoclave bonding [SME PAPER EM-70-126]

01 p0089 A71-11260

Thermal cycling effect on Al-B composites, considering surface roughening and crack initiation

01 p1013 A71-11279

Diffusion bonding cycles for Al-B composite materials fabrication, relating strength enhancement to residual stress relief

01 p1014 A71-11284

Large Al forgings machining cost reduction via stress relief involving mechanical working following quench

01 p0091 A71-11547

Al fatigue testing by cyclic uniaxial tensile load, examining deformation, internal friction ductility and plastic strain

02 p0262 A71-11683

Furnace fluxless brazing of Al with metallic getters, discussing techniques and joint design

02 p2555 A71-11706

Pressurized inert gas metal arc welding of Al, determining voltage, filler metal speed and chamber pressure effects by multiple regression analysis

02 p2555 A71-11709

Multilayer composites preparation by cold rolling packets of alternating Al and Sn foils, determining tensile strength relation to layer thickness

02 p2644 A71-12278

Aluminum compression microstructure under various strain rates and temperatures, discussing dynamic recovery role

02 p2677 A71-12877

Photoelastoplastic analysis of creep and stress of aluminum notched bars and cracked plates under thermal cycle using epoxy resin simulation

03 p0507 A71-13757

Aluminum addition effect on combustion rate of mixtures of ammonium perchlorate with polymethyl methacrylate at different temperatures

03 p0520 A71-13995

Thin Al and plexiglass sheets biaxial stress field effect on fatigue and fracture

04 p0665 A71-14768

Stainless steel-Al joining techniques, describing gas tungsten arc process

04 p0603 A71-14920

Aluminum spot welding specification consistency, examining surface conditions, cleaning procedures, weld schedules and bond design effects

04 p0603 A71-14923

Aluminum bicrystals mechanical properties under high strain rates, considering changes in surface structure, active slip planes and dislocation

04 p0612 A71-15077

Al ingot level pouring casting, considering solidification effect on subsurface segregation and cyclic pattern of macrostructure

04 p0614 A71-15783

Inert gas welding of Al with He as oxidation inhibitor, discussing penetration, welding rate and cost compared to Ar use

04 p0604 A71-15815

Steel wire reinforced Al manufacture and properties, discussing wire-matrix bonding

05 p0764 A71-15922

State definition international standardization for cold rolled Al sheets, examining yield curves and strain energy

05 p0764 A71-15923

Electroformed Al contact solar cells without soldering, investigating process parameters effects on performance

05 p0699 A71-16062

Small scale vacuum stream degassing of molten aluminum for hydrogen removal

05 p0758 A71-16247

Aluminum reinforced epoxy model making, testing and stress analysis for aircraft structures, including creep, photoelastic coating and strain gage effects
05 p0821 A71-16346

Annealed Al bars mechanical properties and stress-strain curves dependence on strain rates under loading
05 p0766 A71-16390

Al single crystals creep deformation, noting thermally activated mechanism at cryogenic temperatures
05 p0769 A71-16879

Pure polycrystalline Al under uniaxial tension, noting vacancy rupture mechanism
06 p1000 A71-17940

Structure changes of Al single and polycrystals with initial cube orientation under cold rolling
06 p0913 A71-18420

Silicon detector measurements of energy deposition in aluminum by monoenergetic electrons
07 p1106 A71-19073

Porosity in gas tungsten arc aluminum weldments and elimination by hydrogen reduction
07 p1119 A71-19969

Hydrogen outgassing from proton irradiated aluminum samples, determining gas evolution and blister formation during annealing
07 p1139 A71-20173

Deformation amplitude effects on dislocation structure and strengthening mechanism of fcc aluminum under cyclic loading
07 p1142 A71-20482

Hydrostatic pressure effects on Al polycrystals stress-strain behavior at room temperature, using magnetostriuctive load cell
07 p1143 A71-20490

W fiber reinforced Al strain distribution under tensile load, using moire grid method
07 p1144 A71-20495

Carbon fiber reinforced Al composites fabrication and evaluation by metallographic examination, considering tensile strength
[PLASTICS INST. PAPER 17]
08 p1322 A71-20930

Tritium and He-3 nuclei measurements in Al targets from Soyuz spacecraft observation
08 p1354 A71-21021

Fluoride overcoated Al reflectance measurements and polarization effects at various angles of incidence, noting utilization in vacuum UV instrumentation
08 p1335 A71-21381

Ribbed aluminum panels airborne sound transmission loss, evaluating structural damping effects
08 p1231 A71-21431

Al electrodes in molten salt electrolytes, investigating electrochemical kinetics by polarization measurements
[ECS PAPER 200]
08 p1250 A71-21470

Al microstructure and strength, investigating prior deformation and temperature effects
08 p1313 A71-21561

Al dislocation mobility at high strain rates, plotting true stress vs true strain
08 p1313 A71-21564

Structural efficiency improvement by materials selection for airframe structures, discussing Al, Ti-Al-V and steel panels
08 p1299 A71-21685

Ultrasonic effects on dislocations and grain boundaries in vacuum annealed polycrystalline Al specimens
09 p1467 A71-22288

Real time and double exposure holographic interferometry measurements of strain on aluminum cylinder under internal pressure, noting discrepancy with strain gage values
09 p1444 A71-22711

Single metal system Al beam leded chips, substrates and crossovers for multilead packaging, describing fabrication techniques
09 p1509 A71-23119

Al and Fe additions effect on transitional phases formation and metastable phase precipitation in Ni-Nb system, using transmission electron microscopy
09 p1471 A71-23124

Crystalline Al stress-strain function parabolic law generalization under combined axial tensile-torsional loading
09 p1480 A71-23700

Aluminum-epoxy joints stress corrosion cracking inhibition and crack tip plastic deformation by scanning electron microscopy
10 p1615 A71-24091

Fatigue crack propagation rates in Al under constant low stress, discussing data processing methods
10 p1629 A71-25053

Al and Pb atoms nuclei inelastic interaction cross section with nuclear active particles, using ionization calorimeter and wide gap spark chambers
11 p1760 A71-25165

Design and fabrication of Borsic aluminum composite fan blades for supersonic turbofan engines, considering 430 F application without severe vibratory stress
[ASME PAPER 71-GT-90]
11 p1771 A71-25997

Al anodizing processes, stressing modern theory of anodic oxidation and anodized Al corrosion
11 p1779 A71-26000

High strain rate effects on Al single crystals deformation, presenting overall and local strain and lattice rotation measurements in impact tested specimens
11 p1779 A71-26014

Grooved Al heat pipes experimental performance in moderate temperature for space vehicle applications
[AIAA PAPER 71-409]
11 p1856 A71-26204

Coarse grain Al sheet deformation, determining dislocations distribution with etching defects method
12 p1919 A71-27691

Torsion creep tests of Al, deriving expression for steady state creep rate as function of temperature and stress
13 p2083 A71-27963

Al matrix-stainless steel composites under tensile loading parallel to reinforcement direction, noting creep behavior at ambient temperature
13 p2089 A71-29413

Creep rupture strength and durability of Al, Ni and Cu irradiated by neutron flux
14 p2258 A71-30004

Thermal emissivity and solar absorptivity of Al coated with surface layers of aluminum oxide and silicon oxide, describing fabrication techniques and performance measurements
14 p2335 A71-30128

Low cycle fatigue strength of high speed rotating aluminum and brass disks, comparing with uniaxial push-pull fatigue test
14 p2328 A71-30418

Mg and Al particles burning in air, water vapor, Cl and nitrous oxide
14 p2337 A71-30614

Ignition initiation, burning time and particle size distribution determination for dispersed Mg and Al particles in condensed system
14 p2337 A71-30615

Burning rate of Al particles suspended in polymer propellant gas flow with inorganic oxidizers
14 p2285 A71-30620

Luneberg lens fabrication technique using thin insulated Al slivers embedded in low density polystyrene foam
14 p2205 A71-31059

Oxidation kinetics of pure Al in dry oxygen as function of pressure and temperature, using manometric method
15 p2426 A71-31408

Al and Cu dynamic plastic deformation at elevated temperatures, discussing relationship between strain rate sensitivity and activation energy
15 p2428 A71-31972

Al and Cu-Al alloys eutectic composites with small interlamellar spacing, characterizing ambient temperature compressive stress strain behavior to failure
15 p2432 A71-32168

Aluminum single crystals tensile deformation and annealing to produce polygonized substructure
15 p2432 A71-32172

Grain size effect on fatigue life during tension and compression tests of alpha brass, copper and aluminum, considering slip character
15 p2437 A71-32578

Ca, Mg, B and Al prominent resonance transitions radiative lifetimes and absolute oscillator strengths
15 p2452 A71-32596

Shock produced stress relaxation in thin walled Al tubes, comparing strain-time profiles with thin shell theory
16 p2647 A71-32923

Time dependent fracture and failure criteria for aluminum under stress pulse loading in uniaxial strain, using exploding foil spallation tests in air and vacuum
16 p2590 A71-32943

Surface deformation in polycrystalline Al samples produced by ultrasound generated cyclic stresses, examining slip bands formation by electron microscope
16 p2591 A71-33224

Anodic dissolution of aluminum bicrystals in electrolytes containing perchloric acid during electropolishing, showing anisotropic layer existence
16 p2592 A71-33371

Pure superconducting Al wire surface inductance measurement as function of temperature, noting penetration depth value
16 p2621 A71-33425

Aluminum effect on nickel diffusion in iron from stainless and aluminum steels study
16 p2599 A71-34053

Boron-aluminum composites fracture behavior, using conventional metallography and scanning electron microscope
16 p2599 A71-34087

Fractographic investigation of fatigue crack propagation in pure monocrystalline and polycrystalline Al
16 p2599 A71-34095

Elastoplastic strain distribution in bent circular Al plate with central hole under concentrated load, giving moire patterns and stress-strain diagram
[SESA PAPER 1822]
17 p2820 A71-34542

Solid state diffusion bonded boron-aluminum composites, discussing mechanical properties, weight and cost reduction and applications
17 p2758 A71-35204

Composite panel of ten-ply unidirectional boron/epoxy laminate adhesively bonded to Al face sheets, discussing ultrasonic inspection technique
17 p2749 A71-35495

Al distribution in gallium aluminum arsenide films obtained by epitaxial growth from liquid phase, showing temperature variation dependence during deposition
18 p2954 A71-36161

Aluminum-boron composite forming and cutting processes covering milling, grinding, abrasive cutoff, drilling, piercing, electrodischarge machining, blanking, punching and shearing
18 p2928 A71-36666

Two dimensional dynamic thermal stresses in Al plate, allowing for Newtonian surface heat exchange
18 p2981 A71-36720

Strain rate dependence of shear stress, plastic cross-slip and stacking fault energy of Al single crystals at 77 K
18 p2937 A71-36749

Fatigue crack propagation in thin aluminum plates under fluctuating tensile loads, concerning Forman model
18 p2938 A71-36851

Cavitation erosion of aluminum at high hydrostatic pressure, using chamber focusing acoustic system
18 p2910 A71-36932

Prestressing effect on yield surfaces of Al and Cu thin walled tubes
19 p3079 A71-37705

Electric contact resistance of various conductive metal coatings on aluminum corrosion free joints
19 p3031 A71-38449

Al, Cu and Ni high temperature creep noting diffusive, shear and dislocation deformation mechanisms
19 p3083 A71-38525

Silicon reactions with aluminum surfaces, using low energy electron diffraction technique
20 p3194 A71-38882

Al electrolytic capacitors characteristics as function of temperature, time and frequency of operation, noting improvement by organic solvents use as electrolyte component
20 p3203 A71-38884

Soyuz observation of tritium and He-3 nuclei in Al targets exposed to space radiation
20 p3280 A71-39601

Lubricated friction of steel ball on commercial tempered aluminum plate as function of time
21 p3396 A71-40100

Steels, aluminums and titaniums ultimate and yield strength statistical distributions in Weibull parameter form, presenting stimulus-response potential failure model
[ASME PAPER 71-VIBR-64]
21 p3396 A71-40307

Vacancy absorption model for fatigue crack propagation in Al based on X ray inspection and transmission electron microscopy
21 p3399 A71-40698

Oxidation resistance and scale fracture healing by Al additions to Co-Cr alloys at high temperatures, using electron probe and scanning electron microscope analyses
21 p3405 A71-41420

Double frustum phenomenon in mushrooming of cylindrical Al projectiles upon high speed impact with hardened steel anvil
21 p3474 A71-41424

LEED studies of oxygen adsorption on (111) and (110) surfaces of Al single crystals
22 p3561 A71-41730

Nondestructive testing evaluation of graphite epoxy composites and adhesive bonded Al composite structures using acoustical holography
22 p3554 A71-41781

Nitrogen ions surface interactions with Al surfaces at and above earth satellite speeds, measuring normal and tangential momentum accommodation coefficients
22 p3577 A71-41980

Pure Al annealed polycrystal electron microscopic observation for fatigue deformation at room and elevated temperatures, noting dislocation loop role in crack initiation and propagation
22 p3564 A71-42497

Irradiation dose effect on alpha particle irradiated Al foil electrical resistivity recovery, using Wheatstone bridge measurement
23 p3689 A71-42934

F, Na and Al origin in galactic cosmic radiation, investigating production as spallation fragments and generation in source
23 p3719 A71-42943

Staircase array and diode stacking moderate power GaAlAs injection laser light sources at room temperature
23 p3685 A71-43504

Lithium additions effect on hydrogen content and mechanical properties of molten aluminum specimens
23 p3691 A71-43522

Surveyor 3 unpainted Al tubing examination by replication electron microscopy for surface damage

ALUMINUM ALLOYS

- due to particle impact and ion bombardment in lunar environment 23 p3766 A71-43821
- Stereophotogrammetric measurements of displacements and strains in Al membrane during explosive forming 24 p3825 A71-44755
- Quartz crystal mass monitor study of monolayer oxygen adsorption on Al films, noting surface roughness variation with deposition temperature 24 p3803 A71-45348
- Leed rotation diagrams for aluminum, obtaining low energy electron diffraction intensity profiles by band structure matching approach 24 p3862 A71-45349

ALUMINUM ALLOYS

- Al-Si alloys corrosion resistance in humid atmosphere and acid medium, investigating effects of refining process and hydrogen content 01 p0097 A71-10040
- Al alloys improved fatigue resistance via thermomechanical processing, considering microstructure and deformation characteristics 01 p0099 A71-10168
- Splat cooled hypoeutectic Al-Cu alloy superplasticity, using tensile tests and electron microscopy 01 p0100 A71-10280
- Periodically modulated phase structure transformations in decomposition of Cu-Ti and Cu-Ti-Al alloys during aging at different temperatures 01 p0101 A71-10670
- Fine structure and lattice constants of Al-W, Al-Mo and Al-Mn alloys at high cooling rates 01 p0101 A71-10675
- Intermetallic Ni-Al volume fraction dependent deformation of single crystals of binary Ni-Al system, using X ray and transmission electron microscopy 01 p0102 A71-10740
- Critical static strength of Duralumin under cyclic impact loads, analyzing statistically load distribution function applicability 01 p0103 A71-11240
- Ti and Ti-Al alloys machinability, discussing physical properties, dynamic deformation behavior and optimal cutting, milling and drilling [SME PAPER EM-70-101] 01 p0089 A71-11254
- Hot forming/die quenching of aluminum and titanium alloy integrally stiffened panels [SME PAPER EM-70-178] 01 p0089 A71-11259
- Airplane materials mechanical properties degradation due to fatigue, discussing breaking strain of Al alloy 01 p0104 A71-11395
- Al alloys low cycle fatigue test under axial load, observing hardening behavior and structure by transmission electron microscopy 01 p0104 A71-11397
- Self ignition temperature of aerogels of Al-Mg alloys during heating of powders 01 p0182 A71-11448
- Self ignition temperature of aerosols of Al-Si powders as function of dispersion and alloy composition 01 p0182 A71-11449
- Al-Zn-Mg-Cu type high strength Al alloys mechanical properties evaluation by fracture mechanics methods 01 p0104 A71-11540
- Quenched Al-Mg alloys, investigating dislocation mechanisms for plastic flow by creep tests at various temperatures 01 p0105 A71-11605
- Discontinuous yielding in annealed Al alloy resulting from negative slope in flow stress-strain rate relationship, discussing impurities diffusion role 01 p0105 A71-11606
- Ni-Al-Ti alloys strength, investigating matrix precipitate lattice parameter mismatch effects 02 p0263 A71-11865
- Ti-Al alloy hot salt stress corrosion cracking due to hydrogen production and absorption 02 p0267 A71-12880
- High strength stress-corrosion resistant Al alloy forgings fabrication processes, noting chemical composition and physical properties 03 p0441 A71-13255
- Al-Zn-Mg alloys intergranular failure due to aqueous stress corrosion cracking, fatigue and exfoliation, analyzing mud-crack pattern 03 p0441 A71-13319
- Strain rate effect on critical shear and cross slip stresses of Al and Al-Mg single crystals, obtaining stacking fault energy 03 p0442 A71-13364
- Transient creep propagation velocity in dead annealed thin walled Al alloy tubes, using constitutive equation for mean stress-strain-time relationship 03 p0508 A71-13761
- Al alloy biaxial shear creep under abrupt temperature and stress changes, noting surface size, shape and location [ASME PAPER 70-WA/APM-41] 03 p0443 A71-14164

- Grain boundary sliding on Mg-Al alloy polycrystalline specimens measured at successive strains during creep under 2800 psi stress 03 p0443 A71-14184
- Water impact erosion on stainless steel, Ni and Al and Ti alloys, observing impact velocity relationship with number 03 p0444 A71-14287
- Low strain cyclic hardening and softening in Al-Mg alloy, comparing measurements by monitoring and tensile testing methods 03 p0444 A71-14315
- Al-Mg alloys secondary creep relationship to mechanical instability during tension 03 p0445 A71-14340
- Al-Zn-Mg ternary alloys stress corrosion cracking resistance relation to mechanical strength decrease, quenching rate increase and solution treatment temperature 04 p0609 A71-14772
- Al-Zn-Mg ternary alloys stress corrosion cracking resistance relation to heat affected zone postannealing aging and cooling rate decrease 04 p0610 A71-14773
- Carbon steel and heat treated duralumin fatigue fracture microstructure observation using electron microscope, determining crack propagation relationships to loading sequence 04 p0610 A71-14880
- Al-Zn-Mg alloys hardness and conductivity behavior as function of aging time and temperature 04 p0610 A71-14884
- Al alloys extrusion and chemical composition relationship to mechanical properties, examining various metallurgical processes 04 p0604 A71-15743
- Al alloys nucleation and precipitation hardening, examining quenching rate effects with hardness measurements and electron microscopy 04 p0613 A71-15744
- AlZnMgCu alloys fracture behavior, examining aging conditions, rolling, forging, cracking, tensile strength and chemical composition 04 p0613 A71-15745
- Al alloys grain boundary precipitation pattern relationship to stress corrosion sensitivity 04 p0613 A71-15746
- Boron fiber-Al alloy composites linear thermal expansion as function of fiber volume fraction and orientation 04 p0615 A71-15788
- Al-Ti alloys segregation substructures, studying nucleant particles relationship to crystal solidification 04 p0615 A71-15791
- Ti-Al and Al alloys and Ni maraging steel creep behavior during high stress, elevated temperatures and rapid heating 04 p0617 A71-15909
- Fiber reinforced Al and Al alloys, discussing physical properties and manufacturing methods 05 p0764 A71-15921
- Fatigue crack propagation in aluminum alloy sheet, determining relationship between propagation rate and stress intensity factor and crack initiation conditions 05 p0766 A71-16296
- Al and Mg alloys mechanical and microstructural changes under low temperature conditions, optimizing casting component ratios 05 p0767 A71-16765
- Austenitic steels and Ti and Al alloys with stress raisers, studying low temperature mechanical properties 05 p0767 A71-16768
- Al-Zn-Mg alloys low temperature mechanical properties dependence on aging treatment 05 p0767 A71-16769
- Overload and underload effects on Al-Mg-Si creep deformation and damage accumulation under single load change 05 p0768 A71-16800
- Protective oxide formation on single phased Cu-Al-Si alloys during high temperature oxidation 05 p0770 A71-17099
- Al-Mg alloy oxide film morphology and composition under various oxidation conditions, using electron microscopy and diffraction 05 p0770 A71-17100
- Polycrystalline Al alloys inelastic deformation under combined stress at elevated temperatures, observing time dependent behavior 05 p0830 A71-17237
- Construction materials characteristic properties significance for design and structural reliability, discussing weldable Al alloys fatigue strength, internal stresses, inhomogeneity and corrosion behavior 06 p0981 A71-17341
- Buckling of cold formed Al alloy thin walled columns under compression, investigating longitudinal half wave formation 06 p0985 A71-17748
- Duralumin with anodic film, examining fatigue and corrosion-fatigue rupture 06 p0911 A71-17935

- Concorde airframe structures, discussing numerically controlled machining of aluminum alloy integral units 06 p0904 A71-17954
- High strength Al alloys stress corrosion resistance testing in various heat treatment conditions, using precracked cantilever beam specimens 06 p0912 A71-18012
- Sintered Al-Ni-Co alloys, investigating magnetic properties and density after heat treatment 06 p0913 A71-18099
- Graphite fiber reinforced Al-Si alloy composite tensile strength and microstructure, observing tension failure modes 06 p0914 A71-18678
- Spacecraft propellant tank development from Al alloy providing excellent weldability, propellant compatibility and strength to weight ratio 07 p1116 A71-18899
- Al alloy rapidly crystallized film structure, studying atomic diffusion mobility effects on formation of supersaturated solid solutions 07 p1130 A71-19299
- Al cast alloys mechanical properties and sensitivity to stress concentration at low temperatures 07 p1131 A71-19366
- Ni-Mn, Ni-Fe and Ni-Fe-Al alloys yield behavior and microstructure as result of ordering and disordering treatments, using center annealing technique 07 p1132 A71-19434
- Mechanical properties of supersaturated Ni-Al alloys aged at 700 F, discussing composition effects on single crystals deformation and polycrystal strength variation 07 p1133 A71-19442
- Binary Ti-Al and ternary Ti-Al-X alloys precipitation strengthening, investigating structure, mechanical properties and deformation behavior 07 p1133 A71-19444
- Single edge notch tension Al alloy specimens mechanical compliance measurement, solving stress functions for various gage length-sample width combinations 07 p1110 A71-19469
- Cerium effect on phase composition and mechanical properties of Nb-Al alloys, plotting isothermal cross sections 07 p1135 A71-19615
- Oxygen effect on mechanical properties of Ti alloys with V and V-Al content, showing strengthening up to 400 C 07 p1136 A71-19631
- Mechanical properties, crack formation sensitivity, corrosion resistance and stress cracking behavior of Al-Zr-Mg alloys welded joints 07 p1136 A71-19633
- Cryogenic tanks manufacture from Al alloys 07 p1118 A71-19801
- Structural materials criteria for cryogenic propellant tanks, discussing chosen alloy composition, heat treatment and general properties 07 p1118 A71-19802
- Mechanical properties at different temperatures and allowable design stress for aluminum alloy 07 p1137 A71-19966
- Fatigue strength of butt, lap and tee welded joints in aluminum alloys under axial stress and repeated bending loads 07 p1119 A71-19971
- Residual stress effects on Al alloys stress corrosion crack growth rates as function of plane strain stress intensity, discussing residual stress elimination methods 07 p1137 A71-19974
- Wrought high strength Al alloy nonequilibrium second phase particles formation effect on mechanical behavior during solidification 07 p1137 A71-19978
- Metastable Al-rich Al-Fe solid solutions decomposition during isothermal and isochronal annealing, from X ray diffraction patterns 07 p1137 A71-19979
- Ternary Al-B-Ti system, investigating Al corner and B effect on grain refinement 07 p1138 A71-19981
- Al alloys thermal fatigue resistance measurement using testing apparatus involving HF induction heating 07 p1142 A71-20325
- Precracked double cantilever beam specimens, measuring resistance to stress corrosion crack propagation as function of overaging in Al alloys 07 p1142 A71-20363
- Creep strain effect on cyclic fatigue life of duralumin at room temperature 07 p1143 A71-20486
- Al-Li alloy precipitation hardening after neutron irradiation, noting yield stress increase after aging at various temperatures 07 p1143 A71-20487
- Additive elements and heat treatment effects on Al-Zn-Mg alloy fracture characteristics, using tensile and stress corrosion tests 07 p1143 A71-20488

Liquid Al binary systems thermodynamic properties, using emf, improved dew point and distribution methods 07 p1143 A71-20489

Neutron irradiation effects on Al-Mg alloys tensile properties, noting yield stress increase and appearance of Luders strain 07 p1143 A71-20492

Al-Si and Al-Sn bearing alloys corrosion resistance to lubricating oils, investigating thrust load, operating time and oxidation factor effects 08 p1304 A71-20996

Recrystallized and overrecrystallized Al alloys, investigating factors controlling anisotropy of mechanical properties 08 p1305 A71-21033

Al-Be-Mg alloys under solution treatment, noting aging and prolonged heating effects on mechanical properties from solid solution decomposition diagram 08 p1305 A71-21034

Aluminum alloy deformations and rupture strength under complex stress at low temperatures, observing anisotropy decrease with temperature 08 p1306 A71-21117

Binding energies between solute atoms and vacancies in dilute Al alloys measured by quantitative transmission electron microscopy 08 p1310 A71-21530

Loop patterns of secondary defect structures in quenched Al based alloys interpreted in terms of internal stress and stacking fault energy 08 p1310 A71-21531

Anomalous dynamic strain aging in supersaturated Al-Cu, Al-Mg and Al-Zn alloy sheet and wire, discussing activation energies and volumes for plastic flow 08 p1310 A71-21534

Dilute Al alloys single crystals amplitude dependent internal frictions measurement, obtaining binding energies between substitutional alloying atoms and dislocations 08 p1310 A71-21535

Al-Cu precipitation hardened alloys, determining microstructure effects on fatigue life and flow stress 08 p1312 A71-21547

Aged Al alloys dislocation substructure effect on mechanical properties at elevated temperatures 08 p1313 A71-21559

Stoichiometric beta NiAl alloy high temperature creep behavior, presenting electron microscopic observations of deformed single crystals dislocation structures 08 p1314 A71-21571

Bubble raft model for atomic configurations in ordered grain boundary and grain boundary dislocation at high temperatures, discussing Al-Mg alloys 08 p1345 A71-21575

Grain boundary sliding and shear deformation in bicrystal Al and Al-Co solid solutions 08 p1345 A71-21576

Ball forming technique application to Al alloys structural part contouring, discussing L-1011 wing panel forming and prestress tooling 08 p1299 A71-21681

Complex Al brazing alloy for honeycomb core joining to Ti alloy face sheets, discussing fillet formation and strength optimization 08 p1299 A71-21686

Al and Mg alloys mechanical properties anisotropy as function of loading conditions, taking into account stress condition effect 09 p1467 A71-22315

Mechanical characteristics of extruded thermally hardened aluminum alloys determined by eddy current method 09 p1468 A71-22326

Al-Mg alloy oxidation, observing Be, B, Mo and Zr addition effects 09 p1468 A71-22656

Underfilm in high humidity environments corrosion of Al alloys coated with paint films, using pH indicating dyes [NACE PAPER 19] 09 p1469 A71-22888

Al alloys HF accelerated fatigue testing, using magnetostrictive transducer excited mechanical resonance and electronic circuitry 09 p1428 A71-22939

Al-Zn-Mg alloys stress corrosion, using electron transmission microscopy for microstructural investigation 09 p1472 A71-23125

Annealed Al-Mg alloys mechanical measurement, noting low temperature tensile strength and yield point variations with specimen composition and temperature 09 p1473 A71-23230

Al-Co alloys, investigating Al and Co intermediate phases formation effect on X ray emission K spectra 09 p1474 A71-23234

Ni-Al alloy strain hardening, observing high intensity ultrasonic irradiation effect on high temperature creep 09 p1475 A71-23315

Prediction of metals heat resistance increase by thermomechanical treatment, considering Ni-Al alloy 09 p1477 A71-23332

Al-Mg alloy positional welding for porosity elimination 09 p1457 A71-23356

Stress corrosion failure prevention in susceptible Al alloys, considering metallurgical structure, environment and stress distribution 09 p1478 A71-23417

Corrosion resistance of adhesive bonded airframe structure components under outdoor weather and salt spray conditions, discussing test results with Al alloy specimens 09 p1459 A71-23690

Precision forging and pressing of Al alloy and Ti alloy parts of aircraft structures at cost effective prices 09 p1459 A71-23691

Thermal, microstructural and X ray analyses of Al-Ti alloys phase diagrams, measuring hardness and conductivity 09 p1480 A71-23704

Buckling coefficient of Al alloy columns with different section profiles, using steel structures stability specifications 10 p1623 A71-23768

Comparative isothermal oxidation of Fe-Cr-Al, Ni-Cr-Al and Co-Cr-Al alloys with protective scales 10 p1624 A71-23971

Metal-metal bonded structures corrosion resistance improvement by use of primers or Al alloy honeycomb core 10 p1626 A71-24110

Low temperature plasticity of Al alloy thin walled tubular specimens under axial tension and internal pressure 10 p1626 A71-24193

Oxidation resistant high temperature Ni-Al system preparation using powder metallurgy and thermomechanical treatments without sintering 10 p1626 A71-24401

Ni-Cr-Ti-Al-Mo system equilibrium conditions, conducting phase analysis by X ray and optical and electron microscopy 10 p1627 A71-24532

Al alloys microstructure and mechanical properties after rapid solidification, considering rapid quenching techniques and resulting metastable variations 10 p1627 A71-24596

Al alloys one step fatigue tests under combined high temperature and structural vibration conditions 10 p1628 A71-24821

Cold and hot working effects on Al alloys elastic properties, discussing crystallographic systems reference points 10 p1628 A71-24822

Al-Cu alloys recrystallization and age hardening irregularities, discussing inhomogeneous and anisotropic effects on ideal characteristics 10 p1628 A71-24823

Rapid melt quenching in Al alloys metastably extended supersaturated solid solutions, discussing strengthening mechanisms, high temperature decomposition and powder metallurgy utilization 10 p1628 A71-25027

Stress-strain curve and single crystal dislocation structure of Al alloys with coherent precipitates, noting screw dislocations predominance 10 p1628 A71-25033

Liquid and solid phase relations in Be-Al-Ti system by chemical, thermal, microscopic and X ray investigation, discussing solubility range of ternary phase and intermetallic compounds 10 p1629 A71-25034

Al alloy and carbon steel low cycle fatigue and fracture surface topography transition from static dimple to striation type by electron fractography 11 p1777 A71-25266

Minimum strength of groove and fillet welded joints in heat treated Al alloy tubular members 11 p1769 A71-25745

Al-Zn-Mg-Cu alloys, investigating minor elements Cr, Mn and Zr effects on quench sensitivity 11 p1780 A71-26018

Cr and Zr additives influence on Al-Zn-Mg-Cu alloys quench sensitivity, discussing mechanical properties and electron microscopic investigation of microstructural characteristics 11 p1780 A71-26021

Mg-Al eutectic alloy and commercial-purity Zr stress relaxation tests and mechanical behavior 11 p1780 A71-26022

Ordered Ti-Al lattice parameters measurement in low and high temperature diffractometer attachment 11 p1780 A71-26023

Strain rate and temperature effects on flow stress of Ni-Al in polycrystalline and single crystal for activation energies and deformation volumes evaluation 11 p1782 A71-26440

Al alloys and steel, determining potential and pH changes during stress corrosion crack propagation by microelectrode technique 11 p1783 A71-26497

Al-Ni alloys rapidly quenched from melt, determining solid solutions mechanical and microstructural properties 12 p1916 A71-26893

Al and Al-Mg alloys average interdislocation internal stress measurement during steady state creep 12 p1916 A71-26895

Al alloys endurance limit determination by accelerated methods, evaluating errors by comparison with conventional tests 12 p1916 A71-26944

Nb and Mo doped Ni-Al alloy with Ni-Nb additions, obtaining diagrams of composition versus heat resistance in high temperature bending tests 12 p1916 A71-26968

Thin film compound Au-Al intermetallic structure of CsCl type with lattice period of 3.140 plus or minus 0.003 Å from electronographic measurement 12 p1917 A71-27308

Fractographic analysis of failure kinetics and crack formation in Al alloys, showing microfatigue intrusions and extrusions for various initial stress levels 12 p1919 A71-27682

Crack extension criterion for time dependent spallation, correlating simple mechanistic model with Al alloys data 12 p1919 A71-27774

Artificial corrosion pits effect on fatigue durability of smooth samples and aircraft duraluminum skin elements 13 p1995 A71-27819

Thermal emf measurement of Ti alloy, steel, bronze and duraluminum subjected to fretting corrosion tests 13 p2082 A71-27820

Fatigue corrosion resistance of duraluminum anodized at various temperatures 13 p2082 A71-27823

Fatigue crack growth rate in plates of anisotropic materials, considering Al and Ti alloys under cyclic loads 13 p2082 A71-27826

Mechanical properties of Ti-Al-Cr and Ti-Al-Cr-Mo alloys annealed below solidus temperatures 13 p2083 A71-27873

Chemical composition effects on microstructure and high temperature properties of cast Cr-Ni-Al steels containing Ti, B, Ce and Zr 13 p2084 A71-28035

Polycrystalline pure Al and Al-Mg alloy strength, investigating temperature and strain rate effects 13 p2084 A71-28112

Refractory and structural steels and Al alloys, obtaining low cyclic plastic deformation and breaking stress curves 13 p2148 A71-28116

High strength Al alloy forgings processing for stress corrosion cracking prevention, including plane relocation and compressive relief techniques 13 p2073 A71-28146

Al-Zn-Mg alloy plates welded with Al-Mg filler metals, observing ghost defects in radiographs 13 p2074 A71-28524

Al alloy matrix-graphite fiber reinforcement composites, discussing strength, temperature properties and processing techniques 13 p2092 A71-28660

High-strength low-cost moderate-conductivity cobalt modified aluminum brass for electrical contacts, terminals and relay springs 13 p2086 A71-28836

DC straight polarity gas tungsten aluminum alloys 13 p2076 A71-29090

Al-Zn-Mg alloys, considering Cu and Cr additions effects on nucleation and incoherent precipitates formation 13 p2088 A71-29406

Quantitative description of solidification structures of Al-Cu, Al-Cu-Ti, Al-Si, Al-Mg and Al-Si-Cu, discussing dendritization index, cooling rate and tensile strength 14 p2257 A71-29842

Discontinuous phase decomposition increase in Co-Ni-Ti alloys by plastic deformation and Al additions, indicating grain boundary diffusion control 14 p2258 A71-30003

X ray interference lines widening in Al-Mo alloy foil obtained from melt by rapid cooling attributed to stress relieving 14 p2258 A71-30008

Notched age hardening Al alloys sheets, obtaining fatigue damage test data and S-N curves 14 p2326 A71-30067

Tenzaloy Al mirrors for IR astronomy, discussing results of Hartmann tests for optical stability 14 p2241 A71-30144

Al-Li alloys precipitation characteristics and time-temperature-transformation curves after solution treatment, water quenching and aging 14 p2259 A71-30393

Vibration fatigue of metallic materials in vacuum and different gas atmospheres, considering fcc metals, Al alloys and steels [DFVLR-SONDERR-62] 14 p2259 A71-30466

ALUMINUM ALLOYS

Al-Mg-Si alloy development with low quenching sensitivity and high tensile strength 14 p2259 A71-30471

Stable eta phase precipitation at dislocations in Al-Zn alloy, using X ray diffraction and electron microscopy 14 p2260 A71-30477

Metal particle agglomeration during burning of Al-Mg alloy in ballistc powder, using high speed burning track microphotography 14 p2260 A71-30619

Particle size effect on self ignition temperature of powdered Al-Mg alloys 14 p2285 A71-30621

Ti-Al-V alloy forgings fatigue strength improvements, discussing surface finish, heat treatments and alpha and beta grain size [AHS PREPRINT 553] 14 p2261 A71-31105

Al-base alloys grains dimension and shape effects on extruded semifinished product mechanical properties and structural stability 15 p2424 A71-31242

Al-Zn-Mg-Li solid solutions isothermal phase diagrams, obtaining Al-rich alloys phase compositions for quenching and aging temperatures 15 p2426 A71-31405

Medium strength corrosion resistant weldable Al-Mg alloy for aircraft jettisonable tanks, napalm containers and jet shroud pipes fabrication 15 p2426 A71-31437

High temperature creep in Al-Zn solid solution, using isothermal tests 15 p2429 A71-31997

Al and Cu-Al alloys eutectic composites with small interlamellar spacing, characterizing ambient temperature compressive stress strain behavior to failure 15 p2432 A71-32168

Explosive and isostatic forming effects on commercial precipitation-hardenable Al-Cu alloy microstructure, tensile properties and fatigue life 15 p2433 A71-32180

Grain refinement in dilute Al alloys, comparing peritectic reaction effect for Ti, Zr and Cr as alloying components 15 p2433 A71-32181

Guinier-Preston zone size and volume fraction effects on polycrystalline Al-Zn alloys yield strength, discussing precipitation strengthening and thermally activated plastic flow 15 p2433 A71-32182

Monograph on ductile fracture covering electron microscopy of fracture surfaces and microstructures of Al alloys 15 p2434 A71-32301

Soviet papers on physical metallurgy of light metal alloys covering high strength, grain size effect, heat treatment, structural dependent properties and melt refining 15 p2434 A71-32326

Al alloys high temperature thermomechanical treatment, discussing mechanical properties, enhanced plasticity and roughness 15 p2434 A71-32327

Grain size effect on corrosion resistance and mechanical properties of Al alloy sheets between final annealing and quenching 15 p2434 A71-32329

Structural inhomogeneity effect on fatigue strength of Al alloys, considering microstructure qualitative estimation on basis of microplastic deformation 15 p2434 A71-32330

Transition metals classification according to effect on structure and physical properties of deformable Al alloys 15 p2434 A71-32331

Fine structure variations of Al alloy after aging, using harmonic analysis for calculating matrix microdeformation for correlation with mechanical properties 15 p2435 A71-32332

Strength, plastic properties, electrical conductivity and fine structure associated with decomposition kinetics of Al alloy supersaturated solid solution 15 p2435 A71-32333

Hydrogen absorption by molten aluminum and Al alloys, considering equilibrium delay in metal-gas system 15 p2435 A71-32334

Al alloys rods and sections extrusion process R and D, using lubricant without press residue 15 p2415 A71-32335

Al alloy spot welding, investigating defects effects on welded joint fatigue strength under dynamic tests by metallographic and X ray examinations 15 p2436 A71-32467

Grade 15 steel vacuum diffusion welding to AMts alloy or AD1 aluminum, using nickel interlayer in joints 15 p2418 A71-32667

Ternary Co-Cr-Al alloy oxidation data, detailing kinetics, products, mechanisms, resistance behavior and rate 16 p2589 A71-32870

Scale factor effect on brittle fracture strength for Ti and Al alloys and high strength steels 16 p2657 A71-33409

Oxygen effect on mechanical properties of Ti alloys with V and V-Al content, showing strengthening up to 400 C 16 p2593 A71-33627

Mechanical properties, crack formation sensitivity, corrosion resistance and stress cracking behavior of Al-Zr-Mg alloys welded joints after prolonged heating 16 p2593 A71-33629

Preliminary corrosion effect on fatigue strength of Al joints, noting insufficient anticorrosive anodic film and additional protection by paint and varnish 16 p2584 A71-33688

Flexural-torsional fatigue fracture of duraluminum, noting dependence on cyclic stress, frequency and medium 16 p2593 A71-33689

Deformable thermally work hardenable Al-Mg-Li alloy, detailing phase composition changes during aging 16 p2594 A71-33711

Al-Mg alloy with Ti, Zr, Mo and B additions under tensile and impact loads, investigating mechanical properties, strength and crack formation 16 p2594 A71-33712

Recrystallized and unrecrystallized deformed semifinished Al base alloy under cyclic and static loads, investigating macrofracture kinetics 16 p2594 A71-33713

Airframe structural uses of Al, Ti and Be alloys, discussing need for structural efficiency improvements by proper heat treatment and stress relieving techniques 16 p2594 A71-33875

Al-Cu-Li-Mn and magnesium/rare-earth-element alloys heat resistance and microhardness, determining strengthening by intermetallics 16 p2597 A71-33926

Neuber elastoplastic analysis of residual notch stresses for improved cumulative damage predictions applied to aluminum alloy under overload [AIAA PAPER 71-776] 16 p2659 A71-34012

Production efficiency prerequisites in extruded Al alloy products manufacture, discussing billet material and processing conditions effects 16 p2584 A71-34091

Storing and plastic deformation effects on artificial aging of Al-Zn-Mg alloy, using thin foil electron microscopy and hardness measurements 17 p2755 A71-34417

Solution chemistry at stress corrosion crack tips in Al alloys, considering factors affecting pH change with time of initially acidic NaCl solutions 17 p2755 A71-34439

Heat treatment effect on fracture behavior of aged Al alloy sheet, investigating toughness dependence on microstructure 17 p2756 A71-34486

Secondary damage in corrosion fatigue of Al alloy tested to failure 17 p2757 A71-34497

Al-Mg-Si alloy vibration creep endurance under single step loading, emphasizing strain and defect accumulation 17 p2757 A71-34593

Limited fatigue strength tests for Al-Mg-Si alloy stress amplitude coefficients under continuous loading, defects, strains and creep accumulation 17 p2757 A71-34596

Electroslag welding of large pressed Al-Mg alloys sections, using electrodes to reduce weld grain size and obtain high mechanical properties 17 p2748 A71-34807

Tension test for filamentary composites, employing hardened Al alloy wedges adhesive bonded to gripping edges 17 p2739 A71-34818

Wrought precipitation hardened Co-base alloy, investigating Ti and Al additives effects on tensile and stress rupture strengths, microstructure and fabricability 17 p2758 A71-35147

Thickness effect on fracture toughness and crack propagation of Al alloy sheets used for aircraft skins 17 p2758 A71-35153

Fatigue crack propagation in Al alloy panels stiffened with bolted and integral stringers, determining stress intensity factor/crack growth rate relationship 17 p2827 A71-35156

Al alloy sheet fatigue crack closure under cyclic tensile loading, deriving expression for crack propagation rate in terms of effective stress amplitude 17 p2828 A71-35162

Hall coefficient and electrical resistivity increase during aging of Al-Zn alloys, suggesting free electron energy reduction due to solute atoms clustering 17 p2759 A71-35227

Al and Mg alloys mechanical and crystal microstructural changes under low temperature conditions, optimizing casting component ratios 17 p2760 A71-35464

Fatigue cracks in tempered and aged Al alloy, using scanning electron microscopy 17 p2760 A71-35474

Environment and frequency effects on fatigue properties of age hardening Al-Cu-Mg alloy 18 p2933 A71-35876

Notch effect on metallographic characteristics of fatigue crack initiation and propagation in Al-Mg alloy 18 p2933 A71-35877

Dezincification of Al-Zn alloys, creating loops and dislocations due to vacancies from Zn evaporation 18 p2935 A71-36199

Salt bath application to steels and Al alloys heat treatment, discussing carburizing, neutral hardening, austempering, martempering, annealing and brazing 18 p2927 A71-36665

Prealloyed Al powder liquid phase sintering without precompacting, discussing oxidation and density control 18 p2928 A71-36667

High strength Al alloys in structural design, taking into account fracture toughness 18 p2937 A71-36849

Aluminum bronze alloy forming dies fabrication and repair, discussing surfacing, hot working grinding, machining and welding methods 18 p2928 A71-36855

Aluminum alloy gas tungsten arc welds, determining defect size and distribution effects on fracture strength 18 p2929 A71-36857

Single crystal Ni-Al solid solutions deformations, examining temperature and concentration dependence of critical cleavage stresses 19 p3076 A71-37120

Phase equilibria of Al-Mg-Li-Mn system in Al-rich region, noting composition effects on mechanical properties 19 p3078 A71-37470

Vertical phase diagrams of Ti-Al-Zr-Mo-Fe alloy system at varying Fe concentrations, showing structural hardening after quenching 19 p3078 A71-37471

Isothermal phase diagrams and composition effects on plasticity in Mo-Ti-Zr-C system in Al-rich region 19 p3078 A71-37472

Al-Cu-Mg monovariant alloys directional solidification, considering criterion for plane front growth breakdown based on constitutional supercooling 19 p3078 A71-37701

Iron precipitation rate from supersaturated Al alloy solid solution in structures with low and high dislocation densities 19 p3079 A71-37702

Stainless steel and Al alloy creep rupture life apparent reduction by frequent beam leveling 19 p3082 A71-38135

Al-Zn-Mg alloy welded joints under repeated static loads, determining shape, filler wire composition and aging effects on fatigue strength 19 p3083 A71-38425

Dynamic tear fracture toughness test and fracture mechanics parameter correlation for high strength Al alloys 20 p3248 A71-38771

Formation and interdependence of quenched induced defect structure in Al-Zn, discussing nucleated loops and screw dislocation developed helical dislocations 20 p3249 A71-39001

Al alloy tensile tests at high temperature and constant elongation and loading rates, noting creep strain 20 p3251 A71-39167

Tensile properties and notch toughness of Al alloys at low temperature, considering fracture toughness and weld strength 20 p3251 A71-39266

Aging conditions effect on stress corrosion resistance in short transverse direction of thick sheet Al alloy, using immersion-emersion tests in air and saline solution 20 p3252 A71-39417

Maximum yielding tensile stress envelope curves as function of structural load index based on compression tests of Al alloy stiffened plane panels 20 p3309 A71-39570

Morphological change of spherical G.P. zones and solute diffusion coefficient in binary Al-Zn alloy during dissolution, using X ray small angle scattering 21 p3395 A71-40022

Hot extrusion properties of free machining Al alloys with low melting point Pb as chip breakers 21 p3384 A71-40026

Eutectic Al alloys parallel alignment formation by stable isothermal boundary surface, investigating microstructure 21 p3396 A71-40029

Fe-Al alloy fine lamellar microstructure from light microscopy and X ray examination 21 p3396 A71-40032

Epitaxial metal film formation on Al-Ni fibers in Al matrix during electropolishing 21 p3387 A71-40456

Thermodynamic activities of Ti and Al in bcc beta phase of Ti-Al system 21 p3398 A71-40465

Aluminum-aluminum nickelide rod eutectic composite elevated temperature stability, presenting coarsening kinetic analysis 21 p3398 A71-40469

Orientation dependent microhardness and columnar and feather crystal structures of directionally cast Al alloys in tensile test bars 21 p3399 A71-40471

Carbon fiber/metal matrix composites fabrication by electrodeposition, discussing aluminum warp sheet lamination and filament wound techniques 21 p3387 A71-40599

Tensile strain response for spallation fracture in metals by impact and electron beam heating of Al, Cu and Ti alloys 21 p3466 A71-40798

Strain rate and temperature effects on polycrystalline Al-Mg alloy strength, considering deformation mechanism 21 p3400 A71-40834

Cryogenic steels, Al and Ti alloys plane strain fracture toughness at room and subzero temperatures, discussing tensile and notch bend results 21 p3401 A71-40915

High strength Al alloys at cryogenic temperatures, presenting plane strain fracture toughness tests results 21 p3401 A71-40916

Specimen design effects on Al and Ti alloy plane strain fracture toughness at room and cryogenic temperatures, discussing crack propagation and rolling directions orientations 21 p3401 A71-40917

Ti-Al-Sn and Al alloys thin sectioned specimens cryogenic fracture strength, discussing surface crack fracture behavior 21 p3401 A71-40918

Low carbon austenitic Cr-Mn steels, noting Ni and Al combined alloying effects on structure and mechanical properties 21 p3403 A71-41101

Preheating effects on crystal lattice orientation, tensile strength and stress corrosion cracking of Al-Zn-Mg alloy thick plates 22 p3559 A71-41516

Duralumin rods deformation and stress propagation study under dynamic pulse loads, using photosensitive epoxy coatings and high speed photography 22 p3537 A71-41612

Weldable Al-Zn-Mg alloys with cathodic polarization protection, noting decrease in stress corrosion crack propagation rate 22 p3560 A71-41625

Stress corrosion testing of Al alloy in NaCl bath under tensile stress, using Weibull distributions 22 p3560 A71-41627

Al alloys tensile deformation and fracture characteristics relation to stress-strain diagrams, discussing strain hardening indices 22 p3560 A71-41642

Thick Al alloy sheet with central slot under cyclic loads, examining striation spacings and fatigue crack propagation rates with electron fractography 22 p3561 A71-41708

AlCu alloy cellular dendritic substructure segregation observation by electron microprobes 23 p3689 A71-42931

Al-Co and Al-Ni alloy rods unidirectionally solidified, discussing compositional range in eutectic structures at high solidification rates 23 p3689 A71-43101

Flash X ray technique for imaging of cavities formation during electron beam welding of Al alloy 23 p3681 A71-43195

Weakly diffracted beam observation of small quenching vacancy loops and Guinier-Preston precipitate zones in Al and Al-Cu, using transmission electron microscopy 23 p3691 A71-43359

Explosive peeling effects on weld fatigue in Ni maraging steel, Fortweld and Al-Zn-Mg alloy 23 p3682 A71-43877

Al-Zn solid solution mean effective and internal stresses and activation area during high temperature creep 23 p3691 A71-43900

Duralumin fatigue process in air and corrosive medium, showing loading frequency and time dependence effects 23 p3692 A71-44027

Heat treatment effect on tensile and bending fatigue strength of Al alloy thin sheet 23 p3693 A71-44217

Hydrogen solubility in alpha phase Ti-Al alloys, using resistometric technique and electron microscopy 23 p3694 A71-44282

Mechanical properties of Al-aluminum intermetallic eutectic alloys after rapid solidification in semicontinuous casting technique, noting flow stress and tensile strength increase 23 p3695 A71-44286

High cycle fatigue resistance improvement of age hardened Al-Zn-Mg-Cu alloys through thermomechanical treatments 23 p3695 A71-44290

Fatigue lifetime of overlapping joint spot welds of Al alloys, investigating shrinkage crack initiation and propagation 24 p3830 A71-44786

Prestraining effect on D16 duraluminum corrosion fatigue and tensile strengths 24 p3838 A71-44856

Statistical analysis of spot welded and adhesive joints of high strength Al alloy sheet in aircraft structures 24 p3831 A71-45012

Free surface equilibrium segregation in solid solutions of Cu-Al alloys single crystals by Auger electron spectroscopy and low energy electron diffraction 24 p3839 A71-45123

Surface segregation, adhesion and friction of monocrystalline Cu-Al, Cu-Sn and Fe-Al alloys from Auger emission spectroscopy and low energy electron diffraction experiments [ASLE PREPRINT 71LC-5] 24 p3839 A71-45287

Liquid Mg-Al alloys thermodynamic properties determination by electrochemical and barometric methods 24 p3840 A71-45372

Hardened cast Al alloys with Cu additions, investigating correlation between mechanical properties and structure at room temperature 24 p3840 A71-45377

ALUMINUM CHLORIDES

Porous glass hyperfiltration membranes stabilization by aluminum chloride solution, noting retreatment need 13 p2026 A71-29377

ALUMINUM COATINGS

Vapor phase aluminization in Ar atmosphere furnace, discussing physicochemical aspects, thermal cycles and deposition kinetics 01 p0099 A71-10267

Al based protective coatings on Nb and Nb alloys considering structure, formation and aluminide component 02 p0271 A71-12941

Ni aluminoboronizing process by circulation method, discussing thermodynamic analysis for saturation possibility and parameters experimental determination 03 p0432 A71-13961

Aluminum high temperature resistant diffusion type coatings structure and chemical composition, outlining turbine blades testing for thermal shock, oxidation and sulfur and sea salt corrosion 09 p1474 A71-23287

Refractory metals and alloys products fabrication for aerospace applications, discussing hydrostatic bulge forming and aluminide coating in Nb alloy nozzle extension production 10 p1618 A71-24766

Al coating of Nb and Nb alloys by pack cementation, discussing coating structural states, heating cycle temperatures and growth kinetics 11 p1781 A71-26295

Nb and Nb alloys coating by hot-dipping in molten Al, investigating critical temperature and growth kinetics 13 p2087 A71-29121

Burn time and acceleration effects on molten metallic material chemical composition near burning surface of aluminized composite solid propellant 19 p3121 A71-38298

Microhardness, thermo-emf and phase composition of Al coatings on Armco iron and steel under furnace and rapid electric heating 21 p3389 A71-41096

Aluminized layer phase and chemical composition of heat resistant iron and nickel alloys 24 p3837 A71-44732

ALUMINUM COMPOUNDS

NT ALUMINATES
NT ALUMINUM CHLORIDES
NT ALUMINUM HYDRIDES
NT ALUMINUM NITRIDES
NT ALUMINUM OXIDES
NT ALUMINUM SILICATES
NT ANDESITE
NT CRYOLITE
NT FELDSPARS
NT KAOLINITE
NT MONTMORILLONITE
NT MUSCOVITE
NT PYROPHYLLITE
NT SAPPHIRE

P-type aluminum gallium arsenide phosphide growth on gallium arsenide phosphide from solution, noting lattice match preservation and heterostructure junction devices 04 p0608 A71-15041

Superconducting niobium aluminide and niobium aluminide-Ge films formation on Nb substrate 05 p0792 A71-16238

Multilayer liquid phase epitaxy heterostructures growth with crystalline solid solutions of aluminum gallium arsenide for injection lasers 09 p1464 A71-23122

Cu-Ti-Al system intermediate phase glasses crystallization from melt in large concentration areas, discussing four-phase reactions 10 p1627 A71-24597

Nickel diffusion in intermetallic compound NiAl as function of temperature and off-stoichiometric composition, noting activation energy changes 11 p1778 A71-25562

P-type Al-Ga-As-p-type Ga-As-n-type Ga-As single heterostructure preparation and properties, discussing effect on injection laser diode characteristics 12 p1914 A71-27027

Temperature dependence of ionization rates in aluminum gallium arsenides for samples with varying Al contents 19 p3117 A71-37486

Low pressure trimethylaluminum vapor and oxygen flat diffusion flame structure, observing separation, formation and growth 19 p3121 A71-38299

Boridosilicide and boridoaluminide diffusion coatings on iron and steel, investigating formation kinetics structure and properties 21 p3390 A71-41171

Room temperature GaAlAs close confinement (single heterojunction) laser diode performance and applications 23 p3684 A71-43503

ALUMINUM HYDRIDES

Lithium tetrafluoro-aluminate equilibrium vapor pressure over solid aluminum fluoride plus solid lithium cryolite examined by weight-loss effusion method 07 p1055 A71-19624

ALUMINUM ISOTOPES

NT ALUMINUM 26
NT ALUMINUM 27
Stress annealing effects on Al 27 NMR lineshapes in pure Al powders fixed and stored at room temperature, considering residual stress 17 p2759 A71-35225

ALUMINUM NITRIDES

Liquid drop role in aluminum nitride whisker growth by aluminum oxide reduction in nitrogen or by direct nitriding 05 p0768 A71-16820

Boron nitride and aluminum nitride particles behavior in Mo matrix, considering solid metallic phase formation 09 p1470 A71-23067

AlN insulating films electrical characteristics for use in charge storage devices, presenting Al-AlN-Au capacitor current-voltage-insulator thickness relationships 09 p1509 A71-23118

Aluminum nitride crystals production by sublimation in resistance furnace with graphite heater 22 p3585 A71-41701

ALUMINUM OXIDES

NT SAPPHIRE
Pressure-bonded trilayer insulator stress analysis, using computer model for explaining alumina component fracturing during fabrication 02 p0256 A71-12249

Breakdown voltage measurement for Cs vapor in cracks in Alumina insulator of pressure bonded sheath tube assemblies 02 p0232 A71-12252

Trilayer niobium-alumina-niobium sheath insulator thermal stability test under electrical load 02 p0232 A71-12253

Ceramic particle compaction as function of size, shape, loading rate and hardness for fused alumina, magnesia and mullite 03 p0448 A71-12973

Whisker growth by vapor phase reactions, detailing thermodynamics, kinetics and supersaturation in aluminum oxide whisker formation 04 p0635 A71-14942

EPR spectrum of tetravalent vanadium ions in gamma irradiated corundum at liquid He temperatures, showing equidistant lines width temperature dependence 04 p0637 A71-15105

Optical properties of corundum for single and multiple layer antireflection achromatic coatings for IR below 5-6 microns 06 p0898 A71-17537

Permanent IR electron radiation effects on hardened MOS integrated inverter circuits, using units with plasma grown and vapor deposited aluminum oxide 07 p1174 A71-19053

X irradiation induced currents across aluminum oxide films sandwiched between thin metal electrodes as function of voltage and time 07 p1174 A71-19056

Mechanical and interface reaction properties of alumina reinforced Ti-Al-V alloy composites fabricated by vacuum diffusion bonding 07 p1137 A71-19965

Fracture toughness of aluminum oxide composite containing ductile Mo fibers 08 p1304 A71-20700

Dispersed alumina inclusions strengthening effect during nichrome alloy sintering 08 p1305 A71-21060

Matrix stacking fault energy effects on steady state creep rate of recrystallized nickel-cobalt-aluminum oxide alloys, showing stress dependence 08 p1315 A71-21578

Artificially grown corundum homogeneous single crystals structure relationship to thermodynamic and kinetic growth conditions 09 p1481 A71-22164

Molten alumina and chromia reactions with refractory metals, calculating isobaric-isothermal potential variations 09 p1466 A71-22165

Pyrolytic aluminum oxide thin films on Si substrate by thermodecomposition, measuring vapor deposition parameters and Si surface preparation effects on dielectric and interface properties 09 p1509 A71-23117

Brittle alumina ceramic tensile and flexural strengths comparison based on statistical surface flaw distribution theory of fracture 09 p1484 A71-23699

Heat resistance, thermal stability, thermal conductivity coefficient and specific heat measured in cylindrical hollow specimens of corundum materials 10 p1634 A71-24200

Alumina trichite reinforcement of nickel base matrix using magnetic alignment and sintering under low pressure below melting point [ONERA-TP-911] 11 p1777 A71-25238

Alumina and titania codeposition from acid copper electrolyte as function of oxide crystalline form, discussing addition agents effects 11 p1779 A71-26011

Total normal emittance under simulated reentry conditions, using emissometer with aluminum oxide reference cavity integral within sample [AIAA PAPER 71-468] 11 p1764 A71-26249

Vanadium oxide thin vapor transport films on single crystal aluminum oxide, using RF sputtering of powdered targets 11 p1809 A71-26397

Magnesia rich magnesium aluminum oxide spinel ceramics, discussing sintering, grain growth inhibition and strength increase 13 p2092 A71-28662

Plastic deformation of aluminum oxide by indentation and abrasion at room temperature, using transmission electron microscopy 13 p2093 A71-28989

Chromatographic separation of molybdenum, niobium and tungsten based on metal ions absorption by aluminum oxide 15 p2367 A71-31647

Single crystal and polycrystalline alumina specimens strengthening by annealing with various metal oxide powders 15 p2438 A71-31975

Compressive creep of aluminum oxide single crystals deformed by dislocation glide and rhombohedral twinning, investigating activation energy and rate controlling mechanism 15 p2439 A71-32439

Crack propagation in brittle solids under constant deformation or thermal shock, verifying behavior by results with polycrystalline aluminum oxides 16 p2590 A71-32941

Laser drilled holes in alumina substrates, studying structure by scanning electron microscopy and X ray diffraction patterns analysis 17 p2763 A71-35738

Thermospheric density determination from ESRO rocket flight produced artificial fluorescent AlO clouds 18 p2914 A71-37060

Ionospheric wind velocity, direction and diffusion coefficient measurements using artificial aluminum oxide luminescent clouds 19 p3091 A71-38629

Trigonal crystal field and spin-orbit interaction matrices for ion energy levels in vanadium corundum in strong g scheme, using symmetry group tensor operators 21 p3427 A71-40075

Quenching effects on glazed and unglazed alumina rods in various media, noting improved flexural and tensile strength, thermal shock resistance and impact resistance 22 p3565 A71-42342

Charge injection in metal-aluminum oxide-silicon dioxide-silicon systems using capacitance voltage technique 22 p3587 A71-42531

Alumina, boron carbide and silicon carbide notched and unnotched impact strength tests, using drop weight technique 22 p3565 A71-42542

Epoxy-alumina trihydrate composite system fracture energy data, noting interdependence of surface

topography, phase dispersion volume fraction, particle size and spacing 23 p3696 A71-43102

ALUMINUM SILICATES

NT ANDESITE
NT KAOLINITE
NT MONTMORILLONITE
NT PYROPHYLLITE

Aluminosilicate separators for silver zinc cells, using compaction and sintering techniques 08 p1235 A71-21096

Nitrogen equilibrium solubility dependence on slag basicity and gas phase nitrogen/carbon monoxide contents in aluminosilicate melts 21 p3399 A71-40470

ALUMINUM 26

Mg 26 isotopic abundance in meteoritic, lunar and terrestrial feldspar by mass spectrometry, suggesting limits on Al 26 in early solar system 06 p0966 A71-17896

ALUMINUM 27

Al 27 for heating working body in heat exchangers of jet engines 06 p0926 A71-18706

ALVEOLAR AIR

Human alveolar-arterial oxygen pressure differences, investigating inert gas effects 04 p0540 A71-15576

Terminal bronchiole diameter changes with volume in isolated air filled lobes of cat lung 07 p1044 A71-20332

Carbohydrate ingestion produced respiratory gas exchange ratio and alveolar ventilation effects on arterial oxygen tension in normal men 07 p1052 A71-20333

Alveolar nitrogen and carbon dioxide tensions changes during compressed air narcosis in constant oxygen partial pressure 08 p1239 A71-20818

Alveolar gas exchanges and cardiovascular functions during breath holding with air, determining resting oxygen consumption 12 p1870 A71-27135

Alveolar air samples of human subjects at various altitudes, determining gas composition and partial pressure 12 p1876 A71-27658

Alveolar and arterial carbon dioxide partial pressure during rebreathing experiments at rest 13 p2007 A71-28435

Pulmonary oxygen toxicity development rate and effects on lung volume and alveolar-arterial gas exchange during oxygen breathing 13 p2024 A71-29501

High altitude pulmonary edema syndrome, investigating increased alveolar-arterial oxygen gradients of humans during treadmill exercise 14 p2184 A71-30279

Alveolar-arterial oxygen pressure gradient derivation as sum of shunt, ventilation/perfusion inequalities and membrane and airway diffusions 15 p2363 A71-31444

Diaphragm mechanics, discussing thoracic pressure-lung volume and air flow relationships of respiratory system during electrophrenic stimulation in men and cats 16 p2530 A71-33239

Alveolar-arterial oxygen pressure difference during controlled hyperventilation and posthyperventilatory phase 19 p3003 A71-38200

Diffusion component of alveolar-arterial oxygen pressure differences in man at rest and during exercise 19 p3009 A71-38556

Variable tidal volume effects on lung test gas washout parameters 19 p3010 A71-38565

Respiratory reflex mechanism of deep breath occurrence after period of airway occlusion in rabbits related to stimulation of vagal receptors 20 p3187 A71-39040

ALVEOLI

Hypertensive heart and pulmonary vascular disease, examining chronic alveolar hypoxia effects 11 p1719 A71-25931

Lung diffusing capacity for oxygen during exercise and alveolar hypoxia measured without blood samples by ear oximeter 13 p2023 A71-29492

Human alveolar wall tissue length-tension characteristics, noting age, sex and expiratory flow relationships 16 p2530 A71-33246

AMALGAMS

U MERCURY AMALGAMS

AMBIENT TEMPERATURE

Physiological effects of heat exchange between human organism and ambient medium by evaporation, radiation, conduction and convection 01 p0028 A71-11597

Human thermoregulatory response to ambient temperature variations, considering deep body and skin temperature interrelations 02 p0202 A71-11667

Rectangular parallelepiped and solid cylinder temperature distributions under time dependent ambient heating or cooling, solving thermal conductivity equation 02 p0333 A71-12647

Rabbit hypothalamic neuron stimulation by changes in ambient temperature 03 p0361 A71-13225

Microwave dual mode reciprocal ferrite phase shifters, deriving insertion phase variations as function of ambient temperature and high average power heating 08 p1262 A71-20760

Temperature analyzer function under ambient temperatures in children 08 p1242 A71-21961

Alternating acceleration and increased ambient temperatures effects on time interval perception and muscular effort estimation 12 p1874 A71-27164

Heat balance of human body submerged in water, determining body temperature reduction as function of ambient temperature 13 p2019 A71-28508

Turbulent gas flame length in motionless air of various ambient temperatures, comparing calculation with measurement 15 p2511 A71-31380

Pilocarpine induced synchronous sweat expulsions, noting frequency linear dependence on ambient temperature with and without generalized sweating 18 p2861 A71-36889

Aerodynamic compensation for ambient medium temperature effect on fluidic standard components and timing devices 19 p2998 A71-37570

Ambient temperature effects on spontaneous rewarming of ground squirrels during awakening after hibernation 22 p3491 A71-42582

AMBIGUITY

Echo location systems theorem concerning ambiguity density relationship to signal bandwidth 14 p2194 A71-30063

AMBIPOLAR DIFFUSION

Ambipolar diffusion coefficients application to analysis of laminar multicomponent ionized boundary layer flow in channel 01 p0070 A71-10795

Partially ionized bounded plasma LF natural oscillations due to ionization processes, ambipolar diffusion and charged particles recombination at walls 02 p0292 A71-12619

Kinetic equations derivation for computer calculation of nonuniform hydrogen plasma decay, considering hydrogen recombination, electron temperature and ambipolar diffusion 03 p0463 A71-13508

Ambipolar diffusion coefficient noting vertical variations 06 p0893 A71-17993

Thermal conditions in asymptotic region of atmospheric pressure Ar arc plasma, considering nonequilibrium ionization due to ambipolar diffusion 10 p1654 A71-24971

Electron-ion recombination and ambipolar diffusion disruption of electron density in cryogenic helium plasma, using cavity resonator measurements 16 p2619 A71-33648

One dimensional ambipolar diffusion parallel to magnetic field lines, considering plasma cloud imbedded in weakly ionized gas with homogeneous field 20 p3215 A71-38737

AMBIT

U FIELD THEORY (PHYSICS)

AMBULANCES

Medical transportation by ambulance, helicopter and fixed wing aircraft, considering vibration damping and acceleration 05 p0715 A71-16932

Patients transportation pathology, discussing accelerations and vibrations in ambulances, helicopters and fixed wing aircraft 06 p0860 A71-18191

Vibration induced paroxysmal and cardiovascular hazards during patients transport to hospital by air or ambulance, discussing therapeutic and preventive treatments 22 p3500 A71-41573

AMIDES

NT ACETAZOLAMIDE
NT POLYIMIDES
NT THIURONIUM
NT UREAS

Embryo chemical sensitization to low radiation doses damage by radiosensitizer iodoacetamide 07 p1037 A71-18963

Cytotoxic and radiosensitizing effect of thiol binding agents iodoacetamide (IAA), N-ethylmaleimide (NEM) and iodoacetic acid (IA) on crypt cells of mice duodenum 07 p1038 A71-18975

Interstellar formamide detection in Sgr direction by microwave emission, showing hyperfine components and rest frequencies 22 p3599 A71-41930

- Chromium and Ni-Cr electrodeposition from amide solvent system, describing water and sulfur ligands effects on plating efficiency 22 p3554 A71-42528
- Ventilatory response to progressively increasing inspired carbon dioxide tensions at ground level and acetazolamide pretreatment before high altitude exposure 23 p3636 A71-44242
- ### AMINES
- NT ANILINE
- NT CATECHOLAMINE
- NT CYSTEAMINE
- NT DIMETHYLHYDRAZINES
- NT FLUOROAMINES
- NT HISTIDINE
- NT HYDROXYLAMINE SULFATE
- NT NITROAMINES
- NT THIURONIUM
- NT TRYPTAMINES
- Hexosamines biosynthesis control mechanism, considering UDP-N-acetylglucosamine function 05 p0706 A71-16217
- Photochemical molecular rearrangement of NN-dimethylphenylethylnylamine into alpha-phenylisobutyronitrile by irradiation at 254 nm 06 p0865 A71-17548
- Radioprotective action of amines and hypoxic agents by blocking oxygen transport to tissues 07 p1032 A71-18931
- DNA modification in *Escherichia coli* exposed to X rays and sensitized by triacetoneamine N-oxyl and oxygen 07 p1033 A71-18939
- Epoxy novolac resin-cured alicyclic anhydride amine-catalyzed ablative polymers molecular structure from computer correlation of analytical data 11 p1789 A71-26033
- Serotonin role in central nervous system activity, stressing sleep/wakefulness cycle regulation 12 p1869 A71-26651
- Mercaptoalkylamine group radiation protection preparations on resistance of rats and mice to lateral acceleration rate 22 p3491 A71-42700
- Aminothiol group radioprotective drugs effect on guinea pigs cardiac function during lateral acceleration 22 p3491 A71-42702
- Sympathomimetic amines effects on central nervous system reflex activity of irradiated and desympathized animals 22 p3492 A71-42708
- Serotonin metabolism of helicopter pilots, showing effects of emotional factors due to flight inexperience 23 p3632 A71-43220
- Brain monoamines localization and metabolism and endocrine function, discussing pituitary secretion and neurotransmitter input 23 p3637 A71-44274
- ### AMINO ACIDS
- NT ASPARTIC ACID
- NT CYSTEINE
- NT GLUTAMIC ACID
- NT GLUTAMINE
- NT GLYCINE
- NT HISTIDINE
- NT METHIONINE
- NT PHENYLALANINE
- NT PYRIDINE NUCLEOTIDES
- NT PYRUVATES
- NT THYROXINE
- NT TRYPTOPHAN
- NT URIDYLIC ACID
- Porphyrins and amino acids chemical bonding under geochemically plausible conditions, considering diagnosis of biogenic compounds and life processes prebiotic chemical evolution 02 p0198 A71-12047
- Synthesized amino esters and ketones with varying distance between functionalities, examining mass spectral fragmentation 02 p0209 A71-12574
- Amino acids synthesis by formaldehyde-ammonia heating and hydrolysis, simulating reactants in weakly reducing atmosphere at volcanic temperatures 03 p0357 A71-13014
- Amino acid synthesis in simulated primitive environments, discussing possible effects of meteoric kinetic energy and lightning-associated shock waves 03 p0358 A71-13015
- Neurochemical factors in auditory stimulation and susceptibility to audiogenic seizures, noting gamma-aminobutyric acid /GABA/ inhibitor 03 p0360 A71-13164
- Gamma-aminobutyric acid /GABA/ penetration through blood-brain barrier for administration in dogs and rats 03 p0362 A71-13236
- Gamma-aminobutyric acid /GABA/ effects on brain serotonin following transaminase inhibitor aminooxyacetic acid administration 03 p0362 A71-13239
- Extraterrestrial abiotic amino acids and hydrocarbons in type II carbonaceous chondrite at Murchison, Australia 03 p0493 A71-14209
- Amino acid content alteration in internal organs in rabbits under HF electromagnetic and ultrasound oscillations 04 p0547 A71-15573
- Decaborane effects on amino acid metabolic patterns of various rat tissues, considering holoenzyme inactivation 05 p0706 A71-16294
- Paper chromatography combination with dinitrophenyl amino acids mass spectrometry for analyzing purine and pyrimidine bases 06 p0865 A71-17574
- Biological radioprotectants in space flights including amino acids, bacterial polysaccharides, hormones and vitamins 06 p0861 A71-18358
- Para-aminopropiophenone and propylene glycol radiation protective effect on hematopoietic stem cells of mice 07 p1036 A71-18959
- Toxicity reduction of aminoethylisothiuronium compounds through n-substitution with amino acids, noting slight decrease in radioprotective effectiveness 07 p1037 A71-18965
- Taurine restorative effect in patients with marked leucopenia induced by radiotherapy 07 p1040 A71-18991
- Amino acid contents of Apollo 11 and 12 fines, discussing laboratory syntheses 07 p1196 A71-19500
- Prenatal exposure to hypoxia, showing prolonged suppression of labeled amino acid incorporation into developing submandibular gland and pancreas in neonatal period 07 p1042 A71-19698
- Murchison meteorite composition analysis, investigating nonprotein amino acids of extraterrestrial origin 07 p1201 A71-20400
- Soil and ground rock amino acids preparation and analysis by desalting method 08 p1251 A71-21891
- Alloisoleucine configuration in blood serum of maple syrup urine disease patients, using gas liquid chromatography 09 p1403 A71-22477
- L-dopa multiinjection timed effects on rat brain norepinephrine metabolites concentrations, observing zero time control rated modifications 09 p1393 A71-22649
- Type III carbonaceous chondrite Murchison meteorite, obtaining amino acids, aliphatic and aromatic hydrocarbons from specimen 09 p1393 A71-22983
- Carbonaceous chondrite and Precambrian chert amino acids detection, using simultaneous optical configuration determination and gas chromatography 09 p1393 A71-22984
- Proteins hydrolysis, investigating temperature effect on reaction, determining optimum conditions for maximum amino acids yields 11 p1728 A71-26066
- Quantitative gas liquid chromatography analysis of amino acids in biological materials, discussing ion exchange techniques 11 p1729 A71-26068
- Dietary pyridoxal deficiency causing amino acid content reduction in liver, kidney, brain and heart tissues 13 p2003 A71-27837
- Hydrocarbons, amino acids and large molecule organic compounds formation in chondrite meteorites by abiogenic reactions 13 p2010 A71-28692
- Nonproteins detection in presence of protein amino acids with Beckman analyzer chromatograms 13 p2026 A71-29478
- Microfossil structures from morphological alterations of proteinoid microspheres due to inclusion of organic or synthetic polyamino acids 14 p2190 A71-30178
- Proteinoids self assembly into primitive cell from observations of polypeptide generation during amino acid heating 14 p2190 A71-30179
- Murchison, Murray and Allende carbonaceous chondrites water extractable amino acids composition 16 p2650 A71-32950
- Long wavelength UV photoproduction of amino acids on primitive earth, using hydrogen sulfide as photon acceptor 18 p2855 A71-36229
- Compounds hydrolyzable to amino acids in aqueous extracts of Apollo 11 and 12 lunar fines, noting presence of glycine and alanine 18 p2855 A71-36230
- Extraterrestrial amino acids identification in carbonaceous chondrite Murray meteorite by gas chromatographic method 19 p3132 A71-37414
- Cystine synthesis in simulated primitive conditions by UV irradiation of methane, ethane, ammonia, water vapor and hydrogen sulfide in spherical vessel 19 p3014 A71-38678
- Cerebral gamma-aminobutyric acid metabolism and hyperbaric oxygen induced seizures in chicks during brain development, noting increased membrane permeability 20 p3186 A71-38970
- Amino acid levels in fasted and fed rats plasma, liver, muscle and kidney during and after exercise, noting glutamine decrease in liver tissue 20 p3186 A71-38982
- Photocatalytic stimulation of UV radiation photolysis of amino acids and pentoses in aqueous solutions by metal oxide soils 21 p3345 A71-40574
- Age dependent changes in free amino acid content and composition of cerebral and carotid arteries in man and dog 21 p3338 A71-41070
- Serotonin and gamma-aminobutyric acid loss and interaction in rat midbrain slices incubated in media containing Na, K and Ca ions 21 p3338 A71-41073
- Radiation damage diagnosis in humans, investigating free amino acid excretion with urine by paper chromatography method 22 p3495 A71-42736
- UV radiation effect on amino acids and peptides in different gas atmospheres in presence of salts and metal oxides 22 p3496 A71-42829
- Early solar system organic matter origin, discussing amino acid synthesis from CO, H and ammonia reaction with N, alumina or clay catalysts 23 p3633 A71-43244
- Prebiotic organic matter in solar system, investigating contamination free amino acid catalytic synthesis from deuterated reactants 23 p3633 A71-43245
- ### AMMETERS
- Fluicid ammeter for measuring electric current in uninsulated wire, using fluicid oscillator sensor 16 p2576 A71-32974
- ### AMMONIA
- Comparative numerical capture and experimental reaction cross sections for ion-molecule ammonia 01 p0028 A71-10476
- Amino acids synthesis by formaldehyde-ammonia heating and hydrolysis, simulating reactants in weakly reducing atmosphere at volcanic temperatures 03 p0357 A71-13014
- Spectrophotometry of methane and ammonia absorption bands indicating decrease toward Jupiter disk edge 03 p0484 A71-13213
- IR microwave double resonance of ammonia during IR vibration-rotation transitions induced by pumping of nitrous oxide laser 03 p0440 A71-14198
- Free radical effect on exchange reaction between ammonia and deuterium in high diluted argon shock tube 04 p0548 A71-14698
- Saturn millimeter wave spectrum and brightness temperature measurements, showing ammonia absorption characteristics in atmosphere 04 p0659 A71-15851
- PH conditional ammonia assimilation deficient mutants isolation and growth properties, studying nitrogen transport in *Hydrogenomonas eutropha* 06 p0857 A71-18672
- Hydrogenomonas eutropha* mutants deficient amination due to ammonia-nitrogen permeation defect 06 p0857 A71-18673
- Equivalent line widths of 5520 Å ammonia band in Jupiter spectrum 07 p1198 A71-19829
- Ammonia inversion radiation at 1.25 cm in direction of three galactic center sources, setting upper limits on densities in other areas 07 p1188 A71-19834
- Kinetic energy dependent charge transfer rates for ion-molecule reactions in ammonia, using cyclotron ejection and impulse methods 08 p1249 A71-20657
- Uranus radio emission model, considering presence of gaseous ammonia at saturation pressure in atmosphere 09 p1519 A71-22526
- Ammonia-parent ion reaction at low energies, comparing numerical and experimental capture cross sections 10 p1573 A71-24416
- ABM control surfaces active oxidation protection, using ammonia as reactive coolant injected through porous W wall matrix [ALAA PAPER 71-391] 11 p1837 A71-25353
- Jupiter equatorial thermal limb darkening data, constructing atmospheric model for ammonia effects on temperature structure 12 p1966 A71-27254
- Titanium-containing steels nitriding in ammonia, discussing hydrogen diffusion layers brittleness, cracking, peeling and thickness 12 p1919 A71-27776

Oscillations in second cavity of ammonia maser containing two resonators successively traversed by molecular beam, studying polarization and radioelectric emission

14 p2254 A71-30440

Hypokinesia effect on formation and elimination of ketones, aldehydes, carbon monoxide and ammonia in rats

15 p2356 A71-31305

Uranus radio emission model, indicating presence of gaseous ammonia at saturation pressure

17 p2807 A71-35501

Hydrazine formation from ammonia in constricted plasma discharge using electron source in selected high energy range

18 p2955 A71-35968

Possible prebiotic synthesis of thymine by heating uracil, paraformaldehyde and hydrazine in ammoniacal solution for three days at 70 C

18 p2855 A71-36231

Hydrogen-oxygen reaction sensitized by ammonia, comparing with nitrogen dioxide and nitrosyl chloride activators

19 p3012 A71-38081

High temperature oxidation of ammonia, carbon monoxide and methane by nitrous oxide in shock tubes, using optical interferometry and UV/IR emissions

19 p3012 A71-38086

Jovian planets methane and ammonium absorption bands spectrophotometric investigation, noting Saturn spectral variations

20 p3290 A71-39311

Vortex flow over helicopter rotor square tips, using visualization technique with ammonia vapor boundary layer flow over diazonium salt solution

21 p3318 A71-40169

Titanium-containing steels nitriding in ammonia, discussing hydrogen diffusion layers brittleness, cracking, peeling and thickness

21 p3424 A71-41097

Time of useful function after mice exposure to life threatening toxic mixtures of carbon monoxide, carbon dioxide and ammonia produced by combustion

22 p3486 A71-41830

Jupiter disk temperature measurement at eight frequencies in 20.5-35.5 GHz range, comparing with saturated ammonia model calculations

22 p3599 A71-41922

Semiempirical model for molecular band mean transmission, applying to ammonia 10 and 16 micron lines

22 p3602 A71-42179

Urine preservatives for urine water recovery system, noting ammonia and organic compound contents in condensate

22 p3506 A71-42809

Jovian geometric albedo at 1800-1950 A decrease explained as absorption by gaseous and solid ammonia in cubic crystal form

23 p3736 A71-43345

Sgr B2 region interstellar gas microwave emission spectrum, observing inversion transitions in metastable rotational levels of ammonia

24 p3872 A71-44916

AMMONIUM CHLORIDES

Photoreduction regulation in *Rhodospirillum rubrum* by ammonium chloride, discussing nitrogen fixation and protein metabolism

16 p2527 A71-33058

Ammonium chloride specific heat measurement near order-disorder transition, comparing results to Ising model behavior

17 p2791 A71-35743

AMMONIUM COMPOUNDS

NT AMMONIUM CHLORIDES

NT AMMONIUM NITRATES

NT AMMONIUM PERCHLORATES

NT AMMONIUM PHOSPHATES

NT HYDROXYLAMMONIUM

PERCHLORATES

High performance superheated subliming solid ammonium carbamate thruster using resistojet technology for specific impulse increase

[WSS/CI PAPER 70-210] 15 p2469 A71-32048

Lithium iodide and tetramethyl ammonium iodide additions effect on radical exchange between phenyl lithium and bromobenzene in diethyl ether

19 p3011 A71-37391

AMMONIUM NITRATES

Reaction mechanism for ammonium nitrate thermal decomposition, discussing chloride catalytic effects

01 p0141 A71-10344

Ammonium nitrate, ammonium perchlorate and nitronium perchlorate as liquid oxidizers for hybrid propellant rocket engines, discussing oxidizer/kerosene mixing ratio

10 p1657 A71-24275

Proton chemical exchanges effects in ammonium nitrate aqueous solution at varying exchange rate, noting geomagnetic field line configurations

10 p1644 A71-24458

Detonation sensitivity of ammonium nitrate containing fertilizers, compared with metadinitrobenzene in powder form

10 p1658 A71-25070

AMMONIUM PERCHLORATES

AP composite solid propellant combustion model based on multiple flame structure surrounding individual oxidizer crystals

03 p0469 A71-13440

Pressure effect on combustion rate of model mixtures of ammonium perchlorate with polystyrene and polymethyl methacrylate

03 p0468 A71-13989

Aluminum addition effect on combustion rate of mixtures of ammonium perchlorate with polymethyl methacrylate at different temperatures

03 p0520 A71-13995

High temperature decomposition kinetics in vacuum of mixed ammonium perchlorate-polystyrene solid fuel, using time of flight mass spectrometer

03 p0469 A71-13997

Radiation effects on thermal decomposition induction period in ammonium perchlorate and other pseudostable inorganic solids

06 p0944 A71-18301

Quench combustion of ammonium perchlorate composite solid propellant sandwich indicating binder-oxidizer interplay

06 p0944 A71-18610

Gas phase model for ammonium perchlorate deflagration at 20-100 atmospheres

06 p0944 A71-18611

Electric field effects on burning rates of composite metallized solid propellant containing ammonium perchlorate

06 p0947 A71-18613

Burning mechanism of condensed ballistite compositions with metallic particles of aluminum, magnesium and ammonium perchlorate

08 p1376 A71-21912

Combustion rate of pure ammonium perchlorate propellants derived from ablation theory

10 p1657 A71-23905

Ammonium nitrate, ammonium perchlorate and nitronium perchlorate as liquid oxidizers for hybrid propellant rocket engines, discussing oxidizer/kerosene mixing ratio

10 p1657 A71-24275

Erosive burning of composite propellants based on ammonium perchlorate, studying oxidizer grain size effect

10 p1658 A71-25122

Compositional and oxidizer particle size effects on combustion instability of plastic propellant based on ammonium perchlorate and polyisobutene

[AIAA PAPER 69-478] 11 p1809 A71-25454

Ammonium perchlorate deflagrations, determining intrinsic stability of one dimensional burning configuration based on flame structure modeling

[AIAA PAPER 70-123] 11 p1809 A71-25455

Phenol furfuraldehyde-ammonium perchlorate solid propellant combustion, investigating burning rate

12 p1944 A71-26742

Ammonium perchlorate propellants sterilizability, using medium resolution mass spectrometer and regression analysis of results in thermal stability studies

[AIAA PAPER 71-718] 14 p2286 A71-30769

Combustion rates of ammonium perchlorate mixtures with organic acids, alcohols, cyclic hydrocarbons, amines, nitroso compounds and nitramines, studying relationship to fuel chemical composition

15 p2366 A71-31370

Liquid KCl and LiF surface films effect on combustion rate of ammonium perchlorate mixtures with polystyrene or polymethyl methacrylate for various initial temperatures

15 p2462 A71-31371

Ammonium perchlorates deflagration rate at 20-100 atm, assessing relative roles of exothermic condensed phase and gas phase reactions by mathematical model

15 p2465 A71-32099

Low temperature condensed phase ammonium perchlorate decomposition effects on ballistic and postheat sterilization properties of CTPB propellant

[AIAA PAPER 71-717] 15 p2465 A71-32282

Ammonium perchlorate combustion characteristics as function of initial temperature by miniature thermocouple measurements

16 p2623 A71-33361

Catalytic role in ammonium perchlorate solid rocket propellants ignition and combustion

17 p2792 A71-34434

Ammonium perchlorate based solid propellants combustion, assuming pyrolysis of solid binder

17 p2792 A71-35549

Radiation induced etch-pit dislocations and thermal decomposition kinetics in ammonium perchlorate crystals

18 p2955 A71-35967

Deflagration behavior of pure and isomorphously doped ammonium perchlorate, using cinephotomicrography of burning samples and scanning electron microscopy of quenched samples

19 p3120 A71-38118

Perchloric acid catalytic pyrolysis relationship to ammonium perchlorate decomposition and combustion from electric conductivity measurements, IR spectroscopy, chemical and thermal analysis

19 p3120 A71-38119

Al and Mg powder dispersed in solid ammonium perchlorate oxidizer, investigating various combustion mechanics

19 p3120 A71-38120

Combustion model of solid composite propellants containing monoperchlorate oxidizers ammonium perchlorate, cyclotetramethylene-tetranitramine and potassium perchlorate

19 p3121 A71-38122

Exothermic decomposition reaction and sublimation mechanism of ammonium perchlorate burning, showing pressure dependence of burning rate

22 p3587 A71-42100

Ammonium perchlorate sublimation using simultaneous differential thermal analysis and thermogravimetry

23 p3641 A71-43116

AMMONIUM PHOSPHATES

High power tunable second harmonic and UV sum frequency generation from rhodamine 6G dye laser and ADP crystal

22 p3556 A71-41803

AMMONOLYSIS

Amino acids synthesis by formaldehyde-ammonia heating and hydrolysis, simulating reactants in weakly reducing atmosphere at volcanic temperatures

03 p0357 A71-13014

AMMUNITION

Fluid amplifiers theory and use as temperature and pressure sensors, discussing applications in chemical and ammunition industries and jet aircraft control

[IEEE PAPER 70-TP-120-IGA] 23 p3630 A71-42921

AMORPHOUS MATERIALS

Amorphous Se p-type conductivity, discussing temperature and crystalline phase dependence

05 p0792 A71-16379

Optical and photoelectrical properties of thin amorphous thallium arsenic sulfide, thallium antimony sulfide and thallium bismuth sulfide films obtained by vacuum deposition

05 p0794 A71-16835

Ion implantation lattice damage effects in crystalline silicon with allowance for optical reflectivity, considering annealing temperature and amorphous layer formation

07 p1175 A71-19062

Amorphous semiconductors theories and models, considering structural, optical and electrical characteristics

07 p1178 A71-19847

Amorphous semiconducting thin films quenching fabrication techniques and electrical properties

07 p1181 A71-20410

Noncrystalline amorphous solids electro-optical effects, studying semiconductor energy band models

07 p1181 A71-20422

Resistance thermometer using amorphous Pd-Si-Cr alloy for enhancing sensitivity at cryogenic temperatures

09 p1444 A71-22714

Measuring instrument for amorphous and polycrystalline materials resistivity and Seebeck coefficient as function of temperature and pressure

09 p1446 A71-22737

Amorphous semiconductors for memory and logic devices, using reversible structural transformations between disordered and ordered states

09 p1509 A71-23114

Laser pulse induced rapid reversible crystallization of amorphous chalcogenide semiconductor films using photon flux model

10 p1655 A71-24044

Amorphous semiconductors, including electrical conductivity, temperature dependence, germanium/silicon structural model and mobility energy

12 p1944 A71-27244

Current oscillations and switching effect in amorphous chalcogenide compound films sputtered thermally on unheated glass and pyroceram substrates

13 p2111 A71-28173

Electron energy spectra of amorphous semiconductors by cell method, replacing conditions for splicing wave functions by extremum integral

13 p2112 A71-28925

Carrier mobility, conductivity and optical absorption in strong electric fields of chalcogenide glasses for switching and memory effect amorphous semiconductors

13 p2112 A71-28926

Amorphous particle rarefied gas in bounded volume, analyzing kinetic equation existence and uniqueness

13 p2103 A71-29146

Elastic static and dynamic piezomechanical characteristics of resin type amorphous materials under pulsed loads, using electromagnetic excitation of torsional vibrations

16 p2659 A71-33996

Amorphous semiconductors electrical switching effects and applications covering computer memory, visual display control and printing 21 p3355 A71-40740

Thermal switching and negative resistance model and measurements of amorphous semiconductor thin films of Ge, Si and chalcogenide glasses 21 p3428 A71-40741

Electron energy spectra of amorphous semiconductors by cell method, replacing wave functions condition extremum integral 21 p3434 A71-41321

Carrier mobility, conductivity and optical absorption in strong electric fields of chalcogenide glasses for switching and memory effect amorphous semiconductors 21 p3434 A71-41323

Coulomb interaction effect between charged traps in amorphous semiconductor, noting state density reduction at Fermi energy 23 p3715 A71-43472

Symbiotic shifts of conductivity compensation effect in glassy chalcogenide semiconductors unaffected by heat treatment of blanks or impurities 23 p3717 A71-44315

AMORPHOUSNESS
U CRYSTALLINITY

AMPLIFICATION
U ELECTRIC CURRENT

AMPHIBIA
NT FROGS

AMPHIBIOUS AIRCRAFT
NT SEAPLANES

Light amphibious passenger STOL P-300 Equator aircraft, using single turbosupercharged engine driving two blade propeller at tail assembly 05 p0696 A71-16132

AMPHIBIOUS VEHICLES
NT AMPHIBIOUS AIRCRAFT

AMPHIBOLES
Kaersutite amphibole formation from pargasite amphibole interaction with basanite, discussing Fe, Ti, K, Mg, Si, Na and Cr contents 10 p1601 A71-24415

Hydrous analog stability in lunar amphibole Apollo samples as function of water vapor pressure and temperature 23 p3743 A71-43648

AMPLIFICATION
NT POWER GAIN
NT SOUND AMPLIFICATION

Planar diffused transistor characterization by equivalent circuit model using input impedance and amplification measurements 01 p0051 A71-10310

Time-pulse converter for semiconductor triodes DC amplification factor measurement 02 p0230 A71-11832

Mechanical characteristics of generalized Rayleigh waves in piezosemiconductors of cubic symmetry, deriving amplification and damping factors for zero diffusion coefficient 02 p0294 A71-11894

Skynet project earth station effective radiated power and gain by dual satellite access measurements 02 p0218 A71-12445

Antenna gain of Space Communications and Tracking terminal from feedhorn radiation pattern and reflector geometry 02 p0219 A71-12448

Cassegrain system far field radiation pattern and gain loss prediction for beam steering by subreflector tilting 02 p0222 A71-12793

Gain/temperature measurement test set for earth station receiving system by radio sources program tracking unit, noting antenna power ratios determination by attenuator 02 p0222 A71-12797

Gain/temperature measurement for earth station antenna and receiving subsystem by FM method, determining Y-factor /noise power proportional increase/ 02 p0222 A71-12798

Vorticity amplification in stagnation flow by stretching, discussing effects on average boundary layer profile 03 p0398 A71-13104

Vectorcardiograms comparison recorded with different electrode leads or amplification systems based on spatial points coordinates correlation coefficients 03 p0371 A71-13115

Planar transistors operating conditions effects on current gain degradation following emitter-base reverse biasing 07 p1076 A71-19560

Gain and radiation properties of phased array antenna with dielectric, using integral method 07 p1078 A71-20070

Kalman filter application as observer of observable signals derivatives, using gain matrix to minimize variance estimate for instrument landing systems 08 p1269 A71-21343

Ground based coherent radar synthetic aperture procedure against uniform velocity targets, discussing

airborne holographic synthetic gain applications to stationary antennas 09 p1405 A71-22697

Model of curved channel multipliers saturation gain at high applied voltages 09 p1446 A71-22736

CW carbon dioxide gasdynamic laser gain for mixture of carbon dioxide, nitrogen and helium 10 p1620 A71-24043

Horizontal electric dipole gain dependence on height above plane lossy earth, deriving radiation intensity expression from Hertzian potential integral representation 11 p1730 A71-25249

Magnetospheric cold plasma dispersive and amplifying combined effects on pearl elements spectral shape, considering wave packet propagation applications 11 p1730 A71-25543

Homogeneous Gaussian beam propagation in inhomogeneous negative absorption media, noting amplification of plane wave 11 p1798 A71-25665

Partly time invariant and periodically time varying gain equations based on Banach algebras spectral mapping theorem and higher order circle criteria 11 p1742 A71-26411

MOS transistor saturation range transconductance, internal resistance and gain factor calculation, allowing for field effect on space charge near drain 12 p1889 A71-27626

Acoustic wave amplification and attenuation in non-homogeneous steady flows applied to air jet discharging in organ pipe 14 p2224 A71-30208

Temperature dependence of current gain in p-n-p transistors due to increased surface recombination rate 14 p2213 A71-30623

Planar and nonplanar transistors noise factor dependence on signal source impedance and emitter current, considering amplification and frequency conversion application 14 p2213 A71-30628

Optimal linear filter gain relation to feedback difference, using Riccati matrix differential equation 14 p2220 A71-30808

Marconi 90 ft space communication antennas and waveguide components, using feed horn radiation patterns to compute gain 15 p2374 A71-31141

Numerical analysis of far field gain pattern of shielded acoustic antenna by Kirchhoff integral, assuming circular symmetry and perfectly absorbing walls 15 p2372 A71-32193

Gain improvement in TWT parametric amplifiers based on slow space charge waves interaction with slow wave structure field by electron beam modulation 15 p2378 A71-32629

Two dimensional linear communication system with crossed channels with different amplification factors and time constant, examining stability with root trajectory method 16 p2549 A71-33569

Signal waves amplifier in medium of high nonlinear electric polarization, considering reflected waves effect on amplification 16 p2544 A71-34131

Microwave amplifiers gain fluctuations effect on Dicke radiometers minimum detectable temperature difference, considering traveling wave tubes and tunnel diode and mixer IF amplifiers 16 p2548 A71-34133

Dynamic amplification ranges of monochromatic signal by semiconductor, solid state and gas lasers in steady operation mode 17 p2750 A71-34270

HCN laser amplifier gain measurement at IR wavelengths in gas mixtures by recording with pyroelectric receiver 17 p2750 A71-34290

Three-frequency parametric traveling wave amplifier amplification and conversion factors calculation by numerical method with allowance for fast and slow space charge wave effects 20 p3206 A71-39812

Pulsed argon ion laser data, presenting excitation mechanisms and time resolved gain measurements 21 p3392 A71-40625

Transverse surface wave amplification in piezosemiconductor, considering cases of total or drift current in thin near-surface semiconducting layer 22 p3585 A71-41707

Bipolar junction transistor doping effects on bandgap decrease and emitter efficiency, explaining current gain temperature dependence 23 p3648 A71-42911

Electron multiplier pulse height distribution for single electron input, investigating relative variance correlation with statistical fluctuations of gain 24 p3811 A71-45329

AMPLIFICATION FACTOR U AMPLIFICATION

AMPLIFIER DESIGN

Linear beat by beat cardiachometer, describing amplifier design and operation 01 p0021 A71-10242

Feedback role in mathematical operation amplifiers for analog computers 01 p0049 A71-10361

Amplifier stability with distributed feedback by root locus trajectories 01 p0059 A71-10605

Broadband cooled parametric amplifier with low noise for satellite communications ground station, discussing performance at room and cryogenic temperatures 01 p0053 A71-10799

Design concepts providing high plate efficiency in high power injected beam crossed field amplifier capable of CW operation with conduction or liquid cooling 01 p0054 A71-10975

YIG C band microwave amplifier using longitudinal pumping, comparing to other systems 02 p0228 A71-11692

Push-pull power amplifiers with class B complementary transistors, describing driver stage 02 p0229 A71-11693

Steady state quantum analysis of linear distributed systems applied to attenuator, maser amplifier and multimaterial-pair networks 02 p0213 A71-12017

Two stage parametric SHF amplifier for Skynet V Naval receiver system 02 p0234 A71-12812

Remotely controlled room temperature microwave parametric amplifier design for shipboard satellite telegraphy terminal 02 p0234 A71-12813

Uncooled low noise microwave parametric amplifier for small receiving earth stations, describing three stage design, gain and bandwidth 02 p0234 A71-12814

Wideband low noise parametric amplifier design, discussing noise temperature improvement by refrigeration at microwave frequencies 02 p0234 A71-12815

Optimal gain tuning elements of cryogenically cooled parametric amplifiers 02 p0235 A71-12833

Surface wave filters, tapped delay line pulse compression networks and amplifiers, discussing design and applications 05 p0728 A71-16915

C band field effect transistor amplifiers with stable power gain, discussing circuit analysis, design parameters and test results 05 p0729 A71-16917

Low distortion gain-controlled 140 MHz IF main amplifiers for 2700-channel microwave repeaters, discussing design and performance 05 p0730 A71-17069

Radiation tolerant monolithic amplifier design, considering IF amplifier 07 p1080 A71-20411

Low noise C band beam lead tunnel diode amplifiers characteristics and application in low cost microstrip reflection amplifiers 08 p1262 A71-20759

K band double-tuned nondegenerate parametric amplifier using single-packaged GaAs varactor diode, discussing design and performance 08 p1262 A71-20763

Wide band low noise millimeter wave parametric amplification using wafer varactor diodes with Schottky barrier junctions 08 p1263 A71-20769

K band cryogenically cooled wideband /600 MHz/ low noise parametric amplifier for millimeter wave satellite communication earth terminals, discussing design 08 p1263 A71-20770

Low noise microstrip microwave mixer-preamplifier on thin polyolefin reinforced with Al, discussing design and manufacture 08 p1263 A71-20771

Microwave amplifier resonant gain frequencies as function of tunnel diode circuit, proposing low input design formulas 08 p1264 A71-21069

Microwave multistage transistor amplifier with IC configuration, discussing design and performance 08 p1265 A71-21287

Uncooled Si nuclear particle detector charge sensitive and pulse shaping amplifier design, discussing spacecraft instrumentation and fabrication requirements 08 p1267 A71-21848

Line fed microelectrode amplifier for electrophysiology, discussing noise reduction 08 p1249 A71-21974

Distributed gain amplifiers synthesis technique permitting use of filter and transmission line design tables 09 p1413 A71-22158

Differential charge amplifier design using ferromagnetic high signal bandwidth isolation with grounded input transducer and output load 09 p1417 A71-22782

Low cost directly coupled differential amplifier with thermodynamic drift stabilization for biological studies 10 p1570 A71-24444

Symmetrical amplitude-frequency characteristics of microwave reflection amplifiers with active resonators connected in series by nonhalf wave transmission line 10 p1584 A71-24879

Ground stations for communication satellites, discussing radio transmitter and receiver systems using low noise parametric amplifiers at low temperatures and extended demodulator threshold 10 p1590 A71-25101

Parametric amplifier design and construction for communication satellite ground station, discussing noise temperature, distortions, bandwidth and antenna gain 10 p1580 A71-25105

Unilateral GaAs traveling wave microwave amplifier based on space charge growth in domain-stabilized transferred electron semiconductors, considering power, noise, gain and efficiency 11 p1736 A71-25234

Computer synthesis of nondegenerate parametric amplifiers with single mesh filter for maximum flat or Chebyshev frequency response applicable to quantum devices 12 p1886 A71-26844

Gain and noise characteristics of reactive phase/amplitude modulation ferrite amplifier as function of pumping power and resonator coupling 12 p1886 A71-26845

Circuit design of double balanced parametric amplifiers regarding low cost and least degradation performance limits 13 p2039 A71-28906

High power multicavity klystron design, investigating cavity voltage, cavity phase, drift length and beam parameter effects 13 p2040 A71-29424

Microstrip microwave amplifier design using common emitter configuration and quarter wave impedance matching transformer 16 p2545 A71-33395

Soviet book on microwave quantum amplifiers covering traveling wave and multicavity masers calculation, design, tests, applications and basic components 17 p2753 A71-34474

Low noise parametric amplifiers for communication satellite ground station radio receivers, considering components characteristics 17 p2709 A71-35513

General purpose pulsed microwave radar receiver, describing balanced mixer and transistorized IF amplifier design and construction 18 p2887 A71-36015

Emission transistor for Eole balloon transmitter power amplifier, discussing trouble-free emission, high output, wide temperature range, lightweight and reliability features 18 p2891 A71-36563

Low noise parametric amplifier design and construction for Intelsat 4 satellite communications earth stations 19 p3027 A71-37496

Maximum efficiency of 10-20 W output semiconductor amplifier at 2.3 GHz, discussing possible replacement of vacuum tubes 20 p3205 A71-39456

Three-pole theory of amplifiers, deriving operational resistances as function of wave resistance and control parameters by current-voltage matrices 20 p3205 A71-39467

Hybrid integrated wideband linear microwave power amplifiers for S and C bands, discussing construction and performance 21 p3357 A71-40817

Transistorized high power telemetry amplifier design, describing test equipment for input and collector load impedance 22 p3519 A71-41632

Supercritical transfer electron amplifier using GaAs CW Gunn diode with cathode doping notch and profiles sloping upward for stabilization 22 p3521 A71-42204

Operational amplifier design with fluidic Schmitt trigger and linear resistor feedback network 23 p3631 A71-44098

Optimal number of parallel connections of transistors in amplifier for improving SNR 24 p3810 A71-45260

AMPLIFIERS

NT BEAM PLASMA AMPLIFIERS
NT BROADBAND AMPLIFIERS
NT CROSSED FIELD AMPLIFIERS
NT CURRENT AMPLIFIERS
NT DIFFERENTIAL AMPLIFIERS
NT DISTRIBUTED AMPLIFIERS
NT FEEDBACK AMPLIFIERS
NT FLUID AMPLIFIERS
NT INTERMEDIATE FREQUENCY AMPLIFIERS
NT JET AMPLIFIERS
NT LIGHT AMPLIFIERS

NT LINEAR AMPLIFIERS
NT MAGNETIC AMPLIFIERS
NT MICROWAVE AMPLIFIERS
NT PARAMETRIC AMPLIFIERS
NT PHOTOMULTIPLIER TUBES
NT POWER AMPLIFIERS
NT PREAMPLIFIERS
NT PUSH-PULL AMPLIFIERS
NT SERVOAMPLIFIERS
NT TRANSISTOR AMPLIFIERS
NT TRAVELING WAVE AMPLIFIERS
NT VOLTAGE AMPLIFIERS

Optimal input stage interaction height in large scale operation of two-stage magnetron amplifier 03 p0385 A71-13791

Chopper amplifier modulator and demodulator circuits analysis, discussing SNR performance 03 p0387 A71-13821

High impedance source with shunt capacitance, discussing periodic output measurement using operational amplifier 03 p0427 A71-13923

Large signal mode tunnel diode amplifier amplitude and phase characteristics by computer study 04 p0556 A71-14622

Resonant self tuning narrow band amplifier, considering transient processes by time domain quantization for differential equations with constant coefficients 04 p0559 A71-15569

Transferred electron devices (TED), reviewing physics of transferred electron effect, theory and design of amplifiers and oscillators 07 p1072 A71-19102

Output pulse amplitude from lithium-drifted detector-amplifier combination under conditions of carrier diffusion and bulk and surface recombination 11 p1802 A71-25804

Differential phase frequency characteristics of low noise or tunnel diode regenerative amplifiers 11 p1738 A71-25941

Electrocardiography from unprepared skin without paste, using integrated stainless steel electrode-buffer amplifiers 13 p2023 A71-29399

HF amplifier statistical gain fluctuations effect on Dicke radiometer sensitivity, using Davenport-Root theory of random processes 16 p2548 A71-34132

Large signal mode tunnel diode amplifier amplitude and phase characteristics by computer study 22 p3521 A71-42262

AMPLITRONS [TRADEMARK]

U PLANOTRONS

AMPLITUDE DISTRIBUTION ANALYSIS

Radar tracking systems stretcher detector circuit output signal amplitude and spectral distribution analysis 01 p0029 A71-10308

Auroral absorption classification of cosmic noise at 32 MHz, plotting time and amplitude distribution diagrams 02 p0243 A71-11769

Wolf numbers monthly fluctuations, giving histogram of fluctuation amplitude distribution 03 p0484 A71-13211

Mode locked pulsed lasers statistical amplitude and phase variations effects on time dependent output intensity and nonlinear optical processes efficiency 03 p0437 A71-13881

Field amplitude distribution parameter in long distance tropospheric communications based on fading depth 05 p0722 A71-16866

Radar echo signal amplitude probability distribution during fully polarizational reception 05 p0723 A71-16873

Out of phase conical horn radiating element amplitude and phase diagrams at short distances 06 p0872 A71-17374

Nose bluntness, angle of attack and oscillation amplitude effect on hypersonic unsteady aerodynamics of slender cones [AIAA PAPER 70-216] 07 p1016 A71-19895

Relative spectral sensitivity/amplitude frequency characteristics/ applicability to describing nonlinear systems 07 p1043 A71-20111

Vibration decrement amplitude dependence study using internal friction method of freely attenuated transverse vibrations, considering energy dissipation 08 p1317 A71-21761

He-Ne ring laser in locking range, studying opposing waves amplitude and phase differences dependence on cavity rotation and oscillation frequency tuning 09 p1461 A71-22382

Expansion bellows fatigue strength based on load and displacement measurements performed during low cycle model tests 09 p1538 A71-22604

Constant, programmed and random amplitude spectral analysis and signal averaging correlation with failure statistics, noting laboratory simulation 09 p1444 A71-22709

Amplitude characteristic polynomial Chebyshev approximation by linear phase nonrecursive digital filter transfer function 09 p1417 A71-23037

Elastic media damping effects on rigid bodies HF vertical and rotational vibrations, considering approximate solution for structural amplitude response 09 p1541 A71-23088

Bounded electromagnetic wave propagation in randomly inhomogeneous medium, calculating correlation in amplitude and phase fluctuations 09 p1407 A71-23109

Amplitude distribution of nuclear burst electromagnetic pulse propagated through atmosphere, deriving two probability distribution functions by central limit theorem 09 p1410 A71-23524

Amplitude discriminating Goto circuit with four tunnel diodes operating on negative and positive half periods as amplitude distribution analyzer at 40 MHz 10 p1582 A71-23954

Amplitude characteristics of Q switched He-Xe laser at 3.5 microns, using rotating reflection prism and velocity equations 10 p1621 A71-24715

Symmetrical amplitude-frequency characteristics of microwave reflection amplifiers with active resonators connected in series by nonhalf wave transmission line 10 p1584 A71-24879

Sensitivity threshold of optical heterodyne receiver as function of laser amplitude spectrum, using photodetector output noise 10 p1622 A71-24882

Linear automatic flight control systems synthesis based on transfer functions and logarithmic amplitude characteristics of open systems 10 p1588 A71-24911

Amplitude curves of reflected wave vertical displacement component in horizontally stratified medium with simple layer velocity pattern 10 p1644 A71-25134

Scalar Gaussian channel information optimal input capacity as function of random variable, assuming finite number of values for amplitude and variance constraints 11 p1730 A71-25374

Industrial helium-neon laser emission noise characteristics, defining amplitude fluctuations by variable proportional to photoelectric multiplier current random modulation factor 13 p2077 A71-27937

Lower ionosphere magnetic fields generated by three dimensional Alfvén waves, examining amplitude and phase spatial distribution and frequency dependence 13 p2059 A71-28254

Radio noise amplitude probability distribution, considering RMS voltage, average voltage and average logarithm of voltage 13 p2031 A71-28861

Surface impedance of sphere based on received electromagnetic field amplitude-frequency characteristics 14 p191 A71-29511

Large amplitude formations and turbulence in Kelvin-Helmholtz instability, comparing with radar observations 14 p2267 A71-29760

Synthesis of slot antenna on metallic wedge for amplitude radiation pattern, determining RMS approximation and fixed phase diagram 14 p2195 A71-30103

Truncated pulse signal height distributions at atmospheric sources 14 p2203 A71-30960

Normal time average holography amplitude range extension by integration over vibration cycle fraction 15 p2404 A71-31270

Interferometric holograms of vibrating body via numerical analysis of oscillations amplitude and phases 15 p2406 A71-31706

Long period quasi-monochromatic geomagnetic micropulsations amplitude spectra and polarization as function of geomagnetic latitude 15 p2397 A71-31760

Amplitude distribution of pulse train with given constant pulse durations in communication channels 18 p2882 A71-36621

Jet turbulence orderly structure enhancement, control and relation to noise, studying response to periodic surging of frequency and amplitude 19 p3056 A71-38204

Laser beams amplitude-phase correction by holographic method, obtaining beams with plane fronts and Gaussian amplitude distribution 20 p3245 A71-39413

Analog statistical analyzer for measuring one dimensional EEG amplitude distribution functions, illustrating reaction response to threshold acoustic stimuli 21 p3344 A71-41067

Probability density and distribution functions of click amplitudes for rectangular IF, determining frequency modulation effect 22 p3513 A71-42386

- Amplitude prediction for terrestrial radar echoes from ground using topographical data 22 p3514 A71-42469
- ## AMPLITUDE MODULATION
- Structure and propagation of large amplitude modulated isolated compression waves in cold three component plasma with negatively charged ions 01 p0132 A71-10676
- Semiconductor lasers direct amplitude, pulse and frequency modulation methods, comparing advantages and limitations 02 p0260 A71-12004
- Holographic amplitude modulation procedure for pulse compression in synthetic aperture radar 02 p0215 A71-12037
- Spacecraft signal amplitude and phase modulation and fault diagnosis by VLF analysis 02 p0218 A71-12447
- Wideband amplitude modulator for quasi-optical waveguide channels, featuring one dimensional rotating wire grating 03 p0378 A71-13804
- Homogeneously broadened pulsed laser mode locking with internal frequency or amplitude modulation 03 p0437 A71-13882
- Second order moment at output of inertialess nonlinear two terminal pair network during amplitude and phase modulation 04 p0550 A71-14620
- Transistorized transmitters constant phase low distortion AM system based on Chireix method, generating AM from two push-pull phase modulated signals 05 p0720 A71-16392
- Reflection point slide velocity of traveling F region ionospheric disturbance by receivers amplitude focusing and echo phase path changes 05 p0741 A71-16440
- Optimal quasi-regular signal detection on amplitude and frequency modulated noise background 05 p0723 A71-17020
- Quantized multiple access voice communications, comparing QPPM-AM and FM performances concerning transmitter power, RF bandwidth, circuit complexity, etc [IEEE PAPER 69-TP-448-COM] 05 p0724 A71-17056
- Stark broadening of hydrogen lines in plasma, noting role of amplitude modulation and nonadiabaticity 06 p0930 A71-17406
- Waveguide cavity CW Gunn microwave oscillator bias voltage controlled amplitude and frequency modulation 07 p1073 A71-19110
- Injection locked microwave oscillators nonlinear differential equation reduction to nonlinear algebraic equation, calculating AM limiting and output power increment as injected signal amplitude functions 07 p1073 A71-19113
- Structure and propagation of large amplitude modulated isolated compression waves in cold three component plasma with negatively charged ions 07 p1170 A71-20138
- Optimal reception of AM signal during nonlinear operation of radio system 07 p1064 A71-20258
- Optimum AM reticle-detector models, discussing image resolution, electrical bandwidth and detection problems 07 p1115 A71-20368
- Blocked and series connected pneumatic fluidic transmission lines, determining amplitude frequency response 07 p1026 A71-20566
- Cosmic rays amplitude hysteresis dependence on sunspot mean heliographic latitude and cluster number 08 p1353 A71-20979
- Long distance PCM-AM pulse regenerator for 4 GHz band and millimeter wave communication 08 p1263 A71-21285
- Periodic subtraction and multiplication systems under amplitude limitation, analyzing detection characteristics at arbitrary correlation coefficients 09 p1405 A71-22464
- Magnetic tape recording systems nonlinear amplitude distortion in terms of transfer function characteristics applied to analog instrumentation 09 p1449 A71-22786
- LF plasma beam density oscillation spectra from microwave emission amplitude modulation 10 p1648 A71-24316
- Combination frequency spectra asymmetry in bounded plasma column resulting from HF AM and PM wave interactions 10 p1651 A71-24637
- TWT amplifiers in radar and communication systems, investigating AM and FM noise theory and reduction 11 p1734 A71-26435
- Interferential spectrometer with selection by amplitude modulation with double passage mirrors arrangement for obtaining double resolution 12 p1905 A71-26811
- Gain and noise characteristics of reactive phase/amplitude modulation ferrite amplifier as function of pumping power and resonator coupling 12 p1886 A71-26845
- Lumped inhomogeneities reflections effect on characteristics of AM signal along transmission line 12 p1883 A71-27624
- Amplitude modulated optical band signal detection, comparing optimal direct photodetection and superheterodyne receivers sensitivities 13 p2029 A71-28365
- Self modulation of amplitude modulated electromagnetic wave propagation in magnetoplasmas, considering interaction effects for ordinary and extraordinary propagation modes 13 p2107 A71-28787
- Microwave responders in FM or AM modes with cavity resonator, considering use in medium distance telemetering or telemonitoring 14 p2215 A71-30911
- Parametric amplification of two laser waves with amplitude and phase modulation under exponential signal growth applied to Raman scattering in picosecond pulse field 15 p2418 A71-31188
- Noise stability at reduced peak signal power of PTM-AM communications using wideband linearly frequency modulated carrier pulses 15 p2368 A71-31228
- Ejected photoelectron count probability distribution due to periodic irradiance modulation of amplitude stabilized light beam 15 p2452 A71-32595
- He-Ne laser emission spectra with AM by reflected Doppler shifted signal and matched/mismatched three-mirror resonator/mobile outer mirror/ 17 p2750 A71-34289
- Nonlinear gain and AM/PM conversion in FDMA communication through satellite repeater, using traveling wave tubes plus postzonal filter 17 p2703 A71-35082
- X-band Gunn oscillator equivalent circuit parameters determination for baseband and RF noise contribution to AM and FM noise 18 p2888 A71-36270
- Electromagnetic wave propagation through magnetoplasma disturbed by acoustic wave, calculating transmitted and reflected waves amplitude modulation 19 p3110 A71-37480
- Modulated electron beam interaction with plasma, showing amplitude growth and traveling wave profile distortion 19 p3114 A71-37856
- Transmission characteristics of communication systems with incoherent carriers through fading and nonfading media, showing advantage of PFM-AM with clipped noise carrier 20 p3201 A71-39913
- Combined AM/PM digital data transmission, using error rate and communication efficiency in bits per cycle of bandwidth vs average SNR as performance criteria 21 p3349 A71-41197
- Second order moment at output of inertialess nonlinear two terminal pair network during amplitude and phase modulation 22 p3510 A71-42260
- Interfering beams amplitude modulation, applying optical heterodyne techniques 22 p3512 A71-42321
- AM crosstalk in unified carrier telemetry system, studying implications for carrier false lock and tracking 22 p3514 A71-42390
- Signal AM-PM conversion by locking oscillator with single external injection 22 p3523 A71-42480
- Second harmonic aperture in ultrashort pulses length measurement by mixing two AM light beams in nonlinear crystals 23 p3683 A71-43397
- Transmission and reaction cavity stabilized Gunn microwave oscillators AM and FM noise spectra, extending calculations based on Kurokawa theory to high modulation frequencies 23 p3653 A71-43967
- ## AMPLITUDE PROBABILITY ANALYSIS
- ### U AMPLITUDE DISTRIBUTION ANALYSIS
- #### AMPLITUDES
- ##### NT PULSE AMPLITUDE
- ##### NT SCATTERING AMPLITUDE
- Phase and amplitude fluctuations in oscillator circuits, determining power spectrum, disturbing voltage and current sources and step and impulse functions 03 p0383 A71-13168
- Portable photoelectric recorder for solar limb vibration frequency spectrum and amplitude measurements 04 p0590 A71-14844
- AC signal amplitude measurements, describing circuit design with DC voltage generation proportional to input AC voltage 06 p0899 A71-17926
- Collisional drift plasma wave instability nonlinear analysis, calculating wave amplitude as function of magnetic field based on two fluid theory 07 p1166 A71-18883
- Laser radiation amplitude and phase fluctuations in complex media, using interferometry 09 p1459 A71-22143
- Round cross section specimens flexural vibration damping decrement, determining amplitude dependent internal friction with allowance for stressed state 09 p1542 A71-23314
- Tunnel diode driven multivibrator, noting triggering signal amplitude and duration effects on output pulse width 11 p1740 A71-26550
- Light beam diffraction by supersonic waves, calculating amplitudes with difference-differential equations 15 p2450 A71-32075
- Vibratory amplitudes and stress levels from metal bellows flow induced vibrations, discussing damping and acoustical resonances effects [ASME PAPER 71-VIBR-22] 21 p3458 A71-40279
- Finite cylinder forced longitudinal axisymmetric vibrations with prescribed surface stresses, reducing problem to quasi-regular infinite system of linear algebraic equations 24 p3880 A71-44723
- ## AMPOULES
- Level ampoule inner surface curvature nonuniformity, noting correction determination in level scale division 04 p0592 A71-14857
- ## AN-24 AIRCRAFT
- Flight stress effects on blood pressure and eye accommodation from frequent takeoffs and landing of AN-24 aircraft 11 p1723 A71-25261
- ## ANABAENA
- Anabaena cylindrica alga chromosomes protein components, noting histone absence 16 p2536 A71-33359
- ## ANAEROBES
- Thermophilic, mesophilic and psychrophilic anaerobes fatty acid composition, discussing results obtained by mass spectral analysis 15 p2360 A71-32050
- Human microflora variation in long term confinement, examining anaerobic and aerobic microorganisms responses 21 p3333 A71-40557
- ## ANALGESIA
- Extraordinary effects of sound on senses, concerning visual functions, nystagmus, galvanic skin response and audioanalgesic use 03 p0359 A71-13158
- ## ANALOG CIRCUITS
- Analog inertial sensor digitizing methods, discussing pulse rebalancing and analog to digital conversion 02 p0279 A71-12453
- Partial differential equations solving device for analog computers 03 p0381 A71-13004
- Analog transducers and tape recorders measurement sensitivity and conversion factor stabilization using push-pull signals 05 p0747 A71-16144
- Analog information systems frequency modulators, describing network design consisting of phase shifting RC network, amplifier and inertialess resistor 09 p1415 A71-22296
- Analog type semiconductor switches for aircraft and spacecraft automatic checkout systems, discussing component transistor types, optoelectronic devices and materials 09 p1418 A71-23041
- Book on nonlinear modulation based on optimum estimation theory covering phase synchronization, analog data transmission, digital and analog systems performance, Markov processes, etc 13 p2029 A71-28041
- Nonlinear analog function generators using semiconductor junctions and combined diode-resistor network 13 p2039 A71-28914
- RC analog fluidic circuits design for arbitrary transfer functions generation 15 p2351 A71-31682
- Transistorized analog multiplication circuit for automatic control system requiring controller input proportional to product of two values 17 p2719 A71-34787
- Panels and cassettes mechanical design for Camac modular construction of electronic analog and digital measuring instruments based on integrated circuits 19 p3029 A71-38065
- Soviet book on rational, irrational and transcendental transfer functions electronic modeling covering mathematical theory and applications to control plants 23 p3648 A71-44185
- ## ANALOG COMPUTERS
- Project DARE/Differential Analyzer Replacement/providing all-digital on-line digital simulation of dynamical systems 01 p0046 A71-10199

- Analog computers seven segment numeral display, describing code converters 01 p0049 A71-10261
- Feedback role in mathematical operation amplifiers for analog computers 01 p0049 A71-10361
- Thermionic Diode Kinetics Experiment with on-line analog computer simulation, investigating thermionic reactor powerplant dynamics and control by non-nuclear means 02 p0195 A71-12258
- Soviet analog computer modifications for iterative and hybrid computations, describing memory system alterations 02 p0228 A71-12489
- Partial differential equations solving device for analog computers 03 p0381 A71-13004
- Analog/hybrid programming of stimulus sequence for cardiac excitation study 04 p0546 A71-15166
- Discrete and analog electrical differentiators accuracy for input functions time derivatives determination, considering systematic errors and application suitability 04 p0599 A71-15567
- Materials fatigue testing using analog computer interfaced with closed loop test system 07 p1216 A71-20203
- Real time remote test site computation and display of complex engine inlet distortion parameters from dynamic pressure signal, using analog computer 09 p1446 A71-22726
- Quasi-analog and hybrid computers, describing ARKUS hybrid integrator effectiveness in solving boundary value problems and ordinary differential equations 10 p1581 A71-24382
- Analog recursive computer with serial digital program for arithmetic unit and storage system control 12 p1884 A71-27150
- Hybrid binary floating point digital differential analyzer technology, noting speed, cost and utility 14 p2207 A71-30021
- Errors in spectral estimates by single-mode filters using analog computer for geoscientific data processing 14 p2246 A71-30482
- Differential equation systems optimal scaling for analog computer, proposing amplitude and time scaling factors and disposition parameters with linear programming 15 p2440 A71-31155
- Analog computer application for determination of charge centers in multilayer gate structure of variable threshold FET, deriving equations yielding position of internally stored charge 15 p2462 A71-32639
- Analog computer analysis of radiocardiograms, determining cardiac function and pulmonary blood volume 20 p3191 A71-38802
- Hybrid electromechanical analog computer real time simulation technique for optimizing vibration response of two degree of freedom system with impact damper [ASME PAPER 71-VIBR-119] 21 p3350 A71-40338
- ANALOG DATA**
- Quantization in data transmission and extraction, considering analog signals transmission in digital form and radar echoes recognition by digital integration systems 01 p0029 A71-10307
- Noiseless linear feedback limitation over bandwidth limited channel capacity in analog data transmission 01 p0064 A71-10906
- Linear delay input effects on analog cross correlator mean performance, plotting output SNR vs integration time 07 p1059 A71-18851
- Analog surveillance radar signal analysis by digital storage and evaluation methods 08 p1252 A71-20745
- Information transmission rate and error probability in analog feedback systems, showing normalized maximum transmission speed dependence on signal to noise ratio 08 p1268 A71-21283
- Magnetic tape recording systems nonlinear amplitude distortion in terms of transfer function characteristics applied to analog instrumentation 09 p1449 A71-22786
- Special purpose analog and digital data acquisition systems for test and instrumentation requirements 09 p1449 A71-22789
- Analog, digital and special data processing equipment interface for aerospace computer system 11 p1735 A71-25844
- MODAPS real time data processing system for modal vibration testing consisting of analog subsystems, digital interfaces and on-line minicomputer 11 p1746 A71-26502
- Vibration data analysis of analog and digital methods for cost comparisons 14 p2221 A71-30057
- Discretization interval in discrete analog filters for optimal processing of complex radar signals, estimating systematic errors 14 p2194 A71-30081
- Optimal inertialess transformation of output signals from several devices, noting method application to analog data processing systems 16 p2550 A71-33892
- Analog error correcting redundancy codes, examining coding and decoding procedures 17 p2701 A71-34967
- Optical grating measuring systems high resolution interpolation using phase analog and digital counter techniques 17 p2745 A71-35293
- Wideband communications theory applied to continuous analog signals using frequency and amplitude modulation 19 p3015 A71-37254
- Incoherent carrier communications system, obtaining message SNR of 60-70 dB for analog signals with compound pulse modulation and carrier clipping 21 p3347 A71-40375
- Surface wave digital and analog signal processing filters for time delayed, frequency or phase coded transmission and reception applications 21 p3357 A71-40811
- Signal to quantizing noise ratios for differential PCM systems used to encode analog signals from Markov processes into digital form 22 p3514 A71-42391
- Analog data computation with hybrid and logic operational elements, applying to periodic function arithmetic mean determination and transistor characteristics representation 22 p3518 A71-42430
- ANALOG SIMULATION**
- Hybrid computer programming for continuous systems simulation 01 p0046 A71-10201
- Critical flutter of wing with rigid aileron studied by analog computer modeling 01 p0169 A71-10606
- Analog device for harmonic functions modeling and electron plasma dispersion function computation 01 p0135 A71-11078
- Large hybrid simulation and analog section replacement by digital model, considering digital simulation techniques for economical solution of special problems class 02 p0227 A71-11797
- Thermionic Diode Kinetics Experiment with on-line analog computer simulation, investigating thermionic reactor powerplant dynamics and control by non-nuclear means 02 p0195 A71-12258
- Thermionic Diode Kinetics Experiment analog simulation results concerning coupling, burnout, startup, etc 02 p0196 A71-12259
- Communication satellite earth station steerable antennas drive train resonance and traction drive wheel slippage control by differential velocity feedback, discussing analog simulation 02 p0222 A71-12790
- Human cardiovascular control system model by analog computer program for various work loads up to submaximal, estimating correspondence to real life 03 p0368 A71-12995
- Flight simulation requirements and design, considering analog computers, myion platforms and visual systems 04 p0566 A71-14996
- Analog and digital methods for interactions between aircraft lifting elements in steady or unsteady supersonic flow [ONERA-TP-850] 04 p0527 A71-15358
- Cochlear nerve fibers two tone inhibition as signal suppressions inherent to bandpass nonlinearities, using modified analog model and mathematical analysis 05 p0712 A71-16280
- Multipath effects on FM communication systems performance, using analog computer simulation 08 p1255 A71-21597
- Radar analog simulators for Polish air traffic controllers training, describing optical and electronic equipment 09 p1428 A71-22950
- Stable system identification by equivalent structure model on analog computer with standard rectangular pulse input signal 09 p1413 A71-23567
- Vestibular system functions physical analog model, predicting responses to motion inputs and possible problems for flight situations 10 p1569 A71-24237
- Stationary and dynamic characteristics of integrators with dosage capacitor for analog frequency measurements, analyzing dynamic response at large modulation depth via analog computer simulation 10 p1589 A71-24502
- Open loop transient analysis of thermionic diode kinetics experiment with analog computer nuclear reactor simulator 11 p1797 A71-25904
- Analog computer power relay analysis simulating flux, coil current, moving mass motion and magnetic and spring forces as function of time 13 p2001 A71-28839
- Analog simulation of cardiac malfunctions associated with A-V conduction block and Wenckebach phenomenon, using P and R wave and internal function generators 13 p2020 A71-29001
- Quasi-point type radar target angular motion simulation by controlling electromagnetic wave phase front in receiving field 14 p2193 A71-29825
- Pin-ended column stability and random behavior under white noise excitation, using analog simulation and application to vertical earthquake and aerospace vibration environments 14 p2330 A71-30683
- Vibration simulation of elastohysteric systems on analog computers using photocurrent-voltage relationship of polycrystalline photoresistors 16 p2658 A71-33978
- Large deflections of thin piecewise prismatic elastic bars by electronic analog computer simulation 16 p2661 A71-34117
- Intelsat 4 communication system simulation by transponder engineering model to test performance objective concerning baseband distortion and intermodulation 17 p2705 A71-35102
- Analog analysis of shape history of ablating graphite nose tips of reentry vehicle, eliminating geometrical instabilities 18 p2984 A71-35953
- Fail operational control moment gyro configuration of four single gimbal gyros, eliminating cross coupling by simple analog steering law [AIAA PAPER 71-936] 19 p3097 A71-37181
- Jet streams simulation method by electrohydrodynamic analog, using principle of mapping free lines of flow 19 p3043 A71-37542
- Hybrid electromechanical analog computer real time simulation technique for optimizing vibration response of two degree of freedom system with impact damper [ASME PAPER 71-VIBR-119] 21 p3350 A71-40338
- Mathematical model for pulse waveform identical with single integrator delta modulator, using analog techniques of angle modulation and sampling 22 p3522 A71-42276
- Laboratory analog simulation of absorption line spectra in cloudy planetary atmospheres, comparing with computational model based on plane parallel atmosphere 23 p3700 A71-43075
- Analog transistor model for IC simulation, discussing static characteristics and switching times 23 p3650 A71-43350
- Soviet book on rational, irrational and transcendental transfer functions electronic modeling covering mathematical theory and applications to control plants 23 p3648 A71-44185
- Analog modeling of enzyme and biochemical systems with fixed and variable functional properties, using operational amplifier integrator 24 p3802 A71-45109
- Algorithm for preparation of nonlinear differential equations for simulation by analog computer in linear form 24 p3807 A71-45156
- ANALOG TO DIGITAL CONVERTERS**
- Analog computers seven segment numeral display, describing code converters 01 p0049 A71-10261
- Weather radar automatic data processing system for digitizing echo reflectivity by Video Integrator and Processor 01 p0050 A71-10594
- Cascade type analog-to-digital converter with successive bit determination by recycling through single operational amplifier and comparator 02 p0231 A71-12038
- Analog inertial sensor digitizing methods, discussing pulse rebalancing and analog to digital conversion 02 p0279 A71-12453
- ECG signal analog to digital conversion at sampling rate and quantizing accuracy for minimal losses and/or distortion 02 p0208 A71-12949
- Canonic synthesis of electronic relays, considering cascade connected isolation box, analog to digital converter and switch 03 p0393 A71-14469
- Blink comparator with automated precision reading for converting rotation angles to digital form for binary star measurements 04 p0534 A71-14853
- Temporal stability of operating points on curves of signals from time interval sensors in angle code converters 06 p0873 A71-17522
- Analog to digital conversion mathematical model, considering comparators dynamic properties effects on optimal algorithms selection 06 p0871 A71-17523

Analog to digital converter optimal algorithm for detecting and correcting errors caused by pulsed noise at input
 06 p0871 A71-17524
 Photogrammetric data digitization system with terrain model measurement and mapping capability
 06 p0901 A71-18294
 Analog to digital converter noise power generation due to quantization and saturation effects under Gaussian input
 07 p1059 A71-18852
 Servo stability of binary code follow-up analog-digital converter with magnetic modulated zero elements
 08 p1261 A71-20736
 ATC automation program for en route and terminal centers, discussing combined nationwide system features, IFR volume and video digitizer data links
 08 p1332 A71-21659
 MODAPS real time data processing system for modal vibration testing consisting of analog subsystems, digital interfaces and on-line minicomputer
 11 p1746 A71-26502
 Analog to digital converters employing subharmonic oscillator phase as recording medium, discussing parametron application as phase comparator
 11 p1743 A71-26541
 German monograph on PHENO hybrid computing elements for nonlinear operations covering ADC and DAC, level and time quantization effects on computational accuracy, etc
 14 p2207 A71-30238
 Variable star brightness measurement, using on-line electronic computer, analog to digital converter and reflector with direct current amplifying photometer
 17 p2741 A71-34990
 Photogrammetric three dimensional digitizer for automatically measuring and recording automotive models dimensions
 17 p2744 A71-35288
 Electronic two axis digitizer, discussing electromagnetic measuring concept, modular design, reliability and economics
 17 p2711 A71-35291
 Large scale MOS IC digital VOR navigation converter, comparing accuracy, size, weight and cost with standard design
 17 p2776 A71-35789
 Digital data acquisition and processing systems for large quantity rapidly generated measurements using reduction computer
 18 p2885 A71-36160
 Fluidics analog to digital signal techniques, discussing data transmission, acquisition and processing
 18 p2851 A71-36206
 Flying spot digitizer angle encoding system, describing multispeed transducer output conversion to digital format
 18 p2925 A71-36914
 Digital techniques for tactical radar signal processing functions, discussing low cost integrated circuitry, moving target indicators, and analog to digital converters
 21 p3348 A71-40588
 Multijunction functional devices for operation as decade digital counter, step voltage generator, analog/digital converter, binary counter, neuristor line, etc
 22 p3520 A71-41706
 Binary parabolic phase coded waveform generation from analog signals by pi-quantization
 23 p3645 A71-43440
 All-electronic synchro-digital converter design using hybrid tracking mode circuit
 24 p3811 A71-45298
ANALOGIES
NT HYDRAULIC ANALOGIES
 Hypothetical analogy between wave formation during explosive welding and Karman vortex street arising in liquid flow around cylinder
 19 p3068 A71-37083
ANALOGS
 Three mass vibrational impact system analysis by mathematical electronic analogs, examining system and excitation parameters influence on vibrational modes and dissipative properties
 05 p0821 A71-16357
 Image restoration from random fluctuations, developing analog procedure from time dependent functions of spatial frequencies and approximation
 09 p1407 A71-23048
 Various configuration thermal contacts, examining conductance with electric analog
 [AIAA PAPER 71-437]
 Maxwell equations analog for gravitational fields, considering Maldybaeva equation as condition for gravitational waves existence in Riemann manifold
 12 p1931 A71-27243
 Newtonian analog construction, examining relativistic homogeneous anisotropic models
 24 p3873 A71-45110
ANALYSIS [MATHEMATICS]
NT ABEL FUNCTION
NT AIRY FUNCTION

NT ANALYTIC FUNCTIONS
NT APERIODIC FUNCTIONS
NT ASYMPTOTES
NT ASYMPTOTIC SERIES
NT BANACH SPACE
NT BESSEL FUNCTIONS
NT BIHARMONIC EQUATIONS
NT BINARY INTEGRATION
NT BLASIUS EQUATION
NT BOREL SETS
NT BURGER EQUATION
NT CALCULUS OF VARIATIONS
NT CAUCHY INTEGRAL FORMULA
NT CAUCHY-RIEMANN EQUATIONS
NT COLLINEARITY
NT COMBINATORIAL ANALYSIS
NT COMPLEX VARIABLES
NT CONFORMAL MAPPING
NT CONJUGATES
NT CONTINUITY [MATHEMATICS]
NT CONVOLUTION INTEGRALS
NT COPLANARITY
NT CUBIC EQUATIONS
NT CURL [VECTORS]
NT DELTA FUNCTION
NT DEPENDENT VARIABLES
NT DIFFERENTIAL CALCULUS
NT DIFFERENTIAL EQUATIONS
NT DUFFING DIFFERENTIAL EQUATION
NT EINSTEIN EQUATIONS
NT ELLIPTIC DIFFERENTIAL EQUATIONS
NT ELLIPTIC FUNCTIONS
NT ENTIRE FUNCTIONS
NT EXISTENCE THEOREMS
NT EXPONENTIAL FUNCTIONS
NT EXTREMUM VALUES
NT FALKNER-SKAN EQUATION
NT FOKKER-PLANCK EQUATION
NT FOURIER ANALYSIS
NT FOURIER SERIES
NT FOURIER TRANSFORMATION
NT FREDHOLM EQUATIONS
NT FUNCTION SPACE
NT FUNCTIONAL ANALYSIS
NT FUNCTIONAL INTEGRATION
NT GAMMA FUNCTION
NT GAUSS EQUATION
NT GREEN FUNCTION
NT HALF PLANES
NT HALF SPACES
NT HANKEL FUNCTIONS
NT HARMONIC ANALYSIS
NT HARMONIC FUNCTIONS
NT HELMHOLTZ VORTICITY EQUATION
NT HILBERT SPACE
NT HILBERT TRANSFORMATION
NT HYPERBOLIC FUNCTIONS
NT HYPERGEOMETRIC FUNCTIONS
NT HYPERPLANES
NT INTEGRAL CALCULUS
NT INTEGRAL EQUATIONS
NT INTEGRAL TRANSFORMATIONS
NT JACOBI INTEGRAL
NT JACOBI MATRIX METHOD
NT KERNEL FUNCTIONS
NT LAGUERRE FUNCTIONS
NT LAPLACE TRANSFORMATION
NT LEBESGUE THEOREM
NT LEGENDRE FUNCTIONS
NT LIAPUNOV FUNCTIONS
NT LIMITS [MATHEMATICS]
NT LINEAR EQUATIONS
NT LIOUVILLE EQUATIONS
NT LIOUVILLE THEOREM
NT LIPSCHITZ CONDITION
NT LOGARITHMS
NT MATHIEU FUNCTION
NT MEASURE AND INTEGRATION
NT MEROMORPHIC FUNCTIONS
NT NEUMANN PROBLEM
NT NONLINEAR EQUATIONS
NT NUMERICAL ANALYSIS
NT NUMERICAL INTEGRATION
NT ORTHOGONAL FUNCTIONS
NT PADE APPROXIMATION
NT PARABOLIC DIFFERENTIAL EQUATIONS
NT PARTIAL DIFFERENTIAL EQUATIONS
NT PERIODIC FUNCTIONS
NT PHASE-SPACE INTEGRAL
NT POISSON EQUATION
NT POWER SERIES
NT QUADRATIC EQUATIONS
NT RATIONAL FUNCTIONS
NT REAL VARIABLES
NT RUNGE-KUTTA METHOD
NT SCHWARZ-CHRISTOFFEL TRANSFORMATION
NT SERIES [MATHEMATICS]
NT SINE SERIES
NT SINGULAR INTEGRAL EQUATIONS
NT SINGULARITY [MATHEMATICS]
NT SPHERICAL HARMONICS
NT STIELTJES INTEGRAL
NT STURM-LIOUVILLE THEORY
NT TAYLOR SERIES
NT TESSERAL HARMONICS

NT TRIGONOMETRIC FUNCTIONS
NT VECTOR ANALYSIS
NT VLASOV EQUATIONS
NT VOLTERRA EQUATIONS
NT VORTICITY
NT WEIERSTRASS FUNCTIONS
NT WEIGHTING FUNCTIONS
NT WHITTAKER FUNCTIONS
NT WIENER HOPF EQUATIONS
NT ZONAL HARMONICS
 Orbiting gyrostats stability elementary cases analysis, examining existing methods and developing new method involving less computational labor
 01 p0163 A71-10123
 Neutral and superneutral equations properties analysis and existence theorems, using successive approximation procedures
 02 p0275 A71-11723
 Linear complexes in three dimensional space considered with canonical transverse system, discussing nonintegral presentation and existence theorem
 12 p1922 A71-27119
 Digital computers for analytic solution of second order nonlinear ordinary differential equations
 18 p2884 A71-36142
ANALYTIC FUNCTIONS
NT ENTIRE FUNCTIONS
 Lubrication hydrodynamics differential equation of ferrous analytic solutions for essential practical cases by use of suitable gap profile expressions
 01 p0085 A71-10121
 N-body problem real singularities in celestial mechanics, considering present status and holomorphic motion
 01 p0154 A71-10384
 Shells with positive Gaussian curvature, deriving p-analytic functions for zero bending stress state and infinitesimal deflections of middle surface
 01 p0168 A71-10415
 Weakly differentiable functional systems related to analytic functions with parametric representation via Stieltjes integral, discussing range theorems
 02 p0276 A71-11724
 Zero bending moment shells of revolution under concentrated load, using boundary value problem for p-analytic functions
 02 p0328 A71-12539
 Quasi-H-analytic function classes sufficient conditions for second order linear hyperbolic type H/Hadamard/ operator
 06 p0918 A71-17575
 Main mixed axisymmetric stress for elastic half space with single line separation between boundary conditions, using p-analytic functions
 06 p1001 A71-18341
 Axisymmetric stress in sphere and space with spherical cavity, using p-analytic functions
 06 p1001 A71-18343
 Axisymmetrical potential theory for two spherical circular disks system, using X-analytic functions for reducing to Fredholm equation
 06 p0928 A71-18345
 Triple integral equations solution based on analytic functions theory, applying to stress-strain state in plate with two equal collinear cracks
 06 p1002 A71-18346
 Analytic functions approximation in complex regions with aid of different systems of functions
 07 p1146 A71-19041
 Analytic function steady approximation with aid of polynomials in given region, considering Dirichlet series
 07 p1146 A71-19042
 Boundary value problems of analytic functions and singular integral equations, considering hydromechanics and elasticity theory applications
 07 p1148 A71-20077
 Polygonal elastic plates natural frequencies investigation by conformal mapping and variational method, transforming holomorphic function into equivalent problem of circular boundary plate
 10 p1691 A71-24813
 Critical stability solutions to ordinary second order differential equations including holomorphic functions with series expansions
 12 p1930 A71-27238
 Automatic numerical evaluation of definite integrals of analytic functions, considering Simpson rule, Gauss quadrature, subdivision and whole interval formulas
 12 p1923 A71-27732
 Conditions for obtaining analytical expressions for eigenvalues and eigenfunctions of homogeneous Fredholm equation
 13 p2096 A71-28015
 System of n plus 1 differential equations with right members in coordinate origin neighborhood represented by holomorphic functions of dependent variables
 16 p2603 A71-33530
 Jacobi polynomial series analytic continuity properties based on relation with corresponding Taylor series
 17 p2764 A71-34421
 Soviet book on theory of elliptic functions covering analytic functions, Jacobi and Liouville theorems,

- modular functions, Weierstrass functions, theta and Jacobi functions 17 p2767 A71-35200
- Regular boundary value problems singularities for linear second order analytic elliptic equations solutions in two independent variables 18 p2942 A71-36925
- Exponential continually discrete analytic functions of complex variable in explicit form, obtaining addition theorem for trigonometric functions 19 p3089 A71-38479
- Holomorphic matrix valued function on connected open subset of complex plane, obtaining conditions for satisfying homogeneous linear differential equation 21 p3410 A71-41185
- Cauchy problem theory covering analytic and nonanalytic functions, Gevrey function spaces, hyperbolic operators and differentiable functions spaces 22 p3566 A71-41513
- ANALYTIC GEOMETRY**
- NT HYPERBOLAS
- NT LOCI
- NT MERCATOR PROJECTION
- NT OBLATE SPHEROIDS
- NT PROLATE SPHEROIDS
- NT S CURVES
- NT SPHEROIDS
- NT TORUSES
- Rigid plane skeletal structures combinational properties, considering analytic geometry criteria and graphs from algorithm 02 p0327 A71-12395
- Body of revolution potential expanded in spherical function series, showing analytical density limited by surface 10 p1679 A71-24934
- Gamma phase composition estimation in Ni base superalloys by phase rule principles and analytic geometry 13 p2089 A71-29407
- Field produced by equilibrium electron distributions on analytic Jordan curve 21 p3419 A71-41082
- ANALYTICAL CHEMISTRY**
- Analytical sensitivity and reproducibility in plasma jet excitation for spectrochemical applications 03 p0465 A71-13970
- Book on hydrazino-hydrazide groups covering experimental details and applications of various analysis methods 05 p0718 A71-17009
- ANALYZERS**
- NT ENGINE ANALYZERS
- NT SIGNAL ANALYZERS
- Adapted multichannel analyzer for cardiology visualizing vectorcardiographic loops 02 p0206 A71-12107
- Optic analyzer dark adaptation dynamics during spatial body position changes, observing restoration speed dependence on physical training 03 p0364 A71-13523
- Photoelectron spectroscopy energy analyzer with spherical retarding field screen, discussing electronic circuit configuration, operational characteristics and spectral resolution 04 p0600 A71-15590
- Small mass spectrometers as substance specific detectors for gas chromatography, differential thermal analysis and thermogravimetry 04 p0601 A71-15916
- Low temperature material properties analyzer with superconducting microwave resonant cavity 07 p1179 A71-20160
- Motor analyzer role in animal orientation to external conditions 08 p1243 A71-21969
- Human visual analyzer excitability shifts due to short duration point light stimuli 08 p1243 A71-21972
- Theoretical and experimental performance studies of quadrupole mass analyzers with round and hyperbolic field forming surfaces, noting resolving power superiority of hyperbolic rods 11 p1760 A71-25219
- Visual and vestibular analyzer interaction, noting reduction in duration of counterrotation illusion and postrotation nystagmus in humans 22 p3505 A71-42797
- ANATOMY**
- NT ADRENAL GLAND
- NT AORTA
- NT ARM [ANATOMY]
- NT ARTERIES
- NT BARORECEPTORS
- NT BLADDER
- NT BLOOD VESSELS
- NT BONES
- NT BRAIN
- NT BRAIN STEM
- NT BRONCHI
- NT BRONCHIAL TUBE
- NT CAPILLARIES [ANATOMY]
- NT CARDIAC VENTRICLES
- NT CARDIOVASCULAR SYSTEM

- NT CEREBELLUM
- NT CEREBRAL CORTEX
- NT CEREBRUM
- NT CHEMORECEPTORS
- NT CHEST
- NT CHOROID MEMBRANES
- NT CIRCULATORY SYSTEM
- NT COCHLEA
- NT COLLAGENS
- NT CONNECTIVE TISSUE
- NT CORNEA
- NT CORTI ORGAN
- NT CRANIUM
- NT DIAPHRAGM [ANATOMY]
- NT DIASTOLE
- NT EAR
- NT ENDOCRINE GLANDS
- NT ERYTHROCYTES
- NT ESOPHAGUS
- NT EYE [ANATOMY]
- NT FEMUR
- NT FINGERS
- NT FLEXORS
- NT FOREARM
- NT FOVEA
- NT GLANDS [ANATOMY]
- NT GLOMERULUS
- NT GRAVIRECEPTORS
- NT HAND [ANATOMY]
- NT HEAD [ANATOMY]
- NT HEART
- NT HEMATOPOIESIS
- NT HEMATOPOIETIC SYSTEM
- NT HIPPOCAMPUS
- NT HUMAN BODY
- NT JOINTS [ANATOMY]
- NT KIDNEYS
- NT KNEE [ANATOMY]
- NT LABYRINTH
- NT LEG [ANATOMY]
- NT LEUKOCYTES
- NT LIMBS [ANATOMY]
- NT LIVER
- NT LUNGS
- NT LYMPHOCYTES
- NT MARROW
- NT MASTOIDS
- NT MECHANORECEPTORS
- NT MIDDLE EAR
- NT MUSCULOSKELETAL SYSTEM
- NT MYOCARDIUM
- NT NECK [ANATOMY]
- NT NOSE [ANATOMY]
- NT OCCIPITAL LOBES
- NT OCULOMOTOR NERVES
- NT ORGANS
- NT OTOLITH ORGANS
- NT PANCREAS
- NT PELVIS
- NT PHARYNX
- NT PHOTORECEPTORS
- NT PINEAL GLAND
- NT PITUITARY GLAND
- NT PROPRIOCEPTORS
- NT PUPILS
- NT RESPIRATORY SYSTEM
- NT RETICULOCYTES
- NT RETINA
- NT SCIATIC REGION
- NT SEMICIRCULAR CANALS
- NT SENSE ORGANS
- NT SKULL
- NT SPLEEN
- NT STOMACH
- NT SYSTOLE
- NT THERMORECEPTORS
- NT THYROID GLAND
- NT TIBIA
- NT TORSO
- NT UTERUS
- NT VASCULAR SYSTEM
- NT VEINS
- NT VERTEBRAE
- NT VERTEBRAL COLUMN
- NT VESTIBULES
- Papers on anatomy and mechanisms of mammalian sensory systems including vision, audition and touch 14 p2183 A71-30251
- Heat removal from space suit, discussing anatomic and physiological features suitable for cooling 20 p3188 A71-39224
- ANDESITE**
- Fe content of clinopyroxene in basalt-basaltic andesite-andesite-latitude of Mogollon Plateau/New Mexico/ 20 p3216 A71-39386
- ANDROMEDA GALAXIES**
- Andromeda galaxy M31 hydrodynamic model, examining kinematical and dynamical functions 01 p0150 A71-10057
- OB stars existence on utmost borders of M 31, using photometric statistics 02 p0312 A71-12465
- Compact galaxies one-magnitude light outburst near M3, discussing photometric statistical data 02 p0313 A71-12469

- Color changes and absorption line variations in M31, M32 and NGC 4472, attempting synthesis of M31 disk population 07 p1197 A71-19814
- Local group stellar systems including Galaxy, Magellanic Clouds, Andromeda galaxy, triangulum and spherical dwarf galaxies 18 p2966 A71-36759
- Spiral structure OB associations in outer regions of Andromeda nebula, investigating blue objects in U and B plates of Schmidt telescope 21 p3451 A71-40723
- ANEOCHIC CHAMBERS**
- Impulsive sound signals perceived noisiness in anechoic chamber, investigating duration, intersignal interval, repetition and frequency effects 05 p0712 A71-16277
- Sound field due to point source inside absorbent lined enclosure for anechoic chamber performance prediction 07 p1160 A71-19587
- Time dependence of radial mechanical driving point impedance of Al cylindrical shell immersed in two anechoic tanks related to chemical reaction 23 p3662 A71-43215
- ANELASTICITY**
- Convective heat transfer in stars from anelastic and Boussinesq approximations, discussing two dimensional solutions, truncated expansions, turbulence and mixing length theories, etc 18 p2968 A71-37038
- Spectral model of warm bubble motion in neutral surroundings from anelastic equations for shallow convection, comparing results with similarity theory and numerical models 23 p3781 A71-43336
- ANEMIAS**
- Erythrocytes diphosphoglycerate increase mechanisms during hypoxia and anemia, studying hemoglobin oxygenation state effects 17 p2685 A71-35368
- Photoplethysmographic analysis of pulse wave velocity in healthy subjects and in patients with hypertension, heart disease, diabetes and anemia 22 p3490 A71-42518
- White rats resistance to acute anoxic, anemic and histotoxic hypoxia during various phases of X radiation sickness, studying adrenal cortex histophysiological state 22 p3494 A71-42731
- ANEMOMETERS**
- NT HOT-FILM ANEMOMETERS
- NT HOT-WIRE ANEMOMETERS
- NT SONIC ANEMOMETERS
- Yaw sphere and thermometer combination, examining proportional vertical heat flux 03 p0422 A71-13231
- Thermoanemometer frequency characteristic determination, simulating turbulent oscillations by plane acoustic waves 05 p0753 A71-16845
- Turbulence measurement by electrothermoanemometry, discussing method errors 05 p0753 A71-16846
- Velocity and density measurements in hypervelocity ballistic projectile turbulent wakes, using hot film anemometers [AIAA PAPER 68-701] 07 p1015 A71-19891
- Jet flow deflection by cross flowing stream applied to low velocity anemometers 07 p1030 A71-20596
- Turbulent velocity pulsations measurement by conduction anemometer with three-electrode sensor 09 p1499 A71-22132
- Turbulent supersonic flow measured by laser anemometry, stressing advantages over optical heterodyning 09 p1453 A71-23693
- Mean wind velocity and turbulence remote measurement with laser anemometry, using intensity modulation technique 10 p1623 A71-25091
- Thermosensitive quartz anemometer operating in vibrational mode, discussing design and applications in low airflow velocity measurement 12 p1906 A71-26826
- Calibration and operation of corona discharge anemometer involving highly stressed anode and large plate cathode 13 p2066 A71-28156
- Wheatstone bridge with thermistors, discussing linearity, sensitivity and applications for temperature difference and flow velocity measurements /anemometers/ 13 p2071 A71-29278
- Thermal diffusion effect on gas flow velocity measurements with anemometers with heat convection signals 14 p2239 A71-29815
- Anemometer measurement optimum averaging time of wind speed for conventional aircraft landings 14 p2270 A71-30394
- Single anemometer wind measurement required for aircraft landing, comparing data from different sampling periods 14 p2270 A71-30395

Fan-produced sound pressure fluctuation in very low speed subsonic wind tunnel test stream, noting resulting anemometer calibration errors
14 p2275 A71-30526

French monograph on thermal microflowmeters covering anemometers, fluid mechanics, Nusselt number, thermocouple flowmeters
17 p2744 A71-35228

Fast response anemometer for measuring atmospheric wind speeds and turbulence components
17 p2745 A71-35327

Laser Doppler anemometer, defining signal transmission region and spectrum bandwidth/amplitude from photocurrent and single moving scattering particle emission
17 p2745 A71-35328

Laser velocimeter for wide range velocity measurement, using photodetector to observe light scattering by particles flowing across fringe pattern
18 p2932 A71-36618

Cooled film anemometer techniques for hypersonic wake temperature and velocity distribution measurements for projectiles in free flight range
21 p3363 A71-40386

Miniature wind tunnel velocity field calibration for testing anemometers, using null method with spherical probe
21 p3384 A71-41380

Ion anemometer for measuring wind velocity magnitude and direction in rarefied Martian atmosphere
22 p3600 A71-41960

Optical anemometers for local nondestructive flow velocity measurements, discussing signal analysis possibilities
23 p3679 A71-43952

ANEMOMETRY
U VELOCITY MEASUREMENT
ANESTHESIA
Human legs thermal response during cooling for refrigeration anesthesia, deriving analytical model for temperature level prediction as function of time
04 p0545 A71-15160

Dynamic respiratory and circulatory responses to hypoxia in anesthetized dogs, recording oxygen partial pressures, heart rate, blood pressure, blood flows, respiratory rate, etc
09 p1396 A71-23358

Helium and nitrogen breathing effects upon intraocular pressure during and after near vacuum exposure in anesthetized and unanesthetized dogs
09 p1400 A71-23359

ANESTHESIOLOGY
Book on clinical physiology techniques and anesthesiology measurements covering electronics, ECG analysis, blood pressure measurement, cardiac function, respiratory mechanics, etc
09 p1398 A71-22459

ANESTHETICS
NT CHLOROFORM
NT CYCLOPROPANE
Sequential dual wavelength IR gas analyzers for anesthetics research and chemical plant process streams analysis
22 p3545 A71-42156

Receptive fields of dark adapted cats striate cortex neurons as function of barbiturate anesthetic level
23 p3634 A71-43871

ANGLE OF ATTACK
NT ZERO ANGLE OF ATTACK
Three dimensional attached compressible laminar boundary layer on slender cones in hypersonic flight at high angles of attack derived by numerical integration
01 p0070 A71-10926

Pressure distributions prediction on blunt bodies at angle of attack, considering bodies of revolution and large angle cones
01 p0004 A71-11580

Aircraft propulsive thrust moment effect on phugoid motion, examining angle of attack and flight path variations with resulting instability
03 p0347 A71-13340

Rocket optimum control synthesis for powered flight phase, determining angle of attack for transfer to maximum velocity by Cauchy problem
05 p0779 A71-16038

Reentry vehicle angle of attack control by mechanically varying center of mass for axial loads
05 p0779 A71-16039

Supersonic flow field around flat plate at various angles of attack, comparing Brieden and Lighthill approximations
05 p0694 A71-16713

Flight range and optimum angle of attack under wind conditions of constant velocity and direction, considering fuel consumption for given distance
06 p0847 A71-18325

Turbulent heat transfer measurements on blunt cone in nitrogen flow at high Mach number under various angles of attack
06 p1008 A71-18499

Angle of attack amplification due to body trim plane rotation, obtaining pertinent relations by method of stationary phase
06 p0980 A71-18509

Finned missiles aerodynamics at high angle of attack, examining body vortex wake region interaction with fins
06 p0980 A71-18511

Three dimensional inviscid compressible flow past sharp shouldered blunt bodies at angle of attack, presenting time dependent finite difference technique
06 p0843 A71-18515

Atmospheric reentry dynamics of spinning body with trim angle of attack
07 p1205 A71-18892

USAF F-4E Stall/Near Stall Investigation, discussing testing requirements, fighter aircraft improvement, spin avoidance and high angle of attack limitations
07 p1019 A71-19095

Nose bluntness, angle of attack and oscillation amplitude effect on hypersonic unsteady aerodynamics of slender cones
07 p1016 A71-19895

Angle of attack vertical variations of free flight trajectory missile, estimating missile, trajectory and atmospheric parameters effects on fluctuations relative to center of mass
08 p1367 A71-22051

Dynamic instability of finned missiles occurring as angle of attack undamping and caused by differential lift from windward and leeward fins
09 p1530 A71-22075

Shock wave shape attached to cone moving in ideal gas studied by Pade-Shanks approximation method, considering angle of attack
09 p1431 A71-22405

Plenum chamber with nozzle wind tunnel model, noting jet flow phenomena at various angles of attack
10 p1590 A71-24865

Tail flutter analysis, considering dihedral, angle of attack and aerodynamic force effects
11 p1706 A71-25188

Lifting surfaces supersonic-hypersonic flutter at angle of attack determined by shock expansion, Newtonian flow and local flow piston theory
11 p1842 A71-25307

Unsteady flow measurement around wing sections during rapid angle of attack variations, emphasizing helicopter rotor blades
12 p1864 A71-27468

Air flow about low aspect ratio delta wing at large angles of attack, deriving lift coefficient
13 p1990 A71-28282

Aircraft flight characteristics dependence on angle of attack, roll and pitch
13 p1997 A71-29043

Dimensionless strength characteristics of convex bodies vs angles of attack in rarefied gas flows by linear regressive analysis using statistical model
13 p1991 A71-29147

Quasi-stationary gliding trajectories of aircraft in planetary atmosphere during constant control of attack and bank angles
13 p2143 A71-29185

Hypersonic flow around delta wing at small angles of attack, using pressure sources method and Fredholm integral equation
13 p1992 A71-29189

Elliptical cones at large angle of attack, calculating three-component real gas properties effects on aerodynamic characteristics
13 p1993 A71-29191

Spacecraft optimal atmospheric reentry trajectory for minimum flight distance, investigating angle of attack control with allowance for load constraints
13 p2143 A71-29229

Air flow past small aspect ratio thick-section wing at small angles of attack, investigating vortex system effect on flow characteristics in absence of lift
13 p1994 A71-29234

Slender cone boundary layer transition under angle of attack at Mach 21 with promoted leeward and fixed windward ray
14 p2335 A71-29887

Supersonic mass flux probe description, discussing inlet geometry, angle of attack and Reynolds and Mach numbers effects on performance
14 p2239 A71-29925

Supersonic potential flow at large distance from slender body of revolution at angle of attack, deriving nonlinear partial differential equations system
15 p2343 A71-31170

Hypersonic wakes behind wedges for various angles of attack, determining near and far wakes
15 p2344 A71-31558

Side forces on ogive cylinder bodies at large incidence as function of Mach number, nose fineness and bluntness ratios for laminar and turbulent boundary layers
15 p2345 A71-31563

Multicomponent nonequilibrium air flow past axisymmetric blunt body, calculating flow distribution at various attack angles with time dependent technique
15 p2512 A71-31575

Low speed testing of VTOL models in wind tunnels, describing method for estimating free air approach velocity and angle of attack
15 p2386 A71-32724

Rarefaction and angle of attack effects on delta wing in hypersonic flow in wind tunnel
16 p2520 A71-33376

Aircraft optimum control synthesis for powered flight phase, determining angle of attack for transfer to maximum velocity by Cauchy problem
16 p2523 A71-33442

Spacecraft reentry trajectory angle of attack control by mechanically varying center of mass for axial loads
16 p2645 A71-33443

Aircraft angle of attack limiter parameters, describing automatic warning system for impending stall
16 p2523 A71-33621

F-4E stall/spin development and flight tests, relating mass distribution and angle of attack aerodynamic design
16 p2524 A71-34008

High speed aircraft maneuvers stability determination by constant angular pitching/rotation velocity, angle of attack and flight speed, using Liapunov method
18 p2849 A71-36176

Dynamic parameters of supersonic flow incident on conical bodies at large angles of attack, considering flow field and entropy distribution
18 p2845 A71-36328

Aerodynamic characteristics of space shuttle configurations over entire flight velocity range, stressing coupling effects of control surfaces at large angles of attack
18 p2972 A71-36437

Heat transfer rate correlation with local surface pressure for blunt cones at angle of attack
20 p3176 A71-39355

Phugoid motion at constant angle of attack without thrust line displacement from aircraft center of gravity, noting longitudinal stability
21 p3324 A71-40168

Heat transfer and pressure distribution of cone shaped model at different angles of attack in hypersonic flow simulating reentry flight in wind tunnel
22 p3480 A71-41965

Windward injection into supersonic stream at angle of attack, minimizing vortex disruption
22 p3481 A71-42787

Angle of attack instrumentation for evaluating aircraft lift performance and phugoid oscillations
23 p3628 A71-43382

Lifting rectangular thin airfoil in symmetrical incompressible steady uniform orthogonal flow at small angle of attack, deriving Weissinger integral equation
23 p3625 A71-43487

Dynamic behavior of dissociating gas supersonic flow past blunt bodies at angle of attack
24 p3790 A71-44775

ANGLES [GEOMETRY]

NT ANGLE OF ATTACK
NT BRAGG ANGLE
NT BREWSTER ANGLE
NT DIHEDRAL ANGLE
NT ELEVATION ANGLE
NT SWEEP ANGLE
Linear algorithms for determining spacecraft relative orbital state using angle data with digital computer
01 p0163 A71-11588

Altitude and azimuth angle values computation using logarithmic and natural haversines table
02 p0280 A71-12899

Blink comparator with automated precision reading for converting rotation angles to digital form for binary star measurements
04 p0534 A71-14853

Action-angle variables for Euler-Poinsot problem of solid body free rotation about stationary point
05 p0783 A71-16996

Unresolved radar targets or multipath distortion determination by measurement of complex indicated angle on two pulses separated by short interval
07 p1058 A71-18843

Radar performance with multipath using complex angle /CA/ method for resolving low angle target, comparing S/N ratio with monopulse system without CA
07 p1058 A71-18844

Optimum tip vertex angles measurement for determining steels tensile strength and yield point from hardness
09 p1467 A71-22314

Rational scale selection for theoretical and experimental graphs, investigating slopes and angles between line segments for various parameters
09 p1439 A71-23347

Parallel plate electrostatic analyzer design, discussing second order focusing, angular aberrations and magnification
12 p1903 A71-26570

Maximum turning angle across oblique shock for fixed density ratio and for fixed upstream Mach number
15 p2392 A71-32125

Action-angle variables for Euler-Poinsot problem of solid body free rotation about stationary point
18 p2948 A71-36796

Optimum synthesis of spatial four-link chain mechanism with pressure angles deviating least from zero degrees for force transmission 24 p3848 A71-44900

Spacecraft orientation angle measurement by inertial sensors, analyzing equipment kinematic efficiency and limitations 24 p3829 A71-45318

ANGULAR ACCELERATION

Guinea pigs vestibular adaptation to repeated angular acceleration dependent on acceleration direction 01 p0012 A71-11056

Nystagmus extinction during repeated exposures to angular accelerations in labyrinthectomized guinea pigs 01 p0014 A71-11139

Rotating accelerometer with magnetic amplifier for angular acceleration detection, investigating static, dynamic and frequency response characteristics 02 p0252 A71-12421

Astronaut visual acuity under angular acceleration, considering vestibular stimulus direction and nystagmus upheating or downbeating 04 p0536 A71-14754

Human rotation perception, discussing man-carrying rotation device, angular acceleration threshold, etc 04 p0541 A71-14756

Earth rotational acceleration and polar secular motion changes, considering correlation with earthquakes 06 p0890 A71-17881

Unsteady viscous incompressible flow over impulsively started rotating disk by acceleration averaging method 07 p1088 A71-19356

Accelerometer for direct measurements of angular acceleration of rotating shafts, using semiconductor transducers 09 p1443 A71-22706

Thresholds comparison for angular acceleration derived by subjective cupulometry and by staircase method, determining thresholds for rotation perception and oculogyral illusion 10 p1570 A71-24605

Human response to and perception of angular acceleration, discussing implications for motion capability in flight simulator [AIAA PAPER 70-350] 10 p1571 A71-24860

Rotation perception in dark and oculogyral illusion, using power law to describe subjective vestibular sensation relation to angular acceleration stimulus pulses 13 p2022 A71-29327

Diffusion electrochemical linear and angular accelerations sensors, noting lack of friction surfaces 15 p2409 A71-32184

Optical tracking task performance and nystagmus during angular acceleration in yaw and pitch, comparing differences due to vertical and horizontal canal response 16 p2535 A71-33107

Angular accelerometer with paddle torsion damper, comparing sensitivity with ordinary inertial instrument 17 p2739 A71-34562

Gross locomotion and cargo handling in simulated artificial gravity environments, studying effects of Coriolis forces, angular accelerations, oculo-vestibular stimuli and traction variations [AIAA PAPER 71-886] 18 p2871 A71-36636

Accelerating rotating disks with variable thickness, presenting shear stress distribution 18 p2982 A71-36771

Optical tracking system for high angular acceleration missile flights, using movable mirrors with motion picture camera interfaced with computer 18 p2900 A71-36906

Angular acceleration measuring device based on closed loop wide bandwidth sensor, discussing theory of operation, performance and applications [AIAA PAPER 71-909] 19 p2995 A71-37160

Stroke number and vestibular nystagmus duration and frequency under successively increasing angular acceleration from tests on guinea pigs 20 p3189 A71-39238

Bull frog activity at rest and response to centripetal acceleration by on-board centrifuge in vestibular space experiment OFO-A 22 p3484 A71-41690

Correlation coefficients between sensitivity thresholds of cupula-endolymphatic system to angular and Coriolis accelerations with human resistance to motion sickness 24 p3795 A71-44532

Coordination structure of human hand arbitrary movements during stimulation of horizontal semicircular canals in vestibular apparatus by negative angular acceleration 24 p3796 A71-44545

ANGULAR CORRELATION

Angular estimation precision in amplitude monopulse off-boresight radar, using linear approximation to error curve 09 p1405 A71-22695

Inelastic scattering alpha-gamma angular correlations from C 12, Mg 24, Ni 58 and Sn 120 decay measurements 23 p3706 A71-43198

ANGULAR DISTRIBUTION

Ball bearing cage life, examining angular misalignment effect 01 p0086 A71-10297

Radio sources fine structure at 81.5 MHz, examining angular structure by interplanetary scintillation 01 p0158 A71-10769

High energy albedo neutrons energy and angular distributions, determining solar neutron flux upper limit 01 p0147 A71-11517

Earth atmosphere X ray absorption, determining photon flux, energy and angular distribution as function of altitude by Monte Carlo method 02 p0299 A71-11776

Asymmetrical cosmic ray showers kinematic interpretation by heuristic model, discussing particle dispersion angular distribution 03 p0476 A71-13843

Negative pi-N NN interactions in emulsion at high energies, plotting angular distributions of secondary particles in cosmic ray showers 03 p0476 A71-13847

Bremsstrahlung photons produced by cosmic ray muons in Fe and Pb at sea level, calculating energy spectra and angular distributions 03 p0477 A71-13863

Cosmic ray shower particles spatial and angular distribution structure near electron-photon cascade core 03 p0478 A71-13867

Inelastic alpha particle scattering experiment for studying energy spectrum and angular distribution of Sc-45 excited states 03 p0462 A71-14417

Angular distribution of atomic oxygen ions produced by electron bombardment of oxygen, showing electron energy dependence 04 p0631 A71-15657

Angular distribution and polarization of solar X-ray bremsstrahlung, taking into account magnetic field effects 05 p0000 A71-16032

Pitch angle distribution of protons and helium ions in magnetosphere from numerical solution of Fokker-Planck equation 06 p0964 A71-17285

Laser produced plasma expansion into vacuum, discussing ion energy angular distributions measurement 06 p0938 A71-18460

Thermal radiation from finite cylindrical particle cloud, determining far field angular distribution by Monte Carlo method [AIAA PAPER 71-78] 06 p1008 A71-18535

Ionospheric low energy electron and proton fluxes near equator from Isis 1 satellite soft particle spectrometer observations, considering energy spectra and pitch angle distribution 07 p1187 A71-19679

Atmospheric excess radiation flux azimuthal asymmetry in equatorial region, discussing angular intensity distribution data from Proton 2 Cerenkov counter 08 p1354 A71-21011

Electron emission from He ion by proton bombardment, calculating double differential cross sections relative to ejection energy and angle 09 p1497 A71-22415

Electron energy spectra construction from Al, Sn and Au target layers transmission angular distribution measurements, using computer calculated spectra for comparison 09 p1497 A71-22688

Solar wind blast wave dependence on initial disturbance energy and angular extent by time dependent two dimensional hydrodynamic flow simulation 10 p1663 A71-24779

Angular, spectral and temporal properties of Cerenkov radiation in cosmic ray extensive air showers 11 p1815 A71-25594

Flow variation effect on velocity and flow angle distribution at exit of shrouded radial flow impeller with backward swept blades, using streamline curvature method [ASME PAPER 71-GT-15] 11 p1703 A71-25961

Quasar 3C 147 angular structure observations, using long baseline interferometer 11 p1830 A71-26113

Water and ice cloud discrimination by angular distribution measurement of various polarization parameters of scattered laser beam radiation, using Mie theory 11 p1776 A71-26298

Preferential orientation of physical galactic pairs, obtaining equatorial plane inclinations and major axes positional angles distribution 12 p1955 A71-26582

Zenith angular air shower distribution by Monte Carlo method, discussing muons horizontal component separation from background events 12 p1951 A71-27385

Zenith angle distribution of atmospheric muons at Mt. Chalcaltaya, considering differential intensity of cosmic ray mesons and horizontally incident cosmic rays 12 p1952 A71-27400

Electric field angular distribution of short radio frequency probe in warm anisotropic plasma under magnetic field 13 p2104 A71-27852

Ground and mountain level measurements of energy and angular distribution of high energy neutrons in lower atmosphere, using double elastic scattering with hydrogen nuclei 13 p2119 A71-27906

High energy sea level cosmic ray neutrons energy spectra, noting angular distribution about zenith and attenuation length in atmosphere 13 p2120 A71-28050

Fireballs existence, discussing maxima in angular distribution due to secondary particles transversal momenta limitation 13 p2058 A71-28062

Fireball transverse momentum effect on angular distribution of secondary particles, considering high energy nuclear interactions 13 p2058 A71-28063

Extensive air showers muons angular distribution, considering high energy nuclear reactions 13 p2126 A71-28097

Fog evolution and droplet radii spectrum determination by scattered laser beam angular distribution measurement 13 p2082 A71-29484

Astronomical radio sources angular structure, using lunar occultations in narrow frequency band at large SNR 15 p2482 A71-31329

Air showers with zenith angles greater than 65 deg recorded by array comprising six scintillation counters, considering angular distribution, intensity and muon content 15 p2475 A71-31786

Atmospheric structure effects on muons zenith angle distribution and maximum intensity direction as function of energy at two different altitudes 15 p2476 A71-31788

Zenith angle distribution of extremely high energy muons from bremsstrahlung showers by emulsion chamber, noting consistency with pion/kaon decay 15 p2476 A71-31790

Angular distribution of high energy cosmic ray muons incident at sea level at large zenith angles, investigating cascade showers initiated by muons 15 p2476 A71-31792

Vertical intensity and angular distribution of cosmic ray muons from observations using scintillator neon flash tube telescopes at three depths 15 p2477 A71-31796

Calculational method for predicting angular distribution of sunlight upwelling flux scattered by atmosphere and reflected by ground, using Monte Carlo data 16 p2562 A71-33130

Spatial and angular distribution of upper atmospheric IR emission layers from Cosmos 65 observation 16 p2563 A71-33449

Atmospheric short wave radiation angular and vertical distribution relation to aerosol scattering parameters, using transport equation 16 p2605 A71-34104

Statistical analysis of radio structure of quasars, considering red shift and anisotropy in angular size distribution 17 p2811 A71-35746

Far field minimum radiation over angular sector for directional broadside array with optimum interelement spacing, considering sidelobe reduction 18 p2875 A71-35972

Molecular beam scattering at solid surfaces, outlining scattered particles angular and velocity distribution measurement 18 p2848 A71-36439

Artificial fog thermodynamic conditions and evolution data, using scattered laser beam angular distribution measurements 19 p3091 A71-38586

Atmospheric excess radiation flux azimuthal asymmetry in equatorial region, discussing angular intensity distribution data from Proton 2 Cerenkov counter 20 p3279 A71-39591

Polarization characteristics of pulsars, considering angular position changes due to interstellar magnetic field using Faraday rotation measurements 20 p3303 A71-39935

Angular distribution of outgoing short wave radiation field intensity as function of sun height on basis of actinometric data from Cosmos 184 satellite 21 p3374 A71-41299

Field ion current angular distribution for large point emitter potentials as function of emitter geometry 22 p3578 A71-42057

Astronomical radio sources angular structure, using lunar occultations in narrow frequency band at large SNR 22 p3606 A71-42604

Asymmetrical cosmic ray showers kinematic interpretation by heuristic model, discussing particle dispersion angular distribution 22 p3594 A71-42644

- Negative pi minus N and NN interactions in emulsion at high energies, plotting angular distributions of secondary particles in cosmic ray showers
22 p3594 A71-42648
- Bremsstrahlung photons produced by cosmic ray muons in Fe and Pb at sea level, calculating energy spectra and angular distributions
22 p3595 A71-42664
- Cosmic ray shower particles lateral and angular distribution structure near electron-photon cascade core
22 p3595 A71-42668
- Equatorial proton and electron pitch angle distributions in loss cone and at large angles from geostationary ATS 5 satellite observation
23 p3720 A71-43165
- Magnetic modulation observation in plasma light scattering spectra experiments, noting dependence on angle between scattering and magnetic field vectors
23 p3713 A71-44150
- Radiative transfer in linearly anisotropic scattering conservative and nonconservative slabs with reflective boundaries, obtaining angular radiation distribution by normal mode expansion technique
24 p3888 A71-44966
- High energy charged particles angular distribution measurements in equatorial region cosmic radiation above atmosphere, using Proton 2 satellite data
24 p3866 A71-45027
- Oxygen viscosity variation under strong magnetic field, comparing angular dependence of Senftleben effect
24 p3802 A71-45116
- Circularly polarized ultrashort radio wave reflection from lunar and planetary surfaces, determining angular scattering spectrum
24 p3805 A71-45313
- ### ANGULAR MOMENTUM
- Galactic interstellar grains alignment by starlight, noting photon intrinsic angular momentum role
01 p0159 A71-10865
- Pulsars as rotating neutron stars with frozen-in magnetic field, accounting for energy and angular momentum losses due to gravitational radiation
02 p0300 A71-12473
- Cosmic photons Planck constant, considering photon absorption dependence on variations of spin angular momentum
03 p0473 A71-13562
- Angular momentum flux from confined gravitational radiator, using linear approximation with Landau-Lifshitz energy-momentum pseudotensor
04 p0625 A71-14731
- Stellar angular momentum, discussing evolution, rotation orbits and relationship between binaries, rotating stars and planetary systems
04 p0647 A71-15240
- Periodic orbits in general three body problem with nonzero angular momenta
04 p0656 A71-15730
- Elliptical and spiral galactic angular momentum and velocity dispersion relations, considering cosmological turbulence during formation
06 p0971 A71-18244
- Spin-orbit coupling and angular momentum transfer between planets and sun by interaction with solar wind
07 p1203 A71-20522
- Angular velocity and momentum vector evolution of isolated bodies in solar system, considering models to trace rotational motion evolution
07 p1203 A71-20525
- Thirring effect experimental measurements in gravitation theory, magnetic suspension system or torsion balance with two rotating disks generating angular momentum
10 p1642 A71-24467
- Star formation angular momentum and magnetic flux problem, investigating collapsing dust cloud theory
11 p1830 A71-26108
- Dust particle angular momentum orientation in comet tails through bombardment by solar wind protons, noting role in scattered light polarization
11 p1832 A71-26182
- Angular momentum meridional transport flux wave number-frequency spectral characteristics in mid-troposphere of Southern Hemisphere
13 p2063 A71-29109
- Inelastic scattering transition densities in single particle operator reduced matrix elements between initial and final nuclear states for nucleon angular momentum calculations
14 p2276 A71-30013
- Angular momentum influence on linear axisymmetric motions of centrally condensed bodies, considering finite amplitude pulsations of rapidly rotating columns
15 p2481 A71-31202
- Constant speed vortex rate sensor, calculating angular momentum dissipation due to shear stresses and response to step signal input
15 p2352 A71-32064
- Angular momentum of rotating Einstein-Rosen bridge, comparing neutron star models
16 p2609 A71-33262
- Elektron 2 and 4 satellites rotary motion with orbital variance of precession parameters and kinetic angular momentum vector, considering gravitational and magnetic effects
16 p2645 A71-33438
- Schuster hypothesis on celestial object relation between angular momentum and magnetic fields
16 p2637 A71-33513
- Pulsars as neutron stars, explaining fast rotation by tendency to conserve angular momentum during compression
17 p2804 A71-34857
- Binary elastic collision integral between particles of disparate mass, determining angular momentum form of Boltzmann equation for Lorentz mixtures
19 p3115 A71-38210
- Solar wind angular momentum flux transport from nonradial velocity components measurements by Mariner 5, noting agreement with comet tail observations
21 p3438 A71-40428
- Angular momentum vector orientation of reentry vehicle at end of spin-up, using heliocoid precession concept to characterize rotational motion during constant thrust
22 p3611 A71-42029
- Spinning and dual spin spacecraft angular momentum and axis control, investigating optimal fuel and small angle reorientation techniques
22 p3611 A71-42045
- Solar wind angular momentum calculation from short term directional, density and velocity fluctuations, using Vela 3 satellite data
22 p3592 A71-42162
- Optimal inner product angular momentum controllers, analyzing performance criteria and feedback control laws
23 p3658 A71-44090
- ### ANGULAR MOTION
- #### U ANGULAR VELOCITY
- #### ANGULAR RESOLUTION
- Compact radio sources of high angular resolution observed via joint U.S.-U.S.S.R. radio interferometry
02 p0307 A71-12086
- Compact radio sources of high angular resolution observed via joint U.S.-U.S.S.R. radio interferometry
08 p1362 A71-21136
- Angular resolution requirements of measurement systems and telescopes for orbital astronomy with applications to faint sources, close stars, spectroscopy, polarimetry, etc
09 p1447 A71-22747
- High accuracy angular precession measurements with autometric gyro for satellite relativity tests, using optical system with reticle coordinates
09 p1452 A71-23595
- Angular discretization effect on calculations of emerging radiation and integrated albedo from model cloudy atmosphere, using multiple scattering with terrestrial particle phase functions
10 p1643 A71-24972
- Lateral separation focus sensors for high angular resolution optical systems, reviewing autocollimating optics and operational patterns
10 p1644 A71-25090
- Phase and log amplitude spectral and angular covariance of scintillation for propagation of two differing plane waves in randomly inhomogeneous medium
11 p1800 A71-26297
- X ray astronomy orthogonal mirror telescopes, noting collecting efficiency, angular resolution and focusing
11 p1766 A71-26307
- High angular resolution of astronomical objects by ground telescopes, considering slowly and rapidly variable defects, atmospheric defects and their reduction
16 p2641 A71-33766
- Optical space observations need in solar physics, stressing 0.2 sec angular resolution for extreme UV and magnetic field measurement
19 p3136 A71-37619
- Image visual observation in coherent diffuse illumination, discussing human eye angular resolution deterioration and depth vision threshold dependence on light characteristics
19 p3074 A71-38195
- Optimal radiant source power for photoelectric two axis autocollimation angle trackers, considering detector threshold sensitivity
19 p3067 A71-38659
- ### ANGULAR VELOCITY
- Hodograph of asymmetrical gyrostator with self excitation, determining angular velocity dependence on flywheel momentum
01 p0163 A71-10656
- Regular optimal motion problem for nonlinear controls reduced to degenerate problem for solving optimal control of solid rotating body angular velocity
01 p0065 A71-11234
- Spinning space stations with mass geometry changes, discussing attitude and angular velocity optimal control
01 p0164 A71-11435
- Traveling angular velocity hodograph equations in solution to gyrostator motion problem
03 p0457 A71-13588
- Kinematic interpretation of body motion about fixed point for case of traveling angular velocity hodograph integrable in closed form
03 p0457 A71-13589
- Vortex angular rate sensor flow characteristics, solving Navier-Stokes equations by numerical technique
03 p0402 A71-14127
- Horizontal clinostat rotation rate for optimal and acceptable weightlessness simulation in plants, comparing with wheat seedlings growth in Biosatellite 2
05 p0712 A71-16150
- Lense-Thirring effect in test masses approaching in same orbit around rotating body, noting correction dependence on central body geometry and angular velocity
05 p0806 A71-16183
- Turbine disks failure under nonuniform heating, deriving expression for critical rpm
05 p0826 A71-16755
- Long base line radio interferometry role in earth rotation rate measurement
06 p0891 A71-17892
- Spectral analysis of five-day pulsations in earth rotational velocity, estimating amplitudes of suspected velocity fluctuations
06 p0896 A71-18452
- Asymmetric missile angular response to spin varying through resonance
06 p0979 A71-18507
- Axisymmetric body rapid rotation under center of gravity velocity vector conditions, solving for plane gliding motion stability in air
07 p1159 A71-19354
- Cosmic ray intensity mean diurnal variation, taking into account angle between solar corotational velocity and earth equatorial plane
07 p1187 A71-19683
- Free flight measurement of aerodynamic coefficients on fixed cruciform fin stabilized bombs, determining aerodynamic forces and moments dependence on angular velocity components
07 p1015 A71-19872
- Time judgment error as function of angular velocity during body rotation
07 p1043 A71-20216
- Angular velocity and momentum vector evolution of isolated bodies in solar system, considering models to trace rotational motion evolution
07 p1203 A71-20525
- Horizontal pendulum angular velocity and motion due to harmonic vibrations at base
07 p1162 A71-20651
- Similarity criterion for volute centrifugal pumps via supersonic model, considering cavitation parameters influence throughout angular velocities range at flow separation
08 p1347 A71-20784
- Earth rotation velocity studies /1956-1966/, noting slowing
08 p1284 A71-21672
- Ephemeride and atomic uniform time scales comparison for earth rotation velocity changes, estimating diurnal and semi-diurnal tides effect
08 p1284 A71-21673
- Heavy solid body motion about stationary point for connected angular velocity vector terminus and trajectory in fixed space
08 p1336 A71-21869
- Angular motion of deformable earth satellite as solid-elastic system with distributed masses, applying automatic control transfer function
09 p1491 A71-22548
- Asymmetric missile nonlinear angular motion, describing quasi-linear relations for frequencies, damping rates and swerving motion amplitude
09 p1532 A71-22906
- Finned configurations with nonlinear aerodynamic properties, obtaining solutions for angular motion at and near resonance
09 p1532 A71-22909
- Dynamic characteristics of two degree of freedom gyroscopes with positional and integral negative feedback for simultaneous angular velocity and displacement measurement
09 p1451 A71-23171
- Fluid rotational stability between coaxial cylinders rotating at same angular velocity in presence of radial temperature gradient
10 p1696 A71-24374
- Cylindrical shock wave in solid body rotating gas for angular variation effects on shock velocity, using similarity method
10 p1593 A71-24405
- Spectral analysis of five day pulsations in earth rotational velocity, estimating periods and amplitudes of suspected velocity fluctuations
12 p1898 A71-26602
- Gyroscopic integrating accelerometer dynamics on high frequency angular vibrating base, determining self oscillations and drift motions
13 p2065 A71-27946

Quasi-point type radar target angular motion simulation by controlling electromagnetic wave phase front in receiving field 14 p2193 A71-29825

Mathematical model for short term adaptation to vestibular stimuli, deriving transfer function relating angular velocities of nystagmus and head rotation 14 p2182 A71-30250

Kinematic interpretation of body motion in Hess solution, discussing axoid vector rolling without slip 14 p2275 A71-30881

Hodograph of asymmetrical gyrost at with self excitation, determining angular velocity dependence on flywheel momentum 14 p2275 A71-30990

Vortex type pneumatic angular rate sensor with vanes and hydrodynamic viscous coupling, determining differential pressure outputs 15 p2352 A71-32063

Constant speed vortex rate sensor, calculating angular momentum dissipation due to shear stresses and response to step signal input 15 p2352 A71-32064

Turbulent gaseous nonmagnetic protogalaxies under external torques, calculating angular velocity distribution 15 p2490 A71-32400

Spacecraft banking control during reentry, deriving dynamic equations of angular motion 16 p2646 A71-33655

Angular position of sun nonoriented artificial earth satellites with angular velocities not exceeding 0.5 deg/sec, using harmonic analysis of magnetometric data 16 p2543 A71-33662

Gas bubble in liquid under surface tension, weightlessness and rotation, determining angular velocity for fluid system disintegration 16 p2560 A71-34142

Galaxy type correlated with rotational velocity using Hubble sequence 18 p2960 A71-35941

High speed aircraft maneuvers stability determination by constant angular pitching/rotation velocity, angle of attack and flight speed, using Liapunov method 18 p2849 A71-36176

Thin circular disk rotating at constant angular velocity, solving three dimensional elasticity problem with formal power series of thickness-diameter ratio [ASME PAPER 71-APM-Q] 18 p2978 A71-36260

Medical physiological requirements of angular velocity and g level for artificial gravity creation by rotating space vehicle, considering human tolerances and vehicle design 18 p2870 A71-36627

Gravitational stimuli due to variations in angular velocity and radius, noting effects on behavioral control [AIAA PAPER 71-871] 18 p2871 A71-36635

Increased artificial gravity avoidance by squirrel monkeys with variations in rotation rate and radius [AIAA PAPER 71-855] 18 p2857 A71-36647

Natural vibrations of two coaxial rotors with unbalanced disk and different angular velocities, solving equations of motion by energy balance method 19 p3156 A71-37536

Equilibrium rotating superdense configurations in general relativity theory, determining integral parameters in low angular velocity approximation 20 p3289 A71-39297

Heavy solid body motion about stationary point for angular velocity vector extremity moving in fixed and body-connected coordinate systems 20 p3270 A71-39368

Numerical analysis for transient elastoplastic thermal stresses on turbine disks at variable rotation speeds 21 p3466 A71-40836

Externally pressurized gas journal bearing whirl instability stabilization system, predicting whirl onset threshold speed 22 p3551 A71-41662

Externally pressurized gas-lubricated foil bearing rotation speed effects on gap topography and clearance variation 22 p3552 A71-41671

Earth angular velocity of rotation vector, discussing rotation rate and polar motion variations 23 p3674 A71-44260

Two rotor gyrocompass with random parameter excitation, calculating angular velocity random variation effects on drift 24 p3825 A71-44700

Rotating disk creep analysis by Van Po Fi-Ozerov nonlinear equation, obtaining numerical solution for total creep equation and time to failure for two angular velocities 24 p3882 A71-44839

Spacecraft motion stabilization about mass center and optimal angular velocity control using minimax technique 24 p3846 A71-45308

Epoxy novolac resin-cured alicyclic anhydride amine-catalyzed ablative polymers molecular structure from computer correlation of analytical data 11 p1789 A71-26033

ANILINE

Electro-optical and high contrast properties of structurally stabilized anil-type nematic liquid crystals in display devices 11 p1729 A71-26070

Toluene and aniline-methylcyclohexane and toluene-aniline nonideal liquid systems, measuring molecular diffusion coefficients as function of concentration by Savart plate birefringent interferometer 24 p3820 A71-45074

ANIMALS

NT ARTHROPODS

NT BATS

NT BEETLES

NT BIRDS

NT CATS

NT CATTLE

NT CHICKENS

NT CHIMPANZEES

NT DOGS

NT DROSOPHILA

NT FISHES

NT FROGS

NT GUINEA PIGS

NT HAMSTERS

NT HUMAN BEINGS

NT INSECTS

NT INVERTEBRATES

NT MAMMALS

NT MICE

NT MONKEYS

NT PARAMECIA

NT PIGEONS

NT PRIMATES

NT PROTOZOA

NT RABBITS

NT RATS

NT RODENTS

NT SHARKS

NT SNAILS

NT SNAKES

NT SPORES

NT TURTLES

NT VERTEBRATES

Movement coordination in animals during walking and running, revealing neurophysiological mechanisms of locomotion control 03 p0356 A71-12987

Sound and sonic booms effects on farm animals physiology and behavior, considering milk production, reproduction, food intake and growth rate 03 p0360 A71-13166

Humans and animals acute hypoxia effects on EEG pattern and behavioral reactions 09 p1390 A71-22210

Interrogation, recording and location system satellite techniques for wildlife tracking and monitoring, describing collar antenna, battery pack and solar cells 14 p2200 A71-30923

Doppler effect satellite location of crystal controlled CW transmitters on earth surface for animal tracking 14 p2200 A71-30924

Biological experiments on plants, animals and bacteria aboard Zond 5, 6 and 7 space probes 20 p3187 A71-39134

Plants and animals reactions to environment gravitational component, showing organisms perception of accelerating force 21 p3326 A71-39970

Soviet book on animals morphophysiological changes in cardiovascular and nervous systems and various internal organs under RF wave exposure 21 p3344 A71-41369

Hyperoxic medium effects on experimental animal cells, tissues and organs morphology, infrastructure and histochemistry 22 p3495 A71-42801

Animal tolerance to carbon monoxide, nitrogen oxide, triethylamine and freon-12 toxic effects after adaptation to hypoxia from tests on albino mice 22 p3496 A71-42810

ANIMATION

U MOTION

ANIONS

Flush-mounted electrostatic probe for plasma properties measurement, calculating negative ions effect on I-V characteristics 09 p1442 A71-22073

German monograph on absorbed anions effect on Ni and Ni-Mo alloys anodic behavior covering temperature dependence, electrons interaction, sulfide ions activation and magnetic properties 10 p1628 A71-24874

Synthesized plasma of interpenetrating positive and negative ion beams, investigating oscillation amplification conditions 12 p1941 A71-27766

D region negative ion densities in chemical equilibrium based on electron density observation, noting role of ozone and carbon dioxide 14 p2228 A71-29533

Mass spectrometric measurements of negative ion concentration in D and lower E regions 19 p3127 A71-38031

Mass spectrometric measurement of negative ion concentration in nighttime D region 19 p3128 A71-38033

Electron transfer cross sections for low energy negative oxygen ion collisions with oxygen molecules measured by single-collision beam technique 23 p3707 A71-43930

Charged particles effect on plasma negative ions, examining Stark effect in energy level 24 p3857 A71-45114

ANISOTROPIC MEDIA

Anisotropic nonhardenable materials steady creep deformation potential as function of mixed invariant of stress and anisotropy tensor 01 p0172 A71-10797

Electromagnetic potentials and Lorentz relation in anisotropic medium, considering Bromwich function and plane wave propagation 02 p0211 A71-11719

Coupled wave equations for magnetoplasma with anisotropic pressure 03 p0463 A71-13346

Electrostatic wave growth rates in anisotropic medium with or without cold plasma 03 p0464 A71-13532

Anisotropic thin rods deformation, extending Nikolai constraints condition on Kirchhoff analogy for isotropic rods 03 p0506 A71-13598

Anisotropic rod elastic curve equilibrium shape for rigidity conditions, considering Goriachev solution to heavy solid body motion about fixed point 03 p0458 A71-13599

Anisotropic materials ductile fracture involving crack initiation and propagation, using Dugdale mathematical model [SESA PAPER 1729] 03 p0507 A71-13760

Anisotropic plasma stability, taking into account self gravitation, finite ion Larmor radius, Hall current and rotation 03 p0465 A71-14263

Electromagnetic instability of counterstreaming electron plasmas with anisotropic temperatures, using Vlasov equation 04 p0633 A71-15032

Wave kinetics in anisotropic plasma of weakly damped magnetosonic vibrations, using Lagrangians of three and four wave interactions 04 p0633 A71-15108

Far field characteristics for diffraction of plane harmonic electromagnetic wave obliquely incident on rectangular wedge in uniaxially anisotropic medium 05 p0781 A71-16414

Supraluminous waves modes in field free two component anisotropic plasma by linearized relativistic Vlasov equation 05 p0791 A71-16939

Rayleigh wave propagation in anisotropic substrates, using light diffraction by surface acoustic waves 05 p0783 A71-17078

Isotropic and slightly anisotropic materials elastic constants evaluation from ultrasonic reflection measurement 05 p0771 A71-17252

Anisotropic tubular Ti alloy samples, noting yield strength and crystal structure dependence on stress-strain state 06 p0912 A71-17937

High amplitude stress wave propagation in anisotropic quartz-phenolic composite, noting strong pulse amplitude attenuation [AIAA PAPER 71-179] 06 p1004 A71-18618

Two dimensional flow MHD in plasmas with anisotropic pressure, considering weak shock waves parameter changes in linear approximation 07 p1168 A71-19726

Failure theory for anisotropic homogeneous materials, discussing interaction factor, resistance, orthotropy and planar stress 07 p1214 A71-20011

Anisotropic materials strength criterion, developing theory from scalar function of two stress tensors 07 p1216 A71-20131

Carbon fiber composites utilization problems for product and tool designers, considering mechanical properties anisotropy, fiber alignment and bundle strength [PLASTICS INST. PAPER 42] 08 p1322 A71-20931

Fabry-Perot resonator with anisotropic medium, deriving reflection mirror shape for optimizing diffraction loss and resonant conditions for extraordinary waves 08 p1289 A71-21284

Anisotropic homogeneous cosmological model, discussing origin of movement and primordial matter chemical composition 08 p1365 A71-21771

ANHYDRIDES

NT PEROXIDES

NT SODIUM PEROXIDES

Anisotropic medium theory of elasticity boundary value problem, considering plane with two closed Liapunov curves without common point

09 p1485 A71-22637

Thick walled anisotropic nonhomogeneous elastic cylinder or plate under axial symmetric time dependent pressure, investigating transient response

09 p1540 A71-23087

Soviet book on problems in anisotropic body elasticity theory, covering orthotropic beams and plates torsion, bending, vibration, stability and boundary value problems, etc

09 p1542 A71-23438

Electromagnetic wave propagation in anisotropic ionospheric plasma with time-varying random electron density irregularities

09 p1506 A71-23586

Variational principles for initial boundary value problem of fully coupled linear thermoelasticity for inhomogeneous anisotropic materials with microstructure

10 p1689 A71-24512

Anisotropic homogeneous two-point double-velocity correlation tensor model for turbulent flow field, deriving relation between micro and macro scale

11 p1748 A71-25153

Dissimilar bonded anisotropic half spaces with flat crack under arbitrary loads, determining stress distribution

11 p1842 A71-25303

Anisotropic bolt bearing specimens failure mode and ultimate load, investigating stress concentrations for failure prediction

[AIAA PAPER 71-354] 11 p1844 A71-25333

Anisotropic material failure under combined loading, predicting strength from uniaxial and shear tests

[AIAA PAPER 71-368] 11 p1845 A71-25342

Coupled vacuum mode equations modified for cylindrical stratification for calculation of propagation characteristics of earth-ionosphere waveguide

11 p1731 A71-25664

Similarity comparisons of isotropic and anisotropic scattering patterns in cloudy atmospheres for haze effects on Mars image contrast, using asymptotic method

11 p1825 A71-25710

Stress-strain states of physically nonlinear anisotropic media, showing boundary value problem equivalent to variational problem

11 p1850 A71-26179

Positive rotational transformations of stress vectors for anisotropic lamina in matrix notation

11 p1852 A71-26393

Epitaxial garnet films magnetic anisotropic models, describing mobile cylindrical domains

12 p1943 A71-26854

Rellich uniqueness theorem for Helmholtz equation for steady state wave propagation in inhomogeneous anisotropic media subject to Sommerfeld radiation

12 p1929 A71-26865

Limiting absorption principle and Schroedinger nonelliptic spectral theory for steady state wave propagation in inhomogeneous anisotropic media

12 p1929 A71-26866

Field aligned anisotropy for auroral ionospheric energetic ions, calculating pitchangle distributions

12 p1899 A71-26885

Fibrous composite structure stress analysis procedures, considering nonisotropy and brittleness effect

[ASME PAPER 71-DE-2] 12 p1977 A71-27321

Three dimensional nonlinear elastic anisotropic body formulating stability at finite subcritical strains with variational principle

12 p1978 A71-27333

Electric field angular distribution of short radio frequency probe in warm anisotropic plasma under magnetic field

13 p2104 A71-27852

Isotropic and anisotropic materials stability criteria and boundary surfaces in invariant stress tensor spaces

13 p2149 A71-28120

Homogeneous anisotropic body elasticity theory, calculating boundary value problem for arbitrary conditions

13 p2153 A71-28422

Anisotropic Heisenberg antiferromagnet sublattice magnetization, obtaining temperature dependence

13 p2100 A71-28675

Elastically and plastically anisotropic single crystals randomly oriented in polycrystalline aggregate, noting initial yield surface in fcc lattice

13 p2155 A71-29063

Extraterrestrial Lyman alpha radiation, showing interplanetary principal anisotropic effects

14 p2307 A71-29731

German monograph on shock waves in anisotropic plasma covering parameters derivation based on kinetic plasma theory and experimental verification possibilities

14 p2280 A71-30235

Asymptotic theory of wave propagation extended to slightly inhomogeneous and slowly varying anisotropic media exhibiting spatial and temporal dispersion

15 p2449 A71-31476

Linear plastic deformation of steel under tension, investigating anisotropy in elastic modulus and strength

15 p2503 A71-31478

Green function or Huygens principle for radiation and diffraction of electromagnetic or acoustic waves in anisotropic media

15 p2449 A71-31869

Anisotropic homogeneous cosmological model, discussing mass motion origin and primordial matter chemical composition

15 p2495 A71-32676

Laser light pulses in anisotropic crystal, investigating nonlinear thermal rotation of polarization plane

16 p2587 A71-33570

Aging theory application to anisotropic strain hardenable metals creep processes description

16 p2659 A71-33984

Stress distribution in isotropic and anisotropic half spaces with crack in interface bonding, reducing boundary value problem to Hilbert problem

17 p2819 A71-34509

Anisotropic composite materials failure surface criteria in three dimensional space, using graphical representation

17 p2824 A71-34817

Free-free bremsstrahlung emission in anisotropic hot electron plasma in magnetic mirror, measuring polarization by Compton scattering

17 p2788 A71-34853

Electric current distributions measurement along monopole antenna in isotropic and anisotropic plasmas generated in large space chamber

17 p2716 A71-35048

LF ferromagnetic resonance in anisotropic polycrystalline thin magnetic films, noting dependence on magnetization inhomogeneity

18 p2955 A71-36940

Hydrodynamic equations for anisotropic plasma in magnetic fields, considering collisionless and collisional transport effects

19 p3111 A71-37634

Absorbance of anisotropically scattering medium compared with measured hemispherical reflectances and transmittances

[ASME PAPER 71-HT-20] 19 p3165 A71-37991

Anisotropic material circular rotating disks of various thickness, calculating stress and deformation

19 p3160 A71-38473

VLF fields of horizontal dipole in waveguide formed between ice covered ground and anisotropic ionosphere of Antarctica

19 p3024 A71-38595

Anisotropic plasma half space moving normal to interface, investigating incident H waves reflection and transmission coefficients

19 p3024 A71-38610

Radiative transfer in inhomogeneous anisotropically scattering spherical shell atmospheres with radial symmetry, using invariant imbedding technique

20 p3287 A71-39082

Flow patterns on Poincare sphere as aid to qualitative study of polarization and intensity of quasi-stationary laser mode in anisotropic resonator

20 p3243 A71-39095

Linear antenna in anisotropic plasma, calculating reactance change with surrounding dielectric layer thickness with allowance for ion depletion

20 p3204 A71-39142

Homogeneous anisotropic body elasticity theory, calculating boundary value problem for arbitrary conditions

21 p3455 A71-40086

Magnetospheric plasma instabilities from velocity distribution anisotropies and nonuniform plasma and magnetic field distributions

21 p3374 A71-41180

Singularities of Green matrix in steady state wave propagation in homogeneous anisotropic media

21 p3416 A71-41245

Transfer equation formulation for radiation field determination in anisotropically scattering medium

22 p3621 A71-42598

Conversion effectiveness of oscillations induced by electron beam in bounded anisotropic plasma into electromagnetic emission

23 p3710 A71-43275

Solid circular plate with diverse elastic moduli in different directions and hole at center, calculating thermoelastic stresses

23 p3777 A71-43422

Anisotropic glass fiber plastic material stress, strain and crack formation threshold measurements under long term static and cyclic axial loads

23 p3696 A71-43424

Three dimensional incompressible anisotropic body with small deformations, calculating elastic stability theory with variational principle

24 p3880 A71-44708

Self similar solution to Cauchy problem of gas dynamics equations in nonisotropic media

24 p3819 A71-44774

Radiative transfer in linearly anisotropic scattering conservative and nonconservative slabs with reflective boundaries, obtaining angular radiation distribution by normal mode expansion technique

24 p3888 A71-44966

Thermal stresses relaxation and distribution in infinite anisotropic viscoelastic cylinder

24 p3884 A71-45002

Three dimensional unbounded anisotropic elastic medium with ellipsoidal inhomogeneity and modulus tensor of piecewise-constant form

24 p3885 A71-45062

Electromagnetic fields in moving anisotropic medium, using network formulation based on radial transmission line representation

24 p3805 A71-45092

Current-optical effects of anisotropic absorption of polarized and unpolarized light in rarefied cosmic media

24 p3860 A71-45106

Refraction of electromagnetic wave with electric field perpendicular to applied magnetic field in anisotropic plasma cylinder cross section

24 p3858 A71-45236

Mo sheet anisotropic dynamic strain aging at high temperatures, noting plastic strain contribution to texture formation and dislocation consolidation

24 p3840 A71-45378

ANISOTROPIC PLATES

Shell theory of anisotropic shells and plates with low shear rigidity, using Timoshenko-type model

01 p0169 A71-10497

Heat conductivity equations for thermal stresses of thin cylindrically anisotropic plates made of reinforced laminar plastics

01 p0169 A71-10499

Book on laminated plate theory covering anisotropic continua, bending, orthotropic plates, energy equations, etc

02 p0330 A71-12844

Shear deformation and rotary inertia in heterogeneous laminated plates of bonded anisotropic layers, discussing bending-extensional coupling

04 p0668 A71-15185

Variable thickness anisotropic annular plates bending on generalized elastic foundation, using numerical method

05 p0823 A71-16423

Bending stress around elliptic elastic inclusions in thin anisotropic plate

05 p0824 A71-16590

Symmetrical elastic bending of anisotropic annular circular plates of variable thickness, solving for line and uniform pressure loads with different boundary conditions

05 p0830 A71-17224

Anisotropic plates bending equations derivation by asymptotic integration from elasticity theory

06 p0985 A71-17754

Circular plates of anisotropic fiber-reinforced materials, calculating axisymmetric bending and buckling

06 p0995 A71-17829

Unsteady temperature fields in thin anisotropic plates with variable coefficient of heat exchange from side surfaces

06 p1009 A71-18730

Unsteady temperature field determination in infinite cylindrically anisotropic plate with circular hole, calculating stress by Volterra equations

07 p1218 A71-20463

Stress analysis of anisotropic plate with square holes under tension, using small parameter method

08 p1374 A71-21947

Stress state elastic equilibrium of ponderable anisotropic half plane with free and ring reinforced elliptic hole near rectilinear boundary

10 p1690 A71-24567

Environmental effects on laminated anisotropic plates thermoelasticity for critical swelling strains, using Hookes law extension of Duhamel-Neumann equations

11 p1783 A71-25332

Composite material structural behavior prediction, emphasizing static, dynamic, buckling and post-buckling response of anisotropic plates laminated from unidirectional plies

11 p1846 A71-25429

Buckling loads of square laminated anisotropic composite plates under compression, including bending-membrane coupling effects

11 p1847 A71-25462

Anisotropic plate with curvilinear holes, noting stress concentrations

12 p1975 A71-27110

Fatigue crack growth rate in plates of anisotropic materials, considering Al and Ti alloys under cyclic loads

13 p2082 A71-27826

- Biaxial plastic extension stability of anisotropic sheets and cylindrical shells, using Hill plasticity theory of orthotropic materials 13 p2156 A71-29074
- German monograph on Mo sheets textures and plastic anisotropy covering recrystallization processes, crystallography, etc 14 p2256 A71-29580
- Soviet book on glass-reinforced plastic plates and shells covering engineering methods for anisotropic plates and shells stability and stress analysis 14 p2327 A71-30245
- Helicopter rotor system vibratory and mechanical stability characteristics, investigating anisotropically mounted flexible swash plate and blade out of track effects [AHS PREPRINT 511] 14 p2178 A71-31082
- Clamped anisotropic symmetrically laminated plate bending, buckling and free vibration exact solution, using Fourier analysis 15 p2506 A71-32013
- Anisotropic bolt bearing specimens failure mode and strength prediction, evaluating relative merits of maximum stress, maximum strain and distortional energy as failure criteria 17 p2824 A71-34820
- Free vibrations frequencies and mode shapes of anisotropic elastic thin plates, using Galerkin method 18 p2983 A71-36931
- Approximate theory for vibration of nonhomogeneous anisotropic layered plates using asymptotic integration of elasticity equations 20 p3310 A71-39782
- Edge supported anisotropic elliptic plate with hole under bending by constant lateral edge load, presenting stress-strain state 24 p3882 A71-44837
- Geometrically nonlinear elastoplastic bending of rectangular flexible plates with various side ratios, using finite difference and strain theory 24 p3883 A71-44849
- Small deflection theory for steady state creep bending of laminated anisotropic rectangular plate under uniform loads, using Galerkin method 24 p3841 A71-44957
- ANISOTROPIC SHELLS**
- Shell theory of anisotropic shells and plates with low shear rigidity, using Timoshenko-type model 01 p0169 A71-10497
- Matrix algorithm using difference-differential method for thin wall moments of varied thickness anisotropic cylindrical shell 02 p0328 A71-12561
- Multilayered anisotropic cylindrical shells free vibration modes 05 p0819 A71-15982
- Anisotropic shell theory with allowance for transverse stresses, using triorthogonal curvilinear coordinates 05 p0821 A71-16367
- Anisotropic shells theory, discussing displacement components 06 p0986 A71-17759
- Anisotropic fiberglass reinforced plastic shell stability under short term and prolonged loading, using geometrically nonlinear formulation and Galerkin method 06 p0994 A71-17825
- Cylindrical anisotropic shells transient deformation processes under external pressure, discussing equations of motion integration 06 p0996 A71-17838
- Stress nonuniformity and initial imperfection influence on cylindrical shell stability 06 p0999 A71-17868
- Stability of rib stiffened and anisotropic shells, including composite and elastic filler structures 06 p1000 A71-17871
- Strength characteristics of thin walled anisotropic shells, using difference-differential method to reduce partial differential equations 06 p1005 A71-18709
- Shallow orthotropic cylindrical shells with weak anisotropy, deriving equations for stress concentration at circular hole 07 p1217 A71-20457
- Stress-strain state of anisotropic circular cylindrical shell with constant thickness, using stepwise linear approximation technique for solving mixed system of partial differential equations 08 p1368 A71-20789
- Momentless theory of anisotropic shells, using three dimensional elasticity theory 08 p1373 A71-21867
- Thermal stress analysis of hinged thin circular cylindrical shells of variable thickness by computerized discrete orthogonalization method 12 p1979 A71-27357
- Soviet book on glass-reinforced plastic plates and shells covering engineering methods for anisotropic plates and shells stability and stress analysis 14 p2327 A71-30245

- Thermal stresses in multilayer anisotropic fiberglass wound conical shell under axisymmetric gradients applicable to structural missile nose cone design 14 p2330 A71-30694
- Nonlinear creep analysis of clamped pressurized circular cylindrical sandwich shells representing stress, membrane force and bending moment as displacement based on Mises criterion 17 p2816 A71-34297
- Anisotropic laminated cylinders under combined axial load, torsion and internal pressure, calculating stresses with Vlasov-Ambartsumyan shell theory 17 p2823 A71-34811
- Partially nonlinear theory of anisotropic shells of uniform thickness, obtaining variational integrals of stress equations of motion 20 p3307 A71-38796
- Membrane theory of anisotropic shells, using three dimensional elasticity theory 20 p3308 A71-39366
- Frequency and buckling stability eigenvalue evaluation for anisotropic circular cylindrical shells under nonuniform lateral prestress 22 p3615 A71-42210
- Two layer anisotropic spherical shell of elastoheterodyne material under uniform pressure, investigating stress-strain state 24 p3880 A71-44710
- Axisymmetric elastic deformation of layered thin anisotropic shells of revolution, using computer integration for arbitrary loads and boundary conditions 24 p3882 A71-44841
- Circular cylindrical laminated anisotropic shells with axisymmetric shape imperfections, investigating upper bound buckling loads 24 p3841 A71-44958
- Stress and displacement solutions to deformation of homogeneous and composite anisotropic near cylindrical bodies, using Almansi algorithm 24 p3885 A71-45061
- ANISOTROPY**
- NT ELASTIC ANISOTROPY**
- NT PLASTIC ANISOTROPY**
- Magnetoelastic anisotropy and low temperature annealing effects on coercive force of ferromagnetic Fe-Ni foils 01 p0138 A71-10669
- Cosmic ray anisotropy fluctuation and propagation function dimensionality relationship, demonstrating essentially one dimensional propagation 02 p0300 A71-12370
- Ionized intergalactic and pregalactic matter 3K microwave background, examining spectrum and degree of anisotropy 02 p0312 A71-12467
- Longitudinal and cross rolling effects on anisotropy of mechanical properties and deep drawability of sintered thin sheet Mo 02 p0257 A71-12518
- Solar flare of 30 March 1969, determining differential rigidity spectral index and small anisotropy 02 p0302 A71-12767
- German monograph on differential solar rotation resulting from anisotropic turbulent viscosity in hydrogen convection zone 02 p0317 A71-12846
- Finite element method for composite materials anisotropic behavior, considering flat sheets plane stress and thin shells membrane and bending deformations 03 p0508 A71-13775
- Solar X-rays emission anisotropy, questioning correlation with optical flares 03 p0480 A71-14047
- Lower F region ionospheric response to internal gravity waves as function of azimuth of wave propagation, noting anisotropy 03 p0420 A71-14534
- Low energy cosmic ray propagation anisotropies in interplanetary medium examined by unidirectional detectors on geostationary satellites 03 p0482 A71-14543
- Elasticity and strength anisotropy changes of unidirectional fiberglass reinforced plastics during winding 05 p0759 A71-16372
- Magnetic disturbances effect on drift behavior and anisotropy parameters of E and F region irregularities 05 p0740 A71-16433
- Electron temperature anisotropy in lower ionosphere, discussing effects of solar UV radiation propagating along geomagnetic field during daytime 05 p0744 A71-17183
- Solar cosmic ray diurnal variations latitude effect explained by two way anisotropy model 06 p0952 A71-18109
- Cosmic ray solar modulation anisotropy during 23 March 1966, 25 May 1967 and 26 January 1968 events in preForbush phase, evaluating multidirectional meson observations 06 p0956 A71-18138
- Superconducting Nb experimental tests for hypothesis concerning relations between anisotropic critical field and dislocation cell structure 07 p1138 A71-19988

- Recrystallized and overrecrystallized Al alloys, investigating factors controlling anisotropy of mechanical properties 08 p1305 A71-21033
- Al and Mg alloys mechanical properties anisotropy as function of loading conditions, taking into account stress condition effect 09 p1467 A71-22315
- Optical resonators with anisotropic elements, altering natural oscillations Q factor and spectrum 09 p1461 A71-22384
- Anisotropy and weldability, considering through-thickness tension decohesion cracking under static nonload conditions in corner and tee joints 09 p1459 A71-23454
- Anisotropy tensor and figurative vector components relation with eigenvector correspondence to eigenstate and eigenmodulus in similitude ratio 10 p1688 A71-24451
- Interplanetary space low energy cosmic ray protons steady state anisotropy based on radial gradient model of outward convection at solar wind speeds 10 p1663 A71-24777
- Nematic liquid crystal ultrasonic measurements at room temperature, showing anisotropy attenuation dependence on magnetic field orientation 11 p1808 A71-26149
- Spiral galaxies orientation anisotropy explanation by hypothetical model of cosmological magnetic field 11 p1831 A71-26166
- Anisotropic instability in velocity distribution of ions in plasmas under external RF electric field 12 p1934 A71-26572
- Diurnal variability of cosmic ray anisotropy calculated from abnormal, ephemeral or nonlinear density gradients 12 p1949 A71-27373
- Anisotropy during cosmic radiation Forbush decreases modulation mechanism onset 12 p1950 A71-27376
- Cosmic ray particles propagation anisotropies in model magnetosphere, suggesting detection interplanetary medium with geostationary satellites 12 p1950 A71-27377
- Cosmic ray anisotropies perpendicular to ecliptic plane from underground muon telescopes in New Mexico and Bolivia 12 p1967 A71-27380
- Satellite-borne anisotropy and energy spectra measurement instruments for cosmic ray electrons and protons and solar and galactic X-rays 12 p1954 A71-27711
- Anisotropy of solar cosmic ray electrons, considering parallel diffusion coefficients for ions and electrons 12 p1954 A71-27712
- Electron temperature anisotropy in lower ionosphere, discussing effects of solar UV radiation propagating along geomagnetic field during daytime at middle latitudes 13 p2059 A71-28240
- Electron thermal anisotropy effect on oblique whistlers preceding strong collisionless shock waves, using linear Vlasov theory 13 p2064 A71-29168
- Solar proton anisotropy measurements, discussing flux directional distribution 14 p2297 A71-29670
- Closed circular cylindrical shell nonlinear problem solvability extended to anisotropic sandwich shell, using mean deflection theory 14 p2332 A71-30866
- Plane parallel inhomogeneous atmosphere, investigating anisotropic light scattering 15 p2448 A71-31332
- Sidereal anisotropy in muon signal observed by cosmic ray telescope above sea level, indicating production by neutral particle and leakage relative to anticoincidence factor 15 p2477 A71-31797
- Fatigue crack propagation anisotropy in hot rolled steel plate, demonstrating crack growth rate sensitivity to microconstituents orientation 15 p2508 A71-32255
- Solar flare radiation data from Pioneer spacecraft, detailing anisotropy, heliocentric longitude gradients, decay time constants and energy spectra 15 p2480 A71-32752
- Anodic dissolution of aluminum bicrystals in electrolytes containing perchloric acid during electropolishing, showing anisotropic layer existence 16 p2592 A71-33371
- Solar modulation origin of sidereal diurnal variation in cosmic ray intensity anisotropies as function of interplanetary field direction, using underground muon telescopes 16 p2628 A71-33931
- Idealized model for anisotropy of metals inelastic characteristics due to plastic prestraining, demonstrating applicability to polycrystalline materials 16 p2659 A71-33989
- Anisotropic carrier redistribution near semiconductor charged surface with energy band bending, discussing relaxation rate 17 p2790 A71-34197

Mechanical and crystallographic structure effect on cold brittleness temperature anisotropy and on exfoliation of Cr alloyed with rare earth elements
17 p2755 A71-34416

Anisotropy instabilities of hydromagnetic wave propagation at small angle perpendicular to magnetic field above ion cyclotron frequency, calculating dispersion relation
17 p2788 A71-34664

Fatigue strength anisotropy in glass fiber materials with epoxy-phenol binders under symmetric and pulsed compression-tension cyclic loads
17 p2762 A71-34783

Statistical analysis of radio structure of quasars, considering red shift and anisotropy in angular size distribution
17 p2811 A71-35746

Large scale atmospheric turbulence, considering anisotropy, thermal stratification, pressure and Coriolis forces effects
18 p2944 A71-36009

Atmospheric temperature effect on solar diurnal variation of muon component, considering asymptotic characteristics of cosmic ray anisotropy
19 p3129 A71-38378

Orientational magneto-optic effect in nickel and ferrosilicon monocrystals, discussing anisotropy influence on frequency dependence
21 p3431 A71-41263

Solar low energy cosmic ray population anisotropy from satellite observations during flare event, describing rise time, decay, field alignment and time constant
22 p3591 A71-41469

Anisotropic solar ground level relativistic proton event of 18 November 1968, determining propagation mechanism characteristics from neutron monitor observations
22 p3591 A71-41470

Relativistic gravity in solar system, predicting Newtonian gravitational constant anisotropy measurements by Cavendish experiments
22 p3575 A71-41920

Anisotropically weighted smoothing theoretical interpretation based on numerical variational analysis for upstream and downstream observations in weather forecasting
22 p3569 A71-42415

Semiinfinite plane parallel inhomogeneous atmosphere anisotropic light scattering
22 p3576 A71-42607

Langmuir paradox problem concerning electron energy distribution function and anisotropy in low pressure DC Hg vapor discharge positive column plasma
23 p3710 A71-43402

Kinetic theory of collisionless system in closed anisotropic cosmologies including rotation effects
23 p3705 A71-44123

Soviet book on computerized finite difference solutions for physically nonlinear plates and shells covering material anisotropy, creep, thermal, radiative and cyclic load effects
23 p3779 A71-44184

Newtonian analog construction, examining relativistic homogeneous anisotropic models
24 p3873 A71-45110

ANNEALING

NT PULSE HEATING

Magnetoelastic anisotropy and low temperature annealing effects on coercive force of ferromagnetic Fe-Ni foils
01 p0138 A71-10669

Composition and annealing temperature effects on recrystallization of vacuum melted thin wire and rod Mo alloys
02 p0265 A71-12521

Nb single crystals, examining structure in initial deformed and annealed states at various low temperatures
02 p0266 A71-12654

Austenitized oil hardened annealed chromium steels with electrolytically isolated carbides, determining structure by X ray analysis
04 p0610 A71-14886

Impurity effects of annealing of radiation defects in p-type silicon, considering annealing temperature
04 p0636 A71-15037

Mo wire annealing with degassing, investigating temperature effect on mechanical properties
04 p0616 A71-15802

Ti alloys welded joints in annealed state and after heat treatment strengthening, noting welding conditions, filler wire composition and edge preparation
05 p0757 A71-16173

Tektite age correction factor determination through annealing of fission tracks, describing experimental technique with reference to etching conditions
05 p0808 A71-16300

Fused titanium carbide structure and property changes during annealing
05 p0769 A71-16863

Recrystallized annealed Ta, examining strain rate effect on mechanical properties
06 p0914 A71-18684

Neutron induced lifetime damage short term annealing dependence on minority carrier density in p-type silicon, considering majority carrier repulsion by positively charged centers
07 p1175 A71-19061

Ion implantation lattice damage effects in crystalline silicon with allowance for optical reflectivity, considering annealing temperature and amorphous layer formation
07 p1175 A71-19062

Annealed Mo creep properties and long term strength, observing temperature and stress effects
07 p1130 A71-19165

Metastable Al-rich Al-Fe solid solutions decomposition during isothermal and isochronal annealing, from X ray diffraction patterns
07 p1137 A71-19979

Stress annealed Ni-base superalloy crystals, investigating orientation and applied uniaxial stress sense effect on coherent gamma prime precipitates morphology
07 p1138 A71-19987

Heavy ion tracks in silicate minerals, using thermal annealing to identify origins
07 p1158 A71-20273

Composition and annealing effects on mechanical and thermoelectric properties of sintered wire W-Re alloys
07 p1143 A71-20493

Radiation-anneal hardening and radiation effects on yield stress temperature dependence in bcc metals
08 p1312 A71-21550

Polycrystalline Nb under plastic deformation and annealing, examining dislocation structure and mechanical properties
08 p1316 A71-21611

Electron microscope investigation of packing defect energy effect on structure of crystal dislocations in hardened metals during annealing and deformation
09 p1473 A71-23226

Molybdenum alloy under annealing and heating by AC electric current, investigating structure change effects on strength properties
09 p1475 A71-23312

Ni-Co strained alloy, examining coercive force as function of annealing time at various temperatures
09 p1475 A71-23313

Deformed Mo single crystals, noting polygonization processes relation to recrystallization during annealing
09 p1476 A71-23318

Annealing and white light illumination effect on I-V characteristics of long Ge diodes irradiated by 5 MeV electrons at 77 K
10 p1583 A71-24144

Prior deformation and subsequent annealing influence on fatigue response of coarse grained alpha Ti, evaluating relative effects of dislocation locking and mechanical twinning
10 p1626 A71-24445

Annealed and cold-worked polycrystalline Fe specimens steady state cyclic stress-strain curves and thin films observation by electron microscopy
11 p1780 A71-26024

Mechanical properties of Ti-Al-Cr and Ti-Al-Cr-Mo alloys annealed below solidus temperatures
13 p2083 A71-27873

Hall effect measurements and electron microscope examination of Te-doped gallium arsenide crystals annealed at various temperatures
13 p2111 A71-28503

Nb single crystals structure and properties after cold rolling and annealing, determining crystallographic parameters of plastic deformation
13 p2086 A71-28579

Fiber strengthening of Cu-Fe-Cr wire by cold drawing and annealing, discussing age hardening process of chromium ferrite needles in ductile Cu matrix
13 p2088 A71-29402

Molybdenum steel annealing, noting carbide phase transformations
15 p2425 A71-31398

Niobium fine structure, examining annealing in vacuum effects on strength
15 p2425 A71-31400

Single crystal and polycrystalline alumina specimens strengthening by annealing with various metal oxide powders
15 p2438 A71-31975

Aluminum single crystals tensile deformation and annealing to produce polygonized substructure
15 p2432 A71-32172

Radiation defects isochronal annealing effects on absorption spectral distribution of gallium arsenide irradiated with fast neutron flux
16 p2620 A71-33184

Deformation conditions and annealing temperature effects on fine structure of Mo single crystals, noting polygonization
16 p2595 A71-33884

Simultaneous degassing and thermal diffusion phenomena in annealed tantalum-oxygen mixed crystals, investigating maximum temperature effect
16 p2599 A71-34094

Stress annealing effects on Al 27 NMR lineshapes in pure Al powders filed and stored at room temperature, considering residual stress
17 p2759 A71-35225

Annealed Mo creep and stress rupture at high temperatures for typical deformation
17 p2760 A71-35661

Niobium dislocation and electronic structure and mechanical properties after plastic deformation and annealing from electron beam studies
17 p2760 A71-35671

Chromium casting steel, investigating annealing effects on alloying elements diffusion
18 p2934 A71-36150

Bubble formation during annealing of W doped with K, Al and Si compounds, using electron microscopy with thin foil and fracture replication techniques
19 p3079 A71-37708

Hydrogen content effect on annealed and work hardened palladium wire tensile properties, determining yield/tensile stress and elongation
20 p3247 A71-38765

Dislocation structures of polycrystalline tungsten after deformation and recovery annealing, observing temperature dependence of critical strain for recrystallization
21 p3399 A71-40472

Ti-Mo base metastable beta Ti alloy tensile properties anomalies at elevated temperatures, examining strain rate and annealing conditions effect
21 p3399 A71-40699

Energy levels and vacancy association of defects in annealed GaAs at 600-1100 C under controlled vapor pressures, using cathodoluminescence measurements
21 p3428 A71-41044

Rough metal surface smoothing through annealing in vacuum, deriving governing equations from Mullins theory of thermal grooving and solid surface capillary morphology
22 p3554 A71-42424

Complex TiC-WC carbides under homogenizing annealing, noting defects, solubility, lattice constant and grain growth
23 p3689 A71-43253

Tungsten and molybdenum oxide crystals shape and size during annealing in various gas atmospheres and vacuum conditions
23 p3690 A71-43255

Electron microscopic study of antiphase domains size and shape in Ni-Mn alloy after annealing
23 p3692 A71-44009

Vacuum annealing and residual gas effects on Mo single crystal dislocation structure and microhardness
23 p3692 A71-44060

ANNIHILATION REACTIONS

NT POSITRON ANNIHILATION

Near space annihilation gamma radiation intensity and spectral energy composition by satellite observation, considering possible antimatter nature of comets and meteor streams
05 p0798 A71-16048

Hydrodynamics of matter-antimatter in contact, discussing coalescence, particles annihilation pressure and energy balance
11 p1821 A71-25539

Geomagnetic horizontal field decrease from magnetospheric tail field annihilation, considering polar ionospheric current generation mechanism
11 p1758 A71-25792

Regular multiplicities of particle production in high energy collisions and antineutron-nucleon annihilation, comparing cosmic ray jet data and pion-nucleon difference
13 p2102 A71-28061

Near space annihilation gamma radiation intensity and spectral energy composition by Cosmos satellite observation, considering possible antimatter nature of comets and meteor streams
16 p2626 A71-33452

ANNUAL VARIATIONS

Geomagnetic field perturbation as function of 11-year solar activity cycle, using magnetic observatory
01 p0073 A71-10921

Global atmosphere energy balance for four seasonal periods, describing production, conversion and loss rates for large scale circulation
01 p0121 A71-11354

Kelvin-Helmholtz instability at magnetopause, initiating semiannual variation of geomagnetic disturbances
01 p0075 A71-11495

Seasonal altitude variation of atomic ion-electron ratio of oxygen/nitrogen species in F1 region, comparing to radar measurements
01 p0076 A71-11507

Endogenous circannual rhythm, discussing free running period, potential zeitgebers, desynchronization and association with circadian rhythm
01 p0020 A71-11571

Semiannual variation in upper atmosphere air density from satellite orbit data
03 p0407 A71-13304

Midlatitude topside ionosphere electron density diurnal variations, discussing F 2 layer seasonal anomaly altitudinal extension

03 p0409 A71-13390

Martian north polar cap observations, discussing physical aspects and seasonal regression curves

03 p0489 A71-13560

Atmospheric reflection latitude and angular dependence on wavelengths from satellite UV measurements, noting ozone content seasonal variation of ozonosphere

03 p0413 A71-14010

Upper atmosphere densities from satellite drag data, noting semiannual variations

03 p0414 A71-14021

Atmospheric density curves by satellite observation, obtaining schematic models for fine structure of semiannual variation

03 p0414 A71-14023

Troposphere and stratosphere mean annual carbon dioxide cycle measurements, describing aircraft collection equipment and procedure

03 p0418 A71-14205

Escaping-earth radiation actinometric measurement by meteorological satellites, discussing seasonal thermal radiation variations in Southern Hemisphere polar regions

04 p0579 A71-14637

Semiannual atmospheric wind and pressure oscillations relation to seasonal meridional baric systems displacements, considering cosinusoidal wave motion variations between Northern and Southern Hemispheres

04 p0621 A71-14639

Noctilucent cloud observations and research covering geographic distribution, annual and diurnal variations, kinematics, volcanic connections, cosmic dust eruptions, etc

04 p0584 A71-15677

Ionospheric absorption measurements noting diurnal, seasonal and solar cycle variations

05 p0740 A71-16429

Ionospheric total electron content determination by Faraday fading of 40 MHz radio transmissions from Explorer 22 satellite, considering seasonal variations

05 p0741 A71-16445

Annual and diurnal variations of temperature inversion over antarctic plateau, discussing wind field structure and ice crystal precipitation

05 p0778 A71-17043

Atmospheric radiating gas components contribution to thermal balance at various altitudes, geographic latitudes and seasons

06 p0923 A71-17509

Solar cosmic ray intensity yearly variation by pressure corrected neutron monitor, discussing atmospheric temperature effects, coronal emission heliolatitude distribution and annual wave amplitude

06 p0953 A71-18117

Seasonal and year-to-year crop radar sensing in agriculture for socioeconomic applications

07 p1095 A71-18825

Midlatitude scintillation diurnal and seasonal variations, using satellite communications data

07 p1095 A71-19003

Ionospheric electron content semiannual variation analysis based on satellite and ground station observations

07 p1096 A71-19009

Solar half cycle total ionospheric electron content and slab thickness diurnal and seasonal variations from Syncom 3 beacon signal

07 p1097 A71-19020

Seasonal factors effect on white rat hypophysis-adrenal cortex system functioning by fluorimetric determination of peripheral blood corticosterone content

07 p1041 A71-19282

Semiannual nutation term determination from diurnal latitudinal observation with zenith telescope over 6 year period

07 p1194 A71-19319

F 2 layer nighttime ionization seasonal fluctuations, considering dependence on geographical longitude and latitude and solar activity levels

07 p1098 A71-19382

Lower ionosphere electron density profile diurnal, seasonal and 11 year variations, tabulating calculated numerical values for 45-70 km altitudes

07 p1099 A71-19383

Twilight helium emission diurnal and seasonal variations relationship to geomagnetic activity and solar depression, using Abastumani observations

07 p1099 A71-19389

Radio wave absorption measurement at constant solar zenith angle of 65 deg, discussing seasonal variation

07 p1101 A71-19408

Aurora polaris activity appearance frequency mean annual values cycle curves

07 p1101 A71-19411

Seasonal variations in F 2 region, using critical frequencies during descending solar activity phase

07 p1102 A71-19672

Cosmic ray intensity annual variations relationship to heliolatitudinal solar activity index HL, providing hysteresis curves for effective angular width parameter estimation

08 p1353 A71-20978

Sq ionospheric current systems longitude and seasonal variations, observing focus positions and electrojet characteristics

08 p1278 A71-21197

Geomagnetic activity winter-summer difference in Northern and Southern Hemisphere middle latitudes

08 p1283 A71-21645

Seasonal variations and migration directions of itinerant ionospheric perturbations detected by ground based backscattering radar

10 p1575 A71-23821

Cosmic particle gradient perpendicular to solar equator plane and semiannual cosmic ray variations, using worldwide neutron monitor network

10 p1660 A71-23839

Sporadic meteors geocentric velocity distribution over celestial sphere by photographic observation and oblique radio sounding, noting annual variations

10 p1668 A71-24029

Meteor-reflected radio wave propagation directivity and diurnal and annual variations, comparing experimental and theoretical calculation results

10 p1576 A71-24033

Circannual biological clock operation without environmental signals based on squirrel hibernation and bird migration studies

10 p1563 A71-24298

Thermosphere heating due to auroral electrojets, discussing thermospheric variations and eddy viscosity

10 p1602 A71-24554

Solar geomagnetic seasonal ionization control of upper ionosphere longitudinal composition variations from polar satellite observations

10 p1602 A71-24555

Seasonal effect on daily periodicity of mice radiosensitivity related to changes in bright/dark daytime proportion and feeding

10 p1565 A71-24654

Midlatitude ionosphere electron production rates during quiet solar activity, deriving seasonally varying electron density profiles

11 p1755 A71-25609

Martian atmospheric pressure carbon dioxide abundance variations correlated with waxing and waning of polar caps or Mars season

11 p1825 A71-25712

Yearly cosmic rays intensity variations in meridional plane from 1955-1969 ionization temperature coefficient recordings as function of solar activity levels

11 p1817 A71-25783

Midlatitude topside ionospheric electron density mean diurnal and seasonal variations from Alouette 1 satellite observation

11 p1757 A71-25784

Sudden commencements occurrence frequency diurnal and seasonal variations from worldwide magnetic storms data

11 p1758 A71-25793

Atmospheric density semiannual variations from satellite observation, comparing with atmospheric models

11 p1760 A71-25824

Diurnal and seasonal variations of scintillations in short wave radio signals transmitted from earth satellites and spacecraft, noting relationship to ionospheric inhomogeneities

12 p1898 A71-26635

Stratospheric seasonal wind reversals morphological classification for comparing atmospheric processes over different rocket sounding stations

12 p1900 A71-27065

Stratospheric wind seasonal reversals over Polish coast of Baltic Sea in 1967-1969 from rocket sounding and upper air synoptic analysis

12 p1900 A71-27067

Atmospheric energy storage and meridional transport, calculating annual cycle in Northern Hemisphere

12 p1925 A71-27193

Earth plasmasphere annual and sunspot cycle variations, considering observations with respect to whistler paths and Pc4 pulsations mean period variations

12 p1902 A71-27669

Radar based values of neutral night exospheric temperature, discussing dominant effect of annual variation

13 p2055 A71-27921

E and F region irregularities random movements over Waltair, India, during IQSY, obtaining diurnal and seasonal variations

13 p2056 A71-27931

Stratosphere and lower mesosphere seasonal climatic temperature profiles calculation from radiation transport and balance equations, noting turbulent heat influxes role in stratification formation

13 p2057 A71-28024

Midlatitude ionospheric signatures from narrow beam HF radar backscatter sounder, discussing diurnal and seasonal occurrences

13 p2031 A71-28782

Seasonal variations in semidiurnal tidal wind velocities in upper atmosphere for Northern Hemisphere radio meteor observations

14 p2231 A71-29720

Normal accelerations experienced by transport aircraft fleet from fatigue load meter data analysis discussing counting rates seasonal variations

14 p2174 A71-29780

Seasonal, irregular and long term earth rotation rate variations

14 p2310 A71-30191

Midlatitude D region electron density winter variability causes consideration based on enhancements, absorption and ionization changes data during stratospheric warming

14 p2237 A71-30944

VLF signal propagation during low and high solar activity, discussing equipment precision, diurnal and seasonal phase variations and phase anomalies correlation

14 p2204 A71-30973

F 2 layer peak electron density diurnal and seasonal variations, noting geomagnetic latitude and solar activity effects

15 p2394 A71-31427

Semiannual nutation term determination from diurnal latitudinal observation with zenith telescope over 6 year period for earth axis

15 p2486 A71-31899

Southern Hemisphere stratosphere and mesosphere meteorological parameters seasonal variation, comparing rocket sounding data with standard models

15 p2400 A71-31968

Mesopause thermal transitions during spring and autumn based on noctilucent cloud observations, discussing stratospheric-mesospheric coupling effects

15 p2400 A71-31988

Cosmic ray annual intensity variations indicating gradient perpendicular to solar equatorial plane

16 p2625 A71-32801

Semiannual density variation in heterosphere as function of height based on satellite drag and atmospheric models

16 p2564 A71-33723

Seasonal temperature and density models for stratosphere and mesosphere from observations by resistance thermometers at Heiss Island Soviet rocket station

16 p2566 A71-33743

Northern high latitude electron trapping boundary position diurnal, seasonal and geomagnetic Kp variations based on ESRO 1/Aurora polar satellite observations

16 p2627 A71-33755

Seasonal and annual longitudinal variations in ionospheric ion distribution, stressing solar geomagnetic control importance

16 p2567 A71-33762

F 2 and E layers peak electron densities semiannual variations, suggesting association with solar activity and charged particles penetration

16 p2568 A71-33785

Seasonal density variations in thermosphere and exosphere, obtaining model from Explorers 19 and 39 drag measurements for comparison withOGO-6 mass spectroscopy

16 p2569 A71-33802

Upper atmosphere neutral species latitudinal and seasonal distributions, using turbulent transport coefficients and photochemical reaction rate constants in finite difference solution

16 p2569 A71-33804

Air density observation near 150 km heights from Cosmos 316 orbit, noting geomagnetic disturbance effects and semiannual variation

16 p2569 A71-33806

Semiannual atmospheric density variation measurements by OV3-6 satellite

16 p2570 A71-33821

Total electron content throughout solar cycle maximum, discussing annual variations

16 p2571 A71-33833

Semiannual ionospheric density variations from Cosmos artificial satellites drag, noting agreement with solar corpuscular radiation geoeffectivity

16 p2571 A71-33841

Exospheric density semiannual variations from June 1968 to December 1970 at altitudes of 900 and 1070 km, using satellite drag determination by orbital period rate of change measurement

16 p2643 A71-33848

COSPAR international reference atmosphere containing seasonal variations, solar flux and altitude models for density, temperature, pressure and wind

16 p2572 A71-33858

Atmospheric boundary layer circulation dynamic interaction with variable depth barotropic ocean surface, studying stream function during annual cycle

16 p2605 A71-33906

Heterosphere semiannual density variation with amplitude as function of height, noting dependence on temperature distribution and sunspot cycle
16 p2574 A71-33963

Seasonal variations of semidiurnal tidal winds in 90-110 km altitude range from harmonic analysis of ionospheric inhomogeneity drift data
16 p2575 A71-34103

Spring and autumn cyclonic circulation in stratosphere and mesosphere up to 95 km, using ionospheric radiosonde and rocket data
17 p2730 A71-34301

Mode conversion and auroral effects observations on polar VLF propagation path, noting seasonal and solar cycle variations
17 p2731 A71-34319

Neutral thermosphere and exosphere structure, discussing density, temperature, composition and diurnal and seasonal variations
17 p2732 A71-34461

VHF wave transhorizonal propagation correlation with daytime E layers in temperature zone, noting height dependence and seasonal and diurnal variations
17 p2707 A71-35445

Atmospheric temperature and density scale height seasonal variations near mesopause, using meteor theory mass and luminosity equations
17 p2737 A71-35740

Solar wind plasma density and flow speed semiannual variations from Vela 3 and 4 satellite observations, noting dependence on heliographic latitude
19 p3124 A71-37351

Semiannual amplitude variations in F2 region for estimating oxygen density dissociation and temperature ratios in lower thermosphere
19 p3048 A71-37398

F2 layer nighttime ionization seasonal fluctuations, considering dependence on geographical longitude and latitude and solar activity levels
19 p3052 A71-37807

Lower ionosphere electron density profile diurnal, seasonal and 11 year variations, tabulating calculated numerical values for 45-70 km altitudes
19 p3052 A71-37808

Twilight helium emission diurnal and seasonal variations relationship to geomagnetic activity and solar depression, using Abastumani observations
19 p3053 A71-37814

Radio wave absorption measurement at constant solar zenith angle of 65 deg, discussing seasonal variation
19 p3053 A71-37832

Aurora Polar activity appearance frequency mean annual values cycle curves
19 p3054 A71-37835

Nighttime sporadic E layer behavior near magnetic equator, discussing occurrence frequency, seasonal variation and solar activity effects
19 p3055 A71-38037

Seasonal distribution of air transportation requirements and utilization rate of transport capacity in passenger traffic
19 p3173 A71-38221

Seasonal, latitudinal and diurnal variations of upper atmospheric structural parameters including density and temperature
19 p3061 A71-38656

F region seasonal anomaly relationship with lower atmosphere composition changes, discussing effects of oxygen/nitrogen relative concentration on ionospheric and atmospheric parameters
20 p3215 A71-38746

Seasonal variations of kinetic energy balance of mean meridional circulation in Northern Hemisphere
20 p3257 A71-39436

Midlatitude solar quiet geomagnetic field dynamics morphology, emphasizing regular diurnal and annual changes and irregular fluctuations
20 p3217 A71-39510

Extrasolar influence on solar activity, considering north-south asymmetry of sunspots distribution and annual June/December sunspots incidence extremes
20 p3294 A71-39540

Incident meteor flux density seasonal variations from radio reflections from trains and light scattering from micrometeoroids
20 p3298 A71-39642

Circumterrestrial dust cloud characteristics from night sky brightness photometric measurements, noting seasonal changes
20 p3219 A71-39646

Neutral upper atmosphere observations, discussing lower thermospheric density and composition diurnal, seasonal and latitudinal variations and solar activity effects
20 p3220 A71-39690

Diurnal and semiannual variations in upper atmosphere density from Cosmos satellite drag observations, noting calculation systematic errors
20 p3223 A71-39707

Semiannual upper atmosphere density variations near solar maximum from satellite drag data, relating height amplitude profile with exospheric temperatures
20 p3223 A71-39710

Neutral-ionized parts interactions in upper atmosphere, discussing ionospheric plasma modulation, solar control and seasonal anomalies in lower ionosphere and ionic reactions
20 p3223 A71-39712

Midlatitude ionospheric electron density and electron temperature measurements by rocket experiments, noting diurnal and seasonal variations
20 p3224 A71-39718

Seasonal stratospheric wind effects on infrasound propagation to U.S. northeast coast from rockets launched at Cape Kennedy
20 p3306 A71-39762

E region electron density and critical frequency seasonal anomaly, allowing for sun zenith angle variations, sunspot activity and earth orbit eccentricity
21 p3371 A71-40034

Ionospheric radio wave absorption winter anomaly concerning seasonal variations of D and lower E region collision frequencies and F region oxygen concentrations
21 p3373 A71-40048

Absorption variation with solar activity and seasons, reexamining vertical incidence absorption measurements at 5.65 MHz/1958 and 1959 at Walaitar
21 p3373 A71-40374

E region irregularities drift and anisotropy at Walaitar during IQSY, inferring trends of diurnal and seasonal variation
21 p3374 A71-40379

Unified international scaling for annual and seasonal precipitations measured by national gages, comparing U.S.S.R. and U.S. reduction coefficients
21 p3383 A71-41377

Error factors of seasonal precipitation measurements by total precipitation gages
21 p3383 A71-41378

Seasonal variations in vertical distribution of ozone at high latitudes, using Murgatroyd model of looped meridional atmospheric circulation
21 p3375 A71-41395

Yearly cosmic rays intensity variations in meridional plane from 1955-1969 ionization temperature coefficient recordings as function of solar activity levels
22 p3591 A71-41551

Midlatitude topside ionospheric electron density mean diurnal and seasonal variations from Alouette 1 satellite observation
22 p3532 A71-41552

Sudden commencements occurrence frequency diurnal and seasonal variations from worldwide magnetic storms data
22 p3533 A71-41561

Sporadic E layer initial height seasonal variations at mean geographic latitudes, considering solar zenith angle and activity effects
22 p3533 A71-41646

Semiannual variation in F2 layer peak height and critical frequencies at midlatitudes, considering vertical ionospheric drifts effects
23 p3665 A71-42973

Blanketing sporadic E layer diurnal and seasonal variations from equatorial stations ionosonde data obtained during IGY, discussing wind shear mechanism
23 p3667 A71-43134

Periodic and isolated /nonperiodic/ ionospheric electron content fluctuations showing noon and midnight peaks and winter increase at high latitudes
23 p3670 A71-43180

Lunar and solar gravitation effects on leveling from formulas and nomogram, noting seasonal maximum effect in southern latitudes and Northern Hemisphere
23 p3670 A71-43302

Spread F configuration irregularities at Nairobi, investigating nocturnal and seasonal variations and magnetic and solar activity effects
23 p3672 A71-43799

ANNULAR FLOW

Three dimensional cascade flow, discussing potential flow, shear flow, flow disturbances and flow approximations for annular cascades
03 p0342 A71-13827

Axial compressor flow characteristics by computerized calculation methods, considering annular duct swirling flow model
03 p0342 A71-13828

Two dimensional annular flow of viscous heat conducting gas between coaxial cylinders, using Navier-Stokes equations
03 p0401 A71-14066

Pressure wave propagation through annular and mist flow patterns, noting virtual mass effects in interphase momentum transport of rarefaction and compression waves
03 p0405 A71-14418

Heat transfer to concentric annular turbulent mercury flow, determining wetting effect, velocity profiles, eddy diffusivity of momentum transfer and friction factors
04 p0570 A71-15172

Ring flow expansion of incompressible viscous fluid in cylindrical channel
04 p0573 A71-15561

Stationary flow of viscoplastic liquid in annular gap with temperature dependent viscosity, taking into account energy dissipation
04 p0579 A71-15799

Viscoelastic fluids flow stability between arbitrary spaced concentric cylinders, noting critical Taylor number dependence on gap size
05 p0735 A71-16715

Free turbulent mixing of heated high speed central hydrogen jet and cold low speed annular air stream coupled with finite rate chemical reactions
[AIAA PAPER 71-5] 06 p0866 A71-18479

Heat transfer and thermal entrance length in annular channel with rounded and sharp inlet edges
07 p1220 A71-18763

Viscous incompressible fluid flow between two cofocal elliptic cylinders, discussing temperature distribution and heat transfer in annulus
07 p1224 A71-20029

Stable ellipsoidal plasma configurations in alternating electrode annular system, considering longitudinal magnetic field strength, electrode voltage and gas discharge chamber pressure
07 p1171 A71-20185

Laminar steady flow and heat transfer of viscous heat conducting gas moving between coaxial cylinders, using Runge-Kutta method
09 p1431 A71-22408

MHD Hg flow between concentric cylinders with nonconductive walls, comparing pressure loss and voltage measurements with theoretical predictions for large Hartmann numbers
10 p1647 A71-23862

Polarographic measurements of secondary Couette flow between coaxial cylinders for diffusion coefficient effects on mean friction factor, using wall flush microelectrodes
10 p1592 A71-23978

Annular free jets application as air curtains, formulating relations for plane and conical jets to calculate deflection of particles
[DFVLR-SONDDR-106] 10 p1596 A71-24938

Hydromagnetic flow of conducting viscous incompressible fluid in rotating straight annular pipe under constant pressure gradient
11 p1804 A71-25433

Smooth annuli correlation equation for friction factor, discussing Prandtl turbulence based Spalding inner velocity profile modification
12 p1896 A71-27053

Viscous dissipation effects on Nusselt number in combined free and forced convection through vertical concentric annuli
13 p2160 A71-28601

Entrance region laminar flow development under suction or blowing at porous inner wall in concentric annular duct
13 p2160 A71-28602

Steady laminar natural convective flow in concentric cylindrical annuli, using finite difference method for Navier-Stokes and energy equations solution
[ASME PAPER 70-WA/HT-9] 13 p2164 A71-28982

Incompressible homogeneous isotropic fluid Couette flow between stationary inner and rotating concentric outer cylinders, examining Weissenberg effect
14 p2226 A71-30445

Book on fluid mechanics covering rotating fluids, flow between concentric cylinders, emulsions, standing waves on water, etc
14 p2226 A71-30554

Discrete tone noise generation by high speed fans and compressor blades, using McCune analysis for linearized three dimensional compressible flow in infinite annulus
15 p2468 A71-31555

Annular ducts finite amplitude spinning acoustic modes propagation and subsonic choking, allowing for nonlinear effects in perturbation procedure
15 p2450 A71-32133

Viscous incompressible flow stability between concentric rotating cylinders, developing nonlinear model of two disturbance interaction
16 p2558 A71-32985

Pressure wave propagation through one and two component annular and mist flows, showing importance of inertial interphase momentum transfer
19 p3171 A71-38293

Hydrodynamic stability of incompressible conducting fluid flow between two moving linearly and rotating coaxial cylinders in longitudinal magnetic field
21 p3367 A71-40688

Two axisymmetric annular flows linear hydrodynamic stability analysis, using Navier-Stokes system
21 p3370 A71-40991

Vibration amplitudes and phases/excitation modes/ during flutter for weakly inhomogeneous annular cascade flow with blade interaction and random inhomogeneity
22 p3615 A71-41846

Forced convection to hydrodynamically and thermally fully developed laminar flow in eccentric annuli, determining energy equation approximate solutions
22 p3620 A71-41880

- Transverse acoustic wave amplification due to mass injection around submerged nozzle in solid propellant rocket engines, noting annular flow role
22 p3589 A71-42034
- Approximate analytic solution for nonstationary heat transfer for viscous incompressible laminar fluid flow in annular cylindrical ducts
22 p3622 A71-42679
- Hydrodynamic model of momentum, heat and mass transport for turbulent flow in straight circular pipes, tabulating velocity profiles and eddy diffusivity
23 p3708 A71-43091
- Steady laminar viscous hydromagnetic flow in annulus with porous walls of different permeability, giving wall friction coefficients and velocity distribution
23 p3708 A71-43099
- Viscous incompressible flow between concentric rotating spheres, investigating hydrodynamic stability
23 p3663 A71-43443
- Free axisymmetric turbulent annular nozzle jet propagation, detailing velocity distribution variation due to momentum loss in stall region
23 p3664 A71-44335
- Thermally driven motion of water with free surface in rotating annulus, investigating steady wave flow by three dimensional nonlinear Navier-Stokes equations numerical integration
24 p3844 A71-44417
- Hydraulic resistance and heat transfer in annular channel with rotating flow, comparing to axial flow
24 p3888 A71-44747
- Mass flow function diagram for axisymmetric isentropic compressible swirling flow in annular duct
24 p3820 A71-44960
- ANNULAR JETS**
U ANNULAR FLOW
U JET FLOW
- ANNULAR PLATES**
Orthotropic annular plates buckling, using finite difference equations and Vianello-Stodola iterative method
01 p0174 A71-10968
- Starting functions solutions for axially symmetric orthotropic annular plates
02 p0329 A71-12689
- Variable thickness anisotropic annular plates bending on generalized elastic foundation, using numerical method
05 p0823 A71-16423
- Symmetrical elastic bending of anisotropic annular circular plates of variable thickness, solving for line and uniform pressure loads with different boundary conditions
05 p0830 A71-17224
- Circular and annular elastic plates elastoplastic bending theory, using Saint Venant conditions and equations of equilibrium and deformation
06 p0993 A71-17812
- Thermal stresses in annular plate of fiberglass reinforced epoxy resin
07 p1209 A71-18919
- Dynamic plastic bending theory of thin circular annular plate with central hole under uniform impulse
10 p1689 A71-24519
- Nonhomogeneous Helmholtz vibration equation for sectorial-annular membranes and plates under arbitrary load, using Fourier method
15 p2508 A71-32231
- Annular plate stability and postbuckling behavior in steady plane axisymmetric temperature field
17 p2822 A71-34598
- Optimal design of axisymmetrical annular plate and cylindrical and spherical shells by maximum principle
17 p2833 A71-35621
- Orthotropic annular plate plastic flow law, establishing yield conditions with plane stress-strain state equations
19 p3155 A71-37527
- Sound radiation from subsonically rotating annular disk source, calculating far field pressure and efficiency
19 p2997 A71-37845
- Thin circular annular Al plate buckling under uniform radial compression
19 p3157 A71-37872
- Free and forced finite amplitude nonlinear oscillations of thin elastic annular plate with free inner and clamped immovable boundaries
21 p3471 A71-41026
- Axisymmetric buckling of annular plate subjected to unequal uniform radial compression along inner and outer edges
22 p3615 A71-42036
- Buckling thermal gradients for rotating orthotropic annular plates under edge pull load
22 p3619 A71-42842
- Forced vibration of internally damped circular and annular plates with clamped boundaries, obtaining driving point and transfer impedances and force transmissibility
23 p3775 A71-43204
- ANNULI**
Numerical solution of Laplace difference equations for circular and irregular annulus
04 p0619 A71-14811

- Elastic deformation of strip, rectangular annulus and cylinder with homogeneous displacement boundary conditions, deriving orthogonality relations for expanded eigenvectors
05 p0828 A71-16993
- Energy dissipation in harmonically oscillating spherical annulus filled with viscous fluid
15 p2391 A71-32104
- Elastic deformation of strip, rectangular annulus and cylinder with homogeneous displacement boundary conditions, deriving orthogonality relations for expanded eigenvectors
18 p2982 A71-36793
- Sliding contact between closed annulus and elastic cylinder, deriving integral expressions
21 p3472 A71-41147
- Heat transfer measurements in differentially heated fluid annulus for nonrotating and rotating flow
23 p3781 A71-43335
- Rough spheres, cylinders and annuli in contact, determining surface roughness and waviness effects on surface geometry under elastic and plastic deformations
23 p3682 A71-43928
- Heat conduction of rarefied air and argon in annuli between coaxial cylinders
23 p3783 A71-44068
- Surface of revolution annular elements thermal radiation and heat exchange for propellant schematization, attachment to missile wall and opening into ambient medium
24 p3889 A71-44970

ANODES

- NT CELL ANODES
NT TUBE ANODES
- Anodic temperature effect on Cs thermionic converter operation under arc regime, obtaining potential jump electron temperature relation near anode
01 p0005 A71-10158
- Quasi-steady MPD accelerators current conduction and power loss mechanism investigation through local anode fall voltage and current density measurements at different arc current levels
06 p0939 A71-18636
- [AIAA PAPER 71-198]
- Anomalous anodic Be dissolution in anhydrous environment, considering chunk effect and multivalent ions production mechanisms
07 p1118 A71-19568
- Electroerosion and electrochemical combined effects on machining surface removal, discussing optimal anodic removal rates and electrolyte concentrations
08 p1296 A71-20852
- Magnetron devices with anode voltage as independent variable, calculating output characteristics based on electron cluster model
09 p1415 A71-22463
- Near anode surface electrode potential region width measurement in Knudsen thermionic converter with Ba-Cs interelectrode medium
14 p2181 A71-29954
- HF anodic oscillation tube tripler circuit optimization under constraints due to heat losses in grid electrode
17 p2714 A71-34572

ANODIC COATINGS

- Duraluminum with anodic film, examining fatigue and corrosion-fatigue rupture
06 p0911 A71-17935
- Preliminary corrosion effect on fatigue strength of Al joints, noting insufficient anticorrosive anodic film and additional protection by paint and varnish
16 p2584 A71-33688

ANODIZING

- Al anodizing processes, stressing modern theory of anodic oxidation and anodized Al corrosion
11 p1779 A71-26000
- Fatigue corrosion resistance of duraluminum anodized at various temperatures
13 p2082 A71-27823
- Sputtered tantalum films oxygen content determination by anodization current efficiency measurements
16 p2621 A71-33187
- Blue edge anodize technique for revealing segregation in Ti alloys without affecting mechanical properties
18 p2938 A71-37058
- Plasma anodization of Si in positive column of DC oxygen glow discharge, considering silicon dioxide growth rate in negative glow, Faraday dark space and anode fall
22 p3581 A71-41809

ANOMALIES**U ABNORMALITIES****ANORTHOSITE**

- Apollo 11 lunar soil sample derived from basaltic and anorthositic rocks, considering basalt origin by melting due to internal radioactive heating
02 p0305 A71-11983
- Lunar anorthosites from Apollo 11 sample 10085 coarse fines, determining major, minor and rare earth elemental abundances
03 p0482 A71-13012

Apollo 11 sample basalts lunar interior origin assumption from comparison with terrestrial massif anorthosite series, using chemical and petrographic analyses
11 p1834 A71-26452

Lunar anorthosite comparison with terrestrial igneous rocks, discussing petrogenetic schemes based on models
12 p1958 A71-26693

Lunar anorthosite crust flotation, fractional crystallization process in seas and mascons genesis based on experimental data and petrogenetic scheme
16 p2636 A71-33505

Potassium-argon age determination for shock-metamorphosed anorthosites of Manicouagan-Mushalagan Lakes structure
19 p3049 A71-37657

Fluorine and other trace elements in lunar plagioclase concentrates from Apollo 11 fines, and anorthosite inclusion from Apollo 12 breccia
20 p3292 A71-39383

Meteoritic material characterization from trace elements in Apollo lunar soil, core samples, breccia and anorthositic fragments by neutron activation analysis
23 p3747 A71-43678

Lunar rocks 12040 and 12013 and anorthosites, determining U-Th distributions with induced fission track maps
23 p3752 A71-43712

Visible and near IR spectral reflectivity measurements of basalt separates, glass and anorthositic fragments from Apollo 12 mare samples
23 p3760 A71-43770

ANOXIA

- Myocardial glycogen stores increase protective role in rat cardiac anoxia studied in isolated perfused heart
03 p0363 A71-13489
- Human body thermography for studying physiological changes due to exercise, anoxia or accelerations
06 p0860 A71-18189
- Anoxic fern spores X ray sensitization, observing diacetyl and isatin effects
07 p1036 A71-18961
- Carbon dioxide absorption of dog blood and plasma under anoxia at simulated high altitudes, deriving equations for protein concentration rated buffer values
07 p1043 A71-20327
- Simulated high altitude chronic hypoxia and long term sideropenic anemia adapted animals, investigating acute anoxia tolerance of myocardium
07 p1044 A71-20331
- Anoxia induced ECG lesion current in conjunction with myocardial phosphorylcreatine collapse, discussing results with air and nitrogen ventilated guinea pigs
13 p2008 A71-28506
- Simple organisms resistance and adaptation to low pressure, anoxia, intense cooling, UV irradiation and Mars conditions
13 p2009 A71-28687
- Hemopoiesis and anoxiobiotic processes comparative characteristics in brain and muscular tissues of heterothermal and homoiothermal rodents during prolonged hypoxia
17 p2679 A71-34221
- Anoxia effect on laboratory animals cardiac action, discussing ECG injury current relation to myocardium phosphorylcreatine content
22 p3484 A71-41568
- White rats resistance to acute anoxic, anemic and histotoxic hypoxia during various phases of X radiation sickness, studying adrenal cortex histophysiological state
22 p3494 A71-42731
- Physiological effects on rats of argon substitution for nitrogen in hermetically sealed chambers under conditions of anoxia and high carbon dioxide concentration
22 p3505 A71-42804

ANTARCTIC REGIONS

- Meteor population radar observation data at Antarctica station, noting monthly variations
01 p0149 A71-10054
- Astronomical-geodetic observations of direction of instantaneous earth rotation vector at South Pole
03 p0406 A71-13007
- Exponential thermal wind spiral equations, discussing planetary boundary layer flow over Antarctic Plateau
03 p0452 A71-13228
- Daytime ionosphere rocket observations at Antarctica, examining electron density profiles
05 p0743 A71-17006
- Polar region atmospheric ozone density profile measurements, using rocket sounding
05 p0743 A71-17007
- Annual and diurnal variations of temperature inversion over antarctic plateau, discussing wind field structure and ice crystal precipitation
05 p0778 A71-17043
- Geomagnetic field secular variations in Drake passage /Antarctic Ocean/, applying absolute magnetic surveys
05 p0747 A71-17215

- Photic stimulation at South Pole by EEG, showing no brain stress, undue tension nor anxiety during hypobaric hypoxia acclimatization 06 p0851 A71-17608
- Antarctic terrain dielectric and loss properties effects on VLF attenuation and phase constants of earth-ionosphere waveguide paths over ice covered regions 06 p0868 A71-17733
- Cosmic ray multiple neutron intensities time variations measurements at Syowa Station /Antarctica/, considering Forbush decrease, diurnal variations, solar protons and storm time increase 06 p0960 A71-18163
- Meteor population radar observation data at Antarctica station, noting monthly variations 08 p1361 A71-21048
- Far ionospheric propagation of round-the-world echo signals from Moscow to Antarctic station Molodezhnaia and back to Moscow 11 p1731 A71-25773
- Antarctic auroral ovals, determining time-longitude coordinates, statistical mean position and polewards and equatorwards boundaries for various Kp 12 p1900 A71-27056
- Harmonic analysis of F 2 region critical frequency in antarctic region, emphasizing solar activity effects 17 p2731 A71-34317
- Antarctic F 2 layer height and critical frequency diurnal variations due to ionospheric neutral winds, ionization maxima and solar effects 17 p2731 A71-34318
- HF radio absorption in antarctic night ionosphere, discussing solar activity effects 17 p2733 A71-34776
- VLF fields of horizontal dipole in waveguide formed between ice covered ground and anisotropic ionosphere of Antarctica 19 p3024 A71-38595
- Far ionospheric propagation of round-the-world echo signals from Moscow to Antarctic station Molodezhnaia and back to Moscow 22 p3509 A71-41541
- ANTARCTICA**
- U ANTARCTIC REGIONS**
- ANTENNA ARRAYS**
- NT ENDFIRE ARRAYS**
- NT LINEAR ARRAYS**
- NT STEERABLE ANTENNAS**
- NT TURNSTILE ANTENNAS**
- NT YAGI ANTENNAS**
- Adaptive retransmission for improving two-way communication between antenna arrays in randomly fading environment, calculating signal to noise ratio 01 p0052 A71-10468
- Stacked dipole antenna arrays with modulated phase velocity, comparing measured and calculated radiation patterns 01 p0052 A71-10474
- Radiator systems field calculation based on waveguide and resonator excitation method, noting field amplitudes in two and three dimensional arrays 01 p0038 A71-11202
- Multielement nonperiodic antenna array synthesis for given main and diffraction lobes of radiation pattern 01 p0057 A71-11214
- Long elevated horizontal line sources mutual impedance coupling, using image theory techniques 01 p0041 A71-11615
- Wellenweber antennas characteristics, calculating input and mutual impedances, total field radiated and power gain 02 p0232 A71-12343
- Short wave signal polarization fading minimization by dispersed reception of circularly polarized components, discussing power gain relation to antenna configuration 02 p0219 A71-12543
- Antenna array radar reflector for simulating objects with given polarization characteristics during radar equipment tuning and calibrating 02 p0233 A71-12634
- Large antenna electrical and mechanical requirements, considering gain/temperature ratio, steerability, housing, design life and erection 02 p0235 A71-12831
- Bonn 100 meter radio telescope, describing frequency range, antenna array, steering accuracy, construction and design 02 p0239 A71-12913
- Optimal synthesis of antenna array radiation patterns with minimum square deviation from zero in sidelobe 04 p0557 A71-14629
- Chebyshev antenna arrays minimum length for given sidelobe levels 04 p0557 A71-14631
- Radiation patterns of diametrically opposed slot antenna arrays on infinitely long cylinders 04 p0559 A71-15878
- Network synthesis of beam-forming matrices feeding linear and rectangular antenna arrays 05 p0719 A71-16145
- Dipole antenna array coupling for circularly polarized radio waves amplitude fluctuations reflected from ionosphere at vertical incidence 05 p0738 A71-16216
- Nonhomogeneous signal fields reception in presence of homogeneous noise using two-element subtractive antenna array, noting S/N improvement 05 p0721 A71-16469
- Axisymmetric multibeam annular antenna array with interacting radiating elements synthesized by partial radiation patterns 05 p0722 A71-16867
- Wideband radar array antenna system with suppressed grating lobes 06 p0867 A71-17712
- Collinear and planar arrays of arbitrarily located parallel elements, determining current and charge distribution, admittances and field patterns 06 p0875 A71-17715
- Phased arrays sidelobe reduction through reflection lobe dispersion 06 p0875 A71-17718
- Phase grating lobes redistribution by aperiodic phased array of line sources with linear variation of element lengths and linear amplitude weighting 06 p0875 A71-17722
- Open cavity radiators radiation fields, describing antenna structure based on backfire principle with dipole array exciter and parasitic reflector 06 p0875 A71-17724
- Chebyshev array directivity for various element spacings and sidelobe ratios, presenting formulas for computer calculations 06 p0875 A71-17725
- Butler matrix antenna array feed network extension to increased number of ports, considering relationship between beams and radiation pattern 06 p0875 A71-17726
- Identical V antennas coplanar array admittance matrix, showing mutual conductance and susceptance as function of spacing 06 p0875 A71-17727
- Airborne X band reflect phased array radar antenna design for simultaneous functions including large volume search, target attack with general surveillance and low altitude assist 06 p0876 A71-18096
- Planar microwave array antenna for scan requirement, discussing tilt angle and element arrangement optimization 06 p0876 A71-18097
- Electromagnetic wave diffraction by multielement and multilayer arrays, discussing asymptotic solution, error estimate and convergence 07 p1060 A71-19180
- Optimal synthesis of linear equidistant antenna arrays with sum and difference radiation patterns, using orthogonal polynomials 07 p1078 A71-20069
- Forward and reverse cross coupling compensation in infinite straight row of radiating elements of antenna array 07 p1078 A71-20071
- Antenna feed waveguides interconnection for compensation of cross coupling between elements of two dimensional array 07 p1079 A71-20072
- Two dimensional concentric ring antenna arrays synthesis, describing radiation pattern formation 08 p1266 A71-21463
- Focused aperture antenna arrays near field radiation patterns, determining minimum focusing distance 08 p1266 A71-21464
- Intersecting dipoles with sinusoidal current distribution, determining input impedance 08 p1266 A71-21469
- Adaptive array processor analysis and optimum design for passive detection of sonar type directional stochastic signals 08 p1256 A71-21602
- Optimum antenna array processing design for target detection in nonuniform clutter background, using decision-theoretic processor with digital computer 08 p1256 A71-21604
- Planar microwave array antenna for scan requirement, discussing tilt angle and element arrangement optimization [AIAA PAPER 70-191] 08 p1229 A71-22030
- Beam compression technique for log periodic dipole antenna array using axial displacement of antenna dipoles feed points 09 p1406 A71-23035
- Satellite communications earth station antennas, describing antenna elements and subsystems analysis, design and performance 09 p1418 A71-23099
- Traveling wave antenna arrays of mismatched elements, calculating element resistances and spacings 09 p1408 A71-23488
- Realizable method of pattern synthesis for broadside array antenna giving arbitrary current distribution 09 p1418 A71-23489
- Geometry optimization of error-free distributed nondirectional aperture array receivers, using signal detectability technique 09 p1408 A71-23491
- Shaped beam radiation patterns synthesis by iterative sampling method with line sources or uniformly spaced antenna arrays 09 p1409 A71-23493
- Radiation nulls suppression and broadband impedance matching of infinite rectangular waveguide phased arrays, giving numerical solutions 09 p1419 A71-23494
- Axial slits circular array pattern in large conducting cylinders fed by waveguides 09 p1419 A71-23497
- Linear antenna arrays synthesis with Z transforms permitting sidelobe reduction and nulls in antenna radiation patterns 09 p1419 A71-23498
- Electric field bounds over phased array antenna aperture, discussing use in predicting array power handling capability 09 p1419 A71-23504
- Lossless radiating antenna element efficiency in circular cylindrical arrays of identical elements, relating to reflection coefficient 09 p1419 A71-23505
- Arbitrary antenna arrays of not necessarily identical elements, deriving maximum realizable gain under impedance matching, and applying to spaced circular arrays 09 p1419 A71-23508
- Dipole antenna array exact design for prescribed radiation patterns in magnetic plane, using current distribution integral 09 p1420 A71-23511
- Modal superpositions for mutual coupling on cylindrical array of waveguide elements 09 p1420 A71-23513
- Earth-ionosphere waveguide model of VLF signals propagation with perturbed ionosphere, considering magnetic dipole transmitting antenna array 09 p1410 A71-23575
- Charged conductors in homogeneous collisionless magnetoactive plasma at hybrid frequencies, investigating antenna array quasi-electrostatic field one dimensional structure 10 p1582 A71-23809
- Iterative synthesis of dipole antenna array for maximum directivity radiation pattern, considering amplitude-phase distributions 10 p1583 A71-24707
- Signal fluctuation effect on directional properties of multidipole receiving antenna, calculating radiation pattern 10 p1583 A71-24708
- Array spacing dependence of ionospheric irregularities horizontal drift and anisotropy, using statistical properties of ground diffraction patterns 11 p1731 A71-25614
- Phase sector direction finder for VHF range, using log periodic dipole arrays 11 p1738 A71-26338
- Single element antenna radiation pattern effect on equidistant linear directional gain, current distribution and array shape 11 p1738 A71-26343
- Cross couplings in wideband antenna arrays, determining scattering coefficients, self/mutual impedances and admittances of two radiating elements 11 p1738 A71-26344
- Dipole elements input impedance of wideband linear antenna arrays, using coupled circuits and induced emf 11 p1738 A71-26345
- Aperture zoning methods for reducing phase errors on radiation patterns of equidistant dimensional arrays with traveling wave slotted waveguide elements 11 p1738 A71-26346
- Linear frequency beam scanning array antenna excited by individual phase shifter, studying rectangular waveguide in magnetic field plane 11 p1741 A71-26552
- Sparse antenna arrays with small sidelobe level, estimating error due to radiation pattern substitution by statistical method 11 p1741 A71-26556
- Quasi-stationary three dimensional array excitation by large phase shift calculated for circular conducting elements 12 p1885 A71-26840
- Coincident radio pulse effects on triggering antenna arrays, considering air shower mechanism 12 p1967 A71-27389
- Adaptive array antennas with control loop, deriving noise expression for maximizing signal to noise ratio 12 p1881 A71-27426
- E- and H-polarized waves diffraction on three antenna arrays crossing at arbitrary angles 12 p1882 A71-27615
- Radio emission measurement from extensive air showers by system of half wave dipoles in complex array of Moscow State University 13 p2127 A71-28106

Strip array excitation by field with large phase shift per period, deriving approximate solution from averaged boundary conditions 13 p2029 A71-28361

Monograph on tolerance effects and performance degradation in microwave aerials covering axial displacement, active array, radiation pattern prediction and mutual coupling 13 p2037 A71-28495

Signal rejection characteristics of receiver preselector and antenna system, requiring receiver mixer efficiency and transmitter parameters 13 p2032 A71-28862

Finite antenna arrays excitation patterns, yielding electromagnetic parameters approaching preselected optimal values 14 p2192 A71-29807

Synthesizing antenna arrays perpendicular to conducting screen by PSK signal theory, discussing optimal binary phasing and radiation patterns numerical data 14 p2211 A71-30104

High efficiency autotrack strip-line-fed dipole antenna array for L and S band airborne telemetry 14 p2198 A71-30905

Optimal omnidirectional antenna array located on cylindrical head section of sounding rocket for L band telemetry 14 p2216 A71-31035

Multiple planar Luneberg lens circular array for airborne electronically scanned X band narrow beam antenna mounted under aircraft nose or fuselage 14 p2216 A71-31038

Tape helix radiators for spacecraft phased antenna arrays, analyzing performance for proposed L band system 14 p2217 A71-31057

Blade antenna linear array design for aircraft-satellite communication, determining mutual influences by array measurements in simulated electrical environment 14 p2206 A71-31062

Collimating optically fed circular antenna array using quadratic phase tapers, emphasizing airborne applications 14 p2206 A71-31064

Near-isotropic six radiator antenna array for large aerospace vehicles, calculating three dimensional radiation distribution 14 p2218 A71-31066

Slotted waveguide arrays in precision Doppler radar antennas, correlating predicted and actual performance 14 p2206 A71-31073

L band aircraft antenna array consisting of circularly polarized elements and static electronic steering circuits for synchronous satellites radio links 14 p2273 A71-31074

Chebyshev antenna array optimum spacing derivation for beamwidth decrease without sidelobe level increase 15 p2368 A71-31142

Electronically scanned cruciform slot-array antenna for satellite controlled navigation aid, discussing circularly polarized wave radiation 16 p2548 A71-34123

Radiator system field calculation method, noting field amplitudes in two and three dimensional arrays 17 p2697 A71-34254

Multielement nonperiodic antenna array synthesis for given main and diffraction lobes of radiation pattern 17 p2698 A71-34265

Horn array electrically respun antenna design, testing and radiation characteristics, noting excitation by feed system consisting of phase shifters and circular switches 17 p2713 A71-34433

Rigorous solution for multiple arm conical log spiral antenna by numerical solution of integral equations, considering current distribution, half power beamwidth, etc 17 p2715 A71-34752

Array design by matrix inversion for specified pattern in far zone field exceeding number of independent excitation voltages 17 p2715 A71-34766

Space-time correlating antenna array forming matched filter for modulated signal reception with interference ejection 17 p2716 A71-34767

Current distribution and driving point admittances computation in curtain antenna array with delta function generator driven electrically long elements 17 p2716 A71-35094

Long baseline atomic clock interferometry with meter wavelength cross polarized antenna arrays for spacecraft propagation experiments 17 p2744 A71-35098

Far field minimum radiation over angular sector for directional broadside array with optimum interelement spacing, considering sidelobe reduction 18 p2875 A71-35972

Isotropic and quasi-isotropic satellite antennas, considering circumferential arrays fed in phase or with progressing phase and systems with orthogonally polarized radiators 18 p2893 A71-36577

Circular loop antenna array of N elements with arbitrary circumference, analyzing by Fourier series expansion 19 p3023 A71-38588

Constrained optimization of array antennas performance for obtaining radiation pattern with desired sidelobe levels 19 p3023 A71-38591

Dipole antenna with parallel parasitic element, investigating resonant length variation as function of spacing with matrix inversion method 19 p3035 A71-38599

Transistor fed active radiating array antennas, showing dependence on elemental mutual coupling 19 p3035 A71-38600

Envelope limiting in control loops of adaptive array antennas, reducing varying noise interference 20 p3195 A71-38863

Book on antenna characteristics covering tabulated data for cylindrical dipoles and monopoles, imperfectly conducting dipoles, circular loop antennas and broadside and endfire arrays 20 p3196 A71-39200

Ionospheric irregularities and reflection points calculation, developing simple ray interference model from large antenna array data 21 p3372 A71-40042

Perturbation procedure application to linear and circular antenna array directivity optimization by phase adjustments under uniform amplitude excitation 21 p3359 A71-41412

Waveguide simulator study of blindness/resonance or surface wave/ effect in phased array antennas 22 p3509 A71-41631

Active synthetic aperture coherent imaging technique to fill and double diameter of sparsely sampled aperture array 22 p3574 A71-41783

Optimal synthesis of antenna array radiation patterns with minimum square deviation from zero in sidelobe 22 p3510 A71-42269

Chebyshev antenna arrays minimum length for given sidelobe levels 22 p3521 A71-42271

Plane electromagnetic wave diffraction on periodic arbitrary profile array, presenting near and far field asymptotic characteristics 22 p3511 A71-42306

Phase distribution randomization in switched antenna array, noting radiation pattern sidelobe compensation application 22 p3522 A71-42312

Arbitrary multipole structure spherical wave propagation in Schwarzschild metric, using Bondi coordinate system and negative powers of r 23 p3704 A71-43826

Extensive air shower radio pulse emission by geomagnetic charge separation mechanism, using antenna and scintillation counters arrays 23 p3646 A71-44012

High power multielement electronically scanned array of microwave low periodic monopole antennas for ionospheric backscattering measurements 23 p3653 A71-44155

Edge effects in finite linear arrays of uniform slits fed by parallel plate waveguides terminated on ground plane 23 p3653 A71-44156

Reflection and scattering properties of two dimensional periodic arrays of loaded dipoles with bandpass filter characteristics as function of frequency 23 p3654 A71-44159

Numerical solution for plane wave scattering by dielectric sheet with imbedded periodic array of conducting strips 23 p3654 A71-44164

Curved wire array to eliminate parasitic circular polarization of variable profile radio telescope antennas, applying to solar observations 23 p3655 A71-44326

Plane electromagnetic wave diffraction on dense periodic array at conducting screen, showing far field asymptotic behavior for E and H polarization 23 p3647 A71-44331

Multicomponent signal arrival angles wave front analysis from antenna array phase and amplitude measurements for radio direction finding 24 p3803 A71-44647

Photon noise limited interferometer transducer for gravitational radiation antenna, using piezoelectric driver to generate subangstrom vibrations 24 p3835 A71-45209

ANTENNA COMPONENTS
NT ANTENNA COUPLERS
NT ANTENNA FEEDS
ANTENNA COUPLERS
NT COUPLING CIRCUITS

Arbitrary lossless antennas radiative, scattering and coupling properties interrelations 06 p0874 A71-17707

Identical V antennas coplanar array admittance matrix, showing mutual conductance and susceptance as function of spacing 06 p0875 A71-17727

Electromagnetic coupling measurement between two antennas in cluttered communications system, emphasizing scale model prediction technique 17 p2703 A71-35078

Numerical method for near field antenna coupling over conducting surface of aerospace vehicles applied to L band slot antennas on F-4 Phantom aircraft 19 p3031 A71-38445

Narrow strongly radiating slot voltage distribution, investigating cavity coupling with integral equation 22 p3522 A71-42305

ANTENNA DESIGN

Spacecraft phased arrays design, considering solid state amplifiers effect on total array performance and transistors and varactors output power efficiency 07 p1069 A71-18813

Pulkovo radio telescope antenna surface precision and electrical characteristics at eight mm, using ground oscillators and solar, lunar and Venusian observations for radiation pattern 07 p1075 A71-19342

Impedance antenna with slow wave structure of zig-zag shaped wires 07 p1079 A71-20260

Loop antenna with finite gap at driving point, deriving admittance, current distribution, radiation pattern and directive gain from variational and Fourier series methods 08 p1265 A71-21296

Plane impedance finite length antenna synthesis, deriving equation for radiation pattern-surface reactance relationship 08 p1266 A71-21461

Two dimensional concentric ring antenna arrays synthesis, describing radiation pattern formation 08 p1266 A71-21463

Wide beam lens antenna synthesis from non-homogeneous dielectric with specified refractive index, using conformal mapping for lens and beam conversion 08 p1266 A71-21466

Linear antenna radiation patterns digital computer simulation, applying algorithm based on Kotelnikov to antenna synthesis 08 p1266 A71-21467

Circularly polarized parabolic reflector UHF antenna with helical feed for direct TV reception from satellite, discussing design and performance 09 p1417 A71-23034

Arbitrary antenna arrays of not necessarily identical elements, deriving maximum realizable gain under impedance matching, and applying to spaced circular arrays 09 p1419 A71-23508

Rudimentary broadband linearly polarized horn antenna design, impedance and radiation characteristics 09 p1419 A71-23509

Multimode slow wave planar spiral antenna design and radiation field characteristics 09 p1420 A71-23510

Dipole antenna array exact design for prescribed radiation patterns in magnetic plane, using current distribution integral 09 p1420 A71-23511

Helios solar probe antenna system for S-band radio communication, discussing electrical and mechanical design 09 p1533 A71-23734

Antenna optimal radiation patterns, discussing antenna synthesis based on desired far field characteristics 10 p1582 A71-23806

Parabolic antenna instantaneous phase center calculations, using radiation patterns from aperture field and current distribution methods 10 p1582 A71-23807

Conical equiangular spiral antenna active region boundary calculation, considering radiation vector 10 p1584 A71-24718

Lightweight parabolic antenna model with inflated Mylar tube torus and central mast interconnected by wires, discussing construction, performance tests and tradeoffs [ALAA PAPER 71-397] 11 p1736 A71-25273

Variance and correlation radius of distortions from transparent dielectric plate, using statistical theory of antennas 11 p1738 A71-26348

Passive two-terminal networks in rod antenna for bandwidth increase, investigating equivalent circuit on digital computer 12 p1886 A71-26987

Antenna analysis method based on transmission line theory, yielding current distribution and input impedance of finite conical antenna 12 p1880 A71-27154

Adaptive array antennas with control loop, deriving noise expression for maximizing signal to noise ratio 12 p1881 A71-27426

Edge geometries and aperture distributions of physically realizable planar antennas 13 p2027 A71-27989

Field correlation diffraction theory of symmetrical microwave Cassegrain antenna, calculating main reflector focused field by spherical wave expansion 13 p2028 A71-27992

Holographic narrow beam VHF antenna design and testing, using X band scale model 13 p2036 A71-27999

Active antennas for frequency range 100 kHz to 250 MHz, discussing transistor circuitry optimization with respect to noise and linearity 14 p2102 A71-29822

Book on antenna admittance problem covering iterative solution of integral equations, Fourier series solution, Wiener Hopf methods, transmission line theory, etc 14 p2193 A71-29932

Parabolic two-mirror antenna design with one small mirror for diffraction fringe effects correction 14 p2196 A71-30637

Raisting ground radio station second antenna system, discussing design for all weather performance 14 p2214 A71-30812

Interrogation, recording and location system satellite techniques for wildlife tracking and monitoring, describing collar antenna, battery pack and solar cells 14 p2200 A71-30923

Structural design, mechanical stability and aircraft compatibility for airborne side-looking radar antennas, using end fed slotted waveguide arrays 14 p2205 A71-31041

Flush mounted aeronautical waveguide antennas with dielectric plug for 5GHz operation 14 p2216 A71-31043

Airborne blade antenna tunable for 26-100 MHz by individual bands, using binary related inductors switched by miniature high vacuum relays 14 p2216 A71-31044

Fincap communication antennas design and environmental tests for vibration, acceleration, waterproofing, salt corrosion, ice formation and compass safe distance 14 p2216 A71-31047

Helicopter aerial design problems, considering antenna multiplicity use of nonmetallic structures and complexity of airborne radio systems 14 p2217 A71-31048

Quasi-isotropic directional, omnidirectional and auxiliary antennas of Helios Solar Probe S band system, discussing design, radiation patterns, adaptability and X band measurements 14 p2217 A71-31052

Light aircraft notch antenna for efficient radiation at HF band lower end and minimal interference with aircraft structure 14 p2217 A71-31053

Aircraft phased arrays for L-band ATC satellite system application, alleviating problems of power budget and vulnerability to multipath and interference 14 p2217 A71-31054

High efficiency narrow beam aircraft Cassegrain antenna design for horizon without excessive ground illumination 14 p2217 A71-31056

Tape helix radiators for spacecraft phased antenna arrays, analyzing performance for proposed L band system 14 p2217 A71-31057

Far field patterns for short active antennas obtained by integration of transistors and passive antennas 14 p2217 A71-31058

L-1011 Tristar antenna arrangement test results, considering weight, aerodynamic and structural design requirements 14 p2218 A71-31060

Civil aircraft antenna design mechanical and environmental aspects and electrical performance, considering serviceability and duplication 14 p2218 A71-31061

Blade antenna linear array design for aircraft-satellite communication, determining mutual influences by array measurements in simulated electrical environment 14 p2206 A71-31062

Short low noise transistorized receiving antennas for rockets with nonconducting hoods and conducting surface 14 p2218 A71-31063

Collimating optically fed circular antenna array using quadratic phase tapers, emphasizing airborne application 14 p2206 A71-31064

Near-isotropic six radiator antenna array for large aerospace vehicles, calculating three dimensional radiation distribution 14 p2218 A71-31066

SIRIO spacecraft cavity backed antenna around apogee motor nozzle operating at 40 and 360 MHz 14 p2218 A71-31069

Aerospace antenna design, calculating one-wavelength circular slot aperture radiation from circular cylindrical surface 14 p2206 A71-31075

Chebyshev antenna array optimum spacing derivation for beamwidth decrease without sidelobe level increase 15 p2368 A71-31142

High directional microwave antennas optical simulation, design and measurement based on coherent optics and holography 15 p2375 A71-31282

Electronically scanned cruciform slot-array aircraft antenna for satellite controlled navigation aid, discussing circularly polarized wave radiation 16 p2548 A71-34123

Dipole coupling, current distribution and impedance of thick dipolar log periodic antennas by 4-term theory 16 p2544 A71-34172

Horn array electrically respun antenna design, testing and radiation characteristics, noting excitation by feed system consisting of phase shifters and circular switches 17 p2713 A71-34433

Transverse feed design for spherical reflector antennas, noting efficiency and field distribution 17 p2700 A71-34751

Worst case criterion for finite circular antenna aperture illuminations effectiveness comparison and optimization in synthesizing ideal radiation pattern 17 p2715 A71-34763

Array design by matrix inversion for specified pattern in far zone field exceeding number of independent excitation voltages 17 p2715 A71-34766

Tuned loop antenna for missile telemetric data transmission, discussing design, implementation and impedance and radiation measurements 17 p2718 A71-35749

Far field radiation patterns and optimum design of horizontal rhombic antenna in warm plasma, using linearized hydrodynamic theory 18 p2875 A71-35969

Omnidirectional one slot aerial energized by dielectric waveguide for hypersonic vehicle-ground communication through ionized shock layer [ONERA-TP-949] 18 p2887 A71-36022

Antenna system design for communication satellite ground station operating in 10.7-35 GHz range 18 p2881 A71-36556

Stabilizing system for retransmission beam of direct TV broadcast satellite, considering rebroadcast antenna, electronic sensor and antenna pointing subsystem 18 p2892 A71-36576

Optimal solutions for antenna synthesis problem for bounded norm of source distribution function and limited error in realization of given directional pattern 18 p2893 A71-36620

Spacecraft conical antenna design for planetary communications, investigating impact on other subsystems [AAS PAPER 71-151] 19 p3018 A71-37953

Gravitational radiation antenna consisting of disk cylinder in radial mode of circular symmetry 19 p3104 A71-38190

Antenna linear array power pattern synthesis, determining optimum nonnegative harmonic approximation to given function in Gauss/weighted least-mean-square/ and Chebyshev senses 19 p3021 A71-38472

Pattern space factor and aperture distribution of continuous line source for maximum directivity 19 p3023 A71-38590

Singular integral equation theory application to design of cylindrical antennas with small length-to-radius ratio 19 p3035 A71-38597

Dipole antenna bandwidth extension by conjugate reactance loading based on periodically loaded transmission line theory 19 p3036 A71-38602

Quadrifilar helix antenna pitch angle and ground plane size optimization based on beam pattern data 19 p3036 A71-38603

Broadband antenna twist reflector with wire grids, deriving design formulas and theoretical performance in terms of polarization attenuation 19 p3036 A71-38606

Active region and truncation point of log periodic dipole antenna as function of length and design parameters 20 p3203 A71-39091

Radiation patterns due to four pyramidal horns used in sum and difference comparison monopulse radar from single horn pattern for design optimization 20 p3203 A71-39092

Synchronous communication satellites stabilization for implementation in 1970-1975 time frame, considering antenna size, power system capacity and vehicle pointing 21 p3348 A71-40480

Computerized numerical optimization for Yagi-Uda antenna array gain, noting nonoptimum in standard traveling-wave design methods 21 p3349 A71-41410

Satellite tracking ground antenna servocontrol, discussing system requirements and automatic and programmed operating modes [DFVLR-SONDDR-125] 22 p3483 A71-41520

Spherical wave technique adaptation to antenna radiation determination by equivalent current sheets 22 p3509 A71-42200

Wave diffraction by air gap multilayered dielectric coated sphere with azimuthal slot for low loss transmission, obtaining radiation pattern 22 p3522 A71-42283

Thin circular frame antenna input admittance computation formulas numerical results comparison, noting insignificant discrepancies 22 p3523 A71-42319

Circularly polarized parabolic SHF antenna with plane and parabolic reflectors, testing radiation pattern performance 22 p3515 A71-42521

German monograph on analysis and design of digital microwave phase shifters for phase controlled antennas covering admittance loaded lines, transmission and reflection behavior 23 p3649 A71-42999

Turnstile loop Yagi and hexafilar contrawound spiral antennas for microwave telemetry rocket data reception, describing design and radiation patterns 23 p3643 A71-43095

ANTENNA FEEDS

Frequency division multiplexing of antenna feeder ducts without resonators using bridge circuits 01 p0054 A71-11084

Cassegrain antenna equivalent parabolic reflector concept for feeds near focus 02 p0233 A71-12424

High efficiency spherical reflector antennas with scanning and multiple feed properties for communication satellite portable earth stations 02 p0233 A71-12792

Multiple beam antenna with fixed spherical reflector and movable dual subreflector feedhorns, comparing with conventional Cassegrain antenna for satellite tracking 02 p0233 A71-12794

Waveguide feeder system design for antenna receive path of Intelsat 3 satellite ground station, considering system noise temperature 02 p0223 A71-12800

Antenna primary feed design and sample and store technique tracking system with conical scan control for Intelsat 3 satellite ground station 02 p0223 A71-12802

Hybrid mode flare feed horns for parabolic antennas, discussing horn parameters and angular aperture effects on gain factor or aperture transmission efficiency 02 p0234 A71-12807

High efficiency feeds for large satellite outtracking earth station antennas, using focal plane distribution 02 p0223 A71-12808

Resonant circularly polarized quadrifilar helix antenna with antiphase feed, noting cardioid shaped radiation patterns 04 p0559 A71-15877

Network synthesis of beam-forming matrices feeding linear and rectangular antenna arrays 05 p0719 A71-16145

Butler matrix antenna array feed network extension to increased number of ports, considering relationship between beams and radiation pattern 06 p0875 A71-17726

Low noise temperature high gain satellite-communication antenna feeds optimal design using step-tapered aperture 06 p0877 A71-18395

Radiation resistance of center fed dipole antenna with transversely displaced feed points, using Schelkunoff moment method 07 p1075 A71-19267

Antenna feed waveguides interconnection for compensation of cross coupling between elements of two dimensional array 07 p1079 A71-20072

Center fed dipole antenna with displaced feed points in warm plasma medium, calculating radiation patterns 08 p1264 A71-21221

Circularly polarized parabolic reflector UHF antenna with helical feed for direct TV reception from satellite, discussing design and performance 09 p1417 A71-23034

Beam compression technique for log periodic dipole antenna array using axial displacement of antenna dipoles feed points 09 p1406 A71-23035

Traveling wave antenna arrays of mismatched elements, calculating element resistances and spacings 09 p1408 A71-23488

Variational formula for input impedance of thin asymmetrical cylindrical dipole antenna 09 p1408 A71-23490

Synthesis of primary electromagnetic fields of transmitting feed antenna for two dimensional circular cylindrical reflector 09 p1418 A71-23492

Single aperture antenna system with multimode log spiral feed 09 p1419 A71-23500

Dipole antenna with displaced feed points, deriving radiation pattern expression with spherical coordinate system 13 p2033 A71-28898

Computerized design of optimally efficient dual-series feed microwave networks for waveguide phased arrays 14 p2209 A71-29566

Resonant dipole antenna with feed points immersed in weakly ionized plasma, investigating performance under electro-acoustic and electromagnetic wave excitation 14 p2193 A71-29858

High efficiency autotrack strip-line-fed dipole antenna array for L and S band airborne telemetry 14 p2198 A71-30905

High speed airborne scanning navigational radar antenna with matched patterns, using offset horn feed reflector and polarization modes for improved visual display 14 p2216 A71-31036

Collimating optically fed circular antenna array using quadratic phase tapers, emphasizing airborne applications 14 p2206 A71-31064

Dual plane monopulse multimode radar antenna feeds, determining input geometry relationship to generated modes by image method 14 p2218 A71-31065

Marconi 90 ft space communication antennas and waveguide components, using feed horn radiation patterns to compute gain 15 p2374 A71-31141

Multimode coaxial feed with circular cross section waveguide and concentric ring shaped radiator for parabolic antennas 16 p2546 A71-33480

Horn array electrically respun antenna design, testing and radiation characteristics, noting excitation by feed system consisting of phase shifters and circular switches 17 p2713 A71-34433

Transverse feed design for spherical reflector antennas, noting efficiency and field distribution 17 p2700 A71-34751

Composite ATS 6 and 7 satellite antenna feed capable of illuminating large space-deployable parabolic antenna 17 p2716 A71-35096

Wide angle microwave antenna radiation beam steering with fixed parabolic reflectors, using adaptive primary feed for intercepted field spatial Fourier transformation 17 p2708 A71-35493

Pleumeur-Bodou /France/ ground station steerable parabolic reflector Cassegrain antenna for communication satellites, discussing specifications and radioelectric and mechanical characteristics 17 p2717 A71-35510

Nonplanar dipole antenna with transversely displaced feed points, considering effects on far field radiation patterns, radiation resistance, power gain, effective aperture and efficiency 18 p2887 A71-35970

Feed point axial displacement effects on radiation resistance and patterns of dipole antenna in weakly ionized plasma 18 p2875 A71-35971

Cassegrain antennas with reflector horn feed for satellite communication, noting gain and noise temperature 18 p2890 A71-36554

Isotropic and quasi-isotropic satellite antennas, considering circumferential arrays fed in phase or with progressing phase and systems with orthogonally polarized radiators 18 p2893 A71-36577

Near field radiation characteristics of corrugated feed by spherical mode expansion method 19 p3018 A71-38218

Transistor fed active radiating array antennas, showing dependence on elemental mutual coupling 19 p3035 A71-38600

Coaxial cable antenna lead with shield or external conductor in form of slotted corrugated metal foil, testing performance 20 p3197 A71-39469

Broadband helical antenna feeds for millimeter wave parabolic reflectors and lenses, determining beamwidths and polarizations as functions of helix parameters and frequency 21 p3359 A71-41408

Electromagnetic wave propagation and radiation pattern of circular corrugated waveguide antenna feeds, considering unity azimuthally dependent modes 22 p3511 A71-42278

Polarization transforming feed horns for rapid scan X-band radar antenna, allowing transmission in various polarization modes and parallel and orthogonal-polarized return reception 23 p3655 A71-44167

Shunt driven circular loop antenna effective length, current distribution and input admittance, comparing to transmission lines 23 p3655 A71-44169

ANTENNA FIELDS

U ANTENNA RADIATION PATTERNS

ANTENNA RADIATION PATTERNS

NT SIDELOBES

Stacked dipole antenna arrays with modulated phase velocity, comparing measured and calculated radiation patterns 01 p0052 A71-10474

Field tests for telemetry receiving systems solar calibration, describing antenna pointing 01 p0033 A71-10891

Pyramidal or conical horn antenna E plane aperture distribution and radiation pattern control by flare angle changes 01 p0054 A71-10973

Long range troposcatter, evaluating antenna directivity effects on signal fading rate and fluctuation 01 p0037 A71-11087

Secondary currents on conducting cylinder near dipole antenna manifested as radio frequency interference, considering effect on radiation pattern 01 p0037 A71-11167

Polarization structure of paraboloid mirror antennas circular emission by geometrical diffraction theory of spherical edge waves 01 p0056 A71-11204

Plane curvilinear radiators synthesis for horizontal or vertical radiation patterns, obtaining current phase amplitude distributions by symmetrical striplines 01 p0056 A71-11205

Multielement nonperiodic antenna array synthesis for given main and diffraction lobes of radiation pattern 01 p0057 A71-11214

Nulls of radiation and input impedance of flush mounted rocket antennas for telemetry and transponder systems 02 p0228 A71-11674

Optimum VLF electromagnetic link between underground terminals with emitter-receiver horizontal antennas, calculating radiation pattern 02 p0211 A71-11717

Wellenweber antennas characteristics, calculating input and mutual impedances, total field radiated and power gain 02 p0232 A71-12343

Antenna gain of Space Communications and Tracking terminal from feedhorn radiation pattern and reflector geometry 02 p0219 A71-12448

Cassegrain system far field radiation pattern and gain loss prediction for beam steering by subreflector tilting 02 p0222 A71-12793

Shaped dual reflector antenna gain prediction based on feedhorn radiation pattern and system geometry 02 p0233 A71-12795

Shaped dual reflector system phase errors due to feedhorn or subreflector axial displacement, examining effects on gain and secondary radiation pattern 02 p0222 A71-12796

Antenna polar diagrams short range measurement, using far field approximation for incident plane waves source and radio star or satellite 02 p0223 A71-12801

Dipole antennas mutual influence near conducting intersecting circular cylinders, using geometrical diffraction theory 03 p0384 A71-13395

Vertical dipole electromagnetic field diffraction by circular aperture in opaque screen with coaxial concentric conducting disk 03 p0379 A71-13963

Stray-source field on plane antenna reflector surface for arbitrary space direction 03 p0387 A71-14335

Optimal synthesis of antenna array radiation patterns with minimum square deviation from zero in sidelobe 04 p0557 A71-14629

Radiation patterns of dielectric rod antennas with axial emission in near field 04 p0557 A71-14630

High altitude rocket-borne radiosonde communication, examining transmission link characteristics, signal losses and antenna radiation patterns 04 p0551 A71-15012

Computer program description of radiation pattern of imperfect paraboloidal reflectors by transforming numerically expressed phase variations in plane electromagnetic wave 04 p0552 A71-15021

Vertical and horizontal VLF fields excited by dipoles of arbitrary orientation and elevation for nighttime ionosphere 04 p0552 A71-15216

Input resistance and effective height of gap excited metallic and dielectric antennas in conductive environment 04 p0558 A71-15220

Resonant circularly polarized quadrifilar helix antenna with antiphase feed, noting cardioid shaped radiation patterns 04 p0559 A71-15877

Radiation patterns of diametrically opposed slot antenna arrays on infinitely long cylinders 04 p0559 A71-15878

Antenna aperture random radiation field representation in expansion in eigenfunctions, comparing results with linear antenna statistical theory 05 p0727 A71-15994

Axissymmetric multibeam annular antenna array with interacting radiating elements synthesized by partial radiation patterns 05 p0722 A71-16867

Cophased two dimensional antennas fields asymptotic expansions in near and far zones with generalization to three dimensional case 05 p0722 A71-16868

Microwave holography application to monopole antenna radiation field mechanism, using liquid crystals for optical reconstruction 05 p0756 A71-17231

Out of phase conical horn radiating element amplitude and phase diagrams at short distances 06 p0872 A71-17374

Arbitrary lossless antennas radiative, scattering and coupling properties interrelations 06 p0874 A71-17707

Monopole antenna with continuous resistive loading, studying broadband characteristics over frequency range by thin film evaporation techniques 06 p0867 A71-17710

Collinear and planar arrays of arbitrarily located parallel elements, determining current and charge distribution, admittances and field patterns 06 p0875 A71-17715

Monopole radiation on ground screens, deriving modified elevation angle to transform quasi-far zone measurements 06 p0868 A71-17716

Phased array antenna element with circular polarization by superposition of complementary dipole and slot, achieving equal E- and H-plane patterns 06 p0875 A71-17719

Log periodic dipole array transient radiation, obtaining radiated pulse envelope time dependence as function of antenna admittance and input pulse frequency spectrum 06 p0875 A71-17720

Optimum line source approximation to desired radiation pattern, deriving least mean squared error expression 06 p0868 A71-17721

Phase grating lobes redistribution by aperiodic phased array of line sources with linear variation of element lengths and linear amplitude weighting 06 p0875 A71-17722

Open cavity radiators radiation fields, describing antenna structure based on backfire principle with dipole array exciter and parasitic reflector 06 p0875 A71-17724

Butler matrix antenna array feed network extension to increased number of ports, considering relationship between beams and radiation pattern 06 p0875 A71-17726

Plasma coated spherical antenna radiation, discussing hot and cold plasmas frequency and electroacoustic wave effects 06 p0875 A71-17730

Doubly shunt loaded short slot antenna, determining optimum capacitive loadings for enhanced radiation or improved directivity 06 p0876 A71-17740

Radiation pattern of narrow beam antenna using artificial dielectric medium with permittivity less than unity 06 p0868 A71-17741

Spherical antenna covered by lossy hot plasma layer, calculating radiation power 06 p0869 A71-18018

Antenna radiation in isotropic plasma near resonance 06 p0937 A71-18311

Pulkovo radio telescope antenna surface precision and electrical characteristics at eight mm, using ground oscillators and solar, lunar and Venusian observations for radiation pattern 07 p1075 A71-19342

Optimum transmitted data volume, orientation accuracy and size of narrow beam parabolic spacecraft antennas, defining optimum parabola for approximate radiation pattern 07 p1078 A71-19871

Directional antenna with parabolic reflector for missile tracking in telemetry band, considering radiation diagrams and design approach 07 p1078 A71-20012

Optimal synthesis of linear equidistant antenna arrays with sum and difference radiation patterns, using orthogonal polynomials 07 p1078 A71-20069

Gain and radiation properties of phased array antenna with dielectric, using integral method
07 p1078 A71-20070

Center fed dipole antenna with displaced feed points in warm plasma medium, calculating radiation patterns
08 p1264 A71-21221

Loop antenna with finite gap at driving point, deriving admittance, current distribution, radiation pattern and directive gain from variational and Fourier series methods
08 p1265 A71-21296

Plane impedance finite length antenna synthesis, deriving equation for radiation pattern-surface reactance relationship
08 p1266 A71-21461

Beam scanning radar antenna, deriving optimum field distributions in aperture
08 p1266 A71-21462

Two dimensional concentric ring antenna arrays synthesis, describing radiation pattern formation
08 p1266 A71-21463

Focused aperture antenna arrays near field radiation patterns, determining minimum focusing distance
08 p1266 A71-21464

Conducting disk with slot dipole at center, determining asymptotic expressions for radiation field far zone
08 p1266 A71-21465

Linear antenna radiation patterns digital computer simulation, applying algorithm based on Kotelnikov to antenna synthesis
08 p1266 A71-21467

Parabolic radio telescope phase errors for field distribution, compensating for mirror system mass deformations
08 p1266 A71-21468

Longitudinal direction positioning error effects on grating lobe field deviation and reduction in uniform linear arrays
08 p1257 A71-21885

Self and mutual admittance, isolation and radiation pattern of slots on infinite cylinder covered by inhomogeneous lossy plasma
08 p1341 A71-21886

Highly directive radio telescope antenna parameters in near zone, using focusing at minimum distance
09 p1414 A71-22218

Linear phased antenna arrays, calculating influence of interaction between radiating elements on radiation pattern
09 p1404 A71-22225

Statistical directivity, radiation pattern, drift dispersion of segmented traveling wave antennas
09 p1414 A71-22226

Cylindrical slot antennas radiation patterns in plane perpendicular to axis, discussing field emission and angular position of each slot for phase multiplier
09 p1415 A71-22458

Envelopes of antenna beams produced by variation of one antenna dimension in radar system
09 p1406 A71-23031

Linear and circular apertures sum and difference radiation patterns for minimum sidelobe power
09 p1407 A71-23108

Realizable method of pattern synthesis for broad-side array antenna giving arbitrary current distribution
09 p1418 A71-23489

Geometry optimization of error-free distributed nondirectional aperture array receivers, using signal detectability technique
09 p1408 A71-23491

Synthesis of primary electromagnetic fields of transmitting feed antenna for two dimensional circular cylindrical reflector
09 p1418 A71-23492

Shaped beam radiation patterns synthesis by iterative sampling method with line sources or uniformly spaced antenna arrays
09 p1409 A71-23493

Radiation nulls suppression and broadband impedance matching of infinite rectangular waveguide phased arrays, giving numerical solutions
09 p1419 A71-23494

Efficiency evaluation of large parabolic antenna reflector by frequency scaling
09 p1409 A71-23496

Axial slits circular array pattern in large conducting cylinders fed by waveguides
09 p1419 A71-23497

Linear antenna arrays synthesis with Z transforms permitting sidelobe reduction and nulls in antenna radiation patterns
09 p1419 A71-23498

Lossless radiating antenna element efficiency in circular cylindrical arrays of identical elements, relating to reflection coefficient
09 p1419 A71-23505

Rudimentary broadband linearly polarized horn antenna design, impedance and radiation characteristics
09 p1419 A71-23509

Multimode slow wave planar spiral antenna design and radiation field characteristics
09 p1420 A71-23510

Dipole antenna array exact design for prescribed radiation patterns in magnetic plane, using current distribution integral
09 p1420 A71-23511

Pulse excited finite length cylindrical monopole antenna mounted vertically on perfectly conducting ground plane, calculating near point electromagnetic fields
09 p1420 A71-23512

Admittance of aperture antenna radiating into lossy warm overdense plasma half space, considering electron energy
09 p1505 A71-23521

Ground metallic plate effect on electric dipole antenna radiation characteristics as function of aperture field
09 p1420 A71-23572

Radiation patterns of radar antennas with single near field cylindrical obstructions, considering directional S band antenna
09 p1420 A71-23678

Antenna optimal radiation patterns, discussing antenna synthesis based on desired far field characteristics
10 p1582 A71-23806

Parabolic antenna instantaneous phase center calculations, using radiation patterns from aperture field and current distribution methods
10 p1582 A71-23807

Atmospheric turbulence parameters determination from radar meteor observation, calculating antenna radiation patterns effect on error
10 p1583 A71-24036

Iterative synthesis of dipole antenna array for maximum directivity radiation pattern, considering amplitude-phase distributions
10 p1583 A71-24707

Signal fluctuation effect on directional properties of multidipole receiving antenna, calculating radiation pattern
10 p1583 A71-24708

Conical equiangular spiral antenna active region boundary calculation, considering radiation vector
10 p1584 A71-24718

Polarization distortion of partially polarized wave emission and reception by two channel horn antennas, noting radio astronomy, radar and optics applications
10 p1584 A71-24876

Flush mounted annular slot missile antenna theory application to near zone field strength instrumentation calibration and plane wave electromagnetic field pulse response determination
10 p1580 A71-25071

Simulated far field patterns of linear and phased arrays without radiation coupling by hybrid analog computer
11 p1735 A71-25851

Single element antenna radiation pattern effect on equidistant linear directional gain, current distribution and array shape
11 p1738 A71-26343

Aperture zoning methods for reducing phase errors on radiation patterns of equidistant dimensional arrays with traveling wave slotted waveguide elements
11 p1738 A71-26346

Single- and two-turn cylindrical spiral antenna, calculating end reflection, current damping and in-phase excitation component effects of radiation characteristics distortion
11 p1741 A71-26553

Sparse antenna arrays with small sidelobe level, estimating error due to radiation pattern substitution by statistical method
11 p1741 A71-26556

Electric and magnetic surface current coefficients of antenna radiating elements in metallic waveguides and resonators by harmonics expansion applied to circular-cylindrical array
12 p1885 A71-26839

Antenna effective area and radiation pattern measurement using emission characteristics of extraterrestrial radio sources, sun and moon
12 p1967 A71-27422

Satellite antenna power density contours on earth, using pattern operator for coordinate transformation
12 p1881 A71-27423

Tacsat 1 telecommunications relay system, discussing UHF-SHF antenna radiation patterns, ground terminal equipment, nutation dampers and attitude and orbital correction procedures
12 p1882 A71-27611

Radiation mechanism of line sources array above finite ground plane, studying maximum field intensity variation and angle
13 p2028 A71-27991

Spherical wave expansion theory application to near field and far field patterns, using analytical, experimental and numerical data
13 p2028 A71-27993

Monograph on tolerance effects and performance degradation in microwave aerials covering axial displacement, active array, radiation pattern prediction and mutual coupling
13 p2037 A71-28495

Feasibility of VHF aeronautical satellite system frequency sharing band used by ATC service, employing spatial separation, antenna directivity and frequency offset
13 p2032 A71-28873

Electromagnetic compatibility, measuring microwave antennas characteristics, including frequency range, gain, beamwidth, voltage standing wave ratio, impedance and radiation patterns
13 p2039 A71-28877

Dipole antenna with displaced feed points, deriving radiation pattern expression with spherical coordinate system
13 p2033 A71-28898

High directivity antennas lateral radiation level, showing field in sidelobe segment approximation by logarithmically normal law
13 p2040 A71-28994

Finite antenna arrays excitation patterns, yielding electromagnetic parameters approaching preselected optimal values
14 p2192 A71-29807

Resonant dipole antenna with feed points immersed in weakly ionized plasma, investigating performance under electro-acoustic and electromagnetic wave excitation
14 p2193 A71-29858

Linear antenna radiation pattern broadening due to atmospheric turbulence
14 p2194 A71-30074

Synthesis of linear antenna with integrated currents for specified ratio of antenna radiation to elementary radiator patterns
14 p2194 A71-30101

Synthesis of slot antenna on metallic wedge for amplitude radiation pattern, determining RMS approximation and fixed phase diagram
14 p2195 A71-30103

Synthesizing antenna arrays perpendicular to conducting screen by PSK signal theory, discussing optimal binary phasing and radiation patterns numerical data
14 p2211 A71-30104

Omnidirectional broadband telemetry antenna array for spacecraft providing near isotropic circular polarized radiation with open line microstrip feed
14 p2199 A71-30907

Four arm conical spiral microwave antenna with circularly polarized hemispherical radiation pattern for satellite and rocket applications
14 p2216 A71-31042

Airborne phased array using computer control for beam steering, investigating row-and-column logic effects on beam shaping and stabilization
14 p2209 A71-31045

Computer program for processing of UHF radiation patterns of ESRO 4 scientific satellite omnidirectional antenna systems
14 p2217 A71-31051

Light aircraft notch antenna for efficient radiation at HF band lower end and minimal interference with aircraft structure
14 p2217 A71-31053

High efficiency narrow beam aircraft Cassegrain antenna design for horizon without excessive ground illumination
14 p2217 A71-31056

Far field patterns for short active antennas obtained by integration of transistors and passive antennas
14 p2217 A71-31058

Near-isotropic six radiator antenna array for large aerospace vehicles, calculating three dimensional radiation distribution
14 p2218 A71-31066

Numerical prediction of radiation patterns for antennas mounted on spacecraft, noting booms and solar cell panels effects
14 p2218 A71-31068

Aerospace antenna design, calculating one-wavelength circular slot aperture radiation from circular cylindrical surface
14 p2206 A71-31075

Polar diagrams computation for large Cassegrain antennas, obtaining sidelobe peaks envelope at wider angles of radiation by near field measurements
15 p2368 A71-31139

Marconi 90 ft space communication antennas and waveguide components, using feed horn radiation patterns to compute gain
15 p2374 A71-31141

Chebyshev antenna array optimum spacing derivation for beamwidth decrease without sidelobe level increase
15 p2368 A71-31142

Microwave antenna far field radiation pattern determination from Brown transmission equation solution
15 p2368 A71-31143

Radiation pattern of linear radiator mounted at quarter-wavelength in front of cylindrical parabolic reflector, discussing calculation procedure based on half-wavelength dipole near field
15 p2369 A71-31415

Numerical analysis of far field gain pattern of shielded acoustic antenna by Kirchhoff integral, as

ANTENNAS

suming circular symmetry and perfectly absorbing walls 15 p2372 A71-32193

Thick unsymmetrically fed dipole antenna radiation pattern measurements and impedance matching 15 p2377 A71-32318

Circular aperture microwave antenna near field calculations based on ray diffraction theory in geometrical optics 15 p2372 A71-32366

Pseudorandom binary codes for improved microwave antenna range measurements by suppressing unwanted reflections 15 p2373 A71-32370

Fixed base two element interferometer for radio astronomy, obtaining beavertail radiation pattern by use of earth rotation 16 p2579 A71-33486

Dipole antenna near electric field, basing calculation method on integral equation for antenna surface charge distribution function 16 p2546 A71-33487

Linear aperture antenna radiation pattern interpolation based on complex-valued function satisfying integral equations system 16 p2546 A71-33497

Harmonic electromagnetic field outside closed surface perfectly conducting antenna, using Kirchhoff formula 16 p2544 A71-34171

Satellite communications use of geostationary orbit, considering ground station antennas radiation patterns, signal processing, stationkeeping, etc 17 p2696 A71-34234

Polarization structure of parabolic reflector antennas circular radiation by geometrical diffraction theory of spherical edge waves 17 p2697 A71-34256

Plane curvilinear radiators synthesis from horizontal or vertical radiation patterns, obtaining current phase amplitude distributions by symmetrical striplines 17 p2697 A71-34257

Multielement nonperiodic antenna array synthesis for given main and diffraction lobes of radiation pattern 17 p2698 A71-34265

Two mirror Cassegrain antenna secondary reflector random fluctuations effects on drift in main lobe direction 17 p2713 A71-34397

Horn array electrically respun antenna design, testing and radiation characteristics, noting excitation by feed system consisting of phase shifters and circular switches 17 p2713 A71-34433

Wideband Cassegrain microwave antenna for space communication, discussing reflecting horn for maximum radiation gain 17 p2715 A71-34686

Slot antennas electromagnetic radiation patterns in conducting ground plane coated with moving isotropic cold plasma sheath 17 p2701 A71-34758

Worst case criterion for finite circular antenna aperture illuminations effectiveness comparison and optimization in synthesizing ideal radiation pattern 17 p2715 A71-34763

Antenna radiation resistance and efficiency in dissipative medium, using concept of modified power density 17 p2701 A71-34764

Radiation pattern of dielectric disk antenna, using computerized analysis of electromagnetic scattering and spherical volume cell 17 p2715 A71-34765

Array design by matrix inversion for specified pattern in far zone field exceeding number of independent excitation voltages 17 p2715 A71-34766

Long conical multimode horn with corrugated surface throat to suppress sidelobes and equalize E and H plane beamwidths 17 p2716 A71-35095

Tuned loop antenna for missile telemetric data transmission, discussing design, implementation and impedance and radiation measurements 17 p2718 A71-35749

Far field radiation patterns and optimum design of horizontal rhombic antenna in warm plasma, using linearized hydrodynamic theory 18 p2875 A71-35969

Nonplanar dipole antenna with transversely displaced feed points, considering effects on far field radiation patterns, radiation resistance, power gain, effective aperture and efficiency 18 p2887 A71-35970

Feed point axial displacement effects on radiation resistance and patterns of dipole antenna in weakly ionized plasma 18 p2875 A71-35971

Far field minimum radiation over angular sector for directional broadside array with optimum interelement spacing, considering sidelobe reduction 18 p2875 A71-35972

Nonplanar dipole antenna with arbitrarily displaced feedpoints, considering far field radiation patterns, radiation resistance, power gain, effective aperture and efficiency 18 p2887 A71-36014

Short helical antenna performance and characteristics, discussing radiation patterns, efficiency, bandwidth and space vehicle use [ONERA-TP-950] 18 p2888 A71-36023

Theoretical signal strength reduction on USAF Eastern Test Range based on missile antenna radiation pattern characteristics 18 p2876 A71-36471

Meter wave aircraft slot antenna for Concorde air to ground communication via satellite, presenting synthetic radiation patterns 18 p2889 A71-36514

Italian SIRIO synchronous satellite for SHF communication, analyzing thermoelastic deformations effect on antenna radiation patterns 18 p2882 A71-36575

Optimal solutions for antenna synthesis problem for bounded norm of source distribution function and limited error in realization of given directional pattern 18 p2893 A71-36620

VOR antenna system with Alford loops above circular conducting ground plate, investigating radiation fields 18 p2894 A71-36827

Corner reflector excitation by vertical or horizontal log-periodic dipole antenna for unidirectional wide-band radiation, deriving far field expression 18 p2895 A71-36994

Minimum spacing between two base station antennas for mobile radio diversity reception 19 p3014 A71-37217

Near field radiation characteristics of corrugated feed by spherical mode expansion method 19 p3018 A71-38218

Antenna azimuthal radiation patterns and meteor radiant distribution effects on wind velocity measurement by radar observation of meteor trains 19 p3145 A71-38372

Parasitic wire elements effects on radiation, impedance and current distribution of antennas, using method of moments 19 p3031 A71-38444

Numerical method for near field antenna coupling over conducting surface of aerospace vehicles applied to L band slot antennas on F-4 Phantom aircraft 19 p3031 A71-38445

Radome lightning protection systems involving electrostatic shield, considering effect on electromagnetic characteristics and radiation patterns of nearby antennas 19 p3031 A71-38450

Radar antenna interference determination based on model using electrical and physical characteristics of reflector type antenna for statistical gain distribution prediction 19 p3021 A71-38458

Antenna linear array power pattern synthesis, determining optimum nonnegative harmonic approximation to given function in Gauss/weighted least-mean-square/and Chebyshev senses 19 p3021 A71-38472

Electromagnetic fields of finite linear antennas in dissipative half space, obtaining antenna patterns from computer results 19 p3023 A71-38589

Pattern space factor and aperture distribution of continuous line source for maximum directivity 19 p3023 A71-38590

Constrained optimization of array antennas performance for obtaining radiation pattern with desired sidelobe levels 19 p3023 A71-38591

Quadrifilar helix antenna pitch angle and ground plane size optimization based on beam pattern data 19 p3036 A71-38603

Excitation asymmetry effects on current distribution and far field of thin dipole radiators 19 p3036 A71-38604

Parabolic reflector aperture antennas with Gaussian distributed random phase deviations, obtaining asymptotic expansion for radiation pattern 19 p3036 A71-38605

Active region and truncation point of log periodic dipole antenna as function of length and design parameters 20 p3203 A71-39091

Radiation patterns due to four pyramidal horns used in sum and difference comparison monopulse radar from single horn pattern for design optimization 20 p3203 A71-39092

Narrow flare angle low permittivity conical dielectric waveguide antenna, examining radiation patterns and propagation characteristics by approximate theory 20 p3196 A71-39380

Broadband helical antenna feeds for millimeter wave parabolic reflectors and lenses, determining beamwidths and polarizations as functions of helix parameters and frequency 21 p3359 A71-41408

Perturbation procedure application to linear and circular antenna array directivity optimization by phase adjustments under uniform amplitude excitation 21 p3359 A71-41412

Spherical wave technique adaptation to antenna radiation determination by equivalent current sheets 22 p3509 A71-42200

Optimal synthesis of antenna array radiation patterns with minimum square deviation from zero in sidelobe 22 p3510 A71-42269

Radiation patterns of dielectric rod antennas with axial emission in near field 22 p3521 A71-42270

Wave diffraction by air gap multilayered dielectric coated sphere with azimuthal slot for low loss transmission, obtaining radiation pattern 22 p3522 A71-42283

Optical modeling of antenna radiation patterns from radio hologram of Fresnel region field 22 p3522 A71-42310

Microwave antenna near field apparent image and phase-amplitude distribution measurement with photocontrolled semiconductor panel 22 p3523 A71-42318

Circularly polarized parabolic SHF antenna with plane and parabolic reflectors, testing radiation pattern performance 22 p3515 A71-42521

Antenna aperture random radiation field representation in expansion in eigenfunctions, comparing results with linear antenna statistical theory 22 p3524 A71-42743

Turnstile loop Yagi and hexafilar contrarotund spiral antennas for microwave telemetry rocket data reception, describing design and radiation patterns 23 p3643 A71-43095

Sandwich wire traveling wave antenna radiation patterns, obtaining attenuation constant 23 p3654 A71-44157

Far field radiation patterns of axially oriented point current sources in presence of dielectric circular cylinders, developing solutions via plane wave scattering 23 p3654 A71-44160

Characteristic modes theory for radiation and scattering by conducting bodies, considering electric and magnetic fields 23 p3660 A71-44161

Characteristic modes computation for conducting bodies of revolution, discussing radiation and scattering patterns convergence 23 p3654 A71-44162

Log spiral antenna with selectable polarization, showing electric field radiation patterns 23 p3654 A71-44165

Aperture field and radiation pattern of conical horns with large flare angles, using vector diffraction formula 23 p3654 A71-44166

Radiation pattern modification factors calculation for TE excited slot antenna in ground plane covered with inhomogeneous plasma reentry sheath 23 p3646 A71-44172

ANTENNAS

NT AIRCRAFT ANTENNAS
NT CASSEGRAIN ANTENNAS
NT CYLINDRICAL ANTENNAS
NT DIPOLE ANTENNAS
NT DIRECTIONAL ANTENNAS
NT HELICAL ANTENNAS
NT HORN ANTENNAS
NT LENS ANTENNAS
NT LOG PERIODIC ANTENNAS
NT LOG SPIRAL ANTENNAS
NT LOOP ANTENNAS
NT MICROWAVE ANTENNAS
NT MISSILE ANTENNAS
NT MONOPOLE ANTENNAS
NT MONOPULSE ANTENNAS
NT MULTIPLE BEAM INTERVAL SCANNERS
NT OMNIDIRECTIONAL ANTENNAS
NT PARABOLIC ANTENNAS
NT RADAR ANTENNAS
NT RADIO ANTENNAS
NT RHOMBIC ANTENNAS
NT SATELLITE ANTENNAS
NT SLOT ANTENNAS
NT SPACECRAFT ANTENNAS
NT SPHERICAL ANTENNAS
NT SPIRAL ANTENNAS
NT STEERABLE ANTENNAS
NT TURNSTILE ANTENNAS
NT TWO REFLECTOR ANTENNAS
NT WAVEGUIDE ANTENNAS
NT YAGI ANTENNAS

Optimum positioning and structure of light hogged antenna masks for radio communications and broadcasting networks 01 p0068 A71-11085

Antenna gain, transmission efficiency and receiving cross sections in dissipative isotropic medium 01 p0041 A71-11614

Adaptive optimal electromagnetic and acoustic detection antenna synthesis, considering signal direction and spatial noise structure
02 p0229 A71-11716

Reflector antenna under wideband noise radiation, determining directivity characteristics by solution for angle range homologous to region of irregular lobes
05 p0728 A71-16008

Soviet book on statistical antenna theory covering large multielement, mirror, laser and synthetic aperture antennas in optics, acoustics, radio astronomy, radio wave propagation, etc
06 p0872 A71-17447

Zigzag antennas current distribution by integral equation analysis
06 p0874 A71-17709

Coaxial cone antenna transient response to incident field along ground plane, using signal generated as step function in time
06 p0875 A71-17717

Optimal antennas statistical synthesis for minimum noise power for given signal gain
14 p2195 A71-30102

Aerospace antennas - IEE Conference, London, June 1971
14 p2215 A71-31034

Antennas scattering coefficients measurement by ground and atmospheric radiation, permitting antenna noise temperature components determination
20 p3205 A71-39803

Reflector antenna under wideband noise radiation, determining directivity characteristics by solution for angle range homologous to region of irregular sidelobes
22 p3524 A71-42757

Antenna impedance measurements using frequency sweep generator and oscillograph
24 p3810 A71-45127

ANTHRACENE
Fluorescence spectra of anthracene ethyl alcohol solution and powdery crystalline anthracene by single and two photon ruby laser excitation
19 p3071 A71-37263

Transient photoconductivity measurements of room temperature electron mobility in deuterated anthracene single crystals, discussing isotope effect
20 p3194 A71-39348

Negative differential conductance of anthracene single crystals in electrolytes, observing N-shaped I-V characteristics
21 p3430 A71-41221

Absorption spectra of benzene, naphthalene and anthracene crystals, noting resonance coupling type effect on vibrational spectrum
24 p3851 A71-45171

ANTHROPOMETRY
Anthropometry for aircraft cockpit and pressure suit design compatible with mission requirements
11 p1724 A71-26115

Human hand anthropometric and biomechanical characteristics, discussing data utilization for human factors engineering
12 p1875 A71-27250

Aircraft pilots anthropometric survey for human factors engineering, discussing measurement techniques and arrangements for training
17 p2692 A71-35198

ANTIBIOTICS
NT PENICILLIN
Subinoculations of bacterial strains under constant, varying and pulsed magnetic fields, producing sensitivity increase or decrease to antibiotics
08 p1247 A71-20856

ANTIBODIES
NT GAMMA GLOBULIN
Radioprotectors and antibody formation in rats, determining ionizing radiation survival rate index for lethal dose and hematological indices
05 p0710 A71-16819

Immunobiological reactivity inhibition in mice under partial adaptation to high altitude hypoxia, observing decreased phagocytic activity, antibody production, hypoplasia and lymph cell number
15 p2356 A71-31289

Human body immune status normalization in prolonged space flight, investigating ribonucleic acid stimulated antibody formation
21 p3332 A71-40554

Pulmonary antibacterial defenses with pure oxygen breathing mice, noting inhibition of early interpulmonary clearance of *Staphylococcus aureus* and enhanced clearance of *Klebsiella pneumoniae*
22 p3487 A71-42241

ANTICOAGULANTS
Antithrombotic agent search, finding anticoagulants useful for Venous system
02 p0200 A71-12418

Blood liquid state control in sanguiferous canal as function of humoral feedback in coagulation, fibrinolytic and anticoagulation systems
13 p2010 A71-28718

ANTICONVULSANTS
Anticonvulsant drugs for counteracting noise effects on central nervous system, discussing audiogenic seizure in mice
03 p0360 A71-13163

Metal ions effect on oxygen toxicity in rats, noting convulsions and lung edema alleviation through mixed Mg-Mn ion treatment
04 p0537 A71-15053

ANTICYCLONES
Anticyclonic eddy formation and emergence within severe thunderstorm observed by radar and surface data, noting wave development along pseudocold front
01 p0118 A71-10588

ANTIDIURETICS
Central nervous system reactions to vasopressin and oxytocin presence in cerebrospinal fluid and blood, discussing respiratory frequency and antidiuretic tests
03 p0363 A71-13485

Antidiuretic action of chlorpropamide in mammalian kidney, considering intrarenal infusions effect on urinary concentration, free water clearance, glomerular filtration and sodium excretion
22 p3486 A71-41939

ANTIDOTES
Antiarrhythmic effects of detergents on digitalis induced arrhythmia in dogs
01 p0010 A71-10392

ANTIFERROMAGNETISM
Ferromagnetic and antiferromagnetic characteristics relation to electromagnetic and spin waves coupling in nonresonant and resonant regions
10 p1656 A71-24317

Anisotropic Heisenberg antiferromagnet sublattice magnetization, obtaining temperature dependence
13 p2100 A71-28675

Magnetostriction in antiferromagnetic, spin flopped and paramagnetic phases of hydrated cesium manganese trichloride, studying volume changes and thermal expansion near phase transition
22 p3585 A71-41885

Antiferromagnetic semiconductors and metals in magnetic field, obtaining Fourier components of electromagnetic fluctuation correlators for dielectric permittivity and magnetic permeability tensors
22 p3586 A71-42062

ANTIFRICTION BEARINGS
NT BALL BEARINGS
NT ROLLER BEARINGS
Aircraft gear pumps bearing elements design for increasing service life
08 p1295 A71-20793

Cermet antifriction and friction powder metallurgy sintered materials for working at high temperatures without lubricants, in vacuum and inert gases
09 p1483 A71-23392

Iron base, white cast iron and high alloy powder metallurgy products for antifriction bearing elements
09 p1478 A71-23393

Three degrees of freedom gyrocompass with common drive and gimbal bearing, exhibiting westerly deviation from drive axis
11 p1763 A71-26188

Dual spin spacecraft bearing assembly flexibility effects on attitude stability, discussing time constant [AIAA PAPER 70-1043]
12 p1973 A71-27569

Redistribution of carbon, copper, nickel and chromium on friction surfaces of powder metallurgy antifriction cermet slide bearings by spectral analysis
15 p2418 A71-32673

Temperature effects on service life of cermet bronze-graphite bearings using different lubricants
15 p2418 A71-32674

Uniaxial gyroscopic stabilizer errors in presence of base random vibration, taking into account dry friction forces in bearings
17 p2738 A71-34560

Low speed angular contact bearings surface geometry effects on friction perturbation torque ripple frequency
18 p2928 A71-36764

Vertical shaft stability on elastic sliding bearings, considering passage through autooscillations zone
24 p3831 A71-45051

Laser beam applications in drilling, shaping and surface finishing of miniature journal and step-type friction bearings, deriving regression equations for optimal process parameters
24 p3834 A71-45162

ANTIGENS
In vitro lymphocyte antigen response measurements in cellular immunity evaluation under adverse logistical conditions, emphasizing RNA and DNA synthesis rates
02 p0199 A71-12390

Antigenic properties of human vascular wall layers in atherosclerosis, using agar precipitation and immunoelectrophoretic measurements
04 p0540 A71-15574

Human heart, kidneys, liver and spleen tissues antigen composition analysis by isolation of pure antibodies
12 p1872 A71-27723

ANTIHISTAMINICS
Antihistamine treatment of hypotension and early transient incapacitation in monkeys under supralethal mixed gamma-neutron radiation
11 p1720 A71-26118

ANTICING ADDITIVES
Ground deicing system for transport aircraft, discussing antifreeze liquid spray application after mechanical snow removal
09 p1428 A71-22948

Gasoline icing inhibitors effect on light aircraft piston engine carburetor icing [SAE PAPER 710371]
10 p1658 A71-24240

ANTIMATTER
NT ANTINEUTRINOS
NT ANTIPARTICLES
NT POSITRONS
Near space annihilation gamma radiation intensity and spectral energy composition by satellite observation, considering possible antimatter nature of comets and meteor streams
05 p0798 A71-16048

Cosmological plasma physics, considering matter, antimatter, electrodynamics, ambiplasma, annihilation and heavy nuclei
07 p1196 A71-19649

Antimatter body size determination, using primary high energy cosmic ray flux
09 p1515 A71-23535

Matter and antimatter separation mechanism in universe based on thermal radiation thermodynamic properties
10 p1665 A71-23739

Antimatter search in primary cosmic rays by balloon-borne cosmic ray telescope formed from gas Cerenkov detector combined with scintillator elements
10 p1659 A71-23748

Radiation measurements near thunderstorms and tornadoes, testing hypothesis of meteoritic matter-antimatter annihilation mechanism for ball lightning
10 p1599 A71-23752

Hydrodynamics of matter-antimatter in contact, discussing coalescence, particles annihilation pressure and energy balance
11 p1821 A71-25539

Lower limit on size of matter and antimatter regions in vanishing baryon number cosmology based on homogeneous intergalactic magnetic field existence
16 p2632 A71-33237

Cosmological implications of microscopic charge-parity violation, considering redefinition of matter and antimatter in time-inverted expansion
16 p2611 A71-33278

Near space annihilation gamma radiation intensity and spectral energy composition by Cosmos satellite observation, considering possible antimatter nature of comets and meteor streams
16 p2626 A71-33452

Energy requirements for antihydrogen production in interstellar photonic drives, discussing feasibility
18 p2956 A71-36683

ANTIMISSILE MISSILES
ABM control surfaces active oxidation protection, using ammonia as reactive coolant injected through porous W wall matrix [AIAA PAPER 71-391]
11 p1837 A71-25353

ANTIMONIDES
NT CADMIUM ANTIMONIDES
NT GALLIUM ANTIMONIDES
NT INDIUM ANTIMONIDES
ANTIMONY
Sb and As base chalcogenide diode structures, determining switching and memory characteristics
13 p2110 A71-27956

Glassy antimony and arsenic chalcogenide diode structures, determining switching and memory characteristics
21 p3435 A71-41343

High purity Sb, In and Ag by vacuum distillation, zone melting and electrolytic refining for semiconductor electronics
24 p3861 A71-45201

ANTIMONY ALLOYS
Thermoelectric properties of quaternary Sb-Bi-Te-Se solid solutions, noting low thermal conductivity
22 p3584 A71-41618

Radioisotope testing methods for dissolution and mass transfer of alloying additives in Pb-Sb alloys during preparation in electromagnetic pumps
22 p3553 A71-41765

ANTIMONY COMPOUNDS
NT CADMIUM ANTIMONIDES
NT GALLIUM ANTIMONIDES
NT INDIUM ANTIMONIDES
Antimony trisulfide semiconductor films, noting chemical composition effects on photosensitive properties
15 p2461 A71-31286

Optical phonons and temperature dependent phase transitions in paraelectric antimony and ferroelectric sulfonide semiconductors, using polarized IR and Raman spectra measurements
21 p3428 A71-40775

SbSI crystal reflection spectra anisotropy and band structure at 90, 273 and 300 K, comparing experimental data with group analysis

23 p3717 A71-43947

ANTINEUTRINOS

Stellar free neutrino and antineutrino emission thermodynamics under hot matter neutronization and hydrodynamic stability during late evolutionary stages

06 p0974 A71-18426

Longitudinal plasmon decay in strong magnetic field into neutrino-antineutrino pair

09 p1527 A71-23533

Cross section for electron and muon neutrino-antineutrino pair production by photons, using intermediate boson theory

11 p1802 A71-25588

Stellar free neutrino and antineutrino emission thermodynamics under hot matter neutronization and hydrodynamic stability during late evolutionary stages

12 p1954 A71-26576

ANTIOXIDANTS

Free radical activity in white mice tissues under hyperbaric oxygenation, examining antioxidants effects

01 p0012 A71-11075

Antitumor properties of jet fuels as function of dissolved oxygen, resin and heteroorganic compound content and temperature, considering antioxidant additives

16 p2623 A71-33579

ANTIPARTICLES

NT ANTINEUTRINOS
NT POSITRONS

Regular multiplicities of particle production in high energy collisions and antineutrino-nucleon annihilation, comparing cosmic ray jet data and pion-nucleon difference

13 p2102 A71-28061

ANTIPODES

Planetary magnetic activity measure based on K indices of antipodal observations

14 p2235 A71-30353

ANTIRADIATION DRUGS

Radioprotectors and antibody formation in rats, determining ionizing radiation survival rate index for lethal dose and hematological indices

05 p0710 A71-16819

Prophylactic radiation protection through lipid toxicants reduction in white rats tissues by high efficiency chemical radioprotectors

06 p0849 A71-17391

Cosmic radiation protection of spacecrews by drugs, extrapolating animal data to humans

06 p0861 A71-18359

Chemical protection against ionizing radiation by thiols and disulfides, discussing hydrogen transfer

07 p1032 A71-18930

Radioprotective action of amines and hypoxic agents by blocking oxygen transport to tissues

07 p1032 A71-18931

Chemical radioprotection by selenium containing compounds in biological and chemical systems tested in irradiated rats

07 p1032 A71-18933

Cysteamine and penicillamine effects on copper ion charge transfer, using electron spin resonance and optical absorption measurements

07 p1033 A71-18935

Structure-function studies of aminothiol radioprotectors on *Escherichia coli* B/r, discussing radiation response at 274 and 77 K

07 p1033 A71-18936

Sulfhydryl cysteamine and disulfide cysteamine effect on bacteriophage survival rate at high anaerobic doses

07 p1033 A71-18938

Lethal radiation in *Escherichia coli* B/r, investigating post irradiation DNA breakdown inhibitors

07 p1033 A71-18940

Sulfur containing organic chelating compounds as radiation protective agents

07 p1034 A71-18941

Cysteine incorporation in *Escherichia coli* B, noting X ray sensitivity and radioprotection

07 p1034 A71-18942

Cysteamine protection of hydroxyurea sensitized Chinese hamster lung cells during X ray exposure

07 p1034 A71-18947

Thiol and disulfide compounds radiation protection capacity at cellular level in tissue culture, using reproductive integrity as protection criteria

07 p1034 A71-18948

Radioprotective drugs relationship to modification of glycolysis in Ehrlich ascites tumor cells

07 p1035 A71-18954

Para-aminopropiophenone and propylene glycol radiation protective effect on hematopoietic stem cells of mice

07 p1036 A71-18959

Hematoporphyrin chlorhydrate radioprotective effects on mice, removing, weighing and fixing spleens for hematopoietic colonies count

07 p1036 A71-18960

Chemical radioprotective effectiveness modification by open skin wounds, discussing results with whole body X ray irradiated mice

07 p1037 A71-18964

Toxicity reduction of aminoethylisothiuronium compounds through n-substitution with amino acids, noting slight decrease in radioprotective effectiveness

07 p1037 A71-18965

Sodium fluoroacetate as radiation protective agent, noting dependence on selective blockade of enzyme asconitase

07 p1037 A71-18967

Temperature effect in sodium fluoroacetate protective action mechanism for mice irradiation

07 p1037 A71-18968

Cysteamine AET, serotonin and mexamine antiradiation drugs, investigating protective effect against fractionated lethal gamma irradiation

07 p1037 A71-18969

Short and long term radiation effects reduction by chemical radioprotectors mixtures, noting improved survival and decrease in leukemia and cancer incidence in X ray irradiated mice

07 p1037 A71-18970

Aminoethylisothiuronium and methoxy-tryptamine synergism quantitative analysis by pharmacological methods of radioprotective effect in X irradiated mice

07 p1038 A71-18971

Central nervous system role in radioprotective contribution of 5-hydroxytryptamine

07 p1038 A71-18972

Rat bone marrow chromosomes radiation protection, using 5-hydroxytryptamine

07 p1038 A71-18973

Mice protection against irradiation damage by adrenochrome monoguanylhydrazones methan-sulphonate

07 p1038 A71-18977

Biochemical mechanism of radioprotective action of aminoethiols in mammals

07 p1039 A71-18979

Rats and mice blood redox potentials injected with cystamine, investigating increased radioprotection

07 p1039 A71-18980

Cellular damage to rat mitochondria and endoplasmic reticulum by injection of radioprotectors, discussing intracellular enzymes passage into plasma

07 p1039 A71-18981

Metabolic effects of sulphur containing cystamine, cystamine and cysteine radioprotective drugs on oxygen uptake in rats

07 p1039 A71-18982

SH containing radioprotectors action on nucleic acid metabolism, discussing DNA synthesis inhibitory effects

07 p1039 A71-18983

Amino-ethyl-S-2-isothiuronium radio protective dose effects on enzyme activity, cardiovascular changes, blood transaminases concentration, bone marrow and peripheral circulation

07 p1040 A71-18986

Disorientation response of survived chicks hatched from eggs injected with radioprotective 2-beta-aminoethylisothiuronium-Br-HBr after incubation

07 p1040 A71-18988

Taurine restorative effect in patients with marked leucopenia induced by radiotherapy

07 p1040 A71-18991

Cystamine effects on lymphocytes chromosomal aberrations in human peripheral blood during local fractionated gamma irradiation

08 p1240 A71-21797

Antihistamine treatment of hypotension and early transient incapacitation in monkeys under supralethal mixed gamma-neutron radiation

11 p1720 A71-26118

Radioprotectants effect on mice against ionizing radiation and tolerance to back-to-chest accelerations in space flight

21 p3330 A71-40345

Radioprotectants effects on mice and guinea pigs physiological reactions to back-to-chest transverse accelerations

21 p3336 A71-41053

Mercaptoalkylamine group radiation protection preparations on resistance of rats and mice to lateral acceleration rate

22 p3491 A71-42700

Aminothiol group radioprotective drugs effect on guinea pigs cardiac function during lateral acceleration

22 p3491 A71-42702

Radiation protection drugs effects on albino rats hypoxia resistance, discussing hypoxic hypoxia response to intraperitoneally and perorally administered cysteamine and aminoethylisothiuronium

22 p3491 A71-42704

Lateral accelerations effect on mice tolerance to toxic doses of aminothiol- and indolylalkylamine- series radiation protection drugs

22 p3491 A71-42706

Antiradiation drugs effects on healthy and irradiated rats gastrointestinal tract evacuatory motor function

22 p3492 A71-42707

Radiation sickness prophylaxis chemical compounds, discussing protection mechanisms, radical inactivation and afflicted cell recovery

22 p3505 A71-42710

Prophylactic medication for radiation damage treatment, covering toxicity, pharmacological properties, metabolism, dosage and physiological action

22 p3505 A71-42711

Chemical agents protective properties on albino mice under gamma-neutron radiation, noting dose and composition effects

22 p3492 A71-42713

Cystamine hydrochloride or vitamin B complex with vitamin C for radiation sickness prevention and therapy

22 p3493 A71-42723

Acceleration tolerance of gamma irradiated mice with and without radioprotectors

22 p3493 A71-42724

Mice acceleration before and after gamma irradiation, determining protective effect of cystamine in adrenaline and amphetamine mixture

22 p3494 A71-42726

Aminothiol class radiation protector influence on tissue damage of white rats under single and two-fold gamma irradiation at various test conditions

22 p3494 A71-42729

Radioprotective effectiveness of cystamine and S beta-aminoethylisothiuronium in mice under combined gamma irradiation and transverse acceleration loads

22 p3494 A71-42730

Prolonged small radiation dosage effects on vestibular analyzer in normal and antiradiation drug protected dogs

22 p3495 A71-42798

ANTISUBMARINE WARFARE

Helicopter handling under ASW flight conditions, discussing sea state effect on low altitude hover stability

13 p1998 A71-29384

ANTISYMMETRY

Boundary conditions of line of symmetry and antisymmetry types for stress-strain state of halved shells

06 p0984 A71-17666

ANTITANK MISSILES

NT SHILLELAGH MISSILES

U.S. tactical missile program evolution since WW II, discussing technology, air defense, assault/antitank weapons, interdiction and battlefield combat support

05 p0818 A71-17149

ANTONOV AIRCRAFT

NT AN-24 AIRCRAFT
NT ANOV AN-24 AIRCRAFT
U AN-24 AIRCRAFT

ANXIETY

Set and uncertainty as factors influencing anticipatory cardiovascular response in humans, monitoring heart rate and vasomotor activity

13 p2011 A71-28809

AORTA

Catheter inserted wire basket device for creation of reversible aortic insufficiency in animal

01 p0022 A71-10248

Aortic and sinus nerves afferent electric impulse under adrenalin and nicotine, considering age peculiarities

03 p0363 A71-13522

Acceleration effects on aortic, coronary and carotid flows in dogs

06 p0855 A71-18380

Left ventricular performance Fourier analysis, obtaining ventricular and ascending aortic pressure and flow from closed and open chest dog measurements

07 p1041 A71-19636

Hemodynamic correlation of Austin Flint murmur and a-wave of apexcardiogram in aortic regurgitation

09 p1392 A71-22589

Carotid pulse wave slope variations in normal subjects, aortic valvular diseases and hypertrophic sub-aortic stenosis

09 p1392 A71-22590

Arterial hypoxia effects on regional blood circulation in anesthetized dogs, measuring aortic blood flow under controlled artificial ventilation and after sinoaortic denervation

09 p1396 A71-23542

Large amplitude wave propagation in arteries, deriving aorta mathematical model consistent with heart pressure and flow pulses and wavefront velocity

12 p1870 A71-26937

Ultrasonic echocardiograms of anterior cusp of mitral valve in aortic valve disease

13 p2002 A71-27814

Vessels mechanical behavior and blood flow dynamics in aorta bifurcation zone, using Navier-Stokes and continuity equations

13 p2019 A71-28657

Sudden death and syncope mechanism in aortic valve stenosis, noting presence of baroreceptors in left ventricular wall

13 p2014 A71-29301

- Energy output of left ventricle and congestive heart failure mechanism, approximating blood velocity in aortic system by mathematical model
15 p2363 A71-31443
- Renal hemodynamic factors in whole kidney glomerulotubular balance in anesthetized dogs by manipulating filtration rate through constriction of aorta, thoracic vena cava, etc
16 p2529 A71-33194
- Energy metabolism disturbance effect on dissolved and undissolved collagen fractions content of aorta connective tissue
17 p2679 A71-34223
- Functioning aortic valve orifice size relation to configuration and flow
17 p2682 A71-35042
- Mucopolysaccharide content and composition of fatty streaks in young male aortas, discussing atherosclerosis effects
18 p2854 A71-35919
- Collagen and elastin transmedial gradients in human aortas as function of age, discussing relationship to atherogenesis
18 p2858 A71-36751
- Second heart sound changes due to position and magnitude variations of aortic or pulmonary component
19 p3001 A71-37233
- Jet and turbulence mechanism of vascular murmurs associated with stenosis for minimum flow Reynolds numbers, using aorta orifice plates in dogs
21 p3336 A71-40864
- DNA synthesis in human aorta endothelium reproduction, reporting intact nuclei and dyed cell membrane samples cytophotometric studies results
23 p3635 A71-44053
- APACHE ROCKET VEHICLE**
Magnus effects on Apache sounding rocket at supersonic speeds, discussing spinning model and static tests
[AIAA PAPER 70-207] 07 p1205 A71-18893
- Nonlinear aerodynamic stability coefficients from free angular motion of rigid bodies, using three degrees of freedom subsonic wind tunnel tests on Apache model
11 p1837 A71-25515
- APATITES**
U CALCIUM PHOSPHATES
U MINERALS
- APERIODIC FUNCTIONS**
Wing aperiodic motion during change from one frequency to another, using Laplace and Fourier transforms to reduce partial to ordinary differential equation
10 p1688 A71-24353
- Random aperiodic signals analysis, using two dimensional Fourier transforms
17 p2709 A71-35790
- APERTURES**
NT IRISES [MECHANICAL APERTURES]
IR astronomical telescope using six independent optical systems with path and phase controls for aperture synthesis
01 p0081 A71-10829
- Horizontal aperture equalization for desired waveform response, describing scanning methods and quantitative effect on noise
02 p0211 A71-11645
- Rectilinear edge aperture filtration, examining mismatch angle effects on video signal amplitude
02 p0248 A71-11828
- Mutual information between radiance of incoherently radiating object plane and field of observing system aperture, obtaining Shannon type formula
04 p0627 A71-15684
- Circular apertures with Besinc correlated illumination, examining far field diffraction properties and intensity distribution
05 p0781 A71-16193
- Laser irradiance pattern from aperture with truncated Gaussian field distribution, evaluating diffraction integral subject to Fresnel approximation
05 p0763 A71-16904
- Aperture concentric diffraction ring differential effects on focal irradiance, using perfect lens half-wave filter model
08 p1333 A71-21178
- Large aperture catadioptric lens system for low light level observation, discussing optical evaluation, thermal properties and mechanical mounting
08 p1289 A71-21372
- Beam scanning radar antenna, deriving optimum field distributions in aperture
08 p1266 A71-21462
- Vertical electric dipole field diffraction by circular aperture in flat conducting screen between two electromagnetically different half spaces
09 p1406 A71-22877
- Ground metallic plate effect on electric dipole antenna radiation characteristics as function of aperture field
09 p1420 A71-23572
- Frequency-contrast characteristics of holographic systems, studying image contrast and angular spread as function of hologram aperture
10 p1611 A71-24529
- German monograph on holographic method to increase effective aperture in optical imaging covering optical systems resolving power increase holography, etc
10 p1613 A71-24875
- Edge geometries and aperture distributions of physically realizable planar antennas
13 p2027 A71-27989
- Optical aperture configurations effect on image performance, discussing large telescope systems design criteria
14 p2242 A71-30147
- Atmospheric turbulence effect on far field diffraction pattern of annular aperture
14 p2275 A71-30465
- Aperture field distribution for excitation of surface waves with high efficiency and gain
15 p2378 A71-32627
- Frequency-contrast characteristics of holographic systems, studying image contrast and angular spread as function of hologram aperture
19 p3066 A71-38257
- Line source excitation for maximum aperture efficiency with given sidelobe level
19 p3035 A71-38596
- Instrument function for central spot distribution of Fabry-Perot etalon with finite aperture, comparing to Airy formula
21 p3379 A71-40636
- Defocused optical system imaging properties and optical transfer function improvement by shaded aperture, discussing necessary conditions and light absorption effect
22 p3548 A71-42551
- Second harmonic aperture in ultrashort pulses length measurement by mixing two AM light beams in nonlinear crystals
23 p3683 A71-43397
- Circular aperture illuminations for high beam efficiency and low sidelobes in search radar antenna applications, using Fredholm integral equation
24 p3809 A71-44990
- APEXES**
Optimum tip vertex angles measurement for determining steels tensile strength and yield point from hardness
09 p1467 A71-22314
- APNEA**
U RESPIRATION
- APOGEES**
High energy three stage booster system for geostationary orbiter, discussing interstage propellant transfer, apogee impulse system and mission rated payload modular configurations
11 p1838 A71-25574
- High energy solid propellants use in Europa 2 launch vehicle perigee-apogee motor, considering synchronous satellite payload increase
16 p2645 A71-33365
- APOLLO APPLICATIONS PROGRAM**
Post-Apollo programs, discussing international participation aspects
01 p0183 A71-10264
- AAP electrical power system simulation for Skylab earth orbit missions, taking environmental effects into account
02 p0190 A71-11795
- Apollo Applications Program command and service module test requirements to achieve reliable hardware for extended missions
[AIAA PAPER 70-378] 03 p0500 A71-14436
- Post Apollo manned space operation, emphasizing Skylab program, space shuttles and long term space station
04 p0689 A71-14927
- Space station, shuttle and tug as post-Apollo space program, discussing objective, designs and systems analysis
19 p3149 A71-37303
- Earth resources experiments package electromagnetic compatibility with Apollo Applications Program
19 p3032 A71-38453
- APOLLO FLIGHTS**
NT APOLLO 6 FLIGHT
NT APOLLO 7 FLIGHT
NT APOLLO 8 FLIGHT
NT APOLLO 9 FLIGHT
NT APOLLO 11 FLIGHT
NT APOLLO 15 FLIGHT
- Telemetry and communications roles in Apollo flight operations, describing data system management
01 p0035 A71-10918
- Apollo Command and Service Module simulation of flight phases in lunar landing missions
02 p0237 A71-11792
- Dynamics and thermodynamics of water and oxygen particles ejected into space by Apollo during translunar flight, using ground based photographic observations
[AIAA PAPER 71-474] 11 p1833 A71-26254
- Apollo lunar and Skylab photographic systems, discussing topographic, panoramic, metric, stellar and multispectral cameras and instrumentation
12 p1907 A71-27257
- Apollo lunar sea geomorphic data agreement with Luna 16 data
15 p2488 A71-33225
- Calcium, potassium and iron loss by astronauts during Apollo space missions, using instrumental neutron activation analysis
16 p2528 A71-33111
- Advantages and drawbacks of pure oxygen and oxygen-nitrogen space breathing, considering decompression sickness in Apollo missions
18 p2863 A71-35907
- Apollo and Luna data related to lunar origin, evolution and processes, discussing mare basalts, interior composition, regolith, breccias, chronology, surface properties, etc
21 p3453 A71-41176
- Telescopic observations of Apollo 8-14 spacecraft, suggesting addition of specular reflecting surfaces or transmitters radiating at optical frequencies
21 p3349 A71-41406
- Apollo 11, 12 and 14 lunar seismometer results suggesting lunar material Q factors up to 3000
21 p3453 A71-41407
- Apollo/Saturn 5 propulsion system design, development, testing and integration
22 p3589 A71-42026
- Lunar plagioclases, tridymite and cristobalite feldspar crystal structure and chemical analyses from Apollo igneous rocks by X ray and electron diffraction
23 p3738 A71-43611
- Minor element concentrations and population sources of Apollo 11 and 12 olivine and plagioclase, using microprobe analyses
23 p3738 A71-43614
- Chemical element composition and mineralogy of powdered lunar surface material, comparing Surveyor, Apollo and Lunik missions data
23 p3748 A71-43682
- Apollo core tube geometry effect on quantity and quality of lunar sample recovery
23 p3757 A71-43750
- IR vibrational spectroscopic analysis of Apollo 11 and 12 rocks and dust isolated silicate minerals, using LF absorption bands
23 p3759 A71-43766
- APOLLO LUNAR SURFACE EXPERIMENTS PACKAGE**
Long seismic reverberations from man-made impacts on moon, using Apollo 12 lunar surface station recordings
01 p0159 A71-10824
- ALSEP magnetometer design and performance
05 p0755 A71-17127
- Solar wind noble gas composition on moon with aluminum foil exposure, confirming absence of lunar atmosphere and magnetic field
11 p1834 A71-26330
- Lunar dynamics and structure data from two lunar seismic stations installed during Apollo 11 and 12 missions as part of ALSEP
12 p1967 A71-27416
- Lunar laser ranging experiments in Japan, detecting returned signals from Apollo 11 retroreflector surface package
16 p2543 A71-33812
- Antenna tracking, RF and bore sight alignment on ships and ground stations using Apollo lunar surface experiments package [ALSEP]
18 p2876 A71-36473
- Apollo lunar surface S band communications and TV systems and equipment, including ground commanded TV assembly
18 p2878 A71-36519
- APOLLO PROGRAM**
Spaceflight astronaut training, discussing guidance and navigation methodology of Apollo Mission Simulators
01 p0067 A71-10516
- Manned space flight network telemetry system modification for Skylab, ERTS and Apollo J missions, giving data flow diagrams and equipment electrical characteristics
01 p0035 A71-10917
- Manned space flight escape systems evolution, examining requirements and devices from X-15 to Apollo program
02 p0320 A71-11977
- Thermal environment loads in lunar ambulation, discussing Apollo EVA suit system and internally produced heat
02 p0207 A71-12386
- Book on geochemical exploration of moon and planets covering orbital, compositional and surface studies, Apollo missions, Lunar Receiving Laboratories and data processing
05 p0813 A71-16950
- Information management system to schedule, control and status work on Apollo/Saturn Program at Kennedy Space Center
[AIAA PAPER 71-239] 07 p1207 A71-19715

Nonflammable self extinguishing nontoxic fluorocarbon elastomers as adhesives and coatings for Apollo program

10 p1632 A71-24097

Apollo lunar orbital missions, discussing remote sensing and photographic equipment for lunar sounding and mass spectrometry, gegenschein experiments and high quality metric photography

10 p1682 A71-24173

Apollo command module guidance computer and environment hybrid simulation for flight software and crew procedures verification

11 p1744 A71-25845

Apollo hybrid simulator for man-machine interface in low orbit lunar landmark tracking

11 p1796 A71-25850

Post Apollo program European participation in space tug design and orbiter model flight tests, considering mini shuttle support applications

11 p1839 A71-26331

Apollo optical retroreflector arrays characteristics and performance for laser range measurements from earth stations, describing multilensed receiver telescope

16 p2642 A71-33831

Apollo real time control center large software systems development management covering implementation, integration, testing, operation and maintenance

17 p2710 A71-34620

Hadamard transform source encoding application to Apollo unified S-band telemetry links, considering possible system performance improvement

18 p2876 A71-36470

Position determination on planetary surface from gravity and star line-of-sight direction measurements, presenting numerical results for Apollo lunar landing missions

[AIAA PAPER 71-900]

19 p3095 A71-37151

Full mission engineering simulator/flight controls integration laboratory utilization in Apollo program, describing equipment for control systems testing, monitoring and troubleshooting

[AIAA PAPER 71-970]

19 p3040 A71-37211

Neutron radiography of Apollo ordnance, describing test facility and equipment

19 p3063 A71-37449

Human response to space environment, discussing prolonged weightlessness, extravehicular work and lunar surface activity

19 p3002 A71-37492

Apollo range instrumentation aircraft, describing C-135A modification with airborne lightweight optical tracking systems

19 p3022 A71-38546

Apollo lunar explorations, reviewing landing, trajectories, hardware, mission problems and scientific studies

20 p3295 A71-39613

Apollo lunar expeditions assessment, discussing rock samples composition, origin, age and relation to earth system

21 p3442 A71-40148

APOLLO SPACECRAFT

Space navigator operations, procedures and computer interface and manually aided onboard Apollo cislunar navigation system possible improvement

01 p0124 A71-10510

Space vehicle onboard navigation and guidance systems capability, considering Apollo transition from direct task interaction and supervision to functional man machine communication

01 p0124 A71-10511

Apollo integrated shell static and dynamic testing, describing data acquisition system techniques

01 p0067 A71-10863

Scientific data transmission systems signal design considerations for Apollo lunar exploration missions

01 p0035 A71-10915

Hybrid real time computer simulation of external visual display cues for Apollo Command and Service Modules

02 p0237 A71-11791

N-body real time trajectory simulation of Apollo Command and Service module G and C systems and mission

02 p0237 A71-11793

Service life and manufacturing yield of Apollo 25-IRIG /inertial reference integrating gyroscope/ ball bearing

02 p0252 A71-12458

Apollo lunar module structural integrity for lunar landing verified by Monte Carlo dynamic analysis

07 p1205 A71-18896

Horizontally coherent supersonic velocity LF sound signals from Apollo rocket vehicles at high elevations

07 p1208 A71-20149

Comparative sting supported and free flight tests in hypersonic wind tunnel on modified Apollo launch configuration

[AIAA PAPER 71-265]

08 p1274 A71-21991

Apollo spacecraft and lunar landing module thermal control surfaces, considering inorganic silicate bonded paint

09 p1533 A71-23426

Adhesives in Apollo command, service and lunar modules primary load carrying structures, electrical potting and sealing medium

10 p1630 A71-24067

Separated flow and time lag effects on sinusoidal gust penetration loads and elastic launch vehicle response of Apollo-Saturn class

[AIAA PAPER 71-344]

11 p1836 A71-25323

Apollo spacecraft qualification vibration test program assessment, discussing structural acoustical excitation method

11 p1745 A71-26441

Apollo program all-up spacecraft thermal vacuum tests, considering component and subsystem reliability analysis, thermal model verification and certification requirements

12 p1894 A71-26682

Apollo cislunar navigation capability and procedures, describing onboard data acquisition and digital processing equipment

13 p2098 A71-29386

Apollo Lunar Module design evolution, considering mission requirements, reliability objectives, environmental factors, manned operation, weight and configuration

15 p2500 A71-31603

Apollo 15-17 CSM design modifications, discussing increased mission duration capability, lunar orbital science instruments operation and weight increase

[AIAA PAPER 71-821]

17 p2812 A71-34723

Apollo/Saturn 5 propulsion system design, development, testing and integration

22 p3589 A71-42026

Apollo command module aerodynamic characteristics in hypersonic low density flow, measuring drag, three component force and heat transfer

22 p3480 A71-42027

Apollo command module land landing capability in case of abort after liftoff, describing Monte Carlo simulation procedure

22 p3573 A71-42776

APOLLO TELESCOPE MOUNT

UV scanning polychromator spectroheliometer on Apollo Telescope Mount, examining temperature distribution on sun

03 p0430 A71-14435

Clean cryogenic vacuum high speed gas pumping system for calibrating spectrometers for use on Apollo telescope mount

07 p1160 A71-19854

ATM for manned solar observation, discussing thermal design, thermal vacuum test philosophy, mathematical models and analytical and test data correlation

[AIAA PAPER 71-433]

11 p1838 A71-26222

Optical ground contamination monitoring devices for Apollo Telescope Mount collecting time-line and integrated data

[AIAA PAPER 71-458]

11 p1764 A71-26240

Apollo Telescope Mount for high resolution solar observation and manned instruments evaluation in space environment, discussing attitude and pointing control systems

15 p2500 A71-31458

Skylab electrical power system located on Orbital Workshop and Airlock Module and on ATM, discussing capabilities, characteristics and limitations

20 p3179 A71-38903

APOLLO 6 FLIGHT

Equatorial convective cloud mesosystems formation from Apollo 6 data, investigating Hadley circulation energy generation

23 p3701 A71-44011

APOLLO 7 FLIGHT

Hurricane Gladys structure and dynamics observations by Apollo 7 spacecraft, satellites and radar, noting large cloud feature

05 p0777 A71-16662

APOLLO 8 FLIGHT

LOX release from Apollo 8 lunar launch vehicle, forming small particle clouds for scattering experiments

06 p0963 A71-17256

APOLLO 9 FLIGHT

ERTS-A imagery, Apollo 9 and high altitude aircraft photography applications to Land Management Bureau, Indian Affairs and Reclamation

09 p1451 A71-23208

Apollo 9 So65 multispectral color space photography for basic land use pattern determinations

12 p1907 A71-27259

APOLLO 11 FLIGHT

Apollo 11 basalts chemistry and petrogenesis by partial melting, considering implications for lunar origin theories

02 p0305 A71-11981

Apollo 11 crystalline igneous rocks mineralogy and petrology, suggesting origin from pyroxenite mantle melting

02 p0305 A71-11982

Apollo 11 lunar soil sample derived from basaltic and anorthositic rocks, considering basalt origin by melting due to internal radioactive heating

02 p0305 A71-11983

Apollo 11 lunar samples dielectric constants, losses and electrical conductivities as function of tempera-

ture and frequency, comparing with terrestrial and simulated lunar rocks

02 p0305 A71-11985

Apollo 11 lunar powder and rock samples optical properties noting similarity over Tranquility base area

02 p0305 A71-11986

Lunar solid state thermal convection throughout interior, noting pressure release production of basaltic magmas consistent with Apollo 11 rocks composition

02 p0305 A71-11988

Apollo 11 lunar rocks excess heat capacity and thermal conductivity at liquid He temperatures due to peaks in vibrational frequency distribution

02 p0306 A71-11989

Lunar anorthosites from Apollo 11 sample 1008, coarse fines, determining major, minor and rare earth elemental abundances

03 p0482 A71-13012

Apollo 11 lunar soil size distribution, examining deficiency in material finer than 15 micrometers

05 p0807 A71-16215

Apollo 11 and 12 lunar rock opaque oxides differences in titanium contents

05 p0807 A71-16298

Refractory elements abundances in chondrites, basaltic achondrites and Apollo 11 fines, emphasizing Ca-Al relationship

06 p0966 A71-17894

Apollo 11 igneous rocks potassium content vs irradiation exposure age, comparing lunar geology models

06 p0966 A71-17897

Apollo 11 flight glass basalt, determining crystallization sequence and phase assemblage of high Ti specimens as oxygen fugacity function

06 p0970 A71-18235

Tranquility Base lunar soil diurnal temperature calculation from one dimensional energy equation, using temperature dependent thermodynamic properties

[AIAA PAPER 71-79]

06 p0977 A71-18536

Lunar radioactive layer effective thickness by radio astronomical methods and from Apollo 11 flight

07 p1193 A71-19312

Amino acid contents of Apollo 11 and 12 fines, discussing laboratory syntheses

07 p1196 A71-19500

Apollo 11 and 12 lunar samples, discussing chemical composition relationship to lunar origin

07 p1196 A71-19605

Lunar magnetic field demagnetization effect hypothesis for explaining Apollo 11 lunar rock samples remanent magnetization

07 p1200 A71-20055

Apollo 11 lunar rocks mineralogical, chemical, isotopic, electrical and magnetic properties

09 p1523 A71-23018

Lunar and terrestrial ilmenite basalt, considering hornfels from Keweenaw Duluth complex in Minnesota and Apollo 11 samples

09 p1529 A71-23657

Apollo 11 lunar samples effect on terrestrial microorganisms, noting pigment production effects of Fe leaching from bulk fines and core samples

10 p1566 A71-23747

Elemental analysis for lunar rocks and regolith, comparing silicon oxide and titanium oxide composition in Apollo 12 and Apollo 11 samples

10 p1672 A71-24389

Xe and Kr isotopes gas extraction and mass spectrometer analyses of Apollo 11 lunar soil, Murray carbonaceous chondrite and atmospheric Xe

10 p1661 A71-24414

Primordial Kr and Xe trapping as possible cause of element abundance trend reversal in Apollo 11 and 12 fines

10 p1673 A71-24428

Thermal conductivity of Apollo 11 lunar fines as function of temperature, pressure and bulk density

[AIAA PAPER 71-477]

11 p1833 A71-26255

Apollo 11 sample basalts lunar interior origin assumption from comparison with terrestrial massif anorthosite series, using chemical and petrographic analyses

11 p1834 A71-26452

Lunar dynamics and structure data from two lunar seismic stations installed during Apollo 11 and 12 missions as part of ALSEP

12 p1967 A71-27416

Methane and deuteromethane released from Apollo 11 and 12 lunar fines by deuterated acid etch, using gas chromatography for carbon compounds separation

13 p2136 A71-28427

Apollo 11 lunar material characteristics and age, emphasizing fine lunar dust

13 p2138 A71-28765

Lunar chronology and evolution from Rb and Sr internal isochrons on Apollo 11 and 12 crystalline rock samples

13 p2142 A71-29142

Ancient lunar magnetic field detection and origin from remanent magnetism in Apollo 11 breccia and basaltic rock samples

14 p2306 A71-29725

- Electrical conductivity measurement of Apollo 11 and 12 lunar surface rocks, using two-probe technique in vacuum furnace 14 p2315 A71-30864
- Apollo 11 and 12 lunar samples compared with deep earth rocks, noting potassium-uranium ratio 14 p2318 A71-31126
- Lunar radioactive layer effective thickness by radio astronomical methods and from Apollo 11 flight 15 p2486 A71-31892
- Glazing lunar craterlet interiors in Apollo 11 observations, comparing solar flash heating and volcanic bomb impact formation 15 p2493 A71-32484
- K-Ar isotope ages of whole sample and feldspar concentrate from Apollo 11 lunar rock 10003 16 p2633 A71-33349
- Lunar laser ranging experiments in Japan, detecting returned signals from Apollo 11 retroreflector surface package 16 p2543 A71-33812
- Electrical conductivities of Apollo 11 and 12 lunar rocks and chondritic meteorites at 300-1100 K 17 p2796 A71-34182
- Apollo 11 and 12 lunar landings, discussing retrieved lunar material, seismographs, solar wind and light reflector for measuring earth-moon distance 18 p2959 A71-35906
- Apollo 11 lunar soil and rock samples under low level beta spectrometry, measuring radon daughter Pb 210 18 p2961 A71-35946
- Apollo 11 and 12 lunar rocks composition, suggesting depletion of K, Rb and Pb in solar nebula prior to final accretion of moon 18 p2963 A71-36228
- Compounds hydrolyzable to amino acids in aqueous extracts of Apollo 11 and 12 lunar fines, noting presence of glycine and alanine 18 p2855 A71-36230
- Apollo 11 lunar crystalline igneous rock samples electrical conductivity temperature dependence, noting age of moon 20 p3295 A71-39619
- Laser ranging to retroreflector array placed on lunar surface during Apollo 11 mission 20 p3296 A71-39622
- Apollo 11 lunar fines and ground terrestrial mafic rock powders effective surface areas and heats of adsorption, using Brunauer-Emmett-Teller Kr adsorption method 21 p3450 A71-40648
- Limited interval definitions of photometric functions of lunar crater walls by photography from orbiting Apollo 11 22 p3603 A71-42187
- Armcolite and ilmenite basalt in Apollo 11 lunar samples, discussing formation process of titanium, potassium and silicon oxides 23 p3734 A71-43247
- Lunar locations and orientations of crystalline rocks, breccia and soil from Apollo 11 and 12 missions, including maps 23 p3737 A71-43603
- Azimuth frequency plots of regolith surface lineaments at Apollo 11 and 12 landing sites 23 p3737 A71-43604
- Tranquillity silicate mineral in crystalline basaltic rocks from Apollo 11 and 12 samples 23 p3737 A71-43605
- Pyroxferroite crystal structure from Apollo lunar Mare Tranquillitatis sample, using X ray counter-diffractometer measurements 23 p3737 A71-43606
- Comparative electron petrography and chemical analysis of Apollo 11 and 12 and terrestrial rocks, noting pyroxene, plagioclase, ilmenite and cristobalite 23 p3738 A71-43608
- Fission track analyses of uranium enriched phases in Apollo 11 and 12 basaltic rocks 23 p3739 A71-43615
- Lexan plastic fission track analysis of uranium distribution in glassy residuum in Apollo 11 rock 10011 23 p3739 A71-43616
- Apollo 11 and 12 rock samples examination, failing to observe radioactive halos 23 p3739 A71-43617
- Zirconium liquid-crystal distribution in phase ilmenite of Apollo 11 and 12 lunar rocks 23 p3739 A71-43618
- Apollo 11 and 12 lunar rocks and soil chemical composition, considering petrogenesis and major and trace elements abundance 23 p3741 A71-43635
- Normative mineralogy of lunar basaltic rocks from Apollo 11 and 12 samples, comparing with terrestrial and meteoritic analogs 23 p3742 A71-43637
- Petrology of Apollo 11 and 12 rock samples with silicate melt inclusions, discussing terrestrial equivalents 23 p3742 A71-43641
- Grain size and modal analyses of lunar regoliths sampled by Apollo 11 and 12, discussing particles origin 23 p3744 A71-43654
- Apollo 11 and 12 unshocked and shocked microbreccias petrology, noting shock compression and shock welding 23 p3745 A71-43658
- Apollo 11 and 12 regolith and breccia samples, discussing shock effects detection and interpretation, chemical composition, grain size distribution and impact origin 23 p3745 A71-43660
- Lunar rocks 12063,9 and 12004,11 opaque mineralogy and textural feature, comparing to Apollo 11 samples 23 p3745 A71-43661
- Nonmare basalts chemical composition and origin from Apollo 11 and 12 sites 23 p3746 A71-43671
- Apollo 11 and 12 lunar rocks and fines, discussing compositional variations and relationships to stony meteorites 23 p3747 A71-43677
- Spark mass spectrometric analysis of major and trace elements abundance in Apollo 11 and 12 lunar rocks and soil samples, comparing with standard basalt 23 p3749 A71-43686
- Apollo 11 and 12 lunar samples elemental composition analysis, using activation and mass spectrometric isotope dilution analysis and emission spectrography 23 p3749 A71-43687
- Apollo 11 and 12 lunar fines 10084 and 12070 trace element determination, using multiclement neutron activation analysis 23 p3749 A71-43690
- Apollo 11 and 12 lunar rock and soil examination, emphasizing Au and Ag excess in soil 23 p3750 A71-43693
- Active and inert gases released by crushing Apollo 11 and 12 samples at room temperature and by low temperature heating 23 p3751 A71-43701
- Lead isotopes volatile transfer in Apollo 11 and 12 lunar soil samples, discussing lunar age estimates 23 p3752 A71-43714
- Neutron activation analysis of Apollo 11 lunar fines, determining Pb 204, U, Bi and Tl contents 23 p3753 A71-43715
- Rare gas concentrations and isotopic abundances in lunar rocks, fines and breccias from Apollo 11 and 12 flights, determining exposure and gas retention ages 23 p3753 A71-43720
- Apollo 11 and 12 lunar samples history of irradiation exposure to galactic cosmic rays and solar wind, using rare gas and Gd isotope measurements 23 p3754 A71-43724
- Apollo 11 and 12 fines cosmogenic He, Ne and Ar radionuclides composition determination, using electron microprobe analysis 23 p3754 A71-43727
- Lunar cosmogenic radionuclides production time and spatial dependence calculations, comparing Apollo 11 and 12 measurements 23 p3754 A71-43729
- Depth profiles of cosmogenic radionuclides in lunar rocks and soil samples from Apollo 11 and 12 flights, considering solar particle flux and spectra 23 p3755 A71-43732
- Tritium activity measurement in Apollo 11 fines, breccia and crystalline rock, comparing with meteoritic values 23 p3755 A71-43735
- Chemical characteristics of carbon compounds in Apollo 11 and 12 lunar fines, using organic solvent extraction, mass spectrometry and gas chromatographic method 23 p3756 A71-43743
- Biological activity in Apollo 11 and 12 core samples searched for after placement in Petri dishes containing media 23 p3757 A71-43747
- Microbial assay of lunar core and surface samples obtained from Apollo 11 and 12 flights 23 p3757 A71-43748
- Ultramicroscopic texture and radiation damage in Apollo 11 and 12 micron sized lunar dust grains compared with meteoritic rocks 23 p3758 A71-43756
- Regular particle morphology and petrostatistics in Apollo 11 and 12 lunar fines and conglomerates, using phase contrast and scanning microscopes 23 p3758 A71-43757
- Elemental abundance analysis of Apollo 11 and 12 lunar materials from Auger electron spectroscopy 23 p3759 A71-43762
- Spectral directional reflectance of Apollo 11 and 12 fines as function of bulk density 23 p3760 A71-43771
- Physical characterization of Apollo 11 and 12 lunar fines and glasses by diffuse reflectance, Raman and X ray spectroscopy and thermally stimulated currents 23 p3760 A71-43773
- Apollo 11 and 12 rocks luminescence under proton, electron, UV and X irradiation 23 p3760 A71-43774
- Polarization characteristics, albedos and optical properties of Apollo 11 and 12 rocks, investigating wavelength dependence and proton irradiation effect 23 p3761 A71-43779
- Apollo 11 and 12 rocks specific heat and thermal conductivity at 2-5 K, comparing elastic properties 23 p3761 A71-43785
- Specific heat of Apollo 11 breccia and Apollo 12 olivine dolerite at 95-340 K 23 p3762 A71-43786
- Dielectric conductivity, relative permittivity and loss tangent of Apollo 11 and 12 rock samples 23 p3762 A71-43787
- Magnetic properties of glass spherules from Apollo 11 and 12 fines, determining oxidation effect 23 p3762 A71-43791
- Apollo 12 fines and Apollo 11 microbreccias and rocks magnetic properties, discussing remanent magnetization 23 p3763 A71-43793
- Apollo 11 and 12 crystalline rocks NRM natural remanent magnetization, discussing magnetizing fields origin 23 p3763 A71-43794
- Spontaneous fission fossil tracks of U, Pu and extinct transuranic elements in pyroxenes of Apollo 11 and 12 soil samples 23 p3764 A71-43803
- Apollo 11 and 12 fines analysis, observing no quarks 23 p3765 A71-43809
- Critique of paper on Apollo 11 ilmenite basalts petrology and lunar bodies origin and form 23 p3769 A71-43886
- Galactic and solar cosmic ray effects on Apollo 11 lunar soil and rock samples, analyzing Xe isotopic anomalies 23 p3772 A71-44016
- Lunar origin hypothesis, discussing Apollo 11 crystalline rocks nature and basalts petrogenesis 23 p3770 A71-44075
- APOLLO 12 FLIGHT**
- Apollo 12 lunar core and soil samples indicating meteoritic trace elements abundance 01 p0148 A71-10003
- Opaque minerals in Apollo 12 rocks, emphasizing spinel compositions 01 p0162 A71-11426
- Lunar seismic reaction to Apollo 12 module launch stage impact, taking into account multistage soil scattering 02 p0304 A71-11921
- Apollo 12 lunar rock 12013 preliminary examination and preparation for instrumental analysis, noting feldspar content and igneous nature 03 p0493 A71-14213
- Petrographic microscope and electron microprobe analysis of Apollo 12 rock 12013, noting bimineralline composition with dominant potassic feldspar plus silica 03 p0493 A71-14214
- Apollo 12 lunar rock 12013 mineralogy, identifying whitlockite, plagioclase, alkali feldspar, ilmenite, quartz and minerals encrusted with quartz 03 p0493 A71-14215
- Apollo 12 lunar rock 12013 petrologic and mineralogic characteristics, discussing data on isotopic Xe and Gd composition 03 p0494 A71-14217
- O, Si, Al and Fe abundances of Apollo 12 lunar rock 12013 from neutron activation analysis 03 p0494 A71-14218
- Apollo 12 lunar rock 12013, discussing major and trace elemental abundances determination by neutron activation analysis 03 p0494 A71-14219
- Ar 40/Ar 39 age determination of Apollo 12 lunar rock 12013 fragments 03 p0494 A71-14220
- Apollo 12 lunar rock 12013 rare earth, alkaline and alkali metal and Sr 87/Sr 86 data, discussing light and dark component composition 03 p0494 A71-14221
- Trace element patterns of Apollo 12 lunar rock 12013 light and dark portions, discussing Rb-Sr age and Li, K, Rb, Sr, Ba and rare earth concentrations 03 p0494 A71-14222
- Apollo 12 lunar rock 12013 origin, determining age by U, Th and Pb isotopic study 03 p0494 A71-14223
- He, Ne, Ar and Xe from stepwise heating of Apollo 12 lunar rock 12013, discussing radiogenic and spallation components and He 3 and Ne 21 cosmic ray exposure ages 03 p0494 A71-14224
- Apollo 12 lunar rock 12013 oxygen 18 and silicon 30 ratios, comparing to terrestrial basalts and gabbros, Apollo 11 rocks and oceanic rhyolite obsidians 03 p0495 A71-14225
- Seismograph recording of Apollo 12 lunar module impact as result of secondary ejecta spray around seismometer or translunar seismic wave propagation 04 p0644 A71-15128

Apollo 12 lunar rock examination, discussing soil mechanics, mineralogical and petrological aspects and surface features and fines 05 p0806 A71-16149

Apollo 11 and 12 lunar rock opaque oxides differences in titanium contents 05 p0807 A71-16298

Rare earth abundance in Apollo 12 basalts and soils and achondritic meteorites, using partial melting model 06 p0966 A71-17899

Apollo 12 Lunar Module high landing accuracy, discussing control actions, trajectory error sources and power descent 07 p1206 A71-19086

Amino acid contents of Apollo 11 and 12 fines, discussing laboratory syntheses 07 p1196 A71-19500

Apollo 12 sample 12023 fines carbon, carbides and methane determination by hydrolysis and vacuum pyrolysis 07 p1196 A71-19541

Apollo 11 and 12 lunar samples, discussing chemical composition relationship to lunar origin 07 p1196 A71-19605

Apollo 12 lightning incident, discussing atmospheric conditions, damage and discharge hazard minimization [SAE PAPER 700938] 07 p1208 A71-19925

Roughrider F-100F aircraft flights in thunderstorms and Apollo 12 launch electric field measurements, comparing patterns and magnitudes of lightning strikes to vehicles 07 p1208 A71-19927

Surveyor 3 spacecraft TV camera surface discoloration patterns caused by lunar soil blown by Apollo 12 exhaust 08 p1363 A71-21219

Apollo 12 crystalline rock samples composition from conventional chemical analysis, suggesting origin in magmatic body with differentiation by crystallization and olivine settling 09 p1529 A71-23654

Elemental analysis for lunar rocks and regolith, comparing silicon oxide and titanium oxide composition in Apollo 12 and Apollo 11 samples 10 p1672 A71-24389

Apollo 12 clinopyroxenes exsolution and epitaxy by electron microprobe and single crystal X ray diffraction 10 p1672 A71-24391

Apollo 12 soils composition and derivation, finding feldspathic orthopyroxene rich rock and chemically comparable glass fragments 10 p1672 A71-24393

Lunar 12 spinel compositional variation and textures as petrogenetic indicators, showing magma differentiation by crystal settling after lunar surface extrusion 10 p1672 A71-24394

Thermoluminescence glow curve and decay characteristics of Apollo 12 fines and soil samples, suggesting lower mean daytime surface temperature at site 10 p1672 A71-24395

Lunar soil 12033 bulk chemical analysis, suggesting mixture of exotic component with local soil in 41/59 proportion 10 p1673 A71-24396

Microcraters on Apollo 12 crystalline rocks and breccia surfaces attributed to primary cosmic particles 10 p1673 A71-24427

Primordial Kr and Xe trapping as possible cause of element abundance trend reversal in Apollo 11 and 12 fines 10 p1673 A71-24428

Surveyor 3 thermal control surfaces analysis from Apollo 12 samples collection, discussing spectral reflectance and lunar dust effects on surface finishes optical properties [AIAA PAPER 71-479] 12 p1920 A71-26759

Lunar dynamics and structure data from two lunar seismic stations installed during Apollo 11 and 12 missions as part of ALSEP 12 p1967 A71-27416

Lunar seismic reaction to Apollo 12 module launch stage impact, taking into account multistage soil scattering 13 p2134 A71-28208

Methane and deuteromethane released from Apollo 11 and 12 lunar fines by deuterated acid etch, using gas chromatography for carbon compounds separation 13 p2136 A71-28427

Surveyor 3 spacecraft attitude change on lunar surface, examining Apollo 12 mission photographs 13 p2145 A71-28699

Lunar chronology and evolution from Rb and Sr internal isochrons on Apollo 11 and 12 crystalline rock samples 13 p2142 A71-29142

Electrical conductivity measurement of Apollo 11 and 12 lunar surface rocks, using two-probe technique in vacuum furnace 14 p2315 A71-30864

Apollo 11 and 12 lunar samples compared with deep earth rocks, noting potassium-uranium ratio 14 p2318 A71-31126

Apollo 12 landing site morphological and textural details from Surveyor 3 photography, considering lunar surface impact and volcanic models 15 p2493 A71-32483

Gravity anomaly and lunar radius measurement at Apollo 12 landing site, using data telemetered to earth from surface module 16 p2636 A71-33507

Electrical conductivities of Apollo 11 and 12 lunar rocks and chondritic meteorites at 300-1100 K 17 p2796 A71-34182

Carbon compounds in Apollo 12 lunar fines and core samples, using pyrolysis, mass spectrometry, ion exchange chromatography and optical and electron microscopy 17 p2801 A71-34649

He, Ne and Ar isotopic distribution and origin in Apollo 12 lunar samples, considering solar wind implantation 17 p2695 A71-35030

Lunar magnetic fields measured by magnetometers placed by Apollo 12 and 14 astronauts, considering permanent fields due to fossil magnetic material and transient fields 17 p2811 A71-35734

Apollo 11 and 12 lunar landings, discussing retrieved lunar material, seismographs, solar wind and light reflector for measuring earth-moon distance 18 p2959 A71-35906

Apollo 11 and 12 lunar rocks composition, suggesting depletion of K, Rb and Pb in solar nebula prior to final accretion of moon 18 p2963 A71-36228

Compounds hydrolyzable to amino acids in aqueous extracts of Apollo 11 and 12 lunar fines, noting presence of glycine and alanine 18 p2855 A71-36230

Scanning electron microscope and petrographic observations of glass particles from Apollo 12 lunar soil sample, revealing surface features and origin 19 p3137 A71-37674

Spectral emittance ranges of Apollo 12 lunar fines dependent on density for 2.5-14 micron wavelengths [ASME PAPER 71-HT-21] 19 p3142 A71-37992

Lunar locations and orientations of crystalline rocks, breccia and soil from Apollo 11 and 12 missions, including maps 23 p3737 A71-43603

Azimuth frequency plots of regolith surface lineaments at Apollo 11 and 12 landing sites 23 p3737 A71-43604

Tranquillity silicate mineral in crystalline basaltic rocks from Apollo 11 and 12 samples 23 p3737 A71-43605

High temperature phase transition and composition of Apollo 12 pigeonite/augite clinopyroxene crystal rock 12021 from X ray diffraction 23 p3738 A71-43607

Comparative electron petrography and chemical analysis of Apollo 11 and 12 and terrestrial rocks, noting pyroxene, plagioclase, ilmenite and cristobalite 23 p3738 A71-43608

Exsolution lamellae structure of Lunar pyroxenes from Apollo 12 samples, using electron microscopy and diffraction 23 p3738 A71-43610

Tridymite structure in lunar pigeonite porphyry 12021 by single crystal X ray diffraction, comparing with meteorite and silica brick 23 p3738 A71-43613

Fission track analyses of uranium enriched phases in Apollo 11 and 12 basaltic rocks 23 p3739 A71-43615

Apollo 11 and 12 rock samples examination, failing to observe radioactive halos 23 p3739 A71-43617

Zirconium liquid-crystal distribution in phase ilmenite of Apollo 11 and 12 lunar rocks 23 p3739 A71-43618

Opaque mineral compositions in Apollo 12 lunar rocks, noting ilmenite, spinels, native iron and troilite 23 p3739 A71-43620

Opaque minerals in Apollo 12 lunar rocks from Oceanus Procellarum by reflected light microscopy and electron microprobe analysis, including ilmenite, chromite and troilite 23 p3739 A71-43622

Luminescence petrography of Apollo 12 lunar igneous rocks, comparing to meteorites and terrestrial basalts 23 p3740 A71-43624

Mineralogical, petrological and chemical features of four Apollo 12 lunar microgabbros 23 p3740 A71-43625

Apollo 12 crystalline rocks mineralogy, petrology and chemical composition, considering magmatic origin 23 p3740 A71-43626

Mineralogy and petrology of Apollo 12 igneous rocks 12004, 12008, 12009 and 12022, noting ilmenite,

olivine and spinel content and metal grains composition 23 p3740 A71-43627

Mineralogy, petrology and chemical composition of Apollo 12 rocks and fines 23 p3740 A71-43628

Petrography and mineral composition of Apollo 12 crystalline rocks 23 p3740 A71-43629

Apollo 12 lunar rocks and fines mineralogy and petrology, using optical and electron microscopy, electron and X ray diffraction and electron probe microanalysis 23 p3741 A71-43630

Gray mottled basaltic rock composition and origin in Apollo 12 lunar soils and breccias 23 p3741 A71-43634

Apollo 11 and 12 lunar rocks and soil chemical composition, considering petrogenesis and major and trace elements abundance 23 p3741 A71-43635

Normative mineralogy of lunar basaltic rocks from Apollo 11 and 12 samples, comparing with terrestrial and meteoritic analogs 23 p3742 A71-43637

Apollo 12 crystalline rocks composition from microprobe analyses, indicating undercooled magmatic fractional crystallization 23 p3742 A71-43639

Petrology of Apollo 11 and 12 rock samples with silicate melt inclusions, discussing terrestrial equivalents 23 p3742 A71-43641

Clinopyroxene crystallization histories of Apollo 12 porphyritic basalt rocks 12021 and 12052 from Oceanus Procellarum 23 p3742 A71-43643

Olivine accumulation in Apollo rock 12040 and basaltic fragments, using textural and microprobe analyses 23 p3742 A71-43644

Crystalline and glassy phases electron probe analysis for picrite basalts, ferrobasalts, feldspathic norites and rhyolites from Apollo 12 lunar soil samples 23 p3743 A71-43645

Apollo 12 basalts petrology and petrogenesis, studying crystallization sequences 23 p3743 A71-43646

Petrography, mineral composition and grain size distribution of Apollo 12 lunar fines 23 p3743 A71-43649

Noritic and anorthositic rock fragment proportions and sources in Apollo 12 soil samples 23 p3743 A71-43650

Size distribution, composition and history of regolith fines at Apollo 12 site 23 p3743 A71-43651

Mineralogical composition, modal distribution and bulk chemical analysis on Apollo 12 lunar fines 23 p3744 A71-43652

Apollo 12 Mare Procellarum soil glasses analyzed by ion and electron microprobe, discussing rock ages 23 p3744 A71-43653

Grain size and modal analyses of lunar regoliths sampled by Apollo 11 and 12, discussing particles origin 23 p3744 A71-43654

Pyroxenes and olivines in lunar rocks from Ocean of Storms, observing plastic deformational processes since crystallization by optical, X ray and electron microprobes 23 p3744 A71-43657

Apollo 11 and 12 unshocked and shocked microbreccias petrology, noting shock compression and shock welding 23 p3745 A71-43658

Impact metamorphism effects in Apollo 12 microbreccias from Oceanus Procellarum 23 p3745 A71-43659

Apollo 11 and 12 regolith and breccia samples, discussing shock effects detection and interpretation, chemical composition, grain size distribution and impact origin 23 p3745 A71-43660

Lunar rocks 12063,9 and 12004,11 opaque mineralogy and textural feature, comparing to apollo 11 samples 23 p3745 A71-43661

Lunar soil samples 12001,1, 12037, 12042,25 and 12070,100 exterior morphology and chemistry, noting environmental temperature decrease, crater formation and meteorite impact 23 p3745 A71-43662

Morphological, physical and chemical characteristics of basaltic and anorthositic glassy spheroids in Apollo 12 lunar fines 23 p3746 A71-43666

Apollo 12 lunar dust sample 12070,128, determining response to effective agents of earth-type chemical weathering 23 p3746 A71-43669

Nonmare basalts chemical composition and origin from Apollo 11 and 12 sites 23 p3746 A71-43671

- Apollo 12 specimens elemental abundance from neutron activation analysis, discussing fractional crystallization, partial melting, rare earth abundances and soil mixing model 23 p3747 A71-43674
- Trace element abundances in Apollo 12 lunar rock and fine samples and mineral separates from Ocean of Storms 23 p3747 A71-43675
- Apollo 12 lunar soils, rocks and core samples, determining rare earth, alkali and alkaline earth elements concentrations 23 p3747 A71-43676
- Apollo 11 and 12 lunar rocks and fines, discussing compositional variations and relationships to stony meteorites 23 p3747 A71-43677
- Primordial radionuclides K, Th and U concentrations in Apollo 12 lunar rocks, breccias and fines, using gamma ray spectrometry 23 p3748 A71-43679
- Apollo 12 lunar soil, breccia and igneous rock samples, determining elemental abundances with spark source mass spectrometry and neutron activation analysis 23 p3748 A71-43680
- Apollo 12 lunar soils and igneous rocks from Ocean of Storms, determining major, minor and trace element composition with chemical, X ray fluorescence and spectrographic techniques 23 p3748 A71-43683
- Bulk elemental composition of Apollo 12 samples of lunar igneous and breccia rocks and soils from instrumental and radiochemical neutron activation analysis 23 p3748 A71-43684
- Apollo 12 lunar rocks and fines under high energy neutron activation analysis, determining O, Si, Al, Mg and Fe abundances 23 p3748 A71-43685
- Spark mass spectrometric analysis of major and trace elements abundance in Apollo 11 and 12 lunar rocks and soil samples, comparing with standard basalt 23 p3749 A71-43686
- Apollo 11 and 12 lunar samples elemental composition analysis, using activation and mass spectrometric isotope dilution analysis and emission spectrography 23 p3749 A71-43687
- Apollo 12 lunar samples 12040,36 and 12064,38 chemical analysis for major elements, discussing titanium, water and iron content 23 p3749 A71-43688
- Apollo 12 lunar samples halogen and trace element composition, investigating chemical and physical processes affecting surface halides, platinum group metals and Hg 23 p3749 A71-43689
- Apollo 11 and 12 lunar fines 10084 and 12070 trace element determination, using multielement neutron activation analysis 23 p3749 A71-43690
- Apollo 12 lunar rocks 12002, 12018, 12021 and 12038 and soil sample 12070 elemental abundances, discussing origin and comparison to meteorites and terrestrial rocks 23 p3749 A71-43691
- Apollo 11 and 12 lunar rock and soil examination, emphasizing Au and Ag excess in soil 23 p3750 A71-43693
- Apollo 12 lunar rock rare earth element abundances, comparing to Icelandic basalt flow 23 p3750 A71-43694
- Rare earth elements and trace elements abundance in Apollo 12 igneous rocks, breccia and lunar soil 23 p3750 A71-43695
- Re isotopic composition measurement in Apollo 12 rocks and regolith samples using neutron bombardment 23 p3750 A71-43697
- Knudsen cell-mass spectrometric study of Apollo 12 samples vaporization process 23 p3750 A71-43700
- Active and inert gases released by crushing Apollo 11 and 12 samples at room temperature and by low temperature heating 23 p3751 A71-43701
- Carbon and sulfur isotope content in Apollo 12 lunar fines 23 p3751 A71-43702
- Apollo 12 lunar dust and rocks carbon and hydrogen amount and isotopic composition determination, using in vacuo outgassing and combustion in oxygen 23 p3751 A71-43703
- Oxygen isotope fractionation in Apollo 12 rocks and soils, noting plagioclase ilmenite isotopic temperature 23 p3751 A71-43704
- Apollo 12 lunar samples 12002,128, 12021,49, 12038,43 and 12070,52 vanadium isotopic composition 23 p3751 A71-43706
- Apollo 12 igneous rocks and fines from Ocean of Storms, presenting rubidium and strontium chronology and chemistry 23 p3752 A71-43709
- Rb-Sr isotopic composition in Apollo 12 regolith samples yielding 4.2-5.1 billion year ages 23 p3752 A71-43710
- Rb, Sr, K, U, Th and Pb concentrations in Apollo 12 lunar soil samples, discussing lunar age estimates 23 p3752 A71-43711
- Lunar rocks 12040 and 12013 and anorthositic, determining U-Th distributions with induced fission track maps 23 p3752 A71-43712
- Age determination of Apollo 12 rocks by U-Th-Pb method 23 p3752 A71-43713
- Lead isotopes volatile transfer in Apollo 11 and 12 lunar soil samples, discussing lunar age estimates 23 p3752 A71-43714
- Isotopic abundances and composition of U and Th in Apollo 12 soil and breccia samples, using mass spectroscopy 23 p3753 A71-43716
- Isotopic composition of U and Th in Apollo 12 lunar rock samples from mass and alpha spectrometry 23 p3753 A71-43717
- Superheavy elements search in lunar fine grains from Apollo 12 mission by measuring kinetic energy spectrum of nuclear fission fragments 23 p3753 A71-43718
- Cosmic ray exposure ages and rare gas concentration profiles in Apollo 12 lunar rocks, discussing spallation products and neutron capture effects 23 p3753 A71-43719
- Rare gas concentrations and isotopic abundances in lunar rocks, fines and breccias from Apollo 11 and 12 flights, determining exposure and gas retention ages 23 p3753 A71-43720
- Isotopic abundances and concentrations of spallogenic Ne, Kr and Xe in Apollo 12 rock 12002, constructing three stage model of irradiation history 23 p3753 A71-43722
- Apollo 11 and 12 lunar samples history of irradiation exposure to galactic cosmic rays and solar wind, using rare gas and Gd isotope measurements 23 p3754 A71-43724
- Apollo 11 and 12 fines cosmogenic He, Ne and Ar radionuclides composition determination, using electron microprobe analysis 23 p3754 A71-43727
- Lunar cosmogenic radionuclides production time and spatial dependence calculations, comparing Apollo 11 and 12 measurements 23 p3754 A71-43729
- Cosmogenic radionuclide concentration and exposure ages of Apollo 12 rock from Ocean of Storms 23 p3754 A71-43730
- Lunar surface erosion and mixing from cosmogenic and primordial radionuclide measurement in Apollo 12 lunar rock and soil samples 23 p3755 A71-43731
- Depth profiles of cosmogenic radionuclides in lunar rocks and soil samples from Apollo 11 and 12 flights, considering solar particle flux and spectra 23 p3755 A71-43732
- Cosmogenic and primordial radionuclides in Apollo 12 surface rocks and fines from nondestructive gamma ray spectrometry 23 p3755 A71-43733
- Solar protons contribution to spallogenic Mn 53 production in Apollo 12 lunar rock and soil from neutron activation analysis 23 p3755 A71-43734
- Radioactive rare gases and tritium in Apollo 12 lunar rocks and in sample return container, noting relationship to solar flare event 23 p3755 A71-43736
- Tritium and argon radioactivities and depth variations in Apollo 12 rocks, discussing solar flare and cosmic ray exposure ages 23 p3755 A71-43737
- Porphyry-like pigments in Apollo 12 lunar soil sample 12023, using spectral analysis involving fluorescence, absorption and magnetic circular dichroism spectrometry 23 p3756 A71-43739
- Apollo 12 lunar surface fines examination noting absence of porphyrins 23 p3756 A71-43740
- Volatilizable organic polymers and hydrocarbons in Apollo 12 lunar core samples 12025 and 12028, using mass spectrometric analysis 23 p3756 A71-43742
- Chemical characteristics of carbon compounds in Apollo 11 and 12 lunar fines, using organic solvent extraction, mass spectrometry and gas chromatographic method 23 p3756 A71-43743
- Organogenic elements and compounds abundances and distribution in Apollo 12 fines 23 p3756 A71-43744
- Long chain alkanes search in Apollo 12 lunar fines, using benzene-methanol extracts 23 p3756 A71-43745
- Apollo 12 lunar dust, rocks and microbreccia microsection examined for evidence of biogenic structure 23 p3757 A71-43746
- Biological activity in Apollo 11 and 12 core samples searched for after placement in Petri dishes containing media 23 p3757 A71-43747
- Microbial assay of lunar core and surface samples obtained from Apollo 11 and 12 flights 23 p3757 A71-43748
- Apollo 12, 14 and 15 lunar core tube sampling 23 p3757 A71-43749
- Apollo 12 fines sample 12057,72 particle size distribution determination procedures, discussing characteristic shapes, glassy agglomerates, smooth opaque particles and volume 23 p3757 A71-43752
- Particle size and shape distributions of Apollo 12 lunar fines by computer evaluation of scanning electron microscope images 23 p3758 A71-43755
- Ultramicroscopic texture and radiation damage in Apollo 11 and 12 micron sized lunar dust grains compared with meteoritic rocks 23 p3758 A71-43756
- Regular particle morphology and petrostatistics in Apollo 11 and 12 lunar fines and conglomerates, using phase contrast and scanning microscopes 23 p3758 A71-43757
- Apollo 12 lunar glass spherules chemical composition, homogeneity, densities and thermal histories, using electron probe analysis 23 p3758 A71-43758
- Neutron diffraction studies of Apollo 12 lunar samples 12070,119, 12071,6 and 12008,7, observing magnetic ordering 23 p3759 A71-43761
- Elemental abundance analysis of Apollo 11 and 12 lunar materials from Auger electron spectroscopy 23 p3759 A71-43762
- Apollo 12 suprathermal ion detector data, considering Apollo 13 S-IVB stage impact 23 p3759 A71-43763
- Mossbauer instrumental analysis of Apollo 12 rock and soil samples, measuring nuclear gamma resonance of iron 57 23 p3759 A71-43764
- Phase analysis of Apollo 12 fines, core tube samples and rocks by Mossbauer studies, noting nearly uniform distribution of major Fe containing phases 23 p3759 A71-43765
- Vacuum pumped Apollo 12 lunar soil sample 12001,118 gas exposure effects, interface microanalysis and adhesion measurements in ultrahigh vacuum system 23 p3759 A71-43767
- Apollo 12 basalts porosity and volume compressibility under hydrostatic pressure 23 p3759 A71-43768
- Grain size distribution and optical and RF electrical properties of Apollo 12 lunar fines and core samples 23 p3759 A71-43769
- Visible and near IR spectral reflectivity measurements of basalt separates, glass and anorthositic fragments from Apollo 12 mare samples 23 p3760 A71-43770
- Spectral directional reflectance of Apollo 11 and 12 fines as function of bulk density 23 p3760 A71-43771
- Physical characterization of Apollo 11 and 12 lunar fines and glasses by diffuse reflectance, Raman and X ray spectroscopy and thermally stimulated currents 23 p3760 A71-43773
- Apollo 11 and 12 rocks luminescence under proton, electron, UV and X irradiation 23 p3760 A71-43774
- Apollo 12 lunar core sample thermoluminescence dependence on radiation dose rates, detecting temperature gradients in regolith by differential thermal analysis 23 p3760 A71-43776
- Natural and X ray excited thermoluminescence in Apollo 12 lunar samples and terrestrial plagioclases 23 p3761 A71-43778
- Polarization characteristics, albedos and optical properties of Apollo 11 and 12 rocks, investigating wavelength dependence and proton irradiation effect 23 p3761 A71-43779
- Apollo 12 multispectral lunar photography experiment using four camera configuration, verifying by ground photoelectric photometry 23 p3761 A71-43780
- Apollo 12 lunar fines 12001,19 thermal conductivity vacuum measurements, using line heat source method 23 p3761 A71-43781
- Elastic wave velocities in Apollo 12 rocks 12052 and 12065 at high pressures, noting basalt-like composition and crystal structure 23 p3761 A71-43783
- Apollo 11 and 12 rocks specific heat and thermal conductivity at 2-5 K, comparing elastic properties 23 p3761 A71-43785
- Specific heat of Apollo 11 breccia and Apollo 12 olivine dolerite at 95-340 K 23 p3762 A71-43786
- Dielectric conductivity, relative permittivity and loss tangent of Apollo 11 and 12 rock samples 23 p3762 A71-43787

Dielectric properties of Apollo 12 samples and lunar interior as function of frequency and temperature 23 p3762 A71-43788

Apollo 12 magnetic measurements of lunar interior electroconductivity simultaneously on lunar surface and in circumlunar orbit 23 p3762 A71-43789

Lunar electrical conductivity profile from joint power spectral density analysis of Apollo 12 and Explorer 35 magnetometer data 23 p3762 A71-43790

Magnetic properties of glass spherules from Apollo 11 and 12 fines, determining oxidation effect 23 p3762 A71-43791

Apollo 12 lunar soil and igneous rocks magnetic properties 23 p3763 A71-43792

Apollo 12 fines and Apollo 11 microbreccias and rocks magnetic properties, discussing remanent magnetization 23 p3763 A71-43793

Apollo 11 and 12 crystalline rocks NRM natural remanent magnetization, discussing magnetizing fields origin 23 p3763 A71-43794

Lunar rocks 12002 and 12022 remanent magnetic moment as evidence for ancient lunar magnetic field 23 p3763 A71-43795

Apollo 12 lunar soil samples magnetic resonance properties, determining temperature, frequency and thermal annealing dependence 23 p3763 A71-43796

Solar and galactic iron group cosmic ray track distributions in Apollo 12 lunar rocks, investigating surface residence times 23 p3764 A71-43800

Primary cosmic ray and spallation track density distribution in Apollo 12 deep core soil samples 23 p3764 A71-43801

Radiation exposure history from fossil tracks in Apollo 12 surface rocks and double core regolith samples, comparing with Saint Severin meteorite 23 p3764 A71-43802

Spontaneous fission fossil tracks of U, Pu and extinct transuranic elements in pyroxenes of Apollo 11 and 12 soil samples 23 p3764 A71-43803

High resolution time averaged energy spectrum and chemical composition of iron group cosmic ray nuclei from fossil tracks in Apollo 12 lunar rocks 23 p3764 A71-43804

Ultraheavy cosmic ray nuclei existence inferred from Apollo 12 lunar rock pigeonite crystal track length distribution 23 p3765 A71-43805

Lunar surface orientation of whole Apollo 12 rocks, considering microcraters distribution 23 p3765 A71-43806

Apollo 11 and 12 fines analysis, observing no quarks 23 p3765 A71-43809

Apollo 12 returned Surveyor 3 component materials analysis for lunar exposure effects by nondestructive and destructive tests 23 p3765 A71-43811

Alpha radioactivity in Surveyor 3 camera visor, calculating upper limit of Po 210 at equilibrium of Oceanus Procellarum 23 p3765 A71-43812

Microbiological analysis for surviving terrestrial microorganisms from Apollo 12 retrieved Surveyor 3 spacecraft electrical cabling 23 p3633 A71-43814

APOLLO 13 FLIGHT

Apollo 13 in flight emergencies and countermeasures, discussing fire in Service Module oxygen tank causes and effects on Spacecraft systems and solutions 07 p1206 A71-19087

Apollo 12 suprathreshold ion detector data, considering Apollo 13 S-IVB stage impact 23 p3759 A71-43763

APOLLO 14 FLIGHT

Apollo 14 communications support by USAF, discussing voice and data relay between spacecraft and control center, global weather support, cartographic and geodetic services, etc 16 p2541 A71-33178

Lunar gravity measurements by Apollo 14 Doppler radio tracking during low altitude orbits, correlating variations with surface features 16 p2641 A71-33771

Lunar magnetic fields measured by magnetometers placed by Apollo 12 and 14 astronauts, considering permanent fields due to fossil magnetic material and transient fields 17 p2811 A71-35734

Apollo 14 Fra Mauro rock fragment samples, determining Ar 40/Ar 39 ages 18 p2961 A71-35945

Gravity determination at Apollo 14 landing site, finding measured value consistent with data from lunar potential models 18 p2964 A71-36283

Physical, chemical, mineralogical and biological analysis of Apollo 14 lunar rocks and fines 19 p3144 A71-38179

Apollo 14 lunar module landing site geology, studying samples from regolith and block ejecta deposit around young crater 19 p3144 A71-38180

Apollo 14 lunar soils chemical element concentrations by atomic absorption spectrophotometry and isotope dilution 20 p3292 A71-39381

Apollo 14 bulk lunar fines sample elemental abundances determination from soils and rocks by activation analysis 20 p3292 A71-39382

Apollo 14 flight Fra Mauro crystalline rocks age measurement, using Ar 40/39 ratio method 22 p3598 A71-41838

Biomedical effects of Apollo 14 space flight, considering weightlessness adaptation 22 p3487 A71-41985

Sequential processor performance prediction error with linear method from Monte Carlo cycle analysis of Apollo 14 early rendezvous profile 23 p3731 A71-43056

[AAS PAPER 71-386]

Lunar impact targeting technique improvement for Apollo 14 mission preflight analyses and flight support operations 23 p3732 A71-43060

[AAS PAPER 71-392]

Rare earth trace elements abundance of Apollo 14 lunar soil samples from Fra Mauro, comparing with chondrites 23 p3735 A71-43248

Apollo 12, 14 and 15 lunar core tube sampling 23 p3757 A71-43749

Climatological studies and weather forecast support for Apollo 14 mission prelaunch, launch, emergency landing and terminal areas 24 p3845 A71-44981

APOLLO 15 FLIGHT

Manned Lunar Roving Vehicle for Apollo 15 expedition, discussing subsystems design features 15 p2384 A71-31746

Lunar roving vehicle for Apollo 15 mission, discussing power, control, navigation and deployment systems in relation to lunar exploration requirements [AIAA PAPER 71-847] 17 p2723 A71-34707

Minkey rendezvous computer program in Apollo 15 CSM aiding guidance, navigation and control system functions 17 p2772 A71-35055

Apollo 12, 14 and 15 lunar core tube sampling 23 p3757 A71-43749

APPENDAGES

NT ARM [ANATOMY]

NT FOREARM

NT HAND [ANATOMY]

NT KNEE [ANATOMY]

NT LEG [ANATOMY]

Motion stability analysis for force-free spinning satellites with flexible appendages by Liapunov direct method [AAS PAPER 71-345] 23 p3772 A71-43018

APPLICATIONS OF MATHEMATICS

Soviet book on chemistry, physics and mathematics of life covering evolution, metabolic processes, biological cycles and rhythms, molecular physiology, cybernetics, etc 04 p0539 A71-15261

Multiple acoustic evoked responses coherence time course using mathematical correlation and Fourier transforms 05 p0714 A71-16922

Similarity methods, partial differential numerical analysis, dispersive wave and perturbation theory applications to mechanics 06 p0920 A71-18220

Noise exposure forecasts for cumulative aircraft noise production single number rating as community response indicator 08 p1249 A71-21817

Applied mathematics and mechanics - Conference, Delft, Netherlands, April 1970 15 p2502 A71-31152

Definitions and axiomatics revision and recommendations for mathematical statistics as applied discipline 19 p3086 A71-37782

Soviet papers on mathematic methods application in programming covering optimal control, game theory, impact problems, thermoelastic waves, etc 22 p3526 A71-41908

APPLICATIONS TECHNOLOGY SATELLITES

NT ATS 1

NT ATS 5

NT ATS 6

NT ATS 7

Carbon dioxide laser intersatellite communication systems as economical alternative to microwave and millimeter systems, noting use onboard ATS satellites 01 p0091 A71-10009

Space research benefits from applications technology satellites and materials utilization, reviewing satellite communication networks, meteorology geodesy, navigation, geology and agriculture 03 p0524 A71-14245

Geostationary radio beacon specifications and observational opportunities on ionospheric satellite ATS-F in 1972 07 p1096 A71-19016

ATS F and G, discussing communications experimental program with deployable 30 ft parabolic antenna [SAE PAPER 700759] 08 p1366 A71-21368

Dioscures project commercial satellite system for telecommunications, air traffic control and navigation, describing simulation method used in cost effectiveness study 09 p1547 A71-22276

Supersonic transport air traffic meteorology, considering high altitude and flight velocities, application technology satellites for lower stratosphere thunderstorms, clear air turbulence, etc 09 p1488 A71-23070

Aeronautical satellites, considering air-ground telecommunication, air traffic control and inertial navigation applications 12 p1971 A71-26825

ATS 1 and 3 satellite VHF transponders for ships and aircraft location, communication and remote sensing, discussing performance test results 14 p2198 A71-30898

Satellite systems for educational TV program distribution, discussing orbit utilization, ground stations and ATS program 16 p2645 A71-33588

Meteorological satellites characteristics, reviewing Tiros,ITOS, Nimbus, ATS, SMS and IGAR programs and vehicles 17 p2812 A71-34244

Electrical performance of Cassegrain antenna reflector for space communication via ATS and deep space research 17 p2700 A71-34747

ATS F and G thermal control, discussing heat pipe, louvers and model tests [ASME PAPER 71-AV-28] 18 p2868 A71-36395

Joint India-U.S. satellite instructional television experiment for national development using ATS-F spacecraft 18 p2988 A71-36502

ATS F and G satellites for half earth surface full time communication coverage, discussing mission objectives 20 p3306 A71-39607

Meteorological and instrumental options for atmospheric vertical temperature soundings from geosynchronous satellites, noting Nimbus 3 and ATS measurements of cloud cover and radiance levels 20 p3240 A71-39674

Cosmic rays cutoff daily variations at ATS geostationary satellite altitude, noting role of magnetospheric tail in lowering cutoff below calculated value 20 p3282 A71-39739

ATS power supply concepts, considering growth capability, control, reliability, thermal dissipation and weight minimization 22 p3588 A71-41958

Atmospheric wind speed estimation, using ATS geostationary satellite cloud photographs 22 p3535 A71-42411

Experimental ATS-1 satellite medical network for geographically and climatically isolated areas, noting impact on emergency treatment and anxiety level reduction [AIAA PAPER 71-1003] 24 p3801 A71-44592

APPROACH

NT INSTRUMENT APPROACH

APPROACH CONTROL

NT RADAR APPROACH CONTROL

Time-synchronized approach control combining aircraft precision navigation and guidance with ATC equipment 02 p0280 A71-12894

Aircraft navigation system requiring computer and display for approach guidance to circular orbit over fixed ground area [AIAA PAPER 69-986] 07 p1156 A71-20305

Noise abatement power cutback takeoff procedures, maximum altitude approaches and preferential runway systems for noise relief 08 p1232 A71-21813

Wind gradient effect on flight characteristics during aircraft landing approach, particularly path deviation 11 p1706 A71-25194

Report on guidance system for approach and landing, discussing airports, aircraft, approach and landing paths, service classes, failure protection and weather penetration 11 p1796 A71-25534

Aircraft approach and landing under low altitude wind shear conditions, discussing flying hazards and glide path correction procedures 11 p1708 A71-26364

Helicopter automatic flight control equipment, discussing autopilot stabilizer, localization system, ground approach guidance coupler and flight director 15 p2446 A71-31916

- Aircraft control design by implicit model-following technique with optimal feedback sampled data and continuous control algorithm, exemplifying STOL aircraft landing approach control
[AIAA PAPER 71-956] 19 p2995 A71-37197
- Aircraft ILS landing approaches, discussing approach area and surface and obstruction clearance surface and limit 21 p3325 A71-40891
- Operational requirements of microwave guidance systems, comparing guidance and position measurement applied to aircraft approach and landing 22 p3572 A71-42092
- APPROACH INDICATORS**
- Aircraft final approach and landing aids, describing ILS, VHF omnidirectional radio range, distance measuring equipment and satellite systems for air navigation 07 p1154 A71-19014
- APPROXIMATION**
- NT BORN APPROXIMATION
- NT BORN-OPPENHEIMER APPROXIMATION
- NT CHEBYSHEV APPROXIMATION
- NT EDDINGTON APPROXIMATION
- NT FINITE DIFFERENCE THEORY
- NT FINITE ELEMENT METHOD
- NT HARTREE APPROXIMATION
- NT LEAST SQUARES METHOD
- NT NEWTON-RAPHSON METHOD
- NT OSEEN APPROXIMATION
- NT PADE APPROXIMATION
- NT PARTICLE IN CELL TECHNIQUE
- NT RAYLEIGH-RITZ METHOD
- NT RELAXATION METHOD [MATHEMATICS]
- NT RITZ AVERAGING METHOD
- NT SCHWARTZ METHOD
- Uniform matter fragmentation under gravitational influence, examining approximate solution for density perturbations 01 p0150 A71-10062
- Bubnov-Galerkin approximation method, reducing Cauchy problem for parabolic equations to ordinary differential system 01 p0111 A71-10436
- Successive approximations method for boundary value problems in plasticity theory of continuous media under complex loading 01 p0171 A71-10652
- Book on approximate methods in optimization problems covering nonlinear extremum, functional analysis, algorithms, optimal control theory and finite dimensional spaces 01 p0113 A71-11323
- Successive approximations of order K iterative methods for calculating inverse matrix, yielding lower and upper bounds 03 p0449 A71-13111
- Approximate minimum energy control for time variable linear system, using mathematical model 03 p0389 A71-13447
- Muon spatial distribution fluctuations at mountain level, using approximate methods 03 p0477 A71-13858
- Total particle number changes, evaluating approximate methods for transition effect calculation 03 p0426 A71-13870
- Convex Taylor series truncations minimization by iterative method based on approximating initial functional 03 p0452 A71-14058
- Finite element method approximations outside variational principle in elasticity problems, examining convergence to exact solution [ASME PAPER 70-WA/APM-34] 03 p0512 A71-14160
- Plane contours problems analytic solution by least squares method approximation, giving matrices of linear equations systems 04 p0602 A71-14605
- Stokes multipliers first approximations for outer expansions of Orr-Sommerfeld flow equation solutions 04 p0570 A71-15096
- Incompressible fluid turbulent boundary layer equations, examining approximate semiempirical calculations 04 p0573 A71-15555
- Periodic orbits representation in trigonometric series with numerical coefficients and truncation for applications 04 p0654 A71-15716
- Structural design analysis approximation for computational cost and computer storage reduction 05 p0824 A71-16575
- Supersonic flow field around flat plate at various angles of attack, comparing Brieden and Lighthill approximations 05 p0694 A71-16713
- Rate sensitive materials impulsively loaded structures by piecewise stationary mode approximate methods 05 p0826 A71-16718
- Partial differential equations approximate solution using Hermitian functions and collocation for improved numerical accuracy 05 p0776 A71-17220
- Continuous monotonic nonlinear controlled systems with time dependent, phase coordinates and nonnegative parameter disturbances, considering Chetaev estimate for restricted approximate solution 06 p0879 A71-17670
- Nonlinear unsteady heat conduction problems, investigating thermophysical property dependence on temperature and body coordinates by half space and approximate methods 06 p1006 A71-17749
- Iterative methods, numerical mathematics, approximation theory - Conference, Oberwolfach, West Germany, November 1968, June and November 1969 06 p0919 A71-18201
- Finite difference theory and other approximation methods convergence determination in nonlinear variational problems 06 p0919 A71-18202
- Dirichlet problem associated with elliptic partial differential equation, discussing integral operator methods for approximating numerical solution 06 p0920 A71-18208
- Numerical approximation of continuous real function in interval by polynomials using appropriate nets, estimating error 06 p0920 A71-18209
- On-line interactive graphical computer program systems for approximation problems, including least squares method 06 p0871 A71-18210
- Triple integrals approximation using cubature formulas symmetrical with respect to parallelepiped center 06 p0921 A71-18344
- High temperature gaseous flow, discussing approximate methods of calculation of turbulent boundary layer [AIAA PAPER 71-163] 06 p0885 A71-18605
- Approximate determination of complex geometry aircraft surfaces in form of discrete points, comparing efficiency to other methods 06 p0848 A71-18714
- Soviet papers on special problems of differential equations and functions theory covering approximation, complex variables, integral operators, etc 07 p1146 A71-19038
- Existence theorem and optimal approximation of functions of many variables by superimposing sums of smaller number of variables in complex region 07 p1146 A71-19039
- Analytic functions approximation in complex regions with aid of different systems of functions 07 p1146 A71-19041
- Analytic function steady approximation with aid of polynomials in given region, considering Dirichlet series 07 p1146 A71-19042
- Minimization with superlinear convergence based on second derivative matrix successive approximation scheme 07 p1146 A71-19176
- Light scattering and attenuation coefficients calculation by small particle approximation, determining applicability limits from comparison with use of exact Mie formulas 07 p1160 A71-19809
- Approximation of Chaplygin equation for subsonic ideal gas plane adiabatic flow, applying to discharge from flat channel with contraction 07 p1016 A71-20083
- Two link approximation of Chaplygin function by coupling to integral equations, applying to ideal gas jet separation flow past symmetrical arc 07 p1016 A71-20084
- Multilink approximation of Chaplygin function in subsonic and supersonic flow regions, deriving coupling conditions relative to modified stream function at approximation nodes 07 p1016 A71-20090
- Digital adaptive spectral filtering canceling undesired power spectra based on measured mean square values ratio and stochastic approximation methods 07 p1082 A71-20408
- Microwave circuits and components design using generalized rational function approximation in finite intervals with Zolotarev functions 08 p1252 A71-20757
- Natural frequencies approximation for vibration modes of stiffened and singly curved panel structures 08 p1369 A71-20810
- Spacecraft motion parameters maximum probability estimates, using approximate weight-matrix inversion techniques 08 p1360 A71-21003
- Derivative approximation techniques for recursive signal detection, using computer program for solving optimum and suboptimum processes signal to noise ratio in effectiveness evaluation 08 p1255 A71-21596
- Curved beams bending stress concentration approximate equations for elliptical, circular and rectangular cross sections, providing behavior prediction superior to exact methods 08 p1373 A71-21749
- Planet density distributions, deriving successive approximations for equilibrium figure equations 08 p1365 A71-21775
- Nonlinear approximation for coherent Green function behavior in randomly fluctuating, unbounded and statistically homogeneous medium, emphasizing large scale fluctuations 08 p1325 A71-21883
- Vertical velocity effects on ionospheric horizontal wind magnitude and direction, solving integral equations system by successive approximations 09 p1435 A71-22428
- Quasi-static problems in nonlinear viscoelasticity theory, comparing integral operator and variable moduli methods for convergence and accuracy of successive approximations 09 p1537 A71-22513
- Polynomial approximation of current along thin isolated asymmetrical cylindrical dipoles 09 p1419 A71-23506
- Proof theorem for Chaplygin successive approximations method, presenting lemma for convergence of solutions to differential equations system 10 p1636 A71-24021
- Approximate trigonometric solution to thermoelastic boundary value problem of plane with doubly periodic system of holes, deriving unsteady temperature and thermostress fields 10 p1687 A71-24195
- Approximate solution for limit load carrying capacity of thin walled tube under combined loadings, deriving formulas describing boundary surface 10 p1688 A71-24385
- Nonstationary linear systems analysis over finite time interval and graphical method for differential equation, comparing exact and approximate solutions for free oscillations 10 p1643 A71-24908
- Analytic approximations in closed form for curves of growth of Doppler-Lorentz broadened lines, considering radiative transport in nonisotropic gases 10 p1646 A71-24991
- Series solution for unbounded mixing of two incompressible homogeneous coaxial fluids with constant properties, using successive approximations method 11 p1748 A71-25159
- Atmospheric wave dynamics in equatorial region, obtaining approximate solution with Coriolis force within perturbation theory 11 p1795 A71-25921
- Approximation of flow around jet flapped airfoil, discussing ground effect on lift coefficient increments 11 p1705 A71-26314
- Optimal control of material point motion in thin spherical layer of central gravitational field, solving by approximation 12 p1957 A71-26631
- Atom rigid rotor problem, applying generalized phase shift rotational excitation treatment in lowest approximation 12 p1932 A71-26949
- Radar cross section data analysis, considering economical approximation techniques in HF and LF ranges 12 p1882 A71-27440
- Second order difference approximations with large viscosity coefficient for primitive barotropic model over spherical geodesic grid, comparing with first order approximations 13 p2097 A71-28231
- Piecewise-linear approximation of nonlinear friction effect on interferometric servosystem stability, deriving formulas for harmonic linearization coefficient of linearity 13 p2041 A71-28375
- Longitudinal wave propagation in ideal elastic bar with viscous stress, calculating approximation to nonlinear wave equations 13 p2153 A71-28483
- Approximation procedures for quasi-static problems solution in thermoviscoelasticity theory, considering time-variable boundaries and inhomogeneous temperature fields 13 p2154 A71-28648
- Integral transformations application to approximate elastic solutions for nonlinear hereditary media, considering elastoplastic deformations under active loads 13 p2154 A71-28649
- Successive approximations method for solving nonlinear elastic problems in transient creep theory, describing stress redistribution 13 p2157 A71-29197
- Approximate calculation for axisymmetric interaction between freely expanding jet and obstacle by reduction to problem of uniform gas flow past sphere 13 p1994 A71-29232
- Approximate method for calculating film cooling effectiveness of flat plate in presence of turbulent boundary layer with injection ratios less than unity 13 p2166 A71-29368
- Approximate method for calculating film cooling effectiveness of flat plate at injection ratios exceeding 3.0 13 p2166 A71-29369

Grid refinement technique generating sequences of approximate solutions to two-point variational problems defined on continuous fields

13 p2096 A71-29380

Approximate methods for optimal control problems solution in terms of functionals differentiable only with respect to direction

14 p2265 A71-29554

Approximate method for nonlinear ordinary differential equations with variable coefficients applied to cylinder oscillation and flexible ring deformation

14 p2324 A71-29881

Time dependent problems involving parabolic and hyperbolic differential equations, discussing formulation for approximate solution by Galerkin methods

14 p2265 A71-30294

Approximate calculation of turbulent boundary layers with adverse pressure gradient, using empirical auxiliary and momentum integral equations and skin friction formula

14 p2226 A71-30400

Nonlinear vibration of changing boundaries structures, approximating boundary values by perturbation technique

14 p2331 A71-30699

Comet and asteroid orbits tangential approximation, determining minimal distances and velocities as function of orbital elements

15 p2482 A71-31303

Finite difference and finite element methods for approximating elliptic boundary value problems solutions

15 p2440 A71-31346

Dirichlet problem for second order linear elliptic differential equations, considering convergence theory results for finite difference approximations

15 p2440 A71-31349

Sufficient stability of difference approximations for initial boundary value problems

15 p2441 A71-31354

Monograph on elliptic differential equations numerical solution covering approximations, relaxation, iterative, integral equation and variational methods, and applications to boundary value problems

15 p2441 A71-31508

Third approximation to Boltzmann equation for heat flux vector of gas of rigid spheres, using Brooker-Green technique

15 p2513 A71-31687

Approximate root locus method in S plane for sampled data systems, mapping constant frequency and constant damping ratio loci onto W plane

15 p2381 A71-31942

Rectangular plates with unidirectional stiffeners, calculating natural frequencies and mode shapes with approximate method

15 p2507 A71-32128

Approximation analysis for laminar two dimensional boundary layer behind plane shock wave moving over infinite flat plate

16 p2556 A71-32914

Stability conditions approximation for assessment of single parameters effect and in making choices

16 p2607 A71-33003

Structural reliability predictions using finite element stress program and partial derivative method involving finite approximations

16 p2583 A71-33294

Root-mean-square and uniform approximations of signals by Fourier and Haar series

16 p2550 A71-33720

Differentiable random processes, deriving approximate determination of correlation functions

17 p2777 A71-34348

Quasi-linear wave equations approximate solution construction by asymptotic methods

17 p2777 A71-34420

Book on asymptotic approximation in three dimensional thin and thick elastic shell theory including interior and Kirchhoff edge zone equations

17 p2822 A71-34770

Nonlinear unsteady heat conduction problems, investigating thermophysical property dependence on temperature and body coordinates by half space and approximate methods

17 p2838 A71-35115

Linear array antenna far field transient time response formulation, using concise vector field integral equations and generalization

17 p2717 A71-35584

Unique linear product approximations of continuous functions of several variables extended to general convex sets

17 p2768 A71-35682

Approximate method for hydrodynamic parameters of supersonic ideal-gas jet, considering isentropic region and theoretical boundary of underexpanded jet

18 p2902 A71-36114

Approximation solution for elliptic boundary value problem with nondifferentiable parameters, considering second order linear partial differential equations in two independent variables

18 p2942 A71-36817

Nonlinear diffraction of weak shock waves near rigid wall with sharp bend, obtaining approximate solution by matched asymptotic expansion method

19 p3043 A71-37100

Second approximation estimates of spatial-temporal signals parameters

19 p3015 A71-37260

Explicit procedure for discrete approximations to general nonlinear fixed-time continuous optimal control problems without intermediate trajectory constraints

19 p3037 A71-37556

Straight-line orbit approximation for plasma response function in system with periodic particle orbits

19 p3113 A71-37750

Radiation heat transfer volume interchange factors approximation for gases with nonuniform temperature, composition or pressure, comparing with exact numerical computations

[ASME PAPER 71-HT-19]

19 p3164 A71-37990

Fracture mechanics for design procedures, producing approximate expressions for stress intensity factors

19 p3158 A71-38019

First and second order density matrices calculation of pure state N fermion systems, using higher random phase approximation

19 p3107 A71-38054

Shallow lattice shell equations approximated by generalization of asymptotic theories for lattice-type disks and plates

19 p3158 A71-38151

Extremal problems approximation conditions in functional optimal value and elements set senses, applying to study of convergence in presence of constraints

19 p3088 A71-38413

Approximate solutions to quasi-linear n dimensional Helmholtz equation by asymptotic methods

19 p3088 A71-38477

Higher order approximation for normal vibration modes in nonlinear two degree of freedom systems

20 p3267 A71-38799

Van der Pol equation periodic solutions using approximation scheme for all Fourier amplitudes

20 p3254 A71-38800

Atmospheric wave dynamics in equatorial region, obtaining approximate solution with Coriolis force within perturbation theory

20 p3256 A71-39212

Spacecraft motion parameters maximum probability estimates, using approximate weight-matrix inversion techniques

20 p3294 A71-39583

BCD Cepheids observations, examining data with quasi-static interpretation approximation for gravity and stellar masses

21 p3441 A71-40065

Approximations to regular solutions by finding distribution function for bonds between unlike molecules, deriving Gibbs energy, enthalpy and entropy

21 p3474 A71-40234

Nonlinear autonomous systems transient response, obtaining approximate solutions by generalized averaging technique based on ultraspherical polynomial expansions

21 p3415 A71-40532

Discrete approximations for continuous fields in solid body nonlinear theory with differential and nonlinear equations replaced by algebraic and linear equations respectively

22 p3616 A71-42218

Galerkin approximation for boundary value problem finite difference scheme optimization by interpolation in Hilbert subspace

22 p3566 A71-42292

One dimensional two phase parabolic free interface /Stefan/ problem numerical solution, using method of lines to approximate partial differential equations at discrete time levels

22 p3575 A71-42294

Stability of finite difference approximation to mixed initial boundary value problems for linear parabolic system of equations

22 p3567 A71-42295

Muon lateral distribution fluctuations at mountain level, using approximate methods

22 p3595 A71-42659

Total particle number changes, evaluating approximate methods for transition effect calculation

22 p3550 A71-42671

Approximate solution for equation in linear normed space by error operator norm optimization, applying to elliptical cylinder type compact sets

23 p3699 A71-43574

Second order approximation algorithm for nonlinear noisy dynamical system state estimation from noise corrupted observations

23 p3656 A71-43854

Analytical function approximation of photofilms characteristic curves, noting validity for all exposure times

23 p3680 A71-44055

Nonlinear wave packet and modulated beam propagation description in approximate heuristic theories, considering chimeras as neoclassical approximation for equations solution

23 p3705 A71-44122

Approximate calculation of cut-off frequencies of H- and Pi-section waveguides using corrugated plane surface theory

23 p3655 A71-44323

Complex configuration shell theory, considering successive approximation method

24 p3876 A71-44403

Nonlinear stochastic systems approximate analysis based on multidimensional nonlinear transforms and distribution functions in Chebyshev-Hermite polynomials, determining dynamic accuracy

24 p3814 A71-44695

Crack theory application to problems with circular boundaries, solving singular integral equations by Aleksandrov-Libatskii approximation method

24 p3880 A71-44721

Rotationally inelastic molecular collisions in atom rigid rotor scattering, considering infinite order approximation of generalized phase shift treatment

24 p3850 A71-44921

APPROXIMATION METHODS

U APPROXIMATION

APSIDAL ANGLES

U ANGLES (GEOMETRY)

APSIDES

NT APOGEES

NT PERIGEEES

NT PERIHELIONS

APT (PICTURE TRANSMISSION)

U AUTOMATIC PICTURE TRANSMISSION

ATTITUDE

Psychopathological causes for French Air Force flying personnel inaptitude, considering motivational problems and age factor

22 p3500 A71-41575

AQUEOUS SOLUTIONS

Corrosion rate of Nb in aqueous solutions as function of temperature, using electrochemical potential measurements

03 p0442 A71-13363

Aqueous acid solution turbulent boundary layer characteristics during alkali solution injection through porous surface in presence of positive pressure gradient

04 p0576 A71-15614

Proton chemical exchanges effects in ammonium nitrate aqueous solution at varying exchange rate, noting geomagnetic field line configurations

10 p1644 A71-24458

Aqueous HCl solutions refractive index calculation from concentration dependence for Venus clouds composition

10 p1680 A71-25012

Diagnostic flow visualization, using chemiluminescent radiation in mixing region between aqueous luminol and potassium ferricyanide solutions

13 p2044 A71-27853

Compounds hydrolyzable to amino acids in aqueous extracts of Apollo 11 and 12 lunar fines, noting presence of glycine and alanine

18 p2855 A71-36230

Lithium iodate hexagonal and tetragonal form crystal growth conditions from aqueous solution and recorded refractivity

23 p3717 A71-43935

ARAGONITE

Calcite and aragonite high pressure Raman line spectra comparisons, testing structural identification theory

07 p1054 A71-19369

ARC CHAMBERS

Atmospheric pressure electrical and thermal conductivities on nitrogen and hydrogen up to 26,000 K from argon arc measurements

12 p1939 A71-27271

Thermal flux model of lithium plasma source at various temperatures and pressures, using arc channel model with conducting cross section

17 p2787 A71-34303

Manual pulsed and continuous arc TIG welding in controlled atmosphere chamber, examining joint quality

19 p3070 A71-38422

ARC DISCHARGES

Saha equilibrium deviations in wall stabilized rare gas arc plasmas under normal pressure, describing numerical method for temperature and density distributions evaluation

01 p0133 A71-10746

Arc discharge plasma response to turbulent gas flow covering wide range of Reynolds numbers measured with Langmuir probes

01 p0136 A71-11479

Cs doped Mg vapor arc discharge, determining electron mobility and diffusion cross section

02 p0286 A71-12180

High current free-burning arc characteristics in air at various pressures, examining dimensions from photographs

04 p0676 A71-15031

Dwell or dark pause measurements of shock tube driver high pressure arc discharge for various gases
05 p0788 A71-16578

Carbon dioxide arc discharge plasma emission spectral absolute intensities under atmospheric pressure, determining molecular band contributions
07 p1162 A71-19131

Diffuse and constricted Ar arc columns continuum emission determination from continuous spectra at 2700-4800 Å
07 p1172 A71-20377

Hollow cathode arc discharge parameters at active zone level, examining gas pressure and electron density
10 p1646 A71-23843

Highly underexpanded plasma jet structure with coaxially superimposed arc discharge, investigating stationary MHD normal shock in jet core (DFVLR-SONDDR-108)
10 p1650 A71-24600

Polymeric ablation materials testing in arc image furnace over various temperatures, pressures and thermal flux
11 p1790 A71-26045

Equations system describing parametric distribution of ionized plasma in thermionic converter gap, discussing current density effects on low voltage arc discharge
12 p1938 A71-27210

Low voltage arc discharge effects on ionized Cs plasma characteristics under high density current conditions
12 p1938 A71-27213

Steady state RF glow, abnormal glow and DC arc discharges in air at atmospheric pressure
12 p1881 A71-27274

Wall-stabilized arc column optimization from energy balance solutions, considering temperature and pressure effects on Ar arcs
12 p1939 A71-27275

Rotating spole in unstable pulsed MPD arc, noting rotation frequency and resemblance to plasma rotation [AIAA PAPER 69-234]
12 p1941 A71-27568

Plasma acceleration in injector with inductive energy storage, discussing arc discharge circuit opening time effect
13 p2108 A71-28856

Unstable collisional drift waves in high density ionized Li arc plasma, possibly causing anomalous losses and fluctuations
14 p2281 A71-30544

Knudsen arc firing potential in plane gas filled diode with hot cathode as function of electrode gap and atom concentration
15 p2455 A71-31739

Interelectrode gap position control of discharge in coaxial gas heater with arc rotated by magnetic field
17 p2676 A71-34309

Low voltage arc discharge development in cesium vapor with glowing spherical plasma cluster formation in electrode gap
19 p3109 A71-37136

Low pressure Cs vapor thermionic converter with lanthanum boride cathode, investigating arc conditions and I-V characteristics
19 p2999 A71-38254

Monograph on electron drift rate measurement in low pressure arc discharge using microwave dragging technique
19 p3116 A71-38549

Equations system describing parametric distribution of ionized plasma in thermionic converter gap, discussing current density effects on low voltage arc discharge
19 p3000 A71-38622

Low voltage arc discharge effects on ionized Cs plasma characteristics under high density current conditions
19 p3117 A71-38625

Controllable overhead arc spark gap discharger system design and characteristics for high power research, communication or industrial electrical installations
19 p3000 A71-38642

Plasma acceleration in inductive energy storage injector, discussing arc discharge circuit opening time effect
21 p3426 A71-41291

Free electron distribution function, atomic level population and ionization rate in low voltage arc near electrodes
23 p3709 A71-43266

Initial development period of low voltage arc discharge in cesium vapor leading to quasi-neutral plasma formation
23 p3710 A71-43269

High current pulsed arc in hydrogen plasma at 400 atm, showing instability with rising pressure and arc length
24 p3854 A71-44519

Dense discharge plasma temperature and ionization distributions in He, H and Ar, investigating pulsed arc emission dependence on current and pressure
24 p3855 A71-44520

ARC HEATING

High pressure arc heater data correlation for laminar and turbulent flows, examining radiation and thermal and electrical conduction effects
03 p0517 A71-13443

Stored arc heated air true temperature, flight and altitude simulation facility in Mach number 8 to 10 region for air breathing propulsion research [AIAA PAPER 71-254]
08 p1273 A71-21983

Water cooled channel flow test device for arc jet material ablation studies, simulating reentry environment of high energy turbulent boundary layer flow [AIAA PAPER 71-260]
08 p1273 A71-21987

Reentry environment simulation at vehicle stations away from stagnation point, using arc heater with supersonic nozzle duct
08 p1274 A71-21988

High enthalpy electric arc plasma jet heaters for simulating entries in hydrogen rich Jovian atmosphere [AIAA PAPER 71-263]
08 p1274 A71-21989

Arc heated duct facilities providing high temperature supersonic turbulent boundary layer flows over large samples for orbital logistic vehicle thermal protection tests
09 p1429 A71-23060

Continuous flow arc heater for reentry vehicle components ground testing, achieving combined high pressure and enthalpy
09 p1429 A71-23061

Arc-heated nonequilibrium arc expansion flow mass spectroscopic analysis, noting reservoir entropy effect [AIAA PAPER 71-621]
15 p2366 A71-31550

High enthalpy plasma jet wind tunnels, considering arc heaters and simulation range extension to higher adiabatic static pressures to avoid nonequilibrium expansion in nozzle
18 p2898 A71-36413

Plasma radiation effects in gas tube electric arc heating, obtaining temperature and heat flux profiles and I-V characteristics from energy transport mathematical model [ASME PAPER 71-HT-18]
19 p3164 A71-37989

Oxygen Schumann-Runge bands system from photographic and photoelectric spectra recording for arc jet heated air and oxygen-noble gas mixtures [AVERET-RR-354]
24 p3850 A71-45088

ARC JET ENGINES

Dynamic I-V characteristics of megawatt pulsed MPD-arc plasma thruster under various axial magnetic fields given for Ar and hydrogen propellants [AIAA PAPER 70-164]
05 p0796 A71-16574

Pulsed megawatt MPD arc thruster exhaust pressure measurements, discussing time dependence, peak dynamic and static pressures, etc [AIAA PAPER 71-196]
06 p0948 A71-18634

Low power MPD arc thruster performance with downstream cathode, using Xe propellant [AIAA PAPER 70-1084]
09 p1511 A71-22903

Closed form formula for plasma thrust from arc jets with self induced magnetic fields, predicting electrode erosion and entrainment
11 p1810 A71-25457

ARC LAMPS

High intensity vacuum UV solar simulator, using high pressure jet pinched xenon arc lamp with magnesium fluoride envelope
11 p1747 A71-26515

Graphite arc radiance temperature measurements with submillisecond resolution, using high speed photoelectric and photographic pyrometers
12 p1905 A71-26812

Krypton arc lamps of high conversion efficiency for optical pumping of neodymium lasers, setting lamp and Nd-YAG rod in prolate ellipsoidal cavity
16 p2585 A71-33140

Flat field condensing system for illuminating film projected on screen using Hg-Xe short arc lamp
18 p2918 A71-36071

Effective flashes by scintillating Xe arc flash tube, considering perception by human eye
22 p3499 A71-41492

ARC MELTING

Arc melted ingot high field superconductor, combining critical density and resistive critical field
10 p1655 A71-24042

Steel structural transformations under arc melting, cooling and electroslog remelting, noting delta ferrite precipitation with hot stage microscope
11 p1776 A71-25168

Metal droplet motion in mercury weld pool in tungsten arc, noting cause by Lorentz force and surface arc plasma jet
11 p1769 A71-25748

Arc melter using Pyrex pipe cross for controlled atmosphere chamber, incorporating Ar jet into electrode holder for dynamic flushing and rapid quenching
13 p2044 A71-28154

Comparative creep rupture properties of tungsten-rhenium consolidated by arc melting and powder metallurgy, considering rupture life and rupture ductility
15 p2427 A71-31818

Creep rupture properties of W-Re arc melted and powder metallurgy materials at 1650 and 2200 C as function of time, void and grain size
15 p2428 A71-31819

Arc melting consolidated W-Re-Hf-C alloy mechanical properties from tensile, creep and bend tests
20 p3247 A71-38766

ARC WELDING

NT GAS TUNGSTEN ARC WELDING

NT PLASMA ARC WELDING

Pressurized inert gas metal arc welding of Al, determining voltage, filler metal speed and chamber pressure effects by multiple regression analysis
02 p0255 A71-11709

Inconel 718 arc welding procedures and weldments mechanical properties, discussing impact strength and ductility improvement by heat treatment
02 p0255 A71-11711

High strength steel weldability with shielded and gas metal arc processes, discussing hardness, tensile, bend, impact and fatigue tests
04 p0603 A71-14922

Temperature gradients and cooling rates of Ti alloy sheet moving arc weld pools, discussing instantaneous solidification
05 p0757 A71-16212

Submerged arc welding process, observing arc motion and metal transfer with X ray high speed photography
06 p0905 A71-18090

Full penetration argon arc welding of titanium alloy plates without edge preparation
09 p1457 A71-23357

Arc weld metal carbon content effects on welded joints mechanical properties in Ni at low and high temperatures, noting crack reduction
09 p1479 A71-23422

Heat affected zone crack filling and weld metal-base metal interactions of high strength alloys in dissimilar gas arc welding
11 p1769 A71-25749

Vacuum arc welding stability in vaporized Mo cathode material as function of current and arc length, describing burner design for material replenishment
11 p1770 A71-25946

Single and multibeam holography application to size, trajectory, distribution, population density and velocity measurements of water and electric arc welding sprays droplets
14 p2243 A71-30299

Arc welding apparatus for chemically active high-melting metals in controlled superpure He atmosphere
14 p2253 A71-30486

Argon arc welding of Ti VT5-L alloy to Ti VT5-L and to wrought alloys OT4 and OT4-1, noting ductile, tough and stress raiser insensitive joints
19 p3070 A71-38421

Ti alloys semiautomatic pulsed arc MIG welding, showing increased productivity and reduced distortion
19 p3070 A71-38423

ARCHES

Nonlinearly elastic rings and arches under hydrostatic pressure, examining equilibrium with sixth order differential equations
02 p0325 A71-12125

Circular shallow prestressed arches with fixed ends, considering initial thrust effect on snap buckling
03 p0505 A71-13545

Circular arches static equilibrium path and dynamic response due to concentrated static and step loading using energy approach
04 p0668 A71-15184

Arches and rings in-plane natural vibration frequencies determination based on Newmark numerical integration method for beams
05 p0820 A71-15985

Critical dynamic snap-through of shallow clamped arches under concentrated loads, using finite difference method
06 p1004 A71-18615

Arbitrary solid cross section frames and arches shakedown analysis including axial forces effects on stress through reduction to linear programming
11 p1849 A71-25678

Heavy hinged nonshallow circular arches stability during buckling sideways with bifurcations in critical load deflection curves
14 p2324 A71-29885

Weight effect on large elastic deflection of thin arches, studying stability via nonlinear differential equation using elastical approach
14 p2330 A71-30686

Symmetric and asymmetric dynamic buckling of shallow elastic arches under uniform loads, using nonlinear finite difference method
14 p2331 A71-30695

Curved finite elements application to circular arches, examining convergence properties of various shape functions used in stress resultant calculations
21 p3474 A71-41425

Shallow two pinned sinusoidal arches stability under random symmetrically distributed lateral loads, observing deformation, buckling and critical value
22 p3612 A71-41429

ARCHITECTURE

- Nonlinear finite element analysis of sandwich arches elastic buckling, using straight beam-column type model 22 p3618 A71-42586
- Plastic buckling stability of hinged arches for perfect and imperfect structures with linear work hardening stress-strain behavior 23 p3776 A71-43372
- Discrete element finite deflection analysis of shallow arches using numerical method of potential energy minimization 24 p3879 A71-44636

ARCHITECTURE

- Architectural and environmental design tools for space system habitability, discussing work and living areas, hygienic facilities, etc [AIAA PAPER 71-879] 18 p2871 A71-36632

ARCS

- Optimal orbital transfer problem by numerical integration of Contensou singular alternating arcs, solving second order differential system followed by quadrature 05 p0812 A71-16730

ARCTIC OCEAN

- Arctic ocean pack ice terrain profiling by airborne laser altimeter and coincident photography, analyzing data for ice development stages interpretation 24 p3833 A71-44986

ARCTIC REGIONS

- Wintertime Arctic F region critical frequency secondary maxima, discussing UT control hypothesis 03 p0408 A71-13386
- Dark adaptation in humans under Arctic conditions, noting role of physiological disorders 08 p1242 A71-21958

- Noctilucent cloud formation from water vapor concentrations in mesosphere and lower thermosphere of arctic and midlatitude regions measured by rocket-borne RF mass spectrometers 14 p2232 A71-29957

- Corpuscular flux intensities in upper atmosphere from meteorological rocket measurements in polar arctic region, discussing altitude-time dependence 16 p2627 A71-33777

- Arctic polar region geomagnetic perturbations during IQSY, noting diurnal variations 19 p3059 A71-38399

- High Arctic latitude thermospheric helium and hydrogen rocket-borne mass spectrometric measurements, showing concentrations and winter bulge 20 p3222 A71-39698

- Mid- and high-latitude ionospheric radio wave transmission from spacecraft during solar cycle, considering latitudinal and longitudinal gradients and electron content change rate 20 p3197 A71-39715

AREA

- Planimetric aerial photographic block adjustment to ground control 08 p1288 A71-21257

AREND-ROLAND COMET

- Photometry of head and tail regions of comets Kosik, Akhmarov-Iurlov-Hassel, Arend-Roland and Mrkos by equidensity method, using Sabatier effect 15 p2484 A71-31668

ARGON

NT ARGON ISOTOPES

- Nitric oxide vibrational relaxation times in Ar from IR emission measurements at high temperature 02 p0287 A71-12495

- Carbon dioxide vibrational relaxation in Ar at high temperature, using shock tube method 02 p0287 A71-12496

- CW ion laser transitions in Ar, Kr and Xe, tabulating threshold data 03 p0438 A71-13896

- Neutral Ar and Ne resonance lines Stark broadening constant from Stark width-oscillator strength product 04 p0630 A71-15651

- SERT II electron bombardment thruster operation with Ar and Hg propellants [AIAA PAPER 71-157] 06 p0947 A71-18599

- Ar-oxygen mixture in undiluted nitrogen, discussing relaxation time change during adiabatic excitation and molecule oscillations deactivation 07 p1163 A71-19276

- Density distribution, heat transfer and drag measurements in rarefied Ar cylindrical Couette flow, comparing results with Navier-Stokes and Burnett equations solutions 07 p1093 A71-20286

- Thermionic converter output improvement by Ar injection at low Cs pressures, noting electron space charge neutralization 08 p1340 A71-21490

- Electron beam current density measurement using neutral Ar atoms electron impact excitation to metastable states 09 p1497 A71-22731

- Nitrogen-oxygen and nitrogen-argon mixtures viscosity, using oscillating disk viscometer to test corresponding states principle validity 09 p1546 A71-23010

- Thermal conductivity of Ar binary mixtures with He, N and Ne, using secondary concentric cylinders cell 09 p1547 A71-23463

- Plane shock wave formation in dense Ar, using molecular dynamics numerical technique 10 p1694 A71-23953

- Ar condensation onset location in supersonic nozzles for nuclear space propulsion systems, using supercooled vapor pressure measurements beyond saturation point 10 p1593 A71-24328

- Gas rich meteorites and carbonaceous chondrites with trapped argon, noting isotopic correlation with neon 10 p1680 A71-24988

- Argon ionization and recombination in solar corona at electron temperatures of 2.0-4.5 times ten to sixth power K 11 p1832 A71-26180

- Ar, N and Ne partial pressure tolerance in dogs, plotting saturation curves 13 p2005 A71-28038

- Ar-oxygen mixture in undiluted nitrogen, discussing relaxation time change during adiabatic excitation and molecule oscillations deactivation 14 p2276 A71-30170

- Thermionic converter output improvement by Ar injection at low Cs pressures 14 p2182 A71-30679

- Molecular rotational excitation during CO ion-Ar interactions by ion beam collision spectroscopy, observing energy loss spectra 15 p2452 A71-32551

- Beam foil excited Ar spectrum between 500 and 1000 Å, tabulating lines with ionization stages based on line intensity variation with beam energy 15 p2368 A71-32601

- Multiply ionized Ar excited valency and inner shell transitions, investigating emission spectrum and energy levels 15 p2368 A71-32747

- Shock tube measurements of vibration-vibration energy exchange probability in nitrogen-carbon monoxide-argon mixtures 16 p2613 A71-32896

- Ionizing shocks in argon produced by pressure driven shock tube, measuring velocity and ionization within and behind nozzle 16 p2616 A71-32904

- Nonequilibrium corner expansion flow of ionized argon induced by normal shock waves in hypervelocity shock tube 16 p2555 A71-32905

- Argon gas ionization behind reflected shock wave front investigation by double probe method with HF multistep pulse voltage 16 p2576 A71-32911

- Temperature stabilization with self controlled water and radiation cooled heat pipes using argon in addition to K heat transfer medium 16 p2663 A71-34039

- Cesium vapor diffusion condensations from laminar argon flows in tubes and turbulent movement on banks, considering boundary layer mist formation effect 17 p2785 A71-34206

- German monograph on spark discharges behavior in nitrogen, carbon dioxide and argon at excess pressure covering Toepfer, Weizel-Rompe and Braginskii laws applicability 17 p2779 A71-34799

- Potassium-argon age determination for shock-metamorphosed anorthositic of Manicouagan-Mushalagan Lakes structure 19 p3049 A71-37657

- K-Ar dating of shock metamorphosed rocks from Brent impact crater /Ontario, Canada/ 19 p3050 A71-37658

- Translational freezing in free expanding jets of Ar, nitrogen and carbon dioxide from molecular beam intensity measurements, deriving perpendicular temperature 19 p3045 A71-37882

- Thermal conductivity anomalous behavior prediction for carbon dioxide, argon, nitrogen, oxygen and methane in critical region [ASME PAPER 71-HT-28] 19 p3165 A71-37998

- Hydrogen bromide effect on argon diluted propane-oxygen flame structure 19 p3167 A71-38100

- Argon arc welding of Ti VT5-L alloy to Ti VT5-L and to wrought alloys OT4 and OT4-1, noting ductile, tough and stress raiser insensitive joints 19 p3070 A71-38421

- Transition probabilities for Ar I, using Coulomb approximation values of radial wave function integral 20 p3271 A71-38776

- Fission track and K-Ar ages of coexisting minerals in drill core from heat-flow boreholes in western central Sierra Nevada batholith 21 p3374 A71-40649

- Thermal conductivity determination of Ar at extremely high temperatures, using temporal development of thermal boundary layer at shock tube wall 22 p3619 A71-41523

- Nitrogen, argon and helium viscosity measurements, obtaining density expansion by statistical analysis 22 p3621 A71-42369

- Ar, Kr and Xe emanation during stepwise heating of lunar rocks under slow neutron irradiation in pile, using mass spectroscopy 23 p3754 A71-43726

- Glass rods loading tests after exposure to hydrogen, nitrogen and argon under high pressure, noting strength improvement by Ar impregnation 24 p3841 A71-44868

- Visible and near UV spectra of vacuum Ar, Kr and Xe microwave discharge lamps with magnesium fluoride windows 24 p3849 A71-45211

ARGON ISOTOPES

- Ar 40/Ar 39 age determination of Apollo 12 lunar rock 12013 fragments 03 p0494 A71-14220

- K-Ar age measurement by optimizing integrated neutron flux and sample size parameters, using graphical method 10 p1601 A71-24411

- Cosmic rays produced He, Ne and Ar isotope concentrations in iron meteorite separated phases, using Rudaust spallation model 10 p1676 A71-24506

- Cosmic ray intensity gradient measurement from Lost City meteorite Ar 37/Ar 39 ratio 15 p2479 A71-32361

- Lost City meteorite Ar isotopes radioactivity measurements, considering cosmic ray flux radial gradient variations during meteoroid orbit 15 p2479 A71-32364

- Argon isotopes retention ages of crystalline lunar rocks 12002, 12051 and 12065 from lunar maria, using neutron activation and stepwise heating experiments 16 p2633 A71-33347

- K-Ar isotope ages of whole sample and feldspar concentrate from apollo 11 lunar rock 10003 16 p2633 A71-33349

- He, Ne and Ar isotopic distribution and origin in Apollo 12 lunar samples, considering solar wind implantation 17 p2695 A71-35030

- Apollo 14 Fra Mauro rock fragment samples, determining Ar 40/Ar 39 ages 18 p2961 A71-35945

- Apollo 14 flight Fra Mauro crystalline rocks age measurement, using Ar 40/39 ratio method 22 p3598 A71-41838

- Tritium and argon radioactivities and depth variations in Apollo 12 rocks, discussing solar flare and cosmic ray exposure ages 23 p3755 A71-43737

ARGON LASERS

- Argon ion CW lasers, discussing design, inverse population, plasma, radiative transition probabilities, pumping, frequency spectra and active medium 01 p0092 A71-10145

- Pulsed Ar ion laser plasma electron density and temperature, discussing Tonks-Langmuir free fall model validity 01 p0096 A71-11623

- High power argon laser single frequency emission, discussing dividing mirror reflection coefficient and degree of gain saturation 03 p0435 A71-13504

- Argon ion laser plasma tube anodic coherent oscillations and noise suppression, using secondary discharge between anode and auxiliary cathode 06 p0906 A71-17306

- Chlorine dioxide induced fluorescence spectra, using argon ion laser 08 p1300 A71-20667

- Exposure time and power effects of CW Ar laser damage to rabbit iris, comparing with pulsed ruby laser effects 10 p1572 A71-25076

- Ionized argon laser optimum performance, comparing master oscillator power amplifier configuration to simple oscillator 11 p1772 A71-25141

- Glow discharge, ion and excited state properties of laser plasmas, including CW conditions for argon 14 p2253 A71-29542

- Combination light scattering in liquids, single crystal and crystal powders, employing long lived argon laser with internal mirrors and large diameter capillaries 14 p2255 A71-30585

- Argon ion laser mode locking in UV lines with intracavity acousto-optic modulator, describing pulse duration and average power 15 p2423 A71-32588

- Long term single frequency stabilization of composite cavity argon laser by mirror separation, using reference He-Ne laser 15 p2423 A71-32611

- Luminous pulse production by internally modulated Ar laser, observing overall modes amplitudes
16 p2587 A71-33381
- Automatic argon ion laser tracking system for high speed rocket sleds, describing apparatus configuration and error correcting devices
18 p2883 A71-36908
- Ar ion laser plasma spectral lines widths and shifts at various pressures and current densities, noting role of ion-neutral charge exchange collisions
18 p2932 A71-37007
- Pulsed argon ion laser data, presenting excitation mechanisms and time resolved gain measurements
21 p3392 A71-40625
- Holographic optical memory breadboard development system based on CW Ar ion laser, discussing component operating, power requirement and cost problems
21 p3380 A71-40922
- Fluorescence of iodine molecule excited at 5017 and 5145 Å by ionized Ar laser, observing magnetic depolarization/Hanle effect/
22 p3555 A71-41623
- Axially constructed Ar laser with segmented graphite line and pumping tube, discussing continuous operation power outputs and electric discharge current optimal magnetic field strength
22 p3556 A71-41704
- ARGON PLASMA**
- Sulfur hexafluoride effects on equilibrium electron concentrations in air and argon plasmas, discussing earth reentry simulation applications
01 p0133 A71-10957
- Shock generated Ar plasma emission spectrum intensity measurements, describing fast-response spectrometer sensitivity calibration method
01 p0134 A71-10997
- Shock tube generated Ar plasma electric conductivity augmentation by electrical discharge through supersonic plasma flow in Faraday tube
01 p0134 A71-10998
- Voltage distribution measurements between electrodes of MHD Faraday nozzle across ionized Ar plasma supersonic flow
01 p0136 A71-11373
- Atomic and ion temperatures in Ar plasma low pressure discharge in metallic tubes with conducting walls
02 p0259 A71-11931
- Tungsten cathode current partitioning in dense Ar plasma, noting electron emitter work function reduction due to ion space charge field
02 p0289 A71-11940
- Nonequilibrium Ar-Cs plasma under rectangular pulse overvoltage, analyzing ionization and recombination kinetics
02 p0289 A71-12177
- Argon plasma column inductive discharge parameters at atmospheric pressure from radial temperature distribution measurements
02 p0290 A71-12181
- Fast electron elastic and inelastic scattering Ar plasma at large Rutherford cross section, obtaining charged particle density
02 p0291 A71-12317
- High Mach number collisionless shock waves in low density argon plasma, measuring electron heating and shock thickness
04 p0631 A71-14685
- Free radical effect on exchange reaction between ammonia and deuterium in high diluted argon shock tube
04 p0548 A71-14698
- Shock-reflection interferometry of electron and mass density profiles of ionized argon end wall thermal layer
04 p0674 A71-14701
- Argon plasma jet local thermodynamic equilibrium at various electron densities, examining Boltzmann excitation and ionization temperatures
04 p0633 A71-14902
- Energy deposition by MHD into supersonic argon plasma flow in shock tube
05 p0787 A71-16537
- Argon ion laser plasma tube anodic coherent oscillations and noise suppression, using secondary discharge between anode and auxiliary cathode
06 p0906 A71-17306
- Thermal Ar plasma with gas additives as standard intensity light source of optically thick spectral lines, using interpolation and Kirchhoff-Planck function
07 p1168 A71-19323
- One dimensional steady supersonic motion of partially ionized two temperature argon-cesium plasma in disk type Hall MHD generator channel
07 p1023 A71-19728
- Wakes in Ar plasma beam, discussing obstacle geometry effects and plasma drift velocity
07 p1169 A71-19805
- Diffuse and constricted Ar arc columns continuum emission determination from continuous spectra at 2700-4800 Å
07 p1172 A71-20377
- High microwave power for studying interactions in high concentration linear Ar discharge plasma waveguide in magnetic field
08 p1339 A71-21479
- HF wave absorption in Ar plasma, observing production in open magnetic trap
08 p1339 A71-21481
- MHD generator with Ar-K plasma, examining electrical insulation behavior
08 p1237 A71-21930
- High pressure laser spark ignition in argon by extraneous plasma source
09 p1460 A71-22235
- Thermal expansion of gas breakdown plasma in argon under heating by high voltage transient pumped carbon dioxide laser
09 p1463 A71-22761
- Brightness temperature measurement in high pressure Ar plasma by comparing reference lamp to plasma radiation intensities
10 p1646 A71-23833
- Thermal conditions in asymptotic region of atmospheric pressure Ar arc plasma, considering nonequilibrium ionization due to ambipolar diffusion
10 p1654 A71-24971
- Preionization and velocity effects in MHD channels containing potassium seeded argon plasma at atmospheric pressure
11 p1804 A71-25488
- Equilibrium compositions and thermodynamic properties tabulated for argon-oxygen plasmas at 0.01 to 10 atm and up to 35,000 K
12 p1986 A71-27187
- Mixed plasmas transport properties at one atmosphere and 5000-35,000 K, considering helium-nitrogen, argon-nitrogen and xenon-nitrogen plasmas
12 p1986 A71-27188
- Wall-stabilized arc column optimization from energy balance solutions, considering temperature and pressure effects on Ar arcs
12 p1939 A71-27275
- Argon plasma jet velocity distribution at MHD channel exit with magnetic quadrupole, using calorimetric plasma velocity measurements and Doppler shift observations
14 p2278 A71-29611
- Thermal load capacity and nozzle shape for guiding and constricting high current plasmas from electric arc data, using Ar as discharge gas
14 p2279 A71-29851
- High microwave power for studying interactions in high density linear Ar discharge plasma waveguide in magnetic field
14 p2282 A71-30666
- Limiting frequency for Ar plasma absorption of HF waves, observing plasma production in open magnetic mirror configuration
14 p2282 A71-30668
- Nonequilibrium Ar-Cs plasma under rectangular pulse overvoltage, analyzing ionization and recombination kinetics
15 p2454 A71-31486
- Argon plasma column inductive discharge parameters at atmospheric pressure from radial temperature distribution measurements
15 p2454 A71-31489
- Viscosity of dissociating oxygen, carbon-air and argon plasmas at high temperature range, including error estimates and expansion up to 12,000 K
15 p2512 A71-31502
- Supersonic arc-heated Ar flow, measuring heavy particle temperature and velocity and electron density profiles by pressure scanned Fabry-Perot interferometer
[AIAA PAPER 71-589] 15 p2454 A71-31534
- Nonequilibrium effects in Ar free jet plasma, using cooled Langmuir probe for electron temperature and ion density measurements through shock wave in front of blunt body
[AIAA PAPER 71-591] 15 p2454 A71-31536
- Ar arc plasma thermochemical nonequilibrium, using finite difference techniques for nonlinear integrodifferential equations
[AIAA PAPER 71-593] 15 p2455 A71-31538
- Steady and unsteady modes of electric arc combustion in Ar and Ar-Cs flows produced by plasma accelerator in closed glass contour
15 p2457 A71-32269
- Resonance radiation field of positive column of low current electric arc burning in nonequilibrium Ar plasma with admixture of K, using optical probe
15 p2457 A71-32270
- Electric arc burning in contracted Ar plasma between two plates, calculating normal current density and I-V characteristic
15 p2457 A71-32271
- Electrical breakdown in transverse magnetic field and Ar plasma flow in pressure range 0.2-1400 mm Hg and velocity range 0-50,000 cm/sec
15 p2457 A71-32272
- Steady state of nonequilibrium Ar-Cs plasma in electric field, attributing instability to plasma radiation effect
15 p2457 A71-32273
- Fast argon plasma flow interaction with strong magnetic fields, describing ionization relaxation phenomena behind magnetically reflected shock fronts
16 p2615 A71-32898
- Ionization profiles of shock heated argon with impurities, using microwave and pulsed Langmuir probe measurements
16 p2616 A71-32912
- Transverse magnetic field effects on Ar cross flow arc in constant velocity mainstream
17 p2788 A71-34868
- Thermal electrodeless plasma generation below RF range through magnetic induction heating, applying to argon glow and arc discharges
17 p2788 A71-34869
- Electrical insulation behavior of MHD generator channel having Ar-K plasma, noting temperature dependence of surface conductivity
17 p2789 A71-35274
- Langmuir probe measurement of ionization density of Ar plasma jet, suggesting electron-ion recombination in probe vicinity
17 p2789 A71-35338
- Externally excited moving striations measurement in low pressure Ar discharge, comparing with ion acoustic wave propagation derivation from model
18 p2948 A71-35859
- Argon plasma electron temperature by laser absorption and electron density measurements
19 p3110 A71-37406
- Gas and electron temperature and thermal nonequilibrium in argon plasma jet from electrodeless induction discharge
19 p3111 A71-37578
- Radial temperature profiles of long induction discharge in argon at atmospheric pressure
19 p3111 A71-37579
- Diagnostic He-Ne laser interferometer for measuring electron concentration in cross section of argon plasma jet
19 p3073 A71-37786
- RF magnetic field radial distribution measurement in thermal argon induction plasma flame
20 p3273 A71-38841
- High pressure laser spark ignition in argon by external plasma source
21 p3394 A71-41115
- Diagnostics of Ar free jet expansion from high pressure inductive arc source into low density wind tunnel, observing background gas effects
22 p3583 A71-42048
- Operating characteristics of arc plasma generator with film and water cooling protected anode
22 p3484 A71-42784
- Boltzmann kinetic equation with electron-ion collision coefficients for isothermal weakly ionized cesium-argon plasma, using nodal point method
23 p3709 A71-43267
- Dense low temperature Ar and Hg plasmas, observing correlation between electrical conductivity and optical emission
23 p3712 A71-43914
- Monochromatic absorption coefficients determination for Ar heated in wall-stabilized arc at high temperatures and pressures
23 p3712 A71-43915
- Carbon dioxide additions effect on electron temperature relaxation and electron concentration distribution in expanding supersonic flow of low temperature Ar plasma
23 p3713 A71-44065
- Local thermodynamic equilibrium deviation theory and application in low density Ar plasma, noting difference in Langmuir probe and spectroscopic electron temperature measurements
23 p3714 A71-44154
- Ar-K and He-R plasma conductivity measurement at atmospheric pressure from equilibrium to nonequilibrium conditions, using electrostatic probes
23 p3714 A71-44275
- ARGON 36**
- U ARGON ISOTOPES**
- ARGON 40**
- U ARGON ISOTOPES**
- ARGUMENTS [MATHEMATICS]**
- U INDEPENDENT VARIABLES**
- ARIEL SATELLITES**
- NT ARIEL 1 SATELLITE**
- NT ARIEL 2 SATELLITE**
- NT ARIEL 3 SATELLITE**
- ARIEL 1 SATELLITE**
- Ionization crests of equatorial anomaly at magnetic L values from Ariel 2 satellite electron probe measurements
11 p1754 A71-25603
- ARIEL 2 SATELLITE**
- Low latitude air density correlation to magnetic disturbance deduced from Ariel 2 satellite spin rate changes
10 p1602 A71-24552

ARIEL 3 SATELLITE

Lumped fifteenth order spherical harmonics in geopotential from Ariel 3 satellite orbital inclination corrected for lunar-solar oscillatory perturbations
16 p2563 A71-33387

ARIES CONSTITUTION

Aries-Taurus region as soft X ray source, determining energy flux and source
14 p2301 A71-30426

ARIP (IMPACT PREDICTION)

U COMPUTERIZED SIMULATION
U IMPACT PREDICTION

ARITHMETIC

NT DOUBLE PRECISION ARITHMETIC
NT FLOATING POINT ARITHMETIC

ARITHMETIC AND LOGIC UNITS

Central data processing unit based on short-rod memories of coated Be-Cu alloy, discussing arithmetic-logic unit operation
01 p0049 A71-10263

Analog recursive computer with serial digital program for arithmetic unit and storage system control
12 p1884 A71-27150

Distributed Fetch sequencing computer technique, discussing system speeds, throughput rates, bus requirement and arithmetic processor demand reduction and task performing capability
17 p2712 A71-35779

Low power nonpulsating arithmetic unit of 16 bit integer numbers for spaceborne applications, using module printed circuit cards
18 p2886 A71-36570

Design method for high speed economical arithmetic units of digital computers, describing functional logic circuits
24 p3806 A71-44396

ARM (ANATOMY)

NT FOREARM

Proprioception role in perception of arm bending and extension during weightlessness and accelerations in aircraft flight along parabolic trajectory
01 p0014 A71-11143

Methodological features of programmed control of human upper extremities movements, using six-channel bioelectric system
17 p2692 A71-35170

ARMATURES

Nonlinear vector potential analysis of aerospace homopolar inductor alternators, considering fully armature currents
03 p0353 A71-13053

ARMED FORCES

NT ARMED FORCES (FOREIGN)

NT ARMED FORCES (UNITED STATES)

NT NAVY

ARMED FORCES (FOREIGN)

British Mediator program for joint civil/military ATC system, discussing air defense relationships [CASIPAPER 72/16]
19 p3100 A71-37603

ARMED FORCES (UNITED STATES)

Satellite design developments by U.S. Navy
02 p0336 A71-11980

Mortality in survivable or partially survivable U.S. Army aircraft accidents, observing death relationship to aircraft duty and seat location and type
23 p3640 A71-44248

ARMOR

Opaque ceramic armor materials for lightweight personnel and equipment ballistic protection applications, discussing mechanical properties and fabrication techniques
09 p1484 A71-23689

Armored cockpit for attack aircraft combat effectiveness, including mold line tumbling plates, terminal ballistic kinematics and integral structural armor [ALAA PAPER 71-778]
17 p2675 A71-35530

AROD (RANGE-ORBIT DETERMINATION)

U AIRBORNE RANGE AND ORBIT DETERMINATION

AROMATIC COMPOUNDS

Organic compounds oxidation inhibition by polycyclic aromatic hydrocarbons, analyzing peroxide radicals charge transfer complex stability
05 p0716 A71-16382

Type III carbonaceous chondrite Murchison meteorite, obtaining amino acids, aliphatic and aromatic hydrocarbons from specimen
09 p1393 A71-22983

Polynuclear aromatic hydrocarbons in Murchison meteorite, determining distribution by gas chromatography and mass spectrometry
17 p2799 A71-34503

AROUSAL

Performance decrement during bimodal vigilance task, discussing arousal and selective attention constructs
04 p0541 A71-14741

Electroencephalographic and motor effects of electrically stimulated reinforcing and negative subcortical structures in sleeping cats
06 p0852 A71-17669

Marmot ketone bodies concentration during activity, deep hibernation and early arousal, discussing increased oxidative metabolism effects
13 p2014 A71-29125

Visual evoked brain potential amplitude and detection efficiency relationship, discriminating between arousal and attention effects
17 p2682 A71-35114

Arousal and activation in nonspecific reticulo-thalamo-cortical systems due to underlying emotion expressed through cortical, visceral and somatomotor channels
21 p3330 A71-40247

ARRAYS

NT ANTENNA ARRAYS

NT ENDFIRE ARRAYS

NT LINEAR ARRAYS

NT PHASED ARRAYS

NT STEERABLE ANTENNAS

NT SYNTHETIC ARRAYS

NT TURNSTILE ANTENNAS

NT YAGI ANTENNAS

Silicon solar cell lightweight integrated array for large arrays, discussing deployment and orientation mechanisms, ribbon coverglass technique and cost estimates
05 p0703 A71-16093

Nonredundant two dimensional square and hexagonal point arrays with optimal autocorrelative properties, considering high resolution imaging systems in holography
07 p1111 A71-19490

Inverse diffraction of plane wave by periodic and doubly periodic arrays, calculating velocity potential and pressure distributions for Neumann and Dirichlet problems
13 p2027 A71-27905

Electronically scanned circular array elements number in receiver design, discussing gain distribution
14 p2206 A71-31072

Diffraction properties of three dimensional asymmetric arrays for reflected and transmitted H- and E-polarized waves
17 p2698 A71-34266

Signed binary numbers multiplication algorithm, describing cellular arrays for twos-complements multiplication method
18 p2894 A71-36831

Cellular array for multiplication and division of two binary numbers, discussing implementation with transistor-transistor logic integrated circuits
18 p2894 A71-36833

Imaging with low redundancy arrays, noting holography role in image processing
22 p3538 A71-41736

ARRESTERS

Civil aircraft arresting on runway overshoots, describing safe deceleration method by use of soft ground arresters
17 p2674 A71-35210

ARRESTING GEAR

Space shuttle vehicles landing with emergency arrestment aids, describing tailhook/cable, net and landing gear/cable engagement methods
18 p2900 A71-36488

ARRHYTHMIA

Antiarrhythmic effects of detergents on digitalis induced arrhythmia in dogs
01 p0010 A71-10392

Computer differential analysis of cardiac rhythm irregularities involving comparison of EKG RR intervals
01 p0025 A71-11154

Antiarrhythmic drugs choice based on excitable tissues biophysics, considering contrast between cardiac muscle and nerve
02 p0201 A71-12419

Cardiac impulse conduction in depressed canine Purkinje fibers, discussing experimental results in connection with reentrant arrhythmias
07 p1041 A71-19638

Orbiting Biosatellite 3 monkey environmental and physiological parameters circadian rhythms, investigating desynchronization or arrhythmia
09 p1395 A71-23241

Cardiac arrhythmias simulated by concealed bundle of His extrasystoles in open chest intact dog hearts
09 p1395 A71-23256

Cardiac arrest or arrhythmia due to coronary arteriosclerosis in young aviator, examining causes, prevention and predictive measures
23 p3637 A71-44250

ARSENATES

High purity lithium hexafluoroarsenate preparation methods and hexafluoroarsenic acid properties
23 p3642 A71-43540

ARSENIC

Arsenic first spark line spectra using high resolution grating spectrograph and Fabry-Perot interferometer
05 p0717 A71-16910

Sb and As base chalcogenide diode structures, determining switching and memory characteristics
13 p2110 A71-27956

Glassy antimony and arsenic chalcogenide diode structures, determining switching and memory characteristics
21 p3435 A71-41343

ARSENIC COMPOUNDS

NT ARSENATES

NT ARSENIDES

NT GALLIUM ARSENIDES

NT INDIUM ARSENIDES

Hologram storage in evaporated thin films of arsenic trisulfides, considering simple diffraction gratings and complex data masks
22 p3542 A71-41811

High purity lithium hexafluoroarsenate preparation methods and hexafluoroarsenic acid properties
23 p3642 A71-43540

ARSENIDES

NT GALLIUM ARSENIDES

NT INDIUM ARSENIDES

Gd-As direct synthesis from components elements and single crystal growth using chemical transport reactions
01 p0138 A71-10404

Hall electron mobility in cadmium arsenide as function of concentration and temperature
01 p0141 A71-11466

Cadmium arsenide alpha and beta phases Hall constant temperature dependence, studying photoelectric and optical properties
07 p1177 A71-19279

Zinc arsenide-zinc telluride ternary system phase diagram investigation by X ray, differential thermal and microstructural analyses and microhardness measurements
16 p2621 A71-33564

Switching effects in diode structure formed by two tungsten point contacts on glassy cadmium germanium arsenide surface
21 p3358 A71-41207

Coherent stimulated recombination radiation emission by p-type cadmium silicon arsenide single crystals in liquid nitrogen cryostat under various pumping levels
21 p3431 A71-41229

Cadmium-tin-arsenide conduction and valence band structure parameter refinement from Faraday effect and absorption spectra of single crystals in polarized light
21 p3433 A71-41319

N-type cadmium germanium arsenide single crystal semiconductor electron and hole effective mass determination from thermoelectric power measurement
21 p3436 A71-41350

Nonlinear optical properties of phase matchable crystal cadmium germanium arsenide for carbon dioxide laser second harmonic generation and parametric interactions
23 p3714 A71-42960

ARTERIES

NT AORTA

Arterial blood pressure changes due to bilateral carotid occlusion or electrical heart pacing, considering effects on kidney blood flow and circumference in dogs
01 p0008 A71-10074

Hydrogen exchange between pial arteries for measuring local cerebral blood flow quantitatively in anesthetized cats
01 p0008 A71-10075

Human blood gases continuous measurement in vivo by mass spectroscopy, considering arterial nitrogen washout and cerebral blood flow determination
01 p0021 A71-10237

Artery wall elasticity relation to Korotkoff sound wave frequency by upper arm blood pressure measurement, using cylindrical rubber tubes and canine specimens
01 p0009 A71-10240

Human coronary arteries fibrinolytic activity, considering histochemical and quantitative methods for arteriosclerosis and occlusion investigations
02 p0200 A71-12416

Adrenal gland blood flow and arterial pressure determination under stochastic pulse excitation of anesthetized dogs centripetal and centrifugal nerves, using analog correlator
03 p0357 A71-12994

Intraluminal pressure effect on stress concentration and deformation of arterial wall in relation to atherosclerosis, using finite element method [ASME PAPER 70-WA/BHF-15]
03 p0373 A71-14113

Local cooling effects on responsiveness of muscular and cutaneous arteries and veins in dogs, noting blood flow redistribution
04 p0538 A71-15091

Simultaneous comparison and calibration of ultrasonic Doppler telemetry and electromagnetic flowmeters implanted on peripheral arteries of dogs
04 p0545 A71-15164

Catheter-flush system for continuous monitoring of central arterial pulse waveform and pressure
04 p0545 A71-15165

Human alveolar-arterial oxygen pressure differences, investigating inert gas effects
04 p0540 A71-15576

Main pulmonary artery velocity profiles in dogs and man, using thin-film resistance anemometer
05 p0706 A71-16324

Middle cerebral artery occlusion effect on cortical blood flow, tissue oxygen pressure and acid base equilibrium in animals under extended ligations
05 p0708 A71-16617

Arterial glucose and lactate levels and heart rate in human males during intermittent running, discussing anaerobic capacity and antioxidative glycolytic processes
05 p0708 A71-16619

Arterial oxygen, carbon dioxide tension, pH and lactic acid changes during rapid descent from altitude to sea level in deep mine
07 p1052 A71-20334

Physiological characteristics in llamas pulmonary circulation at sea level and changes after 5 and 10 weeks at 3,420 m above sea level, noting arterial hypertension
08 p1237 A71-20678

Premature pulmonary valve closure due to severe mitral insufficiency by left atrial V wave retrograde transmission
08 p1240 A71-21888

Cardiac output variations in regulation of arterial oxygen transport during hypoxia
08 p1241 A71-21939

Arterial circulatory system parameter identification from diastolic blood pressure curves by digital filter techniques
09 p1398 A71-22254

Pulmonary arterial blood flow regulation by hydrostatic pressure in low resistance circulatory system
10 p1561 A71-24127

Pulmonary arterial system impedance and transmission properties, noting hypoxia and serotonin infusion vasoconstrictor effects
11 p1719 A71-25929

Large amplitude wave propagation in arteries, deriving aorta mathematical model consistent with heart pressure and flow pulses and wavefront velocity
12 p1870 A71-26937

Arterial tonometry for atraumatic measurement of arterial blood pressure, considering transient effects of drugs or physiological interventions
12 p1874 A71-27140

Hypertension and heart or arterial disease relationships, discussing cause and effect mechanisms in coronary diseases
13 p2004 A71-27866

Alveolar and arterial carbon dioxide partial pressure during rebreathing experiments at rest
13 p2007 A71-28435

High altitude pulmonary edema syndrome, investigating increased alveolar-arterial oxygen gradients of humans during treadmill exercise
14 p2184 A71-30279

Systemic arterial blood pressure response to chronic high altitude and hypoxia effects
14 p2184 A71-30280

Alveolar-arterial oxygen pressure gradient derivation as sum of shunt, ventilation/perfusion inequalities and membrane and airway diffusions
15 p2363 A71-31444

Coronary arteries congenital lesions, discussing major, minor and secondary anomalies relationship to cardiac malformations
15 p2361 A71-32553

Arterial baroreceptor reflex action in rabbits, noting central noradrenergic neuron participation
16 p2528 A71-33075

Arterioles and corneo-scleral shell structural response under various loading conditions, using finite element method for mechanical and hydrostatic stress distribution
16 p2528 A71-33099

Validity and reproducibility of cardiac output determination by thermodilution, using dual thermistor catheter introduced in pulmonary artery
16 p2531 A71-33366

DNA replication in intercostal artery muscle cells during vascular wall physiological regeneration, noting cytophotometric study of polyploidization
16 p2531 A71-33467

Tympanic-cavity nerve plexus electric stimulation effects on cerebral blood circulation and overall arterial pressure in dogs and cats
16 p2533 A71-34108

Nonlinear analysis of arterial flow pulses and shock waves, simulating aortic insufficiency under pathological conditions by mathematical model
16 p2538 A71-34145

Sympathetic response in renal and splanchnic nerves to induced fall and rise of arterial blood pressure in anesthetized rabbits, investigating baroreceptor reflex effect
17 p2685 A71-35367

Patients with selective cine coronary arteriography, statistically correlating vectorcardiographic diagnoses of myocardial infarcts with changes in arteries
18 p2854 A71-36139

Sudden death during physical exertion due to congenital anomalies of coronary arteries
18 p2855 A71-36217

Dynamic characteristics of arterial oxygen tension response to supine submaximal leg exercise in man from harmonic analysis
18 p2856 A71-36239

Dynamic characteristics of arterial blood pressure responses to sinusoidal work load in man from harmonic analysis
18 p2856 A71-36240

Cardiovascular system mathematical model for evaluating system parameters effects on circulatory indices including minute volume and arterial tension
19 p3007 A71-37777

Alveolar-arterial oxygen pressure difference during controlled hyperventilation and posthyperventilatory phase
19 p3003 A71-38200

Diffusion component of alveolar-arterial oxygen pressure differences in man at rest and during exercise
19 p3009 A71-38556

Inspired oxygen concentrations effects on arterial and mixed venous pH, carbon dioxide uptake and oxygen partial pressure in normal subjects
20 p3189 A71-39442

Stagnant asphyxia in cat carotid body during abrupt blood pressure drop by simultaneous carotid artery clamping and tap opening
20 p3190 A71-39443

Human blood pressure in brachial artery during spontaneous night sleep, recording EEG, EKG and horizontal eye movements
21 p3329 A71-40185

Age dependent changes in free amino acid content and composition of cerebral and carotid arteries in man and dog
21 p3338 A71-41070

Oxygen tension distribution in cats glomus caroticum under influence of varying arterial oxygen partial pressure, using platinum microelectrodes
24 p3796 A71-44562

Dimensionless parameters effect on divided blood flow characteristics in large arterial bifurcation
24 p3801 A71-44622

ARTERIOSCLEROSIS
Coronary sclerosis morphology, discussing myocardium microcirculation disturbances
02 p0200 A71-12414

Arterial sclerosis and stenosis physical factors, discussing connective and vascular tissue adaptive responses to mechanical stresses
02 p0200 A71-12415

Human coronary arteries fibrinolytic activity, considering histochemical and quantitative methods for arteriosclerosis and occlusion investigations
02 p0200 A71-12416

Blood cholesterine and protein fraction concentrations in pathogenesis of hypothalamic atherosclerosis patients
02 p0201 A71-12531

Intraluminal pressure effect on stress concentration and deformation of arterial wall in relation to atherosclerosis, using finite element method
[ASME PAPER 70-WA/BHF-15]

03 p0373 A71-14113

Antigenic properties of human vascular wall layers in atherosclerosis, using agar precipitation and immunoelectrophoretic measurements
04 p0540 A71-15574

Early and prognostic signs of arteriosclerosis in aircraft pilots from medical examination records
07 p1045 A71-20541

Age, obliterating arteriopathy and peripheral arterial sclerosis effects on rheographic wave propagation speed to lower limbs
10 p1566 A71-24976

Early diagnosis of atherosclerosis in civil aviation pilots by lipid metabolism and electrocardiographic examinations
15 p2357 A71-31318

Coagulation and fibrinolysis changes after physical exercise in males with atherosclerosis, noting fibrinolytic response differences with age
18 p2853 A71-35918

Mucopolysaccharide content and composition of fatty streaks in young male aortas, discussing atherosclerosis effects
18 p2854 A71-35919

Collagen and elastin transmedial gradients in human aortas as function of age, discussing relationship to atherogenesis
18 p2858 A71-36751

Mid systolic clicks and papillary muscle dysfunction evidence in arteriosclerotic heart disease from ECG, carotid pulse tracing and phonocardiography
23 p3635 A71-44126

Cardiac arrest or arrhythmia due to coronary arteriosclerosis in young aviator, examining causes, prevention and predictive measures
23 p3637 A71-44250

ARTHROPODS
NT BEETLES
NT DROSOPHILA
NT INSECTS
NT SNAILS

Gravity receptors and locomotion orientation in Crustacea, discussing statocyst, stimulation, input and compensatory eye movements with respect to gravitational field
21 p3327 A71-39992

Arthropoda /Daphnia, crawfish, wood lice, cockroaches, flies and ants/ hypoxia survival time and resistance to explosive decompression
24 p3797 A71-44719

ARTICULATION
Isolated synthesized vowel fundamental tone duration, intensity and frequency imitation by human voice
02 p0205 A71-12060

Synthesized glottal consonant imitation by human voice, analyzing stimulus and response intensity levels relationship
02 p0206 A71-12062

Healthy subject speech speed effect on phonation phase length, noting relation to normal articulator phase
16 p2531 A71-33462

Speech intelligibility prediction in time varying aircraft noise based on test score relationship to articulation index for steady state noise
20 p3271 A71-39766

Time varying aircraft noise effect on speech intelligibility, discussing test for relation to articulation index
21 p3343 A71-40709

Transverse accelerations effect on human speech features
24 p3795 A71-44471

ARTIFICIAL SATELLITE
NT VENERA 4 SATELLITE

ARTIFICIAL CLOUDS
Upper atmosphere temperature, wind and diffusion measurements using artificial luminous clouds
01 p0074 A71-11088

Artificial Ba clouds resonance radiation, measuring polarization with photoelectric polarimeter
01 p0075 A71-11333

Ionospheric artificial barium cloud growth and stability, considering ion density, internal electric field and velocity
01 p0077 A71-11508

Rocket-borne Na-K vapor release for upper atmosphere winds profiles and diffusion measurements by ballistic camera photography
03 p0415 A71-14027

German monograph on radiative transport in freely expanding gas clouds covering analytical and numerical calculations and experiments
03 p0418 A71-14369

Isophote evolution in artificial clouds, using photometric analyzer with TV screen as monitor
06 p0867 A71-17704

HF backscatter from ionospheric Ba releases in March 1969 at Alaska, discussing effective cross section
07 p1064 A71-20317

Diborane release into upper atmosphere, considering effectiveness as atmospheric tracer
09 p1489 A71-23450

Electric field, neutral wind velocities and ion collision frequency from artificial ionic clouds motion and deformation in ionospheric E and F regions
10 p1602 A71-24549

Magnetic field aligned currents during 18 March 1969 substorms, observing electric field by Ba plasma cloud motion for magnetic perturbation field
10 p1677 A71-24789

Barium ion cloud experiments for ionospheric vapor release determination from Rubis Rocket trajectory visible markings
11 p1755 A71-25643

Rocket-borne wind measurements at 40-70 km by glass fiber and Cu chaff clouds
12 p1901 A71-27068

Rocket chemical release clouds into atmosphere during IQSY, discussing wind profiles, diffusion coefficients, turbulence, temperatures and atomic O distribution
15 p2396 A71-31615

Upper atmosphere temperatures from barium oxide fluorescence emissions in ion cloud rocket experiments, studying thermal response to geomagnetic disturbances
16 p2562 A71-32808

Thermospheric wind measurement by chemical releases, observing artificial cloud motion and growth
16 p2565 A71-33735

Chemical trimethyl aluminum releases in lower thermosphere for temperature, density, winds, turbulence, diffusion coefficients and atomic oxygen content measurements
16 p2568 A71-33792

Low and midlatitude ionospheric motion determination using barium ion cloud release technique
16 p2570 A71-33827

Belgian report to COSPAR, reviewing experiments with gas release at high altitudes and stratospheric balloons
16 p2667 A71-33870

Lidar observations of artificial warm fog seeding operations, analyzing spatial and temporal variations
17 p2770 A71-35741

Thermospheric density determination from ESRO rocket flight produced artificial fluorescent AIO clouds
18 p2914 A71-37060

Ionospheric wind velocity, direction and diffusion coefficient measurements using artificial aluminum oxide luminescent clouds
19 p3091 A71-38629

Liquid carbon tetrachloride artificial luminescent cloud formation in upper atmosphere, considering injection conditions for rapid vaporization and required concentration

19 p3061 A71-38633

Convective clouds development stimulation by artificial ascending jets forming above stationary heat and momentum source, discussing propagation in atmosphere

19 p3093 A71-38694

Ice forming effectiveness and dispersion of reagent particle aerosols through explosion of Elbrus 2 antiaircraft artillery shells in free and clear atmosphere

19 p3094 A71-38697

Ionospheric electric field strength at equatorial and medium geomagnetic latitudes during twilight from barium-ion cloud drift measurements

20 p3218 A71-39523

Winds and diffusion measurements in lower troposphere using sodium vapor cloud release from Centaur IIB rocket

20 p3221 A71-39692

Magnetic field aligned striations of Ba ion clouds artificially injected into ionosphere, investigating physical processes based on model

20 p3230 A71-39861

Polar cap electric field and relationship to magnetic disturbances from measurements on Ba ion clouds released by rockets

20 p3230 A71-39883

Ion cloud expansion perpendicular to initially homogeneous magnetic field, estimating maximum radius with energy balance and expansion process

23 p3667 A71-43132

Upper atmospheric temperature and density measurements from artificial cloud observations

23 p3667 A71-43139

Barium ion cloud release at 194 km, observing striation formation for instability characteristics evaluation

23 p3669 A71-43170

ARTIFICIAL EARS

Pure tone, air/bone conducting and speech audiometry, considering hearing tests, artificial mastoids, environmental requirements and physical principles

06 p0859 A71-18029

ARTIFICIAL GRAVITY

Control programs realizability for optimal escape trajectories of low thrust vehicles with motion about mass of center and with or without artificial gravity

02 p0319 A71-11905

Space mission reflex vestibular disturbance and motion sickness prevention, examining artificial gravity and drugs

02 p0198 A71-11979

High voltage power supply for NASA orbital gravity substitute electrostatic workbench, including abnormal load and oxygen environment tests

03 p0394 A71-13050

Vestibular problems in long manned space flight, discussing weightlessness and rotating environment for artificial gravity

04 p0541 A71-14753

Elemental maximum energy transport formula for wick heat pipe evaporators under artificial gravity and external acceleration, testing by laboratory centrifuge [AIAA PAPER 71-419]

11 p1857 A71-26210

Control programs reliability for optimal escape trajectories of low thrust vehicles with motion about mass of center and with or without artificial gravity

13 p2144 A71-28192

Artificial g space station configurations, developing movable control mass attitude stabilization system

18 p2971 A71-36277

Medical physiological requirements of angular velocity and g level for artificial gravity creation by rotating space vehicle, considering human tolerances and vehicle design

18 p2870 A71-36627

Gross locomotion and cargo handling in simulated artificial gravity environments, studying effects of Coriolis forces, angular accelerations, oculo-vestibular stimuli and traction variations [AIAA PAPER 71-886]

18 p2871 A71-36636

Manned earth-orbital missions performance assessment experiments, studying effects of artificial and zero gravity spacecraft environments on humans [AIAA PAPER 71-891]

18 p2857 A71-36641

Artificial gravity selection by rats in centrifugal acceleration fields superimposed on weightlessness during sounding rocket flights

18 p2857 A71-36646

Increased artificial gravity avoidance by squirrel monkeys with variations in rotation rate and radius [AIAA PAPER 71-855]

18 p2857 A71-36647

Skylab manned earth orbital artificial gravity experiment, describing mission objectives and requirements [AIAA PAPER 71-861]

18 p2975 A71-36649

Artificial gravity Skylab wobble damping, using ATM control moment gyros [AIAA PAPER 71-862]

18 p2975 A71-36650

Engineering aspects of zero gravity personal hygiene and waste management systems, noting controlled air flows, surface tension and artificial gravity [AIAA PAPER 71-865]

18 p2872 A71-36653

Space shuttle orbital centrifuge systems configuration, comparing artificial gravity experiment performance options

[AIAA PAPER 71-860] 19 p3006 A71-37274

Artificial gravity field produced by rotating spacecraft in earth orbit, examining astronaut physical responses and centrifugal force effects on work tasks

21 p3342 A71-40255

ARTIFICIAL HEART VALVES

Hemodynamic evaluation of heart rate augmentation produced by atrial pacing and isoproterenol in early postoperative phase of cardiac valve surgery

23 p3640 A71-44131

ARTIFICIAL INTELLIGENCE

Artificial intelligence computer programming system for continuum mechanics, discussing capabilities of CONFORM as mathematical language

03 p0382 A71-13548

Information processing in biological and artificial brains, analyzing visual perceptual system

10 p1568 A71-24224

ARTIFICIAL RESPIRATION

U RESUSCITATION

ARTIFICIAL SATELLITES

NT AEROS SATELLITE

NT ALOUETTE SATELLITES

NT ALOUETTE 1 SATELLITE

NT ALOUETTE 2 SATELLITE

NT APPLICATIONS TECHNOLOGY SATELLITES

NT ARIEL 1 SATELLITE

NT ARIEL 2 SATELLITE

NT ARIEL 3 SATELLITE

NT ATS 1

NT ATS 5

NT ATS 6

NT ATS 7

NT BEACON SATELLITES

NT BIOSATELLITE 2

NT BIOSATELLITE 3

NT BIOSATELLITES

NT COMMUNICATION SATELLITES

NT COSMOS SATELLITES

NT EARLY BIRD SATELLITES

NT EARTH RESOURCES TECHNOLOGY SATELLITES

NT ECHO 1 SATELLITE

NT ECHO 2 SATELLITE

NT ELEKTRON SATELLITES

NT ELEKTRON 2 SATELLITE

NT ELEKTRON 4 SATELLITE

NT ENVIRONMENTAL RESEARCH SATELLITES

NT EOSS

NT ESRO SATELLITES

NT ESRO 1 SATELLITE

NT ESRO 2 SATELLITE

NT EXPLORER SATELLITES

NT EXPLORER 12 SATELLITE

NT EXPLORER 22 SATELLITE

NT EXPLORER 26 SATELLITE

NT EXPLORER 28 SATELLITE

NT EXPLORER 31 SATELLITE

NT EXPLORER 33 SATELLITE

NT EXPLORER 35 SATELLITE

NT EXPLORER 37 SATELLITE

NT EXPLORER 38 SATELLITE

NT EXPLORER 40 SATELLITE

NT GEODETIC SATELLITES

NT GEOPHYSICAL SATELLITES

NT GEOS 1 SATELLITE

NT GEOS 2 SATELLITE

NT GEOS-C SATELLITE

NT GRAVITY GRADIENT SATELLITES

NT HEOS A SATELLITE

NT HEOS SATELLITES

NT IMP

NT INJUN SATELLITES

NT INTELSAT SATELLITES

NT ISIS SATELLITES

NT LINCOLN EXPERIMENTAL SATELLITES

NT LUNAR ORBITER

NT LUNAR SATELLITES

NT METEOROLOGICAL SATELLITES

NT MOLNIYA SATELLITES

NT NAVIGATION SATELLITES

NT NIMBUS SATELLITES

NT NIMBUS 2 SATELLITE

NT NIMBUS 3 SATELLITE

NT NIMBUS 4 SATELLITE

NT OAO

NT OGO

NT OGO-B

NT OGO-C

NT OGO-D

NT OGO-E

NT OSO

NT ORBITAL WORKSHOPS

NT OSO-E

NT OSO-F

NT OSO-G

NT OSO-3

NT OUTER PLANETS EXPLORERS

NT PAGEOS SATELLITE

NT PASSIVE SATELLITES

NT PROTON 1 SATELLITE

NT PROTON 2 SATELLITE

NT PROTON 4 SATELLITE

NT RADIO ASTRONOMY EXPLORER SATELLITE

NT RELAY SATELLITES

NT SAN MARCO SATELLITE

NT SAN MARCO 2 SATELLITE

NT SAS-A

NT SKYNET SATELLITES

NT SPUTNIK SATELLITES

NT SYNCHRONOUS METEOROLOGICAL SATELLITE

NT SYNCHRONOUS SATELLITES

NT SYNCOM SATELLITES

NT TELSTAR SATELLITES

NT TIROS SATELLITES

NT VELA SATELLITES

NT VENERA SATELLITES

NT VENERA 6 SATELLITE

Higher geodesy problems, determining earth dimensions and figure, gravitational field and absolute and relative point positions with artificial earth satellites

01 p0159 A71-10809

Numerical analysis of Hill limiting case of restricted three body problem regarding quasi-periodic, ergodic and escape orbits for natural and artificial satellites

01 p0161 A71-11380

Artificial satellite photographic tracking, discussing Baker-Nunn cameras, international projects and future research

03 p0455 A71-14070

Artificial satellites rendezvous, describing common Kepler ellipse in central body field with positioning after time delay

03 p0500 A71-14389

Oblate planet artificial satellite motion, obtaining secular and periodic perturbations to third and second order

04 p0642 A71-14739

Jovian and solar perturbation of hypothetical artificial Callisto satellites, using Delaunay method

09 p1518 A71-22373

Sunlight pressure forces and moments on complex shape artificial earth satellites, assuming uniform incident flux

09 p1492 A71-22374

Artificial earth satellites orientation determined by onboard telemetric measurements, constructing model for rotational motion around center of mass

09 p1531 A71-22569

Artificial earth satellite circular orbit determination from topocentric directions measurement by optical and electronic observations

09 p1408 A71-23176

Simulated artificial satellite position determination, using experienced and inexperienced observers

09 p1528 A71-23547

Restricted three body problem involving two spherical bodies and elongated artificial satellite, considering equations of motion and positions stability

10 p1667 A71-23830

Artificial satellite orbital velocity tangential component time variation from variational calculus direction law

10 p1674 A71-24441

Eccentric satellite observation, considering geodesic determination of coordinate difference between observation station and reference point

11 p1732 A71-25818

Artificial earth satellite observation by Soviet universal and semiautomatic cameras with quartz clocks and four component mirror lens optical system

11 p1762 A71-25829

Induction and wave drag due to Alfvén waves on long cylindrical satellite in ionosphere, investigating radiated power integral

12 p1973 A71-27576

Artificial earth satellite orientation determination from single vector measurements, discussing coordinate systems transition

13 p2145 A71-28204

Oscillating artificial earth satellite orientation determination from geomagnetic field strength vector, using least squares method

13 p2145 A71-28205

Artificial satellites eccentric orbits commensurable with earth rotation, noting resonance effects of geopotential

13 p2135 A71-28354

Artificial satellite illumination by sun, calculating height, time and position of earth shadow by nomogram

13 p2145 A71-28511

Artificial earth satellites initial elliptical orbit calculation, discussing function minimization for optical radar and laser observation

15 p2481 A71-31301

Earth satellite plane periodic oscillations damping with respect to center of mass in orbital plane during motion on elliptical Kepler orbit

16 p2646 A71-33659

Angular position of sun nonoriented artificial earth satellites with angular velocities not exceeding 0.5 deg/sec, using harmonic analysis of magnetometric data

16 p2543 A71-33662

Artificial planetary satellites lifetime estimation from atmospheric drag, discussing critical height-atmospheric density relationship, satellite design and initial orbit height 16 p2638 A71-33671

Compound pendulum in artificial satellite for establishing attitude reference or detecting rotation rate variations 17 p2813 A71-34870

Artificial satellites optical characteristics from amateur observers, discussing brightness and absolute magnitude 20 p3305 A71-38731

Automatic methods for equations of motion solution for artificial satellites orbits 22 p3600 A71-41951

Terrestrial, lunar and planetary dynamical properties and internal constitution, considering data obtained from artificial satellites, lunar and planetary dynamics 22 p3607 A71-42883

Satellites explosion debris distribution and orbital characteristics as data base for earth force field and geopotential resonance phenomena analysis [AAS PAPER 71-351] 23 p3728 A71-43023

Artificial satellite lunar orbit calculation, representing unmodeled accelerations by first order Gauss-Markov sequence with time correlated and random components [AAS PAPER 71-371] 23 p3730 A71-43041

ARYL COMPOUNDS

U AROMATIC COMPOUNDS

ASA

U ACETYSALICYLIC ACID

ASBESTOS

Asbestos applications in aerospace technology, considering chemical and molecular structure, heat and radiation resistance, mechanical properties and reinforcement 05 p0772 A71-16465

Carbon fiber cladding paper for corrosion resistant asbestos laminates, discussing short fibers orientation and acid solutions effects on flexural strength and weight 12 p1921 A71-27014

ASCENT

NT CLIMBING FLIGHT

Inflatable restraint collar for large balloons with heavy loads using winch driven cable launching 02 p0188 A71-11821

ASCENT TRAJECTORIES

Rocket free flight ascent trajectory range error, approximating influence of stabilizers, nose cone and components misalignment along longitudinal axis 04 p0601 A71-14596

KC-135 aircraft climb trajectories for optimum constant lift coefficient, range and fuel amount 22 p3481 A71-42834

Optimal ascent trajectories for delta wing space shuttle flight, using accelerated gradient methods [AAS PAPER 71-328] 23 p3726 A71-43001

ASCORBIC ACID

Ascorbic acid reduction in organs due to thyroid hormones saturation under hypothermia 17 p2680 A71-34646

Cystamine hydrochloride or vitamin B complex with vitamin C for radiation sickness prevention and therapy 22 p3493 A71-42723

ASHES

Cascade mountains volcanic ash deposits elemental abundances correlation by computerized gamma ray spectra analysis of TRIGA reactor activated glass separates 22 p3533 A71-41855

ASPARTATES

Glycine conversion into serine, aspartate and glutamate in cerebrum under normal and hypoxia conditions 09 p1391 A71-22482

ASPARTIC ACID

Transverse acceleration effect on aspartic aminotransferase activity in humans and rats 24 p3795 A71-44528

ASPECT RATIO

NT HIGH ASPECT RATIO

NT LOW ASPECT RATIO

Civil aircraft aspect ratio relationship to commercial viability, considering need for minimum induced drag at wing loading to improve payloads, speeds and ranges 01 p0005 A71-11628

Guide vanes small aspect ratio effect on high pressure stages of axial flow compressors 02 p0186 A71-12558

Wing design criteria imposed by high speed requirement for short takeoff aircraft, considering thin swept-back wing with small aspect ratio for lateral control 12 p1867 A71-27471

Critical aspect ratio of W fibers in metal matrix composites for stress rupture applications 14 p2258 A71-29921

Aspect ratio influence on instability and non-minimum phase effects of longitudinal motion of aircraft relative to negative lift-drag expression transfer functions [DFVLR-SONDDR-127] 16 p2523 A71-33405

Clamped rectangular plate buckling under uniaxial and biaxial compression, obtaining critical loads for various aspect ratios 18 p2979 A71-36360

Acoustic damping of clamped and hinged rectangular panel at natural frequency, noting dependence on aspect ratio 21 p3416 A71-41200

Aerodynamic aspect ratio effects on drag and aircraft performance, noting span loading as major force on wing lifting function 21 p3325 A71-41246

ASPHALT

Asphalt pavement design for heavy multiwheel aircraft, using BISTRO computer program 18 p2897 A71-36000

ASPHERICITY

Paraboloidal, hyperboloidal and flattened spheroidal telescope mirrors testing with optical compensation lenses by Foucault shadow and Ronchi methods 07 p1116 A71-20641

Optical elements aspheric testing, using computer generated synthetic holograms 08 p1290 A71-21388

Aspherization coordinates and error corrections of optical systems with nonspherical surfaces by colliding beam method on digital computer 15 p2406 A71-31620

Aspheric lenses and mirrors testing by single and double exposure two-wavelength visible light holography for obtaining interferogram 20 p3235 A71-39182

Human eye theoretical model with aspherical cornea front and lens back surfaces, computing astigmatism, coma, meridional and sagittal focal lengths by ray tracing method 24 p3798 A71-44978

ASPHYXIA

Oxygen balance of intact and denervated dog spleen during asphyxia, distinguishing splenic contraction and metabolic rate-storage capacity ratio 04 p0538 A71-15087

Asphyxia induced changes in regional cutaneous and visceral sympathetic activity in anesthetized rabbits, noting relationship with ear blood flow increase 06 p0854 A71-18324

Afferent pulsed activity change in peripheral fibers of severed phrenic nerve during air inhalation and under asphyxia 11 p1719 A71-25671

Stagnant asphyxia in cat carotid body during abrupt blood pressure drop by simultaneous carotid artery clamping and tap opening 20 p3190 A71-39443

Hypoxia and hypercapnia induced asphyctic differentiation of cutaneous and visceral sympathetic activity in anesthetized paralyzed rabbits 21 p3334 A71-40629

Time of useful function after mice exposure to life threatening toxic mixtures of carbon monoxide, carbon dioxide and ammonia produced by combustion 22 p3486 A71-41830

ASPIRATION

U VACUUM

ASSAULTING

U ATTACKING [ASSAULTING]

ASSEMBLES

NT SUBASSEMBLIES

Aircraft assembly accuracy parameters, using holes as reference points 02 p0257 A71-12564

Assembling accuracy of three dimensional joints using assembly holes in aircraft construction 04 p0602 A71-14609

ASSEMBLING

NT ORBITAL ASSEMBLY

Soviet book on aircraft gas turbine engine assembly covering organization, specified accuracy, automatic systems, mechanization problems, quality control, etc 04 p0639 A71-15449

Si solar cell cover glass assembly and packaging improvements using Teflon 05 p0702 A71-16079

Aircraft systems assembly methods, discussing rigidity effects on error redistribution in external and internal force field application 08 p1295 A71-20792

Wireless assembly methods for thin and thick film hybrid and monolithic IC, emphasizing flip-chip elements microelectronic devices fabrication and interconnection 22 p3525 A71-41714

ASSEMBLY

Bench-line product assembly analysis, calculating rhythm, cycle and required number of workers 02 p0257 A71-12567

Self adaptive control system for selective assembly process, ensuring matching of size distribution curves within identical batches 12 p1912 A71-27341

ASSESSMENTS

NT TECHNOLOGY ASSESSMENT

ASSIMILATION

Oxygen consumption by nitrogen starved nonsynchronous *Chlorella* culture during different assimilation of nitrogen salts in darkness and light 16 p2531 A71-33461

ASSOCIATIONS

U ORGANIZATIONS

ASSURANCE

Computer aided reliability assurance system /CARAS/ for integrated circuits, correlating process and failure data 12 p1890 A71-26658

Semiconductor neutron hardness assurance by irradiation of wafer, probe, die rejection and anneal screening technique 19 p3034 A71-38520

ASTEROIDS

NT CERES ASTEROID

NT ICARUS ASTEROID

NT VESTA ASTEROID

Asteroids, comets and meteor dynamics in solar system, examining motion and orbital evolution by computer techniques 01 p0155 A71-10437

Minor planets 1969 ephemeris, considering numerical integration of celestial mechanics equations 01 p0155 A71-10438

Hilda minor planet group and Thule model, examining real orbit relation to Schwarzschild type periodic orbits 01 p0155 A71-10441

Minor planet distribution in asteroid belt central area, noting inclination angle, eccentricity, ascending node and perihelion longitude 01 p0155 A71-10442

Juno absolute perturbations due to large planets, using Hill method with digital computer 01 p0156 A71-10549

Photographic and photoelectric photometry of asteroids, discussing luminescence, reflectivities, light curves, colors and phase variations observations 02 p0310 A71-12157

Minor planets precise position tabulations, correcting previously published data 03 p0493 A71-14195

Long period effects in motion of Chicago and Thule, noting commensurability with Jupiter orbit 04 p0652 A71-15705

Comets-minor planets relationship, discussing comas, physical appearance, light variations and condensations 04 p0653 A71-15713

Restricted three body problem of asteroid orbital motion in solar and Jupiter field in three dimensional space 04 p0656 A71-15734

Meteorites as information sources on interplanetary space beyond Martian orbit and asteroid belt, discussing possible magnetic barrier and galactic field modulation 05 p0813 A71-16857

Minor planets mean motions commensurability with Jupiter in restricted three body problem 07 p1202 A71-20515

Asteroids photographic observations for catalog of faint stars positions orientation, correcting observation times to ephemeris time 09 p1525 A71-23338

Approximate determination of 44 minor planets orbits, tabulating orbital elements 09 p1526 A71-23344

Ceres and Pallas orbital commensurability, considering resonance effects 09 p1527 A71-23537

Asteroids or comets orbital elements calculation, using initial heliocentric position and velocity as zero time orbital elements 10 p1668 A71-24023

Lydia asteroid observations, presenting light curves brightness and phase functions near opposition 10 p1669 A71-24177

Star catalogue systematic error corrections from minor planet photographic observations and orbital elements determination 10 p1670 A71-24180

Asteroid ring origin, discussing osculating and corresponding secular orbital elements of mother planet 11 p1820 A71-25245

Meteoroids orbital elements statistically compared to asteroids 11 p1820 A71-25246

Lunar impact cratering in geologic time, deriving meteoritic flux mass approximation and planetesimals origin 13 p2134 A71-28288

Bibliography on lunar and planetary subjects covering astrophysics, comets, cratering, meteors temperature, structure, asteroids, tektites surface features, etc 13 p2135 A71-28293

Triaxial ellipsoid asteroid models, determining light curves and variations 14 p2312 A71-30385

Daniel 1909 IV comet orbit evolution, discussing capture by Jupiter, asteroid collision, brightness, orbit perturbation and nongravitational force effects

15 p2481 A71-31298

Daniel comet collision frequency calculations with asteroids and microasteroids based on trajectory analysis

15 p2481 A71-31299

Daniel comet minimum distance distributions between asteroids, determining minor planet masses

15 p2482 A71-31302

Comet and asteroid orbits tangential approximation, determining minimal distances and velocities as function of orbital elements

15 p2482 A71-31303

Lunar, meteoroid and asteroid surface erosion, investigating hypervelocity impact, solar wind flux and ion sputtering effect

16 p2642 A71-33818

Asteroids and comets bibliography and review, considering celestial mechanics and astrometry, photometry, spectra, polarimetry and radar measurements

17 p2798 A71-34455

Asteroids 457-Alleghania, 649-Josepha, 1038-Tuckia, 1161-Thessalia, 1162-Larissa and 1297-Quadea orbital elements and ephemerides, taking into account planetary perturbations

17 p2809 A71-35581

Diamonds in ureilites and carbonaceous chondrites, discussing formation due to recrystallization during asteroid collisions

17 p2810 A71-35723

Heliocentric energy per mass changes in close planetary encounters, noting relation to cometary and asteroidal material evolution

17 p2811 A71-35744

Stellar catalogs errors assessment from Ceres and Vesta asteroids observations

18 p2962 A71-36109

Asteroid magnetospheres effects on magnetic moments and whistler mode noise propagation in solar wind

18 p2964 A71-36292

Small bodies collisions in solar system, using Newtonian mechanics to indicate formation of meteor and asteroid streams

18 p2967 A71-36923

Requirements and opportunities for comet and asteroid missions including flyby, rendezvous, docking and sample return

[AAS PAPER 71-104] 19 p3139 A71-37906

Grand Tour meteoroid environment analysis, considering different asteroid and cometary particle models

[AAS PAPER 71-110] 19 p3139 A71-37910

Pioneer Jupiter probe missions as precursor to subsequent outer planets exploration, discussing primary objective of asteroid belt and Jupiter radiation belt hazards evaluation

[AAS PAPER 71-111] 19 p3152 A71-37911

Outer planets missions combined zodiacal experiment, examining meteoric, asteroidal and satellite particles distribution and orbits

[AAS PAPER 71-127] 19 p3064 A71-37919

Dust environment estimation in asteroid belt during trans-Martian spacecraft missions, considering cosmological, dynamical and observational evidence

20 p3297 A71-39633

Computer techniques for meteor stream trails recognition, considering stream concept extension to groupings of asteroid orbits

20 p3298 A71-39641

Ephemerides of sun, moon, planets and minor planets for October through December 1971

21 p3442 A71-40153

Apollo type asteroid with high orbital eccentricity and inclination and rough elongated shape, noting ephemerides

21 p3443 A71-40188

Low gravity field phenomena, discussing vertical jump on moon, ball trajectories launched from asteroid and voyage to neutron star

22 p3600 A71-41983

Asteroids flyby approaches during Jupiter missions and Grand Tours, obtaining gravitational deflection of spacecraft trajectories and mass cost estimates

[AAS PAPER 71-360] 23 p3729 A71-43030

Impulsive trajectory optimization for asteroid Eros round trip sample return mission using chemical propulsion

[AAS PAPER 71-369] 23 p3730 A71-43039

Asteroid 1967 observation and ephemeris activity, surveying 1966-1967 literature

24 p3874 A71-45172

Asteroid belt structure by statistical methods, discussing asteroidal zones and agreement with Kuiper hypothesis and protoplanet theory

24 p3874 A71-45173

Computer processed photographic observations of Pluto, 10 Hygiea, 433 Eros and Saturn satellites VII, VIII and IX

24 p3874 A71-45178

ASTHMA

Blood plasma volume reduction by voluntary hyperventilation, associating with hypovolemia of status asthmaticus

04 p0545 A71-15155

ASTIGMATISM

Vestibular habituation retention, showing nystagmic response reduction to repetitive rotatory and caloric tests

04 p0537 A71-14764

Three-mirror telescope third order dioptrics of astigmatism and coma suppression

06 p0901 A71-18313

Astigmatic image distortion in low temperature multiple reflection White cell with aluminum dewar assembly for Martian IR interpretation

18 p2914 A71-35844

ASTRONOMICS

Space shuttle integrated electronic onboard and ground reusable systems design, considering data flow management, checkout, computer decentralization, electronic switching and redundancy

02 p0231 A71-11978

SIRIO satellite project, discussing orbital dynamics, propulsion system, attitude control, onboard and ground electronic equipment

10 p1682 A71-24272

Space shuttle avionics system redundancy, calculating costs for individual line replaceable units

18 p2889 A71-36479

ASTROBEE ROCKET VEHICLES

Astrobees D low cost high performance sounding rocket with long duration radial burning propulsion system for D region and meteorological research

[AIAA PAPER 70-1387] 03 p0498 A71-13670

ASTROBIOLOGY

U EXOBIOLOGY

ASTRODYNAMICS

Papers on mathematical methods in astrodynamics and celestial mechanics for earth-moon trajectories computation, satellite orbit determination and three body problem

16 p2630 A71-33056

Book on astrodynamics covering n body equations of motion, orbital elements, differential corrections, time of flight, ballistic missiles and interplanetary transport

18 p2963 A71-36248

Thrusting lifting orbital vehicle nonlinear longitudinal dynamics in near-circular orbit, deriving orbital elements variation behavior and angle of attack mode period and damping

21 p3454 A71-40094

ASTROGRAPHY

Camera focal distance, optical center position and distortion determination of Zeiss Astrographic objective by moving star pairs method

03 p0428 A71-13941

Mars photographic positions on double short focus astrograph with random error for ascent and declination

07 p1194 A71-19332

Deimos and Phobos position measurements by photographic observations, including refractor and astrograph errors

07 p1194 A71-19333

Deimos photographic observations on Pulkovo normal astrograph during 1967 Mars opposition

07 p1194 A71-19334

Spherical aberration, limiting magnitude, distortion and coordinate determination accuracy of 20-cm two-camera astrograph at Abastumani Astrophysical Observatory

07 p1115 A71-20441

Airborne astrographic camera system for simultaneous determination of multiple object reentry trajectories at Air Force test range

18 p2918 A71-36077

Comet Bennett 1969 head and tail polarization distribution data, using triple astrograph

19 p3145 A71-38524

Climatological European southern observatory in Chile, describing spectroscopic and photometric telescopes, grand prism objective and double astrograph

20 p3210 A71-39527

ASTROMETRY

Precise radio sources positions by Schmidt telescope and AGK 3 reference frame, noting comparison with optical positions

04 p0644 A71-15048

Lunar ephemeris and astrometric corrections from occultation observations, noting FK4 equinox location

08 p1357 A71-20876

Astrometric instruments optimal spatial sampler with parallel slits grill in focal plane, studying error minimization

10 p1608 A71-23825

Independently sampled indirect and direct magnitude measurements, noting linear system effects in astrometry

10 p1575 A71-23845

Double stars astrometry, discussing proper motions, parallaxes and mass ratios of visual binaries

14 p2310 A71-30359

Trigonometric white dwarf star parallax measurements, using astrometric reflector to derive H-R diagram

14 p2316 A71-31007

Schmidt telescope as astrometric instrument, comparing mean error with catalog positions

16 p2578 A71-33322

Asteroids and comets bibliography and review, considering celestial mechanics and astrometry, photometry, spectra, polarimetry and radar measurements

17 p2798 A71-34455

Photoelectric astrometry to determine stellar position, noting application to binary stars

17 p2741 A71-34995

Short term timing stability of Crab pulsar clock from telescope observations at 256 and 405 MHz

19 p3144 A71-38173

Mirror meridian circle of zero expansion glass for reduction of flexure and refraction instrument errors in astrometry

20 p3240 A71-39539

Soviet papers on astrometrical study methods, discussing instrument errors, stellar observation improvement, ambient medium conditions and automation

23 p3770 A71-44254

Astrometrical HF range latitudinal observation error spectrum estimation, showing random dispersion and Chebyshev polynomial expansion parameters for nightly variation

23 p3771 A71-44256

ASTRONAUT LOCOMOTION

Location and Orientation of Lunar Astronauts system using radio frequency ranging and sun azimuth

08 p1331 A71-21241

Human performance in various locomotive tasks under simulated lunar reduced gravity conditions, classifying test stands and equipment

15 p2362 A71-31304

Gross locomotion and cargo handling in simulated artificial gravity environments, studying effects of Coriolis forces, angular accelerations, oculo-vestibular stimuli and traction variations

[AIAA PAPER 71-886] 18 p2871 A71-36636

Mathematical model for underwater simulation of astronaut extravehicular activities in weightless conditions, using computer program

[AIAA PAPER 71-852] 18 p2872 A71-36644

ASTRONAUT MANEUVERING EQUIPMENT

Chemically activated electroadhesive pads on spacecraft surface, allowing astronauts to maneuver or work in zero gravity environments

[AIAA PAPER 71-853] 18 p2872 A71-36645

ASTRONAUT PERFORMANCE

Astronaut visual acuity under angular acceleration, considering vestibular stimulus direction and nystagmus upbeating or downbeating

04 p0536 A71-14754

Medical flight information on astronauts response to space flight environment in confined and unconfined state and during intra- and extravehicular activities

08 p1246 A71-20731

Soyuz 9 cosmonauts physiological monitoring instrumentation and procedures, describing bioinstrumentation harness for data telemetry

09 p1397 A71-22198

Soyuz 9 cosmonauts medical monitoring, discussing physiological changes, vagotonic reactions and work capacity

09 p1389 A71-22199

Soyuz 9 cosmonauts postflight clinical examination, noting muscle pain, eyelid edema, leg muscle atrophy, etc

09 p1389 A71-22200

Weightlessness effects on muscular reflexes, tonus and contractibility in Soyuz 9 astronauts

09 p1389 A71-22202

Soyuz 9 astronaut vertical posture control after 18 day orbital flight, considering cardiovascular disturbances caused by reduced muscle tone and changed interaction between analyzers

09 p1389 A71-22203

Skin tissues automicoflora composition and natural immunity indices changes after 18 day orbital flight from microbiological and immunological examinations

09 p1389 A71-22204

Cosmic rays visual perception by Apollo astronauts during lunar flight, discussing human eye as Cerenkov radiation detector

11 p1716 A71-25237

Light flashes in eyes of dark adapted Apollo astronauts, considering Cerenkov radiation effects from primary cosmic ray single charged particles on retinal elements

12 p1933 A71-27383

Astronauts work-rest schedule principles during space flight, discussing circadian rhythms and desynchronization

15 p2363 A71-31315

Skylab habitability facilities for astronaut work effectiveness and physical well being

15 p2363 A71-31456

Astronaut orthostatic tolerance loss due to weightlessness, describing compensation by periodic lower body negative pressure
[AIAA PAPER 71-859] 18 p2872 A71-36648

Human response to space environment, discussing prolonged weightlessness, extravehicular work and lunar surface activity
19 p3002 A71-37492

Experiences of living on moon, discussing effects on task performance and physical movements and observations of lunar surface, lighting and color
20 p3295 A71-39614

Artificial gravity field produced by rotating spacecraft in earth orbit, examining astronaut physical responses and centrifugal force effects on work tasks
21 p3342 A71-40255

Astronaut work capacity and adaptation during long term flight of space vehicle Soyuz 9
21 p3342 A71-40259

Soviet book on psychology and outer space covering astronauts experiences and emotions during training and flights, daily routine, equipment, food, habits and personal characteristics
21 p3336 A71-40876

Astronaut teleoperators use for space operations cost reduction and future experiments productivity increase
22 p3503 A71-42033

Human adaptive behavior under psychological stress of astronauts tasks posture-motor characteristics, discussing stabilographic platform test results
22 p3503 A71-42041

Voskhod 2 cosmonauts physiological data, presenting heart beat, respiration rates, oculomotor activity and blood composition
22 p3495 A71-42791

Aircraft pilots and astronauts relationship with environment, considering weightlessness, emotional reactions, cabin pressure and temperature control and space survival and rescue
23 p3639 A71-43223

ASTRONAUT TRAINING

Spaceflight astronaut training, discussing guidance and navigation methodology of Apollo Mission Simulators
01 p0067 A71-10516

Physical exercises to increase cosmonaut space environment tolerance, discussing effects of acceleration, altitude and hypoxia
01 p0027 A71-11556

Real time solar flare image production for Skylab astronaut training, using films of H alpha, XUV and X ray solar images
06 p0902 A71-18530

Planetarium use in teaching celestial navigation and space sky simulation
07 p1157 A71-20345

Cosmonauts selection with regard to psychological and physical fitness, discussing clinical examination, hospital tests and training
09 p1397 A71-22192

Astronaut selection and training, considering acceleration, hypoxia, weightlessness and temperature variation tolerance
12 p1873 A71-26951

Human body attitude control in space, using ten body complex geometry system, noting astronaut training jig
14 p2188 A71-29832

Man and equipment instrumentation in simulated space environment, considering training and interface of man and life support systems
14 p2188 A71-30312

Soviet book on space biology and medicine covering cosmonaut selection and training, flight safety, normal life support factors, interplanetary space sojourn, etc
17 p2689 A71-34475

Earth orbital space stations modular design, discussing space shuttle use, crew training and program management
17 p2812 A71-34721

[AIAA PAPER 71-824]

Soviet book on psychology and outer space covering astronauts experiences and emotions during training and flights, daily routine, equipment, food, habits and personal characteristics
21 p3336 A71-40876

ASTRONAUTICS

Soviet astronautics with emphasis on Cosmos satellite program, discussing launching bases, booster rocket designs, radio signals and missions
01 p0164 A71-11456

Astronautics and rocket technology history - Conference, Belgrade, September 1967, covering rocket engines, fuels and materials, ramjet engines, control systems, etc
05 p0816 A71-16500

Aviation and astronautics - Conference, Tel Aviv and Haifa, March 1971
11 p1747 A71-25145

Holography applications in astronautics and astronautics, discussing advantages of three dimensional information in aircraft navigation, space missions and astronomic experiments
15 p2411 A71-32528

Astronautics progress review from earliest space flights to present, discussing stabilization, recovery, ballistic reentry and latitude determination
16 p2634 A71-33396

International cooperation in astronautics, reviewing European satellites launching and world distribution of lunar rock and soil samples
22 p3623 A71-42012

ASTRONAUTS

NT ORBITAL WORKERS

Cosmonaut water supply and regeneration in spacecraft using self contained biological cycle
01 p0025 A71-11150

LOLA /Location and Orientation of Lunar Astronauts/ system using RF ranging and solar sensor, discussing configuration, operation, accuracy and electronics
04 p0623 A71-15303

Scientist-astronauts work in manned space flight program support/backup crews and Skylab missions scientific/medical experiments
07 p1046 A71-19089

Astronaut protection from solar flare high energy protons, discussing spacesuit, spacecraft orientation and solid, electrostatic, magnetic and plasma shielding
13 p2021 A71-29252

Calcium, potassium and iron loss by astronauts during Apollo space missions, using instrumental neutron activation analysis
16 p2528 A71-33111

Astronaut chromosome aberrations, presenting peripheral blood leukocytes cytogenetic tests for pre and post space flight
20 p3188 A71-39227

Medical and technical aspects of air rescue and survival of astronauts in mountainous remote areas, noting dogs use for disaster victims location
22 p3482 A71-41982

ASTRONAVIGATION

Spaceflight astronaut training, discussing guidance and navigation methodology of Apollo Mission Simulators
01 p0067 A71-10516

ASTRONOMICAL CATALOGS

Program and auxiliary tables for stellar azimuth determination by observations near elongation
01 p0159 A71-10810

Extragalactic radio source 3CR catalog, analyzing emission spectra
02 p0300 A71-12087

Mean cosmic density determinations, obtaining field galaxy luminosity function moments with red shift catalogs
02 p0313 A71-12499

Quasars optical positions and magnitude identification for radio sources of 4C catalog
02 p0317 A71-12862

Radio emission upper limits from galaxies in Markarian catalog
02 p0317 A71-12866

Moon surface basic points catalogs differences, estimating position dispersion by residuals of transformations
03 p0484 A71-13216

Stellar magnitude equation from corrected catalog data to determine absolute proper motions relative to galaxies
03 p0484 A71-13218

High galactic latitude faint blue stars from Tonantzintla and Asiago catalogs, finding quasars and subwarfs by spectroscopy and UBV photoelectric photometry
04 p0651 A71-15659

Supernovae as indicators of distances to galaxy clusters based on Karpowicz and Rudnicki catalog and angular measurement
07 p1192 A71-19288

Latitude observation program at Pulkovo from 1968 through 1987 with zenith telescope, noting faint star declination and motion errors in General Catalog
07 p1194 A71-19328

Star maps for recognition and attitude orientation aids as function of stereographic display realism in manned space flight
07 p1157 A71-20348

Eclipsing variable binary system RR Centauri observed photoelectrically in yellow and blue light
08 p1357 A71-20875

Extragalactic radio source 3CR catalog, analyzing emission spectra
08 p1362 A71-21137

Eclipsing binary IZ Persei, examining photoelectric light elements
09 p1527 A71-23528

Venus inferior conjunctions tables from 1960 to 2023, presenting geocentric latitude at conjunction time
09 p1528 A71-23548

Lydia asteroid observations, presenting light curves brightness and phase functions near opposition
10 p1669 A71-24177

Star catalogue systematic error corrections from minor planet photographic observations and orbital elements determination
10 p1670 A71-24180

Intermediate band photometric system for three dimensional star classification based on published stellar spectral energy distribution data
10 p1681 A71-25129

Astronomical catalogs of proper motions and positions, discussing reference systems fundamental declinations and right ascensions measurement principles
12 p1959 A71-26773

Coma galactic cluster, investigating nuclei oblateness, diagrams and tables of variables
12 p1962 A71-26910

Solar cosmic ray flare catalog, using polar region absorption radio burst and proton event data
14 p2299 A71-29986

Double star discovery by common proper motion, using IDS catalog data
14 p2311 A71-30361

Observation errors in double star studies, considering inclusion of corrections in Central Catalog
14 p2311 A71-30370

Red subluminescent stars, presenting catalog identification, proper motions, spectral type, photometric parallax, tangential velocity, UBV photometry, etc
14 p2316 A71-31006

White dwarfs from Catalog of Nearby Stars, indicating radial and tangential velocities, proper motions, positions luminosity and UBV spectra
14 p2317 A71-31009

Lunar center figure position determination by harmonic analysis, comparing with Mills III catalog
15 p2483 A71-31344

Scorpio-Centaurus association and Gould belt proper motion, discussing convergent point in FK4 catalog with maximum likelihood method
15 p2483 A71-31470

Positions and flux densities of radio sources from Fourth Cambridge catalog by pencil beam measurements at 408 MHz, using Molonglo telescope
15 p2485 A71-31697

Astronomical 4C catalog radio sources statistical analysis, showing mean spectral indices dependence on radio emission fluxes and red shifts
15 p2487 A71-32037

Lunar reverse side, cataloging reference points on western libration zone and eastern sector
15 p2495 A71-32682

Stellar ring in Aquila, reducing proper motions of stars in all catalogs to General Catalog system and to Brosche FK 4 system
16 p2632 A71-33327

Stellar catalogs errors assessment from Ceres and Vesta asteroids observations
18 p2962 A71-36109

Stellar proper motions in photographic zenith tubes programs for time service clocks correction, examining catalogs used for astronomical data processing
18 p2962 A71-36110

Selenography and selenodesy with Apollo whole-disk lunar photograph, providing positions catalog in tabular form
18 p2965 A71-36294

Statistical investigation of 1500 galaxies in MCG catalog with weak surface brightness, noting sculpture type spheroidal galaxies in Virgo cluster
20 p3289 A71-39299

Four-color and H beta photometric data tabulation for bright B type stars in Southern Hemisphere
21 p3443 A71-40192

Space distribution of OB stars from revised Victoria H gamma spectrophotometric magnitudes by MK spectral classification
21 p3448 A71-40594

Lunar center figure position determination by harmonic analysis, comparing with Mills III catalog
22 p3607 A71-42619

Extragalactic radio sources catalog from Parkes Australian National Radio Astronomy Observatory 2700 MHz survey of plus/minus 4 deg zone and selected regions
22 p3607 A71-42769

Astronomical radio sources from Parkes catalog, calculating daily and hourly variations in flux density
23 p3722 A71-42937

Goloseyev latitude star catalog, considering observation error distribution and stellar declination estimations
23 p3771 A71-44258

Ohio catalog radio source spectra and positions, presenting flux density and RMS errors
24 p3871 A71-44913

ASTRONOMICAL COORDINATES

Light speed invariance in special theory of relativity concerning Galilean coordinates
01 p0127 A71-10601

Program and auxiliary tables for stellar azimuth determination by observations near elongation
01 p0159 A71-10810

Astronomical-geodetic observations of direction of instantaneous earth rotation vector at South Pole
03 p0406 A71-13007

Mayer formula time determinations from meridian passage instrument, using star program and equalization observations
03 p0422 A71-13009

Astronomically determined latitude, longitude and azimuth reduction to common epoch, discussing secular nonperiodic pole motion due to crust drift
03 p0484 A71-13217

Gravitational waves collision analysis using coordinate system for general relativity
04 p0658 A71-15832

Astronomical-geodetic networks processing in three dimensional rectangular coordinates, considering advantages and accuracy
06 p0889 A71-17674

Stellar intrinsic motions with respect to galaxies, including solar apex coordinates, secular parallax and Oort constants
07 p1194 A71-19331

Small diameter radio sources, determining positions, flux densities and diameters
08 p1357 A71-20870

Planet rotation vector determination, using satellite stellar observations and planetary surface reference points
08 p1365 A71-21776

Geographical latitude from azimuths and zenithal measurements of two stars on hour circle
09 p1438 A71-23180

Stellar UVB photographic photometry of specific Milky Way oblong region
09 p1527 A71-23525

Laplace long period solar inequality effects on lunar ecliptic longitude, considering role in celestial mechanics
10 p1667 A71-23829

Space triangulation corrections of equatorial topocentric coordinates and radius vector of Jupiter in Baker-Nunn net, using Geos A satellite optical and laser observations
11 p1732 A71-25819

Astronomical catalogs of proper motions and positions, discussing reference systems fundamental declinations and right ascensions measurement principles
12 p1959 A71-26773

Artificial earth satellites equatorial topocentric coordinate determination, using photographic distance observations and least squares method
12 p1961 A71-26902

Astronomical latitudes determination under non-setting sun conditions from differences between star azimuths
13 p2056 A71-28011

Coordinate measurement accuracy for star and satellite photographic observation using Zeiss Ascorecord
14 p2250 A71-31121

Planet intrinsic rotation vector determination, using satellite stellar observations and planetary surface reference points
15 p2495 A71-32681

Bright quasi-stellar radio sources B2 1215 plus 30 and ON231, discussing positions and spectrum
16 p2634 A71-33401

M 13 spherical star cluster, determining spatial distribution, center coordinates, radius and dynamic behavior
16 p2634 A71-33428

Differential refraction elimination in stellar triangulation measurements for reference stars catalog and flash coordinates
16 p2642 A71-33801

Graphic method for comet geocentric equatorial coordinates transformation into heliographic coordinates, using trigonometric circle and three stereographic networks with 100 mm radii
17 p2803 A71-34834

Mars, Uranus and Jupiter observations with Sao Paulo Observatory Danjon astrolabe, presenting east and west transits right ascension and declination tables
18 p2961 A71-35943

Book on space science covering celestial coordinates, time and mechanics, planetary atmospheres and interiors, comets, meteors, stellar structure, etc
18 p2963 A71-36246

Correction values to centennial precession, using stellar proper motions
18 p2970 A71-37063

Inertial devices test pads geokinetic reference systems definition, using astronomical data [AIAA PAPER 71-911]
19 p3046 A71-37162

Mars coordinate shift from ecliptic to equator system, considering precession and orientation data
22 p3607 A71-42871

Astronomical azimuth determination for terrestrial objects from observations of star passages across object vertical
24 p3868 A71-44475

Determination method for selenographic coordinates of points on lunar surface, discussing astronomical observations from moon
24 p3870 A71-44813

Selenographic and celestial selenocentric coordinate systems determination and terminology, considering lunar rotation theory
24 p3875 A71-45191

ASTRONOMICAL MAPS

Galactic radio emission sources high resolution observation by telescope, obtaining contour maps with positions and flux densities
02 p0303 A71-11820

Spectraspectroheliograph observations, noting correlations between contour maps of solar continuum intensity and magnetic fields
02 p0315 A71-12693

Contour maps of antenna temperature in W31 region, discussing H I absorption features
07 p1198 A71-19816

Galactic center region far IR map in 75-125 microns spectral interval with 6 minute resolution
07 p1199 A71-19835

Coronal magnetic field geometry maps, using high altitude photospheric field measurements for correlations with active sun
08 p1363 A71-21154

Mercury drawings from refractor observations /1964-1967/
09 p1520 A71-22834

Mercator chart of Mars surface between 70 deg north and 70 deg south latitude from Mariner 6 and 7 photography
09 p1452 A71-23220

Jupiter observation during 1970 visibility period, including drawings, photographs, position and brightness estimates, and red spot
10 p1677 A71-24689

Interstellar CO, constructing strip maps in declination and right ascension across W51, Sgr A and Sgr B2 for 115.2712 line radiation
11 p1818 A71-25201

Venus maps from high resolution radio telescope observations, investigating surface pressure/temperature, planetary atmosphere and water vapor presence
11 p1830 A71-26109

Contour map of galactic radio emission in Cassiopeia and Cepheus region, noting discrete sources
11 p1831 A71-26132

OGO radio astronomy instrument for cosmic noise sky brightness distribution mapping by electrically short antenna ionospheric focusing
11 p1763 A71-26144

Mars surface maps from visual and photographic observations for TV picture interpretation of Mariner orbital flights
11 p1834 A71-26432

Radio mapping of Maffei 1 and 2 galaxies, confirming previously detected small diameter source
13 p2136 A71-28428

Solar chromospheric activity of 8 February 1971, obtaining brightness temperature maps at 400, 800 and 1200 microns
13 p2143 A71-29271

Mars map based on computer cataloged planetary patrol photographs
13 p2143 A71-29342

Data processing technique for radio mapping of sun, discussing unwanted harmonics elimination and noise reduction
15 p2491 A71-32447

Mars Meridiani Sinus region map preparation from computer reconstruction of near and far encounter pictures taken by Mariner 6 and Mariner 7
15 p2492 A71-32464

Cygnus-X region radio photography, presenting radio brightness intensity modulated display supplementing contour map
16 p2630 A71-33124

Water vapor emission map at 22 GHz from W 49, using three-station long baseline radio interferometer data
16 p2631 A71-33179

Radio contour map of Crab nebula at 3.5 mm, giving brightness distribution and flux density
16 p2632 A71-33235

Contour maps of radio source CTB 1 at UHF, suggesting supernova remnant superimposed on broad faint H II region
18 p2962 A71-36153

Interstellar absorption at H alpha line wavelength in Orion nebula, obtaining contour map for comparison with radio intensity
19 p3131 A71-37230

Astronomical geodetic networks equalization, using Laplace azimuths
19 p3056 A71-38174

Astronomical telescopic observations of Mars for map updating, discussing surface colors
19 p3145 A71-38570

Galactic nucleus map and flux at 10 microns scanned with 5.5 arcsec beam on Catalina observatory telescope
20 p3305 A71-39957

Two dimensional maps of circularly polarized solar emission at 7.8 GHz, noting flux density and polarization time dependence before flare
23 p3732 A71-43072

Southern Milky Way isophote maps by near-UV surface photometry, showing brightest areas in Sgr/Scor, Car, Vel/Pup and Cyg
24 p3867 A71-44436

Mars surface mapping, discussing computer reconstruction process for Mariner 6 and 7 TV picture quality improvement
24 p3875 A71-45266

Mariner 9 spacecraft mission, discussing configuration, data handling and TV surface mapping of Mars
24 p3876 A71-45267

ASTRONOMICAL MODELS

Andromeda galaxy M31 hydrodynamic model, examining kinematical and dynamical functions
01 p0150 A71-10057

Radio galaxies emission source, examining Patchy model for prestellar matter magnetic field strength
01 p0150 A71-10063

Solar corona evolution in contraction phase, calculating models based on dissipation theory
01 p0157 A71-10760

Deuterium formation in early solar system by examining autogenetic spallogenic model
01 p0157 A71-10763

Zodiacal light polarized component observation at ecliptic longitudes and latitudes compared to zodiacal cloud model
01 p0158 A71-10773

Lunar arbitrary and free librations and Euler motion of poles, considering hard and elastic models
01 p0158 A71-10807

Sunspot and photosphere electric conductivity relations based on Michard, Mattig and Fricke-Elssasser models
01 p0159 A71-10867

Linear MHD theory of inhomogeneities in axisymmetric models of universe with cosmological magnetic field
01 p0160 A71-11093

Two parameter asymptotic solutions for viscous model of solar wind flow
01 p0147 A71-11511

Regionalized models for earth with oceanic, shield or tectonic crust and upper mantle, taking phase velocities into consideration
02 p0245 A71-11992

Solar activity cycles mechanism, deriving nonlinear equations from quasisymmetric magnetic dynamo models
02 p0307 A71-12081

Galactic models from neutral H line profiles at 21 cm wavelength
02 p0307 A71-12084

Meteorites and earth core composition and models for terrestrial planets internal constitution
02 p0310 A71-12159

Optical thickness of reflecting nebula with given brightness illuminated by star, using three dimensional models
02 p0311 A71-12352

Cosmological models with noninteracting matter and radiation, deriving red shift and luminosity-distance relationship
02 p0312 A71-12464

Pulsars as rotating neutron stars with frozen-in magnetic field, accounting for energy and angular momentum losses due to gravitational radiation
02 p0300 A71-12473

Solar-mass star with carbon core and He envelope, constructing evolution model assuming energy losses due to photons with and without neutrinos
02 p0314 A71-12586

Astrophysical bodies dynamo equations describing large scale magnetic fields generation by small scale cyclonic turbulence in rotating fluid body
02 p0314 A71-12588

Jupiter model construction from improved state equation, considering chemical composition, contraction and rotation
02 p0314 A71-12589

Astronomical model for origins and time variations of compact strong sources radiation over all bands
02 p0315 A71-12663

Solar coronal structure and interplanetary magnetic fields prediction based on magnetic models, testing accuracy at solar eclipses
02 p0315 A71-12694

Solar line blanketing effect data derivation and analysis for model atmosphere computer programs, considering application to spectrally similar stars
02 p0316 A71-12755

Solar faculae semiempirical models, cospatial with strong photospheric magnetic fields constructed from continuum observations
02 p0316 A71-12757

Symmetrical solar wind model solutions with thermal conductivity, showing constant mass and total energy flux conditions relationship to critical line
02 p0303 A71-12771

Solar wind interaction with moon, using two dimensional guiding center model
02 p0303 A71-12772

Diffuse cosmic gamma ray background origin, using simple photon production model
02 p0303 A71-12837

Computerized simulation of disk galaxies evolution, using doubly periodic model for stellar motions
02 p0318 A71-12925

- Galactic spiral structure model, examining nonlinear stellar density waves in plasma cylinder
03 p0484 A71-13205
- Cosmological models with matter and radiation for evolution of universe
03 p0484 A71-13206
- Reflecting and scattering models of line formation in planetary atmospheres allowing for inhomogeneously distributed gas and particles and for anisotropic scattering phase function
03 p0486 A71-13320
- Coherent radiation mechanisms characterizing cosmic masers in molecular lines, sporadic solar radio emission and pulsar radiation
03 p0486 A71-13321
- Nonspherical stellar gravitational collapse to black hole state, discussing event horizon concept
03 p0486 A71-13324
- Mercury microwave and IR observations interpreted for thermophysical models for planetary subsurface, discussing rotation and heating
03 p0492 A71-14069
- Stellar core evolution from He burning phase to oxygen exhaustion in central region, discussing mixing with envelope under various mass conditions
03 p0493 A71-14196
- Thermal emission from IR star shells calculated from circumstellar graphite dust model
03 p0495 A71-14267
- Friedman universe model in centrally symmetric reading system
04 p0644 A71-15123
- Mathematical model of stellar atmospheres using radiation emission by elementary cylinder
04 p0647 A71-15236
- Magnetic stars, discussing stellar magnetic fields, Ap stars, crossover effect, period line width correlation, overabundances and models
04 p0648 A71-15245
- Metal-rich star evolution from main sequence to red giant, examining mass, nuclear reactions and theoretical models
04 p0648 A71-15247
- UV dwarf star evolution, using central and gap star models emphasizing photon-neutrino emission
04 p0648 A71-15250
- UV stellar flux measurements vs theoretical stellar atmosphere models, using rocket and satellite observations
04 p0648 A71-15252
- Coherent emission mechanisms for pulsar models, discussing plasma wave conversion into radio emission
04 p0650 A71-15582
- Nonpulsing pulsar model, discussing idealized neutron star with spin axis aligned with uniform internal magnetic field
04 p0650 A71-15585
- Solar atmosphere semiempirical models taking into account non-LTE conditions
04 p0651 A71-15667
- Pluto-Neptune system implications for solar system evolution theories, discussing deterministic and statistical models and a body problem approaches
04 p0655 A71-15726
- Galactic magnetic field characteristics and cosmic rays origin, discussing gas clumping and star formation
04 p0641 A71-15758
- X ray background angular structure comparison with optical galaxies spatial distribution, ruling out universe models with sources following cosmological mass distribution
04 p0657 A71-15826
- Models for partially mixed stars at He flash time, determining mixture degree effects, carbon production and total mass
05 p0801 A71-15932
- Deizner magnetostatic sunspot model enhancement by surface boundary condition derivation for horizontal pressure difference effect of photosphere
05 p0801 A71-15934
- Pulsars CP 0328, CP 0834, CP 1133 and CP 1919 radio spectra, examining interstellar scintillation model, transverse velocities and line widths
05 p0802 A71-15939
- Solar disk computed continuum and estimated line polarizations compared to BCA photosphere values, discussing metal abundances
05 p0803 A71-16019
- Pulsar number-period distribution, using oblique rotator model under electromagnetic and gravitational torque effects
05 p0804 A71-16106
- Supernova remnant kinematic distance estimates, using molecular absorption line velocities with Schmidt model
05 p0805 A71-16107
- Intergalactic gas photoionization by quasars UV radiation, using Friedman cosmological model
05 p0805 A71-16111
- Vacuum-like state of physical medium as initial state of Friedman cosmology, noting fluctuation instability for conversion into ordinary matter
05 p0806 A71-16180
- Two fluid model solar wind, predicting electron temperature and heat flow
05 p0799 A71-16692
- Closed evolving universe by vanishing pressure, considering eight different models including three cyclic models
05 p0813 A71-16811
- Black hole model for gravitational collapse of universe according to Einstein theory
05 p0813 A71-16956
- Spiral structure of galaxies identified with growing wave propagation in finite thickness axisymmetric disk hydrodynamic theory
05 p0813 A71-17036
- World models with antipoles for deriving cosmological density parameter upper bound
05 p0814 A71-17092
- Galactic cosmic ray solar modulation in interplanetary medium, discussing spherically symmetric model
06 p0949 A71-17275
- Lunar interior electrical conductivity and temperature from various conductivity models, considering interplanetary magnetic source field
06 p0964 A71-17281
- Comet origin based on Lagrange hypothesis and motion analysis, discussing planets short-period families
06 p0965 A71-17625
- Sun daily mean-interplanetary polarized magnetic fields correlation, using source surface model
06 p0968 A71-17920
- Galactic structure derived from neutral hydrogen observations, using kinematic models based on density wave theory
06 p0969 A71-17972
- Black hole model accounting for epsilon Aur eclipsing binary secondary component observations
06 p0970 A71-18031
- Phenomenological one dimensional model of solar cosmic ray propagation for anisotropy and intensity as function of time during early phases of events
06 p0950 A71-18102
- Models for solar wind modulation of galactic cosmic rays by anisotropic diffusion approximation
06 p0951 A71-18104
- Solar cosmic ray diurnal variations latitude effect explained by two way anisotropy model
06 p0952 A71-18109
- Force field model for galactic cosmic rays modulation by solar cycles, noting agreement with Fokker-Planck equation analytic and numerical solutions
06 p0952 A71-18110
- Cosmic plasma dynamics collective phenomena, investigating models, instabilities, nonlinear interactions, wave transformations, turbulence, cosmic rays and radiative acceleration
06 p0972 A71-18330
- Galactic magnetic field observation, investigating cluster polarization, Zeeman effect, pulsar rotation and signal dispersion, interstellar cloud elongation and models
06 p0972 A71-18331
- Interstellar gas and star mass interchange, discussing balance and galactic and stellar evolution models
06 p0972 A71-18334
- Supernovae expansion, investigating hydrodynamic model with interstellar magnetic fields and relativistic particles effects
06 p0973 A71-18335
- Light propagation in mixmaster universe model based on Einstein equations solution
06 p0974 A71-18428
- Solar corona active regions thermal model, taking into account X ray emission and temperature distribution
06 p0963 A71-18439
- Visible brightness of Milky Way for various galactic structure models, discussing star and dust distribution effects
06 p0975 A71-18444
- Extended stellar atmospheres production mechanism involving outward acceleration of material in rarefaction wave following shock wave arrival at atmosphere edge
06 p0976 A71-18472
- Evolutionary cooling sequences and lifetimes for low mass white dwarfs in Hyades cluster, considering near surface convection in models with hydrogen envelopes
07 p1190 A71-18856
- Magnetic stars models on possibility of rotational deceleration by hydromagnetic waves radiation without mass loss
07 p1190 A71-18857
- Maserlike pulsar radiation mechanism using Coulomb bremsstrahlung near strong quantizing magnetic field
07 p1190 A71-18858
- Flux divergence in optically thin outer layers of model moving stellar atmospheres using weighting functions in energy balance equation
07 p1190 A71-18863
- Gum Nebula-fossil Stromgren sphere of Vela X supernova, deriving ionization model from interstellar measurements
07 p1191 A71-18865
- Particle production near Kasner singularity in anisotropic cosmological model
07 p1162 A71-19217
- Vortex perturbations in Friedman cosmological model near zero time, showing perturbation growth associated with increasing Hubble expansion anisotropy
07 p1192 A71-19285
- Ionized gas galactic cluster stabilization model construction, considering ionizing radiation enhanced cosmic flux and quasar PKS 1116 plus 12 absorption spectrum
07 p1198 A71-19830
- Saturn rings radial structure model featuring purely gravitational forces association with primary and perturbers, using planar restricted three body problem formalism
07 p1202 A71-20518
- Homogeneous cosmological models evolution theory, considering Einstein equations analytic solution for lengthy era
07 p1204 A71-20536
- Radiation transport equations for stellar atmosphere model with variable depth magnetic field, considering absorption line formation and polarization characteristics
07 p1205 A71-20637
- Eclipsing variable V701 Cen photoelectric observations in UV tabulated, fitting Russell model solutions to data
08 p1357 A71-20874
- Inner and outer planets groups mass and mean density, considering terrestrial seismic data and lunar, Venus, Mars and Mercury structural models
08 p1358 A71-20888
- Solar burst theories, considering type 3 radiation source model for determination of lower corona plasma waves energy densities
08 p1358 A71-20889
- Homogeneous Newtonian cosmological model, constructing ellipsoidal velocity distributions and kinetic theory
08 p1358 A71-20932
- Newtonian big bang hierarchical cosmological model, considering mean mass density dependence on volume position and size dependence on cluster order
08 p1358 A71-20933
- Population II red giant stars evolution models, investigating relativistic degeneracy, neutrino losses core critical mass and helium flash
08 p1359 A71-20940
- Polytropic models second order pulsations, evaluating stellar pulsational stability and thermal imbalance
08 p1359 A71-20941
- Solar flare model, computing thermal X ray emission
08 p1350 A71-20945
- Interplanetary space cosmic ray density gradient from three dimensional anisotropic diffusion model
08 p1352 A71-20970
- Solar activity cycles mechanism, deriving nonlinear equations from quasi-symmetric magnetic dynamo models
08 p1362 A71-21131
- Galactic models from neutral H line profiles at 21 cm wavelength
08 p1362 A71-21134
- Globular cluster star velocities distribution, examining dynamic evolution models and gravitational effects
08 p1362 A71-21153
- Static cylindrically symmetric universes consisting of Einstein-Maxwell gravitational and electromagnetic fields, discussing central axial mass and charge or current density
08 p1334 A71-21361
- Continuous energy distribution around light maximum of Nova Serpentis 1970 represented by yellow supergiant model, correcting observations for interstellar reddening
08 p1364 A71-21416
- Expanding source model verification for radio outbursts in quasars and Seyfert galaxy nuclei
08 p1365 A71-21424
- Type 2 and 3 solar radio bursts, discussing models without reabsorption
08 p1356 A71-21755
- Type 2 and 3 solar radio burst model, examining exciting agent as electron bunch emitting electron plasma waves
08 p1356 A71-21756
- Anisotropic homogeneous cosmological model, discussing origin of movement and primordial matter chemical composition
08 p1365 A71-21771
- Solar photosphere facula, applying Schuster-Schwarzschild model for molecular lines and bedding level of carbon hydride
08 p1365 A71-21772
- Solar diatomic molecules vibrational degree of freedom model, applying Boltzmann distribution
08 p1365 A71-21773
- Solar activity cycle model, considering dynamo equations with only radial rotation differentiality
08 p1365 A71-21774
- Interstellar dust density, constructing cosmological model with gravitational equations
08 p1366 A71-21785

Universe models topology, examining relation between CT and CP invariance

08 p1366 A71-21786

Linear MHD theory of inhomogeneities in axisymmetric models of universe with cosmological magnetic field

08 p1366 A71-21951

UVB colors and polarization models for reflection nebulae based on Mie scattering functions for exponential size distribution of silicate particles

09 p1517 A71-22332

Comet 1969g spectrum at 3800-8500 Å, noting upper H alpha surface brightness limit consistency with chromospheric resonance fluorescence model

09 p1517 A71-22335

Pulsar model consisting of rotating neutron star with strong magnetic field

09 p1517 A71-22337

X ray spectrum measurement of Scorpius X-1 by Bragg spectrometer, explaining emission or absorption absence by source model with line weakened by electron scattering

09 p1518 A71-22349

Explosive nucleosynthesis in Galaxy, discussing carbon detonation, uniform density models, supernova rates and massive stars

09 p1521 A71-22929

Predicted UV fluxes for main sequence stars, comparing stellar observations with models described by Kucz, Carbon and Gingerich

09 p1522 A71-22962

Homogeneous isotropic relativistic cosmological model of universe, discussing construction

09 p1523 A71-23020

Variable stars radii effective temperature and brightness determination from stellar atmosphere modes

09 p1523 A71-23021

Hot universe model, discussing small scale entropy, matter distribution, adiabatic density perturbations, energy balance, formation of galactic clusters, galaxies, globular clusters and quasars

09 p1527 A71-23531

Quasi-radial hypervelocity approximation of rotating azimuthally dependent solar wind under magnetic field

09 p1515 A71-23709

Milne-Eddington atmosphere, using Unno transfer equations for Stokes parameters

10 p1665 A71-23778

Empirical solar photosphere continuum models, calculating temperature distribution for absolute intensities at center and limb darkening ratios

10 p1666 A71-23779

Brightness temperature from solar UV continuum in 1680 to 600 Å in photosphere-chromosphere transition model

10 p1666 A71-23780

Solar lower chromosphere two dimensional models, using relative RMS line center intensity variations and mean limb darkening curves

10 p1666 A71-23781

Solar simplified geometrical model, observing emission peak center to limb variation of Mg II, H and K lines and optical thickness

10 p1666 A71-23782

Sunspot umbra empirical model, deriving temperature and optical depth relationship from IR continuous limb darkening

10 p1666 A71-23787

Magnetostatic sunspot model with twisted field showing radial dependence of azimuthal component

10 p1666 A71-23789

Gravitational instability of nonhomogeneous cosmological model, establishing density perturbation growth as function of time for model containing matter and radiation

10 p1667 A71-23851

Nonhomogeneous cosmological model with equations describing universe relative density variation, demonstrating thermal instability role in galaxies formation

10 p1667 A71-23856

Astronomy contributions to cosmology, considering universe nature, origin and evolution

10 p1668 A71-24004

Solar wind interaction with field free planetary ionospheres, giving three dissimilar models

10 p1661 A71-24005

Computer simulation model for stars motion in plane of disk-like stellar systems, investigating dynamics of Jeans and gravitational two-stream instability

10 p1670 A71-24181

Book on relativity and discretization in astronomy covering cosmic structures, galactic isopleths equilibrium theory, red shift discretizations, etc

10 p1670 A71-24210

Neutron star matter equations of state involving hyperon formation effects for maximal stable mass models, tabulating moments of inertia

10 p1671 A71-24302

Entropy-free thermodynamics second law based on universe expansion, using homogeneous nonstatic cosmological models

10 p1674 A71-24468

Radiation and gas-dust interactions, examining dispersion relation and instability for cosmological models

10 p1675 A71-24490

Supernovae detonation model, examining nucleosynthesis for solar system abundances

10 p1675 A71-24492

Quiet solar wind two component model, including viscosity, magnetic field and reduced heat conduction

10 p1662 A71-24498

Galactic X ray thermal emission model, discussing origin and location of sources

10 p1662 A71-24675

Cometary nucleus radius, mass, composition and icy-conglomerate model

10 p1677 A71-24687

Interplanetary space low energy cosmic ray protons steady state anisotropy based on radial gradient model of outward convection at solar wind speeds

10 p1663 A71-24777

Laboratory model for radio star scintillation and other diffraction phenomena by thin weak random phase changing screen including earth atmosphere or solar wind

10 p1678 A71-24797

Pulsar oblique magnetic rotator model, noting large amplitude EM traveling wave effects on electron motion

10 p1679 A71-24956

Binary star 112 Herculis elemental abundances by atmospheric model analysis of spectra

10 p1680 A71-25001

Planetary nebulae central stars extended atmospheres, calculating gray and nongray models under hydrostatic, radiative and LTE

11 p1818 A71-25203

Massive stars evolutionary models, exploring convective instability effects

11 p1818 A71-25205

Model for relativistic electrons diffusion from IR sources, determining injected electron spectrum distortion due to inverse Compton losses and X ray spectrum

11 p1814 A71-25294

Gravitational instability picture for galactic rotation, examining numerical model for protogalaxy separation in expanding universe

11 p1820 A71-25535

Planetary nebulae mass ejection by radiation pressure, describing mathematical models for time independent outflowing envelopes

11 p1821 A71-25537

Jupiter far IR emission spectra models, examining atmospheric composition, temperature and structure

11 p1821 A71-25538

Mariner 5 Venus exospheric Lyman alpha measurements for dayside temperature value, using molecular hydrogen photodissociation model

11 p1823 A71-25692

Venus daytime ionospheric models using electron, ion and neutral gas heat conduction with momentum and chemical equations for charged particle densities

11 p1823 A71-25693

Nonuniform density cosmic plasma heating allowing energy losses by radiation and heat conduction, using filament-structured high temperature plasma region model

11 p1828 A71-25765

Planetary formation, obtaining retrograde orbit probability and distances and masses expectation by stochastic model

11 p1830 A71-26110

Spiral galaxies orientation anisotropy explanation by hypothetical model of cosmological magnetic field

11 p1831 A71-26166

Meteor streams dynamic properties, computing mean orbit elements with statistical mathematical model

11 p1835 A71-26458

Bibliography on Gegenschein covering observations, theories, models, review papers, etc

11 p1835 A71-26461

Light propagation in mixmaster universe model based on Einstein equations solution

12 p1955 A71-26578

Solar corona active regions thermal model, considering X ray emission and temperature distribution

12 p1946 A71-26589

Visible brightness of Milky Way for various galactic structure models, discussing star and dust distribution effects

12 p1955 A71-26594

Periodic rotational LF synchrotron model of magnetic neutron star for pulsar radiation

12 p1947 A71-26649

Stellar orbits for nearby stars, examining short arc statistics and galactic field models

12 p1959 A71-26781

Solar coronal heating homopolar generator model, proposing neutrons as energy source

12 p1961 A71-26877

Cosmic IR sources model based on assumption of cosmic ray particles emitting galactic sources sur-

rounded by dust shells absorbing and reemitting energy

12 p1947 A71-26933

Statistical analysis of gravitational instability for isotropic cosmological models, examining density perturbations as random functions of coordinates and comparing with galactic mass statistics

12 p1965 A71-27178

Gravitational field quantum fluctuations role in general theory of relativity and cosmological model

12 p1965 A71-27179

Equations of motion for single trajectory model of nonspiral stationary rotating stellar systems, assuming phase density dependence on motion integrals

12 p1966 A71-27234

Statistical space density and velocity perturbations of galaxies relative to origin of rotation in range of Friedman cosmological model

12 p1966 A71-27235

Jupiter equatorial thermal limb darkening data, constructing atmospheric model for ammonia effects on temperature structure

12 p1966 A71-27254

Cosmic rays origin from pulsar model with particles accelerated by magnetic dipole radiation, producing equal energy spectrum

12 p1948 A71-27365

Galaxy nuclei and quasars model, considering supernova explosions, neutron stars matter accretion and energy radiation

12 p1968 A71-27541

One- and two-component gas models for explaining interstellar gas kinematics and 21 cm line emission brightness temperature dependence on galactic longitude

12 p1970 A71-27747

Krause-Steenbeck solar dynamo eigenvalue evaluation assuming step function differential rotation and delta function alpha-effect for approximation

12 p1971 A71-27749

Linear nonadiabatic pulsations of stellar models, discussing numerical method for eigenvalue problem

13 p1332 A71-27968

Closed universes quantization and gravitational field in general relativity, emphasizing superspace concept and finite-dimensional model quantum theories construction

13 p2100 A71-28395

Expanding metagalaxy closed model with changing gravitational constant, noting matter motion in moving and central reference systems

13 p1336 A71-28423

Solar chromosphere model, explaining spicules origin and relation to small scale nonuniformities

13 p1336 A71-28430

Lunar rocks in large bright rayed craters, calculating thermal abnormality model

13 p2138 A71-28697

Necessary and sufficient global stability criteria for axisymmetric perturbations of stellar dynamic disk models of galaxies

13 p2138 A71-28775

Rotating Jacobi ellipsoid evolution by gravitational waves emission, discussing triaxial nonaxisymmetrical configurations for rapidly rotating pulsars

13 p2140 A71-29000

Compton effect in variable radio sources, considering models of Seyfert galaxies 3C 84 and 3C 120 from baseline interferometry

13 p2141 A71-29100

Early isotropic universe structure evolution, considering non-Friedmannian cosmic expansion stage, metagalactic turbulence and cosmological models

13 p2141 A71-29101

Sunspot deep subphotospheric layer structure, noting evolution, velocity field, visibility and model formulation

13 p2142 A71-29115

Solar neutrino astronomy, investigating interior central temperature, energy generation mechanism and model

13 p2142 A71-29116

Spherical waveguide eigenvalues calculation from two layer model of earth with radially inhomogeneous atmosphere, using Airy functions

14 p2209 A71-29515

Stellar wind flow models associating energy transport with propagation and dissipation of hydrodynamic waves and heat conduction

14 p2297 A71-29586

Cosmological models for creation of hierarchy of clusters within clusters, involving gravitational interactions

14 p2303 A71-29588

Spiral galaxy NGC 2403 neutral hydrogen distribution model fitting of observed velocity profiles

14 p2303 A71-29589

Galactic dynamo generated magnetic field periodic modes based on mathematical model involving cyclonic turbulence and nonuniform rotation of gaseous disk

14 p2303 A71-29591

Jupiter and Saturn magnetic field differences, considering metallic interior models

14 p2304 A71-29599

- Crab Nebula model, discussing electromagnetic field time variation and electron acceleration and synchrotron emission 14 p2304 A71-29632
- Triaxial ellipsoid asteroid models, determining light curves and variations 14 p2312 A71-30385
- Planetary nebulae observations in radio spectrum, determining interstellar extinction, electron temperature recombination theory and models 14 p2312 A71-30388
- Star and galaxy clusters total kinetic energy content, using line of sight velocity data and astronomical models 14 p2312 A71-30390
- Pulsar oblique rotator model wobble and alignment time scales, considering Crab and Vela pulsars precession damping mechanism by internal friction of crust 14 p2313 A71-30428
- BL Lac extragalactic source of radio, IR and visual radiation, estimating upper limit to distance based on spectrum model 14 p2313 A71-30452
- Galactic spirals density wave theory based on three models rotation curve patterns observation 14 p2314 A71-30639
- Spherical stellar system dynamical evolution model, applying constant point mass technique 14 p2314 A71-30640
- Stellar and interstellar magnetic fields effects on plasma instabilities in Colgate cosmic ray model, using computer simulation 14 p2282 A71-30644
- Horizontal and post-horizontal branch hydrogen rich stellar atmospheric models, presenting emergent fluxes and H and He line profiles 14 p2314 A71-30645
- Cosmic ray modulation by solar wind, developing model with time variations based on magnetic bending power 14 p2302 A71-30647
- White dwarf stars effective temperature measurements, matching absolute spectral energy distributions with fluxes from model atmospheres 14 p2317 A71-31013
- White dwarf model atmosphere, discussing DA and non-DA spectral types, surface gravity, mass-radius relation, composition and convection effects 14 p2317 A71-31014
- White dwarf line spectra, constructing atmospheric models and effective temperatures 14 p2317 A71-31015
- Hydrogen deficient white dwarf atmospheres, computing line free flux constant models for He rich compositions with varied metal abundances 14 p2318 A71-31016
- Outer planet large satellite steady state thermal models, indicating interiors at temperatures above ice-ammonia eutectic 14 p2318 A71-31125
- Quasars as nuclei of nascent galaxies, proposing protogalaxy model from spectroscopic or color observations 15 p2482 A71-31328
- Globular star clusters and spherical galaxies stability, proposing rotating gravitating masses spherically symmetrical system model 15 p2482 A71-31331
- Hydrogen burning supermassive stars hydrostatic equilibrium models from numerical integration of stellar structure equations 15 p2485 A71-31718
- Submillimeter background radiation origin possibility from extragalactic discrete sources based on cosmological models 15 p2478 A71-31828
- High density degenerate stellar plasma analysis, obtaining phase transition thresholds, elementary particle stability, thermal energy density and interaction model 15 p2487 A71-32038
- Mars IR spectral geometric albedo of bright and dark regions for surface composition model 15 p2491 A71-32419
- Apollo 12 landing site morphological and textural details from Surveyor 3 photography, considering lunar surface impact and volcanic models 15 p2493 A71-32483
- Anisotropic homogeneous cosmological model, discussing mass motion origin and primordial matter chemical composition 15 p2495 A71-32676
- Solar photosphere and faculae temperature, gas/electron pressures, density and turbulence velocity from Schuster-Schwarzschild model 15 p2495 A71-32677
- Solar diatomic molecules vibrational degree of freedom model, applying Boltzmann distribution 15 p2495 A71-32678
- Solar activity cycle model, considering magnetic dynamo equations with radial rotation differentiability 15 p2495 A71-32679
- Earth tide and nutation correlation, examining internal structure based on model with liquid center and solid inner core 15 p2401 A71-32684
- Self gravitating time independent disk-like stellar system model, investigating mass and velocity distributions 16 p2630 A71-33054
- Crab nebula pulsar model, discussing charged particles acceleration to relativistic energies by intense LF electromagnetic wave 16 p2632 A71-33236
- Angular momentum of rotating Einstein-Rosen bridge, comparing neutron star models 16 p2609 A71-33262
- Relativistic cosmological models with nonzero pressure, considering matter as perfect gas-radiation mixture and isotropic/homogeneous three space 16 p2611 A71-33274
- Einstein field equations solution for universe filled with perfect fluid of position-dependent density 16 p2611 A71-33277
- Gravitation phenomena based on uniformly expanding universe cosmological model for acceleration field 16 p2612 A71-33281
- Cosmic ray nuclei propagation through interstellar medium, solving transfer equation for simple model with allowance for boundary conditions 16 p2625 A71-33325
- Large coronal streamer with active region enhancement during total eclipse on 22 September 1968, giving model of enhancement 16 p2625 A71-33328
- Population II stars evolution models from main sequence to supergiant stage, constructing time constant loci in H-R diagram 16 p2635 A71-33432
- Computer model of eclipsing binary stars tested with photometric B and V observations and orbital elements of RU Ursae Minoris 16 p2635 A71-33436
- Book on relativistic astrophysics, Volume 1, Stars and relativity, covering stellar dynamics, astronomical models, cosmic objects evolution and star clusters 16 p2635 A71-33481
- Schuster hypothesis on celestial object relation between angular momentum and magnetic fields 16 p2637 A71-33513
- Nonlinear correction in Lagrangian density of gravitational field, deriving dusty cosmological model with no singularity 16 p2638 A71-33546
- Universe models topology, examining relation between CT and CP invariance 16 p2638 A71-33547
- Lunar interior thermal history models for setting radioactive heat sources upper limits consistent with proposed temperature distribution 16 p2642 A71-33797
- Lunar surface meteoroid activity from Surveyor 3 sample examination, comparing with predictions by cumulative-flux and near-earth models 16 p2643 A71-33849
- Solar wind modulation effects on galactic protons and cosmic rays, using radial magnetic field mathematical model and Monte Carlo method 17 p2795 A71-34373
- Quasi-closed Einstein universe model, showing orbits rotation similar to perihelions in Schwarzschild field 17 p2778 A71-34630
- Jordan theory of gravitational constant variation, showing nonreducibility to Einstein model 17 p2778 A71-34633
- Fourth order differential gravitational field equations for non-Einsteinian cosmological model, considering linearly expanding universe 17 p2801 A71-34634
- Star formation at interstellar gas cloud stage, discussing gravitational collapse, Bok dust globules, spectroscopic and IR peculiarities and models 17 p2801 A71-34696
- Hydrostatic, dynamic, hydrodynamic and two-component corona models and solar corpuscular radiation, considering heat conductivity and viscosity effects on solar wind dynamic characteristics 17 p2795 A71-34828
- Refutation of greenhouse model of Venus atmosphere from Venus 4 and Mariner 5 data, proposing volcanic activity burst hypothesis 17 p2803 A71-34835
- Luminosity curves for eclipsing Algol-type systems with extended atmospheres based on stellar models 17 p2803 A71-34840
- Lunar microwave thermal emission observation and theoretical predictions based on lunar surface models 17 p2804 A71-35177
- Cosmological singularity, considering homogeneous Newtonian universes expanding or contracting with shear and rotation 17 p2806 A71-35382
- Solar oblateness and Li abundance interpretation by model of thermally driven turbulence terminated at rotating core surface containing partial mass 17 p2806 A71-35385
- Vela X supernova remnant blast wave model and Gum Nebula formation, discussing kinetic and rotational energy transformation into radiation 17 p2807 A71-35414
- Uranus radio emission model, indicating presence of gaseous ammonia at saturation pressure 17 p2807 A71-35501
- Venusian atmospheric models from troposphere, stratosphere and thermosphere models based on satellites data 17 p2807 A71-35502
- Stellar atmospheres mathematical model, considering transfer equation reduction to linear equations set 17 p2808 A71-35556
- Nonstatic model of universe based on Newtonian cosmology, considering central body effects on interstellar dust motion 17 p2809 A71-35600
- Quasars as proto-blackholes in galactic nuclei blackhole model, discussing lifetimes, dust and IR radiation using models 17 p2811 A71-35745
- Neutron star cooling behavior models based on neutrino emission theory, explaining galactic steady state cosmic rays and pulsar radiation 18 p2959 A71-35931
- Massive pulsationally unstable stars dynamic analysis, formation and upper mass limits 18 p2960 A71-35934
- Solar alpha effect dynamo effect model, determining nonaxisymmetric magnetic field generation 18 p2960 A71-35936
- Type II supernovae observations and models, considering photographic light curves and dynamic instabilities in star development, outbursts and ejected matter composition and amounts 18 p2961 A71-35976
- Polynomial Hamiltonian for type VIII and IX vacuum cosmologies, suggesting quantized versions involving fluctuations of 3-space signature and topology 18 p2946 A71-35983
- Cyg X-1 X ray pulsar age determination and emission model speculations based on observation data for supernova remnant and radio counterpart absence explanation 18 p2962 A71-36151
- Variable and magnetic stellar model hypothesis concerning long period modulation due to radial and non-radial oscillation mode coupling beat in dipole magnetic field 18 p2962 A71-36152
- Sagittarius A model involving relativistic electron diffusion from point source due to Compton scattering for observed radio spectra explanation 18 p2957 A71-36155
- Double extragalactic radio sources luminosities and confinement observations, comparing with ram pressure prediction 18 p2963 A71-36156
- Inhomogeneous synchrotron source model calculation for correlation between linear and circular polarization, comparing with quasars observation 18 p2963 A71-36157
- Venus atmospheric model based on Mariner 5 and Venera satellites observation, comparing with optical observation from earth 18 p2965 A71-36293
- Center to limb solar brightness distribution at 1.4 mm, discussing chromospheric models and antenna beam pattern effects 18 p2965 A71-36735
- Solar corona model for structure and dynamic properties, investigating gas-magnetic field interactions 18 p2966 A71-36737
- Solar flare X-ray origin model, discussing charged particle acceleration to relativistic energies, ambient gas heating and thermal and nonthermal X rays 18 p2958 A71-36740
- Truth table analysis of models of Jupiter Great Red Spot, suggesting chromophores welling from below 18 p2967 A71-36926
- Atmospheric rotation on Venus, examining Gierasch model based on radiative drive coupled with response time lags 18 p2967 A71-36930
- Scorpius X-1 cocoon pulsar thermal X ray emission model, describing hot gaseous region around rotating neutron star 18 p2969 A71-37043
- Nonspherical axisymmetric model of minimum type solar corona, investigating light scattering electrons density distribution relation to brightness and polarization 19 p3131 A71-37240
- Stellar atmosphere line formation in magnetic fields, considering Milne-Eddington model 19 p3133 A71-37507
- Solar photosphere and low chromosphere models temperature-height profile 19 p3135 A71-37609
- Quiet sun, active regions and flares far UV space observations interpretation based on models 19 p3136 A71-37615
- Solar limb and disk intensity spectra in chromosphere-corona transition region, calculating models, element abundances structure, electron pressure and hydrostatic equilibrium equations 19 p3136 A71-37617

Solar cosmic ray data, discussing multicharged nuclei relative abundances in photosphere and propagation models 19 p3126 A71-37625

Bianchi type IX universe homogeneous cosmological model, noting oscillatory evolution near singularity and rotating axes of alternating Kasner epochs 19 p3138 A71-37851

Grand Tour meteoroid environment analysis, considering different asteroid and cometary particle models [AAS PAPER 71-110] 19 p3139 A71-37910

Extragalactic Faraday rotation models, examining galactic plane and Galaxy supercluster 19 p3142 A71-38005

Crab Nebula pulsar timing measurement leading to model involving inflation of closed magnetosphere with explosively released plasma 19 p3142 A71-38007

Proposed model with with neutrons as energy source for solar corona, discussing validity based on capture gamma ray flux expectation 19 p3127 A71-38009

Large scale alternating solar magnetic field generation by outer shell convective flow, constructing oscillator hydromagnetic dynamo model 19 p3145 A71-38353

Empirical dimensionless ratios between universal physical constants, supporting steady cosmological expanding universe model 19 p3145 A71-38543

H II region formation from type II supernovae explosion, detecting with fluorescence model 20 p3287 A71-39052

Crab pulsar observations analysis by means of nonaligning or stabilized oblique rotator, discussing starquake theory and stressed magnetic field instability as alternative interpretations 20 p3288 A71-39115

Astronomical models of solar wind interaction with interstellar medium, determining magnetic field effects on shock wave 20 p3278 A71-39139

Critique of quasar model of independent random pulse emitting sources conglomeration from incompatibility with light curve 20 p3289 A71-39294

X ray background model based on photons bremsstrahlung emission by subcosmic metagalactic electrons or protons 20 p3279 A71-39296

Critique of Smith oblique rotator model for Crab pulsar radiation, concerning observation of optical pulse position angle variation and interpulse offset location 20 p3279 A71-39402

MHD models of photospheric layers of sunspots emphasizing magnetic forces distribution 20 p3292 A71-39444

Fast hydrogen clouds in galactic halo related to galaxies formation model 20 p3293 A71-39448

Astronomical models relating sunspots to solar magnetic field existence 20 p3293 A71-39530

Brans-Dicke cosmologies in arbitrary units, deriving power law solutions in flat Friedmann space 20 p3294 A71-39557

Exact solutions to radiation-filled Brans-Dicke cosmologies, using Robertson-Walker metric 20 p3294 A71-39558

Gum Nebula conceived as hydrogen gas mass ionized by UV radiation from supernova explosion related to Vela X remnant, discussing fossil Stromgren sphere model 20 p3294 A71-39572

Two-parametric models of interplanetary dust distribution predictions involving zodiacal light scattering measurements from space probes for in- and out-of-ecliptic missions 20 p3219 A71-39637

Qualitative micrometeoroid model for predicting results of in situ experiments, considering correlation to Pioneer 8 and 9 results 20 p3300 A71-39654

Lunar interior electrical conductivity and temperature three-layer model from magnetic transient response measurement in solar wind 20 p3301 A71-39877

Solar boundary conditions effect on interplanetary propagation of solar flare particles for anisotropic diffusion model 20 p3285 A71-39896

Continuous injection models for secular X ray and radio emission from supernova remnants in Crab Nebula, Cas A and Tycho 20 p3304 A71-39942

Neutron star models, discussing crystalline crust, particle superfluid properties, rotational vortices and relation to Crab Nebula pulsar 20 p3304 A71-39944

Supermassive pulsar model of quasars periodicity and luminosity for Kelvin-Helmholtz contraction, concerning gravitational-rotational energy transformation 20 p3304 A71-39946

Crab Nebula pulsar magnetosphere, considering model of rotating magnetized neutron star rate of energy generation and rotation law exponent 20 p3305 A71-39948

Pulsar radio emission via maser amplification, presenting model based on electrons behavior in intense magnetic field 20 p3285 A71-39949

Critical analysis of big bang cosmological theory, discussing evidence insufficiency and steady state universe possibility 20 p3305 A71-39955

Magnetic A stars accretion model, investigating spectra, abundances, ion capture and braking 21 p3439 A71-40051

Partially thermalized model of stellar system, considering potential and density distribution 21 p3439 A71-40052

Stellar models with He envelopes and carbon-oxygen cores, discussing interior structures and evolution of helium and R CrB stars 21 p3440 A71-40055

Hydrodynamic model of adhering meteors substantiating cosmogonic Laplace-Schmidt hypotheses of solar system planetary formation from cosmic dust 21 p3441 A71-40076

Expanding metagalaxy closed model with changing gravitational constant, noting matter motion in moving and central reference systems 21 p3441 A71-40078

Relativistic and Newtonian neutron star models with nuclear forces in equation of state, using unitary transformations for hard core and soft core potential 21 p3442 A71-40143

Closed formula for relation between luminosity and red shift in expanding Friedman universe for positive cosmological constant, positive space curvature and vanishing pressure 21 p3443 A71-40186

Interstellar medium time dependent model, investigating supernovae and hot stars UV ionization effects on ion production and heating and cloud formation 21 p3445 A71-40248

Computer model for dynamical evolution of isolated disks of stars with initial velocity dispersions corresponding to Toomre criterion, noting instability relative to large scale modes 21 p3445 A71-40410

Young dust-filled planetary nebulae models with hot central stellar black body radiation, evaluating IR radiation absorption and reradiation in H I region 21 p3446 A71-40417

Galaxy active nucleus and quasar fragmentation based on model of rotating supermassive star releasing thermal radiation 21 p3449 A71-40610

Polarized plane electromagnetic waves oblique specular reflection from discretely layered lunar models based on Apollo 11 and 12 data, determining near-surface layers electrical properties 21 p3450 A71-40644

Open star clusters characteristic parameter derivation for boundary potential, radius, stellar mean distance, masses and mean angular velocities based on strip counts 21 p3450 A71-40711

Cosmological models of universe based on expansion-gravitational interaction, including red shift, radio sources, quasars and background radiation measurements 21 p3451 A71-40776

Neutron star matter equation of state and models from energy computations, discussing maximum stable mass 21 p3452 A71-41034

Solar corona current sheet magnetic model, computing polar plume orientations and radial and nonradial streamers 21 p3453 A71-41359

Fireball identification method in accelerator and cosmic ray produced jets, considering model improvement for Lorentz factor determination 21 p3439 A71-41396

Extragalactic radio sources counts for proportional space volume determination, comparing various cosmological models 22 p3596 A71-41445

Solar atmosphere closed magnetic loop system model, determining surface differential rotation rate and angular velocity distribution 22 p3596 A71-41452

Thermal effects in loop prominences formation after solar flares from model computer simulation 22 p3597 A71-41459

Nonuniform density cosmic plasma heating allowing for energy losses by radiation and heat conduction, using filament-structured high temperature plasma region model 22 p3598 A71-41533

Jupiter disk temperature measurement at eight frequencies in 20.5-35.5 GHz range, comparing with saturated ammonia model calculations 22 p3599 A71-41922

Period-age distribution of pulsars, using radio and optically emitting neutron star model 22 p3599 A71-41925

Circinus pulsating X ray source spectrum analysis, considering bremsstrahlung and black body models 22 p3592 A71-41928

Close binary stars monochromatic reflection effect calculation, using surface temperature distribution model 22 p3599 A71-41934

Open clusters membership probabilities and frequency distribution function parameters calculation by fitting relative proper motions to model with maximum likelihood procedure 22 p3601 A71-42161

Cosmic ray and soft X ray steady state models of interstellar gas, determining He/H ions concentration ratio 22 p3601 A71-42167

Nearly diurnal nutation observations from Danjon astrolabe data, comparing theoretical earth models 22 p3602 A71-42172

Dynamic model for Saturn rings radial structure, considering outside composition material, Titan perturbation effect and particle space density 22 p3603 A71-42186

Supernova shell fragmentation as basis for solar system formation model, considering meteoritic materials heavy elements formation by nucleosynthesis is followed by r-process event 22 p3604 A71-42192

Planetary formation from sun ejected charged bodies captured in orbit due to electromagnetic effects, considering Sarvajna model 22 p3604 A71-42334

Interstellar spherical grains surface roughness model, noting far UV radiation extinction enhancement 22 p3605 A71-42340

Statistical analysis of gravitational instability for isotropic cosmological models, examining density perturbations as random functions of coordinates and comparing with galactic mass statistics 22 p3605 A71-42452

Gravitational field quantum fluctuations role in general theory of relativity and cosmological models 22 p3605 A71-42453

Radio source counts interpretation by cosmological evolution models, suggesting luminosity role 22 p3606 A71-42600

Quasars as nuclei of nascent galaxies, proposing test of protogalaxy model from spectroscopic or color observations 22 p3606 A71-42603

Globular star clusters and spherical galaxies stability, modeling as rotating gravitating masses in spherically symmetrical system 22 p3606 A71-42606

Book on cosmology covering stars, galaxies, radio galaxies, universe models, quasars, expansion, intergalactic matter and microwave radiation 22 p3607 A71-42773

Pulsar speedup due to neutron starquakes, deriving self gravitating elastic incompressible sphere model for time prediction 23 p3722 A71-42894

Globular cluster RR Lyræ horizontal branch stellar models, investigating masses luminosities and compositions 23 p3723 A71-42944

Pole-on Be star envelope models, comparing H alpha line profiles with line of sight perpendicular rotation axis 23 p3723 A71-42945

Phase dependent spectra of Cepheids from multifrequency group calculations in radiative transfer model 23 p3723 A71-42946

Mathematical model for solar flares formation based on magnetic/kinetic energy conversion, investigating plasma instability 23 p3719 A71-42950

Solar high energy particles directional and temporal properties, investigating single encounter model with propagating interplanetary shock waves 23 p3720 A71-43153

Mixed world model with arbitrarily moving matter, using coordinate system with matrix of reference point components of three dimensional metric tensor 23 p3736 A71-43404

Lunar surface history model, discussing mascons, chemical composition, isochron ages and seismic and electrical properties of samples 23 p3746 A71-43670

Energy balance in cool quiescent solar prominences, using 6000 km 6000 K isothermal slab model 23 p3767 A71-43843

Lunar gravity estimate from low degree spherical harmonic coefficients in potential model and Lunar Orbiter 4 radio tracking data reduction 23 p3768 A71-43882

Floccule theory three dimensional planetary formation model of collapsing cloud leading to nonplanar system with protoplanets in retrograde orbits
23 p3769 A71-43991

Dissipative processes role in early universe within chaotic cosmology program
23 p3769 A71-43992

Uniform model universes with matter and black body radiation, obtaining radiation temperature dependence on scale factor
23 p3769 A71-43994

Kinetic theory of collisionless system in closed anisotropic cosmologies including rotation effects
23 p3705 A71-44123

Initial singularity removal in model big bang universe compatible with 3K black body radiation in terms of renormalized gravitational theory
23 p3770 A71-44182

Analytical model of eclipsing binary star systems, testing validity through numerical integration error analysis
24 p3867 A71-44437

Stellar density function outside symmetry plane of galactic phase-space model
24 p3868 A71-44461

Spectral characteristics of continuous radio emission of extragalactic binary objects, discussing model of binary radio source formation from dipole nucleus
24 p3869 A71-44801

Semitransparent particle model of Martian surface for reflective power at various incidence and reflection angles, discussing packing density and optical parameters
24 p3869 A71-44808

Fresnel diffraction model appropriateness for stellar occultation by moon
24 p3871 A71-44912

Model computations for Population I star in evolutionary phase from He exhaustion in stellar center up to carbon ignition
24 p3872 A71-45076

Solar radio burst generation model based on effects of strong shock waves during chromospheric flares for geomagnetic storm prediction
24 p3867 A71-45081

Pulsar JP 1933 distance lower limit from 21 cm absorption and galactic rotation model, noting scintillation parameters consistency with observations in thin screen model
24 p3873 A71-45141

Extragalactic astronomical approximate dependences in cosmology of homogeneous isotropic universe from series expansion, considering Einstein field theory and Hoyle matter creation tensor
24 p3874 A71-45175

ASTRONOMICAL OBSERVATORIES

NT OAO
NT OSO
NT OSO-E

Radio astronomy in millimeter and submillimeter ranges, surveying programs and equipment at various observatories
01 p0156 A71-10450

Czech circumzenithal instrument used with astronomical telescope for equal altitude stellar observation, discussing optical system, electronics and measurement results
01 p0082 A71-10872

Pulkovo astronomical expedition in Chile, concerning faint star coordinates and equipment for telescopic, electrophotometric and spectral observations
07 p1083 A71-19326

Pulkovo observatory six channel two slit single photomultiplier rotating photographic plate magnetograph, for solar spectra polarization and radial velocities observation
07 p1109 A71-19337

Stellar image quality at Abastumani on Mount Kanobili, considering image diffraction picture at 755 magnification
07 p1201 A71-20440

Byurakan Astrophysical Observatory instrumentation and research program
09 p1429 A71-23352

IR astronomy high altitude sites, discussing optimal geographic locations, observation conditions criteria, transportation and survival measures
11 p1743 A71-25242

Martian cloud motions from Lowell Observatory plates following local positions of well-defined clouds
11 p1826 A71-25722

Radio astronomy in millimeter and submillimeter ranges, surveying programs and equipment at various observatories
12 p1967 A71-27421

Crimean astrophysical observatory horizontal solar telescope, describing spectrograph spectral bandwidth and dispersion characteristics
14 p2240 A71-29984

Star observation by moon-based telescope for star diameters, multiple components and precise occultation times by distortion and diffraction pattern analysis
14 p2312 A71-30374

Book on space observatories covering atmospheric structure, space astronomy applications, atmospheric attenuation, balloon IR sounding, satellite observation, etc
14 p2316 A71-30895

Skylab as orbital factory, worksite and observatory for experiments in science, technology, materials science and manufacturing
15 p2500 A71-31460

Ruby laser ranging of moon, describing Pic du Midi Observatory laser telemetry station and Luna 17 retroreflectors
16 p2640 A71-33752

Distributed computer system at McDonald observatory, discussing experience with IBM 1800 process control computer time shared operation
17 p2711 A71-35011

Climatological European southern observatory in Chile, describing spectroscopic and photometric telescopes, grand prism objective and double astrograph
20 p3210 A71-39527

Australian National Radio Astronomy Observatory integrated time and frequency system with cesium beam frequency standard and digital computer for real time operation
22 p3547 A71-42498

Goloseyev latitude star catalog, considering observation error distribution and stellar declination estimations
23 p3771 A71-44258

Wanshaff vertical circle flexure determination at Goloseyev, using collimator tube, plane mirror and autocollimation ocular
23 p3680 A71-44262

Odessa observatory meridian circle pivot irregularities effects determination on horizontal axis inclination and azimuth, using Challis method
23 p3680 A71-44263

Goloseyev Wanshaff vertical circle photographic device, discussing photomicroscopes and automatic control unit
23 p3680 A71-44265

Odessa observatory automatic film winding photoelectric system, discussing construction and accuracy
23 p3680 A71-44266

ASTRONOMICAL PHOTOGRAPHY

International joint optical and radio astronomical observations on Saturn rings and disk 1966/
01 p0149 A71-10046

Solar eclipse observations of 7 March 1970, discussing site selection, shadows, corona, prominences, temperature measurements and photographs
01 p0151 A71-10117

Radio sources optical position measurement on Schmidt plates
02 p0314 A71-12578

Vela pulsar optical emission identification using phase selective image tube photographs
02 p0315 A71-12658

Transverse conductivity and temperature dependence of storage time during photographic scanning of astronomical objects with superorthicon camera
03 p0422 A71-13008

Tunable filter reflecting telescope and accessory optics for H alpha monochromatic photography of electron corona during total eclipse
03 p0424 A71-13626

K corona radially and tangentially polarized components coronal differences from 7 March 1970 eclipse photographs analysis
03 p0489 A71-13628

Double photographic techniques for meteors and trails, discussing assembly, control and operation
04 p0589 A71-14831

Star image vibration trail amplitude, determining rms deviation with automatic system
04 p0590 A71-14843

Astrophotographs reduction for wide angle negatives, using linear and eight constants method
04 p0599 A71-15559

Cooperative international program of monochromatic coronal photography with interference filters for 1973-1976
06 p0968 A71-17911

Deimos and Phobos photographic observations with light reducing slit attenuator diaphragm on refractometer
07 p1195 A71-19335

Telescope star photographic magnitude perception maximum capacity, considering effective or equivalent quantum yield and photoemulsion sensitivity
07 p1109 A71-19346

Atmospheric noise effect on solar granulation photographic observation based on cross correlation between identical measurements
07 p1200 A71-20037

Variable emission star BD plus 28.637 deg three color photographic observation data evaluation, giving light curves and H-R position
07 p1201 A71-20435

Photometric field error of Abastumani Schmidt camera determined from Hyad cluster photographs attributed to distance errors from vignetting of optics
07 p1115 A71-20442

Multicolor photographic photometry of NGC 4254 galaxy using electro-optical converter, observing H alpha emission and H II regions at galactic center
07 p1205 A71-20634

International joint optical and radio astronomical observations on Saturn rings and disk 1966/
08 p1361 A71-21040

Telescope plate scanner automated computerized operation, evaluating faint stars identification and color classification for annual motion surveys
09 p1443 A71-22646

Mars yellow clouds extent during near perihelion apparitions since 1877, considering dust storm origin in Southern Hemisphere
09 p1520 A71-22698

Folded all-reflecting Schmidt camera UV image converter system for space astronomy applications, discussing pressure sensitivity effects on UV direct recording emulsion
09 p1447 A71-22751

Venus photographs analysis during synoptic periods, noting inconclusive results on cloud layer and planetary surface structures
09 p1521 A71-22845

Planetary nebulae NGC 1535, 6572, 6543, 7662 and 7009, observing monochromatic photographs and isophotic contours
09 p1521 A71-22870

Rotating photoshutter for astronomical instruments, describing design, electric circuit and operation characteristics
09 p1451 A71-23188

Asteroids photographic observations for catalog of faint stars positions orientation, correcting observation times to ephemeris time
09 p1525 A71-23338

Jupiter observation during 1970 visibility period, including drawings, photographs, position and brightness estimates, and red spot
10 p1677 A71-24689

High resolution UV solar photographs by stratospheric balloon-borne Cassegrain telescope
10 p1680 A71-25018

Scattered stellar clusters region stars and interstellar matter from photographic magnitudes diagrams and color indices, determining absorption fluctuations by color excess technique
10 p1681 A71-25127

Solar radio short and fast-drifting bursts observations with high spectral resolution, describing duration, frequencies bandwidth and polarization
12 p1946 A71-26591

Sunward-pointing secondary tail of comet Tago-Sato-Kosaka observed on astronomical plates
13 p1238 A71-28763

Four stage image intensifier testing for weak astronomical object photography in connection with 42 inch Cassegrain telescope
13 p2070 A71-29138

Mars map based on computer cataloged planetary patrol photographs
13 p1243 A71-29342

Motions in chromospheric limb and disk flares based on H alpha photography
14 p2298 A71-29974

Visual binary star observations by Lallemand electronic camera and photo-electronic image devices
14 p2311 A71-30363

Lallemand camera for photography of visual binaries, avoiding atmospheric motion effects by double image recording
14 p2312 A71-30375

Planetary nebula NGC 7009 narrow band filter photographs and spectra, detailing emission lines, intensity and velocity variations and model
14 p2313 A71-30430

Optical distortion coefficients of objective for astronomical camera
14 p2250 A71-31116

Camera vibration, and refraction anomaly effects on error of designated position for star or satellite
14 p2250 A71-31120

Nucleus brightness of comet Ikeya-Seki from plates in photographic and photovisual spectral regions, indicating relation to solar rotation
15 p2484 A71-31667

Photographic observations of meteors with flares, noting particle, solar and earth atmosphere role
15 p2486 A71-31895

Pleiades flare stars photographic magnitude and brightness data, establishing relation between amplitude and duration
15 p2486 A71-32029

Planetary nebulae nuclei colorimetric, photographic and brightness data, listing temperatures, absolute values and bolometric corrections
15 p2487 A71-32034

Irregular variable BL Lac photographic observations, equating object with radio source VRO 42.22.01
16 p2635 A71-33430

- Astronomical photography of solar eclipse of 7 March 1970 from two locations indicating negative evidence of bulk particle movements above 20 km/sec related to cosmic rays 16 p2642 A71-33810
- Automatic star follower for camera by optically splitting stellar image and measuring radial displacement by comparing signals 17 p2740 A71-34987
- Automatic precise centering on photographic plate star image by movement across scanning slits for orthogonal coordinates and processing in on-line computer 17 p2742 A71-34999
- Jupiter Red Spot and other photographic features in 1969-1970, noting 90-day oscillation in longitude and south tropical zone disturbance 18 p2964 A71-36289
- Doppler velocity field recording method over two dimensional solar active region image, using narrow band filter with video photographic subtraction technique 18 p2924 A71-36730
- Solar chromosphere and corona manifold structure data, using high resolution filter photography 19 p3136 A71-37616
- Bright-dark asymmetry testing in solar granulation photography by objective method 19 p3146 A71-38663
- Stellar proper motion measurement by densitometer automatic scanning of star plates pairs, assessing accuracy 20 p3239 A71-39529
- Statistical analysis of microphotometer scan of solar granulation photographs blurring during partial eclipse of 20 May 1966, correcting image for atmospheric and instrument effects 21 p3439 A71-40053
- Open stellar clusters Tr 14, 15, 16 and eta Carinae Nebula distance determination, using photoelectric and photographic photometry 21 p3441 A71-40064
- Icarus photographic observations, determining general relativity effects on orbital motion 21 p3443 A71-40187
- Photographic photometry of M67 to 200-inch telescope limit for main sequence star evolution track 21 p3446 A71-40414
- Reflecting telescope Schmidt camera photographic color system temperature dependency from cluster NGC 103 photographs 21 p3379 A71-40717
- Interstellar clouds internal structure investigation by photographic photometry, determining maximum density 21 p3451 A71-40718
- Internal structure investigation of interstellar clouds in Cassiopeia, discussing color equation, photographic plate characteristics and accuracy 21 p3451 A71-40719
- Quasar brightness estimates on celestial photographs, noting variability on time scale 21 p3451 A71-40722
- Solar limb high resolution photography at different H-alpha wavelengths, using tunable I-8A and IA Halle filters in tandem for parasitic light elimination 22 p3596 A71-41455
- Quasars light curves and intensity-time tables 23 p3769 A71-43993
- Background illumination effect on stellar magnitude photographic measurement, noting stellar image reduction 23 p3680 A71-44309
- Photographic monitoring of radio sources with flat or peaked spectra, identifying as quasars or unstable galactic nuclei by optical variations 24 p3872 A71-44920
- High resolution Mars photographs obtained with 61-inch reflector telescope 24 p3872 A71-44998
- Martian dust storm observation by telescope in New Mexico, noting brilliant yellow cloud cover 24 p3874 A71-45000
- Deimos and Mars photography observation by 400 mm astrophotographic camera, introducing corrections for irregularities in satellite motion and planet phase 24 p3874 A71-45177
- Computer processed photographic observations of Pluto, 10 Hygiea, 433 Eros and Saturn satellites VII, VIII and IX 24 p3874 A71-45178
- ASTRONOMICAL PHOTOMETRY**
- NT STELLAR SPECTROPHOTOMETRY**
- Spiral galaxy NGC 6946 photometric observations, examining stellar magnitudes, color indices, associations distribution and distance 01 p0149 A71-10055
- Solar active regions lambda 10 830 line from photometric observations, determining optical thickness, Doppler width and radiation source activity 02 p0306 A71-12080
- Planetary surfaces photometry, discussing parameters, phase laws, albedos, spectral reflectivities, phase function theory and light scattering 02 p0309 A71-12156
- Photographic and photoelectric photometry of asteroids, discussing luminescence, reflectivities, light curves, colors and phase variations observations 02 p0310 A71-12157
- OB stars existence on utmost borders of M 31, using photometric statistics 02 p0312 A71-12465
- Compact galaxies one-magnitude light output near M3, discussing photometric statistical data 02 p0313 A71-12469
- Small radio sources emission, examining correlation with optical photometric properties abnormalities 02 p0317 A71-12863
- Photometric maps of reverse side lunar surface from AIM Zond 3 material 03 p0484 A71-13215
- Galilean satellites spectral reflectivity from photometric observations during Jupiter apparitions 03 p0488 A71-13554
- Astronomical objects light polarization recording on magnetic video tape, providing digitized data for computer input 03 p0424 A71-13631
- Normal main sequence B stars, distinguishing features from rapid rotators and supergiants by photometric scheme 05 p0805 A71-16118
- Sco X-1 optical spectroscopic and photometric observations, noting H alpha and H ion emission lines pattern-continuum brightness relationship 05 p0812 A71-16698
- Mariner photometric data, examining variations in Martian surface limb darkening with reciprocity principle 06 p0898 A71-17633
- Type I supernovae brightness curves analysis by photometry 06 p0975 A71-18435
- Background effects on photographic stellar image photometry 06 p0902 A71-18445
- Image tube for extrafocal photometry of faint galaxies, solving small scale sensitivity fluctuation problems 06 p0902 A71-18473
- Planetary nebulae upper distance limits by photometry, including mean nebular parameters and extinction coefficients in galaxy dust model 07 p1191 A71-18999
- Superassociations in late morphological type galaxies, discussing photometric and colorimetric observations 07 p1192 A71-19284
- Photographic observations of meteors with flares, noting particle, solar and earth atmosphere role 07 p1193 A71-19315
- Nuclei reddening of Seyfert galaxies NGC 1068 and 1275 from photoelectric spectrophotometric observations 07 p1197 A71-19813
- Multicolor photographic photometry of NGC 4254 galaxy using electro-optical converter, observing H alpha emission and H II regions at galactic center 07 p1205 A71-20634
- Night sky H beta photometry, showing solar type spectrum at high galactic latitudes and net emission at low latitudes 08 p1350 A71-20946
- Solar active regions lambda 10 830 line from photometric observations, determining optical thickness, Doppler width and radiation source activity 08 p1361 A71-21130
- Solar color index calibration from Mg b triplet photoelectric measurement for dwarfs and Jupiter satellites 09 p1516 A71-22064
- Comet Bennett 1969i IR narrow band filter photometry 09 p1442 A71-22067
- Stellar spatial densities in cluster NGC 6913 area, based on two color photometry and spectral classifications 09 p1524 A71-23185
- Telluric lines from 6327.5 to 6330.0 A in solar spectrum from photoelectric observations 09 p1525 A71-23196
- WX Cep eclipsing system photoelectric components computed in standard UBV colors, obtaining orbital elements 09 p1527 A71-23526
- Titan visual photometric observations, describing measurement procedures and error sources 09 p1528 A71-23549
- Interior umbra observations during lunar eclipses, using photometric analysis 09 p1530 A71-23718
- Solar flares explosive phase in photometric terms for flash onset correlations with 10.7 cm radio and hard X ray bursts, using H alpha film records 10 p1660 A71-23793
- German book on variable stars covering supernovae, novae, pulsating variable stars, symbiotic objects, galactic nebulae, stellar and galactic evolution, astronomical photometry, etc 10 p1675 A71-24479
- Jovian band color variation spectral observations using narrow band photometry 10 p1676 A71-24499
- Solar limb darkening measurement with high temporal resolution and inner corona photometry by white and polarized light during 7 March 1970 eclipse 10 p1678 A71-24829
- Ionized gas and dust distribution in Orion nebula from Balmer line intensities photoelectric measurements 11 p1818 A71-25202
- Jupiter color variations observation by multicolor photoelectric photometry, noting consistency with activity in Jovian atmosphere 11 p1827 A71-25725
- Type I supernovae maximum brightness and occurrence time from photometric analysis 12 p1955 A71-26585
- Background effects in stellar photographic photometry 12 p1903 A71-26595
- Automated and conventional photometry of short period variable star 14 Aurigae, using automatic telescope 12 p1956 A71-26617
- Radio quiet compact galaxy I Zw 1/0051 plus 12/ photometric data, noting variability and brightness levels 12 p1957 A71-26622
- Astronomical photometry and photometric systems, discussing spectral classification, U, V, B, Y, beta system, energy distributions and seven color photography 12 p1903 A71-26774
- Rapid scan astronomical spectrophotometer with 1024 channel for signal averaging on slow change in sky transparency for improving accuracy 12 p1904 A71-26803
- NGC 3351 galaxy core spectrophotometry of optical spectrum covering emission and absorption lines 12 p1960 A71-26831
- Circumterrestrial meteoroid dust cloud properties based on night sky brightness photometric observation 12 p1964 A71-27090
- Solar corona photometry during 22 September 1968 eclipse, determining brightness variations and decrease from limb 12 p1966 A71-27231
- BY Dra stellar flare characteristics by photoelectric observations, noting duration 12 p1971 A71-27750
- Saturn, Titan and ring IR photometric observations, examining brightness temperature albedos, optical thickness and individual particles 13 p2134 A71-28283
- Jovian atmosphere physical properties inferred from eclipses of Galilean satellites, using color photoelectric photometry 13 p2134 A71-28284
- Four eclipse reappearances observations of Jovian satellite Io by area scanning photometer, considering anomalous brightening 13 p2134 A71-28285
- Dark companions and extrasolar planetary system detection, discussing characteristic colorimetric signature method 13 p2134 A71-28291
- Jupiter Galilean satellites narrowband photometric data, observing albedos, spectral reflectivity, rotational phase, and brightness variations 13 p2135 A71-28292
- Iapetus magnitude variations due to orientation changes in poles, comparing visual and photometric observations 13 p2136 A71-28389
- Iapetus photometric observations, obtaining light curve by plotting rotational phase angle against magnitude 13 p2136 A71-28390
- Astronomical photoelectric photometer design features, operation modes and efficiency 13 p2067 A71-28391
- Temperature dependent isophote wavelength in Brill and Planck formulas, comparing uvby and UBV photometric systems 13 p2068 A71-28512
- Narrow-band photometry of comet Bennett, giving intensity profiles and interference filter transmission curve 13 p2138 A71-28761
- Photometric IR observations of Nova Serpentis 1970, showing visual flux decrease 14 p2303 A71-29576
- Binary stars photometry, considering optical, physical and orbital pairs 14 p2312 A71-30373
- Bright comets particles albedo, absorptivity and size observation by combined IR and optical photometry 14 p2314 A71-30649
- Photometric meteor mass calculations from observational data, discussing Fe and Cu photographic luminous efficiency measurements accuracy and interpretation 14 p2314 A71-30651

Albedo-optical thickness relation in photometry of gas and dust comets 15 p2484 A71-31663

Monochromatic photometry of comets for molecular emission bands in head spectra, using wideband and narrowband filters 15 p2484 A71-31665

Cometary nuclei photometry, using focal images of stars with normal exposures as calibration markings in plate characteristics 15 p2484 A71-31666

Photometry of head and tail regions of comets Kosik, Akhmarov-Iurlov-Hassel, Arend-Roland and Mrkos by equidensity method, using Sabatier effect 15 p2484 A71-31668

Lost City /Oklahoma/ meteorite photometric and trajectory data, comparing flight characteristics with other fireballs 15 p2489 A71-32360

Rocket-borne coronagraph photometry of solar corona during solar eclipse of 7 March 1970 16 p2640 A71-33733

Solar corona photometric intensity and polarization measurements during 1970 solar eclipse 16 p2580 A71-33819

Neutral hydrogen interstellar wind parameters from Lyman alpha sky background measurements outside geocorona by photometers on OGO 5 16 p2643 A71-33834

Netherlands space research including solar, stellar and cosmic radiation observations, photometry and satellite geodesy 16 p2666 A71-33858

Lunar surface anomalous brightness during 26 March 1970 photometric and polarimetric observations, discussing possible correlation to solar activity 17 p2797 A71-34183

Asteroids and comets bibliography and review, considering celestial mechanics and astrometry, photometry, spectra, polarimetry and radar measurements 17 p2798 A71-34455

Micrometeoroids bibliography and review, considering ground based photometry and scattering theory, satellite flux measurements, particle collection and craters 17 p2798 A71-34456

Brightness fluctuations in photometric nucleus of Ikeya-Seki comet at 29-31 March 1968 17 p2803 A71-34832

Nova N Her 1963 brightness variations from photometric observations, interpreting data in terms of stellar evolution 17 p2803 A71-34839

Computer controlled pulse counting technique application to astronomical photoelectric photometry for improved telescope efficiency 17 p2740 A71-34989

Variable star brightness measurement, using on-line electronic computer, analog to digital converter and reflector with direct current amplifying photometer 17 p2741 A71-34990

Small digital computers applications to astronomical electronic instrumentation systems of microphotometry and spectroscopy 17 p2743 A71-35010

H beta fluxes of planetary nebulae along southern Milky Way from photoelectric telescope 17 p2809 A71-35593

Galactic star cluster K 4 and Ba 10 observations with RGU photographic photometry, noting distances and types 18 p2960 A71-35938

Photometric and spectroscopic study of NGC 3627 galaxy nucleus during optical observation of radio point galaxies 18 p2963 A71-36192

Supermassive double galaxy spectrographic and photometric data for cluster Abell 1775, showing radial velocity difference, visual magnitude and mass estimates 18 p2969 A71-37041

Cepheid beta Doradus color photometry data, detailing temperature, mean radius, absolute magnitude and surface gravity variations 18 p2971 A71-37070

H alpha emission photometry for galactic H II region, obtaining contour diagrams 19 p3130 A71-37227

Comet Tago-Sato-Kosaka isophotometry, obtaining surface brightness distribution and solar wind velocity estimate 19 p3130 A71-37228

Solar corona photometry during 22 September 1968 eclipse, determining brightness variations and decrease from limb 19 p3132 A71-37383

Circumterrestrial meteoroid properties based on night sky brightness photometric observation 19 p3133 A71-37440

Globular cluster NGC 6541 UVB photometric investigation, determining distance from sun and galactic plane 19 p3143 A71-38164

Pulse, nebula and wisp component in photometric and polarimetric observations of Crab pulsar 20 p3303 A71-39932

Rhea and Titan UVB photoelectric observations, obtaining light curve magnitude variation 21 p3440 A71-40056

Open stellar clusters Tr 14, 15, 16 and eta Carinae Nebula distance determination, using photoelectric and photographic photometry 21 p3441 A71-40064

Critical evaluation of spectroscopic and photometric observations related to radio source 3C 386, suggesting foreground galactic star superposition on radio galaxy 21 p3447 A71-40443

Seyfert galaxy micron photometry measurements, determining IR radiation flux changes with time 21 p3449 A71-40611

Interstellar clouds internal structure investigation by photographic photometry, determining maximum density 21 p3451 A71-40718

Photometric determination of solar granulation rms intensity fluctuation, using ground telescope 22 p3596 A71-41453

Low cost two channel pulse counter /RUFAS/ for astronomical photoelectric occultation observations, describing resolution, data output and computer interfacing 22 p3542 A71-41932

Photometric coefficient of activity in Jupiter atmosphere at 4300, 5500 and 6400 A, giving relative intensities of belts and zones 22 p3603 A71-42183

Photometric study of Jupiter atmospheric activity in yellow light, noting peculiar activity in equatorial area 22 p3603 A71-42184

Photometric study of short term variations of Jupiter atmospheric activity in UV, blue, green, red and near IR spectral ranges 22 p3603 A71-42185

Photometric study of light variation and variable stars in luminous supergiants in Large Magellanic Cloud 23 p3723 A71-42940

Radio galaxies cosmological evolution, discussing rate and spectrophotometric data 23 p3766 A71-43823

Martian surface materials determination by comparing albedo and brightness with spectral and photometric characteristics of crushed reddish volcanic rock and silicate sand mixed with limonite 23 p3770 A71-44052

Cepheid sequence interpretation on gradient diagram based on model atmosphere photometric data 23 p3771 A71-44305

Southern Milky Way isophote maps by near-UV surface photometry, showing brightest areas in Sgr/Scor, Car, Vel/Pup and Cyg 24 p3867 A71-44436

ASTRONOMICAL SATELLITES

NT OSO-3

ASTRONOMICAL SPECTROSCOPY

Satellite with onboard equipment for astronomical IR spectroscopy, considering stabilization accuracy and measurement duration effects on spectral resolution 01 p0163 A71-10395

Laser microspectral investigations of meteorites microregions and nonhomogeneities relevant to astrophysics and nucleosynthesis 01 p0158 A71-10764

Interstellar medium polyatomic molecules formation, destruction and excitation processes by astronomical spectroscopy and interferometry 02 p0209 A71-11867

Luminescence of nebulae with C plus E spectrum, noting hydrogen emission superimposed on continuum due to reflection of stellar radiation by dust 02 p0311 A71-12353

Book on stellar atmospheres covering radiative transfer, opacity, equation of state, LTE, line spectra, atomic levels, etc 03 p0483 A71-13100

High dispersion spectroscopic observations of Venus carbon dioxide bands for deriving rotational temperature 03 p0488 A71-13557

Astronomical spectrometers covering prism, grating, dye filter, plane Fabry-Perot, monochromator, Michelson and coherent detection laser spectrometers 04 p0593 A71-14871

Rocket UV astronomy, discussing atmospheric and interstellar absorption, equipment design and OAO experiments 04 p0649 A71-15253

IR astronomy, considering basic principles, instrumentation energy production and radiation, spectroscopy, detectors and atmospheric absorption and emission 04 p0649 A71-15254

Sco X-1 optical spectroscopic and photometric observations, noting H alpha and H ion emission lines pattern-continuum brightness relationship 05 p0812 A71-16698

ASTRONOMICAL SPECTROSCOPY

High resolution spectroscopy of rotating planets, discussing improvement principles 07 p1107 A71-19204

All-reflection optical device for stellar spectra automatic widening and concurrent night sky spectrum suppression 09 p1442 A71-22068

Spectroscopic observation of comet Bennett near perihelion, noting solar continuum intensity dependence on wavelengths 10 p1681 A71-25062

Saturn satellites spectrophotometric observations at UV, visible and near IR, noting reflection spectra data 11 p1819 A71-25210

Spectroscopic search for water on Mars during 1963-1970, summarizing conclusions concerning quantity and variations with location, season and from year to year 11 p1826 A71-25715

Martian atmospheric water vapor abundance during 10 February-25 April 1969 Mars opposition by spectroscopic observations 11 p1826 A71-25717

Radial velocity differences between components of close visual binary stars by spectroscopic and oscilloscopic measurements 14 p2311 A71-30366

Visual binaries high resolution spectroscopy, obtaining radial velocity changes with Coude spectrograph 14 p2311 A71-30368

Early type close binary systems AO Cas, HD 47129, HD 190918 and HD 193793 spectral observations 14 p2311 A71-30369

Spectroscopic criteria for strong lined white dwarf stars identification on low dispersion objective prism plates 14 p2317 A71-31012

Dachs three axis payload stabilization and attitude control system for spectroscopic comet observation 15 p2499 A71-31218

Quasars as nuclei of nascent galaxies, proposing protogalaxy model from spectroscopic or color observations 15 p2482 A71-31328

Spectroscopic plate emulsion with excellent signal to noise characteristics, investigating baking time response in controlled nitrogen atmosphere 16 p2577 A71-33137

Mars surface harmonics and continental drift from radar and spectroscopic topographic height determination 16 p2638 A71-33519

Meteor spectrum analysis presenting tables for Soviet observations 16 p2639 A71-33694

Coronal line measurements on slit spectrogram during solar eclipse of 7 March 1970, showing fine structure in inner corona 16 p2642 A71-33784

Spectrographic observation of coronal lines in chromosphere during solar eclipse of 7 March 1970 16 p2642 A71-33787

Direct spectra analysis system using refrigerated image isocoon TV camera as detector for astronomical spectrograph 17 p2741 A71-34993

Automated stellar spectrophotometry, defining possible measurements on crowded spectra 17 p2742 A71-35005

Small digital computers applications to astronomical electronic instrumentation systems of microphotometry and spectroscopy 17 p2743 A71-35010

Mass spectrometric studies of origin of light elements Li, Be and B in universe, considering spallation of stellar and galactic gases by high energy particles 18 p2959 A71-35914

Photometric and spectroscopic study of NGC 3627 galaxy nucleus during optical observation of radio point galaxies 18 p2963 A71-36192

Supermassive double galaxy spectrographic and photometric data for cluster Abell 1775, showing radial velocity difference, visual magnitude and mass estimates 18 p2969 A71-37041

Mars surface narrow-band spectrophotometric observation, obtaining spectral reflectivities for geometric albedos calculation 18 p2970 A71-37048

Spectroscopic binary star system with orbital eccentricities less than 5 percent, discussing elliptical or circular orbit possibility 18 p2971 A71-37068

Dumb-bell Nebula forbidden O III line profiles observation with two-etalon scanning Fabry-Perot 19 p3144 A71-38171

Venusian polar tropopause and cloud layer from IR spectral recording in carbon dioxide band near inferior conjunction for crescent regions 20 p3290 A71-39306

Mars short-wave line spectra from measurement with reflector, estimating nitrogen dioxide content in atmosphere 20 p3290 A71-39307

Spiral galaxies N/O abundance gradients across disks from H II regions spectra

21 p3445 A71-40409

Critical evaluation of spectroscopic and photometric observations related to radio source 3C 386, suggesting foreground galactic star superposition on radio galaxy

21 p3447 A71-40443

Echelle gratings in single pass spectrometers, discussing properties, instrument profiles quality and accuracy

22 p3537 A71-41473

Astronomical Cassegrain echelle spectrograph, discussing optical and mechanical design and aberration effects

22 p3542 A71-41933

Quasars as nuclei of nascent galaxies, proposing test of protogalaxy model from spectroscopic or color observations

22 p3606 A71-42603

Classification method for unwidened low dispersion stellar spectra, giving table for weak stars in region around NGC 6913 cluster

23 p3772 A71-44308

Seyfert galaxy NGC 5548 H alpha profile spectroscopic observations, discussing broad emission lines

24 p3870 A71-44901

Sirius B white dwarf star effective temperature, radius and gravitational red shift determination from H-alpha and H-gamma line profile analysis

24 p3871 A71-44908

High dispersion spectroscopic observations of Venus, finding carbon dioxide band rotational temperature

24 p3873 A71-45079

Explorer SAS-D astronomical satellites for UV spectra recording by TV cameras

24 p3876 A71-45275

ASTRONOMICAL TELESCOPES

NT APOLLO TELESCOPES MOUNT

NT PYROHELIOMETERS

NT SPECTROSCOPIC TELESCOPES

NT X RAY TELESCOPES

Digital control system for azimuthal optical telescope, using invariance techniques and photoelectric system to compensate for position and program errors

01 p0081 A71-10727

IR astronomical telescope using six independent optical systems with path and phase controls for aperture synthesis

01 p0081 A71-10829

Czech circumzenithal instrument used with astronomical telescope for equal altitude stellar observation, discussing optical system, electronics and measurement results

01 p0082 A71-10872

Free standing tower astronomical telescope, discussing vibration problems in pedestal design

02 p0239 A71-12500

Reflecting telescope with six meter mirror, describing optical and control systems and structure

02 p0254 A71-12712

Bonn 100 meter radio telescope, describing frequency range, antenna array, steering accuracy, construction and design

02 p0239 A71-12913

Computer controlled eclipse telescope for coronal thermal emission IR spectrum observation

03 p0424 A71-13633

Six meter reflector telescope construction, discussing design, components and control system

04 p0588 A71-14827

Two channel 450 mm TV telescope at Pulkovo Observatory, investigating atmospheric turbulence deformations of stellar images

04 p0588 A71-14828

Duplex telescope system design and functions for photoelectrical stellar brightness measurements

04 p0588 A71-14829

Horizontal ATsU solar telescope and ASP-20 and DFS-3 diffraction spectroscopes, discussing performance, time relay and resolution

04 p0589 A71-14830

Astronomical telescope efficiency improvement, using TV kinescope equipment with superorthicons and videofrequency amplifiers

04 p0589 A71-14832

Stellar photoelectric servo guide with photon counting in mismatch sensor for telescope positioning

04 p0590 A71-14845

Oscillator for guiding clock mechanism of 400 mm photographic telescope, using high stability transistorized multivibrator

04 p0591 A71-14847

Autocollimation control of telescope rotation axis position at arbitrary azimuths

04 p0565 A71-14854

Glass and glass ceramics for large astronomical telescopes, examining fabrication, absorption coefficient and applications

04 p0617 A71-14865

Unequal arm laser interferometer for high precision optics analysis of large astronomical devices

04 p0592 A71-14866

Deformation monitoring of large multilens astronomical objective during assembly, using annular image reflection

04 p0593 A71-14868

Solar telescope coelostat and auxiliary mirror hydropneumatic unloading mechanism

04 p0566 A71-14870

Astronomical telescope automation and remote control, discussing advantages and problems

04 p0597 A71-15255

Automatic telescope instrumentation, considering polychromator, photometer and photoelectric star finders

04 p0597 A71-15256

Variable stars GR 181-202 in galactic cluster IC 1848 field examined by Schmidt telescope

04 p0651 A71-15663

OAQ experiments instrument packages for UV observations from orbit, discussing telescopes pointing accuracy and stability, mission objectives, etc

05 p0755 A71-17129

OAQ continuous observation capability, Project STAR telescopes, solar and X ray instruments and resupply missions based on space shuttle concept

05 p0818 A71-17132

Latitude observations at Pulkovo from 1948 through 1967 with zenith telescope

07 p1194 A71-19327

Pulkovo radio telescope effective frequency range extension beyond minimum 3 cm wavelength into millimeter range, installing high precision reflecting mirror surfaces

07 p1083 A71-19343

Telescope star photographic magnitude perception maximum capacity, considering effective or equivalent quantum yield and photoemulsion sensitivity

07 p1109 A71-19346

Astronomical telescope resolving power in focal plane emphasizing atmospheric turbulence

07 p1109 A71-19347

Altazimuthal telescope mounting with computer controlled guidance, discussing instrumental and methodical error effects on positioning and tracking accuracy

07 p1083 A71-19348

Optical astronomy instrumentation automation including telescopes, computer control, filters and detectors

07 p1114 A71-20051

Spherical aberration, limiting magnitude, distortion and coordinate determination accuracy of 20-cm two-camera astrophotograph at Abastumani Astrophysical Observatory

07 p1115 A71-20441

Image quality degradation studied with interference-polarization filter of Abastumani telescope, discussing photography of solar spectrum around H alpha line and artificial light source

07 p1115 A71-20443

Astronomical IR telescopes image quality and observing efficiency gain

08 p1290 A71-21394

Micrometer screw revolution value determined by method of scale pairs for Bamberg zenith telescope, noting dependence on temperature and declination differences of star pairs

08 p1292 A71-21675

Telescope plate scanner automated computerized operation, evaluating faint stars identification and color classification for annual motion surveys

09 p1443 A71-22646

Large aperture telescope in-orbit maintainability packaging, examining optical systems replacement tolerances and astronauts EVA mode accessibility

09 p1446 A71-22742

Angular resolution requirements of measurement systems and telescopes for orbital astronomy with applications to faint sources, close stars, spectroscopy, polarimetry, etc

09 p1447 A71-22747

Screw run and period error stability of eyepiece micrometer of universal astronomical instruments showing dependence on attitudes in space

09 p1451 A71-23179

Main mirror shape in three mirror telescopes permitting spherical aberration suppression

10 p1608 A71-23820

Astronomical telescopes with Cassegrain two mirror optics, discussing optical aberrations and correction methods and modern testing procedures

10 p1612 A71-24690

X ray astronomy orthogonal mirror telescopes, noting collecting efficiency, angular resolution and focusing

11 p1766 A71-26307

Automated and conventional photometry of short period variable star 14 Aurigae, using automatic telescope

12 p1956 A71-26617

Meteor telescopic observations during Perseid stream activity, determining radiant, stellar magnitudes, length and velocity

12 p1961 A71-26905

Large steerable radio telescope with equatorially mounted parabolic cylinder for lunar occultation, pulsar and scintillation observations

12 p1894 A71-26930

Double resonator ruby maser for observing transitions of interstellar hydroxyl, noting incorporation in modulation radiometer of astronomical telescope

13 p2077 A71-28373

Wollongong University College Cassegrain type 45 cm telescope, describing installation, construction and fabrication

13 p2067 A71-28393

Four foci computer controlled Anglo-Australian reflecting telescope, considering design and applications

13 p2069 A71-28850

Rocket-borne Cassegrain telescope system design for stellar spectra in UV region of EM spectrum between 900 and 3300 A

14 p2238 A71-29727

Automatic telescope guidance system for faint light source tracking, using cumulative photocurrent mismatch signal storage

14 p2271 A71-29994

Optical aperture configurations effect on image performance, discussing large telescope systems design criteria

14 p2242 A71-30147

Star observation by moon-based telescope for star diameters, multiple components and precise occultation times by distortion and diffraction pattern analysis

14 p2312 A71-30374

Astronomical mirror mass balancing system, discussing counterweights and levers arrangement and error and temperature compensation

15 p2411 A71-32526

Schmidt telescope as astrometric instrument, comparing mean error with catalog positions

16 p2578 A71-33322

Martian surface relief details observation from earth distance, showing telescope resolution requirements above dense atmospheric layers

16 p2639 A71-33698

High angular resolution optical telescopes, considering mirror materials, optical coatings and pointing systems

16 p2580 A71-33739

High angular resolution of astronomical objects by ground telescopes, considering slowly and rapidly variable defects, atmospheric defects and their reduction

16 p2641 A71-33766

McDonald Observatory lunar ranging station including telescope matching optics, guiding, timing equipment, pulsed ruby laser system and calibration procedures

16 p2553 A71-33780

Apollo optical retroreflector arrays characteristics and performance for laser range measurements from earth stations, describing multilensed receiver telescope

16 p2642 A71-33831

Computer installations on photometric telescope control system for astronomical observations

17 p2711 A71-34981

Telescope automation using servocontrolled drive with spur gearing and dual opposed motors for data acquisition separation and minimum program interaction

17 p2740 A71-34982

Optical telescopes automatic electronic control by positioning mechanical axis to specified coordinates and tracking guide star

17 p2740 A71-34983

Integrated telescope computer system, including magnetic disk storage, digital encoding, drive control and automatic guiding

17 p2711 A71-34984

Digital computer process controller for telescope with driving system consisting of single worm wheels for tracking and slewing

17 p2740 A71-34985

Computer control of vacuum solar telescopes, taking into account servos/handbox intervention, input-output preprocessor, high speed disk and memory

17 p2740 A71-34986

Computer controlled pulse counting technique application to astronomical photoelectric photometry for improved telescope efficiency

17 p2740 A71-34989

Image dissector photomultiplier for acquisition, guiding, focusing and photometric monitoring in telescope control

17 p2741 A71-34992

GALAXY machine for measuring image position and brightness and converting Schmidt telescope photographic data into computer form, outlining design and development

17 p2741 A71-34996

- GALAXY** measuring engine for automatic measurement of glass photographic plates taken from Schmidt telescopes, discussing performance
17 p2741 A71-34997
- High performance solar prominence telescope, showing objective diameter effect on image contrast
18 p2915 A71-35977
- Precision tracking and pointing of laser beams in space for communication, discussing large space telescope /LST/ applications
18 p2920 A71-36090
- Telescope phase retardation effect on polarization in Zeeman split Fraunhofer line, discussing consequence for solar magnetic field determination
18 p2965 A71-36732
- Astronomical telescopes design and characteristics, reviewing electromagnetic radiation properties
18 p2925 A71-36769
- Spaceborne astronomical telescope image stabilization system, utilizing field splitting technique
18 p2925 A71-36903
- Star sensor telescope, employing digitally coded silicon photocell detector for precise optical image location
18 p2925 A71-36910
- Polarization compensator for Okayama Astrophysical Observatory solar Coude telescope, describing operational and design principles and performance characteristics
19 p3062 A71-37242
- Astronomical telescopic observations of Mars for map updating, discussing surface colors
19 p3145 A71-38570
- Astronomical telescopes image motion, distortion and scintillation, examining atmospheric refractive index and density/temperature variation effects
19 p3010 A71-38571
- True central intensities of Fraunhofer lines, describing solar telescope and Czerny-Turner spectrometer
19 p3146 A71-38661
- StarLifter borne large aperture astronomical telescope for IR and submillimeter observations, discussing design and operation
20 p2324 A71-39173
- Climatological European southern observatory in Chile, describing spectroscopic and photometric telescopes, grand prism objective and double astrogaph
20 p3210 A71-39527
- Astronomical reflecting telescope, discussing frictionless oil pressure bearing design, declination and hour axis drives operation and optical system
20 p2329 A71-39531
- Paraboloid-hyperboloid Cassegrain telescope mirror centering, describing stigmatic point position permanent control in focal plane by geometrical method
21 p3375 A71-40066
- High performance solar prominence telescope components design, considering lenses and diaphragms with special attention to image degrading influences
21 p3378 A71-40523
- Large telescope design - Conference, Geneva, March 1971, covering telescope projects, optical properties, mountings and control and drive systems
22 p3542 A71-42120
- Electronic optical astronomy, describing image detectors and computer controlled microphotometers and telescope setting systems
23 p3678 A71-43542
- Hydrostatic bearings for large optical and radio telescopes, explaining lubricant flow control systems
23 p3661 A71-43862
- Latitudinal observation errors by two zenith telescopes concurrent data, showing distribution function in long term measurement
23 p3771 A71-44255
- Astronomical telescopes stellar image motion dependence on zenith distance, determining RMS value of jitter
23 p3771 A71-44259
- International zenith telescopes micrometer value, determining correction for ocular screw from latitude observations
23 p3680 A71-44261
- High resolution Mars photographs obtained with 61-in reflector telescope
24 p3872 A71-44998
- Mars telescopic observations, emphasizing south polar cap prominences around edge
24 p3872 A71-44999
- Automatic collimator for measuring tube lateral deflection in universal astronomical instruments
24 p3829 A71-45300
- ASTRONOMY**
NT SPACEBORNE ASTRONOMY
Astronomical instrument manufacture - Conference, Pulkovo, U.S.S.R., November 1967
04 p0587 A71-14826
- Astronomical pendulum clock with optical rate and recordable amplitude
04 p0592 A71-14862
- Papers on stellar astronomy, Volume 1, covering observation techniques, spectral classification, stellar atmospheres and line formation and stellar rotation
04 p0645 A71-15226
- Papers on stellar astronomy, Volume 2, covering angular momentum, binaries, white dwarfs, magnetic stars, UV and IR astronomy and theoretical models
04 p0647 A71-15239
- Soviet book on celestial bodies nature and observations covering solar system, variable stars, novae, supernovae, nebula and metagalaxy
04 p0649 A71-15262
- Soviet papers on astronomical devices covering stellar transit and observation, photoelectronic instruments and recordings
04 p0598 A71-15376
- Momentum conservation in metagalactic astronomy, considering magnetoid ejection from active galactic nuclei
04 p0657 A71-15827
- French book on method of equal heights in astronomy covering history, general formulas, universal time and latitude measurements, star catalog, planetary observations, etc
05 p0808 A71-16450
- International Time Bureau /Paris/ astronomical and geophysical research based on universal time and latitude observations of earth rotation
06 p0890 A71-17879
- Orbital environment contamination and effect on optical instruments and astronomical experiments in Skylab Program
06 p0902 A71-18531
- Papers on astronomy and astrophysics, Volume 7, covering electron scattering by diatomic molecules, solar cycle theories, solar radio bursts, cosmic matter, etc
08 p1358 A71-20885
- Book on universe surveying astronomy, measuring tools, solar system, radiation, planets, space exploration, exobiology, astrophysics, Milky Way, galaxies, cosmic evolution, etc
09 p1526 A71-23487
- Book on relativity and discretization in astronomy covering cosmic structures, galactic isopleths equilibrium theory, red shift discretizations, etc
10 p1670 A71-24210
- Papers on lunar astronomy and physics covering motions in space, librations, earth-moon system dynamics, geometrical and optical properties and origin
11 p1822 A71-25683
- Galactic structure historical approach, discussing stellar astronomy foundations, Milky Way, cluster and spiral position, etc
12 p1958 A71-26772
- Celestial mechanics relationship to astronomy, establishing differential equations of earth rotation in relation to terrestrial mantle
14 p2306 A71-29703
- Observational errors respecting orbital visual binaries periods, major axes and total mass, considering random and systematic errors
14 p2312 A71-30371
- Soviet papers on astrophysics, stellar astronomy and celestial mechanics, considering polarimetric and spectrometric data
18 p2962 A71-36105
- Book on space science covering celestial coordinates, time and mechanics, planetary atmospheres and interiors, comets, meteors, stellar structure, etc
18 p2963 A71-36246
- Papers on astronomy and astrophysics covering meteorites and early solar system, dwarf galaxies, IR radiation sources, nearby stars, planetary nebulae, central stars, etc
18 p2967 A71-37026
- Astronomy - Conference, Oberkochen, West Germany, April 1971
20 p3293 A71-39526
- Papers on astronomy covering eclipsing binaries, eclipse functions computations, silicon in sun, Magellanic clouds and stellar kinematics
20 p3300 A71-39819
- Astronomical and earth resources observations accommodation by space shuttle orbital sortie missions, obtaining sensor use rate estimate from worldwide cloud cover statistical distribution
23 p3724 A71-42979
- Gravitational wave astronomy, discussing phenomenon relationship to Einstein relativity theory and detector configurations
23 p3733 A71-43120
- Organization problems of research laboratory for space astronomy experiments, delineating roles of chief scientist, project manager and technical services
23 p3785 A71-43456
- ASTROPHYSICS**
Electromagnetic wave fields in outer space during gravitational collapse of aspherical mass
01 p0160 A71-11064
- Photon-neutrino coupling theory of weak interactions, noting exclusion by astrophysical data for white dwarfs
01 p0130 A71-11272
- Soviet papers on physics of nebulas and variable stars covering luminescence, reflecting and scattering properties, spectrophotometry, computerized simulation, etc
02 p0311 A71-12351
- Soviet book on stellar physics covering evolution, internal structure, mass, luminosity, radius, density, temperature, bolometric magnitude, energy transfer, etc
04 p0645 A71-15225
- Papers on astronomy and astrophysics, Volume 7, covering electron scattering by diatomic molecules, solar cycle theories, solar radio bursts, cosmic matter, etc
08 p1358 A71-20885
- Astrophysical states of matter and phenomena at extreme temperatures and densities, discussing stellar evolution, terminal states of stars, superdense stellar matter, neutron stars, etc
11 p1828 A71-25734
- Physics and astrophysics problem areas justifying intensified research
11 p1799 A71-25918
- Intense magnetic fields in astrophysics, emphasizing flux conservation law and quantum effects
13 p2144 A71-29436
- Astrophysical and aeronic UV molecular photoabsorption cross sections, discussing experimental techniques and associated systematic and random errors
14 p2190 A71-29905
- Crimean astrophysical observatory horizontal solar telescope, describing spectrograph spectral bandwidth and dispersion characteristics
14 p2240 A71-29984
- Book on relativistic astrophysics, Volume 1, Stars and relativity, covering stellar dynamics, astronomical models, cosmic objects evolution and star clusters
16 p2635 A71-33481
- Automation in optical astrophysics - Conference, Edinburgh, August 1970
17 p2740 A71-34980
- Soviet papers on astrophysics, stellar astronomy and celestial mechanics, considering polarimetric and spectrometric data
18 p2962 A71-36105
- Asymptotic approximations to Emden nonlinear differential equations of astrophysics for polytropic gas spheres, using multiple scale technique
18 p2941 A71-36226
- Papers on astronomy and astrophysics covering meteorites and early solar system, dwarf galaxies, IR radiation sources, nearby stars, planetary nebulae, central stars, etc
18 p2967 A71-37026
- Partially thermalized model of stellar system, considering potential and density distribution
21 p3439 A71-40052
- Physics and astrophysics problem areas justifying intensified research, discussing superconductivity, relativity, neutron stars, gravitational waves, etc
22 p3576 A71-42620
- Soviet papers on astrophysics covering variable stars and galactic structure, stellar atmospheres, cometary physics and evolution, stellar and solar spectroscopic observations, etc
23 p3771 A71-44302
- ASYMMETRY**
North-south asymmetry in solar disk microwave bursts sources distribution
03 p0496 A71-14536
- Asymmetric missile angular response to spin varying through resonance
06 p0979 A71-18507
- Rotating asymmetrical disk algorithm using method of local variations in strength and rigidity
07 p1212 A71-19357
- Model of large ionospheric electron density discontinuities, emphasizing horizontal asymmetry association with observed east-west refraction asymmetry
07 p1100 A71-19405
- Geomagnetic disturbance field asymmetry Fourier analysis for amplitude G and local time phase of first diurnal harmonic for IGY
10 p1600 A71-24295
- Model of large ionospheric electron density discontinuities, emphasizing horizontal asymmetry association with observed east-west refraction asymmetry
19 p3053 A71-37829
- Bright-dark asymmetry testing in solar granulation photography by objective method
19 p3146 A71-38663
- Generalized continuum of interleaved microstructures coupled by forces, investigating equations of motion, tensor indices and asymmetrical effects
20 p3309 A71-39566
- ASYMPTOTES**
High latitude neutron monitors during 15 November 1960 solar cosmic ray event, calculating asymptotic directions for protons with magnetospheric model
06 p0959 A71-18161
- Self preserving solutions of Stewart-Townsend and Ogura-Meakoda equations for isotropic turbulence decay, discussing asymptotic nature for small and large wavenumbers
07 p1091 A71-20027
- Asymptotic behavior of boundary layer equations solution for viscous incompressible flow past curvilinear obstacle
14 p2227 A71-30878

Asymptotic behavior of linear and nonlinear equations solutions 17 p2766 A71-34919

Lower bound on distance between vertical asymptotes of second order differential equations solutions involving integral inequality 18 p2941 A71-36227

Asymptotics for nonanalytic second order differential equations solutions 21 p3409 A71-41076

Asymptotic behavior of nonlinear Volterra integrodifferential equation solution, noting application to nuclear reactor dynamics 21 p3409 A71-41077

Optimal impulsive transfer of minimum characteristic velocity between hyperbolic asymptotes associated with real planet 22 p3600 A71-41969

Plane electromagnetic wave diffraction on periodic arbitrary profile array, presenting near and far field asymptotic characteristics 22 p3511 A71-42306

ASYMPTOTIC METHODS

Nonlinear impact buckling of strut, using asymptotic small parameter method 01 p0177 A71-11296

Abel-Tauber theorems predicting asymptotic behavior of source functions for resonance lines formed by frequency redistribution in semiinfinite atmosphere 01 p0131 A71-11350

Two parameter asymptotic solutions for viscous model of solar wind flow 01 p0147 A71-11511

Shadow current method for asymptotic solution to two dimensional problem of electromagnetic wave far diffraction field on ideally conducting plane with infinite rectilinear slot 02 p0210 A71-11629

Heat transfer analysis literature survey, including bibliography of perturbation, asymptotic and integral equations methods 02 p0333 A71-12650

Nonstationary automatic control system asymptotic series solution for equations of perturbed motion, deriving unperturbed motion local stability criteria 03 p0388 A71-13287

Heading of object moving on terrestrial sphere surface with inertial navigation aid, calculating asymptotic stability for position determination on computer 03 p0459 A71-14355

Neumann boundary value problem for region D Helmholtz equation, considering parameter dependence 04 p0619 A71-14649

Diffusely reflected radiation from semiinfinite atmosphere, deriving asymptotic formula including high order scattering terms 04 p0643 A71-14905

Nonlinear integrodifferential equations of heat and mass transfer problems, discussing asymptotic solution method 04 p0688 A71-15542

Thin convex shell of evolution bounded by two parallels minimum vibration frequency using asymptotic method of integration 04 p0671 A71-15556

Perturbation method in nonlinear oscillations theory, using asymptotic recurrence formulas based on Lie transform 05 p0774 A71-16544

Viscous incompressible fluid flow with free boundary at large Reynolds numbers, deriving asymptotic expansion solution for wave motion 05 p0737 A71-16989

Asymptotic formulas for vortex and velocity field far from body in plane viscous incompressible fluid flow 05 p0737 A71-16990

Plane Poiseuille viscoelastic fluids flow stability, using method of inner and outer expansions based on Chun and Schwarz asymptotic solution of Orr-Sommerfeld equation 05 p0737 A71-17102

Thin shallow shell theory, describing asymptotic method for nonlinear equations integration 06 p0988 A71-17776

Elastic plates and shells stability and vibration problems asymptotic solution methods, considering edge effect 06 p0991 A71-17800

Variable thickness truncated hollow cone elastic equilibrium, considering asymptotic analysis of axisymmetric problem 06 p0994 A71-17820

Steady state mixed subsonic-supersonic flow near blunt leading edge in hypersonic internal flow, using asymptotic solution by time-dependent method [AIAA PAPER 71-85] 06 p0843 A71-18542

Spacecraft midcourse guidance technique for lunar and interplanetary trajectories based on matched asymptotic expansions [AIAA PAPER 71-117] 06 p0978 A71-18567

Spacecraft structures vibration testing nonlinear effects, extending asymptotic method for transition through resonance to nonresonant regions [AIAA PAPER 71-211] 06 p1004 A71-18647

Turbulent boundary layer asymptotic theory, taking into account boundary conditions effect on friction and transfer factor laws 07 p1085 A71-18761

Electromagnetic wave diffraction by multielement and multilayer arrays, discussing asymptotic solution, error estimate and convergence 07 p1060 A71-19180

Stationary Navier-Stokes equations solution vorticity asymptotic behavior in three and two dimensional neighborhoods of infinity 07 p1147 A71-19640

Multicomponent gas laminar boundary layer equations, deriving asymptotic formulas for friction coefficient, concentration, temperature and diffusion flows 07 p1089 A71-19734

Lifting surface nonstationary aperiodic motion in incompressible fluid solved by asymptotic method of function parameters, using algorithm for Cauchy problem 08 p1275 A71-20778

High aspect ratio jet flap lifting-line theory, using matched asymptotic expansions method 09 p1381 A71-22083

Weak gravitational field negative energy possibility from energy momentum leakages consideration for asymptotically flat solutions of Einstein equations 09 p1494 A71-22807

Nonstationary automatic control system asymptotic series solution for equations of perturbed motion, deriving unperturbed motion local stability criteria 09 p1424 A71-23262

Asymptotic expression for mutual admittance between axial rectangular slots on large conducting cylinder 09 p1419 A71-23507

Locally illuminated diffracting edge near field calculation in terms of Hankel function asymptotic solution 09 p1409 A71-23514

Asymptotic solution for conical horn modes, comparing with exact solution for eigenfunctions and eigenvalues 09 p1420 A71-23677

Near field asymptotic solution for electromagnetic wave diffraction by perfectly conducting wedge, using steepest descent method 09 p1411 A71-23679

Singular perturbation problems for linear second order elliptic equation, obtaining asymptotic approximations for simple unbounded regions with free boundary layer terms 10 p1636 A71-23934

Unsteady low Mach number flow calculation by singular perturbation method with matched asymptotic expansions, considering application to aerodynamic noise 10 p1549 A71-23936

Asymptotic expression for low energy photoelectron energy loss to ambient thermal electrons 10 p1662 A71-24559

Soviet book on mechanical systems oscillations with allowance for imperfect elasticity covering energy dissipation, linear asymptotic methods, etc 10 p1691 A71-24729

Asymptotic transformations and stability criteria of nonstationary linear automatic control systems using Krylov-Bogolubov slow time concept 10 p1588 A71-24899

Earth oblateness and air drag effects on satellite trajectories by asymptotic method of nonlinear mechanics, obtaining closed form solutions for first order approximation 10 p1678 A71-24928

Circular turbulent liquid jet in external stream, considering Reichardt theory, jet expansion law, asymptotic similarity and constant eddy viscosity hypotheses 10 p1597 A71-24940

Gravitational radiation damping of slowly moving systems, discussing treatment as singular perturbation problem with approximation solution by method of matched asymptotic expansions 11 p1797 A71-25139

Time asymptotic solutions for hypervelocity blunt body flow field with coupled nongray radiation, treating shock as discrete surface [AIAA PAPER 70-865] 11 p1701 A71-25453

Lagerstrom mathematical model for two dimensional viscous flow at low Reynolds number, discussing asymptotic solutions for limit process expansions analysis 11 p1752 A71-26010

Asymptotic solution of second order nonlinear differential equation for autonomous nonlinear resonance system 11 p1743 A71-26536

High Reynolds numbers asymptotic suction boundary layer linear stability analysis for viscous flow, using transformations to hypergeometric functions 12 p1896 A71-26923

Asymptotic solutions for system of nonlinear quasi-normal type differential equations for gyroscopic couplings 12 p1923 A71-27170

Asymptotic methods and Markov processes theory extension to unsteady vibration of nonlinear systems with slowly varying parameters and random perturbation 12 p1930 A71-27173

Three dimensional jet flapped wing matched asymptotic expansion solution for high aspect ratios based on thin airfoil theory assuming inviscid and incompressible flow 12 p1863 A71-27217

Boundary layer separation at free streamline attached to body sharp trailing edge, comparing asymptotic solution with numerical analysis of flow on flat plate 12 p1896 A71-27218

Asymptotic solutions of improved equations for elastic and elastoplastic waves in rods, considering longitudinal waves propagation 12 p1980 A71-27449

Electromagnetic wave diffraction coefficients for discontinuity in curvature from surface field asymptotic description near singularity 14 p2192 A71-29794

Spinning sphere impulsively starting rotation from rest in compressible viscous fluid, calculating boundary layer growth by matched asymptotic expansions method 14 p2225 A71-30295

Nonlinear ordinary first order differential equation solution for mechanical system motion, constructing asymptotic representation 14 p2266 A71-30838

Asymptotic theory of wave propagation extended to slightly inhomogeneous and slowly varying anisotropic media exhibiting spatial and temporal dispersion 15 p2449 A71-31476

Asymptotically optimal rank algorithms for signal resolution at phase and amplitude detectors outputs 15 p2370 A71-31587

Gyroscopic system nonstationary operation mode analysis, utilizing asymptotic method with linear matrix equation 15 p2410 A71-32454

Buckling of axially compressed circular cylindrical shells with localized or random axisymmetric imperfections, deriving asymptotic approximation formulas for stress calculation [ASME PAPER 71-APM-29] 16 p2655 A71-33200

Nonreversibility of Marachkov theorem on asymptotic stability, using scalar equation 16 p2612 A71-33595

Asymptotic expansion of spectral functions expressed by Cauchy integral over smooth open segment 17 p2763 A71-34419

Quasi-linear wave equations approximate solution construction by asymptotic methods 17 p2777 A71-34420

Multicomponent system of elastic plate with hole and built-in viscous-fluid-filled syphon bellows, calculating oscillation by asymptotic methods 17 p2777 A71-34423

Long distance FM signal pulse propagation and maximum compression synthesis in dispersive media, using asymptotic theory for mathematical treatment 17 p2701 A71-34761

Asymptotic formulas for two point boundary value problem of differential equations system, using averaging method 17 p2765 A71-34905

Asymptotic methods for distributed system nonlinear time and space vibrations, discussing system dispersion effect on resonance conditions 17 p2780 A71-34914

Asymptotic solution to nonlinear motion of heavy gyro in gimbal suspension, noting convergence within finite time interval 17 p2746 A71-35606

Self similar numerical and asymptotic solutions of laminar multicomponent isothermal boundary layer equations for large blowing rates 17 p2673 A71-35633

Asymptotic solution of viscous incompressible flow past uniformly heated paraboloid of revolution with constant surface temperature 17 p2730 A71-35800

Compressible similar laminar boundary layer blow-off behavior description from asymptotic analysis, using Prandtl transposition theorem 18 p2901 A71-36032

Monograph on nonlinear first order differential equations adjunction fields and solutions asymptotic behavior, seeking adjoinable solutions 18 p2940 A71-36098

Channel type closed shallow shells stress states calculation, applying asymptotic integration technique to load decomposition 18 p2976 A71-36178

Asymptotic approximations to Emden nonlinear differential equations of astrophysics for polytropic gas spheres, using multiple scale technique 18 p2941 A71-36226

Asymptotic solution of nonlinear Volterra integral equation, examining nonlinear heat conduction and boundary layer heat transfer 18 p2942 A71-36747

Asymptotic expansions for solution of wave motions of viscous incompressible fluid flow with free boundary at large Reynolds number 18 p2909 A71-36789

Asymptotic formulas for vortex and velocity field far from body in plane viscous incompressible fluid flow 18 p2909 A71-36790

Compressible boundary layer equations similarity solutions uniqueness proof, using asymptotic behavior 18 p2909 A71-36814

Swirling flow problem in boundary layer theory, proving existence theorem and asymptotic formula for differential equations solution 18 p2910 A71-36815

Dissipative wave motion asymptotic theory, considering initial boundary value problems for linear partial differential equations 18 p2910 A71-36819

Small strain theory of shells derived from three dimensional equations of equilibrium and compatibility by asymptotic approach 18 p2982 A71-36840

Nonlinear diffraction of weak shock waves near rigid wall with sharp bend, obtaining approximate solution by matched asymptotic expansion method 19 p3043 A71-37100

Turbulent hydrodynamic line stretching problem, considering asymptotic rates as application of central limit theorem for dependent random variables sums 19 p3044 A71-37729

Isolated buoyant thermal motion asymptotic behavior derivation from simplified model, comparing results with experiment 19 p3162 A71-37732

Hydrostatically loaded noncircular pressurized cylindrical shells with nonuniform rings, using asymptotic expansion procedure 19 p3157 A71-37875

Mixed problem for hyperbolic type linear non-homogeneous second order partial differential equation with delayed arguments, obtaining asymptotic solution for derived Cauchy problem 19 p3086 A71-38011

Motion stability for critical case of characteristic equation with purely imaginary roots, deriving solution by nonlinear mechanics asymptotic method 19 p3104 A71-38013

Nonlinear instability theory for wave system in plane Poiseuille flow, deriving asymptotic solution for initial value problem 19 p3046 A71-38203

Plane electromagnetic wave diffraction by dense periodic array with Dirichlet and mixed boundary conditions, determining solution asymptotic behavior 19 p3104 A71-38416

Approximate solutions to quasi-linear n dimensional Helmholtz equation by asymptotic methods 19 p3088 A71-38477

Parabolic reflector aperture antennas with Gaussian distributed random phase deviations, obtaining asymptotic expansion for radiation pattern 19 p3036 A71-38605

Modified asymptotic perturbation expansion method application to free flow rotation effect on boundary layer for hypersonic flow about blunt body 20 p3177 A71-39483

Generalized Riccati equation reduction to integral equation, leading to asymptotic solution of second order linear differential equations 20 p3255 A71-39574

Asymptotic geometric optics methods application to thin shell theory, reducing transport equation to ordinary differential equation 20 p3310 A71-39865

Vortices motion and decay, constructing asymptotic solution to Navier-Stokes equations 21 p3366 A71-40485

Nonself-similar problem of developing plane turbulent jet in unbounded space, obtaining second and third terms of asymptotic series of stream function 21 p3368 A71-40692

Thin elastic plate under dynamic loading, applying asymptotic expansion techniques to three dimensional dynamic elasticity theory 22 p3613 A71-41435

Asymptotic high velocity lift drag ratios for sheet and loop magnetic suspension train tracks 22 p3574 A71-41728

Boundary layer asymptotic solutions for free convection in laminar three dimensional systems, determining rapid mass transfer and centrifugal forces effects 22 p3619 A71-41870

Nonlinear differential equations with retarded argument, proving asymptotic and oscillatory solutions theorems 22 p3568 A71-42692

Asymptotic expansion method for hyperbolic and parabolic differential equations fundamental solutions

featuring validity near surface and in interior of characteristic conoid 23 p3698 A71-43096

Matched asymptotic solutions for optimum lift controlled atmospheric entry of hypersonic lifting vehicles 24 p3876 A71-44609

Validity proof of asymptotic methods in one dimensional dynamic systems described by hyperbolic and parabolic differential equations 24 p3844 A71-45063

ASYMPTOTIC SERIES

Cophased two dimensional antennas fields asymptotic expansions in near and far zones with generalization to three dimensional case 05 p0722 A71-16868

Initial structure of wing-body interaction in steady inviscid supersonic flow, obtaining asymptotic expansion from canonical problem solution 05 p0696 A71-17219

Inviscid incompressible electrically conducting fluid flow past slender profile investigated by asymptotic power expansion of reciprocal magnetic Reynolds number 09 p1382 A71-22135

Passage through resonance of linear oscillator with slowly varying frequency, matching inner and outer asymptotic expansions 14 p2274 A71-29861

Error evaluation for incomplete gamma function calculated by truncated asymptotic series 21 p3408 A71-40852

Asymptotic expansion for hyperbolic Cauchy problem solution, proving correctness 21 p3409 A71-41079

Asymptotic expansion of axisymmetric electromagnetic beams with azimuthal dependence near internal caustic / focal line / 23 p3647 A71-44330

ATHLETES

Trained young runners maximum oxygen consumption rate at sea level and high altitude 16 p2530 A71-33244

World champion marathon runner metabolic responses during submaximal and maximal treadmill running, recording oxygen consumption, heart rate and lactic acid 20 p3185 A71-38890

Habituation and suppression of vestibulo-ocular vertical nystagmic responses to Coriolis stimulation in pentathlon athletes, comparing to pilots and airman trainees 22 p3501 A71-41826

ATHLETES

U RAMJET ENGINES

ATLANTIC OCEAN

Troposphere and stratosphere electric field above Atlantic Ocean, investigating electrode effect role in atmospheric circuit 05 p0738 A71-16220

Communications, navigation and surveillance for aircraft and marine vessels in North Atlantic region, discussing baseline traffic control model 07 p1153 A71-18808

Synoptic climatology of Euroatlantic blocking situations, investigating geographic location and duration 14 p2271 A71-30937

Atlantic Ocean surface temperature distribution data for Gulf Stream meanders and eddies, using Ito's 1 satellite direct readout IR images 17 p2734 A71-35216

Lightning observation by OSO-E satellite, suggesting maximum thunderstorm incidence over North Atlantic Ocean 19 p3061 A71-38675

Aerosol measurements over Atlantic and Indian Oceans, discussing aerosols optical thickness, effective radii, concentrations, sizes and optical properties variations with latitude and meteorological conditions 20 p3257 A71-39328

Synoptic climatology of blocking situations over European-Atlantic region, obtaining middle troposphere circulation patterns by statistical analysis 21 p3411 A71-40826

Latitudinal distribution of integral water drop content of clouds above Pacific, Atlantic and Indian oceans from Cosmos 243 measurements 22 p3568 A71-41653

ATMOSPHERES

Motion equations for neutral matter in head atmosphere of bright comet with high density spherical source and molecular collisions 15 p2484 A71-31661

Density distribution of neutral matter in cometary atmosphere in transition region between hydrodynamic and free molecular flow 15 p2484 A71-31662

ATMOSPHERIC ABSORPTION

U ATMOSPHERIC ATTENUATION

ATMOSPHERIC ATTENUATION

NT AURORAL ABSORPTION

Short wave reflected radiation fluxes in atmosphere with absorption allowance for water vapor, carbon dioxide and ozone 01 p0144 A71-10538

ATMOSPHERIC ATTENUATION

Atmospheric extinction coefficients dependence on wavelength, comparing theoretical prediction to observational data 01 p0119 A71-10832

Pulsed laser emissions in atmosphere, noting backscattered light spatial and temporal structure under various meteorological conditions 01 p0120 A71-11105

Atmospheric UHF attenuation observations by horn antenna 01 p0039 A71-11381

F 2 layer transmission coefficient, describing altitude linear dependence of electron density maximum 02 p0244 A71-11773

Earth atmosphere X ray absorption, determining photon flux, energy and angular distribution as function of altitude by Monte Carlo method 02 p0299 A71-11776

Millimeter and submillimeter radio waves propagation, outlining molecular and aerosol attenuation in real atmosphere together with transmitters and receivers 02 p0212 A71-11872

Ionospheric absorption at solar maximum and minimum, comparing riometer measurements with ray tracing calculations and electron density, collision frequency or temperature profiles 02 p0245 A71-11962

Optical /and IR/ communication systems design, considering effects of atmospheric turbulence, molecular absorption and aerosol scattering 02 p0214 A71-12023

Atmospheric water vapor dimers absorption of microwaves, computing total absorption coefficient 03 p0378 A71-13295

Ionospheric nondeviative absorption diurnal variation describing function suitable for computer methods 03 p0378 A71-13315

Hydrogen Lyman alpha radiation intensity and atmospheric absorption before and during solar eclipse of 20 May 1966, considering D region ion production 03 p0407 A71-13376

Thermal radiation from hot water vapor and carbon dioxide imbedded in cool atmosphere, using extended molecular band models 03 p0518 A71-13649

Atmospheric absorption models of solar X-rays at occultation times, using Solrad satellites 03 p0480 A71-14048

High atmosphere X ray absorption grazing scale height variations from satellite measurement of solar X-ray flux during sunrise and sunset 03 p0480 A71-14049

Aerosol-induced solar radiation attenuation correlation to humidity in atmospheric boundary layer 04 p0641 A71-15119

IR astronomy, considering basic principles, instrumentation energy production and radiation, spectroscopy, detectors and atmospheric absorption and emission 04 p0649 A71-15254

IR laser beam atmospheric absorption, considering heating and cooling effects due to vibrational relaxation 04 p0609 A71-15681

Airborne radiation thermometry corrections for intervening atmospheric absorption and emission and ocean surface nonblackness 04 p0601 A71-15762

Rain and drizzle millimeter wave attenuation and radar scattering cross section calculation 05 p0718 A71-15988

Submillimeter and millimeter waves attenuation in rain, comparing calculation results with measurement 05 p0718 A71-15990

Plasma instabilities role in ionospheric heating and radio wave attenuation 06 p0888 A71-17288

Atmospheric absorption by oxygen, determining metastable molecules absorption cross section at 1095 A 06 p0888 A71-17290

Telecommunications by lasers, considering atmospheric propagation possibilities and limitations 06 p0869 A71-18064

Atmospheric oxygen absorption spectra fluctuations related to presence or absence of jet stream 07 p1151 A71-18912

Calculation methods accuracy for spectral absorption of IR radiation by atmospheric gases, analyzing empirical, numerical integration and spectrum model methods 07 p1151 A71-19148

Atmospheric absorption by clouds, fog and rain on earth-space path at 90 GHz, using sun tracker 07 p1600 A71-19215

Monograph on dual beam parabolic antennas in radio astronomy covering atmospheric effects, EM surface current density and scalar aperture field, etc 07 p1077 A71-19725

Pulsed laser emissions in atmosphere, noting backscattered light spatial and temporal structure under various meteorological conditions 08 p1325 A71-20849

Atmospheric scintillation, refractive and diffusive attenuation of microwaves from outer space at low elevation angles

08 p1364 A71-21421

Aircraft flyover noise samples, obtaining atmospheric absorption coefficients

08 p1231 A71-21425

Atmospheric emission and absorption measurements at millimeter wavelengths, comparing with radiative transfer equation values

08 p1257 A71-21880

Atmospheric attenuation in IR windows near sea level from transmittance spectral curves, discussing continuum absorbance

09 p1437 A71-22740

Atmospheric water vapor dimers microwave absorption, computing total absorption coefficient

09 p1408 A71-23268

Solar spectra of far IR absorption of atmosphere above 4.2 km, using interferometer and cryogenic bolometer measurements

09 p1490 A71-23557

Isolated ionospheric irregularities, describing refraction and diffraction pattern calculations for satellite signals

10 p1578 A71-24463

Atmospheric extinction vs intermediate band color index diagrams, discussing linear correlation and reference star selection

10 p1681 A71-25130

Attenuation and phase velocity of ELF and VLF radio waves propagating under anisotropic ionosphere, discussing geomagnetic field effect

11 p1731 A71-25602

Venus atmosphere mm and cm radio wave propagation calculated from temperature, pressure and chemical composition data

11 p1823 A71-25695

Obliquely incident radio wave absorptions measurements from January-October 1968 vertical ionospheric soundings, correlating diurnal variations with solar zenith angular changes

11 p1732 A71-25787

Atmospheric transmittance vertical structure, using aerosol attenuation and optical densities from aircraft sounding under cloudless conditions

11 p1795 A71-25924

Microwave power transmission from satellite solar energy station to earth, discussing atmospheric attenuation mechanisms and wavelength and power density optimization

13 p2000 A71-28670

Inhomogeneous atmosphere transmittance functions, noting Lindholm line shift in O absorption spectra effects

13 p2063 A71-29019

Transhorizon radio propagation by atmospheric heterogeneities, discussing effect on attenuation, antenna gain reduction and transmission bandwidth

13 p2033 A71-29239

Submillimeter wave region solar radiation atmospheric absorption by Fourier spectrometry and double output Michelson interferometer with Golya cell detectors

14 p2307 A71-29740

Cosmic radio noise absorption measurements at subauroral latitude for ionospheric absorption, discussing ionization regions spatial nonuniformity and horizontal extension

14 p2196 A71-30561

Extensive air showers sidereal-diurnal variation determination, considering atmospheric effects and antisidereal wave vector

14 p2301 A71-30591

Book on space observatories covering atmospheric structure, space astronomy applications, atmospheric attenuation, balloon IR sounding, satellite observation, etc

14 p2316 A71-30895

Solar UV radiation atmospheric absorption during IQSY by ion chamber measurements, considering upper atmosphere oxygen concentration

15 p2396 A71-31616

Atmospheric cosmic ray propagation based on phenomenological model of hadron-nucleus collisions, predicting sea level nucleon, pion and muon energy spectra and ionization profile

15 p2474 A71-31732

Atmospheric laser link with automatic sensitivity control during reception, measuring detector output signal fluctuation reduction characteristics

15 p2372 A71-32319

Statistical analysis of radiometer measurement data of solar emission atmospheric attenuation at 19 GHz

15 p2496 A71-32710

Laser beam atmospheric monochromatic radiation attenuation isolating molecular absorption from total radiant flux attenuation

15 p2451 A71-32757

Solar UV radiation data during 7 March 1970 eclipse from photometers sensitive to narrow bands, discussing sources, atmospheric absorption and D region ionosphere

16 p2627 A71-33773

Nike Apache solar X-ray observations during 7 March 1970 eclipse, determining residual fluxes and atmospheric absorption profiles for ion production rates

16 p2627 A71-33790

Space radio astronomy, discussing frequency range in terrestrial atmosphere, RAE-1 satellite, cosmic and solar emissions and magnetopause generation, propagation and absorption processes

17 p2797 A71-34243

Percent-of-time distributions of attenuation by rain, clouds and atmospheric gases on earth-space paths at frequencies below 30 GHz

17 p2704 A71-35089

Storm models for space-path attenuation calculations using digitized weather radar data for fine structure and surface rainfall data for extrapolation

17 p2704 A71-35090

Refraction, terrain, air attenuation, fog and rain, turbulence and shielding effects on acoustic propagation in lower atmosphere

17 p2734 A71-35235

Atmospheric absorption of 10.6 micron laser beam radiation, noting effect on refractive index

18 p2910 A71-35843

ERTS satellite-based laser communication system, calculating cloud cover effect on clear line-of-sight light transmission probability through atmosphere to ground station

18 p2876 A71-36472

Oxygen telluric lines contours shape analysis, allowing for atmospheric nonisothermicity and inhomogeneity

19 p3090 A71-37978

Atmospheric signal propagation study between satellite and earth, using solar radiometry

19 p3018 A71-38075

Thermospheric atomic oxygen and molecular nitrogen number densities, discussing earth atmospheric absorption of solar UV lines

20 p3214 A71-38727

Atmospheric transmittance vertical structure, using aerosol attenuation and optical densities from aircraft sounding under cloudless conditions

20 p3257 A71-39215

Atmospheric transmissivity measurement from backscattered light intensity, deriving model based on light beam geometry and path

20 p3238 A71-39333

Backscattering patterns in atmospheric opacity measurements, minimizing errors due to atmospheric inhomogeneities and different stratifications

20 p3257 A71-39334

Mars ionosphere radio wave absorption interaction coefficients, studying electron concentration and electron/gas molecular collisions frequency vertical profiles

20 p3297 A71-39629

Extensive air showers attenuation length measurement in Japan 1964-1968, using scintillator

20 p3284 A71-39863

Auroral far UV spectrum and intensity measurements, discussing atmospheric absorption effects on rocket-borne spectrometer sensitivity

21 p3372 A71-40039

Absorption variation with solar activity and seasons, reexamining vertical incidence absorption measurements at 5.65 MHz/1958 and 1959 at Waltair

21 p3373 A71-40374

Line-of-sight microwave multipath fading, predicting attenuation distribution as function of pathlength by piecewise linear approximation of atmospheric refraction index

21 p3349 A71-41196

Magnetospheric VLF transverse wave propagation along geomagnetic field, examining dispersion relation

22 p3533 A71-41797

Atmospheric molecular absorption spectra in IR region, using 15 meter multiple pass absorption cell

22 p3544 A71-42141

Radar systems performance constraints, discussing environmental effects, carrier frequency, aerial directivity, clutter echoes, transmitter power, etc

22 p3509 A71-42199

Atmospheric contrast reduction of aerial images, predicting quality under various target and meteorological conditions

22 p3547 A71-42506

Light wave attenuation in fog, mist, rainfall and snowfall during propagation through atmosphere, deriving semiempirical formulas for attenuation rate relationship to visibility

22 p3569 A71-42523

Atmospheric visibility/light extinction/ measurement from modulated CW laser backscattered signal

22 p3549 A71-42565

Rain and drizzle submillimeter wave attenuation and radar scattering cross section calculation

22 p3515 A71-42737

Submillimeter waves attenuation in rain, comparing calculation with measurement

22 p3515 A71-42739

Visible and IR radiation attenuation in rain and snow, comparing calculation based on Mie diffraction formulas with measurement

22 p3515 A71-42741

Phase integral correction for reflected radio wave absorption in ionosphere, comparing with ray theory

23 p3643 A71-42969

Laboratory analog simulation of absorption line spectra in cloudy planetary atmospheres, comparing with computational model based on plane parallel atmosphere

23 p3700 A71-43075

Atmospheric scattering and absorption effects on balloon altitude spectra observations of auroral X ray penetration into atmosphere

23 p3720 A71-43130

Vertically polarized millimeter and submillimeter wave attenuation measurement in rain

23 p3646 A71-43569

Laser technique for runway and slant visibility range, lower cloud boundary and atmospheric damping coefficient

23 p3701 A71-43889

Radiation attenuation effect on solar photosphere turbulence determination by Goldberg-Unno method

23 p3772 A71-44311

Atmospheric attenuation effects on cloud and precipitation radar reflection coefficient

24 p3845 A71-44880

Long distance atmospheric propagation in earth-ionosphere waveguide, obtaining phase velocities and damping factors

24 p3804 A71-45030

Whistling atmospheric generation mechanism, showing ionic sound excitation by hydromagnetic wave propagation through magnetospheric rapid plasma concentration change regions

24 p3823 A71-45035

Laser IR radiation attenuation in natural and artificial fogs, noting dependence on particle size distribution

24 p3835 A71-45254

Laser IR radiation attenuation in atmospheric precipitation, considering snow, rain and drizzle

24 p3835 A71-45255

Stellar UV cut-off by stathospheric nacelle recorded on photographic film by Schmidt telescope fitted with objective prism, widening spectrum by scanning

24 p3875 A71-45272

ATMOSPHERIC BOUNDARY LAYER

Atmospheric boundary layer nonlinear equations of motion numerical integration for eddies structure and wind direction and latitude effects on turbulence intensities

01 p0113 A71-10351

Doppler radar techniques for turbulent kinetic energy budget in boundary layer, discussing wind profile and turbulence in snow conditions

01 p0117 A71-10577

Low altitude slow aerodynamics, discussing earth surface wind modeling, powered-lift flight efficiency and animal flight

01 p0002 A71-10818

Atmospheric surface layer turbulence spectra and cospectra observations in July-August 1969 at Edithvale, Australia

01 p0120 A71-10858

Atmospheric boundary layer motion and transports applied to mathematical atmospheric circulation models

01 p0121 A71-11355

Wind speed difference quotient conversion to gradients at atmospheric surface layer geometric mean height, considering wind and temperature profiles

03 p0452 A71-13229

Planetary boundary layer flow three dimensional steady state equations applied to air motions over horizontally varying surface roughness, temperature and moisture

03 p0453 A71-13230

Three dimensional numerical model of unstable planetary boundary layer integrated for convecting and turbulent region height, mean lateral shear and Reynolds flux direction

03 p0453 A71-13612

Convective velocity and temperature scales deduced numerically and observationally for unstable planetary boundary layer and for turbulent Rayleigh convection

03 p0453 A71-13613

Aerosol-induced solar radiation attenuation correlation to humidity in atmospheric boundary layer

04 p0641 A71-15119

Soviet monograph on atmospheric boundary layer covering compressible turbulent air flow, diurnal fluctuations, fog, air pollution and lower atmosphere electric field

04 p0621 A71-15399

LF boundary of inertial range in lowest atmospheric layer, comparing turbulence scale and wind velocity components

04 p0622 A71-15632

Unstable atmospheric surface layer wind speed and temperature profiles mathematical representation

05 p0777 A71-16664

Surface roughness and thermal radiation effects on rural and urban boundary layer turbulence and diffusion by wind fluctuations observations
05 p0777 A71-16665

Planetary boundary layer air velocity and temperature measurements from airplane
05 p0777 A71-16666

Turbulent energy balance equation terms for atmospheric boundary layer
05 p0778 A71-16837

Atmospheric diffusion parameters investigated by smoke plumes in atmospheric boundary layer, evaluating turbulent energy dissipation
05 p0778 A71-16838

Atmospheric surface layer turbulence structure simulation model, using laboratory flows for neutrally stable atmosphere
[AIAA PAPER 71-136] 06 p0884 A71-18579

Mesoscale orographic inhomogeneities in vertical air flows past surfaces, noting leeward air waves and upper/lower boundary layers
07 p1149 A71-18793

Atmospheric boundary layer IR transmittance spectra compared to spectrum calculated from transmittance functions
07 p1152 A71-19149

Temperature pulsation in atmospheric boundary layer from meteorological mast under unstable stratification in summer, tabulating dispersion characteristics, turbulent energy dissipation rate, etc
07 p1152 A71-19150

Thermal boundary layer flattening influence on atmospheric cellular convection from satellite observations
07 p1104 A71-20219

Diagnostic numerical model of frontal vertical circulation in atmospheric boundary layer using local parameters
08 p1326 A71-21448

Planetary boundary layer stationary air flow over plane homogeneous surface under geostrophic wind conditions, solving for thermal turbulence field stabilization by iterative method
08 p1330 A71-21874

Mixing length theory of near ground Ekman boundary layer in stationary and diurnal conditions, determining surface drag and wind rotation
09 p1487 A71-22638

Eddy diffusivities and turbulent diffusion characteristics in atmospheric surface layer, using universal function based on similarity theory
09 p1487 A71-22639

Book on atmospheric boundary layer dynamics considering theoretical models of vertical distribution of wind velocity, temperature and humidity
09 p1488 A71-23175

Atmospheric surface layer wind and temperature profile measurements over horizontally uniform flat terrain
09 p1489 A71-23554

Atmospheric surface layer shear/buoyant production, flux divergence and dissipation in terms of turbulent kinetic energy and transport in temperature variance budget
09 p1490 A71-23555

Turbulent mixing and radiative transfer relationship to micrometeorological temperature structure of atmospheric boundary layer
10 p1638 A71-23878

Atmospheric boundary layer numerical modeling, discussing subgrid scale mixing processes and parameterization
10 p1639 A71-25067

Wind speed and potential temperature vertical profile in day/night planetary atmospheres estimated by similarity theory of boundary layer parameters
11 p1826 A71-25719

Atmospheric boundary layer refractive index fluctuations structural characteristics determined from summer vertical wind velocity and temperature profiles
11 p1795 A71-25922

Atmospheric boundary layer refractive index fluctuation isotropy for small turbulence, using intensity distribution photography over collimated laser beam cross section
11 p1762 A71-25923

Wind structure in boundary layer pilot-balloon observation, discussing baseline data processing for digital computer
11 p1796 A71-26560

Atmospheric upper boundary condition in baroclinic forecast, recommending correction using isopycnicity properties of atmospheric processes near 7 km altitude
12 p1924 A71-26738

Large scale structure with unstable stratification, investigating effects on atmospheric ground layer dynamic velocity and turbulent energy production
12 p1924 A71-27101

Vertical variations of Reynolds stress and heat flux in atmospheric surface layer attributed to sub-mesoscale circulations, using sonic, thermometer and drag measurements
13 p2097 A71-28724

Land-sea drag, Ekman parametrization and Monin-Obukhov transfer process in surface boundary layer of atmospheric circulation model
13 p2097 A71-28725

Stability theory for thermal stratified viscous parallel flows at Prandtl number of unity, considering atmospheric boundary layer and jet stream mechanisms
13 p2165 A71-29246

Structural model of mature hurricane, determining heat and moisture transfer, boundary layer dynamics and thermodynamic balance
13 p2097 A71-29250

Wind structure in atmospheric boundary layer, outlining semiempirical laws for mean wind speed variation with height and statistical properties of turbulent fluctuations
13 p2097 A71-29266

Diffusion coefficient as function of height in turbulent atmospheric boundary layer, considering similarity laws between wind tunnel and field data
13 p2051 A71-29432

Time and frequency statistics of turbulent fluctuations of wind, temperature and humidity in atmospheric surface layer
14 p2266 A71-29706

Meteorological tower high resolution CW-FM radar measurements for studies of temperature inversions, waves, thermal plumes and convection in atmospheric boundary layer
14 p2192 A71-29707

Atmospheric turbulence structure, cloud convection, gravity waves, clear air flow and surface/planetary boundary layers
14 p2270 A71-30495

Vertical wind shear calculation in atmospheric surface layer, studying layer thickness effect
15 p2444 A71-31363

Vertical wind shears distribution in atmospheric boundary layer, noting features due to differences in synoptic processes
15 p2444 A71-31364

Atmospheric boundary layer circulation dynamic interaction with variable depth barotropic ocean surface, studying stream function during annual cycle
16 p2605 A71-33906

Radical and formaldehyde daytime concentrations predictions from steady state model of unpolluted surface atmosphere
16 p2575 A71-34048

Spherical microparticles in atmospheric boundary layer and fallout above Pacific Ocean correlated to extraterrestrial origin
17 p2810 A71-35719

Diffusion coefficients determination in planetary boundary layer with radon and ThB, using vertical distribution profile of concentration
18 p2912 A71-36193

Small scale turbulence structure in atmospheric boundary layers over open ocean, noting velocity derivatives probability density function lognormality
19 p3044 A71-37731

Velocity and temperature pulsations as function of stratification parameter in atmospheric boundary layer
19 p3090 A71-37971

Surface layer humidity correlation to height of atmosphere emitting in IR spectral region, determining water vapor content by recording earth radiation angular distribution
19 p3054 A71-37974

Planetary boundary layer stationary air flow over plane homogeneous surface under geostrophic wind conditions, solving for thermal turbulence field stabilization by iterative method
19 p3091 A71-38468

Atmospheric boundary layer refractive index fluctuations structural characteristics determined from summer vertical wind velocity and temperature profiles
20 p3256 A71-39213

Atmospheric boundary layer refractive index fluctuation isotropy for small turbulence, using intensity distribution photography over collimated laser beam cross section
20 p3236 A71-39214

Eddy viscosity in barotropic planetary boundary layer, finding turbulent diffusion coefficient dependence on turbulent kinetic energy
20 p3257 A71-39437

Upper temperature inversion as condition producing pollutants turbulent diffusion in atmospheric boundary layer
22 p3568 A71-41648

Radiative and turbulent heat transfer in atmospheric surface layer, measuring radiative heat flux divergence and temperature fluctuations at different heights
22 p3534 A71-41860

Turbulent energy budget and velocity dissipation spectrum near grass surface as function of atmospheric stability
22 p3569 A71-42546

Wind velocities and directions, air temperature and visibility range in atmospheric boundary layer under fog conditions
22 p3569 A71-42846

ATMOSPHERIC CHEMISTRY

Singlet-D atomic O yield per oxygen ion dissociative recombination from night airglow observations
03 p0408 A71-13382

Ionospheric research covering electron and ion distributions, ion chemistry, neutral atmosphere interactions, thermal structure, electrodynamics, etc
03 p0416 A71-14031

Indeterminacy interval reduction for ionospheric reaction rate constants by imposing supplementary condition on NO/oxygen molecular ion concentrations ratio
06 p0894 A71-18259

Chemical nonequilibrium effects on hypersonic, blunt body shock layers flow in reacting planetary carbon dioxide-nitrogen atmospheres
[AIAA PAPER 71-35] 06 p0866 A71-18496

Earth environment from aviation viewpoint, discussing atmospheric physics and chemistry, flight physiology, radiation, etc
08 p1243 A71-20702

Crossed beam model of nitrogen ion-molecular oxygen reactions in upper atmosphere as function of collision energy
08 p1251 A71-21784

UV photolysis of ozone in presence of molecular oxygen, discussing energy exchange reaction with molecular oxygen
13 p2025 A71-28350

Photochemical ion-molecule reactions in ionosphere by air exhaust device and RF mass spectrometer observation in geophysical rocket experiment
13 p2068 A71-28355

Thermospheric electron heating rate and ion chemistry above Wallops Island during 7 March 1970 solar eclipse, measuring ion composition and concentration
16 p2565 A71-33732

Mathematical model for atmospheric carbon monoxide production from methane
21 p3375 A71-41423

Carbon dioxide photolysis at 1740-2100 A applied to photochemistry of Mars lower atmosphere
23 p3641 A71-43327

Venusian photochemistry, discussing hydrogen source from HCl, loss of water in relation to HCl, carbon dioxide stability and COS and hydrogen sulfide in visible clouds
23 p3736 A71-43341

ATMOSPHERIC CIRCULATION

Meteorological observations during solar eclipse of 7 March 1970 concerning temperature, wind, humidity, pressure, air circulation and optical phenomena
01 p0151 A71-10118

Nonlinear interaction between long planetary waves and zonal circulation in atmospheric model with negative viscosity
01 p0113 A71-10537

Aircraft measurement of vertical and horizontal structures of temperature, moisture, refractivity and turbulence for atmospheric convection patterns, comparing radar structure to meteorological soundings
01 p1116 A71-10561

In- and outflow fields in hurricane Debbie, using airborne radar echoes and ATS 3 satellite pictures
01 p1118 A71-10589

Continuous zonal flow nonlinear baroclinic instability, noting amplitude vacillations and flow-wave interactions
01 p0120 A71-10855

Dynamics of tropical disturbances on Interpolar Convergence Zone (ITCZ), using model covering entire hemisphere
01 p0120 A71-10856

Atmosphere global circulation - Conference, London, August 1969
01 p0121 A71-11351

Global atmospheric circulation, discussing surface irregularities and variable heating role in disturbances
01 p0121 A71-11352

Global atmospheric circulation numerical simulation, discussing modeling factors and applications
01 p0121 A71-11353

Global atmosphere energy balance for four seasonal periods, describing production, conversion and loss rates for large scale circulation
01 p0121 A71-11354

Atmospheric boundary layer motion and transports applied to mathematical atmospheric circulation models
01 p0121 A71-11355

Tropics role in global circulation from satellite photography, discussing convection, cloud clusters, momentum fluxes, etc
01 p0121 A71-11356

Extratropical disturbances role in global atmospheric circulation, examining vertical convective heat transfer and kinetic energy production relationship
01 p0121 A71-11357

Stratospheric thermal structure and circulation, considering temperature, wind and composition fields
01 p0122 A71-11358

Global atmospheric circulation theory relation to flow pattern of free thermal convection in rotating fluid subjected to horizontal temperature gradient
01 p0122 A71-11359

ATMOSPHERIC CIRCULATION

Ionospheric vertical wind role in anomaly of quiet sun diurnal geomagnetic variation at magnetic equator 02 p0243 A71-11764

Ionospheric general circulation model for numerical climate digital simulation and weather forecasting, using fluid flow equations 02 p0277 A71-11808

Atmospheric circulation and earth rotational energy contribution to energy release by intense polar auroras, noting ionospheric current subsonic heating and oxygen emission 02 p0244 A71-11909

Solar granules velocity profiles, establishing horizontal outflow and vertical upflow from filtergrams at 6569.2 Å absorption 02 p0316 A71-12754

Exponential thermal wind spiral equations, discussing planetary boundary layer flow over Antarctic Plateau 03 p0452 A71-13228

Planetary boundary layer flow three dimensional steady state equations applied to air motions over horizontally varying surface roughness, temperature and moisture 03 p0453 A71-13230

Planetary atmosphere circulation kinetic energy, energy transformation and driving temperature gradients, using similarity, dimensional and thermodynamic approaches 03 p0488 A71-13551

Venus equatorial stratosphere structure, presenting approximate radiative dynamical calculation for zonal flow mechanism 03 p0488 A71-13552

Planetary atmospheres motion effect on constant pressure surface height in radio occultation data interpretation 03 p0488 A71-13553

Baroclinic atmospheric model of interaction between zonal circulation and long waves, discussing motion instability and oscillation 04 p0620 A71-14636

Nocturnal intensity and excitation temperature variation of hydroxyl vibrational rotational band in air-glow 04 p0581 A71-15050

Ionization disturbances caused by gravity waves in neutral air propagating through ionosphere in electrostatic field and background wind 06 p0888 A71-17278

Mesosphere and lower thermosphere heat input rates and circulation, calculating worldwide average eddy diffusion coefficient 06 p0892 A71-17978

Solar activity sudden perturbations effect on earth pressure field and atmospheric circulation 06 p0924 A71-18265

Turbulent shear flows transport properties, computing atmospheric and vortex motions by invariant modeling of Reynolds stress term in boundary layer momentum equation [AIAA PAPER 71-217] 06 p0886 A71-18653

Atmospheric circulation integral characteristics prediction from wind intensity, kinetic energy and angular momentum 07 p1150 A71-18873

Upper troposphere-lower stratosphere planetary scale circulation correlation from kinetic energy characteristics analysis 07 p1151 A71-18874

Mean zonal flow effects on Rossby waves in barotropic atmosphere, deriving formulas for energy of spectral components 07 p1151 A71-19146

Helical circulations in unstable planetary boundary layer measurements, using constant volume balloons and air parcel tracking 07 p1103 A71-19761

Clear air turbulence role in general atmosphere circulation, considering energy dissipation, momentum transfer and shear layer producing mesoscale processes 07 p1153 A71-20221

Heat quantity to atmospheric circulation ratio over period of decades, using positive temperature sums for long range forecasting method 08 p1326 A71-21445

Equatorial region stratospheric and upper tropospheric circulation, examining relationships between time variations of winds at both levels 08 p1327 A71-21455

Force moment method estimation of atmospheric circulation effect on earth polar movement 08 p1284 A71-21674

Sounding system constant level superpressure balloons for atmospheric circulation global description at all levels and latitudes in conjunction with satellite observations 08 p1231 A71-21742

Neutral and ionized atmosphere parameter variations and circulation during magnetic storms observed at various heights 09 p1436 A71-22550

Ion and electron drift due to F layer wind and associated polarization fields, causing equatorial atmosphere eastward rotation 09 p1438 A71-22979

Latitudinal variations in adiabatic production and destruction of kinetic energy by meridional and zonal motions of atmosphere 09 p1488 A71-23025

Fluid mechanics of atmospheric environment and flow on swept wings in short and medium range aircraft design, concerning STOL capability in India 09 p1383 A71-23199

Thunderstorms environment analysis from radar and aircraft scanings, determining cumulonimbus cloud air kinematic properties for three dimensional circulation model 09 p1488 A71-23252

Prograde and retrograde 4 day circulation in Boussinesq fluid layer by traveling thermal waves in Venus upper atmosphere 09 p1526 A71-23446

Planetary scale atmospheric motion energy spectra and error prediction from numerical model, using eddy-damped Markovian approximation for two dimensional turbulence 09 p1489 A71-23551

Atmospheric Kelvin waves interaction with mean zonal flow in westerly shear zone, noting momentum flux divergence distribution correlation with observed zonal accelerations 09 p1489 A71-23552

Motion effects on atmospheric density altitude distribution, discussing vertical waves, gravity, temperature and winds 09 p1441 A71-23645

Frequency domain spectral energy equations for large scale atmospheric motions, discussing earth rotation effects on kinetic energy spectrum 10 p1638 A71-23963

Weber differential hydrodynamic equations with earth rotation allowance related to Bjerknes circulation theorem and Ertel variational principle of atmospheric dynamics 10 p1607 A71-25111

Atmospheric vertical particle motion inside convective storms observed by airborne pulse Doppler radar techniques 11 p1794 A71-25378

Neutral air winds and ionospheric continuity equation, calculating midlatitude electron concentration longitudinal variations 11 p1754 A71-25605

Ionospheric evening anomaly geographic distribution and relation to neutral winds global pattern 11 p1755 A71-25612

Southern Hemisphere general atmospheric circulation data, using constant volume balloons dispersion 11 p1755 A71-25641

Venus daytime ionospheric models using electron, ion and neutral gas heat conduction with momentum and chemical equations for charged particle densities 11 p1823 A71-25693

Dynamics of planetary atmospheres large scale motions, using similarity theory and dimensional analysis methods for atmospheric circulation characteristics calculation 11 p1826 A71-25720

Earth atmospheric zonal circulation model, using hydrothermodynamic equations with Newton law for radiative heat sources 11 p1795 A71-25919

Atmospheric wave dynamics in equatorial region, obtaining approximate solution with Coriolis force within perturbation theory 11 p1795 A71-25921

Soviet papers on aviation and synoptic meteorology problems covering vertical motions near cold fronts, cloud development, latitude effect, temperature conditions above mountains, etc 11 p1795 A71-26557

Venusian atmosphere heat transfer processes, calculating radiant fluxes and convective motion model 12 p1958 A71-26640

Unsteady solution of simplified atmospheric dynamics equations, reducing to system of Volterra integral equations of second kind for complex horizontal wind velocity 12 p1924 A71-26734

Atmospheric jet stream reinforcement by cold pseudofronts and convective energy from local source 12 p1924 A71-26824

Lower ionospheric irregularities drift from neutral air motion measurements compared to meteor radar system determination 12 p1900 A71-27057

Stratospheric seasonal wind reversals morphological classification for comparing atmospheric processes over different rocket sounding stations 12 p1900 A71-27065

Long time planetary atmosphere motions, investigating sideband resonance mechanism in Rossby wave packet interactions with weak shear zonal flow 12 p1925 A71-27195

Upper atmospheric winds measurements at 160 and 275 km, finding upward motion difficult to relate to intrinsic atmospheric motions 13 p2056 A71-27930

Lower ionospheric plasma frequencies height determination for actual motions, relating periodic variations to spatial electron density structure 13 p2029 A71-28003

Neutral fluctuations of zonal winds in stratosphere and mesosphere from flow equations, noting flow instability role in generation mechanism 13 p2057 A71-28020

Nonzonal atmospheric motion effects on meteorological elements 26-month oscillations stability in equatorial zone from linear hydrothermodynamic equations 13 p2057 A71-28022

Atmospheric circulation and earth rotational energy contribution to energy release by intense polar auroras, noting ionospheric current subsonic heating and oxygen emission 13 p2058 A71-28196

Venus upper atmosphere retrograde circulation correlation with solar couple effect on thermal semidiurnal atmospheric tide 13 p2134 A71-28286

Atmospheric frontogenesis models with air velocity fields acting on initially large scale temperature distributions 13 p2097 A71-28722

Vertical variations of Reynolds stress and heat flux in atmospheric surface layer attributed to sub-mesoscale circulations, using sonic, thermometer and drag measurements 13 p2097 A71-28724

Land-sea drag, Ekman parametrization and Monin-Obukhov transfer process in surface boundary layer of atmospheric circulation model 13 p2097 A71-28725

Static and quasi-static atmospheric motions, using linearized equations for isothermal compressible atmosphere 13 p2097 A71-29084

Space vehicle observation effect on Mars and Venus conceptions, considering origins of life, runaway greenhouse effect on earth and atmospheric circulation 14 p2308 A71-29909

Long range numerical weather prediction, using two level quasi-geostrophic forced general circulation model with spectral truncation 14 p2269 A71-29945

Long term atmospheric circulation prediction model, considering horizontal grid resolution effect on truncation error 14 p2269 A71-29946

Linear filter to represent diffusion in numerical models of large scale atmospheric circulation 14 p2269 A71-29948

Numerical study of three dimensional structure and energetics of unstable disturbances in pure baroclinic and barotropic zonal currents, using eigenvalue technique 14 p2269 A71-29949

Motions in chromospheric limb and disk flares based on H alpha photography 14 p2298 A71-29974

Noctilucent clouds occurrence frequency relationship to mesospheric circulation 14 p2235 A71-30351

General atmospheric circulation mean time distribution, kinetic energy, regional interactions and mathematical simulation 14 p2236 A71-30492

Atmospheric synoptic and mesoscale motions dynamic theory, including baroclinic instabilities, gravity/planetary waves, tides and sea breezes 14 p2236 A71-30493

Jupiter Red Spot, zonal wind and banded appearance, Venus vertical temperature structure and atmospheric motions, and Mars circulation, dust phenomena and atmosphere stratification 14 p2313 A71-30499

Climate simulation by global atmospheric circulation models including wind, temperature, pressure, water vapor, precipitation, evaporation, soil moisture, snow depth and runoff 14 p2270 A71-30505

White dwarf coronas convection zones thermodynamic calculations, considering high electron degeneracy, and He I and He II ionization 14 p2318 A71-31017

Earth gravitational field anomalies relation to atmospheric circulation and tropical perturbations 15 p2443 A71-31223

Ionospheric drift rate measurements by closed space 2.2 MHz receiver method at vertical and oblique incidence, obtaining atmospheric circulation patterns 15 p2395 A71-31431

Ultrasonic rotameter for turbulent wind velocity circulation measurement, using cylindrical electroacoustic capacitor converter with solid dielectric for radiators and receivers 15 p2444 A71-31447

- Stratospheric circulation synoptic and detailed structure from meteorological rocket network sensors 15 p2396 A71-31614
- Stratospheric circulation, investigating ozone heating role in temperature field formation by numerical experiment 15 p2399 A71-31963
- Coupled radiative transfer-gas dynamic interactions in unsteady wave propagation, two dimensional steady flows and atmospheric motions 15 p2515 A71-32562
- Venusian atmosphere circulation modeling, calculating temperature differences, thermal inertia and wind velocity 15 p2496 A71-32729
- Ionospheric motion boundary value problem, deriving uniqueness of solution 16 p2564 A71-33718
- Ionospheric density diurnal variations and atmospheric rotation data from OV1-15 satellite drag measurements, noting geomagnetic activity effects 16 p2566 A71-33746
- Solar eclipse effects on atmospheric structure, circulation and meridional flow, using rocket measured temperature and wind data for pressure and density variations near stratopause 16 p2567 A71-33764
- Upper atmosphere rotational speed variations from measurements of orbital inclination of satellites 16 p2569 A71-33807
- Escaping photoelectrons effect on polar wind exospheric model, suggesting kinetic pressure predominance at very high altitudes 16 p2569 A71-33814
- Low and midlatitude ionospheric motion determination using barium ion cloud release technique 16 p2570 A71-33827
- Thermospheric circulation and temperature changes due to global scale winds flow through F region ionization anomalies, using time independent dynamic model 16 p2571 A71-33836
- Thermosphere structure and motion from neutral atmospheric density data, noting correlation with enhanced geomagnetic activity 16 p2571 A71-33840
- Atmospheric boundary layer circulation dynamic interaction with variable depth barotropic ocean surface, studying stream function during annual cycle 16 p2605 A71-33906
- Spring and autumn cyclonic circulation in stratosphere and mesosphere up to 95 km, using ionospheric radiosonde and rocket data 17 p2730 A71-34301
- Bibliography on neutral atmospheric dynamics covering waves, winds, turbulence and disturbances in thermosphere and ionospheric effects 17 p2732 A71-34462
- Northern Hemisphere atmospheric vertical velocity computation for all seasons compatible with climatological heating functions, using time averaged thermodynamic energy equation 17 p2770 A71-34803
- Heat exchange between atmosphere and earth surface, calculating nonadiabatic term size and spatial distribution 17 p2734 A71-35193
- Orography, cloudiness and surface temperature effects in six-layer global atmospheric circulation model, giving January simulation data 17 p2770 A71-35804
- Earth upper atmosphere superrotation due to zonally averaged magnetospheric electric fields 18 p2911 A71-35992
- Martian surface topography effects on mean wind from time independent and frictionless thermal wind equation solution for radiative-convective atmospheres at scaling analysis level 18 p2964 A71-36287
- Solar photospheric velocity field measurements, using balloon-borne sodium resonance cell with diffraction limited telescope 18 p2965 A71-36729
- Atmospheric rotation on Venus, examining Gierasch model based on radiative drive coupled with response time lags 18 p2967 A71-36930
- Artificial depression structure from general circulation model synoptic development, reproducing real depression features 19 p3089 A71-37504
- Meteor streams effect on atmospheric motions turbulence intensity based on radar observations 19 p3054 A71-37972
- Atmospheric convective motion model, applying turbulent jet method 19 p3093 A71-38696
- Earth atmosphere wind field motion calculation from displacement of longitudinally elongated cyclones 20 p3277 A71-38736
- Earth atmospheric zonal circulation model, using hydrothermodynamic equations with Newton law for radiative heat sources 20 p3256 A71-39210
- Atmospheric wave dynamics in equatorial region, obtaining approximate solution with Coriolis force within perturbation theory 20 p3256 A71-39212
- Seasonal variations of kinetic energy balance of mean meridional circulation in Northern Hemisphere 20 p3257 A71-39436
- Mars and Venus atmospheres, considering energetics, mean winds, temperature differences, circulations and climates 20 p3296 A71-39624
- Vertical temperature profiles from Nimbus 3 satellite spectral radiance measurements, stressing importance for atmospheric circulation prediction 20 p3258 A71-39666
- E region electron density isopleths height correlation with atmospheric pressure variations, noting sympathetic isobaric surface movements in upper stratosphere 21 p3372 A71-40038
- E region wind and temperature measurements from Nancy incoherent scatter experiments, observing prevailing semidiurnal oscillation with phase propagating downwards 21 p3372 A71-40041
- Solar atmosphere oscillatory component observations at 3 mm wavelengths with two radio telescopes, obtaining power spectra 21 p3447 A71-40424
- Book on numerical weather prediction covering atmospheric wave motions, scale analysis, vorticity and energy, barotropic, baroclinic and multilevel models, etc 21 p3410 A71-40780
- Synoptic climatology of blocking situations over European-Atlantic region, obtaining middle troposphere circulation patterns by statistical analysis 21 p3411 A71-40826
- Soviet book on long wavelength radiative heat exchange in atmosphere covering radiation relationship to circulation, cloud formation and weather prediction 21 p3411 A71-40873
- Atmospheric rotation, anisotropic turbulence and long wave radiative heat transfer effects on cellular heat convection 21 p3412 A71-41387
- Atmospheric wind speed estimation, using ATS geostationary satellite cloud photographs 22 p3535 A71-42411
- Atmospheric circulation finite difference weather prediction model, investigating horizontal grid resolution effects 22 p3535 A71-42412
- Upper atmosphere rotation rate decrease at altitudes above 350 km, determining zonal wind variations by satellite orbits analysis from Hewitt camera observations 23 p3667 A71-43140
- Venusian atmosphere circulation modeling, calculating temperature differences, thermal inertia and wind velocity 23 p3735 A71-43298
- Venusian thermosphere, observing dayside solar radiation absorption generated upward dayside and downward nightside vertical motions 23 p3735 A71-43333
- Isentropic nature of stratospheric air masses motion from balloon measurements of temperature and radiation 23 p3671 A71-43338
- Governing equations numerical integration for Venusian atmosphere circulation, calculating solar heating distribution in spherical polar coordinates 23 p3735 A71-43340
- Global atmospheric research program, discussing circulation, weather forecasts, numerical modelling and observational system 23 p3701 A71-43822
- Planetary atmospheric motions, discussing solar radiation, internal heat sources, planetary rotation and magnetic field effects 23 p3672 A71-43891
- Cumulus clouds photographs above Northern Hemisphere by meteorological satellite during active periods of earth atmospheric circulation 23 p3701 A71-44047
- Atmospheric wind velocity time variations at 80-100 km altitudes from ionospheric drift data, finding planetary oscillation periodicities relationship to solar activity cycle 24 p3822 A71-44349
- ### ATMOSPHERIC COMPOSITION
- #### NT ATMOSPHERIC MOISTURE
- #### NT IONOSPHERIC COMPOSITION
- Nitrous oxide tropospheric abundance from IR solar spectrum altitude variation 01 p0073 A71-10139
- Air carbon dioxide role in rabbits metabolism, using C 14 radioactive tracer technique 01 p0012 A71-11061
- Global ozone distribution from inverted radiance measurements by IR interferometer spectrometer /IRIS/ on Nimbus 3 satellite 01 p0074 A71-11249
- Large fluxes of energetic neutral atomic hydrogen at 800 km preceding geomagnetic disturbance, using sounding rocket electrostatic analyzer 01 p0148 A71-11526
- Altitude distribution of oxygen in atmosphere with eddy diffusion allowance from ARCAS 2 rocket photometric observations 01 p0077 A71-11528
- Satellite sounding of atmospheric pollution by spectral analysis of outgoing thermal radiation 02 p0241 A71-11689
- Venera-borne gas analyzers for parachute descent probing of Venus atmosphere, describing design and operation 02 p0248 A71-11916
- M type supergiants atmospheric metals abundances from high dispersion spectrograms analysis 02 p0308 A71-12095
- Upper stratosphere and mesosphere concentrations of Ne, Ar, and Kr from rocket-borne cryogenic air sampler 02 p0246 A71-12701
- Soviet book on meteorological conditions and supersonic aircraft flight covering atmospheric composition and structure, temperature distribution, wind effects, etc 02 p0278 A71-12840
- Comet brightness fluctuation phenomenon, discussing solar wind interaction with Platt particles in cometary atmosphere 02 p0303 A71-12867
- Ozone atmospheric concentration, dissociation in SST air conditioning systems and biochemical poisoning 03 p0358 A71-13096
- Venus lower atmosphere structure and brightness temperature spectrum analysis for composition, temperature and pressure profiles 03 p0484 A71-13212
- Spectrophotometry of methane and ammonia absorption bands indicating decrease toward Jupiter disk edge 03 p0484 A71-13213
- Neutral upper atmosphere response to solar activity variations, discussing temperature, density and helium/oxygen composition [ALAA PAPER 70-1356] 03 p0409 A71-13577
- Earth atmosphere origin, discussing oxygen and carbon dioxide balance 03 p0409 A71-13697
- Troposphere and stratosphere mean annual carbon dioxide cycle measurements, describing aircraft collection equipment and procedure 03 p0418 A71-14205
- Atmospheric aerosol vertical distribution by lidar system, describing ruby Q switched giant pulse laser design and operation 05 p0720 A71-16221
- Atmospheric aerosol vertical distribution by lidar system, discussing backscatter function, relative humidity, wind velocity, visibility, etc 05 p0720 A71-16222
- Vertical atmospheric ozone distribution from inversion of spectral UV radiation, comparing results with statistical method 05 p0742 A71-16671
- Polar region atmospheric ozone density profile measurements, using rocket sounding 05 p0743 A71-17007
- Isotopic helium atmospheric composition determination, using mixtures of He 3 and He 4 for comparison 06 p0921 A71-17390
- Venus atmosphere and lithosphere thermochemical composition, examining various models 06 p0966 A71-17898
- Subprotonospheric and ion cyclotron whistlers generated by same lightning discharge observed by OV1-10 satellite 06 p0869 A71-17995
- Galactic cosmic rays solar modulation effects on fast neutron flux in atmosphere 06 p0962 A71-18182
- Venusian atmospheric cloud cover, determining nature of particles by optical reflective properties 07 p1191 A71-18907
- Planetary atmospheres structure and dynamics, discussing composition and vertical temperature profile models 07 p1191 A71-18915
- Upper atmosphere H atoms concentration maxima and minima from topside to bottomside ionospheric electron contents ratio, using coupled continuity and thermal equations 07 p1098 A71-19031
- Time-altitude diurnal variations in molecular and atomic oxygen concentrations at 65-200 km from continuity equations 07 p1099 A71-19391
- Natural aerosols effects on atmospheric electron content, comparing theoretical prediction with experiments on artificial aerosols in D region 07 p1100 A71-19404

Atmospheric oxygen evolution and stability, discussing effects of photosynthesis inhibition, hydrogen passage and burial carbon
07 p1102 A71-19540

Atmospheric carbon 14 concentrations during past century, noting radioactive dating implications
07 p1102 A71-19580

Downward atmospheric radiation fluxes incident on Martian surface horizontal plane, tabulating atmospheric composition, surface pressures and temperatures and effective sky temperatures
07 p1199 A71-19874

M type supergiants atmospheric metals abundances from high dispersion spectrograms analysis
08 p1362 A71-21145

Book on ionosphere and magnetosphere covering temperature, composition ionizing radiations, radio communication electron production and loss, etc
08 p1363 A71-21164

Horizontal He distribution in upper atmosphere from OGO 6 mass spectrometer data normalization for altitude by Jacchia model atmosphere
08 p1283 A71-21647

Diurnal variation symmetry of upper atmosphere molecular oxygen concentration in terms of ozone photodissociation
09 p1435 A71-22446

Upper atmospheric composition by nitrogen molecules radiative transition analysis, using laser resonance backscattering effect
09 p1436 A71-22581

Upper atmospheric ion composition during Orionid meteor shower activity by rocket-borne RF mass spectrometer
09 p1437 A71-22680

Ozone flux measurement in atmospheric surface layer by profile method as function of destruction coefficient, friction velocity and concentration
09 p1438 A71-23023

Low temperature laboratory measurements of ozone absorption coefficients for atmospheric standards, using Dobson spectrophotometer and quartz iodine source
09 p1438 A71-23026

Venusian atmosphere carbon dioxide, water, molecular oxygen and nitrogen contents from Venera 5 and 6 data
09 p1523 A71-23144

Ozone distribution measurements in mesosphere and stratosphere by rocket during seasonal ionospheric disturbance and solar eclipse
09 p1490 A71-23562

Tropospheric temperature and aerosol/molecule ratio determination by optical radar measurements, using Doppler broadening in spectral analysis of laser radar echoes
09 p1466 A71-23628

Atmospheric Pb 210 /radium D/ aerosols concentration relationship to solar activity from measurement with blue filter
10 p1599 A71-23859

Xe and Kr isotopes gas extraction and mass spectrometer analyses of Apollo 11 lunar soil, Murray carbonaceous chondrite and atmospheric Xe
10 p1661 A71-24410

Solar geomagnetic seasonal ionization control of upper ionosphere longitudinal composition variations from polar satellite observations
10 p1602 A71-24555

Martian studies during opposition, discussing atmosphere, optical thickness, pressure, brightness phase dependences over land and sea, crust material and dust clouds
10 p1677 A71-24584

Nitrogen, helium, argon and neon containing atmospheres relation to altitude decompression of rats, noting interspecies comparison of metabolic effects
10 p1570 A71-24610

Magnetospheric numerical model with two-monoenergy-component proton distribution function, examining ring current belt formation causing inflation
10 p1663 A71-24782

Nitric oxide diurnal variation model in upper atmosphere incorporating solar flux, absorption cross sections and chemical rate constants
10 p1605 A71-24795

Atomic oxygen and carbon dioxide measurement in lower thermosphere by mass spectroscopy
10 p1606 A71-24803

Electric field, neutral air winds and atmospheric composition changes effects on electron concentration diurnal variation in midlatitude F layer
10 p1607 A71-24922

Atmospheric molecular species, calculating electron impact ionization cross sections and recombination coefficients
10 p1645 A71-24970

Mars atmospheric CO abundances and rotational temperature from Voigt line profiles
10 p1646 A71-24993

Aqueous HCl solutions refractive index calculation from concentration dependence for Venus clouds composition
10 p1680 A71-25012

Muon bundles frequencies from model for propagation of various atmospheric components in combination with theoretical pion spectra
10 p1664 A71-25044

Vertical ozone distribution estimation by umkehr observations, discussing optimum statistical inference technique application
11 p1794 A71-25387

Venus atmosphere chemical composition, determining N, O, water and carbon dioxide concentrations, temperature and pressure
11 p1823 A71-25691

Venus atmosphere composition and structure from microwave spectrum, noting surface pressure and temperature and water vapor
11 p1823 A71-25694

Venus cloud composition, noting partially hydrated iron chloride as principal constituent
11 p1824 A71-25703

Venus cloud hypotheses, discussing chemical composition, vapor pressure, temperatures and spectroscopic abundances
11 p1824 A71-25705

Martian atmospheric pressure carbon dioxide abundance variations correlated with waxing and waning of polar caps or Mars season
11 p1825 A71-25712

Hydrogen-helium gas mixtures high pressure phase behavior, considering solidified gas core under Jupiter and Jovian planets atmospheres
11 p1827 A71-25728

Uranus atmospheric molecular hydrogen abundance from pressure induced overtone spectra, using quadrupole moment and polarizability matrix elements theoretical values
11 p1827 A71-25731

H and He concentrations upper limit for Titan atmosphere from molecular diffusion time constant
11 p1828 A71-25732

Upper atmospheric molecular and atomic N and O diurnal variations correlated to atmospheric heating as function of solar UV radiation from sounding rocket data
11 p1757 A71-25775

Atmospheric boundary layer refractive index fluctuations structural characteristics determined from summer vertical wind velocity and temperature profiles
11 p1795 A71-25922

Neutral H concentration in upper atmosphere during solar minimum, using ion thermal energies from rocket and satellite mass spectrometer, radio and proton whistler measurements
12 p1898 A71-26637

Jupiter occultation of beta Scorpii on 13 May 1971, determining hydrogen/helium ratio
12 p1961 A71-26876

Jovian atmosphere radio observations, discussing helium- and ammonium-hydrogen molecules ratio, brightness temperature spectra and RF wavelength absorbing agents
12 p1964 A71-27087

Atmospheric budget of C/12/O and C/14/O, discussing latitude and altitude effects and tropospheric residence time
12 p1902 A71-27291

Venera-borne gas analyzers for parachute descent probing of Venus atmosphere composition, describing design and operation
13 p2067 A71-28203

Venus carbon dioxide spectrum, observing spatial and temporal variation in abundance
13 p2134 A71-28287

Carbon dioxide concentrations in tropopause, investigating flux from northern troposphere into stratosphere
13 p2063 A71-29112

Tropopause oxygen/nitrogen decrease effect on ion and neutral composition changes in thermospheric region during magnetic storm, using simultaneous ionospheric and atmospheric equations
14 p2229 A71-29665

Super metal rich K giant stars atmospheric model, obtaining abundances and turbulent velocity parameter
14 p2305 A71-29674

Meteorological research on upper atmosphere energy sinks/sources, composition, density, turbulence, winds and thermal structure
14 p2236 A71-30494

Hydrogen deficient white dwarf atmospheres, computing line free flux constant models for He rich compositions with varied metal abundances
14 p2318 A71-31016

Spatially periodic static field mass spectrometers for upper atmosphere composition measurements on board satellite and sounding rocket
15 p2400 A71-32350

High average power flash lamp pumped pulsed dye laser development and application in atmospheric sodium probing
16 p2586 A71-33148

Gaseous chlorine of marine origin in atmosphere based on concentration analysis
16 p2604 A71-33383

Thermospheric composition determination from satellite drag derived densities, comparing with data computed from mass spectroscopic observations
16 p2566 A71-33750

Upper atmospheric composition and density variations with latitude and local time, using OV3-6 satellite measurements
16 p2566 A71-33756

Mass spectroscopy of upper atmosphere neutral composition at equatorial, middle and polar latitudes from meteorological rockets
16 p2566 A71-33758

Upper atmosphere neutral species latitudinal and seasonal distributions, using turbulent transport coefficients and photochemical reaction rate constants in finite difference solution
16 p2569 A71-33804

Upper atmospheric neutral composition diurnal variations as function of altitude, local time and solar activity
16 p2570 A71-33829

Thermospheric dynamics, including global compositional structure, winds and temperature response to solar radiation and vertical mass diffusion
16 p2571 A71-33838

Lower thermosphere atomic nitrogen concentration during maximum solar activity, using rocket-borne radio frequency and time of flight mass spectrometers
16 p2572 A71-33843

Global temperature effects on atmospheric carbon dioxide and aerosols density based on atmospheric model, noting earth surface temperature decrease
16 p2575 A71-34047

Bibliography on upper atmosphere hydrogen covering Lyman alpha and beta and Balmer alpha measurements, non-Maxwellian distribution, diurnal variations and oxygen evolution
17 p2732 A71-34463

Jovian turbopause probe mission, discussing atmospheric composition measurements and nonunivocal system concept [AIAA PAPER 71-833]
17 p2802 A71-34714

Remote sounding of earth atmosphere temperature and composition
17 p2736 A71-35565

Planetary atmospheres composition from ground based IR spectroscopy, including multiple scattering, cloud layers, line formation and absorption
17 p2808 A71-35570

Atmospheric ozone data in tropical regions from Nimbus 3 IR interferometer spectrometer measurements, indicating easterly jet stream existence during summer monsoon period
17 p2771 A71-35810

Twilight aureole visual observation and objective colorimetry from Soyuz spacecraft, noting importance for atmospheric composition determination
18 p2911 A71-36007

Stratospheric ozone reduction through catalytic action of nitrogen oxides from SST exhaust, discussing degrading effect on atmospheric radiation shield
18 p2874 A71-36922

Atmospheric total ozone increase during 1960s, investigating possibility due to southward air flow in troposphere and low stratosphere
19 p3047 A71-37298

Jovian atmosphere radio observations, discussing helium- and ammonium-hydrogen molecules ratio, brightness temperature spectra and RF wavelength absorbing agents
19 p3133 A71-37437

Solar photosphere iron abundance data from Fraunhofer spectrum and EUV line measurements
19 p3135 A71-37610

Venus atmosphere chemical composition, temperature and pressure, discussing model cloud layer, circulation and upper atmospheric structure
19 p3138 A71-37759

Time-altitude diurnal variations in molecular and atomic oxygen concentrations at 65-200 km from continuity equations
19 p3053 A71-37815

Natural aerosols effects on atmospheric electron content, comparing theoretical prediction with experiments on artificial aerosols in D region
19 p3053 A71-37828

Nighttime polar atmospheric structure and temperature variations due to gas kinetic and electron energy changes
19 p3056 A71-38361

Vibrationally excited oxygen molecules formation and decomposition in upper atmosphere, calculating day and night equilibrium concentrations
19 p3057 A71-38373

Atmospheric neutron production by cosmic rays, calculating cadmium-indium ratio
19 p3066 A71-38379

Atmospheric composition and temperature effects on F 1 region ion concentration structure from 140 to 220 km for low solar activity conditions
19 p3058 A71-38382

Chemical composition of atmospheric aerosols from Tokyo region, measuring energy spectrum of neutron irradiated specimens by gamma spectrometer
19 p3094 A71-38698

Atmospheric gases effective electron collision frequency calculations, using momentum transfer cross sections 20 p3271 A71-38743

F region seasonal anomaly relationship with lower atmosphere composition changes, discussing effects of oxygen/nitrogen relative concentration on ionospheric and atmospheric parameters 20 p3215 A71-38746

Atmospheric boundary layer refractive index fluctuations structural characteristics determined from summer vertical wind velocity and temperature profiles 20 p3256 A71-39213

Wide passband techniques for atmospheric total ozone content measurements, discussing choice of ozonometer characteristics and filter parameters 20 p3238 A71-39335

Heavy rare gases adsorption on terrigenous sediments, comparing earth atmospheric composition with meteoritic planetary primordial component 20 p3194 A71-39385

Venus atmosphere chemical composition from gas analysers onboard Venera automatic stations, determining element abundance, water vapor density and cloud layer structure 20 p3296 A71-39625

Global atmospheric ozone distribution from inverted radiance measurements by IR interferometer spectrometer onboard Nimbus 3 satellite 20 p3220 A71-39668

Mesosphere and stratosphere ozone vertical density distribution from sounding rocket data, considering photochemical theory and hydrogenic reductions 20 p3221 A71-39694

Lower thermosphere and mesosphere water vapor and neutral composition spectrometric measurements, estimating hydrogen and oxygen atom recombination coefficient limits with mass analysers 20 p3221 A71-39696

Neutral atmospheric composition and density variations during geomagnetic disturbances from OGO-6 satellite quadrupole mass analyzer measurements 20 p3223 A71-39711

Thermospheric atomic hydrogen concentration temporal variations in situ measurement by Explorer 32 satellite 20 p3232 A71-39898

Brewer bubbler as continuous surface ozone sensor, measuring ozone vertical distribution in atmosphere 21 p3377 A71-40181

Spacecraft cabin artificial atmospheric composition and variation effects on human immunocompetence, examining lymphoid cell immunity reactions after lymphocytes blast transformations 21 p3332 A71-40556

Baric levels determination for weather forecasting from statistical analysis of atmospheric numerical model 21 p3410 A71-40823

Venus survey, discussing mass, radius, rotation, internal structure, magnetic field, radiation belts, surface properties, atmospheric composition, cloud layer, etc 21 p3452 A71-40884

Lunar atmospheric contributions from solar wind, meteoric volatilization, internal degassing and rocket gases, discussing day and night neon concentrations 21 p3453 A71-41182

Upper atmospheric molecular and atomic nitrogen and oxygen diurnal variations correlated to atmospheric heating as function of solar UV radiation from sounding rocket data 22 p3532 A71-41543

Atmospheric trace and pollutant molecules global survey, using airborne/spaceborne high resolution Fourier interference IR spectrometer 22 p3542 A71-41963

German Aeros satellite for upper atmosphere aeronomy research, describing objectives regarding atmospheric composition and density 22 p3610 A71-42008

Beta cephei stars atmospheric He and metal abundances, comparing line spectra data with other early B stars sample 23 p3723 A71-42947

Ozone concentration measurements near sunrise by balloon-borne electrochemical ozonesonde, noting scattered radiation effect 23 p3667 A71-43074

Search for upper atmosphere MgO content, using modified Ebert spectrometer with photomultiplier detection to measure twilight excited scattered and resonance radiation 23 p3670 A71-43191

Atomic oxygen and hydrogen identification in Mars upper atmospheric emission spectra by Mariner UV spectrometer, inferring carbon monoxide presence by self absorption 23 p3735 A71-43330

Mars and Venus carbon dioxide atmospheres, covering solar EUV heating efficiency, upper atmosphere temperature and chemical recombinations 23 p3735 A71-43334

Earth atmosphere gas composition and electron density variations at F region lower boundary explained by stratospheric explosive and diffusive warmings effect on critical frequency 23 p3671 A71-43578

Upper atmosphere minor component distribution rearrangement, investigating transition time to diffusion equilibrium 24 p3823 A71-45031

Ionospheric and neutral atmospheric temperature profile, composition and electron density and energy measurements by MR-12 rocket 24 p3824 A71-45310

ATMOSPHERIC CONDITIONS

U METEOROLOGY

ATMOSPHERIC CONDUCTIVITY

NT IONOSPHERIC CONDUCTIVITY

Electric conductivity dependence on optical depth in photospheres of spectral type F, G and K stars for different gravitational acceleration values on surface 01 p0159 A71-10866

Sunspot and photosphere electric conductivity relationships based on Michard, Mattig and Fricke-El-sasser models 01 p0159 A71-10867

Effective electron collision frequency and RF conductivity along geomagnetic lines in magnetosphere 03 p0377 A71-13272

Atmospheric electrical properties derivation from continuity equation, considering ion concentration, conductivity, space charge density and electric field 03 p0409 A71-13610

Rocket experiments during 1964 solar eclipse, obtaining D region parameters from parachute-borne blunt probe measurements of atmospheric positive and negative conductivities 03 p0416 A71-14033

Atmospheric ionization by vertical gamma and alpha radiation of natural radioactive products, comparing to vertical behavior of conductivity 05 p0799 A71-16843

Electrical conduction in orthogonal coordinates from nondipole nature of geomagnetic field on conductivity tensor of ionospheric dynamo region 19 p3057 A71-38381

ATMOSPHERIC DENSITY

Long period atmospheric fluctuations, investigating large scale disturbance structure from observed data 01 p0119 A71-10852

Space shuttle reentry in quiet and geomagnetic storm perturbed atmosphere with reference to density variations, using San Marco 2 satellite [ICAS PAPER 70-04] 03 p0497 A71-13149

Semiannual variation in upper atmosphere air density from satellite orbit data 03 p0407 A71-13304

Neutral upper atmosphere response to solar activity variations, discussing temperature, density and helium/oxygen composition [ALAA PAPER 70-1356] 03 p0409 A71-13577

Thermospheric neutral particle molecular nitrogen density and temperature measurements by rockets, noting correlations with diurnal, solar cycle and other variations 03 p0414 A71-14020

Upper atmosphere densities from satellite drag data, noting semiannual variations 03 p0414 A71-14021

E layer atmospheric densities from decaying satellites observation, discussing solar activity and geomagnetic correlations 03 p0414 A71-14022

Atmospheric density curves by satellite observation, obtaining schematic models for fine structure of semiannual variation 03 p0414 A71-14023

Diurnal minimum and geomagnetic storms effect on equatorial air density from San Marco 2 satellite drag experiment 03 p0415 A71-14024

Theoretical vs observed atmospheric densities between 350 and 1500 km, using models and satellite observations 03 p0415 A71-14025

Atmospheric density variations determination from Proton 2 braking data for aerodynamic drag coefficient, constructing model for rarefied gas flow-satellite interaction 05 p0804 A71-16043

Rocket-borne beta ray atmospheric densitometer errors due to cosmic rays 05 p0752 A71-16673

Neutral ionospheric temperature profile diurnal variation at Arecibo from incoherent scatter measurements, considering relevance to 1400 hour density maximum 06 p0887 A71-17271

Atmospheric density and rotation measurements below 195 km from high resolution drag analysis of satellite OV1-15 using least squares fitting 06 p0887 A71-17272

Stratospheric small ion density measurements by level flight balloons 07 p1103 A71-19768

High vacuum calibration of cryogenic quartz crystal for atmospheric density 07 p1113 A71-19852

Stochastic Liapunov stability of satellite motion influenced by aerodynamic and gravity gradient torques, considering atmospheric density uncertainty [ALAA PAPER 70-37] 07 p1208 A71-19883

Infrasonic shock wave generation in troposphere by powerful earthquakes, causing upper atmosphere density rise due to heating 08 p1278 A71-21019

Spacecraft autonomous control algorithm to ensure geographically specified landing accuracy, noting atmospheric density 09 p1491 A71-22565

Low latitude atmospheric vertical density variations, comparing solar and geomagnetic activities effects 09 p1436 A71-22578

Midlatitude stratosphere and lower ionosphere density model, discussing vertical, diurnal and seasonal variations effects on spacecraft trajectories 09 p1438 A71-23137

Altitude spectrum of ion formation in interaction of proton flux with atmosphere, using Bragg dissipation function 09 p1514 A71-23153

Motion effects on atmospheric density altitude distribution, discussing vertical waves, gravity, temperature and winds 09 p1441 A71-23645

Low latitude air density correlation to magnetic disturbance deduced from Ariel 2 satellite spin rate changes 10 p1602 A71-24552

Upper atmosphere statistical structure based on analysis of deviations of satellite-determined air densities from theoretical Jacchia model, noting latitudinal, seasonal and diurnal variations 10 p1607 A71-25024

Parachutes for low density atmospheres, describing low and high altitude test results [ALAA PAPER 70-1164] 11 p1707 A71-25525

Spherical harmonics of secular perturbations in artificial satellites motion due to atmospheric gravitation 11 p1829 A71-25808

Solar activity effects on atmospheric density variations from satellite observations, using random process isocorrelation charts 11 p1759 A71-25821

Atmospheric density semiannual variations from satellite observation, comparing with atmospheric models 11 p1760 A71-25824

Solar activity and geomagnetic disturbance effects on upper atmosphere density from ATS 2 satellite orbit observations 12 p1899 A71-26886

Construction, operation and in-flight performance of triaxial bridge accelerometer used in falling sphere experiment for atmospheric density, temperature and pressure determination 13 p2066 A71-28160

Average energy electron capture coefficient dependence on air density, temperature and altitude under gamma radiation 13 p2061 A71-28543

Thermospheric density response to auroral heating during geomagnetic disturbances simulation assuming impulse heat input into small latitude band within auroral ovals 15 p2398 A71-31770

Atmospheric density measurements at 70 to 115 km altitude range from rocket soundings with accelerometer instrumented inflatable spheres 16 p2562 A71-33066

Atmospheric density variations determination from Proton 2 braking data for aerodynamic drag coefficient, constructing model for rarefied gas flow-satellite interaction 16 p2635 A71-33447

Laser radar system for measuring atmospheric density above troposphere, discussing equipment design and construction 16 p2542 A71-33534

Upper atmosphere density fluctuations associated with solar activity and local time values, using Cosmos 14 satellite drag data 16 p2564 A71-33666

Semiannual density variation in heterosphere as function of height based on satellite drag and atmospheric models 16 p2564 A71-33723

Neutral upper atmosphere properties, discussing temperature, density and wind variations during disturbed conditions associated with geomagnetic storms 16 p2565 A71-33727

Thermospheric hydrogen density and temporal variations from Explorer 32 measurements, discussing dependence on exospheric temperature 16 p2565 A71-33731

Upper atmosphere heating at high latitudes, analyzing air density variations from Molniya 1K satellite observations over 2 year period

16 p2565 A71-33740

Ionspheric density diurnal variations and atmospheric rotation data from OVI-15 satellite drag measurements, noting geomagnetic activity effects

16 p2566 A71-33746

Thermospheric composition determination from satellite drag derived densities, comparing with data computed from mass spectroscopic observations

16 p2566 A71-33750

Upper atmospheric composition and density variations with latitude and local time, using OV3-6 satellite measurements

16 p2566 A71-33756

Empirical atmospheric model derivation from midlatitude density data

16 p2566 A71-33759

Global model of atmospheric temperature, chemical composition and density for altitudes from 25 to 1000 km, using satellite drag determined density values

16 p2567 A71-33782

Chemical trimethyl aluminum releases in lower thermosphere for temperature, density, winds, turbulence, diffusion coefficients and atomic oxygen content measurements

16 p2568 A71-33792

Seasonal density variations in thermosphere and exosphere, obtaining model from Explorers 19 and 39 drag measurements for comparison withOGO-6 mass spectroscopy

16 p2569 A71-33802

Air density observation near 150 km heights from Cosmos 316 orbit, noting geomagnetic disturbance effects and semiannual variation

16 p2569 A71-33806

Semiannual atmospheric density variation measurements by OV3-6 satellite

16 p2570 A71-33821

Neutral lower thermosphere density variations at high and middle latitude in Southern Hemisphere from OVI-15 /SPADES/ satellite accelerometer measurements

16 p2570 A71-33824

Neutral atmosphere density profile data from satellite-borne accelerometer experiment, observing gravity waves propagating in north-south direction at high latitudes

16 p2570 A71-33825

Upper atmosphere density determination from Cosmos satellite deceleration data, allowing for diurnal and semiannual variations and solar radio emission intensity effects

16 p2571 A71-33837

Atmospheric density variation response time measurement to geomagnetic activity by satellites-borne low-G accelerometer calibration system, considering atmospheric heating mechanism

16 p2571 A71-33839

Thermosphere structure and motion from neutral atmospheric density data, noting correlation with enhanced geomagnetic activity

16 p2571 A71-33840

Semiannual ionospheric density variations from Cosmos artificial satellites drag, noting agreement with solar corpuscular radiation geoefficiency

16 p2571 A71-33841

Exospheric density semiannual variations from June 1968 to December 1970 at altitudes of 900 and 1070 km, using satellite drag determination by orbital period rate of change measurement

16 p2643 A71-33848

COSPAR international reference atmosphere containing seasonal variations, solar flux and altitude models for density, temperature, pressure and wind

16 p2572 A71-33851

Heterosphere semiannual density variation with amplitude as function of height, noting dependence on temperature distribution and sunspot cycle

16 p2574 A71-33963

Molecular oxygen densities at 80-160 km by rocket sounding with absorption of solar Lyman alpha line and C IV doublet at 1550 A

16 p2574 A71-33966

Upper atmosphere density observation by Q switched ruby laser radar

17 p2753 A71-34748

Upper atmosphere mean temperature, pressure, density and wind distributions as functions of altitude, season and latitude, discussing planetary, infrasonic and internal gravity wave effects

17 p2735 A71-35236

French monograph on ULF geomagnetic field variations covering plasmopause, geomagnetic pulsations, WKB limit and magnetospheric density

17 p2735 A71-35248

Atmospheric temperature and density scale height seasonal variations near mesopause, using meteor theory mass and luminosity equations

17 p2737 A71-35740

Flight test results for CACTUS accelerometer launched by rocket probe at Guiana Space Center,

considering atmospheric density profile in 120-150 km altitude zone

18 p2924 A71-36755

Thermospheric density determination from ESRO rocket flight produced artificial fluorescent AIO clouds

18 p2914 A71-37060

Artificial earth satellite orbital decay rate measurement for upper atmosphere density data, using combined directional observations and orbit data

19 p3048 A71-37394

Semiannual amplitude variations in F 2 region for estimating oxygen density dissociation and temperature ratios in lower thermosphere

19 p3048 A71-37398

Astronomical telescopes image motion, distortion and scintillation, examining atmospheric refractive index and density/temperature variation effects

19 p3010 A71-38571

Seasonal, latitudinal and diurnal variations of upper atmospheric structural parameters including density and temperature

19 p3061 A71-38656

Thermospheric atomic oxygen and molecular nitrogen number densities, discussing earth atmospheric absorption of solar UV lines

20 p3214 A71-38727

Infrasonic shock wave generation in troposphere by powerful earthquakes, causing upper atmosphere density rise due to heating

20 p3219 A71-39599

Lower thermospheric density and molecular nitrogen partial density rocket measurements, obtaining neutral gas temperature vertical distribution and ion density profile

20 p3222 A71-39699

Midlatitude lower thermosphere atomic and molecular oxygen rocket measurements, presenting concentration and vertical distribution data

20 p3222 A71-39700

Upper atmospheric anomalous molecular oxygen distribution, discussing turbulent theory with autocorrelation of density fluctuations

20 p3222 A71-39701

Atmospheric density variations calculation, using aerodynamic drag coefficient data from gas flow-satellite surface interactions

20 p3223 A71-39706

Diurnal and semiannual variations in upper atmosphere density from Cosmos satellite drag observations, noting calculation systematic errors

20 p3223 A71-39707

Long term upper atmosphere density variations correlated with solar flux, using satellite observations

20 p3223 A71-39708

Upper atmosphere density variations and time lag with respect to geomagnetic disturbances, using satellite drag measurements

20 p3223 A71-39709

Semiannual upper atmosphere density variations near solar maximum from satellite drag data, relating height amplitude profile with exospheric temperatures

20 p3223 A71-39710

Neutral atmospheric composition and density variations during geomagnetic disturbances from OGO-6 satellite quadrupole mass analyzer measurements

20 p3223 A71-39711

Equatorial ionospheric density measurements on quiet and perturbed days, using San Marco 2 satellite balance

21 p3373 A71-40047

Upper atmospheric density numerical calculation from draconite period by Perlo program using satellite observation near celestial equator

21 p3374 A71-40655

M superrights hot corona base density determination from radio emissions observations, noting equivalence to solar type 4 microwave bursts

22 p3598 A71-41916

German Aeros satellite for upper atmosphere aeronomy research, describing objectives regarding atmospheric composition and density

22 p3610 A71-42008

Upper atmospheric temperature and density measurements from artificial cloud observations

23 p3667 A71-43139

Onboard computation of Mars atmospheric density and temperature, evaluating error covariance

23 p3774 A71-44095

ATMOSPHERIC DIFFUSION

Rocket-borne Na-K vapor release for upper atmosphere winds profiles and diffusion measurements by ballistic camera photography

03 p0415 A71-14027

Atmospheric diffusion parameters investigated by smoke plumes in atmospheric boundary layer, evaluating turbulent energy dissipation

05 p0778 A71-16838

Mesoscale relative diffusion estimates in low troposphere from tetroon /constant volume balloon/ flights at Nevada Test Site

08 p1326 A71-21449

Eddy diffusivities and turbulent diffusion characteristics in atmospheric surface layer, using universal function based on similarity theory

09 p1487 A71-22639

Monodispersed particle semifinite atmosphere, calculating invariance principles of diffused radiation based on Mie theory

12 p1960 A71-26823

Intensity and polarization of diffusively transmitted sunlight, taking into account various aerosols distributions and normal molecular constituents

12 p1902 A71-27198

Air polluting nitric oxide and soot production by jet aircraft, discussing mixing process and atmospheric dispersion

[AIAA PAPER 70-115]

12 p1946 A71-27560

Cosmic ray components atmospheric diffusion and production based on H quantum, two fireball and aleph model

13 p2122 A71-28064

Diffusion coefficient as function of height in turbulent atmospheric boundary layer, considering similarity laws between wind tunnel and field data

13 p2051 A71-29432

Radio propagation attenuation calculation by tropodiffusion, using meteorological parameters from Brazilian weather stations

14 p2192 A71-29573

Linear filter to represent diffusion in numerical models of large scale atmospheric circulation

14 p2269 A71-29948

Diffuse skylight measurement for atmospheric dust particle concentration, considering sunlight scattering by air molecules and aerosol layers

16 p2567 A71-33767

Thermospheric dynamics, including global compositional structure, winds and temperature response to solar radiation and vertical mass diffusion

16 p2571 A71-33838

Winds and diffusion measurements in lower thermosphere using sodium vapor cloud release from Centaur IIB rocket

20 p3221 A71-39692

ATMOSPHERIC ELECTRICITY

NT AURORAL ELECTROJETS

NT ELECTROJETS

NT EQUATORIAL ELECTROJET

NT IONOSPHERIC CURRENTS

Magnetospheric VLF electric field emissions above electron cyclotron frequency from OGO 5 observation at magnetic equator

01 p0076 A71-11500

Ionspheric vertical drift velocities and east-west electric fields at magnetic equator from incoherent scatter observations

01 p0076 A71-11505

Atmospheric electrical properties derivation from continuity equation, considering ion concentration, conductivity, space charge density and electric field

03 p0409 A71-13610

Troposphere and stratosphere electric field above Atlantic Ocean, investigating electrode effect role in atmospheric circuit

05 p0738 A71-16220

Apollo 12 lightning incident, discussing atmospheric conditions, damage and discharge hazard minimization

[SAE PAPER 700938]

07 p1208 A71-19925

Geomagnetic solar quiet field and terrestrial currents diurnal variations, discussing interrelations and vector polarization

07 p1104 A71-20047

Terrestrial electrical current distribution diagram based on solar quiet variation hodographs

07 p1104 A71-20048

Simultaneous auroral ionospheric electric field measurements by Skylark rockets, deriving plasma drift direction

08 p1279 A71-21208

Polar substorms electric current systems and magnetic effect below and above ionosphere

08 p1279 A71-21211

Electric field formation of field aligned electron density irregularities in magnetosphere

08 p1280 A71-21215

Space charge sign distribution sounding in atmosphere by electrode potential difference measurement

09 p1437 A71-22677

Book on aeronomy covering earth upper atmosphere structure, tidal oscillations, gravity waves, airglow, aurora, ionospheric disturbances, electric currents and turbulence

09 p1437 A71-22778

Lightning return stroke electric field intensity exact expression derivation, obtaining charge moment equation approximation

09 p1488 A71-23443

Neutral wind and ion velocity determination under quiet and disturbed geomagnetic conditions in auroral zone, noting electric field measurements

09 p1440 A71-23600

Electrical processes in stratosphere and mesosphere - Conference, Madrid, September 1969

10 p1603 A71-24698

Vertical and horizontal atmospheric electric fields measurements at balloon altitudes, considering magnetospheric processes effect and potential differences 10 p1603 A71-24699

Inferring ionospheric electric fields at stratospheric levels with tropospheric penetration, using balloon measurements and model atmosphere 10 p1603 A71-24700

Atmospheric electric ring current in higher atmosphere with equatorial flow across magnetic lines, using dipole tensor conductivity model 10 p1603 A71-24701

Atmospheric electrical effects due to aurora, discussing negative space charge, bremsstrahlung flux and electrojet plasma instability 10 p1604 A71-24703

Solar and lunar modulation of geophysical parameters, atmospheric electricity and thunderstorms in complex space-meteorology scope 10 p1604 A71-24706

DC electric fields measurements in magnetosphere at equator, midlatitudes and close to or inside auroral arcs 14 p2237 A71-30955

Atmospheric spectral and structural characteristics, reviewing studies of source phenomena and related electric, magnetic and electromagnetic fields 14 p2237 A71-30965

Atmospheric space charge and distribution measurement through oscillating electric field modulation by sound waves 16 p2562 A71-33067

Japanese space research report to COSPAR, discussing meteorology, atmospheric electricity, ionosphere, magnetosphere, galactic radiation, life sciences and planetology 16 p2666 A71-33860

Ionospheric electric and electromagnetic waves broadband characteristics, investigating auroral hiss and LHR noise 16 p2572 A71-33951

Midlatitude nighttime F region electron concentration enhancements as downward diffusion flux from protonosphere induced by ionospheric substorm associated electric fields 16 p2573 A71-33958

Electrode effect in atmospheric electricity with convection and diffusion, calculating layer thickness dependence on vertical convective transfer velocity 17 p2730 A71-34312

Atmospheric potential gradient measurements during solar eclipse of 7 March 1970, using airborne and ground observations 17 p2731 A71-34321

Bibliography on aurora covering observations, morphology, atomic and molecular processes, electric fields, radio scattering, red arcs and particle precipitation 17 p2732 A71-34467

Earth upper atmosphere superrotation due to zonally averaged magnetospheric electric fields 18 p2911 A71-35992

Quadrupole probe for measuring magnetospheric electric currents, noting transfer impedance dependence on probe motion relative to ambient plasma 18 p2912 A71-36198

Rockets and launch operations protection from atmospheric electricity at Kennedy Space Center, discussing current and future lightning suppression 18 p2913 A71-36451

Excitation and ionization cross sections of atmospheric molecular species by low energy ions in strong auroral and man-made electric fields 19 p3055 A71-38039

Magnetospheric current effects on geomagnetic field structure, noting electron and proton precipitation into auroral zone 19 p3059 A71-38396

Soviet book on cloud electricity covering space charge and electrical characteristics 19 p3091 A71-38533

Rainfall, aerosols and cloud water samples analyzed for chlorides and sulfates content and electrical properties 19 p3092 A71-38687

Ionospheric electric field strength at equatorial and medium geomagnetic latitudes during twilight from barium-ion cloud drift measurements 20 p3218 A71-39523

Peak electron density variations during midlatitude F region storm, investigating electrodynamic drift effects 21 p3372 A71-40037

Ring current location in magnetosphere, noting electromagnetic ion cyclotron instability region as stable proton trapping boundaries 22 p3532 A71-41446

ATMOSPHERIC EMISSION U AIRGLOW

ATMOSPHERIC ENTRY
NT HYPERBOLIC REENTRY
NT HYPERSONIC REENTRY
NT REENTRY
NT SPACECRAFT REENTRY

Spectra of faint optical meteors for chemical abundance, discussing radiative processes during atmospheric entry, Leonid meteors and data acquisition 01 p0161 A71-11275

Soviet book on ballistics of flight vehicles during atmospheric reentry 02 p0319 A71-11844

Soviet book on maneuvering of spacecraft covering trajectory calculation, thrust control, translunar and interplanetary flights, atmospheric reentry, orbital rendezvous, optimal control, etc 02 p0321 A71-12725

Gas ionization in supersonic wake at throat, transition and breakthrough points in hyperballistic firing tunnel for atmospheric reentry study 03 p0462 A71-13131

Space capsule reentry into Martian atmosphere for soft landing, using onboard nonlinear filter and stochastic control for random wind gusts 03 p0500 A71-14479

Mars lander deorbit trajectory sensitivity analysis for fixed flight path and communications angles at atmospheric entry, comparing with Monte Carlo simulation [AIAA PAPER 71-190] 06 p0978 A71-18628

Hyperbolic flow over cones with attached and detached shock waves, using Lax differencing technique and time dependent formulation for reentry flow fields [AIAA PAPER 71-55] 06 p0846 A71-18655

Atmospheric reentry dynamics of spinning body with trim angle of attack 07 p1205 A71-18892

Maximum stagnation temperature on swept wing leading edge for equilibrium glide entry of space shuttle 07 p1013 A71-18902

Radiative heat transfer during entry into shocked Venus model atmosphere 07 p1199 A71-19870

Near equilibrium shock layers nonequilibrium radiant emission calculation, noting application to Mars entry conditions [AIAA PAPER 70-773] 07 p1091 A71-19914

Atmospheric reentry trajectories optimization by differential dynamic programming 08 p1363 A71-21347

Convective plus radiative shock tube model stagnation point heating rate measurements for planetary entry heating rate in air and Venus gas [AIAA PAPER 69-635] 09 p1382 A71-22092

Skipping entry trajectories up to fifth extremal points in planetary atmosphere, using matched asymptotic solution 11 p1837 A71-25483

Test streams and chemical composition effects on ablative composites for hypervelocity heat protection of manned atmospheric entry vehicles 11 p1855 A71-26031

Graphite ablation under high temperatures for large outer planets entry probes, correlating mass loss rates with surface temperatures and specimen nose cone radii [AIAA PAPER 71-418] 11 p1857 A71-26209

Reentry spherical vehicles with variable wall thickness, determining heat flux absorption without surface ablation and wake contamination [AIAA PAPER 71-424] 11 p1858 A71-26215

Computerized automatic control system for atmospheric reentry, combining computational prediction of motion parameters with closed loop feedback 12 p1926 A71-26720

Unsteady vibrations of rotating free solid body entering atmosphere at hypersonic velocity, taking into account nonlinearity of aerodynamic moments 12 p1972 A71-27171

Roll rate variation and lift effect on reentry vehicle impact, comparing analytic treatment with six degree of freedom trajectory simulation 13 p2144 A71-27977

Spacecraft capture by ballistic aerobraking during passage through planet atmosphere, proposing analytic models 13 p2133 A71-27987

Conical body lift/drag ratio increase by wedge shaped nose, noting applications to space vehicles entering atmosphere above escape velocity 13 p1992 A71-29183

Spacecraft trajectory optimization during atmospheric reentry with allowance for total-load restriction, using Pontryagin maximum principle 13 p2143 A71-29195

Vibration amplitudes and transverse acceleration of reentry vehicle during uncontrolled atmospheric descent trajectory 13 p2146 A71-29208

Spacecraft banking control during reentry, deriving dynamic equations of angular motion 16 p2646 A71-33655

Optimal control algorithm for spacecraft descent in atmosphere at speed near escape velocity, using game theory 16 p2646 A71-33702

ATMOSPHERIC ENTRY SIMULATION

Large meteoroids ablation and breakup mathematical model, estimating Mars atmosphere effectiveness as shield against surface impact craters production 16 p2643 A71-33968

Jupiter atmospheric entry probe missions to cloud layers base, discussing tradeoffs between various types of mission trajectories and technologies [AIAA PAPER 71-834] 17 p2801 A71-34713

Jupiter atmospheric entry probe mission, discussing descent depths, atmospheric pressure and temperature effects, data return techniques and Grand Tour Missions [AIAA PAPER 71-832] 17 p2802 A71-34715

Tekites atmospheric and geological history, noting fragmentation and surface sculpturing processes 17 p2811 A71-35728

Optimal lateral guidance switching thresholds for low L/D shuttle vehicle entry, using optimal stochastic control theory for problem formulation in conjunction with dynamic programming [AIAA PAPER 71-914] 19 p3096 A71-37164

Reentry glider approximate optimal atmospheric entry trajectories for maximizing function of terminal velocity, altitude, flight path and heading angle under terminal nonlinear constraints [AIAA PAPER 71-919] 19 p3096 A71-37168

Longitudinal dynamic stability of space shuttle during atmospheric entry, noting magnetic storms effects 19 p3151 A71-37322

Atmospheric entry probe from flyby mission to Jupiter, considering descent trajectory feasibility and instrument package [AAS PAPER 71-142] 19 p3153 A71-37945

Jupiter probe design and communication for deep penetration into atmosphere, concerning mission phases through entry and descent to sample altitudes [AAS PAPER 71-143] 19 p3153 A71-37946

Outer planets atmospheric entry vehicles atmospheric heating, discussing shock and boundary layer physical and chemical effects [AAS PAPER 71-144] 19 p3163 A71-37947

Graphitic ablative heat shield fractions and forebody configurations for probe entry into atmospheres of Saturn, Uranus and Neptune [AAS PAPER 71-145] 19 p3141 A71-37948

Jupiter atmosphere entry probes graphite ablative heat shields performance, indicating convective and radiative blockage and graphite sublimation processes in surface heat balance [AAS PAPER 71-146] 19 p3084 A71-37949

Physical, chemical and biochemical instrumentation and measurements for probe entering Jupiter atmosphere [AAS PAPER 71-148] 19 p3153 A71-37951

Spacecraft entry into planetary atmosphere, considering heating, deceleration and landing 20 p3305 A71-38814

Multihundred watt radioisotope thermoelectric generator heat source survivability in multiple skip reentry 20 p3264 A71-38931

Spacecraft trajectories for reentry at hyperbolic velocity, examining aerodynamic control loads and characteristics in atmospheric skip 20 p3288 A71-39122

Blunt planetary entry probe full scale flight test base pressure measurements, noting insensitivity to angle of attack variations up to 10 degrees 20 p3176 A71-39353

Blunt body heat transfer predictions for atmospheric reentry, discussing coupled effects of real gas behavior and slip/jump boundary conditions 21 p3474 A71-40256

Impulsive retrofire deboost of rocket vehicles initially moving in elliptical orbits for maximum and minimum atmospheric entry angles 22 p3608 A71-41697

Space transportation orbiter design covering thermal protection, aerodynamics and cross range problems during earth reentry 22 p3609 A71-41979

Optimal lift control of hypersonic lifting body during atmospheric entry by singular perturbation method [AAS PAPER 71-366] 23 p3773 A71-43036

Design parameter optimization for two-stage space shuttle atmospheric flight from spherical nonrotating earth by sequential straight line approximation 23 p3774 A71-44115

Matched asymptotic solutions for optimum lift controlled atmospheric entry of hypersonic lifting vehicles 24 p3876 A71-44609

Parabolic velocity atmospheric reentry navigation algorithm for spacecraft control, demonstrating guidance accuracy to landing point 24 p3846 A71-45304

ATMOSPHERIC ENTRY SIMULATION

Combined radiative-convective heating test facility for atmospheric entry simulation [AIAA PAPER 71-255] 08 p1273 A71-21984

High enthalpy electric arc plasma jet heaters for simulating entries in hydrogen rich Jovian atmosphere [AIAA PAPER 71-263] 08 p1274 A71-21989

Wide range nonimmersive RF coil with marginal oscillator for plasma electrical conductivity measurements tested for simulated reentry vehicle
12 p1908 A71-27285

Experimental proof of combustion phenomena in reinforced plastics ablation under simulated atmospheric reentry, using arc plasma jets
12 p1987 A71-27721

Continuous hypersonic wind tunnels with low gas density simulating flow states during reentry phase of space vehicles
18 p2898 A71-36412

Spacecraft reentry into random medium atmosphere, determining optimal control procedure for prescribed arrival region and time with simulation equation
20 p3269 A71-39123

ATMOSPHERIC HEAT BUDGET

Global atmosphere energy balance for four seasonal periods, describing production, conversion and loss rates for large scale circulation
01 p0121 A71-11354

Flux divergence in optically thin outer layers of model moving stellar atmospheres using weighting functions in energy balance equation
07 p1190 A71-18863

Atmospheric energy storage and meridional transport, calculating annual cycle in Northern Hemisphere
12 p1925 A71-27193

Atmospheric optics and radiative transfer, including earth albedo, sky brightness, heat balance, cloud/terrain reflectance, molecular spectroscopy and multiple scattering
14 p2275 A71-30497

Atmospheric energy balance and transfer in lower thermosphere in terms of population temperatures and degrees of freedom (translational, rotational, vibrational, electronic, chemical, etc)
18 p2910 A71-35841

Atmospheric radiative energy budget based on structure and cloudiness distribution data from satellites and in situ observations
20 p3259 A71-39677

Earth-atmosphere system radiation budget, comparing meteorological satellites actinometric data with calculated climatological maps of planetary long wave radiation distribution
20 p3259 A71-39678

ATMOSPHERIC HEATING

Midlatitude atmospheric gravity waves generation by auroral heating during magnetic substorms
02 p0245 A71-11965

F region photoionization heating, investigating energy transfer from ionizing photon to neutral gas atoms and molecules
06 p0893 A71-17982

Equatorial westward propagating wave disturbance model for diagnosing atmosphere response to known diabatic heating distribution
07 p1152 A71-19755

Infrasonic shock wave generation in troposphere by powerful earthquakes, causing upper atmosphere density rise due to heating
08 p1278 A71-21019

Thermospheric heating by solar radiation in Schumann-Runge continuum, taking into account height and atmospheric components distribution
09 p1435 A71-22431

Nimbus 4 satellite selective chopper radiometer data on IR radiation emitted by carbon dioxide, considering stratospheric warming
10 p1598 A71-23743

Atmospheric heating effects on thermoluminescence output variations with depth below Uccia meteorite fusion crust, noting nonuniform cosmic rays shielding
10 p1675 A71-24470

Upper atmospheric molecular and atomic N and O diurnal variations correlated to atmospheric heating as function of solar UV radiation from sounding rocket data
11 p1757 A71-25775

Thermosphere daily variations consisting of diurnal oscillations excited by ozone and EUV heating
12 p1925 A71-27729

Seasonal-climatic vertical distributions of radiative heat sources and sinks calculation for Northern Hemisphere stratosphere and lower mesosphere
13 p2057 A71-28023

Upper atmosphere radiative energy transport equation derivation with allowance for deviations from Kirchhoff law, examining fluorescence mechanism and effect on radiative heating
13 p2057 A71-28025

Equatorial electrojet as supplementary heat source for tropical region upper atmosphere based on thermal energy release calculation
15 p2399 A71-31964

Altitude and amplitude of winter stratospheric warmings from satellite measured radiance changes, considering radiative transfer equation and variable model of temperature structure
16 p2605 A71-33537

Joule heating and winds in upper atmosphere due to geomagnetic disturbances at 140 km altitude, deriving set of nonlinear partial differential equations
16 p2564 A71-33726

Thermospheric electron heating rate and ion chemistry above Wallops Island during 7 March 1970 solar eclipse, measuring ion composition and concentration
16 p2565 A71-33732

Upper atmosphere heating at high latitudes, analyzing air density variations from Molniya 1K satellite observations over 2 year period
16 p2565 A71-33740

Thermospheric dynamics three dimensional model in terms of atmospheric system eigenfunctions, deriving formulas for solar XUV and corpuscular heating during geomagnetic storms
16 p2567 A71-33781

Atmospheric density variation response time measurement to geomagnetic activity by satellites-borne low-G accelerometer calibration system, considering atmospheric heating mechanism
16 p2571 A71-33839

Upper ionosphere electron density scale height data, noting conjugate point sunrise heating effects from Alouette 1 data
17 p2731 A71-34313

Northern Hemisphere atmospheric vertical velocity computation for all seasons compatible with climatological heating functions, using time averaged thermodynamic energy equation
17 p2770 A71-34803

Heating, fusion and atomization of meteoric bodies in earth atmosphere
17 p2810 A71-35724

Outer planets atmospheric entry vehicles atmospheric heating, discussing shock and boundary layer physical and chemical effects
19 p3163 A71-37947

Short path VLF phase and amplitude measurements during stratospheric warming in February 1969, discussing D region electron density changes
19 p3018 A71-38040

Thermospheric wind induction by auroral electrojet heating, considering effects of Joule dissipation of magnetospheric electric fields
20 p3215 A71-38744

Infrasonic shock wave generation in troposphere by powerful earthquakes, causing upper atmosphere density rise due to heating
20 p3219 A71-39599

Upper atmospheric molecular and atomic nitrogen and oxygen diurnal variations correlated to atmospheric heating as function of solar UV radiation from sounding rocket data
22 p3532 A71-41543

Heat balance effects of acousto-gravitational waves in upper atmosphere, concerning infrasonics from earthquakes, polar auroral arcs and magnetic storms
22 p3533 A71-41656

Earth atmosphere gas composition and electron density variations at F region lower boundary explained by stratospheric explosive and diffusive warmings effect on critical frequency
23 p3671 A71-43578

Solar coronal heating neutron theory based on solar gamma ray flux considerations
23 p3770 A71-44014

Stratospheric warmings effect on F 2 region parameters and ionospheric radio wave absorption, assessing time lag
23 p3673 A71-44049

ATMOSPHERIC IMPURITIES

U AIR POLLUTION

ATMOSPHERIC IONIZATION

NT AURORAL IONIZATION

Photoionization coefficients and photoelectron impact excitation efficiencies in daytime ionosphere, noting role in dayglow
01 p0077 A71-11515

Space-time structure of ionospheric regions of anomalous radio wave absorption during auroras, discussing ionization region
02 p0243 A71-11765

Polar ionospheric auroral zone ionization, obtaining ion production function for single electron and proton flux
02 p0244 A71-11772

Tropospheric positive and negative ions mobility distribution measurement from converging channel chamber data
02 p0247 A71-12849

Micrometeorite sputtering in ionosphere producing influx of meteorite atoms and ions in atmosphere, considering temperature dependence of stone meteorite sputtering coefficient
03 p0486 A71-13309

E layer meteor ionization, considering ablation processes effects of meteoroids evaporation and micrometeorites sputtering
03 p0486 A71-13310

Solar X-rays role in D region ionization from ion probe sounding during eclipse of 20 May 1966
03 p0407 A71-13377

Ionospheric photoelectron exchange at magnetic conjugates, considering electron density and impact ionization by inelastic collisions
03 p0408 A71-13381

Slow positive ion and electron production in collisions of protons and hydrogen atoms with gases of planetary atmospheres
03 p0460 A71-13494

Energy spectra of ionization bursts, electromagnetic cascades and nuclear active particles at mountain altitude
03 p0476 A71-13850

Atmospheric ions mobility spectrum measurement describing aspiration capacitor design with various electrode configurations
03 p0431 A71-14500

Midlatitude nighttime D region ionization source considering precipitating energetic electrons
03 p0420 A71-14527

Sporadic E and FEs regions multiples enhancement during squall thunderstorms, noting effects on lower ionospheric ionization
05 p0740 A71-16436

Ionic meteor emission spectra calculation using two-step ionization and excitation model, accounting for atmospheric molecules and vapor atoms collisions
05 p0812 A71-16693

PCA ionization, using range-energy ratio of solar cosmic rays penetrating spirally into polar atmosphere for electron production rate determination
05 p0742 A71-16812

Planetary atmospheres ionosphere formation by cosmic rays, examining ionization of various gases
05 p0799 A71-16817

Atmospheric ionization by vertical gamma and alpha radiation of natural radioactive products, comparing to vertical behavior of conductivity
05 p0799 A71-16843

Sporadic E layer formation based on wind shift theory with drift data
05 p0746 A71-17202

Electron density profiles correction allowing for ionospheric interlayer ionization
05 p0746 A71-17206

Upper atmosphere nitric oxide density measurement by scanning UV spectrometers on Nike-Apache rockets, noting ionization consequences for D region
06 p0888 A71-17273

Ionization disturbances caused by gravity waves in neutral air propagating through ionosphere in electrostatic field and background wind
06 p0888 A71-17278

Ionization in ionosphere E and upper D regions, considering solar short wave radiation, small components, atmospheric dynamics and vertical mass transport
06 p0894 A71-18251

E layer electron concentrations, effective recombination coefficient and ionization sources during solar eclipse, noting soft X radiation intensity
06 p0894 A71-18260

Ionization rate experimental profiles during maximum solar activity compared with calculations, showing additional source of ionization in E region
06 p0895 A71-18272

Nitrogen dioxide and molecular oxygen ions densities in lower ionosphere as function of solar corpuscular radiation
06 p0895 A71-18275

Sporadic ionization occurrences nighttime observation in auroral E region, describing vertical electron concentration profile
06 p0895 A71-18280

Ion-electron recombination coefficient measurement for ionized trails left by rocket exhausts in high atmosphere using radio observation
06 p0895 A71-18314

Ionospheric electron mean content 1964-1969 from density, ionization, slab thickness and solar flux diurnal and equinoctial peaks
07 p1097 A71-19025

Magnetic field generation of rotating stars with partially ionized convective envelopes due to emf arising from convective flow Coriolis acceleration
07 p1193 A71-19294

F 2 layer nighttime ionization seasonal fluctuations, considering dependence on geographical longitude and latitude and solar activity levels
07 p1098 A71-19382

Signal reflection from sporadic E layer, investigating multiplicity relationship to earth surface, ionization level, D region and nighttime absorption
07 p1100 A71-19403

Underlying and interlayer N/b₁ ionization distribution in unobservable region, discussing single and multilayer approximation
07 p1101 A71-19410

Nonequilibrium multicomponent ionization calculations for stagnation merged shock layer of hypersonic blunt body by successive accelerated replacement [AIAA PAPER 69-655]
07 p1015 A71-19890

Forbush decreases effects on radio wave absorption, cosmic ray variations and ionization in lower ionosphere cosmic layer
08 p1353 A71-20981

Thomson scatter measurements of F region ionization drifts vertical velocity at midlatitudes, studying electric field influence
08 p1279 A71-21204

Ionization measurements of high latitude and altitude cosmic rays covering four solar maxima
08 p1355 A71-21628

Middle latitude night E region ionization, describing solar EM and corpuscular radiation absorption effects
08 p1286 A71-21853

F 2 layer nighttime ionization at midlatitudes, investigating conjugate point effects on observation point
09 p1434 A71-22426

E region additional ionization source during solar activity maximum, analyzing ion production function and electron concentration
09 p1435 A71-22440

Lower ionosphere electron concentration space-time variations relation to ionization source intensity fluctuations based on rocket observations and ground sounding data
09 p1435 A71-22442

Meteor trails isotropic diffusion in presence of moving point source of ionization with variable intensity, calculating plasma density on and near trajectory
09 p1518 A71-22447

Atmospheric ions effects on human visual performance, taking into account ozone concentration and humidity
09 p1493 A71-22741

Altitude spectrum of ion formation in interaction of proton flux with atmosphere, using Bragg dissipation function
09 p1514 A71-23153

Night glow emission post twilight decay rates at different seasons by Chamberlain relation, discussing F layer ionization
09 p1441 A71-23644

Pcl propagation in magnetosphere model accounting for ionization gradients aligned along geomagnetic field
10 p1599 A71-23849

Solar cycle effects on diurnal variations of F 2 region critical frequency and maximum ionization height
10 p1600 A71-23884

Meteor trails ionization probability determination based on data since 1948, comparing results of theoretical, semiempirical, experimental and simulation method
10 p1669 A71-24031

Ionization mechanisms for deviation of experimental altitude vs velocity curves of meteor trails, considering various electron and ion emissions and dissociation effects
10 p1669 A71-24032

Tropospheric ionization mechanism for gas to particle condensation embryos existence, using positive and negative ions ground level and altitude profiles
10 p1604 A71-24704

Midlatitude D region considering electron concentration height distribution, ionization process and solar activity effects
10 p1606 A71-24916

Time dependence of atmospheric ionization at polar cap absorption event, obtaining relativistic and non-relativistic solar cosmic rays ionization equations
11 p1754 A71-25586

Neutral wind effects on redistribution of E region ionization and recombination, comparing electron density profiles to vertical ion drift velocities
11 p1755 A71-25613

Laboratory and meteoric cluster ions formation, using mass spectrometric techniques
11 p1802 A71-25630

Universal time effect on E region critical frequency at large solar zenith angles, considering ionization source at midlatitude range
11 p1757 A71-25785

Multicomponent whistler spectra due to discrete ionization inhomogeneities and complex structure nonuniformities forming diffuse whistlers in outer ionosphere
11 p1758 A71-25789

Lower ionosphere ionization response to auroral particle fallout during 1968 substorms, using geomagnetic, VLF and balloon measurements
12 p1899 A71-26642

Equatorial E region cross field instability and ionization irregularities from Nike-Apache rocket measurements
12 p1900 A71-26934

Solar plasma emission capacity, using atmospheric ionization theory
12 p1964 A71-27084

Two dimensional atmospheric model including oxygen and nitrogen photodissociation, recombination and photoionization, investigating solar activity and ionizing radiation effects on temperature stratification
13 p2057 A71-28018

Geomagnetic field effects on directional propagation of LF and VLF radio waves in ionosphere, taking into account ion types effects
13 p2029 A71-28026

Ionospheric anisotropic plasma with mixture of different ions, deriving refractivity at whistler frequencies
13 p2058 A71-28027

Sporadic E layer formation, using wind shear theory and drift data
13 p2059 A71-28257

Electron density profiles correction, taking into account ionospheric interlayer ionization
13 p2060 A71-28261

Vertical electron density profiles correction coefficients, noting computational work decrease and F region frequency discrepancy due to ionization
13 p2060 A71-28262

Short wave skip distance calculation as function of path inclination to ionospheric layer for linear and parabolic ionization distributions
13 p2030 A71-28556

Ionospheric ion formation and neutralization reaction rate coefficients determination by fitting rocket measured electron concentration profiles with computer generated profiles
13 p2062 A71-28560

Geomagnetic tail influence on polar ionosphere proton and electron precipitation, considering ionospheric ionization and polar cap absorption
14 p2300 A71-30034

Physical processes and variations in polar F region, discussing solar photoionization, particle ionization, thermal expansion, electric fields, neutral air winds, ion drag, etc
14 p2234 A71-30038

High latitude upper ionospheric structures and plasma flow in magnetosphere from Alouette/ISIS topside sounders, noting solar UV and particle ionization sources
14 p2234 A71-30042

Cosmic radio noise absorption measurements at subauroral latitude for ionospheric absorption, discussing ionization regions spatial nonuniformity and horizontal extension
14 p2196 A71-30561

Micrometeor mass data from radiometer measurements, detailing Cu and lanthanum hexaboride ionization probability
14 p2315 A71-30652

Atmospheric cosmic ray propagation based on phenomenological model of hadron-nucleus collisions, predicting sea level nucleon, pion and muon energy spectra and ionization profile
15 p2474 A71-31732

VLF atmospherics integrated intensities changes probably due to ionization by meteors
15 p2371 A71-31839

Topside ionosphere structure in high latitudes, discussing electron density profile, corpuscular radiation ionizing effects, polar peak and trough
15 p2400 A71-32349

Upper atmosphere He, Ne, Na and K atoms collisions with molecular oxygen, determining ejected electron energy during fast Na, K, Rb and Cs ionization for meteor phenomena modeling
16 p2639 A71-33695

Corpuscular and solar electromagnetic ionizing radiation simultaneous measurement by sounding rockets, evaluating contribution to lower ionosphere formation
16 p2627 A71-33776

Solar plasma emission capacity, using atmospheric ionization theory
16 p3133 A71-37434

F 2 layer noontime ionization seasonal fluctuations, considering dependence on geographical longitude and latitude and solar activity levels
19 p3052 A71-37807

Signal reflection from sporadic E layer, investigating multiplicity relationship to earth surface, ionization level, D region and nighttime absorption
19 p3053 A71-37827

Underlying and interlayer N/h ionization distribution in unobservable region, discussing single and multilayer approximation
19 p3053 A71-37834

Quiet sun diurnal variations of intertropical F 2 ionization in true heights over Tamarassett meridian
19 p3054 A71-37863

Nighttime D region behavior under ionization by X ray spectrum of Scorpius source
19 p3017 A71-37864

Computer demonstration of ionospheric F region storm causes, noting critical frequency relationship to ionization shift
19 p3055 A71-38038

Ionization rates induced by solar flares charged particles in planetary atmospheres
19 p3142 A71-38047

D region ionization by electron fluxes as explanation for latitudinal radio wave absorption
19 p3057 A71-38370

D region ionization by solar corpuscular streams, considering formation of charged particle concentration profiles
20 p3216 A71-39141

Neutral-ionized parts interactions in upper atmosphere, discussing ionospheric plasma modulation, solar control and seasonal anomalies in lower ionosphere and ionic reactions
20 p3223 A71-39712

D region electron density profiles and ionization models in terms of XUV radiation and minor constituents NO and oxygen, using ground and space measurements
20 p3224 A71-39713

Nighttime equatorial E region ionization and electron density gradient irregularities, noting cross field instability with rocket-borne Langmuir probes
20 p3225 A71-39727

Ion and electron production rate during PCA event, computing electron/ion density, differential proton flux spectrum and ion production rate
20 p3225 A71-39729

Plasmasphere evening ionization anomalies observations from spherical electrostatic analyzers onboard OV3-1 polar orbiting satellite, noting thermal plasma depletion during orbit night sector
20 p3225 A71-39741

Auroral excitation and ionization intensity and rotational and Doppler temperature vertical profiles measurements, emphasizing emission rate profiles
20 p3227 A71-39839

Cosmic ray variations due to atmospheric pressure disturbances and ionizing component variations due to temperature effects, estimating ground observation errors
21 p3437 A71-40074

Universal time effect on E region critical frequency at large solar zenith angles, considering ionization source at midlatitude range
22 p3532 A71-41553

Ionization profiles of upper ionosphere from Alouette 1 vertical sounding data, proposing model for ionosphere shape
22 p3532 A71-41554

Multicomponent whistler spectra due to discrete ionization inhomogeneities and complex structure nonuniformities forming diffuse whistlers in upper ionosphere
22 p3532 A71-41557

Upper atmospheric primary cosmic ray layer ionization, considering secondary particles, X rays, neutrons, tritons and mesons as ionizing agents
22 p3591 A71-41647

Energy spectra of ionization bursts, electromagnetic cascades and nuclear active particles at mountain altitude
22 p3595 A71-42651

Sporadic E layer ionization relation to thundersquall surface pressure disturbance, considering gravity wave propagation
23 p3670 A71-43322

He excitation and ionization in chromospheric flares, performing calculations for 10,000-50,000 K electron temperatures and 0.5-9.0 times 10 to 13th power per cc electron densities
23 p3722 A71-44310

Hydrogen and helium thermal dissociation and ionization at Jupiter and Saturn adiabatic atmospheric models conditions
24 p3850 A71-44809

F 2 region magnetic disturbances conjugacy mechanisms, considering vertical ionization profiles
24 p3823 A71-45029

High DC field induced ionic wind, deriving electric and pneumatic parameters for various electrode configurations
24 p3849 A71-45369

ATMOSPHERIC MODELS

NT BREADBOARD MODELS

NT DYNAMIC MODELS

NT REFERENCE ATMOSPHERES

Auroral ionization relationship to incident magnetospheric electrons based on atmospheric model
01 p0073 A71-10253

Hail cells aloft interactions and radar detectability inferred from surface data, giving statistically random model
01 p0115 A71-10553

Clear air convective process, examining dynamic model with radar patterns
01 p0116 A71-10562

Breaking waves and resulting CAT characteristics from ultrahigh resolution FM-CW radar observation, using model of unstable waves at sheared inversion layer
01 p0116 A71-10565

Lower atmosphere turbulence model derivation from data obtained by Doppler radar windfield measurements in snowfall environment
01 p0117 A71-10578

Radar reflectivity pattern calculation from cumulus cloud growth numerical model, noting similarity with radar data from on-line computer system
01 p0118 A71-10584

Storm reflectivity models using weather radar and surface rainfall data correlations
01 p0118 A71-10585

Updraft vault dynamic in hailstorms using one dimensional cumulonimbus entraining jet model, observing initial conditions steady state

01 p0119 A71-10744

Atmospheric interaction layer large recombination coefficient existence possibility according to corpuscular model of radar head echo

01 p0159 A71-10871

Quiet D region structure exponential model based on E layer reflection measurements

01 p0074 A71-11079

Global atmospheric circulation numerical simulation, discussing modeling factors and applications

01 p0121 A71-11353

Atmospheric boundary layer motion and transports applied to mathematical atmospheric circulation models

01 p0121 A71-11355

Solar flare particles entrance into geomagnetic tail, modifying diffusion model

01 p0147 A71-11494

Compressible corotation of model magnetosphere, considering electric field induced by earth rotation

01 p0077 A71-11514

Atmospheric general circulation model for numerical climate digital simulation and weather forecasting, using fluid flow equations

02 p0277 A71-11808

Solar line blanketing effect data derivation and analysis for model atmosphere computer programs, considering application to spectrally similar stars

02 p0316 A71-12755

Book on stellar atmospheres covering radiative transfer, opacity, equation of state, LTE, line spectra, atomic levels, etc

03 p0483 A71-13100

Solar chromosphere model, investigating radiative transfer effect on temperature structure of plane slab heated by thermal conduction

03 p0483 A71-13186

Sunspots initial appearance east-west asymmetry interpretation by conical atmospheric model, including foreshortening and absorption effects

03 p0483 A71-13188

Kolmogoroff and von Karman constants relationship, using atmospheric model

03 p0452 A71-13227

Atmospheric models integration, discussing elliptic partial differential equation solution

03 p0453 A71-13326

Venus atmosphere rotational model, considering nonlinear instability due to wind shear from solar heat induced convection

03 p0489 A71-13607

Three dimensional numerical model of unstable planetary boundary layer integrated for convecting and turbulent region height, mean lateral shear and Reynolds flux direction

03 p0453 A71-13612

Theoretical vs observed atmospheric densities between 350 and 1500 km, using models and satellite observations

03 p0415 A71-14025

Tropical storms and cyclones development numerical simulation with ten-level model, considering radiational cooling and physical parameters effects

03 p0453 A71-14202

Convective energy transport in stellar atmospheres, computing hot and cool streams thermal structure based on model

03 p0495 A71-14264

Earth hydrogen geocorona models comparison with solar Lyman alpha spectrographic data from Aerobee rocket flight measurements

03 p0496 A71-14509

Solar Lyman alpha emission line absorption by geocoronal atomic hydrogen, comparing observational data with prediction from models

03 p0496 A71-14510

Quiet day magnetic field variations at geosynchronous satellite ATS I, comparing magnetospheric models

03 p0419 A71-14522

Energy conservation in linear atmospheric models using first order kinetic equations

04 p0581 A71-15067

Stratospheric ozone, comparing observations to numerical models of formation, distribution and destruction

04 p0582 A71-15071

UV stellar flux measurements vs theoretical stellar atmosphere models, using rocket and satellite observations

04 p0648 A71-15252

Mercurian atmosphere models, discussing replenishing processes involving chemical reactions in thin and thick models

04 p0650 A71-15583

Solar atmosphere semiempirical models taking into account non-LTE conditions

04 p0651 A71-15667

Numerical weather forecasting model using time dependent boundary values for restricting to acceptable error limits

04 p0622 A71-15676

DA and DB white dwarf atmospheres convection effect on structure based on mixing length theory and constant flux model

04 p0658 A71-15841

Solar disk computed continuum and estimated line polarizations compared to BCA photosphere values, discussing metal abundances

05 p0803 A71-16019

Line formation calculations for different spot models and arbitrary depth dependence of magnetic field vector, interpreting pi component anomalous splitting

05 p0803 A71-16021

Three component model for chromospheric Ca II K line formation, discussing observational agreement

05 p0803 A71-16024

Venusian atmosphere adiabatic and isothermal models from Venera automatic stations data, discussing temperature, pressure, density and cloud layer thickness

05 p0804 A71-16041

Unstable atmospheric surface layer wind speed and temperature profiles mathematical representation

05 p0777 A71-16664

Ionic meteor emission spectra calculation using two-step ionization and excitation model, accounting for atmospheric molecules and vapor atoms collisions

05 p0812 A71-16693

D region exponential model application to high solar activity conditions, using absorption measurement data

05 p0742 A71-16813

Ionospheric transmission model vs current model for examination of low latitude geomagnetic pulsation origin

05 p0743 A71-17002

Planetary boundary layer forecast model, determining horizontal and vertical wind components, temperature, pressure and moisture with numerical variational objective analysis

05 p0778 A71-17049

Diurnal variations of loss factor in D region during polar cap absorption, verifying nighttime D region model by forward propagation data

05 p0744 A71-17185

Sporadic E layers magnetic field variations, examining charged particle redistribution with air turbulence model

05 p0746 A71-17203

Auroral absorption latitudinal distribution diurnal variations, showing existence of two zone model

05 p0746 A71-17205

Venus planetary science, discussing radar and space probe measurements as basis for different atmospheric models

05 p0814 A71-17226

Internal gravity wave propagation in neutral wind stratified atmospheric model

06 p0888 A71-17274

Upper troposphere and lower stratosphere geopotential field short range forecast quasi-geostrophic model

06 p0889 A71-17516

Solar wind torque on earth magnetic dipole based on magnetosphere model analytic solution in rotating reference frame

06 p0891 A71-17885

Venus atmosphere and lithosphere thermochemical composition, examining various models

06 p0966 A71-17898

F I region unsteady model, examining vertical distribution profile of electron concentration on summer day

06 p0895 A71-18273

Lagrangian numerical forecasting barotropic global model using primitive equations with coating set of computation points

06 p0924 A71-18410

Semiimplicit time integration scheme application to grid point atmospheric models of primitive meteorological equations

06 p0924 A71-18411

Relative humidity augmentation for triggering convection in two dimensional numerical cumulus cloud model

06 p0924 A71-18412

Solar corona active regions thermal model, taking into account X ray emission and temperature distribution

06 p0963 A71-18439

Mature severe vortical storm properties, developing atmospheric models for maximum swirling speed and structure

06 p0924 A71-18514

Atmospheric surface layer turbulence structure simulation model, using laboratory flows for neutrally stable atmosphere

06 p0884 A71-18579

Planetary atmospheres structure and dynamics, discussing composition and vertical temperature profile models

07 p1191 A71-18915

Earth atmosphere polytropic equilibrium model density distribution and effective size and mass, taking into account gravitational interactions

07 p1152 A71-19375

Model of large ionospheric electron density discontinuities, emphasizing horizontal asymmetry association with observed east-west refraction asymmetry

07 p1100 A71-19405

Cylindrical shock wave propagation in inhomogeneous exponential atmosphere from extension of method for spherical wave

07 p1089 A71-19742

Equatorial westward propagating wave disturbance model for diagnosing atmosphere response to known diabatic heating distribution

07 p1152 A71-19755

Uranus physically self consistent atmosphere model based on spectroscopic, photometric and radio observational data

07 p1198 A71-19828

Radiative heat transfer during entry into shocked Venus model atmosphere

07 p1199 A71-19870

Nongeostrophic and nonhydrostatic stability of baroclinic fluid for small Richardson numbers

07 p1153 A71-20220

Low latitude geomagnetic substorm development model due to increased resistance in magnetosphere tail current sheath

08 p1278 A71-21017

Dungey model generated by interplanetary magnetic field addition to closed magnetospheric model, discussing adiabatic theory breakdown for model current sheet

08 p1280 A71-21217

Lower limit helium abundance envelope models of hydrogen deficient stars, using mixing length theory

08 p1364 A71-21418

Horizontal He distribution in upper atmosphere from OGO 6 mass spectrometric data normalization for altitude by Jacchia model atmosphere

08 p1283 A71-21647

Numerical weather prediction models, discussing automatic data processing meteorological parameter requirements

08 p1328 A71-21723

Airport pollution dispersion modeling, simulating effect on surrounding areas for abatement strategies calculation

08 p1379 A71-21824

F 2 layer critical frequency and maximum electron concentration statistical characteristics for predicting SW propagation conditions

09 p1435 A71-22427

Uranus radio emission model, considering presence of gaseous ammonia at saturation pressure in atmosphere

09 p1519 A71-22526

Venusian atmospheric models of troposphere, stratosphere and thermosphere based on satellites observation data

09 p1519 A71-22527

High latitude magnetosphere structure, using two dipole model

09 p1437 A71-22665

Upper atmosphere IR emission model with reference to thermal excitation, chemical reactions and electron excitation

09 p1437 A71-22670

Variable stars radii effective temperature and brightness determination from stellar atmosphere models

09 p1523 A71-23021

Linear mountain lee wave model with nonlinear lower boundary condition for arbitrary basic flow and two dimensional topography, computing flow field

09 p1487 A71-23024

Planetary scale atmospheric motion energy spectra and error prediction from numerical model, using eddy-damped Markovian approximation for two dimensional turbulence

09 p1489 A71-23551

Conditional instability of second kind /CISK/ in three dimensional quasi-geostrophic low latitude flow, examining Yamasaki model

09 p1490 A71-23561

Ionospheric drifts at 64-108 km at Birdlings Flat, New Zealand, comparing with meteor wind measurements, chemical release trails and general circulation models

09 p1440 A71-23631

Micropulsations power spectrum from magnetospheric model based on transient current sheets, approximating background frequency dependence and daytime/nighttime spectral line widths

09 p1441 A71-23638

Two group model of stationary plasma flow in magnetosphere with space charges due to inertia drift and forbidden regions

09 p1529 A71-23710

Milne-Eddington atmosphere, using Unno transfer equations for Stokes parameters

10 p1665 A71-23778

Empirical solar photosphere continuum models, calculating temperature distribution for absolute intensities at center and limb darkening ratios

10 p1666 A71-23779

Solar lower chromosphere two dimensional models, using relative RMS line center intensity variations and mean limb darkening curves

10 p1666 A71-23781

Sunspot umbra empirical model, deriving temperature and optical depth relationship from IR continuous limb darkening

10 p1666 A71-23787

Magnetostatic sunspot model with twisted field showing radial dependence of azimuthal component

10 p1666 A71-23789

PC1 propagation in magnetosphere model accounting for ionization gradients aligned along geomagnetic field

10 p1599 A71-23849

Convective heat flow simulation in lower troposphere, using water-heated plate model and shadowgraph photography

10 p1638 A71-23879

Numerical integration of motion equations for two layer atmospheric fronts model with baroclinicity along frontal surface separating two incompressible fluids in stable stratification

10 p1638 A71-23965

Global monsoon atmospheric response model in geostrophic terms for heating input function parameterization, including Himalayas mountains effects

10 p1638 A71-23966

Solar wind interaction with field free planetary ionospheres, giving three dissimilar models

10 p1661 A71-24005

Ionospheric computer model, describing electron and ion densities in middle latitudes as function of latitude, longitude, altitude, season, time and solar activity

10 p1577 A71-24290

Ionospheric irregularities two fluid model, using nonlinear differential equations for longitudinal waves propagating in hot collisional magnetoplasma

10 p1648 A71-24294

Atmospheric model phase ionograms for true height reduction technique tests, using ionosonde data

10 p1602 A71-24461

Tropospheric ionization mechanism for gas to particle condensation embryos existence, using positive and negative ions ground level and altitude profiles

10 p1604 A71-24704

Magnetospheric numerical model with two-monoenergy-component proton distribution function, examining ring current belt formation causing inflation

10 p1663 A71-24782

Nitric oxide diurnal variation model in upper atmosphere incorporating solar flux, absorption cross sections and chemical rate constants

10 p1605 A71-24795

Collisionless ion exosphere kinetic and hydrodynamic models comparison for polar wind supersonic flow characteristics

10 p1605 A71-24796

Magnetospheric model characteristics, discussing auroral phenomena energy sources, magnetotail length, polar cusp, auroral oval and electrojet relationships, polar and magnetospheric substorms

10 p1606 A71-24802

Binary star 112 Herculis elemental abundances by atmospheric model analysis of spectra

10 p1680 A71-25001

Upper atmosphere statistical structure based on analysis of deviations of satellite-determined air densities from theoretical Jacchia model, noting latitudinal, seasonal and diurnal variations

10 p1607 A71-25024

Muon bundles frequencies from model for propagation of various atmospheric components in combination with theoretical pion spectra

10 p1664 A71-25044

Atmospheric boundary layer numerical modeling, discussing subgrid scale mixing processes and parameterization

10 p1639 A71-25067

Planetary nebulae central stars extended atmospheres, calculating gray and nongray models under hydrostatic, radiative and LTE

11 p1818 A71-25203

Martian ionosphere below 80 km, developing positive and negative ion chemistry model

11 p1821 A71-25548

Thermosphere diurnal variations two dimensional model atmosphere characteristic waves, separating density and temperature variations

11 p1756 A71-25649

Mariner 5 Venus exospheric Lyman alpha measurements for dayside temperature value, using molecular hydrogen photodissociation model

11 p1823 A71-25692

Venus daytime ionospheric models using electron, ion and neutral gas heat conduction with momentum and chemical equations for charged particle densities

11 p1823 A71-25693

Venus atmosphere critical refraction model, examining optical effects and ray paths

11 p1823 A71-25696

Atmospheric modeling for earth and Venus heterosphere structure using multicomponent radiative

hydrodynamic equations, determining atmospheric temperature and constituents height variation

11 p1828 A71-25764

N₂/ profiles of upper ionosphere from Alouette 1 vertical sounding data, proposing model for ionosphere shape

11 p1758 A71-25786

Atmospheric density semiannual variations from satellite observation, comparing with atmospheric models

11 p1760 A71-25824

Earth atmospheric zonal circulation model, using hydrothermodynamic equations with Newton law for radiative heat sources

11 p1795 A71-25919

Quantitative UV radiative transfer and photolysis in model Jupiter atmosphere, considering coloration by ammonia and hydrogen sulfide gases in cloud region

11 p1834 A71-26455

Solar corona active regions thermal model, considering X ray emission and temperature distribution

12 p1946 A71-26589

Venusian atmosphere heat transfer processes, calculating radiant fluxes and convective motion model

12 p1958 A71-26640

Venus atmosphere adiabatic and isothermal models, investigating water vapor content, pressure and temperature

12 p1964 A71-27085

Cumulus entrainment and steady state one dimensional convection model

12 p1925 A71-27201

Jupiter equatorial thermal limb darkening data, constructing atmospheric model for ammonia effects on temperature structure

12 p1966 A71-27254

Electrical screening layers around charged clouds, giving numerical model for space charge accumulation, electric field distribution and forces acting on cloud droplets

12 p1925 A71-27290

Cosmic ray particles propagation anisotropies in model magnetosphere, suggesting detection interplanetary medium with geostationary satellites

12 p1950 A71-27377

Hydrodynamic wave modes calculation for solar atmospheric model with ionization effects, noting trapped resonant gravity waves calculation agreement with observed oscillations

12 p1969 A71-27647

Cloud layer role in formation of light and heat regime of two layer Venus atmosphere model, considering sunlight reflection

13 p2131 A71-27808

Equatorial electrojet model instability to gradient instability and electron density irregularities

13 p2055 A71-27922

Diffuse reflection from clouds with horizontal surface striations, using Monte Carlo method to follow photons through simplified models

13 p2056 A71-27975

Two dimensional atmospheric model including oxygen and nitrogen photodissociation, recombination and photoionization, investigating solar activity and ionizing radiation effects on temperature stratification

13 p2057 A71-28018

Extensive air showers muon and electron components primary energy spectrum, using isobar and CKP formula based models

13 p2125 A71-28088

Second order difference approximations with large viscosity coefficient for primitive barotropic model over spherical geodesic grid, comparing with first order approximations

13 p2097 A71-28231

Diurnal variations of loss coefficient in D region during polar cap absorption, verifying nighttime D region model by forward propagation data

13 p2059 A71-28242

Sporadic E layers magnetic field variations, examining charged particle redistribution with air turbulence model

13 p2059 A71-28258

Auroral absorption latitudinal distribution diurnal variations, showing existence of two zone model

13 p2060 A71-28260

Solar chromosphere model, explaining spicules origin and relation to small scale nonuniformities

13 p2136 A71-28430

Magnetospheric two component plasma model, considering thermal and suprathermal spectra

13 p2060 A71-28432

Discrete ionospheric model of supersonic two dimensional low density plasma flow past large bodies, using quasi-neutrality condition

13 p1990 A71-28532

Ion production rates during electron flux-atmosphere interactions based on atmospheric models with different energy and angular distributions

13 p2061 A71-28541

Atmospheric frontogenesis models with air velocity fields acting on initially large scale temperature distributions

13 p2097 A71-28722

Land-sea drag, Ekman parametrization and Monin-Obukhov transfer process in surface boundary layer of atmospheric circulation model

13 p2097 A71-28725

Radio model of brightness temperature and electron density in transition layer of solar active regions, using Laplace transformation and hydrostatic equilibrium equation

13 p2141 A71-29050

Static and quasi-static atmospheric motions, using linearized equations for isothermal compressible atmosphere

13 p2097 A71-29084

Distant geomagnetic tail longitudinal magnetic field gradient model based on pressure balance between internal field and solar wind, discussing tail flux content

13 p2064 A71-29162

Adiabatic flow model of noiseless magnetic neutral sheet of finite width, discussing particle trajectory and charge density distribution

13 p2109 A71-29166

Structural model of mature hurricane, determining heat and moisture transfer, boundary layer dynamics and thermodynamic balance

13 p2097 A71-29250

VLF band signal daytime propagation phase and amplitudes in earth-ionosphere waveguide, using models with geomagnetic field effect

14 p2191 A71-29509

Spherical waveguide eigenvalues calculation from two layer model of earth with radially inhomogeneous atmosphere, using Airy functions

14 p2209 A71-29515

Magnetospheric model calculation for self oscillation period and amplitude dependence on longitude and plasma density estimation from observed geomagnetic pulsation period

14 p2228 A71-29531

Ionic and thermal structure model of daytime Venus ionosphere with solar wind heating based on Mariner 5 flyby mission

14 p2305 A71-29661

Magnetospheric tail models for Uranus type planet with viscous and magnetic coupling compared to geomagnetic configuration

14 p2305 A71-29664

Super metal rich K giant stars atmospheric model, obtaining abundances and turbulent velocity parameter

14 p2305 A71-29674

Shock wave heated atmospheric model computation for solar chromosphere and corona

14 p2306 A71-29684

Jupiter reflected light, examining model having elliptical polarization by surface layer scattering

14 p2306 A71-29730

Atmospheric turbulent shear layer model, giving velocity, stable, unstable and neutral profiles

14 p2267 A71-29759

Atmospheric models of partially trapped waves propagation in layer above tropopause with large stratospheric Scorer parameter

14 p2268 A71-29763

Discrete gust and power spectrum models of atmospheric turbulence, considering energy distribution effect on aircraft dynamic response

14 p2174 A71-29790

Geomagnetic field models validity from satellite data

14 p2231 A71-29903

Solar wind interaction with planetary atmospheres, discussing various models relationship to observational data

14 p2298 A71-29908

Long range numerical weather prediction, using two level quasi-geostrophic forced general circulation model with spectral truncation

14 p2269 A71-29945

Long term atmospheric circulation prediction model, considering horizontal grid resolution effect on truncation error

14 p2269 A71-29946

Polar ionospheric plasma transport, predicting ion density profiles from ionospheric processes models consistent with polar wind theory

14 p2234 A71-30039

Altitude size distribution of atmospheric aerosol from sky radiance measurements in sun aureole region, calculating sunlight forward single scattering

14 p2310 A71-30125

Geomagnetic pulsation effect on charged particles motion, based on Mead magnetosphere analytic model, using Parker perturbation method

14 p2235 A71-30346

Nonequatorial charged particle radial diffusion in asymmetric magnetosphere by third adiabatic invariant violation, using Kosik model

14 p2235 A71-30347

Climate simulation by global atmospheric circulation models including wind, temperature, pressure, water vapor, precipitation, evaporation, soil moisture, snow depth and runoff

14 p2270 A71-30505

Horizontal and post-horizontal branch hydrogen rich stellar atmospheric models, presenting emergent fluxes and H and He line profiles 14 p2314 A71-30645

White dwarf stars effective temperature measurements, matching absolute spectral energy distributions with fluxes from model atmospheres 14 p2317 A71-31013

White dwarf model atmosphere, discussing DA and non-DA spectral types, surface gravity, mass-radius relation, composition and convection effects 14 p2317 A71-31014

Atmospheric primitive equation prediction model, discussing four processor version 15 p2374 A71-31516

Summertime meridional wind component profile construction and hydrodynamic model for semidiurnal fluctuations in upper atmosphere 15 p2399 A71-31962

Venusian atmosphere circulation modeling, calculating temperature differences, thermal inertia and wind velocity 15 p2496 A71-32729

Chromosphere and solar quiet regions transition zone model, investigating radio and UV emission and height dependence of temperature and density 15 p2497 A71-32745

Solar atmospheric model, calculating shock wave dissipation in chromosphere for photosphere central iron line intensity correlation with magnetic field intensity 15 p2497 A71-32746

Mathematical theory of planetary atmosphere oscillations, considering coriolis, magnetic and viscous forces effects 16 p2561 A71-32804

Density distribution of plasmaspheric particles in equatorial plane via model of plasmasphere streaming, noting current system production in lower ionosphere 16 p2562 A71-32806

Polarized light multiple scattering in homogeneous plane parallel planetary atmospheres, considering Rayleigh scattering, test models and phase function obtained by neglecting polarization 16 p2632 A71-33320

Venusian atmosphere adiabatic and isothermal models from Venera automatic stations data, discussing temperature, pressure, density and cloud layer thickness 16 p2635 A71-33445

Charged particles distribution in magnetosphere beyond radiation belts, proposing unstable radiation zone model containing auroral and semitrapped particles 16 p2626 A71-33450

Altitude and amplitude of winter stratospheric warmings from satellite measured radiance changes, considering radiative transfer equation and variable model of temperature structure 16 p2605 A71-33537

Geomagnetic tail natural oscillations, applying model of plasma cylinder with free boundary immersed in interplanetary medium 16 p2564 A71-33673

Thermosphere and exosphere static models with empirical thermal profiles, giving temperature, density and composition as function of height 16 p2564 A71-33722

Semiannual density variation in heterosphere as function of height based on satellite drag and atmospheric models 16 p2564 A71-33723

Solar extreme UV flash spectrum from spectroheliographs aboard Aerobee 170 rocket launched during March 1970 eclipse, comparing with homogeneous and inhomogeneous temperature models 16 p2640 A71-33730

Seasonal temperature and density models for stratosphere and mesosphere from observations by resistance thermometers at Heiss Island Soviet rocket station 16 p2566 A71-33743

Empirical atmospheric model derivation from midlatitude density data 16 p2566 A71-33759

Noctilucent cloud nature from cosmic dust particles collection and detection, discussing mass, absolute falling velocity and model theories 16 p2641 A71-33765

Thermospheric dynamics three dimensional model in terms of atmospheric system eigenfunctions, deriving formulas for solar XUV and corpuscular heating during geomagnetic storms 16 p2567 A71-33781

Global model of atmospheric temperature, chemical composition and density for altitudes from 25 to 1000 km, using satellite drag determined density values 16 p2567 A71-33782

Seasonal density variations in thermosphere and exosphere, obtaining model from Explorers 19 and 39 drag measurements for comparison withOGO-6 mass spectroscopy 16 p2569 A71-33802

Escaping photoelectrons effect on polar wind exospheric model, suggesting kinetic pressure predominance at very high altitudes 16 p2569 A71-33814

Midlatitude E region electron density profile data for various solar activity levels, investigating formation theory and atmospheric models 16 p2570 A71-33822

Striated irregularities in ionospheric ion clouds, using model of ionospheric conductivity profile 16 p2573 A71-33957

Radical and formaldehyde daytime concentrations predictions from steady state model of unpolluted surface atmosphere 16 p2575 A71-34048

Atmospheric optics and geophysics problems modeling arrangement reproducing radiation field within light scattering medium 16 p2605 A71-34106

Three level baroclinic model of short range large scale weather prediction at low latitudes, determining background/steering flow/in tropical disturbances 17 p2769 A71-34300

Storm models for space-path attenuation calculations using digitized weather radar data for fine structure and surface rainfall data for extrapolation 17 p2704 A71-35090

Steady state one dimensional cloud model for cumulus convection, discussing validity range limits 17 p2770 A71-35125

Model interpretation of Pc pulsations during geomagnetic storms, analyzing plane HM-wave resonance in horizontally stratified middle-low geomagnetic latitude lower magnetosphere 17 p2734 A71-35190

Heat exchange between atmosphere and earth surface, calculating nonadiabatic term size and spatial distribution 17 p2734 A71-35193

Reflecting layer model for methane band absorption spectrum in Jovian atmosphere 17 p2807 A71-35412

Venusian atmospheric models from troposphere, stratosphere and thermosphere models based on satellites data 17 p2807 A71-35502

Stellar atmospheres mathematical model, considering transfer equation reduction to linear equations set 17 p2808 A71-35556

Model cloudy atmosphere construction, reviewing computational techniques for radiative transfer analysis 17 p2735 A71-35559

Radiative heat transfer in model water clouds by IR radiation, using method of discrete ordinates 17 p2735 A71-35560

Model radiative transfer across random air-sea interface, determining reflected sky radiance 17 p2736 A71-35562

Orography, cloudiness and surface temperature effects in six-layer global atmospheric circulation model, giving January simulation data 17 p2770 A71-35804

Aerosol size distribution from lidar light scattering polarization properties, constructing inversion model 17 p2770 A71-35806

Tropospheric stratification structure from high resolution FM/CW radar sounder, comparing with internal gravity wave atmospheric models 17 p2771 A71-35808

Venus surface temperature dependence on incident solar flux based on runaway greenhouse nongray calculation, considering water vapor as IR opacity source in models 18 p2964 A71-36285

Martian surface topography effects on mean wind from time independent and frictionless thermal wind equation solution for radiative-convective atmospheres at scaling analysis level 18 p2964 A71-36287

Cartesian diver atmospheric model hypothesis for Jupiter Red Spot longitude, size and intensity variations 18 p2964 A71-36288

Venus atmospheric model based on Mariner 5 and Venera satellites observation, comparing with optical observation from earth 18 p2965 A71-36293

Lifting entry and terminal phase system optimization for 1975 Mars Viking lander, considering graphical tradeoff approach including design parameter and atmosphere model variations 19 p3148 A71-37171

Venus atmosphere adiabatic and isothermal models, investigating water vapor content, pressure and temperature 19 p3133 A71-37435

CAT physical model and formation mechanism, using turbulent zone characteristics and wind velocity spectra 19 p3049 A71-37448

Artificial depression structure from general circulation model synoptic development, reproducing real depression features 19 p3089 A71-37504

Solar photosphere and low chromosphere models temperature-height profile 19 p3135 A71-37609

Solar limb and disk intensity spectra in chromosphere-corona transition region, calculating models, element abundances structure, electron pressure and hydrostatic equilibrium equations 19 p3136 A71-37617

Ion-exosphere in open magnetic field, calculating number density, particle, moment and energy flux distribution from simple mathematical model 19 p3138 A71-37737

Model of large ionospheric electron density discontinuities, emphasizing horizontal asymmetry association with observed east-west refraction asymmetry 19 p3053 A71-37829

Laboratory model for ionospheric perturbations effects on long range VLF paths 19 p3017 A71-37865

Ionospheric E region nighttime model from rocket soundings, obtaining electron density profiles by Langmuir probe and wind measurements by glowing vapor release 19 p3055 A71-38036

Cloud cover areal distribution estimation model using multichannel IR radiometer data from Nimbus 2 satellite 19 p3056 A71-38267

One layer midlatitude beta plane channel model of incompressible fluid for study of systematic error propagation on nearly stationary synoptic scale wave 19 p3090 A71-38268

Magnetospheric field model, assuming magnetostatic problem solution facilitated by equation linearity 19 p3059 A71-38395

Harvard-Smithsonian reference atmosphere model of solar atmosphere, combining photosphere and quiet lower chromosphere 19 p3146 A71-38660

Hydrogen ionization and excitation equilibrium, using slab model atmospheres irradiated from both sides by photospheric, chromospheric and coronal radiation 19 p3146 A71-38664

Atmospheric convective motion model, applying turbulent jet method 19 p3093 A71-38696

Two dimensional magnetospheric model, investigating magnetic line dipole field confinement in empty cavity by tail-like infinitely conducting plasma at constant pressure 20 p3286 A71-38732

Martian lower ionospheric models during solar proton event, determining electron density profiles 20 p3286 A71-38741

Solar proton trajectories calculations in Williams-Mead geomagnetic field model, showing longitude difference in tail region 20 p3216 A71-38747

Earth thermosphere models, discussing shortwave solar radiation as major energy source during quiet conditions, diurnal variations of structure, neutral-charged components interconnection, etc 20 p3216 A71-39117

Plasma layer effect on natural oscillations of magnetosphere tail, using infinite plasma cylinder model immersed in interplanetary plasma 20 p3216 A71-39137

Magnetosphere neutral layer plasma conductivity determination from model of linear magnetic dipole in conducting fluid flow 20 p3216 A71-39138

Southern Hemisphere extended operational meteorological prediction using six level primitive equation model 20 p3256 A71-39202

Earth atmospheric zonal circulation model, using hydrothermodynamic equations with Newton law for radiative heat sources 20 p3256 A71-39210

Three dimensional atmospheric dynamo models in quasi-stationary and stationary approximation for ionospheric and magnetospheric electric fields and currents production during quiet conditions 20 p3217 A71-39512

Lunar and solar daily geomagnetic variation morphology correlation based on atmospheric dynamo model 20 p3217 A71-39515

Diurnal variations of Sq currents in terms of electroconductivity model of ionosphere and geomagnetic field, using two dimensional dynamo theory 20 p3217 A71-39517

Atmospheric dynamo equations derivation based on Maxwell equations and Ohm law with anisotropic and asymmetric electric conductivity tensor for quiet geomagnetic variations explanation 20 p3217 A71-39518

Dynamo equations solution for electrostatic potential, discussing three dimensional model for ionospheric equatorial conditions and Northern-Southern Hemispheres coupling 20 p3218 A71-39519

Dynamo theory for ionospheric thin shell model, considering wind fields determination from diurnal geomagnetic variations 20 p3218 A71-39522

Low latitude geomagnetic substorm development model due to increased resistance in magnetosphere tail current sheath 20 p3219 A71-39597

Venus lower atmosphere model based on surface pressure and temperature from radio astronomical and radar observations 20 p3296 A71-39626

D region electron density profiles and ionization models in terms of XUV radiation and minor constituents NO and oxygen, using ground and space measurements 20 p3224 A71-39713

Ionospheric effective recombination coefficient and reaction rate models for various solar activity periods and day and night conditions 20 p3224 A71-39714

Photoelectron flux and energy spectra effects on ionospheric phenomena, examining sunlit and predawn atmospheric models 20 p3225 A71-39726

D region night airglow OH emissions and IR atmospheric diatomic oxygen bands excitation mechanism with aid of model involving solar photodissociation 20 p3226 A71-39831

Ionospheric model for magnetic perturbation field global distribution during polar magnetic substorm, considering ground level geomagnetic effects from Birkeland and Pedersen currents 20 p3229 A71-39857

Auroral substorm model refinements for proton aurora by classifying substorms according to intensity or magnitude 20 p3284 A71-39858

Plasma transport processes role in E region from midlatitude nocturnal and auroral ionospheric models in terms of transport equations 20 p3232 A71-39893

Sun-earth distance and earth orbital eccentricity effect on E region peak electron density, discussing Chapman-like model 21 p3372 A71-40035

Ionospheric irregularities and reflection points calculation, developing simple ray interference model from large antenna array data 21 p3372 A71-40042

Internal gravity wave parameters calculation from total electron content short term variations, comparing ionospheric disturbance models 21 p3373 A71-40049

Cloud layer role in formation of light and heat regime of two layer Venus atmosphere model, considering sunlight reflection 21 p3441 A71-40077

Atmospheric stratification effects on downward motion of aircraft vortex wakes, developing approximate model 21 p3318 A71-40486

Book on numerical weather prediction covering atmospheric wave motions, scale analysis, vorticity and energy, barotropic, baroclinic and multilevel models, etc 21 p3410 A71-40780

Baric levels determination for weather forecasting from statistical analysis of atmospheric numerical model 21 p3410 A71-40823

Correlation coefficient between winds at 850-30 mb pressure levels over Italy in winter, proposing theoretical model 21 p3411 A71-40825

Mercury visual, radar and radio data, describing rotation, temperature, surface properties, subsurface layers and atmospheric model 21 p3452 A71-40883

Numerical model of three dimensional convection in atmosphere with vertical wind shear, solving system of differential equations 21 p3411 A71-41385

Numerical model of turbulence effect on cumulus cloud mesoscale convective motion 21 p3411 A71-41386

Seasonal variations in vertical distribution of ozone at high latitudes, using Murgatroyd model of looped meridional atmospheric circulation 21 p3375 A71-41395

Thermal effects in loop prominences formation after solar flares from model computer simulation 22 p3597 A71-41459

Atmospheric modeling for earth and Venus heterosphere structure using multicomponent radiative hydrodynamic equations for atmospheric temperature and constituents height variation determination 22 p3598 A71-41532

Ionization profiles of upper ionosphere from Alouette 1 vertical sounding data, proposing model for ionosphere shape 22 p3532 A71-41554

Atmospheric circulation finite difference weather prediction model, investigating horizontal grid resolution effects 22 p3535 A71-42412

Global numerical weather prediction model, using finite difference grid and operators with smoothing techniques 22 p3568 A71-42413

Laboratory analog simulation of absorption line spectra in cloudy planetary atmospheres, comparing with computational model based on plane parallel atmosphere 23 p3700 A71-43075

Equatorial F 2 region lattice model with curved field line geometry for plane stratified atmosphere and time dependent problem solution 23 p3667 A71-43137

Model prediction for magnetospheric electric field dependence on solar wind velocity, comparing results with plasmaspheric measurements for different Kps 23 p3721 A71-43177

Venusian atmosphere circulation modeling, calculating temperature differences, thermal inertia and wind velocity 23 p3735 A71-43298

Ocean and earth tidal effect on semidiurnal lunar atmosphere tide, considering realistic model 23 p3700 A71-43339

Mars and Venus upper atmospheric electron distribution compared with theoretical ionospheric models, considering solar wind as ionization source 23 p3736 A71-43342

Narrow light beam transmission in weakly nonlinear turbulent atmosphere, calculating large scale permittivity inhomogeneity effect on average intensity by model 23 p3645 A71-43564

Small scale electrostatic field penetration from E into F region of ionosphere based on plane stratified model 23 p3671 A71-43577

Atmospheric conditions for hailstone evolution process, using convection theory and kinetic particle model 23 p3701 A71-43909

Kraichnan turbulence theory based on exact solution of model equations presenting strong structural similarities with turbulent Navier-Stokes equations 23 p3701 A71-43976

Vertical equatorial ozone distribution, incorporating oxygen hydrogen reactions and diffuse and advective transport in time dependent meridional model 23 p3673 A71-43987

Cepheid sequence interpretation on gradient diagram based on model atmosphere photometric data 23 p3771 A71-44305

Long range weather prediction based on numerical global atmospheric models, noting application to climatology 24 p3844 A71-44366

Electric conductivity correlation between solar faculae and Bilderberg model of photosphere and chromosphere 24 p3868 A71-44458

Scattered light effect on measured facula-to-photosphere contrast, leading to hotter average facula model 24 p3868 A71-44460

Atmosphere hydrodynamic simulation model for cascade energy transfer in turbulent flow, using Euler gyro equations 24 p3844 A71-44818

Numerical modeling of Venus atmosphere taking into account short wave radiation absorption, boundary layer, mesoscale convection and horizontal friction 24 p3870 A71-44819

Radiative thermal flux model of Venus atmosphere, using Venera data and greenhouse effect 24 p3870 A71-44822

ATMOSPHERIC MOISTURE

Atmospheric refractometry anomaly at high relative humidities observed in controlled environment for causes 01 p0113 A71-10252

Synoptic and moisture content charts from Kosmos-243 satellite measurements of escaping thermal RF flux 01 p0073 A71-10540

Atmospheric total moisture content from Cosmos 243 satellite, describing onboard equipment calibration 01 p0074 A71-11101

Stratospheric and mesospheric water vapor content by satellite-borne spectral measurements 01 p0120 A71-11103

Atmospheric water vapor dimers absorption of microwaves, computing total absorption coefficient 03 p0378 A71-13295

Martian atmospheric water vapor latitude distribution, evaluating high dispersion spectroscopic observations 03 p0488 A71-13555

Atmospheric humidity and cloud moisture determination, considering meteorological satellites radio

measurements errors relation to turbulent sea surface spectral radiant emittance ambiguity 04 p0621 A71-14638

Goethite stability on Mars, considering dehydration-rehydration cycle and time average atmospheric water vapor content 04 p0645 A71-15132

Mars atmospheric water vapor detection during Southern Hemisphere spring and summer season 04 p0645 A71-15139

Soviet monograph on thermal sounding of atmosphere by satellite covering moisture content, cloud surfaces and stratosphere temperatures and thermal radiation distribution 05 p0738 A71-16197

IR radiation absorption by water vapor in atmospheric transmittance windows, discussing fine structure of absorption spectrum 05 p0778 A71-16841

Mars atmospheric data from Mariner flights, discussing north polar haze, bright surface features morphology, multiring structures and water vapor exchange 06 p0965 A71-17627

Adhesive resin metal bond stability, examining surface finish and atmospheric moisture effects at various temperatures on exfoliation 06 p0904 A71-17944

Atmospheric total moisture content from Cosmos 243 satellite, describing onboard equipment calibration 07 p1102 A71-19650

Stratospheric and mesospheric water vapor content by satellite-borne spectral measurements 08 p1277 A71-20847

Atmospheric moisture measurements, using Cosmos 243 satellite radiothermal atmosphere self radiation 08 p1277 A71-21007

Atmospheric moisture field radiometric microwave sounding statistical treatment, noting latitudinal dependence over oceans from Cosmos 243 satellite measurements 09 p1486 A71-22301

Venusian atmosphere carbon dioxide, water, molecular oxygen and nitrogen contents from Venera 5 and 6 data 09 p1523 A71-23144

Atmospheric water vapor dimers microwave absorption, computing total absorption coefficient 09 p1408 A71-23268

Venusian atmosphere subcloud layers intrinsic outgoing thermal radiation and IR spectrum transmissivity from satellite temperature, pressure, moisture content and chemical composition data 10 p1681 A71-25128

Daytime atmospheric water vapor measurements at IR astronomy mountain sites in southwestern U.S. 11 p1793 A71-25243

Low hygrometer calibration for water vapor measurements smaller than 3 mm 11 p1761 A71-25244

Comparative accuracies of vertical atmospheric water vapor profiles by radiosonde and laser backscatter Raman component 11 p1794 A71-25383

Venus water, discussing polar seas, acidity, temperature, wind patterns and clouds 11 p1824 A71-25700

Venus atmosphere adiabatic and isothermal models, investigating water vapor content, pressure and temperature 12 p1964 A71-27085

Latitudinal distribution of integral water content of clouds in droplet form above Pacific, Atlantic and Indian oceans from Cosmos 243 measurements 12 p1924 A71-27098

Structural model of mature hurricane, determining heat and moisture transfer, boundary layer dynamics and thermodynamic balance 13 p2097 A71-29250

Mesospheric extraterrestrial dust and trapped water model of noctilucent cloud formation in high latitude summer conditions, using meridional trajectories 14 p2231 A71-29721

Noctilucent cloud formation from water vapor concentrations in mesosphere and lower thermosphere of arctic and midlatitude regions measured by rocket-borne RF mass spectrometers 14 p2232 A71-29957

Water vapor contamination long lasting effects on stratospheric measurement during balloon flight 14 p2270 A71-30453

Lower thermosphere and ionosphere upper limits of positively ionized water molecules number density, considering desorption and recombination processes 16 p2571 A71-33842

Venus atmosphere adiabatic and isothermal models, investigating water vapor content, pressure and temperature 19 p3133 A71-37435

Indirect reduction of vertical atmospheric water vapor profile from measured outgoing thermal radiation by regularization method 19 p3090 A71-37966

Surface layer humidity correlation to height of atmosphere emitting in IR spectral region, determining water vapor content by recording earth radiation angular distribution

19 p3054 A71-37974

Atmospheric water vapor effects on microwave frequencies refraction index structure

19 p3024 A71-38611

Atmospheric moisture from Cosmos 243 satellite measurements of intrinsic atmospheric radiothermal emission

20 p3218 A71-39587

Atmospheric temperature and water vapor profile calculation from Nimbus satellite IR spectrometer data, noting Southern Hemisphere tropospheric and stratospheric pressure analyses

20 p3258 A71-39667

Atmospheric transmittance measurement errors in determining temperature, water vapor and ozone distributions from satellite remote sensing

20 p3258 A71-39671

Microwave sounding of ocean and earth surface thermal emission and atmospheric water vapor content by Cosmos 243 satellite-borne radiometers

20 p3259 A71-39672

Aircraft sounding of atmospheric microwave radiation transfer compared with IR method, measuring optical Mie characteristics, water vapor content, cloudiness, ice cover, etc

20 p3259 A71-39673

Lower thermosphere and mesosphere water vapor and neutral composition spectrometric measurements, estimating hydrogen and oxygen atom recombination coefficient limits with mass analyzers

20 p3221 A71-39696

Ceramic semiconductor atmospheric humidity detector with hydrophilic properties, using complex capillary porous body composed of crystals and amorphous substance

21 p3383 A71-41237

Stratospheric submillimeter wave emission and water vapor mixing ratios measurements, using Michelson interferometer with phase modulation and Fourier spectroscopy methods

22 p3545 A71-42145

Venusian photochemistry, discussing hydrogen source from HCl, loss of water in relation to HCl, carbon dioxide stability and COS and hydrogen sulfide in visible clouds

23 p3736 A71-43341

Vertical atmospheric humidity profile variations relationship to clouds water vapor content from thermal radio emission measurements onboard Cosmos 243 satellite

23 p3673 A71-44048

Atmospheric vertical humidity profile determination by measuring microwave radiation from satellite

24 p3822 A71-44350

Atmospheric vertical humidity profile from ground measurements of radio wave absorption at 1.35 cm water vapor line

24 p3822 A71-44820

Radio-optical dispersometer for atmospheric water vapor density measurement with increased sensitivity

24 p3809 A71-44985

ATMOSPHERIC NEUTRON FLUX DENSITY

U ATMOSPHERIC RADIATION

U NEUTRON FLUX DENSITY

ATMOSPHERIC NOISE

U ATMOSPHERICS

ATMOSPHERIC OPTICS

Stellar scintillation saturation at large zenith angles, examining atmospheric dispersion and multiple scattering roles

01 p0127 A71-10141

Laser light beam spread in random media, considering atmospheric and oceanographic applications

04 p0609 A71-15682

Statistical optical measurements of solar scintillation due to atmospheric conditions

07 p1111 A71-19489

Photoelectron counting distribution for random medium passage scintillated stochastic light, considering low level amplitude stabilized and chaotic radiation transmission through turbulent atmosphere

07 p1159 A71-19513

IR laser propagation through fog with droplet vaporization, assuming incident electromagnetic radiation as plane harmonic wave

08 p1302 A71-21392

Fredholm integral equations solutions in atmospheric optics, proposing algorithm for optimal parameter regularization values

09 p1487 A71-22378

Atmospheric attenuation in IR windows near sea level from transmittance spectral curves, discussing continuum absorbance

09 p1437 A71-22740

Wave structure and mutual coherence functions of optical wave propagating in turbulent atmosphere, considering signal to noise ratio

10 p1641 A71-23948

Helmholtz reciprocity theorem extension to clear turbulent atmosphere, defining Green functions to

characterize optical propagation in opposite directions between parallel planar apertures

10 p1641 A71-23949

Mars UV polarization and atmospheric opacity measurements, using ground based polarimetric data at near maximum elongation

11 p1825 A71-25709

Atmospheric zero light polarization points, examining solar vertical and various almucentars, horizontal and vertical nonuniformities and albedo variations

11 p1795 A71-25925

Optical anomalies associated with Tungusk meteorite fall in 1908, noting volcanic activity and noctilucent cloud formations

14 p2233 A71-29964

Atmospheric optics and radiative transfer, including earth albedo, sky brightness, heat balance, cloud/terrain reflectance, molecular spectroscopy and multiple scattering

14 p2275 A71-30497

Atmospheric optics and geophysics problems modeling arrangement reproducing radiation field within light scattering medium

16 p2605 A71-34106

Twilight glow spectrophotometry and visual observations from Soyuz 5 spacecraft, determining atmospheric optics and vertical aerosol profile

18 p2911 A71-36006

Atmospheric zero light polarization points, examining solar vertical and various almucentars, horizontal and vertical nonuniformities and albedo variations

20 p3257 A71-39216

Soviet papers on actinometry, atmospheric optics and ozonometry, covering atmospheric ozone contents measurement techniques, radiation balance, atmospheric spectral transmissivity, etc

20 p3257 A71-39326

Aircraft sounding of atmospheric microwave radiation transfer compared with IR method, measuring optical Mie characteristics, water vapor content, cloudiness, ice cover, etc

20 p3259 A71-39673

Atmospheric optical transmission coefficient measurements using steerable laser radar system

21 p3372 A71-40040

Optical phase variations, temperature structure and wind velocity measurements in atmosphere using He-Ne laser beam on 70 m propagation path

22 p3509 A71-41787

Atmospheric contrast reduction of aerial images, predicting quality under various target and meteorological conditions

22 p3547 A71-42506

Atmospheric transmission functions for twilight airglow of alkalis Na, Li and K

23 p3673 A71-43983

Atmospheric aerosol stratification, turbidity, stratospheric layer and purification zone from optical sounding data

24 p3823 A71-44821

ATMOSPHERIC PHYSICS

NT CLOUD PHYSICS

Stellar atmospheric physics - Conference, University of Queensland, Brisbane, Australia, May 1970

01 p0152 A71-10326

Comparative convection levels and energy instabilities in vertical motion, using particle and layer methods

01 p0113 A71-10539

Wolf-Rayet star atmospheres, discussing matter density distribution, light pressure effects on particle motion and H and He ionization levels

01 p0158 A71-10803

Kinetic energy and available potential energy balance in atmospheric stationary disturbances/standing waves/, using atmospheric flow statistics

01 p0119 A71-10853

Upper atmosphere temperature, wind and diffusion measurements using artificial luminous clouds

01 p0074 A71-11088

Magnetospheric processes and structure, discussing solar wind interaction, magnetopause and shock wave formation, geomagnetic tail geometry, etc

03 p0410 A71-13822

Noctilucent clouds, discussing mesosphere thermodynamics and water vapor content, solar rain, etc

03 p0414 A71-14019

Tropospheric diffraction fields computation in atmospheres with modified refractive index increasing monotonically with height, discussing IF and LF ground wave propagation

04 p0552 A71-15020

Radiometeorological measurements of atmospheric structure, using SHF troposcatter synchronously offset beams on great circle propagation path

04 p0584 A71-15545

Atmospheric Coulomb interaction influence on longitude dependence of electron intensity in anomaly region

06 p0963 A71-18255

Extended stellar atmospheres production mechanism involving outward acceleration of material in rarefaction wave following shock wave arrival at atmosphere edge

06 p0976 A71-18472

Gravity oriented satellites librational dynamics in elliptic orbits, emphasizing atmosphere adverse effects [AIAA PAPER 71-89]

06 p0980 A71-18545

Planetary atmospheres structure and dynamics, discussing composition and vertical temperature profile models

07 p1191 A71-18915

Earth environment from aviation viewpoint, discussing atmospheric physics and chemistry, flight physiology, radiation, etc

08 p1243 A71-20702

Upper atmospheric research - Conference, Boulder Colorado, August 1970

08 p1278 A71-21196

Polar substorms electric current systems and magnetic effect below and above ionosphere

08 p1279 A71-21211

Satellite role in future observing systems for global atmospheric research program, describing satellite instrumentation

08 p1328 A71-21721

Observational data characteristics analysis as contributor to knowledge and utilization of all atmospheric physical occurrences

08 p1328 A71-21722

Charge source density during interaction between atmosphere and electron/proton fluxes at prescribed boundary parameters

09 p1513 A71-22675

Unperturbed atmospheric parameters calculation from surface measurements of blunt body at hypersonic speeds under various aerodynamic conditions

09 p1437 A71-22678

Optical observation of structure, composition, thermal spectra and aerosol layers of giant planet atmospheres

09 p1520 A71-22827

Amplitude distribution of nuclear burst electromagnetic pulse propagated through atmosphere, deriving two probability distribution functions by central limit theorem

09 p1410 A71-23524

Soviet book on physics of interaction between atmosphere and ocean covering heat transfer, wave formation, vertical mixing in upper sea layer, etc

10 p1639 A71-24671

Atmospheric electrical structure control by lower ionosphere force, considering interaction between neutral atmosphere tidal circulations and ionospheric plasma in presence of geomagnetic field

10 p1604 A71-24702

Cometary atmosphere photometric data, determining particle distribution and ejection rate, temperature, molecular lifetime, acceleration and emission velocity

11 p1821 A71-25542

Soviet papers on upper atmosphere physics covering thermosphere, dynamic processes and radiative energy transport in stratosphere and mesosphere, and ionospheric parameters radio measurement

13 p2056 A71-28017

Scott effect observation of superrotation of upper atmosphere, relating temperature gradient, magnetic field and gas rotation

13 p2063 A71-29095

Magnetosphere structure, considering geomagnetic field lines configuration in magnetotail

14 p2229 A71-29669

Clear air turbulence mechanics, considering thermal convection, shear layers, Coriolis and centrifugal instability, billons and rotors

14 p2267 A71-29758

Self contained lightweight airborne data acquisition system for atmospheric and meteorological research using analog recorder and telemetry system

14 p2243 A71-30311

General atmospheric circulation mean time distribution, kinetic energy, regional interactions and mathematical simulation

14 p2236 A71-30492

Jupiter Red Spot, zonal wind and banded appearance, Venus vertical temperature structure and atmospheric motions, and Mars circulation, dust phenomena and atmosphere stratification

14 p2313 A71-30499

Book on space observatories covering atmospheric structure, space astronomy applications, atmospheric attenuation, balloon IR sounding, satellite observation, etc

14 p2316 A71-30895

Radiative heat transfer equilibrium in earth, Venus and Mars atmospheres, taking into account interaction with ground

15 p2395 A71-31448

Atmospheric structure effects on moons zenith angle distribution and maximum intensity direction as function of energy at two different altitudes

15 p2476 A71-31788

Atmospheric muons anomalous zenithal distribution at extremely high energy regions

15 p2477 A71-31794

Eole project for atmospheric phenomena studies, describing meteorological satellite/balloons arrangements, equipment and operational methods

15 p2500 A71-31824

Soviet papers on processes in upper layers of atmosphere covering troposphere, stratosphere and mesosphere over Northern and Southern Hemispheres 15 p2399 A71-31961

Stratopause layer atmospheric temperature field characteristics observation, noting association with processes in upper stratosphere and lower mesosphere 15 p2399 A71-31965

Swedish space research activity covering upper atmospheric physics, ionosphere, magnetosphere and solar phenomena 16 p2665 A71-33853

Report to COSPAR on French space program covering ionosphere and magnetosphere physics, meteorology, cosmic rays and earth resources 16 p2666 A71-33861

West German space research activities during 1970 on meteorology, ionospheric physics, solar radiation, cosmic rays and life sciences 16 p2666 A71-33866

Neutral thermosphere and exosphere structure, discussing density, temperature, composition and diurnal and seasonal variations 17 p2732 A71-34461

Manned orbital research modules design for atmospheric physics, weather and earth resources observations and stellar astronomy [AIAA PAPER 71-815] 17 p2814 A71-35426

Non-LTE physics of He atoms in hot stellar atmospheres, presenting numerical results for He I and II line spectra variations explanation 17 p2808 A71-35558

Solar atmosphere mean radial velocity relation to low excitation potential based on Fraunhofer lines blue shifts observations 17 p2808 A71-35576

ESRO sounding rocket program covering atmospheric and ionospheric physics and solar and auroral phenomena 18 p2896 A71-35926

Global atmospheric research with balloons, buoys and orbiting satellites for meteorological and oceanographic data recovery 18 p2913 A71-36486

Friction velocity in stably stratified constant flux layer with known heat flux, using log-linear velocity profile with fixed Monin-Obukhov parameter value 19 p3089 A71-37502

Soviet papers on physical processes in upper earth atmosphere covering ion composition, electron concentration and temperature, luminescent clouds, sporadic E layer, etc 19 p3060 A71-38627

Magnetic field aligned striations of Ba ion clouds artificially injected into ionosphere, investigating physical processes based on model 20 p3230 A71-39861

Stratosphere and mesosphere physics and dynamics, studying composition, radiation fields, temperature, winds, wave phenomena and relations to meteorological theory 20 p3230 A71-39872

Atmospheric physics of cloud formation, rain, hail and snow precipitation, discussing intracloud temperature variations electric fields and air impurities on water condensation 21 p3410 A71-40146

Mariner S-band occultation experimental data compared with theory for accuracy of physical characteristics of Mars and Venus atmosphere, reviewing data reduction and error analysis 23 p3735 A71-43331

Mars atmospheric carbon dioxide dissociation, solving and comparing diffusion equations to Mariner oxygen and carbon dioxide observations 23 p3735 A71-43332

Richardson criterion generalization for atmospheric turbulence onset, considering anisotropic turbulence conditions 24 p3844 A71-44447

ATMOSPHERIC PRESSURE

Power spectra and cross spectra of surface pressure variations in polar regions compared to solar emission, noting Antarctic-Arctic relationship 01 p0119 A71-10741

Meteorological satellite atmospheric parameter observations, discussing instruments and techniques for temperature and pressure profiles, wind patterns and cloud image data 01 p0164 A71-11360

Gravitational fields and atmospheric pressure effects on soils subjected to static and dynamic loading, using aircraft parabolic gravity simulation [AIAA PAPER 69-1009] 01 p0068 A71-11581

Atmospheric pressure pulsed carbon dioxide lasers electrical excitation using double transverse discharge technique 02 p0260 A71-12130

Hypobaric pressure and hypoxic or hyperoxic atmospheres effect on mice resistance to pneumococcal pneumonia 02 p0199 A71-12382

Venus lower atmosphere structure and brightness temperature spectrum analysis for composition, temperature and pressure profiles 03 p0484 A71-13212

Planetary atmospheres motion effect on constant pressure surface height in radio occultation data interpretation 03 p0488 A71-13553

Atmospheric pressure pulsed carbon dioxide laser, investigating gain, peak power and pulse duration as function of gas pressure and discharge voltage 03 p0440 A71-14461

Semiannual atmospheric wind and pressure oscillations relation to seasonal meridional baric systems displacements, considering cosinusoidal wave motion variations between Northern and Southern Hemispheres 04 p0621 A71-14639

Hypersonic shock wave production into air at one atmosphere in tube with electrical discharge gas heating 04 p0566 A71-14970

Nitrogen plasma viscosity at atmospheric pressure, using moving sphere resistance measurement 05 p0786 A71-16225

Atmospheric high pressure axis determination from satellite photographed sea surface sunglint reflection patterns, using model calculations 05 p0778 A71-17045

Power spectra of cosmic ray intensity variations at ground and atmospheric pressure oscillations 06 p0950 A71-17979

Neutron monitor counting rate at Sanae, Antarctica, observing snow and atmospheric pressure and temperature effects 06 p0960 A71-18168

Solar activity sudden perturbations effect on earth pressure field and atmospheric circulation 06 p0924 A71-18265

Optimum design of high peak power transversely excited atmospheric pressure carbon dioxide laser using ballast resistor energy measurements 07 p1121 A71-18749

Upper atmosphere semi-diurnal pressure variations from wind data obtained by radar observation of meteors, discussing seasonal and planetary changes 07 p1151 A71-19147

Barometric pressure and exercise effects on erythropoietin titer in normal and hypoxic rat plasma, noting lactic acid concentration and acid base balance changes 08 p1237 A71-20676

Atmospheric pressure pulsation time spectra on earth surface as function of stratification conditions 08 p1286 A71-21876

Upper atmosphere semi-diurnal pressure variation calculation from hydrodynamic equations similar to atmospheric tides theory 10 p1600 A71-24038

Degradation rate tests on adhesive bonded sandwich panels of temperature resistant composite structural materials at varying atmospheric pressures 10 p1614 A71-24073

Atmospheric pressure carbon dioxide laser electrode design for uniform pulse excitation discharge 10 p1621 A71-24508

Humidity effects on sound velocity in air at constant temperature and normal atmospheric pressure in lower audio frequency range 10 p1642 A71-24815

Aerodynamic infrasound, considering atmospheric pressure variations in seconds to minutes period range 10 p1596 A71-24915

Microbarometric oscillations enhancement due to atmospheric pressure waves generation and cold fronts passage, considering relationship to sporadic E critical frequency 10 p1606 A71-24918

Anomalous winter ionospheric radio wave absorption related to amplitude increases of microbarometric oscillations at ground level 10 p1606 A71-24919

Thermal conditions in asymptotic region of atmospheric pressure Ar arc plasma, considering nonequilibrium ionization due to ambipolar diffusion 10 p1654 A71-24971

Venus atmosphere chemical composition, determining N, O, water and carbon dioxide concentrations, temperature and pressure 11 p1823 A71-25691

Martian surface pressure from 1967-1969 apparition observations, discussing micron bands carbon dioxide abundances 11 p1825 A71-25711

Martian atmospheric pressure carbon dioxide abundance variations correlated with waxing and waning of polar caps or Mars season 11 p1825 A71-25712

Thermal control, pressure survival and structural tradeoffs of Jovian atmospheric probe for mission parametric studies [AIAA PAPER 71-482] 11 p1839 A71-26257

Line formation effective pressure from Venus atmosphere spectra, discussing phase angle variations 11 p1835 A71-26457

Jet stream axis position from cumuliform cloud structural differentiation observed over Central Europe on 22 May 1970, noting coincidence with high pressure near ground 12 p1924 A71-26575

Atmospheric pressure electrical and thermal conductivities on nitrogen and hydrogen up to 26,000 K from argon arc measurements 12 p1939 A71-27271

Steady state RF glow, abnormal glow and DC arc discharges in air at atmospheric pressure 12 p1881 A71-27274

Transversely excited atmospheric pressure carbon dioxide lasers, considering megawatt laser pulse generation 12 p1914 A71-27279

Construction, operation and in-flight performance of triaxial bridge accelerometer used in falling sphere experiment for atmospheric density, temperature and pressure determination 13 p2066 A71-28160

Pulsed atmospheric pressure carbon dioxide laser output pulse characteristics and self mode locking 14 p2253 A71-29799

Cosmic ray nucleon-meson and barometric pressure data continuous recording equipment, comparing system to conventional instruments 14 p2248 A71-30602

Northern Hemisphere upper stratospheric temperature pressure field changes during autumn, using isobar surface charts 15 p2400 A71-31966

Jupiter atmosphere nonequilibrium radiative processes, considering energy balance and pressure and temperature conditions 16 p2637 A71-33516

Mars atmosphere high resolution line spectra, calculating carbon dioxide abundance, rotational temperature and surface pressure 17 p2800 A71-34588

Upper atmosphere mean temperature, pressure, density and wind distributions as functions of altitude, season and latitude, discussing planetary, infrasonic and internal gravity wave effects 17 p2735 A71-35236

Stratospheric pressure surfaces height over polar, middle and tropical latitudes as function of long term solar activity 18 p2944 A71-36220

Artificial depression structure from general circulation model synoptic development, reproducing real depression features 19 p3089 A71-37504

Radial temperature profiles of long induction discharge in argon at atmospheric pressure 19 p3111 A71-37579

Venus atmosphere chemical composition, temperature and pressure, discussing model cloud layer, circulation and upper atmospheric structure 19 p3138 A71-37759

Atmospheric pressure pulsation time spectra on earth surface as function of stratification conditions 19 p3060 A71-38469

Geomagnetic storms association with atmospheric pressure trough development during sporadic solar activity 20 p3214 A71-38729

Venus lower atmosphere model based on surface pressure and temperature from radio astronomical and radar observations 20 p3296 A71-39626

Atmospheric temperature and water vapor profile calculation from Nimbus satellite IR spectrometer data, noting Southern Hemisphere tropospheric and stratospheric pressure analyses 20 p3258 A71-39667

E region electron density isopleths height correlation with atmospheric pressure variations, noting sympathetic isobaric surface movements in upper stratosphere 21 p3372 A71-40038

Cosmic ray variations due to atmospheric pressure disturbances and ionizing component variations due to temperature effects, estimating ground observation errors 21 p3437 A71-40074

Baric levels determination for weather forecasting from statistical analysis of atmospheric numerical model 21 p3410 A71-40823

Air pressure effects on absorption dependence at IR wavelengths, using water vapor transmittance windows 22 p3511 A71-42303

Nimbus 3 satellite IR spectrometer atmospheric pressure height profiles, comparing with nearby radiosonde data 22 p3535 A71-42410

Hypersonic shock wave front motion into air at one atmosphere, measuring reflectivity and curvature for comparison with theory 23 p3626 A71-43929

ATMOSPHERIC RADIATION
NT AIRGLOW
NT AURORAL ARCS
NT AURORAS

NT DAWN CHORUS
 NT DAYGLOW
 NT GEOCORONAL EMISSIONS
 NT IONOSPHERIC NOISE
 NT NIGHTGLOW
 NT RADIO AURORAS
 NT RED ARCS
 NT SKY RADIATION
 NT STRATOSPHERE RADIATION
 NT TWILIGHT GLOW
 NT WHISTLERS
 Long wave radiation earth-atmosphere balance measuring devices, discussing pyrgometer, balometer and tests in Antarctica 01 p0080 A71-10541
 Ionospheric modification by electrons radiant heating, discussing effects on 1.27 micron radiation 01 p0078 A71-11534
 Daytime stratospheric X ray bursts, examining occurrence time, duration, cosmic radio noise and magnetic activity relationship 02 p0299 A71-11775
 Omnidirectional intensity of atmospheric gamma rays at balloon altitudes at various energy thresholds, noting integral spectrum flattening at lower energies 03 p0473 A71-13306
 Earth surface and atmosphere thermal radio emission measurement by radio telescope on Cosmos 243 satellite 03 p0409 A71-13420
 Rocket observations of far IR radiation from upper atmosphere 03 p0415 A71-14026
 Layer boundaries and critical concentrations of anomalous increase of radiation in earth and Venus atmospheres along tangential directions 05 p0738 A71-16044
 Geography of upper atmospheric IR emission layers from Cosmos 65 observation 05 p0738 A71-16045
 Solar stimulated X ray fluorescence by photoelectric ionization in upper atmosphere, discussing effects on X ray astronomy experiments 06 p0949 A71-17268
 Atmospheric radiating gas components contribution to thermal balance at various altitudes, geographic latitudes and seasons 06 p0923 A71-17509
 Radiation fields of various background and atmospheric cloud formations by reflected short wave radiation aircraft measurements 06 p0923 A71-17511
 Atmospheric gamma rays energy spectrum and implication on high energy interactions characteristics 06 p0962 A71-18181
 Atmospheric fast neutron flux, discussing solar proton events and Forbush decreases effects 06 p0963 A71-18183
 Tropospheric and lower stratospheric radiation balance components vertical profiles, using balloon sounding 07 p1151 A71-18913
 Downward atmospheric radiation fluxes incident on Martian surface horizontal plane, tabulating atmospheric composition, surface pressures and temperatures and effective sky temperatures 07 p1199 A71-19874
 Atmospheric high energy gamma rays, pion production and electron energy spectra over Hyderabad, using stack nuclear emulsions 07 p1189 A71-20497
 Atmospheric moisture measurements, using Cosmos 243 satellite radiothermal atmosphere self radiation 08 p1277 A71-21007
 Atmospheric excess radiation flux azimuthal asymmetry in equatorial region, discussing angular intensity distribution data from Proton 2 Cerenkov counter 08 p1354 A71-21011
 Midlatitude VLF discrete emissions generation regions location by dispersion analysis of ground station observations, determining plasma density along path for events 08 p1282 A71-21634
 Fredholm integral equation stabilization methods for atmospheric IR transfer in vertical temperature profile determination 08 p1286 A71-21877
 Atmospheric emission and absorption measurements at millimeter wavelengths, comparing with radiative transfer equation values 08 p1257 A71-21880
 Upper atmosphere IR emission model with reference to thermal excitation, chemical reactions and electron excitation 09 p1437 A71-22670
 Cirrus ice cloud detection from remote emission measurements in far IR by satellite radiometer 09 p1487 A71-23022
 Upper Martian atmosphere UV emission spectrum observation noting carbon dioxide photoionization, ion fluorescent scattering and photon/electron dissociative excitation 10 p1604 A71-24776

Angular discretization effect on calculations of emerging radiation and integrated albedo from model cloudy atmosphere, using multiple scattering with terrestrial particle phase functions 10 p1643 A71-24972
 Cloud radiation measurements by ground based microwave radiometer 11 p1794 A71-25380
 Atmospheric neutron production by cosmic radiation over sunspot cycle, measuring energy spectrum with airplanes and balloon-borne instruments 12 p1950 A71-27382
 Mass spectrum of stopping heavy cosmic ray particles at sea level observed, interpreting flux as deuteron production by high energy protons and neutrons 13 p2122 A71-28067
 Atmospheric scintillation light detection from air shower, determining interaction mean free path of 1-10 million TeV primary particles 13 p2122 A71-28070
 Angular distribution of muon-poor extensive air showers, considering generation by atmospheric nuclei interaction 13 p2123 A71-28073
 Aerosol power law distribution exponent and particle limiting radii from turbid atmosphere outgoing visible radiation polarization high altitude measurements 13 p2063 A71-29111
 Atmospheric and cosmic origin of noctilucent clouds, discussing solar wind effects on H, O and water vapor molecules in mesosphere and thermosphere 14 p2232 A71-29956
 Noctilucent cloud observation from space, discussing instruments, radiation spectrum, global scale formation, time dependent structures and satellite orbit requirements 14 p2232 A71-29963
 Atmospheric VLF electromagnetic emissions and electron instabilities data from satellite observation, detailing source regions, large amplitude electrostatic waves and wave-particle correlation 14 p2202 A71-30952
 Cosmic ray shower size spectrum in atmosphere for muon bremsstrahlung at large zenith angles 15 p2479 A71-31868
 Layer boundaries and critical concentrations of anomalous increase of radiation in earth and Venus atmospheres along tangential directions 16 p2635 A71-33448
 Spatial and angular distribution of upper atmospheric IR emission layers from Cosmos 65 observation 16 p2563 A71-33449
 Upper atmosphere atomic hydrogen H sub alpha emission, correlating intensity and hydroxyl vibration temperature 16 p2564 A71-33665
 Atmospheric short wave radiation angular and vertical distribution relation to aerosol scattering parameters, using transport equation 16 p2605 A71-34104
 Uranus radio emission model, indicating presence of gaseous ammonia at saturation pressure 17 p2807 A71-35501
 Greenhouse effect in gray planetary atmosphere, showing thermal radiation generation and scattering with principles of invariance 18 p2970 A71-37049
 Atmospheric radiant heat influx spectral distribution, evaluating vertical profiles of short wave radiation and aerosol effects 19 p3047 A71-37281
 Upper atmosphere hydroxyl emission nocturnal average vibrational temperature correlation with molecular oxygen emission intensities 19 p3049 A71-37403
 Variable stars atmospheric radiation, investigating unsteady light reflection 19 p3133 A71-37505
 Azimuthal IR radiation distribution of atmospheric brightness cross sections at various zenith angles from balloon programmed-control radiometer data 19 p3054 A71-37969
 Atmospheric pressure and temperature inhomogeneities effects on thermal radiation transmission function of water vapor 19 p3090 A71-37973
 Surface layer humidity correlation to height of atmosphere emitting in IR spectral region, determining water vapor content by recording earth radiation angular distribution 19 p3054 A71-37974
 Fredholm integral equation stabilization methods for atmospheric IR transfer in vertical temperature profile determination 19 p3060 A71-38470
 Atmospheric moisture from Cosmos 243 satellite measurements of intrinsic atmospheric radiothermal emission 20 p3218 A71-39587
 Atmospheric excess radiation flux azimuthal asymmetry in equatorial region, discussing angular intensity distribution data from Proton 2 Cerenkov counter 20 p3279 A71-39591

Atmospheric thermal sounding radiation data interpretation, determining integral Fredholm equation solution, absorption characteristics and temperature profiles 20 p3258 A71-39670
 Aircraft sounding of atmospheric microwave radiation transfer compared with IR method, measuring optical Mie characteristics, water vapor content, cloudiness, ice cover, etc 20 p3259 A71-39673
 Atmospheric radiative energy budget based on structure and cloudiness distribution data from satellites and in situ observations 20 p3259 A71-39677
 Earth-atmosphere system radiation budget, comparing meteorological satellites actinometric data with calculated climatological maps of planetary long wave radiation distribution 20 p3259 A71-39678
 Earth atmosphere radiation fields analysis from Nimbus 3 five-channel scanning radiometer measurements, determining mean planetary albedo and temperature 20 p3259 A71-39679
 Meteorological satellite IR imagery for calculating spectral values of cloudiness radiation contrasts against underlying surface background 20 p3261 A71-39689
 Mesospheric soft corpuscular radiation flux and temperature rocket observations, during solar flare activity 20 p3222 A71-39704
 Antennas scattering coefficients measurement by ground and atmospheric radiation, permitting antenna noise temperature components determination 20 p3205 A71-39803
 Radiating atmosphere - Conference, Queens University, Kingston, Ontario, August 1970 20 p3226 A71-39826
 Solid state modulation for spacecraft horizon sensing via IR carbon dioxide atmospheric radiation, proposing Fabry-Perot structure with controlled plate separation 22 p3537 A71-41475
 Auroral X rays passage through atmosphere, discussing integral spectral measurements with collimated and omnidirectional detectors 22 p3593 A71-42399
 Atmospheric background radiation measurements with balloon-borne Michelson interferometer, noting data reduction and calibration methods 22 p3549 A71-42563
 Long term vertical and horizontal variations of long wave radiation field in free atmosphere over U.S.S.R., using actinometric sounding data 22 p3570 A71-42848
 Absolute transition probabilities derivation for excitation of atmospheric nitrogen molecules and positive ion systems by electrons impact from optical measurement 24 p3850 A71-44371
 Auroral X ray radiation measurements in midnight sector during solar storm of 8 March 1970 24 p3823 A71-45034
ATMOSPHERIC REFRACTION
NT RADIO WAVE REFRACTION
 Atmospheric refractometry anomaly at high relative humidities observed in controlled environment for causes 01 p0113 A71-10252
 Structural properties of atmospheric refractive index, using single mode laser 01 p0120 A71-11102
 Atmospheric refractive index average structural characteristics measurement over 25 km light propagation path, noting diurnal variation 02 p0245 A71-12011
 Laser channel multipath dispersion due to atmospheric inhomogeneities for point and non-zero-area apertures under clear weather conditions 02 p0214 A71-12034
 Lower atmosphere vertical temperature profiles by optical refraction measurements from photographs of equally spaced illuminated targets 03 p0453 A71-13233
 Range and range rate measurement errors between ground station and artificial satellite, investigating atmospheric refraction effects 04 p0661 A71-15003
 Brightness temperature of vertically structured medium in microwave radiometry 04 p0552 A71-15212
 Atmospheric refraction due to ducting and trapping layers based on navigational satellite data 04 p0623 A71-15310
 Atmospheric propagation errors of satellite tracking system in VHF region 07 p1059 A71-19028
 Atmospheric refractive index diurnal and seasonal variations determination by measuring He-Ne laser radiation intensity through turbulent inhomogeneous atmosphere 07 p1061 A71-19374

Model of large ionospheric electron density discontinuities, emphasizing horizontal asymmetry association with observed east-west refraction asymmetry 07 p1100 A71-19405

Tropospheric height integral of refractivity for predicting atmospheric electromagnetic range at arbitrary elevation angle from surface weather data 08 p1257 A71-21881

Electromagnetic propagation errors in radar tracking, photogrammetric cameras and laser range finders due to atmospheric refraction, discussing error compensation techniques 09 p1405 A71-22356

Optical distance correction for fluctuating atmospheric index of refraction in long base line measurements using Lidar with Q switched ruby laser 09 p1495 A71-23451

Cut-off Mach number of sonic bang propagation on ground for flight track in relation to atmospheric parameters 09 p1383 A71-23577

Isolated ionospheric irregularities, describing refraction and diffraction pattern calculations for satellite signals 10 p1578 A71-24463

Venus atmosphere critical refraction model, examining optical effects and ray paths 11 p1823 A71-25696

Atmospheric boundary layer refractive index fluctuations structural characteristics determined from summer vertical wind velocity and temperature profiles 11 p1795 A71-25922

Atmospheric boundary layer refractive index fluctuation isotropy for small turbulence, using intensity distribution photography over collimated laser beam cross section 11 p1762 A71-25923

Optical beam side refraction, determining physical conditions for vertical air temperature gradients at line of sight altitude above earth surface 12 p1902 A71-27484

Ionospheric refraction errors in satellite tracking, computing elevation, range and range rate corrections 16 p2640 A71-33734

Tropospheric range error in EM signal arriving at earth zenith, measuring integral of refractivity through atmosphere from height, pressure, temperature and humidity 16 p2569 A71-33800

Differential refraction elimination in stellar triangulation measurements for reference stars catalog and flash coordinates 16 p2642 A71-33801

Correction method for satellite radio tracking errors due to VHF refraction in atmosphere 16 p2543 A71-33832

Refraction, terrain, air attenuation, fog and rain, turbulence and shielding effects on acoustic propagation in lower atmosphere 17 p2734 A71-35235

Model of large ionospheric electron density discontinuities, emphasizing horizontal asymmetry association with observed east-west refraction asymmetry 19 p3053 A71-37829

Tropospheric refraction effects and field strength dependence on height at frequencies below 10 MHz 19 p3017 A71-37862

Astronomical telescopes image motion, distortion and scintillation, examining atmospheric refractive index and density/temperature variation effects 19 p3010 A71-38571

Atmospheric boundary layer refractive index fluctuations structural characteristics determined from summer vertical wind velocity and temperature profiles 20 p3256 A71-39213

Atmospheric boundary layer refractive index fluctuation isotropy for small turbulence, using intensity distribution photography over collimated laser beam cross section 20 p3236 A71-39214

Mirror meridian circle of zero expansion glass for reduction of flexure and refraction instrument errors in astrometry 20 p3240 A71-39539

Laser remote sensing technique for tropospheric refractivity fluctuation profile measurement with tethered balloon-borne retroreflector tracking by ground based tracker 21 p3374 A71-40977

Line-of-sight microwave multipath fading, predicting attenuation distribution as function of pathlength by piecewise linear approximation of atmospheric refraction index 21 p3349 A71-41196

Hypersonic shock wave front motion into air at one atmosphere, measuring reflectivity and curvature for comparison with theory 23 p3626 A71-43929

Laser beam spot dancing during propagation through turbulent atmosphere, using Kolmogoroff structure function of refractivity and geometrical optics 24 p3834 A71-45208

ATMOSPHERIC SCATTERING

NT TROPOSPHERIC SCATTERING

Stellar scintillation saturation at large zenith angles, examining atmospheric dispersion and multiple scattering roles 01 p0127 A71-10141

Fesenkov photometer for aureole flux observations eliminating solar diffraction 01 p0080 A71-10542

Optical radar system absolute calibration for measuring laser irradiance backscatter function from atmosphere 01 p0094 A71-10874

Absorption line formation in scattering planetary atmospheres with cloud particles 01 p0162 A71-11420

Background noise in optical communication system, considering direct, reflected and scattered radiation sources in atmosphere 02 p0213 A71-12015

Optical /and IR/ communication systems design, considering effects of atmospheric turbulence, molecular absorption and aerosol scattering 02 p0214 A71-12023

Sky brightness scattering indicatrix in effective atmospheric layer free from underlying surface multiple scattering and reflection distortions 02 p0246 A71-12119

Light scattering and polarization measurements in upper atmosphere by modulated searchlight, indicating dust layers 03 p0414 A71-14018

Soviet monograph on visible and IR waves atmospheric propagation covering monochromatic radiation absorption and scattering, laser light beams under turbulence, etc 04 p0551 A71-14800

Diffusely reflected radiation from semiinfinite atmosphere, deriving asymptotic formula including high order scattering terms 04 p0643 A71-14905

Doubly scattered radiation magnitude as function of heights and aerosol concentrations for bistatic laser radar 04 p0609 A71-15761

Mars and Mercury polarization measurements, investigating Rayleigh scattering in atmospheres 05 p0806 A71-16204

LOX release from Apollo 8 lunar launch vehicle, forming small particle clouds for scattering experiments 06 p0963 A71-17256

Atmospheric path effects on spectral radiance intensity in remote airborne multispectral sensors 06 p0898 A71-17559

Polarization of sunlight multiply scattered by atmosphere and cloud particles of Venus from UV to IR 07 p1204 A71-20622

Lidar wavelength optimization for Raman scatter atmospheric studies, taking into account aerosol and weak signal statistical effects 08 p1254 A71-21458

Unsteady scattering patterns analysis, determining atmospheric extinction coefficient by reflected light oscillograms, formulas or signal amplitude time recording 09 p1487 A71-22385

Daytime near horizon atmospheric luminescence measurement by Cosmos 224 satellite, discussing contributions of nitrogen and aerosol and Rayleigh scatterings 09 p1435 A71-22432

Ionospheric radio waves scattering cross sections under time varying random irregularities, considering anisotropic behavior, dielectric tensor and geomagnetic field 09 p1411 A71-23587

Steady state photon transfer through homogeneous semiinfinite isothermal atmosphere with two level atoms, deriving linear integral equation for escape probability distribution 10 p1643 A71-24964

Skylight scattering components from zenith for intensity/polarization variation during twilight and upper atmosphere dust sounding 10 p1607 A71-25114

Similarity comparisons of isotropic and anisotropic scattering patterns in cloudy atmospheres for haze effects on Mars image contrast, using asymptotic method 11 p1825 A71-25710

Visible and IR radiative transfer in water and ice clouds, calculating radiance and polarization from Mie theory 11 p1800 A71-26299

Surviving high energy primary protons of cosmic ray nuclear bursts in atmosphere without air shower at Chacaltaya 12 p1933 A71-27393

Unaccompanied hadron vs primary proton spectra in atmosphere and proton-air inelastic cross sections above 500 GeV from cosmic ray measurements 12 p1951 A71-27394

Inhomogeneous planetary atmosphere resonantly scattered sunlight, calculating intensities with frequency redistribution functions 13 p2100 A71-28346

Skylight polarization dispersion in relation to multiple scattering in molecular atmosphere 13 p2063 A71-29110

Tables of scattering functions and albedo for semiinfinite atmospheres according to nonconservative Rayleigh phase matrix for diffuse radiation computation 14 p2274 A71-30059

Plane parallel inhomogeneous atmosphere, investigating anisotropic light scattering 15 p2448 A71-31332

Semiinfinite atmospheric multiple conservative Rayleigh scattering, describing polarized radiation transfer 15 p2449 A71-31333

Scattering effects on decimeter wavelength quiet sun emissions flux densities, frequencies and brightness temperatures 15 p2485 A71-31716

Calculational method for predicting angular distribution of sunlight upwelling flux scattered by atmosphere and reflected by ground, using Monte Carlo data 16 p2562 A71-33130

Signal to noise ratios for coaxial laser radar system heterodyning signal backscattered from atmospheric aerosol 16 p2541 A71-33138

Standard visibility and scattering coefficient changes due to humidity variation from maritime aerosol particles equilibrium radii calculations 16 p2605 A71-34084

Coherence properties deterioration of laser beam by atmospheric molecular scattering, considering effect on communication system performance 17 p2753 A71-34426

Haze scattering effect on solar radiative heating rate due to water vapor absorption in near IR 17 p2736 A71-35561

Solar radiation field in polluted atmosphere, measuring intensity, polarization and flux due to aerosol scattering for comparison with Mie theory computation 17 p2736 A71-35563

Direct numerical integration for equation of radiative transfer in turbid atmosphere with allowance for scattering on molecules and aerosols 17 p2736 A71-35564

Radiative transfer in terrestrial clouds, inferring colloidal state from measurements of multiple scattering angular and wavelength dependence 17 p2736 A71-35566

Reflection and transmission on plane parallel layers of planetary atmospheres with strongly anisotropic scattering, examining three eigenvalue problems 17 p2736 A71-35567

Absorption spectra formation by diffuse reflection from semiinfinite plane parallel scattering planetary atmosphere, using asymptotic expressions for higher order scattering 17 p2736 A71-35568

Phase and amplitude variations of multipath fading of microwave signals relating atmospheric irregularities 19 p3015 A71-37221

Upper atmosphere dust scattering indicatrix from twilight sky brightness at solar vertical, determining total directed scattering coefficient 19 p3132 A71-37390

Radar returns from convective fields and cells in visually clear atmosphere explained by thermal effects and air motion 19 p3090 A71-37753

Brightness profiles of earth daytime horizon from Soyuz spacecraft photographic photometry, deriving atmospheric scattering coefficient relation to optical thickness vertical distribution 19 p3054 A71-37967

Aerosol scattering coefficient in atmosphere, determining statistical characteristics of vertical and spectral structure 19 p3090 A71-37970

Atmospheric directional scattering coefficients from vertical measurements of IR spectral sky brightness near solar almucantar and direct radiation 19 p3090 A71-37976

Atmospheric gases effective electron collision frequency calculations, using momentum transfer cross sections 20 p3271 A71-38743

Double scattering of plasma stream in bithermal ionosphere, noting ion density perturbation under external magnetic field 20 p3272 A71-38748

Radiative transfer in inhomogeneous anisotropically scattering spherical shell atmospheres with radial symmetry, using invariant imbedding technique 20 p3287 A71-39082

Atmospheric optical stability control in ozone or other selectively absorbing gases measurements, fil-

tering out spurious scattered light from aerosol particles 20 p3257 A71-39331

Altitude variation of atmospheric air scattering coefficient from Soyuz 3 spacecraft measurements, considering aerosol stratification 20 p3259 A71-39676

Monte Carlo method calculation for light pulse reflection from clouds for all orders of multiple scattering 22 p3576 A71-42562

Semiinfinite plane parallel inhomogeneous atmosphere anisotropic light scattering 22 p3576 A71-42607

Semiinfinite atmospheric multiple conservative Rayleigh scattering, describing polarized radiation transfer 22 p3576 A71-42608

Atmospheric scattering and absorption effects on balloon altitude spectra observations of auroral X ray penetration into atmosphere 23 p3720 A71-43130

High power multielement electronically scanned array of microwave log periodic monopole antennas for ionospheric backscattering measurements 23 p3653 A71-44155

E layer vertical velocity fluctuations from scattered signal phase and amplitude correlation measurements, using perturbation technique 23 p3647 A71-44334

ATMOSPHERIC SHELLS

U ATMOSPHERIC STRATIFICATION

ATMOSPHERIC STRATIFICATION

Spatial and temporal structure in turbulent breakdown of shear flows in stably stratified atmosphere from radar images of vertical cross sections 01 p0116 A71-10569

Lidar observation of clear atmospheric structure including lee wave clouds, turbulence, stratification in trade wind inversion layer, etc 01 p0118 A71-10583

Oblique reflection of horizontally and vertically polarized electromagnetic waves from isotropic media with limiting Epstein stratifications 01 p0031 A71-10775

Tropospheric layers radio reflectivity as function of refractivity index and thickness/wavelength ratio 01 p0040 A71-11607

Laser channel multipath dispersion due to atmospheric inhomogeneities for point and nonzerofield apertures under clear weather conditions 02 p0214 A71-12034

Turbulent energy dissipation in lower atmospheric layer on meteorological mast during various temperature stratifications 02 p0246 A71-12112

Atmospheric air columns centers of gravity, determining height from vertically integrated equations of motion 02 p0278 A71-12745

Venus equatorial stratosphere structure, presenting approximate radiative dynamical calculation for zonal flow mechanism 03 p0488 A71-13552

Hydrodynamic equations for isothermal atmosphere stratified by uniform gravitational field, obtaining traveling wave solutions 04 p0570 A71-15030

Pointed body of revolution in gravitationally stratified atmosphere, discussing supersonic boom and minimum drag [DFVLR-SONDDR-97] 05 p0694 A71-16712

Internal gravity wave propagation in neutral wind stratified atmospheric model 06 p0888 A71-17274

Temperature stratification effects on free atmosphere turbulence structure under Archimedean forces, noting energy dissipation buoyancy forces and adiabatic gradients 07 p1150 A71-18796

Long wave radiation balance components vertical profiles, showing temperature stratification effect 07 p1151 A71-18914

Radio wave propagation at frequencies near proton gyrofrequency in horizontally stratified ionosphere, taking into account intermediate coupling 07 p1102 A71-19666

Atmospheric pressure pulsation time spectra on earth surface as function of stratification conditions 08 p1286 A71-21876

Radio ray tracing in complex space, describing plane stratified ionosphere 09 p1411 A71-23731

Numerical integration of motion equations for two layer atmospheric fronts model with baroclinicity along frontal surface separating two incompressible fluids in stable stratification 10 p1638 A71-23965

Finite difference computer algorithm to solve vertical velocity equation of steady air flow about mesoscale obstacle in stably stratified atmosphere 11 p1793 A71-25169

Forced convection in atmosphere boundary layer, considering nonlinear unsteady vertical airflow

velocity increments over temperature spot on earth surface 11 p1793 A71-25170

Turbulent diffusion in stationary thermally stratified atmospheric boundary layer, considering gravitational sedimentation and impurities lifetime 11 p1795 A71-25585

Venus atmosphere composition and structure from microwave spectrum, noting surface pressure and temperature and water vapor 11 p1823 A71-25694

Venus thermal radiation limb darkening measurements, indicating complex atmospheric structure 11 p1824 A71-25699

Atmospheric transmittance vertical structure, using aerosol attenuation and optical densities from aircraft sounding under cloudless conditions 11 p1795 A71-25924

Atmospheric zero light polarization points, examining solar vertical and various albedos, horizontal and vertical nonuniformities and albedo variations 11 p1795 A71-25925

Mesoscale gravity waves and jet stream stability in temperature-stratified atmosphere with small wave perturbations, estimating wave phase velocities and amplitude functions 12 p1924 A71-26736

Large scale structure with unstable stratification, investigating effects on atmospheric ground layer dynamic velocity and turbulent energy production 12 p1294 A71-27101

Jupiter equatorial thermal limb darkening data, constructing atmospheric model for ammonia effects on temperature structure 12 p1966 A71-27254

Three dimensional quasi-stationary problem of local winds in neutrally stratified atmosphere in low latitudes, analyzing Coriolis force role 13 p2096 A71-28016

Two dimensional atmospheric model including oxygen and nitrogen photodissociation, recombination and photoionization, investigating solar activity and ionizing radiation effects on temperature stratification 13 p2057 A71-28018

Stratosphere and lower mesosphere seasonal climatic temperature profiles calculation from radiation transport and balance equations, noting turbulent heat influxes role in stratification formation 13 p2057 A71-28024

Vertically incident radio waves reflection from horizontally stratified ionosphere with random electron density irregularities 14 p2192 A71-29718

Stable laminae in clear air turbulence, noting observations from rawinsonde stations mesoscale network, instrumented and noninstrumented aircraft and ultrasonic radars 14 p2268 A71-29769

Stratospheric circulation synoptic and detailed structure from meteorological rocket network sensors 15 p2396 A71-31614

Matrix solution for wave equation with mode coupling of VLF and ELF radio waves in horizontally stratified layer of anisotropic ionosphere plasma 15 p2373 A71-32444

Solar eclipse effects on atmospheric structure, circulation and meridional flow, using rocket measured temperature and wind data for pressure and density variations near stratosphere 16 p2567 A71-33764

Thermosphere structure and motion from neutral atmospheric density data, noting correlation with enhanced geomagnetic activity 16 p2571 A71-33840

Tropospheric stratification structure from high resolution FM/CW radar sounder, comparing with internal gravity wave atmospheric models 17 p2771 A71-35808

Atmospheric structure near large amplitude Kelvin-Helmholtz billows in upper troposphere, deriving static stability, vertical wind shear and Richardson number 19 p3089 A71-37498

Friction velocity in stably stratified constant flux layer with known heat flux, using log-linear velocity profile with fixed Monin-Obukhov parameter value 19 p3089 A71-37502

Velocity and temperature pulsations as function of stratification parameter in atmospheric boundary layer 19 p3090 A71-37971

Solar semidiurnal atmospheric tide theory based on gravitational action only, taking into account atmospheric stratification 19 p3055 A71-38044

Atmospheric pressure pulsation time spectra on earth surface as function of stratification conditions 19 p3060 A71-38469

Atmospheric transmittance vertical structure, using aerosol attenuation and optical densities from aircraft sounding under cloudless conditions 20 p3257 A71-39215

Atmospheric zero light polarization points, examining solar vertical and various albedos, horizontal and vertical nonuniformities and albedo variations 20 p3257 A71-39216

Unstable thermal stratification and critical Reynolds number effects on dynamic instability of Ekman boundary layer vortex rolls 20 p3257 A71-39438

Ground based studies of Jupiter at optical frequencies, determining atmospheric chemical composition temperature and stratification, aerosol layers structure and flyby/penetration experiments results 20 p3297 A71-39631

Altitude variation of atmospheric air scattering coefficient from Soyuz 3 spacecraft measurements, considering aerosol stratification 20 p3259 A71-39676

High altitude aerosol layer effects on atmospheric UV albedo, correcting ozone scale height spaceborne measurements 20 p3221 A71-39699

Atmospheric stratification effects on downward motion of aircraft vortex wakes, developing approximate model 21 p3318 A71-40486

Equatorial F 2 region lattice model with curved field line geometry for plane stratified atmosphere and time dependent problem solution 23 p3667 A71-43137

Small scale electrostatic field penetration from E into F region of ionosphere based on plane stratified model 23 p3671 A71-43577

Time resolved tropospheric scatter layers from simultaneous bistatic and monostatic radar detection 23 p3646 A71-44174

Atmospheric aerosol stratification, turbidity, stratospheric layer and purification zone from optical sounding data 24 p3823 A71-44821

ATMOSPHERIC TEMPERATURE

NT AURORAL TEMPERATURE

NT IONOSPHERIC TEMPERATURE

Clear air radar structures temperature, wind components and true gust velocities combined with radar data for observed traveling wave features 01 p0030 A71-10560

Carbon dioxide band radiances measured by Nimbus 3 satellite IR spectrometer, noting seasonal temperature changes in stratosphere due to meridional circulation 01 p0119 A71-10743

Atmospheric temperature profile in cloud presence, discussing remote sounding techniques with maximum probability method 01 p0120 A71-10854

Planetary scale Rossby waves, examining vertical structure for zonal flow blocking and polar stratosphere warming 01 p0120 A71-10860

Stratospheric thermal structure and circulation, considering temperature, wind and composition fields 01 p0122 A71-11358

Meteorological satellite atmospheric parameter observations, discussing instruments and techniques for temperature and pressure profiles, wind patterns and cloud image data 01 p0164 A71-11360

Air temperature and wind speed role in finger-freezing time 02 p0197 A71-11669

Reverse flow temperature probe design and calibration for vertical soundings from aircraft, comparing to radiosonde method 02 p0247 A71-11822

Venusian exospheric temperature local time dependence from heat conduction equation for instantaneous heating during Mariner 5 observation 02 p0304 A71-11971

Martian exospheric temperatures diurnal variations during Mariner 4, 6 and 7 observations by solving time dependent heat balance equations 02 p0305 A71-11972

Earth radiation measurement at 10-12 microns by Cosmos 243 satellite-borne radiometer, comparing temperatures for boundary air layers in cloudless conditions 02 p0246 A71-12115

Venus lower atmosphere structure and brightness temperature spectrum analysis for composition, temperature and pressure profiles 03 p0484 A71-13212

Urban heat island induced circulation without synoptic winds, using two dimensional atmospheric model 03 p0453 A71-13232

Lower atmosphere vertical temperature profiles by optical refraction measurements from photographs of equally spaced illuminated targets 03 p0453 A71-13233

Atmospheric temperature remote sounding from satellites using radiometer with selective chopper for carbon dioxide emission 03 p0422 A71-13355

Six channel selective chopper radiometer design and construction for carbon dioxide emission monitoring for remote atmospheric temperature sounding by Nimbus 4 03 p0423 A71-13356

- Atmospheric temperature remote sounding via balloon-borne selective chopper radiometer
03 p0423 A71-13357
- High dispersion spectroscopic observations of Venus carbon dioxide bands for deriving rotational temperature
03 p0488 A71-13557
- Neutral upper atmosphere response to solar activity variations, discussing temperature, density and helium/oxygen composition
[AIAA PAPER 70-1356] 03 p0409 A71-13577
- Thermospheric neutral particle molecular nitrogen density and temperature measurements by rockets, noting correlations with diurnal, solar cycle and other variations
03 p0414 A71-14020
- Lower atmosphere thermal microfluctuation measurement to examine solar seeing area and dome effect
04 p0622 A71-15658
- Fourier data decomposition technique for recovering Doppler temperature, emission line intensity and Doppler shift of central frequency of Fabry-Perot fringes in presence of statistical noise
05 p0748 A71-16265
- Planetary boundary layer air velocity and temperature measurements from airplane
05 p0777 A71-16666
- Atmospheric temperature, computing carbon dioxide concentration effect on radiative heating rates
05 p0742 A71-16677
- Vertical temperature distribution measurements by meteorological satellites distribution measurements applied to numerical weather forecasting
05 p0778 A71-17044
- Nimbus 3 and 4 satellites IR grating spectrometers for remote sensing of vertical temperature and humidity profiles of stratosphere and troposphere near Philippines
05 p0818 A71-17137
- Meteorological satellite data interpretation, including atmospheric layers thermal balance and global absorbed and outgoing radiation distribution mapping
06 p0923 A71-17508
- Solar cosmic ray intensity yearly variation by pressure corrected neutron monitor, discussing atmospheric temperature effects, coronal emission heliolatitude distribution and annual wave amplitude
06 p0953 A71-18117
- Neutron monitor counting rate at Sanae, Antarctica, observing snow and atmospheric pressure and temperature effects
06 p0960 A71-18168
- Atmospheric temperature minima prediction, comparing various correlation methods
07 p1151 A71-18875
- Earth atmosphere thermal sounding problems, considering indirect temperature profile determination, various degrees of cloudiness and Planck function dependence on pressure
07 p1151 A71-18909
- Temperature pulsation in atmospheric boundary layer from meteorological mast under unstable stratification in summer, tabulating dispersion characteristics, turbulent energy dissipation rate, etc
07 p1152 A71-19150
- Laser beam propagation through atmosphere, measuring phase variation dependence on turbulent temperature structure for comparison with prediction
07 p1123 A71-19574
- Tropospheric temperature and aerosol to molecule ratio measurements by optical radar to determine relative concentrations and scattering cross section contributions
07 p1153 A71-20007
- Air temperature effects on internal combustion engines intake process, using similarity theory
08 p1347 A71-20782
- Temperature measurement inaccuracies in 30 to 40 km region by balloonsensors, involving IR cooling of thermistor
08 p1277 A71-20989
- Book on ionosphere and magnetosphere covering temperature, composition ionizing radiations, radio communication electron production and loss, etc
08 p1363 A71-21164
- Heat quantity to atmospheric circulation ratio over period of decades, using positive temperature sums for long range forecasting method
08 p1326 A71-21445
- Radiosonde with radiation sensor, minimizing temperature measurement errors in free atmosphere
08 p1293 A71-21745
- Fredholm integral equation stabilization methods for atmospheric IR transfer in vertical temperature profile determination
08 p1286 A71-21877
- Atmospheric surface layer wind and temperature profile measurements over horizontally uniform flat terrain
09 p1489 A71-23554
- Tropospheric temperature and aerosol/molecule ratio determination by optical radar measurements, using Doppler broadening in spectral analysis of laser radar echoes
09 p1466 A71-23628
- Motion effects on atmospheric density altitude distribution, discussing vertical waves, gravity, temperature and winds
09 p1441 A71-23645
- Turbulent mixing and radiative transfer relationship to micrometeorological temperature structure of atmospheric boundary layer
10 p1638 A71-23878
- Book on electrical equipment deterioration in adverse environments covering climatic action, excessive heat, atmospheric temperature variations, water vapor adsorption and condensation, etc
10 p1583 A71-24478
- Humidity effects on sound velocity in air at constant temperature and normal atmospheric pressure in lower audio frequency range
10 p1642 A71-24815
- Venusian atmosphere subcloud layers intrinsic outgoing thermal radiation and IR spectrum transmissivity from satellite temperature, pressure, moisture content and chemical composition data
10 p1681 A71-25128
- Cometary atmosphere photometric data, determining particle distribution and ejection rate, temperature, molecular lifetime, acceleration and emission velocity
11 p1821 A71-25542
- Upper atmosphere neutral temperature profiles in auroral zone, using aluminum and barium oxide clouds fluorescent emission
11 p1753 A71-25547
- Venus atmosphere chemical composition, determining N, O, water and carbon dioxide concentrations, temperature and pressure
11 p1823 A71-25691
- Jupiter equatorial belt effective temperature during 1965 apparition from limb darkening profile observation
11 p1827 A71-25726
- Atmospheric thermal sounding problem, using regularization and statistical methods and expanding by empirical orthogonal functions
11 p1795 A71-25920
- Atmospheric boundary layer refractive index fluctuations structural characteristics determined from summer vertical wind velocity and temperature profiles
11 p1795 A71-25922
- Soviet papers on aviation and synoptic meteorology problems covering vertical motions near cold fronts, cloud development, latitude effect, temperature conditions above mountains, etc
11 p1795 A71-26557
- Cold front zone meteorological elements, calculating temperature gradients, dew point deficit, and wind vector vertical distribution
11 p1795 A71-26558
- Water vapor dimer effects on atmospheric brightness temperature in cm and mm radiometric investigations from satellites above ocean areas
12 p1901 A71-27099
- Atmospheric viscous dissipation energy relationships, calculating Martian atmosphere thermal structure
12 p1965 A71-27192
- Optical beam side refraction, determining physical conditions for vertical air temperature gradients at line of sight altitude above earth surface
12 p1902 A71-27484
- Two dimensional atmospheric model including oxygen and nitrogen photodissociation, recombination and photoionization, investigating solar activity and ionizing radiation effects on temperature stratification
13 p2057 A71-28018
- Upper atmosphere neutral components temperature differences estimates from gas hydrodynamic equations solution by disturbances method
13 p2057 A71-28019
- Stratosphere and lower mesosphere seasonal climatic temperature profiles calculation from radiation transport and balance equations, noting turbulent heat influxes role in stratification formation
13 p2057 A71-28024
- Construction, operation and in-flight performance of triaxial bridge accelerometer used in falling sphere experiment for atmospheric density, temperature and pressure determination
13 p2066 A71-28160
- Average energy electron capture coefficient dependence on air density, temperature and altitude under gamma radiation
13 p2061 A71-28543
- Temperature effects on cosmic rays muon component variations during cold fronts passage
13 p2131 A71-29485
- Upper atmosphere temperature measurements using red emission Doppler contour width data of atomic oxygen at 6300 A
14 p2229 A71-29673
- Time variable effect on synthetic wind speed and air temperature profiles based on sensible heat flux density and stress at surface layer
14 p2266 A71-29705
- Time and frequency statistics of turbulent fluctuations of wind, temperature and humidity in atmospheric surface layer
14 p2266 A71-29706
- Aircraft instrumentation and data analysis for clear air turbulence, including orthogonal components and temperature and wind distributions
14 p2267 A71-29753
- Mesospheric height-temperature measurements in noctilucent cloud zone of Southern Hemisphere
14 p2232 A71-29958
- Twilight OH emission intensity and rotational temperature in mesosphere as function of solar position below horizon
14 p2232 A71-29959
- Least squares method for inversion of radiative transfer equation, considering atmospheric temperature profiles determination from outgoing radiance
14 p2337 A71-30296
- Aircraft barometric altimeter errors caused by atmospheric temperature deviations from International Standard Atmosphere
14 p2244 A71-30323
- IR scanning vertical temperature profile radiometer forITOS meteorological satellites, describing electronic signal processing
14 p2200 A71-30916
- Satellite atmospheric temperature sounding by radiometric measurements, obtaining vertical temperature profile by mathematical inversion process
14 p2236 A71-30938
- White dwarf stars effective temperature measurements, matching absolute spectral energy distributions with fluxes from model atmospheres
14 p2317 A71-31013
- White dwarf line spectra, constructing atmospheric models and effective temperatures
14 p2317 A71-31015
- Stratospheric circulation, investigating ozone heating role in temperature field formation by numerical experiment
15 p2399 A71-31963
- Stratopause layer atmospheric temperature field characteristics observation, noting association with processes in upper stratosphere and lower mesosphere
15 p2399 A71-31965
- Northern Hemisphere upper stratospheric temperature pressure field changes during autumn, using isobar surface charts
15 p2400 A71-31966
- Mesopause thermal transitions during spring and autumn based on noctilucent cloud observations, discussing stratospheric-mesospheric coupling effects
15 p2400 A71-31988
- Nimbus weather satellite with IR spectrometer, Michelson interferometer and selective chopping radiometer for atmospheric temperature remote sounding
15 p2445 A71-32295
- Uranus and Neptune microwave emission spectra and atmospheric temperatures, comparing with Jupiter and Mars
15 p2490 A71-32410
- Jupiter exospheric temperature diurnal variations for various solar activities and latitudes, using time dependent heat balance equations
15 p2491 A71-32423
- Venusian atmosphere circulation modeling, calculating temperature differences, thermal inertia and wind velocity
15 p2496 A71-32729
- Upper atmosphere temperatures from barium oxide fluorescence emissions in ion cloud rocket experiments, studying thermal response to geomagnetic disturbances
16 p2562 A71-32808
- Jupiter atmosphere nonequilibrium radiative processes, considering energy balance and pressure and temperature conditions
16 p2637 A71-33516
- Neutral upper atmosphere properties, discussing temperature, density and wind variations during disturbed conditions associated with geomagnetic storms
16 p2565 A71-33727
- Middle stratosphere monthly mean temperature maps based on radiosonde measurements, confirming anomalies with satellite IR spectrometer radiances
16 p2641 A71-33755
- Wind and temperature structure in stratosphere at Sonmiani during autumn 1970 from three Dart firings
16 p2567 A71-33763
- Diurnal variation of Venus and Mars exospheric temperatures, using neutral heating efficiency calculation based on molecular theory
16 p2641 A71-33769
- Global model of atmospheric temperature, chemical composition and density for altitudes from 25 to 1000 km, using satellite drag determined density values
16 p2567 A71-33782
- Chemical trimethyl aluminum releases in lower thermosphere for temperature, density, winds, turbulence, diffusion coefficients and atomic oxygen content measurements
16 p2568 A71-33792

Complex monitoring of aerological information on geopotential and temperature of principal isobaric surfaces by static method and optimal interpolation on semiautomatic basis

17 p2769 A71-34299

Mars atmosphere high resolution line spectra, calculating carbon dioxide abundance, rotational temperature and surface pressure

17 p2800 A71-34588

Upper atmosphere mean temperature, pressure, density and wind distributions as functions of altitude, season and latitude, discussing planetary, infrasonic and internal gravity wave effects

17 p2735 A71-35236

Remote sounding of earth atmosphere temperature and composition

17 p2736 A71-35565

Atmospheric temperature and density scale height seasonal variations near mesopause, using meteor theory mass and luminosity equations

17 p2737 A71-35740

Atmospheric energy balance and transfer in lower thermosphere in terms of population temperatures and degrees of freedom /translational, rotational, vibrational, electronic, chemical, etc/

18 p2910 A71-35841

Cepheid beta Doradus color photometry data, detailing temperature, mean radius, absolute magnitude and surface gravity variations

18 p2971 A71-37070

Solar cycle variation of planetary exospheric temperature from heat balance equation solution

19 p3131 A71-37334

Semiannual amplitude variations in F 2 region for estimating oxygen density dissociation and temperature ratios in lower thermosphere

19 p3048 A71-37398

Atmospheric noise temperature variation with frequency in 2.53 mm molecular oxygen rotation line, considering Zeeman effect

19 p3048 A71-37402

Venus atmosphere chemical composition, temperature and pressure, discussing model cloud layer, circulation and upper atmospheric structure

19 p3138 A71-37759

Nighttime polar atmospheric structure and temperature variations due to gas kinetic and electron energy changes

19 p3056 A71-38361

Atmospheric temperature effect on solar diurnal variation of muon component, considering asymptotic characteristics of cosmic ray anisotropy

19 p3129 A71-38378

Atmospheric composition and temperature effects on F 1 region ion concentration structure from 140 to 220 km for low solar activity conditions

19 p3058 A71-38382

Fredholm integral equation stabilization methods for atmospheric IR transfer in vertical temperature profile determination

19 p3060 A71-38470

Astronomical telescopes image motion, distortion and scintillation, examining atmospheric refractive index and density/temperature variation effects

19 p3010 A71-38571

Seasonal, latitudinal and diurnal variations of upper atmospheric structural parameters including density and temperature

19 p3061 A71-38656

Probabilistic weather forecasting for temperature and precipitation, examining feedback and prediction evaluation

20 p3256 A71-39203

Atmospheric thermal sounding problem, using regularization and statistical methods and expanding by empirical orthogonal functions

20 p3256 A71-39211

Atmospheric boundary layer refractive index fluctuations structural characteristics determined from summer vertical wind velocity and temperature profiles

20 p3256 A71-39213

Mars and Venus atmospheres, considering energetics, mean winds, temperature differences, circulations and climates

20 p3296 A71-39624

Ground based studies of Jupiter at optical frequencies, determining atmospheric chemical composition, temperature and stratification, aerosol layers structure and flyby/penetration experiments results

20 p3297 A71-39631

Atmospheric temperature and water vapor profile calculation from Nimbus satellite IR spectrometer data, noting Southern Hemisphere tropospheric and stratospheric pressure analyses

20 p3258 A71-39667

Atmospheric temperature profile from satellite soundings of outgoing radiation in IR carbon dioxide band, using regularization and Chahine methods

20 p3258 A71-39669

Atmospheric thermal sounding radiation data interpretation, determining integral Fredholm equation solution, absorption characteristics and temperature profiles

20 p3258 A71-39670

Atmospheric transmittance measurement errors in determining temperature, water vapor and ozone distributions from satellite remote sensing

20 p3258 A71-39671

Meteorological and instrumental options for atmospheric vertical temperature soundings from geosynchronous satellites, noting Nimbus 3 and ATS measurements of cloud cover and radiance levels

20 p3240 A71-39674

Exospheric evening temperature behavior data, using Fabry-Perot interferometer measurements of atomic oxygen line Doppler broadening

20 p3222 A71-39703

Upper atmospheric temperature and soft solar X-ray time scale fluctuation data, using satellite drag observations and statistical analysis

20 p3280 A71-39705

Auroral excitation and ionization intensity and rotational and Doppler temperature vertical profiles measurements, emphasizing emission rate profiles

20 p3227 A71-39839

Air temperature measurement errors, comparing thermometers with and without meteorological screening

21 p3383 A71-41240

Temperature pulsation measurements by high altitude aircraft in presence of lower troposphere convection elements

21 p3412 A71-41389

Global three dimensional atmospheric temperature mapping by selective chopper radiometer on Nimbus 4 satellite, measuring carbon dioxide IR emission

22 p3533 A71-41629

Water vapor dimer effects on atmospheric brightness temperature in cm and mm radiometric investigations from satellites above oceans

22 p3533 A71-41654

Spacecraft-borne IR sequential filter radiometer design and performance for real time meteorological forecasting and atmospheric temperature measurements

22 p3544 A71-42143

IR atmospheric temperature profiles sounding by selective chopper radiometer launched into polar orbit on Nimbus 4 satellite

22 p3544 A71-42144

Detailed wind velocities and temperature profile measurements by FPS-14 radar/Jimisphere technique for space vehicle and SST applications

22 p3569 A71-42543

Wind velocities and directions, air temperature and visibility range in atmospheric boundary layer under fog conditions

22 p3569 A71-42846

Upper atmospheric temperature and density measurements from artificial cloud observations

23 p3667 A71-43139

Rocket measured exospheric temperatures correlation with global model values based on incoherent scatter measurements

23 p3670 A71-43187

Venusian atmosphere circulation modeling, calculating temperature differences, thermal inertia and wind velocity

23 p3735 A71-43298

Mars and Venus carbon dioxide atmosphere, covering solar EUV heating efficiency, upper atmosphere temperature and chemical recombinations

23 p3735 A71-43334

Onboard computation of Mars atmospheric density and temperature, evaluating error covariance

23 p3774 A71-44095

M stars atmospheric temperature determination from TiO molecular spectrum by vibrational band intensity measurement

23 p3771 A71-44307

Ionospheric and neutral atmospheric temperature profile, composition and electron density and energy measurements by MR-12 rocket

24 p3824 A71-45310

ATMOSPHERIC TIDES

F 2 region critical frequency ionospheric tidal spectrum during solar minimum and maximum at various global locations and solar and lunar day periods

04 p0583 A71-15214

Internal gravity waves in atmospheres with realistic dissipation and temperature, considering thermal tides excited below mesopause

05 p0739 A71-16425

Lunar semimonthly oscillations in solar daily H range related to midday F 2 critical frequency at equatorial stations, analyzing lunar tides in ionosphere

05 p0740 A71-16432

Lunar oscillations in ionospheric absorption measurements, noting tides in f-min during high sunspot years

05 p0740 A71-16434

Dissipative effects on tidal winds at ionospheric heights concerning Lorentz force, molecular viscosity and heat conductivity

08 p1278 A71-21201

Book on aeronomy covering earth upper atmosphere structure, tidal oscillations, gravity waves,

airglow, aurora, ionospheric disturbances, electric currents and turbulence

09 p1437 A71-22778

Jupiter, Saturn and Uranus satellite systems orbital radius and mass correlation, suggesting satellite orbital tidal evolution and energy dissipation at planetary atmospheric boundary layer

11 p1827 A71-25729

Venus upper atmosphere retrograde circulation correlation with solar couple effect on thermal semidiurnal atmospheric tide

13 p2134 A71-28286

Seasonal variations in semidiurnal tidal wind velocities in upper atmosphere for Northern Hemisphere radio meteor observations

14 p2231 A71-29720

Atmospheric synoptic and mesoscale motions dynamic theory, including baroclinic instabilities, gravity/planetary waves, tides and sea breezes

14 p2236 A71-30493

Tidal theory comparison with lower thermospheric wind observations, taking into consideration dissipation and excitation effects

16 p2565 A71-33736

Seasonal variations of semidiurnal tidal winds in 90-110 km altitude range from harmonic analysis of ionospheric inhomogeneity drift data

16 p2575 A71-34103

Solar semidiurnal atmospheric tide theory based on gravitational action only, taking into account atmospheric stratification

19 p3055 A71-38044

Ocean and earth tidal effect on semidiurnal lunar atmosphere tide, considering realistic model

23 p3700 A71-43339

ATMOSPHERIC TURBULENCE

NT CLEAR AIR TURBULENCE

NT GUSTS

NT LOW LEVEL TURBULENCE

Mountain-size atmospheric eddies on leeward slope of Carpathian and Low Tatra mountains, discussing turbulence effects on air navigation

01 p0113 A71-10349

Atmospheric boundary layer nonlinear equations of motion numerical integration for eddies structure and wind direction and latitude effects on turbulence intensities

01 p0113 A71-10351

Spatial and temporal structure in turbulent breakdown of shear flows in stably stratified atmosphere from radar images of vertical cross sections

01 p0116 A71-10569

Doppler radar techniques for turbulent kinetic energy budget in boundary layer, discussing wind profile and turbulence in snow conditions

01 p0117 A71-10577

Lower atmosphere turbulence model derivation from data obtained by Doppler radar windfield measurements in snowfall environment

01 p0117 A71-10578

Free convection in turbulent Ekman layer, discussing kinetic energy budget above surface layer

01 p0119 A71-10742

Atmospheric turbulence characteristic parameters determination by two narrow laser beams

01 p0119 A71-10833

Atmospheric surface layer turbulence spectra and cospectra observations in July-August 1969 at Edithvale, Australia

01 p0120 A71-10858

Scale lengths in atmospheric turbulence from spectra and autocorrelation of vertical air velocity component measured in low flying aircraft

01 p0120 A71-10859

Aerodynamic theory of pressure field induced on lifting surface by isotropic atmospheric turbulence, considering transfer function of Concorde aircraft [ICAS PAPER 70-30]

01 p0002 A71-11019

Global atmospheric circulation, discussing surface irregularities and variable heating role in disturbances

01 p0121 A71-11352

Atmospheric turbulence effects reduction in optical communication by statistical communication theory, considering digital system and waveform estimation

02 p0213 A71-12019

Optical /and IR/ communication systems design, considering effects of atmospheric turbulence, molecular absorption and aerosol scattering

02 p0214 A71-12023

Optical heterodyne receiver design, using nonlinear recursive techniques to estimate atmospheric fluctuation effects on IF signal characteristics

02 p0249 A71-12026

Photosphere and facula turbulent velocities and damping constants from Ni and Fe IR lines analysis

02 p0306 A71-12079

Atmospheric turbulence effects on stellar Michelson interferometry

02 p0308 A71-12099

Turbulent energy dissipation in lower atmospheric layer on meteorological mast during various temperature stratifications

02 p0246 A71-12112

Standard deviation of atmospheric turbulence velocity components over flat arid terrain 02 p0278 A71-12707

Statistical prediction of atmospheric turbulence effects on aeronautical systems 03 p0398 A71-13135

Atmospheric turbulence at cruise altitudes of supersonic transport aircraft, considering gusts probability, thunderstorms and mountain waves 03 p0346 A71-13137

Two channel 450 mm TV telescope at Pulkovo Observatory, investigating atmospheric turbulence deformations of stellar images 04 p0588 A71-14828

Laser beam phase front distortion by atmospheric turbulence, discussing interferometric measurements 04 p0608 A71-15137

LF boundary of inertial range in lowest atmospheric layer, comparing turbulence scale and wind velocity components 04 p0622 A71-15632

Turbulence energy spectra in thick convective cumulonimbus cloud zone, using aircraft measurements 04 p0622 A71-15633

Energy transport over turbulence spectrum of free atmosphere, using aircraft experiments 04 p0622 A71-15634

Lower atmosphere thermal microfluctuation measurement to examine solar seeing area and dome effect 04 p0622 A71-15658

Partially coherent laser beam phase fluctuations using reversing-front interferometer for time integrated irradiance measurement, considering atmospheric turbulence effects 04 p0627 A71-15683

Venera satellites and Mariner 5 radio wave fluctuations and discontinuities of refractive index in Venusian atmosphere, considering atmospheric turbulence 05 p0719 A71-16042

Optical channel capacity and laser signal distortion through turbulent atmosphere 05 p0720 A71-16288

Tropospheric and stratospheric turbulence, discussing energy sources and sinks and energy spectra pattern at different atmospheric conditions 05 p0741 A71-16625

Sporadic E layers magnetic field variations, examining charged particle redistribution with air turbulence model 05 p0746 A71-17203

Stratospheric wind field determination at extreme vertical velocity, noting baric field asymmetry 06 p0923 A71-17512

Macroscale atmospheric vorticity model, using nonlinear system hydrodynamic and adds free motion equations 06 p0923 A71-17513

Wind field from macroscale atmospheric whirlpools/typhoons/ pressure fields by nonlinear hydrodynamic equations 06 p0923 A71-17514

Solar chromosphere mass motion, studying macro turbulence influences on visible spectrum lines high resolution profiles from rocket spectrograms 06 p0967 A71-17904

Flexible aircraft to atmospheric turbulence transfer functions, discussing in-flight measurements [ONERA-TSP-894] 06 p0847 A71-18021

Atmospheric surface layer turbulence structure simulation model, using laboratory flows for neutrally stable atmosphere [AIAA PAPER 71-136] 06 p0884 A71-18579

Soviet papers on atmospheric turbulence and convection covering two dimensional flows, orographic wave formation and air pulsations in rainstorms 07 p1149 A71-18792

Temperature stratification effects on free atmosphere turbulence structure under Archimedean forces, noting energy dissipation buoyancy forces and adiabatic gradients 07 p1150 A71-18796

Atmospheric turbulence steady random process correlation function, spectral density and probability distribution based on aircraft measurements 07 p1150 A71-18797

Phase transitions effect on cloud turbulence behavior from relaxation time, energy and temperature dissipation and supersaturation spectral density 07 p1150 A71-18799

Atmospheric turbulence measurement and detection using non-Doppler radar 07 p1058 A71-18845

Astronomical telescope resolving power in focal plane emphasizing atmospheric turbulence 07 p1109 A71-19347

Atmospheric meteor zone turbulent motions under Archimedes forces based on radio observations 07 p1101 A71-19412

Optical phase variations on short line of sight path through turbulent atmosphere 07 p1159 A71-19512

Photoelectron counting distribution for random medium passage scintillated stochastic light, considering low level amplitude stabilized and chaotic radiation transmission through turbulent atmosphere 07 p1159 A71-19513

Airborne hot wire measurements of small scale structure of atmospheric turbulence 07 p1153 A71-20276

Photosphere and facula turbulent velocities and damping constants from Ni and Fe IR lines analysis 08 p1361 A71-21129

Atmospheric turbulence effects on stellar Michelson interferometry 08 p1362 A71-21149

Planetary boundary layer stationary air flow over plane homogeneous surface under geostrophic wind conditions, solving for thermal turbulence field stabilization by iterative method 08 p1330 A71-21874

Multiwavelength laser beam scintillations and atmospheric turbulence spectra, investigating saturation phenomena, transverse amplitude correlation lengths and signal fluctuations receiver aperture smoothing 09 p1464 A71-22780

Sonic boom and explosion shock wave propagation over long distances through turbulence modeled by sound speed fluctuation, including acoustic scattering effect 09 p1433 A71-22858

Instrument tilt effect on atmospheric turbulence measurements, presenting transformation equations for turbulence characteristics 09 p1488 A71-23028

Solar photosphere turbulent velocity, taking into account instrumental profile effects 09 p1524 A71-23193

Planetary scale atmospheric motion energy spectra and error prediction from numerical model, using eddy-damped Markovian approximation for two dimensional turbulence 09 p1489 A71-23551

Atmospheric surface layer shear/buoyant production, flux divergence and dissipation in terms of turbulent kinetic energy and transport in temperature variance budget 09 p1490 A71-23555

Rigid towed and free flight glider, considering loads and turbulent atmosphere effects 09 p1385 A71-23669

Optical signal heterodyne reception, discussing reduced atmospheric distortion effects 10 p1575 A71-23812

Wave structure and mutual coherence functions of optical wave propagating in turbulent atmosphere, considering signal to noise ratio 10 p1641 A71-23948

Helmholtz reciprocity theorem extension to clear turbulent atmosphere, defining Green functions to characterize optical propagation in opposite directions between parallel planar apertures 10 p1641 A71-23949

Atmospheric turbulence parameters determination from radar meteor observation, calculating antenna radiation patterns effect on error 10 p1583 A71-24036

Atmospheric turbulence effects on sonic boom rise times by statistical theory 10 p1556 A71-24817

Optimum frequency for detection of acoustic sources in upper atmosphere as function of altitude and turbulence 10 p1642 A71-24833

Optimal stochastic control and gust alleviation for jet aircraft response for flight through turbulent upwash field 10 p1557 A71-24870

Mean wind velocity and turbulence remote measurement with laser anemometry, using intensity modulation technique 10 p1623 A71-25091

Binary on-off laser communication channels, calculating atmospheric turbulence effect on Poisson detection error probability 11 p1730 A71-25198

Nonstationary random analysis of flight vehicle response to atmospheric turbulence, using Priestley evolutionary spectral method [AIAA PAPER 71-341] 11 p1836 A71-25320

Validity range of response prediction methods for large flexible aircraft to continuous atmospheric turbulence, discussing power spectral densities and fatigue life [AIAA PAPER 71-342] 11 p1707 A71-25321

Measuring technique for short term laser beam propagation direction fluctuations, discussing atmospheric turbulence effect on initial modulation phase distribution 11 p1774 A71-26047

Wind structure and atmospheric disturbances, noting resolution of pilot-balloon data 11 p1796 A71-26561

Atmospheric currents and turbulence determination from meteor trail photographic observations 12 p1901 A71-27075

Large scale structure with unstable stratification, investigating effects on atmospheric ground layer dynamic velocity and turbulent energy production 12 p1924 A71-27101

Aircraft longitudinal coordinates invariance relative to atmospheric disturbances, giving simultaneous thrust variation, rudder deflection and flap deflection control rules 12 p1867 A71-27339

Laser beam propagation in turbulent atmosphere studied for alignment survey applications, discussing development, construction and testing of centering detectors 12 p1915 A71-27538

Venus atmospheric turbulence from Venera 4, 5, 6 and Mariner 5 observations, discussing scaling laws and normalized signal-amplitude standard deviation 13 p2132 A71-27928

Sporadic E layers magnetic field variations, examining charged particle redistribution with air turbulence model 13 p2059 A71-28258

Atmospheric turbulence effects on focused coaxial carbon dioxide and He-Ne laser beam propagation 13 p2078 A71-28525

Wind resonance in ionosphere under pressure fluctuations, noting turbulent friction factor above 110 km 13 p2060 A71-28533

Turbulence-related accidents frequency and severity during past few years from worldwide synopsis 13 p1997 A71-28885

Focused laser coherent light beam expansion in turbulent atmosphere 13 p2080 A71-29016

Wind structure in atmospheric boundary layer, outlining semiempirical laws for mean wind speed variation with height and statistical properties of turbulent fluctuations 13 p2097 A71-29266

Molieri high energy solution of Schrodinger scattering equation for optical propagation in turbulent atmosphere, noting inconsistency of Born-Rytov approximation 13 p2102 A71-29441

Time and frequency statistics of turbulent fluctuations of wind, temperature and humidity in atmospheric surface layer 14 p2266 A71-29706

Atmospheric turbulence - Conference, London, May 1971 14 p2266 A71-29749

Atmospheric turbulence effect on turbine powered transport aircraft, discussing gust accelerations, avoidance, detection, forecasting and pilot control 14 p2172 A71-29750

Atmospheric turbulence statistical models assessment for aircraft design and operation, considering CAT and thunderstorm turbulence data 14 p2266 A71-29751

Oklahoma and Malaysia thunderstorms comparison based on weather reconnaissance aircraft measurements, considering turbulence patches 14 p2266 A71-29752

Atmospheric turbulence space-time relationships measurements, discussing computerized time series, spatial and phase spectral analysis for sensors data 14 p2267 A71-29754

Atmospheric turbulent shear layer model, giving velocity, stable, unstable and neutral profiles 14 p2267 A71-29759

Atmospheric turbulence over South America from Lufthansa data, noting occurrence, location, strength and dimensions 14 p2268 A71-29766

Stratospheric turbulence correlation to mesoscale horizontal temperature gradient at altitudes flown by SST from Coldscan program 14 p2268 A71-29767

Air turbulence primary and secondary effects on aircraft flight and avoidance criteria considerations 14 p2268 A71-29768

U.S. air carrier accidents due to atmospheric turbulence, considering in-flight weather problems, airborne meteorological radar, CAT detection systems, etc 14 p2172 A71-29770

Flight characteristics under atmospheric turbulence conditions, analyzing analog trace records of airspeed, normal acceleration, altitude, air temperature, control surface and flight attitude parameters 14 p2173 A71-29771

Jet transport aircraft stability and controllability under atmospheric turbulence conditions, discussing longitudinal and lateral-directional characteristics with particular attention to unstable spiral mode 14 p2173 A71-29772

Automatic aircraft landing system modification for improvement of response to air turbulence effects 14 p2271 A71-29773

Pilot subjective evaluation of XB-70 aircraft response to atmospheric turbulence in comparison with measured accelerations 14 p2173 A71-29774

V/STOL aircraft flight path and attitude controls in turbulence, discussing design based on state variable methods of control theory

14 p2173 A71-29776

Jet transport aircraft design for safety under air turbulence conditions, considering cruise altitude limitations and pitch and g excursion reduction by special autopilot mode

14 p2173 A71-29777

Atmospheric turbulence induced aircraft vibrations effects on aircrew performance, discussing physiological and psychological responses

14 p2187 A71-29778

Computerized simulation techniques for investigating aircraft accidents due to atmospheric turbulence

14 p2221 A71-29779

Commercial aircraft piloting in atmospheric turbulence, discussing aircraft characteristics, instrumentation, flying procedures, pilot training and kinesthetic cues

14 p2173 A71-29782

Large subsonic jet aircraft civil pilots performance under physiological and psychological stresses induced during severe atmospheric turbulence

14 p2188 A71-29783

Aircraft structural design requirements based on statistical analysis of air turbulence intensity and gust loads records from large number of research flights

14 p2173 A71-29784

Aircraft gust alleviation, considering movement correction based real time atmospheric turbulence measurement

14 p2174 A71-29785

Atmospheric turbulence effects on handling qualities and structural loads on aircraft

14 p2174 A71-29787

Discrete gust and power spectrum models of atmospheric turbulence, considering energy distribution effect on aircraft dynamic response

14 p2174 A71-29790

Atmospheric turbulence effects on stellar irradiance and phase, discussing electro-optical recording technique and computer generated statistical data

14 p2270 A71-30016

Linear antenna radiation pattern broadening due to atmospheric turbulence

14 p2194 A71-30074

Laser beam scintillation covariance beyond turbulent atmospheric layer in Fresnel and Fraunhofer zones

14 p2254 A71-30423

Atmospheric turbulence effect on far field diffraction pattern of annular aperture

14 p2275 A71-30465

Meteorological research on upper atmosphere energy sinks/sources, composition, density, turbulence, winds and thermal structure

14 p2236 A71-30494

Atmospheric turbulence structure, cloud convection, gravity waves, clear air flow and surface/planetary boundary layers

14 p2270 A71-30495

Imagery of periodic objects through interposed turbulent medium, investigating diffraction images irradiance distribution and contrast

14 p2275 A71-30827

Stratospheric turbulence induced aircraft buffeting dependence on vertical wind shear, Richardson number and thermal stability change from underlying to overlying layer

15 p2444 A71-31365

Stratospheric turbulence induced aircraft buffeting dependence on horizontal temperature and wind distribution

15 p2444 A71-31366

Optical detection of laser or scattered radiation transmitted through turbulent atmosphere, taking into account independent additive background radiation

16 p2608 A71-33145

Venera satellites and Mariner 5 radio wave fluctuations and discontinuities of refractive index in Venusian atmosphere, considering atmospheric turbulence

16 p2542 A71-33446

Atmospheric stability at 30-90 km based on wind and temperature data from grenade experiments

16 p2568 A71-33788

Atmospheric turbulence prediction, discussing gust sensitive aircraft design for structural overload and fatigue failure decreases

[AIAA PAPER 71-775]

16 p2524 A71-34011

Jovian turbopause probe mission, discussing atmospheric composition measurements and nonsurvivable system concept

[AIAA PAPER 71-833]

17 p2802 A71-34714

Communications systems using carbon dioxide laser wave propagation, considering wave extinction by absorption and scattering, scintillations due to atmospheric turbulence, etc

17 p2700 A71-34749

German monograph on lower atmospheric turbulence and monograph coefficients in connection with large scale parameters, deriving climatological flow characteristics from wind measurements

17 p2770 A71-35233

Fast response anemometer for measuring atmospheric wind speeds and turbulence components

17 p2745 A71-35327

Large scale atmospheric turbulence, considering anisotropy, thermal stratification, pressure and Coriolis forces effects

18 p2944 A71-36009

Flight investigation of turbulence effects on aircraft longitudinal flying qualities, evaluating pilot ratings for ILS approach task

[AIAA PAPER 71-905]

19 p2995 A71-37156

Aircraft observed stratospheric gravity waves spectral analysis, noting differentiation between atmospheric turbulence and waves

19 p3089 A71-37500

Solar and stellar chromospheres and coronas production based on turbulence in granulation, photospheric mechanical flux and supergranular network magnetic field structures

19 p3136 A71-37626

Small scale turbulence structure in atmospheric boundary layers over open ocean, noting velocity derivatives probability density function lognormality

19 p3044 A71-37731

Atmospheric meteor zone turbulent motions under Archimedes forces based on radio observations

19 p3054 A71-37836

Meteor streams effect on atmospheric motions turbulence intensity based on radar observations

19 p3054 A71-37972

Gust factor variation as function of height and atmospheric stability, deriving simple power law expression from meteorological tower wind measurements

19 p3091 A71-38289

Difference equations derivation for meteorological turbulent flow prediction, considering errors due to finite difference approximations

19 p3087 A71-38306

Planetary boundary layer stationary air flow over plane homogeneous surface under geostrophic wind conditions, solving for thermal turbulence field stabilization by iterative method

19 p3091 A71-38468

Structural analysis trends, considering strain and force methods, flutter, dynamic response, atmospheric turbulence and random phenomena problems

20 p3308 A71-39400

Synoptic and microscale variance spectrum of horizontal wind velocity at 50 m above ground, comparing with perturbations models

20 p3257 A71-39439

Upper atmospheric anomalous molecular oxygen distribution, discussing turbulent theory with autocorrelation of density fluctuations

20 p3222 A71-39701

Submillimeter plane monochromatic waves propagation in ground layer of turbulent atmosphere, deriving received signals levels fluctuations

20 p3198 A71-39804

Height resolved atmospheric turbulence properties from photometric measurements of airglow intensity fluctuations, discussing detection, separation from noise and statistical analysis

20 p3227 A71-39837

Laser system for atmospheric wind velocity and turbulence, using Doppler frequency shift undergone by radiation beam scattered by particles suspended in flows

21 p3319 A71-40490

Atmospheric and wake turbulence effects on aircraft from discrete gust and spectral interpretations, discussing load production and uncontrollable rolling moments

21 p3321 A71-40507

Far field light diffraction due to circular plane wave apertures rendered partially coherent by atmospheric turbulence

21 p3415 A71-40635

Spectral statistics of seasonal tropospheric wave disturbances in tropical Western Pacific, observing synoptic and planetary scale wind field

21 p3374 A71-41177

Soviet papers on atmospheric turbulence and convection covering cumuli dynamics, wind field microstructure and time characteristics in troposphere and stratosphere

21 p3411 A71-41384

Numerical model of turbulence effect on cumulus cloud mesoscale convective motion

21 p3411 A71-41386

Atmospheric rotation, anisotropic turbulence and long wave radiative heat transfer effects on cellular heat convection

21 p3412 A71-41387

Turbulence energy balance and temperature pulsations in free atmosphere in presence of water phase transformation in clouds of given microstructure

21 p3412 A71-41394

Temporal frequency spectra for spherical wave propagating through atmospheric turbulence, using covariance functions and Taylor hypothesis

22 p3575 A71-41788

Optimal power transfer through atmospheric turbulence by adaptive laser transmitter using beacon waveform to probe channel state

22 p3512 A71-42378

Turbulent energy budget and velocity dissipation spectrum near grass surface as function of atmospheric stability

22 p3569 A71-42546

Mountain induced lee waves, turbulence and wind measurements in Colorado, using aircraft flight data

22 p3569 A71-42548

Collimated laser beam angular deviation in turbulent near earth atmosphere, comparing with interferometric data

23 p3685 A71-43506

Narrow light beam transmission in weakly nonlinear turbulent atmosphere, calculating large scale permittivity inhomogeneity effect on average intensity by model

23 p3645 A71-43564

Collimated light beam transmission in turbulent atmosphere above ground surface, comparing measured coherence function with calculation

23 p3645 A71-43565

Mach-Zehnder interferometric measurement of modulation transfer function of optical instrument disturbed by turbulent atmosphere

23 p3679 A71-43893

Kraichnan turbulence theory based on exact solution of model equations presenting strong structural similarities with turbulent Navier-Stokes equations

23 p3701 A71-43976

Radiation attenuation effect on solar photosphere turbulence determination by Goldberg-Unno method

23 p3772 A71-44311

Turbulent defocusing and displacement fluctuations of focused He-Ne laser beam in atmosphere over paths near ground

23 p3688 A71-44329

Richardson criterion generalization for atmospheric turbulence onset, considering anisotropic turbulence conditions

24 p3844 A71-44447

Atmosphere hydrodynamic simulation model for cascade energy transfer in turbulent flow, using Euler gyro equations

24 p3844 A71-44818

Laser beam spot dancing during propagation through turbulent atmosphere, using Kolmogoroff structure function of refractivity and geometrical optics

24 p3834 A71-45208

ATMOSPHERICS

NT DAWN CHORUS

NT HISS

NT IONOSPHERICS

NT SUDDEN ENHANCEMENT OF ATMOSPHERICS

NT WHISTLERS

Atmosphere effects on antenna noise temperature variations in G/T value for earth station performance in satellite communication system

02 p0222 A71-12799

Attenuation and phase velocities of ELF slow tail atmospherics for easterly and westerly nighttime propagation over Pacific Ocean

04 p0552 A71-15217

Physical factors affecting atmospherics and electromagnetic signal propagation in earth-ionosphere waveguide

07 p1061 A71-19386

Atmospheric noise effect on solar granulation photographic observation based on cross correlation between identical measurements

07 p1200 A71-20037

Lightning flash-ground strokes VHF radio pictures by hyperbolic position fixing system, obtaining three dimensional sferics fixes as function of time

08 p1325 A71-20880

Horizontally and vertically polarized sferic signals from lightning discharges by airborne instrumentation, using pattern recognition approach

08 p1325 A71-20883

Threshold distribution of time intervals between atmospherics contradicting Poisson law

09 p1435 A71-22445

ELF atmospherics pulse trains recordings at widely separated stations for spectral amplitude ratio differentials, using lightning and ionospheric heating mechanisms

09 p1489 A71-23445

Sharp peaking of wave impedance characterizing propagation in earth-ionosphere waveguide from atmospheric radio noise measurements near 2 kHz

13 p2029 A71-28471

Narrow band atmospheric radio noise burst average and rms field strength measurement

13 p2033 A71-28900

Ionospheric VLF signal propagation paths based on earth atmospherics simulation and mathematical models

14 p2228 A71-29513

Atmospherics sources spectral amplitude ratios and group delay times correlation, obtaining VLF iono-

- spheric propagation characteristics from single station observations 14 p2237 A71-30957
- Group delay time differences in locating sources of atmospherics dependent on arrival azimuth, time of day and season 14 p2237 A71-30959
- Truncated pulse signal height distributions of atmospherics sources 14 p2203 A71-30960
- Atmospheric noise statistical characteristics, investigating short term variations, intensities and application to communications 14 p2237 A71-30964
- Atmospherics spectral and structural characteristics, reviewing studies of source phenomena and related electric, magnetic and electromagnetic fields 14 p2237 A71-30965
- Atmospheric and man-made noise measurement techniques, using signal generator as reference standard for absolute amplitudes 14 p2204 A71-30978
- VLF atmospherics integrated intensities changes probably due to ionization by meteors 15 p2371 A71-31839
- Frequency spectrum of lightning discharges, developing mathematical model to account for atmospherics difference between cloud-ground and cloud-cloud discharges 16 p2604 A71-33070
- Physical factors affecting electromagnetic signal propagation in earth-ionosphere waveguide 19 p3017 A71-37811
- Pulse duration of atmospheric radio noise bursts at 3 MHz from lightning flashes, considering effect on data communication 23 p3643 A71-42970
- Long distance atmospherics propagation in earth-ionosphere waveguide, obtaining phase velocities and damping factors 24 p3804 A71-45030
- ### ATOM CONCENTRATION
- Liquid Fe, Co and Ni atomic distributions investigation by X ray diffraction 04 p0612 A71-15036
- Reacting gases atom concentration quantitative measurements with electron spin resonance, discussing microwave power, saturation and modulation amplitude effects 11 p1765 A71-26284
- Propulsion system atom and radical concentrations measurements, using low pressure gas discharge flow system for combustion environment control 11 p1729 A71-26285
- Excited atom density determination for two-photon light absorption in one-dimensional medium, obtaining energy balance equation asymptotic solution and secondary radiation intensity 12 p1914 A71-27028
- Knudsen arc firing potential in plane gas filled diode with hot cathode as function of electrode gap and atom concentration 15 p2455 A71-31739
- Chlorine-fluorine flame, determining adiabatic propagation speed, refractive index field, temperature profile, composition distribution and atom concentrations 19 p3168 A71-38105
- Atomic oxygen concentration from 5577 Å green line emission of airglow and chemiluminescence of nitric oxide 20 p3215 A71-38739
- ### ATOMIC BATTERIES
- ### U RADIOISOTOPE BATTERIES
- ### ATOMIC BEAMS
- Thermoemissive and adsorptive properties of Nb single crystals in Cs atomic beam at various temperatures 01 p0139 A71-11100
- High density cesium beam generation using slot source and nitrogen cooled detector 04 p0632 A71-14796
- Optical hyperfine splitting of Rb resonance lines of atomic beam light source, using Fabry-Perot interferometer 07 p1111 A71-19488
- Thermionic emission and adsorption characteristics of Ta single crystal faces in cesium atom streams, using thermoelectronic and surface ionization methods 15 p2453 A71-32643
- Monatomic gas beams scattering from gas surface interface with randomly distributed energy states, confirming reciprocity or detailed balance principle 19 p3104 A71-38057
- Trapping of neutrals from fast atom beam impinging on molecular hydrogen influx fed electron-cyclotron plasma target 21 p3422 A71-40761
- ### ATOMIC CLOCKS
- Miniaturized Rb atomic frequency source having 1 in 10 to 8th power stability in year and 5 minute warm-up time 02 p0252 A71-12422
- Precision timing system implementation and operation, considering synchronization maintenance by flying cesium beam clocks, satellite, VLF and LF techniques 03 p0429 A71-14270
- Electronic frequency divider with discrete correction of negative quartz clock rate 04 p0592 A71-14859
- Atomic clock synchronization with high accuracy 04 p0596 A71-15208
- Quartz clock nonsystematic and frequency fluctuation statistical properties compared with GBR radio station 04 p0600 A71-15664
- Gravitational constant time variation based on planetary radar echo time delay in comparison with atomic time, discussing accuracy limits 05 p0807 A71-16227
- Navigational precision timing from earth rotation based pendulum to atomic second based quartz oscillator clocks 07 p1156 A71-20341
- Light-microwave signal relation in optical pumping and detection in Rb atomic oscillator 08 p1289 A71-21273
- Ephemeride and atomic uniform time scales comparison for earth rotation velocity changes, estimating diurnal and semidiurnal tides effect 08 p1284 A71-21673
- Time unit definition by atomic clocks, taking into account relativistic effects 11 p1762 A71-25622
- Time-frequency anticollision system for dangerous aircraft detection and avoidance using stable atomic clocks [ONERA-TP-938] 15 p2445 A71-31875
- Atomic clocks on manned space stations, discussing stability in aerospace environment, techniques for earth based timer calibration, reference device, maintenance and corrections 17 p2743 A71-35056
- Long baseline atomic clock interferometry with meter wavelength cross polarized antenna arrays for spacecraft propagation experiments 17 p2744 A71-35098
- Earth clock precision and rotation retardation effects on ephemeris time, comparing with atomic clock 19 p3060 A71-38529
- Universal time and atomic clock earth rotation irregularities measurements checked for Chandler period 20 p3216 A71-39479
- Standard frequency and UTC time signal transmission coherent with SI /atomic/ second 22 p3509 A71-42087
- Radio astronomic intercontinental base interferometry, discussing independent local oscillators requirements and atomic clock frequency standards 23 p3674 A71-43087
- Atomic time standards, discussing Cs 133, hydrogen maser, ammonia maser and rubidium gas cell equipment 24 p3827 A71-44994
- ### ATOMIC COLLISIONS
- Atomic and molecular collisions in gases, considering E and F regions processes, auroras and applications 01 p0129 A71-10133
- Secondary electron emission during RBB, Se and CdTe film bombardment by sodium ions and atoms 01 p0139 A71-11099
- High energy multiple birth inelastic interactions between cosmic ray particles and atomic nucleus targets, using Wilson chamber and ionization calorimeter 01 p0083 A71-11363
- Hydrogen molecule-atom short range interaction energy, calculating multicenter integrals for screening constants 02 p0286 A71-11954
- Cs atom ionization cross section during type II collision with resonantly excited Hg atom 02 p0287 A71-12197
- Thermionic converter electron-cesium atom momentum transfer collision probability, considering scattering cross sections 02 p0287 A71-12227
- He excitation by He, Ne, Ar and Kr collisions, calculating first Born wave cross section 03 p0460 A71-13498
- Neutral atoms collision effects on partially ionized plasmadynamic stability, considering fluid medium model with one dimensional density gradient 03 p0464 A71-13927
- Knocked out atomic electron energy during impact ionization, comparing Thomson and Drawin formulas 03 p0465 A71-13954
- Atomic collision chains in bcc crystal, determining energy loss relation to temperature by computer model with/without perfect lattice thermal oscillations 04 p0630 A71-15103
- Heavy particles collision induced excitation, deexcitation and ionization rates, calculating atomic H quantum level transitions due to H and He atomic collisions at thermal energies 05 p0785 A71-16490
- He-Ne laser atomic scattering theory 06 p0907 A71-17997
- Molecular hydrogen cations collisions with hydrogen and helium, determining dissociation cross section dependence on kinetic energy from threshold to 100 eV 07 p1163 A71-19233
- Frequency shift in hydrogen maser due to atomic collisions with storage bulb surface /wall shift/, investigating temperature dependence 07 p1124 A71-19686
- Triatomic molecules relaxation process, considering translational-vibrational energy exchange in atomic collisions and transition probabilities for carbon dioxide-helium system 08 p1337 A71-20669
- Nitrogen molecule collision with metastable inert gas atoms and ions, investigating energy exchange mechanism 08 p1337 A71-20670
- Carbon monoxide gas phase vibrational relaxation by Fe atoms, using shock tube for determination of decomposition rate of iron carbonyl in dilute mixture with Ar 08 p1337 A71-20672
- Nonadiabatic H-H collisions cross sections in two state time dependent impact parameter approximation, including electron exchange 08 p1337 A71-21193
- Symmetric excited state electron capture cross sections in ion-atom inelastic scattering, using two state approximation formulas 08 p1338 A71-21235
- Electron loss and capture by hydrogen atoms, protons and negative ions during collisions between atoms and molecules in gases, interpreting cross section data 08 p1338 A71-21491
- Slow negative atomic oxygen ion production in collisions between fast protons or hydrogen atoms and gas molecules 09 p1496 A71-22230
- Cross sections for simultaneous ionization and charge transfer in fast proton-helium atom collisions, using Born approximation 09 p1497 A71-22416
- Oxygen and nitrogen molecules nonadiabatic electronic-vibrational interaction effect on vibrational relaxation during collisions with O atoms 09 p1497 A71-22530
- CH molecule line formation mechanism for 4300 Å transition in solar photosphere, studying collisions with hydrogen atoms 09 p1520 A71-22843
- Electron exchange and nuclear symmetry for 2s and 2p collisional excitations of hydrogen by H atom based on symmetrized atomic orbitals set 10 p1644 A71-23925
- He-Ne laser 0.63 micron line collisional broadening dependence on gas temperature 10 p1620 A71-23442
- Collision effects on atomic spectral line profiles, using quantum mechanical description of atomic center-of-mass motion with particular application to lasers 11 p1803 A71-26147
- Hanle cascade effects on atomic lifetime reliability from collisional excitation experiments 11 p1803 A71-26370
- Positron-hydrogen scattering below positronium pickup threshold by Hylleraas bound technique, discussing phase shifts and linear parameters 11 p1803 A71-26372
- Molecular hydrogen cations collisions with hydrogen and helium, determining dissociation cross section dependence on kinetic energy from threshold to 100 eV 12 p1932 A71-26751
- Multiple echo of impurity atom during collisions with solid body surface, contributing to vaporization from layer 12 p1932 A71-27034
- Atom interaction potential with solid body surface, discussing experiments and results 13 p2103 A71-29160
- Gas atoms collisions with linear harmonic oscillator and solid surface simulated by semiinfinite elastically coupled atomic lattice, using combined asymptotic expansions method 13 p2103 A71-29227
- Classical and quantum mechanical theories of gas atom-solid surface scattering with applications to different physical regimes 14 p2276 A71-30405
- Cs atom ionization cross section during type 2 collision with resonantly excited Hg atom 15 p2451 A71-31503
- Monatomic gas interaction with solid phase surface, deriving three dimensional theoretical model including hard spheres collision and surface energy 15 p2451 A71-31675
- Dust grain orientation in interstellar space from Fokker-Planck equation, taking into account collisions with gas atoms and magnetic interactions 15 p2485 A71-31715

Dispersive effect on bremsstrahlung radiation from electron atom collisions in weakly ionized plasma, using Boltzmann transport equation 15 p2456 A71-31850

Energy dependence of collisional time delay functions computed for H/IS/ atoms interacting via hydrogen potential, determining scattering cross sections 16 p2613 A71-32811

Ba atoms excitation and optical transitions line broadening by collisions with Ar atoms behind shock waves, using atomic absorption spectroscopy 16 p2613 A71-32889

Electron loss and capture by hydrogen atoms, protons and negative ions during collisions between atoms and molecules in gases, interpreting cross section data 16 p2614 A71-33042

Upper atmosphere He, Ne, Na and K atoms collisions with molecular oxygen, determining ejected electron energy during fast Na, K, Rb and Cs ionization for meteor phenomena modeling 16 p2639 A71-33695

Nonadiabatic effects in van der Waal line broadening, taking into account mixing between degenerate magnetic sublevels in atomic collisions 19 p3106 A71-37409

Collision effects on line shapes using quantum mechanical description of atomic center of mass motion, considering pressure effects in gas lasers 20 p3271 A71-39069

Close coupling calculation for low energy hydrogen atom-molecule collision, discussing cross section, transition probabilities and elastic scattering 20 p3272 A71-39579

Neutral atoms and ions collision damping constants estimation for spectrum synthesis, using approximate formula based on Stark broadening effect 21 p3442 A71-40160

Atomic hydrogen maser wall shift elimination by operating at temperature to obtain zero average phase shift per atomic collision 21 p3391 A71-40201

Fast charged particles inelastic collisions with atoms and molecules, investigating Bethe differential cross section theory 21 p3418 A71-40675

Fast hydrogen atoms penetration into fusion reactor plasma, calculating collision cross section rates coefficients 21 p3422 A71-40765

Slow negative atomic oxygen ion production in collisions of fast protons and hydrogen atoms with oxygen molecules, measuring scattering cross sections 21 p3419 A71-41109

Penning process for small ionization probability per atomic collision, obtaining ion production constant relationship to temperature 21 p3420 A71-41252

Molecular nitrogen ions collisions with He and Xe gas atoms, discussing processes based on atomic N ion fragment velocity distribution measurements at varying electron energies 21 p3421 A71-41405

Hydrogen three-body recombination and dissociation rates in presence of molecular hydrogen, helium, argon and xenon collision partners 23 p3706 A71-42902

Reduced nebular helium abundances, using capture-cascade and collisional excitation calculations 23 p3733 A71-43081

H transition excitation during atomic hydrogen collision with alkali elements and inert gases, discussing inner electron excitement 23 p3707 A71-43268

Hollow cathode lasers based on negative glow discharge excitation including charge exchange ion-atom collisions and Penning excitation 23 p3686 A71-43955

Electron production cross sections in inelastic atomic collisions, evaluating classical scaling law and quantum mechanical statistical methods against experimental results [AIAA PAPER 71-995] 24 p3850 A71-44587

Low temperature kinetics of metastable He atom pair collisions, investigating temperature dependence of plasma ionization 24 p3856 A71-45054

Molecular oxygen dissociation rate constant determination during interaction with He atoms in cylindrical shock tube 24 p3850 A71-45056

Wave interference phenomena associated with elastic scattering of atoms, considering differential inelastic scattering cross sections anomalies 24 p3851 A71-45166

ATOMIC ENERGY

U NUCLEAR ENERGY

ATOMIC ENERGY LEVELS

Electron excitation coefficient rate of green coronal line by quantum defect method, discussing energy levels of Fe ions 04 p0643 A71-14906

Laser action in visible and near IR on atomic fluorine transitions based on collisional dissociation of hydrogen fluoride 04 p0608 A71-15040

Atomic system ground state energy upper bound, considering internuclear distances and removal of restriction for negative definite potential energy operator 04 p0630 A71-15268

Heavy particles collision induced excitation, deexcitation and ionization rates, calculating atomic H quantum level transitions due to H and He atomic collisions at thermal energies 05 p0785 A71-16490

Evanescent electromagnetic waves quantization by treating transverse triplet wave modes as noninteracting harmonic oscillator, discussing atomic excitation 07 p1159 A71-19548

Powerful solar flare H lines spectrophotometric observation, noting hydrogen atom upper energy levels overexcitation 07 p1188 A71-20033

Hydrogen atoms upper energy levels overexcitation in solar flare, suggesting role of stimulated photorecombinations 07 p1188 A71-20034

Cd atoms excited state populations in nonequilibrium gas discharge plasma 09 p1500 A71-22267

Single to triplet transitions of water vapor as function of scattering angle in electron impact detection 09 p1498 A71-23381

Organic lasers with xanthene dyes solutions, investigating triplet states molecular population effect on output energy characteristics in pumping 10 p1620 A71-24344

Multimode laser with multilevel atoms, deriving Fokker-Planck equation for laser light statistics 10 p1622 A71-24926

Emission spectra, wavelengths and photoelectric intensities of triply-ionized gadolinium, using hollow cathode source with Czerny-Turner vacuum spectrograph 11 p1801 A71-25137

Self consistent field (SCF) calculations of dipyrindine glyoxal and bianthrone photoproduct molecules with triplet ground state, using unrestricted Hartree-Fock theory 11 p1727 A71-25576

Rayleigh-Schrodinger perturbation energies for ground state of two electron atomic Hookes law model through tenth order 11 p1803 A71-26151

Collisional radiative volume recombination and ionization coefficients for quasi-stationary helium, considering singlet and triplet systems as two coupled individual systems 13 p2106 A71-28452

Hydrogen plasma internal magnetic field determination, using spectral characteristic measurements due to level intersection 13 p2108 A71-29030

Strong level crossing signals in stepwise fluorescence, investigating fine and hyperfine structure of atomic Li 14 p2277 A71-30508

Hartree-Fock energy levels, transition probabilities and wave functions for highly ionized atoms in B I isoelectronic sequences, including spin-orbit interactions 15 p2452 A71-32597

Energy dependence of collisional time delay functions computed for H/IS/ atoms interacting via hydrogen potential, determining scattering cross sections 16 p2613 A71-32811

Ion beam-foil produced oxygen spectra in wavelength range between 450 and 2200 Å, determining mean radiative lives of O I - O VI excitation levels 16 p2529 A71-33183

Ab initio calculations on trajectories and nonadiabatic transitions in reactions of hydrogen atomic ions with hydrogen molecules 18 p2949 A71-35897

Nonadiabatic effects in van der Waal line broadening, taking into account mixing between degenerate magnetic sublevels in atomic collisions 19 p3106 A71-37409

Core binding energy difference between bridging and nonbridging oxygen atoms in silicate chain of pyroxenes, using X ray photoelectron spectra 19 p3011 A71-37415

Atomic level interference and hyperfine splitting effects on angular and polarization distributions of resonantly scattered light in magnetic field 21 p3420 A71-41120

Free electron distribution function, atomic level population and ionization rate in low voltage arc near electrodes 23 p3709 A71-43266

ATOMIC EXCITATIONS

He-Cd laser stable long life CW excitation by DC cathodoresis to maintain spatially uniform and optimum Cd vapor concentration 01 p0091 A71-10007

Atomic H excitation by electron impact, deriving cross sections for anomalous recombination lines in H II regions radio frequency spectrum 02 p0317 A71-12872

He excitation by He, Ne, Ar and Kr collisions, calculating first Born wave cross section 03 p0460 A71-13499

Triplet O I excitation in night sky of tropical regions, using photometric measurements of line spectra 03 p0409 A71-13789

Sodium atom excitation by high energy particle collisions behind shock waves, measuring electron and vibrational temperatures 03 p0376 A71-13993

Average energies of ground and excited configurations in highly ionized atoms, using orthogonalized screened hydrogenic radial functions 04 p0630 A71-14999

Heavy particles collision induced excitation, deexcitation and ionization rates, calculating atomic H quantum level transitions due to H and He atomic collisions at thermal energies 05 p0785 A71-16490

O I 1304-Å airglow, observing conjugate excitation withOGO 4 spacecraft 06 p0888 A71-17279

Evanescent electromagnetic waves quantization by treating transverse triplet wave modes as noninteracting harmonic oscillator, discussing atomic excitation 07 p1159 A71-19548

Laser excited atoms quenching by iodine molecules from light pulse induced photodissociation of perfluoropropyl iodide active media 07 p1126 A71-20195

Atomic processes in plasmas including excitation, deexcitation, ionization, recombination, charge transfer, free-free transitions and spectral line broadening for theta pinch parameters determination 07 p1172 A71-20505

Nonequilibrium excitation in recombining nitrogen plasma nozzle flows [AIAA PAPER 70-44] 09 p1498 A71-22093

Cd atoms excited state populations in nonequilibrium gas discharge plasma 09 p1500 A71-22267

Phonon excitations radiated from thermal source in He II below 0.3 K, using carbon film detectors 09 p1497 A71-22418

Electron beam current density measurement using neutral Ar atoms electron impact excitation to metastable states 09 p1497 A71-22731

Bright quiescent solar prominences metastable He excitation, studying electron temperatures and densities in interfilament areas 09 p1525 A71-23197

Condensed state Ni and Pd atoms X ray emission spectra and electron structure 09 p1474 A71-23233

Electron impact excitation rates of bound electronic states of hydrogen, helium and alkali atoms 10 p1645 A71-24543

Atomic nitrogen far UV emission excitation in auroral ionosphere due to electron impact dissociations 10 p1605 A71-24792

Li photoionization cross sections determined from spectral intensity measurements as function of threshold wavelength, discussing radiative electron-recombination into first excited state 10 p1646 A71-24992

He-Zn ion laser, considering charge exchange and Penning collisions as primary excitation sources of Zn II levels 11 p1773 A71-25927

Radiative mean lives and transition probabilities of electronic states in beam foil excited atomic and ionic carbon 11 p1803 A71-26061

Hanle cascade effects on atomic lifetime reliability from collisional excitation experiments 11 p1803 A71-26370

Atom rigid rotor problem, applying generalized phase shift rotational excitation treatment in lowest approximation 12 p1932 A71-26949

Liquid He stable cavities localized excited states, calculating atomic line positions 13 p2101 A71-28796

Fine crystalline substances forced combination scattering at liquid nitrogen temperature, using ultrashort ruby laser pulses for excitation spectra 13 p2080 A71-29022

Atomic Ba excitation, ionization and oxidation during release in sunlight at high altitudes 13 p2026 A71-29038

Laser quantum theoretical analysis, considering atomic thermal motion, photon emission and absorption induced recoil effects on lasing threshold and operating frequency 14 p2253 A71-29574

Electron energy distribution function and ionization rate constant of atoms by electron impact as function of heavy particle temperature 16 p2615 A71-32796

Ba atoms excitation and optical transitions line broadening by collisions with Ar atoms behind shock waves, using atomic absorption spectroscopy

16 p2613 A71-32889

Monatomic mercury gas excitation and ionization mechanisms ahead of and behind shock front, establishing electron gas heating kinetics in relaxation zone

16 p2616 A71-32902

Radiative mean life measurements by low energy beam foil excitation, considering branching ratio of transition probabilities equal to unity

16 p2576 A71-33051

Newton-Raphson method application to iterative solution of atomic excitations and radiative transfer in plasma

17 p2838 A71-35554

Excitation cross sections for resonance states by electron impact on atomic nitrogen and oxygen over aeronomical energy range

18 p2949 A71-36350

Excited state absorption in sulfur hexafluoride traversed by carbon dioxide laser beam

18 p2933 A71-37014

Hydrogen ionization and excitation equilibrium, using slab model atmospheres irradiated from both sides by photospheric, chromospheric and coronal radiation

19 p3146 A71-38664

Pulsed laser oscillation from F atoms in mixed helium-fluorine gases using electric discharge excitation

20 p3244 A71-39107

Glauber and Vainshtein approximations for cross sections of 1s-2p excitation during inelastic electron-atomic hydrogen scattering

20 p3272 A71-39470

Dayglow and twilight emission data, discussing atomic excitation mechanisms, particle production rates, height profiles and temporal variations

20 p3227 A71-39835

Glauber scattering amplitudes for atomic hydrogen excitation by electrons or protons, presenting closed form expressions requiring no numerical integration

21 p3420 A71-41195

Quantum theory of molecular or atomic spontaneous emission while simultaneously undergoing stimulated emissions or absorptions

21 p3421 A71-41401

Analytic approximation for radial integrals and electron excitation cross sections of inert gases, using atomic screening parameters

22 p3577 A71-41620

Intermolecular forces and excited state from atomic line shape experiments, comparing numerical calculations with experimental data

22 p3578 A71-42463

Formaldehyde transitions in ground and excited states at 6 cm, attaining line widths and hyperfine structure at 1-3 kHz

23 p3723 A71-42953

Radiation quenching and depopulation of excited Hg atoms by collisions with ground state hydrogen molecules, using steady state flowing afterglow method

23 p3712 A71-43996

He excitation and ionization in chromospheric flares, performing calculations for 10,000-50,000 K electron temperatures and 0.5-9.0 times 10 to 13th power per cc electron densities

23 p3722 A71-44310

ATOMIC EXPLOSIONS

U NUCLEAR EXPLOSIONS

ATOMIC GASES

U MONATOMIC GASES

ATOMIC PHYSICS

Physics laws and simplifications, discussing Newtonian mechanics, electrodynamics, relativity, atomic physics and quantum theory

07 p1163 A71-19603

Beam foil spectroscopy using van de Graaff accelerator, considering applications to atomic physics research and teaching

08 p1272 A71-21667

Polar cap atomic processes stimulated by photons, electrons and protons, considering particle morphology

10 p1661 A71-24311

Atom rigid rotor problem, applying generalized phase shift rotational excitation treatment in lowest approximation

12 p1932 A71-26949

Shock tube spectroscopy as tool for atomic and molecular research, describing applications in chemical physics, astrophysics, gas dynamics, etc

16 p2578 A71-33152

Relative excitation functions for electron impact with Mg in crossed beam experiment, considering simultaneous ionization of neutral Mg

16 p2614 A71-33331

Radiative heat transfer in atomic lines through shock heated nonhomogeneous gases by analytical frequency integration, using separability approximation

19 p3162 A71-37407

ATOMIC RECOMBINATION

NT OXYGEN RECOMBINATION

Atomic ion-ion recombination total inelastic cross sections calculation by Landau-Zener method, noting agreement with experiment

01 p0129 A71-10366

Hydrogen atoms upper energy levels overexcitation in solar flare, suggesting role of stimulated photorecombinations

07 p1188 A71-20034

Atomic processes in plasmas including excitation, deexcitation, ionization, recombination, charge transfer, free-free transitions and spectral line broadening for theta pinch parameters determination

07 p1172 A71-20505

Recombination emission by atoms or radicals used with population for inversion thermal gas laser production

07 p1128 A71-20529

Nonequilibrium excitation in recombining nitrogen plasma nozzle flows

09 p1498 A71-22093

Two body N atoms recombination rate coefficient, using photometric analysis

09 p1498 A71-23400

ATOMIC SPECTRA

Rapid internal standard identification method for metals by atomic absorption spectrophotometry, using diluted acid solution of specimen

01 p0028 A71-10257

Term splitting of Li I, B I, Na I and other sequences with one electron spectra, using screening parameters obtained from Hartree-Fock calculations

08 p1337 A71-21182

Radiative lifetimes of UV multiplets in atomic C, N and O, using modified phase shift technique

10 p1645 A71-24547

Spectral studies on radiation from molecules, atoms and electrons, demonstrating shock tube applications in opacity measurements

11 p1764 A71-26265

Atomic bond strength of solid solution hardening as function of composition for calcium/strontium difluorides, using vibrational IR and laser Raman spectra

12 p1877 A71-26804

Arc heated plasma expansion through nozzle, observing population inversion of neutral carbon self-absorption UV atomic line

[AIAA PAPER 70-44]

15 p2454 A71-31537

Carbon K alpha band measurements in transition metal carbides, graphite and diamond, using X ray spectrometer with diffraction grating

15 p2430 A71-32149

H atoms generation by photodissociation of molecules evaporated from cometary core, basing analysis on hydrogen atmosphere line spectra

20 p3293 A71-39538

Fluorescence phenomena in celestial bodies, considering atomic lines and molecular bands in stellar and nebulae emissions

22 p3597 A71-41515

Atomic model potentials for spectroscopic and scattering data, using perturbation theory

22 p3578 A71-42420

Moment analysis of atomic spectral lines of Cs-Ar and Cs-He systems, using adiabatic approximation

22 p3578 A71-42462

Intermolecular forces and excited state from atomic line shape experiments, comparing numerical calculations with experimental data

22 p3578 A71-42463

ATOMIC STRUCTURE

Electric quadrupole atomic transitions in muonic PB208, charting X ray spectrum showing transitions

01 p0131 A71-11439

Disordered materials electronic structure band states localization, examining mobility edges

01 p0140 A71-11441

Near stoichiometric binary alloys atomic ordering parameters quantization by field ion microscopy, using direct counting and optical transformation techniques

02 p0297 A71-12736

Interlocking via photoexcitations and deexcitations due to lanthanide rare earths weak line solar spectra and ion atomic structure

06 p0969 A71-17970

Al alloy rapidly crystallized film structure, studying atomic diffusion mobility effects on formation of supersaturated solid solutions

07 p1130 A71-19299

Ni-transition element ternary alloys with bcc and fcc lattices, examining electron structure and ordering processes

07 p1163 A71-19429

Atomic ordered alloy compressive strengthening for fcc and bcc lattices in terms of yielding, work hardening and no hardening stages

07 p1132 A71-19438

Zirconium nitride electronic structure from X ray emission spectra, analyzing chemical bonds

08 p1305 A71-21061

Disordered materials electronic structure, discussing crystal types, amorphous semiconductors and Mott-CFO model

08 p1343 A71-21173

Book on gaseous ionization and plasma electronics covering atomic structure, electron emission, charged particle behavior, self sustaining discharge and breakdown mechanisms

08 p1341 A71-21700

Metals electronic structure effects on hydrogen diffusion mobility

09 p1471 A71-23082

Atomic scale elastic structure equations of state for Thomas-Fermi model extension to high pressures, considering earth core iron-silicates composition

11 p1802 A71-25572

Graphite fiber surfaces atomic composition data, using Auger electron spectroscopy in ultrahigh vacuum low energy electron diffraction system

11 p1788 A71-25633

Coupled and uncoupled versions of Hartree-Fock theory, calculating atomic system linear response to external time dependent perturbation and Green function

11 p1802 A71-26057

Electron structure of transition metals defects, using self consistent method to match resonance and drift integrals to cohesion energy

11 p1808 A71-26342

Alkali and rare earth metal hexaborides energetic structure, discussing semiconducting, semimetallic and metallic compounds on basis of energy bands and effective valence

12 p1944 A71-27094

Atomic and molecular spin in cosmic medium, discussing static/dynamic orientation, resonance mechanism, hyperfine structure and magnetic sublevels

12 p1933 A71-27420

Ni-Pd alloys atomic arrangements and displacements by single crystal X ray diffuse scattering, using computer simulated model

13 p2087 A71-29134

Gas atoms collisions with linear harmonic oscillator and solid surface simulated by semiinfinite elastically coupled atomic lattice, using combined asymptotic expansions method

13 p2103 A71-29227

X ray absorption and atomic number corrections in quantitative microprobe analysis of metals

14 p2277 A71-30476

Refractory and rare metals absolute melting temperature dependence on atomic number, lattice constant, charge negativity and crystallographic, thermodynamic and mechanical parameters

16 p2594 A71-33878

Transition metal carbides and nitrides ordered structures, determining C and N atoms positions with electron and neutron diffractions

16 p2597 A71-33921

Transition metals monocarbides and mononitrides electronic structure, investigating electrical, thermoelectrical and galvanomagnetic properties

16 p2597 A71-33922

Temperature dependent electron structure model of free energy decomposition of beta phase in Ti alloys

16 p2599 A71-34085

Niobium dislocation and electronic structure and mechanical properties after plastic deformation and annealing from electron beam studies

17 p2760 A71-35671

Wavelength prediction for coronal transitions at various atomic configurations, deriving semiempirical expressions from observed data for energy level intervals determination

18 p2965 A71-36733

Neutron diffraction analysis of atomic arrangements in maraging steel, discussing interatomic attractions

19 p3081 A71-37722

Atomic structure constants numerical calculation, obtaining H matrix of complex including spin-orbit interaction and configuration mixing

19 p3142 A71-38155

Diffusion processes electron mechanism in metal-metal and metal-nonmetal systems, using configurational model for valence electrons localization

21 p3403 A71-41159

Transition metal /particularly Ti/ carbide hardness temperature dependence explained from dislocation theory viewpoint, relating hardness to electronic structure

22 p3565 A71-41657

Atomic model potentials for spectroscopic and scattering data, using perturbation theory

22 p3578 A71-42420

Transition metal physicochemical properties explanation by many-electron effects in Hubbard model

23 p3714 A71-42932

Noble and transition metals dilute alloys electronic structure in hybridized tight binding nearly free electron representation, using Harrison-Kanamori pseudopotential theory

24 p3860 A71-45129

Noble or transition metals based dilute alloys electronic structure, describing pure metal band structure by interpolation scheme of hybridized tight binding and nearly free electron orbitals

24 p3860 A71-45130

ATOMIC THEORY

NT HEISENBERG THEORY

Interatomic forces and gas theories from Newton to Lennard-Jones, discussing hypothetical deductive atomic models relation to gas properties

01 p0129 A71-11401

Theoretical equations of state in geophysics, considering systematics approach to laboratory data, seismic velocity profiles, finite strain and atomistic approach

12 p1931 A71-27415

Sum rule functions for expressions of atomic or molecular quantum mechanical properties

16 p2603 A71-33527

ATOMIZATION

U ATOMIZATION

ATOMIZERS

Hollow cone water spray from pressure jet swirl atomizer into uniform air stream, observing drop velocities and trajectories by high speed photography

13 p2049 A71-28753

Liquid fuel atomizers for gas turbine combustion system model experiments, considering droplet sheet photography and molten wax spray technique

13 p2117 A71-28755

Optical measurement of sprays mean droplet size, assessing operating variables effect on air-blast atomizer characteristics

13 p2117 A71-28756

Gas turbine engine startup igniter with modified propellant atomizer enhanced by air injection

13 p2118 A71-28969

ATOMIZING

Quench atomization of iron alloys to powders, using liquid metal two fluid nozzle method

05 p0758 A71-16245

Supersonic combustion ramjet engine with liquid fuel injection, considering atomization process and ignition criteria

05 p0836 A71-16531

Liquid fuel atomization spectrum in nozzles, examining proportion control of droplet size

08 p1348 A71-21262

Two phase mixture nonequilibrium flow mathematical model with allowance for colliding droplets coagulation and atomization based on high speed photographic studies

10 p1551 A71-24380

Gas turbine engine combustion chamber start-up and burning performance, considering air injection and propellant atomization

13 p2117 A71-28968

Atomization drop size distributions in sprays from convergent pneumatic nozzles for molten wax and polyethylene mixtures

13 p2049 A71-29007

Metal powders role in brazing, considering melt atomization and mechanical comminution

13 p2075 A71-29089

Cold flow tests of mixing and atomization characteristics of gas/liquid circular coaxial injector elements in pressurized facilities

[AIAA PAPER 71-672] 14 p2291 A71-30736

Heating, fusion and atomization of meteoric bodies in earth atmosphere

17 p2810 A71-35724

Mass spectrometric investigation of plasma created in atomization of Ni and Y ferrites by laser radiation

19 p3110 A71-37142

Two phase nonequilibrium flow mathematical model with allowance for colliding droplets coagulation and atomization based on high speed photographic studies

24 p3790 A71-44927

ATOMS

NT METASTABLE ATOMS

NT OXYGEN ATOMS

NT RECOIL ATOMS

ATP

U ADENOSINE TRIPHOSPHATE [ATP]

ATROPINE

Gastrointestinal tract reactions to atropine sulfate, acetylcholine and carbacholine in rats after acceleration exposures, using roentgenograms

22 p3495 A71-42796

ATS [SATELLITES]

U APPLICATIONS TECHNOLOGY SATELLITES

ATS 1

Quiet day magnetic field variations at geosynchronous satellite ATS 1, comparing magnetospheric models

03 p0419 A71-14522

Quiet day geomagnetic field measurements at synchronous orbit ATS 1, calculating equatorial component of interaction force between solar wind and earth

07 p1102 A71-19664

Geomagnetic field measurements by ATS 1 in synchronous equatorial orbit, determining pulsations types during magnetically quiet and geomagnetic storm periods

09 p1440 A71-23636

ATS 5

ATS-5 satellite dual swept radiometer features, operation and specifications

01 p0082 A71-10985

ATS 5 satellite millimeter wave earth-space propagation and communications equipment

04 p0551 A71-15009

Magnetopause crossing observation of ATS 5 satellite during magnetic storm

06 p0887 A71-17258

Navigation and communication experiment at L band on board S.S. Manhattan using ATS-5 satellite with biphasic PSK modulation of three tones for ranging

07 p1057 A71-18816

Marine navigation and data communications at L band via synchronous satellite, assessing capabilities by tests on ATS-5 satellite

19 p3102 A71-38070

Dynamic analysis of ATS 5 heat pipe fluid energy dissipation, confirming estimated stability of planned rescue approach configuration

22 p3611 A71-42038

ATS 6

Radio signal receiving system design for group delay experiments with geostationary ATS-F for ionospheric and magnetospheric electron content

07 p1206 A71-19033

Composite ATS 6 and 7 satellite antenna feed capable of illuminating large space-deployable parabolic antenna

17 p2716 A71-35096

ATS 7

Composite ATS 6 and 7 satellite antenna feed capable of illuminating large space-deployable parabolic antenna

17 p2716 A71-35096

ATTACK AIRCRAFT

NT A-7 AIRCRAFT

NT BOMBER AIRCRAFT

NT BUCCANEER AIRCRAFT

NT F-14 AIRCRAFT

NT F-15 AIRCRAFT

NT FIGHTER AIRCRAFT

NT JAGUAR AIRCRAFT

NT TSR-2 AIRCRAFT

Mach 2 Mirage Milan ground attack fighter, noting lift aid moustache, low speed and steep approach handling from short airstrips

02 p0190 A71-12740

Automated design system producing wire format data for cabling avionics subsystem of light attack aircraft

[AIAA PAPER 69-976] 06 p0874 A71-17698

Cheyenne attack helicopter weapons system, discussing night vision capability, armament, fire control and navigation equipment integration

[AHS PREPRINT 530] 14 p2178 A71-31091

Weapons delivery computer for attack helicopters, using planar distributed function generator for general closed form instantaneous solution capability

[AHS PREPRINT 531] 14 p2209 A71-31092

Armored cockpit for attack aircraft combat effectiveness, including mold line tumbling plates, terminal ballistic kinematics and integral structural armor

[AIAA PAPER 71-778] 17 p2675 A71-35530

One man Jaguar aircraft navigation, weapon aiming system and pilot operational tasks, noting internal platform alignment, displays and target attack modes

20 p3261 A71-39825

ATTACKING [ASSAULTING]

Fighting between male mice isolated at early age or reared in small groups, considering ontogenetic and experiential determinants

13 p2011 A71-28805

ATTENTION

Performance decrement during bimodal vigilance task, discussing arousal and selective attention constructs

04 p0541 A71-14741

Overtraining reversal effect on attention process, using choice response and eye fixations compared to criterion trained group

10 p1562 A71-24204

Visual field displacement, examining directed attention and maladaptive adaptation

15 p2363 A71-31949

Visual evoked brain potential amplitude and detection efficacy relationship, discriminating between arousal and attention effects

17 p2682 A71-35114

Physiological mechanisms of human auditory attention, measuring changes in cerebral cortex averaged evoked potential and cochlear nerve response

17 p2693 A71-35575

Visual conspicuity measurements, determining effects of directed attention and relation to visibility

18 p2854 A71-36002

Human factors engineering, discussing industrial, engineering and experimental psychology, human relations, research on attention, perceptual motor skills and control systems laboratory

18 p2864 A71-36296

Visual attention automatization due to repeated stimulus experience, noting fixation rate habituation concomitance with fixations spatial distribution uncertainty reduction

20 p3193 A71-39545

Visual processes involved in flash perception, considering attention attraction at suprathreshold levels, unreliability at threshold levels and latency effects

22 p3497 A71-41477

Flashing lights attention attraction classification based on experimental results conversion into psychometric scale

22 p3498 A71-41486

ATTENUATION

NT ACOUSTIC ATTENUATION

NT ATMOSPHERIC ATTENUATION

NT AURORAL ABSORPTION

NT RADAR ATTENUATION

NT RADIO ATTENUATION

NT SHOCK WAVE ATTENUATION

NT SIDELOBE REDUCTION

NT WAVE ATTENUATION

ATTENUATION COEFFICIENTS

Atmospheric extinction coefficients dependence on wavelength, comparing theoretical prediction to observational data

01 p0119 A71-10832

Light scattering and attenuation coefficients calculation by small particle approximation, determining applicability limits from comparison with use of exact Mie formulas

07 p1160 A71-19809

Acoustic duct lining materials, comparing attenuation constants according to Scott theory

08 p1333 A71-20808

Radiation attenuation volume coefficients for water clouds and fogs thermal sources and laser outputs

16 p2543 A71-33708

Rhodochrosite /manganese carbonate/ complex refractivity determination for correlation between optical reflection, attenuation and scattering coefficients

20 p3269 A71-39185

Physical interpretation of electromagnetic waves attenuation function HF singularity during diffraction over spherical surface, applying to short wave diffraction in tropospheric model

20 p3198 A71-39802

Closed phase lock loop FM demodulator design, determining resonant frequency parameters, attenuation factor and low pass filter elements

23 p3650 A71-43094

Coherent acoustic wave propagation speed and attenuation coefficient in turbulent flow

23 p3703 A71-43209

Sandwich wire traveling wave antenna radiation patterns, obtaining attenuation constant

23 p3654 A71-44157

VLF day and night waveguide modes attenuation coefficients and phase velocities, using moving secondary source formed by mode conversion at sunrise and sunset shadow line

24 p3803 A71-44650

ATTENUATORS

NT POTENTIOMETERS [RESISTORS]

NT PRINTED RESISTORS

NT RESISTORS

NT THERMISTORS

Carbon dioxide lasers IR variable double prism attenuator with gap spacing determination by capacitance measurements

05 p0760 A71-16257

Decision-directed digital adaptive signal equalizer for high speed data transmission, discussing design and advantages

05 p0725 A71-17065

Stepped wideband radio signal power generator with manually controlled signal attenuator

06 p0876 A71-18078

High power light beams attenuator usable as polarizing and depolarizing device, describing design for efficiency and elimination of beam shifting

06 p0908 A71-18081

X band gas tube attenuator for ruby maser saturation protection in pulsed high power radar

07 p1070 A71-18866

Photometric attenuator with linear birefringent polarizers, describing construction and calibration

07 p1110 A71-19468

Symmetric self-calibrating attenuator consisting of rotatable grid between two fixed grids for application at submillimeter wavelengths

09 p1421 A71-23682

Unmodulated microwave oscillations power stabilizer with semiconductor attenuator

13 p2036 A71-28367

High speed rotating optical attenuator for sub-second sawtooth radiance pulse generation for detection, cooling or heating experiments

19 p3063 A71-37249

Precision compact rotary vane microwave attenuator, presenting modified law to extend dynamic attenuation range and reduce rotor section length
24 p3809 A71-45089

ATTITUDE [INCLINATION]

NT PITCH [INCLINATION]

Biocybernetic model of vestibular control system for spatial orientation, considering semicircular canals fluid motion angular velocity sensors and linear displacement perception
03 p0367 A71-12982

Linear coupling between orbital and attitude motions of rigid body, deriving 12th order six degrees of freedom linearized motion equation
09 p1516 A71-22173

Computerized sloshing frequencies of tilting two dimensional tank of flat free surfaces with respect to effective gravity
11 p1752 A71-26198

Preferential orientation of physical galactic pairs, obtaining equatorial plane inclinations and major axes positional angles distribution
12 p1955 A71-26582

Automatic leveling instrument gravity intensity and compensator support tilt angle variations effects on measurement error
15 p2410 A71-32353

Pilots illusory attitude perception causes, suggesting psychological and medical remedies
16 p2534 A71-32830

Herringbone grooved gas lubricated journal bearing load capacity, attitude angle and power loss measurements
17 p2749 A71-35487

Vehicle attitude determination and guidance sensor orientation by vector space matrix method, minimizing errors by weighted least squares affine transformation technique
[AAS PAPER 71-396] 23 p3773 A71-43064

Physiological systems connected with sensory perception of equilibrium and orientation on ground and in air, discussing pilot training and selection
23 p3632 A71-43148

ATTITUDE CONTROL

NT DIRECTIONAL CONTROL

NT LATERAL CONTROL

NT LONGITUDINAL CONTROL

NT SATELLITE ATTITUDE CONTROL

NT THRUST VECTOR CONTROL

NASA modular aerospace computer for attitude control high speed computation, describing implementation with LSI functional characters
01 p0045 A71-10198

Spinning space stations with mass geometry changes, discussing attitude and angular velocity optimal control
01 p0164 A71-11435

Axisymmetric spacecraft fuel optimal reorientation control by reaction jets determined using Pontryagin maximum principle
01 p0165 A71-11586

Motion components about center of mass of body using flywheel attitude control by small parameter method
02 p0279 A71-11906

Cassiopee attitude control device for sounding rocket impulse trajectory correction, discussing spinning nose cones, corrective algorithm and final impact accuracy
[AIAA PAPER 70-1378] 03 p0498 A71-13661

Unguided, attitude stabilized and velocity controlled sounding rockets impact dispersion, discussing system selection and servomechanism
[AIAA PAPER 70-1381] 03 p0498 A71-13664

Skyark sounding rocket attitude control by three axis star pointing system, using strapdown gyro and plus 5 magnitude stellar sensor
[AIAA PAPER 70-1401] 03 p0455 A71-13682

Stellar Tracking Rocket Attitude Positioning System /STRAP/ for sounding rocket payloads three-axis orientation control with accuracy
[AIAA PAPER 70-1402] 03 p0455 A71-13683

Gyro-inertial three axis attitude control systems for sounding rockets, using two degrees of freedom gyro as orientation reference
[AIAA PAPER 70-1405] 03 p0455 A71-13684

Sounding rocket attitude monitoring and control, using digital output roll stabilized gyro platform
[AIAA PAPER 70-1407] 03 p0455 A71-13686

Spacecraft attitude suboptimal control by orthogonal set of amplitude limited PWM reaction control jets, presenting spacecraft controlled motion computer simulation
[AIAA PAPER 70-997] 03 p0499 A71-13722

Spin stabilized spacecraft fuel optimal direction cosine attitude control, considering relation to inertial system
03 p0500 A71-14448

Spinning aerospace vehicle optimal attitude control system by minimizing reaction fuel, noting application of Pontryagin maximum principle
04 p0623 A71-15143

Spacecraft attitude control system with inertia wheels, determining stability by decomposition method
04 p0663 A71-15300

Pulsed plasma thruster system as secondary propulsion unit for spacecraft attitude, station and trajectory control
04 p0638 A71-15325

Attitude and velocity control for VTOL aircraft takeoff and landing operations in hovering flight, discussing simulation devices and testing operations
[DGLR-70-073] 05 p0779 A71-15948

Europa 2 booster rocket third stage attitude control system, describing measuring, controlling and actuating functions dynamic integration and checkout
05 p0815 A71-16134

Cassiopee attitude control system for sounding rockets using stellar and inertial sensors for orientation and pointing
[AIAA PAPER 70-1404] 05 p0780 A71-16416

Delta booster second stage packaged attitude control three-axis system, discussing electronic implementation for gyroscopic action control
05 p0818 A71-17138

Launch vehicle attitude control system for lateral drift minimization and prevention of structural load limit exceeding maneuvers, presenting stability analysis
06 p0979 A71-17338

Kalman-Bucy linear filtering algorithm application to nonlinear estimation of single channel missile attitude control system parameters
07 p1081 A71-18835

Orbiting spacecraft local attitude determination, analyzing second order gyrocompass filter, third order steady state filter and fourth order time varying gyrocompass filter
07 p1207 A71-19531

Spacecraft attitude control microthrusters utilizing catalytically reactive gas mixtures during pulse mode and steady state operation
[AIAA PAPER 70-614] 07 p1183 A71-19859

Representative data of actual forces and moments applicable to large spacecraft attitude control system for typical crew activities obtained through simulation programs
[AIAA PAPER 69-1006] 07 p1208 A71-19866

Missile fluidic attitude control system, discussing integrator, transducer amplifiers and circuits
07 p1028 A71-20583

Missile roll axis attitude control system based on fluid amplifiers, describing fluidic integrator and chain
07 p1028 A71-20584

Switching analysis for high order vehicle systems with magnitude and direction constraints in attitude control for Saturn rocket with sloshing motion
08 p1269 A71-21331

Planar microwave array antenna for scan requirement, discussing tilt angle and element arrangement optimization
[AIAA PAPER 70-191] 08 p1229 A71-22030

Fluidic inertial instruments, describing sensor or transducer components, flight control systems, rate damper systems and attitude control systems
09 p1387 A71-22785

Hybrid coordinate formulation for flexible space vehicle attitude control system design
[AIAA PAPER 70-20] 09 p1532 A71-22907

Ion orientation technique for attitude control based on counterflow sensing in earth upper atmosphere, discussing accuracy
09 p1523 A71-23151

Constant attitude light aircraft flight control system, describing design studies for minimum pilot command requirements
[SAE PAPER 710393] 10 p1555 A71-24257

Aircraft with automatic thrust controller, calculating transfer functions characterizing speed and attitude control modes
10 p1640 A71-24910

Attitude control loop and inertial guidance hardware, studying system dynamic performance hybrid simulation
11 p1796 A71-25846

Reliable brushless direct-drive system design for controlling position and rate of solar power arrays on orbiting spacecraft
12 p1869 A71-27432

Space vehicles solar orientation sensors, discussing construction, configuration and direction finding characteristics
12 p1972 A71-27485

Space shuttle propulsion systems, describing main engine prototype designs, booster attitude and docking control systems
12 p1946 A71-27606

Motion components about center of mass of body using flywheel attitude control by small parameter method
13 p2098 A71-28193

Human body attitude control in space, using ten body complex geometry system, noting astronaut training jig
14 p2188 A71-29832

Catalytic hydrazine thruster design, fabrication and testing for TOPS spacecraft single-axis attitude control simulation program
[AIAA PAPER 71-706] 14 p2294 A71-30763

Algorithm providing three-gimballed inertial system all-attitude capability by protecting against gimbal lock
14 p2272 A71-30802

Dachs three axis payload stabilization and attitude control system for spectroscopic comet observation
15 p2499 A71-31218

Apollo Telescope Mount for high resolution solar observation and manned instruments evaluation in space environment, discussing attitude and pointing control systems
15 p2500 A71-31458

High performance low cost space shuttle propulsion systems airbreathing engines, attitude control thruster and orbital maneuvering
[AIAA PAPER 71-656] 15 p2470 A71-32292

Goddard trajectory determination system, discussing attitude dynamics, data preparation, differential correction and orbit information
15 p2495 A71-32645

Skylab pointing and control system using control moment gyros and cold gas reaction thruster system to provide attitude control
17 p2813 A71-35064

French monograph on DC/DC transformers with controllable output voltage covering ion beam electrostatic deviation during attitude control, equivalent transformer circuits, etc
17 p2677 A71-35234

Ion propulsion R and D at ONERA, discussing ionizer test control procedures, attitude control simulation and neutral fraction measurements
[DGLR-71-027] 17 p2793 A71-35536

Space shuttle attitude control propulsion and orbit maneuver, considering high and low chamber pressure gaseous systems
18 p2973 A71-36456

Breadboard attitude control system for scale model space station using control moment gyros
[AIAA PAPER 71-935] 19 p3097 A71-37180

Double gimbal control moment gyro systems for spacecraft attitude control, providing three axis attitude stabilization, precision pointing control and maneuverability
[AIAA PAPER 71-937] 19 p3097 A71-37182

Optimized momentum and attitude control system /MACS/ for Skylab class space stations employing control moment gyro and reaction jet elements
[AIAA PAPER 71-938] 19 p3098 A71-37183

Gravity gradient desaturation of momentum exchange attitude control system, considering control moment gyros and reaction wheels
[AIAA PAPER 71-940] 19 p3098 A71-37185

Gimballed reaction wheel for spacecraft accurate attitude stabilization and control
[AIAA PAPER 71-950] 19 p3098 A71-37191

Twinn wheel momentum bias/reaction jet spacecraft attitude control system, presenting mathematical model, stability analysis and design
[AIAA PAPER 71-951] 19 p3099 A71-37192

Integrated system for precision attitude determination and pointing control of spacecraft gimballed payloads
[AIAA PAPER 71-962] 19 p3099 A71-37203

Gyro and star tracker precision attitude determination system, assessing computational and other error effects on system performance
[AIAA PAPER 71-964] 19 p2996 A71-37205

Skewed and orthogonal redundant reaction wheels comparison for outer planet exploration spacecraft attitude control based on reliability analysis
[AAS PAPER 71-157] 19 p3101 A71-37926

Attitude control propulsion system for booster and orbiter of space shuttle in European participation package
21 p3454 A71-40159

Optical orientation determination and star pattern recognition for Skylab in solar inertial attitude by digital and hybrid simulations
[AAS PAPER 71-397] 23 p3732 A71-43065

Analysis and stability of multiloop attitude control systems for flexible spacecraft
23 p3773 A71-44091

German book on adaptive control systems covering flight attitude control, jet engine thrust, marine surface navigation, identification, etc
23 p3660 A71-44187

ATTITUDE GYROS

NT GYRO HORIZONS

Two-gyro attitude control system with conical suspension, analyzing vehicle motion asymptotic stability in circular orbit
01 p0081 A71-10634

Gyro-inertial three axis attitude control systems for sounding rockets, using two degrees of freedom gyro as orientation reference
[AIAA PAPER 70-1405] 03 p0455 A71-13684

ATTITUDE INDICATORS

NT GYRO HORIZONS

San Marco satellite attitude determination from on-board aerodynamic drag measurements, using least squares method for three components calculation
01 p0122 A71-10390

Optimum orientation and accuracy of redundant sensor arrays in space navigation, guidance and attitude reference systems
[AIAA PAPER 71-59] 06 p0925 A71-18518

ESRO 1 small scientific satellite attitude measurement system, discussing design and flight test results
07 p1154 A71-18840

Spacecraft attitude measurement using spatial coherence of laser or star light beam, discussing feasibility and detection equipment
12 p1927 A71-27429

Compound pendulum in artificial satellite for establishing attitude reference or detecting rotation rate variations
17 p2813 A71-34870

Integrated system for precision attitude determination and pointing control of spacecraft gimbaled payloads
[AIAA PAPER 71-962] 19 p3099 A71-37203

Right ascension and declination accuracy for Sirio satellite attitude determination in transfer orbit, describing computer program
19 p3150 A71-37312

ATTITUDE STABILITY

NT DIRECTIONAL STABILITY

NT GYROSCOPIC STABILITY

NT LATERAL STABILITY

NT LONGITUDINAL STABILITY

Gimbaled reaction boom attitude control systems for gravity gradient stabilization of earth-pointing satellites, investigating performance by dynamic model simulation
01 p0165 A71-11585

Spacecraft attitude control system with inertia wheels, determining stability by decomposition method
04 p0663 A71-15300

Space vehicle attitude stabilization system, using sensor with hysteresis relay characteristic for vibration damping
05 p0780 A71-16049

Spinning symmetric satellite roll-yaw resonant attitude instabilities in circular orbit
[AIAA PAPER 71-88] 06 p0980 A71-18544

Inertia effects on coupled librations and stability bounds of axisymmetric gravity oriented satellites in circular orbits, using integral manifold
11 p1838 A71-26195

Dual spin spacecraft bearing assembly flexibility effects on attitude stability, discussing time constant
[AIAA PAPER 70-1043] 12 p1973 A71-27569

Asymptotic stability of equilibrium position of vibrating linear mechanical systems with semidefinite damping matrix applicable to satellite attitude stabilization
15 p2502 A71-31174

Space vehicle attitude stabilization system, using sensor with hysteresis relay characteristic for vibration damping
16 p2605 A71-33453

ESRO activity in low thrust electric propulsion systems development for attitude stabilization and stationkeeping, using colloid and field emission thruster concepts
[DGLR-71-035] 17 p2794 A71-35541

Wideband stabilizer design for high acuity aerial reconnaissance camera to obtain high degree of attenuation to roll and pitch rotational motion inputs
18 p2919 A71-36087

Artificial g space station configurations, developing movable control mass attitude stabilization system
18 p2971 A71-36277

Double gimbal control moment gyro systems for spacecraft attitude control, providing three axis attitude stabilization, precision pointing control and maneuverability
[AIAA PAPER 71-937] 19 p3097 A71-37182

Electromagnetic actuator for momentum desaturation of control moment gyros used for attitude stabilization and control of space stations
[AIAA PAPER 71-939] 19 p3098 A71-37184

Gimbaled reaction wheel for spacecraft accurate attitude stabilization and control
[AIAA PAPER 71-950] 19 p3098 A71-37191

Dual-spin vs three-axis stabilization and control systems for synchronous communication satellite design
21 p3454 A71-40477

Three-axis and dual-spin stabilization systems for future synchronous communication satellites, considering reliability, mission flexibility and growth potential
21 p3455 A71-40479

Attitude stiffness and pointing accuracy of three-axis and dual-spin stabilization system for future synchronous communication satellites
21 p3455 A71-40481

German monograph on locking process in earth satellites with passive magnetic attitude control cover-

ing satellite rotational motion mathematical model, stability analysis, etc
21 p3455 A71-40773

Earth-orbiting space vehicle attitude motion under constantly acting disturbances based on mathematical total stability of equilibrium
22 p3608 A71-41968

Spin stabilized lunar satellite attitude determination, using Kalman filter for processing telemetered sun aspect angle measurements from satellite sensor
22 p3573 A71-42780

Attitude stability of dual spin spacecraft with energy dissipation in flexible momentum wheel having two degrees of freedom
[AAS PAPER 71-347] 23 p3772 A71-43020

ATTRITION [MATERIALS]

U COMMUNITION

AUDIO EQUIPMENT

NT MICROPHONES

Electroencephalophone for stereophonic display of four channel EEG physiological signals from skull quadrants
09 p1397 A71-22252

AUDIO FREQUENCIES

HF stability audio multichannel oscillators design and operation, comparing frequency synthesizer systems for optimal circuitry characteristics
09 p1417 A71-23029

Humidity effects on sound velocity in air at constant temperature and normal atmospheric pressure in lower audio frequency range
10 p1642 A71-24815

Field strength standards and calibrations for frequencies from audio to 1 GHz range, discussing uncertainties
14 p2205 A71-30980

Stress determination by vibration measurement in cantilever specimens fatigue tests with audio frequency loading, taking into account end restraint elasticity
19 p3160 A71-38347

AUDIO VISUAL EQUIPMENT

U TRAINING DEVICES

U VISUAL AIDS

AUDIOMETRY

Electrophysiological audiometry noting average brain response in man
06 p0858 A71-17295

Pure tone, air/bone conducting and speech audiometry, considering hearing tests, artificial mastoids, environmental requirements and physical principles
06 p0859 A71-18029

Quick-check audiometry reliability for testing hearing ability according to fitness regulations, comparing to complete tone and speech audiometry
14 p2188 A71-29821

Comparative residual and reversed microinterval masking signals and human auditory perception capacity measurements using sound level estimates
22 p3490 A71-42579

AUDITORY DEFECTS

F-100 pilots acute HF hearing loss due to noise ground environment and excessive in-flight noise exposure
09 p1400 A71-23249

Nonauditory and auditory physiological effects of noise, discussing hearing conservation, noise measurement and noise hazard
11 p1726 A71-26511

Aircraft noise effect on hearing impairment of cockpit crews in civil aviation, using audiometric evaluation
19 p3008 A71-38222

AUDITORY PERCEPTION

Extraauditory effects of sound on senses, concerning visual functions, nystagmus, galvanic skin response and audioanalgesic use
03 p0359 A71-13158

Neurophysiological aspects of human optical and acoustical perception, discussing pattern recognition and cognizance role in optical image evaluation
03 p0373 A71-14331

Impulsive sound signals perceived noisiness in anechoic chamber, investigating duration, intersignal interval, repetition and frequency effects
05 p0712 A71-16277

Auditory meatus sound pressure levels measurements in subjects with fabricated human ear molds with canal modifications, considering frequency responses and resonance
05 p0712 A71-16279

Acoustic intensity and exposure time duration for threshold lesion in cat brain
05 p0712 A71-16283

Auditory illusions, investigating phonemic restorations, verbal transformations and perceptual organization
07 p1051 A71-20212

Human panel comparison of aircraft engine noise tape recordings with synthetic broadband noise approximating pure jet
09 p1398 A71-22255

Neurophysiological auditory information processing, considering mechanical transformation of

two dimensional pressure-time signal and three dimensions for presentation to nervous system
10 p1562 A71-24228

Speech processing and recognition, considering progressive data reduction by ear and physiological limitations imposed information rate time variation
10 p1568 A71-24230

Vibrotactile information transmission, discussing skin mechano-receptive systems and similarities or differences between auditory and tactile characteristics
10 p1563 A71-24231

Auditory analyzer functional changes in flight crews as result of long flights and emotional stress, noting cumulative effects of various harmful factors
10 p1569 A71-24340

Intramodal and crossmodal sensory transfer of visual and auditory temporal patterns in normal young adults
13 p2022 A71-29326

Acoustic nerve, cochlear nucleus and superior olivary complex central projection, investigating ascending auditory system organization
14 p2183 A71-30255

Gundefender earplug evaluation tests, using temporary threshold shift reduction and modified rhyme techniques for speech intelligibility measurement in noise
15 p2364 A71-32196

Frequency and level dependent discrepancy between free field and pressure thresholds at low frequencies due to physiological noise produced under earcap
17 p2681 A71-34699

Physiological mechanisms of human auditory attention, measuring changes in cerebral cortex averaged evoked potential and cochlear nerve response
17 p2693 A71-35575

Human response to auditory stimuli start and cessation, noting time lag and perception duration
19 p3001 A71-37283

Prediction methods for human aircraft noise perception, assessing weighted sound pressure level or complex loudness-noisiness computation scales
21 p3325 A71-40866

Noy curves in perceived noise levels, noting relative noisiness dependence on relative intensities
21 p3325 A71-40867

Comparative residual and reversed microinterval masking signals and human auditory perception capacity measurements using sound level estimates
22 p3490 A71-42579

Contrast effects in loudness judgments, using category scale and maximally extensive number response language
23 p3638 A71-43111

Human auditory adaptation to medium intensity noise complex action under relative isolation and hypokinesia conditions from monaural hearing threshold measurement
24 p3799 A71-44400

AUDITORY SENSATION AREAS

Methionine S 35 uptake rate changes in auditory analyzer receptors and neurons due to sonic stimulation in guinea pigs
06 p0850 A71-17393

AUDITORY SIGNALS

External acoustic signals for human cyclic movements temporal structure control
02 p2025 A71-12058

Human voice imitation of tonal signals pitch interval
02 p2026 A71-12061

Impulsive sound signals perceived noisiness in anechoic chamber, investigating duration, intersignal interval, repetition and frequency effects
05 p0712 A71-16277

Cochlear auditory patterns degrees of freedom along spatial axis, considering displacement of basilar membrane and mechanical coupling
05 p0706 A71-16281

Horizontally coherent supersonic velocity LF sound signals from Apollo rocket vehicles at high elevations
07 p1208 A71-20149

Circuit selection for LF three octave acoustic signal bandpass filters, taking into account time constants
08 p1261 A71-20738

Muscle reflex action role in contralateral remote masking at high auditory signal sound pressure levels
08 p1246 A71-20803

Cortical potentials evoked by weak acoustic signals below hearing threshold in man
10 p1564 A71-24440

Human auditory signal detection related to averaged evoked potential in scalp by electrophysiological measurements
16 p2534 A71-32951

Cochlear nucleus and posterior clivus neurons impulse activity due to tonal signals in anesthetized cats auditory system
16 p2532 A71-33899

Comparative residual and reversed microinterval masking signals and human auditory perception capacity measurements using sound level estimates
22 p3490 A71-42579

AUDITORY STIMULI

Conditioned reflexes in cats with mesencephalic reticular formation subject to food-signaling acoustic stimulation
01 p0007 A71-10034

Guinea pigs head and eye movements produced by vestibular apparatus stimulation via static pressure changes
01 p0010 A71-10347

Auditory averaged evoked potential as measure correlating with degree of psychopathology in schizophrenia
01 p0011 A71-10765

Step-wise discriminant analysis in auditory evoked potential variability in schizophrenia
01 p0011 A71-10766

Orientiation reflex in healthy and nervous human subjects from peripheral vessels blood pressure fluctuations in response to acoustic signals
01 p0012 A71-11055

Rodents bimodal cochlear microphonic response to high frequencies recorded from round window membrane
01 p0016 A71-11346

Reaction time diurnal variations to optical and acoustic stimuli, investigating disturbed natural sleep-waking rhythm effects
02 p0197 A71-11684

Moderate acoustic stimuli effects, discussing subjective noise ratings relation with physiological and mental state changes
02 p0208 A71-12838

Audiogenic stress effects on susceptibility to cyto-destructive and oncogenic virus infections and host defense mechanisms
03 p0359 A71-13152

Protective brain function in epileptical convulsive seizures during sonic stimulation in rats
03 p0359 A71-13159

Acoustic priming of audiogenic seizures in mice, noting high susceptibility to convulsions under intense sound
03 p0360 A71-13160

Genetics and temporal audiogenic seizures in mice, noting age and exposure effects on susceptibility
03 p0360 A71-13161

Neurochemical factors in auditory stimulation and susceptibility to audiogenic seizures, noting gamma-aminobutyric acid /GABA/ inhibitor
03 p0360 A71-13164

Sound duration effect on brain activity of cats, studying EEG and behavioral responses
03 p0361 A71-13189

Acoustic stimulation effect on electroretinogram of man
03 p0361 A71-13191

Bias free loudness judgments by modification of vision studies method, considering physical correlate theory of stimulus intensity
05 p0712 A71-16282

Multiple acoustic evoked responses coherence time course using mathematical correlation and Fourier transforms
05 p0714 A71-16922

Topography of acoustically evoked potentials triggered by alpha activity in man
05 p0710 A71-16942

Methionine S 35 uptake rate changes in auditory analyzer receptors and neurons due to sonic stimulation in guinea pigs
06 p0850 A71-17393

Intermittent noise effects on performance of visual search tasks of varying complexity, measuring test subjects target detection time under various noise/time ratio conditions
10 p1562 A71-24206

Critical period and habituation in control precision performance response to startle due to pistol shots
11 p1723 A71-25181

Temporal and spectral stimuli combinations effects on judged noisiness of aircraft sounds by college students
12 p1868 A71-27531

Behavioral arousal and EEG thresholds changes during sleep due to electrical and audio stimulation
13 p2005 A71-28379

Humans and animals vestibular stimuli effect on external respiration function and respiration center neuron activity
13 p2007 A71-28413

Habituation and dishabituation of human vertex response, using auditory or somatosensory stimuli
13 p2012 A71-28890

Repetitive stimulation effects on auditory evoked potentials in cochlear nucleus, inferior colliculus and medical geniculate body of unanesthetized cats
13 p2012 A71-28892

Conditioned auditory reflex behavior in rats under influence of acceleration, noting ontogenetic effects
15 p2356 A71-31249

Blood circulation in auditory analyzer cortical section relationship to bioelectrical activity, using various frequencies pure tones as stimuli
15 p2360 A71-32531

Sounds effects on natural nocturnal sleep of healthy humans with normal hearing
17 p2679 A71-34479

Visual and auditory evoked potentials enhancement in cats using cryogenic blockage of nonspecific thalamo-cortical system in inferior thalamic peduncle region
17 p2682 A71-35112

Orientation reflexes neuronal activity due to various stimuli, noting hippocampus reaction to sound and light
17 p2685 A71-35361

Reaction times distributions in visual or auditory mode single and multiple motor response units
17 p2686 A71-35433

Fear measurement and mastery, investigating relationship between experience and electrodermal arousal in responses to stimulus words of varying relevance
18 p2862 A71-36944

Human response to auditory stimuli start and cessation, noting time lag and perception duration
19 p3001 A71-37283

Analog statistical analyzer for measuring one dimensional EEG amplitude distribution functions, illustrating reaction response to threshold acoustic stimuli
21 p3344 A71-41067

Analog computer analysis of EEG wave asymmetry for organism functional state detection illustrated on human reaction response to threshold acoustic stimuli
21 p3344 A71-41068

Auditory stimulus conditioning of human skin resistance responses on escape-avoidance schedule
22 p3497 A71-42862

Proactive reaction time inhibition as indicator of immediate memory retention intensity in subjects receiving interpolated acoustic stimuli
23 p3634 A71-43865

Trace reflex formation in response to acoustic stimulus with verbal reinforcement, determining cross correlation connections between induced activity of auditory and motor areas
24 p3796 A71-44547

Eye movements and visual images evoked by verbal stimuli, considering hereditary factors contribution to image formation
24 p3796 A71-44548

AUDITORY TASKS

Signal detection payoff in symmetrical auditory task, studying effect on rates and error analysis
07 p1045 A71-20384

Multiple suprathreshold visual and auditory monitoring tasks, evaluating vigilance decrement, in individual differences, intertask relationships and channel capacity
12 p1874 A71-27248

AUGER EFFECT

Secondary emission analog for improved Auger spectroscopy to eliminate objectionable feature of electron spectra taken with retarding potential analyzer
18 p2922 A71-36579

K-LL Auger spectra of nitrogen, oxygen, carbon monoxide, nitrogen oxide, water and carbon dioxide, using double focusing electrostatic electron spectrometer
21 p3345 A71-40235

AUGMENTATION

NT THRUST AUGMENTATION

Nightglow 6300 A emission latitude wide enhancement at Mt. Abu, India
06 p0893 A71-17990

Large coronal streamer with active region enhancement during total eclipse on 22 September 1968, giving model of enhancement
16 p2625 A71-33328

AURIGA CONSTELLATION

Hydroxyl emission at T Tauri stars positions in Taurus-Auriga region, discussing radial velocities of stars and dust clouds
19 p3144 A71-38172

AURORAL ABSORPTION

Auroral absorption of HF radar waves over high latitude ionospheric paths
01 p0041 A71-11610

Polar aurora pulsations of 4-12 sec intensity with associated cosmic radio noise absorption, using photometric measurements
02 p0242 A71-11761

Space-time structure of ionospheric regions of anomalous radio wave absorption during auroras, discussing ionization region
02 p0243 A71-11765

Auroral absorption classification of cosmic noise at 32 MHz, plotting time and amplitude distribution diagrams
02 p0243 A71-11769

Atmospheric circulation and earth rotational energy contribution to energy release by intense polar auroras, noting ionospheric current subsonic heating and oxygen emission
02 p0244 A71-11909

Auroral absorption latitudinal distribution diurnal variations, showing existence of two zone model
05 p0746 A71-17205

Time structure of auroral radio absorption from magnetically conjugate and closely spaced observations
06 p0892 A71-17977

Ionospheric radio wave absorption above polar aurora during solar activity minimum, discussing diurnal and annual behavior
09 p1435 A71-22429

Atmospheric circulation and earth rotational energy contribution to energy release by intense polar auroras, noting ionospheric current subsonic heating and oxygen emission
13 p2058 A71-28196

Auroral absorption latitudinal distribution diurnal variations, showing existence of two zone model
13 p2060 A71-28260

Auroral absorption and DR currents development during magnetic storms, discussing corpuscular fluxes arrival from magnetospheric tail into lower ionosphere
13 p2062 A71-28563

Conjugate and closely-spaced riometer observations of auroral radio absorption, considering explanation by alternation of particle precipitation between Northern and Southern Hemispheres
14 p2192 A71-29667

IQSY data analysis of pulse reflection measurements from midlatitude station, determining polar cap and auroral absorption
15 p2396 A71-31611

Equatorial and precipitating solar proton fluxes interrelationship in magnetosphere from riometer absorption in auroral and polar cap regions
19 p3125 A71-37360

Auroral zone proton measurements during slowly varying cosmic noise absorption, obtaining energy spectrum by rocket soundings
19 p3125 A71-37418

Auroral pulsations physical correlation with cosmic noise absorption, using statistical correlation analysis
20 p3215 A71-38734

AURORAL ACTIVITY

U AURORAS

AURORAL ARCS

NT RED ARCS

Rocket-borne mass spectrometer observation of NO in auroral arc
01 p0077 A71-11522

Parallel and perpendicular electric fields in auroral arcs from rocket-borne experiment
03 p0406 A71-13303

Polar auroral arc orientations spatial and diurnal distribution and morphological characteristics for grouping into four types, discussing aurora borealis
05 p0744 A71-17188

Small scale spatially periodic auroral arc distortion observations, using low light level TV reception
06 p0893 A71-17981

Morphology and dynamics of low intensity monochromatic midlatitude auroral arcs of 6300 A /O I/, comparing results with observation during IGY
07 p1103 A71-19766

Oxygen red-green line emission intensity in quiet auroral arc, using rocket-borne photometers
11 p1754 A71-25551

Multiple midlatitude auroral arcs during geomagnetic storm recovery phase /8-9 March 1970/, noting correlation with recorded geomagnetic field intensity variations
12 p1902 A71-27670

Auroral arc orientation spatial and diurnal distribution, location and morphological characteristics, grouping into four types
13 p2059 A71-28245

Equatorward moving fast auroral waves recorded with image intensifier-TV system
14 p2229 A71-29660

Auroral substorms development phases, noting auroral arcs latitudinal shifting during genesis phase
19 p3059 A71-38394

E x B plasma instability in auroral arcs, deriving dispersion relation
21 p3373 A71-40045

Electric current shear at auroral arcs due to electron precipitation into lower ionosphere
22 p3536 A71-42623

Magnetospheric substorms observations by satellite and balloon-borne X ray detectors, considering auroral arc brightening and energetic electron flux enhancement in magnetotail
23 p3668 A71-43163

Geomagnetic bay-like disturbances formation and decay during multiple midlatitude 6300 A auroral arc after magnetic storm, observing time variation of current system pattern
23 p3672 A71-43981

Geophysical data analysis for high latitude negative geomagnetic disturbances revealing geomagnetic pulsations during auroral arcs passage
24 p3823 A71-45037

AURORAL ECHOES

Auroral radio reflections mechanism in terms of auroral plasma instability processes, identifying ion acoustic wave characteristics among other echo components

20 p3199 A71-39852

Radio and optical aurora correlation and control by polar electrojet, using VHF backscatter and geomagnetic recordings

20 p3229 A71-39853

Proton precipitation satellite observation, comparing with simultaneous ground based measurement of auroral radar echoes

20 p3285 A71-39887

AURORAL ELECTROJETS

Position finding for auroral electrojet using magnetometer measurements onboard Black Brant 3 rockets

01 p0075 A71-11331

Auroral electrojet electric fields from plasma electron density and collision frequency profiles measurements via Black Brant rockets variable frequency impedance probes

01 p0075 A71-11332

Auroral oval electrojet poleward expansion correlation to energetic electron enhancement in magnetotail during substorm from satellite observation

03 p0419 A71-14518

Polar magnetic disturbances in electrojet, studying Hall conductivity, electric field behavior and auroral ionosphere ionization

07 p1101 A71-19415

HF Hall current instability, discussing short wavelength backscatter for equatorial and auroral electrojets in disturbed ionosphere

08 p1279 A71-21205

Hourly changes in auroral conjugate location from ionospheric absorption and riometer magnetograms, noting electrojet triangulation

08 p1279 A71-21210

Thermosphere heating due to auroral electrojets, discussing thermospheric variations and eddy viscosity

10 p1602 A71-24554

Low latitude DS ionospheric current component and auroral electrojet intensity for intense geomagnetic storms, considering particle observations by ATS 5 synchronous satellite

10 p1605 A71-24790

Latitudinal profiles of geomagnetic H and Z components due to return current of auroral zone electrojet during polar substorms

11 p1756 A71-25757

Pitch angle distribution effects of auroral electrojet on scattering and absorption of fast precipitated electrons in upper atmosphere, using computerized Monte Carlo technique

13 p2119 A71-27794

German monograph on determination of instantaneous position of polar electrojet for rocket launching parameters computation

18 p2911 A71-35920

German monograph on calibrating induction coil and proton precession magnetometers for polar electrojet rocket experiments

18 p2915 A71-35922

Polar magnetic disturbances in electrojet, studying Hall conductivity, electric field behavior and auroral ionosphere ionization

19 p3054 A71-37839

Electrojet currents association with visible aurorae, using sounding rockets with rubidium vapor magnetometers

20 p3215 A71-38733

Thermospheric wind induction by auroral electrojet heating, considering effects of Joule dissipation of magnetospheric electric fields

20 p3215 A71-38744

Auroral zone X ray events in midnight sector associated with substorm and electron precipitation following electrojet, using balloon-borne detector measurements

20 p3284 A71-39851

Infrasonic waves correlation to supersonic auroral motions and polar electrojet during substorm periods

20 p3229 A71-39859

Polar cap magnetic variation mechanism based on electric field aligned continuity of Hall current auroral electrojets, noting ionospheric electron density gradients effects

20 p3230 A71-39862

AURORAL EMISSION

U AURORAS

U LIGHT EMISSION

AURORAL IONIZATION

Auroral ionization relationship to incident magnetospheric electrons based on atmospheric model

01 p0073 A71-10253

ESRO 1 satellite hydrogen and ionized nitrogen auroral emissions photometric measurements, discussing electron/proton phenomena relation to geomagnetic activity

03 p0406 A71-13248

Longitudinal drift of auroral ionization in substorm recorded at different stations

07 p1099 A71-19388

Polar magnetic disturbances in electrojet, studying Hall conductivity, electric field behavior and auroral ionosphere ionization

07 p1101 A71-19415

Solar wind origin of auroral ions from low energy hydrogen and helium ion spectral measurements

10 p1664 A71-24791

Lower ionosphere ionization response to auroral particle fallout during 1968 substorms, using geomagnetic, VLF and balloon measurements

12 p1899 A71-26642

High latitude measurements of low energy electron precipitation by Auroral 1 satellite, explaining anomalous high level F region ionization near dark pole

14 p2299 A71-30031

Longitudinal drift of auroral ionization in substorm recorded at different stations

19 p3052 A71-37813

Polar magnetic disturbances in electrojet, studying Hall conductivity, electric field behavior and auroral ionosphere ionization

19 p3054 A71-37839

Stable auroral red arc excitation observations by HF radar scattering, scanning photometers and Alouette 1 satellite, noting local electron concentration increase

19 p3054 A71-38034

Excitation and ionization cross sections of atmospheric molecular species by low energy ions in strong auroral and man-made electric fields

19 p3055 A71-38039

Auroral electrons temporal and spatial structure from ground based optical observations and rocket-borne electron detector measurements

20 p3228 A71-39849

Low energy hydrogen and helium ions composition of primary aurora precipitation from rocket-borne spectrometer experiment, suggesting direct solar wind origin of primaries

20 p3301 A71-39850

AURORAL IRRADIATION

ATS-5 satellite-borne auroral electron and proton energy spectrum measuring instrument using cylindrical coordinate electrostatic analyzer

08 p1294 A71-21845

Auroral X ray radiation measurements in midnight sector during solar storm of 8 March 1970

24 p3823 A71-45034

AURORAL SPECTROSCOPY

Nitrogen Vegard-Kaplan and second positive band systems emission, using rocket-borne spectrometer in UV aurora

07 p1102 A71-19670

Differential secondary electron flux measurement in aurora with Aerobee rocket spectrometer

08 p1282 A71-21635

Auroral protons and substorm resonance concept, eliminating discrepancy between hydrogen emission spectroscopic and direct measurements

09 p1513 A71-22674

High altitude low latitude aurora, observing intense spectral bands and lines and excitation due to optical resonance, atom- and molecule- electron collisions

09 p1441 A71-23643

Auroral pulsation analysis from rocket soundings, investigating oxygen green linear excitation sources

11 p1753 A71-25549

Insufficient auroral electron spectra and pitch angle distributions from ground based altitude luminosity profiles

13 p2054 A71-27802

Auroral spectroscopy, considering grating spectrometers, Fabry-Perot and Michelson spectrometers, filter photometers, etc

13 p2058 A71-28039

Upper atmosphere aeronomy historical review, considering meteor trails, radio waves, auroral photography, terrestrial magnetic field and spectroscopy

14 p2229 A71-29704

IR spectrum of aurora, reviewing past and current experimental approaches

20 p3228 A71-39842

Stable auroral red and hydrogen arcs simultaneous spectrographic triangulation, noting correlation

20 p3232 A71-39895

Auroral far UV spectrum and intensity measurements, discussing atmospheric absorption effects on rocket-borne spectrometer sensitivity

21 p3372 A71-40039

Atmospheric scattering and absorption effects on balloon altitude spectra observations of auroral X ray penetration into atmosphere

23 p3720 A71-43130

Night airglow oxygen Herzberg I bands covariation with O I 5577 A line, evaluating NASA 1968 airborne auroral measurements

23 p3670 A71-43186

AURORAL TEMPERATURE

Midlatitude atmospheric gravity waves generation by auroral heating during magnetic substorms

02 p0245 A71-11965

Auroral electron temperature, noting field aligned energy transport current effects

12 p1899 A71-26887

Thermospheric density response to auroral heating during geomagnetic disturbances simulation assuming impulse heat input into small latitude band within auroral ovals

15 p2398 A71-31777

Auroral plasma particle discharge during motion in strong magnetic field, discussing magnetospheric instability due to temperature anisotropy

24 p3867 A71-45309

AURORAL ZONES

Nighttime polar aurora zone during IGY and IQSY related to magnetic activity

02 p0242 A71-11759

Ionospheric stability in nighttime and daytime auroral zone with E layer corpuscular stream disturbances

02 p0243 A71-11762

Polar ionospheric auroral zone ionization, obtaining ion production function for single electron and proton flux

02 p0244 A71-11772

Langmuir probe DC detector for rocket quasi-static and AC electric field measurements in auroral zone ionosphere

03 p0406 A71-13302

Bremsstrahlung X rays-radar echoes relation in southern auroral zone, discussing electron precipitation role

03 p0408 A71-13388

Churchill research range auroral sounding rocket launcher facility, describing design, construction and performance

03 p0397 A71-14275

Auroral oval transverse magnetic disturbance, examined as field aligned current models

03 p0419 A71-14523

Auroral zone electron and proton energy spectra measurements, using sounding rockets with electrostatic analyzers

03 p0419 A71-14524

Resonant proton drift in axisymmetric rotating magnetosphere, discussing flow from boundary or tail to auroral region

05 p0800 A71-17178

Geocentric distances to subsolar point on magnetospheric boundary as function of magnetic activity state, discussing auroral oval position

05 p0744 A71-17180

Auroral sporadic E layer events relationship to pi type irregular magnetic pulsations generation in Arkhangelsk region

05 p0744 A71-17187

Magnetotail plasma sheet electron and proton energy spectra and angular distribution over auroral zone, comparing Vela satellite and rocket measurements

06 p0887 A71-17260

Vertical profile of electron collisions effective frequencies in auroral ionosphere E region

06 p0895 A71-18279

Ionospheric electron density irregularity effects on communication satellite scintillation in auroral zone, using Doppler and Faraday measurements

07 p1098 A71-19035

Stable midlatitude red arc in night sky south of auroral zones, reviewing observed features, ionospheric behavior and formation theories

07 p1098 A71-19322

Aurora polaris activity appearance frequency mean annual values cycle curves

07 p1101 A71-19411

Pc 3-4 period range geomagnetic micropulsations simultaneous recordings at Canadian stations spanning auroral and polar regions

07 p1102 A71-19665

Simultaneous auroral ionospheric electric field measurements by Skylark rockets, deriving plasma drift direction

08 p1279 A71-21208

Auroral electron and proton precipitation patterns observed at Fort Churchill, discussing particle energies

08 p1282 A71-21636

Pi 2 type geomagnetic pulsations relationship to auroral zone morphological features

09 p1435 A71-22448

Neutral wind and ion velocity determination under quiet and disturbed geomagnetic conditions in auroral zone, noting electric field measurements

09 p1440 A71-23600

Auroral zone electron energy spectra local time dependence from polar satellite observations

09 p1515 A71-23632

Auroral zone magnetic substorm correlation to magnetospheric plasma drift

09 p1441 A71-23640

Morphology, dynamics and time variations of auroral zone electron precipitation events from balloon measurements of bremsstrahlung X rays

10 p1662 A71-24535

Atomic nitrogen far UV emission excitation in auroral ionosphere due to electron impact dissociations

10 p1605 A71-24792

Polar substorm energy from auroral region size and brightness photographic observations, discussing total flux dependence on magnetic field disturbance intensity 10 p1606 A71-24917

Upper atmosphere neutral temperature profiles in auroral zone, using aluminum and barium oxide clouds fluorescent emission 11 p1753 A71-25547

Latitudinal profiles of geomagnetic H and Z components due to return current of auroral zone electrojet during polar substorms 11 p1756 A71-25757

German low altitude polar orbiting research satellite AZUR orbital characteristics and bearing on auroral zone substorm phenomena 12 p1899 A71-26833

Particle precipitation at auroral heights, examining ground based observations evidence for existence of protons, neutrons and electrons 12 p1947 A71-26864

Antarctic auroral ovals, determining time-longitude coordinates, statistical mean position and polewards and equatorwards boundaries for various Kp 12 p1900 A71-27056

Auroral zone X ray events due to electron precipitation, considering relationship to polar magnetic substorms 13 p2119 A71-27797

Midnight sector balloon measurements of X ray bremsstrahlung from electrons precipitating in auroral zone during polar magnetic substorms 13 p2119 A71-27798

Resonant proton drift in asymmetric rotating magnetosphere, discussing flow from boundary or tail to auroral zone 13 p2128 A71-28235

Geocentric distances to subsolar point of magnetospheric boundary as function of magnetic activity state, discussing auroral oval position 13 p2059 A71-28237

Auroral sporadic E layer events relationship to Pi 1 type irregular magnetic pulsations generation in Arkhangelsk region 13 p2059 A71-28244

Concentration and transport from auroral zone of minor constituents in mesosphere and lower thermosphere during anomalous midlatitude radio absorption periods 14 p2230 A71-29711

Auroral precipitation electron energetic and angular distributions as function of geomagnetic activity from Cosmos 261 measurements 14 p2230 A71-29713

High latitude regions of low energy electron precipitation from OGO 4 satellite auroral particle experiment 14 p2300 A71-30032

Low energy electron precipitation effects on upper atmosphere based on polar cap and auroral oval electron spectrum comparison 14 p2300 A71-30035

Electron flux rigidities in polar aurora region, using stratospheric nighttime X ray and cosmic radio noise absorption measurements 14 p2302 A71-30595

Electron and proton precipitation observations in auroral, polar cap and outer radiation zones by electrostatic analyzers on earth satellite Injun 5 15 p2397 A71-31756

Low energy auroral thermal electrons flux after geomagnetic substorm, entering magnetosphere from solar wind 16 p2629 A71-33953

German monograph on rocket measurements in auroral zone with proton magnetometer covering magnetosphere, spin-lattice and spin-spin relaxation time and data processing 18 p2910 A71-35885

Local time dependence of auroral zone electron precipitation X ray events from balloon measurements of bremsstrahlung 18 p2911 A71-35894

Auroral zone proton measurements during slowly varying cosmic noise absorption, obtaining energy spectrum by rocket soundings 19 p3125 A71-37418

Aurora Polaris activity appearance frequency mean annual values cycle curves 19 p3054 A71-37835

Magnetic perturbations in near polar region and morning-night sectors of auroral oval as function of current sources and modulation by universal time 19 p3059 A71-38397

Auroral electrons and protons precipitation patterns from ESR0 1A northern polar cap observations, identifying electron energy zones 19 p3060 A71-38574

Auroral zone ionosphere time lag observations, noting delay in cosmic noise absorption pulsations to fast bremsstrahlung X rays, luminosity and micropulsations 20 p3215 A71-38740

Solar proton enhancement over auroral zone observed aboard near earth polar orbiting ESR0 2 satellite 20 p3282 A71-39735

Auroral morphology, covering static and dynamic ovals, polar cap and dayside auroras, auroral zones, substorms and electron precipitation 20 p3227 A71-39838

Auroral zone X ray events in midnight sector associated with substorm and electron precipitation following electrojet, using balloon-borne detector measurements 20 p3284 A71-39851

Magnetospheric plasma convection electric field double-probe measurement at high latitude by Injun-5 satellite, noting east-west velocity reversals or discontinuities at auroral zone 20 p3230 A71-39882

Night and daytime auroral zone ionospheric electric field measurement by rocket-borne Langmuir probe, noting components parallel and perpendicular to magnetic field 20 p3231 A71-39884

Power spectral analyses of auroral light and X ray pulsations, discussing damping due to velocity dispersions of electrons with various energies 21 p3373 A71-40069

High latitude auroral particle precipitation patterns and connections to plasma sheet, ring current, cusp and radiation belt sources, using rocket and satellite observations 21 p3439 A71-41179

Auroral X rays passage through atmosphere, discussing integral spectral measurements with collimated and omnidirectional detectors 22 p3593 A71-42399

Localized abnormal geomagnetic disturbance near polar cap and simultaneous ionospheric variation during auroral zone weak magnetic activity periods 22 p3536 A71-42625

Low energy particle plasma sheet and convection electric field distributions over auroral zones and polar caps from satellite Injun 5 observation 23 p3669 A71-43168

Auroral conjugacy observations over Alaska and south of New Zealand, noting correlation with geomagnetic field lines 23 p3671 A71-43325

Auroral charged particle fluxes electrodynamic interaction with atmosphere, determining ion formation rate and electron concentration and conductivity 24 p3866 A71-45032

AUROMAS
NT AURORAL ARCS
NT RADIO AURORAS
NT RED ARCS
Auroral magnetoionospheric perturbations processes, discussing space charge electric field structure and plotted altitude dependences 01 p0073 A71-10070
Atomic and molecular collisions in gases, considering E and F regions processes, auroras and applications 01 p0129 A71-10133
Rapid geomagnetic field variations relationship with auroral luminosity fluctuations at 4278 A 01 p0076 A71-11501
Auroral vacuum UV spectra and 3914 A emission from sounding rocket data 01 p0076 A71-11502
Far UV equatorial airglow and aurora intensities and occurrence frequencies from satellite observation 01 p0076 A71-11504
Visual, photographic and photoelectric observations of polar auroras and hydrogen emission at conjugate points 02 p0242 A71-11757
Diurnal variations of polar aurora-magnetic activities correlation at high latitudes 02 p0242 A71-11758
Regularities of polar auroras and ionospheric disturbances during solar cycle with decreased low energy corpuscular flux 02 p0242 A71-11760
ESR0 1 satellite hydrogen and ionized nitrogen auroral emissions photometric measurements, discussing electron/proton phenomena relation to geomagnetic activity 03 p0406 A71-13248
Geomagnetic tail configuration during substorms from Imp 4 magnetic field and auroral index measurements 03 p0419 A71-14516
Field aligned currents and high potential drop space charge regions above aurora associated with electron acceleration 03 p0419 A71-14525
Auroral oval continuity during winter /1969-1970/ from jet aircraft ionospheric instrumentation, showing band distribution along geomagnetic pole 03 p0419 A71-14526
Primary auroral electron flux angular distribution measurement by rocket probe, showing particle precipitation and trapping by electrostatic double layers in ionosphere 04 p0584 A71-15896
Zone of unstable radiation in magnetosphere localizing auroral and quasi-captured particles 05 p0798 A71-16046
Auroral ionosphere, examining low energy proton fluxes parallel to geomagnetic field lines of force 05 p0738 A71-16160
Polar auroras emission bursts at 6300 and 5577 A, noting diurnal variation with electrophotometer 05 p0746 A71-17209
Auroral luminosity and X ray bremsstrahlung quasi-periodic pulsations data analysis by power spectrum and cross correlation methods 06 p0949 A71-17265
Auroral phenomena, using dimensional analysis to examine MHD equations for fields and plasmas in magnetosphere 06 p0888 A71-17286
Electrostatic fields parallel to geomagnetic field role in charged particles acceleration mechanism to auroral energies, considering electron and proton precipitation 06 p0893 A71-17989
Sporadic ionization occurrences nighttime observation in auroral E region, describing vertical electron concentration profile 06 p0895 A71-18280
Penetrating electron flux relation to magnetic perturbations and auroral substorms development 07 p1185 A71-19392
Aurora polaris activity appearance frequency mean annual values cycle curves 07 p1101 A71-19411
Energetic electron and proton precipitation measurements by sounding rocket-borne particle detectors in pulsating aurora 07 p1186 A71-19669
Polar auroras, lower magnetosphere and geomagnetic perturbations, as effect of corpuscular fluxes penetration into lower ionosphere 07 p1104 A71-20046
H Lyman alpha auroras during May 18-27, 1967 magnetic disturbance from satellite observation 08 p1283 A71-21637
Polarization characteristics of 42 MHz oblique backscatter from breakup auroras 08 p1272 A71-21639
Auroral X radiation at magnetoconjugate points Kerguelen/Archangel region, using balloon-borne spectrometers 09 p1438 A71-23146
Lower ionospheric region parameters during 24 and 30 March 1968 substorms, determining auroral electron precipitation effects 09 p1440 A71-23630
Polar caps magnetic field variations, considering relationship to auroral phenomenon and ionospheric conductivity variations 10 p1600 A71-24314
Balloon sonde for auroral luminosity measurements and comparison of auroral emissions, X rays and ionospheric absorptions 10 p1602 A71-24530
Spatial distribution of aurorae in O and molecular nitrogen ion emissions 10 p1602 A71-24533
Atmospheric electrical effects due to aurora, discussing negative space charge, bremsstrahlung flux and electrojet plasma instability 10 p1604 A71-24703
Magnetospheric model characteristics, discussing auroral phenomena energy sources, magnetotail length, polar cusp, auroral oval and electrojet relationships, polar and magnetospheric substorms 10 p1606 A71-24802
A type red aurora in polar region accompanied by sporadic F2 layer 11 p1754 A71-25608
Outer radiation belt energetic electron flux intensity correlation with auroral activity and Kp index 11 p1816 A71-25760
Field aligned anisotropy for auroral ionospheric energetic ions, calculating pitchangle distributions 12 p1899 A71-26885
Precipitation energy flux of continuous noontime aurora, using airborne ionospheric and optical measurements 13 p2054 A71-27801
Properties of higher latitude region of structured low energy electron precipitation in noon hemisphere, relating radiation with optical emissions in dayside auroral oval 13 p2119 A71-27911
Polar auroras emission bursts at 6300 and 5577 A, noting diurnal variation with electrophotometer 13 p2060 A71-28264
Auroral color variations and human color perception, noting visual appearance agreement with calculations based on normal spectrum 13 p2060 A71-28348
Ring current as source region for proton auroras, calculating energetic proton lifetimes for model magnetosphere 13 p2064 A71-29167

Pulsating aurora observations, noting light intensity, diurnal variations and power spectra

14 p2229 A71-29671

Low energy electron and proton fluxes in geomagnetic tail of equatorial magnetosphere forming plasma sheet related to auroral oval

14 p2299 A71-30029

Low energy precipitating auroral particle fluxes over magnetic poles delineating polar cap, noting electron precipitated flux

14 p2299 A71-30030

Auroral electrons interaction with atmosphere from Fokker-Planck equation, considering angular diffusion, energy loss and geomagnetic field convergence effects

14 p2235 A71-30345

Pitch angle diffusion of electrons in postbreakup auroral glow, measuring electron intensities by Petrel sounding rocket

15 p2394 A71-31423

Electron intensities measurement in pulsating aurora on ESRO Skylark rocket launched from Sweden

15 p2394 A71-31424

Classification changes in IQSY Auroral Atlas, considering symbolism, synoptic map plotting and data reduction

15 p2396 A71-31608

Oxygen /super 1S/ effective lifetime measurements in pulsating aurora, discussing mechanisms, quenching coefficients and heights

15 p2397 A71-31762

Lyman alpha emission cross sections for collisions of hydrogen ion and atom beams with thin target nitrogen and oxygen relevant to proton auroral analysis

15 p2397 A71-31763

Auroral 1.2-4 second periodicity X ray pulsations during magnetic storms, using omnidirectional detector at balloon altitude

15 p2474 A71-31775

Charged particles distribution in magnetosphere beyond radiation belts, proposing unstable radiation zone model containing auroral and semitrapped particles

16 p2626 A71-33450

Altitude variation of forbidden line of 5577 A and 3914 A auroral emissions intensities ratio from rocket sounding

16 p2566 A71-33748

Auroral 4278 A positive nitrogen ions emission relation to low energy electron precipitation, using polar orbiting Aurorae satellite photometer and particle detector data

16 p2568 A71-33794

Rocket-borne electron spectrometer measurements of low energy electrons during auroral events, noting influx sudden enhancement

16 p2570 A71-33820

Stable auroral red arcs generation at plasmopause from ion cyclotron wave turbulent dissipation of ring current proton energy

16 p2572 A71-33947

Pulsating auroral patches with sudden intensity dependent spatial expansion, noting relation to triggering instabilities of precipitating electron beam

16 p2573 A71-33954

Mode conversion and auroral effects observations on polar VLF propagation path, noting seasonal and solar cycle variations

17 p2731 A71-34319

Pitch distribution of protons precipitated from auroral radiation region measured by scintillation detector aboard Cosmos 261 satellite in Northern Hemisphere

17 p2731 A71-34320

Bibliography on aurora covering observations, morphology, atomic and molecular processes, electric fields, radio scattering, red arcs and particle precipitation

17 p2732 A71-34467

Statistical analysis of polar auroras visual observation, discussing solar activity effects

17 p2733 A71-34836

Polar auroras visual observations, plotting diurnal changes in height and occurrence frequency

17 p2803 A71-34837

ESRO sounding rocket program covering atmospheric and ionospheric physics and solar and auroral phenomena

18 p2896 A71-35926

Electron and proton fluxes intercorrelation in recovery phase of auroral substorm

19 p3125 A71-37362

Balloon-measured magnetospheric electric fields comparison with all sky camera pictures of large scale visible auroral form motions, noting relationship

19 p3047 A71-37363

Infrasonic pulsations of optical auroral luminosity in 3914 A positive molecular nitrogen ion and 5577 A O I emission measurement by double photometer system

19 p3048 A71-37395

Polar auroras production by electric fields and electron precipitation from magnetospheric magnetic storms

19 p3052 A71-37761

Penetrating electron flux relation to magnetic perturbations and auroral substorms development

19 p3127 A71-37816

Aurora Polaris activity appearance frequency mean annual values cycle curves

19 p3054 A71-37835

Auroral radio noise from electrostatic oscillations excited by fast proton beams

19 p3018 A71-38046

Charged particles eruptions effects on relation of magnetic perturbations to integral auroral luminance intensity from whole sky photometry measurements

19 p3059 A71-38398

Auroral luminosity patterns over northern Scandinavia based on ESRO all-sky camera recordings, noting relationship to electron and proton precipitation

19 p3060 A71-38573

Magnetic activity effect on pitch angle distribution of low energy auroral electrons from ESRO 1A measurements

19 p3060 A71-38575

Far UV auroral luminosity profile using calibrated EUV spectrometer, noting nitrogen band emission

20 p3225 A71-39731

Auroral morphology, covering static and dynamic ovals, polar cap and dayside auroras, auroral zones, substorms and electron precipitation

20 p3227 A71-39838

Auroral excitation and ionization intensity and rotational and Doppler temperature vertical profiles measurements, emphasizing emission rate profiles

20 p3227 A71-39839

Auroral conjugacy and time dependent geometry via all sky cameras and image orthicon TV onboard conjugate-flying aircraft

20 p3228 A71-39840

Equatorial modulation in pulsating aurora, discussing electron measurements with channel multipliers and electrostatic analyzers aboard ESRO Skylark S29/2

20 p3228 A71-39841

IR auroral/airglow study covering hydroxyl emission and dipole moment function determination and atmospheric nitrogen vibrational temperature measurement

20 p3240 A71-39843

Electric fields effects on ions temperature and electron densities of auroral ionosphere

20 p3228 A71-39844

Proton auroras ionization and excitation cross sections of atmospheric constituents by energetic hydrogen ions and atoms, presenting recent measurements and H emission laboratory results

20 p3228 A71-39845

Auroral electron and proton precipitation patterns, noting LF radio noise emissions relationship to low energy electron flux through Cerenkov process

20 p3228 A71-39846

Low energy auroral particle measurements from polar satellites, obtaining electron and proton precipitations location, and angular and energy distributions

20 p3228 A71-39847

Auroral electron and proton precipitation patterns, measuring airglow emissions

20 p3284 A71-39848

VLF emissions and low energy electrons relation to other auroral phenomena from satellite-borne data associating midnight maximum with particles from plasma sheet

20 p3229 A71-39855

Auroral substorm model refinements for proton aurora by classifying substorms according to intensity or magnitude

20 p3284 A71-39858

Infrasonic waves correlation to supersonic auroral motions and polar electrojet during substorm periods

20 p3229 A71-39859

Large and small scale auroral formation dynamics, covering precipitating electron and proton acceleration and plasma instabilities role

20 p3229 A71-39860

Steady state magnetospheric convection pattern from synoptic maps of magnetic disturbance and auroral motions

20 p3230 A71-39879

Magnetotail plasma sheet variations association with auroral display features during substorms from all sky photography

20 p3230 A71-39880

Artificial auroral experiment by Aerobee rocket-borne electron accelerator generated monoenergetic electron beam injection onto magnetospheric field

20 p3231 A71-39885

Ground based optical observation of raylike artificial auroras produced by rocket-borne accelerator generated electron beams, using image orthicon TV system

20 p3231 A71-39886

Plasma transport processes role in E region from midlatitude nocturnal and auroral ionospheric models in terms of transport equations

20 p3232 A71-39893

Magnetosphere-ionosphere electric coupling for polar magnetic disturbances and auroral break-up origin, discussing thermal particles precipitation due to transient electric field

21 p3375 A71-41354

Outer radiation belt energetic electron flux intensity correlation with auroral activity and Kp index

22 p3591 A71-41528

Precipitation measurements in polar cap electron aurora, discussing neutral point entry, acceleration mechanisms, flux, pitch angle and magnetospheric models

23 p3669 A71-43169

TV data acquisition system for auroral and ionospheric research, noting visual and subvisual detection sensitivity

23 p3677 A71-43515

Tables for aurora correlation with solar radio bursts at 185 MHz

23 p3769 A71-43908

Night enhancements in 6300 A line at Sanae related to diurnal excursion of auroral oval, observing ionospheric blackout and high energy electrons precipitation

23 p3672 A71-43980

AUSFORMING

High velocity metal working, discussing airfoil forging, ausforming of bearing race blanks, tooling, etc [SME PAPER MF-70-228]

01 p0090 A71-11267

Titanium-steel continuously reinforced composites strength to weight ratings, describing ausforming process and fatigue tests

08 p1316 A71-21587

AUSTENITE

Stainless steel sputter deposits equilibrium phases, determining deposition temperature ranges for austenite and ferrite formation

02 p0267 A71-12884

Nitrogen austenite solute-solute binding energy derivation from experimental data for comparison with carbon austenite

03 p0441 A71-13314

Steels prior austenite and martensite grain size control by thermal cycling

03 p0446 A71-14492

Microstructure changes during austenite isothermal decomposition in Fe-Mo-C alloys

04 p0614 A71-15778

Austenite-martensite transformation effects on Fe-Ni-Co alloys low temperature thermal conductivity

05 p0768 A71-16771

Chemical composition effect of low carbon alloys metallic matrix on wear resistance in abrasive medium, showing austenitic manganese alloys superiority to martensitic or ferritic alloys

07 p1136 A71-19630

Maraging steels thermal embrittlement, discussing austenite grain boundaries inclusions, carbide networks precipitation and carbon concentration

08 p1305 A71-21027

Martensitic transformation-induced plasticity in austenitic Fe alloys, examining strain rate and chemical composition effects

08 p1312 A71-21554

Fe-Ni-Co alloy strengthening by martensite to austenite transformation taking into account microstructure

08 p1313 A71-21556

Aging behavior of Nb-containing Fe-Ni alloys, considering austenite and martensite in twinned and massive form

13 p2089 A71-29412

Precipitation kinetics and austenite formation during aging of Fe-Ni-Mo and Fe-Ni-Co-Mo maraging alloys from dilatometry, electrical resistivity measurement and electron microscopy

14 p2257 A71-29838

Austenite and carbide chromium manganese steel boron distribution obtained by tracing elements

15 p2425 A71-31397

Chemical composition effect of low carbon alloys metallic matrix on abrasive wear resistance, showing austenitic manganese alloys superiority to martensitic or ferritic alloys

16 p2593 A71-33626

Strength and toughness optimization in high strength stainless steels by austenitizing and removing delta ferrite by isothermal transformation

17 p2756 A71-34491

Plastic deformation effects on austenite thermal stabilization in Fe-Ni-C alloy, considering temperature dependence

19 p3079 A71-37704

Alloy steels supercooled austenite nitriding in ammonia flow, examining diffusion layers by X ray analysis and hardness tests

21 p3404 A71-41164

Alloying elements effects on high-carbon steels phase transformation under shock loading to form martensite-austenitic structure

24 p3840 A71-45376

AUSTENITIC STAINLESS STEELS

Cryogenic austenitic steels embrittlement dependence on nitrogen content, noting second phase precipitation role

01 p0098 A71-10086

Steels and weld metal alloying for stable austenitic structure under long term cryogenic conditions, investigating optimal Cr, Ni, Mn and nitrogen combinations

01 p0085 A71-10087

Plastic deformation and phase transformation in textured austenitic stainless steel, considering stacking fault energy contribution

01 p0101 A71-10737

Austenitic Cr-Ni-Nb stabilized steel, evaluating high temperature oxidation and creep process interaction

01 p0104 A71-11603

Homogenization and dehomogenization phenomena at high temperature of Cr-Ni austenitic steels, discussing electron microscope microstructural examinations after heat treatment

01 p0105 A71-11617

Hardening effects of various Ta proportions in Fe-Ni-Ta alloys, noting austenitic nature after homogenization and quenching at high temperature

01 p0105 A71-11619

Austenitic stainless steels point defect migration sensitivity, measuring dislocation damping during recovery after quenching

02 p0267 A71-12883

Austenitized oil hardened annealed chromium steels with electrolytically isolated carbides, determining structure by X ray analysis

04 p0610 A71-14886

Carburization time, temperature and rates in austenitic stainless steels, discussing complex carburized structures

04 p0602 A71-14897

Austenitic steel containing C, Cr and Mn, investigating W, Mo, V and Nb effect on structure and mechanical properties

04 p0616 A71-15804

German monograph on Co-free heat resistant austenitic steel alloys precipitation hardening and creep strength properties as function of chemical composition

05 p0764 A71-15973

Nitrogen-alloyed austenitic steels precipitation hardening, discussing aging and strengthening rates

05 p0767 A71-16767

Austenitic steels and Ti and Al alloys with stress raisers, studying low temperature mechanical properties

05 p0767 A71-16768

Austenitic stainless steel intergranular corrosion model for thermodynamic analysis leading to grain boundary diffusion and Cr concentration profiles determination

07 p1134 A71-19566

Austenitic stainless steel dislocation structures during fatigue deformation under cyclic loading, observing slip lines and lattice strain morphology

07 p1136 A71-19699

Intrinsic stacking fault energy temperature dependence in austenitic Fe-Cr-Ni alloys determination from dislocation mode measurements by high temperature transmission electron microscopy

07 p1138 A71-19984

Yield point temperature dependence in heat resistant austenitic alloys, showing tendency to brittle failure under short term overloads

09 p1468 A71-22598

Chromium and titanium alloyed austenitic steels, examining short and long time application as turbine engine parts

09 p1475 A71-23295

High temperature austenitic steels, Ni and Co alloys machining, considering deformation resistance and strain hardening

09 p1456 A71-23297

High temperature steel and alloys metallurgical processes for stationary and aircraft gas turbine engine components, discussing production-quality control-research interrelationship

09 p1456 A71-23301

Stress and structure effects on creep rate of two austenitic steels in quenched state, considering decorated stacking faults

09 p1479 A71-23624

Hot deformation of superrefractory austenitic Ni alloy, considering elastic and plastic limits

09 p1479 A71-23625

Crystal imperfections effect on MC carbide precipitation on coherent twin boundaries and regions close to grain boundaries in austenitic steels, using electron microscopy

11 p1780 A71-26027

Metal carbide grain boundary precipitates effect on austenitic stainless steels high temperature fatigue fracture behavior

11 p1782 A71-26439

C and Ni contents effects on water quenched tempered austenitic chromium nickel-stainless steels intercrystalline corrosion

12 p1919 A71-27777

Grain boundary precipitation in austenitic steels during creep deformation and ordinary aging treatment

13 p2086 A71-28623

Plastic strain development at fatigue crack tip in mild carbon and stainless austenitic steels from electron and optical microscopy

14 p2257 A71-29841

Crack propagation resistance-cyclic fracture strength relation for austenitic and Mn-Cr-V steels, considering thermomechanical working effects

16 p2592 A71-33408

Cryogenic austenitic steels embrittlement dependence on nitrogen content, noting second phase precipitation role

16 p2593 A71-33642

Steels and weld metal alloying for stable austenitic structure under long term cryogenic conditions, investigating optimal Cr, Ni, Mn and nitrogen combinations

16 p2584 A71-33643

Austenitic high nitrogen chromium-nickel steels plastic deformation and heat treatment in plasma arc furnaces

16 p2596 A71-33910

Cr-Ni austenitic steels thermomechanical destabilization using cyclic strain hardening

18 p2934 A71-36173

Mo effect on high temperature strength, heat resistance, plasticity and toughness of austenitic Cr-Mn-Ni-Al steel

19 p3077 A71-37465

High strength Cr-Mo-Co stainless steels with improved toughness and ductility by austenitizing temperature selection

19 p3079 A71-37707

High strength metastable austenitic steels fractography, showing alloy composition, strain rate and temperature effects

19 p3080 A71-37717

Stress concentration and defects effect on crack initiation and propagation in austenitic steels thermal fatigue

20 p3307 A71-39022

Solution temperature and Ti/C ratio effects on Cr-Ni-Ti austenitic steels creep properties, including precipitation, deformation, rupture and coalescence

20 p3250 A71-39025

Soviet book on austenitic boron steels and alloys for welded structures, covering boron influence on steels and alloys structure and properties, with special reference to weldability

20 p3251 A71-39090

Austenitic stainless steels susceptibility to intergranular corrosion under unwelded, welded and heat treated conditions in process environments

20 p3241 A71-39341

Explosively shock strengthened austenitic stainless steel, investigating mechanical properties at elevated temperatures

21 p3398 A71-40462

Dislocation structures in austenitic steel fatigued at various stress cycles and tensioned at various strains, using transmission electron microscopy

21 p3400 A71-40833

Dislocation arrays effects on heat treated austenitic stainless steel susceptibility to intercrystalline corrosion in sulfuric and nitric acids and cracking in magnesium chloride

21 p3402 A71-41087

Alloying effects on crack propagation resistance of precipitation hardening austenitic steel

21 p3402 A71-41091

Nitrogen alloying effects on relaxation resistance of Cr-Mn austenitic steel

21 p3402 A71-41092

Alloying effects on corrosion cracking of Cr-Ni austenitic stainless steels, testing in chloride solutions

21 p3402 A71-41094

Cr and Cr-Ni ferritic and austenitic steels, investigating high temperature nitriding for intensifying nitrogen diffusion saturation

21 p3389 A71-41098

C and Ni contents effects on water quenched tempered austenitic chromium nickel-stainless steels intercrystalline corrosion

21 p3403 A71-41100

Low carbon austenitic Cr-Mn steels, noting Ni and Al combined alloying effects on structure and mechanical properties

21 p3403 A71-41101

High heat resistance of austenitic Cr-Ni-V-B steel by polygonization and recrystallization, using thermomechanical treatment

21 p3403 A71-41102

Mo, W and Al alloying additives effects on mechanical properties and wear resistance of austenitic high Mn electroslag melted steel

21 p3403 A71-41106

Austenitic stainless steels diffusion layer formation and structure by gaseous carburization with FeAl-ammonium chloride powder mixture, describing elements redistribution

21 p3390 A71-41166

Ni-Cr-Mo-Co steel microstructures after austenitizing, quenching and tempering, correlating with mechanical properties

22 p3560 A71-41594

Tempering anomalies of austenitic stainless steels partially transformed into martensite, using dilatometry, resistivity and internal friction measurements

22 p3562 A71-42244

LF eddy current bridge to measure small magnetic permeability changes in weakly ferromagnetic materials, applying to nondestructive tests of austenitic stainless steels

23 p3681 A71-43193

Austenitic Fe-Ni-Ti steel strengthening by precipitation hardening and subsequent aging at 600 C

23 p3690 A71-43282

Scanning electron microscopic observation of fracture surface of austenitic stainless steels for stress corrosion cracking in magnesium chloride and calcium chloride solution

23 p3693 A71-44073

Stable austenitic stainless steels and fcc metals plastic deformation flow curve model, presenting stress-strain relation

23 p3695 A71-44284

AUSTRALIA

Magnetic disturbances effect on F2 critical frequencies in Australasian zone during IGY-IGC, correlating to equatorial electrojet

05 p0741 A71-16438

AUSTRALITES

Flanged australite and australasian microtektites chemical compositions, using electron microprobe analysis

01 p0162 A71-11427

Australian tektites population polygons of bulk specific gravity and refractive index, indicating variations in chemical composition

04 p0582 A71-15133

AUTOCATALYSIS

Hemoglobin-sodium nitrite reaction in absence of oxygen, discussing methemoglobin formation by autocatalysis

03 p0363 A71-13486

Lithium deuteride nuclear fuel autocatalytic burning via proton and beryllium isotope resonance in fusion chain reactions

24 p3847 A71-44497

AUTOCLAVING

Secondary fabrication of boron reinforced aluminum matrix composite sheets for aerospace sub-components, detailing joining and autoclave bonding [SME PAPER EM-70-126]

01 p0089 A71-11260

AUTOCOLLIMATORS

U COLLIMATORS

AUTOCORRELATION

Instrument for measuring cross and autocorrelation functions with capability of extracting signal masked by noise by averaging operations

01 p0079 A71-10313

Autocorrelation function for gravity anomaly stochastic field outside earth spherical surface

01 p0127 A71-10358

Autocorrelation of weather radar precipitation patterns by incoherent optical method

01 p0030 A71-10599

Auto and cross correlation function computation from waveform polarity by flexible one bit digital correlator for frequencies to 25 MHz

02 p0211 A71-11644

Photospheric magnetic field direction autocorrelation showing differential and rigid rotation properties at various heliographic latitudes

02 p0316 A71-12751

Two mode He-Ne gas laser irradiance autocorrelation function measurement, comparing time-to-amplitude converter techniques with frequency domain measurements

05 p0760 A71-16268

Autocorrelation functions of anomalous gravitational and magnetic fields for ocean lines, relating Mohorovičić boundary and Curie isotherm

06 p0894 A71-18268

Nonredundant two dimensional square and hexagonal point arrays with optimal autocorrelative properties, considering high resolution imaging systems in holography

07 p1111 A71-19490

Radio wave propagation through extensive weakly scattering medium, presenting typical results for scintillation index, scintillation visibility and spatial autocorrelation function

07 p1196 A71-19576

Coherent optical target recognition through phase distorting medium, using holography, Fourier transform and autocorrelation functions

08 p1335 A71-21377

Cyclic block code structures for generating binary sequences with good autocorrelation properties

09 p1407 A71-23110

Continuous identification algorithm for system containing two delays for signal represented by stationary

- random process with autocorrelation function approximation 10 p1585 A71-24160
- Structural system frequency response measurements under environmental noise conditions, discussing autocorrelation function for transient excitation damping 11 p1797 A71-25182
- Thermal fluctuations in earth upper atmosphere, related to satellite deceleration and X ray solar radiation changes by autocorrelation and cross correlation analyses 11 p1817 A71-25822
- Autocorrelation functions of quasi-uniform solar radiation field reflected from earth with scattering allowance, using stationary random theory 12 p1901 A71-27097
- Output autocorrelation functions of zero memory nonlinear devices excited by signal plus Gaussian noise and interference 13 p2039 A71-28869
- Optico-acoustic autocorrelator for linear FM signals spatial compression, discussing design and performance 14 p2194 A71-30085
- Digital generation algorithm for random number sequences with specified autocorrelation and probability density function, illustrating computation accuracy and versatility 17 p2719 A71-34745
- Autocorrelation functions of quasi-uniform solar radiation field reflected from earth, using stationary random theory and allowing for scattering 22 p3533 A71-41652
- Mode-locked laser ultrashort pulse duration measurement from field intensities autocorrelation functions 23 p3685 A71-43562
- Diffuse cosmic X rays small scale structure, comparing Wolfe-Burbridge theoretical autocorrelation functions for galaxies clusters and superclusters with experimental value 23 p3722 A71-44013
- AUTOGYROS**
- Stowable aircrew vehicle escape rotoseat autogyro, providing controllable flight for pilot after ejection 04 p0532 A71-15418
- Jet flaps application to autogyro rotor, using pressure jump for air centrifugation 21 p3324 A71-41399
- AUTOIONIZATION**
- Plasma accelerator self ionizing current free stable radiative shock wave structure in hydrogen, using time resolved spectroscopic measurements 04 p0548 A71-14696
- Diatomic molecular autoionization model, calculating limit of high vibrational and electronic principal quantum numbers 07 p1164 A71-19687
- Coronal line observation of autoionizing states by dielectronic recombination in solar spectrum 07 p1198 A71-19827
- Autoionic mass spectroscopy, discussing emitters, ion sources and mass spectra of deuterized benzene, chlorobenzene and chloroform molecules during electron ionization and autoionization 10 p1611 A71-24383
- Hydrogen autoionization rates for molecular vibrational transitions near threshold, using internal conversion model 22 p3578 A71-42464
- AUTOKINESIS**
- Visual movement aftereffect storage absence of patterned surround for fixated visible target 15 p2364 A71-31984
- Autokinetic motion of luminous target, relating apparent visual movement to experienced displacement 17 p2694 A71-35739
- Canadian Forces experiments on aircraft flashing lights covering warning signals, navigation and anticollision displays and autokinetic phenomenon 22 p3499 A71-41491
- AUTOMATA THEORY**
- Finite automata systems invariance with respect to control actions 01 p0061 A71-10708
- Controller characteristic adaptive control by disturbance of plant operation under random nonmanipulated action, considering cognitive system as Markovian automation-nature game 03 p0389 A71-13516
- Automaton concept in cybernetics, emphasizing synchronous switching circuit operation with asynchronous input data 12 p1884 A71-27045
- Real time computable partial recursive functions of n variables with expectancy estimate on Minsky machines 13 p2096 A71-28976
- Algorithm determining sequential machine error partition representing inessential errors 14 p2206 A71-29521
- German monograph on experiments with stochastic automata covering noisy sequential nonanticipating

- channels with finite input/output alphabets, statistical decision functions, etc 17 p2719 A71-34774
- Error correction in autonomous linear finite automata with correcting codes 17 p2711 A71-34979
- Algorithms and operator matrix language for infinite linear automata analysis, synthesis and identification 19 p3024 A71-37223
- Time-bounded grammars and languages capable of simulation by Turing acceptors in automata theory 20 p3202 A71-39050
- Composition analysis of automata with unreliable components, illustrating possibility of comparative estimate of different variants of automaton structural scheme 22 p3516 A71-41857
- AUTOMATIC CONTROL**
- NT ADAPTIVE CONTROL
- NT AUTOMATIC FLIGHT CONTROL
- NT AUTOMATIC FREQUENCY CONTROL
- NT AUTOMATIC GAIN CONTROL
- NT AUTOMATIC LANDING CONTROL
- NT CASCADE CONTROL
- NT DYNAMIC CONTROL
- NT FEEDBACK CONTROL
- NT FEEDFORWARD CONTROL
- NT LEARNING MACHINES
- NT NUMERICAL CONTROL
- NT OFF-ON CONTROL
- NT OPTIMAL CONTROL
- NT PROPORTIONAL CONTROL
- NT SELF ADAPTIVE CONTROL SYSTEMS
- NT SELF ALIGNMENT
- NT SEQUENTIAL CONTROL
- NT TIME OPTIMAL CONTROL
- Nonlinear automatic control systems steady random processes approximate analysis by integral linearization of functions and operators 01 p0058 A71-10100
- Digital simulation of steam boiler by process control computer using coefficients directly calculable from transfer function of continuous system 01 p0049 A71-10324
- Structural analysis of invariant automatic control systems characterized by coordinate pairs coupled through disturbed load operator 01 p0058 A71-10406
- Nonlinear pulsed automatic control systems absolute stability with unsteady linearity by Pontryagin principle, considering forced and free motions 01 p0058 A71-10428
- Transient response of pulse frequency modulation automatic control systems for zero or nonzero initial conditions, using signal Laplace transforms 01 p0059 A71-10528
- Computer methods for calculating sensitivity of amplitude and phase frequency response functions in automatic control systems to system parameter changes 01 p0059 A71-10529
- Automatic control systems invariance theory - Conference, Kiev, May-June 1966, Volume 1 01 p0059 A71-10701
- Automatic control systems invariance theory, discussing Poncellet principle, perturbation measurement, etc 01 p0060 A71-10702
- Automatic control and information systems epsilon invariance, generalizing Kotelnikov theorem on continuous signals reduction 01 p0060 A71-10703
- Multiloop discrete automatic control system invariant with respect to external perturbations 01 p0060 A71-10704
- Controlled parameters invariance in automatic systems with bounded-coordinate components 01 p0060 A71-10706
- Automatic control with twofold invariance properties, describing use as nonsearch self adaptive system 01 p0061 A71-10707
- Finite automata systems invariance with respect to control actions 01 p0061 A71-10708
- Invariant automatic control structure for nonlinear plant, using inverse method 01 p0061 A71-10710
- Automatic control systems analysis and synthesis, applying invariance conditions second form 01 p0061 A71-10711
- Automatic feedback control systems performance correction for errors due to weakly damped components effects 01 p0061 A71-10712
- Quasi-invariant automatic feedback control system, deriving basis for determination of perturbation compensating components parameters 01 p0061 A71-10713
- Dynamic errors estimation for nearly invariant automatic control systems, discussing parameter-change sensitivity 01 p0061 A71-10715
- Invariant automatic control system performance improvement by signal predistortion for reproducibility increase 01 p0062 A71-10717

- Automatic control systems without disturbance feedback, examining invariance under positive-zero-negative error transition 01 p0062 A71-10720
- Rapid-response automatic control systems synthesis, using compensation signals based on external disturbances 01 p0063 A71-10722
- Pulsed analog and digital control systems invariance conditions at discrete times, using Laplace transform method 01 p0063 A71-10726
- Invariance in automatic control systems nonlinear differential equations of motion 01 p0064 A71-10730
- PERL programming language for on-line control of industrial processes and scientific experiments 01 p0051 A71-11186
- Relay corrector for widening automatic control systems stability via jump-change in signal amplification factor 01 p0065 A71-11236
- Final state automatic control system structural properties, considering second stage synthesis, passage from initial state, degeneracy conditions and coordinate selection 01 p0065 A71-11245
- Automated machinery for reinforced plastic structural products manufacture by filament winding [SME PAPER EM-70-135] 01 p0089 A71-11261
- Soviet book on gyroscopes in geodesy and aerial photography based on structural analysis for automatic control systems, covering gyro error, theodolites, etc 01 p0083 A71-11321
- Automatic instrument for star detection and azimuth derivation, scanning nighttime zenith star field [AIAA PAPER 69-861] 01 p0126 A71-11584
- Holographic filters for optical automatic pattern recognition systems, discussing reconnaissance target and fingerprint 02 p0247 A71-11702
- Computer controlled mass spectrometer system, processing spectral information data for on-line graphic system output 02 p0253 A71-12550
- Fluidic sensors for automatic control systems parameter measurement 02 p0196 A71-12625
- Earth station antennas structural parameters and performance prediction, considering autotrack loop stability optimization by multiple lag compensation using single axis model 02 p0223 A71-12803
- Satellite ground station autotracking receivers, discussing antenna position control systems 02 p0239 A71-12816
- Human behavior during machine control learning, modeling habit development as automatic control system 03 p0368 A71-12997
- Biological and medical cybernetics approach to closed systems construction for continuous automatic monitoring and control of human physiological processes under harmful conditions 03 p0368 A71-13000
- Trailing edge flap automatic control for glider performance improvement 03 p0346 A71-13020
- Automatic test equipment with digital computer for control, discussing software schemes and tradeoff analysis 03 p0381 A71-13079
- Nonstationary automatic control system asymptotic series solution for equations of perturbed motion, deriving unperturbed motion local stability criteria 03 p0388 A71-13287
- Automatic antisurge control of axial compressor using partial gas recycling bypass method 03 p0469 A71-13370
- Dynamic automatic control and servo systems with distributed parameters, discussing synthesis and precision 03 p0389 A71-13373
- Linear control systems searchless automatic optimization on basis of ideal reviewing model 03 p0389 A71-13519
- Computer controlled eclipse telescope for coronal thermal emission IR spectrum observation 03 p0424 A71-13633
- Automatic temperature control for cryostats operating at 1-300 K, describing mechanical, electrical and combined devices 03 p0429 A71-14302
- Locking characteristics of automatic phase control circuits in noisy environment 03 p0391 A71-14311
- Spacecraft and aircraft automatic control man machine interface, bionics and traffic control systems 03 p0455 A71-14393
- Soviet book on frequency method of calculating nonlinear systems covering continuous and pulsed automatic control 03 p0393 A71-14425

- Photoelectric automatic logger with perforated tape recorder, discussing block diagram 04 p0589 A71-14837
- Semiautomatic device for vertical circle limb photographs measurement, involving beam splitting with subsequent comparison of modulated components 04 p0591 A71-14850
- Automatic micrometer for measurement of limb graduations and scales, basing method on Archimedes rotating spiral principle 04 p0591 A71-14851
- Semiautomatic photoelectric apparatus for limb graduations using pivoted optical arrangement, discussing accuracy, measurement rate and reliability improvement methods for similar instruments 04 p0591 A71-14852
- Autocollimation control of telescope rotation axis position at arbitrary azimuths 04 p0565 A71-14854
- Automatic amplitude control of transistorized quartz clock master oscillator 04 p0592 A71-14860
- Automatic transistor noise factor measurement equipment consisting of noise source, signal amplifier, synchronizing oscillator, controllable attenuator and automatic control circuits 04 p0557 A71-15078
- Soviet book on aviation automation covering automatic control systems in piston, turbojet and turboprop engines, navigation, air temperature and pressure 04 p0529 A71-15223
- Astronomical telescope automation and remote control, discussing advantages and problems 04 p0597 A71-15255
- Automatic telescope instrumentation, considering polychromator, photometer and photoelectric star finders 04 p0597 A71-15256
- Automated radar calibration system using star tracker and computerized control 04 p0554 A71-15318
- Linear digital computer simulation and process control, considering state space method 05 p0730 A71-16126
- Unmanned Soviet spacecraft Luna 16 mission, describing landing techniques, sample taking and experiment conduction 05 p0805 A71-16147
- Automatic systems design, describing optimization method for nonlinear nonstationary system acted upon by fluctuation signals and disturbances 05 p0731 A71-16793
- Automatic control systems with parametric invariance, describing method for quick response increase 05 p0731 A71-16797
- Frequency stability of automatic control system with hydraulic actuating mechanism external load, taking into account fluid compressibility 05 p0705 A71-17033
- Absolute stability of closed automatic control system with nonlinear components, discussing frequency criterion 05 p0732 A71-17172
- Ultrasonic position sensor for automatic control, using short pulses for azimuth and range resolution 06 p0896 A71-17321
- Parameter estimation of mixed autoregressive moving-average /ARMA/ time series using output data 06 p0878 A71-17332
- Automatic phase control system with separating capacitance containing low and high frequency electric filters 06 p0866 A71-17375
- Pulsed phase locked automatic phase control system linear model, discussing optimal white noise filtration with integrating filter 06 p0867 A71-17377
- Soviet book on Liapunov functions covering autonomous linear and nonlinear systems, asymptotic and absolute stability, etc 06 p0916 A71-17442
- Teleautomatic data processing systems with computer control, synthesizing optimal structure 06 p0871 A71-17495
- Single loop automatic control system with lag, determining time constant and transfer functions critical values for real positive first and second derivative elements 06 p0879 A71-17520
- Computer controlled time division multiple access control system for U.S. Army Satellite Communication Agency, discussing tests and operational details 07 p1057 A71-18820
- Aircraft automatic landing improvement through use of space diversity ILS receiving system 07 p1153 A71-18830
- Soviet book on automatic control systems synthesis covering dynamic characteristics optimization, based on quality indices and computerized design 07 p1081 A71-19048
- Automatic regulators of wire tension during coil winding 07 p1108 A71-19310
- Altazimuthal telescope mounting with computer controlled guidance, discussing instrumental and methodical error effects on positioning and tracking accuracy 07 p1083 A71-19348
- Control function synthesis by linearization for maintenance of uniform motion of driven component in mechanical system including motor, variator and operating machine 07 p1116 A71-19358
- Automatic control in space - Conference, Toulouse, March 1970 07 p1154 A71-19526
- Continuous flow oxygen regulators construction, performance and testing SAE standard, covering automatic, adjustable and preset types [SAE-AS-1197] 07 p1049 A71-19648
- Lunar Module physical characteristics and control system function, emphasizing automated vs manual flight degree and astronaut overriding capability 07 p1208 A71-19915
- Fluid logic automatic control systems troubleshooting, discussing circuit and components design for quick malfunction analysis and repair 07 p1023 A71-19995
- Active control moments construction of solid body rotating about stationary point 07 p1161 A71-20268
- Automatic system for indirect blood pressure measurement in carotid compression test, discussing applications 08 p1247 A71-20827
- Papers on modern practice in servo design covering digital techniques, applications of analog and hybrid computers and thyristors, reliability engineering, etc 08 p1268 A71-21195
- Automatic procedure for determining cloud motion from geosynchronous satellite pictures based on cross correlation, discussing real time operational system 08 p1327 A71-21454
- ATC automation program for en route and terminal centers, discussing combined nationwide system features, IFR volume and video digitizer data links 08 p1332 A71-21659
- Time shared digital computer-based data acquisition and control system for multiple remote laboratories, using modular programming, multiprocessing and language processors 08 p1260 A71-21851
- Signaling sensitivity leveling by introduction of automatic defect indicator into defectoscope 08 p1273 A71-21904
- Liapunov matrix equation for linear and nonlinear automatic control systems stability 08 p1325 A71-21976
- Nonlinear automatic control systems stabilization by seeking Liapunov function satisfying certain integral relationships 08 p1270 A71-21977
- Nonstationary automatic control systems analysis using frozen coefficients and weighting functions 08 p1270 A71-21978
- Nonlinear automatic control system stability with random stationary parameters 08 p1271 A71-22024
- Complex automatic systems with random switch-off, developing failure sequence models 09 p1422 A71-22119
- Spacecraft autonomous control algorithm to ensure geographically specified landing accuracy, noting atmospheric density 09 p1491 A71-22565
- Telescope plate scanner automated computerized operation, evaluating faint stars identification and color classification for annual motion surveys 09 p1443 A71-22646
- ATC electronic automation systems development for air safety improvements 09 p1491 A71-22953
- Soviet book on navigation and control covering data processing, optimal stochastic self guidance, instrument errors, mean energy consumption and stabilization loop time lag 09 p1491 A71-23163
- Nonstationary automatic control system asymptotic series solution for equations of perturbed motion, deriving unperturbed motion local stability criteria 09 p1424 A71-23262
- Differential equations construction for controlled systems and controller starting from programmed motion stability requirement 09 p1495 A71-23432
- Computer controlled electromechanical system for luminous projection on world map of satellite orbits, using Ne-He laser beam 09 p1430 A71-23627
- Soviet papers on cybernetics problems covering control and communication for information handling machines and biological nervous systems 10 p1585 A71-24155
- Iterative algorithms for regression function saddle point and applications in reliability and automatic control theories 10 p1585 A71-24156
- Respiratory system self regulation and coordinated activity interference by biocontrolled stimulator incorporation into natural nerve links 10 p1567 A71-24165
- Automated fueling for Kennedy jet airport, using computer controlled underground bulk storage-satellite tank pipeline system 10 p1589 A71-24300
- Asymptotic transformations and stability criteria of nonstationary linear automatic control systems using Krylov-Bogoliubov slow time concept 10 p1588 A71-24899
- Distribution functions of initial and established intervals of stochastic and Poisson sequences in automatic control, reliability and communications theories 10 p1588 A71-24902
- Stability indices of automatic control system from open circuit logarithmic frequency characteristics, determining poles of transfer function 10 p1588 A71-24905
- Differential equations of root loci motions for stationary linear automatic control design by hodograph and Evan method 10 p1637 A71-24906
- Aircraft with automatic thrust controller, calculating transfer functions characterizing speed and attitude control modes 10 p1640 A71-24910
- Soviet book on optimal, multiply connected and adaptive control systems covering variational methods, dynamic programming, functional analysis and statistical methods 11 p1742 A71-26098
- Soviet book on aircraft and rocket engines control automation, discussing nuclear power plant/fuel systems design and control simulation methods 11 p1814 A71-26403
- Frequency phase multistable elements, discussing automatic control, telemechanics and digital measurement applications 11 p1739 A71-26465
- Automated facility for electronic equipment production reliability environmental testing, discussing human engineering and test and failure mode designs 11 p1746 A71-26512
- Parametrically invariant automatic control systems with linear controllers, using compensating devices based on certain transfer function qualifications 12 p1890 A71-26721
- Equivalent-to-adaptive parametrically invariant automatic control, discussing compensation, variable structure, autooscillator, HF nonlinear, ultracoarse and nonsearching self adjusting systems 12 p1890 A71-26723
- Automatic control application to liquid metal and semiconductor materials, plasma flows, charged particle beams and similar media interacting with magnetic fields 12 p1936 A71-26972
- Automatic control systems with nonlinear hysteresis characteristics, deriving frequency conditions for absolute system stability 12 p1892 A71-27025
- Plant and compensator parameters deviations effect on accuracy of complex unitary-code programmed automatic control system with delay line digital compensator 12 p1893 A71-27342
- Variable structure automatic control system dynamic properties, using frequency response method 13 p2041 A71-27943
- Variable structure automatic control system synthesis, giving roots distribution of characteristic equation for fluttering mode 13 p2041 A71-28636
- Automatic control systems preventive inspection intervals examined from cost optimization viewpoint for various failure distribution rules 13 p2042 A71-28641
- Four foci computer controlled Anglo-Australian reflecting telescope, considering design and applications 13 p2069 A71-28850
- Quantization by levels effect on steady state processes in digital automatic control systems 13 p2044 A71-28918
- Soviet book on multiloop automatic control systems covering matrix notation, stability and accuracy, invariance principle, compensating cross couplings, etc 14 p2218 A71-29527
- Automatic amplitude control dynamic performance of system with oscillating frequency determination by ring gain bandpass behavior 14 p2210 A71-29809
- Complex automatic systems with random switch-off, developing failure sequence models 14 p2220 A71-29997
- Fluidic cabin pressure automatic control systems for military and civil aircraft, discussing design, operation and performance 14 p2182 A71-30308
- Sinusoidal vibration tests using narrowband tracking filters, considering automatic servocontrols and feedback loop optimum matching 14 p2175 A71-30310

Computer controlled acoustic data acquisition system with real time control of 16 high intensity acoustic generators

14 p2208 A71-30315

French ATC, discussing automatic coordinator systems, computer utilization and flight plan data processing

14 p2272 A71-30382

Maastricht Automatic Data Processing and Display ATC system with digital computers for aiding controllers in issuing instructions and making decisions

14 p2272 A71-30383

Airborne phased array using computer control for beam steering, investigating row-and-column logic effects on beam shaping and stabilization

14 p2209 A71-31045

Automatic camera for international synchronous observations of geodetic satellites

14 p2250 A71-31117

Nonlinear multiple component automatic control systems equations and frequencies for absolute stability

15 p2378 A71-31292

Automatic coordinate compensation for systematic and random distortions of photographs on stereophotogrammetric devices

15 p2406 A71-31619

Nonlinear multidimensional automatic control systems structural synthesis

15 p2379 A71-31844

Automatic system for random vibration spectra control, consisting of spectrum shaper/analyzer and multidimensional controller

15 p2379 A71-31845

Maastricht automatic data processing and display system concept for automatic management of reception and data transmission and information visualization

15 p2384 A71-31888

Stability criterion for cross coupled symmetrical two dimensional nonlinear control systems allowing different slopes for Popov lines

15 p2380 A71-31938

Discrete group symmetric linear control systems reduction to elementary cell, generalizing Fourier transform to groups without operational constraints

15 p2381 A71-31978

Noise rejection in step type extremal self oscillating system with variable control period, estimating process precision

15 p2381 A71-31981

Mathematical theory of control systems synthesis, considering Shannon functions asymptotic behavior

15 p2442 A71-31992

Centerless grinding control high precision automatic invariant systems synthesis, outlining machine tool working elements inductive setters

15 p2415 A71-32185

Gradual failure effects on operational reliability of centralized automatic control machine

15 p2374 A71-32192

Atmospheric laser link with automatic sensitivity control during reception, measuring detector output signal fluctuation reduction characteristics

15 p2372 A71-32319

Two-spool turbojet engine nozzle diameter adjustment system for increasing thrust, fuel economy and reliability, describing automatic clamshell shutter control mechanism

15 p2471 A71-32527

N-order continuous linear automatic control system compensation method, using model of sampled systems with duration modulation

16 p2549 A71-33377

Numerical identification of linear automatic control system, starting from pulse response

16 p2549 A71-33378

Automatic control systems sensitivity, including literature survey

16 p2550 A71-33703

Algebraic structure and design of automatic systems using partitions in set of states of finite automation

16 p2545 A71-33705

Potential benefits accruing to air superiority fighters by integrating automatic feedback control system technology into design, using F-4 as baseline configuration

[AIAA PAPER 71-764]

16 p2523 A71-34002

Frequency stabilized He-Ne laser wave secondary length standard for automatic measurements, discussing electronic control, accuracy, line width, pressure, current and magnetism effects

16 p2588 A71-34119

Computerized automatic control of aircraft electrical system using remote power controllers and multiplexed data bus for wiring reduction and reliability improvement

17 p2677 A71-34700

Automated lunar landing missions with modified Mars Viking spacecraft, discussing propulsion and subsystems modifications, science payload and lunar exploration capabilities

[AIAA PAPER 71-822]

17 p2812 A71-34724

Optimum diagnostics algorithm for complex automatic control system state detection based on Bayesian rule successive application for minimum time requirement

17 p2720 A71-34959

Control reliability in automated system of discrete production management

17 p2721 A71-34961

Redundancy utilization in automatic control systems synthesis, considering dynamic characteristics sensitivity

17 p2721 A71-34965

Optical telescopes automatic electronic control by positioning mechanical axis to specified coordinates and tracking guide star

17 p2740 A71-34983

Integrated telescope computer system, including magnetic disk storage, digital encoding, drive control and automatic guiding

17 p2711 A71-34984

Computer control of vacuum solar telescopes, taking into account servos/handbox intervention, input-output preprocessor, high speed disk and memory

17 p2740 A71-34986

Automatic star follower for camera by optically splitting stellar image and measuring radial displacement by comparing signals

17 p2740 A71-34987

Computer controlled pulse counting technique application to astronomical photoelectric photometry for improved telescope efficiency

17 p2740 A71-34989

Computer controlled encoding device with laser flying spot scanning for automatic photographic image measurement

17 p2741 A71-34998

Soviet papers on exact analytical methods for studying nonlinear automatic control systems covering synthesis, stability, quality and dynamics problems

17 p2783 A71-35126

Parameter space sections method for nonlinear automatic control systems analysis, reducing initial system by linear transformation of variables to first and second order equations

17 p2783 A71-35127

Second order and degenerate third order nonlinear automatic control systems analysis by point mapping method, considering global stability and self oscillation mode

17 p2783 A71-35128

N-dimensional phase spaces of nonlinear nth order automatic control systems at parameter space sections /hyperplanes/, considering nonlinearities effects in servomechanisms

17 p2783 A71-35129

Frequency criteria for absolute stability of equilibrium states and processes in nonlinear automatic control systems

17 p2783 A71-35130

Nonlinear automatic control systems stability during large modulus-limited deviations based on method of sections and direct Liapunov method

17 p2783 A71-35131

Nonlinear automatic control systems synthesis based on structure and parameter values selection, formulating quality criteria

17 p2783 A71-35132

On-off automatic control systems, using nonlinear finite difference equations for switching times and coordinate values determination

17 p2721 A71-35133

Dynamic response as function of time of nonlinear nonautonomous second order control system to external disturbances, using moving phase plane method

17 p2721 A71-35135

Nonlinear automatic control systems sensitivity to changes in prescribed operating conditions and component parameters

17 p2784 A71-35136

French monograph on variable-structure automatic control systems covering algorithms, stability, nonlinear hypersurface slip, minimum time, switching elements, analog simulation, etc

17 p2767 A71-35249

Automatic control system output signal changes due to finite variations, noting expansion into Taylor series

17 p2723 A71-35344

Automatic system for follow-up balancing of digital bridge, noting fast response rate

17 p2723 A71-35711

Avionic and missile computer control systems, describing universal function unit design and digital processing requirements

17 p2711 A71-35775

Remote power controller as static circuit protection device for aircraft and spacecraft automatically controlled electrical wiring system, discussing performance improvement

17 p2678 A71-35782

Autoexposure system for tracking telescopes, describing photometer and camera shuttle automatic control subsystems

18 p2919 A71-36088

Book on stability theory covering Liapunov functions, variable structure automatic control systems and differential equations solutions in Banach space

18 p2947 A71-36250

Computer programs for functional analysis, planning and control of space stations and shuttles operation

18 p2885 A71-36459

Telecommunications satellite data acquisition from automatic beacons, discussing Role program

18 p2988 A71-36543

Automatic fringe counting pulsed ultrasonic interferometer for transit time measurement, using phase sensitive multiple echo detection

18 p2922 A71-36586

Optical tracking system for high angular acceleration missile flights, using movable mirrors with motion picture camera interfaced with computer

18 p2900 A71-36906

Automatic argon ion laser tracking system for high speed rocket sleds, describing apparatus configuration and error correcting devices

18 p2883 A71-36908

Optical target detection and position error signal system for boost phase missiles, using TV with digital computer controlled dual tracking electronics

18 p2883 A71-36911

Direct digital control technology for optical tracking systems, discussing advantage and deficiencies

18 p2883 A71-36913

Three-channel monopulse tracking receiver for automatic steering of satellite tracking antennas, noting gain controlled IF amplifier module

18 p2884 A71-36996

Computerized automatic estimation techniques application to real time aircraft tracking in ATC system design

[AIAA PAPER 71-926]

19 p3096 A71-37172

Automatic control systems with nonlinear hysteresis characteristics, deriving frequency conditions for absolute system stability

19 p3038 A71-37694

Automated test capability for digital modules, describing test generation, circuit analysis and simulation programs

19 p3030 A71-38406

Ti alloys semiautomatic pulsed arc MIG welding, showing increased productivity and reduced distortion

19 p3070 A71-38423

Automatic regulation of volumetric blood flow rate during artificial blood circulation, using electromechanical system for controlling arterial pump of cardiopulmonary machine

19 p3010 A71-38641

Automated meteorological radar information operation methods for cloud fields, discussing data analysis and processing

19 p3094 A71-38702

Miniature self regulating rapid cooling Joule-Thomson cryostat, noting purging of accumulated contaminants

20 p3184 A71-39274

Computer use in automatic tracking radar systems design, describing adaptive radar hardware

20 p3200 A71-39902

Random vibration testing digital computer control system and experiment design, considering discrete Fourier transform techniques application

[ASME PAPER 71-VIBR-30]

21 p3360 A71-40285

Flight test experiment to evaluate mechanized automatic control system to minimize wake turbulence effects on aircraft

21 p3321 A71-40509

Automatic balance control device for regulating vibration caused by rotating ill-balanced mass system

21 p3388 A71-40755

Cybernetics and automatic control of space systems with pursuit process, using trajectory approximation with mathematical model graphs

21 p3452 A71-40857

Stability and quality diagrams of linear discrete automatic control systems with time constant parameters

21 p3361 A71-41142

Statistical methods for calculating cross correlation function integrals of input and output coordinates of automatic control system in presence of random noise at input

22 p3525 A71-41437

Statistical analysis of digital automatic control system with unreliable communication channel, determining system mean square error

22 p3525 A71-41439

Graph-analytical method of determining optimal adjustment of real differentiating units and components introduced into single loop automatic control system with time lag

22 p3525 A71-41440

Temperature field of thermochemical sensor in automatic control systems, developing thermal energy transport models for circular disk with energy source at center

22 p3537 A71-41443

Satellite tracking ground antenna servocontrol, discussing system requirements and automatic and programmed operating modes

[DFVLR-SONDDR-125]

22 p3483 A71-41520

Automatic control theory application to pneumatic self vibration /hammer/ occurrence criteria derivation

for externally-pressurized gas- lubricated thrust collar bearings
22 p3551 A71-41660
Soviet book on multivariable automatic control system synthesis with adaptation to computer covering methodology, algorithms, transfer function approximation and stability problem
22 p3525 A71-41799
Soviet book on automatic control and computer components reliability, explaining redundancy principles and test and repair procedures
22 p3526 A71-41820
Soviet book on nonlinear sampled-data control systems with PFM and PDM covering mathematical description, transient analysis and system stability problems
22 p3526 A71-41821
Recurrent finitely converging algorithms for solving inequalities in automatic control systems involving adaptive filters
22 p3526 A71-41858
Mathematical models for computerized ATC automatic aircraft flight tracking logics without tracks smoothing
22 p3573 A71-42396
Frequency conversion/division, multiplication and shifting/ application to multistable phase- frequency elements design
22 p3524 A71-42573
Synthesis models and methods for large scale automated control systems with human elements, discussing mathematical models and computerized design
22 p3528 A71-42858
IBM 9020 multiprocessing computer application to ATC, discussing control sectors for inflight control at air route traffic control centers in U.S.
23 p3702 A71-43888
Automatic control - Conference, St. Louis, August 1971
23 p3657 A71-44076
Sequential zero-pole placement technique for multivariable control systems, developing algorithm for computing closed loop transfer function matrix
23 p3660 A71-44120
Goloseyev Wanshaff vertical circle photographic device, discussing photomicroscopes and automatic control unit
23 p3680 A71-44265
Odessa observatory automatic film winding photoelectric system, discussing construction and accuracy
23 p3680 A71-44266
Trends in automatic control field in last two decades, emphasizing optimal control and performance criteria selection
[AIAA PAPER 71-1001] 24 p3813 A71-44591
Automatic control systems optimal nonlinear digital filter design, using theoretical numerical grid
24 p3813 A71-44680
Nonlinear automatic control system statistical optimization using similarity theory
24 p3813 A71-44681
Statistically optimal automatic control system synthesis with phase coordinate vector
24 p3814 A71-44685
Orthogonal method for studying nonlinear automatic control systems in presence of random perturbations, discussing applicability limits
24 p3815 A71-44701
Computer systems design for complex process control, constructing models with differential equations and Boolean functions
24 p3806 A71-44714
Curie point region automatic thermal stabilization effectiveness of cylindrical/disk shaped segnetoceramic elements in electrostrictive constant magnetic field converters
24 p3828 A71-45164
Automatic eddy current system to detect fastener hole cracks consisting of scanner unit, control box, recorder and mounting hardware
24 p3831 A71-45281
AUTOMATIC CONTROL VALVES
NT PRESSURE REGULATORS
Hydraulic system self acting valves natural vibration dynamic characteristics, showing energy transfer by phase shift of variable hydrostatic compression component
17 p2677 A71-34349
AUTOMATIC DATA PROCESSING
U DATA PROCESSING
AUTOMATIC FLIGHT CONTROL
NT AUTOMATIC LANDING CONTROL
Themis project automatic navigation program, examining optimum stochastic feedback error analysis and sensitivity algorithms
01 p0125 A71-10525
Flight testing of automatic orbital operations system for satellites and space probes
[DGLR 70-080] 05 p0779 A71-15958
Concorde automatic flight control, noting reduced weight and speed accuracy limit at Mach 2
05 p0751 A71-16325

VTOL aircraft avionics systems, discussing automatic flight control and navigation systems integration
06 p0925 A71-17925
Variable camber flap automatic control equipment for glider, considering combinations of mechanical, electrical and electronic approaches
06 p0847 A71-18250
Optimum automatic flight control techniques in horizontal guidance of aircraft at terminal
07 p1156 A71-20306
V/STOL aircraft automatic flight controls and electronic head down displays, discussing handling qualities, lift effectiveness and autostabilization
10 p1554 A71-23944
Automatic control system for fighter aircraft sideslip correction, using rudder position sensor, transverse accelerometer and high pass filter for anticipatory sideslip reduction
10 p1556 A71-24288
Soviet papers on automatic control for flight vehicles, Part I, covering dynamics of linearized systems, deterministic and random inputs, stability, oscillations, thrust control, etc
10 p1588 A71-24897
Linear automatic flight control systems synthesis based on transfer functions and logarithmic amplitude characteristics of open systems
10 p1588 A71-24911
V/STOL aircraft instruments, deck display and automatic flight controls for takeoff and landing operation
13 p2098 A71-29132
Controlled aircraft motion under strict kinematic constraints in terms of simple subsystems, noting pilots role in Newmark theory
14 p2177 A71-31024
European Airbus automatic pilot and flight control system, including computers in electromechanical subassemblies
15 p2446 A71-31914
Concorde aircraft automatic landing and flight control system objective, design, reliability and certification tests
15 p2446 A71-31915
Helicopter automatic flight control equipment, discussing autopilot stabilizer, localization system, ground approach guidance coupler and flight director
15 p2446 A71-31916
Soviet book on aircraft automatic control systems covering linear theory, design, autopilot, man machine performance, operation modes, etc
17 p2771 A71-34473
Automatic flight control accommodation to dynamic characteristics variations of airframe, providing uniform response for all flight conditions
19 p2996 A71-37296
Automation in third generation ATC requiring distributed management and spacing functions delegation to pilot
19 p3100 A71-37602
Automatic ATC display systems, discussing electronic flight progress strip for telemetry reproduction
19 p3102 A71-38300
Large crane heavy lift helicopter stability and controllability, considering effects of slung loads, performance improvement, automatic flight control and physical size
19 p2998 A71-38651
Automatic flight control systems, discussing pilot as systems manager or retained in control loop
24 p3845 A71-44454
American development in automatic flight control, noting FAA requirements, pilot involvement and visibility enhancement
24 p3846 A71-44455
AUTOMATIC FREQUENCY CONTROL
Solid state circuit digital frequency discriminator with low pass filter in ESRO stations telemetry receivers AFC and antisideband system
05 p0720 A71-16326
Phase locked AFC theory, analyzing equation by bifurcation methods
05 p0731 A71-16984
Operating mode of semiconductor AFC mixer of radar receiver under large signal
06 p0874 A71-17546
Wideband submillimeter range backward wave tubes automatic frequency control system, using combination of passive standard and open cavity
06 p0876 A71-18079
Pulsed phase detectors for phase comparisons of pulse sequences having arbitrary frequency ratios, designing circuit to prevent false locking in AFC systems
07 p1061 A71-19509
Transistorized DC amplifiers operational characteristics, discussing principal electrical parameters and application in phase lock AFC loops
08 p1263 A71-20786
Automatic control circuits for millimeter wave backward wave tube frequency tuning and supply voltage regulation
08 p1267 A71-21804

Phase regulated AFC system design for millimeter and submillimeter wave backward wave tubes
08 p1267 A71-21805
Optimal phase regulated AFC system for FM signal filtration in presence of internal noise
09 p1404 A71-22155
Dynamic frequency and phase characteristics of oscillatory circuit dependent linearly on time variable capacitance
10 p1643 A71-24907
Time optimal phase locked AFC system synthesis based on Pontryagin maximum principle, comparing computerized and experimental transient response
12 p1882 A71-27514
Phase locked AFC system, calculating phase detector response effects on dynamic properties
15 p2370 A71-31592
Microwave acoustic delay device incorporated in phase discriminator for AFC, FM noise meters and pseudo-superhetrodyne receivers
18 p2893 A71-36599
Phase locked AFC theory, analyzing equation by bifurcation methods
18 p2896 A71-36784
Estimation-correlation principle application to harmonic signal receiver with unknown carrier frequency, using searching phase locked AFC circuit as estimation unit
22 p3512 A71-42313
AUTOMATIC GAIN CONTROL
AGC system with transfluxor as gain control element and output-level memory device
01 p0054 A71-11086
Low level optical signal transient response measuring instrument with nsec resolution and automatic photomultiplier current gain control
02 p0249 A71-12131
Transistor amplifiers automatic gain control open loop amplitude characteristics, discussing output level stabilization relation to signal source coupling and negative feedback
02 p0233 A71-12544
Optimal gain tuning elements of cryogenically cooled parametric amplifiers
02 p0235 A71-12833
Low distortion gain-controlled 140 MHz IF main amplifiers for 2700-channel microwave repeaters, discussing design and performance
05 p0730 A71-17069
Invariant control system with optimum gain and time lag adjustment for compensating parameter changes under random disturbance
06 p0879 A71-17519
Transistorized microwave amplifier/limiter for upper part of decimeter wave range, suggesting limitation in automatic gain control transistors
16 p2547 A71-33499
Three-channel monopulse tracking receiver for automatic steering of satellite tracking antennas, noting gain controlled IF amplifier module
18 p2884 A71-36996
Bayesian learning algorithm derivation for statistically optimum adaptive gain control in Rayleigh-distributed signal reception
20 p3206 A71-38874
Laser amplifier with range variable automatic gain control in Fabry-Perot cavity with allowance for oscillation
22 p3556 A71-41807
Range finder receiver based on Si avalanche detector coupled to tunnel diode circuit, with automatic gain control through tunnel diode bias control
23 p3677 A71-43518
Transistorized AGC circuit for use with ultrasonic Doppler-cardiogram recording system to retain signal characteristics under strong fluctuations
24 p3801 A71-44543
AUTOMATIC LANDING CONTROL
Aircraft all weather automatic landing system, discussing component weights and reliability connected with problem area
02 p0279 A71-12274
All-weather automatic landing electronic technology, describing flight automation landing system for VC 10 BAC 111 and Concorde aircraft
02 p0279 A71-12275
Helicopter automatic and manual low visibility landing systems evaluation by hybrid computer simulation
06 p0880 A71-18423
Two dimensional aircraft automatic landing motions control processes by simulation without use of moving cockpit simulator
07 p1084 A71-20066
Transport aircraft all weather automatic landing operation, examining guidance system and independent monitors
[SAE PAPER 710441] 13 p2098 A71-28323
Automatic landing systems independent monitor for L-1011 aircraft, providing pilot confidence under reduced visibilities
13 p2098 A71-28324
Trident aircraft autopilot for automatic landings in blind conditions, discussing operational problems
13 p2098 A71-29261

- Automatic aircraft landing system modification for improvement of response to air turbulence effects
14 p2271 A71-29773
- Caravelle aircraft all-weather Sud Lear automatic landing system operation and performance
15 p2446 A71-31913
- Concorde aircraft automatic landing and flight control system objective, design, reliability and certification tests
15 p2446 A71-31915
- Automatic landing systems using inertial navigation derived translational state information, discussing evaluation by simulation of transport aircraft operating with conventional instrument landing system
[AIAA PAPER 71-795] 16 p2605 A71-34020
- Soviet book on air transportation covering ATC, automatic landing and information display systems
17 p2774 A71-35194
- Lockheed L-1011 development, discussing flying stabilizer design, direct lift control and autoland system
[AIAA PAPER 71-782] 17 p2675 A71-35532
- Cost effective high speed projectile trajectory plotting system for gunnery range instrumentation, applying to aircraft path recording during automatic landing control
18 p2924 A71-36613
- L-1011 aircraft automatic landing safety and performance improvement through direct lift control, discussing flight control system integration
[AIAA PAPER 71-906] 19 p3095 A71-37157
- Performance limitation of simplified radio-inertial lateral control guidance system subject to stochastic gusts for automatic landing
[AIAA PAPER 71-957] 19 p3099 A71-37198
- Performance monitor for aircraft automatic landing systems safety control
[AIAA PAPER 71-958] 19 p3099 A71-37199
- European automatic flight control systems for landing in category IIIA conditions, discussing triplex system in Trident and simplex in Caravelle
24 p3846 A71-44456
- Landing control algorithm using onboard digital computer for spacecraft hyperbolic velocity reentry, discussing simulation test results
24 p3846 A71-45303
- AUTOMATIC PATTERN RECOGNITION**
U PATTERN RECOGNITION
- AUTOMATIC PICTURE TRANSMISSION**
Picture transmission by Fourier transform based data reduction system, considering law of module probability and spatial distribution, statistical analysis and degradation
05 p0722 A71-16746
- Frequency memories application to earth-satellite-aircraft UHF communications, repeater apparatus and multiple access transmission of half tone images in worldwide satellite communication
18 p2881 A71-36553
- APT weather satellite cloud pictures over sea southwest of Kyushu showing striated cloud pattern transformation into closed cellular pattern, discussing lower atmospheric layer moisture budget
22 p3568 A71-41859
- AUTOMATIC PILOTS**
Digital computers in aviation electronics, discussing automatic control loop in automatic pilot
03 p0382 A71-13687
- Feedback control system parameters optimization by target model method, with automatic pilot example
04 p0560 A71-15205
- Eigen proportional control method for second order system with time varying parameters, applying to aircraft autopilot systems
06 p0925 A71-18308
- Lunar module digital autopilot design, considering attitude state estimator, reaction control system and thrust vector control
[AIAA PAPER 70-991] 07 p1154 A71-18897
- Automatic Carrier Landing System with linear adaptive aircraft Navigation Computer, investigating effectiveness in reducing system errors due to nonlinearities and noise effects
07 p1157 A71-20405
- Subsonic tactical missile hydraulic and fluidic autopilot systems for directional control, considering costs, reliability, vulnerability, maintainability, weight and mobility
[SME PAPER MS-70-524] 07 p1024 A71-20547
- Large flexible booster launch vehicle autopilots automated design and optimization by computerized technique in frequency and time domain
08 p1332 A71-21337
- Self adjusting autopilot synthesis with capability for control plant changing parameters and structural vibrations effects compensation
12 p1927 A71-26732
- Trident aircraft autopilot for automatic landings in blind conditions, discussing operational problems
13 p2098 A71-29261
- European Airbus automatic pilot and flight control system, including computers in electromechanical subassemblies
15 p2446 A71-31914

- Helicopter automatic flight control equipment, discussing autopilot stabilizer, localization system, ground approach guidance coupler and flight director
15 p2446 A71-31916
- Soviet book on aircraft automatic control systems covering linear theory, design, autopilot, man machine performance, operation modes, etc
17 p2771 A71-34473
- ATC avionics equipment, discussing inertial area navigation, autopilots, airborne data acquisition, altitude reporting, collision avoidance, CAT, satellite communications, etc
17 p2771 A71-34615
- BAC 111 autopilot development, discussing computer compatible system for digital representation of airborne flight test data and direct transmission to ground-based computers
18 p2946 A71-36672
- Sight line autopilot (SLAP) for side-firing aircraft pointing accuracy improvement, using optimal regulator theory to generate control gains
[AIAA PAPER 71-960] 19 p3099 A71-37201
- German VAK 191B combat VTOL aircraft development program, describing prototype ground tests, autopilot preoptimization and hover flight tests
22 p3482 A71-41517
- AUTOMATIC ROCKET IMPACT PREDICTORS**
U COMPUTERIZED SIMULATION
U IMPACT PREDICTION
- AUTOMATIC TEST EQUIPMENT**
Aircraft structures fatigue testing device using programmed control of electrical inputs to electrodynamic vibration stand, noting load cycle effects and damage accumulation
01 p0168 A71-10409
- Automatic support systems for advanced maintainability - IEEE Conference, St. Louis, October 1970
03 p0394 A71-13076
- Multiple dialect automatic test language for avionics industry, considering software design
03 p0381 A71-13077
- Automatic test equipment with digital computer for control, discussing software schemes and tradeoff analysis
03 p0381 A71-13079
- Automatic testing of electro-optical systems including TV, IR and laser applications
03 p0395 A71-13082
- Automatic RF and microwave test equipment for communication, navigation, radar and tactical systems
03 p0395 A71-13083
- Automatic digital test unit for avionics systems
03 p0396 A71-13085
- Software cost estimates for automatic test equipment for avionics support analysis
03 p0396 A71-13086
- User requirements of Versatile Avionic Shop Test /VAST/ computer controlled automatic test equipment, including documentation, compatibility, assurance plan, etc
03 p0396 A71-13087
- Long range goals for avionics automatic test equipment /ATE/ involving complex computer
03 p0396 A71-13088
- Monte Carlo simulation model program, evaluating automatic test equipment design influence
03 p0381 A71-13089
- Economic evaluation of automatic support systems for maintainability of low quantity high technology space programs
03 p0396 A71-13091
- Automatic electric network topological and electrical characteristic analysis, using mixed method for computational accuracy and speed
04 p0560 A71-14746
- Automatic excitation forces generation for aircraft structure ground vibration tests using digital computer [ONERA-TP-870] 04 p0669 A71-15352
- Computerized outgassing analyzer for nuclear rocket graphite fuel elements at various temperatures in vacuum
05 p0780 A71-16243
- Test instrumentation for inertial gyros performance evaluation, describing turntables, holding fixtures, electronic equipment, automation, environment simulation, etc
[AGARDGRAPH-128] 05 p0750 A71-16305
- Soviet book on machines and instruments for programmed fatigue tests
05 p0734 A71-17025
- Digital electronic equipment logic networks computer controlled tester, describing method for test patterns synthesis
06 p0879 A71-17322
- Automated vision tester for evaluating space environment effects and multiphasic health screening
07 p1046 A71-18805
- Automatic test equipment for sorting large quantity resistors based on nonlinearity measurement
07 p1076 A71-19554
- Universal materials testing system control using digital computer and changeable programs
07 p1069 A71-20201

- Engineering data integrated test system with sensor based digital computer for data collection and test control
07 p1069 A71-20202
- Materials fatigue testing using analog computer interfaced with closed loop test system
07 p1216 A71-20203
- Automatic materials testing device for thermal fatigue and strength under programmed loading
08 p1271 A71-20838
- Analog type semiconductor switches for aircraft and spacecraft automatic checkout systems, discussing component transistor types, optoelectronic devices and materials
09 p1418 A71-23041
- Materials microstrain determination using automatic capacitance bridge gage and analog or hybrid computer for measurement signal processing
10 p1609 A71-23916
- User-oriented conversational language computer program for Jet Propulsion Laboratory digital control random excitation environmental test system for spacecraft
11 p1736 A71-26498
- Airborne Doppler radar receiver transmitter failure testing by Versatile Avionics Shop Test computer controlled system
13 p2031 A71-28778
- Miss/stick oscilloscope techniques in signal and switching relay testing with automated human-interactive time-and-level-measurement machine
13 p2001 A71-28840
- Mechanical properties and strain rates determination at high temperature, using automatic loading system with strain gage dynamometer and oscillograph
13 p2045 A71-29375
- Computer real time data monitoring and control software in satellite integration support and test operations, noting test oriented language
14 p2208 A71-30339
- Gas turbine engine condition analysis by digital computer and fault isolation techniques
[SAE PAPER 710448] 14 p2289 A71-30532
- Army aircraft automatic inspection and maintenance monitoring system, considering feasibility, technology approach and effectiveness
[AIAA PAPER 71-649] 14 p2177 A71-30726
- Onboard computer for aircraft engine testing, monitoring and data reduction, emphasizing automatic in-flight recording for post-flight displays
[AIAA PAPER 71-651] 14 p2290 A71-30727
- Automated ultrasonic inspection system for L-1011 adhesive bonded fuselage panels using through transmission technique
[SME PAPER IQ-71-746] 15 p2417 A71-32437
- Automatic testing machine for materials corrosive strength under varying and combined complex static or dynamic stresses
16 p2580 A71-33687
- GALAXY measuring engine for automatic measurement of glass photographic plates taken from Schmidt telescopes, discussing performance
17 p2741 A71-34997
- Automated endurance testing of 2-15 kW Brayton power conversion system, using rotating unit, heat exchanger, electronic voltage regulator, parasitic speed control
20 p3180 A71-38907
- Complex electronic modules automatic checkout, discussing processing time and cost reduction for large printed circuit logic boards test and diagnostic programs
[ASME PAPER 71-VIBR-115] 21 p3362 A71-40335
- Abbreviated test language for avionics systems, discussing program organization, statement formats, vocabulary and syntax diagrams
21 p3351 A71-40812
- Mobile monitoring and testing meteorological laboratory design and equipment for automated station network, considering pressure sensors, thermohygrometer and wind measurement
21 p3365 A71-41381
- Computer controlled modular automatic test equipment for DC-10 aircraft maintenance, discussing system block diagram
22 p3519 A71-41518
- Mobile concept and automated checkout applications in Apollo/Saturn 5 Launch Complex 39, discussing performance
22 p3611 A71-42044
- Computerized bacterial identification system to process Apollo spacecraft sample laboratory test results in NASA Planetary Quarantine Lunar Information System
22 p3504 A71-42233
- Computer operated RF automatic test system for HF radio receiver spurious response measurements, giving test results
22 p3514 A71-42389
- Maximum bubble pressure automatic capillary electrometer for salt solutions and organic compounds electroosorption, comparing with Lippmann instrument and capacitance bridge
22 p3548 A71-42529

True stress calculation from automatic diagram plotted in coordinates for cylindrical specimen testing under uniaxial tension

22 p3550 A71-42851

Static and dynamic measurement errors in contact and contactless sensors of automatic dimensional control of finished product sorting

23 p3679 A71-43866

Digital algorithm for automatic aircraft engine monitoring system, using Boolean algebra and events/states theory

23 p3679 A71-43897

AUTOMATIC TYPEWRITERS

On-line machine language dynamic debugger for Operating System 360, using graphic display terminal or operator typewriter

01 p0045 A71-10193

AUTOMATION

ATC automation, using conflict prediction algorithm based on airspace assignment to aircraft entering system

02 p0278 A71-11698

Spectrophotometric instrumentation in physics and chemistry, discussing developments in automation, accuracy and measurement time

03 p0429 A71-14326

Photointerpretation automation, discussing computer pattern input system, image scanning and correlation, optical image transformations, trainable logic techniques, etc

06 p0900 A71-18095

Automatic cartography, describing data conversion, EDP and instrumentation

06 p0895 A71-18291

Automatic cartography, using plotting machine digital output via attached shaft encoders

06 p0895 A71-18292

Machine analysis of biological structures and processes - Conference, Pushchino, U.S.S.R., May 1968

06 p0863 A71-18690

Automatic cytophotometric techniques including microphotometer, ultramicrospectrophotograph, radiographic analyzer, microinterferometers, cytofluorometer and differential microfluorometer

06 p0864 A71-18693

System automation evolutionary process in terminal Air Traffic Control environment

07 p1155 A71-19717

National Airspace System air traffic control automation man machine considerations, noting controller productivity increase, input difficulties and symbology clutter

07 p1049 A71-19720

Optical astronomy instrumentation automation including telescopes, computer control, filters and detectors

07 p1114 A71-20051

ATC automation system design, considering controllers decision time savings

10 p1640 A71-24271

Automation in cardiology, discussing analog and digital computer techniques for on-line hemodynamic analysis and collection and manipulation of cardiovascular data

13 p2016 A71-27868

Automated orifice drilling optimal treatment routines, including proper timing and adequate total depth allowance

13 p2074 A71-28941

ATC data automation, discussing flight plant processing system /FPPS/, radar data processing system /RDPS/ and signal automatic control system /SATCO/

15 p2446 A71-32523

Geophysical map preparation by automatic procedure using polynomial representation of fields in iteration process

16 p2563 A71-33460

Automation in optical astrophysics - Conference, Edinburgh, August 1970

17 p2740 A71-34980

Telescope automation using servocontrolled drive with spur gearing and dual opposed motors for data acquisition separation and minimum program interaction

17 p2740 A71-34982

Operator performance improvement in monitoring automated processes by alternating displays, discussing simulated radar and sonar CRT display laboratory tests

22 p3501 A71-41636

Molins 24 integrated automatic complete-processing system for small light-metal parts, using numerically controlled machine tools integrated with palletized feeder system

23 p3681 A71-43473

AUTOMOBILE ENGINES

Soviet book on automotive and jet aircraft engine fuel chemical stabilizers under storage, transit and operational conditions, examining additives in relation to stability ratings

06 p0942 A71-17433

Lanthanum cobalt oxide as potential auto exhaust catalyst from studies of activity in gas phase

07 p1055 A71-19545

Chemical kinetic calculation of nitric oxide formation in spark ignition automobile engines and gas turbine combustors

14 p2190 A71-30454

Nickel-zinc batteries for use in hybrid heat engine/electric systems of low pollutant passenger cars, increasing service life by aerospace technology

20 p3181 A71-38936

Turbine propulsion system smoking and exhaust gas emission, discussing aircraft and automobile pollution emission

20 p3277 A71-39452

AUTOMOBILES

VTOL air system for automobile travel replacement noting noise, cost, pollution and traffic congestion reduction

22 p3624 A71-42527

AUTOMORPHISMS

Static electromagnetic fields in general relativity obtained for space-time metrics of group G automorphisms, considering Rainich unified field theory equations

16 p2610 A71-33265

AUTONOMIC NERVOUS SYSTEM

NT SYMPATHETIC NERVOUS SYSTEM

Previous heavy work effect on central hemodynamics and autonomic nervous system, discussing ensuing heart rate changes

04 p0545 A71-15156

Target aiming function /TAF/ susceptibility to vagotonic vegetative imbalance in male subjects after experimental kinetosis

07 p1047 A71-19464

Somatic and autonomic responses in vestibular tolerance of human subjects, using Coriolis acceleration test

13 p2007 A71-28414

Human hypoxic ventilatory drive data for high altitude breathing, noting motivation reduction inversely related to time and altitude

14 p2185 A71-30288

Ventilatory control in acute hypoxia, detailing polycythemia effects on respiratory chemoreceptor sensitivity

14 p2185 A71-30289

Lowered cardiac output and arterial pressure response to exercise after autonomic heart blockade in man, noting retained work capability

15 p2358 A71-31454

Optical organs and autonomic nervous system fatigue assessment by blink method associated with eyelids, oculomotor muscles, retina and cerebrum

17 p2687 A71-34356

Respiratory reflex mechanism of deep breath occurrence after period of airway occlusion in rabbits related to stimulation of vagal receptors

20 p3187 A71-39040

Auditory stimulus conditioning of human skin resistance responses on escape-avoidance schedule

22 p3497 A71-42862

AUTONOMY

Discrete time finite dimensional autonomous linear systems, investigating controllability and pole assignment to closed loop transfer matrix by choice of state variable feedback gain

09 p1424 A71-23465

Autonomous dynamic systems optimal control problems solution by reduction to operator equation, using Pontryagin maximum principle

10 p1636 A71-24352

Limit cycle bounds in phase plane for self sustained vibrations of autonomous systems, using Poincare-Bendixon theorem

11 p1841 A71-25179

Suboptimal control of nonlinear autonomous dynamical systems via linear approximation by hyperplanes

15 p2379 A71-31823

Nonlinear autonomous systems transient response, obtaining approximate solutions by generalized averaging technique based on ultraspherical polynomial expansions

21 p3415 A71-40532

AUTOPILOTS

U AUTOMATIC PILOTS

AUTOPSIES

Autopsies compared to ECG for diagnosis accuracy for acute recurrent myocardial infarction

05 p0711 A71-16951

AUTOROTATION

Helicopter optimal autorotation landing parameters for touchdown at zero speed, including rotor rpm drop due to flow separation on blades

23 p3627 A71-43090

AUTOTROPHS

NT HYDROGENOMONAS

Chemoautotroph Thiobacillus neapolitanus growth inhibition by histidine, methionine, phenylalanine and threonine under imbalance conditions

04 p0537 A71-14776

Autotrophic cultivation of cereals with high photosynthetic activity under intensive illumination as biological components in life support systems

13 p2017 A71-28405

Biologically mineralized human waste products utilization in nutrient solutions for higher and lower autotrophs cultivation

22 p3507 A71-42819

AUXILIARY ELECTRIC POWER UNITS

U AUXILIARY POWER SOURCES

AUXILIARY EQUIPMENT [COMPUTERS]

NT PLOTTERS

NT PRINTERS [DATA PROCESSING]

Handwritten graphical data computer input device with pen position coordinate measurement from acoustic signal propagation delay time in piezoelectric solid plate

21 p3376 A71-40122

AUXILIARY POWER SOURCES

NT CHEMICAL AUXILIARY POWER UNITS

NT NUCLEAR AUXILIARY POWER UNITS

NT SNAP 8

NT SNAP 15

NT SNAP 19

NT SNAP 21

NT SNAP 23

NT SNAP 27

NT SOLAR AUXILIARY POWER UNITS

NT SPACE POWER UNIT REACTORS

Aircraft emergency evacuation illumination standards, considering independent power source, crash survivable installation, operation initiation and exit visibility

01 p0004 A71-10030

Small gas turbines for aircraft auxiliary power unit, considering compressor and combustor design, noise, fuel consumption and specific weight problems

01 p0006 A71-10751

Electric power source requirements of USAF aircraft, missile and spacecraft electrical systems

03 p0351 A71-13036

L-1011 aircraft auxiliary power unit with lightweight free turbine engine, giving fuel economy and lower pneumatic pressures

03 p0353 A71-13725

Fuel cell technology in astronautics, reviewing design and operational characteristics, functional and economic merits as spacecraft power supply sources

05 p0705 A71-16140

Integrated drive AC generator for aircraft, discussing design improvements in power-weight ratio

07 p1023 A71-19494

Optimum mounting angles for direct solar radiation flux on solar battery on circular orbit satellite

09 p1386 A71-22673

Helicopter auxiliary power unit /APU/ life cycle cost computation

12 p1988 A71-26679

Optimization of military VTOL aircraft secondary power systems, considering alternate power source for aircraft hydraulics, pneumatic drives, etc

13 p1998 A71-28326

Gas turbine auxiliary power unit accessories, discussing high energy igniters, cables and connectors, thermocouples and speed and temperature monitoring equipment

13 p2071 A71-29262

Gaseous oxygen/gaseous hydrogen auxiliary propulsion engines, considering cold flow experiments with nonreactive simulant gases

14 p2291 A71-30737

Satellite auxiliary electric propulsion systems survey for program managers and systems engineers, considering cost and component reliability

14 p2292 A71-30747

Low pressure gaseous hydrogen/gaseous oxygen APS rocket engines operating with propellant stored as liquids and fed to thruster without pressure augmentation

15 p2467 A71-31326

NERVA nuclear rocket engine for space propulsion and long duration auxiliary power generation

15 p2448 A71-32285

Space shuttle auxiliary propulsion subsystems for attitude control, orbit maneuvering and power supply, discussing design requirements with emphasis on fail-operational and fail-safe criteria

17 p2795 A71-35624

AUXILIARY PROPULSION

High pressure gaseous hydrogen oxygen auxiliary propulsion systems /APS/ thruster design and cold flow and hot fire testing for space shuttle requirements

15 p2470 A71-32291

AVALANCHE DIODES

Silicon avalanche photodiode detectors for near IR laser pulse receivers, discussing quantum efficiencies, internal gains and room temperature responsivities

01 p0092 A71-10011

Microwave negative resistance diode avalanche region, deriving four element incremental signal model

01 p0055 A71-11168

Temperature compensated semiconductor transducers for dynamic pressure measurements, using Si Zener diodes

01 p0057 A71-11289

Microplasma low temperature noise spectra in Si and Ge avalanche diodes 03 p0387 A71-13981

Pulse rise, fall times and peak current values in sawtooth-voltage generator relaxation circuits with avalanche transistors 03 p0387 A71-13998

High efficiency LF operating modes in avalanche diodes under low current density 04 p0558 A71-15147

Transistors and Zener diodes temperature dependence and normal and accelerated life tests 05 p0728 A71-16289

Singly tuned IMPATT diodes, examining noise and power saturation 05 p0729 A71-16919

Microwave circuit with coupled TEM bars for L band Si avalanche diodes 05 p0729 A71-16920

Silicon junction avalanche diodes as S band oscillators and amplifiers, presenting peak power efficiency and gain data 05 p0729 A71-16921

Temperature compensated Zener diodes noise voltage measurements in ELF domain 05 p0729 A71-17000

Avalanche diodes as solid state noise sources, observing planar silicon junctions breakdown voltages 06 p0940 A71-17324

Neutron radiation damage on high efficiency microwave avalanche diode sources /TRAPATT oscillators/ 07 p1071 A71-19068

Avalanche transit time devices operational modes principles and characteristics, giving data on experimental circuits 07 p1072 A71-19101

Large signal microwave equivalent circuits analysis of IMPATT diodes, allowing carrier multiplication by impact ionization at every point in diode 07 p1072 A71-19108

Avalanche diodes TRAPATT mode initial conditions by computer analysis 07 p1072 A71-19109

X band IMPATT oscillator, discussing frequency stability, rms noise deviation, admittance characteristics, output power loss, temperature effects and power stability 07 p1073 A71-19111

Broadband IMPATT diode multistage transmission amplifiers computer aided design and X band performance 07 p1073 A71-19114

Power amplification with anomalous mode Si p-n-n mesa structure avalanche diodes under input driving power at system resonance frequency 07 p1073 A71-19116

One watt CW high efficiency X band avalanche diode amplifier with in-band and second harmonic impedance control 07 p1073 A71-19117

Microwave oscillator circuit with cap structures for testing millimeter wave IMPATT diodes 07 p1073 A71-19119

Frequency variation with temperature in coaxial cavity avalanche transit time microwave oscillators explained by diode junction capacitance and cavity length changes with temperature 07 p1074 A71-19120

Avalanche diodes Evans circuit /low pass filter located one half wavelength from diode/ analytic theory, developing expressions for efficiency and diode impedance 07 p1074 A71-19121

Metal ceramic microstrip L band oscillator circuit with high efficiency silicon avalanche diodes in capacitively loaded TEM coupled lines 07 p1074 A71-19122

Compact microstrip high power high efficiency L band avalanche diode oscillator 07 p1074 A71-19123

Phase locked avalanche transit time oscillators FM noise spectra 07 p1074 A71-19124

Packaged microwave avalanche diodes negative resistance properties three-parameter characterization at low current densities 07 p1074 A71-19125

Random gain statistics of avalanche diode optical detectors, analyzing simple optical binary receivers 07 p1074 A71-19216

X band multiple IMPATT oscillator combining 12 packaged diodes in waveguide cavity for 10.5 watt CW output at 9.1 GHz, noting clean spectrum 07 p1075 A71-19266

Avalanche transistor emitter current voltage characteristics, using Kirchhoff equations for equivalent circuit 07 p1077 A71-19798

IMPATT and Gunn microwave oscillators injection phase locking, discussing stationary state synchronization theory and phase vs frequency deviation measurements 08 p1263 A71-20990

Si step-junction avalanche diodes conduction current pulse waveforms during large signal operation, using numerical calculation 08 p1265 A71-21290

Microwave diode technology, discussing Schottky barrier, p-i-n junction, varactor, tunnel, bulk effect and avalanche diodes performance and applications 08 p1266 A71-21622

Varactor-tuned avalanche microwave source, using interchangeable iris shims at output cavity for passive stabilization, power output and tuning variability 09 p1418 A71-23155

Avalanche diode microwave oscillator stabilized by two external resonant circuits, investigating self oscillation characteristics 10 p1582 A71-23808

IMPATT diode oscillators noise and injection phase locking, discussing theoretical refinements of original simple model by Read 10 p1584 A71-24818

IMPATT oscillators noise properties at large RF amplitudes, deriving expression for noise current as function of threshold current 11 p1733 A71-26369

Microwave radiometers transfer calibrations by noise injection through avalanche diode directional coupler similar to plasma tube 11 p1739 A71-26438

P-i-n avalanche diode trapped plasma avalanche triggered transit /TRAPATT/ oscillations characteristics and voltage waveform under square wave driving current, using computer program 12 p1887 A71-27046

Si p-n-n junction avalanche diode, investigating experimental evidence of microwave generation at subharmonics of transit time excitation and trapped-plasma mode 12 p1887 A71-27047

Temperature compensation for frequency changes stabilization of avalanche transit time diode microwave oscillator, using loop circuits and high dielectric constant ceramics 13 p2036 A71-27938

Voltage regulating diodes, discussing development and principal characteristics of Epi-Z family of Zener diodes 13 p2037 A71-28575

Small signal impedance of avalanche region in microwave IMPATT diode 14 p2215 A71-30833

IMPATT diode oscillator for CW Doppler radar, microwave detection and communications systems, emphasizing cost reduction 15 p2377 A71-32522

Time domain model of device-circuit characteristics of TRAPATT diode microwave oscillator 15 p2378 A71-32699

Optoelectronic elements for information system applications, discussing photomultipliers, photodiodes, photoresistors, avalanche and photoparametric diodes response and bandwidth characteristics 17 p2752 A71-34391

High power efficiency solid state UHF sources, comparing Gunn and avalanche diodes performance 17 p2715 A71-34685

Silicon IMPATT microwave oscillators, calculating CW power as function of frequency by scaling approximation 18 p2888 A71-36129

Self consistent one dimensional large signal analysis of Read type IMPATT diode oscillator, taking into account device-circuit interaction 18 p2888 A71-36130

High efficiency avalanche diode microwave oscillator design guidelines based on oscillation mode theory, covering CW and pulsed operations 18 p2888 A71-36131

IMPATT diode amplifiers and oscillators AM and FM noise spectra and SNR prediction for comparison with experiment 18 p2888 A71-36271

Avalanche diode microwave oscillator design, comparing coaxial lumped, lumped element, microstrip and waveguide circuits 18 p2893 A71-36600

Spurious effects on stabilizing circuits with loaded Zener diodes for reference voltage source 18 p2893 A71-36800

Harmonic generation in trapped-plasma-mode IMPATT diode microwave oscillators with waveguide-coaxial cavity 18 p2894 A71-36828

Microwave avalanche diodes, considering drift velocity and power efficiency limitations of IMPATT mode 18 p2894 A71-36976

Fabrication and noise performance of high power Schottky barrier GaAs IMPATT diodes with double epitaxial layer structure on low-etch-pit density substrates 18 p2895 A71-36982

Harmonic extraction from high power efficiency avalanche diodes, discussing circuit in terms of multiple reflection triggering process 18 p2895 A71-36983

Experimental comparison between double drift and single drift region mm wave IMPATT diodes on room temperature metal heat sinks 18 p2895 A71-36984

IMPATT diode microwave oscillator temperature effect on operation, comparing with Read diode small signal admittance characteristics 18 p2895 A71-36986

One- and two-sided abrupt junction IMPATT diodes, investigating Si junction type effects on avalanche region and diode design 18 p2895 A71-36987

Temperature variations effect on TRAPATT microwave oscillator parameters, considering upper temperature limit dependence on heat dissipated in diode and heat sink thermal resistance 18 p2895 A71-36988

FM noise in output spectrum of low level operating IMPATT diode microwave oscillators 19 p3029 A71-38217

High peak power microwave oscillators, discussing pulsed limited space charge accumulation and TRAPATT diodes pulsed radiation sources performance 19 p3029 A71-38294

GaAs and silicon IMPATT diodes applications and performance, discussing power levels, amplifier applications, injection locked oscillators and microwave signal source 21 p3357 A71-40818

Avalanche Si photodiode current pulse formation frequency governing mechanism, considering roles of free carriers and electron tunneling 21 p3358 A71-41344

Performance levels prediction for airborne solid state phased array radar transmission sources, considering TRAPATT devices 22 p3509 A71-41630

Spherical avalanche diodes in silicon and silicon-germanium mixed crystals, describing IR detection properties 22 p3543 A71-42125

Background LF noise of semiconducting diode voltage regulators with breakdown due to avalanche effect 22 p3523 A71-42472

X band GaAs diffused IMPATT diodes for high CW efficiencies 22 p3523 A71-42483

Single cavity multiple device microwave oscillator with 12 IMPATT diodes combined output power, presenting proof for circuit configuration stable operation free from moding problems 22 p3524 A71-42631

IMPATT diodes noise performance lower limits, deriving optimization theorem for GaAs diodes under assumption of equal ionization coefficients for electrons and holes 22 p3524 A71-42632

Linear and nonlinear models for computer aided circuit design involving Zener diodes, providing for thermal effects 22 p3524 A71-42762

IMPATT diode development for millimeter wave applications including oscillators, sweep generators and Doppler radar 22 p3524 A71-42763

Reactive impedance matching of Gunn or IMPATT diodes for microwave oscillators by dielectric tuning 23 p3650 A71-43071

Large amplitude high efficiency TRAPATT oscillation mode in Si avalanche diodes, using resonant cavity for voltage and current waveforms analysis 23 p3650 A71-43352

Range finder receiver based on Si avalanche diode detector coupled to tunnel diode circuit, with automatic gain control through tunnel diode bias control 23 p3677 A71-43518

Wideband microwave amplifier with two antiparallel high efficiency avalanche diode pairs, presenting fishbone shaped tuning plate for bandwidth widening 23 p3653 A71-43961

Silicon avalanche diodes for microwave TRAPATT amplifiers and self excited oscillators with IMPATT triggering 23 p3653 A71-43964

X band microwave oscillator design for matched cavity reactance and maximized power by coupling Gunn and IMPATT diodes to coaxial transmission line 24 p3807 A71-44362

AVANCES

U ADVANCED VIDICON CAMERA SYSTEM [AVCS]

Transistor collector pulse response characteristics measurement at high voltages in avalanche multiplication region, considering dissipated power curve 01 p0051 A71-10282

Electron-photon showers, discussing cascade theory equilibrium spectra, avalanches and radio emission 03 p0475 A71-13840

Electron-photon showers, discussing cascade theory, equilibrium spectra, avalanches and radio emission 22 p3594 A71-42641

AVERAGE
NT MEAN
 Equations of motion averaging method, constructing series representation of function
 [AAS PAPER 71-334] 23 p3727 A71-43007

AVIATION
U AERONAUTICS
AVIATORS
U AIRCRAFT PILOTS
AVIONICS
 Avionics system maximizing pilot chances of surviving mission and destroying selected target by removing mental limitations
 01 p0124 A71-10506
 Aeronautical electronic equipment, discussing static transformer, radiotelephone sets, angle of approach meter, etc
 03 p0383 A71-13018
 Multiple dialect automatic test language for avionics industry, considering software design
 03 p0381 A71-13077
 Versatile Avionic Shop Test (VAST) general purpose digital tester, discussing hardware and software
 03 p0395 A71-13084
 Automatic digital test unit for avionics systems
 03 p0396 A71-13085
 Software cost estimates for automatic test equipment for avionic support analysis
 03 p0396 A71-13086
 User requirements of Versatile Avionic Shop Test (VAST) computer controlled automatic test equipment, including documentation, compatibility, assurance plan, etc
 03 p0396 A71-13087
 Long range goals for avionics automatic test equipment (ATE) involving complex computer
 03 p0396 A71-13088
 Digital computers in aviation electronics, discussing automatic control loop in automatic pilot
 03 p0382 A71-13687
 Army avionics technology transfer to civil aviation, discussing communication systems, flight control and landing aids
 04 p0557 A71-15017
 Lightning induced voltages in aircraft wing structures, examining induced voltage across load impedances in electric circuits
 06 p0874 A71-17581
 Automated design system producing wire format data for cabling avionics subsystem of light attack aircraft
 [AIAA PAPER 69-976] 06 p0874 A71-17698
 VTOL aircraft avionics systems, discussing automatic flight control and navigation systems integration
 06 p0925 A71-17925
 Avionics subsystem design improvements for aeronautical systems, considering standardization, weight impact, environmental control, maintainability and equipment growth
 07 p1069 A71-18829
 Navy avionic modular multiprocessed digital computer operating system reliability, comparing totally software and partly hardware approaches
 07 p1067 A71-18833
 Draw-through cooling of electronic equipment in subsonic and supersonic commercial jet transports, discussing internal circulation system design
 [SAE-AIR-64A] 07 p1077 A71-19642
 Late model F-4 air superiority aircraft and electronic flight control systems protection against lightning discharges damage to electric and electronic systems
 07 p1021 A71-19940
 Lightning and surge protection devices for survivability of aircraft electrical systems
 07 p1021 A71-19941
 Avionics for gliders and touring aircraft, considering safety and VHF radio equipment
 08 p1261 A71-20684
 Performance test methods and equipment for aircraft avionics and weapons systems, discussing computer integration with radar and phototheodolite range instrumentation system
 08 p1260 A71-21660
 Avionics for gliders and touring aircraft, surveying available electronic equipment for 1971
 08 p1294 A71-21768
 Soviet book on aircraft ground support and onboard radio equipment operation and reliability increase by redundancy and rational methods, discussing preventive maintenance
 10 p1583 A71-24670
 Avionics growth, discussing use of digital computers, solid state transducers, integrated circuits, electronic flight instruments, area navigation and collision avoidance systems
 12 p1906 A71-26878
 Airborne radio communication systems, stressing electronic equipment design reliability
 12 p1878 A71-26880
 Airborne Doppler radar receiver transmitter failure testing by Versatile Avionics Shop Test computer controlled system
 13 p2031 A71-28778

Interface IC circuits for driving high voltage transistor switches from low level logic inputs, noting avionics application
 13 p2039 A71-28910
 Heat exchanger miniaturization for avionics applications, discussing design and fabrication
 [HEAT EXCH. CONF. PAPER 15] 15 p2376 A71-31636
 Computer program for prediction of repair time elements for versatile avionic shop test
 16 p2545 A71-33314
 Avionics systems for weapons control in F-14 fighter aircraft, discussing track multiple targets, sighting aids, radar, computer navigation, communications and built-in self testing
 16 p2527 A71-34155
 ATC avionics equipment, discussing inertial area navigation, autopilots, airborne data acquisition, altitude reporting, collision avoidance, CAT, satellite communications, etc
 17 p2771 A71-34615
 Comet 4 installation and experimental program, investigating avionics systems integration techniques
 17 p2774 A71-35070
 Avionic and missile computer control systems, describing universal function unit design and digital processing requirements
 17 p2711 A71-35775
 Space shuttle avionics system redundancy, calculating costs for individual line replaceable units
 18 p2889 A71-36479
 Streamer discharges effects on integrated aircraft antenna and associated avionics, emphasizing RF interference and component damage
 19 p3033 A71-38462
 Complex airborne electronic system design for interference minimization, considering electromagnetic compatibility
 19 p3033 A71-38464
 Reliability controlled maintenance plan for avionics equipment based on mean time between failures
 20 p3203 A71-39087
 Avionics combined display system for area navigation, discussing design, color map projection, overlays, CRT unit and viewability
 21 p3413 A71-40137
 Abbreviated test language for avionic systems, discussing program organization, statement formats, vocabulary and syntax diagrams
 21 p3351 A71-40812

AVOIDANCE
NT COLLISION AVOIDANCE
 Increased artificial gravity avoidance by squirrel monkeys with variations in rotation rate and radius
 [AIAA PAPER 71-855] 18 p2857 A71-36647

AXES [COORDINATES]
U COORDINATES
AXES [REFERENCE LINES]
NT AXES OF ROTATION
NT EARTH AXIS
 Optimal axis alignment for strapdown inertial guidance system, suggesting alternate method of raised mounting pads and cylindrical alignment pins
 02 p0279 A71-12456

AXES OF ROTATION
NT EARTH AXIS
 Local invariants under axial rotation, deriving recurrence relations for time series expansions and perturbation methods
 01 p0154 A71-10387
 Uniaxial satellite rotational motion, examining magnetic and gravitational torque effects on gyro dynamic properties
 02 p0320 A71-11975
 Heavy gyroscope equations of motion solution, assuming center of mass on major axis
 03 p0457 A71-13584
 Symmetry axis motion of solid body with ellipsoidal cavity filled with ideal incompressible uniformly turbulent fluid
 03 p0458 A71-13596
 Autocollimation control of telescope rotation axis position at arbitrary azimuths
 04 p0565 A71-14854
 Euler problem on permanent axes of rotation with extension to spinning gyrost
 04 p0662 A71-15195
 Dynamically symmetrical satellite optimal transfer into steady axial rotation state with simultaneous alignment of symmetry axis, considering control jets moments
 05 p0779 A71-16037
 Missile roll axis attitude control system based on fluid amplifiers, describing fluidic integrator and chain
 07 p1028 A71-20584
 Four axis Zeiss camera unit for satellite small circle arc orbit observations, determining axial parameters equalization by least squares method and rotation rates
 11 p1762 A71-25830
 Equivalent width of metallic lines for pole-on main sequence stars, examining effect of rotational axis inclination with respect to line of sight on washout of lines
 16 p2633 A71-33334

Dynamically symmetrical satellite optimal transfer into steady axial rotation state with simultaneous alignment of symmetry axis, considering control jets moments
 16 p2605 A71-33441
 Fixed sphere on axis of unbounded rotating fluid /R greater than unity/, suggesting flow of Taylor column type
 17 p2726 A71-34576
 Bianchi type IX universe homogeneous cosmological model, noting oscillatory evolution near singularity and rotating axes of alternating Kaser epochs
 19 p3138 A71-37851
 Stability of plane rotating galaxies in magnetic field parallel to axis of rotation, showing linearized MHD equations self conjugate for radial disturbance case
 20 p3289 A71-39298
 Spinning and dual spin spacecraft angular momentum and axis control, investigating optimal fuel and small angle reorientation techniques
 22 p3611 A71-42045
 Three-legged slewing about nonorthogonal axes, solving single-axis reorientations by two successive rotations about arbitrary fixed lines
 [AAS PAPER 71-389] 23 p3773 A71-43057

AXIAL COMPRESSION LOADS
 Buckling of ring stiffened conical shells under axial compression, determining critical loads
 01 p0168 A71-10342
 Cylindrical shell stability under combined axial compression and heating, using finite difference method
 01 p0170 A71-10646
 Axial compression of thin circular epoxy resin disks with three dimensional stress state produced by cementing to rigid platens, using triaxial analysis
 01 p0109 A71-11008
 Postbuckling behavior of open cylindrical shells under uniform axial compression loads, solving finite difference equations by Newton-Raphson method
 03 p0505 A71-13539
 Open cylindrical shells with end eccentricity or initial deflection imperfections, investigating buckling under axial compression by Newton-Raphson method
 03 p0505 A71-13544
 Thin walled cylindrical shells with filler, determining stability under axial compression by computer calculation
 03 p0514 A71-14360
 Nondestructive test with high resolution instrumentation for observing long thin walled cylinder lateral displacements prior to buckling under axial compression
 04 p0669 A71-15297
 Local axisymmetric dimple imperfection effects on buckling load of circular cylindrical shell under axial compression
 [AIAA PAPER 70-103] 05 p0823 A71-16557
 Axisymmetric stability of fluid filled cylindrical shells under rapid axial compression
 05 p0824 A71-16592
 Stability loss of cylindrical shell at upper bound of buckling load under axial compression
 06 p0983 A71-17365
 Cylindrical shells buckling under subcritical loads, considering internal and external hydrostatic pressure and axial compression
 06 p0988 A71-17779
 Closed circular cylindrical shell stability and buckling during axial compression, using energy method in geometrically nonlinear formulation
 06 p0994 A71-17824
 Design criteria for buckling prediction of elliptical and circular cylindrical shells under axial compression from asymmetric and axisymmetric shape imperfections distribution
 [AIAA PAPER 71-145] 06 p1003 A71-18588
 Axially compressed ring and stringer stiffened cylindrical shells minimum weight design, considering configuration instability
 [AIAA PAPER 71-147] 06 p1003 A71-18590
 Uniaxial compression effect on dispersion of helicon wave in n-type semiconductors, considering strain potential constants determination
 07 p1176 A71-19269
 Imperfect elliptical cylindrical shells buckling under axial compression, demonstrating imperfection sensitivity
 07 p1213 A71-19888
 Optimal design parameters in minimization of reinforcement elements weight in cylindrical glass fiber reinforced orthotropic plastic shells under axial compression
 09 p1539 A71-22826
 Imperfect thin walled circular cylindrical shells under axial compression with relaxed boundary conditions, determining deformations with differential equations
 09 p1541 A71-23089
 Cylindrical body stability under axial compression with small elongations and shears, determining critical buckling force
 09 p1542 A71-23437
 Cylindrical Duralloy shells critical strain measurement in axial compression under creep conditions
 10 p1690 A71-24575

Buckling load scatter reduction in axially compressed thin walled circular shells as function of manufacturing accuracy [DFVLR-SONDDR-92] 12 p1974 A71-26869

Buckling of circular cylindrical shells with axisymmetric imperfection distributions under axial compression 12 p1983 A71-27573

Axial compression buckling of elastic core filled circular cylindrical shells with transverse shear flexibility, noting solid propellant rocket cases design application 13 p2148 A71-27984

Minimum weight design of circular cylindrical shell hinged at ends under axial compression, using random search method with self learning 13 p2152 A71-28280

Cylindrical liquid filled shells under rapid axial compression along generatrix, examining dynamic deformation characteristics 13 p2156 A71-29072

Stability loss, critical load and wave numbers for smooth conical and cylindrical shells of fiberglass reinforced plastics under uniform axial compression 13 p2157 A71-29181

Elastic deformation and plastic buckling of rectangular column with initial deflection under axial compression 13 p2157 A71-29287

Buckling and postbuckling loads of initially imperfect orthotropic cylindrical shells under axial compression and internal pressure, using potential energy principle 16 p2651 A71-33025

Buckling of axially compressed circular cylindrical shells with localized or random axisymmetric imperfections, deriving asymptotic approximation formulas for stress calculation [ASME PAPER 71-APM-29] 16 p2655 A71-33200

Heated tank under axial compression and internal pressure, noting fuel expenditure effects on stress-strain state 16 p2658 A71-33620

Closed circular cylindrical shell stability under dynamic axial compressive loading with static internal pressure 16 p2658 A71-33719

Eccentrically stiffened thin cylindrical panels instability under uniform axial compression, uniform hoop compression and uniform shear 16 p2661 A71-34150

Slender elastic column dynamic buckling under constant compressive axial end displacement, considering damping effects 17 p2818 A71-34506

Finite oval cylindrical shells with clamped boundaries, investigating stability and elastic buckling under axial compression for comparison with circular cylindrical shells [SESA PAPER 1832] 17 p2819 A71-34536

Cylindrical shell with continuous filler, calculating stability and axisymmetric buckling in axial compression 17 p2830 A71-35321

Clamped rectangular plate buckling under uniaxial and biaxial compression, obtaining critical loads for various aspect ratios 18 p2979 A71-36360

Nickel base alloy under axisymmetric tension compression tests, obtaining breaking load diagrams and fatigue and creep curves 18 p2937 A71-36716

Longitudinal edge stiffness and internal pressure effects on buckling and initial postbuckling behavior of axially compressed stringer reinforced cylindrical panels, discussing imperfection sensitivity 19 p3157 A71-37873

Inelastic buckling process of axially compressed cylindrical shells with edge constraints, using variational principle and Rayleigh-Ritz method 19 p3158 A71-38182

In-plane boundary conditions effect on buckling loads of axially compressed simply supported ring stiffened cylindrical shells 19 p3159 A71-38270

Cylindrical shell stability under radial pressure or axial compression from load-distributing filler model solution 20 p3308 A71-39166

Buckling load reduction for axially compression loaded geometrically perfect cylindrical shells by wall temperature gradients induced partial yielding 21 p3469 A71-41006

Critical coefficients of axial compressive forces with variable intensity for approximate stability analysis of vertical bars 21 p3472 A71-41151

Longitudinal rib reinforced cylindrical shell under axial compression loads, determining equilibrium stability with approximation of transcendental equations 23 p3780 A71-44222

Thin soft layer under steady creep conditions, considering axisymmetric problem of simultaneous tension and torsion 24 p3877 A71-44409

Power series analysis of circular cylindrical shells stability under biaxial compression, expressing critical loadings 24 p3878 A71-44612

Buckling stability and critical loads of thin elastic cylindrical shells with hollow core in axial compression 24 p3882 A71-44844

Metal cylindrical shells plastic collapse under axial compression, deriving theoretical load/deflection relationship 24 p3883 A71-44875

Stress-strain curve of unidirectional fiber reinforced composite Al and N-CI wire under axial compression loads, discussing buckling and shear instabilities 24 p3842 A71-45229

AXIAL COMPRESSORS U TURBOCOMPRESSORS AXIAL FLOW

Buoyancy effect on boundary layer flow over heated horizontal circular cylinder immersed in uniform axial free stream, considering successively greater displacements 03 p0519 A71-13731

MHD channel flow with axial conduction and third kind boundary condition, investigating thermal entry region heat transfer 04 p0684 A71-15506

Velocity profiles of steady axial flow of homogeneous incompressible Newtonian liquid between infinitely long parallel eccentric circular cylinders 05 p0735 A71-16611

Boundary layer development on slender rod in axial shear flow for different profiles 05 p0694 A71-16711

Axial and swirling mean flow effects on sound transmission and generation in hard walled ducts 06 p0945 A71-17620

Tangential velocity and total temperature distribution axial and radial gradients from secondary flow functions and turbulent energy equations 06 p0883 A71-18321

Axial Mach number distribution of supersonic flow in rocket nozzle with Rao optimum contour 07 p1093 A71-20366

Velocity and static pressure redistribution in distorted flow field upstream of axial flow compressors [AIAA PAPER 69-485] 10 p1553 A71-24856

Tangential velocity profile in steady incompressible electrically conducting viscous axial flow between concentric rotating cylinders with radial magnetic field, solving Navier-Stokes equations 11 p1752 A71-26048

Eigenvalues of axially uniform fluid waveguide with eccentric annulus cross section and acoustically hard boundaries 12 p1928 A71-26700

Axial flow fan noise, investigating louvers effects on sound field 12 p1945 A71-26704

Large axial compressor flow straightening stator blades unsteady pressure measurements with short response time detectors 12 p1945 A71-27469

Cylindrical duct stationary uniform axial flow effects on propagation of acoustic vibration modes of wavelength smaller than damping length [ONERA-TP-969] 12 p1981 A71-27479

Aerofoil cascades with axial velocity change in incompressible flow, determining turbine blade force dependence on circulation 13 p1990 A71-28467

Multistage axial flow compressors on digital computer, testing gas dynamic design in final adjustment phase 13 p2115 A71-28584

Monograph on potential flow interaction between blade rows in axial flow compressors covering mathematical model, numerical analysis and experiment 13 p1990 A71-28883

Properties of arbitrarily thick turbulent boundary layer for incompressible axial flow past long cylinder [ASME PAPER 71-FE-25] 13 p1995 A71-29462

Aerodynamics of axial and axial tangential blade swirler twisted jet near nozzle, testing effectiveness of equivalent problem of heat conduction theory 15 p2388 A71-31522

Potential vortex with turbulent viscous core and axial velocity excess or deficiency, using integral method with quasi-cylindrical flow approximations to describe core flow [AIAA PAPER 71-615] 15 p2393 A71-32278

Mach number effects on axial flow transonic compressor characteristics, using empirical corrections based on measured three dimensional grid characteristics 15 p2471 A71-32715

Viscous trailing vortices decay downstream of non-free axial flow fan, assuming steady axisymmetric incompressible laminar flow 17 p2725 A71-34191

Space time structure of acoustic waves propagating in cylindrical duct with weakly absorbing walls and axial inviscid time dependent fluid flow [ONERA-TP-965] 18 p2946 A71-36030

Vortex flow through axial, axially radial and other three dimensional axisymmetric channels, using finite difference model for flow equations solution 20 p3211 A71-39465

Class of steady viscous incompressible axisymmetric nonrotating flows with axial velocity component dependent on distance along axis from reference point 23 p3663 A71-43489

Flow acceleration coefficient effect at inlet on centrifugal compressor wheel characteristics during axial-radial rotation 23 p3626 A71-43555

Axial flow compressors stable operation, using rotating guide vanes regulation 23 p3626 A71-43554

AXIAL FLOW COMPRESSORS U TURBOCOMPRESSORS AXIAL FLOW PUMPS NT TURBINE PUMPS

Rotating blade/rotors and stationary/stators/rows in axial flow molecular pump, deriving overall and individual transmission probabilities 09 p1455 A71-23058

Experimental materials for axial flow vane pumps operating under cavitation conditions, considering separated flow around impeller blades 20 p3241 A71-39169

AXIAL FLOW TURBINES

Axial turbomachine rotating blades, calculating three dimensional boundary layer thickness for laminar flow 01 p0069 A71-10337

Turbulence level effects on aerodynamic losses of axial flow turbomachines, discussing boundary layer of blades 03 p0340 A71-13143

Axial turbomachines boundary layer flow, describing two dimensional cascade calculation methods 03 p0340 A71-13146

Soviet book on air driven microturbines covering design, operation, energy losses, efficiency, economy and applications 06 p0848 A71-17446

Multistage axial flow turbine off-design performance prediction, exploring inlet temperature and pressure and exit pressure variation effects [ASME PAPER 70-PWR-2] 07 p1184 A71-20195

Axial turbomachine three dimensional cascade flow calculation from dynamics vector equations 09 p1383 A71-23601

Coupled vibration modes for nonrotating blade-disk system in axial flow turbines and fans calculated by finite element method [AIAA PAPER 71-375] 11 p1845 A71-25348

Soviet book on theory of aircraft blade machines covering axial flow, centrifugal and composite turbines and compressors, thermodynamic efficiency, control turbocompressor matching, etc 11 p1814 A71-26401

Variable elasticity algorithm for axial flow turbine disks with allowance for plasticity, creep and loading history 12 p1979 A71-27351

Cascade approximation of unsteady forces acting on blades of axial flow turbomachines, using perturbation potential combined with slip condition [ONERA-TP-944] 12 p1946 A71-27713

Quasi-axisymmetric and superposed fine fluctuating structure of ideal incompressible vortex flows in axial flow turbines, assuming infinite mutual blade proximity [ONERA-TP-945] 12 p1866 A71-27714

Nonlinear limit rotation velocity and circulation induced by wheel in axial flow turbomachine for incompressible ideal fluid, using iterative numerical algorithm [ONERA-TP-946] 12 p1866 A71-27715

Measurement errors in testing single stage air driven axial flow compressors and turbines 13 p2115 A71-28582

Axial flow turbines comparative performance tests under steady and pulse flow conditions for turbocharger application 14 p2169 A71-29819

Axial flow steam and gas turbines performance estimations over ranges of loading, velocity/blade ratio, Reynolds number and aspect ratio 15 p2469 A71-31733

Performance test facility for pulsed axial flow gas turbine of turbocharger unit on large diesel engines 15 p2469 A71-31943

End play influence on dynamic bending vibration stresses induced by aerodynamic forces in axial flow turbine rotor blades in case of resonant vibrations 15 p2508 A71-32298

German monograph on accelerating grids in wind tunnel and axial flow turbine, covering plane/secondary flows past cascades and stator/rotor blading 15 p2347 A71-32303

Axial flow gas turbines blade cascades forming arrays with convergent channels, discussing contours design

16 p2521 A71-33615
Siren wail in turbine axial stage due to nonuniform pressure fields behind blade cascades

18 p2843 A71-36180
Axial flow turbines, calculating effects of axial clearance between stator and rotor bladings on rotor impulse blades bending vibration strength

18 p2979 A71-36299
Vibration analysis of simulated axial flow turbine disks by holography, illustrating advantages of full field modal and deflection information

[ASME PAPER 71-VIBR-105] 21 p3377 A71-40330
Quasi-steady three dimensional ideal compressible fluid flow between convex and concave sides of neighboring blade profiles in axial flow turbine

21 p3322 A71-40687
Noise sources in axial flow fans, considering radiation from turbulent boundary layers, scattering of incident turbulence and secondary flow influence

21 p3323 A71-40710
Streamline curvature analysis of compressible subsonic, transonic and supersonic cascade flows in axial turbine blades

23 p3665 A71-44347

AXIAL LOADS

NT AXIAL COMPRESSION LOADS

Glass fiber reinforced plastics strain properties under multiaxial loads, considering long and short time loading, temperature and environmental conditions

01 p0109 A71-10696
Al alloys low cycle fatigue test under axial load, observing hardening behavior and structure by transmission electron microscopy

01 p0104 A71-11397
Al fatigue testing by cyclic uniaxial tensile load, examining deformation, internal friction ductility and plastic strain

02 p0262 A71-11683
Metal and glass composites with similar residual stress states under axial loading, examining yielding and fracture behavior

03 p0443 A71-14186
Axially loaded finite stringer bonded to infinite elastic sheet, considering adhesive shear flow

03 p0514 A71-14350
Two-member composite cylinders, predicting residual stress and axial loading behavior by elastoplastic analysis for comparison with experiment

04 p0666 A71-14893
Eccentrically reinforced cylindrical shells stability equations under axisymmetric loading

06 p0993 A71-17813
Numerical algorithms of elastic stability solutions for thin walled axisymmetrically loaded shells of revolution with finite difference schemes

06 p0999 A71-17864
Gas turbine rotor axial load determination, using static pressure distribution

08 p1348 A71-21268
Two frequency axial loading fatigue testing machine using torsional/linear vibration transducer

09 p1426 A71-22500
Thick walled anisotropic nonhomogeneous elastic cylinder or plate under axial symmetric time dependent pressure, investigating transient response

09 p1540 A71-23087
Crystalline Al stress-strain function parabolic law generalization under combined axial tensile-torsional loading

09 p1480 A71-23700
Low temperature plasticity of Al alloy thin walled tubular specimens under axial tension and internal pressure

10 p1626 A71-24193
Deformability and strength of soft fiber reinforced plastics under biaxial tension, determining low temperature critical tensile stresses and elongation ratios

10 p1634 A71-24194
Cylinder roller bearing for heavy axial and radial loads, determining carrying capacity by sliding surfaces

10 p1617 A71-24683
Buckling of axially compressed imperfect isotropic cylindrical shells with edge constraints, deriving two point boundary value problem numerical solution by shooting method

[AIAA PAPER 71-358] 11 p1844 A71-25337
Arbitrary solid cross section frames and arches shakedown analysis including axial forces effects on stress through reduction to linear programming

11 p1849 A71-25678
Specimen sample mounting stress effects on fatigue durability scatter in axial load tests

12 p1976 A71-27116
High altitude balloon gore meridional stresses effects on film response by analyzing cylindrical elastic membrane under uniform hydrostatic pressure and axial loads

12 p1976 A71-27121
Nonlinear equations of motion for cylindrical elastoplastic shell under axial impact

12 p1980 A71-27452

Girder system transverse bending under axial and lateral loads, deriving stability conditions by direct Liapunov method

13 p2153 A71-28519
Composite materials elastic-plastic behavior under uniaxial loading, determining stress-strain relationships by dislocation theory

14 p2321 A71-29688
In-plane boundary effects on buckling and critical stress of axially loaded cylindrical panels

14 p2331 A71-30697
Fatigue testing machine for axial and torsional loadings at low temperatures in vacuum

15 p2384 A71-31858
Thin walled tubes under external and internal pressures axial loads and torques, showing load capacity limit dependence

15 p2428 A71-31860
Boundary conditions of elastic deformations of constrained circular cylinders under axial load, discussing modulus dependence on Poisson ratio

15 p2505 A71-32007
Statistical methods application to buckling of axially loaded columns, considering entire spectrum of elastic, elastoplastic and fully plastic ranges

16 p2654 A71-33123
Stress, slip and damping of clamped elastic plate with finite friction under alternating axial load, using finite element method

16 p2581 A71-33174
Single crystal Ni-base superalloy anisotropic hollow cylinder creep under biaxial loading, studying rate dependence on crystallographic axis orientation and stresses ratio

[ASME PAPER 71-APM-1] 16 p2591 A71-33222
Pin connected beam under axial loading, discussing resultant constraint forces, bending moments and lateral displacements

16 p2661 A71-34116
Equivalent reinforcement of contact area between spherical shell and radial outlet cylindrical pipe under internal pressure and axial force

17 p2817 A71-34332
Hinged bar dynamic buckling under harmonic axial load, using Timoshenko beam theory with longitudinal vibration effects

17 p2832 A71-35400
Circular inclusion effects in infinite viscoelastic plate under monotonically increasing uniaxial tension, considering stress distribution

19 p3157 A71-37798
Clamped oval cylindrical thin walled shells elastic buckling under axial loads, solving stability equations by Fourier method and higher order difference technique

19 p3157 A71-37876
Creep testing machines load axiality, investigating bending strains allowable limits excess as function of tensile stress and temperature

19 p3082 A71-38134
Partial thickness cracks of preselected depths and shapes by axial and flexural fatigue methods, yielding preferred propagation path

20 p3248 A71-38780
Axially loaded slender beam mass and deformation effect on constrained bending motion system stability and dynamic response

21 p3469 A71-41010
Vertical bar longitudinal bending equation under axial forces, obtaining relation between extreme free angle and deflection

21 p3472 A71-41148
Anisotropic glass fiber plastic material stress, strain and crack formation threshold measurements under long term static and cyclic axial loads

23 p3696 A71-43424
Axisymmetric elastic deformation of layered thin anisotropic shells of revolution, using computer integration for arbitrary loads and boundary conditions

24 p3882 A71-44841
Cylindrical and weakly concave shells, testing critical pressure relationship to axial tension load with celuloid models

24 p3884 A71-44898
Elastoplastic deformation of Zn single crystals under uniaxial tensile loads, noting critical stresses relationship to current pulses

24 p3838 A71-45100

AXIAL STRAIN
Al alloy biaxial shear creep under abrupt temperature and stress changes, noting surface size, shape and location

[ASME PAPER 70-WA/APM-41] 03 p0443 A71-14164
Nonlinear elastic membranes large axisymmetric deformation, deriving initial value problem with differential equations

04 p0667 A71-15183
Axisymmetric normal loading of lateral surface of finite length elastic solid cylinder

05 p0824 A71-16595
Spheroidal cavity effects on elastic medium under axisymmetric stress field, using Legendre potential functions

07 p1212 A71-19253

Stress annealed Ni-base superalloy crystals, investigating orientation and applied uniaxial stress sense effect on coherent gamma prime precipitates morphology

07 p1138 A71-19987
Elastic and elastic-plastic surface strain fields around skewed circular holes in flat plate under uniaxial tension

08 p1372 A71-21654
Stressed state in region of strain raisers /round holes/ in plate subjected to two axial tension associated with plastic yield

08 p1372 A71-21703
Uniaxial, equal biaxial and unequal homogeneous biaxial strain rates of viscoelastic materials under isothermal tensile test conditions

09 p1481 A71-22141
Isotropic incompressible viscoelastic solid deformation field under uniaxial and equal biaxial relaxation, determining constitutive equation

09 p1534 A71-22142
Prolonged storage effect on polycarbonates mechanical properties, measuring tensile strength, elastic modulus, yield point and breakdown strains under uniaxial tension

09 p1483 A71-22825
Mo fibers surface state and reactions under uniaxial stress from electron work function measurements

09 p1471 A71-23080
Anisotropic material failure under combined loading, predicting strength from uniaxial and shear tests

[AIAA PAPER 71-368] 11 p1845 A71-25342
Axisymmetric deformation differential equations system for nonlinearly elastic shells under vertical loadings, considering various Euler buckling boundary problems

11 p1848 A71-25567
Boundary value problems of steady state thermoelasticity and axisymmetric Boussinesq stress concentration for half space in linear Cosserat elasticity

12 p1974 A71-26942
Axisymmetrically strained thin elastic shells of revolution with temperature dependent random elastic characteristics

12 p1979 A71-27358
Nonlinear heredity theory related to Volterra-Freschet heredity theory under uniaxial tension, giving expression for polymers deformation relaxation processes

13 p2092 A71-28650
Deformation work for strained copper during tensile testing until fracture as function of slenderness in neck

15 p2427 A71-31700
Axially symmetric thermal stress distributions in infinite elastic solid containing flat circular external crack

16 p2654 A71-33169
Axisymmetrical elasticity theory for vertical finite length cylinder with mixed boundary conditions on top and bottom end surfaces, obtaining stress and displacement expressions

17 p2822 A71-34779
Elastic viscous plastic waves profiles of finite uniaxial strain, obtaining constitutive equations

21 p3465 A71-40788
Axisymmetric contact problem of elastic half space stress-strain state, seeking displacements in Hankel integral expansion form

24 p3885 A71-45222

AXIAL STRESS
Elastic plane with hypertrochoid hole under axial tension, determining stress concentration at hole boundary due to irregularities

01 p0168 A71-10424
Reinforced cylindrical shells under external pressure, investigating longitudinal tensile stresses effect on stability

01 p0175 A71-11040
Two dimensional stressed state of isotropic plate with elastically reinforced elliptical hole under biaxial tension

02 p0326 A71-12290
Spherical shell segments stresses and displacement due to arbitrary axisymmetric surface tractions and edge boundary conditions, using axisymmetric elasticity solutions

[ASME PAPER 70-WA/APM-27] 03 p0512 A71-14159
Thin Al and plexiglass sheets biaxial stress field effect on fatigue and fracture

[ASME PAPER 70-PVP-17] 04 p0665 A71-14768
Stress intensity factors for infinite sheet rectangular cut-out with symmetrical edge internal cracks under axial tension

04 p0670 A71-15387
Relation uniaxial stressed state relationship to internal geometry of flexible shell

06 p0993 A71-17814
Rib reinforced cylindrical shell stability under annular and axial stresses, determining eigenvalue of homogeneous integral equation

06 p0993 A71-17816
Smooth cylindrical shell stability, considering internal pressure effect on critical axial stresses

06 p0993 A71-17819

Pure polycrystalline Al under uniaxial tension, noting vacancy rupture mechanism 06 p1000 A71-17940

Uniaxial stress effect on morphology changes of coherent gamma prime precipitates in nickel base superalloy crystals 06 p0914 A71-18682

Uniaxial elastic stresses effect on ferromagnetic resonance parameters in polycrystalline ferrites 07 p1177 A71-19497

Materials bending fatigue strength calculations for biaxial tension compared with experiments, showing agreement 09 p1538 A71-22596

Macroscopically ductile and brittle fracture via electron microscope photographs, considering brittle fracture and embrittlement temperature under uniaxial and multiaxial stress 10 p1627 A71-24595

Principal axial stresses determination from bonded wire resistance strain gages with known cross sensitivities, deriving expressions from concentric Mohr circles 14 p2239 A71-29834

Finned solid cylinders surface layers, determining residual axial stresses distribution and amount with induction sensor 15 p2503 A71-31480

Thermal buckling of elastic plates exposed to random temperature field producing biaxial stress concentration 15 p2504 A71-31834

Cylindrical shell under internal pressure, detailing axial thermal stresses relaxation 15 p2505 A71-31861

Failure and forming limit diagrams in biaxial tension for sheet metal with preexisting inhomogeneities based on Marciniak concept 15 p2505 A71-31945

Loading history effect on optical and mechanical properties of polymethyl methacrylate under uniaxial tension 16 p2600 A71-32815

Two phase fiber reinforced composites under polyaxial stresses, predicting plastic behavior by deformation theory 17 p2823 A71-34810

AXIOMS

Thermodynamics axioms for work and energy under volume-area continuity conditions, discovering local power density in velocity field 18 p2948 A71-36812

Quantum mechanics axiom system construction from physical theories, using imbedding operation 19 p3103 A71-37276

Definitions and axiomatics revision and recommendations for mathematical statistics as applied discipline 19 p3086 A71-37782

Polycrystalline body macrohomogeneous plastic deformation, deriving basic postulates for slippage and plane relationships to tangential stress and shear strength dependence on elastic deformation 23 p3777 A71-43576

AXISYMMETRIC BODIES

Axially symmetric bodies impact landing on water surface, deriving acceleration for comparison with measurement 01 p0178 A71-11398

Starting functions solutions for axially symmetric orthotropic annular plates 02 p0329 A71-12689

Axissymmetrically loaded shells of revolution made of work hardening materials, determining inelastic finite deformations and buckling loads by incremental variational method 03 p0505 A71-13543

Symmetry axis motion of solid body with ellipsoidal cavity filled with ideal incompressible uniformly turbulent fluid 03 p0458 A71-13596

Condensate film thickness and Nusselt number on axisymmetric vertical plates and cylinders, correcting for variable gravity and body form [ASME PAPER 70-HT-P] 03 p0519 A71-13699

Axissymmetric satellite optimal reorientation into prescribed rotary motion by gas operated control jets, considering space navigation problems 05 p0815 A71-16036

Dynamically symmetrical satellite optimal transfer into steady axial rotation state with simultaneous alignment of symmetry axis, considering control jets moments 05 p0779 A71-16037

Axissymmetric body stationary motions around sphere, investigating secular and ordinary stability 05 p0809 A71-16473

Applicability limits of equations of theory of three-layer plates and shells of axisymmetric structure 06 p0987 A71-17766

Closed axisymmetric vessel filled with viscous incompressible fluid, calculating integral heat release coefficients in free convection 07 p1222 A71-19196

Axisymmetric phase object holographic interferometry, showing light beam refraction effect on interference pattern 07 p1108 A71-19237

Axisymmetric body rapid rotation under center of gravity velocity vector conditions, solving for plane gliding motion stability in air 07 p1159 A71-19354

Reacting and nonreacting gases laminar boundary layer flows over two dimensional and axisymmetric bodies at zero lift, comparing numerical methods 07 p1015 A71-19860

Displacement function and principal stress differences in transverse plane of symmetry of axially symmetric photoelastic body 08 p1372 A71-21653

Optimal orientation control of axisymmetric rotating space vehicle, using cyclic sliding mode theory 09 p1532 A71-22659

Stability of regular motions of dynamically symmetrical body with equatorial symmetry plane in Newtonian force field of spherical planet by Liapunov second method 09 p1526 A71-23346

Circular stagnation line position on axisymmetrical blunt bodies with circular sharp edge 09 p1384 A71-23672

Numerical solution of axisymmetric minimum drag bodies in hypersonic viscous gas flow, obtaining coefficient of friction by local variations method 10 p1551 A71-24370

Arbitrary plates and axisymmetric bodies creep analysis by finite element method 10 p1691 A71-24820

Unsteady hypersonic flow around melting axisymmetric blunt bodies of revolution with profile depending on wall temperature, calculating temperature distribution and wall pressure 10 p1698 A71-25087

Axissymmetric ablating graphite nosetip analysis code, demonstrating shape change, heating distribution and internal conduction coupling [AIAA PAPER 71-413] 11 p1856 A71-26206

Axissymmetric phase object holographic interferometry, showing light beam refraction effect on interference pattern 12 p1903 A71-26755

Minimum volume design of sandwich axisymmetric plates obeying Mises criterion, using calculus of variations 13 p2146 A71-27782

Approximate limiting loads with minimum yield stress for axisymmetric rigid-plastic body of arbitrary shape, using computerized static equilibrium method 13 p2150 A71-28137

Linear isotropic and centro-symmetric second-grade elastic material and special case with coupling stress, calculating stress field of long straight screw and edge dislocations 14 p2327 A71-30290

Axissymmetric bodies torsion problems solution by superimposing elasticity equations, using point matching technique 14 p2329 A71-30463

Exponentially varying thickness thin plate volume minimization for simultaneous stress and deflection constraints under axisymmetric load, using digital computer 14 p2330 A71-30691

Three dimensional elasticity theory solutions for isotropic axisymmetric bodies of revolution by p-analytic and generalized analytic functions 14 p2333 A71-30889

Multicomponent nonequilibrium air flow past axisymmetric blunt body, calculating flow distribution at various attack angles with time dependent technique [AIAA PAPER 71-595] 15 p2512 A71-31575

Two dimensional axisymmetric shell analytical model for liquid propellant launch vehicle longitudinal vibration modes and steady state response calculation 16 p2653 A71-33092

Axissymmetric satellite optimal reorientation into prescribed rotary motion by gas operated control jets, considering space navigation problems 16 p2645 A71-33440

Dynamically symmetrical satellite optimal transfer into steady axial rotation state with simultaneous alignment of symmetry axis, considering control jets moments 16 p2605 A71-33441

Axissymmetric blunted body heating by high temperature plasma flow as function of geometry, pressure and stagnation enthalpy 17 p2669 A71-34207

Numerical method for limit analysis of axisymmetric shells of revolution, considering truncated conical shells and pressure vessels with rigid circular plates 17 p2818 A71-34400

Hypersonic small perturbation flow past two dimensional or axisymmetric slender bodies supporting logarithmic shock waves 17 p2670 A71-34658

Three dimensional boundary layers on axisymmetric bodies with large positive and negative crossflows, using finite difference method 17 p2727 A71-34875

Circular contact area in theory of elasticity with allowance for surface structure of bodies in contact solving Hertz axisymmetrical problem of elastic bodies 17 p2833 A71-35616

Elastoplastic thermal stress analysis in axisymmetric bodies by finite element method, calculating residual stresses 21 p3466 A71-4084

Blunt and hemispherical base axisymmetric bodies in Mach 4 free stream, investigating turbulent near wakes generation 21 p3324 A71-40999

Axisymmetric imperfect conical shells vibration analysis using time average holographic interferometry technique 21 p3382 A71-41028

Shock layer pressure distribution for axisymmetric bodies moving at supersonic velocity in gas at rest, deriving nonstationary analog of Newton-Busemann formula 22 p3481 A71-42864

Sonic line position measurement in supersonic flow behind detached shock wave preceding axisymmetric or plane blunt bodies 23 p3625 A71-43092

Hypersonic axisymmetric slender body near wake shear layer determination by shock expansion method for numerical computation accuracy and efficiency 23 p3626 A71-44194

Flare induced laminar boundary layer/shock wave interactions on axisymmetric bodies at zero incidence in supersonic flow under adiabatic conditions 24 p3789 A71-44604

Nonlinear theory of wave resistance in supersonic ideal gas flow past finite flat axisymmetric bodies, establishing drag relation to flow rate deficit 24 p3790 A71-44773

Ideal weight of axisymmetric fuselage shells, taking into account load distribution and cabin pressurization 24 p3885 A71-45180

AXISYMMETRIC DEFORMATION

U AXIAL STRAIN

AXISYMMETRIC FLOW

NT ANNULAR FLOW

Free and impinging axisymmetric turbulent jet characterization model providing continuous transition from nozzle exit through fully developed region [ASME PAPER 70-WA/FLCS-6] 03 p0401 A71-14082

Axissymmetric supersonic overexpanded ideal gas jet calculation, using finite difference method based on buildup principle 03 p0346 A71-14573

Nonlinear two dimensional free boundary problem of axisymmetric fluid flow in tubes with surface solidification, obtaining numerical solution based on finite difference equations 04 p0677 A71-15454

Started supersonic axisymmetric parallel diffuser, examining wall static pressure and heat transfer 04 p0528 A71-15489

Round cylinder in viscous fluid axisymmetrically disturbed flow, calculating dynamic and temperature conditions with difference method 04 p0571 A71-15496

Two dimensional and axisymmetric flow film cooling effectiveness in supersonic turbulent boundary layer, using Eckert reference enthalpy method 04 p0571 A71-15496

Axissymmetric turbulent wakes with zero excess momentum, noting mean and pulsation velocity and Reynolds shear stresses 04 p0577 A71-15624

Minimum mixing losses of axisymmetric turbulent wakes in profiled wall channels 04 p0578 A71-15629

Nonstationary isentropic low density flows with axial or central symmetry, suggesting characteristics with flow rate and sound speed variation as in stationary source flow 07 p1014 A71-19729

Viscous incompressible axisymmetrical flow, examining vortices near stagnation point of infinite flat obstacle 07 p1089 A71-19737

Three dimensional axisymmetric flows in tornado-like vortex boundary layer, determining nonlinear radial and vertical velocity distribution components 07 p1152 A71-19753

Rarefied monatomic gas flow in axisymmetric jet exhaustion into vacuum, noting expansion to low densities at thermodynamic nonequilibrium 07 p1090 A71-19894

Stability of two concentrically flowing fluids in straight circular tube, investigating axisymmetric and asymmetric disturbances by small perturbation method 07 p1093 A71-20282

Two axisymmetric jets impingement in fluid amplifiers, discussing velocity profiles of radial jet 07 p1029 A71-20592

Inviscid incompressible vortex-free axisymmetric pipe flow near arbitrary shape body symmetrically located near axis 09 p1431 A71-22180

Turbulent flow in initial section of convergent axisymmetric nozzle based on logarithmic velocity law 09 p1431 A71-22409

Axisymmetric steady diabatic flow equations exact solutions 09 p1434 A71-23545

Integral equation for solving potential incompressible fluid flow past blade cascade on axisymmetric current surface in variable thickness layer 10 p1593 A71-24369

Vortex layer near circular cone surface in supersonic axisymmetric steady flow of homogeneous inviscid gas 10 p1551 A71-24372

Linear theory of weakly perturbed supersonic plane axisymmetric flows of gas-particles mixture, deriving partial differential equation for perturbation potential 10 p1551 A71-24373

Numerical solution of nonuniform enthalpy mixed axisymmetric gas flow in curvilinear regions with upper boundary and discontinuity using build-up method 10 p1551 A71-24376

Coaxial jets development and mixing in axisymmetric twisted turbulent ring air flow injected through inlets 10 p1594 A71-24560

Velocity distributions in axisymmetric air jets submerged in coaxial oscillating stream measured by hot-wire anemometer 11 p1748 A71-25156

Steady three dimensional subsonic nonviscous flow through turbomachine with arbitrary hub and shroud shapes and finite blade number, using iterative blade to blade procedure [ASME PAPER 71-GT-2] 11 p1702 A71-25948

Axisymmetrical incompressible and compressible fluid flow inverse problem formulation and solution with application to turbine blade design 11 p1752 A71-26051

Hypersonic reentry heat shielding problem, considering axisymmetric laminar boundary layer flow with local coolant mass injections at multiple stations 13 p1990 A71-29127

Two coaxial axisymmetric subsonic gas jets of different density mixed during expulsion from convergent nozzles with high compression, using flow rate ratio 13 p2050 A71-29215

Numerical method for two dimensional or axisymmetric heated flows allowing for dissipation extended to viscous flow, using Navier-Stokes equations in streamwise coordinates 13 p2118 A71-29280

Properties of arbitrarily thick turbulent boundary layer for incompressible axial flow past long cylinder [ASME PAPER 71-FE-25] 13 p1995 A71-29462

Axisymmetric flow effects on surface mass injection at supersonic and hypersonic speeds, streamline inclinations and surface pressures generation by turbulent viscous dissipation 14 p2223 A71-29874

Axisymmetrical three component flow equations for incompressible viscous fluid in cylinder with rotating disk 14 p2227 A71-30855

Compressible laminar plane axisymmetric boundary layer flows in Laval nozzles, studying temperature, density and velocity distribution relations 15 p2386 A71-31164

Pade fractions use in calculation of axisymmetric flow of perfect gas past blunt body of revolution, obtaining stream function Taylor expansion terms 15 p2346 A71-32122

Flow measurements in axisymmetric turbulent wake of sphere in low speed wind tunnel 15 p2346 A71-32123

Ducted axisymmetric jet mixing flow, investigating flow separation and reattachment as function of diameter and velocity 15 p2392 A71-32252

Steady inhomogeneous axisymmetric nozzle flow, determining pattern by simultaneous solution of radial equilibrium and continuity equations 16 p2521 A71-33614

Viscous trailing vortices decay downstream of non-free axial flow fan, assuming steady axisymmetric incompressible laminar flow 17 p2725 A71-34191

Binary laminar boundary layer in hypersonic axisymmetric stagnation point flow with temperature dependent material properties, presenting exact and approximate calculation methods 17 p2671 A71-35422

Supersonic jet interaction with turbulent wake, calculating plane and axisymmetric flow behind body butt face 17 p2672 A71-35630

Time dependent calculation of mixed two dimensional or axisymmetric transonic flows in nozzle, writing equations of motion with transformed spatial variables 18 p2906 A71-36323

Axisymmetric plane transonic flow past convex corner point, obtaining characteristics by mapping into hodograph plane 19 p2991 A71-37103

Linear theory of weakly perturbed supersonic plane axisymmetric flows of gas-particles mixture, deriving partial differential equation for perturbation potential 20 p3175 A71-38898

Vortex flow through axial, axially radial and other three dimensional axisymmetric channels, using finite difference model for flow equations solution 20 p3211 A71-39465

Steady axisymmetric incompressible flow past sphere at low Reynolds numbers, reducing equations of motion to ordinary differential equations 20 p3212 A71-39506

Axisymmetric small Rossby number flow driven by axially distributed heat sources, examining core multiboundary layer structure 20 p3212 A71-39507

Compressible circular free jet instability allowing for turbulent boundary layer thickness, considering influence of axisymmetry on spatial growth rate and disturbance phase velocity 21 p3365 A71-40013

Shock fronts diffraction and reflection with vortices generation at discontinuities, predicting wave shape and strength distribution in two dimensional or axisymmetric situations 21 p3365 A71-40016

Rotationally symmetric quasi-cylindrical viscous incompressible vortex flow, using method of weighted residuals approximating axial velocity and circulation profiles by series of exponentials 21 p3369 A71-40951

Two axisymmetric annular flows linear hydrodynamic stability analysis, using Navier-Stokes system 21 p3370 A71-40991

Two phase flow in asymmetrically roughened ducts, investigating secondary flow effects on heat transfer characteristics 21 p3477 A71-40995

Axially symmetric flow in half space above rotating disk, proving boundary value problem solution existence by fixed point technique 22 p2531 A71-42402

Free axisymmetric turbulent annular nozzle jet propagation, detailing velocity distribution variation due to momentum loss in stall region 23 p3664 A71-44335

Rotating fluid axisymmetric flow into point sink, investigating Rossby number 24 p3817 A71-44419

Generalized eddy viscosity model application to quiescent and coflowing axisymmetric turbulent jets mixing 24 p3818 A71-44626

Mass flow function diagram for axisymmetric isentropic compressible swirling flow in annular duct 24 p3820 A71-44960

Critical streamline length in axisymmetric and plane ideal gas flows past conical bodies as function of Mach number and form parameter 24 p3790 A71-45058

Axisymmetric hypersonic flow of nonequilibrium ionized monatomic radiating inviscid gas past blunt body, using Clarke-Ferrari kinetic model 24 p3790 A71-45224

AXISYMMETRY
U SYMMETRY
AXLES
U SHAFTS [MACHINE ELEMENTS]
AZIDES [INORGANIC]
Hydrazine-hydrazine azide blending for propellant performance improvement and freezing point reduction, presenting engine test data 22 p3588 A71-42778

AZIMUTH
Program and auxiliary tables for stellar azimuth determination by observations near elongation 01 p0159 A71-10810
Altitude and azimuth angle values computation using logarithmic and natural haversines table 02 p0280 A71-12899
Satellite tracking by radio direction finder, noting periodic azimuth deviations related to ionospheric Faraday effect 03 p0377 A71-13169
Autocollimation control of telescope rotation axis position at arbitrary azimuths 04 p0565 A71-14854
Coherent optical system for range and azimuth ambiguity simulation in radar systems 04 p0551 A71-15010
Gyrocompass strapdown three coil synchro sensor magnetometer in conjunction with vertical gyro, eliminating azimuth detector inertial platforms 07 p1156 A71-20340

Geographical latitude from azimuths and zenithal measurements of two stars on hour circle 09 p1438 A71-23180

Quasi-radial hypervelocity approximation of rotating azimuthally dependent solar wind under magnetic field 09 p1515 A71-23709

Meteor trails azimuth angle measurement by radar interferometry, describing system advantages with respect to receiver noise, angular resolution and calibration 10 p1576 A71-24053

Geodetic geographic coordinate transformations and ellipsoid heights, azimuth and length determination from synchronous photographic observations and distance measurements of artificial satellites 11 p1759 A71-25813

Geodetic azimuth between two remote points on earth surface based on synchronous satellites positions and photographs 11 p1759 A71-25817

Astronomical latitudes determination under non-setting sun conditions from differences between star azimuths 13 p2056 A71-28011

Alidade level instead of superposed level for azimuth determination by astronomical universal 15 p2395 A71-31465

Polarization direction finder determining electromagnetic waves azimuth on basis of field intensity vectors 19 p3014 A71-37074

Astronomical geodetic networks equalization, using Laplace azimuths 19 p3056 A71-38174

Star comparator automatic azimuth system using long evacuated tunnel transfer to underground inertial guidance laboratory 19 p3102 A71-38328

Binary moving-window integrator radar target azimuth measurement error determination, presenting target detection probability curves obtained by digital simulation 21 p3348 A71-40725

Odesa observatory meridian circle pivot irregularities effects determination on horizontal axis inclination and azimuth, using Challis method 23 p3680 A71-44263

Astronomical azimuth determination for terrestrial objects from observations of star passages across object vertical 24 p3868 A71-44475

AZINES
NT CYANURATES
Fluoro-alkyl s-triazines as high temperature lubricants and energy transfer fluids for aerospace systems [ASLE PREPRINT 70LC-5] 08 p1322 A71-21155

AZOLES
NT ACETAZOLAMIDE
NT INDOLES
NT OXAZOLE
NT TRYPTOPHAN

AZUR SATELLITE
Azur research satellite scientific instruments and objectives and design parameters 01 p0164 A71-11334
Mission objectives and orbit parameters of Azur satellite, considering satellite control and data transmission as function of ground support system 10 p1589 A71-23927
German low altitude polar orbiting research satellite AZUR orbital characteristics and bearing on auroral zone substorm phenomena 12 p1899 A71-26833
Azur satellite mission report, discussing major anomalies, energy supply, position control, temperature behavior and orbit [DGLR-71-008] 15 p2501 A71-32779
Azur satellite flight data evaluation, discussing heat balance and temperature monitoring [DGLR-71-013] 15 p2501 A71-32780
In-flight operation of Azur satellite magnetic attitude control system during period between booster separation and steady orbital motion 15 p2501 A71-32782
Azur satellite structure and mechanism requirements, design and tests, noting damping characteristics and Yo-Yo system [DGLR-71-014] 15 p2501 A71-32783
German space operations center for performing ground operations for Azur research satellite 16 p2553 A71-33747
Radiation belt proton intensities and energy spectra measurements by Azur satellite solid state detector telescope with energy level discrimination electronics 19 p3125 A71-37417
Premidnight asymmetry in directional 40 keV ionospheric electron flux profiles in magnetic local time observed on Azur satellite 23 p3721 A71-43185

B

B STARS

- Star origin position in Galaxy, computing meridional galactic orbits for nearby late B types
01 p0161 A71-11385
- OB stars existence on utmost borders of M 31, using photometric statistics
02 p0312 A71-12465
- Be stars IR emission, noting thermal free-free radiation superposed upon stellar continuum
03 p0483 A71-13185
- Hertzsprung-Russell diagram calibration in terms of age and mass for main sequence B and A stars
04 p0646 A71-15234
- Be star rarefied gaseous envelopes emitting or absorbing region size determination, noting application to other rotating stellar systems
04 p0659 A71-15843
- Normal main sequence B stars, distinguishing features from rapid rotators and supergiants by photometric scheme
05 p0805 A71-16118
- O-B stars velocity distribution in synthetic association, proposing method for space velocities mean value determination
07 p1192 A71-19289
- O and B type stars galactic Keplerian parameters statistical distributions based on galaxy point model
11 p1820 A71-25248
- He I absorption line profiles in normal main sequence B star spectra, discussing He abundance and LTE
11 p1821 A71-25536
- He I lines in OB spectra, examining main sequence stars
11 p1830 A71-26111
- Faint O-B5 type blue stars data, listing absolute spectrophotometric gradients and Balmer series discontinuities
15 p2487 A71-32032
- H II regions near O and R stars effect on interstellar electron density in solar vicinity
20 p3294 A71-39542
- Four-color and H beta photometric data tabulation for bright B type stars in Southern Hemisphere
21 p3443 A71-40192
- Be star theta Corona Borealis UVBY H alpha filter observations, noting spectroscopic changes of light variation due to particles in stellar atmosphere
21 p3443 A71-40193
- B star in galactic north pole region, noting high radial velocity
21 p3448 A71-40517
- Space distribution of OB stars from revised Victoria H gamma spectrophotometric magnitudes by MK spectral classification
21 p3448 A71-40594
- Spiral structure OB associations in outer regions of Andromeda nebula, investigating blue objects in U and B plates of Schmidt telescope
21 p3451 A71-40723
- Pole-on Be star envelope models, comparing H alpha line profiles with line of sight perpendicular to rotation axis
23 p3723 A71-42945
- Beta Sco occultation by Jupiter, interpreting UV light curve
23 p3733 A71-43124
- B stars spectra, calculating C III ions spontaneous electric dipole transitions and oscillator strengths in vacuum UV region
23 p3767 A71-43829
- B-52 AIRCRAFT**
LAMS flight control systems for turbulence induced fatigue damage reduction in B-52 and C-5A aircraft, using mathematical models
02 p0188 A71-11660
- B-52 LAMS test vehicle structural modification and instrumentation in flight phase
02 p0188 A71-11661
- B-70 AIRCRAFT**
Pilot subjective evaluation of XB-70 aircraft response to atmospheric turbulence in comparison with measured accelerations
14 p2173 A71-29774
- B-103 AIRCRAFT**
U BUCCANEER AIRCRAFT
BABBITT METAL
U BEARING ALLOYS
BAC AIRCRAFT
NT BAC 111 AIRCRAFT
NT TSR-2 AIRCRAFT
NT VC-10 AIRCRAFT
Aerial land rover for special needs of developing countries as passenger and freight aircraft, crop spraying and dusting, aerial survey and fire fighting
21 p3325 A71-40701
- BAC TSR 2 AIRCRAFT**
U TSR-2 AIRCRAFT

BAC 111 AIRCRAFT

- BAC 111 autopilot development, discussing computer compatible system for digital representation of airborne flight test data and direct transmission to ground-based computers
18 p2946 A71-36672

BACILLUS

- Chemoautotroph *Thiobacillus neapolitanus* growth inhibition by histidine, methionine, phenylalanine and threonine under imbalance conditions
04 p0537 A71-14776

BACKGROUND NOISE

- Background nonequivalence during long term photopic dark adaptation
01 p0008 A71-10143
- Notch power ratio noise tests on magnetic tape recorder/reproducer using direct recording in baseband
01 p0034 A71-10910
- M-dimensional gradient extremal system under non-random and random noises of inertial control plant, using difference equation
01 p0064 A71-10922
- Optical components and technology for acquisition, tracking, transmit-beam offset and background noise discrimination functions in optical space communications
02 p0213 A71-12007
- Background noise in optical communication system, considering direct, reflected and scattered radiation sources in atmosphere
02 p0213 A71-12015
- Signal parameter estimation during pulse sequence reception on background of nonstationary additive noise
04 p0549 A71-14614
- Polar chorus background hiss generation, investigating VLF wave characteristics responsible for harder electron precipitation from magnetosphere
05 p0743 A71-17004
- Optimal quasi-regular signal detection on amplitude and frequency modulated noise background
05 p0723 A71-17020
- Noise stability during complex signals reception and lag measurement on fluctuating noise background
06 p0866 A71-17371
- Coherent light photoelectric detection probability in background light passing through narrow band filter of rectangular or Lorentz frequency characteristics
07 p1059 A71-18848
- Optical data storage photodetector output signal to noise and signal to background ratios, using Fourier transform amplitude and phase holograms
08 p1287 A71-21186
- Detectable information rate changes of photon counter with finite observation time and background noise
08 p1289 A71-21286
- Single and dual channel weak signal adaptive detectors theoretical performance under statistically undefined noise background
08 p1256 A71-21601
- Optimal temporal and spatial temporal resolution for unknown parameter of interfering signal on white noise background
09 p1404 A71-22219
- Maximum likelihood estimates for deterministic signal parameter during optimal reception on stationary normal noise background
09 p1405 A71-22465
- Correlation estimates and optimal detector for incomplete a priori information signal reception on random and white noise background
10 p1579 A71-24878
- Asymptotically optimal detection/discrimination algorithms for weak signals on correlated noise background
14 p2195 A71-30105
- Neural spikes and LF components separation from background noise, describing feedback amplifiers circuit
15 p2356 A71-31251
- Optimal Bayesian system for simultaneous discrimination and parameter estimation of several signals in noise background
15 p2370 A71-31585
- Signal detection in noise, investigating quantiles position optimization in nonparametric test statistics
15 p2370 A71-31588
- Signal detection in stationary, Markov and other noise background, discussing functional method of statistical and probabilistic representation
15 p2370 A71-31589
- Two stage noncoherent rank detector of fluctuating radar signals in noise with unknown distribution
15 p2373 A71-32630
- Integrating discrete signal receiver with weighting proportional to signal, evaluating operational quality in presence of external stationary correlated noise
16 p2542 A71-33488
- Signal detection on Gaussian noise background, deriving error probabilities and optimal processing algorithms
19 p3015 A71-37224

- Probability functional formulas for quasi-determinate signal on unsteady normal noise background for use in false alarm and correct detection
20 p3199 A71-39815

- Accuracy in maximum likelihood estimate for correlation function parameter of random process in signal reception on normal noise background
20 p3199 A71-39816

- Signal parameter estimation accuracy in nonoptimal reception on pulse background with random uniformly distributed initial phase
20 p3199 A71-39817

- Holography review covering photon, grain and speckle noises limitations, large 3D picture production and various applications
21 p3381 A71-40930

- Semiconductor surface layer noise generation physical model with allowance for relaxation effects due to traps in space charge region
21 p3432 A71-41301

- Signal parameter estimation during pulse sequence reception on background of nonstationary additive noise
22 p3510 A71-42254

- Background LF noise of semiconducting diode voltage regulators with breakdown due to avalanche effect
22 p3523 A71-42472

- Signal filtration algorithms and parameter estimation in additive non-Gaussian noise background by conditional Markov process theory
23 p3644 A71-43290

- Second order approximation algorithm for nonlinear noisy dynamical system state estimation from noise corrupted observations
23 p3656 A71-43854

- Laser vibration noise produced by piezoelectric transducer induced forced vibrations of resonator mirror, determining translational and rotational amplitude limits for laser output fluctuation
23 p3686 A71-43999

- Algorithms for discrete message signal reception in background non-Gaussian additive noise with unknown statistical characteristics
23 p3647 A71-44321

BACKGROUND RADIATION

- Radio sources, cosmic rays and X ray background origin, discussing synchrotron mechanism, Compton scattering and red shifts
01 p0144 A71-10770
- Diffuse galactic X ray background intensity as function of galactic scattering and discrete sources
01 p0145 A71-11345
- Sky radiation background in far UV spectral region, calculating stellar component
02 p0304 A71-11913
- Background emission characteristics, discussing cosmic electrons, X rays and radiation sources
02 p0300 A71-12092
- Ionized intergalactic and pregalactic matter 3K microwave background, examining spectrum and degree of anisotropy
02 p0312 A71-12467
- Diffuse cosmic gamma ray background origin, using simple photon production model
02 p0303 A71-12837
- X ray sources location and grouping into supernova remnants and loose cluster categories, accounting for galactic background
03 p0483 A71-13187
- Radio sky background temperature measurement with telescope, using moon as screen
03 p0487 A71-13472
- Extragalactic LF background radiation spectra, using model for free-free absorption in galactic disk
03 p0473 A71-13563
- X ray sources at various flux levels, evaluating contribution to background radiation
03 p0481 A71-12469
- Cosmic objects relativistic plasma X ray and gamma ray background radiation increase, considering bremsstrahlung effect on radiation spectrum
04 p0657 A71-15747
- Metagalactic background X rays origin, hypothesizing electron leakage from radio galaxy
04 p0657 A71-15748
- X ray background angular structure comparison with optical galaxies spatial distribution, ruling out universe models with sources following cosmological mass distribution
04 p0657 A71-15826
- Pulsars relationship to very high energy cosmic ray electron propagation, examining far IR background and radiation sources
05 p0797 A71-15941
- Radiation fields of various background and atmospheric cloud formations by reflected short wave radiation aircraft measurements
06 p0923 A71-17511
- Background effects on photographic stellar image photometry
06 p0902 A71-18445
- IR system with moving space filter, calculating detector output and noise due to background radiation
07 p1058 A71-18828

- Isotropic diffuse cosmic X rays and gamma radiation background origin
07 p1184 A71-19321
- X ray and far IR measurement inconsistency from Centaurus A, discussing metagalactic submillimeter background
07 p1185 A71-19546
- Isotropic component of diffuse gamma ray background, discussing possible dense intergalactic medium coexistence with universal cosmic ray flux
07 p1185 A71-19549
- Low energy cosmic X ray observations, examining diffuse background and absolute flux values
08 p1349 A71-20936
- Radio background in universe due to synchrotron radiation, X ray and photon backgrounds due to cosmic electrons inverse Compton effect
08 p1351 A71-20960
- High energy electron background flux in F 2 layer, discussing grouped particle acceleration
08 p1354 A71-21012
- Background emission characteristics, discussing cosmic electrons, X rays and radiation sources
08 p1355 A71-21142
- Long wave cosmic radio background emission in circumpolar space by Luna 11 and 12 satellites, observing increase in earth magnetosphere tail
09 p1513 A71-22576
- Cosmic X ray astronomy, discussing supernova, variable and extragalactic radiation sources, diffuse background radiation and Crab Nebula measurements
09 p1522 A71-22976
- Lyman alpha sky background measurements by OGO 5 satellite, discussing absolute emission rate, spatial variations and origin
10 p1601 A71-24439
- IR astronomical background radiation measurements at very near IR and longer wavelengths for interplanetary, galactic and intergalactic sources
10 p1677 A71-24582
- X ray astronomy, including celestial sources emission, discrete cosmic sources, recording techniques, isotropic background and shielding
10 p1681 A71-25117
- Cosmic background radiation ground based measurements at two high altitude sites, using radiometric technique
11 p1815 A71-25300
- Background effects in stellar photographic photometry
12 p1903 A71-26595
- Cosmic microwave background measurements at 8 mm wavelength, examining isotropy
12 p1956 A71-26614
- Milky Way galaxy radio halo, investigating background brightness distribution and local spiral arm magnetic field structure
12 p1963 A71-27078
- Zenith angular air shower distribution by Monte Carlo method, discussing muons horizontal component separation from background events
12 p1951 A71-27385
- Line emission in X ray background in galactic plane and at galactic pole based on rocket flight data
13 p2120 A71-28005
- Sky radiation background stellar component in far UV spectral region, determining intensity with Venera instruments
13 p2133 A71-28200
- Cosmic X ray background observations, using rocket-borne proportional counter
13 p2131 A71-29269
- Galactic IR background emission mechanisms, considering electrons, protons and cosmic rays role
13 p2131 A71-29272
- Pulsar signature on diffuse X ray background, converting fraction of luminosity into k series photons
14 p2297 A71-29584
- Soft X ray background source, discussing north polar galactic spur as supernova outburst remnant
14 p2298 A71-29732
- Cosmic gamma ray background flux for photon energies greater than 100 MeV, considering Compton collisions
14 p2301 A71-30435
- Radiometric errors in cosmic background radiation measurement
14 p2204 A71-30970
- Transparency of extragalactic space to very high energy photons, considering background gamma rays effects
15 p2472 A71-31198
- Cosmic ray secondary background of balloon-borne X ray scintillation astronomical telescopes for equatorial latitudes with reference to shutter technique and NaI/Tl crystal
15 p2406 A71-31751
- Night sky submillimeter wave diffuse background radiation telescopic measurements above 120 km
15 p2399 A71-31827
- Submillimeter background radiation origin possibility from extragalactic discrete sources based on cosmological models
15 p2478 A71-31828
- Line emission in diffuse X ray background at high galactic latitudes, interpreting rocket observations
15 p2480 A71-32760
- Optical detection of laser or scattered radiation transmitted through turbulent atmosphere, taking into account independent additive background radiation
16 p2608 A71-33145
- Earth velocity vector right ascension, declination and magnitude determination from cosmic 3 K background radiation anisotropy
16 p2563 A71-33402
- Gamma radiation flux distribution and spectral composition from Cosmos satellite observation, analyzing background effects
16 p2626 A71-33451
- Background phonon X ray and gamma quanta intensities dependence on solar activity from Geiger counter recordings in outer space
16 p2626 A71-33675
- Neutral hydrogen interstellar wind parameters from Lyman alpha sky background measurements outside geocorona by photometers on OGO 5
16 p2643 A71-33834
- Ideal laser gyro sensitivity against background of natural emission fluctuations
17 p2737 A71-34411
- Ground noise reduction with balancing units, discussing transmission line driving and receiving end applications
17 p2716 A71-34859
- Statistical detection theory applied to images against background of laser produced speckle, using flying-spot type scanning machine
17 p2754 A71-35324
- Milky Way galaxy radio halo, investigating background brightness distribution and local spiral arm magnetic field structure
19 p3133 A71-37428
- Extragalactic background soft X ray diffuse flux consistent with absorption by Small Magellanic Cloud
20 p3278 A71-39108
- Interplanetary medium thermal emission detection, presenting diffuse background radiation upper limits in intermediate IR from sounding rocket data
20 p3288 A71-39114
- X ray background model based on photons bremsstrahlung emission by subcosmic metagalactic electrons or protons
20 p3279 A71-39296
- High energy electron background flux in F 2 layer, discussing grouped particle acceleration
20 p3280 A71-39592
- Interplanetary H scattered solar Lyman alpha background observations by Vela 7 and OGO 3 satellites, showing 27 day correlation with intensity curve
20 p3300 A71-39736
- Diffuse background 0.1-1 MeV gamma ray component observed by balloon-borne counter system, finding no positive evidence for cosmic component existence
20 p3283 A71-39752
- Isotopic X ray photography application to welded joint flaw detection in atomic power plant with radiation background
22 p3540 A71-41763
- Atmospheric background radiation measurements with balloon-borne Michelson interferometer, noting data reduction and calibration methods
22 p3549 A71-42563
- Solar soft X-rays scattering in upper atmosphere, providing background against cosmic X rays
23 p3721 A71-43363
- Cosmic X ray astronomy, considering discrete sources and isotropic background X radiation
23 p3768 A71-43863
- Background illumination effect on stellar magnitude photographic measurement, noting stellar image reduction
23 p3680 A71-44309
- Night sky far IR background radiation measurements by rocket-borne superfluid HE cooled radiometer, determining average signal strength equivalency to black body temperature of 3.1 K
24 p3822 A71-44752
- BACKINGS**
U BACKUPS
BACKSCATTERING
- Optical radar system absolute calibration for measuring laser irradiance backscatter function from atmosphere
01 p0094 A71-10874
- Pulsed laser emissions in atmosphere, noting backscattered light spatial and temporal structure under various meteorological conditions
01 p0120 A71-11105
- HF radar wave Doppler shift by ionosphere effect in retransmitted and backscatter signals
01 p0040 A71-11524
- Lower ionosphere partially reflecting regions, describing vertical thickness distribution based on 1.75 MHz backscatter soundings
01 p0040 A71-11525
- Radar target backscattering characteristics description using scattering matrix invariants
04 p0619 A71-15329
- Cloud fine structure using backscattered laser radiation, incorporating multiple scattering effects into data processing system
06 p0921 A71-17381
- Terrain backscatter characteristics in EHF band, establishing average radar cross sections for various incidence angles
06 p0867 A71-17713
- Backscattered radiation energy during laser beam scanning of diffusely scattering surface
07 p1123 A71-19309
- HF backscatter from ionospheric Ba releases in March 1969 at Alaska, discussing effective cross section
07 p1064 A71-20317
- Pulsed laser emissions in atmosphere, noting backscattered light spatial and temporal structure under various meteorological conditions
08 p1325 A71-20849
- HF Hall current instability, discussing short wavelength backscatter for equatorial and auroral electrojets in disturbed ionosphere
08 p1279 A71-21205
- Polarization characteristics of 42 MHz oblique backscatter from breakup auroras
08 p1272 A71-21639
- HF backscattering by plane electromagnetic wave at oblique incidence from perfectly conducting right circular cone, applying geometrical theory of diffraction
08 p1257 A71-21884
- Quantum mechanical theory of nonrelativistic fast electron backscattering from continuous media, considering scattering cross sections
09 p1496 A71-22236
- Backscatter from nonuniform dielectric coated cylinders in terms of inner surface admittance, using transmission line approach
09 p1410 A71-23515
- Average radar backscattering cross section calculation for conducting obstacles for arbitrary transmitter and receiver antenna polarizations, obtaining results for straight wires, circular loops and helices
09 p1410 A71-23516
- Radar backscattering from thin metallic conductive films, giving results for Al and Ni from anechoic chamber measurements
09 p1410 A71-23517
- Thin metallic disk radar cross sections for near resonance frequencies backscatter, comparing experimental and computer results
09 p1410 A71-23518
- Seasonal variations and migration directions of itinerant ionospheric perturbations detected by ground based backscattering radar
10 p1575 A71-23821
- Comparative accuracies of vertical atmospheric water vapor profiles by radiosonde and laser backscatter Raman component
11 p1794 A71-25383
- Electromagnetic backscatter cross section for HF irradiated turbulent dielectric media by rigorous and heuristic derivations
13 p2028 A71-27998
- Midlatitude ionospheric signatures from narrow beam HF radar backscatter sounder, discussing diurnal and seasonal occurrences
13 p2031 A71-28782
- Meteorologic bistatic radar equation for randomly distributed targets, applying to raindrops, refractivity perturbations, etc
14 p2197 A71-30830
- Signal to noise ratios for coaxial laser radar system heterodyning signal backscattered from atmospheric aerosol
16 p2541 A71-33138
- Short narrow light pulse reflection from thick turbid medium with strong anisotropic scattering, obtaining backscattering signal power from unsteady transport equation solution
16 p2544 A71-34105
- Backscattered laser radar pulses and downward IR flux enhancements in clear air around small cumulus clouds, discussing hygroscopic aerosols for increased radiance
17 p2707 A71-35381
- Linearly polarized lidar light scattering in spherically symmetrical uniformly distributed cloud water drops, investigating multiple backscattering effects on depolarization
17 p2770 A71-35807
- Time dependent multiple backscattering of pulsed light for linearly polarized incident radiation
17 p2709 A71-35809
- Backscattering laser Doppler velocimeter for water flow and moving opaque object measurements, discussing velocity resolution and optical geometry
19 p3072 A71-37552
- Electromagnetic wave arbitrary incidence on conducting circular disk for polarization parallel and perpendicular to incidence plane, calculating backscattering cross section for comparison with measurement
20 p3194 A71-38840
- Backscattering patterns in atmospheric opacity measurements, minimizing errors due to atmospheric inhomogeneities and different stratifications
20 p3257 A71-39334

Solar wind origin in active regions by radar exploration, noting signal backscattering from coronal plasma turbulent pulsations

20 p3281 A71-39732

Terrain and atmospheric parameters affecting radar system design at microwave frequencies, discussing radar backscatter cross section and attenuation

20 p3200 A71-39904

Optical properties of graphite-iron-silicate grain mixtures from Mie theory for spherical particles, noting models consistency with interstellar extinction and backscattering observations

21 p3444 A71-40242

Quantum mechanical theory of nonrelativistic fast electron backscattering from continuous media, considering scattering cross sections

21 p3419 A71-41118

Light sources selection and design for visibility range sensors employing backscattering

21 p3382 A71-41236

Ionospheric transverse inclinations from radio wave propagation characteristics obtained by circular oblique backscatter sounding scans

22 p3532 A71-41556

Ocean surface condition correlation to radar backscattering cross sections and wind velocity from scatterometer data

22 p3569 A71-42545

Atmospheric visibility /light extinction/ measurement from modulated CW laser backscattered signal

22 p3549 A71-42565

Low loss images from smooth solid specimens in surface scanning electron microscope by collecting backscattered electrons

23 p3674 A71-42959

BACKUPS

Third Chance flight control system, discussing aircraft control capability with backup hydraulic system after loss of dual main hydraulic systems due to combat damage

13 p1998 A71-29382

BACKWARD WAVE TUBES

Interelectrode focusing voltage effect on electron beam and tube efficiency in TW and backward wave tubes with electrostatic focusing systems

03 p0385 A71-13793

Wideband submillimeter range backward wave tubes automatic frequency control system, using combination of passive standard and open cavity

06 p0876 A71-18079

Efficiency deterioration of M type backward wave oscillators /M-BWO/ from cyclotron wave interactions

07 p1080 A71-20453

Automatic control circuits for millimeter wave backward wave tube frequency tuning and supply voltage regulation

08 p1267 A71-21804

Phase regulated AFC system design for millimeter and submillimeter wave backward wave tubes

08 p1267 A71-21805

Millimeter backward wave oscillators, discussing cooling, operating characteristics, frequency pulling and pushing, life and reliability

11 p1739 A71-26436

Hybrid M-type microwave oscillators including backward and traveling wave tubes with crossed fields in large amplitude mode, considering power efficiency and frequency control

12 p1888 A71-27620

BACKWARD WAVES

Three diffracting light beams parametric interaction, applying variational method to theory of backward wave parametric oscillator

08 p1334 A71-21181

Phase velocity modulated backward wave antenna with slow wave structure, consisting of dipoles spaced along antenna length

09 p1415 A71-22295

Backward propagation method for ultrasonic image reconstruction, examining resolution in near field for high contrast objects

22 p3541 A71-41784

BACKWASH

Backflow region and shock interaction in rotating and swirling gas streams and jets in supersonic nozzle with separation and thrust effects

22 p3480 A71-42682

BACTERIA

NT BACILLUS
NT ESCHERICHIA
NT HYDROGENOMONAS
NT KLEBSIELLA
NT PSEUDOMONAS
NT STAPHYLOCOCCUS
NT STEAROTERMOPHILUS
NT STREPTOCOCCUS
NT STREPTOMYCETES

UV effect on airborne bacteria survival in simulated Martian dust clouds

01 p0019 A71-11557

Bacteria and mammalian cells radiosensitization, using phenylglyoxal and various carbonyl compounds

07 p1034 A71-18944

Subinoculations of bacterial strains under constant, varying and pulsed magnetic fields, producing sensitivity increase or decrease to antibiotics

08 p1247 A71-20856

Division cycle of *Myxococcus xanthus*, considering kinetics of cell growth and protein synthesis

09 p1396 A71-23473

Space flight biological effects on lysozyme bacteria and human cells in culture

12 p1872 A71-26641

Hypoxia effects on organism resistance and immunobiological reactivity, noting bacterial and protozoa infections aggravation

13 p2006 A71-28401

Bacteria and yeast strains, fungus specimens and seaweed species high vacuum resistance, noting microorganisms interplanetary transport in outer space

13 p2009 A71-28689

Germ survival and transport possibility in outer space, discussing spore survival under UV radiation

13 p2010 A71-28691

Biological experiments on plants, animals and bacteria aboard Zond 5, 6 and 7 space probes

20 p3187 A71-39134

Human microbial flora and immunologic response in long term space missions, describing environmental parameters and factors and work-rest schedules effects

21 p3332 A71-40553

Microflora simplification effects on immunocompetent organism systems, observing shifts in guinea pigs lymphoid tissue with limited flora

21 p3332 A71-40555

Human microflora variation in long term confinement, examining anaerobic and aerobic microorganisms responses

21 p3333 A71-40557

Bacterial contamination in confined sealed space during long term human occupation, observing hemolytic microflora spreading dynamics on bodies, clothes, wall and air

21 p3343 A71-40560

Bacterial spores survival under simulated lunar surface conditions, comparing results with vegetable cells experiments

21 p3334 A71-40567

Extraterrestrial life detection methods, discussing bacterial cultures growth dynamics in nutrient media and iron porphyrin proteins and ATP content increase

21 p3334 A71-40570

Halophilic bacteria electron transport chain, studying protein, phospholipids, flavoproteins and cytochromes sedimentation properties by electron microscopy and light scattering technique

21 p3334 A71-40593

Computerized bacterial identification system to process Apollo spacecraft sample laboratory test results in NASA Planetary Quarantine Lunar Information System

22 p3504 A71-42233

Electron transport chain of extremely halophilic bacteria, investigating cytochrome oxidase activity dependence on pH

23 p3633 A71-43525

BACTERICIDES

Mechanical sterilization and cleansing of Goldmann applanation tonometer prisms contaminated with coliphage, comparing with germicidal immersion

13 p2020 A71-29036

BACTERIOLOGY

Halophilic bacteria growth in freeze-thaw environment, investigating cooling and warming rates and solute concentrations

09 p1388 A71-22131

Gas exchange metabolic fluctuations of nitrogen fixation, hydrogen evolution and photoreduction in *Rhodospirillum rubrum* as function of culture conditions and age

16 p2528 A71-33059

BACTERIOPHAGES

Bacteriophage Q beta ribonucleic acid variants, considering fluorescence determination of replication inhibition by ethidium bromide

04 p0548 A71-15267

Sulfhydryl cysteamine and disulfide cysteamine effect on bacteriophage survival rate at high anaerobic doses

07 p1033 A71-18938

BAFFLES

Sound pressure radiation from infinite plate with rigid or pressure release baffles perpendicular to surface, using steepest descent method

02 p0325 A71-11997

Liquid sloshing in liquid propellant containing orbiting vehicle stabilized by active control system, examining expression for ring baffle slosh damping under reduced gravity

09 p1532 A71-22913

Far field sound radiation pattern from vibrating circular piston set in nonrigid baffle for sonar detectors

11 p1798 A71-25186

Alpha particle gas densitometric response to planet atmospheric density profiles in terms of radioactive

source energy distribution, considering contoured baffle models

11 p1763 A71-26079

Multiple port baffles tests using stoichiometric propane-air mixtures

13 p2116 A71-28746

Average and pulsating velocity distributions during subsonic air jet interaction with plane baffle, describing jet dissipation geometrical pattern

14 p2225 A71-30223

Baffled piston sound source radiation impedance from numerical solution of Fredholm integral equation for vibrating disk in finite rigid concentric baffle

19 p3104 A71-37849

Photometric measurements of light attenuation on baffles in visible, considering sensor location and surface coating

20 p3234 A71-39174

BAGGAGE

Frankfurt terminal baggage conveyor system, describing passenger capacity and luggage handling equipment

13 p2045 A71-29312

Baggage handling network, describing automobile luggage check, inbound, connecting, customs claim and recheck systems

19 p3041 A71-38025

Airport design for passenger and baggage handling efficiency, considering choice between continuous and batching type intra-airport transit system

22 p3529 A71-42072

BAGS

NT BAGS

BAINITE

Bainite structure effects on Cr-Mo-V steels creep and rupture strength

07 p1134 A71-19520

BAINITIC STEEL

Low carbon Mn-Mo-Ni steel dilatometric measurements with RPI Gleebie machine, examining bainitic transformation

04 p0617 A71-15913

Tempered martensite and lower bainite in high purity carbon steels, discussing impact toughness due to internal twinning, grain boundary precipitation and carbide morphology

15 p2432 A71-32173

BAKEOUT

U BAKING

U DEGASSING

BAKER-NUNN CAMERA

Optical spacecraft tracking, using pulsed ruby lasers at Baker-Nunn camera stations of Smithsonian Astrophysical Observatory for retroreflector-equipped satellites ranges

21 p3349 A71-41404

BAKING

Spectroscopic plate emulsion with excellent signal to noise characteristics, investigating baking time response in controlled nitrogen atmosphere

16 p2577 A71-33137

BALANCED AMPLIFIERS

U PUSH-PULL AMPLIFIERS

BALANCING

Flexible rotating shafts high speed, rigid body and modal balancing machines

[ASME PAPER 71-VIBR-73] 21 p3460 A71-40311

Flexible rotor multiplane field balancing analysis, investigating test validity and accuracy and sensing instruments effects

[ASME PAPER 71-VIBR-74] 21 p3460 A71-40312

Flexible rotor balancing by exact point speed influence coefficient method

[ASME PAPER 71-VIBR-91] 21 p3386 A71-40324

BALL BEARINGS

Photographic measuring method for angular misalignment associated with broken ball bearing

01 p0086 A71-10296

Ball bearing cage life, examining angular misalignment effect

01 p0086 A71-10297

Elastohydrodynamic oil film measurements for rolling point contact of ball bearing under starvation using optical interferometry

01 p0087 A71-10481

Ball bearings with irregular surfaces, analyzing static equilibrium conditions

01 p0088 A71-10635

Service life and manufacturing yield of Apollo 25-IRIG /inertial reference integrating gyroscope/ ball bearing

02 p0252 A71-12458

Unwanted gimbal rotation friction torques in gyro wheel bearings due to lubrication viscous friction, ball wedging and contamination

02 p0253 A71-12459

Ball bearing dynamics, considering motion equations for four degree of freedom balls and six degree of freedom separator

[ASME PAPER 70-LUB-H] 03 p0432 A71-13708

Film lubrication for angular contact ball bearings, taking rolling and spinning into account

04 p0604 A71-15768

Lubricant and ball steel effects on fatigue life / pit formation after repeated stress cycles/
[ASME PAPER 70-LUB-16] 07 p1118 A71-19507

Control of time varying mechanical torque normal to ball bearing pair common spin axis by cross torque control through misalignment coupling
[ASLE PREPRINT 70LC-9] 08 p1298 A71-21156

EHD lubricant film thickness and friction forces effects on ball and roller bearings selection and design
[ASME PAPER 71-DE-3] 12 p1911 A71-27322

Thin solid films on ball bearing surfaces, measuring electrical conductivity
13 p2072 A71-27817

Static load and stress distribution in rolling element bearings, using elastic contact area analysis method
[ASLE PREPRINT 71AM 1D-1] 13 p2076 A71-29487

Yield pressure, starting torque, consistency and rheology of lubricating greases at low temperature in ball bearings
[ASLE PREPRINT 71AM 1B-2] 13 p2076 A71-29489

Long-life self-contained solid lubricated ball bearing systems operating under combined high-temperature, high-speed, high-load conditions
14 p2252 A71-30192

Structural design of gyroscope ball bearings, considering additional sliding friction force moment
17 p2739 A71-34561

Friction force moment in ball bearing without lubrication in presence of angular vibrations of one race
17 p2748 A71-34563

Oil for lubricating ball bearings in spacecraft antenna despin system, investigating weight loss, sorption, surface migration and contamination danger
20 p3184 A71-39352

Contactless oscillography of static and kinetic moments of friction in ball bearings in aggressive gas media, discussing experimental assembly design
22 p3529 A71-42489

Mo and Co alloying effects on high temperature chromium ball bearing steels contact strength
23 p3692 A71-44037

Radial thrust bearing balls ovality effect on axial vibration of rapidly rotating turbine engine rotor
24 p3864 A71-45006

Unlubricated instrument ball bearing axial vibration frequency and amplitude effect on fretting corrosion at constant temperature and humidity
[ASLE PREPRINT 71LC-7] 24 p3832 A71-45289

BALLISTIC CAMERAS
N interval trajectory estimation computer program minimum variance adjustment technique, discussing airborne astrophotographic camera system for reentry bodies position determination
04 p0556 A71-15330

Ballistic measurement system for photographing satellites, illustrating minimum brightness relation to satellite distance
20 p3240 A71-39536

BALLISTIC MISSILES
NT INTERCONTINENTAL BALLISTIC MISSILES
NT MINUTEMAN ICBM
NT SHORT RANGE BALLISTIC MISSILES
Ballistic reentry warheads atmospheric interception, investigating defensive nuclear bursts effects
01 p0163 A71-10268

Multistage rocket propelled ballistic missiles and space boosters design and trajectory optimization, using SWORD computer program
04 p0556 A71-15292

Nonguided finned rocket initial stability problem, evaluating axis and tangent trajectory
05 p0817 A71-16638

Angle of attack vertical variations of free flight trajectory missile, estimating missile, trajectory and atmospheric parameters effects on fluctuations relative to center of mass
08 p1367 A71-22051

Instrument orientation optimization for ballistic missile applications, emphasizing acceleration induced velocity and position errors
11 p1796 A71-26410

French National Strategic Force sea-ground and ground-ground ballistic missiles characteristics and performances
16 p2646 A71-34099

Book on astrodynamics covering n body equations of motion, orbital elements, differential corrections, time of flight, ballistic missiles and interplanetary transport
18 p2963 A71-36248

Estimation error covariance matrices of linearized Kalman tracker for ballistic reentering missiles, observing strong coupling of range and range rate with ballistic coefficient
23 p3646 A71-44083

BALLISTIC RANGES
Geodetic survey adjustment and accuracy improvement using satellite radar range and ballistic camera data
04 p0583 A71-15302

Sequential electric spark technique for hypersonic projectiles turbulent wake velocity measurements at ballistic ranges in free flight regime
21 p3362 A71-40385

Hypersonic turbulent wake density measurements in free flight hyperballistic ranges by electron beam fluorescence probe technique
21 p3363 A71-40389

Laser optical system for hyperballistic range hypersonic velocity models surface erosion measurement, describing instrumentation of front-lighted, silhouette and stereo stations
23 p3677 A71-43513

BALLISTIC TRAJECTORIES
Angle of attack vertical variations of free flight trajectory missile, estimating missile, trajectory and atmospheric parameters effects on fluctuations relative to center of mass
08 p1367 A71-22051

Spacecraft capture by ballistic aerobraking during passage through planet atmosphere, proposing analytic models
13 p2133 A71-27987

Roll moment of inertia to static margin ratio effect on yaw of repose angle magnitude in ballistic match of projectiles
14 p2325 A71-29890

Analytic solution to range deviations along descending branch of free flight trajectory of ballistic vehicle in planetary atmosphere
24 p3872 A71-45015

BALLISTIC VEHICLES
Exact expression for minimum range sensitivity deorbit from elliptical orbits for ballistic atmospheric entry vehicle, considering retrovelocity
07 p1199 A71-19873

Iterative processing technique for limited measurement sets, discussing Kalman filter reaching steady state during ballistic target tracking
08 p1269 A71-21340

Switched mode adaptive terminal control for propulsive landing of nonlifting gravity turn ballistic vehicle under uncertain atmospheric conditions
[AIAA PAPER 71-903] 19 p3095 A71-37154

BALLISTICS
NT INTERIOR BALLISTICS
NT TERMINAL BALLISTICS
Soviet book on ballistics of flight vehicles during atmospheric reentry
02 p0319 A71-11844

Ballistic data reduction for drag coefficient of spherical projectiles, using time distance relation for constant coefficient
03 p0341 A71-13467

ONERA hypersonic wind tunnels used for ballistic and aerodynamic research kinetic heating problems and control surface efficiency
[ONERA-TP-877] 06 p0841 A71-18025

Soviet book on long range rocket ballistics covering control system, dynamics, firing distance, motion equations, stage separation and nominal trajectories
13 p2146 A71-29438

BALLOON FLIGHT
Primary cosmic rays heavy ion tracks from balloon-borne emulsion
04 p0641 A71-15368

Extraterrestrial gamma ray and neutron flux and energy spectrum at balloon altitudes over equatorial latitudes, using pulse shape discriminator during solar flare
06 p0962 A71-18177

Fast neutron energy spectrum and flux, using balloon flight neutron detector with charged particle rejection scheme and pulse shape discriminator for gamma rays separation
06 p0962 A71-18178

Heavy cosmic rays slowing in balloon-borne stack, discussing high resolution measurement and synthesis in rapid neutron capture
08 p1354 A71-21038

Balloon flight instrumentation for solar cell I-V measurements, using semiconductor selection circuits and RF telemetry
09 p1446 A71-22734

Balloonborne radiometric instrumentation for solar and thermal radiations upward and downward flux measurements, discussing net radiation balance as function of solar elevation
09 p1515 A71-23558

Vertical air motions measurement by balloon radar tracking, discussing method of radar noise error reduction by ascent rate smoothing technique
11 p1794 A71-25385

Inflation of initially spherical balloon of elastic rubber-like material, discussing tensile instability
11 p1707 A71-25445

Southern Hemisphere general atmospheric circulation data, using constant volume balloons dispersion
11 p1755 A71-25641

In-flight deployment balloon launching system with load lowering friction brake, discussing flight test results
14 p2175 A71-30071

Local time variations of power spectra of magnetospheric electric field from balloon flight data
13 p2397 A71-31758

Auroral 1.2-4 second periodicity X ray pulsations during magnetic storms, using omnidirectional detector at balloon altitude
15 p2474 A71-31775

Cosmic ray rigidities spectra measurements above geomagnetic cutoff using balloon-borne emulsion plates in superconducting magnet field
15 p2407 A71-31805

Azimuthal IR radiation distribution of atmospheric brightness cross sections at various zenith angles from balloon programmed-control radiometer data
19 p3054 A71-37969

Crab Nebula pulsar NP 0532 pulsed gamma emission from balloon flight measurements with spark chamber equipped gamma ray telescope
20 p3283 A71-39754

BALLOON SOUNDING
Gas-Cerenkov balloon-borne detector for low energy gamma rays, calculating efficiency and angular response by Monte Carlo program
01 p0083 A71-11222

Mountainous region vertical air flow research, describing superpressure balloon and precise pressure radiosonde system
02 p0189 A71-12420

Celestial sources far IR radiation detection using balloon-borne telescope
02 p0315 A71-12657

Omnidirectional intensity of atmospheric gamma rays at balloon altitudes at various energy thresholds, noting integral spectrum flattening at lower energies
03 p0473 A71-13306

Atmospheric temperature remote sounding via balloon-borne selective chopper radiometer
03 p0423 A71-13357

Balloon-borne observation of X ray sources in northern sky, including Sco, Cyg and SN 1572
05 p0797 A71-15931

Impulse drive strip-chart recorder with low battery drain for high altitude balloon flights
05 p0755 A71-17143

Balloon-borne telescopes to detect pulsed gamma rays from Crab Nebula, graphing data and diagramming telescope
06 p0950 A71-18034

High energy albedo neutron production by cosmic ray collisions, investigating balloon altitude flux variations near atmospheric top
06 p0962 A71-18179

Balloon heliophysics, discussing equipment and working program of first Soviet stratospheric solar station
07 p1195 A71-19336

Helical circulations in unstable planetary boundary layer measurements, using constant volume balloons and air parcel tracking
07 p1103 A71-19761

Stratospheric small ion density measurements by level flight balloons
07 p1103 A71-19768

Solar constant and spectral energy distribution standard values by high altitude aircraft, balloon and spacecraft measurements
07 p1199 A71-20005

Temperature measurement inaccuracies in 30 to 40 km region by balloonsensors sensors, involving IR cooling of thermistor
08 p1277 A71-20989

Mesoscale relative diffusion estimates in low troposphere from tetron /constant volume balloon/ flights at Nevada Test Site
08 p1326 A71-21449

Vector wind shears statistical analysis at various altitudes, using balloon sounding measurements
08 p1327 A71-21457

Magnetospheric electric fields properties via simultaneous balloon flights between plasmapause and polar cap, indicating fields and bulk plasma flow turbulence
08 p1282 A71-21632

Rawin system performance and technical features, describing radio direction finder design, operation, capabilities and carrier balloons
08 p1330 A71-21741

Sounding system constant level superpressure balloons for atmospheric circulation global description at all levels and latitudes in conjunction with satellite observations
08 p1231 A71-21742

Diffuse cosmic X ray observations, discussing balloon and OSO-3 data
09 p1514 A71-22934

Auroral X radiation at magnetocorjugate points Kerguelen/Archangel region, using balloon-borne spectrometers
09 p1438 A71-23146

Solar impulsive hard X-ray burst structure and location determination with balloon-borne modulation collimator, noting nonthermal electron origin
10 p1660 A71-23795

Solar spectrum observations in water band at 1.87 micron by stratospheric balloon sounding

10 p1667 A71-23863

Twilight airglow measurements of hydroxyl and molecular oxygen bands by balloon-borne instruments including IR grating spectrometer and filter photometers

10 p1601 A71-24400

Balloon sonde for auroral luminosity measurements and comparison of auroral emissions, X rays and ionospheric absorptions

10 p1602 A71-24530

Morphology, dynamics and time variations of auroral zone electron precipitation events from balloon measurements of bremsstrahlung X rays

10 p1662 A71-24535

Magnetometer for indicating position of constant level meteorological balloons provided with solar sensors

10 p1612 A71-24759

Granular features of solar surface, describing television equipment used aboard balloon for image in 1.2-2 microns region

10 p1680 A71-25004

Upper level wind measurements by Doppler equipped aircraft and jimsphere balloon radar tracking, presenting measured data rms variation and power spectral density

11 p1794 A71-25384

Wind structure in boundary layer pilot-balloon observation, discussing baseline data processing for digital computer

11 p1796 A71-26560

Wind structure and atmospheric disturbances, noting resolution of pilot-balloon data

11 p1796 A71-26561

Meteoritic aerosols optical manifestation from photometric measurements on stratospheric balloons, demonstrating Orionids effects on twilight sky brightness

12 p1960 A71-26832

Wind profile data in Cape Kennedy area from FPS-16 radar/jimsphere master tapes

13 p2098 A71-29346

Vertical distribution of small ion density and of electric polar conductivity and ion temperature profiles in atmosphere at 1.5-19 km from balloon measurements

13 p2065 A71-29425

Water vapor contamination long lasting effects on stratospheric measurement during balloon flight

14 p2270 A71-30453

Balloon-borne transistorized stratospheric cosmic ray probe, describing simultaneous gas discharge and dual coincidence telescope counters data transmission

14 p2247 A71-30596

High energy X ray flux from source in Centaurus Crux detected by balloon sounding

14 p2303 A71-30654

Rapid fluctuations in high energy X ray flux from source in Centaurus Crux from balloon sounding

14 p2303 A71-30655

Cosmic ray secondary background of balloon-borne X ray scintillation astronomical telescopes for equatorial latitudes with reference to shutter technique and NaI/Tl crystal

15 p2406 A71-31751

High energy primary cosmic ray program of Goddard Space Flight Center involving charge composition and energy spectra studies in balloon and satellite experiments

15 p2478 A71-31804

Balloon-borne ionization spectrometer for high energy cosmic ray measurement, discussing calibration and accuracy

15 p2407 A71-31811

Balloon-borne magnetic spectrograph for primary cosmic ray particle trajectory and rigidities measurement

15 p2407 A71-31812

Balloon X ray astronomy techniques and observations, noting collimated scintillation counter instrumentation and PCM telemetry

16 p2641 A71-33754

Brazilian space research planning effort and activities covering rocket and satellite meteorology, satellite tracking, balloon experiments and ground based geophysical observations

16 p2667 A71-33869

Cyg X-1 X ray intensity and energy spectrum variation data, using balloon-borne telescope

16 p2629 A71-34076

Stratospheric extraterrestrial particles identification from balloon-collected electron microscope photographs, suggesting cometary origin

16 p2644 A71-34127

Local time dependence of auroral zone electron precipitation X ray events from balloon measurements of bremsstrahlung

18 p2911 A71-35894

Cosmic X ray astronomy by rocket and balloon soundings and discrete emission source measurements, considering energy spectra

18 p2957 A71-36212

Global atmospheric research with balloons, buoys and orbiting satellites for meteorological and oceanographic data recovery

18 p2913 A71-36486

Balloon observations of solar protons on 29-30 September 1968 over Iceland with GM telescopes and scintillation detectors, considering energy spectrum and time behavior

18 p2958 A71-36744

Pulsed X ray emission from NP 0532 at 20-200 keV measured by balloon flown sun sensor controlled azimuth stabilized detectors

18 p2958 A71-36760

X ray source Cygnus X-1 location measurement by balloon, noting agreement with Uhuru data

18 p2959 A71-37052

Cosmic ray nuclear interactions in 10-300 GeV energy range, using balloon-borne emulsion target, spark chambers and ionization spectrometer

19 p3124 A71-37286

Pulsed gamma radiation detection from Crab Nebula by balloon-borne telescope

19 p3124 A71-37333

Balloon-measured magnetospheric electric fields comparison with all sky camera pictures of large scale visible auroral form motions, noting relationship

19 p3047 A71-37363

Solar brightness temperature measurements using balloon-borne Michelson interferometer

19 p3135 A71-37613

Upper atmosphere supplementary electron flux data following geomagnetic disturbance from high altitude balloon experiments

19 p3129 A71-38357

Hybrid thin film radiosonde transmitter design for atmospheric temperature and humidity data transmission from meteorological sounding balloon to ground station

19 p3035 A71-38539

Dynamic energy spectra of nonthermal electrons in solar flares from balloon-borne high resolution hard X ray observations

19 p3130 A71-38673

U.S.S.R. and U.S. balloon measurements of direct solar radiation integral fluxes, deriving solar constant values

20 p3260 A71-39683

Diffuse background 0.1-1 MeV gamma ray component observed by balloon-borne counter system, finding no positive evidence for cosmic component existence

20 p3283 A71-39752

Spectrum and galactic isotropy of diffuse cosmic X rays by balloon-borne detector

21 p3438 A71-40605

Laser remote sensing technique for tropospheric refractivity fluctuation profile measurement with tethered balloon-borne retroreflector tracking by ground based tracker

21 p3374 A71-40977

Balloon Sonde I experiment, discussing telemetry from flying body and temperature effects on earth IR radiation measurement

22 p3535 A71-42053

Alcyon project PTA 1, considering balloon stabilization efficiency during night-day transition and system reliability

22 p3483 A71-42400

Ozone concentration measurements near sunrise by balloon-borne electrochemical ozonesonde, noting scattered radiation effect

23 p3667 A71-43074

Orion constellation hot stars UV spectra observation by photography from stratospheric balloon gondola using geomagnetic field for stabilization

23 p3735 A71-43249

Isentropic nature of stratospheric air masses motion from balloon measurements of temperature and radiation

23 p3671 A71-43338

Balloon-borne far IR survey of sky portions in Galactic plane

23 p3736 A71-43539

Balloon flight detected gamma ray source Lib gamma-1, discussing possible identification with PKS 1514-24 radio galaxy

24 p3865 A71-44444

Balloon measurement of solar flux and brightness temperature in 12-24 micron range

24 p3873 A71-45142

BALLOONS

NT HIGH ALTITUDE BALLOONS

NT METEOROLOGICAL BALLOONS

Numerical stress-strain calculation for design of high pressure fiberglass-reinforced plastic balloons

01 p0176 A71-11048

Inflatable restraint collar for large balloons with heavy loads using winch driven cable launching

02 p0188 A71-11821

Balloon position determination in Venusian atmosphere, using ranging measurement and radiated signal polarization

04 p0623 A71-15014

Balloon and glider vertical speed indicators, considering barometric devices and electric variometer

06 p0901 A71-18248

Airships and balloons potential commercial use in Canada, discussing cargo, passenger and military applications

07 p1019 A71-19916

BALLUTES

Expandable structures for midair pilot rescue device with hot air filled BALLUTE, discussing BALLUTE material development

11 p1707 A71-25278

BALMER SERIES

Algol type variables, investigating gradient Balmer discontinuity and diameter variations

04 p0651 A71-15662

Strong and weak emission red shifts of N galaxy 3C 390.3 in Balmer lines, indicating nonisothermal source and gas ejection

05 p0807 A71-16216

Hydrogen-allow electron collision cross sections, calculating Jovian upper atmosphere Lyman alpha and Balmer H alpha emission

06 p0929 A71-17679

Theoretical and observed Balmer alpha distributions over solar cycle by Lyman beta scattering on hydrogen in upper atmosphere

07 p1187 A71-19671

Balmer emission lines in hydrogen cloud in bright galactic nucleus

09 p1518 A71-22351

Ionized gas and dust distribution in Orion nebula from Balmer line intensities photoelectric measurements

11 p1818 A71-25202

Planetary nebulae continuous UV spectrum, discussing glow process, electron temperature and density and Balmer discontinuity

12 p1955 A71-26584

Galactic nebula YM 29 radiometric observations showing thermal source, mass and Balmer line fluxes comparable to planetary nebula

14 p2314 A71-30643

Faint O-B5 type blue stars data, listing absolute spectrophotometric gradients and Balmer series discontinuities

15 p2487 A71-32032

AO Algol-type variables W Del, T L Mi, RZ Cas, and delta Lib gradient variation and Balmer discontinuity, detailing luminosity and radius ratio effects

16 p2634 A71-33427

Real time system for solar spectrophotometry, noting application for scanning H alpha and other Balmer series lines profiles in solar flare regions

17 p2741 A71-34994

Deuterium Balmer line intensities and overpopulations measurements relationship to thermal equilibrium in pinch discharges

21 p3421 A71-40142

Hydrogen plasma Balmer spectrum measurement for emission coefficients, comparing results with theories

22 p3583 A71-42373

BANACH SPACE

Halley method of tangential hyperbolas in Banach space, deriving local existence, uniqueness and convergence theorems

04 p0620 A71-15668

Iterative solution of nonlinear operator equations in Banach spaces, proving existence, uniqueness and convergence theorems

06 p0920 A71-18211

Eigenvectors spectral structure analysis of monotonic and completely continuous nonlinear operator equations in separable real reflexive Banach space

07 p1149 A71-20646

Nonlinear stability of incompressible laminar flows involving perturbation in Banach space

10 p1591 A71-23914

Partly time invariant and periodically time varying gain equations based on Banach algebras spectral mapping theorem and higher order circle criteria

11 p1742 A71-26411

Dual methods for calculating minimum of convex function on intersection of convexes, considering reflexive Banach space and normalized vector space

13 p2095 A71-28822

Calculus of variations sudden expansion and decentralization, minimizing convex junctional on closed group in reflexive Banach space

13 p2095 A71-28824

Linear unbiased estimates of mathematical expectation of random process optimal in sense of norm of symmetrical Banach space

17 p2765 A71-34861

Linear differential equations solutions stability in Banach space for finite and infinite dimensional cases, generalizing Liapunov theorems

17 p2781 A71-34922

Optimality conditions for trajectory in Banach space, considering generalized controls

18 p2896 A71-36188

- Book on stability theory covering Liapunov functions, variable structure automatic control systems and differential equations solutions in Banach space 18 p2947 A71-36250
- Linear functional equations bounded solutions stability by reflexive Banach space mapping, applying to elliptical and parabolic differential equations ill-posed problems 18 p2941 A71-36351
- Nonlinear eigenvalue problem solution in real Banach space, investigating continua existence and elliptic equations application 18 p2942 A71-36818
- Optimality criterion for convergence of iterative solution of linear time optimal problem in reflexive Banach space 19 p3088 A71-38414
- BAND STRUCTURE OF SOLIDS**
- Disordered materials electronic structure band states localization, examining mobility edges 01 p0140 A71-11441
- Electron transfer in ion microscope field ionization, analyzing band and periodic surface structure effects, ionization probability and collision formalism 02 p0288 A71-12734
- Multiple valued Sasaki effect concerning electron transitions in multivalley Ge semiconductors 07 p1181 A71-20537
- Submillimeter wave oscillations possibility by Bloch oscillation of conduction electrons in ideal crystal with periodic energy band structure 08 p1343 A71-21280
- Luders bands motion in steel and iron, studying plastic zone velocity dependence on stress, composition, grain size, dislocation substructure and temperature 08 p1308 A71-21517
- Electron-electron interaction effects on electronic states density in electron gas impurity bands, using matrix method 10 p1644 A71-23772
- Electron structure of transition metals defects, using self consistent method to match resonance and drift integrals to cohesion energy 11 p1808 A71-26342
- LF hot-electron noise during quasi-elastic scattering in semiconductor with simple band structure, evaluating convective fluctuations contribution to noise temperature 13 p2112 A71-29082
- Carbon K alpha band measurements in transition metal carbides, graphite and diamond, using X ray spectrometer with diffraction grating 15 p2430 A71-32149
- High resolution energy spectra and valence band structure vs carbon content in homogeneous titanium carbides 15 p2430 A71-32150
- Soft X ray spectra measurements of vanadium carbides in homogeneity range on ultralong wave spectrometer, showing three zone energy structure of valence band 15 p2430 A71-32151
- Semiconductor heterostructure junction diode lasers for operation at room temperature, discussing energy band structure and mass communications application 16 p2587 A71-33471
- UV photoemission measurements on hexagonal ZnO cleaved in vacuum, determining Zn 3d states location 17 p2791 A71-34854
- Magneto-optical oscillatory absorption spectrum of tin oxide crystal at 1.3 K observed beyond band-band absorption edge with peaks as function of magnetic field 21 p3431 A71-41235
- Exchange interaction in excitons for arbitrary band structure of semiconductors in effective mass approximation allowing correction 21 p3431 A71-41262
- Sn-N-GaAs semiconductor surface barrier structure electrical properties measurement over wide electron density range, determining energy band diagram and current flow mechanism 21 p3433 A71-41313
- Cadmium-tin-arsenide conduction and valence band structure parameter refinement from Faraday effect and absorption spectra of single crystals in polarized light 21 p3433 A71-41319
- Anisotropic transport coefficients valence band model of TiSe, measuring electric conductivity, Hall effect and thermo-emf as function of temperature 21 p3434 A71-41328
- Bipolar junction transistor doping effects on bandgap decrease and emitter efficiency, explaining current gain temperature dependence 23 p3648 A71-42911
- SbSI crystal reflection spectra anisotropy and band structure at 90, 273 and 300 K, comparing experimental data with group analysis 23 p3717 A71-43947
- Noble or transition metals based dilute alloys electronic structure, describing pure metal band structure by interpolation scheme of hybridized tight binding and nearly free electron orbitals 24 p3860 A71-45130
- Leed rotation diagrams for aluminum, obtaining low energy electron diffraction intensity profiles by band structure matching approach 24 p3862 A71-45349
- BANDPASS FILTERS**
- Passband circuits improving radio telemetry channel potential in atmospheric sounding system 01 p0080 A71-10543
- Interference passband filters with wide angle lenses for multispectral photography, discussing design and applications 01 p0081 A71-10827
- PCM telemetry signal encoding, investigating aliasing and pulse width errors dependence on frequency band occupied by bandpass signal 01 p0032 A71-10881
- Tunable filter reflecting telescope and accessory optics for H alpha monochromatic photography of electron corona during total eclipse 03 p0424 A71-13626
- Microwave bandpass filter design with couplings between nonadjacent resonant circuits for generating attenuation pole and increasing slope steepness 03 p0387 A71-13875
- Interdigital converter for excitation and reception of acoustic surface waves on piezoelectric materials in bandpass filter design 03 p0388 A71-14574
- Bandpass limiter output envelope fluctuations dependence on input form and bandwidth 05 p0730 A71-17061
- Noise bandwidth of optimum second order and bandpass Butterworth, Bessel and Chebyshev filters for communication and radar systems 07 p1081 A71-19539
- Temporal registration efficiency of rectangular pulse by position of front at ideal band filter output 07 p1064 A71-20259
- Group delay and amplitude equalized bandpass elliptic function filters for ground stations of communications satellite system 07 p1082 A71-20412
- Circuit selection for LF three octave acoustic signal bandpass filters, taking into account time constants 08 p1261 A71-20738
- Slot transmission line bandpass and bandstop filters and hybrid couplers for microwave IC applications, presenting experimental performance data 08 p1262 A71-20761
- Four-cavity elliptic waveguide microwave bandpass filter design and performance prediction from mathematical model 08 p1262 A71-20762
- Target detection improvement in reconnaissance by black and white TV system, using narrow band filters for conversion to multispectral sensor system 08 p1287 A71-21240
- Signal-white noise mixture filtration, determining maximum SNR position and magnitude and filter bandwidth 09 p1416 A71-22466
- Electromagnetic wave propagation in circular waveguide loaded with coaxial dielectric cylinders, calculating band pass characteristics 09 p1406 A71-23039
- Spectrum economy by passing signal through symmetrical bandpass filter using FSK keyer 10 p1574 A71-23769
- Magnetically tunable microwave bandpass and bandstop filters with yttrium-iron garnet /YIG/ single crystal 11 p1737 A71-25625
- Linear passive network steady state FM distortion numerical calculation, applying to Chebyshev-response bandpass filter 14 p2197 A71-30806
- Microwave IC bandpass filters, utilizing dielectric resonators for high Q values 16 p2548 A71-33559
- UHF head for 225-400 MHz AM receiver, emphasizing choice of ring mixer and passband filter switching principle 16 p2548 A71-34124
- Single sideband mechanical filters for voice multiplex transmission in radio and telephone systems, discussing material characteristics 17 p2714 A71-34608
- High spectral resolution image recording instrument with postrecording bandpass selection, discussing signature data base and sensor modes 18 p2917 A71-36066
- Stochastic passband model of tropospheric communications channel, denoting random frequency duration above threshold level 19 p3022 A71-38501
- Wide passband techniques for atmospheric total ozone content measurements, discussing choice of ozonometer characteristics and filter parameters 20 p3238 A71-39335
- Microwave narrow bandpass filters design using microstrip lines 21 p3354 A71-40733
- Coupled resonator AT cut quartz crystal bandpass filter design in ladder configuration with low sensitivity and simple manufacturing methods 21 p3360 A71-40810
- Bragg imaging with optical heterodyne detection and bandpass filtering, considering resolution, SNR and dynamic range 22 p3540 A71-41777
- High performance bandpass and low pass interference filter for IR region above 40 microns, discussing metallic mesh and reflecting element properties 22 p3544 A71-42136
- Bandpass filter harmonic signal phase shift distortion effect on transient response in PSK of multichannel transmission 23 p3644 A71-43286
- Low noise IR range radiometer, including impedance matching and narrow band filtering 23 p3678 A71-43534
- Incoherent light bandpass filter to amplify detail contrast of optical system 23 p3679 A71-44010
- Reflection and scattering properties of two dimensional periodic arrays of loaded dipoles with bandpass filter characteristics as function of frequency 23 p3654 A71-44159
- BANDS**
- Radio link diversity reception improvements by multiple baseband combinations in one or several stages 03 p0380 A71-14333
- BANDWIDTH**
- NT BROADBAND**
- NT SPECTRAL LINE WIDTH**
- Radio telemetry transmitter receiver systems notch noise testing for relationships between spectral power density, video and IF bandwidths and peak deviation 01 p0034 A71-10908
- Parametric amplifier with nonlinear capacitance varying as quadratic function of voltage, deriving power gain, bandwidth and noise figure from equivalent circuit 03 p0383 A71-13270
- Wideband signal processing via multiple narrow band channels, discussing performance limitations due to amplitude and phase distortion and spurious outputs 04 p0555 A71-15341
- Resonant self tuning narrow band amplifier, considering transient processes by time domain quantization for differential equations with constant coefficients 04 p0559 A71-15569
- Bandpass limiter output envelope fluctuations dependence on input form and bandwidth 05 p0730 A71-17061
- Band limiting effects on PCM/split phase signal detection, considering signal to noise ratio degradation 07 p1061 A71-19263
- Singly resonant optical parametric oscillator allowable pump bandwidth 07 p1126 A71-20179
- Spectral bandwidth of Q switched giant pulse laser as function of single pass gain, optical switch and resonator loss 10 p1619 A71-23955
- Power spectrum symmetry effect on radar signal correlation function and bandwidth 10 p1580 A71-25107
- SHF lithium tantalum oxide optical modulator for optical detector evaluation, discussing bandwidth and phase modulation characteristics 12 p1903 A71-26790
- Passive two-terminal networks in rod antenna for bandwidth increase, investigating equivalent circuit on digital computer 12 p1886 A71-26987
- Echo location systems theorem concerning ambiguity density relationship to signal bandwidth 14 p2194 A71-30063
- Restrictions on signals effective bandwidth, determining uniform upper bounds for use in design of systems with minimum distortion 16 p2542 A71-33458
- Critique of paper on additional signal power for optimum performance of PCM binary signal detection under channel band limiting effect in white noise 20 p3196 A71-38870
- Flat thin films in stripline cavity resonator with TEM mode, expressing bandwidth and resonance as frequency difference 20 p3239 A71-39426
- Information producing capabilities of various combinations of SNR, bandwidth and contrast in simulated digital encoding TV systems 21 p3347 A71-40130
- BANG-BANG CONTROL**
- U OFF-ON CONTROL**
- BANKING FLIGHT**
- U TURNING FLIGHT**
- BARDEEN APPROXIMATION**
- U BARRIER LAYERS**

U ELECTRICAL PROPERTIES
U SURFACE PROPERTIES

BARIUM

- Artificial Ba clouds resonance radiation, measuring polarization with photoelectric polarimeter
01 p0075 A71-11333
- Energy deposition, vacuum expansion and vaporization of barium in two phase jets, using combustion and solid state shock waves
05 p0836 A71-16538
- HF backscatter from ionospheric Ba releases in March 1969 at Alaska, discussing effective cross section
07 p1064 A71-20317
- Atomic Ba excitation, ionization and oxidation during release in sunlight at high altitudes
13 p0206 A71-29038
- Ba atoms excitation and optical transitions line broadening by collisions with Ar atoms behind shock waves, using atomic absorption spectroscopy
16 p2613 A71-32889
- Low and midlatitude ionospheric motion determination using barium ion cloud release technique
16 p2570 A71-33827
- Magnetic field aligned striations of Ba ion clouds artificially injected into ionosphere, investigating physical processes based on model
20 p2320 A71-39861
- Barium ion cloud release at 194 km, observing striation formation for instability characteristics evaluation
23 p3669 A71-43170

BARIUM ALLOYS

- Au-Ba intermetallic compound electron work function temperature dependence
07 p1179 A71-19922

BARIUM COMPOUNDS

- NT BARIUM FLUORIDES
NT BARIUM OXIDES
NT BARIUM TITANATES
- Orthorhombic-tetragonal phase transition in barium sodium niobate, investigating expansion curve discontinuities due to crystallographic changes from dilatometric studies
20 p2375 A71-38816

BARIUM FLUORIDES

- Barium titanate-fluorine substitutional solid solutions production and X ray analysis, examining Curie point behavior
09 p1506 A71-22166

BARIUM OXIDES

- Upper atmosphere temperatures from barium oxide fluorescence emissions in ion cloud rocket experiments, studying thermal response to geomagnetic disturbances
16 p2562 A71-32808

BARIUM TITANATES

- Microwave permittivity dispersion in segnetoelectrics as function of single crystal domains size, considering barium titanate dielectric spectrum resonance
01 p0138 A71-10433
- Barium titanate single crystals domain structure and electrical properties at room temperature under uniaxial tensile stresses, measuring dielectric hysteresis loops
04 p0637 A71-15104
- Monolithic optically written and electrically read semiconductor-ferroelectric memory device employing single crystal barium titanate
07 p1067 A71-19261
- Barium titanate-fluorine substitutional solid solutions production and X ray analysis, examining Curie point behavior
09 p1506 A71-22166
- Ferroelectric barium titanate ceramics technology for capacitor fabrication
09 p1483 A71-23394
- Barium titanate pyroelectric receivers for giant pulse laser emission measurements
12 p1915 A71-27756
- Dielectric properties of barium titanate with Nb, noting metal oxide additives effects on conductivity
13 p2092 A71-28661
- Polycrystalline barium titanates solid solutions with fluorine displacement of oxygen atoms, observing IR absorption spectra
20 p2376 A71-39151
- Quadratic and linear electro-optical effect dispersion in flux grown crystals of barium titanate
22 p3585 A71-41729
- Barium strontium lanthanum titanate thermistor bolometer for IR thermal detector, using positive temperature coefficient of resistance
22 p3543 A71-42126
- Permittivity increase in fluor-substituted barium titanate solid solutions for ceramic capacitor microminiaturization
24 p3859 A71-44387
- Barium titanate single crystal solid solution electro-optic characteristics at 6328 Å and temperatures above Curie point, determining temperature dependences
24 p3860 A71-44667

BAROCLINIC WAVES

- Continuous zonal flow nonlinear baroclinic instability, noting amplitude vacillations and flow-wave interactions
01 p0120 A71-10855

- Rayleigh, baroclinic and Rossby waves instabilities effects on stellar structure during differential rotation
03 p0486 A71-13322

- Baroclinic atmospheric model of interaction between zonal circulation and long waves, discussing motion instability and oscillation
04 p0620 A71-14636

- Nongeostrophic and nonhydrostatic stability of baroclinic fluid for small Richardson numbers
07 p1153 A71-20220

- Baroclinic instability problem analytical solutions for models with linear wind profiles, presenting growth rate variations and unstable waves phase velocity
10 p1638 A71-23962

- Numerical integration of motion equations for two layer atmospheric fronts model with baroclinicity along frontal surface separating two incompressible fluids in stable stratification
10 p1638 A71-23965

- Numerical study of three dimensional structure and energetics of unstable disturbances in pure baroclinic and barotropic zonal currents, using eigenvalue technique
14 p2269 A71-29949

- Book on numerical weather prediction covering atmospheric wave motions, scale analysis, vorticity and energy, barotropic, baroclinic and multilevel models, etc
21 p3410 A71-40780

- Thermally driven motion of water with free surface in rotating annulus, investigating steady wave flow by three dimensional nonlinear Navier-Stokes equations numerical integration
24 p3844 A71-44417

BAROCLINITY

- Atmospheric upper boundary condition in baroclinic forecast, recommending correction using isopycnicity properties of atmospheric processes near 7 km altitude
12 p1924 A71-26738
- Atmospheric synoptic and mesoscale motions dynamic theory, including baroclinic instabilities, gravity/planetary waves, tides and sea breezes
14 p2236 A71-30493
- Three level baroclinic model of short range large scale weather prediction at low latitudes, determining background/steering flow/ in tropical disturbances
17 p2769 A71-34300
- Lower boundary condition effects on quasi-geostrophic baroclinic instability, showing vertical wind shear as function of pressure and wavelength
22 p3569 A71-42544

BAROMETERS

- Balloon and glider vertical speed indicators, considering barometric devices and electric variometer
06 p0901 A71-18248
- Simple sensitive multichannel servo system thermobarometer for volume changes corrections, noting adaptation to five channel closed circuit respiratory apparatus
12 p1874 A71-27138
- OMB-3P optical microbarometer for high altitude networks, discussing transmission-multiplier mechanism and instrument errors
15 p2406 A71-31468
- Barometric altimetry system inadequacies and approach/landing accidents, noting pitot static components blocking hazards
23 p3628 A71-43384

BAROMETRIC PRESSURE

U ATMOSPHERIC PRESSURE

BARORECEPTORS

- Small signal characteristics mathematical models of carotid sinus baroreceptors of rabbits
12 p1870 A71-27133
- Arterial baroreceptor reflex action in rabbits, noting central noradrenergic neuron participation
16 p2528 A71-33075
- Sympathetic response in renal and splanchnic nerves to induced fall and rise of arterial blood pressure in anesthetized rabbits, investigating baroreceptor reflex effect
17 p2685 A71-35367
- Bulbar and baroreceptor inhibition of spinal and supraspinal sympathetic reflex discharges recorded in cats from renal nerve
18 p2857 A71-36689
- High blood pressure and age effect on human baroreflex arc controlling pulse interval sensitivity, showing systolic pressure response to phenylephrine intravenous injection
24 p3794 A71-44434

BAROTRAUMA

- Barotrauma from aerospace medicine viewpoint, discussing oxygen absorption, barosinusitis, abdominal distention and aerodontalgia
08 p1238 A71-20706

BAROTROPIC FLOW

- One dimensional unsteady barotropic fluid flow based on Euler equations, describing rarefied plasma nonlinear motions
03 p0462 A71-13289
- Mean zonal flow effects on Rossby waves in barotropic atmosphere, deriving formulas for energy of spectral components
07 p1151 A71-19146

- One dimensional unsteady barotropic fluid flow based on Euler equations, describing rarefied plasma nonlinear motions
09 p1504 A71-23265

- Flow theorem as circulation extension for closed curves in autobarotropic fluids in meteorology and hydrography
10 p1639 A71-25113

- Steady barotropic motion of ideal fluid, determining conditions for unit vector serviceability as velocity direction field
11 p1753 A71-26566

- Two phase supersonic barotropic flow with solid particles around thin profile with allowance for elastic particle collisions
12 p1864 A71-27450

- Numerical study of three dimensional structure and energetics of unstable disturbances in pure baroclinic and barotropic zonal currents, using eigenvalue technique
14 p2269 A71-29949

- Atmospheric boundary layer circulation dynamic interaction with variable depth barotropic ocean surface, studying stream function during annual cycle
16 p2605 A71-33906

- Steady barotropic motion of ideal fluid, determining conditions for unit vector serviceability as velocity direction field
17 p2729 A71-35503

- Eddy viscosity in barotropic planetary boundary layer, finding turbulent diffusion coefficient dependence on turbulent kinetic energy
20 p3257 A71-39437

- Book on numerical weather prediction covering atmospheric wave motions, scale analysis, vorticity and energy, barotropic, baroclinic and multilevel models, etc
21 p3410 A71-40780

BAROTROPISM

- Second order difference approximations with large viscosity coefficient for primitive barotropic model over spherical geodesic grid, comparing with first order approximations
13 p2097 A71-28231

BARRICADES

U BARRIERS

BARRIER LAYERS

- Alloyed p-n junction diode with deep impurities, discussing barrier capacitance frequency dependence
01 p0057 A71-11462
- Reinforced Ni-based composites, discussing barrier coating for tungsten fibers
05 p0769 A71-16860
- Semiconductor thermocell junction polishing effects on bilateral layers tensile strength and electrical contact resistance
07 p1023 A71-19145
- Schottky barrier diode shot noise, examining dependence on potential barrier gap thickness, height and permittivity, impurity distribution, Schottky layer thickness and semiconductor dielectric constant
07 p1075 A71-19225
- Wideband transistor amplifier frequency response at low frequencies, discussing gain increase, thermal pull-in effect, barrier layer geometry and switching control functions
12 p1887 A71-27042
- Current controlled unstable pulse oscillator, discussing depletion layer transistors and upper frequency limit as function of thermal loads and switching times
12 p1887 A71-27043

- Characteristics of field effect and surface barrier GaAs transistor (MESFET) operating at 4.2 K, noting very low temperature hyperfrequency amplifier application
14 p2212 A71-30439

- Diffusive p-type Si valve photocells, investigating barrier capacitance
17 p2713 A71-34565

- Photovoltaic and electron-voltaic properties of diffused and Schottky barrier GaAs diodes, considering irradiance in 0.001-10,000 microwatt/sq cm range
19 p3027 A71-37484

- Specific contact resistance at zero bias as measure of ohmic or rectifying behavior of metal-semiconductor barrier under operating conditions
19 p3117 A71-37485

- Thin film Au-CdS-Al type metal-semiconductor barriers, determining barrier height from temperature dependence measurements of I-V characteristics
19 p3118 A71-37488

- Molybdenum hemicarbide layer as diffusion barrier between metal and disilicide, investigating system thermal stability
21 p3399 A71-40526

BARRIERS

- Ta and W single crystals yield stress temperature dependence, confirming asymmetric Peierls barrier
08 p1307 A71-21507

BARS

NT ELASTIC BARS
NT PRISMATIC BARS

- Notched steel bars fatigue strength improvement via compressive self stresses/residual stresses/
01 p0167 A71-10172

- Torsion computation for bar with rectangular cross section by analogy with electrical networks, comparing with Saint Venant results
01 p0167 A71-10340
- Fibrous body optimum material distribution, considering arbitrary density continuous three dimensional bar network
01 p0177 A71-11285
- Repeated bending and torsion of viscoplastic bars and circular cylinders, using hereditary nonlinear integral equations
02 p0322 A71-11688
- Nonlinear heat conduction of contacting bars with boundary conditions of fourth kind, using small parameter method
02 p0332 A71-12529
- Variational equation of motion for thin walled open section bars coupled flexure and torsion, considering thermal effects
[ASME PAPER 70-WA/APM-51]
03 p0513 A71-14169
- Annealed Al bars mechanical properties and stress-strain curves dependence on strain rates under loading
05 p0766 A71-16390
- Flexible bar as spatial filter for measuring wave number-frequency spectra of distributed random processes
05 p0822 A71-16405
- Stress analysis of orthotropic twisted bars under tension applied at ends
06 p0985 A71-17747
- Conical bar with yield point lag, investigating elastoplastic wave propagation with Rabotnov model
13 p2155 A71-29064
- Steel bar under longitudinal impact, deriving flexural half waves length formulas for critical force
13 p2158 A71-29435
- Orthotropic bar under compression loads, calculating Eulerian values for critical force
17 p2817 A71-34335
- Circumferential notch effect on distribution of compressive self stresses produced by shallow skin layer expansion in round steel bars, using finite element method
[SESA PAPER 1831]
17 p2819 A71-34529
- Optimal bar design for tangential load transmission into sheet, determining stress distribution
17 p2821 A71-34591
- Orthotropic thin walled bars with rigidly connected rectangular elements, applying displacement under torsion with allowance for shear to H beam
17 p2823 A71-34782
- Torsion free, rigid and elastic stiffness matrices of thin walled bars, noting transformation to eccentric nodal points
17 p2832 A71-35399
- Universal dispersion curve for steady state sinusoidal flexural wave propagation in plates and bars, using Poisson ratio as single parameter
21 p3463 A71-40535
- Vertical bar longitudinal bending equation under axial forces, obtaining relation between extreme free angle and deflection
21 p3472 A71-41148
- Critical coefficients of axial compressive forces with variable intensity for approximate stability analysis of vertical bars
21 p3472 A71-41151
- Bar forces in statically determinate planar truss due to arbitrary loads at joints, describing computer program for sequential solution
22 p3517 A71-41869
- Nonlinear theory of tensile instability /necking/ of homogeneous isotropic bar obeying Ramberg-Osgood law
22 p3618 A71-42588
- BARYCENTER**
U CENTER OF GRAVITY
- BARYONS**
Baryon isobars average mass data in cosmic ray interactions, using particle angular measurements in backward direction of center mass system
11 p1818 A71-26427
- Cosmic ray shower evolution model based on passive baryon existence and direct energy transfer to gamma quanta hypotheses
14 p2302 A71-30593
- Lower limit on size of matter and antimatter regions in vanishing baryon number cosmology based on homogeneous intergalactic magnetic field existence
16 p2632 A71-33237
- BASALT**
Apollo 11 basalts chemistry and petrogenesis by partial melting, considering implications for lunar origin theories
02 p0305 A71-11981
- Apollo 11 lunar soil sample derived from basaltic and anorthositic rocks, considering basalt origin by melting due to internal radioactive heating
02 p0305 A71-11983
- Lunar solid state thermal convection throughout interior, noting pressure release production of basaltic magmas consistent with Apollo 11 rocks composition
02 p0305 A71-11988
- Archaean volcanics geochemistry and modern basalts chemical and geographic characteristics, considering trace element model
06 p0892 A71-17895
- Rare earth abundance in Apollo 12 basalts and soils and achondritic meteorites, using partial melting model
06 p0966 A71-17899
- Apollo 11 flight glass basalt, determining crystallization sequence and phase assemblage of high Ti specimens as oxygen fugacity function
06 p0970 A71-18235
- Craters on lunar crater Copernicus inner walls, discussing origin based on size distribution frequency comparison with terrestrial basalt flow collapse craters
07 p1196 A71-19542
- Lunar and terrestrial ilmenite basalt, considering hornfels from Keweenaw Duluth complex in Minnesota and Apollo 11 samples
09 p1529 A71-23657
- Kaersutite amphibole formation from pargasite amphibole interaction with basanite, discussing Fe, Ti, K, Mg, Si, Na and Cr contents
10 p1601 A71-24415
- Tumor theory of crust formation and moon-earth consolidation, showing fractional crystallization of basaltoid silicate melts
10 p1681 A71-25112
- Apollo 11 sample basalts lunar interior origin assumption from comparison with terrestrial massif anorthosite series, using chemical and petrographic analyses
11 p1834 A71-26452
- Variable abyssal basalt populations, considering chemical analyses variations for ridges as function of ocean floor spreading rate
13 p2063 A71-29139
- Coarse grained lunar basalt from Oceanus Procellarum, examining ground mass and subsolidus cooling history
14 p2313 A71-30427
- Terrestrial basalts and lunar rocks volatile element concentrations comparison, noting relationship to abundance in chondrites
16 p2633 A71-33348
- Crystallization behavior and chemical compositions of Apollo 11 lunar basalts including olivine and silica normative varieties
16 p2637 A71-33512
- Central Colorado basaltic lava flows tertiary paleomagnetic transition zone data, illustrating whole rock K-Ar dating difficulties
18 p2911 A71-35949
- Seismic wave velocity measurements in pahoe-hoe basalt flows in lava beds, comparing with laboratory dilatational velocities
19 p3052 A71-37685
- Fe content of clinopyroxene in basalt-basaltic andesite-andesite-latitude of Mogollon Plateau /New Mexico/
20 p3216 A71-39386
- Dribble spires in Snake River Plain, Idaho, discussing basalt lava features and remnants in lunar
22 p3533 A71-41839
- Lunar rocks composition, age, history and evolution, comparing to terrestrial basalts
22 p3599 A71-41943
- Armstrongite and ilmenite basalt in Apollo 11 lunar samples, discussing formation process of titanium, potassium and silicon oxides
23 p3734 A71-43247
- Tranquillity silicate mineral in crystalline basaltic rocks from Apollo 11 and 12 samples
23 p3737 A71-43605
- Fission track analyses of uranium enriched phases in Apollo 11 and 12 basaltic rocks
23 p3739 A71-43615
- Gray mottled basaltic rock composition and origin in Apollo 12 lunar soils and breccias
23 p3741 A71-43634
- Normative mineralogy of lunar basaltic rocks from Apollo 11 and 12 samples, comparing with terrestrial and meteoritic analogs
23 p3742 A71-43637
- Clinopyroxene crystallization histories of Apollo 12 porphyritic basalt rocks 12021 and 12052 from Oceanus Procellarum
23 p3742 A71-43643
- Olivine accumulation in Apollo rock 12040 and basaltic fragments, using textural and microprobe analyses
23 p3742 A71-43644
- Crystalline and glassy phases electron probe analysis for picrite basalts, ferrobasalts, feldspathic norites and rhyolites from Apollo 12 lunar soil samples
23 p3743 A71-43645
- Apollo 12 basalts petrology and petrogenesis, studying crystallization sequences
23 p3743 A71-43646
- Petrogenesis and crystallization of protohypersthene basalts in lunar maria lava lakes, deducing eruption temperatures
23 p3743 A71-43647
- Morphological, physical and chemical characteristics of basaltic and anorthositic glassy spheroids in Apollo 12 lunar fines
23 p3746 A71-43666
- Nonmare basalts chemical composition and origin from Apollo 11 and 12 sites
23 p3746 A71-43671
- Lunar rock volatile and siderophile elements, comparing with terrestrial and meteoritic basalts
23 p3746 A71-43672
- Apollo 12 lunar rock rare earth element abundances, comparing to Icelandic basalt flow
23 p3750 A71-43694
- Visible and near IR spectral reflectivity measurements of basalt separates, glass and anorthositic fragments from Apollo 12 mare samples
23 p3750 A71-43770
- Critique of paper on Apollo 11 ilmenite basalts petrology and lunar bodies origin and form
23 p3759 A71-43886
- Lunar origin hypothesis, discussing Apollo 11 crystalline rocks nature and basalts petrogenesis
23 p3770 A71-44075
- Thermal conductivity, diffusivity and specific heat of lunar soil and basalt analogs, using Luna 16 samples
24 p3873 A71-45103
- BASE FLOW**
Thrust-minus-drag optimization by base bleed and/or boattailing, using computer program
01 p0004 A71-11589
- Base flow prediction for axially symmetric cylindrical vehicle with supersonic single central jet by two stream interaction model, comparing Thor flight data
[AIAA PAPER 71-643]
14 p2290 A71-30720
- Base flow characteristics in four-nozzle rocket exhaust as functions of nozzle axis interspaces, nozzle exit section-base surface distance and Mach number
18 p2903 A71-36117
- Planar supersonic near wake flow field problem with variable viscosity and base injection, investigating boundary errors spatial decay rate
18 p2906 A71-36321
- Inclined wedges in rarefied hypersonic flow conditions, investigating base and wake pattern geometrical and aerodynamic characteristics
18 p2849 A71-36756
- Two dimensional supersonic base flow with small Mach number recirculation zone, determining jet line by variational principle of Poisson equation
20 p3176 A71-39414
- BASE HEATING**
In-flight base heating and thermal environment measurements from Thor Delta launch vehicle using six strap-on solid propellant motors
[AIAA PAPER 71-644]
14 p2320 A71-30721
- BASE PRESSURE**
Base pressure variation by mass injection in turbulent supersonic axisymmetric near wake at high Mach numbers
03 p0399 A71-13457
- Turbulent base pressure on conical afterbodies in supersonic axisymmetric flow, including initial deflection effect
[AIAA PAPER 70-555]
03 p0344 A71-14450
- Hypersonic flight test base pressure results at high Reynolds numbers for slender cone in turbulent flow, noting implications for ground test simulation
[AIAA PAPER 71-134]
06 p0883 A71-18578
- Wind tunnel testing of base pressure model attached to long cylindrical body extended and supported far upstream
[AIAA PAPER 71-268]
08 p1274 A71-21994
- Base pressure measurement behind wedge-parallelepipeds and cone-cylinder models of variable geometry
13 p2049 A71-29199
- Low thrust jet effect on base pressures on boat-tailed afterbodies in Mach number 0.8-1.2 flow
14 p2169 A71-29889
- Inert and reactive gas injection in near wake behind afterbodies in supersonic flow, considering influence on base pressure and temperature
14 p2336 A71-30213
- Supersonic flow base pressure correlation based on reduced Reynolds number in mixing region
15 p2346 A71-31211
- Base pressure of cluster rocket exhaust with several jets simultaneously ejecting from nozzles
18 p2903 A71-36116
- Blunt planetary entry probe full scale flight test base pressure measurements, noting insensitivity to angle of attack variations up to 10 degrees
20 p3176 A71-39353
- BASES (FOUNDATIONS)**
U FOUNDATIONS
- BATCH PROCESSING**
Batch/Time-Sharing Monitor for achieving balance of digital computer systems efficiency and responsiveness, discussing performance modeling and empirical measurements
01 p0043 A71-10178
- Queueing model of statistical multiplexer buffer behavior for batch Poisson arrivals and single constant output, applying to time sharing computer buffer design
05 p0724 A71-17063

- Manned space flight data processing system data storage, describing data base structure, direct access display and batch processing
[AIAA PAPER 71-237] 07 p1068 A71-19713
- Digital fluidic metering system for composition control of liquid batch mixing from circuit design to final product 07 p1028 A71-20581
- Carbon fiber reinforced plastics mechanical properties, discussing batch processing and specimen geometry variables effects on laminates [PLASTICS INST. PAPER 24] 08 p1318 A71-20893
- Batch fabricated three dimensional planar coaxial microelectronic interconnection and packaging technique for semiconductor chips 12 p1890 A71-27771
- BATHS**
NT SALT BATHS
- BATS**
Fog droplet and rain effects on propagation of echo location signals from bats 10 p1638 A71-24423
- BATTERIES**
U ELECTRIC BATTERIES
- BATTERY CHARGES**
Pulse charging methods for improved storage batteries performance in space power supply systems, noting solar array voltage variations use in spinning satellites 16 p2526 A71-32847
- BATTERY SEPARATORS**
U SEPARATORS
- BAUSCHINGER EFFECT**
Turbine disks cyclic nonisothermal deformation with allowance for Bauschinger effect, determining stress-strain state and residual microstresses 02 p0323 A71-11747
- Quasi-stationary one dimensional thermoplastic stress strain state in cylindrical fuel tank during emptying process, allowing for Bauschinger effect 13 p2157 A71-29196
- Elastoplastic buckling of structures, considering strain hardening materials, slip and Bauschinger effect 16 p2650 A71-33024
- Prestrain directional effects in steel tension and compression test specimens, noting Bauschinger and work hardening effects 18 p2937 A71-36834
- BAYES THEOREM**
Dynamic programming and Bayes algorithm for self organizing and self adjusting Markovian systems 03 p0389 A71-13515
- Radar detection problem, using pseudo Bayes techniques to determine likelihood ratio computational algorithms for stochastic process 04 p0551 A71-15007
- Bayesian modeling of nonstationary Poisson process with probabilistic lambda in time 11 p1791 A71-25252
- Maximum entropy principle for prior distribution determination in Bayesian reliability estimation, comparing with statistical decision theory 11 p1772 A71-26164
- Service life testing and reliability estimation, using ordinary and empirical Bayes approach in failure model with gamma probability distribution 12 p1910 A71-26685
- Bayesian time to failure distribution for graphical estimation of component burn-in time and reliability prediction, comparing with Weibull technique failure rates 12 p1911 A71-26686
- Noisy image visual discrimination and detection, investigating Bayes criterion ideal statistical method validity for pattern recognition 14 p2197 A71-30815
- Bayesian estimate of signal parameters in random noise background under mutually exclusive hypotheses about statistical properties 15 p2370 A71-31584
- Optimal Bayesian system for simultaneous discrimination and parameter estimation of several signals in noise background 15 p2370 A71-31585
- Nonparametric Bayes risk estimation for measurement classification, using nearest neighbor error rate and Parzen probability density function estimators 16 p2602 A71-32822
- Monte Carlo Bayesian analysis technique applied to decision problem concerning population of single-use item in state of operational readiness 16 p2582 A71-33288
- Sequential analysis and Bayesian demonstration in hypothesis testing, considering weight ratios based on objective lower level program reliability test information 16 p2582 A71-33289
- Bayes theorem tests based on experimental observations, considering binomial, exponential and normal sampling distribution of priors as family of natural conjugates 16 p2582 A71-33290
- Bayesian decision theory, discussing choice of possible systems to convert wind into electrical energy 16 p2582 A71-33291

Nonlinear filters synthesis by digital computer technique, discussing density storage and Bayes law computation problems 16 p2549 A71-33351

Linear dynamic systems state estimation, using empirical Bayes decision theory to develop filter set 17 p2825 A71-34897

Optimum diagnostics algorithm for complex automatic control system state detection based on Bayesian rule successive application for minimum time requirement 17 p2720 A71-34959

Gyro drift rate acceptance test design to reflect system performance, using Bayes philosophy for derivation of test cost, product yield and quality [AIAA PAPER 71-968] 19 p3068 A71-37209

Single-shot joint detection-estimation for discrete and continuous data and generalization to Bayesian system identification, considering optimal nonlinear estimator realization 20 p3201 A71-38847

Bayesian learning algorithm derivation for statistically optimum adaptive gain control in Rayleigh-distributed signal reception 20 p3206 A71-38874

Bayesian estimates in nonlinear filtration of nonstationary non-Gaussian radio signals, deriving second central moments and parameter estimate errors 20 p3198 A71-39807

Optimal design procedure as experimental design finite decision problem, using Bayes and minimax techniques 21 p3408 A71-40879

Cloud classification from various radar data independent characteristics, using statistical theory of Bayes hypotheses 24 p3844 A71-44878

BAYESIAN STATISTICS

U BAYES THEOREM

BGGKY HIERARCHY

Nonlinear heat transfer in plane rarefied isothermal Couette gas flow, using BGK model 16 p2561 A71-34143

Longitudinal electron oscillations damping in ionized plasma, obtaining wave dispersion relation from BGK model 22 p3583 A71-42372

BCC LATTICES

U BODY CENTERED CUBIC LATTICES

BCH CODES

Two algorithms for decoding beyond Bose-Chaudhuri-Hocquenhem bound 08 p1258 A71-21314

Block code construction for binary single, double and triple error correction, including cyclic BCH, circulant and nonlinear codes 14 p2200 A71-30919

BE-B

U EXPLORER 22 SATELLITE

BEACON EXPLORER B

U EXPLORER 22 SATELLITE

BEACON SATELLITES

NT EXPLORER 22 SATELLITE

Satellite beacon experiments applications - Conference, Lindau uber Norheim, West Germany, June 1970 07 p1095 A71-19001

Receiving equipment for direct differential Doppler frequency measurement via beacon satellites observation 07 p1059 A71-19012

Geostationary radio beacon specifications and observational opportunities on ionospheric satellite ATS-F in 1972 07 p1096 A71-19016

Ionosphere and magnetosphere daily electron content change measurement, describing satellite beacon experiment 07 p1096 A71-19017

Low angle signal strength enhancements from ionospheric beacon satellite BE-B transmissions 07 p1096 A71-19018

Total electron content over New Delhi by satellite beacons, discussing solar activity effects, electron production rates and seasonal variations 07 p1097 A71-19019

BEACONS

NT RADAR BEACONS

NT RADIO BEACONS

NT RADIO DIRECTION FINDERS

Low profile optical system producing annular cone of radiation from point source for high speed aircraft beacon 07 p1107 A71-19203

Telecommunications satellite data acquisition from automatic beacons, discussing Eole program 18 p2988 A71-36543

BEAM COLUMNS

U BEAMS (SUPPORTS)

U COLUMNS (SUPPORTS)

BEAM CURRENTS

Current interception in TWT electron beam affecting minimum noise factor level 03 p0386 A71-13803

BEAM PLASMA AMPLIFIERS

Microwave plasma device development, noting beam plasma amplifiers and quiescent source 07 p1167 A71-19257

Microwave signal attenuation in LF oscillation beam plasma discharge, comparing to braking cyclotron absorption effect 10 p1653 A71-24890

Electromagnetic wave amplification using coaxial line matching with plasma waveguide by charged particle beam 24 p3853 A71-44508

BEAM SPLITTERS

Beam splitter prisms with dielectric multilayer coatings 06 p0907 A71-17534

Y-shaped microwave power splitter, using dielectric wedge partially extending into rectangular metallic waveguide 11 p1733 A71-26349

Interference spectroscopy and spectrometry techniques, describing transverse achromatic light source beam splitting and frequency analysis of photographed fringes 14 p2238 A71-29804

Two beam holographic interferometer based on spherical mirrors with laser beam splitting by semitransparent plate and image reconstruction in monochromatic and nonmonochromatic light 15 p2402 A71-31257

Beam splitting photocell for pulsed laser power and energy measurement 19 p3072 A71-37551

Far IR spectrum analysis using Michelson interferometer with beam splitter 23 p3676 A71-43400

Jones reflection and transmission matrices representation for beam splitters, investigating reversibility and action on incident light amplitude and/or phase 24 p3849 A71-45210

Laser mode suppression arrangements consisting of Michelson interferometers with polarization prism as beam splitting element 24 p3835 A71-45264

BEAM SWITCHING

Holography development, discussing three dimensional images, fine grain recording emulsions and beam switching during reconstruction 06 p0897 A71-17369

Space-DMA or space-TDMA techniques conserving spectrum and increasing communication satellite channel capacity, discussing spot beams and switchings 08 p1254 A71-21326

Beam vector control from ion bombardment thrusters with dual grid electrostatic, movable screen electrode and discharge chamber extraction systems [AIAA PAPER 71-691] 14 p2293 A71-30751

Laser beam CW self-induced frequency modulation and switching observation in liquids with low surface tension 15 p2420 A71-32381

Two spot beam switching without storage at satellite for time division multiple access system in satellite communication, giving switching algorithm 22 p3514 A71-42482

BEAM WAVEGUIDES

Light beam deflection due to temperature gradient in laminar gas flow in shielding pipe for laser communication, considering beam waveguide design 02 p0284 A71-11869

Beam waveguides for optical transmission, considering cost, attenuation, dispersion and flexibility 02 p0249 A71-12009

Coherent light propagation guidance by helicoidal guide, calculating transverse electric field distribution for luminous beam variations 05 p0722 A71-16705

Dielectric thin optical film waveguides excitation for integrated optical circuitry by Gaussian laser beams 07 p1123 A71-19213

Regular beamguides of second kind consisting of nonidentical nonequidistant correctors, calculating energy losses 13 p2029 A71-28362

Beamguides with inhomogeneities regulated for constant radiation losses of waves-analogs of modes 14 p2211 A71-30077

Resonant excitation of thin film dielectric optical waveguide through supercritical layer by limited light beam with arbitrary amplitude-phase distribution 15 p2375 A71-31227

Optimum pulse width and information carrying capacity for dielectric single mode glass optical waveguides under distortion due to attenuation and phase velocity dispersion 16 p2541 A71-33127

Stabilizing system for retransmission beam of direct TV broadcast satellite, considering rebroadcast antenna, electronic sensor and antenna pointing subsystem 18 p2892 A71-36576

- Optical coupling of degenerative modes in two parallel dielectric waveguides, applying to slab guides and fibers crosstalk problem 19 p3014 A71-37214
- Optical dielectric slab waveguides with core thickness variations, computing crosstalk due to light scattering in terms of guided mode radiation loss 19 p3014 A71-37215
- Double heterostructure GaAs injection laser mode reflectivity and waveguide properties, discussing threshold current density and wavelength dependence on mirror reflectivity 24 p3832 A71-44433
- BEAMS [RADIATION]**
- NT ATOMIC BEAMS
- NT ELECTRON BEAMS
- NT ION BEAMS
- NT LIGHT BEAMS
- NT MICROBEAMS
- NT MOLECULAR BEAMS
- NT NEUTRAL BEAMS
- NT NEUTRON BEAMS
- NT PARTICLE BEAMS
- NT PHOTON BEAMS
- NT PION BEAMS
- NT PROTON BEAMS
- NT RADAR BEAMS
- Weakly divergent electromagnetic wave beam propagation in optically nonlinear laminarly inhomogeneous medium, considering absorption coefficient and self focusing 01 p0037 A71-11201
- Double beam microphotometer for simultaneous measurement of negatives, reducing processing time and density fluctuations 02 p0251 A71-12358
- Optimum beam ratio producing maximum contrast photographic reconstructions from double exposure holographic interferograms 03 p0424 A71-13639
- Laser light beam spread in random media, considering atmospheric and oceanographic applications 04 p0609 A71-15682
- Irregular waveguide and horn construction using asymptotic two beam sum theory 05 p0719 A71-15998
- German monograph on beam shift at total reflection covering Goos-Hanchen optical effect, acoustics, quantum mechanics, plasma physics, Brewster law, holography, etc 05 p0780 A71-16122
- Delay time between beams reflected from different parts of meteor trail, using phase invariant and frequency scanning methods 06 p0869 A71-18263
- Group delay times criterion of multibeam propagation of ionospheric radio echoes for communications systems 06 p0869 A71-18281
- Finite amplitude helical instability effect on microwave beam phase propagated through plasma column 07 p1166 A71-18888
- Monograph on dual beam parabolic antennas in radio astronomy covering atmospheric effects, EM surface current density and scalar aperture field, etc 07 p1077 A71-19725
- Envelopes of antenna beams produced by variation of one antenna dimension in radar system 09 p1406 A71-23031
- Beam compression technique for log periodic dipole antenna array using axial displacement of antenna dipoles feed points 09 p1406 A71-23035
- Shaped beam radiation patterns synthesis by iterative sampling method with line sources or uniformly spaced antenna arrays 09 p1409 A71-23493
- Homogeneous Gaussian beam propagation in inhomogeneous negative absorption media, noting amplification of plane wave 11 p1798 A71-25665
- Measuring technique for short term laser beam propagation direction fluctuations, discussing atmospheric turbulence effect on initial modulation phase distribution 11 p1774 A71-26047
- Monoenergetic beam relaxation dynamics in plasma, describing oscillation excitation and diffusion allowing for instability 12 p1942 A71-27769
- Continuous relative phase control between reference and object beams in holographic interferometry 13 p2066 A71-28161
- Antenna and radome constructions/shape effects on minimizing cross polarization produced by flat, cylindrical, conical and paraboloidal randoms in linear and circular beams 14 p2216 A71-31039
- Matched/mismatched crossed beam interference field combination with sinusoidal holographic diffraction grating, studying metric properties and moire-obtured bands 15 p2410 A71-32404
- Holograms of physical objects, calculating irradiance statistical distribution from reference-object beam powers ratio 15 p2412 A71-32594
- Nitrogen beam foil spectrum analysis, calculating transitions and decay times 15 p2452 A71-32598
- Focused ultrasonic nondestructive tests search units, describing focal distance, beam diameter and lens/crystal radius optimum ratio 16 p2581 A71-32863
- Weakly divergent electromagnetic wave beam propagation in optically nonlinear laminarly inhomogeneous medium, considering absorption coefficient and self focusing 17 p2697 A71-34253
- Time division multiple access system with narrow beam coverage 18 p2880 A71-36348
- Pulsar radiation beaming due to strong magnetic field, computing Compton scattering and opacity 20 p3285 A71-39953
- Irregular waveguide and horn construction using asymptotic two beam sum theory 22 p3515 A71-42747
- Asymptotic expansion of axisymmetric electromagnetic beams with azimuthal dependence near internal caustic/focal line/ 23 p3647 A71-44330
- Circular aperture illuminations for high beam efficiency and low sidelobes in search radar antenna applications, using Fredholm integral equation 24 p3809 A71-44990
- BEAMS [SUPPORTS]**
- NT BOX BEAMS
- NT CANTILEVER BEAMS
- NT CURVED BEAMS
- NT I BEAMS
- NT RECTANGULAR BEAMS
- Nonlinear viscoelastic beam with hereditary properties, analyzing forced harmonic vibration propagation 01 p0169 A71-10638
- Impulsively loaded rigid plastic continua deformation lower bounds calculation, considering beams and plates 01 p0173 A71-10943
- Short beams vibrational analysis extended to stability analysis, using Timoshenko theory 01 p0174 A71-10966
- Coupled vibrations of thin walled beams of open cross section using finite element method 01 p0175 A71-11015
- Composite beam of three thin plates reinforced by thin electric ribs, calculating stress strain state by Fourier transforms 01 p0176 A71-11044
- Free lateral vibration of viscoelastic metallic beam under axial creep, considering elastic deformation 02 p0324 A71-11996
- Thin walled lipped-channel and trapezoidal section beams under end moment loading, deriving differential equations and strain energy for end plates 02 p0330 A71-12950
- Small forced flexural elastoplastic vibrations of structural beam, deriving approximate partial differential equation based on stress-strain relation 03 p0502 A71-13403
- Elastic instability of transversely isotropic Timoshenko beam, deriving buckling coefficients curves vs parameter measuring shear deformation effect 03 p0504 A71-13452
- Elastic metal thin beams transverse resonant free vibrations, analyzing viscoelastic coatings damping effects [ASME PAPER 70-DE-D] 03 p0507 A71-13710
- Beams and plates deflection optical measurement using moire gap effect generalized to include linear and rotational mismatches [SESA PAPER 1703] 03 p0507 A71-13754
- Beam structures plastic shakedown sufficient conditions derivation in terms of bending moments 03 p0510 A71-13947
- Periodic beam structure vibration response, using formulation for flexural wave propagation groups [ASME PAPER 70-WA/DE-3] 03 p0511 A71-14139
- Buckled beam nonlinear vibration under harmonic excitation, solving governing partial differential equation by Galerkin and harmonic balance methods [ASME PAPER 70-WA/APM-48] 03 p0512 A71-14167
- Infinite elastic beam normal impact by seminfinitesimal elastic rod, using Timoshenko beam and one dimensional bar theory to describe elastic waves [ASME PAPER 70-WA/APM-54] 03 p0513 A71-14171
- Nonlinear partial differential equation solution for natural free-free vibrations of beam structures [ASME PAPER 70-WA/APM-55] 03 p0513 A71-14172
- Polish book on impact in discrete mechanical systems covering beams, curved rods, plates, nonlinear damping, numerical analysis, subjected to shock loading 03 p0513 A71-14297
- Steel-concrete composite beam creep numerical analysis by reduction to elastic problem with initial strains 04 p0669 A71-15198
- Minimum weight design for beams and frames with compliance constraints from constitutive relation 04 p0671 A71-15754
- Naturally twisted and orthotropic cylindrical beam bending by transverse load 04 p0673 A71-15886
- Slender beams transverse vibration, including nonlinear bending inertia in motion equation 05 p0825 A71-16716
- Deflection-optimal elastic beams design for distributed dynamic loading 05 p0825 A71-16717
- Support systems relative efficiency in external damping free-free configuration production for flexing beam 05 p0828 A71-16967
- Haunched beam design optimization for lightest weight, analyzing failure modes under assumption of elastically rigid perfectly plastic material 06 p0981 A71-17301
- Natural transverse vibrations of beam with variable cross section and parameters exhibiting small random deviations 06 p0983 A71-17368
- Long thin circular cylindrical shell circumferential wave functions reduction to beam type transverse vibration equation, including rotary inertia 06 p0984 A71-17618
- Circular and elliptical holes and inclusions effects on stress concentration in elastic beams under uniform compression 06 p1002 A71-18414
- Spring supported beam-column nth vibration and buckling eigenvalues, discussing Monte Carlo simulation for evaluating perturbation method accuracy for variance calculation [AIAA PAPER 71-149] 06 p1004 A71-18591
- Natural frequency bounds for clamped beam with linearly varying compressive load and constant end load by Rayleigh-Ritz, Bazley-Fox second projection and Kato methods 08 p1368 A71-20806
- Periodically supported beams response to random loading, using space-harmonic analysis 08 p1371 A71-21429
- Beams torsional rigidity under thermal stress due to arbitrary temperature distribution 09 p1534 A71-22103
- Nonhomogeneous orthotropic beam Saint Venant bending, using finite element method 09 p1534 A71-22104
- Dynamic response of beams to transverse impact, considering deflection curve 09 p1541 A71-23205
- Soviet book on problems in anisotropic body elasticity theory, covering orthotropic beams and plates torsion, bending, vibration, stability and boundary value problems, etc 09 p1542 A71-23438
- Creep analysis for thermoplastic beams under bending and struts under buckling 10 p1685 A71-23942
- Operational research methods application to beam theory, deriving general deformation equation for beams with constant or variable moments of inertia and isotatic or hyperstatic systems 10 p1687 A71-24289
- Hinged sandwich beams loaded by concentrated masses, calculating natural vibration frequencies with and without allowance for rotatory mass inertia 10 p1690 A71-24571
- Dynamic analysis of vibrating beams on viscoelastic supports, using Galerkin approximate method 10 p1694 A71-25088
- High speed tracked air cushion vehicles dynamic interactions with guideways, considering model of lumped double-sprung vehicle masses traveling in tandem along simply supported beams [AIAA PAPER 71-386] 11 p1846 A71-25350
- Carbon fiber reinforcement in carbon fiber/glass fiber mat sandwich beams increasing tensile and compressive strength 11 p1846 A71-25412
- Stress redistribution and static interioelastic instability of rotating beams and disks of low modulus high yield strength materials 11 p1848 A71-25495
- Optimal elastic beam structural design for given deflection in presence of body forces, considering rod under centrifugal loads 11 p1849 A71-25680
- Modified interaction equation for biaxially bent beam columns of hollow tubular sections yielding satisfactory prediction of ultimate strength 12 p1973 A71-26699
- Vibration damping of simply supported sandwich beam with viscoelastic core, using energy method [ASME PAPER 71-DE-C] 12 p1977 A71-27318

Statically determinate beams optimal design, considering displacement and stress constraints in optimality conditions derivation 12 p1983 A71-27596

Minimum weight design of statically determinate wide flange beams, using Lagrange multipliers 13 p2151 A71-28210

Center of rigidity position determination in cross section of thin walled beam under nonuniform temperature due to creep 13 p2154 A71-28642

Distributed inertial forces due to cyclic loading in minimum volume beams cross sectional stress calculations 13 p2154 A71-28643

Optimal design of minimum volume beams of variable height under bilateral restrictions on stresses and displacements 13 p2154 A71-28645

Elastic stability of compressed beams, giving method for evaluating neutral axis form and critical load in buckling 13 p2157 A71-29321

Transient creep of thin walled composite beam under bending and tensile loads in nonuniform temperature field by increment method 14 p2321 A71-29538

Stress analysis of thin walled framed cylindrical beams under deformation beyond proportionality limit by iteration method 14 p2321 A71-29540

Optimal structural design of minimum weight trusses and beam cross sections for given load using computerized nonlinear programming method 14 p2321 A71-29541

Transverse free vibrations of beam with one end fixed and other supported on bilinear spring and carrying concentrated mass 14 p2323 A71-29847

Optimized thin walled elements in elastic planar frame structures minimum weight design 14 p2324 A71-29872

Stability and longitudinal vibrations of elastic beam under rapid monotonously increasing and impulsive loading assuming free end 14 p2326 A71-30194

Free vibrations of beam-like structures, deducing equations of motion 15 p2502 A71-31419

Elastic structure dynamic stability problem, determining optimum inequality relating energy functional to displacement, and considering beam column with various boundary conditions 15 p2506 A71-32015

Pulsed laser double exposure holographic interferometry for measuring transverse wave propagation in beams 15 p2413 A71-32790

Pin connected beam under axial loading, discussing resultant constraint forces, bending moments and lateral displacements 16 p2661 A71-34116

Optimality condition for statically indeterminate beams minimum deflection design, using principle of stationary mutual complementary energy 16 p2661 A71-34148

Transverse vibrations of beam with bilinear support spring and nonlinear constraint, using single degree of freedom system analysis [SESA PAPER 1745] 17 p2820 A71-34543

Weightless elastoplastic beam dynamic bending under moving concentrated load, calculating deformation by reduction to Cauchy problem 17 p2822 A71-34780

Small forced flexural elastoplastic vibration of structural beam, deriving approximate partial differential equation based on stress-strain relation 17 p2825 A71-35013

Clamped-clamped sandwich beam with thin face sheets and soft viscoelastic core, investigating forced, damped, nonlinear and LF flexural vibrations 17 p2826 A71-35032

Low rigidity stretched prismatic beam bending under tension by force couple 17 p2831 A71-35345

Chebyshev polynomial expansions application to beams and columns with large deflections, discussing accuracy 17 p2832 A71-35424

Saint Venant principle generalization for transient creep and stress relaxation analysis in rectilinear thin walled multiply connected beam under torsion 17 p2833 A71-35612

Timoshenko beam transverse vibration with time dependent boundary and normal loads, using Laplace transform method [ASME PAPER 71-APM-F] 18 p2977 A71-36253

Cantilever column critical dynamic instability load under nonconservative follower force including thermomechanical coupling effect from boundary value problem formulation [ASME PAPER 71-APM-L] 18 p2977 A71-36255

Simply supported Bernoulli-Euler beam resting on elastic foundation and carrying equally spaced moving

mass particles, calculating lateral response dynamic stability by Galerkin method 18 p2978 A71-36256

Generalized vectorial equation of motion for vibrating nonprismatic thin space beams, discussing boundary conditions, rotary inertia and shear deformation [ASME PAPER 71-APM-F] 18 p2978 A71-36259

Laminated composite beam microstructure continuum model, calculating equations of motion and boundary conditions with Hamilton principle [ASME PAPER 71-APM-S] 18 p2978 A71-36261

Beam column with probabilistic material and geometric properties, axial loads and boundary conditions, obtaining free vibration and natural frequency stochastic equations 18 p2979 A71-36358

Elastic beam dynamic buckling stability under transverse follower force, considering force direction dependence on cross sectional twist angle [DFVLR-SONDDR-137] 18 p2980 A71-36679

Nonstationary resonance analysis of forced flexural elastoplastic vibrations of beam of hardening/softening material under cyclic strain 18 p2981 A71-36709

Bending tests of beam with different creep characteristics in tension and compression 18 p2981 A71-36717

Thin walled beam structures under external torsional loading, calculating distribution of longitudinal and shear stresses 18 p2982 A71-36808

Stress and deflection analysis of plates reinforced with discrete stiffeners in form of simple beams and twisting elements, determining bending moments 18 p2983 A71-36845

Constant stiffness beam-columns analysis in pressure piping systems calculations for nuclear industry, using initial parameter method 19 p3102 A71-37073

Torsion of hollow beam consisting of two homogeneous isotropic rods with different elastic properties and simply connected cross sections, solving by conformal mapping 19 p3155 A71-37387

Linearly deformable beams with distributed parameters and lumped inclusions, determining natural transverse vibration frequencies and mode shapes 19 p3155 A71-37535

Constitutive equation coefficients determination for nonlinear vibrations of viscoelastic beam by perturbation and optimal linearization method 19 p3158 A71-38060

Transient response of Euler-Bernoulli and Timoshenko beams and cylindrical shells with moving loads 19 p3158 A71-38183

Elastic beam-columns with initial curvature and pinned or clamped ends under transient axial and distributed lateral loads, deriving upper displacement bounds 19 p3159 A71-38184

Shear envelope of thin walled beam with semicircular cross section under creep 19 p3159 A71-38186

Lumped parameter models for description of continuous one dimensional and Bernoulli-Euler beam vibration, compared on basis of maximum system strain energy [ASME PAPER 71-VIBR-5] 21 p3456 A71-40268

Nonlinear free and forced vibration response and stability of simply supported restrained buckled beams, using analog computer simulation [ASME PAPER 71-VIBR-17] 21 p3458 A71-40277

Deflection equations and bending stress for forced vibration of beam with time dependent boundary condition [ASME PAPER 71-VIBR-32] 21 p3458 A71-40286

Beams with multiple constrained viscoelastic layer coatings, presenting damped vibrational response prediction for various materials, geometries, wavelengths and temperatures [ASME PAPER 71-VIBR-40] 21 p3459 A71-40290

Transversely vibrating hollow cylindrical beam sound radiation and response to acoustic excitation, predicting resonant frequencies [ASME PAPER 71-VIBR-84] 21 p3461 A71-40320

Optimum geometry and vibration damping ability of laminated three layer elastic-viscoelastic-elastic beam at resonance [ASME PAPER 71-VIBR-102] 21 p3461 A71-40328

Bending resonance frequencies of beams for known external forces 21 p3463 A71-40550

Axially loaded slender beam mass and deformation effect on constrained bending motion system stability and dynamic response 21 p3469 A71-41010

Nonlinear elastic deflection analysis of beams in space, deriving geometric curvature, free center line torsion and cross section twist angle 21 p3471 A71-41022

Maximum vector values for stability and rigidity of elastic systems under modulo limited disturbances, applying to beam deflection and second derivative 21 p3473 A71-41154

Stress concentration in layers of sandwich beams with holes under bending and tension 21 p3473 A71-41155

Regular and singular perturbation solutions for beam bending under axial forces and shaft warping torsion 22 p3616 A71-42210

Motion equations derived for slender beam transverse vibrations on continuous viscoelastic foundation, considering nonlinearities from external couplings, longitudinal displacements and curvature 22 p3617 A71-42500

Stability of edge reinforced circular plate under uniform radial load, considering flexural and extensional stiffness of reinforcing beam 22 p3618 A71-42501

Stiffness and consistent mass matrices for beam bending finite element containing integration parameters 23 p3776 A71-43370

Dynamic flexures in beam during massive extended load motion with allowance for inertial forces, using Bubnov-Galerkin method 23 p3778 A71-44040

Global-local finite element combined Ritz method for beam and plate vibration analysis 24 p3880 A71-44638

Critical bending moments for elastic beams weakened by elliptical crack in tensile stress region 24 p3882 A71-44840

Geometrically nonlinear integral solutions to equilibrium equations of curvilinear beam under uniform pressure, using Weierstrass functions 24 p3883 A71-44850

BEAMSHAPING

U COLLIMATION

BEARING [DIRECTION]

Guinea pigs vestibular adaptation to repeated angular acceleration dependent on acceleration direction 01 p0012 A71-11050

Triangulation position fix techniques employing lines of bearing, n-locus, least square fits and resection by intersection method 02 p0280 A71-12900

Radio direction finding of celestial bodies from moving platform, determining plane rotation effects on angle measurements 09 p1532 A71-22660

Stabilization of solid body orientation with twin gyros under slave engine drive, producing control moments to gimbal axis 13 p2145 A71-28930

Electro-optic direction sensor, discussing single axis star tracking application [AIAA PAPER 71-966] 19 p3100 A71-37200

Bearing axis wobble for dual spin vehicle in terms of rotor static and dynamic unbalance and platform mass geometry and inertias 20 p3306 A71-39350

Nikolajev-Helwan space direction determination between satellite tracking stations at long distances using simultaneous circle method 21 p3374 A71-41050

BEARING ALLOYS

Bearing materials for ultrahigh vacuum applications, discussing various metals and alloys friction and wear characteristics 05 p0757 A71-16140

Al-Si and Al-Sn bearing alloys corrosion resistance to lubricating oils, investigating thrust load, operating time and oxidation factor effects 08 p1304 A71-20990

Lead bronze and Babbitt metal composite material detailing antifriction efficiency and wear resistance in bearings 15 p2417 A71-32660

BEARINGS

NT ANTIFRICTION BEARINGS

NT BALL BEARINGS

NT FOIL BEARINGS

NT GAS BEARINGS

NT JOURNAL BEARINGS

NT LIQUID BEARINGS

NT ROLLER BEARINGS

NT THRUST BEARINGS

Papers on bearings covering types, materials, lubricants, applications, etc 01 p0088 A71-10810

Plain bearing oil whirl onset speed, using matrix manipulation for unbalanced shaft self induced vibration amplitudes prediction 03 p0431 A71-13072

MHD conducting lubricant composite slider bearing in transverse magnetic field, calculating conductivity effect on load capacity 04 p0602 A71-14801

Bearing vibration monitoring for wear and damage detection 04 p0603 A71-15671

Numerical control automation in aircraft bearing production for small batch runs 04 p0603 A71-15672

Shock pulse measurements for detecting damage to ball and roller bearings due to fatigue 04 p0604 A71-15673

Gyroscope bearings friction moments constant and variable components experimental determination by method of compensation, using test equipment based on electric spring principle 05 p0758 A71-16355

Synthesized hydrocarbon oil antiwear and extreme pressure additives effects on bearing spinning torque and endurance 06 p0904 A71-17580

Gyroscope in gimbal system with elastic rotor bearings, determining dynamic stability in Newtonian central force field 06 p0899 A71-17929

High speed low power loss spiral groove bearings self sealing grease lubricants with high shear stability and good boundary lubrication [ASLE PREPRINT 70LC-6] 08 p1322 A71-21157

Stationary motion stability of shaft in cylindrical MHD finite length bearing, assuming incompressible lubrication and small lubrication clearance 09 p1453 A71-22139

Three greases in oscillatory bearings under various conditions of speed, load and angle of oscillation, determining effects on fretting corrosion prevention [ASLE PREPRINT 71AM 1B-1] 13 p2076 A71-29490

Variable gap and chamber width effect on load bearing capacity of radial hydrostatic bearing with capillary throttling 16 p2584 A71-33616

Counterrotating antenna without mechanical contact, using magnetic bearings for spin stabilized geostationary telecommunications satellites 18 p2892 A71-36574

Material, design and operating principles of rotary seals used in gas ducts, bearing elements and fuel systems of aircraft gas turbine engines 19 p3069 A71-38015

Spontaneous hot zone formation in oil flow through small pipes, showing significance in pressure losses and plain bearings calculations 19 p3046 A71-38275

Low temperature viscous lubricants from mixed pentaerythritol esters for precision inertial guidance gyroscope bearings and instrument applications 20 p3254 A71-39800

Distributed mass and elastic damping finite element model for turborotor system on fluid film bearings [ASME PAPER 71-VIBR-56] 21 p3385 A71-40301

Single mass flexible rotor in elastic bearings mounted on damped flexible supports, analyzing dynamic unbalance response and transient motions [ASME PAPER 71-VIBR-72] 21 p3460 A71-40310

Friction, wear and adhesion of filler and matrix polymer composite bearing materials including glass, carbon, lamellar solids, metal powders, carbons, nylons, PTFE, polyimides, etc 21 p3405 A71-40602

Hydrostatic bearings for large optical and radio telescopes, explaining lubricant flow control systems 23 p3661 A71-43862

Disk fillets stressed state, determining concentration coefficient and bearing capacity effect 23 p3780 A71-44221

Pressure distribution in narrow porous metal bearings solved with Bessel functions in cylindrical coordinates, finding lower load capacity 24 p3830 A71-44950

BEAT
U SYNCHRONISM
BEAT FREQUENCIES

Subsidiary resonance response time decay behavior in ionosphere, showing occurrence of principal resonances at higher orders 01 p0077 A71-11523

Topside ionosphere plasma resonance due to electrostatic wave echoes, comparing electron temperature dependent beat pattern with ray tracing calculations 03 p0421 A71-14540

Stark induced quantum beats in H Ly alpha emission, using beam foil excited hydrogen 05 p0785 A71-16701

Annular gas laser beat frequency as function of Doppler shift emission, examining mirrors feedback, cavity Q and pumping variational effects 07 p1122 A71-19137

Mode locked picosecond laser pulse duration measurement by beat frequency detection 07 p1123 A71-19211

Ring laser beat frequency response near parametric resonance 07 p1125 A71-19810

He-Ne laser spontaneous emission intensity in N synchronized longitudinal modes as function of intermediate beat frequency and longitudinal magnetic field strength 07 p1127 A71-20376

Beat and synchronization modes of opposed waves in rotating gas ring laser, examining frequency response asymptotic behavior 09 p1460 A71-22222

Optical parametric oscillator, observing simultaneous oscillation and second harmonic and difference frequency generation 09 p1493 A71-22760

Production rates for beat and sum frequencies mixing from interaction of two parallel laser beams with free electrons, using nonrelativistic radiation theory 09 p1465 A71-23546

Velocity measurements for slowly moving pendulum bob with incandescent filament lamp, detecting Doppler shifted beam interference beat frequency with photomultiplier 10 p1574 A71-23738

Mode multiplicity effect on ring laser independent beat and synchronized beat regimes 11 p1774 A71-26004

Vacuum tube frequency meters to measure oscillator stability, calculating beat period modulation characteristics 12 p1883 A71-27619

BED REST

Clinical, physiological and metabolic changes in human body during 120 day bed rest 06 p0855 A71-18371

Human renal diluting capacity, examining prolonged absolute bed rest effects 09 p1401 A71-23365

Psychobiological stress of prolonged weightlessness /bed rest/ in man in terms of adaptive homeostatic state and decreased sensory-motor-muscular input 11 p1725 A71-26120

Psychobiological effects of prolonged bed rest in young healthy volunteers from EEG recording, psychological testing and psychomotor performance 13 p2022 A71-29363

Nasal vascular system reactions during 120-day bed rest hypokinesia under drug affected metabolism 20 p3188 A71-39229

Shin muscle electrical activity during standing after 120 day bed rest hypokinesia from EMG measurement 20 p3188 A71-39230

Bed rest effects on human hemodynamic and gaseous metabolism, observing increased cardiac output and decreased oxygen consumption and carbon dioxide production 20 p3188 A71-39231

Summation dial vectorial representation of stationary and nonstationary time series data, relating rhythms in bed rest study 20 p3190 A71-39480

Human vascular and extravascular fluid changes during six days bedrest based on fluid volume and ideal body weight from individual heights 21 p3331 A71-40354

Prolonged bed rest effects on EEG sleep patterns in young healthy subjects with and without exercise 23 p3631 A71-43109

BEDS [PROCESS ENGINEERING]

Conductive and radiative axial heat transfer in packed/stagnant beds at 20-750 C, giving temperature profiles 22 p3620 A71-41877

BEEFLES

Circadian rhythm in dermestid beetles *Trogoderma glabrum* Herbst as response to compulsory constant light and temperature conditions 01 p0020 A71-11567

BEHAVIOR
NT HUMAN BEHAVIOR

Sound duration effect on brain activity of cats, studying EEG and behavioral responses 03 p0361 A71-13189

Stress and behavior regulation, investigating pituitary-adrenal system operation 07 p1043 A71-20213

Pargyline behavioral effects in primates, concerning therapeutic use for decabornane intoxication 08 p1239 A71-20819

Rhesus monkeys concurrent avoidance and appetitive behavior patterns with counter discontinuities in shock proximity indicator tests 10 p1573 A71-25136

Behavioral arousal and EEG thresholds changes during sleep due to electrical and audio stimulation 13 p2005 A71-28379

Squirrel monkey physiological and behavioral thermoregulation elements interrelationships, considering mean skin and medial preoptic hypothalamic temperatures 18 p2862 A71-36896

Observing behavior in squirrel monkeys under multiple schedule of reinforcement availability 22 p3497 A71-42861

BELL AIRCRAFT
NT UH-1 HELICOPTER
BELLMAN THEORY

Bellman function for time optimal problem under Lipschitz condition 05 p0782 A71-16981

Optimal terminal control stochastic synthesis for linear systems by Bellman second order nonlinear partial differential equations 14 p2220 A71-30872

Self similar invariant group solutions to Bellman nonlinear partial differential equation for optimal correction problems of control systems motion with random disturbances 16 p2549 A71-32935

High order optimality conditions of singular controls, considering Pontryagin maximum principle, Bellman dynamic programming and functional analysis 16 p2550 A71-33701

Bellman function for time optimal problem under Lipschitz condition 18 p2942 A71-36781

BELLOWS

Bellows for aerospace feed line ducting, discussing liquid propellant rocket engines, cryogenic valves, etc 01 p0007 A71-11433

Expansion bellows fatigue strength based on load and displacement measurements performed during low cycle model tests 09 p1538 A71-22604

Multicomponent system of elastic plate with hole and built-in viscous-fluid-filled siphon bellows, calculating oscillation by asymptotic methods 17 p2777 A71-34423

Flow induced vibrations of metal bellows with internal cryogenic fluid flow, noting effects of heat transfer, liquid state properties, external damping and condensation [ASME PAPER 71-VIBR-14] 21 p3457 A71-40276

Vibratory amplitudes and stress levels from metal bellows flow induced vibrations, discussing damping and acoustical resonances effects [ASME PAPER 71-VIBR-22] 21 p3458 A71-40279

BELTRAMI FLOW

Gromeka-Beltrami ideal incompressible fluid flow in semiinfinite circular cylindrical tube 14 p2225 A71-30221

BENARD CELLS

Steady nonlinear regime of Benard convection in uniformly rotating fluid, using two-dimensional primitive equation numerical model with rigid boundaries 15 p2393 A71-32638

Unstable nonlinear systems transient behavior analysis with two-time perturbation method applied to Benard and Taylor flow problems 17 p2730 A71-35797

Bright-dark asymmetry testing in solar granulation photography by objective method 19 p3146 A71-38663

Photometric determination of solar granulation rms intensity fluctuation, using ground telescope 22 p3596 A71-41453

Radar observation of convective process in clear air, presenting turreted top cell contour tracings from PPI sequence 23 p3700 A71-43088

Power spectrum analysis of solar granular intensity fluctuations and velocities, noting asymmetry behavior of Ba II line in individual convection cells 23 p3767 A71-43834

BENDING
NT ELASTIC BENDING

German monograph on nonlinear flexural-torsional stress analysis of thin walled rods with open profiles covering fork supported and cantilever beam systems 01 p0166 A71-10112

Metal sheet plate and bar fabrication, calculating minimum bend radii from ductility ratings 01 p0087 A71-10457

Arbitrary shape and variable thickness cylindrical shell bending numerical solution by replacement of circular cylindrical strip elements 01 p0177 A71-11324

Anisotropic polycrystalline carbon fiber tensile strength and bending behavior, interpreting inelastic characteristics from single filament experiments 02 p0273 A71-11945

Plane nonhomogeneous strain fields deformation tensor determination by moire equations for fringe pitch and angle measurement, considering rectangular block bending 03 p0508 A71-13772

Local distributed load effects on bending of fiberglass reinforced plastic laminar orthotropic cylindrical shell 06 p0986 A71-17761

Elastoplastic conical shells strain under longitudinal impact by large rigid body, analyzing plastic bending 06 p0996 A71-17842

Flat triangular elements for shell analysis, describing membrane and bending displacements by identical quadratic polynomials [AIAA PAPER 71-114] 06 p1003 A71-18564

Semiempirical bending, axial and torsional flexibility coefficients for structural joint assemblies, noting dependence on assembly diameter 07 p1209 A71-18903

Tapered cantilevered beams design, determining end deflection and bending stress magnitude by graphical method 07 p1213 A71-19693

Corrugated blank cross section distortion under bending on three roller mill 08 p1295 A71-20795

Machining electrode materials, investigating high melting transition metals electroerosive stability and bending strength on basis of electrochemical theory 08 p1296 A71-20853

Low alloy Mo mechanical characteristics relation to structural states obtained during tensile and bending tests 08 p1316 A71-21613

Stress analysis of elastic bending plates by holographic interferometry, comparing results to theory 08 p1373 A71-21752

Transverse bending of hinged or clamped rectangular plates with different tensile and compressive resistance 08 p1373 A71-21945

Mechanical strength and elastic properties under tension and bending of boron fibers, noting dependence on surface defects 09 p1482 A71-22823

Ferrous and nonferrous sheet metals neck formation prevention for increasing elongation in tensile tests, using continuous plastic bending method 09 p1479 A71-23697

Linear viscoelastic materials, investigating failure and bending as function of time in response to load under creep conditions 13 p2154 A71-28522

Stress intensity factors for deep cracks in single edge cracked bend and compact tension specimens 14 p2322 A71-29739

Column buckling under initially random bending and twisting, comparing numerical analysis accuracy with Bernoulli-Euler results 14 p2330 A71-30692

Stress-strain dependence on surface deflection and nonlinearity during bending of elliptic flat plate under plastic deformation 16 p2659 A71-33994

Stress distribution over elements of boss or collar tightened flange joints of circular thin walled shells during bending 17 p2829 A71-35306

Molybdenum mechanical characteristics relation to structural states obtained during tensile and bending tests 17 p2760 A71-35673

Circular cylindrical shells creep buckling in pure bending, deriving formula for critical time 18 p2980 A71-36674

Bending tests of beam with different creep characteristics in tension and compression 18 p2981 A71-36717

High temperature four point bending vacuum furnace machine testing thin refractory sheets, noting strain rate, velocity jump and relaxation on tantalum carbide 19 p3063 A71-37554

Testing apparatus contribution to bending in tension specimens, noting instrument errors role 19 p3065 A71-38133

High precision displacement functions for finite element models of rotational shell and plate bending problems 21 p3470 A71-41019

Finite element method for stress intensity factors calculation in cracked plates under bending 22 p3614 A71-41639

Stiffness and consistent mass matrices for beam bending finite element containing integration parameters 23 p3776 A71-43374

Solid powder metallurgy tungsten alloys, determining scale factor effect on bending strength and fatigue limit 23 p3693 A71-44226

High purity Be single crystal transverse bending tests, plotting yield stress and bending angle vs temperature 24 p3836 A71-44673

Edge supported anisotropic elliptic plate with hole under bending by constant lateral edge load, presenting stress-strain state 24 p3882 A71-44837

BENDING DIAGRAMS

Temperature induced bending of rectangular plate, obtaining stress-strain state 10 p1687 A71-24196

Bending strain diagram conversion into tensile strain diagram, considering elastic limit values correlation for Cu-Ni-Al alloy 22 p3561 A71-41698

BENDING FATIGUE

TiC and ZrC samples with different porosities, examining bending strength at various temperatures 01 p0102 A71-10786

Test equipment with axial mode closed loop machine for cyclic deformation and fatigue in pure bending [SESA PAPER 1726] 03 p0507 A71-13756

Fatigue strength of butt, lap and tee welded joints in aluminum alloys under axial stress and repeated bending loads 07 p1119 A71-19971

Six position machine for fatigue testing in corrosive medium of circular rotating metal specimen with cantilever bending 09 p1426 A71-22327

Low-cycle fatigue curve determination for plane elastoplastic bending with flexible loading, deriving rated fatigue life 09 p1536 A71-22502

Materials bending fatigue strength calculations for biaxial tension compared with experiments, showing agreement 09 p1538 A71-22596

Creep analysis for thermoplastic beams under bending and struts under buckling 10 p1685 A71-23942

Stress threshold for crack growth in rotating shaft bending fatigue 10 p1693 A71-25058

Metals mechanical properties under vacuum conditions, discussing alternate bending tests of Cu and Al specimens under range of oxygen pressures 11 p1777 A71-25389

Room temperature rated coercive force measurements of Ni sheet specimens in torsional bending cycles for saturation value, using ballistic method 11 p1778 A71-25563

Sheet metal fatigue test method for transverse 100-1000 Hz bending at normal and high temperatures, applying to 1.5 mm Ti alloy sheet 15 p2505 A71-31864

Flexural-torsional fatigue fracture of duraluminum, noting dependence on cyclic stress, frequency and medium 16 p2593 A71-33689

Resolved stress formula for shafts under simultaneous tangential bending and torsion acting at dangerous points of cross section 18 p2981 A71-36721

Stress intensity factors analysis of strip with longitudinal crack subject to tension and bending along edges and tension of rectangular plates with central crack 22 p3614 A71-41709

Heat treatment effect on tensile and bending fatigue strength of Al alloy thin sheet 23 p3693 A71-44217

BENDING MOMENTS

I-beam plastic moment under shear force, using empirical curve for interaction between bending moment and shear force 01 p0174 A71-11000

Repeated bending and torsion of viscoplastic bars and circular cylinders, using hereditary nonlinear integral equations 02 p0322 A71-11688

Stability loss of circular cylindrical shells under bending beyond elastic limit 02 p0325 A71-12287

Zero bending moment shells of revolution under concentrated load, using boundary value problem for p analytic functions 02 p0328 A71-12539

Beam structures plastic shakedown sufficient conditions derivation in terms of bending moments 03 p0510 A71-13947

Stiff rings attached to elastic cylinders, analyzing stresses and deformations under concentrated loads and bending moments about radial and tangential axes [ASME PAPER 70-WA/PVP-1] 03 p0510 A71-14099

Slender beams transverse vibration, including nonlinear bending inertia in motion equation 05 p0825 A71-16716

Shell shape without bending stresses due to external load 05 p0828 A71-16891

Structural hysteresis in split rod fir tree turbine blade attachment under centrifugal forces and cyclic bending moments 07 p1211 A71-19162

Elastoplastic tubular rods rotation under constant bending moments, solving for large rotational angles 07 p1212 A71-19352

Stress-strain state of rectangular transversely isotropic plate with clamped edge under uniformly distributed load, considering bending moments 07 p1218 A71-20473

Curved beams bending stress concentration approximate equations for elliptical, circular and rectangular cross sections, providing behavior prediction superior to exact methods 08 p1373 A71-21749

Nomograms for normal stresses and bending moments in thin circular cylindrical shell under uniformly distributed local load 08 p1374 A71-22054

Low-cycle fatigue curve determination for plane elastoplastic bending with flexible loading, deriving rated fatigue life 09 p1536 A71-22502

Vibrating cylindrical shell with circular plate, discussing bending moments, deflections and frequencies from Lagrangian 09 p1540 A71-23056

Stability analysis of rigid frames and trusses, including effect of bending moments and shear forces before buckling 12 p1976 A71-27161

Long circular cylindrical shell stability under action of bending moments at end face, deriving neutral equilibrium equations 12 p1981 A71-27495

Radial free vibration frequency of pressurized orthotropic shells with bending terms 14 p2325 A71-29884

Shear deformations effect on circular plates from Reissner theory, expressing bending moments and shear forces as functions of lateral deflection and stress function 15 p2507 A71-32117

Thin plate theory approach with discrete triangular approximation of moment and displacement surfaces for plate bending analysis 16 p2652 A71-33087

Pin connected beam under axial loading, discussing resultant constraint forces, bending moments and lateral displacements 16 p2661 A71-34116

Precatastrophic extension effects on local stresses in cracked plates under bending fields, using stress freezing and slicing for photoelastic experiments [SESA PAPER 1820] 17 p2820 A71-34549

Traveling waves propagation in elastic shell of revolution subjected to bending moment 17 p2833 A71-35618

Structural hysteresis in gas turbine blade herringbone scarf joints under centrifugal forces and cyclic bending moments 17 p2834 A71-35658

Large deformation stress and mechanical resistance of thin glass circular plates by bending test involving concentric rings 18 p2940 A71-36697

Cyclic bending stress distribution in fir tree turbine blade root for arbitrary loading phase 18 p2980 A71-36705

Stress and deflection analysis of plates reinforced with discrete stiffeners in form of simple beams and twisting elements, determining bending moments 18 p2983 A71-36845

Space shuttle boost vehicle with various degrees of aerodynamic stability, discussing control laws effects on rigid body bending moment tradeoff [AIAA PAPER 71-918] 19 p3147 A71-37167

Variable thickness plate under cylindrical bending, considering stress concentration around circular hole 19 p3160 A71-38542

Deflection equations and bending stress for forced vibration of beam with time dependent boundary condition [ASME PAPER 71-VIBR-32] 21 p3458 A71-40286

Thin skewed plates bending and twisting at constant temperature moment, obtaining angle skew effects on torque-twist relation 21 p3463 A71-40592

Specimen support effects on three point bending tests of fiber-plastic composites, suggesting small diameter roller 21 p3405 A71-40596

Steel with various intensity stress risers under bending loads, showing difference in crack nucleation and propagation resistance 23 p3778 A71-44036

Factorial determinants in solving space contours, considering bending and torsional moments in structural analysis 24 p3881 A71-44800

Critical bending moments for elastic beam weakened by elliptical crack in tensile stress region 24 p3882 A71-44847

Cross section behavior of tube under plastic bending based on hollow rod treatment 24 p3883 A71-44848

Strain hardening narrow strip lateral instability under bending in plane of maximum rigidity, deriving critical moment formula 24 p3883 A71-44854

Thin walled tube under combined bending and torsion, considering stress distribution and curvature behavior 24 p3883 A71-44892

BENDING THEORY

Photoelastic analysis using stress freezing to evaluate closure and precatastrophic crack extension in plates under cylindrical bending 01 p0167 A71-10295

Cracked rectangular plate bending under uniform transverse load, discussing crack geometry and propagation 02 p0321 A71-11681

Biorthogonal relation for bending of uniformly loaded clamped sector plates with boundary functions along curved edge 02 p0327 A71-12397

Stress concentration in buckling proof clamped sandwich rod with multicut rectangular cross section under torsional bending 03 p0504 A71-13527

Shell of revolution bending deformation, assessing Trefftz approximation error 03 p0506 A71-13597

Bending of cylindrical shells with and without intermediate supports under arbitrarily distributed and discontinuous loads, using arbitrary parameter method [ASME PAPER 70-WA/PVP-2] 03 p0510 A71-14100

Pure bending and flexure in plane stress with moment stress effects taken into account, considering Saint Venant principle 04 p0672 A71-15769

Variable thickness anisotropic annular plates bending on generalized elastic foundation, using numerical method 05 p0823 A71-16423

Rib reinforced circular cylindrical shells, analyzing elementary and zero bending stress states 06 p0982 A71-17351

Anisotropic plates bending equations derivation by asymptotic integration from elasticity theory 06 p0985 A71-17754

Orthotropic shallow shells nonlinear theory, examining inverse bending problems 06 p0988 A71-17778

Circular and annular elastic plates elastoplastic bending theory, using Saint Venant conditions and equations of equilibrium and deformation 06 p0993 A71-17812

Circular plates of anisotropic fiber-reinforced materials, calculating axisymmetric bending and buckling 06 p0995 A71-17829

Complex form plates bending and oscillations under various boundary conditions, discussing procedure for coordinate sequences construction 06 p0997 A71-17853

Multilayer plates and shells, considering bending, stability, boundary layer stress state, rigid filters theory and local strength 06 p0998 A71-17857

Deformation theory of dynamic bending, buckling and stability of plates and shells beyond elastic limit 06 p0999 A71-17865

Rectangular plate bending with mixed boundary conditions, using paired trigonometric series 06 p1005 A71-18708

Infinite circular cylindrical shell with elastic stiffener ring, calculating transient axisymmetric bending stress under radial impulse 07 p1213 A71-19907

Asymmetric three layer cylindrical shells with orthotropic layers under deflection due to high temperature, deriving differential bending equations 07 p1217 A71-20456

Bending stiffness matrix for sandwich folded plate, reproducing core shearing deformations 08 p1367 A71-20748

Heat exchanger circular rigid tube sheets calculation by thin plates bending theory, using stepped profile circular plates stress analysis 08 p1374 A71-22053

Nonhomogeneous orthotropic beam Saint Venant bending, using finite element method 09 p1534 A71-22104

Unknowns elimination from partial linear equations system with constant coefficients, applying to differential equations for bending transversely isotropic plate under normal external load 09 p1535 A71-22257

Bending analysis of clamped and simply supported isotropic skew plates under uniformly distributed load 09 p1540 A71-22995

Viscoelastic rectangular sandwich plate bending, stability, deflection and critical load calculation, assuming core stress-strain relation governed by Maxwell-Thompson differential equation 09 p1540 A71-22998

Book on elastic plate theory covering bending and transverse shear effects, boundary problems, rectangular isotropic, structurally orthotropic, circular and annular plates under various loads 09 p1544 A71-23701

Nonconforming displacement triangular finite element derivation for plate bending problems, considering constant bending moment element 10 p1685 A71-23939

Operational research methods application to beam theory, deriving general deformation equation for beams with constant or variable moments of inertia and isostatic or hyperstatic systems 10 p1687 A71-24289

Dynamic plastic bending theory of thin circular annular plate with central hole under uniform impulse 10 p1689 A71-24519

Inextensible elastic Cosserat surfaces finite deformation mechanisms, applying theory to flexure of rectangular plate into closed circular cylinder and helical strip 11 p1849 A71-25681

Modified interaction equation for biaxially bent beam columns of hollow tubular sections yielding satisfactory prediction of ultimate strength 12 p1973 A71-26699

Dynamic stress and strain concentration in flat plate at sharp change of section, assuming diffuse bending wave field 12 p1973 A71-26703

Bending problems of elastoplastic plate rigidly clamped over edges, deriving theorems on existence, uniqueness and convergence of approximate solutions 12 p1974 A71-26962

Shallow laminated shells nonlinear bending equations, using variational principle with allowance for transverse shear strain of layers 12 p1975 A71-27104

Nonlinear elastic shells free vibrations, obtaining phase trajectories with finite bending within Hooke's law 12 p1975 A71-27106

Thin walled stiffened Duralumin box spars bending stress-strain states under unsteady creep 12 p1981 A71-27496

Asymmetric structure elastic transversely isotropic sandwich panels bending equations, taking into account transverse shear strain and stability 12 p1981 A71-27497

Spar box structure under pure bending noting flexural rigidity and stress and stability analysis with Karman nonlinear equations 12 p1981 A71-27498

Bending stress in conical shell subjected to thermal and pressure loadings with uniform spatial distribution, using perturbation method 12 p1983 A71-27594

Stretching, twisting, pure bending and flexure of pretwisted elastic rectangular plates of rectangular cross section 13 p2147 A71-27783

Rectangular plate bending elements displacement functions representation by trigonometric expressions, using finite element method 13 p2147 A71-27790

Morera and Maxwell stress functions determination by integrodifferential equations of deformation continuity for bending of thin plates 13 p2148 A71-27891

Load bearing capacity of thin walled box shaped rod of strain hardening material during bending beyond elastic limit 13 p2153 A71-28294

Girder system transverse bending under axial and lateral loads, deriving stability conditions by direct Liapunov method 13 p2153 A71-28519

Elastoplastic plates and shallow shells with rigid orthotropic filler, bending and buckling beyond elastic limit 13 p2156 A71-29066

Multiple Fourier method for plate bending compared with least squares and boundary collocation solutions 14 p2325 A71-29888

Bending equations solution for arbitrarily shaped quadrilateral plates with simply supported edges, using finite difference method 14 p2329 A71-30485

Rods instability with cross sectional stress concentration depending properties, presenting buckling and bending problems 16 p2648 A71-32990

Elastic plate with part-through surface crack, determining stress intensity factor for remote tensile and bending loads [ASME PAPER 71-APM-20] 16 p2655 A71-33209

Large plastic strains in fiber in sheet bending for wide angle range, using Hill theory 17 p2816 A71-34298

Dugdale mathematical model for cylindrical bending of thin plates, finding resulting plastic zone dependence on applied moment and normal coordinate [SESA PAPER 1854A] 17 p2819 A71-34538

Time dependent bending of circular cross sectioned rod under constant load compression and creep 17 p2821 A71-34564

Weightless elastoplastic beam dynamic bending under moving concentrated load, calculating deformation by reduction to Cauchy problem 17 p2822 A71-34780

German monograph on corner singularities in oblique plates calculation with aid of displacement and stress functions, covering bending theory 17 p2823 A71-34796

German monograph on plane, arbitrarily curved and bending resistant trusses calculations allowing for elastic and plastic deformation 17 p2823 A71-34800

Rectangular plate with two adjacent sides clamped and two supported, solving bending problems with linear algebraic vector equations 17 p2824 A71-34846

Rectangular flexible plate displacement theory, solving boundary value problems with fractional step method 17 p2824 A71-34848

Finite element procedure for plate large deflection by considering effects of element membrane forces

due to initial deflection and bending on stiffness matrices 17 p2825 A71-34872

Bending of circular conical shell with discretely reinforced end cross section, deriving accurate closed form solution within limits of working model 17 p2828 A71-35302

Thermal stressed state and bending theory of rectangular plate by initial function method, allowing for distributed transverse load 17 p2829 A71-35304

Low rigidity stretched prismatic beam bending under tension by force couple 17 p2831 A71-35345

Chebyshev polynomial expansions application to beams and columns with large deflections, discussing accuracy 17 p2832 A71-35424

Cylindrical steel and Ni alloy specimens bearing strength in inhomogeneous stress states under cyclic elastoplastic bending and loading to failure 17 p2760 A71-35668

Hyperelastic compressible isotropic elliptical and circular cylinders simple bending, studying second order effects 18 p2977 A71-36195

Membrane and bending stresses analysis around elliptic hole in long thin circular cylindrical shell, using perturbation technique 20 p3309 A71-39776

Morera and Maxwell stress functions determination by integrodifferential equations of deformation continuity for bending of thin plates 21 p3455 A71-40085

Bending of semiinfinite rectangular plates clamped at long edges 21 p3464 A71-40770

Axially loaded slender beam mass and deformation effect on constrained bending motion system stability and dynamic response 21 p3469 A71-41010

Vertical bar longitudinal bending equation under axial forces, obtaining relation between extreme free angle and deflection 21 p3472 A71-41148

Regular and singular perturbation solutions for beam bending under axial forces and shaft warping in torsion 22 p3616 A71-42214

Inertia-loaded elastic thin circular ring in rigid cavity with small initial clearance, calculating deformation by nonlinear bending theory 22 p3616 A71-42215

Plastic shells under finite bending, deriving large deflection theory from nonlinear continuum mechanics by yield criterion Lagrangian formulation 23 p3775 A71-43317

Multicore circular sandwich plates under various symmetrical loading and boundary conditions, deriving bending equations 24 p3879 A71-44619

Stiffness matrix algorithm for triangular plate bending elements using hierarchy of interpolation polynomials 24 p3879 A71-44637

Geometrically nonlinear elastoplastic bending of rectangular flexible plates with various side ratios, using finite difference and strain theory 24 p3883 A71-44849

Small deflection theory for steady state creep bending of laminated anisotropic rectangular plate under uniform loads, using Galerkin method 24 p3841 A71-44957

Three dimensional stress field error estimates in linear plate bending, using Prager-Synge hypercircle elasticity theorem 24 p3884 A71-44964

BENDING VIBRATION

Turbine blades coupled bending vibrations in centrifugal field, deriving vibration equations including previously neglected centrifugal coupling terms 01 p0166 A71-10120

Flexible Storable Tubular Extendible Member /STEM/ in-plane bending vibrations under solar heating 01 p0173 A71-10941

Natural frequencies of cantilever turbine blade with asymmetric aerofoil under coupled bending-torsion vibrations, using Ritz-Galerkin method for equations of motion 01 p0143 A71-11014

Flexural-torsional vibration stability of thin walled elastic bars under longitudinal periodic force, using parametric resonance theory 02 p0321 A71-11687

Turbomachine blades torsional-bending vibrations aerodynamic damping, noting natural frequency shift 03 p0340 A71-13141

Cantilever beam bending vibration, measuring driving point impedance and natural frequencies at low strain amplitudes for Mg alloy, Mn-Cu and coated Al beams 03 p0502 A71-13299

Small forced flexural elastoplastic vibrations of structural beam, deriving approximate partial differential equation based on stress-strain relation

03 p0502 A71-13403

Carbon steel specimens size effect on energy dissipation and damping characteristics under transverse flexural vibrations

03 p0503 A71-13412

Static tension effect on damping capacity of drawn rods under flexural vibrations, considering materials with strong magneto-mechanical hysteresis

03 p0503 A71-13413

Logarithmic damping of flexural oscillations produced by residual fretting stresses in circular plates

03 p0503 A71-13415

Test equipment for damping ability of vibration absorbing coatings on prismatic rods under pure bending, using electromagnetic vibration induction system and optical recorder

03 p0396 A71-13417

Thin gas turbine disk strength under axisymmetric flexural vibrations, noting agreement of calculated and experimental rotor rpm danger zone

04 p0671 A71-15639

Energy dissipation during torsional and flexural vibrations of steel and duralumin specimens subjected to plastic deformation, accounting for discrepancies due to methodical errors

04 p0671 A71-15640

Thin elastic orthotropic oval cylindrical shells nonlinear flexural vibration based on assumed modes, using Galerkin method

05 p0819 A71-15979

Tapered cantilever beam with variable bending rigidity and concentrated mass, investigating nonlinear flexural vibration

05 p0820 A71-15986

Turbine blades flexural vibration modes, noting frequency parameter dependence on angular velocity, disk radius and stagger angle

05 p0796 A71-16648

Free flight space vehicle nonlinear bending vibrations due to harmonic and pulse excitation

05 p0825 A71-16679

Multilayer asymmetric plates deflection, stability and vibrations, deriving nonlinear bending equations with allowance for transverse shear strains

06 p0995 A71-17833

Three dimensional bending vibration analysis of homogeneous elastic circular cylindrical shell with both ends restrained

06 p1001 A71-18230

Partial differential equation solution for aircraft hydraulic lines flexural vibration by Bubnov-Galerkin method, reducing to Duffing equation analysis

08 p1286 A71-20783

Static tensile stresses effect on magnetized ferromagnetic materials damping properties explained by anisotropic microplastic strains dissipating energy during bending vibration

08 p1306 A71-21120

Rotating cantilever beams flexural vibrations, developing tables for frequency equation determination

08 p1370 A71-21306

Free flexural vibrations of orthotropic rectangular plates subjected to large amplitude free or forced oscillations, using von Karman nonlinear equations

08 p1370 A71-21307

Shrouded aircraft engine turbine blades vibration stresses found minimum by setting up paired blades with fixed tension along shroud

09 p1538 A71-22595

Energy dissipation during independent flexural-torsional vibrations of rods, noting alternating shear stress superposition effect on damping

09 p1538 A71-22629

Round cross section specimens flexural vibration damping decrement, determining amplitude dependent internal friction with allowance for stressed state

09 p1542 A71-23314

Flexural vibration analysis of rectangular isotropic and orthotropic polygonal elastic plates with constant or variable thickness, considering mass distribution and boundary conditions

10 p1625 A71-24019

Infinitely small flexural oscillations of initially stretched incompressible elastic circular cylinder, showing stretch effect on wave propagation velocity

10 p1689 A71-24521

Lumped parameter torsional and flexural system synthesis for vibratory characteristics, using transfer matrices

10 p1692 A71-24925

Spherical shell containing through crack, calculating in-plane and Kirchhoff bending stresses under periodic transverse vibrations

10 p1693 A71-25054

Frequency equation of flexural vibration of fluid filled circular cylindrical shells, using linear elasticity

12 p1974 A71-26928

Bending and torsional oscillations in rectangular specimens of femur and tibia, calculating elastic and shear moduli of compact bone tissues

13 p2019 A71-28658

Twist-bending vibration of ring of rectangular cross section for entire range of length-to-diameter ratios, using Rayleigh shell theory

14 p2328 A71-30414

Laminated plate flexural mode free vibration analysis by asymptotic method, obtaining phase velocity for comparison with experiment

14 p2330 A71-30684

Isotropic elastic thin oval rings nonlinear free and forced flexural vibrations calculation by Galerkin method

15 p2503 A71-31436

Clamped anisotropic symmetrically laminated plate bending, buckling and free vibration exact solution, using Fourier analysis

15 p2506 A71-32013

End play influence on dynamic bending vibration stresses induced by aerodynamic forces in axial flow turbine rotor blades in case of resonant vibrations

15 p2508 A71-32298

Circular rings coupled twist bending vibrations, considering rotatory inertia and shearing deformation effects

15 p2510 A71-32517

Missiles free flexural vibrations on moving or stationary launching pad calculated by matrix method

16 p2656 A71-33340

Rotary inertia and shear deformation effects on three dimensional flexural vibrations of circular ring on elastic foundation

16 p2657 A71-33421

Logarithmic decrement of flexural, longitudinal and torsional vibration damping of various size rods, taking into account surface layer energy loss

16 p2659 A71-33979

Finite length thin circular cylindrical shells with clamped or simply supported edges, calculating flexural free vibration natural frequencies

17 p2822 A71-34643

Small forced flexural elastoplastic vibration of structural beam, deriving approximate partial differential equation based on stress-strain relation

17 p2825 A71-35013

Static tension effect on damping capacity of stretched rods under flexural vibrations, considering materials with strong magneto-mechanical hysteresis

17 p2826 A71-35020

Logarithmic damping of bending oscillations produced by residual fretting stresses in circular plates

17 p2826 A71-35022

Clamped-clamped sandwich beam with thin face sheets and soft viscoelastic core, investigating forced, damped, nonlinear and LP flexural vibrations

17 p2826 A71-35032

Axial flow turbines, calculating effects of axial clearance between stator and rotor bladings on rotor impulse blades bending vibration strength

18 p2979 A71-36299

Fundamental frequency of large amplitude bending vibration of elastic and isotropic rectangular plates, considering effects of transverse shear and rotatory inertia

18 p2980 A71-36496

Nonstationary resonance analysis of forced flexural elastoplastic vibrations of beam of hardening/softening material under cyclic strain

18 p2981 A71-36709

Dynamic properties of turbine wheels under bending vibrations, classifying resonant frequencies on basis of vibration modes

18 p2981 A71-36722

Coriolis coupled bending vibrations of hingeless helicopter rotor blades, noting out-of-plane component contribution to aerodynamic coupling

19 p3154 A71-37294

Vertical statically unbalanced rotating shaft with two degrees of freedom, investigating internal damping, flexural vibrations and equation of motion

19 p3154 A71-37348

Coupled bending-bending vibration of pretwisted tapered cantilever blades, obtaining equations of motion

[ASME PAPER 71-VIBR-78] 21 p3460 A71-40315

Shear deformation and rotatory inertia effects on flexural vibration frequencies of pretwisted, nonpretwisted and tapered cantilever beams

[ASME PAPER 71-VIBR-79] 21 p3461 A71-40316

Bending resonance frequencies of beams for known external forces

21 p3463 A71-40550

Flexural vibration of rectangular orthotropic plates under in-plane hydrostatic forces

21 p3464 A71-40768

Holographic interferometry application to plate Poisson ratio determination and bending vibration analysis

22 p3539 A71-41741

Flexural wave propagation in thin curved rod oscillating in plane, calculating frequency and velocity from boundary conditions according to Saint Venant

22 p3617 A71-42574

Flexural vibration of transversely isotropic composite material curved beams, deriving curvature effects on natural frequency

24 p3878 A71-44616

BENDS [PHYSIOLOGY]

U DECOMPRESSION SICKNESS

BENZENE

Benzene, benzene-d sub 6 and sulfur dioxide radiative lifetime measurement comparison, investigating internal conversion behavior

14 p2190 A71-30576

Shock compressed tetranitromethane mixtures with various benzene ethyl iodide proportions, investigating lateral discharge wave effects on detonation process structure

15 p2511 A71-31382

Lithium iodide and tetramethyl ammonium iodide additions effect on radical exchange between phenyl lithium and bromobenzene in diethyl ether

19 p3011 A71-37391

Absorption spectra of benzene, naphthalene and anthracene crystals, noting resonance coupling type effect on vibrational spectrum

24 p3851 A71-45171

BERYLLIUM

NT BERYLLIUM 7

NT BERYLLIUM 10

NT BERYLLIUM 10

Be mechanical and physical properties, corrosion behavior, toxicity, fabrication and application as aircraft and spacecraft structural material

01 p0104 A71-11539

Be mirrors thermal dimensional instabilities dependence on crystalline anisotropy, discussing X ray quality control technique

03 p0424 A71-13637

Pressure and strain rate effects on polycrystalline Be shear strength, determining activation energy for dislocation motion

03 p0445 A71-14463

Europa 2 booster payload increase by using beryllium-containing solid fuels in perigee and apogee stages

05 p0815 A71-15969

Be impact strength temperature dependence and fracture structure, noting grain boundaries cohesion role

05 p0768 A71-16773

Ti-Be composites produced by powder coextrusion, discussing microprobe studies to determine microstructure thermal stability

05 p0000 A71-17104

Anomalous anodic Be dissolution in anhydrous environment, considering chunk effect and multivalent ions production mechanisms

07 p1118 A71-19568

Be films evaporated in vacuum on W single crystals, investigating adsorption and electron emission by field emission microscopy

07 p1178 A71-19918

Thermal conductivity, electrical resistivity and specific heat of hot pressed beryllium

10 p1624 A71-23908

Spark sintering powder metallurgy using alternating and direct current plus pressure, discussing use in Be components production for aerospace applications

10 p1618 A71-24765

C-5A airplane Be brakes, considering critical design weight environment for optimum load carrying capacity

[SAE PAPER 710427] 13 p1996 A71-28313

Be sheet plastic bend ductility and yield strength, considering purity and processing effects

13 p2088 A71-29403

Compression rolled and hot upset Be sheet stress-strain behavior and deformation dynamics, emphasizing temperature and strain rate effects on polycrystalline flow stress

13 p2088 A71-29404

Be droplet burning rate in oxygen-argon mixtures, using laser ignition technique

[WSS/CI PAPER 71-23] 15 p2464 A71-31632

Be, U and W shear strength measurements, detailing strain, strain rate and pressure effects

[ASME PAPER 70-WA/PT-2] 15 p2434 A71-32260

Fabrication, texture, alloying, substructure and fracture effects on bend ductility and toughness of beryllium sheet

15 p2436 A71-32509

T Tauri stars Li, Be and B autogenic generation, considering underabundance in surrounding gas

16 p2626 A71-33433

Beryllium impurities effects on ductile-brittle transition temperature, investigating fracture characteristics deformation mechanism

19 p3076 A71-37121

Cell structure development during room temperature tensile deformation of beryllium after prism slip by combined X ray diffraction-transmission electron microscopy

20 p3249 A71-39002

Burning rates of single laser ignited beryllium droplets, considering particle size effect

21 p3475 A71-40862

Beryllium reflector plate failure in NASA Plum Brook Reactor, discussing irradiation induced mechanical and physical property changes and internal/external stress effects

21 p3414 A71-40904

Increased microplastic deformation resistance, relaxation stability and aging of beryllium by cyclic heat treatment 23 p3690 A71-43281

Apollo 11 and 12 lunar dust and rocks, determining Be and Cr contents by gas chromatography for comparison with crystalline rocks 23 p3751 A71-43707

Solar atmosphere electron densities from ion emission line intensities in Be isoelectronic sequence 23 p3721 A71-43839

Zone refined Be crystals under room temperature compression, examining lattice defects with X ray synergy method 23 p3695 A71-44287

High purity Be single crystal transverse bending tests, plotting yield stress and bending angle vs temperature 24 p3836 A71-44673

Beryllium preparation from liquid beryllium iodides, describing apparatus 24 p3840 A71-45373

BERYLLIUM ALLOYS

Liquid and solid phase relations in Be-Al-Ti system by chemical, thermal, microscopic and X ray investigation, discussing solubility range of ternary phase and intermetallic compounds 10 p1629 A71-25034

Airframe structural uses of Al, Ti and Be alloys, discussing need for structural efficiency improvements by proper heat treatment and stress relieving techniques 16 p2594 A71-33875

Metallography of 700 C precipitation hardening in Fe-Ni alloy containing Be, using transmission electron microscopy 21 p3404 A71-41417

Thermoelastic coefficient development by tempering for Ni-Fe alloy containing Be 22 p3563 A71-42325

BERYLLIUM COMPOUNDS

NT BERYLLIUM HYDRIDES

NT BERYLLIUM NITRIDES

NT BERYLLIUM OXIDES

Device for rapid direct analysis of beryllium ores and concentrates in transport containers, using radiometric method 09 p1427 A71-22506

Structure and properties of beryllium compounds from solid state stable electron configuration formation viewpoint, discussing classification based on chemical bond 16 p2597 A71-33920

Beryllium preparation from liquid beryllium iodides, describing apparatus 24 p3840 A71-45373

BERYLLIUM HYDRIDES

Beryllium hydride pyrolytic decomposition kinetics noting temperature range, time distribution, linear growth rate and X ray irradiation 07 p1182 A71-19241

BERYLLIUM ISOTOPES

NT BERYLLIUM 7

NT BERYLLIUM 9

NT BERYLLIUM 10

BERYLLIUM NITRIDES

Heat capacity and thermodynamic properties of alpha beryllium nitride from 20 to 315 K, using precision calorimeter 04 p0674 A71-14726

BERYLLIUM OXIDES

High power microwave phase shifter, using beryllium oxide filler ceramic dielectrics to obtain thermal coupling between ferrite element and waveguide wall 17 p2713 A71-34396

BERYLLIUM 7

Cosmic ray Be 7 equilibrium concentration, examining electron capture and radioactive decay 05 p0798 A71-16114

BERYLLIUM 9

Enhanced low energy nuclear resonance reaction cross section estimation, finding Be 9 isotope reaction with proton for clean controlled thermonuclear reactor 24 p3847 A71-44495

BERYLLIUM 10

Criticism of paper on spallation cross section for Be 10 production from oxygen high energy fragmentation in meteorites 22 p3508 A71-42350

BESSEL FUNCTIONS

NT HANKEL FUNCTIONS

Bessel equation solutions for electromagnetic and acoustic wave equations in form of Hankel functions 08 p1333 A71-20740

Elliptical motion series representation, presenting methods for estimating values of Bessel functions, Fourier and Hansen coefficients 09 p1486 A71-23336

Simultaneous dual integral equations coupled pairs with constant coefficients involving Bessel functions of orders zero and unity 13 p2094 A71-28484

Matrix trace method for identities relating eigenvalues of singular ordinary differential operators and zero Bessel functions 16 p2603 A71-33593

Integrable linear differential equations application to Ricatti equation and Bessel, Legendre and other functions relations in celestial mechanics [AAS PAPER 71-333] 23 p3727 A71-43006

Recurrence techniques for generation of Bessel functions of complex order and argument 23 p3648 A71-43966

BETA PARTICLES

Rocket-borne beta ray atmospheric densitometer errors due to cosmic rays 05 p0752 A71-16673

Ce 138 excited states identification in beta decay spectra of Pr 138m and Pr 138 sources, using proton target bombardment 07 p1163 A71-19547

Radioactive decay energy conversion of beta particle emitting cerium 144 into high voltage electricity in coaxial cylinder cell 15 p2447 A71-32211

Thermoluminescent dosimeter for skin basal layer dose measurement in mixed beta and gamma radiation fields 17 p2693 A71-35450

Radioisotopic power applications of beta and gamma emitting Co 60, noting powder ceramic fabrication of dense wafers for irradiation to convert natural Co 59 20 p3265 A71-38938

BETATRONS

X ray monitoring process optimization with pmb-6 betatron, discussing intensifying screens thickness and composition effects on defects detectability 22 p3553 A71-41762

BIAS

NT RESPONSE BIAS

Temperature and bias circuit frequency modulation in CW X band Gunn oscillators 18 p2888 A71-36132

BIBLIOGRAPHIES

Soviet bibliography concerning lunar surface physical properties, covering ground and orbiters observations data 01 p0148 A71-10045

Carbon dioxide laser bibliography/1964-1969/ with chronologically listed references, author index and subject index 01 p0092 A71-10370

Bibliography of bibliographies, manuals and books covering photointerpretation and remote sensing 01 p0084 A71-11379

Heat transfer literature/1969/ covering conduction, boundary layer, channel and separated flows, convection, mass transfer, radiation, etc 01 p0181 A71-11402

Sparse matrices inverses and eigenvectors computation methods, giving bibliography 02 p0276 A71-11802

Nonideal plasma thermodynamics data, discussing particle interactions, Coulomb potential, stability, etc 02 p0288 A71-11888

Heat transfer analysis literature survey, including bibliography of perturbation, asymptotic and integral equations methods 02 p0333 A71-12650

Postbuckling theory and applications covering perfect structure prebuckling state stability, cylindrical shells under axial compression, etc 04 p0664 A71-14734

Lunar studies bibliography covering shape, EM properties, structure, gravitational fields, chemical composition, origin, surface features, etc 05 p0809 A71-16463

Relativistic gravitation theory and experimentation, surveying literature on gravity waves, EM propagation, gyroscopic precession, etc 07 p1158 A71-19096

Soviet bibliography concerning lunar surface physical properties, covering ground and orbiters observations data 08 p1360 A71-21039

Research bibliography on resins and additives covering polyesters, epoxies and new polymers with improved corrosion, fire and heat resistance 11 p1788 A71-25431

Bibliography on Gegenschein covering observations, theories, models, review papers, etc 11 p1835 A71-26461

Pyrophoric materials literature, discussing nature, behavior, production, safe handling and fire control 13 p2158 A71-27854

Bibliography on lunar and planetary subjects covering astrobibliography, comets, cratering, meteors temperature, structure, asteroids, tektites surface features, etc 13 p2135 A71-28293

Multicategory bibliographic classification of human behavior computer simulation models 14 p2189 A71-30461

Bibliographic references of articles on solar terrestrial research during IQSY, including geophysical

phenomena, international projects and background material 15 p2397 A71-31617

Pattern recognition machine construction for written alphanumeric symbols and human voice identification, providing bibliography 15 p2372 A71-32316

Josephson and IC type superconducting tunneling junction neuristor devices performance tests, presenting bibliography 15 p2377 A71-32317

Optimal control of distributed parameter systems described by integral and partial differential equations, providing theory and bibliography 16 p2549 A71-33354

Automatic control systems sensitivity, including literature survey 16 p2550 A71-33703

Bibliography and review of noble gases isotopic abundance in meteorites and lunar material, considering cosmic ray interactions, radiation ages and extinct radionuclides 17 p2798 A71-34451

Bibliography and review of age determination of meteorites and lunar samples, considering chondrites, achondrites and iron meteorites 17 p2798 A71-34452

Bibliography and review of meteorites not classified as chondrites, considering achondrites, stony irons and iron meteorites 17 p2798 A71-34453

Chondrites bibliography and review, considering classification, metamorphism, ages and thermal history, achondrites and organic compounds 17 p2798 A71-34454

Asteroids and comets bibliography and review, considering celestial mechanics and astrometry, photometry, spectra, polarimetry and radar measurements 17 p2798 A71-34455

Micrometeoroids bibliography and review, considering ground based photometry and scattering theory, satellite flux measurements, particle collection and craters 17 p2798 A71-34456

Bibliography and review of solar system bodies surfaces, considering remote sensing at UV, optical, IR, microwave and radio wavelengths, in situ lunar measurement and surface exploration 17 p2798 A71-34458

Bibliography and review of solar activity relevant to sun-planet relationships, considering magnetic fields, transient events, corona and solar wind 17 p2799 A71-34459

Bibliography and review of interplanetary magnetic fields and plasmas, considering solar wind properties, magnetosheath, bow shock and magnetospheric tail 17 p2799 A71-34460

Bibliography on neutral atmosphere dynamics covering waves, winds, turbulence and disturbances in thermosphere and ionospheric effects 17 p2732 A71-34462

Bibliography on upper atmosphere hydrogen covering Lyman alpha and beta and Balmer alpha measurements, non-Maxwellian distribution, diurnal variations and oxygen evolution 17 p2732 A71-34463

Airglow research review and bibliography covering past four years observations of nightglow, twilight, dayglow and metals in upper atmosphere 17 p2732 A71-34466

Bibliography on aurora covering observations, morphology, atomic and molecular processes, electric fields, radio scattering, red arcs and particle precipitation 17 p2732 A71-34467

Bibliography on magnetosphere covering structure, magnetopause, geomagnetic tail, plasma sheet, convection plasmopause, storm and substorms, ring current and energetic particles 17 p2732 A71-34468

Soviet papers on higher nervous activity physiology, Part 1, Basic laws and mechanisms of conditioned reflex activity covering inhibition, and bioelectrical effects, with bibliography 17 p2684 A71-35357

Microwave radiation biological effects review and bibliography covering protein activity, genetic, central nervous system and cardiovascular effects 18 p2864 A71-35956

Air piracy/hijacking/ bibliography, considering national and international law, extradition, punishment, prevention and safety insurance for passengers and crews 22 p3622 A71-41617

Asteroid 1967 observation and ephemeris activity, surveying 1966-1967 literature 24 p3874 A71-45172

BICARBONATES

U CARBONATES

BICRYSTALS

Aluminum bicrystals mechanical properties under high strain rates, considering changes in surface structure, active slip planes and dislocation 04 p0612 A71-15077

BIHARMONIC EQUATIONS

Weak periodic solutions of hyperbolic partial differential equation with quadratic dissipative term for biharmonic waves

02 p0276 A71-12000

Thermal stresses in finite circular cylinder heated axisymmetrically over curved surface, constructing thermoelastic displacement potential and biharmonic Love function

09 p1536 A71-22452

Biharmonic problems solution in elasticity theory for piecewise homogeneous doubly connected media with interface in conformal mapping of ring onto doubly connected region

19 p3160 A71-38486

Random analogs of boundary value problems class for biharmonic functions, demonstrating unique solution existence

21 p3410 A71-41189

Biharmonic operator eigenvalues for rectangular domain, presenting bilateral a posteriori estimation methods based on discrete analysis and approximate separation of variables

24 p3842 A71-44476

BILLETS

Stress-strain state of annular billet under local plastic bending by forces in cross sectional plane

13 p2154 A71-28646

Production efficiency prerequisites in extruded Al alloy products manufacture, discussing billet material and processing conditions effects

16 p2584 A71-34091

BIMETALS

Thin walled two layer bimetallic shells of revolution under large deformation, analyzing equilibrium by zero moment theory

06 p0998 A71-17856

Titanium-steel bimetal part fabrication using explosive and drop forging

08 p1295 A71-20840

Bimetallic refractory metal joints electron beam welding and aging for applications to in-pile thermionic converters

11 p1769 A71-25857

Mechanical design of frictionless bimetal actuated lower system for spacecraft thermal control [ASME PAPER 71-AV-39]

18 p2870 A71-36406

Bimetallic plated high strength steel, noting transition zone effects on mechanical properties

23 p3692 A71-44026

BINARY ALLOYS

Fine structure and lattice constants of Al-W, Al-Mo and Al-Mn alloys at high cooling rates

01 p0101 A71-10675

Near stoichiometric binary alloys atomic ordering parameters quantization by field ion microscopy, using direct counting and optical transformation techniques

02 p0297 A71-12736

Nb-impurity binary solid solutions, calculating interdiffusion and heterodiffusion coefficients

02 p0270 A71-12930

Nb binary solid solutions with various Ti, Mo and Zr percentages, examining structure and mechanical properties

02 p0270 A71-12931

Nb binary alloys room temperature brittleness in hydrogen atmosphere

02 p0270 A71-12932

Nb high purity binary alloys preparation and processing

02 p0270 A71-12933

Hole effect on residual resistivity of crystalline binary ordered substitution alloy with bcc lattice

03 p0467 A71-13952

Near equiatomic Ta-Ru alloys phase transformations by resistance and susceptibility changes and X ray powder patterns of cooled structure

04 p0614 A71-15777

Binary Ti alloys hydrogenation-dehydrogenation treatment effect on alloying element activity

04 p0615 A71-15801

Vapor deposition rates from liquid binary alloy targets under ion sputtering

05 p0757 A71-16235

Computer calculation of phase diagrams from thermochemical data for Cr-Mo and Mg-Cd systems

07 p1054 A71-19519

Mossbauer effect study of 475 C decomposition of binary Fe-Cr alloys, considering fluctuations about average composition

07 p1138 A71-19985

Aging effect on tensile mechanical properties and hardness of high purity binary Ni-Cr alloys at 290-530 C

07 p1138 A71-19986

InAs-AlAs pseudobinary system solidus boundary determination from pellet phase diagram

08 p1344 A71-21472

Fcc binary alloys cross slip difficulty due to solute atoms and small short range order regions

08 p1309 A71-21527

Single crystal TiC-VC alloys mechanical properties, considering room temperature hardness, high tem-

perature deformation and brittle to ductile transition temperature

08 p1316 A71-21589

Isothermal transformation of metastable beta Ti-Mo alloys, considering contraction start point coincidence with point of quenched omega transformation to aged omega in TTT diagram

10 p1625 A71-24006

Zr effect on Ti-Mo beta alloy stability, considering Zr suppression and retardation of omega precipitation on basis of TTT diagram and tensile tests

10 p1625 A71-24007

Diffusion processes in Mo-W thermionic emitters of massive couple type and piece of Mo substrate with vapor-deposited W layer respectively

11 p1709 A71-25864

Monovariant eutectic Co-Cr-C ternary systems, determining pseudobinary and near-pseudobinary phases by differential thermal and microprobe analyses and optical microscopy

11 p1780 A71-26025

Dutch monograph on Cr-W interdiffusion in solid state concerning Kirkendall effect and relation between chemical and self diffusion

11 p1783 A71-26488

Ni-Cr and Ni-W alloys high temperature strength properties, considering stacking fault energy, diffusion velocity, Young modulus and dislocation locking

12 p1919 A71-27762

Molybdenum-niobium alloys single crystals electron work function in vacuum from emission patterns and anisotropy

16 p2595 A71-33881

Binary and ternary metal compounds superconductivity parameters comparison, considering crystal structure, valence electron concentration, component position and processing techniques

16 p2622 A71-33925

Superhigh cooling rate effects during crystallization of solidified binary alloys, achieving superconductive properties

16 p2598 A71-33998

Binary alloy solidification in electroslag remelting process, determining temperature distribution and solidus, mushy and liquidus zones by heat transfer analysis

19 p3079 A71-37706

Intermetallic formation in Au-Al systems via diffusion couples, determining activation energy, silicon effect and tensile strength

19 p3119 A71-38513

Ambient gas effects on Au-Al bonds life in integrated circuit package

19 p3119 A71-38514

Ti-Fe and Ti-Cr binary alloys microsegregation genetic trend measurement by electron probe microanalysis, observing critical cooling rate from beta phase

22 p3562 A71-41945

Co-Mn binary alloy phase diagram redetermination, noting sigma phase formation after heavy deformation

23 p3689 A71-42933

Structure, hardness, density and electrical resistance of binary alloys V-Ti, V-Cr, V-Al and V-Sn

23 p3691 A71-43283

Thermodynamic properties of Ti-Mo alloys, using triple Knudsen cell technique

23 p3694 A71-44279

Sodium role in accelerated oxidation behavior /sulfidation/ of Ni-base superalloys and binary alloys coated with sodium sulfate or carbonate

23 p3695 A71-44288

Mo-W, Ta-W and Nb-W alloys X ray analysis at high temperatures, calculating interdiffusion coefficients and temperature effects on W concentration

24 p3836 A71-44671

BINARY CODES

PL/I compiler for system programming in high speed binary machine object code

01 p0045 A71-10194

Block code for retransmission of information damaged by noise bursts for feedback digital communication systems

01 p0034 A71-10905

Decoding n-bit Johnson code to decimal numbers using n 2-input 2-output comparator circuits

01 p0037 A71-11175

Binary error correcting codes in asynchronous systems for separate message transmission, discussing decoding and spacing

01 p0039 A71-11315

Iterative and cascaded codes for single and grouped error detection

01 p0039 A71-11317

Image recognition process based on binary digit codes descriptions, developing algorithm for minimal system of characteristics

05 p0726 A71-17019

Digital asynchronous information transmission, describing schemes for coding binary into ternary signals

05 p0724 A71-17058

Servo stability of binary code follow-up analog-digital converter with magnetic modulated zero elements

08 p1261 A71-20736

Lower bounds for minimum weight of binary cyclic code vectors of composite length, using factorization

08 p1324 A71-21321

Binary pseudorandom codes sequences correlation properties in PSK telemetry

09 p1404 A71-22154

Power spectral density /PSD/ analysis of multilevel binary coded signals for high density PCM recording

09 p1412 A71-22784

Cyclic and multiresidue AN codes, determining single error correcting range

09 p1412 A71-23103

Hybrid decoding technique for symmetrical binary input channels, using bootstrap algorithm across convolutionally encoded information streams

11 p1730 A71-25375

Binary periodic convolutional codes with lower bound everywhere stronger than Wagner on definite decoding minimum distance

11 p1731 A71-25758

Block code construction for binary single, double and triple error correction, including cyclic BCH, circulant and nonlinear codes

14 p2200 A71-30919

Binary, uncoded and M-ary FSK with convolutional codes for low powered planetary entry probes communicating to earth

14 p2200 A71-30921

Pseudorandom binary codes for improved microwave antenna range measurements by suppressing unwanted reflections

15 p2373 A71-32370

Error estimates in transmission of pulse code telemetering signals by nonredundant binary code through asymmetric channel

16 p2543 A71-33706

Mean-square-error determination for binary code data transmission in symmetrical channels with slowly changing parameters, noting dependence on fading level

17 p2702 A71-34974

Binary coding and phase displacement modulation of digital data in radio transmission

22 p3514 A71-42471

Binary parabolic phase coded waveform generation from analog signals by pi-quantization

23 p3645 A71-43440

Binary nonconsecutive one code for time-tag data compression in digital communication, noting transmission power and bandwidth requirements reduction

24 p3803 A71-44651

Error correcting binary block code decoding on Q-ary output channels /weighted erasure decoding/, considering applications

24 p3806 A71-44936

Rate 1/2 convolutional error correcting binary codes with complementary generators, discussing synthesis and search procedure for largest free distance

24 p3807 A71-44937

BINARY DATA

Radio signal reception error in cadence synchronization of binary data transmission systems with indeterminate signal arrival time

02 p0212 A71-11834

Signal optimization for binary data transmission system with noiseless feedback channel, considering receiver signal energy and structure

04 p0560 A71-14743

Iterative method for good aperiodic binary sequences in radar range resolution

07 p1148 A71-19769

Optimal error correcting code structure selection for binary data transmission systems synchronization, using criterion of minimum false detection probability

08 p1260 A71-21979

Cyclic block code structures for generating binary sequences with good autocorrelation properties

09 p1407 A71-23110

Large high speed binary multiplier units design

12 p1884 A71-27152

Fast versatile iterative parallel binary comparator array, proposing cell output states assignment

13 p2037 A71-28475

Binary data compression for satellite-borne instrumentation for space physics measurements, discussing redundancy reduction technique

13 p2033 A71-29274

Binary pulse sequences correlation and synchronization, developing effectiveness criteria with two stage measures

14 p2201 A71-30927

Binary intensity holographic information storage system, investigating nonlinearity effects

15 p2412 A71-32591

Telegraphy binary data transmission through channels with frequency-selective fading, investigating noise stability improvement by programmed carrier frequency variation and receiver passband shifting

17 p2698 A71-34394

- Binary relation algebra application to diagnostics tests for system involving redundant subsystems
17 p2720 A71-34960
- Iterative clustering technique for minimizing probability of differences between binary data reconstructions from cluster codes and initial data
17 p2711 A71-35047
- FSK L-level or duobinary system performance evaluation under intersymbol interference, using limiter-discriminator without postdetection filter as detector
17 p2707 A71-35479
- German monograph on nonlinear distortion correction of binary bipolar signals in Gaussian noise covering receiver, decision theory and error probabilities
18 p2874 A71-35959
- Error occurrence due to perturbations in space communication channels for digital data transmission, describing binary channels models based on Markov chains
18 p2881 A71-36567
- Binary sequences generated by conventional pseudorandom shift register sequences for communication and system identification
18 p2881 A71-36568
- Critique of paper on additional signal power for optimum performance of PCM binary signal detection under channel band limiting effect in white noise
20 p3196 A71-38870
- Ear inherent channel capacity estimation by applying Shannon equations for binary signal transmission
20 p3191 A71-39769
- Binary moving-window integrator radar target azimuth measurement error determination, presenting target detection probability curves obtained by digital simulation
21 p3348 A71-40725
- Computer technique for synthesizing binary holograms used in wave beams analysis in quasi-optical communication channels
22 p3546 A71-42320
- BINARY DIGITS**
Image recognition process based on binary digit codes descriptions, developing algorithm for minimal system of characteristics
05 p0726 A71-17019
- Serial binary multiplication computation speed, considering recoding algorithm with cellular array multipliers
18 p2894 A71-36829
- Signed binary numbers multiplication algorithm, describing cellular arrays for twos-complements multiplication method
18 p2894 A71-36831
- Cellular array for multiplication and division of two binary numbers, discussing implementation with transistor-transistor logic integrated circuits
18 p2894 A71-36833
- BINARY FLUIDS**
Laminar and turbulent mixing of two parallel streams of dissimilar fluids, using similarity transformation
[ASME PAPER 70-WA/APM-37]
03 p0403 A71-14162
- Inviscid binary gas mixture steady supersonic two dimensional flow past convex corner, taking into account spontaneous condensation
03 p0345 A71-14559
- Translatory vapor bubbles motion in binary liquid mixtures under heat and mass transfers
04 p0687 A71-15534
- Binary fluids boiling heat and mass transfer in boundary layer, discussing bubble growth rate, surface roughness effects and burnout heat flux
07 p1221 A71-18791
- Group properties of laminar boundary layer equations for incompressible binary fluid under various magnetic field distributions and reaction rates
13 p2048 A71-28735
- Dielectric relaxation time in Debye binary liquid, comparing liquid filled coaxial transmission line step response measurements with Debye model
14 p2215 A71-30985
- Binary fluid mixtures density gradients near critical point due to gravity effect, deriving expression as linear function of height with thermodynamic equilibrium as starting point
21 p3345 A71-40236
- BINARY INTEGRATION**
Hybrid binary floating point digital differential analyzer technology, noting speed, cost and utility
14 p2207 A71-30021
- BINARY MIXTURES**
NT BINARY FLUIDS
NT EUTECTIC ALLOYS
NT EUTECTICS
Thermal conductivity of binary gas mixtures with/without hydrogen to 1100 K, using molecular kinetic theory and structure model
03 p0520 A71-13749
- Binary liquid metal forced convection boiling heat transfer, determining axial and radial temperature distribution in two phase flow
04 p0676 A71-15173
- Binary gas mixture rarefied hypersonic flow structure near blunt body, investigating diffusive effects on recovery temperature dependence
04 p0528 A71-15488
- Methane and ethane binary mixtures with chlorine, determining main combustion products under flame propagation
07 p1054 A71-19280
- Two phase mixture spark ignition dynamics, investigating probabilistic character and ignition energy
07 p1224 A71-20068
- Binary gas mixtures shock tube flow kinetic theory, indicating shock wave formation, contact layer diffusion and expansion wave dispersion
07 p1093 A71-20287
- Bismuth oxide and iron oxide equimolar mixtures solid state reactions, determining rates from integrated X ray diffraction and activation energies
08 p1318 A71-20699
- Fe-S condensates structure and phase transformations during heating, noting importance for antifriction materials synthesis
08 p1322 A71-21062
- Fe powder concentration in Ni powder by spectral analysis, examining particle size and HF generator spark condensation effects
08 p1306 A71-21066
- Nitrogen-oxygen and nitrogen-argon mixtures viscosity, using oscillating disk viscometer to test corresponding states principle validity
09 p1546 A71-23010
- Thermal conductivity of Ar binary mixtures with He, N and Ne, using secondary concentric cylinders cell
09 p1547 A71-23463
- Spherical shell potential extension to shells of differing diameters for intermolecular forces in globular molecules, considering binary gaseous mixtures
11 p1801 A71-25369
- Thermodynamical properties computation for binary mixture in equilibrium at constant pressure and temperature based on Gibbs free energy
11 p1851 A71-26380
- Inhibiting mechanism of ethane in hydrogen-oxygen mixtures ignition, discussing lower limits, carbon monoxide effect and chain lengthening reactions
11 p1730 A71-26566
- Diagnostic flow visualization, using chemiluminescent radiation in mixing region between aqueous luminol and potassium ferricyanide solutions
13 p2044 A71-27853
- Partially ionized binary gas mixture temperature development during nonequilibrium ion formation, solving heat and ionization balance equations
13 p2062 A71-28573
- Gasoline-air combustion zone extent as function of inlet temperature for plane turbulent flame in square-section channel
13 p2163 A71-28960
- Grid-induced turbulence effect on flameout characteristics of kerosene-air flames stabilized by bluff bodies of different sizes
13 p2163 A71-28961
- Combustion process in mixing zone of kerosene-air mixture and hot combustion products, deriving flameout time relation to characteristic temperature in mixing region
13 p2163 A71-28964
- Jet induced flame stabilization in combustible kerosene-air mixture flow of variable composition, discussing stable burning range and excess air content
13 p2163 A71-28965
- Diffusive separation of binary gas mixture in free jet expelled into vacuum, comparing theory and experimental results
13 p2050 A71-29216
- Stochastic modification of binary fluid mixtures hydrodynamic dissipative equations, considering nonequilibrium entropy
13 p2051 A71-29354
- Pressure recovery performance of straight-wall two dimensional diffusers with subsonic air-water mixtures, studying gas volume flow ratio and diffuser geometry effects
[ASME PAPER 71-FE-20]
13 p2052 A71-29458
- Alkali metal, alkaline earth metal nitrates and sodium perchlorate mixed with powdered magnesium burned in rarefied air
14 p2338 A71-30616
- Reagents for photometric determination of rare earth elements of yttrium subgroup in binary mixtures with La or Ce
15 p2367 A71-31646
- Thermodynamic properties of dilute solutions of oxygen in liquid Fe-Co and Fe-Ni binary mixtures, obtaining Gibbs energy variation with temperature
15 p2432 A71-32174
- Binary laminar boundary layer in hypersonic axisymmetric stagnation point flow with temperature dependent material properties, presenting exact and approximate calculation methods
17 p2671 A71-35422
- Microphase separation in homopolymer-block copolymer mixtures as function of composition, molecular weight and interaction parameters
17 p2695 A71-35525
- Spectroscopic analysis of continuous light emission from molecular oxygen-nitrogen mixtures in Mach 9 shock waves, stressing radiative reaction role
19 p3106 A71-37462
- Flow parameters behind shock waves propagating in carbon dioxide-nitrogen mixtures at Mach numbers from 5 to 10
19 p3044 A71-37583
- Mg-Ge alloys liquid and two phase mixtures thermodynamic properties at 660-1130 C, using galvanic cell with magnesium chloride electrolyte
19 p3080 A71-37715
- Shock induced ignition in explosive homogeneous hydrogen-oxygen gaseous mixtures
19 p3171 A71-38130
- Composition effects on binary gas mixtures thermal conductivity coefficient, considering Hirschfelder-Eucken formula
24 p3886 A71-44369
- BINARY STARS**
NT COMPANION STARS
NT ECLIPSING BINARY STARS
Computer program for orbital elements of spectroscopic binaries and probable error computation
01 p0152 A71-10352
- Orbital elements of spectroscopic binary Zeta Scuti by computer program and spectrograph observations, tabulating results
01 p0152 A71-10353
- Blue supergiants evolution, discussing chemical composition of atmospheres, mass, binary nature and cluster association
01 p0153 A71-10375
- Zero moments surface in problem of two immovable centers taking into account cosmic dust accumulation before binary apex moving forward with periastron of bright component
03 p0484 A71-13220
- Close binary star evolution, discussing mass exchange in system with 7 solar mass primary
03 p0490 A71-13939
- Blink comparator with automated precision reading for converting rotation angles to digital form for binary star measurements
04 p0534 A71-14853
- German monograph on mass transfer between close binaries from hydrodynamic standpoint
04 p0644 A71-15099
- Close binaries evolution, atmospheres structure and three body problem
04 p0647 A71-15241
- Binary star radial velocity measurement, discussing formation, evolution, motion frequency and H-R diagrams
04 p0647 A71-15242
- Double star system with neutron star in pair with matter-losing star, discussing X ray sources variability causes
06 p0976 A71-18455
- Cosmic plasma stream capture by magnetic dipole of neutron star in binary system
07 p1192 A71-19287
- Book on dwarf novae covering light variations, spectra, binary systems, absolute magnitude, mass, gas streams, outburst, etc
08 p1363 A71-21165
- Photoelectric stellar image analyzer for measuring close binary stars separation, collecting data by image coherent superposition
08 p1290 A71-21393
- Stellar X ray sources as close binary stars and old novae, calculating radiation by deceleration process
09 p1528 A71-23544
- Collapsed or neutron star companions of bright binary stars, explaining low luminosity of more massive component
10 p1665 A71-23740
- Binary star 112 Herculis elemental abundances by atmospheric model analysis of spectra
10 p1680 A71-25001
- Binary alpha Virginis interferometric data, noting distance, luminosity brightness ratio, angular size and diameter, orbits mass, temperature and gravity
11 p1830 A71-26107
- Neutron star formation from supernova explosion in close binary system
11 p1832 A71-26171
- Mass exchange during main sequence evolution of close binaries with shell hydrogen burning
11 p1832 A71-26185
- Binary system of neutron star paired with matter-losing star, discussing X ray emission variability causes
12 p1956 A71-26605
- Lunar occultation photoelectric observations, emphasizing double star nature
14 p2306 A71-29685
- Visual double stars observation techniques coordination - Conference, Nice, September 1969
14 p2310 A71-30356
- Photoelectric scanning photometer for visual binaries measurement, using on-line computer for data sampling and acquisition from three photon counters
14 p2246 A71-30357

Lunar occultation application to small separation double stars discovery and measurement

14 p2246 A71-30358

Double stars astrometry, discussing proper motions, parallaxes and mass ratios of visual binaries

14 p2310 A71-30359

Double and triple stars common proper motion, discussing white dwarf or degenerate components

14 p2310 A71-30360

Double star discovery by common proper motion, using IDS catalog data

14 p2311 A71-30361

Visual binary star observations by Lallemand electronic camera and photo-electronic image devices

14 p2311 A71-30363

Double star measurements precision obtainable in space with stable and perfect instrument, comparing to ground observations

14 p2246 A71-30364

Visual binary stars spectroscopic observations, discussing spectra, luminosity, parallax and radial velocities of mass center and individual stars

14 p2311 A71-30365

Radial velocity differences between components of close visual binary stars by spectroscopic and oscilloscopic measurements

14 p2311 A71-30366

Visual double stars spectroscopy, discussing stellar mass and parallax determination

14 p2311 A71-30367

Visual binaries high resolution spectroscopy, obtaining radial velocity changes with Coude spectrograph

14 p2311 A71-30368

Early type close binary systems AO Cas, HD 47129, HD 190918 and HD 193793 spectral observations

14 p2311 A71-30369

Observation errors in double star studies, considering inclusion of corrections in Central Card Catalog

14 p2311 A71-30370

Observational errors respecting orbital visual binaries periods, major axes and total mass, considering random and systematic errors

14 p2312 A71-30371

Orbit computation and measurement errors of visual binaries by wire micrometer distance method

14 p2312 A71-30372

Binary stars photometry, considering optical, physical and orbital pairs

14 p2312 A71-30373

Lallemand camera for photography of visual binaries, avoiding atmospheric motion effects by double image recording

14 p2312 A71-30375

Pulsars 0527 and 0531 as remnants of binary star supernova explosion, considering mass exchange and measured proper motion of 0531 and Crab Nebula

14 p2315 A71-30657

Galactic discrete X ray sources identification with black nebulae, H II regions, close binary stars, Wolf-Rayet stars and planetary nebulae

15 p2482 A71-31330

Neutron stars with pulsar characteristics in binary systems, discussing matter accretion relationship to X ray source evolution

15 p2483 A71-31342

Wolf-Rayet stars evolution due to stellar matter mixing and escape from nuclei

17 p2800 A71-34571

Photoelectric astrometry to determine stellar position, noting application to binary stars

17 p2741 A71-34995

Mass transfer in close binaries, determining gaseous ring formation conditions and properties from ejected particle trajectories computation

17 p2809 A71-35594

Close binary systems evolutionary processes, considering mass transfer and gas dynamics

18 p2968 A71-37033

Spectroscopic binary star system with orbital eccentricities less than 5 percent, discussing elliptical or circular orbit possibility

18 p2971 A71-37068

Spectroscopic binary system with invisible major mass components, considering relativistic companion star

19 p3134 A71-37508

Close binary star system: U Gem, VV Pup and UX UMa, calculating gas streams trajectory movement

19 p3134 A71-37509

Black holes in binary star systems from orbital eccentricity observations

19 p3142 A71-38006

Binary stars survey at Nice observatory, presenting expression for probable period and parallax of newly discovered binaries

19 p3143 A71-38156

White dwarfs production in small mass binary systems, deriving formulas for final mass and orbital velocity with application to blue stragglers

19 p3143 A71-38160

Binary systems formation probability during triple encounters, considering random initial conditions

20 p3290 A71-39301

Observation probability of orbital motion and mass transfer of pulsars in close binary systems, excluding supernova explosion origin for runaway velocities

20 p3304 A71-39943

Close binary stars monochromatic reflection effect calculation, using surface temperature distribution model

22 p3599 A71-41934

Pulsar characteristics suppression in neutron stars of binary systems, discussing matter accretion relationship to X ray source evolution

22 p3606 A71-42617

To passage in front of binary star beta Scorpii on 14 May 1971, presenting satellite trajectory calculations and appulse time

23 p3733 A71-43150

BINARY SUMMATORS

U ADDING CIRCUITS

BINARY SYSTEMS [DIGITAL]

U DIGITAL SYSTEMS

BINARY SYSTEMS [MATERIALS]

NT BINARY ALLOYS

NT BINARY FLUIDS

NT BINARY MIXTURES

NT EUTECTIC ALLOYS

NT EUTECTICS

Two-phase composites stability at various temperatures, noting failure regularities dependence on components mechanical properties relationship

01 p0106 A71-10083

Phase relationships in magnesium ferrite-magnesium chromate systems subjected to annealing in air and hydrogen atmospheres

01 p0107 A71-10403

Cadmium-copper fibrous eutectic alloy morphology, describing sample preparation and crystallographic examinations by optical and electron microscopes

01 p0103 A71-11018

Fine coherent precipitate morphologies by spinodal mechanism, reviewing clustering in binary solid solutions

03 p0446 A71-14491

Two-phase detonations, discussing importance of stripping mechanism and droplets deformation in reaction zone fuel consumption

05 p0834 A71-16515

Binary A15 phases transition elements compositional variations effects on atomic ordering

07 p1163 A71-19430

Liquid Al binary systems thermodynamic properties, using emf, improved dew point and distribution methods

07 p1143 A71-20489

Effective dielectric constant of macroscopically homogeneous and isotropic two phase composites in terms of sample geometry

10 p1655 A71-23922

Binary phase systems stress analytic method for water saturated elastic porous medium

10 p1685 A71-23993

Binary interstitial solid solutions thermodynamic properties calculation with Kirkwood expansion, allowing crystal first order partition function measurement without degeneracy error

13 p2087 A71-29133

Grain refinement in dilute Al alloys, comparing peritectic reaction effect for Ti, Zr and Cr as alloying components

15 p2433 A71-32181

Two-phase composites stability at various temperatures, studying mechanical properties dependence on second phase proportion

16 p2593 A71-33639

Tungsten-oxygen system surface reactions in vacuum, emphasizing interfacial geometry variations, faceting and oxide nucleation

17 p2694 A71-34667

Diffusion processes electron mechanism in metal-metal and metal-nonmetal systems, using configurational model for valence electrons localization

21 p3403 A71-41159

BINAURAL HEARING

Earmuff hearing protectors evaluation for attenuation of narrow band noise on experienced subjects

14 p2188 A71-30196

BINDERS [ADHESIVES]

U ADHESIVES

BINDERS [MATERIALS]

NT PROPELLANT BINDERS

Polymer binder effect photoviscoelastic stress analysis near discontinuous reinforcing fibers, comparing results with finite element method for time dependence

[SESA PAPER 1630]

03 p0507 A71-13755

WC-Co system binder phase composition and properties, studying W content as function of initial carbide grain size, Co content, sintering and quenching time

09 p1466 A71-22170

Discrete phase vs binder strength of inorganic brittle polycrystalline powder metallurgy materials, including alumina and magnesia

09 p1483 A71-23398

Impact composite materials with reactive resins as binders for polyester fabric, determining peel resistance, tensile shear strength and high temperature aging effect

11 p1786 A71-25416

Polymer binder setting degree effect on maximum strength of fiberglass cross reinforced plastic, analyzing compressive, bending, hardness, impact, thermal and porosity properties

16 p2601 A71-33682

Tungsten carbide-cobalt alloys, investigating binder metal mechanical properties relationship to composition by chemical analysis and X ray inspection

19 p3083 A71-38475

BINDING

Dilute Al alloys single crystals amplitude dependent internal frictions measurement, obtaining binding energies between substitutional alloying atoms and dislocations

08 p1310 A71-21535

Van der Waal bound lamellar solids interlayer binding energy computational model, discussing talc and pyrophyllite equilibrium stacking arrangements and force constants

10 p1573 A71-24541

BINOCULAR VISION

Visual slant averaging mechanism evidence from binocular disparator tests, considering gradient slant perception theory and neurophysiological averaging mechanism

04 p0546 A71-15170

Binocular synchronization data, suggesting visual coordination dependent on continuous eye movement and retinal feedback timing

05 p0712 A71-16218

Monocular and binocular vision comparison under moderate whole body Gz sinusoidal vibration stress environments

06 p0858 A71-17606

Nonius horopter theory and mathematical model, discussing binocular disparity and monocular visual direction criterion

09 p1399 A71-23016

Visual latencies at photopic levels as function of binocular differences in retinal illuminance, using Limulus adaptation model and ERG correspondence

16 p2527 A71-32867

Light adaptation and visual latency, discussing temporal resolving properties of eye as function of binocular differences and target background contrast

16 p2527 A71-32868

Stereoscopic effects and apparent shape or position of moving objects at relativistic speeds under binocular observation

16 p2535 A71-33166

Risk additivity in portfolios from experiments on accommodation role in binocular rivalry control

17 p2684 A71-35254

Visual perceptual masking under binocular and dichoptic conditions separating peripheral and central interference effects

21 p3342 A71-40225

Inhibitory binocular receptive fields in dorsal nucleus of lateral geniculate body for dominant and nondominant eye in cats, using moving slit and flash spot stimulation

21 p3335 A71-40669

Flash light angular size, adaptation luminance, pulse shape and color effects on Blondel-Rey constant tested on observers with good binocular vision

22 p3498 A71-41483

Successively presented flashing lights detection, discrimination and brightness measurements with four channel binocular Maxwellian viewing system

22 p3498 A71-41488

Passive and active extraocular muscle forces in strabismus, giving horizontal binocular alignment during fixation or eye movement

22 p3489 A71-42442

Eye vergence movement control, describing effective target configurations and binocular units receptive field disparities

22 p3489 A71-42447

Crossed retinal pathways in Siamese cats due to neuroanatomical defect impairing binocular vision and stereoscopic depth perception

23 p3633 A71-43546

BIOASSAY

Laser microprobe emission spectroscopy of biological matrix elements, investigating bovine albumine effect on spectrum analysis

07 p1113 A71-19785

Tissue typing instrumentation with fluorochromatic cytotoxicity assay for quantitative data analysis, eliminating visual counting

07 p1050 A71-20050

Lipid, protein and carbohydrate concentrations in *Chlorella* biomass from pyrolysis and aluminogel column chromatography

13 p2017 A71-28407

Redundancy in receptive neuronal nets, examining structural and functional organization of generalized biological analyzer peripheral section

17 p2690 A71-34956

- Activation impulse blocking in nerve, using inhomogeneous Lillie electrochemical model
19 p3006 A71-37282
- Physical, chemical, mineralogical and biological analysis of Apollo 14 lunar rocks and fines
19 p3144 A71-38179
- Apollo 12 lunar surface samples analysis for organic compounds by mass spectroscopy and pyrolysis-gas chromatography
23 p3756 A71-43741
- Microbial assay of lunar core and surface samples obtained from Apollo 11 and 12 flights
23 p3757 A71-43748

BIOASTRONAUTICS

- Biomedical experiments and man machine relationship on Soyuz 9 record endurance flight
01 p0164 A71-11457
- Space base biomedical center based on Integrated Medical and Behavioral Laboratory Measurement System (IMBLMS)/concept
04 p0546 A71-15280
- Exobiology in astronautics, surveying extraterrestrial life possibilities, conditions and forms
17 p2686 A71-35438
- Space station biological/medical laboratories, discussing physiology, pathology, hematological, static and dynamic equilibrium, neuropsychic, dietetic, radiobiological, hygiene and prophylaxis departments
19 p3006 A71-37308
- Life science and space research - Conference, Leningrad, May 1970
21 p3332 A71-40551
- Prolonged manned space flight infectious disease hazards, discussing confinement, zero gravity, high oxygen content, personal hygiene, waste disposal and preflight immune status
21 p3333 A71-40561
- Artificial ecological regenerative life support system design for space environments, discussing biotechnological properties
21 p3343 A71-40563
- Soviet papers on cosmic biology, Volume 16, covering man and animal physiology under extremal loads, spacecraft life support systems and extraterrestrial life detection, etc
22 p3505 A71-42789
- Voshkod 2 cosmonauts physiological data, presenting heart beat, respiration rates, oculomotor activity and blood composition
22 p3495 A71-42791

BIOCHEMISTRY

- NT BACTERIOLOGY**
- NT ENZYMOLOGY**
- Cardiovascular and biochemical effects of chronic intermittent neurogenic stimulation, noting alaphamethyltyrosine antihypertension agent
03 p0359 A71-13157
- Soviet book on chemistry, physics and mathematics of life covering evolution, metabolic processes, biological cycles and rhythms, molecular physiology, cybernetics, etc
04 p0539 A71-15261
- Integratism in life biology, discussing reductionism and organismism at biopolymer macromolecule construction and conformational levels
06 p0852 A71-17683
- Biochemical mechanism of radioprotective action of aminoethiols in mammals
07 p1039 A71-18979
- German papers on plasma physics, metal corrosion, organic chemistry, molecular biology, etc
07 p1160 A71-19601
- Chemical release from traumatized tissue in dogs under cross circulation with lethal cardiac depression response
11 p1720 A71-26119
- Functional-biochemical shifts in rats central nervous system during initial stage of increased oxygen pressure exposure
13 p2002 A71-27810
- Oxygen exposure effect on food consumption/ utilization efficiency, growth and biochemical parameters
13 p2015 A71-29360
- Intense muscular work adaptation in rats, reducing biochemical and adaptive changes and enhancing anabolic processes
14 p2186 A71-30552
- Adrenal medulla biochemistry and morphology, discussing epinephrine synthesis control by glucocorticoid hormones
14 p2187 A71-30809
- Ion-membrane hydrogen oxygen fuel cell, using microbially or biochemically produced hydrogen by enzymatic reactions
16 p2527 A71-33550
- Biological and biochemical cyclic phenomena, including circadian rhythms
20 p3190 A71-39475
- Soviet monograph on coacervates and protoplasm covering colloidal-chemical properties, enzyme catalysts and multiphase cell and organism simulation
21 p3336 A71-40870

- Nonaqueous biosystems unlikelihood from consideration of enzymatic activity possibility and liquid water unique ability for complexity required by carbonaceous biosystems
22 p3487 A71-42229
- Chlorella biomass chemical composition stability during prolonged cultivation with nitrates recycling medium
22 p3507 A71-42818
- Analog modeling of enzyme and biochemical systems with fixed and variable functional properties, using operational amplifier integrator
24 p3802 A71-45109

BIOCONTROL SYSTEMS

- Impulsive activity of neuron populations in cerebral sections controlling psychic and motor functions in man
01 p0014 A71-11149
- Soviet papers on movement control covering rate regulation, human rhythms, finger coordination, etc
02 p0203 A71-12051
- Human temporal performance of homogeneous discrete motor acts sequence, suggesting central nervous mechanism for movement rate generation
02 p0204 A71-12052
- Human muscular control patterns during forearm precision cyclic bending on ergograph
02 p0204 A71-12053
- Human discrete and continuous rhythmical movements rate control
02 p0204 A71-12054
- External acoustic signals for human cyclic movements temporal structure control
02 p0205 A71-12058
- Biological movement control systems from structural linguistics viewpoint
02 p0206 A71-12063
- Data processing analog for human vertical position regulation via afferent nervous system control of skeletal muscles
02 p0206 A71-12064
- Bioelectric control, man and automatic systems - Conference, Yerevan, U.S.S.R., September 1968
03 p0365 A71-12976
- Muscle activity control mechanism in animals locked into external feedback loop, relating exciting stimulus to muscles stressed state
03 p0367 A71-12980
- Human equilibrium maintenance system analogy to multiput/multioutput controller, considering motion of projection of center of gravity onto horizontal plane
03 p0356 A71-12981
- Biocybernetic model of vestibular control system for spatial orientation, considering semicircular canals fluid motion angular velocity sensors and linear displacement perception
03 p0367 A71-12982
- Mathematical model for eye crystalline lens accommodation control interaction with pupil, deriving dynamic equations from human/cat experiments with/without neurological control
03 p0356 A71-12984
- Pupil neurological control system for reaction to light and accommodation process by statistical eye noise analysis and microelectrode recordings of brain stem neurons
03 p0367 A71-12985
- Adaptation mechanism of human movement control as motor neuron reaction to external stimuli, considering peripheral arch, cerebrosplinal canal and feedback
03 p0356 A71-12986
- Movement coordination in animals during walking and running, revealing neurophysiological mechanisms of locomotion control
03 p0356 A71-12987
- Human motor reactions sequential systems control characteristics, considering effects of external stimulus and repetition time interval
03 p0357 A71-12988
- Complex biomechanical system control, discussing adjustments to perturbation from movement performance
03 p0357 A71-12989
- Biocontrol devices for artificial respiration and blood circulation, using information from organism
03 p0367 A71-12991
- Human cardiovascular control system model by analog computer program for various work loads up to submaximal, estimating correspondence to real life
03 p0368 A71-12995
- Biological and medical cybernetics approach to closed systems construction for continuous automatic monitoring and control of human physiological processes under harmful conditions
03 p0368 A71-13000
- Psychophysiological, strict engineering-psychological and systems engineering analyses, solving engineering-psychological problems in large control systems for human operators
03 p0369 A71-13001
- Decision making heuristic program reflecting human brain function in problems with listed requirements and unspecified goal
03 p0369 A71-13002

- Coronary perfusion pressure, heart performance and homeometric autoregulation in intact dogs
03 p0361 A71-13224
- Accommodation model concerning nervous control of ciliary muscle
03 p0373 A71-14378
- Ascending pathways from spinal thermosensitive region to hypothalamic temperature control center, considering spinothalamic tract impulse frequency temperature response and bilateral RF coagulations
04 p0539 A71-15094
- Cerebral cortex regulation of internal organ functions, examining neural and neurohumoral channels, hormones and vascular changes
05 p0709 A71-16802
- Human brain electric activity during kinesthetic analysis of excitations by radiocarpal joint movements, considering cortical regulation
05 p0709 A71-16803
- Ventricular controllers automatism suppression by HF electric stimulation, examining energy metabolism inhibitors effects
08 p1240 A71-21793
- Central regulation mechanisms of acidic-alkaline equilibrium in ontogenesis, discussing midbrain intraterine and respiratory postnatal development
08 p1241 A71-21937
- Cardiac output variations in regulation of arterial oxygen transport during hypoxia
08 p1241 A71-21939
- Visceral system regulation processes investigation in human organism during manual labor and environmental adaptation, using multichannel biotelemetry and computer processing
08 p1241 A71-21941
- Respiratory system self regulation and coordinated activity interference by biocontrolled stimulator incorporation into natural nerve links
10 p1567 A71-24165
- Resistance and mathematical modeling of human body control concerning brain, cardiovascular, arteriolar muscle contraction and protein metabolism systems
10 p1571 A71-24955
- Predictive stochastic optimal control model for saccadic eye movements in visual target tracking based on target motion estimate
11 p1723 A71-25142
- Body fluid osmolality control of food intake initiation in rehydrated rats injected with hypertonic sodium chloride solution
11 p1719 A71-26073
- Instantaneous postural reaction of cattle to brain concussion indicating mechanoreceptor HF discharge impulse pathophysiological mechanism
11 p1720 A71-26122
- Coronary blood flow regulation, discussing local and remote control mechanisms and disturbance effects due to obstructive arteriosclerosis
13 p2003 A71-27860
- Mycardium cells contractile activity control with frequency dependent self regulatory mechanism
13 p2006 A71-28383
- Blood liquid state control in sanguiferous canal as function of humoral feedback in coagulation, fibrinolytic and anticoagulation systems
13 p2010 A71-28718
- Food choice, consumption control and metabolism, discussing homeostatic alimentary theories, nerve signals and appetite regulation
13 p2010 A71-28719
- Whole body blood flow autoregulation relationship to hypertension in reflex dogs
13 p2013 A71-28953
- Biosynthesis control of melatonin and other methoxyindoles in mammalian pineal organ
14 p2182 A71-29631
- Human blood pH and gas composition regulation mechanism under response to carbon dioxide partial pressure changes in inhaled air
15 p2357 A71-31316
- Regulation patterns of external respiration rate in man during physical exertion, showing load dependent pulmonary ventilation in accord with minimum energy expenditure principle
15 p2358 A71-31321
- Central nervous system self regulating properties analysis by automatic control theory, using parametric functional model of brain electrical activity
16 p2538 A71-34107
- Hypothermia effects on cat and dog vascular tonus vasomotor reflex regulation, suggesting role of inhibition due to changed afference from cooled tissues
16 p2533 A71-34111
- Human motor control behavior sampling hypothesis of open loop system at voluntary effort initiation, discussing validity based on ankle rotation physiological test
17 p2690 A71-34741
- Methodological features of programmed control of human upper extremities movements, using six-channel bioelectric system
17 p2692 A71-35170

Brain locking activity structural organization, discussing cerebral processes and control contact mechanisms activating conditioned reflexes

17 p2684 A71-35358

Stimulus control during conditional discrimination development at various training stages, using two key situation and two visual dimensions

17 p2686 A71-35499

Monograph on peripheral chemoreceptors and central chemosensitive area control of ventilation during chronic blood acid base changes and hypoxia in mammals

18 p2852 A71-35869

Afferent nerve impulse traffic from atrial A-type receptor fibers in cats in relation to heart rate control

18 p2857 A71-36688

Local skin thermoregulation mechanism in man controlled by cooperative bradykinin biosynthesis, using IR thermometry recording of thermal stimulus

18 p2859 A71-36868

Brown fat thermogenesis regulation, emphasizing adipose tissue and afferent nerves control by experimental system approach, using intact unanesthetized unrestrained animals

18 p2859 A71-36872

Retinal adaptation to prism-displaced hand image in terms of sensorimotor coordination central control change

19 p3006 A71-37543

Proposed prism adaptation model suggesting visual motor control loop as linear system comprising independent subsystems

19 p3007 A71-37544

Visual target pursuit tracking test confirming error amending by central mechanism without sensory feedback

19 p3007 A71-37545

Stop test method to study acceleration in movement control processes in man, considering elbow joint movements in normal and pathological tremors in Parkinson disease afflicted subjects

19 p3007 A71-37569

Gravity sensors and intracellular conduction mechanisms in animals, noting contradictory hypotheses on function of hair cell in labyrinth

21 p3328 A71-40009

Cardiac automatic rhythms, discussing diastolic depolarization in Purkinje fibers and factor controlling automaticity

21 p3330 A71-40250

Cardiac sympathetic nervous control of right ventricular pressure-flow dynamics in outflow tract in anesthetized dogs

22 p3484 A71-41522

Vestibulo-colic reflex control of head movement in seated man under sinusoidal and stepwise rotational velocity stimulation, comparing with ocular stabilization

22 p3501 A71-41822

Eye movement control - Conference, University of the Pacific, San Francisco, November 1969

22 p3488 A71-42432

Eye movement neurophysiology, discussing ocular proprioception, oculomotor muscle sensory receptor role, extraocular muscle afferent and efferent innervation and central nervous system control effect

22 p3488 A71-42433

Human ocular control system supranuclear disorder syndromes and signs in terms of physiological concepts

22 p3488 A71-42438

Cat and human eye movement control system measurements, studying isolated oculomotor muscles and globe restraining tissues dynamics

22 p3489 A71-42441

Passive and active extraocular muscle forces in strabismus, giving horizontal binocular alignment during fixation or eye movement

22 p3489 A71-42442

Saccadic eye movement control system behavior simulation model evaluation, considering oculomotor pathways

22 p3504 A71-42443

Versional eye movement control system models, considering dual mode control, intermittency, plant dynamics and pattern recognition

22 p3489 A71-42444

Vergence eye movements control, discussing transient and frequency responses

22 p3489 A71-42446

Eye vergence movement control, describing effective target configurations and binocular units receptive field disparities

22 p3489 A71-42447

Neural control organization in vestibulo-ocular reflex arc, considering afferent and oculomotor neural signals

22 p3490 A71-42449

Arterial blood pressure spontaneous fluctuations due to cutaneous circulation adjustments by thermoregulatory system

23 p3632 A71-43142

Human motor system control mechanism for stretch reflex loop gain with simplified central nervous system computation

23 p3639 A71-43354

Circumscribed eccentric afterimages effect on visual oculomotor control system, examining central transfer functions

23 p3635 A71-43971

BIODYNAMICS

Complex biomechanical system control, discussing adjustments to perturbation from movement performance

03 p0357 A71-12989

Optic analyzer dark adaptation dynamics during spatial body position changes, observing restoration speed dependence on physical training

03 p0364 A71-13523

Biomechanical systems dynamic response - ASME Conference, New York, November-December 1970

04 p0542 A71-14785

Dynamic response with feedback characterization of human musculoskeletal frameworks by linegraph-flow graph procedure

05 p0713 A71-16485

Human skin biomechanical properties, observing extensibility, resiliency and elasticity

05 p0710 A71-16807

Human biodynamics during deceleration, impact and blast, discussing body positions and protective restraints for crash safety, aircraft ejection, etc

08 p1244 A71-20707

Human biomechanical and vegetative reactions to hypnotic suggestion of gravitational effects

08 p1243 A71-21971

Biological oscillating propulsion systems, investigating plate propeller, boundary layer control, low drag fuselage shapes and VTOL engine installations

10 p1569 A71-24235

Human hand anthropometric and biomechanical characteristics, discussing data utilization for human factors engineering

12 p1875 A71-27250

Animal urinary bladder mechanical properties from controlled stretch tests, identifying viscoelastic, elastostatic and creep elements

14 p2186 A71-30566

German monograph on conversion of human muscular work into flywheel mechanical kinetic energy covering testing and analysis of biomechanical relationships

15 p2364 A71-32308

Man machine system dynamic properties and biomechanical model concepts, determining random vibration effects on sitting and working human body

15 p2366 A71-32728

Arterioles and corneo-scleral shell structural response under various loading conditions, using finite element method for mechanical and hydrostatic stress distribution

16 p2528 A71-33099

Vibration effects on human body, discussing neurophysiological data, safe exposure limits, therapeutic applications, motion sickness, muscular responses and biomechanical effects

21 p3342 A71-40147

Mechanical properties of muscular organs, presenting mathematical model for biological fluid flow analysis

21 p3336 A71-40984

Man machine system dynamic properties and biomechanical model concepts, determining random vibration effects on sitting and working human body

23 p3639 A71-43299

BIOELECTRIC POTENTIAL

Dorsomedial nucleus electric impulse stimulation in anesthetized cats with oscillogram recorded response potentials of cortex preoral gyrus, indicating relay transmission function

01 p0008 A71-10091

Auditory averaged evoked potential as measure correlating with degree of psychopathology in schizophrenia

01 p0011 A71-10765

Step-wise discriminant analysis in auditory evoked potential variability in schizophrenia

01 p0011 A71-10766

Open and closed eyes electroretinogram, discussing lamellar electrode placed on lower eyelid

01 p0024 A71-11077

Bioelectric potential in gap between abutting cardiac muscle cells, using differential equation for active to inactive cell transmission

01 p0025 A71-11177

Isopotential maps comparison of thorax with vectorcardiograms from superficial potential distribution zones

02 p0207 A71-12111

Small-tipped microelectrode minimizing capacitive artifacts during current passage through bath in membrane potential measurement

03 p0372 A71-13912

Topography of acoustically evoked potentials triggered by alpha activity in man

05 p0710 A71-16942

Surface negative slow EEG potential /CNV/ in human brain after total sleep loss

06 p0850 A71-17428

Human cardiac intraventricular conduction measurements, using right and left bundle branch potentials during catheterization

07 p1044 A71-20351

Latency fluctuations and quantal transmitter release influence on end plate potential amplitude distribution, using frog muscle synaptic delays

07 p1045 A71-20445

Vestibular stimulation effects on bioelectrical activity in retina, optic tract, geniculate, visual cortex and ectosylvian gyrus in anesthetized cats

09 p1390 A71-22215

Computer aided statistical model of visual evoked potential in man as normality criterion for pathological indicator

09 p1397 A71-22253

W-formed summated evoked potential to light stimulus in healthy subjects significant to Wilcoxon test

09 p1393 A71-23012

Cortical potentials evoked by weak acoustic signals below hearing threshold in man

10 p1564 A71-24440

Extraprimary /briefly latent/ postsynaptic negative component of evoked visual potential in cortex of nembutal anesthetized rabbits, using Alvar biophase oscillator

13 p2004 A71-27894

Visual cortex neurons impulse activity and postsynaptic potential changes due to light stimuli from quasi-intracellular recordings

13 p2005 A71-28381

Evoked brain potentials averaging in real time with computer linked by long distance communication lines

13 p2017 A71-28385

Repetitive stimulation effects on auditory evoked potentials in cochlear nucleus, inferior colliculus and medial geniculate body of unanesthetized cats

13 p2012 A71-28892

Electroencephalographic and evoked cortical potential correlates of reaction time and visual discrimination in humans

13 p2022 A71-29345

Fly *Lucilia sericata* olfactory receptor and unit action potentials response to odor stimulation by homologous compounds

14 p2186 A71-30569

Readiness potential, vertex positive wave and contingent negative variation recordings for evaluation of neural events associated with visually stimulated perception

15 p2359 A71-31953

Spectral sensitivities of discrete slow potentials and threshold level nerve spikes in *Limulus* ommatidium as function of hyperpolarizing current

16 p2527 A71-32869

Human auditory signal detection related to averaged evoked potential in scalp by electrophysiological measurements

16 p2534 A71-32951

Human visual evoked cortical potential spectral sensitivity measurement, comparing results with psychophysical data

17 p2680 A71-34652

Visual and auditory evoked potentials enhancement in cats using cryogenic blockage of nonspecific thalamo-cortical system in inferior thalamic peduncle region

17 p2682 A71-35112

Visual evoked potentials and cortical recovery cycle data for normal and psychiatric subjects of various ages

17 p2682 A71-35113

Visual evoked brain potential amplitude and detection efficiency relationship, discriminating between arousal and attention effects

17 p2682 A71-35114

Physiological mechanisms of human auditory attention, measuring changes in cerebral cortex averaged evoked potential and cochlear nerve response

17 p2693 A71-35575

Mitosis control assuming existence of functional relationship between potential level and mitotic activity, using classical membrane potential theory

18 p2853 A71-35893

Monophasic action potential recording of intact human heart, using bipolar electrode catheter for explanation of ECG abnormalities

18 p2853 A71-35910

Sagittal path of moving electrical center of human heart from measurements of surface ECG potentials

18 p2853 A71-35911

Human visual cerebral cortex potentials evoked by sinusoidally modulated field under stabilized and unstabilized conditions

19 p3004 A71-38279

Visual evoked potential relationship to apparent size reduction of invariant retinal image

19 p3004 A71-38281

Primary biological receptor element analogous electronic model for potential and afferent pulse train responses to stimuli

20 p3191 A71-38894

- Simultaneous measurement of transverse and longitudinal bioelectric potential differences in plants without direct contact with tissues, using vibrating reed electrometer 21 p3375 A71-39985
- Corned-retinal potential as generator of occipital alpha rhythm in human electroencephalogram modulated at 10 Hz by tremor in extraocular muscles 21 p3329 A71-40176
- Heart excitation and membrane permeability effects on two component action potentials in human atrial muscle strips, using microelectrodes 21 p3336 A71-40865
- Human cerebral EEG phenomena and evoked potential relationships to eye and retinal image movements 22 p3488 A71-42437
- Muscular bioelectric potential input processing into digital computer, describing amplitude, frequency and time domain analysis of electromyogram signals 24 p3801 A71-44542
- Averaged evoked potentials of human cortex in response to visual stimuli 24 p3796 A71-44549
- Postsynaptic de- and hyperpolarization potential development mechanisms in wakeful cats cortical neurons during LF thalamic structure stimulation 24 p3797 A71-44720
- Simultaneous recordings of ERG and visually evoked cortical potential to stimuli of differing luminance and pattern, comparing spatial frequency characteristics 24 p3801 A71-44977
- Averaged potentials in vertex and occipital region of human cranium evoked by emotional visual stimuli 24 p3798 A71-45057
- Postsynaptic potentials in adjacent synaptic regions of tonic fiber of rabbit external eye muscle 24 p3798 A71-45066
- BIOELECTRICITY**
- Midbrain reticular neurons discharges in response to electrical stimulation of posterior ventral nucleus of thalamus 01 p0008 A71-10072
- Percutaneous vitreous carbon electrodes long term effects, considering mechanical stability, bioelectrical signal receptivity, low interface impedance and surrounding epidermis growth 01 p0021 A71-10238
- Neuron pairs discharge sequence temporal correlation in cats association cortex during natural sleep and wakefulness 01 p0011 A71-10849
- Cardiac cells electrical interaction mathematical simulation, calculating gap region resistance and current 01 p0025 A71-11176
- Bioelectric control, man and automatic systems - Conference, Yerevan, U.S.S.R., September 1968 03 p0365 A71-12976
- Neuromuscular spindles sensory information processing, determining fibers selective data transmission functions by frequency meter and model for electrical and mechanical properties 03 p0366 A71-12977
- Heat rotation induced eye movements in cats by neuron level determination, considering vestibular apparatus of signal transmission loop for mathematical model 03 p0356 A71-12983
- Gap in atrioventricular conduction in humans by catheter technique for recording electrical activity of His bundle 03 p0363 A71-13488
- Ascending neuron vestibulo-ocular reflex arc, emphasizing medial longitudinal fasciculus 04 p0537 A71-14763
- Intestinal muscle electrical behavior as series of loosely coupled oscillators, demonstrating slow wave frequency gradient and propagation velocity by computerized simulation 04 p0544 A71-15089
- Hippocampal, neocortical and somatic effects of HF electrical stimulation of mesencephalic reticular formation during different stages of sleep in cats 05 p0707 A71-16424
- Retinal neurons receptive field center, examining excitation and direct inhibition interaction 05 p0707 A71-16596
- Human brain electric activity during kinesthetic analysis of excitations by radiocarpal joint movements, considering cortical regulation 05 p0709 A71-16803
- Hypokinesia and acceleration effects on plasma proteins displacement and bioelectric activity of striated muscles of rats 06 p0853 A71-17960
- Nervous and muscular tissues excitability during subthreshold rhythmic stimulation, discussing mathematical model for compounding polarization induced electrotonic fluctuations 07 p1050 A71-20115
- Biological memory and perception processes electronic simulation by keyboard structure reenacting word reception, storage and delivery 07 p1051 A71-20118
- Neuroelectric signal analysis using real time nerve spike recognition and separation based on nuclear instrumentation techniques 08 p1249 A71-21839
- Rhodopsin dissociation and retina photochemical and bioelectrical processes after light flashes of various intensity 09 p1388 A71-22124
- Hind limb antagonistic muscles bioelectric activity dependence on animal rotation direction and head fixation 09 p1388 A71-22196
- Electroencephalogram analysis, using analog computers for biopotential data reduction 09 p1398 A71-22489
- Hyperthermia effects on conduction velocity of nerve fibers and peripheral motor neuron-muscular activity in man 09 p1399 A71-22924
- Chemical thermoregulation muscular electricity activity during shivering and thermoregulation tonus change after cold adaptation, discussing oxygen consumption rise 10 p1564 A71-24486
- Neural transmission to vestibular nuclei of semicircular canal response to rotational stimulation, discussing test methods and results with decerebrated or anesthetized cats 10 p1566 A71-25042
- Cortico- and subcorticograms rhythm dynamics in sleeping and awake cats by spectral analysis and EEG integration 12 p1871 A71-27486
- Human brain subcortical formations slow electrical processes during memory tests 13 p2005 A71-28377
- Natural sleep and wakefulness stages neurophysiology based on bioelectric activity spectral and correlation analyses 13 p2005 A71-28380
- Cat single optic nerve fibers receptive field, observing functional organization and conduction velocity 13 p2008 A71-28458
- Cat type I and II optic nerve fibers response to flicker stimulation, noting receptive field organization, conduction velocity and temporal and spatial information processing 13 p2008 A71-28459
- Analog simulation of cardiac malfunctions associated with A-V conduction block and Wenckebach phenomenon, using P and R wave and internal function generators 13 p2020 A71-29001
- Space crew members muscle tone, determining weightlessness effect by rigidity and bioelectric activity 15 p2357 A71-31317
- Femoral nerve afferent muscle fibers bioelectric activity in anesthetized cats, determining effect of blood circulation level on receptors functional activity 15 p2358 A71-31323
- Cortical and subcortical electrical activity during electrically and drug induced convulsive seizures in cats, correlating with spinal monosynaptic reflex variations 15 p2359 A71-31957
- Human operator work quality evaluation with EEG data based on brain electrical activity as function of central nervous system 15 p2365 A71-32530
- Blood circulation in auditory analyzer cortical section relationship to bioelectrical activity, using various frequencies pure tones as stimuli 15 p2360 A71-32531
- Gas exchange, thermoregulatory muscle tone and electrical activity in rat muscles in hyperoxic atmosphere 15 p2360 A71-32533
- Individual neurons activity during stereotaxic operations on Parkinsonism and hyperkinesia syndromes, describing microelectrodes for extracellular recording 15 p2365 A71-32535
- Adrenalectomy influence on electrical activity of cortex and subcortical areas in rats under hyperbaric oxygen, using implanted electrode electroencephalographic recordings 16 p2528 A71-33118
- Temperature effects on spontaneous electrical and contractile activity of smooth muscle cells of portal vein in rats 16 p2533 A71-34110
- Cat thalamus ventrolateral nucleus neuronal discharges during waking and slow and fast wave sleeps 17 p2680 A71-34689
- Methodological features of programmed control of human upper extremities movements, using six-channel bioelectric system 17 p2692 A71-35170
- Deep cerebral structures and cortex electrical activity in apes, noting biopotentials during orientation/defense reactions and light signals responses 17 p2683 A71-35246
- Soviet papers on higher nervous activity physiology, Part I, Basic laws and mechanisms of conditioned reflex activity covering inhibition, and bioelectrical effects, with bibliography 17 p2684 A71-35357
- Bioelectrical aspects of conditioned reflex activity, discussing changes in cortex background, cortical and cerebral biopotentials and alpha- rhythm depression reactions 17 p2685 A71-35362
- Bulbar and baroreceptor inhibition of spinal and supraspinal sympathetic reflex discharges recorded in cats from renal nerve 18 p2857 A71-36689
- Activation impulse blocking in nerve, using inhomogeneous Lillie electrochemical model 19 p3006 A71-37282
- Human respiratory muscles electrical activity, discussing correlation analysis of interferential electromyograms from external intercostal muscles during breathing exercises 19 p3003 A71-38198
- Phrenic nerve activity correlation with ventilation in anesthetized cats, analyzing relationship between phrenic impulse rate and integrated electrical activity 20 p3192 A71-38983
- Motor and vestibular analysors and frontal hypothalamus role in gravitational loads compensation during orthostasis, noting respiration, arterial pressure and brain bioelectric activity changes 20 p3188 A71-39223
- Shin muscle electrical activity during standing after 120 day bed rest hypokinesia from EMG measurement 20 p3188 A71-39230
- Nervous system functional characteristics based on neuron structure and electrical transmission from electron microscopy, electrophysiology and biochemical analysis 21 p3329 A71-40145
- Electrical heart activity and ECG mathematical model with nonlinear oscillator system construction for normal and abnormal rhythms 21 p3336 A71-40986
- Motor stereotype formation with different muscular loads, noting muscle electrical activity and static tension changes 21 p3337 A71-41062
- Gas metabolism and electrical activity of skeletal muscles of rats in He/O medium at room temperature, noting rectal temperature drop 22 p3496 A71-42803
- Brain monoamines localization and metabolism and endocrine function, discussing pituitary secretion and neurotransmitter input 23 p3637 A71-44274
- Bioelectrical activity of monkeys cortex and deep cerebral structures under lasting rhythmic photostimulation 24 p3793 A71-44411
- BIOENGINEERING**
- NT ANTHROPOMETRY
- NT BIOMINSTRUMENTATION
- NT BIOMETRICS
- NT BIOTELEMETRY
- NT BODY MEASUREMENT [BIOLOGY]
- NT CARDIOGRAPHY
- NT ELECTROCARDIOGRAPHY
- NT ELECTROENCEPHALOGRAPHY
- NT ELECTROMYOGRAPHY
- NT ELECTRORETINOGRAPHY
- NT PLETHYSMOGRAPHY
- High speed real time interpretive language for biological calculations with PDP-8 computer 01 p0049 A71-10244
- Complex biomechanical system control, discussing adjustments to perturbation from movement performance 03 p0357 A71-12989
- Psychophysiological, strict engineering- psychological and systems engineering analyses, solving engineering-psychological problems in large control systems for human operators 03 p0369 A71-13001
- Arterial circulatory system parameter identification from diastolic blood pressure curves by digital filter techniques 09 p1398 A71-22254
- Aerospace research bionics and bioengineering, considering adaptation of man to environment and matching of man and machine 10 p1568 A71-24221
- Automatic regulation of volumetric blood flow rate during artificial blood circulation, using electromechanical system for controlling arterial pump of cardiopulmonary machine 19 p3010 A71-38641
- Artificial ecological regenerative life support system design for space environments, discussing biotechnological properties 21 p3343 A71-40563
- BIOGENESIS**
- U BIOLOGICAL EVOLUTION
- BIOINSTRUMENTATION**
- NT BIOTELEMETRY

Manganese dioxide depolarizer for biomedical electrodes, discussing electrochemical and toxicological characteristics

01 p0021 A71-10239

Intracranial pressure measurement by miniature transducer with modifications for baseline reading and calibration checking throughout implantation period, giving circuit diagram

01 p0021 A71-10241

Linear beat by beat cardiostachometer, describing amplifier design and operation

01 p0021 A71-10242

Catheter inserted wire basket device for creation of reversible aortic insufficiency in animal

01 p0022 A71-10248

Transducer for measuring mandibular dynamic movements during speech

01 p0079 A71-10346

Metabolic rate and ergometric data recording by analog and digital systems

01 p0026 A71-11409

Electro-optic monitoring method for single isolated heart cell activity

02 p0202 A71-11672

Real time contourgram for monitoring ECG waveform data, describing cardiac measurement and data display

02 p0199 A71-12384

Human respiratory parameters telemetry, discussing transducer development for ventilatory volume measurement

03 p0370 A71-13068

Microcathodes measurement of oxygen tension on arterioles external surface in hamster cheek pouch and hamster/rat cremaster muscle for blood flow regulation mechanism

03 p0363 A71-13487

Fluorim oscillators as sensors for carbon dioxide concentration detection in exhaled breathing gases, noting frequency dependence on gas properties [ASME PAPER 70-WA/FLCS-10]

03 p0372 A71-14086

Catheter-flush system for continuous monitoring of central arterial pulse waveform and pressure

04 p0345 A71-15165

Strain gage for in vivo recording of single and tetanic responses of skeletal muscles in mice during work in isometric regime

06 p0855 A71-18378

Strain gage attachment to rat heart ventricle in situ with fine stainless steel pins

06 p0862 A71-18391

Tissue typing instrumentation with fluorochromatic cytotoxicity assay for quantitative data analysis, eliminating visual counting

07 p1050 A71-20050

Automatic system for indirect blood pressure measurement in carotid compression test, discussing applications

08 p1247 A71-20827

Neuroelectric signal analysis using real time nerve spike recognition and separation based on nuclear instrumentation techniques

08 p1249 A71-21839

Soyuz 9 cosmonauts physiological monitoring instrumentation and procedures, describing bioinstrumentation harness for data telemetry

09 p1397 A71-22198

Electroencephalophone for stereophonic display of four channel EEG physiological signals from skull quadrants

09 p1397 A71-22252

Low cost directly coupled differential amplifier with thermodynamic drift stabilization for biological studies

10 p1570 A71-24444

Space research utilization in medicine, discussing remote blood pressure measurements, seismocardiography visual analysis, sterilization procedures and equipment for physically handicapped

10 p1571 A71-24754

Percutaneous access to implanted electrodes, discussing metal plaque-needle system and connection to instruments

11 p1724 A71-25436

Waist seal design providing discrete anatomical placement, subject comfort, ingress/egress ease and size accommodation for lower body negative pressure devices

11 p1725 A71-26130

Arterial or venous blood oxygen tension continuous measurement, describing electrode cuvette design with response time of less than 3 sec

16 p2535 A71-33248

Biological instrumentation and soil sampler aboard Viking lander for 1975 mission to Mars

16 p2537 A71-33808

Anatomical load sensing method, determining torso pain thresholds by sensitivity tests [SESA PAPER 1823A]

17 p2689 A71-34539

Medical screening techniques, discussing sensitive, specific, reliable, fail-safe and self calibrating instrumentation systems

17 p2689 A71-34609

Redundancy in receptive neuronal nets, examining structural and functional organization of generalized biological analyzer peripheral section

17 p2690 A71-34956

Monophasic action potential recording of intact human heart, using bipolar electrode catheter for explanation of ECG abnormalities

18 p2853 A71-35910

Thermomodulation method instrument using cold indicator depot with heat exchanger for standardization of heart-time-volume measurements

18 p2872 A71-36692

Phonocardiograph design and calibration for accurate measuring and recording of cardiac vibration displacements, velocities and accelerations

19 p3005 A71-37231

Frequency phonocardiography technique for heart sounds and murmurs registration, producing analog voltage proportional to frequency by zero crossing detector

19 p3006 A71-37234

Continuous recording of human rectal temperature under extreme environmental conditions, using battery powered thermographs with thermistor probes

20 p3192 A71-39041

Lung scanning, describing moving detectors, electronic apparatus adjustment and choice of radionuclide and labelled compound

20 p3192 A71-39072

Miniature biopotential transmitter suitable for telemetry, giving EEG and circuit and performance characteristics

21 p3342 A71-40184

Aquanuts tremor response measurement by muscle force transducer during compression and decompression in 520-foot saturation dive, noting differences among individuals

21 p3331 A71-40350

Transistorized AGC circuit for use with ultrasonic Doppler-cardiogram recording system to retain signal characteristics under strong fluctuations

24 p3801 A71-44543

Miniature battery operated electromagnetic blood flowmeter for data acquisition from unrestrained animals

24 p3801 A71-44783

BIOLOGICAL ACTIVITY

U ACTIVITY [BIOLOGY]

BIOLOGICAL ANALYSIS

U BIOASSAY

BIOLOGICAL CELLS

U CELLS [BIOLOGY]

BIOLOGICAL CLOCKS

U RHYTHM [BIOLOGY]

BIOLOGICAL EFFECTS

NT RELATIVE BIOLOGICAL EFFECTIVENESS [RBE]

Laser systems radiation hazards, considering operational requirements, personnel protective equipment, biological effects and exposure levels

01 p0021 A71-10008

Short term pure oxygen exposure effects on rats proximal convoluted tubular cell structure

01 p0011 A71-10768

Space flight biological effects on parasitic wasp *Habrobracon*, investigating genetic, mutational, biochemical, behavioral and physiological parameters

01 p0019 A71-11553

Lower fasting blood glucose levels in high altitude acclimatization

02 p0197 A71-11664

Unsymmetrical dimethylhydrazine/UDMH effect on canine blood coagulation, blood-aqueous barrier and cornea

02 p0199 A71-12383

Soyuz 9 prolonged space flight biomedical effects on human organism, emphasizing weightlessness

03 p0365 A71-14392

Limitations of electron and X ray microscopy concerning damage of biological molecules by observation

04 p0596 A71-15140

Magnetic field effects on biological systems, discussing ergometer measurements of human subjects muscular contractions

05 p0714 A71-16896

UV light starvation prevention, describing biological effects and illumination equipment for working areas

06 p0858 A71-17528

Spacecraft cabin rare gas-oxygen atmosphere decompression effects on animal metabolic rates

06 p0853 A71-17956

Orbital space flight effects on dry barley seeds, noting increased intracellular rearrangements

09 p1392 A71-22564

Apollo 11 lunar samples effect on terrestrial microorganisms, noting pigment production effects of Fe leaching from bulk fines and core samples

10 p1566 A71-23747

Supernova explosion or solar outburst theory of climatic effects on mass extinction of organisms at Cretaceous-Tertiary boundary

10 p1673 A71-24422

Thermal and nonthermal effects of microwave and RF radiation in biological systems, discussing dielectric constant and conductivity for high water content tissues

11 p1716 A71-25281

Low power density modulated RF energy illumination effects on mammalian biological functions, noting possible hazards to personnel

11 p1716 A71-25282

Microwave radiation nonthermal and cumulative biological effects, discussing dose/irradiation safety standards

11 p1717 A71-25283

Negative heart rate response during low level microwave irradiation of dorsal head in rabbits

11 p1717 A71-25284

Microwave radiation nonthermal biological damage, describing beetle pupae irradiation and radiant heating experiments

11 p1717 A71-25285

Microwave biological exposure systems implementation in limited space, describing focused prolate spheroid, absorber-lined horn and compact range illumination system

11 p1723 A71-25288

Space flight biological effects on lysogenic bacteria and human cells in culture

12 p1872 A71-26641

Book on electromagnetic fields and life environment covering biological effects of radio waves, protection, radiation sources, permissible intensities, working conditions

12 p1873 A71-26868

German book on rescue systems for space emergencies covering mission failure, biological problems, escape vehicles, orbital operations safety and spacecraft transfer

12 p1972 A71-27185

Biological tests of laser protective filters for eye as function of optical density and wavelength by sensitivity of in vivo ocular tissue response

13 p2020 A71-29035

Microwave exposure effects on organisms and biological functions responses and thermal stresses as function of specific frequencies, power density and environmental temperature

13 p2021 A71-29325

Psychobiological effects of prolonged bed rest in young healthy volunteers from EEG recording, psychological testing and psychomotor performance

13 p2022 A71-29363

German book on radiation climate of earth covering EM, corpuscular IR radiation sources, spectral composition, biological effects, etc

14 p2298 A71-29941

High-mountain altitudes inhibition of inflammation and wound healing in rabbits

16 p2531 A71-33522

Biological effects of inert gases in elevated pressure respiratory mixtures on human central nervous system

16 p2536 A71-33577

Cosmic and telluric radiation biological effects on parameria, discussing relationship between dosage and growth rate

16 p2532 A71-33757

Functional systems changes in intact and anesthetized rats during increasing hypoxia in decompression chamber

16 p2532 A71-33911

Deep cerebral structures and cortex electrical activity in apes, noting biopotentials during orientation/defense reactions and light signals responses

17 p2683 A71-35246

Muscle contraction model under biological factors action, considering circular cylindrical vessel equilibrium under internal and external pressures

17 p2694 A71-35616

Microwave radiation biological effects review and bibliography covering protein activity, genetic, central nervous system and cardiovascular effects

18 p2864 A71-35956

Book on biological effects of radiation covering ionizing radiation properties and effects at molecular, cellular and tissue levels

19 p3002 A71-38048

Signals convergence of various sensory modalities as function of impulse reactions of individual brain neurons in mammals

19 p3003 A71-38197

Double standard for national levels of exposure and biological hazards of microwave radiation, comparing Soviet work to U.S.

19 p3008 A71-38442

Biological experiments on plants, animals and bacteria aboard Zond 5, 6 and 7 space probes

20 p3187 A71-39134

Tissular and cellular biological resistance as indices for organism resistance to adverse effects, noting increase due to muscular training and cold adaptation

20 p3187 A71-39219

Medical, zoological and biological effects of ELF signals in atmosphere, comparing with EEG alpha and gamma rhythm

20 p3193 A71-39478

Geoelectric effects on plants geotropic reaction chain, discussing hormone auxin asymmetric distribution due to gravity

21 p3340 A71-39984

Integrative action of central nervous system in converting gravity sensation into crustacean equilibrium reactions

21 p3327 A71-39993

Biosatellite 2 onboard experiments studying weightlessness effects on biological processes and interaction with radiation from Sr 85 gamma ray source

21 p3341 A71-40007

Book on high power laser radiation covering heating, melting, vaporization, particle emission, plasma production, gas and transparent material breakdown and biological effects

22 p3558 A71-42426

Medical preparations use and avoidance by spacecraft and aircraft crew members, discussing aftereffects, allergies and health requirements

22 p3491 A71-42705

Lateral accelerations effect on mice tolerance to toxic doses of aminothiols and indolylalkylamine-series radiation protection drugs

22 p3491 A71-42706

Antiradiation drugs effects on healthy and irradiated rats gastrointestinal tract evacuatory motor function

22 p3492 A71-42707

Hyperoxia pathological effects on albino rats subcutaneous connective tissue, noting oxidizing enzyme activity depression and cellular metabolism suppression

22 p3496 A71-42802

Toxic biological effects of life functions gaseous products in albino rats

22 p3506 A71-42811

Simulation chamber for experimental investigation of organisms reactions to Mars environment

22 p3507 A71-42827

Erythropoietic activity dosage in polycythemic mice after intermittent hypobaric hypoxia

23 p3632 A71-43216

Hypobaric hypoxia effect on polycythemic mice erythropoietic hyperactivity, evaluating iron content in peripheral erythrocytes

23 p3632 A71-43217

Extrarenal production of erythropoietin in biphrextomized rats after hypobaric hypoxia

23 p3632 A71-43218

Serotonin metabolism of helicopter pilots, showing effects of emotional factors due to flight inexperience

23 p3632 A71-43220

Cosmic ray biological effects and admissible dose level normalization in space flight from prolonged tests on dogs

24 p3798 A71-44890

Biological effects of ionizing radiation and non-radiative factors on radiation damage from satellite space flight tests on dogs and plants

24 p3798 A71-44891

Solar activity effects on biosphere, examining solar-geomagnetic and medico-biological indexes relationships and clinico-statistical evidence of human organism effects

24 p3799 A71-45197

BIOLOGICAL EVOLUTION

NT ABIOTIC GENESIS

Life detection for space missions based on detecting optical asymmetry in biogenic molecules by gas chromatography involving diastereomeric esters synthesis

01 p0029 A71-11562

Gas-liquid chromatographic milligram preparative separation of steranes and triterpanes from hydrocarbon fraction of Green River oil shale

11 p1729 A71-26067

Deleterious mutations and neutral substitutions, discussing molecular evolution model for DNA and proteins

13 p2013 A71-29096

Missions beyond solar system for studying origin and evolution of life, planets and stars [AAS PAPER 71-163]

19 p3141 A71-37960

Gravity receptor evolution in invertebrates, considering cilia role in reception and transduction into responses

21 p3327 A71-39991

Biogenicity and significance of oldest stromatolites from optical microscopic and carbon isotopic studies

22 p3533 A71-41616

Polymerized and hydrolyzed polypeptides from condensed amino acid adenylates for prebiological synthesis model

22 p3508 A71-42232

Apollo 12 lunar dust, rocks and microbreccia microsection examined for evidence of biogenic structure

23 p3757 A71-43746

BIOLOGICAL MODELS

U BIONICS

BIOLOGICAL RHYTHM

U RHYTHM [BIOLOGY]

BIOLOGY

Machine analysis of biological structures and processes - Conference, Pushchino, U.S.S.R., May 1968

06 p0863 A71-18690

Matched spatial filters for holographic image recognition in biological studies

06 p0903 A71-18695

Memoscope for communications between operator and machine during biological image studies

06 p0864 A71-18696

Follow-up scanning systems and reading volume reduction in biological image descriptions facilitating computer aided microstructure analysis

06 p0871 A71-18697

Industrial bioscience research laboratory information flow, product ideas, procedural innovations and scientific/technical literature reading

08 p1378 A71-20775

Quantitative gas liquid chromatography analysis of amino acids in biological materials, discussing ion exchange techniques

11 p1729 A71-26068

Existence of life under extreme environmental conditions, discussing biological temperature limits and adaptability to lack of water

11 p1721 A71-26321

Soviet papers on biological and medical cybernetics covering control principles in living organisms, heuristic programming, higher nervous activity models, learning problems, etc

17 p2691 A71-35164

BIO-LUMINESCENCE

Luciferin fermentative oxidation method for adenosine triphosphate determination in extraterrestrial life detection, using extract of firefly luminescent organs

13 p2009 A71-28683

Biochemical luminescence reaction for ferroporphyrin proteins determination in extraterrestrial life detection

13 p2009 A71-28684

BIOMECHANICS

U BIODYNAMICS

BIOMEDICAL DATA

Physiological data telemetry link using time division multiplex method

01 p0024 A71-10981

Biomedical experiments and man machine relationship on Soyuz 9 record endurance flight

01 p0164 A71-11457

Medical data acquisition - Conference, Nancy, France, June, 1969

02 p0206 A71-12106

Computerization of medical records of ophthalmology clinic

02 p0206 A71-12109

Medical data processing techniques in electrocardiography and effort vectorcardiography facilitating clinical observations

02 p0207 A71-12110

Real time contourgram for monitoring ECG waveform data, describing cardiac measurement and data display

02 p0199 A71-12384

Long term human biomedical and behavioral characteristics research, enhancing enhanced physiological fitness in space

04 p0543 A71-14933

FM converter for tape recording of LF biological data

04 p0545 A71-15163

Organic free radical photographic films for biomedical microimaging

07 p1110 A71-19475

Correlation and spectrum analysis of simultaneous EEG data in mono and dizygotic twins using computer and FFT algorithm

08 p1246 A71-20746

Soyuz 9 cosmonauts physiological monitoring instrumentation and procedures, describing bioinstrumentation harness for data telemetry

09 p1397 A71-22198

Soyuz 9 cosmonauts medical monitoring, discussing physiological changes, vagotonic reactions and work capacity

09 p1389 A71-22199

Respiration parameters digital recording system, describing analog signal recording and processing, analog to digital conversion and digital readout equipment and techniques

11 p1724 A71-25595

Stochastic identification method for transforming ECG and VCG data to approximate diagnosis, using computerized dipole models

13 p2020 A71-29002

Eight channel micropowered miniature biomedical PAM/FM telemetry system for implantation in research subjects aboard orbiting space station

14 p2189 A71-30930

Computerized registry of traumatic injuries with IBM 360/44 system for use in mortality, paired patient and accidental risk factor analyses

16 p2535 A71-33109

Summation dial vectorial representation of stationary and nonstationary time series data, relating rhythms in bed rest study

20 p3190 A71-39480

Physiological deterioration of monkey onboard Biosatellite 3 and unexpected demise, presenting collected data for response analysis

21 p3333 A71-40564

Biomedical effects of Apollo 14 space flight, considering weightlessness adaptation

22 p3487 A71-41985

BIOMETRICS

NT ANTHROPOMETRY

NT BODY MEASUREMENT [BIOLOGY]

NT CARDIOGRAPHY

NT ELECTROCARDIOGRAPHY

NT ELECTROENCEPHALOGRAPHY

NT ELECTROMYOGRAPHY

NT ELECTRORETINOGRAPHY

NT MAGNETOCARDIOGRAPHY

NT PLETHYSMOGRAPHY

Fiberoptic indicator-dilation assessment of myocardial function

03 p0362 A71-13329

Soviet book on biometry covering correlation coefficients, rectilinear/curvilinear regression, non-parametric statistics, diversity indices, algorithms, dispersion and statistical analysis and probability

04 p0546 A71-15263

Design, construction and performance of photoelectric isometric force transducer for muscle mechanics

06 p0862 A71-18392

High sensitivity portable two channel apparatus for brain temperature measurements using small glass insulated thermistors

06 p0863 A71-18469

Erythrocytometric curve analysis by conductometric granulometric method

06 p0863 A71-18692

Automatic cytophotometric techniques including microphotometer, ultramicrospectrophotograph, radiographic analyzer, microinterferometers, cytofluorometer and differential microfluorometer

06 p0864 A71-18693

Cytophotometric method using digital computer program and scanning microscope

06 p0864 A71-18694

Respiration parameters digital recording system, describing analog signal recording and processing, analog to digital conversion and digital readout equipment and techniques

11 p1724 A71-25595

Partial oxygen tension in blood and biological fluids measurement with enclosed electrode polarographic sensor

12 p1876 A71-27744

Equipment for prolonged measurement of oxygen consumption, respiratory quotient and insensitive perspiration in man, noting cost reduction and operation simplification

13 p2021 A71-29316

Rapid scanning dual wavelength spectrophotometer for recording oxidation-reduction and membrane bound reactions in turbid suspensions of biological materials

18 p2922 A71-36580

Dynamic sampling calorimeter for continuous measurement of human radiative, convective and evaporative heat loss, enabling closed loop control system analysis

22 p3503 A71-42155

Metric characteristics of horizontal saccadic eye movements in normal humans from electrooculographic recordings, discussing dysconjugacies mechanisms

23 p3635 A71-43972

BIONICS

Artery wall elasticity relation to Korotkoff sound wave frequency by upper arm blood pressure model, using cylindrical rubber tubes and canine specimens

01 p0009 A71-10240

Neuron network modeling by stable rhythmic impulsion system, considering vestibular nystagmus

01 p0025 A71-11137

Cardiac cells electrical interaction mathematical simulation, calculating gap region resistance and current

01 p0025 A71-11176

Human body temperature regulation feedback control system model by electric circuit analog, discussing digital simulation for static and dynamic responses

02 p2023 A71-11805

Data processing analog for human vertical position regulation via afferent nervous system control of skeletal muscles

02 p2026 A71-12064

Identification problems in mathematical model of respiratory function

02 p2026 A71-12108

Photosynthesis models, discussing photoenergetics of molecular systems

02 p2021 A71-12714

Neuromuscular spindles sensory information processing, determining fibers selective data transmission

sion functions by frequency meter and model for electrical and mechanical properties

03 p0366 A71-12977

Human neuromuscular activity description by model for muscle spindles functions, considering systems parameters oscillations relation to mean muscle stress

03 p0366 A71-12978

Muscle simulation by information theory for statistical analysis of behavior based on gas thermodynamics methods, showing stress relation to motor units excitation

03 p0366 A71-12979

Human equilibrium maintenance system analogy to multiinput/multioutput controller, considering motion of projection of center of gravity onto horizontal plane

03 p0356 A71-12981

Biocybernetic model of vestibular control system for spatial orientation, considering semicircular canals fluid motion angular velocity sensors and linear displacement perception

03 p0367 A71-12982

Mathematical model for eye crystalline lens accommodation control interaction with pupil, deriving dynamic equations from human/cat experiments with/without neurological control

03 p0356 A71-12984

Human cardiovascular control system model by analog computer program for various work loads up to submaximal, estimating correspondence to real life

03 p0368 A71-12995

Human behavior during machine control learning, modeling habit development as automatic control system

03 p0368 A71-12997

Human motor skills acquisition during manual control problem solving, modeling operator as single channel data processing system

03 p0368 A71-12998

Human operator thinking and decision making model for man-machine interaction

03 p0368 A71-12999

Human left ventricle mathematical models, determining physiological response oriented mechanical parameters with diagnostic significance [ASME PAPER 70-WA/BHF-14]

03 p0373 A71-14112

German monograph on frequency filter behavior of human retina regarding electric pulses, using ganglion model

03 p0373 A71-14372

Accommodation model concerning nervous control of ciliary muscle

03 p0373 A71-14378

Spacecraft and aircraft automatic control man machine interface, bionics and traffic control systems

03 p0455 A71-14393

Biological heuristic programming in cybernetics, discussing solid state logic elements limiting factors in modeling

03 p0383 A71-14394

Semicircular canal ducts dynamic response characteristics, using suspended liquid filled inner tube for endolymph simulation

04 p0542 A71-14789

Vestibular system semicircular canals mathematical model determination of galvanic stimulation and directional preponderance, considering visual, postural and vehicle orientation feedback loops

04 p0543 A71-14790

Cochlear nerve fibers two tone inhibition as signal suppressions inherent to bandpass nonlinearities, using modified analog model and mathematical analysis

05 p0712 A71-16280

Concentric layer model for estimating energy expenditure of left ventricle

05 p0713 A71-16486

Retinal electronic model with about 700 photoreceptors and output cells and new interconnections technique

05 p0715 A71-17079

Multifactor correlation analysis of systemic circulation effects on brain blood filling level, using linear regression equations

06 p0855 A71-18373

Human temperature control computer simulation, considering sudomotor, vasomotor and metabolic as error signals from hypothalamic and cutaneous thermoreceptors

07 p1048 A71-19585

Vision mathematical model based on homogeneous medium thermal conductivity equation

07 p1043 A71-20112

Electronic model of color recognition by human eye using spectral filter-photosensor system

07 p1051 A71-20122

Model experiment for purposeful motor behavior in cells or elements medium, assuming cell to cell system movement, adjacent cell visibility and different reaction to nearby cells

07 p1051 A71-20124

Biophysical model of life origin on earth using primordial gas-small organic molecule-macromolecule-protocell transformations

07 p1043 A71-20125

Mathematical model for brain arteries hemodynamic resistance, using blood pressure data

09 p1390 A71-22261

Synchronous combinative time pulse polylogical structural elements for computer simulation of human neuron functions, discussing circuit design

09 p1398 A71-22271

Nonius horopter theory and mathematical model, discussing binocular disparity and monocular visual direction criterion

09 p1399 A71-23016

Excitable myocardium cell simplified model based on artificial membrane excitation phenomena, using hybrid computer complex analog section

10 p1567 A71-24166

Principles and practice of bionics - NATO/AGARD Conference, Free University of Brussels, Belgium, September 1968

10 p1568 A71-24220

Aerospace research bionics and bioengineering, considering adaptation of man to environment and matching of man and machine

10 p1568 A71-24221

Nervous system modeling, considering cybernetic brain functions, neuroheuristic programming and modes of distributed information processing pertinent to neuropsychological experiments

10 p1568 A71-24222

Adaptive flight control systems, emphasizing bionics approach to self organizing systems

10 p1682 A71-24227

Mathematical neuronal model for functional learning system networks, representing brain pattern recognition, learning and size invariance mechanisms

10 p1569 A71-24233

Biological oscillating propulsion systems, investigating plate propeller, boundary layer control, low drag fuselage shapes and VTOL engine installations

10 p1569 A71-24235

Heart electric generator system simulation by bipolar or multipolar generators

10 p1569 A71-24238

Absolute and relative visual movement perception quantitative models relevant to length perception theory

10 p1570 A71-24603

Resistance and mathematical modeling of human body control concerning brain, cardiovascular, arterial muscle contraction and protein metabolism systems

10 p1571 A71-24955

Flight helmets speech intelligibility evaluation using in-flight manikin recording

10 p1572 A71-25069

Microwave energy dissipation as heat in eye, using agar for eye model construction

10 p1572 A71-25078

Discrete control input system oscillations, resembling eye pupil diameter changes, hand tremors and aiming fluctuations during rifle sighting experiments

11 p1723 A71-25166

Model of retinal information in cats from physiological and anatomical evidence, considering processing of contrast and eye movement information

11 p1723 A71-25254

Nonlinear axisymmetric solution for cardiovascular system pulsatile flow, using long rigid tube and velocity profile representation

11 p1726 A71-26485

Large amplitude wave propagation in arteries, deriving aorta mathematical model consistent with heart pressure and flow pulses and wavefront velocity

12 p1870 A71-26937

Multicomponent exponential curves analysis by Post-Widder equation, providing continuous distribution function of time constants in inhomogeneous systems

12 p1870 A71-27129

Small signal characteristics mathematical models of carotid sinus baroreceptors of rabbits

12 p1870 A71-27133

Human body thermal behavior modeling, obtaining steady state analytical solution for various boundary conditions and parameters

12 p1875 A71-27563

Human inner organic system simulation by digital computer, using overall quantitative heuristic model

12 p1876 A71-27742

Grating pattern vision models, examining single neural network and multiple channel stimulus information processing

13 p2018 A71-28461

Superposition model of spontaneous activity of cerebellar Purkinje cells for spike triggering

13 p2014 A71-29289

Mathematical and mechanical models of human thermal system thermodynamic/transport processes and external regulation devices for single elements and entire body

13 p2023 A71-29400

Heat transfer through human peripheral tissue based on one dimensional steady state continuum model combining effects of conduction, convection, vascular heat exchange and metabolism

13 p2025 A71-29502

Human body attitude control in space, using ten body complex geometry system, noting astronaut training jig

14 p2188 A71-29832

Electromagnetic field action on living organism simulated with infinite homogeneous cylinder in infinite cylindrical solenoid EM media

14 p2182 A71-30026

Biomathematical model and least square estimation from time series data of discrete particle population in stochastic compartmental system

14 p2265 A71-30181

Multicategory bibliographic classification of human behavior computer simulation models

14 p2189 A71-30461

Energy output of left ventricle and congestive heart failure mechanism, approximating blood velocity in aortic system by mathematical model

15 p2363 A71-31443

Inertial properties of segmented cadaver trunk for mathematical model of spinal response to impact in seat ejection acceleration injuries in high speed aircraft

16 p2528 A71-33117

Central nervous system self regulating properties analysis by automatic control theory, using parametric functional model of brain electrical activity

16 p2538 A71-34107

Nonlinear analysis of arterial flow pulses and shock waves, simulating aortic insufficiency under pathological conditions by mathematical model

16 p2538 A71-34145

Mathematical fatigue models based on permeability variations in synaptic membranes and feedback regulation due to working organ metabolic changes

17 p2687 A71-34354

German monograph on extrapolation procedure based on Taylor series expansion and on algorithm for identification and prediction of eye pursuit movements

17 p2690 A71-34790

Rotational ocular nystagmus phases induced by head rotation, developing vestibulo-ocular system mathematical model

17 p2691 A71-35045

Neurobionics, considering data processing in brain and central nervous system

17 p2691 A71-35165

Mathematical models of distance perception under flight conditions according to visible brightness of luminous surface

17 p2691 A71-35166

Adaptive mathematical model of human operator during pursuit tracking, synthesizing brain in accordance with arbitrary reasonability criterion

17 p2692 A71-35169

Mathematical model of human visual system light adaptive signal transformation

17 p2692 A71-35171

Visual adaptation mathematical model, studying relation of brightness static transformation into luminance

17 p2692 A71-35174

Conjugate eye movement stimulator and monitor for human experimentation in closed loop, open loop and variable feedback modes of operation

17 p2693 A71-35392

Muscle contraction model under biological factors action, considering circular cylindrical vessel equilibrium under internal and external pressures

17 p2694 A71-35616

Human visual system biological model for pattern recognition based on spatial filtering covering Fourier transform modification for application to discrete case

17 p2694 A71-35793

Modeling human disorientation and motion sickness in rotating spacecraft, stressing sensors dynamic response

18 p2872 A71-36654

[AIAA PAPER 71-870] Mathematical model for human thermal system, checking accuracy

18 p2873 A71-36899

Human operator models parameter estimation by stochastic approximation, considering continuous and sampled data models

19 p3007 A71-37648

Cardiovascular system mathematical model for evaluating system parameters effects on circulatory indices including minute volume and arterial tension

19 p3007 A71-37777

Thermal behavior simulation of cooling biological system, describing heat generation and transfer at normothermic to hibernating body temperatures with mathematical model

19 p3003 A71-38199

Signal propagation in model neuron network in terms of differential equations system, representing retina major cell types in planar model

19 p3003 A71-38276

Primary biological receptor element analogous electronic model for potential and afferent pulse train responses to stimuli
20 p3191 A71-38894

Small pressure wave transmission in abdominal venae cavae of dogs in mathematical model development for viscoelastic behavior of large veins
20 p3187 A71-38987

Spacecraft manual control investigation, using human operator models described by linear transfer function with variable coefficients
20 p3193 A71-39226

Pulmonary nitrogen washout and carbon monoxide uptake, developing dynamic mathematical models for volume and distensibility distributions in airways and alveoli
20 p3193 A71-39441

Cortical responses of awake cat to narrow-band FM noise stimuli, proposing neuronal model
20 p3190 A71-39767

Soviet monograph on coacervates and protoplasm covering colloidal-chemical properties, enzyme catalysts and multiphase cell and organism simulation
21 p3336 A71-40870

Human perceptual motor skill development in tracking performance, using feedback control system gain and effective time delay as measures
21 p3343 A71-40909

Bioholographic animal information processing model, considering nervous system as diffractive medium and neural network as Fourier analyzer
21 p3380 A71-40923

Mechanical properties of muscular organs, presenting mathematical model for biological fluid flow analysis
21 p3336 A71-40984

Electrical heart activity and ECG mathematical model with nonlinear oscillator system construction for normal and abnormal rhythms
21 p3336 A71-40986

Computerized electrostatic field model of biological cell membrane
22 p3487 A71-42119

Saccadic eye movement control system behavior simulation model evaluation, considering oculomotor pathways
22 p3504 A71-42443

Versional eye movement control system models, considering dual mode control, intermittency, plant dynamics and pattern recognition
22 p3489 A71-42444

Oculomotor neural organization models, considering vestibular ocular reflex, saccadic eye movements and smooth pursuit systems
22 p3504 A71-42450

Evoked and background activities interaction in computerized self zeroing neuron model
24 p3801 A71-44550

Human eye theoretical model with aspherical cornea front and lens back surfaces, computing astigmatism, coma, meridional and sagittal focal lengths by ray tracing method
24 p3798 A71-44978

Analog modeling of enzyme and biochemical systems with fixed and variable functional properties, using operational amplifier integrator
24 p3802 A71-45109

BIOPAQS
Preservative phenol derivative effects on toxic gas evolution from stored urine in sealed vessels
22 p3506 A71-42808

BIOPHYSICS
Antiarrhythmic drugs choice based on excitable tissues biophysics, considering contrast between cardiac muscle and nerve
02 p0201 A71-12419

Soviet book on chemistry, physics and mathematics of life covering evolution, metabolic processes, biological cycles and rhythms, molecular physiology, cybernetics, etc
04 p0539 A71-15261

Biophysical nature of human memory, investigating electrosensibility phase modulators and variations by supralintensive light stimulus to eye and adjustment reflex
09 p1391 A71-22484

Humid operative temperature as index for biophysical thermometry and thermal comfort sensation prediction
18 p2861 A71-36887

BIOREGENERATION
U REGENERATION (PHYSIOLOGY)
BIOREGENERATIVE LIFE SUPPORT SYSTEMS
U CLOSED ECOLOGICAL SYSTEMS
BIOSATELLITE 2
Horizontal clinostat rotation rate for optimal and acceptable weightlessness simulation in plants, comparing with wheat seedlings growth in Biosatellite 2
05 p0712 A71-16150

Biosatellite 2 onboard experiments studying weightlessness effects on biological processes and interaction with radiation from Sr 85 gamma ray source
21 p3341 A71-40007

BIOSATELLITE 3
Biosatellite 3 reduced gravity environmental laboratory with subhuman primate on 30 day mission, discussing ground base tests, simulated and actual flight
09 p1400 A71-23238

Biosatellite 3 monkey sleep and wake states based on visual and computer analysis of telemetered EEG data from earth orbital flight
09 p1395 A71-23242

Macaca nemestrina monkey bone density change during Biosatellite 3 mission
21 p3330 A71-40343

Physiological deterioration of monkey onboard Biosatellite 3 and unexpected demise, presenting collected data for response analysis
21 p3333 A71-40564

BIOSATELLITES
NT BIOSATELLITE 2
NT BIOSATELLITE 3
Frequency spectra and cosinor for circadian rhythms in rodents and in man during Gemini and Vostok flights, considering future biosatellites
01 p0020 A71-11569

Biosatellite hydrogen oxygen fuel cell/silver zinc battery combination power system for long aerospace missions, discussing optimal design tradeoff
04 p0535 A71-15286

Biosatellite postflight experiment evaluating effects of forced electrolyte imbalance in Macaca nemestrina
08 p1239 A71-20821

Three day mission biosatellite environmental thermal control system design and flight performance [ASME PAPER 71-AV-33]
18 p2869 A71-36400

Microorganisms under closed environmental ecological conditions with reference to astronauts in infectious diseases, discussing bacteria growth in Biosatellite 2 and earth based closed chamber experiments
21 p3343 A71-40562

BIOSENSORS
U BIOINSTRUMENTATION
BIOSIMULATION
U BIONICS
BIOSPHERE
U EARTH HYDROSPHERE
U LOWER ATMOSPHERE
BIOSYNTHESIS
Diet effects on hepatic fatty acid synthesis in rats and mice, noting linoleate content role
01 p0011 A71-10848

Biosynthesis of inosinic acid in transfer RNA in Escherichia coli by polynucleotide modification
03 p0375 A71-13173

Hexosamines biosynthesis control mechanism, considering UDP-N-acetylglucosamine function
05 p0706 A71-16217

Pineal gland endocrine functions, discussing melatonin synthesis and secretion in response to environmental illumination
05 p0712 A71-17108

Organic compounds biosynthesis in simulated Mars atmosphere, using UV irradiation for photocatalytic production from CO and water mixtures
09 p1403 A71-22647

DNA synthesis rhythm in aorta endothelial cells nuclei during direct division, noting effects of amitosis by autoradiography
12 p1872 A71-27752

Hypothermia effect on lipid synthesis of hamster tissue following intravenous injection of acetate-C 14
14 p2182 A71-29582

Biosynthesis control of melatonin and other methoxyindoles in mammalian pineal organ
14 p2182 A71-29631

Local skin thermoregulation mechanism in man controlled by cooperative bradykinin biosynthesis, using IR thermometry recording of thermal stimulus
18 p2859 A71-36868

Peptides formation from glycine in presence of trimetaphosphate, investigating mechanism
21 p3345 A71-40175

Glycerides metabolism in rats brain under normal conditions and during hypoxia, showing diglycerides role in triglycerides and phospholipids biosynthesis
21 p3337 A71-41056

Rat brain carbohydrates biosynthesis from organic acid products under normal conditions and during central nervous system disturbances, investigating butyric acid participation
21 p3337 A71-41058

Stimulatory effects of hypobaric hyperoxia on lipid synthesis in rat liver and adipose tissues under free feeding
22 p3486 A71-41825

BIOTECHNOLOGY
Bioelectric potential in gap between abutting cardiac muscle cells, using differential equation for active to inactive cell transmission
01 p0025 A71-11177

Human factors engineering in man machine systems, evaluating biotechnology and aeronautical medicine relationship
05 p0715 A71-16935

Laser systems for biomedical applications, considering ophthalmology, dermatology, surgery, biological and cellular research, analytical and diagnostic medicine
07 p1049 A71-19782

Radioisotope thermoelectric generators in micro/milliwatt power range for biomedical applications
20 p3192 A71-38912

BIOTELEMETRY
Mammalian hair effectiveness as insulation, using biotelemetry for deep body temperature measurement
01 p0023 A71-10886

Electronic instrumentation for monitoring intragastric pH, temperature, motility and electrical activity
01 p0023 A71-10887

Temperature telemetry for pyrogenic drugs testing on dogs
01 p0023 A71-10977

Physiological data telemetry link using time division multiplex method
01 p0024 A71-10981

Design criteria for implantable biotelemetry systems, discussing RF signal transmission through conductive body tissue
01 p0024 A71-10982

Dog blood flow telemetric measurement with TV system using ultrasonic signals Doppler effect
01 p0024 A71-11059

Military parachutists physiological and force field responses to aerospace recovery environment, using multichannel FM/FM telemetry for heart rates
02 p0207 A71-12389

Biological and medical cybernetics approach to closed systems construction for continuous automatic monitoring and control of human physiological processes under harmful conditions
03 p0368 A71-13000

Biotelemetry - Conference, Erlangen, West Germany, November 1968
03 p0369 A71-13058

Biotelemetry objectives, principles, implementation and applications, discussing wire and wireless systems, radio frequency selection, transmitting power and modulation methods
03 p0369 A71-13059

Biotelemetry data acquisition and electrode technology, discussing physiological measurements and pickup techniques for conversion into electrical signals
03 p0369 A71-13060

In-flight ECG telemetry for aircraft pilots diagnostics, discussing characteristic recordings and measuring probes development for simultaneous parameters transmission
03 p0370 A71-13062

Biotelemetry in aviation medicine, discussing telemetric methods and applications for continuous observation of physiological processes under environmental exercise and stress conditions
03 p0370 A71-13063

In-flight telemetric ECG recordings of aircraft pilots during normal, abnormal and aerobatic flight, analyzing heart rate variations as function of stresses
03 p0370 A71-13064

Telemetric ECG recordings of workers under high and strongly varying temperature conditions, discussing heart rate variations under heat stress
03 p0370 A71-13065

ECG telemetric data computerized processing, describing cardiac data acquisition, long distance telephone transmission, analog to digital converter, central processor and output devices
03 p0370 A71-13066

In-flight EEG recordings telemetry for pilot aptitude testing, showing pilot error relationship to brain oversteering
03 p0370 A71-13067

Human respiratory parameters telemetry, discussing transducer development for ventilatory volume measurement
03 p0370 A71-13068

Semiconductor devices for continuous blood pressure telemetry
03 p0370 A71-13069

Direct continuous radiotelemetry of blood pressure measurements taken from aorta, pulmonary artery and inside heart during normal activity of test subjects
03 p0371 A71-13070

Simultaneous comparison and calibration of ultrasonic Doppler telemetry and electromagnetic flowmeters implanted on peripheral arteries of dogs
04 p0545 A71-15164

Electrically rotating chair transmitting medicobiological information of functional state of vestibular analyzer and statokinetic stability
05 p0715 A71-17027

Multichannel EEG radio telemetry for remote recording of biological activity from subjects in motion and within human body
05 p0715 A71-17110

Light and drugs effect on diurnal body temperature from radio telemetry of adult male rats
05 p0715 A71-17111

- Telemetric techniques for pharmacological effects of body temperature, motor activity and food and fluid intake on rat brain, describing recording and monitoring equipment 05 p0716 A71-17112
- Bioelectric activity of cerebral cortex in man under neuroemotional stress, using multichannel radioelectroencephalography 06 p0856 A71-18464
- Optimal contactless kinetocardiography recording LF patient chest vibrations, comparing short wave method 06 p0863 A71-18468
- Multiple sensor heart rate telemetry using automatic data acquisition and management in squirrel ecology 07 p1049 A71-19626
- Biotelemetric contactless recording of animal movements using centimeter band standing waves 09 p1397 A71-22216
- Jet pilots flight stresses assessment via biotelemetric transmission of pulse rate, respiratory rate, electrocardiographic data, flight altitude and velocity 10 p1567 A71-23880
- Astronaut electrode-amplifier helmet harness for cable and radiotelemetry acquisition of EEG, EGO, EMG and blood pressure data on noninterference basis 10 p1570 A71-24475
- ECG miniaturized single channel biotelemetry transmitter, discussing lightweight design and power supply 10 p1570 A71-24487
- Compact head mounted six channel IC telemeter for artifact free EEG recording during laughter 13 p2020 A71-28889
- Cardiovascular telemetry total implants, describing measurement problems, equipment design, low current operation, size and thermal and temporal stability 16 p2534 A71-33071
- Telemetric accelerometer for assessing mental performance under industrial working conditions for work characterized by periodically repeated stereotyped movements 17 p2688 A71-34363
- Radiotelemetric equipment for continuous subcutaneous measurements of circadian body temperature rhythm in rats 21 p3335 A71-40634
- Miniaturized multichannel FM/AM biological telemetry system for simultaneous transmission of EEGs, EMGs, EOGs and EKGs 22 p3500 A71-41574
- Pulmonary circulation pressure and flow telemetry of free ranging intact animals, describing instrumentation and technique for transduction and transmission 23 p3640 A71-44243
- BIOTIN**
- Cystamine hydrochloride or vitamin B complex with vitamin C for radiation sickness prevention and therapy 22 p3493 A71-42723
- BIPROPELLANTS**
- U LIQUID ROCKET PROPELLANTS**
- BIRDS**
- NT CHICKENS**
- NT PIGEONS**
- Bird strikes incidence and prevention, discussing velocity effects, migration role and uses of distress calls, falconry and radar 06 p0848 A71-18664
- Bird impact hazard to general aircraft, discussing structural damage, flight safety and testing procedures 10 p1557 A71-24997
- Materials and structural design development by high velocity impact testing due to transport and subsonic military aircraft susceptibility to bird collision damage 14 p2221 A71-29642
- F 101 30,000 lb thrust augmented turbofan engine for B-1 bomber, considering maintainability and bird ingestion tolerance 19 p3122 A71-37491
- BIREFRINGENCE**
- Q switched laser wave birefringence thermal variations in liquids, calculating optical anisotropy temperature dependence 02 p0261 A71-12172
- Streaming birefringence theory, discussing incompressible fluids, shear and Couette flows, fading memory, deformations 05 p0784 A71-17244
- Neodymium glass lasers, investigating pump-induced birefringence effect on polarization and radiation distribution 06 p0907 A71-17398
- Photometric attenuator with linear birefringent polarizers, describing construction and calibration 07 p1110 A71-19468
- Photometric method for birefringence parameters determination in photoelastic stress distribution measurements, using proposed photosensitivity calibration standards 10 p1611 A71-24354

- Wide field high resolution birefringent filter based on Fabry-Perot etalon and Lyot-Ohman filter, discussing limitations and applications 12 p1904 A71-26802
- Lossless KDP Pockels cell modulator for high power laser Q switching based on tuned face electro-optical crystal 12 p1905 A71-26813
- Gas laser birefringence observation in active elements under pumping action, using light beam components polarization intensity measurements 14 p2255 A71-30586
- Dynamic polariscope for birefringent materials stress wave low cost analysis 18 p2923 A71-36611
- Isotropic materials with memory, discussing induced birefringence theory to account for memory and nonlinearity effects in dielectric properties dependence on deformation history 19 p3118 A71-37525
- Neodymium-glass lasers active elements thermal-stress-induced birefringence effects on energetic and polarization characteristics 19 p3072 A71-37767
- Stress state determination in birefringent elastic material for plane dynamic problems, by photoelasticimetric and interferometric techniques 21 p3376 A71-40103
- Reflected shadow method for constrained zone photoelastic observation around cracks in birefringent transparent plate under plane stress 22 p3549 A71-42555
- Nonmagnetic dielectric artificial birefringence determination, using permittivity additivity with bivalent symmetrical tensor 24 p3877 A71-44408
- BIREFRINGENT COATINGS**
- Two and three dimensional static and dynamic photoelasticity and birefringent coating techniques applications in linear fracture mechanics 13 p2152 A71-28217
- Birefringent coating method for stress analysis of fiber-reinforced laminated composites, developing subsurface stress-surface strain relation [SESA PAPER 1837A] 17 p2761 A71-34528
- Stress analysis of photosensitive coatings and transparent birefringent materials, applying holography to optical polarization method 22 p3537 A71-41614
- BISMUTH**
- Vacuum deposited Bi thin films on glass substrates at liquid He temperature, investigating characteristics of critical thickness 03 p0466 A71-13291
- Thin bismuth films thermal and electrical conductivities and thermoelectric power measurements, examining preparation methods 21 p3435 A71-41338
- Thermomagnetic recording by Curie point writing in thin manganese-bismuth films for magneto-optic mass memories 22 p3587 A71-42473
- BISMUTH ALLOYS**
- In-Bi alloys electrical conductivity measurement for compositions covering characteristic points of phase diagram at temperatures from liquidus line to 850 C 02 p0294 A71-11895
- Thermoelectric properties of quaternary Sb-Bi-Te-Se solid solutions, noting low thermal conductivity 22 p3584 A71-41618
- In-Bi whisker growth by squeeze technique, measuring crystal structure by X ray analysis and melting point method 23 p3689 A71-42956
- Thin film oxide, ferroelectric and bismuth titanate dielectrics for high capacitance microwave IC technology 23 p3651 A71-43429
- Nd-Bi phase diagrams from thermal differential, metallographic and X ray analyses, discussing carrier concentration and mobilities, Hall coefficients, conductivity and thermal emf 23 p3692 A71-44022
- BISMUTH COMPOUNDS**
- NT BISMUTH OXIDES**
- NT BISMUTH TELLURIDES**
- Bismuthide chemistry research, presenting equilibrium diagrams with all elements 16 p2622 A71-33923
- Laser Curie point writing characteristics and diffraction efficiencies of MnBi thin films for holographic recording 19 p3062 A71-37143
- Heat treated thallium bismuth sulfide, selenide and telluride amorphous and polycrystalline thin films electrical conductivity, differential thermal emf and forbidden bandwidth 20 p3276 A71-39076
- BISMUTH OXIDES**
- Bismuth oxide and iron oxide equimolar mixtures solid state reactions, determining rates from integrated X ray diffraction and activation energies 08 p1318 A71-20699

- BISMUTH TELLURIDES**
- Refractive index and reflectivity of BiTeBr and BiTeI single crystals from interference measurements in transmission spectra 12 p1944 A71-27545
- Bismuth telluride single crystals thermal conductivity and thermoelectric power temperature dependence 2.3-100 K, discussing magnetic field effects 21 p3433 A71-41314
- BISPENOLS**
- Difunctional epoxy resins from dihydroxydiphenyl sulfone /bisphenol S/, obtaining increased heat resistance and thermal stability 11 p1787 A71-25424
- BISTABLE AMPLIFIERS**
- U FLIP-FLOPS**
- BISTABLE CIRCUITS**
- Fluidic proportional amplifier circuit with two bistable element stages, using pulse width modulation techniques 07 p1027 A71-20579
- Boundary layer pressure distributions for supersonic fluidics bistable devices 07 p1029 A71-20589
- Flowmeter based on oscillating bistable fluid amplifier, discussing Mach number, Reynolds number and Strouhal number effects on measuring characteristics 15 p2352 A71-32066
- BISTATIC REFLECTIVITY**
- Synthetic aperture holographic techniques in continuous wave bistatic radars for moving targets 03 p0381 A71-14477
- Coupling effect on monostatic-bistatic radar equivalence for monochromatic wave and short pulse scattering 07 p1060 A71-19260
- Synthetic aperture Doppler free coherent bistatic radar for high resolution maps of tropospheric radio scatterers 12 p1881 A71-27286
- Meteorologic bistatic radar equation for randomly distributed targets, applying to raindrops, refractivity perturbations, etc 14 p2197 A71-30830
- Bistatic radar frequency spectra and cross sections dependence on surface scattering laws, studying echo bandwidth 17 p2702 A71-35026
- Electromagnetic wave scattering from turbulent plasma at 31 GHz, determining cross section dependence on bistatic angle and electron density 19 p3017 A71-37868
- Bistatic radar scattering cross section from slightly rough perfectly conducting infinite surface, using Fourier transform 19 p3024 A71-38609
- BIT SYNCHRONIZATION**
- PCM telemetry receiving stations testing, comparing bit error probabilities of coherent and noncoherent methods of synchronizing pseudonoise sequences 01 p0033 A71-10890
- NRZ PCM signal conditioning, bit and group synchronization and decommutation techniques 01 p0034 A71-10901
- PCM telemetry bit synchronizer/signal conditioner, discussing bit acquisition, error and slippage rates 01 p0053 A71-10907
- Radio signal reception error in cadence synchronization of binary data transmission systems with indeterminate signal arrival time 02 p0212 A71-11834
- Synchronous digital communication system with each station clock rate established by phase locked oscillator input average, calculating two-station network dynamic stability 05 p0729 A71-17051
- Phase-coherent communication systems with phase locked loops for data detector synchronization, calculating noisy timing effects on detection efficiency 05 p0724 A71-17059
- Absolute value type early-late gate bit synchronizer steady state phase noise performance evaluation by Fokker-Planck method 05 p0730 A71-17060
- PCM bit synchronization and signal detection by nonlinear filter theory, giving optimum sequential estimator 07 p1061 A71-19536
- Optimal error correcting code structure selection for binary data transmission systems synchronization, using criterion of minimum false detection probability 08 p1260 A71-21979
- Automaton concept in cybernetics, emphasizing synchronous switching circuit operation with asynchronous input data 12 p1884 A71-27045
- Modular digital TDM switch for radially distributed clock synchronization, discussing design and control 13 p2034 A71-29318
- Digital communication system frame synchronizer performance analysis, using mean time formula and state transition matrices 14 p2201 A71-30925

Synchronization of high-speed digital data communication systems with continentwide interconnected switching centers, discussing elastic storage buffering to compensate for transmission time delay variations 17 p2712 A71-35784

Bit and scanning field synchronizations of time multiplex for air traffic control 18 p2946 A71-36513

Signal shape matched suboptimum self bit synchronizer for high SNR and timing error variance, reducing jitter 20 p3203 A71-38862

Bit synchronization in high SNR digital communication system, using Kalman filtering algorithm 22 p3513 A71-42383

BITS

Bits round-off and approximate division error effects in data compressor design, suggesting best maximum error criteria 01 p0050 A71-10878

Cascade type analog-to-digital converter with successive bit determination by recycling through single operational amplifier and comparator 02 p0231 A71-12038

PCM telemetry bit error probability confidence intervals and Bayesian posterior distributions derivation, using statistical method 04 p0554 A71-15327

Bit error probability estimation from sync word error rate data 07 p1062 A71-19538

Accuracy requirements determination method for digital controller coefficients, discussing bits needed 11 p1792 A71-26415

Bit error rate detector for testing digital data links, using analog network mathematical model 22 p3519 A71-42764

Elastic surface waves bi-phase modulated encoding and decoding at 10 Mbit/sec using Y-cut quartz 23 p3645 A71-43436

BLACK BODY RADIATION

Body radiative properties, examining degree of blackness dependence on surface roughness factor 02 p0331 A71-12188

Emissivity and temperature measurement of assembled microscopic particles in black body cavity 04 p0676 A71-14954

Planck formula correction for small cavity black body radiation, considering application to far IR standard sources 04 p0676 A71-14955

Airborne radiation thermometry corrections for intervening atmospheric absorption and emission and ocean surface nonblackness 04 p0601 A71-15762

Extragalactic radio sources relativistic electrons interaction with cosmic black body radiation, noting effect on sources lifetime and X ray background 04 p0641 A71-15838

Galaxies and universe evolution, discussing expansion, isotropic black body radiation, present matter distribution, radio source population density and galactic nuclei instability 04 p0661 A71-15895

Monte Carlo calculations of intrinsic radiation and blackness degree of nonisothermal cavities with non-specific temperature profile 06 p0897 A71-17529

Radiant heat transfer from heated cylindrical enclosure with black/gray walls to absorbing gas or gas having black particles, calculating absorption coefficients 07 p1224 A71-20018

Radiation patterns and scattering cross sections of plane black disks excited by electromagnetic and acoustic waves 14 p2194 A71-30079

Body radiative properties, examining degree of blackness dependence on surface roughness factor 15 p2512 A71-31495

Black radiation absorption by isothermal gas in entire spectrum, discussing Hottel empirical formula 17 p2836 A71-34214

Normal emission factors of dielectric materials at 1000-1500 C, using black bodies in study of thermal radiation of refractory materials 20 p3254 A71-39960

Young dust-filled planetary nebulae models with hot central stellar black body radiation, evaluating IR radiation absorption and reradiation in H I region 21 p3446 A71-40417

Highly compact X ray source spectrum fitted by black body model at 15 million K 23 p3732 A71-43076

Uniform model universes with matter and black body radiation, obtaining radiation temperature dependence on scale factor 23 p3769 A71-43994

Initial singularity removal in model big bang universe compatible with 3K black body radiation in terms of renormalized gravitational theory 23 p3770 A71-44182

BLACK BRANT SOUNDING ROCKETS

NT BLACK BRANT 3 SOUNDING ROCKET
NT BLACK BRANT 4 SOUNDING ROCKET

Intense X radiation source in Cetus region observation by Black Brant rocket 04 p0640 A71-15049

BLACK BRANT 3 SOUNDING ROCKET

Black Brant 3B sounding rocket design and development, discussing payload capability, static and dynamic stability, flight and ground handling loads [AIAA PAPER 70-1396] 03 p0499 A71-13677

BLACK BRANT 4 SOUNDING ROCKET

Black Brant 4 rocket second stage motor, investigating high altitude ignition problems by postflight analysis [AIAA PAPER 70-1384] 03 p0470 A71-13667

BLACKBURN B-103 AIRCRAFT

U BUCCANEER AIRCRAFT

BLACKOUT (PHYSIOLOGY)

Jet fighter pilot blackout episode report, correlating laboratory data with flight profile and events sequence 12 p1871 A71-27634

BLACKOUT (PROPAGATION)

NT ATMOSPHERICS
NT COSMIC NOISE
NT DAWN CHORUS
NT ELECTROMAGNETIC NOISE
NT HISS
NT IONOSPHERIC NOISE
NT IONOSPHERICS
NT SHOT NOISE
NT SUDDEN ENHANCEMENT OF ATMOSPHERICS
NT THERMAL NOISE
NT WHISTLERS

Communication blackout during missile and spacecraft high altitude flight, considering convective effects on gas breakdown by microwaves 14 p2206 A71-31071

Kerr-Newman black hole as generic final state of gravitational collapse developed from Schwarzschild geometry and mass, angular momentum and charge parameters 16 p2631 A71-33177

Quasars as proto-blackholes in galactic nuclei blackhole model, discussing lifetimes, dust and IR radiation using models 17 p2811 A71-35745

Black holes in binary star systems from orbital eccentricity observations 19 p3142 A71-38006

Night enhancements in 6300 A line at Sanae related to diurnal excursion of auroral oval, observing ionospheric blackout and high energy electrons precipitation 23 p3672 A71-43980

BLADDER

Sodium counterflow from serosal to mucosal surface of short-circuited acid-killed turtle bladder 01 p0015 A71-11182

Animal urinary bladder mechanical properties from controlled stretch tests, identifying viscoelastic, elastostatic and creep elements 14 p2186 A71-30566

BLADDERS [MECHANICS]

U DIAPHRAGMS [MECHANICS]

BLADE TIPS

Helicopter downwash velocities, noise and airloads, examining rotor tip modification effects 04 p0527 A71-15410

Transonic compressor rotors blade camberline shape optimization by various tip diffusion factor-ratio combinations 07 p1184 A71-20200

Marginal vortex effects on aerodynamics of helicopter lifting surfaces, considering blade form and noise spectrum tested in hydrodynamic tunnel 12 p1864 A71-27473

Combination tone noise generation from turbofans with supersonic fan blade tip speed, determining sound power distribution among engine rotation frequency harmonics [AIAA PAPER 71-730] 14 p2295 A71-30777

BLADES

Reversible transonic fluid flow through cylindrical blades cascade by hodographic singularities solution of potential and stream function 01 p0003 A71-11023

Creep effect on cooled blades elastoplastic stress-strain relationship using computer programs 02 p0323 A71-11741

Helicopter rotor stall characteristics, investigating blade flexibility, unsteady aerodynamics and variable inflow effects [AHS PREPRINT 520] 14 p2171 A71-31086

Aerodynamics of axial and axial tangential blade swirler twisted jet near nozzle, testing effectiveness of equivalent problem of heat conduction theory 15 p2388 A71-31522

Two dimensional supersonic flow pattern, velocity and loss in shock waves in front of blade cascade 22 p3479 A71-41842

Blade cascade design for meridional flow, using finite difference method for universal computer program 23 p3626 A71-43550

BLADES [CUTTERS]

Contoured silicone internal pressure bag mandrels for helicopter rotor blades fabrication 10 p1615 A71-24096

BLANKING [CUTTING]

Rectangular, square and circular cross section blanks dynamic metal cutting process by method of characteristics 08 p1295 A71-20794

High temperature blank heating and cutting during magnetic alloy machining for optimal cutter stability 08 p1296 A71-20844

BLANKS

Energy balance during ring blanks widening by electromagnetic pulses, establishing theoretical limit of mechanical efficiency 06 p0906 A71-18712

BLASIUS EQUATION

Existence theorems for compressible boundary layer problems, discussing Blasius differential equation and Falkner-Skan class of similarity solutions 06 p0881 A71-17638

Existence proof for Blasius equation and initial conditions system solution, using Luke results with integrals of incomplete gamma function 20 p3255 A71-39035

BLAST LOADS

Annealed steels strengthening and structural changes under explosive shock wave 01 p0085 A71-10037

Stress wave propagation in plates from explosive loading, discussing wave front interaction and scab formation 07 p1215 A71-20091

Blast wave propagation following explosions at center of generalized Roche model, discussing core radius and envelope thickness 09 p1431 A71-22371

BLASTOFF

U ROCKET LAUNCHING

BLEACHING

Thermal and bleaching waves as diffusion phenomena in opposite limits, discussing laser heating [AIAA PAPER 71-109] 06 p0928 A71-18559

Bleached hologram lifetime extension, decreasing light induced decay rate by gelatin hardening 12 p1905 A71-26815

Reversal bleaching process for low flare light and high diffraction efficiencies and SNR in holograms 14 p2241 A71-30134

Iodine vapor bleaching under molecular electronic-vibrational transition due to ruby laser intense monochromatic radiation 15 p2421 A71-32409

BLEED-OFF

U PRESSURE REDUCTION

BLIND LANDING

Kalman filter simulation for estimating aircraft position and velocity from airborne digital computer data in zero-zero landing system 06 p0924 A71-17697

Blind landing by mobile beams and Doppler systems, superseding heavy infrastructure ILS 06 p0925 A71-17951

VFR flying under bad weather conditions, discussing flight through and above cloud layers, need for radiotelephone communication and ground radar support 08 p1231 A71-21767

Trident aircraft autopilot for automatic landings in blind conditions, discussing operational problems 13 p2098 A71-29261

Holographic display for blind landing system with variable image perspective over wide field of view, using collimated or cylindrical laser beam 18 p2945 A71-36061

Military pilot handling characteristics, discussing combat operations, accident prevention and blind landing 22 p3504 A71-42239

BLINDNESS

NT FLASH BLINDNESS

Vision loss from windshield tinting in night visual flying accident 08 p1247 A71-20824

BLOCKING

Cardiac impulse conduction measurements noting delay, block and one way block in excised canine Purkinje fibers with depressed responsiveness 07 p1041 A71-19637

Blocked and series connected pneumatic fluidic transmission lines, determining amplitude frequency response 07 p1026 A71-20566

Horizontal flat plate moving transversely in rotating stratified fluid, calculating boundary layer blocking conditions for entire Rossby and Russell numbers range 12 p1897 A71-27222

Synoptic climatology of Euroatlantic blocking situations, investigating geographic location and duration 14 p2271 A71-30937

BLOOD

NT ERYTHROCYTES

NT LEUKOCYTES

NT LYMPHOCYTES NT RETICULOCYTES

Human blood gases continuous measurement in vivo by mass spectrography, considering arterial nitrogen washout and cerebral blood flow determination

01 p0021 A71-10237

Renin level in renal venous and peripheral blood in patients with renovascular hypertension

01 p0010 A71-10391

Carbohydrate-peptide bond and residue chain structure of group blood substances, using alkali decomposition of monosaccharides

01 p0013 A71-11091

Blood cholesterol and protein fraction concentrations in pathogenesis of hypothalamic atherosclerosis patients

02 p0201 A71-12531

Glucose intestinal absorption, blood glucose and hematocrit in hamsters, relating physiologic modifications to pregnancy

02 p0201 A71-12608

Central nervous system reactions to vasopressin and oxytocin presence in cerebrospinal fluid and blood, discussing respiratory frequency and antidiuretic tests

03 p0363 A71-13485

Blood lactate levels in human males after bicycle rides, considering altitude effects on oxygen consumption and glycolytic and aerobic activity

05 p0709 A71-16623

Human physical exercise with stepwise increasing load noting working capacity, cardiovascular and respiratory system performance and blood composition interrelations

05 p0709 A71-16805

K, Na, Ca and I electrolytes content in thyroid gland and blood during experimental hypothyroidism in rabbits

06 p0852 A71-17668

Rats and mice blood redox potentials injected with cystamine, investigating increased radioprotection

07 p1039 A71-18980

Hyperventilation and isoproterenol infusion, investigating T wave abnormalities, arterial blood gases and plasma electrolyte concentration

07 p1042 A71-19837

Microwave irradiation effects on peripheral blood and bone marrow in dogs and rabbits

07 p1053 A71-20539

Acute hydrazine hydrate poisoning morphological effects on internal organs and blood in guinea pigs, noting pronounced changes in liver and kidneys

09 p1393 A71-22921

Carbon dioxide tension in pulmonary arterial blood before/during prolonged rebreathing in oxygen mixtures at rest and exercise

10 p1558 A71-23895

Human blood cholinergic complex during various physiological states, noting nonmediator action of acetylcholine

13 p2006 A71-28384

Blood liquid state control in splanchnic canal as function of humoral feedback in coagulation, fibrinolytic and anticoagulation systems

13 p2010 A71-28718

Chronic hypoxia effects on blood oxygen and carbon dioxide tensions and pH changes in unanesthetized chickens at high altitude compared to sea level control

14 p2186 A71-30565

Pyruvate and lactate concentrations in muscle tissue and blood at rest and during exercise

14 p2187 A71-31136

Hypoxic hypoxia and hypercapnia effect on calcium, inorganic phosphorus and total protein in rats blood during hypodynamic syndrome

15 p2356 A71-31306

Peripheral blood and bone marrow morphological composition in dogs subjected to chronic and repeated gamma irradiation

15 p2357 A71-31308

Human blood pH and gas composition regulation mechanism under response to carbon dioxide partial pressure changes in inhaled air

15 p2357 A71-31316

Lactic acid production rate in human blood during supramaximal exercise, noting relationship to oxygen consumption

17 p2685 A71-35366

Biochemical measurements of human urine and blood changes during simulated oxygen-helium dives to 1500 feet

21 p3331 A71-40353

Dogs peripheral blood reaction to complex action of transverse accelerations and gamma irradiation

22 p3494 A71-42727

Vibration influence on peripheral blood reaction to gamma radiation in dogs, using clinico-hematological indices

22 p3494 A71-42728

Radiation effects on rats peripheral blood state in low pressure environment with sea level value oxygen tension

22 p3494 A71-42732

Water-salt metabolism in human blood and urine under high temperature conditions after residence in different climatic zone

24 p3794 A71-44414

Serotonin /5-oxytryptamine/ extraction from rat whole blood in series analysis, using acidic butanol instead of ordinary butanol

24 p3801 A71-44541

BLOOD CIRCULATION

NT BRAIN CIRCULATION

NT CARBOXYHEMOGLOBIN

NT CORONARY CIRCULATION

NT INTRAVASCULAR SYSTEM

NT ISCHEMIA

NT PULMONARY CIRCULATION

Soviet book on blood hydrodynamics covering circulatory system structure, rheology and mathematical models, pulsating flows, concentration effects and mass transfer

02 p0203 A71-11846

Biocontrol devices for artificial respiration and blood circulation, using information from organism

03 p0367 A71-12991

Circulatory response to beta adrenergic blockade during muscular work, causing reduction in cardiac frequency, exercise tolerance and oxygen consumption

05 p0709 A71-16622

Air blast effects on pulmonary ventilation, gas exchange, venous-arterial shunt and blood gas parameters

06 p0851 A71-17601

LF vibration effects on human beings, discussing circulatory reactions

06 p0859 A71-18188

Carboxyhemoglobin changes in circulating blood volume during lower body negative pressure exposure

06 p0854 A71-18363

Arm to tongue blood circulation time for heart disease and failure diagnosis in aged people

07 p1043 A71-20215

Polarographic blood oxygen measurement by principle of oxygen liberation into physical solution by potassium ferricyanide

07 p1053 A71-20337

Arterial circulatory system parameter identification from diastolic blood pressure curves by digital filter techniques

09 p1398 A71-22254

Cerebrospinal knee and flexor reflex suppression observations in rabbits and cats during blood circulation disorders

09 p1391 A71-22480

Arterial blood and muscle lactates in cold water swimming rats indicating reduced circulation endurance factors

09 p1396 A71-23360

Parabolic dialysis, examining uses as in vivo diffusible substances test and alternative for conventional chronic hemodialysis

09 p1401 A71-23370

Arterial hypoxia effects on regional blood circulation in anesthetized dogs, measuring aortic blood flow under controlled artificial ventilation and after sinoaortic denervation

09 p1396 A71-23542

Chemical release from traumatized tissue in dogs under cross circulation with lethal cardiac depression response

11 p1720 A71-26119

Age effects on whole blood viscosity with Wells-Brookfield microviscometer, investigating role of hematocrit and plasma protein

11 p1722 A71-26362

Nervous/cardiovascular systems and blood composition changes in moderate duration military transport flights

12 p1874 A71-27163

High altitude aerobic working capacity limitations, examining oxygen transport system and circulator factors

14 p2183 A71-30276

Vago sympathetic nerve trunk stimulation effects on pulmonary blood volume changes magnitudes and pattern in isolated perfused lungs

14 p2187 A71-31135

Circulation parameters in vascular network by bloodless zonal ultrasonic sphygmography based on acoustic bioecho location

17 p2689 A71-34648

Cutaneous circulation control by venous thermoregulatory reactions to temperature variations, using dog saphenous veins perfused with autologous blood or Krebs-Ringer solution

18 p2862 A71-36898

Cardiovascular system mathematical model for evaluating system parameters effects on circulatory indices including minute volume and arterial tension

19 p3007 A71-37777

Heart maximal aerobic and anaerobic power and stroke volume, discussing cardiac output and blood oxygen capacity measurements in subalpine population subjects

20 p3185 A71-38887

Human retinal blood circulation changes and vision disturbance under transversely directed acceleration, using dark chamber teleophthalmoscopy

20 p3188 A71-39228

Real time multitrack half tone recorder for displaying three dimensional information on instantaneous blood velocity measurement by Doppler effect

21 p3377 A71-40132

Vasomotor effects of vagus nerve on canine lung blood content in response to electrical stimulation of vagosympathetics

22 p3490 A71-42581

Minute blood and stroke volumes dynamics during prolonged hypokinesia by acetylene method

24 p3796 A71-44536

External respiration, gas exchange and blood circulation during passive orthostatic tests

24 p3796 A71-44537

Local and central body temperature effects on human cutaneous venomotor reflexes, monitoring venous wall tension by measuring hand dorsal veins pressure during temporary arrest of hand circulation

24 p3797 A71-44777

BLOOD COAGULATION

Unsymmetrical dimethylhydrazine (UDMH)/ effect on canine blood coagulation, blood-aqueous barrier and cornea

02 p0199 A71-12383

High altitude blood coagulation, determining hypercoagulability relationship to altered pulmonary hemodynamics

14 p2183 A71-30278

Coagulation and fibrinolysis changes after physical exercise in males with atherosclerosis, noting fibrinolytic response differences with age

18 p2853 A71-35918

BLOOD FLOW

Arterial blood pressure changes due to bilateral carotid occlusion or electrical heart pacing, considering effects on kidney blood flow and circumference in dogs

01 p0008 A71-10074

Arterial branches pulsating flow and wave propagation in large blood vessels, considering flow measurements from simulated model experiments

01 p0008 A71-10111

Dog blood flow telemetric measurement with TV system using ultrasonic signals Doppler effect

01 p0024 A71-11059

Vasodilation, oxygen, potassium and osmolality effects on exercise hyperemia in dog gracilis muscle

01 p0015 A71-11184

Human skin blood flow and venous tone in middle finger and forearm during leg muscle exercise to exhaustion

01 p0016 A71-11410

Cutaneous blood flow in anesthetized pig forelimb modified by brain temperature changes

02 p0197 A71-11671

Cardiovascular system blood flow mathematical model parameter optimization by simulation on hybrid computer, using OPTRAN program

02 p0203 A71-11807

Blood pressure and velocity waveform recording for patients during cardiac catheterization, interpreting relationships to vascular impedance

02 p0201 A71-12915

Healthy subjects physical training effects on blood flow and enzymatic activity in skeletal muscle

02 p0201 A71-12916

Adrenal gland blood flow and arterial pressure determination under stochastic pulse excitation of anesthetized dogs centripetal and centrifugal nerves, using analog correlator

03 p0357 A71-12994

Mixed venous oxygen tension oxide determination by nitrogen-carbon rebreathing method, considering pulmonary blood flow and oxygen carrying capacity

03 p0360 A71-13182

Oxygen tension, blood flow, redox potential and temperature variations in cerebrum and musculus gastrocnemius of rats during high mountain adaptation

03 p0361 A71-13190

Gamma-aminobutyric acid (GABA) penetration through blood-brain barrier for administration in dogs and rats

03 p0362 A71-13236

Microcathodes measurement of oxygen tension on arterioles external surface in hamster cheek pouch and hamster/rat cremaster muscle for blood flow regulation mechanism

03 p0363 A71-13487

Ascending aorta blood flow sequential velocity measurement using conical hot-film probe with linearized constant temperature anemometer circuit [ASME PAPER 70-WA/BHF-13]

03 p0373 A71-14111

Angiotensin I infusion effect on intrarenal blood flow distribution, using krypton 85 method and autoradiography

04 p0538 A71-15088

Local cooling effects on responsiveness of muscular and cutaneous arteries and veins in dogs, noting blood flow redistribution

04 p0538 A71-15091

Simultaneous comparison and calibration of ultrasonic Doppler telemetry and electromagnetic flowmeters implanted on peripheral arteries of dogs

04 p0545 A71-15164

Living human tissue thermal behavior analytical modeling including internal heat generation and blood flow effects

04 p0539 A71-15460

Syncope as temporary suspension of consciousness due to cerebral blood supply failure, considering cardiac rhythm disturbances, blood flow obstructions and heart disease

04 p0541 A71-15915

Main pulmonary artery velocity profiles in dogs and man, using thin-film resistance anemometer

05 p0706 A71-16324

Middle cerebral artery occlusion effect on cortical blood flow, tissue oxygen pressure and acid base equilibrium in animals under extended ligations

05 p0708 A71-16617

Lung volume direction and change rate effects on pulmonary vascular conductance and arterial flow in isolated dog lung lobe

05 p0711 A71-16952

Cinearteriographically demonstrated coronary artery disease severity correlation with myocardial blood flow response to treadmill exercise or isoproterenol infusion

06 p0852 A71-17874

Hydrodynamic model of human red blood cell rotation in flow toward sizing orifice, predicting volume distribution

07 p1045 A71-20446

Mathematical model for brain arteries hemodynamic resistance, using blood pressure data

09 p1390 A71-22261

Coronary blood flow measurements during strenuous upright exercise, using nitrous oxide method

09 p1400 A71-23362

Book on gravity and acceleration effects on lungs covering breathing mechanics, ventilation distribution, blood flow, gas exchange, arterial oxygen saturation and pulmonary shunting

09 p1402 A71-23620

Stroke-pulmonary blood volume relation and vascular recruitment and distensibility in dogs, allowing independent control of flow, heart rate and left atrial pressure

10 p1561 A71-24123

Gradual unilateral hypoxia effects on pulmonary blood flow partition, noting interaction with hypercapnia

10 p1561 A71-24125

Pulmonary arterial blood flow regulation by hydrostatic pressure in low resistance circulatory system

10 p1561 A71-24127

Aging effects on blood pressure-flow relations and cardiac output/ventricular end diastolic pressure, discussing pulmonary vascular bed capacity dependence on increasing flow during supine exercise

10 p1561 A71-24128

Heart rate and diastolic inflow coronary resistance extravascular component, discussing heart artificial stimulation and pharmacological maximal dilation effects

10 p1565 A71-24679

Isotonic training effects on circulation for limb muscular strength characteristics, using peak blood flow and venous compliance measurements

11 p1719 A71-26071

Leg position effect on human calf muscle blood flow during standardized heavy rhythmic exercise

11 p1722 A71-26358

Nonlinear axisymmetric solution for cardiovascular system pulsatile flow, using long rigid tube and velocity profile representation

11 p1726 A71-26485

Nonbleeding blood flow measurement by magnetorheography, using electromagnetic flowmeter principle

12 p1874 A71-27137

Coronary blood flow regulation, discussing local and remote control mechanisms and disturbance effects due to obstructive arteriosclerosis

13 p2003 A71-27860

Pulmonary circulation regulating factors, examining heart disease effects on lung capillary blood flow

13 p2003 A71-27861

Vessels mechanical behavior and blood flow dynamics in aorta bifurcation zone, using Navier-Stokes and continuity equations

13 p2019 A71-28657

Whole body blood flow autoregulation relationship to hypertension in reflex dogs

13 p2013 A71-28953

Carbon dioxide reduction and hemoglobin saturation rates of blood flow in curved channel membrane exchanger

13 p2013 A71-29004

Coronary blood flow response to acute and chronic hypoxia, observing vascular smooth muscle relaxation relation to released adenosine

14 p2184 A71-30281

Coronary vasculature development under hypoxia and pulmonary hypertension as possible cause of right ventricle phasic flow contour changes

14 p2184 A71-30282

High altitude acclimatized humans, noting decreased coronary blood flow and increased oxygen extraction

14 p2184 A71-30283

Short term high altitude exposure, determining coronary blood flow reduction relationship to cardiac output and stroke volume

14 p2184 A71-30284

Energy output of left ventricle and congestive heart failure mechanism, approximating blood velocity in aortic system by mathematical model

15 p2363 A71-31443

Human muscle blood flow measurement by Xe 133 clearance method during rhythmic exercise, noting work load effects

15 p2358 A71-31455

Cardiac output and regional blood flow in hypoxic woodchucks, noting no change in heart rate, diaphragm, kidney, liver, stomach and intestines

16 p2529 A71-33189

Physiologic and pathologic cardiomegaly, noting myocardial blood flow oxygen uptake and lengthening and widening of coronary vessels

16 p2531 A71-33423

M-cholinergic and adrenergic subcortical structures blockage effects on blood flow rate in dog pulmonary circulation system

16 p2534 A71-34113

Nonlinear analysis of arterial flow pulses and shock waves, simulating aortic insufficiency under pathological conditions by mathematical model

16 p2538 A71-34145

Nitrogen and oxygen exit rate from subcutaneous gas pockets in rats during tissue blood flow elevation due to cobalt chloride injection

17 p2678 A71-34174

Statistical evaluation of Doppler ultrasonic blood flowmeter, determining correlation between Doppler signal zero crossing density and fluid flow velocity

17 p2689 A71-34448

Left ventricular aneurysm electrocardiographic features and postresection changes based on ECG statistical analysis

18 p2854 A71-36138

Regional cerebral blood flow, tissue oxygen, EEG activity and behavioral reaction at high pressure

19 p3009 A71-38557

Automatic regulation of volumetric blood flow rate during artificial blood circulation, using electromechanical system for controlling arterial pump of cardiopulmonary machine

19 p3010 A71-38641

Cell volume analyzer for sensing individual blood cells and plotting number as function of size

20 p3191 A71-38824

Monograph on blood flow rates instantaneous measurement from ultrasound signals of Doppler flowmeter, discussing steady laminar flow test results

20 p3193 A71-39262

Potassium concentrations and osmolality levels changes effects on vascular resistance in subcutaneous adipose tissue blood flow

20 p3189 A71-39379

Cutaneous and intestinal blood flow differentiation during hypothalamic heating and cooling in anesthetized dogs

21 p3335 A71-40632

Coronary blood flow at increased arterial carbonic acid partial pressure, noting induced hypercapnia

21 p3335 A71-40633

Jet and turbulence mechanism of vascular murmurs associated with stenosis for minimum flow Reynolds numbers, using aorta orifice plates in dogs

21 p3336 A71-40864

Atrial shortening during volume loading by infusion in animal, using Frank-Starling approach

22 p3485 A71-41718

Frequency analysis of blood circulation rhythms and oxygen tension fluctuations in cerebra of rabbits, cats, monkeys and men

22 p3490 A71-42580

Pulmonary circulation pressure and flow telemetry of free ranging intact animals, describing instrumentation and technique for transduction and transmission

23 p3640 A71-44243

Dimensionless parameters effect on divided blood flow characteristics in large arterial bifurcation

24 p3801 A71-44622

Pulmonary blood flow and carbon monoxide diffusing capacity uneven distribution measurements, determining body position effects

24 p3798 A71-44782

Miniature battery operated electromagnetic blood flowmeter for data acquisition from unrestrained animals

24 p3801 A71-44783

BLOOD PLASMA

Lower fasting blood glucose levels in high altitude acclimatization

02 p0197 A71-11664

Blood plasma nonesterified fatty acids mobilization in relation to work load severity during and after prolonged exercise in men

04 p0544 A71-15154

Blood plasma volume reduction by voluntary hyperventilation, associating with hypovolemia of status asthmaticus

04 p0545 A71-15155

Hypokinesia and acceleration effects on plasma proteins displacement and bioelectric activity of striated muscles of rats

06 p0853 A71-17960

X ray influence on protein and mineral content of blood serum in dogs

06 p0858 A71-18728

Cellular damage to rat mitochondria and endoplasmic reticulum by injection of radioprotectors, discussing intracellular enzymes passage into plasma

07 p1039 A71-18981

Carbon dioxide absorption of dog blood and plasma under anoxia at simulated high altitudes, deriving equations for protein concentration rated buffer values

07 p1043 A71-20327

Barometric pressure and exercise effects on erythropoietin titer in normal and hypoxic rat plasma, noting lactic acid concentration and acid base balance changes

08 p1237 A71-20676

Bone tissue optical density and blood serum and urine calcium content of Soyuz 9 crew members during and after flight

09 p1389 A71-22201

Alloisoleucine configuration in blood serum of maple syrup urine disease patients, using gas liquid chromatography

09 p1403 A71-22477

Blood serum protein displacement in force direction in albumin injected rats under centrifuging acceleration

09 p1393 A71-22919

Blood plasma hyperosmolality and pulmonary vascular resistance in cats, infusing hyperosmolar solutions of sodium chloride, mannitol, urea, glucose, thiourea and ethylene glycol

09 p1396 A71-23258

Fluorometric microvolumetric test for unconjugated 11-hydroxycorticosteroids distribution in plasma, noting concentrations in capillary and venous blood

11 p1718 A71-25627

Blood plasma volume decrease, red cell mass and survival measurements in aquanauts of Teklite I at prolonged habitation

11 p1720 A71-26123

Isocarbic metabolic acidosis effects on blood plasma, electrochemical potential differences and cerebrospinal fluid pH

11 p1722 A71-26361

Age effects on whole blood viscosity with Wells-Brookfield microviscometer, investigating role of hematocrit and plasma protein

11 p1722 A71-26362

Partial oxygen tension in blood and biological fluids measurement with enclosed electrode polarographic sensor

12 p1876 A71-27744

Proton release association with whole blood oxygenation at constant plasma pH and carbon dioxide partial pressure, using alkaline titration

13 p2007 A71-28433

Physiological and biochemical characterization of natriuretic hormone in human urine and blood plasma

13 p2013 A71-28952

Bivalent metal salts effect on blood serum albumin crystallization by isolating pure protein

16 p2531 A71-33468

Dehydration effects on blood parameters in Somali donkeys and zebu steers, observing increases in plasma osmolality, sodium chloride, hemoglobin, packed cell volume, etc

17 p2681 A71-34940

Ouabain insensitive effects of metabolism on ion and water content of red blood cells

17 p2681 A71-34943

Physical training effects on human plasma glutamic-oxalacetic transaminase, creatine phosphokinase and lactic dehydrogenase enzyme levels

17 p2683 A71-35143

Afferent mechanisms of orthostasis in space flight, discussing plasma fluid volume reduction and cardiovascular adjustments on passive tilting

18 p2856 A71-36634

Renin, plasma norepinephrine and epinephrine responses to work loads of various intensities, evaluating sympathetic nervous system as stimulus for secretion

19 p3008 A71-38551

Physiological responses of burro Equus asinus to oxygen lack in mountain altitudes, studying red blood cell and plasma volumes

19 p3005 A71-38560

Plasma renin activity in hypertonic and normotonic persons exposed to exogenous stress, comparing with measurements at rest and in orthostasis

20 p3183 A71-38893

Amino acid levels in fasted and fed rats plasma, liver, muscle and kidney during and after exercise, noting glutamine decrease in liver tissue

20 p3186 A71-38982

Comparative abdomen and head shield effect during gamma irradiation of dogs on protein fractions in blood serum, noting increased globulins and glutamate aspartate transferases

20 p3188 A71-39222

Human vascular and extravascular fluid changes during six days bedrest based on fluid volume and ideal body weight from individual heights

21 p3331 A71-40354

Water immersion effect on plasma renin activity, urinary aldosterone excretion and renal sodium and potassium handling in normal man

22 p3485 A71-41720

Rat plasma creatine phosphokinase activity, hypothermia and stress, considering cold restraint

22 p3486 A71-41938

Glutamicoaspartic and glutamicoalanine aminotransferase activity in blood serum of dogs under gamma irradiation with shielded abdomen or head, observing hyperfermentemia

22 p3493 A71-42720

Solute diffusion coefficients dependence on protein concentrations in human plasma from experiment, presenting equation for prediction

23 p3637 A71-44253

Age effects on plasma aldosterone levels, red cell, plasma and total blood volume at sea level and high altitude

24 p3797 A71-44781

BLOOD PRESSURE

NT HYPERTENSION

NT HYPOTENSION

NT SYSTOLIC PRESSURE

Arterial blood pressure changes due to bilateral carotid occlusion or electrical heart pacing, considering effects on kidney blood flow and circumference in dogs

01 p0008 A71-10074

Artery wall elasticity relation to Korotkoff sound wave frequency by upper arm blood pressure model, using cylindrical rubber tubes and canine specimens

01 p0009 A71-10240

Orientation reflex in healthy and nervous human subjects from peripheral vessels blood pressure fluctuations in response to acoustic signals

01 p0012 A71-11055

Blood pressure changes in heart cavities and large vessels of dogs exposed to accelerations

01 p0013 A71-11126

Blood pressure and velocity waveform recording for patients during cardiac catheterization, interpreting relationships to vascular impedance

02 p0201 A71-12915

Adrenal gland blood flow and arterial pressure determination under stochastic pulse excitation of anesthetized dogs centripetal and centrifugal nerves, using analog correlator

03 p0357 A71-12994

Semiconductor devices for continuous blood pressure telemetry

03 p0370 A71-13069

Direct continuous radiotelemetry of blood pressure measurements taken from aorta, pulmonary artery and inside heart during normal activity of test subjects

03 p0371 A71-13070

Coronary perfusion pressure, heart performance and homeometric autoregulation in intact dogs

03 p0361 A71-13224

Catheter-flush system for continuous monitoring of central arterial pulse waveform and pressure

04 p0545 A71-15165

Four-electrode impedance plethysmograph system for evaluating conduction variations of upper and lower body segments relative to blood volume displacement

06 p0853 A71-17958

Left ventricular performance Fourier analysis, obtaining ventricular and ascending aortic pressure and flow from closed and open chest dog measurements

07 p1041 A71-19636

Left ventricular function analysis by atrial pacing in subjects with normal and elevated left ventricular filling pressure, relating stroke volume to end diastolic pressure

07 p1044 A71-20352

Automatic system for indirect blood pressure measurement in carotid compression test, discussing applications

08 p1247 A71-20827

Arterial circulatory system parameter identification from diastolic blood pressure curves by digital filter techniques

09 p1398 A71-22254

Book on clinical physiology techniques and anesthesiology measurements covering electronics, ECG analysis, blood pressure measurement, cardiac function, respiratory mechanics, etc

09 p1398 A71-22459

Blood pressure measurement by catheter gages, analyzing error due to wave reflection at catheter tip

09 p1399 A71-22972

In-flight monkey cardiovascular observations, discussing central venous pressure, urine volume, electrolyte imbalances and heart rate

09 p1395 A71-23244

Stroke-pulmonary blood volume relation and vascular recruitment and distensibility in dogs, allowing independent control of flow, heart rate and left atrial pressure

10 p1561 A71-24123

Aging effects on blood pressure-flow relations and cardiac output/ventricular end diastolic pressure, discussing pulmonary vascular bed capacity dependence on increasing flow during supine exercise

10 p1561 A71-24128

Space research utilization in medicine, discussing remote blood pressure measurements, seismocardiography visual analysis, sterilization procedures and equipment for physically handicapped

10 p1571 A71-24754

Flight stress effects on blood pressure and eye accommodation from frequent takeoffs and landing of AN-24 aircraft

11 p1723 A71-25261

Cardiovascular system response to swimming exercise by dogs, measuring left ventricular internal diameter and pressure, cardiac output and heart rate

12 p1873 A71-27130

Blood pressure measurement with Doppler ultrasonic flowmeter, providing sensitive and accurate noninvasive approach for continuous measurement of systemic arterial pressure

12 p1874 A71-27139

Arterial tonometry for atraumatic measurement of arterial blood pressure, considering transient effects of drugs or physiological interventions

12 p1874 A71-27140

Cardiac output and arterial pressure control in presence or absence of functional nervous system, discussing dog experiments

13 p2003 A71-27839

Preavoidance blood pressure elevations accompanied by heart rate decreases in dogs

13 p2008 A71-28516

Diastolic and mean blood pressure responses to exercise after beta-adrenergic blockade in normal and labile hypertensive subjects, using Trascior

13 p2014 A71-29320

Systemic arterial blood pressure response to chronic high altitude and hypoxia effects

14 p2184 A71-30280

Factors affecting respiratory waves formation, modulating arterial blood pressure recordings and photoplethysmograms

14 p2185 A71-30411

Left ventricular power as product of pressure and volume change rate, relating peak values to end diastolic mass

14 p2187 A71-30709

Lowered cardiac output and arterial pressure response to exercise after autonomic heart blockade in man, noting retained work capability

15 p2358 A71-31454

Hypoxia effects on cardiovascular reflexes during hypoxia, measuring response of heart rate to lower body negative pressure

16 p2529 A71-33191

Efferent vagal activity increase prior to intermittent cardiac block due to rise in blood pressure

16 p2529 A71-33192

Tympanic-cavity nerve plexus electric stimulation effects on cerebral blood circulation and overall arterial pressure in dogs and cats

16 p2533 A71-34108

Oxygen pulmonary diffusion capacity estimation by rebreathing procedure based on gas-blood partial-oxygen-pressure equilibration

17 p2678 A71-34173

Venous and arterial blood gases in hibernating and normothermic ground squirrels, showing venous oxygen and carbon dioxide partial pressures reduction in hibernation

17 p2681 A71-34941

Sympathetic response in renal and splanchnic nerves to induced fall and rise of arterial blood pressure in anesthetized rabbits, investigating baroreceptor reflex effect

17 p2685 A71-35367

Dynamic characteristics of arterial blood pressure responses to sinusoidal work load in man from harmonic analysis

18 p2856 A71-36240

Human physiological responses to rotating environment, evaluating heart rates, blood pressure, pulmonary functions, visual observations and vital capacities

[AIAA PAPER 71-890] 18 p2856 A71-36639

Brain temperature change effects on cardiovascular responses, examining heart rate and systemic arterial blood pressure

18 p2860 A71-36880

Cardiovascular system mathematical model for evaluating system parameters effects on circulatory indices including minute volume and arterial tension

19 p3007 A71-37777

Pulmonary diastolic pressure relation to left ventricle and atrium of patient with diagnostic heart catheterization at rest

19 p3004 A71-38296

Autoclave chronic catheter system and restraining box for blood sampling and pressure measurement for hibernating marmots

19 p3010 A71-38568

Motor and vestibular analysis and frontal hypothalamus role in gravitational loads compensation during orthostasis, noting respiration, arterial pressure and brain bioelectric activity changes

20 p3188 A71-39223

Active vasodilation in gracilis muscle vascular bed due to perfusion pressure changes

20 p3189 A71-39378

Stagnant asphyxia in cat carotid body during abrupt blood pressure drop by simultaneous carotid artery clamping and tap opening

20 p3190 A71-39443

Human blood pressure in brachial artery during spontaneous night sleep, recording EEG, EKG and horizontal eye movements

21 p3329 A71-40185

Altitude and cold acclimatization effects on human basal heart rate, blood pressure, respiration and breath-holding

21 p3330 A71-40349

Long term effects of hypoxic stimulus suppression upon heart rate, cardiac output and pulmonary artery pressure of highlanders, observing bradycardia

23 p3631 A71-43117

Arterial blood pressure spontaneous fluctuations due to cutaneous circulation adjustments by thermoregulatory system

23 p3632 A71-43142

Posture and lower body negative pressure effects on human heart rate and blood pressure

23 p3636 A71-44241

Pulmonary circulation pressure and flow telemetry of free ranging intact animals, describing instrumentation and technique for transduction and transmission

23 p3640 A71-44243

Respiratory carbon dioxide and oxygen partial pressure effects on intraocular and blood pressure in rabbits under Somnifen narcosis

24 p3793 A71-44368

High blood pressure and age effect on human baroreflex arc controlling pulse interval sensitivity, showing systolic pressure response to phenylephrine intravenous injection

24 p3794 A71-44434

BLOOD VESSELS

NT AORTA

NT ARTERIES

NT CAPILLARIES [ANATOMY]

NT GLOMERULUS

NT VEINS

Arterioles, arteriovenous anastomoses and efferent veins functional behavior in anesthetized white mice ears

01 p0007 A71-10035

Arterial branches pulsating flow and wave propagation in large blood vessels, considering flow measurements from simulated model experiments

01 p0008 A71-10111

Newly formed blood vessels ultrastructure in newborn pups and adult rabbits

01 p0012 A71-11081

Cytophotometric study of DNA content in fibroblasts from human blood vessel walls, discussing cell proliferation and ploidy

09 p1392 A71-22609

Extrinsic factors in pathogenesis of congenital heart diseases, considering morphogenetic processes in heart and great vessels development

13 p2002 A71-27811

Vessels mechanical behavior and blood flow dynamics in aorta bifurcation zone, using Navier-Stokes and continuity equations

13 p2019 A71-28657

Left ventricular aneurysm electrocardiographic features and postresection changes based on ECG statistical analysis

18 p2854 A71-36138

Morphological changes in dogs brain vessels under transverse accelerations

24 p3796 A71-44546

BLOWDOWN WIND TUNNELS

Turbulent boundary layer separation at low supersonic Mach numbers based on blowdown wind tunnel tests

05 p0735 A71-16582

Two dimensional test facility in blowdown wind tunnel transonic section, discussing porous sidewall boundary layer control effects on airfoils geometric characteristics

[AIAA PAPER 71-293] 09 p1428 A71-22957

Intermittent hypersonic wind tunnels, considering pressure and vacuum storage, blowdown tunnels and pressure tubes

18 p2897 A71-36409

BLOWERS

Blower suction line random vibrations due to distributed random pressure, investigating various isolation arrangements for vibration reduction

20 p3308 A71-39085

BLOWING

- Blowing air conditions and flow parameters effects on film cooling efficiency for rotating cylinder
 - 01 p0178 A71-10416
- Numerical analysis of complex boundary layer at axisymmetric stagnation point with massive blowing
 - 01 p0071 A71-10964
- Film cooling in gaseous medium, assuming turbulent boundary layer at blowing point
 - 02 p0333 A71-12645
- Uniformly blown turbulent boundary layer on flat plate, investigating unheated solid starting length effect on heat transfer
 - 04 p0572 A71-15500
- Nonuniform blowing and surface temperature turbulent boundary layer, investigating heat transfer
 - 04 p0684 A71-15502
- Plasma blowing and suction through channel wall electrodes in two dimensional stationary flow, taking into account Hall effect
 - 09 p1502 A71-22537
- Wind tunnel stability tests of wing with different blowing nozzle arrangements on bottom overpressure surface at 18 and 30 m/sec air speeds
 - 09 p1384 A71-23663
- Blowing and suction effects on laminar boundary layer flow of quiet fluid over permeable rotating cone, discussing skin friction and heat transfer
 - 10 p1594 A71-24406
- Optimal blowing wall jet prediction for suppressing separation from high lift aerofoils with incomplete mixing of upstream boundary layer
 - 11 p1704 A71-26196
- Blowing and wall curvature effects on gas flow separation and critical pressure gradient in Couette flow examples
 - 13 p1993 A71-29193
- Self similar numerical and asymptotic solutions of laminar multicomponent isothermal boundary layer equations for large blowing rates
 - 17 p2673 A71-35633
- Compressible similar laminar boundary layer blow-off behavior description from asymptotic analysis, using Prandtl transposition theorem
 - 18 p2901 A71-36032

BLOWOUTS

- Blowout characteristics prediction analysis for safety fuses with current limiting feature
 - 08 p1233 A71-21075

BLUE GREEN ALGAE

- Blue green algae activity in Kratz-Myers medium, noting C 14 uptake changes for monocultures and mixed cultures of *Anacystis nidulans* and *Synechocystis aquatilis*
 - 06 p0858 A71-17392
- Heterotrophic growth in dim light of blue green alga *Agmenellum quadruplicatum* and *Lyngbya lagerheimii* with glucose as carbon source
 - 09 p1402 A71-23472
- Cell free extracts with high nitrogenase activity from blue green alga *Anabaena cylindrica* by sonic oscillation and French press treatment
 - 09 p1402 A71-23475
- Blue-green algae *Microcystis aeruginosa* central zone cellular structure electron microscopic investigation, noting absence of distinct boundary between central and peripheral regions
 - 23 p3640 A71-44054

BLUFF BODIES

- Compressibility correction for subsonic flows past bluff bodies, considering boundary distortion and pressure distribution shift
 - 11 p1701 A71-25149
- Grid-induced turbulence effect on flameout characteristics for kerosene-air flames stabilized by bluff bodies of different sizes
 - 13 p2163 A71-28961
- Aerodynamic behavior of bodies in wake of two dimensional bluff bodies, discussing loads
 - 13 p1994 A71-29265
- Hypersonic flow theory evolution, considering friction and high temperature effects and flows about slender, blunt and bluff bodies
 - 19 p2992 A71-37455
- Turbulence and flow pattern in wake of bluff body flame stabilizers, using hot-wire anemometer measurements and Prandtl-Kolmogorov model
 - 19 p3168 A71-38102

BLUNT BODIES

- Nongray equilibrium radiative heat transfer in viscous radiating shock layer around blunt body entering high temperature nonisothermal carbon dioxide-nitrogen atmosphere
 - 01 p0180 A71-10938
- Pressure distributions prediction on blunt bodies at angle of attack, considering bodies of revolution and large angle cones
 - 01 p0004 A71-11580
- Three dimensional incompressible flow behind blunt obstacle at leading edge of flat plate compared with mathematical model by Oseen linearization
 - 03 p0341 A71-13434

Uniform flow stability near two dimensional stagnation region formed by blunt body immersion in cross flow

Hypersonic viscous air flow past blunt bodies with radiation, obtaining solution for Navier-Stokes equations by finite difference scheme

Blunt body problem with detached shock, considering methods of lines and integral relations agreement for wide range of Mach numbers

Hypersonic flow with nonequilibrium oxygen dissociation around blunt and conical bodies, considering temperature, pressure, density and compressibility factor behind normal shock

Two dimensional incompressible laminar boundary layer flow along ablative blunt body in irradiant environment

Free stream turbulence enhanced stagnation line heat and mass transfer on two dimensional blunt body

Binary gas mixture rarefied hypersonic flow structure near blunt body, investigating diffusive effects on recovery temperature dependence

Blunt body stagnation point heat transfer in hypersonic flow, describing gas dynamic equations flow field viscosity and conductivity

Blunt body nose protection from radiation-convective heat transfer, using porous injection of radiation absorbing substance

Steady two dimensional ideal gas flow past blunt body at incident infinite Mach number, obtaining gas dynamic variable asymptotic expansions as kappa approaches infinity

Supersonic blunt body flow relaxation processes, calculating bow shock for various flow regimes and reaction rates

Steady state supersonic flow of combustible gas mixture around solid blunt bodies

Nongray absorption and radiation cooling on smooth symmetric blunt bodies included in modified Maslen flow field method for radiation and large blowing

Lateral vibration effects on heaving airfoil blunt trailing edge vortex shedding flows, examining base cavity damping by flow visualization

Chemical nonequilibrium effects on hypersonic, blunt body shock layers flow in reacting planetary carbon dioxide-nitrogen atmospheres

Turbulent heat transfer measurements on blunt cone in nitrogen flow at high Mach number under various angles of attack

Three dimensional inviscid compressible flow past sharp shouldered blunt bodies at angle of attack, presenting time dependent finite difference technique

Steady state mixed subsonic-supersonic flow near blunt leading edge in hypersonic internal flow, using asymptotic solution by time-dependent method

Solid particle impurity effects on hypersonic shock tube flow, determining error in blunt body measurements

Soviet book on gas flow past blunt bodies, Part I, Flow analysis and calculation methods covering finite difference theory, algorithms, etc

Soviet book of gas dynamic function tables for two and three dimensional flows past blunt bodies

Hypersonic radiating gas inviscid flow past blunt bodies, using spherical harmonics approximation

Interaction between radiation from shock wave region and oncoming cold air flow in hypersonic flow past blunt body

Dissociating airflow over two dimensional blunt body, determining laminar boundary layer chemical reaction suppression effects on heat exchange

Nonequilibrium multicomponent ionization calculations for stagnation merged shock layer of hypersonic blunt body by successive accelerated replacement

Nose bluntness, angle of attack and oscillation amplitude effect on hypersonic unsteady aerodynamics of slender cones

Unsteady analogy for hypersonic flows past blunt bodies with shock deformation

Trajectories prediction for subsonic spin stabilized projectiles via water tunnel tests, considering blunt nose and tail and rounded nose right circular cylinders

Aerodynamic effects of bluntness on slender cones in free flight tests at Mach 17

Unsteady analogy for hypersonic flows past blunt bodies with shock deformation

Trajectories prediction for subsonic spin stabilized projectiles via water tunnel tests, considering blunt nose and tail and rounded nose right circular cylinders

Aerodynamic effects of bluntness on slender cones in free flight tests at Mach 17

Unperturbed atmospheric parameters calculation from surface measurements of blunt body at hypersonic speeds under various aerodynamic conditions

Circular stagnation line position on axisymmetrical blunt bodies with circular sharp edge

Mass entrainment products effect on radiative and convective heat transfer during decomposition of graphite blunt body in steady hypersonic flow of radiating air

Unsteady hypersonic flow around melting axisymmetric blunt bodies of revolution with profile depending on wall temperature, calculating temperature distribution and wall pressure

Aerodynamic forces and hinge moments of delta cruciform control surface in blunt-nosed canard configuration for subsonic, transonic and supersonic flows

Time asymptotic solutions for hypervelocity blunt body flow field with coupled nongray radiation, treating shock as discrete surface

Hypersonic reentry flow over blunt nosed bodies, using water oxygen mixture to achieve simulation at lower stagnation temperatures

Emmons spot theory extension for boundary layer flow on blunt bodies, deducing spot formation rate dependence on transition Reynolds and Mach numbers

Radiative emission effects on viscous flow in shock structure of low density hypersonic flow around blunt body

Rarefied hypersonic flow in blunt body bow region, measuring density and rotational temperature fields by electron beam method

Unsteady large particle numerical solutions to vortical equations of plane and axisymmetric inviscid gas flow past blunt body for subsonic and hypersonic velocities

Closed system of macroequations for mass and energy conservation along symmetry axis of steady rarefied supersonic gas flow in front of blunt body

Differential equation describing nonstationary reflection of symmetrical shock front from spherical and cylindrical blunt bodies

Multicomponent gas nonequilibrium viscous flow near blunt body stagnation point, presenting shock layer parameter variations effects on heat exchange

Exothermic hypersonic blunt body flow periodic instability mechanism, using ballistic range with schlieren photographic equipment

Multicomponent nonequilibrium air flow past axisymmetric blunt body, calculating flow distribution at various attack angles with time dependent technique

Inviscid supersonic flow field structure over blunt delta wing, determining attack angle effects on shock layer surface pressure distributions and streamline patterns

Velocity profiles of oscillating flow in wake of blunt based body, using finite difference solutions of vorticity transport and Poisson equations

Nonequilibrium dissociating gas flow past blunt body using time dependent shock layer analysis

Pade fractions use in calculation of axisymmetric flow of perfect gas past blunt body of revolution, obtaining stream function Taylor expansion terms

Two dimensional viscous hypersonic flow past thin, needle shaped and highly blunted bodies with strong boundary layer interaction on outer stream

Axisymmetric blunted body heating by high temperature plasma flow as function of geometry, pressure and stagnation enthalpy

Secondary floating shock generation in supersonic ideal gas flow about blunt bodies, investigating body configuration and flight regime effects

Low density hypersonic flow around blunt bodies, considering total pressure and flow velocity on stagnation point line

18 p2846 A71-36417

Shock layer parameters of supersonic viscous gas flow past blunt bodies of heat insulated and cooled surfaces, using Navier-Stokes equations

19 p2991 A71-37089

Nonspherical nose bluntness effects on slender vehicle dynamics, considering conical geometry as approximate nose shape after ablation due to turbulent heating

[AIAA PAPER 71-931]

19 p3148 A71-37176

Hypersonic flow theory evolution, considering friction and high temperature effects and flows about slender, blunt and bluff bodies

19 p2992 A71-37455

Supersonic flow past steady and oscillating blunt bodies of revolution, using singularity transformation and series truncation methods

19 p2993 A71-37878

Blunt planetary entry probe full scale flight test base pressure measurements, noting insensitivity to angle of attack variations up to 10 degrees

20 p3176 A71-39353

Heat transfer rate correlation with local surface pressure for blunt cones at angle of attack

20 p3176 A71-39355

Unsteady analogy for hypersonic flows past blunt bodies with shock deformation

20 p3176 A71-39362

Modified asymptotic perturbation expansion method application to free flow rotation effect on boundary layer for hypersonic flow about blunt body

20 p3177 A71-39483

Blunt body heat transfer predictions for atmospheric reentry, discussing coupled effects of real gas behavior and slip/jump boundary conditions

21 p3474 A71-40256

Arc driven hypersonic wind tunnels total enthalpy measurement from blunt body gas cap emission, using rapid scan spectrometer for gray gas continua

21 p3364 A71-40403

Blunt and hemispherical base axisymmetric bodies in Mach 4 free stream, investigating turbulent near wakes generation

21 p3324 A71-40999

Heat transfer and pressure distribution on biconic and hemispherical geometries with sharp and blunt noses in Mach 15-20 flow

22 p3480 A71-41964

Sonic line position measurement in supersonic flow behind detached shock wave preceding axisymmetric or plane blunt bodies

23 p3625 A71-43092

Chemically reacting gas mixture supersonic flow characteristics around blunt body, using differential equations

23 p3784 A71-44336

Dynamic behavior of dissociating gas supersonic flow past blunt bodies at angle of attack

24 p3790 A71-44775

Axisymmetric hypersonic flow of nonequilibrium ionized monatomic radiating inviscid gas past blunt body, using Clarke-Ferrari kinetic model

24 p3790 A71-45224

BLUNTNESS

U ELLIPTICITY

BLURRING

Statistical analysis of microphotometer scan of solar granulation photographs blurring during partial eclipse of 20 May 1966, correcting image for atmospheric and instrument effects

21 p3439 A71-40053

BO-105 HELICOPTER

Rotary wing and VTOL aircraft controllability requirements definition through in-flight simulation of visual and kinetic impressions and environmental conditions by BO-105 helicopter

05 p0696 A71-16135

BOATTAILS

Thrust-minus-drag optimization by base bleed and/or boattailing, using computer program

01 p0004 A71-11589

Low thrust jet effect on base pressures on boat-tailed afterbodies in Mach number 0.8-1.2 flow

14 p2169 A71-29889

BODIES

Calculation method for flow about bodies with injection, presenting parameters approximation formulas derived from Cauchy problem solution for Helmholtz equation

24 p3789 A71-44478

BODIES OF REVOLUTION

NT CELESTIAL SPHERE

NT CONICAL BODIES

NT CYLINDRICAL BODIES

NT PARABOLIC BODIES

NT POINCARÉ SPHERES

NT ROTATING CYLINDERS

NT ROTATING SPHERES

NT SLENDER CONES

NT SPHERES

NT TORUSES

Torsion of solid bounded by one sheet of hyperboloid of two sheets of revolution under mixed boundary conditions, using Legendre transform

01 p0173 A71-10843

Wind motion apparatus for reproducing coning and spinning motions of bodies of revolution, using six-component strain gage balance for aerodynamic forces

01 p0002 A71-10930

Shallow shells of revolution of strain-hardening material, deriving stress strain state by rigid plastic body model

01 p0175 A71-11039

Elastic waves excitation by pressure wave in shells of revolution, investigating acoustic medium effects on frontal discontinuities intensity

01 p0176 A71-11148

Monograph on plane shock wave interactions covering supersonically moving two dimensional thin airfoils, slender bodies of revolution and thin wings

01 p0003 A71-11227

Rayleigh-Gans-Born approximation application to thermal radiation of reflecting convex plasma sphere, cylinder and ellipsoid

02 p0288 A71-11633

Stress-strain state variability associated with optimal local heating of shallow shells of revolution

02 p0322 A71-11727

Unsteady heat conduction in multilayer body of revolution with convective heat transfer on curvilinear surfaces, considering radiation on inner surface

02 p0330 A71-11730

Thermoelastic stresses in closed laminar orthotropic shells of revolution subjected to axisymmetric loads and temperature gradients

02 p0322 A71-11735

Laminar orthotropic circular cylindrical shell stress state under inversely symmetrical loading

02 p0322 A71-11737

Thin shells of revolution local stability under nonuniform stressed state development under heating

02 p0324 A71-11755

Temperature fields without induced stress, considering relation between thermal and dislocation stresses in shells of revolution

02 p0325 A71-12283

Boundary value problems solution in elasticity theory of isotropic homogeneous body configurations close to ellipsoid of revolution, obtaining stress-strain state by approximate method

02 p0325 A71-12285

Zero bending moment shells of revolution under concentrated load, using boundary value problem for analytic functions

02 p0328 A71-12539

Two dimensional axisymmetric laminar boundary layer on blown wing and body of revolution, using sixth-order polynomial for velocity distribution

02 p0186 A71-12554

Nonlinear aerodynamic moments for arbitrary motions of bodies of revolution in free flight

[AIAA PAPER 70-205]

03 p0341 A71-13435

Axisymmetrically loaded shells of revolution made of work hardening materials, determining inelastic finite deformations and buckling loads by incremental variational method

03 p0505 A71-13543

Shell of revolution bending deformation, assessing Trefftz approximation error

03 p0506 A71-13597

Laminar boundary layer on spinning bodies of revolution in oncoming stream, using implicit finite difference technique

[AIAA PAPER 70-1377]

03 p0341 A71-13660

Thin shells of revolution formed of closed box sections, using numerical integration and stiffness matrix for solution

[ASME PAPER 70-PVP-12]

04 p0665 A71-14770

Incompressible Newtonian fluid laminar through flow between two surfaces of revolution rotating at various velocities about common axis

04 p0570 A71-15176

Thin convex shell of evolution bounded by two parallel minimum vibration frequency using asymptotic method of integration

04 p0671 A71-15556

Turbulent pressure pulsations at surface of floating body of revolution moving unsteadily in sea water during boundary layer development

04 p0576 A71-15613

Spherical or conical shells of revolution axisymmetric oscillations, analyzing zero moment equations system spectrum

05 p0822 A71-16377

Orthotropic shells of revolution free vibration theory, including transverse shear and rotary inertia effects

05 p0823 A71-16495

Pointed body of revolution in gravitationally stratified atmosphere, discussing supersonic boom and minimum drag

[DFVLR-SONDDR-97]

05 p0694 A71-16712

Supersonic flow field downstream of turbofan aircraft engine fan nozzle over bodies of revolution,

using boundary layer theory and method of characteristics

05 p0796 A71-17150

Weight-optimal cylindrical shells of revolution with uniform strength edge reinforcement, discussing pressure vessel design

06 p0982 A71-17356

Axisymmetric problem solution method for ring shaped body of revolution in elasticity theory

06 p0983 A71-17366

Limiting analysis for upper estimate of carrying capacity of shell of revolution under load concentrated at center, evaluating stability loss

06 p0987 A71-17771

Geometrically nonlinear thin nonshallow shells of revolution, deriving axisymmetrical elastic deformation equations

06 p0988 A71-17780

Multilayer conical and spherical shells of revolution axisymmetric elastic deformation, deriving stress-strain state equations with allowance for transverse shear

06 p0990 A71-17795

Thin elastic shell of revolution with negative Gaussian curvature, discussing free nonaxisymmetric oscillations

06 p0992 A71-17811

Heavy liquid shells of revolution, determining equilibrium form in gravitational and surface tension forces from condition of minimal functional of total free energy

06 p0994 A71-17827

Shells of revolution of different forms, discussing numerical solution of inverse problem

06 p0995 A71-17832

Axisymmetric isotropic shells of revolution, using matrix-operator notation for differential equations systems solution

06 p0995 A71-17835

Thin walled two layer bimetallic shells of revolution under large deformation, analyzing equilibrium by zero moment theory

06 p0998 A71-17856

Numerical algorithms of elastic stability solutions for thin walled axisymmetrically loaded shells of revolution with finite difference schemes

06 p0999 A71-17864

Slender bodies of revolution with cylindrical afterbodies in subsonic wind tunnel, examining vortex systems and aerodynamic forces

06 p0842 A71-18048

Plane or axisymmetric revolution geometry elasticity problems using finite element method and Fourier series

06 p1002 A71-18421

Prismatic shells vibration, buckling and stress analysis, applying computer solutions to complex bodies of revolution

[AIAA PAPER 71-112]

06 p1003 A71-18562

Separation patterns over inclined body of revolution from symmetry-plane boundary layer solutions, discussing bubble type

[AIAA PAPER 71-130]

06 p0845 A71-18574

Stress-strain state of large inhomogeneous bodies of revolution, considering deformation due to arbitrary surface and mass forces in temperature field

07 p1210 A71-19158

Large inhomogeneous bodies of revolution three dimensional strain state under symmetrical cyclic loads

07 p1210 A71-19159

Surface construction of body of revolution in supersonic gas flow from distribution of velocity vector modulus along generatrix of body, using Frankl method of characteristics

07 p1016 A71-20089

Thin cylindrical shell of revolution delaminations detection model, using free vibration natural frequency parameter under clamped-clamped conditions

07 p1216 A71-20135

Physically nonlinear bodies of revolution, investigating stress-strain state by small parameter and perturbation methods

07 p1219 A71-20650

Composite elongated ellipsoid of revolution under torsion, determining stress-strain state, boundary conditions and elastic displacements

08 p1368 A71-20800

Spherical wave scattering on thin conducting truncated bodies of revolution, deriving equations system for field pattern

08 p1254 A71-21460

Shells of revolution under combined thermal and mechanical loading, presenting analytical basis of BOSOR 3 digital stress analysis program

09 p1533 A71-22079

Reinforced shells of revolution carrying capacity upper limit subjected to internal adiabatic ideal gas flow

09 p1538 A71-22632

Filament winding geodesic characteristics of shells of revolution made of glass fiber reinforced plastics

09 p1482 A71-22815

Photoelasticity methods applied to model of beam of revolution under simple torsion constructed by stress freezing technique 10 p1684 A71-23837

Spherical and paraboloid shells of revolution internal and external forces correlation, considering boundary value problem differential solution 10 p1686 A71-23996

Coaxial shells of revolution connected by meridional ribs, deriving elastic equilibrium conditions, stress-strain components and contact forces under thermal and mechanical loads 10 p1688 A71-24358

Hydrodynamic Stokes flow around body of revolution, using least squares method for fluid sticking on wall 10 p1594 A71-24455

Boundary value problem concerning stability and oscillations of shells of revolution through reduction to Cauchy problem based on direct integration of equilibrium equations 10 p1690 A71-24569

Orthotropic shells of revolution with concentrated masses and oscillator inclusions and reinforced by stringers and ribs, calculating free vibration by Ritz method 10 p1690 A71-24570

Body of revolution potential expanded in spherical function series, showing analytical density limited by surface 10 p1679 A71-24934

Unsteady hypersonic flow around melting axisymmetric blunt bodies of revolution with profile depending on wall temperature, calculating temperature distribution and wall pressure 10 p1698 A71-25087

Nonlinear dynamic analysis of shells of revolution under symmetric and asymmetric loads, obtaining solutions for shallow cap buckling 11 p1847 A71-25465

Dynamic response of rotationally symmetric open-ended thin shells of revolution under transient impulsive and thermal loadings, using FORTRAN 4 finite difference program 11 p1847 A71-25466

Aerodynamic characteristics of slender body of revolution traveling in long tube with circular cross section, deriving static and dynamic stability derivatives formulas 11 p1702 A71-25477

Prestress vibration hardening of shells of revolution for circumferential 0 and 1 wave number, using VALORS and BALORS programs 11 p1848 A71-25486

Soviet book on thermal stresses in bodies of revolution of arbitrary shape covering energy conservation equations and heat equations solutions 11 p1850 A71-26096

Generalization of restricted three body problem in formulation with principal gravitating body constituting flattened ellipsoid 12 p1964 A71-27177

Oscillation theorem for natural vibrations of thin shells of revolution, considering boundary value problem eigenvalues 12 p1977 A71-27304

Axisymmetrically strained thin elastic shells of revolution with temperature dependent random elastic characteristics 12 p1979 A71-27358

Axisymmetric deformation of thin elastic shell of revolution under combined effect of static surface load and nonuniform heating 12 p1979 A71-27359

Spherical or conical shells of revolution axisymmetric oscillations, analyzing zero moment equations system spectrum 12 p1981 A71-27463

Flow field model for steady asymmetric vortex system shed from slender body of revolution in coning motion [AIAA PAPER 70-52] 12 p1865 A71-27552

Shells of revolution plastic deformation problem, applying rigid viscoplastic strain hardenable material model 12 p1984 A71-27686

Axial wave propagation in linearly elastic membrane shells of revolution, using dynamic finite element technique 13 p2147 A71-27786

Static problems of shells of revolution under local loads, solving by stable numerical process 13 p2152 A71-28276

Cylindrical shells of revolution with various boundary conditions, calculating free vibrations with differential equations 13 p2156 A71-29067

Stress-strain state of thin walled ellipsoidal shell of revolution with arbitrarily oriented crack 13 p2156 A71-29069

Pressure, velocity and potential distribution of flow around arbitrarily shaped body of revolution during arbitrary motion in perfect liquid 13 p1992 A71-29187

Analytic optimization of Cassegrain antennas of revolution used in satellite telecommunications 13 p2033 A71-29241

Error in determining pressure and loading distribution on surface of slender bodies of revolution 13 p1994 A71-29323

Critical load of shallow shell of revolution as function of geometric and material parameters 14 p2321 A71-29624

Elastic plastic shells of revolution deflection analysis by numerical integration with computer program 14 p2324 A71-29870

Critical loads and stability loss equations near edge of thin convex clamped elliptical shell of revolution under uniform external compression loads 14 p2325 A71-30024

Closed membrane shell of revolution finite creep due to uniform pressure, applying large deformation incremental theory 14 p2328 A71-30396

Elastic deformation of double cavity hyperboloid of revolution under variable loads applied to boundaries 14 p2332 A71-30846

Load carrying capacity of edge clamped spherical shells of revolution with Tresca yield condition under uniform internal pressure 14 p2332 A71-30848

Strength analysis of shells of revolution and plates under axisymmetrical loads for rigidly plastic material with Tresca yield condition 14 p2332 A71-30849

Transonic flow past bodies of revolution, using finite difference scheme 14 p2171 A71-30876

Soviet papers on three dimensional structures covering strength and stability of compound curvature shells, bodies of revolution and multilayer plates 14 p2332 A71-30888

Three dimensional elasticity theory solutions for isotropic axisymmetric bodies of revolution by p-analytic and generalized analytic functions 14 p2333 A71-30889

Momentless axisymmetric stress state and stability loss in thin convex shells of revolution in linear approximation 14 p2333 A71-30891

Supersonic potential flow at large distance from slender body of revolution at angle of attack, deriving nonlinear partial differential equations system 15 p2343 A71-31170

Near field flow pattern of inclined slender body of revolution, using Witham far field theory of supersonic flow [AIAA PAPER 71-626] 15 p2344 A71-31554

Pade fractions use in calculation of axisymmetric flow of perfect gas past blunt body of revolution, obtaining stream function Taylor expansion terms 15 p2346 A71-32122

Thin metallic body of revolution under electromagnetic pulse, predicting transient induced currents with radiation condition in finite difference solution 15 p2372 A71-32368

German monograph on iterative procedure for sectional parameters of shells of revolution with meridian form under peripheral loads described by harmonic functions 15 p2509 A71-32374

Drag coefficients of bodies of revolution from wind tunnel shock induced steady flow data, considering blast loading experiments in shock tube 16 p2519 A71-32878

Sun as flattened ellipsoid of revolution, showing flatness effects on planet motion in relativity theory framework 16 p2612 A71-33567

Nonlinear theory for rotating shallow shells of revolution, deriving edge zone boundary layer solutions for differential equations 16 p2660 A71-34071

Concave thin shell of revolution lowest natural vibration spectra frequency corresponding to simple inflection point 17 p2817 A71-34341

Numerical method for limit analysis of axisymmetric shells of revolution, considering truncated conical shells and pressure vessels with rigid circular plates 17 p2818 A71-34400

Laminar boundary layer on wing profiles and bodies of revolution, calculating flow characteristics based on integral momentum relation 17 p2670 A71-34424

Filament wound shell of revolution optimum configuration, deriving equations for orthotropic filament axes coincidence with principal stress trajectories 17 p2830 A71-35317

Finite element analysis codes for complex two layered linear elastic shells of revolution under static and dynamic loads 17 p2831 A71-35351

Traveling waves propagation in elastic shell of revolution subjected to bending moment 17 p2833 A71-35618

Photoelastic analysis of cylindrical shells of revolution with one hemispheric closed end and reinforcing

flanges at opposite end rim, examining boundary conditions effects 18 p2981 A71-36718

Natural axisymmetric vibration of thin elastic shell of revolution, deriving eigenvalues convergence to spectrum lower bound by asymptotic method 19 p3154 A71-37097

Supersonic flow past steady and oscillating blunt bodies of revolution, using singularity transformation and series truncation methods 19 p2993 A71-37878

Oscillation theorem for natural vibrations of thin shells of revolution, considering boundary value problem eigenvalues 19 p3159 A71-38264

Acoustical field from streamlined body of revolution moving in homogeneous gaseous medium past seminfinitesimal rigid screen, using Wiener-Hopf method for diffraction radiation 20 p3175 A71-38809

Axial vibration transmission characteristics of shells of revolution, stressing shell mass and thickness, internal damping and edge restraint effects [ASME PAPER 71-VIBR-7] 21 p3457 A71-40270

Thin elastic shell of revolution under asymmetric loads, calculating time dependent transient response with implicit backward and explicit central differencing schemes 21 p3467 A71-40960

Slender body of revolution in supersonic and subsonic air flow, calculating boundary conditions with Lagrange formulation 21 p3323 A71-40963

High precision displacement functions for finite element models of rotational shell and plate bending problems 21 p3470 A71-41019

Paraboloidal shells of revolution inextensional vibrations comparison to Sanders theory, using finite element method 21 p3471 A71-41030

Elastic shells of revolution displacement analysis, using incremental variational theory with finite element method 22 p3613 A71-41434

Orthotropic shells of revolution limit analysis, considering yield conditions and flow rules 22 p3614 A71-41605

Ideally conducting and dielectric coaxial bodies of revolution, investigating joint excitation by TM wave 22 p3522 A71-42304

Natural frequencies and vibration modes of perforated cylindrical, conical and spherical shells of revolution, using Ritz method 22 p3617 A71-42488

Characteristic modes computation for conducting bodies of revolution, discussing radiation and scattering patterns convergence 23 p3654 A71-44162

Stress state of arbitrary contour body of revolution under torsion using finite difference method 23 p3779 A71-44218

Thin elastic shell of revolution with waves along parallel, considering small free nonaxisymmetric vibrations 24 p3877 A71-44406

Curved finite element for elastic-plastic analysis of thin toroidal shells of revolution with discontinuous meridional slope under axisymmetric loadings 24 p3879 A71-44634

Approximate periodic Green matrix solution to equilibrium equations in displacements for shell of revolution under linear loads 24 p3881 A71-44826

Axisymmetric elastic deformation of layered thin anisotropic shells of revolution, using computer integration for arbitrary loads and boundary conditions 24 p3882 A71-44841

Equivalent stiffening of circular hole in convex shell of revolution by short shell under symmetric and antisymmetric loads 24 p3882 A71-44845

Surface of revolution annular elements thermal radiation and heat exchange for propellant schematization, attachment to missile wall and opening into ambient medium 24 p3889 A71-44970

Shell of revolution natural vibration spectrum, investigating moment and momentless type systems of differential equations 24 p3886 A71-45342

BODY CENTERED CUBIC LATTICES

Hole effect on residual resistivity of crystalline binary ordered substitution alloy with bcc lattice 03 p0467 A71-13952

Atomic collision chains in bcc crystal, determining energy loss relation to temperature by computer model with/without perfect lattice thermal oscillations 04 p0630 A71-15103

Metals and alloys with bcc structure, investigating ductile-to-brittle transition by ultrasonic MHz technique 05 p0770 A71-17251

Atomic ordered alloy compressive strengthening for fcc and bcc lattices in terms of yielding, work hardening and no hardening stages

07 p1132 A71-19438

Fast neutron irradiation effects on Mo recovery stages 1 to 3 in bcc metals using electrical resistivity measurements

07 p1143 A71-20491

Bcc metals plastic deformation, discussing active slip systems, stress asymmetry, dislocation dynamics, interstitial and substitutional alloys, defect configurations, etc

08 p1307 A71-21502

Interstitial role in bcc metals slip anisotropy at low temperatures, examining stress differential effect in Nb-oxygen solid solutions

08 p1307 A71-21505

Bcc metals low temperature strength, examining solution softening in Fe-Mo alloys

08 p1307 A71-21506

Bcc Ti-V single crystals deformation modes and resolved shear stresses as function of temperature and composition

08 p1307 A71-21510

Plastic anisotropy in bcc metal crystals, measuring flow strength for various plane strain compression states

08 p1308 A71-21513

Interstitial impurities effects on relation of activation energy to effective stress in iron, low carbon steel and other bcc metals

08 p1308 A71-21514

Bcc metals slip band formation, investigating deformation and fraction behavior

08 p1308 A71-21515

Segmented slip theory of hardening application to bcc metals, discussing dislocation locking and virtual athermal dislocation model

08 p1308 A71-21516

Internal friction solid solution weakening of bcc group V-B alloys

08 p1309 A71-21524

Bcc metals single and multilayer stacking faults, twin boundaries and screw dislocations observations, using central force atomic model

08 p1310 A71-21537

Guinier-Preston zone formation by mixed substitutional-interstitial solute-atom clustering in bcc metals, considering steel strengthening

08 p1311 A71-21541

Radiation-anneal hardening and radiation effects on yield stress temperature dependence in bcc metals

08 p1312 A71-21550

Tensile data for dispersion hardened iron containing thorium spherulites analyzed in terms of Orwan theory, considering bcc materials yield strength

09 p1466 A71-22172

Elastic stresses during local deformation in Nb-Mo, Ni-Cr, Cu-Al and pure bcc metals, using X ray analysis

13 p2085 A71-28225

Face shear and thickness twist waves in bcc crystal plates, presenting numerical computation results for Fe and W

15 p2426 A71-31418

Yield point thermal component in bcc metals at low temperatures as function of hydrostatic compression, noting interionic reaction potential nonsparsity

16 p2596 A71-33889

Cobalt and lanthanum with face and body centered lattices, studying plastic deformation during allotropic transformations under sliding friction and gripping

16 p2584 A71-33895

Thermodynamic activities of Ti and Al in bcc beta phase of Ti-Al system

21 p3398 A71-40465

Temperature and strain rate effects on yield and flow stress of bcc Ti-Mo alloy over 77-824 K range

21 p3404 A71-41414

Diffusion acceleration in bcc Ti due to imperfections of fine structure created during polymorphous transformation

24 p3840 A71-45379

BODY COMPOSITION [BIOLOGY]

Ar-Ag arc, microwave discharge and plasma torch techniques in emission spectroscopy of trace elements in biological materials

03 p0377 A71-14421

Amino acid content alteration in internal organs in rabbits under HF electromagnetic and ultrasound oscillations

04 p0547 A71-15573

Walking effects on body composition and cardiovascular function of middle aged men

06 p0862 A71-18388

Dipeptidyl aminopeptidase I /cathepsin C/ properties, subcellular localization and polypeptide degradation in rat liver and bovine spleen and pituitary glands

13 p2025 A71-28179

Marmot ketone bodies concentration during activity, deep hibernation and early arousal, discussing increased oxidative metabolism effects

13 p2014 A71-29125

Calcium, potassium and iron loss by astronauts during Apollo space missions, using instrumental neutron activation analysis

16 p2528 A71-33111

Human power output during short duration exercise, relating to body size and composition

17 p2686 A71-35434

Hamster body fat, water and density measurements by dilution method and air displacement technique, comparing to determination by direct chemical analysis upon sacrificing

19 p3005 A71-38555

Physiological relationship of young to old men, considering body composition, aerobic capacity and capillary-muscle fiber ratio

22 p3485 A71-41717

Total body adipose tissue mass and composition variations, examining hyperglycemic, obese, exercised and centrifuged animals

23 p3637 A71-44299

BODY FLUIDS

NT BLOOD

NT CEREBROSPINAL FLUID

NT ENDOLYMPH

NT ERYTHROCYTES

NT LEUKOCYTES

NT LYMPH

NT LYMPHOCYTES

NT RETICULOCYTES

NT SWEAT

NT URINE

Anatomy and function of normal pericardium including removal effect in mammals, fish and amphibians

03 p0362 A71-13328

Human mitral valve fluid mechanics, confirming existence of vortex forms during diastasis by vitro flow patterns

[ALAA PAPER 71-102]

06 p0863 A71-18556

Internal osmotic balance and stress induced body fluid osmolality changes due to food or water deprivation, reporting on experimental results with rats

08 p1240 A71-21750

Body fluid osmolality control of food intake initiation in rehydrated rats injected with hypertonic sodium chloride solution

11 p1719 A71-26073

Partial oxygen tension in blood and biological fluids measurement with enclosed electrode polarographic sensor

12 p1876 A71-27744

Peristaltic pumping mechanism as progressive wave train of transverse wall displacement in plane two dimensional channel

15 p2366 A71-32559

High altitude exposure effects on concentration and total quantity of electrolytes in human serum and extracellular space

19 p3009 A71-38562

Sodium and cations elimination by kidneys during water-salt metabolism changes due to high temperature and hypodynamia

20 p3189 A71-39232

Human vascular and extravascular fluid changes during six days bedrest based on fluid volume and ideal body weight from individual heights

21 p3331 A71-40354

BODY KINEMATICS

Krylov-Bogoliubov integration theory for first-order perturbation analysis of multidimensional harmonic oscillator applied to body motion in earth gravity

01 p0151 A71-10113

Sight of body and active locomotion effects on perceptual adaptation to tilted vision in male subjects

01 p0010 A71-10398

Successive approximations method for boundary value problems in plasticity theory of continuous media under complex loading

01 p0171 A71-10652

Solid body motion about fixed point on pseudoeuclidean Lobachevskii plane under external forces, using Euler angle analogy

03 p0457 A71-13423

Equations of motion of gyroscopic body having fixed point, determining conditions for existence of quadratic invariant correlation

03 p0457 A71-13583

Differential equations of spherical motion of heavy solid body with ellipsoidal cavity filled with liquid, deriving stationary solutions

03 p0457 A71-13586

Integrodifferential equations of motion of body with fixed point, obtaining solution and geometrical interpretation

03 p0457 A71-13587

Kinematic interpretation of body motion about fixed point for case of traveling angular velocity hodograph integrable in closed form

03 p0457 A71-13589

Heavy gyrostad motion problem, using Mozalevskaia particular solution characterized by algebraic invariant relation

03 p0458 A71-13593

Solid body motion kinematics about fixed point for Euler-Poisson equations

03 p0458 A71-13594

Body motion with liquid filled cavities in central Newtonian force field, using hodography

03 p0458 A71-13595

Perturbed motion equations of body with liquid filled cylindrical cavity reinforced by elastically clamped ribs, solving boundary value problems

03 p0460 A71-14356

Computer simulation of human body kinematics under rapid decelerations

04 p0542 A71-14786

Four-electrode impedance plethysmograph system for evaluating conduction variations of upper and lower body segments relative to blood volume displacement

06 p0853 A71-17958

Rigid body motion implicit representation in curved finite elements

07 p1214 A71-19910

Heavy solid body motion about stationary point for connected angular velocity vector terminus and trajectory in fixed space

08 p1336 A71-21869

Biotelemetric contactless recording of animal movements using centimeter band standing waves

09 p1397 A71-22216

Conformally variable body, formulating differential equations of motion in moving coordinate system using Hamilton-Ostrogradskii form of least action principle

09 p1495 A71-23434

Body profile low frequency oscillations in transonic gas flow, investigating nonlinear differential equation boundary value problem by approximation method

10 p1550 A71-24363

Solid body finite rotation theory involving formal operations on quaternions

10 p1642 A71-24576

Free solid body carrying heavy pendulum, calculating oscillations as function of geometrical and inertial characteristics during motion under tangential force

12 p1929 A71-27117

Massive body gravitational to inertial mass ratio from equilibrium assembly model of particle interactions

13 p2139 A71-28997

Kinematic interpretation of body motion in Hesse solution, discussing axoid vector rolling without slip

14 p2275 A71-30881

Lunar forced motions and free oscillations, considering inertia moments effects on rotational and translational movements

16 p2636 A71-33502

Fatigue effects on standing broad jump and other body movements patterns

18 p2873 A71-36975

Heavy solid body motion about stationary point for angular velocity vector extremity moving in fixed and body-connected coordinate systems

20 p3270 A71-39368

Viscometric motions of continuous bodies, studying kinematics and dynamics of d'Alembert, homogeneous and circulation preserving groups

20 p3309 A71-39567

Free flight model accelerations, forces and trajectory measurements in short duration facilities, using optical methods and digital recording

21 p3362 A71-40383

Existence theorem derivation for moving surface of one dimensional geometrical and kinematic compatibility condition

21 p3415 A71-40658

BODY MEASUREMENT [BIOLOGY]

NT ANTHROPOMETRY

Fat lean cellular and bone mineral mass determination in living bodies, using radiation absorption spectrometry

02 p0210 A71-12954

Atrial and ventricular dimensional analysis in animals and man, discussing angiocardigraphic, biplane, X ray, indicator dilution, radioisotopic and noninvasive methods

05 p0715 A71-16925

Shielding effectiveness of different body portions during repeated proton irradiation on dogs

06 p0861 A71-18360

Mean whole body intracellular pH and buffer capacity for arterial carbon dioxide tension in ventilated dogs

10 p1558 A71-23896

Drug effects on LF whole body vibration response of dogs administered with phenobarbital, phenox-ybenzamine and morphine

11 p1720 A71-26121

Stereophotogrammetric measurement of body and limb volume changes after prolonged space mission

22 p3502 A71-41861

BODY SIZE [BIOLOGY]

Human power output during short duration exercise, relating to body size and composition

17 p2686 A71-35434

BODY TEMPERATURE

- Automatic temperature monitor and proportional solid state DC controller for electrophysiological use
01 p0022 A71-10247
- Mammalian hair effectiveness as insulation, using biotelemetry for deep body temperature measurement
01 p0023 A71-10886
- Human heat exchange and body overheating mechanism at high ambient temperatures at sea level and lowered pressures
01 p0013 A71-11134
- Thermal state symptoms characterizing limit of human tolerance to heat loads at rest and during physical exercise
01 p0014 A71-11135
- Mammal species body temperature during 24 hr periodic light cycle, using statistical data analysis
01 p0020 A71-11570
- Human thermoregulatory response to ambient temperature variations, considering deep body and skin temperature interrelations
02 p0202 A71-11667
- Human body temperature regulation feedback control system model by electric circuit analog, discussing digital simulation for static and dynamic responses
02 p0203 A71-11805
- Body heat loss in water immersion, using heat transfer model
02 p0207 A71-12387
- Sweating responses in men during intermittent hard treadmill work, considering regulation by skin/core temperatures, neuromuscular reflexes and vein/muscle thermoreceptors
04 p0544 A71-15151
- Conditioned reflex gas exchange shifts in persons under repeated local thermal stimuli
04 p0540 A71-15572
- Polymorphic nucleus leukocytes pyrogenic protein fraction effects on rabbits hypothalamus thermal control structures
05 p0707 A71-16386
- Muscular heat production effect on contraction during cold adaptation tests
05 p0710 A71-16806
- Light and drugs effect on diurnal body temperature from radio telemetry of adult male rats
05 p0715 A71-17111
- Telemetric techniques for pharmacological effects of body temperature, motor activity and food and fluid intake on rat brain, describing recording and monitoring equipment
05 p0716 A71-17112
- Human body thermography for studying physiological changes due to exercise, anoxia or accelerations
06 p0860 A71-18189
- High sensitivity portable two channel apparatus for brain temperature measurements using small glass insulated thermistors
06 p0863 A71-18469
- Mammalian tolerance to low body temperatures, discussing limits to spontaneous unassisted recovery and recovery assisted with reanimation and resuscitation procedures
07 p1041 A71-19523
- Hyperresponsiveness in hibernating mammals, discussing responsiveness increase with body temperature decrease as compensating mechanism for sensitivity loss
07 p1041 A71-19524
- Human temperature control computer simulation, considering sudomotor, vasomotor and metabolic as error signals from hypothalamic and cutaneous thermoreceptors
07 p1048 A71-19585
- Human body temperature regulation, investigating mild exercise dehydration effects
07 p1044 A71-20349
- Physiological effects of cooling measured by men wearing air and water cooling garment under external heat loads or large metabolic heat
08 p1248 A71-21232
- Oxygen deficiency and body temperature effects on work capacity of human subjects in hot humid environment
09 p1399 A71-22922
- Rats hypoxia tolerance, noting smoke effects on survival, respiratory rate, body temperature and glycolytic parameters
09 p1396 A71-23364
- Body temperature effects on intracellular carbon dioxide dissociation, pH and buffer capacity in hypothermic and hyperthermic dogs
10 p1559 A71-23897
- Organic thermoregulator control signal generation as function of body peripheral to central temperature ratios, using skin temperature rise measurements
10 p1564 A71-24485
- Chemical thermoregulation muscular electricity activity during shivering and thermoregulation tonus change after cold adaptation, discussing oxygen consumption rise
10 p1564 A71-24486

- Thermomodulation and indocyanine green dye technique comparison for cardiac output measurement in man
11 p1724 A71-25435
- Body temperature regulation and heat dissipation responses during continuous and intermittent exercise in man
11 p1721 A71-26354
- Human body thermal behavior modeling, obtaining steady state analytical solution for various boundary conditions and parameters
12 p1875 A71-27563
- Cerebrum temperature variations and tissue insulating and heat conducting properties in ether anesthetized dogs with heads cooled by water stream
13 p2004 A71-28029
- Helium for nitrogen substitution effects on body temperature of rats exposed to high carbon dioxide concentrations at different ambient temperatures
13 p2006 A71-28402
- Heat balance of human body submerged in water, determining body temperature reduction as function of ambient temperature
13 p2019 A71-28508
- Isolation technique for recording low level ECG and deep body temperature signals in animals exposed to large amplitude RF fields
13 p2020 A71-28864
- Mathematical and mechanical models of human thermal system thermodynamic/transport processes and external regulation devices for single elements and entire body
13 p2023 A71-29400
- Cold environment exposure effect on mouse resistance to infection with *Klebsiella pneumoniae*
16 p2528 A71-33115
- Human body temperature regulation under various hydration regimes during exercise, noting changes related to sweating
16 p2530 A71-33243
- Human sweating regulation at rest, evaluating thermal inputs effects on thermoregulatory center and internal hypothalamic and skin temperatures
17 p2683 A71-35247
- Adenosine triphosphate addition effects on heat production in intact muscular fibers by calorimetry
17 p2686 A71-35388
- Human thermoregulator set point under physical exercise, using behavioral indicator
17 p2686 A71-35388
- Young guinea pigs thermal adaptation tests at different temperatures and environmental conditions, observing threshold temperature shifting for shivering and heat polypnea
18 p2858 A71-36863
- Human thermoregulation, discussing experimental determination of equation for mean body temperature calculation in neutral and warm environments
18 p2858 A71-36866
- Brain temperature change effects on cardiovascular responses, examining heart rate and systemic arterial blood pressure
18 p2860 A71-36880
- Physiological strains due to industrial heat stress, investigating heart rate and body temperature
18 p2860 A71-36882
- Exercise temperature plateau shift and sweat rate during moderate CO poisoning associated with resetting of thermoregulating centers by low oxygen tensions
18 p2861 A71-36886
- Humid operative temperature as index for biophysical thermometry and thermal comfort sensation prediction
18 p2861 A71-36887
- Temperature effects on spinal excitation and inhibition in cats, investigating spinal motoneurons discharge frequency
18 p2861 A71-36890
- Thermoregulation under stringent low temperature conditions, considering internal body temperature maintenance by homeothermic organism
18 p2861 A71-36891
- Convective and conductive heat loss analysis of underwater swimmers and divers exercising in cold water
18 p2861 A71-36892
- Skeletal muscles shivering thermogenesis during cold adaptation, investigating thermoregulation effects on organ and system heat production
18 p2862 A71-36895
- Mathematical model for human thermal system, checking accuracy
18 p2873 A71-36899
- Guinea pig thermoregulation of shivering and nonshivering thermogenesis, showing intrahypothalamic noradrenaline injection effects on threshold temperature elevation
18 p2862 A71-36901
- Thermal behavior simulation of cooling biological system, describing heat generation and transfer at normothermic to hibernating body temperatures with mathematical model
19 p3003 A71-38199

- Postexercise elevated tissue temperatures contributions to oxygen consumption in rats, suggesting hypothalamic adjustment
20 p3186 A71-38981
- Continuous recording of human rectal temperature under extreme environmental conditions, using battery powered thermographs with thermistor probes
20 p3192 A71-39041
- Heat removal from space suit, discussing anatomic and physiological features suitable for cooling
20 p3188 A71-39224
- Radiotelemetric equipment for continuous subcutaneous measurements of circadian body temperature rhythm in rats
21 p3335 A71-40634
- Mean body temperature computation in neutral and hot environments from rectal and skin temperatures
22 p3485 A71-41723
- Dynamic sampling calorimeter for continuous measurement of human radiative, convective and evaporative heat loss, enabling closed loop control system analysis
22 p3503 A71-42155
- Ambient temperature effects on spontaneous rewarming of ground squirrels during awakening after hibernation
22 p3491 A71-42582
- Sparrows pinealectomy effect on circadian rhythms of body temperature in light and darkness from radio telemetric monitoring
23 p3633 A71-43547
- Hyperoxia effects on thermoregulation and neurochemical functions, showing temperature increases in cerebrum and decreases in cortical and subcortical formations
23 p3633 A71-43582
- Local and central body temperature effects on human cutaneous venomotor reflexes, monitoring venous wall tension by measuring hand dorsal veins pressure during temporary arrest of hand circulation
24 p3797 A71-44777
- Moderate heat exposure effects on human circadian variations in body temperature, heart and metabolic rates and water loss
24 p3797 A71-44779

BODY TEMPERATURE [NON-BIOLOGICAL]

U TEMPERATURE

BODY TEMPERATURE REGULATION

U THERMOREGULATION

BODY VOLUME [BIOLOGY]

- Variable tidal volume effects on lung test gas washout parameters
19 p3010 A71-38565

BODY WEIGHT

- Sex differences in rat body weight regulation due to lateral hypothalamic lesions
11 p1720 A71-26074
- Postflight metabolism and renal function of Soyuz 6, 7 and 8 crewmembers, associating weight loss during flight with water and salt discharges
13 p2006 A71-28409
- Hemodynamic changes in healthy pilots with excess weight investigated by mechanocardiograph, showing decreased cardiac output, left ventricle strength and volume rate
15 p2357 A71-31319
- Human body weight and skin sweat gland water loss rates effects on thermoregulation
18 p2858 A71-36864
- Human vascular and extravascular fluid changes during six days bedrest based on fluid volume and ideal body weight from individual heights
21 p3331 A71-40354
- Diurnal water and food intake and body weight changes pattern in rats with hypothalamic lesions
22 p3486 A71-41936
- Death rates, median life span and weight in mice exposed to gamma radiation after intra-abdominal injections of cysteamine
22 p3505 A71-42712
- Hypokinesia effects on gas exchange and oxygen consumption in rats, noting weight losses
24 p3795 A71-44526

BODY-WING AND TAIL CONFIGURATIONS

- Wing-body interference in supersonic inviscid flow, extending Stewartson approach to arbitrary smooth convex cylinder
01 p0002 A71-10774
- Lift of slender aircraft with rectangular cross section fuselage and high wing
03 p0342 A71-13737
- Initial structure of wing-body interaction in steady inviscid supersonic flow, obtaining asymptotic expansion from canonical problem solution
05 p0696 A71-17219
- Slender, conical, plane and cambered wing-body combinations with different volume distributions in supersonic flow, comparing experimental with theoretical aerodynamic characteristics [DFVLR-SONDDR-86]
06 p0841 A71-17418
- Wing-canard configurations nonlinear vortex interactions, using Sacks method of vortex sheet simulation with discrete vortices distribution [AIAA PAPER 71-95]
06 p0844 A71-18550

- Three dimensional inviscid supersonic flow fields with primary and embedded shock and expansion waves determined over and behind wings and wing-body configurations
[ALAA PAPER 71-99] 06 p0844 A71-18554
- Transverse and torsional vibrations of fuselage-wing combination with wing tip fuel tanks, calculating mass and stiffness matrix for elastic beam
07 p1022 A71-20364
- Wing-fuselage-tail interacting low speed flutter, considering mechanical tuning and aerodynamic interference couplings
[ALAA PAPER 71-326] 11 p1842 A71-25306
- Minimum drag surface shape of thick lifting delta wing integrated with conical fuselage for supersonic cruising speed
[ONERA-TP-947] 12 p1866 A71-27716
- Minimum drag wing-fuselage combination for supersonic speeds and prescribed lifting force, longitudinal moment and volume, using method of successive approximations
13 p1992 A71-29182
- Optimum vertical surface configuration for STOL transports, considering structural weight and performance requirements
[ALAA PAPER 71-769] 16 p2524 A71-34006
- Supersonic flow field computation for wing-body combinations by shock-capturing finite difference techniques, discussing improvement based on Runge-Kutta method
18 p2844 A71-36303
- BOEING AIRCRAFT**
- NT B-52 AIRCRAFT
- NT BOEING 737 AIRCRAFT
- NT BOEING 747 AIRCRAFT
- NT BOEING 707 AIRCRAFT
- NT C-135 AIRCRAFT
- NT CH-46 HELICOPTER
- NT CH-47 HELICOPTER
- Supersonic transport fuel tank environments and sealant requirements, describing Boeing laboratory environment approach
09 p1385 A71-23424
- BOEING 737 AIRCRAFT**
- Boeing 737 aircraft takeoff and landing performance, emphasizing high lift systems and stopping capability
07 p1018 A71-19083
- Turbulent boundary layer pressure fluctuations in-flight measurements on Boeing 737 aircraft, obtaining power spectral densities and RMS pressure fluctuations for various Mach numbers
08 p1231 A71-21426
- BOEING 747 AIRCRAFT**
- Boeing 747 flight loads measurements, describing aircraft instrumentation with strain gages and pressure pickups
03 p0348 A71-13766
- Hydraulic systems in Boeing 747 aircraft, considering piston design
05 p0705 A71-16131
- Link 747 simulator design and operation, describing cockpit layout, motion picture system and malfunction insertion and display unit
06 p0881 A71-18665
- Space shuttle development and certification test program comparison with large aircraft and spacecraft programs, considering Boeing 747 aircraft and Apollo Saturn S-IC stage
[ALAA PAPER 71-306] 09 p1531 A71-22619
- Boeing 747 aircraft passenger handling measures in Frankfurt airport, discussing loading, unloading, baggage claim and customs control
09 p1430 A71-23696
- Boeing 747 crew members training program, describing ground training, classrooms, inertial navigation system and cockpit trainers
[SAE PAPER 71-0473] 13 p1996 A71-28339
- Boeing 747 aircraft integrated data system program for reducing engine maintenance and operating costs
[ALAA PAPER 71-648] 14 p2290 A71-30725
- Reliability implications of Boeing 747 program, considering problem detection and identification, parts fabrication and installation, airline operating variables, etc
16 p2522 A71-33285
- Carousel IV inertial navigation system of Boeing 747 aircraft, discussing informational capabilities, accuracy and reliability
16 p2606 A71-34079
- Statistical analysis of error sources and magnitudes in Boeing 747 weight values obtained by onboard aircraft weighing system and by manual calculations
[SAE PAPER 897] 17 p2676 A71-35813
- Link 747 simulator with six degrees of motion system for engineers and pilot training
18 p2900 A71-36970
- Boeing 747 digital computer type flight simulator with four degrees of movement for engineer and pilot training
18 p2901 A71-36971
- Boeing 747 aircraft hydraulic system design, discussing thin wall high pressure tubing, swaged sleeves and welded joints
20 p3183 A71-39148

- Boeing 747, Lockheed C-5A and other aircraft vortex wake characteristics by tower flyby technique
21 p3320 A71-40498
- On-condition monitoring of aircraft hydraulic systems for component deterioration, applying to Boeing 747, L-1011 and DC 10 aircraft
22 p3483 A71-42075

BOEING 707 AIRCRAFT

- Ti intermediate diagonal tension field shear beam analysis and design for Boeing SST, using Rayleigh-Ritz method
[ALAA PAPER 71-340] 11 p1843 A71-25319

BOGOLIUBOV THEORY

- Bogoliubov electronic excitations anomalous scattering and tunneling in superconductor intermediate state, noting pair production one direction step function changes
07 p1181 A71-20207
- Krylov-Bogoliubov averaging method in optimal satellite motion programming of transfer orbit and low thrust correction
10 p1587 A71-24843
- Bogoliubov generalization principle applicability conditions for second order hyperbolic equations with functionally perturbed argument, using Wendroff-Bellman lemma
11 p1792 A71-26154
- Gyroscopic systems equations of motion solution by Bogoliubov averaging method, considering free gyroscope on rotating base
13 p2065 A71-27952
- Bogoliubov averaging method application to non-linear stochastic systems described by ordinary and partial differential equations and differential-difference equations
15 p2449 A71-31829
- Monograph on statistical theory for weak homogeneous turbulence covering mathematical model, wave correlation functions, Bogoliubov expansion method, kinetic equation, nonlinear interactions, etc
17 p2727 A71-34771

BOILERS

- Digital simulation of steam boiler by process control computer using coefficients directly calculable from transfer function of continuous system
01 p0049 A71-10324
- Spacecraft propane boiler system, obtaining heat transfer behavior under simulated aerospace conditions
14 p2319 A71-29726
- Helical induction boiler feed electromagnetic pump design, fabrication and testing for potassium Rankine cycle space power system
[GESP-455] 15 p2415 A71-32202
- Tantalum/stainless steel mercury boilers for SNAP 8, evaluating performance
15 p2448 A71-32219
- Unalloyed tantalum as containment material in mercury Rankine cycle SNAP 8 system boiler for 5 year service life
15 p2448 A71-32221
- Book on external corrosion and deposits on boiler tubes and gas turbine blades covering mineral matter in fuels, oxidation, additives, etc
18 p2935 A71-36247

BOILING

- NT FILM BOILING
- NT LEIDENFROST PHENOMENON
- NT NUCLEATE BOILING
- Boiling under weightlessness, examining gravitational effects on bubbles formation frequency and diameters
02 p0331 A71-11922
- Binary liquid metal forced convection boiling heat transfer, determining axial and radial temperature distribution in two phase flow
04 p0676 A71-15173
- Boiling cryogenic gas-liquid cross-current heat exchanger unit surface power transmission optimization
04 p0626 A71-15463
- Heat transfer - Conference, Versailles, August-September 1970, Volume 5, Boiling
04 p0686 A71-15526
- Heat transfer - Conference, Versailles, August-September 1970, Volume 6, Boiling and condensation
04 p0687 A71-15533
- Cryogenic liquids boiling peculiarities concerning heated surface material thermophysical properties effects on cavity stability, density and heat transfer rate
04 p0688 A71-15537
- Boiling layer microcharacteristics, investigating temperature pulsations near wall attachment and sub-cooled liquid two phase boundaries
07 p1221 A71-18788
- Boiling in two-phase layer on heated wall in relation to thermal exchange mechanisms
07 p1221 A71-18790
- Binary fluids boiling heat and mass transfer in boundary layer, discussing bubble growth rate, surface roughness effects and burnout heat flux
07 p1221 A71-18791

- Vapor bubbles radius at heating surface separation moment at boiling under free convection and forced motion through channel
07 p1221 A71-18929

- Boiling of relativistic heat conducting fluid in normal space-time manifold for nonstrict hyperbolic system, using Eckart scheme
10 p1694 A71-238

- Boiling under weightlessness, examining gravitational effects on bubbles formation frequency and diameters
13 p2159 A71-28299

- Local forced convection heat transfer data and empirical correlations for boiling Hg in single wetted tube with composite helical inserts
[GESP-450] 15 p2447 A71-32206

- Perfectly effective boiling fin design in horizontally right circular cylinder shape, deriving formulas at peak heat flux operation
15 p2514 A71-32206

- Saturated Hg vapor pressure at 650-900 K by boiling point method
19 p3162 A71-37591

- Bulk boiling studies with motion picture camera and quartz envelope of KIO 220/2500-2 tube for heat releasing surface
24 p3890 A71-45022

BOILING WATER REACTORS

- Cooled porous plug burner for flame recombination of oxygen and hydrogen, noting boiling water reactor off-gas application
03 p0517 A71-13367

BOLIDES

- Bolide spectrum on 6 June 1969, determining stellar magnitude and periodic pulsations and asynchronous flares characteristics along trajectory
12 p1965 A71-27225
- Bolide spectrum on 6 June 1969, determining stellar magnitude and periodic pulsations and asynchronous flares characteristics along trajectory
19 p3132 A71-37384

BOLKOW AIRCRAFT

- NT BO-105 HELICOPTER
- BOLKOW BO-105 HELICOPTER**
- U BO-105 HELICOPTER

BOLOGRAMS**U BOLOMETERS**

- Thermistor bolometer characteristics, considering resistance-performance relationship, radiation and Wheatstone bridge potentials
20 p3233 A71-38965
- Rollin InSb hot electron bolometer performance and calibration
22 p3543 A71-42124
- Barium strontium lanthanum titanate thermistor bolometer for IR thermal detector, using positive temperature coefficient of resistance
22 p3543 A71-42124

BOLTS

- Soviet book on bolting and coupling elemental threads used in aircraft industry covering configurations selection, cutting, tolerance requirements and quality control
02 p0258 A71-12723
- Flange joint moments magnitude due to bolts nonuniform tightening during assembly based on probability theory
07 p1116 A71-19358
- Bolted joint assemblies under sustained loading, examining joint and fastener coating, bolt design and strength level and shear and tension stress effects
08 p1371 A71-21412
- Anisotropic bolt bearing specimens failure modes and ultimate load, investigating stress concentrations for failure prediction
[ALAA PAPER 71-354] 11 p1844 A71-25334
- Anisotropic bolt bearing specimens failure modes and strength prediction, evaluating relative merits of maximum stress, maximum strain and distortional energy as failure criteria
17 p2824 A71-34820

BOLTZMANN DISTRIBUTION

- Solar diatomic molecules vibrational degree of freedom model, applying Boltzmann distribution
08 p1365 A71-21773
- Magnetic corrections to Boltzmann distribution function by power expansion, determining current density in system of free electrons accelerated by crossed electric and magnetic fields
13 p2109 A71-29288
- Solar diatomic molecules vibrational degree of freedom model, applying Boltzmann distribution
15 p2495 A71-32678

BOLTZMANN TRANSPORT EQUATION

- Cauchy problem for linearized Boltzmann equation, using collision operator eigenfunction series
01 p0109 A71-10027
- Direct computerized simulation Monte Carlo method for numerical solution of Boltzmann equation in rarefied gas dynamics
01 p0113 A71-11472
- Multicomponent gaseous mixtures and plasmas transport analysis improved formalism consisting of N

- moment Boltzmann equation and N parameter distribution function representation
02 p0290 A71-12229
- Boundary value problem for linear Boltzmann equation in kinetic theory, proving existence and uniqueness theorems
[ONERA-TP-820] 02 p0276 A71-12338
- Relativistic kinetic theory of particles with magnetic dipole moment in external EM field, deriving transport equations for distribution function
03 p0463 A71-13425
- Boltzmann equation solution for isotropic heat velocity distribution in molecular gas kinetics
03 p0401 A71-13907
- Metal galvanomagnetic properties for specific Fermi surface and conduction electron scattering model, solving linearized Boltzmann equation
05 p0792 A71-16317
- Classical multiatomic gases kinetic theory, considering generalized Boltzmann equations
05 p0785 A71-16779
- Relativistic velocity particles diffusion in cloud of scattering centers in centrifugal motion from Boltzmann equation solution by method of extensions
06 p0963 A71-18229
- Linearized Boltzmann equation analytic solutions for rarefied gas dynamic problems, using ellipsoid model
07 p1093 A71-20285
- Boundary condition effects on thermomagnetic torque from moment method solution for Boltzmann equation for diatomic molecular gas in magnetic field and cylindrical geometry
09 p1502 A71-22853
- Inhomogeneous rotating self-gravitating system kinetic theory, linearizing collisionless Boltzmann equation to two dimensional linear integral equation for obtaining small oscillation modes
10 p1641 A71-24278
- Boltzmann equation for shock wave structure, comparing errors of variational principles and moment methods of approximation
10 p1593 A71-24279
- Solar cycle time variations in trapped radiation belt proton flux, deriving proton transport equation from Boltzmann equation
10 p1663 A71-24785
- Cosmic ray transport equation for solar sources, using Fisk numerical method by applying transformation of independent variable $U/r, T$
10 p1664 A71-24801
- Fully ionized gas under electric and magnetic fields, calculating electron velocity distribution and runaway rate as function of time from Boltzmann equation
10 p1654 A71-24975
- Neutron transport equation in five dimensional tensor form, applying finite differencing by integration method via use of divergence theorem
11 p1791 A71-25741
- Thermionic converters performance in ignited mode from transport equations for diffusion region, determining electron concentration, potential and temperature
11 p1711 A71-25879
- Cosmic ray propagation in interplanetary space, deriving steady state transport equation with energy losses
11 p1817 A71-26172
- Three dimensional turbulent boundary layer calculations, using two dimensional method based on turbulent energy equation empirical conversion into shear stress transport equation
11 p1753 A71-26443
- Sound dispersion in monatomic gases from viewpoint of linearized hydrodynamic, Boltzmann and model equations
12 p1930 A71-27190
- Electromagnetic longitudinal cascades development numerical treatment based on Boltzmann equation, discussing Monte Carlo computing times for primary energy total electron counts
12 p1933 A71-27387
- Third harmonic component generation in reflected and transmitted waves from magnetoplasma slab, using Boltzmann transport equation and Maxwell equation
13 p2109 A71-29243
- Reactor shielding design in U.S. based on Boltzmann transport equation solutions and Monte Carlo method
13 p2099 A71-29254
- Boltzmann equation applicability to rarefied multiatomic gases if distribution function is identical with integral of free molecular motion
14 p2276 A71-29561
- Galactic cosmic ray transport equation numerical solution for interplanetary region, considering modulation, diffusion, convection and energy loss effects
14 p2301 A71-30387
- Boltzmann equation approximate solution for molecular velocity distribution function perturbations by inelastic collisions
15 p2386 A71-31158
- Boltzmann kinetic equation for imperfect gases in pair collision approximation, including terms proportional to time and coordinate derivatives and van der Waal constants
15 p2387 A71-31193
- Third approximation to Boltzmann equation for heat flux vector of gas of rigid spheres, using Brooker-Green technique
15 p2513 A71-31687
- Classical polyatomic gases kinetic theory, considering generalized Boltzmann equation solution
16 p2614 A71-33031
- Cauchy problem for nonlinear Boltzmann equation in general relativity, utilizing energy inequalities
16 p2612 A71-34059
- German monograph on electron motion in cesium plasma covering Boltzmann equation, radiative transfer, mathematical model, electron velocity distribution, etc
17 p2787 A71-34485
- Linearized Boltzmann equation solution for rarefied gas dynamics, discussing analytical, variational and numerical methods
17 p2784 A71-35572
- Rarefied gas dynamic models with velocity dependent collision frequencies, investigating linearized Boltzmann equations
17 p2729 A71-35573
- Kramer problem for steady linear Boltzmann equation in kinetic theory of gases, noting solution existence
18 p2947 A71-36190
- Shock wave structure prediction by nonlinear kinetic models with Monte Carlo solutions of full Boltzmann equation
18 p2907 A71-36334
- Temperature dependence of electrical resistance in mixed superconducting-normal systems, solving transport equation
18 p2954 A71-36746
- Spatial relaxation of electron energy distribution with inelastic and Coulomb collisions, integrating Boltzmann equation
18 p2949 A71-36969
- Binary elastic collision integral between particles of disparate mass, determining angular momentum form of Boltzmann equation for Lorentz mixtures
19 p3115 A71-38210
- High pressure collisional plasma instabilities caused by spatial gradients from quasi-stationary state transport equations derivation
22 p3580 A71-41585
- Semilinear hyperbolic systems analogous to differential-integral Boltzmann equations of gas dynamics, developing solutions existence for nonnegative initial data
22 p3531 A71-42690
- Boltzmann kinetic equation with electron-electron collision coefficients for isothermal weakly ionized cesium-argon plasma, using nodal point method
23 p3709 A71-43267
- Iterative solution for radiant energy transport equation by Wiener Hopf operator equations, investigating convergence conditions
23 p3699 A71-43573
- Chaos propagation derivation from Boltzmann equation for dilute gas with intermolecular forces and collisions in pairs
23 p3705 A71-43873
- Hydrodynamic equations for ions and electrons of ionized collision plasma in strong nonuniform magnetic field from Boltzmann kinetic equations
24 p3855 A71-44521
- Boundary conditions determined for hydrodynamic equations from solution of Boltzmann kinetic equation in Knudsen layer, obtaining distribution function in Enskog function superposition form
24 p3821 A71-45226
- BOLTZMANN-VLASOV EQUATION**
Gravitational stability analysis based on Boltzmann-Vlasov collisionless kinetic equation solution by trajectory integration method in plasma physics
07 p1173 A71-20531
- BOMBER AIRCRAFT**
NT B-52 AIRCRAFT
NT B-70 AIRCRAFT
NT F-100 AIRCRAFT
Strategic bomber B-1A program, discussing airframe and engine contractors, design, characteristics performance, electronic equipment and armament
18 p2850 A71-36757
F 101 30,000 lb thrust augmented turbofan engine for B-1 bomber, considering maintainability and bird ingestion tolerance
19 p3122 A71-37491
Variable geometry B-1A bomber aircraft, discussing size, payloads, speed, altitude range and runway takeoff
19 p2996 A71-37516
- BOMBS [ORDNANCE]**
Free flight measurement of aerodynamic coefficients on fixed cruciform fin stabilized bombs, determining aerodynamic forces and moments dependence on angular velocity components
07 p1015 A71-19872
- BOMBS [PRESSURE GAGES]**
U PRESSURE GAGES
BOMBS [SAMPLERS]
U SAMPLERS
BONDING
NT ADHESIVE BONDING
NT CERAMIC BONDING
NT EXPLOSIVE WELDING
NT METAL BONDING
NT METAL-METAL BONDING
NT RESIN BONDING
Epoxy resin reinforcement by various fiberglass types, discussing effects of bond-enhancing agents, fatigue strength properties, etc
01 p0108 A71-10691
Adhesive bonding and detachable joints in multilayered fiber reinforced plastic structures, discussing joint strength test methods, fiber and load force orientation effects, etc
01 p0108 A71-10692
Optical bonding agent for calcite prism on Pioneer F/G mission, emphasizing optical and mechanical properties resistance to Jupiter high energy particles
01 p0081 A71-10835
Pressure-bonded trilayer insulator stress analysis, using computer model for explaining alumina component fracturing during fabrication
02 p0256 A71-12249
High modulus boron-epoxy composite aircraft structures adhesive bonding, discussing mechanical properties, manufacturing techniques and quality control
[SAE PAPER 710110] 06 p0904 A71-17624
Metallic soaps polarity and micellar bond energy effects on pliable lubricants structure and properties
07 p1144 A71-19491
Bonded rod of two semiinfinite elastic bars subjected to end impulse, formulating motion equations and initial and boundary conditions
07 p1217 A71-20367
Ultrasonic bonding techniques discussing high frequency activated adhesives, equipment and automated processes
10 p1615 A71-24092
Glass transition temperature and specific heat of Apiezon N and T greases used as thermal bonding agent at cryogenic temperatures
20 p3253 A71-39267
Holographic inspection of bond between inert solid propellant grain and polymer liner, using double exposure to record surface deformation of fiberglass case
22 p3549 A71-42570
- BONE MARROW**
Bone marrow physiological regeneration after chronic gamma irradiation, noting effect on fission processes and chromosome apparatus of cells
01 p0014 A71-11146
Amino-ethyl-S-2-isothiuronium radio protective dose effects on enzyme activity, cardiovascular changes, blood transaminases concentration, bone marrow and peripheral circulation
07 p1040 A71-18986
Microwave irradiation effects on peripheral blood and bone marrow in dogs and rabbits
07 p1053 A71-20539
Rapid erythroblast multiplication in vitro by incubation of rabbit blood buffy coat and marrow cells, giving autoradiographic results
10 p1566 A71-25014
Erythrocytes life span and bone marrow production in dogs subjected to gamma irradiation in doses simulating prolonged space flight conditions
15 p2356 A71-31307
Peripheral blood and bone marrow morphological composition in dogs subjected to chronic and repeated gamma irradiation
15 p2357 A71-31308
Abdomen shielding effects on chromosome aberrations in bone marrow cells of guinea pigs and rats under gamma irradiation
22 p3493 A71-42719
- BONES**
NT CEREBRUM
NT CRANIUM
NT FEMUR
NT MARROW
NT MASTOIDS
NT PELVIS
NT SCIATIC REGION
NT SKULL
NT TIBIA
NT VERTEBRAE
Transducer for measuring mandibular dynamic movements during speech
01 p0079 A71-10346
Elastic behavior of bone as two phase composite material, using ultrasonically measured hydroxyapatite moduli
[ASME PAPER 70-WA/BHF-3] 03 p0373 A71-14110
Metabolic processes in bone tissues as basis for fighting bone disease, emphasizing enzymes role
05 p0710 A71-16858
Bone tissue optical density and blood serum and urine calcium content of Soyuz 9 crew members during and after flight
09 p1389 A71-22201

Primate restraint harness of nylon jacket and cotton
cot on aluminum frame padded seat for bone resorp-
tion and calcium metabolism studies
09 p1398 A71-22476

Structural development in rat bone under earth
gravity, hypergravity and simulated weightlessness,
discussing physical dimensions, density, rigidity,
microhardness and ash content
[AIAA PAPER 71-895] 18 p2856 A71-36640

Macaca nemestrina monkey bone density change
during Biosatellite 3 mission
21 p3330 A71-40343

BOOLEAN ALGEBRA

NT BOOLEAN FUNCTIONS

Boolean algebra and flow diagram nomenclature for
sequential logic design
13 p2035 A71-28912

Binary relation algebra application to diagnostics
tests for system involving redundant subsystems
17 p2720 A71-34960

Permanent logical faults identification in discrete
combination devices by practical behavior in response
to given input sets, using one of Boolean algebras
19 p3025 A71-37571

Computerized algorithm for redundant configura-
tion system reliability function generation from Boolean
an algebra transmission function
22 p3517 A71-42107

BOOLEAN FUNCTIONS

Chow parameters of switching functions in
threshold logic, discussing basic properties and alter-
native definitions
13 p2035 A71-28975

Computer systems design for complex process con-
trol, constructing models with differential equations
and Boolean functions
24 p3806 A71-44714

BOOMS [EQUIPMENT]

Spacecraft deployable booms, discussing structural
design, self loading, weight, stowage volume and ther-
mal stability requirements
[AIAA PAPER 71-396] 11 p1841 A71-25272

RAE satellite flexible boom vibration, obtaining an-
tenna boom static deflection, natural frequencies and
thermal bending effects
[ASME PAPER 71-DE-J] 12 p1977 A71-27319

Thermal flutter of satellite storable tubular exten-
sible members, determining static flexural and torsional
vibrations due to solar radiation
12 p1984 A71-27736

Thermally induced torque of circular thin walled
open section booms, predicting steady state behavior
13 p2148 A71-27980

Long thin spacecraft antennas and gravity gradient
booms, explaining solar induced oscillations with
lumped parameter and Lagrangian equation models
15 p2504 A71-31598

Maximum nutation-precession angles of spin stabl-
ized satellites during extension of long flexible booms
15 p2500 A71-32046

Planar librational motion prediction for gravity
gradient satellite with extendible booms during
deployment
22 p3610 A71-42014

BOOST

U ACCELERATION (PHYSICS)

BOOSTER RECOVERY

Computerized synthesis for fly-back system of first
stage winged booster for earth-to-orbit reusable space
transportation system
[FZA-456] 22 p3611 A71-42032

BOOSTER ROCKET ENGINES

Europa 3C light alloy space booster powered by
Rolls-Royce engines using kerosene and LOX
05 p0816 A71-16403

High energy three stage booster system for geo-
stationary orbiter, discussing interstage propellant
transfer, apogee impulse system and mission rated
payload modular configurations
11 p1838 A71-25574

Space shuttle propulsion systems, describing main
engine prototype designs, booster attitude and docking
control systems
12 p1946 A71-27606

Solid propellants based on low cost hydroxyl ter-
minated polybutadiene binders meeting burning rate,
mechanical properties and processing requirements
for large booster motors
[AIAA PAPER 71-708] 14 p2286 A71-30764

Propulsion system design and performance require-
ments for space shuttle booster and orbiter vehicle,
considering low cost, long life, reliability, safety and
minimum maintenance
[AIAA PAPER 71-657] 15 p2471 A71-32577

Rocket engine burning oxygen and hydrogen propel-
lants at 3000 psia combustion chamber pressure for
space shuttle booster and orbiter stages
[AIAA PAPER 71-659] 16 p2624 A71-33106

Dynamic stability analysis, ground testing and cor-
rective accumulator devices for POGO oscillations in
space booster structure
22 p3609 A71-41992

BOOSTER ROCKETS

Space shuttle technology, discussing wind tunnel
studies, aerothermal and operational flight mechanics,

model characteristics, orbiter configurations and
booster-orbiter separation
07 p1209 A71-20227

Large flexible booster launch vehicle autopilots au-
tomated design and optimization by computerized
technique in frequency and time domain
08 p1332 A71-21337

Earth-to-orbit space shuttle booster and orbiter unit
design considerations including low development cost,
risk and time, weight and payloads
11 p1840 A71-26529

Reusable space shuttle optimization, discussing
earth-to-orbit transportation, economic aspects,
booster vehicles design, propellant cryogenic tanks
and thermal protection
[AIAA PAPER 71-805] 17 p2814 A71-35430

Space shuttle with two stage booster and orbiter
reusable vehicles, discussing performance, structural
design and flight control system
[AIAA PAPER 71-804] 17 p2814 A71-35431

Space shuttle booster configuration design, compar-
ing stowed, fixed straight and delta wing approaches,
discussing air breathing engines, stage mating, fins,
etc
18 p2972 A71-36444

Missile vibrations during acceleration calculated in
matrix form for Saturn 5/Apollo booster configuration
20 p3306 A71-39412

Computerized synthesis for fly-back system of first
stage winged booster for earth-to-orbit reusable space
transportation system
[FZA-456] 22 p3611 A71-42032

BOOSTGLIDE VEHICLES

Space shuttle optimal lifting trajectory analysis, ex-
amining boost launch system performance increase
22 p3608 A71-41955

BOOTS [FOOTWEAR]

Permanent magnets for footwear restraint and mo-
bility in zero gravity spacecraft, testing neutral
buoyancy and six degree of freedom simulation ef-
fects
[IEEE PAPER 2.2] 07 p1048 A71-19607

BOLANES

Decaborane effects on amino acid metabolic pat-
terns of various rat tissues, considering holoenzyme
inactivation
05 p0706 A71-16294

BORATES

Soviet book on Mg, Ca, Fe and Sn high temperature
borates formation covering optimum synthesis condi-
tions, properties, stability analysis, etc
02 p0208 A71-11800

Photomagnetic effect in ferric borate, noting
photoinduced change, radiation sensitivity and tem-
perature effects
12 p1943 A71-26857

BOREL SETS

Measurability and nonmeasurability of composition
function, considering Borel sets
03 p0451 A71-13784

Admissible translations of probability measures on
sigma algebra of Borel sets of Hilbert space
07 p1147 A71-19200

Weighted distribution functions of normal
processes, calculating stochastic mixture components
in Borel sets
10 p1637 A71-24903

BORES

U CAVITIES

BORESIGHTS

Angular estimation precision in amplitude
monopulse off-boresight radar, using linear approxi-
mation to error curve
09 p1405 A71-22695

Lens test facility calibrating Mipir radar boresight
lenses by measuring deviations due to gravitational ef-
fects
18 p2897 A71-36072

Antenna tracking, RF and boresight alignment on
ships and ground stations using Apollo lunar surface
experiments package /ALSEP/
18 p2876 A71-36473

Algorithms for directional antenna boresight orien-
tation estimation errors relative to spacecraft attitude
sensor, based on measurement of received signal
strength
22 p3525 A71-42775

Precision pointing correction /boresight calibration/
of microwave antennas, using sun as test source
23 p3654 A71-44158

BORIDES

NT CHROMIUM BORIDES

NT TITANIUM BORIDES

Boride coatings for Fe-Si alloy, testing corrosion and
wear resistances in aqueous salt, acid and alkali solu-
tions
01 p0097 A71-10039

Diffusion boride protective coatings on Nb, Ta, Mo
and W against carbon diffusion from carburizing
agents
01 p0100 A71-10401

Boride composites with high strength and thermal
resistance suitable as nose cap and leading edge
materials for reusable lifting reentry systems
[AIAA PAPER 70-278] 01 p0109 A71-11282

Soviet book on boride coatings on iron and steels
covering physicochemical interactions and properties
02 p0263 A71-11848

Tungsten boride sintering bonds with molten Ni ar
function of wettability low dihedral angle, discussing
cermet porosity range
07 p1130 A71-19297

Grain growth inhibition in niobium diboride by TiN
addition
07 p1144 A71-19390

Electrodeposition of coherent coatings of zirconium
diboride from solution of zirconium tetrafluoride and
boron oxide in molten eutectic mixture of NaF-KF
LiF
07 p1118 A71-19567

Steel coatings produced by boriding, investigating
structure and wear resistance properties
07 p1118 A71-19583

Refractory metals and carbides and borides, in-
vestigating laws governing electrodes erosion during
electric spark breakdown
07 p1139 A71-20205

Refractory transition metals diborides thermoelec-
trical properties for use in cathode materials
07 p1144 A71-20653

Hf, Ta, W and Re solubility in La and Ce hex-
aborides from lattice parameters, microhardness and
X ray and metallographic analyses
09 p0509 A71-23066

Transition metal diborides chemical stability after
treatment with oxygenless acid in nitrogen and air at-
mosphere
12 p1877 A71-27124

Boride coated steels and cast iron surfacing with
nonconsumable tungsten electrode for higher abrasive
wear resistance
12 p1917 A71-27125

Disintegration energy of hard compounds /carbides,
nitrides and borides/ related to wear resistance and
microhardness of alloys
13 p2072 A71-27818

Electrical conductivity, thermal emf, expansion and
Hall coefficient of hot compressed powdered
diborides of group IV and V transition metals
13 p2084 A71-28036

Surfacing materials based on transition metal
borides with boron carbide additions, testing brittle-
ness, hardness and abrasive wear resistance
15 p2431 A71-32163

Low temperature heat capacities from 1.5 to 15 K
for transition metal borides and solid solution
15 p2437 A71-32649

Abrasive capability, shape and strength of refrac-
tory powders of fused titanium and niobium carbides
and calcium boride compared with synthetic corun-
dum
16 p2592 A71-33574

Pulsed high perveance electron gun with hot
lanthanum boride cathode
20 p3204 A71-39156

Refractory diborides in oxidizing environments,
considering mechanical strength, thermal stability, ox-
idation resistance, heat conductivity, thermal expan-
sion, specific heat and electrical resistance
21 p3405 A71-40138

Boridosilicide and boridoaluminide diffusion
coatings on iron and steel, investigating formation
kinetics structure and properties
21 p3390 A71-41171

Two temperature region oxidation of zirconium
diboride, showing formation of continuous surface
film and quadratic crystallized discontinuous layer
22 p3563 A71-42246

Diboride-nitride system dry friction and wear re-
sistance at room temperature
23 p3681 A71-43254

Vacuum fusion sintered rhodium borides melting
point, microhardness and conductivity and thermal
emf temperature dependences determination by ther-
mal metallographic and X ray analyses
23 p3717 A71-44024

Platinoid boride production, determining reaction
sintering temperature with thermal metallographic and
X ray analysis
24 p3838 A71-44735

Externally pressurized air lubricated bearing boring
spindle performance tests, considering circular accu-
racy, maintenance, tool life and cost effectiveness
22 p3552 A71-41675

Single Born scattering theory applicability to critical
electron density fluctuations
07 p1171 A71-20293

Turbulent plasma flame incoherent scatter calcula-
tion by modified first order Born approximation, con-
sidering attenuation due to absorption and scatter by
energy conservation
07 p1171 A71-20294

Rayleigh-Gans-Born approximation application to
thermal radiation of reflecting convex plasma sphere,
cylinder and ellipsoid
02 p0288 A71-11633

He excitation by He, Ne, Ar and Kr collisions, cal-
culating first Born wave cross section
03 p0460 A71-13498

Single Born scattering theory applicability to critical
electron density fluctuations
07 p1171 A71-20293

Turbulent plasma flame incoherent scatter calcula-
tion by modified first order Born approximation, con-
sidering attenuation due to absorption and scatter by
energy conservation
07 p1171 A71-20294

Cross sections for simultaneous ionization and charge transfer in fast proton-helium atom collisions, using Born approximation 09 p1497 A71-22416

Plasma in strong electric and magnetic field with allowance for inelastic electron collisions with neutral particles, showing resonant oscillations from Born approximation 12 p1937 A71-27183

Moliere high energy solution of Schroedinger scattering equation for optical propagation in turbulent atmosphere, noting inconsistency of Born-Rytov approximation 13 p2102 A71-29441

Electromagnetic wave scattering on inhomogeneities by Born approximation, estimating maximum error for small correlation radius 14 p2194 A71-30100

Plasma in strong electric and magnetic field with allowance for inelastic electron collisions with neutral particles, showing resonant oscillations from Born approximation 22 p3584 A71-42460

BORN-MAYER EQUATION
U BORN APPROXIMATION
BORN-OPPENHEIMER APPROXIMATION
Born-Oppenheimer approximation for elastic and inelastic electron scattering by diatomic molecules 08 p1337 A71-20886

German monograph on comparison between quantum mechanical approximate methods through projection of approximated eigenfunctions covering Schroedinger equation, wave functions, Born-Oppenheimer approximation, etc 20 p3271 A71-39042

BORON
NT BORON ISOTOPES
Viscoelastic behavior of boron fiber-epoxy resin composites at high temperature from torsion pendulum study, proposing linear model for damping peak effect 01 p0107 A71-10460

Boron addition distribution in iron microstructure, using nuclear track radiography 01 p0103 A71-11072

Polymide/boron reinforced plastic structures fabrication, discussing use in leading edges [SME PAPER EM-70-133] 01 p0090 A71-11263

Thermal cycling effect on Al-B composites, considering surface roughening and crack initiation 01 p0103 A71-11279

Boron vs graphite fiber reinforced composites, noting design application role 01 p0104 A71-11280

Diffusion bonding cycles for Al-B composite materials fabrication, relating strength enhancement to residual stress relief 01 p0104 A71-11284

Ni aluminoboronizing process by circulation method, discussing thermodynamic analysis for saturation possibility and parameters experimental determination 03 p0432 A71-13961

Boron fiber-Al alloy composites linear thermal expansion as function of fiber volume fraction and orientation 04 p0615 A71-15788

Particulate B fuels combustion and ignition working models in air at ambient pressures, using levitation cell and pulsed Nd doped laser [WSS/CI PAPER 70-13] 06 p0943 A71-17659

Lightning protective coatings for boron and graphite fiber reinforced plastics 07 p1021 A71-19944

High intensity electric current damage in boron and graphite filament reinforced epoxy resin composites 07 p1145 A71-19945

Ternary Al-B-Ti system, investigating Al corner and B effect on grain refinement 07 p1138 A71-19981

Mechanical strength and elastic properties under tension and bending of boron fibers, noting dependence on surface defects 09 p1482 A71-22823

Composite materials for compressor blades in aircraft engines, considering boron and carbon fiber reinforced materials 09 p1456 A71-23286

B and C polymer laminated film composites efficiency for stability designed structures, considering weight reduction by planar reinforcements [AIAA PAPER 71-353] 11 p1783 A71-25331

Boron and graphite fiber market competition, considering aerospace application 11 p1860 A71-25400

Boron-epoxy structural skins design for F-14 honeycomb horizontal stabilizer, using computer program 11 p1786 A71-25420

Rocket propellant performance improvement with boron, giving boiling temperature vs pressure and calculation methods for combustion products composition 11 p1809 A71-25573

Boron filaments and whiskers as reinforcements in high strength composite materials 11 p1790 A71-26336

Boron or phosphorus doping of silicon, noting microhardness increase and friction coefficient reduction 12 p1911 A71-26820

Ti, B and graphite fiber composites application to aircraft design, discussing mechanical properties and market competition 12 p1918 A71-27676

Carbon and boron fiber reinforced plastics adhesive bonded and bolted joints, presenting results of hole deformation tests [DFVLR-SONDDR-96] 13 p2093 A71-29306

Hybrid boron-graphite filaments in epoxy matrix composite, describing increased tensile strength and modulus of elasticity 14 p2261 A71-29638

Ignition and combustion tests of storable boron/magnesium/hexane slurry injected directly in high speed air stream [AIAA PAPER 71-723] 14 p2286 A71-30773

Austenite and carbide chromium manganese steel boron distribution obtained by tracing elements 15 p2425 A71-31397

Boron solubility in molybdenum, showing grain size decrease, plastic deformation change and elongation 15 p2425 A71-31399

Amorphous boron powder total burning time in premixed laminar boron-propane-oxygen-nitrogen flames at atmospheric pressure, noting variation as function of oxygen initial partial pressure 15 p2511 A71-31472

Boron combustion characteristics as function of temperature, pressure and gaseous fuel mixture ratio, using color photography [WSS/CI PAPER 71-19] 15 p2464 A71-31628

Boron particles ignition theory and shock tube experiments, measuring ignition delay as function of temperature, pressure, gas composition and particle size [WSS/CI PAPER 71-20] 15 p2464 A71-31629

Silicon-boron melts, investigating B and C concentration effects on carbide layer thickness on graphite/melt interface 15 p2439 A71-32144

Boron and graphite fiber reinforced plastics machining, discussing tools, operating parameters and process limitations [SME PAPER MR-71-820] 15 p2416 A71-32429

Tensile strength of boron, silicon carbide coated boron, silicon carbide, stainless steel and tungsten fibers after exposure to air, argon and aluminum at high temperatures 15 p2435 A71-32440

Ca, Mg, B and Al prominent resonance transitions radiative lifetimes and absolute oscillator strengths 15 p2452 A71-32596

Ultrasonic pulse technique for plane transverse and longitudinal stress wave dispersion in boron fiber reinforced epoxy composite, determining group velocity dependence on frequency and elastic moduli [ASME PAPER 71-APM-27] 16 p2600 A71-33202

Tauri stars Li, Be and B autogenic generation, considering underabundance in surrounding gas 16 p2626 A71-33433

Boron-aluminum composites fracture behavior, using conventional metallography and scanning electron microscope 16 p2599 A71-34087

High modulus graphite-boron composites design and application to lightweight structures, illustrating sandwich construction for race boat main boom stiffness and compressive strength 17 p2762 A71-35203

Solid state diffusion bonded boron-aluminum composites, discussing mechanical properties, weight and cost reduction and applications 17 p2758 A71-35204

Composite panel of ten-ply unidirectional boron/epoxy laminate adhesively bonded to Al face sheets, discussing ultrasonic inspection technique 17 p2749 A71-35495

Boron-epoxy composite wing box beam design, describing preliminary weight estimation from layouts [SAWE PAPER 891] 17 p2834 A71-35815

Boron, carbon, sapphire and glass fiber composite materials, considering brittleness, anisotropic properties, filament winding and plastic and metallic matrices 18 p2939 A71-35915

Aluminum-boron composite forming and cutting processes covering milling, grinding, abrasive cutoff, drilling, piercing, electrodischarge machining, blanking, punching and shearing 18 p2928 A71-36666

Microradiographic and acoustic evaluation of fracture in boron filament aluminum matrix composite under tensile stress 19 p3081 A71-37903

Boron powder combustion at elevated pressures, observing preignition metastable surface reactions, self sustained diffusion burning and decay 19 p3170 A71-38116

Carbon and boron fibers and whisker reinforced plastics fabrication, properties and costs, noting materials and optimum matrix combination 21 p3405 A71-40600

Microwave photoconductivity of boron single crystals under pulsed illumination, determining temperature effects on carrier mobility, recombination coefficients and relaxation times 21 p3428 A71-41202

Beta rhombohedral boron whiskers production from hydrogen reduction of boron bromide and chloride by vapor-liquid-solid mechanism 22 p3564 A71-42533

BORON ALLOYS
Boron additive effects on Ti thermal conductivity and expansion 01 p0102 A71-10787

Groups IV-VIII transition metals reaction with Re and B, studying ternary compounds formation by X ray and metallographic analyses 07 p1140 A71-20233

V-Mn-B, Mo-Mn-B and W-Mn-B systems phase equilibria, describing diagrams isothermal sections at specific temperature 09 p1470 A71-23065

Equilibrium diagrams for Nb-Zr-B alloys, establishing solidus surface, Zr/B isothermal and vertical sections 11 p1782 A71-26474

Boron solubility in Mo-W solid solution, discussing microstructure, electrical and mechanical properties for range of alloying ratios 12 p1918 A71-27660

Ti-Co-B and Ti-Re-B systems diagrams of isothermal sections at 800 and 1400 C 13 p2083 A71-28008

Solid state solubility of B in Nb, determining binary Nb-B alloys phase diagram by microscopic, X ray and thermal analyses 13 p2085 A71-28224

Isothermal sections at 1400 C of systems niobium-titanium-boron and niobium-molybdenum-boron by X ray analysis 15 p2437 A71-32672

Si-B-C alloy phase diagram near SiC-B cross section, noting B solubility limit, microhardness and electrical resistivity 16 p2592 A71-33565

Phase diagrams of ternary systems Ta-Fe-B and Ta-Ni-B using X ray and metallographic analyses 16 p2592 A71-33575

Ti-W-B, Hf-Ta-B and Ta-W-B alloys isothermal phase diagrams at 1400 C, using X ray analysis and metallographic techniques 19 p3076 A71-37112

Soviet book on austenitic boron steels and alloys for welded structures, covering boron influence on steels and alloys structure and properties, with special reference to weldability 20 p3251 A71-39090

BORON CARBIDES
Boron carbonitride formation, describing chemical synthesis 09 p1470 A71-23064

Boron modifications and carbides formation by vapor deposition on tantalum filaments 12 p1943 A71-27093

Combustion characteristics of single boron carbide particles, studying minimum gas temperatures for self-ignition and burning times [WSS/CI PAPER 71-21] 15 p2464 A71-31630

Hot pressed boron carbide and titanium diboride for use as indenter materials for tungsten carbide hardness measurements at high temperatures 15 p2409 A71-32165

Ion machining techniques for cutting accurate and repeatable pumping grooves in gas bearing component materials typified by boron carbide 22 p3551 A71-41665

Alumina, boron carbide and silicon carbide notched and unnotched impact strength tests, using drop weight technique 22 p3565 A71-42542

BORON CHLORIDES
Pressure dependent absorption of carbon dioxide laser by boron chloride, considering saturation and line overlapping effects 22 p3556 A71-41805

BORON COMPOUNDS
NT BORANES
NT BORATES
NT BORIDES
NT BORON CARBIDES
NT BORON CHLORIDES
NT BORON HYDRIDES
NT BORON NITRIDES
NT BORON PHOSPHIDES
NT CHROMIUM BORIDES
NT DIBORANE
NT TITANIUM BORIDES
Transition metal borides X ray emission K alpha band, establishing asymmetry index, bandwidth and maximum power shift deviations from B 05 p0770 A71-17169

- Filamentary composites for primary aircraft structural applications, emphasizing boron-epoxy material 10 p1618 A71-24770
- Diffusion coefficients determination in planetary boundary layer with radon and ThB, using vertical distribution profile of concentration 18 p2912 A71-36193
- Boron silicide coatings wear resistance in vacuum and air, determining shipping rate and working medium influence on friction process in active surface layers 24 p3830 A71-44859

BORON HYDRIDES

NT BORANES

- Boron and carbon hydrides and carbon deuteride molecular ions radiative lifetime measurements, computing absolute oscillator strengths 08 p1250 A71-20671
- Pargylene behavioral effects in primates, concerning therapeutic use for decaborane intoxication 08 p1239 A71-20819

BORON ISOTOPES

- Relative abundances and mass measurements of Li and B isotopes in primary low energy cosmic rays 22 p3593 A71-42339
- Li, B, Mg and Ti isotopic abundances and search for trapped solar wind Li in Apollo 11 and 12 rocks 23 p3752 A71-43708

BORON NITRIDES

- Boron carbonitride formation, describing chemical synthesis 09 p1470 A71-23064
- Boron nitride and aluminum nitride particles behavior in Mo matrix, considering solid metallic phase formation 09 p1470 A71-23067

BORON PHOSPHIDES

- Epitaxial boron phosphides single crystals growth, using thermal decomposition and reduction for deposition on hexagonal silicon carbide substrates basal plane 07 p1180 A71-20174

BOROSILICATE GLASS

- Arc melter using Pyrex pipe cross for controlled atmosphere chamber, incorporating Ar jet into electrode holder for dynamic flushing and rapid quenching 13 p2044 A71-28154
- Lead borosilicate glass with crystalline opacifiers, observing microstructure and reflectance 13 p2093 A71-28990

BOSE-CHAUDHURI-HOCQUENGHEM CODES

U BCH CODES

BOSE-KEINSTEIN STATISTICS

U QUANTUM STATISTICS

BORON FIELDS

- Cross section for electron and muon neutrino-antineutrino pair production by photons, using intermediate boson theory 11 p1802 A71-25588

BOSONS

NT ALPHA PARTICLES

NT MESONS

NT PHOTONS

NT PIONS

- Feynman path integration for multiply connected space systems of indistinguishable particles, considering bosons and fermions propagators 10 p1644 A71-24214
- Production cross section of Lee-Wick hypothetical massive electromagnetic bosons by muons at high energy, giving Feynman diagrams 17 p2785 A71-34750

BOTANY

NT GEOBOTANY

BOUGUER LAW

- Spectrophotometers photometric accuracy measurement technique, using Bouguer law and optical fields superposition 14 p2240 A71-30123

- Quasi-specular and Lambert reflection of short radio waves from lunar surface dependent on central portion of near side 16 p2543 A71-33668

BOUNDARIES

NT FLUID BOUNDARIES

NT FREE BOUNDARIES

NT GAS-SOLID INTERFACES

NT GRAIN BOUNDARIES

NT JET BOUNDARIES

NT LIQUID-LIQUID INTERFACES

NT LIQUID-SOLID INTERFACES

NT LIQUID-VAPOR INTERFACES

- Plane EM waves at two dimensional periodic media boundaries, obtaining reflection and refraction for harmonics 05 p0723 A71-17029

- Large elastic deformations of incompressible materials shells with inclusion of transverse normal strain, considering thickness change at boundaries 12 p1976 A71-27159

BOUNDARY LAYER COMBUSTION

- Gas dynamics of fuel boundary layer combustion and surface pyrolysis in hybrid rocket motors 01 p0178 A71-10131

- Flame propagation along interface between fuel slab /polymers, aluminum and tungsten powders/ and oxidizer slab /inorganic salts and oxides/ 03 p0521 A71-14278

- Gas dynamic analysis of hybrid boundary layer combustion with nonequilibrium surface pyrolysis, using Rayleigh analogy 05 p0837 A71-16539

- Axisymmetric wake diffusion flame response to HF periodic velocity oscillations at combustor boundaries 08 p1375 A71-20863

- Single boundary layer flame sheet model for continuous diffusion chemical lasers, obtaining integrated zero power gain, laser power and efficiency [ALAA PAPER 71-28] 11 p1774 A71-25928

- Coolant combustion effects in transpiration cooling of gas turbine components, using hydrogen, ammonia and nitrogen coolants [ASME PAPER 71-GT-72] 11 p1855 A71-25986

- Combustion dynamics, including fire spread in solid fuels, ignition, turbulent/laminar fields and boundary layer, stagnation point and opposed jet burning 19 p3166 A71-38077

- Ethyl alcohol combustion effect on laminar boundary layer structure near flat plate, assuming thermal cracking of fuel 19 p3169 A71-38113

BOUNDARY LAYER CONTROL

- NT POROUS BOUNDARY LAYER CONTROL
- STOL and boundary layer control aircraft takeoff and landing distance, considering jet suction action influence on lift and drag coefficients 04 p0529 A71-14595

- Phantom and Buccaneer aircraft boundary layer control, examining lift from trailing and leading edges 06 p0847 A71-17953

- Potential flow past cylinder with sources and sinks singularities, deriving formulas for aerodynamic characteristics of infinite span wings with boundary layer control 08 p1227 A71-20777

- Optimization of slot angle, slot positioning and flow quantity affecting boundary layer control in energy transfer over airfoil profiles 09 p1383 A71-23201

- Biological oscillating propulsion systems, investigating plate propeller, boundary layer control, low drag fuselage shapes and VTOL engine installations 10 p1569 A71-24235

- Optimally controlled boundary layer equations reduction to ordinary differential equations 12 p1898 A71-27490

- Separation control of two dimensional air flow with turbulent boundary layer along circular cylindrical wall by jets or suction 13 p2051 A71-29433

- High entrainment constant area multiple nozzle ejectors with two mixing tube lengths for boundary layer control, estimating performance with analytical model [ASME PAPER 71-FE-34] 13 p2053 A71-29469

- Plane laminar incompressible jet flow along parabola with no external stream, using second order boundary layer theory [ASME PAPER 71-APM-MM] 18 p2904 A71-36268

- Submerged vehicle drag reduction and turbulence transition damping by MHD boundary layer control, using Lorentz force and optimum magnetic field 20 p3214 A71-39963

- Strongly curved wall jets development in thick boundary layer upstream of blowing slot, discussing calculation method, correction for shear stresses and comparison with experimental results 24 p3819 A71-44952

BOUNDARY LAYER FLOW

NT BOUNDARY LAYER SEPARATION

NT REATTACHED FLOW

NT SECONDARY FLOW

NT SEPARATED FLOW

- Axial turbomachine rotating blades, calculating three dimensional boundary layer thickness for laminar flow 01 p0069 A71-10337

- Fluid flow turbulent boundary layer development in channel inlet under injection, obtaining friction coefficient and dynamic characteristics at subsonic velocities 01 p0070 A71-10794

- Ambipolar diffusion coefficients application to analysis of laminar multicomponent ionized boundary layer flow in channel 01 p0070 A71-10795

- Atomic and molecular transport coefficients for various species injected into boundary layer on ablating or transpiration cooled surface 01 p0130 A71-10958

- Numerical analysis of complex boundary layer at axisymmetric stagnation point with massive blowing 01 p0071 A71-10964

- Atmospheric boundary layer motion and transports applied to mathematical atmospheric circulation models 01 p0121 A71-11355

- Near separation flow in laminar compressible boundary layer on cold wall near zero skin friction, suggesting added terms for previous expansion 02 p0332 A71-12378

- Frictionless rotationally symmetrical free super-sonic gas jets with thermodynamic relaxation, applying approximate method for shape and flow parameters at boundary 02 p0241 A71-12407

- Two free homogeneous turbulent coaxial air jet mixing, showing mass transfer between boundary layers and interface presence 02 p0185 A71-12409

- Shear flow turbulent friction in boundary layer, deriving Navier-Stokes equation integrodifferential formulation 02 p0241 A71-12411

- Mass transfer and Biot diffusion in MHD flows with mixed boundary reaction kinetics, considering Hartmann and plate problems 02 p0293 A71-12632

- Channel flow boundary layers, discussing parabolic differential equations, pressure gradients, friction coefficients, Stanton numbers, velocity and temperature profiles, etc 02 p0241 A71-12644

- Flat plate film boiling heat transfer under forced boundary layer convection, examining nonstationary wall temperature effects 02 p0333 A71-12646

- Nitrogen plasma flow over flat plate, comparing probe and probeless methods for boundary layer concentration profile measurement 02 p0254 A71-12648

- Boundary layer solution for unsteady compressible incompressible flow past body, discussing momentum conservation equation solution by series expansion 02 p0241 A71-12848

- Flow characteristics in turbomachine blade cascades with transonic regime, emphasizing shock-boundary layer interaction phenomena 03 p0340 A71-13140

- Turbulence level effects on aerodynamic losses of axial flow turbomachines, discussing boundary layer of blades 03 p0340 A71-13143

- Axial turbomachines boundary layer flow, describing two dimensional cascade calculation methods 03 p0340 A71-13146

- Turbulent boundary layer structure and prediction, considering various turbulence onset theories 03 p0340 A71-13147

- Plane laminar flow stability along flexible boundary, obtaining numerical and asymptotic solutions 03 p0399 A71-13198

- Exponential thermal wind spiral equations, discussing planetary boundary layer flow over Antarctic Plateau 03 p0452 A71-13228

- Planetary boundary layer flow three dimensional steady state equations applied to air motions over horizontally varying surface roughness, temperature and moisture 03 p0453 A71-13230

- Buoyancy effect on boundary layer flow over heated horizontal circular cylinder immersed in uniform axial free stream, considering successively greater displacements 03 p0519 A71-13731

- Fluid-loaded rectangular plates and membranes random vibration excitation by turbulent boundary layer flow [ASME PAPER 70-WA/DE-15] 03 p0511 A71-14147

- Boundary layer flow field exposed to oscillating stream, determining third term of Fourier series expansion 03 p0405 A71-14295

- Reflected shock wave interaction with boundary layer and contact surface in shock tube, examining flow uniformity 04 p0568 A71-14703

- Boundary layer equations existence and convergence theorems, using von Mises transformation for conversion into parabolic differential equation boundary value problem 04 p0568 A71-14810

- Soviet book on friction and heat transfer covering interaction of bodies with internal/external liquid/gas laminar/turbulent boundary layer flows 04 p0571 A71-15264

- Two dimensional incompressible laminar boundary layer flow along ablative blunt body in irradiant environment 04 p0679 A71-15467

- Air flow turbulence effect on heat transfer and boundary layer growth around flat plate, aerodynamic profile and cylinder 04 p0681 A71-15483

- Hypersonic laminar cavity heat transfer, including upstream boundary layer thickness, unequal core and wall temperature effects 04 p0528 A71-15491

- Fuel rod bundle boundary layer in longitudinal fluid flow, investigating turbulent temperature and pressure pulsations 04 p0684 A71-15504
- Thermal radiation-conduction interaction in horizontal fluid layer, obtaining temperature profiles with Mach-Zehnder interferometer 04 p0685 A71-15515
- Axisymmetrical, optically thick nonNewtonian, power law boundary layer with injection and suction, obtaining similarity transformations for simultaneous convection and radiation 04 p0685 A71-15516
- Dissociated diatomic gas nonequilibrium boundary layer flow over catalytic flat plate, examining velocity profiles, temperature and concentration 05 p0735 A71-16389
- Incompressible turbulent boundary layer flow over steadily rotating flat plate blade, discussing centrifugal pumping and shear stress 05 p0694 A71-16581
- Air injection into turbulent boundary layer flow through porous plate, examining heat transfer and shielding efficiency 05 p0838 A71-16783
- French book on fluid mechanics, Volume 3, covering nonsteady phenomena, boundary layer and viscous flow 06 p0882 A71-18019
- Laminar incompressible flow heat transfer in inlet between parallel plates at constant temperature, considering pressure gradient effect on boundary layer velocity profile [AIAA PAPER 71-36] 06 p1008 A71-18497
- Interaction theory for supersonic separated and reattaching turbulent boundary layers, comparing to real flow past compression ramp [AIAA PAPER 71-128] 06 p0844 A71-18572
- Two dimensional turbulent boundary layer flows numerical methods with simplicity and accuracy [AIAA PAPER 71-164] 06 p0885 A71-18606
- Finite difference calculation for two dimensional compressible turbulent boundary layer flow with heat transfer, using mixing length concept [AIAA PAPER 71-165] 06 p0885 A71-18607
- Nonadiabatic compressible turbulent boundary layer heat transfer to rough surfaces under arbitrary pressure gradient [AIAA PAPER 71-166] 06 p0885 A71-18608
- Hydromagnetic boundary layer free convection past vertical flat plate, discussing flow rates, temperature profiles and skin friction for high and low Prandtl numbers 07 p1165 A71-18744
- Friction, heat transfer and mass transfer theory of flow represented by two dimensional parabolic boundary layer equations 07 p1085 A71-18766
- Three dimensional axisymmetrical flows in tornado-like vortex boundary layer, determining nonlinear radial and vertical velocity distribution components 07 p1152 A71-19753
- Reacting and nonreacting gases laminar boundary layer flows over two dimensional and axisymmetrical bodies at zero lift, comparing numerical methods 07 p1015 A71-19860
- Elastic-viscous liquid laminar free convection flow along nonuniformly heated vertical flat plate, using momentum integral method for boundary layer velocity and temperature distributions 07 p1091 A71-20031
- Unsteady boundary layers on sphere or cone moving along axis, determining skin friction angular response 07 p1016 A71-20098
- Wind tunnel boundary interference on V/STOL model calculated in test section with solid vertical and slotted horizontal walls, using image method and Fourier transforms [AIAA PAPER 70-575] 08 p1229 A71-22029
- Incompressible laminar boundary layer flow with mass and heat sources, calculating thermal and friction stress distribution 08 p1277 A71-22037
- Boundary layer flow with large mass injection rate, presenting numerical method with rapid convergence for increasing blowing parameter 09 p1430 A71-22108
- Hypersonic strong interaction flow over inclined surface, using asymptotic expansion in powers of hypersonic interaction parameter for boundary layer equations reduction 09 p1382 A71-22109
- Steady boundary layer flow in viscous liquid thin down variable incline for large Reynolds and Froude numbers 09 p1432 A71-22451
- Incompressible viscous fluid nonsteady three dimensional flow, obtaining velocity field and pressure distribution in boundary layer 09 p1433 A71-23092
- Asymptotic far field velocity component in Prandtl boundary layer equations for steady laminar two dimensional flow past rigid body 09 p1486 A71-23578
- In-flight profile drag measurement of gliders with total and static pressure sensors in boundary layer wake, using moments method 09 p1384 A71-23667
- Heterogeneous chemical reaction for visualization of wall streamlines on moving obstacle, discussing boundary layer structure at large Prandtl and Schmidt numbers 10 p1591 A71-23835
- Laminar incompressible boundary layer flow over thin Joukowski, parabolic and slender wedge airfoils, using small perturbation and quasi-similarity theories 10 p1549 A71-23957
- Linear coastal hydrostatic boundary layers of lake with no horizontal motion, discussing flow conditions under wind stress and interior velocity 10 p1600 A71-23961
- Numerical solution of nonuniform enthalpy mixed axisymmetric gas flow in curvilinear regions with upper boundary and discontinuity using build-up method 10 p1551 A71-24376
- Friction drag and energy losses of steady plane incompressible boundary layer flow of viscous liquid on nonconducting wall in MHD channel 10 p1649 A71-24377
- Blowing and suction effects on laminar boundary layer flow of quiet fluid over permeable rotating cone, discussing skin friction and heat transfer 10 p1594 A71-24406
- Laminar incompressible boundary layer flow stability, emphasizing wall curvature and flexibility effects 10 p1594 A71-24548
- Turbulent shear flows, examining zero and negative entrainment in boundary layers 10 p1595 A71-24626
- Universal equations of two dimensional incompressible unsteady laminar boundary layer 10 p1597 A71-25017
- Pulsating incompressible two dimensional laminar boundary layer flow past insulated plate at zero incidence, calculating skin friction and surface temperature 10 p1697 A71-25084
- Convective heat transfer in three dimensional stagnation point boundary layer flow characterized by real gas properties 10 p1698 A71-25098
- Forced convection in atmosphere boundary layer, considering nonlinear unsteady vertical air flow velocity increments over temperature spot on earth surface 11 p1793 A71-25170
- Axisymmetric incompressible boundary layer flow, temperature distribution and heat exchange near critical point of rotating body with varying surface temperature 11 p1854 A71-25239
- Boundary layer equation for free convective diffusion on flat vertical plate in translation motion in viscous incompressible fluid 11 p1854 A71-25240
- Flat plate trailing edge problem solution consistent with second order boundary layer theory, establishing laminar wake evolution nature and upstream influence 11 p1701 A71-25469
- Dust devil vortex model, considering boundary layer velocity profiles and thickness and integrated radial and vertical mass flows 11 p1794 A71-25470
- Compressible laminar boundary layer flow including second order longitudinal surface curvature effects, deriving flow equations from Navier-Stokes equations 11 p1750 A71-25473
- Interaction theory for supersonic separated and reattaching turbulent boundary layers, comparing to real flow past compression ramp [AIAA PAPER 71-128] 11 p1702 A71-25476
- Prandtl first order boundary layer equations for two dimensional laminar incompressible flow past circulation controlled circular lifting rotor 11 p1702 A71-25494
- Three dimensional boundary layer flow and velocity profiles in mixed diffuser with equal angle walls [ASME PAPER 71-GT-40] 11 p1704 A71-25973
- Asymptotic expansions for viscous flow along right angle corner, satisfying layer equations and boundary conditions 11 p1752 A71-26104
- Hele-Shaw flow viscous tails from airfoil, observing high Reynolds number trailing edge flow for separation and initiation of Kutta condition 11 p1705 A71-26447
- Soviet book on MHD flows in channels covering one dimensional theory, viscous fluids, boundary layers, electric fields, laminar flow, etc 12 p1940 A71-27294
- Emmons spot theory extension for boundary layer flow on blunt bodies, deducing spot formation rate dependence on transition Reynolds and Mach numbers 12 p1865 A71-27557
- Equilibrium air boundary layer flows at three dimensional stagnation points, discussing flow characteristics and real gas heat transfer parameters [AIAA PAPER 70-809] 12 p1866 A71-27582
- Boundary layers velocity distribution measurements, using scattered laser radiation Doppler shift 13 p2078 A71-28574
- Compressible laminar boundary layer flow over semiinfinite isothermal porous flat plate in nearly quasi-steady motion, considering skin friction and heat transfer 13 p2048 A71-28600
- Transformed boundary layer equation solution for power law fluid flows of Falkner-Skan type by gamma functions series [ASME PAPER 71-FE-35] 13 p2053 A71-29470
- Numerical solution of coupled boundary layer equations describing strongly cooled turbulent flow of gas between parallel plates with property variation [ASME PAPER 71-FE-38] 13 p2166 A71-29473
- Existence theorem for nonlinear boundary value problems involving two dimensional incompressible boundary layer equations 14 p2264 A71-29523
- Conducting incompressible liquid in transverse magnetic field, considering plane steady motion of isothermal MHD boundary layer 14 p2278 A71-29604
- Group-invariant properties of boundary layer flow differential equation for electrically conducting liquid in magnetic field 14 p2279 A71-29629
- Spectral lines self reversal effects on plasma temperature and density measurement in MHD duct boundary layer 14 p2279 A71-30046
- Boundary layer effect on sound transmission in acoustically treated circular duct with shear flow, reducing governing equations to two-point boundary value problem 14 p2224 A71-30199
- Similarity solution of boundary layer equations for nonuniform external flow 14 p2225 A71-30217
- Shear stress distribution and local heat flux at surface of axisymmetric bodies for laminar and turbulent boundary layer flow 14 p2170 A71-30219
- High velocity boundary layer on flat plate, deriving equations analytical solution by flow variables expansion in powers of inversely squared Mach numbers 14 p2226 A71-30441
- Surface curvature effects in nonsimilar second order boundary layer solutions for subsonic plane flow over cylinder with separation 14 p2170 A71-30442
- Asymptotic behavior of boundary layer equations solution for viscous incompressible flow past curvilinear obstacle 14 p2227 A71-30878
- Gray air flow in turbulent optically thin boundary layer, determining radiant energy transport by Patankar-Spalding finite difference procedure 14 p2236 A71-30932
- Surface renewal and penetration model in heat and momentum transfer analogy for incompressible turbulent boundary layer flow 14 p2227 A71-30935
- Laminar boundary layer of free vortex and source flow, obtaining similarity transform of Navier-Stokes equation 14 p2228 A71-31027
- Compressible laminar plane axisymmetrical boundary layer flows in Laval nozzles, studying temperature, density and velocity distribution relations 15 p2386 A71-31164
- Velocity profile of steady two dimensional incompressible laminar boundary layer flow with suction or injection, noting wall shear function 15 p2388 A71-31441
- Recovery factor for highly accelerated adiabatic compressible laminar boundary layer flow 15 p2391 A71-32114
- Surface liquid film wave motion effect on air supersonic turbulent boundary layer flow field, discussing film thickness, heat transfer rates and wall temperatures [AIAA PAPER 71-623] 15 p2515 A71-32544
- Two dimensional viscous hypersonic flow past thin, needle shaped and highly blunted bodies with strong boundary layer interaction on outer stream 15 p2347 A71-32569
- Air injection into turbulent boundary layer flow through porous plate, examining heat transfer and shielding efficiency 16 p2662 A71-33035
- Wall shear stress, momentum and displacement thickness of shock induced boundary layer interaction in tube and over flat plate, using integral method [ASME PAPER 71-APM-21] 16 p2559 A71-33208
- Laminar boundary layer flow at stagnation point with intensive injection of different absorbing medium, calculating temperature profiles and thermal fluxes 17 p2725 A71-34215
- Boundary effects on gaseous detonation velocity deficit and limit using approximation into boundary layer equations, comparing to experimental data 17 p2837 A71-34437

Viscous incompressible fluid flow downstream of paraboloid of revolution described by matching boundary layer approximations to potential flow solutions 17 p2727 A71-34673

German monograph on pressure changes as boundary layer effect in tube wind tunnels covering test equipment and experimental design, Becker theory, pipe flow, etc 17 p2670 A71-34792

Electron density and temperature distribution in boundary layer flow of reflected shock tunnel conical nozzle 17 p2727 A71-34877

Three dimensional laminar compressible boundary layer flow solution by numerical integration 17 p2728 A71-34894

Supersonic turbulent two dimensional boundary layer flows wall flux and velocity/temperature profiles prediction 17 p2729 A71-35283

Interior region of incompressible turbulent boundary layer with pressure gradient on permeable wall, discussing local similitude hypothesis 17 p2729 A71-35346

One dimensional flow with boundary layer, considering numerical solution of Navier-Stokes equation at large Reynolds number 17 p2729 A71-35466

Intermittency signals correlation, determining lateral motion of two dimensional jet boundaries 18 p2901 A71-35854

Boundary velocity and temperature field of unsteady natural periodic convection over three dimensional obstacle for arbitrary Prandtl numbers 18 p2984 A71-35950

Incompressible turbulent shear boundary layer equations of motion, developing integrodifferential formulation of Navier-Stokes theory 18 p2904 A71-36184

Adversely heated fluid flow layers between rigid boundaries, studying thermal instability due to formation of stationary secondary rolls [ASME PAPER 71-APM-00] 18 p2985 A71-36269

Adverse pressure gradient effects on compressible turbulent boundary layer flow in parallel duct at Mach 4 and high Reynolds number 18 p2904 A71-36297

Laminar boundary layer flow analysis from nonlinear difference equations solution by Newton method, using block-tridiagonal factorization 18 p2905 A71-36313

Laminar boundary layer flow theory for arbitrary curved surfaces, predicting shear stress, thickness and velocity and pressure distributions 18 p2844 A71-36319

Initial flow past circular cylinder in viscous incompressible fluid calculation by numerical integration using boundary layer coordinates 18 p2908 A71-36341

Incompressible two dimensional turbulent hyper-sonic boundary layer flow velocity, pressure, temperature and density distributions 18 p2908 A71-36429

Swirling flow problem in boundary layer theory, proving existence theorem and asymptotic formula for differential equations solution 18 p2910 A71-36815

Rotating disk flow system for Fe vaporizing into cold Ar atmosphere, investigating effect of condensation in boundary layer on mass transfer 19 p3162 A71-37727

Discharge coefficient formula for supersonic nozzles at low throat Reynolds numbers, investigating boundary layer thickness for various nozzle geometries 19 p2993 A71-37896

Laminar boundary layer flows on bodies with suction or injection, solving equations using Goertler series solution for impermeable wall 20 p3210 A71-39027

Sloping flat plate impulsively started constant velocity motion through slightly diffusive viscous density-stratified fluid, investigating transient and oscillatory viscous boundary layer flow 20 p3212 A71-39503

Second order viscoelastic fluid two dimensional stagnation point flow, solving boundary layer equations 20 p3213 A71-39564

Water tunnel study of turbulent boundary layers structure in incompressible fluid with longitudinal pressure gradient at inlet section of converging and diverging nozzles 20 p3213 A71-39789

Semibounded jets in laminar and turbulent flows, discussing boundary layers skin and stream regions, step flow velocities, temperatures and self similar problems 20 p3214 A71-39794

Vortex flow over helicopter rotor square tips, using visualization technique with ammonia vapor boundary layer flow over diazonium salt solution 21 p3318 A71-40169

Galerkin/spectral/ method accuracy for numerical simulation of incompressible boundary flows, testing scalar-convection and Taylor-Green vortex decay problems 21 p3367 A71-40638

Time dependent analysis of swirling flow boundary layers in rotating container using modified Oseen method 21 p3367 A71-40639

Unsteady boundary layer of viscous incompressible rotating fluid flow due to infinite flat plate accelerated motion, calculating velocity and skin friction 21 p3367 A71-40657

Turbulent viscosity, energy dissipation and diffusion parameters of steady plane boundary layer flows of incompressible fluids with transverse shift in closed system of differential equations 21 p3368 A71-40691

Uniform inlet flow inside centrifugal turbomachinery diffusers with flat parallel side walls, measuring pressure distribution and boundary layer velocity profiles 21 p3323 A71-40757

Viscoelastic boundary layer flow solutions, using second order constitutive equation 21 p3370 A71-40989

Surface roughness and mass transfer influence on boundary layer and friction coefficient for turbulent flow over flat plate 21 p3371 A71-40997

Existence and uniqueness of boundary layer equations similarity solution for viscous incompressible fluid flow past paraboloid 22 p3531 A71-42197

Plane MHD boundary layer growth and separation in viscous incompressible flow past cylinder under abrupt motion and transverse magnetic field 22 p3584 A71-42685

Circle, half plane and cylinder theorems for slow viscous flows involving hydrodynamic singularities under rigid boundary 23 p3625 A71-43237

Differential equations system for convective incompressible fluid flow boundary layer temperature profile description, analyzing solution existence and uniqueness 23 p3781 A71-43306

Heat exchange between two fluid streams in concurrent, countercurrent, laminar or turbulent boundary layer flow separated by flat plate, determining temperature distribution 23 p3783 A71-44193

Turbulent stress distribution relationship to averaged characteristics of incompressible fluid boundary layer flow with positive pressure gradient 24 p3818 A71-44748

Incompressible turbulent boundary layer with suction and surface injection computation by implicit finite difference method and turbulent kinetic energy equation for mixing length flow 24 p3820 A71-44954

BOUNDARY LAYER NOISE

U AERODYNAMIC NOISE

U BOUNDARY LAYERS

BOUNDARY LAYER SEPARATION

Rotating stall in axial flow compressor high pressure stages, taking into account boundary layer separation 01 p0003 A71-11063

Boundary layer separation at free streamline attachment to sharp trailing edge of flat plate, deducing terminal velocity profile for two dimensional flow 02 p0185 A71-12376

Solution singularity of laminar boundary layer structure near separation point 02 p0240 A71-12379

Minimum suction rate preventing laminar boundary layer separation from curvilinear porous surface in jet flow 02 p0186 A71-12553

Leading edge bluntness and boundary layer displacement effects on attached and separated laminar boundary layers in high temperature hypersonic flow over compression corner [AIAA PAPER 68-68] 03 p0341 A71-13437

Flow patterns modification through space charges, demonstrating laminarization of turbulent flow and boundary layer separation prevention 04 p0569 A71-14985

Leading edge bluntness and boundary layer displacement effects on attached and separated laminar boundary layers in high temperature hypersonic flow over compression corner [AIAA PAPER 68-68] 05 p0735 A71-16561

Turbulent boundary layer separation at low supersonic Mach numbers based on blowdown wind tunnel tests 05 p0735 A71-16582

Incompressible fluid boundary layer with negative pressure gradient near separation point, discussing stability characteristics and velocity profiles 05 p0736 A71-16847

Supersonic turbulent boundary layer separation on flat plate by forward facing step, measuring mean flow field characteristics [AIAA PAPER 71-127] 06 p0844 A71-18571

Slender cone hypersonic laminar three dimensional boundary layer separation at angle of attack, proposed helical vortex model 06 p0845 A71-18579

Separation patterns over inclined body of revolution from symmetry-plane boundary layer solutions discussing bubble type [AIAA PAPER 71-130] 06 p0845 A71-18579

Heat and mass exchange coefficients and critical separation for turbulent boundary layer during nonequilibrium blowing under nonisothermal conditions 07 p1087 A71-18579

Viscosity effects on three dimensional supercritical flow around circular half cones on flat plate, examining turbulent boundary layer separation 07 p1014 A71-19707

Landau viscous incompressible boundary layer separation formula comparison with Chudov finite difference method 07 p1090 A71-19707

Boundary layer separation in unsteady pipe flows examining velocity profiles under influence of periodic pressure fluctuations 07 p1093 A71-20282

Boundary layer discontinuity on helicopter rotor blade in hovering using flow visualization [AIAA PAPER 69-197] 07 p1017 A71-20304

Compressible boundary layer separation near zero skin friction by Kaplin perturbation technique, studying nonlinear integral equation with Abel kernel 09 p1432 A71-22451

Incident thermal flux parameters and wall temperature effects on flow characteristics in preseparator zone of laminar boundary layer and separation point location 10 p1551 A71-24366

Supersonic boundary layer flow profile distortions due to oblique shock during separation 10 p1552 A71-24598

Optimal blowing wall jet prediction for suppression of separation from high lift aeroflows with incomplete mixing of upstream boundary layer 11 p1704 A71-26199

Newtonian limit of hypersonic flow over elliptical cylinder, finding standoff distance by Freeman result 12 p1863 A71-27051

Boundary layer separation at free streamline attached to body sharp trailing edge, comparing asymptotic solution with numerical analysis of flow on flat plate 12 p1896 A71-27210

Laminar boundary layer equations for rotating plate with surface of arbitrary curvilinear shape, determining external flow pressure gradient leading to separation 12 p1865 A71-27508

Hypersonic cruise vehicles viscous interactions areas, examining compression corners, shock interactions, laminar and turbulent flow, boundary layer separation, etc [AIAA PAPER 70-781] 12 p1865 A71-27552

Two dimensional turbulent boundary layer before rectangular step, investigating heat exchange in separation regions 13 p2048 A71-28577

Laminar boundary layer separation by free stream with large amplitude oscillating velocity, using multiple hot-wire anemometer arrays 13 p2050 A71-29244

Shock wave strength for laminar boundary layer separation at transonic speeds with external flow free stream Mach number near one 14 p2324 A71-29888

Flat plate span effects on ramp induced adiabatic laminar boundary layer separation at supersonic and hypersonic speeds, measuring surface pressure distribution [AIAA PAPER 71-559] 15 p2344 A71-31557

Incompressible laminar boundary layer on parabolic profile at angle of attack, noting singularity in all vanishing shear stress/separation/points [ASME PAPER 71-APM-31] 16 p2520 A71-33198

Two dimensional laminar separation bubbles in high Reynolds number flow fields, using finite difference solutions to Navier-Stokes equations 16 p2561 A71-34162

Negative pressure gradient effect on separation of supersonic flow over notches, comparing theory with wind tunnel determination 17 p2671 A71-34898

Time and space variable magnetic field effects on plane unsteady MHD boundary layer flow separation 17 p2789 A71-35343

Flow distribution behind laminar boundary layer separation point in supersonic flow, calculating plateau region pressure 17 p2672 A71-35629

Unsteady laminar boundary layers flow around three dimensional bodies, using finite difference techniques and power series expansion of time square root [ONERA-TP-941] 18 p2901 A71-36019

Pressure distribution over deflected flap as function of boundary layer separation, flap geometry Reynolds number and Mach number 18 p2972 A71-36433

- Transverse curvature effect on singularity at separation for laminar boundary layer from analogy with flat-plate compressible boundary layer
19 p3044 A71-37726
- Numerical analysis of plane transonic flows past shock free airfoils without boundary layer separation using inverse method of complex characteristics
19 p2994 A71-38307
- French monograph on laminar boundary layer on circular cone at angle of incidence in supersonic stream, calculating separation from parabolic equations by numerical integration
19 p2994 A71-38647
- Heat and mass exchange coefficients and critical separation for turbulent boundary layer with secondary fluid injection under nonisothermal conditions
20 p3210 A71-38897
- Potential flow and laminar boundary layer separation about profiled circular disks, calculating streamlines
20 p3175 A71-39029
- Flap span length effects on boundary layer separation, giving streamwise pressure distributions
21 p3323 A71-40967
- Heat transfer in turbulent boundary layer separation zones ahead of step, using local flow parameters at wall boundary layer limit
24 p3887 A71-44746
- BOUNDARY LAYER STABILITY**
- Plane steady boundary layer stability, describing numerical solution procedures for boundary value problem
01 p0072 A71-11292
- Discrete vortex formation above perforated flat plate in wind tunnel, examining unsteady boundary layer
03 p0345 A71-14568
- Linearized equation for stability and heat transfer of two dimensional incompressible laminar boundary layer in water flow
04 p0679 A71-15469
- Incompressible fluid boundary layer with negative pressure gradient near separation point, discussing stability characteristics and velocity profiles
05 p0736 A71-16847
- Incompressible boundary layers with specific velocity distribution, studying stability on straight and yawing wings
05 p0736 A71-16849
- Three dimensional boundary layer with Pohlhausen velocity distribution, examining stability on yawing wing
05 p0736 A71-16850
- Plane incompressible boundary layer stability in presence of pressure gradient and suction
05 p0736 A71-16851
- Boundary layer nonlinear stability theory, considering hydrodynamic problems associated with laminar flow transition into turbulent flow
07 p1086 A71-18777
- Gortler instability of laminar boundary layer flow on concave wall with finite length effect for perturbation vortices
10 p1592 A71-23958
- High Reynolds numbers asymptotic suction boundary layer linear stability analysis for viscous flow, using transformations to hypergeometric functions
12 p1896 A71-26923
- Laminar boundary layer perturbation by sinusoidal wall roughness, analyzing effect on transition nature and position
12 p1864 A71-27470
- Laminar boundary layer centrifugal Gortler instability over concave wall, depending on velocity profile inflection points
13 p2046 A71-27840
- Neutral stability of laminar free boundary layer in mixing incompressible MHD half jets at low Reynolds number
13 p2103 A71-27842
- Modified brute force technique application boundary layer stability
13 p2050 A71-29203
- Thermal boundary layer instability near heated vertical flat plate in poorly conducting liquid under horizontal DC electric field
14 p2337 A71-30407
- Ekman boundary layer energy stability, determining effective Reynolds number critical value by Euler-Lagrange equations numerical integration
14 p2226 A71-30410
- Perturbed two dimensional laminar boundary layers of incompressible conducting fluid flow along insulated concave wall in transverse magnetic field, investigating three dimensional instability
17 p2788 A71-34642
- Natural convection boundary layer stability on vertical flat plate with uniform heat flux, using numerical computer solutions for large Grashof number range
20 p3314 A71-39501
- Linear stability equations for two dimensional compressible supersonic boundary layer with three dimensional disturbances including thickness growth term
21 p3370 A71-40992
- Vertical laminar natural convection boundary layer stability during thermal expansion at large Prandtl number
24 p3886 A71-44422
- Laminar-turbulent boundary layer transition at Mach number 2-10, observing stabilizing effect of transition Reynolds number at increasing heat transfer intensity
24 p3818 A71-44745
- BOUNDARY LAYER TRANSITION**
- Free convection in turbulent Ekman layer, discussing kinetic energy budget above surface layer
01 p0119 A71-10742
- Temperature sensitive paint and thermocouple techniques comparison for boundary layer transition data, considering aerodynamic heating and transition Reynolds numbers
03 p0518 A71-13468
- Electromagnetic cascade-material boundary crossing transition effect analysis by perturbation theory in terms of differential shower particle flux
03 p0478 A71-13871
- Shock induced exothermic reactions on boundary layer transition in shock tube, investigating free stream thermal energy release effects
04 p0572 A71-15503
- Hypersonic lifting entry vehicle turbulent heat transfer and boundary layer transition at various angles of attack and Reynolds numbers
06 p0844 A71-18555
- Disturbances within hypersonic transitional boundary layer in Mach 7 gun tunnel observed with hot-wire anemometer, comparing results with surface heat transfer measurement
06 p0886 A71-18637
- Pressure gradient and roughness effects on laminar, transition and turbulent boundary layer in hypersonic shock tunnel
08 p1377 A71-22031
- Mixing length theory of near ground Ekman boundary layer in stationary and diurnal conditions, determining surface drag and wind rotation
09 p1487 A71-22638
- Asymptotic stability of rapidly rotating horizontally bounded fluid heated from below, considering conductive state and Ekman layers
10 p1595 A71-24618
- Traveling shock waves interaction with orifice inside ducts, noting anomalous phenomena probably due to unsteady boundary layer growth or time lag
10 p1596 A71-24923
- Laminar boundary layer perturbation by sinusoidal wall roughness, analyzing effect on transition nature and position
12 p1864 A71-27470
- Supersonic boundary layer transition on adiabatic wall, discussing wind tunnel size, surface roughness and freestream disturbances effects
12 p1865 A71-27554
- Flow visualization of free convection laminar-to-turbulent transition along vertical heated plate in water induced by two dimensional forced disturbances
12 p1987 A71-27739
- Land-sea drag, Ekman parametrization and Monin-Obukhov transfer process in surface boundary layer of atmospheric circulation model
13 p2097 A71-28725
- Slender cone boundary layer transition under angle of attack at Mach 21 with promoted leeward and fixed windward ray
14 p2335 A71-29887
- Ekman boundary layer energy stability, determining effective Reynolds number critical value by Euler-Lagrange equations numerical integration
14 p2226 A71-30410
- Turbulent boundary layer transition in shock tube with thickness inhomogeneity regions, using schlieren photographs
16 p2559 A71-33404
- Space shuttle aerothermodynamics, discussing heat transfer measurements, phase change patterns, electron beam flow visualization and boundary layer transition
18 p2847 A71-36430
- Streamwise wall curvature and transition effects in turbulent boundary layers, using modified eddy viscosity and mixing length concepts
19 p3045 A71-37891
- Laminar-turbulent transition zone in boundary layer about bodies moving in gas at high Reynolds number, using statistical physics methods
19 p3046 A71-38481
- Unstable thermal stratification and critical Reynolds number effects on dynamic instability of Ekman boundary layer vortex rolls
20 p3257 A71-39438
- Perturbation velocity of laminar wake downstream of two dimensional body in boundary layer, considering transition behind trip wire
21 p3322 A71-40640
- Laminar boundary layer transition prediction techniques, evaluating empirical formulations and Schlichting-Tollmien stability methods
24 p3817 A71-44581
- Laminar-turbulent boundary layer transition at Mach number 2-10, observing stabilizing effect of transition Reynolds number at increasing heat transfer intensity
24 p3818 A71-44745
- Combustion and chemical reactions near wall, in forced convection, boundary layer transition, radiation and ablation of missile reentry
24 p3890 A71-45148
- BOUNDARY LAYERS**
- NT ATMOSPHERIC BOUNDARY LAYER
- NT COMPRESSIBLE BOUNDARY LAYER
- NT HYPERSONIC BOUNDARY LAYER
- NT LAMINAR BOUNDARY LAYER
- NT SUPERSONIC BOUNDARY LAYERS
- NT THERMAL BOUNDARY LAYER
- NT THREE DIMENSIONAL BOUNDARY LAYER
- NT TURBULENT BOUNDARY LAYER
- Boundary layer thickness measurement behind shock wave front using oscillogram of electrostatic probe current
01 p0078 A71-10160
- Nonsimilarity boundary layer solutions applicable locally and independently of information from other streamwise positions
01 p0070 A71-10928
- Unsteady light field spatial moments in turbid medium boundary layer with intense anisotropic scattering during illumination by narrow beam
02 p0277 A71-12116
- Hydrogen fuel injection into hot oncoming air flow, investigating boundary layer chemical behavior at stagnation point of diffusion flame
02 p0334 A71-12857
- Boundary layer theory extended to cross vorticity transport in outer flow approaching two dimensional stagnation point
03 p0398 A71-13103
- Vorticity amplification in stagnation flow by stretching, discussing effects on average boundary layer profile
03 p0398 A71-13104
- Boundary position and thickness between geomagnetic field and solar wind plasma, simulating interaction with magnetosphere
03 p0473 A71-13107
- Casing /end wall/ boundary layers in multistage axial flow compressors, discussing velocity distributions
03 p0340 A71-13144
- Boundary layer growth effects on two dimensional flow field in low pressure test gas of circular and rectangular shock tubes
04 p0568 A71-14667
- Boundary layer higher order effects on zero-lift drag of short slender bodies, emphasizing shock generated vorticity
04 p0569 A71-15029
- Pressure boundary layer profile numerical solution for transient and steady hydrodynamic gas film under high speed and small trailing edge thickness
04 p0570 A71-15178
- Boundary layer development on slender rod in axial shear flow for different profiles
05 p0694 A71-16711
- Plasma boundary layer temperature distribution near conducting surfaces by measuring current voltage characteristics
05 p0790 A71-16776
- Flat plate wake displacement sources in potential flow, considering high Reynolds numbers outside boundary layer
05 p0695 A71-16960
- Planetary boundary layer forecast model, determining horizontal and vertical wind components, temperature, pressure and moisture with numerical variational objective analysis
05 p0778 A71-17049
- Boundary layer construction near free edge of laminar plates by asymptotic integration of three dimensional equations of elasticity theory
06 p0997 A71-17849
- MHD oscillating flow along infinite unmagnetized conducting plane porous wall, deriving temperature field in boundary layer
06 p0937 A71-18231
- Ionizational and electron thermal nonequilibrium effects in insulator boundary layer of potassium-seeded nitrogen MHD accelerator
06 p0939 A71-18581
- MHD boundary layers with nonequilibrium ionization and recombination at finite rates
06 p0939 A71-18582
- Wall flow boundary layer, observing external turbulent field effect on velocity and temperature distribution and heat exchange
07 p1086 A71-18771
- High velocity liquid flow past rough plate surface, investigating boundary layer cavitation effects on convective heat and mass transfer
07 p1086 A71-18774
- Heat and mass transfer investigation in nucleate boiling boundary layer by salt depositions
07 p1221 A71-18787

Binary fluids boiling heat and mass transfer in boundary layer, discussing bubble growth rate, surface roughness effects and burnout heat flux

07 p1221 A71-18791

Helical circulations in unstable planetary boundary layer measurements, using constant volume balloons and air parcel tracking

07 p1103 A71-19761

Nonequilibrium electron temperature, concentration and reflection in reentry boundary layers, discussing heat transfer and ionization energy diffusion

[AIAA PAPER 69-82] 07 p1015 A71-19879

Fluidic rotational speed sensor, using boundary layers attached to rotating disk surfaces to deflect fluid jets

07 p1031 A71-20604

Plasma configurations kinetic description by differential equations based on Vlasov and Maxwell equations, obtaining boundary layer distribution between plasma and magnetic field

08 p1340 A71-21492

Ground boundary layer effects of fixed ground plane for powered STOL wind tunnel model, discussing flow breakdown criteria, contraction lag, strut fairing interference, etc

[AIAA PAPER 71-266] 08 p1232 A71-21992

Boundary layer model of laminar viscous flow around high speed slender bodies with surface mass transfer

[AIAA PAPER 68-719] 09 p1381 A71-22084

Power density spectrum of longitudinal velocity fluctuations in pretransition pulsed boundary layer

10 p1591 A71-23836

Pulsed subsonic wind tunnel, calculating instantaneous flow velocity with allowance for boundary layer thickness at walls

10 p1549 A71-23855

Singular perturbation problems for linear second order elliptic equation, obtaining asymptotic approximations for simple unbounded regions with free boundary layer terms

10 p1636 A71-23934

Boundary layer equations for radiating and absorbing gas flow at large Reynolds numbers

10 p1593 A71-24367

Approximate solution for limit load carrying capacity of thin walled tube under combined loadings, deriving formulas describing boundary surface

10 p1688 A71-24385

Compressible flow in two dimensional boundary layers in arbitrary pressure gradient, using turbulent energy equation for skin frictions and free stream Mach numbers

10 p1598 A71-25082

Prandtl equations derivation, initial value problem and similarity theory models for steady plane incompressible laminar flow

11 p1749 A71-25302

Turbulent diffusion in stationary thermally stratified atmospheric boundary layer, considering gravitational sedimentation and impurities lifetime

11 p1795 A71-25585

MHD waves incident at density step, calculating reflection, refraction and transmission coefficients and coupling modes

11 p1807 A71-26429

Boundary layer suction optimization to achieve normal velocity component distribution for local Reynolds number equal to critical value at transition point

12 p1896 A71-26973

Horizontal flat plate moving transversely in rotating stratified fluid, calculating boundary layer blocking conditions for entire Rossby and Russell numbers range

12 p1897 A71-27222

Shock heated Ar thermal conductivity measurements by following temperature boundary layer with time resolved interferograms with HF laser stroboscope light source

12 p1986 A71-27578

Momentum thickness of boundary layer of circular cylinder in cross flow at high Reynolds numbers from static pressure and skin friction measurements

12 p1867 A71-27738

Eigenvalue, shooting and parallel shooting methods for solving Falkner-Skan boundary layer equation with positive or negative wall shear

13 p2047 A71-28230

Multicomponent ionized gas mixtures chemically equilibrated flows over nonporous and ablating surfaces, using Navier-Stokes and Prandtl equations for asymptotically thin boundary layer

13 p2048 A71-28570

Data correlation and effectiveness prediction from film cooling injection geometries, considering finitely thick slot lip and boundary layers

13 p2161 A71-28751

Kinetic theory of two dimensional boundary layer between plasma and magnetic field, using computer for vector potential differential equations solution

13 p2109 A71-29214

Boundary layer equations based on eddy viscosity model for turbulent free shear flow, solving numerically in Crocco coordinate plane

[ASME PAPER 71-FE-17] 13 p2052 A71-29456

Heterogeneous fluid flow-chemical processes in interaction in low density plasma flow two phase boundary layer seeding, using physicochemical model

14 p2279 A71-29878

Electrode size effects on voltage loss and boundary layer conductivity of combustion driven MHD generator

14 p2287 A71-29880

Monograph on boundary layer theory covering unsteady heat transfer from rotating disk, thermal free convection in corners, etc

14 p2223 A71-29934

Retreating blade stall experiments on model helicopter rotor, considering series of pressure distribution and boundary layer events

[AHS PREPRINT 521] 14 p2172 A71-31087

Pressure fluctuations in acoustic field of boundary layer under slot suction, considering vortex formation and separation on edges

15 p2389 A71-31713

Viscous boundary layer induced shock decay from analysis of disturbances generated by power law bodies in otherwise uniform two dimensional flow

15 p2392 A71-32115

Plasma boundary layer temperature distribution near conducting surfaces from I-V characteristics of gas gap

16 p2618 A71-33028

Plasma configurations kinetic description by differential equations based on Vlasov and Maxwell equations, obtaining boundary layer distribution between plasma and magnetic field

16 p2618 A71-33043

Layer boundaries and critical concentrations of anomalous increase of radiation in earth and Venus atmospheres along tangential directions

16 p2635 A71-33448

Richardson number relationship to vertical heat diffusion coefficients in boundary layer

16 p2605 A71-34070

Boundary shock waves in electrically conducting gas under magnetic field, deriving Rankine-Hugoniot jump relations analogs and Prandtl relation

16 p2560 A71-34128

Convective flow at stagnation point relation to radiation flux decrease as result of absorption in cold boundary layer

17 p2671 A71-35259

Parabolic boundary layer equations for heat convection problems with unknown wall boundary conditions, noting solution by deterministic and nondeterministic optimization methods

17 p2838 A71-35355

Finite difference method application to three dimensional boundary layer calculation on sphere-segment surfaces in supersonic flow

17 p2672 A71-35632

Double-diaphragm shock tube optimal parameters with allowance for boundary layer effect behind shock wave propagating in central chamber

17 p2730 A71-35634

Detonation wave with dual front structure, calculating attenuation in Chapman-Jouquet regime by boundary shock layer method

17 p2839 A71-35635

Hyperbolic and parabolic system three dimensional boundary layer equations, discussing characteristics and subcharacteristics roles in influence and dependence zones determination

18 p2902 A71-36039

Supersonic jets expansion in variable cross section channel, emphasizing boundary layer behavior

18 p2903 A71-36119

Asymptotic solution of nonlinear Volterra integral equation, examining nonlinear heat conduction and boundary layer heat transfer

18 p2942 A71-36747

Dissolution rate of vertical nickel cylinder in liquid aluminum under free convection, showing fluid boundary layer mass transfer role

19 p3079 A71-37709

Spatial distribution, ion density and space potential measurements in plasma boundary layer at conducting sphere

19 p3112 A71-37738

Unsteady burning rate response of condensed phase fuel plate adjacent to reacting gaseous boundary layer with oscillating external flow

19 p3123 A71-38095

Axisymmetric small Rossby number flow driven by axially distributed heat sources, examining core multiboundary layer structure

20 p3212 A71-39507

Supersonic and hypersonic viscous gas flows with boundary layer induced pressure gradients, investigating disturbance upstream propagation by asymptotic theory

21 p3322 A71-40680

Boundary layer disturbances influence on three dimensional hypersonic flow about infinite triangular

flat plate, investigating pressure effects on heat transfer and friction coefficients

21 p3322 A71-40681

Radiation role in nonequilibrium boundary layer during atmospheric reentries at speeds exceeding escape velocity

21 p3368 A71-40694

Chemical kinetics and fluid mechanics interaction effects in stagnation point boundary layer

21 p3475 A71-40860

Hypersonic flat plate under impulsive loads, calculating time dependent transient wall shear stress and boundary layer induced pressure

21 p3369 A71-40961

Roughness role in liquid He-solid boundary thermal resistance, calculating heat transfer coefficient

21 p3416 A71-41122

Helicopter wake and boundary layer effects on rotor aerodynamic performance in hovering, low and high speed forward flight

[AIAA PAPER 71-581] 22 p3479 A71-41500

Random parietal environment representation by homogeneous distribution of independent sources, using boundary layer model

[ONERA-TP-933] 22 p3576 A71-42500

Transverse current conduction through MHD generator seeded hot plasma flow, showing Joule heating dominance in cathode boundary layer due to thermal instability

22 p3584 A71-42596

Shear flow effects on sound propagation in rigid rectangular ducts, taking into account boundary layer thickness

23 p3704 A71-43212

Boundary layer solution for initial flow around impulsively started sphere in viscous fluid at high Reynolds numbers

23 p3664 A71-44144

Two dimensional incompressible turbulent wall jet in moving stream, describing viscous flow characteristics and various boundary layer parameters

24 p3818 A71-44605

Magnetospheric midday boundary width dependence on geomagnetic dipole axis orientation, discussing different positions for magnetosphere boundary

24 p3824 A71-45319

BOUNDARY LUBRICATION

High speed low power loss spiral groove bearings self sealing grease lubricants with high shear stability and good boundary lubrication

[ASLE PREPRINT 70LC-6] 08 p1322 A71-21157

Mathematical models for boundary lubrication, computing specific liquid lubricant/surface wear rates in machine element design

15 p2414 A71-31950

BOUNDARY VALUE PROBLEMS

NT NEUMANN PROBLEM

Elliptic boundary value methods applied to parabolic initial boundary problems

01 p0111 A71-10320

Neutron linear transport theory boundary value problems, using Green function approach

01 p0111 A71-10333

Electrodynamics boundary value problems numerical solutions, explaining algorithms used

01 p0052 A71-10419

Variational and boundary value problems for functionals depending on functions with deviating argument

01 p0111 A71-10488

Gas dynamic equations of arbitrary materials detonation without allowance for transport phenomena, deriving stability criteria from boundary value problem steady solution

01 p0070 A71-10490

Elastic boundary value problem of viscoelastic cylindrical body with temperature and time variations and relaxation kernel

01 p0169 A71-10492

Boundary value problem of elasticity theory for reinforced plastics with internal stresses due to shrinkage

01 p0107 A71-10495

Boundary value problems in thermoelastic equilibrium of unbounded isotropic plate with slits and foreign circular inclusion

01 p0170 A71-10643

Successive approximations method for boundary value problems in plasticity theory of continuous media under complex loading

01 p0171 A71-10652

Stress concentration and free surface shape at sliding contact for elastic semiinfinite cylinder, discussing mixed boundary value problem

01 p0171 A71-10658

Orthogonal polynomials method for integral equations solution in two dimensional mixed boundary value problems of elasticity theory

01 p0171 A71-10660

Torsion of solid bounded by one sheet of hyperboloid of two sheets of revolution under mixed boundary conditions, using Legendre transform

01 p0173 A71-10643

Transient heat conduction of solids obeying Fourier law, deriving numerical solution for boundary value problem by Laplace transformation

01 p0180 A71-10937

Axisymmetric mixed boundary value problem of thermoelasticity for hot stamp penetration into transversely isotropic half space, deriving contact stresses

01 p0175 A71-11036

Thin nonlinear elastic bar small longitudinal oscillations, solving boundary value problem for disturbances propagation

01 p0176 A71-11050

Linear stability of finite difference approximations to no-slip boundary conditions in nonsteady fluid flow

01 p0071 A71-11161

Downstream boundary condition on stream function, discussing sufficiency conditions in finite difference methods

01 p0071 A71-11162

Plane steady boundary layer stability, describing numerical solution procedures for boundary value problem

01 p0072 A71-11292

Multiple scattering boundary value problem for two parallel circular cylinders

01 p0041 A71-11613

Coupled Riemann-Hilbert boundary value problems for thermoelastic state near thermally insulated crack in inhomogeneous elastic medium

02 p0322 A71-11734

Closed cylindrical shell response to random sound in contained fluid, investigating cylinder end acoustic boundary conditions with coupled oscillator theory

02 p0239 A71-11998

Boundary value problems solution in elasticity theory of isotropic homogeneous body configurations close to ellipsoid of revolution, obtaining stress-strain state by approximate method

02 p0325 A71-12285

Two dimensional mixed boundary value problems solution in elasticity theory by linear differential operators, applying to Dirichlet and Neumann problems

02 p0326 A71-12293

Boundary value problem for linear Boltzmann equation in kinetic theory, proving existence and uniqueness theorems

[ONERA-TP-820] 02 p0276 A71-12338

German monograph on polygonal thin plates calculation by differential equations method for two dimensional boundary value problems solution

02 p0327 A71-12399

Elastic body problems, determining eigenfunctions homogeneous geometrical and static boundary conditions

02 p0328 A71-12405

Initial Dirichlet boundary value problem parabolic and elliptic equations of order 2b, discussing existence and uniqueness proofs

02 p0276 A71-12532

Zero bending moment shells of revolution under concentrated load, using boundary value problem for p analytic functions

02 p0328 A71-12539

Perforated thick shallow spherical shell, solving boundary value problem for external loads

02 p0329 A71-12671

Successive approximation procedure for discrete time nonlinear systems data smoothing, developing Newton method algorithm for two point boundary value problem

02 p0277 A71-12726

Unstable linear initial value problem numerical solution, using Riccati equations of invariant imbedding

02 p0277 A71-12727

Initial value problems differential equations discontinuities, describing step-size adjustment for fourth order Runge-Kutta methods

02 p0277 A71-12728

Total impedance plethysmography boundary value problems, developing computer program based on Jacobi iterative method

03 p0367 A71-12993

Partial differential equation approximate solution by matrix transformation, reducing boundary or mixed problem to n independent linear ordinary differential equations

03 p0449 A71-13117

Minimization of unconstrained function of several variables by gradient dependent techniques, discussing applications to boundary value problems in optimal control

[AJAA PAPER 69-951] 03 p0450 A71-13444

Initial value method for Fredholm integral equations with displacement kernels on infinite interval, using invariant imbedding

03 p0450 A71-13622

Two-point boundary value problems for linear differential equation systems, describing adjoints and complementary functions methods

03 p0451 A71-13624

Boundary value problems transformation into initial value problems, obviating homogeneity in boundary conditions

03 p0451 A71-13715

Shells and plate disk structures elastoplasticity analysis problems, considering limit loads, large deflections, boundary state theory, optical design, etc

03 p0510 A71-13944

Elastoplastic stress analysis for samples with notches and holes under tension, discussing boundary condition calculation by finite element method

03 p0510 A71-13949

Boundary value problem for pluriparabolic differential equations

03 p0451 A71-13965

Pressurized toroid modified linear membrane theory, presenting approximate solutions for derived boundary value problem by variational calculus methods

[ASME PAPER 70-WA/APM-49]

03 p0512 A71-14168

Shallow shell theory boundary value problems, calculating stress concentration for domes and shells with holes

03 p0513 A71-14230

Axisymmetric mixed boundary problem for elastic infinite cone, obtaining solution by assuming zero shearing stresses

03 p0513 A71-14234

Three dimensional mixed boundary value problems, obtaining solutions for elastic body differential equilibrium equations

03 p0513 A71-14235

Nonlinear control systems optimization methods formulation according to deterministic and random disturbances and initial conditions

03 p0391 A71-14402

Boundary value problems solution by partial absorption method for elastic oscillations in inhomogeneous media, discussing Hilbert space methods

04 p0665 A71-14809

Monograph on bounds for vibration frequencies and buckling loads of clamped uniform thin elastic plates covering stability, harmonic and biharmonic functions

04 p0667 A71-14899

Free boundary value problems in elasticity, applying plane linear theory to electroelasticity

04 p0667 A71-15175

MHD generalized Couette flow by splitting linear time dependent flow into simultaneous solution of boundary and initial value problems

04 p0571 A71-15201

Soviet monograph on singular integral equations and boundary value problems involving Cauchy kernels

04 p0619 A71-15400

Steady heat conduction with generation, discussing boundary value problem transformation by change of variables

04 p0677 A71-15453

MHD channel flow with axial conduction and third kind boundary condition, investigating thermal entry region heat transfer

04 p0684 A71-15506

Radiative/convective heat transfer in moving media, reducing boundary problem to integral equations

04 p0685 A71-15514

Quasi-linear elliptic boundary point solutions, deriving modulus of continuity estimates

04 p0619 A71-15552

Numerical weather forecasting model using time dependent boundary values for restricting to acceptable error limits

04 p0622 A71-15676

Initial value or boundary value problems in mathematical physics, solving by process of condition elimination

05 p0780 A71-16178

Isotropic circular plate natural vibrations for inhomogeneous boundary conditions, using net point method to derive finite difference equations

05 p0821 A71-16353

Elliptical boundary value problems with conditions not in direction normal to boundary, deriving theorems on homomorphisms and Green formula

05 p0774 A71-16418

Variational principle for generalized theory of heat conduction with finite wave speed, reducing nonlinear boundary value problem to ordinary differential equation

05 p0837 A71-16567

Internal combustion engine exhaust system sound radiation, discussing pressure wave effects, energy flux and boundary conditions

05 p0796 A71-16604

Finite difference and initial value solutions of nonlinear boundary problems for ordinary differential equations, generating algorithms by quasi-linearization method

05 p0775 A71-16646

Unsteady heat conductivity problems with nonlinear boundary conditions, using perturbation method

05 p0838 A71-16782

Diffraction on strip, investigating for Dirichlet boundary conditions, deriving excited current density and scattered pattern

05 p0722 A71-16869

Differential equations system continuability theorem for specific initial conditions

05 p0775 A71-16885

Two-point boundary value problems approximation for differential equation systems with discontinuity in right-side derivatives

05 p0775 A71-16886

Boundary value problem for second order elliptic equation with discontinuous coefficients, discussing solvability conditions and boundary characteristics

05 p0775 A71-16887

Thin shallow shell theory boundary value problem, discussing reduction to Fredholm integral equations system

05 p0828 A71-16893

Cantilever plates calculation, satisfying boundary conditions by coordinate sequence construction

05 p0828 A71-16894

Initial conditions selection for optimal control of systems with time lag

05 p0782 A71-16982

Structural stability of incompressible elastic rod of variable rigidity flattened along axis, reducing boundary value problem to equation with continuous operator

05 p0828 A71-16987

Complex configuration solid bodies boundary value problems numerical solution algorithm using R functions

05 p0775 A71-17013

Mathematical physics multidimensional boundary value problems seminumerical solution, using differential-difference method and integral transformations

05 p0783 A71-17014

Linear boundary value problem for first order partial differential equations of composite type with two real characteristics, deriving index formula

05 p0775 A71-17015

One dimensional Markovian process residence probability in region with variable boundaries

05 p0732 A71-17021

Hyperbolic heat conduction equation with small relaxation time parameter, studying convergence for Cauchy and boundary value problem

05 p0839 A71-17035

Circular disks or cylinders with temperature boundary conditions, discussing iterative solution and computer program for transient thermoelastic stresses

05 p0829 A71-17117

Fibrous composite materials stress and deformation analysis, using point matching numerical method and boundary point least squares method

05 p0829 A71-17119

Variational principles for linear initial value problems with sources on and within boundaries, using time convolutions

05 p0776 A71-17218

Symmetrical elastic bending of anisotropic annular circular plates of variable thickness, solving for line and uniform pressure loads with different boundary conditions

05 p0830 A71-17224

Mixed boundary value problem in elasticity theory for piecewise homogeneous isotropic plate with slits, reducing to integral equations

06 p0983 A71-17361

Partial differential equations mixed boundary value problems with unsteadiness over part of boundary reduced to Cauchy problem

06 p0916 A71-17385

Boundary value problems for singular elliptic partial differential operators, with application to region bounded by smooth manifold

06 p0916 A71-17386

Plasma feedback system boundary conditions, describing electrical properties, dispersion relation and mode interaction

06 p0931 A71-17455

Nonlinear boundary value problems numerical solutions using spline and Hermitian functions in Ritz-Galerkin setting

06 p0917 A71-17565

Initial value problems involving linear ordinary differential equations, deriving theorems for Runge-Kutta and Adams methods effectiveness

06 p0917 A71-17566

Boundary conditions of line of symmetry and antisymmetry types for stress-strain state of halved shells

06 p0984 A71-17666

Second order dynamic relay system with unstable linear part, investigating constant disturbance effects with point mapping and bifurcation theory

06 p0927 A71-17672

Log periodic dipole antennas Maxwell equations solution in cylindrical coordinates for all boundary conditions

06 p0874 A71-17706

Nonstationary temperature fields and thermal stresses in plates and shells for discontinuous boundary conditions

06 p0991 A71-17799

Critical parameters and vibration frequencies of homogeneous closed circular rings connected to thin shells determined for various boundary conditions

06 p0996 A71-17844

Complex form plates bending and oscillations under various boundary conditions, discussing procedure for coordinate sequences construction

06 p0997 A71-17853

Polyvibrating equation boundary value problem solution in Fourier series form, obtaining Green function

06 p0928 A71-18226

Recursively defined infinite system convergence solutions for initial and boundary value inequalities, applying to differential game stability problems

06 p0920 A71-18237

Main mixed axisymmetric stress for elastic half space with single line separation between boundary conditions, using p-analytic functions

06 p1001 A71-18341

Rectangular plate bending with mixed boundary conditions, using paired trigonometric series

06 p1005 A71-18708

Turbulent boundary layer asymptotic theory, taking into account boundary conditions effect on friction and transfer factor laws

07 p1085 A71-18761

Integral equation solution for air flow over mountain shape, considering boundary value problems of Helmholtz equation

07 p1149 A71-18794

Boundary condition iteration methods in chemical process plant optimal design and control, considering simplicity and ease of programming, computation time and storage requirements

07 p1054 A71-18800

Numerical solution of nonsell adjoint boundary value problems of electrodynamics using finite difference scheme and iterative processes

07 p1159 A71-19179

Difference scheme for solution of static boundary value problem differential equations of elasticity theory

07 p1211 A71-19181

Forced thickness-stretch vibrations of plated elastic plate, involving time derivatives in boundary conditions

07 p1212 A71-19589

Thin shallow elastic shells boundary value problem, deriving existence and multiplicity of equilibrium state critical points for bending and buckling

07 p1213 A71-19639

Elasticity theory equations for homogeneous boundary value problem, deriving solution existence conditions by Fourier method validity demonstration

07 p1213 A71-19799

Conductive heat transfer with nonlinear boundary condition, reducing to linear boundary value problem through variational principle

07 p1224 A71-19902

Three-part mixed boundary problem concerning equilibrium of semiinfinite two dimensional elastic medium containing Griffith cracks parallel to free boundary

07 p1214 A71-20021

Boundary value problems and applications in fluid and gas mechanics - Conference, Kazan, U.S.S.R., May 1969

07 p1091 A71-20076

Boundary value problems of analytic functions and singular integral equations, considering hydromechanics and elasticity theory applications

07 p1148 A71-20077

Inverse boundary value problems in hydroaeromechanics, involving profile construction from given velocity or pressure distribution and supersonic flow boundaries determination

07 p1091 A71-20078

Riemann surfaces use in plane boundary value problems and singular integral equations, considering plane elasticity and filtration theories

07 p1148 A71-20079

Stress distribution boundary value problem for long isotropic elastic cylinder with strip cracks due to internal pressure

07 p1215 A71-20100

Bonded rod of two semiinfinite elastic bars subjected to end impulse, formulating motion equations and initial and boundary conditions

07 p1217 A71-20367

Fokker-Planck boundary value solutions to transient phase error response of nonlinear phase locked tracking systems

07 p1082 A71-20428

Boundary value problem solution of nonlinear differential equation system with delayed arguments

07 p1149 A71-20644

Solid mechanics boundary value problems solution by cylindrical functions addition theorem in polar and curvilinear orthogonal coordinates

07 p1162 A71-20648

Arbitrarily shaped waveguide analysis computer program EHPOL for polynomial approximation to eigenfunctions of Helmholtz equation, considering homogeneous Neumann and Dirichlet boundary conditions

08 p1261 A71-20752

Point matching techniques, discussing effects of metal boundary on divergence of series and error from numerical examples of rectangular waveguide and scattering

08 p1252 A71-20755

Flat rectangular plate under plane stress, solving boundary condition problems with displacements and stresses from two neighboring edges

08 p1369 A71-20846

Komkov class of boundary value problems and associated variational principles, discussing necessary conditions for basic functional or potential extremal behavior

08 p1323 A71-20878

Free boundary problems for heat equation involving interface coinciding initially with fixed face, proving existence, uniqueness and continuous dependence theorems

08 p1324 A71-20879

Steady state thermoelastic mixed boundary value problem for elastic layer, obtaining temperature, stresses and displacements in finite integrals through Hankel transforms

08 p1370 A71-21238

Laser resonator mode representation with oblate spheroidal vector wave function through boundary value problem formulation

08 p1301 A71-21293

Bessel transform and corresponding inversion formula, showing relationship to Fourier, Watson and Kontorovich-Lebedev transforms for boundary value problems solution

08 p1324 A71-21355

Boundary problem for displacement equilibrium equations of elastic body using iterative methods, demonstrating convergence of difference equation solution

08 p1372 A71-21706

Boundary value problem of end effect in MHD channel with semiinfinite electrodes for arbitrary Reynolds numbers

09 p1499 A71-22130

Boundary value problems in noncylindrical domains investigated by Green matrix

09 p1484 A71-22176

Boundary value problems solution, using Runge-Kutta method with computer for eigenfunctions of ordinary differential equations

09 p1484 A71-22177

Nonshallow spherical shells of small shear modulus materials, examining boundary conditions and axisymmetric deformation

09 p1535 A71-22184

Variational and boundary value problems in regular regions containing manifolds with dimensionabilities lower than n minus one

09 p1485 A71-22289

Mixed boundary value problem solution for ring in class of functions with given singularities, using Keldysh-Sedov formulas

09 p1485 A71-22525

Anisotropic medium theory of elasticity boundary value problem, considering plane with two closed Liapunov curves without common point

09 p1485 A71-22637

Boundary condition effects on thermomagnetic torque from moment method solution for Boltzmann equation for diatomic molecular gas in magnetic field and cylindrical geometry

09 p1502 A71-22853

Contact heat conduction boundary value problems, applying parabolic potentials method to Volterra singular integral equation systems

09 p1545 A71-22876

Imperfect thin walled circular cylindrical shells under axial compression with relaxed boundary conditions, determining deformations with differential equations

09 p1541 A71-23089

Soviet papers on differential equations and application covering control and system stability, elastic theory, boundary value problems, etc

09 p1495 A71-23428

Steady electromagnetic oscillation amplitude calculation from solution kernel to Maxwell equations boundary value problems through orthogonal coordinate transformation to Fredholm integral equations

09 p1495 A71-23431

Heat conduction differential equation boundary value problem, obtaining closed solution to Cauchy problem in integral form with finite limits by reflection method

09 p1547 A71-23435

Second order dynamic relay system with unstable linear part, investigating constant disturbance effects with point mapping and bifurcation theory

09 p1424 A71-23458

Higher dimensional wave equation boundary value control, investigating hyperbolic problems in several space dimensions with application of Holmgren and John uniqueness theorems

09 p1424 A71-23467

Synthesis of primary electromagnetic fields of transmitting feed antenna for two dimensional circular cylindrical reflector

09 p1418 A71-23492

Kinetic theory of electromagnetic waves obliquely incident upon plasma slab considered as boundary value problem

09 p1409 A71-23499

Fourth order boundary problems with discontinuous boundary conditions, considering circular plate transverse vibrations

09 p1543 A71-23614

Dynamic behavior of circular and rectangular membrane panels with time and space dependent boundary conditions for aerospace structures

09 p1544 A71-23736

Perfectly plastic and viscoplastic materials relation between permanent deflection and response time in boundary value problems

10 p1684 A71-23931

Spherical and paraboloid shells of revolution internal and external forces correlation, considering boundary value problem differential solution

10 p1686 A71-23996

Nonlinear second order differential system two point boundary problems, establishing eigenvalues and associated solutions boundedness and oscillations

10 p1636 A71-24130

Approximate trigonometric solution to thermoelastic boundary value problem of plane with doubly periodic system of holes, deriving unsteady temperature and thermosress fields

10 p1687 A71-24195

Body profile low frequency oscillations in transonic gas flow, investigating nonlinear differential equation boundary value problem by approximation method

10 p1550 A71-24363

Variational principles for initial boundary value problem of fully coupled linear thermoelasticity for inhomogeneous anisotropic materials with microstructure

10 p1689 A71-24512

Boundary value problem concerning stability and oscillations of shells of revolution through reduction to Cauchy problem based on direct integration of equilibrium equations

10 p1690 A71-24569

Fourth order partial differential equations boundary value problems solution by Monte Carlo techniques

10 p1637 A71-24601

Temperature distribution in composite media sections involving solid interfacial sources, using Vodicica orthogonality equations

10 p1697 A71-24694

Reissner variational theorem for boundary values in linear anisotropic and nonhomogeneous elasticity

10 p1691 A71-24809

Optimum one term series solution for multidimensional heat conduction problem with initial profiles

10 p1698 A71-25086

Detonation wave of gas in circular cylinder with nonsimultaneous axisymmetric initiation at plane boundary, obtaining solution for small perturbation flow behind detonation front

11 p1853 A71-25152

In-plane boundary conditions influence on clamped conical shells buckling under external pressure, using displacement method based on Donnell stability equations

11 p1841 A71-25158

Prandtl equations derivation, initial value problem and similarity theory models for steady plane incompressible laminar flow

11 p1749 A71-25302

Elastic boundary conditions effect on natural frequencies and resonant displacement of thin isotropic circular cylindrical shell under concentrated load with harmonic time history

[AIAA PAPER 71-335]

11 p1843 A71-25314

Numerical solution procedures evaluation for geometrically nonlinear structural analysis by direct stiffness method, noting capability of self correcting initial value formulation

[AIAA PAPER 71-356]

11 p1844 A71-25335

Existence theorems in micropolar elastostatics three dimensional boundary value problems relating to isotropic and homogeneous bodies equilibrium

11 p1847 A71-25442

Axisymmetric deformation differential equations system for nonlinearly elastic shells under vertical loadings, considering various Euler buckling boundary problems

11 p1848 A71-25567

Solid circular Ti shaft torsion boundary value problem solution, using elastic-viscoplastic materials thermodynamics and constitutive relations

11 p1849 A71-25801

Mixed boundary value problem for fiber reinforced materials, analyzing shear response in multiply admissible kinematic deformations

11 p1850 A71-26105

Elliptical equation boundary value problems solution, using finite difference representation

11 p1792 A71-26156

Criticism of paper on synchrotron sources energy spectra formation, examining time dependent spectrum on boundary conditions

11 p1832 A71-26170

Stress-strain states of physically nonlinear anisotropic media, showing boundary value problem equivalent to variational problem

11 p1850 A71-26179

Boundary value problems of steady state thermoelasticity and axisymmetric Boussinesq stress concentration for half space in linear Cosserat elasticity

12 p1974 A71-26942

Error estimate for solution of approximately linear elastic boundary value problems of shells with no strain energy functional, discussing stress-strain relations

12 p1974 A71-26943

Stationary points of functional corresponding to boundary value problem with free boundary

12 p1930 A71-27167

Oscillation theorem for natural vibrations of thin shells of revolution, considering boundary value problem eigenvalues

12 p1977 A71-27304

Elastic body displacement equilibrium equations, using variable direction iteration methods for boundary value problems

12 p1978 A71-27329

Thin delta wing in hypersonic inviscid flow at small angles of attack, calculating motion equations and boundary conditions at small perturbations

12 p1863 A71-27330

Boundary value problems solution convergence, using point integrators in synchronous dynamic mode

12 p1884 A71-27335

Two dimensional periodic and doubly periodic boundary value problems solution in theory for stable oscillations of elastic and viscoelastic bodies perforated by circular holes

12 p1980 A71-27447

Nonlinear heat conduction problems, obtaining boundary conditions with approximate method

12 p1987 A71-27664

Thin walled elastic isotropic shallow shell with thermal boundary conditions, obtaining thermoelastic solution in series form

12 p1984 A71-27687

Error estimates for class of least squares methods for 2mth order elliptic boundary value problems solution approximation

13 p2093 A71-27803

Adjoint Green operator use in parabolic problems with normal boundary conditions

13 p2094 A71-27804

Nonlinear elasticity displacement equations, presenting three dimensional boundary value problem formulation and solution by small parameter method

13 p2150 A71-28130

Forced axisymmetric vibrations of composite cylindrical shell with spherical bottom, obtaining influence coefficients and inhomogeneous boundary conditions

13 p2150 A71-28141

Strip array excitation by field with large phase shift per period, deriving approximate solution from averaged boundary conditions

13 p2029 A71-28361

Homogeneous anisotropic body elasticity theory, calculating boundary value problem for arbitrary conditions

13 p2153 A71-28422

HF diffraction of plane electromagnetic waves by ideally conducting iris diaphragm, developing boundary value problem asymptotic solution

13 p2029 A71-28448

Stratified fluid flow over barrier, obtaining stationary solution for initial value problem

13 p2047 A71-28481

Existence and uniqueness of solution to Dirichlet boundary value problem of invariant in nonclassical theory of elasticity concerning behavior of media with memory

13 p2154 A71-28651

Viscoelastic and elastic shells boundary value problems relation, studying natural and forced oscillations of isotropic viscoelastic shells

13 p2155 A71-28656

Electromagnetic wave reflection from interface between moving and stationary electron plasma, giving boundary conditions at velocity discontinuity surface

13 p2108 A71-28855

Cylindrical shells of revolution with various boundary conditions, calculating free vibrations with differential equations

13 p2156 A71-29067

Boundary value problems solution for composite cylinder consisting of three different layers with nonideal thermal contacts

13 p2165 A71-29086

Boundary conditions formulation for energy and mass transfer in weakly rarefied gas flows past bodies

13 p1991 A71-29149

Acoustic refraction by two dimensional shear layer in duct, considering sound propagation and initial value problem solution

13 p2051 A71-29248

Differential equations analytic theory - Conference, Kalamazoo, April-May 1970

13 p2096 A71-29422

Existence theorem for nonlinear boundary value problems involving two dimensional incompressible boundary layer equations

14 p2264 A71-29523

Rectangular cross section MHD channel spatial electrical field distribution, obtaining electrostatic potential, boundary conditions and efficiency

14 p2278 A71-29612

Horizontal conducting fluid cylinder ultrasonic oscillations in crossed electric and magnetic fields, obtaining boundary value problem

14 p2278 A71-29614

Electromagnetic flowmeters readings for boundary effects of current equalization

14 p2279 A71-29616

Dispersion and boundary equation concerning space-charge wave propagation under diffusion effect in Gunn semiconductors with anisotropic conductivity and finite thickness

14 p2283 A71-29793

Arbitrary periodic composite structure system with local interactions, obtaining macroscopic properties from unit cell boundary value problems

14 p2323 A71-29812

Hyperelastic continuous bodies with periodic structure, developing macroscopic model based on boundary value problem for unit cell

14 p2323 A71-29813

Couette flow two point boundary value problem solution using Navier-Stokes and Barnett viscous gas equations

14 p2224 A71-30185

Thin walled cylindrical elastic shell with rectangular holes at equal intervals along straight line, deriving boundary conditions expression by R-functions

14 p2326 A71-30190

Boundary layer effect on sound transmission in acoustically treated circular duct with shear flow, reducing governing equations to two-point boundary value problem

14 p2224 A71-30199

Incompressible plastic shells behavior, discussing deformation, energy dissipation rate, equilibrium equations and boundary conditions

14 p2328 A71-30380

Nonlinear vibration of changing boundaries structures, approximating boundary values by perturbation technique

14 p2331 A71-30699

Dirichlet, neumann and mixed boundary value problems relative to wave equation for rectangle, discussing solution based on singularity theorem

14 p2266 A71-30810

Stress concentration and free surface shape at sliding contact for elastic semiinfinite cylinder, discussing mixed boundary value problem

14 p2333 A71-30992

Orthogonal polynomials method for integral equations solution in two dimensional mixed boundary value problems of elasticity theory

14 p2333 A71-30994

Two dimensional hypersonic boundary layer equations solution upper and lower bounds determination as initial value problem

15 p2386 A71-31161

Finite difference and finite element methods for approximating elliptic boundary value problems solutions

15 p2440 A71-31346

Integral equation methods application to exterior boundary value problems solution for Laplace and Helmholtz equations

15 p2441 A71-31350

Sufficient stability of difference approximations for initial boundary value problems

15 p2441 A71-31354

Harmonic mixed boundary value problem exact solution for rectangle with slit, outlining finite difference techniques convergence

15 p2441 A71-31356

Finite difference methods application to numerical weather prediction problems, describing frontal depression growth and boundary conditions for short gravity wave suppression

15 p2443 A71-31357

Variational principles application to continuum mechanics boundary and initial value problems, discussing examples in elastostatics, piezoelectricity and hydroelasticity

15 p2441 A71-31416

Monograph on elliptic differential equations numerical solution covering approximations, relaxation, iterative, integral equation and variational methods, and applications to boundary value problems

15 p2441 A71-31508

Initial value problem in quasi-static thermoelasticity, using heat equation and Somigliana tensor

15 p2504 A71-31698

Collocation method application to linear boundary value problems for system of differential equations

15 p2442 A71-31831

Existence and uniqueness theorem for n-point boundary value problems of nonlinear ordinary differential equations, using Polya condition

15 p2442 A71-31871

Boundary conditions of elastic deformations of constrained circular cylinders under axial load, discussing modulus dependence on Poisson ratio

15 p2505 A71-32007

Soviet book on plane elasticity theory boundary value problems solution on digital and analog computers

15 p2508 A71-32276

Linear two-point boundary value problem solution through integral transformation into Cauchy system with Green function as auxiliary dependent variable

15 p2443 A71-32441

Book on hodograph equations covering plane transonic flow, Tricomi boundary value problems, weak shocks and pressure density relations

15 p2394 A71-32766

Rods stability under nonconservative loads, applying Liapunov functions to boundary value problems

16 p2607 A71-32977

Hilbert space valued systems and elliptic boundary value problems stability, employing circle criterion

16 p2549 A71-32978

Hydrodynamic stability, determining velocity field bounds in laminar boundary layer by Nagumo-Westphal theory of parabolic differential operators [DFVLR-SONDDR-131]

16 p2557 A71-32982

Perturbation method for solving nonstationary heat conduction problems with nonlinear boundary conditions

16 p2662 A71-33034

Fluid mechanics problem of nonuniform meshes and complex boundary conditions, using finite element method

16 p2559 A71-33097

Linear elastic body stress field singularities, investigating local geometry and boundary condition effects

16 p2654 A71-33175

Cosmic ray nuclei propagation through interstellar medium, solving transfer equation for simple model with allowance for boundary conditions

16 p2625 A71-33325

Geodetic boundary value problem reformulation, using measured gravity values on known earth surface and potential theory

16 p2563 A71-33476

Isotropic elastic body steady vibrations with moment stresses, solving two dimensional boundary value problem

16 p2658 A71-33716

Ionospheric motion boundary value problem, deriving uniqueness of solution

16 p2564 A71-33718

Linear heat transfer boundary value problem series solution in Cartesian and cylindrical coordinate systems

16 p2663 A71-33904

Magnetohydrodynamic model system numerical integration as initial value problem, using finite difference scheme or differential equation conversion method

16 p2620 A71-34081

Mixed boundary value problem of hereditary elasticity theory, discussing existence and uniqueness of solution

17 p2818 A71-34425

Current distribution on grid type dipole antenna in warm isotropic plasma, using direct source approach and boundary value analysis

17 p2698 A71-34430

Book on linear and ordinary celestial mechanics covering perturbed two body motion, numerical methods, canonical theory and initial value problems

17 p2799 A71-34471

Viscous incompressible flow along right angle corner, using algebraic nature of asymptotic flow field for numerical analysis boundary conditions

17 p2726 A71-34504

Displacement field of constant thickness elastic disk with stress boundary conditions, using finite difference technique

17 p2818 A71-34505

Invariant imbedding for two point boundary value problems for difference equations, noting conversion to initial value problem

17 p2764 A71-34519

Metal strips with holes under tensile loads, determining plastic region boundaries with photostress method

17 p2821 A71-34592

Direct variational methods for solving parabolic boundary value problems of arbitrary order in space variables, considering Dirichlet problem solution

17 p2764 A71-34640

Electromagnetic wave propagation into time varying medium, considering boundary value transmission problems

17 p2701 A71-34760

Axisymmetrical elasticity theory for vertical finite length cylinder with mixed boundary conditions on top and bottom end surfaces, obtaining stress and displacement expressions

17 p2822 A71-34779

Isotropic compressible homogeneous body with small deformations superposed on finite elastic deformation, deriving equations of motion and boundary conditions

17 p2823 A71-34788

Boundary value problems solution for second order finite difference equations, applying second order orthonormal polynomials and related functions

17 p2764 A71-34843

Rectangular flexible plate displacement theory, solving boundary value problems with fractional step method

17 p2824 A71-34848

Boundary value problem for Laplace equations, noting conditions for convergence of solutions sequence

17 p2765 A71-34867

Elastic bar boundary conditions, noting bending stiffness

17 p2825 A71-34886

Stress hybrid finite element model for boundary conditions in solid continua with nodal values as final set of matrix equations

17 p2825 A71-34893

Asymptotic formulas for two point boundary value problem of differential equations system, using averaging method

17 p2765 A71-34905

Functional analysis of nonlinear nonautonomous and autonomous periodic oscillations by treating equations and periodicity conditions for initial displacements and velocities as generalized operator equation

17 p2782 A71-34936

Difference analog of nonlinear hydrodynamic boundary value problem from Navier-Stokes steady state theory

17 p2728 A71-35241

Axisymmetric dynamic deformation of elastic solid, obtaining characteristic properties and solutions of mixed initial and boundary value problems

17 p2831 A71-35353

Parabolic boundary layer equations for heat convection problems with unknown wall boundary conditions, noting solution by deterministic and nondeterministic optimization methods

17 p2838 A71-35355

Bounded plane circular three body problem stability, analyzing Jacobi integral and canonical equations

17 p2807 A71-35496

Three dimensional bounded circular three body problem solution in form of Taylor power series of time and vicinity values for canonical elliptical elements

17 p2807 A71-35497

Bounded circular three body problem stability, deriving Jacobi integral and canonical equations with Poincare variables

17 p2807 A71-35498

Two dimensional steady viscous gas transonic flow Navier-Stokes equations, establishing uniqueness of solutions to boundary value problems

17 p2673 A71-35646

Methods construction for initial value problem solution, using fifth and sixth order algorithms with Adams-Moulton correctors

17 p2768 A71-35686

Integral equation method for solving mixed boundary value problems

17 p2769 A71-35798

Impulsively started time-dependent rotational Couette flow stability analysis by initial value problem and quasi-steady approaches

18 p2902 A71-36038

Existence and uniqueness of weak solution of wave equation with nonlinear boundary condition, using Galerkin method

18 p2940 A71-36094

Unstable two point boundary value problems solution by decomposition into lower order differential equations sequence for computer integration, giving illustrative examples

18 p2940 A71-36143

Stress-strain behavior of tapered circular cylindrical shell, applying equalization calculation to boundary value problem

18 p2976 A71-36179

Timoshenko beam transverse vibration with time dependent boundary and normal loads, using Laplace transform method

[ASME PAPER 71-APM-F] 18 p2977 A71-36253

Cantilever column critical dynamic instability load under nonconservative follower force including thermomechanical coupling effect from boundary value problem formulation

[ASME PAPER 71-APM-L] 18 p2977 A71-36255

Transonic flow numerical analysis, discussing initial conditions and imbedded shocks choice for computation efficiency

18 p2905 A71-36307

Boundary conditions discretization on fluid flow moving discontinuities for analytical or numerical integration

18 p2906 A71-36315

Planar supersonic near wake flow field problem with variable viscosity and base injection, investigating boundary errors spatial decay rate

18 p2906 A71-36321

Numerical solution algorithm for parabolic free boundary problem in statistical decision theory, comparing convergence with asymptotic expansions

18 p2941 A71-36352

Finite difference approximation application to linear two-point boundary value problem differential equation for testing finite point suitability for infinity before computation

18 p2941 A71-36354

Elastodynamics three dimensional mixed initial and boundary value problems, presenting infinite series solution

18 p2979 A71-36359

Photoelastic analysis of cylindrical shells of revolution with one hemispheric closed end and reinforcing flanges at opposite end rim, examining boundary conditions effects

18 p2981 A71-36718

Initial conditions selection for optimal control of systems with time lag

18 p2948 A71-36782

Structural stability of incompressible elastic rod of variable rigidity flattened along axis, reducing boundary value problem to equation with continuous operator

18 p2982 A71-36787

Approximation solution for elliptic boundary value problem with nondifferentiable parameters, considering second order linear partial differential equations in two independent variables

18 p2942 A71-36817

Dissipative wave motion asymptotic theory, considering initial boundary value problems for linear partial differential equations

18 p2910 A71-36819

Regular boundary value problems singularities for linear second order analytic elliptic equations solutions in two independent variables

18 p2942 A71-36925

Plane transonic gas flows through Laval nozzle and symmetrical wedge-shaped profile, solving boundary value problem by reduction to singular integral equation

19 p2991 A71-37101

Specific optimal techniques in control and estimation, emphasizing fixed configuration optimization with time variant parameters and two point boundary value problem

19 p3036 A71-37237

Cylindrical shells under uniform external pressure loads, determining boundary conditions effects on natural frequencies and vibration mode shapes

19 p3155 A71-37529

Shallow spherical shell under uniform external pressure loads, obtaining boundary conditions effects on stress-strain state

19 p3155 A71-37530

Boundary value problems solution in optimal control theory, discussing gradient descent method in state space

19 p3037 A71-37534

Noniterative scheme for treating two-point boundary value problems for single and multipoint linear constant systems, requiring solution of $2n$ differential equations

19 p3086 A71-37559

Homogeneous turbulence decay calculation from multipoint velocity correlations or spectral equivalents at initial time

19 p3044 A71-37730

On-off temperature control system with distributed parameters under boundary conditions, investigating symmetric self oscillation

19 p3163 A71-37780

Nonlinear differential equations and boundary conditions describing behavior of electrically polarizable finitely deformable heat conducting continuum interacting with electric field

19 p3118 A71-37793

Ergodic boundary in time evolution of two dimensional incompressible Navier-Stokes equations solution at large Reynolds numbers

19 p3045 A71-37841

Forced axisymmetric motion of circular viscoelastic plate, including effects of rotatory inertia, transverse shear and time dependent boundary conditions

19 p3157 A71-37848

Buckling and initial postbuckling behavior of clamped thin shallow spherical sandwich shells under axisymmetrical loads

19 p3159 A71-38185

Nonlinear instability theory for wave system in plane Poiseuille flow, deriving asymptotic solution for initial value problem

19 p3046 A71-38203

Oscillation theorem for natural vibrations of thin shells of revolution, considering boundary value problem eigenvalues

19 p3159 A71-38264

In-plane boundary conditions effect on buckling loads of axially compressed simply supported ring stiffened cylindrical shells

19 p3159 A71-38276

Hybrid computer continuous space methods for time dependent partial differential equations involving solution of sequence of two point boundary value problems

19 p3025 A71-38292

Hypercircle method application to elliptic variational problems, obtaining bounds for error in boundary value problems approximation

19 p3087 A71-38307

Error behavior in numerical solution of elliptic differential equations boundary value problems by least squares approximation

19 p3087 A71-38304

Numerical solutions of boundary value problems for linear elliptic partial differential equations by function theoretic methods

19 p3087 A71-38308

Convergence rate of finite difference schemes applied to initial value problems for hyperbolic equations

19 p3088 A71-38312

Natural oscillations existence in cross section of cylindrical waveguide with resonant cavity based on Hilbert space operators, solving boundary value problem

19 p3019 A71-38336

Electromagnetic wave propagation in comb type waveguides, obtaining boundary value electrodynamic problem rigorous solution

19 p3020 A71-38342

Convergence estimation of locally one dimensional scheme for multidimensional heat conduction boundary value problem solution on nonuniform grids using maximum principle

19 p3171 A71-38415

Plane electromagnetic wave diffraction by dense periodic array with Dirichlet and mixed boundary conditions, determining solution asymptotic behavior

19 p3104 A71-38416

Third basic problem solution in elasticity theory satisfying boundary condition and Lamé equation system with two arbitrary vectors

19 p3160 A71-38484

Error analysis for stable implicit difference methods for heat equation with derivative boundary condition

20 p3254 A71-38758

Principal boundary value problems solution for Helmholtz equation in half space with spherical cavities, reducing problems to infinite systems of algebraic equations

20 p3268 A71-38808

Generalized finite Hankel transform method for engineering problems with complicated boundary conditions

20 p3255 A71-39034

Existence proof for Blasius equation and initial conditions system solution, using Luke results with integrals of incomplete gamma function

20 p3255 A71-39035

Finite thickness infinite slab with radiation from time dependent source, solving nonhomogeneous boundary value problem for linear transport equation

20 p3269 A71-39079

Electromagnetic wave transmission through conducting plasma slab, reducing nonlocal wave interaction two point boundary value problem to Cauchy system

20 p3274 A71-39080

Thin shallow spherical shell weakened by circular hole, calculating stressed state from boundary value problem solution

20 p3308 A71-39165

Variational methods application to high order dynamic systems resonance boundary value problem

20 p3309 A71-39487

Steady state thermoelastic mixed boundary value problem for elastic layer with one face stress free and other face resting on rigid frictionless foundation

20 p3309 A71-39495

Stability problem in hydrodynamics of perturbed heterogeneous shear flow, solving initial value problem for Couette flow

20 p3213 A71-39783

Supercavitating bounded flow of weightless fluid past slender bodies, deriving singular integral equations in terms of pressure gradient and cavern thickness derivative

20 p3213 A71-39787

Modified Newton-Raphson stiffness matrices and initial value formulations to geometrically nonlinear structural analysis for beam and plane stress triangular elements

20 p3311 A71-39870

Homogeneous anisotropic body elasticity theory, calculating boundary value problem for arbitrary conditions

21 p3455 A71-40086

One phase Stefan problem for unidimensional heat conduction in plane infinite slab of thermally isotropic material with prescribed flux on fixed boundary
21 p3474 A71-40210

Positive solutions for nonlinear elliptic boundary value problems with convex nonlinearities
21 p3407 A71-40211

Approximate controllability for boundary value control of higher dimensional wave equation
21 p3360 A71-40253

Blunt body heat transfer predictions for atmospheric reentry, discussing coupled effects of real gas behavior and slip/jump boundary conditions
21 p3474 A71-40256

Book on complex variable methods in elasticity, covering boundary value problems for half planes and circular regions
21 p3456 A71-40264

Limiting polarization of radio waves emerging obliquely from ionosphere into free space, describing numerical integration method and boundary conditions
21 p3348 A71-40525

Continuous analog iterative methods and solution of nonlinear two point boundary value problems, producing convergent series of iterates
21 p3408 A71-40585

Radiant monatomic gas flux boundary conditions derivation, considering all points in local thermodynamic equilibrium
21 p3475 A71-40660

Projective numerical solution of integral equations arising in boundary value problems of electric and magnetic field theory
21 p3416 A71-40846

Nonlinear static structural mechanical problems solution, using self correcting initial value formulations
21 p3467 A71-40959

Slender body of revolution in supersonic and subsonic air flow, calculating boundary conditions with Lagrange formulation
21 p3323 A71-40963

Steady slow free molecule flow past sphere, obtaining distribution function and surface boundary conditions
21 p3370 A71-40987

Continuum dislocation theory, discussing initial stress couple problem, slip motion and dislocation rate tensor
21 p3468 A71-41000

Generalized radiation cooling of convex solid, demonstrating existence of unique stable positive solution to boundary value problem related to temperature distribution
21 p3477 A71-41184

Random analogs of boundary value problems class for biharmonic functions, demonstrating unique solution existence
21 p3410 A71-41189

Electromagnetic wave reflection from interface between moving and stationary electron plasmas, giving boundary conditions at velocity discontinuity surface
21 p3426 A71-41288

Elastic continuous medium with nonlocal interactions, calculating surface waves dispersion equations with boundary solutions
21 p3417 A71-41366

Uniqueness theorems and boundary conditions for problem related to Navier-Stokes equations
21 p3566 A71-41514

Point-matching method application to electromagnetic scattering from quadrilateral conducting cylinders in resonance range, using computer programs
22 p3510 A71-42205

Edge supported cylindrically curved panels flutter, investigating in-plane boundary conditions and geometry effects on natural frequency
22 p3616 A71-42216

Galerkin approximation for boundary value problem finite difference scheme optimization by interpolation in Hilbert subspace
22 p3566 A71-42292

One dimensional two phase parabolic free interface /Stefan/ problem numerical solution, using method of lines to approximate partial differential equations at discrete time levels
22 p3575 A71-42294

Stability of finite difference approximation to mixed initial boundary value problems for linear parabolic system of equations
22 p3567 A71-42295

Weak row sum criterion for nonlinear equation systems, applying to discrete two point boundary value problems and linear equation systems
22 p3567 A71-42374

Axially symmetric flow in half space above rotating disk, proving boundary value problem solution existence by fixed point technique
22 p3531 A71-42402

Nonaxisymmetric boundary value problem solution for transversely isotropic half space with circular

separation line between boundary conditions, determining tangential stresses
22 p3617 A71-42576

Viscous hydrodynamic equations functional type boundary value problem, investigating uniqueness theorem for elliptic equations
22 p3531 A71-42629

Approximate solutions to Stefan nonlinear heat and mass transfer problem under various boundary conditions and phase transformation temperature
22 p3622 A71-42687

Spheroid with two dielectric separated halves and mixed boundary conditions, determining spreading currents Lf electromagnetic field
22 p3484 A71-42879

Boundary value problem for plane wave scattering by spherical cap, obtaining scattering cross section for Helmholtz resonator and hemispherical shell
23 p3703 A71-43208

Boundary displacement conditions in linear elasticity with friction, using minimization of nondifferentiable convex functional and variational inequalities
23 p3775 A71-43239

Micropolar elasticity plane problems equilibrium equations system solution, considering elastic half space deformation and steady thermoelasticity
23 p3775 A71-43316

Boundary value problems solution for reaction pressure to elastic base circular plate bending under uniformly distributed load
23 p3777 A71-43910

Inverse problem for heat conductivity equation in semiinfinite region with Tikhonov specific initial and boundary conditions
23 p3782 A71-44062

Temperature distribution in current carrying cylindrical conductor with nonlinear boundary condition of emission by Stefan-Boltzmann law
23 p3783 A71-44070

Boundary layer solution for initial flow around impulsively started sphere in viscous fluid at high Reynolds numbers
23 p3664 A71-44144

Heat generating granular layer tube, obtaining temperature distribution across cross section and boundary conditions
23 p3719 A71-44338

Nongray radiative heat transfer in finite slab with discrete absorption coefficient and specularly and diffusely reflecting boundary surfaces of uniform temperature
24 p3886 A71-44372

Boundary value problems of forced vibration of nonconservatively loaded dynamic elastic system, using William method
24 p3878 A71-44554

Modified perturbation method for solving optimal control boundary value problems with state variable inequality constraints, noting application to reentry trajectories
24 p3876 A71-44608

Multicore circular sandwich plates under various symmetrical loading and boundary conditions, deriving bending equations
24 p3879 A71-44619

Transonic flows about two dimensional airfoils, calculating far field boundary conditions with coordinate transformation
24 p3789 A71-44620

Stochastic process optimal control in presence of constraints, solving two-point boundary value problem by successive approximation method
24 p3814 A71-44688

Boundary value problems eigenvalues determination with differential equations for lifting surfaces vibration theory
24 p3818 A71-44706

Crack theory application to problems with circular boundaries, solving singular integral equations by Aleksandrov-Libatskii approximation method
24 p3880 A71-44721

Finite difference scheme for elasticity theory boundary value problem in curvilinear region, estimating solution convergence rates
24 p3881 A71-44771

Numerical analysis of electromagnetic wave diffraction on inhomogeneous transmitting bodies, reducing Maxwell equations boundary value problem to differential equations solution
24 p3804 A71-44772

Multiple scattering theory of radiative transfer boundary value problems, showing Neumann intensity expansion coefficients relation to singular normal modes
24 p3848 A71-44788

Boundary value problem of plane electromagnetic wave interaction with inhomogeneous warm plasma column, using matching method
24 p3856 A71-44794

Finite plane strain inflation of compressible hollow circular cylinder, using perturbation method for nonlinear boundary value problem
24 p3884 A71-44955

Mixed boundary elasticity solutions for plane with cut on real axis, using Riemann surface
24 p3885 A71-45102

Spatial characteristics based difference scheme application to axisymmetric problems of elastic wave propagation, allowing for solid or hollow circular cylinder boundary conditions
24 p3885 A71-45221

Boundary conditions determined for hydrodynamic equations from solution of Boltzmann kinetic equation in Knudsen layer, obtaining distribution function in Enskog function superposition form
24 p3821 A71-45226

BOUSSINESQ APPROXIMATION
Prograde and retrograde 4 day circulation in Boussinesq fluid layer by traveling thermal waves in Venus upper atmosphere
09 p1526 A71-23446

Boundary value problems of steady state thermoelasticity and axisymmetric Boussinesq stress concentration for half space in linear Cosserat elasticity
12 p1974 A71-26942

Boussinesq stratified fluid zonal flow with vertical and horizontal shear, studying stability to hydrostatic neutral wave perturbations
12 p1925 A71-27194

Thermal turbulence at infinite Prandtl number of horizontally infinite fluid layer heated from below, using Boussinesq equations
13 p2162 A71-28776

Stationary nonparallel plane flow stability with horizontal shear to three dimensional nondivergent disturbances in Boussinesq fluid, using Arnold method
15 p2393 A71-32637

Global hydrodynamic stability theory, discussing energy methods and nonlinear Boussinesq equations for disturbed motion
16 p2558 A71-32995

Convective heat transfer in stars from anelastic and Boussinesq approximations, discussing two dimensional solutions, truncated expansions, turbulence and mixing length theories, etc
18 p2968 A71-37038

Thermal convection induced perturbations in unstably stratified horizontal shear Couette flow of Boussinesq fluid in rectangular channel heated from below
21 p3475 A71-40641

BOW SHOCK WAVES
U BOW WAVES
U SHOCK WAVES
BOW WAVES
Stationary waves produced by earth bow shock, calculating cyclotron radiation amplitude and polarization characteristics by thin current sheet model
01 p0075 A71-11490

Directed proton fluxes measurements in bow shock, magnetosheath and solar wind byOGO 5 satellite ion spectrometer
01 p0147 A71-11491

Magnetic field fluctuations in magnetosheath from Pioneer observations, noting bow shock correlation
01 p0075 A71-11492

Supersonic blunt body flow relaxation processes, calculating bow shock for various flow regimes and reaction rates
05 p0835 A71-16525

Solar wind upstream waves ahead of earth bow shock by dual satellite observations
05 p0741 A71-16629

Earth bow shock configuration model from dual satellite observation
05 p0742 A71-16632

Shock wave bisector rule improvement, applying to asymptotic behavior of bow shock attached to airfoil in two dimensional supersonic flow
06 p0841 A71-17420

Comparison of experimental and gas dynamic fluid parameter jumps across earth bow shock, suggesting reappraisal of gas dynamic analog from satellite observation
07 p1103 A71-19678

Magnetosonic waves generation by interaction of bow shock with frozen tangential discontinuities in solar wind
09 p1521 A71-22866

Lunar shadow effects on bow wave mechanism during 7 March 1971 solar eclipse, considering traveling ionospheric disturbance measurements from satellite
10 p1600 A71-23885

Thermalization processes in earth bow shock with emphasis on ion heating, using electromagnetic dispersion relation for ion-ion streaming instability
13 p2054 A71-27908

Solar wind-Mercury interaction, discussing planet physical properties, magnetized wind parameters and bow shock wave existence
13 p2120 A71-27924

Solar wind ion thermalization in earth bow shock by counterstreaming instability related to interplanetary magnetic field
15 p2399 A71-31774

Earth bow shock internal structure based on correlated observations of magnetic field, ELF magnetic

fluctuations and suprathermal electrons by OGO 5 satellite

16 p2628 A71-33943

Bibliography and review of interplanetary magnetic fields and plasmas, considering solar wind properties, magnetosheath, bow shock and magnetospheric tail

17 p2799 A71-34460

Earth bow shock multiple crossings identification by magnetic field experiment onboard Pioneer 8 at geocentric distances

20 p3320 A71-39878

Suprathermal electron beam induced HF wave instability in solar wind upstream from earth bow shock, interpreting OGO 5 observations

23 p3720 A71-43158

Magnetopause and bow shock location from IMP measurements, discussing solar wind momentum flux induced orbit-to-orbit changes in boundary positions

23 p3667 A71-43159

Solar eclipse induced atmospheric gravity waves interference, considering resulting bow wave discrepancy with wavelike ionospheric disturbance

23 p3670 A71-43190

BOX BEAMS

Aircraft structural parameters optimization satisfying flutter velocity constraint and minimum mass, applying to box beam design

17 p2825 A71-34874

Constrained torsion of spar box fastened along isolated parts of wing span, noting structural failure due to tangential stress distribution

17 p2830 A71-35313

Boron-epoxy composite wing box beam design, describing preliminary weight estimation from layouts [SAWE PAPER 891]

17 p2834 A71-35815

BOXES

Spar box structure under pure bending noting flexural rigidity and stress and stability analysis with Karman nonlinear equations

12 p1981 A71-27498

BRADYCARDIA

Long term effects of hypoxic stimulus suppression upon heart rate, cardiac output and pulmonary artery pressure of highlanders, observing bradycardia

23 p3631 A71-43117

BRAGG ANGLE

Optico-acoustical deflector with high resolving capability, using Bragg light diffraction by ultrasonic waves

04 p0604 A71-14627

Bragg diffracted light intensity increase from standing resonating acoustic wave, considering applicability for laser communication multiplexing and demultiplexing

05 p0720 A71-16269

Monograph on optical imaging of ultrasonic fields by acoustic Bragg diffraction covering heuristic plane wave and ray approach scattered fields

07 p1111 A71-19575

Stimulated emission of laser oscillation in periodic structures of gelatin films with distributed feedback by backward Bragg scattering

09 p1463 A71-22762

Cut metal crystal orientation planes and dislocation structure determination, using Bragg reflection of monochromatic X ray beam

09 p1452 A71-23319

Kinematic theory of resonant gamma rays diffraction by single crystals, calculating differential cross sections of Bragg scattering for total degeneracy and Zeeman splitting

21 p3420 A71-41123

Bragg imaging with optical heterodyne detection and bandpass filtering, considering resolution, SNR and dynamic range

22 p3540 A71-41777

Phase aberrations in Bragg imaging for sound components projecting out of plane normal to light beam

22 p3540 A71-41778

Brillouin scattering effect on noise of Bragg imaging in ultrasonic band at room temperature, using convergent illuminating light beam

22 p3541 A71-41779

Optico-acoustical deflector with high resolving capability, using Bragg light diffraction by ultrasonic waves

22 p3558 A71-42267

BRAIN

NT BRAIN STEM

NT CEREBELLUM

NT CEREBRAL CORTEX

NT CEREBRUM

NT HIPPOCAMPUS

Conditioned reflexes in cats with mesencephalic reticular formation subject to food-signaling acoustic stimulation

01 p0007 A71-10034

Midbrain reticular neurons discharges in response to electrical stimulation of posterior ventral nucleus of thalamus

01 p0008 A71-10072

Interhemispherical synthesis of conditioned reflex motor reactions at different running angles in mice

01 p0011 A71-11051

Respiratory neuron structure in lateral zone of medulla oblongata in cats

01 p0013 A71-11097

Cutaneous blood flow in anesthetized pig forelimb modified by brain temperature changes

02 p0197 A71-11671

Decision making heuristic program reflecting human brain function in problems with listed requirements and unspecified goal

03 p0369 A71-13002

In-flight EEG recordings telemetry for pilot aptitude testing, showing pilot error relationship to brain oversteering

03 p0370 A71-13067

Protective brain function in epileptic convulsive seizures during sonic stimulation in rats

03 p0359 A71-13159

Sound duration effect on brain activity of cats, studying EEG and behavioral responses

03 p0361 A71-13189

Glutaminase isoenzyme activators in mitochondrial brain fractions of rabbits

03 p0361 A71-13235

Gamma-aminobutyric acid (GABA) effects on brain serotonin following transaminase inhibitor aminooxyacetic acid administration

03 p0362 A71-13239

Bioenergetics of brain in vertebrates, concerning oxidative metabolism in neurones, glia and mitochondria structure

03 p0362 A71-13240

Brain electrodes rapid implantation method, using preassembled, stereotactically loaded, preconnected and pretested electrode and pedestal assemblies

04 p0538 A71-15059

Respiratory and circulatory responses in anesthetized cats to medullary ventral surface perfusion with mock cerebrospinal fluid of varying K concentration or 2 percent procaine solutions

04 p0540 A71-15577

Acoustic intensity and exposure time duration for threshold lesion in cat brain

05 p0712 A71-16283

EEG wave phase durations over human brain surface, examining asymmetry distribution level

05 p0709 A71-16801

Human brain electric activity during kinesthetic analysis of excitations by radiocarpal joint movements, considering cortical regulation

05 p0709 A71-16803

Telemetric techniques for pharmacological effects of body temperature, motor activity and food and fluid intake on rat brain, describing recording and monitoring equipment

05 p0716 A71-17112

Electrophysiological audiometry noting average brain response in man

06 p0858 A71-17295

Electroencephalographic and motor effects of electrically stimulated reinforcing and negative subcortical structures in sleeping cats

06 p0852 A71-17669

High sensitivity portable two channel apparatus for brain temperature measurements using small glass insulated thermistors

06 p0863 A71-18469

Bromouridine as radiosensitizing agent improving effectiveness of radiation therapy of malignant brain tumor cells

07 p1040 A71-18990

Oxidative and hydrolytic enzymes localization in rhesus monkey brain, investigating glutaraldehyde fixation effect with histochemistry

07 p1042 A71-20017

Central regulation mechanisms of acidic-alkaline equilibrium in ontogenesis, discussing midbrain intraterine and respiratory postnatal development

08 p1241 A71-21937

Mathematical model for brain arteries hemodynamic resistance, using blood pressure data

09 p1390 A71-22261

Brain norepinephrine synthesis pharmacological inhibition, discussing effects of ovariectomy to decrease sensitivity

09 p1391 A71-22472

Cerebrospinal knee and flexor reflex suppression observations in rabbits and cats during blood circulation disorders

09 p1391 A71-22480

Photoperiodic effects on insect brain circadian clock control, investigating eclosion cycle initiation, stimulant hormone release and termination as functions of dark phase

09 p1392 A71-22648

L-dopa multinection timed effects on rat brain norepinephrine metabolites concentrations, observing zero time control rated modifications

09 p1393 A71-22649

Nervous system modeling, considering cybernetic brain functions, neuroheuristic programming and modes of distributed information processing pertinent to neuropsychological experiments

10 p1568 A71-24222

Information processing in biological and artificial brains, analyzing visual perceptual system

10 p1568 A71-24224

Mathematical neuronal model for functional learning system networks, representing brain pattern recognition, learning and size invariance mechanisms

10 p1569 A71-24233

Human brain subcortical formations slow electrical processes during memory tests

13 p2005 A71-28377

Brain subcortical structure neuronal assemblies impulse activity during sleeping and dreaming in patients treated with implanted electrodes

13 p2005 A71-28378

Evoked brain potentials averaging in real time with computer linked by long distance communication lines

13 p2017 A71-28385

Localized focused ultrasonic beam action on brain portions without skull trepanation in animals and man, visualizing sonic field by Tepler effect

15 p2356 A71-31291

Cellular respiration and high altitude adaptation effect on cytochrome content and on oxidation and oxidative phosphorylation parameters of brain homogenates in rats

15 p2357 A71-31310

Human operator work quality evaluation with EEG data based on brain electrical activity as function of central nervous system

15 p2365 A71-32530

Visual evoked brain potential amplitude and detection efficiency relationship, discriminating between arousal and attention effects

17 p2682 A71-35114

Neurobionics, considering data processing in brain and central nervous system

17 p2691 A71-35165

Rat brain acetylcholine levels circadian rhythm correlated to spontaneous motor activity and sleep-awake cycle

17 p2684 A71-35326

Brain locking activity structural organization, discussing cerebral processes and control contact mechanisms activating conditioned reflexes

17 p2684 A71-35358

Bulbar and baroreceptor inhibition of spinal and supraspinal sympathetic reflex discharges recorded in cats from renal nerve

18 p2857 A71-36689

Squirrel monkeys midbrain reticular formation direct thermal stimulation effects on physiological or behavioral thermoregulatory responses

18 p2858 A71-36860

Circadian rhythm maturation of brain norepinephrine and serotonin in rat, relating spontaneous motor activity and sleep-wakefulness mechanism

19 p3003 A71-38071

Signals convergence of various sensory modalities as function of impulse reactions of individual brain neurons in mammals

19 p3003 A71-38197

Electroencephalographic evaluation of brain functions disturbances in response to stress in flying personnel, relating fatigue and rest periods allocation

19 p3008 A71-38223

Protein content in cytoplasm of neurons and glial satellite cells in supraoptical and red nuclei of white rat brains during natural and paradoxical phase deprived sleep

19 p3005 A71-38545

Brain polysomes disaggregation and tryptophan elevation in immature rats and adult animals after L-dopa administration

20 p3186 A71-38979

Aminazine and chloral hydrate effects on metabolism intensity of rats brain gangliosides components including N-acetylneuramine acid and N-acetylgalactosamine

21 p3337 A71-41055

Glycerides metabolism in rats brain under normal conditions and during hypoxia, showing diglycerides role in triglycerides and phospholipids biosynthesis

21 p3337 A71-41056

Gangliosides and cerebroside content in rat brain under normal conditions, during hypoxia and under small X ray doses action

21 p3337 A71-41057

Rat brain carbohydrates biosynthesis from organic acid products under normal conditions and during central nervous system disturbances, investigating butyric acid participation

21 p3337 A71-41058

Thyroxine effects on brain glutaminase isoenzymes interaction and deamidation in mitochondrial fractions, comparing with sodium phosphate, bicarbonate and aspartate

21 p3338 A71-41069

Serotonin and gamma-aminobutyric acid loss and interaction in rat midbrain slices incubated in media containing Na, K and Ca ions

21 p3338 A71-41073

Differential lipid and phospholipid composition of white matter in brain, cervical, thoracic and lum-

bosacral sections of spinal cord and sciatic nerve in dogs

21 p3338 A71-41074

Gangliosides inhibitory effects on active Ca ion transport in rat brain mitochondria, using succinate as respiratory substrate

21 p3338 A71-41075

Brain monoamines localization and metabolism and endocrine function, discussing pituitary secretion and neurotransmitter input

23 p3637 A71-44274

Morphological changes in dogs brain vessels under transverse accelerations

24 p3796 A71-44546

BRAIN CIRCULATION

Hydrogen exchange between pial arteries for measuring local cerebral blood flow quantitatively in anesthetized cats

01 p0008 A71-10075

Human blood gases continuous measurement in vivo by mass spectrography, considering arterial nitrogen washout and cerebral blood flow determination

01 p0021 A71-10237

Hypoxia effects on cerebral vascular autoregulation to arterial perfusion pressure in dogs

01 p0015 A71-11185

Gamma-aminobutyric acid /GABA/ penetration through blood-brain barrier for administration in dogs and rats

03 p0362 A71-13236

Phospholipid dynamics of blood entering and leaving brain during unilateral desympathectomy in dogs

03 p0362 A71-13238

Syncope as temporary suspension of consciousness due to cerebral blood supply failure, considering cardiac rhythm disturbances, blood flow obstructions and heart disease

04 p0541 A71-15915

Middle cerebral artery occlusion effect on cortical blood flow, tissue oxygen pressure and acid base equilibrium in animals under extended ligations

05 p0708 A71-16617

Multifactor correlation analysis of systemic circulation effects on brain blood filling level, using linear regression equations

06 p0855 A71-18373

Blood circulation in auditory analyzer cortical section relationship to bioelectrical activity, using various frequencies pure tones as stimuli

15 p2360 A71-32531

Tympanic-cavity nerve plexus electric stimulation effects on cerebral blood circulation and overall arterial pressure in dogs and cats

16 p2533 A71-34108

Brain temperature change effects on cardiovascular responses, examining heart rate and systemic arterial blood pressure

18 p2860 A71-36880

Regional cerebral blood flow, tissue oxygen, EEG activity and behavioral reaction at high pressure

19 p3009 A71-38557

Age dependent changes in free amino acid content and composition of cerebral and carotid arteries in man and dog

21 p3338 A71-41070

Hypothermia effect on brain nutritive processes and regulator activity, considering changes in brain blood supply, respiration and carbohydrate metabolism

22 p3486 A71-41940

Frequency analysis of blood circulation rhythms and oxygen tension fluctuations in cerebra of rabbits, cats, monkeys and men

22 p3490 A71-42580

BRAIN DAMAGE

Chronic posttraumatic changes in central nervous system in pugilists from brain damage due to head injuries

01 p0010 A71-10393

C 14 incorporation from labeled glucose into cerebral glycogen of normal and X ray irradiated rats

01 p0011 A71-10850

Impact induced closed brain injuries pathomorphology, considering dura mater, cortical contusions, neuron and glial damage, brain stem lesions and hemorrhages

04 p0537 A71-14787

Globus pallidus damage in cats, investigating effects on conditioned motor reflexes, learning and memory

10 p1564 A71-24466

Instantaneous postural reaction of cattle to brain concussion indicating mechanoreceptor HF discharge impulse pathophysiological mechanism

11 p1720 A71-26122

Tolerance tests including EEG, glucose test, thermal stress and G stress for aircrew fitness assessment after cranio-cerebral incidents

12 p1871 A71-27633

Brain stem mechanisms underlying visual discrimination in rhesus monkeys subjected to bilateral lesions of the inferotemporal cortex, posterior thalamus or midbrain

13 p2011 A71-28807

BRAIN STEM

Pupil neurological control system for reaction to light and accommodation process by statistical eye noise analysis and microelectrode recordings of brain stem neurons

03 p0367 A71-12985

Brain stem mechanisms underlying visual discrimination in rhesus monkeys subjected to bilateral lesions of the inferotemporal cortex, posterior thalamus or midbrain

13 p2011 A71-28807

Vestibular apparatus effect on brain stem somatic activity

21 p3328 A71-39998

BRAKES [FOR ARRESTING MOTION]

NT AERODYNAMIC BRAKES

NT AIRCRAFT BRAKES

NT BALLUTES

NT DRAG CHUTES

NT LEADING EDGE SLATS

NT TRAILING-EDGE FLAPS

NT WHEEL BRAKES

NT WING FLAPS

Statics and aerodynamics of lifting decelerators /parawings and sailwings/ at supersonic and hypersonic speeds

01 p0002 A71-10927

[ALAA PAPER 68-945]

BRAKING

Atmospheric density variations determination from Proton 2 braking data for aerodynamic drag coefficient, constructing model for rarefied gas flow-satellite interaction

05 p0804 A71-16043

Spacecraft optimal impulsive braking by onboard engine to ensure maximum angle of atmospheric reentry

09 p1519 A71-22567

Atmospheric density variations determination from Proton 2 braking data for aerodynamic drag coefficient, constructing model for rarefied gas flow-satellite interaction

16 p2635 A71-33447

Braking performance of runway surfaces and skidding resistance of aircraft tires, considering load and inflation pressure, tread materials and weather conditions effects

22 p3529 A71-42234

BRANCHING [MATHEMATICS]

Branching model of scientific information propagation and influence networks, exemplifying problem of hypersonic flow around blunted bodies

02 p0335 A71-11854

Branching of periodic solutions of second order nonlinear ordinary differential equations similar to Duffing equation

06 p0918 A71-17643

Nonlinear global strong cellular branching solutions stability of Navier-Stokes equations

16 p2558 A71-32997

Bifurcating systems analysis in structural stability problems, discussing perturbation patterns in nonlinear branching theory

16 p2650 A71-33018

Branch points of root locus curves for rational transfer functions and transfer functions with recovery time

22 p3566 A71-41854

Bifurcation /branch point/ theorems and limit cycles for integral curves of hard excitation nonlinear systems

22 p3527 A71-42675

Branched trajectory optimization algorithm using steepest descent method applied to space shuttle vehicle mission design

23 p3726 A71-43000

BRANCHING [PHYSICS]

Helicopter vibrational behavior prediction in flight with known aerodynamic loads, using branch modes method

09 p1385 A71-23606

Small autooscillations of high order differential equations system, investigating bifurcation occurrence relationship to zero equilibrium position stability change

23 p3699 A71-43572

BRASSES

Tungsten wire reinforced brass composites, studying multiple necking phenomena during tensile tests

04 p0615 A71-15794

High-strength low-cost moderate-conductivity cobalt modified aluminum brass for electrical contacts, terminals and relay springs

13 p2086 A71-28836

Low cycle fatigue strength of high speed rotating aluminum and brass disks, comparing with uniaxial push-pull fatigue test

14 p2328 A71-30418

Grain size effect on fatigue life during tension and compression tests of alpha brass, copper and aluminum, considering slip character

15 p2437 A71-32578

Notch effect on stainless steel and alpha brass rods and plates ductility and fracture strength

16 p2591 A71-32947

Mechanical properties of explosively clad plates, considering stainless steel/mild steel and brass/mild steel composites

17 p2757 A71-34663

BRAYTON CYCLE

Brayton space power system for NASA manned space missions, discussing control system requirements, design and performance

15 p2354 A71-32203

Brayton power system electrical subsystem and component performance tests, discussing engine control package, DC supply, inverters and instrumentation

15 p2354 A71-32204

Electrically-heated Brayton power conversion system, comparing performance tests with prediction

15 p2354 A71-32212

Performance tests of two identical Brayton cycle heat exchanger units consisting of recuperator, heat sink exchanger and ducting in combination with turbine

15 p2355 A71-32213

Steady state and transient performance of Brayton cycle alternator and electronic controls for space power

15 p2355 A71-32215

Steady state and transient interactions due to thermal integration of isotope Brayton space power and life support systems

15 p2364 A71-32220

Hot performance tests of three identical Brayton rotating units on gas bearings

15 p2355 A71-32226

Pressure ratios and surface effects on regenerative heat exchanger in Brayton gas turbine cycles with intercooling or reheating

16 p2663 A71-34037

Brayton cycle 2-15 kW power system for space application and potential gains from component improvements, discussing current status

20 p3180 A71-38906

Automated endurance testing of 2-15 kW Brayton power conversion system, using rotating unit, heat exchanger, electronic voltage regulator, parasitic speed control

20 p3180 A71-38907

Brayton cycle power conversion system using He-Xe gas mixture, discussing compressor net engine and turbine static efficiencies

20 p3180 A71-38908

Post test inspection of Brayton Rotating Unit for closed Brayton cycle electric power conversion system for long space missions

20 p3180 A71-38909

Electrical subsystem of 2-15 kW Brayton power conversion system consisting of speed controller, alternator voltage regulator, DC power supply, etc

20 p3180 A71-38910

Motor starting techniques for 2-15 kW Brayton space power system with turbine driven radial flow compressor and Lundell type alternator

20 p3180 A71-38911

Nuclear reactor Brayton cycle space power system design point characteristics, discussing cycle parameters, working fluid, turbine inlet temperature, operating pressure level, etc

20 p3262 A71-38913

Reactor powered Brayton cycle power conversion system, evaluating performance at different turbine inlet temperatures and power levels by computer simulation

20 p3262 A71-38914

Low temperature space radiator to reject thermal power from isotope Brayton cycle power system for future space missions

20 p3181 A71-38917

Reactor power systems for earth orbital space station, considering thermoelectric and Brayton cycle power conversion modules

20 p3262 A71-38919

Isotope Brayton four module adaptable compact power system for space station, using plutonium 238 fuel and lithium hydride shielding for neutron attenuation

20 p3263 A71-38922

Brayton cycle electric space power supply systems, describing shielded reactor and heat exchanger design

20 p3263 A71-38924

BRAZIL

Earth remote sensing in Brazil, discussing program organization and data acquisition related to NASA environmental resources technology satellites

16 p2570 A71-33826

BRAZING

NT ULTRASONIC SOLDERING

Furnace fluxless brazing of Al with metallic getters, discussing techniques and joint design

02 p0255 A71-11706

Combined vacuum furnace brazing with diffusion welding for joining high strength Ni base superalloys

02 p0255 A71-11708

Heat and corrosion resistant vacuum tight ceramic to metal brazed seals

07 p1119 A71-19972

Complex Al brazing alloy for honeycomb core joining to Ti alloy face sheets, discussing fillet formation and strength optimization 08 p1299 A71-21686

Powders and torch techniques for brazing, including Mn-Ni-Co, Cu-Mn-Ni, Zr-Ti-Be, Ti-Cu-Ni and Zr-Be alloys 11 p1769 A71-25746

Spreading, wettability, diffusion and aggressive properties of nickel base brazing filler metals on stainless steels 11 p1769 A71-25750

Metal powders role in brazing, considering melt atomization and mechanical comminution 13 p2075 A71-29089

Diffusion bonding in production of shuttle type vehicles, considering fluxless brazing of refractory superalloys for heat shielding [SME PAPER AD-71-246] 18 p2927 A71-36660

Refractory, superalloy and composite materials brazing process for space shuttle orbiter heat shield 18 p2928 A71-36854

Water cooled reactor Zircaloy brazing filler metals, investigating corrosion resistance, joint strength and brazing capability 18 p2928 A71-36856

Brazing roughness effects on rectangular plate fin heat exchanger surfaces heat transfer and flow friction characteristics, noting fin surface geometry influence [ASME PAPER 71-HT-29] 19 p3166 A71-37999

Vacuum brazing for nozzle guide vanes repair in aircraft gas turbine engines, noting economic advantages 19 p3069 A71-38313

Steam turbine blades induction brazing with programmed cycle, describing coil design 19 p3070 A71-38315

Metallurgical and mechanical properties of Ti-Al-V joints produced by thin film diffusion brazing with copper 19 p3070 A71-38316

Brazing filler metals as cost effective replacement for Au-Ni in aircraft gas turbine engine component 21 p3387 A71-40621

BREADBOARD MODELS

Service support for hardware engineering models from breadboard to preproduction stages, determining spare parts location, quantity and cost requirements 09 p1430 A71-23477

Breadboard simulation model of laser space communications system consisting of carbon dioxide laser, transmitter telescope, GaAs phase modulator and attenuator 20 p3196 A71-39116

Holographic optical memory breadboard development system based on CW Ar ion laser, discussing component operating, power requirement and cost problems 21 p3380 A71-40922

BREAKAWAY

U BOUNDARY LAYER SEPARATION

BREKDOWN

Solid metal plates breakdown mechanism at high temperatures and supersonic plasma jet action 05 p0768 A71-16778

Hydrodynamic lubrication temporary breakdown during initiation of extrusion process 10 p1618 A71-24924

Metal specific work breakdown during crack propagation, investigating thermal effect of plastic deformation with thermocouples 15 p2413 A71-31479

BREATHING

Decompression urticaria response in subjects after inert gas breathing at constant ambient pressure, noting osmosis mechanism 08 p1246 A71-20813

Skin cooling effect on awake exercising dog ventilation, noting carbon dioxide response curve, arterial partial pressure and hyperpnea 09 p1396 A71-23366

Ventilation and heart rate responses to muscular exercise by work load ramp function changes studies 11 p1722 A71-26359

High oxygen tension during severe exercise, studying effects on humoral and nervous ventilation changes 11 p1722 A71-26363

Reflex increase in ventilation induced by vibrations applied to cat triceps surae muscles, noting muscular and articular receptors role 17 p2678 A71-34175

Spontaneous deep sighing breath physiological regulation in rats as lung inflation response due to vagally mediated mechanoreflex 17 p2679 A71-34176

Breathing capacity increase without rise in oxygen consumption due to active and passive muscular work and heavy energy expenditure 17 p2681 A71-34821

Human respiratory muscles electrical activity, discussing correlation analysis of interferential electromyograms from external intercostal muscles during breathing exercises 19 p3003 A71-38198

Respiratory reflex mechanism of deep breath occurrence after period of airway occlusion in rabbits related to stimulation of vagal receptors 20 p3187 A71-39040

Hyperbaric normoxic breathing helium, nitrogen and neon gas mixture effects on EEG and reaction time in man 21 p3342 A71-40347

Altitude and cold acclimatization effects on human basal heart rate, blood pressure, respiration and breath-holding 21 p3330 A71-40349

BREATHING APPARATUS

NT UNDERWATER BREATHING APPARATUS

Respiratory gas reaction mechanism on potassium superoxide in closed circuit breathing apparatus 13 p2021 A71-29113

Fatigue measurements in hot working conditions on subjects wearing self contained breathing apparatus in heat chamber 17 p2688 A71-34361

Advantages and drawbacks of pure oxygen and oxygen-nitrogen space breathing, considering decompression sickness in Apollo missions 18 p2863 A71-35907

BREATHING MODE

U BREATHING VIBRATION

Optimal respiration mode based on controlled artificial feedback characteristics, making resistance to inhalation dependent on duration 17 p2680 A71-34644

BRECCIA

Annular structures on earth, moon and Mars, explaining cosmic origin on basis of lens-shaped subsurface breccia 02 p0310 A71-12298

Microcraters on Apollo 12 crystalline rocks and breccia surfaces attributed to primary cosmic particles 10 p1673 A71-24427

Apollo 11 lunar rock and microbreccia examination for natural remanent magnetization, emphasizing viscous magnetization effect in terrestrial magnetic field 14 p2303 A71-29534

Water, carbon and rare gases in lunar crater breccias based on meteorites nature 15 p2494 A71-32490

Progressive metamorphism and classification of shocked and brecciated crystalline rocks at impact craters 19 p3050 A71-37665

Detritus and breccias occurrence, composition, shock metamorphism, ejection mode and deposition at terrestrial single impact crater formations based on petrographic observation 19 p3051 A71-37667

Lunar breccia, considering welded or sintered breccias, glassy breccias containing xenocrysts and xenoliths, instant rock breccias and recrystallized breccias 19 p3137 A71-37675

Lunar locations and orientations of crystalline rocks, breccia and soil from Apollo 11 and 12 missions, including maps 23 p3737 A71-43603

Apollo 12 lunar igneous rocks and breccia opaque minerals examined by optical and electron microprobe techniques 23 p3739 A71-43621

Gray mottled basaltic rock composition and origin in Apollo 12 lunar soils and breccias 23 p3741 A71-43634

Apollo 12 lunar soil and breccia core tube and surface samples optical and electron microscope and microprobe analysis, relating data to geologic processes 23 p3744 A71-43656

Apollo 11 and 12 unshocked and shocked microbreccias petrology, noting shock compression and shock welding 23 p3745 A71-43658

Impact metamorphism effects in Apollo 12 microbreccias from Oceanus Procellarum 23 p3745 A71-43659

Apollo 11 and 12 regolith and breccia samples, discussing shock effects detection and interpretation, chemical composition, grain size distribution and impact origin 23 p3745 A71-43660

Lunar breccia sample matrix composition characteristics examination by transmission electron microscope, suggesting condensation from rock volatilized by meteorite impact heat 23 p3745 A71-43663

Meteoritic material characterization from trace elements in Apollo lunar soil, core samples, breccia and anorthositic fragments by neutron activation analysis 23 p3747 A71-43678

Apollo 12 lunar soil, breccia and igneous rock samples, determining elemental abundances with spark source mass spectrometry and neutron activation analysis 23 p3748 A71-43680

Trace elements concentration and metallic particles analysis from Apollo 12 lunar igneous rocks, soils and breccias, noting relation to sample location and exposure age 23 p3748 A71-43681

Bulk elemental composition of Apollo 12 samples of lunar igneous and breccia rocks and soils from instrumental and radiochemical neutron activation analysis 23 p3748 A71-43684

Rare earth elements and trace elements abundance in Apollo 12 igneous rocks, breccia and lunar soil 23 p3750 A71-43692

Isotopic abundances and composition of U and Th in Apollo 12 soil and breccia samples, using mass spectroscopy 23 p3753 A71-43716

Apollo 12 lunar soil samples trapped rare gas analysis, observing solar wind He local variation from breccia 23 p3754 A71-43723

Inert gases release from breccia 10065 by lunar rock vacuum crushing at room temperature, suggesting breccia formation from gas-rich parent materials 23 p3754 A71-43725

Tritium activity measurement in Apollo 11 fines, breccia and crystalline rock, comparing with meteoritic values 23 p3755 A71-43735

BRECHES

U CLOSURES

BREEDER REACTORS

German monograph on creep buckling tests of finned and unfinned thin walled pipes of heat resistant breeder reactor cladding materials 21 p3464 A71-40781

BREMSSTRAHLUNG

Bremsstrahlung effect on charged particle motion in nonuniform magnetic field 01 p0132 A71-10677

Bremsstrahlung X rays-radar echoes relation in southern auroral zone, discussing electron precipitation role 03 p0408 A71-13388

Bremsstrahlung photons produced by cosmic ray muons in Fe and Pb at sea level, calculating energy spectra and angular distributions 03 p0477 A71-13863

Theta pinch plasma enhanced radiation at far IR wavelengths, observing emission exceeding thermal bremsstrahlung 03 p0465 A71-14189

Impulsive solar flare X rays spectral characteristics, examining electron energy, bremsstrahlung, microwave bursts and particle escape, collisions and injection 05 p0797 A71-15937

Angular distribution and polarization of solar X-ray bremsstrahlung, taking into account magnetic field effects 05 p0000 A71-16032

H-He partially ionized plasma bremsstrahlung, radiative and dielectric recombination, discrete levels excitation and collisional ionization 05 p0787 A71-16489

Auroral luminosity and X ray bremsstrahlung quasi-periodic pulsations data analysis by power spectrum and cross correlation methods 06 p0949 A71-17265

Maserlike pulsar radiation mechanism using Coulomb bremsstrahlung near strong quantizing magnetic field 07 p1190 A71-18858

Solar radio waves varying component local sources relationship with sunspots development, describing characteristics based on thermal bremsstrahlung and cyclotron/synchrotron fast electrons radiation 07 p1195 A71-19339

Bremsstrahlung effect on charged particle motion in nonuniform magnetic field 07 p1170 A71-20139

Electron trapping in dielectrics, providing effective light and inexpensive spacecraft bremsstrahlung shield and lower average radiation energy at synchronous altitudes 07 p1164 A71-20625

Time and spectral distribution of hard X ray radiation during solar flare, using nonrelativistic electron bremsstrahlung model 07 p1189 A71-20638

Plasma electrons heating by interaction with ultrashort laser pulses, considering hard bremsstrahlung generation 09 p1460 A71-22245

Morphology, dynamics and time variations of auroral zone electron precipitation events from balloon measurements of bremsstrahlung X rays 10 p1662 A71-24535

Atmospheric electrical effects due to aurora, discussing negative space charge, bremsstrahlung flux and electrojet plasma instability 10 p1604 A71-24703

Milky Way Galaxy X ray sources, discussing bremsstrahlung, synchrotron radiation, Compton ef-

fect optical objects, supernova remnants and X ray astronomy
12 p1959 A71-26780

X ray flux variability of massive elliptical galaxy M87 from rocket flight measurement, considering synchrotron, inverse Compton and thermal bremsstrahlung
12 p1962 A71-26931

Midnight sector balloon measurements of X ray bremsstrahlung from electrons precipitating in auroral zone during polar magnetic substorms
13 p2119 A71-27798

Solar and geophysical morphology of radio burst of active sun, treating bremsstrahlung, gyro, synchrotron and Cerenkov radiation and plasma waves
13 p2137 A71-28514

Galactic LF nonthermal radio emission origin, considering mechanisms of synchrotron radiation from cosmic ray electrons and enhanced bremsstrahlung
14 p2304 A71-29593

Flux estimates of gamma quanta with energies of 5 TeV from celestial objects due to bremsstrahlung and inverse Compton scattering of relativistic electrons
14 p2299 A71-29985

Zenith angle distribution of extremely high energy muons from bremsstrahlung showers by emulsion chamber, noting consistency with pion/kaon decay
15 p2476 A71-31790

Dispersive effect on bremsstrahlung radiation from electron atom collisions in weakly ionized plasma, using Boltzmann transport equation
15 p2456 A71-31850

Cosmic ray shower size spectrum in atmosphere for muon bremsstrahlung at large zenith angles
15 p2479 A71-31868

Free-free bremsstrahlung emission in anisotropic hot electron plasma in magnetic mirror, measuring polarization by Compton scattering
17 p2788 A71-34853

Local time dependence of auroral zone electron precipitation X ray events from balloon measurements of bremsstrahlung
18 p2911 A71-35894

Virgo XR-1 X rays observation with rocket-borne proportional counters, noting photo index or bremsstrahlung temperature consistency with spectrum
18 p2959 A71-37050

GX 17 X ray observation, noting exponential spectrum characteristic of thermal bremsstrahlung and resemblance with Sco X-1 radiation
18 p2959 A71-37054

Plasma diagnostics based on IR continuum intensity due to bremsstrahlung emission from plasma
19 p3113 A71-37765

Flare stars X ray emission by fast electrons nonthermal bremsstrahlung
19 p3128 A71-38157

X ray background model based on photons bremsstrahlung emission by subcosmic metagalactic electrons or protons
20 p3279 A71-39296

Electrons heating by matter interaction with ultrashort laser pulses, considering hard bremsstrahlung generation
21 p3394 A71-41134

Bremsstrahlung photons produced by cosmic ray muons in Fe and Pb at sea level, calculating energy spectra and angular distributions
22 p3595 A71-42664

Magnetic fields, bremsstrahlung and synchrotron emission in impulsive flare of 24 October 1969
23 p3721 A71-43849

Suprathermal proton bremsstrahlung cross section calculation, using Weizsacker-Williams method
24 p3865 A71-44905

BREWSTER ANGLE

Ray transformation after passing through optical resonator with Brewster prism, calculating spectral energy losses dependence by geometrical optics method
09 p1464 A71-23072

Nd-YAG folded center lasers Q switching and cavity dumping, using fused silica and Brewster cut intracavity acousto-optic modulator
11 p1773 A71-25798

Longitudinal modes in standing wave gas laser with Brewster windows in presence of active level emission capture
17 p2753 A71-34412

BRIGHTNESS

Telescopic and photographic meteors brightness distribution curves
01 p0149 A71-10051

Image transmission in isotropic photooptical channels, examining object-image brightness relationship
02 p0211 A71-11830

Cloud brightness as function of illumination and underlying surface conditions, relating macrooptical parameters and microstructure
02 p0277 A71-12113

Brightness field spatial structure of solar radiation reflected from earth by Cosmos 149 satellite, discussing homogeneity and isotropy
02 p0246 A71-12114

Optical thickness of reflecting nebula with given brightness illuminated by star, using three dimensional models
02 p0311 A71-12352

Comet brightness fluctuation phenomenon, discussing solar wind interaction with Platt particles in cometary atmosphere
02 p0303 A71-12867

Zodiacal light brightness measurement in three mutually perpendicular directions, tabulating data
06 p0966 A71-17677

Type I supernovae brightness curves analysis by photometry
06 p0975 A71-18435

Statistical analysis for parabolic approximation of phase dependence observations of integral Mars brightness
06 p0975 A71-18446

Telescopic and photographic meteors brightness distribution curves
08 p1361 A71-21045

Gaussian shaped laser pulse holographic brightness analysis, presenting theoretical and experimental holographic coherence length curves for Q switched laser oscillator and amplifier system
08 p1290 A71-21390

Mars border-disk brightness comparison noting atmospheric transparency effects
09 p1520 A71-22837

Solar surface radiation brightness and intensity for different disk regions and wavelengths
09 p1526 A71-23419

Mars 1969 opposition effects, describing Syrtis Major, Arabia and disk brightness, color and spectrum
11 p1835 A71-26456

Parabolic approximation of total Mars brightness phase dependence observations, using statistical analysis
12 p1955 A71-26596

Four eclipse reappearances observations of Jovian satellite Io by area scanning photometer, considering anomalous brightening
13 p2134 A71-28285

Turbulent flame boundaries and maximum brightness surface position in gasoline-air mixtures, using photography and gas analysis measurements of carbon dioxide concentrations
13 p2162 A71-28955

Flame propagation speed, combustion zone extent and distance from front to maximum brightness surface in turbulent gasoline-air flames
13 p2162 A71-28956

Triaxial ellipsoid asteroid models, determining light curves and variations
14 p2312 A71-30385

Brightness variations of satellite during passage in circular orbit as function of distance, phase and atmospheric extinction
14 p2318 A71-31122

Brightness dependence on heliocentric distance of cometary hydroxyl and hydrogen halos, using three step production mechanism
14 p2318 A71-31124

Laser radiation source time and spatial coherence effect on brightness distribution of image produced by hologram
15 p2402 A71-31254

Nucleus brightness of comet Ikeya-Seki from plates in photographic and photovisual spectral regions, indicating relation to solar rotation
15 p2484 A71-31667

Io brightness anomaly after eclipse by Jupiter
15 p2491 A71-32421

Forbidden O II spectra brightness ratio measurements across Orion nebula, determining electron density variations
16 p2631 A71-33229

Radio contour map of Crab nebula at 3.5 mm, giving brightness distribution and flux density
16 p2632 A71-33235

Visual integral brightness estimates of Ikeya-Seki 1967n comet observed at Dyushambe from 9 January to 18 April 1968
17 p2803 A71-34833

Center to limb solar brightness distribution at 1.4 mm, discussing chromospheric models and antenna beam pattern effects
18 p2965 A71-36735

Solar chromospheric plage area related to peak K coronal brightness at limb
18 p2966 A71-36738

Dwarf elliptical and irregular galaxies of small intrinsic size, small absolute luminosity and low surface brightness
18 p2967 A71-37028

Comet Tago-Sato-Kosaka isophotometry, obtaining surface brightness distribution and solar wind velocity estimate
19 p3130 A71-37228

Bright-dark asymmetry testing in solar granulation photography by objective method
19 p3146 A71-38663

Statistical investigation of 1500 galaxies in MCG catalog with weak surface brightness, noting sculpture type spheroidal galaxies in Virgo cluster
20 p3289 A71-39299

Statistical processing of phase dependence of Martian integral brightness at 0.3-1.1 microns, noting abrupt reflectivity decrease
20 p3290 A71-39308

Scorpius X-1 radio emission detection at 1415 MHz, discussing brightness distribution
21 p3441 A71-40068

Successfully presented flashing lights detection, discrimination and brightness measurements with four channel binocular Maxwellian viewing system
22 p3498 A71-41488

Martian surface materials determination by comparing albedo and brightness with spectral and photometric characteristics of crushed reddish volcanic rock and silicate sand mixed with limonite
23 p3770 A71-44052

Mach bands appearance in red/green triangular wave intensity distributions generated on CRT, quantifying perceived brightness distribution by matching with variously positioned light slit
24 p3800 A71-44468

Comet brightness variations correlation with geomagnetic field and solar corpuscular flux variations in interplanetary space
24 p3870 A71-44814

BRIGHTNESS DISCRIMINATION

Contour effects on brightness paradox, investigating contrast and perception of luminance gradients in space by constant sum estimation method
03 p0365 A71-14377

Human vigilance performance in brightness discrimination task under hypoxia, considering reaction time in signal detection
04 p0541 A71-14740

Mathematical model of visual information of edge contrast effects in human eye as functions of image brightness and viewing angle
07 p1051 A71-20123

Darkness adapted human eye, investigating absolute light perception threshold dependence on light stimulus gradient
09 p1391 A71-22487

Planetary surface smoothness factor determination by disk brightness, Mars red light and phase curves methods, indicating superiority of visual observation
09 p1520 A71-22828

Chromatic visual acuity measurement for gratings with bars of equal luminance and different colors
10 p1560 A71-23985

Comparative contrast and cues for illumination effects on perception of surface lightness, using target cast shadow experiments
12 p1872 A71-26613

Human visual system gate type lateral interaction to luminous intensity, noting visual field response to monocular viewing
13 p2018 A71-28460

Luminance and luminous flux discrimination in light and dark reared rats after early visual deprivation
13 p2011 A71-28810

Human visual perception response to brightness under sinusoidal current, suggesting interaction with retinal neural structures
17 p2680 A71-34656

Long duration brightness change in electroluminescent panel detection during monitoring task, discussing role of payoffs and signal ratios
17 p2690 A71-34705

Mathematical models of distance perception under flight conditions according to visible brightness of luminous surface
17 p2691 A71-35166

Visual adaptation mathematical model, studying relation of brightness static transformation into luminance
17 p2692 A71-35174

BRIGHTNESS TEMPERATURE

Planetary and lunar thermal radio emission and brightness temperature measurements using sensitive receivers and large aperture radio telescopes
02 p0309 A71-12155

Radio sources LF spectra distortions at critical value brightness temperature, noting induced Compton scattering effect on ambient gas thermal electrons
02 p0317 A71-12865

Venus lower atmosphere structure and brightness temperature spectrum analysis for composition, temperature and pressure profiles
03 p0484 A71-13212

Radio sky background temperature measurement with telescope, using moon as screen
03 p0487 A71-13472

Brightness temperature of vertically structured medium in microwave radiometry
04 p0552 A71-15212

Saturn millimeter wave spectrum and brightness temperature measurements, showing ammonia absorption characteristics in atmosphere
04 p0659 A71-15851

Mars, Jupiter, Saturn and Uranus millimeter wave radiation brightness temperatures, considering search for variations with time or phase angle

04 p0660 A71-15860

Solar chromosphere structure and Lyman continuum, examining brightness and kinetic temperatures, limb variations, radiative transfer and models

05 p0803 A71-16023

Atlas of 21 cm H I emission line profiles of outer part of Galaxy in Galactic anticenter region, plotting brightness temperature vs radial velocity

06 p0964 A71-17348

Theoretical submillimeter spectrum of Venusian radiation, determining brightness temperature

07 p1193 A71-19313

Light and radial velocity curves of binary HD 175514, obtaining spectroscopic and photometric orbital elements

07 p1204 A71-20633

Variable stars radii effective temperature and brightness determination from stellar atmosphere modes

09 p1523 A71-23021

Lunar equatorial region IR emission directional characteristics from brightness temperature measurements, developing cratered soil thermal model for negative surface relief studies

09 p1530 A71-23713

Brightness temperature from solar UV continuum in 1680 to 600 Å in photosphere-chromosphere transition model

10 p1666 A71-23780

Brightness temperature measurement in high pressure Ar plasma by comparing reference lamp to plasma radiation intensities

10 p1646 A71-23833

Jovian atmosphere radio observations, discussing helium- and ammonium-hydrogen molecules ratio, brightness temperature spectra and RF wavelength absorbing agents

12 p1964 A71-27087

Microwave emission from North Sea and North Atlantic at surface wind speeds of 5-25 m/sec, measuring brightness temperature

12 p1902 A71-27199

Uranus radio emission measurements at 8.22 mm wavelength, noting brightness temperature and atmospheric properties

12 p1965 A71-27226

Quiet sun and new moon brightness temperatures simultaneous measurements as function of frequency and wavelength

12 p1969 A71-27648

Chromospheric millimetric emission through 250 GHz atmospheric passband on isophoto maps, showing higher brightness temperatures compared with solar disk

12 p1969 A71-27649

One- and two-component gas models for explaining interstellar gas kinematics and 21 cm line emission brightness temperature dependence on galactic longitude

12 p1970 A71-27747

Saturn, Titan and ring IR photometric observations, examining brightness temperature albedos, optical thickness and individual particles

13 p2134 A71-28283

Radio model of brightness temperature and electron density in transition layer of solar active regions, using Laplace transformation and hydrostatic equilibrium equation

13 p2141 A71-29050

Planetary disks brightness temperature measurement using 22 m radio telescope with indium antimonide detector at 1.4 mm

13 p2141 A71-29102

Solar chromospheric activity of 8 February 1971, obtaining brightness temperature maps at 400, 800 and 1200 microns

13 p2143 A71-29271

Type 4 source movement out to 6 solar radii from solar center based on 80 MHz brightness temperature observations

14 p2306 A71-29694

Scattering effects on decimeter wavelength quiet sun emissions flux densities, frequencies and brightness temperatures

15 p2485 A71-31716

Theoretical submillimeter spectrum of Venusian radiation, determining brightness temperature

15 p2486 A71-31893

Heat balance and 8.22 mm radio emission of Mars, evaluating surface thermal and electrical parameters including brightness temperature

15 p2490 A71-32411

Uranus radio emission measurement at 8.22 mm, obtaining brightness temperature

15 p2490 A71-32412

Mars and Jupiter radio emission at 2.3 mm and 8.15 mm, determining brightness temperature and electrical and thermal waves soil penetration depth ratio

15 p2490 A71-32413

Mars microwave brightness temperature measurements, defining planetary spectra

15 p2490 A71-32415

Mars microwave spectrum, discussing brightness temperature increase towards short wavelengths in terms of surface material thermal, electrical or chemical properties

15 p2490 A71-32417

Saturn radio emission and brightness temperature measurements, determining rings optical thickness upper limit

16 p2639 A71-33692

Uranus radio emission measurements at 8.22 mm wavelength, noting brightness temperature and atmospheric properties

19 p3132 A71-37378

Jovian atmosphere radio observations, discussing helium- and ammonium-hydrogen molecules ratio, brightness temperature spectra and RF wavelength absorbing agents

19 p3133 A71-37437

Solar brightness temperature measurements using balloon-borne Michelson interferometer

19 p3135 A71-37613

Thermal radio emission of Jovian planets at atmospheres, deriving brightness temperature [AAS PAPER 71-109]

19 p3139 A71-37909

Saturn planetary system optical and radio observations during 1966, discussing Janus satellite, D ring, rarefied envelope and brightness temperature distribution

20 p3297 A71-39632

Microwave emission measurement of earth surface from Cosmos 243 satellite, detecting radio brightness temperature dependence on latitude and local features

20 p3260 A71-39685

Radio telescopic observations of Jupiter, Venus and radio source 3C 273 at 2 and 8 mm wavelengths, determining brightness temperatures and radiation flux densities

21 p3445 A71-40258

Water vapor dimer effects on atmospheric brightness temperature in cm and mm radiometric investigations from satellites above oceans

22 p3533 A71-41654

Small scale structure of extragalactic compact radio sources at 6 and 18 cm, obtaining magnetic field strengths and maximum brightness temperatures

22 p3598 A71-41912

Solar K-line profile absolute intensity calibration from elements of fine structure on surface, determining brightness temperature

23 p3767 A71-43836

Radio brightness temperature relationship to sea surface state, noting ocean storm regions determination from radiometric satellite data

23 p3673 A71-44050

Balloon measurement of solar flux and brightness temperature in 12-24 micron range

24 p3873 A71-45142

BRILLOUIN EFFECT

Rayleigh-Brillouin light scattering in compressed hydrogen, hydrogen deuteride and deuterium, noting discrepancy between observed and theoretical spectra

08 p1301 A71-20743

Single mode laser pumping generator of stimulated Brillouin scattering pulse in water

09 p1462 A71-22399

Stimulated Mandelstam-Brillouin, Rayleigh line wing and thermal light scattering, discussing fine structure, glass fracture and components shift

10 p1621 A71-24837

Nonlinearities effects on inorganic liquid laser output, investigating Raman and Brillouin scatterings and self focusing

18 p2933 A71-37012

Molecular iodine vapor absorption filter for stray laser light in Brillouin and Raman scattering

21 p3393 A71-41042

Brillouin scattering effect on noise of Bragg imaging in ultrasonic band at room temperature, using convergent illuminating light beam

22 p3541 A71-41779

BRILLOUIN ZONES

Highly ordered pressure-annealed pyrolytic graphite majority carrier electrons and holes locations in Brillouin zone from measurements in magnetic fields

08 p1344 A71-21363

BRISTOL-SIDDELEY OLYMPUS 593 ENGINE

Olympus 593 Concorde engine combustion system, discussing operating conditions, combustion performance criticality and altitude relighting

13 p2116 A71-28740

Olympus 593 supersonic engine lubricants tests, defining requirements in terms of bulk thermal stability, resistance to hot bearing breakdown, oil mist coking, etc

14 p2250 A71-29826

BRITISH AIRCRAFT CORP AIRCRAFT

U BAC AIRCRAFT

BRITTLE MATERIALS

Fracture location in brittle solids, using stress wave propagation in slender rod

09 p1538 A71-22699

Soviet book on metal alloys plasticity gaps covering crystallization, thermomechanical treatment, heat induced brittleness zones formation, etc

09 p1472 A71-23161

Discrete phase vs binder strength of inorganic brittle polycrystalline powder metallurgy materials, including alumina and magnesia

09 p1483 A71-23398

Brittle alumina ceramic tensile and flexural strengths comparison based on statistical surface flaw distribution theory of fracture

09 p1484 A71-2369

Brittle materials ultrasonic machining, discussing abrasive particle shape, size, temperature and pressure effects on process accuracy, speed, quality and efficiency

10 p1617 A71-24131

Brittle fracture mechanism models and connections with rheological properties of material, deriving relations for Griffith energy criterion

10 p1688 A71-24381

Crack propagation in chromium steel butt weld sheets, discussing dendrite macrostructural effects on brittle resistance and toughness

11 p1770 A71-25945

Electric discharge machining process for hard and brittle materials, based on metal erosion by interrupted electric spark

13 p2075 A71-28946

Low alloy high strength steels undetected fabrication originated anomalies, causing brittle behavior and crack propagation susceptibility [SME PAPER EM-71-706]

15 p2435 A71-32435

Crack propagation in brittle solids under constant deformation or thermal shock, verifying behavior by results with polycrystalline aluminum oxides

16 p2590 A71-32941

Brittle fracture under stress concentrations, calculating scale factor based on technical cohesive strength statistical theory

17 p2833 A71-35619

Brittle ceramic materials strength, showing porosity effect dependence on Weibull homogeneity parameter value

23 p3698 A71-44225

BRITTLENESS

Turbine disks and shafts for low temperature operation, examining brittle fracture tendency by acceleration testing

01 p0098 A71-10078

Cracked metals brittle fracture statistical analysis, discussing plastic deformation under load

01 p0166 A71-10080

Cr-Si steels cold shortness tests, identifying low temperature failure mechanisms

01 p0098 A71-10082

Materials and welded joints brittle fracture resistance estimation from impact bending tests

01 p0085 A71-10084

Weibull density functions applied to fracture location distribution in brittle solids

01 p0167 A71-10294

Critical ductile-brittle transition temperature and microstructure under deep drawing of sintered and vacuum melted Mo

02 p0257 A71-12519

Nb binary alloys room temperature brittleness in hydrogen atmosphere

02 p0270 A71-12932

Physical-metallurgical nature of brittle fracture of steels from phenomenological and atomic/dislocation approach

03 p0516 A71-14576

Brittle fracture mechanics, discussing shape, stress and dynamic toughness factors, crack-defect interaction and crack barriers

03 p0516 A71-14578

Brittle fracture resistance of mild steel after low cycle fatigue damage

03 p0516 A71-14579

Fracture toughness tests and brittle failure of high strength structural steels under thermomechanical treatment

03 p0447 A71-14581

Steel brittle fracture tests using explosive charge stress wave absorption measurements

03 p0517 A71-14583

Low temperature steel welded joints resistance to brittle fracture, discussing Niblink dynamic loading, deep notch static loading and Charpy V tests

03 p0433 A71-14585

Hugoniot elastic limit and dynamic compression strength for brittle bodies, considering hydrostatic stress and porous specimens

04 p0617 A71-14750

Notched tensile tests for measuring metal ductile-brittle transition temperature, deriving proportionality law

04 p0666 A71-14877

Steels brittle fracture susceptibility by notch impact bending test, considering plastic deformation zone and crack propagation

04 p0610 A71-14889

Reversible hydrogen brittleness of steels in terms of dislocation theory

04 p0612 A71-15550

- Inverse variational principles of brittle body fracture derived by extending inverse variational principles of mechanics and thermodynamics
05 p0825 A71-16609
- Solid deformable body combined brittle and plastic elements model for strain analysis
05 p0827 A71-16758
- Metals and alloys with bcc structure, investigating ductile-to-brittle transition by ultrasonic MHz technique
05 p0770 A71-17251
- Brittle fracture propagation velocity and branching, using high speed photography, electrical and ultrasonic methods
06 p0981 A71-17296
- Brittle plates with statistically distributed cracks, examining limiting equilibrium under tension and compression
06 p1000 A71-17941
- Dissolved hydrogen effects on mechanical properties, modulus of elasticity, lattice constants and X ray lines of Ti alloys, showing cold brittleness at high strain rates
07 p1130 A71-19298
- Rhenium effect on tungsten sensitivity to brittle fracture, measuring amplitude dependence of internal friction at temperatures from 77 to 1273 K
07 p1141 A71-20247
- Low temperature impact toughness test as criteria for metal susceptibility to brittle fracture
09 p1468 A71-22509
- Brittle materials tensile strength testing method, using thermal contraction loading device
09 p1479 A71-23698
- Adhesive fracture blister tests, using energy balance for treating stress singularities in brittle elastic materials
10 p1631 A71-24077
- Macroscopically ductile and brittle fracture via electron microscope photographs, considering brittle fracture and embrittlement temperature under uniaxial and multiaxial stress
10 p1627 A71-24595
- Epoxy resin fatigue behavior from double torsion technique, considering stable crack movement in brittle materials
11 p1785 A71-25401
- Ductility and susceptibility to brittle fracture of alloys under stress at low temperatures
12 p1919 A71-27685
- Crack kinematics for bodies with time dependent deformation and strength characteristics in brittle fracture, discussing tip region, crack models and energy equation
13 p2149 A71-28123
- Notch analysis of fracture, discussing elasticity theory of stress concentration and applications to brittle inhomogeneous materials and fatigue crack propagation
13 p2151 A71-28215
- Brittle structures and materials fracture strength, using linear fracture mechanics as analytical basis for testing
14 p2258 A71-29895
- Materials selection in product design, considering performance, cost, schedule and materials characteristics requirements, with special attention to brittle materials
14 p2340 A71-29899
- Industrial Ti and beta-Ti alloy hydrogen thermodynamic and effects on brittleness
15 p2424 A71-31238
- Low carbon high chromium steel, emphasizing nitrogen content effects on temper brittleness
15 p2427 A71-31529
- Steel structural elements resistance reserve to brittle fracture, considering critical temperatures and breaking stresses
15 p2504 A71-31852
- Brittle plates with stochastic distribution of cracks under biaxial tensile-compressive stresses, obtaining critical load
15 p2504 A71-31853
- Steels resistance to brittle fracture at various temperatures, determining failure stress and transition temperatures for nonuniform stress distribution
15 p2428 A71-31855
- Strain rate effect on crack growth within subcritical load range, deriving expressions for rate-independent and rate-dependent quasi-brittle solids
16 p2590 A71-32946
- Turbine wheels and shafts for low temperature operation, examining brittle fracture by acceleration testing
16 p2593 A71-33634
- Cracked metals brittle fracture statistical analysis, discussing plastic deformation under loading
16 p2658 A71-33636
- Cold hardened Cr-Si steels strength/plasticity thermal dependence and brittleness from short torsion and compression tests, identifying low temperature failure mechanisms
16 p2593 A71-33638
- Materials and welded joints low temperature operation reliability prediction by estimating brittle fracture resistance from impact bending tests
16 p2584 A71-33640
- High strength structural stainless steels with good toughness and little crack sensitivity, noting brittleness due to oxidation, precipitation and carbide network
16 p2597 A71-33916
- Mechanical and crystallographic structure effect on cold brittleness temperature anisotropy and on exfoliation of Cr alloyed with rare earth elements
17 p2755 A71-34416
- Deformation temperature effects on microstructure and mechanical properties of low alloy Mo, considering cold brittleness temperature and associated plasticity
17 p2755 A71-34418
- Combined brittle and plastic elements model for strain analysis of nonelastic deformed solid
17 p2832 A71-35457
- Machine components resistance to low temperature brittle failure, considering threaded joints, gears and shafts for strength and plasticity characteristics
17 p2832 A71-35463
- Dynamic yield and absorptivity of steel during brittle fracture propagation under neutron irradiation
18 p2934 A71-35987
- Beryllium impurities effects on ductile-brittle transition temperature, investigating fracture characteristics deformation mechanism
19 p3076 A71-37121
- Alpha Ti at blue brittle temperature, observing strain rate dependent work hardening effects on necking strain
21 p3398 A71-40464
- Brittle transition temperature of steels by Vickers hardness testing, comparing with tensile properties and impact fracture process in Charpy impact test
21 p3388 A71-40751
- Inelastic transverse strain coefficient and Poisson ratio dependences on plastic and brittle properties
23 p3780 A71-44227
- Recrystallized metalceramic W plastic deformation effects on brittleness temperature threshold, revealing relationship to impurity segregations at grain boundaries
24 p3837 A71-44674
- Homogenizing annealed TiC-WC carbides properties at room temperature, investigating microhardness, microbrittleness and resistivity
24 p3838 A71-44740
- BROADCASTING**
- Magnetic disk storage media for recording and reproducing wideband instrumentation data
01 p0082 A71-10893
- Type IV solar radio emission broadband intensity fluctuations explained by MHD pulsations in flux tubes in corona
01 p0162 A71-11387
- Two-terminal pair broadband matching circuits losses from method for LF series-shunt coupler with uniform scattering
03 p0386 A71-13810
- Wideband signal processing via multiple narrow band channels, discussing performance limitations due to amplitude and phase distortion and spurious outputs
04 p0555 A71-15341
- Reflector antenna under wideband noise radiation, determining directivity characteristics by solution for angle range homologous to region of irregular lobes
05 p0728 A71-16008
- Broadband radiated man-made electromagnetic noise measurement for communication systems performance determination, noting instrumentation problems
05 p0721 A71-16468
- Gunn diodes impedance measurement at bias voltage above threshold, using broadband equivalent circuit model for mount and package
07 p1072 A71-19103
- White dwarf G195-19 circular polarization measurements of continuum radiation in broad band, using electro-optically switched polarimeter
07 p1198 A71-19832
- Microwave wideband and multiband radome design for strength, environmental and electrical requirements, achieving transmission efficiencies with dielectric and wall thickness selection
14 p2216 A71-31037
- Broadband varactor tuned X band Gunn oscillator, investigating output power and temperature stability
17 p2717 A71-35340
- Type I supernova broadband identification, examining interstellar medium spectra
17 p2806 A71-35384
- Physical nature and measurement of broadband noise, considering rms value directly proportional to square root of frequency bandwidth
19 p3020 A71-38428
- Dipole antenna bandwidth extension by conjugate reactance loading based on periodically loaded transmission line theory
19 p3036 A71-38602
- Broadband antenna twist reflector with wire grids, deriving design formulas and theoretical performance in terms of polarization attenuation
19 p3036 A71-38606
- Wide passband techniques for atmospheric total ozone content measurements, discussing choice of ozonometer characteristics and filter parameters
20 p3238 A71-39335
- Multiple pure tone and broadband noise generation in high speed turbobans, noting analytical model
20 p3277 A71-39773
- Broadband random vibration simulation of force environment action on multimode structure [ASME PAPER 71-VIBR-2]
21 p3362 A71-40266
- Mean value theorem for broadband matching of source with known resistance and parasitic capacitance matched to load resistance
22 p3510 A71-42247
- BROADCASTING AMPLIFIERS**
- Broadband cooled parametric amplifier with low noise for satellite communications ground station, discussing performance at room and cryogenic temperatures
01 p0053 A71-10799
- Wideband low noise parametric amplifier design, discussing noise temperature improvement by refrigeration at microwave frequencies
02 p0234 A71-12815
- L band DME and TACAN improvements, emphasizing use of static broadband amplifiers
02 p0235 A71-12905
- Solid state transferred electron broadband amplifiers in electronic countermeasure memory systems for radar pulse replica retransmission, comparing with low noise traveling wave tubes
04 p0558 A71-15361
- Broadband hybrid UHF integrated power amplifiers providing high output, noting integration techniques, design, fabrication and characterization
04 p0559 A71-15876
- Broadband IMPATT diode multistage transmission amplifiers computer aided design and X band performance
07 p1073 A71-19114
- K band cryogenically cooled wideband /600 MHz/ low noise parametric amplifier for millimeter wave satellite communication earth terminals, discussing design
08 p1263 A71-20770
- Wideband UHF amplification in bulk n-type GaAs during domain generation, comparing cut-off and Gunn frequency
09 p1507 A71-22223
- Microwave amplification using negative resistance device in prototype filter equalization networks, permitting realization of wideband amplifiers for C band and superhigh frequencies
11 p1736 A71-25140
- Broadband multicavity multimegawatt klystron design for superpower amplifiers in radars and particle accelerators
11 p1734 A71-26433
- Wideband transistor amplifier frequency response at low frequencies, discussing gain increase, thermal pull-in effect, barrier layer geometry and switching control functions
12 p1887 A71-27042
- Interdigital broadband hybrid junction transducer terminated in negative resistances for acoustic surface waves amplification
13 p2037 A71-28476
- Hybrid integrated wideband linear microwave power amplifiers for S and C bands, discussing construction and performance
21 p3357 A71-40817
- Wideband microwave amplifier with two antiparallel high efficiency avalanche diode pairs, presenting fishbone shaped tuning plate for bandwidth widening
23 p3653 A71-43961
- BROADCASTING**
- Optimum positioning and structure of light hogged antenna masts for radio communications and broadcasting networks
01 p0068 A71-11085
- Satellite regional broadcasting and telephony/data services cost model
02 p0221 A71-12781
- Direct broadcast television service by satellite transmission, calculating trees and woods effects on attenuation and suggesting receiving system design modification
09 p1408 A71-23384
- Communication satellite TV and sound broadcasting system design without unreasonable cost
17 p2697 A71-34237
- Satellite broadcasting defined by UN, discussing community and home direct reception modes and educational TV potentialities and problems
17 p2697 A71-34238
- Global broadcasting from space, suggesting international cooperation and UN role
17 p2841 A71-34250
- Satellite instructional TV experiment for direct community broadcasting to Indian villages [AIAA PAPER 71-844]
17 p2700 A71-34709

Low elevation angle tropospheric fading relationship to satellite communications and broadcasting at frequencies between 1 and 20 GHz

17 p2703 A71-35083

Queueing theory approach to communication satellite network design, applying to ocean air traffic control and worldwide military broadcast systems

17 p2721 A71-35106

Satellite TV broadcasting development in European community, giving cost estimation procedure and program reception methods

18 p2876 A71-36504

Stabilizing system for retransmission beam of direct TV broadcast satellite, considering rebroadcast antenna, electronic sensor and antenna pointing subsystem

18 p2892 A71-36576

Direct broadcast satellite TV communications, discussing international regulations and legal aspects

18 p2989 A71-36578

BROMIDES

NT CHROMIUM BROMIDES

NT POTASSIUM BROMIDES

Ethylene oxide and methyl bromide sporadic activity compared for spacecraft sterilization of *B. subtilis* var niger spores

01 p0027 A71-11565

Lowered ignition temperature and fire propagation of polyester containing bromides

07 p1182 A71-19243

IR and Raman spectra vibrational analysis of crystalline and fluidic oxalyl bromide, explaining observations by two geometrical isomers existence

11 p1727 A71-25363

HBr positive ion formation by Ar ion beam collision with HBr, using predissociation to establish dissociation limit

13 p2026 A71-29039

Hydrogen bromide effect on argon diluted propane-oxygen flame structure

19 p3167 A71-38100

BROMINE

Emission line spectra of halogens ClI, BrI and II in 4-micron region

05 p0717 A71-16911

Bromine dissociation rates in presence of He, Ne, Ar, Kr and Xe, determining rate constant expressions from light absorption measurements behind incident shock waves

13 p2027 A71-29508

BROMINE COMPOUNDS

NT BROMIDES

NT CHROMIUM BROMIDES

NT POTASSIUM BROMIDES

Lithium iodide and tetramethyl ammonium iodide additions effect on radical exchange between phenyl lithium and bromobenzene in diethyl ether

19 p3011 A71-37391

BRONCHI

Terminal bronchiole diameter changes with volume in isolated air filled lobes of cat lung

07 p1044 A71-20332

BRONCHIAL TUBE

NT PHARYNX

Pulmonary oxygen toxicity, considering composition of endobronchial saline extracts of rats and edema development

13 p2015 A71-29362

BRONZES

Oxide bronzes as oxygen reduction catalysts in batteries and fuel cells, considering effects of varying compositions and crystal faces

03 p0374 A71-13054

Cu and Al bronze civil transformation kinetics, using electron photoemission microscopy

03 p0444 A71-14337

Electrochemical properties of Na-W bronzes for use as electrocatalysts in acid electrolyte fuel cells

09 p1387 A71-23648

Metal finishing tests on bronze in presence and absence of surface active agents, considering abrasive working

13 p2072 A71-27816

Thermal emf measurement of Ti alloy, steel, bronze and duraluminum subjected to fretting corrosion tests

13 p2082 A71-27820

Optimal electron beam welding of Nb alloy to bronze, showing high mechanical properties due to deep Cu diffusion

14 p2253 A71-30491

Lead bronze and Babbitt metal composite material, detailing antifriction efficiency and wear resistance in bearings

15 p2417 A71-32666

Temperature effects on service life of cermet bronze-graphite bearings using different lubricants

15 p2418 A71-32674

Aluminum bronze alloy forming dies fabrication and repair, discussing surfacing, hot working grinding, machining and welding methods

18 p2928 A71-36855

BROWNIAN MOVEMENTS

Fluctuations in parametrically excited subharmonic oscillator, deriving steady state probability distribution for amplitude and phase transitions analogous to Brownian motion of particle in potential well

20 p3203 A71-39094

BRUSHES

Molybdenum disulfide treated graphite brushes in electric contact with copper slip rings at high rates in dry pure inert gas atmospheres

07 p1120 A71-20275

BUBBLES

Liquid film formation at base of bubbles and effects on heat transfer during nucleate boiling

01 p0181 A71-11404

Boiling under weightlessness, examining gravitational effects on bubbles formation frequency and diameters

02 p0331 A71-11922

Acoustic velocity in water, examining air bubble effects on pressure pulse attenuation

03 p0459 A71-13720

Planned optical coincidence system for level bubble end image superimposition and transmittance to passage instrument ocular part

04 p0591 A71-14856

Translatory vapor bubbles motion in binary liquid mixtures under heat and mass transfers

04 p0687 A71-15534

Gas bubble statics in physical systems and organism tissues during decompression

06 p0855 A71-18374

Vapor bubbles radius at heating surface separation moment at boiling under free convection and forced motion through channel

07 p1221 A71-18923

Vapor bubbles during nucleate boiling, deriving formation frequency relationship with departure diameter

07 p1222 A71-19197

Bubble of energetic charged particles embedded in interstellar or intergalactic magnetic field and in gas, discussing dynamic effects on radio astronomy observation

07 p1197 A71-19815

Gas bubble growth and dissolution due to pressure fluctuations in turbulent diffusion liquid flow

07 p1094 A71-20475

Acoustic beam attenuation through liquid medium under ultrasonically excited cavitation, taking into account bubble configuration

09 p1434 A71-23668

Surface roughness ensuring turbulent reattachment at low Reynolds numbers on airfoil sections with separation near leading edge resulting in bubbles [ONERA-TP-923]

10 p1549 A71-23762

Closed steady streamline creeping flow in cylindrical cavity applied to bubble or plug flow in pulmonary and peripheral capillaries

10 p1571 A71-24614

Short N wave refraction and diffraction by gas-filled soap bubble, discussing measurements to explain peaking and rounding in sonic boom pressure signature

10 p1642 A71-24811

Cavitation in liquids with dissolved gases by acoustic wave induced oscillating pressure, discussing gas bubble formation through rectified diffusion process

10 p1597 A71-24942

Cavitation microstreaming near spherical drop or bubble performing translational harmonic oscillations in liquid at rest

11 p1749 A71-25183

Boiling under weightlessness, examining gravitational effects on bubbles formation frequency and diameters

13 p2159 A71-28209

Flow visualization by cathodic hydrogen bubble technique, using electric pulsing for regular pattern formation for flow distortion tracing [ASME PAPER 71-FE-36]

13 p2053 A71-29471

Large gas bubble migration in rotating liquid without gravity, noting velocity dependence on stagnation point distance and radius of curvature

15 p2392 A71-32119

Boiling at solid heated surfaces, discussing nucleation, bubble formation, pool boiling factors, heat transfer correlation and forced convection

15 p2515 A71-32565

Dynamic bubble growth and diameter at detachment during liquid boiling at heating surfaces, using force equilibrium, laser Mach-Zehnder interferometer and temperature measurements

16 p2663 A71-34038

Gas bubble in liquid under surface tension, weightlessness and rotation, determining angular velocity for fluid system disintegration

16 p2560 A71-34142

Two dimensional laminar separation bubbles in high Reynolds number flow fields, using finite difference solutions to Navier-Stokes equations

16 p2561 A71-34165

Vapor bubble growth on heated surface with random temperature distribution and liquid microfilm for water and boiling potassium

17 p2836 A71-34306

Liquid Zr drops combustion in oxygen-nitrogen atmospheres, examining critical conditions for gas formation with homogeneous bubble nucleation theory

17 p2837 A71-34511

Free jet expansion of liquid-gas bubble mixture suspended in glycerine

17 p2728 A71-34891

Bubble formation during annealing of W doped with K, Al and Si compounds, using electron microscopy with thin foil and fracture replication techniques

19 p3079 A71-37708

High speed neutral buoyancy bubble generators for aerodynamic flow visualization, investigating tip vortex from wing or helicopter rotor blade

19 p3064 A71-37725

Spherical cap bubbles in water and mineral oil at various dynamic viscosities, measuring laminar and turbulent wakes character, rise speed and shape

21 p3365 A71-40017

Scanning ultrasonic imaging technique for in vivo monitoring of microscopic bubble formation in decompression sickness, presenting image displays

22 p3504 A71-42250

Spectral model of warm bubble motion in neutral surroundings from anelastic equations for shallow convection, comparing results with similarity theory and numerical models

23 p3781 A71-43336

Transportation lag simulation by fluidic transmission lines and bubble tubes

24 p3793 A71-45086

Shock wave structure in liquid-gas bubble mixture with varying volumetric gas content, bubble size, shock strength and liquid viscosity

24 p3820 A71-45128

BUCCANEER AIRCRAFT

Phantom and Buccaneer aircraft boundary layer control, examining lift from trailing and leading edges

06 p0847 A71-17953

BUCKLING

NT CREEP BUCKLING

NT ELASTIC BUCKLING

NT EULER BUCKLING

NT THERMAL BUCKLING

Buckling of ring stiffened conical shells under axial compression, determining critical loads

01 p0168 A71-10342

Circular shallow cylindrical panel stability and creep buckling under hydrostatic pressure

01 p0171 A71-10649

Buckling under compressive loads of incompressible neo-Hookean plates

01 p0171 A71-10659

Buckling in fiber reinforced plastic thin walled shell structures, discussing structural stability problems and methods for prevention of buckling

01 p0172 A71-10698

Orthotropic annular plates buckling, using finite difference equations and Vianello-Stodola iterative method

01 p0174 A71-10968

Nonlinear impact buckling of strut, using asymptotic small parameter method

01 p0177 A71-11296

Simply supported cylindrical shell buckling under linearly varying lateral pressure

01 p0178 A71-11399

Buckling analysis of rectangular waffle plates with multiple sizes of ribs in each stiffening direction, considering stability and design

01 p0178 A71-11583

Doubly curved thin shallow shells nonlinear stability, using piecewise linearization for postbuckling load-displacement curves

03 p0501 A71-13073

Marguerre equations for deflection and buckling of partially and fully loaded spherical caps, noting inaccuracy of finite difference approximation

03 p0503 A71-13428

Clamped shallow spherical and conical shells axisymmetric dynamic buckling under step loads of infinite duration, showing similarity with static buckling

03 p0504 A71-13455

Stress concentration in buckling proof clamped sandwich rod with multicut rectangular cross section under torsional bending

03 p0504 A71-13527

Postbuckling behavior of open cylindrical shells under uniform axial compression loads, solving finite difference equations by Newton-Raphson method

03 p0505 A71-13539

Axisymmetrically loaded shells of revolution made of work hardening materials, determining inelastic finite deformations and buckling loads by incremental variational method

03 p0505 A71-13543

Open cylindrical shells with end eccentricity or initial deflection imperfections, investigating buckling under axial compression by Newton-Raphson method

03 p0505 A71-13544

Circular shallow prestressed arches with fixed ends, considering initial thrust effect on snap buckling

03 p0505 A71-13545

Buckled beam nonlinear vibration under harmonic excitation, solving governing partial differential equation by Galerkin and harmonic balance methods [ASME PAPER 70-WA/APM-48]

03 p0512 A71-14167

- Postbuckling theory and applications covering perfect structure prebuckling state stability, cylindrical shells under axial compression, etc 04 p0664 A71-14734
- Ellipsoidal pressure vessel heads failure mode analysis, considering buckling under internal pressure and design formula with safety factors [ASME PAPER 70-PVP-26] 04 p0665 A71-14769
- Monograph on bounds for vibration frequencies and buckling loads of clamped uniform thin elastic plates covering stability, harmonic and biharmonic functions 04 p0667 A71-14899
- Rectangular and circular thin orthotropic plates thermal buckling approximate solution using Rayleigh-Ritz energy method 05 p0819 A71-15978
- Eccentrically stringer-reinforced rectangular plates buckling under linearly varying longitudinal compression, using Galerkin method 05 p0819 A71-15980
- Local axisymmetric dimple imperfection effects on buckling load of circular cylindrical shell under axial compression [AIAA PAPER 70-103] 05 p0823 A71-16557
- Circular cylindrical shells buckling with different elastic moduli in tension and compression under arbitrary axial and lateral pressure 05 p0823 A71-16558
- Axial buckling tests on machined integrally ring stiffened cylindrical shells 05 p0823 A71-16559
- Stability loss of cylindrical shell at upper bound of buckling load under axial compression 06 p0983 A71-17365
- Circular cylindrical orthotropic fiberglass-reinforced shell buckling under longitudinal impact, assuming initial surface imperfections 06 p0985 A71-17684
- Buckling of cold formed Al alloy thin walled columns under compression, investigating longitudinal half wave formation 06 p0985 A71-17748
- Cylindrical shells buckling under subcritical loads, considering internal and external hydrostatic pressure and axial compression 06 p0988 A71-17779
- Closed circular cylindrical shell stability and buckling during axial compression, using energy method in geometrically nonlinear formulation 06 p0994 A71-17824
- Circular plates of anisotropic fiber-reinforced materials, calculating axisymmetric bending and buckling 06 p0995 A71-17829
- Prismatic shells vibration, buckling and stress analysis, applying computer solutions to complex bodies of revolution [AIAA PAPER 71-112] 06 p1003 A71-18562
- Design criteria for buckling prediction of elliptical and circular cylindrical shells under axial compression from asymmetric and axisymmetric shape imperfections distribution [AIAA PAPER 71-145] 06 p1003 A71-18588
- Nonlinear finite difference computer program applied to elliptic cylinder collapse under uniform external pressure, comparing with theoretical bifurcation buckling [AIAA PAPER 71-146] 06 p1003 A71-18589
- Spring supported beam-column with vibration and buckling eigenvalues, discussing Monte Carlo simulation for evaluating perturbation method accuracy for variance calculation [AIAA PAPER 71-149] 06 p1004 A71-18591
- Dynamic elastic-plastic buckling of rectangular plates in sustained flow involving mass impact 07 p1211 A71-19251
- Imperfect elliptical cylindrical shells buckling under axial compression, demonstrating imperfection sensitivity 07 p1213 A71-19888
- Plastic strains, thermal residual stresses and buckling of rectangular cross section plates and beams subjected to asymmetric heating and cooling 08 p1375 A71-22056
- Nonlinear elastoplastic ring buckling under compression 09 p1534 A71-22145
- Asymmetric buckling of spherical caps with asymmetrical imperfections, using nonlinear relaxation technique for treatment of finite difference representation of differential equations 09 p1541 A71-23090
- Clamped shallow spherical caps under uniform pressure, computing axisymmetric buckling 09 p1541 A71-23091
- Cylindrical body stability under axial compression with small elongations and shears, determining critical buckling force 09 p1542 A71-23437
- Buckling coefficient of Al alloy columns with different section profiles, using steel structures stability specifications 10 p1623 A71-23768
- Creep analysis for thermoplastic beams under bending and struts under buckling 10 p1685 A71-23942
- Thin simply supported polygonal and rhombic plates critical hydrostatic buckling loads and free vibration frequency calculation by conformal mapping and power series expansion 10 p1686 A71-24018
- Multilayer sandwich plates with transverse shear resistant inner layers and bending and twisting moment resistant outer layers, calculating critical buckling loads by finite elements 10 p1686 A71-24020
- Optimal prestressing against buckling of structures with reserve capacity, using energy methods of structural analysis 10 p1689 A71-24514
- In-plane boundary conditions influence on clamped conical shells buckling under external pressure, using displacement method based on Donnell stability equations 11 p1841 A71-25158
- Buckled rectangular panels response to random excitation via single degree of freedom nonlinear vibration equation 11 p1841 A71-25196
- Cylindrical shells panel flutter analysis for internal stress and supersonic flow, considering still air buckling data useful for determining buckling loads [AIAA PAPER 71-328] 11 p1842 A71-25308
- Initially curved thin elastic plates, predicting large deflection and postbuckling behavior with finite element procedure [AIAA PAPER 71-357] 11 p1844 A71-25336
- Buckling of axially compressed imperfect isotropic cylindrical shells with edge constraints, deriving two point boundary value problem numerical solution by shooting method [AIAA PAPER 71-358] 11 p1844 A71-25337
- Composite material structural behavior prediction, emphasizing static, dynamic, buckling and post-buckling response of anisotropic plates laminated from unidirectional plies 11 p1846 A71-25429
- Nonlinear dynamic analysis of shells of revolution under symmetric and asymmetric loads, obtaining solutions for shallow cap buckling 11 p1847 A71-25465
- Buckling load scatter reduction in axially compressed thin walled circular shells as function of manufacturing accuracy [DFVLR-SONDDR-92] 12 p1974 A71-26869
- Buckling of eccentrically stiffened multilayered circular cylindrical shells with different orthotropic moduli in tension and compression 12 p1982 A71-27572
- Buckling of circular cylindrical shells with axisymmetric imperfection distributions under axial compression 12 p1983 A71-27573
- Edge restraint effects on postbuckling behavior of thin flat plates under uniformly distributed compressive loads, noting buckling load and stiffness increase 13 p2153 A71-28466
- Elastic deformation and plastic buckling of rectangular column with initial deflection under axial compression 13 p2157 A71-29287
- Circular cylindrical thin walled shells buckling, determining postbuckling patterns development by high speed cinematography [DFVLR-SONDDR-99] 13 p2157 A71-29305
- Elastic stability of compressed beams, giving method for evaluating neutral axis form and critical load in buckling 13 p2157 A71-29321
- Stress analysis of thin walled framed structures of variable cross section by second order differential buckling equations, using matrix method 14 p2321 A71-29539
- Vertically cantilevered column weight and follower force effects on flutter and buckling instabilities respectively 14 p2330 A71-30685
- Clamped shallow spherical cap buckling and initial postbuckling behavior under axisymmetric band type loads, using numerical analysis 14 p2330 A71-30690
- Column buckling under initially random bending and twisting, comparing numerical analysis accuracy with Bernoulli-Euler results 14 p2330 A71-30692
- Work hardening material planar frame inelastic load deformation and buckling, using finite difference method and variational principle 14 p2330 A71-30693
- In-plane boundary effects on buckling and critical stress of axially loaded cylindrical panels 14 p2331 A71-30697
- Simply supported skew plates buckling under uniform in-plane stresses, obtaining numerical results for various ratios and angles 14 p2331 A71-30698
- Viscoplastic cylindrical shell dynamic buckling during axial impact of rigid mass, discussing constitutive equations 14 p2331 A71-30841
- Buckling under compressive loads of incompressible neo-Hookean plates for homogeneous initial deformation, using variational principle 14 p2333 A71-30993
- Snap buckling instability of shallow shell type structures subject to random transverse load 15 p2502 A71-31417
- Finite element midincrement stiffness matrices in postbuckling analysis of imperfect strut and rectangular plate 15 p2503 A71-31420
- Clamped anisotropic symmetrically laminated plate bending, buckling and free vibration exact solution, using Fourier analysis 15 p2506 A71-32013
- Rods instability with cross sectional stress concentration dependent properties, presenting buckling and bending problems 16 p2648 A71-32990
- Plastic structures buckling and instability phenomena, using elementary models with limited number of degrees of freedom and associated yield profiles 16 p2649 A71-32999
- Optimal structural design for nonconservative systems under buckling, noting application to minimal weight nonprismatic elastic bar shape determination 16 p2649 A71-33012
- Elastoplastic buckling of structures, considering strain hardening materials, slip and Bauschinger effect 16 p2650 A71-33024
- Buckling and postbuckling loads of initially imperfect orthotropic cylindrical shells under axial compression and internal pressure, using potential energy principle 16 p2651 A71-33025
- Statistical methods application to buckling of axially loaded columns, considering entire spectrum of elastic, elastoplastic and fully plastic ranges 16 p2654 A71-33123
- Buckling of axially compressed circular cylindrical shells with localized or random axisymmetric imperfections, deriving asymptotic approximation formulas for stress calculation [ASME PAPER 71-APM-29] 16 p2655 A71-33200
- Shear modulus, flexure and buckling of web stiffened sandwich structures, using core layer model based on continuum theory [ASME PAPER 71-APM-8] 16 p2656 A71-33217
- Annular plate stability and postbuckling behavior in steady plane axisymmetric temperature field 17 p2822 A71-34598
- Long laminar plate and cylindrical panels with hinged lateral edges under buckling by normal uniformly distributed load, calculating deflection as monotonic pressure functions 17 p2823 A71-34781
- Cylindrical shell with continuous filler, calculating stability and axisymmetric buckling in axial compression 17 p2830 A71-35321
- Toroidal shell stability analysis for asymmetric buckling based on small deflection theory linearized relations, deriving upper critical pressure by Bubnov-Galerkin method 17 p2831 A71-35323
- Hinged bar dynamic buckling under harmonic axial load, using Timoshenko beam theory with longitudinal vibration effects 17 p2832 A71-35400
- Postbuckling elastic characteristics of structures under combined loading near special critical point 17 p2832 A71-35420
- Clamped rectangular plate buckling under uniaxial and biaxial compression, obtaining critical loads for various aspect ratios 18 p2979 A71-36360
- Thin circular annular Al plate buckling under uniform radial compression 19 p3157 A71-37872
- Longitudinal edge stiffness and internal pressure effects on buckling and initial postbuckling behavior of axially compressed stringer reinforced cylindrical panels, discussing imperfection sensitivity 19 p3157 A71-37873
- Inelastic buckling process of axially compressed cylindrical shells with edge constraints, using variational principle and Rayleigh-Ritz method 19 p3158 A71-38182
- Buckling and initial postbuckling behavior of clamped thin shallow spherical sandwich shells under axisymmetrical loads 19 p3159 A71-38185
- In-plane boundary conditions effect on buckling loads of axially compressed simply supported ring stiffened cylindrical shells 19 p3159 A71-38270
- Nonlinear free and forced vibration response and stability of simply supported restrained buckled beams, using analog computer simulation [ASME PAPER 71-VIBR-17] 21 p3458 A71-40277

Shallow spherical cap and deep thin spherical shell buckling, solving integral equations by iterative procedure

21 p3463 A71-40542

Buckling load reduction for axially compression loaded geometrically perfect cylindrical shells by wall temperature gradients induced partial yielding

21 p3469 A71-41006

Nonlinear periodically oscillating motions in shell theory, examining buckling characteristics of thin walled structures under dynamic and shock loads action

21 p3473 A71-41152

Shallow two pinned sinusoidal arches stability under random symmetrically distributed lateral loads, observing deformation, buckling and critical value

22 p3612 A71-41429

Koiter theory for structural snap-through buckling behavior, using discretized matrix procedure based on finite element idealization

22 p3613 A71-41436

Axisymmetric buckling of annular plate subjected to unequal uniform radial compression along inner and outer edges

22 p3615 A71-42036

Frequency and buckling stability eigenvalue evaluation for anisotropic circular cylindrical shells under nonuniform lateral prestress

22 p3615 A71-42210

Plastic buckling stability of hinged arches for perfect and imperfect structures with linear work hardening stress-strain behavior

23 p3776 A71-43372

Radial edge displacement effect on circular cylindrical shells compressive buckling stress, noting opposite effects for different length/radius ratio ranges [AIAA PAPER 71-984]

24 p3878 A71-44580

Geometrically nonlinear circular plate under nonuniformly distributed radial force, calculating loading rate and end condition effects on buckling, deflection and stress

24 p3884 A71-44899

Circular cylindrical laminated anisotropic shells with axisymmetric shape imperfections, investigating upper bound buckling loads

24 p3841 A71-44958

Stochastically imperfect columns on nonlinear elastic foundations, obtaining approximate asymptotic expression for buckling stresses and lateral displacement autocorrelation

24 p3884 A71-44962

Stress-strain curve of unidirectional fiber reinforced composite Al and N-CI wire under axial compression loads, discussing buckling and shear instabilities

24 p3842 A71-45229

BUDGETING

Computer aided network analysis for multiple project planning facilitating readjustments and budgeting

02 p0336 A71-12122

Ossa R and D program noting budget allocations, satellite programs and international projects

04 p0690 A71-14934

R and D money optimal reallocation due to total research budget decrement, based on computer program

05 p0840 A71-16743

Satellite project cost estimation, evaluating formulae for budget, tender offer and contractual expense

23 p3785 A71-43459

BUFFER STORAGE

Earth satellites ferrite core buffer storage replacement by magnetic tape unit noting design, performance, volume and operation [DGLR-70-082]

05 p0726 A71-15952

Queueing model of statistical multiplexer buffer behavior for batch Poisson arrivals and single constant output, applying to time sharing computer buffer design

05 p0724 A71-17063

Large capacity ferrite core buffer memory for spacecraft telemetry temporary data storage, using access circuitry with multiplex and thin film circuits

09 p1421 A71-23735

BUFFERS [CHEMISTRY]

Carbon dioxide absorption of dog blood and plasma under anoxia at simulated high altitudes, deriving equations for protein concentration rated buffer values

07 p1043 A71-20327

Mean whole body intracellular pH and buffer capacity for arterial carbon dioxide tension in ventilated dogs

10 p1558 A71-23896

Body temperature effects on intracellular carbon dioxide dissociation, pH and buffer capacity in hypothermic and hyperthermic dogs

10 p1559 A71-23897

Equilibration rate of uncatalyzed carbon dioxide hydration reaction in open system at constant carbon dioxide partial pressure, examining buffering capacity effect

10 p1559 A71-23898

Respiratory acid-base disturbances, studying deviations of bicarbonate ion vs pH pathway followed by buffered solution on carbon dioxide titration

13 p2007 A71-28434

BUFFETING

Swept wing fighter aircraft transonic buffet onset lift coefficient from camber and trailing edge deflection, considering design variations

02 p0186 A71-12679

Vibration and buffeting effects on man, discussing aerospace environments, biomechanics, human tolerances and performance, etc

08 p1244 A71-20709

F-8D aircraft transonic flight and wing tunnel tests for buffet onset prediction, considering effects of g level and fluctuation amplitude and frequency [AIAA PAPER 70-341]

10 p1557 A71-24863

Miniature pressure transducers for wind tunnel aircraft models buffet phenomena measurements, discussing calibration, frequency and pressure range, sensitivity and accuracy

14 p2245 A71-30335

Stratospheric turbulence induced aircraft buffeting dependence on horizontal temperature and wind distribution

15 p2444 A71-31366

Cone-cylinder-cone missile type body in transonic buffeting environment determining static and fluctuating wall pressure distribution [ONERA-TP-942]

18 p2843 A71-36020

BUILDING MATERIALS

U CONSTRUCTION MATERIALS

BULGARIA

Night airflow measurements over Bulgaria, showing midnight minimum, maximum between 0100 and 0200 hours local time, steady airflow periods and random fluctuations

10 p1599 A71-23877

BULGING

Axisymmetric bulge region formed in long uniform plasma column by reduction of external magnetic field

01 p0134 A71-11004

BULK MODULUS

Ta alloys single crystals elastic compliance constants over temperature range, deriving bulk and shear moduli and anisotropy factor

01 p0100 A71-10373

Polycrystalline NbC and TaC Young, shear and bulk moduli determination at high temperature, noting porosity and temperature effects

11 p1781 A71-26294

Thermal expansion coefficient and bulk modulus of lunar rocks 10020, 10046, 10057 and 12022,95

23 p3761 A71-43782

BULKHEADS

Aircraft fuselage design with marine type bulkhead construction, discussing advantages in cabin decompression and fire hazards reduction

20 p3178 A71-38752

BUMPERS

Construction and hypervelocity impact tests of penetration resistive dual bumper wall for spacecraft meteoroid protection [AIAA PAPER 71-339]

11 p1843 A71-25318

BUNCHING

NT ELECTRON BUNCHING

BUNDLES

Brachial plexus bundle structural and histological characteristics in man and monkey, noting lack of intraneural network in monkey

23 p3634 A71-43911

BUOYANCY

Thermal instabilities in rapidly rotating fluids with buoyancy force and depth gradient, noting geophysical analogy of self gravitating sphere

03 p0409 A71-13727

Buoyancy effect on boundary layer flow over heated horizontal circular cylinder immersed in uniform axial free stream, considering successively greater displacements

03 p0519 A71-13731

Buoyancy effects on transient free convection heat transfer in revolving tube for zero to 100 g centrifugal acceleration [ASME PAPER 70-HT-10]

03 p0521 A71-14292

Destabilizing buoyancy forces effect on weak homogeneous shear flow turbulence in gases, discussing turbulence decay with time and turbulence energy growth

12 p1896 A71-26940

Equation for motion of buoyant free vortices in inviscid fluid subjected to gravity [AIAA PAPER 71-604]

15 p2388 A71-31543

Consecutive toroidally circulating buoyant elements interactions by numerical simulation, including vortex formation process effects

18 p2901 A71-35954

High speed neutral buoyancy bubble generators for aerodynamic flow visualization, investigating tip vortex from wing or helicopter rotor blade

19 p3064 A71-37725

Isolated buoyant thermal motion asymptotic behavior derivation from simplified model, comparing results with experiment

19 p3162 A71-37732

Buoyant centrifugal force effect on combustion of homogeneous propane-air mixtures at stoichiometric proportions, using steel pipe as centrifuge

19 p3167 A71-38101

Buoyancy effects on heat transfer coefficients in liquid nitrogen film boiling in vertical flow

20 p3313 A71-39228

Buoyancy and surface-tension induced fluid instabilities in open and closed vertical circular cylindrical containers from series solution by Jeffreys-Goldstein method

21 p3367 A71-40084

Film boiling liquid hydrogen vertical flow system, determining buoyancy effects on hydrodynamic and heat transfer characteristics

21 p3476 A71-40085

BUOYS

Global atmospheric research with balloons, buoyancy and orbiting satellites for meteorological and oceanographic data recovery

18 p2913 A71-36454

BURGER EQUATION

Nonlinear acoustics propagation theoretical solutions by weak shock theory and Burger equation, noting differences in exactness and complexity of methods

05 p0784 A71-17151

Burger model equations for MHD turbulence with analog in gas dynamics for nondissipative case

09 p1432 A71-22707

Dissipation and nonlinearity effects on linear three-dimensional wave front, obtaining Burger equation for gas dynamics

09 p1433 A71-23053

BURNERS

Cooled porous plug burner for flame recombination of oxygen and hydrogen, noting boiling water reactor off-gas application

03 p0517 A71-13361

Combustion instability data with same solid propellants by T-burner and L super asterisk burner, discussing theoretical models of transient combustion

05 p0837 A71-16570

Pulsed T-burner testing of oscillatory combustion and droplet damping of aluminized solid propellants as function of frequency and sample properties [AIAA PAPER 71-634]

14 p2289 A71-30711

Comparative variable area, pulsed and modified T-burners for testing oscillatory combustion and stability of propellants containing aluminum [AIAA PAPER 71-635]

14 p2289 A71-30711

Acoustic damping of small amplitude waves by nonburning particles in T burners and rocket motors, noting propellant seeding with zirconium oxide [AIAA PAPER 71-633]

15 p2471 A71-32577

Monograph on flame form and temperature field of burners with nozzle for oxygen addition, using water model

17 p2837 A71-34799

Combustion driven acoustic oscillations in gas fired burner of premixed methane, nitrogen and oxygen, noting mixture ratio and flow rate effects

19 p3123 A71-38095

Fuel rich premixed hydrogen-oxygen flame stabilization on cooled porous plate burners at 10 mm Hg

19 p3168 A71-38107

Flat diffusion flame structure experimental investigation on Parker-Wolfhard burner, comparing results with perturbation solutions theoretical predictions

24 p3888 A71-44935

BURNING

U COMBUSTION

BURNING PROCESS

U COMBUSTION

BURNING RATE

Combustion velocity of burning liquid fuel droplets as function of number and distance

01 p0182 A71-11447

Thermal radiation effects on M-2 double base solid propellant ignition, deflagration and burning rate

02 p0298 A71-12851

Pressure effect on combustion rate of model mixtures of ammonium perchlorate with polystyrene and polymethyl methacrylate

03 p0468 A71-13989

Aluminum addition effect on combustion rate of mixtures of ammonium perchlorate with polymethyl methacrylate at different temperatures

03 p0520 A71-13995

Burning velocities in 50 percent hydrogen-air mixtures

03 p0376 A71-14282

Burning rate manual determination for solid propellant rocket motors with sliverless grains

03 p0522 A71-14451

Gas phase reactions near solid-gas interface of deflagrating double base propellant causing abrupt changes in burning rate-pressure curve [AIAA PAPER 70-124]

05 p0837 A71-16571

Composite propellant transient burning rates continuous measurement during rapid depressurization [AIAA PAPER 71-173]

06 p0944 A71-18612

Electric field effects on burning rates of composite metallized solid propellant containing ammonium perchlorate [AIAA PAPER 71-174]

06 p0947 A71-18613

Pressure wave distortion effects on combustor acoustic mode instability based on model with burning rate related to Reynolds number

07 p1224 A71-19906

Ballistic modification of nitric ester based propellant combustion by lead compounds, concerning burning rate-pressure relation

08 p1346 A71-20860

Flame structure in laminar condensed systems, noting burning rate dependence on pressure and specimen layer thickness, composition and mechanical condition

08 p1376 A71-21906

Solid propellant instantaneous burning rates prediction methods based on flame structure model and steady state burning data as functions of pressure and initial temperature

[AIAA PAPER 70-667] 09 p1510 A71-22905

Burning rate temperature sensitivity of composite solid propellants, using granular diffusion flame model

09 p1510 A71-22911

Combustion rate of pure ammonium perchlorate propellants derived from ablation theory

10 p1657 A71-23905

Erosive burning of composite propellants based on ammonium perchlorate, studying oxidizer grain size effect

10 p1658 A71-25122

Photographic study of burning metallized composite propellant, noting burning rate augmentation by heat transfer from alumina particles retained on propellant surface

[AIAA PAPER 69-173] 11 p1809 A71-25502

Phenol furaldehyde-ammonium perchlorate solid propellant combustion, investigating burning rate

12 p1944 A71-26742

Gasoline-air mixtures normal combustion velocity by photographic observations of flame propagation in transparent tubes

12 p1986 A71-27499

Transient nature of fuel droplet combustion, discussing burning rates and flame to drop diameter ratio

13 p2161 A71-28614

Combustion chamber design with flame stabilizers, deriving gas flow, energy conservation equations and propellant combustion rates

13 p2163 A71-28967

Gas turbine engine combustion chamber start-up and burning performance, considering air injection and propellant atomization

13 p2117 A71-28968

Continuous burning rate measurement for metallized composite solid propellants, using optical sensor for servo tracking propellant surface

14 p2244 A71-30328

Burning rate of Al particles suspended in polymer propellant gas flow with inorganic oxidizers

14 p2285 A71-30620

Fast burning rates in thin film solid composite propellants composed of McCormick-Selph 510, 164 monopropellant, oxidizer and polyvinyl chloride binder

[AIAA PAPER 71-655] 14 p2285 A71-30730

HF stability and combustion product flow characteristics of laminar burning in cylindrical tube, considering longitudinal and radial instabilities

14 p2338 A71-30856

Combustion rates of ammonium perchlorate mixtures with organic acids, alcohols, cyclic hydrocarbons, amines, nitroso compounds and nitrates, studying relationship to fuel chemical composition

15 p2366 A71-31370

Liquid KCl and LiF surface films effect on combustion rate of ammonium perchlorate mixtures with polystyrene or polymethyl methacrylate for various initial temperatures

15 p2462 A71-31371

Burning rate of compressed charges of potassium perchlorate with lead dinitrophenolate at constant pressure

15 p2462 A71-31372

Gunpowder mean burning rate at constant pressure with periodic variation of heat influx into flame zone

15 p2462 A71-31374

Gunpowder unsteady burning as closed dynamic system, studying frequency characteristics and transient processes

15 p2462 A71-31375

Inflammability, burning rates and exothermal decomposition of compact hydroxylamine and hydrazine sulfate and chloride with/without copper chloride additions, plotting pressure variations curves

15 p2463 A71-31377

Be droplet burning rate in oxygen-argon mixtures, using laser ignition technique

[WSS/CI PAPER 71-23] 15 p2464 A71-31632

Al particles combustion kinetics in propellant flames, showing gas composition and pressure effects on burning rate

[WSS/CI PAPER 71-24] 15 p2464 A71-31633

Burning velocity measurement of laminar conical hydrogen-air flames on 10.3 mm diam water cooled

nozzle burner, using schlieren and particle tracking techniques

15 p2465 A71-32085

Ammonium perchlorates deflagration rate at 20-100 atm, assessing relative roles of exothermic condensed phase and gas phase reactions by mathematical model

15 p2465 A71-32099

Electric field effects on town gas and hydrocarbon flame reaction rate, burning velocity and propagation speed due to free electrons in flame front

17 p2840 A71-35704

Unsteady burning rate response of condensed phase fuel plate adjacent to reacting gaseous boundary layer with oscillating external flow

19 p3123 A71-38095

Solid propellant combustion pressure oscillations amplification, developing mathematical model as function of reaction rate constant, chamber pressure, frequency and solid properties

19 p3123 A71-38096

Inhibitory effects of halogen compounds on hydrogen-air and hydrogen-nitrous oxide flames, measuring burning velocities and temperature/ composition profiles

19 p3013 A71-38106

Aerothermodynamics and scale modeling techniques for prediction of plastic burning rates, using Spalding mass transfer theory and dimensional analysis

19 p3171 A71-38250

Burning rates of single laser ignited beryllium droplets, considering particle size effect

21 p3475 A71-40862

Acceleration dependent burning rate increases of aluminized composite solid propellants induced by combined erosive and acceleration

21 p3436 A71-40943

Small hybrid rocket engine using aromatic amines mixture as fuel and nitric acid as oxidizer, discussing regression rate relations and internal ballistics design

22 p3589 A71-42019

Exothermic decomposition reaction and sublimation mechanism of ammonium perchlorate burning, showing pressure dependence of burning rate

22 p3587 A71-42100

Spherical hydrocarbon fuel droplet combustion in air, considering mass burning rates and flame zone locations as function of drop size

[AIAA PAPER 71-989] 24 p3887 A71-44584

Fuel droplet burning rate variation with ambient temperature and oxygen concentration in combustion gas environment

24 p3887 A71-44606

Solid propellant combustion simplified laminar flame theory, calculating pressure effect on burning rate, surface energy loss and temperature effects

24 p3888 A71-44938

Limiting chemical reaction rate of graphite and carbon containing material combustion at high temperatures

24 p3890 A71-45108

Self similar solution for unsteady powder combustion rate with decreasing pressure, generalizing to rate dependence on pressure and initial temperature

24 p3891 A71-45217

Solid fuel combustion in presence of unsteady heat propagation in heated layer, solving fuel heat conduction equation for sudden combustion rate change

24 p3891 A71-45218

BURNING TIME

Flame propagation process, investigating transfer in turbulent flow, combustion times and burning in channel

07 p1220 A71-18778

Ignition initiation, burning time and particle size distribution determination for dispersed Mg and Al particles in condensed system

14 p2337 A71-30615

Alkali metal, alkaline earth metal nitrates and sodium perchlorate mixed with powdered magnesium burned in rarefied air

14 p2338 A71-30616

Amorphous boron powder total burning time in premixed laminar boron-propane-oxygen-nitrogen flames at atmospheric pressure, noting variation as function of oxygen initial partial pressure

15 p2511 A71-31472

Combustion characteristics of single boron carbide particles, studying minimum gas temperatures for self-ignition and burning times

[WSS/CI PAPER 71-21] 15 p2464 A71-31630

Monosized oil droplet streams combustion in stationary free flames, examining burning times and constants

19 p3169 A71-38112

Aluminum particles ignition by focused laser flux in controlled oxygen-Argon environment, observing by cinephotomicrography throughout entire burning time

19 p3169 A71-38114

Burn time and acceleration effects on molten metallic material chemical composition near burning surface of aluminized composite solid propellant

19 p3121 A71-38298

Low thrust long burning solid rocket propellant motor for orbit insertion maneuvers, discussing design, static tests, nozzle composition, igniter and performance

22 p3589 A71-42016

BURNOUT

Hybrid rocket propulsion engine combustion efficiency, burnout patterns and operating conditions, using nitric acid oxidizer

02 p0298 A71-12070

Polyfraction Mg particles suspension in active gaseous medium, studying ignition and burnout

08 p1376 A71-21909

BURNS [INJURIES]

Heparin efficacy in burns, considering healing time, pain relief, etc

02 p0207 A71-12391

Book on eye injuries covering mechanical traumata, neuro-ophthalmology, chemical, thermal, radiation, electrical and sonic injuries, etc

05 p0711 A71-17010

Laser thermal/photochemical burns and electric shock prevention by preemployment/regular physical examinations and safety requirement education

09 p1402 A71-23412

Skin surface burns effect on neurosecretory processes in hypothalamus supraoptic and paraventricular nuclei and neurosecretory admission into hypophysis

17 p2680 A71-34647

BURNTHROUGH [FAILURE]

Bayesian time to failure distribution for graphical estimation of component burn-in time and reliability prediction, comparing with Weibull technique failure rates

12 p1911 A71-26686

BURSTS

NT RADIO BURSTS

NT SOLAR RADIO BURSTS

NT TYPE 2 BURSTS

NT TYPE 3 BURSTS

NT TYPE 4 BURSTS

Polar auroras emission bursts at 6300 and 5577 Å, noting diurnal variation with electrophotometer

05 p0746 A71-17209

Spectrum analysis and probability distribution of burst noise pulses of silicon planar bipolar transistors consistent with Markov two state process

10 p1574 A71-23773

Burst-like signal detectability evaluation in terms of optimum detector performance and probability theory

12 p1882 A71-27442

Bursting phenomenon measurement in turbulent boundary layer by hot wire, noting spottiness, HF intermittency and energy balance dynamics

18 p2985 A71-36036

BUS CONDUCTORS

Digital wire line system data bus design, calculating transmission performance of noise environment shielded twisted pair cable by linear filter model

14 p2198 A71-30904

Distributed Fetch sequencing computer technique, discussing system speeds, throughput rates, bus requirement and arithmetic processor demand reduction and task performing capability

17 p2712 A71-35779

Aerospace data bus for multiplexed transmission within vehicles, considering control and sequencing methods terminal concepts, capability noise reduction and reliability

17 p2712 A71-35785

BUTADIENE

Ionization potentials of cyclobutadiene, using photoelectron spectrum measurement

03 p0377 A71-14373

Fractography of thermoset resins toughened with Hycar carboxyl terminated butadiene acrylonitrile, using electron microscope

11 p1785 A71-25406

BUTENES

Butene hydroperoxides structure and intermolecular reactions from NMR spectra, discussing peroxide radical addition, OH group signals shifts and self association

12 p1877 A71-27751

BUTT JOINTS

High strength steel butt welds surface geometry effect on fatigue durability under cyclic loads, using photoelastic analysis

04 p0602 A71-14881

Polymer adhesive protective coatings for improving fatigue resistance of butt and lap welded joints in thin Al sheet construction

09 p1478 A71-23355

Crack propagation in chromium steel butt weld sheets, discussing dendrite macrostructural effects on brittle resistance and toughness

11 p1770 A71-25945

Thin sheet Nb-Zr alloy welds, detailing residual stresses in butt joints

15 p2413 A71-31204

BUTYLENE

U BUTENES

BUTYRIC ACID

Neurochemical factors in auditory stimulation and susceptibility to audiogenic seizures, noting gamma-aminobutyric acid /GABA/ inhibitor

03 p0360 A71-13164

Gamma-aminobutyric acid /GABA/ penetration through blood-brain barrier for administration in dogs and rats

03 p0362 A71-13236

Gamma-aminobutyric acid /GABA/ effects on brain serotonin following transaminase inhibitor aminooxyacetic acid administration

03 p0362 A71-13239

Rat brain carbohydrates biosynthesis from organic acid products under normal conditions and during central nervous system disturbances, investigating butyric acid participation

21 p3337 A71-41058

BYPASSES

Automatic antisurge control of axial compressor using partial gas recycling bypass method

03 p0469 A71-13370

Cylindrical post shunt impedance in rectangular waveguide, evaluating approximate theory for free space thin wire conductor

03 p0378 A71-13808

Two-terminal pair broadband matching circuits losses from method for LF series-shunt coupler with uniform scattering

03 p0386 A71-13810

C

C BAND

C-band radar network calibration, using GEOS 2 satellite worldwide tracking data

04 p0554 A71-15319

C band field effect transistor amplifiers with stable power gain, discussing circuit analysis, design parameters and test results

05 p0729 A71-16917

Low noise C band beam lead tunnel diode amplifiers characteristics and application in low cost microstrip reflection amplifiers

08 p1262 A71-20759

Elliptic-function low pass microwave filters and other C sections applications including broadband impedance transformers

08 p1262 A71-20766

C and higher band pulse modulated signal generation with nanosecond duration, using TEM- mode pulse-forming network

10 p1577 A71-24211

Microwave amplification using negative resistance device in prototype filter equalization networks, permitting realization of wideband amplifiers for C band and superhigh frequencies

11 p1736 A71-25140

C band SYDAC system compatible with conventional ILS, considering transmission sensitivity to ground reflection and lateral obstacles

15 p2445 A71-31910

C-5 AIRCRAFT

LAMS flight control systems for turbulence induced fatigue damage reduction in B-52 and C-5A aircraft, using mathematical models

02 p0188 A71-11660

C-5 military transport stability augmentation for pitch and yaw inertia at low speed, using pilot evaluation on cockpit simulator

02 p0190 A71-12684

Variable weight composite materials for aircraft optimal adhesive bonding structural designs, discussing C-5A tow weight saving Ti honeycomb applications

10 p1686 A71-24084

C-5A cargo box side wall deformations, examining square plates center deflections with elastic beams

10 p1557 A71-24871

C-5A airplane Be brakes, considering critical design weight environment for optimum load carrying capacity

13 p1996 A71-28313

[SAE PAPER 710427] Boeing 747, Lockheed C-5A and other aircraft vortex wake characteristics by tower flyby technique

21 p3320 A71-40498

C-130 AIRCRAFT

Multispectral scanner and data system with 24 channels for NASA C-130 earth resources survey aircraft

18 p2920 A71-36361

C-131 AIRCRAFT

Total in-flight simulator /TIFS/ in variable stability C-131 aircraft, describing potential as design tool

17 p2675 A71-35529

C-135 AIRCRAFT

Apollo range instrumentation aircraft, describing C-135A modification with airborne lightweight optical tracking systems

19 p3022 A71-38546

KC-135 aircraft climb trajectories for optimum constant lift coefficient, range and fuel amount

22 p3481 A71-42834

C-142 AIRCRAFT

U XC-142 AIRCRAFT

CABIN ATMOSPHERES

NT SPACECRAFT CABIN ATMOSPHERES

Air conditioning of passenger cabin in SST, noting heat exchanges due to radiation, convection and evaporation

03 p0371 A71-13094

Heat tolerance for resting subjects in event of air conditioning system failure in SST passenger cabin

03 p0371 A71-13095

Pilot performance under helicopter cabin high temperature and humidity

04 p0547 A71-15422

Human nitrogen and water-salt metabolisms and respiratory activity during prolonged confinement in small volume chamber with cyclic varying hypoxic air

22 p3495 A71-42799

Toxic gaseous compounds effects on low pressure tolerance of rats under hypoxic hypoxia in atmosphere containing polymer decomposition products

22 p3506 A71-42806

CABLES

Nonlinear mathematical model for dynamical behavior of extensible towing cable subjected to aerodynamic forces generated by uniform flow field, discussing system stability

14 p2171 A71-31026

Common mode choke for reduction of current unbalance in cable to improve electromagnetic interference performance

19 p3000 A71-38432

CABLES (ROPES)

Cable-connected spinning and orbiting satellite spring-mass system, deriving in-plane motion equations by Hamilton principle for numerical analysis

01 p0165 A71-11587

Inflatable restraint collar for large balloons with heavy loads using winch driven cable launching

02 p0188 A71-11821

Nonlinear analysis of cable and truss structures, using computerized stiffness matrix method

08 p1367 A71-20749

CADMIUM

NT CADMIUM ISOTOPES

Mercuric oxide-cadmium batteries optimum cell design for low temperature operating conditions and elevated temperature storage life

03 p0351 A71-13038

Ti alloys crack initiation by solid Cd coating under tensile stress with intimate contact, noting time and temperature effects

03 p0441 A71-13318

Cd atoms excited state populations in nonequilibrium gas discharge plasma

09 p1500 A71-22267

Helium role in populating upper levels of cadmium gas laser in discharge tube

09 p1462 A71-22401

Steel alloys solid Cd embrittlement, discussing crack propagation rate temperature dependence and Cd surface diffusion as controlling effect

11 p1777 A71-25447

Cd ion laser with He-Ne, suggesting Cd ion excitation by Penning process

18 p2929 A71-35981

Helium-cadmium laser discharge, discussing possible He trapping mechanisms and improved tube design to eliminate He cleanup

18 p2933 A71-37013

Atmospheric neutron production by cosmic rays, calculating cadmium-indium ratio

19 p3066 A71-38379

Positive column He-Cd/plus/ laser discharge, determining electron temperature and density

22 p3558 A71-42345

CADMIUM ALLOYS

Cadmium-copper fibrous eutectic alloy morphology, describing sample preparation and crystallographic examinations by optical and electron microscopes

01 p0103 A71-11018

Mg-Cd single crystals deformation by prismatic slip as function of testing temperature and state of order

07 p1132 A71-19437

Polycrystalline thin film CdSe-CdS and CdSe-CdTe solid solution semiconductor alloys Hall mobility and carrier concentration dependence on substrate temperature

23 p3715 A71-43433

CADMIUM ANTIMONIDES

IR absorption edge measurement in cadmium antimonide crystals grown with various perfection degrees, considering forbidden band and phonon spectrum anisotropy

01 p0138 A71-10432

CADMIUM COMPOUNDS

NT CADMIUM ANTIMONIDES

NT CADMIUM SELENIDES

NT CADMIUM SULFIDES

NT CADMIUM TELLURIDES

Hall electron mobility in cadmium arsenide as function of concentration and temperature

01 p0141 A71-11466

Cadmium arsenide alpha and beta phases Hall constant temperature dependence, studying photoelectric and optical properties

07 p1177 A71-19279

Energy spectrum parameters from Burstein-Moss effect observation in thin CdO layers, explaining absorption edge shape at various electron concentrations

16 p2622 A71-34029

Switching effects in diode structure formed by tungsten point contacts on glassy cadmium germanium arsenide surface

21 p3358 A71-41200

Coherent stimulated recombination radiation emission by p-type cadmium silicon arsenide single crystals in liquid nitrogen cryostat under various pumping levels

21 p3431 A71-41220

Cadmium-tin-arsenide conduction and valence band structure parameter refinement from Faraday effect and absorption spectra of single crystals in polarized light

21 p3433 A71-41319

N-type cadmium germanium arsenide single crystal semiconductor electron and hole effective mass determination from thermoelectric power measurement

21 p3436 A71-41350

CADMIUM ISOTOPES

Self locked He-Cd 114 laser pulse velocity behavior, discussing stability

02 p0260 A71-11948

Gas laser operating on mixture of He and Cd 114 for excitation of scattered light spectra

19 p3073 A71-37792

CADMIUM NICKEL BATTERIES

U NICKEL CADMIUM BATTERIES

CADMIUM SELENIDES

Polycrystalline semiconductors Hall effect by grain structure model for low and high resistivity boundaries, giving vapor deposited cadmium selenide film data

01 p0137 A71-10283

Photoelectrical and thermoelectrical properties of CdS, CdS-CdSe and CdSe single crystals epitaxial films

05 p0793 A71-16823

Stimulated emission wavelength tuning from GaAs and CdSe electron beam pumping laser crystals as a function of time and current

07 p1128 A71-20393

Semiconductor zinc selenide and zinc cadmium selenide crystals thin photon absorption coefficients, noting forbidden bandwidth relation

13 p2077 A71-27954

Surface conductivity and current carrier mobility vs surface potential in CdSe single crystal films deposited on mica base by vacuum vaporization

15 p2461 A71-31511

Spectral dependence of GaAs-CdSe alloys optical reflection coefficient

17 p2790 A71-34203

MnSe-CdSe mixed crystals growth investigation by elements, binary compounds and solid solutions vapor transport properties

21 p3427 A71-40214

Two photon absorption coefficients of ZnSe and zinc cadmium selenide crystals for ruby laser radiation, showing energy gap reduction effect

21 p3395 A71-41340

Current amplification in CdS and CdSe single crystals and thin films by fast electron bombardment

24 p3859 A71-44386

CADMIUM SULFIDES

I-V characteristics of low and high resistance p(SiC)-n(CdS)/ junctions prepared by different methods

01 p0139 A71-11116

CdS-CuS n-p junction solar converters, noting long wave sensitivity dependence on light extrinsic absorption

02 p0190 A71-11896

Semiconductor cadmium sulfide crystal structure changes during high power electron beam and optical pumping, using stimulated emission spectra measurements

03 p0439 A71-13984

CdS single crystals green edge emission and optical flash spectra, discussing wavelength, UV excitation intensity and temperature effects

03 p0468 A71-14384

CdS single crystals with Cu and Cl additives, observing optical flash and thermoluminescence in IR band

03 p0468 A71-14385

CdS thin film grain boundaries and stacking faults effects on electrical resistivity

05 p0791 A71-16055

CdS solar cells thermal stability and performance, discussing satellite applications

05 p0699 A71-16056

Copper sulfide-cadmium disulfide thin film solar cells degradation under simulated orbital conditions, determining electrochemically induced copper filament growth as electric shorts causes

05 p0699 A71-16057

Integrated high voltage CdS solar batteries with interconnected cells in series without grid

05 p0699 A71-16058

- CdS solar cells performance under simulated synchronous orbit conditions, describing test equipment 05 p0702 A71-16081
- CdS laser wavelength and relative threshold excitation levels as function of temperature based on band edge absorption effects 05 p0763 A71-16498
- Thin CdS condensate layer formation mechanism during films slow vacuum deposition onto glass or polystyrene sublayer bases 05 p0793 A71-16821
- CdS single crystals treatment in salt melts to obtain given conductivity and photosensitivity, discussing LiCl, Ag, Cu, Na, Cd and In concentration effects 05 p0793 A71-16822
- Photoelectrical and thermoelectrical properties of CdS, CdS-CdSe and CdSe single crystals epitaxial films 05 p0793 A71-16823
- Li concentration effect on CdS single crystals brittle fracture anisotropy by metallographic techniques 06 p0941 A71-18083
- Gas phase composition effect on CdS deposits crystalline perfection by Knudsen effusion apparatus and mass spectrometry 06 p0942 A71-18084
- Electron beam pumped CdS laser, investigating output pulse time duration based on laser oscillation quenching model 08 p1302 A71-21433
- Transverse excitation of elastic ultrasonic waves in CdS piezoelectric plates, considering conductivity effect on damping 12 p1944 A71-27544
- Optical losses and quantum efficiencies of electron beam pumped CdS lasers, determining extinction coefficient from dependence of threshold current on resonator length 12 p1915 A71-27639
- Preferential pairing detection in CdS at 4.2 K through electron radiation damage of donor-acceptor pair green edge emission, discussing resulting wavelength shift 14 p2284 A71-29818
- Cadmium sulfide pulsed laser spectrum analysis, discussing output stabilization by mode selection and electron beam scanning 14 p2253 A71-30092
- Self focusing effect of Q switched single mode ruby laser emission in CdS crystal, noting 60 kW minimum threshold power 16 p2588 A71-33645
- Thin film Au-CdS-Al type metal-semiconductor barriers, determining barrier height from temperature dependence measurements of I-V characteristics 19 p3118 A71-37488
- Copper sulfide-cadmium sulfide photovoltaic solar cell electronic processes observation at heterojunction, noting electron trapping and hole injection roles in long term stability 19 p3119 A71-38140
- Copper sulfide-cadmium sulfide thin film solar cells under simulated orbital conditions, including thermal cycling, constant illumination and temperature effects 20 p3182 A71-38946
- Spontaneous emission decreases at CdS and GaAs lasing onset observed visually in internal reflection cavity under electron beam pumping 20 p3243 A71-39007
- Low temperature phonon assisted edge emission bands in pure cadmium sulfide crystals 20 p3276 A71-39008
- Surface acoustic waves in layered substructure of piezoelectric epitaxial film of cadmium sulfide on germanium substrate 21 p3429 A71-41208
- CdS crystals faces damage caused by picosecond light pulses from free oscillating Nd-glass laser 21 p3432 A71-41305
- Au diffusion parameters in CdS determined under Cd and sulfur vapor atmospheres at 540-1000 C, explaining profile difference by dissociative mechanism 21 p3433 A71-41315
- CdS single crystal acoustoelectric domain determination, using light diffraction method 21 p3436 A71-41364
- Macromolecular binding agent effect on electrophotographic properties of high resistance layers containing photoconductive CdS 22 p3586 A71-42405
- Photoconductive CdS disintegration effect on heterophase electrophotographic layer electric and photoelectric properties, noting optimal properties relationship to grain diameter 22 p3586 A71-42406
- Current amplification in CdS and CdSe single crystals and thin films by fast electron bombardment 24 p3859 A71-44386
- Adhesion, recombination and electron-band curvature nomograms for space charge region in photosensitive CdS single crystals 24 p3859 A71-44388
- Solar to electric energy conversion efficiency and electrical properties of photoconverters using compressed sintered CdS 24 p3808 A71-44390
- CADMIUM TELLURIDES**
- CdTe thin film solar cell characterization, showing low carrier concentration of base layer and improved stability at elevated temperatures 05 p0699 A71-16059
- Electrical, photoelectrical and optical properties of crystalline cadmium telluride-indium telluride alloys, discussing temperature dependence, spectral characteristics and photoconductivity 05 p0793 A71-16824
- CdTe thin film anomalous photovoltaic effect and piezoeffect dependence on real state 07 p1176 A71-19271
- Thin polycrystalline CdTe film photovoltaic effect dependence on monochromatic light incidence angle 07 p1176 A71-19272
- Cadmium telluride epitaxial films on potassium bromide, investigating external gases effects on photovoltaic properties 07 p1179 A71-19919
- Cadmium mercury telluride solid solutions electron energy spectrum at low temperatures, calculating electron mobility in crystals with zero forbidden band 13 p2110 A71-27955
- Junction conversion and fabrication of Hg-Cd-Te n-p photovoltaic detectors by proton bombardment 13 p2066 A71-28043
- Multielement IR photoconductive detector arrays of InSb and mercury cadmium telluride operating at cryogenic temperatures 18 p2923 A71-36606
- Electroabsorption spectra of cadmium telluride at photon energies smaller than forbidden band width, observing energy levels 21 p3429 A71-41212
- Solid solution electron energy spectrum at low temperatures, considering electron mobility in cadmium-mercury telluride crystals with zero forbidden band 21 p3435 A71-41342
- Large photomagnetic effect in semiconductor films using multilayered Cd-Te p-n microjunctions 23 p3716 A71-43484
- Photorecombination model explaining kinetics of negative photoconductivity effect during illumination of impurity region in high resistivity p-type ZnTe-CdTe single crystals at room temperatures 23 p3717 A71-43948
- Phase composition and defect structure of thin film CdTe islet compensates on NaCl and KBr cleavage faces 23 p3718 A71-44316
- Cd doped thin polycrystalline CdTe films rectification mechanism and DC conductivity, discussing light, electric field and temperature effects 24 p3861 A71-45248
- HgTe-CdTe thin films structural and optical properties, measuring absorption spectra in UV, IR and visible regions to determine Te contents effect 24 p3862 A71-45251
- CADMIUM 114**
- U CADMIUM ISOTOPES**
- CALCITE**
- Calcite and aragonite high pressure Raman line spectra comparisons, testing structural identification theory 07 p1054 A71-19369
- CALCIUM**
- Three component model for chromospheric Ca II K line formation, discussing observational agreement 05 p0803 A71-16024
- Streptomyces sp chitinase purification and properties by column chromatography, noting calcium component 11 p1728 A71-26064
- Calcium H and K line anomaly in faint meteor spectra, discussing brightness correlation with aerodynamic flow and resonant charge exchange with ionized nitrogen 12 p1957 A71-26626
- Solar Ca II K line core formation, discussing models for high spatial resolution spectra 13 p2140 A71-29045
- Integral equations for source functions of Ca II H, K and IR triplet lines for transfer through homogeneous stellar atmosphere 14 p2276 A71-30298
- Hypoxic hypoxia and hypercapnia effect on calcium, inorganic phosphorus and total protein in rats blood during hypodynamic syndrome 15 p2356 A71-31306
- Ca, Mg, B and Al prominent resonance transitions radiative lifetimes and absolute oscillator strengths 15 p2452 A71-32596
- Solar atmosphere structure inhomogeneities, describing Ca II H and K line spectra profiles 15 p2497 A71-32743
- Ca and Mg light emission and ionization cross section measurements at simulated meteor conditions, using photomultiplier and optical filters 17 p2798 A71-34374
- Calcium abundance in solar corona, using measured values for total intensity of continuum and integrated intensities ratio 23 p3768 A71-43845
- CALCIUM CARBONATES**
- NT ARAGONITE**
- NT CALCITE**
- CALCIUM CHLORIDES**
- Scanning electron microscopic observation of fracture surface of austenitic stainless steels for stress corrosion cracking in magnesium chloride and calcium chloride solution 23 p3693 A71-44073
- CALCIUM COMPOUNDS**
- NT ARAGONITE**
- NT CALCITE**
- NT CALCIUM CHLORIDES**
- NT CALCIUM FLUORIDES**
- NT CALCIUM OXIDES**
- NT CALCIUM PHOSPHATES**
- NT PEROVSKITES**
- CALCIUM FLUORIDES**
- Dy-ion-doped calcium fluoride laser with monochromatic pumping, examining mode selection and coupling 08 p1303 A71-21791
- Energy transmission mechanism in calcium fluoride-europium ion plus holmium ion system, investigating luminescence and absorption spectra 09 p1461 A71-22388
- Photochromic calcium fluoride preparation by rare earth additive coloration techniques 09 p1509 A71-23120
- Calcium difluoride powder under sintering, examining optical transparency and morphological features 19 p3069 A71-38049
- CALCIUM METABOLISM**
- Bone tissue optical density and blood serum and urine calcium content of Soyuz 9 crew members during and after flight 09 p1389 A71-22201
- Primate restraint harness of nylon jacket and cotton cot on aluminum frame padded seat for bone resorption and calcium metabolism studies 09 p1398 A71-22476
- Calcium, potassium and iron loss by astronauts during Apollo space missions, using instrumental neutron activation analysis 16 p2528 A71-33111
- Calcium ions effects on electrophysiological properties of portal vein muscle cells in rats 16 p2533 A71-34109
- Gangliosides inhibitory effects on active Ca ion transport in rat brain mitochondria, using succinate as respiratory substrate 21 p3338 A71-41075
- CALCIUM OXIDES**
- Lime refractory fabrication and properties for high temperature applications, describing production of calcium oxide grain by sintering process from commercial calcium hydroxide 21 p3405 A71-40246
- CALCIUM PHOSPHATES**
- Rare earth element concentrations in zircons and apatites separated from dacites and granites, explaining partition coefficients between phenocrysts and groundmass by crystal structure 03 p0407 A71-13338
- Apollo 12 lunar rock 12013 mineralogy, identifying whitlockite, plagioclase, alkali feldspar, ilmenite, quartz and minerals encrusted with quartz 03 p0493 A71-14215
- Undoped and Nd doped synthetic fluorapatite single crystals heat capacity, thermal expansion and thermal conductivity measurements, yielding Debye temperature 07 p1180 A71-20164
- Fluorapatite single crystals absorption spectra and luminescent characteristics under activation by rare earth ions, noting line widening dependence on crystal composition 09 p1507 A71-22390
- Frequency doubling of 2.06 micron holmium doped oxyapatite laser output by proustite single crystal 15 p2423 A71-32610
- Hydrogen atoms trapped in gamma irradiated calcium phosphates, studying radiation yields, electron paramagnetic resonance line widths, dose saturation and relaxation 16 p2538 A71-32873
- CALCULATION**
- U COMPUTATION**
- CALCULATORS**
- Multichannel scaler as interface between edge scan unit and calculator to generate optical transfer functions 13 p2066 A71-28159
- CALCULUS**
- NT ASYMPTOTIC SERIES**
- NT COLLINEARITY**
- NT CONTINUITY [MATHEMATICS]**
- NT COPLANARITY**
- NT CURL [VECTORS]**
- NT DIFFERENTIAL CALCULUS**
- NT FOURIER SERIES**

NT INTEGRAL CALCULUS
 NT LIMITS [MATHEMATICS]
 NT PADE APPROXIMATION
 NT POWER SERIES
 NT SERIES [MATHEMATICS]
 NT SINE SERIES
 NT TAYLOR SERIES
 NT VECTOR ANALYSIS
 NT VORTICITY
CALCULUS OF VARIATIONS
 Thin elastic plates generalized variational equations derivation from virtual displacements and forces principles for arbitrary subdomains, observing node displacement continuity condition 01 p0166 A71-10124
 Matrix perturbation methods for nonlinear perturbed systems, involving variational equations solution of regularized Keplerian motion 01 p0154 A71-10380
 Dynamic problems linear variation equations associated with one and two particle motion in force field 01 p0111 A71-10385
 Space navigation variation problem, examining perturbation differential equation for semimajor axis and eccentricity and momentum and eccentric anomaly relationship 01 p0122 A71-10389
 Variational and boundary value problems for functionals depending on functions with deviating argument 01 p0111 A71-10488
 Incorrectly posed variational problems with non-linear unbounded operators, demonstrating solution by regularization method and beta convergence 01 p0112 A71-10489
 Canonical transformations for method of variations applied to differential equations describing satellite orbit perturbations 01 p0156 A71-10544
 Variational bounds on phase shifts for electromagnetic wave scattering by dielectric obstacles in waveguides 01 p0056 A71-11199
 Elastic plate plane stress analysis by Euler variational method for arbitrary geometric shapes and loading, obtaining isotropic and orthotropic solutions 02 p0330 A71-12747
 Book on optimal control theory covering dynamic programming, calculus of variations, Pontryagin maximum principle and iterative techniques 02 p0236 A71-12773
 Second order variational endpoint condition numerical application used for low thrust minimum fuel orbital transfer problems 03 p0450 A71-13445
 Variational methods applied to shells transition into plastic state during cylindrical bending, giving critical load formulas 03 p0509 A71-13873
 Three body plane restricted problem axisymmetric periodic solutions, establishing linear equations of variation 04 p0652 A71-15703
 Optimal process control with various delay times, discussing maximum principle variant and calculus of variations 06 p0879 A71-17671
 Variational methods application to optimal heating of thin elastic shells, using elastic-energy functional minimization as optimality criterion 06 p1006 A71-17767
 Thin walled prismatic shell constrained torsion problem, applying Reissner mixed variational method 06 p0992 A71-17806
 Finite difference theory and other approximation methods convergence determination in nonlinear variational problems 06 p0919 A71-18202
 Ground state energy approximate eigenvalues calculation for electron in stationary finite electric dipole field by variational approach 07 p1163 A71-19684
 Trajectory measurement program optimization, constructing algorithm for variational problems 08 p1360 A71-21001
 Variational difference schemes construction by approximation method of finite elements 09 p1485 A71-22369
 Variational approaches to steady state heat conduction, discussing relationship between variational and differential problems 09 p1545 A71-22453
 Variational formula for input impedance of thin asymmetrical cylindrical dipole antenna 09 p1408 A71-23490
 Book on mathematical theory nonlinear control processes covering dynamic programming, calculus of variations, etc 09 p1486 A71-23724
 Variational formulation for minimum weight of structures with given yield stress, considering homogeneous isotropic material, plasticity condition and collapse mechanism 10 p1685 A71-23977

Reissner variational theorem for boundary values in linear anisotropic and nonhomogeneous elasticity 10 p1691 A71-24809
 Variational criterion for stationary mode elastic structural oscillation, considering coincidence with normal modes for materials with stress-strain homogeneous function relationship 10 p1692 A71-25048
 Variational formulation for hydrodynamic stability based on local potential motion, determining transition from laminar to turbulent flow 11 p1749 A71-25441
 Stress-strain states of physically nonlinear anisotropic media, showing boundary value problem equivalent to variational problem 11 p1850 A71-26179
 S wave scattering from H and He positron systems at low energies, applying Kohn and Harris variational methods 11 p1803 A71-26373
 Soviet book on variational methods in mathematical physics covering energy method, Ritz process, Bubnov-Galerkin method and least squares method 12 p1931 A71-27292
 Minimum volume design of sandwich axisymmetric plates obeying Mises criterion, using calculus of variations 13 p2146 A71-27782
 Structural properties of equilibrium solutions of quadratic matrix equation, using variational interpretation of associated Riccati equation, transform techniques and Parseval formula 13 p2095 A71-28815
 Numerical solution of nonclassical problem of calculus of variations, reducing nonlinear integral equation with Green function 13 p2095 A71-28819
 Calculus of variations sudden expansion and decentralization, minimizing convex functional on closed group in reflexive Banach space 13 p2095 A71-28824
 Criterion on types of extrema of singular solutions of conditional equations in calculus of variations from Euler function behavior with respect to integration path 13 p2096 A71-29322
 Calculus of variations application to optimal control theory, outlining method for optimal control problems transformation into equivalent classical Lagrange problems 17 p2764 A71-34443
 Linearized Boltzmann equation solution for rarefied gas dynamics, discussing analytical, variational and numerical methods 17 p2784 A71-35572
 Nonlinear time varying systems digital integration simulation techniques by variational equations approach, discussing accuracy, execution time and limitations 18 p2884 A71-36141
 Optimization problems for control processes described by ordinary differential equations, solving by variational methods 19 p3086 A71-37555
 Partially nonlinear theory of anisotropic shells of uniform thickness, obtaining variational integrals of stress equations of motion 20 p3307 A71-38796
 Variational methods application to high order dynamic systems resonance boundary value problem 20 p3309 A71-39487
 Dual variational formulation for rigid plastic structure minimum cost design, applying to sandwich and fiber-reinforced plates [ASME PAPER 71-VIBR-110] 21 p3462 A71-40333
 Field adsorption of inert gas atoms at metal surface from variational calculation 21 p3419 A71-40887
 Functional methods in numerical solution of heat transfer problems, including finite element and local variation methods 22 p3621 A71-42290
 Anisotropically weighted smoothing theoretical interpretation based on numerical variational analysis for upstream and downstream observations in weather forecasting 22 p3569 A71-42415
 Boundary displacement conditions in linear elasticity with friction, using minimization of nondifferentiable convex functional and variational inequalities 23 p3775 A71-43239
 First order variational equations of Hamiltonian systems with two degrees of freedom for symmetric periodic orbit 23 p3699 A71-43240
 Second variation for general space trajectories in terms of pseudo-Hamiltonian of Pontryagin, applying to singular arc optimality in space vehicle escape maneuver 23 p3768 A71-43857
 Noether invariance and conservation laws theorems extension to nonlocal calculus of variations, obtaining coordinate and point transformations effects on dependent functions domain space 23 p3700 A71-44177

Variational formulation for stability of parallel flows with imposed temperature gradient 23 p3783 A71-44180
 Critique of variational formulation approach in finite displacement analysis, considering applicability requirements and limitations 24 p3880 A71-44639
 Dynamic system optimal weighting function determination, using variational methods for statistical criteria 24 p3813 A71-44677
CALDERAS
 Caudron subsidence in lunar post-mare crater contiguous pair, discussing compatibility with volcanic origin hypothesis 19 p3137 A71-37680
 Morphological features of crater Copernicus as lunar caldera, observing agreement with volcanic origin 19 p3137 A71-37681
CALIBRATING
NT WIND TUNNEL CALIBRATION
 Accelerometers and dynamic pressure transducers calibration, using laser interferometer system 01 p0082 A71-10862
 Optical radar system absolute calibration for measuring laser irradiance backscatter function from atmosphere 01 p0094 A71-10874
 L and S band paraboloidal dish antenna stellar calibration technique using absolute flux density from Cassiopeia A or Cygnus A 01 p0032 A71-10888
 Field tests for telemetry receiving systems solar calibration, describing antenna pointing 01 p0033 A71-10891
 VHF/UHF telemetry antenna stellar calibration using radio stars 01 p0054 A71-10909
 Low brightness spacecraft photometer calibration using moonlit earth radiance as reference 02 p0249 A71-12075
 Calibration of condenser microphone micrometeoroid sensor, using bead drop and hypervelocity impact tests 03 p0422 A71-13284
 Spherical and cylindrical electrostatic probes for point ion density measurements in continuum flowing plasmas in hypersonic wake, discussing shock tube program for calibration 03 p0423 A71-13441
 Rugged stable differential Pt resistance thermometer for Lunar Heat Flow Program, discussing construction, calibration and environmental test 03 p0427 A71-13917
 Linearly polarized light measurements of solar spectral lines Zeeman effects, describing calibration method based on Fraunhofer lines broadening due to magnetic fields 04 p0642 A71-14903
 Simultaneous comparison and calibration of ultrasonic Doppler telemetry and electromagnetic flowmeters implanted on peripheral arteries of dogs 04 p0545 A71-15164
 Telemetry systems prelaunch calibration tests, considering bit error rate, intermodulation distortion and antenna tracking 04 p0554 A71-15317
 Automated radar calibration system using star tracker and computerized control 04 p0554 A71-15318
 C-band radar network calibration, using GEOS 2 satellite worldwide tracking data 04 p0554 A71-15319
 Electron accelerator with broad stable beam for calibration of spectrometers and channel electron multipliers 04 p0599 A71-15587
 Transducer with single crystal Ge for high heat flux measurement, noting calibration by direct conduction 04 p0599 A71-15589
 Pressure effects on calibration characteristics of hot-film anemometers, discussing heat loss from sensing element 04 p0601 A71-15765
 Vacuum UV monochromators calibration by molecular branching ratio technique based on electron transition probabilities 05 p0717 A71-16907
 Dynamic pressure reduction method errors in vacuum gages calibration 05 p0754 A71-16949
 Mariner Mars 1969 TV cameras instrument design and calibration techniques 06 p0898 A71-17632
 Unified approach to dosimetry in radiological protection, discussing practical application and instrument calibration to existent standards 06 p0859 A71-18030
 Heat transfer from circular cylindrical hot wire and film anemometer probes, examining calibration steadiness 07 p1106 A71-18783
 Hot-wire anemometer calibration, measuring shear stress and turbulence distributions in circular channel 07 p1106 A71-18785

- High vacuum calibration of cryogenic quartz crystal for atmospheric density 07 p1113 A71-19852
- Clean cryogenic vacuum high speed gas pumping system for calibrating spectrometers for use on Apollo telescope mount 07 p1160 A71-19854
- Plastic track detectors calibration for heavy charged particles in cosmic ray experiments, considering track etching rates as function of particle charge and velocity 07 p1113 A71-20042
- USAF Camera Calibration Facility, describing precision multibank collimator for measuring focal length, distortion, prism effect, fiducial center and other camera parameters 08 p1272 A71-21258
- Micrometer screw revolution value determined by method of scale pairs for Bamberg zenith telescope, noting dependence on temperature and declination differences of star pairs 08 p1292 A71-21675
- Ocular micrometer screw revolution value of instruments of astronomical universal type from scale pair outside of meridian 08 p1292 A71-21676
- Accuracy, calibration, maintenance and optimum design of scientific instruments for meteorological measurements 08 p1293 A71-21735
- Nondestructive monitoring calibration and alignment with standard specimens conforming with metrological regulations 08 p1300 A71-21895
- Fatigue life gages performance test using calibration program for cryogenic temperature applications 09 p1444 A71-22716
- Full photographic spectral range spaceborne cameras photometric calibration, involving determination of absolute magnitude and illuminance spatial variation in image plane 09 p1447 A71-22744
- Error analysis of random and system degradation between calibrations for complex instrumentation by digital computer models 09 p1449 A71-22790
- Pyrolytic graphite microcalorimeter for X ray absorbed dose measurement, exploiting for calibration self heating 10 p1608 A71-23742
- Geomagnetic field inclination determination by incoherently scattered signal Faraday rotation calibration and simultaneous ionosonde measurements of ionospheric electron density 10 p1605 A71-24798
- Trisonic wind tunnel calibration tests results including second throat effects, Mach number and static pressure distributions, flow inclination and aerodynamic characteristics 10 p1590 A71-24819
- Quark flux measurement by simulating fractional charge particle pulses, testing calibration procedures by comparing simulated and genuine quarklike events 10 p1613 A71-24957
- Low hygrometer calibration for water vapor measurements smaller than 3 mm 11 p1761 A71-25244
- Optimum calibration of turbine flow sensors AC voltage signals with volume proportional frequency by weighted least squares techniques 11 p1762 A71-25934
- Pulsed optical range finders, predicting transmitter pulse waveshape effects on calibration, precision and efficiency by probability density function 12 p1903 A71-26792
- Sapphire windowed argon filled tungsten ribbon filament lamp in vacuum UV for application in photomultiplier quantum efficiency calibration 12 p1904 A71-26801
- Calibration test rig for high accuracy liquid hydrogen flowmeter, discussing design and operation 12 p1906 A71-26836
- Optimal shapes and sizes of marker signs used in calibrating aerial photographs 12 p1906 A71-26971
- Substrate materials thermal characteristics determination for thin films resistance thermometers calibration, using pulse heating technique 12 p1908 A71-27593
- Hot-wire flowmeters calibration for low density flow measurements, describing method for hot wire end loss determination 12 p1908 A71-27595
- Calibration and operation of corona discharge anemometer involving highly stressed anode and large plate cathode 13 p2066 A71-28156
- Lunar mapping metric camera subsystems stellar calibration for photography maximum usability in photogrammetric data reduction 13 p2071 A71-29348
- Small turbine type flowmeters for liquid hydrogen, discussing design, inspection, calibration and reliability 14 p2239 A71-29926
- Fluctuating pressure measurements in jet engine testing, using miniature transducers with calibration and data acquisition equipment 14 p2244 A71-30325
- Aircraft flight load measurements in high temperature environment, determining optimal strain gage installation and calibration 14 p2248 A71-30681
- Field testing for radio telemetry receiving systems calibration, including tape recorder degradation effects during data processing 14 p2198 A71-30903
- Absolute calibration of radio sources with variable flux density in microwave region 14 p2316 A71-30976
- Preferred frequencies for RF measurement and calibration based on Renard number series 14 p2205 A71-30986
- Balloon-borne ionization spectrometer for high energy cosmic ray measurement, discussing calibration and accuracy 15 p2407 A71-31811
- Deep Space Communications System low noise microwave receiver, discussing operating noise temperature calibration, error analysis and programming 15 p2372 A71-32311
- Laser interferometer application in machine tool calibration, digital readout and feedback system, discussing advantages and limitations [SME PAPER IQ-71-745] 15 p2421 A71-32433
- Dispersionless delay line design producing signal frequency shifts for calibration tests of wideband Doppler shift measuring equipment 15 p2373 A71-32632
- Radiative energy transfer equations solution in magnetic field, facilitating magnetograph calibration 15 p2496 A71-32740
- Peak contour positions of rotation lines of hydrogen chloride as function of spectral slitwidth for wavenumber calibration of far IR spectrometers 16 p2577 A71-33134
- Prism IR spectrometer calibration, using linear equation and dispersion formula for derivation of numerical calibration table 16 p2577 A71-33135
- Dynamic small perturbation calibration of constant temperature hot-wire anemometers for turbulence measurements in Karman vortex streets, comparing static method 16 p2581 A71-34166
- Instrument calibration, discussing statistical estimation of relationship and experimental design for precision improvement 17 p2738 A71-34526
- Direct in-orbit alignment of integrated optical strapdown inertial guidance system for space application, considering self contained prelaunch alignment and calibration 17 p2774 A71-35071
- In situ metal-gas secondary standard assembly for ultrahigh vacuum gage calibration, using repeatable pressure generation from binary erbium- hydrogen system 17 p2744 A71-35140
- Preston skin friction measuring tube calibration, presenting Patel analytic method simplification 17 p2729 A71-35284
- German monograph on calibrating induction coil and proton precession magnetometers for polar electrojet rocket experiments 18 p2915 A71-35922
- Platinum resistance thermometers calibration normalized in resistance-difference ratios 18 p2916 A71-36047
- Operational calibration of airborne IR spectrometer over hydrogeologically significant terrains, obtaining radiance spectra 18 p2920 A71-36363
- Integrated test concept for terminal guidance subsystems and components evaluation, laboratory calibration and simulation tests [AIAA PAPER 71-969] 19 p3040 A71-37210
- Mass flow rate measurements and calibration in heterogeneous medium with hot wires tested on Freon mixtures 19 p3163 A71-37894
- Simultaneous calibration of gas analyzers and meters for continuous process gas stream composition monitoring 19 p3010 A71-38566
- Direct measurements of cosmic dust particles in near earth environment and interplanetary space, noting reliability and calibration 20 p3300 A71-39655
- Transient calibration method for piezoelectric accelerometer in high g-level range [ASME PAPER 71-VIBR-43] 21 p3377 A71-40293
- Quantitative schlieren system for shock wave velocity, density ratio and relaxation time measurements, discussing electro-optical modification and calibration technique 21 p3364 A71-40404
- Compensation type reference pyrohelometer design and calibration, considering accuracy, constant characteristics and turbidity effects 21 p3384 A71-41383
- Rollin InSb hot electron bolometer performance and calibration 22 p3543 A71-42124
- Atmospheric background radiation measurements with balloon-borne Michelson interferometer, noting data reduction and calibration methods 22 p3549 A71-42563
- Interplanetary navigation TV camera in-flight calibration, discussing instrument error sources elimination 22 p3573 A71-42771
- Magnetron manometer calibration to .001 picotorr for hydrogen, using condensate pump 23 p3674 A71-43273
- Precision calibration system with adjustable temperature extended radiance source for long wavelength IR radiometer, discussing performance tests 23 p3676 A71-43512
- Aeronautical radio navigation aids photo-optical calibration, describing photogrammetric procedure and ground equipment for checking out airport ILS systems 23 p3702 A71-43587
- Solar K-line profile absolute intensity calibration from elements of fine structure on surface, determining brightness temperature 23 p3767 A71-43836
- Precision pointing correction /boresight calibration/ of microwave antennas, using sun as test source 23 p3654 A71-44158
- Photographic recording for graduated circle readings during stellar observation, discussing method, errors and system 23 p3680 A71-44264
- Gravimeters calibration by inclination method with astronomical theodolite, tabulating relative errors and temperature corrections 24 p3826 A71-44767
- CALIFORNIA**
Rotaformidae of upper cretaceous Nassellarina /radiolaria/ from Great Valley Sequence, California Coast Ranges 07 p1104 A71-20013
- CALIFORNIUM**
NT CALIFORNIUM ISOTOPES
CALIFORNIUM ISOTOPES
Portable Cf 252 neutron radiographic camera, noting reactor fuel and concrete polymer content measurements 07 p1119 A71-19950
- CALIFORNIUM 252**
U CALIFORNIUM ISOTOPES
CALORIC REQUIREMENTS
Exercise-induced human protein catabolism not due to caloric deficit 19 p3008 A71-38552
- CALORIC STIMULI**
Gravity effects on human caloric and rabbits rotational nystagmus, noting semicircular canals role 04 p0542 A71-14757
- Vestibular habituation retention, showing nystagmic response reduction to repetitive rotatory and caloric tests 04 p0537 A71-14764
- Lateral and anterior semicircular canal neural reactions to caloric stimulation in frogs, indicating hydrodynamic interactions 16 p2532 A71-33912
- Controlled caloric stimulation of labyrinths in man by water at various temperatures 22 p3504 A71-42583
- CALORIMETERS**
Mean heat transfer coefficients determination at surface front of built-in alpha calorimeter from wall temperature data 01 p0179 A71-10611
- High temperature calorimetry of solids for heat capacity and thermal processes thermodynamic and thermokinetic characteristics, considering calorimeter design engineering 01 p0083 A71-11226
- Small size calorimetric probe for measuring enthalpy, temperature and pressure in high velocity dense plasma flow 02 p0290 A71-12194
- Transmitter system for Skeynet spacecraft performance tests using calibrated automatic level control and microwave calorimeters 02 p0218 A71-12442
- Calorimetric method for measuring high signal reflection coefficients at microwave frequencies 04 p0586 A71-14656
- Calorimeter for quantitative differential thermal analysis at high temperatures 04 p0595 A71-14958
- Calorimeter for ruby or neodymium laser output energy measurement 05 p0748 A71-16254

- Plasma torch stagnation point heat transfer measurements, using heat pipe calorimetry [AIAA PAPER 71-81] 06 p0902 A71-18538
- Pyrolytic graphite microcalorimeter for X ray absorbed dose measurement, exploiting for calibration self heating 10 p1608 A71-23742
- Calorimetric determination of reactor gamma source heating as function of specimens thickness and atomic number, discussing slab and cylindrical geometrical effects 11 p1797 A71-26078
- Heat flux measurement in high pressure arc heated wind tunnel flow by swept null point calorimetry, describing calorimeter configurations and test results [AIAA PAPER 71-428] 11 p1763 A71-26217
- Small size calorimetric probe for measuring enthalpy, temperature and pressure in high velocity dense plasma flow 15 p2454 A71-31500
- Temperature decay method for determining superinsulation thermal conductivity, equating insulation heat transfer rate to calorimeter plate heat loss 20 p3312 A71-39273
- Dynamic sampling calorimeter for continuous measurement of human radiative, convective and evaporative heat loss, enabling closed loop control system analysis 22 p3503 A71-42155

CALORIMETRY

U HEAT MEASUREMENT

CALUTRONS

U CYCLOTRONS

CAMBER

- Variable camber flap automatic control equipment for glider, considering combinations of mechanical, electrical and electronic approaches 06 p0847 A71-18250
- Transonic compressor rotors blade camberline shape optimization by various tip diffusion factor-ratio combinations 07 p1184 A71-20200
- Cascading turbomachine blade row coupled flutter, correlating camber angle, cascade condition and elasticity 13 p2157 A71-29128

CAMBERED WINGS

- Cambered and symmetric wing profiles and flap configurations, discussing wind tunnel tests at moderate Reynolds numbers 02 p0185 A71-11950

CAMERA SHUTTERS

- Deimos and Phobos photographic observations with light reducing slit attenuator diaphragm on refractometer 07 p1195 A71-19335
- Electro-optical shutter with low control voltage /3 kV/ for ruby laser consisting of Pockels cell and Porro prism 07 p1125 A71-19808
- Rotating photoshutter for astronomical instruments, describing design, electric circuit and operation characteristics 09 p1451 A71-23188
- Camera shutter spatial frequency spectrum and components light scattering effects on negatives quality based on composite image representation systems theory 11 p1767 A71-26469
- Autoexposure system for tracking telescopes, describing photometer and camera shuttle automatic control subsystems 18 p2919 A71-36088

CAMERA TUBES

NT IMAGE DISSECTOR TUBES

NT IMAGE ORTHICONS

NT ORTHICONS

NT RETURN BEAM VIDICONS

NT VIDICONS

- High reliability low energy camera tubes for video communication in space missions, considering vidicons with photoconducting layer with large time constant 17 p2739 A71-34683

- Image amplifier camera resolution as function of light level based on photon statistics and cathode quantum efficiency 17 p2746 A71-35762

- High performance image isocan camera tube, noting resolution, contrast, service life, cost and TV applications 22 p3548 A71-42510

CAMERAS

NT BAKER-NUNN CAMERA

NT BALLISTIC CAMERAS

NT FRAMING CAMERAS

NT HIGH SPEED CAMERAS

NT LALLEMAND CAMERAS

NT SCHMIDT CAMERAS

NT TELEVISION CAMERAS

- Pulsed laser holography, discussing illumination source and holocameras for high contrast recording with Q switched ruby lasers 04 p0597 A71-15363

- Close range photogrammetry with simple cameras, using calibration device and digital data processing 06 p0901 A71-18288

- EROS program mapping cameras, discussing wide angle, narrow angle and telescopic imaging 08 p1288 A71-21243

- USAF Camera Calibration Facility, describing precision multibank collimator for measuring focal length, distortion, prism effect, fiducial center and other camera parameters 08 p1272 A71-21258

- Full photographic spectral range spaceborne cameras photometric calibration, involving determination of absolute magnitude and illuminance spatial variation in image plane 09 p1447 A71-22744

- Artificial earth satellite observation by Soviet universal and semiautomatic cameras with quartz clocks and four component mirror lens optical system 11 p1762 A71-25829

- Four axis Zeiss camera unit for satellite small circle arc orbit observations, determining axial parameters equalization by least squares method and rotation rates 11 p1762 A71-25830

- Apollo lunar and Skylab photographic systems, discussing topographic, panoramic, metric, stellar and multispectral cameras and instrumentation 12 p1907 A71-27257

- Vibration effects on image resolution and accuracy of Zeiss RMK AR 15/23 aerial camera, using aircraft vibration simulator for testing 12 p1907 A71-27263

- Satellite paralactical mounted camera installation for adjusting axis parallel to earth rotation axis 13 p2070 A71-29120

- Lunar mapping metric camera subsystems stellar calibration for photography maximum usability in photogrammetric data reduction 13 p2071 A71-29348

- X ray telescopes and neutron cameras telephoto lenses for satellites and space stations, discussing optical design and correction methods 14 p2246 A71-30391

- Optical distortion coefficients of objective for astronomical camera 14 p2250 A71-31116

- Automatic camera for international synchronous observations of geodetic satellites 14 p2250 A71-31117

- Photographic observations of Pageos satellite during 1968 with PO-2 camera 14 p2250 A71-31118

- Trace length analysis of Pageos and Echo 2 satellites by camera observations 14 p2318 A71-31119

- Camera vibration, and refraction anomaly effects on error of designated position for star or satellite 14 p2250 A71-31120

- Satellite IR photography, discussing camera systems, photointerpretation, applications in glaciology, hydrology, oceanography, geology, volcanology and environmental protection 15 p2408 A71-31835

- Optical center position on negative and lens distortion of satellite camera verified on zenith area photos of stellar coordinate measurements 16 p2575 A71-32835

- High resolution 16mm pulse mode cine reconnaissance camera design features, discussing dynamic balance and reaction forces cancellation 17 p2746 A71-35761

- Ruby laser sources of short duration and high energy emission in holography, considering oscillator amplifier illuminator, contour spacings, transmission holocameras, etc 18 p2930 A71-36057

- Aerial cameras performance prediction by computer simulation technique with random number generation 18 p2917 A71-36069

- Airborne astrographic camera system for simultaneous determination of multiple object reentry trajectories at Air Force test range 18 p2918 A71-36077

- Image recording system low light /IRSILL/ camera design for long range attitude and events /LORAE/ telescopes in short missile instrumentation 18 p2919 A71-36086

- Wideband stabilizer design for high acuity aerial reconnaissance camera to obtain high degree of attenuation to roll and pitch rotational motion inputs 18 p2919 A71-36087

- Solid state light emitting diodes in aerial camera data recording system for enhanced spectral matching, increased photo conversion efficiency and lower power drive 18 p2920 A71-36089

- Stellar calibration of lunar mapping camera for precision metric photography and time correlated postflight attitude determination 18 p2925 A71-36916

- Calibrated IR thermographic camera development and applications in medicine, X ray beam energy and reactor cooling rod measurements 22 p3545 A71-42148

- Color photography of magnetic particle and penetrant indications, discussing light sources, camera types, filter and film selection, exposure and spectral characteristics of indications 24 p3829 A71-45282

CAMS

- Flexible laminated cam ring for high speed variable displacement vane pumps 01 p0091 A71-11544

- Cam profile selection for adjustment in computing resolving unit of aneroid sensors of altimeters 13 p2069 A71-28949

CANADAIR CF-104 AIRCRAFT

U F-104 AIRCRAFT

CANALS

- Mariner 6 and 7 Mars color TV recording of crater chaotic terrain and canals, using wide and narrow angle cameras 20 p3297 A71-39622

CANARD CONFIGURATIONS

- Aft vs canard horizontal tail locations for fighter/attack configuration at sub and supersonic speeds, obtaining lift coefficient, L/D and longitudinal stability [AIAA PAPER 71-8] 06 p0848 A71-18482

- Wing-canard configurations nonlinear vortex interaction, using Sacks method of vortex sheet simulation with discrete vortices distribution [AIAA PAPER 71-95] 06 p0844 A71-18550

- Impact dispersion reduction of uncontrolled solid rocket ZENITH with CUCKOO booster by canard control, noting flight path angle error by tracking radar 09 p1533 A71-23598

- Aerodynamic forces and hinge moments of delta cruciform control surface in blunt-nosed canard configuration for subsonic, transonic and supersonic flows 11 p1701 A71-25161

- Canard space shuttle reusable launch vehicle wing geometry variations effect on flyback systems weight, noting influence of aspect ratio and wing area 18 p2974 A71-36484

CANCER

NT LEUKEMIAS

- Short and long term radiation effects reduction by chemical radioprotectors mixtures, noting improved survival and decrease in leukemia and cancer incidence in X ray irradiated mice 07 p1037 A71-18970

- 6-azauridine effect on radiation induced inhibition of Yoshida sarcomas, Ehrlich carcinomas, benzopyrene-induced carcinomas and spontaneous mammary carcinomas growth and transplantability 07 p1039 A71-18978

- Aircraft piston and turbine engine soot extracts canerogenic activity in hybrid mice 12 p1872 A71-27724

CANNONS

U GUNS [ORDNANCE]

CANONICAL FORMS

- Canonical theory of dynamics, examining independent variable transformations for perturbed two body problem 01 p0154 A71-10379

- Canonical transformations for method of variations applied to differential equations describing satellite orbit perturbations 01 p0156 A71-10544

- Two-rotor gyrocompass equations of motion under perturbation, demonstrating reducibility to canonical form 03 p0430 A71-14354

- Generalized von Zeipel treatment of lunar and artificial satellite theories, generating single canonical transformation by variable separation technique 04 p0654 A71-15719

- Canonical linear Hamiltonian systems normalization algorithm, applying to restricted three body problem 05 p0810 A71-16547

- Nonrecursive solution for discrete Riccati equation by finding eigenvalues and eigenvectors of canonical state-costate equations 06 p0878 A71-17335

- Time varying multivariable system transformation to phase variable canonical form 08 p1324 A71-21329

- Second order hyperbolic partial differential equation in canonical form solution by iterative method 09 p1485 A71-22277

- Analytical lunar ephemeris main problem solution by canonical perturbation theory based on Lie transforms and echeloned series processing 10 p1674 A71-24431

- Canonical perturbation theory formulation applied to Poincare-von Zeipel method 10 p1679 A71-24935

- Linear complexes in three dimensional space considered with canonical transverse system, discussing nonintegral presentation and existence theorem 12 p1922 A71-27119

- Computational approach to maximum principle in control theory, considering canonical problem 13 p2035 A71-28996

- Sensitivity functions of phase canonical form for single input linear time invariant controllable systems, using frequency domain techniques 15 p2382 A71-32442

- Canonical quantization, discussing Schroedinger equation, Hamilton-Jacobi theory, Feynman integrals and sandwich conjecture 16 p2609 A71-33258
- Book on linear and ordinary celestial mechanics covering perturbed two body motion, numerical methods, canonical theory and initial value problems 17 p2799 A71-34471
- Multidimensional canonical formalism based on field system state description with potentials and momenta 17 p2778 A71-34635
- Shell analysis in curvilinear coordinates, obtaining edge effect equation with canonical kinematic unknowns in plane sections law 17 p2830 A71-35314
- Bounded plane circular three body problem stability, analyzing Jacobi integral and canonical equations 17 p2807 A71-35496
- Three dimensional bounded circular three body problem solution in form of Taylor power series of time and vicinity values for canonical elliptical elements 17 p2807 A71-35497
- Closed loop control of nonlinear systems in potentially large neighborhood of nominal trajectory, reducing nonlinear differential equations to related canonical linear form 19 p3037 A71-37239
- Canonical approximation of state correlation matrix and threshold crossings of variable systems with random turbulence type input vectors representing flight environment 21 p3408 A71-40614
- Canonical transformations application to spinning satellite with nutation damper [AAS PAPER 71-346] 23 p3728 A71-43019
- Thermally loaded rod structures optimization, presenting method for estimating canonical equations influence parameters 24 p3842 A71-44642
- Kruskal transformation canonization of perturbed periodic systems with Hamiltonian 24 p3843 A71-44789
- Classical Poincare-von Zeipel canonical perturbation theory extension to adiabatically perturbed systems with slow dependence on time or dynamic variables 24 p3848 A71-44790
- CANOPIES**
- Snatch force during lines-first deployment of aerodynamic decelerator, including effects of canopy skirt acceleration and suspension wave propagation characteristics [AIAA PAPER 70-1171] 09 p1385 A71-22915
- CANT**
- U SLOPES**
- CANTILEVER BEAMS**
- Bending-torsional flutter stability of cantilevered bar subjected to transverse follower force of fluid jet, using Frobenius method 01 p0166 A71-10125
- Nonautonomous vibrations of self excited cantilever beam with tangential force 01 p0177 A71-11295
- Ni maraging steel cantilever beams intergranular stress corrosion cracking in aqueous solutions, noting heat treatment effects 02 p0267 A71-12881
- Cantilever beam bending vibration, measuring driving point impedance and natural frequencies at low strain amplitudes for Mg alloy, Mn-Cu and coated Al beams 03 p0502 A71-13299
- Instantaneous deflection and velocity distribution curves of cantilever beam with uniformly varying length in constant gravity field by numerical methods 03 p0504 A71-13465
- Cantilever beam resonant frequencies measurement using electrodynamic vibration exciter 04 p0672 A71-15823
- Tapered cantilever beam with variable bending rigidity and concentrated mass, investigating nonlinear flexural vibration 05 p0820 A71-15986
- Complex modulus of elasticity relation to viscoelastic cantilever beams stress or strain under forced vibration, considering fiber reinforced plastics 05 p0826 A71-16738
- Dynamic stress measurement of cantilever beams, frame structures and rings under impulsive loads 07 p1210 A71-19046
- Tapered cantilevered beams design, determining end deflection and bending stress magnitude by graphical method 07 p1213 A71-19693
- Precracked double cantilever beam specimens, measuring resistance to stress corrosion crack propagation as function of overaging in Al alloys 07 p1142 A71-20363
- Rotating cantilever beams flexural vibrations, developing tables for frequency equation determination 08 p1370 A71-21306
- Vibrational characteristics of pretwisted cantilever beams with uniform rectangular cross section, investigating slenderness ratio effect on natural frequencies 09 p1543 A71-23661
- Dynamic programming for designing beams and plates under steady creep with minimum weight, discussing cantilever beam optimization 11 p1853 A71-26564
- Vibrating cantilever beam dynamic stress photoelastic determination based on photomechanics and optic-stress laws 14 p2324 A71-29850
- Nonuniform cross section tapered, stepped rectangular and I section cantilever beams elastic lateral stability 14 p2330 A71-30689
- Coupled natural frequencies in rectangular cross section pretwisted cantilever beams flexural vibrations 15 p2503 A71-31442
- Jet engine thrust induced nonconservative effects in aeroelastic analysis of vertical takeoff, using cantilever beam torsion and bending differential equations 16 p2650 A71-33019
- Forced transverse vibration damping of end loaded elastic cantilever beam, determining hysteresis loop contour from resonance curves 16 p2658 A71-33977
- Nonlinear elastic bending of nonhomogeneous cantilever beam under stepwise and triangular pulse loads of finite duration 17 p2821 A71-34578
- Cantilever bar free and forced transverse vibrations amplitude dependent damping, considering longitudinal tensile force effect and hysteresis 17 p2825 A71-35015
- Pretwisted cantilever airfoil cross section turbine and compressor blades vibration natural frequencies and mode shapes 17 p2828 A71-35282
- Dynamic programming to design beams and plates under steady creep with minimum weight, applying to cantilever beam 17 p2832 A71-35505
- Dynamic loading of cantilever beams by magnetomotive and explosive loads and high bullet speed impact, noting elastic and plastic deformation modes 18 p2981 A71-36770
- Rigid body longitudinal impact against free end of variable cross sectioned viscoelastic cantilever beam, obtaining solution as rapidly converging Fourier series 19 p3160 A71-38485
- Experimental stress intensity coefficients for contoured double cantilever beams, using Irwin-Kies method based on compliance with respect to crack length 20 p3307 A71-38779
- Stability of rotating unsymmetrically mass distributed cantilever shaft with unsymmetrical rotor, determining unstable region boundaries by theoretical analysis and experiment 21 p3385 A71-40303
- Shear deformation and rotary inertia effects on flexural vibration frequencies of pretwisted, nonpretwisted and tapered cantilever beams [ASME PAPER 71-VIBR-79] 21 p3461 A71-40316
- Parametric instability in first spatial and temporal modes of cantilevered elastic columns with longitudinal inertia and end mass 21 p3462 A71-40531
- Vibration characteristics of cantilever beam about nonlinear equilibrium state, showing flexibility and prestressed state effect 21 p3468 A71-40968
- Elastic stability of prismatic and cantilever bars in torsion 21 p3472 A71-41150
- CANTILEVER MEMBERS**
- NT CANTILEVER BEAMS**
- NT CANTILEVER PLATES**
- Cylindrical cantilever shells/silos/ under wind loads by semimembrane analysis, discussing cross section distortion and stress prediction [ASME PAPER 70-WA/APM-7] 04 p0667 A71-15182
- Optimal structural design for nonconservative elastic stability of cantilever column, obtaining critical load 07 p1212 A71-19473
- Dynamic stability of cantilever under pulsating scanning load 07 p1218 A71-20474
- Critical velocity of fluid flow in cantilever tube, applying Galerkin method to modal type analysis 11 p1748 A71-25163
- Vertically cantilevered column weight and follower force effects on flutter and buckling instabilities respectively 14 p2330 A71-30685
- Helicopter stability, using Lockheed rotor system with gyro coupled to cantilevered blades 15 p2348 A71-31599
- Cantilever column critical dynamic instability load under nonconservative follower force including ther-
- momechanical coupling effect from boundary value problem formulation [ASME PAPER 71-APM-L] 18 p2977 A71-36255
- Rectangular cantilever plate free vibration under in-plane acceleration loads, calculating frequencies and mode shapes by Ritz method and computer technique 19 p3157 A71-37850
- Stress determination by vibration measurement in cantilever specimens fatigue tests with audio frequency loading, taking into account end restraint elasticity 19 p3160 A71-38347
- Three dimensional surface displacement measurement by hologram interferometry, applying to cantilever 20 p3235 A71-39187
- Coupled bending-bending vibration of pretwisted tapered cantilever blades, obtaining equations of motion [ASME PAPER 71-VIBR-78] 21 p3460 A71-40315
- CANTILEVER PLATES**
- Cantilever plates calculation, satisfying boundary conditions by coordinate sequence construction 05 p0828 A71-16894
- Optimal design with geometric constraints for simply supported Tresca plastic disk and cantilever plate under concentrated force 05 p0830 A71-17223
- Vibration natural frequencies and mode shapes of cantilever plate mounted on rotating disk periphery, using finite element technique 13 p2147 A71-27788
- Natural vibration parameters of cantilevered isotropic plates, using finite difference method with matrix form solution 17 p2829 A71-35308
- CANTILEVER WINGS**
- U WINGS**
- CAPACITANCE**
- Alloyed p-n junction diode with deep impurities, discussing barrier capacitance frequency dependence 01 p0057 A71-11462
- Parametric amplifier with nonlinear capacitance varying as quadratic function of voltage, deriving power gain, bandwidth and noise figure from equivalent circuit 03 p0383 A71-13270
- Elevated temperature strain gages using capacitance changes as indication, discussing design and response tests 03 p0426 A71-13770
- Resonators sequence delay system with external capacitance link, calculating dispersion characteristic and coupling resistance 03 p0386 A71-13802
- Tunnel diode trigger circuit, calculating effect of junction capacitance variation and small inductance on switching time 05 p0730 A71-17082
- Automatic phase control system with separating capacitance containing low and high frequency electric filters 06 p0866 A71-17375
- Doubly shunt loaded short slot antenna, determining optimum capacitive loadings for enhanced radiation or improved directivity 06 p0876 A71-17740
- Si surface barrier radiation detectors depletion region low energy proton irradiation damage determination from capacitance-voltage curves and capacitance recovery techniques 07 p1071 A71-19071
- Planar-epitaxial IC resistors p-n junction parasitic effects on cut-off frequency, obtaining design formulas for capacitance and geometry 08 p1264 A71-21074
- Varactor capacitance variations compensation for temperature dependent diffusion potentials and dielectric constants changes 08 p1265 A71-21299
- I-V and capacitance characteristics of silicon diodes prepared by diffusive melting, considering recombination processes in p-n junctions 09 p1414 A71-22290
- Variable capacitance signal transducers characteristics, circuitry and pulse width modulation 09 p1448 A71-22771
- GaAs single crystals conductivity and surface capacitance under transverse electric field at low temperatures 10 p1657 A71-24322
- Junction thermal behavior and energy losses in active contactless bipolar transistor switch loaded by capacitive impedance 11 p1739 A71-26377
- Dielectric layer surface electric charge movement determination by measuring metal-insulator-semiconductor /MIS/ capacity response at very low frequency 12 p1942 A71-26829
- I-V and capacitance characteristics of chalcogenide-glass based matrix-film diode sandwich and film-face switching structures with/without memory 13 p2112 A71-28922
- Rectangular section microstrip lumped capacitance calculation by matrix methods 14 p2210 A71-29571

- Capacitance/voltage characteristics of MOS capacitors before/after 25 MeV proton irradiation
14 p2210 A71-29797
- Heat sink requirements in transistor devices, examining temperature dependence of thermal resistivity and electrical capacitance
14 p2284 A71-30631
- Parametric regeneration amplifier with capacitor modulation by signal voltage only
15 p2378 A71-32633
- Plane diode electrode gap differential capacitance for operation with anode negative voltage, current saturation and space charge limitation
16 p2548 A71-33709
- Diffusive p-type Si valve photocells, investigating barrier capacitance
17 p2713 A71-34565
- Long small bore metal tube internal diameter calculation from capacitances comparison with cylindrical coaxial probes
18 p2922 A71-36581
- Mean value theorem for broadband matching of source with known resistance and parasitic capacitance matched to load resistance
22 p3510 A71-42247
- Impedance and capacitance frequency dependence of p-n junction diodes at microwave frequencies with high injection levels
23 p3650 A71-43308
- Capacitance and conductivity in metal dielectric semiconductor during majority current carrier population depletion by pulsed voltage, discussing concentration and mobility determination
24 p3859 A71-44376
- ### CAPACITANCE SWITCHES
- I-V and capacitance characteristics of chalcogenide-glass based matrix-film diode sandwich and film-fase switching structures with/without memory
21 p3433 A71-41317
- ### CAPACITORS
- Design principles for sensitive elements of capacitive sensors for distance measurement via electrostatic induction effects
01 p0079 A71-10527
- MOS capacitors as low mass micrometeoroid detectors in near-earth space, discussing fabrication and environmental tests
01 p0083 A71-11310
- Metallized capacitors types and properties, considering extra thin dielectric films and high field strength
02 p0230 A71-11817
- Heat pipe improvement of capacitor energy storage and I-V, analyzing in terms of heat loss vs conducted heat
03 p0352 A71-13045
- Radio sets integrated selection components, noting ceramic capacitors and filters and coil circuits
03 p0388 A71-14336
- Minority carrier bulk lifetime from large signal response time of MOS capacitor in deep inversion
03 p0388 A71-14474
- Periodically reverse switched capacitor network theory, deriving equivalent resonant transfer circuit and expression for voltage transfer ratio
04 p0561 A71-15699
- Four-ring stable capacitor for reference standard and application to precision angle measurement
07 p1080 A71-20315
- Interdigital capacitors frequency response and application to lumped element microwave integrated circuits
08 p1261 A71-20753
- Autoparametric oscillator with tunnel diode and variable capacitors, considering effective frequency range extension
09 p1414 A71-22258
- AlN insulating films electrical characteristics for use in charge storage devices, presenting Al-AIN-Au capacitor current-voltage-insulator thickness relationships
09 p1509 A71-23118
- Ferroelectric barium titanate ceramics technology for capacitor fabrication
09 p1483 A71-23394
- Soviet book on large pulsed currents and magnetic fields technology covering condenser bank discharge systems and components design, electrical characteristics and structural details
10 p1557 A71-24014
- Optimization of mechanical characteristics of asynchronous capacitor microengine designs with asymmetric stator circuit for prolonged continuous operation with negligible steel wear
13 p2002 A71-28929
- Low frequency noise spectra measurement in varicaps by frequency modulation of harmonic oscillator, noting application to diode and p-n transistors
15 p2369 A71-31232
- Step voltage generator design based on periodic release of prespecified charge fractions by storage condenser using dosing capacitor
18 p2893 A71-36624

- Dielectrophoresis force measurements and wedge shaped capacitor separation properties in satellite zero gravity conditions
19 p3103 A71-37278
- Al electrolytic capacitors characteristics as function of temperature, time and frequency of operation, noting improvement by organic solvents use as electrolyte component
20 p3203 A71-38884
- Semiconductor materials compensated trapping levels analysis, applying thermally simulated capacitor discharge technique
21 p3431 A71-41231
- Energy requirement measurements for bridge wire igniters at low voltage, using capacitor discharge
22 p3587 A71-41448
- Current-voltage hysteresis and memory properties of silicon-silicon nitride capacitors as function of oxide layer and stacking fault traps
22 p3516 A71-41684
- Mica selection quality criteria for capacitors, outlining electrical, physical and optical properties standards
22 p3520 A71-41712
- Conventional components in hybrid circuits, using leadless inverted device, SOT-23 transistor and multilayer ceramic capacitors
23 p3655 A71-43349
- Thin film oxide, ferroelectric and bismuth titanate dielectrics for high capacitance microwave IC technology
23 p3651 A71-43429
- Current controlled diodes used as voltage variable capacitors in oscillators
23 p3652 A71-43832
- Permittivity increase in fluor-substituted barium titanate solid solutions for ceramic capacitor microminiaturization
24 p3859 A71-44387
- Impurity redistribution errors in C-V characteristics of MOS capacitors due to Si thermal oxidation
24 p3809 A71-44993
- ### CAPE KENNEDY LAUNCH COMPLEX
- Kennedy Space Center Meteorological Tower Facility, describing equipment and data acquisition mission
02 p0277 A71-12528
- Information management system to schedule, control and status work on Apollo/Saturn Program at Kennedy Space Center
[AIAA PAPER 71-239]
07 p1207 A71-19715
- Lightning and static electricity hazards at Kennedy Space Center, discussing meteorological aspects
07 p1084 A71-19948
- Binomial distribution models for thunderstorm activity at Cape Kennedy
08 p1326 A71-21452
- Rockets and launch operations protection from atmospheric electricity at Kennedy Space Center, discussing current and future lightning suppression
18 p2913 A71-36451
- Space station facilities and launch and prelaunch operations at Kennedy Space Center, discussing statistical analysis for activity optimization and integrated mission management concept
18 p2899 A71-36474
- Airline operations approach to Cape Kennedy launch processing system for reduced hardware and operational costs of shuttle support
18 p2899 A71-36475
- ### CAPILLARIES [ANATOMY]
- Capillary density relationship to maximal oxygen uptake, indicating endurance training effects on human skeletal muscle
16 p2530 A71-33245
- Physiological relationship of young to old men, considering body composition, aerobic capacity and capillary-muscle fiber ratio
22 p3485 A71-41717
- ### CAPILLARY CIRCULATION
- #### U CAPILLARY FLOW
- #### CAPILLARY FLOW
- Capillary ball game phenomenon under weightlessness, showing photographs of mercury droplet reflection from fluid boundary
02 p0239 A71-11925
- Capillary plasma heating source processes, using textolite and fiberglass-reinforced textolite dielectric discharge chambers
02 p0292 A71-12556
- Vaporization heat transfer mechanism from capillary wick covered heated surface, considering applicability to heat pipes
03 p0353 A71-13615
- Spacecraft propellant expulsion systems, comparing capillary with conventional techniques
[AIAA PAPER 70-685]
07 p1183 A71-19856
- Computerized capillary model for fluid restrictors in multipoint concurrent air flow measurements
07 p1025 A71-20563
- Hyperemic skeletal muscle capillaries restricted diffusion, obtaining permeability data for chromium 51 labeled EDTA and inulin in exercising human forearm
08 p1237 A71-20677

- Closed steady streamline creeping flow in cylindrical cavity applied to bubble or plug train in pulmonary and peripheral capillaries
10 p1571 A71-24614
- Capillary pressure and contact angle drop of two fluid flow separated by parallel plate interface
11 p1750 A71-25443
- Capillary and electro-osmotic flow pumping in heat pipes, discussing capacity increase
[AIAA PAPER 71-423]
11 p1857 A71-26214
- Pulmonary circulation regulating factors, examining heart disease effects on lung capillary blood flow
13 p2003 A71-27861
- Isothermal flow under capillary forces in heat pipe with zero gravity, deriving relation between flow rate and duct parameters
13 p2050 A71-29219
- Electrical insulation failure in dielectric fluid layer due to electrocapillary instability, presenting critical potential difference approximate and exact calculation
15 p2376 A71-31932
- Factors affecting tissue oxygen supply in old people, showing capillary circulation disturbance role in hypoxia development during aging
17 p2679 A71-34220
- Vaporization heat transfer in saturated liquid capillary flow through wick structure, describing test facility and procedure
[ASME PAPER 71-HT-35]
19 p3166 A71-38000
- Maximum bubble pressure automatic capillary electrometer for salt solutions and organic compounds electrosorption, comparing with Lippmann instrument and capacitance bridge
22 p3548 A71-42529
- ### CAPILLARY TUBES
- Cryogenic heat pipes with parallel capillary channel wicks
[ASME PAPER 70-WA/ENER-1]
03 p0520 A71-14106
- Nonlinear axisymmetric solution for cardiovascular system pulsatile flow, using long rigid tube and velocity profile representation
11 p1726 A71-26485
- Evaporative injector system for capillary column gas chromatography for solutes in dilute solution
20 p3194 A71-39257
- ### CAPILLARY WAVES
- #### NT BAROCLINIC WAVES
- #### NT GRAVITY WAVES
- #### NT RIPPLES
- Stimulated light scattering by capillary waves on incompressible fluid surface or by Rayleigh waves on surface of isotropic solid body with small opticoelastic moduli
02 p0285 A71-12505
- ### CAFSULES [SPACECRAFT]
- #### U SPACE CAPSULES
- ### CAPTIVE TESTS
- #### NT STATIC TESTS
- Captive trajectory techniques for six degree of freedom external store separation wind tunnel testing, noting capability for missile guidance system simulation
[AIAA PAPER 71-282]
08 p1275 A71-22007
- External store surface pressure distributions during captive flight aboard F-4B aircraft, considering carrying aircraft effects on flow field about airborne ordnance
[AIAA PAPER 71-295]
08 p1232 A71-22015
- Design provisions for captive fired testing of solid rocket motors, describing equipment and procedures for monitoring motor phenomena during testing
[AIAA PAPER 71-678]
14 p2292 A71-30742
- ### CAPTURE CROSS SECTIONS
- #### U ABSORPTION CROSS SECTIONS
- ### CAPTURE EFFECT
- Three body gravitational capture of interstellar dust in solar system, examining zodiacal cloud
01 p0158 A71-10771
- Zone of unstable radiation in magnetosphere localizing auroral and quasi-captured particles
05 p0798 A71-16046
- Heavy cosmic rays slowing in balloon-borne stack, discussing high resolution measurement and synthesis in rapid neutron capture
08 p1354 A71-21038
- Diffusion-ion capture and heat transfer by phonons in solid and liquid metals
09 p1494 A71-22882
- Negative pion capture in nuclei, examining charged particle emission energy spectra
10 p1644 A71-24538
- Spacecraft capture by ballistic aerobraking during passage through planet atmosphere, proposing analytic models
13 p2133 A71-27987
- Solar neutrino detection using capture reaction in perchloroethylene medium
15 p2478 A71-31803
- Longitudinal modes in standing wave gas laser with Brewster windows in presence of active level emission capture
17 p2753 A71-34412

- Reduced nebular helium abundances, using capture-cascade and collisional excitation calculations
23 p3733 A71-43081
- Rapid neutron capture products evidence on peculiar A star surfaces from observation of promethium and heaviest elements abundance
24 p3865 A71-44567
- Nonadiabatic and atmosphere induced energy losses as causes of proton capture in geomagnetic field
24 p3867 A71-45320
- CARAVELLE AIRCRAFT**
U SE-210 AIRCRAFT
CARBAMATES [TRADENAME]
NT URETHANES
- CARBIDES**
NT BORON CARBIDES
NT CHROMIUM CARBIDES
NT HAFNIUM CARBIDES
NT MOLYBDENUM CARBIDES
NT NIOBIUM CARBIDES
NT SILICON CARBIDES
NT TANTALUM CARBIDES
NT TITANIUM CARBIDES
NT TUNGSTEN CARBIDES
NT URANIUM CARBIDES
NT VANADIUM CARBIDES
NT ZIRCONIUM CARBIDES
- Transition metals powders and carbides sintering by high temperature hot pressing in homogeneity region, determining optimum conditions and activation energy
02 p0256 A71-12276
- Transition metals carbides and nitrides homogeneity regions relation to nonlocalized valence electrons in lattice and configuration stabilizing ability
02 p0264 A71-12280
- Transition metal carbides and nitrides, observing metallic and nonmetallic sublattice dynamic characteristics by X ray diffraction
02 p0266 A71-12672
- Austenitized oil hardened annealed chromium steels with electrolytically isolated carbides, determining structure by X ray analysis
04 p0610 A71-14886
- Carbide particles mean interparticle spacing and low alloyed steels dislocation density determination by planar and volume methods for metal matrix
04 p0612 A71-15076
- Thermophysical properties of solids at high temperatures concerning zirconium carbide, corundum, metals and Ba-Cs system
04 p0612 A71-15578
- Monograph on cobalt base superalloys covering mechanical properties relation to microstructure, carbides, heat treatment, aging, intermetallic precipitation and dislocation
05 p0765 A71-16198
- One chamber vacuum furnace for dewax, presinter and sinter of cemented carbides, referring to Cox chart for system design
05 p0758 A71-16248
- Group 4 and 5 transition metal carbides thermal expansion determined on quartz dilatometer at various temperatures
05 p0768 A71-16789
- Powdered Ni-carbide composites compressibility, noting mixture and pressure effects on compact density
05 p0769 A71-16859
- Elastic and thermodynamic properties of transition metal carbides, comparing Debye temperatures obtained from elastic constant to those obtained from specific heat data
06 p0915 A71-18687
- Apollo 12 sample 12023 fines carbon, carbides and methane determination by hydrolysis and vacuum pyrolysis
07 p1196 A71-19541
- Cubic iron carbide identification from iron meteorites by X ray powder photography and electron microscopy
07 p1200 A71-20057
- Refractory metals and carbides and borides, investigating laws governing electrodes erosion during electric spark breakdown
07 p1139 A71-20205
- Iron-iron carbide structure dissolution behavior from electron transmission microscopy, observing carbide, matrix, general and interface attack modes
07 p1056 A71-20361
- Mass spectrometric determination of vapor phase dissociation energies of scandium dicarbide and scandium tetracarbide
08 p1250 A71-20673
- High temperature liquid propellant oxidative-erosion resistant ablative composites containing in situ reaction formed refractory metal carbides for rocket nozzles
08 p1318 A71-20696
- Crystal imperfections effect on MC carbide precipitation on coherent twin boundaries and regions close to grain boundaries in austenitic steels, using electron microscopy
11 p1780 A71-26027
- Metal carbide grain boundary precipitates effect on austenitic stainless steels high temperature fatigue fracture behavior
11 p1782 A71-26439
- Disintegration energy of hard compounds/carbides, nitrides and borides/ related to wear resistance and microhardness of alloys
13 p2072 A71-27818
- Austenite and carbide chromium manganese steel boron distribution obtained by tracing elements
15 p2425 A71-31397
- Molybdenum steel annealing, noting carbide phase transformations
15 p2425 A71-31398
- Soviet papers on refractory carbides covering high purity and alloy products electrical, thermal, thermodynamic, mechanical, chemical, wear and abrasive properties
15 p2429 A71-32137
- D-transition metal carbides properties based on electron configuration localization model
15 p2429 A71-32138
- Titanium, vanadium and niobium carbohydrides, investigating electronic structure effects on atomic behavior
15 p2429 A71-32140
- Ti, Zr, Nb, Cr, Mo and W carbides compaction, investigating effects of compression, duration, pressing number, moisture and plasticizer contents and stress distribution
15 p2415 A71-32141
- Carbide coating formation on graphite from vapor-gas phase, calculating thermodynamics and kinetics by digital computer for comparison with experiment
15 p2438 A71-32143
- Optimum temperature for Zr and Mo soldering of graphite materials with formation of carbide interlayer for ensuring maximum heat resistance
15 p2439 A71-32145
- Carbon K alpha band measurements in transition metal carbides, graphite and diamond, using X ray spectrometer with diffraction grating
15 p2430 A71-32149
- Rare earth metals di- and sesqui-carbides physical characteristics, establishing changing properties patterns during phase transitions
15 p2461 A71-32153
- Thermal coefficient of resistivity of carbides and solid solutions of Ti, Zr, Hf, V and Nb, noting inverse dependence of covalent bond in Me-Me band
15 p2430 A71-32154
- Hot pressed transition metal carbide samples microhardness measurement, interpreting results in terms of atomic electron configurations
15 p2431 A71-32162
- Nickel and cobalt pseudobinary eutectic alloys reinforced by refractory metal monocarbides whiskers, studying mechanical properties, solidification and phase equilibria
15 p2432 A71-32169
- Vaporization thermodynamics of lanthanum carbides from Knudsen effusion mass spectrometry
16 p2538 A71-32812
- Transition metal carbides and nitrides ordered structures, determining C and N atoms positions with electron and neutron diffractions
16 p2597 A71-33921
- Transition metals monocarbides and mononitrides electronic structure, investigating electrical, thermoelectrical and galvanomagnetic properties
16 p2597 A71-33922
- Alloying elements effects on martensite decomposition and carbide phase formation during tempering of chromium steels
21 p3401 A71-41085
- Transition metal /particularly Ti/ carbide hardness temperature dependence explained from dislocation theory viewpoint, relating hardness to electronic structure
22 p3565 A71-41657
- Total-to-open porosity ratio for carbide-iron type materials sintering, noting relative density and chemical composition effects
24 p3838 A71-44736
- Temperature dependence of external friction coefficient between high-melting carbides in vacuum at constant normal load and slipping rate
24 p3830 A71-44863
- CARBOHYDRATE METABOLISM**
NT HYPERGLYCEMIA
Myocardial infarction acute stage, noting carbohydrate metabolism disturbances
06 p0849 A71-17291
- Carbohydrate metabolism and electrolyte changes in human muscle tissue during heavy exercise
06 p0856 A71-18387
- Carbohydrate ingestion produced respiratory gas exchange ratio and alveolar ventilation effects on arterial oxygen tension in normal men
07 p1052 A71-20333
- Mitochondrial oxidation of substrates coupled with phosphorylation studied using organelles isolated from red and white skeletal muscles of rabbit, noting enzyme activity of fatty acids
08 p1238 A71-20682
- Absorption and incorporation rates of C 14 glucose in rats under acute hypoxia
08 p1242 A71-21964
- Hypothermia effect on brain nutritive processes and regulator activity, considering changes in brain blood supply, respiration and carbohydrate metabolism
22 p3486 A71-41940
- CARBOHYDRATES**
NT ADENINES
NT ADENOSINE DIPHOSPHATE [ADP]
NT ADENOSINE TRIPHOSPHATE [ATP]
NT ADENOSINES
NT CELLULOSE
NT CHOLINE
NT FATS
NT GALACTOSE
NT GLUCOSE
NT GLUCOSIDES
NT GLYCOKENASE
NT HEXOKINASE
NT HEXOSES
NT MONOSACCHARIDES
NT NUCLEOSIDES
NT PENTOSE
NT POLYSACCHARIDES
NT RIBOSE
NT SUGARS
- Carbohydrate-peptide bond and residue chain structure of group blood substances, using alkali decomposition of monosaccharides
01 p0013 A71-11091
- Space diets for maximum energy consisting of fats and proteins from biological systems and carbohydrates from chemical systems
01 p0027 A71-11573
- Biological radioprotectants in space flights including amino acids, bacterial polysaccharides, hormones and vitamins
06 p0861 A71-18358
- Potential foods synthesis for long duration space missions by physicochemical methods, discussing regeneration of carbohydrates from metabolic waste carbon dioxide and electrolytic byproduct hydrogen
07 p1056 A71-20375
- Lipid, protein and carbohydrate concentrations in Chlorella biomass from pyrolysis and aluminogel column chromatography
13 p2017 A71-28407
- Yeasts growth on synthetic carbohydrates with crude formose sugars, discussing application as regenerating food in long term closed life support system
19 p3011 A71-37576
- Rat brain carbohydrates biosynthesis from organic acid products under normal conditions and during central nervous system disturbances, investigating butyric acid participation
21 p3337 A71-41058
- Monosaccharides effect on catalytic synthesis of carbohydrates from formaldehyde
24 p3800 A71-44527
- CARBON**
NT CARBON ISOTOPES
NT CARBON 12
NT CARBON 13
NT CARBON 14
NT CHARCOAL
- Diffusion boride protective coatings on Nb, Ta, Mo and W against carbon diffusion from carburizing agents
01 p0100 A71-10401
- Carbon-carbon composites nondestructive testing following various processing steps, discussing material variations and discrete discontinuities
01 p0090 A71-11278
- Anisotropic polycrystalline carbon fiber tensile strength and bending behavior, interpreting inelastic characteristics from single filament experiments
02 p0273 A71-11945
- Carbon fiber reinforced epoxy composites, evaluating application as helicopter tail rotor blade material
02 p0273 A71-12477
- Carbon fiber reinforced plastics, discussing mechanical and nondestructive testing for performance factors
02 p0274 A71-12482
- Carbon fiber surface treatment for reinforced plastic composites interlaminar strength increase, using wet oxidation process based on hypochlorous acid
02 p0274 A71-12485
- Carbon fiber composites, examining epoxy resin matrix effects on mechanical performance and heat tolerance
02 p0274 A71-12486
- Carbon fiber-epoxy resin composites in aircraft industry, examining fatigue life, cost, specific moduli and mechanical properties
02 p0275 A71-12488
- Carbon fiber surface reactivity relationship to various organic compounds using gas-solid chromatography, evaluating molecular absorption enthalpies
02 p0209 A71-12537

Welded joint structural stability determination by measuring decarburized steel layer thickness after carbon diffusion into lower activity region

03 p0432 A71-13690

Ni coated carbon fibers tensile properties, examining thickness, stress-strain curve, plasticity and grain size

03 p0448 A71-14185

Submicron sectioning apparatus for studying slow carbon self diffusion in dense polycrystalline tungsten carbide

03 p0429 A71-14187

Carbon base multifiber yarns for metal matrix composites reinforcement, considering fiber strength degradation minimization methods

03 p0449 A71-14419

Thermal lattice expansion measurements on carbon powders up to graphitization temperatures, using X ray diffraction

04 p0618 A71-14960

Cross sections for single-electron capture by C/4 plus/ from He, Ne and Ar target gases

04 p0630 A71-15656

Cu and Ni electroless deposition on carbon fibers for composites

05 p0759 A71-16927

Carbon fibers for low weight aircraft plastic structural materials

06 p0915 A71-17743

Relative biological effectiveness of multicharged C ions during single irradiation of *Chlorella*, noting dose dependent mutability

06 p0854 A71-18366

Photoionization cross section in resonance continuum of C I, using wall stabilized arc arc

07 p1111 A71-19487

Apollo 12 sample 12023 fines carbon, carbides and methane determination by hydrolysis and vacuum pyrolysis

07 p1196 A71-19541

Interstitial solid solution hardening in pure Ni and Ni-C alloys, noting mechanism and C concentration effects

07 p1138 A71-19980

Alloying addition effects on wetting of carbon by liquid metals, using sessile drop technique [PLASTICS INST. PAPER 19]

08 p1296 A71-20911

C solubility in Mo-W solid solution at various temperatures

08 p1306 A71-21063

Ternary Mo-Hf-C alloys thermomechanical and mechanical property relationship, obtaining yield strength at various temperatures

08 p1313 A71-21557

High temperature tensile strength testers for metallic and carbon filaments

09 p1446 A71-22735

Arc weld metal carbon content effects on welded joints mechanical properties in Ni at low and high temperatures, noting crack reduction

09 p1479 A71-23422

Macroheterogeneous carbon materials elastic characteristics during heat treatment process

10 p1634 A71-24203

Mo-Ti-C ternary alloy, examining solid state solubility, equilibrium conditions and microhardness

10 p1628 A71-24647

Mo-Fe-C ternary system, investigating various concentrations, microhardness measurements, solid state solubility and ductility

10 p1628 A71-24648

Atomic N and C photoionization cross sections by shock tube vacuum UV spectrometry

10 p1646 A71-24990

B and C polymer laminated film composites efficiency for stability designed structures, considering weight reduction by planar reinforcements [AIAA PAPER 71-353]

11 p1783 A71-25331

Carbon fiber reinforced plastics industrial engineering applications, noting cost effectiveness, strength and elasticity

11 p1861 A71-25407

Radiative mean lives and transition probabilities of electronic states in beam foil excited atomic and ionic carbon

11 p1803 A71-26061

Entry vehicle carbon vapor thermochemistry uncertainties effects on nose tip ablation response concerning stagnation point surface recession and temperature levels

11 p1857 A71-26207

Lightweight oxidation resistant carbon-carbon composites for space shuttle leading edge components thermal protection

11 p1790 A71-26231

Carbon and oxygen inclusions effects on polycrystalline molybdenum rupture due to precipitation and chemisorption

11 p1781 A71-26323

Extraterrestrial and earth life genesis, discussing carbon foundation, planetary conditions, water prerequisite and space exploration

13 p2009 A71-28679

Carbon deposition rates in gas turbine engine combustion chambers with airstream-mechanical propellant atomization

13 p2118 A71-28970

Mo and W single crystals mechanical properties, considering C and iron group additions influence

14 p2255 A71-29516

Carbon-carbon spacecraft reentry heatshields evaluation and selection by nondestructive and destructive tests on flight cones

14 p2262 A71-29647

Porous carbon and graphite substrates chemical vapor deposition carbon infiltration process, discussing isothermal and thermal and pressure gradients techniques

14 p2262 A71-29652

Hollow carbon microspheres from pitch material, emphasizing applications in porous composites

14 p2263 A71-29657

Carbonaceous chondrites total nitrogen and carbon abundances, using gas chromatography

15 p2486 A71-31990

Silicon-boron melts, investigating B and C concentration effects on carbide layer thickness on graphite/melt interface

15 p2439 A71-32144

Carbon K alpha band measurements in transition metal carbides, graphite and diamond, using X ray spectrometer with diffraction grating

15 p2430 A71-32149

Water, carbon and rare gases in lunar crater breccias based on meteorites nature

15 p2494 A71-32490

Anisotropic carbon-graphite materials and metals temperature dependence of thermal expansion coefficients, noting approximation by Debye heat capacity function

16 p2601 A71-33710

Mo single crystal growth by vacuum melting without oil vapors, noting reduced carbon content and increased ductility

16 p2595 A71-33880

Transition metal carbides and nitrides ordered structures, determining C and N atoms positions with electron and neutron diffractions

16 p2597 A71-33921

High porosity carbon-graphite materials thermal and electrical conductivities at high temperatures by potentiometric method

17 p2761 A71-34208

Carbon and nitrogen abundances in howardites, enstatite and hypersthene achondrites

17 p2800 A71-34515

Hydrogen discharge from Fe-C alloys in absolute suction metal mold, finding discharge decrease with increasing carbon content

18 p2926 A71-36300

Carbon effects on strength, ductility, brittle transition and plastic strains of tungsten at high temperatures

18 p2936 A71-36713

Cast electron-beam remelted Mo, investigating carbon and zirconium carbide additions effects on structure and low-temperature plasticity

18 p2937 A71-36723

Carbon impurity effects on molybdenum ingot formation, detailing crystal growth, size reduction and length

19 p3077 A71-37277

Interstitial solute thermomigration of C in Ti, V, Fe, Co, Ni and Pd, using radioactive tracer technique

19 p3079 A71-37710

Carbon and methyl radical formation, studying emission intensities and chemi-ionization rates in hydrogen-oxygen flames with hydrocarbons

19 p3013 A71-38090

Ion beam deposition of insulating carbon thin films on room temperature substrates, considering transparency, index of refraction, insulating capacity, glass scratching ability, etc

20 p3241 A71-39011

Solution temperature and Ti/C ratio effects on Cr-Ni-Ti austenitic steels creep properties, including precipitation, deformation, rupture and coalescence

20 p3250 A71-39025

Soviet monograph on carbon deposits in jet engines covering distribution, formation, fuel properties, reduction and removal and harmful effects in gas turbines

21 p3437 A71-40871

Photochemical mechanism of atomic carbon production in Mars and Venus atmospheres, comparing dayglow emissions with Mariner results

23 p3734 A71-43157

Apollo 12 samples total C and N abundances suggesting indigenous lunar material with solar wind component

23 p3750 A71-43698

B stars spectra, calculating C III ions spontaneous electric dipole transitions and oscillator strengths in vacuum UV region

23 p3767 A71-43829

Evolutionary meaning of nitrogen and carbon sequences in Wolf-Rayet stars

23 p3770 A71-44064

Interstitial solute carbon distribution in martensite, using generalized perfect lattice gas statistical mechanics

23 p3694 A71-44281

Carbon ion and free electrons three body recombination rate coefficient measurement in carbon monoxide flows

24 p3802 A71-44660

Model computations for Population I star in evolutionary phase from He exhaustion in stellar center up to carbon ignition

24 p3872 A71-45076

CARBON ARCS

Photon intensities of UV spectral lines from energetic magnetically confined vacuum carbon arc, using monochromator double ion chamber detector system

09 p1502 A71-22811

Viscosity of dissociating oxygen, carbon-air and carbon plasmas at high temperature range, including error estimates and expansion up to 12,000 K

15 p2512 A71-31502

CARBON COMPOUNDS

NT ARAGONITE

NT BORON CARBIDES

NT CALCITE

NT CARBIDES

NT CARBONATES

NT CHROMIUM CARBIDES

NT HAFNIUM CARBIDES

NT LEXAN (TRADEMARK)

NT MOLYBDENUM CARBIDES

NT NIOBIUM CARBIDES

NT POLYCARBONATES

NT SILICON CARBIDES

NT SODIUM CARBONATES

NT TANTALUM CARBIDES

NT TITANIUM CARBIDES

NT TUNGSTEN CARBIDES

NT URANIUM CARBIDES

NT VANADIUM CARBIDES

NT ZIRCONIUM CARBIDES

Boron and carbon hydrides and carbon deuteride molecular ions radiative lifetime measurements, computing absolute oscillator strengths

08 p1250 A71-20671

CH molecule line formation mechanism for 4300 A transition in solar photosphere, studying collisions with hydrogen atoms

09 p1520 A71-22843

Carbon suboxide polymers formation in Martian atmosphere, examining carbon monoxide photolysis and radiolysis processes enhanced by solar ionizing radiation

15 p2491 A71-32420

Carbon compounds in Apollo 12 lunar fines and core samples, using pyrolysis, mass spectrometry, ion exchange chromatography and optical and electron microscopy

17 p2801 A71-34649

Carbon difluoride in ablating air-teslon laminar boundary layers by spectrally and spatially resolved UV thermal radiation measurements

19 p3163 A71-37881

Flash photolysis produced gaseous carbon difluoride IR spectrum analysis by rapid scan IR spectroscopy

19 p3011 A71-38053

Carbon and noncarbon polymers based high temperature elastomeric materials chemical structure and physical properties

19 p3085 A71-38068

Slow and explosive gas phase oxidation of carbon suboxide and monoxide over various pressure and temperature ranges, noting branching reactions

19 p3167 A71-38088

Crystal lattice vibration and molecular libration effects on solid carbon tetrachloride heat capacity at 0-20 and 200-230 K

22 p3585 A71-42059

Nonaqueous biosystems unlikelihood from consideration of enzymatic activity possibility and liquid water unique ability for complexity required by carbonaceous biosystems

22 p3487 A71-42229

CH radical 10 cm line frequency determination by photographic Fabry-Perot interferometry

23 p3733 A71-43082

Indigenous gases and hydrolyzable carbon compounds in Apollo 11 and 12 samples through gas chromatographic and mass spectrometric examination, noting meteoric impact and solar wind implantation as probable origins

23 p3755 A71-43738

Chemical characteristics of carbon compounds in Apollo 11 and 12 lunar fines, using organic solvent extraction, mass spectrometry and gas chromatographic method

23 p3756 A71-43743

Limiting chemical reaction rate of graphite and carbon containing material combustion at high temperatures

24 p3890 A71-45108

CARBON DIOXIDE

Carbon dioxide clathrate in Martian ice cap suggested from hydrate stability relative to solid phase and water ice as function of temperature
01 p0148 A71-10002

Carbon dioxide band radiances measured by Nimbus 3 satellite IR spectrometer, noting seasonal temperature changes in stratosphere due to meridional circulation
01 p0119 A71-10743

Air carbon dioxide role in rabbits metabolism, using C 14 radioactive tracer technique
01 p0012 A71-11061

Carbon dioxide IR absorption bands at elevated pressures, deriving transmission function
01 p0130 A71-11104

Carbon dioxide molecules dissociative excitation processes by low energy electrons, examining light emission mechanism in VUV
02 p0261 A71-12318

Carbon dioxide vibrational relaxation in Ar at high temperature, using shock tube method
02 p0287 A71-12496

Venus spectra 10488 A carbon dioxide band from high dispersion spectroscopy
03 p0488 A71-13556

High dispersion spectroscopic observations of Venus carbon dioxide bands for deriving rotational temperature
03 p0488 A71-13557

Mars atmosphere carbon dioxide condensate cloud layer implications, considering temperature lapse rate and water condensation at lower levels
03 p0489 A71-13608

Thermal radiation from hot water vapor and carbon dioxide imbedded in cool atmosphere, using extended molecular band models
03 p0518 A71-13649

CW laser output in carbon dioxide and nitrous oxide induced by vibrational energy transfer from excited carbon monoxide
03 p0438 A71-13893

Troposphere and stratosphere mean annual carbon dioxide cycle measurements, describing aircraft collection equipment and procedure
03 p0418 A71-14205

Mars atmosphere carbon dioxide photodissociation via pressure independent one step process
03 p0497 A71-14548

Pure carbon dioxide planetary atmospheres, calculating photochemical instability from atmospheric model
03 p0377 A71-14549

Rate constant measurement for atomic hydrogen reaction with carbon dioxide yielding OH and CO, considering near IR emission spectroscopy applicability
04 p0548 A71-14697

Venus high dispersion spectra used for line positions and constants of carbon dioxide 7820 and 7883 A bands
04 p0629 A71-14806

Diurnal variations due to actual heat output, oxygen consumption and carbon dioxide production in rats undergoing eating habit changes
04 p0539 A71-15157

Venus high resolution spectra interpretation for sub II band of carbon dioxide isotope
04 p0659 A71-15859

Ozone in Mars solid carbon dioxide polar cap, using UV reflection-absorption spectra
04 p0661 A71-15897

Solar line spectra wavelength improvement in 7780 to 7925 A range, using carbon dioxide bands
05 p0803 A71-16020

Shock waves in nitrogen, carbon dioxide and mixtures, measuring Mach number for deviation evaluation from vibrational and dissociation equilibria
05 p0835 A71-16522

Carbon dioxide refractivity measurement, determining dielectric constant, Verdet constant and Rayleigh scattering cross section by dispersion formula
05 p0717 A71-16908

Cross sections for fluorescence production in carbon dioxide photoionization by 58.4 nm radiation, deriving emission spectra
06 p0963 A71-17255

Intrarenal vascular pattern in carbon dioxide death of rhesus monkeys and dogs, observing sympathetic vasoconstriction
06 p0851 A71-17610

Carbon dioxide arc discharge plasma emission spectral absolute intensities under atmospheric pressure, determining molecular band contributions
07 p1162 A71-19131

D region oxygen photoionization rates decrease due to carbon dioxide absorption
07 p1103 A71-19673

Scattered light depolarization measurement near carbon dioxide critical temperature, using He-Ne laser
07 p1127 A71-20379

Intermediates structure and IR spectrum in OH reaction with CO by vacuum UV photolysis, studying

refractive product absorptions and valence force potentials

Vibrationally excited carbon dioxide deactivation by collisions with CO, determining rate constants by laser fluorescence method
08 p1336 A71-20661

MnO oxidation reduction kinetics measurement in carbon monoxide/dioxide atmospheres by gravimetry and electrical conductivity
08 p1250 A71-20665

Carbon dioxide IR absorption bands at elevated pressures, deriving transmission function
08 p1318 A71-20698

Carbon dioxide 7883 and 7820 A band strengths compared in Venus atmosphere
08 p1337 A71-20848

Organic impurities effects on carbon dioxide dissociation activation energy, considering magnitude dependence on experimental conditions and data reduction techniques
08 p1338 A71-21396

Carbon dioxide flow vacuum condensation on cryogenic pump surface, noting flow temperature and directivity effects on condensation rate
08 p1251 A71-21783

Ultrasound propagation velocity dependence on high pressure and temperature in carbon dioxide, considering Rao rule applicability to highly compressed gases
09 p1544 A71-22268

Venusian atmosphere carbon dioxide, water, molecular oxygen and nitrogen contents from Venera 5 and 6 data
09 p1492 A71-22529

Carbon dioxide tolerance after hyperbaria adaptation of rhesus monkeys in upright position
09 p1523 A71-23144

Quantum yield of carbon dioxide photolysis at 1470 A concerning Mars and Venus atmospheres
09 p1395 A71-23250

Ice, solid carbon dioxide and alcohols oxygen K spectra from long wave X ray spectroscopy
09 p1403 A71-23377

Nimbus 4 satellite selective chopper radiometer data on IR radiation emitted by carbon dioxide, considering stratospheric warming
09 p1498 A71-23479

Equilibration rate of uncatalyzed carbon dioxide hydration reaction in open system at constant carbon dioxide partial pressure, examining buffering capacity effect
10 p1598 A71-23743

Spectral transmittance of pressure induced and intrinsic absorption of IR energy by carbon dioxide and water due to Fermi bands and asymmetric molecules
10 p1559 A71-23898

Air and carbon dioxide intensive injection effect on turbulent boundary layer of subsonic channel air flow
10 p1644 A71-23950

Upper Martian atmosphere UV emission spectrum observation noting carbon dioxide photoionization, ion fluorescent scattering and photon/electron dissociative excitation
10 p1551 A71-24378

Atomic oxygen and carbon dioxide measurement in lower thermosphere by mass spectroscopy
10 p1604 A71-24776

High resolution measurement of carbon dioxide broadened half widths for water vapor lines in fundamental band
10 p1606 A71-24803

Half widths calculation for carbon dioxide broadened water vapor absorption lines in nu sub 2 fundamental, considering dipole-quadrupole interactions
10 p1645 A71-24965

CO absorption spectrum in carbon dioxide atmosphere, comparing self- and nitrogen- broadened half widths
10 p1645 A71-24966

CO half-width calculations for carbon dioxide broadened fundamental and first overtone bands from Anderson-Tsao-Curnutte theory
10 p1645 A71-24968

CO Fourth Positive band system excitation cross sections by electron impact on carbon monoxide and carbon dioxide
10 p1645 A71-24969

Venus life forms, describing algae grown in pure carbon dioxide under pressure in acidic nutrient media at high temperatures
11 p1727 A71-25366

Martian surface pressure from 1967-1969 apparition observations, discussing micron bands carbon dioxide abundances
11 p1724 A71-25701

Martian atmospheric pressure carbon dioxide abundance variations correlated with waxing and waning of polar caps or Mars season
11 p1825 A71-25711

Relative elevation differences on Mars surface revealed by near IR carbon dioxide bands spectroscopic observations
11 p1825 A71-25712

Mars surface pressure and elevation differences determined by spectroscopic observation of carbon dioxide band

Carbon dioxide cations emission bands in Mars and Venus dayglows, suggesting fluorescent scattering and photoionization as main excitation sources
11 p1825 A71-25714

Nonreacting and reacting ideal gases expansion between interconnected chambers, considering nitrogen and carbon dioxide simultaneous pressure measurements
11 p1827 A71-25724

Energy dependence of integral scattering cross sections of noble gas atoms in carbon dioxide
12 p1877 A71-27550

Collision excited carbon dioxide molecule vibrational relaxation rate constant based on statistical model
13 p2102 A71-27809

Venus carbon dioxide spectrum, observing spatial and temporal variation in abundance
13 p2102 A71-27885

Venus cloud height at equatorial and polar latitudes, using carbon dioxide band distribution intensity
13 p2134 A71-28287

German monograph on gaseous detonations stability covering carbon dioxide thermal decomposition, initial temperature/pressure, reflected shock waves and water adsorption
13 p2138 A71-28593

Carbon dioxide reduction and hemoglobin saturation rates of blood flow in curved channel membrane exchanger
13 p2049 A71-28878

Rotational line overlap effect on laser IR radiation absorption in high pressure carbon dioxide, comparing calculated absorption coefficient with measurements
13 p2013 A71-29004

Carbon dioxide free jet plumes issuing from supersonic nozzle into high vacuum, measuring densities and temperature
13 p081 A71-29337

Performance tests of electron bombardment ion thruster, using xenon, krypton argon, neon, nitrogen, helium and carbon dioxide
13 p2026 A71-29355

Nitrogen-carbon dioxide system molecular resonant energy exchange vibration-vibration probability measurement by shock tube and IR emission monitoring, noting temperature effects
14 p2287 A71-29922

Carbon dioxide photodissociation in vacuum UV, using time-of-flight spectroscopy and metastable photofragment detection by electron emission from metal surfaces
14 p2276 A71-30399

Inert gases, hydrogen, deuterium and carbon dioxide flow in plane parallel glass slots over various Knudsen numbers, calculating slippage constants and volumetric discharge
14 p190 A71-30571

Carbon dioxide electron impact energy loss spectrum and molecular orbit calculations, discussing fourth positive bands production in Mars upper atmosphere UV dayglow
14 p2227 A71-30673

Carbon dioxide frosts spectral absolute reflectance measurements at 0.5-12 microns, applying results to problems associated with cryogenically cooled surfaces
15 p2398 A71-31766

Global temperature effects on atmospheric carbon dioxide and aerosols density based on atmospheric model, noting earth surface temperature decrease
15 p2514 A71-32098

Population inversion damping on vibrational-rotational transitions of carbon dioxide molecule during interaction with monochromatic radiation pulse, using two level model
15 p2354 A71-32205

German monograph on spark discharges behavior in nitrogen, carbon dioxide and argon at excess pressure covering Toepler, Weizel-Rompe and Braginskii laws applicability
16 p2575 A71-34047

Molecular hydrogen sorption pumping by cold carbon dioxide cryodeposits, showing adsorbed molecules surface diffusion into disordered frost structure
17 p2752 A71-34387

Ultrasound propagation velocity dependence on high pressure and temperature in carbon dioxide, considering Rao rule applicability to highly compressed gases
17 p2779 A71-34799

Mars, Venus and earth atmospheres, considering abundance of volatiles such as carbon dioxide, water, oxygen, nitrogen, argon, carbon monoxide, chlorine and fluorine
17 p695 A71-35138

Carbon dioxide IR radiation measurements of duration of constant reflected shock temperature in over-tailored shock tunnel

19 p3041 A71-37893

Supercritical carbon dioxide free convective heat transfer, investigating heater surface material and flow effects

[ASME PAPER 71-HT-27] 19 p3165 A71-37997

Far IR collision induced spectrum in carbon dioxide, observing temperature and pressure dependence in gas phase and absorption in liquid

19 p3106 A71-38051

Amino silica gels absorption properties with respect to carbon dioxide, hydrogen sulfide and water vapor, comparing affinity

20 p3193 A71-39233

Inspired oxygen concentrations effects on arterial and mixed venous pH, carbon dioxide uptake and oxygen partial pressure in normal subjects

20 p3189 A71-39442

Atmospheric temperature profile from satellite soundings of outgoing radiation in IR carbon dioxide band, using regularization and Chahine methods

20 p3258 A71-39669

Gas dynamic model for coupled vibrational and radiative nonequilibrium in carbon dioxide, obtaining macroscopic collisional and radiative transfer equations

21 p3418 A71-40233

Diamond radiation counters for C 14 containing carbon dioxide in extraterrestrial life detection, noting radioactivity curves as function of sample microflora

21 p3378 A71-40571

Solid state modulation for spacecraft horizon sensing via IR carbon dioxide atmospheric radiation, proposing Fabry-Perot structure with controlled plate separation

22 p3537 A71-41475

Global three dimensional atmospheric temperature mapping by selective chopper radiometer on Nimbus 4 satellite, measuring carbon dioxide IR emission

22 p3533 A71-41629

Time of useful function after mice exposure to life threatening toxic mixtures of carbon monoxide, carbon dioxide and ammonia produced by combustion

22 p3486 A71-41830

Electromagnetic radiation in stagnation flow region, determining temperature distribution absorption coefficient of carbon dioxide at rest between two parallel plates

22 p3621 A71-42024

Martian polar caps heat balance, noting albedo differences due to irregularities in solid carbon dioxide cover

22 p3603 A71-42190

Electron impact excited carbon monoxide and dioxide 1260-5000 A spectral emission, discussing cross sections of Cameron and fourth positive bands

23 p3706 A71-42904

Carbon dioxide spectral emission at 1260-4500 A from electron impact excitation, discussing cross sections and Mars atmosphere application

23 p3706 A71-42905

Carbon dioxide absorption temperature dependence in 1750-1200 A region, calculating electron densities and transition moments

23 p3641 A71-43326

Carbon dioxide photolysis at 1740-2100 A applied to photochemistry of Mars lower atmosphere

23 p3641 A71-43327

Carbon dioxide photolysis at 1849 A and various pressures, suggesting gas dissociation at wavelengths with appreciable absorption

23 p3641 A71-43328

Carbon dioxide UV absorption and dissociation processes and reaction kinetics of dissociation products

23 p3642 A71-43329

Mars atmospheric carbon dioxide dissociation, solving and comparing diffusion equations to Mariner oxygen and carbon dioxide observations

23 p3735 A71-43332

Mars and Venus carbon dioxide atmospheres, covering solar EUV heating efficiency, upper atmosphere temperature and chemical recombinations

23 p3735 A71-43334

Venusian photochemistry, discussing hydrogen source from HCl, loss of water in relation to HCl, carbon dioxide stability and COS and hydrogen sulfide in visible clouds

23 p3736 A71-43341

Carbon dioxide additions effect on electron temperature relaxation and electron concentration distribution in expanding supersonic flow of low temperature Ar plasma

23 p3713 A71-44065

Chronic hypoxia exposure effects on human ventilatory response to carbon dioxide and oxygen deficiency

24 p3797 A71-44780

Martian height gradients from 1.6 micron carbon dioxide band intensity, using telescopes with prismatic quartz spectrometer

24 p3869 A71-44807

N-heptane, carbon dioxide and Freon 13 droplet vaporization measurements at supercritical pressure, comparing with film theory calculation

24 p3890 A71-45072

High dispersion spectroscopic observations of Venus, finding carbon dioxide band rotational temperature

24 p3873 A71-45079

CARBON DIOXIDE CONCENTRATION

Low compensation point species capacity for carbon dioxide fixation, suggesting reduced photosynthesis role

02 p0201 A71-12475

Earth atmosphere origin, discussing oxygen and carbon dioxide balance

03 p0409 A71-13697

Fluoride oscillators as sensors for carbon dioxide concentration detection in exhaled breathing gases, noting frequency dependence on gas properties [ASME PAPER 70-WA/FLCS-10]

03 p0372 A71-14086

Atmospheric temperature, computing carbon dioxide concentration effect on radiative heating rates

05 p0742 A71-16677

High environmental carbon dioxide effects on cardiac depression and respiratory rate in rhesus monkeys and chimpanzees

06 p0851 A71-17612

Carbon dioxide and carbon monoxide atmospheric distribution dependence on combined effects of photochemical production, loss and transport in mesosphere and upper stratosphere

06 p0893 A71-17980

Carbon dioxide concentration control in sealed chamber with animals during atmosphere regeneration by Chlorella

06 p0860 A71-18356

Carbon dioxide absorption of dog blood and plasma under anoxia at simulated high altitudes, deriving equations for protein concentration rated buffer values

07 p1043 A71-20327

Helium for nitrogen substitution effects on body temperature of rats exposed to high carbon dioxide concentrations at different ambient temperatures

13 p2006 A71-28402

Turbulent flame boundaries and maximum brightness surface position in gasoline-air mixtures, using photography and gas analysis measurements of carbon dioxide concentrations

13 p2162 A71-28955

Carbon dioxide concentrations in tropopause, investigating flux from northern troposphere into stratosphere

13 p2063 A71-29112

Hypercapnia in rat, measuring carbon dioxide concentration effect on tidal and minute volumes, respiratory rate, pH depression, blood gases, hematocrit and percent oxyhemoglobin saturation

13 p2015 A71-29364

Ion exchange resin carbon dioxide removal and concentration system for space cabin environments, describing monitoring and control instrumentation

14 p2189 A71-30313

Mars atmosphere high resolution line spectra, calculating carbon dioxide abundance, rotational temperature and surface pressure

17 p2800 A71-34588

Hydrogen depolarized fuel cell for space station prototype carbon dioxide concentrator, describing modular design concept and operation

18 p2870 A71-36404

Physiological effects on rats of argon substitution for nitrogen in hermetically sealed chambers under conditions of anoxia and high carbon dioxide concentration

22 p3505 A71-42804

CARBON DIOXIDE LASERS

Carbon dioxide laser intersatellite communication systems as economical alternative to microwave and millimeter systems, noting use onboard ARTS satellites

01 p0091 A71-10009

Carbon dioxide laser bibliography (1964-1969) with chronologically listed references, author index and subject index

01 p0092 A71-10370

Output properties of electrically pulsed carbon dioxide laser as functions of partial gas pressure and discharge voltage

01 p0092 A71-10372

Carbon dioxide laser vs electron beam welding, examining weldability of high thermal conductivity metals

01 p0087 A71-10452

Similar gas discharges for carbon dioxide lasers, including thermal effects and particle distributions over energy levels

01 p0093 A71-10682

Giant pulses composed of shorter pulse trains obtained in Q switched carbon dioxide laser with transverse modes

02 p0259 A71-11880

High power carbon dioxide laser radiation absorption on vaporized and heated quartz

02 p0260 A71-11944

Atmospheric pressure pulsed carbon dioxide laser electrical excitation using double transverse discharge technique

02 p0260 A71-12130

Discharge current oscillations attributed to acoustic wave excitation by Q switched carbon dioxide laser

02 p0261 A71-12344

Carbon dioxide laser optical pumping by resonant emission from alkali metal lamp

03 p0434 A71-13294

Transversely excited atmospheric pressure carbon dioxide laser mode locking with Ge acoustic-optic modulator

03 p0434 A71-13477

High power carbon dioxide electric discharge mixing laser with vibrationally excited nitrogen providing population inversion

03 p0434 A71-13480

Carbon dioxide laser stable mode locking with resonated internal electro-optic phase modulator driven at frequencies near axial mode interval

03 p0434 A71-13481

Carbon dioxide laser plasma lensing effect used as mirror curvature compensation for maximum output power

03 p0436 A71-13641

CW carbon dioxide lasers low voltage excitation, using cold cathode transverse glow discharges

03 p0436 A71-13642

Constant dispersion rotating grating Q switch for carbon dioxide laser with simultaneous band selection and cavity adjustment

03 p0436 A71-13652

Carbon dioxide laser induced thermal lensing (focusing) reduction in liquid carbon disulfide with DC electric field

03 p0436 A71-13877

CW carbon dioxide laser beam IR absorption by sulfur hexafluoride, investigating saturation parameter relationship to pressure, temperature and relaxation time

03 p0437 A71-13879

Reactive Q switching in carbon dioxide multimode multipass laser with movable end mirror, measuring pulse rates and amplitudes

03 p0438 A71-13892

Scaled-off carbon dioxide laser power output and efficiency test during continuous operation over one year

03 p0438 A71-13894

Ablative materials performance in high radiative heat flux environments produced by CW carbon dioxide laser [AIAA PAPER 70-864]

03 p0449 A71-14437

Atmospheric pressure pulsed carbon dioxide laser, investigating gain, peak power and pulse duration as function of gas pressure and discharge voltage

03 p0440 A71-14461

Helium effects on dissociation and population inversion dynamics in pulsed carbon dioxide lasers

04 p0605 A71-14628

IR lasers, discussing carbon dioxide CW and Q-switched operation and semiconductor lasers

04 p0606 A71-14712

Carbon dioxide laser output power and efficiency as function of tube length, discussing bore diameter and cavity insertion losses effects

04 p0606 A71-14716

Carbon dioxide lasers for wideband data transmission in space

04 p0556 A71-15648

Carbon dioxide lasers signature, considering 10.4 micron band P/20 and P/16 lines dominant modes for wide gain curve and operating conditions

05 p0760 A71-16255

Carbon dioxide laser with simultaneous active rotating mirror Q switch and passive absorbing gas cell

05 p0760 A71-16256

Carbon dioxide lasers IR variable double prism attenuator with gap spacing determination by capacitance measurements

05 p0760 A71-16257

Carbon dioxide laser gyro flowing gas system, considering stability, locking frequencies and ease of construction

05 p0761 A71-16271

Carbon dioxide laser gyro with cavity configuration for polarization isotropy and enhanced competition effects, considering high gain and mechanical imperfection tolerance

05 p0761 A71-16272

Carbon dioxide laser frequency doubling by Te crystal reflector output element, discussing shortcomings for conversion efficiency enhancement by power density increase

05 p0761 A71-16273

Spontaneous mode locking in high pressure carbon dioxide laser with nanosecond pulse separations

05 p0763 A71-16496

Carbon dioxide laser beam thermal focusing effects on deflection in absorbing gas

05 p0763 A71-16902

Mode locked high pressure carbon dioxide lasers subnanosecond pulse widths measurement based on photon flux and fast shutter in semiconductor

06 p0907 A71-17310

- Fusion reactor plasma feedback stabilization by nonlinear interaction of two carbon dioxide IR laser beams to produce difference frequency near hybrid resonance
06 p0931 A71-17457
- Carbon dioxide laser with Ge Brewster windows equipped sealed gas discharge tube, comparing with NaCl and KBr windows
06 p0908 A71-18080
- Electric discharge carbon dioxide lasers, obtaining increased power output with convective cooling process
[AIAA PAPER 71-63] 06 p0909 A71-18522
- Carbon dioxide electric discharge lasers physics, discussing electron energy distributions and excitations, gain and saturation intensity
[AIAA PAPER 71-64] 06 p0909 A71-18523
- Electric discharge carbon dioxide mixing laser, presenting model with chemical, vibrational and thermal nonequilibrium effects
[AIAA PAPER 71-66] 06 p0909 A71-18525
- Carbon dioxide laser excitation using nonequilibrium MHD generator
[AIAA PAPER 71-67] 06 p0938 A71-18526
- Pulsed carbon dioxide laser amplifier, examining spatial and temporal refractive index variations with interferometric measurements
06 p0910 A71-18667
- Multipass carbon dioxide pulsed laser mode competition and self locking
06 p0910 A71-18668
- Small sealed low power carbon dioxide lasers, noting signature variations as function of mirror distance variations
06 p0910 A71-18669
- Optimum design of high peak power transversely excited atmospheric pressure carbon dioxide laser using ballast resistor energy measurements
07 p1121 A71-18749
- Single frequency carbon dioxide laser cavity length computer aided selection for reduced line competition, considering heterodyne communications systems
07 p1121 A71-18811
- Pulsed laser emissions in carbon dioxide under high pressure, discussing onset inversion and pulse duration
07 p1121 A71-19128
- Carbon dioxide dissociation plasma composition as function of gas mixture, flow rate, pressure and discharge current in sealed and flow-through laser systems
07 p1122 A71-19134
- Similar gas discharges for carbon dioxide lasers, including thermal effects and particle distributions over energy levels
07 p1125 A71-20143
- Carbon dioxide laser heterodyne plasma density length product measuring with microsecond response in Astron controlled fusion experimental area
07 p1126 A71-20166
- Flow-through carbon dioxide lasers population inversion relation to individual gas components and electron velocity distribution functions
07 p1126 A71-20187
- Fog removal by high power carbon dioxide lasers, evaluating possibility of clearing airport runways
[AIAA PAPER 69-670] 07 p1153 A71-20308
- Carbon dioxide lasers passive Q switching by saturable absorbers, using four state kinetic model
07 p1128 A71-20390
- Carbon dioxide laser IR pulse transmission under moderate pressure conditions using four state model of molecular laser passive Q switching and double resonance
07 p1128 A71-20391
- Mode locked pulsing from carbon dioxide-nitrogen-helium multipass laser by cavity end reflector sinusoidal modulation along axis
07 p1128 A71-20395
- Carbon dioxide laser IR pulses self focusing in liquid carbon disulfide, calculating nonlinear refractive index
07 p1128 A71-20396
- Carbon dioxide laser molecular upper level vibrational relaxation time measurement
07 p1128 A71-20527
- Nitrogen-carbon dioxide electric discharge mixing laser /EDML/ used as pulse amplifier, using high flow rate for waste heat removal
07 p1129 A71-20618
- Sparks induced in gases by transversely excited atmospheric pressure carbon dioxide IR pulsed lasers, observing plasma filament forward propagation
07 p1129 A71-20619
- Carbon dioxide-nitrogen CW laser AC excitation in optical cavity, considering power output
08 p1301 A71-20997
- Carbon dioxide laser Ge windows thermal runaway characteristics
08 p1302 A71-21391
- Carbon dioxide laser population inversion using chemical reaction of burning with gas combustion products of vibrationally excited polyatomic molecules
08 p1302 A71-21499
- Nuclear reaction products effect on population inversion in gas lasers, considering neutron irradiation enhancement of carbon dioxide laser output
08 p1303 A71-21668
- Carbon dioxide lasers gas discharges positive column, studying electron energy distribution by probe method
09 p1461 A71-22381
- Single longitudinal mode operation and mode locking of pulsed high pressure transversely excited carbon dioxide laser by saturable absorbers
09 p1463 A71-22758
- Doppler jitter stabilization of carbon dioxide laser without internal modulation to inverted Lamb dip in extracavity absorption cell
09 p1463 A71-22759
- Thermal expansion of gas breakdown plasma in argon under heating by high voltage transient pumped carbon dioxide laser
09 p1463 A71-22761
- Carbon dioxide laser optical pumping by resonant emission from alkali metal lamp
09 p1464 A71-23266
- Carbon dioxide lasers for industrial material processing, discussing machine tool reliability, maintenance, various automation approaches and economic efficiency
09 p1457 A71-23403
- Carbon dioxide production laser for automatic resistors trimming without current carrying capability reduction, noting accuracy, flexibility and speed
09 p1465 A71-23405
- Polyethylene plastic packet with chemical pellets, describing welding, cutting and small hole punching by CW carbon dioxide laser
09 p1458 A71-23410
- Carbon dioxide laser performance quantitative analysis, considering electron to optical energy conversion via electric discharge in carbon dioxide-nitrogen-helium mixture
09 p1465 A71-23481
- Spontaneous self locking axial modes in transversely excited high pressure carbon dioxide laser of helical geometry, measuring emission pulses in MW power range
09 p1465 A71-23483
- Uniform continuous electric discharge in large volume high pressure near-sonic carbon dioxide-nitrogen-helium flowstream, describing closed cycle continuous laser amplifier channel design
09 p1505 A71-23485
- Stable single mode cavity resonators of high Fresnel number with increased fundamental transverse mode for carbon dioxide laser oscillators
09 p1466 A71-23727
- Gas dynamic CW laser with supersonic hot moist carbon dioxide-nitrogen as working fluid, discussing laser gain vs water content
10 p1619 A71-23760
- Transverse gas flow effects on deuterium fluoride-carbon dioxide chemical laser output, discussing amplifier medium homogeneity factor
10 p1619 A71-23834
- Molecular gases dissociation due to pulsed carbon dioxide laser radiation, observing luminescence temporal, spatial and spectral characteristics prior to breakdown
10 p1620 A71-24040
- CW carbon dioxide gasdynamic laser gain for mixture of carbon dioxide, nitrogen and helium
10 p1620 A71-24043
- Collision induced spectral cross relaxation radiative saturation and Lamb dip formation in carbon dioxide molecular lasers, using rate equations
10 p1620 A71-24151
- Cross-excited electrically pulsed carbon dioxide laser investigating self mode locking as function of cavity length, operating pressure and bleachable absorber sulfur hexafluoride
10 p1620 A71-24152
- Atmospheric pressure carbon dioxide laser electrode design for uniform pulse excitation discharge
10 p1621 A71-24508
- Poloidal magnetic field measurements in toroidal pinch by Thomson scattered carbon dioxide laser beam
10 p1651 A71-24631
- Carbon dioxide laser coherent radiation in IR region from Young double slit interference experiments, noting emergent beam spatial phase shift
10 p1622 A71-24959
- Carbon dioxide laser design and characteristics, discussing lasing action, spectral properties of continuous and Q switching output power
10 p1623 A71-25089
- Time delay in pulsed optical carbon dioxide laser pumping mechanism in high current gaseous discharge
11 p1773 A71-25796
- Carbon dioxide plasma discharge current changes from Q switched laser irradiation, studying excitation and relaxation mechanisms
11 p1774 A71-25933
- Plasma electron density measurements by carbon dioxide laser as function of discharge current, using interferometry and scattering methods
12 p1912 A71-26573
- Amplitude-phase distortions of optical beam during nonlinear amplification in carbon dioxide laser with periodic correction
12 p1913 A71-26846
- Capacitor discharge excited atmospheric pressure carbon dioxide-nitrogen-helium pulsed IR laser, investigating laser output dependence on gas flow and electrical parameters
12 p1913 A71-26976
- External circuit inductance effect on transverse discharge excited atmospheric pressure carbon dioxide-helium-nitrogen laser small signal gain
12 p1914 A71-26978
- Similarity laws for gas discharges in carbon dioxide lasers verified by longitudinal electric field measurements
12 p1914 A71-27209
- Transversely excited atmospheric pressure carbon dioxide lasers, considering multimegawatt laser pulse generation
12 p1914 A71-27279
- Electron energy distribution functions in carbon dioxide laser plasmas, using Langmuir probes
12 p1940 A71-27280
- Carbon dioxide laser pulse shape, duration and power dependence on repetition rate during continuous pumping
13 p2077 A71-28366
- Monograph on carbon dioxide laser gain observations covering spectroscopy, energy levels, radiative transitions, molecular collisions, power efficiency, etc
13 p2078 A71-28494
- Atmospheric turbulence effects on focused coaxial carbon dioxide and He-Ne laser beam propagation
13 p2078 A71-28525
- Transversely excited atmospheric pressure carbon dioxide laser operation at 9.6 microns, describing proper gas mixture for power adjustment
13 p2079 A71-28674
- Microsphere formation by melting spinning refractory oxide rod tip in carbon dioxide laser focused emission
13 p2079 A71-28905
- Small-signal gain radial variation in cylindrical electrically excited carbon dioxide laser amplifier, characterizing discharge properties by modified Schottky analysis
13 p2080 A71-29330
- High intensity tunable InSb spin flip stimulated Raman scattering from pulsed high pressure carbon dioxide laser radiation pumping
13 p2081 A71-29336
- Simultaneous mode locking and pulse coupling of carbon dioxide laser achieved by single internal GaAs element, discussing possible application to pulse code modulation
13 p2081 A71-29341
- Pulsed atmospheric pressure carbon dioxide laser output pulse characteristics and self mode locking
14 p2253 A71-29799
- Convectively cooled carbon dioxide-nitrogen-helium electric discharge laser theory based on excitation and relaxation processes, comparing with experiment
[AIAA PAPER 71-588] 15 p2419 A71-31574
- Carbon dioxide laser flow-through discharge, measuring electron density and collision rates with heavy particles as function of tube parameters
15 p2419 A71-31741
- Carbon dioxide laser beam machining, describing accessories for cutting, drilling, scribing and welding
[SME PAPER MR-71-807] 15 p2416 A71-32431
- Repetitive passive Q switching of single frequency carbon dioxide laser with intracavity saturable absorber, developing nonlinear model
15 p2423 A71-32602
- Plasma induced random noise and striation oscillations in carbon dioxide lasers as function of operational parameters
15 p2423 A71-32608
- Compact pulsed carbon dioxide laser with uniform volume excitation, obtaining output energy as function of discharge voltage, gas composition and pressure
15 p2424 A71-32698
- Carbon dioxide laser population inversion based on chemical combustion reaction producing gas of vibrationally excited polyatomic molecules
16 p2585 A71-33047
- Molecular spectral coincidences of carbon monoxide and carbon dioxide IR lasers for atmospheric pollutant detection by sensing of resonant absorption, thermal emission or fluorescence
16 p2585 A71-33129
- Stark effect saturable absorber modulation of passively Q switched carbon dioxide laser, using difluoroethane, difluoroethylene, methyl fluoroform, trichloroethylene and vinyl chloride
16 p2586 A71-33147
- Theta pinch deuterium plasma heating by carbon dioxide laser as function of pulse duration and energy
16 p2587 A71-33188

IR carbon dioxide laser amplifier with fundamental mode output power in excess of 500 w, describing multistage mirror section design and test results

16 p2587 A71-33491

Single mode carbon dioxide laser action from quasi-optical mirror emission channels

16 p2588 A71-33894

Minimum output power required for CW carbon dioxide laser drilling of thin stainless steel sheets in vacuum and air, using cylindrical source model

17 p2750 A71-34369

Transversely excited atmospheric pressure pulsed carbon dioxide laser with helical electrode, discussing diverging lens effect due to cavity transverse electric discharges

17 p2750 A71-34370

Carbon dioxide laser single wavelength operation in TEM mode without intracavity dispersive elements

17 p2751 A71-34379

Communications systems using carbon dioxide laser wave propagation, considering wave extinction by absorption and scattering, scintillations due to atmospheric turbulence, etc

17 p2700 A71-34749

Transversely excited carbon dioxide lasers gain measurements for linear and helical electrodes at various gas mixtures and pressures as function of time

17 p2754 A71-35404

Papers on quantum electronics, Volume 1, covering carbon dioxide and YAG lasers, quantum counter action and interference holography

18 p2930 A71-36144

Carbon dioxide laser, discussing mixture composition, vibrational energy levels, excitation and relaxation mechanisms, output characteristics, CW and Q switching, mode locking and applications

18 p2930 A71-36147

Carbon dioxide-helium mixture IR laser action and power gain increase by nitrogen addition

18 p2932 A71-37006

Gas dissociation in carbon dioxide laser by IR absorption method, investigating role in population inversion

18 p2932 A71-37008

Carbon dioxide laser radiation frequency doubling, using Te for second harmonic generation

18 p2933 A71-37010

Te coefficient for frequency doubling with pulsed carbon dioxide lasers, considering peak second harmonic generation conversion efficiency due to absorption of fundamental

18 p2933 A71-37011

Excited state absorption in sulfur hexafluoride traversed by carbon dioxide laser beam

18 p2933 A71-37014

Carbon dioxide laser high efficiency driven Q switching, using Stark effect in molecular gases

18 p2933 A71-37015

Pulsed combustion heated carbon dioxide gas dynamic laser with expansion separation, showing composition and stagnation pressure dependent gain and energy variations

19 p3071 A71-37144

Relaxation processes in Michelson interferometer as integral part of carbon dioxide laser cavity in phase Q switching regime

19 p3071 A71-37389

Carbon dioxide laser, measuring focal length of gas defocusing lens in active medium as function of gas pressure and discharge tube diameter

19 p3073 A71-37771

Mode selection of transition frequencies in carbon dioxide laser with Fabry-Perot interferometer in resonator

19 p3073 A71-37790

Vacuum deposition of silica and alumina thin films on silicon substrate MOS diodes, using CW carbon dioxide laser

19 p3074 A71-38233

Machining integrated circuit metal film masks with continuously operating carbon dioxide laser and high pressure pulsed He-Ne laser

19 p3069 A71-38234

Similarity laws for gas discharges in carbon dioxide lasers verified by longitudinal electric field measurements

19 p3075 A71-38621

Unidirectional regenerative ring carbon dioxide laser power amplifier tests for below and above threshold operations, noting saturation role in performance

20 p3242 A71-38843

Electric discharge carbon dioxide laser gas temperature, electron and current densities radial distribution from mathematical model

20 p3242 A71-38844

Papers on semiconductor, carbon dioxide and dye lasers

20 p3243 A71-39065

Carbon dioxide lasers, covering molecular structure, IR spectra and laser transitions, population inversion mechanisms, gas discharge and longitudinal flow

20 p3243 A71-39067

Electro-optic mode locking of dual polarization carbon dioxide laser using intracavity birefringence modulation

20 p3244 A71-39096

Small signal gain and saturation intensity measurement of carbon dioxide laser as function of gas flow velocity

20 p3244 A71-39099

Carbon dioxide laser triggered pressurized spark gap producing high voltage fast risetime pulses for use in IR radiation control by electro-optic shutters

20 p3244 A71-39106

Breadboard simulation model of laser space communications system consisting of carbon dioxide laser, transmitter telescope, GaAs phase modulator and attenuator

20 p3196 A71-39116

Temperature dependent extracavity and intracavity etalon effects in optical materials for carbon dioxide lasers

20 p3245 A71-39178

Millimeter and submillimeter laser action in symmetric tip molecules optically pumped via parallel absorption bands

20 p3246 A71-39759

Carbon dioxide laser signatures prediction from multiple application of optical resonant equation by computer program, studying line competition effects

20 p3247 A71-39771

Electrode configuration and power output for transverse flow carbon dioxide laser consisting of two parallel water cooled copper tubes perpendicular to gas flow

21 p3391 A71-40182

Transversely excited and atmospheric carbon dioxide laser, measuring time behavior of refraction index profile and lensing effects on resonator

21 p3392 A71-40547

Optical mixing and higher harmonics generation by free carriers in semiconductors, using carbon dioxide laser

21 p3393 A71-40663

IR holography with cholesteric liquid crystals as recording medium and carbon dioxide laser as light source, discussing demagnification and image reconstruction

21 p3379 A71-40703

Cylindrical plasma column light scattering diagnostics by focusing carbon dioxide laser beam on center

22 p3580 A71-41601

Interferometric measurement of gas temperature in positive column of discharges used for carbon dioxide lasers

22 p3574 A71-41725

Carbon dioxide, nitrogen and water vapor hot mixture expansion through Laval nozzle, showing population inversion on carbon dioxide laser transition

22 p3556 A71-41726

Pressure dependent absorption of carbon dioxide laser by boron chloride, considering saturation and line overlapping effects

22 p3556 A71-41805

Partial quenching of radiation from ionized inert gases during bases irradiation by IR produced with carbon dioxide lasers

22 p3581 A71-41808

P-type germanium photon drag detectors with carbon dioxide lasers, discussing response speed and sensitivity

22 p3543 A71-42129

Mode locked transversely excited atmospheric carbon dioxide laser with Ge ultrasonic diffraction cell active loss modulator generating 10.6 micron wavelength pulses

22 p3557 A71-42132

Pulsed atmospheric pressure carbon dioxide laser, studying pulse power and shape as functions of energy storage capacitor value, charging voltage and gas composition

22 p3557 A71-42159

Helium effects on dissociation and population inversion dynamics in pulsed carbon dioxide lasers

22 p3558 A71-42268

Nonlinear optical properties of phase matchable crystal cadmium germanium arsenide for carbon dioxide laser second harmonic generation and parametric interactions

23 p3714 A71-42960

Plasma generation with transversely excited high pressure carbon dioxide laser and solid targets, describing optical emission spectral characteristics

23 p3712 A71-43932

Multimode different-phase discharge carbon dioxide laser output power characteristics as function of discharge current and number of modes

23 p3686 A71-44000

Intercavity scanning for mode selection of carbon dioxide laser in transversely degenerate resonator by localized electron-beam-trigger excitation

23 p3687 A71-44132

Explosion-pumped gas dynamic carbon dioxide laser, obtaining high pulse energy by common hydrocarbon fuels

23 p3687 A71-44135

Wideband phase-matched carbon dioxide laser second harmonic generation in GaAs thin film waveguide through dielectric dispersion

23 p3687 A71-44136

Transition selection with adjustable outcoupling for laser device applied to carbon dioxide

23 p3688 A71-44294

High repetition rate TEA carbon dioxide laser up to 1000 pps with average power output up to 65 W

23 p3688 A71-44298

Carbon dioxide-helium-nitrogen laser with nonlinearly absorbing cell, presenting emission pulse duration and rate

24 p3834 A71-45111

Low cost CW carbon dioxide laser power meter using joule heating technique

24 p3835 A71-45213

CARBON DIOXIDE REMOVAL

Long term lunar surface environment, discussing radiation, thermal and meteoroid protection, water budget, carbon dioxide removal and air lock design

11 p1726 A71-26534

Extraterrestrial life detection by tagged carbon dioxide extraction from substrate in radioactive glucose containing soil nutrient media

13 p2068 A71-28685

Ion exchange resin carbon dioxide removal and concentration system for space cabin environments, describing monitoring and control instrumentation

14 p2189 A71-30313

Carbon dioxide elimination across human skin, investigating perspiration effects

14 p2186 A71-30567

Oxygen generation system for 90-day space station simulator, considering carbon dioxide removal and reduction and water electrolysis

18 p2867 A71-36385

Self contained one man module cell design and tests of electrochemical carbon dioxide concentrating system for space applications

18 p2867 A71-36388

Granular lithium hydroxide as carbon dioxide absorbent for closed cycle life support systems, considering porosity, carrier gas and water vapor pressure and bed temperature

22 p3508 A71-41773

Spacecraft closed loop oxygen recovery system using electrochemical carbon dioxide concentrator, Sabatier reactor and water electrolysis subsystem

22 p3503 A71-42017

CARBON DIOXIDE TENSION

NT HYPERCAPNIA

NT HYPOCAPNIA

Respiratory mechanics and ventilatory response to carbon dioxide during positive pressure breathing in conscious man

06 p0861 A71-18379

Arterial oxygen, carbon dioxide tension, pH and lactic acid changes during rapid descent from altitude to sea level in deep mine

07 p1052 A71-20334

Alveolar nitrogen and carbon dioxide tensions changes during compressed air narcosis in constant oxygen partial pressure

08 p1239 A71-20818

Carbon dioxide tension in pulmonary arterial blood before/during prolonged rebreathing in oxygen mixtures at rest and exercise

10 p1558 A71-23895

Mean whole body intracellular pH and buffer capacity for arterial carbon dioxide tension in ventilated dogs

10 p1558 A71-23896

Body temperature effects on intracellular carbon dioxide dissociation, pH and buffer capacity in hypothermic and hyperthermic dogs

10 p1559 A71-23897

Proton release association with whole blood oxygenation at constant plasma pH and carbon dioxide partial pressure, using alkaline titration

13 p2007 A71-28433

Alveolar and arterial carbon dioxide partial pressure during rebreathing experiments at rest

13 p2007 A71-28435

Chronic hypoxia effects on blood oxygen and carbon dioxide tensions and pH changes in unanesthetized chickens at high altitude compared to sea level control

14 p2186 A71-30565

Human blood pH and gas composition regulation mechanism under response to carbon dioxide partial pressure changes in inhaled air

15 p2357 A71-31316

Venous and arterial blood gases in hibernating and normothermic ground squirrels, showing venous oxygen and carbon dioxide partial pressures reduction in hibernation

17 p2681 A71-34941

Bed rest effects on human hemodynamic and gaseous metabolism, observing increased cardiac output and decreased oxygen consumption and carbon dioxide production

20 p3188 A71-39231

- Human expiratory oxygen and carbon dioxide partial pressure and dissociation curves for intrapulmonary gas mixing, using mass spectrometry
21 p3328 A71-40098
- Intracellular pH and carbon dioxide combining curve of muscle tissue in dogs, using DMO method
21 p3335 A71-40631
- Ventilatory response to progressively increasing inspired carbon dioxide tensions at ground level and acetazolamide pretreatment before high altitude exposure
23 p3636 A71-44242
- Respiratory carbon dioxide and oxygen partial pressure effects on intracellular and blood pressure in rabbits under Somnifen narcosis
24 p3793 A71-44368
- CARBON DISULFIDE**
Carbon disulfide absorption spectrum measurement in far UV region
01 p0129 A71-10251
- Carbon dioxide laser induced thermal lensing/focusing/reduction in liquid carbon disulfide with DC electric field
03 p0436 A71-13877
- Carbon dioxide laser IR pulses self focusing in liquid carbon disulfide, calculating nonlinear refractive index
07 p1128 A71-20396
- High power carbon disulfide-oxygen combustion pulsed laser, discussing foreign gases effects on performance and energy transfer mechanism
16 p2586 A71-33165
- CARBON FIBERS**
Graphite fiber reinforced Al-Si alloy composite tensile strength and microstructure, observing tension failure modes
06 p0914 A71-18678
- Charpy notched impact strength of carbon fiber reinforced epoxy resin composites over temperature range
[PLASTICS INST. PAPER 20] 08 p1318 A71-20891
- Carbon fiber reinforced epoxy resin fatigue and crack propagation behavior in air, moisture and oil environments, using tensile, bending and torsion test methods
[PLASTICS INST. PAPER 49] 08 p1318 A71-20892
- Carbon fiber reinforced plastics mechanical properties, discussing batch processing and specimen geometry variables effects on laminates
[PLASTICS INST. PAPER 24] 08 p1318 A71-20893
- Carbon fiber reinforced carbon base composites manufacture by thermal decomposition of carbon fiber reinforced thermosetting resins, discussing polymer matrix shrinkage control
[PLASTICS INST. PAPER 36] 08 p1319 A71-20894
- Carbon fibers structural features, confirming model of slowly undulating ribbons of sp² carbons as basic structural elements by high resolution dark field micrographs
[PLASTICS INST. PAPER 9] 08 p1319 A71-20895
- Carbon fiber reinforced polymers for self lubricating materials applications, discussing friction and wear characteristics under fresh and sea water, alcohols, mineral oils, etc
[PLASTICS INST. PAPER 31] 08 p1319 A71-20896
- Tensile, shear, bulk density and electrical properties of pitch based strain graphitized glassy carbon fibers
[PLASTICS INST. PAPER 13] 08 p1319 A71-20897
- Carbon fiber-metal composites fabrication and properties, discussing coating, compaction, electroforming, mixed metal powder hot working and liquid metal infiltration techniques
[PLASTICS INST. PAPER 14] 08 p1319 A71-20898
- Carbon fiber and carbon fiber-polytetrafluoroethylene composites high temperature mechanical properties
[PLASTICS INST. PAPER 35] 08 p1319 A71-20899
- High strength flexible carbon fabrics from oxidized polyacrylonitrile yarns for reinforced plastic laminates
[PLASTICS INST. PAPER 39] 08 p1319 A71-20900
- Microstructure crystallites and voids of polyacrylonitrile based carbon fibers, using X ray diffraction and electron microscopy measurements
[PLASTICS INST. PAPER 8] 08 p1320 A71-20901
- Filament wound carbon fiber reinforced plastics components fabrication and performance tests
[PLASTICS INST. PAPER 47] 08 p1296 A71-20902
- Carbon fiber and carbon fiber-polyester composites chemical resistance to acid and alkaline solutions at various concentrations and temperatures
[PLASTICS INST. PAPER 32] 08 p1320 A71-20903
- Carbon fibers, light metal alloys and composites, studying moduli of elasticity and shear thermal variations
[PLASTICS INST. PAPER 16] 08 p1320 A71-20904
- Carbon fiber reinforced plastics applications for aero-engine components, considering mechanical and thermal properties and environmental conditions
[PLASTICS INST. PAPER 45] 08 p1347 A71-20905
- Graphite fiber reinforced plastics adhesion and orientation effects on mechanical properties
[PLASTICS INST. PAPER 27] 08 p1320 A71-20906
- Composite materials with metallic matrix and carbon fibers, discussing production techniques and mechanical properties
[PLASTICS INST. PAPER 15] 08 p1320 A71-20907
- Epoxy resin matrix properties influence on carbon fiber composites performance, discussing test methods for measuring mechanical and fatigue properties over temperature and frequency range
[PLASTICS INST. PAPER 22] 08 p1320 A71-20908
- Carbon fibers production by polyacrylonitrile fibers spinning, discussing stretching temperature effects on mechanical properties
[PLASTICS INST. PAPER 12] 08 p1320 A71-20909
- High performance graphitized carbon/carbon composites, discussing mechanical properties improvement by fiber content optimization and heat treatment
[PLASTICS INST. PAPER 37] 08 p1321 A71-20910
- Cross-ply carbon fiber reinforced epoxy resin laminates fatigue behavior under axial loading, discussing various failure mechanisms
08 p1321 A71-20912
- High modulus graphite fiber reinforced composites tensile and compressive test methods and results
[PLASTICS INST. PAPER 23] 08 p1321 A71-20913
- Carbon fiber/carbon composites produced by moulded carbon technique, discussing mechanical properties and applications in rocket motors
[PLASTICS INST. PAPER 38] 08 p1348 A71-20914
- Fiber content effect on mechanical properties of carbon felt/carbon matrix composites
[PLASTICS INST. PAPER 40] 08 p1321 A71-20915
- Thermosetting and thermoplastic carbon fiber composites fabrication molding techniques, forms provisions and new uses
[PLASTICS INST. PAPER 33] 08 p1321 A71-20916
- Carbon fibers and composites nondestructive testing, discussing defect detection problems in ultrasonics, X ray diffraction and X radiography methods
[PLASTICS INST. PAPER 52] 08 p1296 A71-20918
- Carbon fiber composites engineering applications, discussing mechanical properties, weight and economic considerations
[PLASTICS INST. PAPER 30] 08 p1297 A71-20919
- Heat resistant extended life carbon fiber/polyimide resin composites, noting aerospace applications
[PLASTICS INST. PAPER 34] 08 p1321 A71-20920
- High voltage electron microscopy of internal defects in carbon fibers, considering fiber strength
[PLASTICS INST. PAPER 10] 08 p1297 A71-20921
- High speed ball impact tests and fracture energy of carbon fiber reinforced plastics
[PLASTICS INST. PAPER 25] 08 p1322 A71-20922
- Tensile, flexural and compressive shear, impact and fatigue characteristics of carbon fiber-epoxy resin composites
[PLASTICS INST. PAPER 26] 08 p1322 A71-20923
- Carbon fiber evaluation of structural reinforcement potentialities for rocket motor cases and pressure vessels filament winding
[PLASTICS INST. PAPER 48] 08 p1297 A71-20924
- High strength and modulus continuous carbon fibers, discussing preparation and quality control
[PLASTICS INST. PAPER 5] 08 p1297 A71-20925
- Pyrolysis products of polyacrylonitrile fibers in low pressure apparatus, using mass spectrometer
[PLASTICS INST. PAPER 4] 08 p1250 A71-20926
- Carbon fiber reinforced plastics potential aerospace structural applications, considering weight saving, mechanical properties, thermal expansion, stress concentration, impact resistance, corrosion and lightning problems
[PLASTICS INST. PAPER 43] 08 p1369 A71-20927
- High modulus carbon fiber wettability by matrix resin
[PLASTICS INST. PAPER 21] 08 p1322 A71-20928
- Cost aspects of carbon fiber reinforced composites in aircraft structures, suggesting increased aviation market for carbon fiber
[PLASTICS INST. PAPER 46] 08 p1378 A71-20929
- Carbon fiber reinforced Al composites fabrication and evaluation by metallographic examination, considering tensile strength
[PLASTICS INST. PAPER 17] 08 p1322 A71-20930
- Carbon fiber composites utilization problems for product and tool designers, considering mechanical properties anisotropy, fiber alignment and bundle strength
[PLASTICS INST. PAPER 42] 08 p1322 A71-20931
- Tribological characteristics of carbon fiber reinforced thermoplastics, noting improved sliding wear against metal surfaces
[PLASTICS INST. PAPER 12] 09 p1481 A71-22344
- Thermoplastics reinforcement with carbon, silicon nitride and silicon carbide fibers, noting fiber aspect ratio
[PLASTICS INST. PAPER 5] 09 p1482 A71-22345
- Composite materials for compressor blades in aircraft engines, considering boron and carbon fiber reinforced materials
09 p1456 A71-23286
- Microstructural defects responsible for tensile strength reduction in carbon fibers subjected to high temperature graphitization, using transmission electron microscopy
09 p1483 A71-23653
- Graphite fiber reinforced ablative composites fabricated into rocket propulsion test units for oxidative liquid high temperature and pressure environments
09 p1459 A71-23685
- Carbon fiber strength/microstructure relationship, examining failure mechanism initiated by graphite crystallites shearing
10 p1634 A71-24446
- Thornel graphite fibers modulus of elasticity, mechanical properties, applications and price
10 p1635 A71-24773
- Short carbon and glass fiber reinforced composites, calculating modulus of elasticity from mathematical model
10 p1635 A71-24806
- Thermal conductivity prediction during ablation of phenolic-carbon and phenolic-graphic composites for heating and cooling conditions
[AIAA PAPER 71-380] 11 p1783 A71-25304
- Graphite fibers mechanical properties based on rayon and polyacrylonitrile, considering tensile, flexural, compressive and shear strength
11 p1784 A71-25398
- Carbon fiber-epoxy resin composites Young modulus, thermal and electrical conductivities as function of fiber alignment and porosity
11 p1784 A71-25399
- Boron and graphite fiber market competition, considering aerospace application
11 p1860 A71-25400
- Graphite epoxy composites fatigue testing, including loaded and unloaded shear, hardness and tensile strength in wet and dry environments
11 p1785 A71-25402
- Carboxyl terminated butadiene-acrylonitrile/epoxy carbon fiber composites fracture energy, noting fracture strength, short beam shear strength and tensile strength at cryogenic temperatures
11 p1785 A71-25403
- Carbon fiber reinforced high interlaminar shear strength composites, noting applications to advanced engineering structures
11 p1785 A71-25408
- Graphite fiber resin composites physical and mechanical properties at ambient and cryogenic temperatures, discussing unidirectional ring and bar specimens and filament wound pressure vessels
11 p1785 A71-25409
- Carbon fiber reinforcement in carbon fiber/glass fiber mat sandwich beams increasing tensile and compressive strength
11 p1846 A71-25412
- Composite materials fiber-matrix interfacial behavior, determining polymer concentration on graphite fibers surface by Raman spectroscopy and composite shear strength increase
11 p1787 A71-25430
- Plastics reinforcement by combining high plastic deformation and fracture resistances with stiffness, discussing ceramics, whiskers, carbon and glass fibers
11 p1788 A71-25654
- Boron and carbon fracture and debonding in epoxy matrix, using acoustic emission analysis
11 p1772 A71-26392

High hyperthermal ablation performance of reinforced carbon-carbon composites for reentry nose tip application
[AIAA PAPER 71-416] 12 p1920 A71-26764

Microcrack formation in carbon fiber-resin matrix composites under thermal stress 12 p1920 A71-27013

Carbon fiber cladding paper for corrosion resistant asbestos laminates, discussing short fibers orientation and acid solutions effects on flexural strength and weight 12 p1921 A71-27014

Izod impact testing of carbon fiber reinforced plastics, considering fiber volume loading, surface treatment and specimen and notch geometry 12 p1921 A71-27015

Tensile strength and fracture toughness of carbon fiber polyester composites, using mechanical testing and scanning electron microscopy 13 p2092 A71-28625

Mechanical properties of carbon fibers thinly coated with TiC by chemical vapor deposition from hydrogen, methane and titanium tetrachloride vapor mixture 13 p2092 A71-28627

Carbon and boron fiber reinforced plastics adhesive bonded and bolted joints, presenting results of hole deformation tests [DFVLR-SONDDR-96] 13 p2093 A71-29306

Fabrication and properties of carbon reinforced carbon matrix composites 14 p2261 A71-29639

Carbon/carbon composites, describing manufacturing techniques for fiber reinforced matrix structures 14 p2261 A71-29640

Mechanical and thermal properties of chemical vapor deposited carbon composite felt material for reentry heat shielding 14 p2262 A71-29648

Carbon/graphite cloth reinforced aromatic/heterocyclic resins ablative composites pyrolysis kinetics by computer code analysis 14 p2262 A71-29649

Graphite fiber composite structures nondestructive testing, discussing liquid penetrants, X ray radiography sonic methods, acoustic emission and IR tests 15 p2414 A71-31816

Polyacrylonitrile and rayon precursor graphite fibers diameter relation to Young modulus and tensile strength 15 p2438 A71-31817

Boron and graphite fiber reinforced plastics machining, discussing tools, operating parameters and process limitations [SME PAPER MR-71-820] 15 p2416 A71-32429

Carbon fiber surface reactivity from gas chromatographic measurement, discussing adsorption isotherm of various vapors 16 p2541 A71-34049

Mechanical properties, fracture and limited high temperature oxidation resistance of carbon fiber reinforced Ni composites 16 p2599 A71-34086

Welded, bearing and interlocking joints and adhesive bonding in carbon fiber reinforced plastics, discussing anisotropy, thermal expansion and electrochemical corrosion problems 17 p2748 A71-34344

High modulus graphite composites application for structural weight reduction and stiffness requirement without strength loss 17 p2762 A71-35202

Boron, carbon, sapphire and glass fiber composite materials, considering brittleness, anisotropic properties, filament winding and plastic and metallic matrices 18 p2939 A71-35915

Filament wound carbon/carbon composite heat shields, describing fabrication process involving winding, carbonization, pyrolytic carbon infiltration and graphitization [SME PAPER EM-71-204] 18 p2939 A71-36664

Carbon fiber reinforced plastics, reviewing properties, performance, development, applications and potential cost reduction 18 p2940 A71-36765

Uniaxially aligned glass and carbon fiber reinforced nylon composites prepared from caprolactam by anionic polymerization 19 p3083 A71-37339

Carbon-fiber-reinforced carbon composites for high temperature applications, describing filament orientation, matrix composition and heat treatment effects on ablation performance 19 p3085 A71-38350

Evaporated pure Ni coatings effects on carbon fiber fracture strength and microstructure at room temperature 20 p3248 A71-38815

Carbon-carbon composites fabrication by electrostatic fiber deposition/flooding, using liquid impregnation-carbonization cycles with coal tar pitch 21 p3384 A71-40140

Glass-fiber/glass-bead/resin beam stiffness and strength improvement with sandwiching between layers of unidirectional carbon fiber composite 21 p3405 A71-40597

Nondestructive testing of carbon fiber reinforced composites with resin matrices [CFRP], suggesting ultrasonics for void detection 21 p3387 A71-40598

Carbon fiber/metal matrix composites fabrication by electrodeposition, discussing aluminum warp sheet lamination and filament wound techniques 21 p3387 A71-40599

Carbon and boron fibers and whisker reinforced plastics fabrication, properties and costs, noting materials and optimum matrix combination 21 p3405 A71-40600

Carbon fiber reinforced plastics, considering aerospace and medical applications 21 p3406 A71-40702

Carbon fibers grown on graphite by thermal decomposition of hydrocarbons, investigating external morphology and structure 21 p3406 A71-40837

Graphite high modulus fiber material tensile strength, modulus of elasticity and elongation measurement method and equipment 23 p3696 A71-42898

Fibrous carbon structure determination by high resolution electron microscopy, establishing relationship between graphite planes and catalyst particles orientation 23 p3696 A71-43141

Carbon fiber reinforced plastics featuring high strength and Young modulus and low density for engineering applications 24 p3840 A71-44363

CARBON ISOTOPES

NT CARBON 12
NT CARBON 13
NT CARBON 14

Carbon kinetic isotope fractionation into carbon dioxide and organic compounds in meteorite-like Fischer-Tropsch reaction with nickel-iron or magnetite catalyst 03 p0483 A71-13013

Terrestrial and stony meteorite carbon, investigating similarity in isotopic composition 07 p1201 A71-20399

N stars Y CVn, RY Dra and 19 Psc IR synthetic cyanide radical spectrum analysis, determining C 12/C 13 ratio 18 p2969 A71-37044

Biogenicity and significance of oldest stromatolites from optical microscopic and carbon isotopic studies 22 p3533 A71-41616

Carbon and sulfur isotope content in Apollo 12 lunar fines 23 p3751 A71-43702

Apollo 12 lunar dust and rocks carbon and hydrogen amount and isotopic composition determination, using in vacuo outgassing and combustion in oxygen 23 p3751 A71-43703

Apollo 11 and 12 lunar samples O 18/O 16, Si 30/Si 28, D/H and C 13/C 12 ratio determination, examining whole rocks, breccias, soils, plagioclases and fines 23 p3751 A71-43705

CARBON MONOXIDE

CO chemical laser power output augmentation by selective depopulation of CO lower vibrational levels by energy transfer to added gases 02 p0262 A71-12709

Solar photosphere temperature constancy in thin CO layer from equivalent spectral line width determination 03 p0484 A71-13208

CW laser output in carbon dioxide and nitrous oxide induced by vibrational energy transfer from excited carbon monoxide 03 p0438 A71-13893

Hydrogen peroxide decomposition acceleration by carbon monoxide, discussing reaction mechanisms and rate coefficients 03 p0376 A71-14280

Laser power from carbon monoxide supersonic expansion in nitrogen and argon mixtures, comparing to carbon dioxide gas dynamic lasers 04 p0608 A71-15042

Carbon monoxide fundamental band spectral absorptivity distributions at various high temperatures and optical densities 04 p0549 A71-15512

CO laser emission lines and nitrogen oxides absorption lines spectral coincidences observations 05 p0762 A71-16339

Gas dynamic coupling effect on vibrational deexcitation of carbon monoxide at 1400 to 2200 K range in shock tube 05 p0835 A71-16523

IR object IRC plus 10216 carbon monoxide emission at 2.6 mm, noting spectral line width, thermal emission and mass 05 p0812 A71-16695

Carbon dioxide and carbon monoxide atmospheric distribution dependence on combined effects of

photochemical production, loss and transport in mesosphere and upper stratosphere 06 p0893 A71-17980

N and CO thermal conductivity shock tube measurements, discussing pressure distribution and high temperature effects 06 p1007 A71-18075

Lasers operating on rotation vibration of chemically formed carbon monoxide, discussing excitation methods 06 p0908 A71-18312

Hydrogen and carbon monoxide coadsorption on platinum single crystal surface, examining interactions and species formation by thermal flash and electron impact techniques in ultrahigh vacuum 07 p1055 A71-19844

Vibrationally excited carbon dioxide deactivation by collisions with CO, determining rate constants by laser fluorescence method 08 p1250 A71-20665

Carbon monoxide gas phase vibrational relaxation by Fe atoms, using shock tube for determination of decomposition rate of iron carbonyl in dilute mixture with Ar 08 p1337 A71-20672

MnO oxidation reduction kinetics measurement in carbon monoxide/dioxide atmospheres by gravimetry and electrical conductivity 08 p1318 A71-20698

Equivalent widths of CO lines in interstellar absorption spectrum of zeta Ophiuchi 08 p1360 A71-20982

Electrochemical detection of hydrogen, carbon monoxide and hydrocarbons in inert or oxygen atmospheres, using electrical biasing technique 08 p1250 A71-21473

Metastable radiative lifetimes of molecular states of nitrogen and CO, using time of flight and high resolution electron gun techniques 09 p1497 A71-22417

Reaction dynamics for CO ion plus deuterium to yield COD ion plus D, noting polarization forces role 09 p1497 A71-22702

Vibrational relaxation of CO and hydrogen atom effects in nonequilibrium nozzle flow using shock tunnel IR detection system 09 p1404 A71-23379

Hydrogen-nickel reaction in presence of CO adsorbed gas, increasing total desorption cross section and eliminating monotonic relation between uptake and H ion current 10 p1573 A71-24540

CO absorption spectrum in carbon dioxide atmosphere, comparing self- and nitrogen-broadened half widths 10 p1645 A71-24968

CO half-width calculations for carbon dioxide broadened fundamental and first overtone bands from Anderson-Tsao-Curnutte theory 10 p1645 A71-24969

Mars atmospheric CO abundances and rotational temperature from Voigt line profiles 10 p1646 A71-24993

Interstellar CO, constructing strip maps in declination and right ascension across W51, Sgr A and Sgr B2 for 115.2712 line radiation 11 p1818 A71-25201

CO Fourth Positive band system excitation cross sections by electron impact on carbon monoxide and carbon dioxide 11 p1727 A71-25366

CO exposure effects on human psychomotor performance for blood carboxyhemoglobin saturation levels, using sleep monitored EEG methods 11 p1726 A71-26509

Inhibiting mechanism of ethane in hydrogen-oxygen mixtures ignition, discussing lower limits, carbon monoxide effect and chain lengthening reactions 11 p1730 A71-26566

Carbon monoxide methods for studying diffusing capacity of human lungs 12 p1869 A71-26654

Atmospheric budget of C12/O and C14/O, discussing latitude and altitude effects and tropospheric residence time 12 p1902 A71-27291

Vibrational energy transfer from excited nitrogen to CO and NO, describing flow tube measurements 12 p1934 A71-27760

Position, exercise and lung volume effects on healthy males pulmonary diffusing capacity for CO at rest and during exercise 13 p2015 A71-29493

Hypokinesia effect on formation and elimination of ketones, aldehydes, carbon monoxide and ammonia in rats 15 p2356 A71-31305

Stoichiometric hydrogen-carbon monoxide-oxygen mixtures detonation wave propagation at critical Mach number, noting explosion limit chemical kinetics role 15 p2465 A71-32088

Power output of stable sealed off CO lasers with semiconfocal cavities and totally reflecting spherical and dielectrically coated flat mirrors 15 p2420 A71-32387

- Molecular rotational excitation during CO ion-Ar interactions by ion beam collision spectroscopy, observing energy loss spectra 15 p2452 A71-32551
- Temperature measurements in shock heated carbon monoxide by IR emission-absorption technique 15 p2411 A71-32554
- Carbon monoxide gas dynamic laser oscillation generation, observing maximum power and vibrational exchange among single diatomic species states 15 p2422 A71-32583
- CW gain measurements on rotation-vibration P branch transitions of CO molecular laser, calculating gas temperature, Einstein coefficient and population densities 15 p2423 A71-32609
- Pulsed output, delay time and rotational-vibrational transitions of high pressure transverse discharge CO laser 15 p2424 A71-32613
- Shock tube measurements of vibration-vibration energy exchange probability in nitrogen-carbon monoxide-argon mixtures 16 p2613 A71-32896
- Vibrational relaxation of CO by Fe atoms in Ar shock tube following iron pentacarbonyl decomposition 16 p2539 A71-32897
- Pure carbon monoxide dissociation rate behind incident shock wave in high temperature environment, using two wavelength IR emission data 16 p2539 A71-32909
- Molecular spectral coincidences of carbon monoxide and carbon dioxide IR lasers for atmospheric pollutant detection by sensing of resonant absorption, thermal emission or fluorescence 16 p2585 A71-33129
- Effective cross sections for charged and excited particles formation from He, Ne and Ar ion collisions with CO molecules, using mass spectrometry 16 p2614 A71-33646
- Carbon monoxide in metastable state, considering quenching and radiative lifetime 16 p2615 A71-34089
- CO lasing processes using small signal single pass gain measurements on flowing CO-air-He laser 17 p2751 A71-34378
- Vibrational population distribution in high power liquid nitrogen cooled CO laser by emission spectroscopy 17 p2754 A71-35751
- Collisional broadening of IR absorption lines in vibration-rotation bands of carbon monoxide and hydrochloric acid 19 p3106 A71-37374
- Vibrational relaxation behind incident shock waves in CO based on shock tube pressure measurements at 2400-6000 K 19 p3106 A71-37880
- Temperature dependent differential quenching rates of vibrationally excited CO fluorescence by ortho and para hydrogen, using Born-Bethe approximation 19 p3107 A71-38052
- Water vapor effect on vibrational relaxation of CO in shock tubes, measuring IR emissions 19 p3012 A71-38084
- High temperature oxidation of ammonia, carbon monoxide and methane by nitrous oxide in shock tubes, using optical interferometry and UV/IR emissions 19 p3012 A71-38086
- Kinetic modeling of vibrational state populations in high power direct discharge excited CO laser, using iterative technique 20 p3243 A71-39005
- Low vibrational level CO transitions of flowing electrochemically excited liquid nitrogen cooled helium-air-methane-carbon monoxide laser in Q switched operation 20 p3244 A71-39100
- Pulmonary nitrogen washout and carbon monoxide uptake, developing dynamic mathematical models for volume and distensibility distributions in airways and alveoli 20 p3193 A71-39441
- IR spectroscopy of CO using tunable PbS₂ diode laser, measuring Doppler linewidth and room temperature absorption coefficient at line center 20 p3246 A71-39757
- Ionized carbon monoxide in cometary tails, estimating time scale in recombination of ions into C and O atoms 21 p3442 A71-40155
- Deactivation and radiative lifetime of CO Cameron forbidden transition spectral bands produced by photon absorption 21 p3418 A71-40232
- CO relaxation measurement in unsteady expansion wave, removing metal carbonyls by passing gas through liquid oxygen cooled trap 21 p3418 A71-40237
- Carbon monoxide laser emission from helium-air-cyanogen mixture 21 p3393 A71-41043
- Germanium single crystal surface conductivity, observing carbon monoxide adsorption effects at various pressures 21 p3435 A71-41341
- Mathematical model for atmospheric carbon monoxide production from methane 21 p3375 A71-41423
- Time of useful function after mice exposure to life threatening toxic mixtures of carbon monoxide, carbon dioxide and ammonia produced by combustion 22 p3486 A71-41830
- Electron impact excited carbon monoxide and dioxide 1260-5000 Å spectral emission, discussing cross sections of Cameron and fourth positive bands 23 p3706 A71-42904
- Electrical CO laser performance prediction from pumping mechanism based on vibrational energy exchange under thermal nonequilibrium conditions 23 p3683 A71-42954
- Electrically excited gas dynamic CO laser using glow discharge in supersonic nozzle plenum 23 p3683 A71-42958
- Atomic oxygen and hydrogen identification in Mars upper atmospheric emission spectra by Mariner UV spectrometer, inferring carbon monoxide presence by self absorption 23 p3735 A71-43330
- Gas interaction with lunar fines, investigating carbon monoxide, nitrogen, oxygen, argon and water vapor adsorption 23 p3758 A71-43754
- Effective excitation cross sections of molecular CO ion bands in comet tails due to He ions collisions with CO molecules, considering deviation from adiabatic hypothesis 23 p3708 A71-44314
- Carbon ion and free electrons three body recombination rate coefficient measurement in carbon monoxide flows 24 p3802 A71-44607
- Pulmonary carbon monoxide diffusing capacity of sea level and high altitude dwellers at various altitudes, noting early postnatal lung growth effects 24 p3797 A71-44778
- Pulmonary blood flow and carbon monoxide diffusing capacity uneven distribution measurements, determining body position effects 24 p3798 A71-44782
- CARBON MONOXIDE POISONING**
- CO pulmonary diffusing capacity rebreathing measurements at rest and while exercising, noting relationship to oxygen consumption 04 p0545 A71-15162
- Jet aircraft flight decks pressurization, tobacco smoking and carbon monoxide levels, discussing potential dangers 09 p1400 A71-23247
- Toxicological evaluation of CO in humans and other mammals, considering pilot performance prediction for aircraft environment 13 p2012 A71-28902
- Exercise temperature plateau shift and sweat rate during moderate CO poisoning associated with resetting of thermoregulating centers by low oxygen tensions 18 p2861 A71-36886
- CARBON STEELS**
- Carbon steel specimens size effect on energy dissipation and damping characteristics under transverse flexural vibrations 03 p0503 A71-13412
- Cu-Al alloy, Ti and low carbon steel under LF flexural stress, testing parameters effect on fatigue resistance 03 p0445 A71-14339
- Heat treated low carbon steel fatigue tests at low cycle tension compression loads, determining durability relationships to load and total work to fracture 04 p0666 A71-14878
- Carbon steel and heat treated duraluminum fatigue fracture microstructure observation using electron microscope, determining crack propagation relationships to loading sequence 04 p0610 A71-14880
- Austenitic steel containing Cr, Mn, and Ni, investigating W, Mo, V and Nb effect on structure and mechanical properties 04 p0616 A71-15804
- Low carbon Mn-Mo-Ni steel dilatometric measurements with RPI Gleeble machine, examining bainitic transformation 04 p0617 A71-15913
- High carbon Cr and Mn steels martensitic transformation points, ascertaining short range order occurrence by electron microscopic study 07 p1130 A71-19278
- Loading frequency effect on carbon steel energy dissipation at large stress amplitudes, deriving strain rate relations 07 p1142 A71-20478
- Interstitial impurities effects on relation of activation energy to effective stress in iron, low carbon steel and other bcc metals 08 p1308 A71-21514
- Low carbon steel welds, investigating low cycle deformation and rupture resistance as function of weld zones 08 p3136 A71-21609
- Al alloy and carbon steel low cycle fatigue and fracture surface topography transition from static mode to striation type by electron fractography 11 p1777 A71-25266
- Cr and V diffusion plating influence on principal characteristics of highly alloyed martensitic and carbon steels 12 p1912 A71-27690
- Carbon steel fatigue crack tip plastic zone substructure by X ray microbeam technique, determining dislocation density, stress intensity and crack propagation rate interrelationships 13 p2155 A71-28789
- Plastic strain development at fatigue crack tip in mild carbon and stainless austenitic steels from electron and optical microscopy 14 p2257 A71-29841
- High chromium low carbon steel, detailing oxygen content effects on high temperature reduction intercrystalline corrosion and grain growth 15 p2427 A71-31528
- Low carbon high chromium steel, emphasizing nitrogen content effects on temper brittleness 15 p2427 A71-31529
- Tempered martensite and lower bainite in high purity carbon steels, discussing impact toughness due to internal twinning, grain boundary precipitation and carbide morphology 15 p2432 A71-32173
- Closed die forgings of vacuum remelted carbon and low alloy steels to improve transverse ductility and microcleanness for aircraft industry 17 p2749 A71-35336
- Carburizing steels cold forging, investigating pressure requirement relationship to compressive stress from comparison of backward extrusion and laboratory compression tests 18 p2935 A71-36669
- Vacuum-melted low-carbon low-manganese steel, investigating Ni and Cr additions effects on recrystallization textures 19 p3079 A71-37703
- Carbon activity, free energy entropy and enthalpy in fcc solid solution of Fe-Ni-C alloy 19 p3080 A71-37714
- Low, medium and high carbon steels hardenability determination from composition, using charted data 20 p3251 A71-39336
- Multiplying factors charts for hardenability prediction of Cr, Ni, Si, Mo and Mn steels containing carbon 20 p3251 A71-39337
- Intermittent stress creep tests on low carbon steel, commercially pure iron, Cr-Mo steel and commercially pure tantalum, noting static-to dynamic transition 21 p3400 A71-40835
- Carbon and stainless steels chemical composition effects on diffusion layer structure and fatigue strength after diffusive boring 21 p3403 A71-41162
- Vacuum contactless metallization of carbon steels, stainless steels and nickel alloys, considering Si, Cr and Al coatings 21 p3390 A71-41172
- Decarbonization monitoring of ball bearing steel bars, describing defectoscopy based on eddy current higher harmonics method 22 p3553 A71-41768
- Carbon effects on fracture phenomena in martensitic transformation of steels under heat and thermomechanical treatments 22 p3563 A71-42322
- Exponential type equation for carbon steel stretched sample necking profile curve 23 p3780 A71-44228
- Alloying elements effects on high-carbon steels phase transformation under shock loading to form martensite-austenitic structure 24 p3840 A71-45376
- CARBON TETRACHLORIDE**
- Cysteine prevention of fatty liver induced by carbon tetrachloride and ethionine 07 p1040 A71-18987
- Liquid carbon tetrachloride artificial luminescent cloud formation in upper atmosphere, considering injection conditions for rapid vaporization and required concentration 19 p3661 A71-38633
- CARBON TETRACHLORIDE POISONING**
- Continuous and intermittent effect of carbon tetrachloride breathing on pathomorphological and histochemical structure of liver in test animals 01 p0013 A71-11129
- CARBON TETRAFLUORIDE**
- Liquefied gas solutions of methane in carbon tetrafluoride and propylene, calculating pressure and temperature dependence of density 15 p2462 A71-31246

CARBON 12

Atmospheric budget of C/12/O and C/14/O, discussing latitude and altitude effects and tropospheric residence time 12 p1902 A71-27291

CARBON 13

Interstellar formyl radical and carbon 13 formyl ion search in galactic radio sources 13 p2142 A71-29103

CARBON 14

C 14 incorporation from labeled glucose into cerebral glycogen of normal and X ray irradiated rats 01 p0011 A71-10850
Atmospheric carbon 14 concentrations during past century, noting radioactive dating implications 07 p1102 A71-19580

Atmospheric budget of C/12/O and C/14/O, discussing latitude and altitude effects and tropospheric residence time 12 p1902 A71-27291

Hypothermia effect on lipid synthesis of hamster tissue following intravenous injection of acetate-C 14 14 p2182 A71-29582

Diamond radiation counters for C 14 containing carbon dioxide in extraterrestrial life detection, noting radioactivity curves as function of sample microflora 21 p3378 A71-40571

CARBONACEOUS METEORITES

NT MURRAY METEORITE
NT ORGUEIL METEORITE

Solar Hg abundance low value by photosphere spectrum absence of Hg I lines, comparing higher content in carbonaceous chondrites 02 p0306 A71-12048

Carbon kinetic isotope fractionation into carbon dioxide and organic compounds in meteorite-like Fischer-Tropsch reaction with nickel-iron or magnetite catalyst 03 p0483 A71-13013

Prairie Network bright meteors, discussing constraints on meteoroid structure, photometric and dynamic masses and classical single body theory variations 03 p0490 A71-13934

Extraterrestrial abiotic amino acids and hydrocarbons in type II carbonaceous chondrite at Murchison, Australia 03 p0493 A71-14209

Type III carbonaceous chondrite Murchison meteorite, obtaining amino acids, aliphatic and aromatic hydrocarbons from specimen 09 p1393 A71-22983

Carbonaceous chondrite and Precambrian chert amino acids detection, using simultaneous optical configuration determination and gas chromatography 09 p1393 A71-22984

Carbonaceous chondrites natural remanent magnetization, revealing grey spinel oxide, Ni-Fe and iron sulfide as principal opaque minerals 10 p1674 A71-24429

Gas rich meteorites and carbonaceous chondrites with trapped argon, noting isotopic correlation with neon 10 p1680 A71-24988

Chemical analysis and petrography of Murchison meteorite compared to Murray meteorite 11 p1836 A71-26483

Petrographic study of Allende carbonaceous chondrite by high voltage transmission electron microscopy, comparing substructure with terrestrial rocks 14 p2308 A71-29912

Murchison, Murray and Allende carbonaceous chondrites water extractable amino acids composition 16 p2630 A71-32950

Carbonaceous chondrites chemical and mineralogical composition densities and structure due to condensation at various temperatures within early solar nebula 17 p2799 A71-34512

Murchison meteorite heterocyclic compounds contents, using gas chromatography-mass spectrometry 17 p2801 A71-34650

Meteorites, covering impact on earth, craters, as-troblems, tektites, carbonaceous chondrites properties, collisions, fragmentation, etc 17 p2809 A71-35714

Diamonds in ureilites and carbonaceous chondrites, discussing formation due to recrystallization during asteroid collisions 17 p2810 A71-35723

Carbonaceous chondrite fission producing super-heavy element decay half life 22 p3605 A71-42398

CARBONACEOUS ROCKS

NT COAL

Permeability and porosity of Precambrian Onverwacht cherts and other low permeability rocks, discussing geological origin of rock-contained organic compounds 18 p2913 A71-36768

CARBONATES

NT ARAGONITE

NT CALCITE

NT LEXAN (TRADEMARK)

NT POLYCARBONATES

NT SODIUM CARBONATES

Alkaline fuel cells electrochemical regeneration for controlling carbonate concentration in electrolyte for performance improvement 03 p0353 A71-13057

Respiratory acid-base disturbances, studying deviations of bicarbonate ion vs pH pathway followed by buffered solution on carbon dioxide titration 13 p2007 A71-28434

Ions association constant with water in propylene carbonate from proton magnetic resonance measurements 13 p2026 A71-29040

Frequencies, rotational constants, molecular structure and moments of inertia of five isotopic species of vinylene carbonate from microwave spectrum analysis 19 p3011 A71-37373

Rhodochrosite /manganese carbonate/ complex refractivity determination for correlation between optical reflection, attenuation and scattering coefficients 20 p3269 A71-39185

Bicarbonate requirement for elimination of lag period of chemoautotrophically grown *Hydrogenomonas eutropha* 21 p3329 A71-40213

Free radical induced high temperature oxidation degradation curtailment of polyphenyl ethers by oxides, hydroxides and carbonates of alkali metals and Na [ASLE PREPRINT 71LC-11] 24 p3842 A71-45290

CARBONIC ACID

Carbonic acid effect on isolated skeletal muscle, discussing membrane potential and ion content measurements 05 p0710 A71-16941

Oxygen consumption and carbonic acid output in hypothermic rats cooled under diethyl ether anesthesia, investigating physiological indices during hypothermia 06 p0852 A71-17667

Coronary blood flow at increased arterial carbonic acid partial pressure, noting induced hypercapnia 21 p3335 A71-40633

CARBONIZATION

Graphitizing and nongraphitizing substances carbonization, observing cokes chemical structure changes and thermal decomposition 15 p2368 A71-32733

EPR spectra and spin-lattice relaxation time in coal pitch and polyvinyl chloride during low temperature carbonization 17 p2763 A71-35245

CARBONYL COMPOUNDS

Bacteria and mammalian cells radiosensitization, using phenylglyoxal and various carbonyl compounds 07 p1034 A71-18944

Carbon monoxide gas phase vibrational relaxation by Fe atoms, using shock tube for determination of decomposition rate of iron carbonyl in dilute mixture with Ar 08 p1337 A71-20672

Gaseous chromium carbonyl or aqueous chromium salt spray additives behavior photometric investigations in premixed hydrogen-oxygen-nitrogen flames 16 p2540 A71-33374

Interstellar carbonyl sulfide transition at 109.5 GHz, noting column density 21 p3447 A71-40447

Carbonyl fluorine thermal decomposition in excess Ar behind incident and reflected shock waves, analyzing reaction rate variation with temperature and total pressure 24 p3802 A71-44941

CARBORUNDUM (TRADEMARK)

Canyon Diablo iron meteorite optical microscopic and X ray structural analysis finding moissanite /or carborundum/ 17 p2810 A71-35722

CARBOXYHEMOGLOBIN

Carboxyhemoglobin changes in circulating blood volume during lower body negative pressure exposure 06 p0854 A71-18363

CARBOXYHEMOGLOBIN TEST

CO exposure effects on human psychomotor performance for blood carboxyhemoglobin saturation levels, using sleep monitored EEG methods 11 p1726 A71-26509

CARBOXYL GROUP

Fractography of thermoset resins toughened with Hycar carboxyl terminated butadiene acrylonitrile, using electron microscope 11 p1785 A71-25406

CARBOXYLIC ACIDS

NT ACETIC ACID

NT ACETYL SALICYLIC ACID

NT ALANINE

NT ASPARTIC ACID

NT IODOACETIC ACID

NT LACTIC ACID

NT OXALIC ACID

NT TRYPTOPHAN

Mass spectroscopic determination of geometric isomers of alpha, beta-unsaturated carboxylic acids, noting various modes of fragmentation 01 p0028 A71-11304

Alpha-beta unsaturated carboxylic acids geometric isomers determination by mass spectroscopy 11 p1727 A71-25230

Chronic inability of succinate for protection against paralysis of rats exposed to hyperbaric oxygen toxicity, correlating thermocontrol response 11 p1720 A71-26124

Perfluorinated monocarboxylic fatty acids additives for controlling lubricating oils spreading on metals and antifriction properties improvement 15 p2438 A71-31680

CARBURETORS

Gasoline icing inhibitors effect on light aircraft piston engine carburetor icing [SAE PAPER 710371] 10 p1658 A71-24240

CARBURIZING

High stress cycles and impact fatigue behavior of common case hardened carburized gear steels under loading 03 p0441 A71-13253

Carburization time, temperature and rates in austenitic stainless steels, discussing complex carburized structures 04 p0602 A71-14897

Regeneratively cooled stainless steel thrust chamber failure related to internal carburization by fuel decomposition and propellant combustion 11 p1810 A71-25505

Carburizing steels cold forging, investigating pressure requirement relationship to compressive stress from comparison of backward extrusion and laboratory compression tests 18 p2935 A71-36669

Mechanical properties of carburized cermet steel with hypereutectic structure after water quenching and tempering at 300 C 19 p3076 A71-37113

Multiplying factors charts for hardenability prediction of Cr, Ni, Si, Mo and Mn steels containing carbon 20 p3251 A71-39337

Eutectoidal decomposition of tantalum dicarbide, noting X ray phase identification during carburization of tantalum ribbons 20 p3252 A71-39961

CARCINOMA

U CANCER

CARDIAC VENTRICLES

Right heart ventricle activity in patients with hypertension recorded by electrokymograph 01 p0014 A71-11138

Abnormal left ventricular contour with late systolic murmur at apex preceded by click and with abnormal T waves in electrocardiogram 02 p0197 A71-11694

Mitral valve muscular fibers, investigating pathological changes of myocardium of left heart ventricle 02 p0198 A71-11695

Gap in atrioventricular conduction in humans by catheter technique for recording electrical activity of His bundle 03 p0363 A71-13488

Left ventricular volume and cardiac work evaluation by thermoluminescence technique, employing thermocatheter for temperature measurement [ASME PAPER 70-WA/TEMP-2] 03 p0372 A71-14102

Human left ventricle mathematical models, determining physiological response oriented mechanical parameters with diagnostic significance [ASME PAPER 70-WA/BHF-14] 03 p0373 A71-14112

Concentric layer model for estimating energy expenditure of left ventricle 05 p0713 A71-16486

Atrial and ventricular dimensional analysis in animals and man, discussing angiocardigraphic, biplane, X ray, indicator dilution, radioisotopic and noninvasive methods 05 p0715 A71-16925

Digitalis-induced bundle branch ventricular tachycardia from electrode catheter recordings of dogs specialized conducting tissues 06 p0852 A71-17873

Right and left ventricular systolic time intervals from high fidelity pulmonary arterial pulse wave measurements 06 p0852 A71-17875

Strain gage attachment to rat heart ventricle in situ with fine stainless steel pins 06 p0862 A71-18391

Myocardial ventricle contraction in high altitude hypoxia adaptation, using barochamber trained rats 06 p0857 A71-18467

Acetylcholine endogenous formation in rabbit myocardium effect on ventricle rhythm guides automatic activity suppression by HF excitations 07 p1040 A71-19281

Left ventricular performance Fourier analysis, obtaining ventricular and ascending aortic pressure and flow from closed and open chest dog measurements 07 p1041 A71-19636

Primary T wave derived from ECG waveform dependent intrinsic ventricular recovery properties 07 p1050 A71-19840

Human cardiac intraventricular conduction measurements, using right and left bundle branch potentials during catheterization 07 p1044 A71-20351

Left ventricular function analysis by atrial pacing in subjects with normal and elevated left ventricular filling pressure, relating stroke volume to end diastolic pressure 07 p1044 A71-20352

Frog ventricles myocardial fibers spontaneous activity in Ringer solution due to ion conductivity variations 08 p1239 A71-21057

Ventricular controllers automatism suppression by HF electric stimulation, examining energy metabolism inhibitors effects 08 p1240 A71-21793

Premature pulmonary valve closure due to severe mitral insufficiency by left atrial V wave retrograde transmission 08 p1240 A71-21888

Rat left ventricle isolated papillary muscles contractile force in pressure chamber under high altitude adaptation 09 p1388 A71-22125

Excitation-contraction coupling of papillary muscles from hypertrophied right ventricles of cats with pulmonary artery artificial stenosis 09 p1395 A71-23257

Rats under various exercise programs, determining cardiac ventricle and gastrocnemius muscles calcium activated adenosine triphosphatase activities 09 p1400 A71-23361

Transthoracic measurements of left and right ventricular systolic pressures in anesthetized mice, using fiber optics and strain gage manometer techniques 09 p1401 A71-23371

Aging effects on blood pressure-flow relations and cardiac output/ventricular end diastolic pressure, discussing pulmonary vascular bed capacity dependence on increasing flow during supine exercise 10 p1561 A71-24128

Canine heart rate Frank-Starling mechanism effects on ventricular volumes during natural and artificial cardiac pacing 10 p1565 A71-24681

Left ventricular enlargements, comparing vectorcardiographic spatial magnitude and electrocardiographic precordial QRS voltage measurements 11 p1725 A71-26428

Cardiovascular system response to swimming exercise by dogs, measuring left ventricular internal diameter and pressure, cardiac output and heart rate 12 p1873 A71-27130

Ventricular septal defect, discussing incidence, human physiological responses, morbidity and mortality in various age groups 13 p2004 A71-27862

Ventricular mass estimation using electrocardiographic parameters 13 p2021 A71-29302

Coronary vasculature development under hypoxia and pulmonary hypertension as possible cause of right ventricle phasic flow contour changes 14 p2184 A71-30282

High altitude residents cardiovascular evaluations, showing right ventricular enlargement and reactive pulmonary hypertension 14 p2184 A71-30285

Myocardial ischemia observations, utilizing morphologic and pathophysiologic correlations with cinecoronary arteriography, left ventriculography and hemodynamic examination 14 p2185 A71-30287

Left ventricular power as product of pressure and volume change rate, relating peak values to end diastolic mass 14 p2187 A71-30709

Energy output of left ventricle and congestive heart failure mechanism, approximating blood velocity in aortic system by mathematical model 15 p2363 A71-31443

Left ventricular posterior wall motion measurements in myocardial infarction, using ultrasonic echogram time-motion data 15 p2365 A71-32536

Concealed and supernormal atrioventricular conduction data, using His bundle electrogram recordings 15 p2366 A71-32539

Atrioventricular and intraventricular conduction disturbances in acute myocardial infarction, discussing heart block 15 p2361 A71-32540

Right ventricular end-diastolic volume as index of myocardial fiber length and correlation with ventricular work at rest and exercise with and without right ventricular failure 15 p2361 A71-32541

LVET/EICT ratio usefulness compared to EICT for left ventricular contractility in patients with mitral valve disease 15 p2361 A71-32659

Spatial ECG ventricular gradient ECG morphology, noting use in stimulus intraventricular conduction disturbances recording 17 p2690 A71-34823

Human ventricular activation correlation with canine model in chronic myocardial infarction 17 p2682 A71-35041

Myocardial inotropism index, using left ventricle time varying pressure/volume ratio in systole 17 p2683 A71-35121

Electrocardiographic evidence of false complete bilateral bundle branch block with impaired atrioventricular conduction in patient with hypertensive heart disease 18 p2853 A71-35912

Correlative ECG survey of surgically proven constrictive pericarditis involving left ventricle with T wave inversion 18 p2853 A71-35913

Left ventricular aneurysm electrocardiographic features and postresection changes based on ECG statistical analysis 18 p2854 A71-36138

Canine ventricular myocardium as cardiac beta-adrenergic receptor, describing binding of norepinephrine to microsomal particles 19 p3002 A71-37900

Pulmonary diastolic pressure relation to left ventricle and atrium of patient with diagnostic heart catheterization at rest 19 p3004 A71-38296

Cardiac sympathetic nervous control of right ventricular pressure-flow dynamics in outflow tract in anesthetized dogs 22 p3484 A71-41522

Ejection fraction relation to left ventricular dimensional changes in patients with heart disease, using angiocardigrams 23 p3635 A71-44128

Diagnostic import of QRS notching in HF ECG of living subjects with heart disease, noting notch count correlation with ventricular enlargement 23 p3636 A71-44130

CARDIOGRAMS

Optimal contactless kinetocardiography recording LF patient chest vibrations, comparing short wave method 06 p0863 A71-18468

Hemodynamic correlation of Austin Flint murmur and a-wave of apexcardiogram in aortic regurgitation 09 p1392 A71-22589

Ultrasonic echocardiograms of anterior cusp of mitral valve in aortic valve disease 13 p2002 A71-27814

Analog computer analysis of radiocardiograms, determining cardiac function and pulmonary blood volume 20 p3191 A71-38802

CARDIOGRAPHY

NT ELECTROCARDIOGRAPHY

NT MAGNETOCARDIOGRAPHY

Left ventricular volume determination by high speed cineangiocardiology, using optical scanning and automatic data processing 02 p0203 A71-11705

Gravitational acceleration effects on hemodynamics, describing mechanocardiographic equipment 02 p0198 A71-11900

Atrial and ventricular dimensional analysis in animals and man, discussing angiocardiology, biplane, X ray, indicator dilution, radioisotopic and noninvasive methods 05 p0715 A71-16925

Dog cardiac output measurement by using ethyl ether dissolved in saline solution as indicator, comparing to Fick method results 06 p0856 A71-18389

Chest and cardiovascular system optimal radiologic facilities, discussing X ray examination, catheterization-angiocardiology and nuclear radiology laboratories 07 p1053 A71-20354

Informative precordial palpation taking into account location, timing, duration and amplitude 08 p1241 A71-21889

Hemodynamic changes in healthy pilots with excess weight investigated by mechanocardiograph, showing decreased cardiac output, left ventricle strength and volume rate 15 p2357 A71-31319

Human radioisotopic angiocardiology, emphasizing identification and physiological diagnosis of congenital and acquired cardiovascular defects 15 p2361 A71-32537

Resting and postexercise apexcardiogram correlation with maximal treadmill stress test, noting mean a-wave ratios 21 p3332 A71-40406

CARDIOLOGY

Adapted multichannel analyzer for cardiology visualizing vectorcardiographic loops 03 p0206 A71-12107

Analog/hybrid programming of stimulus sequence for cardiac excitation study 04 p0546 A71-15166

Clinical and hemodynamic profile of cardiogenic shock after acute myocardial infarction 04 p0541 A71-15914

Cardiac output during submaximal bicycle exercise in children and teen-agers, discussing oxygen transport function of blood 06 p0857 A71-18722

Cardiac impulse conduction measurements noting delay, block and one way block in excised canine Purkinje fibers with depressed responsiveness 07 p1041 A71-19637

Cardiac impulse conduction in depressed canine Purkinje fibers, discussing experimental results in connection with reentrant arrhythmias 07 p1041 A71-19638

Cardiac arrhythmias simulated by concealed bundle of His extrasystoles in open chest intact dog hearts 09 p1395 A71-23256

Thermomodulation and indocyanine green dye technique comparison for cardiac output measurement in man 11 p1724 A71-25435

Cardiology - Conference, London, September 1970 13 p2003 A71-27858

Automation in cardiology, discussing analog and digital computer techniques for on-line hemodynamic analysis and collection and manipulation of cardiovascular data 13 p2016 A71-27868

Automated data acquisition and analysis during cardiac catheterization, using photokymographic and analog magnetic tape recording system in conjunction with digital computer 13 p2020 A71-29003

Upright tilt stress effects on cardiac cycle phases in healthy subjects, using noninvasive techniques 15 p2358 A71-31453

Efferent vagal activity increase prior to intermittent cardiac block due to rise in blood pressure 16 p2529 A71-33192

Spatial ECG ventricular gradient ECG morphology, noting use in stimulus intraventricular conduction disturbances recording 17 p2690 A71-34823

Papers on exercise and cardiac death covering coronary athero- and arteriosclerosis, congenital anomalies, myocarditis, tumors and physical exertion 18 p2855 A71-36213

Acute fatal nontraumatic collapse during physical exertion due to circulatory diseases 18 p2855 A71-36215

Frequency phonocardiography technique for heart sounds and murmurs registration, producing analog voltage proportional to frequency by zero crossing detector 19 p3006 A71-37234

Cardiac automatic rhythms, discussing diastolic depolarization in Purkinje fibers and factor controlling automaticity 21 p3330 A71-40250

CARDIOTACHOMETERS

Linear beat by beat cardi tachometer, describing amplifier design and operation 01 p0021 A71-10242

CARDIOVASCULAR SYSTEM

NT AORTA

NT ARTERIES

NT BLOOD VESSELS

NT CAPILLARIES [ANATOMY]

NT CARDIAC VENTRICLES

NT DIASTOLE

NT ERYTHROCYTES

NT GLOMERULUS

NT HEART

NT HEMATOPOIESIS

NT HEMATOPOIETIC SYSTEM

NT LEUKOCYTES

NT LYMPHOCYTES

NT MYOCARDIUM

NT RETICULOCYTES

NT SYSTOLE

NT VEINS

Blood pressure changes in heart cavities and large vessels of dogs exposed to accelerations 01 p0013 A71-11126

Cardiovascular and ventilatory responses to room air and pure oxygen breathing under various exercise work load conditions 01 p0016 A71-11407

Cardiovascular system blood flow mathematical model parameter optimization by simulation on hybrid computer, using OPTRAN program 02 p0203 A71-11807

Human cardiovascular control system model by analog computer program for various work loads up to submaximal, estimating correspondence to real life 03 p0368 A71-12995

Cardiovascular and biochemical effects of chronic intermittent neurogenic stimulation, noting alphamethyltyrosine antihypertension agent 03 p0359 A71-13157

Anatomy and function of normal pericardium including removal effect in mammals, fish and amphibians 03 p0362 A71-13328

Pulsus alternans study by noninvasive techniques for assessing cardiovascular function in hemodynamics and muscular physiology

03 p0372 A71-13492

Cardiovascular and respiratory systems affect innervation in cats investigating pericardial, expiratory and pneumo-vascular mechanoreceptors

05 p0707 A71-16343

Human physical exercise with stepwise increasing load noting working capacity, cardiovascular and respiratory system performance and blood composition interrelations

05 p0709 A71-16805

Epinephrine infusion in man, examining systolic time intervals and sympathetic stimulation in cardiovascular dynamics

06 p0850 A71-17440

Walking effects on body composition and cardiovascular function of middle aged men

06 p0862 A71-18388

Cardiovascular responses of hypoxic hypoxia in mongrels with catecholamine induced coronary dilatation

06 p0857 A71-18723

Amino-ethyl-S-2-isothiuronium radio protective dose effects on enzyme activity, cardiovascular changes, blood transaminases concentration, bone marrow and peripheral circulation

07 p1040 A71-18986

Hybrid computer simulation for cardio-circulatory assist device, discussing atrium to aorta and ventricle to aorta optimal output, time tension index and flow control

07 p1048 A71-19584

Chest and cardiovascular system optimal radiologic facilities, discussing X ray examination, catheterization-angiographic and nuclear radiology laboratories

07 p1053 A71-20354

Cardiopulmonary and circulatory mechanisms, adaptation limits and response to aerospace flight stress

08 p1238 A71-20720

Tarahumara Indian runners cardiovascular system physical conditioning for endurance extremes

08 p1240 A71-21887

Soyuz 9 astronaut vertical posture control after 18 day orbital flight, considering cardiovascular disturbances caused by reduced muscle tone and changed interaction between analyzers

09 p1389 A71-22203

Soyuz 9 spacecraft astronaut cardiovascular and respiratory systems responses to orthostatic effect after 18-day orbital flight from EKG measurements and sphygmography

09 p1389 A71-22208

Soyuz 9 spacecraft simulator prolonged confinement effect on human cardiovascular system functional state

09 p1390 A71-22209

Weightlessness, high acceleration and aerospace vehicle maneuvering effects on cardiovascular and vestibular systems, discussing disorientation, space sickness and blood circulation

09 p1398 A71-22357

Adrenergic neurons in intramural cardiac ganglia in rabbits, using histochemical luminescent microscopy

09 p1391 A71-22533

In-flight monkey cardiovascular observations, discussing central venous pressure, urine volume, electrolyte imbalances and heart rate

09 p1395 A71-23244

Central nervous system role in body metabolism effects on cardiac output, measuring 2,4-dinitrophenol/DNP dosage effect on arterial pressure and oxygen consumption in dogs

09 p1396 A71-23541

Cardiovascular functional reactions in pilot trainees during training flights, presenting case histories

10 p1570 A71-24341

Chemical release from traumatized tissue in dogs under cross circulation with lethal cardiac depression response

11 p1720 A71-26119

Nonlinear axisymmetric solution for cardiovascular system pulsatile flow, using long rigid tube and velocity profile representation

11 p1726 A71-26485

Cardiovascular responses to submaximum and maximum effort cycling and running on bicycle ergometer and motor driven treadmill, using carbon dioxide rebreathing method

12 p1873 A71-27128

Cardiovascular system response to swimming exercise by dogs, measuring left ventricular internal diameter and pressure, cardiac output and heart rate

12 p1873 A71-27130

Alveolar gas exchanges and cardiovascular functions during breath holding with air, determining resting oxygen consumption

12 p1870 A71-27135

Nervous/cardiovascular systems and blood composition changes in moderate duration military transport flights

12 p1874 A71-27163

Mild hypertension risks, presenting results of case studies over ten year period of mortality rate associated with cardiovascular diseases

13 p2004 A71-27865

Automation in cardiology, discussing analog and digital computer techniques for on-line hemodynamic analysis and collection and manipulation of cardiovascular data

13 p2016 A71-27868

Set and uncertainty as factors influencing anticipatory cardiovascular response in humans, monitoring heart rate and vasomotor activity

13 p2011 A71-28809

Metabolic, ventilator and cardiovascular response during free swimming and treadmill walking, relating oxygen consumption to work intensity

13 p2024 A71-29500

Hypoxia, high altitude and heart - Conference, Aspen, Colorado, January 1970

14 p2183 A71-30275

Cardiac activity changes during prolonged hypodynamia, discussing clinical and experimental investigations results with humans and animals

15 p2358 A71-31320

Lowered cardiac output and arterial pressure response to exercise after autonomic heart blockade in man, noting retained work capability

15 p2358 A71-31454

Human radioisotopic angiocardiology, emphasizing identification and physiological diagnosis of congenital and acquired cardiovascular defects

15 p2361 A71-32537

Cortical neurodynamics during vestibular afferent activity and associated cardiovascular and respiratory reactions, noting EEG correlation to hemodynamics

16 p2527 A71-32828

Cardiovascular telemetry total implants, describing measurement problems, equipment design, low current operation, size and thermal and temporal stability

16 p2534 A71-33071

Hypoxia effects on cardiovascular reflexes during hypoxia, measuring response of heart rate to lower body negative pressure

16 p2529 A71-33191

Cardiovascular responses to hypothalamic, spinal cord and stellate ganglion stimulation as function of intensity, pulse duration and frequency in cats

16 p2531 A71-33367

Cardiovascular and respiratory systems, motor and muscular activity, metabolism and body energetics functional changes due to prolonged weightlessness

16 p2531 A71-33676

Histochemical investigation of enzymes activity during various cardiac cycle phases in frogs, noting effects of ion concentration

16 p2533 A71-33913

Pulmonary blood volume changes in cat due to neurogenic, pharmacological and mechanical effects on cardiovascular system, noting pulmonary function role

16 p2533 A71-34112

Afferent mechanisms of orthostasis in space flight, discussing plasma fluid volume reduction and cardiovascular adjustments on passive tilting

18 p2856 A71-36634

Cardiovascular system mathematical model for evaluating system parameters effects on circulatory indices including minute volume and arterial tension

19 p3007 A71-37777

Instrumental learning of cardiovascular and visceral responses and behavioral, physiological and biochemical consequences in relation to psychosomatic therapy

20 p3190 A71-39548

Jet and turbulence mechanism of vascular murmurs associated with stenosis for minimum flow Reynolds numbers, using aorta orifice plates in dogs

21 p3336 A71-40864

Soviet book on animals morphophysiological changes in cardiovascular and nervous systems and various internal organs under RF wave exposure

21 p3344 A71-41369

Vibration induced paroxysmal and cardiovascular hazards during patients transport to hospital by air or ambulance, discussing therapeutic and preventive treatments

22 p3500 A71-41573

Atrial shortening during volume loading by infusion in animal, using Frank-Starling approach

22 p3485 A71-41718

Cardiovascular system functional disorders relationship to nervous activity disturbances

24 p3795 A71-44472

CARET WINGS

Hypersonic aerodynamic characteristics of flat delta and caret wing models at high incidence angles for space shuttles

03 p0344 A71-14445

Caret wing serial tests in Mach 8 to 15 hypersonic flow, including three component force, spanwise direction pressure distribution and shock wave angular measurements by flow visualization

07 p1016 A71-20015

Flat delta and caret wings aerodynamic performance over incidence angle and Mach number range suitable for lifting reentry

16 p2519 A71-32877

Design shock wave correspondence to strong oblique shock, discussing off design behavior of caret wing

17 p2671 A71-35280

Supersonic aircraft propulsion by external heat addition, discussing numerical method for suitable caret wing design

17 p2793 A71-35396

CARGO

NT AIR CARGO

NT BAGGAGE

CARGO AIRCRAFT

NT C-5 AIRCRAFT

NT C-130 AIRCRAFT

NT C-131 AIRCRAFT

NT C-135 AIRCRAFT

Cargo aircraft crew safety and survival, describing restraint, escape, flight deck interior doors, fire and smoke hazards and personnel environmental protection

[SAE-ARP-1139] 07 p1019 A71-19643

Nuclear surface effect vehicle and subsonic aircraft for transoceanic cargo shipping, discussing mobile reactor safety tests under high speed impact conditions

[AIAA PAPER 70-1221] 09 p1492 A71-22779

Air cargo volume development trends, examining worldwide airport terminal capacities and pallet/ containerization systems modular design and operation

10 p1699 A71-24824

Soviet Mil V-12 heavy lift helicopter for civil and military missions, noting turbine engines, rotor configuration, cargo hold and navigation system

14 p2175 A71-30420

Mil Mi-12 Soviet giant rigid rotor helicopter with 30,000 kg load or 250 passenger capacity

20 p3178 A71-39375

CARGO SHIPS

Army/Navy operational evaluation of offshore containerhips discharge by CH-54 helicopters

[AHS PREPRINT 573] 14 p2180 A71-31114

CARGO SPACECRAFT

Space shuttle cargo handling systems, considering space logistics, space missions, vehicle traffic, satellite maintenance, rescue modules, etc

[AIAA PAPER 71-319] 09 p1427 A71-22615

System engineering techniques application to end-to-end space shuttle cargo handling system

18 p2899 A71-36466

Spacecraft housekeeping relation to logistics elements of maintenance and up and down cargo supply

18 p2899 A71-36467

Orbital cargo transfer simulation techniques involving zero-g aircraft and water immersion

18 p2899 A71-36469

Intravehicular manual cargo transfer, using water immersion technique for zero gravity simulation

[AIAA PAPER 71-851] 18 p2871 A71-36642

Weightlessness simulation for orbital man machine experimentation, discussing teterboard and cargo transfer examples

[AIAA PAPER 71-850] 18 p2871 A71-36643

CARIBOU AIRCRAFT

U DHC 4 AIRCRAFT

CARNOT CYCLE

Chemical energy conversion into mechanical work, examining irreversible mixing, Van Hoff box and Carnot cycle

05 p0717 A71-16785

Carnot cycles generalization for thermodynamic systems with stationary gravitational fields, deriving temperature, thermodynamic equilibrium and entropy definitions for general relativistic systems

11 p1798 A71-25738

Chemical energy conversion into mechanical work, examining irreversible mixing, vant Hoff box and Carnot cycle

16 p2540 A71-33037

CAROTENE

Carotenoid depleted Drosophila circadian rhythm and visual receptors photosensitivity, discussing photopigment effects

09 p1394 A71-23160

CAROTID SINUS REFLEX

Arterial blood pressure changes due to bilateral carotid occlusion or electrical heart pacing, considering effects on kidney blood flow and circumference in dogs

01 p0008 A71-10074

Carotid sinus hypotension in dogs under fasting/digestion conditions, considering effect on splanchnic circulation and vasoconstrictor response

04 p0538 A71-15090

Hypoxemia reflex neurogenic vasoconstrictor factors competition with local vasodilator mechanisms in skeletal muscle

08 p1237 A71-20680

Carotid pulse wave slope variations in normal subjects, aortic valvular diseases and hypertrophic sub-aortic stenosis

09 p1392 A71-22590

Myocardial oxygen reduction by stimulating carotid sinus nerves and angina pectoris treatment application

11 p1718 A71-25437

Small signal characteristics mathematical models of carotid sinus baroreceptors of rabbits
12 p1870 A71-27133

Stagnant asphyxia in cat carotid body during abrupt blood pressure drop by simultaneous carotid artery clamping and tap opening
20 p3190 A71-39443

Oxygen tension distribution in cats glomus caroticum under influence of varying arterial oxygen partial pressure, using platinum microelectrodes
24 p3796 A71-44562

CARRIER FREQUENCIES

Instrumentation tape recorder time base error effects on signal carrier amplitude and spectral purity
01 p0033 A71-10896

Satellite communication system earth station transmitter with FDM-FM and SPADE carriers, noting intermodulation effect on channel capacity
02 p0223 A71-12810

Narrow band FM modems with high carrier frequency stability for satellite communication terminals with small dish antennas
02 p0234 A71-12820

Image polarity in holography and carrier frequency photography
04 p0601 A71-15696

Suppressed RF carrier tracking for two channel interplex phase modulated telemetry
07 p1066 A71-20427

Threshold carrier to noise ratio for phase lock demodulators, using computerized prediction model
10 p1574 A71-23764

Optimal continuous recording of amplitude-phase distributions on spatial carrier frequency for light wave modulation and optical antenna simulation
12 p1878 A71-26841

Carrier suppression in angle modulated transponding telemetry by first order stationary stochastic processes
12 p1880 A71-27074

Error probability and reception stability in synchronous detection of phase manipulated signals with additive Gaussian noise at multiplied carrier frequency
16 p2542 A71-33498

Telegraphy binary data transmission through channels with frequency-selective fading, investigating noise stability improvement by programmed carrier frequency variation and receiver passband shifting
17 p2698 A71-34394

Holography with single transverse longitudinal mode pulsed ruby laser, emphasizing carrier frequency shift as limiting factor on depth of field
17 p2745 A71-35587

Spectrum limitation of FM carrier in case of accidental overloading of modulating signal arising in Intelsat 4 communication system
18 p2891 A71-36559

Doppler carrier frequency shift measurement accuracy
20 p3198 A71-39808

Radar systems performance constraints, discussing environmental effects, carrier frequency, aerial directivity, clutter echoes, transmitter power, etc
22 p3509 A71-42199

Estimation-correlation principle application to harmonic signal receiver with unknown carrier frequency, using searching phase locked AFC circuit as estimation unit
22 p3512 A71-42313

CARRIER INJECTION

Si diffusion p-n junctions at high injection levels in strong electric fields, discussing I-V characteristics, minority carrier lifetime, barrier capacitance, etc
03 p0384 A71-13374

Nonequilibrium injected carrier distribution effect on bipolar drift mobility in compensated semiconductors
03 p0467 A71-13983

Injection locked microwave oscillators nonlinear differential equation reduction to nonlinear algebraic equation, calculating AM limiting and output power increment as injected signal amplitude functions
07 p1073 A71-19113

Nonlinear planar transistor model, analyzing majority carrier current flow fields in base due to injection of emitter and collector p-n junctions
12 p1888 A71-27612

Multilayered semiconductor structures with p-n junctions, discussing I-V characteristics, noninjection component effects, carrier transport and negative resistance
13 p2111 A71-28920

Carrier scattering related to orbiting and resonance states in screening impurity donor center of weakly doped homeopolar n-type semiconductor under injection
13 p2112 A71-28928

Silicon planar transistors at low injection levels, showing current transfer function temperature dependence
14 p2213 A71-30624

Equivalent circuit parameters of microwave planar power transistors at high injection levels, indicating parameters frequency dependence determination
14 p2213 A71-30627

Switching on p-n-p-n structure under high injection level in both bases, noting current concentration and voltage steady state buildup
16 p2546 A71-33496

I-V characteristics of compensated semiconductors during nonequilibrium carrier injection from contacts
16 p2622 A71-34028

He ion beam space charge neutralization by thermal electrons injection
17 p2784 A71-34200

Self generated turbulence in insulating liquids during unipolar charge carrier injection, describing charge transport by Lagrangian diffusion process
19 p3044 A71-37736

Evaporative injector system for capillary column gas chromatography for solutes in dilute solution
20 p3194 A71-39257

Carrier scattering related to orbiting and resonance states in screened field of impurity donor center in weakly doped homeopolar n-type semiconductor under injection
21 p3434 A71-41331

Charge injection in metal-aluminum oxide-silicon dioxide-silicon systems using capacitance voltage technique
22 p3587 A71-42531

Negative resistance in high resistance compensated semiconductor diodes with double injection associated with diffusion growth
23 p3652 A71-43482

Transistor current gain as function of emitter current for low injection levels
24 p3807 A71-44381

Nondiffusion theory for I-V characteristics of monolayer and quasi-monolayer photosensitive semiconductors with various carrier injection levels
24 p3859 A71-44385

CARRIER MOBILITY

NT ELECTRON MOBILITY

NT HOLE MOBILITY

Minority current carrier mobility in anisotropic semiconductors, using Demer and photomagnetic effects
01 p0139 A71-11035

Carrier mobility dependence on channel transverse electric field in MOS transistor
02 p0231 A71-11841

Gunn diodes I-V characteristics width as function of carrier concentration/mobility and diode length, noting role of impact ionization in strong electric field
02 p0231 A71-11877

High resistance semiconductors minority carriers mean diffusion length based on induced charge dependence on applied voltage during illumination by absorbable light
02 p0294 A71-11898

Nonequilibrium injected carrier distribution effect on bipolar drift mobility in compensated semiconductors
03 p0467 A71-13983

Oscillatory systems slow monotonic motion due to carrying elements performing HF low amplitude relative oscillations
06 p0897 A71-17364

Microwave measurements of semiconductors and semiconductor films including resistivity, permittivity and carrier mobility
06 p0873 A71-17538

Carrier mobility in noncompensated highly doped semiconductors, presenting derivation from Rogachev expression for scattering Coulomb center screening charge density
07 p1175 A71-19218

Nonhomogeneous arbitrarily formed semiconductor layers, using Van der Pauw method for measuring conductivity and Hall mobility
07 p1175 A71-19221

GaAs lasers p-n junction active region thickness from minority carrier mobility and spontaneous emission measurements in threshold current determination
09 p1460 A71-22305

Integrated circuits semiconductor components, determining effects of heat energy production/withdrawal and strong field on electric current carriers mobility and concentration
09 p1416 A71-22496

Inhomogeneous semiconductor model leading to anomalously high apparent mobility
09 p1510 A71-23486

Carrier mobility, conductivity and optical absorption in strong electric fields of chalcogenide glasses for switching and memory effect amorphous semiconductors
13 p2112 A71-28926

Surface conductivity and current carrier mobility vs surface potential in CdSe single crystal films deposited on mica base by vacuum vaporization
15 p2461 A71-31511

Carrier diffusion length change in damaged gamma irradiated silicon solar cells by numerical analysis, using experimentally obtained voltage or current
17 p2677 A71-35050

Free carrier surface density and mobility in large MOS transistors from conductivity and Hall measurements
19 p3028 A71-37564

Microwave photoconductivity of boron single crystals under pulsed illumination, determining temperature effects on carrier mobility, recombination coefficients and relaxation times
21 p3428 A71-41202

Impurity photoconductivity, generation-recombination noise and temperature dependences of Hall coefficient and equilibrium carrier mobility in p-type cobalt-doped germanium
21 p3429 A71-41213

High resistivity Fe-doped GaAs, investigating carrier lifetime dependence on Fe atoms concentration
21 p3431 A71-41234

Electrical conductivity and thermoelectric power measurements for polycrystalline beta-SiC heavily doped with nitrogen, estimating electron effective mass and carrier mobility at high temperatures
21 p3433 A71-41307

Carrier mobility, conductivity and optical absorption in strong electric fields of chalcogenide glasses for switching and memory effect amorphous semiconductors
21 p3434 A71-41323

GaAs-InAs solid solutions single crystal ingots, investigating optical absorption and reflection spectra, energy gap width and carrier mobility temperature dependence
21 p3435 A71-41335

Polycrystalline thin film CdSe-CdS and CdSe-CdTe solid solution semiconductor alloys Hall mobility and carrier concentration dependence on substrate temperature
23 p3715 A71-43433

Space charge density and carrier mobility in disordered regions of p-n microjunctions
23 p3717 A71-43486

Nd-Bi phase diagrams from thermal differential, metallographic and X ray analyses, discussing carrier concentration and mobilities, Hall coefficients, conductivity and thermal emf
23 p3692 A71-44022

Current carrier mobility and concentration measurements in inversion metal dielectric semiconductor channels by Hall method
24 p3808 A71-44384

CARRIER MODULATION

U MODULATION

CARRIER ROCKETS

U LAUNCH VEHICLES

CARRIER SYSTEMS

U WIRELESS COMMUNICATIONS

CARRIER WAVES

Constant bandwidth FM subcarrier oscillators signal preemphasis for FM and PM transmitters
01 p0033 A71-10897

Wall loss influence on energy flow center velocity of rectangular carrier pulses in circular waveguide for long distance transfer
01 p0056 A71-11195

Balanced modulators and multipliers, using feedback control for suppressing carrier leak
02 p0236 A71-12425

Squaring loops for establishing coherent carrier reference for bi-phase PSK modulation, deriving optimal presquaring filter
05 p0730 A71-17075

Wideband subcarrier frequencies demodulation technique for uncoded or coded PSK telemetry over large input SNR range for deep space interplanetary communication
08 p1254 A71-21316

Walsh orthogonal functions application in signal processing and as carrier waves in telemetry data transfer systems
14 p2199 A71-30909

Noise stability at reduced peak signal power of PTM-AM communications using wideband linearly frequency modulated carrier pulses
15 p2368 A71-31228

Communication satellite ground station transmitting equipment, discussing carrier waves, FM, frequency converters and microwave amplifiers characteristics
17 p2717 A71-35515

Distance measurement system with onboard transponder, discussing subcarrier and pseudorandom code signal techniques synthesis
18 p2879 A71-36532

Incoherent carrier communications system, obtaining message SNR of 60-70 dB for analog signals with compound pulse modulation and carrier clipping
21 p3347 A71-40375

AM crosstalk in unified carrier telemetry system, studying implications for carrier false lock and tracking
22 p3514 A71-42390

CARTESIAN COORDINATES

- Elastic theory problems, deriving continuum spectral models in Cartesian coordinate system
02 p0327 A71-12404
- Three dimensional traverse in geocentric Cartesian coordinates for connection of two adjacent satellite observation stations
03 p0418 A71-14324
- Astronomical-geodetic networks processing in three dimensional rectangular coordinates, considering advantages and accuracy
06 p0889 A71-17674
- Numerical integration for continuously thrusting spacecraft optimal trajectory, considering rectangular Cartesian and polar cylindrical coordinates characteristics
[AIAA PAPER 69-903] 07 p1191 A71-18891
- Favorable construction of elementary figures of cosmic triangulation in three dimensional Cartesian coordinates, determining errors
09 p1404 A71-22272
- Singularities in linear elliptic partial differential equations, considering Cartesian and cylindrical polar coordinate problems
15 p2440 A71-31348
- Falling body problem solution, considering curvilinear motion effects of earth rotation axis
15 p2450 A71-32039
- Small deflection analysis within Cartesian coordinate system applicable to elastic-plastic rectangular plates bending under Tresca yield criterion
16 p2654 A71-33122
- Radially symmetric shocked flows computation method, using momentum equation in conservation form in original Cartesian coordinates
21 p3368 A71-40848
- Geophysical cartesian coordinate system transformation, using vector-matrix formalism
21 p3375 A71-41355
- Half space with periodic continuous distributed dislocations and plastic distortions, calculating stress fields and free surface orientation with cartesian coordinate system
22 p3613 A71-41432
- Linear regression optimal filtering application to aircraft target tracking
23 p3659 A71-44094
- CARTOGRAPHY**
U MAPPING
- CARTRIDGE ACTUATED DEVICES**
U ACTUATORS
U EXPLOSIVE DEVICES
- CASCADE CONTROL**
Cascade type analog-to-digital converter with successive bit determination by recycling through single operational amplifier and comparator
02 p0231 A71-12038
- Canonic synthesis of electronic relays, considering cascade connected isolation box, analog to digital converter and switch
03 p0393 A71-14469
- Transistorized amplifiers synthesis with multiloop feedback
05 p0728 A71-16871
- Lossless two-port cascade network synthesis using computer-oriented technique
08 p1258 A71-21344
- MOS transistor cascade amplifiers, discussing monolithic integrated circuits
09 p1416 A71-22492
- Electronically tunable compact X band triplexer, consisting of four port nonreciprocal directional YIG filters in cascade
09 p1418 A71-23416
- Cascade connection of nonlinear block and time invariant finite dimensional system, discussing stabilization by controlled state variable feedback
17 p2722 A71-35213
- CASCADE FLOW**
Plane linear cascades of thin curved profiles, obtaining potential flow velocities and lifting force on leading edge
01 p0001 A71-10339
- Reversible transonic fluid flow through cylindrical blades cascade by hodographic singularities solution of potential and stream function
01 p0003 A71-11023
- Plane diffuser cascade losses at low main stream pressures, discussing Reynolds number role
01 p0003 A71-11062
- Flow characteristics in turbomachine blade cascades with transonic regime, emphasizing shock-boundary layer interaction phenomena
03 p0340 A71-13140
- Axial turbomachines boundary layer flow, describing two dimensional cascade calculation methods
03 p0340 A71-13146
- Two dimensional cascade flow, discussing methods of flow field idealization, nonviscous incompressible flow theoretical methods, compressibility and viscosity effects
03 p0342 A71-13826

- Three dimensional cascade flow, discussing potential flow, shear flow, flow disturbances and flow approximations for annular cascades
03 p0342 A71-13827
- Cascade flow test data, considering blade section performance in transonic and supersonic axial flow compressors
03 p0343 A71-13829
- Electromagnetic cascade-material boundary crossing transition effect analysis by perturbation theory in terms of differential shower particle flux
03 p0478 A71-13871
- Low speed two dimensional axial flow compressor cascade data, considering lift drag ratio and minimum loss coefficient
[ASME PAPER 70-WA/GT-10] 03 p0343 A71-14118
- Cascade thermoelectric cooler/heat pump/transient response for various geometries, materials and environmental conditions
03 p0355 A71-14320
- Gas-particle mixture cascade flow over turbine blades, considering momentum/heat transfer and particle trajectories
[AIAA PAPER 70-712] 06 p0841 A71-17701
- Gas turbine cascade radial gap inverse heat transfer, calculating release coefficients
06 p1006 A71-18002
- Pressure distribution over blade in cascade nozzle for incompressible and compressible particulate gas flow
[AIAA PAPER 71-82] 06 p0883 A71-18539
- Three dimensional transonic shear flow structure in turbomachine cascade, using time dependent numerical solution
[AIAA PAPER 71-83] 06 p0843 A71-18540
- Gas-particle mixture cascade flow over turbine blades, considering momentum/heat transfer and particle trajectories
[AIAA PAPER 70-712] 07 p1017 A71-20311
- Low aspect ratio compressor blade cascade performance at blade span center, discussing pressure loss, angle of attack and staggering
07 p1017 A71-20624
- Radial flow energy losses in rotating cylindrical cascade of inward-flow turbine wheel, determining profile losses and exit blade angle
08 p1349 A71-22044
- Oscillating airfoil wake interaction with fixed cascade, considering two dimensional incompressible inviscid small perturbation flow theory
09 p1511 A71-22943
- Axial turbomachine three dimensional cascade flow calculation from dynamics vector equations
09 p1383 A71-23601
- Integral equation for solving potential incompressible fluid flow past blade cascade on axisymmetric current surface in variable thickness layer
10 p1593 A71-24369
- High subsonic flow two dimensional turbine cascade design by approximate hodograph method, noting pressure distribution measurements
[ASME PAPER 71-GT-34] 11 p1704 A71-25971
- Time dependent asymptotic solution for transonic flows in hyperbolic nozzle and turbine cascades with oblique shock
[ASME PAPER 71-GT-42] 11 p1704 A71-25975
- Supersonic turbine design, presenting performance data for film cooled blunt leading edge rotor blades measured in two dimensional cascade experiments
[ASME PAPER 71-GT-76] 11 p1704 A71-25990
- Turbomachine blade cascades in supersonic flow, noting wave configurations, entropy and counter pressure variations
12 p1864 A71-27475
- Cascade approximation of unsteady forces acting on blades of axial flow turbomachines, using perturbation potential combined with slip condition
[ONERA-TP-944] 12 p1946 A71-27713
- Hydraulic analogy for visualization of flow through moving plane cascade for rotor section of compressor stage
12 p1898 A71-27720
- Aerofoil cascades with axial velocity change in incompressible flow, determining turbine blade force dependence on circulation
13 p1990 A71-28467
- Supercavitating flow past straight cascade with arbitrary blade shapes, considering lift and drag coefficients, cavitation number, cavity shape and exit flow conditions
[ASME PAPER 71-FE-6] 13 p1995 A71-29448
- Two dimensional jet flap cascades, presenting stream deflection angles as function of jet to mainstream momentum flux
[ASME PAPER 71-FE-14] 13 p1995 A71-29453
- Finite element method application to transonic viscous flow through cascades and channels
[AIAA PAPER 71-602] 15 p2388 A71-31542
- Cascading turbomachine blades vibrations measurement in subsonic and sonic high temperature gas flows, describing test facility
16 p2553 A71-33993

- Stream lines construction in meridional plane of blade nozzle annular cascades of steam and gas turbines in subsonic and supersonic flow
17 p2670 A71-34446
- Siren wail in turbine axial stage due to nonuniform pressure fields behind blade cascades
18 p2843 A71-36180
- Cascade displacements and stresses in nozzle ring guide vanes with sectional diaphragm under axial and circumferential flow
18 p2980 A71-36706
- Incompressible potential cascade flow interaction, presenting approximate method based on blade profile flow expression by power series with distance between cascades as parameter
21 p3322 A71-40685
- Two dimensional supersonic flow pattern, velocity and loss in shock waves in front of blade cascade
22 p3479 A71-41842
- Vibration amplitudes and phases/excitation modes during flutter for weakly inhomogeneous annular cascade flow with blade interaction and random inhomogeneity
22 p3615 A71-41846
- Blade cascade design for meridional flow, using finite difference method for universal computer program
23 p3626 A71-43550
- Streamline curvature analysis of compressible subsonic, transonic and supersonic cascade flows in axial turbine blades
23 p3665 A71-44347
- Flow models for turbomachinery, averaging equations for flow through blade cascades across pitch
23 p3627 A71-44348
- Navier-Stokes equations solutions expressing flow conditions through blade cascade
24 p3817 A71-44523
- Plane cascades efficiency and exit blade angles dependence on cooling air admitted to air-gas flow area from exhaust nozzle guide vanes
24 p3864 A71-45009
- CASCADE WIND TUNNELS**
Glass fiber rotor blades design with longitudinal pressure tapings for cascade wind tunnel and turbomachinery flow research applications
11 p1772 A71-26316
- Schlieren visualization for supersonic annular fixed cascade and freon compressor wind tunnels, using vane holding cylinder devices
[ONERA-TP-948] 12 p1867 A71-27717
- CASCADES**
Iterative and cascaded codes for single and grouped error detection
01 p0039 A71-11317
- Transient effects due to electromagnetic cascades in lead during copper wall passage in ionization chamber
01 p0084 A71-11370
- N-port networks interconnection by NASAP-70 transfer function capability for large scale circuit problems, considering Laemmel and Cascade Parameter methods
03 p0390 A71-14309
- Electron collision cascades in braking medium, deriving integral equations for energy structure, displacement and ionization yield
04 p0629 A71-14914
- Cascade and single stage rotating rig data comparison with aerodynamic predictions based on intrablade analysis, including wall boundary layer model
[ASME PAPER 71-GT-13] 11 p1703 A71-25959
- Handle cascade effects on atomic lifetime reliability from collisional excitation experiments
11 p1803 A71-26370
- Cascaded inertial vibration isolation systems, using rigid masses interconnected by air spring type isolator elements
11 p1853 A71-26492
- Electromagnetic longitudinal cascades development numerical treatment based on Boltzmann equation, discussing Monte Carlo computing times for primary energy total electron counts
12 p1933 A71-27387
- Cascading turbomachine blade row coupled flutter, correlating camber angle, cascade condition and elasticity
13 p2157 A71-29128
- Flexible blades cascade at various pitch angles and Reynolds numbers
15 p2343 A71-31203
- Plane sound waves transmission and reflection through finite plates single cascade by Wiener Hopf technique
21 p3437 A71-40537
- Plane acoustic wave transmission problem through finite chord plate array in subsonic gas flow, using factorization method in diffraction theory
21 p3322 A71-40686
- Monte Carlo model of muon and active component distribution in nuclear cascade in extensive cosmic ray shower
22 p3595 A71-42650
- Reduced nebular helium abundances, using capture-cascade and collisional excitation calculations
23 p3733 A71-43081

- Transonic airfoil cascade analytical design, determining efficiency from velocity distribution
24 p3791 A71-45381
- ASCADs [FLUID DYNAMICS]**
U FLUID DYNAMICS
- ASCODE MOSFET**
U FIELD EFFECT TRANSISTORS
- ASE BONDED PROPELLANTS**
Low modulus solid propellants family for low thrust-to-mass ratio fully case bonded end-burning motors, using polymer network theory for binder formulation
[AIAA PAPER 71-654] 14 p2285 A71-30729
- ASE HISTORIES**
Aerial stowaway clinical case covering unconsciousness, deafness, hypoxia, hypothermia, acidosis and other effects due to 9 hr flight in unpressurized landing gear cell
04 p0544 A71-15058
Case histories of pilot failure during training or operational flight due to cerebral cortical dysfunction
13 p2023 A71-29365
Case histories of aircraft damage due to wind acting on airport surfaces, discussing wind and hail protection
17 p2675 A71-35442
Potential epilepsy determination in flight personnel, suggesting systematic EEG with hyperventilation and photic stimulation tests and personal history data of head trauma and unconsciousness
21 p3331 A71-40357
USAF aeromedical consultation service experience on vertigo cases covering symptoms and related diseases
21 p3331 A71-40358
Psychophysiological and conversion mechanisms as unconscious expression of student pilot motivation decrease for further flight training, presenting case histories
22 p3502 A71-41837
- ASES [CONTAINERS]**
NT ROCKET ENGINE CASES
Microwave transistor case design, considering RF parasitics, thermal dissipation, environmental mechanical factors, ceramic technology and sealing
15 p2377 A71-32500
- CASING**
Casing /end wall/ boundary layers in multistage axial flow compressors, discussing velocity distributions
03 p0340 A71-13144
Casing material effects on velocity of low speed phase prior to detonation onset of high density PETN, testing steel, Plexiglas, Duralumin and brass
15 p2511 A71-31390
- CASSEGRAIN ANTENNAS**
Cassegrain antenna equivalent parabolic reflector concept for feeds near focus
02 p0233 A71-12424
Cassegrain system far field radiation pattern and gain loss prediction for beam steering by subreflector tilting
02 p0222 A71-12793
Multiple beam antenna with fixed spherical reflector and movable dual subreflector feedhorns, comparing with conventional Cassegrain antenna for satellite tracking
02 p0233 A71-12794
Cassegrain antenna electrical and structural design and control system for microwave propagation and communication research, using moon reflected signals as atmospheric probes
02 p0234 A71-12806
Field correlation diffraction theory of symmetrical microwave Cassegrain antenna, calculating main reflector focused field by spherical wave expansion
13 p2028 A71-27992
Analytic optimization of Cassegrain antennas of revolution used in satellite telecommunications
13 p2033 A71-29241
High efficiency narrow beam aircraft Cassegrain antenna design for horizon without excessive ground illumination
14 p2217 A71-31056
Polar diagrams computation for large Cassegrain antennas, obtaining sidelobe peaks envelope at wider angles of radiation by near field measurements
15 p2368 A71-31139
Two mirror Cassegrain antenna secondary reflector random fluctuations effects on drift in main lobe direction
17 p2713 A71-34397
Wideband Cassegrain microwave antenna for space communication, discussing reflecting horn for maximum radiation gain
17 p2715 A71-34686
Electrical performance of Cassegrain antenna reflector for space communication via ATS and deep space research
17 p2700 A71-34747
Second Pleumeur-Bodou /France/ ground station for Telstar satellite communication, discussing equipment specifications, Cassegrain antenna and parabolic reflector
17 p2708 A71-35509
- Pleumeur-Bodou /France/ ground station steerable parabolic reflector Cassegrain antenna for communication satellites, discussing specifications and radioelectric and mechanical characteristics
17 p2717 A71-35510
Cassegrain antennas with reflector horn feed for satellite communication, noting gain and noise temperature
18 p2890 A71-36554
- CASSEGRAIN OPTICS**
Complementary field component of radiation from Cassegrain subreflector
01 p0055 A71-11172
Optical design of image selector for Cassegrain telescope recording difference spectrum of targets in focal plane
03 p0425 A71-13646
Third order aberrations in Cassegrain type telescopes and coma correction in servo-stabilized images
07 p1107 A71-19202
Astronomical telescopes with Cassegrain two mirror optics, discussing optical aberrations and correction methods and modern testing procedures
10 p1612 A71-24690
Wollongong University College Cassegrain type 45 cm telescope, describing installation, construction and fabrication
13 p2067 A71-28393
Four stage image intensifier testing for weak astronomical object photography in connection with 42 inch Cassegrain telescope
13 p2070 A71-29138
Rocket-borne Cassegrain telescope system design for stellar spectra in UV region of EM spectrum between 900 and 3300 Å
14 p2238 A71-29727
Star EV Lac polarimetric observations during flare, using Cassegrainian reflector
15 p2487 A71-32031
Paraboloid-hyperboloid Cassegrain telescope mirror centering, describing stigmatic point position permanent control in focal plane by geometrical method
21 p3375 A71-40066
Astronomical Cassegrain echelle spectrograph, discussing optical and mechanical design and aberration effects
22 p3542 A71-41933
- CASSIOPEIA A**
Cassiopeia A galactic supernova remnant, discussing flocculi formation from material ejected from outer layers before explosion
20 p3304 A71-39941
- CASSIOPEIA CONSTELLATION**
UV and visual spectra of gamma Cassiopeiae from rocket spectrograph and OAO observations
02 p0314 A71-12585
Eclipsing system GG Cas, presenting photoelectric data
09 p1527 A71-23527
Contour map of galactic radio emission in Cassiopeia and Cepheus region, noting discrete sources
11 p1831 A71-26132
Eclipsing binaries among Wolf-Rayet AO Cassiopeia and U Geminorum stars from photometric observations
20 p3300 A71-39821
Internal structure investigation of interstellar clouds in Cassiopeia, discussing color equation, photographic plate characteristics and accuracy
21 p3451 A71-40719
Cosmic soft X rays in energy range 0.14-7 keV from rocket soundings with thin polypropylene window proportional counters, covering field of view in Cygnus-Cassiopeia region
22 p3593 A71-42330
- CASTIGLIANO VARIATIONAL THEOREM**
Statically indeterminate rod system design, using linear strengthened materials strain diagrams and Castigliano principle
09 p1538 A71-22650
- CASTING**
NT INVESTMENT CASTING
Soviet book on crystallite boundaries in cast metals and alloys covering solute distribution, lattice imperfections, fracture mechanisms, etc
02 p0763 A71-11845
Al ingot level pouring casting, considering solidification effect on subsurface segregation and cyclic pattern of macrostructure
04 p0614 A71-15783
Cast Mo alloy at low temperatures, investigating elasticity, plasticity and tensile strength characteristics
08 p1316 A71-21615
Solidification process for unidirectionally cast airfoil shaped turbine components from Ni superalloys, discussing mold withdrawal
08 p1299 A71-21682
Gas turbine components precision casting, discussing high temperature alloys and casting techniques in manufacture of components subject to high thermal and mechanical stresses
09 p1456 A71-23293
- Cast cobalt base superalloys extrusion and forging, noting hot deformation effects on tensile properties, stress rupture strength and ductility
11 p1778 A71-25854
Low cost metal matrix composite fabrication, discussing plasma spraying and continuous casting
14 p2263 A71-29655
Manufacturing processes in orbital workshop, considering metal and optical lenses casting crystal growth and gravity lack effects
16 p2606 A71-32856
Chromium casting steel, investigating annealing effects on alloying elements diffusion
18 p2934 A71-36150
Carbon impurity effects on molybdenum ingot formation, detailing crystal growth, size reduction and length
19 p3077 A71-37277
Gas turbine blades cast heat treated superalloys high temperature mechanical properties during aging
21 p3403 A71-41103
Ni-based alloy strength characteristics dependence on heat treatment during melting and casting in vacuum and in air
23 p3691 A71-43425
Heat resistant ZrSi₂ alloy precision and ground cast specimens, determining short and long term strength and fatigue
23 p3780 A71-44236
- CASTINGS**
NT INGOTS
Heat flow in unidirectional solidification of vacuum cast alloy turbine blades, using analog thermal model
05 p0758 A71-16244
Al and Mg alloys mechanical and microstructural changes under low temperature conditions, optimizing casting component ratios
05 p0767 A71-16765
Microporosity morphology relationship to grain size and boundaries in alloys solidification and pores removal kinetics from castings by sintering
07 p1119 A71-19977
Cast ZrC hot hardness measurement by static tests at high temperatures, comparing with hot-pressed samples
15 p2431 A71-32161
Sealing porous metal castings and powdered parts, discussing impregnation by vacuum-pressure and internal circulatory methods and sealant types
18 p2928 A71-36838
Ni-Cu alloy castings solidification experiments on catalytically clean metals to avoid heterogeneous nucleation
21 p3387 A71-40460
Orientation dependent microhardness and columnar and feather crystal structures of directionally cast Al alloys in tensile test bars
21 p3399 A71-40471
Statistical analysis of endurance limits for castings and forgings of die forged and cast steel, using rotating beam fatigue tests
21 p3388 A71-40754
Cr-Ni alloy heat treated cast specimens microstructure, metallographic, X ray and spectral investigation, noting chemical inhomogeneity
24 p3836 A71-44484
- CASTOR OIL**
Complex calcium-based lubricants preparation based on hydrogenated castor oil or free fatty acids, considering saturation effect on structure and properties
13 p2091 A71-28227
- CATALASE**
Gaseous medium composition and multiple freezing temperature effects on catalase activity
22 p3497 A71-42831
- CATALOGS [PUBLICATIONS]**
NT ASTRONOMICAL CATALOGS
- CATALYSIS**
NT AUTOCATALYSIS
Mass spectrometric technique for investigation of hydrazine catalytic decomposition on heated platinum at low pressure, considering advantages of quadrupole spectrometer
11 p1765 A71-26280
Bronsted relationship between adsorption heat and activation energy in electrocatalysis of purified orthophosphoric acid and phase-oxide-free noble metals
21 p3345 A71-40540
- CATALYSTS**
NT ELECTROCATALYSTS
Lanthanum cobalt oxide as potential auto exhaust catalyst from studies of activity in gas phase
07 p1055 A71-19545
Monopropellant hydrazine propulsion catalysts evaluation, considering catalyst durability improvement and breakup
07 p1183 A71-19858
Iridium-based long life hydrazine catalyst with multiple cold start capability, describing development program for substrate evaluation and physical properties and process optimization
[AIAA PAPER 71-704] 14 p2286 A71-30761

Fibrous carbon structure determination by high resolution electron microscopy, establishing relationship between graphite planes and catalyst particles orientation

23 p3696 A71-43141

CATALYTIC ACTIVITY

Reaction mechanism for ammonium nitrate thermal decomposition, discussing chloride catalytic effects

01 p0141 A71-10344

Oxide bronzes as oxygen reduction catalysts in batteries and fuel cells, considering effects of varying compositions and crystal faces

03 p0374 A71-13054

Sulfur trioxide catalytic formation in gases from fuel-rich propane-air flames containing sulfur

03 p0376 A71-14279

Catalytic decomposition of sodium chlorate using cobalt oxide catalysts

04 p0549 A71-15750

Hydrogen-oxygen catalytic ignition system steady state model for predicting temperature and concentration profiles

05 p0795 A71-16350

Dissociated diatomic gas nonequilibrium boundary layer flow over catalytic flat plate, examining velocity profiles, temperature and concentration

05 p0735 A71-16389

Spacecraft attitude control microthrusters utilizing catalytically reactive gas mixtures during pulse mode and steady state operation

[AIAA PAPER 70-614]

07 p1183 A71-19859

Metastable state gas flow experiment, investigating laminar boundary layer change in presence of flat plate surface catalytic reaction

11 p1705 A71-26276

Catalytic effect of lanthanide hydroxides on formaldehyde conversion to pentoses and hexoses at 110°C in life support systems

13 p2018 A71-28408

Template catalysis of acetyl transfer reactions, showing triple helices formation by polyuridylic acid with adenosine derivatives

13 p2026 A71-29479

Frequency analysis of open loop transfer function, determining combustion instability for catalytic monopropellant thrusters

[AIAA PAPER 71-701]

14 p2286 A71-30759

Liquid hydrazine catalytic reactor startup characteristics as function of catalyst adsorbed gas condition and temperature by high speed motion picture observation

[AIAA PAPER 71-702]

14 p2294 A71-30760

Catalytic hydrazine thruster design, fabrication and testing for TOPS spacecraft single-axis attitude control simulation program

[AIAA PAPER 71-706]

14 p2294 A71-30763

Metal additives catalytic effect on free radicals recombination rates in hydrogen-oxygen-nitrogen flames

15 p2515 A71-32552

Catalytic role in ammonium perchlorate solid rocket propellants ignition and combustion

17 p2686 A71-35574

Polyester formation by *Escherichia coli* ribosome catalyzed alpha-hydroxy acid incorporation into polymer chain

17 p2686 A71-35574

Stratospheric ozone reduction through catalytic action of nitrogen oxides from SST exhaust, discussing degrading effect on atmospheric radiation shield

18 p2874 A71-36922

Metal additives catalytic effects on premixed hydrogen-oxygen-nitrogen flames free radical recombination rates, discussing heterogeneous and homogeneous schemes

19 p3012 A71-38082

Perchloric acid catalytic pyrolysis relationship to ammonium perchlorate decomposition and combustion from electric conductivity measurements, IR spectroscopy, chemical and thermal analysis

19 p3120 A71-38119

Photocatalytic stimulation of UV radiation photolysis of amino acids and pentoses in aqueous solutions by metal oxide sols

21 p3345 A71-40574

Monosaccharides effect on catalytic synthesis of carbohydrates from formaldehyde

24 p3800 A71-44527

CATARACTS

Mathematical analysis of eye transparency, discussing light scattering from normal corneal stroma, swollen opaque corneas and cataractous lens

08 p1240 A71-21371

Coagulative and delayed cumulative cataract production by microwaves investigated by hypothermic technique

10 p1572 A71-25077

Cataract production from microwave radiation exposure by lens nutrition alteration and surface shape changes

11 p1718 A71-25292

Ultrasonic softening of lens material to facilitate aspiration, using in vivo rabbit lenses for cataracts production

15 p2365 A71-32348

CATECHOLAMINE

Hypothalamus and adrenal glands catecholamines relationship for hypophysectomized rats

03 p0362 A71-13293

Cardiovascular responses of hypoxic hypoxia in mongrels with catecholamine induced coronary dilation

06 p0857 A71-18723

Control and prolonged exercised rats adrenal and plasma catecholamine, corticosterone and epinephrine level comparisons using fluorometric analysis

07 p1044 A71-20330

L-dopa multinection timed effects on rat brain norepinephrine metabolites concentrations, observing zero time control rated modifications

09 p1393 A71-22649

Diurnal rhythm of adrenaline secretion in subjects with different working habits, comparing catecholamine excretion under relaxation conditions

11 p1721 A71-26355

Diurnal variations in catecholamine excretion, alertness and performance of subjects with different working habits

11 p1722 A71-26356

Systolic and diastolic blood pressures and urinary catecholamines under stress in normotensive and hypertensive subjects

15 p2358 A71-31451

Psychophysiological reactions to understimulation and overstimulation, noting catecholamine output, heart rate and performance efficiency in humans

21 p3329 A71-40177

Adrenaline, noradrenaline and catecholamine excretion in railroad men during daytime and nighttime work

24 p3799 A71-45085

CATENARY CURTAINS

U CURTAINS

CATHETERIZATION

Catheter inserted wire basket device for creation of reversible aortic insufficiency in animal

01 p0022 A71-10248

Blood pressure and velocity waveform recording for patients during cardiac catheterization, interpreting relationships to vascular impedance

02 p0201 A71-12915

Left ventricular volume and cardiac work evaluation by thermomodulation technique, employing thermocatheter for temperature measurement

[ASME PAPER 70-WA/TEMP-2]

03 p0372 A71-14102

Catheter-flush system for continuous monitoring of central arterial pulse waveform and pressure

04 p0545 A71-15165

Digitalis-induced bundle branch ventricular tachycardia from electrode catheter recordings of dogs specialized conducting tissues

06 p0852 A71-17873

Human cardiac intraventricular conduction measurements, using right and left bundle branch potentials during catheterization

07 p1044 A71-20351

Chest and cardiovascular system optimal radiologic facilities, discussing X ray examination, catheterization-angiocardiographic and nuclear radiology laboratories

07 p1053 A71-20354

Blood pressure measurement by catheter gages, analyzing error due to wave reflection at catheter tip

09 p1399 A71-22972

Automated data acquisition and analysis during cardiac catheterization, using photokymographic and analog magnetic tape recording system in conjunction with digital computer

13 p2020 A71-29003

Validity and reproducibility of cardiac output determination by thermomodulation, using dual thermistor catheter introduced in pulmonary artery

16 p2531 A71-33366

Electrical medical apparatus with electrodes and intracardiac catheters, considering electric current danger threshold, electrocution hazards and safety precautions

17 p2693 A71-35486

Monophasic action potential recording of intact human heart, using bipolar electrode catheter for explanation of ECG abnormalities

18 p2853 A71-35910

Autoclave chronic catheter system and restraining box for blood sampling and pressure measurement for hibernating marmots

19 p3010 A71-38568

Early systolic clicks shown due to mitral valve prolapse by phonocardiography, cardiac catheterization and angiography

23 p3635 A71-44127

CATHODE RAY TUBES

Alphanumeric character generation from resistive storage of time derivatives for CRT displays

01 p0047 A71-10216

Three dimensional dynamic CRT display for simulation, using VECTRAN /Vector transformer/ digital computing device for control

01 p0084 A71-11394

Filter effect on CRT display resolution and relation to photometric and color contrast

02 p0249 A71-12073

Beam-combining prism/magnifier eyepiece configuration with miniature CRT for superimposing magnified virtual image upon user visual field

04 p0597 A71-15362

Cathode ray tubes as real time display device in various types of professional equipment, describing functional performance and related tube design aspects

06 p0872 A71-17319

Current-sensitive single-gun polychromatic CRT phosphor screen operational characteristics

14 p2215 A71-31031

Forty channel magnetography system including CRT display, digital controlled heliostat, real time computer and optical transducer

17 p2740 A71-34989

Autoplotter for radar echoes on CRT screen, using video tape recorder for ship navigation use

19 p3017 A71-37700

Data display units as man machine interface elements in data processing operations, discussing combined alphanumeric/graphic CRT units

20 p3202 A71-38883

Display devices components in highly interactive man machine systems, noting drawbacks of CRT

20 p3233 A71-39059

Cathode ray tube, including electron beam peak power, resolution elements, luminescent materials, fabrication techniques, contrast preservation and reliability

20 p3234 A71-39062

Book on electronic components covering radio, cathode ray and microwave tubes, telecommunications, ceramic materials, light conversion to electricity, integrated circuits, etc

20 p3205 A71-39757

Bicolor cathode ray display tubes with triple-layer bombarding electron beam energy-dependent red-green fluorescent screen

21 p3347 A71-40109

Display devices in aircraft cockpit providing pilots with information from various sources, considering head-up display and CRT

21 p3376 A71-40120

Computerized multiparametric data three dimensional CRT graphic display involving isometric viewing and intensity modulation

21 p3350 A71-40123

Contrast level reading tests of CRT and self luminous display devices with optical filters at high ambient light for cockpit applications

21 p3376 A71-40127

Three dimensional graphics software package for CRT and storage tube displays and plotters, describing coordinate transformation

21 p3347 A71-40130

Deformographic storage display tube system, describing construction, development, design, performance and operating principles

21 p3352 A71-40135

Avionics combined display system for area navigation, discussing design, color map projection, overlays, CRT unit and viewability

21 p3413 A71-40137

Character size, case and symbol generation effects on CRT display search time

22 p3503 A71-42195

Electronic techniques in optoelectronics, discussing CRT, image tubes, semiconductor tubes and lasers

22 p3559 A71-42467

Mach bands appearance in red/green triangular wave intensity distributions generated on CRT, quantifying perceived brightness distribution by matching with variously positioned light slit

24 p3800 A71-44468

Cathode ray tube graphical display system as digital computer output terminal, using analog memory for flickerfree image

24 p3806 A71-44652

CATHODES

NT COLD CATHODE TUBES

NT COLD CATHODES

NT HOLLOW CATHODES

NT HOT CATHODES

NT PHOTOCATHODES

NT PHOTOMULTIPLIER TUBES

NT THERMIONIC CATHODES

High energy batteries electronic discharge mechanisms, examining use of semiconductor cathodes

03 p0352 A71-13042

Cathode tip shape influence on temperature and velocity fields in gas tungsten arc welding, noting effect on weldment area and penetration

04 p0603 A71-14924

Electron bombardment ion thruster using hollow cathode and two-grid ion accelerating geometry, discussing performance tests

[AIAA PAPER 71-158]

06 p0947 A71-18600

- Electrochemical metal machining tool profile two dimensional steady state problem, solving for cathode surface changes as function of interelectrode potential 08 p1296 A71-20854
- Hollow cathode arc discharge parameters at active zone level, examining gas pressure and electron density 10 p1646 A71-23843
- Vacuum arc welding stability in vaporized Mo cathode material as function of current and arc length, describing burner design for material replenishment 11 p1770 A71-25946
- Plasma state and IV characteristics of thermionic converter, discussing cathode emitting area increases and patchiness effects 14 p2182 A71-30680
- Gas laser construction and processing techniques, considering operating temperature, cathode processing, bore design and Brewster window material 14 p2255 A71-30706
- Cathode damage of nanosecond atmospheric arcs on silver, gold, tungsten and palladium contacts, using scanning electron microscope 15 p2376 A71-32022
- Electrolytic production of metal powder in continuously operating facility, using vibrating cathodes with chambers filled with granulated anode metal 19 p3068 A71-37105
- Numerical calculation of electron guns with converging spherical beams near cathode and electron-optic systems decelerating at collector 20 p3204 A71-39157
- CATIONS**
- NT FERRIC ION
- NT MANGANESE IONS
- NT METAL IONS
- Cations partitioning between coexisting single and multistate phases in pyroxenes and olivines 06 p0894 A71-18236
- Polycation effect on tumor cells, describing growth rate inhibitions, X ray sensitivity and DNA interference 07 p1035 A71-18951
- Lithium-like and sodium-like positive ions electron impact ionization, calculating cross sections and reaction rates with binary encounter model 11 p1801 A71-25211
- Carbon dioxide cations emission bands in Mars and Venus dayglows, suggesting fluorescent scattering and photoionization as main excitation sources 11 p1827 A71-25724
- Synthesized plasma of interpenetrating positive and negative ion beams, investigating oscillation amplification conditions 12 p1941 A71-27766
- HBr positive ion formation by Ar ion beam collision with HBr, using predissociation to establish dissociation limit 13 p2026 A71-29039
- Sodium and cations elimination by kidneys during water-salt metabolism changes due to high temperature and hypodynamia 20 p3189 A71-39232
- Nitrogen and neon cations number density time dependence during plasma decay in neon-nitrogen mixtures 23 p3711 A71-43881
- Absolute transition probabilities derivation for excitation of atmospheric nitrogen molecules and positive ion systems by electrons impact from optical measurement 24 p3850 A71-44371
- CATS**
- Conditioned reflexes in cats with mesencephalic reticular formation subject to food-signaling acoustic stimulation 01 p0007 A71-10034
- Dorsomedial nucleus electric impulse stimulation in anesthetized cats with oscillogram recorded response potentials of cortex preoral gyrus, indicating relay transmission function 01 p0008 A71-10091
- Cats photopic and scotopic spectral sensitivity functions from dark adaptation curves, using behavioral tracking procedure 01 p0009 A71-10232
- Hippocampal, neocortical and somatic effects of HF electrical stimulation of mesencephalic reticular formation during different stages of sleep in cats 05 p0707 A71-16424
- Visual image propagation from retina to higher level formations in multichannel system of cat visual analyzer 10 p1561 A71-24163
- Cat pupillary system static and dynamic response determination under light and electrical stimulation, using TV pupilometer and on-line computer 17 p2691 A71-35044
- Cats preoptic and skin temperature change effects on posterior hypothalamic neurons 18 p2861 A71-36888
- Stagnant asphyxia in cat carotid body during abrupt blood pressure drop by simultaneous carotid artery clamping and tap opening 20 p3190 A71-39443
- Feline retinal neurons, noting span and density of branching amacrine cell protrusions and ganglion cells diversity 23 p3633 A71-43581
- Oxygen tension distribution in cats glomus caroticum under influence of varying arterial oxygen partial pressure, using platinum microelectrodes 24 p3796 A71-44562
- CATTLE**
- Air-photo interpretation to inventory kind of cattle-raising operation practiced on farms of southern Ontario 08 p1282 A71-21437
- Purine and pyrimidine derivatives of cattle hypothalamus determined by gel filtration and subsequent spectral analysis and chromatography 21 p3338 A71-41071
- CAUCHY INTEGRAL FORMULA**
- Soviet monograph on singular integral equations and boundary value problems involving Cauchy kernels 04 p0619 A71-15400
- Asymptotic expansion of spectral functions expressed by Cauchy integral over smooth open segment 17 p2763 A71-34419
- Quadrature formula for Cauchy integrals 19 p3086 A71-37883
- CAUCHY PROBLEM**
- Cauchy problem for linearized Boltzmann equation, using collision operator eigenfunction series 01 p0109 A71-10027
- Bubnov-Galerkin approximation method, reducing Cauchy problem for parabolic equations to ordinary differential system 01 p0111 A71-10436
- Cauchy problem for nonlinear integrodifferential equations with time lag argument, estimating iterative solution existence and uniqueness 01 p0112 A71-10491
- Cauchy problem solution for Laplace equation, constructing algorithms based on successive approximations 02 p0276 A71-12538
- Cauchy problem solution for elasticity theory dynamic system in Euclidean space arbitrary region 03 p0510 A71-13962
- Cauchy problem for parabolic system with discontinuous coefficients 05 p0775 A71-17034
- Hyperbolic heat conduction equation with small relaxation time parameter, studying convergence for Cauchy and boundary value problem 05 p0839 A71-17035
- Partial differential equations mixed boundary value problems with unsteadiness over part of boundary reduced to Cauchy problem 06 p0916 A71-17385
- Lifting surface nonstationary aperiodic motion in incompressible fluid solved by asymptotic method of function parameters, using algorithm for Cauchy problem 08 p1275 A71-20778
- Mechanical systems partial differential equations solution through reduction to infinite systems of ordinary differential equations, considering Cauchy problem power series solution 09 p1492 A71-22523
- Heat conduction differential equation boundary value problem, obtaining closed solution to Cauchy problem in integral form with finite limits by reflection method 09 p1547 A71-23435
- Boundary value problem concerning stability and oscillations of shells of revolution through reduction to Cauchy problem based on direct integration of equilibrium equations 10 p1690 A71-24569
- Modified Chaplygin algorithm application to bilateral approximate solution of limiting Cauchy problem, discussing convergence and error estimation 11 p1792 A71-26155
- Parabolic systems solutions asymptotic behavior with dissipation in half space greater than zero, considering Cauchy problem 13 p2094 A71-27805
- Optimal control systems with discontinuities in right members of differential equations, considering solution to Cauchy problem 13 p2040 A71-27896
- Cauchy problem solution for elliptic equations of fourth order in two independent variables, improving Henrici, Pucci and Colton results 14 p2266 A71-30811
- Linear two-point boundary value problem solution through integral transformation into Cauchy system with Green function as auxiliary dependent variable 15 p2443 A71-32441
- Cauchy problem for nonlinear Boltzmann equation in general relativity, utilizing energy inequalities 16 p2612 A71-34059
- Numerical algorithm for Cauchy problem nonlinear partial differential integral equations solution by invariant imbedding 16 p2604 A71-34082
- Weightless elastoplastic beam dynamic bending under moving concentrated load, calculating deformation by reduction to Cauchy problem 17 p2822 A71-34780
- Mixed problem for hyperbolic type linear nonhomogeneous second order partial differential equation with delayed arguments, obtaining asymptotic solution for derived Cauchy problem 19 p3086 A71-38011
- Electromagnetic wave transmission through conducting plasma slab, reducing nonlocal wave interaction two point boundary value problem to Cauchy system 20 p3274 A71-39080
- Pointwise bounds in Cauchy problem for fourth order quasi-linear equation using a priori inequality, applying Rayleigh-Ritz technique to elliptic partial differential equations 20 p3255 A71-39573
- Asymptotic expansion for hyperbolic Cauchy problem solution, proving correctness 21 p3409 A71-41079
- Cauchy problem theory covering analytic and nonanalytic functions, Gevrey function spaces, hyperbolic operators and differentiable functions spaces 22 p3566 A71-41513
- Equilibrium equations of elastic plates, reducing to Cauchy problem by use of invariant imbedding 22 p3618 A71-42584
- Calculation method for flow about bodies with injection, presenting parameters approximation formulas derived from Cauchy problem solution for Helmholtz equation 24 p3789 A71-44478
- Self similar solution to Cauchy problem of gas dynamics equations in nonisotropic media 24 p3819 A71-44774
- CAUCHY-RIEMANN EQUATIONS**
- Plane adiabatic Prig gas flow, reducing hodograph equations in elliptic regions to Cauchy-Riemann equations via Baeklund transformations 23 p3662 A71-43121
- CAUSTICS**
- U ALKALIES
- CAVITATION**
- U CAVITATION FLOW
- CAVITATION CORROSION**
- Metals erosion by cavitation and liquid impingement, discussing test methods and resistance prediction 03 p0404 A71-14174
- Cavitation and jet impingement erosion, discussing materials response and exposure time effects 03 p0404 A71-14285
- Accelerated cavitation damage in Na, examining pressure and temperature effects 03 p0443 A71-14286
- Metallographic specimens etching by cavitation damage, testing performance by ultrasonic vibration technique 03 p0445 A71-14420
- Pressure and temperature variation effects on vibratory cavitation damage tests conducted in water 04 p0604 A71-15767
- Ultrasonic cleaning by cavitation disintegration of highly adhesive surface coatings, discussing cleaning liquid, field parameters and external static pressure effects on process efficiency 10 p1617 A71-24135
- Metals crystallization in ultrasonic field, investigating structural change as function of energy and impedance factors and cavitation effects in fine grain formation 10 p1626 A71-24136
- Cavitation erosion of aluminum at high hydrostatic pressure, using chamber focusing acoustic system 18 p2910 A71-36932
- Cavitation damage in water to unalloyed metals and Ni superalloy, using ultrasonic vibratory testing with magnetostrictive transducer 19 p3081 A71-37904
- Cavitation damage resistance of Fe, Ni and Co alloys in liquid sodium and mercury 23 p3692 A71-43906
- Liquid properties and ambient pressure effects on cavitation erosion in thin film 24 p3819 A71-44946
- CAVITATION FLOW**
- Unsteady cavitation flow, presenting physical mechanism of cavity formation in liquid flow and formulation of governing equations 01 p0069 A71-10110
- Nonlinear problem of fully and partially cavitating flow past oblique flat plates, solving via conformal mapping theory and Riemann-Hilbert method 03 p0398 A71-13106
- Electroacoustical device for recording gas and vapor cavitation resistance in liquids 04 p0617 A71-14599
- Scale effect in cavitation flow, discussing flow parameters and model size effects on similar flows 04 p0570 A71-15063

Hypersonic laminar cavity heat transfer, including upstream boundary layer thickness, unequal core and wall temperature effects

04 p0528 A71-15491

High velocity liquid flow past rough plate surface, investigating boundary layer cavitation effects on convective heat and mass transfer

07 p1086 A71-18774

Various configuration fluid jet amplifiers, investigating cavitation conditions in water tunnels and open duct

07 p1023 A71-19198

Ultrasonic cavitation noise spectra in liquid helium and nitrogen, comparing He I and II

07 p1160 A71-19951

Ideal fluid jets theory, discussing cavitation flows calculation, jet flow and plane steady potential incompressible fluid flow

07 p1091 A71-20080

Cavitation flow of fluid with free surface past flat plate between parallel walls

07 p1092 A71-20081

Cavitation flow of fluid with free surface past under water wing with jet flap, solving equations of motion for thin foil with jet emergent from trailing edge

07 p1092 A71-20086

Heavy fluid flow past partially cavitating flat plate with cavity closed by fictitious plate, considering lifting force under gravity

07 p1092 A71-20087

Similarity criterion for volute centrifugal pumps via supersonic model, considering cavitation parameters influence throughout angular velocities range at flow separation

08 p1347 A71-20784

Rocket fuel lines disruptive cavitation oscillations, considering rocket body mechanical vibrations and fuel line oscillation frequency characteristics

08 p1366 A71-21753

Acoustic beam attenuation through liquid medium under ultrasonically excited cavitation, taking into account bubble configuration

09 p1434 A71-23668

Cavitation in liquids with dissolved gases by acoustic wave induced oscillating pressure, discussing gas bubble formation through rectified diffusion process

10 p1597 A71-24942

Cavitation microstreaming near spherical drop or bubble performing translational harmonic oscillations in liquid at rest

11 p1749 A71-25183

Cavity cross sections deformation in heavy ideal liquid, deriving nonlinear system of equations for time dependence within framework of small perturbation theory

13 p2047 A71-28279

Structure and shape of vortex wake associated with oblique flow past multiblade hinged rotor, using cavitation method

13 p1993 A71-29217

Circular lead specimens in water flow, determining external magnetic field effects on cavitation and erosion

14 p2278 A71-29613

Rocket body longitudinal autooscillation modes, taking into account pipeline fluid discontinuous cavitation oscillations

16 p2644 A71-32834

Runner and cavitation characteristics of hydraulic machine with finite blade number and ideal frictionless incompressible working fluid determination by potential theory

17 p2727 A71-34668

Numerical solution for two dimensional steady state fluid flow in square cavity by optimum time step formulation

17 p2728 A71-34880

Directional hydraulic control switching fluid amplifier at various Reynolds numbers, including cavitation effects

18 p2851 A71-36205

Experimental materials for axial flow vane pumps operating under cavitation conditions, considering separated flow around impeller blades

20 p3241 A71-39169

Stability characteristics and general transient motion of vertical finite width three lobe journal bearing, assuming incompressible fluid with cavitation [ASME PAPER 71-VIBR-76]

21 p3385 A71-40314

Perturbation and projection operator algorithms for Navier-Stokes equations for incompressible flow in rectangular cavities and injection into cylindrical ducts

23 p3662 A71-43238

Wall effects and correction rules for cavitation flow past wedge in closed water tunnel, deriving drag coefficient from various theoretical models

23 p3663 A71-43442

Cavity cross sections perturbed motion equations

24 p3819 A71-44840

Rocket fuel lines disruptive cavitation oscillations, considering rocket body mechanical vibrations and fuel line oscillation frequency characteristics

24 p3876 A71-44926

CAVITIES

Supersonic and transonic flow including effects of pressure oscillations within cavity, predicting rectangular cavities drag from mathematical model

01 p0002 A71-10931

Cavity fluid oscillation near convecting field, calculating onset velocity as hydrodynamic stability problem

03 p0399 A71-13438

Geometry and oncoming boundary layer characteristics effects on heat transfer rate in reattached wall of cavity exposed to hypersonic flow

03 p0517 A71-13464

Body motion with liquid filled cavities in central Newtonian force field, using holography

03 p0458 A71-13595

Projectile entry into water vertically from air, predicting cavity shape as function of time based on hydraulic flow model

[ASME PAPER 70-WA/FE-8] 03 p0402 A71-14129

Acoustic shock wave scattering by cylindrical cavities in inviscid fluid medium, noting shielding effect, peak excitation and inverse logarithmic decay

[ASME PAPER 70-WA/AFM-57] 03 p0459 A71-14173

Perturbed motion equations of body with liquid filled cylindrical cavity reinforced by elastically clamped ribs, solving boundary value problems

03 p0460 A71-14356

Multicavity thin walled containers of spheres and intersecting plane partitions, comparing structural properties with single sphere of equal overall volume

03 p0515 A71-14366

Monte Carlo calculations of intrinsic radiation and blackness degree of nonisothermal cavities with non-specific temperature profile

06 p0897 A71-17529

Stress wave propagation from spherical cavity in isotropic nonhomogeneous elastic medium in contact with vacuum at infinity, obtaining closed form solution

06 p1001 A71-18228

Axisymmetric stress in sphere and space with spherical cavity, using p-analytic functions

06 p1001 A71-18343

Spheroidal cavity effects on elastic medium under axisymmetric stress field, using Legendre potential functions

07 p1212 A71-19253

Steady state temperature field for infinite space with spherical cavities distributed along straight line, reducing problem to infinite system of algebraic equations

10 p1695 A71-24359

Heat transfer in cylindrical cavity with circulating flow as function of time and Peclet number

10 p1696 A71-24615

Stress distribution in infinite elastic solid containing spherical cavity and external crack, discussing displacement components for axisymmetric loading

12 p1974 A71-26740

Cylindrical cavities in infinite series, examining shear wave diffraction

12 p1975 A71-27109

Elastic wave diffraction in infinite series of spherical cavities with centers on straight line

13 p2100 A71-28275

Two stage creep cavity growth by grain boundary sliding as shear crack and Griffith-Orowan fracture, using energy balance argument

13 p2085 A71-28504

Coupled thermoelastic problem of homogeneous isotropic elastic half space with embedded spherical cavity

22 p3613 A71-41566

Inertia-loaded elastic thin circular ring in rigid cavity with small initial clearance, calculating deformation by nonlinear bending theory

22 p3616 A71-42215

Finite plates coincidence effect occurrence with sound waves, examining backing cavity and incidence angle influence

22 p3576 A71-42538

Coupled plate-cavity acoustic system response at LF and spatially uniform pressure, using plate finite elements and acoustic volume-displacement theory

22 p3617 A71-42540

Flash X ray technique for imaging of cavities formation during electron beam welding of Al alloy

23 p3681 A71-43195

CAVITY RESONATORS

Transverse gain inhomogeneity effect on monopulse duration and development in multimode spherical laser resonator

01 p0094 A71-11026

Spectral properties of solid state laser with cavity lengthened by optical delay line

01 p0095 A71-11096

He-Ne IR laser resonator as quadratic receiver for modulated filtered laser emission, noting strong LF noise

01 p0096 A71-11218

Multiple region hydrogen maser using Teflon coated cylindrical vessel to reduce atom-wall collision frequency shift

01 p0096 A71-11220

Self excited cavity oscillators with tunnel anode parametric diodes and nonequilibrium medium, noting single and multimodes, energy capabilities and frequency interactions

02 p0231 A71-18740

Cavity resonator length effect on lasing threshold, output energy, pulse power and duration and spectral width of giant single pulse mode laser with passive Q switch

02 p0259 A71-19330

Fabry-Perot laser cavity resonant modes, noting host medium movement effects on diffraction loss and light beam intensity distribution

02 p0260 A71-12147

Finite amplitude sound interaction with Helmholtz resonator, attributing losses to viscous damping and orifice jet flow kinetic energy dissipation

03 p0456 A71-13279

Weak nonlinear absorption effects shown by passive optical elements placed in laser resonator cavity with large angular emission divergence

03 p0435 A71-13511

Optical plate induced helicoidal steady light field in laser cavity, imparting structure to isotropic transparent material medium

03 p0436 A71-13787

Mirror-coupled oscillations of open resonant cavities for arbitrary coupling coefficients

03 p0385 A71-13799

He-Ne laser with hemispherical nontunable internal cavity resonator formed by mirrors bonded to discharge tubes

03 p0439 A71-13999

Hologram and optical elements insertion in Q switched laser for generation switching, using YAG /Nd/ basic laser

03 p0439 A71-14176

Carbon dioxide laser gyro with cavity configuration for polarization isotropy and enhanced competition effects, considering high gain and mechanical imperfection tolerance

05 p0761 A71-16272

Large optical cavity low loss n-type GaAs injection laser with reduced degradation

05 p0763 A71-16499

Open cavity radiators radiation fields, describing antenna structure based on backfire principle with dipole array exciter and parasitic reflector

06 p0875 A71-17724

Micropulsations dynamic properties and resonant cavity modes, obtaining coupled toroidal and poloidal modes solution

06 p0969 A71-17976

Solar photosphere oscillations, suggesting convection zone acting as resonant cavity

06 p0971 A71-18243

Quarter wave tube in off- and near-resonance regimes, dissipating energy by jet formation during flow emergence from cavity into duct

06 p0881 A71-18543

Single frequency carbon dioxide laser cavity length computer aided selection for reduced line competition, considering heterodyne communications systems

07 p1121 A71-18811

Frequency saturation effects in transferred electron /Gunn/ microwave oscillators mechanical tuning characteristics in conventional waveguide cavities

07 p1072 A71-19105

Gas laser gain and loss coefficients measurement, using resonator staged calibrator plate for optimal and nonoptimal conditions

07 p1122 A71-19139

Thermocompensated cavity resonator for SHF wavelength measurements

07 p1075 A71-19302

Low temperature material properties analyzer with superconducting microwave resonant cavity

07 p1179 A71-20160

Book on nonresonant feedback in lasers covering multimode cavity, emission spectra, generation in cloud, quasi-concentric resonator, etc

08 p1301 A71-21226

Fabry-Perot resonator with anisotropic medium, deriving reflection mirror shape for optimizing diffraction loss and resonant conditions for extraordinary waves

08 p1289 A71-21284

Laser resonator mode representation with oblate spheroidal vector wave function through boundary value problem formulation

08 p1301 A71-21293

Spectral properties of solid state laser with cavity lengthened by optical delay line

08 p1303 A71-21954

Klystron output resonator efficiency optimization under excitation of plasma with Pi-shaped charge concentration based on performance analysis as function of plasma width

09 p1415 A71-22360

Optical resonators with anisotropic elements, altering natural oscillations Q factor and spectrum
 09 p1461 A71-22384

Ray transformation after passing through optical resonator with Brewster prism, calculating spectral energy losses dependence by geometrical optics method
 09 p1464 A71-23072

Stable single mode cavity resonators of high Fresnel number with increased fundamental transverse mode for carbon dioxide laser oscillators
 09 p1466 A71-23727

Cross-excited electrically pulsed carbon dioxide laser investigating self mode locking as function of cavity length, operating pressure and bleachable absorber sulfur hexafluoride
 10 p1620 A71-24152

Spurious spikes in microwave circulators due to hybrid resonant modes of ferrite post open-resonator structure
 10 p1583 A71-24212

Superregenerative linear mode amplification in Q switched He-Xe laser as function of resonator phase, length and signal angle
 10 p1621 A71-24713

Symmetrical amplitude-frequency characteristics of microwave reflection amplifiers with active resonators connected in series by nonhalf wave transmission line
 10 p1584 A71-24879

Emission dynamics of pulsed laser with optical delay line in resonator
 10 p1622 A71-24885

He-Ne laser cavity amplifier performance analysis, indicating usefulness as scanning interferometer for high resolution analysis of other laser outputs
 11 p1776 A71-26430

Thermal noise measurement of superconducting coaxial lambda/2 resonator at 2.46 GHz with ruby traveling wave maser and tunnel diode amplifier setup
 12 p1887 A71-27010

Coulomb forces detrimental effects on electron bunching in three-resonator klystron, defining buncher optimal parameters for different perveance values
 12 p1888 A71-27614

Cavity mirror transmittance variation effect on output power and pulse length of single-pulse Nd-doped glass laser with nonuniform inverted population distribution
 13 p2077 A71-27855

Electron density distribution determination from microwave resonant frequencies of parallel plate cavity containing cold, collisionless, isotropic plasma
 13 p2105 A71-27994

Book on laser physics covering radiation theory, atomic system interactions, Fresnel diffraction, Gaussian beam, Lamb theory and cavity engineering
 13 p2078 A71-28429

Cylindrical microwave cavity partially containing cold nonuniform plasma enclosed by quartz tube, calculating resonant frequency by exact, multistrata and series methods
 13 p2029 A71-28500

Heat transfer within resonant cavities at subsonic and supersonic flow, discussing wind tunnels, test procedures and data reduction
 [ASME PAPER 71-FE-9] 13 p2166 A71-29450

TM, TE and combination cavity modes choice for plasma column electron density distribution determination by perturbation methods
 14 p2279 A71-29859

Laser cavity analysis for etalon effects on mode, using signal flow graphs
 14 p2254 A71-30143

Microcavity parametric oscillations in stationary ultrasonic field
 14 p2275 A71-30438

Oscillations in second cavity of ammonia maser containing two resonators successively traversed by molecular beam, studying polarization and radioelectric emission
 14 p2254 A71-30440

Field components, frequency, quality and filling factors effects of storage quartz bulbs in maser microwave cavities
 14 p2254 A71-30563

Double cavity tuning of Gunn oscillators at mm wavelengths achieving output power improvements
 14 p2215 A71-30831

Microwave responders in FM or AM modes with cavity resonator, considering use in medium distance telemetering or telemonitoring
 14 p2215 A71-30911

Pressure and velocity distributions in gas filled cavity undergoing resonant acoustic oscillations due to heat addition
 15 p2392 A71-32126

Microwave resonator Q factor measurement by reflection coefficient method, using swept signal generator to eliminate incidental FM problem
 15 p2376 A71-32310

Far IR coupled cavity HCN laser interferometer for measuring low density transient plasma
 15 p2410 A71-32384

Power output of stable scaled off CO lasers with semiconfocal cavities and totally reflecting spherical and dielectrically coated flat mirrors
 15 p2420 A71-32387

Room with windows and open doors under sonic boom, determining cavity resonance model for impulsive loading conditions
 15 p2450 A71-32514

Ionization measurement in detonation and shock waves in reactive gas mixtures by microwave cavity techniques
 15 p2411 A71-32556

Multiple laser cavities in single lasing medium, describing spatial separation of single giant pulses
 15 p2422 A71-32584

Argon ion laser mode locking in UV lines with intracavity acousto-optic modulator, describing pulse duration and average power
 15 p2423 A71-32588

Long term single frequency stabilization of composite cavity argon laser by mirror separation, using reference He-Ne laser
 15 p2423 A71-32611

Cavity loss dependent erbium glass laser line oscillations in lower threshold region under Q switch and long pulse conditions
 15 p2424 A71-32612

Magnetospheric resonator properties bounded by ionosphere/earth system lines of force, examining nonuniform plane wave generation and standing wave pulsation period
 15 p2401 A71-32731

Large signal saturation effects in cyclotron resonance oscillators, using helical electron beam-cavity interaction model
 16 p2545 A71-33394

Open microwave resonators self oscillations damping, using Sommerfeld radiation conditions
 16 p2546 A71-33479

He-Ne IR laser resonator as quadratic detector for modulated filtered laser radiation, noting strong LF noise
 17 p2750 A71-34269

Crystal laser elliptic cavity size determination for maximum emission efficiency, using photochemical method for energy transfer measurement
 17 p2754 A71-35748

Harmonic generation in trapped-plasma-mode IMPATT diode microwave oscillators with waveguide-coaxial cavity
 18 p2894 A71-36828

Fluid mechanics of human whistling as function of resonant cavity and orifice jet velocities, comparing Rayleigh bird call and Pfeifentone
 18 p2910 A71-36935

Oscillatory variation of optical length of pulsed laser resonators during lasing, testing with ruby laser in free emission mode
 19 p3073 A71-37791

Integral equation for determination of nonuniform gain profile effect on resonant modes of ion laser cavity, considering ring modes at high current densities
 19 p3074 A71-38228

Natural oscillations existence in cross section of cylindrical waveguide with resonant cavity based on Hilbert space operators, solving boundary value problem
 19 p3019 A71-38336

Shielded enclosure resonance effects reduction on cavity impedance measurement by technique analogous to wave traps for notching out RF signal at selected frequencies
 19 p3032 A71-38459

Diffraction loss equality in field distribution at confocal laser resonator mirrors with circular coupling holes
 20 p3242 A71-38850

Flat thin films in stripline cavity resonator with TEM mode, expressing bandwidth and resonance as frequency difference
 20 p3239 A71-39426

Electron density measurement in microwave cavity resonator as function of plasma parameter or time, using digital control system
 20 p3274 A71-39428

Elliptical cylinder pump cavity design for solid state laser with ideal beam geometry
 20 p3246 A71-39493

Emissive molecular beam masers, discussing cavity resonators, spectroscopy, amplifiers characteristics, oscillators behavior and electrostatics
 20 p3247 A71-39873

Resonant oscillations effect on heat transfer across mixing length in cavities spanned by low speed turbulent shear layers
 21 p3371 A71-41033

Laser amplifier with range variable automatic gain control in Fabry-Perot cavity with allowance for oscillation
 22 p3556 A71-41807

Laser beam focusing at various distances from caustic surfaces by spherical resonator formed by mirrors or lenses
 22 p3557 A71-42063

Single cavity multiple device microwave oscillator with 12 IMPATT diodes combined output power, presenting proof for circuit configuration stable operation free from moding problems
 22 p3524 A71-42631

Large amplitude high efficiency TRAPATT oscillation mode in Si avalanche diodes, using resonant cavity for voltage and current waveforms analysis
 23 p3650 A71-43352

Neodymium glass laser emission kinetics control with positive and negative feedback by introducing nonlinear media into plane-parallel resonator with two positive lenses
 23 p3684 A71-43418

Laser resonator natural field amplitude fluctuation calculation based on two- and four-level models for photon number dispersion
 23 p3685 A71-43560

Traveling wave laser with confocal, plane and semiconcentric resonators, calculating emission field spatial-temporal structure and inversion distribution
 23 p3685 A71-43561

Transmission and reaction cavity stabilized Gunn microwave oscillators AM and FM noise spectra, extending calculations based on Kurokawa theory to high modulation frequencies
 23 p3653 A71-43967

Intercavity scanning for mode selection of carbon dioxide laser in transversely degenerate resonator by localized electron-beam-trigger excitation
 23 p3687 A71-44132

X band microwave oscillator design for matched cavity reactance and maximized power by coupling Gunn and IMPATT diodes to coaxial transmission line
 24 p3807 A71-44362

Transverse instability of charged particle beam in segmented linear accelerators due to beam encounter with wall
 24 p3855 A71-44522

Pulsed modulation of continuous laser resonator Q factor, recording output on oscillograph
 24 p3834 A71-45045

Low loss mode selection and wavelength regulation of gas lasers with electro-optical intracavity resonator
 24 p3834 A71-45163

HF dispersion, power and energy storage in periodic slow wave waveguides of resonator chains coupled through openings
 24 p3805 A71-45257

CEILOMETERS

U CLOUD HEIGHT INDICATORS

CELESTIAL BODIES

NT A STARS

NT ACHONDrites

NT ANDROMEDA GALAXIES

NT AREND-ROLAND COMET

NT ASTEROIDS

NT AUSTRALITES

NT B STARS

NT BINARY STARS

NT BOLIDES

NT CARBONACEOUS METEORITES

NT CASSIOPEIA A

NT CEPHEID VARIABLES

NT CERES ASTEROID

NT CHONDRITES

NT COMETS

NT CRAB NEBULA

NT DEIMOS

NT DWARF STARS

NT EARLY STARS

NT EARTH [PLANET]

NT ECLIPSING BINARY STARS

NT EXTARS

NT GALAXIES

NT GEMINID METEORIODS

NT GIACOBINI-ZINNER COMET

NT GIANT STARS

NT HOT STARS

NT IAPETUS

NT ICARUS ASTEROID

NT INFRARED STARS

NT IRON METEORITES

NT JUPITER [PLANET]

NT KAPOETA ACHONDrite

NT LEONID METEORIODS

NT MAGNETIC STARS

NT MAIN SEQUENCE STARS

NT MARS [PLANET]

NT MERCURY [PLANET]

NT METEORITES

NT METEOROID DUST CLOUDS

NT METEOROID SHOWERS

NT METEORIODS

NT MICROMETEORIODS

NT MILKY WAY GALAXY

NT MOON

NT MRKOS COMET

NT MURRAY METEORITE

NT NATURAL SATELLITES

NT NEBULAE

NT NEPTUNE [PLANET]

NT NEUTRON STARS

NT NOVAE

NT O STARS

- NT ORGUEIL METEORITE
 NT ORIONID METEORIDS
 NT PERSEID METEORIDS
 NT PHOBOS
 NT PLANETARY NEBULAE
 NT PLANETS
 NT PLUTO [PLANET]
 NT PROTOSTARS
 NT PULSARS
 NT QUASARS
 NT RADIO GALAXIES
 NT RADIO METEORS
 NT RADIO SOURCES [ASTRONOMY]
 NT RADIO STARS
 NT SATURN [PLANET]
 NT SCHWASSMANN-WACHMANN COMET
 NT SOLAR SYSTEM
 NT SPIRAL GALAXIES
 NT SPORADIC METEORIDS
 NT STAR CLUSTERS
 NT STARS
 NT STONY METEORITES
 NT SUN
 NT SUPERGIANT STARS
 NT SUPERNOVAE
 NT T TAURI STARS
 NT TEKTTITES
 NT TUNGUSK METEORITE
 NT URANUS [PLANET]
 NT VARIABLE STARS
 NT VENUS [PLANET]
 NT VESTA ASTEROID
 NT VIRGO STAR CLUSTER
 NT WHITE DWARF STARS
 NT ZETA AURIGAE STAR
 NT ZODIACAL DUST
 Celestial body gravitational field from satellite photogrammetry 01 p0083 A71-11326
 Soviet book on celestial bodies nature and observations covering solar system, variable stars, novae, supernovae, nebula and metagalaxy 04 p0649 A71-15262
 Cosmic objects relativistic plasma X ray and gamma ray background radiation increase, considering bremsstrahlung effect on radiation spectrum 04 p0657 A71-15747
 Celestial bodies position determination, discussing optical observation, interferometry, radar, lasers and applications 05 p0811 A71-16650
 Radio direction finding of celestial bodies from moving platform, determining plane rotation effects on angle measurements 09 p1532 A71-22661
 Astrophysical objects magnetic field generation, examining behavior at large dynamo numbers 10 p1676 A71-24494
 Spherical celestial bodies with linear equatorial velocities, deriving anomalous rotation law 11 p1833 A71-26260
 Flux estimates of gamma quanta with energies of 5 TeV from celestial objects due to bremsstrahlung and inverse Compton scattering of relativistic electrons 14 p2299 A71-29985
 Solar neutrinos and compact luminous objects, discussing unsolved problems and theoretical-observational discrepancies 14 p2309 A71-30015
 Schuster hypothesis on celestial object relation between angular momentum and magnetic fields 16 p2637 A71-33513
 Extragalactic objects luminosity upper limits in hard gamma ray band, using Cosmos 208 scintillation Cerenkov telescope 17 p2796 A71-35736
 Celestial body mass determination in many body problem, using Kalman-Bucy filtering for Taylor series approximation linearized problem 18 p2960 A71-35935
 Fluorescence phenomena in celestial bodies, considering atomic lines and molecular bands in stellar and nebulae emissions 22 p3597 A71-41515
 Graphic mission analysis for outer planet missions, considering spacecraft and celestial bodies relative positions, sensor and spacecraft relative orientation [AAS PAPER 71-378] 23 p3731 A71-43048
 Motion equations numerical integration step as function of celestial object location and velocity in interplanetary probe orbit computation 24 p3869 A71-44799
- CELESTIAL MECHANICS**
 Quasi-stationary spherical various mass star system, applying ergodic theory in stellar dynamics 01 p0150 A71-10058
 Celestial mechanics - Conference, Oberwolfach, West Germany, October 1970, Volume 2 01 p0153 A71-10376
 Poincare hydrodynamic analogy in celestial mechanics, relating differential equations for dynamic systems with two degrees of freedom and two and three dimensional flow 01 p0154 A71-10383
- N-body problem real singularities in celestial mechanics, considering present status and holomorphic motion 01 p0154 A71-10384
 Asteroids, comets and meteor dynamics in solar system, examining motion and orbital evolution by computer techniques 01 p0155 A71-10437
 Minor planets 1969 ephemeris, considering numerical integration of celestial mechanics equations 01 p0155 A71-10438
 Gravitational theory with variable constant, examining local energy momentum tensor conservation law and celestial mechanics effects 01 p0155 A71-10440
 Mechanical systems free motion, comparing effects of external and delayed action internal forces 01 p0155 A71-10446
 Hamiltonian systems properties in relation to Poincare function and canonical variables in bilinear form, discussing periodic orbits 01 p0128 A71-10668
 Celestial mechanics, Volume 1, Dynamical principles and transformation theory covering quasi-periodic motions, many body problems, Lie groups, etc 02 p0316 A71-12774
 Dynamic problems of two dimensions with semisurface of section, examining charged particles motion in axisymmetric magnetic field 04 p0627 A71-15706
 Deep resonance problem of conservative periodic Hamiltonian reduction to ideal form in celestial mechanics 04 p0657 A71-15736
 FORTRAN-based list processor subroutines for computing Poisson series used in celestial mechanics 04 p0660 A71-15890
 Perturbation theory of celestial mechanics, using expansions of negative powers of mutual distances between two bodies 05 p0810 A71-16546
 Capture and control of derelict spacecraft drifting through gravitational field of solar system by pursuit craft 06 p0927 A71-17642
 Vortex perturbations in Friedman cosmological model near zero time, showing perturbation growth associated with increasing Hubble expansion anisotropy 07 p1192 A71-19285
 Short period comets opposition at recent apparitions, investigating nongravitational forces effects in motions 07 p1202 A71-20513
 Rendezvous operations near second lunar libration point, using Halo orbiting relay satellite for communication with spacecraft behind moon 09 p1521 A71-22912
 Celestial mechanics n body equations simultaneous integration, using Taylor-Steffensen numerical method 09 p1525 A71-23335
 Celestial mechanics, discussing fourth order linear differential equation for Hansen coefficients 09 p1486 A71-23340
 Laplace long period solar inequality effects on lunar ecliptic longitude, considering role in celestial mechanics 10 p1667 A71-23829
 Restricted three body problem involving two spherical bodies and elongated artificial satellite, considering equations of motion and positions stability 10 p1667 A71-23830
 Analytic theories in celestial mechanics, checking by exact differential equations form based on Von Zeipel method 13 p2135 A71-28353
 Celestial mechanics and nonlinear dynamics in Poisson series, discussing Echeloned Series Processor for computer programming 13 p2034 A71-28355
 Celestial mechanics relationship to astronomy, establishing differential equations of earth rotation in relation to terrestrial mantle 14 p2306 A71-29703
 Lunar origin dynamics, discussing orbit evolution by tidal friction and celestial mechanical theory 14 p2307 A71-29901
 Hamiltonian systems properties in relation to Poincare function and canonical variables in bilinear form, discussing periodic orbits 14 p2276 A71-31001
 Scorpio-Centaurus association and Gould belt proper motion, discussing convergent point in FK4 catalog with maximum likelihood method 15 p2483 A71-31470
 Papers on mathematical methods in astrodynamics and celestial mechanics for earth-moon trajectories computation, satellite orbit determination and three body problem 16 p2630 A71-33056
 Lunar forced motions and free oscillations, considering inertia moments effects on rotational and translational movements 16 p2636 A71-33502
- Swiss space research, surveying international cooperative scientific activity relative to upper atmosphere satellite geodesy, solar wind, lunar samples analysis, IR and UV astronomy and celestial mechanics 16 p2665 A71-33852
 Asteroids and comets bibliography and review, considering celestial mechanics and astrometry, photometry, spectra, polarimetry and radar measurements 17 p2798 A71-34455
 Book on linear and ordinary celestial mechanics covering perturbed two body motion, numerical methods, canonical theory and initial value problems 17 p2799 A71-34471
 Averaging method for nonlinear oscillations in celestial mechanics, radio engineering and electronics and for time lag, random forces and integrodifferential equations 17 p2779 A71-34904
 Orbital elements oscillations in celestial mechanics two body problem with slowly decreasing mass described by nonlinear nonautonomous differential equations system, obtaining approximate solutions 17 p2804 A71-34912
 Soviet papers on astrophysics, stellar astronomy and celestial mechanics, considering polarimetric and spectrometric data 18 p2962 A71-36105
 Planets masses based on observational or analytical methods, discussing systematic errors effects [AAS PAPER 71-106] 19 p3139 A71-37907
 Automated algebraic manipulation in celestial mechanics, discussing use of Poisson series in perturbation theory problem 19 p3088 A71-38400
 Nearby high velocity stars energy and momentum data, determining orbital properties and integrals of motion 21 p3440 A71-40062
 Three body problem involving large mass ratio by backward numerical integration in constant density resisting medium 22 p3601 A71-42164
 Integrable linear differential equations application to Riccati equation and Bessel, Legendre and other functions relations in celestial mechanics [AAS PAPER 71-333] 23 p3727 A71-43006
 Gravitational system dynamics, discussing massive-light star mixtures with collisions and systems with equal mass objects 24 p3869 A71-44803
 Saturn ring motion stability factors for atomized material resistance to gravitational field, discussing ring thickness, density and other parameters 24 p3869 A71-44810
- CELESTIAL NAVIGATION**
NT ASTRONAVIGATION
 Planetaria as celestial navigation instruction aids, discussing astronomical simulation capabilities, celestial coordinate systems, special effect projectors, etc 01 p0022 A71-10519
 Navigational precision timing from earth rotation based pendulum to atomic second based quartz oscillator clocks 07 p1156 A71-20341
 Planetarium use in teaching celestial navigation and space sky simulation 07 p1157 A71-20345
 Celestial and satellite navigation sensitivity for Lunar roving vehicle /LRRV/ position fix 07 p1157 A71-20414
 Coupled control of space vehicle orientation with reference to three celestial bodies, reducing plane vibrations to dynamic third order system 09 p1491 A71-22547
 Selenographic position determination method based on stellar observations 09 p1530 A71-23714
- CELESTIAL OBSERVATION**
U ASTRONOMY
CELESTIAL REFERENCE SYSTEMS
 Star maps for recognition and attitude orientation aids as function of stereographic display realism in manned space flight 07 p1157 A71-20348
 Photographic quasi-draconic period measurements from satellite transit across topocentric celestial equator tested on Echo 2 and Pages A 11 p1732 A71-25828
 Misalignment estimation software system [MESS/ for in-flight celestial and inertial reference attitude sensor alignment and calibration on OAO [AAS PAPER 71-357] 23 p3648 A71-43027
- CELESTIAL SPHERE**
 Sporadic meteors geocentric velocity distribution over celestial sphere by photographic observation and oblique radio sounding, noting annual variations 10 p1668 A71-24029
 High order conditional algebraic equations in determination from azimuthal radar observation sporadic meteor density distribution over celestial sphere, discussing solution procedure and convergence 10 p1576 A71-24030

CELL ANODES

Anode sheath width for collisionless thermionic converter with Ba plus Cs filler, assuming linear potential variation

01 p0005 A71-10157

High energy density solid state electrolyte cell with lithium anode

03 p0351 A71-13033

Electrolytic production of metal powder in continuously operating facility, using vibrating cathodes with chambers filled with granulated anode metal

19 p3068 A71-37105

High voltage solid state electrolytic cell battery with Li anodes, testing storage and discharge characteristics

20 p3181 A71-38935

CELL DIVISION

Cytophotometric study of DNA content in fibroblasts from human blood vessel walls, discussing cell proliferation and ploidy

09 p1392 A71-22609

Division cycle of *Myxococcus xanthus*, considering kinetics of cell growth and protein synthesis

09 p1396 A71-23473

DNA synthesis rhythm in aorta endothelial cells nuclei during direct division, noting effects of amitosis by autoradiography

12 p1872 A71-27752

Centrally parietal chromatophore in green coccal algae, noting individual cell division and total number increase throughout ontogeny

16 p2531 A71-33465

DNA replication in intercostal artery muscle cells during vascular wall physiological regeneration, noting cytophotometric study of polyploidization

16 p2531 A71-33467

Mammalian cells cultivation at suboptimal temperatures, considering reproduction and cytophysiological changes

20 p3188 A71-39220

Mechanical vibrations effects on mouse embryos growth and development, investigating critical frequencies and accelerations

23 p3637 A71-44246

CELLOPHANE

Cellulose application as zinc silver oxide battery separator, considering chemical stability, cellophane properties, polymerization and crystallinity

08 p1234 A71-21093

CELLS

Rigid cellular plastics mechanical properties based on model assuming pentagonal dodecahedron cell form

04 p0667 A71-14894

Volume diffusion role in Ni-Cr eutectic and cast alloys cellular structure growth

04 p0615 A71-15793

CELLS [BIOLOGY]

NT CARBOXYHEMOGLOBIN

NT CHROMOSOMES

NT COLLAGENS

NT ERYTHROCYTES

NT FIBROBLASTS

NT HEMATOPOIESIS

NT HEMOGLOBIN

NT LEUKOCYTES

NT LYMPHOCYTES

NT MACROPHAGES

NT MITOCHONDRIA

NT NEURONS

NT OXYHEMOGLOBIN

NT RETICULOCYTES

Visual cells outer segments structure and retinal photoreception characteristics, describing open thermodynamic system

01 p0009 A71-10231

Double beam monochromatic differential cinespectrophotometer for recording oxidation/reduction reactions in intercellular pigments

01 p0021 A71-10243

Feedback circuit for constant current stimulation through intracellular microelectrode

01 p0021 A71-10245

Short term pure oxygen exposure effects on rats proximal convoluted tubular cell structure

01 p0011 A71-10768

Bone marrow physiological regeneration after chronic gamma irradiation, noting effect on fission processes and chromosome apparatus of cells

01 p0014 A71-11146

Cardiac cells electrical interaction mathematical simulation, calculating gap region resistance and current

01 p0025 A71-11176

Bioelectric potential in gap between abutting cardiac muscle cells, using differential equation for active to inactive cell transmission

01 p0025 A71-11177

Self-sustaining coacervates photochemical formation, discussing enzyme-like properties and abiogenesis

01 p0017 A71-11453

Space flight effects on survival, mutation and cell development of *Chlorella* cells suspensions onboard Zond 5 spacecraft

01 p0019 A71-11554

Biological clocks self oscillating mechanism as temperature dependent component of circadian clocks in multicellular organisms, assuming small enzyme concentrations

01 p0020 A71-11566

Electro-optic monitoring method for single isolated heart cell activity

02 p0202 A71-11672

Retinal electronic model with about 700 photoreceptors and output cells and new interconnections technique

05 p0715 A71-17079

Ultrastructure changes of membrane and sarcoplasmic reticulum of myocardial cells in squirrels during hibernation

06 p0850 A71-17412

Electron microscopic studies of nerve membrane fine structure, discussing cell membrane multienzyme and macromolecular energy and information transduction, protein synthesis and nucleic acids interrelations

06 p0850 A71-17500

Computer applications in analysis of biological structures, considering tissues, cells, chromosomes, proteins and lipids

06 p0863 A71-18691

Molecular mechanisms of bacterial cell radiosensitization and protection, discussing radiation produced free radicals interactions

07 p1031 A71-18927

Radiation damage to HeLa cells at liquid nitrogen temperature and dry fern spores at room temperature

07 p1033 A71-18937

Bacteria and mammalian cells radiosensitization, using phenylglyoxal and various carbonyl compounds

07 p1034 A71-18944

Age dependent changes in mammalian cells radiosensitivity, emphasizing endogenous nonprotein sulphhydryl effects

07 p1034 A71-18945

Drug-radiation damage interaction relationship to radiosensitization in mammalian cells

07 p1034 A71-18946

Cysteamine protection of hydroxyurea sensitized Chinese hamster lung cells during X ray exposure

07 p1034 A71-18947

Polycation effect on tumor cells, describing growth rate inhibitions, X ray sensitivity and DNA interference

07 p1035 A71-18951

L-erythro-alpha, beta-dihydroxybutyraldehyde radiosensitizing effect on adenocarcinoma Ehrlich ascites tumor cells

07 p1035 A71-18952

Radioprotective drugs relationship to modification of glycolysis in Ehrlich ascites tumor cells

07 p1035 A71-18954

Ehrlich ascites tumor cell membrane potassium and electrophoretic mobility loss, investigating radiation effects under radiosensitizing and radioprotecting drugs

07 p1036 A71-18956

Mitomycin C radiosensitizing effect on hematopoietic colony forming cells, using technique based on bone marrow cells spleen colonies forming ability

07 p1036 A71-18958

Para-aminopropiophenone and propylene glycol radiation protective effect on hematopoietic stem cells of mice

07 p1036 A71-18959

Human kidney cell generation and life cycle parameters, considering thyroxine effects

07 p1041 A71-19594

Vertebrate retina receptive field structure, suggesting interaction between receptor, horizontal and bipolar cells

07 p1046 A71-20623

Orbital space flight effects on dry barley seeds, noting increased intracellular rearrangements

09 p1392 A71-22564

Excitable myocardium cell simplified model based on artificial membrane excitation phenomena, using hybrid computer complex analog section

10 p1567 A71-24166

Cardiac hypertrophy in animals, discussing increased cardiac work load compensation and muscle cell alterations

10 p1565 A71-24674

Rapid erythroblast multiplication in vitro by incubation of rabbit blood buffy coat and marrow cells, giving autoradiographic results

10 p1566 A71-25014

Space flight biological effects on lysogenic bacteria and human cells in culture

12 p1872 A71-26641

Ventral spinocerebellar tract cellular level control transmission to motoneurons, considering monitoring of inhibitory interneurons output against excitatory input

12 p1869 A71-26705

Beef liver cell nuclei acoustic absorption at various frequencies, determining relation to protein content

12 p1928 A71-27535

Myocardium cells contractile activity control with frequency dependent self regulatory mechanism

13 p2006 A71-28383

Superposition model of spontaneous activity of cerebellar Purkinje cells for spike triggering

13 p2014 A71-29289

Proteinoids self assembly into primitive cell from observations of polypeptide generation during amino acid heating

14 p2190 A71-30179

Mammalian neurons, neuroendocrine transducer/pinealocytes and adrenomedullary chromaffin/ and endocrine cells communication properties, noting signal transmission

14 p2182 A71-30180

Immunobiological reactivity inhibition in mice under partial adaptation to high altitude hypoxia, observing decreased phagocytic activity, antibody production, hypoplasia and lymph cell number

15 p2356 A71-31289

Diurnal variations of mitotic activity in thyroid epithelial cells of different follicle size

15 p2356 A71-31290

Anabaena cylindrica alga chromosomes protein components, noting histone absence

16 p2536 A71-33359

Calcium ions effects on electrophysiological properties of portal vein muscle cells in rats

16 p2533 A71-34109

Temperature effects on spontaneous electrical and contractile activity of smooth muscle cells of portal vein in rats

16 p2533 A71-34110

Cat thalamus ventrolateral nucleus neuronal discharges during waking and slow and fast wave sleeps

17 p2680 A71-34689

Somatic cell mitosis control by simulated changes in electrical transmembrane potential difference

18 p2853 A71-35892

Retina photosensitive cells properties and functions compared with films photosensitive chemicals, emphasizing retinal image transformation

18 p2864 A71-36068

Book on biological effects of radiation covering ionizing radiation properties and effects at molecular, cellular and tissue levels

19 p3002 A71-38048

Chlorella extracellular metabolites, identifying indole nature biologically active substances

19 p3004 A71-38544

Cell volume analyzer for sensing individual blood cells and plotting number as function of size

20 p3191 A71-38824

Cell contacts in canine duodenal smooth muscle layers, using perfusion with glutaraldehyde fixative

20 p3187 A71-38985

Tissular and cellular biological resistance as indices for organism resistance to adverse effects, noting increase due to muscular training and cold adaptation

20 p3187 A71-39219

Mammalian cells cultivation at suboptimal temperatures, considering reproduction and cytophysiological changes

20 p3188 A71-39220

Cryogenics applications to cryosurgery and long term low temperature storage of living cells and tissues

20 p3189 A71-39252

Gravity sensors and intracellular conduction mechanisms in animals, noting contradictory hypotheses on function of hair cell in labyrinth

21 p3328 A71-40009

Space conditions exposure of lysogenic strains of *Escherichia coli* and monolayer cultures of human cells aboard Zond 5 and 7 flights

21 p3333 A71-40565

Living organisms life-sustaining possibility under simulated Martian temperature, humidity and atmospheric composition conditions, emphasizing unicellular organisms radiation resistance

21 p3334 A71-40572

Computerized electrostatic field model of biological cell membrane

22 p3487 A71-42119

Hyperoxic medium effects on experimental animal cells, tissues and organs morphology, infrastructure and histochemistry

22 p3495 A71-42801

Blue-green algae *Microcystis aeruginosa* central zone cellular structure electron microscopic investigation, noting absence of distinct boundary between central and peripheral regions

23 p3640 A71-44054

Nonactomyosin component differentiation in potassium chloride insoluble myofibrillaments in vertebrate smooth muscle cells

24 p3794 A71-44424

Visual masking effects in cat striate cortex single cell activity, using moving slit and diffuse flashing light stimuli

24 p3799 A71-45140

CELLULOSE

Cellulose, explosives and propellants thermal surface ignition, using heat transport and chemical kinetic equations

06 p0944 A71-18298

Cellulose application as zinc silver oxide battery separator, considering chemical stability, cellophane properties, polymerization and crystallinity

08 p1234 A71-21093

CELLULOSE NITRATE

Shape effect of compressed solid fuel on thermal ignition delay time in heated gas flow for pyroxyline

03 p0520 A71-13993

Principal stresses separation in nitrocellulose transparent material with photoelastoplastic properties, using scattered light method

14 p2322 A71-29700

CELSIUS TEMPERATURE SCALE

U TEMPERATURE SCALES

CEMENTATION

One chamber vacuum furnace for dewax, presinter and sinter of cemented carbides, referring to Cox chart for system design

05 p0758 A71-16248

Al coating of Nb and Nb alloys by pack cementation, discussing coating structural states, heating cycle temperatures and growth kinetics

11 p1781 A71-26295

CEMENTS

Load-deformation characteristics in tension, compression and bending of two thin cement laminates reinforced with short random glass fibers, discussing stiffness and residual strain

11 p1790 A71-26384

Cement systems based on metal oxides and organic compounds, stressing acidity factor for organic component selection

13 p2090 A71-28007

Soviet book on hydrodynamics of nonstationary motions of viscoplastic media covering mechanical properties of clay, mortar, cement, lubricating oil, petroleum and disperse media, etc

21 p3369 A71-40872

CENTAUR LAUNCH VEHICLE

Centaur/shuttle integration and operations, considering ground tanking modes and in-flight propellant transfer

18 p2973 A71-36477

Winds and diffusion measurements in lower thermosphere using sodium vapor cloud release from Centaur IIB rocket

20 p3221 A71-39692

CENTAUR PROJECT

Shuttle/Centaur injection stage, considering application to comet rendezvous mission via Jovian powered swingby

[AAS PAPER 71-113]

19 p3139 A71-37912

CENTAUR VEHICLE

U CENTAUR LAUNCH VEHICLE

CENTAURUS CONSTELLATION

Nova-like X ray source near or in Centaurus constellation, presenting energy spectra measured by sounding rockets in Japan during August 1969

05 p0808 A71-16452

X ray and far IR measurement inconsistency from Centaurus A, discussing metagalactic submillimeter background

07 p1185 A71-19546

High energy X ray flux from source in Centaurus Crux detected by balloon sounding

14 p2303 A71-30654

Rapid fluctuations in high energy X ray flux from source in Centaurus Crux from balloon sounding

14 p2303 A71-30655

Scorpio-Centaurus association and Gould belt proper motion, discussing convergent point in FK4 catalog with maximum likelihood method

15 p2483 A71-31470

Large amplitude periodic X ray pulsations from Centaurus X-3, observing abrupt source intensity and pulse rate changes

17 p2798 A71-34375

Cen X-3 source X ray flux periodic variations due to white dwarf star radial vibrations based on nonrotating model

21 p3449 A71-40613

CENTER OF GRAVITY

Soviet book on rocket flight dynamics covering center of mass motion characteristics, guided missiles, external ballistics, multistage design and flight optimization

02 p0320 A71-12724

Atmospheric air columns centers of gravity, determining height from vertically integrated equations of motion

02 p0278 A71-12745

Human equilibrium maintenance system analogy to multiput/multioutput controller, considering motion of projection of center of gravity onto horizontal plane

03 p0356 A71-12981

Heavy gyroscope equations of motion solution, assuming center of mass on major axis

03 p0457 A71-13584

Gyrostatic system with center of mass in uniform circular motion, deriving rotary motion equations invariant

03 p0460 A71-14386

Reentry vehicle angle of attack control by mechanically varying center of mass for axial loads

05 p0779 A71-16039

Axially symmetric body rapid rotation under center of gravity velocity vector conditions, solving for plane gliding motion stability in air

07 p1159 A71-19354

Gyrostat with center of gravity on ellipsoid axis, determining motion by two invariant algebraic equations

07 p1209 A71-20645

Angle of attack vertical variations of free flight trajectory missile, estimating missile, trajectory and atmospheric parameters effects on fluctuations relative to center of mass

08 p1367 A71-22051

Aerodynamic moment on satellite with asymmetrically positioned solar cell platforms, analyzing motion around center of mass for diffuse scattering flow

09 p1531 A71-22568

Concorde aircraft fuel system and fuel pumps, considering center of gravity and center of pressure relationship to maintain trim

09 p1512 A71-23581

Eye movement tendencies, investigating rectilinear, horizontal or vertical and center of gravity fixation effects on visual perception

10 p1570 A71-24602

Plane rigid airfoil with fixed center of gravity, discussing motion in turbulent air and gust loads

10 p1557 A71-24947

Ion-ion mutual neutralization cross sections, measuring range of barycentric energies by superimposed beam technique

12 p1932 A71-27005

Onboard weighing system for gross weight determination and center of gravity location of Alouette helicopter, using load sensors, electrical circuits and visual indicators

14 p2175 A71-30320

Spacecraft reentry trajectory angle of attack control by mechanically varying center of mass for axial loads

16 p2645 A71-33443

Controlled motion dynamics of spacecraft performing maneuvers, applying point transformation to third-order nonlinear system moving about center of mass in lateral motion

16 p2646 A71-33658

Earth satellite plane periodic oscillations damping with respect to center of mass in orbital plane during motion on elliptical Kepler orbit

16 p2646 A71-33659

Graviplane flight theory, spacecraft center of mass motion in central gravitational field with continuous mass geometry variation

16 p2646 A71-33661

Transfer function and temporal behavior interrelations for linear network, characterizing circuit delay and rise time by center of gravity and inertial moment of pulse response

16 p2550 A71-34139

V/STOL aircraft with vectored thrust propulsion systems, noting weight and center of gravity-lift-thrust relationship changes effect on performance

[SAWE PAPER 894]

17 p2676 A71-35817

Mass, center of gravity and moment of inertia measurements curtailment by tolerance and regression analyses and Monte Carlo method

[SAWE PAPER 883]

17 p2834 A71-35820

Center of gravity and moment of inertia measurement system based on standards of comparison principles

[SAWE PAPER 880]

17 p2835 A71-35822

Mass and center of gravity determining system model, describing equipment, operation principles, calibration data and techniques accuracy and errors

[SAWE PAPER 879]

17 p2725 A71-35824

Analog mass center estimator for spinning drag-free orbiting satellite, using free-falling proof mass shielded from external forces inside satellite cavity as reference

[AIAA PAPER 71-947]

19 p3148 A71-37188

Collision effects on line shapes using quantum mechanical description of atomic center of mass motion, considering pressure effects in gas lasers

20 p3271 A71-39069

Crab Nebula pulsar timing observations, correcting arrival times to solar system barycenter and dispersion effect

20 p3302 A71-39929

Phugoid motion at constant angle of attack without thrust line displacement from aircraft center of gravity, noting longitudinal stability

21 p3324 A71-40168

Differential correction for redetermination of satellite observation stations geodetic coordinates as related to earth center of gravity and terrestrial potential coefficients

22 p3534 A71-42023

Lunar center figure position determination by harmonic analysis, comparing with Mills III catalog

22 p3607 A71-42619

Translational and rotational vibrational motion correlation of solid body mass center in Newtonian force field

24 p3872 A71-45047

CENTER OF PRESSURE

Concorde aircraft fuel system and fuel pumps, considering center of gravity and center of pressure relationship to maintain trim

09 p1512 A71-23581

CENTIGRADE TEMPERATURE SCALE

U TEMPERATURE SCALES

CENTRAL NERVOUS SYSTEM

NT BRAIN

NT BRAIN STEM

NT CEREBELLUM

NT CEREBRAL CORTEX

NT CEREBRUM

NT HIPPOCAMPUS

NT SPINAL CORD

NT SPINE

NT THALAMUS

Chronic posttraumatic changes in central nervous system in pugilists from brain damage due to head injuries

01 p0010 A71-10393

Human temporal performance of homogeneous discrete motor acts sequence, suggesting central nervous mechanism for movement rate generation

02 p0204 A71-12052

Anticonvulsant drugs for counteracting noise effects on central nervous system, discussing audiogenic seizure in mice

03 p0360 A71-13163

Central nervous system reactions to vasopressin and oxytocin presence in cerebrospinal fluid and blood, discussing respiratory frequency and antidromic tests

03 p0363 A71-13485

Mean period spontaneous EEG as psychophysiological characteristics of higher nervous activity in human individuals

06 p0858 A71-17600

Central nervous system role in radioprotective contribution of 5-hydroxytryptamine

07 p1038 A71-18972

Clinical aspects of aerospace neurology, considering central nervous system diseases among flying personnel

08 p1238 A71-20723

Central regulation mechanisms of acid-alkaline equilibrium in ontogenesis, discussing midbrain intraterine and respiratory postnatal development

08 p1241 A71-21937

Central nervous system functions under high oxygen concentrations at normal and elevated pressures

08 p1241 A71-21938

Cerebrospinal knee and flexor reflex suppression observations in rabbits and cats during blood circulation disorders

09 p1391 A71-22480

Central nervous system role in body metabolism effects on cardiac output, measuring 2,4-dinitrophenol/DNP dosage effect on arterial pressure and oxygen consumption in dogs

09 p1396 A71-23541

Signal transformation laws of central nervous system motor command patterns construction from sensory impulse streams

10 p1569 A71-24236

Central nervous system responsiveness changes after exhausting physical exercise, giving electroencephalogram and sensorimotor reaction records

11 p1719 A71-25668

Serotonin role in central nervous system activity, stressing sleep/wakefulness cycle regulation

12 p1869 A71-26651

Functional-biochemical shifts in rats central nervous system during initial stage of increased oxygen pressure exposure

13 p2002 A71-27810

Human operator work quality evaluation with EEG data based on brain electrical activity as function of central nervous system

15 p2365 A71-32530

Biological effects of inert gases in elevated pressure respiratory mixtures on human central nervous system

16 p2536 A71-33577

Central nervous system self regulating properties analysis by automatic control theory, using parametric functional model of brain electrical activity

16 p2538 A71-34107

Neurobiology, considering data processing in brain and central nervous system

17 p2691 A71-35165

Squirrel monkey physiological and behavioral thermoregulation elements interrelationships, considering mean skin and medial preoptic hypothalamic temperatures

18 p2862 A71-36896

Firing frequency of single trochlear nerve fibers during eye movements in alert monkey

19 p3001 A71-37413

- Conditioned motor reactions characterizing higher nervous activity, using logokinetic method
19 p3006 A71-37447
- Test equipment for evaluating human higher nervous activity, noting use for radiotelegraphist selection
19 p3007 A71-37775
- Integrative action of central nervous system in converting gravity sensation into crustacean equilibrium reactions
21 p3327 A71-39993
- Central nervous tissue sensitivity, considering direct sensing of gravitational stimuli of vibratory character
21 p3328 A71-39997
- Rat brain carbohydrates biosynthesis from organic acid products under normal conditions and during central nervous system disturbances, investigating butyric acid participation
21 p3337 A71-41058
- Orthodromic and antidromic impulsion role in functional state changes of contralateral cerebropinal center during mixed nerve prolonged stimulation by rectangular pulses
21 p3337 A71-41059
- Soviet book on experimental research on human higher nervous activity from growth aspect covering normal and pathological states, cerebral cortex interaction with central nervous system
21 p3339 A71-41374
- Central pathway connection between vestibular and oculomotor nuclei through pons responsible for horizontal eye movements induced by visual and vestibular stimuli
22 p3488 A71-42436
- Sympathomimetic amines effects on central nervous system reflex activity of irradiated and desympathized animals
22 p3492 A71-42708
- Human expired air toxicity effect on mice neurohumoral changes stimulating inhibitory reactions in central nervous system
22 p3506 A71-42813
- Human motor system control mechanism for stretch reflex loop gain with simplified central nervous system computation
23 p3639 A71-43354
- CENTRAL NERVOUS SYSTEM STIMULANTS**
Microwave irradiation of animals, noting analeptic effect and increased alertness
11 p1718 A71-25293
- CENTRAL PROCESSING UNITS**
Centralized inquiry-response systems for information retrieval, analyzing voice-data communications interaction
01 p0048 A71-10220
- Central data processing unit based on short-rod memories of coated Be-Cu alloy, discussing arithmetic-logic unit operation
01 p0049 A71-10263
- Microcomputer design using standard interfacing module for balanced electronic logic amounts in central processor and peripheral controllers
22 p3518 A71-42207
- CENTRIFUGAL COMPRESSORS**
Centrifugal compressor impeller exit flow velocity distribution distortion based on equations of motion involving entropy gradient terms
03 p0343 A71-13831
- Two stage compressors with subsonic and supersonic air velocity and high camber rotor blades, discussing strength against centrifugal force
05 p0796 A71-16647
- Turbocharged diesel engine precompressed inlet air cooling by evaporation cooling, considering water injection effects on centrifugal compressor
08 p1347 A71-20781
- Pressure increase, dry air consumption and power requirements effects of water quantity fed into centrifugal compressor
08 p1347 A71-20833
- Centrifugal compressor vaneless diffuser, estimating energy losses with hydrodynamic model
08 p1348 A71-21266
- Axial-radial and radial compressor stage optimum exit blade angle, considering flow rate control by variable pitch nozzle guide vanes
08 p1220 A71-22049
- Papers on centrifugal compressors covering fluid dynamics and small high pressure ratio radial compressors design and performance
10 p1550 A71-24215
- Centrifugal compressor fluid dynamics, discussing unresolved problems governing design and performance prediction
10 p1550 A71-24216
- High pressure ratio radial outflow compressor analysis, design, construction and testing
10 p1550 A71-24217
- High pressure ratio centrifugal compressors for small gas turbine engines, investigating power and specific fuel consumption variation with pressure and temperature
10 p1658 A71-24218
- Small high pressure ratio single-stage centrifugal compressor design, testing and efficiency
10 p1550 A71-24219
- Reynolds number effects on centrifugal compressor performance characteristics, discussing power losses in compressor, impeller and diffuser stages and compressor adiabatic efficiency
11 p1703 A71-25967
- Soviet book on theory of aircraft bladed machines covering axial flow, centrifugal and composite turbines and compressors, thermodynamic efficiency, control turbocompressor matching, etc
11 p1814 A71-26401
- Centrifugal blowers optimum blade number for maximum efficiency, discussing design measures for shock and friction loss minimization
20 p3277 A71-38750
- Inlet conditions for centrifugal compressor impeller covering pressure, temperature and velocity measurements on quasi-three dimensional model
22 p3480 A71-42035
- Centrifugal compressor bladeless diffuser parameters, flow kinematics and energy losses, noting effects of friction coefficient and expansion angle
23 p3626 A71-43551
- Medium compressibility effect on gas dynamic characteristics and aerodynamic forces and moments in centrifugal compressor end stage bladed diffuser
23 p3626 A71-43552
- Flow acceleration coefficient effect at inlet on centrifugal compressor wheel characteristics during axial-radial rotation
23 p3626 A71-43553
- Centrifugal superchargers high pressure wheels efficiency improvement, considering blade profiling
23 p3626 A71-43556
- Compressors and turbines centripetal stages operational characteristics, investigating airflow rate and pressure ratio effects on power
24 p3790 A71-45380
- CENTRIFUGAL FORCE**
Turbine blades coupled bending vibrations in centrifugal field, deriving vibration equations including previously neglected centrifugal coupling terms
01 p0166 A71-10120
- Dynamic behavior of liquids in partially filled mobile tanks under almost centrifugal force fields
01 p0069 A71-10396
- Centrifugal and Coriolis force in general relativity, discussing paradox associated with terms in mass shell test particles equations of motion
03 p0489 A71-13564
- Relativistic velocity particles diffusion in cloud of scattering centers in centrifugal motion from Boltzmann equation solution by method of extensions
06 p0963 A71-18229
- Incompressible unsteady viscous fluid flow through circular cross section curved pipe, noting centrifugal effects in interior
06 p0882 A71-18316
- Structural hysteresis in split root fir tree turbine blade attachment under centrifugal forces and cyclic bending moments
07 p1211 A71-19162
- Viscous incompressible fluid partly filling rotating cylindrical cavity, considering motion under centrifugal forces in adjoining unperturbed free surface region
07 p1093 A71-20467
- Centrifugal force effect on pigeon head nystagmus, acting on semicircular canal via otoliths or cupula
09 p1388 A71-22123
- Centrifugal particle separation limit in free vortex, stressing particle interference with vortex flow and viscous effects
11 p1750 A71-25467
- Optimal elastic beam structural design for given deflection in presence of body forces, considering rod under centrifugal loads
11 p1849 A71-25680
- Low cost solar array unfolded by centrifugal spinning force, considering application to spin and 3-axis stabilized spacecraft
16 p2526 A71-32852
- Structural hysteresis in gas turbine blade herringbone scarf joints under centrifugal forces and cyclic bending moments
17 p2834 A71-35658
- Jovian magnetospheric plasma densities, discussing roles of centrifugal ejection, solar wind plasma injection and photoelectron diffusion
18 p2964 A71-36291
- Artificial gravity selection by rats in centrifugal acceleration fields superimposed on weightlessness during sounding rocket flights
18 p2857 A71-36646
- Buoyant centrifugal force effect on combustion of homogeneous propane-air mixtures at stoichiometric proportions, using steel pipe as centrifuge
19 p3167 A71-38101
- Artificial gravity field produced by rotating spacecraft in earth orbit, examining astronaut physical responses and centrifugal force effects on work tasks
21 p3342 A71-40255
- Jet flaps application to autogyro rotor, using pressure jump for air centrifugation
21 p3324 A71-41399
- Boundary layer asymptotic solutions for free convection in laminar three dimensional systems, determining rapid mass transfer and centrifugal forces effects
22 p3619 A71-41870
- Liquid flow and heat transfer in thermosiphons in centrifugal and Coriolis force fields
24 p3888 A71-44931
- Liquid particles motion over variable profile turbine rotor blade edge, concave and fanning surfaces as function of Coriolis and centrifugal force
24 p3819 A71-44932
- CENTRIFUGAL PUMPS**
Miniature centrifugal pump for circulating liquid He in flow loop, testing performance
02 p0255 A71-12129
- Impeller radial forces in volute casing centrifugal pumps, using potential theory
03 p0431 A71-13145
- Similarity criterion for volute centrifugal pumps via supersonic model, considering cavitation parameters influence throughout angular velocities range at flow separation
08 p1347 A71-20784
- Centrifugal pump channels flow velocity measurement by optical method, noting flow separation near blade exits
08 p1230 A71-22048
- Vapor-liquid mixture steady flow from centrifugal injectors, determining kinetic energy loss relationship to phase separation
16 p2624 A71-33608
- Soviet book on high pressure centrifugal pumps design and calculation covering industrial applications, systems engineering, components, etc
21 p3391 A71-41371
- Centrifugal pump pressure characteristics calculation by pressure quality coefficient dependence on relative flow rate, assuming arbitrary number of blades
22 p3554 A71-41848
- High rpm effect on centrifugal pump efficiency, considering hydraulic, volume and mechanical losses
22 p3554 A71-41849
- Flow rate and heating analysis of centrifugal pumps with variable cross section impeller blade ring inlet
22 p3554 A71-41850
- Centrifugal wheel flow swirl effect on pressure/flow rate characteristic in input zone
23 p3626 A71-43555
- Photogrammetric flow rate determination in centrifugal pump impeller, using rotating camera
24 p3825 A71-44754
- CENTRIFUGES**
NT HUMAN CENTRIFUGES
Partially ionized rotating plasma centrifuge for isotope and element separation, controlling velocity distribution of conducting magnetic fluid by isorotation law
05 p0788 A71-16607
- Space shuttle orbital centrifuge systems configuration, comparing artificial gravity experiment performance options
19 p3006 A71-37274
- CENTRIFUGING**
Heat transfer through phase change in metallic heat carrier exposed to strong centrifugation encountered in turbine blades
04 p0639 A71-15462
- Accelerometers linearity variations by centrifuge tests
05 p0750 A71-16313
- Accelerometer precision centrifuge test data reduction by inversion method, extracting odd second order coefficients
13 p2072 A71-29506
- Bull frog activity at rest and response to centripetal acceleration by on-board centrifuge in vestibular space experiment OFO-A
22 p3484 A71-41690
- CENTRIFUGING STRESS**
Time judgment error as function of angular velocity during body rotation
07 p1043 A71-20216
- Blood serum protein displacement in force direction in albumin injected rats under centrifuging acceleration
09 p1393 A71-22919
- External oblique inguinal hernia due to acrobatic flying centrifugal accelerations, considering anatomical, clinical and medico-legal aspects
17 p2681 A71-34822
- Chronic centrifugation effects on water intake and urine output in mice, considering food intake and growth rate
20 p3186 A71-38984
- Vestibulo-colic reflex control of head movement in seated man under sinusoidal and stepwise rotational velocity stimulation, comparing with ocular stabilization
22 p3501 A71-41822

Respiratory function and gas metabolism shift under high transverse accelerations in reclined centrifuged subjects
22 p3495 A71-42795

CENTRIPETAL FORCE

Element and isotope separation effects under centripetal acceleration in rotating plasma, using mass spectrometric diagnostics
22 p3580 A71-41584

Bull frog activity at rest and response to centripetal acceleration by on-board centrifuge in vestibular space experiment OFO-A
22 p3484 A71-41690

CEPHALOPODS

NT SNAILS

CEPHEID VARIABLES

Cepheid radius-temperature variation functions phase shift
02 p0308 A71-12101

Classical Cepheids nature and evolution, discussing relation between periods and luminosity in galaxies, characteristics in scattered clusters, brightness curves
03 p0485 A71-13260

Cepheids in Milky Way spherical component, emphasizing brightness and color curves and spectral characteristics
03 p0485 A71-13261

RR Lyr type stars kinematic behavior, line of sight velocities, spectral energy distribution and temperature
03 p0485 A71-13263

RR Lyr type dwarf stars, discussing brightness curves, color indices, effective temperatures, line of sight velocities and spectral classes
03 p0485 A71-13265

Population I Cepheids studies applied to galactic rotation and solar motion parameters estimation, discussing stellar distances inaccuracy effects
04 p0643 A71-14908

Reddening effects in determining intrinsic color of supernight and cepheid variable stars
04 p0646 A71-15235

UBV photometry of RR Lyrae variables in metal rich globular cluster NGC 6171
04 p0649 A71-15372

Cepheids normal color index-spectrum relation, noting light variation phases and color-color diagrams reddening lines
06 p0975 A71-18436

WX Cep eclipsing system photoelectric components computed in standard UBV colors, obtaining orbital elements
09 p1527 A71-23526

Cepheids broadband photometric study of temperature and blanketing variations as function of turbulent velocity and gravity, using atmospheric models
11 p1818 A71-25206

RR Lyrae type variable star statistical population indices evaluation based on space and radial velocities and position
11 p1820 A71-25247

Cepheids normal color index-spectrum relation, noting brightness variation phases and two-color diagrams reddening lines
12 p1955 A71-26586

Cepheids period and luminosity relation, using Kraft method
12 p1962 A71-26906

Cepheids UBV spectrum analysis, examining brightness shapes and color index curves
12 p1962 A71-26907

Long period Cepheids, obtaining brightness curves distribution for minimum, maximum and fixed phase stellar magnitudes
12 p1962 A71-26908

Blue edge of RR Lyrae instability strip, examining convection, radiation and surface boundary conditions effects
13 p2133 A71-27969

Central Galactic region star distribution, considering RR Lyrae and metal-rich stars
15 p2495 A71-32704

Cepheid beta Doradus color photometry data, detailing temperature, mean radius, absolute magnitude and surface gravity variations
18 p2971 A71-37070

Photometric and spectroscopic observations of pulsating stars, noting shock waves in atmospheres of W Virginis and RR Lyrae
20 p3292 A71-39446

BCD Cepheids observations, examining data with quasi-static interpretation approximation for gravity and stellar masses
21 p3441 A71-40065

RR Lyrae variables period-frequency distribution in Oosterhoff types I and II globular clusters, interpreting in terms of pulsation theory
21 p3445 A71-40413

SV Cephei variable photoelectric UBV observation showing existence of quasi-periodic minima with changing characteristics
21 p3451 A71-40715

Stellar evolution on horizontal branch and parameters of state of RR Lyrae stars in globular clusters of various ages
21 p3451 A71-40720

RR Lyrae stars instability strip for halo population variables, presenting linear nonadiabatic approximate pulsation calculations with emphasis on blue edges location in H-R diagram
22 p3602 A71-42171

Globular cluster RR Lyrae horizontal branch stellar models, investigating masses luminosities and compositions
23 p3723 A71-42944

Phase dependent spectra of Cepheids from multifrequency group calculations in radiative transfer model
23 p3723 A71-42946

Beta cephei stars atmospheric He and metal abundances, comparing line spectra data with other early B stars sample
23 p3723 A71-42947

Cepheid sequence interpretation on gradient diagram based on model atmosphere photometric data
23 p3771 A71-44305

Evolved Cepheid-type stars vibrational stability against nonradial perturbations from quasi-adiabatic approximation of radiative dissipation
24 p3872 A71-45077

CEPHEUS CONSTELLATION

Contour map of galactic radio emission in Cassiopeia and Cepheus region, noting discrete sources
11 p1831 A71-26132

CERAMAL PROTECTIVE COATINGS

U CERMETS

U PROTECTIVE COATINGS

CERAMALS

U CERMETS

CERAMIC BONDING

Nb-sheathed insulators of three coaxial cylinders with ceramic bonding for thermionic converter, discussing pressure bonding techniques and stress relieving properties
02 p0232 A71-12248

Heat and corrosion resistant vacuum tight ceramic to metal brazed seals
07 p1119 A71-19972

Electron beam welding of metal-metal and metal-ceramic joints and sapphire sealing under vacuum
11 p1745 A71-26399

Ceramic rod supported helix derived traveling wave tubes, considering titanium carbide for internal attenuators due to zero temperature coefficient of resistivity
14 p2214 A71-30702

CERAMIC COATINGS

Ceramic fiber external insulation thermal protection systems for space shuttles, considering use with Al and Ti
12 p1985 A71-26763

Flame or plasma sprayed ceramic coating porosity estimation, using statistical distribution of breakdown voltage in coating
15 p2438 A71-31285

CERAMICS

NT PORCELAIN

Interdigital Rayleigh wave transducer on piezoelectric ceramics with comb-to-comb polarization
01 p0055 A71-11174

High strength ceramics for high temperature applications, reviewing oxides, nitrides and carbides
01 p0109 A71-11601

Ceramic fibers formation by particles mechanical deformation by extrusion in W matrix, describing grain structure of various extruded metal oxides
02 p0273 A71-12149

Ceramic particle compaction as function of size, shape, loading rate and hardness for fused alumina, magnesia and mullite
03 p0448 A71-12973

Glass ceramics manufacture, chemical composition and properties, and applications
03 p0448 A71-14352

Thermal expansion of dilute binary composites concerning ceramic-glass, glass-metal, metal-metal and organic-metal systems
03 p0449 A71-14458

Glass and glass ceramics for large astronomical telescopes, examining fabrication, absorption coefficient and applications
04 p0617 A71-14865

Ceramic and metallic whiskers mechanical properties, discussing failure and deformation mechanisms
04 p0611 A71-14946

Test stand for endurance and creep testing of plastics, glazed ceramics and other brittle materials
04 p0567 A71-15645

Piezoelectric ceramic transducer vibration measurement under mechanical loading, noting displacement as function of thickness and time
04 p0601 A71-15835

High strength metal and ceramic reinforcement fibers, discussing properties and fabrication for plastic composites
06 p0916 A71-18088

Fracture toughness of aluminum oxide composite containing ductile Mo fibers
08 p1304 A71-20700

Stress profiles measurement in opaque tempered glass and ion exchanged glass-ceramic flat plates from length change during etching
09 p1480 A71-22115

Organo-ceramic composites for thermal protection of aerospace vehicles, discussing heat sink property
09 p1483 A71-23206

Solid state sintering of metal ceramics, discussing diffusion-viscous, pure diffusion and activation mechanisms
09 p1457 A71-23390

Ferroelectric barium titanate ceramics technology for capacitor fabrication
09 p1483 A71-23394

Opaque ceramic armor materials for lightweight personnel and equipment ballistic protection applications, discussing mechanical properties and fabrication techniques
09 p1484 A71-23689

Brittle alumina ceramic tensile and flexural strengths comparison based on statistical surface flaw distribution theory of fracture
09 p1484 A71-23699

Plastics reinforcement by combining high plastic deformation and fracture resistances with stiffness, discussing ceramics, whiskers, carbon and glass fibers
11 p1788 A71-25654

Magnesia rich magnesium aluminum oxide spinel ceramics, discussing sintering, grain growth inhibition and strength increase
13 p2092 A71-28662

Constant load tensile creep tests on polycrystalline ceramics, determining high density alumina applied stress and strain rate
16 p2553 A71-33384

High power microwave phase shifter, using beryllium oxide filler ceramic dielectrics to obtain thermal coupling between ferrite element and waveguide wall
17 p2713 A71-34396

Ceramic fibrous materials for high temperature insulation, discussing practical approach to obtain lower thermal conductivity
18 p2939 A71-36668

Papers on ultrasonic transducer materials covering magnetostrictive metals and alloys and piezoelectric crystals and ceramics
20 p3236 A71-39253

Magnetostrictive metals and piezomagnetic ceramics as transducer materials for ultrasonic wave generation, detection and filtration
20 p3236 A71-39254

Piezoelectric crystals and ceramics for acoustic power detectors and radiators, considering crystal symmetry and coupling factor effect on piezoelectricity
20 p3253 A71-39255

Capacitive thermometry characteristics of dielectric crystallized titanate-containing glass ceramic at cryogenic temperatures
20 p3253 A71-39279

Substrate influence on circuit board conformal coatings electrical insulation resistance, discussing test results with epoxy/glass and ceramic substrates and various coating materials
21 p3353 A71-40438

Ceramic semiconductor atmospheric humidity detector with hydrophilic properties, using complex capillary porous body composed of crystals and amorphous substance
21 p3383 A71-41237

Gyro wheels cleaning by ion bombardment applied to ceramic gas bearings, comparing with chemical cleaning
22 p3552 A71-41674

High temperature structural application of refractory fiber reinforced ceramic composites
22 p3565 A71-42287

Brittle ceramic materials strength, showing porosity effect dependence on Weibull homogeneity parameter value
23 p3698 A71-44225

Temperature and frequency effects on permittivity and dielectric loss angle tangent in glasses and pyroceramics
24 p3859 A71-44379

Curie point region automatic thermal stabilization effectiveness of cylindrical/disk shaped segnetoceramic elements in electrostrictive constant magnetic field converters
24 p3828 A71-45164

CEREBELLUM

Cerebellum substrate for memory list processing in brain assuming Perceptron mechanism
01 p0015 A71-11313

Cerebellum efferent visceral field functional organization in cats
08 p1240 A71-21794

Superposition model of spontaneous activity of cerebellar Purkinje cells for spike triggering
13 p2014 A71-29289

CEREBRAL CORTEX

Hydrogen exchange between pial arteries for measuring local cerebral blood flow quantitatively in anesthetized cats

01 p0008 A71-10075

Dorsomedial nucleus electric impulse stimulation in anesthetized cats with oscillogram recorded response potentials of cortex preoral gyrus, indicating relay transmission function

01 p0008 A71-10091

Neuron pairs discharge sequence temporal correlation in cats association cortex during natural sleep and wakefulness

01 p0011 A71-10849

EEG dynamics and visual cortex neuron responses in cats to conditioned optical stimulus during defensive reflex formation

01 p0011 A71-11052

Temporary connection of neurons in visual and associative cortical regions of hemispheres in cats

01 p0012 A71-11053

Cortical vestibular projection zones in formation of conditioned reflexes and spatial orientation of cats

01 p0012 A71-11054

Impulsive activity of neuron populations in cerebral sections controlling psychic and motor functions in man

01 p0014 A71-11149

Slow cortical potentials associated with human motor and mental acts differentiated via spatial distribution

01 p0015 A71-11220

Olfactory tract terminal distribution in prepyriform cortex

01 p0017 A71-11455

Vestibular nerve projection to association fields of cerebral cortex in Rhesus monkey under alpha chloralose and without anesthetic agent

04 p0537 A71-14765

Impact induced closed brain injuries pathomorphology, considering dura mater, cortical contusions, neuron and glial damage, brain stem lesions and hemorrhages

04 p0537 A71-14787

Cerebral oxygenation and metabolism during progressive hyperthermia

04 p0538 A71-15092

Motor cortex sensory input in animals and man, using evoked responses recording

05 p0706 A71-16319

Bilateral and single median nerve electrical stimulation, observing summated cortical responses from homologous scalp derivations

05 p0706 A71-16322

Vestibular apparatus cortical zone projections on striopallidal complex in cats

05 p0707 A71-16387

Cerebral cortex regulation of internal organ functions, examining neural and neurohumoral channels, hormones and vascular changes

05 p0709 A71-16802

Visual cortex inhibitory neurons, examining pause discharges in rabbits during light stimulation

06 p0849 A71-17383

Somatosensory and viscerosensory stimulation effects on cortex neuron amygdala complex and convergent interrelations

06 p0849 A71-17384

Training effect on oxygen tension dynamics in rats brain cortex under progressive high altitude hypoxia conditions, noting adaptation influence on motor activity and survival rate

06 p0850 A71-17394

Bioelectric activity of cerebral cortex in man under neuroemotional stress, using multichannel radioelectroencephalography

06 p0856 A71-18464

Seasonal factors effect on white rat hypophysis-adrenal cortex system functioning by fluorimetric determination of peripheral blood corticosterone content

07 p1041 A71-19282

Brain cortical-subcortical functions in psychic processes, indicating developments in psychotherapy

08 p1241 A71-21940

Vestibular stimulation effects on bioelectrical activity in retina, optic tract, geniculum, visual cortex and octosylvian gyrus in anesthetized cats

09 p1390 A71-22215

Pyridine nucleotide concentration in cerebral hemispheres of rats under hyperoxia

09 p1391 A71-22534

Contour density effects on evoked critical response, discussing improved photopic visibility, spatial summation area and retina interaction

10 p1559 A71-23983

Cortical potentials evoked by weak acoustic signals below hearing threshold in man

10 p1564 A71-24440

Spatial and temporal patterned light flashes effects on dark adapted subjects, discussing cortical response changes in contrast depth

10 p1565 A71-24680

Intraocular pressure self regulating nervous system components, discussing fluctuation sensors, cortical centers to eye impulse conveyors and glaucoma diagnostic applications

11 p1716 A71-25199

Cortico- and subcorticograms rhythm dynamics in sleeping and awake cats by spectral analysis and EEG integration

12 p1871 A71-27486

Unanesthetized rabbits visual cortex cells neuron activity during sound-rhythmic light flashes association

12 p1871 A71-27487

Anesthetized cats visual cortex responses to prolonged light stimuli, studying dependence on photopic retina cone and rod apparatus

12 p1871 A71-27489

Somatosensory cortical and cuneate evoked responses and EEG amplitude/frequency changes due to hypovolemic shock

13 p2003 A71-27836

Extraprimary/briefly latent/ postsynaptic negative component of evoked visual potential in cortex of nembutal anesthetized rabbits, using Alvar biophase oscillator

13 p2004 A71-27894

Visual cortex neurons impulse activity and postsynaptic potential changes due to light stimuli from quasi-intracellular recordings

13 p2005 A71-28381

Visual discrimination learning by monkeys with inferotemporal cortex lesions, using positive reinforcers and electric shock punishments

13 p2011 A71-28804

Brain stem mechanisms underlying visual discrimination in rhesus monkeys subjected to bilateral lesions of the inferotemporal cortex, posterior thalamus or midbrain

13 p2011 A71-28807

Evoked cortical responses to taste solutions of acid and salt applied to human tongue surface, using averaging technique

13 p2012 A71-28887

Visual evoked cortical response in man related to rate, spatial frequency and wavelength of alternating barred pattern with background illumination

13 p2012 A71-28888

Electroencephalographic and evoked cortical potential correlates of reaction time and visual discrimination in humans

13 p2022 A71-29345

Case histories of pilot failure during training or operational flight due to cerebral cortical dysfunction

13 p2023 A71-29365

Alpha rhythm activity, periodicity and mean frequency in cortex regions of healthy humans based on EEG frequency and correlation analyses

14 p2186 A71-30551

Subcortical-cortical EEG recording of unrestrained chimpanzees sleep cycles, using computer analysis and biotelemetry techniques

15 p2359 A71-31951

Visually evoked cortical responses and visual acuity, discussing ocular convergence and accommodation effects

15 p2359 A71-31955

Cerebral ischemia effects on sensorimotor cortex function in cats, recording spontaneous EEG and pyramidal response to cortex electrical stimulation

15 p2359 A71-31956

Cortical and subcortical electrical activity during electrically and drug induced convulsive seizures in cats, correlating with spinal monosynaptic reflex variations

15 p2359 A71-31957

Blood circulation in auditory analyzer cortical section relationship to bioelectrical activity, using various frequencies pure tones as stimuli

15 p2360 A71-32531

Adrenalectomy influence on electrical activity of cortex and subcortical areas in rats under hyperbaric oxygen, using implanted electrode electroencephalographic recordings

16 p2528 A71-33118

Factor analysis of phase discrimination in mental fatigue during diurnal variation of cortical functions in railroad traffic control center operators

17 p2688 A71-34362

Hypothalamus and cerebral cortex electrical stimulation effects on temperature homeostasis under hyperoxia

17 p2680 A71-34645

Human visual evoked cortical potential spectral sensitivity measurement, comparing results with psychophysical data

17 p2680 A71-34652

Visual and auditory evoked potentials enhancement in cats using cryogenic blockage of nonspecific thalamo-cortical system in inferior thalamic peduncle region

17 p2682 A71-35112

Visual evoked potentials and cortical recovery cycle data for normal and psychiatric subjects of various ages

17 p2682 A71-35113

Deep cerebral structures and cortex electrical activity in apes, noting biopotentials during orientation/defense reactions and light signals responses

17 p2683 A71-35246

Brain locking activity structural organization, discussing cerebral processes and control contact mechanisms activating conditioned reflexes

17 p2684 A71-35358

Photoc and electric release of afterdischarges in rats visual cortex, showing retina and Corpus geniculatum laterale role

17 p2686 A71-35489

Physiological mechanisms of human auditory attention, measuring changes in cerebral cortex averaged evoked potential and cochlear nerve response

17 p2693 A71-35575

Rhesus monkeys electrocortical events recorded during foreperiod of reaction time tasks

18 p2853 A71-35895

Activity correlation of adjacent neurons of cat cerebral cortex somatosensory zone, considering distribution of same direction /cophase/ and different direction /counterphase/ of background rhythms

19 p3001 A71-37392

Functional relation of primary responses and unit spike activity at subcortical visual centers in cats

19 p3001 A71-37443

Human visual cerebral cortex potentials evoked by sinusoidally modulated field under stabilized and unstabilized conditions

19 p3004 A71-38279

Visually evoked cerebral cortex responses to on- and off-set of patterned light and contour density and sharpness in humans

19 p3004 A71-38282

Cerebral gamma-aminobutyric acid metabolism and hyperbaric oxygen induced seizures in chicks during brain development, noting increased membrane permeability

20 p3186 A71-38970

Cortical responses of awake cat to narrow-band FM noise stimuli, proposing neuronal model

20 p3190 A71-39767

Arousal and activation in nonspecific reticulothalamo-cortical systems due to underlying emotion expressed through cortical, visceral and somatomotor channels

21 p3330 A71-40247

Normal females electrophysiological changes during sensory isolation of water tank variety from EEG, EMG, EOG, EKG and electrodermal measurements, considering cortical activities reduction

21 p3330 A71-40346

Soviet book on experimental research on human higher nervous activity from growth aspect covering normal and pathological states, cerebral cortex interaction with central nervous system

21 p3339 A71-41374

Receptive fields of dark adapted cats striate cortex neurons as function of barbiturate anesthetic level

23 p3634 A71-43871

Quantitative variation in anesthetized cats striate cortex receptive fields as function of light and dark adaptation

23 p3634 A71-43872

Bioelectrical activity of monkeys cortex and deep cerebral structures under lasting rhythmic photostimulation

24 p3793 A71-44411

Averaged evoked potentials of human cortex in response to visual stimuli

24 p3796 A71-44549

Postsynaptic de- and hyperpolarization potential development mechanisms in wakeful cats cortical neurons during LF thalamic structure stimulation

24 p3797 A71-44720

Simultaneous recordings of ERG and visually evoked cortical potential to stimuli of differing luminance and pattern, comparing spatial frequency characteristics

24 p3801 A71-44977

Visual masking effects in cat striate cortex single cell activity, using moving slit and diffuse flashing light stimuli

24 p3799 A71-45140

CEREBRAL VASCULAR ACCIDENTS

Hypoxia effects on cerebral vascular autoregulation to arterial perfusion pressure in dogs

01 p0015 A71-11185

Middle cerebral artery occlusion effect on cortical blood flow, tissue oxygen pressure and acid base equilibrium in animals under extended ligations

05 p0708 A71-16617

Simulated airline pilot cerebral incapacitation etiology, incidence and detection, noting unimpaired crew members conduct and reaction times during approach for landing

22 p3501 A71-41824

CEREBROSPINAL FLUID

Central nervous system reactions to vasopressin and oxytocin presence in cerebrospinal fluid and blood, discussing respiratory frequency and antidiuretic tests

03 p0363 A71-13485

Respiratory and circulatory responses in anesthetized cats to medullary ventral surface perfusion with mock cerebrospinal fluid of varying K concentration or 2 percent procaine solutions

04 p0540 A71-15577

Cerebrospinal fluid changes due to isocarbic hypoxia, discussing electrochemical potential, lactate concentration and anaerobic glycolysis

11 p1722 A71-26360

Isocarbic metabolic acidosis effects on blood plasma, electrochemical potential differences and cerebrospinal fluid pH

11 p1722 A71-26361

Ventral spinocerebellar tract cellular level control transmission to motoneurons, considering monitoring of inhibitory interneurons output against excitatory input

12 p1869 A71-26705

Ventilatory acclimatization to chronic hypoxia in high altitude natives by cerebrospinal fluid pH decrease

17 p2683 A71-35144

CEREBRUM

Oxygen tension, blood flow, redox potential and temperature variations in cerebrum and musculus gastrocnemius of rats during high mountain adaptation

03 p0361 A71-13190

Rheoencephalography of cerebral hemodynamics during mental work, showing left hemisphere hyperemia

08 p1242 A71-21960

Cerebral lipid fractions, examining relation between physiological functions and metabolism

09 p1391 A71-22481

Glycine conversion into serine, aspartate and glutamate in cerebrum under normal and hypoxia conditions

09 p1391 A71-22482

Biological learning, considering EEG wave activity association with structural change underlying information storage in cerebral tissue

10 p1562 A71-24226

Cerebral speech mechanisms division into cortical centers and basal ganglia centers

10 p1563 A71-24229

Tolerance tests including EEG, glucose test, thermal stress and G stress for aircrew fitness assessment after cranio-cerebral incidents

12 p1871 A71-27633

Cerebrum temperature variations and tissue insulating and heat conducting properties in other anesthetized dogs with heads cooled by water stream

13 p2004 A71-28029

Small spotted dogfish shark epiphysis cerebri, determining light sensitivity and properties

13 p2008 A71-28456

Higher nervous activity physiology, discussing induction, protective and conditioned inhibition mechanisms in cerebrum and electrophysiological indices

17 p2684 A71-35359

Regional cerebral blood flow, tissue oxygen, EEG activity and behavioral reaction at high pressure

19 p3009 A71-38557

Frequency analysis of blood circulation rhythms and oxygen tension fluctuations in cerebra of rabbits, cats, monkeys and men

22 p3490 A71-42580

CERENKOV COUNTERS

Gas-Cerenkov balloon-borne detector for low energy gamma rays, calculating efficiency and angular response by Monte Carlo program

01 p0083 A71-11222

Atmospheric excess radiation flux azimuthal asymmetry in equatorial region, discussing angular intensity distribution data from Proton 2 Cerenkov counter

08 p1354 A71-21011

Cerenkov detectors and He filled spark chambers with large interelectrode spaces in high energy nuclear interaction studies, noting cosmic ray applications

10 p1612 A71-24667

Large Cerenkov detectors in absorption spectrometers during high mountain cosmic ray measurements

10 p1612 A71-24668

Nuclear component analysis of primary cosmic radiation by Cerenkov spectrometer onboard Cosmos 228 satellite

11 p1817 A71-25780

Large air shower Cerenkov detectors system, discussing energy spectra from vertical arrays, delayed muons and radio pulse detection rates

12 p1950 A71-27384

Cosmic ray telescopes with scintillation and Cerenkov counters for 2 to 8 BeV energy range, describing structural details and operational specifications

14 p2247 A71-30597

Large volume Cerenkov detector design for cosmic ray energy total absorption spectrometer measurements

14 p2247 A71-30599

Cosmic ray muon intensity measurements in water at large depths by Cerenkov counter

15 p2475 A71-31781

Atmospheric excess radiation flux azimuthal asymmetry in equatorial region, discussing angular intensity distribution data from Proton 2 Cerenkov counter

20 p3279 A71-39591

Nuclear component analysis of primary cosmic radiation by Cerenkov spectrometer onboard Cosmos 228 satellite

22 p3591 A71-41548

CERENKOV EFFECT U CERENKOV RADIATION CERENKOV RADIATION

Excited waves due to transverse disturbance normal to boundary in dielectric half of isotropic Vlasov plasma with Cerenkov instability

05 p0789 A71-16658

Cerenkov energy losses of rigid cylindrical uniformly charged bunch moving at constant speed through homogeneous isotropic dispersive dielectric

09 p1498 A71-23574

Cosmic rays visual perception by Apollo astronauts during lunar flight, discussing human eye as Cerenkov radiation detector

11 p1716 A71-25237

Angular, spectral and temporal properties of Cerenkov radiation in cosmic ray extensive air showers

11 p1815 A71-25594

Light flashes in eyes of dark adapted Apollo astronauts, considering Cerenkov radiation effects from primary cosmic ray single charged particles on retinal elements

12 p1933 A71-27383

Parametric dissipative plasma instability in HF electric field, showing plateau formation in velocity distribution function causes Cerenkov dissipation decrease

12 p1941 A71-27765

Arrival time distribution of electrons and Cerenkov light in extensive air showers, showing detector feasibility for age classification

13 p2122 A71-28071

Cerenkov light distribution calculation from gamma ray initiated air shower model obtained from Monte Carlo computer program

13 p2125 A71-28093

Solar and geophysical morphology of radio burst of active sun, treating bremsstrahlung, gyro, synchrotron and Cerenkov radiation and plasma waves

13 p2137 A71-28514

Auroral electron and proton precipitation patterns, noting LF radio noise emissions relationship to low energy electron flux through Cerenkov process

20 p3228 A71-39846

Crab Nebula cosmic gamma rays from air shower emitted Cerenkov light detection, using synchrotron Compton scattering model

20 p3285 A71-39922

Plasma resonator excitation by Cerenkov emission from density modulated uncompensated charged particle beam

24 p3854 A71-44512

CERES ASTEROID

Ceres perturbation by Neptune, comparing Laplace-Newcomb and Hill methods

01 p0156 A71-10448

Ceres and Pallas orbital commensurability, considering resonance effects

09 p1527 A71-23537

CERIUM

NT CERIUM ISOTOPES

NT CERIUM 144

Cerium effect on phase composition and mechanical properties of Nb-Al alloys, plotting isothermal cross sections

07 p1135 A71-19615

Ce, Pr and Nd solubility in Cr, investigating temperature dependence, microhardness, deoxidation and alpha phase by X ray, metallographic and durometric analyses

07 p1144 A71-20652

Zinc and misch metal in Mg alloys, detailing rare earth metals distributions in various phases

16 p2594 A71-33714

Lattice and grain boundary diffusion of Ce and Nd in Ni using radioactive tracer sectioning technique

21 p3398 A71-40468

CERIUM COMPOUNDS

Hf, Ta, W and Re solubility in La and Ce hexaborides from lattice parameters, microhardness and X ray and metallographic analyses

09 p1509 A71-23066

CERIUM ISOTOPES

NT CERIUM 144

Ce 138 excited states identification in beta decay spectra of Pr 138m and Pr 138 sources, using proton target bombardment

07 p1163 A71-19547

CERIUM 144

Radioactive decay energy conversion of beta particle emitting cerium 144 into high voltage electricity in coaxial cylinder cell

15 p2447 A71-32211

CERMETS

Kr 85 disposition following Mo-uranium oxide cermet fuels irradiation in test chamber

02 p0296 A71-12240

Gas and fluid flow through flat and cylindrical porous cermets walls, determining permeation energy loss and radial flow hydraulic resistance

02 p0240 A71-12277

Thin film cermet resistive elements physical controls electrical properties, physical controls, thermal and radiation stability

07 p1071 A71-19075

Tungsten boride sintering bonds with molten Ni as function of wettability low dihedral angle, discussing cermet porosity range

07 p1130 A71-19297

Cermet antifriction and friction powder metallurgy sintered materials for working at high temperatures without lubricants, in vacuum and inert gases

09 p1483 A71-23392

Aircraft power plants sealing materials, emphasizing porous cermet seals heat resistance under thermal cyclic loads

12 p1895 A71-27688

Titanium carbide based cermet materials with alloy steel binder, investigating production conditions, hardness, machining and quenching properties

15 p2429 A71-32139

Redistribution of carbon, copper, nickel and chromium on friction surfaces of powder metallurgy antifriction cermet slide bearings by spectral analysis

15 p2418 A71-32673

Temperature effects on service life of cermet bronze-graphite bearings using different lubricants

15 p2418 A71-32674

Microhardness dependent saturation of glass powders by iron, nickel and titanium during sintering of cermet metal matrix materials in vacuum

16 p2601 A71-33573

Ni-Cr-Mo cermet alloys sinterability, physicochemical properties and microstructure

19 p3075 A71-37109

Cermet iron chromosilicidization and sinter compactness effects on depth and structure, noting wear, corrosion and thermal resistance

19 p3075 A71-37110

Physicochemical properties of cermet sintered thermoelectric materials, considering n- and p-type samples of Si-Ge alloys

19 p3075 A71-37111

Mechanical properties of carburized cermet steel with hypereutectic structure after water quenching and tempering at 300 C

19 p3076 A71-37113

Nickel-chromium system powders physicochemical properties, noting use as high temperature cermet packing materials

23 p3690 A71-43256

CERTIFICATION

Airworthiness and Air Registration Board, discussing aims, objectives, technical changes and national and international control

03 p0524 A71-13734

Concorde progress toward certification, discussing SST airworthiness requirements, flight test program, takeoff and landing operational experience and stability problems at high incidence

05 p0696 A71-16487

Space shuttle development and certification test program comparison with large aircraft and spacecraft programs, considering Boeing 747 aircraft and Apollo Saturn S-1C stage

09 p1531 A71-22619

Business jet aircraft noise certification, discussing test programs and cost reduction

10 p1555 A71-24249

Light aircraft steel landing gear springs structural design at Cessna, considering certification requirements

10 p1555 A71-24262

Apollo program all-up spacecraft thermal vacuum tests, considering component and subsystem reliability analysis, thermal model verification and certification requirements

12 p1894 A71-26682

Airport certification and safety inspection procedures and minimum safety standards

13 p1267 A71-28305

Concorde flight simulator at Toulouse, discussing flight control system, air navigation and certification

15 p2384 A71-31881

Aircraft engine noise test methods for acoustic certification, investigating jet and compressor silencing, absorbent materials, rotor and propeller noise and psychoacoustic tests

15 p2385 A71-31890

Concorde aircraft automatic landing and flight control system objective, design, reliability and certification tests

15 p2446 A71-31915

French flight test center role in development and certification of Concorde aircraft, considering cooperation with industry

17 p2675 A71-35526

V/STOL airworthiness certification, considering standards developed by FAA in cooperation with industry
[CASI PAPER 72/21] 19 p2997 A71-37607
Airport certification and safety inspection program mandated by Airport and Airway Development Act of 1971 23 p3661 A71-43235

CESIUM

NT CESIUM ISOTOPES
NT CESIUM VAPOR
NT CESIUM 133

Thermoemissive and adsorptive properties of Nb single crystals in Cs atomic beam at various temperatures 01 p0139 A71-11100

Cs atom ionization cross section during type II collision with resonantly excited Hg atom 02 p0287 A71-12197

Electropolished and single crystal surface effects on work function of macroscopic tungsten emitter in cesiated converter 02 p0295 A71-12204

Bare and cesiated work function of covapor deposited tungsten-rhenium electrodes from vacuum emission vehicle Schottky plots 02 p0295 A71-12205

Cesiated work functions of directed monocrystalline Re thermionic emitter from saturated electron emission currents over temperature range 02 p0295 A71-12207

Electron emission formulation for cesiated metal surfaces in thermionic converter in terms of work function, using Swanson-Strayer correlation 02 p0295 A71-12210

Thermionic converter electron-cesium atom momentum transfer collision probability, considering scattering cross sections 02 p0287 A71-12227

Cesium consumption rates and content in thermionic converter components affecting system performance indicated via integral adsorption reservoir 02 p0195 A71-12245

Liquid Cs graphite integral reservoir effect on thermionic converter performance 02 p0196 A71-12271

Desorption and migration of Cs adsorbed on W surface under electric field, using field emission microscope 02 p0296 A71-12340

High density cesium beam generation using slot source and nitrogen cooled detector 04 p0632 A71-14796

Na-Cs unpolarized and spin exchange differential scattering cross sections calculation by phenomenological and difference potential methods 04 p0630 A71-15654

Cs thermoelectric power near critical temperature and pressure, determining dense plasma electron-neutral elements interaction effects 11 p1715 A71-26153

Cs atom ionization cross section during type 2 collision with resonantly excited Hg atom 15 p2451 A71-31503

Thermionic emission and adsorption characteristics of Ta single crystal faces in cesium atom streams, using thermoelectronic and surface ionization methods 15 p2453 A71-32643

Hg condensation characteristics on Cs substrate in high velocity nitrogen carrier gas, formulating one dimensional flow model based on two phase three component gas dynamics 22 p3620 A71-41876

CESIUM ALLOYS

Ce-CeN system phase diagrams investigated by differential thermal, X ray and metallographic analysis 09 p1481 A71-22186

CESIUM COMPOUNDS

NT CESIUM FLUORIDES
NT CESIUM IODIDES

Ordered intermetallic CsCl compounds thermodynamic properties determination, noting linear relationship between intrinsic disorder and formation heat 07 p1131 A71-19428

Magnetostriction in hydrated cesium manganese chloride, examining dimensional changes as function of magnetic field and temperature through antiferromagnetic, spin flopped and paramagnetic phases 11 p1807 A71-25559

Magnetostriction in antiferromagnetic, spin flopped and paramagnetic phases of hydrated cesium manganese trichloride, studying volume changes and thermal expansion near phase transition 22 p3585 A71-41885

CESIUM DIODES

Anode sheath width for collisionless thermionic converter with Ba plus Cs filler, assuming linear potential variation 01 p0005 A71-10157

Thermionic converter integrated Cs reservoir module power efficiency and service life, considering diode technology 02 p0196 A71-12270

Cs plasma thermionic diode, using Penning effect for ionization rate increase via Hg or Cd seeding 05 p0705 A71-16170

CESIUM ENGINES

Cs ion microrocket engine development, discussing Cs fueling device, ionizer heating, fabrication and control methods [ONERA-TP-847] 04 p0639 A71-15351
Ionizer, neutralizer and ion optics of cesium contact ion thruster, examining porous W materials technology [DGLR-71-033] 17 p2793 A71-35535

CESIUM FLUORIDES

Thermal dissociation rate of excited CsF, calculating ion-ion recombination rates 21 p3346 A71-40888

CESIUM HALIDES

NT CESIUM FLUORIDES

NT CESIUM IODIDES

CESIUM IODIDES

IR spectra temperature dependence of CsI crystals doped with sulfate and carbonate anions and Pb and Cd cations, observing intensive absorption bands 24 p3860 A71-44665

CESIUM ION

Cs ions surface diffusion/migration/ in presence of blocking electric field on emitter surface, examining contact-ionization ion sources 08 p1342 A71-21914

Sudden thermionic emission in surface ionization at near threshold temperatures of cesium activated tungsten single crystals 09 p1494 A71-22879

Temperature field influence on hysteresis in Cs surface ionization on metal surfaces, observing adsorption phase fine structure and ion current density increase 10 p1657 A71-24542

Cs ions surface diffusion/migration/ in presence of retarding electric field on emitter surface, showing temperature effects 17 p2789 A71-35258

Cesium ion sampling measurements in DC and RF plasma discharges, using mass spectrometry 24 p3851 A71-44429

CESIUM ISOTOPES

NT CESIUM 133

Resonance line radiation polarization of potassium and cesium isotopes excited by electron impact 09 p1496 A71-22187

CESIUM PLASMA

Nonequilibrium Ar-Cs plasma under rectangular pulse overvoltage, analyzing ionization and recombination kinetics 02 p0289 A71-12177

Thermionic converter Cs plasmas electron temperature and density gradients spectroscopic measurements compared with prediction from energy transport analysis and ionization coefficients 02 p0194 A71-12226

Compressible magnetofluid dynamics studies in cesium shock tube 04 p0632 A71-14690

Molecular ion recombination coefficient of decaying plasma formed by UV irradiation of Cs vapor in inert gas, using microwave diagnostic method 04 p0634 A71-15115

Collisional drift instability remote feedback suppression in Q machine Cs plasma by microwave modulation at upper hybrid frequency 06 p0932 A71-17464

Photoresonant cesium plasma ionization, discussing pumping spectra, electron gas, molecular-atomic ion ratio and dynamics 06 p0936 A71-17591

Low temperature confined cesium plasma, observing ion-acoustic oscillation excitation effects on transfer process and ionization 07 p1167 A71-19236

One dimensional steady supersonic motion of partially ionized two temperature argon-cesium plasma in disk type Hall MHD generator channel 07 p1023 A71-19728

Cs ion beam space charge and current neutralization by electron capture for partially ionized plasma formation, investigating longitudinal electrostatic wave excitation 07 p1171 A71-20193

Thermionic converter output improvement by Ar injection at low Cs pressures, noting electron space charge neutralization 08 p1340 A71-21490

Hot Cs plasma parametric resonance in variable electric field related to plasma heating 09 p1499 A71-22229

Physical properties of Cs discharge plasma with incandescent electrode, considering Cs atoms ionization near cathode by thermal electrons accelerated by potential jump 10 p1650 A71-24528

Measured and calculated comparison of thermionic converter cesium plasma electron densities, using rate equations taking into account collision, diffusion and photoabsorption processes 11 p1712 A71-25889

Low temperature confined Cs plasma, observing ion-acoustic oscillation excitation effects on transfer process and ionization 12 p1935 A71-26754

Low voltage arc discharge effects on ionized Cs plasma characteristics under high density current conditions 12 p1938 A71-27213

Diffusion measurement of highly ionized thermal Cs plasma in magnetic field by Langmuir probe, determining density profile 13 p2106 A71-28450

Thermionic converter output improvement by Ar injection at low Cs pressures 14 p2182 A71-30679

Nonequilibrium Ar-Cs plasma under rectangular pulse overvoltage, analyzing ionization and recombination kinetics 15 p2454 A71-31486

Steady and unsteady modes of electric arc combustion in Ar and Ar-Cs flows produced by plasma accelerator in closed glass contour 15 p2457 A71-32269

Steady state of nonequilibrium Ar-Cs plasma in electric field, attributing instability to plasma radiation effect 15 p2457 A71-32273

Cesium spectral lines luminescence and population during helium-cesium discharge plasma decay 15 p2458 A71-32407

Photoresonance cesium plasma development and decay, determining density spatial-temporal behavior and recombination and polar diffusion coefficients by probe measurements 17 p2787 A71-34287

German monograph on electron motion in cesium plasma covering Boltzmann equation, radiative transfer, mathematical model, electron velocity distribution, etc 17 p2787 A71-34485

Electric fields effects on ionization and recombination rate in non-LTE Cs plasma 18 p2852 A71-36967

Physical properties of Cs discharge plasma with incandescent electrode, considering Cs atoms ionization near cathode by thermal electrons accelerated by potential jump 19 p3116 A71-38255

Low voltage arc discharge effects on ionized Cs plasma characteristics under high density current conditions 19 p3117 A71-38625

Interelectrode spacing effects on nonequilibrium cesium plasmas in close spaced thermionic converters 20 p3179 A71-38876

Highly ionized hot Cs plasma parametric resonance in alternating electric field related to plasma heating 21 p3424 A71-41107

Nonlinear effects on spatial growth of cesium plasma wave excited by electron beam of varying density and velocity 22 p3584 A71-42535

Weakly ionized cesium plasmas produced in sealed diodes, examining LF instabilities with fluid equations 23 p3708 A71-43083

Boltzmann kinetic equation with electron-electron collision coefficients for isothermal weakly ionized cesium-argon plasma, using nodal point method 23 p3709 A71-43267

Cesium ion sampling measurements in DC and RF plasma discharges, using mass spectrometry 24 p3851 A71-44429

Microwave radiation intensity and spectral frequencies of Knudsen discharge in cesium plasma 24 p3858 A71-45244

CESIUM VAPOR

Low pressure Cs vapor discharge in positive column, determining electron energy distribution function 02 p0289 A71-11956

Cs doped Mg vapor arc discharge, determining electron mobility and diffusion cross section 02 p0286 A71-12180

Cs vapor filled cracks breakdown in thermionic trilayer insulators, calculating electron reflection and ion recombination kinetics on surfaces 02 p0232 A71-12239

Breakdown voltage measurement for Cs vapor in cracks in Alumina insulator of pressure bonded sheath tube assemblies 02 p0232 A71-12252

Cs vapor thermionic diodes with low temperature dual mode characteristics applicable as switching elements in DC to AC power conditioner 02 p0196 A71-12267

Velocity distribution measurement of Cs gas flow from orifice in near-free molecule regime, using apparatus based on time of flight method 09 p1432 A71-22682

Cesium vapor thermal conductivity measurements with miniature vacuum mode thermionic diode, investigating net accommodation coefficient dependence on surface temperature 11 p1714 A71-25901

- Spectral emission and level populations of diffusion and principal series lines of cesium vapor in 5 mm discharge plasma diode with hot cathode
12 p1941 A71-27549
- Sound velocity measurements in superheated Cs vapors, using least squares method for analytic relationships on saturation line and isobars
13 p2099 A71-27881
- Cesium vapor diffusion condensations from laminar argon flows in tubes and turbulent movement on banks, considering boundary layer mist formation effect
17 p2785 A71-34206
- Low voltage arc discharge development in cesium vapor with glowing spherical plasma cluster formation in electrode gap
19 p3109 A71-37136
- Cs and Hg vapors compressibility factor in supercritical range as function of density, considering charged particles and atoms polarization interactions in ionized metal vapors
19 p3111 A71-37590
- Low pressure Cs vapor thermionic converter with lanthanum boride cathode, investigating arc conditions and I-V characteristics
19 p2999 A71-38254
- Initial development period of low voltage arc discharge in cesium vapor leading to quasi-neutral plasma formation
23 p3710 A71-43269
- Transients determined for Cs vapor discharge phases, observing current fluctuations between steady states in negative resistance zone above 0.2 torr
24 p3858 A71-45246
- CESIUM 133**
Population inversion in Cs133 ground state hyperfine levels, using CW GaAs laser at 77 K for optical pumping
12 p1913 A71-26977
- Atomic time standards, discussing Cs 133, hydrogen maser, ammonia maser and rubidium gas cell equipment
24 p3827 A71-44994
- CESSNA AIRCRAFT**
Cessna Citation twin turbofan business aircraft design, performance characteristics, communications, navigation and automatic flight control equipment and flight evaluation
09 p1385 A71-22112
- CF-104 AIRCRAFT**
U F-104 AIRCRAFT
- CH-3 HELICOPTER**
Model following technique for optimal control applied to hovering motion of CH-3 helicopter
20 p3178 A71-39000
- CH-46 HELICOPTER**
Integral spar inspection system for making CH-46 rotor blade fail-safe
[AHS PREPRINT 551] 14 p2180 A71-31103
- CH-47 HELICOPTER**
Turbine engine fuel control stability on CH-47C helicopter, using flight tests and lag damper simulation
[AHS PREPRINT 560] 14 p2297 A71-31107
- Boeing 347 helicopter program consisting of analysis, vibration simulation, wind tunnel, whirl tower and bench tests
[AHS PREPRINT 571] 14 p2180 A71-31112
- Tapered roller bearing lubrication, considering application to CH-47 Boeing helicopter transmission
17 p2749 A71-35300
- CH-53 HELICOPTER**
U H-53 HELICOPTER
- CH-54 HELICOPTER**
Army/Navy operational evaluation of offshore containerships discharge by CH-54 helicopters
[AHS PREPRINT 573] 14 p2180 A71-31114
- CH-113 HELICOPTER**
U CH-46 HELICOPTER
- CHAFF**
Rocket-borne wind measurements at 40-70 km by glass fiber and Cu chaff clouds
12 p1901 A71-27068
- CHAINS**
Optimum synthesis of spatial four-link chain mechanism with pressure angles deviating least from zero degrees for force transmission
24 p3848 A71-44900
- CHALCOGENIDES**
NT ALUMINUM OXIDES
NT BARIUM OXIDES
NT BERYLLIUM OXIDES
NT BISMUTH OXIDES
NT BISMUTH TELLURIDES
NT CADMIUM SELENIDES
NT CADMIUM SULFIDES
NT CADMIUM TELLURIDES
NT CALCIUM OXIDES
NT CARBON DIOXIDE
NT CARBON DISULFIDE
NT CARBON MONOXIDE
NT CHLORINE OXIDES
NT CHROMITES
NT CHROMIUM OXIDES
NT COBALT OXIDES
NT COESITE

- NT COPPER OXIDES
NT COPPER SELENIDES
NT COPPER SULFIDES
NT DISULFIDES
NT ENSTATITE
NT GALLIUM SELENIDES
NT HAFNIUM OXIDES
NT HEAVY WATER
NT HYDROGEN PEROXIDE
NT HYDROGEN SULFIDE
NT ILMENITE
NT INDIUM SULFIDES
NT INDIUM TELLURIDES
NT INORGANIC PEROXIDES
NT IRON OXIDES
NT LANTHANUM OXIDES
NT LEAD OXIDES
NT LEAD SELENIDES
NT LEAD SULFIDES
NT LEAD TELLURIDES
NT LITHIUM OXIDES
NT MAGNESIUM OXIDES
NT MAGNETITE
NT MANGANESE OXIDES
NT MERCURY OXIDES
NT MERCURY TELLURIDES
NT METAL OXIDES
NT MOLYBDENUM DISULFIDES
NT MOLYBDENUM OXIDES
NT MOLYBDENUM SULFIDES
NT MUSCOVITE
NT NICKEL OXIDES
NT NIOBIUM OXIDES
NT NITRIC OXIDE
NT NITROGEN DIOXIDE
NT NITROGEN OXIDES
NT NITROGEN TETROXIDE
NT NITROUS OXIDES
NT OXIDES
NT PEROXIDES
NT PHOSPHORUS OXIDES
NT POLYSULFIDES
NT POTASSIUM OXIDES
NT PYROXENES
NT QUARTZ
NT RUTILE
NT SAPPHIRE
NT SCANDIUM OXIDES
NT SELENIDES
NT SILICON DIOXIDE
NT SILICON OXIDES
NT SILVER OXIDES
NT SODIUM PEROXIDES
NT SULFIDES
NT SULFUR OXIDES
NT TANTALUM OXIDES
NT TELLURIDES
NT THORIUM OXIDES
NT TIN OXIDES
NT TIN TELLURIDES
NT TITANIUM OXIDES
NT TROLITE
NT TUNGSTEN OXIDES
NT URANIUM OXIDES
NT VANADIUM OXIDES
NT YTTRIUM OXIDES
NT ZINC OXIDES
NT ZINC SELENIDES
NT ZINC SULFIDES
NT ZINC TELLURIDES
NT ZINCBLENDE
NT ZIRCONIUM OXIDES
- Zinc chalcogenides core electron energy levels measurement by X ray induced photoemission, noting agreement with observed auger transitions
05 p0792 A71-16318
- Laser pulse induced rapid reversible crystallization of amorphous chalcogenide semiconductor films using photon flux model
10 p1655 A71-24044
- Sb and As base chalcogenide diode structures, determining switching and memory characteristics
13 p2110 A71-27956
- Current oscillations and switching effect in amorphous chalcogenide compound films sputtered thermally on unheated glass and pyroceram substrates
13 p2111 A71-28173
- I-V and capacitance characteristics of chalcogenide-glass based matrix-film diode sandwich and film-face switching structures with/without memory
13 p2112 A71-28922
- Carrier mobility, conductivity and optical absorption in strong electric fields of chalcogenide glasses for switching and memory effect amorphous semiconductors
13 p2112 A71-28926
- I-V and capacitance characteristics of chalcogenide-glass based matrix-film diode sandwich and film-face switching structures with/without memory
21 p3433 A71-41317
- Carrier mobility, conductivity and optical absorption in strong electric fields of chalcogenide glasses for switching and memory effect amorphous semiconductors
21 p3434 A71-41323

- Glassy antimony and arsenic chalcogenide diode structures, determining switching and memory characteristics
21 p3435 A71-41343
- Symbatic shifts of conductivity compensation effect in glassy chalcogenide semiconductors unaffected by heat treatment of blanks or impurities
23 p3717 A71-44315
- Joule heating effect on static negative differential resistance and switching of chalcogenide thin films
24 p3862 A71-45353
- CHANCE-VOUGHT MILITARY AIRCRAFT**
U MILITARY AIRCRAFT
- CHANNEL CAPACITY**
Data transmission systems using information feedback techniques to achieve high bit rates /channel capacity/
01 p0064 A71-10902
- Noiseless linear feedback limitation over bandedlimited channel capacity in analog data transmission
01 p0064 A71-10906
- Frequency division multiplexing methods for wideband optical communications systems, calculating approximate information capacity
02 p0214 A71-12022
- Traffic capacity of Gaussian communications channel with Rayleigh fading, examining coder transmission coefficient under discrete control mode
03 p0378 A71-13394
- Optical channel capacity and laser signal distortion through turbulent atmosphere
05 p0720 A71-16288
- Randomly used shared communication channels capacity, calculating probability function dependence on frequency assignment policy
05 p0721 A71-16467
- Dynamic data processing systems with feedback and internal noise, evaluating carrying capacities, limiting parameters and optimal transfer function
05 p0732 A71-17164
- Intelsat 4 satellite optimum channel capacity as function of earth station performance
07 p1056 A71-18809
- Information rates attainable in optical communication channel
07 p1110 A71-19481
- Fading microwave radio channel baseband gain and noise stability, assuming nonuniform frequency selective fading effects
07 p1066 A71-20426
- Space-DMA or space-TDMA techniques conserving spectrum and increasing communication satellite channel capacity, discussing spot beams and switchings
08 p1254 A71-21326
- Frequency signal structure selection to ensure maximum information capacity for given SNR at receiver output in discrete information transmission
08 p1257 A71-21980
- Dynamic data processing systems with feedback and internal noise, evaluating carrying capacities, limiting parameters and optimal transfer function
12 p1893 A71-27455
- Optimum pulse width and information carrying capacity for dielectric single mode glass optical waveguides under distortion due to attenuation and phase velocity dispersion
16 p2541 A71-33127
- German monograph on experiments with stochastic automata covering noisy sequential nonanticipating channels with finite input/output alphabets, statistical decision functions, etc
17 p2719 A71-34774
- Wideband fiber waveguide communication systems for optical frequencies, considering information carrying capacity limitation by components available for repeaters and terminal equipment
18 p2883 A71-36995
- Performance characteristics and reuse intervals of high capacity mobile radio systems with dynamic channel assignment, using computer simulations
19 p3014 A71-37216
- Traffic capacity of systems for search and analysis of radio signals with random duration
19 p3015 A71-37258
- Ear inherent channel capacity estimation by applying Shannon equations for binary signal transmission
20 p3191 A71-39769
- CHANNEL FLOW**
NT OPEN CHANNEL FLOW
Shock wave propagation in channel with MHD interaction between compressed gas and nonuniform magnetic field
01 p0132 A71-10662
- Vertical fluid-filled channel with uniform internal heat source, analyzing steady plane-parallel convective motion
01 p0179 A71-10665
- Slowly varying plane flows of highly conducting inviscid quasi-neutral gas plasma in channel with solid metallic walls as electrodes
01 p0133 A71-10790
- Steady supersonic conducting gas flow in channel with nonconducting walls, calculating electric and gas

dynamic parameters for different imposed magnetic field geometries

01 p0133 A71-10791

Ambipolar diffusion coefficients application to analysis of laminar multicomponent ionized boundary layer flow in channel

01 p0070 A71-10795

Inviscid fluid flow in cylindrical channel excited by internal hydrodynamic energy source, calculating velocity and density distribution

01 p0071 A71-11045

Steady isothermal plane gas flow between infinite parallel plates at arbitrary Knudsen numbers, obtaining linear differential equations of mass transfer

01 p0071 A71-11114

Supersonic electrically conducting gas flow in flat channel with dielectric walls in inhomogeneous magnetic field

02 p0289 A71-11926

Diffusion with convection in flow between parallel walls, using Von Mises transformation

02 p0332 A71-12410

Sweptback turboblasts in parallel wall channel, investigating thickness, camber and leading edge curvature effects on flow and pressure distributions and vortex movement

02 p0186 A71-12606

Channel flow boundary layers, discussing parabolic differential equations, pressure gradients, friction coefficients, Stanton numbers, velocity and temperature profiles, etc

02 p0241 A71-12644

German monograph on heat transfer in Prandtl-Eyring fluid flows through flat channels with allowance for dissipation and asymmetrical thermal boundary

02 p0241 A71-12675

Rarefied gas linearized Poiseuille flow between parallel plates, using variational methods for Boltzmann equation

03 p0398 A71-13102

Nonuniform flow in straight channel inlet section initiated by Fourier expandable nonuniform profile, linearizing Navier-Stokes equations about mean velocity

[ASME PAPER 70-WA/FE-27] Superfluid flow through parallel channel, obtaining critical velocity measurements by phase coupling

03 p0404 A71-14199

Incompressible two dimensional inviscid stably stratified fluid flow over vertical step in channel bounded by rigid horizontal lid

03 p0453 A71-14201

Multielectrode MHD channels, investigating relaxation effects on two dimensional current distribution and plasma properties

03 p0466 A71-14319

Viscous incompressible conducting fluid steady flow in rectangular channel under normal external magnetic field

03 p0466 A71-14554

Conducting fluid flow in rectangular channel with electrodes under longitudinal magnetic field

03 p0466 A71-14555

Viscous incompressible conducting fluid steady laminar flow in rectangular channel with two insulating and two arbitrarily conducting walls under external magnetic field

03 p0466 A71-14556

Plane potential incompressible fluid flow in channel with rough bottom and variable surface pressure, allowing for gravitational and surface tension forces

03 p0406 A71-14567

Incident shock tube flow interaction with one dimensional MHD channel flow

04 p0632 A71-14687

Ionizing shock wave propagation through MHD channel flow, determining induction emf current and electron density and concentration

04 p0632 A71-14691

Heat transfer intensification under forced one and two phase flow in channels

04 p0675 A71-14782

Wall static pressure and convective heat transfer measurements in subsonic, transonic and supersonic regions in heated air turbulent flow through variable cross section channel

04 p0680 A71-15476

MHD channel flow with axial conduction and third kind boundary condition, investigating thermal entry region heat transfer

04 p0684 A71-15506

Ring flow expansion of incompressible viscous fluid in cylindrical channel

04 p0573 A71-15561

Minimum mixing losses of axisymmetric turbulent wakes in profiled wall channels

04 p0578 A71-15629

Dynamic model of flow separation of plane fluid past body in channel with eddy wake formation

04 p0578 A71-15630

Tubular powder channel gas velocity distribution and pressure buildup during burning

04 p0638 A71-15680

Soviet papers on energy transfer in channels covering aerothermoptics, hydrodynamics, light propagation, free convection and thermoconvective waves

04 p0628 A71-15807

Free convective flow in plane channel by boundary layer approximation, deriving continuity equations for viscous stress tensor

04 p0689 A71-15814

Turbulent boundary layer development and heat transfer in parallel wall passage entrance region, comparing measurement results with computer solution

04 p0689 A71-15920

Velocity profiles of steady axial flow of homogeneous incompressible Newtonian liquid between infinitely long parallel eccentric circular cylinders

05 p0735 A71-16611

Heat transfer from finite flat plate in channel flow for vanishing Prandtl number, using Fourier transform and Wiener-Hopf technique

[DFVLR-SONDDR-98] Plane steady laminar flow into channel between two semiinfinite parallel plates, constructing asymptotic solution for large Reynolds number

05 p0736 A71-16966

Steady two dimensional flow past flat plate in rectangular channel for low Reynolds number

05 p0738 A71-17249

Channel flow and flow past bodies turbulent/laminar reverse transition for friction drag and heat transfer reduction

06 p0881 A71-17584

Anomalous viscous fluid in channel with nonconducting walls, considering magnetic field effect on heat transfer

06 p0937 A71-17738

Convective heat transfer in coolant with constant velocity in ring channel with heat sources, deriving expressions for flow and wall temperature

06 p1006 A71-18004

Laminar flow heat transfer between plane parallel plates under generalized Graetz conditions, retaining longitudinal conduction term

06 p1007 A71-18306

Laminar incompressible flow heat transfer in inlet between parallel plates at constant temperature, considering pressure gradient effect on boundary layer velocity profile

[AIAA PAPER 71-36]

06 p1008 A71-18497

Chemically reacting viscous supersonic laminar flow in two dimensional divergent plane channel, developing approximate system of parabolic partial differential equations

[AIAA PAPER 71-44]

06 p0866 A71-18505

Flow between parallel plates of dissimilar surface texture, obtaining mixing length models velocity profiles, skin friction coefficients and zero shear stress position

07 p1086 A71-18773

Flow field behind two dimensional roughness element in rectangular channel, discussing wall effects, reattachment point position, velocity distribution and turbulence intensity

07 p1086 A71-18775

Flame propagation process, investigating transfer in turbulent flow, combustion times and burning in channel

07 p1220 A71-18778

Two dimensional turbulent channel flow, determining local mean wall shear stress from velocity gradient

07 p1087 A71-18784

Incompressible turbulent circulatory fluid flow in plane curvilinear channel, deriving energy balance equations

07 p1088 A71-19199

Weakly ionized gas discharge three dimensional unsteady motion of viscous incompressible gas discharge plasma in homopolar device curvilinear channel, emphasizing secondary overflow during acceleration

07 p1167 A71-19235

Unsteady MHD channel flow between two semiinfinite harmonically oscillating and perfectly conducting solids, determining fluid velocity profile curves

07 p1169 A71-20032

Turbulent pipe, channel and plane Couette flow by Prandtl model equations, comparing with experimental data

07 p1092 A71-20278

Finite element solution of plane Poiseuille rarefied gas flow between parallel infinite plates

07 p1093 A71-20284

Computerized simulation of inlet channel flow passage cross section effect on internal combustion engine filling

08 p1347 A71-20830

Cellular convection in horizontal gas layer between solid walls and heated from below

08 p1376 A71-21789

Velocity profile in viscous sublayer at wall based on maximum stability principle applied to Karman constant for turbulent channel flow

08 p1277 A71-21950

Water cooled channel flow test device for arc jet material ablation studies, simulating reentry environment of high energy turbulent boundary layer flow

08 p1273 A71-21987

Flow in channel with abrupt asymmetric widening, calculating expanding flow velocity profile by Prandtl semiempirical turbulence theory

08 p1277 A71-22041

Centrifugal pump channels flow velocity measurement by optical method, noting flow separation near blade exits

08 p1230 A71-22048

Boundary value problem of end effect in MHD channel with semiinfinite electrodes for arbitrary Reynolds numbers

09 p1499 A71-22130

Three dimensional end effects on MHD flow in rectangular channel with nonconducting walls

09 p1499 A71-22133

Laminar flow of viscous electrically conducting fluid in traveling magnetic field, examining channel flow in traveling wave field of one directional and two directional inductor

09 p1499 A71-22134

Nonlinear MHD equations solution for laminar flow of electrically conducting fluid in cylindrical channel in traveling magnetic field

09 p1499 A71-22191

Plasma blowing and suction through channel wall electrodes in two dimensional stationary flow, taking into account Hall effect

09 p1502 A71-22537

Electrohydrodynamic flow in plane channel with conducting walls and axial emitter electrode, determining velocity and pressure profiles distortion

09 p1502 A71-22538

Power augmented lift STOL aircraft operating costs reduction by channel wing concept, discussing aerodynamic theory and structural applications to high lift flaps aircraft

09 p1385 A71-22592

Rarefied gas thermal creep flow between parallel plates, using Boltzmann equation relaxation model for all Knudsen numbers

09 p1433 A71-23055

Quasi-one dimensional approximation equations derivation for electrohydrodynamic channel flows with small interaction parameter, obtaining I-V characteristics

10 p1649 A71-24365

Friction drag and energy losses of steady plane incompressible boundary layer flow of viscous liquid on nonconducting wall in MHD channel

10 p1649 A71-24377

Air and carbon dioxide intensive injection effect on turbulent boundary layer of subsonic channel air flow

10 p1551 A71-24378

Steady two dimensional MHD laminar flow between two parallel circular porous disks in transverse magnetic field, determining velocity, pressure and shear stress distribution

10 p1649 A71-24408

Flow instability and secondary circulation in pressure-driven rotating rectangular channel

10 p1595 A71-24617

Flow patterns within centrifugal and mixed flow impeller channel, examining velocity distributions, blade surface pressure and flow behavior

[ASME PAPER 71-GT-41]

11 p1704 A71-25974

Glass fiber rotor blades design with longitudinal pressure tapings for cascade wind tunnel and turbomachinery flow research applications

11 p1772 A71-26316

Radiating laminar convective flow in vertical heated channel, noting radiation effects on temperature and velocity

11 p1860 A71-26446

Laminar incompressible entry flow in plane channel based on modern boundary layer theory

12 p1897 A71-27223

Soviet book on MHD flows in channels covering one dimensional theory, viscous fluids, boundary layers, electric fields, laminar flow, etc

12 p1940 A71-27294

Spectral density of friction pulsations in turbulent channel wall flow for various length to height ratios and Reynolds numbers, using electrochemical method

12 p1897 A71-27306

Electrohydrodynamic ideal incompressible fluid flow in flat and circular channels, determining electric potential and field distribution

12 p1941 A71-27520

Viscous convergent-divergent nozzle flow slender channel approximation, discussing nozzle geometry, Reynolds number and wall temperature effects

[AIAA PAPER 69-654]

12 p1865 A71-27556

Local and mean heat transfer at initial thermal segment for stabilized turbulent air flow in circular tubes and rectangular channels

13 p2159 A71-28419

Optimal control of oscillations of electrically conducting fluid by magnetic field in plane channel with free boundaries, using dynamic programming

13 p2107 A71-28728

Carbon dioxide reduction and hemoglobin saturation rates of blood flow in curved channel membrane exchanger

13 p2013 A71-29004

Exact method for low Peclet number thermal entry region heat transfer in channel flow, considering transverse nonuniformity of fluid velocity and axial conduction

13 p2164 A71-29009

Transonic gas flow measurement during sudden expansion from circular nozzle into coaxial cylindrical channel, emphasizing flow attachment

13 p1993 A71-29192

Gas flow in plane channel due to longitudinal temperature gradient at arbitrary Knudsen number, using linearized Boltzmann kinetic model equation

13 p1993 A71-29194

Steady flow of electrically conducting incompressible viscous fluid in rotating parallel-plate channel under constant transverse magnetic field

13 p2110 A71-29296

Electric circuits calculation in MHD problems such as MHD channel flow, electrodynamic plasma, etc

14 p2277 A71-29558

Laminar incompressible fully developed pulsating flow between parallel flat plates effects on local time-average heat flux

14 p2334 A71-29603

MHD flow in rectangular channel with two conducting walls, investigating velocity structure

14 p2278 A71-29607

Argon plasma jet velocity distribution at MHD channel exit with magnetic quadrupole, using calorimetric plasma velocity measurements and Doppler shift observations

14 p2278 A71-29611

Rectangular cross section MHD channel spatial electrical field distribution, obtaining electrostatic potential, boundary conditions and efficiency

14 p2278 A71-29612

Flow transition to laminar drag law for thin cylinder freely suspended in Hg in rotating vertical cylindrical MHD channel

14 p2279 A71-29615

Electrode voltage of rectangular cross section MHD channel in conductive flowmeter, investigating magnetic field inhomogeneity and velocity profile effects

14 p2279 A71-29617

Stationary Gaussian Markovian form randomly fluctuating pressure gradient effects on steady incompressible channel flow velocity

14 p2223 A71-29924

Vortex induced shear and secondary flow through row of spheres, curved channel, turbine blades, rotating impeller, suction pipe and upstream boundary layers

14 p2224 A71-30176

Heat transfer in rarefied gases, considering gas at rest between flat plates, concentric spheres and cylinders and flowing through tubes, nozzles and between parallel plates

14 p2336 A71-30242

MHD three dimensional flow between rotating and stationary disks in transverse magnetic field with uniform suction at stationary disk

14 p2283 A71-30839

German monograph on similarity transformations application to MGD channel flows covering mechanical, electromagnetic and thermodynamic equations

14 p2283 A71-30863

Shock wave propagation in channel with MHD interaction between compressed gas and nonuniform magnetic field

14 p2283 A71-30995

Vertical fluid-filled channel with uniform internal heat source, analyzing steady plane-parallel convective motion

14 p2339 A71-30998

Finite element method application to transonic viscous flow through cascades and channels

[AIAA PAPER 71-602]

15 p2388 A71-31542

Slip flow development in parallel plate channel entrance, discussing center line velocity and excess pressure distributions

15 p2393 A71-32262

Peristaltic pumping mechanism as progressive wave train of transverse wall displacement in plane two dimensional channel

15 p2366 A71-32559

Axial flow gas turbines blade cascades forming arrays with convergent channels, discussing contours design

16 p2521 A71-33615

Viscous incompressible fluid flow between two rotating nonconcentric cylinders, presenting transverse velocity profiles

17 p2725 A71-34177

Supersonic jet expansion in variable geometry channels, obtaining pressure dependence on injection rate and similarity parameters

17 p2669 A71-34216

German monograph on electron production effect on channel breakdown in nitrogen, showing positive space charge accumulation near anode in gas discharge

17 p2788 A71-34775

Reynolds magnetic number effect on MHD channel conducting gas flow current distribution, taking into account Hall effect

17 p2790 A71-35642

Compressible electrically conducting gas boundary layer on MHD channel electrode, deriving equations for ambipolar region with finite ionization and recombination rates

17 p2790 A71-35644

Electric and magnetic fields effect on turbulent boundary layer of conducting gas near electrode in MHD channel with insulated walls

18 p2951 A71-36113

Supersonic jets expansion in variable cross section channel, emphasizing boundary layer behavior

18 p2903 A71-36119

Laminar and turbulent incompressible entry flows in channel with jets along walls, determining filling length

18 p2904 A71-36135

Weakly interacted laminar MHD flow growth in entrance region of plane channel with wall conductances investigated by momentum integral method

[ASME PAPER 71-APM-A]

18 p2951 A71-36251

Steady inviscid fluid flows in plane channel and in axially symmetric nozzle, considering external magnetic field effects with electroconductive fluid

18 p2907 A71-36327

MHD channels end effects at finite magnetic Reynolds numbers, discussing wall conductivity and external magnetic field geometry effects

19 p3108 A71-37078

Gas flow velocity measurements in channel, using electromagnetic technique

19 p3061 A71-37090

Laser light beam attenuation, considering turbulent pulsation effects in closed channel fluid flow axial region

19 p3071 A71-37279

Spectral density of friction pulsations in turbulent channel wall flow for various length to height ratios and Reynolds numbers, using electrochemical method

19 p3046 A71-38262

Perturbed problem of rotational steady compressible flow in three dimensional channel at upstream infinity/shear flow/, using linearization by current functions

20 p3211 A71-39419

Flow instability in stagnation point region of circular cylinder in turbulent channel flow, using hydrogen bubble method for flow visualization

20 p3211 A71-39454

Vortex flow through axial, axially radial and other three dimensional axisymmetric channels, using finite difference model for flow equations solution

20 p3211 A71-39465

Velocity and resistance profiles for unsteady turbulent flow in rough pressure channels, using Prandtl hypothesis

20 p3214 A71-39797

Stepwise change in wall roughness effects on turbulent shear flow through two dimensional channel, measuring mean velocity, turbulent intensity and shear stress

21 p3365 A71-40015

Laminar-turbulent inverse transition in divergent radial flow between two parallel flat disks

21 p3366 A71-40101

Unsteady viscous compressible flow through straight channel with flat porous walls under time varying pressure

21 p3367 A71-40591

Thermal convection induced perturbations in unstably stratified horizontal shear Couette flow of Boussinesq fluid in rectangular channel heated from below

21 p3475 A71-40641

Electrically conducting fluid flow resistance in plane insulated channel in presence of transverse magnetic field, determining pressure, velocity and electric potential distributions

21 p3422 A71-40677

Nonstationary ideal gas flow in variable section axisymmetric channel, noting flow disturbances during sudden changes in conditions at outlet section

21 p3368 A71-40696

Spectral density functions of velocity pulsations and frequency dependent stability in turbulent plane and axisymmetric channel air flows at different Reynolds numbers

21 p3368 A71-40697

Heat transfer and temperature field calculation in turbulent flows through channels of noncircular cross sections, allowing for secondary flow

22 p3619 A71-41871

Laminar Couette flow between parallel plates with mechanical energy dissipation and temperature dependent viscosity, determining velocity and temperature distribution

22 p3531 A71-42683

Rivlin-Ericksen fluid steady flow between parallel plates with uniform suction at lower wall, detailing velocity field, skin friction and flow coefficient

23 p3663 A71-43492

Isentropic ideal compressible vortical gas flow in axisymmetric channel, determining stream function and gas density

23 p3625 A71-43549

Random fluctuating longitudinal pressure gradient effect on steady incompressible channel flow for arbitrary power spectrum and probability density

23 p3664 A71-43597

Sound wave propagation from two dimensional acoustic source in subsonic fluid moving between two reflecting parallel walls

23 p3705 A71-44149

Supersonic aircraft shape for shock waves minimization based on channel configuration with converging inlet and diverging outlet section

24 p3791 A71-44572

Hydraulic resistance and heat transfer in annular channel with rotating flow, comparing to axial flow

24 p3888 A71-4474

Flow instability due to viscosity variation in high pressure two dimensional laminar flow of Newtonian fluid between rigid parallel plates

24 p3819 A71-44945

Perturbations generated by two dimensional supersonic channel flows with walls oscillating with harmonic time dependence and small pressure amplitude computed, using linearized method of characteristics

24 p3819 A71-44951

Hydraulic resistance of laminar isothermal flow of fluid with structural viscosity in circular cylindrical rigid channel

24 p3821 A71-45227

CHANNELS

Channel form determination from circles family envelopes, discussing turbine duct geometries

06 p0641 A71-18009

CHANNELS (DATA TRANSMISSION)

Coherent binary reception channels noiseproof qualities in presence of fluctuating noise and single concentrated bursts

01 p0030 A71-10473

Low cost error control technique for bulk data transmission over channels with noisy feedback link

01 p0034 A71-10903

Linear information feedback methods for white Gaussian noise channels

01 p0064 A71-10904

Output format coding for telemetry data compressor channel and frame identification

01 p0036 A71-10984

Gaussian message optimal transmission through channel with white Gaussian noise in presence of total feedback

01 p0064 A71-11152

Soviet papers on digital information transmission via channels with memory

01 p0039 A71-11314

Continuous signal discretization for communication channels maximum information compression rates

02 p0211 A71-11826

Isotropic photooptical channels transfer functions analysis, using two dimensional Fourier transforms

02 p0211 A71-11829

Image transmission in isotropic photooptical channels, examining object-image brightness relationship

02 p0211 A71-11830

Noise stability in single-channel FM transmission system via maximum SNR obtained with optimal predistortion

02 p0212 A71-11836

Phase meter channels correlation effect on mean phase difference measurements accuracy in heterodyne oscillators

02 p0212 A71-11837

Optical scatter channel transmission characteristics, using mathematical model consistent with radiative transfer theory and probability-computing receiver

02 p0249 A71-12012

Free space optical channel analog and digital communication theory, considering SNR, M-ary signaling, error probabilities and information rates, etc

02 p0213 A71-12018

Direct detection, heterodyne and optimum receivers for optical scattering channels in digital communication

02 p0214 A71-12020

Wideband amplitude modulator for quasi-optical waveguide channels, featuring one dimensional rotating wire grating

03 p0378 A71-13804

Gigabit PCM data communications system using functional circuits with microstrip interconnect

05 p0719 A71-16152

Equipment and procedures for group servicing of parallel data transmission channels with error correcting codes and automatic interrogation of erroneous sequences

07 p1061 A71-19510

Computer display channel for en route air traffic control flexible real time data processing and display subsystem

07 p1156 A71-19721

Reproduction quality of information transmitted by error correcting codes for stationary symmetrical channel without storage

08 p1251 A71-20732

Information loss in transmission by group error correcting codes in stationary symmetric channel without storage

08 p1252 A71-20733

Short wave communication channel quality estimate for discrete signal transmission based on signal level variations calculation with allowance for ionospheric parameters

08 p1252 A71-20773

Telephone channel phase-frequency distortions effects on discrete signal transmission quality from phase-delay-time frequency characteristics criterion

08 p1253 A71-20774

Complex and envelope covariance for Rician fading communication channel, deriving equation for unsymmetric power spectrum

10 p1574 A71-23767

ECG miniaturized single channel biotelemetry transmitter, discussing lightweight design and power supply

10 p1570 A71-24487

Binary on-off laser communication channels, calculating atmospheric turbulence effect on Poisson detection error probability

11 p1730 A71-25198

Scalar Gaussian channel information optimal input capacity as function of random variable, assuming finite number of values for amplitude and variance constraints

11 p1730 A71-25374

Hybrid decoding technique for symmetrical binary input channels, using bootstrap algorithm across convolutionally encoded information streams

11 p1730 A71-25375

Digital FM techniques for combined time and frequency division multiplexing, improving telemetry sampling channel bandwidth utilization

14 p2193 A71-30020

Discrete and continuous channel stochastic coding processes and resulting communication system properties

15 p2372 A71-32320

ATC satellites providing communications channels between aircraft and ground control stations and aircraft localization

16 p2605 A71-32849

Two dimensional linear communication system with crossed channels with different amplification factors and time constant, examining stability with root trajectory method

16 p2549 A71-33569

Error estimates in transmission of pulse code telemetering signals by nonredundant binary code through asymmetric channel

16 p2543 A71-33706

Telegraphy binary data transmission through channels with frequency-selective fading, investigating noise stability improvement by programmed carrier frequency variation and receiver passband shifting

17 p2698 A71-34394

Error correcting codes in binary symmetrical communication channel with additive white noise at large SNR

17 p2702 A71-34972

Mean-square-error determination for binary code data transmission in symmetrical channels with slowly changing parameters, noting dependence on fading level

17 p2702 A71-34974

Forty channel magnetography system including CRT display, digital controlled heliostat, real time computer and optical transducer

17 p2740 A71-34988

FDMA single channel per carrier satellite communication system voice processing and modulation techniques, discussing analog frequency modulation and phase shift keying

17 p2704 A71-35086

SPADE system digital channel unit applicability to services other than voice transmission, discussing narrow- and wide-band data transmissions and bit-error-rate performance

17 p2706 A71-35104

Redundant solid state sequencer programmable via core memory, using two identical channels to prevent wrong output

18 p2885 A71-36449

Error occurrence due to perturbations in space communication channels for digital data transmission, describing binary channels models based on Markov chains

18 p2881 A71-36567

Amplitude distribution of pulse train with given constant pulse durations in communication channels

18 p2882 A71-36621

Stochastic passband model of tropospheric communications channel, denoting random frequency duration above threshold level

19 p3022 A71-38501

Critique of paper on additional signal power for optimum performance of PCM binary signal detection under channel band limiting effect in white noise

20 p3196 A71-38870

Statistical analysis of digital automatic control system with unreliable communication channel, determining system mean square error

22 p3525 A71-41439

Computer technique for synthesizing binary holograms used in wave beams analysis in quasi-optical communication channels

22 p3546 A71-42320

Signal design and error rate of impulse noise channel, analyzing error probability of smear-desmeared standard data channels through Rice integral evaluation

22 p3513 A71-42381

Primary sensor transfer function selection to minimize rms error in information transmission over telemetry channel for subsequent digital processing

23 p3648 A71-43294

Uniform signal energy distribution in wideband synchronous data transmission channels using linear sequential filters with scramblers

23 p3647 A71-44345

CHAPLYGIN EQUATION

Plane nonsteady gas dynamic flows, reducing to system of time dependent equations system, presenting Chaplygin equation generalization

03 p0401 A71-13908

Geometrical solutions to central motion and space vehicle dynamics, including Chaplygin problem, position and velocity transfer and comet tail separation

05 p0810 A71-16584

Approximation of Chaplygin equation for subsonic ideal gas plane adiabatic flow, applying to discharge from flat channel with contraction

07 p1016 A71-20083

Two link approximation of Chaplygin function by coupling to integral equations, applying to ideal gas jet separation flow past symmetrical arc

07 p1016 A71-20084

Multilink approximation of Chaplygin function in subsonic and supersonic flow regions, deriving coupling conditions relative to modified stream function at approximation nodes

07 p1016 A71-20090

Tricomi problem for elliptic-hyperbolic Chaplygin equation extended to mixed Lavrentev-Bitsadze equation

10 p1635 A71-23802

Proof theorem for Chaplygin successive approximations method, presenting lemma for convergence of solutions to differential equations system

10 p1636 A71-24021

Modified Chaplygin algorithm application to bilateral approximate solution of limiting Cauchy problem, discussing convergence and error estimation

11 p1792 A71-26155

Hydrodynamic analogy for postulates in special relativity theory, analyzing steady and potential flow of inviscid compressible medium for Chaplygin gas with unreal time

12 p1932 A71-27547

CHAPMAN SHEAR LAYER

U SHEAR LAYERS

CHAPMAN-ENSKOG THEORY

Maxwellian distribution function calculation for molecules during initial phase of chemical reaction by successive approximations and Chapman-Enskog method

03 p0376 A71-14065

Space-time and time correlation functions for classical many body system, proving Chapman-Enskog equivalence to correlation function methods

05 p0786 A71-16864

CHAPMAN-JOUGET FLAME

U CHEMICAL EQUILIBRIUM

U DETONATION

U FLAME PROPAGATION

CHARACTER RECOGNITION

World four dimensional and space three dimensional characters and psychophysical sensations dependence on Weber-Fechner law and tritestimulus principle in psychology

09 p1530 A71-23730

Pattern recognition machine construction for written alphanumeric symbols and human voice identification, providing bibliography

15 p2372 A71-32316

Isolated lower case letters visual recognition, investigating perceptual similarities and common properties serving as cues

17 p2680 A71-34655

CHARACTERISTIC EQUATIONS

U EIGENVALUES

U EIGENVECTORS

CHARACTERISTIC FUNCTIONS

U EIGENVALUES

U EIGENVECTORS

CHARACTERISTIC METHOD

U METHOD OF CHARACTERISTICS

CHARACTERIZATION

Characterization of high purity metals by residual resistivity ratio, using nondestructive eddy current decay method

18 p2938 A71-36992

CHARACTERS

U SYMBOLS

CHARCOAL

Activated charcoal effects moss development alterations on artificial agar substrate

11 p1721 A71-26319

CHARGE CARRIERS

NT FREE ELECTRONS

NT HOLES [ELECTRON DEFICIENCIES]

NT MAJORITY CARRIERS

NT MINORITY CARRIERS

Microwave Gunn diodes I-V characteristics as function of carrier concentration

01 p0057 A71-11213

P-n junction formation in zinc mercury telluride samples, using heat treatment to control carrier concentration

01 p0140 A71-11464

Carrier mobility dependence on channel transverse electric field in MOS transistor

02 p0231 A71-11841

CdTe thin film solar cell characterization, showing low carrier concentration of base layer and improved stability at elevated temperatures

05 p0699 A71-16059

Field effect transistors with nonuniform doping profiles along channel, calculating carrier accumulation and space charge limited current flow by two dimensional model analysis

05 p0791 A71-16166

Gallium phosphide current carriers radiative recombination, discussing electro- and photoluminescence phenomena

06 p0940 A71-17350

Surface illuminated semiconductor excess current carriers nonstationary distribution and space charge, solving equation system by operational technique

06 p0942 A71-18185

Polycrystalline semiconductors grain boundaries effect on conductivity, Hall mobility and current carriers concentration

06 p0942 A71-18187

Lamb wave interaction with current carriers in cubic symmetry piezosemiconductors, obtaining amplification factor

06 p0942 A71-18352

Carrier mobility in noncompensated highly doped semiconductors, presenting derivation from Rogachev expression for scattering Coulomb center screening charge density

07 p1175 A71-19218

SHF electric fields effects on free carrier redistribution in semiconductors and surface effect influence on sample conductivity

07 p1177 A71-19496

Intermetallic III-V compound semiconductor films and layers charge carrier transport phenomena and optical properties

07 p1178 A71-19850

Charging carriers of MOS structure interface states, considering effect on static transistor characteristics

08 p1265 A71-21291

Nonlinear theory of intrinsic semiconductors electromagnetic wave transmission under skin effect conditions, determining reflectance and carrier temperature

08 p1344 A71-21442

Three dimensional model of semiconductor diode current dependence on charge carrier diffusion length and surface recombination rate

09 p1414 A71-22189

Electron entrainment by photons during intraband light absorption by free carriers in Ge semiconductors

09 p1507 A71-22232

Carrier concentration, radiation dose and temperature effects on radiation defect formation in Si and Ge during gamma irradiation

10 p1655 A71-24138

Output pulse amplitude from lithium-drifted detector-amplifier combination under conditions of carrier diffusion and bulk and surface recombination

11 p1802 A71-25804

Semiconductors high carrier densities at low temperatures, showing possible soft plasma branch and electron sound

12 p1944 A71-27770

Complex permittivity of spherical conducting particles in dielectric host medium, showing dependence of real and imaginary parts

13 p2038 A71-28611

Electron-hole scattering effect on carrier heating and I-V characteristics in semiconductors, using relaxation time and self consistent analysis

13 p2111 A71-28921

Thermal suppression of photoconductivity in crystals with two impurity types, showing carrier concentration decrease in conduction band in narrow temperature range

13 p2112 A71-28924

Variances and covariances calculation for fluctuating numbers of semiconductor conduction electrons in terms of noise

14 p2211 A71-30292

Thermal noise in space charge limited solid state diodes with field dependent mobility and hot carriers

14 p2284 A71-30502

Poisson equation for space charge layer of reverse-biased p-n junction in p-n-p-n structure with allowance for two types of moving current carriers

16 p2546 A71-33495

Switching on p-n-p-n structure under high injection level in both bases, noting current concentration and voltage steady state buildup

16 p2546 A71-33496

Microwave Gunn diodes I-V characteristics as function of carrier concentration and power efficiency

17 p2713 A71-34264

Self generated turbulence in insulating liquids during unipolar charge carrier injection, describing charge transport by Lagrangian diffusion process

19 p3044 A71-37736

Gunn diodes stable high field domains parameters and behavior, considering hole effects in various carriers

19 p3028 A71-37861

Nonlinear Faraday effect in nonparabolic semiconductors subjected to strong electromagnetic field and steady magnetic field, deriving distribution function of charge carriers

20 p3276 A71-39010

Electron drag by photons during intraband light absorption by free carriers in n-Ge semiconductors

21 p3428 A71-41111

Electron-hole scattering effect on carrier heating and I-V characteristics in semiconductors, using relaxation time and self consistent analysis

21 p3433 A71-41308

Auger recombination coefficient determination for nonequilibrium carriers in n-type InAs from photoconductivity and light absorption under laser excitation at high levels, noting electron mobility

21 p3433 A71-41310

Thermal suppression of photoconductivity in crystals with two impurity types, showing carrier concentration decrease in conduction band in narrow temperature range

21 p3434 A71-41320

Semiconducting plasma carrier density gradient instability, investigating threshold curve for n-type germanium

21 p3434 A71-41330

Avalanche Si photodiode current pulse formation frequency governing mechanism, considering roles of free carriers and electron tunneling

21 p3358 A71-41344

Multiple layer liquid epitaxial growth of lead tin tellurides from Pb-Sn solution, determining low carrier concentrations by Hall effect and capacitance measurements

22 p3585 A71-41810

Scale effect in semiconductor magnetoresistance due to carrier separation across plate thickness under perpendicular magnetic field

23 p3715 A71-43476

Dynamic carrier density instabilities for semiconductor-metal electronic phase transition by Frenkel-Poole effect in semiconductor with donors

23 p3716 A71-43478

Current carrier mobility and concentration measurements in inversion metal dielectric semiconductor channels by Hall method

24 p3808 A71-44384

Experimental verification for electrostatic field gradient effects on charge carrier concentration in diffused regions of semiconductors

24 p3863 A71-45359

Luminescence time decay in optically excited thin direct gap semiconductor with surface losses, establishing phase shift method for carrier lifetime and semiconductor surface properties

24 p3863 A71-45360

CHARGE DISTRIBUTION

Lower limit of neutral line in geomagnetic tail merging, noting inconclusiveness of direct spacecraft observations

03 p0421 A71-14551

Field effect transistors with nonuniform doping profiles along channel, calculating carrier accumulation and space charge limited current flow by two dimensional model analysis

05 p0791 A71-16166

Nonraining clouds electric fields and charge distribution, calculating convection influence by numerical means

05 p0777 A71-16675

Collinear and planar arrays of arbitrarily located parallel elements, determining current and charge distribution, admittances and field patterns

06 p0875 A71-17715

Silicon dioxide space charge distribution dependence on photoinjected currents in MOS structures, showing charge effects on I-V characteristics

07 p1174 A71-19055

Ion diffusion and conduction to cloud droplets, determining resulting mean charge distribution for polar conductivities fixed ratio

07 p1152 A71-19757

MOS transistors and bipolar microcircuits mobile charge density, observing p-n junction effects

07 p1079 A71-20175

Large Z primary cosmic rays charge spectra, using semiautomatic photometer

08 p1350 A71-20953

Galactic cosmic ray propagation earth-source distance determination by observing charge spectrum

08 p1354 A71-21018

Differential charge amplifier design using ferromagnetic high signal bandwidth isolation with grounded input transducer and output load

09 p1417 A71-22782

Potential and ion charge distribution in proximity to conducting sphere moving in low density collisionless ion-electron plasma

12 p1958 A71-26647

Electrical screening layers around charged clouds, giving numerical model for space charge accumulation, electric field distribution and forces acting on cloud droplets

12 p1925 A71-27290

ECG measuring locations number and positions for determination of time varying total body QRS surface potential distribution

13 p2016 A71-28149

Lightning problem from electrodynamic viewpoint, considering vertical discharge channel, charge distribution, current and nonuniform inducing fields

13 p2097 A71-28394

Adiabatic flow model of noiseless magnetic neutral sheet of finite width, discussing particle trajectory and charge density distribution

13 p2109 A71-29166

Atmospheric space charge and distribution measurement through oscillating electric field modulation by sound waves

16 p2562 A71-33067

Dipole antenna near electric field, basing calculation method on integral equation for antenna surface charge distribution function

16 p2546 A71-33487

Anisotropic carrier redistribution near semiconductor charged surface with energy band bending, discussing relaxation rate

17 p2790 A71-34197

General media electrical properties from current and charge distributions and impedance characteristics of electrically thin cylindrical antennas

17 p2715 A71-34759

Electron beam for determining plasma potential and charge density as function of radius of inertially confined tenuous plasma cylinder

20 p3273 A71-39009

Electron removal from neutralizing emitter in cylindrical ion beam, determining I-V characteristics of plane diode with positive charge distribution

20 p3272 A71-39152

Electron guns pervance increase by transverse and longitudinal charge compression, reviewing beam formation theory

20 p3204 A71-39154

Galactic cosmic ray propagation earth-source distance determination by observing charge spectrum

20 p3280 A71-39598

Neutron irradiation effects on Si p-n junction field effect transistors I-V characteristics, charge distribution in space charge region and transconductance

22 p3586 A71-42297

Pulsar radio emission from expanding charge sheets moving relativistically along dipolar magnetic field near neutron star polar caps, calculating energy distribution

22 p3604 A71-42336

Minority carriers charge distribution at boundary between neutral base and collector transition region of one dimensional n-p-n transistors

23 p3653 A71-43965

Capacitance and conductivity in metal dielectric semiconductor during majority current carrier population depletion by pulsed voltage, discussing concentration and mobility determination

24 p3859 A71-44376

Current and charge saturation effects on channel electron multipliers in continuous and pulse operation

24 p3811 A71-45330

Experimental verification for electrostatic field gradient effects on charge carrier concentration in diffused regions of semiconductors

24 p3863 A71-45359

CHARGE EXCHANGE

NT RESONANCE CHARGE EXCHANGE
Dense plasma cluster charge exchange in supersonic Mg jet, examining pair collision model, particle scattering, target thickness and Q switching

02 p0292 A71-12614

MOSFET transistors instabilities due to charge exchange near oxide-silicon interface states, determining energy levels distribution and time constants

05 p0791 A71-16165

Anomalous low magnetospheric He alpha/proton flux ratio in terms of electrostatic radial diffusion taking into account charge exchange and pitch angle loss processes

06 p0964 A71-17284

Zinc electrode kinetics noting exchange reactions, anodic behavior in alkaline solutions and capacitance

08 p1233 A71-21080

Cross sections for simultaneous ionization and charge transfer in fast proton-helium atom collisions, using Born approximation

09 p1497 A71-22416

He-Zn ion laser, considering charge exchange and Penning collisions as primary excitation sources of Zn II levels

11 p1773 A71-25927

Stellar electric charges, determining sign and magnitude by exchange processes between stars and surroundings

12 p1971 A71-27763

Cosmic rays neutron spectrum at sea level, using charge exchange reaction

15 p2479 A71-31867

Ar ion laser plasma spectral lines widths and shifts at various pressures and current densities, noting role of ion-neutral charge exchange collisions

18 p2932 A71-37007

Reversible charge exchange reactions effects on ionization equilibrium of nitrogen in interstellar space

21 p3445 A71-40412

He-Cd CW laser transitions, describing charge exchange and Penning ionization-excitation processes

21 p3393 A71-41038

Semiconductor surface relaxation behavior with allowance for inhomogeneity and charge exchange between slow states and space charge

21 p3434 A71-41322

Hollow cathode lasers based on negative glow discharge excitation including charge exchange ion-atom collisions and Penning excitation

23 p3686 A71-43955

CHARGE SEPARATION

U POLARIZATION [CHARGE SEPARATION]

CHARGE TRANSFER

Organic compounds oxidation inhibition by polycyclic aromatic hydrocarbons, analyzing peroxide radicals charge transfer complex stability

05 p0716 A71-16382

He-Zn vapor lasers excitation mechanism, presenting Penning and charge transfer cross sections

06 p0910 A71-18670

Atomic processes in plasmas including excitation, deexcitation, ionization, recombination, charge transfer, free-free transitions and spectral line broadening for theta pinch parameters determination

07 p1172 A71-20505

Kinetic energy dependent charge transfer rates for ion-molecule reactions in ammonia, using cyclotron ejection and impulse methods

08 p1249 A71-20657

Metastable oxygen ion distribution and related optical emission rates in aurora, discussing line intensities, charge transfer efficiency and ionization peaks

09 p1441 A71-23642

Cross sections of metastable H formation by charge transfer of hydrogen ion beam on helium, argon, nitrogen and oxygen targets

11 p1803 A71-26371

Dielectric layer surface electric charge movement determination by measuring metal-insulator-semiconductor (MIS) capacity response at very low frequency

12 p1942 A71-26829

Thermal ion-atom charge transfer effects on ionization equilibrium of interstellar oxygen in H I regions, using Bahcall-Wolf orbiting approximation

13 p2132 A71-27966

Laser radiation second harmonic generation susceptibility in molecular crystals due to charge transfer accompanied lowest energy electronic transitions

15 p2421 A71-32402

Rare gas ions molecular and dissociative charge transfer reactions with nitrogen, using statistical phase-space theory of chemical reactions

16 p2538 A71-32813

Plasma mobility, diffusion, electron energy distribution, surface phenomena, elastic collisions, charge transfer, etc

16 p2617 A71-32954

Plasma heat transport associated with matter, momentum, energy and electrical charges transfer

16 p2617 A71-32956

Electrosensing liquid level gage using electrochemical charge transfer through fluid

17 p2744 A71-35290

Charged particles transport in thermionic converter near-emitter plasma, determining potential and electron density profiles

18 p2953 A71-36968

Self generated turbulence in insulating liquids during unipolar charge carrier injection, describing charge transport by Lagrangian diffusion process

19 p3044 A71-37736

CHARGED PARTICLES

NT ALPHA PARTICLES
NT ANIONS
NT ARGON PLASMA
NT BETA PARTICLES
NT CATIONS
NT CESIUM PLASMA
NT COLD PLASMAS
NT COLLISIONLESS PLASMAS
NT CONDUCTION ELECTRONS
NT COSMIC PLASMA
NT DEUTERIUM PLASMA

NT DEUTERONS
 NT ELECTRON PLASMA
 NT ELECTRONS
 NT FERRIC ION
 NT FREE ELECTRONS
 NT HIGH ENERGY ELECTRONS
 NT HIGH TEMPERATURE PLASMAS
 NT HOT ELECTRONS
 NT INNER RADIATION BELT
 NT MAGNETICALLY TRAPPED PARTICLES
 NT MANGANESE IONS
 NT METAL IONS
 NT N ELECTRONS
 NT OUTER RADIATION BELT
 NT PHOTOELECTRONS
 NT POLARONS
 NT POSITRONS
 NT PROTON BELTS
 NT PROTONS
 NT RADIATION BELTS
 NT RECOIL PROTONS
 NT SOLAR PROTONS
 NT STELLAR WINDS

Charged particle motion in magnetic dipole field, investigating singularity and topological flow nature

01 p0127 A71-10382

Bremsstrahlung effect on charged particle motion in nonuniform magnetic field

01 p0132 A71-10677

Miniature multigrid probes for measuring energy spectra of charged particles and absolute plasma densities, comparing results to microwave measurements

02 p0247 A71-11637

Charged particle motion in self consistent continuous wave spectrum from Vlasov and Poisson equations solution

02 p0289 A71-11955

Transformation properties of radiation field and electromagnetic energy fluxes of relativistic charged particles in magnetic field

02 p0312 A71-12362

Equilibrium, highly imperfect, partially ionized Hg and Li vapor plasmas, examining charged and neutral particle interaction forming charged clusters

02 p0292 A71-12617

Partially ionized bounded plasma LF natural oscillations due to ionization processes, ambipolar diffusion and charged particles recombination at walls

02 p0292 A71-12619

Charged particles momenta and spatial arrangement during cosmic ray particles nuclear interactions, describing recording equipment

03 p0476 A71-13845

Static charged dust distributions, investigating general relativity field equations with electromagnetic stress tensor

04 p0625 A71-14732

Ionospheric electron and ion temperatures and charged particle concentration from satellite and space probe observations

04 p0640 A71-14775

Charged particle trajectory under dipole magnetic field, deriving Stoermer orbit existence and uniqueness proof

04 p0625 A71-15081

High energy cosmic ray particle charge and direction detector on Proton 3 satellite

04 p0596 A71-15122

Charged particles-noble gases interactions with resultant vacuum UV radiation, considering conservation of energy principle and Jesse effect

04 p0630 A71-15652

Dynamic problems of two dimensions with semisurface of section, examining charged particles motion in axisymmetric magnetic field

04 p0627 A71-15706

Poisson-Boltzmann equation solution for potential of charged sphere with radius not larger than Debye radius

05 p0781 A71-16383

Charged particle power radiation in homogeneous magnetoplasma

05 p0790 A71-16660

Photoemulsions densitometric characteristics for protonogram analysis, during fast charged particle interaction with single crystals

05 p0754 A71-17031

Charged particle acceleration by electrical mechanism in magnetosphere, evaluating particle flux penetration into ionosphere

05 p0800 A71-17177

Sporadic E layers magnetic field variations, examining charged particle redistribution with air turbulence model

05 p0746 A71-17203

Charged particle beam interaction with electrostatic surface waves in plasma layer

06 p0929 A71-17317

Magnetic storm of 31 October 1968, observing charged particle increase at geomagnetic equator

06 p0961 A71-18172

Muon momentum spectra and charge ratio at 60 deg in east-west plane

06 p0961 A71-18176

Charged particle balance equations for stratosphere and mesosphere, noting particle composition investigation and formation and annihilation processes

06 p0963 A71-18261

Radial microdistribution of absorbed dose in heavy charged particle track, allowing for delta electron emission

06 p0963 A71-18365

Plasma produced by pulsating fast electron beam, observing electron temperature and charged particle concentration

07 p1167 A71-19232

Charged particles interactions with shock fronts or MHD discontinuities, indicating contributory effects to cosmic rays acceleration

07 p1184 A71-19376

Ring currents and polar magnetic substorms during intensive charged particle flux period in nighttime magnetosphere

07 p1101 A71-19414

Computational model for post acceleration propagation of solar flare charged particles

07 p1185 A71-19652

Diffusion coefficient estimation for energetic charged particles across magnetic fields from mathematical model

07 p1186 A71-19662

Bubble of energetic charged particles embedded in interstellar or intergalactic magnetic field and in gas, discussing dynamic effects on radio astronomy observation

07 p1197 A71-19815

Bremsstrahlung effect on charged particle motion in nonuniform magnetic field

07 p1170 A71-20139

Plasma with oriented charged particle fluxes macroscopic parameter measurement by multigrid probes facing and reversed to drift, noting graphical data processing

07 p1171 A71-20183

Charged particles acceleration in pulsed magnetic field, deriving distribution function by diffusion coefficient and turbulence spectrum determination

08 p1351 A71-20963

Book on gaseous ionization and plasma electronics covering atomic structure, electron emission, charged particle behavior, self sustaining discharge and breakdown mechanisms

08 p1341 A71-21700

Positive and negative charged particle beam steady one dimensional motion analysis based on continuity, motion and Maxwell equations, allowing for electrostatic particle interactions

09 p1496 A71-22265

Adiabatic drawing of quasi-captured charged particles by geomagnetic trap field during phase recovery period of magnetic storm

09 p1513 A71-22572

Elongation characteristics of modulation type charged particle traps and analyzers, discussing ions and electrons trapping

09 p1513 A71-22668

Charge source density during interaction between atmosphere and electron/proton fluxes at prescribed boundary parameters

09 p1513 A71-22675

Proton energy change effects on charged particles propagating in interplanetary space, using low energy solar flare proton fluxes observations

09 p1514 A71-22801

Near earth motion equations for electrically charged dust particles in gravitating dipole magnetic fields, using zero-relative-velocity surfaces and energy integral

09 p1437 A71-22832

Cosmic rays propagation in solar wind, presenting statistical theory of interplanetary magnetic field effect on charged particles transport

09 p1515 A71-23461

Cerenkov energy losses of rigid cylindrical uniformly charged bunch moving at constant speed through homogeneous isotropic dispersive dielectric

09 p1498 A71-23574

Neutrino magnetic moment spin precession effects on solar magnetic fields, discussing electromagnetic field-charged particles interaction

09 p1528 A71-23593

Stochastic scattering process charged particle flux by Lagrange expansion based on Fokker-Planck equation

09 p1529 A71-23594

Polar cap lower ionosphere mapping by solar and magnetospheric charged particles, considering disturbances in polar regions

10 p1661 A71-24312

Charged particles velocity distribution effect on plasma flow in transverse nonuniform magnetic field, observing configuration/trajectory distortion and particle dispersion

10 p1649 A71-24319

Mesosphere charged particles concentration and mobility measurements, using rocket-borne aspiration probes

10 p1604 A71-24705

Quark flux measurement by simulating fractional charge particle pulses, testing calibration procedures by comparing simulated and genuine quarklike events

10 p1613 A71-24957

Planetary distribution of primary cosmic rays and residual charged particles over atmosphere from Cosmos 208 and 228 satellite data

11 p1816 A71-25761

Energy transfer during charged particles passage through material media as function of spatial distribution, discussing electron production rates

11 p1802 A71-25769

One dimensional charged particle continuity equation solution in low energy neutral plasma with current flows

11 p1804 A71-26374

Charge particle motion and radiation in strong plane and spherical electromagnetic waves with nonthermal astrophysical applications

12 p1877 A71-26616

Collisionless motion of solar wind ions in helical magnetic field, giving transfer function of charged particles

12 p1947 A71-26636

Plasma production by pulsating fast electron beam, observing electron temperature and charged particle concentration

12 p1934 A71-26750

Automatic control application to liquid metal and semiconductor materials, plasma flows, charged particle beams and similar media interacting with magnetic fields

12 p1936 A71-26972

Energetic charged particle motion in magnetosphere, considering radiation belt dynamics

12 p1949 A71-27372

Lower ionosphere charged particle concentrations and collision frequencies determination by LF impedance probe

13 p2058 A71-28028

Charged particle temperature distribution in outer ionosphere, disregarding collisional energy exchange

13 p2058 A71-28207

Charged particles acceleration by electric field in magnetosphere, evaluating injected particles flux into ionosphere under quiet conditions

13 p2128 A71-28234

Sporadic E layers magnetic field variations, examining charged particle redistribution with air turbulence model

13 p2059 A71-28258

Charged particles magnetic scattering on cyclotron instability waves of radiation belt plasma, estimating proton relaxation time

13 p2129 A71-28552

Plane one dimensional steady compressible ideally charged gas flow characteristics in electric field

13 p2107 A71-28567

Electrostatic spray generated charged colloids adaptation to thruster with metal capillary needles under AC voltage, evolving low thrust propellants

13 p2118 A71-29503

Soviet book on inhomogeneous plasma instabilities covering spatial gradients, charged particles collisions, temperature effects, steady electric fields and magnetic shear

14 p2279 A71-29942

Trapped charged particle cyclotron, bounce and drift motion in distorted geomagnetic field

14 p2300 A71-30033

Upper F region transpolar plasma distribution from Alouette 1 data, relating results to satellite measurements of magnetospheric low energy charged particles

14 p2234 A71-30041

Geomagnetic pulsation effect on charged particles motion, based on Mead magnetosphere analytic model, using Parker perturbation method

14 p2235 A71-30346

Nonequatorial charged particle radial diffusion in asymmetric magnetosphere by third adiabatic invariant violation, using Kosik model

14 p2235 A71-30347

Energy dependence of cosmic ray muon charge ratio at large zenith angles, using large aperture and high resolution cosmic ray momentum spectrograph

15 p2475 A71-31779

High energy primary cosmic ray program of Goddard Space Flight Center involving charge composition and energy spectra studies in balloon and satellite experiments

15 p2478 A71-31804

Plasma decay due to charged particles recombination, linearizing nonlinear equations describing diffusion of singly ionized two-component gas undergoing recombination

15 p2456 A71-31999

Thermal electron density fluctuations in weakly ionized gas from viewpoint of particle diffusion in single charged particle phase space, considering incoherent scattering

15 p2458 A71-32392

Guiding center equations for charged particle motion and statistical fluctuations of plasma in magnetic field, using Krylov-Bogoliubov transformation

15 p2458 A71-32393

Crab nebula pulsar model, discussing charged particles acceleration to relativistic energies by intense LF electromagnetic wave

16 p2632 A71-33236

Energy-radiation problems in relativity theory, considering electromagnetic waves, Einstein equations, momentum tensors and moving charged particles

16 p2609 A71-33259

Charged particles distribution in magnetosphere beyond radiation belts, proposing unstable radiation zone model containing auroral and semitrapped particles

16 p2626 A71-33450

Effective cross sections for charged and excited particles formation from He, Ne and Ar ion collisions with CO molecules, using mass spectrometry

16 p2614 A71-33646

Fast charged particles measurement in magnetosphere belt by Cerenkov counter mounted on Cosmos 137 satellite indicating presence of high energy electrons

16 p2626 A71-33664

German monograph on self consistent ring current models of geomagnetic field interaction with charged particles

17 p2733 A71-34789

Anomalous microwave heating of electrons in magnetized plasma, showing resonances dependence on magnetic fields and charged particles concentration

17 p2790 A71-35735

Pulsar radiation generation by charged particles nonlinear Thomson scattering of strong LF electromagnetic wave and nonthermal radio emission

18 p2960 A71-35940

Solar flare X-ray origin model, discussing charged particle acceleration to relativistic energies, ambient gas heating and thermal and nonthermal X rays

18 p2958 A71-36740

Ion charge composition in plasma-electron beam system in strong longitudinal magnetic field, noting multiply charged ions production under high temperature conditions

19 p3109 A71-37132

Charged particles elastic interaction and recombination in low temperature weakly ionized potassium plasma

19 p3109 A71-37135

Plasma heating and compression with nonadiabatic charged particle motion in uniform magnetic field

19 p3109 A71-37137

Heavily ionized particles search at sea level for magnetic monopoles existence evidence in highest energy cosmic rays

19 p3124 A71-37285

Pulsars electromagnetic radiation, considering bunch of relativistic charged particles

19 p3134 A71-37513

Solar cosmic ray data, discussing multicharged nuclei relative abundances in photosphere and propagation models

19 p3126 A71-37625

Plasma cyclotron wave excitation with charged particle beam, determining unstable oscillations frequency range and spatial and time development with nonlinear analysis

19 p3111 A71-37633

Charged particles interactions with shock fronts or MHD discontinuities, indicating contributory effects to cosmic rays acceleration

19 p3127 A71-37801

Ring currents and polar magnetic substorms during intensive charged particle flux period in nighttime magnetosphere

19 p3054 A71-37838

Homogeneous collisionless plasma in external electric field, considering evolution in time of charged particles distribution functions

19 p3114 A71-37858

Ionization rates induced by solar flares charged particles in planetary atmospheres

19 p3142 A71-38047

Electric fields for solid and liquid fuels dispersion and trajectory manipulation of charged particles to control mixing with air, vaporization and burning

19 p3171 A71-38193

Charged particle acceleration by nonstationary sinusoidal electric fields in earth magnetosphere based on mathematical model

19 p3129 A71-38377

Charged particles eruptions effects on relation of magnetic perturbations to integral auroral luminance intensity from whole sky photometry measurements

19 p3059 A71-38398

Charged particles interaction with geomagnetic field, discussing plasma equations of motion, ionospheric current induction, transition layer and magnetotail rotation

20 p3216 A71-39118

Fast charged particle flux measurement in inner radiation belt by Cosmos 137 satellite in January-February 1967

20 p3278 A71-39140

D region ionization by solar corpuscular streams, considering formation of charged particle concentration profiles

20 p3216 A71-39141

Charged particle motion in constant magnetic field under random electric field, deriving maximum energy and diffusion coefficient

20 p3269 A71-39163

Air shower pion/proton and neutral/charged ratios at mountain altitude, using cloud chamber, Cerenkov counter and spectrometer measurements

20 p3279 A71-39323

High resolution charged particle detector with wire cathode for synchrotron applications, discussing design and advantages

20 p3238 A71-39423

Flow velocity measurement in electromagnetically driven unsteady shock tube from charged particles extraction, using ionization gages

20 p3239 A71-39432

Primary cosmic rays high energy gamma ray intensity spectrometric measurements onboard Cosmos 208 satellite, allowing for charged particles effects

20 p3283 A71-39753

Relativistic primary cosmic rays chemical composition between Be and Fe from charge spectrum obtained with Cerenkov counters

20 p3284 A71-39756

Fast charged particles inelastic collisions with atoms and molecules, investigating Bethe differential cross section theory

21 p3418 A71-40675

Charged particles acceleration in homogeneous magnetic field varying periodically with time /Alfven magnetic pumping/

21 p3424 A71-41117

Planetary distribution of primary cosmic rays and residual charged particles over atmosphere from Cosmos 208 and 228 satellite data

22 p3591 A71-41529

Energy transfer during charged particles passage through material media as function of spatial distribution, discussing electron production rates

22 p3577 A71-41537

Charged pions differential photoproduction cross section description by theoretical model

22 p3578 A71-42060

Charged particles momenta and spatial arrangement during cosmic ray particles nuclear interactions, describing recording equipment

22 p3594 A71-42646

Coulomb interaction effect between charged traps in amorphous semiconductor, noting state density reduction at Fermi energy

23 p3715 A71-43472

Aqueous etchant for charged particle tracks revelation in olivines

23 p3737 A71-43544

Plasma resonator excitation by Cerenkov emission from density modulated uncompensated charged particle beam

24 p3854 A71-44512

Transverse instability of charged particle beam in segmented linear accelerators due to beam encounter with wall

24 p3855 A71-44522

Manned spacecraft hazard from charged particles radiation during solar flares and trapped particles by geomagnetic field, recommending protection methods

24 p3865 A71-44887

High energy charged particles angular distribution measurements in equatorial region cosmic radiation above atmosphere, using Proton 2 satellite data

24 p3866 A71-45027

Auroral charged particle fluxes electrodynamic interaction with atmosphere, determining ion formation rate and electron concentration and conductivity

24 p3866 A71-45032

Charged particles effect on plasma negative ions, examining Stark effect in energy level

24 p3857 A71-45114

CHARGING

Helicopter charging mechanisms, considering engine and rain precipitation charging

07 p1020 A71-19933

Electrostatic charging noise measurement, reduction and flight test verification

07 p1021 A71-19937

Overcharging effects on ion source with volume ionization, considering two dimensional ionization chamber model with lengthwise distributed neutral plasma component

13 p2109 A71-29202

CHARPY IMPACT TEST

Charpy notched impact strength of carbon fiber reinforced epoxy resin composites over temperature range [PLASTICS INST. PAPER 20]

08 p1318 A71-20891

Transition temperature behavior in plane strain fracture toughness tests on A517-F steel, comparing with Charpy tests

20 p3248 A71-38770

Charpy impact test measurement of maraging steel thermal embrittlement, observing fracture mode and toughness changes with heat treatment

21 p3398 A71-40467

Brittle transition temperature of steels by Vickers hardness testing, comparing with tensile properties and impact fracture process in Charpy impact test

21 p3388 A71-40751

Ni-steels toughness improvement at cryogenic temperatures by accelerated cooling, using Charpy V-notch and static and dynamic fracture tests at 139.7-671.7 R

21 p3400 A71-40881

CHARRING

Nonequilibrium modeling of pyrolysis gas products flow through char layer of ablative heat shield

14 p2334 A71-29876

CHARTS

NT FLOW CHARTS

NT GRAPHS [CHARTS]

NT METEOROLOGICAL CHARTS

NT MOLLIER DIAGRAM

Star charts as orientation and navigation aids in manned space flight

01 p0125 A71-10517

Interactive computer graphic system for compiling air navigational data on two dimensional aeronautical charts

08 p1258 A71-21236

Worldwide aeronautical charts maintenance for weapon systems support, discussing data sources

08 p1281 A71-21254

Standard printing color identification system for DOD mapping, charting and geodesy services standardization

08 p1281 A71-21259

Isoline charts showing F 2 layer critical frequency deviations and negative disturbance zones during solar eclipse of 22 September 1968

19 p3058 A71-38385

CHEBYSHEV APPROXIMATION

Square root function approximation in interval, using Heron iteration and Chebyshev method

06 p0919 A71-18206

Approximation theory applications to differential and integral equations, considering nonlinear Chebyshev method in connection with hyperbolic and heat transfer equations

06 p0919 A71-18207

Tchebycheffian spline functions, solving Hermite-Birkhoff interpolation as stochastic prediction and filtering

07 p1147 A71-19325

Amplitude characteristic polynomial Chebyshev approximation by linear phase nonrecursive digital filter transfer function

09 p1417 A71-23037

Steady convergence analysis of generalized Chebyshev successive interpolation process, using functions of interpolative classes

10 p1635 A71-23801

Closed-loop nonlinear systems synthesis, using mapping in Chebyshev series converging everywhere, multidimensional linearization and Volterra singular integral equations

10 p1587 A71-24744

Nonlinear systems optimal control computational method, using Chebyshev algorithm

12 p1868 A71-27592

Chebyshev and extremal approximations for monotonically increasing or decreasing variable

13 p2094 A71-28272

Phase hologram nonlinearities effects, determining signal to noise power ratio in terms of Chebyshev series coefficients

13 p2069 A71-28714

Iteration parameters ordering in Chebyshev cyclic iteration method

14 p2265 A71-29557

German monograph on Fourier-Chebyshev approximation of primary functions, giving quadrature method

17 p2764 A71-34484

Chebyshev polynomial expansions application to beams and columns with large deflections, discussing accuracy

17 p2832 A71-35424

Antenna linear array power pattern synthesis, determining optimum nonnegative harmonic approximation to given function in Gauss/weighted least-mean-square/ and Chebyshev senses

19 p3021 A71-38472

Chebyshev polynomials computation of nonlinear oscillations of conservative autonomous system with single degree of freedom

23 p3777 A71-43493

Astrometrical HF range latitudinal observation error spectrum estimation, showing random dispersion and Chebyshev polynomial expansion parameters for nightly variation

23 p3771 A71-44256

CHECKOUT

On-line machine language dynamic debugger for Operating System 360, using graphic display terminal or operator typewriter

01 p0045 A71-10193

Majority decoding schemes for cyclic and decyclic codes, using successive application of separate checks

01 p0039 A71-11318

Apollo Applications Program command and service module test requirements to achieve reliable hardware for extended missions
[AIAA PAPER 70-378] 03 p0500 A71-14436

Electronic equipment maintenance simplification by proceduralized troubleshooting method for malfunction isolation and tests and checks selection and sequencing, noting technician training cost reduction
17 p2689 A71-34702

TOTAL checkout computer language for future space vehicles, considering objectives, characteristics and merits
18 p2885 A71-36447

Mobile concept and automated checkout applications in Apollo/Saturn 5 Launch Complex 39, discussing performance
22 p3611 A71-42044

Qualification tests for equatorial ELDO Europa Launch Site with MSRV, discussing checkout system and performance
23 p3661 A71-43474

CHECKOUT EQUIPMENT
U TEST EQUIPMENT
CHELATE COMPOUNDS
U CHELATES
CHELATES

Sulfur containing organic chelating compounds as radiation protective agents
07 p1034 A71-18941

Luminescence excitation in chelates under pulsed ruby and neodymium laser radiation action, examining two photon absorption mechanism
07 p1122 A71-19130

CHEMICAL ANALYSIS
NT ELECTROPHOTOMETRY
NT GAS ANALYSIS
NT GAS SPECTROSCOPY
NT MICROANALYSIS
NT NEUTRON ACTIVATION ANALYSIS
NT OZONOMETRY
NT PAPER CHROMATOGRAPHY
NT POTENTIOMETRIC ANALYSIS
NT QUANTITATIVE ANALYSIS
NT SPECTROSCOPIC ANALYSIS
NT URINALYSIS
NT VOLUMETRIC ANALYSIS

Rapid identification of steels and other metals by chemical, instrumental and organoleptic methods
01 p0183 A71-10256

Surveyor lunar probes alpha scattering chemical analysis technique tested on rocks of known composition
02 p0305 A71-11984

High purity hafnium titanate, discussing preparation and DTA, electron microscopy wet chemical and X ray analyses
02 p0275 A71-12595

Chemical test method for composition analysis of Ni-Cd electrodes
03 p0374 A71-13028

ESCA /Electron Spectroscopy for Chemical Analysis/ spectrometer using small digital computer as process regulator
03 p0428 A71-13925

Book on hydrazino-hydrazide groups covering experimental details and applications of various analysis methods
05 p0718 A71-17009

Computerized method of interpreting low resolution mass spectra in organic chemical analysis, describing inference maker program applications and results
09 p1403 A71-22471

Apollo 12 crystalline rock samples composition from conventional chemical analysis, suggesting origin in magmatic body with differentiation by crystallization and olivine settling
09 p1529 A71-23654

Mesosiderites silicate textures and compositions and metal-silicate relationships from mineralogical, petrographical and chemical data
10 p1602 A71-24504

Chemical analysis and petrography of Murchison meteorite compared to Murray meteorite
11 p1836 A71-26483

Transition metal diborides chemical stability after treatment with oxygenless acid in nitrogen and air atmosphere
12 p1877 A71-27124

Variable abyssal basalt populations, considering chemical analyses variations for ridges as function of ocean floor spreading rate
13 p2063 A71-29139

Apollo 12 sample zoned olivines, determining Fe, Mg, Si, Ca, Mn and Cr distributions by electron probe analysis
14 p2315 A71-30865

Meteoritic material magnetic fraction determination by chemical analysis for spherules in soil surrounding meteorite craters at Henbury, Australia
15 p2488 A71-32351

Lost City /Oklahoma/ meteorite mineralogical and chemical investigations, comparing with Pribram and Uuera meteorites
15 p2489 A71-32365

Computer controlled data handling system for quadrupole mass spectrometer performing on-line chemical analysis of rocket chamber combustion gases [JPL-TR-32-1518] 16 p2578 A71-33182

Cosmic radiation and gas retention ages of Chassigny achondrite by measuring Al, K and noble gases contents and production rates in meteorites
17 p2800 A71-34514

Chromatographic paper extraction of residual thiosulfate in processed photographic film
19 p3062 A71-37247

Charlevoix structure impatite description, discussing meteoritic impact origin from petrographic and chemical data
19 p3049 A71-37656

Physical, chemical, mineralogical and biological analysis of Apollo 14 lunar rocks and fines
19 p3144 A71-38179

Rainfall, aerosols and cloud water samples analyzed for chlorides and sulfates content and electrical properties
19 p3092 A71-38687

Moon surface electrical conductivity, seismic transmission properties, dust components, chemical analysis and comparison to earth
20 p3295 A71-39615

Heat release from elemental decay in radioactive layer from radio astronomical observations and lunar rock chemical analysis
20 p3295 A71-39620

Comparative electron petrography and chemical analysis of Apollo 11 and 12 and terrestrial rocks, noting pyroxene, plagioclase, ilmenite and cristobalite
23 p3738 A71-43608

Mineralogical composition, modal distribution and bulk chemical analysis on Apollo 12 lunar fines
23 p3744 A71-43652

Apollo 12 lunar soil and breccia core tube and surface samples optical and electron microscope and microprobe analysis, relating data to geologic processes
23 p3744 A71-43656

Apollo 12 lunar samples 12040,36 and 12064,38 chemical analysis for major elements, discussing titanium, water and iron content
23 p3749 A71-43688

Apollo 11 and 12 lunar dust and rocks, determining Be and Cr contents by gas chromatography for comparison with crystalline rocks
23 p3751 A71-43707

Elemental abundance analysis of Apollo 11 and 12 lunar materials from Auger electron spectroscopy
23 p3759 A71-43762

Group analysis of impurities in water regenerated from liquid human wastes
24 p3800 A71-44529

CHEMICAL ATTACK
NT INTERGRANULAR CORROSION

Vapor phase interaction of methanol and carbon tetrachloride with Ti thin films, discussing Ti stress corrosion cracking implications
01 p0102 A71-10812

Reactive molecule and atom attack of refractory materials in dissociated gases at filament temperatures up to sublimation threshold
03 p0374 A71-13124

Iron-iron carbide structure dissolution behavior from electron transmission microscopy, observing carbide, matrix, general and interface attack modes
07 p1056 A71-20361

Surface chemical characteristics of monomeric liquid epoxy resins
10 p1632 A71-24085

CHEMICAL AUXILIARY POWER UNITS
Electric power system for satellites, considering energy conversion, storage and processing from chemical, solar and nuclear sources
17 p2676 A71-34227

CHEMICAL BONDS
NT COVALENT BONDS
NT HYDROGEN BONDS

K-beta and L-alpha X ray spectral emission bands of high melting vanadium compounds, considering chemical bonds
02 p0263 A71-11892

Porphyryns and amino acids chemical bonding under geochemically plausible conditions, considering diagenesis of biogenic compounds and life processes prebiotic chemical evolution
02 p0198 A71-12047

Bovine pituitary proteinase I action on oxidized B chain of insulin, noting preference for specific bonds
05 p0718 A71-17105

Semiconductors isoelectronic impurity states, using semiempirical delta-potential method to calculate bonding energy for GaP containing nitrogen as impurity
07 p1175 A71-19220

Metallic soaps polarity and micellar bond energy effects on pliable lubricants structure and properties
07 p1144 A71-19491

Zirconium nitride electronic structure from X ray emission spectra, analyzing chemical bonds
08 p1305 A71-21061

Binding energies between solute atoms and vacancies in dilute Al alloys measured by quantitative transmission electron microscopy
08 p1310 A71-21530

Atomic bond strength of solid solution hardening as function of composition for calcium/strontium difluorides, using vibrational IR and laser Raman spectra
12 p1877 A71-26804

Complex molecules forced vibrations as material points system with quasi-elastic valence bonds
15 p2452 A71-32624

Atomic bond rupture and molecular mechanisms of polymer fracture, using EPR spectroscopy
16 p2600 A71-32944

Chemical bonds types in intermetallic, metal-like and nonmetallic compounds, stressing model based on valence electrons configuration localization
16 p2622 A71-33919

Structure and properties of beryllium compounds from solid state stable electron configuration formation viewpoint, discussing classification based on chemical bond
16 p2597 A71-33920

Molecular bond rupture and strain energy release rates correlation during ozone cracking of rubber from electron paramagnetic resonance and stress elongation measurements
18 p2939 A71-36244

Ambient gas effects on Au-Al bonds life in integrated circuit package
19 p3119 A71-38514

Approximations to regular solutions by finding distribution function for bonds between unlike molecules, deriving Gibbs energy, enthalpy and entropy
21 p3474 A71-40234

Filler quantity and type effects on mechanical energy losses in polymers, discussing molecular interaction and chemical bond influences
23 p3697 A71-44205

Proton irradiation damage on lunar surface, considering solar wind sputtering, reduction, chemical bond breakage and electron paramagnetic resonance
24 p3867 A71-44423

CHEMICAL CLEANING
Aircraft industrial cleaning agents, processes and techniques applied to components in course of manufacturing and assembly phases, emphasizing emulsion and alkaline methods
16 p2584 A71-33542

CHEMICAL COMPOSITION
NT CARBON DIOXIDE CONCENTRATION

Cr-Tb alloys phase transformations and diagrams dependence on temperature and composition, using physicochemical analysis
01 p0100 A71-10418

Flanged australite and australasian microtektites chemical compositions, using electron microprobe analysis
01 p0162 A71-11427

Water intake effects on human thermal sweat rate and composition in environmental chamber at specific temperature and humidity
02 p0202 A71-11670

Venera-borne gas analyzers for parachute descent probing of Venus atmosphere, describing design and operation
02 p0248 A71-11916

Apollo 11 basalts chemistry and petrogenesis by partial melting, considering implications for lunar origin theories
02 p0305 A71-11981

Flame propagation and inhibition in polymers and unsaturated polyester resins, considering component and composition effect on flammability
02 p0275 A71-12492

Composition and annealing temperature effects on recrystallization of vacuum melted thin wire and rod Mo alloys
02 p0265 A71-12521

Alkoxy derived yttria stabilized hafnia composition, using DTA, X ray diffraction, electron microscopy and emission spectrographic analysis
02 p0275 A71-12596

Chemical test method for composition analysis of Ni-Cd electrodes
03 p0374 A71-13028

Apollo 11 and 12 lunar rocks physical and mechanical properties and chemical composition compared with terrestrial rocks
03 p0487 A71-13421

C, N and O nuclei abundances in radiation belt near geomagnetic equator, using data obtained byOGO-5 satellite in 1968
03 p0473 A71-13475

High energy nucleon passage through lower atmosphere during chemical composition changes of primary cosmic rays, using Proton satellite observations
03 p0476 A71-13851

Spectrographic method for simultaneous determination of constituents in hard metals by rotating disk solution technique
03 p0375 A71-13972

Carbon/oxygen and nitrogen/oxygen ratios in cosmic rays, considering energy dependence interstellar ionization loss and necessity for two component source model

03 p0480 A71-14051

Compton scattering in quasars, discussing gamma rays effects on core chemical abundances

03 p0481 A71-14266

Glass ceramics manufacture, chemical composition and properties, and applications

03 p0448 A71-14352

Al alloys extrusion and chemical composition relationship to mechanical properties, examining various metallurgical processes

04 p0604 A71-15743

Old subjant delta Pavonis composition, suggesting metal rich state

04 p0658 A71-15839

Saturn rings spectral reflectivity measurement and compositional implications concerning water frosts and silicates

04 p0659 A71-15857

German monograph on Co-free heat resistant austenitic steel alloys precipitation hardening and creep strength properties as function of chemical composition

05 p0764 A71-15973

Glass lasers characteristics and applications, discussing material compositions, ion imbeddings and manufacturing techniques

05 p0761 A71-16327

Alloys constitution research, discussing experimental methods in phase diagram investigations of multicomponent systems

06 p0910 A71-17340

Muscovite mica substrate surface composition as function of preparation and processing, using Auger electron spectroscopy

06 p0941 A71-17408

Tektites earth vs possible lunar or cometary origins, taking into account chemical composition

06 p0968 A71-17963

Stellar chemical composition and structural evolution, discussing mass/luminosity relationship, evolution sequences during hydrogen and helium combustion stages, etc

06 p0970 A71-18200

Binary A15 phases transition elements compositional variations effects on atomic ordering

07 p1163 A71-19430

Adsorbed formaldehyde levels from vaporized paraformaldehyde on various surfaces as function of relative humidity and chemical concentration

07 p1055 A71-19593

Apollo 11 and 12 lunar samples, discussing chemical composition relationship to lunar origin

07 p1196 A71-19605

Chemical composition effect of low carbon alloys metallic matrix on wear resistance in abrasive medium, showing austenitic manganese alloys superiority to martensitic or ferritic alloys

07 p1136 A71-19630

High transition temperature superconducting materials thin films composition control by sputtering from hot pressed powder mixture ingots targets

07 p1178 A71-19849

Martensitic high strength steels composition effect on environmentally induced delayed failure

07 p1139 A71-19990

TiH metallographic and lattice parameters variation with hydrogen content

07 p1139 A71-19993

Elastic modulus as function of chemical composition and structure of binary alloys Mo-Re and Ni-Re

07 p1141 A71-20248

Composition and annealing effects on mechanical and thermoelectric properties of sintered wire W-Re alloys

07 p1145 A71-20493

Unactivated dry charged zinc-silver oxide cells storage life, determining chemical composition changes at various temperatures and time lengths

08 p1235 A71-21100

High temperature alloys oxidation resistance and strength characteristics, considering influence of various alloying compositions via use of oxide mapping method

08 p1314 A71-21573

Ni-Cr-Al alloys high temperature oxidation resistance, studying effects of Cr/Al ratio and chemical composition

08 p1315 A71-21574

Composition, microstructure, heat treatment and properties of Ni alloy with high rupture strength and hot corrosion resistance for turbine blade applications

08 p1299 A71-21687

Heat resistance in air of Co-Cr alloys as function of chemical composition

08 p1317 A71-21763

Galaxy chemical evolution, discussing stellar mass loss, supernova explosions, white dwarf formations, nucleosynthesis, cosmochronology, etc

09 p1521 A71-22869

Ultrahigh tensile steels for landing gear and other aircraft design applications, discussing composition, mechanical properties, quality requirements, manufacture and testing

09 p1454 A71-22996

Composition and composition inhomogeneity effects on plated wire memory elements strain sensitivity, considering tension and torsion sensitivities

09 p1509 A71-23115

Cr alloys alloying elements Os, Re, Fe, Co and Mn effect on lattice constant and elastic properties, using acoustic measurements

09 p1473 A71-23229

Aluminum high temperature resistant diffusion type coatings structure and chemical composition, outlining turbine blades testing for thermal shock, oxidation and sulfur and sea salt corrosion

09 p1474 A71-23287

Welding rods chemical composition and welding procedures for heat resistant austenitic and martensitic steels for gas turbines, considering maraging steels heat treatment influence

09 p1456 A71-23291

Apollo 12 crystalline rock samples composition from conventional chemical analysis, suggesting origin in magmatic body with differentiation by crystallization and olivine settling

09 p1529 A71-23654

Lunar soil 12033 bulk chemical analysis, suggesting mixture of exotic component with local soil in 41/59 proportion

10 p1673 A71-24396

Cometary nucleus radius, mass, composition and icy-conglomerate model

10 p1677 A71-24687

Luna 16 lunar rock samples mechanical properties and chemical and mineralogical compositions for regolith origin determination

10 p1681 A71-25116

Nickel diffusion in intermetallic compound NiAl as function of temperature and off-stoichiometric composition, noting activation energy changes

11 p1778 A71-25562

Venus atmosphere chemical composition, determining N, O, water and carbon dioxide concentrations, temperature and pressure

11 p1823 A71-25691

Venus cloud hypotheses, discussing chemical composition, vapor pressure, temperatures and spectroscopic abundances

11 p1824 A71-25705

Petrography, chemistry and mineralogy of El Paso meteorite

11 p1835 A71-26481

Morphology, mineralogy and chemistry of Ashmore meteorite

11 p1835 A71-26482

Spaceborne optical sensors cleanliness requirements, considering particle size distribution, shape, population densities, chemical composition and origin [AIAA PAPER 71-471]

12 p1873 A71-26758

Nb and Mo doped Ni-Al alloy with Ni-Nb additions, obtaining diagrams of composition versus heat resistance in high temperature bending tests

12 p1916 A71-26968

Comet Bennett light polarization data, determining color index and chemical composition

12 p1965 A71-27227

Sulfur hexafluoride equilibrium composition, thermodynamic functions, transport properties and application to simplified enthalpy flow arc model

12 p1939 A71-27267

Long term aged heat resistant Ni base alloys, investigating gamma prime phase chemical composition

12 p1917 A71-27298

Cosmic ray diffusion from discrete sources in random galactic location, studying chemical constituents anisotropy and age with scattering model

12 p1948 A71-27367

Chemical composition effects on microstructure and high temperature properties of cast Cr-Ni-Al steels containing Ti, B, Ce and Zr

13 p2084 A71-28035

Chemical composition change in cosmic particles at energies near 10,000 TeV from angular measurements of extensive air shower axis inclinations

13 p2123 A71-28072

High energy hadrons energy flow fluctuations and chemical composition of cosmic rays in air shower cores, comparing to Monte Carlo calculations

13 p2123 A71-28079

Venera-borne gas analyzers for parachute descent probing of Venus atmospheric composition, describing design and operation

13 p2067 A71-28203

Iron and stony iron meteorites chemical classification, noting Ni, Ga, Ge and Ir concentrations and metal phases

13 p2134 A71-28290

Semiquantitative X ray nondestructive analysis of metal alloys, noting critical nature of sampling

13 p2074 A71-28438

Superconductive Nb-Al alloy critical temperature as function of chemical composition and heat treatment

13 p2085 A71-28576

Apollo 12 sample zoned olivines, determining Fe, Mg, Si, Ca, Mn and Cr distributions by electron probe analysis

14 p2315 A71-30865

Monograph on planetary nebulae covering structure, luminosity, spectra, origin, chemical composition, temperature, magnetic fields, etc

15 p2481 A71-31148

Antimony trisulfide semiconductor films, noting chemical composition effects on photosensitive properties

15 p2461 A71-31286

Combustion rates of ammonium perchlorate mixtures with organic acids, alcohols, cyclic hydrocarbons, amines, nitroso compounds and nitramines, studying relationship to fuel chemical composition

15 p2366 A71-31370

Al-Zn-Mg-Li solid solutions isothermal phase diagrams, obtaining Al-rich alloys phase compositions for quenching and aging temperatures

15 p2426 A71-31405

Niobium and zirconium carbides enthalpy and specific heat dependence on temperature and composition

15 p2431 A71-32156

Zirconium dioxide reactions with chromium, molybdenum and tungsten carbides, studying reaction products, phase composition, sintering temperatures and chemical separation

15 p2432 A71-32166

Udimet 700 superalloy gamma phase precipitate particle size, volume fraction and chemical composition as function of time and temperature

15 p2433 A71-32176

Primary high purity Mg refining technique, composition, oxidation and structure

15 p2435 A71-32338

Chemical composition effect on corrosion resistance of Mg-Li system with alloying additions

15 p2435 A71-32339

Lost City /Oklahoma/ meteorite chemical and mineral composition analysis by X ray diffraction and optical emission spectroscopy

15 p2489 A71-32362

Niobium-zirconium system alloys Debye-Waller factor temperature and concentration dependence, noting nonmonotonocities due to phonon spectra

15 p2437 A71-32625

Radiation flux calculation and divergence in regions with stepwise temperature and chemical composition distribution

16 p2661 A71-32798

Microstructure and chemical composition of lunar soil sample collected by Luna 16

16 p2630 A71-32838

Chemical composition effect of low carbon alloys metallic matrix on abrasive wear resistance, showing austenitic manganese alloys superiority to martensitic or ferritic alloys

16 p2593 A71-33626

Meteorite structure and chemical composition, describing investigation methods, origin and evolution

16 p2639 A71-33691

Global model of atmospheric temperature, chemical composition and density for altitudes from 25 to 1000 km, using satellite drag determined density values

16 p2567 A71-33782

Yttrium effect on phase composition of V-Ga alloys from microstructural, X ray structural and microdrometric analysis

16 p2622 A71-33909

Ternary systems chemical composition of contacting and equilibrium states due to directional flow in multicomponent diffusion layer, noting relationship to phase diagrams

16 p2541 A71-33929

Cuban tektite classification based on age, discussing physical properties and chemical composition

17 p2797 A71-34275

Carbonaceous chondrites chemical and mineralogical composition densities and structure due to condensation at various temperatures within early solar nebula

17 p2799 A71-34512

Kyle /Texas/ chondrite classification based on chemical composition, mineralogy and structure

17 p2800 A71-34513

Carbon and nitrogen abundances in howardites, enstatite and hypersthene achondrites

17 p2800 A71-34515

Nazareth /Texas/ meteorite chemical composition and structure, showing Neumann bands in kamacite fields

17 p2800 A71-34516

Stony meteorites relicts in mesozoic formation of central Urals, discussing chemical and mineralogical composition and structure

17 p2800 A71-34517

Carbon compounds in Apollo 12 lunar fines and core samples, using pyrolysis, mass spectrometry, ion exchange chromatography and optical and electron microscopy

17 p2801 A71-34649

Murchison meteorite heterocyclic compounds contents, using gas chromatography-mass spectrometry

17 p2801 A71-34650

Lunik 16 soil samples physical properties, rock types, chemical analysis, mineral composition and petrology, comparing to Apollo project
17 p2805 A71-35332

Microphase separation in homopolymer-block copolymer mixtures as function of composition, molecular weight and interaction parameters
17 p2695 A71-35525

Thin layer silica gel chromatography applied to cosmic dust chemical composition
17 p2811 A71-35730

Mineral and chemical composition of Krasnyi Kluch meteorite, characterizing as recrystallized chondrite containing chondrules
17 p2811 A71-35731

Manua Islands /Samoa/ lavas chemical composition, geology and probable history
18 p2911 A71-35887

Composition and daily fluctuations of trace contaminants during 90-day space station simulator test [ASME PAPER 71-AV-17]
18 p2867 A71-36384

High intensity molecular beams properties, measurement and production methods, considering kinetic energy, chemical composition and technology applications
18 p2908 A71-36438

Interstellar dust clouds physical and chemical constitution, discussing molecular gas chemical composition and abundances
18 p2968 A71-37037

Comet Bennet light polarization data, determining color index and chemical composition
19 p3132 A71-37379

Phase equilibria of Al-Mg-Li-Mn system in Al-rich region, noting composition effects on mechanical properties
19 p3078 A71-37470

Isothermal phase diagrams and composition effects on plasticity in Mo-Ti-Zr-C system in Al-rich region
19 p3078 A71-37472

Venus atmosphere chemical composition, temperature and pressure, discussing model cloud layer, circulation and upper atmospheric structure
19 p3138 A71-37759

Carbon and noncarbon polymers based high temperature elastomeric materials chemical structure and physical properties
19 p3085 A71-38068

Chlorine-fluorine flame, determining adiabatic propagation speed, refractive index field, temperature profile, composition distribution and atom concentrations
19 p3168 A71-38105

Burn time and acceleration effects on molten metallic material chemical composition near burning surface of aluminized composite solid propellant
19 p3121 A71-38298

Tungsten carbide-cobalt alloys, investigating binder metal mechanical properties relationship to composition by chemical analysis and X ray inspection
19 p3083 A71-38475

Chemical composition of atmospheric aerosols from Tokyo region, measuring energy spectrum of neutron irradiated specimens by gamma spectrometer
19 p3094 A71-38698

Mineral composition optimization of nutrient medium for Hydrogenomonas, using steepest ascent method for mathematical planning of experiments
20 p3193 A71-39236

Low, medium and high carbon steels hardenability determination from composition, using charted data
20 p3251 A71-39336

Tantalum and niobium ternary oxides recovery from liquid potassium solution, determining composition and crystallographic modifications by chemical and X ray diffraction analyses
20 p3194 A71-39372

Apollo 14 lunar soils chemical element concentrations by atomic absorption spectrophotometry and isotope dilution
20 p3292 A71-39381

Venus atmosphere chemical composition from gas analysers onboard Venera automatic stations, determining element abundance, water vapor density and cloud layer structure
20 p3296 A71-39625

Ground based studies of Jupiter at optical frequencies, determining atmospheric chemical composition, temperature and stratification, aerosol layers structure and flyby/penetration experiments results
20 p3297 A71-39631

High altitude balloon cosmic dust collection, considering individual particle chemical composition and ablation
20 p3299 A71-39653

Relativistic primary cosmic rays chemical composition between Be and Fe from charge spectrum obtained by Cerenkov counters
20 p3284 A71-39756

Optical constants of beta-phase NiAl, PdAl and nickel gallium aluminide, noting chemical composition and electron density effects on photon energy absorption
21 p3426 A71-40033

Soviet monograph on Canyon Diablo/Arizona/ meteorite covering chemical composition, minerals, isotope composition, history, geology and impact recrystallization
21 p3452 A71-40874

Chemical composition and size distribution of particulate matter in solid propellant combustor of boron loaded rocket motor
21 p3436 A71-40944

Alloying effects on crack propagation resistance of precipitation hardening austenitic steel
21 p3402 A71-41091

Elements distribution in ternary alloy system during simultaneous saturation and burning-out of two components and successive diffusion into third
21 p3403 A71-41161

Carbon and stainless steels chemical composition effects on diffusion layer structure and fatigue strength after diffusive boriding
21 p3403 A71-41162

High energy nucleon passage through lower atmosphere during chemical composition changes of primary cosmic rays, using Proton satellite observations
22 p3595 A71-42652

Chlorella biomass chemical composition stability during prolonged cultivation with nitrates recycling medium
22 p3507 A71-42818

Solar system organic compounds detection and evolution, considering element, isotope and pigment composition, optical activity and polymerization
22 p3496 A71-42824

Synthetic fibers and plastics development, chemical composition, physical and mechanical properties, production growth rates and applications
23 p3696 A71-43107

Physical properties, mineralogy and chemical composition of lunar regolith sample returned by unmanned Lunik 16 probe
23 p3737 A71-43602

Optical, chemical and structural properties of lunar bytownite twin from U stage, microprobe and X ray measurements
23 p3738 A71-43612

Mineralogical, petrological and chemical features of four Apollo 12 lunar microgabbros
23 p3740 A71-43625

Apollo 12 crystalline rocks mineralogy, petrology and chemical composition, considering magmatic origin
23 p3740 A71-43626

Mineralogy, petrology and chemical composition of Apollo 12 rocks and fines
23 p3740 A71-43628

Apollo 11 and 12 lunar rocks and soil chemical composition, considering petrogenesis and major and trace elements abundance
23 p3741 A71-43635

Apollo 11 and 12 crystalline rocks petrographical analysis and textural-mineralogical-chemical group classification, considering local stratigraphic reconstruction
23 p3742 A71-43638

Size distribution, composition and history of regolith fines at Apollo 12 site
23 p3743 A71-43651

Lunar fines samples 10084,148 and 12070,98, investigating grain size, mineral and chemical composition and optical properties
23 p3744 A71-43655

Lunar breccia sample matrix composition characteristics examination by transmission electron microscope, suggesting condensation from rock volatilized by meteorite impact heat
23 p3745 A71-43663

Nonmare basalts chemical composition and origin from Apollo 11 and 12 sites
23 p3746 A71-43671

Chemical element composition and mineralogy of powdered lunar surface material, comparing Surveyor, Apollo and Lunik missions data
23 p3748 A71-43682

Bulk elemental composition of Apollo 12 samples of lunar igneous and breccia rocks and soils from instrumental and radiochemical neutron activation analysis
23 p3748 A71-43684

Carbon and sulfur isotope content in Apollo 12 lunar fines
23 p3751 A71-43702

High resolution time averaged energy spectrum and chemical composition of iron group cosmic ray nuclei from fossil tracks in Apollo 12 lunar rocks
23 p3764 A71-43804

Aluminized layer phase and chemical composition of heat resistant iron and nickel alloys
24 p3837 A71-44732

Total-to-open porosity ratio for carbide-iron type materials sintering, noting relative density and chemical composition effects
24 p3838 A71-44736

CHEMICAL COMPOUNDS

Metals and intermetallic chemical compounds, examining heat and oxidation resistance, magnetic and

semiconductor properties, superconductivity and electron emissivity

16 p2597 A71-33924

Recording device with Fourier hologram memory based on optical spatial filtration principle for identifying chemical compounds by IR absorption spectra
19 p3064 A71-37773

Negative ion and compound formation in premixed fuel-rich laminar atmospheric pressure hydrogen-oxygen-nitrogen flames with molybdenum and potassium atoms
19 p3167 A71-38092

Radiation sickness prophylaxis chemical compounds, discussing protection mechanisms, radical inactivation and afflicted cell recovery
22 p3505 A71-42710

CHEMICAL EFFECTS

Binary Ti alloys hydrogenation-dehydrogenation treatment effect on alloying element activity
04 p0615 A71-15801

Austenitic steel containing C, Cr and Mn, investigating W, Mo, V and Nb effect on structure and mechanical properties
04 p0616 A71-15804

O-barenylacetic and methyl-o-barencarboxylic acids effects on mice radiosensitivity to fast neutrons and gamma rays
07 p1038 A71-18976

Glass fiber reinforced thermoplastics with increased room temperature mechanical properties, noting effect of heat, aging and chemical environment exposure
07 p145 A71-19692

Martensitic high strength steels composition effect on environmentally induced delayed failure
07 p1139 A71-19990

Chemosensitivity in normal, hypoxia and hypocapnia cases, using rebreathing techniques to construct isoxic carbon dioxide response curves and isocapnic oxygen response curves
07 p1052 A71-20329

Ni plastic properties and creep measurement under deformation by tension at room temperature, noting effect of impurities content
09 p1473 A71-23231

Al-Zn-Mg-Cu alloys, investigating minor elements Cr, Mn and Zr effects on quench sensitivity
11 p780 A71-26018

Oxygen effects on SiC electrical properties by comparison of photoluminescence spectra of alpha-SiC crystals grown by sublimation in Ar atmosphere
21 p3436 A71-41348

CHEMICAL ELEMENTS

NT ACTINIDE SERIES

NT ALKALI METALS

NT ALKALINE EARTH METALS

NT ALUMINUM

NT ALUMINUM ISOTOPES

NT ALUMINUM 26

NT ALUMINUM 27

NT ANTIMONY

NT ARGON

NT ARGON ISOTOPES

NT ARSENIC

NT BARIUM

NT BERYLLIUM

NT BERYLLIUM 7

NT BERYLLIUM 9

NT BERYLLIUM 10

NT BISMUTH

NT BORON

NT BORON ISOTOPES

NT BROMINE

NT CADMIUM

NT CADMIUM ISOTOPES

NT CALCIUM

NT CALIFORNIUM ISOTOPES

NT CARBON

NT CARBON ISOTOPES

NT CARBON 12

NT CARBON 13

NT CARBON 14

NT CERIUM

NT CERIUM ISOTOPES

NT CERIUM 144

NT CESIUM

NT CESIUM ISOTOPES

NT CESIUM VAPOR

NT CESIUM 133

NT CHARCOAL

NT CHLORINE

NT CHROMIUM

NT COBALT

NT COBALT ISOTOPES

NT COBALT 60

NT COPPER

NT DEUTERIUM

NT DEUTERIUM PLASMA

NT DYSPROSIUM

NT ERBIUM

NT EUROPIUM

NT FLUORINE

NT GADOLINIUM

NT GALLIUM

NT GERMANIUM

NT GOLD

NT HAFNIUM
NT HALOGENS
NT HELIUM
NT HELIUM ATOMS
NT HELIUM ISOTOPES
NT HOLMIUM
NT HYDROGEN
NT HYDROGEN ATOMS
NT HYDROGEN IONS
NT HYDROGEN ISOTOPES
NT HYDROGEN PLASMA
NT INDIUM
NT IODINE
NT IRON
NT IRON 57
NT ISOTOPES
NT KRYPTON ISOTOPES
NT LANTHANUM
NT LEAD [METAL]
NT LEAD ISOTOPES
NT LIGHT ELEMENTS
NT LIQUID HELIUM
NT LIQUID HYDROGEN
NT LIQUID NITROGEN
NT LIQUID POTASSIUM
NT LIQUID SODIUM
NT LITHIUM
NT LITHIUM ISOTOPES
NT LUTETIUM
NT MAGNESIUM
NT MAGNESIUM ISOTOPES
NT MANGANESE
NT MANGANESE ISOTOPES
NT MERCURY [METAL]
NT MERCURY VAPOR
NT METALLOIDS
NT NEODYMIUM
NT NEODYMIUM ISOTOPES
NT NEON
NT NEON ISOTOPES
NT NICKEL
NT NITROGEN
NT NITROGEN ATOMS
NT NITROGEN IONS
NT NUCLIDES
NT ORTHO HYDROGEN
NT OXYGEN ISOTOPES
NT OXYGEN 18
NT PALLADIUM
NT PARA HYDROGEN
NT PLATINUM
NT PLUTONIUM
NT PLUTONIUM 238
NT POLONIUM 210
NT POTASSIUM
NT POTASSIUM ISOTOPES
NT POWDERED ALUMINUM
NT PRASEODYMIUM
NT PROMETHIUM
NT RADIOACTIVE ISOTOPES
NT RADON
NT RADON ISOTOPES
NT RARE EARTH ELEMENTS
NT RARE GASES
NT RHODIUM
NT RUBIDIUM
NT RUBIDIUM ISOTOPES
NT RUTHENIUM
NT SAMARIUM
NT SCANDIUM ISOTOPES
NT SELENIUM
NT SILICON
NT SILICON ISOTOPES
NT SILVER
NT SODIUM
NT SODIUM VAPOR
NT STRONTIUM
NT STRONTIUM ISOTOPES
NT SULFUR
NT SULFUR ISOTOPES
NT TECHNETIUM
NT TELLURIUM
NT TERBIUM
NT THALLIUM
NT THORIUM
NT THORIUM ISOTOPES
NT TIN
NT TITANIUM
NT TITANIUM ISOTOPES
NT TRACE ELEMENTS
NT TRANSURANIUM ELEMENTS
NT TRITIUM
NT URANIUM
NT URANIUM ISOTOPES
NT URANIUM 235
NT VANADIUM
NT XENON
NT XENON ISOTOPES
NT XENON 133
NT YTTRIUM
NT ZINC
NT ZIRCONIUM

Cosmic radiation origin, discussing inner and extragalactic energy density and elements distribution
02 p0300 A71-12372

Re intermetallic compounds structure and physical properties, examining chemical reactivity with transition metals as function of elements periodic table position
07 p1140 A71-20236

Chemical elements abundance in ordinary chondrites, terrestrial magma and lunar rocks, considering Alven theory of solar system origin
10 p1665 A71-23741

Dust grain condensation and primordial elements transport into interplanetary space during early stage solar evolution
11 p1819 A71-25222

Terrestrial basalts and lunar rocks volatile element concentrations comparison, noting relationship to abundance in chondrites
16 p2633 A71-33348

Apollo 14 bulk lunar fines sample elemental abundances determination from soils and rocks by activation analysis
20 p3292 A71-39382

Elements distribution in ternary alloy system during simultaneous saturation and burning-out of two components and successive diffusion into third
21 p3403 A71-41161

Element and isotope separation effects under centripetal acceleration in rotating plasma, using mass spectrometric diagnostics
22 p3580 A71-41584

Ti alloy microarea alloying element concentration quantitative analysis by EPMA program, obtaining working curves for Al, Fe, Cr, Mo and V
22 p3561 A71-41944

Minor element concentrations and population sources of Apollo 11 and 12 olivine and plagioclase, using microprobe analyses
23 p3738 A71-43614

CHEMICAL ENERGY

NT ENERGY OF FORMATION

Energy sources for rockets and satellites, comparing chemical, solar and nuclear supplies
02 p0282 A71-12302

Chemical energy conversion into mechanical work, examining irreversible mixing, Van Hoff box and Carnot cycle
05 p0717 A71-16785

Chemical energy conversion into mechanical work, examining irreversible mixing, vant Hoff box and Carnot cycle
16 p2540 A71-33037

Thermal or chemical energy conversion to electromagnetic radiation by laser, discussing atomic or molecular processes and thermodynamic limitations
20 p3242 A71-38939

CHEMICAL ENGINEERING

NASA qualitative reliability technology applications to chemical industry
04 p0602 A71-14802

Boundary condition iteration methods in chemical process plant optimal design and control, considering simplicity and ease of programming, computation time and storage requirements
07 p1054 A71-18800

Soviet book on gas phase chemical reactions rate constants determination covering elementary processes kinetics empirical methods
17 p2694 A71-34522

On-line identification for nonlinear system from noisy measurements, applying stochastic algorithm to hybrid simulation of chemical process models
20 p3207 A71-38974

CHEMICAL EQUILIBRIUM

NT ACID BASE EQUILIBRIUM

Thermodynamic calculation of chemical equilibrium of rocket propellants and gun powders using computer program in Fortran IV
01 p0141 A71-10343

Detonation front at Chapman-Jouguet velocity demonstration by numerical transient flow calculations
05 p0834 A71-16510

Vitamin K3 effect on redox equilibria in red cell, discussing radiosensitizer mechanism
07 p1039 A71-18985

Equilibration rate of uncatalyzed carbon dioxide hydration reaction in open system at constant carbon dioxide partial pressure, examining buffering capacity effect
10 p1559 A71-23898

Lighter-than-iron elements in earth iron core, assuming formation timed chemical equilibrium with mantle
10 p1607 A71-24986

Critique of paper on earth core-mantle chemical equilibrium, considering upper mantle element abundance, oxidation state and volatiles nature
10 p1607 A71-24987

Sulfur hexafluoride equilibrium composition, thermodynamic functions, transport properties and application to simplified enthalpy flow arc model
12 p1939 A71-27267

Chemically nonequilibrium laminar boundary layer profiles in axisymmetric hypersonic conical nozzle at

high air stagnation temperature, calculating wall friction, displacement and momentum loss thickness
13 p1989 A71-27904

Fluorine chemical shift tensor measurements in magnesium fluoride, using multiple pulse NMR technique
13 p2025 A71-28031

Multicomponent ionized gas mixtures chemically equilibrated flows over nonporous and ablating surfaces, using Navier-Stokes and Prandtl equations for asymptotically thin boundary layer
13 p2048 A71-28570

Relaxation distance for sharp cone behavior from chemical nonequilibrium laminar boundary layer effects on simulated space shuttle configuration during reentry
13 p2146 A71-29504

D region negative ion densities in chemical equilibrium based on electron density observation, noting role of ozone and carbon dioxide
14 p2228 A71-29533

Sodium oxide-titanium dioxide-water ternary system, determining sodium titanates formation regions in equilibria in 300 C isotherm
15 p2367 A71-31902

German textbook on fundamentals of thermodynamics covering energy conversion, reversible/irreversible processes, chemical/molecular thermophysics, statistical analysis, probability theory, etc
15 p2516 A71-32767

Chemical equilibria susceptibility to gravitational field effects, suggesting coincidence with conditions derived from relativistic thermodynamics
16 p2540 A71-33257

Time dependent corrections to one component monatomic systems equilibrium rate of reactions and temperature change, using moment method for integrating nonlinear Boltzmann equation
17 p2785 A71-34945

Nitrogen equilibrium solubility dependence on slag basicity and gas phase nitrogen/carbon monoxide contents in aluminosilical melts
21 p3399 A71-40470

Molecular gas dissociation equilibrium and carbon monoxide overtone line widths dependences on magnetic field strength in sunspots
24 p3868 A71-44459

CHEMICAL EXPLOSIONS

NT GAS EXPLOSIONS

Explosion shock wave induced short wave radio emission, deriving time related gas ionization state of wave front
02 p0284 A71-11927

Liquid rocket propellants characteristics study for explosive yield prediction, using mathematical model and critical mass method
04 p0637 A71-15345

Explosion products population inversion by combining vibrational chemical excitation with thermal ignition
06 p0865 A71-17402

Thermal decomposition rates and explosion of dinitroxydiethyl nitramine from heat release measurements at various pressures
15 p2462 A71-31376

Critique of paper on explosive hazards of large solid rocket motors, suggesting extrapolation of fractional TNT equivalent
18 p2955 A71-36284

Impact and explosive craters production in same target material under controlled laboratory conditions, determining depth of burst simulating impingement
19 p3156 A71-37682

CHEMICAL FUELS

NT AIRCRAFT FUELS
NT GASOLINE
NT HYDROCARBON FUELS
NT HYDROGEN FUELS
NT JET ENGINE FUELS
NT METAL FUELS
NT SLURRY PROPELLANTS

CHEMICAL KINETICS

U REACTION KINETICS

CHEMICAL LASERS

CO chemical laser power output augmentation by selective depopulation of CO lower vibrational levels by energy transfer to added gases
02 p0262 A71-12709

CW chemical laser operation with HF and DF in subsonic electric discharge mixing device, obtaining 5.5 w output
03 p0434 A71-13479

Dye lasers operational principles and characteristics, considering dyes molecular structure, optical pumping, continuous operation, wavelength selection and applications
05 p0761 A71-16330

CW chemical operation in IR for hydrogen fluoride, deuterium fluoride, hydrogen fluoride-carbon dioxide and deuterium fluoride-carbon dioxide systems
06 p0909 A71-18493

CW electric discharge mixing chemical lasers, identifying molecular transitions responsible for radiation from output spectral distribution measurements
06 p0909 A71-18652

Chemical energy conversion in lasers, discussing vibrational inversions in diatomic and multiautomic molecules and chain reactions

07 p1121 A71-19098

Hydrogen fluoride elimination chemical laser from difluoromethylamine using temperatures below 268 K and flash photolysis

07 p1123 A71-19372

Plasma refractive index effects in pulsed HCN lasers, calculating stable cavity mirror curvatures con- striction as function of electron density by ray matrix approach

07 p1124 A71-19795

High energy narrow pulsed HF chemical laser emission from transverse multiple electrode nitrogen fluoride and nitric tetrafluoride discharge

07 p1128 A71-20397

Continuous wave HCl chemical laser, achieving large specific gain through high speed flow, rapid mixing and transverse geometry

09 p1465 A71-23480

Transverse gas flow effects on deuterium fluoride-carbon dioxide chemical laser output, discussing amplifier medium homogeneity factor

10 p1619 A71-23834

Pulsed HF chemical laser output as function of fluorine source, flow rate and output coupling

10 p1620 A71-24153

Nitrogen laser pumped cresyl violet dye laser output increase through excitation transfer from added intermediary dye

11 p1773 A71-25926

Single boundary layer flame sheet model for continuous diffusion chemical lasers, obtaining integrated zero power gain, laser power and efficiency

[ALAA PAPER 71-28]

11 p1774 A71-25928

Einstein relations for stimulated luminescence, and application to high pressure chemical laser power gain and population inversion calculation

12 p1913 A71-26966

Cross field magnetic discharge stabilization of plasma column in flowing CW electrically initiated chemical laser

12 p1940 A71-27278

Continuous chemical laser, emphasizing strong coupling in cavity between radiation and chemistry

[ALAA PAPER 71-574]

15 p2419 A71-31565

CW chemical lasers research, summarizing three lasing principles and advantages over electrically or thermally excited lasers

16 p2586 A71-33163

Deuterium fluoride overtone vibration-rotation chemical laser emission, studying frequency doubling and rate constant ratios

17 p2753 A71-34801

Pulsed chain reaction chemical lasers using flash photolysis of hydrogen-fluorine-helium mixtures

17 p2754 A71-35750

Vibrational energy distribution and emission lines of fluorine atoms plus chloroform reactions in chemical laser, using equal gain measurements

19 p3071 A71-37331

Einstein relations for stimulated luminescence, and application to high pressure chemical laser power gain and population inversion calculation

19 p3075 A71-38265

High repetition line selectable compact electrically pulsed hydrogen fluoride lasers operating on sulfur fluoride and hydrogen mixture

20 p3242 A71-38825

Pulsed laser emission chemically pumped by exothermic chain reaction between hydrogen and fluorine mixed with He initiated by flash photolysis

21 p3391 A71-40238

Gain and spectral characteristics of transverse flow CW chemical laser with hydrogen and deuterium fluorides active medium

21 p3393 A71-41041

Chemical laser action at atmospheric pressure from vibrational rotational transitions of HF produced by multiple transverse spark discharges in propane-helium-sulfur fluoride mixtures

22 p3556 A71-41727

High power tunable second harmonic and UV sum frequency generation from rhodamine 6G dye laser and ADP crystal

22 p3556 A71-41803

Time dependent progress of vibrational rotational transitions in chemical laser using hydrogen- fluorine mixture investigated by oscillography with IKM-1 monochromator

23 p3684 A71-43405

R-branch multiline performance of transversely excited pulsed HF chemical laser

23 p3688 A71-44297

Continuous chemical laser model for constant gain method exposure, emphasizing strong radiation-chemistry coupling, molecular J-shift, output power limiting behavior and lasing efficiency

24 p3832 A71-44373

Chemical lasers diatomic and multiautomic molecules dissociation in nonequilibrium conditions, discussing vibrational energy exceeding gas temperature

24 p3834 A71-45112

Fluidic element fabrication techniques, discussing concrete and epoxy molds and stainless steel chemical milling

07 p1121 A71-20562

Photochemical machining, describing parts design, line width and corner radii relation to metal thickness and base materials

[SME PAPER MR-71-812]

15 p2416 A71-32428

Photochemical machining applied to thin complex flat metal parts manufacture, discussing tooling, prototype, production costs and dimensional requirements

[SME PAPER MR-71-813]

15 p2416 A71-32430

CHEMICAL MILLING

U CHEMICAL MACHINING

CHEMICAL PROPERTIES

NT ACIDITY

NT HEAT OF COMBUSTION

NT HEAT OF FORMATION

NT HEAT OF SOLUTION

NT HEAT OF VAPORIZATION

NT SALINITY

NT THERMOCHEMICAL PROPERTIES

Fiber reinforced materials industrial applications

based on various matrix-fiber combinations, considering manufacturing processes, chemical and mechanical properties, etc

01 p0107 A71-10316

Sanitary, chemical and toxic properties of polymeric materials in isolation chamber with contaminated outgassing atmosphere at moderate temperature

01 p0024 A71-11128

Soviet book on chemistry of titanium covering intermetallic compounds, hydroxides, dioxide, titanates, halides, sulfates, titanium ores, deposit sites, etc

02 p0209 A71-11847

Physical, chemical and electrical properties of silicon nitride thin films deposited pyrolytically on Si substrates, analyzing deposition process effects

03 p0468 A71-14001

Glass ceramics manufacture, chemical composition and properties, and applications

03 p0448 A71-14352

Re intermetallic compounds structure and physical properties, examining chemical reactivity with transition metals as function of elements periodic table position

07 p1140 A71-20236

Carbon fiber and carbon fiber-polyester composites chemical resistance to acid and alkaline solutions at various concentrations and temperatures

[PLASTICS INST. PAPER 32]

08 p1320 A71-20903

Electrochemical properties of Na-W bronzes for use as electrocatalysts in acid electrolyte fuel cells

09 p1387 A71-23648

Electrical properties, chemical resistance and reinforced plastics applications of telechelic ultrahigh vinyl polybutadiene resins

11 p1786 A71-25422

Physicochemical properties of powdered Al and Al-Mg-Zn alloy combustion products from chemical, electron microscopic and X ray analysis

14 p2191 A71-30617

Graphitizing and nongraphitizing substances carbonization, observing cokes chemical structure changes and thermal decomposition

15 p2368 A71-32733

Physicochemical properties and applications of lubricant materials based on organic compounds, discussing developments in inorganic lubricants

16 p2600 A71-32839

Chemical properties of titanium, zirconium and hafnium germanides exposed to acids, oxidizers, complex salts, alkaline solutions and water

19 p3075 A71-37106

Perfluoropolyether fluid lubricant physical and chemical properties at high and low temperatures, explaining metals effects on thermal stability by topochemical reaction mechanism

19 p3083 A71-37424

Silicon difluoride reactions and properties, describing production from commercial silicon tetrafluoride and versatility of reactions with organic and inorganic compounds

19 p3011 A71-37647

Transition metal physicochemical properties explanation by many-electron effects in Hubbard model

23 p3714 A71-42932

Nickel-chromium system powders physicochemical properties, noting use as high temperature cermet packing materials

23 p3690 A71-43256

High purity lithium hexafluoroarsenate preparation methods and hexafluoroarsenic acid properties

23 p3642 A71-43540

Morphological, physical and chemical characteristics of basaltic and anorthositic glassy spheroids in Apollo 12 lunar fines

23 p3746 A71-43666

Chemical characteristics of carbon compounds in Apollo 11 and 12 lunar fines, using organic solvent extraction, mass spectrometry and gas chromatographic method

23 p3756 A71-43743

CHEMICAL PROPULSION

Deep space shuttles operating modes and vehicle types, considering chemical vs nuclear propulsion, direct vs near-orbit rendezvous, refueling, etc

01 p0165 A71-11593

Optimal control of composite spacecraft propulsion system incorporating high thrust-weight ratio chemical engine and low thrust ion engine

09 p1512 A71-23138

Propulsion system atom and radical concentrations measurements, using low pressure gas discharge flow system for combustion environment control

11 p1729 A71-26285

Impulsive trajectory optimization for asteroid Eros round trip sample return mission using chemical propulsion

[AAS PAPER 71-369]

23 p3730 A71-43039

CHEMICAL REACTIONS

NT AMMONOLYSIS

NT ATOMIC RECOMBINATION

NT CARBONIZATION

NT CHLORINATION

NT DEHYDROGENATION

NT DEIONIZATION

NT DENITROGENATION

NT DEOXIDIZING

NT ELECTROCHEMICAL OXIDATION

NT ENDOTHERMIC REACTIONS

NT EXOTHERMIC REACTIONS

NT FLUORINATION

NT GLYCOLYSIS

NT HYDROGENATION

NT HYDROGENOLYSIS

NT HYDROLYSIS

NT ION RECOMBINATION

NT METAL-WATER REACTIONS

NT NITRIDING

NT OXIDATION

NT OXYGEN RECOMBINATION

NT OXYGENATION

NT PHOSPHORYLATION

NT PHOTOCHEMICAL REACTIONS

NT PHOTOCROMISM

NT PHOTODECOMPOSITION

NT PHOTOLYSIS

NT PHOTOSYNTHESIS

NT PYROLYSIS

NT RADIOLYSIS

NT REDUCTION [CHEMISTRY]

NT SABATIER REACTION

NT SULFATION

NT THERMAL DISSOCIATION

NT TITRATION

Reaction mechanism for ammonium nitrate thermal decomposition, discussing chloride catalytic effects

01 p0141 A71-10344

Chemically interacting gases transfer properties at varying temperatures, determining collision parameters by viscosity, diffusion coefficients, molecular beam scattering and vibrational relaxation time

02 p0286 A71-12186

Hydrocarbon fuels high temperature oxidation behind shock waves, investigating reaction process by combustion products IR emissions and density gradient

02 p0298 A71-12860

Propellant low temperature preignition reactions during simulated engine shutdown conditions, discussing IR spectroscopic observation method

02 p0298 A71-12861

Maxwellian distribution function calculation for molecules during initial phase of chemical reaction by successive approximations and Chapman-Enskog method

03 p0376 A71-14065

Rate constant measurement for atomic hydrogen reaction with carbon dioxide yielding OH and CO, considering near IR emission spectroscopy applicability

04 p0548 A71-14697

Laminar boundary layer on porous plane plate situated in plasma jet, examining transfer phenomena with chemical reaction

04 p0572 A71-15507

Shock waves and chemical reactions due to plane, cylindrical and spherical point explosions in combustible gaseous mixtures

05 p0833 A71-16503

Single pulse shock tube in high temperature chemical reaction kinetics, considering shock reflection theory

05 p0836 A71-16527

Transonic flow with chemical reactions, analyzing one and two dimensional problem by small perturbation method

05 p0717 A71-16534

Chemiluminescent NO-O reaction spectral radiant intensity and absolute rate constant redetermination in premixed gaseous free jet and hydrogen flame atmosphere

05 p0837 A71-16568

CHEMICAL MACHINING

NT ELECTROCHEMICAL MACHINING

Gas phase reactions near solid-gas interface of deflagrating double base propellant causing abrupt changes in burning rate-pressure curve
[AIAA PAPER 70-124] 05 p0837 A71-16571

Laminar or turbulent chemically reacting gas mixture flow in circular tube, examining heat transfer with enthalpy equation
05 p0838 A71-16791

N-t-butyliminoacetone nitrile formation by reaction between adduct from sodium bisulphite, formaldehyde, t-butylamine and potassium cyanide
06 p0865 A71-17549

Europium hexaboride-high melting point metals reaction for intermetallic compounds production, noting evaporation kinetics
06 p0913 A71-18087

Free turbulent mixing of heated high speed central hydrogen jet and cold low speed annular air stream coupled with finite rate chemical reactions
[AIAA PAPER 71-5] 06 p0866 A71-18479

Chemically reacting viscous supersonic laminar flow in two dimensional divergent plane channel, developing approximate system of parabolic partial differential equations
[AIAA PAPER 71-44] 06 p0866 A71-18505

Spalding-Patankar finite difference method application to combined free and forced convection turbulent boundary layer with variable fluid properties and chemical reaction
07 p1054 A71-18769

Chemical reaction kinetics optimal problem numerical solution based on Pontryagin maximum principle and gradient method
07 p1147 A71-19185

Dissociating airflow over two dimensional blunt body, determining laminar boundary layer chemical reaction suppression effects on heat exchange
07 p1015 A71-19748

Laser applications in chemical research, exploring fast chemical processes, isotope enrichment and molecular reactions and structure observations
07 p1124 A71-19790

Spacecraft attitude control microthrusters utilizing catalytically reactive gas mixtures during pulse mode and steady state operation
[AIAA PAPER 70-614] 07 p1183 A71-19859

Reacting and nonreacting gases laminar boundary layer flows over two dimensional and axisymmetric bodies at zero lift, comparing numerical methods
07 p1015 A71-19860

Reactant-product structure of turbulent multicomponent mixture with first order reactions at large wavenumbers
07 p1091 A71-20020

Chemical reaction rate microscopic reversibility, observing rotational vibrational and/or translational states dependence of products reactants
08 p1250 A71-20666

Zinc-zinc oxide electrode chemistry, describing interaction with strongly alkaline solution of alkaline battery system
08 p1233 A71-21078

Molten alumina and chromia reactions with refractory metals, calculating isobaric-isothermal potential variations
09 p1466 A71-22165

Boltzmann kinetic equations for gas mixtures reacting according to detail balance principle
09 p1496 A71-22376

Reactive equilibrium hypersonic gas flow over slender pointed body, neglecting rate chemistry
09 p1383 A71-23054

Book on homogeneous flows aerothermochemistry covering chemical reactions, heat and mass transfer, entropy production, species continuity, momentum and energy equation
09 p1547 A71-23674

Heterogeneous chemical reaction for visualization of wall streamlines on moving obstacle, discussing boundary layer structure at large Prandtl and Schmidt numbers
10 p1591 A71-23835

Probability of quasi-chemical reactions between point defects in semiconductors due to ionizing radiation
10 p1655 A71-24139

Proton chemical exchanges effects in ammonium nitrate aqueous solution at varying exchange rate, noting geomagnetic field line configurations
10 p1644 A71-24458

Hydrogen-nickel reaction in presence of CO adsorbed gas, increasing total desorption cross section and eliminating monotonic relation between uptake and H ion current
10 p1573 A71-24540

Prolonged perceptual deprivation effects on behavioral, physiological and chemical reactions, discussing EEG mean frequency changes
11 p1724 A71-25362

Gas dynamic effects of reaction center in explosive gas mixture, using model and numerical computation
[AIAA PAPER 70-147] 11 p1854 A71-25452

Glass fiber reinforced plastics, discussing adhesion, wetting and adsorption effects on chemical reactions in glass-resin interfaces
11 p1788 A71-25657

Butene hydroperoxides structure and intermolecular reactions from NMR spectra, discussing peroxide radical addition, OH group signals shifts and self association
12 p1877 A71-27751

Temperature, concentration and heat conductivity profiles of chemically reacting gas mixtures with thermal gradient, using classical transfer equations
13 p2025 A71-27884

Chemical reactions occurrence during gas supersonic expansion into vacuum, calculating gas temperature, pressure and density
13 p2025 A71-28774

German monograph on bimolecular reactions of H and O atoms in shock waves with hydrogen peroxide and dioxide and nitrous oxide
13 p2102 A71-28881

Simultaneous partial differential equations, applying to one directional diffusion in finite porous slab accompanied by chemical reaction
13 p2025 A71-29011

Thermal unimolecular processes falloff data calculation based on Rice-Ramsperger-Kassel or Rice-Ramsperger-Kassel-Marcus theories
13 p2025 A71-29037

Template catalysis of acetyl transfer reactions, showing triple helices formation by polyuridylic acid with adenosine derivatives
13 p2026 A71-29479

Three body ion-neutral association reactions of NO ions with oxygen, nitrogen and carbon dioxide, noting temperature effect on rate constant
13 p2026 A71-29507

Thermodynamic equilibrium constants of Fe-MgO-SiO₂-O₂ system reactions at one atmosphere and 900-1300 C
14 p2190 A71-29875

Shock wave caused chemical reactions between solids and cryogenic liquids, discussing shock sensitivity tester for liquid propellant- structural material systems
14 p2222 A71-30546

Nonstationary perturbation propagation in gaseous medium with irreversible internal process /chemical reactions or excitations with one degree of freedom of molecules/
14 p2338 A71-30823

Chemically interacting gases transfer properties at various temperatures, determining collision parameters and interaction cross sections and energies
15 p2451 A71-31494

Nonreacting and equilibrium chemically reacting gas turbulent boundary layer flows through hypervelocity nozzles, comparing calculation with experiment
[AIAA PAPER 71-597] 15 p2512 A71-31577

Zirconium dioxide reactions with chromium, molybdenum and tungsten carbides, studying reaction products, phase composition, sintering temperatures and chemical separation
15 p2432 A71-32166

Nickel sponge preparation by liquid nickel sulfide reaction with NiO under reduced pressure at various temperatures
15 p2433 A71-32178

Gas dynamics of explosions, considering electromagnetic fields and chemical reactions effects on blast wave propagation in unbounded media
15 p2515 A71-32567

Elementary reactions in hydrocarbon combustion, using shock tube as chemical reactor to determine rate of reaction in 1600 to 2100 K range
16 p2539 A71-32892

Book on chemical reactions under plasma conditions covering thermodynamics, equilibrium states, transport properties and experimental production
16 p2617 A71-32952

Plasma chemistry, discussing low and high temperature plasmas, nuclear fusion reactions and chemical molecular and nuclear synthesis
16 p2539 A71-32963

Nonequilibrium plasma chemical reaction kinetics problems, discussing time dependence, dissociation and recombination theories in pulsed EM field, equations and numerical calculations
16 p2539 A71-32965

Chemical reactions in electrical discharges, discussing H, O, N, halogens and free radicals, hydrides, halides and fluorinated compound synthesis and ion-molecule reactions
16 p2540 A71-32966

Plasma jet chemical reactions, discussing temperature and quenching effects, molecular and gas decomposition and endothermic compounds formation
16 p2540 A71-32967

Low temperature plasma chemical processes, investigating molecular and atomic ionization, reactions under equilibrium and nonequilibrium conditions and specific energy production
16 p2540 A71-32968

Combustion flame plasma reactions, considering collisional and chemical ionization, ion decay, electron temperatures and additives
16 p2540 A71-32969

Shock wave generated plasmas elementary reactions, discussing shock tubes and noble and diatomic gases chemiionization
16 p2540 A71-32970

Plasma generation by photon irradiation, radiolytic mechanism and high energy particle bombardment, discussing ionized media chemical reactions
16 p2540 A71-32971

Laminar or turbulent chemically reacting gas mixture flow in circular tube, examining heat transfer with enthalpy equation
16 p2662 A71-33041

Soviet book on gas phase chemical reactions rate constants determination covering elementary processes kinetics empirical methods
17 p2694 A71-34521

Viscous relaxing gas hypersonic flow around sphere in presence of nonequilibrium chemical reactions in shock layer
17 p2673 A71-35637

Nonequilibrium processes, discussing chemical reactions between electronically, vibrationally, rotationally and translationally excited reagents
18 p2873 A71-35831

IR chemiluminescence from HCl formed in atomic hydrogen reaction with sulfur dichloride, noting energy distribution among reaction products
18 p2874 A71-35832

Vibrationally excited hydroxyl formation by atomic hydrogen reaction with ozone, using Fourier transform spectroscopy
18 p2874 A71-35833

Electronic to vibrational energy transfer in mercury vapor reaction with hydrogen fluoride, studying IR emission and scattering cross section
18 p2874 A71-35834

Reaction rate of vibrationally excited hydroxyl with ozone, obtaining hydroxyl emission spectra by Fourier transform spectroscopy
18 p2874 A71-35836

IR chemiluminescence of atomic nitrogen reaction with molecular oxygen, obtaining quantum efficiency
18 p2874 A71-35838

Chemically activated electroadhesive pads on spacecraft surface, allowing astronauts to maneuver or work in zero gravity environments
[AIAA PAPER 71-853] 18 p2872 A71-36645

Chondrite classification, primordial matter composition and early solar system chemical processes, discussing cosmic gas condensation and refractory element fractionation
18 p2967 A71-37027

Silicon difluoride reactions and properties, describing production from commercial silicon tetrafluoride and versatility of reactions with organic and inorganic compounds
19 p3011 A71-37647

Hydrogen-oxygen reaction sensitized by ammonia, comparing with nitrogen dioxide and nitrosyl chloride activators
19 p3012 A71-38081

Chemi-ionization induced by cyanogen in stoichiometric atmospheric pressure carbon monoxide-oxygen-nitrogen flames
19 p3013 A71-38089

Nitrogen atoms chemiluminescent reaction spectra with carbon tetrachloride, ethylene and methylene chloride, noting application to artificial clouds formation
19 p3014 A71-38634

Airglow optical emission processes covering resonance scattering, fluorescence, chemical association, ionic reactions and excitation transfer
20 p3226 A71-39827

Configuration space theory of nonrelativistic three body scattering covering transition amplitudes of three-three chemical reaction rates
22 p3577 A71-41651

Organic synthesis in simulated Jovian atmosphere by passing semicorona discharge through methane-ammonia mixture
22 p3602 A71-42180

Apparatus for optical diagnostics of helioelectrochemical conversion reaction phototransformation kinetics including diffusion coefficient measurement in liquid phase
22 p3484 A71-42845

Time dependence of radial mechanical driving point impedance of Al cylindrical shell immersed in two anechoic tanks related to chemical reaction
23 p3662 A71-43215

Early solar system organic matter origin, discussing amino acid synthesis from CO, H and ammonia reaction with N, alumina or clay catalysts
23 p3633 A71-43244

Apollo 12 lunar dust sample 12070,128, determining response to effective agents of earth-type chemical weathering
23 p3746 A71-43669

Kinetic equations derivation for rarefied chemically reacting monatomic or stable molecular gases
23 p3707 A71-43924

Morphological and cytochemical changes in red and mixed skeletal muscles of animals exposed to hypokinesia
23 p3636 A71-44237

Chemically reacting gas mixture supersonic flow characteristics around blunt body, using differential equations
23 p3784 A71-44336

Limiting chemical reaction rate of graphite and carbon containing material combustion at high temperatures
24 p3890 A71-45108

Combustion and chemical reactions near wall, in forced convection, boundary layer transition, radiation and ablation of missile reentry
24 p3890 A71-45148

CHEMICAL REACTORS
Liquid hydrazine catalytic reactor startup characteristics as function of catalyst adsorbed gas condition and temperature by high speed motion picture observation
[AIAA PAPER 71-702] 14 p2294 A71-30760

Turbojet engine combustor nitric oxide formation prediction based on adiabatic micromixed perfectly stirred reactor model analysis
[AIAA PAPER 71-713] 15 p2470 A71-32286

Internal ballistics equations of powder solid fuel rocket motor treated as homogeneous chemical reactor
24 p3890 A71-45107

CHEMICAL RELAXATION
U MOLECULAR RELAXATION

CHEMICAL SHIFT
U CHEMICAL EQUILIBRIUM

CHEMICAL TESTS
NT CHEMICAL ANALYSIS
NT ELECTROPHOTOMETRY
NT GAS ANALYSIS
NT GAS SPECTROSCOPY
NT MICROANALYSIS
NT NEUTRON ACTIVATION ANALYSIS
NT OZONOMETRY
NT PAPER CHROMATOGRAPHY
NT POTENTIOMETRIC ANALYSIS
NT QUANTITATIVE ANALYSIS
NT SALT SPRAY TESTS
NT SPECTROSCOPIC ANALYSIS
NT URINALYSIS
NT VOLUMETRIC ANALYSIS

CHEMILUMINESCENCE
Chemiluminescent NO-O reaction spectral radiant intensity and absolute rate constant redetermination in premixed gaseous free jet and hydrogen flame atmosphere
05 p0837 A71-16568

Biological tissues ultraweak chemiluminescence, discussing nature, characteristics and measurement
11 p1724 A71-25672

Diagnostic flow visualization, using chemiluminescent radiation in mixing region between aqueous luminol and potassium ferricyanide solutions
13 p2044 A71-27853

IR chemiluminescence from HCl formed in atomic hydrogen reaction with sulfur dichloride, noting energy distribution among reaction products
18 p2874 A71-35832

IR chemiluminescence of atomic nitrogen reaction with molecular oxygen, obtaining quantum efficiency
18 p2874 A71-35838

Vibrational temperature of nitric oxide in upper atmosphere, computing collisional, radiative and chemiluminescent excitation rates
18 p2910 A71-35840

Nitrogen atoms chemiluminescent reaction spectra with carbon tetrachloride, ethylene and methylene chloride, noting application to artificial clouds formation
19 p3014 A71-38634

CHEMISORPTION
Chemisorption layer kinetics of oxygen on thin Ta films at room temperature and low pressures
03 p0441 A71-13359

Chemisorption and sticking probability of nitrogen on Ta films, considering relationship to temperature and pressure
03 p0441 A71-13360

Chemisorption rate and physical adsorption of nitrogen on Ta films as function of temperature
03 p0441 A71-13361

Nitrogen chemisorption and absorption on polycrystal Ta ribbons, using static method in ultrahigh vacuum
06 p0940 A71-17298

Nitrogen chemisorption on Ta by field emission microscopy, taking into account work function changes
06 p0940 A71-17299

Chemisorption energies of organics on Pb surface by extended Hueckel molecular orbital technique
07 p1055 A71-19845

Hydrogen and nitrogen chemisorbed species interactions on 100° tungsten crystals, using flash desorption methods
07 p1056 A71-19846

Hydrogen recombination and molecule formation by nonactivated chemisorption on iron grains surfaces
10 p1573 A71-25006

Metallic Ni trace effects on oxygen chemisorption forms on nickel oxide in various temperature regions
15 p2367 A71-31901

CHEMISTRY
Bismuthide chemistry research, presenting equilibrium diagrams with all elements
16 p2622 A71-33923

CHEMONUCLEAR PROPULSION
U CHEMICAL PROPULSION
U NUCLEAR PROPULSION

CHEMORECEPTORS
Hypoxia-hypercapnia interplay as respiratory chemoreceptors stimulants and depressants by investigating arterial oxygen and carbon dioxide tensions effects on phrenic nerve activity
06 p0854 A71-18061

Respiratory responses and hyperventilation mechanism during static muscular work in maximal voluntary contraction, noting chemoreceptor and alarm-defense reaction
13 p2008 A71-28436

Ventilatory control in acute hypoxia, detailing polycythemia effects on respiratory chemoreceptor sensitivity
14 p2185 A71-30289

Temperature, odor mixing and stimulation frequency effects on olfactory receptor potential of fly *Lucilia sericata*
14 p2186 A71-30568

Fly *Lucilia sericata* olfactory receptor and unit action potentials response to odor stimulation by homologous compounds
14 p2186 A71-30569

Monograph on peripheral chemoreceptors and central chemosensitive area control of ventilation during chronic blood acid base changes and hypoxia in mammals
18 p2852 A71-35869

Respiratory chemoreceptors and acid-base alterations effects on adrenocortical activation during hypoxia in dogs
20 p3187 A71-38986

CHEMOTHERAPY
Antiarrhythmic drugs choice based on excitable tissues biophysics, considering contrast between cardiac muscle and nerve
02 p0201 A71-12419

Cardiovascular and biochemical effects of chronic intermittent neurogenic stimulation, noting alphanethyltyrosine antihypertension agent
03 p0359 A71-13157

Light and drugs effect on diurnal body temperature from radio telemetry of adult male rats
05 p0715 A71-17111

Disorientation response of survived chicks hatched from eggs injected with radioprotective 2-beta-aminoethylisothiuronium-Br-HBr after incubation
07 p1040 A71-18988

Pargyline behavioral effects in primates, concerning therapeutic use for decarboxine intoxication
08 p1239 A71-20819

Drug effects on LF whole body vibration response of dogs administered with phenobarbital, phenox-ybenzamine and morphine
11 p1720 A71-26121

Humoral smooth muscle acting factor and phenyl-piperazinylmethyl cyclohexanone effects on decompression sickness production and prevention in thin mice
21 p3331 A71-40352

Hemodynamic evaluation of heart rate augmentation produced by atrial pacing and isoproterenol in early postoperative phase of cardiac valve surgery
23 p3640 A71-44131

CHEST
Chest and cardiovascular system optimal radiologic facilities, discussing X ray examination, catheterization-angiographic and nuclear radiology laboratories
07 p1053 A71-20354

CHICKENS
Disorientation response of survived chicks hatched from eggs injected with radioprotective 2-beta-aminoethylisothiuronium-Br-HBr after incubation
07 p1040 A71-18988

CHILDREN
Cardiac output during submaximal bicycle exercise in children and teen-agers, discussing oxygen transport function of blood
06 p0857 A71-18722

CHILE
Pulkovo astronomical expedition in Chile, concerning faint star coordinates and equipment for telescopic, electrophotometric and spectral observations
07 p1083 A71-19326

CHILLING
U COOLING

CHIMES
U AUDITORY SIGNALS

CHIMPANZEES
NT HUMAN BEINGS
NT MONKEYS
Subcortical-cortical EEG recording of unrestrained chimpanzees sleep cycles, using computer analysis and biotelemetry techniques
15 p2359 A71-31951

First and last rapid eye movement (REM) sleep differences in unrestrained chimpanzee
18 p2853 A71-35891

CHINOOK HELICOPTER
U CH-47 HELICOPTER

CHIPS
Single metal system Al beam leaded chips, substrates and crossovers for multilead packaging, describing fabrication techniques
09 p1509 A71-23119

Hybrid circuit heat sensitive semiconductor chips mounting methods for preventing thermal degradation
21 p3356 A71-40744

Beam-lead nitride-passivated IC seal junction chip reliability evaluation by life tests for optimum packaging into functional modules
21 p3357 A71-40813

Beam-lead devices, discussing comparison to conventional transistor chip, reliability, applications and assembly techniques
21 p3357 A71-40815

CHIRP
NT CHIRP SIGNALS

CHIRP SIGNALS
Chirped optical pulses nature, properties, generation and applications in pulse shape measurement in nonlinear wave propagation, ultrashort pulse generation and adiabatic population inversions
07 p1160 A71-19778

Lens-prism model for holographic image processing in space-frequency domains with chirp signal interferometric compression
09 p1452 A71-23565

Swept frequency or chirp signals for data transmission and pulse compression, considering long range air ground communication in HF band
22 p3510 A71-42277

CHLORAL
Aminazine and chloral hydrate effects on metabolism intensity of rats brain gangliosides components including N-acetylneuraminic acid and N-acetylglucosamine
21 p3337 A71-41055

CHLORATES
Chlorates use in breathable oxygen production for aircrews
06 p0860 A71-18193

Oxygen supply to air transported patients by chemical compounds, suggesting use of permanganates and chlorates
22 p3500 A71-41571

CHLORELLA
Chlorella ration effect on internal organs of protein-deficient mice compared with casein and soybean rations
01 p0025 A71-11145

Space flight effects on survival, mutation and cell development of Chlorella cells suspensions onboard Zond 5 spacecraft
01 p0019 A71-11554

Carbon dioxide concentration control in sealed chamber with animals during atmosphere regeneration by Chlorella
06 p0860 A71-18356

Intensive Chlorella cultivation for controlling toxic gaseous contaminants in atmosphere
06 p0861 A71-18357

Relative biological effectiveness of multicharged C ions during single irradiation of Chlorella, noting dose dependent mutability
06 p0854 A71-18366

Lipid, protein and carbohydrate concentrations in Chlorella biomass from pyrolysis and aluminogel column chromatography
13 p2017 A71-28407

Oxygen consumption by nitrogen starved nonsynchronous Chlorella culture during different assimilation of nitrogen salts in darkness and light
16 p2531 A71-33461

Chlorella extracellular metabolites, identifying indole nature biologically active substances
19 p3004 A71-38544

Combined action of vibration and gamma irradiation on sporulation dynamics, survival rate and mutability of chlorella
20 p3193 A71-39237

Chlorella viability and mutability aboard Soyuz and Zond spacecraft, noting trend toward growth of anomalies in autosporeulation
21 p3343 A71-40566

Chlorella biomass chemical composition stability during prolonged cultivation with nitrates recycling medium
22 p3507 A71-42818

CHLORIDES
NT ALUMINUM CHLORIDES

NT AMMONIUM CHLORIDES
NT BORON CHLORIDES
NT CALCIUM CHLORIDES
NT CARBON TETRACHLORIDE
NT COPPER CHLORIDES
NT DICHLORIDES
NT HYDROCHLORIC ACID
NT HYDROCHLORIDES
NT IRON CHLORIDES
NT LEAD CHLORIDES
NT MAGNESIUM CHLORIDES
NT POTASSIUM CHLORIDES
NT SILICON TETRACHLORIDE
NT SODIUM CHLORIDES
NT TETRACHLORIDES

Ordered intermetallic CsCl compounds thermodynamic properties determination, noting linear relationship between intrinsic disorder and formation heat

07 p1131 A71-19428

Thermal dissociation rates of alkali chlorides reinterpeted in terms of chloride ion collisional detachment rate

21 p3346 A71-40889

Crystal lattice vibration and molecular liberation effects on solid carbon tetrachloride heat capacity at 0-20 and 200-230 K

22 p3585 A71-42059

CHLORINATION

Mo, W and Mo-W alloys chlorination kinetics, investigating temperature and pressure effects on reaction rate from electron micrographs

18 p2938 A71-37002

Calculation method for standard potentials and enthalpies of metals during oxidation and chlorination, representing molar functions dependence on temperature

19 p3082 A71-38153

CHLORINE

Emission line spectra of halogens Cl I, Br I and I I in 4-micron region

05 p0717 A71-16911

Methane and ethane binary mixtures with chlorine, determining main combustion products under flame propagation

07 p1054 A71-19280

Cl chondrites approximating primordial solar system matter condensable fractions based on isotopic/elemental abundance continuity, fractionation patterns and chondrules absence

14 p2306 A71-29708

Laminar flame speeds in chlorine-fluorine mixtures, predicting low temperature isothermal rates and spontaneous ignition limits

15 p2465 A71-32090

Gaseous chlorine of marine origin in atmosphere based on concentration analysis

16 p2604 A71-33383

Chlorine-fluorine flame, determining adiabatic propagation speed, refractive index field, temperature profile, composition distribution and atom concentrations

19 p3168 A71-38105

Cl abundance in sun, discussing low noise photoelectric scan

23 p3767 A71-43833

CHLORINE COMPOUNDS

NT ALUMINUM CHLORIDES
NT AMMONIUM CHLORIDES
NT AMMONIUM PERCHLORATES
NT BORON CHLORIDES
NT CALCIUM CHLORIDES
NT CARBON TETRACHLORIDE
NT CHLORATES
NT CHLORIDES
NT CHLORINE FLUORIDES
NT CHLORINE OXIDES
NT CHLOROSILANES
NT COPPER CHLORIDES
NT DICHLORIDES
NT HYDROCHLORIC ACID
NT HYDROCHLORIDES
NT HYDROXYLAMMONIUM
PERCHLORATES
NT IRON CHLORIDES
NT LEAD CHLORIDES
NT MAGNESIUM CHLORIDES
NT NITRONIUM PERCHLORATE
NT PERCHLORATES
NT POTASSIUM CHLORIDES
NT POTASSIUM PERCHLORATES
NT SILICON TETRACHLORIDE
NT SODIUM CHLORIDES
NT TETRACHLORIDES

Nitrogen atoms chemiluminescent reaction spectra with carbon tetrachloride, ethylene and methylene chloride, noting application to artificial clouds formation

19 p3014 A71-38634

CHLORINE FLUORIDES

Metal powders hypergolic ignition in gaseous chlorine trifluoride, examining use in air augmented rockets primary combustors

07 p1183 A71-19875

Chlorine trifluoride standard heat of formation by fluorine flame calorimetry, deriving from measured enthalpies of reactions

07 p1056 A71-20656

ClF diluted solutions in Ne, investigating thermal decomposition mechanism behind shock waves by mass spectroscopy

15 p2367 A71-31874

CHLORINE OXIDES

Chlorine dioxide induced fluorescence spectra, using argon ion laser

08 p1300 A71-20667

CHLOROETHYLENE

Solar neutrino detection using capture reaction in perchloroethylene medium

15 p2478 A71-31803

CHLOROFORM

Vibrational energy distribution and emission lines of fluorine atoms plus chloroform reactions in chemical laser, using equal gain measurements

19 p3071 A71-37331

CHLOROPHYLLS

Remote sensing of chlorophyll and temperature in marine and fresh waters by spectroradiometer and differential and IR filter radiometers onboard airplane

22 p3534 A71-41986

CHLOROPLASTS

Isolated tobacco chloroplasts disintegration, measuring simultaneous particle size and photochemical reduction rate changes by electron micrography

04 p0539 A71-15269

Hill reaction of disintegrating chloroplasts in vitro, investigating transient color sensitivity /red-blue effect/

04 p0539 A71-15270

Saturating flash delayed luminescence from chloroplasts, considering relationship to oxygen evolution

24 p3799 A71-45382

CHLOROSILANES

Fluorochlorosilane preparation and identification by Raman laser spectroscopy, establishing line to vibration mode relation

14 p2189 A71-29746

CHOICE

U SELECTION

CHOKES

Ground noise reduction with balancing units, discussing transmission line driving and receiving end applications

17 p2716 A71-34859

CHOKES (RESTRICTIONS)

Common mode choke for reduction of current unbalance in cable to improve electromagnetic interference performance

19 p3000 A71-38432

CHOLESTEROL

Mortality of myocardial infarction patients on diet low in saturated fats and cholesterol

01 p0015 A71-11299

Blood cholesterol and protein fraction concentrations in pathogenesis of hypothalamic atherosclerosis patients

02 p0201 A71-12531

Thermally induced helical inversion absence in single component cholesteric liquid crystals indicating impurity compensation

02 p0296 A71-12571

Cholesteric liquid crystal pitch from IR transmission measurements

02 p0209 A71-12572

Chlorophenoxyisobutyric acid action on human cholesterol metabolism, suggesting cholesterol synthesis inhibition

07 p1044 A71-20353

Human crystalline lens protein and lipid discussing cholesterol accumulation with age

09 p1390 A71-22421

Electrical conduction in cholesteryl acetate, propionate and stearate in solid, liquid crystal and isotropic liquid states characterized by I-V measurements

11 p1807 A71-25564

Cholesteric liquid crystal mixtures optical characteristics, measuring reflection, transmission and extinction ratio

12 p1942 A71-26800

Cholesterol and esterified cholesterol distribution in human skin from analysis on fat, epidermis, corium, subcutaneous tissue and serum by chromatographic/colorimetric methods

20 p3185 A71-38892

Cholesterol liquid crystals technique for thermal analysis of microcircuits, multilayer circuit boards, semiconductor devices and other electronic components

21 p3355 A71-40738

CHOLINE

Acetylcholine endogenic formation in rabbit myocardium effect on ventricle rhythm guides automatic activity suppression by HF excitations

07 p1040 A71-19281

High motor stresses effects on muscle acetylcholine content, cholinesterase activity and localization, solitary contractions fusion and pessimal weakening

14 p2186 A71-30553

Rat brain acetylcholine levels circadian rhythm correlated to spontaneous motor activity and sleep-awake cycle

17 p2684 A71-35326

Gastrointestinal tract reactions to atropine sulfate, acetylcholine and carbacholine in rats after acceleration exposures, using roentgenograms

22 p3495 A71-42794

Cholinesterase activity and acetylcholine level dependence on adrenaline dose injected in heart during rats experimental myocardiodystrophy

24 p3800 A71-44500

CHOLINERGICS

Human blood cholinergic complex during various physiological states, noting nonmediator action of acetylcholine

13 p2006 A71-28384

M-cholinergic and adrenergic subcortical structures blockage effects on blood flow rate in dog pulmonary circulation system

16 p2534 A71-34113

ACh retina application effects, showing second retinal neuron cholinergic receptors desensitization

17 p2686 A71-35490

CHOLINESTERASE

Ionized air exposure effects on acetylcholine content and cholinesterase activity in mice, noting cholinergic and serotonic interaction

13 p2006 A71-28404

High motor stresses effects on muscle acetylcholine content, cholinesterase activity and localization, solitary contractions fusion and pessimal weakening

14 p2186 A71-30553

Cholinesterase activity and acetylcholine level dependence on adrenaline dose injected in heart during rats experimental myocardiodystrophy

24 p3800 A71-44500

CHONDRITES

NT CARBONACEOUS METEORITES

NT MURRAY METEORITE

NT ORGUEIL METEORITE

Chondrites Li content, using atomic absorption spectroscopy

01 p0162 A71-11429

Isotopic Rb/Sr age and initial chondritic ratio for silicate inclusions in Colomera iron meteorite

02 p0318 A71-12902

Al and Si abundances of Italian chondrites by instrumental pile neutron activation analysis

02 p0318 A71-12903

Fe, Si, Mg, Ca, Al, Ti, Mn, K and P concentration differences in L and H group common chondrites

03 p0487 A71-13337

Na and Mn homogeneity in chondritic meteorites, discussing accretion processes, metamorphisms, weathering effects and specimens size

04 p0659 A71-15855

Refractory elements abundances in chondrites, basaltic achondrites and Apollo 11 fines, emphasizing Ca-Al relationship

06 p0966 A71-17894

Shock reheated chondrites metal phases, discussing postshock cooling thermal histories by metallographic and electron microprobe studies

09 p1519 A71-22643

Chemical elements abundance in ordinary chondrites, terrestrial magma and lunar rocks, considering Alven theory of solar system origin

10 p1665 A71-23741

Orgueil carbonaceous chondrite organic matter, detecting homologous compounds, optically active species, isotopes, bacteria and organized elements

10 p1565 A71-24612

Potassium-Argon dating analyses of neutron irradiated meteorites, discussing Chainpur chondrite chondrules gas retention ages

10 p1679 A71-24984

Clear taenite formation in bronzite and hypersthene chondrites studied by metallographic and electron microprobe

10 p1680 A71-24985

Rare earth and heavy elements determination in olivine hypersthene and enstatite chondrites by spark source mass spectroscopy, noting Fe meteorite silicate inclusions composition

11 p1819 A71-25225

Mineralogy, petrology, chemistry and microstructure of Valdinizza meteorite

11 p1835 A71-26480

Petrography, chemistry and mineralogy of El Paso meteorite

11 p1835 A71-26481

Morphology, mineralogy and chemistry of Ashmore meteorite

11 p1835 A71-26482

Hydrocarbons, amino acids and large molecule organic compounds formation in chondritic meteorites by abiogenic reactions

13 p2010 A71-28692

Chemical fractionations in meteorites, considering trace elements abundance in L chondrites and implications for cosmochemistry 13 p2141 A71-29097

Equilibrium temperatures, pressures and oxygen fugacities of equilibrated chondrites in meteorites 13 p2141 A71-29098

Cl chondrites approximating primordial solar system matter condensable fractions based on isotopic/elemental abundance continuity, fractionation patterns and chondrules absence 14 p2306 A71-29708

Carbonaceous chondrites total nitrogen and carbon abundances, using gas chromatography 15 p2486 A71-31990

Lost City /Oklahoma/ and Suchy Dul /Czechoslovakia/ bronzite chondrites stable rare gas concentration determination 15 p2488 A71-32354

Lost City /Oklahoma/ chondrites, determining alkali, alkaline earth and rare earth element concentrations and Rb-Sr model age 15 p2489 A71-32355

Lost City /Oklahoma/ meteorite classification as type H5 chondrite based on bulk chemical composition, mineralogy and petrography 15 p2489 A71-32356

Terrestrial basalts and lunar rocks volatile element concentrations comparison, noting relationship to abundance in chondrites 16 p2633 A71-33348

Electrical conductivities of Apollo 11 and 12 lunar rocks and chondritic meteorites at 300-1100 K 17 p2796 A71-34182

Chondrites bibliography and review, considering classification, metamorphism, ages and thermal history, achondrites and organic compounds 17 p2798 A71-34454

Kyle /Texas/ chondrite classification based on chemical composition, mineralogy and structure 17 p2800 A71-34513

De Kalb /Missouri/ chondrite structure and mineral composition, noting olivine and bronzite presence 17 p2800 A71-34518

Mineral and chemical composition of Krasnyi Kliuch meteorite, characterizing as recrystallized chondrite containing chondrules 17 p2811 A71-35731

Chondrite classification, primordial matter composition and early solar system chemical processes, discussing cosmic gas condensation and refractory element fractionation 18 p2967 A71-37027

Crustal and meteoritic abundances of elements and water, considering chondritic and achondritic composition 19 p3055 A71-38145

Carbonaceous chondrite fission producing super-heavy element decay half life 22 p3605 A71-42398

Rare earth trace elements abundance of Apollo 14 lunar soil samples from Fra Mauro, comparing with chondrites 23 p3735 A71-43248

CHONDRULE
Potassium-Argon dating analyses of neutron irradiated meteorites, discussing Chainpur chondrite chondrules gas retention ages 10 p1679 A71-24984

Mineral and chemical composition of Krasnyi Kliuch meteorite, characterizing as recrystallized chondrite containing chondrules 17 p2811 A71-35731

CHOPPERS [ELECTRIC]
U ELECTRIC CHOPPERS

CHORDS [GEOMETRY]
Direction of chord in space from synchronous photographic satellite observations, considering optimum satellite altitude 12 p1900 A71-26969

CHOROID MEMBRANES
Chorioretinal temperature increases from naked solar eclipse observations for various observation angles and pupil diameters, considering solar irradiance and atmospheric transmittance spectra 11 p1726 A71-26484

CHORUS [DAWN PHENOMENON]
U DAWN CHORUS

CHORUS PHENOMENON
U DAWN CHORUS

CHROMATES
Phase relationships in magnesium ferrate-magnesium chromate systems subjected to annealing in air and hydrogen atmospheres 01 p0107 A71-10403

CHROMATOGRAPHY
Gel permeation chromatography for polymer molecules size /hydrodynamic volume/ separation 04 p0548 A71-15265

Streptomyces sp chitinase purification and properties by column chromatography, noting calcium component 11 p1728 A71-26064

Quantitative gas liquid chromatography analysis of amino acids in biological materials, discussing ion exchange techniques 11 p1729 A71-26068

Nonproteins detection in presence of protein amino acids with Beckman analyzer chromatograms 13 p0206 A71-29478

Chromatographic separation of molybdenum, niobium and tungsten based on metal ions absorption by aluminum oxide 15 p2367 A71-31647

CHROME
U CHROMIUM

CHROMITES
Chromite and ilmenite analysis in pallasites, mesosiderites, achondrites and meteorites with electron microprobe 14 p2310 A71-30173

Surface morphology of free-growing ilmenites and chromites from lunar vuggy rocks by scanning electron microscopy and electron microprobe 23 p3745 A71-43665

CHROMIUM
Dislocation pinning by interstitial atoms during Cr and Cr-Ce strain aging, using amplitude dependent internal friction technique 02 p0263 A71-11897

Cr and Mo thin film coatings on Si-Fe, examining effect on plastic deformation and mechanical properties 02 p0266 A71-12655

Presulfidized Ni alloys and Cr oxidation rates 04 p0615 A71-15787

Austenitic stainless steel intergranular corrosion model for thermodynamic analysis leading to grain boundary diffusion and Cr concentration profiles determination 07 p1134 A71-19566

Ce, Pr and Nd solubility in Cr, investigating temperature dependence, microhardness, deoxidation and alpha phase by X ray, metallographic and durometric analyses 07 p1144 A71-20652

Vacuum deposited Cr film formation as function of condensation rate 09 p1469 A71-22847

Cr specimens containing Y, investigating microscopic breakdown at high temperatures as function of deformation during vacuum rolling 09 p1474 A71-23235

Cr plastic properties, investigating recovery and recrystallization effects from La and Y additions 09 p1476 A71-23316

Cr and V diffusion plating influence on principal characteristics of highly alloyed martensitic and carbon steels 12 p1912 A71-27690

Al-Zn-Mg alloys, considering Cu and Cr additions effects on nucleation and incoherent precipitates formation 13 p2088 A71-29406

Nickel alloys susceptibility to pores formation in tungsten inert gas welding in argon-nitrogen mixture, considering influence of Cr, Mo and W 14 p2260 A71-30487

Fe-Ni alloys with Cr, investigating heat treatment effect on thermoelastic coefficient 15 p2426 A71-31482

Vacuum deposited thin Cr films on glass substrate, describing hydrogen adsorption effects 19 p3076 A71-37116

Vacuum deposited thin Cr films on glass, investigating substrate temperature and inert gas pressure effects on texture 19 p3076 A71-37117

Vacuum-melted low-carbon low-manganese steel, investigating Ni and Cr additions effects on recrystallization textures 19 p3079 A71-37703

Diffusion layer structure and phase composition during quenched and annealed steel saturation by Cr at high heating rates 21 p3404 A71-41170

Chromium and Ni-Cr electrodeposition from amide solvent system, describing water and sulfur ligands effects on plating efficiency 22 p3554 A71-42528

Porous materials prepared from electrolytic Cr powder, noting high permeability and strength and filter applications 23 p3689 A71-43252

Apollo 11 and 12 lunar dust and rocks, determining Be and Cr contents by gas chromatography for comparison with crystalline rocks 23 p3751 A71-43707

Stress and magnetic field induced spin density wave polarization vectors rotation in Cr single crystals, accounting for Young modulus temperature and magnetic field dependence 24 p3861 A71-45131

CHROMIUM ALLOYS
NT CHROMIUM STEELS

Cr-Tb alloys phase transformations and diagrams dependence on temperature and composition, using physicochemical analysis 01 p0100 A71-10418

Cr-alloyed Fe powders fine crystalline structure from X ray analysis 01 p0102 A71-10789

Cr-chromium nitride fusion phase diagram analysis, establishing nonvariant eutectic and dissociative transformations 02 p0266 A71-12673

Substructures and properties of Ni, Chromel A, Inconel 600 and TD-NiCr following explosive shock load deformation, using electron microscope 02 p0268 A71-12889

Volume diffusion role in Ni-Cr eutectic and cast alloys cellular structure growth 04 p0615 A71-15793

Thoria dispersed Ni-Cr alloy hypersonic entry ablation model, accounting for Cr oxidation [ALAA PAPER 71-34] 06 p1009 A71-18654

Cr alloys endurance and dynamic creep under HF tension-compression loads at room temperature 07 p1129 A71-19154

High temperature oxidation of Cr-Ti-Si coatings on Nb alloy 07 p1135 A71-19619

Mossbauer effect study of 475 C decomposition of binary Fe-Cr alloys, considering fluctuations about average composition 07 p1138 A71-19985

Aging effect on tensile mechanical properties and hardness of high purity binary Ni-Cr alloys at 290-530 C 07 p1138 A71-19986

Ni-Cr thoria dispersion strengthened alloys, determining texture effects on high temperature mechanical properties 08 p1311 A71-21545

Co-Ni-Cr-Mo alloys hardening mechanisms, noting martensitic transformation role 08 p1312 A71-21551

Heat resistance in air of Co-Cr alloys as function of chemical composition 08 p1317 A71-21763

High chromium Ni-Cr alloys use and improvement, discussing refractoriness in oxidizing atmospheres and chemical corrosion in combustion products deposits 09 p1470 A71-23043

High temperature precipitation hardening of Ni-Cr alloys, discussing effect on creep rupture strength 09 p1470 A71-23044

Cr alloys alloying elements Os, Re, Fe, Co and Mn effect on lattice constant and elastic properties, using acoustic measurements 09 p1473 A71-23229

Polygonization and recrystallization processes in Fe-Cr alloy, using electron diffraction and microscopy 09 p1476 A71-23322

Ni-Cr alloys hardened by Nb and Ta, examining precipitation and plastic deformation mechanisms 09 p1479 A71-23622

Co-Cr and Ni-Cr eutectic alloys with single crystal TaC fiber reinforcement, discussing unidirectional solidification 09 p1479 A71-23623

Fine structure and heat resistance of thin Ni-Cr alloys specimens after prolonged exposure to high temperatures under tensile loads 09 p1480 A71-23703

Comparative isothermal oxidation of Fe-Cr-Al, Ni-Cr-Al and Co-Cr-Al alloys with protective scales 10 p1624 A71-23971

Ternary compositions for high temperature alloys Ni-Cr-Al and Co-Cr-Al, using superimposed oxidation data on phase diagrams /oxide mapping/ 10 p1625 A71-23972

Manganese and silicon effects on oxidation and scale mechanisms of Co-Cr alloys, using thermogravimetric, metallographic and microprobe techniques 10 p1625 A71-23973

Ni-Cr-Ti-Al-Mo system equilibrium conditions, conducting phase analysis by X ray and optical and electron microscopy 10 p1627 A71-24532

Crystallographic relationships between Ni- and Cr-rich solid solutions, noting preferred interface interfaces in Ni-Cr eutectic alloy 11 p1778 A71-25532

TD NiCr nickel based alloy high temperature oxidation control, discussing thoria dispersion effect on Ni-Cr oxidation properties 11 p1779 A71-26015

Dutch monograph on Cr-W interdiffusion in solid state concerning Kirkendall effect and relation between chemical and self diffusion 11 p1783 A71-26488

High chromium hot corrosion resistant superalloys in sheet form, noting precipitation hardening and creep resistance equivalent to Nimonic alloys 12 p1916 A71-26922

Mo-Zr-Cr alloy samples cast annealed and quenched at 1500 C, calculating phase equilibrium diagram 12 p1918 A71-27528

Ni-Cr and Ni-W alloys high temperature strength properties, considering stacking fault energy, diffusion velocity, Young modulus and dislocation locking 12 p1919 A71-27762

Mechanical properties of Ti-Al-Cr and Ti-Al-Cr-Mo alloys annealed below solidus temperatures

13 p2083 A71-27873

Cr and Cr-Y alloy interstitial residual content and dynamic dislocation-interstitial interactions at various temperatures and strain rates

13 p2085 A71-28578

Oxidation and nitrogen absorption protection of Cr alloy by Ni alloy claddings applied by gas pressure bonding

13 p2087 A71-29122

Nucleation, growth and spinodal decomposition during aging in Fe-Cr alloys, using Mossbauer spectroscopy

13 p2089 A71-29414

Beta stabilizing Mo and Cr effects on mechanical properties of welded and heat treated Ti alloys

14 p2260 A71-30490

Molten Co-Cr alloy structural transitions at increasing temperatures, relating to change in solid state with increasing Cr content

15 p2425 A71-31393

Solidus-liquidus surfaces and isothermal phase diagrams of quaternary system of Cr with Ti, Zr, Nb and Ta, showing Laves phase interactions and continuous solid solutions

15 p2426 A71-31407

Ternary Co-Cr-Al alloy oxidation data, detailing kinetics, products, mechanisms, resistance behavior and rate

16 p2589 A71-32870

Ternary Co-Cr-Al alloy oxidation resistance composition selection, using oxide maps superimposed on phase diagram

16 p2590 A71-32872

Randomly distributed domain structure of ordered Ni-Cr alloy, using electron microscopy and neutron diffraction

17 p2755 A71-34413

Mechanical and crystallographic structure effect on cold brittleness temperature anisotropy and on exfoliation of Cr alloyed with rare earth elements

17 p2755 A71-34416

Co-Cr-W alloy sulfidation at high temperatures, performing weight gain, metallographic X ray and electron probe analysis

17 p2758 A71-35149

Ni-Cr alloys sulfidation at 700 C from inert and radioactive marker techniques

18 p2938 A71-37003

Phase diagram of Ti-Cr alloys for temperatures from 800 to 1600 C

19 p3077 A71-37466

Cr diffusion into Ni-Cr alloys in presence of calorized layer, noting increased diffusive mobility

21 p3390 A71-41167

Si addition effect on Ni-Cr alloy calorized layer depth, microhardness, phase structure, chemical composition and scaling resistance

21 p3390 A71-41168

Oxidation resistance and scale fracture healing by Al additions to Co-Cr alloys at high temperatures, using electron probe and scanning electron microscope analyses

21 p3405 A71-41420

Isothermal martensite transformations in Fe-Ni-Cr alloys, explaining kinetics difference in terms of elastic parameters small variations

23 p3688 A71-42925

Nickel-chromium system powders physicochemical properties, noting use as high temperature cermet packing materials

23 p3690 A71-43256

Ni-Cr single crystals plastic deformation, presenting work hardening characteristics and critical resolved shear stress

23 p3694 A71-44278

Precipitation hardenable Cr-Cu liquid phase sintered powder composite, showing matrix properties variations

23 p3695 A71-44291

Cr-Ni alloy heat treated cast specimens microstructure, metallographic, X ray and spectral investigation, noting chemical inhomogeneity

24 p3836 A71-44484

Hydrogen solubility in liquid Cr, Ni and Co alloys containing Si for various concentrations and temperatures

24 p3840 A71-45371

CHROMIUM BORIDES

Chromium carbides or borides high melting wear resistant surfacing material for machine components subjected to abrasive wear

15 p2418 A71-32669

CHROMIUM BROMIDES

Faraday rotation near ferromagnetic critical temperature of chromium bromide, discussing scaling laws validity and experimental confirmation

04 p0637 A71-15796

CHROMIUM CARBIDES

Neutron irradiation effect on lattice parameters and distortion energy of titanium and chromium carbides, using X ray analysis

15 p2430 A71-32152

Zirconium dioxide reactions with chromium, molybdenum and tungsten carbides, studying reaction products, phase composition, sintering temperatures and chemical separation

15 p2432 A71-32166

Chromium carbides or borides high melting wear resistant surfacing material for machine components subjected to abrasive wear

15 p2418 A71-32669

Intergranular corrosion of chromium carbide sensitized Ni base alloys, noting surface effect during solution heat treatment

22 p3560 A71-41626

CHROMIUM COMPOUNDS

NT CHROMATES

NT CHROMITES

NT CHROMIUM BORIDES

NT CHROMIUM BROMIDES

NT CHROMIUM CARBIDES

NT CHROMIUM OXIDES

Gaseous chromium carbonyl or aqueous chromium salt spray additives behavior photometric investigations in premixed hydrogen-oxygen-nitrogen flames

16 p2540 A71-33374

Chromium sesquioxide instability towards oxygen at high temperature, using spring thermobalance

18 p2937 A71-36763

CrN discovery in iron meteorites, determining carlsbergite mineral composition by electron microprobe

23 p3770 A71-44015

CHROMIUM OXIDES

NT CHROMITES

Chromium oxide electric conductivity activation energy and active oxygen, discussing perchloric acid and ammonium perchlorate vapors effect

07 p1182 A71-19247

Oxidation/vaporization kinetics of chromium oxide hot pressed and sintered pellets

09 p1480 A71-22113

Molten alumina and chromia reactions with refractory metals, calculating isobaric-isothermal potential variations

09 p1466 A71-22165

Oxidation kinetics and scale morphology of chromium oxide forming thoriated and unthoriated Ni alloys, discussing rate controlling processes effects

16 p2590 A71-32871

CHROMIUM STEELS

Cr-Ni steel elastic properties under intercrystalline corrosion, examining temperature effects on internal friction, electric resistivity and vibration frequency

01 p0096 A71-10038

Cr-Si steels cold shortness tests, identifying low temperature failure mechanisms

01 p0098 A71-10082

Mechanical properties, long term strength and corrosion resistance of low alloy chromium steel with nitrogen

01 p0103 A71-11069

Ferritic steel with 17 percent Cr, examining dynamic behavior under high speed tension test regarding heterogeneity of plastic deformation, stress peak, etc

01 p0105 A71-11616

Chromium steel surface diffusion saturation by sublimated Mo, examining process kinetics

03 p0442 A71-13400

Austenitized oil hardened annealed chromium steels with electrolytically isolated carbides, determining structure by X ray analysis

04 p0610 A71-14886

Austenitic steel containing C, Cr and Mn, investigating W, Mo, V and Nb effect on structure and mechanical properties

04 p0616 A71-15804

Molybdenizing effects on Cr-Ni-Ti steel strength and stability in liquid Li

05 p0768 A71-16772

High carbon Cr and Mn steels martensitic transformation points, ascertaining short range order occurrence by electron microscopic study

07 p1130 A71-19278

Bainite structure effects on Cr-Mo-V steels creep and rupture strength

07 p1134 A71-19520

Optimal heat resistance, mechanical properties and microstructure of steam pipe Cr-Mo-V steel

07 p1135 A71-19618

Intrinsic stacking fault energy temperature dependence in austenitic Fe-Cr-Ni alloys determination from dislocation mode measurements by high temperature transmission electron microscopy

07 p1138 A71-19984

Deformation-induced martensitic transformation effects on Fe-Ni-Cr-C alloy plastic behavior

08 p1313 A71-21555

Cr steel cyclic strength and elastic properties after combined high temperature thermomechanical treatment and cold working

09 p1471 A71-23079

Phosphorus segregation to prior austenite grain boundaries in ferrite, considering effect on Ni-Cr-C-P steel temper embrittlement

09 p1471 A71-23123

Chromium and titanium alloyed austenitic steels, examining short and long time application as turbine engine parts

09 p1475 A71-23295

Crack propagation in chromium steel butt weld sheets, discussing dendrite macrostructural effects on brittle resistance and toughness

11 p1770 A71-25945

C and Ni contents effects on water quenched tempered austenitic chromium nickel-stainless steels intercrystalline corrosion

12 p1919 A71-27777

Si, Mo and Cu effects on pitting corrosion of Cr-Ni steel

13 p2082 A71-27831

Chemical composition effects on microstructure and high temperature properties of cast Cr-Ni-Al steels containing Ti, B, Ce and Zr

13 p2084 A71-28035

Stress relief cracking in Cr-Mo steel, considering correlation with embrittlement of water quenched base metal tempered at low temperature

13 p2086 A71-29091

Austenite and carbide chromium manganese steel boron distribution obtained by tracing elements

15 p2425 A71-31397

Strengthening mechanism of Cr-Ni and Ni maraging steels related to dislocation stress field

15 p2427 A71-31524

High chromium low carbon steel, detailing oxygen content effects on high temperature reduction intercrystalline corrosion and grain growth

15 p2427 A71-31528

Low carbon high chromium steel, emphasizing nitrogen content effects on temper brittleness

15 p2427 A71-31529

Crack propagation resistance-cyclic fracture strength relation for austenitic and Mn-Cr-V steels, considering thermomechanical working effects

16 p2592 A71-33408

Cold hardened Cr-Si steels strength/plasticity thermal dependence and brittleness from short torsion and compression tests, identifying low temperature failure mechanisms

16 p2593 A71-33638

Austenitic high nitrogen chromium-nickel steels plastic deformation and heat treatment in plasma arc furnaces

16 p2596 A71-33910

Chromium casting steel, investigating annealing effects on alloying elements diffusion

18 p2934 A71-36150

Cr-Ni austenitic steels thermomechanical destabilization using cyclic strain hardening

18 p2934 A71-36173

Chromium stainless steels fine structure, noting quenching and tempering temperatures effects

19 p3076 A71-37118

Cr-Mo-V steel creep strength tests extrapolation by parametric approach, discussing optimum regression dependence

20 p3250 A71-39019

Creep tests effect on Cr-Mo-V steels mechanical properties during alternating stress fatigue testing, considering preliminary static prestressing

20 p3250 A71-39023

Intermittent stress creep tests on low carbon steel, commercially pure iron, Cr-Mo steel and commercially pure tantalum, noting static-to-dynamic transition

21 p3400 A71-40835

Alloying elements effects on martensite decomposition and carbide phase formation during tempering of chromium steels

21 p3401 A71-41085

Hardness, internal friction, microstress, martensite lattice and density changes during aging of precipitation hardening Fe-Cr-Ni steel, using dilatometric and X ray analysis

21 p3402 A71-41086

Nitrogen alloying effects on relaxation resistance of Cr-Mn austenitic steel

21 p3402 A71-41092

Alloying effects on corrosion cracking of Cr-Ni austenitic stainless steels, testing in chloride solutions

21 p3402 A71-41094

Cr and Cr-Ni ferritic and austenitic steels, investigating high temperature nitriding for intensifying nitrogen diffusion saturation

21 p3389 A71-41098

C and Ni contents effects on water quenched tempered austenitic chromium nickel-stainless steels intercrystalline corrosion

21 p3403 A71-41100

Low carbon austenitic Cr-Mn steels, noting Ni and Al combined alloying effects on structure and mechanical properties

21 p3403 A71-41101

High heat resistance of austenitic Cr-Ni-V-B steel by polygonization and recrystallization, using thermomechanical treatment

21 p3403 A71-41102

Fine structure dislocation and phase composition of Cr-Mo steel at elevated temperature in steam pipe applications, noting recrystallization stability 23 p3690 A71-43277

Boron addition effects on scaling resistance of Ni-Cr steel at high temperatures 23 p3690 A71-43278

Mo and Co alloying effects on high temperature chromium ball bearing steels contact strength 23 p3692 A71-44037

Strain hardening effect of Ni, Mn and Mo in Cr steel after high temperature annealing 23 p3693 A71-44216

CHROMOSOMES

Bone marrow physiological regeneration after chronic gamma irradiation, noting effect on fission processes and chromosome apparatus of cells 01 p0014 A71-11146

Rat bone marrow chromosomes radiation protection, using 5-hydroxytryptamine 07 p1038 A71-18973

Cystamine effects on lymphocytes chromosomal aberrations in human peripheral blood during local fractionated gamma irradiation 08 p1240 A71-21797

Chromosome radiation injury preservation in generations of X ray irradiated cells of human diploid strains 08 p1242 A71-21966

Spaceflight effects on dry crepis capillaris seeds in five day orbit, showing chromosome rearrangements and increased mutagenic sensitivity 09 p1392 A71-22563

Chromosome mapping of *Pasteurella pseudotuberculosis* by interrupted mating, indicating chromosome transfer in more than one linkage group 09 p1396 A71-23474

Anabaena cylindrica alga chromosomes protein components, noting histone absence 16 p2536 A71-33359

Brain polysomes disaggregation and tryptophan elevation in immature rats and adult animals after L-dopa administration 20 p3186 A71-38979

Astronaut chromosome aberrations, presenting peripheral blood leukocytes cytogenetic tests for pre and post space flight 20 p3188 A71-39227

Specific banding patterns for identification and structural detection of human chromosomes, using differential staining method 21 p3336 A71-40853

Abdomen shielding effects on chromosome aberrations in bone marrow cells of guinea pigs and rats under gamma irradiation 22 p3493 A71-42719

Lymphocyte chromosome aberrations by inhaled ozone in Chinese hamster, indicating mutagen damage 24 p3799 A71-45150

CHROMOSPHERE

Solar chromospheric flares observations tabulation /1969/ and H alpha line width curves graph 01 p0144 A71-10870

Solar core to surface energy transfer mechanism, discussing chromosphere spectrographic, photoelectric and telescopic observations 02 p0312 A71-12373

Solar chromosphere model, investigating radiative transfer effect on temperature structure of plane slab heated by thermal conduction 03 p0483 A71-13186

Chromospheric flare north-south asymmetry aspects, calculating radio flux density correlation indices 03 p0417 A71-14193

Solar chromosphere structure and Lyman continuum, examining brightness and kinetic temperatures, limb variations, radiative transfer and models 05 p0803 A71-16023

Three component model for chromospheric Ca II K line formation, discussing observational agreement 05 p0803 A71-16024

Solar chromosphere mass motion, studying macroturbulence influences on visible spectrum lines high resolution profiles from rocket spectrograms 06 p0967 A71-17904

Eclipse observations interpretation for transition region between extreme limb and low chromosphere 06 p0967 A71-17905

Solar chromosphere and corona wave motions, presenting solar radio emission fluctuations correlation functions 07 p1199 A71-20010

Spectrophotometric observation of solar weak chromospheric flare of 15 June 1964, determining flare origin 07 p1188 A71-20039

Zeta Aurigae chromospheric lines observed radial velocities mean variations, taking into account H ion gas acceleration, K star mass ejection and rotation 08 p1364 A71-21417

Solar chromosphere and prominences observations during total eclipse of 12 November 1966 by slitless spectrograph, using grazing incidence method 08 p1365 A71-21423

Brightness temperature from solar UV continuum in 1680 to 600 A in photosphere-chromosphere transition model 10 p1666 A71-23780

Solar lower chromosphere two dimensional models, using relative RMS line center intensity variations and mean limb darkening curves 10 p1666 A71-23781

Solar chromospheric emission line identification at 4097.3 A, discussing N III transition 10 p1666 A71-23783

Turbulent photosphere and chromosphere, investigating finite resistivity effects on solar flare phenomena 11 p1832 A71-26173

Star Arcturus chromospheric Lyman alpha emission observation by rocket-borne precision pointing telescope and UV spectrometer 12 p1957 A71-26625

Chromospheric millimetric emission through 250 GHz atmospheric passband on isophoto maps, showing higher brightness temperatures compared with solar disk 12 p1969 A71-27649

Solar chromosphere model, explaining spicules origin and relation to small scale nonuniformities 13 p1316 A71-28430

Solar chromospheric flares in 1969, constructing tables of observation data commencement and end time and H alpha line maximum width 13 p1218 A71-28480

Solar quiet region chromosphere K emission line behavior, identifying surface characteristics for width absolute magnitude relation 13 p1240 A71-29046

Solar chromospheric activity of 8 February 1971, obtaining brightness temperature maps at 400, 800 and 1200 microns 13 p1243 A71-29271

Shock wave heated atmospheric model computation for solar chromosphere and corona 14 p2306 A71-29684

Solar active regions velocity field at different levels, discussing transition region from photosphere to chromosphere 14 p2308 A71-29973

Motions in chromospheric limb and disk flares based on H alpha photography 14 p2298 A71-29974

Chromospheric flare on 11 July 1966, comparing solar radio emissions at 10 cm and 1.5 m wavelengths 14 p2298 A71-29976

Unipolar sunspot magnetic field and electric currents, comparing chromosphere and photosphere total field vector 14 p2298 A71-29978

Solar prominences formation, discussing coronal thermal instability, chromospheric heat balance, magnetic field and gas heating 15 p2482 A71-31334

Chromosphere and solar quiet regions transition zone model, investigating radio and UV emission and height dependence of temperature and density 15 p2497 A71-32745

Spectrographic observation of coronal lines in chromosphere during solar eclipse of 7 March 1970 16 p2642 A71-33787

Metallic lines in high-dispersion spectrograms in 1966 Peruvian eclipse for lower chromosphere excitation temperature 17 p2799 A71-34476

Solar corona studies at Kiev University during 1952, 1954, 1961, 1965 and 1968 solar eclipses, showing coronal fine structure relation to chromosphere 17 p2802 A71-34827

Center to limb solar brightness distribution at 1.4 mm, discussing chromospheric models and antenna beam pattern effects 18 p2965 A71-36735

Solar chromospheric plage area related to peak K coronal brightness at limb 18 p2966 A71-36738

UV studies of solar atmosphere in quiet and active regions, considering low and high chromosphere, transition zone, quiet corona and inhomogeneity 18 p2968 A71-37034

Solar photosphere and low chromosphere models temperature-height profile 19 p3135 A71-37609

Solar chromosphere and corona manifold structure data, using high resolution filter photography 19 p3136 A71-37616

Solar limb and disk intensity spectra in chromosphere-corona transition region, calculating models, element abundances structure, electron pressure and hydrostatic equilibrium equations 19 p3136 A71-37617

Electron temperatures for lithium-like ions O VI, Ne VIII and Mg X formation in solar chromosphere and corona, using rocket spectrometric measurements 19 p3136 A71-37618

Solar and stellar chromospheres and coronas production based on turbulence in granulation, photospheric mechanical flux and supergranular network magnetic field structures 19 p3136 A71-37626

Stellar chromosphere detection through H, K and metastable He lines observation, noting importance for solar physics 19 p3136 A71-37627

Nonlinear coupling between thermal conduction and radiative transfer in solar chromosphere by iterative method 19 p3143 A71-38159

Harvard-Smithsonian reference atmosphere model of solar atmosphere, combining photosphere and quiet lower chromosphere 19 p3146 A71-38660

Solar X-ray line emission, using crystal spectrometers during large chromospheric flare 19 p3130 A71-38672

Oscillations of visible chromosphere boundary and regularity in position of spicule groups along limb, studying H alpha filtergrams 22 p3597 A71-41456

Morphological relationships in solar chromospheric H alpha fine structure involving bushes, fibrils, threads and filaments 22 p3597 A71-41457

Spiral topology of chromospheric fibrils and filaments in H alpha near sunspots, noting similarity with axisymmetric force free magnetic field configuration 22 p3597 A71-41458

Solar prominences formation, discussing coronal thermal instability, chromospheric heat balance, magnetic field and gas heating 22 p3606 A71-42609

Solar chromosphere spectrum analysis, measuring H alpha line relative shifts variation with altitude 22 p3607 A71-42872

Solar chromospheric data for 1952, 1958, 1962 and 1966 eclipses, showing helium abundance in prominences 23 p3767 A71-43842

He excitation and ionization in chromospheric flares, performing calculations for 10,000-50,000 K electron temperatures and 0.5-9.0 times 10 to 13th power per cc electron densities 23 p3722 A71-44310

Electric conductivity correlation between solar faculae and Bilderberg model of photosphere and chromosphere 24 p3868 A71-44458

Transverse magnetic field measurement over sunspot in chromosphere, noting fan-shaped field line divergence 24 p3870 A71-44817

CHRONIC CONDITIONS

Soviet army medical appraisal of chronic microwave field induced affections, noting evaluation procedures inadequacy 16 p2534 A71-32827

Human fatigue with emphasis on chronic conditions unrelieved by rest or sleep, recommending elimination of conditions resulting in excessive stress, anxiety or boredom 17 p2687 A71-34353

Human ventricular activation correlation with canine model in chronic myocardial infarction 17 p2682 A71-35041

Chronic hypercapnia effects on oxygen affinity and 2,3-diphosphoglycerate in red cell from tests on guinea pigs 20 p3189 A71-39440

Wheat seedling responses to chronic acceleration, considering total height, coleoptile diameter, root length, sensitivity to growth retardation and histological changes 21 p3341 A71-40001

Chronic acceleration effects on animals, considering growth rate, food intake, oxygen metabolism and life expectancy 21 p3328 A71-40003

CHRONOGRAPHS

U CHRONOMETERS

CHRONOLOGY

Tektite age correction factor determination through annealing of fission tracks, describing experimental technique with reference to etching conditions 05 p0808 A71-16300

Marine sediment age by fission track dating of volcanic glass shards, noting agreement with K-Ar, paleomagnetic and paleontologic ages 10 p1601 A71-24430

Lunar surface age determination by crater age classification system, using Lunar Orbiter 4 photographs 15 p2493 A71-32488

Myocardial ischemic lesions age, discussing validity of histopathological criteria and margin of error 15 p2361 A71-32542

Long range thermoluminescent dating of meteorites and tektites, discussing dependence on thermal release of trapped carriers, radiation saturation and instrumental errors 16 p2638 A71-33518

Cuban tektite classification based on age, discussing physical properties and chemical composition 17 p2797 A71-34275

Cosmic radiation and gas retention ages of Chassigny achondrite by measuring Al, K and noble gases contents and production rates in meteorites 17 p2800 A71-34514

Potassium-argon age determination for shock-metamorphosed anorthosites of Manicouagan-Mushalagan Lakes structure

19 p3049 A71-37657

Cosmic ray exposure ages and rare gas concentration profiles in Apollo 12 lunar rocks, discussing spallation products and neutron capture effects

23 p3753 A71-43719

CHRONOMETERS

Relativistic correction for planet perihelion rotation within Einstein gravitation theory, using proper magnitudes in terms of chronometric invariants

01 p0159 A71-10920

CHRONOPHOTOGRAPHY

Biosatellite 3 onboard camera time lapse photography of monkey sleep/wake activity patterns during weightlessness

09 p1394 A71-23240

CHRONOTRONS

U PULSE RATE

U TIME LAG

CHUGGING

U COMBUSTION STABILITY

CINEFLUOROGRAPHY

U MOTION PICTURES

U RADIOGRAPHY

CINEMATOGRAPHY

Pure hydrocarbon droplets heating, expansion, vapor phase fuel storage and gasification in oxidizing gas at elevated pressures, using high speed cinematography

06 p1007 A71-18300

Circular cylindrical thin walled shells buckling, determining postbuckling patterns development by high speed cinematography [DFVLR-SONDDR-99]

13 p2157 A71-29305

CINERADIOGRAPHY

U MOTION PICTURES

U RADIOGRAPHY

CINESPECTROGRAPHS

Double beam monochromatic differential cinespectrophotometer for recording oxidation/reduction reactions in intercellular pigments

01 p0021 A71-10243

CIRCADIAN RHYTHMS

Circadian work-rest cycles in isolated humans

01 p0017 A71-11411

Biological clocks self oscillating mechanism as temperature dependent component of circadian clocks in multicellular organisms, assuming small enzyme concentrations

01 p0020 A71-11566

Circadian rhythm in dermestid beetles *Trogoderma glabrum* Herbst as response to compulsory constant light and temperature conditions

01 p0020 A71-11567

Circadian rhythms synchronization changes in human biological and physiological functions during transmeridian flights

01 p0020 A71-11568

Frequency spectra and cosinor for circadian rhythms in rodents and in man during Gemini and Vostok flights, considering future biosatellites

01 p0020 A71-11569

Endogenous circannual rhythm, discussing free running period, potential zeitgebers, desynchronization and association with circadian rhythm

01 p0020 A71-11571

Reaction time diurnal variations to optical and acoustic stimuli, investigating disturbed natural sleep-waking rhythm effects

02 p0197 A71-11684

Light-dark cycle strength as Zeitgeber for circadian rhythms in isolated man

03 p0364 A71-14249

Time zone change effects on worldwide schedule flight crews sleep patterns, considering biological functions Circadian rhythm changes

04 p0544 A71-15057

Human circadian rhythms in continuous darkness, noting social cues entrainment sufficiency

06 p0849 A71-17303

Circadian patterns of deer mice oxygen consumption in constant dark and thermally neutral zone

06 p0856 A71-18381

Circadian rhythms from aerospace medicine viewpoint, discussing cycle stability and flexibility, air and space travel, etc

08 p1238 A71-20704

Sleep period time displacement effect on sleep using EEG recordings

08 p1239 A71-20816

Photoperiodic effects on insect brain circadian clock control, investigating eclosion cycle initiation, stimulant hormone release and termination as functions of dark phase

09 p1392 A71-22648

Carotenoid depleted *Drosophila* circadian rhythm and visual receptors photosensitivity, discussing photopigment effects

09 p1394 A71-23160

Orbiting Biosatellite 3 monkey environmental and physiological parameters circadian rhythms, investigating desynchronization or arrhythmia

09 p1395 A71-23241

Biosatellite 3 neurophysiological data analysis by digital computer presenting maps of parietal cortex spectra, responsive states transient changes, circadian rhythms and EEG activity

09 p1395 A71-23243

Circannual biological clock operation without environmental signals based on squirrel hibernation and bird migration studies

10 p1563 A71-24298

Diurnal rhythm of adrenaline secretion in subjects with different working habits, comparing catecholamine excretion under relaxation conditions

11 p1721 A71-26355

Diurnal variations in catecholamine excretion, alertness and performance of subjects with different working habits

11 p1722 A71-26356

Cortico- and subcortical rhythms dynamics in sleeping and awake cats by spectral analysis and EEG integration

12 p1871 A71-27486

Diurnal rhythms of human physiological functions and performance during frequently alternating sleep-work cycles

13 p2006 A71-28410

Rat liver and lung collagenase activity Circadian rhythm, noting maximum enzyme activity in early morning and minimum during afternoon and early evening

13 p2010 A71-28788

Rat 24 hour clock inborn nature, discussing dependence on alternating light-dark periods for time measurement

13 p2010 A71-28801

Circadian rhythm of leaves of *Phaseolus angularis* plants in controlled carbon dioxide and humidity environment

13 p2015 A71-29475

Diurnal variations of mitotic activity in thyroid epithelial cells of different follicle size

15 p2356 A71-31290

Astronauts work-rest schedule principles during space flight, discussing circadian rhythms and desynchronization

15 p2363 A71-31315

Rat brain acetylcholine levels circadian rhythm correlated to spontaneous motor activity and sleep-awake cycle

17 p2684 A71-35326

Circadian rhythm maturation of brain norepinephrine and serotonin in rat, relating spontaneous motor activity and sleep-wakefulness mechanism

19 p3003 A71-38071

Biological and biochemical cyclic phenomena, including circadian rhythms

20 p3190 A71-39475

Molecular nature of circadian oscillations mechanism, suggesting nucleic acids implication

20 p3190 A71-39476

Circadian rhythms of human renal excretions in polar, temperate and equatorial regions

20 p3190 A71-39477

Pinto beans circadian leaf movements in simulated weightless environment, relating rotational treatment time to rhythm phase

21 p3341 A71-40006

Radiotelemetric equipment for continuous subcutaneous measurements of circadian body temperature rhythm in rats

21 p3335 A71-40634

Circadian rhythm relation to aircraft pilot safe performance

23 p3632 A71-43232

Circadian rhythm in isolated *Aplysia* eye due to retinal neurons population interaction

23 p3633 A71-43545

Sparrows pinealectomy effect on circadian rhythms of body temperature in light and darkness from radio telemetric monitoring

23 p3633 A71-43547

Human skin cold receptor diurnal activity rhythm

24 p3795 A71-44499

Moderate heat exposure effects on human circadian variations in body temperature, heart and metabolic rates and water loss

24 p3797 A71-44779

CIRCLES [GEOMETRY]

NT GREAT CIRCLES

Precise Brorfelde transit circle reading by photoelectric scanning, determining diameter and group corrections

06 p0899 A71-17967

Wanshaff vertical circle flexure determination at Goloseyev, using collimator tube, plane mirror and autocollimation ocular

23 p3680 A71-44262

Photographic recording for graduated circle readings during stellar observation, discussing method, errors and system

23 p3680 A71-44264

Goloseyev Wanshaff vertical circle photographic device, discussing photomicroscopes and automatic control unit

23 p3680 A71-44265

CIRCUIT BOARDS

High density MOS memory circuits, using multilayer ceramic substrate board for demonstration

17 p2712 A71-35787

Multilayer printed circuit board development, design and production for high reliability and cost effectiveness, emphasizing multidisciplinary communication

21 p3352 A71-40436

High density packaging effects on multilayer interconnection board reliability tested in thermal environments

21 p3352 A71-40437

Substrate influence on circuit board conformal coatings electrical insulation resistance, discussing test results with epoxy/glass and ceramic substrates and various coating materials

21 p3353 A71-40438

Cholesterol liquid crystals technique for thermal analysis of microcircuits, multilayer circuit boards, semiconductor devices and other electronic components

21 p3355 A71-40738

Multilayer printed circuit boards defects detection by temperature field monitoring

22 p3520 A71-41764

Plated through holes interconnection in nine layer phased array antenna printed circuit board, using numerically controlled drilling and plastic encased preform solder system

22 p3525 A71-42765

Printed circuit board components and connections survival under severe vibration and G forces, considering resonant frequency, mounting methods and lead wire strain relief

23 p3652 A71-43538

CIRCUIT DIAGRAMS

Switching bipolar transistor dynamic model equivalent circuit diagram characterization by parameters

02 p0228 A71-11655

Basic digital circuits with integrated TTL and MOS structural elements, giving diagrams for dual counters, frequency dividers, adders and shift registers

02 p0231 A71-11862

Nondissipatively-regulated DC to DC converter design, describing circuit technique and magnetic-semiconductor combinations

03 p0352 A71-13046

Traveling wave tubes electric simulation, giving block diagram for circuit model

03 p0386 A71-13806

Rectangular diagrams for solving linear RLC networks by digital computer graphics

03 p0390 A71-14308

AC signal amplitude measurements, describing circuit design with DC voltage generation proportional to input AC voltage

06 p0899 A71-17926

Tunnel diode output voltage converter circuit diagram and waveforms

07 p1080 A71-20360

Transistorized gas laser discharge current stabilizer using double feedback circuit, discussing schematic diagram and operation principles

08 p1303 A71-21807

Hydropulsion equipment for fatigue tests, presenting schematic diagrams and technical data

09 p1427 A71-22510

Topological unistor graph solutions to linear equations of electronic circuits by structural conjugate numbers on digital computer

11 p1792 A71-26376

Unijunction transistors operation principles, electrical parameters, structural features and circuit applications

11 p1740 A71-26548

Linear sawtooth voltage phantastion type generator, presenting operation time diagrams and circuit advantages

12 p1906 A71-26900

Electrical waveform sampling circuits without switched feedback amplifiers, discussing advantages of open loop configuration with circuit diagrams

12 p1891 A71-26997

Circuit design of double balanced parametric amplifiers regarding low cost and least degradation performance limits

13 p2039 A71-28906

Millimeter band plasma microwave radiation receivers for emission measurement, presenting schematic diagrams for superheterodyne

24 p3825 A71-44507

Operational principles and circuit diagram of transistorized preamplifier for Si p-i-n gamma quanta radiant flux detector, noting noise properties and possible improvements

24 p3810 A71-45151

CIRCUIT PROTECTION

Late model F-4 air superiority aircraft and electronic flight control systems protection against lightning discharges damage to electric and electronic systems

07 p1021 A71-19940

Lightning and surge protection devices for survivability of aircraft electrical systems 07 p1021 A71-19941

LF transistor power amplifier protection from power overloads in case of short circuit at output 12 p1889 A71-27625

Self adhesion in relay contacts, discussing cold weld conditions and prevention by dry oxygen addition 13 p2074 A71-28835

Solid state voltage regulator with hybrid tunnel-diode/transistor circuit discriminator for overload protection, discussing operation, circuit diagram and performance 17 p2716 A71-34786

Aircraft electric power system design with reliability, simplicity, low cost, weight and size, discussing automatic circuit protection and energy power 17 p2678 A71-35780

Remote power controller as static circuit protection device for aircraft and spacecraft automatically controlled electrical wiring system, discussing performance improvement 17 p2678 A71-35782

Sealed and vented fusing devices, testing vacuum effects on performance at high and low temperatures 19 p3035 A71-38536

Hybrid circuit heat sensitive semiconductor chips mounting methods for preventing thermal degradation 21 p3356 A71-40744

Circuits for scintillation counters signals identification, describing protective measures against electrical interference and background radiation 23 p3677 A71-43526

CIRCUIT RELIABILITY

Pad relocation technique by DC wafer probe tests for interconnecting LSI arrays of imperfect yield 01 p0044 A71-10186

Hybrid microcircuits reliability, discussing test data regarding receiving and sample inspection, environmental and performance testing, etc 01 p0053 A71-10733

Thin film methods applied to microwave integrated circuits for compactness, reliability and low cost 01 p0053 A71-10736

Reliability test for fluidic digital comparison device 01 p0006 A71-10925

Pulse-fed transistorized discrete devices reliability properties estimation by model, taking into account structural properties 01 p0057 A71-11232

Electronic circuit analysis using parametric reliability criteria based on progressive failures, applying statistical computerized simulation method 02 p0230 A71-11840

Reliability evaluation for electrical connectors used in electronic equipment based on probability and environment considerations 07 p1076 A71-19555

RF distributed transistors for high reliability and power operation, discussing failure physics 07 p1076 A71-19559

Planar transistors operating conditions effects on current gain degradation following emitter-base reverse biasing 07 p1076 A71-19560

Plastics for long life microcircuit encapsulation, investigating materials properties and failure mechanisms for device reliability assessment 07 p1077 A71-19561

Plastics for long life microcircuit encapsulation, investigating water absorption and resin-to-lead adhesion effects on reliability 07 p1077 A71-19562

Satellite electronic equipment reliability engineering, considering circuit and system design, components screening, assembly and test procedures and quality assurance plans 07 p1207 A71-19563

Electronic equipment reliability prediction, considering confidence limits 07 p1077 A71-19564

Power station electronic control equipment and integrated circuit computer reliability data analysis, emphasizing combined mathematical prediction and observation 07 p1077 A71-19565

Microelectronic circuits reliability in aircraft engine control applications, discussing testing and selection for severe temperature and vibration environments [SAE PAPER 700822] 08 p1265 A71-21369

Semiconductor integrated circuit fabrication optimization, considering defect density, component number, crystal size and cost analysis 09 p1416 A71-22490

Integrated circuits electrical parameters and design joint optimization, describing technological analysis, physical component characteristics, operating conditions and design factors 09 p1422 A71-22493

In-core thermionic reactor network reliability analysis, assuming component failures as equally probable stochastic events 11 p1713 A71-25893

Total reliability requirement procedure for design, development and production of medium- and large-scale integrated circuits 12 p1884 A71-26660

Continuous loading method for accelerated reliability testing of circuit components 13 p2072 A71-27830

Regenerative system reliability, examining oscillation mode selector 13 p2040 A71-28995

Failures detection in combinational digital switching circuits due to component malfunction 13 p2036 A71-29291

Coupling effects between reliability components of integrated circuits by modeling failures in structures 15 p2377 A71-32345

Traveling wave tube for reflex type amplifier on-board space communication satellite, discussing prototype reliability and performance 17 p2714 A71-34682

Redundant modules introduction in microelectronic systems for increased reliability 17 p2716 A71-34954

Communication satellite ground station electric power generation and distribution equipment characteristics, emphasizing reliability 17 p2724 A71-35517

Statistical evaluation of switching elements reliability, considering permanent and temporary failure rates 17 p2718 A71-35627

Aircraft electric power system design with reliability, simplicity, low cost, weight and size, discussing automatic circuit protection and energy power 17 p2678 A71-35780

Aerospace data bus for multiplexed transmission within vehicles, considering control and sequencing methods terminal concepts, capability noise reduction and reliability 17 p2712 A71-35785

AN/ARC-144 solid state ultrareliable UHF multimode aircraft transceiver, discussing tuning, frequency synthesis and broadband power amplifier 20 p3196 A71-39209

C-MOS integrated circuit technology emphasizing reliability, design, failure mechanisms and performance parameters [DFVLR-SONDDR-100] 21 p3355 A71-40737

Leadless electronic packaging system for MOS LSI for low cost, high reliability and heat transfer advantages 21 p3356 A71-40745

Plastic encapsulated IC reliability tests, relating results to failure mechanism 21 p3356 A71-40747

Beam-lead nitride-passivated IC seal junction chip reliability evaluation by life tests for optimum packaging into functional modules 21 p3357 A71-40813

Beam-lead devices, discussing comparison to conventional transistor chip, reliability, applications and assembly techniques 21 p3357 A71-40815

Spacecraft tape recorder design for five years minimum continuous unattended reliable operation, describing quality control and environmental/life testing procedures 22 p3608 A71-41507

Computer-aided statistical analysis correlation method for prediction of electronic circuit component part variability effects on performance and reliability 22 p3517 A71-42102

Computer predictions of postirradiation reliability of electrical circuits, using Sceptre program and component tests 22 p3518 A71-42111

Multiple component logic circuit reliability analysis using Karnaugh diagram procedure for simplification 24 p3807 A71-45299

CIRCUITS

NT ADDING CIRCUITS

NT ANALOG CIRCUITS

NT BISTABLE CIRCUITS

NT CIRCULATORS [PHASE SHIFT CIRCUITS]

NT COINCIDENCE CIRCUITS

NT COMPARATOR CIRCUITS

NT COUNTING CIRCUITS

NT COUPLING CIRCUITS

NT DELAY CIRCUITS

NT DIGITAL INTEGRATORS

NT DISCRIMINATORS

NT ELECTRIC BRIDGES

NT EQUIVALENT CIRCUITS

NT FEEDBACK CIRCUITS

NT FLIP-FLOPS

NT FLUID SWITCHING ELEMENTS

NT GATES [CIRCUITS]

NT INTEGRATED CIRCUITS

NT ITERATIVE NETWORKS

NT LC CIRCUITS

NT LIMITER CIRCUITS

NT LINEAR CIRCUITS

NT LOGIC CIRCUITS

NT MAGNETIC CIRCUITS

NT MATRICES [CIRCUITS]

NT MEDIUM SCALE INTEGRATION

NT MICROWAVE CIRCUITS

NT MIXING CIRCUITS

NT MONOSTABLE MULTIVIBRATORS

NT MULTIVIBRATORS

NT NEGATIVE RESISTANCE CIRCUITS

NT OHMS LAW

NT PHANTASTRONS

NT PHASE DETECTORS

NT PHASE SHIFT CIRCUITS

NT PNEUMATIC CIRCUITS

NT POWER SUPPLY CIRCUITS

NT PRINTED CIRCUITS

NT RC CIRCUITS

NT RL CIRCUITS

NT RLC CIRCUITS

NT SCALERS

NT SWITCHING CIRCUITS

NT THRESHOLD GATES

NT TRANSISTOR CIRCUITS

NT TRANSMISSION CIRCUITS

NT TRIGGER CIRCUITS

NT VARACTOR DIODE CIRCUITS

NT WHEATSTONE BRIDGES

NT WIRE BRIDGE CIRCUITS

Cylindrical post shunt impedance in rectangular waveguide, evaluating approximate theory for free space thin wire conductor 03 p0378 A71-13808

Two-terminal pair broadband matching circuits losses from method for LF series-shunt coupler with uniform scattering 03 p0386 A71-13810

Electric circuit theory - IEEE Conference, University of Minneapolis, May 1970 03 p0390 A71-14304

Conventional components in hybrid circuits, using leadless inverted device, SOT-23 transistor and multilayer ceramic capacitors 23 p3655 A71-43349

CIRCULAR CONES

Circular cone with cross shaped wings in supersonic flow, determining flow characteristics, velocities and pressure 02 p0185 A71-11958

Symmetrical wave excitation by electric dipole of conical surface ideally conducting along hyperbolic spirals, obtaining solution by integral transformation 05 p0727 A71-15996

Hypersonic boundary layer of spinning circular cone at angle of attack, using finite difference method [AIAA PAPER 71-57] 06 p0843 A71-18516

Equilibrium positions of multiple pairs of vortices in wakes of circular and elliptic bodies 07 p1087 A71-18901

HF backscattering by plane electromagnetic wave at oblique incidence from perfectly conducting right circular cone, applying geometrical theory of diffraction 08 p1257 A71-21884

Vortex layer near circular cone surface in supersonic axisymmetric steady flow of homogeneous inviscid gas 10 p1551 A71-24372

Steady supersonic isoeenergetic flow of thermally and calorically perfect gas past circular cones at zero angle of attack, using dimensional perturbation method 12 p1863 A71-26939

Axisymmetric problem solution in theory of elasticity and thermoelasticity for semiinfinite circular cones truncated along spherical surface 12 p1980 A71-27361

Unsteady hypersonic self similar gas flow and drag on circular cone accelerated according to power law, using small perturbation theory 13 p1993 A71-29205

Hypersonic shockless gas flow past circular cone and cylindrical surfaces, reducing Vallander equations to nonlinear integral 14 p2169 A71-30183

French monograph on laminar boundary layer on circular cone at angle of incidence in supersonic stream, calculating separation from parabolic equations by numerical integration 19 p2994 A71-38647

Solar rudder for spacecraft steering in form of right circular cone with ideally reflecting surface 20 p3306 A71-39136

Symmetrical wave excitation by electric dipole of conical surface ideally conducting along hyperbolic spirals, obtaining solution by integral transformation 22 p3524 A71-42745

Circular conical shell initial deformation under impulsive load, using Timoshenko theory 24 p3883 A71-44852

CIRCULAR CYLINDERS

Hollow circular cylinder with variable inner radius, solving nonlinear viscoelasticity dynamic load problem 01 p0168 A71-10422

Thermal stresses on curved surface of initially stressed circular cylinder with smooth rigid insulated cover 01 p0172 A71-10839

Impulsively started time dependent transonic flow of ideal compressible gas past circular cylinder, using finite difference method

01 p0003 A71-11160

Arbitrary shape and variable thickness cylindrical shell bending numerical solution by replacement of circular cylindrical strip elements

01 p0177 A71-11324

Cylindrical shells finite element analysis by rectangular cylindrical elements replacement of actual structure

01 p0177 A71-11325

Multiple scattering boundary value problem for two parallel circular cylinders

01 p0041 A71-11613

Repeated bending and torsion of viscoplastic bars and circular cylinders, using hereditary nonlinear integral equations

02 p0322 A71-11688

Laminar orthotropic circular cylindrical shell stress state under inversely symmetrical loading

02 p0322 A71-11737

Electromagnetic scattering by oblique circular cylinder, deriving field equations

02 p0215 A71-12145

Stability loss of circular cylindrical shells under bending beyond elastic limit

02 p0325 A71-12287

Prebuckling deformations influence on circular cylindrical shell buckling under external pressure, applying Galerkin method to Donnell equations

02 p0329 A71-12602

Incompressible fluid filled circular cylindrical shells loaded by pressure ring at center, obtaining yield point load

03 p0500 A71-13022

Initial phase of unsteady laminar flow from cylindrical vessel through circular cylindrical tube

03 p0398 A71-13105

Incompressible elastoviscous unsteady fluid flow past circular cylinder, confining calculations to non-zero vorticity region near cylinder

03 p0398 A71-13108

Unsteady flow induced by circular cylinder impulsive motions, examining vortices formation and interaction

03 p0399 A71-13197

Dipole antennas mutual influence near conducting intersecting circular cylinders, using geometrical diffraction theory

03 p0384 A71-13395

Buoyancy effect on boundary layer flow over heated horizontal circular cylinder immersed in uniform axial free stream, considering successively greater displacements

03 p0519 A71-13731

Natural convection inside horizontal circular cylinder, selecting fluid, geometry and thermal boundary condition for high Prandtl and Grashof numbers

03 p0519 A71-13732

Laminated circular cylindrical shells under axisymmetric mechanical and thermal loads, including transverse isotropy and shear deformation effects in stress analysis theory

[ASME PAPER 70-WA/APM-53]

03 p0513 A71-14170

Circular cylindrical shell with trapezoidal stringers reinforcement system along length, calculating strain during oscillation

03 p0514 A71-14359

Thin circular cylindrical plate reinforced by longitudinal rigid stringers, deriving computer algorithm for calculating forced vibration

03 p0515 A71-14367

Circular cylinder creep deformation under complex varying loading, comparing computation and test results

[ONERA-TP-846]

04 p0669 A71-15353

Round cylinder in viscous fluid asymmetrically disturbed flow, calculating dynamic and temperature conditions with difference method

04 p0571 A71-15492

Local heat transfer to transverse circular cylinder at low Reynolds numbers, using iterative finite difference approach

04 p0683 A71-15493

Circular cylindrical shell reinforced by ring ribs, investigating dynamic characteristics under impulsive loading

04 p0672 A71-15756

Plane wave diffraction by double grating of thin circular cylinders, determining field polarization in directions parallel and perpendicular to axis

05 p0718 A71-15995

Orthotropic sandwich and homogeneous single layer circular cylindrical shells optimal design

05 p0822 A71-16419

Circular cylindrical shells buckling with different elastic moduli in tension and compression under arbitrary axial and lateral pressure

05 p0823 A71-16558

Circular disks or cylinders with temperature boundary conditions, discussing iterative solution and computer program for transient thermoelastic stresses

05 p0829 A71-17117

Rib reinforced circular cylindrical shells, analyzing elementary and zero bending stress states

06 p0982 A71-17351

Circular cylindrical orthotropic fiberglass-reinforced shell buckling under longitudinal impact, assuming initial surface imperfections

06 p0985 A71-17684

Compressive contact interaction problem for elastic circular cylindrical shell lying in circular cylindrical cavity of elastic body

06 p0987 A71-17764

Circular cylindrical sandwich shell natural vibrations reduced to shell and filler contact problem, using two and three dimensional models

06 p0990 A71-17792

Closed circular cylindrical shell stability and buckling during axial compression, using energy method in geometrically nonlinear formulation

06 p0994 A71-17824

Vertical circular cylindrical tank with shallow spherical shell bottom filled partially by ideal incompressible liquid, calculating joint oscillations

06 p0994 A71-17826

Thin circular cylindrical shell thermoelastic vibrations, deriving differential equations of motion with allowance for shear, rotatory and translational inertia

06 p0996 A71-17840

Circular cylindrical shell stability with ribs of variable cross sections, using method based on semimentless theory

06 p0997 A71-17850

Three dimensional bending vibration analysis of homogeneous elastic circular cylindrical shell with both ends restrained

06 p1001 A71-18230

Vortex streets behind circular cylinders at Reynolds numbers 50-160, discussing transition

06 p0842 A71-18322

Design criteria for buckling prediction of elliptical and circular cylindrical shells under axial compression from axisymmetric and axisymmetric shape imperfections distribution

[AIAA PAPER 71-145]

06 p1003 A71-18588

Dynamic response of pressurized thin circular cylindrical shells under moving loads

[AIAA PAPER 71-175]

06 p1004 A71-18614

Heat transfer from circular cylindrical hot wire and film anemometer probes, examining calibration steadiness

07 p1106 A71-18783

Fluid flow around two parallel circular cylinders moving in ideal liquid, deriving exact solution for flow velocity and kinetic energy

07 p1089 A71-19736

Infinite circular cylindrical shell with elastic stiffener ring, calculating transient axisymmetric bending stress under radial impulse

07 p1213 A71-19907

Wind tunnel experiments on vortex shedding from circular cylinders in oscillating free stream

07 p1090 A71-19908

Axisymmetric wave propagation in semiinfinite hollow elastic circular cylinders subjected to pressure step loading, obtaining asymptotic solutions for strains by double integral transforms

07 p1214 A71-19954

Elastic harmonic waves propagation in composite circular elastic cylinder

07 p1214 A71-19956

Steady state thermal stresses and deformations in infinite hollow circular cylinder by sinusoidal internal heat source and Newtonian radiation boundary condition outer surface cooling

07 p1214 A71-20026

Thin single layer orthotropic circular cylindrical shell shear coupled traveling wave reflections, determining stresses in terms of particle velocities

07 p1216 A71-20134

Stress-strain state of anisotropic circular cylindrical shell with constant thickness, using stepwise linear approximation technique for solving mixed system of partial differential equations

08 p1368 A71-20789

Book of tables and graphs for circular cylindrical shells free vibrations

08 p1370 A71-21234

Surface current density and electromagnetic scattering from finite tubular cylinder solved numerically by approximate product integration method

08 p1256 A71-21691

Trajectories prediction for subsonic spin stabilized projectiles via water tunnel tests, considering blunt nose and tail and rounded nose right circular cylinders

[AIAA PAPER 71-296]

08 p1275 A71-22016

Nomograms for normal stresses and bending moments in thin circular cylindrical shell under uniformly distributed load

08 p1374 A71-22054

Pressure drag and cross flow force coefficients of inclined circular cylinder in supercritical flow

09 p1382 A71-22098

Thermal stresses in finite circular cylinder heated axisymmetrically over curved surface, constructing thermoelastic displacement potential and biharmonic Love function

09 p1536 A71-22452

Circular cylindrical shell initial geometrical imperfections effect on stability under nonuniform composite loading

09 p1537 A71-22518

Circular cylindrical shell under radial local load, determining maximum stresses in center and boundary

09 p1538 A71-22651

Spring supported circular cylinder stability in wake flow of similar cylinder at various spacings using quasi-static aerodynamic derivatives and flutter theory

09 p1539 A71-22942

Imperfect thin walled circular cylindrical shells under axial compression with relaxed boundary conditions, determining deformations with differential equations

09 p1541 A71-23089

Lossless radiating antenna element efficiency in circular cylindrical arrays of identical elements, relating to reflection coefficient

09 p1419 A71-23505

Asymptotic expression for mutual admittance between axial rectangular slots on large conducting cylinder

09 p1419 A71-23507

Rough circular rod effective surface impedance and propagation constant, discussing guided electromagnetic wave attenuation on structure

10 p1578 A71-24399

Infinitely small flexural oscillations of initially stretched incompressible elastic circular cylinder, showing stretch effect on wave propagation velocity

10 p1689 A71-24521

Detonation wave of gas in circular cylinder with nonsimultaneous axisymmetric initiation at plane boundary, obtaining solution for small perturbation flow behind detonation front

11 p1853 A71-25152

Longitudinal, flexural and elastic waves propagation in infinite orthotropic circular cylinders

11 p1850 A71-26176

Uniformly and nonuniformly spaced circular cylinders contacting two planes, calculating conductive heat transfer coefficient under vacuum conditions

[AIAA PAPER 71-436]

11 p1858 A71-26224

Vortex shedding characteristics of circular cylinders at low Reynolds numbers from experiment on tapered models wake structure

12 p1897 A71-27220

Natural frequencies of finite circular cylinders in axially symmetric longitudinal vibration, using Rayleigh-Ritz method to derive differential equations for expansion functions coefficients

12 p1981 A71-27482

Long circular cylindrical shell stability under action of bending moments at end face, deriving neutral equilibrium equations

12 p1981 A71-27495

Buckling of eccentrically stiffened multilayered circular cylindrical shells with different orthotropic moduli in tension and compression

12 p1982 A71-27572

Buckling of circular cylindrical shells with axisymmetric imperfection distributions under axial compression

12 p1983 A71-27573

Axisymmetric stressed-state problem of finite length hollow circular cylinder in Fourier and Fourier-Dini series form

12 p1984 A71-27692

Momentum thickness of boundary layer of circular cylinder in cross flow at high Reynolds numbers from static pressure and skin friction measurements

12 p1867 A71-27738

Axial compression buckling of elastic core filled circular cylindrical shells with transverse shear flexibility, noting solid propellant rocket cases design application

13 p2148 A71-27984

Circular cylinder thermal stressed state, considering interaction between temperature and deformation fields

13 p2152 A71-28273

Circular cylindrical thin walled shells buckling, determining postbuckling patterns development by high speed cinematography

[DFVLR-SONDDR-99]

13 p2157 A71-29305

Freestream density field in nonequilibrium dissociating nitrogen flow over circular cylinder, using free piston shock tunnel and optical interferometry measurements

14 p2169 A71-29884

Torsion of circular composite rods of sectors with different shear moduli and radial cracks

14 p2326 A71-30193

Free convection in horizontally positioned, water filled circular cylindrical cavity

14 p2336 A71-30228

Two dimensional electromagnetic scattering by conducting corrugated circular cylinders, determining surface current by matrix and integral equation methods

14 p2195 A71-30248

Transient and steady state creep of circular cylindrical shells loaded by internal pressure, using strain hardening hypotheses and finite difference method

14 p2328 A71-30379

Monograph on crack problems in mathematical theory of thermoelasticity covering crack effects on stress distribution in circular cylinders, thick plates and infinite solid bodies

14 p2329 A71-30501

Microwave scattering by DC magnetized ferrimagnetic circular cylinder in rectangular waveguide

14 p2212 A71-30512

Mechanical support system role in determination of aeroelastic stability of leeward cylinder immersed in wake using undamped flutter theory

14 p2334 A71-31021

Boundary conditions of elastic deformations of constrained circular cylinders under axial load, discussing modulus dependence on Poisson ratio

15 p2505 A71-32007

Circular cylindrical shell with elliptic hole, calculating stress concentration around hole under torsion

15 p2506 A71-32014

Cylindrical membrane aeroelastic stability and flutter analysis at high supersonic or low hypersonic Mach numbers

15 p2506 A71-32019

Perfectly effective boiling fin design in horizontal right circular cylinder shape, deriving formulas at peak heat flux operation

15 p2514 A71-32264

Elements movement and stability loss of circular cylindrical shells during snap, using Gauss least constraint principle

16 p2651 A71-33027

Imperfect circular cylindrical shell under external hydrostatic pressure loads, determining free and resonant vibration modes

16 p2651 A71-33062

Oscillating circular cylinder wake fluctuating velocity measurement at low Reynolds numbers, using hot-wire anemometer

[ASME PAPER 71-APM-33] 16 p2520 A71-33196

Buckling of axially compressed circular cylindrical shells with localized or random axisymmetric imperfections, deriving asymptotic approximation formulas for stress calculation

[ASME PAPER 71-APM-29] 16 p2655 A71-33200

Approximate calculation of pressure distribution, separation points and drag on circular cylinder in viscous liquid flow, using ideal fluid jet model

16 p2560 A71-33597

Stability loss of circular cylindrical shell with stepped wall thickness of central reinforcing sleeve under annular loading, determining critical load by thin shell theory

16 p2657 A71-33600

Critical loads and stability of longitudinally compressed circular cylindrical shells with eccentric ring and stringer reinforcement

16 p2657 A71-33603

Isotropic elastic circular cylinders longitudinal stress waves, presenting dispersion relation /Pochhammer equation/ numerical solutions

16 p2658 A71-33625

Closed circular cylindrical shell stability under dynamic axial compressive loading with static internal pressure

16 p2658 A71-33719

Stress-strain state of circular cylindrical shell hinged at edges under local radial loads

17 p2817 A71-34340

Finite length thin circular cylindrical shells with clamped or simply supported edges, calculating flexural free vibration natural frequencies

17 p2822 A71-34643

Axisymmetrical elasticity theory for vertical finite length cylinder with mixed boundary conditions on top and bottom end surfaces, obtaining stress and displacement expressions

17 p2822 A71-34779

Isotropic circular cylindrical shell stability with longitudinal hinges under uniform external pressure, determining critical load

17 p2831 A71-35322

Muscle contraction model under biological factors action, considering circular cylindrical vessel equilibrium under internal and external pressures

17 p2694 A71-35616

Circular cylinder resistance in oscillating stream of second order fluid, calculating flow distribution

18 p2843 A71-36042

Stress-strain behavior of tapered circular cylindrical shell, applying equalization calculation to boundary value problem

18 p2976 A71-36179

Hyperelastic compressible isotropic elliptical and circular cylinders simple bending, studying second order effects

18 p2977 A71-36195

Viscous fluid flow past circular cylinder, using trigonometric representation of vorticity based on truncated Stokes-Picard and Oseen-Picard methods

18 p2844 A71-36316

High subsonic potential flow calculation past circular cylinder by integral relations method

18 p2844 A71-36326

Initial flow past circular cylinder in viscous incompressible fluid calculation by numerical integration using boundary layer coordinates

18 p2908 A71-36341

Allen and Vincenti blockage corrections for drag coefficients on circular cylinder in wind tunnel

19 p3041 A71-37888

Plane electromagnetic wave diffraction by circular cylinder with longitudinal slot, determining scattered field by Riemann-Hilbert method

19 p3020 A71-38417

Flow instability in stagnation point region of circular cylinder in turbulent channel flow, using hydrogen bubble method for flow visualization

20 p3211 A71-39454

Viscous fluid stirring due to small amplitude rigid circular cylinder rotation, calculating steady flow velocity relationship to Reynolds number

20 p3177 A71-39481

Membrane and bending stresses analysis around elliptic hole in long thin circular cylindrical shell, using perturbation technique

20 p3309 A71-39776

Static thrust loss of circular cylinder due to sink effects of turbulent jet discharging along surface line

21 p3317 A71-40012

Karman vortex street geometry calculation for single circular cylinder, using pressure drag coefficient, Strouhal number and Kronauer criterion

[ASME PAPER 71-VIBR-11] 21 p3457 A71-40273

Karman vortex street induced fluctuating lift forces on single circular cylinder, deriving relationship between lift coefficient and steady state pressure drag coefficient

[ASME PAPER 71-VIBR-12] 21 p3457 A71-40274

Wake formation behind circular cylinders undergoing self excited and forced transverse oscillations

[ASME PAPER 71-VIBR-25] 21 p3458 A71-40282

Flow induced vibration suppression by perforated concentric shroud around circular cylinder, investigating porosity and shroud/cylinder diameter ratio effects

[ASME PAPER 71-VIBR-28] 21 p3458 A71-40283

Fluctuating aerodynamic force measurement on stationary circular cylinder spanning wind tunnel, using direct method without support interference

21 p3363 A71-40393

Effective momentum ratio for Lamb circular cylinder double vortex, Hill spherical vortex, Thomson straight line paired vortices and Helmholtz circular ring vortex

21 p3321 A71-40541

Rotating viscous fluid flow between concentric circular cylinders, predicting velocity field dependence on position and time during inner cylinder sudden stop

21 p3366 A71-40543

Hydroelastic coupled oscillations of partially filled circular cylindrical liquid container with flexible bottom and elastic side wall

21 p3366 A71-40545

Numerical analysis of steady state creep of simply supported circular cylindrical shells by combined Newton and finite difference methods

21 p3463 A71-40752

Closed form solution for quasi-static thermal stress field due to moving point heat source in circular disk, noting application to welding problems

21 p3467 A71-40966

Circular cylindrical shells analysis by Koiter strain energy method for small finite deflections, considering simplifying modifications of energy functionals

21 p3468 A71-40976

Circular cylindrical shell under longitudinal parametric load, obtaining nonstationary responses with deformation theory

21 p3471 A71-41029

Elastoplastic indentation of half space by infinitely long rigid circular cylinder, using finite element method

21 p3474 A71-41426

Insulating circular cylinder steady axial motion in conducting fluid permeated by uniform transverse magnetic field, determining flow along cylinder at field tangency points

22 p3583 A71-42198

Point-matching method application to electromagnetic scattering from quadrilateral conducting cylinders in resonance range, using computer programs

22 p3510 A71-42205

Electromagnetic scattering by imperfectly conducting circular and square cylinders, using matrix technique based on conformal transformation from polygonal to circular cross section

22 p3512 A71-42361

Plane wave diffraction by double grating of thin circular cylinders, determining field polarization in directions parallel and perpendicular to axis

22 p3515 A71-42744

Thin closed circular cylindrical shell under arbitrary loading

23 p3778 A71-44039

Far field radiation patterns of axially oriented point current sources in presence of dielectric circular cylinders, developing solutions via plane wave scattering

23 p3654 A71-44160

Transmission coefficient calculations for infinite grating of conducting circular cylinders, considering parallel and perpendicular polarizations

23 p3655 A71-44170

Longitudinal rib reinforced cylindrical shell under axial compression loads, determining equilibrium stability with approximation of transcendental equations

23 p3780 A71-44222

Free elastic vibrations and waves in laminated orthotropic circular cylinders

24 p3878 A71-44561

Isothermal gas rotation in circular cylinder, calculating symmetric normal frequency modes

[AIAA PAPER 71-999] 24 p3818 A71-44590

Power series analysis of circular cylindrical shells stability under biaxial compression, expressing critical loadings

24 p3878 A71-44612

Circular cylindrical shell critical stress level leading to stability loss during high speed clogging process based on kinetic energy method

24 p3884 A71-44897

Finite plane strain inflation of compressible hollow circular cylinder, using perturbation method for nonlinear boundary value problem

24 p3884 A71-44955

Circular cylindrical laminated anisotropic shells with axisymmetric shape imperfections, investigating upper bound buckling loads

24 p3841 A71-44958

Total temperature thermocouple probe based on circular cylinder recovery temperature with combined advantages of hot wire and shielded probe, discussing design and applications

24 p3826 A71-44971

Azimuthal guiding surface wave attenuation with curvature applied to dielectric clad circular cylinder, including impedance tables

24 p3804 A71-44991

Spatial characteristics based difference scheme application to axisymmetric problems of elastic wave propagation, allowing for solid or hollow circular cylinder boundary conditions

24 p3885 A71-45221

CIRCULAR ORBITS

NT STATIONARY ORBITS

Orbiting gyrostats stability elementary cases analysis, examining existing methods and developing new method involving less computational labor

01 p1613 A71-10123

Satellites initial circular orbit determination from incomplete observations

01 p0155 A71-10444

Two-gyro attitude control system with conical suspension, analyzing vehicle motion asymptotic stability in circular orbit

01 p0081 A71-10634

Dynamical investigation of deformable gyrostats stability in circular orbit subject to gravitational torques, noting equilibrium states and damping effects

04 p0662 A71-15142

Hamiltonian of two center libration, including resonant circular orbits and Garfinkel formalism

04 p0620 A71-15739

Gyrostat in circular orbit in Newtonian force field, solving for optimal rotational motion stabilization

05 p0817 A71-16997

Spinning symmetric satellite roll-yaw resonant attitude instabilities in circular orbit

[AIAA PAPER 71-88] 06 p0980 A71-18544

Parameter estimates effectiveness from independent discrete and continuous navigation measurements of circular orbital plane

09 p1491 A71-22543

Artificial earth satellite circular orbit determination from topocentric directions measurement by optical and electronic observations

09 p1408 A71-23176

Minimum propellant optimal rendezvous maneuver of two cosmic vehicles on circular orbits, considering tracking vehicle motion equations

10 p1672 A71-24335

Sensitivity algorithms and application to attitude estimation of rigid body satellite in circular earth orbit

10 p1587 A71-24747

Topocentric satellite trajectory approximation along circular orbit by n-degree equation, using coordinate-time relation

11 p1829 A71-25809

Optimal symmetric minimum-impulse rendezvous between close near-circular noncoplanar orbits

13 p2139 A71-28820

Equations of motion of infinitesimal particles attracted by Newtonian gravitation of two mutual revolving masses in circular orbits

13 p2101 A71-29114

Approximate analytical method for nonlinear coupled equations of axisymmetric satellite librations in circular orbit, using constant Hamiltonian

14 p2319 A71-29892

Optimal two impulse minimum transfer of particle between coplanar circular orbits under perturbations in flight plane

14 p2310 A71-30187

Brightness variations of satellite during passage in circular orbit as function of distance, phase and atmospheric extinction 14 p2318 A71-31122

Equilibrium position stability of nonlinear two body satellite system in circular orbits in gravitational central force field, using linearized equations of motion 15 p2499 A71-31176

Circular orbit patterns for continuous whole earth surface coverage with five satellites 16 p2630 A71-32840

Elliptical and circular orbit satellite injection capabilities of Europa 2 launch vehicle, considering geostationary orbit and launcher performance 16 p2645 A71-33364

Optimal transfer in central field between coplanar circular orbits, allowing for errors in velocity changes and phase variables 18 p2962 A71-36107

Gyrostad in circular orbit in Newtonian force field, solving for optimal rotational motion stabilization 18 p2976 A71-36797

Spectroscopic binary star system with orbital eccentricities less than 5 percent, discussing elliptical or circular orbit possibility 18 p2971 A71-37068

Energy optimal single impulse transfer from hyperbolic trajectory to circular orbit 20 p3288 A71-39119

Satellite circular orbit trajectory plane time optimal relocation, examining turn angle angular position and modulus of maximum lateral acceleration 20 p3288 A71-39121

Earth gravitational field fine structure via circular orbit satellite perturbations 20 p3220 A71-39660

Thrusting lifting orbital vehicle nonlinear longitudinal dynamics in near-circular orbit, deriving orbital elements variation behavior and angle of attack mode period and damping 21 p3454 A71-40094

Probe for circular polar Mercury orbit, obtaining missions values 22 p3600 A71-42010

Diamond launch vehicle multistage development for placing satellites in low perigee and high eccentricity and high and low circular orbits 22 p3610 A71-42020

Circular sun synchronous earth satellites, investigating swathing patterns control by orbit selection and modification [AAS PAPER 71-353] 23 p3728 A71-43025

Fuel optimal transfer from circular orbit space station to rendezvous with vehicles in different circular orbits [AAS PAPER 71-365] 23 p3729 A71-43035

Near circular orbit elements determination as functions of spacecraft initial speed and coordinates deviation by mathematical expectation procedure 24 p3876 A71-45317

CIRCULAR PLATES

Cylindrical shells and circular plates optimal limiting and adaptable loads calculation by Pontryagin maximum principle 01 p0170 A71-10639

Variable thickness circular plate uniformly clamped along edge, calculating critical force from eigenfunctions and eigenvalues of equation with one independent variable 01 p0171 A71-10650

Axial compression of thin circular epoxy resin disks with three dimensional stress state produced by cementing to rigid platens, using triaxial analysis 01 p0109 A71-11008

Circular elastoplastic plates, solving adaptation theory kinematic equations by linear programming procedures 02 p0324 A71-11751

Stress-strain state of thin circular plate with variable thickness along circumference under bending due to uniformly distributed load, using small p 02 p0326 A71-12289

Secondary jet action on circular horizontal plate located above parallel screen, using Poisson equation 02 p0186 A71-12552

Circular plates forced vibrations, considering internal damping and free and supported boundaries in thin plate wave equation solutions 03 p0502 A71-13300

Logarithmic damping of flexural oscillations produced by residual fretting stresses in circular plates 03 p0503 A71-13415

Circular plates strain wave analysis by Laplace transform method, using MacDonald functions approximation 03 p0515 A71-14383

Clamped circular plates axisymmetric nonlinear resonant frequency response under uniform static pressure 04 p0668 A71-15187

Rectangular and circular thin orthotropic plates thermal buckling approximate solution using Rayleigh-Ritz energy method 05 p0819 A71-15978

Isotropic circular plate natural vibrations for inhomogeneous boundary conditions, using net point method to derive finite difference equations 05 p0821 A71-16353

Circular disks or cylinders with temperature boundary conditions, discussing iterative solution and computer program for transient thermoelastic stresses 05 p0829 A71-17117

Symmetrical elastic bending of anisotropic annular circular plates of variable thickness, solving for line and uniform pressure loads with different boundary conditions 05 p0830 A71-17224

Stress state analysis in rigidly clamped circular plate bent by edge loads, using three dimensional elasticity theory 06 p0989 A71-17786

Circular and annular elastic plates elastoplastic bending theory, using Saint Venant conditions and equations of equilibrium and deformation 06 p0993 A71-17812

Circular plates of anisotropic fiber-reinforced materials, calculating axisymmetric bending and buckling 06 p0995 A71-17829

Plastic deformation of circular plates and shells from material with different yield and strengthening moduli in tension and compression 07 p1211 A71-19164

Circular membranes and plates with arbitrary hole distribution, deriving natural vibrations frequency characteristic equations by infinite determinants 07 p1218 A71-20464

Viscoelastic plates forced motion under dynamic loads by Valani method, considering elastic and layered elastic-viscoelastic circular plates 08 p1368 A71-20801

Buckling of thin elastic circular plates under steady state asymmetric temperature distribution 08 p1370 A71-21304

Design and spark erosion production for circular Fresnel zone plates under He-Ne laser illumination, considering plates as optical reference elements 08 p1289 A71-21374

Heat exchanger circular rigid tube sheets calculation by thin plates bending theory, using stepped profile circular plates stress analysis 08 p1374 A71-22053

Vibrating cylindrical shell with circular plate, discussing bending moments, deflections and frequencies from Lagrangian 09 p1540 A71-23056

Fourth order boundary problems with discontinuous boundary conditions, considering circular plate transverse vibrations 09 p1543 A71-23614

Dynamic behavior of circular and rectangular membrane panels with time and space dependent boundary conditions for aerospace structures 09 p1544 A71-23736

Circular plates with radially symmetric membrane stresses and thickness, investigating stability under peripheral-moving load excitations 10 p1692 A71-24995

Thermal stresses in circular plate with cylindrical orthotropy and reinforced edge, determining temperature and stress distributions 12 p1979 A71-27356

Circular viscoelastic plate under in-plane forces, determining increase in curvature as function of time 12 p1983 A71-27574

Free vibrations of isotropic nonhomogeneous circular plates, deriving closed form expressions for nodal frequencies 12 p1983 A71-27587

Circular elastic ideally plastic plate deformation due to circumferentially distributed rectangular pulse loading 13 p2156 A71-29075

Imperfect circular disks large amplitude free transverse vibration calculation by Galerkin procedure 14 p2326 A71-30064

Thermoelastic stress analysis of circular perforated plate under point heat source 14 p2326 A71-30195

Axisymmetric vibrations of heterogeneous isotropic composite clamped circular plates based on Kirchhoff theory 14 p2327 A71-30205

Large circular plate residual stresses due to local spot heating and cooling, investigating effects of yield strain, heat input rate and peak temperature 14 p2329 A71-30462

Shear deformations effect on circular plates from Reissner theory, expressing bending moments and shear forces as functions of lateral deflection and stress function 15 p2507 A71-32112

Time average holographic interferometric fringes of circular plate vibrating in two rationally related modes 15 p2412 A71-32593

Circular plates finite amplitude response under pulse loading, presenting nonlinear equations finite difference solution 16 p2650 A71-33014

General solution of cylindrical fourth order differential equation with zero index representing circular disk and ring plate problems in elasticity theory 16 p2602 A71-33400

Uniformly extended elastic circular plate with rectilinear slot under normal tensile loads at boundary 16 p2660 A71-34115

Circular plate deflection weakened by hole and under constant external pressure, obtaining successive approximation method solution convergence 17 p2816 A71-34329

Jet induced secondary flow interaction with circular plate, showing ring vortex effects on pressure distribution 17 p2669 A71-34334

Displacement field of constant thickness elastic disk with stress boundary conditions, using finite difference technique 17 p2818 A71-34505

Elastoplastic strain distribution in bent circular Al plate with central hole under concentrated load, giving moire patterns and stress-strain diagram [SESA PAPER 1822] 17 p2820 A71-34542

Axisymmetric nonlinear buckling equations for composite thin circular elastic plates of isotropic or orthotropic layers under radial compression 17 p2821 A71-34580

Circular symmetry stressed state for flat disk with flat circular crack, detailing potential and elasticity theories 17 p2824 A71-34844

Logarithmic damping of bending oscillations produced by residual fretting stresses in circular plates 17 p2826 A71-35022

Equilibrium bifurcation for nonlinearly elastic incompressible body during finite subcritical homogeneous deformation, obtaining characteristic equations for cylindrical shell, circular and rectangular plates, etc 17 p2832 A71-35609

Calculation method for zenith and azimuth directional sensitivity characteristics of cylindrical cosmic ray telescopes with circular recording surfaces 17 p2746 A71-35650

Plastic deformation of circular plates and shells of material with different yield and hardening moduli in tension and compression from creep theory relationships 17 p2834 A71-35660

Thin circular disk rotating at constant angular velocity, solving three dimensional elasticity problem with formal power series of thickness-diameter ratio [ASME PAPER 71-APM-Q] 18 p2978 A71-36260

Large deformation stress and mechanical resistance of thin glass circular plates by bending test involving concentric rings 18 p2940 A71-36697

Elastic circular plate with hole traversed by tube filled with viscous fluid, studying system motion 19 p3043 A71-37539

Displacement in circular plate with radial slit under transverse forces 19 p3156 A71-37796

Forced axisymmetric motion of circular viscoelastic plate, including effects of rotatory inertia, transverse shear and time dependent boundary conditions 19 p3157 A71-37848

Thin circular annular Al plate buckling under uniform radial compression 19 p3157 A71-37872

Pressure pulse shape effect on final plastic deformation of simply supported thin circular plate 19 p3158 A71-38181

Anisotropic material circular rotating disks of various thickness, calculating stress and deformation 19 p3160 A71-38473

Isotropic viscoelastic plates of variable thickness subjected to mechanical and thermal stress, considering circular and rectangular plates vibration by external thermal shock 19 p3160 A71-38480

Electromagnetic plane wave monostatic scattering incident to thin circular metallic disk, calculating spectral and transient response from far field amplitude and phase data 19 p3036 A71-38608

Free and forced nonlinear vibrations of rigidly clamped thin circular plate, deriving ordinary differential equations 20 p3307 A71-38795

Electromagnetic wave arbitrary incidence on conducting circular disk for polarization parallel and perpendicular to incidence plane, calculating backscattering cross section for comparison with measurement 20 p3194 A71-38840

Potential flow and laminar boundary layer separation about profiled circular disks, calculating streamlines 20 p3175 A71-39029

Laminar-turbulent inverse transition in divergent radial flow between two parallel flat disks 21 p3366 A71-40101

Von Karman equations analogs solution for nonlinear large amplitude vibrations of circular plate on uniform elastic foundation [ASME PAPER 71-VIBR-9] 21 p3457 A71-40271

Clamped circular elastic plate nonlinear free vibrations, obtaining mode shapes and amplitude-frequency relationships

21 p3471 A71-41025

Numerical computation of potential vortex induced laminar boundary layer on circular disks, using two layer asymptotic expansion

22 p3530 A71-41886

Stability of edge reinforced circular plate under uniform radial load, considering flexural and extensional stiffness of reinforcing beam

22 p3618 A71-42592

Forced vibration of internally damped circular and annular plates with clamped boundaries, obtaining driving point and transfer impedances and force transmissibility

23 p3775 A71-43204

Solid circular plate with diverse elastic moduli in different directions and hole at center, calculating thermoelastic stresses

23 p3777 A71-43422

Boundary value problems solution for reaction pressure to elastic base circular plate bending under uniformly distributed load

23 p3777 A71-43910

Critical compression loads and stability equations for clamped and hinged circular three layer plates with light filler, using Bessel functions

23 p3778 A71-44043

Multicore circular sandwich plates under various symmetrical loading and boundary conditions, deriving bending equations

24 p3879 A71-44619

Nonlinear vibrations of circular plate with variable boundary contact on rigid base

24 p3881 A71-44831

Geometrically nonlinear circular plate under nonuniformly distributed radial force, calculating loading rate and end condition effects on buckling, deflection and stress

24 p3884 A71-44899

CIRCULAR POLARIZATION

Distribution function for two circularly polarized modes in laser with axial magnetic field derived by master equation transformation to Fokker-Planck equation

01 p0094 A71-10745

Solar local SHF emission sources circular polarization, discussing sunspot clusters effects

02 p0306 A71-12076

Short wave signal polarization fading minimization by dispersed reception of circularly polarized components, discussing power gain relation to antenna configuration

02 p0219 A71-12543

Center limb linearized impulsiveness calculations for type 2 solar bursts recorded with circular polarization features

02 p0302 A71-12762

Jupiter decimetric emission circular polarization, observing equatorial magnetic field strength in radiation belt

02 p0317 A71-12868

Sunspot spectrograms analysis, observing wavelength shift in Zeeman triplet circular components and magnetic splitting inequality under different circular polarizations

03 p0484 A71-13210

Propagation modes and circularly polarized wave production in circular waveguides with anisotropic walls

03 p0384 A71-13317

Whistler-mode waves circular polarization measurement byOGO 6 satellite, noting application to hiss, chorus and ion density studies

03 p0421 A71-14538

Tribedral metallic post corner reflector for radar echo enhancement, reflecting same sense rotation as incident circularly polarized signal

04 p0559 A71-15879

Circular polarization measurement in various lines, finding magnetic field strength influenced by line absorption coefficient variations from photosphere to spot and faculae

05 p0803 A71-16025

Coronal condensations emission changes after microwave solar bursts, discussing circular polarization and flare mechanism based on collisionless dissipation of magnetic energy

05 p0804 A71-16029

Dipole antenna array coupling for circularly polarized radio waves amplitude fluctuations reflected from ionosphere at vertical incidence

05 p0738 A71-16216

Phased array antenna element with circular polarization by superposition of complementary dipole and slot, achieving equal E- and H-plane patterns

06 p0875 A71-17719

White dwarf G195-19 circular polarization measurements of continuum radiation in broad band, using electro-optically switched polarimeter

07 p1198 A71-19832

Magnetic white dwarf G195-19 circularly polarized light, confirming handedness and approximate magnitude

07 p1199 A71-19833

Circularly polarized He-Ne ring laser operation, noting no traveling waves coupling via amplifying medium and locking due to cavity imperfections

07 p1127 A71-20388

Radio telescope measurements of circular polarization and total flux of Jupiter at 13.1 cm wavelength

08 p1357 A71-20871

Solar local SHF emission sources circular polarization, discussing sunspot clusters effects

08 p1361 A71-21126

Radiative instability of nonequilibrium plasmas in magnetic traps, considering circularly polarized oscillations propagating along magnetic field

09 p1500 A71-22241

Pulsar radiation circular polarization component Stokes parameter, noting average value different from zero

09 p1522 A71-22978

Crab Nebula emissions on 4 and 6 November 1970, observing optical circular polarization

09 p1522 A71-22981

Circularly polarized parabolic reflector UHF antenna with helical feed for direct TV reception from satellite, discussing design and performance

09 p1417 A71-23034

Ionospheric scintillation effects on fading of oppositely circularly polarized VHF signals in space communications

09 p1410 A71-23522

Nonlinear Landau damping of circularly polarized electromagnetic cyclotron waves, calculating interaction matrix for particular electron velocity distribution functions

10 p1652 A71-24656

Circular polarization in white dwarf G99-37 continuum radiation as function of wavelength

12 p1956 A71-26609

Periodic variations in circular polarization of continuum radiation of white dwarf G195-19 from 3800 to 5400 A

12 p1956 A71-26610

Jupiter circularly polarized visible light measurements, using photoelastic polarimeter

14 p2306 A71-29729

Quasars circular polarization measurements at 21 cm, noting synchrotron self absorption

14 p2307 A71-29867

Polarization Fourier spectrometer for circular dichroism spectroscopy, stressing IR application

14 p2242 A71-30156

Omnidirectional broadband telemetry antenna array for spacecraft providing near isotropic circular polarized radiation with open line microstrip feed

14 p2199 A71-30907

Four arm conical spiral microwave antenna with circularly polarized hemispherical radiation pattern for satellite and rocket applications

14 p2216 A71-31042

Circular polarization and fadeout of moving solar type 4 burst related to magnetic arch and synchrotron emitting electrons deceleration

15 p2473 A71-31693

Moving type 4 solar radio burst observation on 10 October 1969 with radioheliograph, noting circular polarization, movement direction, speed and structure

15 p2473 A71-31694

Ion motion effect on first order oscillations in infinite homogeneous two-component cold plasma in constant magnetic field and circularly polarized external field

15 p2459 A71-32651

Scattered light circular polarization data from Jupiter and other planets indicating nonmagnetic origin

17 p2805 A71-35377

Solar radio bursts circular polarization data, presenting single and multiple inversion analysis at microwave frequencies

19 p3128 A71-38170

White dwarf stars broadband circular polarization and normal/quadratic Zeeman effect

20 p3304 A71-39940

Radiative instability of nonequilibrium plasmas in magnetic traps, considering circularly polarized oscillations propagating along magnetic field

21 p3424 A71-41130

Spatial dispersion effect on circular polarized cyclotron radiation spontaneous emission coefficient in nonequilibrium plasma

22 p3583 A71-42326

Ambient medium, reabsorption and Faraday rotation effects on circular polarization degree of synchrotron radiation, using transfer equation

22 p3593 A71-42335

Circularly polarized parabolic SHF antenna with plane and parabolic reflectors, testing radiation pattern performance

22 p3515 A71-42521

Deterministic signal with normal noise, considering field representation as superposition of two circularly polarized components of directly opposite rotation

22 p3515 A71-42758

Two dimensional maps of circularly polarized solar emission at 7.8 GHz, noting flux density and polarization time dependence before flare

23 p3732 A71-43072

White dwarfs EG 248, GR 289 and EG 250 spectra with circular polarization, detailing violet lines, absolute magnitudes, color and luminosity

23 p3733 A71-43079

Linearly and circularly polarized electromagnetic field effective scattering surfaces relationships determination as value proportional to reflected and transmitted rms flux density ratio

23 p3644 A71-43285

Curved wire array to eliminate parasitic circular polarization of variable profile radio telescope antennas, applying to solar observations

23 p3655 A71-44326

Optical pulsar NP 0532 circular polarization upper limit from measurements throughout light curve

24 p3872 A71-44918

Circularly polarized ultrashort radio wave reflection from lunar and planetary surfaces, determining angular scattering spectrum

24 p3805 A71-45313

CIRCULAR SHELLS

Shallow shells of revolution of strain-hardening material, deriving stress strain state by rigid plastic body model

01 p0175 A71-11039

Thin circular cylindrical perforated shell, analyzing stress distribution around circular hole by coordinate transformation and partial differential equations

02 p0326 A71-12346

Thin circular cylindrical shell stability subjected to axisymmetric thermal pulse, describing buckling process by mathematical model

05 p0820 A71-16186

Local axisymmetric dimple imperfection effects on buckling load of circular cylindrical shell under axial compression

05 p0823 A71-16557

Circular cylindrical shell stability under uniform tension, taking into account support flexibility and temperature difference

06 p0990 A71-17794

Rectangular plate and circular cylindrical shell segment under rotating moment and dynamic loads evaluated by Green function

10 p1691 A71-24812

German monograph on circular cylindrical shells theory comparative studies covering energy and equilibrium methods, tensor representation, reinforced shells, etc

10 p1692 A71-24912

Thin circular cylindrical shells thermoelastic behavior under one directional radiant heating, comparing measured displacements and strains with calculated values based on measured temperature distributions

11 p1841 A71-25187

Natural vibration analysis method for circular cylindrical shell based on three dimensional theory of elasticity and energy principle, discussing boundary conditions effect

11 p1852 A71-26405

Buckling load scatter reduction in axially compressed thin walled circular shells as function of manufacturing accuracy

12 p1974 A71-26869

Thermal stress analysis of hinged thin circular cylindrical shells of variable thickness by computerized discrete orthogonalization method

12 p1979 A71-27357

Local plastic deformation analysis of spherical and cylindrical shells subjected to yield point loads through rigid boss, using nonlinear programming

13 p2147 A71-27787

Stress-strain state of strain hardenable rigid-viscoplastic shells of revolution, presenting example calculation for conical shell with uniformly distributed load

13 p2150 A71-28132

Minimum weight design of circular cylindrical shell hinged at ends under axial compression, using random search method with self learning

13 p2152 A71-28280

Heavy hinged nonshallow circular arches stability during buckling sideways with bifurcations in critical load deflection curves

14 p2324 A71-29885

Frequency equations for trains of axisymmetric harmonic waves traveling in infinitely long three layered elastic circular cylindrical shells and rods

14 p2327 A71-30202

Closed circular cylindrical shell nonlinear problem solvability extended to anisotropic sandwich shell, using mean deflection theory

14 p2332 A71-30866

Dynamic midsurface displacements of thin circular cylindrical shell under uniform membrane stress state and three dimensional surface loads

16 p2656 A71-33214

Nonlinear creep analysis of clamped pressurized circular cylindrical sandwich shells representing

stress, membrane force and bending moment as displacement based on Mises criterion

17 p2816 A71-34297

Circular cylindrical shell stability under combined axial tensile /compressive/ loads and torque, verifying theory by experiments on stainless steel shell

17 p2817 A71-34336

Bending of circular conical shell with discretely reinforced end cross section, deriving accurate closed form solution within limits of working model

17 p2828 A71-35302

Stresses in smooth circular cylindrical shell under radial local load applied on small area

17 p2828 A71-35303

Stress distribution over elements of boss or collar tightened flange joints of circular thin walled shells during bending

17 p2829 A71-35306

Dynamic response of oddly stiffened circular cylindrical shells, using modified variational method

18 p2980 A71-36495

Circular cylindrical shells creep buckling in pure bending, deriving formula for critical time

18 p2980 A71-36674

Elastic field and stress distribution in composite circular rotating disk under constant normal pressure

19 p3159 A71-38187

Radial edge displacement effect on circular cylindrical shells compressive buckling stress, noting opposite effects for different length/ radius ratio ranges [AIAA PAPER 71-984]

24 p3878 A71-44580

Ideal weight of axisymmetric fuselage shells, taking into account load distribution and cabin pressurization

24 p3885 A71-45180

CIRCULAR TUBES

Heat transfer in nongray radiating gas turbulent flow in circular tube

01 p0181 A71-11403

Hot-wire anemometer calibration, measuring shear stress and turbulence distributions in circular channel

07 p1106 A71-18785

Three dimensional scattering and surface current density measurements on circular tube illuminated by electromagnetic wave

08 p1256 A71-21689

Periodically supported and damped closed circular beam structure, determining frequency response matrix

08 p1374 A71-22026

Velocity profiles for flows with laminar heat transfer in circular tube and rectangular duct inlet region with wall suction and injection

10 p1597 A71-25064

Sharp circular edged orifice dynamic characteristics under high amplitude periodic fluid flow conditions, discussing hydraulic resistance coefficients

12 p1898 A71-27506

Laminar flow breakdown in circular tubes, noting disturbance level effect on intermittent flow parameters and turbulent zone length distribution

13 p2046 A71-27827

Circular thin glass tube waveguide containing cold cylindrically stratified plasma, calculating electromagnetic wave propagation

13 p2029 A71-28499

Gromeka-Beltrami ideal incompressible fluid flow in semiinfinite circular cylindrical tube

14 p2225 A71-30221

Eddy diffusivity of mass in air measurement discrepancies in circular duct, considering axial concentration and radial distributions

14 p2339 A71-30934

Finite element method stress analysis for evaluating localized stress distributions in thick walled circular tube with step change in thermal expansion [SESA PAPER 1841A]

17 p2819 A71-34534

Design and performance testing of arterial wick circular heat pipes for OAO-C spacecraft [ASME PAPER 71-AV-26]

18 p2868 A71-36393

Elastic circular plate with hole traversed by tube filled with viscous fluid, studying system motion

19 p3043 A71-37539

Convective heat transfer between laminar fluid flow and circular flat tubes, considering wall thermophysical properties effect

22 p3619 A71-41873

CIRCULATION

NT ATMOSPHERIC CIRCULATION

NT BLOOD CIRCULATION

NT BRAIN CIRCULATION

NT CARBOXYHEMOGLOBIN

NT CORONARY CIRCULATION

NT INTRAVASCULAR SYSTEM

NT ISCHEMIA

NT PERIPHERAL CIRCULATION

NT PULMONARY CIRCULATION

CIRCULATORS [PHASE SHIFT CIRCUITS]

Circulation adjustment of m-port waveguide single junction circulator by scattering matrix eigenvalues

01 p0056 A71-11197

Broadband mini ferrite T circulator and isolator for X band

03 p0384 A71-13274

Spurious spikes in microwave circulators due to hybrid resonant modes of ferrite post open-resonator structure

10 p1583 A71-24212

Coplanar-guide and slot-guide junction circulators on ferrite substrate magnetized perpendicular to surface

13 p2037 A71-28473

Ferrimagnetic components in microwave IC, considering junction circulators, planar phase shifters, etc

16 p2547 A71-33551

Series stabilization reflection type tunnel diode microwave amplifier synthesis with allowance for real circulator reactance

24 p3810 A71-45259

CIRCULATORY SYSTEM

NT AORTA

NT ARTERIES

NT BLOOD VESSELS

NT CAPILLARIES [ANATOMY]

NT GLOMERULUS

NT VASCULAR SYSTEM

NT VEINS

Soviet book on blood hydrodynamics covering circulatory system structure, rheology and mathematical models, pulsating flows, concentration effects and mass transfer

02 p0203 A71-11846

Respiratory and circulatory responses in anesthetized cats to medullary ventral surface perfusion with mock cerebrospinal fluid of varying K concentration or 2 percent procaine solution

04 p0540 A71-15577

Cardiopulmonary and circulatory mechanisms, adaptation limits and response to aerospace flight stress

08 p1238 A71-20720

Dynamic respiratory and circulatory responses to hypoxia in anesthetized dogs, recording oxygen partial pressures, heart rate, blood pressure, blood flows, respiratory rate, etc

09 p1396 A71-23358

Pulmonary arterial system impedance and transmission properties, noting hypoxia and serotonin infusion vasoconstrictor effects

11 p1719 A71-25929

Cardiac output and arterial pressure control in presence or absence of functional nervous system, discussing dog experiments

13 p2003 A71-27839

Circulatory fatigue during shift work, determining pulse rate/oxygen intake at two different loads on bicycle ergometer

17 p2687 A71-34358

Noisy environment effects on circulatory, respiratory and metabolic parameters during physical exercise, measuring heart rate, systolic blood pressure, oxygen intake and respiratory quotient

20 p3185 A71-38889

Dynamic characteristics of human respiratory and circulatory adaptation to muscular exercise, using systems analysis approach

23 p3634 A71-43905

CIRCUMLUNAR TRAJECTORIES

Circumlunar space flight effects on spiderwort, dry seeds and onion bulbs germinating capacity, growth stimulation and chromosome rearrangements

08 p1247 A71-21025

Long wave cosmic radio background emission in circumlunar space by Luna 11 and 12 satellites, observing increase in earth magnetosphere tail

09 p1513 A71-22576

Circumlunar trajectories with return to earth atmosphere, comparing various methods

09 p1519 A71-22662

Circumlunar space flight effects on spiderwort, dry seeds and onion bulbs germinating capacity, growth stimulation and chromosome rearrangements

20 p3193 A71-39605

CIRRUS CLOUDS

Wind foot cirrus cloud pattern relationship to tropospheric jet streams based on high resolution satellite color photographs

04 p0621 A71-15275

Cirrus ice cloud detection from remote emission measurements in far IR by satellite radiometer

09 p1487 A71-23022

CISLUNAR SPACE

Picogram dust particle flux measurements in selenocentric cislunar and interplanetary space by Mariner 4, OGO 3 and Explorer 35

03 p0491 A71-14014

Earth-moon test range for testing earth environmental characteristics in cislunar space, discussing administrative benefits

04 p0649 A71-15296

Dust particle measurements in selenocentric and cislunar space /1967-1969/ by Lunar Explorer 35 and OGO 3

20 p3298 A71-39640

Space shuttle operations analysis for cislunar space, including transfer trajectory inclination and long term effects [AAS PAPER 71-300]

23 p3724 A71-42976

CITIES

Aircraft noise propagation in city streets due to intertown V/STOL and helicopter ports, using small scale models

20 p3178 A71-39264

CIVIL AVIATION

NT YAK 40 AIRCRAFT

Civil aircraft aspect ratio relationship to commercial viability, considering need for minimum induced drag at wing loading to improve payloads, speeds and ranges

01 p0005 A71-11628

V/STOL aircraft in civil air transportation, discussing safety, reliability, maintainability and propulsion system concepts

03 p0348 A71-13576

Civil aviation safety - Conference, Beirut, September-October 1970

04 p0690 A71-14990

Hijacking and acts of violence against civil aircraft, concerning draft convention by legal committee of International Civil Aviation Organization

04 p0691 A71-14997

Army avionics technology transfer to civil aviation, discussing communication systems, flight control and landing aids

04 p0557 A71-15017

Air charter flights legal status, considering public, private and international laws and civil responsibility

06 p1009 A71-17422

Revision of 1929 Warsaw Convention Articles 3 and 25 relative to air carrier liability, discussing possible U.S. secession

06 p1009 A71-17424

Air transport popularization possibilities, considering group rates and fare adjustments

06 p1009 A71-17586

French statistical system for civil air transport operations from airport viewpoint

06 p1009 A71-17587

Civil aviation medicine practice, discussing airman certification for flight fitness, government legislation, accidents and carrier operations

08 p1245 A71-20728

Civil aviation aircraft mean flight time overhaul schedules, considering statistical evaluation of relationship between operational characteristics and time between overhauls

08 p1230 A71-20797

Commercial aviation stratospheric water vapor injections influence on radiation budget, ozone, polar night cloudiness and potential climatic effects

08 p1286 A71-21822

V/STOL civil aircraft, considering rotor lift and variable sweep wings

10 p1556 A71-24850

Psychoreactive action caused by flying accident in group, discussing repercussions in civil and military aviation fields

10 p1572 A71-24982

Crosswind components measurement for different runways of important German civil airports

10 p1639 A71-25041

Weather minimum standards for civil aircraft, considering cloud ceilings, visibility, wind velocity and direction, onboard and ground-based flight control equipment and aircraft characteristics

12 p1924 A71-27141

Soviet airlines operations planning, discussing principal objectives, methodology and organizational principles

12 p1988 A71-27144

MAC malfunction detection, analysis and recording system applications in commercial airlines, emphasizing real time response for maintenance function [SAE PAPER 710425]

13 p1995 A71-28311

Commercial airlines flight training program, using simulation and improved techniques for safety and economy [SAE PAPER 710475]

13 p2044 A71-28340

Commercial V/STOL and jet VTOL transport, discussing Do-31 test results, landing approach, air traffic control automation and electronic control

13 p1997 A71-29131

Roentgenological analysis of paranasal sinuses in civil aviators, studying facial cavities infection

13 p2023 A71-29367

Book on air law and civil air policy covering international regulation, air traffic market, passenger and cargo services, etc

14 p2340 A71-29938

Air transport and travel expansion rate, discussing motivations and cost

14 p2340 A71-30159

Circumstances inducing growth in different air transport sectors, discussing transportation cost, aviation capital requirement and business and leisure air travel

14 p2340 A71-30160

Long haul international air transport, analyzing traffic growth rates

14 p2340 A71-30161

Civil aviation customer /operator, passenger and community/ needs, describing STOL and V/STOL aircrafts

14 p2340 A71-30162

Computer aided design program for civil transport aircraft configuration, performance, propulsion, weight and costs to meet given specifications

14 p2175 A71-30398

Soviet Mil V-12 heavy lift helicopter for civil and military missions, noting turbine engines, rotor configuration, cargo hold and navigation system

14 p2175 A71-30420

Inertial navigation systems improvements for commercial air transportation, noting digital computer program revision and increased functional capability [SAE PAPER 710458]

14 p2272 A71-30534

Civil aircraft antenna design mechanical and environmental aspects and electrical performance, considering serviceability and duplication

14 p2218 A71-31061

Flightworthy 25-foot diameter propotor wind tunnel test, considering civil and military need for VTOL transportation [AHS PREPRINT 501]

14 p2177 A71-31077

Civil and military aviation operational problems, including cloud masses and CAT detection, landing aids and radar navigation

15 p2446 A71-31917

Canadian R and D on fixed wing civil STOL aircraft, discussing augmentor wing concept using jet powered lift augmentor system

16 p2523 A71-33470

Future aviation development constraints on manufacturer and purchaser, design, test costs, noise, airport location and multinational operation [AIAA PAPER 71-799]

16 p2667 A71-34024

Civil V/STOL aircraft projects, discussing design, lift fan engines, weights, flight performance, noise levels, safety and comfort standards

16 p2525 A71-34101

Navigation and communication satellites development for civil aviation and shipping, examining technical, organizational, operational and cost problems

17 p2771 A71-34240

Psychosociological and medical evaluation of private pilots to promote flight safety

17 p2690 A71-34824

Civil aircraft arresting on runway overshoots, describing safe deceleration method by use of soft ground arresters

17 p2674 A71-35210

Military and civil aircraft navigation systems development, emphasizing self contained airborne equipment

17 p2775 A71-35374

Civil aviation and merchant marine satellites, considering aircraft and surface vessel antenna characteristics and modulation techniques for optimum communication channel frequencies

17 p2775 A71-35582

Air transportation safety review covering weather knowledge, aircraft structures, instrumentation, radio aids and power plants

18 p2849 A71-36175

Civil aircraft market analysis, examining replacement cycle and used aircraft market based on aircraft histories

18 p2989 A71-36676

German glossary of commercial air traffic with english equivalents

18 p2989 A71-36962

Civil aircraft future propulsion requirements, considering larger engine sizes, higher takeoff thrusts and lower noise levels [CASI PAPER 72/10]

19 p3122 A71-37600

Civil V/STOL aircraft engines requirements, considering noise reduction, thrust, multifunction propulsion/blowing, lift and booster fan engines [CASI PAPER 72/19]

19 p3122 A71-38021

Airport congestion as constraint on air travel, considering runway capacity and adjusted demand

19 p3042 A71-38028

Aircraft noise effect on hearing impairment of cockpit crews in civil aviation, using audiometric evaluation

19 p3008 A71-38222

Civil aircraft cockpit lighting evaluation guidelines

19 p2999 A71-38241

Flashing civil aviation lights history, progress and photometric characteristics, discussing navigation and landing aids

22 p3499 A71-41489

UK military and civil ATC coordination, discussing Mediator plan for modernization of communication and navigation equipment and techniques

22 p3570 A71-41519

Federal Aviation Act amendment prohibiting controlling interest in air carrier without Civil Aeronautics Board approval

22 p3624 A71-42070

Airlines procedures in conducting pilot training programs within ICAO recommendations and German regulations

23 p3639 A71-43230

Solid state airborne weather radar for civil aviation, discussing design, weight and power requirement reduction

23 p3647 A71-44273

Future transportation technology impact, considering system design evaluation criteria and civil aviation and urban mass transit systems contributions [AIAA PAPER 71-1010]

24 p3892 A71-44594

Civil aviation research and development policy review covering aircraft noise, congestion, ATC, runway capacity and airport development problems [AIAA PAPER 71-1024]

24 p3892 A71-44602

CLADDING
Oxidation and nitrogen absorption protection of Cr alloy by Ni alloy claddings applied by gas pressure bonding

13 p2087 A71-29122

Mechanical properties of explosively clad plates, considering stainless steel/mild steel and brass/mild steel composites

17 p2757 A71-34663

CLAMPS
Inflatable restraint collar for large balloons with heavy loads using winch driven cable launching

02 p0188 A71-11821

Biorthogonal relation for bending of uniformly loaded clamped sector plates with boundary functions along curved edge

02 p0327 A71-12397

Woven textile structures tensile strength tests at high strain rates, using unbreakable compact clamp system

22 p3564 A71-41590

CLARK Y AIRFOIL
U AIRFOIL PROFILES
CLASSIC AIRCRAFT

U IL-62 AIRCRAFT
CLASSICAL MECHANICS
NT ASTRODYNAMICS

NT CELESTIAL MECHANICS
NT KEPLER LAWS
NT ORBITAL MECHANICS

Energy relations in physical space of general relativity theory and inertia space of Newtonian classical mechanics

03 p0458 A71-13605

Classical and relativistic forces of inertia based on exact solution of Einstein nonlinear gravitational field equations, using general covariance principle

04 p0628 A71-15903

Book on dynamic characteristics of aerosol particles in terms of classical mechanics covering continuum approximation, single particles heat and mass transfer, diffusion, dispersion, etc

09 p1431 A71-22284

Gravitational field equations in classical Newtonian mechanics within framework of macroscopic gravitation theory

09 p1523 A71-23074

Rumanian book on distribution theory applications in mechanics covering physical point motions, variable mass, concentrated and distributed loads, elasticity theory equilibrium, motion equations, etc

15 p2501 A71-31147

General nonorthogonal coordinate systems operation techniques, modifying matrix theory for vector equations handling in classical mechanics

15 p2442 A71-32111

Classical Poincare-von Zeipel canonical perturbation theory extension to adiabatically perturbed systems with slow dependence on time or dynamic variables

24 p3848 A71-44790

CLASSIFICATIONS
NT DICHOTOMIES
NT HIERARCHIES
NT INDEXES [DOCUMENTATION]

Classification of electromagnetic wave scattering fluctuating objects from statistical scattering matrices, obtaining incident wave polarization

01 p0038 A71-11208

Auroral absorption classification of cosmic noise at 32 MHz, plotting time and amplitude distribution diagrams

02 p0243 A71-11769

Fog phenomena systematics, describing physical classification according to substrate and function

02 p0277 A71-12371

Solar flare classification based on X ray intensity, offering geophysical significance advantage [AIAA PAPER 70-1370]

02 p0301 A71-12697

Morgan two dimensional stellar spectral system with luminosity classes, comparing to Harvard scheme

04 p0646 A71-15230

Orthogonal transforms and feature selection using pattern, Harr, Walsh, Fourier and Karhunen-Loeve spaces for providing efficient classification algorithms in pattern recognition

08 p1258 A71-21354

Discrete solar proton event three digit classification system, covering proton intensity, riometer absorption and neutron monitor increase

10 p1660 A71-23799

Man machine systems classification, suggesting machine-only system for decision making

10 p1567 A71-23998

Collisional plasma background influence on classification of two stream instability, considering lines of equal asymptotic growth rates in parameter space

10 p1651 A71-24635

Image classification by optical and electro-optic processing methods for spatial signal perception and treatment in natural form

14 p2248 A71-30816

Classification changes in IQSY Auroral Atlas, considering symbolism, synoptic map plotting and data reduction

15 p2396 A71-31608

Classification by curvature tensor of relativistic Riemann space-time gravitational metric field

16 p2611 A71-33276

Classification reliability of electromagnetic wave scattering fluctuating objects from statistical scattering matrices, obtaining incident wave polarization

17 p2698 A71-34260

Lunar maps classification, nomenclature and scales sequence

21 p3448 A71-40549

High vacuum ion source classification according to ionization technique, using pervance and current flow parameters

22 p3589 A71-42055

Meteorological formation classification problems from radar data, discussing optimal solution with discrete selection space

24 p3844 A71-44877

Cloud classification from various radar data independent characteristics, using statistical theory of Bayes hypotheses

24 p3844 A71-44878

Thunderclouds and torrential clouds classification from radar data, developing algorithm model with Bayes method

24 p3845 A71-44884

CLASSIFIERS
Linear pattern classifiers design, using error correction and least mean square adaptive algorithms

03 p0383 A71-14480

CLASSIFYING
Pattern classification as linear programming problem, presenting optimal algorithm

09 p1412 A71-22969

Flexible runway surfaces classification by LCN method, calculating for Ilyushin aircraft

11 p1745 A71-26201

Identities required for classification of Newman-Penrose formalism equations, using tensor description

16 p2612 A71-34068

Chondrites bibliography and review, considering classification, metamorphism, ages and thermal history, achondrites and organic compounds

17 p2798 A71-34454

Automatic classification of targets characterized by radar returns at discrete set of frequencies in Rayleigh region and first resonance range

17 p2747 A71-35773

Uncataloged meteorites presumed to have fallen in Poland, using historical records reporting meteoritic metal for metallurgical applications

19 p3137 A71-37645

Progressive metamorphism and classification of shocked and brecciated crystalline rocks at impact craters

19 p3050 A71-37665

Soviet papers on radar meteorology covering formations classification, signal intensity measurement, detection probability, efficiency and errors

24 p3844 A71-44876

CLATHRATES
Carbon dioxide clathrate in Martian ice cap suggested from hydrate stability relative to solid phase and water ice as function of temperature

01 p0148 A71-10002

CLAYS
Hydroponic plant cultivation with keramzit substrate, investigating replacement time effect and regenerative power of nutrient solution

22 p3506 A71-42816

CLEANERS
NT AIR FILTERS
CLEANING

Ultrasonic cleaning by cavitation disintegration of highly adhesive surface coatings, discussing cleaning liquid, field parameters and external static pressure effects on process efficiency

10 p1617 A71-24135

Gyro wheels cleaning by ion bombardment applied to ceramic gas bearings, comparing with chemical cleaning

22 p3552 A71-41674

CLEANLINESS
Spaceborne optical sensors cleanliness requirements, considering particle size distribution, shape, population densities, chemical composition and origin [AIAA PAPER 71-471]

12 p1873 A71-26758

Hydraulic system cleanliness - ASTM Conference, Toronto, June 1970

19 p2999 A71-38318

Hydraulic system and fluid cleanliness maintenance, discussing contamination sources and prevention techniques including filtration, dehydration and degasification
19 p2999 A71-38319

CLEAR AIR TURBULENCE

Clear air radar structures temperature, wind components and true gust velocities combined with radar data for observed traveling wave features
01 p0030 A71-10560

Clear air convective process, examining dynamic model with radar patterns
01 p0116 A71-10562

CAT wind structure and velocity dynamics, using Doppler radar techniques
01 p0116 A71-10564

Breaking waves and resulting CAT characteristics from ultrahigh resolution FM-CW radar observation, using model of unstable waves at sheared inversion layer
01 p0116 A71-10565

CAT radar observation from instrumented and uninstrumented jet fighter flights, analyzing data statistically for spatial correspondence of ground and airborne observations
01 p0116 A71-10566

Thin CAT layer detection in lower stratosphere by L band radar complemented by radiosonde and U-2 aircraft probes
01 p0116 A71-10567

Mesoscale meteorological structure during radar CAT detection at Wallops Island during January-March 1968 and 1969
01 p0118 A71-10568

CAT layer simultaneous radar and instrumented aircraft observations, noting eddy dissipation rate computation from radar reflectivity measurement
01 p0116 A71-10570

Lidar observation of clear atmospheric structure including lee wave clouds, turbulence, stratification in trade wind inversion layer, etc
01 p0118 A71-10583

Clear turbulent atmosphere effects on optical transmission characteristics and communication system design
02 p0213 A71-12010

Clear air turbulence effects on flight and structural response of aircraft, using gust loads model [ONERA-TP-867]
03 p0346 A71-13136

Clear air convective processes radar observations, discussing development stages of convective field and individual cells
03 p0453 A71-13609

Synthetic endfire hologram radar for small target and clear air turbulence detection
03 p0381 A71-14476

Clear air turbulence due to large amplitude Kelvin-Helmholtz billows, noting simultaneous measurements by instrumented aircraft and radar
04 p0621 A71-15043

Shearing gravity waves /Kelvin-Helmholtz/ instability in isothermal layer model discontinuous interface application to CAT
05 p0777 A71-16667

Clear air turbulence role in general atmosphere circulation, considering energy dissipation, momentum transfer and shear layer producing mesoscale processes
07 p1153 A71-20221

Turbulent/total flight mile ratio in high altitude clear air turbulence /HICAT/ program
07 p1022 A71-20314

High sensitivity S band meteorological radar detecting clear air echoes from low horizontal layers and high altitude turbulence
12 p1880 A71-27156

Aircraft instrumentation and data analysis for clear air turbulence, including orthogonal components and temperature and wind distributions
14 p2267 A71-29753

Stratospheric air flow patterns and CAT measurements onboard aircraft over and downwind of Western U.S. mountain terrain
14 p2267 A71-29755

Clear air turbulence mechanics, considering thermal convection, shear layers, Coriolis and centrifugal instability, billons and rotors
14 p2267 A71-29758

Large amplitude formations and turbulence in Kelvin-Helmholtz instability, comparing with radar observations
14 p2267 A71-29760

High power 10 cm radar as CAT detector, comparing with radar and aircraft data coincident in space and time
14 p2267 A71-29761

Synoptic scale processes effect on high level clear air turbulence production, considering Kelvin-Helmholtz instability role in flow transition
14 p2268 A71-29762

Thunderstorm, CAT, weather and mountain wave induced turbulence forecasting and analysis for transport aircraft
14 p2268 A71-29764

Airborne equipment for CAT detection ahead of aircraft, considering pulsed Doppler laser and IR detectors
14 p2268 A71-29765

Stable laminar in clear air turbulence, noting observations from rawinsonde stations mesoscale network, instrumented and noninstrumented aircraft and ultrasensitive radars
14 p2268 A71-29769

Atmospheric turbulence structure, cloud convection, gravity waves, clear air flow and surface/planetary boundary layers
14 p2270 A71-30495

Hydrodynamic instability generation by stable layer tilting at high altitude, considering clear air turbulence
15 p2445 A71-32712

ATC avionics equipment, discussing inertial area navigation, autopilots, airborne data acquisition, altitude reporting, collision avoidance, CAT, satellite communications, etc
17 p2771 A71-34615

Clear air turbulence in midstratosphere, analyzing heat and momentum transports and temperature fluctuations spectra
18 p2943 A71-36008

CAT physical model and formation mechanism, using turbulent zone characteristics and wind velocity spectra
19 p3049 A71-37448

Synoptic aerological conditions for occurrence of CAT, considering in-flight registrations and observations under jet stream conditions over North Atlantic
19 p3089 A71-37751

Synoptic-aerological conditions of CAT under jet streams, using aircraft measurements
19 p3090 A71-37752

Radar returns from convective fields and cells in visually clear atmosphere explained by thermal effects and air motion
19 p3090 A71-37753

Simultaneous radar and instrumented aircraft observations in clear air turbulent layer for eddy dissipation rates calculation
20 p3256 A71-39207

Aircraft wake turbulence relation to CAT, discussing flight control loss, jumbo jets trailing vortex wakes breakup and detection and safe aircraft spacing
21 p3325 A71-40704

CAT energy budget and physical mechanisms in relation to aviation and atmospheric processes incorporating long range numerical prediction model
21 p3411 A71-41178

Radar observation of convective process in clear air, presenting turret top cell contour tracings from PPI sequence
23 p3700 A71-43088

CLEARANCES

Piecewise linear analysis of two connecting structures including connections with clearance, applying to engine crankshafts and pin-and-eye problems
05 p0829 A71-17116

Time dependent clearance changes effects on aerodynamic characteristics of sectorially grooved gas bearings, describing lift and drag coefficients calculation
14 p2252 A71-30227

Axial flow turbines, calculating effects of axial clearance between stator and rotor bladings on rotor impulse blades bending vibration strength
18 p2979 A71-36299

Gas bearing ground clearance effects on pivoted pad resonance, pitching vibration mode, static journal displacement and friction
22 p3551 A71-41661

Externally pressurized gas-lubricated foil bearing rotation speed effects on gap topography and clearance variation
22 p3552 A71-41671

Inertia-loaded elastic thin circular ring in rigid cavity with small initial clearance, calculating deformation by nonlinear bending theory
22 p3616 A71-42215

CLEAVAGE

Cleavage fracture equations of motion solved for constant moment, force and deflection, discussing plate crack propagation
01 p0167 A71-10291

Crack growth relation to grain boundaries, considering transgranular cleavage in plain carbon steels and ductile intergranular fracture in Al-Zn alloy
03 p0447 A71-14497

Cross and single polarized light techniques revealing coarse grained fractures cleavage facets
07 p1111 A71-19582

Single crystal Ni-Al solid solutions deformations, examining temperature and concentration dependence of critical cleavage stresses
19 p3076 A71-37120

Phase composition and defect structure of thin film CdTe islet compensates on NaCl and KBr cleavage faces
23 p3718 A71-44316

CLIMATE

Supernova explosion or solar outburst theory of climatic effects on mass extinction of organisms at Cretaceous-Tertiary boundary
10 p1673 A71-24422

Earth orbital radiation variations effect on climate, noting minor temperature, wind and hydrological changes
16 p2562 A71-33069

Meteorological planning study for 1973 African solar eclipse observation site selection
16 p2572 A71-33844

Weather and climate modification, reviewing techniques for meteorological processes control, cloud and precipitation modification, ascending flow stimulation, etc
23 p3701 A71-43450

CLIMATOLOGY

NT MICROCLIMATOLOGY

Conference report on impact of man on global environment, assessing actions covering climatic and ecological effects, pollution monitoring, etc
02 p0246 A71-12350

Earth macroclimate mean zonally averaged state equilibrium solution, using thermohydrodynamic equations
08 p1325 A71-20882

Linear vector differential Fridman equations for cosmic and telluric effects on earth atmosphere facilitating dynamic climate forecasts
10 p1639 A71-25115

Climate simulation by global atmospheric circulation models including wind, temperature, pressure, water vapor, precipitation, evaporation, soil moisture, snow depth and runoff
14 p2270 A71-30505

Synoptic climatology of Euroatlantic blocking situations, investigating geographic location and duration
14 p2271 A71-30937

Northern Hemisphere atmospheric vertical velocity computation for all seasons compatible with climatological heating functions, using time averaged thermodynamic energy equation
17 p2770 A71-34803

German monograph on lower atmospheric turbulence and gustiness coefficients in connection with large scale parameters, deriving climatological flow characteristics from wind measurements
17 p2770 A71-35233

Climatological European southern observatory in Chile, describing spectroscopic and photometric telescopes, grand prism objective and double astrophotograph
20 p3210 A71-39527

Synoptic climatology of blocking situations over European-Atlantic region, obtaining middle troposphere circulation patterns by statistical analysis
21 p3411 A71-40826

Climatic changes periodicity in Italy, considering cause by sirocco enhancement
21 p3411 A71-40827

Long range weather prediction based on numerical global atmospheric models, noting application to climatology
24 p3844 A71-44366

Climatological studies and weather forecast support for Apollo 14 mission prelaunch, launch, emergency landing and terminal areas
24 p3845 A71-44981

SST operation climatic impact assessment program, considering carbon dioxide, water vapor, contrails, particulates, nitrogen oxides and carbon monoxide
24 p3823 A71-44982

CLIMBING FLIGHT

Optimal motion of multistage body of variable mass during vertical climb with allowance for weight limitations
10 p1683 A71-24845

Minimal time climb velocity optimization for stratospheric and tropospheric jet aircraft flights
22 p3482 A71-41972

KC-135 aircraft climb trajectories for optimum constant lift coefficient, range and fuel amount
22 p3481 A71-42834

CLINICAL MEDICINE

Medical data processing techniques in electrocardiography and effort vectorcardiography facilitating clinical observations
02 p0207 A71-12110

Aerial stayaway clinical case covering unconsciousness, deafness, hypoxia, hypothermia; acidosis and other effects due to 9 hr flight in unpressurized landing gear cell
04 p0544 A71-15058

Flight surgeons guidance criteria for flying personnel, detailing individual areas examination, documentation and clinical findings
08 p1245 A71-20719

Clinical aspects of aerospace neurology, considering central nervous system diseases among flying personnel
08 p1238 A71-20723

Preventive and clinical medicine effect on aircrew health maintenance
08 p1245 A71-20725

- Pilots hypoxic hypoxia occurrence and treatment
08 p1249 A71-21959
Book on clinical physiology techniques and
anesthesiology measurements covering electronics,
ECG analysis, blood pressure measurement, cardiac
function, respiratory mechanics, etc
09 p1398 A71-22459
German book on clinical pathophysiology of
respiration covering respiratory physiology, pulmon-
ary gas exchange, respiratory control, hypoxia,
hyperoxia, pressure breathing, etc
09 p1394 A71-23069
Clinical value of electroencephalogram following
sleep deprivation in detecting abnormalities in neu-
rological patients
09 p1395 A71-23248
Acoustic holography for simultaneous three-
dimensional image and internal structure insight, discussing
applications to submarine exploration and medical
diagnostics
13 p2071 A71-29299
Neutron radiography and dosimetry as clinical diag-
nostic tool, calculating resolution through tissues for
simulated human arm
17 p2693 A71-35449
Antecedent clinical statistics of myocardial infar-
ction and sudden death in actively employed middle
aged men, noting cardiac rate, rhythm and conduction
abnormalities
22 p3485 A71-41798
Cardiac arrest or arrhythmia due to coronary ar-
teriosclerosis in young aviator, examining causes,
prevention and predictive measures
23 p3637 A71-44250
- CLOCK PARADOX**
Clock paradox problem resolution in relativity
theory, considering space travel effects on time mea-
surement and aging process
20 p3271 A71-39571
- CLOCKS**
NT ATOMIC CLOCKS
NT CHRONOMETERS
Clock corrections determinations by stars pairs situ-
ated symmetrically around zenith, obtaining formulas
by various methods
03 p0484 A71-13219
Oscillator for guiding clock mechanism of 400 mm
photographic telescope, using high stability
transistorized multivibrator
04 p0591 A71-14847
Automatic amplitude control of transistorized
quartz clock master oscillator
04 p0592 A71-14860
Astronomical pendulum clock with optical rate and
recordable amplitude
04 p0592 A71-14862
Pendulum clock with contactless drive for
isochronal autooscillation period, outlining pulse am-
plitude and duration stabilization
04 p0592 A71-14863
Satellites for time dissemination, discussing clock
synchronization and signal propagation
07 p1154 A71-19011
Clock correction for Danjon prism astrolabe deter-
mination method description and verification
08 p1284 A71-21678
Hipp pendulum controller electromechanical clock,
considering dry and viscous friction dynamic models
12 p1932 A71-27525
Rat 24 hour clock inborn nature, discussing depen-
dence on alternating light-dark periods for time mea-
surement
13 p2010 A71-28801
One way UHF clock synchronization, using geosta-
tionary communication satellites with propagation
delays calculated from orbital elements
20 p3239 A71-39460
- CLOGGING**
U PLUGGING
- CLOSED CIRCUIT TELEVISION**
Visual devices for training simulators, discussing
film and closed circuit TV systems and components
15 p2385 A71-31889
On-orbit payload handling for space shuttles, in-
cluding manipulator arms for drawing docking vehi-
cles together, closed circuit TV and airclocking
[AIAA PAPER 71-811] 17 p2814 A71-35427
- CLOSED CYCLES**
Aircraft jet engine application of electric discharge
machining for repetitive continuous production, con-
sidering automated closed cycle equipment
[SME PAPER MR-71-143] 18 p2927 A71-36658
Post test inspection of Brayton Rotating Unit for
closed Brayton cycle electric power conversion
system for long space missions
20 p3180 A71-38909
Closed cycle refrigeration system for cryogenic
cooling of IR illuminator in helicopter mounted U.S.
Army NVASS Night Vision System for night recon-
naissance
20 p3184 A71-39275
- CLOSED ECOLOGICAL SYSTEMS**
Mass balance stability in closed life support
systems, using mathematical model
01 p0024 A71-11127
Cosmonaut water supply and regeneration in
spacecraft using self contained biological cycle
01 p0025 A71-11150
Optimum mineral medium for algae Chlorella and
Scenedesmus cultivation in closed ecological system
09 p1393 A71-22923
Space flight factors effects on human physiology
and psychology, discussing spacecraft gaseous me-
dium control, food supply, closed ecological systems
and weightlessness effects
13 p2016 A71-27876
Closed cycle life support water electrolysis system
using solid plastic sheet electrolyte/ion exchange
membrane/of sulfonated perfluoro polymer
[ASME PAPER 71-AV-9] 18 p2866 A71-36376
Microflora simplification effects on immunocom-
petent organism systems, observing shifts in guinea
pigs lymphoid tissue with limited flora
21 p3332 A71-40555
Bacterial contamination in confined sealed space
during long term human occupation, observing
hemolytic microflora spreading dynamics on bodies,
clothes, wall and air
21 p3343 A71-40560
Prolonged manned space flight infectious disease
hazards, discussing confinement, zero gravity, high
oxygen content, personal hygiene, waste disposal and
preflight immune status
21 p3333 A71-40561
Microorganisms under closed environmental
ecological conditions with reference to astronauts in-
fectious diseases, discussing bacteria growth in Bio-
satellite 2 and earth based closed chamber experi-
ments
21 p3343 A71-40562
Artificial ecological regenerative life support system
design for space environments, discussing
biotechnological properties
21 p3343 A71-40563
Spacecraft closed loop oxygen recovery system
using electrochemical carbon dioxide concentrator,
Sabatier reactor and water electrolysis subsystem
22 p3503 A71-42017
Manned 90 day test of closed chamber regenerative
life support system simulator, describing subsystems,
crew nutrition, hygiene, maintenance and leisure ac-
tivities
22 p3503 A71-42043
Humans under constant diet feeding in closed
ecological system, demonstrating instability in
elimination process of various elements
22 p3506 A71-42817
- CLOSED LOOP SYSTEMS**
U FEEDBACK CONTROL
- CLOSURES**
Photoelastic analysis using stress freezing to evalu-
ate closure and precatastrophic crack extension in
plates under cylindrical bending
01 p0167 A71-10295
Polyester resin model fatigue crack closure, deter-
mining residual stress distribution and crack opening
and closing force by photoelastic research
04 p0670 A71-15390
- CLOTH**
U FABRICS
- CLOTHING**
NT BOOTS [FOOTWEAR]
NT COTTON FIBERS
NT FLIGHT CLOTHING
NT HELMETS
NT PRESSURE SUITS
NT PROTECTIVE CLOTHING
NT SPACE SUITS
Digital simulation mathematical model describing
simultaneous energy and mass transfer process in
clothing-airspace-skin system
02 p0203 A71-11806
Maximal sweat evaporative heat loss and permitted
work load measurements as function of temperature
and clothing insulation
18 p2872 A71-36861
- CLOUD CHAMBERS**
Semiautomatic stereophotographic processing of
particle interaction data from Wilson chamber
01 p0083 A71-11364
Nuclear interaction examination, using Wilson mag-
netic chamber for multiple particle production
03 p0461 A71-13836
X ray films in emulsion chambers, discussing elec-
tron-photon cascades
03 p0426 A71-13839
Sound attenuation by warm air fog, using droplet
measurements in Wilson cloud chamber
09 p1490 A71-23556
Extensive air showers cores structure observed with
plastic scintillators and multiplate cloud chamber at
2770 m
13 p2124 A71-28082
Near sea level cosmic ray high energy interactions
from data recorded by interleaved stack of cloud and
ionization chambers and carbon and iron plates
19 p3124 A71-37287
Nuclear interaction examination, using Wilson mag-
netic chamber for multiple particle production
22 p3579 A71-42637
- X ray films in emulsion chambers, discussing elec-
tron-photon cascades
22 p3550 A71-42640
- CLOUD COVER**
Transient response measurements of multiple scat-
tered laser radiation from clouds as function of view
field
02 p0260 A71-12032
Mars atmosphere carbon dioxide condensate cloud
layer implications, considering temperature lapse rate
and water condensation at lower levels
03 p0489 A71-13608
Venus halo as photometric evidence for hexagonal
ice in cloudtops
04 p0660 A71-15862
Venusian atmospheric cloud cover, determining na-
ture of particles by optical reflective properties
07 p1191 A71-18907
Earth atmosphere thermal sounding problems, con-
sidering indirect temperature profile determination,
various degrees of cloudiness and Planck function de-
pendence on pressure
07 p1151 A71-18909
Atmospheric absorption by clouds, fog and rain on
earth-space path at 90 GHz, using sun tracker
07 p1060 A71-19215
Polarization of sunlight multiply scattered by at-
mosphere and cloud particles of Venus from UV to IR
07 p1204 A71-20622
VFR flying under bad weather conditions,
discussing flight through and above cloud layers, need
for radiotelephone communication and ground radar
support
08 p1231 A71-21767
Energy distribution in dark and light details on
Venus spectrograms, considering relation to clouds in
upper atmosphere
09 p1520 A71-22838
Spectrographic measurements of Jovian Red Spot
and Southern Tropical Zone molecular absorption
bands related to cloud cover density and depth
09 p1520 A71-22839
Aqueous HCl refractive indices measured for room
temperature to Venus cloud temperature and various
concentrations
09 p1522 A71-22937
Venus water, discussing polar seas, acidity, tem-
perature, wind patterns and clouds
11 p1824 A71-25700
Venus cloud pattern contrast, using photoelectric
scans with narrow band interference filter sequences
11 p1824 A71-25702
Venus cloud composition, noting partially hydrated
iron chloride as principal constituent
11 p1824 A71-25703
Jupiter cloud structure observations near 8.5
microns from thermal flux measurement along polar
and equatorial scans
11 p1827 A71-25727
Saturn cloud layer molecular absorption from spec-
tral /photographic and photoelectric/ observations
11 p1827 A71-25730
Venus subcloud layer, investigating radiant heat
transfer in convective lower atmosphere
12 p1958 A71-26646
Latitudinal distribution of integral water content of
clouds in droplet form above Pacific, Atlantic and In-
dian oceans from Cosmos 243 measurements
12 p1924 A71-27098
Earth surface formations and clouds angular
brightness distribution based on reflected solar radia-
tion intensity
12 p1901 A71-27102
Cloud layer role in formation of light and heat
regime of two layer Venus atmosphere model, con-
sidering sunlight reflection
13 p2131 A71-27808
Venus cloud height at equatorial and polar latitudes,
using carbon dioxide band distribution intensity
13 p2138 A71-28593
Aircraft hazards due to frequent low cloud occur-
rences at Kenya airport, forecasting weather with
statistical analysis and radiosounding
13 p2097 A71-29106
Sky brightness measurements during total solar
eclipses, discussing solar elevation, cloud cover and
albedo effects
14 p2309 A71-30117
Atmospheric turbulence structure, cloud convec-
tion, gravity waves, clear air flow and surface/planeta-
ry boundary layers
14 p2270 A71-30495
Hydrodynamic instability generation by stable layer
tilting at high altitude, considering clear air turbulence
15 p2445 A71-32712
Planetary atmospheres composition from ground
based IR spectroscopy, including multiple scattering,
cloud layers, line formation and absorption
17 p2808 A71-35570
Earth radiance analysis by IR interferometric spec-
trometer of Nimbus 3 satellite, noting cloud cover as
dominant variable
18 p2912 A71-36065
ERTS satellite-based laser communication system,
calculating cloud cover effect on clear line-of- sight

light transmission probability through atmosphere to ground station

18 p2876 A71-36472

Cloud cover areal distribution estimation model using multichannel IR radiometer data from Nimbus 2 satellite

19 p3056 A71-38267

Automated meteorological radar information operation methods for cloud fields, discussing data analysis and processing

19 p3094 A71-38702

Venusian polar tropopause and cloud layer from IR spectral recording in carbon dioxide band near inferior conjunction for crescent regions

20 p3290 A71-39306

Cloud amount and cloud cover interpretation from satellite data compared with ground, noting radiometric limitations

20 p3258 A71-39549

Cloud cover charts for North Atlantic-European-North African region, comparing satellite and ground station visual observations

20 p3258 A71-39552

Spectrophotometry and photography of earth twilight aureole, clouds and underlying surface from manned Soyuz 5 and 7 spacecraft

20 p3240 A71-39675

Cloud layer role in formation of light and heat regime of two layer Venus atmosphere model, considering sunlight reflection

21 p3441 A71-40077

Rapid retrograde rotation of Y shaped cloud formations in Venus upper atmosphere, discussing correlation with slow ground rotation

21 p3441 A71-40106

Height variations of Venusian cloud tops at planet equatorial and polar regions

21 p3449 A71-40608

Martian surface clouds distribution in graph, noting statistical correlation with surface radar altitude

21 p3450 A71-40712

Venus survey, discussing mass, radius, rotation, internal structure, magnetic field, radiation belts, surface properties, atmospheric composition, cloud layer, etc

21 p3452 A71-40884

Latitudinal distribution of integral water drop content of clouds above Pacific, Atlantic and Indian oceans from Cosmos 243 measurements

22 p3568 A71-41653

Astronomical and earth resources observations accommodation by space shuttle orbital sortie missions, obtaining sensor use rate estimate from worldwide cloud cover statistical distribution

[AAS PAPER 71-303] 23 p3724 A71-42979

Martian dust storm observation by telescope in New Mexico, noting brilliant yellow cloud cover

24 p3872 A71-45000

CLOUD GLACIATION

Cirrus ice cloud detection from remote emission measurements in far IR by satellite radiometer

09 p1487 A71-23022

Venus water ice clouds existence possibility from high altitude IR spectra and ground based spectroscopic observations

22 p3603 A71-42189

CLOUD HEIGHT INDICATORS

Cloud base height estimation methods involving vertical radar, laser, stereotelemeter and ceilograph measurements with instrument error analyses

10 p1639 A71-25100

Earth and ocean surface state and cloud height determination using airborne laser radar observations

16 p2568 A71-33786

GaAs injection laser radar for measuring cloud height, determining required laser output power as function of state of atmosphere and receiver sensitivity

21 p3394 A71-41238

Emitted signal delay time effect on operational precision of semiconductor laser radar for measuring lower cloud boundary heights

21 p3394 A71-41239

Laser radar for lower cloud boundary measurements, using information theory for potentials evaluation

22 p3550 A71-42850

CLOUD PHOTOGRAPHS

Wind speed field estimations from wind direction, using satellite cloud photographs

01 p0119 A71-10851

Maximum wind speed estimation in tornadoes and waterspouts, using cloud deck height and funnel cloud photographs

03 p0453 A71-14203

Simultaneous meteorological satellite IR radiation measurements and cloud photographs for superposition and mutual interpretation

05 p0752 A71-16676

Computer pattern recognition technique for determining cloud motions in real time from ATS satellite photographs

08 p1326 A71-21453

Latent heat convective transport from lower to tropical upper troposphere, noting periodic energy fluctuations from time lapse synchronous satellite cloud photographs

09 p1489 A71-23553

Martian cloud motions from Lowell Observatory plates following local positions of well-defined clouds

11 p1826 A71-25722

Noctilucent cloud morphology and kinematics from photographic observations near Moscow

14 p2233 A71-29971

CLOUD PHOTOGRAPHY

Cloud and precipitation boundaries in convective storms studied by stereophotogrammetry and radar, discussing radar echo motion within cloud envelope

01 p0118 A71-10586

Meteorological satellite atmospheric parameter observations, discussing instruments and techniques for temperature and pressure profiles, wind patterns and cloud image data

01 p0164 A71-11360

Contour signal characteristics for cloud form recognition by computer using learning algorithm and photographic data

02 p0225 A71-11691

Photographic observation of noctilucent cloud occurrence over geographical location during sounding rocket flight

02 p0246 A71-12706

Meteorological satellite systems, discussing earth image transmission by TV cameras IR photography, data processing and cloud pictures

05 p0817 A71-16641

Nimbus meteorological satellite program, discussing global cloud cover mapping and automatic picture taking, radioisotopic thermoelectric generator, sounder instrumentation and remote sensors

05 p0818 A71-17133

Environmental satellite data on-line processing and extraction procedures, including visible and IR imagery mapping and cloud pictures analysis

07 p1067 A71-18806

Earth twilight aureole and cloud spectra from satellite photometry

08 p1285 A71-21792

Mars yellow clouds extent during near perihelion apparitions since 1877, considering dust storm origin in Southern Hemisphere

09 p1520 A71-22698

Earth optical radiation environment observation from satellites, reviewing solar spectra, near IR cloud spectra and vacuum UV radiometer scans

09 p1437 A71-22739

Statistical diameter size distribution of random circles on plane or spheres in space from satellite and aircraft measurements for aerial and cloud photography

12 p1929 A71-27100

Cloud amount and cloud cover interpretation from satellite data compared with ground, noting radiometric limitations

20 p3258 A71-39549

Statistical diameter size distribution of random circles on plane or spheres in space from satellite and aircraft measurements for aerial and cloud photography

22 p3537 A71-41655

APT weather satellite cloud pictures over sea southwest of Kyushu showing striated cloud pattern transformation into closed cellular pattern, discussing lower atmospheric layer moisture budget

22 p3568 A71-41859

Lower atmosphere wind and cloud velocity measurements by combined stereophotogrammetry and balloon visual observation

22 p3542 A71-41862

Atmospheric wind speed estimation, using ATS geostationary satellite cloud photographs

22 p3535 A71-42411

Equatorial convective cloud mesosystems formation from Apollo 6 data, investigating Hadley circulation energy generation

23 p3701 A71-44011

Cumulus clouds photographs above Northern Hemisphere by meteorological satellite during active periods of earth atmospheric circulation

23 p3701 A71-44047

CLOUD PHYSICS

Updraft vault dynamic in hailstorms using one dimensional cumulonimbus entraining jet model, observing initial conditions steady state

01 p0119 A71-10744

Ionospheric artificial barium cloud growth and stability, considering ion density, internal electric field and velocity

01 p0077 A71-11508

Cloud brightness as function of illumination and underlying surface conditions, relating macrooptical parameters and microstructure

02 p0277 A71-12113

Noctilucent cloud particle size composition and origin from sounding rocket flight and control collecting surfaces

02 p0246 A71-12702

Soviet book on nephelanalysis for synoptic forecasting covering meteorological satellite observations and

network characteristics, photointerpretation, data processing, cloud identification, weather charts, etc

02 p0278 A71-12842

Turbulence energy spectra in thick convective cumulonimbus cloud zone, using aircraft measurements

04 p0622 A71-15631

Noctilucent cloud observations and research covering geographic distribution, annual and diurnal variations, kinematics, volcanic connections, cosmic dust eruptions, etc

04 p0584 A71-15677

Thunderstorms anvil cloud high level outflow mapping by Doppler radar at various heights and elevation angles

05 p0721 A71-16669

Nonraining clouds electric fields and charge distribution, calculating convection influence by numerical means

05 p0777 A71-16675

Solar radiation fluxes at earth surface in presence of cumulus clouds, relating fluxes to cloud magnitude and sunshine duration by regression relations

06 p0889 A71-17648

Relativistic velocity particles diffusion in cloud of scattering centers in centrifugal motion from Boltzmann equation solution by method of extensions

06 p0963 A71-18229

Ion diffusion and conduction to cloud droplets, determining resulting mean charge distribution from polar conductivities fixed ratio

07 p1152 A71-19757

Spatial correlations between inside cumulus cloud conditions and precipitation onset and intensity from modification experiments from aircraft penetration measurements

08 p1326 A71-21450

Computer pattern recognition technique for determining cloud motions in real time from ATS satellite photographs

08 p1326 A71-21453

Automatic procedure for determining cloud motion from geosynchronous satellite pictures based on cross correlation, discussing real time operational system

08 p1327 A71-21454

Submillimeter wave extinction in clouds and fogs, using spectrometric results of water optical properties

09 p1408 A71-23375

Power spectra and electrostatic mechanism of thunder from intercloud and cloud to ground lightning using analog and digital methods

09 p1489 A71-23441

Pre-main sequence T Tauri stellar evolution, discussing mass loss rates and star formation by interstellar cloud violent hydrodynamic compression

09 p1528 A71-23592

Soviet book on noctilucent clouds covering propagation region, occurrence frequency, morphology, dynamics, color, spectrum, composition, relation to solar and ionospheric phenomena, etc

10 p1604 A71-24734

Angular discretization effect on calculations of emerging radiation and integrated albedo from model cloudy atmosphere, using multiple scattering with terrestrial particle phase functions

10 p1643 A71-24972

Venus ferrous chloride hydrate cloud production, examining geochemical problems

11 p1824 A71-25704

Venus cloud hypotheses, discussing chemical composition, vapor pressure, temperatures and spectroscopic abundances

11 p1824 A71-25705

Cloud activity on Mars near autumn equinox of Northern Hemisphere, comparing 1937 and 1969 oppositions

11 p1826 A71-25721

Water and ice cloud discrimination by angular distribution measurement of various polarization parameters of scattered laser beam radiation, using Mie theory

11 p1776 A71-26298

Visible and IR radiative transfer in water and ice clouds, calculating radiance and polarization from Mie theory

11 p1800 A71-26299

Cloud shape data, comparing meteorological satellite measurements and ground based visual observations

11 p1795 A71-26559

Jet stream axis position from cumuloniform cloud structural differentiation observed over Central Europe on 22 May 1970, noting coincidence with high pressure near ground

12 p1924 A71-26575

Electrical screening layers around charged clouds, giving numerical model for space charge accumulation, electric field distribution and forces acting on cloud droplets

12 p1925 A71-27290

Diffuse reflection from clouds with horizontal surface striations, using Monte Carlo method to follow photons through simplified models

13 p2056 A71-27975

Light pulses reflection from water and ice in clouds, using Monte Carlo technique for all orders of multiple scattering

13 p2031 A71-28795

Neutral gas cloud expansion into vacuum explained by high altitude rocket released metal vapor molecules collisions and release mechanism characteristics

14 p2223 A71-29662

Mesospheric extraterrestrial dust and trapped water model of noctilucent cloud formation in high latitude summer conditions, using meridional trajectories

14 p2231 A71-29721

Mesospheric /noctilucent/ cloud physics - Conference, Riga, November 1968

14 p2231 A71-29955

MHD processes of upper atmosphere in mesospheric cloud formation, discussing solar wind-magnetic field interactions and equilibrium for Pikelner bomb

14 p2232 A71-29960

Mesospheric cloud statistics compared with 200 MHz solar radio emission during summers of 1958-1966

14 p2232 A71-29961

Noctilucent cloud observation from space, discussing instruments, radiation spectrum, global scale formation, time dependent structures and satellite orbit requirements

14 p2232 A71-29963

Noctilucent cloud data statistical treatment by meteor observation double counting method

14 p2233 A71-29966

Soviet research program relative to climatology, physical nature, morphology and dynamics of mesospheric clouds, discussing observational and experimental methods

14 p2233 A71-29968

Noctilucent clouds observations and data acquisition, considering cloud amount and thickness calculations

14 p2233 A71-29969

Ice crystal and cloud drop nuclei origin and physical characteristics, discussing nucleation pollution products, weather modification and microphysical processes

14 p2270 A71-30496

Atmospheric optics and radiative transfer, including earth albedo, sky brightness, heat balance, cloud/terrain reflectance, molecular spectroscopy and multiple scattering

14 p2275 A71-30497

Cloud energy dissipation coefficient determination by ruby laser device, applying to water content and liquid particle concentration, vapor cloud and aerosol concentration

15 p2445 A71-31449

Carbon suboxide polymers formation in Martian atmosphere, examining carbon monoxide photolysis and radiolysis processes enhanced by solar ionizing radiation

15 p2491 A71-32420

Gravitating continuous medium instability in presence of delta shaped point density perturbations, discussing cloud structure development in interstellar gas

15 p2495 A71-32642

Noctilucent cloud nature from cosmic dust particles collection and detection, discussing mass, absolute falling velocity and model theories

16 p2641 A71-33765

Radiative heat transfer in model water clouds by IR radiation, using method of discrete ordinates

17 p2735 A71-35560

Physics of clouds and active effects - Soviet Conference, Tiflis, U.S.S.R., May 1969

19 p3091 A71-38679

Droplet clouds microstructure and phase state occurrence as function of temperature, size distribution and water content based on experimental data

19 p3091 A71-38680

Cumulus clouds macro- and microstructural parameters measurements including convective flow, temperature, water content, droplet concentration and size

19 p3091 A71-38681

Fronts and frontal clouds evolution theory as nonstationary two dimensional problem with allowance for dynamics and thermodynamics

19 p3091 A71-38682

Theoretical model for initial stage of cloud condensation developing at constant air cooling rate

19 p3092 A71-38684

Cloud particle electrification mechanism with allowance for secondary collisions between particles

19 p3092 A71-38685

Dissolved and mixed water vapor condensation aerosol nuclei thermodynamic properties from aircraft and ground-based cloud measurement data

19 p3092 A71-38686

Rainfall, aerosols and cloud water samples analyzed for chlorides and sulfates content and electrical properties

19 p3092 A71-38687

Cloud elements evolution, investigating electrical charges effects on ice crystal growth rate in water vapor by laboratory experiment

19 p3092 A71-38688

Precipitation formation and regulation from supercooled and frontal clouds, noting crystalline cloud seeding effects

19 p3092 A71-38689

Vertical motions, turbulent heat exchange and radiative heat input role in stratus clouds evolution, deriving humidity and heat transfer equations as functions of time

19 p3093 A71-38690

Convective clouds development stimulation by artificial ascending jets forming above stationary heat and momentum source, discussing propagation in atmosphere

19 p3093 A71-38694

Stationary ascending and descending jets velocities in nonstationary cloud layer, discussing cumulus clouds breakup rate

19 p3093 A71-38695

Radar measurements of vertical structure and motion trajectories of cumulus-rain clouds, studying vertical flows velocities and radar echo characteristics

19 p3094 A71-38701

Cloud physics, comparing observational and theoretical values of wave parameter determining heat influx properties

19 p3094 A71-38703

Cloud particles coagulation kinetics, using integral equation for distribution function

19 p3095 A71-38704

UV photochemistry of lower Jovian clouds, using experimental simulation

21 p3447 A71-40427

Monte Carlo method calculation for light pulse reflection from clouds for all orders of multiple scattering

22 p3576 A71-42562

Convective cloud dissipation after rainfall, calculating temporal behavior of temperature fields, water content, moisture and air motion rate

22 p3569 A71-42847

Internal velocity field role in massive star formation, discussing cloud fragmentation and mass function

23 p3723 A71-42941

Laboratory analog simulation of absorption line spectra in cloudy planetary atmospheres, comparing with computational model based on plane parallel atmosphere

23 p3700 A71-43075

Atmospheric conditions for hailstone evolution process, using convection theory and kinetic particle model

23 p3701 A71-43909

Equatorial convective cloud mesosystems formation from Apollo 6 data, investigating Hadley circulation energy generation

23 p3701 A71-44011

CLOUD SEEDING

Warm fog modification by condensation nucleus seeding, discussing droplet concentrations, cloud height and aerosol content effects on salt seeding material optimal size and dosage

09 p1488 A71-23253

Cloud control and modification through seeding with hygroscopic compounds

14 p2271 A71-30611

Lidar observations of artificial warm fog seeding operations, analyzing spatial and temporal variations

17 p2770 A71-35741

Precipitation formation and regulation from supercooled and frontal clouds, noting crystalline cloud seeding effects

19 p3092 A71-38689

Artificial crystallization and dispersion in supercooled stratus clouds, observing growth, stabilization and disintegration stages in crystallization zones expansion

19 p3093 A71-38691

Tropical cumulus clouds seeding experiments with silver iodide smoke, discussing cloud growth and precipitation increase

19 p3093 A71-38693

CLOUDS

NT ARTIFICIAL CLOUDS

NT CIRRUS CLOUDS

NT CLOUDS [METEOROLOGY]

NT CUMULONIMBUS CLOUDS

NT CUMULUS CLOUDS

NT ELECTRON CLOUDS

NT HYDROGEN CLOUDS

NT NOCTILUCENT CLOUDS

NT PLASMA CLOUDS

NT STRATUS CLOUDS

Radar target optimal detection algorithms in cloud of passive reflectors, noting space surveillance regularities

05 p0722 A71-16870

Ellipsoidal level surface gas cloud expansion into vacuum

05 p0783 A71-16991

Thermal radiation from finite cylindrical particle cloud, determining far field angular distribution by Monte Carlo method

[AIAA PAPER 71-78] 06 p1008 A71-18535

Ellipsoidal level surface gas cloud expansion into vacuum

18 p2948 A71-36791

Interstellar dust clouds physical and chemical constitution, discussing molecular gas chemical composition and abundances

18 p2968 A71-37037

CLOUDS [METEOROLOGY]

NT ARTIFICIAL CLOUDS

NT CIRRUS CLOUDS

NT CUMULONIMBUS CLOUDS

NT CUMULUS CLOUDS

NT NOCTILUCENT CLOUDS

NT STRATUS CLOUDS

Atmospheric temperature profile in cloud presence, discussing remote sounding techniques with maximum probability method

01 p0120 A71-10854

Free nonlinear air convective motion in two dimensional cloud banks along vertical wind shift

02 p0277 A71-11690

Q switched ruby laser facility for measuring light pulse transmission spatial and temporal response through clouds

02 p0213 A71-12013

Cloud brightness as function of illumination and underlying surface conditions, relating macrooptical parameters and microstructure

02 p0277 A71-12113

Holographic measurement of moving cloud droplets size distribution from aircraft using Q switched ruby laser

04 p0596 A71-14968

Cloud drop size distribution from spectral transmission measurements, using spectroradiometer

04 p0621 A71-15073

Optically thick clouds reflected light radiance and polarization for haze and nimbostratus models

05 p0781 A71-16252

Turbulent diffusion of impurity from infinite linear source in clouds and fog, allowing for particle entrainment

05 p0776 A71-16422

Hurricane Gladys structure and dynamics observations by Apollo 7 spacecraft, satellites and radar, noting large cloud feature

05 p0777 A71-16662

Artificially produced holes closing in clouds, investigating role of water vapor and droplets turbulent diffusion by mathematical model

05 p0777 A71-16668

Cloud fine structure using backscattered laser radiation, incorporating multiple scattering effects into data processing system

06 p0921 A71-17381

Light reflection during plane cloud layer light scattering, studying zenith angles and angular brightness distribution

06 p0923 A71-17510

Radiation fields of various background and atmospheric cloud formations by reflected short wave radiation aircraft measurements

06 p0923 A71-17511

Radiation temperature fields and cloud distributions seasonal and latitude characteristics by meteorological earth satellite data

06 p0924 A71-17517

Phase transitions effect on cloud turbulence behavior from relaxation time, energy and temperature dissipation and supersaturation spectral density

07 p1150 A71-18799

Cloud droplet growth by condensation, deriving equation solution computational stability

07 p1152 A71-19756

Soviet book on fog, cloud and humidity measuring instruments, discussing artificial fog formation and natural fog dispersion problems

07 p1114 A71-20298

Cloud radiation measurements by ground based microwave radiometer

11 p1794 A71-25380

Cloud height distribution pattern, developing analogy between diffusion and quantum motions

12 p1924 A71-26737

Cloud formation two dimensional model simulation by numerical integration of hydrodynamic and thermodynamic equations, considering condensation, evaporation, coagulation and water drops terminal fall velocity

12 p1925 A71-27196

Optical effects observation by air traveler during takeoff, including haze or cloud droplet scattering, halos, shock wave shadows, shallow watercolors and twilight wedge

13 p2022 A71-29350

Height sign change prediction for lower cloud boundary from pressure Laplacian sign at earth surface

15 p2443 A71-31359

Storm clouds tops maximum height and vertical velocity calculation, allowing for entrainment and vertical wind shear

15 p2444 A71-31362

Onboard meteorological pulse radars for cloud formations detection, navigational aids, ground reference points determination and relief surveillance

15 p2371 A71-31920

Radiation attenuation volume coefficients for water clouds and fogs thermal sources and laser outputs

16 p2543 A71-33708

Percent-of-time distributions of attenuation by rain, clouds and atmospheric gases on earth-space paths at frequencies below 30 GHz

17 p2704 A71-35089

Model cloudy atmosphere construction, reviewing computational techniques for radiative transfer analysis

17 p2735 A71-35559

Radiative heat transfer in model water clouds by IR radiation, using method of discrete ordinates

17 p2735 A71-35560

Radiative transfer in terrestrial clouds, inferring colloidal state from measurements of multiple scattering angular and wavelength dependence

17 p2736 A71-35566

Orography, cloudiness and surface temperature effects in six-layer global atmospheric circulation model, giving January simulation data

17 p2770 A71-35804

Linearly polarized lidar light scattering in spherically symmetrical uniformly distributed cloud water drops, investigating multiple backscattering effects on depolarization

17 p2770 A71-35807

Combined lidar and radiometric techniques for high layer cumulus and cirrus clouds IR emissivity determination

19 p3089 A71-37501

Water and ice clouds spectral brightness coefficients in IR region of spectra from aircraft measurements

19 p3090 A71-37977

Soviet book on cloud electricity covering space charge and electrical characteristics

19 p3091 A71-38533

Physics of clouds and active effects - Soviet Conference, Tiflis, U.S.S.R., May 1969

19 p3091 A71-38679

Droplet clouds microstructure and phase state occurrence as function of temperature, size distribution and water content based on experimental data

19 p3091 A71-38680

Cloud condensation nuclei supersaturation spectrum and aerosol particle concentration variations with height

19 p3092 A71-38683

Electric charge generation in storm clouds, considering water droplets, ice crystals and air movements role in precipitation and charge separation mechanism

20 p3256 A71-39071

Atmospheric radiative energy budget based on structure and cloudiness distribution data from satellites and in situ observations

20 p3259 A71-39677

Earth surface characteristics measurements with remote sensors, proposing overland albedo measurements for clues as to ground type [clouds, vegetation, sand and snow]

20 p3260 A71-39684

Meteorological satellite IR imagery for calculating spectral values of cloudiness radiation contrasts against underlying surface background

20 p3261 A71-39689

Atmospheric physics of cloud formation, rain, hail and snow precipitation, discussing intracloud temperature variations electric fields and air impurities on water condensation

21 p3410 A71-40146

Soviet book on long wavelength radiative heat exchange in atmosphere covering radiation relationship to circulation, cloud formation and weather prediction

21 p3411 A71-40873

Turbulence energy balance and temperature pulsations in free atmosphere in presence of water phase transformation in clouds of given microstructure

21 p3412 A71-41394

Linear system model for multiple scattering light transmission through optically thick clouds, calculating optical effects by four dimensional linear superposition integral

22 p3575 A71-41789

APT weather satellite cloud pictures over sea southwest of Kyushu showing striated cloud pattern transformation into closed cellular pattern, discussing lower atmospheric layer moisture budget

22 p3568 A71-41859

Weather and climate modification, reviewing techniques for meteorological processes control, cloud and precipitation modification, ascending flow stimulation, etc

23 p3701 A71-43450

Electrooptical measurement of high altitude rain cloud droplets size, shape and distribution

23 p3676 A71-43507

Laser technique for runway and slant visibility range, lower cloud boundary and atmospheric damping coefficient

23 p3701 A71-43889

Vertical atmospheric humidity profile variations relationship to clouds water vapor content from thermal radio emission measurements onboard Cosmos 243 satellite

23 p3673 A71-44048

Cloud classification from various radar data independent characteristics, using statistical theory of Bayes hypotheses

24 p3844 A71-44878

Radio echoes from clouds and precipitation, determining detection threshold, station potential and statistical distribution numerical characteristics

24 p3844 A71-44879

Atmospheric attenuation effects on cloud and precipitation radar reflection coefficient

24 p3845 A71-44880

Cloud and precipitation effects on radio echoes intensity measurement, discussing pulse dimensions influence on average signal magnitude

24 p3845 A71-44881

Radio echo average power measurement errors due to clouds

24 p3845 A71-44882

Thunderclouds and torrential clouds classification from radar data, developing algorithm model with Bayes method

24 p3845 A71-44884

Radar vs visual observation of cloudiness and hazardous weather phenomena, emphasizing storm warnings

24 p3845 A71-44885

CLUMPS

Iterative clustering technique for minimizing probability of differences between binary data reconstructions from cluster codes and initial data

17 p2711 A71-35047

Lunar evolution theory, discussing terrestrial cluster dynamics during earth accumulation

24 p3870 A71-44811

CLUSTERS

U CLUMPS

CLUTCHES

High precision safety couplings performance, discussing flexible clutches enhancing effects

15 p2413 A71-31481

CLUTTER

Fluctuating radar target detection in clutter by sidelobe blanking system, discussing false alarm adaptive threshold procedure

07 p1154 A71-18842

Constant false alarm rate (CFAR) operation of airborne pulse Doppler radar in nonhomogeneous and point clutter, using similar critical region test

07 p1065 A71-20421

Frequency agile waveforms effects on detection and tracking radars performance, decorrelating distributed clutter echoes

08 p1253 A71-20798

Moving target indicator (MTI) performance improvement in presence of rain, chaff or other broadband clutter disturbances by adaptation for canceler setting optimization

08 p1254 A71-21338

Optimum antenna array processing design for target detection in nonuniform clutter background, using decision-theoretic processor with digital computer

08 p1256 A71-21604

Omnidirectional radar moving target detection from clutter, using Doppler filter system

09 p1407 A71-23047

Two-frequency moving target indicator Doppler radar system, predicting efficiency to clutter drift under stochastic echo and clutter signals

10 p1578 A71-24591

Vertical plane dual beam properties of doubly curved shaped reflector, considering surveillance radar antenna modification to improve performance with ground clutter

13 p2028 A71-27990

Radar target detection in nonGaussian sea clutter, calculating trimmed-mean detector performance under Rayleigh fluctuation

14 p2197 A71-30805

Clutter signals simulation with predetermined auto- and cross correlation, describing mathematical method for filter weighting function

16 p2541 A71-33424

IF nonlinearities effect on Gaussian clutter rejection associated with noncoherent MTI radar receiver

17 p2708 A71-35483

Resolution and clutter performance of simultaneous Doppler and acceleration measurement with coherent pulse trains

20 p3195 A71-38855

Doppler distortions of clutter and resolution performance of pulse trains with large time bandwidth products

20 p3195 A71-38861

Signal processing techniques for clutter suppression in moving target indicator radar

20 p3200 A71-39908

Radar systems performance constraints, discussing environmental effects, carrier frequency, aerial directivity, clutter echoes, transmitter power, etc

22 p3509 A71-42199

Model aspects of sea echoes and clutter unsteadiness on radar

22 p3514 A71-42470

COAGULATION

NT BLOOD COAGULATION

Two phase mixture nonequilibrium flow mathematical model with allowance for colliding droplets coagulation and atomization based on high speed photographic studies

10 p1551 A71-24380

Time decrease of acoustically irradiated aerosol concentration involving coagulation processes

17 p2784 A71-35347

Cloud particles coagulation kinetics, using integral equation for distribution function

19 p3095 A71-38704

Ice particles initial concentration effect on coagulation growth kinetics, considering distribution function variation with time

19 p3095 A71-38705

Co-Ni-Ti alloy intermittent decomposition kinetics observation by light and electron microscopy, noting finely divided phase coagulation

24 p3836 A71-44670

Two phase nonequilibrium flow mathematical model with allowance for colliding droplets coagulation and atomization based on high speed photographic studies

24 p3790 A71-44927

COAL

EPR spectra and spin-lattice relaxation time in coal pitch and polyvinyl chloride during low temperature carbonization

17 p2763 A71-35245

COALESCENCE

U COALESCING

COALESCING

Hydrodynamics of matter-antimatter in contact, discussing coalescence, particles annihilation pressure and energy balance

11 p1821 A71-25539

Droplet pair collision efficiencies and coalescence parameters, computing flow fields from nonlinear time dependent Navier-Stokes equations

17 p2770 A71-35805

COANDA EFFECT

Ground effect vehicles limiting volumetric dissipations from air cushion and propulsion systems with fluid boundary by Coanda effect

07 p1019 A71-19923

Two dimensional discrete fluidic element with Coanda effect, calculating switching discharge, jet gap and circulation zone length

09 p1386 A71-22654

Propulsion, guidance and stability of ground effect vehicle with perimetric Coanda fluid boundary

13 p1997 A71-29308

Fluid jets along curved or straight walls with non-zero external potential flow, analyzing Coanda effect

15 p3290 A71-32055

COARSENESS

Stability and coarseness of one- and two-channel invariant control systems for various forms of parameter deviations

12 p1893 A71-27340

Aluminum-aluminum nickelide rod eutectic composite elevated temperature stability, presenting coarsening kinetic analysis

21 p3398 A71-40469

COASTING FLIGHT

German monograph on linear theory of optimization problems for low thrust rockets covering orbital calculations, flight characteristics and Coast Arc problem

14 p2319 A71-30233

Branched space trajectory optimization by steepest descent method with coasting arcs, obviating numerical integration for accuracy increase and computing time reduction

23 p3725 A71-42985

COATING

NT ANODIZING

NT ENCAPSULATING

NT METALLIZING

YIG with thin piezosemiconductor coating, investigating transverse surface wave amplification and velocity

01 p0140 A71-11288

Backscatter from nonuniform dielectric coated cylinders in terms of inner surface admittance, using transmission line approach

09 p1410 A71-23515

Electron beam vapor deposited CoCrAlY coating composition optimization with ballistic impact and furnace/long term burner rig oxidation tests

14 p2257 A71-29636

Frequency dependent conductor coating matrices for lossy cylindrical conductors with circular section, using diffusion equation

20 p3197 A71-39450

COATINGS

- NT ALUMINUM COATINGS
- NT ANODIC COATINGS
- NT BIREFRINGENT COATINGS
- NT CERAMIC COATINGS
- NT ENAMELS
- NT ENCAPSULATING
- NT GLASS COATINGS
- NT GOLD COATINGS
- NT INORGANIC COATINGS
- NT MAGNETIC FILMS
- NT METAL COATINGS
- NT METALLIZING
- NT NICKEL COATINGS
- NT PAINTS
- NT PLASTIC COATINGS
- NT PRIMERS [COATINGS]
- NT PROTECTIVE COATINGS
- NT SPRAYED COATINGS
- NT THERMAL CONTROL COATINGS
- Discrete coatings, surface diffusion and thermomechanical surface treatments for metal fatigue strengthening
 - 01 p0099 A71-10169
- Test equipment for damping ability of vibration absorbing coatings on prismatic rods under pure bending, using electromagnetic vibration induction system and optical recorder
 - 03 p0396 A71-13417
- Cylindrical shell spacecraft thermal control coating system optimization, using truncated series representation [ASME PAPER 70-WA/AUT-13]
 - 03 p0499 A71-14151
- Si solar cells with titanium oxide antireflection coatings, discussing environmental test results
 - 05 p0700 A71-16064
- Si solar cells with antireflection titanium dioxide layer, comparing performance with conventional adhesive cover system
 - 05 p0700 A71-16065
- Si solar cell performance improvement from use of achromatic antireflective coatings
 - 05 p0701 A71-16077
- Beam splitter prisms with dielectric multilayer coatings
 - 06 p0907 A71-17534
- Optical properties of corundum for single and multiple layer antireflection achromatic coatings for IR below 5-6 microns
 - 06 p0898 A71-17537
- Two layer antireflection coatings on glass for He-Ne lasers, calculating optimal film thicknesses for various substrates and wavelengths
 - 06 p0907 A71-18038
- Integrating sphere coatings bidirectional reflectance characteristics, describing reflectometer data for smoked magnesium oxide and Au coated sandpaper samples [AIAA PAPER 71-77]
 - 06 p0902 A71-18534
- Solid state laser with different diffuse coatings on external reflector of pumping source, measuring energy output
 - 07 p1125 A71-19812
- Bolted joint assemblies under sustained loading, examining joint and fastener coating, bolt design and strength level and shear and tension stress effects
 - 08 p1371 A71-21412
- Selective optical coatings efficiency and thermal properties under solar radiation and radiative heat exchange
 - 09 p1510 A71-23418
- Spacecraft thermal control coatings for long duration exposure to near-earth orbital conditions, determining optical properties degradation and solar absorptance [AIAA PAPER 71-454]
 - 11 p1859 A71-26237
- Thermal conductivity and coating emittance measurements by stationary substrate heater method suitable for materials applied by flame vaporization
 - 15 p2512 A71-31501
- Carbide coating formation on graphite from vapor-gas phase, calculating thermodynamics and kinetics by digital computer for comparison with experiment
 - 15 p2438 A71-32143
- SiO antireflection coatings for GaAs injection lasers, discussing single layer quarter-wave coatings for loss minimization and bandwidth maximization
 - 16 p2585 A71-33136
- High angular resolution optical telescopes, considering mirror materials, optical coatings and pointing systems
 - 16 p2580 A71-33739
- Visual detection of stars in spacecraft environment, considering window cleanliness and antireflection coating effect on light scattering
 - 18 p2864 A71-36278
- Structure born noise reduction by viscoelastic coatings, examining effects of thickness, density, bending and shear induced loss factors, moduli and Poisson ratio [ASME PAPER 71-VIBR-29]
 - 21 p3414 A71-40284
- Substrate influence on circuit board conformal coatings electrical insulation resistance, discussing

test results with epoxy/glass and ceramic substrates and various coating materials

21 p3353 A71-40438

COAXIAL CABLES

- Complex permittivity and impedance of dielectric samples in coaxial lines and rectangular waveguides by moving probe and resonant Q factor measurements
 - 02 p0229 A71-11713
- Pulse response of unshielded coaxial umbilical cable connector mounted flush with missile skin
 - 10 p1585 A71-25072
- Undesirable electromagnetic interference minimization in electrical equipment by filtering, shielding, balancing lines, hot/neutral lines twisting and coaxial cables
 - 15 p2369 A71-31506
- Telecommunication developments covering coaxial cables, waveguides, error elimination, information theory, sound transmission and radars
 - 19 p3016 A71-37340
- Nonreflecting dielectric support washers design in coaxial-stripline junctions, calculating VSWR as function of dimensions and frequency
 - 19 p3019 A71-38335
- Coaxial cable antenna lead with shield or external conductor in form of slotted corrugated metal foil, testing performance
 - 20 p3197 A71-39469
- Hot-wire anemometer remote operation, discussing coaxial cable length, terminal connection and bridge current
 - 22 p3541 A71-41794
- Electromagnetic wave amplification using coaxial line matching with plasma waveguide by charged particle beam
 - 24 p3853 A71-44508

COAXIAL FLOW

- Two free homogeneous turbulent coaxial air jet mixing, showing mass transfer between boundary layers and interface presence
 - 02 p0185 A71-12409
- Nuclear light bulb reactor and coaxial flow reactor for gas core nuclear rocket engines [AIAA PAPER 70-708]
 - 03 p0456 A71-14427
- Parallel nonuniform supersonic flow of two coaxial gas jets past sphere
 - 03 p0345 A71-14562
- Supersonic flow past notch in lateral body surface or in two closely lying coaxial bodies, applying turbulent jet theory to separation zone
 - 04 p0528 A71-15626
- Near and far noise fields from coaxial interacting supersonic jet flows [AIAA PAPER 71-152]
 - 06 p0884 A71-18594
- Coaxial jets development and mixing in axisymmetric twisted turbulent ring air flow injected through inlets
 - 10 p1594 A71-24560
- Series solution for unbounded mixing of two incompressible homogeneous coaxial fluids with constant properties, using successive approximations method
 - 11 p1748 A71-25159
- Transonic gas flow measurement during sudden expansion from circular nozzle into coaxial cylindrical channel, emphasizing flow attachment
 - 13 p1993 A71-29192
- Coaxial free mixing flow calculations, using turbulent kinetic energy method
 - 21 p3369 A71-40958
- Volume fraction analysis of coaxial flow gas core nuclear rocket for mass flow ratios, fuel radius and density, using free jet computer code and eddy viscosity equations
 - 22 p3573 A71-41638
- Flow field generation by coaxial turbulent jets, determining velocity distribution, turbulence intensities and shear stresses by hot-wire anemometers
 - 23 p3627 A71-44198

COAXIAL PLASMA ACCELERATORS

- Plasma jet electron temperature and distribution behind pulsed coaxial accelerator exit section
 - 02 p0290 A71-12182
- MPD thruster, discussing electrodes, coaxial magnetic nozzle, accelerator and tests
 - 02 p0283 A71-12311
- Plasma jet two stage acceleration in coaxial systems, superposing additional discharge current
 - 07 p1167 A71-19234
- Pulsed coaxial plasma accelerator, measuring longitudinal gas pressure distribution, particle emission and magnetic fields characteristics under various operating conditions
 - 08 p1341 A71-21498
- Plasma jet two stage acceleration in coaxial systems, superposing additional discharge current
 - 12 p1934 A71-26752
- Equations system describing plasmoid acceleration process in coaxial injector with inductive energy storage
 - 12 p1938 A71-27205
- Plasma jet electron temperature and distribution behind pulsed coaxial electromagnetic accelerator exit section, studying time variation
 - 15 p2454 A71-31490

Pulsed coaxial plasma accelerator, measuring longitudinal gas pressure distribution, particle emission and magnetic fields characteristics under various operating conditions

16 p2618 A71-33046

Coaxial electrodynamic plasma acceleration, investigating triple electron and ion recombinations effects

19 p3108 A71-37129

Dense plasma focus conjectured as short finite two dimensional Z pinch forming near or at end of coaxial plasma accelerator

19 p3116 A71-38248

Equations system describing plasmoid acceleration process in coaxial injector with inductive energy storage

19 p3117 A71-38617

COAXIAL TRANSMISSION

U COAXIAL CABLES

U TRANSMISSION

COBALT

NT COBALT ISOTOPES

NT COBALT 60

Liquid Fe, Co and Ni atomic distributions investigation by X ray diffraction

04 p0612 A71-15036

Highly ionized line spectra of Fe, Co, Ni and Cu belonging to Na I and Mg I isoelectronic sequences

05 p0717 A71-16909

Co oxidation rate measurements over temperature range 475-1325 C at various oxygen pressures, determining oxide formation kinetic law and activation energy

07 p1139 A71-20225

Oscillopolarographic determination conditions for Co, Ni, and Fe, giving statistical treatment of results

09 p1454 A71-22501

Thermomagnetic modulated Kerr effect readout and magneto-optical laser recording at high output on cobalt base metallic films

10 p1613 A71-25108

Dispersion hardened Co strength and plasticity temperature dependence, determining Ti and Nb carbides additives effects

15 p2434 A71-32237

Cobalt and lanthanum with face and body centered lattices, studying plastic deformation during allotropic transformations under sliding friction and gripping

16 p2584 A71-33895

Graphite solubility in Co and Ni, discussing solution energies and entropies

19 p3081 A71-37723

COBALT ALLOYS

Tensile and stress rupture tests of Co base alloy bars extruded from prealloyed powders made by Ar gas atomization

01 p0100 A71-10480

Crystalline structural changes during decomposition of supersaturated solid solution of Ta in Co

01 p0101 A71-10608

Decomposition structure of supersaturated solid solution in Co-Nb alloy, showing beta phase transformation inhibition

01 p0101 A71-10671

High strength and plasticity maraging steels of Fe-Ni-Co-Mo system, noting surface crack sensitivity in tension

01 p0103 A71-11071

Monograph on cobalt base superalloys covering mechanical properties relation to microstructure, carbides, heat treatment, aging, intermetallic precipitation and dislocation

05 p0765 A71-16198

Co-ti alloy hardness recovery, noting dependence on solid solution structure after low temperature aging

05 p0768 A71-16855

High strength multiphase Co-Ni-Cr-Mo alloy hardening, noting deformation and aging induced strengthening

06 p0913 A71-18098

High strength and plasticity maraging steels of Fe-Ni-Co-Mo system, noting surface crack sensitivity in tension

08 p1305 A71-21036

Ordered states effects on mechanical properties of Va-Co-Ni ternary alloys, considering creep behavior difference between ordered and disordered structures

08 p1309 A71-21526

Co-Ni-Cr-Mo alloys hardening mechanisms, noting martensitic transformation role

08 p1312 A71-21551

Co-Cr-W alloy systems equilibrium and precipitation effects, investigating microstructural properties at elevated temperatures

08 p1314 A71-21569

Co base superalloys fracture toughness microstructural aspects, considering effects of interdiffusion carbides and carbide precipitation on aging at elevated temperatures

08 p1314 A71-21572

Matrix stacking fault energy effects on steady state creep rate of recrystallized nickel-cobalt-aluminum oxide alloys, showing stress dependence

08 p1315 A71-21578

Paired dislocations after high temperature deformation in precipitation hardened Co-Ti alloy
08 p1315 A71-21582

Heat resistance in air of Co-Cr alloys as function of chemical composition
08 p1317 A71-21763

WC-Co system binder phase composition and properties, studying W content as function of initial carbide grain size, Co content, sintering and quenching time
09 p1466 A71-22170

Thermal fatigue tests of high temperature Ni and Co base alloys by fluidized bed technique
09 p1469 A71-22812

Discontinuous decomposition and aging kinetics of supersaturated solid solutions of tungsten in cobalt, comparing to precipitation theories
09 p1469 A71-22848

Al-Co alloys, investigating Al and Co intermediate phases formation effect on X ray emission K spectra
09 p1474 A71-23234

Dispersion hardened Ni and Co alloys production by powder metallurgy, noting elastic distortion due to particle strengthened base material
09 p1474 A71-23294

High temperature austenitic steels, Ni and Co alloys machining, considering deformation resistance and strain hardening
09 p1456 A71-23297

High temperature Fe, Co and Ni alloys for gas turbine components, considering tensile and creep rupture strength increase by thermal mechanical processing
09 p1475 A71-23298

High temperature Ni and Co alloys powder metallurgy, discussing production, preparation, pressing and sintering
09 p1456 A71-23300

High temperature Ni and Co alloys for stationary gas turbines and jet engine parts, considering microstructure and mechanical behavior under stress and temperature
09 p1475 A71-23302

Ni-Co strained alloy, examining coercive force as function of annealing time at various temperatures
09 p1475 A71-23313

Co-Cr and Ni-Cr eutectic alloys with single crystal TaC fiber reinforcement, discussing unidirectional solidification
09 p1479 A71-23623

Ternary compositions for high temperature alloys Ni-Cr-Al and Co-Cr-Al, using superimposed oxidation data on phase diagrams/oxide mapping/
10 p1625 A71-23972

Manganese and silicon effects on oxidation and scale mechanisms of Co-Cr alloys, using thermogravimetric, metallographic and microprobe techniques
10 p1625 A71-23973

Cast cobalt base superalloys extrusion and forging, noting hot deformation effects on tensile properties, stress rupture strength and ductility
11 p1778 A71-25854

Monovariant eutectic Co-Cr-C ternary systems, determining pseudobinary and near-pseudobinary phases by differential thermal and microprobe analyses and optical microscopy
11 p1780 A71-26025

Magnetization discontinuities in cobalt-rare earth particles at discrete imperfection levels as function of chemical, mechanical and heat treatment, noting Co-Y rectangular loop
12 p1943 A71-26861

Ti-Co-B and Ti-Re-B systems diagrams of isothermal sections at 800 and 1400 C
13 p2083 A71-28008

High strength corrosion resistant multiphase Co-Ni-Cr-Mo alloys with fcc structure hardened to hcp by mechanical deformation
13 p2084 A71-28148

Discontinuous phase decomposition increase in Co-Ni-Ti alloys by plastic deformation and Al additions, indicating grain boundary diffusion control
14 p2258 A71-30003

Potentiometric measurement of temperature effects on electrical resistance and Hall effect in Ni-Co alloys
14 p2259 A71-30188

Magnetic properties of sintered cobalt-rare earth alloy magnets using Sm, Pr, La or Ce misch metal for microwave device applications
14 p2284 A71-30703

Magnetic properties measurement of Co-rare earth permanent magnets, using Nb-Sn superconducting solenoid
14 p2284 A71-30704

Hysteresis loop measurements and functional measurements correlation on periodic permanent magnet stacks of TWT ring magnets of Sm-Co alloy
14 p2285 A71-30705

Molten Co-Cr alloy structural transitions at increasing temperatures, relating to change in solid state with increasing Cr content
15 p2425 A71-31393

Molten Co-Sn alloys, detailing vaporization rate, vapor pressure and partial and integral isothermal and isobaric formation potentials
15 p2425 A71-31394

Ni-Co alloys electrical resistivity dependence on temperature after mechanical and thermal treatments
15 p2429 A71-31994

Nickel and cobalt pseudobinary eutectic alloys reinforced by refractory metal monocarbides whiskers, studying mechanical properties, solidification and phase equilibria
15 p2432 A71-32169

Ternary Co-Cr-Al alloy oxidation data, detailing kinetics, products, mechanisms, resistance behavior and rate
16 p2589 A71-32870

Ternary Co-Cr-Al alloy oxidation resistant composition selection, using oxide maps superimposed on phase diagram
16 p2590 A71-32872

Wrought precipitation hardened Co-base alloy, investigating Ti and Al additives effects on tensile and stress rupture strengths, microstructure and fabricability
17 p2758 A71-35147

Co-Cr-W alloy sulfidation at high temperatures, performing weight gain, metallographic X ray and electron probe analysis
17 p2758 A71-35149

Ni-Co alloy fine structure under plastic deformations, determining stacking fault energy effects with X ray diffraction lines
19 p3076 A71-37119

Tungsten carbide-cobalt alloys, investigating binder metal mechanical properties relationship to composition by chemical analysis and X ray inspection
19 p3083 A71-38475

Solid Ni-Co and Ni-Cu alloys, investigating hydrogen solubility
21 p3398 A71-40466

Co-Ni alloy interdiffusion coefficient determination as function of concentration by magnetic transformation effect
21 p3399 A71-40700

Ferromagnetic Co phase nondestructive determination in hard powdered-metal alloys by permanent magnet ponderomotive force measurement based on relationship to ferromagnetic alpha phase
22 p3561 A71-41775

Co-Mn binary alloy phase diagram redetermination, noting sigma phase formation after heavy deformation
23 p3689 A71-42933

Al-Co and Al-Ni alloy rods unidirectionally solidified, discussing compositional range in eutectic structures at high solidification rates
23 p3689 A71-43101

Cavitation damage resistance of Fe, Ni and Co alloys in liquid sodium and mercury
23 p3692 A71-43906

Mo and Co alloying effects on high temperature chromium ball bearing steels contact strength
23 p3692 A71-44037

Mo additions to Co rich ductile permanent magnet alloys, obtaining higher coercive forces and energy products
23 p3694 A71-44283

Ni-Co maraging steels with improved combination of mechanical and magnetic properties at elevated temperatures
24 p3836 A71-44441

Tensile and creep rupture strength and microstructure of Co-Fe-Ta alloys at elevated temperatures
24 p3836 A71-44442

High temperature aging, structural stability and tensile properties of hot rolled Co-W heat resistant alloy for space applications
24 p3836 A71-44443

Co-Ni-Ti alloy intermittent decomposition kinetics observation by light and electron microscopy, noting finely divided phase coagulation
24 p3836 A71-44670

Hydrogen solubility in liquid Cr, Ni and Co alloys containing Si for various concentrations and temperatures
24 p3840 A71-45371

COBALT COMPOUNDS NT COBALT OXIDES

Magnetostriiction in cobalt and nickel-cobalt ferrites from room temperature to 300 C
15 p2426 A71-31514

COBALT ISOTOPES NT COBALT 60

Co 59-neutron reaction tensor spin-spin potential, using polarized targets of Ho 165 and Co 59 for nuclear spin-spin effect measurement
18 p2949 A71-36681

COBALT OXIDES

Cobalt 60 oxides as thermionic fuels, discussing high temperature properties, fabrication and irradiation techniques
02 p0280 A71-12256

Lanthanum cobalt oxide as potential auto exhaust catalyst from studies of activity in gas phase
07 p1055 A71-19545

COBALT 60

Cobalt 60 oxides as thermionic fuels, discussing high temperature properties, fabrication and irradiation techniques
02 p0280 A71-12256

Mouse Ehrlich ascites tumor cells, examining Co-60 gamma ray influence in presence of radiosensitizing 5,8-dihydroxypsoralen
07 p1035 A71-18953

Large cobalt 60 gas cooled radioisotope heat source, including test loop, operations, control and safety
20 p3265 A71-38937

Radioisotopic power applications of beta and gamma emitting Co 60, noting powder ceramic fabrication of dense wafers for irradiation to convert natural Co 59
20 p3265 A71-38938

COCHLEA

Rodents bimodal cochlear microphonic response to high frequencies recorded from round window membrane
01 p0016 A71-11346

Cochlear sensory epithelium and Corti organ degeneration after noise exposure in guinea pigs and cats, using scanning electron microscopy
02 p0199 A71-12364

Inner ear basilar membrane motions estimation for lower hearing threshold, using nonlinear model
02 p0201 A71-12474

Cochlear nerve fibers two tone inhibition as signal suppressions inherent to bandpass nonlinearities, using modified analog model and mathematical analysis
05 p0712 A71-16280

Cochlear auditory patterns degrees of freedom along spatial axis, considering displacement of basilar membrane and mechanical coupling
05 p0706 A71-16281

Cochlear/vestibular apparatus, ganglion cells, spinal roots and nerve trunk damage from ionizing radiation based on neural elements transirradiation in neoplasms
10 p1566 A71-25039

Direct electrical stimulation of musculus tensor tympani on click elicited responses in cochlea and cochlear nucleus
13 p2003 A71-27832

Repetitive stimulation effects on auditory evoked potentials in cochlear nucleus, inferior colliculus and medial geniculate body of unanesthetized cats
13 p2012 A71-28892

Acoustic nerve, cochlear nucleus and superior olivary complex central projection, investigating ascending auditory system organization
14 p2183 A71-30255

Cochlear nucleus and posterior clivus neurons impulse activity due to tonal signals in anesthetized cats auditory system
16 p2532 A71-33899

Physiological mechanisms of human auditory attention, measuring changes in cerebral cortex averaged evoked potential and cochlear nerve response
17 p2693 A71-35575

Intracochlear electric potential of anesthetized cats recorded with potassium filled glass micropipets, determining magnitude and phase of responses
20 p3191 A71-39768

COCKPIT SIMULATORS

C-5 military transport stability augmentation for pitch and yaw inertia at low speed, using pilot evaluation on cockpit simulator
02 p0190 A71-12684

Moving cockpit flight simulator design with force and rotational acceleration vectors at pilot head location
03 p0396 A71-13343

Cockpit simulator motion effects on ILS approach pilot guidance errors, using Erdmann model [DGLR-70-071]
05 p0779 A71-15956

Link 747 simulator design and operation, describing cockpit layout, motion picture system and malfunction insertion and display unit
06 p0881 A71-18665

Boeing 747 crew members training program, describing ground training, classrooms, inertial navigation system and cockpit trainers [SAE PAPER 710473]
13 p1996 A71-28339

Flight crew training ground school programs, featuring automated instruction in cockpit classroom with audio visual machines [SAE PAPER 710478]
13 p2017 A71-28343

Aircraft-simulating cockpit procedure trainer statistical data and development problems concerning safety, economy and efficiency performance
15 p2384 A71-31883

COCKPITS

Combat aircraft cockpit temperature control system design and operation
01 p0004 A71-10270

Airline experience with dual inertial systems as sole means of navigation, considering equipment reliability, cockpit design, training, etc
01 p0124 A71-10509

Aerospace Recommended Practice criteria for flight deck crew escape systems applicable to all commercial aircraft propulsion systems, design speeds and payloads
[SAE-ARP-808A] 07 p1019 A71-19646

Jet aircraft flight decks pressurization, tobacco smoking and carbon monoxide levels, discussing potential dangers
09 p1400 A71-23247

Anthropometry for aircraft cockpit and pressure suit design compatible with mission requirements
11 p1724 A71-26115

Armored cockpit for attack aircraft combat effectiveness, including mold line tumbling plates, terminal ballistic kinematics and integral structural armor
[ALAA PAPER 71-778] 17 p2675 A71-35530

Civil aircraft cockpit lighting evaluation guidelines
19 p2999 A71-38241

Display devices in aircraft cockpit providing pilots with information from various sources, considering head-up display and CRT
21 p3376 A71-40113

CODES

Traffic capacity of Gaussian communications channel with Rayleigh fading, examining code transmission coefficient under discrete control mode
03 p0378 A71-13394

PAM/FM radio telemetry coder including electronic commutator for sampling and sequential time control, discussing design, operation, performance and reliability
06 p0870 A71-18399

Algorithms for constructing minimized abstract automatic subunits and two switch types as basis for arbitrary linear block encoder
13 p2035 A71-28915

Parallel pressure multiplexer and encoder for aerodynamic testing, employing zero pressure detectors coupled with IC digital electronics and reference pressure signal
14 p2222 A71-30342

Computer controlled encoding device with laser flying spot scanning for automatic photographic image measurement
17 p2741 A71-34998

Ternary delta modulation evolution from binary system by addition of encoder-analyzer, calculating SNR
20 p3202 A71-39468

CODES

Matched filter output response computation for combined Barker codes, considering Doppler mismatch
04 p0551 A71-15013

Explicit formulas for Euclidean geometry and Berlekamp subcodes weight enumerators for second order binary Reed-Muller codes
14 p2209 A71-30828

Decoding of linear codes combinations for non-identical domains of correct reception, noting dependence on signal structure
17 p2702 A71-34973

Iterative clustering technique for minimizing probability of differences between binary data reconstructions from cluster codes and initial data
17 p2711 A71-35047

Three phase code transformation task reliability and correlation, representing general factor analytic intellectual abilities and personality characteristics
20 p3192 A71-39073

Ternary code and three value logic in digital computers, considering economic advantages, signal distinguishability and numerical interpretation of p digit abstract alphabet
22 p3516 A71-41856

CODING

NT DECODING

NT REDUNDANCY ENCODING

NT SIGNAL ENCODING

Touch sensitive X-Y position encoder for computer display input using surface wave piezoelectric transducer
01 p0047 A71-10214

Instruction Set Design System /ISDS/ program for computer order code selection
01 p0047 A71-10217

Output format coding for telemetry data compressor channel and frame identification
01 p0036 A71-10984

Weak magnetic field measurement using magnetometer with digital technique time coding
02 p0247 A71-11722

Multiplex spectrometer for eclipse spectra photoelectric observation, using pseudorandom binary sequences as encoding pattern
03 p0424 A71-13634

Digital asynchronous information transmission, describing schemes for coding binary into ternary signals
05 p0724 A71-17058

Phase shift measurement by digital encoding via time interval, angle of rotation and voltage conversions
06 p0876 A71-18076

Catastrophic error propagation and minimum weight codewords in convolutional codes
07 p1069 A71-20417

Lower bounds for minimum weight of binary cyclic code vectors of composite length, using factorization
08 p1324 A71-21321

Transform coding techniques using orthogonal matrices to implement bandwidth or dimensionality reduction for image processing in digital communication systems
08 p1259 A71-21591

Holographic method for coding and decoding three dimensional information
13 p2067 A71-28443

Coding for feedback communication system with additive white Gaussian noise, using mean-square estimation error
13 p2034 A71-29379

Communication satellites unique word coding with algorithm, reducing false detection probability by error correlation technique
14 p2201 A71-30926

Recorder circuit quick response enhancement in Grey code pulse counter, realizing parallel decoding in binary digits at high speeds
15 p2374 A71-31294

Discrete and continuous channel stochastic coding processes and resulting communication system properties
15 p2372 A71-32320

Random images transmission rates, comparing line-by-line and two dimensional encoding
16 p2541 A71-32819

Visual search performance as function of color coding for information location tested on aeronautical charts
17 p2689 A71-34703

Incoherent radiation distribution analysis by image multiplex coding with SNR gain applied to IR region [ONERA-TP-972] 18 p2916 A71-36031

Hadarnad transform source encoding application to Apollo unified S-band telemetry links, considering possible system performance improvement
18 p2876 A71-36470

Serial binary multiplication computation speed, considering recoding algorithm with cellular array multipliers
18 p2894 A71-36829

Impulse skin temperature encoding in primate cutaneous thermoreceptors in dynamic thermal conditions
18 p2860 A71-36877

Flying spot digitizer angle encoding system, describing multispeed transducer output conversion to digital format
18 p2925 A71-36914

Failure analysis of memory organization in self repair memory system, using various coding and modularization techniques on subsystems
21 p3350 A71-40365

Presentation modality as encoding variable in short term memory, obtaining mean recall score as function of trials
23 p3639 A71-43113

Elastic surface waves bi-phase modulated encoding and decoding at 10 Mbit/sec using Y-cut quartz
23 p3645 A71-43436

Code conversion and coincidence circuits design for positional digital control systems with combinatorial code producing feedback elements
24 p3805 A71-45154

COEFFICIENT OF FRICTION

Elastic body-vibrating surface interaction, examining friction coefficient under various modes
01 p0088 A71-10626

Gear drives operating in vacuum conditions, calculating friction coefficient with dimensional analysis
02 p0258 A71-12598

Friction coefficient in anti-friction polytetrafluoroethylene compounds with lead, bronze or graphite
02 p0275 A71-12600

Hollow annular inserts for stress concentration and alternating stress range reduction around holes in thin flat plates, taking friction coefficient into account [ASME PAPER 70-DE-L] 03 p0506 A71-13706

Film thickness effect on solid powdered graphite, molybdenum disulphide and calcium fluoride lubricants friction coefficients
07 p1116 A71-18998

Multicomponent gas laminar boundary layer equations, deriving asymptotic formulas for friction coefficient, concentration, temperature and diffusion flows
07 p1089 A71-19734

Service life of solid molybdenum sulfide based plastic coatings with different binders under high vacuum friction investigated by mass spectroscopy
09 p1454 A71-22819

Arbitrary direction harmonic vibration effects on kinetic friction coefficient between sliding bodies
11 p1767 A71-25267

Friction and wear of steels, Ti, Al, Cu and copper beryllium in sliding over hardness range of steel plates in vacuum and air
11 p1771 A71-26143

Boron or phosphorus doping of silicon, noting microhardness increase and friction coefficient reduction
12 p1911 A71-26820

Friction coefficient and wear of steel in vacuum and air at low and room temperatures
13 p2072 A71-27870

Plane Couette flow with suction/injection at stationary plate, obtaining motion and continuity equations, pressure distribution and friction coefficient
13 p2047 A71-28520

Lead bronze and Babbitt metal composite material, detailing anti-friction efficiency and wear resistance in bearings
15 p2417 A71-32666

Copper on copper friction coefficient dependence on oxygen pressure, investigating exoelectron emission from differently oxidized copper surface layers
18 p2928 A71-36750

Heat transfer to transpired turbulent boundary layer, reviewing theoretical models and experimental results for friction coefficient and Stanton number [ASME PAPER 71-HT-44] 19 p3166 A71-38003

Mean velocity profile and wall friction coefficients of perturbed turbulent boundary layer on flat plate
21 p3366 A71-40511

Mechanical and frictional properties of sintered copper matrix glass compacts, considering lubricating or seizure preventing effects of glass presence
21 p3406 A71-40759

Surface roughness and mass transfer influence on boundary layer and friction coefficient for turbulent flow over flat plate
21 p3371 A71-40997

Centrifugal compressor bladeless diffuser parameters, flow kinematics and energy losses, noting effects of friction coefficient and expansion angle
23 p3662 A71-43551

Temperature effects on niobium carbide friction process in vacuum conditions, considering surface layer microhardness and X ray and metallographic analyses
23 p3692 A71-44030

Temperature dependence of external friction coefficient between high-melting carbides in vacuum at constant normal load and slipping rate
24 p3830 A71-44863

COEFFICIENTS

NT ACCOMMODATION COEFFICIENT

NT AERODYNAMIC COEFFICIENTS

NT ATTENUATION COEFFICIENTS

NT COEFFICIENT OF FRICTION

NT COHERENCE COEFFICIENT

NT CORRELATION COEFFICIENTS

NT COUPLING COEFFICIENTS

NT DIFFUSION COEFFICIENT

NT DISCHARGE COEFFICIENT

NT FLOW COEFFICIENTS

NT HEAT TRANSFER COEFFICIENTS

NT INFLUENCE COEFFICIENT

NT IONIZATION COEFFICIENTS

NT NOZZLE THRUST COEFFICIENTS

NT RECOMBINATION COEFFICIENT

NT REGRESSION COEFFICIENTS

NT SCATTERING COEFFICIENTS

NT STRUCTURAL INFLUENCE COEFFICIENTS

Linear homogeneous nth order ordinary differential equations reduction to equations with constant coefficients by transformation of independent variables
01 p0110 A71-10317

First exchange energy inhomogeneity term numerical coefficient approximate derivation
07 p1164 A71-19690

Jacobi series coefficient relation to convergent series sum singularities in lemniscate bounded domain
07 p1149 A71-20643

Te coefficient for frequency doubling with pulsed carbon dioxide lasers, considering peak second harmonic generation conversion efficiency due to absorption of fundamental
18 p2933 A71-37011

Quasi-fluid mechanical formulation generation for ionized gases dispersive transport coefficients by linear dynamic response function technique
21 p3423 A71-40800

Extracting coefficients of nonlinear differential equations from data on oscillating systems, using time derivative methods
21 p3409 A71-41015

COENZYMES

NT CYTOCHROMES

Acetyl-coenzyme A synthetase in aerobic yeast cells localization in microsomal fraction by density gradients
14 p2187 A71-31003

COERCIVITY

Magnetoelectric anisotropy and low temperature annealing effects on coercive force of ferromagnetic Fe-Ni foils
01 p0138 A71-10669

Hard metals and WC-Co alloy stress and heat treatment effect on coercive force, crack formation energy and abrasive resistance
06 p0911 A71-17342

Ni-Co strained alloy, examining coercive force as function of annealing time at various temperatures

09 p1475 A71-23313

Base metal impurity effects on coercive force and contact properties of miniature multilayered diffused reed switches

13 p2038 A71-28837

Lattice defect mechanism for high coercive force remanence production in meteorites and lunar samples by cosmic ray exposure

14 p2308 A71-29913

Bloch-wall Permalloy films coercive force effects on low frequency creep, using high resolution Bitter pattern observation technique

15 p2461 A71-32003

Mn-Ge solid solutions coercive force and magnetization, investigating temperature dependence and heat treatment effects

21 p3432 A71-41264

Ferrite coercimeter with attached electromagnet and compensation winding, deriving analytical expressions for demagnetization and compensation currents

22 p3521 A71-41767

Mo additions to Co rich ductile permanent magnet alloys, obtaining higher coercive forces and energy products

23 p3694 A71-44283

COESITE

Coesite-stishovite content in Ries crater nonporous crystalline rocks of variable composition and degree of shock metamorphism

19 p3050 A71-37660

COGNITION

Redundancy information effect on human performance in forced pace cognitive tasks under overload stimulus presentation rates

16 p2536 A71-33679

Human violent exercise burst effect on cognitive task, noting mild hypoxia irrelevance to skills decrements

17 p2686 A71-35436

COHERENCE

Q switched monomode ruby laser coherence length measurements, using holography at various beam intensities

01 p0096 A71-11374

Laser data on coherence and radiance, deriving from manufacturer specifications for application selection

02 p0261 A71-12325

Gaussian shaped laser pulse holographic brightness analysis, presenting theoretical and experimental holographic coherence length curves for Q switched laser oscillator and amplifier system

08 p1290 A71-21390

Wave structure and mutual coherence functions of optical wave propagating in turbulent atmosphere, considering signal to noise ratio

10 p1641 A71-23948

Second-order degree of coherence measurement by compact wave front shearing interferometer

16 p2577 A71-33131

Single mode ruby laser spatiotemporal coherence characteristics with emission moment controlled by Q switch operating on modulated ultrasonic traveling waves

23 p3683 A71-43395

Spatiotemporally coherent pulsed Ne and Ti vapor lasers superradiation, showing coherence time dependence on pulse length and gas pressure

23 p3683 A71-43395

COHERENCE COEFFICIENT

Multiple acoustic evoked responses coherence time course using mathematical correlation and Fourier transforms

05 p0714 A71-16922

He-Ne laser coherence measurement by Young interference method, noting dependence on resonator mirror alignment

07 p1127 A71-20378

Holographic evaluation of low power ruby laser emitted wave spatial coherence factor via fringe visibility measurements

23 p3679 A71-43894

COHERENT ACOUSTIC RADIATION

Active synthetic aperture coherent imaging technique to fill and double diameter of sparsely sampled aperture array

22 p3574 A71-41783

Coherent acoustic wave propagation speed and attenuation coefficient in turbulent flow

23 p3703 A71-43209

COHERENT ELECTROMAGNETIC RADIATION

NT COHERENT LIGHT

Coherent binary reception channels noiseproof qualities in presence of fluctuating noise and single concentrated bursts

01 p0030 A71-10473

Real noise stability of coherent FM receiver for case of spectrum limited signals due to passage through channel and selective networks

07 p1061 A71-19508

Doppler geodetic measurements, discussing ionospheric wave diffraction errors, refractive index and electromagnetic wave propagation

11 p1732 A71-25831

Radio interferometry techniques and instrumental advances, examining transionospheric waves coherence properties and ionospheric source distribution

13 p2031 A71-28783

Cosmic radio emission coherent generation mechanism, involving derelativization and relativization of particles in small space

15 p2483 A71-31343

Coherent electromagnetic excitation of optical transition levels by fluorescence measurement, obtaining dipole moment and relaxation times

18 p2929 A71-35903

Radio pulses from pulsars based on model of coherent synchrotron radiation from magnetosphere trapped charged particles

20 p3285 A71-39951

N-type In-Sb continuous coherent microwave oscillation under transverse magnetic field, discussing helical frequency instability on threshold and growing wave conditions

22 p3586 A71-42347

Cosmic radio emission coherent generation mechanism involving derelativization and relativization of particles in small space

22 p3606 A71-42618

Ionospheric integral electron concentration data from Elektron 1 and 3 satellites, using coherent radio wave measurements

24 p3866 A71-45028

COHERENT LIGHT

Frequency stability of molecular beam laser with stimulated coherent emission

01 p0093 A71-10681

Coherent optical data processing system imaging qualities photographic film requirements

01 p0050 A71-10900

Truncated periodic targets modulation in partially coherent light, deriving diffraction image formulas

02 p0260 A71-12146

Spatial and temporal coherence effects in holography, giving general formula for reconstructed virtual image

02 p0251 A71-12148

Coherent light wave propagation in two level system, discussing wave periodicity, deviation from sinusoidal form, interaction with medium and energy loss and gain effects

02 p0215 A71-12319

He-Ne laser light beam double slit experiments, investigating multimode operation effect on spatial coherence

03 p0440 A71-14177

Two point resolution in Fourier holography with partially coherent recording and illuminating light

03 p0429 A71-14180

Partially coherent laser beam phase fluctuations using reversing-front interferometer for time integrated irradiance measurement, considering atmospheric turbulence effects

04 p0627 A71-15683

Surface roughness determination by spatially coherent laser light speckles correlation and spectral distribution on film records

04 p0609 A71-15689

Coherent light propagation guidance by helicoidal guide, calculating transverse electric field distribution for luminous beam variations

05 p0722 A71-16705

Coherent light photoelectric detection probability in background light passing through narrow band filter of rectangular or Lorentz frequency characteristics

07 p1059 A71-18848

Coherent noise elimination in coherent light imaging systems by time averaging noise concentrations through lens rotation about optical axis

07 p1107 A71-19208

Coherent optical data processing principles, discussing lens, diffraction, focused wave front, intensity vs amplitude and spectrum analyzer

07 p1067 A71-19627

Coherent optical data processing techniques, discussing diffraction phenomena, spectral analysis and holography

07 p1067 A71-19629

Organic dye lasers flash lamp pumped system for tunable coherent light production in visible and near IR spectrum

07 p1125 A71-19796

Frequency stability of molecular beam laser with stimulated coherent emission

07 p1125 A71-20142

Semiconductor injection lasers, discussing energy characteristics of state density distribution, coherent emission, etc

07 p1126 A71-20252

Coherent optical target recognition through phase distorting medium, using holography, Fourier transform and autocorrelation functions

08 p1335 A71-21377

Strongly coherent Nd doped glass laser development by decreasing cavity Fresnel number, discussing maximized radiance and infrared output

09 p1465 A71-23564

Direct optical measurements of strains, using spatially coherent light with moire technique

10 p1611 A71-24280

Mutual coherence effects in time varying radiation fields on two beam interferometric optical discrimination response

11 p1800 A71-26306

Higher order laser light coherence effects on photoelectron distribution detected by third order photoeffect

12 p1913 A71-26961

Spacecraft attitude measurement using spatial coherence of laser or star light beam, discussing feasibility and detection equipment

12 p1927 A71-27429

Focused laser coherent light beam expansion in turbulent atmosphere

13 p2080 A71-29016

Combined heterodyning, beam forming and cross correlation of broadband multichannel signal from multidimensional phased array, using coherent optical system

14 p2241 A71-30142

Laser radiation source time and spatial coherence effect on brightness distribution of image produced by hologram

15 p2402 A71-31254

Fourier transform holography with partially coherent light from incoherent quasi-monochromatic source, considering bias problem

15 p2402 A71-31256

High gain parametric generation of coherent light in ammonium dihydrogen phosphate crystal continuously tunable across visible spectrum with UV harmonic of Nd-YAG laser

15 p2420 A71-32383

Elastic materials Poisson ratio measurement by moire method in coherent and incoherent light

16 p2575 A71-32825

Insufficient spatial and temporal coherence effects on holographic image reconstruction by injection laser, noting application to optical data processing

16 p2577 A71-33142

Quantitative measurement of speckle contrast for illumination with laser oscillating simultaneously in multilongitudinal modes on rough surface, determining coherence length

16 p2589 A71-34130

Two dimensional pictorial information Fourier transform generation by coherent optics method, applying to imageries in earth sciences

17 p2737 A71-34271

Coherence properties deterioration of laser beam by atmospheric molecular scattering, considering effect on communication system performance

17 p2753 A71-34426

Picosecond duration coherent light pulse propagation in resonant medium, discussing basic equation, self induced transparency, Bloch equations, soluble model and higher conservation laws

17 p2754 A71-35375

Spatial coherence measurement for two points of pseudothermal light source by comparing photocathode luminous intensity probability density and photoelectron distribution moments

17 p2754 A71-35585

High coherence Q switched spatially filtered Nd-glass laser operating in fundamental mode for high power

17 p2754 A71-35747

Partially spatially coherent illumination influence on measurement of correlation function of two dimensional patterns, obtaining formula for optical filtering

18 p2929 A71-35973

High resolution holographic image deburring methods involving coherent optical analog processing and Fourier transform division filter

18 p2918 A71-36079

Coherence in image plane of incoherent optical system, considering illumination conditions and component impulse response

18 p2920 A71-36104

Coherent optical fields properties, discussing equivalence of quantum and classical descriptions

18 p2932 A71-36959

Two dimensional objects three dimensional image possibility based on self-reproduction effect for arbitrary periodic distribution function of transparency, using coherent light source

19 p3064 A71-37770

Photosystem resolution of coherent laser illuminated objects, discussing experimental investigation of image quality dependence on relative aperture

19 p3073 A71-38194

Image visual observation in coherent diffuse illumination, discussing human eye angular resolution deterioration and depth vision threshold dependence on light characteristics

19 p3074 A71-38195

Fourier transform holograms as complex matched filter for pattern recognition and signal detection in coherent optical systems

19 p3066 A71-38239

Long object photography with lens array in non-coherent light and subsequent integrated image focus holography in laser beam for reconstruction in white light

19 p3068 A71-38708

Laser beam spatial coherence properties dependence on transverse mode structure for given longitudinal mode

20 p3245 A71-39350

Pseudotransfer function for interference contrast of coherent illuminated phase edge object

20 p3245 A71-39427

Ultrarapid color holography using continuous synchronized coherent light sources of different wavelengths

21 p3378 A71-40514

Far field light diffraction due to circular plane wave apertures rendered partially coherent by atmospheric turbulence

21 p3415 A71-40635

Coherent optical processing system coupled to electronic readout system incorporating image orthicon TV camera, small digital computer and cell generator

21 p3381 A71-40929

Light flux spatial coherence in visual reception, considering aventurine spots perception as point light source

21 p3344 A71-41065

Computer synthesis of holograms and spatial filters for coherent optical data processing systems, noting large computational volume required for three dimensional objects

22 p3539 A71-41746

Real time coherent optical data processing, describing spatial filtering and reactive processor and image converter designs

22 p3540 A71-41750

Visible coherent radiation generation mechanism in ionized oxygen and nitrogen, considering free radical stabilized on discharge tube wall and metastable atom creation

23 p3706 A71-42889

Collimated light beam transmission in turbulent atmosphere above ground surface, comparing measured coherence function with calculation

23 p3645 A71-43565

Holographic evaluation of low power ruby laser emitted wave spatial coherence factor via fringe visibility measurements

23 p3679 A71-43894

Laser beam spot dancing during propagation through turbulent atmosphere, using Kolmogoroff structure function of refractivity and geometrical optics

24 p3834 A71-45208

COHERENT RADAR

Coherent laser synthetic aperture radar at microwave frequencies for airborne ground point target mapping

02 p0215 A71-12044

Coherent optical system for range and azimuth ambiguity simulation in radar systems

04 p0551 A71-15010

Ground based coherent radar synthetic aperture procedure against uniform velocity targets, discussing airborne holographic synthetic gain applications to stationary antennas

09 p1405 A71-22697

Synthetic aperture Doppler free coherent bistatic radar for high resolution maps of tropospheric radio scatterers

12 p1881 A71-27286

Target movement effects on airborne coherent side-looking synthetic aperture imaging radar during scan rate and compression ratio increases

14 p2197 A71-30798

Coherent microwave holographic radar systems, discussing mono and bistatic versions, far field performance, pulse compression techniques and signal processing

22 p3540 A71-41751

COHERENT RADIATION

NT COHERENT ACOUSTIC RADIATION

NT COHERENT ELECTROMAGNETIC RADIATION

NT COHERENT LIGHT

Coherent optical sources in form of lasers and parametric oscillators with usable power for communications

02 p0260 A71-12002

Coherent radiation mechanisms characterizing cosmic masers in molecular lines, sporadic solar radio emission and pulsar radiation

03 p0486 A71-13321

Coherent emission mechanisms for pulsar models, discussing plasma wave conversion into radio emission

04 p0650 A71-15582

Squaring loops for establishing coherent carrier reference for bi-phase PSK modulation, deriving optimal presquaring filter

05 p0730 A71-17075

High power continuous and pulsed coherent radiation generation by gas lasers, discussing transmission by proton generators and transforming engines [AIAA PAPER 71-106]

06 p0946 A71-18557

Phase locked automatic direction finder /ADF/ flight test results, indicating signal to noise threshold reduction by coherent detection

07 p1057 A71-18815

Incomplete separation influence of composite signal components on noise stability of coherent communication systems

07 p1064 A71-20257

Dominant diagrams of renormalization method in coherent random wave propagation

07 p1065 A71-20322

Coherent radiative phenomena with nontrivial zero-pi pulses propagation behavior in attenuating media

08 p1334 A71-21194

Approximate photocount statistics for superposition of coherent and chaotic radiation of Gaussian, triangular, square and Lorentzian shaped spectra

09 p1462 A71-22686

Scalar wave equation of mutual coherence propagation in turbulent medium with stochastic permittivity using local independence approximation

10 p1641 A71-24398

Carbon dioxide laser coherent radiation in IR region from Young double slit interference experiments, noting emergent beam spatial phase shift

10 p1622 A71-24959

Type 2 and 3 solar radio burst generation, proposing coherent synchrotron electron deceleration mechanism

12 p1954 A71-27710

Pulsed lasers coherence measurements by holographic techniques, considering high fraction of near field pattern with appreciable coherence

15 p2419 A71-31255

Refraction and absorption length of coherent laser radiation propagating in high temperature cylindrical plasma column

15 p2458 A71-32390

High resolution microdensitometry image interpretation and manipulation by digital computer, discussing radiation coherence problems

17 p2742 A71-35002

Coherent neutral sheet radiation from pulsars, examining relationship between pulsation-driving energy source and mechanisms for pulsed emission

18 p2958 A71-36928

Coherent stimulated recombination radiation emission by p-type cadmium silicon arsenide single crystals in liquid nitrogen cryostat under various pumping levels

21 p3431 A71-41229

Flat modulation transfer functions obtained by spatial filtering of high aspect ratio annular apertures images in coherent optical processor

22 p3549 A71-42552

He-Ne laser coherent radiation photodetection by variable diaphragm photomultiplier, analyzing photocurrent spectra as function of diaphragms aperture size and shape

23 p3687 A71-44175

COHERENT SCATTERING

Positive pions coherent production by negative pions with aid of nuclear photoemulsions

03 p0461 A71-13853

Stacking fault formation in Nb deformed by filing, determining coherent scattering regions with X ray diffraction

12 p1917 A71-27299

Positive pions coherent production by negative pions with aid of nuclear photoemulsions

22 p3579 A71-42654

COHERENT SOUND

U COHERENT ACOUSTIC RADIATION

U SOUND WAVES

COHERENT SOURCES

U COHERENT RADIATION

U RADIATION SOURCES

COHERENT TRANSMISSION

U COHERENT RADIATION

COHESION

Fcc metals cohesion strengths, using fracture technique with subsequent cold welding

02 p0267 A71-12879

Elasticity theory two dimensional contact problems, examining cohesion or friction in contact area

03 p0513 A71-14229

Cohesive strength of metal coatings obtained by simultaneous vacuum condensation of strengthening phase and matrix material vapors

07 p1130 A71-19157

Cohesive strength of flame sprayed metallic coatings of various thicknesses

08 p1297 A71-21064

Electron structure of transition metals defects, using self consistent method to match resonance and drift integrals to cohesion energy

11 p1808 A71-26342

Adhesive strength of metal coatings obtained by simultaneous vacuum condensation of strengthening phase and matrix material vapors

17 p2760 A71-35655

Polymethyl methacrylate samples resistance to crack propagation, detailing modulus of cohesion effects

24 p3841 A71-45050

COHOMOLOGY

U HOMOLOGY

COILS

Automatic regulators of wire tension during coil winding

07 p1108 A71-19310

Wide range nonimmersive RF coil with marginal oscillator for plasma electrical conductivity measurements tested for simulated reentry vehicle

12 p1908 A71-27285

Steam turbine blades induction brazing with programmed cycle, describing coil design

19 p3070 A71-38315

Design parameters optimization for flat spiral coils printed on dielectric substrates based on equivalent circuit analysis, emphasizing coil shape effects on Q and inductance

22 p3520 A71-41715

COINCIDENCE CIRCUITS

Fluidic coincidence position sensors, using wall attachment amplifiers and nozzle displacement

07 p1030 A71-20601

Charge sensitive low power amplifier and fast coincidence system for solid state detectors and random counting rates in Skylab application

08 p1267 A71-21849

Radio particle correlation of extensive air showers at large zenith angles, using twofold coincident 44 MHz receiver trigger-scintillator system

13 p2127 A71-28108

Coincidence adders with digit by digit alteration of direct and inverse signals, discussing synthesis and reliability

15 p2376 A71-32183

Code conversion and coincidence circuits design for positional digital control systems with combinatorial code producing feedback elements

24 p3805 A71-45154

COINING

Aircraft structure fatigue life improvement via material stress coining inside and around holes and slots

01 p0085 A71-10170

COKE

Graphitizing and nongraphitizing substances carbonization, observing cokes chemical structure changes and thermal decomposition

15 p2368 A71-32733

COKE AIRCRAFT

U AN-24 AIRCRAFT

COLD ACCLIMATIZATION

Shivering and heat polyneuropathy threshold temperature shift in guinea pigs, considering thermal adaptation under cool environment exposure

03 p0364 A71-14250

Muscular heat production effect on contraction during cold adaptation tests

05 p0710 A71-16806

Chemical thermoregulation muscular electricity activity during shivering and thermoregulation tonus change after cold adaptation, discussing oxygen consumption rise

10 p1564 A71-24486

Sympathetic nervous system in short term adaptation to cold, observing oxygen consumption, urinary noradrenaline proportion and excretion

17 p2681 A71-34698

Thyroidectomy and cold adaptation effects on hibernating hamsters thermoregulation and heat transfer coefficient

18 p2860 A71-36881

Skeletal muscles shivering thermogenesis during cold adaptation, investigating thermoregulation effects on organ and system heat production

18 p2862 A71-36895

Tissular and cellular biological resistance as indices for organism resistance to adverse effects, noting increase due to muscular training and cold adaptation

20 p3187 A71-39219

Altitude and cold acclimatization effects on human basal heart rate, blood pressure, respiration and breath-holding

21 p3330 A71-40349

Cold pressor response tests under altitude acclimatization and simultaneous hypoxic acclimatization and cold in man

22 p3502 A71-41831

Elevated basal metabolism in man under simultaneous altitude hypoxia and cold acclimatization

23 p3636 A71-44239

COLD CATHODE TUBES

NT PHOTOMULTIPLIER TUBES

Ion sources with oscillating electrons, discussing operating principles and characteristics of sources with cold and incandescent cathodes and Penning ionization chamber

08 p1343 A71-22043

Continuous cold cathode forward wave reentrant beam crossed field amplifiers with cut-off electrode, investigating AM and PM noises and phase coherence 11 p1739 A71-26434

Inertialless glow discharge ignition in triatron controllable crossed field cold cathode tube, comparing with magnetic coil initiation 19 p3028 A71-37785

COLD CATHODES

CW carbon dioxide lasers low voltage excitation, using cold cathode transverse glow discharges 03 p0436 A71-13642

Cold cathode ionization gages dynamic pressure response as function of gas pulse mean speed and gas type, using magnetron test measurements 10 p1610 A71-24182

Cold cathode pulsed gas laser construction with glass plasma tube allowing operation with oxygen and variety gases 14 p2255 A71-30882

He-Ne laser discharge tube using water cooled mercury cathode with supplementary molybdenum anode 19 p3073 A71-37789

VLF plasma oscillations in spherical magnetized cold cathode DC discharge, determining frequency relationship to current/voltage, gas pressure, magnetic field strength and cathode diameter 20 p3273 A71-38880

Electric parameters of cold hollow cathode discharge and effect, controlling electron free paths by electric or magnetic field 23 p3710 A71-43276

COLD DRAWING

Fiber textures formation in polycrystalline Zr from cold forging and cold drawing, observing fully developed recrystallization 10 p1629 A71-25028

Fiber strengthening of Cu-Fe-Cr wire by cold drawing and annealing, discussing age hardening process of chromium ferrite needles in ductile Cu matrix 13 p2088 A71-29402

Spherulitic linear polyethylene rod cold drawing, observing fibrous structure formation by light and electron microscopy and X ray scattering 19 p3084 A71-37650

COLD FLOW TESTS

Open cycle gas core nuclear rocket engine, considering reactor critical experiments and cold and hot flow tests [AIAA PAPER 71-641] 14 p2273 A71-30718

Cold flow tests of mixing and atomization characteristics of gas/liquid circular coaxial injector elements in pressurized facilities [AIAA PAPER 71-672] 14 p2291 A71-30736

Gaseous oxygen/gaseous hydrogen auxiliary propulsion engines, considering cold flow experiments with nonreactive simulant gases [AIAA PAPER 71-673] 14 p2291 A71-30737

Gaseous oxygen/hydrogen injector element modeling based on composition profile measurements for cold flows [AIAA PAPER 71-674] 14 p2291 A71-30738

Gas injectors characteristics investigation by cold flow simulation, using flow field visualization techniques and velocity and mass concentration profiles measurements [AIAA PAPER 71-675] 14 p2291 A71-30739

Dual Flex nozzle concept, discussing design equations derivation, cold flow testing, fabrication and static tests [AIAA PAPER 71-749] 14 p2296 A71-30843

Cold flow analysis of liquid propellant sprays from rocket engine injectors, relating propellant mixing and combustion performance 15 p2465 A71-32044

COLD FORMING

U COLD WORKING

COLD GAS

Collision free ionizing wave propagation into cold low density ionized gas, showing wave oscillations damping due to ion velocities phase mixing 07 p1171 A71-20289

Pneumatic and hydraulic fluidic power control systems, discussing moving part position servos and cold gas reaction systems 07 p1028 A71-20585

Extraterrestrial Lyman alpha radiation source attributed to solar Lyman alpha scattering on cold interplanetary hydrogen penetrating to inner solar system 09 p1526 A71-23462

Cold combustible gas mixture ignition temperature at flat plate forward stagnation point, investigating inert gas concentration, activation energy and first Damkohler number effects 17 p2837 A71-34436

Cold gas rocket propulsion systems design parameters, determining performance and weight formulae 21 p3437 A71-41050

COLD HARDENING

Dissolved hydrogen effects on mechanical properties, modulus of elasticity, lattice constants and X ray lines of Ti alloys, showing cold brittleness at high strain rates 07 p1130 A71-19298

Cold prestraining effect on steady state creep strength and rate of precipitation hardened heat resistant steel 09 p1477 A71-23331

Recrystallization of heat treated Fe-Ni alloys microstructures after hammer hardening 16 p2598 A71-34051

COLD PLASMAS

Structure and propagation of large amplitude modulated isolated compression waves in cold three component plasma with negatively charged ions 01 p1332 A71-10676

Self similar unsteady waves in cold plasma containing magnetic field, determining plasma oscillations 01 p1335 A71-11095

Collisionless damping of electromagnetic waves in regions with strong homogeneity of cold plasma 02 p0291 A71-12509

Electrostatic wave growth rates in anisotropic medium with or without cold plasma 03 p0464 A71-13532

Far field diffraction of unidirectional surface wave by conducting rectangular wedge in cold anisotropic plasma, showing frequency dependent transmission coefficient 03 p0465 A71-13953

Nonlinear electron beam bunching in zero temperature plasma during modulation by two frequencies, using klystron model 04 p0631 A71-14625

Low temperature weakly ionized molecular plasma kinetic equation in electric field, considering free electron distribution function for molecule-electron inelastic collisions 04 p0634 A71-15114

Surface wave conversion to longitudinal oscillations near strong discontinuity in resonant cold magnetoactive plasma 06 p0937 A71-18355

Vacuum spectrum modification theory for inverse Compton scattering in cold collisionless plasma 07 p1165 A71-18855

Cold bounded nonuniform magnetoplasma harmonic generations model for small collision frequencies 07 p1166 A71-18889

Magnetoactive cold plasma wave interaction theory, investigating energy transfer 07 p1167 A71-19230

Low temperature confined cesium plasma, observing ion-acoustic oscillation excitation effects on transfer process and ionization 07 p1167 A71-19236

Structure and propagation of large amplitude modulated isolated compression waves in cold three component plasma with negatively charged ions 07 p1170 A71-20138

Input impedance of cylindrical and helical antennas in cold lossy magnetoplasma, discussing sensitivity to current distribution 07 p1065 A71-20323

Low temperature plasma radiation transfer equation, discussing constraints to applicability in real radiation transfer problems 08 p1339 A71-21055

Self similar unsteady waves in cold plasma containing magnetic field, determining plasma oscillations 08 p1342 A71-21953

Homogeneous equilibrium low temperature dense helium plasma ionization composition and radiative energy losses, calculating ionization potential 09 p1501 A71-22380

Low temperature plasma electron velocity distribution function perturbation due to exothermal chemical reactions 09 p1501 A71-22389

Electromagnetic wave propagation through bounded time-space periodic cold plasma under plane wave incidence, calculating transmitted and reflected components 09 p1503 A71-22986

Soviet papers on low temperature plasma physics covering production and diagnostic techniques, electrokinetic and optical characteristics, electromagnetic and shock effects, metal plasmas, etc 10 p1648 A71-24188

Cold Hg plasma in composite HF and magnetostatic field near electron cyclotron resonance, obtaining electron and ion energy spectra 10 p1650 A71-24527

Steady state streaming of cold magnetospheric plasma in magnetic equatorial plane near plasmopause 10 p1650 A71-24557

Nonhomogeneous plane parallel cold plasma flows in external magnetic field, deriving energy transfer between two sliding plasmas 10 p1651 A71-24634

One dimensional Gaussian electrostatic wave packet nonlinear time development due to weak resonant broad beam introduction into cold uniform plasma 10 p1652 A71-24658

Variable density cold inhomogeneous plasma small amplitude free electrostatic oscillations investigation by Green function of differential equation 10 p1652 A71-24662

Magnetohydrodynamic Kelvin-Helmholtz problem in Hall plasma, discussing case of hot unmagnetized fluid juxtaposed to cold magnetized plasma 10 p1653 A71-24664

Electromagnetic wave conversion into plasma waves in cold anisotropic plasma with two dimensional inhomogeneity 10 p1654 A71-24893

Metastable atom destruction, collision-radiative recombination and electron heating in low temperature decaying helium plasmas, using spectroscopic resonance line measurements 10 p1654 A71-24896

Magnetospheric cold plasma dispersive and amplifying combined effects on pearl elements spectral shape, considering wave packet propagation applications 11 p1730 A71-25543

Magnetoactive cold electron plasma wave interaction theory, investigating energy transfer 12 p1934 A71-26748

Low temperature confined Cs plasma, observing ion-acoustic oscillation excitation effects on transfer process and ionization 12 p1935 A71-26754

Electron beam high frequency modulation effects on hot ions production in cold plasma 12 p1938 A71-27207

Low temperature plasma collisional-radiative ionization and recombination coefficients, discussing nonequilibrium factors affecting electron density change rate 12 p1939 A71-27270

Cold plasma convection production by ion driven LF drift instability, noting tokamaks and stellarators stabilization 13 p2104 A71-27850

Electron density distribution determination from microwave resonant frequencies of parallel plate cavity containing cold, collisionless, isotropic plasma 13 p2105 A71-27994

Circular thin glass tube waveguide containing cold cylindrically stratified plasma, calculating electromagnetic wave propagation 13 p2029 A71-28499

Cylindrical microwave cavity partially containing cold nonuniform plasma enclosed by quartz tube, calculating resonant frequency by exact, multiterm and series methods 13 p2029 A71-28500

Low temperature plasma radiation transfer equation, computing problems with absorption coefficient accounting for re-emission 14 p2280 A71-30168

Soviet monograph on wave propagation in cold and hot magnetoplasmas covering particle collisions, plasma control and instability and plasma-particle interactions 14 p2280 A71-30246

Low temperature plasma MHD waves propagation in inhomogeneous magnetic fields, comparing numerical solutions with experimental results 14 p2282 A71-30559

Satellite measurements of cold plasma density and plasmopause in magnetosphere, comparing Whistler, Langmuir probe and ion trap data 14 p2237 A71-30951

Electromagnetic wave energy absorption in inhomogeneous cold magnetoactive plasma cylindrical columns 15 p2455 A71-31735

Ion cyclotron harmonic waves development in simulated low density and temperature space plasma, determining propagation upper and lower bounds 15 p2491 A71-32448

Ion motion effect on first order oscillations in infinite homogeneous two-component cold plasma in constant magnetic field and circularly polarized external field 15 p2459 A71-32651

Radiation from electrostatic waves in thin current sheet in geomagnetic tail into cold magnetized plasma, noting wave damping for wide frequency range 16 p2562 A71-32805

Plasma chemistry, discussing low and high temperature plasmas, nuclear fusion reactions and chemical molecular and nuclear synthesis 16 p2539 A71-32963

Low temperature plasma reactions, discussing electron impact and collisions, ion formation, molecular excitation and thermal dissociation, vibrational relaxation, recombination, etc 16 p2539 A71-32964

Low temperature plasma chemical processes, investigating molecular and atomic ionization, reactions under equilibrium and nonequilibrium conditions and specific energy production 16 p2540 A71-32968

Quasi-neutral inhomogeneity /particle cloud/ in collisionless hot or cold plasmas without magnetic field 16 p2619 A71-33521

- Electron-ion recombination and ambipolar diffusion disruption of electron density in cryogenic helium plasma, using cavity resonator measurements 16 p2619 A71-33648
- Van Allen radiation belts and plasma sheet energy loss control, using cold plasma injection 16 p2629 A71-33976
- Nonthermal electron population of energy levels in cool dense helium afterglow for small principal quantum number, using Saha equation and optical spectroscopy techniques 16 p2620 A71-34044
- Cold plasma flow rate determination from emission inhomogeneities, using time of flight method and high speed streak photography for instantaneous velocity measurements 17 p2787 A71-34286
- Slot antennas electromagnetic radiation patterns in conducting ground plane coated with moving isotropic cold plasma sheath 17 p2701 A71-34758
- Charged particles elastic interaction and recombination in low temperature weakly ionized potassium plasma 19 p3109 A71-37135
- Plasma guns hot and cold plasma separation, describing diverter operation principles 19 p3112 A71-37639
- Linear and nonlinear two-stream instability under relative motion between cold plasma components from Hamiltonian derivation for plasmons 19 p3112 A71-37744
- Electrical microwave probe for measuring HF potential oscillations in low temperature plasma 19 p3064 A71-37787
- Flow around obstacle in plasma with ions cold relative to electrons and with directed subsonic, considering relative density measurement 19 p3115 A71-38207
- Radiation resistance of small filamentary loop antenna in cold collisionless uniform multicomponent magnetoplasma, assuming uniform current distribution along loop 19 p3023 A71-38594
- Electron beam HF modulation effects on hot ions production in cold plasma 19 p3117 A71-38619
- Numerical procedure for electromagnetic field penetration through inhomogeneous cold plasma slab with collisions, using Riccati type differential equation 20 p2273 A71-39004
- Electromagnetic wave conversion into plasma waves in cold anisotropic plasma with two dimensional inhomogeneity 21 p3425 A71-41273
- Metastable atom destruction, collision-radiative recombination and electron heating in low temperature decaying helium plasmas, using spectroscopic resonance line measurements 21 p3425 A71-41276
- Electron beam heating of cold plasma in magnetic trap as function of plasma density, showing two stream instability due to Cerenkov effect 21 p3425 A71-41285
- Nonlinear electron beam bunching in zero temperature plasma during modulation by two frequencies, using klystron model 22 p3583 A71-42265
- Steady state transition layer between cold solar plasma flow and geomagnetic field in one dimensional model 22 p3536 A71-42622
- I-V characteristics of weakly ionized cold plasma plane layer with electron-atom collisions 22 p3584 A71-42875
- Dense low temperature Ar and Hg plasmas, observing correlation between electrical conductivity and optical emission 23 p3712 A71-43914
- Strong magnetic field effects on acoustic oscillations and instability in stationary inhomogeneous low temperature plasma flow in crossed fields 23 p3712 A71-43917
- Low temperature plasma radiation flux heated absorbing fluid, investigating convective heat transfer to semitransparent wall 24 p3856 A71-44893
- Zero temperature relativistic plasma ground state energy calculation using Fermi momentum and Green function 24 p3857 A71-45115
- COLD PLATES**
U COLD SURFACES
COLD ROLLING
Multilayer composites preparation by cold rolling packets of alternating Al and Sn foils, determining tensile strength relation to layer thickness 02 p0264 A71-12278
- Metal shaping process during angle steel ream-type rolling, determining metal particles velocity fields, strain energy and total metal pressure on rollers 02 p0257 A71-12566
- Groove depth /residual deformation/ in vibrational rolling of Ti cylindrical samples, considering impression force, cylinder and steel spheres diameters 02 p0258 A71-12641
- State definition international standardization for cold rolled Al sheets, examining yield curves and strain energy 05 p0764 A71-15923
- Structure changes of Al single and polycrystals with initial cube orientation under cold rolling 06 p0913 A71-18420
- Nb single crystals structure and properties after cold rolling and annealing, determining crystallographic parameters of plastic deformation 13 p2086 A71-28579
- Cold rolled recrystallized Ni-Fe alloy, considering short range order structure effect on elastic limit 13 p2087 A71-29264
- Structural disorientation dependent recrystallization of cold rolled and annealed Mo single crystals 14 p2258 A71-30006
- Hot rolled powder metallurgy Mo, noting texture during annealing and cold rolling 15 p2425 A71-31396
- Neutron irradiated Mo single crystals polygonization after cold rolling, using X ray topology methods 16 p2596 A71-33886
- Pressure distribution during cold rolling of metallic powders of stainless steels, iron, titanium and copper, using dynamometer mounted in roll 19 p3075 A71-37107
- COLD STRENGTH**
Cr-Si steels cold shortness tests, identifying low temperature failure mechanisms 01 p0098 A71-10082
- Cold hardened Cr-Si steels strength/plasticity thermal dependence and brittleness from short torsion and compression tests, identifying low temperature failure mechanisms 16 p2593 A71-33638
- Cast electron-beam remelted Mo, investigating carbon and zirconium carbide additions effects on structure and low-temperature plasticity 18 p2937 A71-36723
- Mo alloy under impact tests, investigating notch sharpness effects on cold shortness threshold and strength 23 p3693 A71-44231
- COLD SURFACES**
Near separation flow in laminar compressible boundary layer on cold wall near zero skin friction, suggesting added terms for previous expansion 02 p0332 A71-12378
- Gas removal from system by condensation onto cold surface /cryopumping/, noting pumping speed, ultimate pressure and applications 20 p3270 A71-39248
- COLD TOLERANCE**
Skin temperature and metabolism changes magnitude, duration and variability in unacclimatized male subjects during cold stress 02 p0208 A71-12836
- Mammalian tolerance to low body temperatures, discussing limits to spontaneous unassisted recovery and recovery assisted with reanimation and resuscitation procedures 07 p1041 A71-19523
- Halophilic bacteria growth in freeze-thaw environment, investigating cooling and warming rates and solute concentrations 09 p1388 A71-22131
- Cold environment exposure effect on mouse resistance to infection with Klebsiella pneumoniae 16 p2528 A71-33115
- Human temperature tolerance during exposure to hot and cold environments, using skin temperature as indicator 18 p2859 A71-36875
- Convective and conductive heat loss analysis of underwater swimmers and divers exercising in cold water 18 p2861 A71-36892
- COLD TRAPS**
Liquid nitrogen cold trap for oil diffusion pump 05 p0757 A71-16232
- Lunar surface rocks Hg content under daytime temperatures volatilization conditions, considering cold trap and lunar atmosphere 12 p1958 A71-26692
- COLD WALLS**
U COLD SURFACES
U WALLS
COLD WATER
Arterial blood and muscle lactates in cold water swimming rats indicating reduced circulation endurance factors 09 p1396 A71-23360
- COLD WEATHER**
Cold climate clothed human windchill tables, considering various heat transfer modes and skin temperature 20 p3192 A71-39205
- COLD WEATHER TESTS**
Traumatic vasospastic disease in forest workers with Raynaud phenomena, considering cold vasodilation and occupational vibration vasoconstriction by finger blood circulation tests 05 p0708 A71-16616
- Cold pressor response tests under altitude acclimatization and simultaneous hypoxic acclimatization and cold in man 22 p3502 A71-41831
- COLD WELDING**
Fcc metals cohesion strengths, using fracture technique with subsequent cold welding 02 p0267 A71-12879
- Self adhesion in relay contacts, discussing cold weld conditions and prevention by dry oxygen addition 13 p2074 A71-28835
- COLD WORKING**
NT COLD ROLLING
NT EXPLOSIVE FORMING
Cr steel cyclic strength and elastic properties after combined high temperature thermomechanical treatment and cold working 09 p1471 A71-23079
- Cold and hot working effects on Al alloys elastic properties, discussing crystallographic systems reference points 10 p1628 A71-24822
- Fiber textures formation in polycrystalline Zr from cold forging and cold drawing, observing fully developed recrystallization 10 p1629 A71-25028
- Annealed and cold-worked polycrystalline Fe specimens steady state cyclic stress-strain curves and thin films observation by electron microscopy 11 p1780 A71-26024
- Temperature dependence of flow stress of cold worked heavily deformed doped W 11 p1781 A71-26296
- Cold worked pure Mo recrystallization kinetics, indicating dependence on deformation mode and techniques 15 p2433 A71-32177
- Carburizing steels cold forging, investigating pressure requirement relationship to compressive stress from comparison of backward extrusion and laboratory compression tests 18 p2935 A71-36669
- Cold work peak characteristics in undeformed aged niobium-nitrogen alloys from internal friction spectrum 20 p3252 A71-39464
- Microstructural characteristics of Fe-Ni alloy plastic deformation at 20-500 C during cold and hot rolling, noting intergranular shear processes 21 p3402 A71-41095
- COLLAGENS**
Rat liver and lung collagenase activity Circadian rhythm, noting maximum enzyme activity in early morning and minimum during afternoon and early evening 13 p2010 A71-28788
- Energy metabolism disturbance effect on dissolved and undissolved collagen fractions content of aorta connective tissue 17 p2679 A71-34223
- Collagen and elastin transmedial gradients in human aortas as function of age, discussing relationship to atherogenesis 18 p2858 A71-36751
- Optical second harmonic generation in excised tissues by Q switched ruby laser irradiation, observing narrow band emission line in collagenous tissues 22 p3559 A71-42567
- COLLAPSE**
Runaway pulsar formation and ejection in supernova collapse, fragmentation, condensation, radiation and disruption 04 p0643 A71-15046
- Thick walled noncircular cylinders shape showing full plasticization at collapse 04 p0673 A71-15885
- Computerized nonlinear collapse analysis of elliptical cylinders and cones under axial compression 05 p0823 A71-16555
- Limit analysis of dissipation power and collapse load of rigid perfectly plastic continua with piecewise linear yield surface, using linear programming 17 p2816 A71-34324
- COLLECTORS**
U ACCUMULATORS
COLLIMATION
Laser beam reflection from arbitrary geometric surface, considering reverse problem of response of flat or curved mirror to incident collimated light 18 p2929 A71-36055
- Auroral X rays passage through atmosphere, discussing integral spectral measurements with collimated and omnidirectional detectors 22 p3593 A71-42399
- Collimated laser beam angular deviation in turbulent near earth atmosphere, comparing with interferometric data 23 p3685 A71-43506
- COLLIMATORS**
Stellar spectrograph with image converter, obtaining optimal ratio between telescope and collimator diameters 04 p0589 A71-14833

Autocollimation control of telescope rotation axis positioning at arbitrary azimuths 04 p0565 A71-14854

Optics and metrological characteristics of optimal photoelectric autocollimators 06 p0897 A71-17535

Rotating modulation collimator as astronomical X ray camera, discussing data reduction techniques for image synthesis 07 p1109 A71-19455

USAF Camera Calibration Facility, describing precision multibank collimator for measuring focal length, distortion, prism effect, fiducial center and other camera parameters 08 p1272 A71-21258

Lateral separation focus sensors for high angular resolution optical systems, reviewing autocollimating optics and operational patterns 10 p1644 A71-25090

Operating principles of spaceflight simulators, considering star coordinates errors in collimator simulator of stellar sky 19 p3062 A71-37150

Optimal radiant source power for photoelectric two axis autocollimation angle trackers, considering detector threshold sensitivity 19 p3067 A71-38659

Wanshaff vertical circle flexure determination at Goloseyev, using collimator tube, plane mirror and autocollimation ocular 23 p3680 A71-44262

Automatic collimator for measuring tube lateral deflection in universal astronomical instruments 24 p3829 A71-45300

COLLINEARITY

Antiplane stress distribution around single or collinear cracks in nonwork hardening elastoplastic material under uniform load 07 p1212 A71-19350

COLLISION AVOIDANCE

American ATA prototype aircraft collision avoidance equipment and proposed noncooperative system 01 p0125 A71-10753

ATC automation, using conflict prediction algorithm based on airspace assignment to aircraft entering system 02 p0278 A71-11698

ATA Collision Avoidance System based on time and frequency synchronization via ground stations or other aircraft 02 p0280 A71-12895

Collision avoidance system flight test and evaluation program for airline industry CAS specification 02 p0280 A71-12896

Air traffic control using collision risk equations, noting data handling automation, airborne collision avoidance devices and geostationary satellites 04 p0624 A71-15646

Bird strikes incidence and prevention, discussing velocity effects, migration role and uses of distress calls, falconry and radar 06 p0848 A71-18664

Aircraft midair collision avoidance, discussing Elimination Range Zero system operation procedures and cost 07 p1154 A71-19079

Three-phase time-ordered functional organization for ground based collision avoidance, discussing information flow, display capability and dynamic simulation model [AIAA PAPER 71-240] 07 p1155 A71-19716

Airline collision avoidance system test and evaluation program, considering range, rate and altitude accuracy, communications reliability, synchronization and system integration with air traffic control 08 p1331 A71-21167

Aircraft collision avoidance dynamical system, determining barriers between possible capture regions by optimal control problem solution 08 p1331 A71-21322

Digital simulation facility for airborne collision avoidance system effects on ATC terminal automation, discussing operation, hardware and software equipment 10 p1590 A71-24774

Two flash threshold measurement of comparison stimulus duration of Bloch law for anticollision strobe lights 11 p1725 A71-26116

Midair collisions analysis for civil-military integrated ATC air space, discussing near miss volume, random heading aircraft density and pilots evasive action vs avoidance percentages 12 p1927 A71-27599

Radar avoidance action logic for converging aircraft safe passage, discussing near miss and collision situations 12 p1927 A71-27600

Time-frequency anticollision system for dangerous aircraft detection and avoidance using stable atomic clocks [ONERA-TP-938] 15 p2445 A71-31875

Helicopter radar equipment for obstacle avoidance in all-weather low altitude flight, describing components installation, cockpit display and controls 15 p2446 A71-31919

Time and frequency synchronization for EROS airborne collision avoidance system, considering impact on aeronautical communication, navigation and surveillance [CASI PAPER 72/17] 19 p3100 A71-37604

Canadian Forces experiments on aircraft flashing lights covering warning signals, navigation and anticollision displays and autokinetic phenomenon 22 p3499 A71-41491

Strobe lighting for aircraft midair collision hazard reduction, comparing Collision Avoidance System and Pilot Warning Indicator effectiveness 22 p3499 A71-41493

Aircraft anticollision flashing lights, discussing current practices within national and international air traffic regulations regarding flash frequency, color and light sources 22 p3483 A71-41499

COLLISION RATES

Chemically interacting gases transfer properties at varying temperatures, determining collision parameters by viscosity, diffusion coefficients, molecular beam scattering and vibrational relaxation time 02 p0286 A71-12186

Electron transfer in ion microscope field ionization, analyzing band and periodic surface structure effects, ionization probability and collision formalism 02 p0288 A71-12734

Atomic collision chains in bcc crystal, determining energy loss relation to temperature by computer model with/without perfect lattice thermal oscillations 04 p0630 A71-15103

Helicopter fuselage design for crashworthiness under specific conditions 04 p0532 A71-15416

Collisional effects on Taylor and Kelvin instabilities in composite medium, considering longitudinal wave propagation mode 05 p0788 A71-16627

Collision effects on temporal plasma wave echoes, using free particle model 05 p0790 A71-16661

Hard-sphere gas three-particle collision integrals, using binary collision expansion 05 p0785 A71-16704

Ionized gases quantum transport cross sections and collision integrals, considering energy and temperature ranges for attractive and repulsive screened Coulomb potentials 07 p1224 A71-20283

Nitrogen molecules vibrational excitation effect on elastic collisions frequency in nitrogen plasma 10 p1646 A71-23819

Diffusion and acoustic ion waves in weakly ionized plasma as function of exciting/collision frequency ratio 13 p2110 A71-29372

Chemically interacting gases transfer properties at various temperatures, determining collision parameters and interaction cross sections and energies 15 p2451 A71-31494

Random walk theory applied to electron motion in early stage of He breakdown in electric field, based on integral and differential cross section data 15 p2452 A71-31921

Collision integral for classical electron plasma, concerning Born-Bogoliubov-Green-Kirkwood-Yvon equations for long range interaction potential and motions of multiple particles 16 p2619 A71-33650

Droplet pairs collision efficiencies and coalescence parameters, computing flow fields from nonlinear time dependent Navier-Stokes equations 17 p2770 A71-35805

Fully ionized plasma expansion from spherical source into vacuum, deriving equations of motion and collision integrals 19 p3115 A71-38212

Partially ionized plasma expansion from spherical source into vacuum, obtaining equations of motion, collision integrals and recombination rate coefficient 19 p3115 A71-38213

Electron concentration and collisions number fluctuations effect on D region profiles based on radio waves partial reflection data 19 p3057 A71-38365

Molecular gas mixtures inelastic collision integral spectra, describing internal degrees of freedom with correlation functions 21 p3420 A71-41271

Boltzmann kinetic equation with electron-electron collision coefficients for isothermal weakly ionized cesium-argon plasma, using nodal point method 23 p3709 A71-43267

Identification of 417 Å line in solar EUV spectrum, calculating collision strengths and recombination rates for Fe XV 24 p3873 A71-45143

COLLISION RATES

F region reflected radio wave heating effect, considering electron temperature, collision frequency and heat conductivity 01 p0040 A71-11531

ELF and VLF radio attenuation for propagation below inhomogeneous isotropic ionosphere with realistic vertical variation models for electron density and collision frequency 02 p0212 A71-11964

Thermionic converter electron-cesium atom momentum transfer collision probability, considering scattering cross sections 02 p0287 A71-12227

Effective electron collision frequency and RF conductivity along geomagnetic lines in magnetosphere 03 p0377 A71-13272

Ionospheric electron collision frequency and concentration height distribution during annular solar eclipse of 20 May 1966 03 p0407 A71-13378

Locally slowly varying magnetoplasma, determining electron concentration and collision frequency by wave propagation experiment 04 p0633 A71-15034

Electron density and collision frequency in plasma under RF modulation, solving energy balance equation 05 p0787 A71-16290

Kinetic theory approximate method application to model equation with velocity dependent collision frequency, obtaining solution for Kramers problem and expression for slip coefficient 06 p0931 A71-17450

Vertical profile of electron collisions effective frequencies in auroral ionosphere E region 06 p0895 A71-18279

Cold bounded nonuniform magnetoplasma harmonic generations model for small collision frequencies 07 p1166 A71-18889

Ion-molecule collision charge transfer and momentum transfer relaxation rates, using ion cyclotron resonance heterodyning method 07 p1054 A71-19371

Plasma concentration and heavy particle-electron collision frequency in open cylindrical cutoff resonator based on frequency shift and passband broadening data 07 p1171 A71-20184

Electron-ion plasma in HF electric and constant magnetic field, determining relaxation times and collision frequency for temperature compensation 09 p1502 A71-22539

Electromagnetic pulse propagation through inhomogeneous plasma, discussing electron collision frequency effects 09 p1504 A71-22987

Electron collision frequency energy dependence influence on electrical conductivity of weakly ionized plasmas, considering Taylor series expansion around probable plasma electron velocity 10 p1623 A71-23875

Weakly ionized plasma instabilities in high frequency field exceeding electron collision frequency, considering waves parametric excitations 12 p1937 A71-27204

Particle interaction with wedge surface in supersonic two phase flow, determining incidence coordinates and collision frequency as function of initial conditions 12 p1866 A71-27665

Lower ionosphere charged particle concentrations and collision frequencies determination by LF impedance probe 13 p2058 A71-28028

Conductivity tensor of turbulent plasma from coherent response to external test wave, introducing effective collision frequencies 13 p2109 A71-29244

Daniel comet collision frequency calculations with asteroids and microasteroids based on trajectory analysis 15 p2481 A71-31299

Carbon dioxide laser flow-through discharge, measuring electron density and collision rates with heavy particles as function of tube parameters 15 p2419 A71-31741

Microwave probing of electron number density and collision frequency in slightly ionized plasmas 15 p2458 A71-32395

Conductivity measurement of shock generated nitrogen plasma in transverse magnetic field, considering vibrationally excited molecules role in electron collision frequency 16 p2616 A71-32899

Rarefied gas dynamic models with velocity dependent collision frequencies, investigating linearized Boltzmann equations 17 p2729 A71-35573

Collision rates in photon and relativistic particle gases, noting importance for cosmic radio and X ray sources processes calculations 18 p2949 A71-36100

- Weakly ionized plasma instabilities in high frequency field exceeding electron collision frequency, considering waves parametric excitations 19 p3117 A71-38616
- Atmospheric gases effective electron collision frequency calculations, using momentum transfer cross sections 20 p3271 A71-38743
- Ionospheric radio wave absorption winter anomaly concerning seasonal variations of D and lower E region collision frequencies and F region oxygen concentrations 21 p3373 A71-40048
- Particle interaction with wedge surface in supersonic two phase flow, determining incidence coordinates and collision frequency as function of initial conditions 24 p3790 A71-44930
- Hot electrons in semiconductors within crossed and parallel electric and quantizing magnetic fields, examining collision frequencies and energy relaxation 24 p3861 A71-45165
- COLLISION WARNING DEVICES**
U COLLISION AVOIDANCE
U WARNING SYSTEMS
- COLLISIONLESS PLASMAS**
 Monograph on nonlinear theory of one dimensional homogeneous collisionless plasma resonance covering charged particle motion in sinusoidal and standing potential waves 01 p0131 A71-10101
- Transverse wave instability of unmagnetized collisionless plasma subjected to shear flow 01 p0136 A71-11477
- Ray tracing in warm collisionless magnetoplasmas based on wave dispersion relation, discussing satellite communication 01 p0137 A71-11612
- High Mach number collisionless shock waves in low density argon plasma, measuring electron heating and shock thickness 04 p0631 A71-14685
- Monochromatic wave propagation along cylindrical helical line, showing tubular waveguide formation from wave field and collisionless plasma interaction 04 p0633 A71-15107
- Collisionless electrostatic shock formation and structure, using one dimensional two species numerical simulation code 04 p0634 A71-15174
- Collisionless plasma density measurement by spherical probe, considering probe to Debye radius ratio 04 p0635 A71-15260
- Collisionless plasma shock longitudinal wave propagation perpendicular to magnetic field, demonstrating ion acoustic/electron Bernstein modes instability 05 p0789 A71-16655
- Inhomogeneous collisionless low beta plasma drift wave instability dynamic stabilization, considering AC electric field parallel to confining field 06 p0933 A71-17474
- Dynamic stabilization of two stream ion instability in collisionless plasma 06 p0934 A71-17483
- Collisionless plasma density determination valid for probe/Debye radii finite ratio, using positive ion current-voltage characteristics 06 p0936 A71-17680
- Vacuum spectrum modification theory for inverse Compton scattering in cold collisionless plasma 07 p1165 A71-18855
- Inhomogeneous collisionless plasma stability, showing small pressure gradient effects 07 p1167 A71-19228
- Collision free ionizing wave propagation into cold low density ionized gas, showing wave oscillations damping due to ion velocities phase mixing 07 p1171 A71-20289
- Magnetic field effects on collisionless plasma sheath near planar electrode, solving electric and magnetic potentials nonlinear differential equations by numerical scheme 07 p1171 A71-20290
- Noncollisional plasma LF instabilities, discussing flute-like, drift wave and trapped particle modes from spatially confined plasma Vlasov equation 07 p1173 A71-20509
- High beta plasmas instabilities, discussing collisionless bounce model of theta pinch and diagnostic measurements 07 p1173 A71-20511
- Nonlinear collisionless magnetoplasma waves and ionospheric irregularities electric field intensity, defining nonlinear oscillations domain by pseudopotential well 08 p1339 A71-21206
- Supersonic collisionless plasma flow around flat plate and expansion into vacuum, using Poisson equation 09 p1500 A71-22233
- Electron gun diode design for beam-collisionless plasma interaction nonlinear evolution, studying delta function beam velocity distribution 09 p1502 A71-22754
- Collisionless plasma steady flow past thin symmetrical semiinfinite wedge, considering dispersion due to finite Larmor radius 09 p1504 A71-23052
- High beta collisionless shock wave turbulence, discussing frequency and wavenumber spectra and turbulence level measurements by light scattering technique 09 p1504 A71-23255
- Charged conductors in homogeneous collisionless magnetoactive plasma at hybrid frequencies, investigating antenna array quasi-electrostatic field one dimensional structure 10 p1582 A71-23809
- Wave propagation with frequency inferior to gyrofrequency of ions in collisionless hydrogen plasma, showing Alfvén wave reflection on discontinuity surface parallel to magnetic field 10 p1599 A71-23846
- Observation range determination numerically for cyclotron resonances of effective scattering cross section of light wave by collisionless plasma in magnetic field 10 p1646 A71-23848
- Electrostatic waves high order interaction in collisionless plasma, deriving coupling constants from energy conservation and invariance under time reversal 10 p1647 A71-23888
- Stationary shock wave propagation perpendicular to magnetic field in Vlasov collisionless plasmas 10 p1647 A71-23892
- Transverse spatial particle diffusion in plasma under random oscillations, examining interaction between collisionless plasma and longitudinal wave 10 p1649 A71-24318
- Inhomogeneous collisionless plasma instabilities under dense blanket of neutral gas, investigating Alfvén type oscillation 10 p1650 A71-24628
- Magnetic mirror confined microwave heated plasmas stability based on uniform collisionless plasma model 10 p1651 A71-24632
- Collisionless ion exosphere kinetic and hydrodynamic models comparison for polar wind supersonic flow characteristics 10 p1605 A71-24796
- Shock wave propagation in electronically excited hot plasma in electromagnetic field, assuming negligible electron-ion collisions 10 p1653 A71-24828
- Pulsed magnetic piston produced shock waves propagation along field in collisionless hydrogen plasma 10 p1654 A71-24894
- Potential and ion charge distribution in proximity to conducting sphere moving in low density collisionless ion-electron plasma 12 p1958 A71-26647
- Inhomogeneous collisionless plasma stability, showing small pressure gradient effects 12 p1934 A71-26746
- Drift waves dynamic stabilization in collisionless plasma, considering AC electric field effects on low frequency instabilities 12 p1935 A71-26914
- Collisionless plasma with thermal ions in magnetic field absence, investigating stationary ion shock wave propagation 12 p1941 A71-27767
- Electron density distribution determination from microwave resonant frequencies of parallel plate cavity containing cold, collisionless, isotropic plasma 13 p2105 A71-27994
- Isomagnetic potential discontinuity of electrostatic character in collisionless plasma shock waves, studying Mach number effect 13 p2105 A71-28169
- Magnetic pumping of collisionless turbulent plasma with LF Alfvén and magnetosonic waves, assuming high initial plasmon energy 13 p2105 A71-28175
- Collisionless plasma thermal shock wave, showing heat in electron component transportable along magnetic field at lower rates than thermal velocity 13 p2106 A71-28425
- Rarefied collisionless plasma, obtaining hydrodynamic equations for magnetic viscosity and thermal conductivity 13 p2106 A71-28564
- Helicon and magnetoacoustic waves instability during passage through hot collisionless plasma with current transverse to weak external magnetic field 13 p2107 A71-28851
- Book on shock waves in collisionless plasmas covering basic equations and classification of shock structures, magnetosonic waves, shocks and solitons, electrostatic shocks and solitons, etc 13 p2108 A71-28896
- Electric field potential near sphere moving through rarefied collisionless plasma in condensation zone, determining ion and electron concentrations 13 p1991 A71-29159
- Electron thermal anisotropy effect on oblique whistlers preceding strong collisionless shock waves, using linear Vlasov theory 13 p2064 A71-29168
- Collisionless plasmas stationary flow hydrodynamic equations applied to plasma waves analysis 14 p2280 A71-30211
- Anomalous microwave energy dissipation and electron heating in collisionless plasma without decay at high collision frequencies 14 p2281 A71-30539
- Collisionless magnetic slow shocks laminar wave train structure, using two-fluid hydromagnetics with ion cyclotron radius dispersion 14 p2282 A71-30558
- Strong magnetic fields effects on neutron stars or white dwarfs, considering Thomson scattering in fully ionized collisionless plasma 14 p2315 A71-30858
- Superhigh frequency microwave absorption region localization in collisionless plasmas by plasma parameters measurement in toroidal magnetic field 15 p2370 A71-31737
- Longitudinal ionic wave excitation by grid in collisionless Q machine plasma 15 p2456 A71-31820
- Potential measurements in collisionless plasma sheath of conducting plate, evaluating electrostatic vs emissive and floating emissive probes 15 p2458 A71-32391
- Finite ion temperature effect on large amplitude magnetosonic disturbances and collisionless shock waves formation in plasmas, using one dimensional macroparticle code 15 p2458 A71-32394
- Collisionless small amplitude shocks in plasmas, considering wave dispersion and critical Mach number effects 15 p2459 A71-32561
- Relativistic kinetic theory of large amplitude transverse Alfvén wave, discussing propagation in collisionless plasma 15 p2459 A71-32653
- Electrical plasma probes, discussing ion-surface effects, geometry, cleaning procedures, collisionless regime and electron/ion current 16 p2617 A71-32961
- Quasi-neutral inhomogeneity /particle cloud/ in collisionless hot or cold plasmas without magnetic field 16 p2619 A71-33521
- Collisionless turbulent plasmas nonequilibrium electric fields determination from hydrogen spectral lines Stark broadening 16 p2619 A71-33549
- Transverse shock waves fine structure and saturation of ion-acoustic turbulence in collisionless plasma, using magnetic field probe and MHD equations 16 p2619 A71-33649
- Nonisothermal collisionless low beta plasma with electron temperature greater than ion, investigating low frequency potential modes for Kelvin-Helmholtz instability 16 p2620 A71-34167
- Temporal echo oscillations in collisionless relativistic electron plasma 17 p2786 A71-34198
- LF resonances for radially inhomogeneous collisionless plasma sphere impinged by plane electromagnetic waves 17 p2708 A71-35485
- Bernstein mode wave instability growth rate in collisionless shocks propagating perpendicular to magnetic field, including pressure gradient effects 18 p2950 A71-35928
- Vlasov-Poisson equations of collisionless plasma flow around conducting cylinder without magnetic effects, using nonrestrictive hybrid simulation techniques [ONERA-TP-958] 18 p2951 A71-36025
- Hydrodynamic equations for anisotropic plasma in magnetic fields, considering collisionless and collisional transport effects 19 p3111 A71-37634
- Finite-beta stabilization of collisionless trapped particle mode in toroidal plasma confinement devices, using magnetic well dug by plasma diamagnetism 19 p3112 A71-37742
- Collisionless plasma Vlasov and Poisson equations numerical solution based on Fourier-Fourier transform, comparing with particle motion simulation 19 p3113 A71-37748
- Collisionless plasma shock front microstructure, examining isomagnetic discontinuity with high spatial resolution probes 19 p3045 A71-37853
- Electron density inhomogeneity behavior, examining thermal electron motion and collisionless plasma initial condition effects 19 p3114 A71-37857
- Homogeneous collisionless plasma in external electric field, considering evolution in time of charged particles distribution functions 19 p3114 A71-37858

Finite Larmor radius equations for collisionless plasmas in magnetic fields, noting application to axisymmetric systems stability 19 p3115 A71-38209

Ion and electron drift waves propagation and stability in nonhomogeneous plasma containing impurity ions 19 p3115 A71-38214

Debye potential well formation in collisionless current carrying plasma, noting wave-particle resonant interaction role 19 p3115 A71-38216

Radiation resistance of small filamentary loop antenna in cold collisionless uniform multicomponent magnetoplasma, assuming uniform current distribution along loop 19 p3023 A71-38594

Collisionless shock waves downstream state, using Rankine-Hugoniot type relation model 19 p3117 A71-38650

Pressure anisotropy effects on plasma wave coupling and modification for dispersion in collisionless beam-plasma systems 20 p3273 A71-39045

Collisionless plasma thermal shock wave, showing heat in electron component transportable along magnetic field at lower rates than thermal velocity 21 p3421 A71-40083

Weak discontinuities propagation speeds, equations and eigenvectors in uniform collisionless plasma 21 p3421 A71-40209

Supersonic collisionless plasma flow around flat plate and expansion into vacuum, using Poisson equation 21 p3424 A71-41113

HF electric field influence on collisionless electron gas acoustoelectric effect, emphasizing electron scattering mechanism 21 p3431 A71-41232

Pulsed magnetic piston produced shock waves propagation along field in collisionless plasma 21 p3425 A71-41274

Nonelectrostatic helicon and magnetoacoustic waves instability during passage through hot collisionless plasma with current transverse to weak external magnetic field 21 p3425 A71-41280

Low density collisionless plasma stabilization in ion-accelerating external DC electric field 21 p3426 A71-41293

Laminar collisionless shock propagation perpendicular to magnetic field into hot plasma, calculating temperature effects on leading edge growth rate 22 p3579 A71-41580

High Alfvén Mach number collisionless plasma flow in weak magnetic field, investigating momentum transfer mechanisms and coupling lengths 22 p3581 A71-41890

Inhomogeneous high-beta collisionless plasma temperature gradient effects on ion-acoustic and Alfvénic drift instabilities 22 p3583 A71-41907

Strong current z discharge collisionless plasma, investigating ions distribution functions fine structure 23 p3708 A71-42890

Plane collisionless plasma diode between two hot emitters, considering potential distributions 24 p3808 A71-44551

COLLISIONS

NT ATOMIC COLLISIONS

NT COULOMB COLLISIONS

NT INELASTIC COLLISIONS

NT IONIC COLLISIONS

NT METEORITE COLLISIONS

NT MIDAIR COLLISIONS

NT MOLECULAR COLLISIONS

NT PARTICLE COLLISIONS

Two massive arbitrarily shaped hard bodies spatial collision, determining kinetic energy loss, motion and deformation of impact point 17 p2818 A71-34347

Two dimensional elliptic restricted three body problem, considering regularization mechanism and periodic collision orbits 21 p3441 A71-40095

COLLOCATION

Collocation method predicting oscillatory subsonic pressure distributions on interfering parallel lifting surfaces, considering approach more economical than finite element method [AIAA PAPER 71-329] 11 p1701 A71-25309

Collocation method application to linear boundary value problems for system of differential equations 15 p2442 A71-31831

First kind Fredholm integral equation approximation by numerical quadrature formulas plus collocation, using singular value decomposition for solution 22 p3567 A71-42296

COLLOIDAL GENERATORS

Ground test reactor design based on colloid fueled reactor concept [AIAA PAPER 70-688] 07 p1158 A71-19862

COLLOIDAL PROPELLANTS

Colloid microthruster system life test, discussing design and steady state performance [AIAA PAPER 70-1110] 07 p1184 A71-19864

Two component solid gas vortex flows with end wall injection eliminating boundary layer losses for colloid core nuclear rocket engine concept [AIAA PAPER 71-637] 14 p2273 A71-30715

COLLOIDS

NT AEROSOLS

NT COLLOIDAL PROPELLANTS

NT FOG

Electrofluiddynamic colloid generator performance characteristics, considering power output limitation due to electric breakdown [ASME PAPER 70-WA/ENER-5] 03 p0355 A71-14108

Subdomain magnetic particles ferrofluid colloidal dispersions, for energy conversion devices, viscous dampers, accelerometers, gyroscope supports and specific gravity meters [IEEE PAPER 27.2] 07 p1178 A71-19611

Electrostatic spray generated charged colloids adaptation to thruster with metal capillary needles under AC voltage, evolving low thrust propellants 13 p2118 A71-29503

High thrust density colloid emitting source development as basic microthruster for electrostatic propulsion systems [AIAA PAPER 71-694] 14 p2293 A71-30753

Radiative transfer in terrestrial clouds, inferring colloidal state from measurements of multiple scattering angular and wavelength dependence 17 p2736 A71-35566

Soviet monograph on coacervates and protoplasm covering colloidal-chemical properties, enzyme catalysts and multiphase cell and organism simulation 21 p3336 A71-40870

COLOR

Hill reaction of disintegrating chloroplasts in vitro, investigating transient color sensitivity /red-blue effect/ 04 p0539 A71-15270

Standard printing color identification system for DOD mapping, charting and geodesy services standardization 08 p1281 A71-21259

Liquid crystals of cholesteryl nonanoate with cholesteryl chloride or cholesteryl propionate, examining color dependence on temperature 09 p1442 A71-22270

Lunar surface optical properties, examining albedo, color, brightness variation and polarization 11 p1822 A71-25688

MgO single crystals dominant coloration in solar spectral region by electron hole pair diffusion, trapping and recombination [AIAA PAPER 71-450] 11 p1808 A71-26234

Mars 1969 opposition effects, describing Syrtis Major, Arabia and disk brightness, color and spectrum 11 p1835 A71-26456

Galactic brightness, color distribution and ellipticity data from photometry and colorimetry observations 15 p2486 A71-32028

Three dimensional display with multicolor capability, continuously variable intensity and random accessed flying spot, exhibiting fixed or moving objects 20 p3234 A71-39063

Cholophor /passive polarization switched liquid crystal screen/ for laser power enhancement in multicolor displays 20 p3234 A71-39064

Color and music distraction for operator in isolated environment and counteract psychophysiological activity impairment 20 p3193 A71-39225

COLOR BLINDNESS

U COLOR VISION

COLOR CENTERS

Photochromic calcium fluoride preparation by rare earth additive coloration techniques 09 p1509 A71-23120

COLOR PERCEPTION

U COLOR VISION

COLOR PHOTOGRAPHY

Direction indicating color schlieren system displaying radial refractive index gradients, comparing with knife edge monochrome image resolution 03 p0423 A71-13459

K corona radially and tangentially polarized components color differences from 7 March 1970 eclipse photographs analysis 03 p0489 A71-13628

Aerial photographic film color separation tests 04 p0585 A71-14644

Color schlieren system with wedge type interference filter between high quality lenses pair for obtaining undistorted real image 04 p0598 A71-15364

Photometric observations of lunar surface regions, noting color variations with phase change 05 p0809 A71-16461

Multicolor photographic photometry of NGC 4254 galaxy using electro-optical converter, observing H alpha emission and H II regions at galactic center 07 p1205 A71-20634

Aerial color negative system for processing Ektachrome aero film type 8442 to obtain negative transparency with fourfold effective film speed increase 08 p1288 A71-21261

Solar color index calibration from Mg b triplet photoelectrical measurement for dwarfs and Jupiter satellites 09 p1516 A71-22064

Telescope plate scanner automated computerized operation, evaluating faint stars identification and color classification for annual motion surveys 09 p1443 A71-22646

High temperature measurement by photographic technique using radiation-sensitive color film for unpredictable exposure conditions 09 p1444 A71-22712

Multicolor photographic photometry of flare stars in Orion aggregate based on two UBV photoelectric sequences 10 p1680 A71-25061

Scattered stellar clusters region stars and interstellar matter from photographic magnitudes diagrams and color indices, determining absorption fluctuations by color excess technique 10 p1681 A71-25127

Jupiter color variations observation by multicolor photoelectric photometry, noting consistency with activity in Jovian atmosphere 11 p1827 A71-25725

Astronomical photometry and photometric systems, discussing spectral classification, U, V, B, Y, beta system, energy distributions and seven color photography 12 p1903 A71-26774

Photography date effects on intensive study sites airphoto interpretations, using color and color-IR films 12 p1907 A71-27258

Apollo 9 So65 multispectral color space photography for basic land use pattern determinations 12 p1907 A71-27259

Black and white television scanning ability of color differentiation and gray tone identification by signal fluctuations in aerial imagery 12 p1907 A71-27261

Color and color IR films for soil identification, performing optical density measurements on film transparencies with densitometer 13 p2071 A71-29394

Dwelling unit estimation with color IR photos, applying aerial photointerpretation to urban analysis 13 p2064 A71-29396

Space photos for land use and forestry, considering IR color photographs from Apollo 9 flight 13 p2064 A71-29398

Diseased plants and crop loss per field from aerial IR-color photography 14 p2236 A71-30576

Aerial color photography in forestry for species identification, reforestation areas development, watershed studies and land planning 17 p2737 A71-34272

Multispectral color aerial photography for identification of farm crops and tree species, using broadband camera filters 17 p2737 A71-34274

Urban environmental quality analysis using color IR aerial photography, considering film sensitivity and haze penetration 18 p2911 A71-36062

Pseudocolor image enhancement by two-separation photographic process, considering transformation curve alterations in CIE space by changes of photographic materials, filters and exposures 18 p2918 A71-36080

Ultrarapid color holography using continuous synchronized coherent light sources of different wavelengths 21 p3378 A71-40514

Reflecting telescope Schmidt camera photographic color system temperature dependency from cluster NGC 103 photographs 21 p3379 A71-40717

Bicolor projections analogs with red and green McCollough aftereffects 23 p3635 A71-43975

Color photography of magnetic particle and penetrant indications, discussing light sources, camera types, filter and film selection, exposure and spectral characteristics of indications 24 p3829 A71-45283

COLOR TELEVISION

Concorde economic flight testing methods, discussing Blagnac flight simulator mobile cabin visualization and color TV terrain model 12 p1868 A71-27608

Mariner 6 and 7 Mars color TV recording of craters, chaotic terrain and canals, using wide and narrow angle cameras 20 p3297 A71-39628

COLOR VISION

Background nonequivalence during long term photopic dark adaptation 01 p0008 A71-10143

Color matching discrepancies, considering rod blue qualities under photopic conditions, luminance level and trichromatic stimulus unsuitability for large field additive colorimetry 01 p0010 A71-10273

Eye wavelength/color discrimination ability measurements for linear dispersion spectra 01 p0016 A71-11390

Color sensations and retinex theory, discussing mathematics of lightness scheme and biologic correlate of reflectance 05 p0753 A71-16901

Book on visual perception covering physics of light, rods and cones, color vision, brightness psychophysiology, stimulus generalization, etc 06 p0850 A71-17409

Electronic model of color recognition by human eye using spectral filter-photosensor system 07 p1051 A71-20122

Temporal masking effects with perception of color matching double flashes 09 p1394 A71-23015

Chromatic visual acuity measurement for gratings with bars of equal luminance and different colors 10 p1560 A71-23985

Monocular vision field structural color in violet and yellow region under increasing light frequency and periodic electric stimulation 10 p1560 A71-23990

Book on color and pattern vision physiology covering retinal induction, electrical excitation of eye, optical illusion, figural aftereffect, movement sensation, etc 12 p1870 A71-26769

Human color vision investigation by psychophysical methods, discussing spectral sensitivity, pigment absorption and defective color vision as function of stimulus wavelength 12 p1873 A71-26863

Auroral color variations and human color perception, noting visual appearance agreement with calculations based on normal spectrum 13 p2060 A71-28348

Human nervous reactions to monochromatic red, yellow green and blue light for optimal color climate in spacecraft cabins 13 p2018 A71-28411

Color conversion model of equivalences under various illuminants, reducing problem to chromatic adaptation with nonlinear von Kries formulation 15 p2412 A71-32599

Visual search performance as function of color coding for information location tested on aeronautical charts 17 p2689 A71-34703

Mathematical models of color data coding and decoding, studying light emissions transformations in visual organs and engineering systems 17 p2692 A71-35173

Human cone visual pigments kinetic equation testing by comparing photolysis rate at equilibrium to regeneration rates 18 p2854 A71-36001

Colored light sources luminosity determination by Helmholtz-Kohlrausch effect, discussing brilliant and fluorescent stimuli 18 p2854 A71-36003

Color perception with achromatic stimulation by changing intensity of stationary light source to produce flicker colors 18 p2864 A71-36004

Subjects with strabismic amblyopia, investigating defects in cone or rod mechanisms of dark adaptation by using colored filters 18 p2854 A71-36011

Hue shifts by intermittent stimulation, suggesting interaction between stimulus intermittency and temporal color coding in visual system 19 p3004 A71-38283

Wavelength discrimination from color naming by young adults with normal visual acuity and color vision 19 p3004 A71-38285

Bicolor cathode ray display tubes with triple-layer bombarding electron beam energy-dependent red-green fluorescent screen 21 p3347 A71-40109

Red and green light emitting GaP junction diodes and monolithic arrays for display devices, discussing fabrication and properties 21 p3352 A71-40110

Flash light angular size, adaptation luminance, pulse shape and color effects on Blondel-Rey constant tested on observers with good binocular vision 22 p3498 A71-41483

Color defective vision and aviation color signal light flashes recognition, indicating Farnsworth Lantern performance prediction test superiority 22 p3499 A71-41490

Human visual system color and edge-sensitive channels confirmation by psychological tests of tuning for orientation 23 p3640 A71-43548

Bicolor projections analogs with red and green McCollough aftereffects 23 p3635 A71-43975

Visual pigments in color blind subjects, using retinal densitometry 24 p3794 A71-44464

Red/green pigments in normal color vision, describing analytical anomaloscope for measuring protanope and deuteranope sensitivity curves 24 p3794 A71-44465

COLORADO

Colorado Land Use and Environmental Resource Inventory Project /CLARI/ by computer methods, saving information retrieval time and cost 08 p1281 A71-21253

COLORATION

U COLOR COLORIMETRY

Color matching discrepancies, considering rod blue qualities under photopic conditions, luminance level and trichromatic stimulus unsuitability for large field additive colorimetry 01 p0010 A71-10273

Suprassociations in late morphological type galaxies, discussing photometric and colorimetric observations 07 p1192 A71-19284

Soviet lunar surface rocks physical properties ground observation including colorimetry, spectrophotometry and polarimetry 07 p1193 A71-19311

Atmospheric extinction vs intermediate band color index diagrams, discussing linear correlation and reference star selection 10 p1681 A71-25130

Colorimetry of Mars surface from dual beam area scanner, considering light and dark areas contrast during 1969 opposition 11 p1824 A71-25706

Comet Bennett light polarization data, determining color index and chemical composition 12 p1965 A71-27227

Dark companions and extrasolar planetary system detection, discussing characteristic colorimetric signature method 13 p2134 A71-28291

Soviet lunar surface rocks physical properties ground observation including colorimetry, spectrophotometry and polarimetry 15 p2485 A71-31891

Planetary nebulae nuclei colorimetric, photographic and brightness data, listing temperatures, absolute values and bolometric corrections 15 p2487 A71-32034

Twilight aureole visual observation and objective colorimetry from Soyuz spacecraft, noting importance for atmospheric composition determination 18 p2911 A71-36007

Comet Bennet light polarization data, determining color index and chemical composition 19 p3132 A71-37379

COLUMBIUM

U NIOBIUM

COLUMNS [SUPPORTS]

NT TAPERED COLUMNS

Elastic column optimization, examining material distribution for minimum volume without buckling 03 p0501 A71-13023

Optimal design of one end-clamped elastic column subject to conservative concentrated compressive loads 03 p0501 A71-13110

Elastic columns under transient loading, ascertaining stability by Liapunov function direct method 03 p0505 A71-13540

Buckling of cold formed Al alloy thin walled columns under compression, investigating longitudinal half wave formation 06 p0985 A71-17748

Spring supported beam-column nth vibration and buckling eigenvalues, discussing Monte Carlo simulation for evaluating perturbation method accuracy for variance calculation [AIAA PAPER 71-149] 06 p1004 A71-18591

Optimal structural design for nonconservative elastic stability of cantilever column, obtaining critical load 07 p1212 A71-19473

Buckling coefficient of Al alloy columns with different section profiles, using steel structures stability specifications 10 p1623 A71-23768

Elastic deformation and plastic buckling of rectangular column with initial deflection under axial compression 13 p2157 A71-29287

Nonconservative dynamic instability of columns under distributed tangential force, using analog computer 13 p2158 A71-29430

Pin-ended column stability and random behavior under white noise excitation, using analog simulation and application to vertical earthquake and aerospace vibration environments 14 p2330 A71-30683

Vertically cantilevered column weight and follower force effects on flutter and buckling instabilities respectively 14 p2330 A71-30685

Column buckling under initially random bending and twisting, comparing numerical analysis accuracy with Bernoulli-Euler results 14 p2330 A71-30692

Angular momentum influence on linear axisymmetric motions of centrally condensed bodies, considering finite amplitude pulsations of rapidly rotating columns 15 p2481 A71-31202

Elastic structure dynamic stability problem, determining optimum inequality relating energy functional to displacement, and considering beam column with various boundary conditions 15 p2506 A71-32015

Nonlinear coupled parametric response of crooked thin walled columns under harmonic longitudinal load 15 p2507 A71-32095

Statistical methods application to buckling of axially loaded columns, considering entire spectrum of elastic, elastoplastic and fully plastic ranges 16 p2654 A71-33123

Snap-through buckling of three hinged deep trusses and wire restrained column under critical quasi-static loading based on elastica theory of prismatic bars 17 p2815 A71-34294

Slender elastic column dynamic buckling under constant compressive axial end displacement, considering damping effects 17 p2818 A71-34506

Chebyshev polynomial expansions application to beams and columns with large deflections, discussing accuracy 17 p2832 A71-35424

Book on optimum structural design covering single element optimizations, load transmission, slender columns, cost-weight tradeoffs and statically indeterminate structures 18 p2977 A71-36249

Notched fixed-pinned columns under concentric and eccentric compressive loads, presenting failure analysis based on stress intensity concept and methods of limit analysis 18 p2983 A71-36852

Constant stiffness beam-columns analysis in pressure piping systems calculations for nuclear industry, using initial parameter method 19 p3102 A71-37073

Elastic beam-columns with initial curvature and pinned or clamped ends under transient axial and distributed lateral loads, deriving upper displacement bounds 19 p3159 A71-38184

Asymptotic solution to dynamic buckling of thin slowly compressed eccentric elastic columns, using two time scheme 23 p3776 A71-43373

Stochastically imperfect columns on nonlinear elastic foundations, obtaining approximate asymptotic expression for buckling stresses and lateral displacement autocorrelation 24 p3884 A71-44962

COMA

Comets-minor planets relationship, discussing comas, physical appearance, light variations and condensations 04 p0653 A71-15713

Comets structural features via visual observations, emphasizing inner coma structures and expanding envelopes surrounding nucleus 09 p1526 A71-23351

COMBAT

Military helicopter design and weaknesses correction, considering man/machine combat survivability and operational accidents reduction 04 p0534 A71-15447

Armored cockpit for attack aircraft combat effectiveness, including mold line tumbling plates, terminal ballistic kinematics and integral structural armor [AIAA PAPER 71-778] 17 p2675 A71-35530

Real time reconnaissance cockpit display system for airborne sensor systems, providing night combat imagery 17 p2747 A71-35772

Secondary visual tracking tasks utility in simulated lag effect in simulated combat aircraft dynamics 18 p2873 A71-36973

Aircraft performance and optimal energy flight path control in combat environment 19 p2997 A71-37724

Zero sum differential game solution for aerial combat problem, applying direct gradient methods 23 p3699 A71-44103

COMBINATORIAL ANALYSIS

NT FACTORIALS
NT PARTITIONS [MATHEMATICS]

- Combinatorial extremum problem distribution among units of hierarchical control system
02 p0236 A71-12623
- Failure diagnosis and localization algorithm for combinational circuits of functional elements, considering arbitrary combinations and essential fault presence
21 p3361 A71-41141
- Code conversion and coincidence circuits design for positional digital control systems with combinational code producing feedback elements
24 p3805 A71-45154

COMBINED STRESS

- Polyethyl methacrylate lifetime under simultaneous mechanical stresses and ionizing radiation
01 p0106 A71-10044
- Ductile Ni deformation and fracture, examining simultaneous cyclic and monotonic strain effects
01 p0098 A71-10164
- Discrete search method for stiffened cylindrical shell stability under combined uniform axial compression and lateral pressure loads
01 p0174 A71-10963
- Moire technique calculation of transverse strain directly from longitudinal strain distribution across sections of symmetry in grooved tensile bar
01 p0174 A71-11007
- Axial compression of thin circular epoxy resin disks with three dimensional stress state produced by cementing to rigid platens, using triaxial analysis
01 p0109 A71-11008
- Stress separation data for axisymmetric and three dimensional data from frozen stress photoelastic model slices
01 p0174 A71-11010
- Micropolar elastic body with spherical inclusion, investigating thermal and couple stresses
01 p0181 A71-11286
- Coupled stresses effect on dynamic stress concentration produced by traveling loads on elastic Cosserat plate
03 p0509 A71-13905
- Plastic wave propagation of combined stresses due to longitudinal impact of pretorqued tube
04 p0668 A71-15190
- Isotropic elastic spherical shells stability under combined axial compression and local loads
05 p0824 A71-16593
- Self-consistent polycrystalline model for combined stress state time dependent creep, examining flow potential existence
05 p0830 A71-17236
- Reinforced cylindrical minimum weight shells under combined axial compression and internal pressure, examining strength and buckling modes
06 p0982 A71-17357
- Shells of revolution under combined thermal and mechanical loading, presenting analytical basis of BOSOR 3 digital stress analysis program
09 p1533 A71-22079
- Limit load carrying capacity of thin walled tube under combined forces, including pressure effects by variational method of plasticity theory
10 p1688 A71-24384
- Approximate solution for limit load carrying capacity of thin walled tube under combined loadings, deriving formulas describing boundary surface
10 p1688 A71-24385
- Linearly elastic cylindrical shells dynamic stability under combined axial and radial stochastic excitations, using Liapunov analysis
11 p1842 A71-25312
- Transient creep of thin walled composite beam under bending and tensile loads in nonuniform temperature field by increment method
14 p2321 A71-29538
- Combined mechanical and cyclic thermal stresses effect on plastic deformation buildup in E1435 alloy preceding breakdown
15 p2433 A71-32236
- Automatic testing machine for materials corrosive strength under varying and combined complex static or dynamic stresses
16 p2580 A71-33687
- Circular cylindrical shell stability under combined axial tensile/compressive/loads and torque, verifying theory by experiments on stainless steel shell
17 p2817 A71-34336
- Anisotropic laminated cylinders under combined axial load, torsion and internal pressure, calculating stresses with Vlasov-Ambartsumyan shell theory
17 p2823 A71-34811
- Resolved stress formula for shafts under simultaneous tangential bending and torsion acting at dangerous points of cross section
18 p2981 A71-36721
- Low temperature test facility for cryogenic and rocket materials under combined tension and torsion
18 p2900 A71-36726
- Thin walled tube under combined bending and torsion, considering stress distribution and curvature behavior
24 p3883 A71-44892

COMBUSTIBILITY
U FLAMMABILITY

COMBUSTIBLE FLOW

- One dimensional unsteady flows of combustible gas mixtures with detonation waves generation, noting electromagnetic effects
05 p0833 A71-16502
- Shock waves and chemical reactions due to plane, cylindrical and spherical point explosions in combustible gaseous mixtures
05 p0833 A71-16503
- Two dimensional supersonic turbulent burning mixing layer, measuring physical properties and growth rate
06 p0943 A71-17657
- [WSS/CI PAPER 70-16]
- Multiphase two dimensional mixing and combustion of flow fields suspended in gaseous medium for propulsion systems problems, obtaining governing equations
11 p1854 A71-25509
- [AIAA PAPER 70-145]
- Soviet papers on combustion processes in turbulent and laminar flows of kerosene and gasoline mixtures, stressing gas turbine engines problems
13 p2162 A71-28954
- Flame propagation rate in gasoline-air flow with tubular and grid-induced turbulence during two-stage burning process
13 p2162 A71-28959
- Jet induced flame stabilization in combustible kerosene-air mixture flow of variable composition, discussing stable burning range and excess air content
13 p2163 A71-28965
- Artificially induced unsteady flows effects on flame stabilization by model opposed jet stabilizer employing premixed propane-air combustible flow and opposed air jet
17 p2840 A71-35706
- Combustion dynamics, including fire spread in solid fuels, ignition, turbulent/laminar fields and boundary layer, stagnation point and opposed jet burning
19 p3166 A71-38077
- COMBUSTION
- NT AFTERBURNING
- NT BOUNDARY LAYER COMBUSTION
- NT DEFLAGRATION
- NT FUEL COMBUSTION
- NT HYDROCARBON COMBUSTION
- NT METAL COMBUSTION
- NT PROPELLANT COMBUSTION
- NT SOLID PROPELLANT IGNITION
- NT SPONTANEOUS COMBUSTION
- NT SUPERSONIC COMBUSTION
- French book on thermodynamics and gas dynamics covering theoretical and applied thermodynamics, air compressors, combustion, internal combustion engines, water vapor, compressible fluid cooling, etc
09 p1545 A71-22965
- Combustion and heat transfer in gas turbine systems - Conference, Cranfield, England, April 1969
13 p2116 A71-28739
- High power carbon disulfide-oxygen combustion pulsed laser, discussing foreign gases effects on performance and energy transfer mechanism
16 p2586 A71-33165
- Combustion - Conference, University of Utah, Salt Lake City, August 1970
19 p3166 A71-38076
- COMBUSTION CHAMBERS
- Tubular gas turbine engine combustor design by combining turbulent flame speed, microvolume burning and stirred reactor models
02 p0299 A71-12852
- Oscillatory combustion mechanism variations with geometrical configuration changes, considering variable cross sectional area and straight tube combustors
03 p0517 A71-13354
- Supersonic and subsonic combustion modes in constant area ramjet combustors, deriving dimensionless parameter for varying flow ratios as combustion stability criterion
03 p0521 A71-14148
- [ASME PAPER 70-WA/AV-4]
- Swirling flow in short cylindrical combustion chambers with diaphragm-free inlet section, examining momentum loss
03 p0405 A71-14382
- Wankel engine chamber gas leakage determination based on exit slot sample gas analysis, considering air to working fluid ratio
04 p0638 A71-14598
- Solid propellant rocket chamber unstable motion, discussing pressure and velocity coupling
06 p0946 A71-18297
- Swirling effects on turbulent flow recirculation zone behavior in gas turbine main burners
06 p0946 A71-18477
- [AIAA PAPER 71-2]
- Unstable liquid propellant rocket engine nonlinear behavior, considering stability of cylindrical combustor with distributed steady state combustion process and multiforce quasi-steady nozzle
06 p0948 A71-18644
- [AIAA PAPER 71-208]
- Gas temperature in combustion chamber and jet nozzle exit, and gas jet velocity resulting from various pressures, temperatures and air excess factors combinations
06 p0948 A71-18702

Metal powders hypergolic ignition in gaseous chlorine trifluoride, examining use in air augmented rockets primary combustors
07 p1183 A71-19875

Pressure wave distortion effects on combustor acoustic mode instability based on model with burning rate related to Reynolds number
07 p1224 A71-19906

Combustor design for minimum exhaust smoke emission from aircraft gas turbine jet engines, considering air pollution
08 p1347 A71-20867

Combustion chamber radiant heat transfer measurements, describing radiometer
08 p1288 A71-21270

Book on aircraft gas turbine engine technology covering combustion chambers, exhaust systems, lubricating oils, thrust augmentation, inlet ducts and overhaul procedures
08 p1348 A71-21625

Liquid fuel rocket combustor longitudinal pressure oscillations nonlinear analysis, using multiple scales technique
09 p1544 A71-22107

Fuel evaporation in combustion chambers L-shaped and annular vaporizers, determining operational parameters effect on evaporation ratio
10 p1658 A71-25123

Gas turbine engine combustor stability dynamic model, representing premixing and combustion chambers as Helmholtz resonators for stability criteria derivation
11 p1813 A71-25987

Combustion chamber flame tube cooling by swirling air flow, determining radial and longitudinal temperature distributions for various swirler hub ratios and jet angles
11 p1813 A71-26052

Gas field nonuniformity as function of turbine engine combustion chamber design parameters, discussing hot tube circumferential holes total area effect
12 p1945 A71-27501

Two dimensional inviscid heated flows in terms of pressure, density, speed, direction and heating rate applied to supersonic duct combustion chambers
12 p1987 A71-27735

Combustion chambers unstable acoustic oscillations, calculating equations for nonlinear growth and decay rate and limiting amplitude
13 p2160 A71-28613

Noise emission and acoustic efficiency in pulsating combustors, considering sound pressure level
13 p2113 A71-28618

Olympus 593 Concorde engine combustion system, discussing operating conditions, combustion performance criticality and altitude relighting
13 p2116 A71-28740

Statistical analyses for tube-annular and annular combustion chamber temperature profiles
13 p2116 A71-28741

RB 162 turbojet engine combustors for VTOL aircraft, achieving ignition by two pressure jet atomizers operative during starting cycle
13 p2116 A71-28742

Annular vaporizing combustion chambers, considering aerodynamic control of fuel distribution and mechanical simplifications
13 p2116 A71-28744

Diffusion and thermal mechanism ignition theories, applying to altitude relighting of gas turbine engine combustors
13 p2116 A71-28745

Air mass flow rate in can type gas turbine combustion chambers
13 p2117 A71-28747

Annular vaporizing combustion chamber with film cooling, determining flame temperature under supersonic flight conditions
13 p2117 A71-28749

Liquid fuel atomizers for gas turbine combustion system model experiments, considering droplet sheet photography and molten wax spray technique
13 p2117 A71-28755

Gas dynamic antechambers flame stabilization at various flow rates and temperatures, calculating mixing factor vs flow and jet parameters
13 p2163 A71-28966

Combustion chamber design with flame stabilizers, deriving gas flow, energy conservation equations and propellant combustion rates
13 p2163 A71-28967

Gas turbine engine combustion chamber start-up and burning performance, considering air injection and propellant atomization
13 p2117 A71-28968

Carbon deposition rates in gas turbine engine combustion chambers with airstream-mechanical propellant atomization
13 p2118 A71-28970

Gas turbine engine combustion chamber outlet, noting gas flow temperature field peripheral nonuniformity
13 p2118 A71-28972

Head end secondary flows in solid propellant rocket motor combustion chamber due to transverse acoustic waves in quiescent fluid

14 p2335 A71-29877

Reattachment of single two dimensional turbulent air jet, investigating gas flow characteristics in combustion chambers

14 p2170 A71-30419

Analytical model of compressor sensitivity to transient and distorted transient flows, considering inlet duct, compressor stages and combustor up to turbine nozzles

[AIAA PAPER 71-670]

14 p2291 A71-30734

Analytical model for performance and pollutant emissions of gas turbine combustors, predicting gas composition and temperature

[AIAA PAPER 71-711]

14 p2294 A71-30765

Modular concept mathematical model for combustion and pollution formation processes in jet engine combustors, including turbulent mixing and reaction kinetics

[AIAA PAPER 71-714]

14 p2294 A71-30766

Nitric oxide formation analytical model for gas turbine combustion chamber, considering influence of primary zone equivalence ratio, combustor residence time and initial fuel droplet size

[AIAA PAPER 71-715]

14 p2191 A71-30767

Soviet book on liquid rocket engines covering combustion chambers, fuel supply systems, static and dynamic characteristics, control and reliability

15 p2466 A71-31296

Pressure gain resonant combustion chambers in gas turbines, discussing thermal efficiency and power output

15 p2467 A71-31445

Turbojet engine combustor nitric oxide formation prediction based on adiabatic micromixed perfectly stirred reactor model analysis

[AIAA PAPER 71-713]

15 p2470 A71-32286

Gas generator with high thrust-weight ratio, discussing thermodynamic cycles, mass flow rates and combustion chamber

15 p2471 A71-32571

Aerodynamic flame stabilization by secondary air jets obliquely directed toward combustion chamber main flow, comparing with mechanical devices characteristics

[DFVLR-SONDDR-120]

15 p2472 A71-32719

Rocket engine burning oxygen and hydrogen propellants at 3000 psia combustion chamber pressure for space shuttle booster and orbiter stages

[AIAA PAPER 71-659]

16 p2624 A71-33106

Jet engine combustion chamber design, considering air supply and geometrical criteria

16 p2624 A71-33344

Turbulent homogeneous air-fuel mixtures pulsating combustion in plane chambers with nozzle and plate stabilizers, noting influence of fuel type and mixture composition

16 p2663 A71-33360

Swirling flow in gas turbine engine combustion chamber forward part, considering air flow characteristics behind blade swirler

16 p2624 A71-33606

Gas turbine engine combustion chamber outlet gas temperature field peripheral nonuniformity, detailing jets disruptive capacity effects in mixing zone

16 p2625 A71-33609

Time constant dependence of hybrid rocket combustion chamber on engine parameters and structure

16 p2625 A71-33619

Gas turbine with high velocity combustor, pure impulse compressor and turbine and isothermal burner

17 p2793 A71-34590

Vibrational combustion study of powder, using Helmholtz resonators with connected auxiliary combustion chamber

17 p2839 A71-35697

Nitroglycerin powder combustion acoustic instability, determining mean pressure and sample and combustion chamber geometry effects

17 p2840 A71-35700

Solid fuel vibrational combustion devices and operational analysis, considering various chamber configurations

17 p2840 A71-35702

Free fuel droplet spherical combustion in freely falling chamber under zero gravity condition

19 p3169 A71-38111

Homogeneous fuel combustors with multistage reaction rate controlled system, determining linear relationships and heat release

21 p3437 A71-41049

Thermal combustion produced biocomplex vegetable waste mineralization effect on furnace working surface oxide film

22 p3507 A71-42821

Operating variables effect on pollutant exhaust from jet aircraft turbine engines, discussing combustor design techniques for emissions reduction

23 p3718 A71-43600

Operational characteristics of starting igniters for gas turbine engine combustion chambers

24 p3864 A71-45003

COMBUSTION CONTROL

Diffusion controlled combustion of liquid fuel droplet in oxygen-steam oxidizer mixture

03 p0468 A71-13996

Accelerating flame front generation and propagation controlling mechanism in porous propellant

[AIAA PAPER 71-210]

06 p0948 A71-18646

Solid propellant rocket motor combustion control by fluidic vortex valve, considering thrust variation

[AIAA PAPER 70-643]

07 p1183 A71-18904

Turbulent diffusion flame laminarization by superimposed rotating flow field, discussing boundary layer stabilizing effect of external centrifugal force field

10 p1695 A71-24048

Propulsion system atom and radical concentrations measurements, using low pressure gas discharge flow system for combustion environment control

11 p1729 A71-26285

Solid impulse control using solid quench system and wafer demand gas generator for solid propellants

14 p2297 A71-30844

Dynamic coupling response between convectively controlled burning process and nonsteady flow field with pressure, density and gas velocity periodic variations

23 p3782 A71-43593

COMBUSTION EFFICIENCY

Hybrid rocket propulsion engine combustion efficiency, burnout patterns and operating conditions, using nitric acid oxidizer

02 p0298 A71-12070

Motor design parameters effects on solid propellant extinguishment predicted from mathematical combustion model

[AIAA PAPER 70-664]

03 p0469 A71-14442

Continuous combustion gas turbine with stepwise heat release, investigating ideal thermal efficiency cycle of gas overexpansion, cooling and compression

13 p2115 A71-28583

Olympus 593 Concorde engine combustion system, discussing operating conditions, combustion performance criticality and altitude lighting

13 p2116 A71-28740

Combustion efficiencies of staged rocket motor consisting of gas generator, secondary combustor and converging-diverging nozzle

[AIAA PAPER 71-739]

14 p2296 A71-30782

Combustion acceleration of molar oxygen-methane mixtures in cylindrical chamber during flame-shock wave interaction, using motion picture techniques

15 p2511 A71-31381

Cold flow analysis of liquid propellant sprays from rocket engine injectors, relating propellant mixing and combustion performance

15 p2465 A71-32044

COMBUSTION HEAT

U HEAT OF COMBUSTION

COMBUSTION INSTABILITY

U COMBUSTION STABILITY

COMBUSTION PHYSICS

Solid fuels and propellants heterogeneous ignition mechanism, using local similarity and related methods

02 p0333 A71-12853

Spherical hydrogen-oxygen diffusion flame structure, discussing combustion processes chemical kinetics

02 p0210 A71-12856

Air-acetylene and air-propane-butane flames absorption spectra, determining distribution of free Ca and Na atoms and OH hydroxyl radicals

03 p0518 A71-13501

Turbulence intensity in combustion zone of stabilized air-kerosene flame from annular burner, using He diffusion measurements

03 p0520 A71-13994

Burning velocities in 50 percent hydrogen-air mixtures

03 p0376 A71-14282

Supersonic combustion thermogasdynamics analysis, presenting combustion processes via pressure-velocity diagram

04 p0676 A71-14986

Supersonic combustion process heat transfer, using momentum integral method for turbulent boundary layer equations

04 p0683 A71-15485

Monopropellant /isopropyl nitrate/ detonation limits, characteristics and properties

05 p0795 A71-16516

Gaseous mixtures turbulent combustion, considering turbulent flame propagation velocity

05 p0836 A71-16536

German monograph on ignition and combustion processes in rapidly flowing gas mixtures covering supersonic flow, ramjet parameters, flow heating, etc

05 p0838 A71-16900

Hypersonic ramjet reaction mechanisms for H combustion, discussing computational models, operation principles and atomic, radical and molecular collisions

06 p0865 A71-17410

Combustion research for air breathing engines, discussing combustion stability in thrust augmentors, aircraft fire detection, MHD and external burning

[AIAA PAPER 71-1]

Mg slurry fuel mixing, ignition and combustion characteristics for injection into high speed air flow

[AIAA PAPER 71-6]

06 p1007 A71-18480

Quench combustion of ammonium perchlorate composite solid propellant sandwich indicating binder-oxidizer interplay

[AIAA PAPER 71-170]

06 p0944 A71-18610

Flame propagation process, investigating transfer in turbulent flow, combustion times and burning in channel

07 p1220 A71-18778

Diffusion flame stability, investigating critical dependencies for ignition point coordinates for fuel gas burning

07 p1220 A71-18779

Liquid fuel droplets in heterogeneous detonation of dilute sprays, noting deformation and fragmentation in reaction zone

07 p1222 A71-19189

Zirconium droplet combustion in oxygen-rich gas mixtures, observing transient burning phenomena, oxidation conditions and luminosity-time records

07 p1223 A71-19623

Two phase mixture spark ignition dynamics, investigating probabilistic character and ignition energy

07 p1224 A71-20068

Combustion kinetics of premixed laminar graphite dust-oxygen-nitrogen flames with/without hydrocarbon

08 p1346 A71-20866

Flame structure in laminar condensed systems, noting burning rate dependence on pressure and specimen layer thickness, composition and mechanical condition

08 p1376 A71-21906

Al particle burning in oxygen and water vapor, examining surface oxide film role in ignition mechanism

08 p1376 A71-21908

Gaseous fuel mixtures containing nitrogen oxides, discussing combustion mechanism

09 p1403 A71-22531

Combustion research laboratory at Purdue University consisting of buildings, housing test cells, data acquisition system, propellant storage and instrument service area

09 p1427 A71-22727

Burning rate temperature sensitivity of composite solid propellants, using granular diffusion flame model

09 p1510 A71-22911

Thermal ignition theory review, discussing mathematical problem statement, ignition characteristics approximate calculation methods, heat transfer mechanisms, geometrical and critical conditions, experimental tests, etc

10 p1695 A71-24050

Shock tunnel extremely high enthalpy and pressure for scramjet engine combustion research

11 p1860 A71-26267

Shock induced combustion by firing spheres or cone cylinders into air- or oxygen-hydrogen mixtures, taking shadow photographs of resulting disturbances

11 p1860 A71-26268

One dimensional premixed turbulent flame energy equation as function of heat release rate curve, temperature, velocity, composition and density

12 p1983 A71-26741

Gasoline-air mixtures normal combustion velocity by photographic observations of flame propagation in transparent tubes

12 p1986 A71-27499

Shock wave ignition of liquid fuel droplet in oxidizing atmosphere, discussing combustion process

[AIAA PAPER 70-9]

12 p1986 A71-27566

Experimental proof of combustion phenomena in reinforced plastics ablation under simulated atmospheric reentry, using arc plasma jets

12 p1987 A71-27721

Nitric oxide formation kinetics in shock induced combustion processes, considering hydrogen-oxygen-nitrogen reaction

13 p2113 A71-28616

Nonresonant noise from turbulent nonpremixed flames, discussing burner diameter, impingement angle and equivalence ratio effects on acoustic power radiated

[AIAA PAPER 71-732]

14 p2295 A71-30779

Combustion generated aerodynamic noise, considering sound radiation from open turbulent flames, spectral content, power output and origin

[AIAA PAPER 71-735]

14 p2338 A71-30780

Turbulent gas flame length in motionless air of various ambient temperatures, comparing calculation with measurement

15 p2511 A71-31380

Hydrocarbon flame radicals excitation nature observation by photoelectric measurements, noting irrelevance to electron-ion recombination

15 p2463 A71-31389

Unenclosed laminar jet diffusion flame phenomenological analysis predicting flame height relationship to fuel flow rate and atmospheric density and oxygen concentration

[WSS/CI PAPER 71-12]

15 p2513 A71-31622

- Boron combustion characteristics as function of temperature, pressure and gaseous fuel mixture ratio, using color photography [WSS/CIPAPER 71-19] 15 p2464 A71-31628
- Combustion characteristics of single boron carbide particles, studying minimum gas temperatures for self-ignition and burning times [WSS/CIPAPER 71-21] 15 p2464 A71-31630
- Al particles combustion kinetics in propellant flames, showing gas composition and pressure effects on burning rate [WSS/CIPAPER 71-24] 15 p2464 A71-31633
- Nonpremixed and premixed combustion theory in laminar flows, considering diffusion flame-reaction time ratio and activation energy effects 15 p2515 A71-32564
- Mathematical model for combustion processes, obtaining computerized approximate solutions for momentum, heat and mass transfer partial differential equations 16 p2663 A71-33362
- Monograph on flame form and temperature field at burners with nozzle for oxygen addition, using water model 17 p2837 A71-34795
- Combustion systems ionic wind velocities, investigating gauze parameters, magnetic fields and mixture inhomogeneity effects 17 p2785 A71-35703
- Concentration profiles around burning droplet, assuming constant binary diffusion coefficients for all species 17 p2840 A71-35705
- Combustion dynamics, including fire spread in solid fuels, ignition, turbulent/laminar fields and boundary layer, stagnation point and opposed jet burning 19 p3166 A71-38077
- Chemi-ionization induced by cyanogen in stoichiometric atmospheric pressure carbon monoxide-oxygen-nitrogen flames 19 p3013 A71-38089
- Boron powder combustion at elevated pressures, observing preignition metastable surface reactions, self sustained diffusion burning and decay 19 p3170 A71-38116
- Low pressure trimethylaluminum vapor and oxygen flat diffusion flame structure, observing separation, formation and growth 19 p3121 A71-38299
- Soviet book on fuel burning process physicochemical fundamentals covering combustion gases thermophysical and thermochemical characteristics, methane, formaldehyde and carbon monoxide combustion reaction kinetics, etc 20 p3194 A71-39089
- Exothermic decomposition reaction and sublimation mechanism of ammonium perchlorate burning, showing pressure dependence of burning rate 22 p3587 A71-42100
- Limiting chemical reaction rate of graphite and carbon containing material combustion at high temperatures 24 p3890 A71-45108
- Combustion and chemical reactions near wall, in forced convection, boundary layer transition, radiation and ablation of missile reentry 24 p3890 A71-45148
- ### COMBUSTION PRODUCTS
- Combustion residues particle size and distribution during rocket plume impingement on Al surface 01 p0183 A71-11594
- Sulfur trioxide catalytic formation in gases from fuel-rich propane-air flames containing sulfur 03 p0376 A71-14279
- Safe escape from toxic combustion products environment, discussing time of environmental deterioration dependence on consolidated biokinetic forces 04 p0543 A71-15055
- Explosion products population inversion by combining vibrational chemical excitation with thermal ignition 06 p0865 A71-17402
- Plastics thermal decomposition, investigating combustion products and toxicity 06 p0916 A71-18089
- Back mixing effects on hydrocarbons combustion, comparing well-stirred reactor with flat flame soot yields 07 p1181 A71-19240
- Methane and ethane binary mixtures with chlorine, determining main combustion products under flame propagation 07 p1054 A71-19280
- Oxygen-kerosene fuel combustion products, calculating thermal and physical constants 08 p1346 A71-21263
- Carbon dioxide laser population inversion using chemical reaction of burning with gas combustion products of vibrationally excited polyatomic molecules 08 p1302 A71-21499
- Water vapor condensation effects on methane-air combustion gases for aerodynamic test medium [AIAA PAPER 71-258] 08 p1377 A71-21986

- Optimal inlet parameters of MHD generator channel employing kerosene-gaseous oxygen combustion products 09 p1386 A71-22136
- High chromium Ni-Cr alloys use and improvement, discussing refractoriness in oxidizing atmospheres and chemical corrosion in combustion products deposits 09 p1470 A71-23043
- Nonequilibrium recombination of dissociated combustion products of hydrogen in oxygen enriched heated air in supersonic nozzle 10 p1696 A71-24381
- Rocket propellant performance improvement with boron, giving boiling temperature vs pressure and calculation methods for combustion products composition 11 p1809 A71-25573
- Air polluting nitric oxide and soot production by jet aircraft, discussing mixing process and atmospheric dispersion [AIAA PAPER 70-115] 12 p1946 A71-27560
- Combustion process in mixing zone of kerosene-air mixture and hot combustion products, deriving flameout time relation to characteristic temperature in mixing region 13 p1263 A71-28964
- Chemical kinetic calculation of nitric oxide formation in spark ignition automobile engines and gas turbine combustors 14 p2190 A71-30454
- Physicochemical properties of powdered Al and Al-Mg-Zn alloy combustion products from chemical, electron microscopic and X ray analysis 14 p2191 A71-30617
- HF stability and combustion product flow characteristics of laminar burning in cylindrical tube, considering longitudinal and radial instabilities 14 p2338 A71-30856
- Thermal fatigue cracking of gas turbine blades in fuel combustion product flow, investigating surface composition, microhardness and structure under simulated loads 15 p2469 A71-32227
- Aircraft pollutant emission regulation, discussing low smoke combustors and fuel dumping problem 15 p2516 A71-32246
- Jet engines nitric oxide air pollutant emission formation, developing gas turbine combustor models [AIAA PAPER 71-712] 15 p2470 A71-32289
- Carbon dioxide laser population inversion based on chemical combustion reaction producing gas of vibrationally excited polyatomic molecules 16 p2585 A71-33047
- Computer controlled data handling system for quadrupole mass spectrometer performing on-line chemical analysis of rocket chamber combustion gases [JPL-TR-32-1518] 16 p2578 A71-33182
- Materials stability testing in high temperature propane-butane combustion product flow, selecting compact silicon carbide for structural use in redox medium 17 p2761 A71-34310
- Combustion products and temperature distributions along axis of hexane/air diffusion flame 18 p2984 A71-35867
- Ethyl alcohol combustion effect on laminar boundary layer structure near flat plate, assuming thermal cracking of fuel 19 p3169 A71-38113
- Soviet monograph on carbon deposits in jet engines covering distribution, formation, fuel properties, reduction and removal and harmful effects in gas turbines 21 p3437 A71-40871
- Time of useful function after mice exposure to life threatening toxic mixtures of carbon monoxide, carbon dioxide and ammonia produced by combustion 22 p3486 A71-41830
- Human waste product utilization possibility through mineralization by wet combustion method 22 p3507 A71-42820
- Thermal combustion produced biocomplex vegetable waste mineralization effect on furnace working surface oxide film 22 p3507 A71-42821
- Emissivity calculation for radiant heat flux from isothermal gas mixture of hydrocarbon fuel combustion products 23 p3718 A71-43918
- Fuel droplet burning rate variation with ambient temperature and oxygen concentration in combustion gas environment 24 p3887 A71-44606
- Condensate particle crystallization retardation effect on energy characteristics of jet engine, calculating nonequilibrium flows of two phase combustion products in nozzle 24 p3864 A71-45004
- ### COMBUSTION STABILITY
- #### NT FLAME STABILITY
- Supersonic and subsonic combustion modes in constant area ramjet combustors, deriving dimensionless parameter for varying flow ratios as combustion stability criterion [ASME PAPER 70-WA/AV-4] 03 p0521 A71-14148

- Stability criteria for longitudinal combustion instability tested for generality using data from various solid propellant formulations [AIAA PAPER 69-480] 05 p0837 A71-16569
- Combustion instability data with same solid propellants by T-burner and L super asterisk burner, discussing theoretical models of transient combustion 05 p0837 A71-16570
- Powder combustion unsteady processes equations, taking into account nonadiabatic flame front and chemical reactions incompleteness 06 p1005 A71-17389
- Unstable liquid propellant rocket engine nonlinear behavior, considering stability of cylindrical combustor with distributed steady state combustion process and multiorifice quasi-steady nozzle [AIAA PAPER 71-208] 06 p0948 A71-18644
- Solid propellant combustion instability, considering burning propellant mass flux response to periodic thermal radiation [AIAA PAPER 71-209] 06 p0948 A71-18645
- Pressure wave distortion effects on combustor acoustic mode instability based on model with burning rate related to Reynolds number 07 p1224 A71-19906
- Liquid fuel rocket combustor longitudinal pressure oscillations nonlinear analysis, using multiple scales technique 09 p1544 A71-22107
- Combustion reactions development with velocity gradient downstream steady shock wave, considering aerodynamic field in supersonic wind tunnel 10 p1694 A71-23813
- Stable limit cycles and triggering limits of first radial mode in nonlinearly unstable liquid propellant rocket motors, using wave equation and Galerkin method 11 p1836 A71-25162
- Compositional and oxidizer particle size effects on combustion instability of plastic propellant based on ammonium perchlorate and polyisobutene [AIAA PAPER 69-478] 11 p1809 A71-25454
- Ammonium perchlorate deflagrations, determining intrinsic stability of one dimensional burning configuration based on flame structure modeling [AIAA PAPER 70-123] 11 p1809 A71-25455
- Gas turbine engine combustor stability dynamic model, representing premixing and combustion chambers as Helmholtz resonators for stability criteria derivation [ASME PAPER 71-GT-73] 11 p1813 A71-25987
- Solid propellant combustion stability theory for two dimensional disturbances, considering process as elastic body transformation into gaseous combustion products 13 p2159 A71-28138
- Monograph on solid propellant rockets combustion instability covering pressure oscillations at acoustic frequencies, swirling nozzle flow, chamber pressure, etc 14 p2287 A71-29577
- Pulsed T-burner testing of oscillatory combustion and droplet damping of aluminized solid propellants as function of frequency and sample properties [AIAA PAPER 71-634] 14 p2289 A71-30713
- Comparative variable area, pulsed and modified T burners for testing oscillatory combustion and stability of propellants containing aluminum [AIAA PAPER 71-635] 14 p2289 A71-30714
- Turbopropulsion systems thrust augmentor combustion instability, discussing physical causes due to various pressure oscillation modes [AIAA PAPER 71-697] 14 p2293 A71-30756
- Turbojet and turbofan augmentors combustion instability, discussing pressure oscillations elimination by screech liner and flameholder design [AIAA PAPER 71-698] 14 p2294 A71-30757
- Acoustic absorbers for combustion instability prevention, discussing design theory and experimental results [AIAA PAPER 71-699] 14 p2294 A71-30758
- Frequency analysis of open loop transfer function, determining combustion instability for catalytic monopropellant thrusters [AIAA PAPER 71-701] 14 p2286 A71-30759
- Combustion instability with wave motion coupling in solid propellant rocket motors due to energy gain and loss mechanisms within chamber [AIAA PAPER 71-753] 14 p2296 A71-30787
- Solid propellant rocket engine design, discussing combustion instability technology applications in damping and driving mechanisms influence determination [AIAA PAPER 71-754] 14 p2296 A71-30788
- Minuteman 2 third stage rocket engine instrumentation performance evaluation for oscillatory combustion characteristics analysis [AIAA PAPER 71-755] 14 p2248 A71-30789
- Acoustic liner design for propellant combustion instability and jet aircraft noise suppression, discussing cross flow and oscillatory pressure effects [AIAA PAPER 71-757] 14 p2296 A71-30791
- HF stability and combustion product flow characteristics of laminar burning in cylindrical tube, considering longitudinal and radial instabilities 14 p2338 A71-30856

Analytical model of oscillatory combustion in aircraft engine augmentors [AIAA PAPER 71-700] 15 p2466 A71-31324

Nonlinear combustion stability problems in liquid propellant rocket engines, describing unsteady combustion response by Crocco time lag hypothesis 15 p2467 A71-31471

Solid propellant rocket engines combustion instability, reexamining Culick analysis of longitudinal oscillations with pressure and velocity coupling 15 p2467 A71-31473

Acoustic damping of small amplitude waves by non-burning particles in T burners and rocket motors, noting propellant seeding with zirconium oxide [AIAA PAPER 71-633] 15 p2471 A71-32574

Turbulent combustion stability in rocket engine with allowance for walls reflecting acoustic waves excited by flame 16 p2663 A71-33605

Soviet papers on fuel vibrational combustion in model devices covering applications to gases, powder and coal particles 17 p2839 A71-35694

Exhaust pipe or diffusion kinetic flame type relaxation autooscillatory fuel combustion system, calculating vibrational frequency, amplitude and mode 17 p2839 A71-35695

Cylindrical shaped powder samples vibrational combustion, observing acoustic instability with high speed motion picture photography 17 p2839 A71-35698

Cylindrical powder samples combustion stability, noting gaseous and condensed phase interaction effects on sound emission 17 p2840 A71-35699

Nitroglycerin powder combustion acoustic instability, determining mean pressure and sample and combustion chamber geometry effects 17 p2840 A71-35700

Nonlinear combustion instability in liquid propellant rocket engines, describing unsteady combustor flow with single wave equation 19 p3122 A71-38093

One dimensional nonsteady combustion processes accompanying self sustained detonation waves initiated by merger of two weak shock waves, using Lax finite difference method 19 p3170 A71-38127

Solid propellant rocket motor stable operation region, describing propellant response function to pressure and velocity fluctuations [ONERA-TP-1016] 22 p3588 A71-41956

COMBUSTION TEMPERATURE

Bipropellant droplet supercritical steady combustion temperature measurements in zero gravity near critical point, comparing high and low pressures models for ambient gas solubility 01 p0141 A71-11309

Aluminum addition effect on combustion rate of mixtures of ammonium perchlorate with polymethyl methacrylate at different temperatures 03 p0520 A71-13995

Solid propellant oxidizers hydroxylammonium perchlorate and hydrazine nitroform self deflagration, determining combustion temperatures and burning rate pressure relationships 06 p0944 A71-18299

Gas temperature in combustion chamber and jet nozzle exit, and gas jet velocity resulting from various pressures, temperatures and air excess factors combinations 06 p0948 A71-18702

Internal combustion engine gas temperature measurement, using ultrasonic wave frequency shift method 11 p1810 A71-25269

Rocket propellant performance improvement with boron, giving boiling temperature vs pressure and calculation methods for combustion products composition 11 p1809 A71-25573

High altitude probe design and optimization, discussing hybrid propellant propulsion system peak altitude payloads and combustion temperatures 11 p1811 A71-25575

Ammonium perchlorate combustion characteristics as function of initial temperature by miniature thermocouple measurements 16 p2623 A71-33361

COMBUSTION VIBRATION

Oscillatory combustion mechanism variations with geometrical configuration changes, considering variable cross sectional area and straight tube combustors 03 p0517 A71-13354

Axisymmetric wake diffusion flame response to HF periodic velocity oscillations at combustor boundaries 08 p1375 A71-20863

Missile component vibration environments generation by Minuteman 2 and 3 third stage motors solid propellant oscillatory burning [AIAA PAPER 71-756] 14 p2296 A71-30790

Turbulent homogeneous air-fuel mixtures pulsating combustion in plane chambers with nozzle and plate

stabilizers, noting influence of fuel type and mixture composition 16 p2663 A71-33360

Vibrational combustion study of powder, using Helmholtz resonators with connected auxiliary combustion chamber 17 p2839 A71-35697

Cylindrical shaped powder samples vibrational combustion, observing acoustic instability with high speed motion picture photography 17 p2839 A71-35698

Self excitation and amplitude limitation of powder vibratory combustion, considering pressure and sample length effects 17 p2840 A71-35701

Solid fuel vibrational combustion devices and operational analysis, considering various chamber configurations 17 p2840 A71-35702

Vibratory flame propagation and pressure measurements in short closed tubes and vessels, using high speed schlieren cinematography and quartz piezoelectric transducer 19 p3167 A71-38097

Combustion driven acoustic oscillations in gas fired burner of premixed methane, nitrogen and oxygen, noting mixture ratio and flow rate effects 19 p3123 A71-38098

Combustion oscillator for MHD energy conversion, using products flow modulation by traveling pressure wave 19 p2998 A71-38099

Film ablative cooled gas pressure feed liquid rocket engine unstationary process analysis with digital computer, detailing engine dynamics, heat transfer and temperature profile 22 p3589 A71-42054

Aerodynamic combustion noise generation from premixed or diffusion open turbulent flames, using fluid mechanics and Lighthill method 23 p3781 A71-43448

COMBUSTION WAVES

U FLAME PROPAGATION

COMBUSTORS

U COMBUSTION CHAMBERS

COMET 4 AIRCRAFT

Comet 4 installation and experimental program, investigating avionics systems integration techniques 17 p2774 A71-35070

COMETS

NT AREND-ROLAND COMET

NT GIACOBINI-ZINNER COMET

NT MRKOS COMET

NT SCHWASSMANN-WACHMANN COMET

Asteroids, comets and meteor dynamics in solar system, examining motion and orbital evolution by computer techniques 01 p0155 A71-10437

Comet Tempel-Tuttle elements, discussing association with Leonids meteor shower 01 p0159 A71-10808

Comet head physical processes, discussing atomic and molecular distributions, gas ejection velocity and temperature, UV optical thickness, photodissociation, etc 02 p0308 A71-12097

Computer program for processing elliptical polarization observations of nebulae and comets 02 p0251 A71-12360

Comet brightness fluctuation phenomenon, discussing solar wind interaction with Platt particles in cometary atmosphere 02 p0303 A71-12867

Comet distributions near Jupiter orbit 03 p0487 A71-13375

Photoelectric measurements of four comets, discussing instrumental data transformations to international UVB system 03 p0490 A71-13943

Planetary system effects on long period comets orbital characteristics, presenting eccentricities and reciprocal semimajor axes calculations 04 p0642 A71-14738

Comets-minor planets relationship, discussing comas, physical appearance, light variations and condensations 04 p0653 A71-15713

Long period comets orbital orientations and perihelion distances, discussing Oort evolutionary theory modification 04 p0659 A71-15858

Geometrical solutions to central motion and space vehicle dynamics, including Chaplygin problem, position and velocity transfer and comet tail separation 05 p0810 A71-16584

Comet origin based on Lagrange hypothesis and motion analysis, discussing planets short-period families 06 p0965 A71-17625

Tektites earth vs possible lunar or cometary origins, taking into account chemical composition 06 p0968 A71-17963

Cometary nebulae and globules, discussing ionized and neutral gas densities, temperatures and morphological classifications 06 p0974 A71-18433

Nearly parabolic comets orbital orientation relation to sun peculiar motion direction, noting repulsive particles capture mechanism 06 p0976 A71-18449

Multiple impulsive spacecraft trajectory optimization technique application to comet rendezvous problem, using computer program [AIAA PAPER 71-93] 06 p0977 A71-18548

Short period comets opposition at recent apparitions, investigating nongravitational forces effects in motions 07 p1202 A71-20513

Comet head physical processes, discussing atomic and molecular distributions, gas ejection velocity and temperature, UV optical thickness, photodissociation, etc 08 p1362 A71-21147

Comet Bennett 1969i IR narrow band filter photometry 09 p1442 A71-22067

Suzuki-Sato-Seki and other 1970 comets, discussing position observation and ephemeris calculation 09 p1516 A71-22069

Comet 1969g spectrum at 3800-8500 A, noting upper H alpha surface brightness limit consistency with chromospheric resonance fluorescence model 09 p1517 A71-22335

Comets structural features via visual observations, emphasizing inner coma structures and expanding envelopes surrounding nucleus 09 p1526 A71-23351

Comets gaseous atmospheres related to 1970 OAO discovery of vast hydrogen atmosphere, indicating molecular hydrogen abundance and gas production rate 10 p1665 A71-23745

Sodium D line flare emission on solar surface vs comet scattering, using photoelectric observation in undisturbed center disk region 10 p1660 A71-23791

Asteroids or comets orbital elements calculation, using initial heliocentric position and velocity as zero time orbital elements 10 p1668 A71-24023

Shock and turbulent ray interactions of plasma streams with neutral gas cloud, noting comet tail similarity 10 p1652 A71-24653

Cometary nucleus radius, mass, composition and icy-conglomerate model 10 p1677 A71-24687

Spectroscopic observation of comet Bennett near perihelion, noting solar continuum intensity dependence on wavelengths 10 p1681 A71-25062

Cometary atmosphere photometric data, determining particle distribution and ejection rate, temperature, molecular lifetime, acceleration and emission velocity 11 p1821 A71-25542

Dust particle angular momentum orientation in comet tails through bombardment by solar wind protons, noting role in scattered light polarization 11 p1832 A71-26182

Comet orbits correction, including differential coefficients perturbations based on Kulikov equation for difference between computed and true radius vector 11 p1833 A71-26328

Cometary nebulae and globules, discussing ionized and neutral gas densities, temperatures and morphological classifications 12 p1955 A71-26583

Nearly parabolic comets orbital orientation relation to sun peculiar motion direction, noting repulsive particles capture mechanism 12 p1955 A71-26599

Ground based and airborne IR observation of comets over various wavelengths, determining flux distribution, luminous outbursts and color temperature 12 p1956 A71-26621

Comet Bennett light polarization data, determining color index and chemical composition 12 p1965 A71-27227

Comets Alcock 1963 III and Everhart 1964 IX brightness bursts, obtaining time curves for gas evolution 12 p1965 A71-27228

Bibliography on lunar and planetary subjects covering astrobology, comets, cratering, meteors temperature, structure, asteroids, tektites surface features, etc 13 p2135 A71-28293

Narrow-band photometry of comet Bennett, giving intensity profiles and interference filter transmission curve 13 p2138 A71-28761

Sunward-pointing secondary tail of comet Tago-Sato-Kosaka observed on astronomical plates 13 p2138 A71-28763

Comets, observational report 1970 13 p2138 A71-28764

Bright comets particles albedo, absorptivity and size observation by combined IR and optical photometry 14 p2314 A71-30649

Brightness dependence on heliocentric distance of cometary hydroxyl and hydrogen halos, using three step production mechanism

14 p2318 A71-31124

Dachs three axis payload stabilization and attitude control system for spectroscopic comet observation

15 p2499 A71-31218

Soviet papers on irregular forces of comet motion, emphasizing Daniel comet-asteroid collisions, orbit evolution, brightness, orbital distances, etc

15 p2481 A71-31297

Daniel 1909 IV comet orbit evolution, discussing capture by Jupiter, asteroid collision, brightness, orbit perturbation and nongravitational force effects

15 p2481 A71-31298

Daniel comet collision frequency calculations with asteroids and microasteroids based on trajectory analysis

15 p2481 A71-31299

Daniel comet minimum distance distributions between asteroids, determining minor planet masses

15 p2482 A71-31302

Comet and asteroid orbits tangential approximation, determining minimal distances and velocities as function of orbital elements

15 p2482 A71-31303

Absolute magnitudes of 1965-1969 comets, including orbit elements, perihelion coordinates and maximum values of reduced head diameter and tail length

15 p2483 A71-31339

Soviet papers on cometary physics covering photometric observations, morphology, composition, internal dynamics, atmosphere, density, albedo, photographic techniques, etc

15 p2484 A71-31660

Motion equations for neutral matter in head atmosphere of bright comet with high density spherical source and molecular collisions

15 p2484 A71-31661

Density distribution of neutral matter in cometary atmosphere in transition region between hydrodynamic and free molecular flow

15 p2484 A71-31662

Albedo-optical thickness relation in photometry of gas and dust comets

15 p2484 A71-31663

Physical characteristics of comet Encke from visual observations, indicating nucleus of porous refractory material and ice structure

15 p2484 A71-31664

Monochromatic photometry of comets for molecular emission bands in head spectra, using wideband and narrowband filters

15 p2484 A71-31665

Cometary nuclei photometry, using focal images of stars with normal exposures as calibration markings in plate characteristics

15 p2484 A71-31666

Nucleus brightness of comet Ikeya-Seki from plates in photographic and photovisual spectral regions, indicating relation to solar rotation

15 p2484 A71-31667

Photometry of head and tail regions of comets Kosik, Akhamarov-Lurlov-Hassel, Arend-Roland and Mrkos by equidensity method, using Sabatier effect

15 p2484 A71-31668

Coordinate transformations of shape and position of cometary tails on orbit plane suitable for digital computer

15 p2485 A71-31669

Comet Honda 1968 c, determining osculating hyperbolic orbit from osculating elements

16 p2634 A71-33426

Comet origin hypotheses, examining orbit axes and perihelions distribution

16 p2639 A71-33693

Intra-Mercurial planets and comets discovered during solar eclipses, discussing size, orbital eccentricity, albedo and equilibrium temperature

16 p2642 A71-33830

Asteroids and comets bibliography and review, considering celestial mechanics and astrometry, photometry, spectra, polarimetry and radar measurements

17 p2798 A71-34455

Comet dust polydispersion, showing particle distribution near nuclei similar to meteor streams

17 p2803 A71-34829

Cometary dissociative recharging and recombination dissociation of water and hydrogen peroxide molecules in comets, giving empirical relation for effective cross sections

17 p2803 A71-34830

Honda 1968 comet activity from photographic and visual brightness observations, establishing relation between brightness fluctuations and solar activity

17 p2803 A71-34831

Brightness fluctuations in photometric nucleus of Ikeya-Seki comet at 29-31 March 1968

17 p2803 A71-34832

Visual integral brightness estimates of Ikeya-Seki 1967n comet observed at Dyushambe from 9 January to 18 April 1968

17 p2803 A71-34833

Graphic method for comet geocentric equatorial coordinates transformation into heliographic coordinates, using trigonometric circle and three stereographic networks with 100 mm radii

17 p2803 A71-34834

Lyman alpha resonant radiation in regions distant from cometary tails due to additional atomic hydrogen production from dust particles

17 p2809 A71-35595

Heliocentric energy per mass changes in close planetary encounters, noting relation to cometary and asteroidal material evolution

17 p2811 A71-35744

Book on space science covering celestial coordinates, time and mechanics, planetary atmospheres and interiors, comets, meteors, stellar structure, etc

18 p2963 A71-36246

Comet Tago-Sato-Kosaka isophotometry, obtaining surface brightness distribution and solar wind velocity estimate

19 p3130 A71-37228

Comet Bennet light polarization data, determining color index and chemical composition

19 p3132 A71-37379

Comets Alcock 1963 III and Everhart 1964 IX brightness bursts, obtaining time curves for gas evolution

19 p3132 A71-37380

Matter effluence forming comet Bennett 1969 i tail, calculating particle ejection acceleration as function of intrinsic anomaly of nucleus

19 p3138 A71-37783

Requirements and opportunities for comet and asteroid missions including flyby, rendezvous, docking and sample return

[AAS PAPER 71-104]

19 p3139 A71-37906

Grand Tour meteoroid environment analysis, considering different asteroid and cometary particle models

[AAS PAPER 71-110]

19 p3139 A71-37910

Shuttle/Centaur injection stage, considering application to comet rendezvous mission via Jovian powered swingby

[AAS PAPER 71-113]

19 p3139 A71-37912

Guidance and navigation requirements for rendezvous missions to two short period comets

[AAS PAPER 71-116]

19 p3101 A71-37913

Ultrapanetary probes for exploration beyond solar system, discussing heliosphere, cometary, interstellar and stellar mission categories propulsion system selection

[AAS PAPER 71-164]

19 p3141 A71-37961

Laser radar observation of comet Bennett dust at 40-90 km, deducing particle size from rate of descent

19 p3142 A71-38041

Comet Bennett 1969 head and tail polarization distribution data, using triple astrophotograph

19 p3145 A71-38524

Numerical integration of element T /transit time through perihelion/ in perturbations of near parabolic comet orbits

20 p3291 A71-39321

IAU Executive Committee, General Assembly and commissions reports on astronomy, including manuscripts preparation guidelines, handbook, etc

20 p3315 A71-39425

H atoms generation by photodissociation of molecules evaporated from cometary core, basing analysis on hydrogen atmosphere line spectra

20 p3293 A71-39538

Sporadic and cometary meteor particles concentration along earth orbit, using optical and radiant measurements

20 p3299 A71-39650

Comet Bennett 1969i nucleus light polarimetric observations, noting vibration direction

21 p3440 A71-40060

Ionized carbon monoxide in cometary tails, estimating time scale in recombination of ions into C₂ atoms

21 p3442 A71-40155

Microwave water emission in Comet Bennett, deriving column density for various temperatures of cometary gas

21 p3443 A71-40190

Absolute magnitudes of 1965-1969 comets, including orbit elements, perihelion coordinates and maximum values of reduced head diameter and tail length

22 p3606 A71-42614

Solar electric propulsion application to Halley Comet flythrough and rendezvous missions, describing trajectory characteristics and payload capabilities

[AAS PAPER 71-363]

23 p3729 A71-43033

Cometary nucleus disintegration rate as function of orbital elements, calculating lifetimes for Encke and Halley type comets

23 p3772 A71-44313

Effective excitation cross sections of molecular CO ion bands in comet tails due to He ions collisions with CO molecules, considering deviation from adiabatic hypothesis

23 p3708 A71-44314

Cometary nucleus outbursts and splitting moments spatial distribution, indicating solar radiation and tidal action effects

24 p3868 A71-44457

Comet brightness variations correlation with geomagnetic field and solar corpuscular flux variations in interplanetary space

24 p3870 A71-44814

Orbital elements of Encke comet from 1953-1954, 1957, 1960-1961 and 1963-1964 apparitions, finding secular acceleration coefficient

24 p3874 A71-45176

COMFORT

Helicopter pilot and passenger comfort/vibration tolerance criteria

04 p0532 A71-15420

Air transportation systems ride vibration environments in relation to human comfort

04 p0532 A71-15421

COMMAND AND CONTROL

Command system and associated algorithm for synthesis of integrated microcircuits composed of components with memories

01 p0051 A71-10090

Skyнет telemetry and command stations configuration and equipment functions, discussing antenna subsystem parabolic reflector and positioning, PCM demodulation and computer systems

02 p0217 A71-12431

OA0 2 design and performance features concerning pointing accuracy and stability, command capability, data handling, thermal environment, orbit constraints, ultraviolet spectroscopy, etc

05 p0818 A71-17128

Intelsat 3 Ground Control System functions, design and operation of tracking, telemetry and command stations subsystems

06 p0870 A71-18394

Computer controlled ground based command and data acquisition software system for OA0-A2 spacecraft remote control stations, discussing interface with monitor and interrupt capabilities

08 p1259 A71-21658

Aircraft integrated command and control system, discussing vertical, aerodynamic and horizontal situations, flight mechanics, power setting, telecommunications, etc

15 p2349 A71-31878

COMMAND GUIDANCE

First order digital phase locked loops analysis for single channel command system, using random walk techniques

08 p1270 A71-21351

Apollo command module guidance computer and environment hybrid simulation for flight software and crew procedures verification

11 p1744 A71-25845

Interceptor aircraft optimal nonlinear command guidance scheme for reduction of airborne computation load with forward prediction of interceptor and target state vectors

19 p3096 A71-37166

COMMAND MODULES

N-body real time trajectory simulation of Apollo Command and Service module G and C systems and mission

02 p0237 A71-11793

Soyuz spacecraft command cabin equipment, describing control panel, command signal systems and routine operations

03 p0497 A71-13196

Adhesives in Apollo command, service and lunar modules primary load carrying structures, electrical potting and sealing medium

10 p1630 A71-24067

Apollo command module guidance computer and environment hybrid simulation for flight software and crew procedures verification

11 p1744 A71-25845

Apollo command module aerodynamic characteristics in hypersonic low density flow, measuring drag, three component force and heat transfer

22 p3480 A71-42027

Apollo command module land landing capability in case of abort after liftoff, describing Monte Carlo simulation procedure

22 p3573 A71-42776

COMMAND SERVICE MODULES

Apollo Command and Service Module simulation of flight phases in lunar landing missions

02 p0237 A71-11792

Apollo 15-17 CSM design modifications, discussing increased mission duration capability, lunar orbital science instruments operation and weight increase

17 p2812 A71-34723

Minkey rendezvous computer program in Apollo 15 CSM aiding guidance, navigation and control system functions

17 p2772 A71-35055

COMMAND SYSTEMS

U COMMAND GUIDANCE

COMMAND-CONTROL

U COMMAND AND CONTROL

COMMERCIAL AIRCRAFT

NT A-300 AIRCRAFT

NT BOEING 737 AIRCRAFT
 NT BOEING 747 AIRCRAFT
 NT BOEING 767 AIRCRAFT
 NT COMET 4 AIRCRAFT
 NT DC 10 AIRCRAFT
 NT DH 121 AIRCRAFT
 NT EUROPEAN AIRBUS
 NT F-28 TRANSPORT AIRCRAFT
 NT IL-62 AIRCRAFT
 NT L-1011 AIRCRAFT
 NT SUPERSONIC COMMERCIAL AIR TRANSPORT

NT TU-134 AIRCRAFT
 NT TU-144 AIRCRAFT
 NT VC-10 AIRCRAFT
 German monograph on commercial jet aircraft maintenance systems covering changes and adaptations for performance improvement
 01 p0004 A71-10114

German monograph on systems analysis of future jet and fan propulsion systems for VTOL commercial aircraft weight and cost reduction
 01 p0142 A71-10115

Commercial transport aircraft maintenance simulation Monte Carlo Modeling techniques, considering application to airline operations
 [SAE PAPER 700345] 01 p0067 A71-10128

Civil aircraft aspect ratio relationship to commercial viability, considering need for minimum induced drag at wing loading to improve payloads, speeds and ranges
 01 p0005 A71-11628

Navigation and traffic control of VTOL commercial transport aircraft, discussing noise, G forces, turbulent wakes, approach profiles and V-ports
 04 p0624 A71-15429

Design objectives for subsonic, transonic and supersonic civil transport flying characteristics based on MIL-F-8785, considering aircraft control
 [SAE-ARP-8428] 07 p1019 A71-19645

Commercial aviation stratospheric water vapor injections influence on radiation budget, ozone, polar night cloudiness and potential climatic effects
 08 p1286 A71-21822

Ground deicing system for transport aircraft, discussing antifreeze liquid spray application after mechanical snow removal
 09 p1428 A71-22948

Commercial V/STOL aircraft area navigation system requirements, discussing airborne computer, flight plan data storage and control subsystems and horizontal orientation display
 10 p1639 A71-24150

FAA flying and handling qualities program, discussing development of optimum and minimum acceptable flight characteristics criteria for new civilian and military aircraft designs
 [SAE PAPER 710372] 10 p1554 A71-24241

Pan American reliability program effect on airline maintenance, considering cost effectiveness, aircraft performance, data collection and analysis
 12 p1910 A71-26671

Military/commercial STOL transport design, discussing performance, payload and equipment requirements with emphasis on production cost benefits
 [SAE PAPER 710468] 13 p1996 A71-28336

V/STOL and supersonic commercial aircraft developments, comparing man and machine performance as information processing systems for aircraft control and navigation
 13 p2018 A71-28486

Cost efficient sound limit expenditures per parameter unit in commercial transport aircraft design
 13 p2167 A71-28945

Commercial aircraft piloting in atmospheric turbulence, discussing aircraft characteristics, instrumentation, flying procedures, pilot training and kinesthetic cues
 14 p2173 A71-29782

Airborne integrated data system capabilities based on flight tests with commercial aircraft
 14 p2208 A71-30319

Commercial vs military design criteria for STOL transport aircraft, noting landing and takeoff distances and noise levels
 [SAE PAPER 710465] 14 p2176 A71-30536

STOL commercial aircraft propulsion systems, considering two stream augmentor wing engine and high bypass ratio three stream engine
 [AIAA PAPER 71-746] 15 p2467 A71-31325

Commercial SST aircraft engine noise during takeoff, discussing exhaust geometries for suppression
 15 p2468 A71-31595

French SNECMA M56 turbofan engine design for medium capacity airliners, featuring low specific fuel consumption and low noise level
 15 p2471 A71-32692

Commercial ATC, considering VFR, flight control and inertial navigation
 22 p3570 A71-42078

Takeoff and landing performance evaluation for commercial STOL aircraft, noting high bypass ratio turbofans and high lift systems use
 22 p3483 A71-42286

Airlines procedures in conducting pilot training programs within ICAO recommendations and German regulations
 23 p3639 A71-43230

Corporate aircraft operations in Latin America, discussing communication and navigation, fuel, paper work, food, vaccinations and weather
 23 p3629 A71-43391

COMMERCIAL AVIATION
 U CIVIL AVIATION
 U COMMERCIAL AIRCRAFT

COMMUNITION
 NT CRUSHING
 NT GRINDING [COMMUNITION]
 Metal powders role in brazing, considering melt atomization and mechanical comminution
 13 p2075 A71-29089

COMMUNICATING
 NT AIRCRAFT COMMUNICATION
 NT GROUND-AIR-GROUND COMMUNICATIONS

NT INFORMATION DISSEMINATION
 NT INTERSTELLAR COMMUNICATION
 NT POINT TO POINT COMMUNICATIONS
 NT UNDERGROUND COMMUNICATION
 NT VERBAL COMMUNICATION
 Information and technology transfer in multinational corporate R and D, discussing mechanisms of communication, use of common technical language and impediments due to attitude differences
 07 p1225 A71-19450

Vibrotactile information transmission, discussing skin mechano-receptive systems and similarities or differences between auditory and tactile characteristics
 10 p1563 A71-24231

COMMUNICATION
 NT INFORMATION DISSEMINATION
 NT UNDERWATER COMMUNICATION
 NT VERBAL COMMUNICATION

COMMUNICATION CABLES
 NT BEAM WAVEGUIDES
 NT COAXIAL CABLES
 NT PLASMA GUIDES
 NT WAVEGUIDES
 Surge voltages produced by transient currents on signal conductors in shielded cables
 07 p1022 A71-19946

Digital wire line system data bus design, calculating transmission performance of noise environment shielded twisted pair cable by linear filter model
 14 p2198 A71-30904

Satellite communication system selection vs underground cable or hybrid systems, based on power requirements and economics
 17 p2700 A71-34678

TV broadcasting by satellite to isolated users via cable transmission, estimating cost and satellite optimal radiating power
 18 p2877 A71-36507

Intercontinental point to point radio communication, discussing Hertzian beam /radio relay links/ and satellite communication comparison with underground and submarine cables
 19 p3016 A71-37343

COMMUNICATION EQUIPMENT
 NT ADVANCED VIDICON CAMERA SYSTEM [AVCS]

NT CLOSED CIRCUIT TELEVISION
 NT RADIO RECEIVERS
 NT SATELLITE TELEVISION
 NT SPACECRAFT TELEVISION
 NT SUPERHETERODYNE RECEIVERS
 NT TRANSMITTER RECEIVERS

Test laboratory for Skyнет spacecraft communications subsystems at microwave frequencies
 02 p0238 A71-12443

Skyнет types III and IV ground stations design, discussing signal flow, antenna system, SNR, tracking and transmitter channels and test facilities
 02 p0221 A71-12784

Earth station modifications for INTELSAT IV operation, discussing transmission parameters, distortion control, amplifier design, etc
 02 p0221 A71-12786

Satellite communications system earth station operation and reliability, discussing staffing, main and supporting communication equipment maintenance, utilities and redundancy
 02 p0224 A71-12825

Earth station communication system planning for Intelsat 4, discussing telephony and TV transmission
 02 p0225 A71-12830

Communication technology development relation to NASA programs, discussing receivers, microwave tubes, solid state transmitters, lasers, information retrieval and frequency sharing
 03 p0388 A71-14412

ATS 5 satellite millimeter wave earth-space propagation and communications equipment
 04 p0551 A71-15009

Aerospace technology application to oceanic instrumentation and communication requirements
 04 p0583 A71-15307

Gigabit PCM data communications system using functional circuits with microstrip interconnect
 05 p0719 A71-16152

Incomplete separation influence of composite signal components on noise stability of coherent communication systems
 07 p1064 A71-20257

Intelsat 4 transmission subsystems design, discussing alternative high power amplifier configurations, redundancy and emergency routing of transmitted RF carriers
 12 p1894 A71-26992

Communication electronic equipment electromagnetic compatibility characteristics derived from spectrum signature data, discussing application to systems design
 13 p2032 A71-28876

Airborne vidicoder visual communication system for transmitting single frame TV information in digital form from air to ground over narrow and wideband circuits
 17 p2709 A71-35760

Operator-computer communication devices with graphic data display, discussing construction and operation
 18 p2884 A71-35879

Gridistor microwave FET for space communication equipment, combining advantages of FET and bipolar transistors
 18 p2892 A71-36565

Phase locked loop oscillator applications in communication and instrumentation, discussing tracking receivers, FM and FSK detection, laser modes, pulse width modulation, etc
 18 p2884 A71-36997

Co-site analysis model automated for evaluation EM compatibility of single site employing large number of transmitting and receiving equipments
 19 p3032 A71-38457

Independent sideband transmitter checkout and maintenance for maximum communication circuit performance
 21 p3353 A71-40519

ATC integrated communication, navigation and identification system, discussing design, economics, technology and flexibility
 22 p3571 A71-42086

Computerized simulation of maintenance man hour loading for communication system based on repair, failure and availability distributions
 22 p3554 A71-42113

COMMUNICATION SATELLITES
 NT EARLY BIRD SATELLITES
 NT INTELSAT SATELLITES
 NT MOLNIYA SATELLITES
 NT RELAY SATELLITES
 NT SYNCOM SATELLITES

Geostationary communication satellites system with timed orbital motions for avoiding serial sun transit outages and eclipses
 01 p0030 A71-10471

Skyнет satellite communications system configuration and specifications, discussing geostationary satellite multiple access, SSMA transmission system, power budgets, reliability and repeater specifications
 02 p0217 A71-12428

Skyнет communication systems, describing long distance strategic communication links between ground and mobile air/helicopter stations via wide and narrow band pathways
 02 p0218 A71-12439

Skyнет satellites in orbit communications, repeaters testing, describing test facilities, spacecraft communication subsystems operation, terminals calibration and atmospheric losses
 02 p0218 A71-12440

Microwave radiometry for earth terminal and communication satellite performance measurements, including gain, tracking, noise temperature, radome attenuation, power and transfer characteristics
 02 p0218 A71-12446

Regional European communications satellite system operation, discussing coverage area, performance requirements, meteorological aspects of propagation, etc
 02 p0221 A71-12782

Cost optimal direct broadcast and redistribution satellite systems
 02 p0221 A71-12783

Communication satellite earth station technology, considering steerable antenna subsystems, high power amplifiers, terminal equipment and frequency bands allocation
 02 p0222 A71-12787

Electric power supplies for communication satellite earth stations, considering methods for power availability and stability
 02 p0222 A71-12788

Communication satellite autotracking by step track technique for exclusion of tracking feeds and multiple receiver channels in earth stations
 02 p0222 A71-12789

Communication satellite earth station steerable antennas drive train resonance and traction drive wheel

slippage control by differential velocity feedback, discussing analog simulation

02 p0222 A71-12790

Communication satellite ground station steerable antenna autotracking, evaluating on-line optimal search techniques by digital simulation

02 p0222 A71-12791

High efficiency spherical reflector antennas with scanning and multiple feed properties for communication satellite portable earth stations

02 p0233 A71-12792

Atmosphere effects on antenna noise temperature variations in G/T value for earth station performance in satellite communication system

02 p0222 A71-12799

Frequency selective conical scanning for direction finding earth station antennas for communication satellite automatic tracking, using waveguide mode conversion

02 p0223 A71-12809

Satellite communication system earth station transmitter with FDM-FM and SPADE carriers, noting intermodulation effect on channel capacity

02 p0223 A71-12810

Earth station mixers design as wideband millimeter wave up- and down-converters for satellite communication systems

02 p0234 A71-12818

Ground station central control and monitoring of satellite communications systems

02 p0224 A71-12822

Ground station power control in multiple access satellite communication system

02 p0224 A71-12823

Large earth station control for satellite communications system, including traffic capacity, TV transmission path breaks and logic equipment

02 p0224 A71-12824

Satellite communications system earth station operation and reliability, discussing staffing, main and supporting communication equipment maintenance, utilities and redundancy

02 p0224 A71-12825

Communication satellite systems ground stations operating personnel training, outlining basic and specialized study and on-job training program

02 p0224 A71-12826

Military earth communication station maintenance, noting mobility, environment, logistics and reliability

02 p0224 A71-12827

Large earth station operation and maintenance for international communications, noting control consoles, static tracking, aerial flexibility, transmitter reliability, etc

02 p0224 A71-12828

Antenna steering systems for satellite communications, discussing tracking, mechanical drives and subreflector servo

02 p0235 A71-12832

Ground based data derivation and transmission system for multicontrol satellite communication system

02 p0225 A71-12834

Nondegenerate parametric amplifiers above X band for satellite communication systems, discussing circuitry, varactors, diode packaging and solid state pump sources improvements

02 p0235 A71-12906

Satellites applications in French space programs, discussing telecommunication, meteorology, air navigation aids, space geodesy and earth resources

02 p0337 A71-12918

Television satellites orbital transfer from low to geostationary orbit using ion propulsion

03 p0378 A71-13742

Large multipurpose synchronous communication satellite, discussing design versatility, applications and operating characteristics

04 p0663 A71-15311

Remote area voice, teletype and data communication using satellites for providing links with central terminals, considering economic feasibility by cost analysis

04 p0555 A71-15338

Satellite voice communication by suppressed clock pulse duration modulation technique, using optimum digital modulation and processing for maximum traffic and cost effectiveness

04 p0555 A71-15340

Synchronous orbit satellite links in tandem for government and military telephone communications, discussing subjective evaluation for acceptability

05 p0725 A71-17070

European telecommunications satellite project, discussing INTELSAT and telephony-telegraphy-telex system

06 p1010 A71-17999

Communication satellite systems for long distance telephone connections, comparing transmission possibilities between links and terrestrial extensions

06 p0869 A71-18013

Intelsat 4 satellite optimum channel capacity as function of earth station performance

07 p1056 A71-18809

Pulse gated binary modulation (PGBM)/ visible laser communications for earth orbital missions

07 p1056 A71-18810

Radio amateur satellites contribution to space research and communications

07 p1057 A71-18814

Digital multiple access communications for commercial transmission via Intelsat satellites

07 p1057 A71-18817

Defense Satellite Communications System Phase II design and implementation, considering earth, space and control subsystems

07 p1057 A71-18818

Error free SATCOM computer to computer data communication via satellite link

07 p1058 A71-18822

Ionospheric electron density irregularity effects on communication satellite scintillation in auroral zone, using Doppler and Faraday measurements

07 p1098 A71-19035

Statistical model for interference to terrestrial radio relay systems from geostationary satellites

07 p1060 A71-19214

Passive airborne computer augmented aircraft antenna pointing control system for communication satellites tracking

[AIAA PAPER 71-233]

07 p1077 A71-19710

Communication satellite station at Fucino /Italy/, testing receiving and transmitting equipment transmission quality

07 p1063 A71-20041

Group delay and amplitude equalized bandpass elliptic function filters for ground stations of communications satellite system

07 p1082 A71-20412

Space-DMA or space-TDMA techniques conserving spectrum and increasing communication satellite channel capacity, discussing spot beams and switchings

08 p1254 A71-21326

Multisatellite communications system transmission capacity, comparing time division with Walsh multiplexing

08 p1269 A71-21334

Satellite communications systems international planning, discussing Intelsat system limitations

09 p1548 A71-23354

Luneberg lens antenna theory and gain for communication satellite radio links, discussing shielding from hostile space environment

10 p1583 A71-24450

Symphonic communication satellite power supply system voltage control, discussing controlled system properties based on closed circuit frequency characteristics

10 p1683 A71-24642

Ground stations for communication satellites, discussing radio transmitter and receiver systems using low noise parametric amplifiers at low temperatures and extended demodulator threshold

10 p1590 A71-25101

Communication satellite ground station radio receiver and transmitter systems including parametric amplifier and phase lock demodulators applications

10 p1590 A71-25102

Measurement system for communication satellite ground station equipment including parametric amplifier, wideband receiver, power oscillators, and radio transmitters and receivers

10 p1590 A71-25103

Parametric amplifier design and construction for communication satellite ground station, discussing noise temperature, distortions, bandwidth and antenna gain

10 p1580 A71-25105

Threshold-extension phase-lock demodulator design for optimizing satellite communication ground station systems, using FM carriers

10 p1580 A71-25106

Australian satellite domestic telecommunications network design, discussing population distribution, existing systems and Intelsat 3 F-4

11 p1730 A71-25264

Symphonic Franco-German satellite telecommunications system, describing orbital launching operations

11 p1840 A71-26523

Project Symphonie status in January 1971, discussing booster stages, ground stations, thermal control, stabilization, power supply system, telecommunication equipment and telecontrol system

11 p1840 A71-26524

Communication satellites telephone, telex and high speed data transmission systems engineering, discussing intercontinental TV, synchronous orbit injection and solar panel deployment

12 p1973 A71-27610

Feasibility of VHF aeronautical satellite system frequency sharing band used by ATC service, employing spatial separation, antenna directivity and frequency offset

13 p2032 A71-28873

Sirio B European communication satellite, discussing electronic equipment for simultaneous multichannel telephony and color TV transmission

14 p2319 A71-29820

German-French Symphony synchronous communication satellites, discussing frequency and time division multiple access subsystems characteristics

14 p2193 A71-29824

Communication satellites electric propulsion economic tradeoff studies, considering propellant requirements for north-south stationkeeping, and near-synchronous orbit maneuvers

[AIAA PAPER 71-683]

14 p2292 A71-30746

Communication satellites use as educational medium, discussing program organization, student and faculty involvement, course contents and methods

14 p2341 A71-30829

Nationwide man machine remote employment/personal services system including synchronous communication satellite, information and control network and remote terminals

14 p2199 A71-30914

Communication satellites unique word coding with algorithm, reducing false detection probability by error correlation technique

14 p2201 A71-30926

Intelsat 4 satellite Spade communication system, using common reserve circuits and repeaters

15 p2373 A71-32640

ATC satellites providing communications channels between aircraft and ground control stations and aircraft localization

16 p2605 A71-32849

European geostationary telecommunication satellite stabilization using ion thrusters

16 p2623 A71-32851

Incore thermionic reactor as low cost power supply for direct-to-home TV satellite, converting thermal power to electrical without moving masses

16 p2526 A71-32853

Solar electric propulsion and transfer system for higher payloads of SECOM communication satellites, using Europa 2 launcher

16 p2644 A71-32855

Millimeter broadband high power traveling wave transmitter tubes with stub voltage tuning for ground stations of satellite communication systems

16 p2545 A71-32975

Symphonic communication satellite subsystem, discussing geostationary positions, launchers, frequency ranges and transmission zones

16 p2543 A71-33583

International Telecommunications Satellite Consortium, reviewing legal order, organization structural framework, objectives and financial aspects

16 p2664 A71-33584

Optimum power parameters and economic efficiency of Soviet communication satellite system, comparing with terrestrial multichannel communication

17 p2696 A71-34231

European telecommunication and TV distribution satellite system, including telephony, telegraphy, telex and wideband data transmission

17 p2696 A71-34232

Communication satellite systems integration into general telecommunication network, considering telephone circuit data transmission characteristics, routing and signal processing

17 p2696 A71-34235

Communication satellite systems vs conventional terrestrial methods, emphasizing economic comparison

17 p2697 A71-34236

Communication satellite TV and sound broadcasting system design without unreasonable cost

17 p2697 A71-34237

Navigation and communication satellites development for civil aviation and shipping, examining technical, organizational, operational and cost problems

17 p2771 A71-34240

Copyright protection of communication satellite transmitted radio and TV programs, discussing involvement of UN agencies and other international organizations

17 p2841 A71-34248

UN leadership in space communications international cooperation, emphasizing communication satellite systems application to educational TV

17 p2841 A71-34249

Maritime operational and frequency requirements for satellite system having worldwide coverage

17 p2697 A71-34251

Multifunctional communications satellite for TV distribution and trunk line, domestic, aeronautical, maritime, small user and space vehicle services

17 p2699 A71-34613

Satellite communication technology in next decade covering Intelsat 4 characteristics, meteorological satellites, navigation aids, multichannel telephone and TV circuits and frequency assignment

17 p2699 A71-34677

Satellite communication system selection vs underground cable or hybrid systems, based on power requirements and economics

17 p2700 A71-34678

European regional satellite communication system, discussing TV coverage, spot beam antennas, frequency reuse, speech interpolation and circuits allocation

17 p2700 A71-34679

Time division multiplexing system for ATS, discussing surveillance geostationary satellite feasibility, delta modulation for data transmission and aircraft equipment

17 p2772 A71-34680

Discusses communication satellite system for air traffic control and navigation, discussing aircraft antenna beam electronic scanning by computerized control

17 p2714 A71-34681

Traveling wave tube for reflex type amplifier on-board space communication satellite, discussing prototype reliability and performance

17 p2714 A71-34682

Advanced communications satellites system engineering, including configuration based on active body stabilization, rechargeable hydrogen oxygen fuel cells and ion engines

[AIAA PAPER 71-843]

17 p2812 A71-34710

First generation domestic communications satellite system, discussing various proposals for FCC authorization

[AIAA PAPER 71-842]

17 p2700 A71-34711

Communications capability of Canadian domestic satellite system, outlining performance parameters of satellite and earth stations

17 p2703 A71-35080

Transmission performance of thin route satellite communication system for northern Canada, comparing FM, PCM and delta modulation techniques

17 p2703 A71-35081

Low elevation angle tropospheric fading relationship to satellite communications and broadcasting at frequencies between 1 and 20 GHz

17 p2703 A71-35083

Reduced cost ground stations for satellite communications system and applicability to small nations, using single channel per carrier FM and companders

17 p2704 A71-35087

Transponder configurations for communication satellites using frequencies above 10 GHz, discussing service type, modulation method and equipment

17 p2705 A71-35092

Satellite-to-aircraft links propagation characteristics, considering specular reflected signals, diffuse scattering and scattering function

17 p2705 A71-35097

Intelsat 4 communication system simulation by transponder engineering model to test performance objective concerning baseband distortion and intermodulation

17 p2705 A71-35102

Comparison of demand assignment multiple access/modulation techniques for satellite communication using high quality telephone channels

17 p2706 A71-35103

Multiple access satellite digital communication system with onboard distribution center, discussing time frame synchronization methods

17 p2706 A71-35105

Queueing theory approach to communication satellite network design, applying to ocean air traffic control and worldwide military broadcast systems

17 p2721 A71-35106

Satellite voice communications system for small terminals in remote areas, discussing feasibility, design, cost and frequency allocation

17 p2706 A71-35123

Intelsat satellite-earth station communications technology, considering microwave line of sight techniques

17 p2707 A71-35333

Second Pleumeur-Bodou /France/ ground station for Telstar satellite communication, discussing equipment specifications, Cassegrain antenna and parabolic reflector

17 p2708 A71-35509

Pleumeur-Bodou /France/ ground station steerable parabolic reflector Cassegrain antenna for communication satellites, discussing specifications and radioelectric and mechanical characteristics

17 p2717 A71-35510

Low noise parametric amplifiers for communication satellite ground station radio receivers, considering components characteristics

17 p2709 A71-35513

Communication satellite ground station receiver-demodulator equipment using frequency double transposition and compression

17 p2717 A71-35514

Communication satellite ground station terminal equipment, discussing carrier current telephone, video and sound TV apparatus

17 p2717 A71-35516

Communication satellite ground station electric power generation and distribution equipment characteristics, emphasizing reliability

17 p2724 A71-35517

Remote control and surveillance equipment for communication satellite ground station, discussing console and engineering service circuit designs

17 p2709 A71-35518

Communication satellite ground station equipment modifications for second station compatible with Intelsat 3

17 p2709 A71-35519

Civil aviation and merchant marine satellites, considering aircraft and surface vessel antenna characteristics and modulation techniques for optimum communication channel frequencies

17 p2775 A71-35582

Technological environment for international communications law, examining system design, radio spectrum resource management and communication satellites

18 p2986 A71-36164

Unilateralism in U.S. satellite communications policy, suggesting international cooperation for frequency spectrum management

18 p2986 A71-36165

Juridical and institutional aspects of problems raised by TV programs content transmitted by communication satellites, noting applicability of international law

18 p2986 A71-36166

South American contributions to satellite communication juridical problems solution, suggesting adherence to international law

18 p2987 A71-36170

International satellite broadcasting practices and laws, discussing effect on free information dissemination

18 p2987 A71-36171

Satellite TV broadcasting development in European community, giving cost estimation procedure and program reception methods

18 p2876 A71-36504

Radio tracking of aircraft by two geostationary satellites, discussing measurement, navigation and position errors

18 p2945 A71-36508

ESRO part of joint ATC communication experiment for L band satellite use, giving voice and data transmission and distance measurement techniques tests results

18 p2945 A71-36510

Satellite telecommunications problems, discussing frequency assignment and power efficiency

18 p2877 A71-36515

European regional satellite communication system, discussing TV coverage, spot beam antennas, frequency reuse, speech interpolation and circuits allocation

18 p2877 A71-36516

European 12 GHz regional satellite telecommunications systems, discussing band assignment limitation and frequency reuse

18 p2877 A71-36517

Italian SIRIO experimental SHF telecommunications satellite, noting trapped radiation and high energy electron experiments

18 p2974 A71-36521

Franco-German Symphonie communication satellite, discussing missions and subsystems design features

18 p2974 A71-36522

Data transmission system of Franco-German Symphonie communication satellite

18 p2889 A71-36523

Franco-German Symphonie communication satellite reliability measures, describing component selection methods

18 p2889 A71-36524

Symphonie telecommunication satellite attitude control system, describing operational principle based on gyroscopic inertial reference and redundant IR sensors

18 p2974 A71-36525

Large synchronous communication satellite launching by propulsion stages assembling in orbit through automatic rendezvous maneuvers

18 p2975 A71-36526

Satellite time and frequency dissemination, discussing deficiencies of HF broadcasts for navigation and communication systems

18 p2878 A71-36530

Range and range rate measuring equipment for PCM-TDMA satellite communications system data feed and orbit observation

18 p2879 A71-36533

Communication satellite components reliability assurance method, discussing production and qualification tests

18 p2890 A71-36538

Telecommunications satellite data acquisition from automatic beacons, discussing Eole program

18 p2988 A71-36543

Multiple access to communication satellites by time division multiplexing

18 p2879 A71-36544

Propagation model type effect on modulation and multiple access techniques choice for regional European communication satellite system

18 p2880 A71-36550

Frequency memories application to earth-satellite-aircraft UHF communications, repeater apparatus and multiple access transmission of half tone images in worldwide satellite communication

18 p2881 A71-36553

COMMUNICATION SATELLITES

Cassegrain antennas with reflector horn feed for satellite communication, noting gain and noise temperature

18 p2890 A71-36554

Communication satellites automatic tracking system, noting low cost

18 p2881 A71-36555

Antenna system design for communication satellite ground station operating in 10.7-35 GHz range

18 p2881 A71-36556

Parametric amplifiers for ground station low-noise receivers in communication satellite systems, considering frequency range extension effect on noise temperature and passband requirements

18 p2890 A71-36557

Spectrum limitation of FM carrier in case of accidental overloading of modulating signal arising in Intelsat 4 communication system

18 p2891 A71-36559

Digital filtering in PCM communication systems with active repeater satellites and space vehicle telemetry

18 p2881 A71-36569

High power microwave CW tubes and power amplifier requirements for communication satellites

18 p2892 A71-36571

Telecommunication satellites photoelectric power systems, discussing solar generators with silicon cells

18 p2851 A71-36572

High power nickel cadmium battery for geostationary communications satellites for replacement in Intelsat 4 series

18 p2852 A71-36573

Counterrotating antenna without mechanical contact, using magnetic bearings for spin stabilized geostationary telecommunications satellites

18 p2892 A71-36574

Italian SIRIO synchronous satellite for SHF communication, analyzing thermoelastic deformations effect on antenna radiation patterns

18 p2882 A71-36575

Stabilizing system for retransmission beam of direct TV broadcast satellite, considering rebroadcast antenna, electronic sensor and antenna pointing subsystem

18 p2892 A71-36576

Direct broadcast satellite TV communications, discussing international regulations and legal aspects

18 p2899 A71-36578

French space programs, discussing European and international activities, telecommunication, meteorology, data collecting, natural resources and air and sea traffic control

18 p2975 A71-36573

Synchronous three-axes stabilized communication satellites attitude control system with double gimbaled reaction wheel control actuator, obtaining 0.1 degree pointing accuracy with pitch and roll sensors

[AIAA PAPER 71-949]

19 p3098 A71-37190

Book on communication satellites technology covering satellite transponders, spacecraft antennas and subsystems, high power transmission, launch vehicles, digital techniques, earth stations, etc

19 p3149 A71-37271

Systems planning and operation of European applications satellites, noting Sirio and Symphonie programs

19 p3172 A71-37329

Intercontinental point to point radio communication, discussing Hertzian beam /radio relay links/ and satellite communication comparison with underground and submarine cables

19 p3016 A71-37343

Telecommunications satellites, discussing Intelsat series, multiple access, radio navigation, weather satellites and earth resources satellites

19 p3017 A71-37493

International Telecommunication Union report on telecommunication and peaceful uses of outer space, covering space programs, communication satellites, UN role, etc

19 p3172 A71-37517

Radio satellite scintillation producing small scale ionospheric irregularities, determining characteristic size variation with latitude by autocorrelation method

19 p3055 A71-38043

Technical parameters and performance tradeoffs of ESRO preoperational aeronautical satellite program

19 p3153 A71-38067

Marine navigation and data communications at L band via synchronous satellite, assessing capabilities by tests on ATS-5 satellite

19 p3102 A71-38070

Cryogenic refrigeration requirements of low noise microwave amplifiers in satellite communications, discussing solid state masers and liquid helium parametric amplifiers

20 p3204 A71-39251

One way UHF clock synchronization, using geostationary communication satellites with propagation delays calculated from orbital elements

20 p3239 A71-39460

Broadband point-to-point communication satellite systems for 1970s, discussing R and D effort, economics and international and domestic applications

20 p3197 A71-39606

ATS F and G satellites for half earth surface full time communication coverage, discussing mission objectives 20 p3306 A71-39607

Papers on communication satellites for 1970s covering various national domestic systems, aeronautical service, ERTS data transmission and collection problems, etc 21 p3347 A71-40473

Italian Sirio synchronous satellite for SHF propagation and communication experiments on fading statistics, frequency dependence, path diversity and TV transmission 21 p3347 A71-40474

Technical characteristics, capabilities and applications of future geostationary communication satellites for U.S. internal commercial communications services 21 p3448 A71-40475

Dual-spin vs three-axis stabilization and control systems for synchronous communication satellite design 21 p3454 A71-40477

Three axis and dual-spin attitude control subsystems for communications satellites, considering flywheel stabilization advantage 21 p3454 A71-40478

Three-axis and dual-spin stabilization systems for future synchronous communication satellites, considering reliability, mission flexibility and growth potential 21 p3455 A71-40479

Synchronous communication satellites stabilization for implementation in 1970-1975 time frame, considering antenna size, power system capacity and vehicle pointing 21 p3348 A71-40480

Attitude stiffness and pointing accuracy of three-axis and dual-spin stabilization system for future synchronous communication satellites 21 p3455 A71-40481

Satellite navigation, surveillance and communication service requirements for maritime transportation industry, discussing initial services 22 p3572 A71-42093

Two spot beam switching without storage at satellite for time division multiple access system in satellite communication, giving switching algorithm 22 p3514 A71-42482

Common channel signaling system for demand assigned multiple access satellite communication, discussing design features and applications to PCM-TDMA 22 p3514 A71-42520

Intelsat 1, 2, 3 and 4 satellite network development for world telecommunication coverage, discussing expected future replacement and modulation and multiple access technologies 23 p3643 A71-43250

COMMUNICATION SYSTEMS
U TELECOMMUNICATION
COMMUNICATION THEORY
NT SYLLABLES
NT WORDS [LANGUAGE]
 Chi-square distributions fitted to observed telecommunication variables distributions 01 p0041 A71-11609

Optical communications for terrestrial and space applications, assessing state of art of optics devices, systems and theory 02 p0212 A71-12001

Quantum mechanical communication theory of optical receivers, using statistical detection and estimation theory 02 p0213 A71-12016

Free space optical channel analog and digital communication theory, considering SNR, M-ary signaling, error probabilities and information rates, etc 02 p0213 A71-12018

Atmospheric turbulence effects reduction in optical communication by statistical communication theory, considering digital system and waveform estimation 02 p0213 A71-12019

Optimal and nonoptimal signal reception under conditions of incomplete a priori information based on approximation by Markov processes in white noise 05 p0730 A71-16000

Arbitrary patterns recognition by parallel processing, deriving mathematical instructions for signal processing based on statistical communication theory 05 p0726 A71-16391

Statistical properties of radio communication system polarization reception coefficient as function of receiving antenna and signal polarization characteristics 09 p1405 A71-22294

Soviet papers on cybernetics problems covering control and communication for information handling machines and biological nervous systems 10 p1585 A71-24155

Atmospheric turbulence effects on sonic boom rise times by statistical theory 10 p1556 A71-24817

Interference threshold probabilities of pseudorandom frequency hopped signals in conventional spread spectrum communications relative to Gaussian receiver bandwidth 12 p1881 A71-27428

Echo location systems theorem concerning ambiguity density relationship to signal bandwidth 14 p2194 A71-30063

Computer communication asynchronous time division multiplexing, studying communication channel sharing, data buffering and demultiplexing design 14 p2201 A71-30929

Book on detection of signals in noise covering statistical theory principles and applications in digital communications, radar and sonar 15 p2369 A71-31507

Bayesian estimate of signal parameters in random noise background under mutually exclusive hypotheses about statistical properties 15 p2370 A71-31584

Optimal Bayesian system for simultaneous discrimination and parameter estimation of several signals in noise background 15 p2370 A71-31585

Conditional distribution density formation for signal-noise mixture based on learning sampling with dependent values 15 p2370 A71-31586

Passive and active radar detection theory and practice, considering advances in sensors, signal generators, processors and filters 15 p2371 A71-31907

Discrete and continuous channel stochastic coding processes and resulting communication system properties 15 p2372 A71-32320

Synchronous data transmission system digital signal harmonic analysis based on stochastic process theory, applying to amplitude and phase modulation 15 p2372 A71-32321

Error correcting codes in binary symmetrical communication channel with additive white noise at large SNR 17 p2702 A71-34972

Book on synchronous communications theory covering statistical detection, decision and estimation and source and channel encoding 17 p2707 A71-35218

Wideband communications theory applied to continuous /analog/ signals using frequency and amplitude modulation 19 p3015 A71-37254

Optimal and nonoptimal signal reception under conditions of incomplete a priori information based on approximation by Markov processes in white noise 22 p3527 A71-42749

COMMUNITIES
NT MOUNTAIN INHABITANTS
COMMUTATION
 Variable voltage and frequency thyristor inverter, describing series commutation power stage 03 p0352 A71-13047

Precommutative bounded and symmetrical unbounded operators extension to commutative bounded and self adjoint operators 04 p0618 A71-14648

Semiconductor thermoelectric battery p-n cell elements joining with mercury amalgam for commutating 14 p2181 A71-29953

Transistorized trigger generator with improved commutation, using inductor circuit limiting collector voltage front durations 15 p2375 A71-31234

Internal commutation of telephonic channels with variable destination in time division multiple access system 18 p2880 A71-36547

COMMUTATORS
NT DECOMMUTATORS
 P-n junction controlled discrete microwave commutation diodes performance calculation and design optimization 11 p1741 A71-26554

Decimeter range diode commutation devices, calculating speed, wideband capability, noise level and maximum power 11 p1741 A71-26555

Four phase reluctance motor design for electromagnetic torque variation, examining function of commutation frequency and phase time constants 17 p2677 A71-35710

Stepping electromotor in self commutation mode with local feedback, examining dynamics with phase plane method 23 p3655 A71-43293

COMPACTING
 Ceramic particle compaction as function of size, shape, loading rate and hardness for fused alumina, magnesia and mullite 03 p0448 A71-12973

Powdered Ni-carbide composites compressibility, noting mixture and pressure effects on compact density 05 p0769 A71-16859

Stress reduction in metal powders compaction at different temperatures and deformation rates 08 p1305 A71-21059

Sponge iron sintered powder compacts deformation behavior from uniaxial compression tests, proposing plasticity prediction criteria 09 p1466 A71-22169

Ti, Zr, Nb, Cr, Mo and W carbides compaction, investigating effects of compression, duration, pressing number, moisture and plasticizer contents and stress distribution 15 p2415 A71-32141

Hot compaction of tungsten and pseudoalloys powders in terms of volumetric-viscous flow dependence on isothermal exposure time, using Kovachenko-Samsonov equation 16 p2592 A71-33572

Nichrome powder microstructure characteristics effect on hot compaction kinetics, considering temperature, pressure and preliminary heat treatment effects 19 p3075 A71-37108

Cermet iron chromosulfidization and sinter compactness effects on depth and structure, noting wear, corrosion and thermal resistance 19 p3075 A71-37110

COMPACTNESS
U VOID RATIO
COMPANION STARS
 Black hole model accounting for epsilon Aur eclipsing binary secondary component observations 06 p0970 A71-18031

Epsilon Aur eclipsing binary primary star mass and evolutionary stage considered to interpret secondary 06 p0970 A71-18032

Algol secondary component gravity darkening observations, examining IR light curve 09 p1527 A71-23530

Collapsed or neutron star companions of bright binary stars, explaining low luminosity of more massive component 10 p1665 A71-23740

Dark companions and extrasolar planetary system detection, discussing characteristic colorimetric signature method 13 p2134 A71-28291

Double and triple stars common proper motion, discussing white dwarf or degenerate components 14 p2310 A71-30360

Dust disk around secondary component of Epsilon Aurigae, noting role in system eclipse 15 p2494 A71-32550

Spectroscopic binary system with invisible major mass components, considering relativistic companion star 19 p3134 A71-37508

Radio stars classes, discussing red dwarf flare, red supergiants, blue dwarf companion, novae, pulsars and X ray stars 21 p3448 A71-40582

Sirius B white dwarf star effective temperature, radius and gravitational red shift determination from H-alpha and H-gamma line profile analysis 24 p3871 A71-44908

COMPARATOR CIRCUITS
 Decoding n-bit Johnson code to decimal numbers using n 2-input 2-output comparator circuits 01 p0037 A71-11175

Analog to digital converters employing subharmonic oscillator phase as recording medium, discussing parametron application as phase comparator 11 p1743 A71-26541

Star comparator automatic azimuth system using long evacuated tunnel transfer to underground inertial guidance laboratory [AIAA PAPER 71-925] 19 p3102 A71-38328

COMPARATORS
 Blink comparator with automated precision reading for converting rotation angles to digital form for binary star measurements 04 p0534 A71-14853

Shape and dimensions of magnetoresistance sensors as transducers in magnetic induction comparators field measurement error analysis 04 p0599 A71-15571

Analog to digital conversion mathematical model, considering comparators dynamic properties effects on optimal algorithms selection 06 p0871 A71-17523

Pulkovo radio telescope reflector adjustment by phase comparator, using centimeter wave transmitting-receiving antenna for sun, moon and Venus observations 07 p1083 A71-19344

Fast versatile iterative parallel binary comparator array, proposing cell output states assignment 13 p2037 A71-28475

COMPARTMENTATION
U COMPARTMENTS
COMPARTMENTS
NT AIR LOCKS
NT AIRCRAFT COMPARTMENTS
NT ANECHOIC CHAMBERS
NT COMMAND MODULES
NT PRESSURE CHAMBERS
NT PRESSURIZED CABINS

NT SPACECRAFT CABINS
 NT TEST CHAMBERS
 NT VACUUM CHAMBERS
 Earth international compartmentalization into equal area elements on reference sphere for spherical functions utilization 10 p1601 A71-24460

COMPASSES
 NT GYROCOMPASSES
 NT MAGNETIC COMPASSES
 NT SOLAR COMPASSES
 Aircraft radio compass navigation errors due to loop antenna inclinations during maneuvering 08 p1331 A71-20787

COMPATIBILITY
 Geometrically nonlinear shell dynamics, basing equations of motion and compatibility on variational principles 03 p0514 A71-14346
 Power series uniformization by transformations of perturbation functions irregular part, considering compatibility problem 06 p0919 A71-18197
 Light aircraft standard fuel flight evaluation, discussing compatibility with grades 80/87 and 100/130 certified engines and comparative operational fuel consumption [SAE PAPER 70-10369] 10 p1657 A71-24239

COMPENSATION
 Hybrid computers solution of linear differential equations, analyzing Taylor series /derivatives/ use for compensation 01 p0048 A71-10224
 Quasi-invariant automatic feedback control system, deriving basis for determination of perturbation compensating components parameters 01 p0061 A71-10713
 Head spatial position effects on vestibular compensation rates in rabbits 01 p0012 A71-11074
 Wind compensation method for launching sounding rockets susceptible to nonlinear wind effects, using data generated by six degree of freedom trajectory digital simulation program [AIAA PAPER 70-1390] 03 p0498 A71-13672
 N-order continuous linear automatic control system compensation method, using model of sampled systems with duration modulation 16 p2549 A71-33377

COMPENSATORS
 Complex control systems using self adjustment compensation of error signals according to input derivative 01 p0063 A71-10723
 Photoelastic compensator of urethane rubber, describing construction and applications 01 p0082 A71-11009
 Fluidic pneumatic control system compensator for digital signal processing 07 p1026 A71-20567
 Algorithmic analysis of detection characteristics of periodic compensation systems used in moving targets signal detection 09 p1404 A71-22153
 Optimal fixed dimensionality dynamic compensator design for linear time-invariant closed-loop system based on quadratic cost and gain criteria 11 p1742 A71-26414
 Time coordinate compensator for time variable spectrometers operating on long plastic scintillators with two terminal photomultipliers 14 p2247 A71-30579
 Automatic leveling instrument gravity intensity and compensator support tilt angle variations effects on measurement error 15 p2410 A71-32353
 Polarization compensator for Okayama Astrophysical Observatory solar Coude telescope, describing operational and design principles and performance characteristics 19 p3062 A71-37242
 Compensator design for linear controllers for time varying nonlinear systems, using digital computer oriented approach 22 p3577 A71-42676
 Pole placement design of dynamic compensators for linear time invariant multivariable systems, using transfer function matrices 23 p3660 A71-44119
 Transistor compensation stabilizers design and fabrication with enhanced voltages 24 p3807 A71-44382

COMPENSATORY TRACKING
 Human tracking of external targets and body point projections, examining visual feedback role 02 p0205 A71-12057
 Human operator adaptive response characteristics to step changes in compensatory tracking system dynamics 02 p0207 A71-12349
 Vestibular nystagmus and display luminance effects on hand-eye coordination in compensatory tracking of aircraft instrument 02 p0207 A71-12381

Two dimensional adaptive pattern-recognizing model of human operator in visual-manual compensatory tracking task 07 p1053 A71-20406
 Two dimensional adaptive model of human operator control in visual-manual compensatory tracking task using pattern recognition 17 p2691 A71-35046

COMPILATION [COMPUTERS]
 U COMPILERS
 COMPILER PROGRAMS
 U COMPILERS
 COMPILERS
 PL/I compiler for system programming in high speed binary machine object code 01 p0045 A71-10194
 Computer program for compiling interpreter coded test instructions from high order pseudoEnglish language 03 p0381 A71-13078
 Algol 60 object time error messages detection with test run in-core load-and-go compiler 13 p2035 A71-29014
 Compiler program generation for ordinary differential equations system automatic numerical solution by Taylor series method 20 p3254 A71-38754

COMPLEMENTS [MATHEMATICS]
 Two-point boundary value problems for linear differential equation systems, describing adjoints and complementary functions methods 03 p0451 A71-13624

COMPLEX NUMBERS
 Digital multiplier based on cellular logic iterative arrays for complex numbers processing 13 p2037 A71-28470
 Analysis and synthesis of linear optical systems involving polarization effects by Pauli algebra of complex second order matrices 20 p3267 A71-38775

COMPLEX SYSTEMS
 Complex dielectric structure simulation for microwave scattering purposes using rotating target and zone technique 01 p0051 A71-10255
 Motion stabilization for nonlinear control systems with critical zero and imaginary roots, using Liapunov classical theory 01 p0128 A71-10667
 Complex servo systems with feedback loop and anticipating path, demonstrating equivalence to systems based on error measurements 01 p0062 A71-10719
 Complex control systems using self adjustment compensation of error signals according to input derivative 01 p0063 A71-10723
 Invariance in nonminimum phase complex combined control systems synthesis, using root hodograph method 01 p0063 A71-10724
 Complex programmed control systems invariance for discrete times, synthesizing compensating filter with specific transfer function 01 p0063 A71-10725
 Complex control nonlinear systems invariance and stability conditions, discussing harmonic balance analysis method 01 p0063 A71-10729
 Complex systems potential effectiveness theory, establishing reliability, noise resistance and controllability limits 01 p0065 A71-11230
 Complex automatic systems with random switch-off, developing failure sequence models 09 p1422 A71-22119
 Radio ray tracing in complex space, describing plane stratified ionosphere 09 p1411 A71-23731
 Complex real time hybrid computer simulator for captive two blade rotor platform dynamic problem solving 11 p1744 A71-25847
 Handbook on radar cross sections, Volume 2, covering scattering from planar surfaces, complex bodies, rough surfaces, ionized media, plasmas, radar targets and various objects 11 p1733 A71-26009
 Synthesis of high speed digital computer non-searching adaptive control program to ensure closed system required dynamic characteristics for complex linear unsteady control plant 12 p1926 A71-26731
 Complex automatic systems with random switch-off, developing failure sequence models 14 p2220 A71-29997
 Motion stabilization for nonlinear control systems with zero and imaginary roots, using Liapunov classical theory 14 p2221 A71-31000
 Russian papers on complex control systems covering hierarchical structures, automatic, optimal, self adaptive, multidimensional and nonlinear systems analysis and synthesis 15 p2379 A71-31842

Series and parallel complex systems reliability maximization by allocating optimum numbers of stocked spare parts 15 p2415 A71-32343
 Mathematical models to optimize successive fault finding programs in complex control systems with/without recovery 15 p2382 A71-32618
 Complex systems with n independently failing subsystems, minimizing expected cost per unit usage by assigning replacement age 16 p2552 A71-33312
 Statistical limits on reliability, informativeness, controllability and self organization of complex systems, determining minimum redundancy requirements for suppressing interfering factors 17 p2720 A71-34953
 Optimum diagnostics algorithm for complex automatic control system state detection based on Bayesian rule successive application for minimum time requirement 17 p2720 A71-34959
 Economic acceptability, structure and decomposition of multilevel optimal control for complex systems 18 p2896 A71-35916
 Computer algorithm for simulating dynamic systems by functional graphs, noting extension to complex systems 18 p2884 A71-35917
 Complex airborne electronic system design for interference minimization, considering electromagnetic compatibility 19 p3033 A71-38464
 Criterion selection and minimum margin search for optimization of complex electronic circuit parameters described by mathematical models 19 p3039 A71-38503
 Interaction measure for optimal multivariable feedback control system design for complex blending processes, noting paradoxical solution 20 p3207 A71-38993
 Mixed decomposition and convergence of gradient type coordinating algorithm for two-level complex control system using interconnection variables and Lagrange parameters 20 p3208 A71-39472
 Ionization amplitude calculation method, using extrapolation from complex energies approach 21 p3418 A71-40249
 Optimal redundancy and availability allocation for MTBF and time to repair in multistage system, using dynamic programming 22 p3518 A71-42116
 Synthesis models and methods for large scale automated control systems with human elements, discussing mathematical models and computerized design 22 p3528 A71-42858

COMPLEX VARIABLES
 NT AIRY FUNCTION
 NT ANALYTIC FUNCTIONS
 NT BESSEL FUNCTIONS
 NT CAUCHY INTEGRAL FORMULA
 NT CONFORMAL MAPPING
 NT CONJUGATES
 NT ELLIPTIC FUNCTIONS
 NT ENTIRE FUNCTIONS
 NT EXPONENTIAL FUNCTIONS
 NT GAMMA FUNCTION
 NT HANKEL FUNCTIONS
 NT HARMONIC FUNCTIONS
 NT HYPERBOLIC FUNCTIONS
 NT HYPERGEOMETRIC FUNCTIONS
 NT LAGUERRE FUNCTIONS
 NT LEGENDRE FUNCTIONS
 NT LIOUVILLE THEOREM
 NT LOGARITHMS
 NT MATHEU FUNCTION
 NT MEROMORPHIC FUNCTIONS
 NT ORTHOGONAL FUNCTIONS
 NT RATIONAL FUNCTIONS
 NT SCHWARZ-CHRISTOFFEL TRANSFORMATION
 NT SINGULARITY [MATHEMATICS]
 NT SPHERICAL HARMONICS
 Unresolved radar targets or multipath distortion determination by measurement of complex indicated angle on two pulses separated by short interval 07 p1058 A71-18843
 Radar performance with multipath using complex angle /CA/ method for resolving low angle target, comparing S/N ratio with monopulse system without CA 07 p1058 A71-18844
 Soviet papers on special problems of differential equations and functions theory covering approximation, complex variables, integral operators, etc 07 p1146 A71-19038
 Analytic functions approximation in complex regions with aid of different systems of functions 07 p1146 A71-19041
 Plane electromagnetic wave propagation and reflection in presence of substances with arbitrary complex permittivity 07 p1066 A71-20543

Maximum likelihood method for accuracy of spacecraft trajectory determination by complex expressions in multidimensional geometric representation 12 p1957 A71-26629

Design principles of complex value converters with selfbalancing circuits based on generalized graph of essential information transformations 12 p1892 A71-27024

Inhomogeneous plasma, describing linear wave transformation with fourth order differential equation with variable coefficients 12 p1942 A71-27768

Radiation field description with spatial complex variables, considering application to scattering and waveguide problems 14 p2209 A71-29567

Phase-only complex valued spatial filter for holographic wave front construction involving amplitude and phase modulations, investigating performance 17 p2745 A71-35590

Two dimensional stress tensor invariants for finite elastic deformations of thin plate using initial complex coordinates 19 p3156 A71-37541

Exponential continually discrete analytic functions of complex variable in explicit form, obtaining addition theorem for trigonometric functions 19 p3089 A71-38479

Stationary covariance generation of matrix of rational functions of complex variable, solving factorization equation via algebraic Riccati equation 20 p3207 A71-38990

Book on complex variable methods in elasticity, covering boundary value problems for half planes and circular regions 21 p3456 A71-40264

Homogeneous mountain mass and canyon thermoelastic stress analysis in curvilinear coordinate system by complex variables 23 p3776 A71-43421

Recurrence techniques for generation of Bessel functions of complex order and argument 23 p3648 A71-43966

Complex variable solutions to electrochemical machining with two dimensional straight sided tool 23 p3682 A71-44142

COMPLEXITY

NT TASK COMPLEXITY

COMPLIANCE (ELASTICITY)

U MODULUS OF ELASTICITY

COMPONENT RELIABILITY

Aircraft all weather automatic landing system, discussing component weights and reliability connected with problem area 02 p0279 A71-12274

Reliability prediction for machine parts subjected to cyclic stresses, using statistical analysis of fatigue data for failure rate calculation 02 p0327 A71-12367

Structural design for component low cycle fatigue resistance, emphasizing material cyclic stress-strain behavior 03 p0501 A71-13252

Radio electronic equipment components reliability, using image recognition theory 03 p0384 A71-13422

Cryotron elementary storage cells work region determination by phase transition characteristic form, discussing component reliability 03 p0382 A71-13520

VC-10 aircraft ILS electronic equipment reliability tests 04 p0559 A71-15873

Electronic components failure rate distribution 04 p0559 A71-15875

Gas turbine engines materials and components equivalent service life estimation 05 p0796 A71-16753

Machine components resistance to low temperature failure, considering threaded joints, gears and shafts for strength and plasticity characteristics 05 p0827 A71-16764

Aging process effects on thermoelectric semiconductor physical stability for cryogenic applications 05 p0793 A71-16799

Automatic systems multipositional elements reliability, analyzing output errors and transition states stability 05 p0729 A71-17039

Digital computer components reliability determination, using bypass algorithm 06 p0870 A71-17492

Intelsat 3 satellite mechanical and electronic components fabrication, emphasizing quality and reliability assurance procedures and assembly techniques 06 p0905 A71-18403

Long life spacecraft tape recorders, considering digital and analog equipment and life and reliability testing of components and complete units 07 p1106 A71-18812

Microcircuits component vulnerability, deriving time independent nonlinear terminal I-V characteristics, electrical switching response and ionizing radiation induced transient response 07 p1070 A71-19059

F-104D aircraft side stick control system design and function, curriculum maneuvers and component reliability 07 p1018 A71-19092

Reliability evaluation for electrical connectors used in electronic equipment based on probability and environment considerations 07 p1076 A71-19555

Satellite electronic equipment reliability engineering, considering circuit and system design, components screening, assembly and test procedures and quality assurance plans 07 p1207 A71-19563

Miner-Sediakin failure models for element operation without manufacturing process stability restrictions 08 p1300 A71-22019

Components field failure rates assessment methods for ground support equipment 09 p1454 A71-22618

Semiconductor element design flexibility, providing greater reliability and reduced size/weight for space vehicles and missiles 09 p1445 A71-22722

Book on reliability mathematics covering fundamental statistical concepts, logic diagrams, mathematical models, component reliability prediction, system prediction, reliability growth, assessment methods, etc 09 p1485 A71-22958

Soviet book on reliability and efficiency prediction of radio electronic devices covering a priori and posteriori random quality indices, mathematical and physical models and applications 10 p1582 A71-23900

Elementary component constant failure rate for systems with prolonged operation without maintenance, determining mathematical model for confidence levels and dependability figures 10 p1617 A71-24266

Airborne electronics reliability testing in temperature controlled chamber 10 p1589 A71-24604

Satellite power supply systems, discussing solar cell generators with emphasis on reliability 10 p1683 A71-24641

Reliability test extent, duration, confidence limits and failure rate computed by nomograms 11 p1737 A71-25623

Nonrepairable elements reliability under external influences, discussing linear damage accumulation hypothesis 11 p1768 A71-25659

Particle impact noise detection of loose particles in electronic component cavities, discussing implementation, cost savings and reliability improvement 12 p1884 A71-26659

Reliability analysis as essential input in trade studies for selecting system component designs, emphasizing NERVA program 12 p1928 A71-26664

Risk assessment associated with reliability demonstration testing, considering fixed price procurement and cost effectiveness 12 p1910 A71-26677

Bayesian time to failure distribution for graphical estimation of component burn-in time and reliability prediction, comparing with Weibull technique failure rates 12 p1911 A71-26686

Adaptive control systems components stability and accuracy requirements, demonstrating functional multipliers and quorum elements operation by functional diagrams, transient equations and signal waveforms 12 p1890 A71-26717

Force springs flexural pivots and miniature incandescent lamp tests failure distribution analysis for comparing mechanical vs electrical components [ASME PAPER 71-DE-34] 12 p1911 A71-27326

Continuous loading method for accelerated reliability testing of circuit components 13 p2072 A71-27830

Computer methods for automatic diagnosis program applied to future manned space vehicles, discussing cost relationship to fault isolation techniques and component reliability 13 p2044 A71-27940

Reduction gearbox reliability problems from development and service experience with PT6A turboprop engine [SAE PAPER 710433] 13 p2073 A71-28318

Solar arrays for satellite electrical power supply, discussing mathematical model for reliability calculation 13 p2002 A71-29273

Failures detection in combinational digital switching circuits due to component malfunction 13 p2036 A71-29291

Satellite auxiliary electric propulsion systems survey for program managers and systems engineers, considering cost and component reliability [AIAA PAPER 71-685] 14 p2292 A71-30747

Fail-safe helicopter rotor control design, discussing damage tolerant components, redundant system, failure warning and maintenance [AHS PREPRINT 550] 14 p2179 A71-31102

SNAP 8 turbine-alternator as nuclear-electric space power converter, discussing rotating machinery components design and 10,000 hr endurance testing results 15 p2447 A71-32208

Noise equivalent resistance of thermionic tubes as stability and reliability criterion 16 p2545 A71-33073

Concorde lightweight disk brakes, discussing operating costs, weight and volume factors, design philosophy, structural materials, component life, maintenance and reliability 16 p2522 A71-33226

DC-10 design dispatch and component reliability through flight test and follow-up fault isolation programs 16 p2522 A71-33297

Synthesis method for combining individual part repair time distributions for maintainability prediction using computer 16 p2552 A71-33301

Soviet book on space radio telemetry systems characteristics, design, requirements and operation conditions covering noise stability, reliability and redundant codes 17 p2699 A71-34521

High reliability low energy camera tubes for video communication in space missions, considering vidicons with photoconducting layer with large time constant 17 p2739 A71-34683

Gas turbine engines materials and components equivalent service life estimation 17 p2793 A71-35452

Machine components resistance to low temperature brittle failure, considering threaded joints, gears and shafts for strength and plasticity characteristics 17 p2832 A71-35463

Integrated drive generator for aircraft electrical power systems, improving weight, life and reliability 17 p2678 A71-35781

Franco-German Symphonie communication satellite reliability measures, describing component selection methods 18 p2889 A71-36524

Commercial production of high reliability components in plane transistors, bipolar integrated circuits and printed circuits technologies 18 p2889 A71-36535

High reliability integrated complementary MOS circuit fabrication chain in Concerto satellite program, discussing technological process with account of physicochemical data 18 p2890 A71-36536

Scanning electron microscope examination of components and materials quality and reliability in satellite onboard equipment 18 p2890 A71-36537

Communication satellite components reliability assurance method, discussing production and qualification tests 18 p2890 A71-36538

Low noise microwave transistor, describing geometry and diffusions optimization, power gain, reliability and base resistance 18 p2892 A71-36564

Electronic component products improvement history, discussing electron tubes, future trends and reliability 19 p3027 A71-37345

Outer planet exploration spacecraft subsystems reliability and ten year flight requirements for planet orbiting and flyby missions [AAS PAPER 71-112] 19 p3140 A71-37934

Simulation model for optimal cost time-independent component replacement of complex system subject to probabilistic deterioration 19 p3069 A71-38288

Hydraulic fluid filtering and maintenance techniques, discussing component life optimization and adverse environment handling problems 19 p3000 A71-38325

Streamer discharges effects on integrated aircraft antenna and associated avionics, emphasizing RF interference and component damage 19 p3033 A71-38462

Reliable plastic encapsulated semiconductor devices design, production and evaluation, noting application to IC 19 p3033 A71-38509

Ni-Cr thin film resistors reliability, describing deposits on silicon dioxide, intermetallic formation and electromigration 19 p3034 A71-38515

Discrete semiconductor devices test program assessing environmental screening for improved component reliability 19 p3034 A71-38517

Collector/base current ratio degradation in bipolar transistors, describing mechanisms characteristics and protective techniques 19 p3034 A71-38522

Emitter avalanche stress on gated silicon planar n-p-n transistors, investigating degradation phenomena 19 p3034 A71-38523

Component performance of three loop Rankine cycle test rig using lithium, potassium and NaK-78 as working fluids 20 p3263 A71-38923

Reliability controlled maintenance plan for avionics equipment based on mean time between failures 20 p3203 A71-39087

Fracture mechanics application to proof testing for components life determination, exemplifying concept by flawed pressure vessel 20 p3308 A71-39459

Test unit number selection for lowest total life test cost, considering operating test environments and component reliability 21 p3386 A71-40368

Multilayer printed circuit board development, design and production for high reliability and cost effectiveness, emphasizing multidisciplinary communication 21 p3352 A71-40436

High density packaging effects on multilayer interconnection board reliability tested in thermal environments 21 p3352 A71-40437

Silicon gate process effect on MOS circuits application, noting bipolar compatibility, circuit layout compactness and reliability 21 p3354 A71-40729

Reliable thin film switching circuits fabrication by deposition on suitable substrates 21 p3354 A71-40732

Semiconductor components reliability assurance under assumption of failure rate decrease with time for IC quality and performance improvement 21 p3356 A71-40746

Redundancy optimization of series-parallel k-out-of-n systems for maximum reliability subject to multiple cost constraints 21 p3388 A71-40878

Reliability requirements in LSI technology, considering multilevel metallization and test vehicles for process control 22 p3519 A71-41633

Soviet book on automatic control and computer components reliability, explaining redundancy principles and test and repair procedures 22 p3526 A71-41820

Composition analysis of automata with unreliable components, illustrating possibility of comparative estimate of different variants of automaton structural scheme 22 p3516 A71-41857

ATS power supply concepts, considering growth capability, control, reliability, thermal dissipation and weight minimization 22 p3588 A71-41958

Validity study of mathematical models representing failure rate variations of electronic components, considering thermal and electrical stresses 22 p3517 A71-42109

Computer predictions of poststradial reliability of electrical circuits, using Sceptre program and component tests 22 p3518 A71-42111

Computerized simulation of reliability and in-flight subsystem maintenance for increased space mission success probability, using priority and waiting queue method 22 p3518 A71-42112

Hazard rate functions of systems with identically distributed subsystem failure times in sequential or simultaneous operation 22 p3566 A71-42118

Tracking servosystems errors of indicator-receiver of amplitude radio interferometers for recording electromagnetic field pattern extremes 22 p3521 A71-42275

Electric circuit component failure prediction and probability distribution in troubleshooting search 23 p3638 A71-42900

Thick film hybrid microcircuits for spacecraft electronic systems component reliability 23 p3650 A71-43123

Multiple component logic circuit reliability analysis using Karnaugh diagram procedure for simplification 24 p3807 A71-45299

COMPONENTS

Electronic components - Conference, Washington, D.C., May 1970 19 p3035 A71-38535

COMPOSITE MATERIALS

NT CERMENTS

NT COMPOSITE PROPELLANTS

NT LAMINATES

NT METAL MATRIX COMPOSITES

NT REINFORCED PLASTICS

NT THREE DIMENSIONAL COMPOSITES

NT WHISKER COMPOSITES

Two-phase composites stability at various temperatures, noting failure regularities dependence on components mechanical properties relationship 01 p0106 A71-10083

Fiber reinforced materials technology, reviewing basic principles, existing technologies and future trends, various composite materials characteristics, etc 01 p0107 A71-10315

Fiber reinforced materials industrial applications based on various matrix-fiber combinations, considering manufacturing processes, chemical and mechanical properties, etc 01 p0102 A71-10316

Glass fiber reinforced durometer and hard foam sandwich structures deformation characteristics under static loads, presenting theoretical and experimental results 01 p0172 A71-10700

Composite Ni coatings, adding mullite crystals to enhance oxidation resistance 01 p0102 A71-10784

Materials for spacecraft design requirements, considering composite and refractory metals, Ti and heat resistant alloys 01 p0102 A71-10816

High modulus graphite fiber composites, considering production, properties, utilization, availability and price/performance [SME PAPER EM-70-114] 01 p0109 A71-11251

Composite fiber-reinforced structures fabrication methods [SME PAPER EM-70-112] 01 p0089 A71-11256

Modular ratios effect on structural composites, predicting property values from structural measurements 01 p0103 A71-11276

Fiber reinforced composites application in aerospace and aircraft, discussing boron and graphite and cost effectiveness 01 p0103 A71-11277

Carbon-carbon composites nondestructive testing following various processing steps, discussing material variations and discrete discontinuities 01 p0090 A71-11278

Boron vs graphite fiber reinforced composites, noting design application role 01 p0104 A71-11280

Composite materials structure cost effectiveness demonstrated in aircraft relief crew compartment panels 01 p0177 A71-11281

Boride composites with high strength and thermal resistance suitable as nose cap and leading edge materials for reusable lifting reentry systems [AIAA PAPER 70-278] 01 p0109 A71-11282

Homogeneous and composite polycrystalline materials macroscopic thermoelastic characteristics determination based on structural model 02 p0324 A71-11750

Composite materials with high strength short discontinuous fibers, considering manufacturing processes and mechanical properties 02 p0273 A71-12478

Unidirectionally fiber reinforced composite materials, discussing compressive strength 02 p0274 A71-12481

Carbon fiber reinforced plastics and metals structural components design, discussing properties, processing and applications 02 p0330 A71-12910

Composite materials testing, standards and design, considering flat laminates, honeycombs and construction weight savings 03 p0448 A71-13535

Composite materials interaction stresses by ideal model with linearly elastic isotropic homogeneous inclusions and matrix, solving by finite element method 03 p0505 A71-13536

Photoelastic study of stress wave propagation in composites under fiber matrix strip directed impulsive loading with exploding wire [SESA PAPER 1708] 03 p0507 A71-13758

Composite viscoelastic materials fracture energy determination using equations for line crack in linear materials from spherical flaw theory and Griffith concept [SESA PAPER 1647] 03 p0508 A71-13764

Thin web shear test device demonstrated on aluminum foil and glass fiber composites 03 p0508 A71-13765

Continuous filament composite materials fabrication and tests for dynamic deformation, fracture and wave propagation properties, considering axially reinforced cylindrical body compression 03 p0508 A71-13768

Finite element method for composite materials anisotropic behavior, considering flat sheets plane stress and thin shells membrane and bending deformations 03 p0508 A71-13775

Elastic behavior of bone as two phase composite material, using ultrasonically measured hydroxyapatite moduli [ASME PAPER 70-WA/BHF-3] 03 p0373 A71-14110

Metal and glass composites with similar residual stress states under axial loading, examining yielding and fracture behavior 03 p0443 A71-14186

Thermal expansion of dilute binary composites containing ceramic-glass, glass-metal, metal-metal and organic-metal systems 03 p0449 A71-14458

Composite material of ductile matrix and straight reinforcing fibers, deriving yield condition 04 p0669 A71-15196

Plane wave propagation in layer direction in fiber reinforced viscoelastic materials 04 p0669 A71-15202

Sandwich metal construction with welded Norsial corrugated core for light weight and strength, discussing fabrication and application to hypersonic research vehicles 04 p0603 A71-15207

Graphite/epoxy composite structural spacecraft panels, discussing design analysis and fabrication procedure 04 p0618 A71-15344

Composite materials of highly conductive metal fibers randomly distributed in low conductive matrices, investigating parameters affecting thermal conductivity from stochastic models 04 p0678 A71-15458

Ferromagnetic dielectric composites physicochemical properties, considering thermal conductivity, density, linear expansion, resistivity, thermal stability and magnetic permeability 04 p0618 A71-15570

Transverse elastic modulus and Poisson coefficient of composite materials as function of reinforcement, structure and fiber radius 05 p0771 A71-16360

Interlayer rigidity effects on strength of fiber reinforced composite materials under plane loads 05 p0771 A71-16366

Stress wave scattering in fiber reinforced composite material, using model of parallel elastic cylinders embedded in unbounded elastic medium 05 p0826 A71-16719

Powdered Ni-carbide composites compressibility, noting mixture and pressure effects on compact density 05 p0769 A71-16859

Creep testing machine for plastics and composites 05 p0772 A71-16929

Tensometer for measuring strain rate effects on composites mechanical properties 05 p0734 A71-16930

Composite materials plasticity limit calculation using variational principles 05 p0773 A71-16992

Ti-Be composites produced by powder coextrusion, discussing microprobe studies to determine microstructure thermal stability [AIME PAPER F-70-3] 05 p0000 A71-17104

Fibrous composite materials stress and deformation analysis, using point matching numerical method and boundary point least squares method 05 p0829 A71-17119

Matrix and round inclusion two component composite equilibrium, considering crack effect on strength 06 p1000 A71-17938

Mechanical property data for silicon nitride-silicon carbide fiber ceramic composites having high fracture values 06 p0916 A71-18035

Fiber composites reinforcement obtained in oriented solidification by structural precipitation hardening of matrix [ONERA-TP-920] 06 p0913 A71-18094

Unidirectional discontinuous fiber composite longitudinal strength calculation based on perturbation effect and distortional energy criterion, using finite element method 06 p1001 A71-18100

Unidirectional fiber reinforced orthotropic composite materials elastic constants calculation as function of two isotropic components characteristics 06 p1001 A71-18309

Graphite fiber reinforced Al-Si alloy composite tensile strength and microstructure, observing tension failure modes 06 p0914 A71-18678

Deformation-thermal diffusion processes relation for thin coated composite materials under variable thermal stresses 07 p1210 A71-19156

Lightning protection for dielectric composites, analyzing damage from shock waves, vaporization pressure, magnetic forces and burning 07 p1021 A71-19942

Rail shear test theoretical and experimental analysis, comparing high modulus reinforced composites test data with predicted values from lamination theory 07 p1215 A71-20128

Laminate analogy predicting elastic and thermal expansion properties of short fiber reinforced composites, extending to two and three dimensional woven fabric composites 07 p1215 A71-20129

Unidirectional fiber reinforced composite longitudinal shear deformation, deriving analytical expression for stress distribution

07 p1216 A71-20132

Fiber reinforced materials machining, considering deformation and stress fields, forces required for continuous machining

07 p1120 A71-20133

AL particle size and filler volume optimization effects on epoxy composite dynamic response

07 p1139 A71-20136

Strain rate effect on fiber reinforced unidirectional epoxy composites tensile stress, noting steel, boron, beryllium and graphite/epoxy strands

07 p1139 A71-20137

Heterogeneity effects on thin composite cylindrical shells axisymmetric vibration characteristic, considering material and geometric symmetry deviations influence on frequency spectra

08 p1368 A71-20805

Carbon fiber and carbon fiber-polyester composites high temperature mechanical properties

[PLASTICS INST. PAPER 35]

08 p1319 A71-20899

Carbon fiber and carbon fiber-polyester composites chemical resistance to acid and alkaline solutions at various concentrations and temperatures

[PLASTICS INST. PAPER 32]

08 p1320 A71-20903

Carbon fibers, light metal alloys and composites, studying moduli of elasticity and shear thermal variations

[PLASTICS INST. PAPER 16]

08 p1320 A71-20904

Composite materials with metallic matrix and carbon fibers, discussing production techniques and mechanical properties

[PLASTICS INST. PAPER 15]

08 p1320 A71-20907

Epoxy resin matrix properties influence on carbon fiber composites performance, discussing test methods for measuring mechanical and fatigue properties over temperature and frequency range

[PLASTICS INST. PAPER 22]

08 p1320 A71-20908

High performance graphitized carbon/carbon composites, discussing mechanical properties improvement by fiber content optimization and heat treatment

[PLASTICS INST. PAPER 37]

08 p1321 A71-20910

High modulus graphite fiber reinforced composites tensile and compressive test methods and results

[PLASTICS INST. PAPER 23]

08 p1321 A71-20913

Carbon fiber/carbon composites produced by moulded carbon technique, discussing mechanical properties and applications in rocket motors

[PLASTICS INST. PAPER 38]

08 p1348 A71-20914

Fiber content effect on mechanical properties of carbon felt/carbon matrix composites

[PLASTICS INST. PAPER 40]

08 p1321 A71-20915

Thermosetting and thermoplastic carbon fiber composites fabrication molding techniques, forms provisions and new uses

[PLASTICS INST. PAPER 33]

08 p1321 A71-20916

Carbon fibers and composites nondestructive testing, discussing defect detection problems in ultrasonics, X ray diffraction and X radiography methods

[PLASTICS INST. PAPER 52]

08 p1296 A71-20918

Carbon fiber composites engineering applications, discussing mechanical properties, weight and economic considerations

[PLASTICS INST. PAPER 30]

08 p1297 A71-20919

High modulus carbon fiber wettability by matrix resin

[PLASTICS INST. PAPER 21]

08 p1322 A71-20928

Cost aspects of carbon fiber reinforced composites in aircraft structures, suggesting increased aviation market for carbon fiber

[PLASTICS INST. PAPER 46]

08 p1378 A71-20929

Carbon fiber composites utilization problems for product and tool designers, considering mechanical properties anisotropy, fiber alignment and bundle strength

[PLASTICS INST. PAPER 42]

08 p1322 A71-20931

Friction-wear characteristics of self lubricating composites under sliding conditions in air and vacuum

[ASLE PREPRINT 70LC-17]

08 p1298 A71-21160

Tetra-Core structural composite material, discussing fabrication techniques, test results, potential and applications

08 p1369 A71-21225

Unidirectionally aligned fiber phase solidified eutectic composites model, discussing high temperature rupture and creep properties

08 p1323 A71-21585

Elastic characteristics of graphite plastics and graphite materials impregnated with synthetic resins, considering aging effect on elastic modulus

09 p1483 A71-22824

Reinforced composite materials with curved fibers, considering one dimensional stress-strain relation and misalignment effect

09 p1539 A71-22917

Composite material dynamic processes based on diffusing mixtures continuum theory

09 p1540 A71-23085

Organo-ceramic composites for thermal protection of aerospace vehicles, discussing heat sink property

09 p1483 A71-23206

Composite materials for compressor blades in aircraft engines, considering boron and carbon fiber reinforced materials

09 p1456 A71-23286

Metallic and nonmetallic composite materials in jet engine component design, discussing integral blade/disk, reinforcement hoop, rotors and airfoils

09 p1456 A71-23307

Subsonic velocities erosion behavior of polymeric coatings and composites, considering void content and reinforcement influence on composite structure

09 p1483 A71-23425

Graphite fiber reinforced ablative composites fabricated into rocket propulsion test units for oxidative liquid high temperature and pressure environments

09 p1459 A71-23685

Effective dielectric constant of macroscopically homogeneous and isotropic two phase composites in terms of sample geometry

10 p1655 A71-23922

Single ply sandwich composite prepregs for use with honeycomb reinforcement, noting one step curing for light weight structural panels

10 p1630 A71-24065

Degradation rate tests on adhesive bonded sandwich panels of temperature resistant composite structural materials at varying atmospheric pressures

10 p1614 A71-24073

Variable weight composite materials for aircraft optimal adhesive bonding structural designs, discussing C-5A tow weight saving Ti honeycomb applications

10 p1686 A71-24084

Polyblends and composites - Conference, New York, June 1969

10 p1634 A71-24767

Composite morphology and mechanical properties relationship, considering reinforcing effect, filamentous systems, whisker growth ladder molecules synthesis and material production

10 p1635 A71-24768

Composites fabrication techniques, component materials and nature, emphasizing fiber orientation and matrix properties

10 p1618 A71-24769

High temperature honeycomb woven fiberglass reinforced polyimide resin, asbestos reinforced composites and high modulus graphite materials, discussing specific strength and stiffness

10 p1618 A71-24771

Three dimensional composite reinforcement principles, discussing thermal strain reduction and mechanical properties

10 p1691 A71-24772

Short carbon and glass fiber reinforced composites, calculating modulus of elasticity from mathematical model

10 p1635 A71-24806

B and C polymer laminated film composites efficiency for stability designed structures, considering weight reduction by planar reinforcements

[AIAA PAPER 71-353]

11 p1783 A71-25331

Composites under transverse normal tensile loading micromechanics failure criteria based on distortion energy theory, taking into account multiaxial stress concentration

[AIAA PAPER 71-355]

11 p1784 A71-25334

Failure analysis of notched unidirectional composites under tensile load parallel to fiber, considering Griffith-Irwin-Orowan fracture theory applicability

[AIAA PAPER 71-369]

11 p1784 A71-25343

Stress rupture behavior of S glass/epoxy multifilament strands, developing tensile and creep test apparatus installed in controlled environment building

11 p1784 A71-25397

Graphite epoxy composites fatigue testing, including loaded and unloaded shear, hardness and tensile strength in wet and dry environments

11 p1785 A71-25402

Carboxyl terminated butadiene-acrylonitrile/epoxy carbon fiber composites fracture energy, noting fracture strength, short beam shear strength and tensile strength at cryogenic temperatures

11 p1785 A71-25403

Longitudinal tensile strength of unidirectional fibrous glass/polymeric matrix composites under high loading rates

11 p1785 A71-25405

Carbon fiber reinforced high interlaminar shear strength composites, noting applications to advanced engineering structures

11 p1785 A71-25408

Graphite fiber resin composites physical and mechanical properties at ambient and cryogenic temperatures, discussing unidirectional ring and bar specimens and filament wound pressure vessels

11 p1785 A71-25409

Epoxy resin in fiber reinforced composite prepregs, characterizing by thermomechanical analysis and gel permeation chromatography

11 p1786 A71-25411

Impact composite materials with reactive resins as binders for polyester fabric, determining peel resistance, tensile shear strength and high temperature aging effect

11 p1786 A71-25416

Longitudinal and transverse residual stresses arising in lamination fabrication process of cross-ply fiber composites

11 p1786 A71-25421

Representative Thorneil fiber aircraft fuselage component nondestructive testing and repair, and Thorneil fiber, polysulfone and polyamide-imide composites fabrication and evaluation

11 p1787 A71-25427

Prototype graphite fiber/plastic fuselage component design, test and performance prediction, using structural analysis methods

11 p1787 A71-25428

Composite material structural behavior prediction, emphasizing static, dynamic, buckling and post-buckling response of anisotropic plates laminated from unidirectional plies

11 p1846 A71-25429

Composite materials fiber-matrix interfacial behavior, determining polymer concentration on graphite fibers surface by Raman spectroscopy and composite shear strength increase

11 p1787 A71-25430

Fiber reinforced composites, predicting mechanical properties, stress-strain behavior, interface failure, creep and fatigue by mathematical model

11 p1849 A71-25655

Resin matrix composite airfoils in gas turbine engines, considering performance, fabrication and cost

[ASME PAPER 71-GT-47]

11 p1770 A71-25980

Boron-glass-epoxy lightweight composite gear case for aircraft engine reduction gearbox, describing design, molding, machining and testing

[ASME PAPER 71-GT-85]

11 p1771 A71-25993

Test streams and chemical composition effects on ablative composites for hypervelocity heat protection of manned atmospheric entry vehicles

11 p1855 A71-26031

Thermosetting polyphenylene resins synthesis and use in reinforced ablative composites, discussing polymerization and curing

11 p1789 A71-26036

Resin systems for ablative composites, correlating hyperthermal performance characteristics via thermogravimetric, mechanical flexural and ablation tests

11 p1789 A71-26039

High performance ablative composites thermal physical characteristics from differential equations, describing thermochemical ablation-in depth and boundary layer transport processes

11 p1856 A71-26041

Mixed boundary value problem for fiber reinforced materials, analyzing shear response in multiply admissible kinematic deformations

11 p1850 A71-26105

Lightweight oxidation resistant carbon-carbon composites for space shuttle leading edge components thermal protection

[AIAA PAPER 71-446]

11 p1790 A71-26231

Boron filaments and whiskers as reinforcements in high strength composite materials

11 p1790 A71-26336

Graphite materials for nosetip/reentry applications, discussing isostatically pressed short fiber-pitch composites and binderless graphites, ablation data and NDT procedures

[AIAA PAPER 71-417]

11 p1790 A71-26341

Viscous model for stress wave propagation perpendicular to plates of bilaminar composite material

11 p1851 A71-26381

Stress analysis near free surfaces in thin composite plates with unidirectionally oriented elastic isotropic fibers, applying boundary point least squares technique

11 p1851 A71-26382

Bounds for effective dielectric constant of fiber reinforced materials, using Miller geometry of matrix and inclusion

11 p1782 A71-26388

Strain concentration around holes in composite plate by moire techniques

11 p1851 A71-26389

- High hyperthermal ablation performance of reinforced carbon/carbon composites for reentry nosetip application
[AIAA PAPER 71-416] 12 p1920 A71-26764
- Soviet book on spherical bottoms weakened by openings covering shell stress/strain, elastic-plastic deformations, reinforcing elements and composite materials
12 p1977 A71-27293
- Air Force development programs with graphite reinforced composites, discussing matrix materials and cost and weight savings
[ASME PAPER 71-DE-13] 12 p1921 A71-27323
- Impulsive energy deposition generated stress waves in composite media formed by two plane layers with interfacial molecular bond joining
12 p1983 A71-27575
- Fiber composites monofilament and strand tests, considering fracture, fatigue, stress, corrosion and microstructure
12 p1921 A71-27635
- Fiber reinforcements for structural composites, considering glass, polycrystals, vapor deposition, whiskers and metals
12 p1922 A71-27636
- Ti, B and graphite fiber composites application to aircraft design, discussing mechanical properties and market competition
12 p1918 A71-27676
- Fibrous composite materials experimental failure studies at high temperatures and cyclic loading
12 p1922 A71-27683
- Compression strength theory for monodirectional reinforced homogeneous anisotropic and piecewise homogeneous materials, using microvolume stability loss failure mechanism
12 p1922 A71-27684
- Fiber reinforced composite materials plastic behavior shear stress theory, determining yield criteria and plastic strain rates associated with various failure modes
12 p1984 A71-27773
- Critical equilibrium of two component composite material with crack propagating along diameter of round inclusion
13 p2090 A71-27824
- Refractory composite inorganic materials technology, covering gas phase, single crystal and hydrothermal synthesis, physicochemical analysis and fabrication methods
13 p2090 A71-28006
- Filament reinforced composite materials, considering spacecraft and missile applications mechanical and physical properties
13 p2144 A71-28166
- Composite materials application to space shuttles, considering resulting weight reduction
13 p2144 A71-28167
- Filamentary composite reinforced metal aircraft structures, considering boron/epoxy in combination with aluminum
13 p2151 A71-28168
- Composites nature and assembly from inspection standpoint, discussing maturing process and comparison with ordinary metals
13 p2091 A71-28439
- Graphite epoxy composites fiber microstructure and surface condition, noting tensile fracture, crack propagation and brittleness
13 p2092 A71-28594
- Fabrication and properties of carbon reinforced carbon matrix composites
14 p2261 A71-29639
- Carbon/carbon composites, describing manufacturing techniques for fiber reinforced matrix structures
14 p2261 A71-29640
- Carbon-carbon spacecraft reentry heatshields evaluation and selection by nondestructive and destructive tests on flight cones
14 p2262 A71-29647
- Mechanical and thermal properties of chemical vapor deposited carbon composite felt material for reentry heat shielding
14 p2262 A71-29648
- Three dimensional orthogonally woven reinforced felt-yarn composite for low density thermal insulation and chemical vapor deposition
14 p2262 A71-29651
- Advanced composite vs conventional material components in cost comparison for aircraft parts
14 p2263 A71-29656
- Composite materials elastic-plastic behavior under uniaxial loading, determining stress-strain relationships by dislocation theory
14 p2321 A71-29688
- Advanced filamentary composite materials behavior, discussing limited ductility, sensitivity to stress concentrations, fatigue and viscoelastic properties
14 p2264 A71-29897
- Unidirectional fiber composites impact resistance, showing matrix modulus, fabrication process, fiber and void volume ratios and microresidual stress effects
14 p2264 A71-29920
- Shape instabilities for eutectic alloys composite microstructure at elevated temperatures
14 p2259 A71-30413
- Elastic properties of orthotropic composite disks of fiber-reinforced materials, comparing actual stress in composite with permissible stress of fiber and matrix
14 p2329 A71-30472
- Composite materials application to V/STOL prop/rotors, determining material properties parametric effect on frequencies and weight by Southwell coefficients
[AHS PREPRINT 554] 14 p2180 A71-31106
- Notched unidirectional composites failure mechanics under tensile load in fiber direction, considering debonding, plasticity and strength
15 p2428 A71-31971
- Interfiber stress model for elastic matrix-fiber reinforced composites under inplane shear and transverse normal loading
15 p2507 A71-32096
- Mechanics of laminated filamentary composite orthotropic material used for cover skin in advanced aircraft component design
15 p2507 A71-32109
- Al and Cu-Al alloys eutectic composites with small interlamellar spacing, characterizing ambient temperature compressive stress strain behavior to failure
15 p2432 A71-32168
- Fiber reinforced materials with oriented armoring, calculating stress-strain state under transverse shear
15 p2439 A71-32235
- Composite materials fabrication primary and secondary aerospace and aeropropulsion structural components
[SME PAPER EM-71-710] 15 p2416 A71-32434
- Lead bronze and Babbitt metal composite material, detailing antifriction efficiency and wear resistance in bearings
15 p2417 A71-32666
- Two-phase composites stability at various temperatures, studying mechanical properties dependence on second phase proportion
16 p2593 A71-33639
- Composite materials reinforced by brittle sapphire and ductile copper whisker crystals, noting surface defects effect on mechanical properties
16 p2601 A71-33917
- Advanced composites as future aircraft structural materials, discussing design concepts, service experience, manufacturing methods and quality assurance
[AIAA PAPER 71-779] 16 p2660 A71-34014
- Boron-aluminum composites fracture behavior, using conventional metallography and scanning electron microscope
16 p2599 A71-34087
- Titanium and composite fabrication for F-14 aircraft, discussing hot forming, chemical milling and electron beam welding
16 p2585 A71-34156
- Fibrous composites with multiple and variable shear strength interfaces to improve longitudinal shear and transverse tensile strengths and toughness
17 p2817 A71-34342
- Strain rate effects on composite material tensile and flexural properties measured by load sensors and streak photography
17 p2737 A71-34345
- Fiber to matrix modulus of elasticity ratio for two dimensional plane stress composite by finite element and moire strain analyses
[SESA PAPER 1826A] 17 p2761 A71-34527
- Gross static material elastic constants for layered composite materials, using photoelastic models
[SESA PAPER 1845A] 17 p2761 A71-34531
- Method of producing transparent model composite materials for photo-orthotropic-elastic studies, allowing preparation of larger laminates
17 p2820 A71-34540
- Two phase fiber reinforced composites under polyaform stresses, predicting plastic behavior by deformation theory
17 p2823 A71-34810
- Dynamic compressive strength and failure of steel reinforced epoxy composites, discussing strain rate sensitivity
17 p2762 A71-34813
- Elastic stress waves propagation in photoelastic layered composite materials, indicating wave front steady state
17 p2824 A71-34816
- Anisotropic composite materials failure surface criteria in three dimensional space, using graphical representation
17 p2824 A71-34817
- Tension test for filamentary composites, employing hardened Al alloy wedges adhesive bonded to gripping edges
17 p2739 A71-34818
- Aluminum powder filled epoxy composites, investigating particle size and filler percent effects on damping properties and elastic modulus
17 p2762 A71-34819
- Composite materials and structures - Conference, Colorado Springs, May 1971
17 p2762 A71-35201
- High modulus graphite composites application for structural weight reduction and stiffness requirement without strength loss
17 p2762 A71-35202
- High modulus graphite-boron composites design and application to lightweight structures, illustrating sandwich construction for race boat main boom stiffness and compressive strength
17 p2762 A71-35203
- Low thermal flux lightweight glass fiber composite tubing for cryogenic propulsion plumbing systems
17 p2762 A71-35206
- Stress wave propagation in quartz-phenolic composite, measuring particle velocity by velocity interferometer
17 p2762 A71-35207
- Bunched parallel reinforcing fibers of equal size and varying tensile strength, deriving critical loads and stresses under gradual failure
17 p2763 A71-35451
- Deformation-thermal diffusion processes relation for thin coated composite materials under variable thermal stresses
17 p2834 A71-35654
- Composite materials effect on supersonic aircraft weight, design and performance
[SAWE PAPER 888] 17 p2676 A71-35818
- Weight reduction potential of composite materials in aerospace structures, proposing weight estimation technique
[SAWE PAPER 887] 17 p2834 A71-35819
- Design, analysis and testing of F-111 complex fuselage full scale section of composite materials, noting weight savings
[SAWE PAPER 889] 17 p2835 A71-35825
- Boron, carbon, sapphire and glass fiber composite materials, considering brittleness, anisotropic properties, filament winding and plastic and metallic matrices
18 p2939 A71-35915
- Loaded crack ending at bimaterial composite interface, analyzing crack tip stress field singularity order dependence on material elastic constants
[ASME PAPER 71-APM-O] 18 p2978 A71-36258
- Incompressible fiber reinforced composite materials finite plane deformation continuum theory and stress analysis without restriction concerning elasticity, plasticity or viscoelasticity behavior
[ASME PAPER 71-APM-V] 18 p2978 A71-36264
- Composite materials and structures analysis and design, examining elastic constants, thermal expansion coefficients, viscoelastic moduli, conductivities and failure modes
18 p2979 A71-36274
- Filament wound carbon/carbon composite heat shields, describing fabrication process involving winding, carbonization, pyrolytic carbon infiltration and graphitization
[SME PAPER EM-71-204] 18 p2939 A71-36664
- Composite materials plasticity limit calculation using variational principles
18 p2940 A71-36792
- Refractory, superalloy and composite materials brazing process for space shuttle orbiter heat shield
18 p2928 A71-36854
- Maximum acoustic attenuation in lead-wool-polyurethane and nickel-Cerrobend composites for different compositions, frequencies and pressures
18 p2948 A71-36933
- Microscopically homogeneous and isotropic two phase composite material shear modulus formula derivation
19 p3155 A71-37481
- Carbon-fiber-reinforced carbon composites for high temperature applications, describing filament orientation, matrix composition and heat treatment effects on ablation performance
19 p3085 A71-38350
- Carbon-carbon composites fabrication by electrostatic fiber deposition/flocking, using liquid impregnation-carbonization cycles with coal tar pitch
21 p3384 A71-40140
- Macroscopically isotropic and homogeneous two phase composite materials elastic constants determination, discussing approximate formulas and validity
21 p3463 A71-40583
- Glass-fiber/glass-bead/resin beam stiffness and strength improvement with sandwiching between layers of unidirectional carbon fiber composite
21 p3405 A71-40597
- Elastomeric rocket motor thermal insulants ablation, considering composite properties, heat transfer, compounding and tests
21 p3406 A71-40603
- Modulus of elasticity and Poisson ratio of composite material with anisotropic or isotropic fibers arranged in rectangular or square array
21 p3464 A71-40772
- Shock stress waves dispersion in laminated composite materials
21 p3465 A71-40790
- Pulse attenuation in composite materials, discussing stress waves geometric dispersion and compressive fracturing effects
21 p3465 A71-40791

Composites and mechanical systems dynamic behavior prediction, calculating Hugoniot with effective modulus

21 p3465 A71-40792

Dynamic photoelasticity for stress wave propagation in anisotropic fiber reinforced composites, using birefringent models and pulsed ruby laser beam

21 p3471 A71-41027

High temperature structural application of refractory fiber reinforced ceramic composites

22 p3565 A71-42287

Grainy composite material structural analysis, presenting statistical mathematical model

23 p3698 A71-44224

Porous fiber reinforced composite low density heat insulating materials thermal conductivity measurements, showing energy transport by heat transfer mechanisms

23 p3784 A71-44341

Fiber-reinforced composites mechanical properties based on analytical treatment as homogeneous orthotropic bodies

24 p3841 A71-44573

Flexural vibration of transversely isotropic composite material curved beams, deriving curvature effects on natural frequency

24 p3878 A71-44616

Composite materials thermal diffusivity at high temperatures by quasi-stationary and monotonic methods, determining validity domain of differential heat conduction equation without heat sources

24 p3889 A71-44967

Stress-strain curve of unidirectional fiber reinforced composite Al and N-Cl wire under axial compression loads, discussing buckling and shear instabilities

24 p3842 A71-45229

COMPOSITE PROPELLANTS

AP composite solid propellant combustion model based on multiple flame structure surrounding individual oxidizer crystals

03 p0469 A71-13440

Quench combustion of ammonium perchlorate composite solid propellant sandwich indicating binder-oxidizer interplay

[AIAA PAPER 71-170] 06 p0944 A71-18610

Composite propellant transient burning rates continuous measurement during rapid depressurization

[AIAA PAPER 71-173] 06 p0944 A71-18612

Electric field effects on burning rates of composite metallized solid propellant containing ammonium perchlorate

[AIAA PAPER 71-174] 06 p0947 A71-18613

Burning rate temperature sensitivity of composite solid propellants, using granular diffusion flame model

09 p1510 A71-22911

Erosive burning of composite propellants based on ammonium perchlorate, studying oxidizer grain size effect

10 p1658 A71-25122

Composite propellant flame temperature and emission spectra during depressurization by rarefaction waves, using rapid scanning spectrometer

[AIAA PAPER 70-663] 12 p1945 A71-27564

Depressurization extinguishment of composite solid propellants for thrust termination, considering flame structure, surface characteristics and restart capability

[DFVLR-SONDDR-129] 13 p2113 A71-28615

Solid composite propellant mixing influence on viscosity, pot life and motor reject rates based on bench scale production

[AICHE PAPER 32D] 13 p2113 A71-28894

Continuous burning rate measurement for metallized composite solid propellants, using optical sensor for servo tracking propellant surface

14 p2244 A71-30328

Fast burning rates in thin film solid composite propellants composed of McCormick-Selph 510, 164 monopropellant, oxidizer and polyvinyl chloride binder

[AIAA PAPER 71-655] 14 p2285 A71-30730

Combustion rates of ammonium perchlorate mixtures with organic acids, alcohols, cyclic hydrocarbons, amines, nitroso compounds and nitramines, studying relationship to fuel chemical composition

15 p2366 A71-31370

Combustion model of solid composite propellants containing monopropellant oxidizers ammonium perchlorate, cyclotetramethylene-tetranitramine and potassium perchlorate

19 p3121 A71-38122

Burn time and acceleration effects on molten metallic material chemical composition near burning surface of aluminized composite solid propellant

19 p3121 A71-38298

Acceleration dependent burning rate increases of aluminized composite solid propellants induced by combined erosive and acceleration

21 p3436 A71-40943

COMPOSITE STRUCTURES

NT LAMINATES

Composite fiber-reinforced structures fabrication methods

[SME PAPER EM-70-112] 01 p0089 A71-11256

Metal matrix composites fabrication techniques, discussing isostatic hot pressing, explosive processing and in situ fibering

[SME PAPER EM-70-125] 01 p0090 A71-11264

Load limit surfaces for composite plates with long elastic plastic fibers site bonded or imbedded in low strength matrix

03 p0504 A71-13429

Elastic metal thin plates transverse resonant free vibrations, analyzing viscoelastic coatings damping effects

[ASME PAPER 70-DE-E] 03 p0506 A71-13709

Elastic metal thin beams transverse resonant free vibrations, analyzing viscoelastic coatings damping effects

[ASME PAPER 70-DE-D] 03 p0507 A71-13710

Orthotropic photoelastic analysis of residual stresses in filament-wound composite ring structures, comparing with boring-out and cut-through methods

03 p0508 A71-13773

Two-member composite cylinders, predicting residual stress and axial loading behavior by elastoplastic analysis for comparison with experiment

04 p0666 A71-14893

Steel-concrete composite beam creep numerical analysis by reduction to elastic problem with initial strains

04 p0669 A71-15198

Fiber reinforced cryogenic pressure vessels design, manufacture and testing for space and terrestrial applications, comparing glass fibers to carbon fibers

04 p0618 A71-15650

Inhomogeneously reinforced composite structures strengthening by internal stress matching

05 p0771 A71-16365

Combined deformation of reinforcing elements and polymer binder in monodirectional composite structure, determining stress distribution

06 p0915 A71-17380

High modulus boron-epoxy composite aircraft structures adhesive bonding, discussing mechanical properties, manufacturing techniques and quality control

[SAE PAPER 710110] 06 p0904 A71-17624

Composite hollow cylinders of heteromaterials, discussing stress-strain state

06 p0984 A71-17650

Elastic composite liquid filled shell containers, calculating natural vibration with Ritz method

06 p0992 A71-17809

Ni-W eutectic alloy unidirectional solidification to obtain composite structure in Ni-W solid solution

06 p0915 A71-18689

Composite plastic aircraft structures lightning protection, considering hazard to composite materials and use of metal filled or plasma sprayed coatings and metal foil coverings

07 p1021 A71-19943

Torsional wave propagation in elastic circular composite cylinders, introducing correction factors for approximate theory

07 p1214 A71-19955

Elastic harmonic waves propagation in composite circular elastic cylinder

07 p1214 A71-19956

Bonded rod of two semiinfinite elastic bars subjected to end impulse, formulating motion equations and initial and boundary conditions

07 p1217 A71-20367

Asymmetric three layer cylindrical shells with orthotropic layers under deflection due to high temperature, deriving differential bending equations

07 p1217 A71-20456

Composite elongated ellipsoid of revolution under torsion, determining stress-strain state, boundary conditions and elastic displacements

08 p1368 A71-20800

Structural element for discrete element idealization of missile and liquid propellant as one composite structure

[AIAA PAPER 70-23] 09 p1430 A71-22087

Statically indeterminate rod system design, using linear strengthened materials strain diagrams and Castigliano principle

09 p1538 A71-22650

Subsonic velocities erosion behavior of polymeric coatings and composites, considering void content and reinforcement influence on composite structure

09 p1483 A71-23425

Unidirectional fibrous composites brittle and ductile failures prediction under tension and torsion, comparing results with tests on glass-epoxy composites

10 p1686 A71-24017

Weather stress tests for determining optimum adhesive system for bonding reinforced fiberglass panels to Al extrusions held by steel beams

10 p1616 A71-24114

Temperature distribution in composite media sections involving solid interfacial sources, using Vodicica orthogonality equations

10 p1697 A71-24694

Frequency equation for harmonic waves with circumferential nodes traveling in composite traction

free circular cylindrical shells, using IBM 7094 computer

11 p1847 A71-25461

Air cooled turbine blades activated diffusion brazing and gas pressure welding, using composite finned configuration model

[ASME PAPER 71-GT-32] 11 p1770 A71-25969

Fibrous composite structure stress analysis procedures, considering nonisotropy and brittleness effect

[ASME PAPER 71-DE-2] 12 p1977 A71-27321

Graphite-epoxy composite skins for commercial aircraft flight spoiler, discussing multiangle ply design and fabrication

12 p1921 A71-27413

Combined deformation of reinforcing elements and polymer binder in monodirectional composite structure, determining stress distribution

12 p1921 A71-27462

Forced axisymmetric vibrations of composite cylindrical shell with spherical bottom, obtaining influence coefficients and inhomogeneous boundary conditions

13 p2150 A71-28141

Free elastically joined composite rod under tracking forces, calculating stability and oscillations by numerical method

13 p2154 A71-28644

Thermal transients in composite cylinders, solving diffusion equation by Laplace transform technique

13 p2164 A71-28987

Aboveground liquid storage tanks design with fiberglass-reinforced composites based on pressure vessels requirements

[DFVLR-SONDDR-93] 13 p2157 A71-29307

Oscillation and stability of free composite body with elastically suspended masses, simulating liquid sloshing in cavity by equivalent mechanical model

14 p2321 A71-29537

Filament wound pressure vessels and composites flaw detection nondestructive tests with X rays and thermography

14 p2262 A71-29644

Arbitrary periodic composite structure system with local interactions, obtaining macroscopic properties from unit cell boundary value problems

14 p2323 A71-29812

Torsion of circular composite rods of sectors with different shear moduli and radial cracks

14 p2326 A71-30193

Axisymmetric vibrations of heterogeneous isotropic composite clamped circular plates based on Kirchhoff theory

14 p2327 A71-30205

Geometrical parameters and load carrying capacity of fiberglass reinforced plastic composites with elastoplastic adhesive bonding, deriving relations for stress distribution

14 p2264 A71-30270

Graphite fiber composite structures nondestructive testing, discussing liquid penetrants, X ray radiography sonic methods, acoustic emission and IR tests

15 p2414 A71-31816

Composite rocket engine casing thermal flux approximation from multilayer plate heat conduction

17 p2837 A71-34568

Axisymmetric nonlinear buckling equations for composite thin circular elastic plates of isotropic or orthotropic layers under radial compression

17 p2821 A71-34580

Composite piezoelectric transducer subjected to current flow in semiconducting boundary layer under polarization gradient, determining mechanical response by Laplace transform

17 p2739 A71-34669

Rectangular composite prismatic bar with T shaped cross section, calculating torsion with summary representation method

17 p2824 A71-34847

Composite materials and structures - Conference, Colorado Springs, May 1971

17 p2762 A71-35201

Gradient shape influence on connectivity in two phase graded structures, considering polyphase structure of filament reinforced composites

17 p2763 A71-35226

Composite materials and structures analysis and design, examining elastic constants, thermal expansion coefficients, viscoelastic moduli, conductivities and failure modes

[AIAA PAPER 71-366] 18 p2979 A71-36274

Composite structures development, discussing wing, fuselage, aeropropulsion and missile development, weight savings of hardware and fighter empennage applications

[AIAA PAPER 71-367] 18 p2979 A71-36275

Stress field singularities at interface corners in bonded dissimilar isotropic elastic materials under plane force field applied to wedge subregion

18 p2983 A71-36843

Elastic field and stress distribution in composite circular rotating disk under constant normal pressure

19 p3159 A71-38187

Dynamic response of elastic cylindrical shell-solid core composite under time dependent loading from Laplace transform 21 p3467 A71-40949

Nondestructive testing evaluation of graphite epoxy composites and adhesive bonded Al composite structures using acoustical holography 22 p3554 A71-41781

Two-component composite cylindrical body thermoelectric stresses near junction-surface edge under plane deformation conditions 23 p3776 A71-43420

Numerical solution for plane wave scattering by dielectric sheet with imbedded periodic array of conducting strips 23 p3654 A71-44164

Photoelastic analysis of thermal stresses in polyurethane rubber ring reinforced polymers, cermets and rubber-metal composites 24 p3883 A71-44895

Stress and displacement solutions to deformation of homogeneous and composite anisotropic near cylindrical bodies, using Almansi algorithm 24 p3885 A71-45061

COMPOSITE WRAPPING
Winding equipment for continuous production of large diameter cylindrical filaments of reinforcing materials and polyester resins 11 p1768 A71-25418

COMPOSITES
U COMPOSITE MATERIALS
COMPOSITION [PROPERTY]
NT ATMOSPHERIC COMPOSITION
NT ATMOSPHERIC MOISTURE
NT ATOM CONCENTRATION
NT BODY COMPOSITION [BIOLOGY]
NT CARBON DIOXIDE CONCENTRATION
NT CHEMICAL COMPOSITION
NT CONCENTRATION [COMPOSITION]
NT GAS COMPOSITION
NT IONOSPHERIC COMPOSITION
NT LUNAR COMPOSITION
NT METEORIC COMPOSITION
NT METEOROID CONCENTRATION
NT MOISTURE CONTENT
NT PLANETARY COMPOSITION
NT PLASMA COMPOSITION
Computer solutions of one dimensional flow of constant composition and specific heat ratio fluids, using influence coefficients 03 p0405 A71-14440
Ni-Fe alloy films composition gradients produced by W boats evaporation, noting vapor pressures effect 05 p0791 A71-16230
Mossbauer effect study of 475 C decomposition of binary Fe-Cr alloys, considering fluctuations about average composition 07 p1138 A71-19985
Minima and maxima in composition dependence of thermal diffusion factor and conductivity of gas mixtures 16 p2614 A71-33104
Composition transformations at interface levels in iron-nickel alloys as function of thermal treatment, using potentiokinetic method 16 p2598 A71-34050
Maximum acoustic attenuation in lead-wool-polyurethane and nickel-Cerrobend composites for different compositions, frequencies and pressures 18 p2948 A71-36933

COMPOUND HELICOPTERS
Compound and VTOL aircraft and prototype compact downtown V-ports for short haul air transportation improvement and expansion 03 p0348 A71-13619
AH-56A Cheyenne compound helicopter icing spray rig tests, discussing ice protection systems design and operating performance 04 p0534 A71-15438
Electromechanical control system synthesis for compound hingeless rotor helicopter, using root locus method with transfer functions from airframe motion linear model 14 p2179 A71-31096
[AHS PREPRINT 536]
High performance UH-1 compound helicopter high speed flight research, considering rotor loads, stability, control and flying qualities 14 p2180 A71-31111
[AHS PREPRINT 570]
AH-56A compound helicopter rigid rotor stability and handling qualities, using flight, whirl tower and wind tunnel tests 14 p2180 A71-31115
[AHS PREPRINT 574]

COMPRESSED AIR
Explosive forming using compressed air as power source for safety and lower cost 01 p0091 A71-11549
Alveolar nitrogen and carbon dioxide tensions changes during compressed air narcosis in constant oxygen partial pressure 08 p1239 A71-20818
Water vapor effects on shock compressed air in thermodynamic equilibrium by computer program, noting temperature and electron concentration reduction 18 p2984 A71-35857

COMPRESSED GAS
NT HIGH PRESSURE OXYGEN
Shock wave propagation in channel with MHD interaction between compressed gas and nonuniform magnetic field 14 p2283 A71-30995
High pressure pneumatic lines dynamics, considering equation of state for real gas with given compressibility function 16 p2527 A71-33618
Oblique shock-combustion wave polar investigation of stationary two dimensional flow of fuel mixture in compressed gas 18 p2985 A71-36133

COMPRESSIBILITY
Density and compressibility of oxygen in critical region, using capacitance measurements 05 p0781 A71-16703
Isotropic compressible homogeneous body with small deformations superposed on finite elastic deformation, deriving equations of motion and boundary conditions 17 p2823 A71-34788
Cs and Hg vapors compressibility factor in supercritical range as function of density, considering charged particles and atoms polarization interactions in ionized metal vapors 19 p3111 A71-37590
Heat stresses in elastic compressible material plate strip subjected to finite deformation 20 p3308 A71-39038
Apollo 12 basalt porosity and volume compressibility under hydrostatic pressure 23 p3759 A71-43768

COMPRESSIBILITY EFFECTS
Fredholm method for reversible transonic flow in computing aircraft wing and turbomachine or helicopter blade airfoils for compressibility law 01 p0003 A71-11022
Hydraulic servomechanism with piston-type control valve, examining oil compressibility and sustained oscillations effects on system stability 01 p0007 A71-11378
Contraction coefficient of orifice for subsonic and supersonic flows, including velocity-of-approach and compressibility effects upstream and downstream [ASME PAPER 70-WA/FM-1] 03 p0402 A71-14103
Turbulent boundary layer equations for heat and mass transfer in incompressible and compressible flows, using eddy viscosity formulation 04 p0680 A71-15479
Fe powder filled tubular shell compression by magnetic fields and pulse sequences 05 p0759 A71-17168
Uniaxial compression effect on dispersion of helicon wave in n-type semiconductors, considering strain potential constants determination 07 p1176 A71-19269
Compressibility effect on turbulent pipe flow shear stress distribution, presenting high subsonic Mach number theoretical results from Kjellstrom-Hedberg momentum equation integration 07 p1088 A71-19423
Mercury intrusion porosimetry application to pore size and shape measurements for porous solids, discussing solid and air compressibilities, surface tension, contact angle, etc 09 p1453 A71-22168
Compressibility correction for subsonic flows past bluff bodies, considering boundary distortion and pressure distribution shift 11 p1701 A71-25149
Shear stress and eddy viscosity distribution in Mach 20 compressible turbulent boundary layer, using mixing length flow theory 11 p1751 A71-25499
Rigid spherical projectile hypervelocity impact with compressible strain-hardening target material, obtaining analytic solution based on dynamic cavity expansion and deep penetration theories 12 p1982 A71-27570
Static and quasi-static atmospheric motions, using linearized equations for isothermal compressible atmosphere 13 p2097 A71-29084
Army rotorcraft performance data, discussing hovering and forward flight performance out of ground and level flight power requirements and drag and compressibility effects 14 p2177 A71-31076
[AHS PREPRINT 500]
Tensile stress and compressive effects on grain boundary precipitate morphology in Ni-base superalloy during creep 15 p2433 A71-32179
Plasma flow wave propagation, investigating compressibility, radiation and finite electrical conductivity effects with plane asymptotic solution combinations 16 p2618 A71-33173
Yield point thermal component in bcc metals at low temperatures as function of hydrostatic compression, noting interionic reaction potential nonisothermicity 16 p2596 A71-33889
Incompressible materials weak compressibility effect in elastic theory, deriving displacement equation

with average pressure function for any Poisson coefficient values 17 p2818 A71-34350
Medium compressibility effect on gas dynamic characteristics and aerodynamic forces and moments in centrifugal compressor end stage bladed diffuser 23 p3626 A71-43552
Finite plane strain inflation of compressible hollow circular cylinder, using perturbation method for nonlinear boundary value problem 24 p3884 A71-44955

COMPRESSIBLE BOUNDARY LAYER
Adiabatic compressible turbulent boundary layer equations for two dimensional and axisymmetric flow, discussing methods of solution based on eddy viscosity formulation [AIAA PAPER 69-687] 01 p0071 A71-10933
Near separation flow in laminar compressible boundary layer on cold wall near zero skin friction, suggesting added terms for previous expansion 02 p0332 A71-12378
Compressible turbulent boundary layers with fluid injection, considering transpiration cooling, skin friction coefficient, etc 03 p0398 A71-13128
Compressible turbulent boundary layer skin friction measurements on adiabatic flat plate, discussing drag balance calibration [ASME PAPER 70-WA/FE-26] 03 p0403 A71-14134
Temperature profiles in high velocity compressible turbulent boundary layer over flat plate without pressure gradients 04 p0681 A71-15480
Turbulent compressible two dimensional boundary layer flows with heat transfer, pressure gradients and wall blowing or suction 04 p0681 A71-15482
Existence theorems for compressible boundary layer problems, discussing Blasius differential equation and Falkner-Skan class of similarity solutions 06 p0881 A71-17638
Finite difference calculation for two dimensional compressible turbulent boundary layer flow with heat transfer, using mixing length concept [AIAA PAPER 71-165] 06 p0885 A71-18607
Nonadiabatic compressible turbulent boundary layer heat transfer to rough surfaces under arbitrary pressure gradient 06 p0885 A71-18608
Cross flow profiles for compressible turbulent boundary layers with and without flow reversal via hodograph models family 08 p1229 A71-22033
Compressible boundary layer separation near zero skin friction by Kaplan perturbation technique, studying nonlinear integral equation with Abel kernel 09 p1432 A71-22455
Low Prandtl number laminar compressible boundary layer flow over flat plate, obtaining recovery temperature profile and heat transfer by matched asymptotic expansions method 10 p1597 A71-25066
Compressible laminar boundary layer flow including second order longitudinal surface curvature effects, deriving flow equations from Navier-Stokes equations 11 p1750 A71-25473
Compressible similar laminar boundary layer equations for zero wall shear and mass addition, describing heat transfer reduction and boundary layer growth by asymptotic analysis 11 p1750 A71-25479
Compressible turbulent boundary layer interaction with wedge or corner induced oblique shock waves, using transformation methods 11 p1750 A71-25481
Compressible laminar boundary layer flow over semiinfinite isothermal porous flat plate in nearly quasi-steady motion, considering skin friction and heat transfer 13 p2048 A71-28600
Instrument for skin friction measurements in adiabatic turbulent compressible boundary layers [ASME PAPER 71-FE-27] 13 p2072 A71-29463
Transformation of compressible turbulent and laminar boundary layers with and without wall blowing [ASME PAPER 71-FE-37] 13 p2166 A71-29472
Spinning sphere impulsively starting rotation from rest in compressible viscous fluid, calculating boundary layer growth by matched asymptotic expansions method 14 p2225 A71-30295
Shear stress, eddy viscosity and mixing length distributions in compressible turbulent boundary layers with air and carbon dioxide injection 14 p2228 A71-31025
Compressible turbulent boundary layers closed form solution by extending Buri momentum integral analysis of incompressible turbulent boundary layers 14 p2228 A71-31129
Friction in compressible turbulent boundary layers at isothermal adiabatic wall 15 p2510 A71-31163

- Compressible laminar plane axisymmetric boundary layer flows in Laval nozzles, studying temperature, density and velocity distribution relations
15 p2386 A71-31164
- Recovery factor for highly accelerated adiabatic compressible laminar boundary layer flow
15 p2391 A71-32114
- Two dimensional compressible turbulent boundary layer with time dependent mean velocity and density fields, deriving momentum and kinetic energy integral equations
17 p2727 A71-34876
- Compressible electrically conducting gas boundary layer on MHD channel electrode, deriving equations for ambipolar region with finite ionization and recombination rates
17 p2790 A71-35644
- Adverse pressure gradient effects on compressible turbulent boundary layer flow in parallel duct at Mach 4 and high Reynolds number
18 p2904 A71-36297
- Compressible three dimensional nonsimilar laminar boundary layers numerical analysis using two layer heuristic model
18 p2845 A71-36336
- Compressible boundary layer equations similarity solutions uniqueness proof, using asymptotic behavior
18 p2909 A71-36814
- Transverse curvature effect on singularity at separation for laminar boundary layer from analogy with flat-plate compressible boundary layer
19 p3044 A71-37726
- Linear stability equations for two dimensional compressible supersonic boundary layer with three dimensional disturbances including thickness growth term
21 p3370 A71-40992
- Mach number distribution along critical streamline in compressed layer in front of cylinder in supersonic flow
24 p3790 A71-45101
- COMPRESSIBLE FLOW**
- Multiple spark camera for unsteady compressible flow investigations, considering geometrical optical design, parallax, spark producing electric circuitry, etc
01 p0078 A71-10106
- Shock formation in cylindrical and two dimensional tubes investigated numerically by FLIC method for compressible fluid flow
01 p0069 A71-10130
- Compressible gas jet flow from vessel with parallel walls pointing in opposite directions, solving Chaplygin equations for stream functions
01 p0069 A71-10420
- Boundary layer solution for unsteady compressible incompressible flow past body, discussing momentum conservation equation solution by series expansion
02 p0241 A71-12848
- Modified Coles compressibility transformation for wake mapping with Howarth-Dorodnitsin scaling suppression
03 p0400 A71-13460
- Compressible flow similarity parameters, establishing dimensionless relations for radial turbomachines design
03 p0343 A71-13830
- Compressible subsonic and supercritical flows, developing flowmeter orifice expansion factors [ASME PAPER 70-WA/FM-3]
03 p0402 A71-14105
- Compressible magnetofluid dynamics studies in cesium shock tube
04 p0632 A71-14690
- Compressible flow with closed streamlines at large Reynolds numbers, considering viscous and heat conduction cumulative secondary effects
04 p0569 A71-14987
- Finite amplitude instability of compressible laminar wake with strongly amplified disturbances, discussing nonlinear theory in terms of von Karman equation
04 p0569 A71-15028
- Turbulent boundary layer equations for heat and mass transfer in incompressible and compressible flows, using eddy viscosity formulation
04 p0680 A71-15479
- Wall stability of parallel elastic plate duct in contact with inviscid compressible fluid flow
04 p0573 A71-15563
- Compressible flow density measurement using optical polarization interferometry with birefringent devices
04 p0601 A71-15918
- Subsonic compressible flow equations solution in terms of velocity potential, obtaining reliable convergence
05 p0737 A71-17115
- Three dimensional inviscid compressible flow past sharp shouldered blunt bodies at angle of attack, presenting time dependent finite difference technique [AIAA PAPER 71-56]
06 p0843 A71-18515
- Compressible turbulent flows free mixing based on two dimensional viscous flow equations [AIAA PAPER 71-4]
07 p1088 A71-19701
- Compressible turbulent boundary layers integral solution based on entrainment theory
07 p1090 A71-19903
- Acoustic propagation through variable area duct with steady compressible flow, transforming governing equations into two decoupled linear ordinary differential equations
07 p1160 A71-19952
- Prandtl-Glauert pressure distribution rule improvement subsonic planar flow
07 p1017 A71-20312
- Compressible two dimensional laminar and turbulent free jet characteristics, presenting unitary method with similarity transformation
07 p1029 A71-20593
- Numerical solution of quasi-one dimensional viscous heat conducting compressible Laval nozzle flows by time dependent finite difference scheme
09 p1545 A71-22454
- Exact numerical solution for laminar compressible boundary layers with nonuniform wall temperatures compared with Luxton-Young approximate method results, noting skin friction effects
09 p1545 A71-22940
- Critical speeds for inviscid compressible potential flow past thin elastic cylindrical shells, using long wave approximation
10 p1689 A71-24565
- Nonuniform transonic shear compressible flow past symmetric airfoil, using linearized small disturbance theory
10 p1552 A71-24761
- Compressible flow in two dimensional boundary layers in arbitrary pressure gradient, using turbulent energy equation for skin frictions and free stream Mach numbers
10 p1598 A71-25082
- Loads induced on infinite aspect ratio wing by straight infinite free vortex in subsonic compressible freestream, using planar lifting surface theory
11 p1702 A71-25474
- Axisymmetrical incompressible and compressible fluid flow inverse problem formulation and solution with application to turbine blade design
11 p1752 A71-26051
- Steady supersonic isoeenergetic flow of thermally and calorically perfect gas past circular cones at zero angle of attack, using dimensional perturbation method
12 p1863 A71-26939
- Hydrodynamic analogy for postulates in special relativity theory, analyzing steady and potential flow of inviscid compressible medium for Chaplygin gas with unreal time
12 p1932 A71-27547
- Conjugate steady convective aerodynamic heating of plate in longitudinal compressible gas flow, taking into account boundary layer enthalpy distribution
13 p1989 A71-27890
- Turbulent boundary layers calculation downstream of compressible relaxing slot injection flows, using finite difference method based on eddy viscosity model
13 p2046 A71-27986
- Compressible viscous gas supersonic flow, observing near wake region behind perpendicular trailing face of plate with motion, state, energy and continuity equations
13 p2047 A71-28421
- Plane one dimensional steady compressible ideally charged gas flow characteristics in electric field
13 p2107 A71-28567
- Compressible rarefied gas Couette flow over plane wall, calculating mean free path with Boltzmann equation relaxation model
13 p2051 A71-29357
- Properties of arbitrarily thick turbulent boundary layer for incompressible axial flow past long cylinder [ASME PAPER 71-FE-25]
13 p1995 A71-29462
- Small spherical solid or liquid particles deceleration, melting and shattering due to spherical and conical bodies in compressible hypersonic shock layer flow field [AIAA PAPER 69-712]
14 p2334 A71-29873
- Rotational effects on laminar subsonic compressible viscous flow across shaft face seals, noting leakage rates and pressure profiles
14 p2251 A71-29936
- Film cooling as solid surfaces protection in high temperature environments, considering two and three dimensional secondary compressible and incompressible flow geometries
14 p2337 A71-30244
- Discrete tone noise generation by high speed fans and compressor blades, using McCune analysis for linearized three dimensional compressible flow in infinite annulus [AIAA PAPER 71-617]
15 p2468 A71-31555
- Compressible transonic flow about two dimensional airfoils, developing inviscid nonlinear potential equations by relaxation procedures [AIAA PAPER 71-569]
15 p2345 A71-31562
- Inviscid compressible transonic flow field equations for perfect gas in conical rocket nozzles, measuring wall and center line pressures
15 p2390 A71-32040
- Unsteady compressible flow measurement, determining local lift coefficient from pressure distribution along airfoil
16 p2520 A71-33342
- Three dimensional laminar compressible boundary layer flow solution by numerical integration
17 p2728 A71-34894
- Gust loading on two dimensional thin airfoil in compressible flow, deriving closed-form lift expression
17 p2671 A71-35285
- Compressible similar laminar boundary layer blow-off behavior description from asymptotic analysis, using Prandtl transposition theorem
18 p2901 A71-36032
- Streamlines geometry in hydromagnetic inviscid nonheat conducting compressible flow in magnetic field, taking into account force vectors and energy/mass distributions
18 p2951 A71-36183
- Viscous compressible flow around slender body in hypersonic slip flow regime, using finite difference method
18 p2908 A71-36344
- Numerical methods for unsteady compressible flows, considering method of characteristics, Lax-Wendroff and particle-in-cell method
19 p2992 A71-37456
- Laminar compressible wakes instability behind planar and axisymmetric slender bodies, solving integral conservation equations for fluctuation amplitude variations
19 p2993 A71-37879
- Computer algorithm for simulation of one dimensional unsteady compressible fluid flow in presence of area change, wall friction, heat transfer and entropy gradients
19 p3025 A71-38291
- Perturbed problem of rotational steady compressible flow in three dimensional channel at upstream infinity/shear flow/, using linearization by current functions
20 p3211 A71-39419
- Compressible circular free jet instability allowing for turbulent boundary layer thickness, considering influence of axisymmetry on spatial growth rate and disturbance phase velocity
21 p3365 A71-40013
- Conjugate steady convective aerodynamic heating of plate in longitudinal compressible gas flow, taking into account boundary layer enthalpy distribution
21 p3317 A71-40080
- Compressible viscous gas supersonic flow, observing near wake region behind perpendicular trailing face of rectangular plate with motion, state, energy and continuity equations
21 p3318 A71-40081
- Unsteady viscous compressible flow through straight channel with flat porous walls under time varying pressure
21 p3367 A71-40591
- Isentropic ideal compressible vortical gas flow in axisymmetric channel, determining stream function and gas density
23 p3625 A71-43549
- Compressible flow across shaft face seals and narrow slots, examining fluid inertia, viscous friction and entrance losses
23 p3663 A71-43592
- Streamline curvature analysis of compressible subsonic, transonic and supersonic cascade flows in axial turbine blades
23 p3665 A71-44347
- Compressible viscous flow calculation, deriving finite element analog of Navier-Stokes and energy equations
24 p3818 A71-44617
- Mass flow function diagram for axisymmetric isentropic compressible swirling flow in annular duct
24 p3820 A71-44960
- Compressible gas flow in two dimensional porous wall, calculating heat transfer and mass flow by conformal mapping for Laplace equation solution
24 p3889 A71-44972
- COMPRESSIBLE FLUIDS**
- Compression shock wave development in compressible media, deriving wave amplitude/time relationship via velocity distribution approximation by discontinuous Mach wave series
01 p0069 A71-10122
- Spherical elastic shell axisymmetric vibrations in compressible fluid with free surface
01 p0071 A71-11046
- Lagrangian invariants of inviscid compressible fluid applied to hydrodynamic equations
02 p0239 A71-11923
- Acoustic turbulence spectrum in compressible fluid with potential motion, using complex traveling wave amplitudes in hydrodynamic equations
02 p0239 A71-11924
- Free convection in compressible viscous heat conducting liquid near critical point, discussing temperature gradients, layer heights, density distribution and inhomogeneity effect
02 p0331 A71-12190

Plane and cylindrical MHD wave propagation in conducting compressible fluid under Hall effect, examining flow perturbation

02 p0291 A71-12533

Navier-Stokes equations numerical integration in Eulerian coordinates, applying results to compressible and incompressible fluids steady flow

[AIAA PAPER 70-2] 03 p0399 A71-13426

Free convection in compressible viscous heat conducting fluid, determining parameters leading to onset

03 p0521 A71-14233

Free transverse oscillations of closed prismatic shell of flexible rectangular panels filled with compressible inviscid liquid

04 p0573 A71-15564

Frequency stability of automatic control system with hydraulic actuating mechanism external load, taking into account fluid compressibility

05 p0705 A71-17033

Dynamic stability of cylindrical shell with freely supported edges partly filled with ideal compressible fluid and undergoing steady longitudinal vibrations

06 p0997 A71-17846

Gravity stratified compressible fluid spin-up in sphere, analyzing by increase in container angular velocity and linearization about uniform rotation

06 p0883 A71-18320

Unsteady interaction of compressible fluid and flat circular deforming elastic membrane analyzed coupled computer program method

[AIAA PAPER 70-75] 09 p1430 A71-22085

Hydrodynamic equations for behavior of thermally conducting viscous compressible fluid in first post-Newtonian approximation to general relativity, obtaining conservation laws

09 p1518 A71-22338

Viscous compressible fluid response to incident gravitational wave, deriving governing equations in linearized approximation to general relativity

10 p1676 A71-24496

Relativistic MHD waves based on ideal fluid compressibility and statistical mechanics for given space-time

10 p1650 A71-24586

Ideal compressible fluid slow motion in permanent and nonpermanent regime, discussing velocity field geometrical interpretation

11 p1748 A71-25173

Relativistic fluid thermodynamics for compressible fluid reversible adiabatic flow, using variational principle to derive stress-energy tensor

11 p1798 A71-25739

Inviscid compressible fluid jet flow, calculating instability boundaries characteristics by linear perturbation analysis and numerical solution

12 p1897 A71-27219

Compressible electrically conducting liquid two dimensional steady state laminar flow calculations in MHD duct

13 p2109 A71-29294

Ideally conducting compressible liquid flow near arbitrary geometrical thin profile form in transverse magnetic field

14 p2278 A71-29608

Gas-filled spherical cavity in infinite compressible liquid, deriving radial oscillations by numerical solution

14 p2225 A71-30229

Gravitational instability of heat conducting compressible fluid relative to class of axisymmetric perturbations, considering viscosity, magnetic field and uniform rotation

14 p2226 A71-30397

Free convection in compressible viscous heat conducting liquid near critical point, discussing temperature gradients, layer heights, density distribution and inhomogeneity effect

15 p2512 A71-31497

Dirichlet problem in hodograph plane of compressible fluid flow from aircraft, helicopter blades or turbine blade airfoils

17 p2672 A71-35470

Main parameters of free supersonic jets of ideal compressible fluid, comparing with numerical calculations and experimental data

19 p2991 A71-37081

Nonlinear hydrodynamic field equations transformations into complex wave equations for application to ideal compressible fluids

20 p3211 A71-39031

Numerical analysis of natural frequency spectrum of elastic plate free vibrations in compressible inviscid fluid

20 p3310 A71-39784

Plane steady irrotational flow of ideal compressible fluid around jet profile, obtaining Kutta-Joukowski theorem

21 p3322 A71-40580

Turbulent fluids constitutive equations verification by Truesdell principle of material indifference in incompressible and compressible fluids

21 p3367 A71-40652

Vertical magnetic field effects on stability of variable density compressible inviscid fluid, solving by variational principle

21 p3415 A71-40666

Quasi-steady three dimensional ideal compressible fluid flow between convex and concave sides of neighboring blade profiles in axial flow turbine

21 p3322 A71-40687

Soviet monograph on unsteady motion of compressible fluids covering acoustic and shock wave reflection from solid boundaries, impact penetration and pressure propagation

21 p3369 A71-40869

Ideal compressible fluid plane unsteady vortex-free self-similar flow, obtaining particular solutions families similar to Riemann waves and Prandtl-Meyer flows

22 p3532 A71-42866

Spherical projectile hypervelocity impact on compressible fluid, showing viscous effects on velocity and stress distribution behind shock front

24 p3877 A71-44426

COMPRESSING

Gaseous squeeze-film bearings analysis for large squeeze numbers

05 p0759 A71-16975

Two dimensional supersonic turbulent free shear layer recompression process from flow model numerical calculation

21 p3371 A71-40998

COMPRESSION BUCKLING

U BUCKLING

COMPRESSION LOADS

NT AXIAL COMPRESSION LOADS

NT IMPACT LOADS

Stability of longitudinally hinged isotropic cylindrical shells under external pressure, using finite difference method

01 p0170 A71-10645

Buckling under compressive loads of incompressible neo-Hookean plates

01 p0171 A71-10659

Simply supported cylindrical shell buckling under linearly varying lateral pressure

01 p0178 A71-11399

Stress distribution in gelatin disk and rectangular plate compressed between horizontal slabs, using tangential difference method

02 p0328 A71-12512

Continuous elastic filler effects on axisymmetric stability loss in cylindrical shell under subcritical compression loads, using three dimensional linearized equations

02 p0329 A71-12665

Optimal design of one end-clamped elastic column subject to conservative concentrated compressive loads

03 p0501 A71-13110

Nb-Mo alloys single crystals deformed in compression, considering work hardening and slip relation to temperature, Mo content and stress level

03 p0441 A71-13313

Eccentrically stringer-reinforced rectangular plates buckling under linearly varying longitudinal compression, using Galerkin method

05 p0819 A71-15980

Creep and long term strength of unidirectionally reinforced plastics under compression

05 p0771 A71-16361

Orthotropic cylindrical shell stability under variable compression loads, considering glass fiber reinforced plastic tube

05 p0822 A71-16368

Circular cylindrical shells buckling with different elastic moduli in tension and compression under arbitrary axial and lateral pressure

05 p0823 A71-16558

Deformation stability of three dimensional body with rheological properties under compression

05 p0824 A71-16591

Buckling of cold formed Al alloy thin walled columns under compression, investigating longitudinal half wave formation

06 p0985 A71-17748

Equilibrium stability of orthotropic cylindrical shell under longitudinal compression, discussing critical stresses

06 p0986 A71-17762

Axisymmetric stability loss of thin long cylindrical shell with elastic filler under uniformly distributed compressive forces over shell ends

06 p0987 A71-17770

Cylindrical shell compression stability in presence of creep, determining initial surface dent effects

06 p0992 A71-17805

Thin plates and shell with various yield stress materials, observing limiting equilibrium under tension and compression loads

06 p0992 A71-17810

Cr-Ni stainless steel tensile and compressive stresses effect on hydrogen permeability at elevated temperatures

06 p0912 A71-17946

Cr alloys endurance and dynamic creep under HF tension-compression loads at room temperature

07 p1129 A71-19154

Tubular Mg and Ti alloy samples under tension and compression load, observing creep properties

07 p1211 A71-19195

Conical shell stability under dynamic longitudinal compression

07 p1218 A71-20472

Natural frequency bounds for clamped beam with linearly varying compressive load and constant end load by Rayleigh-Ritz, Bazley-Fox second projection and Kato methods

08 p1368 A71-20806

Tubular compression members, examining residual stress profile effects on strength reduction

08 p1370 A71-21411

Hot extruded W-Cu pseudobonds under tension and compression, determining impact strength and plasticity

08 p1316 A71-21614

Nonlinear elastoplastic ring buckling under compression

09 p1534 A71-22145

Theory of plates under finite initial elastic deformation, applying to rectangular plate stability under compressions in two mutually perpendicular directions

09 p1537 A71-22521

Honeycomb sandwich core elastic modulus measurement under transverse compression

09 p1470 A71-22994

TiNi martensitic transformations-fatigue strength relation at room temperature, observing hysteresis in tensile compressive loading cycle to maximum stress

09 p1477 A71-23349

Stress-strain curves for plastics with or without fiber reinforcements under impulsive compressive loading cycles, using split Hopkinson pressure bar apparatus

10 p1630 A71-23921

Buckling of axially compressed imperfect isotropic cylindrical shells with edge constraints, deriving two point boundary value problem numerical solution by shooting method

11 p1844 A71-25337

Buckling loads of square laminated anisotropic composite plates under compression, including bending-membrane coupling effects

11 p1847 A71-25462

Optimum buckling load of cylindrical shells under lateral pressure using Rayleigh-Ritz method

11 p1848 A71-25484

Approximate critical stresses during longitudinal compression of nonmetallic rods of medium flexibility, using stability loss curve tangent to Euler hyperbola

13 p2091 A71-28295

Edge restraint effects on postbuckling behavior of thin flat plates under uniformly distributed compressive loads, noting buckling load and stiffness increase

13 p2153 A71-28466

Complex loading history effect on elastoplastic deformation trajectories delay trail characteristic angles and length variation, determining plastic strain vector components in Euclidean space

13 p2155 A71-28652

Elastic stability of compressed beams, giving method for evaluating neutral axis form and critical load in buckling

13 p2157 A71-29321

Uniaxially reinforced W-Cu matrix composite material dynamic compressive load properties, considering strain rates and yield stress

14 p2257 A71-29643

Plasticity theory for materials with different mechanical properties in tension and compression, deriving yield criteria and flow rules by tensorial expansions

14 p2322 A71-29736

Critical loads and stability loss equations near edge of thin convex clamped elliptical shell of revolution under uniform external compression loads

14 p2325 A71-30024

Pisa University Aeronautical Institute activities /1960-1970/, considering supersonic and subsonic flow research, thin stiffened shells fatigue under compressive or tensile loads, etc

14 p2222 A71-30822

Buckling under compressive loads of incompressible neo-Hookean plates for homogeneous initial deformation, using variational principle

14 p2333 A71-30993

Brittle plates with stochastic distribution of cracks under biaxial tensile-compressive stresses, obtaining critical load

15 p2504 A71-31853

Soviet book on multilayered media elasticity theory three dimensional problems covering Fourier and Hankel integral transformations, compression, bending, normal and tangential loads, etc

15 p2506 A71-32020

Elastic rods and rings stability under compression beyond elasticity limit, determining equilibrium branching characteristics near bifurcation point

16 p2647 A71-32927

Critical loads and stability of longitudinally compressed circular cylindrical shells with eccentric ring and stringer reinforcement

16 p2657 A71-33603

- Orthotropic bar under compression loads, calculating Eulerian values for critical force
17 2817 A71-34335
- Time dependent bending of circular cross sectioned rod under constant load compression and creep
17 2821 A71-34564
- Long laminar plate and cylindrical panels with hinged lateral edges under buckling by normal uniformly distributed load, calculating deflection as monotonic pressure functions
17 2823 A71-34781
- Three layer trapezoidally corrugated panels with skin under longitudinal compression, determining local stability and stress-strain diagrams
17 2830 A71-35320
- Hot pressed W-Cu pseudobinary strength and ductility under tension and compression
17 2760 A71-35674
- Elastic buckling load of cylindrical shells with dimple imperfections under external pressure, applying perturbation expansion to Karman-Donnell equations
18 2982 A71-36839
- Notched fixed-pinned columns under concentric and eccentric compressive loads, presenting failure analysis based on stress intensity concept and methods of limit analysis
18 2983 A71-36852
- Nonlinear behavior of compressed elastic and elastoplastic rods in presence of large deformations, determining bearing capacity by step method
20 3269 A71-39164
- Two stage rotor-piston vacuum pump, determining minimum work of gas compression
20 3183 A71-39171
- Fiber reinforced tube under lateral compression between two flat dies, determining finite deformation from nonlinear elastic and elastoplastic shearing response analysis
20 3311 A71-39966
- Pulse attenuation in composite materials, discussing stress waves geometric dispersion and compressive fracturing effects
21 3465 A71-40791
- Two dimensional cylindrical stress propagation over viscoelastoplastic body arbitrary cylindrical surface under instantaneous compression load, using finite difference method
22 3613 A71-41564
- Axisymmetric buckling of annular plate subjected to unequal uniform radial compression along inner and outer edges
22 3615 A71-42036
- Asymmetrical metal fatigue cracks development under infrequent compression cycles alternating with fundamental cycles of tension
23 3774 A71-42896
- Asymptotic solution to dynamic buckling of thin slowly compressed eccentric elastic columns, using two time scheme
23 3776 A71-43373
- Singly and nonsingly connected thin elastic rectangular plate stability analysis under arbitrary compression load on surface
23 3777 A71-43423
- Strength and deformation characteristics of glass plastic under torsional and compressive shear loads, investigating temperature effects on elastic modulus
23 3697 A71-44204
- Zone refined Be crystals under room temperature compression, examining lattice defects with X ray synergy method
23 3695 A71-44287
- Radial edge displacement effect on circular cylindrical shells compressive buckling stress, noting opposite effects for different length/radius ratio ranges
[AIAA PAPER 71-984]
24 3878 A71-44580
- COMPRESSION TESTERS**
U COMPRESSION TESTS
COMPRESSION TESTS
- Aluminum compression microstructure under various strain rates and temperatures, discussing dynamic recovery role
02 20267 A71-12877
- Compressive contact interaction problem for elastic circular cylindrical shell lying in circular cylindrical cavity of elastic body
06 20987 A71-17764
- Cancellous bones mechanical properties from compression testing of human femora, vertebrae and cranial bones
06 20863 A71-18561
[AIAA PAPER 71-111]
[PLASTICS INST. PAPER 23]
- Tensile-compressive testing apparatus for low cycle load at high temperatures
08 21321 A71-20913
- Cruciform biaxial fatigue under alternate tensile and compressive forces, using finite element analysis and photoelastic-coating techniques
09 21426 A71-22499
- Elastic characteristics of multilayer structures with honeycomb fillers, discussing deflection, tensile and compression tests
10 21685 A71-23941
- 12 21980 A71-27362

- Compressive creep of aluminum oxide single crystals deformed by dislocation glide and rhombohedral twinning, investigating activation energy and rate controlling mechanism
15 2439 A71-32439
- Consistency examination of thermal activation analysis in Nb, determining strain rate sensitivity of pure Nb and Nb-Mo single crystals subjected to compression at 178 and 273 K
17 2759 A71-35223
- Supersonic cylindrical freon compressor with low blade height for elementary compression and flow visualization aerodynamic and thermodynamic tests
17 2793 A71-35467
- Carburizing steels cold forging, investigating pressure requirement relationship to compressive stress from comparison of backward extrusion and laboratory compression tests
18 2935 A71-36669
- Prestrain directional effects in steel tension and compression test specimens, noting Bauschinger and work hardening effects
18 2937 A71-36834
- Acoustic emission test facility with constant strain rate compressive sample deformation
20 3208 A71-38823
- Maximum yielding tensile stress envelope curves as function of structural load index based on compression tests of Al alloy stiffened plane panels
20 3309 A71-39570
- Stress-strain curves of dual slip orientation in Ge single crystals deformed in compression, using interference, optical and electron microscopy
21 3397 A71-40457
- Mechanical properties of various polymeric solids under compressive loading cycles of 100 microsec duration and under steady state compressive loads
21 3406 A71-41427
- COMPRESSION WAVES**
- Structure and propagation of large amplitude modulated isolated compression waves in cold three component plasma with negatively charged ions
01 20132 A71-10676
- German monograph on plane ideal gas flows calculation with allowance for unsteady gaslight walls and compression shocks using difference methods
02 20240 A71-12400
- Radiation effects on compression shock in hot gases, considering hypersonic flow around blunt body during planetary atmosphere entry
04 20526 A71-15101
- Compression waves produced in viscous heat conducting gas by impulsive one dimensional piston start and by wall temperature change
05 20831 A71-16477
- Plane compression waves propagation into constant state nonviscous fluid, considering shock formation of pressure pulses and overpressure as function of time
07 21091 A71-19961
- Structure and propagation of large amplitude modulated isolated compression waves in cold three component plasma with negatively charged ions
07 21170 A71-20138
- Mach reflection of strong shock waves by sharp compressive corner in real gas in hypersonic tube, using laser Mach-Zehnder interferometer
11 21752 A71-26190
- Particle displacements during resonance motion of shear and compression waves in linearly viscoelastic flat plate of finite thickness
14 22332 A71-30851
- Electron density gradient and radial compression waves in pulsed IR laser gas discharge tube
16 22585 A71-32795
- Shock wave attenuation along uniform perforated tube, considering rarefaction and compression waves in resulting unsteady flow
16 22554 A71-32883
- Hanging compression shock wave in plane supersonic ideal gas flow past body with broken generatrix
20 3176 A71-39371
- COMPRESSION STRENGTH**
- Unidirectionally fiber reinforced composite materials, discussing compressive strength
02 20274 A71-12481
- Hugoniot elastic limit and dynamic compression strength for brittle bodies, considering hydrostatic stress and porous specimens
04 20617 A71-14750
- Elastic and compression strength characteristics of fiberglass-reinforced plastics prepared by cold solidification
05 20771 A71-16364
- Theoretical model of elastic medium with diverse tensile and compression resistances under finite deformation
08 21373 A71-21944
- Transverse bending of hinged or clamped rectangular plates with different tensile and compressive resistance
08 21373 A71-21945
- Low compression set and volume swell of vulcanizates of fluorocopolymer at elevated temperatures for sealing applications
10 21632 A71-24099

- Carbon fiber reinforcement in carbon fiber/glass fiber mat sandwich beams increasing tensile and compressive strength
11 21846 A71-25412
- Hereditary elastic body model with various tensile and compressive strengths, using elasticity theory with differing moduli
12 21982 A71-27519
- Compression strength theory for monodirectional reinforced homogeneous anisotropic and piecewise homogeneous materials, using microvolume stability, loss failure mechanism
12 21922 A71-27680
- Stainless steel wire fibers in refractory castables, noting flexural and compressive strength improvements
13 20993 A71-28666
- Dynamic compressive strength and failure of steel reinforced epoxy composites, discussing strain rate sensitivity
17 2762 A71-34813
- Theoretical estimation of tensile strength, elastic modulus and deformation of cubical diamond specimens under tension and compression
22 33565 A71-42873
- COMPRESSOR BLADES**
- Turbine and compressor blade profiles grinding, formulating mathematical rules for shaping links adaptable to programmed control
02 20258 A71-12569
- Axial flow compressors radiated sound reduction by segmented stator blades
03 20353 A71-13283
- Cascade flow test data, considering blade section performance in transonic and supersonic axial flow compressors
03 20343 A71-13829
- Low aspect ratio compressor blade cascade performance at blade span center, discussing pressure loss, angle of attack and staggering
07 21017 A71-20624
- Vibrational tumbling effects on steel compressor blades surface roughness, cold hardening, residual stresses and fatigue strength
08 21295 A71-20842
- Axial compressor blades surface finish and fatigue strength restoration by vibrational tumbling
08 21295 A71-20843
- Probabilistic estimate of aerodynamic imbalance of aircraft gas turbine rotors due to production errors in compressor blade angle
08 21349 A71-22045
- Axial-radial and radial compressor stage optimum exit blade angle, considering flow rate control by variable pitch nozzle guide vanes
08 21230 A71-22049
- Composite materials for compressor blades in aircraft engines, considering boron and carbon fiber reinforced materials
09 21456 A71-23286
- Axial compressor subsonic stages theoretical and experimental investigation, discussing blade design, calculation and experimental methods and results
10 21554 A71-24958
- Cascade and single stage rotating rig data comparison with aerodynamic predictions based on intrablade analysis, including wall boundary layer model [ASME PAPER 71-GT-13]
11 21703 A71-25959
- Impeller blade loading vorticity on stream surface of revolution for mixed flow compressor, using annular cascade theory [ASME PAPER 71-GT-17]
11 21703 A71-25962
- Quasi-three dimensional method for radial flow compressor blade loadings computation, presenting combined meridional plane and blade to blade solutions for adaptation to computer [ASME PAPER 71-GT-60]
11 21704 A71-25982
- Large axial compressor flow straightening stator blades unsteady pressure measurements with short response time detectors
12 21945 A71-27469
- Milling, band grinding, final manual polishing and tumbler polishing effect on fatigue life and surface finish of steel compressor blades
12 21912 A71-27680
- Monograph on potential flow interaction between blade rows in axial flow compressors covering mathematical model, numerical analysis and experiment
13 21990 A71-28883
- Accelerated semiempirical method determining metallurgical processing techniques effects on steel and titanium alloy compressor blades fatigue life, comparing results with experimental data
14 22522 A71-30269
- Vibration analysis for static and rotating objects by stroboscopic holography, considering axial flow compressor blades and two-mass system with torsional vibration
15 22404 A71-31273
- Discrete tone noise generation by high speed fans and compressor blades, using McCune analysis for linearized three dimensional compressible flow in infinite annulus [AIAA PAPER 71-617]
15 22468 A71-31555

Dynamic stress on rotor blades of aircraft engine axial compressor stages with low hub/diameter ratio 16 p2624 A71-33345

Linear radial loads effect on stress and strain of hyperboloidal rotor disk applied to aircraft engine compressors with two stream flow of working medium 17 p2822 A71-34597

Pretwisted cantilever airfoil cross section turbine and compressor blades vibration natural frequencies and mode shapes 17 p2828 A71-35282

Multiple tone generation by axial flow transonic compressors, considering shock waves production and propagation associated with supersonic elements of blading 18 p2848 A71-36497

Holographic interferometry application to vibration mode pattern analysis of steam turbine and centrifugal compressor blades and disks 19 p3067 A71-38419

Centrifugal blowers optimum blade number for maximum efficiency, discussing design measures for shock and friction loss minimization 20 p3277 A71-38750

Segmented stator vanes performance in axial flow compressor, noting radiated sound reduction 20 p3175 A71-39093

Compressor blade hodography and profile equations for subsonic two dimensional flow calculated on graphic visualization console 20 p3176 A71-39420

Failure and crack formation in gas turbine engine compressor disks under variable stresses from fatigue tests, considering safety factors 23 p3779 A71-44210

COMPRESSOR EFFICIENCY

Axial flow compressor design emphasizing component efficiency 03 p0470 A71-13825

Jet propulsion optimization by energy and energy for minimum total cost flux by varying unit compressor pressure ratio 08 p1348 A71-21300

Small high pressure ratio single-stage centrifugal compressor design, testing and efficiency 10 p1550 A71-24219

Compressor surge effect on mixed compression inlet flow from numerical solution of one dimensional unsteady inviscid flow equations in variable area duct [AIAA PAPER 69-484] 10 p1553 A71-24855

Centrifugal blowers optimum blade number for maximum efficiency, discussing design measures for shock and friction loss minimization 20 p3277 A71-38750

High rpm effect on centrifugal pump efficiency, considering hydraulic, volume and mechanical losses 22 p3554 A71-41849

COMPRESSOR ROTORS

Transonic compressor rotors blade camberline shape optimization by various tip diffusion factor-ratio combinations 07 p1184 A71-20200

Loads on compressor, ventilator and turbine rotor disks having large central holes, giving formulas for stress distributions 12 p1945 A71-26952

Hydraulic analogy for visualization of flow through moving plane cascade for rotor section of compressor stage 12 p1898 A71-27720

Turbomachinery rotor and stator row aerodynamic interaction, describing discrete tone noise generation from far field measurements 15 p2450 A71-32134

Two stage rotor-piston vacuum pump, determining minimum work of gas compression 20 p3183 A71-39171

COMPRESSORS

NT CENTRIFUGAL COMPRESSORS

NT SUPERCHARGERS

NT SUPERSONIC COMPRESSORS

NT TRANSONIC COMPRESSORS

NT TURBOCOMPRESSORS

Secondary losses in plane compressor grid with low aspect vanes, discussing flow characteristics dependence on fins, protruding elements and smoothed junctions 06 p0846 A71-18705

Equation derived for operation of turboprop engine with high pressure compressor controlling gas temperature at turbine front 08 p1347 A71-20831

Light rays bundle compression devices performance based on phase space treatment using Liouville theorem, comparing linear tapers and lenses performance to compressor with graded refractive index distribution 08 p1335 A71-21373

French book on thermodynamics and gas dynamics covering theoretical and applied thermodynamics, air compressors, combustion, internal combustion engines, water vapor, compressible fluid cooling, etc 09 p1545 A71-22965

Air bypass behind compressor into variable area exhaust nozzle, obtaining energy losses from gas turbine jet engine indices 13 p2115 A71-28586

Pilot vacuum pump with piston-rotor compression action to enhance pumping performance, comparing to single stage pumps 22 p3554 A71-42490

COMPTON EFFECT

Radio sources LF spectra distortions at critical value brightness temperature, noting induced Compton scattering effect on ambient gas thermal electrons 02 p0317 A71-12865

Gas heating near quasars, Seyfert galaxies nuclei and pulsars by induced Compton effect 02 p0317 A71-12872

Compton scattering in quasars, discussing gamma rays effects on core chemical abundances 03 p0481 A71-14266

Radiation intensity produced by inverse Compton effect between solar flux and Van Allen belt trapped high energy electrons 04 p0640 A71-14875

X ray source Sco X-1 gamma radiation due to Compton synchrotron process, comparing flux observation for synchrotron origin validity 05 p0799 A71-16476

Vacuum spectrum modification theory for inverse Compton scattering in cold collisionless plasma 07 p1165 A71-18855

Electromagnetic radiation pumping by stimulated Compton scattering near pulsars, determining secondary emission frequencies from energy and momentum conservation laws 07 p1192 A71-12922

Radio background in universe due to synchrotron radiation, X ray and photon backgrounds due to cosmic electrons inverse Compton effect 08 p1351 A71-20960

Magnetic Compton spectrometer for high intensity pulsed gamma ray environments and nuclear device spectral measurement 08 p1294 A71-21840

Compton scattering of relativistic electrons in cosmic plasma waves as source of HF radio emission from metagalactic objects 09 p1521 A71-22926

Model for relativistic electrons diffusion from IR sources, determining injected electron spectrum distortion due to inverse Compton losses and X ray spectrum 11 p1814 A71-25294

Compton electrons produced ring current effects on geomagnetic fields for gamma quantum source and air molecular interactions, considering exact analytical model 11 p1817 A71-25777

Stimulated Compton effect in compact radio sources, giving formulas for energy flow between relativistic electron and radiation field 11 p1831 A71-26169

X ray flux variability of massive elliptical galaxy M87 from rocket flight measurement, considering synchrotron, inverse Compton and thermal bremsstrahlung 12 p1962 A71-26931

Universe UV radiation intensity, estimating inverse Compton effect interaction of cosmic relativistic electrons with relic radiation 12 p1948 A71-27079

Quantum electrodynamics on null planes in Minkowski space, discussing applications to lasers, wave packet construction, Heisenberg and Furry pictures and Compton scattering 13 p2080 A71-28998

Compton effect in variable radio sources, considering models of Seyfert galaxies 3C 84 and 3C 120 from baseline interferometry 13 p2141 A71-29100

Flux estimates of gamma quanta with energies of 5 TeV from celestial objects due to bremsstrahlung and inverse Compton scattering of relativistic electrons 14 p2299 A71-29985

Cosmic gamma ray background flux for photon energies greater than 100 MeV, considering Compton collisions 14 p2301 A71-30435

Fokker-Planck equation for Compton scattering in hot plasma, considering energy exchange rates for scattering in relativistic Maxwellian plasma 14 p2283 A71-30859

Gamma rays in Crab Nebula pulsar, considering synchrotron radiation and inverse Compton scattering as production mechanisms 17 p2796 A71-35335

Compton synchrotron spectra of gamma rays produced in Crab Nebula by photons scattered by relativistic electrons, assuming magnetic field due to pulsar 18 p2963 A71-36154

Sagittarius A model involving relativistic electron diffusion from point source due to Compton scattering for observed radio spectra explanation 18 p2957 A71-36155

Universe UV radiation intensity, estimating inverse Compton effect interaction of cosmic relativistic electrons with relic radiation 19 p3126 A71-37429

Gas heating by LF radiation due to Compton scattering near quasars, Seyfert galaxies nuclei and pulsars 20 p3289 A71-39293

Crab Nebula and pulsar gamma ray emission from synchrotron or inverse Compton mechanism 20 p3301 A71-39919

Pulsar radiation beaming due to strong magnetic field, computing Compton scattering and opacity 20 p3285 A71-39953

Compton electrons produced ring current effects on geomagnetic fields for gamma quantum source and air molecular interactions, considering exact analytical model 22 p3532 A71-41545

COMPUTATION

NT ORBIT CALCULATION

Sparse matrices inverses and eigenvectors computation methods, giving bibliography 02 p0276 A71-11802

Electronic computation - Conference, Purdue University, Lafayette, Indiana, August 1970 09 p1412 A71-23273

Continuous machines basic properties, introducing tau computation and tau computable sets union, intersection, difference and parallel product 18 p2886 A71-36824

COMPUTER COMPONENTS

NT COMPUTER GRAPHICS

Modular computer design for long term missions, discussing reliability estimation 01 p0046 A71-10205

Digital structures simulation system as computer systems design aid, discussing basic building blocks, flow charts, task assignments, cost and performance constraints, etc 01 p0048 A71-10222

Basic digital circuits with integrated TTL and MOS structural elements, giving diagrams for dual counters, frequency dividers, adders and shift registers 02 p0231 A71-11862

Partial differential equations solving device for analog computers 03 p0381 A71-13004

Computer operators activity analysis, suggesting computer center layout 04 p0547 A71-15847

Digital computer components reliability determination, using bypass algorithm 06 p0870 A71-17492

Field distribution in multiple-opening ferromagnetic digital computer elements, using linear approximation integral method 06 p0872 A71-17497

Memory materials and components - Conference, Washington, D.C., September 1970 07 p1177 A71-19606

Plated wire storage element for military and aerospace scratch pad, main and mass memories of various speeds 07 p1077 A71-19608

Integrated dynamic digital computer elements, examining regenerative information storage, internal duration determination by clock pulse frequency and switching 09 p1411 A71-22494

Semiconductor random access memory components, discussing LSI circuits developments for RAM applications cost effectiveness in computer main-frame memories 13 p2035 A71-28772

Soviet book on automatic control and computer components reliability, explaining redundancy principles and test and repair procedures 22 p3526 A71-41820

COMPUTER DESIGN

Multiprogrammed and time shared multiaccess digital computers operating systems design, discussing dynamic memory protection structures 01 p0043 A71-10179

Structured or array logic configurations based on transistorized matrices with programmable interconnections for large scale integration in computer design 01 p0044 A71-10182

LSI device standardized set for implementing digital computer systems of varying functional complexities 01 p0044 A71-10183

Binary cellular logic circuit array multiplication unit based on functional module concept adaptable to LSI implementation, discussing design methodology 01 p0044 A71-10185

Fast computers design, describing program modifications for performance improvement 01 p0045 A71-10195

Real time systems design principles for processor organization, logic circuits, fault detection and diagnostic tests to facilitate high degree of reliability and maintainability 01 p0046 A71-10203

Modular computer design for long term missions, discussing reliability estimation

01 p0046 A71-10205

Digital structures simulation system as computer systems design aid, discussing basic building blocks, flow charts, task assignments, cost and performance constraints, etc

01 p0048 A71-10222

Aerospace digital computer partitioning based on MOS MSI technology using functional building blocks /FBB/

03 p0384 A71-13281

Real time processor design for sequential control of all-digital multiline data set

[IEEE PAPER 70-TP-375-COM]

05 p0725 A71-17067

Hybrid computer systems, describing interface, analog output and program design

06 p0871 A71-17744

Stored-programmed special purpose computer for double precision arithmetic realization of digital filters, discussing design, implementation and testing

07 p1067 A71-18733

Computer display channel for en route air traffic control flexible real time data processing and display subsystem

[AIAA PAPER 71-247]

07 p1156 A71-19721

Associative digital processor with associative memory for high speed ATC data processing, discussing design and operation

07 p1068 A71-19997

Microprogramming by Computer Design Language for describing digital computer functional configuration and sequential operation

07 p1069 A71-20404

Digital computer modular LSI control logic design using multifunctional binary decoder with transistor array read-only memory for odd and even parity error detection

08 p1260 A71-21663

Book on digital computers in engineering covering systems, man machine communication, numerical analysis, network analysis program, circuits, devices, control, etc

10 p1581 A71-24476

Floating point arithmetic units design for large high speed digital computer

12 p1884 A71-27151

Optimum configuration/cost design of computer graphics systems, using mathematical model involving response time prediction by queueing analysis

15 p2374 A71-31181

Avionic and missile computer control systems, describing universal function unit design and digital processing requirements

17 p2711 A71-35775

Microprogrammable hardware interpreter design in LSI multiprocessing system, emulating instruction set with software functions

17 p2712 A71-35776

Hardware executive control with associative memory for avionic digital computer system, comparing computation speed, cost and reliability with software method

17 p2712 A71-35778

Minerva digital computing system with learning cells and electronic microcircuit elements capable of self organizing similar to human intelligence

19 p3025 A71-37420

High reliability computers via multiprocessing for long duration space missions, discarding quad redundant and majority voter approaches

[AAS PAPER 71-158]

19 p3152 A71-37927

Subnanosecond digital computer with emitter-coupled fully integrated circuit packaging concept

21 p3351 A71-40748

Ternary code and three value logic in digital computers, considering economic advantages, signal distinguishability and numerical interpretation of p digit abstract alphabet

22 p3516 A71-41856

Microcomputer design using standard interfacing module for balanced electronic logic amounts in central processor and peripheral controllers

22 p3518 A71-42207

Two dimensional holography application to fault-tolerant high density mass data storage design for digital information retrieval system

22 p3548 A71-42517

Cost effective general purpose minicomputer FDP-11/45 design and technology using Schottky TTL/MSI, semiconductor memories, multiple buses, microprogramming and floating point units

22 p3519 A71-42761

MINSK 22M computer modifications, discussing peripheral switching, interrupt, timing, operation termination and storage, readout, etc

23 p3648 A71-43355

Design method for high speed economical arithmetic units of digital computers, describing functional logic circuits

24 p3806 A71-44396

Computer systems design for complex process control, constructing models with differential equations and Boolean functions

24 p3806 A71-44714

COMPUTER GRAPHICS NT PLOTTERS

On-line machine language dynamic debugger for Operating System 360, using graphic display terminal or operator typewriter

01 p0045 A71-10193

Real time graphic display monitoring of time sharing computer systems operational state

01 p0046 A71-10207

Touch sensitive X-Y position encoder for computer display input using surface wave piezoelectric transducer

01 p0047 A71-10214

Computer output microfilm /COM/ technology, describing recorders and applications

01 p0047 A71-10218

Computer microfilm data recorder for output speed increase and information retrieval, discussing cost reduction

01 p0048 A71-10219

Three dimensional dynamic CRT display for simulation, using VECTRAN /Vector Transformer/ digital computing device for control

01 p0084 A71-11394

Thermionic converter with oriented W electrodes, discussing computerized data acquisition system for mapping I-V performance

02 p0193 A71-12215

Computer controlled mass spectrometer system, processing spectral information data for on-line graphic system output

02 p0253 A71-12550

Rectangular diagrams for solving linear RLC networks by digital computer graphics

03 p0390 A71-14308

Computerized human body anatomical geometrical model with life size skeleton and organs scaling for radiation dosage analyses in space missions

04 p0546 A71-15282

Ionospheric response to internal gravity waves isotropic spectrum, presenting computer produced tonal value plots

06 p0893 A71-17986

On-line interactive graphical computer program systems for approximation problems, including least squares method

06 p0871 A71-18210

Memoscope for communications between operator and machine during biological image studies

06 p0864 A71-18696

Computer graphic search for stiffly stable methods of high orders for ordinary differential equations

07 p1067 A71-18738

Computer generated motion pictures to simulate real events, discussing design problems and airfield simulation with GPSS software package

07 p1111 A71-19511

Airplane wing high lift and flap designs by interactive computer graphics system

[AIAA PAPER 71-227]

07 p1019 A71-19705

Two dimensional aircraft automatic landing motions control processes by simulation without use of moving cockpit simulator

07 p1084 A71-20066

Interactive computer graphic system for compiling air navigational data on two dimensional aeronautical charts

08 p1258 A71-21236

Computer generated profile maps to fill military need for rapidly produced, easily interpreted terrain map

08 p1280 A71-21242

Interactive computer graphics in cartography, considering on-line updating of digital topographic map file by human decision making

08 p1281 A71-21248

Man machine interactive computer graphics for design molding during evolution by computer with nonlinear programming algorithm

09 p1412 A71-23276

Interactive computer graphics technology industrial applications, emphasizing structural analysis and engineering master drawings

10 p1580 A71-23758

Man-machine interactive scanned-display computer graphics system implemented on Honeywell DDP-224 computer

10 p1581 A71-23967

Computer generated visual simulation of three dimensional objects, using geometric modeling technique for mathematical representation of photographic process

10 p1581 A71-24775

Optimum configuration/cost design of computer graphics systems, using mathematical model involving response time prediction by queueing analysis

15 p2374 A71-31181

Mars Meridiani Sinus region map preparation from computer reconstruction of near and far encounter pictures taken by Mariner 6 and Mariner 7

15 p2492 A71-32464

Mathematically oriented digital computer system implemented on IBM 360 with graphic remote consoles for engineering problems

17 p2710 A71-34622

Automatic electronics design, analyzing visual and graphic devices for initial data preparation, introduction, operator computer interaction and results extraction

18 p2887 A71-35878

Operator-computer communication devices with graphic data display, discussing construction and operation

18 p2884 A71-35879

Static converters of computer graphic information using photoreceivers with linearly decreasing and increasing spatial sensitivity

18 p2884 A71-35882

Visual displays preview, noting miniature eight-character alphanumeric, tabular, video, telephone and graphical displays

18 p2924 A71-36619

Computer program for generation and automatic plotting of perfect and twinned electron diffraction patterns for cubic crystal structures

19 p3118 A71-37719

Data display units as man machine interface elements in data processing operations, discussing combined alphanumeric/graphic CRT units

20 p3202 A71-38885

Frequency domain computer graphics technique for linear time-invariant multivariable feedback control system design

20 p3207 A71-38997

Computer aided aircraft design, analysis and production, discussing Numerical Master Geometry program developed by British Aircraft Corporation

20 p3241 A71-39543

Picture processing using general purpose digital computer simulation for reduction of processing time and special purpose hardware investments

21 p3376 A71-40111

Handwritten graphical data computer input device with pen position coordinate measurement from acoustic signal propagation delay time in piezoelectric solid plate

21 p3376 A71-40122

Computerized multiparametric data three dimensional CRT graphic display involving isometric viewing and intensity modulation

21 p3350 A71-40123

Computerized interactive stereographics by treating line identification as primitive, enabling rapid access to stereo pair for speed advantage

21 p3376 A71-40124

Computer generated buffered displays for psychological experiments involving interception, tracking, steering, memory and calculation tasks

21 p3341 A71-40136

Graphical display of digital computer simulated steady state unbalanced turborotor response for lumped and distributed parameter models, using GATRAN language

[ASME PAPER 71-VIBR-42]

21 p3459 A71-40292

Vortex wake development and aircraft dynamics, using computer graphics and flow visualization techniques

21 p3319 A71-40497

Binary computer holograms construction, discussing two and three dimensional objects, wave propagation, plotter instrumentation, photographic reduction and diffusers

21 p3380 A71-40921

Computer synthesis of holograms and spatial filters for coherent optical data processing systems, noting large computational volume required for three dimensional objects

22 p3539 A71-41746

Interactive graphical computer system with remote on-line consoles for engineering problem modeling and analysis, giving illustrative examples

22 p3516 A71-41868

One and two dimensional function values calculation for curve systems by continued fraction interpolation from point grids, using computer program

22 p3518 A71-42394

Computerized screen construction for surfaces with net characterized by singularity-free and curve-edges properties

22 p3518 A71-42395

Graphic mission analysis for outer planet missions, considering spacecraft and celestial bodies relative positions, sensor and spacecraft relative orientation

[AAS PAPER 71-378]

23 p3731 A71-43048

Grand Tour mission satellite planetary imaging analyses and science scan platform pointing requirements, utilizing computer graphic techniques

[AAS PAPER 71-379]

23 p3731 A71-43049

Computer graphic interactive flight path design program for planetary flyby missions

[AAS PAPER 71-380]

23 p3702 A71-43050

Light pen optical writing and erasing with bistable phosphor storage tubes using screen photoconductivity

23 p3651 A71-43437

Cathode ray tube graphical display system as digital computer output terminal, using analog memory for flickerfree image

24 p3806 A71-44652

COMPUTER METHODS

U COMPUTER PROGRAMS

COMPUTER PROGRAMMING

NT LANGUAGE PROGRAMMING

NT MICROPROGRAMMING

NT MULTIPROGRAMMING

NT ON-LINE PROGRAMMING

Programming language translator system, describing syntactic specifications for input-output relationships

01 p0045 A71-10190

PL/I compiler for system programming in high speed binary machine object code

01 p0045 A71-10194

MOBSSL-UAF block structured simulation language for digital and hybrid computers

01 p0046 A71-10200

Hybrid computer programming for continuous systems simulation

01 p0046 A71-10201

On-line software checkout facility for special purpose computers used in developing spaceborne programs

01 p0048 A71-10227

High speed real time interpretive language for biological calculations with PDP-8 computer

01 p0049 A71-10244

PERL programming language for on-line control of industrial processes and scientific experiments

01 p0051 A71-11186

Multiple dialect automatic test language for avionics industry, considering software design

03 p0381 A71-13077

Artificial intelligence computer programming system for continuum mechanics, discussing capabilities of CONFORM as mathematical language

03 p0382 A71-13548

Programming language for computerized circuit design and analysis, considering techniques for input statements translation

03 p0382 A71-14306

Biological heuristic programming in cybernetics, discussing solid state logic elements limiting factors in modeling

03 p0383 A71-14394

Analog/hybrid programming of stimulus sequence for cardiac excitation study

04 p0546 A71-15166

Computer programmable flow coefficient formulas for standard constrictions, orifice gages and Venturi nozzles

10 p1595 A71-24640

Optimal models for time shared computer systems with real time multiprogramming

10 p1581 A71-24727

German monograph on nonnumerical transformation of tensor equations by computers, applying to shallow shell theory

10 p1692 A71-25038

Digital computerization for cylindrical shells post-buckling stability analysis, discussing FORMAC and REDUCE formula manipulation systems

11 p1845 A71-25341

Experiment planning, using digital computer in real time with programmed algorithm

12 p1883 A71-26713

Plant and compensator parameters deviations effect on accuracy of complex unitary-code programmed automatic control system with delay line digital compensator

12 p1893 A71-27342

Hill-Brown differential equations for satellite coordinates transformed for integration with analytical programming language

13 p2135 A71-28352

Celestial mechanics and nonlinear dynamics in Poisson series, discussing Echeloned Series Processor for computer programming

13 p2034 A71-28355

Probabilistic cyclic queue model of overhead time and channel utilization in multiprogrammed computer systems under demand memory paging

13 p2035 A71-28973

Principal program languages application and classical mathematical notation

14 p2206 A71-29562

Angular function computation in Mie theory of light scattering, considering sequential computer programming economics

14 p2207 A71-30150

German book on simulation systems for digital computers covering programming language requirements, program structures and comparative analysis

14 p2207 A71-30263

Real time systems programming techniques based on modular programs, integrated data stores, multiprocessing and special computer languages

14 p2208 A71-30381

Large software systems development management, discussing pending disaster early identification, relationship to hardware, integrating contractor and programming tools

17 p2710 A71-34619

Interactive digital computing systems survey, describing one language AMTRAN system as example

17 p2710 A71-34621

Redundant solid state sequencer programmable via core memory, using two identical channels to prevent wrong output

18 p2885 A71-36449

Syntactical characterization of tautologies for deductive systems and theories based on formalized algorithmic languages

18 p2942 A71-36822

Optimal models for time shared computer systems with real time multiprogramming

19 p3025 A71-37692

Modular component computational algorithm for sequential least squares estimation /filtering/ with process noise for straightforward computer code conversion

20 p3201 A71-38757

Abbreviated test language for avionic systems, discussing program organization, statement formats, vocabulary and syntax diagrams

21 p3351 A71-40812

Symbolic ALGOL programming of partial differential equations applied to three dimensional MHD runs

21 p3351 A71-40847

COMPUTER PROGRAMS

NT COMPILERS

NT COMPUTER SYSTEMS PROGRAMS

NT INPUT/OUTPUT ROUTINES

NT OPERATING SYSTEMS [COMPUTERS]

NT SUBROUTINES

Computer programs parallel processable tasks recognition techniques survey, discussing algorithms

01 p0043 A71-10177

Operational memory share supervisor program with storage protection feature for real time multitask digital process control and teleprocessing of electrical power utility system

01 p0043 A71-10181

Fast computers design, describing program modifications for performance improvement

01 p0045 A71-10195

Hybrid executive programs for simulation, discussing I/O processing, potentiometer evaluation, data conversions, etc

01 p0046 A71-10202

Instruction Set Design System /ISDS/ program for computer order code selection

01 p0047 A71-10217

Hybrid computer simulation program for analyzing large circuits intractable by conventional methods using PACTOLUS language

01 p0048 A71-10225

Error bounds for inverted nonsingular matrices using interval arithmetic in ALGOL-60

01 p0049 A71-10325

Computer program for orbital elements of spectroscopic binaries and probable error computation

01 p0152 A71-10352

Orbital elements of spectroscopic binary Zeta Scuti by computer program and spectrograph observations, tabulating results

01 p0152 A71-10353

Asteroids, comets and meteor dynamics in solar system, examining motion and orbital evolution by computer techniques

01 p0155 A71-10437

Computer methods for calculating sensitivity of amplitude and phase frequency response functions in automatic control systems to system parameter changes

01 p0059 A71-10529

Radar weather echo data processing by digital computer, providing economical means for analyzing large quantities of data

01 p0050 A71-10596

Interstellar gas cloud spherically symmetrical collapse, considering computer program for density, temperature, flow velocity, cooling rate and gravity force

01 p0157 A71-10758

Algorithm and computer program generating formats and logic equations for addressable remote multiplexed time division telemetry systems

01 p0050 A71-10880

Instrumentation System Margin Analysis Program /ISMAP/ for ICBM telemetry data acquisition systems performance tests

01 p0032 A71-10882

Error model and digital computer simulation programs for technical management of missile development and testing

01 p0068 A71-10883

Computerized data management program for Minuteman radio telemetry instrumentation systems

01 p0050 A71-10884

Flow field of two dimensional nozzle exhaust to vacuum, describing computer program based on BGK equation and plotting exhaust region density, temperature and velocity

[AIAA PAPER 69-658] 01 p0002 A71-10932

Heart rhythm coordinate curves for continuous EKG analysis using digital computer

01 p0025 A71-11153

Computer differential analysis of cardiac rhythm irregularities involving comparison of EKG RR intervals

01 p0025 A71-11154

Computer analysis of microwave circuit parameters effects on limited space charge accumulation oscillation in CW transferred electron devices

01 p0055 A71-11169

Manual tracking systems identification and real time display, developing software system

01 p0027 A71-11437

Thrust-minus-drag optimization by base bleed and/or boattailing, using computer program

01 p0004 A71-11589

MOS multiphase LSI circuits design using computer program

02 p0228 A71-11651

Contour signal characteristics for cloud form recognition by computer using learning algorithm and photographic data

02 p0225 A71-11691

Computer source code generation for symbolic partial differentiation program for continuous system digital simulation

02 p0226 A71-11778

Fast on-line block-diagram-based DARE II digital simulation program for use on PDP-9 computer with CRT display console

02 p0226 A71-11779

Digital hybrid systems simulator /DIHYSYS/ program, examining subsystems sampling and execution time and applications

02 p0226 A71-11780

Real time six degree of freedom aircraft flight digital simulation using SL-1 continuous system simulation language

02 p0226 A71-11786

Digital simulation computer program in FORTRAN IV for radar systems performance evaluation in various environments

02 p0211 A71-11796

Cardiovascular system blood flow mathematical model parameter optimization by simulation on hybrid computer, using OPTTRAN program

02 p0203 A71-11807

Digital simulation program in GPSS language for airline operations including aircraft maintenance, flight scheduling, terminal space, equipment, work forces utilization, etc

02 p0227 A71-11809

Computerization of medical records of ophthalmology clinic

02 p0206 A71-12109

Pressure-bonded trilayer insulator stress analysis, using computer model for explaining alumina component fracturing during fabrication

02 p0256 A71-12249

Computer program for processing elliptical polarization observations of nebulas and comets

02 p0251 A71-12360

Solar general magnetic field determination by measuring visually small displacements on photographic plate

02 p0316 A71-12752

Total impedance plethysmography boundary value problems, developing computer program based on Jacobi iterative method

03 p0367 A71-12993

Computer program for compiling interpreter code test instructions from high order pseudo-English language

03 p0381 A71-13078

Automatic test equipment with digital computer for control, discussing software schemes and tradeoff analysis

03 p0381 A71-13079

Versatile Avionic Shop Test /VAST/ general purpose digital tester, discussing hardware and software

03 p0395 A71-13084

Software cost estimates for automatic test equipment for avionic support analysis

03 p0396 A71-13086

User requirements of Versatile Avionic Shop Test /VAST/ computer controlled automatic test equipment, including documentation, compatibility, assurance plan, etc

03 p0396 A71-13087

Long range goals for avionics automatic test equipment /ATE/ involving complex computer

03 p0396 A71-13088

Sounding rockets aerodynamic heating effects approximate prediction methods using computer programs

[AIAA PAPER 70-1399] 03 p0518 A71-13680

Computer algorithm for state variables equations used in linear and nonlinear, active and passive electronic circuits analysis

03 p0389 A71-13807

Axial compressor flow characteristics by computerized calculation methods, considering annular duct swirling flow model

03 p0342 A71-13828

Computer controlled laser machining system for cutting integrated circuit masks in thin films deposited as fused silica substrates

03 p0433 A71-14342

Heading of object moving on terrestrial sphere surface with inertial navigation aid, calculating asymptotic stability for position determination on computer

03 p0459 A71-14355

Thin walled cylindrical shells with filler, determining stability under axial compression by computer calculation

03 p0514 A71-14360

Computer program TENSOR for numerical solutions of shell theory

03 p0515 A71-14396

Computer solutions of one dimensional flow of constant composition and specific heat ratio fluids, using influence coefficients

03 p0405 A71-14440

Steady state node simplification technique for thermal radiation in gray enclosures, including computer program

03 p0522 A71-14446

Large signal mode tunnel diode amplifier amplitude and phase characteristics by computer study

04 p0556 A71-14622

Computer program description of radiation pattern of imperfect paraboloidal reflectors by transforming numerically expressed phase variations in plane electromagnetic wave

04 p0552 A71-15021

Data system environment simulator /DASYS/ for real time test bed capability for software development and testing

04 p0556 A71-15294

Strapdown inertial guidance and software technologies for cosmic speed aerospace vehicles and low speed air, marine and ground transport

04 p0623 A71-15301

Automated radar calibration system using star tracker and computerized control

04 p0554 A71-15318

Intercept Ground Optical Recording telescope and Mobile Optical Tracking System for electro-optical photography, discussing measurement and system errors and CAMDAT computer program

04 p0554 A71-15320

N interval trajectory estimation computer program minimum variance adjustment technique, discussing airborne astrogatic camera system for reentry bodies position determination

04 p0556 A71-15330

Soviet monograph on universal program for finite difference solution of Dirichlet problem of Poisson equation with enhanced accuracy formulas

04 p0619 A71-15450

Two dimensional motion stability near sun-perturbed earth-moon triangular libration points, using computerized high order treatment

04 p0653 A71-15708

Hori and Deprit perturbation theories comparison based on Poisson brackets, giving computer program determining functions through sixth order for equivalence proof

04 p0660 A71-15889

Satellite flight trajectories construction, proposing algorithms for computer and automatic curve plotter

05 p0779 A71-16040

R and D money optimal reallocation due to total research budget decrement, based on computer program

05 p0840 A71-16743

Time sharing program for digital logic circuits simulation

05 p0726 A71-16959

Circular disks or cylinders with temperature boundary conditions, discussing iterative solution and computer program for transient thermoelastic stresses

05 p0829 A71-17117

Permanent magnet system as nonlinear computer problem, using Newton method and equivalent circuits with lumped parameters

05 p0705 A71-17174

Digital electronic equipment logic networks computer controlled tester, describing method for test patterns synthesis

06 p0879 A71-17322

Efficient evasion strategies for vehicle pursuit-evasion games with imperfect information, using computer solution

06 p0846 A71-17331

Global computer processing scheme for aerological radiosonde observation, using coded telegrams as primary information data

06 p0922 A71-17502

Automatic computer verification of diurnal temperature and geopotential observations on principal isobaric surfaces by statistical data analysis, describing computer algorithm

06 p0922 A71-17504

Computer estimation of correctness of tropopause determination from singular points based on criteria from global meteorological network

06 p0922 A71-17505

Computer algorithm for distribution functions of meteorological element on isobaric surface

06 p0922 A71-17506

Photointerpretation automation, discussing computer pattern input system, image scanning and correlation, optical image transformations, trainable logic techniques, etc

06 p0900 A71-18095

On-line interactive graphical computer program systems for approximation problems, including least squares method

06 p0871 A71-18210

Agricultural information and advisory service, utilizing remote sensing, computer sciences, research programs, educational involvement, satellites and aircraft

06 p1010 A71-18408

Worldwide remote sensing with satellites, high flying aircraft and computer data processing, discussing application in less developed countries

06 p0896 A71-18409

Multiple impulsive spacecraft trajectory optimization technique application to comet rendezvous problem, using computer program

[AIAA PAPER 71-93] 06 p0977 A71-18548

Prismatic shells vibration, buckling and stress analysis, applying computer solutions to complex bodies of revolution

[AIAA PAPER 71-112] 06 p1003 A71-18562

Nonlinear finite difference computer program applied to elliptic cylinder collapse under uniform external pressure, comparing with theoretical bifurcation buckling

[AIAA PAPER 71-146] 06 p1003 A71-18589

Machine analysis of biological structures and processes - Conference, Pushchino, U.S.S.R., May 1968

06 p0863 A71-18690

Computer applications in analysis of biological structures, considering tissues, cells, chromosomes, proteins and lipids

06 p0863 A71-18691

Cytophotometric method using digital computer program and scanning microscope

06 p0864 A71-18694

Follow-up scanning systems and reading volume reduction in biological image descriptions facilitating computer aided microstructure analysis

06 p0871 A71-18697

Follow-up scanning system input of microobject data with maximum contraction for biological computer analysis, noting karyotype or blood formula applications

06 p0864 A71-18698

Vortex flow theory, developing computer program for various separation flows

07 p1086 A71-18776

Structures electromagnetic scattering and multipath transmission effects on aircraft instrument landing system localizer signals, using computer program

07 p1153 A71-18831

Ionospheric columnar electron content, describing data processing and analysis programs

07 p1096 A71-19008

Computer generated motion pictures to simulate real events, discussing design problems and airfield simulation with GPSS software package

07 p1111 A71-19511

Aerospace Recommended Practice for gas turbine engine steady state performance presentation for digital computer programs, describing engine type, operating and control characteristics

[SAE-ARP-681B] 07 p1183 A71-19647

Space shuttle integrated information management system, emphasizing software element requirements and data processor hardware

[AIAA PAPER 71-222] 07 p1155 A71-19703

Extendable Computer System Simulator, discussing simulators as tools for integrated information systems design

[AIAA PAPER 71-228] 07 p1068 A71-19706

Complex digital computer systems effectiveness measurement, using simulation program with programming language SIMSCRIPT

[AIAA PAPER 71-229] 07 p1068 A71-19707

General purpose software inventory under single executive for application oriented information systems

[AIAA PAPER 71-236] 07 p1225 A71-19712

Spacecraft minimum impulse (or fuel) ellipse-ellipse transfer, discussing computer survey results of 630 trajectories

07 p1199 A71-19899

Universal materials testing system control using digital computer and changeable programs

07 p1069 A71-20201

Digital computer program for optimum design of narrow band klystron, discussing beam interception and power conversion efficiency

08 p1261 A71-20742

Arbitrarily shaped waveguide analysis computer program EHPOL for wavenumber approximation to eigenfunctions of Helmholtz equation, considering

homogeneous Neumann and Dirichlet boundary conditions

08 p1261 A71-20752

Cylindrical shells with arbitrary cross sectional contour, thickness and longitudinal stiffener spacing under tension or compression, presenting computer algorithm for determining stress-strain state

08 p1368 A71-20790

Trajectory measurement program optimization, constructing algorithm for variational problems

08 p1360 A71-21001

Trajectory measurement optimal program, using least squares method

08 p1360 A71-21002

Computer program for determining roving vehicle position and heading on lunar surface by landmarks

08 p1332 A71-21348

Derivative approximation techniques for recursive signal detection, using computer program for solving optimum and suboptimum processes signal to noise ratio in effectiveness evaluation

08 p1255 A71-21596

Computer controlled ground based command and data acquisition software system for OAO-A2 spacecraft remote control stations, discussing interface with monitor and interrupt capabilities

08 p1259 A71-21658

Shells of revolution under combined thermal and mechanical loading, presenting analytical basis of BOSOR 3 digital stress analysis program

09 p1533 A71-22079

Boundary value problems solution, using Runge-Kutta method with computer for eigenfunctions of ordinary differential equations

09 p1484 A71-22177

Heuristic search algorithm for highest and lowest values of functions, considering Algol program

09 p1485 A71-22313

Computer program for space and airborne optical imaging systems evaluation, emphasizing image motion compensation role

09 p1411 A71-22748

Probable solar flare doses on interplanetary mission calculated by MCFIARE computer program using Monte Carlo methods

09 p1399 A71-22809

Reactor shield weight optimization using FASTER-III Monte Carlo computer program for neutron and gamma ray transport

09 p1539 A71-22810

Computer algorithm for optimal linear impulse corrections to satellite orbit under inequality type constraints

09 p1424 A71-23135

Element stiffness matrix generator in terms of material and geometric properties by computer algorithm, using displacement functions, transformation matrices and strain energy expression

09 p1542 A71-23281

Statistically indeterminate modified structures automated design reanalysis by displacement method, using matrix formulations, numerical computation and computer operations

09 p1542 A71-23282

Structural design constraints check by computer single program algorithm, resembling similar human activity

09 p1413 A71-23284

Computer program for selected gases outgassing rates calculation, tabulating and plotting for NERVA fuel elements gas evaluation

09 p1492 A71-23348

Automatic computer program synthesis based on theorem proving approach for construction of recursive and iterative programs operating on natural numbers, lists and trees

10 p1581 A71-23968

Low speed airfoil characteristics calculation by digital computer, using Theodoresen conformal transformation method for potential flow pressure distribution

[SAE PAPER 710389] 10 p1550 A71-24253

Reversible point integrator circuits synthesis, using AB-102 universal ALGOL computer program

10 p1581 A71-24355

Numerical errors in computer programmed structural analysis calculations, using finite element displacement method for exact solutions and error sources identification

10 p1693 A71-25051

Strain energy calculation of V notched crack in elastic continuum from finite element computer programs applied to fractures in solid propellant rocket motor cartridges or grains

10 p1693 A71-25056

Book on computer calculation of phase diagrams covering quantitative computation of phase equilibrium and lattice stability parameters of refractory metal systems

11 p1777 A71-25197

Computer controlled source data preparation Keycheck system, discussing real-time software support for documents audio/visual error detection

11 p1734 A71-25638

PERLO program for analysis of satellite orbital period changes to determine celestial equator crossings from sequence of positions

11 p1829 A71-25825

Computer program algorithm for satellite photographic observation data processing based on measurement at one station

11 p1733 A71-25833

BeO reflected-fast-spectrum liquid-metal-cooled thermionic reactor, discussing two dimensional transport perturbation theory computer code for temperature coefficients evaluation

11 p1712 A71-25887

Thermionic converter electrostatic sheath analysis, using discontinuous distribution functions for emitted, plasma and trapped particles, and computer program

11 p1713 A71-25891

Thermionic converter nonsaturation effect in diode I-V characteristics from computerized analysis for plasma transport phenomena and sheath-electrode-plasma interactions

11 p1713 A71-25892

Quasi-vacuum mode thermionic converter for space and remote terrestrial power supplies, describing computer codes for design optimization

11 p1713 A71-25899

Computer acquired performance mapping of fixed spaced planar diode with etched Re emitter and Nb collector over wide operating temperature range

11 p1737 A71-25907

FORTAN 4 computer program for gamma ray energy spectra, determining peak locations, peak areas and elemental abundances

11 p1729 A71-26069

User-oriented conversational language computer program for Jet Propulsion Laboratory digital control random excitation environmental test system for spacecraft

11 p1736 A71-26498

Computer programs for random noise vibration test digital control, describing data base and logic programs

11 p1736 A71-26499

Computer program for interpretation of residual gas analyzer mass spectra, considering vacuum environmental testing of spacecraft

11 p1730 A71-26505

Statistical estimation in monitoring and control systems analysis, discussing algorithm construction for computer solution of nonlinear differential equations system

12 p1891 A71-26724

Synthesis of high speed digital computer non-searching adaptive control program to ensure closed system required dynamic characteristics for complex linear unsteady control plant

12 p1926 A71-26731

Waveform and spectral analysis program for electronic system designs, discussing fast Fourier transform modular staging and noise control applications

12 p1884 A71-27148

Analog recursive computer with serial digital program for arithmetic unit and storage system control

12 p1884 A71-27150

Computer program for aerodynamic forces on flexible plate undergoing transient motion in shear flow, applying to panel flutter

12 p1866 A71-27559

Computerized use of transient thermal resistance and power pulses superposition to calculate instantaneous transistor junction temperatures for various pulse conditions

13 p2038 A71-28770

MACE /management aid to compatibility engineering/, consisting of analysis routines for IBM 7030 and Univac 1108 computers

13 p2032 A71-28871

Hybrid computer program for data reduction or on-line analysis of nystagmus during closed loop experiment involving visual and/or vestibular function

13 p2022 A71-29359

Algorithm for calculating optimal covering of regions in plane, assembling computer program

14 p2264 A71-29552

Atmospheric turbulence space-time relationships measurements, discussing computerized time series, spatial and phase spectral analysis for sensors data

14 p2267 A71-29754

German book on simulation systems for digital computers covering programming language requirements, program structures and comparative analysis

14 p2207 A71-30263

Real time radar instrumentation data processing and control system, discussing computer selection, software requirements and configuration, etc

14 p2196 A71-30338

Computer real time data monitoring and control software in satellite integration support and test operations, noting test oriented language

14 p2208 A71-30339

French ATC, discussing automatic coordinator systems, computer utilization and flight plan data processing

14 p2272 A71-30382

Computer aided design program for civil transport aircraft configuration, performance, propulsion, weight and costs to meet given specifications

14 p2175 A71-30398

Inertial navigation systems improvements for commercial air transportation, noting digital computer program revision and increased functional capability [SAE PAPER 710458]

14 p2272 A71-30534

Nonuniform cross section tapered, stepped rectangular and I section cantilever beams elastic lateral stability

14 p2330 A71-30689

Computer program for processing of UHF radiation patterns of ESRO 4 scientific satellite omnidirectional antenna systems

14 p2217 A71-31051

Diffraction technique for three dimensional frequency spectra of photographic images using computer program based on Fourier transformation of optical density distribution

15 p2406 A71-31645

Computerized assistance in EEG analysis and interpretation, describing computer program for time and effort reduction in EEG recording

15 p2365 A71-32449

Finite element method application to potential flow field problems governed by Laplace equation in fluid mechanics, developing computer program [ASME PAPER 71-APM-22]

16 p2520 A71-33207

Computer program for prediction of repair time elements for versatile avionic ship test

16 p2545 A71-33314

Mathematical model for combustion processes, obtaining computerized approximate solutions for momentum, heat and mass transfer partial differential equations

16 p2663 A71-33362

Computer algorithm for diode detector static and dynamic I-V characteristics calculation by trial and error process with piecewise linear approximation

16 p2546 A71-33399

Satellite flight trajectories construction, proposing algorithms for computer and automatic curve plotter

16 p2605 A71-33444

Large software systems development management, discussing steps including program design before analysis, documentation, testing, monitoring and cost effectiveness

17 p2709 A71-34618

Large software systems development management, discussing pending disaster early identification, relationship to hardware, integrating contractor and programming tools

17 p2710 A71-34619

Apollo real time control center large software systems development management covering implementation, integration, testing, operation and maintenance

17 p2710 A71-34620

Electromagnetic wave multiple scattering by collinear spheres, computing radar cross sections with recursion relation for computer solution

17 p2701 A71-34757

Automatic pattern recognition of urban development changes from aerial photographs, using computer program and nonlinear registration technique for cell pairs partitioning

17 p2711 A71-35043

Minkey rendezvous computer program in Apollo 15 CSM aiding guidance, navigation and control system functions

17 p2772 A71-35055

Red blood cell image hologram reconstruction and superresolution based on coherent physical optics, using computer program

17 p2693 A71-35586

Ray trace equations for conic surfaces, noting application in computer programs for unusual systems

17 p2768 A71-35592

Higher order computer language architecture for aerospace software production problems, discussing real time constraints, hardware tradeoffs, memory, computer design and logic circuitry

17 p2712 A71-35777

Analytical weight determination of articulated shaft driven helicopter main rotor blades, presenting computer program [SAWE PAPER 893]

17 p2835 A71-35826

Computer program formulation of equations of state of electronic circuits, using state variable method with mixed coordinate basis

18 p2896 A71-35883

Computer algorithm determining transfer function of linear electronic circuit in autonomous quadrupole form with zero initial conditions

18 p2887 A71-35884

Computer programs for functional analysis, planning and control of space stations and shuttles operation

18 p2885 A71-36459

Consumable usage as function of mission time computed with computer program simulating NASA Skylab mission

18 p2885 A71-36461

Reentry vehicles trajectory reconstruction by computer program and Kalman filter estimation theory, analyzing instrument errors

[AIAA PAPER 71-933] 19 p3097 A71-37178

Right ascension and declination accuracy for Sirius satellite attitude determination in transfer orbit, describing computer program

19 p3150 A71-37312

Computer program for generation and automatic plotting of perfect and twinned electron diffraction patterns for cubic crystal structures

19 p3118 A71-37719

Air traffic congestion and delay Monte Carlo digital simulation in FORTRAN, exemplifying two-runway airport operation under instrument flight rules

19 p3041 A71-38024

Orbit computation and tracking system for Iris satellite using differential correction program

19 p3142 A71-38066

Computer programs for nonlinear finite element analysis with applications to large displacement and small strain problems

19 p3088 A71-38309

Large stiffness matrices building and manipulation, including structural analysis computer programs input determination, coupling techniques and eigenvalue problems solution

19 p3161 A71-38654

Shuttle convective heat transfer involving similar axial temperature gradients in piston and cylinder, calculating interaction with wall conduction by finite difference computer program

20 p3312 A71-39281

Radiation condenser computer program generalization to include effective radiative steady state node multiple enclosure simplification shield for thermal analysis optimization

20 p3314 A71-39357

Trajectory measurement optimal program, using least squares method

20 p3294 A71-39582

Carbon dioxide laser signatures prediction from multiple application of optical resonant equation by computer program, studying line competition effects

20 p3247 A71-39771

Three dimensional graphics software package for CRT and storage tube displays and plotters, describing coordinate transformation

21 p3347 A71-40133

Third order oscillatory system optimal terminal-state control synthesis by quadratic functional minimization iterative procedure algorithm, using ODR-1204 computer program

21 p3359 A71-40164

Fortran source listing for computer program approximating system reliability

21 p3351 A71-40371

Upper atmospheric density numerical calculation from draconite period by Perlo program using satellite observation near celestial equator

21 p3374 A71-40655

Elastic viscous plastic effects calculation in materials, describing method permitting constitutive equations introduction into computer programs for continuum mechanics equations solution

21 p3465 A71-40787

Computer program for nonuniform thickness ring structure stress distribution under uniform radial line load based on reinforced circular cylindrical shell interaction under hydrostatic pressure

22 p3516 A71-41866

GWU-FAP computer program for rigid frame elastic-inelastic analysis based on finite element method and plastic initial strain concept

22 p3516 A71-41867

Bar forces in statically determinate planar truss due to arbitrary loads at joints, describing computer program for sequential solution

22 p3517 A71-41869

Relcomp conversational time-sharing computer program for rapid calculation of reliability and MTBF of systems with serial and redundant units

22 p3517 A71-42103

Bias network analysis computer program for reliability analysis suited to failure mode, criticality, drift and catastrophic failures prediction

22 p3517 A71-42104

Computerized reliability optimization system program for electronic equipment design and management methods to achieve high reliability and low cost

22 p3517 A71-42105

Point-matching method application to electromagnetic scattering from quadrilateral conducting cylinders in resonance range, using computer programs

22 p3510 A71-42205

Computer program for on-line determination of minimal realizations of transfer function matrices, using Rosenbrock system matrix formulation

22 p3526 A71-42285

One and two dimensional function values calculation for curve systems by continued fraction interpolation from point grids, using computer program

22 p3518 A71-42394

- Viking Mars 1975 mission analysis software system for trajectory optimization, describing condensed format print and contour plot program
[AAS PAPER 71-311] 23 p3725 A71-42987
- Misalignment estimation software system /MESS/ for in-flight celestial and inertial reference attitude sensor alignment and calibration on OAO
[AAS PAPER 71-357] 23 p3648 A71-43027
- Blade cascade design for meridional flow, using finite difference method for universal computer program
23 p3626 A71-43550
- Computer programs based on least squares numerical analysis for complex internal friction spectra due to Snoek and grain boundary relaxation
23 p3648 A71-43927
- Automated analysis of high resolution IR astronomical spectra by computer program, presenting procedures for spectral line width, depth and frequency determination
24 p3867 A71-44438
- Hermite polynomials application to stiffness matrix determination in plate finite element method for disk under plane stress, presenting digital computer program flow diagram
24 p3880 A71-44641
- Computer program for recirculating fluid flows applied to concentration curves obtained by gas injection on pipe center line with fully developed turbulent flow
24 p3820 A71-44956
- ### COMPUTER SIMULATION
- #### U COMPUTERIZED SIMULATION
- #### COMPUTER STORAGE DEVICES
- NT BUFFER STORAGE
NT CORE STORAGE
NT CRYOGENIC COMPUTER STORAGE
NT DELAY LINES [COMPUTER STORAGE]
NT FLIP-FLOPS
NT MAGNETIC CORES
NT MAGNETIC DISKS
NT MAGNETIC TAPES
NT RANDOM ACCESS MEMORY
NT REGISTERS [COMPUTERS]
NT SHIFT REGISTERS
- System logic and usage recorder for storage area monitoring and data reduction
01 p0045 A71-10197
- Silicon-on-sapphire complementary MOS circuits for high speed associative memory arrays, discussing system, circuit and device processing concepts
01 p0047 A71-10209
- High performance LSI main frame MOS flip-flops memory module for digital computers
01 p0047 A71-10210
- Orthoferrite cylindrical magnetic domains in memory and logic devices, considering conductor, angelfish and in-plane rotating field circuits
01 p0047 A71-10211
- Mass fabrication of three hole integrated Permalloy sheet magnetic memories
01 p0047 A71-10212
- Mated magnetic film memory design employing continuous vacuum deposition fabrication
01 p0047 A71-10213
- Central data processing unit based on short-rod memories of coated Be-Cu alloy, discussing arithmetic-logic unit operation
01 p0049 A71-10263
- MOS transistors as high speed switches in magnetic film memory selection matrix, discussing requirements for drive current pulse yield, signal power and dissipation
02 p0229 A71-11815
- Stapleblock fabrication method for low mass, high strength ferrite core memory storage blocks in space travel applications
02 p0232 A71-12071
- Soviet analog computer modifications for iterative and hybrid computations, describing memory system alterations
02 p0228 A71-12489
- Computer memory reduction through Fortran higher level language, discussing tradeoff between costs saved and additional logic hardware
[AIAA PAPER 69-963] 03 p0382 A71-13450
- Cryotron elementary storage cells work region determination by phase transition characteristic form, discussing component reliability
03 p0382 A71-13520
- Holography developments concerning interferometry, microscopy, display systems, data storage and ultrasonic tests
04 p0587 A71-14724
- Holographic optical memory and computer output applications for rapid bulk data storage, considering various laser visualization systems
06 p0908 A71-18067
- Holography and shapes recognition, considering optical memory, information density advantages and optical correlators
06 p0900 A71-18068
- Monolithic optically written and electrically read semiconductor-ferroelectric memory device employing single crystal barium titanate
07 p1067 A71-19261
- Unstable high speed optronic /photoelectric/ flip-flop memory elements with positive optical feedback
07 p1075 A71-19303
- Memory materials and components - Conference, Washington, D.C., September 1970
07 p1177 A71-19606
- Plated wire storage element for military and aerospace scratch pad, main and mass memories of various speeds
[IEEE PAPER 7.6] 07 p1077 A71-19608
- Associative digital processor with associative memory for high speed ATC data processing, discussing design and operation
07 p1068 A71-19997
- Convolutional code words minimum distance-arbitrary length relationship for path memory performance measurement
08 p1258 A71-21313
- Amorphous semiconductors for memory and logic devices, using reversible structural transformations between disordered and ordered states
09 p1509 A71-23114
- Composition and composition inhomogeneity effects on plated wire memory elements strain sensitivity, considering tension and torsion sensitivities
09 p1509 A71-23115
- Automatic generator for finite rectangular/isoparametric element stiffness and mass matrices, discussing memory requirements and computation time optimization
09 p1542 A71-23280
- Thin holographic recording and retrieval from semipermanent optical memories
11 p1762 A71-25624
- Adaptive self-organizing and -learning control systems with long and short term memory retention, using logic random searches to find parameter values
[ASME PAPER 71-DE-22] 12 p1892 A71-27324
- Sb and As base chalcogenide diode structures, determining switching and memory characteristics
13 p2110 A71-27956
- Semiconductor random access memory components, discussing LSI circuits developments for RAM applications cost effectiveness in computer main-frame memories
13 p2035 A71-28772
- Semiconductor lasers with fast electron pencil beam excitation for high capacity computer storage application
14 p2207 A71-30110
- Real time systems programming techniques based on modular programs, integrated data stores, multiprocessing and special computer languages
14 p2208 A71-30381
- Electrical fiber plates as high resolution conductive arrays for storage and display in electron beam addressed systems
14 p2250 A71-31033
- Channel P MOS memory elements, discussing factors governing electrical energy dissipation and consumption
17 p2715 A71-34684
- Higher order computer language architecture for aerospace software production problems, discussing real time constraints, hardware tradeoffs, memory, computer design and logic circuitry
17 p2712 A71-35777
- High density MOS memory circuits, using multilayer ceramic substrate board for demonstration
17 p2712 A71-35787
- GaAs laser arrays for beam addressable memories, discussing efficiency, junction width, beam spread and polarization
18 p2929 A71-35957
- Ferrite core memories for information storage of digital computer onboard Eole satellite, discussing design and reliability measures
18 p2891 A71-36560
- Channel P doped MOS memory elements, discussing factors governing electrical energy dissipation and consumption
18 p2891 A71-36561
- Capacitive memory storage for filtration of repetitive pulse radio signals mixed with additive noise
19 p3022 A71-38500
- Failure analysis of memory organization in self repair memory system, using various coding and modularization techniques on subsystems
21 p3350 A71-40365
- Fast read only memory design implemented in MOS and bipolar technology, noting low access times
21 p3355 A71-40735
- Memory cell fault tolerant sequential machine synthesis, considering masking feasibility and lower bounds on minimum redundancy
21 p3351 A71-41036
- Carrier mobility, conductivity and optical absorption in strong electric fields of chalcogenide glasses for switching and memory effect amorphous semiconductors
21 p3434 A71-41323
- Glassy antimony and arsenic chalcogenide diode structures, determining switching and memory characteristics
21 p3435 A71-41343
- Current-voltage hysteresis and memory properties of silicon-silicon nitride capacitors as function of oxide layer and stacking fault traps
22 p3516 A71-41684
- Two dimensional holography application to fault-tolerant high density mass data storage design for digital information retrieval system
22 p3548 A71-42517
- Cost effective general purpose minicomputer PDP 11/45 design and technology using Schottky TTL/MSI, semiconductor memories, multiple buses, microprogramming and floating point units
22 p3519 A71-42761
- Radio-optics prospects in signal and information processing, image reconstruction, data transmission, computer storage, display and holographic movies and TV
23 p3681 A71-44344
- Cathode ray tube graphical display system as digital computer output terminal, using analog memory for flickerfree image
24 p3806 A71-44652
- Large random access computer store based on redundancy in form of error correcting codes, discussing use for manufacturing yield improvements
24 p3806 A71-44655
- ### COMPUTER SYSTEMS PROGRAMS
- #### NT INPUT/OUTPUT ROUTINES
- #### NT OPERATING SYSTEMS [COMPUTERS]
- Switch series data checking and sequence identification in program controlled computer systems, exemplifying tape reading procedure
11 p1734 A71-25637
- EDITOR program for writing, reading, copying or altering data on file disk via display station
13 p2035 A71-29015
- ### COMPUTER TECHNIQUES
- Computer for speaking and answering verbal questions, using continuous frequency spectrum analysis and phonemes spectra in memory storage
06 p0871 A71-18057
- Environmental satellite data on-line processing and extraction procedures, including visible and IR imagery mapping and cloud pictures analysis
07 p1067 A71-18806
- Error free SATCOM computer to computer data communication via satellite link
07 p1058 A71-18822
- Soviet book on computer calculation of three-layer elastic plates and shells covering programs, initial equations, input number language, numerical solution, etc
07 p1210 A71-19047
- Book on computer methods of structural analysis concentrating on frame systems, stiffness matrix techniques and Fortran IV
07 p1210 A71-19099
- Computer calculation of phase diagrams from thermochemical data for Cr-Mo and Mg-Cd systems
07 p1054 A71-19519
- Computer aided automatic fault data logging, classification, analysis and reporting methods in integrated ATC system
07 p1155 A71-19556
- Multiple sensor heart rate telemetry using automatic data acquisition and management in squirrel ecology
07 p1049 A71-19626
- Optical astronomy instrumentation automation including telescopes, computer control, filters and detectors
07 p1114 A71-20051
- Computer algorithms for scattering matrix of rectangular waveguide splitters in H plane
07 p1079 A71-20073
- Engineering data integrated test system with sensor based digital computer for data collection and test control
07 p1069 A71-20202
- Computer calculation of high Reynolds number viscous and inviscid flow over arbitrary shaped two dimensional bodies and airfoils
07 p1017 A71-20313
- Correlation and spectrum analysis of simultaneous EEG data in mono and dizygotic twins using computer and FFT algorithm
08 p1246 A71-20746
- Computer plotting of living units, business and industrial plant location for public utilities planning
08 p1280 A71-21246
- Colorado Land Use and Environmental Resource Inventory Project /CLARI/ by computer methods, saving information retrieval time and cost
08 p1281 A71-21253
- Lossless two-port cascade network synthesis using computer-oriented technique
08 p1258 A71-21344
- Hologram imagery and aberrations computer based analysis, considering hologram geometries and nonchromatic aberrations
08 p1290 A71-21387
- Optical elements aspheric testing, using computer generated synthetic holograms
08 p1290 A71-21388

Crop species and soil condition computerized identification from film optical density differences, using multibase and multimulsion photography 08 p1282 A71-21436

Automatic adaptive pattern recognition in photomapping 08 p1259 A71-21438

EEG analyzer voltage peaks recording on computer, using digital readout for simultaneous initial and terminal stage markings 08 p1248 A71-21446

Computer pattern recognition technique for determining cloud motions in real time from ATS satellite photographs 08 p1326 A71-21453

Computer processing in communications - Conference, Polytechnic Institute of Brooklyn, April 1969 08 p1255 A71-21590

Performance test methods and equipment for aircraft avionics and weapons systems, discussing computer integration with radar and phototheodolite range instrumentation system 08 p1260 A71-21660

Computer aided statistical model of visual evoked potential in man as normality criterion for pathological indicator 09 p1397 A71-22253

Computerized method of interpreting low resolution mass spectra in organic chemical analysis, describing inference maker program applications and results 09 p1403 A71-22471

Computerized finite element techniques for stress and structural analysis for space communication and radar applications 10 p1684 A71-23756

Materials microstrain determination using automatic capacitance bridge gage and analog or hybrid computer for measurement signal processing 10 p1609 A71-23916

Computerized interactive scheduling system for modeling, optimizational and priority requirements for NASA manned space flight network 10 p1581 A71-24297

Quasi-analog and hybrid computers, describing ARKUS hybrid integrator effectiveness in solving boundary value problems and ordinary differential equations 10 p1581 A71-24382

Real time high resolution mass spectroscopy using digital computer techniques for data acquisition, processing and presentation 11 p1761 A71-25220

On-line computer technique for pulmonary ventilation continuous/automatic measurement of cardiac patients exercise and work tolerances 11 p1734 A71-25255

System design and optimization computer subroutines based on biological mutation and selection principles, using random number generator 11 p1734 A71-25639

Twin spool turbojet engine dynamic response, discussing simulator predictions, digital computer control, nozzle area variations and operating trajectories [ASME PAPER 71-GT-14] 11 p1812 A71-25960

Computer aided reliability assurance system /CARAS/ for integrated circuits, correlating process and failure data 12 p1890 A71-26658

Computerized system evaluation and feedback data for assurance at hardware level, including reject and failure report documentation 12 p1890 A71-26673

Digital computer analysis of orthogonal ECG and VCG from patients with myocardial infarction 12 p1875 A71-27287

Computer analysis for normal ranges of orthogonal lead ECG parameters derived from modified axial lead systems 13 p2016 A71-27812

Three vs 12 lead electrocardiogram input for computer assisted interpretation 13 p2016 A71-27813

Automation in cardiology, discussing analog and digital computer techniques for on-line hemodynamic analysis and collection and manipulation of cardiovascular data 13 p2016 A71-27868

Computer methods for automatic diagnosis program applied to future manned space vehicles, discussing cost relationship to fault isolation techniques and component reliability 13 p2044 A71-27940

Evoked brain potentials averaging in real time with computer linked by long distance communication lines 13 p2017 A71-28385

Primary component corrections for global cosmic ray variations from latitudinal expeditions, discussing method adaptation to computer 13 p2128 A71-28528

Computer phase hologram synthesis simplified modification, using EM field vector transformation for points 13 p2070 A71-29029

Integral kinetic equation for flow distribution past body and surface heat flow, noting representation in form for computer solution 13 p1991 A71-29156

Computer algorithm for liquid sloshing in rotating cavities, using finite difference scheme 13 p2050 A71-29211

Mars map based on computer cataloged planetary patrol photographs 13 p2143 A71-29342

Experimental computer-aided system evolution to integrate technology plans and evaluate potential resource allocations for mission-oriented technology programs 14 p2339 A71-29853

Atmospheric turbulence effects on stellar irradiance and phase, discussing electro-optical recording technique and computer generated statistical data 14 p2270 A71-30016

Hybrid computer solutions for optimal control of time varying systems with parameter uncertainties, exemplifying minimax load relief for large launch vehicles 14 p2319 A71-30019

Special purpose computer mechanization of inertial attitude reference computation and transformation of body axis information into desired reference frame 14 p2271 A71-30317

Photoelectric scanning photometer for visual binaries measurement, using on-line computer for data sampling and acquisition from three photon counters 14 p2246 A71-30357

Gas turbine engine condition analysis by digital computer and fault isolation techniques [SAE PAPER 710448] 14 p2289 A71-30532

Liquid hydrogen fueled space vehicle fluorine-hydrogen main tank injection pressurization system performance prediction by computerized analysis [AIAA PAPER 71-645] 14 p2290 A71-30722

Onboard computer for aircraft engine testing, monitoring and data reduction, emphasizing automatic in-flight recording for post-flight displays [AIAA PAPER 71-651] 14 p2290 A71-30727

Computer communication asynchronous time division multiplexing, studying communication channel sharing, data buffering and demultiplexing design 14 p2201 A71-30929

Error reduction in automatic systems using computers and measuring network parameters over broad frequency ranges 14 p2205 A71-30983

Airborne phased array using computer control for beam steering, investigating row-and-column logic effects on beam shaping and stabilization 14 p2209 A71-31045

Ritz-Trefftz algorithm application to optimal state regulator problem computer processing to improve speed of solution and storage requirements 15 p2374 A71-31182

Computer quantitation of ST segment response to graded exercise in untrained and trained subjects, continuously recording amplitude of selected points on ECG waveform 15 p2358 A71-31452

Soviet book on plane elasticity theory boundary value problems solution on digital and analog computers 15 p2508 A71-32276

Computer analysis of ECG compared to cardiologist conclusions, noting discordance in rhythm analysis 15 p2366 A71-32543

Analog computer application for determination of charge centers in multilayer gate structure of variable threshold FET, deriving equations yielding position of internally stored charge 15 p2462 A71-32639

Computerized registry of traumatic injuries with IBM 360/44 system for use in mortality, paired patient and accidental risk factor analyses 16 p2535 A71-33109

Computer controlled data handling system for quadrupole mass spectrometer performing on-line chemical analysis of rocket chamber combustion gases [JPL-TR-32-1518] 16 p2578 A71-33182

Hybrid computer use for dynamic system probabilistic modeling, determining hydraulic actuator output statistics 16 p2549 A71-33295

Synthesis method for combining individual part repair time distributions for maintainability prediction using computer 16 p2552 A71-33301

Digital computer techniques for transient data processing and test control 17 p2709 A71-34544

Computer controlled durability and low cycle fatigue testing, using digital random sequencing technique 17 p2821 A71-34555

Computerized automatic control of aircraft electrical system using remote power controllers and multiplexed data bus for wiring reduction and reliability improvement 17 p2677 A71-34700

Computer installations on photometric telescope control system for astronomical observations 17 p2711 A71-34981

Integrated telescope computer system, including magnetic disk storage, digital encoding, drive control and automatic guiding 17 p2711 A71-34984

Digital computer process controller for telescope with driving system consisting of single worm wheels for tracking and slewing 17 p2740 A71-34985

Computer control of vacuum solar telescopes, taking into account servos/handbox intervention, input-output processor, high speed disk and memory 17 p2740 A71-34986

Computer controlled pulse counting technique application to astronomical photoelectric photometry for improved telescope efficiency 17 p2740 A71-34989

Automatic precise centering on photographic plate star image by movement across scanning slits for orthogonal coordinates and processing in on-line computer 17 p2742 A71-34999

Computerized microphotometry of stellar spectrograms for converting input density data to intensity scales, coding tube sensitometer plates, wedge/strip spectrograms and step wedges 17 p2742 A71-35006

Small digital computers applications to astronomical electronic instrumentation systems of microphotometry and spectroscopy 17 p2743 A71-35010

Distributed Fetch sequencing computer technique, discussing system speeds, throughput rates, bus requirement and arithmetic processor demand reduction and task performing capability 17 p2712 A71-35779

BITSIM computer simulation technique for application to real time airborne photoreconnaissance imagery data transmission system design and performance analysis 18 p2917 A71-36070

Computer best least square filtering and approximation by radial filter of noisy imagery using discrete array transmission from photographic film 18 p2884 A71-36081

Eye-point-of-regard system including eye and head movements devices and analog computer for pilot scanning and display research 18 p2864 A71-36091

Digital computers for analytic solution of second order nonlinear ordinary differential equations 18 p2884 A71-36142

Unstable two point boundary value problems solution by decomposition into lower order differential equations sequence for computer integration, giving illustrative examples 18 p2940 A71-36143

Digital data acquisition and processing systems for large quantity rapidly generated measurements using reduction computer 18 p2885 A71-36160

Computerized solutions of gas turbine engines motion equations, considering Euler, fourth order and fifth order Runge-Kutta, Adams, Bashforth and implicit methods 18 p2957 A71-36809

Aircraft industry license norms and standards, describing indexing procedures, storage techniques and data recovery operations with computer 18 p2886 A71-36810

Computer interpretation of Mossbauer effect spectra with iterative, integration and comparison procedure 18 p2887 A71-36858

Computer-based aircraft tracking with aid of twin radar air traffic control system, discussing components and operation 18 p2883 A71-36993

Computerized automatic estimation techniques application to real time aircraft tracking in ATC system design [AIAA PAPER 71-926] 19 p3096 A71-37172

Strapdown guidance systems computerized test system consisting of minicomputer and cathode ray display tube with keyboard control over all system elements [AIAA PAPER 71-967] 19 p3040 A71-37208

Stability theorem for predictor-corrector methods for differential equations systems solution using computer 19 p3085 A71-37421

Grand Tour missions centralized data handling, describing computer aided telemetry system and self testing and repairing control computer [AAS PAPER 71-152] 19 p3025 A71-37954

Airfield surface system digital simulation model application to airport planning for airline operations 19 p3041 A71-38022

Computer demonstration of ionospheric F region storm causes, noting critical frequency relationship to ionization shift 19 p3055 A71-38038

Frequency power and resolution effects on ultrasonic holography for medical diagnosis involving information processing on computer

19 p3066 A71-38240

Hybrid computer continuous space methods for time dependent partial differential equations involving solution of sequence of two point boundary value problems

19 p3025 A71-38292

Automated algebraic manipulation in celestial mechanics, discussing use of Poisson series in perturbation theory problem

19 p3088 A71-38400

Computer aided digital transform natural image processing, using Fourier, Hadamard and Haar matrix algebra

19 p3026 A71-38404

Automated information systems for electromagnetic compatibility analysis using computer

19 p3030 A71-38438

Computer automated systems development for electromagnetic compatibility analysis, noting interactive processing in near real time mode

19 p3030 A71-38439

Electromagnetic fields of finite linear antennas in dissipative half space, obtaining antenna patterns from computer results

19 p3023 A71-38589

Compiler program generation for ordinary differential equations system automatic numerical solution by Taylor series method

20 p3254 A71-38754

Analog computer analysis of radiocardiograms, determining cardiac function and pulmonary blood volume

20 p3191 A71-38802

Automatic pulsating locator beacons and receivers to determine emergency transmitters locations, using satellites with computer analysis

20 p3261 A71-38865

Computer control of multiple site track correlation, describing coarse fine method for implementation and accuracy

20 p3202 A71-38973

Time resolved gain measurements of pulsed two level laser system, using computer for curve analysis

20 p3245 A71-39179

Natural convection boundary layer stability on vertical flat plate with uniform heat flux, using numerical computer solutions for large Grashof number range

20 p3314 A71-39501

Computer techniques for meteor stream trails recognition, considering stream concept extension to groupings of asteroid orbits

20 p3298 A71-39641

Fast time digital computer simulation model for evaluation of man-machine interface /display/ problem of ATC system including personnel and equipment

21 p3412 A71-40112

Computerized touch display for ATC tasks compared to conventional keyboard tabular display performance

21 p3413 A71-40114

Computerized tabular data display with cross-bar addressed glow discharge panel, discussing system details

21 p3350 A71-40115

ATC display devices with computer-derived alphanumeric labels on radar screen, examining feasibility and effectiveness

21 p3413 A71-40118

Book on fitting equations to data by computer analysis of multifactor data for scientists and engineers, covering independent variables selection and least squares method

21 p3406 A71-40166

Computer implementation for Hansen theory of general perturbations, constructing program based on automatic Poisson series processor

21 p3445 A71-40257

Mechanical elements and systems optimal design, discussing variational and programming techniques application to machine elements design optimization [ASME PAPER 71-VIBR-62]

21 p3385 A71-40306

Computerized analysis of fluid film behavior, load capacity and center locus of journal bearing under dynamic load

[ASME PAPER 71-VIBR-86]

21 p3386 A71-40322

Computer-aided study of journal bearing performance under cyclic loads, determining bearing load for circular, linear and elliptical orbits of journal center

[ASME PAPER 71-VIBR-87]

21 p3386 A71-40323

Tracking meteorological satellite receiving antenna orientation data computer calculation, obtaining methods for geographic picture gridding

21 p3410 A71-40824

Computer algorithms for gamma algebra of electromagnetic form factors in terms of Chebyshev polynomials with photon 4-momentum

21 p3415 A71-40842

Helium, neon, nitrogen, oxygen, argon, carbon dioxide and monoxide and methane thermodynamic

and transport properties calculation using computer program for state equations

21 p3351 A71-40893

Algorithms for calculating temperature fields of electronic devices on computers, considering solid body in shape of bounded cylinder

22 p3519 A71-41442

Lame function generation within ellipsoidal coordinates by computerized formula manipulation techniques

22 p3565 A71-41501

Computer controlled modular automatic test equipment for DC-10 aircraft maintenance, discussing system block diagram

22 p3519 A71-41518

Digital picture processing and holography, considering spatial filtering computer simulation and image synthesis

22 p3539 A71-41745

Shell structure computer analysis capability assessment covering U.S. industrial concerns, government agencies and universities research activities

22 p3516 A71-41864

Computer controlled multichannel high speed data acquisition and processing system featuring redundant data deletion, arbitrary number of predeterminations and printing output in full English statements

22 p3517 A71-42108

Computer predictions of postradiation reliability of electrical circuits, using Sceptre program and component tests

22 p3518 A71-42111

Computerized electrostatic field model of biological cell membrane

22 p3487 A71-42119

Computerized bacterial identification system to process Apollo spacecraft sample laboratory test results in NASA Planetary Quarantine Lunar Information System

22 p3504 A71-42233

Aeronautics future, discussing aircraft noise reduction, computer techniques and aircraft design

22 p3482 A71-42237

Large signal mode tunnel diode amplifier amplitude and phase characteristics by computer study

22 p3521 A71-42262

Computer technique for synthesizing binary holograms used in wave beams analysis in quasi-optical communication channels

22 p3546 A71-42320

Computer operated RF automatic test system for HF radio receiver spurious response measurements, giving test results

22 p3514 A71-42389

Mathematical models for computerized ATC automatic aircraft flight tracking logics without tracks smoothing

22 p3573 A71-42396

Rotated pattern detection by optical spatial filtering with superposed holograms, obtaining optimal rotation angle for triangle with digital computer

22 p3546 A71-42475

Digital computer holography, discussing generation, reconstruction, applications in optical spatial filtering and surface testing and sampling and quantization effects

22 p3546 A71-42479

Computer controlled image orthon tube for low light level spectroscopy of metastable excited ions transient absorption spectra

22 p3549 A71-42558

Compensator design for linear controllers for time varying nonlinear systems, using digital computer oriented approach

22 p3577 A71-42676

Orbital spacecraft trajectory and attitude dynamics, using computerized state model for mission planning, orbit determination, satellite geodesy and reentry analysis

[AAS PAPER 71-344]

23 p3727 A71-43017

Automatic multi-satellite ephemeris maintenance by mathematical procedures, describing computer automated scheduling system program

[AAS PAPER 71-355]

23 p3728 A71-43026

Management information techniques, discussing project reports, meetings, decision process, work breakdown, planning schedules and computerization

23 p3785 A71-43457

Electronic optical astronomy, describing image detectors and computer controlled microphotometers and telescope setting systems

23 p3678 A71-43542

Computer acquired I-V characteristics of thermionic fixed spaced planar diodes

23 p3630 A71-43596

Particle size and shape distributions of Apollo 12 lunar fines by computer evaluation of scanning electron microscope images

23 p3758 A71-43755

Computer generation of sensitivity functions for nonlinear sampled data control systems, discussing simulator components and computational time economy problems

23 p3648 A71-43859

IBM 9020 multiprocessing computer application to ATC, discussing control sectors for inflight control at air route traffic control centers in U.S.

23 p3702 A71-43888

Laser use in computer technology, reporting lithium and barium sodium niobate single crystals capacity for data storage

23 p3686 A71-43959

Trap states existence in OSO type satellites, considering damping mechanism and computer results

23 p3773 A71-44092

Soviet book on computerized finite difference solutions for physically nonlinear plates and shells covering material anisotropy, creep, thermal, radiative and cyclic load effects

23 p3779 A71-44184

Digital computer applications to physics problems, giving examples of plasma research and methane molecule properties determination based on quantum mechanics

24 p3847 A71-44355

Automated analysis of high resolution IR astronomical spectra by computer program, presenting procedures for spectral line width, depth and frequency determination

24 p3867 A71-44438

Evoked and background activities interaction in computerized self zeroing neuron model

24 p3801 A71-44550

Nonlinear structural frame analysis by dynamic relaxation for use with computers

24 p3879 A71-44632

Feedback controlled computerized queueing system, deriving generating functions for system state probabilities corresponding to different service time types

24 p3806 A71-44653

Waiting time distribution in computer controlled queueing system with Poisson input, deriving formulas on basis of total probability and Markov chain theory

24 p3806 A71-44654

Isodensity mapping with digital computer symbol selection and cathode ray X-Y plotter, showing photographic image display and enhancement of density or height information

24 p3826 A71-44787

Mars surface mapping, discussing computer reconstruction process for Mariner 6 and 7 TV picture quality improvement

24 p3875 A71-45266

Ultrasonic flaw detection analytical and experimental wave propagation procedure including dynamic photoelasticity and elastic wave computer codes in nondestructive testing

24 p3831 A71-45282

COMPUTERIZED DESIGN

Computer aided design system for integrated circuits including layouts and logic simulation

01 p0058 A71-10249

Search procedures selection from heuristic methods of solving design development problems by computer

01 p0087 A71-10408

Computerized analysis of seal temperature, elastic displacements and seal force balance in iterative design method for gas turbine mainshaft seals

01 p0142 A71-10479

MOS multiphase LSI circuits design using computer program

02 p0228 A71-11651

Optical communication systems cost and weight optimization by COPTRAN program

02 p0214 A71-12028

High speed homopolar alternators as static frequency converter supplies, optimizing design parameters by computer geometric programming

03 p0352 A71-13052

Computer design of magnetron gun forming electron beam of specific pervance and oscillatory energy in converging magnetic field

03 p0385 A71-13796

Computer aided design for fluidic-pneumatic sequential control circuits synthesis, discussing algorithms and computer programs

[ASME PAPER 70-WA/FLCS-17]

03 p0354 A71-14090

High speed automated network design method for optimum value determination of system parameters, using sensitivity analysis and hybrid computer optimization techniques

03 p0390 A71-14305

Programming language for computerized circuit design and analysis, considering techniques for input statements translation

03 p0382 A71-14306

Multistage rocket propelled strategic ballistic missiles and space boosters design and trajectory optimization, using SWORD computer program

04 p0556 A71-15292

Automated design system producing wire format data for cabling avionics subsystem of light attack aircraft

[AIAA PAPER 69-976]

06 p0874 A71-17698

Single frequency carbon dioxide laser cavity length computer aided selection for reduced line competition, considering heterodyne communications systems
07 p1121 A71-18811

Soviet book on automatic control systems synthesis covering dynamic characteristics optimization, based on quality indices and computerized design
07 p1081 A71-19048

Broadband IMPATT diode multistage transmission amplifiers computer aided design and X band performance
07 p1073 A71-19114

Guided weapons modeling techniques, discussing use of mathematical models for analog, digital and hybrid computerized design of missile systems
07 p1207 A71-19419

Computerized transonic airfoil design from predetermined supercritical velocity distribution, obtaining equivalent incompressible flow through streamline and potential line network transformation
07 p1017 A71-20304

Microprogramming by Computer Design Language for describing digital computer functional configuration and sequential operation
07 p1069 A71-20404

Digital computer program for optimum design of narrow band klystron, discussing beam interception and power conversion efficiency
08 p1261 A71-20742

Automated network design optimization trends and role in computer aided design of lumped- distributed and microwave networks, emphasizing adjoint network method
08 p1268 A71-20767

Lens geometry history covering computerized design, prototype testing, optical shop aids and laser interferometry
08 p1333 A71-21177

Multistage gas turbine design optimization, using parameter and component analysis with computer calculations
08 p1348 A71-21267

Large flexible booster launch vehicle autopilots automated design and optimization by computerized technique in frequency and time domain
08 p1332 A71-21337

Lossless two-port cascade network synthesis using computer-oriented technique
08 p1258 A71-21344

Soviet book on research and design work optimization and automation based on mathematical methods and computer techniques
08 p1299 A71-21650

Direct search algorithm for automated optimum structural design with spiral stiffened cylindrical shell application
09 p1533 A71-22077

Multiple reflections method for complex reflection and transmission coefficients of microwave transmission line permitting use of digital computers
09 p1413 A71-22151

Computer program for space and airborne optical imaging systems evaluation, emphasizing image motion compensation role
09 p1411 A71-22748

Aircraft wings automated preliminary structural design and weight determination procedures based on external shape, aerodynamic loads and fuel mass interaction
09 p1541 A71-23274

Man oriented program system for industrial facilities engineering design with modular structure, operating in time sharing mode
09 p1412 A71-23275

Man machine interactive computer graphics for design molding during evolution by computer with nonlinear programming algorithm
09 p1412 A71-23276

Civil Engineering Systems Laboratory remote terminal interactive time sharing computer facility, discussing consulting engineer design office experiences and computing center management
09 p1412 A71-23277

Structural design constraints check by computer single program algorithm, resembling similar human activity
09 p1413 A71-23284

Interactive computer graphics technology industrial applications, emphasizing structural analysis and engineering master drawings
10 p1580 A71-23758

British Aircraft Corporation Numerical Master Geometry system using parameter surface mathematics and digital computer
10 p1580 A71-23759

Automated optimal weight fully stressed large scale structural design of aircraft, using matrix- mathematical programming technique
11 p1844 A71-25340

Self acting herringbone journal bearings optimization program for maximum radial load capacity and wide operating range via groove configurations
11 p1769 A71-25836

Six degree of freedom hybrid digital computer program for complex flight control and associated mode logic design and training
11 p1736 A71-25852

Quasi-vacuum mode thermionic converter for space and remote terrestrial power supplies, describing computer codes for design optimization
11 p1713 A71-25899

Microstrip microwave circuit design by complex admittance measurement and computer modeling
12 p1892 A71-27149

Computerized minimum weight design of elastic redundant trusses under multiple static loads, using algorithms for generating upper and lower bounds for configuration
12 p1980 A71-27409

Automated low cost structural-mechanical design and optimization of wing pivot systems for variable geometry aircraft
12 p1980 A71-27410

Customized MOS arrays computer aided preliminary layout design methodology, using four phase clocking schemes
12 p1890 A71-27772

Thick film flat spiral inductor filter design for television signals, using linear analysis computer program
13 p2039 A71-28913

Computerized circuit design and optimization methods with allowance for constraints and error criteria
13 p2036 A71-29292

Microwave meander line /coupled parallel commensurate conductors array/ network analysis and synthesis, using equivalent circuit transformation for computerized design
14 p2219 A71-29565

Computerized design of optimally efficient dual-series feed microwave networks for waveguide phased arrays
14 p2209 A71-29566

Computer aided design program for civil transport aircraft configuration, performance, propulsion, weight and costs to meet given specifications
14 p2175 A71-30398

Exponentially varying thickness thin plate volume minimization for simultaneous stress and deflection constraints under axisymmetric load, using digital computer
14 p2330 A71-30691

Computer aided design of P-I-N diodes equipped S band phase shifter for phased array antennas, discussing optimization problems
15 p2375 A71-31414

Computing geometric airplane aerodynamic characteristics during preliminary and detailed design processes
15 p2348 A71-31597

Structural synthesis and analysis concepts, discussing design philosophy, failure modes, load conditions, algorithms and computer aided design
16 p2653 A71-33093

Nonlinear filters synthesis by digital computer technique, discussing density storage and Bayes law computation problems
16 p2549 A71-33351

Computer designed optimal or suboptimal feedback controllers, considering least-pth and minimax cost functions
18 p2886 A71-36832

Computerized calculation of field configurations in automated design of electromagnetic transducers
19 p3038 A71-37774

Design algorithm for gyrotropic waveguide consisting of symmetrical rectangular coaxial with magnetized ferrite rods
19 p3019 A71-38333

Computerized design of large multivariable control systems using inverse Nyquist array method
20 p3202 A71-38994

German monograph on filters based on coupled lines, covering computerized design, numerical approximation, rounding errors and matrix correction method
20 p3208 A71-39263

Computer aided aircraft design, analysis and production, discussing Numerical Master Geometry program developed by British Aircraft Corporation
20 p3241 A71-39543

Computer use in automatic tracking radar systems design, describing adaptive radar hardware
20 p3200 A71-39902

Graphical display of digital computer simulated steady state unbalanced turbomotor response for lumped and distributed parameter models, using GATRAN language
21 p3459 A71-40292

Nonlinear mixed integer programming for automated design and structures optimization, describing penalty function technique and recovery scheme to satisfy integer requirements
21 p3350 A71-40336

Radiative-conductive heat transfer systems optimum thermal design, using nonlinear programming with mathematical model based on nodal analysis
21 p3474 A71-40339

Logarithmic rate meter computer aided design, taking into account components tolerances for desired accuracy over selected frequency range
21 p3379 A71-40650

Computerized optimal design of L band phase shift networks for broadband performance
21 p3361 A71-40816

Computerized numerical optimization for Yagi-Uda antenna array gain, noting nonoptimum in standard traveling-wave design methods
21 p3349 A71-41410

Computerized step-jump and time-transient dynamic analysis application to gimbal mounted Rayleigh-step gas-lubricated thrust bearing design
22 p3552 A71-41672

Computerized design procedures for externally pressurized flexibly mounted gas lubricated journal bearings, predicting steady state performance, vibration capacity and translational stability
22 p3552 A71-41676

Soviet book on multivariable automatic control system synthesis with adaptation to computer covering methodology, algorithms, transfer function approximation and stability problem
22 p3525 A71-41799

Interactive graphical computer system with remote on-line consoles for engineering problem modeling and analysis, giving illustrative examples
22 p3516 A71-41868

Interactive computerized design system for undergraduate aerospace engineering, using remote time sharing computer terminals
22 p3517 A71-41991

Computerized synthesis for fly-back system of first stage winged booster for earth-to-orbit reusable space transportation system
22 p3611 A71-42032

Computer-aided statistical analysis correlation method for prediction of electronic circuit component part variability effects on performance and reliability
22 p3517 A71-42102

Bias network analysis computer program for reliability analysis suited to failure mode, criticality, drift and catastrophic failures prediction
22 p3517 A71-42104

Computerized reliability optimization system program for electronic equipment design and management methods to achieve high reliability and low cost
22 p3517 A71-42105

Computerized system redundancy optimization formulation as zero-one type variables integer programming problem, obtaining algorithmic solution for maximum reliability
22 p3517 A71-42106

Computerized algorithm for redundant configuration system reliability function generation from Boolean algebra transmission function
22 p3517 A71-42107

Design technique based on frequency response loci associated with characteristic transfer functions for linear time-invariant multivariable feedback control system
22 p3526 A71-42284

Design and performance optimization of series mode step recovery diode frequency multipliers, using computer aided analysis
22 p3523 A71-42358

Nonlinear and syllabic companded digital delta modulation systems, discussing SNR measurement and computer simulation for optimum design
22 p3514 A71-42392

Linear and nonlinear models for computer aided circuit design involving Zener diodes, providing for thermal effects
22 p3524 A71-42762

Synthesis models and methods for large scale automated control systems with human elements, discussing mathematical models and computerized design
22 p3528 A71-42858

Microwave bipolar transistors computer aided design, describing optimization and synthesis procedures and RF performance
23 p3649 A71-43067

Field effect devices mathematical modeling for computer aided circuit design, using unified approach
23 p3649 A71-43069

COMPUTERIZED SIMULATION
NT ANALOG SIMULATION
NT DIGITAL SIMULATION

Flight simulator ancillary features using computer data storing and processing capabilities for flight instructor decision making process improvement
01 p0066 A71-10018

Hybrid executive programs for simulation, discussing I/O processing, potentiometer evaluation, data conversions, etc
01 p0046 A71-10202

Hybrid computer simulation program for analyzing large circuits intractable by conventional methods using PACTOLUS language
01 p0048 A71-10225

Radar reflectivity pattern calculation from cumulus cloud growth numerical model, noting similarity with radar data from on-line computer system
01 p0118 A71-10584

Direct computerized simulation Monte Carlo method for numerical solution of Boltzmann equation in rarefied gas dynamics

01 p0113 A71-11472

Computer simulation - Conference, Denver, June 1970

02 p0225 A71-11777

Digital hybrid systems simulator /DHYSYS/ program, examining subsystems sampling and execution time and applications

02 p0226 A71-11780

Inertially stabilized tactical missile control system performance analysis using hybrid computer simulation methods

02 p0226 A71-11785

Saturn V second stage longitudinal oscillation from structure and propulsion system interaction examined by transfer function simulator subroutine /TRANSIM/ computer program

02 p0318 A71-11788

Hybrid computer structural response simulation for helicopter fuselage, using matrix displacement method

02 p0227 A71-11790

Hybrid real time computer simulation of external visual display cues for Apollo Command and Service Modules

02 p0237 A71-11791

AAP electrical power system simulation for Skylab earth orbit missions, taking environmental effects into account

02 p0190 A71-11795

Missile six degree of freedom simulation by hybrid computer, discussing roll and pitch dynamics

02 p0227 A71-11798

Computer simulation - Conference, Denver, June 1970

02 p0227 A71-11804

Cardiovascular system blood flow mathematical model parameter optimization by simulation on hybrid computer, using OPTRAN program

02 p0203 A71-11807

Electronic circuit analysis using parametric reliability criteria based on progressive failures, applying statistical computerized simulation method

02 p0230 A71-11840

Computerized simulation of disk galaxies evolution, using doubly periodic model for stellar motions

02 p0318 A71-12925

Monte Carlo simulation model program, evaluating automatic test equipment design influence

03 p0381 A71-13089

Computer simulation for evaluating equipment effect on weapon mission success, considering failure time, repair cycle, operational and maintenance parameters

03 p0431 A71-13090

Spacecraft attitude suboptimal control by orthogonal set of amplitude limited PWM reaction control jets, presenting spacecraft controlled motion computer simulation

[AIAA PAPER 70-997]

03 p0499 A71-13722

Computerized statistical simulation of steady state, ergodic, self oscillatory processes in plane magnetron

03 p0386 A71-13811

NERVA XE-Prime test series, discussing computer simulation full power and high specific impulse operation and startup under varying initial conditions

[AIAA PAPER 70-709]

03 p0456 A71-14428

Computerized simulation of disturbance torques of spin stabilized spacecraft in near earth orbit

03 p0500 A71-14433

Computer simulation of human body kinematics under rapid decelerations

04 p0542 A71-14786

Hybrid computer simulation of three degree of freedom surface to air missile trajectory, obtaining cluster of points for position errors

04 p0642 A71-14798

Computer simulation of thermal diffusivity measurements by flash method, considering errors due to boundary conditions

04 p0607 A71-14964

Computerized Monte Carlo models of distributed parameter systems of partial differential equations with moving nonlinear boundaries

04 p0619 A71-15150

Linear digital computer simulation and process control, considering state space method

05 p0730 A71-16126

Metal powders sintering computer simulated dynamic volume diffusion model based on Laplace equation, comparing calculated growth rates with electron microscope data

06 p0903 A71-17344

Hybrid computer simulation for cardio-circulatory assist device, discussing atrium to aorta and ventricle to aorta optimal output, time tension index and flow control

07 p1048 A71-19584

Extendable Computer System Simulator, discussing simulators as tools for integrated information systems design

[AIAA PAPER 71-228]

07 p1068 A71-19706

Complex digital computer systems effectiveness measurement, using simulation program with programming language SIMSCRIPT

[AIAA PAPER 71-229]

07 p1068 A71-19707

On-line computer systems performance characteristics determination through functional simulation, using FORTRAN IV program packages

[AIAA PAPER 71-230]

07 p1068 A71-19708

Two dimensional aircraft automatic landing motions control processes by simulation without use of moving cockpit simulator

07 p1084 A71-20066

Cyclic stress-strain behavior prediction by mathematical model and computer simulation, applying to Al alloy fatigue

07 p1216 A71-20204

Man-machine considerations in all-weather low-altitude navigation system design, discussing computer generation of roll command guidance, visual display and pilot modeling

07 p1157 A71-20344

HF plasma instabilities driving mechanisms and distribution types, considering beam plasma computer simulation example

07 p1173 A71-20508

Computerized simulation of inlet channel flow passage cross section effect on internal combustion engine filling

08 p1347 A71-20830

Interactive Saturn flight program simulator for real time graphics operations of navigation, guidance, engine control, event sequencing and communications

08 p1272 A71-21237

Airport pollution dispersion modeling, simulating effect on surrounding areas for abatement strategies calculation

08 p1379 A71-21824

Computer simulation of strongly ionized potassium and hydrogen plasmas relaxation during rapid electrode cooling by He atoms, noting population inversions

08 p1342 A71-21913

Synchronous combinative time pulse polylogical structural elements for computer simulation of human neuron functions, discussing circuit design

09 p1398 A71-22271

Dioscures project commercial satellite system for telecommunications, air traffic control and navigation, describing simulation method used in cost effectiveness study

09 p1547 A71-22276

Si Read diode computer simulated large-signal operation, determining temperature effect on microwave oscillating efficiency

09 p1417 A71-22966

Structural design constraints check by computer single program algorithm, resembling similar human activity

09 p1413 A71-23284

Computer simulation model for stars motion in plane of disk-like stellar systems, investigating dynamics of Jeans and gravitational two-stream instability

10 p1670 A71-24181

Computerized simulation of lateral inhibitory networks for figural aftereffects, discussing light and dark adaptation mechanism

10 p1563 A71-24232

Computer generated visual simulation of three dimensional objects, using geometric modeling technique for mathematical representation of photographic process

10 p1581 A71-24775

Computer simulation of stress corrosion cracking, considering electrochemical oxidation mechanism for crack propagation

11 p1847 A71-25449

Thermodynamic properties of interstitial solid solutions with fcc metals from atomically discrete model by computer simulation

11 p1778 A71-25531

Hybrid computer Monte Carlo technique for simulation and optimization of system with random parameters

11 p1735 A71-25843

Apollo command module guidance computer and environment hybrid simulation for flight software and crew procedures verification

11 p1744 A71-25845

Attitude control loop and inertial guidance hardware, studying system dynamic performance hybrid simulation

11 p1796 A71-25846

Complex real time hybrid computer simulator for captive two blade rotor platform dynamic problem solving

11 p1744 A71-25847

Hybrid simulation to increase hit possibility of rocket fired from military tanks at moving targets

11 p1735 A71-25848

Apollo hybrid simulator for man-machine interface in low orbit lunar landmark tracking

11 p1796 A71-25850

Simulated far field patterns of linear and phased arrays without radiation coupling by hybrid analog computer

11 p1735 A71-25851

Hybrid computer operating system for piloted aircraft simulation and optimization studies

11 p1736 A71-25853

Computer aided statistical analysis of irregular quasi-optical transmission lines containing random inhomogeneities

11 p1733 A71-26347

Planetary system formation, examining particulate matter aggregation within dust cloud and gas around sun by computer simulation

11 p1835 A71-26459

Design analogies of aerospace and commercial systems, describing computerized simulation method for system design evaluation and reliability improvement

12 p1909 A71-26663

Solar energy absorptance changes in spacecraft thermal control surfaces exposed to particulate radiation at simulated synchronous altitude, using computerized model

[AIAA PAPER 71-453]

12 p1928 A71-26761

Pulmonary gas exchange studied in computer models with series inequality of ventilation

12 p1870 A71-27131

Cloud formation two dimensional model simulation by numerical integration of hydrodynamic and thermodynamic equations, considering condensation, evaporation, coagulation and water drops terminal fall velocity

12 p1925 A71-27196

Human inner organic system simulation by digital computer, using overall quantitative heuristic model

12 p1876 A71-27742

Computer simulation of fading records in spaced antenna ionospheric drift experiment, detecting mean direction and diffraction pattern velocity with correlation analysis

13 p2054 A71-27800

Air showers nuclear active and muon components simulation in space and time, using different shower models based on isobar-fireball concept

13 p2125 A71-28090

Computer simulation of automatic voice communication link intelligibility measurement, using speech recognition techniques

13 p2032 A71-28872

Computerized simulation techniques for investigating aircraft accidents due to atmospheric turbulence

14 p2221 A71-29779

Flight vehicle equations of motion for computer simulation, calculating optimal servosystem parameters and optimal range control by hybrid computer scheme

14 p2319 A71-30001

SIMCON simulation of physical systems using IBM 360/91 computer illustrated by satellite attitude control application

14 p2207 A71-30022

Multicategory bibliographic classification of human behavior computer simulation models

14 p2189 A71-30461

Nuclear space power systems computer simulation for preliminary system and mission analysis, considering Brayton, Rankine and thermionic systems

[AIAA PAPER 71-689]

14 p2208 A71-30749

Performance predictions for Viterbi decoding algorithm by simulation on UNIVAC 1108

14 p2200 A71-30922

Simulation equipment installation with link to Concorde flight simulator, discussing functional and operational features

15 p2384 A71-31885

Spiral density wave structure in computer simulations of evolution of galaxies, showing azimuthal dependence on gravitational and radial forces

15 p2497 A71-32769

Precision area navigation system, considering position and velocity continuous measurement in three dimensional space, system components and simulation program

17 p2771 A71-34616

Robots structural description and computer modeling based on various algorithms

17 p2691 A71-35167

Dynamic system impulse response model for goodness of fit and linearity hypothesis tests by computer simulation

17 p2722 A71-35181

Computer simulation of strongly ionized potassium and hydrogen plasmas relaxation during rapid electrode cooling by He atoms, noting population inversions

17 p2788 A71-35257

Computer simulation of error probability performances of binary coherent PSK system under thermal noise and intersymbol and interchannel radio interferences effects

17 p2707 A71-35476

Aircraft loading system consisting of onboard weight and balance equipment and fully mechanized

cargo pallet transfer, using computerized simulation model for parametric evaluation [SAWE PAPER 900] 17 p2676 A71-35811

Computer algorithm for simulating dynamic systems by functional graphs, noting extension to complex systems 18 p2884 A71-35917

Aerial cameras performance prediction by computer simulation technique with random number generation 18 p2917 A71-36069

Computer simulation model for experimental data in post-Skylab space station design 18 p2973 A71-36458

Long duration orbital simulator for technical planning activities, discussing capabilities, options, accuracy and central processing unit usage 18 p2885 A71-36460

Pneumatic isolation system for inertial instrument testing, using computer simulation model to evaluate physical parameter variation effect on pad suspension dynamic behavior [AIAA PAPER 71-910] 19 p3040 A71-37161

Boeing computer simulator for logic design confirmation and failure diagnostic programs, providing for propagation delays and feedback simulation [AAS PAPER 71-162] 19 p3025 A71-37959

Airport facilities operational planning, discussing computer simulation parking systems and arrivals building 19 p3041 A71-38026

Airfield performance evaluation by simulation, providing statistical measures and computer generated motion picture for visual display of simulated future activity 19 p3041 A71-38027

Computer algorithm for simulation of one dimensional unsteady compressible fluid flow in presence of area change, wall friction, heat transfer and entropy gradients 19 p3025 A71-38291

Automated test capability for digital modules, describing test generation, circuit analysis and simulation programs 19 p3030 A71-38406

Simulator for operating decision rules for control of airborne IR forest fire detection system 19 p3066 A71-38409

Reactor powered Brayton cycle power conversion system, evaluating performance at different turbine inlet temperatures and power levels by computer simulation 20 p3262 A71-38914

Rechargeable cylindrical hydrogen-oxygen fuel cell for synchronous satellites, determining energy density as function of current, pressure and electrolytes with computer model 20 p3182 A71-38947

Tubular compact air cooled thermoelectric module endurance and performance tests and computer simulation for space reactor power system 20 p3266 A71-38954

Long life radioisotope thermoelectric generator, discussing mathematical model to simulate expected performance profiles 20 p3266 A71-38958

On-line identification for nonlinear system from noisy measurements, applying stochastic algorithm to hybrid simulation of chemical process models 20 p3207 A71-38974

Variable thickness ice film water-to-cryogen heat exchanger design, presenting mathematical model for performance calculation by modified integration digital analog simulator computer program 20 p3314 A71-39291

Lumped parameter simulation model for flexible turbine rotor dynamics in nonspinning coordinate system, discussing bearing constraints modeling methods and eigenanalysis applicability [ASME PAPER 71-VIBR-71] 21 p3385 A71-40309

Computer method to simulate dynamic behavior of two dimensional machine systems with linkage elements [ASME PAPER 71-VIBR-111] 21 p3386 A71-40334

Nonlinear flight dynamic simulation using wind tunnel and aircraft model as analog function generator and computer for motion equation processing and command orientation 21 p3363 A71-40392

Computer simulation of crack propagation in plane strain and plane stress geometries, solving continuum mechanics equations in two space dimensions and time 21 p3351 A71-40797

Monograph on satellite airport system modeling for large metropolitan areas covering systems analysis methodology and computer algorithms for optimization [SU-TR-71-1] 21 p3365 A71-40799

Particle model measurements of collision and heating times in two dimensional thermal computer plasma 21 p3423 A71-40843

Soviet monograph on astronomical foundation of meteor communications, covering radio wave scatter-

ing by meteor trails and computer simulation of signal time-amplitude characteristics 21 p3349 A71-41373

Thermal effects in loop prominences formation after solar flares from model computer simulation 22 p3597 A71-41459

Hybrid computer simulation of nonlinear ion-acoustic shocks in diaphragms 22 p3577 A71-41896

Computerized simulation of reliability and in-flight subsystem maintenance for increased space mission success probability, using priority and waiting queue method 22 p3518 A71-42112

Computerized simulation of maintenance man hour loading for communication system based on repair, failure and availability distributions 22 p3554 A71-42113

Fano and stack algorithms comparison by computer simulation of two sequential decoding algorithms 22 p3512 A71-42379

Nonlinear and syllabic companded digital delta modulation systems, discussing SNR measurement and computer simulation for optimum design 22 p3514 A71-42392

Viking vehicle structural flexibility and propellant sloshing effects on thrust vector control dynamics, obtaining computer simulated responses for hybrid and discrete coordinate models [AAS PAPER 71-348] 23 p3773 A71-43021

Optical orientation determination and star pattern recognition for Skylab in solar inertial attitude by digital and hybrid simulations [AAS PAPER 71-397] 23 p3732 A71-43065

Synthesis procedure for feedback parameter adaptive control systems, discussing computer simulation data 23 p3658 A71-44081

Real time interactive simulation of multifunction phased array radar, using digital computer links 23 p3648 A71-44272

Two dimensional radiative heat transfer in absorbing-emitting medium bounded by nonisothermal gray walls from Monte Carlo simulation, showing gas emissive power distribution 23 p3784 A71-44276

Computer model of microchannel electron multiplier plates in imaging devices using Monte Carlo method 24 p3811 A71-45328

COMPUTERS

NT AIRBORNE/SPACEBORNE COMPUTERS

NT ANALOG COMPUTERS

NT COUNTING RATE COMPUTERS

NT DIGITAL COMPUTERS

NT HYBRID COMPUTERS

NT IBM COMPUTERS

NT IBM 360 COMPUTER

NT ILLIAC 4 COMPUTER

NT PDP COMPUTERS

NT PDP 8 COMPUTER

NT RCA SPECTRA 70 COMPUTER

NT SEQUENTIAL COMPUTERS

NT SITE DATA PROCESSORS

Time shared computer display system design with analog drive signal generator and digital information channeling processor 01 p0045 A71-10196

Computer systems performance simulation, discussing data collection and preparation and language selection 05 p0727 A71-17048

Power station electronic control equipment and integrated circuit computer reliability data analysis, emphasizing combined mathematical prediction and observation 07 p1077 A71-19565

On-line computer systems performance characteristics determination through functional simulation, using FORTRAN IV program packages [AIAA PAPER 71-230] 07 p1068 A71-19708

Computers - Conference, Houston, November 1970 14 p2207 A71-30017

Reliability analysis of universal computer system with identical elementary computers interconnected by communication channels 17 p2710 A71-34958

Redundant strapdown Inertial Measurement Unit processor recovery requirements, investigating IMU information loss effects during recovery on spacecraft mission 17 p2772 A71-35058

Generalized computing machines deductive systems, introducing sequence of partial functions 18 p2886 A71-36823

Continuous machines basic properties, introducing tau computation and tau computable sets union, intersection, difference and parallel product 18 p2886 A71-36824

Continuous machine arithmetical properties, introducing tau generable set 18 p2886 A71-36825

COMSAT PROGRAM

Satellite broadcasting to West African countries, discussing communications policies, NASA tracking

stations in Africa and U.S.- Nigeria agreement for Comsat and Intelsat programs 18 p2987 A71-36169

CONCAVITY

Inviscid incompressible two phase concave type corner flows embedded with small spherical particles, examining streamlines, critical collision conditions and approximate viscous effects 10 p1598 A71-25081

CONCENTRATION [COMPOSITION]

NT ATMOSPHERIC MOISTURE

NT ATOM CONCENTRATION

NT CARBON DIOXIDE CONCENTRATION

NT MASCONS

NT METEOROID CONCENTRATION

NT MOISTURE CONTENT

Anomalous Cu concentration profile due to migrating Cu ions-GaAs crystal defects interaction 05 p0794 A71-16877

Hydrazine concentration measurement in potassium hydroxide, describing instrument design and operation 06 p0900 A71-18014

Multicomponent gas laminar boundary layer equations, deriving asymptotic formulas for friction coefficient, concentration, temperature and diffusion flows 07 p1089 A71-19734

Laser induced Raman scattering as diagnostic technique for measuring specie concentrations in gas mixtures [AIAA PAPER 70-224] 07 p1125 A71-19897

Interstitial solid solution hardening in pure Ni and Ni-C alloys, noting mechanism and C concentration effects 07 p1138 A71-19980

Germanium distribution coefficient in GaAs epitaxial crystals by radiotracer, mass spectroscopy and electron probe analysis noting total impurity concentration from Hall mobility 07 p1180 A71-20176

Etchant type, concentration and temperature effect on various plastics track etching ratio and sensitivity 07 p1145 A71-20272

Gas concentration determination for mixture by UV energy absorption measured in terms of photomultiplier tube output current, describing oxygen sensor 08 p1287 A71-20987

Fe powder concentration in Ni powder by spectral analysis, examining particle size and HF generator spark condensation effects 08 p1306 A71-21066

Temperature, concentration and heat conductivity profiles of chemically reacting gas mixtures with thermal gradient, using classical transfer equations 13 p2025 A71-27884

Concentration and transport from auroral zone of minor constituents in mesosphere and lower thermosphere during anomalous midlatitude radio absorption periods 14 p2230 A71-29711

Nitrogen and sulfur dioxide reactions in isolation, determining rate by concentration measurements using light absorption technique 15 p2465 A71-32082

Radical and formaldehyde daytime concentrations predictions from steady state model of unpolluted surface atmosphere 16 p2575 A71-34048

Turbulent He jet time resolved velocity and He mass fraction measurements, using hot-wire anemometry and digital recording techniques 17 p2670 A71-34878

Concentration profiles around burning droplet, assuming constant binary diffusion coefficients for all species 17 p2840 A71-35705

Light wave Rayleigh interferometer for concentration gradient measurements in liquid systems with mass transport 18 p2917 A71-36052

Concentration effects of Nb and Ta on strengthening in tetrahedral section of W-Mo-Nb-Ta system at temperatures from 20 to 1100 C 19 p3078 A71-37473

Co-Ni alloy interdiffusion coefficient determination as function of concentration by magnetic transformation effect 21 p3399 A71-40700

Ti alloy microarea alloying element concentration quantitative analysis by EPMA program, obtaining working curves for Al, Fe, Cr, Mo and V 22 p3561 A71-41944

Liquid laser output wavelength dependence on rhodamine dye concentration, comparing experimental data with Stepanov theory 23 p3684 A71-43417

CONCENTRATORS

Multiplexer concentrators for data telecommunication systems with erratic information flow, concerning statistical assumptions, transient response, queuing tails and message clustering 12 p1880 A71-27072

CONCENTRIC CYLINDERS

Nonlinear heat transfer in rarefied gas between concentric cylinders, using modified discrete ordinate method based on BGK model equation

01 p0182 A71-11405

Nonstationary rotating MHD viscoplastic medium between coaxial cylinders in crossed electric and magnetic fields, determining zone interface position and stress distribution

03 p0464 A71-13601

Two dimensional annular flow of viscous heat conducting gas between coaxial cylinders, using Navier-Stokes equations

03 p0401 A71-14066

Couette flow stability between coaxial rotating cylinders, calculating eigenvector in first approximation small perturbation equations

03 p0404 A71-14231

Viscoelastic fluids flow stability between arbitrary spaced concentric cylinders, noting critical Taylor number dependence on gap size

05 p0735 A71-16715

Rarefied gas Couette flow between concentric cylinders and heat transfer from wire to external cylinder, applying momentum method

05 p0736 A71-16723

Axisymmetric vibration frequencies, form shapes and apparent masses for vertical fluid filled coaxial cylindrical shells resting on spherical spherical shell

06 p0986 A71-17763

Circular cylindrical shells on coaxial rings coupled by finite number of spokes as structural analytical models for engine casings, deriving formulas for arbitrary loads

08 p1374 A71-22040

Laminar steady flow and heat transfer of viscous heat conducting gas moving between coaxial cylinders, using Runge-Kutta method

09 p1431 A71-22408

Electromagnetic wave propagation in circular waveguide loaded with coaxial dielectric cylinders, calculating band pass characteristics

09 p1406 A71-23039

Thermal conductivity of Ar binary mixtures with He, N and Ne, using secondary concentric cylinders cell

09 p1547 A71-23463

Polarographic measurements of secondary Couette flow between coaxial cylinders for diffusion coefficient effects on mean friction factor, using wall flush microelectrodes

10 p1592 A71-23978

Fluid rotational stability between coaxial cylinders rotating at same angular velocity in presence of radial temperature gradient

10 p1696 A71-24374

Tangential velocity profile in steady incompressible electrically conducting viscous axial flow between concentric rotating cylinders with radial magnetic field, solving Navier-Stokes equations

11 p1752 A71-26048

Steady laminar natural convective flow in concentric cylindrical annuli, using finite difference method for Navier-Stokes and energy equations solution [ASME PAPER 70-WA/HT-9]

13 p2164 A71-28982

Incompressible homogeneous isotropic fluid Couette flow between stationary inner and rotating concentric outer cylinders, examining Weissenberg effect

14 p2226 A71-30445

Book on fluid mechanics covering rotating fluids, flow between concentric cylinders, emulsions, standing waves on water, etc

14 p2226 A71-30554

Heat transfer through stationary monatomic rarefied gas in annular space between coaxial cylinders, using two-flow Maxwellian function for approximate molecular velocity distribution

16 p2661 A71-32832

Cellular convective fluid flow stability regions between concentric cylinders, considering nonuniqueness features with asymptotic stationary solution

16 p2557 A71-32983

Viscous incompressible flow stability between concentric rotating cylinders, developing nonlinear model of two disturbance interaction

16 p2558 A71-32985

Nonlinear global strong cellular branching solutions stability of Navier-Stokes equations

16 p2558 A71-32997

Oscillatory modes of perturbation in onset of flow instability for Newtonian liquid between concentric rotating cylinders with transverse pressure gradient

20 p3212 A71-39484

Gortler-Taylor vortices visualization in liquids between rotating concentric cylinders using pulverized aluminum

20 p3213 A71-39781

Rotating viscous fluid flow between concentric circular cylinders, predicting velocity field dependence on position and time during inner cylinder sudden stop

21 p3366 A71-40543

Axisymmetric stress and strain states calculation for linear elastic field in cylindrical tight fits between hub and shaft

21 p3463 A71-40656

Hydrodynamic stability of incompressible conducting fluid flow between two moving linearly and rotating coaxial cylinders in longitudinal magnetic field

21 p3367 A71-40688

Radiant flux from finite cylindrical volume to coaxial screen calculated under quasi-homogeneous medium and arbitrary optical thickness assumptions

23 p3782 A71-43920

Heat conduction of rarefied air and argon in annuli between coaxial cylinders

23 p3783 A71-44068

Taylor vortex flow stability between rotating concentric cylinders, using fifth order amplitude expansions in matrix form

24 p3817 A71-44420

CONCORDE AIRCRAFT

Concorde role in air traffic market, discussing operating costs and profit potential

02 p0190 A71-12746

Medicophysiological problems in Concorde SST relative to altitude and speed, noting risks of cosmic radiation, ozone in atmosphere, decompression, wing loss and high temperatures

03 p0371 A71-13093

Ground and airborne aircraft flight simulation methods, discussing simulator layouts and application to Concorde project

04 p0566 A71-15206

Concorde automatic flight control, noting reduced weight and speed accuracy limit at Mach 2

05 p0751 A71-16325

Concorde progress toward certification, discussing SST airworthiness requirements, flight test program, takeoff and landing operational experience and stability problems at high incidence

05 p0696 A71-16487

Concorde airframe structures, discussing numerically controlled machining of aluminum alloy integral units

06 p0904 A71-17954

Concorde aircraft Olympus 593 two-spool turbojet engine, discussing variable nozzle and intake assembly, afterburner and control system

07 p1183 A71-19081

Concorde airworthiness requirements and Air Registration Board participation in flight test program, considering supersonic flight characteristics

09 p1385 A71-23579

Concorde thermal fatigue test installation, controlling temperature by transfer temperature variation in single heat exchanger block

09 p1430 A71-23580

Concorde aircraft fuel system and fuel pumps, considering center of gravity and center of pressure relationship to maintain trim

09 p1512 A71-23581

Concorde aircraft components electrochemical marking, considering stamping and engraving unacceptability for highly stressed thin material parts

09 p1459 A71-23582

Concorde environmental testing, considering endurance tests, thermal shock rigs and plant for simulating air supply from compressor stages of aircraft gas turbine engines

09 p1430 A71-23583

ATC regulations considered for Concorde introduction to passenger service, discussing landing and takeoff characteristics

11 p1706 A71-25232

Concorde aircraft construction methods, materials and design

12 p1867 A71-26882

Space shuttle comparison with transport aircraft, discussing high thermal resistant and cryogenic insulator material concepts, with application to Concorde structural computations

12 p1973 A71-27605

Concorde economic flight testing methods, discussing Blagnac flight simulator mobile cabin visualization and color TV terrain model

12 p1868 A71-27608

Olympus 593 pure jet twin shaft engine development program for Concorde, discussing engine evolution, design considerations and flight development [SAE PAPER 710422]

13 p2114 A71-28309

Olympus 593 Concorde engine combustion system, discussing operating conditions, combustion performance criticality and altitude re-lighting

13 p2116 A71-28740

Concorde SST flight test equipment installation with PCM recording and visual instruments

14 p2174 A71-30055

Concorde power plant fire protection system, describing prototype engine bay overheat detection system and additional UV optical fire detection system

14 p2288 A71-30300

TU-144-Concorde differences, discussing design philosophy engine mounting and thrust, wing span and

profiles, gross weight, fuselage cross sections landing gear, droop nose, etc

15 p2349 A71-31873

Concorde aircraft engine noise emission and reduction, examining acoustic measurements in takeoff and approach phases, reduced thrust and retractable silencer

15 p2469 A71-31877

Concorde flight simulator at Toulouse, discussing flight control system, air navigation and certification

15 p2384 A71-31881

Simulation equipment installation with link to Concorde flight simulator, discussing functional and operational features

15 p2384 A71-31885

Concorde aircraft automatic landing and flight control system objective, design, reliability and certification tests

15 p2446 A71-31915

French contribution to air transportation, discussing international cooperation on supersonic Concorde, medium range airbus and short range Mercure

15 p2350 A71-32688

Concorde flight characteristics, discussing performance flight test data relationship to design

15 p2350 A71-32690

Concorde lightweight disk brakes, discussing operating costs, weight and volume factors, design philosophy, structural materials, component life, maintenance and reliability

16 p2522 A71-33226

French flight test center role in development and certification of Concorde aircraft, considering cooperation with industry

17 p2675 A71-35526

Thermal ground testing of Concorde and Veras, considering static and fatigue testing in heat environment

18 p2899 A71-36464

Meter wave aircraft slot antenna for Concorde air to ground communication via satellite, presenting synthetic radiation patterns

18 p2889 A71-36514

Concorde aircraft navigation system comprising triple inertial systems, dual VOR/DME, dual ILS and dual ADF

19 p3100 A71-37599

Concorde droop nose for takeoff and landing visibility improvement, describing design and operation

19 p2997 A71-38343

Atmospheric wind, temperature, turbulence, hydrometeors, ozone, cosmic radiation and radio activity effects on commercial SST Concorde flight

21 p3325 A71-40829

International cooperation in aerospace projects, discussing Concorde program organization

22 p3623 A71-42011

CONCRETES

Steel-concrete composite beam creep numerical analysis by reduction to elastic problem with initial strains

04 p0669 A71-15198

CONDENSATES

Condensate film thickness and Nusselt number on axisymmetric vertical plates and cylinders, correcting for variable gravity and body form

03 p0519 A71-13699

Moving condensate film effect on velocity profile and mass transfer rate from gas-vapor mixture by Crank-Nicholson method

06 p1006 A71-18070

Metal and alloys condensates corrosion tests based on recording changes in electrical resistance

15 p2427 A71-31651

Condensate removal devices for potassium vapor Rankine space power turbines to prevent blade erosion and efficiency degradation

20 p3262 A71-38918

Phase composition and defect structure of thin film CdTe islet compensates on NaCl and KBr cleavage faces

23 p3718 A71-44316

Condensate particle crystallization retardation effect on energy characteristics of jet engine, calculating nonequilibrium flows of two phase combustion products in nozzle

24 p3864 A71-45004

CONDENSATION

Mars atmosphere carbon dioxide condensate cloud layer implications, considering temperature lapse rate and water condensation at lower levels

03 p0489 A71-13608

Spacecraft propellant condensation on low temperature surfaces near cesium ion thruster exhaust, considering neutral atoms impingement and charge exchange

03 p0522 A71-14455

Inviscid binary gas mixture steady supersonic two dimensional flow past convex corner, taking into account spontaneous condensation

03 p0345 A71-14559

Heat transfer - Conference, Versailles, August-September 1970, Volume 6, Boiling and condensation

04 p0687 A71-15533

Liquid metals vapor drag and electromagnetic fields effects on laminar film condensation, using finite difference method

04 p0688 A71-15539

Interstellar gas cloud equilibrium and gravitational stability, examining evaporation, condensation, thermal balance and pressure

04 p0658 A71-15837

Thin CdS condensate layer formation mechanism during films slow vacuum deposition onto glass or polystyrene sublayer bases

05 p0793 A71-16821

Water vapor condensation due to heterogeneous nucleation in nozzles, considering flows seeded with inorganic smoke and metallic ions

[ASME PAPER 70-FE-22]

05 p0737 A71-16974

Cloud droplet growth by condensation, deriving equation solution computational stability

07 p1152 A71-19756

Condensed water vapor in supersonic nozzle flow, describing dispersion coefficient measurement

08 p1275 A71-21269

Carbon dioxide flow vacuum condensation on cryogenic pump surface, noting flow temperature and directivity effects on condensation rate

09 p1544 A71-22268

Kinetic theory of transient condensation and evaporation at plane surface, using Maxwell moment formulation

09 p1545 A71-22852

Mafic silicates condensation in primordial solar nebula, explaining meteoritic abundance patterns by two component elemental volatility model and trace element distribution

09 p1521 A71-22932

Ar condensation onset location in supersonic nozzles for nuclear space propulsion systems, using supercooled vapor pressure measurements beyond saturation point

10 p1593 A71-24328

Nozzle area rated two component flow properties, combining integrated solution equations into single transcendental equation for equilibrium condensation

10 p1550 A71-24336

Plane stationary shock wave propagation through one component vapor-liquid mixture, calculating profile and mixture parameters under evaporation and condensation

10 p1593 A71-24348

Reassessment of Cotter model startup in Li heat pipe, modifying model by moving sonic point to end of hot zone and including wall friction and condensation

11 p1715 A71-25914

Laboratory approach to circumstellar mineral condensation, demonstrating fractional condensation

15 p2486 A71-31989

Cesium vapor diffusion condensations from laminar argon flows in tubes and turbulent movement on banks, considering boundary layer mist formation effect

17 p2785 A71-34206

Exit stream velocity increase in propulsion units by adding latent heat of vaporization by condensation in supersonic nozzle

17 p2728 A71-34882

Method of characteristics application to supersonic jet and nozzle gas flow with allowance for equilibrium and nonequilibrium condensation

17 p2673 A71-35636

Rotating disk flow system for Fe vaporizing into cold Ar atmosphere, investigating effect of condensation in boundary layer on mass transfer

19 p3162 A71-37727

Cloud condensation nuclei supersaturation spectrum and aerosol particle concentration variations with height

19 p3092 A71-38683

Theoretical model for initial stage of cloud condensation developing at constant air cooling rate

19 p3092 A71-38684

Dissolved and mixed water vapor condensation aerosol nuclei thermodynamic properties from aircraft and ground-based cloud measurement data

19 p3092 A71-38686

Spatially periodic inhibition of gold vapor condensation by intense optical standing wave using Q switched laser radiation

20 p3245 A71-39403

Hypersonic wind tunnel air condensation detection by light scattering instrumentation, discussing stagnation temperature condensation

21 p3364 A71-40405

Hg condensation characteristics on Cs substrate in high velocity nitrogen carrier gas, formulating one dimensional flow model based on two phase three component gas dynamics

22 p3620 A71-41876

Liquid metal MHD cycles for spacecraft power supply systems, proposing counterflow condensation at nozzle outlet

22 p3574 A71-42431

CONDENSATION PUMPS

Liquid-vapor interactions in constant area steam-water condensing ejector mixing section, measuring axial static and stagnation pressure profiles

[ASME PAPER 71-FE-21]

13 p2032 A71-29459

Gas removal from system by condensation onto cold surface /cryopumping/, noting pumping speed, ultimate pressure and applications

20 p3270 A71-39248

Ultrahigh vacuum by condensate pump, defining vacuum level by mass spectrometric determination of residual gas content

23 p3661 A71-43271

Hydrogen evacuation with He condensation pump in ultrahigh vacuum region

23 p3661 A71-43272

Magnetron manometer calibration to .001 picotorr for hydrogen, using condensate pump

23 p3674 A71-43273

CONDENSATION TRAILS

U CONTRAILS

CONDENSER RADIATORS

U CONDENSERS [LIQUIFIERS]

U HEAT RADIATORS

CONDENSERS

Electrodynamic plasma accelerator with single phase salient pole magnetoelectric generator and storage condenser, giving component characteristics and transient processes equations systems

04 p0535 A71-15812

Plane grid condenser movement through magnetized plasma, calculating resistance by quasi-hydrodynamic approximation for plasma dielectric tensor

06 p0936 A71-17731

Step voltage generator design based on periodic release of prespecified charge fractions by storage condenser using dosing capacitor

18 p2893 A71-36624

Radiation condenser computer program generalization to include effective radiative steady state node multiple enclosure simplification shield for thermal analysis optimization

20 p3314 A71-39357

CONDENSERS [LIQUIFIERS]

Multitube condensers of various geometries, investigating tube flow stability, distribution and gravitational effects

04 p0688 A71-15538

CONDENSING

NT FILM CONDENSATION

Liquid-phase nucleus condensation of supersaturated vapor in drawer, using statistical method

01 p0180 A71-11089

Kinetic equations of quasi-steady homogeneous condensation of water vapor in supersonic nozzle two phase flow

01 p0182 A71-11443

Acoustic attenuation in condensing vapor, using continuumlike formulation allowing for phase exchange process

01 p0182 A71-11470

CONDITIONED RESPONSES

U CONDITIONING [LEARNING]

CONDITIONING [LEARNING]

Conditioned reflexes in cats with mesencephalic reticular formation subject to food-signaling acoustic stimulation

01 p0007 A71-10034

Interhemispherical synthesis of conditioned reflex motor reactions at different running angles in mice

01 p0011 A71-11051

Temporary connection of neurons in visual and associative cortical regions of hemispheres in cats

01 p0012 A71-11053

Cortical vestibular projection zones in formation of conditioned reflexes and spatial orientation of cats

01 p0012 A71-11054

Behaviorally induced hypertension in squirrel monkey following conditioned key-pressing response schedules

01 p0015 A71-11330

Human behavior during machine control learning, modeling habit development as automatic control system

03 p0368 A71-12997

High intensity sonic boom effects on heart rate of dogs, noting conditioning benefit

03 p0358 A71-13097

Visual pattern perception learning, recognition upon subsequent encountering and unfavorable conditions

05 p0716 A71-17243

Relevant cue placement effects in concept identification tasks employing enforced verbal encoding

07 p0148 A71-19514

Human conditioned reflexes to time and EEG responses under acute hypoxia

08 p1243 A71-21970

Globus pallidus damage in cats, investigating effects on conditioned motor reflexes, learning and memory

10 p1564 A71-24466

Rhesus monkeys concurrent avoidance and appetitive behavior patterns with counter discontinuities in shock proximity indicator tests

10 p1573 A71-25136

Conditioned reflexes developed by prolonged training in two genetic strains of mice during adaptation to altitude hypoxia

15 p2356 A71-31248

Conditioned auditory reflex behavior in rats under influence of acceleration, noting ontogenetic effects

15 p2356 A71-31249

Sense organs conditioned reflex and physiology, investigating mechanisms and functional localization of discrimination function and differentiating inhibition

15 p2360 A71-32529

Radio telemetry stimulator for conditioning large animals by applying high voltage short duration pulses to skin surface

16 p2534 A71-33050

Higher nervous activity physiology, discussing induction, protective and conditioned inhibition mechanisms in cerebrum and electrophysiological indices

17 p2684 A71-35359

Direct and reverse conditioned connections including defense reflexes, response to indifferent stimuli and electrophysiological manifestations

17 p2685 A71-35360

Bioelectrical aspects of conditioned reflex activity, discussing changes in cortex background, cortical and cerebral biopotentials and alpha-rhythm depression reactions

17 p2685 A71-35362

Physicochemical aspects of conditioned reflexes, including membrane mechanisms, effectiveness of synapses, mediation processes, ribonucleotides function and subcellular structures dynamics

17 p2685 A71-35364

Conditioned reflex activity, demonstrating development of individual signals systems interrelation

17 p2685 A71-35365

Stimulus control during conditional discrimination development at various training stages, using two key situation and two visual dimensions

17 p2686 A71-35499

Conditioned motor reactions characterizing higher nervous activity, using logokinetic method

19 p3006 A71-37447

Instrumental learning of cardiovascular and visceral responses and behavioral, physiological and biochemical consequences in relation to psychosomatic therapy

20 p3190 A71-39548

Incentive goal and extensive stimulation experience effects on proportion increase of hypothalamic electrode sites yielding elicited eating and drinking behavior

21 p3336 A71-40706

Auditory stimulus conditioning of human skin resistance responses on escape-avoidance schedule

22 p3497 A71-42862

CONDITIONS

NT ADIABATIC CONDITIONS

NT CHRONIC CONDITIONS

NT FLIGHT CONDITIONS

NT KUTTA-JOUKOWSKI CONDITION

NT LIPSCHITZ CONDITION

NT NONEQUILIBRIUM CONDITIONS

NT RUNWAY CONDITIONS

CONDUCTING FLUIDS

Steady supersonic conducting gas flow in channel with nonconducting walls, calculating electric and gas dynamic parameters for different imposed magnetic field geometries

01 p0133 A71-10791

One dimensional motion of unsteady incompressible conducting free jet in transverse magnetic field, noting computer solution by characteristics method

01 p0133 A71-10792

Self gravitating fluid spheroid oscillations in hydrostatic equilibrium with magnetic fields using variational principle

01 p0129 A71-11336

Supersonic electrically conducting gas flow in flat channel with dielectric walls in inhomogeneous magnetic field

02 p0289 A71-11926

Plane and cylindrical MHD wave propagation in conducting compressible fluid under Hall effect, examining flow perturbation

02 p0291 A71-12533

Mean and pulsation characteristics of velocity and temperature in turbulent conducting jets under longitudinal and transverse magnetic fields

02 p0292 A71-12626

Inviscid ideally conducting fluid flow past thin foil in transverse magnetic field, using small parameter method

02 p0186 A71-12629

Mercury droplet dynamics in conducting liquid within electromagnetic field under reduced gravitation

02 p0293 A71-12631

Uniform magnetic field effects on electroconducting fluids turbulent flow and heat transfer characteristics

02 p0293 A71-12649

Conducting fluids Rayleigh-Taylor instability in vertical magnetic field, taking into account Hall currents

03 p0463 A71-13473

Unsteady MHD forced flow of viscous incompressible electrically conducting fluid against rotating disk

03 p0459 A71-13902

Varying electrical resistivity incompressible fluid flow with Hall effect in presence of thin airfoil

03 p0343 A71-13903

Viscous incompressible conducting fluid steady flow in rectangular channel under normal external magnetic field

03 p0466 A71-14554

Conducting fluid flow in rectangular channel with electrodes under longitudinal magnetic field

03 p0466 A71-14555

Viscous incompressible conducting fluid steady laminar flow in rectangular channel with two insulating and two arbitrarily conducting walls under external magnetic field

03 p0466 A71-14556

MHD conducting lubricant composite slider bearing in transverse magnetic field, calculating conductivity effect on load capacity

04 p0602 A71-14801

Input resistance and effective height of gap excited metallic and dielectric antennas in conductive environment

04 p0558 A71-15220

Conducting and ferromagnetic liquids thermoelectroconvective waves, considering disturbance propagation process in equilibrium state with constant entropy gradient

04 p0628 A71-15809

Hydrodynamic stability of viscous conducting fluid plane Couette-Poiseuille flow in transverse magnetic field by linear theory, considering complete spectrum of small disturbances

07 p1169 A71-19727

Unsteady viscous incompressible electrically conducting fluid flow past accelerated conductor or insulator flat plate in uniform transverse magnetic field

07 p1169 A71-20022

Pressure shocks propagation through electrically and thermally conducting viscous gas in presence of uniform magnetic field

07 p1169 A71-20025

Viscous conducting fluid MHD fluctuating flow over porous flat plate with time dependent suction, determining skin friction and transient velocity profiles

07 p1169 A71-20028

Plane steady state MHD shock wave structure in infinitely conducting fluid under magnetic field perpendicular to shock velocity, introducing quadratic artificial viscosity factor

07 p1174 A71-20616

Nonlinear MHD equations solution for laminar flow of electrically conducting fluid in cylindrical channel in traveling magnetic field

09 p1499 A71-22191

MHD equations for charged conducting fluid behavior in first postNewtonian approximation to general relativity, obtaining conservation laws

09 p1518 A71-22339

Conducting fluid in transverse magnetic field at low Reynolds numbers, deriving laminar boundary layer universal equations in Crocco or Mises variables

10 p1648 A71-24028

Pseudo-stationary shock wave in plane MHD flow of conducting gases, deriving existence theorem for linear relations between vorticity and current density

10 p1648 A71-24281

Mixing layer of turbulent flows in homogeneous nonconducting and conducting incompressible fluids, extending approximate solution to flow in longitudinal magnetic field

10 p1593 A71-24366

Induced electrostatic field in forced Hg vortex of ideal viscous electrically conducting fluid under axial magnetic field

10 p1649 A71-24456

Waves generated by obstacle steady motion along axis of uniformly rotating electrically conducting homogeneous fluid, using Lighthill technique

10 p1595 A71-24624

Hydromagnetic flow of conducting viscous incompressible fluid in rotating straight annular pipe under constant pressure gradient

11 p1804 A71-25433

Second order correlation functions of velocity and magnetic field for homogeneous unsteady isotropic hydromagnetic turbulence in incompressible conducting fluid

11 p1805 A71-25599

Optimal control of oscillations of electrically conducting fluid by magnetic field in plane channel with free boundaries, using dynamic programming

13 p2107 A71-28728

Gravitohydromagnetic instability of static and counterstreaming composite systems composed of infinitely conducting fluids, using normal mode analysis

13 p2108 A71-29164

Quasi-one dimensional nonlinear model of electrohydrodynamic stability and control of current carrying seminsulating jets at supercritical and subcritical regimes

13 p2118 A71-29249

Compressible electrically conducting liquid two dimensional steady state laminar flow calculations in MHD duct

13 p2109 A71-29294

Acceleration covariance in turbulent flow of isotropic homogeneous incompressible viscous conducting fluid

13 p2109 A71-29295

Steady flow of electrically conducting incompressible viscous fluid in rotating parallel-plane channel under constant transverse magnetic field

13 p2110 A71-29296

Conducting incompressible liquid in transverse magnetic field, considering plane steady motion of isothermal MHD boundary layer

14 p2278 A71-29604

Ideally conducting compressible liquid flow near arbitrary geometrical thin profile form in transverse magnetic field

14 p2278 A71-29608

Incompressible conducting fluid plane jet expansion in homogeneous slipstream, deriving partial differential equations for nonconduction approximation

14 p2278 A71-29610

Horizontal conducting fluid cylinder ultrasonic oscillations in crossed electric and magnetic fields, obtaining boundary value problem

14 p2278 A71-29614

Group-invariant properties of boundary layer flow differential equation for electrically conducting liquid in magnetic field

14 p2279 A71-29629

Gravitational instability of heat conducting compressible fluid relative to class of axisymmetric perturbations, considering viscosity, magnetic field and uniform rotation

14 p2226 A71-30397

Vertical magnetic field and Coriolis forces effect on equilibrium of heavy viscous incompressible infinitely conducting rotating fluid

15 p2453 A71-31183

Plane and cylindrical waves three dimensional propagation, investigating finite electrical fluid conductivity and radiation effects in MGD

16 p2618 A71-33172

Velocity and magnetic field equations of electroconductive fluid vortex motion due to annular receptacle insulating walls rotation

16 p2620 A71-34057

Boundary shock waves in electrically conducting gas under magnetic field, deriving Rankine-Hugoniot jump relations analogs and Prandtl relation

16 p2560 A71-34128

Thin elastic shallow cylindrical panel in steady conducting supersonic gas flow, detailing magnetic field effects on static and dynamic stability and flutter

17 p2816 A71-34326

Perturbed two dimensional laminar boundary layers of incompressible conducting fluid flow along insulated concave wall in transverse magnetic field, investigating three dimensional instability

17 p2788 A71-34642

Transverse magnetic field influence on heat transfer of conductive fluid/mercury in electrically insulated pipe subjected to uniform heat flux

17 p2788 A71-34660

Thermoelectric materials thermodynamic properties, developing coldness as universal function of viscous heat conducting fluids

17 p2837 A71-34694

Partial differential equations governing second order correlation functions for velocity and magnetic field in isotropic conducting turbulent flow

17 p2789 A71-35443

Nonuniform self propagation of cylindrical imploding shock waves in electrically conducting gas

18 p2951 A71-36005

Steady inviscid fluid flows in plane channel and in axially symmetric nozzle, considering external magnetic field effects with electroconductive fluid

18 p2907 A71-36327

MHD equations of motion solved for conducting fluid interaction with electromagnetic field in porous media in range of Darcy law

18 p2953 A71-36948

Viscous incompressible conducting fluid at constant flow rate under magnetic field variation, investigating laminar unsteady MHD Couette flow problem with approximate solution

19 p3108 A71-37092

Ideally conducting magnetostatic equilibria and associated time dependent resistive flows from two dimensional solution for MHD equations

19 p3115 A71-38211

Uniformly moving homogeneous isotropic non-dispersive conducting medium with arbitrarily distributed electromagnetic radiation sources, deriving solution in four dimensional covariant form

20 p3196 A71-39083

Magnetosphere neutral layer plasma conductivity determination from model of linear magnetic dipole in conducting fluid flow

20 p3216 A71-39138

MHD power generator for converting heat into electricity by interacting magnetic field with flowing electrically conducting fluid

21 p3436 A71-40020

Magnetic field stabilizing effect on free shear layer of electrically conducting fluid at small Reynolds number

21 p3421 A71-40637

Electrically conducting fluid flow resistance in plane insulated channel in presence of transverse magnetic field, determining pressure, velocity and electric potential distributions

21 p3422 A71-40677

Hydrodynamic stability of incompressible conducting fluid flow between two moving linearly and rotating coaxial cylinders in longitudinal magnetic field

21 p3367 A71-40688

Insulating circular cylinder steady axial motion in conducting fluid permeated by uniform transverse magnetic field, determining flow along cylinder at field tangency points

22 p3583 A71-42198

Electrification induced instabilities, breakup and drop size of charged cylindrical liquid jets, using small perturbation method

23 p3663 A71-43445

Plane vortex sheet in inviscid incompressible finitely conducting fluid under uniform magnetic field, considering hydromagnetic stability

23 p3663 A71-43490

Stability of dissipative shear flow of inviscid incompressible electrically conductive fluid in presence of magnetic field, deriving instability modes phase velocity limiting conditions from MHD equations

24 p3855 A71-44645

CONDUCTING MEDIA

U CONDUCTORS

CONDUCTION BANDS

Electron states in highly doped semiconductors, describing energies in conduction and forbidden bands

02 p0297 A71-12616

One conduction band semiconductor surface drift waves in presence of current carrier drift

05 p0794 A71-16836

Thermal suppression of photoconductivity in crystals with two impurity types, showing carrier concentration decrease in conduction band in narrow temperature range

13 p2112 A71-28924

Thermal suppression of photoconductivity in crystals with two impurity types, showing carrier concentration decrease in conduction band in narrow temperature range

21 p3434 A71-41320

Illumination effects on drain current for p channel enhancement type MOS transistor, attributing photoresponse to electron excitation in conduction band

22 p3523 A71-42481

CONDUCTION ELECTRONS

Sasaki effect in doped semiconductors at low temperatures concerning conduction anisotropy and intervalley impurity electron scattering

01 p0139 A71-10777

Submillimeter wave oscillations possibility by Bloch oscillation of conduction electrons in ideal crystal with periodic energy band structure

08 p1343 A71-21280

Variances and covariances calculation for fluctuating numbers of semiconductor conduction electrons in terms of noise

14 p2211 A71-30292

Crystal lattice drag by conduction electrons and Onsager relationship between electroacoustic coefficients valid for arbitrary topology of Fermi surface

21 p3428 A71-41127

Auroral charged particle fluxes electrodynamic interaction with atmosphere, determining ion formation rate and electron concentration and conductivity

24 p3866 A71-45032

CONDUCTIVE HEAT TRANSFER

Heat conduction effect on propagation of laser radiation absorption shock wave

01 p0092 A71-10068

Heat conductivity equations for thermal stresses of thin cylindrically anisotropic plates made of reinforced laminar plastics

01 p0169 A71-10499

Nonlinear heat conduction problems, applying finite difference equation stability

01 p0179 A71-10616

Heat conduction approximate averaging equation, determining mean unstationary temperature of arbitrary nuclear fuel element

01 p0179 A71-10617

Ultrasonic sound velocity dispersion in various hydro and gas suspensions, considering viscosity and heat conduction effects

01 p0127 A71-10618

Transient heat conduction of solids obeying Fourier law, deriving numerical solution for boundary value problem by Laplace transformation

01 p0180 A71-10937

Three dimensional ablation calculated for reentry sphere-cone taking into account shape changes and internal heat conduction
[AIAA PAPER 70-199] 01 p0180 A71-10952

Shear wave propagation into heat conducting viscoelastic fluids, considering steady one dimensional flow stability 01 p0181 A71-11188

Unsteady heat conduction in multilayer body of revolution with convective heat transfer on curvilinear surfaces, considering radiation on inner surface 02 p0330 A71-11730

Thermoelastic axisymmetric problem for half space applied to steady temperature field and stress concentration in infinite body with heat conducting plane circular crack 02 p0322 A71-11733

Nonlinear heat conduction of contacting bars with boundary conditions of fourth kind, using small parameter method 02 p0332 A71-12529

Cylindrical wall with variable heat conductivity coefficient, solving temperature distribution by asymptotic method 02 p0333 A71-12540

Temperature distribution in heat conducting cylindrical laser rod at large pumping pulse repetition rates 03 p0435 A71-13512

Cylindrical sample longitudinally isothermal zone unsteady temperature field calculation from heat conduction equation with allowance for temperature dependence of thermodynamic properties 03 p0520 A71-13960

Two dimensional annular flow of viscous heat conducting gas between coaxial cylinders, using Navier-Stokes equations 03 p0401 A71-14066

Free convection in compressible viscous heat conducting fluid, determining parameters leading to onset 03 p0521 A71-14233

Transient heat conduction in dual-layer insulated plate exposed to pulse heating, discussing temperature response [AIAA PAPER 70-14] 03 p0522 A71-14439

Heat conduction equation for thermal diffusivity measurements by flash method in two layer composites 04 p0595 A71-14965

Heat transfer - Conference, Versailles, August-September 1970, Volume 1, Conduction and heat exchangers 04 p0677 A71-15451

One dimensional transient heat conduction analysis by iterative isotherm migration method, discussing boundary conditions, stability, truncation error and relative efficiency 04 p0677 A71-15452

Steady heat conduction with generation, discussing boundary value problem transformation by change of variables 04 p0677 A71-15453

Heated jet injection into isothermal turbulent boundary layer, investigating temperature distribution downstream with conduction model 04 p0572 A71-15499

MHD channel flow with axial conduction and third kind boundary condition, investigating thermal entry region heat transfer 04 p0684 A71-15506

Thermal radiation-conduction interaction in horizontal fluid layer, obtaining temperature profiles with Mach-Zehnder interferometer 04 p0685 A71-15515

Laminar turbulent tube flow heat transfer, investigating internal radiation exchange and wall heat conduction and generation effects 04 p0685 A71-15519

Turbulent mixing at homogeneous wakes boundary, using heat conduction theory equivalence 04 p0578 A71-15628

Heat conduction three dimensional problem in radiation heated thin crystalline plates with temperature dependent thermophysical characteristics 05 p0831 A71-16184

Compression waves produced in viscous heat conducting gas by impulsive one dimensional piston start and by wall temperature change 05 p0831 A71-16477

Variational principle for generalized theory of heat conduction with finite wave speed, reducing nonlinear boundary value problem to ordinary differential equation 05 p0837 A71-16567

Unsteady heat conductivity problems with nonlinear boundary conditions, using perturbation method 05 p0838 A71-16782

Phonon distribution function kinetic equation solution, determining two dimensional lattice heat conductivity 05 p0794 A71-16876

Elastic plate with heat conducting rectilinear crack, determining steady state temperature field and stresses 05 p0827 A71-16889

Hyperbolic heat conduction equation with small relaxation time parameter, studying convergence for Cauchy and boundary value problem 05 p0839 A71-17035

Homogeneous rod heat transfer inverse problem, considering temperature distribution determination 06 p1005 A71-17325

Nonlinear unsteady heat conduction problems, investigating thermophysical property dependence on temperature and body coordinates by half space and approximate methods 06 p1006 A71-17749

Unsteady heat conduction in thermally coupled spherical regions, discussing duration, penetration depth and temperature histories 06 p1006 A71-18071

Laminar flow heat transfer in circular pipes, including longitudinal conduction term in Graetz problem 06 p1007 A71-18305

Laminar flow heat transfer between plane parallel plates under generalized Graetz conditions, retaining longitudinal conduction term 06 p1007 A71-18306

Unsteady heat conduction due to radiative energy transfer in dispersed powders, hydrosols and aerosols 06 p1009 A71-18729

Heat transfer by radiation, convection and molecular thermal conductivity in gray absorbing medium flat layer bounded by parallel diffusively radiating planes 07 p1219 A71-18757

One dimensional nonstationary temperature field in solid body with linearly related heat conductivity and capacity 07 p1221 A71-18921

Conductive heat transfer with nonlinear boundary condition, reducing to linear boundary value problem through variational principle 07 p1224 A71-19902

Normal shock wave stability in perfect gas with viscosity and heat conduction under arbitrary small one dimensional disturbances, formulating eigenvalue problem 07 p1224 A71-20288

Thermal conductivity coefficients of heat conducting pastes in transistor application 08 p1318 A71-20845

Three dimensional nonlinear heat conduction problem solving by perturbation theory and finite integral transform 08 p1377 A71-21927

Variational approaches to steady state heat conduction, discussing relationship between variational and differential problems 09 p1545 A71-22453

Contact heat conduction boundary value problems, applying parabolic potentials method to Volterra singular integral equation systems 09 p1545 A71-22876

Steady one dimensional temperature field of cylindrical shell spacecraft, allowing for heat conduction and convective and radiative heat transfer within shell 09 p1546 A71-23148

Heat conduction effect on propagation of laser radiation absorption shock wave 09 p1464 A71-23263

Heat conduction differential equation boundary value problem, obtaining closed solution to Cauchy problem in integral form with finite limits by reflection method 09 p1547 A71-23435

Boiling of relativistic heat conducting fluid in normal space-time manifold for nonstrict hyperbolic system, using Eckart scheme 10 p1694 A71-23831

Global monsoon atmospheric response model in geostrophic terms for heating input function parameterization, including Himalayas mountains effects 10 p1638 A71-23966

Thin isotropic plates with time and temperature dependent surface heat exchange coefficients, presenting heat conduction equations 10 p1695 A71-24361

Soviet papers on heat and mass transfer covering conduction, transport in capillary and dispersed systems, irreversible thermodynamics, material drying, etc 10 p1696 A71-24481

Quiet solar wind two component model, including viscosity, magnetic field and reduced heat conduction 10 p1662 A71-24498

Asymptotic stability of rapidly rotating horizontally bounded fluid heated from below, considering conductive state and Ekman layers 10 p1595 A71-24618

Solar wind heat conduction evaluation by electron energy equation dimensional analysis 10 p1663 A71-24778

Solids evaporation into vacuum, considering interconnected problems of heat conduction and evaporation front boundary conditions 10 p1697 A71-25063

Optimum one term series solution for multidimensional heat conduction problem with initial profiles 10 p1698 A71-25086

One dimensional heat conduction with freezing or melting in bodies with variable cross sectional areas, using phase boundary rate of propagation equations 10 p1698 A71-25099

Axisymmetric ablating graphite nosetip analysis code, demonstrating shape change, heating distribution and internal conduction coupling [AIAA PAPER 71-413] 11 p1856 A71-26206

Variable conductance heat pipes feedback mechanisms for spacecraft electrical temperature control system design, using steady state analysis based performance model [AIAA PAPER 71-421] 11 p1857 A71-26212

Variable conductance inert gas type heat pipe for spacecraft electronic equipment fine temperature control, noting design to eliminate start-up problems [AIAA PAPER 71-422] 11 p1857 A71-26213

Uniformly and nonuniformly spaced circular cylinders contacting two planes, calculating conductive heat transfer coefficient under vacuum conditions [AIAA PAPER 71-436] 11 p1858 A71-26224

Spacecraft radiator thermal scale model, using forced convection, conduction and radiation heat transfer 11 p1860 A71-26517

Heat conduction effects on small amplitude plane harmonic wave propagation in transversely isotropic elastic Zn single crystals 12 p1985 A71-26925

Nonlinear heat conduction problems, obtaining boundary conditions with approximate method 12 p1987 A71-27664

Pyrolytic graphite heat conductivity coefficients in direction perpendicular to deposition surface at high temperatures 13 p2090 A71-27883

Temperature, concentration and heat conductivity profiles of chemically reacting gas mixtures with thermal gradient, using classical transfer equations 13 p2025 A71-27884

Modified heat conductivity solutions for region with moving boundary, applying to crystallization front or crack propagation 13 p2159 A71-28037

Approximate determination of first characteristic root of equation for plate, hollow sphere and hollow cylinder, using variational method for heat conduction problem 13 p2159 A71-28184

Combined conductive and radiative heat transfer in absorbing and scattering materials, using two-flux model for transport and local energy balance equations solution 13 p2164 A71-28983

Heat conduction role in leading edge heating of wing in hypersonic flight, using conducting plate theory 13 p2165 A71-29282

Stellar wind flow models associating energy transport with propagation and dissipation of hydrodynamic waves and heat conduction 14 p2297 A71-29586

Static strain measurements on Ti specimen subjected to different conductive heating rates, testing various gages 14 p2239 A71-29833

German monograph on network method application for conductive and radiative energy transfer coupling problems 14 p2336 A71-30231

Two dimensional unsteady heat conduction in solid with subliming surface, replacing original boundary value problem by ordinary integrodifferential equation 14 p2338 A71-30933

Perturbation method for solving nonstationary heat conduction problems with nonlinear boundary conditions 16 p2662 A71-33034

Nonlinear unsteady heat conduction problems, investigating thermophysical property dependence on temperature and body coordinates by half space and approximate methods 17 p2838 A71-35115

Three dimensional nonlinear heat conduction problem solving by perturbation theory and finite integral transformation method 17 p2838 A71-35271

Solar-type dwarf star rotation effect on stellar wind structure and thermal regime, obtaining time independent solutions with heat conduction 17 p2796 A71-35577

General Stefan problem for heat conduction with melting and free boundary problems occurring in control and statistical decision theories 17 p2841 A71-35794

Asymptotic solution of nonlinear Volterra integral equation, examining nonlinear heat conduction and boundary layer heat transfer 18 p2942 A71-36747

Convective and conductive heat loss analysis of underwater swimmers and divers exercising in cold water 18 p2861 A71-36892

Supersonic spherical viscous heat conducting gas discharge into vacuum, solving Navier-Stokes equations by buildup method

19 p3042 A71-37087

Turbulent boundary layer jet flow calculation using equivalent heat conduction theory

19 p3161 A71-37128

Small parameter method application to quasi-linear problems solution in nonstationary heat conduction with substantial nonlinearities and weak perturbation, analyzing error

19 p3162 A71-37584

Transient simultaneous conductive and radiative heat transfer in plane gray layer bounded by black walls, yielding nonlinear integrodifferential equation [ASME PAPER 71-HT-22]

19 p3165 A71-37993

Variable thermal conductance wall based on working fluid evaporation and condensation [ASME PAPER 71-HT-39]

19 p3166 A71-38001

Convergence estimation of locally one dimensional scheme for multidimensional heat conduction boundary value problem solution on nonuniform grids using maximum principle

19 p3171 A71-38415

Heat conduction equation coupling to wave equation in adjacent regions from operational method solution of Volterra equation reduced problem

19 p3171 A71-38532

Initial viscous heat conducting gas dynamic state one dimensional decay problem solution, using kinetic theory with Boltzmann equation

19 p3046 A71-38541

Shuttle convective heat transfer involving similar axial temperature gradients in piston and cylinder, calculating interaction with wall conduction by finite difference computer program

20 p3312 A71-39281

One phase Stefan problem for unidimensional heat conduction in plane infinite slab of thermally isotropic material with prescribed flux on fixed boundary

21 p3474 A71-40210

Radiative-conductive heat transfer systems optimum thermal design, using nonlinear programming with mathematical model based on nodal analysis [ASME PAPER 71-VIBR-120]

21 p3474 A71-40339

Thermal stresses in infinite elastic plate with circular hole and single heat source, considering steady state heat conduction

21 p3464 A71-40753

Solar wind theory, discussing thermal conduction and MHD wave energy supply mechanisms of large scale solar corona expansion

21 p3439 A71-41183

Conductive and radiative axial heat transfer in packed/stagnant beds at 20-750 C, giving temperature profiles

22 p3620 A71-41877

Combined radiative and conductive heat transfer prediction in semitransparent solids by Taylor series expansion, defining radiative conductivity

22 p3620 A71-41883

Bounded plasma ionization instability inhomogeneity scale evaluation, assuming negligible electron energy losses due to heat conduction as compared to elastic losses

23 p3712 A71-43923

Nonsteady heat conduction of multilayer cylindrical and conical shells in periodic radiation flux, calculating temperature distribution

23 p3783 A71-44067

Heat conduction of rarefied air and argon in annuli between coaxial cylinders

23 p3783 A71-44068

Composite materials thermal diffusivity at high temperatures by quasi-stationary and monotonic methods, determining validity domain of differential heat conduction equation without heat sources

24 p3889 A71-44967

Conductive heat transfer and temperature jump in polyatomic gas between parallel plates evaluated by variational principle based on linearized integro-differential equation

24 p3889 A71-44969

Two dimensional stationary temperature fields calculation for temperature independent heat conduction

24 p3890 A71-45068

Solid fuel combustion in presence of unsteady heat propagation in heated layer, solving fuel heat conduction equation for sudden combustion rate change

24 p3891 A71-45218

CONDUCTIVITY

Erythrocytometric curve analysis by conductometric granulometric method

06 p0863 A71-18692

Nonhomogeneous arbitrarily formed semiconductor layers, using Van der Pauw method for measuring conductivity and Hall mobility

07 p1175 A71-19221

Conductivity in microwave Permalloy thin films without external magnetic field comparing Fuchs-Sondheimer theory

10 p1656 A71-24213

GaAs single crystals conductivity and surface capacitance under transverse electric field at low temperatures

10 p1657 A71-24322

Nonuniform conductivity effect on cosmic magnetic fields structure with zero Lorentz force, using Maxwell equations and Ohm law

14 p2274 A71-29982

CONDUCTORS

NT AIRCRAFT ANTENNAS

NT ANTENNAS

NT BUS CONDUCTORS

NT CASSEGRAIN ANTENNAS

NT DIPOLE ANTENNAS

NT DIRECTIONAL ANTENNAS

NT ELECTRIC CONDUCTORS

NT ELECTRIC WIRE

NT ELECTROLYTES

NT EXPLODING WIRES

NT HELICAL ANTENNAS

NT HORN ANTENNAS

NT ION EXCHANGE MEMBRANE ELECTROLYTES

NT LENS ANTENNAS

NT LOG PERIODIC ANTENNAS

NT LOG SPIRAL ANTENNAS

NT LOOP ANTENNAS

NT MICROWAVE ANTENNAS

NT MISSILE ANTENNAS

NT MONOPOLE ANTENNAS

NT MONOPULSE ANTENNAS

NT MULTIPLE BEAM INTERVAL SCANNERS

NT OMNIDIRECTIONAL ANTENNAS

NT PARABOLIC ANTENNAS

NT PHOTOCONDUCTORS

NT RADAR ANTENNAS

NT RADIO ANTENNAS

NT RHOMBIC ANTENNAS

NT SLOT ANTENNAS

NT SPIRAL ANTENNAS

NT STEERABLE ANTENNAS

NT SUPERCONDUCTORS

NT THERMAL CONDUCTORS

NT TURNSTILE ANTENNAS

NT TWO REFLECTOR ANTENNAS

NT WAVEGUIDE ANTENNAS

NT YAGI ANTENNAS

Moving magnetic field lines identification, applying to moving nonrigid conductor

08 p1283 A71-21648

Charged conductors in homogeneous collisionless magnetoactive plasma at hybrid frequencies, investigating antenna array quasi-electrostatic field one dimensional structure

10 p1582 A71-23809

Isolated symmetrical cylindrical dipole antennas in homogeneous conducting media

12 p1880 A71-27153

Harmonic electromagnetic field outside closed surface perfectly conducting antenna, using Kirchhoff formula

16 p2544 A71-34171

Arbitrary cross sectional semiinfinite conductor, investigating electromagnetic wave diffraction

17 p2701 A71-34754

Slot antennas electromagnetic radiation patterns in conducting ground plane coated with moving isotropic cold plasma sheath

17 p2701 A71-34758

Kinematic-dynamo equations for stationary unsheared conducting nonrotating sphere dynamo action in isotropic velocity turbulence

18 p2969 A71-37046

Ideally conducting and dielectric coaxial bodies of revolution, investigating joint excitation by TM wave

22 p3522 A71-42304

CONES

NT ABLATIVE NOSE CONES

NT CIRCULAR CONES

NT CONICAL BODIES

NT NOSE CONES

NT ROCKET NOSE CONES

NT SLENDER CONES

Supersonic overexpanded jet flow past cone, determining impingement point by method of characteristics

01 p0002 A71-10613

Axissymmetric mixed boundary problem for elastic infinite cone, obtaining solution by assuming zero shearing stresses

03 p0513 A71-14234

Coaxial cone antenna transient response to incident field along ground plane, using signal generated as step function in time

06 p0875 A71-17717

Supersonic axisymmetric wake-like and two dimensional shear nonuniform free stream flows effects on inviscid flow fields and aerodynamic coefficients of sharp and spherically blunted cones [AIAA PAPER 71-51]

06 p0843 A71-18512

Hypersonic flow over cones with attached and detached shock waves, using Lax differencing technique and time dependent formulation for reentry flow fields [AIAA PAPER 71-55]

06 p0846 A71-18655

Viscosity effects on three dimensional supersonic flow around circular half cones on flat plate, examining turbulent boundary layer separation

07 p1014 A71-19743

Cone roll dynamics-ablation patterns coupling in hypersonic wind tunnels [AIAA PAPER 70-562]

07 p1208 A71-19868

Large angle cones supersonic aerodynamic and wake characteristics at low Reynolds numbers, including model support interference effects [AIAA PAPER 71-264]

08 p1228 A71-21990

German monograph on spatial elasticity problems solution by multidimensional Fourier transformation covering stress concentration on hollow and solid cones for given load distribution

15 p2509 A71-32300

Holographic interferometry measurements of mean and localized fluctuating wake density field of cones fired at Mach 6 at ballistic range, using pulsed laser [AIAA PAPER 71-564]

16 p2520 A71-33105

Ray trace equations for conic surfaces, noting application in computer programs for unusual systems

17 p2768 A71-35592

Lame equation perturbation solution and applications to problems involving elliptic cones or infinite sectors

20 p3177 A71-39497

Circular conical diffuser inlet velocity profile effect on efficiency, presenting experimental results for different cone angles and expansion ratios

20 p3177 A71-39799

Aperture field and radiation pattern of conical horns with large flare angles, using vector diffraction formula

23 p3654 A71-44166

CONFERENCES

Flight training simulators - Conference, London, October 1970

01 p0065 A71-10012

Structural stability at low temperatures - Conference, Kiev, February 1970

01 p0097 A71-10076

High fatigue resistance in metals and alloys - Conference, Atlantic City, July 1969

01 p0098 A71-10161

Information processing - Conference, Las Vegas, November 1969

01 p0041 A71-10176

Ultrasonics for industry - Conference, London, October 1970

01 p0086 A71-10301

Stellar atmospheric physics - Conference, University of Queensland, Brisbane, Australia, May 1970

01 p0152 A71-10326

Celestial mechanics - Conference, Oberwolfach, West Germany, October 1970, Volume 2

01 p0153 A71-10376

Role of man in navigation - Conference, Colorado Springs, July 1970

01 p0122 A71-10501

Radar meteorology - Conference, Tucson, November 1970

01 p0113 A71-10551

Reinforced plastics - Conference, Freudenstadt, West Germany, October 1970

01 p0108 A71-10688

Automatic control systems invariance theory - Conference, Kiev, May-June 1966, Volume 1

01 p0059 A71-10701

Electronic components - IEEE-EIA Conference, Washington, D.C., May 1970

01 p0053 A71-10731

Pre-main sequence stellar evolution - Conference, Liege, Belgium, June-July 1969

01 p0157 A71-10757

Telemetry - Conference, Los Angeles, October 1970

01 p0031 A71-10876

Telemetry - IEEE Conference, Los Angeles, April 1970

01 p0036 A71-10976

Atmosphere global circulation - Conference, London, August 1969

01 p0121 A71-11351

Biological rhythms and space nutrition - COSPAR Conference, Prague, May 1969, Life sciences and space research

01 p0017 A71-11551

Pattern recognition - Conference, New York City, June 1969

02 p0225 A71-11701

Computer simulation - Conference, Denver, June 1970

02 p0225 A71-11777

Computer simulation - Conference, Denver, June 1970

02 p0227 A71-11804

Science studies, prediction and information procurement - Conference, Kiev, December 1967

02 p0334 A71-11851

Medical data acquisition - Conference, Nancy, France, June, 1969

02 p0206 A71-12106

Aircraft pavement design - Conference, London, November 1970

02 p0237 A71-12162

- Thermionic conversion - IEEE Conference, Carmel, October 1969 02 p0191 A71-12201
- Applied mechanics - Conference, Bucharest, June 1969 02 p0284 A71-12401
- Thrombosis and coronary heart disease - Conference, Porvoo, Finland, September 1969 02 p0199 A71-12413
- Skynet - IEE Conference, London, April 1970 02 p0216 A71-12426
- Inertial guidance problems - Conference, Cambridge, Mass., January 1970 02 p0252 A71-12451
- Reinforced plastics - Conference, Brighton, October 1970 02 p0273 A71-12476
- Field-ion, field emission microscopy - Conference, University of Florida, March 1970 02 p0287 A71-12732
- Earth station technology - IEE Conference, London, October 1970 02 p0219 A71-12776
- Niobium - Conference, Paris, October 1969 02 p0268 A71-12926
- Air accident investigation and litigation - Conference, Dallas, March 1970 03 p0522 A71-12961
- Bioelectric control, man and automatic systems - Conference, Yerevan, U.S.S.R., September 1968 03 p0365 A71-12976
- Power sources - Conference, Atlantic City, May 1970 03 p0349 A71-13026
- Biotelemetry - Conference, Erlangen, West Germany, November 1968 03 p0369 A71-13058
- Automatic support systems for advanced maintainability - IEEE Conference, St. Louis, October 1970 03 p0394 A71-13076
- Heterogenous kinetics at elevated temperatures - Conference, Philadelphia, September 1969 03 p0374 A71-13121
- Flow research on blading - Conference, Baden, Switzerland, March 1969 03 p0339 A71-13139
- Physiological effects of noise - Conference, Boston, December 1969 03 p0358 A71-13151
- Heat transfer - ASME/AICHE Conference, Minneapolis, August 1969 03 p0518 A71-13614
- Internal aerodynamics/turbomachinery - Conference, Cambridge University, England, July 1967 03 p0342 A71-13823
- Cosmic ray physics - Conference, Leningrad, October 1969 03 p0473 A71-13832
- Material testing - Conference, Budapest, October 1970, Section 3, Spectrochemical analysis 03 p0375 A71-13968
- Space research on thermosphere H and He properties - COSPAR Conference, Prague, May 1969 03 p0410 A71-14002
- Erosion resistance characterization and determination - ASTM Conference, Atlantic City, June 1969 03 p0443 A71-14284
- Electric circuit theory - IEEE Conference, University of Minneapolis, May 1970 03 p0390 A71-14304
- Decision and control /adaptive processes/ - IEEE Conference, Pennsylvania State University, November 1969 03 p0393 A71-14478
- Ultrafine-grain metals - Conference, Raquette Lake, New York, August 1969 03 p0445 A71-14486
- Fractures - Conference, Marienbad, Czechoslovakia, October 1970, Part 2 03 p0516 A71-14577
- Fractures - Conference, Marienbad, Czechoslovakia, October 1970, Part 3 03 p0433 A71-14584
- Precision electromagnetic measurements - Conference, Boulder, June 1970 04 p0585 A71-14651
- Shock tubes - Conference, University of Toronto, June 1969 04 p0562 A71-14661
- Laser technology - Conference, Rochester, New York, November 1969 04 p0605 A71-14707
- Vestibular function on earth and in space - Conference, Uppsala, May 1968 04 p0536 A71-14751
- Petroleum mechanical engineering and pressure vessels and piping - ASME Conference, Denver, September 1970 04 p0665 A71-14767
- Convective heat and mass transfer - ASME Conference, New York, November-December 1970 04 p0674 A71-14777
- Biomechanical systems dynamic response - ASME Conference, New York, November-December 1970 04 p0652 A71-14785
- Quantum optics - NATO Conference, Musselburgh, Scotland, July 1969 04 p0607 A71-14803
- Space technology and earth problems - AAS Conference, Las Cruces, New Mexico, October 1969 04 p0579 A71-14817
- Astronomical instrument manufacture - Conference, Pulkovo, U.S.S.R., November 1967 04 p0587 A71-14826
- Material testing - Conference, Budapest, October 1970, Metal physics and test methods, Volume 1, Part 1 04 p0665 A71-14876
- Material testing - Conference, Budapest, October 1970, Metal physics and test methods, Volume 2, Part 2 04 p0666 A71-14885
- Thermophysical properties of solids at high temperatures - Conference, Salford, England, July-September 1970, Part I 04 p0594 A71-14953
- Civil aviation safety - Conference, Beirut, September-October 1970 04 p0690 A71-14990
- Maritime and aeronautical technology - Conference, Paris, May 1970 04 p0571 A71-15204
- Space sciences - Conference, Santa Maria, California, October 1970, Part I 04 p0662 A71-15276
- Space sciences future applications for mankind - Conference, Santa Maria, California, October 1970 04 p0553 A71-15316
- Environmental effects on VTOL design - Conference, Arlington, Texas, November 1970 04 p0529 A71-15401
- Heat transfer - Conference, Versailles, August-September 1970, Volume 1, Conduction and heat exchangers 04 p0677 A71-15451
- Heat transfer - Conference, Versailles, August-September 1970, Volume 2, Forced convection 04 p0679 A71-15466
- Heat transfer - Conference, Versailles, August-September 1970, Volume 3, Forced convection and radiation 04 p0681 A71-15484
- Heat transfer - Conference, Versailles, August-September 1970, Volume 4, Natural convection and rheology 04 p0685 A71-15521
- Heat transfer - Conference, Versailles, August-September 1970, Volume 5, Boiling 04 p0686 A71-15526
- Heat transfer - Conference, Versailles, August-September 1970, Volume 6, Boiling and condensation 04 p0687 A71-15533
- Heat transfer - Conference, Versailles, August-September 1970, Volume 7, Combined heat transfer and measuring techniques 04 p0688 A71-15540
- Turbulent flows - Conference, Kiev, June 1967 04 p0573 A71-15601
- Periodic orbits, stability and resonances - Conference, Sao Paulo, Brazil, September 1969 04 p0651 A71-15701
- High alloy weldability evaluation methods - Conference, Philadelphia, April 1969 04 p0616 A71-15906
- Solar cells - IEEE Conference, Seattle, August 1970 05 p0697 A71-16053
- Upper atmosphere electromagnetic probing - Conference, Calcutta, July 1969 05 p0739 A71-16426
- Astronautics and rocket technology history - Conference, Belgrade, September 1967, covering rocket engines, fuels and materials, ramjet engines, control systems, etc 05 p0816 A71-16500
- Gas dynamics of explosions - Conference, Novosibirsk, U.S.S.R., August 1969 05 p0832 A71-16501
- Geoscience electronics - IEEE Conference, Washington, D.C., April 1970 05 p0754 A71-17126
- Aerodynamic noise - Conference, Loughborough, England, September 1970 05 p0783 A71-17152
- Feedback and dynamic control of plasmas - Conference, Princeton, June 1970, Volume 1 06 p0931 A71-17451
- Nonlinear problems numerical solutions - Conference, Philadelphia, October 1968 06 p0917 A71-17563
- Advances in differential and integral equations - Conference, University of Wisconsin, August 1968 06 p0918 A71-17637
- Shell and plate theory - Conference, Dnepropetrovsk, U.S.S.R., September 1969 06 p0985 A71-17751
- Earthquake displacement fields and earth rotation - Conference, London, Canada, June 1969 06 p0889 A71-17876
- Cosmic rays - Conference, Budapest August-September 1969, Volume 2, Solar cosmic rays, modulation of galactic radiation, magnetospheric and atmospheric effects 06 p0950 A71-18101
- Iterative methods, numerical mathematics, approximation theory - Conference, Oberwolfach, West Germany, November 1968, June and November 1969 06 p0919 A71-18201
- Static seals - IME Conference, London, December 1970 06 p0905 A71-18214
- Applied mechanics - Harvard University, June 1970 06 p0927 A71-18219
- Interstellar gas dynamics - Conference, Yalta, September 1969 06 p0971 A71-18326
- Aerospace science and agricultural development - Conference, Madison, Wisconsin, November 1969 06 p0895 A71-18405
- Machine analysis of biological structures and processes - Conference, Pushchino, U.S.S.R., May 1968 06 p0863 A71-18690
- Sounding rockets and experimental results - Conference, Cardiff, Wales, April 1970 06 p0903 A71-18717
- Heat and mass transfer in turbulent boundary layers - Conference, Herceg Novi, Yugoslavia, September 1968, Volume 1 07 p1219 A71-18751
- Electronics and aerospace systems - IEEE Conference, Washington, D.C., October 1970 07 p1056 A71-18801
- Radiation protection and sensitization - Conference, Rome, May 1969 07 p1031 A71-18926
- Satellite beacon experiments applications - Conference, Lindau uber Northeim, West Germany, June 1970 07 p1095 A71-19001
- Nuclear and space radiation effects - NASA/IEEE Conference, University of California at San Diego, July 1970 07 p1070 A71-19051
- Flight tests - Conference, Beverly Hills, September 1970 07 p1017 A71-19076
- Ordered alloys structural applications and physical metallurgy - Conference, Lake George, New York, September 1969 07 p1131 A71-19426
- Dormancy and survival - Conference, England, September 1968 07 p1041 A71-19521
- Automatic control in space - Conference, Toulouse, March 1970 07 p1154 A71-19526
- Reliability in electronics - IEE Conference, London, December 1969 07 p1076 A71-19551
- Memory materials and components - Conference, Washington, D.C., September 1970 07 p1177 A71-19606
- Perception - Conference, New York, October 1970 07 p1042 A71-19694
- Lasers - Conference, New York, May 1969 07 p1124 A71-19776
- Vacuum science and technology - Conference, Washington, D.C., October 1970 07 p1160 A71-19842
- Lightning and static electricity - Conference, San Diego, December 1970 07 p1019 A71-19926
- Boundary value problems and applications in fluid and gas mechanics - Conference, Kazan, U.S.S.R., May 1969 07 p1091 A71-20076
- Rhenium in modern technology - Conference, Moscow, October 1968, Part 2 07 p1140 A71-20231
- Electronics - Conference, Chicago, December 1970 07 p1080 A71-20401
- Solar system evolutionary problems - Conferences, University of Rome, November 1968 and February 1969 07 p1202 A71-20512
- Fluidics - Conference, Coventry, March 1970, Volumes 1, 2, 3 07 p1024 A71-20551
- Microwave theory and techniques - IEEE Conference, Newport Beach, California, May 1970 08 p1261 A71-20751
- Cosmic ray physics - Conference, Leningrad, November 1969 08 p1350 A71-20951
- Zinc-silver oxide batteries - Conference, Montreal, October 1968 08 p1233 A71-21076
- Theoretical physics - NSF Conference, University of Notre Dame, South Bend, Indiana, April 1970 08 p1333 A71-21172
- Upper atmospheric research - Conference, Boulder, Colorado, August 1970 08 p1278 A71-21196

Photogrammetry and aerial photography - Conference, Denver, October 1970 08 p1280 A71-21239

System sciences - Conference, Honolulu, January 1971 08 p1268 A71-21312

Strength of metals and alloys - Conference, Pacific Grove, California, August-September 1970 08 p1306 A71-21501

Computer processing in communications - Conference, Polytechnic Institute of Brooklyn, April 1969 08 p1255 A71-21590

Earth studies by astronomy and geophysics methods - Conference, Poltava, U.S.S.R., October 1967 08 p1283 A71-21670

Meteorological observations and instrumentation - Conference, Washington, D.C., February 1969 08 p1327 A71-21714

Aircraft and environment - Conference, New York, February 1971, Part I 08 p1378 A71-21811

Nuclear science and power systems - IEEE Conference, New York, November 1970 08 p1267 A71-21838

Epoxy resins - ACS Conference, San Francisco, April 1968 09 p1482 A71-22404

Instrumentation - Conference, Pittsburgh, October 1970, Part 2, Advances in Instrumentation 09 p1443 A71-22705

Space Optics - ESSA-USAF Conference, Santa Barbara, September 1969 09 p1446 A71-22738

Aerospace instrumentation - ISA Conference, Seattle, May 1970, Volume 3 09 p1448 A71-22767

Aerospace instrumentation - Conference, Las Vegas, May 1969, Volume 2 09 p1449 A71-22781

Cryogenic engineering - Conference, West Berlin, May 1970 09 p1545 A71-23002

Photogrammetry - Conference, Washington, D.C., March 1971 09 p1438 A71-23207

Electronic computation - Conference, Purdue University, Lafayette, Indiana, August 1970 09 p1412 A71-23273

Laser welding, machining and safety - Conference, Pennsylvania State University, July 1969 09 p1457 A71-23401

Electromagnetic wave propagation - Conference, Graz, Austria, June 1970 09 p1410 A71-23569

Applied mechanics - Conference, Bucharest, June 1969 09 p1496 A71-23610

Satellite, rocket and Thomson scatter data application to communications - IEE Conference, London, January 1971 10 p1575 A71-23864

Thermophysical properties of solids at high temperatures - Conference, University of Salford, England, April 1970 10 p1624 A71-23906

Aerospace adhesives and elastomers - Conference, Dallas, Texas, October 1970, Volume 2 10 p1630 A71-24063

Pulmonary circulation - Conference, Prague, June 1969 10 p1560 A71-24121

Phase and frequency instabilities in electromagnetic wave propagation - NATO/AGARD Conference, Ankara, Turkey, October 1967 10 p1576 A71-24185

Astrophysics - Conference, University of Nice, France, April 1969 10 p1670 A71-24186

Principles and practice of bionics - NATO/AGARD Conference, Free University of Brussels, Belgium, September 1968 10 p1568 A71-24220

Electrical processes in stratosphere and mesosphere - Conference, Madrid, September 1969 10 p1603 A71-24698

Parameter estimation - Conference, Prague, June 1970 10 p1586 A71-24735

Polyblends and composites - Conference, New York, June 1969 10 p1634 A71-24767

Control optimization methods - Conference, Novosibirsk, U.S.S.R., June 1968 10 p1637 A71-24839

Aviation and astronautics - Conference, Tel Aviv and Haifa, March 1971 11 p1747 A71-25145

Mass spectroscopy - Conference, Kyoto, September 1969 11 p1819 A71-25217

Relativity - Conference, Cincinnati, June 1969 11 p1798 A71-25279

Reinforced plastics - Conference, Washington, D.C., February 1971 11 p1784 A71-25392

Planetary atmospheres - Conference, Marfa, Texas, October 1969 11 p1823 A71-25690

Thermodynamics - Conference, Cardiff, Wales, April 1970 11 p1828 A71-25733

Hybrid computation - Conference, Brussels, August-September 1970 11 p1734 A71-25839

Thermionic conversion - IEEE Conference, Miami Beach, October 1970 11 p1709 A71-25856

Ablative plastics - ACS Conference, San Francisco, March-April 1968 11 p1789 A71-26029

Laser interaction and related plasma phenomena - U.S. Army Conference, Hartford, June 1969 11 p1775 A71-26080

Experimental techniques in propulsion and energetics research - NATO/AGARD Conference, Munich, September 1967 11 p1764 A71-26263

Environment sciences - Conference, Los Angeles, April 1971 11 p1745 A71-26490

Engineering for space environment - ASCE/AIAA, Conference, Houston, April 1970 11 p1747 A71-26526

Reliability - IEEE Conference, Washington, D.C., January 1971 12 p1908 A71-26655

Adaptive systems - Conference, Moscow, March 1970 12 p1926 A71-26714

Galaxy structure and evolution - NATO Conference, Athens, September 1969 12 p1958 A71-26771

Magnetism and magnetic materials - IEEE-AIP Conference, Miami Beach, November 1970 12 p1943 A71-26853

Photography and navigation - Conference, Columbus, Ohio, May 1970 12 p1907 A71-27255

Cosmic rays - Conference, La Paz, Bolivia, July 1970, Volume 1 12 p1948 A71-27364

Cardiology - Conference, London, September 1970 13 p2003 A71-27858

Cosmic rays - Conference, Budapest, August-September 1969, Volume 3, High energy interactions and extensive air showers 13 p2120 A71-28048

Technical, sales/marketing and management - Conference, Coronado, California, May 1971 13 p2091 A71-28164

Space simulation - Conference, Gaithersburg, Maryland, September 1970 13 p2044 A71-28302

Combustion and heat transfer in gas turbine systems - Conference, Cranfield, England, April 1969 13 p2116 A71-28739

Optimization - Conference, Nice, June-July 1969 13 p2043 A71-28811

Relay advances - Conference, Oklahoma State University, April 1971 13 p2000 A71-28834

Electromagnetic compatibility - IEEE Conference, San Antonio, October 1970 13 p2031 A71-28860

Aerospace medicine - Conference, Houston, April 1971 13 p2014 A71-29300

Differential equations analytic theory - Conference, Kalamazoo, April-May 1970 13 p2096 A71-29422

Theoretical and applied mechanics - Conference, Tokyo, November 1968 13 p2158 A71-29426

Aerospace materials - Conference, Anaheim, California, April 1971 14 p2261 A71-29633

Atmospheric turbulence - Conference, London, May 1971 14 p2266 A71-29749

Mesospheric/noctilucent/ cloud physics - Conference, Riga, November 1968 14 p2231 A71-29955

Computers - Conference, Houston, November 1970 14 p2207 A71-30017

Polar ionosphere and magnetospheric processes - Conference, Kjeller, Norway, April 1969 14 p2299 A71-30027

Dynamic testing - Conference, London, January 1971 14 p2251 A71-30033

Aviation within total transport system - Conference, London, May 1971 14 p2340 A71-30158

Space stations - AAS Conference, Anaheim, California, June 1970 14 p2320 A71-30256

Hypoxia, high altitude and heart - Conference, Aspen, Colorado, January 1970 14 p2183 A71-30275

Instrumentation in aerospace industry - Conference, Las Vegas, May 1971 14 p2243 A71-30300

Visual double stars observation techniques coordination - Conference, Nice, September 1969 14 p2310 A71-30350

Electron device techniques - IEEE Conference, New York, September 1970 14 p2214 A71-30700

Telemetering - IEEE Conference, Washington, D.C., April 1971 14 p2197 A71-30890

Radio science - Conference, Ottawa, August 1969, Volume 1, Ionosphere, magnetosphere, radio noise 14 p2201 A71-30939

Radio science - Conference, Ottawa, August 1969, Volume 2 14 p2203 A71-30960

White dwarfs - Conference, Fife, Scotland, August 1970 14 p2316 A71-31004

Display devices - IEEE Conference, New York, December 1970 14 p2249 A71-31028

Aerospace antennas - IEE Conference, London, June 1971 14 p2215 A71-31034

Applied mathematics and mechanics - Conference, Delft, Netherlands, April 1970 15 p2502 A71-31152

Holography applications - Conference, Besancon, France, July 1970 15 p2402 A71-31252

Numerical analysis of partial differential equations - Conference, London, June 1970 15 p2440 A71-31345

Education in creative engineering - Conference, MIT, April 1970 15 p2348 A71-31593

Cosmic rays - Conference, Budapest, August 1969, Volume 4, Muons and neutrinos techniques 15 p2474 A71-31776

Fluidics - Conference, Prague, June-July 1971 15 p2351 A71-32051

Aircraft and environment - Conference, Washington, D.C., February 1971, Part 2 15 p2516 A71-32240

Shock tubes - Conference, London, July 1971 16 p2554 A71-32876

Continuous systems stability and instability - Conference, Herrenalb, West Germany, September 1969 16 p2648 A71-32976

Matrix methods of structural analysis and design - Conference, Tokyo, August 1969 16 p2651 A71-33076

Optical methods in gas dynamic research - Conference, Syracuse University, New York, May 1970 16 p2586 A71-33151

Relativity and gravitation - Conference, Technion City, Israel, July 1969 16 p2609 A71-33255

Reliability and maintainability - ASME/SAE/AIAA Conference, Anaheim, California, June 1971 16 p2582 A71-33284

Moon and planets - NATO Conference, University of Newcastle-upon-Tyne, England, April 1970 16 p2636 A71-33501

Organizing space activities for world needs - Conference, New York, October 1968 16 p2664 A71-33580

Refractory and rare metals single crystals - Conference, Moscow, December 1968 16 p2594 A71-33876

Steels and alloys structure and properties - Conference, Moscow, May 1968 16 p2596 A71-33914

Methodology of fatigue assessment - Conference, Kyoto, September 1969 17 p2687 A71-34352

Advanced testing techniques - ASTM Conference, Philadelphia, June 1969 17 p2820 A71-34552

Millimeter system, devices and guides - Conference, Los Angeles, August 1970, Volume 14 17 p2714 A71-34601

Space radio communication - Conference, Paris, March 1971 17 p2699 A71-34676

Nonlinear oscillations - Conference, Kiev, August-September 1969 17 p2779 A71-34903

Automation in optical astrophysics - Conference, Edinburgh, August 1970 17 p2740 A71-34980

Space shuttle, space station and nuclear shuttle navigation - Conference, Huntsville, Alabama, February 1971 17 p2772 A71-35051

Communications - IEEE Conference, Montreal, June 1971 17 p2703 A71-35076

Aircraft structures damage tolerance - ASTM Conference, Philadelphia, June 1970 17 p2826 A71-35151

Composite materials and structures - Conference, Colorado Springs, May 1971 17 p2762 A71-35201

Transport theory applications - Conference, Oxford University, September 1970 17 p2808 A71-35551

Aerospace electronics - IEEE Conference, Dayton, Ohio, May 1971 17 p2746 A71-35752

Photo-optical instrumentation - Conference, Anaheim, California, September 1970 18 p2916 A71-36051

Fluid power transmissions and control systems - Conference, Hanover, West Germany, April 1971 18 p2850 A71-36201

Fluid dynamics numerical methods - Conference, University of California at Berkeley, September 1970 18 p2904 A71-36301

Flow mechanics with emphasis on reentry problems - Conference, Goettingen, West Germany, March 1971, Volume 1 18 p2845 A71-36407

Space technology - Conference, Cocoa Beach, Florida, April 1971, Volumes 1 and 2 18 p2972 A71-36442

Space communication - Conference, Paris, March-April 1971, Volumes 1 and 2 18 p2876 A71-36501

Electro-optics - Conference, Brighton, England, March 1971 18 p2923 A71-36601

Behavioral thermoregulation - Conference, Lyons, France, September 1970 18 p2858 A71-36859

Optical tracking systems - Conference, El Paso, Texas, January 1971 18 p2882 A71-36902

Magnetic thin films - Conference, Prague, September 1970 18 p2954 A71-36936

Nonlinear functional analysis - Conference, University of Wisconsin, Madison, October 1970 18 p2943 A71-36951

Orbiting stations and space shuttles - Conference, Rome, April 1971 19 p3149 A71-37301

Solar studies with emphasis on space observations - Conference, London, April 1970 19 p3135 A71-37608

Meteorite impact and volcanism - Conference, Houston, October 1970 19 p3049 A71-37651

Metallographic techniques - Conference, Cleveland, November 1970 19 p3081 A71-37901

Combustion - Conference, University of Utah, Salt Lake City, August 1970 19 p3166 A71-38076

Elevated temperature testing problem areas - ASME-ASTM Conference, Toronto, June 1970 19 p3065 A71-38131

Laser engineering applications - Conference, Tel Aviv, June 1970 19 p3074 A71-38226

Numerical solution of partial differential equations - Conference, University of Maryland, College Park, May 1970 19 p3087 A71-38301

Hydraulic system cleanliness - ASTM Conference, Toronto, June 1970 19 p2999 A71-38318

Engineering for conservation of mankind - IEEE Conference, Sacramento, May 1971 19 p3030 A71-38401

Electromagnetic compatibility - IEEE Conference, Anaheim, California, July 1970 19 p3030 A71-38426

Reliability physics - IEEE Conference, Las Vegas, April 1970 19 p3033 A71-38504

Electronic components - Conference, Washington, D.C., May 1970 19 p3035 A71-38535

Physics of clouds and active effects - Soviet Conference, Tiflis, U.S.S.R., May 1969 19 p3091 A71-38679

Energy conversion engineering - Conference, Boston, August 1971 20 p3261 A71-38901

Multivariable control system design and applications - IEE Conference, Manchester, England, September 1971 20 p3207 A71-38988

Heat resistant material properties under power and chemical plant conditions - Conference, Mala Fatra, Czechoslovakia, September 1971 20 p3249 A71-39013

Aerospace fluid power - Conference, Detroit, Michigan, October 1970 20 p3183 A71-39147

Cryogenic engineering - Conference, Boulder, Colorado, June 1970 20 p3312 A71-39265

IAU Executive Committee, General Assembly and commissions reports on astronomy, including manuscripts preparation guidelines, handbook, etc 20 p3315 A71-39425

Interdisciplinary cycle research - Conference, Noordwijk, Netherlands, June 1970 20 p3190 A71-39474

Solar regular daily geomagnetic variations - Conference, Potsdam, East Germany, April 1970 20 p3216 A71-39508

Astronomy - Conference, Oberkochen, West Germany, April 1971 20 p3293 A71-39526

Space research - COSPAR Conference, Leningrad, May 1970 20 p3219 A71-39612

Radiating atmosphere - Conference, Queens University, Kingston, Ontario, August 1970 20 p3226 A71-39826

Crab Nebula - IAU Conference, Victoria University of Manchester, England, August 1970 20 p3301 A71-39917

Displays - IEE Conference, Loughborough University of Technology, England, September 1971 21 p3376 A71-40107

Holographic applications in mechanics - ASME Conference, University of Southern California at Los Angeles, August 1971 21 p3377 A71-40226

Instrumentation in aerospace simulation facilities - Conference, Rhode-Saint-Genese, Belgium, June 1971 21 p3362 A71-40380

Electronic packaging and production - Conference, Anaheim and New York, February and June 1971 21 p3352 A71-40435

Tabular listing of frequency allocations for space services and radio astronomy made at Extraordinary Administrative Radio Conference 21 p3348 A71-40476

Aircraft wake turbulence and detection - Conference, Seattle, September 1970 21 p3318 A71-40482

Life science and space research - Conference, Leningrad, May 1970 21 p3332 A71-40551

Microelectronics - Conference, Munich, November 1970 21 p3353 A71-40726

Shock waves and mechanical properties of solids - Conference, Raquette Lake, New York, September 1970 21 p3464 A71-40784

Electronics - Conference, San Francisco, August 1971 21 p3356 A71-40801

Materials research - Conference, Kyoto, September 1970 21 p3400 A71-40830

Cryogenic fracture toughness testing - ASTM-ASME Conference, Toronto, June 1970 21 p3401 A71-40914

Holographic developments - Conference, Boston, April 1971 21 p3380 A71-40919

Fluid and solid mechanics - Conference, University of Notre Dame, South Bend, Indiana, August 1971 21 p3468 A71-40982

Flashing lights perception and application - Conference, London, April 1971 22 p3497 A71-41476

Gas bearing - Conference, University of Southampton, England, March 1971, Volumes 1 and 2 22 p3550 A71-41658

Holography applications - Conference, Washington, D.C., October 1969 22 p3538 A71-41731

Acoustical holography - Conference, Newport Beach, California, July 1970, Volume 3 22 p3540 A71-41776

Navigation role in airways systems development - Conference, Saddle Brook, New Jersey, April 1971 22 p3570 A71-42077

Large telescope design - Conference, Geneva, March 1971, covering telescope projects, optical properties, mountings and control and drive systems 22 p3542 A71-42120

Infrared techniques - Conference, University of Reading, Reading, Berkshire, England, September 1971 22 p3542 A71-42121

Eye movement control - Conference, University of the Pacific, San Francisco, November 1969 22 p3488 A71-42432

Electronic imaging systems - Conference, Palo Alto, California, April 1970 22 p3547 A71-42502

Cosmic ray physics - Conference, Leningrad, October 1969 22 p3594 A71-42633

Corporate aircraft safety - Conference, Washington, D.C. April 1971 23 p3627 A71-43226

Theoretical and applied mechanics - Conference, Haifa, September 1971 23 p3775 A71-43368

Corporate aircraft safety - Conference, San Antonio, May 1970 23 p3628 A71-43379

Space program management - Conference, Paris and Neuilly-sur-Seine, February 1970 23 p3784 A71-43451

Electro-optical systems design - Conference, Anaheim, May 1971 23 p3684 A71-43501

Photogrammetry of moving objects - Conference, Saint-Mande, France, September 1970 23 p3678 A71-43586

Lunar science - Conference, Houston, January 1971, Volume 1, Mineralogy and petrology, Volume 2, Chemical and isotope analyses, Volume 3, Physical properties/Surveyor 3 23 p3737 A71-43601

Automatic control - Conference, St. Louis, August 1971 23 p3657 A71-44076

Radiation protection biological aspects - Conference, Kyoto, October 1969 23 p3638 A71-44325

Photogrammetry of moving objects - Conference, Saint Mande, France, September 1970, Part 3 24 p3825 A71-44753

Heat transfer - Conference, Versailles, August-September 1970, Volume 9 24 p3890 A71-45146

Thin films of Te compounds with Zn an Ga subgroup metals - Conference, Vilnius, U.S.S.R., December 1969, Part 3 24 p3861 A71-45247

CONFIDENCE LIMITS

PCM telemetry data transmission bit error probability confidence intervals upper bounds based on Markov chain model analysis 01 p0032 A71-10877

Social quantitative benefit vs risk assessment of new technologies, considering atomic power safety 02 p0336 A71-12120

PCM telemetry bit error probability confidence intervals and Bayesian posterior distributions derivation, using statistical method 04 p0554 A71-15327

Gaussian probability density functions covariance matrices dimension-reducing mapping using confidence spaces 04 p0619 A71-15331

Electronic equipment reliability prediction, considering confidence limits 07 p1077 A71-19564

Model concepts and mathematical methods for planned economy conditions and goals representation, considering prediction reliability 11 p1860 A71-25257

Amplitude-quantized random noise contaminated unknown signal sample, deriving conditional probability density function of combined output error and signal confidence interval 12 p1880 A71-27157

Exact confidence intervals for probability and sampling quantiles of random quantity from beta distribution law 17 p2763 A71-34302

Statistical limits on reliability, informativeness, controllability and self organization of complex systems, determining minimum redundancy requirements for suppressing interfering factors 17 p2720 A71-34953

Orthogonal method for studying nonlinear automatic control systems in presence of random perturbations, discussing applicability limits 24 p3815 A71-44701

CONFIGURATION MANAGEMENT

Book on configuration management in aerospace industry covering documentation, identification, accounting, etc 09 p1548 A71-22672

CONFIGURATIONS

Complex configuration shell theory, considering successive approximation method 24 p3876 A71-44403

CONFINEMENT

Soyuz 9 spacecraft simulator prolonged confinement effect on human cardiovascular system functional state 09 p1390 A71-22209

Monograph on free and confined vortex gas burner flow characteristics covering pressure distribution, velocity, power law, mass flow in boundary layers, etc 13 p2047 A71-28496

Fighting between male mice isolated at early age or reared in small groups, considering ontogenetic and experiential determinants 13 p2011 A71-28805

Bounded flow incident on cylindrical body in transverse magnetic field, determining constraints effects on dynamic and structural characteristics 14 p2278 A71-29609

CONFORMAL MAPPING

German monograph on invariant curves of annulus differentiable mappings covering existence theorem for closed curve within annulus transformed by mapping

01 p0110 A71-10127

Polygonal elastic plates natural frequencies investigation by conformal mapping and variational method, transforming holomorphic function into equivalent problem of circular boundary plate

10 p1691 A71-24813

Schwarz-Christoffel conformal transformation inversion for electrostatic field integral equation formulation, applying to stepped-guide junction

14 p2212 A71-30515

Conformal transformation of multiply connected plane domain of Poincaré standardization

17 p2672 A71-35469

Satellite applications to cartographic and geodetic surveys, discussing photographic difficulties

19 p3047 A71-37302

Torsion of hollow beam consisting of two homogeneous isotropic rods with different elastic properties and simply connected cross sections, solving by conformal mapping

19 p3155 A71-37387

Biharmonic problems solution in elasticity theory for piecewise homogeneous doubly connected media with interface in conformal mapping of ring onto doubly connected region

19 p3160 A71-38486

Complex solutions blocking in sectorial second order differential equations with polynomials, involving conformal mapping

21 p3410 A71-41191

Electromagnetic scattering by imperfectly conducting circular and square cylinders, using matrix technique based on conformal transformation from polygonal to circular cross section

22 p3512 A71-42361

Function construction procedure for ring-shaped structure conformal mapping onto doubly connected regions with simple contours, applying to prismatic rod torsion problem

23 p3776 A71-43419

Plane electromagnetic wave diffraction by infinitely conductive grating at nonorthogonal incidence angles, using conformal mapping technique

24 p3847 A71-44357

CONFORMAL TRANSFORMATIONS

U CONFORMAL MAPPING

CONGENITAL ANOMALIES

Coronary arteries congenital lesions, discussing major, minor and secondary anomalies relationship to cardiac malformations

15 p2361 A71-32553

Sudden death during physical exertion due to congenital anomalies of coronary arteries

18 p2855 A71-36217

Myocardial blood flow and oxidative metabolism in cyanotic congenital heart disease patients, using lactate/pyruvate ratios and coronary sinus catheterization

22 p3484 A71-41521

CONGENITAL CONDITIONS

U CONGENITAL ANOMALIES

CONICAL BODIES

NT SLENDER CONES

Longitudinal elastic wave propagation equations of motion in cone with small apex angle, using perturbation theory

03 p0456 A71-12974

Turbulent base pressure on conical afterbodies in supersonic axisymmetric flow, including initial direction effect

[AIAA PAPER 70-555]

03 p0344 A71-14450

Hypersonic flow past freely vibrating hemisphere-cylinder-cone, noting Reynolds and Mach numbers dependence and conical stabilizer aperture angle

03 p0345 A71-14571

Hypersonic flow with nonequilibrium oxygen dissociation around blunt and conical bodies, considering temperature, pressure, density and compressibility factor behind normal shock

04 p0525 A71-14982

Conical body laminar boundary layer heat transfer problem in supersonic flow, using quasi-linearization and implicit finite difference method

04 p0527 A71-15487

Turbulent heat transfer measurements on blunt cone in nitrogen flow at high Mach number under various angles of attack

[AIAA PAPER 71-38]

06 p1008 A71-18499

Incompressible hypersonic laminar boundary layer flow over sharp cone, based on asymptotic inner and outer flow field expansion

07 p1015 A71-19892

Unsteady boundary layers on sphere or cone moving along axis, determining skin friction angular response

07 p1016 A71-20098

Aerodynamic characteristics of conical and pyramidal configurations with various planforms by

slender body theory, replacing three dimensional flow by two dimensional flow

08 p1227 A71-20776

Steel conical disks two dimensional stressed state determined with deformations at elastic and elastoplastic strains using digital computers

08 p1369 A71-21116

Three dimensional laminar boundary layer on cone at incidence in supersonic flow evaluated by pressure distribution technique, comparing heat transfer, Pitot probe measurements, etc

[AIAA PAPER 70-48]

09 p1381 A71-22088

Mean flow measurement of cone laminar supersonic wake

09 p1381 A71-22091

Shock wave shape attached to cone moving in ideal gas studied by Pade-Shanks approximation method, considering angle of attack

09 p1431 A71-22405

Asymptotic solution for conical horn modes, comparing with exact solution for eigenfunctions and eigenvalues

09 p1420 A71-23677

Low frequency electromagnetic wave scattering by metallic cone, noting dipole moment contribution

12 p1879 A71-27054

Antenna analysis method based on transmission line theory, yielding current distribution and input impedance of finite conical antenna

12 p1880 A71-27154

Thermal buckling and snapping of flat rings and of shallow conical rings under axisymmetric temperature distribution

[ASME PAPER 71-DE-B]

12 p1977 A71-27317

Crosshatched ablation patterns on conical bodies, presenting wind tunnel test results on Mach number, local static pressure and temperature ratio effects

12 p1987 A71-27591

Supersonic flow around porous-wall conical body with uniform gas injection through wall, deriving equations for pressure at contact surface

13 p1990 A71-28182

Monograph on heat transfer from rotating heated surface with induced turbulent boundary layers covering disk, cone and sphere geometries

13 p2162 A71-28882

Conical bar with yield point lag, investigating elastoplastic wave propagation with Rabotnov model

13 p2155 A71-29064

Conical body lift/drag ratio increase by wedge shaped nose, noting applications to space vehicles entering atmosphere above escape velocity

13 p1992 A71-29183

Base pressure measurement behind wedge-parallelepipeds and cone-cylinder models of variable geometry

13 p2049 A71-29199

Viscous flow fields around pointed cones at angle of attack in nonuniform supersonic flow, using axisymmetric analog for three dimensional boundary layer

[AIAA PAPER 71-624]

15 p2344 A71-31552

Free flight static and dynamic stability tests on lightweight cone shaped models in longshot tunnel at hypersonic speeds, using spark recording

16 p2519 A71-32879

Cone-cylinder-cone missile type body in transonic buffeting environment determining static and fluctuating wall pressure distribution

[ONERA-TP-942]

18 p2843 A71-36020

Dynamic parameters of supersonic flow incident on conical bodies at large angles of attack, considering flow field and entropy distribution

18 p2845 A71-36328

Conical ablation surface models in hypersonic wind tunnel tests, describing Mach number and nosetip bluntness effects on cross hatching

21 p3476 A71-40965

Critical streamline length in axisymmetric and plane ideal gas flows past conical bodies as function of Mach number and form parameter

24 p3790 A71-45058

CONICAL FLARE

U CONES

CONICAL FLOW

Soviet book on nonlinear conical gas flow theory covering flows with different characteristics past bodies of various geometries and positions

02 p0187 A71-12719

Diverging flow structure in conical diffuser using two Townsend turbulent parameters

03 p0399 A71-13456

Supersonic inviscid flow fields associated with conical premixed flame sheet

03 p0521 A71-14242

Hypersonic conical flow with attached shock waves over delta wings

03 p0344 A71-14243

Vortex breakdown in swirling conical flows, determining swirl angle distribution, flow rates and Reynolds number effects

[AIAA PAPER 71-52]

06 p0843 A71-18513

Conical diffusers swirling inlet flow effects on pressure recovery and outlet flow profile

[AIAA PAPER 71-84]

06 p0883 A71-18541

High accuracy hypersonic low density cone drag measurements, using method with advantages of free jet and wind tunnel electromagnetic balance

[AIAA PAPER 71-133]

06 p0845 A71-18577

Laminar swirling jet flow through vertical circular cone, assuming velocity singularities on axis

07 p1092 A71-20049

Flowfield isentropes in conical gas flow with singular current surfaces

08 p1227 A71-21864

Magnetically suspended laminar supersonic cone wake stability from hot wire fluctuation and spectral components amplitude/phase measurements

11 p1702 A71-25472

Truncated conical diffusers with various geometrical configurations and incompressible inlet flow conditions, noting reduced pressure recovery

13 p2047 A71-28406

Hollow cone water spray from pressure jet swirling atomizer into uniform air stream, observing droplet velocities and trajectories by high speed photography

13 p2049 A71-28752

Flow and heat transfer measurements in dihedral simulating patterns about supersonic conical edge and shock wave interaction line, using thermodynamic coating technique

13 p1992 A71-29174

Elliptical cones at large angle of attack, calculating three-component real gas properties effects on aerodynamic characteristics

13 p1993 A71-29191

Short conical diffusers with radial splitters for flow stabilization with high pressure recovery performance

14 p2225 A71-30304

Tube or duct confined submerged turbulent jet exit cone angle calculation for various expansion area ratios

15 p2390 A71-32016

Conical converging nozzle flow of perfect monatomic gas in rarefied near continuum, transition and near free molecular regimes, using finite difference methods

15 p2390 A71-32045

Burning velocity measurement of laminar conical hydrogen-air flames on 10.3 mm diam water cooled nozzle burner, using schlieren and particle tracking techniques

15 p2465 A71-32085

Aperture angle effect on flow separation in inlet section of diffuser with cylindrical to conical channel transition

16 p2521 A71-33611

Dynamic parameters of supersonic flow incident on conical bodies at large angles of attack, considering flow field and entropy distribution

18 p2845 A71-36328

Flow field isentropes in conical ideal gas flow with singular stream surfaces

20 p3176 A71-39363

Heat transfer and pressure distribution of cone shaped model at different angles of attack in hypersonic flow simulating reentry flight in wind tunnel

22 p3480 A71-19655

Approximate solution for position and strength of shock waves about cones in steady supersonic flow

24 p3790 A71-44624

CONICAL INLETS

Supersonic conical inlet additive drag formula, using flow data in freestream

10 p1553 A71-24866

CONICAL NOZZLES

Optimum two fluid mixing chamber length for energy efficiency of conical diffusers in straight pipe jet pump systems

03 p0399 A71-13369

Surface roughness effects on gas to wall heat transfer in conical converging diverging nozzles, using heated air

04 p0675 A71-14780

Cone shaped diffusers effectiveness, noting inlet conditions effect on pressure recovery coefficient

05 p0694 A71-16750

Inviscid incompressible flow velocity distribution in conical configurations with water as working fluid, using method of integral relations

05 p0737 A71-17103

Chemically nonequilibrium laminar boundary layer profiles in axisymmetric hypersonic conical nozzle at high air stagnation temperature, calculating wall friction, displacement and momentum loss thickness

13 p1989 A71-27904

Electron density and temperature distribution in boundary layer flow of reflected shock tunnel conical nozzle

17 p2727 A71-34877

Turbulent boundary layer and heat transfer measurements along cooled conical convergent-divergent nozzle

[ASME PAPER 71-HT-4]

19 p2993 A71-37982

Highly uniform inlet velocity profile influence on conical diffuser characteristics

20 p3177 A71-39798

- Inlet circulation and swirl effect and optimum vane angle for maximum efficiency of subsonic straight conical diffusers
20 p3177 A71-39875
- Conical diffusers outlet flow profile and performance, investigating swirling inlet flow effects on pressure recovery
21 p3323 A71-40950
- Conical nozzle roughness on heat transfer in supersonic region
22 p3622 A71-42785
- CONICAL SCANNING**
- Antenna primary feed design and sample and store technique tracking system with conical scan control for Intelsat 3 satellite ground station
02 p0223 A71-12802
- Frequency selective conical scanning for direction finding earth station antennas for communication satellite automatic tracking, using waveguide mode conversion
02 p0223 A71-12809
- Low level target locating by monopulse and conical scanning radar, solving balance equation
17 p2708 A71-35482
- Scanning microwave landing guidance system coordinates choice, discussing signal format, antennas planar or conical beams and V-STOL application
22 p3572 A71-42090
- CONICAL SHELLS**
- Buckling of ring stiffened conical shells under axial compression, determining critical loads
01 p0168 A71-10342
- Axisymmetric and unsymmetric free vibrations of orthotropic sandwich cylindrical or conical shells under various boundary conditions
02 p0325 A71-11999
- Clamped shallow spherical and conical shells axisymmetric dynamic buckling under step loads of infinite duration, showing similarity with static buckling
03 p0504 A71-13455
- Spherical or conical shells of revolution axisymmetric oscillations, analyzing zero moment equations system spectrum
05 p0822 A71-16377
- Computerized nonlinear collapse analysis of elliptical cylinders and cones under axial compression
05 p0823 A71-16555
- Sandwich panels with conical shell or elongated honeycomb fillers, calculating stability and elastic properties
06 p0986 A71-17757
- Multilayer conical and spherical shells of revolution axisymmetric elastic deformation, deriving stress-strain state equations with allowance for transverse shear
06 p0990 A71-17795
- Variable thickness truncated hollow cone elastic equilibrium, considering asymptotic analysis of axisymmetric problem
06 p0994 A71-17820
- Elastic momentless conical tank with spherical bottom partially filled by liquid, calculating axisymmetric oscillation
06 p0995 A71-17828
- Elastoplastic conical shells strain under longitudinal impact by large rigid body, analyzing plastic bending
06 p0996 A71-17842
- Axisymmetric deformed state of three layer circular conical shell with rigidly clamped edges, obtaining equilibrium equations by Bubnov-Galerkin method
06 p0997 A71-17851
- Sheet blanks shaping into conical products by rolling, discussing stress-strain state in blank and time dependent rolling process
06 p0906 A71-18711
- Cylindrical, conical and spherical shells natural frequencies and vibration modes determination using matrix series
07 p1212 A71-19365
- Conical shell stability under dynamic longitudinal compression
07 p1218 A71-20472
- Shallow conical shells local heat treatment, determining optimal temperature fields
09 p1546 A71-23084
- In-plane boundary conditions influence on clamped conical shells buckling under external pressure, using displacement method based on Donnell stability equations
11 p1841 A71-25158
- Orthotropic conical shell subjected to torsion, using Ritz approximate energy method for linear stability problem solution
11 p1848 A71-25618
- Plastic conical shell with variable thickness, calculating load carrying capacity under cyclic mechanical and thermal loads
12 p1979 A71-27353
- Spherical or conical shells of revolution axisymmetric oscillations, analyzing zero moment equations system spectrum
12 p1981 A71-27463
- Bending stress in conical shell subjected to thermal and pressure loadings with uniform spatial distribution, using perturbation method
12 p1983 A71-27594
- Stress concentration at circular hole in conical shell, using Bubnov-Galerkin method in conjunction with linear thin shell theory
13 p2150 A71-28135
- Thermal stresses in multilayer anisotropic fiberglass wound conical shell under axisymmetric gradients applicable to structural missile nose cone design
14 p2330 A71-30694
- Thin conical shell under longitudinal impact, deriving theory for transverse and rotary inertias and transverse shear deformation effects
15 p2506 A71-32017
- Initial interaction phase between thin shallow conical shell vibrating axisymmetrically and ideal incompressible fluid, determining hydrodynamic pressure effects
16 p2560 A71-33901
- Conical shell with circular hole, determining stress function and normal deflection in torsion
17 p2817 A71-34338
- Numerical method for limit analysis of axisymmetric shells of revolution, considering truncated conical shells and pressure vessels with rigid circular plates
17 p2818 A71-34400
- Bending of circular conical shell with discretely reinforced end cross section, deriving accurate closed form solution within limits of working model
17 p2828 A71-35302
- Metal-reinforced glass plastic composite conical shell with positive Gaussian curvature, estimating reliability and stability based on static tests
17 p2830 A71-35316
- Thin truncated conical shells axisymmetric free vibrations, considering shear deformation and rotary inertia effects
21 p3462 A71-40528
- Axisymmetric imperfect conical shells vibration analysis using time average holographic interferometry technique
21 p3382 A71-41028
- Natural frequencies and vibration modes of perforated cylindrical, conical and spherical shells of revolution, using Ritz method
22 p3617 A71-42488
- Free axisymmetric torsional vibrations of thick hollowed conical frustums cantilevered at small end, considering conicity and cone thickness effects
22 p3618 A71-42590
- Nonsteady heat conduction of multilayer cylindrical and conical shells in periodic radiation flux, calculating temperature distribution
23 p3783 A71-44067
- Cyclic symmetrical deformation of thin elastic conical shells of revolution of variable thickness with meridional ribs under physical and thermal loads
24 p3882 A71-44843
- Circular conical shell initial deformation under impulsive load, using Timoshenko theory
24 p3883 A71-44852
- Conical and cylindrical shell deformation with nonlinear one dimensional wave processes, describing algorithm for method of characteristics application
24 p3885 A71-45341
- CONICS**
- NT HYPERBOLAS**
- CONJUGATE POINTS**
- Conjugate mirror point locations for world geomagnetic contour maps, noting use for particle tracing
01 p0077 A71-11516
- Visual, photographic and photoelectric observations of polar auroras and hydrogen emission at conjugate points
02 p0242 A71-11757
- Ionospheric photoelectron exchange at magnetic conjugates, considering electron density and impact ionization by inelastic collisions
03 p0408 A71-13381
- Conjugate observations of ionospheric absorption associated with electron precipitation during sudden commencement of magnetic storm
03 p0419 A71-14520
- O I 1304-A airglow, observing conjugate excitation withOGO 4 spacecraft
06 p0888 A71-17279
- Time structure of auroral radio absorption from magnetically conjugate and closely spaced observations
06 p0892 A71-17977
- Hourly changes in auroral conjugate location from ionospheric absorption and riometer magnetograms, noting electrojet triangulation
08 p1279 A71-21210
- F 2 layer nighttime ionization at midlatitudes, investigating conjugate point effects on observation point
09 p1434 A71-22426
- Auroral X radiation at magnetocojugate points Kerguelen/Archangel region, using balloon-borne spectrometers
09 p1438 A71-23146
- Conjugate approximations for piecewise functions of stress analysis using finite element method
11 p1792 A71-26103
- Short wave radio reception and signal paths at magnetically conjugate point in Southern Hemisphere, using 40-110 msec delay times
13 p2030 A71-28536
- Conjugate and closely-spaced riometer observations of auroral radio absorption, considering explanation by alternation of particle precipitation between Northern and Southern Hemispheres
14 p2192 A71-29667
- Conjugate photoelectrons existence from rocket measurements during total solar eclipse of 7 March 1970
16 p2570 A71-33823
- Upper ionosphere electron density scale height data, noting conjugate point sunrise heating effects from Alouette I data
17 p2731 A71-34313
- Magnetically conjugate range-time observations of E region radio aurora by pulsed VHF radar echoes
18 p2875 A71-35963
- Auroral conjugacy and time dependent geometry via all sky cameras and image orthicon TV onboard conjugate-flying aircraft
20 p3228 A71-39840
- Formulas derived for object conjugate points coordinates and holographic image
23 p3675 A71-43304
- Predawn effect on hot and cold electrons at magnetocojugate point in F 2 layer, discussing electron shock wave speed and thermal collisionless wave energy dissipation
24 p3824 A71-45321
- CONJUGATES**
- NT CONJUGATE POINTS**
- Conjugate direction minimization procedure based on sequences and inferred second partial derivative matrix inverse
01 p0112 A71-10962
- Design charts relating time response characteristics to parameters of closed loop transfer functions possessing conjugate pair of poles
13 p2042 A71-28706
- Conjugate functions theory variational application to solid mechanics, generalizing concept of potential for nonlinear behavior laws in viscosity and plasticity
14 p2329 A71-30447
- Bayes theorem tests based on experimental observations, considering binomial, exponential and normal sampling distribution of priors as family of natural conjugates
16 p2582 A71-33290
- Stability of plane rotating galaxies in magnetic field parallel to axis of rotation, showing linearized MHD equations self conjugate for radial disturbance case
20 p3289 A71-39298
- N-step conjugate gradient minimization algorithm for nonquadratic functions, giving numerical example of application to double precision arithmetic
24 p3842 A71-44623
- F 2 region magnetic disturbances conjugacy mechanisms, considering vertical ionization profiles
24 p3823 A71-45029
- CONJUGATION**
- Digital computer operated from remote terminal for signal analysis including Fourier transform, complex multiplication and conjugation
05 p0727 A71-17144
- CONJUNCTION**
- Venus inferior conjunctions tables from 1960 to 2023, presenting geocentric latitude at conjunction time
09 p1528 A71-23548
- CONNECTIONS**
- U JOINTS (JUNCTIONS)**
- CONNECTIVE TISSUE**
- NT COLLAGENS**
- NT MARROW**
- Energy metabolism disturbance effect on dissolved and undissolved collagen fractions content of aorta connective tissue
17 p2679 A71-34223
- Hyperoxia pathological effects on albino rats subcutaneous connective tissue, noting oxidizing enzyme activity depression and cellular metabolism suppression
22 p3496 A71-42802
- CONNECTORS**
- NT ELECTRIC CONNECTORS**
- NT UMBILICAL CONNECTORS**
- NT UNIONS (CONNECTORS)**
- Magnetic pulse technique connecting Al pipe with steel pipe, determining mechanical and physical parameters
06 p0906 A71-18713
- CONNECTORS [ELECTRIC]**
- U ELECTRIC CONNECTORS**
- CONOIDS**
- U CONICAL BODIES**

CONSCIOUSNESS

Physiological interaction between conscious and unconscious trace processes during time count by pairing acoustic, tactile, proprioceptive and photic stimuli
06 p0850 A71-17599

CONSECUTIVE EVENTS

Uniform convergence of frequencies of events in independent tests sequence to probabilities of occurrence
17 p2764 A71-34573

CONSERVATION

Engineering for conservation of mankind - IEEE Conference, Sacramento, May 1971
19 p3030 A71-38401

CONSERVATION EQUATIONS

Energy conservation in linear atmospheric models using first order kinetic equations
04 p0581 A71-15067

Ejector pump with gas-air jet, deriving momentum conservation equation
06 p0882 A71-18010

Mode conversion in inhomogeneous plasma, discussing conservation laws relationships to differential equation invariants
09 p1501 A71-22535

Soviet book on thermal stresses in bodies of revolution of arbitrary shape covering energy conservation equations and heat equations solutions
11 p1850 A71-26096

Conservation theorem of velocity circulation along moving contours in continuous steady ideal gas flows
12 p1863 A71-27305

Combustion chamber design with flame stabilizers, deriving gas flow, energy conservation equations and propellant combustion rates
13 p2163 A71-28967

Closed system of macroequations for mass and energy conservation along symmetry axis of steady rarefied supersonic gas flow in front of blunt body
13 p1991 A71-29151

Elastic stability theory for perfectly elastic materials with couple stresses, deriving exact functional for overall conservative systems of forces and couples
16 p2648 A71-32989

Laminar compressible wakes instability behind planar and axisymmetric slender bodies, solving integral conservation equations for fluctuation amplitude variations
19 p2993 A71-37879

Conservation theorem of velocity circulation along moving contours in continuous steady ideal gas flows
19 p3046 A71-38258

Laser heating of D-T plasma, deriving average equations of momentum and energy conservation with allowance for thermonuclear fusion heat
20 p3275 A71-39471

Radially symmetric shocked flows computation method, using momentum equation in conservation form in original Cartesian coordinates
21 p3368 A71-40848

Numerically simulated turbulent velocity flow field, covering Navier-Stokes and energy conservation equations
21 p3371 A71-40996

CONSERVATION LAWS

Gravitational theory with variable constant, examining local energy momentum tensor conservation law and celestial mechanics effects
01 p0155 A71-10440

Hydrodynamic equations for behavior of thermally conducting viscous compressible fluid in first post-Newtonian approximation to general relativity, obtaining conservation laws
09 p1518 A71-22338

MHD equations for charged conducting fluid behavior in first postNewtonian approximation to general relativity, obtaining conservation laws
09 p1518 A71-22339

Gas dynamic solutions of plane shock wave propagation in moving medium, considering conservation laws
09 p1525 A71-23198

Intense magnetic fields in astrophysics, emphasizing flux conservation law and quantum effects
13 p2144 A71-29436

Turbulent flow asymmetrical mechanics equations derivation from conservation laws, discussing Navier-Stokes equation, angular momentum and transport theory
14 p2227 A71-30877

Lunar surface structural evolution from energy conservation considerations, discussing earth primitive continent acquisition from moon
15 p2493 A71-32485

Landau-Lifshitz pseudotensor analogs of ten mechanical conservation laws in Einstein theory of gravitation
16 p2611 A71-33275

Heat and fictitious forces in variable rest mass relativistic particle dynamics for thermal energy conservation laws interpretation
19 p3162 A71-37641

Wave and elementary particles equations invariance properties relationship with respect to Lie group and conservation laws
19 p3105 A71-38579

Convergence of progressive shock wave solutions for higher order equations of conservation laws with dissipation and dispersion terms, proving shock curves existence
21 p3414 A71-40141

Photon mass terrestrial and extraterrestrial limit measurements, discussing speed of light frequency dependence, Coulomb law analog in magnetostatics energy conservation, etc
21 p3418 A71-40674

Lorentz invariant theory for relativistic gravity testing, deriving conservation laws and parameter constraints from parametrized post-Newtonian equations of motion
22 p3575 A71-41919

Noether invariance and conservation laws theorems extension to nonlocal calculus of variations, obtaining coordinate and point transformations effects on dependent functions domain space
23 p3700 A71-44177

Invariance theory for nonlocal variational principles, covering energy forms and identities, weak coordinate invariance, integral balance and conservation laws
23 p3700 A71-44179

CONSOLES

NT REMOTE CONSOLES

CONSONANTS [SPEECH]

Synthesized global consonant imitation by human voice, analyzing stimulus and response intensity levels relationship
02 p0206 A71-12062

CONSTANTAN

Centerline loss, transient sink temperature and thermal conductivity design constant considerations for thin foil copper-Gardon heat flux sensors
11 p1764 A71-26251

CONSTANTS

NT GRAVITATIONAL CONSTANT

NT GRUNEISEN CONSTANT

NT PLANCKS CONSTANT

NT SOLAR CONSTANT

NT TIME CONSTANT

Dimensions in physical science, discussing fundamentals and constants in dimensional analysis, operational measurements and numerical quantities
22 p3577 A71-42677

Light velocity measurements by optical and microwave techniques, noting electromagnetic constant error and role in distance measurement and physical theories development
24 p3827 A71-44996

CONSTELLATIONS

NT ARIES CONSTELLATION

NT AURIGA CONSTELLATION

NT CASSIOPEIA CONSTELLATION

NT CENTAURUS CONSTELLATION

NT CEPHEUS CONSTELLATION

NT CORONA BOREALIS CONSTELLATION

NT CYGNUS CONSTELLATION

NT ORION CONSTELLATION

NT SAGITTARIUS CONSTELLATION

NT SCORPIUS CONSTELLATION

NT TAURUS CONSTELLATION

Balloon-borne observation of X ray sources in northern sky, including Sco, Cyg and SN 1572
05 p0797 A71-15931

CONSTITUTIONAL DIAGRAMS

U PHASE DIAGRAMS

CONSTITUTIVE EQUATIONS

Thin reinforced laminates configurations with elastic behavior of homogeneous orthotropic or isotropic material, considering flat plates and thin shells constitutive equations
03 p0505 A71-13537

Elastoviscoplastic materials infinitesimal theory extension to thermodynamic processes by limit transition, deriving constitutive equations
03 p0510 A71-13946

Cosserat surfaces and variable thickness elastic plates linear isothermal theory, deriving constitutive equations corresponding to isotropic three dimensional plate bending and stretching
05 p0831 A71-17250

Isotropic incompressible viscoelastic solid deformation field under uniaxial and equal biaxial relaxation, determining constitutive equation
09 p1534 A71-22142

Solid circular Ti shaft torsion boundary value problem solution, using elastic-viscoplastic materials thermodynamics and constitutive relations
11 p1849 A71-25801

Rarefied gas Poiseuille flow in parallel plates, cylindrical tube and annulus geometries, deriving subsonic flow velocity profiles by third order constitutive relations
14 p2227 A71-30574

Elastic properties relativistic theory, defining deformation tensor and constitutive laws
15 p2442 A71-31904

Gases refractive behavior, discussing constitutive properties, wave propagation, Lorentz electron theory of dispersion, spectral interferometry and hook method
16 p2608 A71-33156

Error estimates in thin elastic shell linear theory, modifying three dimensional displacement field
17 p2815 A71-34224

Plastic nonlinear creep behavior theory reformulation, obtaining constitutive relations based on experimental data
19 p3084 A71-37524

Constitutive equation coefficients determination for nonlinear vibrations of viscoelastic beam by perturbation and optimal linearization method
19 p3158 A71-38060

Thermodynamics second law restrictions on constitutive equations of electromagnetic theory for nonlinear materials with long-range gradually fading memory, considering dissipation principle consequences
20 p3270 A71-39485

Nonassociated constitutive equations for rigid viscoplastic plates and thin rotationally symmetric shells under dynamic loading with Huber-Mises yield condition
20 p3310 A71-39777

Yield conditions and flow rules derivation from hypoelasticity, regarding constitutive equation as linear transformation on six dimensional inner product space of symmetrical tensors
21 p3455 A71-40090

Turbulent fluids constitutive equations verification by Truesdell principle of material indifference in incompressible and compressible fluids
21 p3367 A71-40652

Elastic viscous plastic effects calculation in materials, describing method permitting constitutive equations introduction into computer programs for continuum mechanics equations solution
21 p3465 A71-40787

Elastic viscous plastic waves profiles of finite uniaxial strain, obtaining constitutive equations
21 p3465 A71-40788

Iron response to dynamic loads, discussing pressure induced phase changes, constitutive equation relationship to dislocation processes and dynamic fracture criteria
21 p3399 A71-40789

Strain rate dependent constitutive relation for shock propagation in porous materials, discussing relaxation time
21 p3465 A71-40794

Viscoelastic boundary layer flow solutions, using second order constitutive equation
21 p3370 A71-40989

Nonlocal thermodynamics constitutive theory of continuous systems with global energy balance in terms of classical thermostatics
23 p3782 A71-43868

Nonlinear theory of nonlocal continuum mechanics, considering global energy balance, constitutive equations and Clausius-Duhem inequality
23 p3705 A71-43869

CONSTRAINTS

NT METEOROLOGICAL PARAMETERS

Continuum internal thermodynamic constraints effect on materials response, assuming workless stress tensor
03 p0506 A71-13694

Time optimal control of systems with magnitude and impulse limited constraints on control forces
05 p0782 A71-16983

Constrained function extremization, taking into account modified quasi-linearization algorithm
05 p0776 A71-17088

Elastic plates and members deformation with constraints on deflections, determining strain state with dynamic programming
06 p0984 A71-17651

Optimal control sufficient conditions with state and control constraints
07 p1082 A71-19771

Normalized hodographic mapping for constrained trajectory families, discussing mapping concepts, information content and applications
07 p1199 A71-19884

Linear one dimensional systems with infinite degrees of freedom, examining optimal constrained control
09 p1421 A71-22118

Primate restraint harness of nylon jacket and cotton cot on aluminum frame padded seat for bone resorption and calcium metabolism studies
09 p1398 A71-22476

Hamilton-Jacobi type theorem on equations of motion with factors of constraints, giving proof for stationary mechanical systems
12 p1923 A71-27529

Statically determinate beams optimal design, considering displacement and stress constraints in optimality conditions derivation
12 p1983 A71-27596

- Bounded flow incident on cylindrical body in transverse magnetic field, determining constraints effects on dynamic and structural characteristics
14 p2278 A71-29609
- Linear one dimensional systems with infinite degrees of freedom, examining optimal constrained control
14 p2219 A71-29996
- Constrained optimization problems solution combining modified pattern search methods and polynomial constraints in aircraft design parameters selection
16 p2603 A71-33721
- Numerically stable algorithm for solving least squares problems with linear equalities and inequalities as additional constraints
17 p2769 A71-35693
- Time optimal control of systems with magnitude and impulse limited constraints on control forces
18 p2896 A71-36783
- Physical constraints on universe topology near collapsed-ordinary stars interaction in general relativity theory
19 p3105 A71-38583
- Necessary conditions of optimality for control problems with state variable inequality constraints, using separating hyperplane theorem
21 p3359 A71-40207
- Elastic trusses optimal design under multiple mechanical constraint conditions, describing steepest descent method with constraint error compensation
21 p3470 A71-41021
- CONSTRUCTIONS**
- Computer programmable flow coefficient formulas for standard constrictions, orifice gages and Venturi nozzles
10 p1595 A71-24640
- Eigenvalues lower bounds determination for arbitrary shape region, presenting domain constriction method
21 p3416 A71-41014
- CONSTRUCTION**
- Radome design and production, considering construction, materials, shape, manufacturing techniques and technological problems
14 p2218 A71-31067
- CONSTRUCTION MATERIALS**
- Lightweight structural elements fabrication from fiber reinforced plastic materials [prepregs], discussing manufacturing methods, structural design, production and testing of parts, etc
01 p0172 A71-10690
- Materials for spacecraft design requirements, considering composite and refractory metals, Ti and heat resistant alloys
01 p0102 A71-10816
- Airplane materials mechanical properties degradation due to fatigue, discussing breaking strain of Al alloy
01 p0104 A71-11395
- Radiative properties of construction properties and working media, noting importance to radiative heat transfer calculation
03 p0519 A71-13747
- Sandwich metal construction with welded Norsial corrugated core for light weight and strength, discussing fabrication and application to hypersonic research vehicles
04 p0603 A71-15207
- Aircraft light alloys fatigue characteristics for component endurance evaluation
05 p0767 A71-16757
- Construction materials characteristic properties significance for design and structural reliability, discussing weldable Al alloys fatigue strength, internal stresses, inhomogeneity and corrosion behavior
06 p0981 A71-17341
- Metallic construction materials creep rupture behavior, discussing primary, secondary and tertiary creep metallurgical and physical processes
06 p0911 A71-17346
- Intermetallic compounds structural component applications, considering crystal growth, alloy constitution and development, mechanical properties and processing technology
07 p1131 A71-19427
- Structural materials criteria for cryogenic propellant tanks, discussing chosen alloy composition, heat treatment and general properties
07 p1118 A71-19802
- Plastics and metals as construction materials in aircraft, missile and rocket design
07 p1215 A71-20044
- Carbon fiber reinforced plastics potential aerospace structural applications, considering weight saving, mechanical properties, thermal expansion, stress concentration, impact resistance, corrosion and lightning problems
[PLASTICS INST. PAPER 43]
08 p1369 A71-20927
- Tetra-Core structural composite material, discussing fabrication techniques, test results, potential and applications
08 p1369 A71-21225
- Large spaceborne telescope primary mirrors materials under microstructural loads, considering low expansion ceramics and metallics applications
09 p1446 A71-22743
- Complex alloying of structural steels, stressing structural changes, electron interactions and phase transition changes
09 p1470 A71-23075
- Glass fiber reinforced plastics aerospace applications covering radomes, dielectric panels, aircraft ducting, secondary structures, furnishings, mouldings and tooling
11 p1788 A71-25652
- Concorde aircraft construction methods, materials and design
12 p1867 A71-26882
- Material properties, impregnation, shaping, hardening and structural design in mass production of reinforced laminates for aircraft construction
12 p1920 A71-26954
- Flame retardant silicone elastomers for use as aircraft construction materials, describing fabrication techniques, mechanical, aging and weathering properties
12 p1921 A71-27412
- Aircraft industry materials development, discussing innovations in governmental programs management, procurement specifications and Department of Defense contracting procedures
12 p1918 A71-27677
- Materials evaluation system for aerospace structural application
12 p1919 A71-27678
- Materials selection in product design, considering performance, cost, schedule and materials characteristics requirements, with special attention to brittle materials
14 p2340 A71-29899
- Shock wave caused chemical reactions between solids and cryogenic liquids, discussing shock sensitivity tester for liquid propellant- structural material systems
14 p2222 A71-30546
- Impact sensitivity tester for engineering materials in liquid and gaseous oxygen at high pressures
14 p2222 A71-30548
- Intermetallic compounds application in structural materials, emphasizing role in superalloys development for gas turbine engine parts and high temperature environments
15 p2427 A71-31531
- Variously thick standard production heavy plate constructional steels stress condition and elastic energy margin effects on cold brittleness
15 p2414 A71-31652
- Structural materials low temperature testing using cryogenic chambers, high power tensile test machines, semiconductor thermometers and resistance wire strain gauges
15 p2408 A71-31854
- Endurance limit of construction materials under fast and thermal neutron irradiation in reactor channel
16 p2598 A71-33986
- German monograph on structural steels tensile and yield strength, detailing strain rate and testing machine effects
17 p2818 A71-34483
- German book on welding conditions and material composition effects on structural changes and heat-affected zone mechanical properties of high strength structural steels
17 p2748 A71-34851
- Light alloys fatigue characteristics for aircraft components endurance evaluation
17 p2759 A71-35456
- Structural steels fatigue resistance, investigating processing technique, chemical composition, plastic and hot working and heat treatment effects
18 p2934 A71-36149
- Experimental materials for axial flow vane pumps operating under cavitation conditions, considering separated flow around impeller blades
20 p3241 A71-39169
- Economical alternative construction materials selection for partmaking cost reduction while maintaining quality
20 p3251 A71-39338
- Structural support system for large log-periodic antenna, discussing asbestos-cement pressure pipes and fiberglass rods as construction materials for antenna critical electrical characteristic needs
20 p3210 A71-39871
- Soviet papers on construction materials stress state dynamics, thermoelasticity and statics modeling problems, using optical polarization methods
22 p3614 A71-41609
- High temperature structural application of refractory fiber reinforced ceramic composites
22 p3565 A71-42287
- Sintered construction material with high SiC content, investigating thermal stability in nitrogen, air, carbon dioxide and water vapor above 2000 K
23 p3696 A71-44020
- Strength and plasticity characteristics of hardened multilayer structural steels, investigating layer thickness effect
24 p3837 A71-44729
- Structural materials ability for irreversible conversion of mechanical to thermal energy from free longitudinal vibrations attenuation measurements in rod
24 p3817 A71-45200
- CONSUMPTION**
- NT FUEL CONSUMPTION
NT OXYGEN CONSUMPTION
NT WATER CONSUMPTION
CONTACT POTENTIALS
- External-internal gear stages contact ratio on basis of gear wheels working drawing geometrical quantities
03 p0431 A71-13025
- Contact potential measurements of work function dependence on adsorption of alkali metals on Ta/110 and W/100/ crystals under ultrahigh vacuum
09 p1497 A71-22701
- CONTACT RESISTANCE**
- Thermal contact resistance as function of time during static load
07 p1116 A71-18917
- Semiconductor thermocell junction polishing effects on bilateral layers tensile strength and electrical contact resistance
07 p1023 A71-19145
- Dry reed sealer transfer contact design, operation and embodiment, noting Au diffused and Rh contacts with hydrogen gas
13 p2038 A71-28838
- Peroxide-alkaline polishing solution for GaAs, evaluating optical quality, surface damage, polishing rate and metallic contact resistance
18 p2955 A71-37004
- Specific contact resistance at zero bias as measure of ohmic or rectifying behavior of metal- semiconductor barrier under operating conditions
19 p3117 A71-37485
- Electric contact resistance of various conductive metal coatings on aluminum corrosion free joints
19 p3031 A71-38449
- X band Gunn diode oscillator pulsed operation starting delay time relationship to CW operation frequency/temperature characteristics, suggesting contact resistance role
21 p3359 A71-41411
- CONTACTORS**
- Rolling contact body displacement effect on bearings rigidity with allowance for inner ring transverse vibration
08 p1295 A71-20689
- Spring loaded intermittent contact devices vibrating system parameters for computer programmed transfer matrix solution, noting gravity loaded variant
12 p1931 A71-27480
- CONTACTS (ELECTRIC)**
- U ELECTRIC CONTACTS
- CONTAINERS**
- Multicavity thin walled containers of spheres and intersecting plane partitions, comparing structural properties with single sphere of equal overall volume
03 p0515 A71-14366
- Gas discharge from curvilinear walled vessel of finite width and from symmetrical vessel with rectilinear parallel walls
07 p1092 A71-20082
- Air cargo volume development trends, examining worldwide airport terminal capacities and pallet/ containerization systems modular design and operation
10 p1699 A71-24824
- C-5A cargo box side wall deformations, examining square plates center deflections with elastic beams
10 p1557 A71-24871
- Exchange regulation of standardized container loading units in air freight transportation
19 p3173 A71-38220
- CONTAMINANTS**
- NT TRACE CONTAMINANTS
- Portable direct reading spectrometer for monitoring oxygen-hydrogen containing contaminants in gas tungsten arc welding process
02 p0247 A71-11712
- Apollo 11 and 12 lunar soil samples common contaminant identified as disisopropyl disulfide, using chromatograph mass spectrometer
05 p0716 A71-16453
- Gas turbine engines emission characteristics, discussing methods for pollutants reduction
08 p1349 A71-21820
- Corrosive contaminants, oxygen, humidity and temperature environment simulation
11 p1746 A71-26496
- Agena rocket engine pollutants, considering pollution control by scrubbers, engine system modification and micrometeorological data gathering
[AIAA PAPER 71-716]
14 p2294 A71-30768
- Long mission duration manned spacecraft contaminant control system design, discussing catalytic, oxidation, chemisorption and charcoal adsorption removal techniques and computerized performance prediction
[ASME PAPER 71-AV-19]
18 p2867 A71-36386

Oxygen contamination effect on GaP solar cell electroluminescence and photoluminescence characteristics from electrical and mass spectroscopic analysis data

19 p2998 A71-38143

Miniature self regulating rapid cooling Joule-Thomson cryostat, noting purging of accumulated contaminants

20 p3184 A71-39274

CONTAMINATION

NT FUEL CONTAMINATION

NT SPACECRAFT CONTAMINATION

Nb surface contamination by oxidation during electrolytic polishing and vacuum annealing

02 p0269 A71-12928

Surface roughness and contamination, drop volume and liquid subcooling effects on Leidenfrost temperature

04 p0675 A71-14783

Reflecting oven for very high temperatures under gas pressure, describing apparatus, heat source and possible contamination

10 p1613 A71-25040

Contamination degrading effects on optical surfaces, discussing application to real time monitors data analysis

[AIAA PAPER 71-460]

11 p1800 A71-26242

Optical surfaces contamination analysis by holographic interferometry, using fringe patterns for contaminant film thickness and uniformity

14 p2244 A71-30330

Water vapor contamination long lasting effects on stratospheric measurement during balloon flight

14 p2270 A71-30453

Fluid contamination and protective filter in hydraulic power components for design service life

18 p2851 A71-36204

Hydraulic system and fluid cleanliness maintenance, discussing contamination sources and prevention techniques including filtration, dehydration and degasification

19 p2999 A71-38319

Hydraulic servo equipment filtration systems design, discussing contamination effects and servo components physical characteristics effects on tolerance level

19 p2999 A71-38320

Hydraulic components and equipment contamination control and effects on system efficiency, discussing filter ratings and location

19 p2999 A71-38321

Hydraulic equipment fluid contamination control, discussing sample bottle cleaning, fluid sampling, component tolerance profiles and filtration performance specifications

19 p2999 A71-38322

Hydraulic fluids contribution to system contamination, discussing precipitate formation due to reaction with water, filtration inability and contaminant elimination

19 p2999 A71-38323

ASTM Committee F-7-C status report on contamination methods including sampling, processing samples and particulate analysis

19 p3000 A71-38324

Microbial contamination of human skin and upper respiratory tract during long term isolation in sealed environment

21 p3333 A71-40559

Bacterial contamination in confined sealed space during long term human occupation, observing hemolytic microflora spreading dynamics on bodies, clothes, wall and air

21 p3343 A71-40560

Re and Os abundance and meteoritic contamination levels in Apollo 11 and 12 rocks, fines and breccia

23 p3750 A71-34396

CONTINENTAL DRIFT

Critique of Ethiopian Afar depression formation as oceanic crust resulting from Arabia drift, considering plate tectonics analysis for bifurcated spreading zones

04 p0582 A71-15126

Stokes earth shape formula derivation without removing continental masses for regularization requirement

09 p1438 A71-23181

Mars surface harmonics and continental drift from radar and spectroscopic topographic height determination

16 p2638 A71-33519

CONTINENTS

NT AFRICA

NT AUSTRALIA

NT EUROPE

NT SOUTH AMERICA

Lunar surface structural evolution from energy conservation considerations, discussing earth primitive continent acquisition from moon

15 p2493 A71-32485

CONTINUITY [MATHEMATICS]

Quasi-linear elliptic boundary point solutions, deriving modulus of continuity estimates

04 p0619 A71-15552

Continuous time stochastic optimal control systems necessary and sufficient dynamic programming conditions for optimality

04 p0562 A71-15871

Differential equations system continuability theorem for specific initial conditions

05 p0775 A71-16885

Numerical approximation of continuous real function in interval by polynomials using appropriate nets, estimating error

06 p0920 A71-18209

Neutral functional differential equations, discussing forward and backward continuation

06 p0921 A71-18239

Grid refinement technique generating sequences of approximate solutions to two-point variational problems defined on continuous fields

13 p2096 A71-29380

Jacobi polynomial series analytic continuity properties based on relation with corresponding Taylor series

17 p2764 A71-34421

Continuity and smoothness properties of piecewise optimal control at junction between singular and nonsingular subarcs, developing necessary conditions

17 p2723 A71-35296

Unique linear product approximations of continuous functions of several variables extended to general convex sets

17 p2768 A71-35682

Nonlinear eigenvalue problem solution in real Banach space, investigating continua existence and elliptic equations application

18 p2942 A71-36818

CONTINUITY EQUATION

Moving plasma hydrodynamic equations of motion, continuity and energy in axially symmetric coordinate system

03 p0464 A71-13904

Continuity and balance equations of acoustic energy in nonuniform fluid flows

07 p1160 A71-19588

Strain continuity equations in statics using equivalent integrodifferential form

07 p1218 A71-20465

Electron continuity equation for lower F 2 layer near dip equator, estimating photoionization and recombination rates

08 p1278 A71-21203

Stored gas retrorocket total impulse expression, deriving from fluid continuity equation in closed duct

08 p1366 A71-21308

Book on homogeneous flows aerothermochemistry covering chemical reactions, heat and mass transfer, entropy production, species continuity, momentum and energy equation

09 p1547 A71-23674

Ionospheric dynamic behavior, describing time dependent continuity and ion, electron and neutral particle motion equations

10 p1606 A71-24914

Neutral air winds and ionospheric continuity equation, calculating midlatitude electron concentration longitudinal variations

11 p1754 A71-25605

Numerical integration of unsteady continuity equation for electron-ion gas concentration distribution in F 2 region

11 p1757 A71-25770

One dimensional charged particle continuity equation solution in low energy neutral plasma with current flows

11 p1804 A71-26374

Continuity equation properties for incoherent fluid, obtaining linear partial differential equation

19 p3105 A71-38584

Midlatitude ionospheric data comparison to F 2 critical frequency from continuity equation and neutral air winds

21 p3372 A71-40043

Morera and Maxwell stress functions determination by integrodifferential equations of deformation continuity for bending of thin plates

21 p3455 A71-40085

Numerical integration of unsteady continuity equation for electron-ion gas concentration distribution in F 2 region

22 p3532 A71-41538

Elastic and inelastic thin shell nonlinear theory derivation by integrating material continuity equations of motion over shell thickness

23 p3775 A71-43318

Ideal gas and liquid droplets two phase flow continuity and motion one dimensional equations, describing relations between velocity, density, pressure and bulk component concentrations

24 p3818 A71-44709

CONTINUOUS NOISE

Electromagnetic field measurements for continuous noise sources and traversed ionospheric region parameters, using ground, rocket and satellite techniques

09 p1440 A71-23629

CONTINUOUS RADIATION

NT MODULATED CONTINUOUS RADIATION

He-Cd laser stable long life CW excitation by D-C cathaphoresis to maintain spatially uniform and optimum Cd vapor concentration

01 p0091 A71-10003

Argon ion CW lasers, discussing design, inverse population, plasma, radiative transition probabilities, pumping, frequency spectra and active medium

01 p0092 A71-10181

CW chemical laser operation with HF and DF subsonic electric discharge mixing device, obtaining 5.5 w output

03 p0434 A71-13475

CW carbon dioxide lasers low voltage excitation using cold cathode transverse glow discharges

03 p0436 A71-13641

CW ion laser transitions in Ar, Kr and Xe, tabulating threshold data

03 p0438 A71-13890

AlAs-GaAs heterojunction laser threshold current and CW operation at room temperature as function of p- and n-type emitter regions

03 p0439 A71-13981

Gas laser technology developments, discussing CW noble gas ion lasers, high output IR carbon dioxide lasers, metal vapor and pure helium lasers

04 p0605 A71-14711

IR lasers, discussing carbon dioxide CW and Q-switched operation and semiconductor lasers

04 p0606 A71-14712

CW sounding for HF adaptive control for data transmission with ionospheric phase error

04 p0552 A71-15145

Continuous nitrogen and oxygen ion spectra due to photoionization and free ion transfers at high temperatures

05 p0838 A71-16788

CW microwave reflection-type amplification from circuit stabilized epitaxial GaAs transferred electron devices, observing gain and hysteresis

05 p0729 A71-16918

Planetary nebulae continuous UV spectrum, discussing glow process, electron temperature and density and Balmer discontinuity

06 p0974 A71-18430

CW chemical operation in IR for hydrogen fluoride, deuterium fluoride, hydrogen fluoride-carbon dioxide and deuterium fluoride-carbon dioxide systems

06 p0909 A71-18490

High power continuous and pulsed coherent radiation generation by gas lasers, discussing transmission by proton generators and transforming engines

06 p0946 A71-18557

CW electric discharge mixing chemical lasers, identifying molecular transitions responsible for radiation from output spectral distribution measurements

06 p0909 A71-18552

Noise spectra of CW hollow cathode zinc ion lasers compared with conventional discharges, noting gain per unit length on transitions

06 p0910 A71-18662

Linearly polarized CW signal transmission through near solar corona, measuring Faraday rotation

07 p1191 A71-19030

One watt CW high efficiency X band avalanche diode amplifier with in-band and second harmonic impedance control

07 p1073 A71-19117

Thermally induced modifications of high power CW laser beam, considering heat losses by forced and free convection

07 p1122 A71-19207

CW GaAs semiconductor laser fabrication by liquid epitaxy, noting Ag plating role in output power

07 p1126 A71-20196

Diffuse and constricted Ar arc columns continuum emission determination from continuous spectra at 2700-4800 A

07 p1172 A71-20377

CW helium-air-carbon monoxide laser with low flow rate and liquid nitrogen cooling, observing emission below 5 microns

07 p1128 A71-20398

Electrophotometric and spectral observations of continuous airglow spectrum

07 p1105 A71-20438

Modified waveguide magnetrons for continuous 1.3 mm waves, discussing construction and operation

07 p1081 A71-20454

YAG-Nd laser rods CW pumping by cooled and room temperature GaAsP diodes, determining threshold temperature dependence

07 p1129 A71-20621

Carbon dioxide-nitrogen CW laser AC excitation in optical cavity, considering power output

08 p1301 A71-20997

Spectral mode and CW operation of stripe geometry double heterostructure GaAs junction lasers above room temperature

09 p1463 A71-22763

Spectral mode, band to band carrier decay, pulsed and CW operation of laser quality In-Ga-P

09 p1463 A71-22765

Giant elliptical galaxy Maffei I continuous radiation emission data at 1415 MHz, examining radio luminosity magnitude

09 p1523 A71-22982

GaAs junction laser continuous operation, investigating reflectivity dependence of temperature rise, stimulated light output and power efficiency

09 p1464 A71-22988

Polyethylene plastic packet with chemical pellets, describing welding, cutting and small hole punching by CW carbon dioxide laser

09 p1458 A71-23410

Q switched and continuous laser collimated radiation exposure limits for eye cornea and skin, discussing environmental contamination

09 p1402 A71-23414

Continuous wave HCl chemical laser, achieving large specific gain through high speed flow, rapid mixing and transverse geometry

09 p1465 A71-23480

Gas dynamic CW laser with supersonic hot moist carbon dioxide-nitrogen as working fluid, discussing laser gain vs water content

10 p1619 A71-23760

High power single mode CW tunable spin-flip Raman laser in InSb using CO pump

10 p1620 A71-24041

CW carbon dioxide gasdynamic laser gain for mixture of carbon dioxide, nitrogen and helium

10 p1620 A71-24043

Parasitic noise reduction in CW Nd-YAG laser output

10 p1620 A71-24154

Exposure time and power effects of CW Ar laser damage to rabbit iris, comparing with pulsed ruby laser effects

10 p1572 A71-25076

Carbon dioxide laser design and characteristics, discussing lasing action, spectral properties of continuous and Q switching output power

10 p1623 A71-25089

Oxygen and carbon dioxide continua absorption cross sections in Schumann and far UV regions by photoelectric technique with vacuum monochromator

11 p1801 A71-25364

Single boundary layer flame sheet model for continuous diffusion chemical lasers, obtaining integrated zero power gain, laser power and efficiency [AIAA PAPER 71-28]

11 p1774 A71-25928

InP pulsed and CW millimeter wave oscillators at frequencies above 30 GHz

11 p1739 A71-26367

Continuous cold cathode forward wave reentrant beam crossed field amplifiers with cut-off electrode, investigating AM and PM noises and phase coherence

11 p1739 A71-26434

Planetary nebulae continuous UV spectrum, discussing glow process, electron temperature and density and Balmer discontinuity

12 p1955 A71-26584

Circular polarization in white dwarf G99-37 continuum radiation as function of wavelength

12 p1956 A71-26609

Periodic variations in circular polarization of continuum radiation of white dwarf G195-19 from 3800 to 5400 Å

12 p1956 A71-26610

Precipitation energy flux of continuous nighttime aurora, using airborne ionospheric and optical measurements

13 p2054 A71-27801

Continuous visible operation of semiconductor laser at room temperature, discussing lasing thresholds

13 p2081 A71-29340

Glow discharge, ion and excited state properties of laser plasmas, including CW conditions for argon

14 p2253 A71-29542

CW 28 micron signal resonant regenerative amplification in pulsed water vapor laser, showing pulse to pulse frequency coherence

14 p2255 A71-30832

Continuous chemical laser, emphasizing strong coupling in cavity between radiation and chemistry [AIAA PAPER 71-574]

15 p2419 A71-31565

Carbon monoxide-helium-oxygen laser emission continuous self mode locking and temporal structure for various optical cavity lengths

15 p2420 A71-32379

Laser beam CW self-induced frequency modulation and switching observation in liquids with low surface tension

15 p2420 A71-32381

Singly ionized magnesium CW laser oscillation in He-Mg discharge at micron wavelengths with possible extension to visible and UV spectrum

15 p2420 A71-32386

CW laser transitions in Se II, investigating current saturation behavior and output power and structure

15 p2422 A71-32581

CW gain measurements on rotation-vibration P branch transitions of CO molecular laser, calculating gas temperature, Einstein coefficient and population densities

15 p2423 A71-32609

IR stars and galaxies measurements, determining 3.5 mm continuum radiation intensity

15 p2498 A71-32775

Continuous nitrogen and oxygen ion spectra due to photoionization and free ion transfers at high temperatures, calculating absorption coefficient

16 p2662 A71-33040

CW chemical lasers research, summarizing three lasing principles and advantages over electrically or thermally excited lasers

16 p2586 A71-33163

Semiconductor laser continuous emission conditions at room temperature, assuming output power drop with increasing current due to p-n junction heating

16 p2587 A71-33492

Low noise operation of CW devices with GaAs vapor grown p-n junctions, observing optimum AM SNR of minus 140 dB

17 p2713 A71-34445

Gasdynamic lasers optically active medium two-flow model, deriving solutions for CW generators and quantum amplifiers

17 p2754 A71-35397

High intensity continuous gas discharge line source for extreme UV with low electromagnetic interference

18 p2914 A71-35845

Silicon IMPATT microwave oscillators, calculating CW power as function of frequency by scaling approximation

18 p2888 A71-36129

High efficiency avalanche diode microwave oscillator design guidelines based on oscillation mode theory, covering CW and pulsed operations

18 p2888 A71-36131

Carbon dioxide laser, discussing mixture composition, vibrational energy levels, excitation and relaxation mechanisms, output characteristics, CW and Q switching, mode locking and applications

18 p2930 A71-36147

High power microwave CW tubes and power amplifier requirements for communication satellites

18 p2892 A71-36571

Plasma diagnostics based on IR continuum intensity due to bremsstrahlung emission from plasma

19 p3113 A71-37765

High-power high-efficiency CW X band Gunn oscillators on diamond heat sinks, noting operation in waveguide cavities

19 p3029 A71-38219

Spectral measurements of nitrogen continuum radiation behind incident shocks at high speeds, suggesting free bound neutral atom-electron interactions origin

19 p3172 A71-38718

Visible thermal tuning CW parametric oscillator using barium sodium niobate as nonlinear material

20 p3241 A71-38788

Polarization flip with hysteresis effect at zero magnetic field in CW far IR HCN laser

20 p3244 A71-39098

Water cooled hollow cathode design for continuous emission HCN lasers

20 p3246 A71-39494

Early stars UV continuum brightness from rocket-borne photoelectric spectrophotometer, estimating total interstellar flux density

21 p3444 A71-40244

Venus 3-4 micron region continuum absorption from high resolution spectra of Venus and sun

21 p3448 A71-40448

Ultrarapid color holography using continuous synchronized coherent light sources of different wavelengths

21 p3378 A71-40514

He-Cd CW laser transitions, describing charge exchange and Penning ionization-excitation processes

21 p3393 A71-41038

Axially constructed Ar laser with segmented graphite line and pumping tube, discussing continuous operation power outputs and electric discharge current optimal magnetic field strength

22 p3556 A71-41704

Tunable CW optical parametric oscillator optimum operating conditions, using barium, sodium and lithium niobate crystals parametric fluorescence tuning curves for comparison

22 p3557 A71-41863

Continuous chemical laser model for constant gain method exposure, emphasizing strong radiation-chemistry coupling, molecular J-shift, output power limiting behavior and lasing efficiency

24 p3832 A71-44373

Low cost CW carbon dioxide laser power meter using Joule heating technique

24 p3835 A71-45213

CONTINUOUS WAVE RADAR

Synthetic aperture holographic techniques in continuous wave bistatic radars for moving targets

03 p0381 A71-14477

Meteorological tower high resolution CW-FM radar measurements for studies of temperature inversions, waves, thermal plumes and convection in atmospheric boundary layer

14 p2192 A71-29707

Electromagnetic compatibility performance of pulse Doppler radar receivers, considering CW or synchronous pulse interference

19 p3020 A71-38430

Book on pulse, CW, Doppler, pulse Doppler and space radar theory, operation and maintenance, describing equipment, tracking and siting

22 p3509 A71-41621

CONTINUOUS WAVES

U CONTINUOUS RADIATION

CONTINUUM FLOW

Approximate bridging relations for heat transfer, surface shear and drag in transitional regime between free molecule and continuum flows

07 p1087 A71-18894

Atmospheric attenuation in IR windows near sea level from transmittance spectral curves, discussing continuum absorbance

09 p1437 A71-22740

Continuous flow arc air heater for reentry vehicle components ground testing, achieving combined high pressure and enthalpy

[AIAA PAPER 71-259]

09 p1429 A71-23061

Conical converging nozzle flow of perfect monatomic gas in rarefied near continuum, transition and near free molecular regimes, using finite difference methods

15 p2390 A71-32045

Monograph on dynamic viscous pressure interaction in hypersonic flow covering boundary layer effect on oscillating body unsteady pressure distribution in continuum hypersonic flow

17 p2671 A71-35217

Flow field and model wall on slender bodies in low density hypersonic flows ranging from free molecular flow to continuum flow

18 p2846 A71-36418

Rarefied gas flow characteristics through pipe orifice in intermediate range of rarefaction between free molecular flow and continuum flow

18 p2849 A71-37023

Continuum dislocation theory, discussing initial stress couple problem, slip motion and dislocation rate tensor

21 p3468 A71-41000

CONTINUUM MECHANICS

Nondissipative micromorphic media field equations derivation, applying variational principle to theory of deformable bodies

01 p0177 A71-11372

Plastic deformation continuum model, including first and second strain gradients

02 p0321 A71-11679

Stochastic wave propagation in continuously randomly inhomogeneous media, surveying analytical methods

02 p0219 A71-12545

Monograph on corrections to Holtsmark continuum model for plasma fluctuations covering probability distributions, quantum mechanical corrections for hot plasmas, etc

02 p0293 A71-12843

Artificial intelligence computer programming system for continuum mechanics, discussing capabilities of CONFORM as mathematical language

03 p0382 A71-13548

Continuum internal thermodynamic constraints effect on materials response, assuming workless stress tensor

03 p0506 A71-13694

Rarefied gas flow through long square tubes, solving continuum differential equation with noncontinuum slip boundary conditions

[ASME PAPER 70-WA/PID-1]

03 p0402 A71-14098

Inextensible fiber-reinforced plastic-rigid solid, applying continuum theory to derive kinematic properties, yield condition and flow rule

03 p0514 A71-14349

German monograph on field equations solution for Cosserat continua in planar strip type regions covering stress analysis

03 p0515 A71-14370

Flat products skin milling work determination from microgrid deformation graphs, using continuum mechanics equations

04 p0602 A71-14607

Shock structure in crystalline solids, including dissipative processes, discontinuities, continuum mechanics and lattice dynamics

04 p0664 A71-14662

Metal fatigue crack initiation and propagation by continuum mechanics approach, considering dislocation, stress and deformation conditions and load cycle effects

04 p0666 A71-14888

Soviet book on continuum medium covering dynamic, thermodynamic and electrodynamic equations mechanic problems, three dimensional space, internal degrees of freedom, etc

04 p0626 A71-15373

Stationary edge dislocation interaction with partially bonded bimetallic interface, noting isotropic elastic continuum approximation

04 p0670 A71-15383

Consistent finite element model for two dimensional continuum problems on basis of virtual work principle
04 p0672 A71-15770

Continual systems analytical mechanics, discussing least constraint variational and Ostrogradskii-Hamilton principle applications in shell stability, filtration, plasticity and dislocation theories
05 p0828 A71-16895

Book on dynamic characteristics of aerosol particles in terms of classical mechanics covering continuum approximation, single particles heat and mass transfer, diffusion, dispersion, etc
09 p1431 A71-22284

Models for nonferromagnetic solid body mechanics allowing for relationships among mechanical, thermal and electromagnetic processes
09 p1509 A71-23076

Composite material dynamic processes based on diffusing mixtures continuum theory
09 p1540 A71-23085

Solids continuum mechanics and fracture criteria, emphasizing intermixed elastic, plastic or viscoelastic types materials behavior idealization
13 p2151 A71-28214

Numerical integration procedure for calculating mixed phase transformation in continuum mechanics for given volume and internal energy increments
13 p2100 A71-28232

Conjugate functions theory variational application to solid mechanics, generalizing concept of potential for nonlinear behavior laws in viscosity and plasticity
14 p2329 A71-30447

Continuous system nonconservative stability examined by finite element Ritz method with extended Hamilton principle
14 p2330 A71-30687

Complex media and plasticity theory deformation models based on central friction mechanism, discussing elastic spring analog
14 p2332 A71-30879

Rumanian book on distribution theory applications in mechanics covering physical point motions, variable mass, concentrated and distributed loads, elasticity theory equilibrium, motion equations, etc
15 p2501 A71-31147

Variational principles application to continuum mechanics boundary and initial value problems, discussing examples in elastostatics, piezoelectricity and hydroelasticity
15 p2441 A71-31416

Stochastic wave propagation in continuous randomly inhomogeneous media, surveying analytical methods
15 p2373 A71-32501

Fracture mechanics macroscopic aspects in terms of continua mechanics to provide practical criteria for fracture toughness estimates
15 p2510 A71-32557

Gravitating continuous medium instability in presence of delta shaped point density perturbations, discussing cloud structure development in interstellar gas
15 p2495 A71-32642

Static stability criterion dynamic extension for nonlinear continua under conservative loads, using Liapunov functions
16 p2607 A71-32980

Mechanical continuous system equilibrium stability under follower forces, discussing viscous damping destabilizing effects
16 p2608 A71-33007

Variational principles in solid continua mechanics, describing finite element models
16 p2651 A71-33078

Continuum mechanics in differential forms, discussing material and spatial coordinates, compatibility conditions energy balance, entropy inequality and invariance principles
16 p2613 A71-34146

Tensional thermoelasticity theory of continuum media, analyzing material particle interactions by stress tensor and equations of motion
17 p2815 A71-34187

Limit analysis of dissipation power and collapse load of rigid perfectly plastic continua with piecewise linear yield surface, using linear programming
17 p2816 A71-34324

Hybrid techniques combining continuum and finite element methods, noting application to stress concentration singularities
17 p2831 A71-35354

Microcracks analysis by micropolar continua theory, presenting solution for circular hole in infinite plate
17 p2832 A71-35421

Laminated composite beam microstructure continuum model, calculating equations of motion and boundary conditions with Hamilton principle [ASME PAPER 71-APM-S]
18 p2978 A71-36261

Incompressible fiber reinforced composite materials finite plane deformation continuum theory and stress analysis without restriction concerning elasticity, plasticity or viscoelasticity behavior [ASME PAPER 71-APM-V]
18 p2978 A71-36264

Thermodynamics axioms for work and energy under volume-area continuity conditions, discovering local power density in velocity field
18 p2948 A71-36812

Nonlinear differential equations and boundary conditions describing behavior of electrically polarizable finitely deformable heat conducting continuum interacting with electric field
19 p3118 A71-37793

Continuum mechanical approach to velocity dispersion of longitudinal plane waves in elastic solid containing dislocations
19 p3118 A71-37794

Generalized continuum of interleaved microstructures coupled by forces, investigating equations of motion, tensor indices and asymmetric effects
20 p3309 A71-39566

Elastic viscous plastic effects calculation in materials, describing method permitting constitutive equations introduction into computer programs for continuum mechanics equations solution
21 p3465 A71-40787

Computer simulation of crack propagation in plane strain and plane stress geometries, solving continuum mechanics equations in two space dimensions and time
21 p3351 A71-40797

Fiber reinforced elastic materials steady state plane wave propagation by modeling constituents as continua undergoing individual motions
21 p3469 A71-41004

Lower bound deformation theorem for rigid plastic continua and structures under impulsive loading, using kinematically admissible velocity field
22 p3614 A71-41608

Discrete approximations for continuous fields in solid body nonlinear theory with differential and nonlinear equations replaced by algebraic and linear equations respectively
22 p3616 A71-42218

Plastic shells under finite bending, deriving large deflection theory from nonlinear continuum mechanics by yield criterion Lagrangian formulation
23 p3775 A71-43317

Nonlocal thermodynamics constitutive theory of continua systems with global energy balance in terms of classical thermostatics
23 p3782 A71-43868

Nonlinear theory of nonlocal continuum mechanics, considering global energy balance, constitutive equations and Clausius-Duhem inequality
23 p3705 A71-43869

CONTINUUMS

Seminfinite isotropic linear Cosserat continuum surface under impulsive loading, calculating displacements with Laplace transformation
04 p0672 A71-15834

Cracks in Cosserat continuum, investigating couple-stress effects on stress concentration
13 p2153 A71-28521

Cosserat continuum elastic tensor potentials applied to Kirchhoff theory of wave diffraction
20 p3269 A71-39033

Micropolar continuum, potential energy, stresses and constitutive relations for buckling of large rectangular grid frameworks under axial load
21 p3469 A71-41009

Calcium abundance in solar corona, using measured values for total intensity of continuum and integrated intensities ratio
23 p3768 A71-43845

CONTOURS

Ground relief representation by contour lines and by profiles, noting error possibilities
01 p0074 A71-11328

Electronic contour line recorder with intermittent line setting capacity and interpolation frequency regulation
01 p0083 A71-11329

Minimum suction rate preventing laminar boundary layer separation from curvilinear porous surface in jet flow
02 p0186 A71-12553

Contour effects on brightness paradox, investigating contrast and perception of luminance gradients in space by constant sum estimation method
03 p0365 A71-14377

Plane contours problems analytic solution by least squares method approximation, giving matrices of linear equations systems
04 p0602 A71-14605

Manual vs automatic contouring, comparing accuracy and economy
08 p1281 A71-21256

Two dimensional incompressible laminar boundary layer with longitudinal surface curvature, examining equations with particular attention to pressure boundary conditions and pressure gradient formulation
09 p1433 A71-23098

Optical field contouring techniques using holographic interferometry for obtaining objects shapes on contour maps
21 p3382 A71-40940

Rotating disks optimal design allowing for creep from additional coupling imposition and contour displacement
23 p3780 A71-44220

Factorial determinants in solving space contours, considering bending and torsional moments in structural analysis
24 p3881 A71-44800

CONTRACT MANAGEMENT

Technical work evaluation in cost-plus contracts for management control
01 p0184 A71-11190

Space shuttle program plans, economics, operational characteristics, contracting and management planning
04 p0689 A71-14929

Aerospace contractor management program projected through 1975 in terms of system engineering, configuration and financial management, with Minuteman Missile as example
04 p0691 A71-15291

Contractor claim of value of delayed payments under government contracts as adjustment for stretch-out, discussing tenability
14 p2341 A71-31131

Cost control over changes in major weapons systems between letting of contract and final hardware delivery
14 p2342 A71-31134

Cost effective integrated logistics support documentation system for military contractors
23 p3661 A71-43196

Satellite project cost estimation, evaluating formulae for budget, tender offer and contractual expense
23 p3785 A71-43459

Project management by contractual procedures for ELDO space research
23 p3786 A71-43466

Quality control for space programs hardware suppliers, discussing contractual aspects
23 p3786 A71-43468

CONTRACT NEGOTIATION

Defense industry pricing and contracting for inflation, considering statistical analysis and direct cost estimation
14 p2342 A71-31132

Maintenance aids evaluation for government contracting and decision making, including cost model based on life cycle economics
16 p2552 A71-33311

Negotiations of BEA/BOAC productivity agreements in aircraft industry
18 p2926 A71-35924

Government and public agencies procurement policy evolution from legal obligations to economic impact consideration
23 p3786 A71-43464

Incentive contract with contractor profit based on achievement in cost, schedule and technical performance
23 p3786 A71-43467

NASA NHB reliability engineering provisions for aeronautical and space system contractors, considering criteria for program management, system engineering, manufacturing and facilities
23 p3682 A71-43497

CONTRACTION

Contraction coefficient of orifice for subsonic and supersonic flows, including velocity-of-approach and compressibility effects upstream and downstream [ASME PAPER 70-WA/FM-1]
03 p0402 A71-14103

Myocardium cells contractile activity control with frequency dependent self regulatory mechanism
13 p2006 A71-28383

Continuously stratified fluid flow into contraction, assuming constant upstream dynamic pressure and density gradient/Long model/
17 p2726 A71-34661

CONTRACTORS

Aerospace contractor management program projected through 1975 in terms of system engineering, configuration and financial management, with Minuteman Missile as example
04 p0691 A71-15291

Industrial project management, defining functions and responsibilities of program director, contractor, subcontractor and manufacturer
23 p3785 A71-43460

Industrial project management executive work team for space programs, emphasizing responsibilities of prime contractor
23 p3786 A71-43461

CONTRACTS

NT SUBCONTRACTS

NASA patents and licensing policy, discussing contractor rights and invention handling
04 p0690 A71-14939

CONTRAILS

Differential radiometer with ultranarrow interference filter for daytime tracking of high altitude chemical vapor trails
03 p0424 A71-13636

CONTRALATERAL FUNCTIONS

Orthodromic and antidromic impulsion role in functional state changes of contralateral cerebrospinal center during mixed nerve prolonged stimulation by rectangular pulses

21 p3337 A71-41059

CONTRAST

NT IMAGE CONTRAST
NT PHASE CONTRAST

Meteorological satellite IR imagery for calculating spectral values of cloudiness radiation contrasts against underlying surface background

20 p3261 A71-39689

Contrast effects in loudness judgments, using category scale and maximally extensive number response language

23 p3638 A71-43111

CONTROL

Generalized control theory, discussing criterion function, pareto-optimal set determination, information structure, etc

01 p0112 A71-10846

Approximate minimum energy control for time variable linear system, using mathematical model

03 p0389 A71-13447

Linear control systems searchless automatic optimization on basis of ideal reviewing model

03 p0389 A71-13519

Neural pulse frequency modulated error sampled control system stability, considering model limitations and modifications

03 p0390 A71-14307

Decision and control /adaptive processes/ - IEEE Conference, Pennsylvania State University, November 1969

03 p0393 A71-14478

Simultaneous identification and control by separation method of two separate problems solution, one being set of unknown parameters estimation

03 p0394 A71-14485

Linear, nonlinear and stochastic real control systems optimization by numerical techniques, considering gradient methods and linear programming

05 p0730 A71-16250

Control systems root contours boundary lines, dividing a plane into realizability regions for system characteristic equation complex conjugate roots

06 p0878 A71-17337

Second order dynamic relay system with unstable linear part, investigating constant disturbance effects with point mapping and bifurcation theory

06 p0927 A71-17672

Control of time varying mechanical torque normal to ball bearing pair common spin axis by cross torque control through misalignment coupling

[ASLE PREPRINT 70LC-9] 08 p1298 A71-21156

Second order dynamic relay system with unstable linear part, investigating constant disturbance effects with point mapping and bifurcation theory

09 p1424 A71-23458

Parameter optimization in linear control systems subject to random disturbances, using hybrid computer

11 p1735 A71-25840

Absolute instability of nonlinear control systems, applying circular criterion to systems with nonstationary nonlinearities

19 p3037 A71-37568

CONTROL DATA [COMPUTERS]

Direct digital control system for random excitation environmental testing, discussing interfacing of TIME/DATA time series processor and minicomputer

11 p1736 A71-26500

Analog recursive computer with serial digital program for arithmetic unit and storage system control

12 p1884 A71-27150

Telemetry system for control data transmission, noting pulse comparison with feedback signal

13 p2031 A71-28633

CONTROL DEVICES

U CONTROL EQUIPMENT

CONTROL EQUIPMENT

NT CRYOSTATS

NT PRESSURE REGULATORS

NT SERVOAMPLIFIERS

NT TELEOPERATORS

NT THERMOSTATS

Polynomial finite difference description of first order nonlinear dynamic control plants with incomplete information

01 p0058 A71-10405

Second order nonlinear control system control law derivation by Liapunov direct method, defining region of undisturbed motion asymptotic stability

01 p0058 A71-10407

Computerized optimization of nonlinear dynamic control system subjected to random disturbances, using Monte Carlo method for quality functional

01 p0058 A71-10426

Transient response of pulse frequency modulation automatic control systems for zero or nonzero initial conditions, using signal Laplace transforms

01 p0059 A71-10528

Computer methods for calculating sensitivity of amplitude and phase frequency response functions in automatic control systems to system parameter changes

01 p0059 A71-10529

Invariance in nonminimum phase complex combined control systems synthesis, using root hodograph method

01 p0063 A71-10724

Extremal control systems operation, analyzing search and scanning phases

01 p0064 A71-10840

M-dimensional gradient extremal system under non-random and random noises of inertial control plant, using difference equation

01 p0064 A71-10922

Reliability prediction method effectiveness for control plant with efficiency represented by canonical forms

01 p0064 A71-10924

Perturbed motion stabilization in nonlinear control system with applicable equation containing zero root and imaginary roots

01 p0128 A71-11158

Pulse transmission control equipment for Q switched ruby laser output

01 p0095 A71-11171

Single channel step-type extremal systems with inertial control plants, proposing automatic optimizer

01 p0065 A71-11235

Relay corrector for widening automatic control systems stability via jump-change in signal amplification factor

01 p0065 A71-11236

Final state automatic control system structural properties, considering second stage synthesis, passage from initial state, degeneracy conditions and coordinate selection

01 p0065 A71-11245

Neural pulse frequency modulation model limitations and modification for error sampled control system stability analysis

01 p0038 A71-11312

Three dimensional dynamic CRT display for simulation, using VECTRAN /Vector Transformer/ digital computing device for control

01 p0084 A71-11394

Digital optimal feedback control device, discussing design requirements, algorithm, block diagram, flow chart and measurement results

02 p0236 A71-12150

Pulse frequency modulated pulsed control systems, deriving sufficient conditions for limit boundedness /dissipativity/

02 p0236 A71-12621

Combinatorial extremum problem distribution among units of hierarchical control system

02 p0236 A71-12623

Large earth station control for satellite communications system, including traffic capacity, TV transmission path breaks and logic equipment

02 p0224 A71-12824

Rationalized design of integrated circuits for control systems, noting cost reduction and quality improvement

03 p0388 A71-14575

Soviet radio telescope tracking control system, describing feedback sensors, digital computer, servomotors, actuators and control panels

04 p0565 A71-14848

Ti alloy research, describing transparent atmosphere chamber design and dilatometer control modifications

04 p0604 A71-15908

Control system synthesis and analysis, using time and frequency domain methods

06 p0878 A71-17427

Coded control circuit for digital frequency synthesizer

06 p0870 A71-17494

Relay type pulsed control systems performance, determining noise effects by statistical analysis

06 p0879 A71-17927

Computer controlled time division multiple access control system for U.S. Army Satellite Communication Agency, discussing tests and operational details

07 p1057 A71-18820

Power station electronic control equipment and integrated circuit computer reliability data analysis, emphasizing combined mathematical prediction and observation

07 p1077 A71-19565

Fluidic control systems, discussing basic concepts, static and dynamic, input, transfer and output characteristics of fluidic devices

07 p1023 A71-20002

Nonlinear control systems with transport lag, obtaining parameter plane equations for stability analysis

07 p1082 A71-20369

Gas-liquid fluidic timing control device, discussing media combination, oscillator complete clock, bubble counter and pressure gages

07 p1031 A71-20605

Precision temperature controller using resistive sensor and Wheatstone bridge in heater loop, discussing prototype design for gyroscope application

08 p1287 A71-20986

Control and instrumentation fluidics, describing equipment, circuits and applications to jet engine controls, missile guidance, flight control, ordnance and machine tool control

09 p1386 A71-22775

Metals ultrasonic welding, discussing welded elements interactions in terms of thermal and diffusive phenomena, sample preparation, transducers, electric generators and process control systems

10 p1617 A71-24134

Accuracy requirements determination method for digital controller coefficients, discussing bits needed

11 p1792 A71-26415

Computer programs for random noise vibration test digital control, describing data base and logic programs

11 p1736 A71-26499

Digital control systems for electrodynamic vibration exciters, discussing computer ranged instrumentation amplifier, digitally controlled sine wave oscillator and FFT processor

11 p1746 A71-26503

Fluidic cabin pressure automatic control systems for military and civil aircraft, discussing design, operation and performance

14 p2182 A71-30308

Real time radar instrumentation data processing and control system, discussing computer selection, software requirements and configuration, etc

14 p2196 A71-30338

Functional control system synthesis based on transition dynamics to hypersurface in form of differential equations

15 p2380 A71-31848

Performance category III all-weather capability ILS landing equipment standards, discussing high directivity antennas and transmission and control system redundancy techniques for reliability

15 p2445 A71-31909

Helicopter automatic flight control equipment, discussing autopilot stabilizer, localization system, ground approach guidance coupler and flight director

15 p2446 A71-31916

Brayton space power system for NASA manned space missions, discussing control system requirements, design and performance

15 p2354 A71-32203

Book on fluidic systems design covering analog and digital control, application to aircraft, spacecraft, computers, tracking devices and equivalent circuits

16 p2526 A71-33475

Transistorized analog multiplication circuit for automatic control system requiring controller input proportional to product of two values

17 p2719 A71-34787

Computer installations on photometric telescope control system for astronomical observations

17 p2711 A71-34981

Telescope automation using servocontrolled drive with spur gearing and dual opposed motors for data acquisition separation and minimum program interaction

17 p2740 A71-34982

Digital computer process controller for telescope with driving system consisting of single worm wheels for tracking and slewing

17 p2740 A71-34985

Computer control of vacuum solar telescopes, taking into account servos/handbox intervention, input-output processor, high speed disk and memory

17 p2740 A71-34986

Image dissector photomultiplier for acquisition, guiding, focusing and photometric monitoring in telescope control

17 p2741 A71-34992

Integrated vehicular information management systems consisting of computers, multiprocessors, multiplexers, dedicated subsystem processors, sensors and effectors

17 p2743 A71-35057

Automatic system for follow-up balancing of digital bridge, noting fast response rate

17 p2723 A71-35711

German TDMA system based on satellite repeater, discussing network configuration, transmission parameters, control, frame/burst format and field trial

18 p2875 A71-36050

Fluid amplifiers in logic circuits and control and monitoring systems, discussing operating principles and performance features

18 p2850 A71-36137

Hydraulic resistance control and actuation switch system designs and classifications, using bridge half components and loop combinations

18 p2850 A71-36203

Bulk semiconductor microwave control components, considering dielectric and conductive properties of plasma state

18 p2894 A71-36980

Active precession control devices for spin stabilized spacecraft, noting energy dissipation effect [AIAA PAPER 71-952] 19 p3148 A71-37193

Jump phenomena of nonlinear control systems subjected to nonstationary Gaussian random inputs, using statistical linearization method 19 p3036 A71-37236

Semiconductor instability effects on reflection and transmission coefficients of microwave control devices 19 p3026 A71-37252

Monograph on strong signal behavior of control systems containing multiphase rectifier, covering stability of high power sources 19 p3039 A71-38550

Multivariable control system design and applications - IEE Conference, Manchester, England, September 1971 20 p3207 A71-38988

Computerized design of large multivariable control systems using inverse Nyquist array method 20 p3202 A71-38994

Wing tip vortex control device, discussing design, operation and effectiveness 20 p3175 A71-39084

Low cost Ti substitutions for Ni and alloys in corrosion resistant applications, prosthetic devices and pollution control equipment 20 p3251 A71-39339

Sampled data control systems with pulse frequency modulation and time lag element, determining error response 22 p3527 A71-42493

Computer generation of sensitivity functions for nonlinear sampled data control systems, discussing simulator components and computational time economy problems 23 p3648 A71-43859

Physics and technology discoveries utilization in industrial control, considering semiconductors, thin films, lasers, holography, cryogenics, etc 24 p3827 A71-45071

Apparatus for dynamically equivalent ground tests of satellite instrumentation and attitude control system 24 p3817 A71-45273

CONTROL MOMENT GYROSCOPES

Free three degrees of freedom gyroscope motion with exponential attenuation of rotor kinetic moment 01 p0079 A71-10532

Nonlinear control law for increased powered stabilization system accuracy in single-axis gyrostabilizer 01 p0079 A71-10533

Probability method for gyroscope instrumental errors associated with inaccurate fabrication and components assembly, classifying external moments 01 p0080 A71-10534

Active control moments construction of solid body rotating about stationary point 07 p1161 A71-20268

Semipassive and active nutation dampers in orbiting dual spin spacecraft, using single axis control moment gyro 13 p2144 A71-27976

Stabilization of solid body orientation with twin gyros under slave engine drive, producing control moments to gimbal axis 13 p2145 A71-28935

ST-224 redundant inertial measurement system, using conventional gimbaled platforms, each with three skewed single-degree-of-freedom control gyro and one caged gyro 17 p2773 A71-35060

Control moment gyro for attitude pointing control system of Skylab space station 17 p2743 A71-35063

Skylab pointing and control system using control moment gyros and cold gas reaction thruster system to provide attitude control 17 p2813 A71-35064

Breadboard attitude control system for scale model space station using control moment gyros [AIAA PAPER 71-935] 19 p3097 A71-37180

Double gimbal control moment gyro systems for spacecraft attitude control, providing three axis attitude stabilization, precision pointing control and maneuverability [AIAA PAPER 71-937] 19 p3097 A71-37182

Optimized momentum and attitude control system /MACS/ for Skylab class space stations employing control moment gyro and reaction jet elements [AIAA PAPER 71-938] 19 p3098 A71-37183

Electromagnetic actuator for momentum desaturation of control moment gyros used for attitude stabilization and control of space stations [AIAA PAPER 71-939] 19 p3098 A71-37184

Gravity gradient desaturation of momentum exchange attitude control system, considering control moment gyros and reaction wheels [AIAA PAPER 71-940] 19 p3098 A71-37185

Spacecraft pointing control system with momentum exchange controllers, considering near optimal control policy for control moment gyro system 22 p3608 A71-41966

Dynamic unbalances effects for axially symmetrical dual spin space station with rigid or low coupling interconnections, considering control moment gyros use 22 p3612 A71-42770

CONTROL SIMULATION

Random parameter plant control, considering recursion formulas, optimal strategy and computerized simulation 03 p0391 A71-14379

Human temperature computer simulation, considering sudomotor, vasomotor and metabolic as error signals from hypothalamic and cutaneous thermoreceptors 07 p1048 A71-19585

Aircraft electronic control systems, considering hydraulic servocontrol, force simulation and reliability models 07 p1156 A71-20064

Digital simulator for training ATC officers, considering authenticity and working and geographical environments 09 p1428 A71-22954

Aircraft motion and traffic control at air corridors intersections for minimum flight schedule deviation under random disturbance due to weather, using statistical simulation 10 p1639 A71-24158

Automatic control, safety and dynamics of thermionic reactor experiment under simulated spacecraft load requirements 11 p1712 A71-25888

Soviet book on aircraft and rocket engines control automation, discussing nuclear power plant/fuel systems design and control simulation methods 11 p1814 A71-26403

Catalytic hydrazine thruster design, fabrication and testing for TOPS spacecraft single-axis attitude control simulation program [AIAA PAPER 71-706] 14 p2294 A71-30763

Dynamic system impulse response model for goodness of fit and linearity hypothesis tests by computer simulation 17 p2722 A71-35181

Time optimal self alignment methods for inertial platforms, using mathematical model based on torque iteration and bang bang misalignment angles control 21 p3413 A71-40544

Comparative qualitative simulation of pulse frequency modulation control with/without error signal derivatives 23 p3656 A71-43867

Real time interactive simulation of multifunction phased array radar, using digital computer links 23 p3648 A71-44272

CONTROL STABILITY

Structural analysis of invariant automatic control systems characterized by coordinate pairs coupled through disturbed load operator 01 p0058 A71-10406

Amplifier stability with distributed feedback by root locus trajectories 01 p0059 A71-10605

Motion stabilization for nonlinear control systems with critical zero and imaginary roots, using Liapunov classical theory 01 p0128 A71-10667

Automatic control systems invariance theory, discussing Poncelet principle, perturbation measurement, etc 01 p0060 A71-10702

Automatic control and information systems epsilon invariance, generalizing Kotelnikov theorem on continuous signals reduction 01 p0060 A71-10703

Multiloop discrete automatic control system invariant with respect to external perturbations 01 p0060 A71-10704

Controlled parameters invariance in automatic systems with bounded-coordinate components 01 p0060 A71-10706

Finite automata systems invariance with respect to control actions 01 p0061 A71-10708

Dynamic errors estimation for nearly invariant automatic control systems, discussing parameter-change sensitivity 01 p0061 A71-10715

Linear continuous receiver and control systems resolution and statistical epsilon invariance 01 p0062 A71-10716

Automatic control systems without disturbance feedback, examining invariance under positive-zero-negative error transition 01 p0062 A71-10720

Complex programmed control systems invariance for discrete times, synthesizing compensating filter with specific transfer function 01 p0063 A71-10725

Pulsed analog and digital control systems invariance conditions at discrete times, using Laplace transform method 01 p0063 A71-10726

Complex control nonlinear systems invariance and stability conditions, discussing harmonic balance analysis method 01 p0063 A71-10729

Nonlinear precision attitude control system stability analysis algorithm based on quadratic Liapunov function 02 p0278 A71-11648

Control system for resonant mechanical loads with feedback, examining stability conditions and oscillation damping by Coulomb friction 03 p0431 A71-13074

Stochastic stability for optimum systems with general search control law for boundary parameters under vector stochastic differential equation 03 p0389 A71-13518

Limit cycle oscillations in satellite attitude control system, producing control moment by pulse modulated controller 03 p0499 A71-14074

Optimal synthesis of rational composite system for gyrostabilizer stabilization 05 p0751 A71-16588

Frequency stability of automatic control system with hydraulic actuating mechanism external load, taking into account fluid compressibility 05 p0705 A71-17033

Coordinatograph control system transfer function and interpolation error calculation 05 p0732 A71-17040

Two countable systems of differential inequalities, applying to stability of feedback controls synthesizing equilibrium solutions to linear quadratic differential games 06 p0919 A71-18198

Nonlinear control systems with transport lag, obtaining parameter plane equations for stability analysis 07 p1082 A71-20369

Servo stability of binary code follow-up analog-digital converter with magnetic modulated zero elements 08 p1261 A71-20736

Nonlinear absolutely stable regulator design in parameter space, using computer simplex search 08 p1324 A71-21319

Stability of model tracking adaptive control systems with reduced state feedback and measurement noise 08 p1269 A71-21336

Action reproduction accuracy of nonlinear controlled systems with constraints and delays, considering stability degree 08 p1336 A71-21861

Optimal asymptotic stability laws of control systems with unstable plant, using piecewise coordinate functions 08 p1270 A71-21949

Linear optimal stochastic control systems described by covariance matrix correlating errors and estimates of state variables, analyzing instability under parameter variations [AIAA PAPER 70-36] 09 p1421 A71-22076

Nonlinear control systems absolute instability, establishing general frequency criteria 09 p1421 A71-22117

Nonlinear control systems absolute stability range in parameter space 09 p1422 A71-22121

Soviet papers on differential equations and application covering control and system stability, elastic theory, boundary value problems, etc 09 p1495 A71-23428

Optimal control stabilization under continuous small disturbances applied to aircraft stability in horizontal flight under vertical gust loads 10 p1586 A71-24726

Approximate analytical formulas for free oscillations of nonstationary linear control systems using canonical transformations 10 p1643 A71-24898

Asymptotic transformations and stability criteria of nonstationary linear automatic control systems using Krylov-Bogolubov slow time concept 10 p1588 A71-24899

Stability and coordinate bounds of motion of linear dynamic systems over finite time intervals by solutions of differential equations 10 p1643 A71-24900

Random response of stationary linear system to pulse noise in time with independent amplitudes 10 p1588 A71-24901

Stability indices of automatic control system from open circuit logarithmic frequency characteristics, determining poles of transfer function 10 p1588 A71-24905

Discrete control input system oscillations, resembling eye pupil diameter changes, hand tremors and aiming fluctuations during rifle sighting experiments 11 p1723 A71-25166

Variable sweep wing aircraft angular motion mathematical model, analyzing inertial moments influence on control dynamics 11 p1708 A71-25661

Sun sensor design accuracy and stability parameters for spacecraft ultrafine guidance, comparing bias error with solar simulator measurements 11 p1767 A71-26334

Fluid interface Rayleigh-Taylor type instability, considering control as optimal regulator problem 11 p1742 A71-26413

Approximate stability criteria-system parameter relationships facilitating higher order adaptive systems synthesis 12 p1890 A71-26722

Optimal stabilization system synthesis for multidimensional linear control plant in presence of random perturbation 12 p1892 A71-27176

Stability and coarseness of one- and two-channel invariant control systems for various forms of parameter deviations 12 p1893 A71-27340

Optimal output regulator for linear time invariant systems with reference vector and quadratic cost functional 12 p1893 A71-27430

Nonlinear sampled data control systems stabilization, eliminating intersample ripples by zero-order hold 13 p2042 A71-28702

Closed loop circuit stability determination based on predetermined area requirement for characteristic equation roots 13 p2043 A71-28793

Variable structure control system synthesis with roots of equation of perturbed motion of characteristic point in dead zone 13 p2096 A71-28934

Nonlinear control systems absolute instability, establishing general frequency criteria 14 p2219 A71-29995

Nonlinear control systems absolute stability range in parameter space, using system of inequalities 14 p2220 A71-29999

Unsteady controlled object dynamic characteristics evaluation for search-free self adjusting systems and telemetric information processing improvements 14 p2220 A71-30814

Motion stabilization for nonlinear control systems with zero and imaginary roots, using Liapunov classical theory 14 p2221 A71-31000

Turbine engine fuel control stability on CH-47C helicopter, using flight tests and lag damper simulation [AHS PREPRINT 560] 14 p2297 A71-31107

Nonlinear multiple component automatic control systems equations and frequencies for absolute stability 15 p2378 A71-31292

Nonlinear control systems stochastic stability frequency conditions based on one and multidimensional cases 15 p2379 A71-31293

Quality degradation and sensitivity standard of plant parameter definition accuracy in optimal open control system 15 p2379 A71-31520

Mathematical model of multidimensional system stability for random vibration spectra control, including white noise generators, spectrum shaper/analyzer and summator 15 p2380 A71-31847

Stability criterion for cross coupled symmetrical two dimensional nonlinear control systems allowing different slopes for Popov lines 15 p2380 A71-31938

Pulse frequency modulated control systems stability analysis by Liapunov method, introducing discrete correction into modulation law 15 p2381 A71-31979

Linearly increasing input signal tracking in nonlinear control systems with pulse frequency modulation, discussing error determination, asymptotic stability and equations of motion 15 p2381 A71-31980

Stability control of magnetic suspension with stabilizer allowing for energy dissipation in electromagnet, using Lagrange-Maxwell electromechanical equations 15 p2353 A71-32080

Nonoscillating and quasi-oscillating conditions of time optimal second order nonlinear control systems with piecewise-continuous right hand sides 15 p2382 A71-32620

Dynamic stability and reliability analysis of pulse width modulated control systems by point-to-point mapping method 15 p2382 A71-32621

Optimal stabilization of self adjusting control system for nonstationary plant in limited time by linear model using Lagrange multipliers 15 p2382 A71-32622

Synthesis algorithms for model reference adaptive control systems using Liapunov second and Popov hyperstability methods 15 p2382 A71-32623

Self excited and transient oscillations parameters determination in nonlinear control systems, using control area concept 15 p2383 A71-32697

Linear two shaft turbojet model development and conditions for stability, observability, controllability and feedback loop parameters 15 p2383 A71-32711

Pulsed relay control system for stabilizing spacecraft orientation in flight, allowing for changes in characteristics of guidance sensor systems and slave mechanisms 16 p2646 A71-33660

Closed linear systems optimal stabilization, determining transfer function from Wiener Hopf equation 16 p2550 A71-33900

Limit cycle of nonlinear oscillations of third order differential equations dependent on Euclidean phase space with central restoring control force 17 p2763 A71-34293

Two dimensional nonlinear discrete /pulse frequency modulation/ control system stability, using Liapunov direct method and mathematical model 17 p2721 A71-35134

Object motion stabilization, determining minimum control actions number for linear and nonlinear systems 18 p2947 A71-36777

Control strategies for space shuttle transition at 45,000-150,000 ft, emphasizing terminal conditions and stability and control boundaries [AIAA PAPER 71-921] 19 p3147 A71-37170

Twin wheel momentum bias/reaction jet spacecraft attitude control system, presenting mathematical model, stability analysis and design 19 p3099 A71-37192

Discrete closed loop system stability with Kalman filter by determining z plane poles of special augmented transition matrix 19 p3036 A71-37235

Liapunov direct method for transient multimachine power-system stability analysis using multivariable control modeling 20 p3207 A71-38991

Action reproduction accuracy of nonlinear controlled systems with constraints and delays, estimating maximum error and stability degree 20 p3208 A71-39360

Three axis and dual-spin attitude control subsystems for communications satellites, considering flywheel stabilization advantage 21 p3454 A71-40478

Relative motion interaction dynamics in rocket biaxial control with azimuth and elevation servos, using Mathieu equation and stability criterion 22 p3526 A71-41971

French monograph on extrapolation type extremal control systems speed and stability performance improvement based on Jacob step duration modulation method 22 p3526 A71-42067

Stable feedback control of single variable nonlinear plants with arbitrary uncertainties, ensuring system error convergence to guaranteed stability 23 p3657 A71-43943

Active flutter mode control system synthesis for flight test, showing mass balancing as possible artificial symmetrical wing destabilization 23 p3629 A71-44106

Single- and multivariable discrete nonlinear control systems with pulse amplitude modulation, deriving frequency criteria for stochastic stability in mean 24 p3812 A71-44397

CONTROL SURFACES

NT AERIAL RUDDERS

NT AILERONS

NT ELEVATORS [CONTROL SURFACES]

NT ELEVONS

NT FLAPS [CONTROL SURFACES]

NT GUIDE VANES

NT HORIZONTAL TAIL SURFACES

NT JET FLAPS

NT JET VANES

NT LEADING EDGE SLATS

NT RUDDERS

NT SPOILERS

NT TABS [CONTROL SURFACES]

NT TRAILING-EDGE FLAPS

NT WING FLAPS

Aerodynamic forces on control surfaces in subsonic range, investigating pressure distribution on harmonically oscillating wing 03 p0344 A71-14347

Wings with control surfaces in unsteady subsonic flow, applying lifting surface theory [ONERA-TP-889] 04 p0526 A71-15355

Unsteady coefficient measurements to corroborate theory for coefficient distribution about little elongated two dimensional wings with control surfaces 05 p0694 A71-16737

Frequency and amplitude during longitudinal control surface pumping by pilots in precise flight path handling for aircraft design [AIAA PAPER 70-567] 06 p0847 A71-17699

CONTROL THEORY

ONERA hypersonic wind tunnels used for ballistic and aerodynamic research kinetic heating problems and control surface efficiency [ONERA-TP-877] 06 p0841 A71-18025

Apollo spacecraft and lunar landing module thermal control surfaces, considering inorganic silicate bonded paint 09 p1533 A71-23426

Inclined engine cold circular jet effects on tail control surfaces aerodynamic characteristics, considering aircraft longitudinal stability [DFVLR-SONDDR-104] 10 p1552 A71-24593

Aerodynamic forces and hinge moments of delta cruciform control surface in blunt-nosed canard configuration for subsonic, transonic and supersonic flows 11 p1701 A71-25161

ABM control surfaces active oxidation protection, using ammonia as reactive coolant injected through porous W wall matrix [AIAA PAPER 71-391] 11 p1837 A71-25353

Solar energy absorbance changes in spacecraft thermal control surfaces exposed to particulate radiation at simulated synchronous altitude, using computerized model [AIAA PAPER 71-453] 12 p1928 A71-26761

Hypersonic flight load bearing refractory alloy control surface protective coatings, emphasizing oxidation screening tests 14 p2262 A71-29646

German monograph on incompressible potential flow field calculation about thick rectangular wings with control surfaces and ground effects 15 p2347 A71-32307

Oscillating thin wing with control surfaces in two dimensional compressible subsonic flow, calculating aerodynamic forces based on kernel function method [DFVLR-SONDDR-132] 16 p2519 A71-33013

Aerodynamic characteristics of space shuttle configurations over entire flight velocity range, stressing coupling effects of control surfaces at large angles of attack 18 p2972 A71-36437

Aerodynamic control surfaces optimal location for flexible aircraft disturbed by random wind gusts, using matrix minimum principle and calculus of variations 19 p2998 A71-38713

Control surfaces and direct jet force flutter suppression system shown to increase flutter speed of wing 23 p3630 A71-44108

CONTROL SYSTEMS

U CONTROL

CONTROL THEORY

Noninferior performance index vectors in multicriteria optimal control theory 07 p1147 A71-19472

Development program for multiple access real time tactical information distribution system, designing and constructing tactical air control system test facility [AIAA PAPER 71-243] 07 p1156 A71-19718

Optimal control sufficient conditions with state and control constraints 07 p1082 A71-19771

Book on stochastic processes covering random events, Markov chains, fixed terminal time, discounted cost problem, optimal control and stability theory 08 p1268 A71-21310

Numerical results for optimal trajectory control and filtering using Kalaba method 08 p1269 A71-21327

Block decomposition of linear time invariant multivariable control systems 08 p1269 A71-21328

Time varying multivariable system transformation to phase variable canonical form 08 p1324 A71-21329

Finite difference description for dynamic control plants with unknown disturbances based on integral transformation and extrapolation, applying to automatic control systems synthesis 08 p1270 A71-21975

Nonstationary automatic control systems analysis using frozen coefficients and weighting functions 08 p1270 A71-21978

Control sets bound structure, discussing invariance theorems 09 p1422 A71-22377

Dynamic control plants parametric identification theory for linear and nonlinear systems 09 p1423 A71-22874

Control systems optimization via heuristic approach based on Pontryagin maximum principle and pseudotrajectory concept 09 p1423 A71-22968

Nonlinear sampled data feedback control systems periodic mode of oscillations, using state variable approach 09 p1423 A71-23033

Differential equations construction for controlled systems and controller starting from programmed motion stability requirement 09 p1495 A71-23432

Higher dimensional wave equation boundary value control, investigating hyperbolic problems in several space dimensions with application of Holmgren and John uniqueness theorems

09 p1424 A71-23467

Optimal control theory of systems with time and state variables dependent coefficients, considering systems described by measure delay-differential equations

09 p1486 A71-23468

Book on mathematical theory nonlinear control processes covering dynamic programming, calculus of variations, etc

09 p1486 A71-23724

Optimal control problems with phase constraints, using v technique and abstract multipliers technique

10 p1585 A71-23755

Soviet book on variable structure system theory covering nonlinear automatic control, stability, optimization, adaptive systems, incomplete information processes, linear filters, etc

10 p1585 A71-24147

Dynamical nonlinear systems observability definition and necessary and sufficient criterion for checking

10 p1587 A71-24743

Q factor of control systems as mathematical expectation of functional on input signal set with prescribed probabilistic measure and random initial conditions

10 p1588 A71-24904

Resistance and mathematical modeling of human body control concerning brain, cardiovascular, arteriolar muscle contraction and protein metabolism systems

10 p1571 A71-24955

Optimal characteristics for single-input single-output memoryless time invariant nonlinear dynamic systems

11 p1742 A71-25751

Conflicting and relaxed minimax controls for Weierstrass E condition or Pontryagin maximum principle

11 p1792 A71-25752

Optimal fixed dimensionality dynamic compensator design for linear time-invariant closed-loop system based on quadratic cost and gain criteria

11 p1742 A71-26414

Nonlinear control systems dominating oscillation modes, investigating parameter variations effect by root locus technique

11 p1743 A71-26425

Equivalent-to-adaptive parametrically invariant automatic control, discussing compensation, variable structure, autooscillatory, HF nonlinear, ultracoarse and nonsearching self adjusting systems

12 p1890 A71-26723

Statistical estimation in monitoring and control systems analysis, discussing algorithm construction for computer solution of nonlinear differential equations system

12 p1891 A71-26724

Marks searchless self adjusting control system calculation, using method of total motion separation into characteristic components

12 p1891 A71-26726

Adaptive control systems probability characteristics in presence of random inputs, discussing improvements by coefficients and interpolation methods

12 p1891 A71-26727

Logical dynamic control systems, interpreting structural properties in categories of logic-operator matrices and predicate systems

12 p1893 A71-27338

Stability and coarseness of one- and two-channel invariant control systems for various forms of parameter deviations

12 p1893 A71-27340

Linear system programmed maxmin transfer time problem solvability, investigating control process theory with time inversion

12 p1931 A71-27523

Optimal nonlinear control with fixed time and compact convex target set, using gradient method

12 p1923 A71-27728

Modal control systems with confluent eigenvalues, using system mode controllability matrix

13 p2042 A71-28701

Control of distributed parameter systems, presenting analysis method using arbitrary set of space modes with time dependent coefficients

13 p2042 A71-28707

Book on multivariable control systems covering dynamical, linear continuous and time-discrete systems

13 p2043 A71-28792

Linear control of systems governed by second order equations, discussing games in operational partial differential equations

13 p2095 A71-28823

Computational approach to maximum principle in control theory, considering canonical problem

13 p2035 A71-28996

Transmitter clock phase lock loop for PCM-TDMA satellite communication system, applying to control system design having time lag

13 p2034 A71-29392

Infimum principle for dynamic optimal control with nonscalar valued cost criteria, rederiving Kalman-Bucy filter

14 p2219 A71-29627

Closed-loop control of discrete time systems with uncertainty, discussing minimax reachability of target sets and tubes

14 p2219 A71-29698

Controlled aircraft motion under strict kinematic constraints in terms of simple subsystems, noting pilots role in Newmark theory

14 p2177 A71-31024

Hingeless rotor helicopter stability and control characteristics, considering induced flow field, flapwise bending modes and blade-fuselage dynamic coupling

[AHS PREPRINT 54]

14 p2179 A71-31098

Output probability distributions and covariance functions of nonlinear transformations of Gaussian stochastic processes occurring in signal detection and control theory

15 p2379 A71-31822

Hierarchical systems compromise controls selection by decomposition method

15 p2379 A71-31843

Necessary and sufficient conditions for optimality for singular control problems with totally singular extremal path

15 p2380 A71-31900

Suboptimal feedback control law for second order nonlinear systems with quadratic performance index, determining power series coefficients

15 p2381 A71-31941

Soviet book on discrete control systems covering linear and nonlinear systems synthesis and analysis, digital computer techniques, one and multidimensional pulsed systems optimization, etc

15 p2381 A71-31976

Discrete control system optimization in terms of power requirements minimization, using Pontryagin maximum principle

15 p2381 A71-31977

Discrete group symmetric linear control systems reduction to elementary cell, generalizing Fourier transform to groups without operational constraints

15 p2381 A71-31978

Mathematical theory of control systems synthesis, considering Shannon functions asymptotic behavior

15 p2442 A71-31992

Optimality conditions for nonlinear distributed parameter control systems described by functionals of evolutionary and stationary equations of mathematical physics

15 p2382 A71-31993

Sensitivity functions of phase canonical form for single input linear time invariant controllable systems, using frequency domain techniques

15 p2382 A71-32442

Minimum dimensionality determination for control process stabilizing linear mechanical system, obtaining necessary and sufficient conditions for stabilization

16 p2607 A71-32933

Control system stability with nonlinear feedback in steady equilibrium state

16 p2548 A71-32934

Self similar invariant group solutions to Bellman nonlinear partial differential equation for optimal correction problems of control systems motion with random disturbances

16 p2549 A71-32935

Optimal control of distributed parameter systems described by integral and partial differential equations, providing theory and bibliography

16 p2549 A71-33354

Central nervous system self regulating properties analysis by automatic control theory, using parametric functional model of brain electrical activity

16 p2538 A71-34107

Coupled nonlinear control system optimization by noniterative perturbation method

16 p2551 A71-34170

Calculus of variations application to optimal control theory, outlining method for optimal control problems transformation into equivalent classical Lagrange problems

17 p2764 A71-34443

Linear dynamic system recursive state estimation for set-membership description of uncertainty under unknown input disturbances and observation errors

17 p2718 A71-34734

Multivariable control system state variable feedback decoupling theory generalization to include output subset, using matrices

17 p2718 A71-34736

Distributed parameter systems described by parabolic differential equations in Hilbert space, discussing existence of optimal control based on quadratic cost criteria

17 p2719 A71-34738

Optimal structure and parameter adaptive estimation for continuous and discrete data Gaussian process models with linear dynamics

17 p2719 A71-34739

Linear time-invariant dynamic feedback system suboptimal control by lower order generalized aggregated model for reducing computational complexity

17 p2719 A71-34740

Linear system optimal stochastic control and observation strategies simultaneous determination without quadratic cost by dynamic programming

17 p2719 A71-34742

Monograph on parametric errors estimation for dynamic models of linear time invariant control systems

17 p2720 A71-34793

Infinite-time linear dynamic system suboptimal control derivation from lower dimension models, exemplifying by flexible-bodied rocket vehicle pitch plane dynamics

17 p2720 A71-34871

Control reliability in automated system of discrete production management

17 p2721 A71-34961

Redundancy encoding with error correcting codes for controlling results of rational operations series in residual classes system

17 p2710 A71-34976

Optimal control of plant with varying parameters, obtaining suboptimal systems with feedback loops

17 p2722 A71-35214

French monograph on variable-structure automatic control systems covering algorithms, stability, nonlinear hypersurface slip, minimum time, switching elements, analog simulation, etc

17 p2767 A71-35249

Geometric theory of linear multivariable systems extension by controllable output subspace introduction

17 p2723 A71-35295

General Stefan problem for heat conduction with melting and free boundary problems occurring in control and statistical decision theories

17 p2841 A71-35794

Continuous deflection strategies in game problems with motion encounters, discussing absorption sets

18 p2948 A71-36778

Phase locked AFC theory, analyzing equation by bifurcation methods

18 p2896 A71-36784

Operator solutions of nonlinear equations in linear feedback optimal control

18 p2943 A71-36956

Boundary value problems solution in optimal control theory, discussing gradient descent method in state space

19 p3037 A71-37534

Reliability engineering techniques for design control of electromagnetic compatibility, employing statistical theory

19 p3030 A71-38437

Pulse transfer functions for aperiodic and weakly oscillating control objects identification

19 p3039 A71-38640

Feedback system estimation algorithm, comparing performance to algorithm based on stochastic control separation principle

19 p3039 A71-38715

Simultaneous identification and feedback control optimization using predictor updating scheme

20 p3206 A71-38972

Computer control of multiple site track correlation, describing coarse fine method for implementation and accuracy

20 p3202 A71-38973

State feedback decoupling sensitivity of time invariant linear multivariable system, using Liapunov matrix equations

20 p3207 A71-38992

Decomposition matrix Cauer model for multivariable control systems analysis and design

20 p3207 A71-38995

Suboptimal control with nearly isocost surfaces involving plants subject to large set point changes

20 p3207 A71-38996

Parameter estimation algorithms for state variable models of multivariable linear control systems from noisy input-output records

20 p3208 A71-38999

Mixed decomposition and convergence of gradient type coordinating algorithm for two-level complex control system using interconnection variables and Lagrange parameters

20 p3208 A71-39472

Necessary conditions of optimality for control problems with state variable inequality constraints, using separating hyperplane theorem

21 p3359 A71-40207

Minimal time function of optimal feedback controls for normal and semidynamical systems

21 p3359 A71-40252

Approximate controllability for boundary value control of higher dimensional wave equation

21 p3360 A71-40253

Optimal control laws existence for stochastic systems with minimized cost functional, considering trajectory information for controller decisions
21 p3360 A71-40254

Controllability and optimal control for linear system with discontinuous restriction on control function
21 p3361 A71-41137

Envelope process transfer function calculation for self adaptive systems parametric control dynamic characteristics
21 p3361 A71-41138

Automatic control theory application to pneumatic self vibration /hammer/ occurrence criteria derivation for externally-pressurized gas- lubricated thrust collar bearings
22 p3551 A71-41660

Soviet book on nonlinear sampled-data control systems with PFM and PDM covering mathematical description, transient analysis and system stability problems
22 p3526 A71-41821

Discrete system high order optimality sufficient conditions and methods for singular and nonsingular controls study
22 p3527 A71-42854

Control system synthesis from transient process estimates with Liapunov functions, proposing optimality criteria based on Gaussian minimum constraint principle extension
22 p3527 A71-42855

Control system effectiveness improvement, using redundancy and self adaptive techniques
23 p3655 A71-43291

Distributed parameter system optimal feedback control with quadratic performance indices dependence on discrete point states, applying to uniform bar temperature control
23 p3656 A71-43853

Deterministic system optimal control with single control and several cost functionals by Pontryagin maximum principle
23 p3656 A71-43858

Necessary and sufficient conditions for optimal control problems equivalence, considering time functions for disturbing influence of external forces
23 p3656 A71-43861

Singular optimal control theory generalization using appropriate transformations, considering stability results for bang-bang solutions
23 p3657 A71-43941

Error insensitive proportional integral derivative /P-I-D/ tracking controller design using optimal linear regulator theory
23 p3657 A71-43946

German book on adaptive control systems covering decision processes and application examples
23 p3660 A71-44188

Algorithm for dual compromise control problems arising from each subsystem of inner level in multilevel static hierarchical system
24 p3812 A71-44393

Single- and multivariable discrete nonlinear control systems with pulse amplitude modulation, deriving frequency criteria for stochastic stability in mean
24 p3812 A71-44397

Integral quadratic control quality estimates in terms of system coefficients with allowance for system oscillation characteristics
24 p3812 A71-44483

Trends in automatic control field in last two decades, emphasizing optimal control and performance criteria selection
24 p3813 A71-44591
[AIAA PAPER 71-1001]

Suboptimal control laws calculation, using functional form of variables for algorithm
24 p3813 A71-44615

Dual control theory for distributed systems with time lag described by partial differential equations, considering controller and algorithms synthesis
24 p3814 A71-44686

Accuracy analysis of statistically optimal dynamic system with modulus bounded control for discrete and continuous information input, using Fokker-Planck-Kolmogoroff equation
24 p3814 A71-44689

Optimal linear final parameter control synthesis for dynamic systems with given accuracy, using multivariate statistical analysis
24 p3814 A71-44690

Optimal dynamic accuracy of control systems with random signals and parameter oscillations, using sensitivity theory
24 p3815 A71-44697

Orthogonal method for studying nonlinear automatic control systems in presence of random perturbations, discussing applicability limits
24 p3815 A71-44701

Optimal stochastic control law derivation for linear regulator with quadratic performance criterion from limiting form of transfer function
24 p3816 A71-45134

CONTROL UNITS [COMPUTERS]
Digital computer modular LSI control logic design using multifunctional binary decoder with transistor

array read-only memory for odd and even parity error detection
08 p1260 A71-21663

Hardware executive control with associative memory for avionic digital computer system, comparing computation speed, cost and reliability with software method
17 p2712 A71-35778

Microcomputer design using standard interfacing module for balanced electronic logic amounts in central processor and peripheral controllers
22 p3518 A71-42207

CONTROL VALVES
Fluidic instrument pressure regulator, noting pressure sensing circuit, confined jet amplifier and control valve
[ASME PAPER 70-WA/FLCS-4]
03 p0428 A71-14080

Control valves aerodynamically generated sound pressure level prediction, using empirical method
[ASME PAPER 70-WA/FE-28]
03 p0403 A71-14136

Solid propellant rocket motor combustion control by fluidic vortex valve, considering thrust variation
[AIAA PAPER 70-643]
07 p1183 A71-18904

Moving parts pneumatic control, discussing valves adaptation to control language and functional requirements
07 p1023 A71-19996

CONTROLLABILITY
Complex systems potential effectiveness theory, establishing reliability, noise resistance and controllability limits
01 p0065 A71-11230

Heavy supersonic aircraft controllability, noting irreversible boost control system and stability
03 p0454 A71-13195

Wing upper surface air suction influence on aircraft longitudinal controllability, considering control stick forces for deflected flaps and angle of attack
04 p0528 A71-14594

VTOL handling qualities criteria for civil IFR qualifications, taking into account pilot abilities
04 p0533 A71-15427

Complete system associated with given control, discussing trajectories uniform approximation and nonlinear controllability conditions based on linear partial differential equation
04 p0620 A71-15865

Nonlinear time varying systems global and local controllability, deriving conditions related to linear systems controllability
04 p0561 A71-15867

Nonlinear systems bang-bang controllability by differential geometry approach
04 p0562 A71-15872

Pilot training flight simulators without visual or motion cues, discussing validity for aircraft handling qualities assessment and pilot role in simulation process
[DGLR-70-070]
05 p0733 A71-15968

Hypersonic vehicles low speed handling qualities, describing test flights approach and landing operations
05 p0697 A71-16680

Rigid heat conductors, using controllable states for heat flux-temperature gradient materials response function measurements
05 p0837 A71-16721

Air cushion vehicle technology, considering economics, propulsion, structures, controllability, flexible skirt systems and R and D
[SAE PAPER 710183]
08 p1231 A71-21713

Lifting body vehicle handling qualities, considering X-24A, M2-F3 and HL-10 reentry vehicles flight characteristics and simulation requirements
[AIAA PAPER 71-310]
09 p1532 A71-22622

Discrete time finite dimensional autonomous linear systems, investigating controllability and pole assignment to closed loop transfer matrix by choice of state variable feedback gain
09 p1424 A71-23465

Necessary and sufficient controllability conditions for linear nonstationary system with deterministic inputs described by two differential equations
10 p1586 A71-24387

Multivariable linear systems parameter reduction, assuming minimum controllability and observability
[DFVLR-SONDDR-89]
12 p1922 A71-27007

Aircraft handling rating scales efficiency, noting difficulty in understanding and interpreting pilot opinion
12 p1875 A71-27253

Controllability and optimal control for linear system with discontinuous restriction on control function
13 p2041 A71-28009

Modal control systems with confluent eigenvalues, using system mode controllability matrix
13 p2042 A71-28701

Helicopter handling under ASW flight conditions, discussing sea state effect on low altitude hover stability
13 p1998 A71-29384

Commercial aircraft piloting in atmospheric turbulence, discussing aircraft characteristics, instrumentation, flying procedures, pilot training and kinesthetic cues
14 p2173 A71-29782

Atmospheric turbulence effects on handling qualities and structural loads on aircraft
14 p2174 A71-29787

Noise effect on signal parameter control in linear measurement devices
14 p2194 A71-30082

Handling qualities and control sensitivity of high performance helicopters, considering pitch and collective control
[AHS PREPRINT 542]
14 p2179 A71-31099

Handling qualities of V/STOL research vehicles during steep terminal area approaches, discussing powered lift fan VTOL aircraft limitations and instrument landing approach
[AHS PREPRINT 544]
14 p2179 A71-31101

AH-56A compound helicopter rigid rotor stability and handling qualities, using flight, whirl tower and wind tunnel tests
[AHS PREPRINT 574]
14 p2180 A71-31115

Rigid rotor hub flapping stiffness tailoring for controllability, considering length and fatigue/structural strength
15 p2348 A71-31601

Liapunov approach to nonlinear dynamic systems controllability, deriving conditions for linear dynamic systems
15 p2380 A71-31935

Lateral-directional handling qualities and roll control power requirements for executive jet and military class II airplanes in landing approach flight phase
[AIAA PAPER 71-771]
16 p2524 A71-34007

Controllable phase locked frequency splitting in two-frequency lasers by anisotropic or nonreciprocal resonator elements
17 p2751 A71-34380

Geometric theory of linear multivariable systems extension by controllable output subspace introduction
17 p2723 A71-35295

German monograph on field effect transistors as controllable resistors with applications in adjustable amplifiers and dampers, covering nonlinear harmonic distortion and control dynamics
18 p2887 A71-35961

Approximate controllability for boundary value control of higher dimensional wave equation
21 p3360 A71-40253

Controllability and optimal control for linear system with discontinuous restriction on control function
21 p3361 A71-41137

Controllability conditions for linear differential equations of dynamic system
22 p3568 A71-42696

SST handling qualities, takeoff speeds and performance evaluation on six degree of freedom flight simulator
23 p3627 A71-42922

CONTROLLED ATMOSPHERES
NT CABIN ATMOSPHERES
NT INERT ATMOSPHERE
NT SPACECRAFT CABIN ATMOSPHERES

Carbon dioxide concentration control in sealed chamber with animals during atmosphere regeneration by Chlorella
06 p0860 A71-18356

Intensive Chlorella cultivation for controlling toxic gaseous contaminants in atmosphere
06 p0861 A71-18357

Arc melter using Pyrex pipe cross for controlled atmosphere chamber, incorporating Ar jet into electrode holder for dynamic flushing and rapid quenching
13 p2044 A71-28154

Endogenous short period rhythms in rotational movements of unifoliate leaves of Phaseolus angularis Wight grown under controlled environmental conditions
13 p2015 A71-29476

Arc welding apparatus for chemically active high-melting metals in controlled superpure He atmosphere
14 p2253 A71-30486

Local shielding chambers for welding circumferential and longitudinal seams in Ti alloys with minimum residual oxygen concentrations
14 p2253 A71-30489

Manual pulsed and continuous arc TIG welding in controlled atmosphere chamber, examining joint quality
19 p3070 A71-38422

Protective xenon atmospheres in sealed silicon-germanium alloy thermoelectric generators, discussing leakage and pressure levels
20 p3265 A71-38934

Blue-green algae survival or growth ability tests under simulated Precambrian atmospheric conditions
22 p3487 A71-42230

CONTROLLED FUSION
One dimensional laser heating of stationary plasma for application to controlled thermonuclear reactions
07 p1165 A71-18880

Fusion energy technology, discussing controlled reactor construction and operation
07 p1169 A71-20000

Soviet papers on plasma physics and controlled thermonuclear synthesis problems covering interac-

tions with charged particle beams, stability, HF properties, etc
24 p3853 A71-44501

CONTROLLED STABILITY

U CONTROL
U STABILITY

CONTROLLERS

NT SERVOAMPLIFIERS
NT SERVOMECHANISMS
NT SERVOMOTORS

Controller characteristic adaptive control by disturbance of plant operation under random non-manipulated action, considering cognitive system as Markovian automation-nature game
03 p0389 A71-13516

Optimal controller analytical design procedures using dynamic programming and Liapunov function
03 p0392 A71-14404

Parametrically invariant automatic control systems with linear controllers, using compensating devices based on certain transfer function qualifications
12 p1890 A71-26721

Gradual failure effects on operational reliability of centralized automatic control machine
15 p2374 A71-32192

Modal control for linear multivariable time-invariant systems incorporating multiloop single input proportional controllers
18 p2896 A71-36235

Optimal zero-memory regulator for linear system with stochastic jump parameters, considering Bayes and minimax controllers
19 p3039 A71-38711

Controller design for linear closed loop system with transport delay, discussing simplified procedure with correction by zero-pole cluster outside bandpass
19 p3040 A71-38717

Signal quantization induced low amplitude oscillations in digital control systems, discussing relationship to digital controller programming form
21 p3361 A71-40980

Compensator design for linear controllers for time varying nonlinear systems, using digital computer oriented approach
22 p3577 A71-42676

Error insensitive proportional integral derivative (P-I-D) tracking controller design using optimal linear regulator theory
23 p3657 A71-43946

Optimal inner product angular momentum controllers, analyzing performance criteria and feedback control laws
23 p3658 A71-44090

Dual control theory for distributed systems with time lag described by partial differential equations, considering controller and algorithms synthesis
24 p3814 A71-44686

CONVAIR MILITARY AIRCRAFT

U MILITARY AIRCRAFT

CONVECTION

NT FORCED CONVECTION

NT FREE CONVECTION

Solar magnetic fine structure production by gas motion in supergranular convection
02 p0316 A71-12753

Nonraining clouds electric fields and charge distribution, calculating convection influence by numerical means
05 p0777 A71-16675

Convection schemes finite difference formulation for nonlinear instability prevention by absolute spatial conservation rather than flux form
06 p0917 A71-17552

Rayleigh and phase change instability for olivine-spinel mantle convection
07 p1105 A71-20450

Blue edge of RR Lyrae instability strip, examining convection, radiation and surface boundary conditions effects
13 p2133 A71-27969

Constant profile solutions stability for nonlinear wave equations with convection and dissipation
16 p2608 A71-33023

Large scale convection solar magnetic field patterns calculations based on rotating thin spherical shells, noting solar cycle activity
19 p3147 A71-38667

Dead ended compartments concentration and current distributions calculation in space hydrogen-oxygen fuel cells, using mathematical model with convective diffusion equation
21 p3326 A71-41249

CONVECTION CURRENTS

Comparative convection levels and energy instabilities in vertical motion, using particle and layer methods
01 p0113 A71-10539

Aircraft measurement of vertical and horizontal structures of temperature, moisture, refractivity and turbulence for atmospheric convection patterns, comparing radar structure to meteorological soundings
01 p0116 A71-10561

Clear air convective process, examining dynamic model with radar patterns
01 p0116 A71-10562

Convective thunderstorm propagation from Doppler radar velocities at leading edges
01 p0117 A71-10571

Free nonlinear air convective motion in two dimensional cloud banks along vertical wind shift
02 p0277 A71-11690

Clear air convective processes radar observations, discussing development stages of convective field and individual cells
03 p0453 A71-13609

Turbulence energy spectra in thick convective cumulonimbus cloud zone, using aircraft measurements
04 p0622 A71-15633

Relative humidity augmentation for triggering convection in two dimensional numerical cumulus cloud model
06 p0924 A71-18412

Noise-producing subsonic jet turbulence eddies between anemometer measurements of convection velocity as functions of frequency
06 p0884 A71-18596

Soviet papers on atmospheric turbulence and convection covering two dimensional flows, orographic wave formation and air pulsations in rainstorms
07 p1149 A71-18792

Thermal boundary layer flattening influence on atmospheric cellular convection from satellite observations
07 p1104 A71-20219

Model and glass tank furnaces for earth upper mantle convection movements simulation, studying fluid dynamics and geodynamic processes
07 p1105 A71-20449

Ion currents to cylindrical electrodes in mobility dominated plasma flow from thin sheath theory involving convection currents
09 p1505 A71-23374

Ice forming nuclei in atmosphere during severe convective storms from aged background aerosol and soil particles aerosolized by storm turbulence
12 p1925 A71-27197

Clear air turbulence mechanics, considering thermal convection, shear layers, Coriolis and centrifugal instability, billons and rotors
14 p2267 A71-29758

Nonadiabatic convection parameters calculation allowing for vertical wind shear, determining effect on thunderstorm maximum possible duration, gusts and precipitation quantity
15 p2444 A71-31361

Heating effects on wing tip vorticity diffusion rate in gas vortex, causing outward radial convection and increased kinematic viscosity
15 p2512 A71-31556

Steady nonlinear regime of Benard convection in uniformly rotating fluid, using two-dimensional primitive equation numerical model with rigid boundaries
15 p2393 A71-32638

Electrode effect in atmospheric electricity with convection and diffusion, calculating layer thickness dependence on vertical convective transfer velocity
17 p2730 A71-34312

Steady state one dimensional cloud model for cumulus convection, discussing validity range limits
17 p2770 A71-35125

Radar returns from convective fields and cells in visually clear atmosphere explained by thermal effects and air motion
19 p3090 A71-37753

Temperature pulsation measurements by high altitude aircraft in presence of lower troposphere convection elements
21 p3412 A71-41389

Convective cloud dissipation after rainfall, calculating temporal behavior of temperature fields, water content, moisture and air motion rate
22 p3569 A71-42847

Low energy particle plasma sheet and convection electric field distributions over auroral zones and polar caps from satellite Injun 5 observation
23 p3669 A71-43168

Ion current sheath-convection effects with flush mounted electrostatic probes in high pressure flowing plasmas
24 p3826 A71-44792

CONVECTIVE FLOW

Vertical fluid-filled channel with uniform internal heat source, analyzing steady plane-parallel convective motion
01 p0179 A71-10665

Optically thin medium convective instability, examining radiant pressure and magnetic field effects
01 p0158 A71-10804

Diffusion with convection in flow between parallel walls, using Von Mises transformation
02 p0332 A71-12410

Venus atmosphere rotational model, considering nonlinear instability due to wind shear from solar heat induced convection
03 p0489 A71-13607

Convective velocity and temperature scales deduced numerically and observationally for unstable planetary boundary layer and for turbulent Rayleigh convection
03 p0453 A71-13613

Severe storm mass and energy convective transport characteristics, using ATS-3 cloud photographs and three layer model
03 p0454 A71-14204

Convective mass transfer, velocity and concentration fields during nonNewtonian fluid motion in circular pipe with diffusion flow at wall
04 p0579 A71-15798

DA and DB white dwarf atmospheres convection of effect on structure based on mixing length theory and constant flux model
04 p0658 A71-15841

Solar photosphere oscillations, suggesting convection zone acting as resonant cavity
06 p0971 A71-18243

Elastico-viscous liquid laminar free convection flow along nonuniformly heated vertical flat plate, using momentum integral method for boundary layer velocity and temperature distributions
07 p1091 A71-20031

Two and three dimensional thermals and steady and starting plumes convective fluid motion formulas, using vorticity integration method
07 p1104 A71-20223

Solar granular or convective motion velocities vs photospheric oscillations for Doppler shifts in line spectra
10 p1665 A71-23776

Plane unsteady convective motion of viscous incompressible liquid in infinite horizontal vessel of rectangular cross section due to wall temperature fluctuations
10 p1696 A71-24375

Forced convection in atmosphere boundary layer, considering nonlinear unsteady vertical airflow velocity increments over temperature spot on earth surface
11 p1793 A71-25170

Massive stars evolutionary models, exploring convective instability effects
11 p1818 A71-25205

Atmospheric vertical particle motion inside convective storms observed by airborne pulse Doppler radar techniques
11 p1794 A71-25378

Radiating laminar convective flow in vertical heated channel, noting radiation effects on temperature and velocity
11 p1860 A71-26446

Venus subcloud layer, investigating radiant heat transfer in convective lower atmosphere
12 p1958 A71-26646

Atmospheric jet stream reinforcement by cold pseudofronts and convective energy from local source
12 p1924 A71-26824

Cumulus entrainment and steady state one dimensional convection model
12 p1925 A71-27201

Rotation-convection model of solar equatorial acceleration and temperature, assuming inhomogeneous isotropic latitude dependent turbulent energy transport
12 p1968 A71-27644

Helium-rich white dwarfs convective envelopes, acoustic noise generation and corona formation
12 p1970 A71-27746

Cold plasma convection production by ion driven LF drift instability, noting tokamaks and stellarators stabilization
13 p2104 A71-27850

Wall shear stress and static pressure of developing turbulent flow in square ducts with convective accelerating core for various Reynolds numbers
13 p2048 A71-28595

Steady laminar natural convective flow in concentric cylindrical annuli, using finite difference method for Navier-Stokes and energy equations solution
13 p2164 A71-28982

LF hot-electron noise during quasi-elastic scattering in semiconductor with simple band structure, evaluating convective fluctuations contribution to noise temperature
13 p2112 A71-29082

Convection stability in arbitrarily shaped fluid containers heated from below with temperature gradient above critical value
14 p2337 A71-30408

Plane horizontal fluid film convective stability with free boundaries in vertical circular cylinder for periodic modulation of vertical temperature gradient or gravitational field
14 p2338 A71-30873

Vertical fluid-filled channel with uniform internal heat source, analyzing steady plane-parallel convective motion
14 p2339 A71-30998

White dwarf coronas convection zones thermodynamic calculations, considering high electron degeneracy, and He I and He II ionization
14 p2318 A71-31017

Communication blackout during missile and spacecraft high altitude flight, considering convective effects on gas breakdown by microwaves
14 p2206 A71-31071

Cellular convective fluid flow stability regions between concentric cylinders, considering nonuniqueness features with asymptotic stationary solution 16 p2557 A71-32983

Convective motions in differentially rotating thin spherical shells, explaining solar differential rotation 16 p2630 A71-33055

Thermospheric convective instability as interpretation of north polar cap high speed winds observed by satellite at 200 km altitude during magnetic storm of May 1967 16 p2572 A71-33847

Convective flow at stagnation point relation to radiation flux decrease as result of absorption in cold boundary layer 17 p2671 A71-35259

Plate temperature fluctuations effect on convective flow and heat transfer from horizontal plate, presenting solutions for LF and HF 17 p2838 A71-35419

Main sequence A and early F stars with shallow convective envelopes, investigating particle diffusion effects on element abundance data 18 p2960 A71-35939

Finite difference technique for convective flow equations involving shock wave propagation, discussing heuristic analysis for truncation error 18 p2907 A71-36338

Stellar convective shell plane gas layer, noting time dependence of energy flux 19 p3134 A71-37514

Isolated buoyant thermal motion asymptotic behavior derivation from simplified model, comparing results with experiment 19 p3162 A71-37732

Large scale alternating solar magnetic field generation by outer shell convective flow, constructing oscillator hydromagnetic dynamo model 19 p3145 A71-38353

Atmospheric convective motion model, applying turbulent jet method 19 p3093 A71-38696

Steady state magnetospheric convection pattern from synoptic maps of magnetic disturbance and auroral motions 20 p3230 A71-39879

Magnetospheric plasma convection electric field double-probe measurement at high latitude by Injun-5 satellite, noting east-west velocity reversals or discontinuities at auroral zone 20 p3230 A71-39882

Boundary vorticity method for finite amplitude convection in plane Poiseuille flow with isothermally heated and cooled plates, using Boussinesq approximation 21 p3477 A71-40993

Soviet papers on atmospheric turbulence and convection covering cumuli dynamics, wind field microstructure and time characteristics in troposphere and stratosphere 21 p3411 A71-41384

Numerical model of three dimensional convection in atmosphere with vertical wind shear, solving system of differential equations 21 p3411 A71-41385

Numerical model of turbulence effect on cumulus cloud mesoscale convective motion 21 p3411 A71-41386

Longitudinal, transverse and vertical wind distribution microstructure during convection from airborne experiments 21 p3412 A71-41388

Radar observation of convective process in clear air, presenting turreted top cell contour tracings from PPI sequence 23 p3700 A71-43088

Differential equations system for convective incompressible fluid flow boundary layer temperature profile description, analyzing solution existence and uniqueness 23 p3781 A71-43306

Spectral model of warm bubble motion in neutral surroundings from anelastic equations for shallow convection, comparing results with similarity theory and numerical models 23 p3781 A71-43336

Dynamic coupling response between convectively controlled burning process and nonsteady flow field with pressure, density and gas velocity periodic variations 23 p3782 A71-43593

Steady acceleration sensor system with two electrode chambers in closed circuit, producing convective flow by electrolyte density gradients 24 p3828 A71-45099

CONVECTIVE HEAT TRANSFER

Spherical alcohol droplet vaporization in acoustically disturbed medium, considering convective heat and mass transfer 01 p0179 A71-10798

Reinforced tube bundles thermal efficiency and convective heat transfer, discussing inter-rib cavity depth effects 01 p0181 A71-11229

Extratropical disturbances role in global atmospheric circulation, examining vertical convective heat transfer and kinetic energy production relationship 01 p0121 A71-11357

Physiological effects of heat exchange between human organism and ambient medium by evaporation, radiation, conduction and convection 01 p0028 A71-11597

Pipe bends effects on heat transfer coefficient of turbulent forced convection 02 p0330 A71-11650

Unsteady axisymmetric temperature and stress distribution in multilayer cylinder in convective heat transfer with temperature-varying medium 02 p0322 A71-11729

Unsteady heat conduction in multilayer body of revolution with convective heat transfer on curvilinear surfaces, considering radiation on inner surface 02 p0330 A71-11730

Unsteady convective heat transfer in pipes in presence of heat flux density and flow rate aperiodic variations 02 p0331 A71-11885

Free convection in compressible viscous heat conducting liquid near critical point, discussing temperature gradients, layer heights, density distribution and inhomogeneity effect 02 p0331 A71-12190

Laminar boundary layer convective heat transfer with constant wall temperature, using Gaussian quadrature formulas 02 p0332 A71-12394

Laminar natural convective heat transfer from base plates of vertical rectangular fin arrays, taking temperature and fin geometry effects into account 02 p0333 A71-12603

Natural convective heat transfer from fin edges in vertical rectangular arrays, noting temperature and fin thickness effects 02 p0333 A71-12604

Natural convective heat transfer from fin-flat in vertical rectangular arrays, comparing duct and open channel coefficients 02 p0333 A71-12605

Flat plate film boiling heat transfer under forced boundary layer convection, examining nonstationary wall temperature effects 02 p0333 A71-12646

Adiabatic temperature gradient requirement for neutral convection mode in general relativity of star in hydrostatic equilibrium 03 p0486 A71-13330

Variable viscosity effect on laminar forced convective heat transfer in rectangular duct, using ethylene glycol and aqueous solutions 03 p0518 A71-13616

Radiative and convective heat transfer from conducting fins on plane surface, describing interactions among heat conduction and radiant exchange [ASME PAPER 70-HT-F] 03 p0519 A71-13701

Laminar flow of liquid in duct with zero heat resistance of walls, calculating temperature distribution during radiative convective heating 03 p0519 A71-13745

Free convection in compressible viscous heat conducting fluid, determining parameters leading to onset 03 p0521 A71-14233

Convective energy transport in stellar atmospheres, computing hot and cool streams thermal structure based on model 03 p0495 A71-14264

Buoyancy effects on transient free convection heat transfer in revolving tube for zero to 100 g centrifugal acceleration [ASME PAPER 70-HT-10] 03 p0521 A71-14292

Convective heat and mass transfer - ASME Conference, New York, November-December 1970 04 p0674 A71-14777

Vibration effects on free convection heat transfer from fluid filled horizontal cylinder 04 p0675 A71-14784

Direct measurement of convective heat transfer coefficient by realizing proportionality to sublimation rate of naphthalene ball near body surface 04 p0545 A71-15158

Binary liquid metal forced convection boiling heat transfer, determining axial and radial temperature distribution in two phase flow 04 p0676 A71-15173

Heat transfer - Conference, Versailles, August-September 1970, Volume 2, Forced convection 04 p0679 A71-15466

Wall static pressure and convective heat transfer measurements in subsonic, transonic and supersonic regions in heated air turbulent flow through variable cross section channel 04 p0680 A71-15476

Heat transfer - Conference, Versailles, August-September 1970, Volume 3, Forced convection and radiation 04 p0681 A71-15484

Radiative/convective heat transfer in moving media, reducing boundary problem to integral equations 04 p0685 A71-15514

Axisymmetrical, optically thick nonNewtonian, power law boundary layer with injection and suction, obtaining similarity transformations for simultaneous convection and radiation 04 p0685 A71-15516

Thermal radiation absorbing and emitting medium in flow between parallel plates, examining heat transfer for simultaneous radiation and convection 04 p0685 A71-15517

Blunt body nose protection from radiation-convective heat transfer, using porous injection of radiation absorbing substance 04 p0685 A71-15518

Mach-Zehnder interferometer measurements of average temperature and heat transfer rate in free convection on heated vertical flat plate 04 p0599 A71-15522

Two phase heat transfer in thermosyphon counterflow under simulated gravities of 0.1 to 100 earth gravity, measuring critical heat flow rates and convection coefficients 04 p0687 A71-15531

Conducting and ferromagnetic liquids thermoconvective waves, considering disturbance propagation process in equilibrium state with constant entropy gradient 04 p0628 A71-15809

Steady laminar convection in infinite layer of heated homogeneous fluid between constant temperature rigid plate and thermal insulator 05 p0838 A71-16962

Laminar flow convective heat and mass transfer on end walls of vortex chambers 06 p1005 A71-17737

Thermoelastic equilibrium of multiply connected plate during convective heat exchange 06 p0989 A71-17788

Convective heat transfer in coolant with constant velocity in ring channel with heat sources, deriving expressions for flow and wall temperature 06 p1006 A71-18004

Forced convective heat transfer in laminar flow fluid of vanishing viscosity in constant wall temperature pipe, discussing velocity distribution effects 06 p0882 A71-18073

Thermal shock physiological effects, determining skin-air convective heat exchange coefficient 06 p0860 A71-18190

Electric discharge carbon dioxide lasers, obtaining increased power output with convective cooling process [AIAA PAPER 71-63] 06 p0909 A71-18522

Heat transfer by radiation, convection and molecular thermal conductivity in gray absorbing medium flat layer bounded by parallel diffusively radiating planes 07 p1219 A71-18757

High velocity liquid flow past rough plate surface, investigating boundary layer cavitation effects on convective heat and mass transfer 07 p1086 A71-18774

Free convection turbulent flow under supercritical conditions, investigating convection heat transfer and flow patterns 07 p1220 A71-18780

Evolutionary cooling sequences and lifetimes for low mass white dwarfs in Hyades cluster, considering near surface convection in models with hydrogen envelopes 07 p1190 A71-18856

Natural convection heat transfer between two isothermal concentric spheres, using water and silicone oils as convective fluids 07 p1222 A71-18995

Natural convection heat transfer coefficients from isothermal flat surfaces, using Boelter-Schmidt type heat flux meters 07 p1222 A71-18996

Two dimensional thermal convection through shallow layer with vertical shear using numerical model 07 p1152 A71-19752

Convective and nonconvective heat release in mesoscale parameterization improving numerical weather prediction 08 p1326 A71-21447

Cellular convection in horizontal gas layer between solid walls and heated from below 08 p1376 A71-21789

Hydrodynamically stabilized turbulent viscous incompressible fluid flow in circular tube, examining nonstationary convective heat transfer by numerical methods 08 p1276 A71-21923

Combined radiative-convective heating test facility for atmospheric entry simulation [AIAA PAPER 71-255] 08 p1273 A71-21984

Convective heat transfer coefficient for supersonic flow past sphere, considering kinetic heating by flow 08 p1378 A71-22047

Elastic half space two dimensional unsteady temperature and stress fields under induction heating and convective heat transfer 09 p1537 A71-22519

Latent heat convective transport from lower to tropical upper troposphere, noting periodic energy fluctua-

tions from time lapse synchronous satellite cloud photographs 09 p1489 A71-23553

Convective heat flow simulation in lower troposphere, using water-heated plate model and shadowgraph photography 10 p1638 A71-23879

Mass entrainment products effect on radiative and convective heat transfer during decomposition of graphite blunt body in steady hypersonic flow of radiating air 10 p1696 A71-24364

Convective heat transfer in three dimensional stagnation point boundary layer flow characterized by real gas properties 10 p1698 A71-25098

Tornado producing thunderstorms upper level outflow synoptic and dynamic processes from ATS 3 pictures, discussing convective warming effects 11 p1794 A71-25381

Spacecraft radiator thermal scale model, using forced convection, conduction and radiation heat transfer 11 p1860 A71-26517

Venusian atmosphere heat transfer processes, calculating radiant fluxes and convective motion model 12 p1958 A71-26640

Unsteady mass exchange during laminar MHD free convection on vertical plate, deriving time dependence expression for external magnetic field 12 p1938 A71-27242

Conjugate steady convective aerodynamic heating of plate in longitudinal compressible gas flow, taking into account boundary layer enthalpy distribution 13 p1989 A71-27890

Critical Rayleigh numbers for natural convection of water confined in square cells, noting heat transfer modes [ASME PAPER 70-WA/HT-7] 13 p2164 A71-28981

Vibration effect on heat transfer by natural convection from oscillating horizontal wire in air 13 p2164 A71-28984

Flow direction effect on combined forced and free convective heat transfer from cylinders to air 13 p2164 A71-28985

Thermal diffusion effect on gas flow velocity measurements with anemometers with heat convection signals 14 p2239 A71-29815

Monograph on boundary layer theory covering unsteady heat transfer from rotating disk, thermal free convection in corners, etc 14 p2223 A71-29934

Radiative and convective heat transfer for stagnation point flow of emitting carbon dioxide and nitrogen gas mixture, assuming thermodynamic equilibrium in shock layer 14 p2335 A71-30212

Free convection in compressible viscous heat conducting liquid near critical point, discussing temperature gradients, layer heights, density distribution and inhomogeneity effect 15 p2512 A71-31497

Convectively cooled carbon dioxide-nitrogen-helium electric discharge laser theory based on excitation and relaxation processes, comparing with experiment [AIAA PAPER 71-588] 15 p2419 A71-31574

Flow stability in differentially heated inclined rectangular box of small depth/length ratio, examining thermal convection and transition to turbulent flow as function of inclination angle 15 p2513 A71-31930

Local forced convection heat transfer data and empirical correlations for boiling Hg in single wetted Ta tube with composite helical inserts [GESP-450] 15 p2447 A71-32216

Cooling fin shape optimization for minimum volume, considering convective and radiative heat exchange for assumed temperature distribution 17 p2837 A71-34442

Convective mass or heat transfer to or from uniform or size distributed drops, bubbles or solid particles at high Peclet and low particle Reynolds numbers 17 p2837 A71-34690

Sunspot convective heat transfer in terms of magnetic field convection theory, considering motion in photosphere 17 p2802 A71-34826

Laminar convective heat transfer rates on hemisphere cylinder in rarefied hypersonic flow, comparing experimental results with Cheng, Davis and Lees theories 17 p2671 A71-34902

Hydrodynamically stabilized turbulent viscous incompressible fluid flow in circular tube, examining unsteady convective heat transfer by numerical methods 17 p2729 A71-35267

Parabolic boundary layer equations for heat convection problems with unknown wall boundary conditions, noting solution by deterministic and nondeterministic optimization methods 17 p2838 A71-35355

Plate temperature fluctuations effect on convective flow and heat transfer from horizontal plate, presenting solutions for LF and HF 17 p2838 A71-35419

Convective heat exchange coefficient determination for human body immersed in turbulent water flow, using fractional calorimetry 18 p2858 A71-36862

Respiratory aspects of hyperbaric thermal environments, considering heat exchange by convection 18 p2860 A71-36878

Convective and conductive heat loss analysis of underwater swimmers and divers exercising in cold water 18 p2861 A71-36892

Convective heat transfer in stars from anelastic and Boussinesq approximations, discussing two dimensional solutions, truncated expansions, turbulence and mixing length theories, etc 18 p2968 A71-37038

High power radar identification of preferred areas of shower development, analyzing thermal convective areas distribution 19 p3089 A71-37503

Isolated buoyant thermal motion asymptotic behavior derivation from simplified model, comparing results with experiment 19 p3162 A71-37732

Turbulent forced-convection heat transfer coefficient for supercritical fluid, extending Prandtl mixing length concept [ASME PAPER 71-HT-26] 19 p3165 A71-37996

Supercritical carbon dioxide free convective heat transfer, investigating heater surface material and flow effects [ASME PAPER 71-HT-27] 19 p3165 A71-37997

French monograph on similar solutions of laminar boundary layer problem in supersonic flow covering finite difference methods and convective heat flux 19 p2994 A71-38648

Convective clouds development stimulation by artificial ascending jets forming above stationary heat and momentum source, discussing propagation in atmosphere 19 p3093 A71-38694

German monograph on free convective heat transfer from heated tubes in air in presence of bounding walls parallel to tube axis 20 p3311 A71-39043

Heat transfer by radiation, conduction and convection, including various types of thermal insulation 20 p3311 A71-39244

Shuttle convective heat transfer involving similar axial temperature gradients in piston and cylinder, calculating interaction with wall conduction by finite difference computer program 20 p3312 A71-39281

Free convective heat transfer in cryogenic liquid filled enclosure, studying effects of vibration near resonant frequency 20 p3314 A71-39292

Gravity induced free convection effects in melting phenomena for thermal control, predicting temperature distributions and solid-liquid interface profiles by two dimensional model 20 p3314 A71-39354

Conjugate steady convective aerodynamic heating of plate in longitudinal compressible gas flow, taking into account boundary layer enthalpy distribution 21 p3317 A71-40080

Time periodic convection development in incompressible viscous fluid with distributed heat sources 21 p3475 A71-40689

Thermal stress distribution and temperature profiles in nearly opaque spherical shell under radiant and convective heating flux 21 p3476 A71-40942

Atmospheric rotation, anisotropic turbulence and long wave radiative heat transfer effects on cellular heat convection 21 p3412 A71-41387

Convective heat transfer between laminar fluid flow and circular flat tubes, considering wall thermophysical properties effect 22 p3619 A71-41873

Finite element method application to convective heat transfer between parallel planes for arbitrary surface temperatures and Nusselt number 22 p3619 A71-41874

Laminar free convective heat transfer on vertical cylinder with concentration gradients, considering mass transfer effects prediction 22 p3620 A71-41882

Thermal radiation effect on laminar boundary layer of nonabsorbing fluid for plane heat emitting surface under natural and forced convection 22 p3622 A71-42680

Laminar incompressible flow velocities and heat transfer by radiation and convection in inlet section of parallel plate duct 23 p3781 A71-43313

Laminar convective heat transfer from rotating isothermal disk in uniform forced stream, using pressure distribution measurements 23 p3781 A71-43314

Convective heat transfer by laminar and turbulent free convection in air on large horizontal and vertical planes 23 p3781 A71-43324

Fluid flow friction and combined free and forced convective heat transfer characteristics in rotating curved circular tube, using finite difference scheme and iterative solution 23 p3783 A71-44199

Forced convection steady heat transfer across laminar incompressible constant-property boundary layers over wedges with step discontinuity in surface temperature 23 p3784 A71-44196

Free convection heat transfer from vertical flat plate with sinusoidal wall temperature distribution [AIAA PAPER 71-988] 24 p3887 A71-44583

Low temperature plasma radiation flux heated absorbing fluid, investigating convective heat transfer to semitransparent wall 24 p3856 A71-44893

CONVERGENCE

Partial differential equations hybrid computer solution by extended space technique for overcoming slow convergence of Galerkin method 01 p0048 A71-10223

Partial differential equations finite difference approximation, applying convergence theorems with probabilistic method 01 p0111 A71-10318

Incorrectly posed variational problems with nonlinear unbounded operators, demonstrating solution by regularization method and beta convergence 01 p0112 A71-10489

Quadratically convergent algorithms for function minimization tested by numerical examples 01 p0112 A71-10847

Pontryagin space and convergence of Bubnov-Galerkin method for equations with involution operators 01 p0112 A71-11092

Diffraction on smooth convex body, constructing convergent series for homogeneous wave equation solution 01 p0038 A71-11203

Optimal control discrete time matrix Riccati equation, establishing convergence, uniqueness and stability properties 02 p0275 A71-11673

Fourier series in almost periodic Bohr functions, examining uniform convergence definitiveness 03 p0450 A71-13294

Iterative functional minimization methods using Lagrange multipliers, examining convergence 03 p0452 A71-14059

Linear integrodifferential time lag systems quick response problem approximate iterative solution, considering convergence and controllability conditions 03 p0452 A71-14060

Navier-Stokes equations numerical solution method, considering stability and convergence of scheme and system of difference equations 03 p0452 A71-14175

Boundary layer equations existence and convergence theorems, using von Mises transformation for conversion into parabolic differential equation boundary value problem 04 p0568 A71-14810

Kalman filtering sequential estimates convergence theorems for identifying modeling errors 04 p0561 A71-15328

Various free stream turbulence levels at nonconverging and converging walls, investigating foreign gas film cooling 04 p0683 A71-15501

Halley method of tangential hyperbolas in Banach space, deriving local existence, uniqueness and convergence theorems 04 p0620 A71-15668

Von Zeipel procedure convergence for proving theorem pertaining to conditionally periodic motion equations with small change in Hamiltonian 04 p0661 A71-15892

Controlled objects convergence game, constructing optimal minimax pursuer strategy 05 p0782 A71-16979

Differential game of convergence, constructing extremal strategy for ensuring motion encounter with given set 05 p0783 A71-17011

Differential descent method modifications, comparing convergence rates and insensitivity to computer computational errors 05 p0775 A71-17012

Hyperbolic heat conduction equation with small relaxation time parameter, studying convergence for Cauchy and boundary value problem 05 p0839 A71-17035

Kincaid iterative solution for multidimensional systems of nonlinear equations, noting quadratic convergence as function of initial vectors 05 p0775 A71-17046

Dynamic relaxation method for solving simultaneous linear differential equations, comparing asymp-

- otic rate of convergence with degenerate Chebyshev approximation 05 p0776 A71-17122
- Finite difference theory and other approximation methods convergence determination in nonlinear variational problems 06 p0919 A71-18202
- Nonlinear equations solution, considering Newton method and Henrici algorithm disadvantages and quadratic convergent procedure 06 p0919 A71-18203
- Iterative solution of nonlinear operator equations in Banach spaces, proving existence, uniqueness and convergence theorems 06 p0920 A71-18211
- One step iterative solution for linear equations by summation methods, discussing convergence improvement 06 p0920 A71-18213
- Recursively defined infinite system convergence solutions for initial and boundary value inequalities, applying to differential game stability problems 06 p0920 A71-18237
- Weighted least squares nonlinear estimation problem, presenting partial step algorithm for convergence region enlargement [AIAA PAPER 71-121] 06 p0921 A71-18658
- Minimization with superlinear convergence based on second derivative matrix successive approximation scheme 07 p1146 A71-19176
- Electromagnetic wave diffraction by multielement and multilayer arrays, discussing asymptotic solution, error estimate and convergence 07 p1060 A71-19180
- Jacobi series coefficient relation to convergent series sum singularities in lemniscate bounded domain 07 p1149 A71-20643
- Elastic solutions convergence in nonlinear problems of viscoelastic incompressible media, formulating and proving uniqueness theorem for certain conditions 08 p1369 A71-21053
- Simple algorithms for accelerating convergence and averting divergence in Kalman filters, using feedback from measurement residuals 08 p1324 A71-21333
- Mixed player convergence game of conflicting controlled motion under phase constraint 08 p1336 A71-21860
- Mean periodic exponential functions with certain trigonometric properties, proving summation and euclidean convergence theorems 08 p1325 A71-22018
- Frequency counted measurements and phase locking to noisy oscillators, showing counted frequency method sample variance slow convergence to actual variance 10 p1574 A71-23763
- Steady convergence analysis of generalized Chebyshev successive interpolation process, using functions of interpolative classes 10 p1635 A71-23801
- Convergence rates of multistep iterative procedures for finding zero of nonlinear function defined on R to n th power 11 p1792 A71-25932
- Bending problems of elastoplastic plate rigidly clamped over edges, deriving theorems on existence, uniqueness and convergence of approximate solutions 12 p1974 A71-26962
- Boundary value problems solution convergence, using point integrators in synchronous dynamic mode 12 p1884 A71-27335
- Minimization of convex functions without derivative calculation, proving superlinear convergence 13 p2094 A71-27895
- Convergence and accuracy of modified Gauss-Seidel finite difference scheme, calculating one dimensional Navier-Stokes shock structure 13 p2051 A71-29429
- Iterative solution for quasi-linear heat equation, examining convergence for equation describing self similar heat wave from instantaneous plane source 14 p2334 A71-29564
- Iris-type discontinuity problems in waveguides and periodic structures, investigating numerical solutions convergence 14 p2212 A71-30513
- Linear positive convolutive operators, considering convergence problem 15 p2439 A71-31144
- Bubnov-Galerkin method convergence prediction, discussing J spaces and orthonormal bases 15 p2439 A71-31154
- Dirichlet problem for second order linear elliptic differential equations, considering convergence theory results for finite difference approximations 15 p2440 A71-31349
- Fluid flow equations problems, describing stability and convergence theory for finite difference approximations 15 p2441 A71-31353
- Harmonic mixed boundary value problem exact solution for rectangle with slit, outlining finite difference techniques convergence 15 p2441 A71-31356
- Mathematical modeling and convergence analysis of nonscanning self adaptive control systems for linear objects, using Liapunov second method 15 p2379 A71-31519
- Averaging of nonlinear integrodifferential equations, demonstrating uniform convergence of sequence by successive approximations 15 p2442 A71-31521
- Algorithm convergence for sparse nonlinear equations system solution with Jacobian satisfying Lipschitz condition 15 p2442 A71-32313
- Self adjoint expansion of Laplace operator with point spectrum, establishing uniform convergence and Riesz summability conditions of spectral decomposition 16 p2603 A71-33999
- Short convergents without risk of detachment, deducing corresponding distribution on provisional wall from velocity field 16 p2521 A71-34054
- Diffraction on smooth convex body, constructing convergent series for homogeneous wave equation solution 17 p2697 A71-34255
- Convergence characteristics of sequential and combined conjugate gradient restoration algorithms for mathematical programming, studying constrained function minimization 17 p2764 A71-34520
- Rapid convergence method application to linear system with odd almost periodic coefficients 17 p2779 A71-34907
- Classes of n dimensional functions nonlinear matrix mapping, emphasizing block-Jacobi and block-Gauss-Seidel process convergence for continuous surjective M functions 17 p2767 A71-35524
- Convergence and error estimates for finite difference methods for approximately positive solutions of mildly nonlinear eigenvalue problems 17 p2768 A71-35683
- Orders of convergence for iterative procedures for finding zero of nonlinear function, considering secant and Steffenson method 17 p2768 A71-35685
- Convergence rate for finite element method, considering Neumann problem for second-order elliptic differential equations with constant coefficients in m dimensional Euclidean space 17 p2769 A71-35688
- Global convergence of iterative schemes by Newton-Gauss-Seidel method, considering discrete approximations of elliptic partial differential equations 17 p2769 A71-35689
- Orthogonal matrix estimate by iterative algorithm with given order of convergence 17 p2769 A71-35692
- Numerical solution algorithm for parabolic free boundary problem in statistical decision theory, comparing convergence with asymptotic expansions 18 p2941 A71-36352
- Weakly singular integrals numerical compound quadrature error bound and convergence rate estimate by applying Peano theorem with modification for avoiding singularity 18 p2941 A71-36355
- Convergence theorem for singular integrands numerical quadratures, assuming domination near singularity by monotone integrable function 18 p2941 A71-36356
- Convergence of Broyden single-rank iterative solution for nonlinear equations systems involving approximation to Jacobian matrix 18 p2941 A71-36357
- Controlled objects convergence game, constructing optimal minimax pursuer strategy 18 p2948 A71-36779
- Convergence theory for Newton-like iterative methods to solve nonlinear equations in abstract spaces, presenting error analysis 18 p2943 A71-36955
- Model-reference feedback control system, investigating effects of equivalence lack between reference and plant on iterative process convergence by linear transformation 19 p3038 A71-37778
- Convergence rate of finite difference schemes applied to initial value problems for hyperbolic equations 19 p3088 A71-38312
- Extremal problems approximation conditions in functional optimal value and elements set senses, applying to study of convergence in presence of constraints 19 p3088 A71-38413
- Optimality criterion for convergence of iterative solution of linear time optimal problem in reflective Banach space 19 p3088 A71-38414
- Convergence estimation of locally one dimensional scheme for multidimensional heat conduction boundary value problem solution on nonuniform grids using maximum principle 19 p3171 A71-38415
- Sequence convergence of similarity transformations in matrix balancing for accurate eigenvalues computation 20 p3254 A71-38756
- Rapidly converging second order optimal tracking algorithms for adaptive equalization on basis of estimated bounds for eigenvalues of signal plus noise correlation matrix 20 p3201 A71-38872
- Mixed strategy convergence game of conflicting controlled motion under phase constraint 20 p3270 A71-39359
- Mixed decomposition and convergence of gradient type coordinating algorithm for two-level complex control system using interconnection variables and Lagrange parameters 20 p3208 A71-39472
- Iterative method for linearly elastic structure undamped vibration natural frequency determination with fast convergence 20 p3311 A71-39965
- Convergence of progressive shock wave solutions for higher order equations of conservation laws with dissipation and dispersion terms, proving shock curves existence 21 p3414 A71-40141
- Continuous analog iterative methods and solution of nonlinear two point boundary value problems, producing convergent series of iterates 21 p3408 A71-40585
- Rapidly converging iterative solution to radial Schroedinger equation in oscillatory region 21 p3408 A71-40845
- Periodic functions complete orthogonal sequences class as linear combinations of Fourier expansions, obtaining convergence theorem 21 p3410 A71-41083
- Curved finite elements application to circular arches, examining convergence properties of various shape functions used in stress resultant calculations 21 p3474 A71-41425
- Recurrent finitely converging algorithms for solving inequalities in automatic control systems involving adaptive filters 22 p3526 A71-41858
- Mathematical modeling and convergence analysis of nonscanning self adaptive control systems for linear objects, using Liapunov second method 22 p3528 A71-42884
- Factor methods convergence for abstract equations with nonlinear entirely continuous operators 23 p3699 A71-43570
- Iterative solution for radiant energy transport equation by Wiener Hopf operator equations, investigating convergence conditions 23 p3699 A71-43573
- Convergence improvement in parallel tangents/penalty function solutions for missile trajectory optimization with terminal constraints, comparing with steepest descent method 23 p3659 A71-44102
- Convergence and strain accuracy of finite element solutions for nodal displacements in plane elastic mesh 24 p3842 A71-44633
- Finite difference scheme for elasticity theory boundary value problem in curvilinear region, estimating solution convergence rates 24 p3881 A71-44771
- Pseudomoments estimation of convergence rate in central limit theorem for random variables series 24 p3843 A71-44874

CONVERGENT NOZZLES

- Shock wave propagation through converging nozzle, predicting real gas dissociation and vibrational excitation effects for comparison with shock tube measurement 05 p0735 A71-16528
- Turbulent flow in initial section of convergent axisymmetric nozzle based on logarithmic velocity law 09 p1431 A71-22409
- Flow field properties of impinging free jets from circular convergent nozzle, measuring velocity, surface pressure and momentum flux 10 p1552 A71-24616
- Atomization drop size distributions in sprays from convergent pneumatic nozzles for molten wax and polyethylene mixtures 13 p2049 A71-29007
- Two coaxial axisymmetric subsonic gas jets of different density mixed during expulsion from convergent nozzles with high compression, using flow rate ratio 13 p2050 A71-29215
- Thrust and flow rate control in choked convergent nozzles by potential vortex generation, verifying swirling nozzle flow analytical model 15 p2391 A71-32061

CONVERGENT-DIVERGENT NOZZLES

Turbulent boundary layer air flow through supersonic convergent-divergent nozzle with heat transfer, considering relationship between temperature and velocity profiles

01 p0180 A71-10950

Surface roughness effects on gas to wall heat transfer in conical converging diverging nozzles, using heated air

04 p0675 A71-14780

Transonic gas flows in axisymmetric small throat curvature radius Laval nozzle with appreciable flow parameters variation in transverse direction

07 p1014 A71-19732

Inviscid air nonequilibrium shock layer properties correlation based on plenum entropy, predicting composition of downstream converging-diverging nozzle expanding air flow

[AIAA PAPER 70-866] 07 p1090 A71-19905

Numerical solution of quasi-one dimensional viscous heat conducting compressible Laval nozzle flows by time dependent finite difference scheme

09 p1545 A71-22454

Viscous flow in supersonic de Laval nozzle, measuring gas density and rotational temperatures by electron beam techniques

[AIAA PAPER 70-810] 12 p1865 A71-27555

Viscous convergent-divergent nozzle flow slender channel approximation, discussing nozzle geometry, Reynolds number and wall temperature effects

[AIAA PAPER 69-654] 12 p1865 A71-27556

Direct Laval nozzle design problem solution using finite difference method

13 p1991 A71-29170

Combustion efficiencies of staged rocket motor consisting of gas generator, secondary combustor and converging-diverging nozzle

[AIAA PAPER 71-739] 14 p2296 A71-30782

Compressible laminar plane axisymmetric boundary layer flows in Laval nozzles, studying temperature, density and velocity distribution relations

15 p2386 A71-31164

Plane transonic gas flows through Laval nozzle and symmetrical wedge-shaped profile, solving boundary value problem by reduction to singular integral equation

19 p2991 A71-37101

Turbulent boundary layer and heat transfer measurements along cooled conical convergent-divergent nozzle

[ASME PAPER 71-HT-4] 19 p2993 A71-37982

Two phase critical flow of saturated and subcooled high pressure liquid nitrogen through convergent-divergent nozzle, comparing with water

21 p3369 A71-40894

Stationary collisional shock observation in continuous supersonic plasma wind tunnel involving Q device modified into magnetic de Laval nozzle

21 p3426 A71-41403

Carbon dioxide, nitrogen and water vapor hot mixture expansion through Laval nozzle, showing population inversion on carbon dioxide laser transition

22 p3556 A71-41726

Hypersonic nozzle convergent section heat transfer optimization by Euler method, using Lagrange undetermined multiplier and pipe flow approximation

22 p3622 A71-42781

CONVERSION TABLES

Microwave front end designs for low noise operation, discussing FET applications and mixer conversion loss reductions

11 p1731 A71-25673

CONVERTAPLANES

U V/STOL AIRCRAFT

CONVERTERS

Queueing model for analyzing video scan converter

01 p0047 A71-10215

Time-pulse converter for semiconductor triodes DC amplification factor measurement

02 p0230 A71-11832

Nondissipatively-regulated DC to DC converter design, describing circuit technique and magnetic-semiconductor combinations

03 p0352 A71-13046

Spacecraft electric power transformation and control techniques enhancement, using DC to DC converter, voltage converter/regulator and solar array reorientation system

03 p0352 A71-13049

Electronic time scale converters for frequency synthesizers

04 p0592 A71-14861

FM converter for tape recording of LF biological data

04 p0545 A71-15163

Current/voltage converter for measurements at floating potential with respect to ground, using Wheatstone bridge type circuit

04 p0560 A71-15894

Tunnel diode output voltage converter circuit diagram and waveforms

07 p1080 A71-20360

Electrodynamic transducer design for structural vibration testing system, using low power steering

signal converter to generate large scale electromechanical loads

09 p1386 A71-22606

Approximate optimal control synthesis, eliminating use of nonlinear functional converter for switching units design

09 p1423 A71-22607

Amplitude-frequency characteristics of physically similar piezoelectric accelerometric converters

09 p1450 A71-22798

Book on thyristor phase-controlled converters and cycloconverters covering operation, control and performance

13 p1998 A71-27941

Dual phase asynchronous or hysteretic micromotors powering with two transistorized static DC to AC voltage converter circuits

13 p1999 A71-28629

Probabilistic analysis of random pulse signal gating on time selective zero lag converter with rectangular pulse input

23 p3647 A71-44322

CONVEYORS

Material point motion in conveyor horizontal pipe drums with screw surface on inner walls, using law of addition

13 p1998 A71-28297

Frankfurt terminal baggage conveyor system, describing passenger capacity and luggage handling equipment

13 p2045 A71-29312

CONVOLUTION INTEGRALS

Noncoherent optical analog image processing by corrective convolution integral techniques for removal of blur, defocus and noise

01 p0081 A71-10828

Hybrid decoding technique for symmetrical binary input channels, using bootstrap algorithm across convolutionally encoded information streams

11 p1730 A71-25375

Convolution-type integral equations over arbitrary finite segment number with kernels, showing solvability in spaces, applications and correctness

12 p1982 A71-27519

Differentiability of nonlinear Volterra integral equations of second kind with convolutional weakly singular kernels

15 p2442 A71-31870

Step-change single blow transient temperature response synthesis by data reduction with aid of operational calculus and half-line convolution integral equation theory

20 p3314 A71-39488

Convolution integral equation unique solution in second kind Fredholm equation form, applying to plane polarized electromagnetic wave diffraction on infinitely thin band

24 p3804 A71-44769

CONVOLUTIONS [MATHEMATICS]

U CONVOLUTION INTEGRALS

CONVULSIONS

Protective brain function in epileptical convulsive seizures during sonic stimulation in rats

03 p0359 A71-13159

Acoustic priming of audiogenic seizures in mice, noting high susceptibility to convulsions under intense sound

03 p0360 A71-13160

Audioconditioned convulsive response [ACCR] characterization, investigating age, auditory conditioning and environmental noise effects on sound-induced seizures in mice

03 p0360 A71-13162

Cortical and subcortical electrical activity during electrically and drug induced convulsive seizures in cats, correlating with spinal monosynaptic reflex variations

15 p2359 A71-31957

EEG study of hyperoxic convulsions in Macacus nemestrinus and Papio primates, considering preventive effect of Diazepam and derivatives

21 p3339 A71-41418

Vibration induced paroxysmal and cardiovascular hazards during patients transport to hospital by air or ambulance, discussing therapeutic and preventive treatments

22 p3500 A71-41573

COOLANTS

NT ENGINE COOLANTS

NT ORGANIC COOLANTS

Coolants Prandtl number effect on pressure drop, heat transfer and friction of rough surfaces

04 p0675 A71-14779

Convective heat transfer in coolant with constant velocity in ring channel with heat sources, deriving expressions for flow and wall temperature

06 p1006 A71-18004

Turbulent boundary layers transpiration cooling prediction with coolant fluid serving as heat sink within structure wall and as protective film

07 p1220 A71-18768

ABM control surfaces active oxidation protection, using ammonia as reactive coolant injected through porous W wall matrix

[AIAA PAPER 71-391] 11 p1837 A71-23553

Coolant combustion effects in transpiration cooling of gas turbine components, using hydrogen, ammonia and nitrogen coolants

[ASME PAPER 71-GT-72] 11 p1855 A71-25986

Hypersonic reentry heat shielding problem, considering axisymmetric laminar boundary layer flow with local coolant mass injections at multiple stations

13 p1990 A71-29122

Coolant thermophysical properties effect on heat transfer intensity in porous metals, analyzing differential equations

17 p2835 A71-34204

Mercury properties, chemistry, safety, handling and corrosion in nuclear coolant applications

19 p3102 A71-37071

COOLERS

Cascade thermoelectric cooler/heat pump/transient response for various geometries, materials and environmental conditions

03 p0355 A71-14320

COOLING

NT AIR COOLING

NT EVAPORATIVE COOLING

NT FILM COOLING

NT GAS COOLING

NT LIQUID COOLING

NT QUENCHING [COOLING]

NT RADIANT COOLING

NT REGENERATIVE COOLING

NT SUPERCOOLING

NT SURFACE COOLING

NT SWEAT COOLING

NT THERMOELECTRIC COOLING

NT THERMOMAGNETIC COOLING

Body heat loss in water immersion, using heat transfer model

02 p0207 A71-12387

Tissue cooling with liquid nitrogen, determining film boiling transition temperature and heat transfer rates

[ASME PAPER 70-WA/HT-16] 03 p0372 A71-14096

Local cooling effects on responsiveness of muscular and cutaneous arteries and veins in dogs, noting blood flow redistribution

04 p0538 A71-15091

Human legs thermal response during cooling for refrigeration anesthesia, deriving analytical model for temperature level prediction as function of time

04 p0545 A71-15160

Quantitative acoustic vibration effects on cooldown rate of bodies from room temperature to liquid nitrogen or helium temperature

04 p0686 A71-15525

Glass textolite materials strength during cooling under tensile, high rate tension and impact loads

05 p0771 A71-16362

Ti alloys beta phase solid solution decomposition during cooling and plastic deformation at low temperatures

05 p0767 A71-16770

Nonadiabatic gas acoustic oscillation instability, examining heat release fluctuations

05 p0838 A71-16777

Plate critical surface temperature in case of stabilization by supersonic boundary layer cooling

05 p0695 A71-16852

Cooling models for flare produced plasmas in solar corona, considering collisional, radiative and conductive mechanisms

06 p0968 A71-17913

Draw-through cooling of electronic equipment in subsonic and supersonic commercial jet transports, discussing internal circulation system design

[SAE-ISR-64A] 07 p1077 A71-19642

S-IVB liquid rocket engine and propellant feed systems restart shutdown in orbital operations

[AIAA PAPER 70-672] 07 p1183 A71-19857

Physiological effects of cooling measured by men wearing air and water cooling garment under external heat loads or large metabolic heat

08 p1248 A71-21232

Time optimal control for massive solids heating or cooling from initial into prescribed finite state with constraints

10 p1695 A71-24159

Steel structural transformations under arc melting, cooling and electroslag remelting, noting delta ferrite precipitation with hot stage microscope

11 p1776 A71-25168

M stars mass loss, determining dust shells radii and densities with IR observations of circumstellar emission

11 p1818 A71-25204

Nickel alloys crystallization at superhigh cooling rates by dropping liquid metals on rotating copper cylinders to obtain films

12 p1917 A71-27301

Unidirectionally and cross rolled titanium alloys elastic properties anisotropy during cooling, discussing Young modulus distribution

15 p2428 A71-31857

Turbine disks failure under radial temperature drop, studying effects on load bearing capacity for thermal stresses

17 p2832 A71-35454

Densely packaged microelectronics thermal control, using immersion cooling in dielectric fluids 17 p2718 A71-35786

Finger freezing time correlation with cooling rate, discussing effects of indeterminate skin supercooling 18 p2860 A71-36883

Cooling history of magma containing apatite growth forms on basis of morphological variations in glassy and crystalline rocks 19 p3051 A71-37673

Heat removal from space suit, discussing anatomic and physiological features suitable for cooling 20 p3188 A71-39224

Physiological responses to head and neck vs trunk and leg cooling under hyperthermic stress 21 p3331 A71-40356

Ti-Fe and Ti-Cr binary alloys microsegregation genetic trend measurement by electron probe microanalysis, observing critical cooling rate from beta phase 22 p3562 A71-41945

High temperature gas turbine engines rotor blades cooling, deriving generalized dimensionless relations for heat transfer data extension from static tests to operational conditions 23 p3718 A71-44066

COOLING FINNS

Laminar natural convective heat transfer from base plates of vertical rectangular fin arrays, taking temperature and fin geometry effects into account 20 p3333 A71-12603

Natural convective heat transfer from fin edges in vertical rectangular arrays, noting temperature and fin thickness effects 20 p3333 A71-12604

Natural convective heat transfer from fin-flat in vertical rectangular arrays, comparing duct and open channel coefficients 20 p3333 A71-12605

Thin shallow annular radiating fins for heat removal from sphere or polyhedron with isothermal surfaces, determining optimal weight and geometrical parameters 12 p1986 A71-27331

Perfectly effective boiling fin design in horizontal right circular cylinder shape, deriving formulas at peak heat flux operation 15 p2514 A71-32264

Optimal radiative capacity of star shaped radiator with mirror reflecting surfaces for vacuum cooling of elongated finned bodies 17 p2836 A71-34311

Cooling fin shape optimization for minimum volume, considering convective and radiative heat exchange for assumed temperature distribution 17 p2837 A71-34442

Brazing roughness effects on rectangular plate fin heat exchanger surfaces heat transfer and flow friction characteristics, noting fin surface geometry influence [ASME PAPER 71-HT-29] 19 p3166 A71-37999

COOLING SYSTEMS

Closed system for air cooling of image converter tubes and superorthicons for wear light flux, using refrigerator or dry ice 20 p0080 A71-10622

Closed hermetic air cooling system for high temperature gas turbines 20 p0143 A71-11246

Nuclear rocket nozzle cooling passages, discussing heat transfer and friction correlations for single-phase hydrogen turbulent flow [AIAA PAPER 70-661] 20 p0456 A71-14444

Spacecraft cryogenic cooling systems, discussing passive, phase change and closed cycle coolers and refrigerators 20 p0535 A71-15343

Gas turbine air cooling systems hydraulic characteristics by graph-analytical method 20 p0945 A71-18001

Optimal weight of aerodynamic heat protection layers of stressed skin and optimal efficiency of cooling system for hypersonic aircraft compartments 20 p1375 A71-20836

Miniature cryogenic systems for cooling IR detectors in upper atmosphere involving earth surface, air-glow and OH emission measurements 20 p1545 A71-23004

Hydrocarbon fuel for hypersonic vehicle cooling, discussing use of endothermic reactions to achieve maximum heat sinks [AIAA PAPER 68-997] 20 p1658 A71-24852

Heat transfer coefficients of various jet systems impinging on gas turbine blade inner surfaces, discussing cooling flow rates and solid particles injection into air flow [ASME PAPER 71-GT-9] 20 p1811 A71-25955

Coated abrasive grinding of Ti alloys using water, various soluble cutting oils and inorganic phosphate solutions as coolants and lubricants 20 p1771 A71-26142

Optimal shape of single radiative cooling elements without self irradiation relative to cross sections and linear generatrices of radiator 20 p2165 A71-29179

Radiative cooling system for nearly spherical or polyhedral bodies using radially attached diverging conical elements 17 p2836 A71-34307

Complex form plates with energy sources in combined cooling system, calculating temperature field 17 p2836 A71-34422

Fan jet first stage turbine blade air cooling, describing design, heat transfer data, efficiency and temperature distribution 18 p2956 A71-35904

Specular reflecting passive radiators for synchronous satellite radiation detectors cooling [ASME PAPER 71-AV-30] 18 p2869 A71-36397

Feasibility assessment of hypersonic transports with actively cooled airframe structure, considering liquid hydrogen fuel use as coolant 19 p2995 A71-37123

Space shuttle structural heat problems, discussing shield design configurations and cooling systems 19 p3150 A71-37311

Closed cycle refrigeration system for cryogenic cooling of IR illuminator in helicopter mounted U.S. Army NVASS Night Vision System for night reconnaissance 20 p3184 A71-39275

Paramagnetic cycles for low temperature superconducting magnet cooling, discussing refrigerator, cryogenic pumps, regenerators and adjustable heat source and sink 21 p3476 A71-40898

Cryogenic temperature cooling systems for IR detectors, describing Joule-Thomson liquefier and liquid transfer devices 22 p3544 A71-42139

Thermal radiative cooling system characteristics determination allowing surface material thermal conductivity and blackness degree dependence on temperature 23 p3782 A71-43919

Space vehicle radiative cooling system rib temperature field calculation, taking into account material heat conductivity temperature dependence 24 p3889 A71-45023

Ni-Zr alloy crystallization at large cooling rates obtained by melt droplets blowing with compressed He jet onto rotating Cu cylinder surface 24 p3840 A71-45374

COORDINATION

Technical resources pooling among airlines for investment and maintenance cost cut of aircraft fleets 24 p0690 A71-14992

COORDINATE SYSTEMS

U COORDINATES

COORDINATE TRANSFORMATIONS

Recurrent Lagrange multipliers coordinate transformation for optimal low thrust Earth- Jupiter trajectories 20 p0160 A71-10947

Satellite orientation determination from single vector measurements, discussing coordinate systems transition 20 p0319 A71-11917

International geomagnetic reference field 1965 geomagnetic potential rate of change and transformation to dipole coordinates 20 p0888 A71-17282

Mathematical model for perpendicular coordinate transformation from pattern to sensation in central visual field 20 p1050 A71-20106

Curved space-time mathematical structure /quasi-groups/, investigating 10-parametric classes of coordinate systems and Poincare groups 20 p1334 A71-21358

Steady electromagnetic oscillation amplitude calculation from solution kernel to Maxwell equations boundary value problems through orthogonal coordinate transformation to Fredholm integral equations 20 p1495 A71-23431

Tensor inertia conversion from principal to rotated coordinates system, obtaining negative products in aircraft [DFVLR-SONDDR-111] 20 p1557 A71-24949

Geodetic geographic coordinate transformations and ellipsoid heights, azimuth and length determination from synchronous photogrammetric observations and distance measurements of artificial satellites 21 p1759 A71-25813

Artificial earth satellite orientation determination from single vector measurements, discussing coordinate systems transition 21 p2145 A71-28204

Gas dynamic and irrotational flow equations system transformation into Cauchy-Riemann equations via Beltrami coordinate transformation for simple representation of transonic flows [DFVLR-SONDDR-124] 21 p2228 A71-31127

Coordinate transformations of shape and position of cometary tails on orbit plane suitable for digital computer 21 p2485 A71-31669

Spinning and point particles motion from Einstein equations based on covariance with general coordinate transformations 16 p2610 A71-33270

Geometric object concept in third principle of relativity, obeying identity functional equations for infinitesimal general coordinate transformations 16 p2611 A71-33273

Graphic method for comet geocentric equatorial coordinates transformation into heliographic coordinates, using trigonometric circle and three stereographic networks with 100 mm radii 17 p2803 A71-34834

Quaternion representation of successive rotations in space vehicle control, locating final position of coordinate frame with respect to original position 17 p2773 A71-35066

Linear, affine and projective coordinate transformation from one mapping plane to another with quick maximum error estimation 17 p2734 A71-35187

Potential function transformation under coordinate rotations, deriving coefficients for Laplace equation series expansion 19 p3138 A71-37755

Mathematical feature selection transformations by multidimensional rotations, considering character recognition experiment 19 p3026 A71-38490

Delta wing problem reduction to Laplace equation solution, using perturbation technique to solve Lame equation resulting from elliptic conal coordinates transformation 20 p3177 A71-39498

Three dimensional graphics software package for CRT and storage tube displays and plotters, describing coordinate transformation 21 p3347 A71-40133

Mars coordinate shift from elliptic to equator system, considering precession and orientation data 22 p3607 A71-42871

Noether invariance and conservation laws theorems extension to nonlocal calculus of variations, obtaining coordinate and point transformations effects on dependent functions domain space 23 p3700 A71-44177

Transonic flows about two dimensional airfoils, calculating far field boundary conditions with coordinate transformation 24 p3789 A71-44620

COORDINATES

NT ASTRONOMICAL COORDINATES

NT CARTESIAN COORDINATES

NT GEOCENTRIC COORDINATES

NT GEODETIC COORDINATES

NT INERTIAL COORDINATES

NT LAGRANGE COORDINATES

NT PLANETOCENTRIC COORDINATES

NT POLAR COORDINATES

Numerical method for stress distribution around openings in shells, using orthogonal coordinate system 20 p0321 A71-11649

Static axially symmetric gravitational field equations, presenting Weyl solutions for standard coordinates 20 p0625 A71-14730

Navier-Stokes equation solution in cylindrical coordinates, using finite difference scheme with brute force matrix methods 20 p0572 A71-15551

Cantilever plates calculation, satisfying boundary conditions by coordinate sequence construction 20 p0828 A71-16894

Optimal solutions to control problem with bounded coordinates 20 p0731 A71-17016

Nonlinear unsteady heat conduction problems, investigating thermophysical property dependence on temperature and body coordinates by half space and approximate methods 20 p1006 A71-17749

Earth rotation pole coordinates from International Latitude Service stations and International Polar Motion Service data 20 p0890 A71-17878

Automatic coordinate measuring and recording devices for photogrammetric restitution equipment 20 p0901 A71-18293

Geomagnetic latitude-longitude coordinates, examining field lines intersections at height of 100 km 20 p1285 A71-21757

Coordinate conditions necessary for Einstein gravitation equations system completion 20 p1336 A71-21796

Mathematical model for calculating plates of variable thickness referred to curvilinear triorthogonal coordinate system 20 p1536 A71-22411

Hybrid coordinate formulation for flexible space vehicle attitude control system design [AIAA PAPER 70-20] 20 p1532 A71-22907

Structural system analysis by partial decomposition of flexibility and stiffness matrices, obtaining coor-

- dinate deformations for computer and hand applications
10 p1691 A71-24693
- Covariance matrix of coordinate fluctuations of instantaneous radar center of reflection from set of scatterers
10 p1578 A71-24709
- Distant artificial cosmic objects coordinate determination by image converter/closed TV system screen photography and TV observations of space probes
14 p2309 A71-29992
- Entropy layer in hypersonic flows, determining body configuration from shock wave shape described by coordinates power function
14 p2171 A71-30875
- Absolute magnitudes of 1965-1969 comets, including orbit elements, perihelion coordinates and maximum values of reduced head diameter and tail length
15 p2483 A71-31339
- General nonorthogonal coordinate systems operation techniques, modifying matrix theory for vector equations handling in classical mechanics
15 p2442 A71-32111
- Optimal phase trajectories of coordinates of electrodynamic vibration test stand, analyzing motion of moving part and optimal control signal along coil
15 p2353 A71-32190
- Physical meaning of fifth coordinate in five dimensional field theory, discussing relationship as parameter metric of de Sitter four dimensional space-time manifold
16 p2608 A71-33223
- Scalar function expansion in relativistic invariant functions in pseudoeuclidian space, deriving direct and inverse formulas for spherical, hyperbolic and Lobachevskii coordinates
16 p2612 A71-33459
- Coordinate conditions necessary for Einstein gravitation equations system
16 p2612 A71-33548
- Nonlinear unsteady heat conduction problems, investigating thermophysical property dependence on temperature and body coordinates by half space and approximate methods
17 p2838 A71-35115
- Shell analysis in curvilinear coordinates, obtaining edge effect equation with canonical kinematic unknowns in plane sections law
17 p2830 A71-35314
- Satellite attitude control principles for studies requiring satellite orientation relative to orbital coordinate system
19 p3062 A71-37149
- Operating principles of spaceflight simulators, considering star coordinates errors in collimator simulator of stellar sky
19 p3062 A71-37150
- Statistical methods for calculating cross correlation function integrals of input and output coordinates of automatic control system in presence of random noise at input
22 p3525 A71-41437
- Scanning microwave landing guidance system coordinates choice, discussing signal format, antennas planar or conical beams and V/STOL application
22 p3572 A71-42090
- Reproduction accuracy of holographic model, discussing coordinates origin and X-Y-Z errors
23 p3675 A71-43303
- Formulas derived for object conjugate points coordinates and holographic image
23 p3675 A71-43304
- Mixed world model with arbitrarily moving matter, using coordinate system with matrix of reference point components of three dimensional metric tensor
23 p3736 A71-43404
- Stationary or moving objects spatial coordinates determination by three and four dimensional terrestrial photogrammetry, using phototheodolite stereophotographic pictures
23 p3671 A71-43590
- Invariance theory for nonlocal variational principles, covering energy forms and identities, weak coordinate invariance, integral balance and conservation laws
23 p3700 A71-44179
- Spherically symmetric Gaussian coordinate systems completeness in spaces analogous to Lemaître and Kruskal spaces in general relativity
24 p3848 A71-44658
- COORDINATION**
- Human fingers coordination during teletype operation, examining temporal characteristics
02 p0205 A71-12055
- Coordinatograph control system transfer function and interpolation error calculation
05 p0732 A71-17040
- Eye-head coordination in monkeys by recordings from neck and eye muscles, noting central neural command role
18 p2856 A71-36232
- Coordination structure of human hand arbitrary movements during stimulation of horizontal semicircular canals in vestibular apparatus by negative angular acceleration
24 p3796 A71-44545
- COPILOTS**
- U AIRCRAFT PILOTS**
- COPLANARITY**
- Weierstrass condition for optimality in coplanar elliptic orbit transfer involving velocity impulse control variables, discussing switching relations at corner of optimal trajectory
12 p1963 A71-27061
- COPOLYMERS**
- A-B-A block copolymers statistical thermodynamics, describing postulated microstructure theoretical model for phase transition prediction
02 p0273 A71-12450
- Imide-pyrone copolymers preparation by solution polymerization, considering base/acid degradation resistance and thermal stability in air and vacuum
04 p0549 A71-15749
- Phenylated imide-quinoxaline copolymers, describing synthesis and thermal and solubility properties
11 p1787 A71-25425
- Styrene-methyl methacrylate and -acrylonitrile copolymers linear and mass regression rates in hybrid rocket fuels combustion
15 p2464 A71-31640
- Microphase separation in homopolymer-block copolymer mixtures as function of composition, molecular weight and interaction parameters
17 p2695 A71-35525
- Polyethylene, polypropylene and copolymers sliding friction viscoelastic nature, obtaining relationship between sliding force, adhesion bond shear strength and contact area
19 p3068 A71-37425
- COPPER**
- Cu compatibility with refractory Ta-W alloy interface at high temperature, noting eutectic formation
01 p0100 A71-10374
- Cu addition effects in solid solution on grain boundary sliding in Al at constant shear stress, considering accompanying crystal dislocations
01 p0102 A71-10739
- Anomalous Cu concentration profile due to migrating Cu ions-GaAs crystal defects interaction
05 p0794 A71-16877
- Highly ionized line spectra of Fe, Co, Ni and Cu belonging to Na I and Mg I isoelectronic sequences
05 p0717 A71-16909
- Cu and Ni electroless deposition on carbon fibers for composites
05 p0759 A71-16927
- W fibers reinforced Cu matrix work hardening rates as function of fiber diameter and volume fraction, using isolated tension pile-up model
09 p1535 A71-22279
- Nonelastic unloading microstrains in Cu crystals after stage II macroscopic prestraining, discussing stresses action on dislocations
09 p1468 A71-22700
- Polycrystalline copper and magnetic films thin intermediate layers, showing prevention of epitaxial growth
12 p1943 A71-26855
- Al-Zn-Mg alloys, considering Cu and Cr additions effects on nucleation and incoherent precipitates formation
13 p2088 A71-29406
- Uniaxially reinforced W-Cu matrix composite material dynamic compressive load properties, considering strain rates and yield stress
14 p2257 A71-29643
- Creep rupture strength and durability of Al, Ni and Cu irradiated by neutron flux
14 p2258 A71-30004
- Al and Cu dynamic plastic deformation at elevated temperatures, discussing relationship between strain rate sensitivity and activation energy
15 p2428 A71-31972
- Thermoelastic stress generation in Cu and Ta samples by linear accelerator produced monochromatic MeV electron pulses, comparing measurements with wave theory predictions
15 p2414 A71-31973
- Grain size effect on fatigue life during tension and compression tests of alpha brass, copper and aluminum, considering slip character
15 p2437 A71-32578
- Triple Knudsen cell method to determine thermodynamic activity of Cu in bcc solid solution of Ti-Cu alloys
17 p2756 A71-34488
- Copper on copper friction coefficient dependence on oxygen pressure, investigating exoelectron emission from differently oxidized copper surface layers
18 p2928 A71-36750
- Surface properties and environmental effects on fatigue striations development and crack initiation in Cu single crystals
19 p3077 A71-37412
- Prestressing effect on yield surfaces of Al and Cu thin walled tubes
19 p3079 A71-37705
- Copper single crystals fatigue as statistical work hardening phenomenon
19 p3081 A71-38072
- Al, Cu and Ni high temperature creep noting diffusive, shear and dislocation deformation mechanisms
19 p3083 A71-38525
- Mechanical and frictional properties of sintered copper matrix glass compacts, considering lubricating or seizure preventing effects of glass presence
21 p3406 A71-40759
- Vacuum apparatus for fatigue tests at room and low temperatures, giving results for annealed copper
22 p3538 A71-41700
- COPPER ALLOYS**
- NT BRASSES**
- NT BRONZES**
- Splat cooled hypoeutectic Al-Cu alloy superplasticity, using tensile tests and electron microscopy
01 p0100 A71-10280
- Periodically modulated phase structure transformations in decomposition of Cu-Ti and Cu-Ti-Al alloys during aging at different temperatures
01 p0101 A71-10670
- Cadmium-copper fibrous eutectic alloy morphology, describing sample preparation and crystallographic examinations by optical and electron microscopes
01 p0103 A71-11018
- Cu-Ni-Mn alloys hardening by heat treatment, describing various critical temperature measurement methods and micrographic analysis
01 p0105 A71-11622
- Cu-Al alloy, Ti and low carbon steel under LF flexural stress, testing parameters effect on fatigue resistance
03 p0445 A71-14339
- AlZnMgCu alloys fracture behavior, examining aging conditions, rolling, forging, cracking, tensile strength and chemical composition
04 p0613 A71-15745
- Protective oxide formation on single phased Cu-Al-Si alloys during high temperature oxidation
05 p0770 A71-17099
- Al-Cu precipitation hardened alloys, determining microstructure effects on fatigue life and flow stress
08 p1312 A71-21547
- Hot extruded W-Cu pseudoalloys under tension and compression, determining impact strength and plasticity
08 p1316 A71-21614
- Refining process of Fe-NiCu-Mn alloys, discussing aging kinetics, hardening mechanism and strength properties
11 p1781 A71-26159
- Fretting corrosion relationship to mechanical vibrations damping capacity for Fe and Cu alloys, noting energy dissipation
13 p2082 A71-27822
- Elastic stresses during local deformation in Nb-Mo, Ni-Cr, Cu-Al and pure bcc metals, using X ray analysis
13 p2085 A71-28225
- Fiber strengthening of Cu-Fe-Cr wire by cold drawing and annealing, discussing age hardening process of chromium ferrite needles in ductile Cu matrix
13 p2088 A71-29402
- Impact strength of Cu, Cu-Ni alloy and superalloy matrices reinforced with W fibers, studying temperature, heat treatment and fiber content and toughness effects
14 p2258 A71-29919
- Al and Cu-Al alloys eutectic composites with small interlamellar spacing, characterizing ambient temperature compressive stress strain behavior to failure
15 p2432 A71-32168
- Explosive and isostatic forming effects on commercial precipitation-hardenable Al-Cu alloy microstructure, tensile properties and fatigue life
15 p2433 A71-32180
- Triple Knudsen cell method to determine thermodynamic activity of Cu in bcc solid solution of Ti-Cu alloys
17 p2756 A71-34488
- Hot pressed W-Cu pseudoalloys strength and ductility under tension and compression
17 p2760 A71-35674
- Slip line deformation of ordered and disordered Cu-Au intermetallic single crystals from microstrain and electron micrographic studies
20 p3249 A71-38967
- Cu-rich alloys with high damping capacity at low stress amplitudes for structures and machines, noting damping stability improvement in Mn-Cu alloy by Cd addition
21 p3396 A71-40331
- Ni-Cu-Nb age hardenable steel mechanical properties, examining hot rolling and heat treatment effects
21 p3387 A71-40455
- Ni-Cu alloy castings solidification experiments on catalytically clean metals to avoid heterogeneous nucleation
21 p3387 A71-40460
- Solid Ni-Co and Ni-Cu alloys, investigating hydrogen solubility
21 p3398 A71-40466

- Resistance NOR Ti BOND joining of Ti shapes, forming TiCu eutectic at Cu plated Ti joint interface 21 p3387 A71-40620
- Tensile strain response for spallation fracture in metals by impact and electron beam heating of Al, Cu and Ti alloys 21 p3466 A71-40798
- Bending strain diagram conversion into tensile strain diagram, considering elastic limit values correlation for Cu-Ni-Al alloy 22 p3561 A71-41698
- AlCu alloy cellular dendritic substructure segregation observation by electron microprobes 23 p3689 A71-42931
- Weakly diffracted beam observation of small quenching vacancy loops and Guinier-Preston precipitate zones in Al and Al-Cu, using transmission electron microscopy 23 p3691 A71-43359
- Precipitation hardenable Cr-Cu liquid phase sintered powder composite, showing matrix properties variations 23 p3695 A71-44291
- Free surface equilibrium segregation in solid solutions of Cu-Al alloys single crystals by Auger electron spectroscopy and low energy electron diffraction 24 p3839 A71-45123
- Surface segregation, adhesion and friction of monocrystalline Cu-Al, Cu-Sn and Fe-Al alloys from Auger emission spectroscopy and low energy electron diffraction experiments [ASLE PREPRINT 71LC-5] 24 p3839 A71-45287
- COPPER CHLORIDES**
- Inflammability, burning rates and exothermal decomposition of compact hydroxylamine and hydrazine sulfate and chloride with/without copper chloride additions, plotting pressure variations curves 15 p2463 A71-31377
- COPPER COMPOUNDS**
- NT COPPER CHLORIDES
- NT COPPER OXIDES
- NT COPPER SELENIDES
- NT COPPER SULFIDES
- CuH lines in sunspot spectra and solar isotopic ratio of Cu obtained from Cu I lines 06 p0969 A71-17971
- Cuprous halides nonlinear properties in near and medium IR regions 08 p1302 A71-21435
- Rapidly quenched CuAu ordered state development on low temperature annealing, presenting Young modulus variation as function of heat treatment time 09 p1477 A71-23350
- Cu-Ti-Al system intermediate phases crystallization from melt in large concentration areas, discussing four-phase reactions 10 p1627 A71-24597
- Copper-indium-tellurides homogeneity region components solubility in different cross sections of concentration triangle at room temperature 23 p3717 A71-44023
- COPPER OXIDES**
- Copper oxide-magnesium thermal cells open circuit voltage drop in latter discharge stages, discussing cuprous iron activity at cathode 02 p0197 A71-12959
- COPPER SELENIDES**
- Copper gallium diselenide point contact diodes I-V characteristics temperature and illumination dependence, considering high temperature and photoelectric devices applications 21 p3434 A71-41327
- COPPER SULFIDES**
- CdS-CuS n-p junction solar converters, noting long-wave sensitivity dependence on light extrinsic absorption 02 p0190 A71-11896
- Copper sulfide-cadmium disulfide thin film solar cells degradation under simulated orbital conditions, determining electrochemically induced copper filament growth as electric shorts causes 05 p0699 A71-16057
- Copper sulfide-cadmium sulfide photovoltaic solar cell electronic processes observation at heterojunction, noting electron trapping and hole injection roles in long term stability 19 p3119 A71-38140
- Copper sulfide-cadmium sulfide thin film solar cells under simulated orbital conditions, including thermal cycling, constant illumination and temperature effects 20 p3182 A71-38946
- CORDITE**
- U COLLOIDAL PROPELLANTS
- U DOUBLE BASE PROPELLANTS
- CORE FLOW**
- Plane Couette flow turbulence, discussing wall region shear and core homogeneity 03 p0400 A71-13546
- Viscous core of incompressible swirling flow through nozzle using momentum-integral equations [AIAA PAPER 70-51] 11 p1750 A71-25468
- Static pressure recovery and core region velocity profile in rectangular wall diffusers with uniform shear flow [ASME PAPER 71-GT-5] 11 p1751 A71-25951
- Wall shear stress and static pressure of developing turbulent flow in square ducts with convective accelerating core for various Reynolds numbers 13 p2048 A71-28595
- Potential vortex with turbulent viscous core and axial velocity excess or deficiency, using integral method with quasi-cylindrical flow approximations to describe core flow [AIAA PAPER 71-615] 15 p2393 A71-32278
- Axisymmetric small Rossby number flow driven by axially distributed heat sources, examining core multiboundary layer structure 20 p3212 A71-39507
- Viscous vortex rings of small cross section, considering velocity in ideal fluid with arbitrary vorticity in core and arbitrary circumferential velocity 21 p3366 A71-40484
- Self induction function and stability for vortex with finite core at aircraft wing, confirming Crow theory 21 p3320 A71-40502
- CORE SAMPLING**
- Nuclear tracks high density in Apollo core small silicate crystals, discussing extralunar dust and photospheric iron-hydrogen ratio 07 p1189 A71-18740
- Lunar drilling equipment design from probe data, describing powered hand drill, 3 meter coring device and Apollo lunar surface drill 15 p2385 A71-32497
- Carbon compounds in Apollo 12 lunar fines and core samples, using pyrolysis, mass spectrometry, ion exchange chromatography and optical and electron microscopy 17 p2801 A71-34649
- Volatilizable organic polymers and hydrocarbons in Apollo 12 lunar core samples 12025 and 12028, using mass spectrometric analysis 23 p3756 A71-43742
- Biological activity in Apollo 11 and 12 core samples searched for after placement in Petri dishes containing media 23 p3757 A71-43747
- Apollo 12, 14 and 15 lunar core tube sampling 23 p3757 A71-43749
- Apollo core tube geometry effect on quantity and quality of lunar sample recovery 23 p3757 A71-43750
- Phase analysis of Apollo 12 fines, core tube samples and rocks by Mossbauer studies, noting nearly uniform distribution of major Fe containing phases 23 p3759 A71-43765
- Grain size distribution and optical and RF electrical properties of Apollo 12 lunar fines and core samples 23 p3759 A71-43769
- Apollo 12 lunar core sample thermoluminescence dependence on radiation dose rates, detecting temperature gradients in regolith by differential thermal analysis 23 p3760 A71-43776
- Nuclear track densities in lunar core and fine samples, relating erosion history, solar activity and surface stirring 23 p3764 A71-43799
- Radiation exposure history from fossil tracks in Apollo 12 surface rocks and double core regolith samples, comparing with Saint Severin meteorite 23 p3764 A71-43802
- CORE STORAGE**
- Minimum core storage forms for radiant heat transfer doubly subscripted nonsymmetric equations, giving simple modifications for interchange between emitting and reflecting surfaces 03 p0522 A71-14454
- Earth satellites ferrite core buffer storage replacement by magnetic tape unit noting design, performance, volume and operation [DGLR-70-082] 05 p0726 A71-15952
- Redundant solid state sequencer programmable via core memory, using two identical channels to prevent wrong output 18 p2885 A71-36449
- CORES**
- NT EARTH CORE
- NT HONEYCOMB CORES
- NT LUNAR CORE
- NT MAGNETIC CORES
- NT REACTOR CORES
- Fcc crystal strengthening, examining short range core defect dislocations 08 p1310 A71-21538
- CORIOLIS EFFECT**
- Centrifugal and Coriolis force in general relativity, discussing paradox associated with terms in mass shell test particles equations of motion 03 p0489 A71-13564
- Mathematical models for heat transfer by laminar free convection to rotating central plate passing through synchronously rotating surroundings, considering Coriolis effect 03 p0518 A71-13617
- Rotating streaming plasma stability, including ion Larmor finite radius effects in presence of coriolis forces 05 p0788 A71-16628
- Coriolis vestibular reaction testing of pilot trainees, evaluating brief vestibular disorientation test validity and reliability at 10 and 15 rpm test conditions 08 p1247 A71-20823
- Coriolis effects on endolymph shift direction in semicircular canals of man under rotation with head movements in sagittal plane, involving nystagmus and illusory sensations 09 p1392 A71-22640
- Phase lag in periodic Coriolis star nystagmus between Coriolis input and corresponding ocular component in cats 10 p1559 A71-23923
- Three dimensional quasi-stationary problem of local winds in neutrally stratified atmosphere in low latitudes, analyzing Coriolis force role 13 p2096 A71-28016
- Soviet book on vestibular reactions covering functional relationship between stimulus parameters and labyrinth nonauditory part, adaptation to Coriolis forces and response to ionizing radiation 13 p2008 A71-28672
- Vertical magnetic field and Coriolis forces effect on equilibrium of heavy viscous incompressible infinitely conducting rotating fluid 15 p2453 A71-31183
- Mathematical theory of planetary atmosphere oscillations, considering coriolis, magnetic and viscous forces effects 16 p2561 A71-32804
- Large scale atmospheric turbulence, considering anisotropy, thermal stratification, pressure and Coriolis forces effects 18 p2944 A71-36009
- Gross locomotion and cargo handling in simulated artificial gravity environments, studying effects of Coriolis forces, angular accelerations, oculo-vestibular stimuli and traction variations [AIAA PAPER 71-886] 18 p2871 A71-36636
- Coriolis forces influence on rotating spacecraft design, estimating relationships between coriolis force, artificial g, rotational radius and speed and velocity of motion [AIAA PAPER 71-889] 18 p2871 A71-36638
- Coriolis coupled bending vibrations of hingeless helicopter rotor blades, noting out-of-plane component contribution to aerodynamic coupling 19 p3154 A71-37294
- Earth rotation effect on mesoscale wave characteristics, considering Coriolis force influence in homogeneous inertly stratified jet stream 21 p3375 A71-41393
- Habituation and suppression of vestibulo-ocular vertical nystagmic responses to Coriolis stimulation in pentathlon athletes, comparing to pilots and airman trainees 22 p3501 A71-41826
- Correlation coefficients between sensitivity thresholds of cupula-endolymphatic system to angular and Coriolis accelerations with human resistance to motion sickness 24 p3795 A71-44532
- Human adaptation to Coriolis and linear accelerations, investigating habituation effect 24 p3795 A71-44533
- Coriolis acceleration effect on human organism from optic functions and retinal hemodynamics study 24 p3795 A71-44534
- Liquid flow and heat transfer in thermosiphons in centrifugal and Coriolis force fields 24 p3888 A71-44931
- Liquid particles motion over variable profile turbine rotor blade edge, concave and fanning surfaces as function of Coriolis and centrifugal force 24 p3819 A71-44932
- CORNEA**
- Unsymmetrical dimethylhydrazine (UDMH)/ effect on canine blood coagulation, blood-aqueous barrier and cornea 02 p0199 A71-12383
- Laser ocular effects, discussing corneal/retinal/lens lesion production, damage thresholds and application to clinical ophthalmological problems 07 p1049 A71-19792
- TV monitoring and digital data recording of human corneal reflection during voluntary eye movements, considering visual perception studies application 07 p1051 A71-20210
- Illumination level effect on corneo-retinal potential and electro-oculography (EOG) recording 08 p1246 A71-20812
- Mathematical analysis of eye transparency, discussing light scattering from normal corneal stroma, swollen opaque corneas and cataractous lens 08 p1240 A71-21371
- Corneal transparency in metabolic activity absence, using acid mucopolysaccharide depletion and prolonged gamma irradiation 09 p1393 A71-22985
- Corned-retinal potential as generator of occipital alpha rhythm in human electroencephalogram modulated at 10 Hz by tremor in extraocular muscles 21 p3329 A71-40176

HF signals adaptation dependence from human cornea potential measurements by presenting narrow band chromatic stimuli to subjects under photopic, mesopic and scotopic adaptation conditions
24 p3794 A71-44467

Human eye theoretical model with aspherical cornea front and lens back surfaces, computing astigmatism, coma, meridional and sagittal focal lengths by ray tracing method
24 p3798 A71-44978

CORNERS

Supersonic laminar boundary layer structure near convex corners for large turning angles
01 p0069 A71-10461

Laminar corner boundary layer secondary flow, taking into account velocity and skin friction distributions
03 p0404 A71-14239

Inviscid binary gas mixture steady supersonic two dimensional flow past convex corner, taking into account spontaneous condensation
03 p0345 A71-14559

Supersonic reactive gas flow free expansion over sharp corner into region of constant pressure, using linearized theory and numerical method of characteristics
05 p0836 A71-16535

Mathematical model for secondary flow in turbulent boundary layer in corners and salients, confirming existence of transversal pressure gradient variation
10 p1592 A71-23979

Asymptotic expansions for viscous flow along right angle corner, satisfying layer equations and boundary conditions
11 p1752 A71-26104

Laminar free convection heat transfer in vertical rectangular corner, considering velocity and temperature distribution
13 p2161 A71-28621

Two dimensional transonic potential flow near convex corner
14 p2225 A71-30215

Inviscid transonic rotational flow expansion around convex corner, applying to supersonic boundary layer over flat plate ending at sharp corner
14 p2226 A71-30444

Axisymmetric plane transonic flow past convex corner point, obtaining characteristics by mapping into hodograph plane
19 p2991 A71-37103

Two dimensional supersonic moist air expansion around sharp corner, investigating water vapor condensation by homogeneous nucleation
21 p3369 A71-40952

Irregularly shaped thin elastic plates under uniform transverse or point loads with singularities resulting from loading or corner conditions
22 p3618 A71-42591

Stress concentrations and singularities at interface corners, presenting procedure for standardized mathematical formulation of conditions for different physical problems
23 p3777 A71-43494

CORONA BOREALIS CONSTELLATION

Be star theta Corona Borealis UVBY H alpha filter observations, noting spectroscopic changes of light variation due to particles in stellar atmosphere
21 p3443 A71-40193

CORONA DISCHARGES

U ELECTRIC CORONA

CORONAGRAPHS

Meteorological, optical and coronagraphical observations of total solar eclipse of 7 March 1970
01 p0151 A71-10116

Solar eclipse observations of 7 March 1970, discussing site selection, shadows, corona, prominences, temperature measurements and photographs
01 p0151 A71-10117

Mauna Loa coronagraph observations before, during and after 7 March 1970 solar eclipse
06 p0968 A71-17912

Mariner 6 and 7 UV spectrometers, describing technical details, operating characteristics and calibration of planetary coronagraph and Ebert-Fastie monochromator used for Martian atmosphere analysis
11 p1766 A71-26301

Emission characteristics above solar limb in four EUV lines, comparing with K-coronameter measurements to estimate element abundances
19 p3130 A71-38671

Monochromatic observations of coronal loop, using isophotal map from coronagraph through Fabry-Perot interferometer
23 p3768 A71-43846

CORONARY CIRCULATION

Eating and digestion effects on conscious dog coronary and visceral vasoactivity
01 p0015 A71-11183

Coronary artery heart disease detection in aircraft pilots to age 45 during physical examinations
02 p0208 A71-12392

Coronary sclerosis morphology, discussing myocardium microcirculation disturbances
02 p0200 A71-12414

Human coronary arteries fibrinolytic activity, considering histochemical and quantitative methods for arteriosclerosis and occlusion investigations
02 p0200 A71-12416

Coronary perfusion pressure, heart performance and homeometric autoregulation in intact dogs
03 p0361 A71-13224

ECG changes and coronary risk of acquired bundle branch block in healthy population
03 p0363 A71-13490

Human heart rates long term measurement by cumulative counters activation by electrical signals from precordial electrodes
04 p0544 A71-15153

Cinearteriographically demonstrated coronary artery disease severity correlation with myocardial blood flow response to treadmill exercise or isoproterenol infusion
06 p0852 A71-17874

Acceleration effects on aortic, coronary and carotid flows in dogs
06 p0855 A71-18380

Cardiovascular responses of hypoxic hypoxia in mongrels with catecholamine induced coronary dilation
06 p0857 A71-18723

Coronary blood flow measurements during strenuous upright exercise, using nitrous oxide method
09 p1400 A71-23362

Heart rate and diastolic inflow coronary resistance extravascular component, discussing heart artificial stimulation and pharmacological maximal dilation effects
10 p1565 A71-24679

Coronary hemodynamic responses to postural changes in hemorrhaged dogs involving head-up and head-down tilts
11 p1720 A71-26114

Coronary blood flow regulation, discussing local and remote control mechanisms and disturbance effects due to obstructive arteriosclerosis
13 p2003 A71-27860

Sitting and supine position effect on exercise tolerance, heart rate, systolic pressure and respiration rate in male subjects with coronary insufficiency, noting onset of angina pectoris
13 p2014 A71-29303

Systemic arterial blood pressure response to chronic high altitude and hypoxia effects
14 p2184 A71-30280

Coronary blood flow response to acute and chronic hypoxia, observing vascular smooth muscle relaxation relation to released adenosine
14 p2184 A71-30281

Coronary vasculature development under hypoxia and pulmonary hypertension as possible cause of right ventricle phasic flow contour changes
14 p2184 A71-30282

High altitude acclimatized humans, noting decreased coronary blood flow and increased oxygen extraction
14 p2184 A71-30283

Short term high altitude exposure, determining coronary blood flow reduction relationship to cardiac output and stroke volume
14 p2184 A71-30284

Myocardial ischemia and necrosis without major coronary arteries obstruction, investigating possible deranged hemoglobin-oxygen transport
14 p2185 A71-30286

Myocardial ischemia observations, utilizing morphologic and pathophysiologic correlations with cinecoronary arteriography, left ventriculography and hemodynamic examination
14 p2185 A71-30287

Concealed and supernormal atrioventricular conduction data, using His bundle electrogram recordings
15 p2366 A71-32539

Atrioventricular and intraventricular conduction disturbances in acute myocardial infarction, discussing heart block
15 p2361 A71-32540

Coronary arteries congenital lesions, discussing major, minor and secondary anomalies relationship to cardiac malformations
15 p2361 A71-32553

Physiologic and pathologic cardiomegaly, noting myocardial blood flow oxygen uptake and lengthening and widening of coronary vessels
16 p2531 A71-33423

Patients with selective cine coronary arteriography, statistically correlating vectorcardiographic diagnoses of myocardial infarcts with changes in arteries
18 p2854 A71-36139

Acute fatal nontraumatic collapse during physical exertion due to circulatory diseases
18 p2855 A71-36215

Diastolic heart sounds and filling waves in coronary artery disease, relating graphic abnormalities and clinical, arteriographic and hemodynamic findings
19 p3002 A71-37550

Right and left heart and pulmonary blood volume determination, using radiocardiograms and analog computer analysis
20 p3191 A71-38801

Coronary blood flow at increased arterial carbonic acid partial pressure, noting induced hypercapnia
21 p3335 A71-40633

Coronary dilating substances of low molecular weight separated through dialysis from hypothalamic protein carriers
21 p3338 A71-41072

Myocardial blood flow and oxidative metabolism in cyanotic congenital heart disease patients, using lactate/pyruvate ratios and coronary sinus catheterization
22 p3484 A71-41521

Midsystolic clicks and papillary muscle dysfunction evidence in arteriosclerotic heart disease from ECG, carotid pulse tracing and phonocardiography
23 p3635 A71-44126

Preclinical coronary heart disease detection by near maximal treadmill exercise ECG
23 p3636 A71-44129

Cardiac arrest or arrhythmia due to coronary arteriosclerosis in young aviator, examining causes, prevention and predictive measures
23 p3637 A71-44250

CORONAS

NT ELECTRIC CORONA

NT SOLAR CORONA

Galactic radio corona existence, measuring northern galactic hemisphere sky brightness and cosmic ray distribution
03 p0483 A71-13204

Helium-rich white dwarfs convective envelopes, acoustic noise generation and corona formation
12 p1970 A71-27746

White dwarf coronas convection zones thermodynamic calculations, considering high electron degeneracy, and He I and He II ionization
14 p2318 A71-31017

Solar and stellar chromospheres and coronas production based on turbulence in granulation, photospheric mechanical flux and supergranular network magnetic field structures
19 p3136 A71-37626

M supergiants hot corona base density determination from radio emissions observations, noting equivalence to solar type 4 microwave bursts
22 p3598 A71-41916

CORPUSCULAR RADIATION

NT BETA PARTICLES

NT CYCLOTRON RADIATION

NT ELECTRON BEAMS

NT ELECTRON PRECIPITATION

NT ELECTRON RADIATION

NT ION CYCLOTRON RADIATION

NT PRIMARY COSMIC RAYS

NT SOLAR CORPUSCULAR RADIATION

NT SOLAR COSMIC RAYS

NT SOLAR PROTONS

Regularities of polar auroras and ionospheric disturbances during solar cycle with decreased low energy corpuscular flux
02 p0242 A71-11760

Ionospheric stability in nighttime and daytime auroral zone with E layer corpuscular stream disturbances
02 p0243 A71-11762

Polar region semitransparent sporadic ionospheric layers nighttime temporal and cyclic ionization variations, determining solar activity effects and corpuscular stream densities by ionogram
02 p0243 A71-11767

Cosmic ray neutron component intensity increases dependence on corpuscular stream velocity before Forbush effects
06 p0954 A71-18124

Polar auroras, lower magnetosphere and geomagnetic perturbations, as effect of corpuscular fluxes penetration into lower ionosphere
07 p1104 A71-20046

Solar activity effects on midlatitude upper atmosphere corpuscular radiation intensity studied by rocket sounding
09 p1513 A71-22580

Latitude dependence of upper atmosphere corpuscular radiation intensity, analyzing sounding data from Indian Ocean area
12 p1947 A71-26645

Nucleon-nucleon interactions produced energetic penetrating particles /muons/ in cosmic ray showers, studying neon flash tube technique
12 p1948 A71-27186

Penetrating particle observations on showers produced at 70 mwe underground, revealing weakly ionized group in quark flux contradiction
12 p1951 A71-27396

Ionospheric continuity in F 2 region during partial solar eclipses, using EUV radiation and additional corpuscular source of ionization
13 p2053 A71-27792

Auroral absorption and DR currents development during magnetic storms, discussing corpuscular fluxes arrival from magnetospheric tail into lower ionosphere
13 p2062 A71-28563

German book on radiation climate of earth covering EM, corpuscular IR radiation sources, spectral composition, biological effects, etc
14 p2298 A71-29941

High energy penetrating component of cosmic radiation at mountain level recorded in underground ionization calorimeter, showing muon production in vertical and horizontal direction
15 p2476 A71-31787

Topside ionosphere structure in high latitudes, discussing electron density profile, corpuscular radiation ionizing effects, polar peak and trough
15 p2400 A71-32349

Corpuscular and solar electromagnetic ionizing radiation simultaneous measurement by sounding rockets, evaluating contribution to lower ionosphere formation
16 p2627 A71-33776

Corpuscular flux intensities in upper atmosphere from meteorological rocket measurements in polar arctic region, discussing altitude-time dependence
16 p2627 A71-33777

Hard X ray pulsations limits in higher energy range from Cyg X-1, comparing with Crab Nebula pulsar
20 p3279 A71-39407

Mesospheric soft corpuscular radiation flux and temperature rocket observations, during solar flare activity
20 p3222 A71-39704

Fast hydrogen atoms penetration into fusion reactor plasma, calculating collision cross section rates coefficients
21 p3422 A71-40765

Manned spacecraft hazard from charged particles radiation during solar flares and trapped particles by geomagnetic field, recommending protection methods
24 p3865 A71-44887

CORRECTION
NT OPTICAL CORRECTION PROCEDURE
Alouette 2 ionograms frequency interpolation correction allowing measurement accuracy comparable to sounder system resolution
05 p0725 A71-17083

Correction factors for small values of logarithm of Debye length ratio to mean impact parameter in electrical conductivity of fully ionized plasma
12 p1936 A71-26950

Methods construction for initial value problem solution, using fifth and sixth order algorithms with Adams-Moulton correctors
17 p2768 A71-35686

CORRELATION
NT ANGULAR CORRELATION
NT AUTOCORRELATION
NT CORRELATION COEFFICIENTS
NT CORRELATION DETECTION
NT CROSS CORRELATION
NT DATA CORRELATION
NT SIGNAL ANALYSIS
NT STATISTICAL CORRELATION
Laser optical field intensity correlation function determination from photoelectric counting distribution measurements
03 p0436 A71-13876

Turbulent plasma correlation functions for decay and nondecay spectra, deriving descriptive equations by perturbation theory series summation
03 p0464 A71-13932

Reflected electromagnetic wave polarization parameters, obtaining correlation functions for radar echoes
04 p0557 A71-14632

Third order correlations in grid turbulence, investigating high pass filtering effect at small cut-off frequencies
04 p0569 A71-15027

Intensity correlation functions as parameters for cosmic radiation activity
04 p0640 A71-15086

Soviet book on biometry covering correlation coefficients, rectilinear/curvilinear regression, nonparametric statistics, diversity indices, algorithms, dispersion and statistical analysis and probability
04 p0546 A71-15263

Interplanetary magnetic field sectors correlated to solar coronal active centers and condensations in metric wavelengths from radio observations
05 p0802 A71-16015

Space-time and time correlation functions for classical many body system, proving Chapman-Enskog equivalence to correlation function methods
05 p0786 A71-16864

Correlated noise linear filtering problem analysis, introducing concept of invariant directions for Riccati equation
06 p0877 A71-17328

Midlatitude wind vector longitudinal and transverse components correlation functions for different isobaric surfaces in summer and winter
06 p0924 A71-17647

Atmospheric turbulence steady random process correlation function, spectral density and probability distribution based on aircraft measurements
07 p1150 A71-18797

Atmospheric temperature minima prediction, comparing various correlation methods
07 p1151 A71-18875

Binary pseudorandom codes sequences correlation properties in PSK telemetry
09 p1404 A71-22154

Time series analysis techniques concerning correlation, auto and cross power spectral density, amplitude and period histograms, real time pattern recognition and filtering
09 p1405 A71-22783

Second order correlation functions of velocity and magnetic field for homogeneous unsteady isotropic hydromagnetic turbulence in incompressible conducting fluid
11 p1805 A71-25599

Spatial and temporal density fluctuations correlation in stars
12 p1955 A71-26581

Spatial filter synthesis for real time combined subtraction and correlation in coherent optical data processing system
12 p1905 A71-26808

Correlation function of modulation of radar sounding signals with nonwhite nonstationary Gaussian noise, obtaining target range and velocity maximum likelihood estimates
12 p1882 A71-27616

Optical pattern recognition by correlation measurements, detecting by zero in intensity distribution
13 p2069 A71-28715

Data correlation and effectiveness prediction from film cooling injection geometries, considering finitely thick slot lip and boundary layers
13 p2161 A71-28751

Longitudinal space-time correlation function of turbulent near wall pressure pulsations with hydrodynamic wavelength exceeding boundary layer thickness at streamlined model
13 p2049 A71-28846

Gaussian processes discrimination, considering correlation functions in integral control of nonlinear filter for image recognition
13 p2039 A71-28917

Direct measurement of spatial velocity correlation functions in turbulent flow by conditional probability of scattered light
15 p2449 A71-31866

Differentiable random processes, deriving approximate determination of correlation functions
17 p2777 A71-34348

Partial differential equations governing second order correlation functions for velocity and magnetic field in isotropic conducting turbulent flow
17 p2789 A71-35443

Partially spatially coherent illumination influence on measurement of correlation function of two dimensional patterns, obtaining formula for optical filtering
18 p2929 A71-35973

Computer control of multiple site track correlation, describing coarse fine method for implementation and accuracy
20 p3202 A71-38973

Book on statistical mechanics of turbulent fluid flows covering gas oscillations, correlation function, Reynolds equation, laminar flow, particle dispersion, etc
20 p3213 A71-39774

Accuracy in maximum likelihood estimate for correlation function parameter of random process in signal reception on normal noise background
20 p3199 A71-39816

Optical correlation for surveillance and pulse Doppler radar receivers signal processing
20 p3200 A71-39910

Canonical approximation of state correlation matrix and threshold crossings of variable systems with random turbulence type input vectors representing flight environment
21 p3408 A71-40614

Molecular gas mixtures inelastic collision integral spectra, describing internal degrees of freedom with correlation functions
21 p3420 A71-41271

Correlation functions characteristics of wind velocity field in troposphere and stratosphere up to 25 km based on bihourly radiosonde data
21 p3412 A71-41390

Spectra and correlation functions for ion sound turbulence, calculating anomalous resistivity for plasma in external electric field
22 p3579 A71-41582

Equilibrium neutral gas and plasma electron number density fluctuation determination, deriving correlation functions from Liouville equation
22 p3530 A71-41894

Reflected electromagnetic wave polarization parameters, obtaining correlation functions for radar echoes
22 p3510 A71-42272

Correlation system of equations for mathematical expectations and phase coordinate correlation moments for accuracy analysis in flight vehicle dynamics problems
24 p3792 A71-44692

CORRELATION COEFFICIENTS

Vectorcardiograms comparison recorded with different electrode leads or amplification systems based on spatial points coordinates correlation coefficients
03 p0371 A71-13115

SNR of harmonic signal mixed with narrow band noise, measuring correlation coefficients
04 p0550 A71-14615

Binary sequences with relaxed Barker criterion, examining correlation coefficients
07 p1149 A71-20418

Soft X ray radiation correlations to radio emission flux at various frequencies in 20th solar activity cycle
09 p1515 A71-23529

Integral coefficient of correlation between gravitational and magnetic fields with geological element
14 p2235 A71-30189

Harmonic residuum of solar quiet, considering mean deviation and correlation coefficients
20 p3217 A71-39514

Correlation coefficient between winds at 850-30 mb pressure levels over Italy in winter, proposing theoretical model
21 p3411 A71-40825

Electron-electron correlation effects in photoabsorption induced double electron ejection process, using many body perturbation theory
22 p3577 A71-41628

SNR of harmonic signal mixed with narrow band Gaussian noise, measuring correlation coefficients
22 p3510 A71-42255

Areal precipitation correlation with 850 mb geopotential height over Northern Hemisphere
22 p3535 A71-42414

Correlation coefficients between sensitivity thresholds of cupula-endolymphatic system to angular and Coriolis accelerations with human resistance to motion sickness
24 p3795 A71-44532

CORRELATION DETECTION

Equatorial ionosphere correlation data regarding VHF telemetry disturbances and satellite tracking, determining antenna ground spacing
01 p0074 A71-11307

Nd 147 decay gamma-gamma directional correlations, using coaxial Ge/Li and NaI/Tl detectors in conjunction with multichannel coincidence configuration
02 p0285 A71-11646

Correlation measurements by laser in turbulent gas flow, determining phase structure velocity distributions and coherence lengths
03 p0435 A71-13529

Subsequences of pseudorandom sequences for correlation detection, discussing algorithms for weight distribution moments determination
05 p0724 A71-17062

Noise rejection of two channel asynchronous storage circuit with internal detection for weak signal reception
08 p1252 A71-20734

Correlation detection systems, calculating DC component effects on output signal to noise ratio
08 p1253 A71-21281

Solar activity effects on atmospheric density variations from satellite observations, using random process isocorrelation charts
11 p1759 A71-25821

Optico-acoustic autocorrelator for linear FM signals spatial compression, discussing design and performance
14 p2194 A71-30085

Communication satellites unique word coding with algorithm, reducing false detection probability by error correlation technique
14 p2201 A71-30926

Optimal discrete time detection of radar signal parameters in nonGaussian correlated and noncorrelated noise, using Markov model
15 p2373 A71-32619

Space-time correlating antenna array forming matched filter for modulated signal reception with interference rejection
17 p2716 A71-34767

Output correlation functions of periodic signals limiting in random noise passing through zero memory devices, using Hermite polynomials method
20 p3195 A71-38857

Estimation-correlation principle application to harmonic signal receiver with unknown carrier frequency, using searching phase locked AFC circuit as estimation unit
22 p3512 A71-42313

CORRELATION FUNCTIONS
U CORRELATION
CORRELATORS
Instrument for measuring cross and autocorrelation functions with capability of extracting signal masked by noise by averaging operations
01 p0079 A71-10313

Auto and cross correlation function computation from waveform polarity by flexible one bit digital correlator for frequencies to 25 MHz
02 p0211 A71-11644

Correlator circuit for low level signal extraction from noise and for analysis of frequency spectrum of complex AC signals

03 p0377 A71-13241

Linear delay input effects on analog cross correlator mean frequency, plotting output SNR vs integration time

07 p0109 A71-18851

Holographic matched filter correlator using liquid gate precision plate holder to eliminate necessity for hologram movement

19 p3065 A71-38238

CORROSION

NT CAVITATION CORROSION

NT ELECTROCHEMICAL CORROSION

NT FRETTING CORROSION

NT FUEL CORROSION

NT INTERGRANULAR CORROSION

NT SCALE [CORROSION]

NT STRESS CORROSION

Heterogeneous kinetics at elevated temperatures - Conference, Philadelphia, September 1969

03 p0374 A71-13121

Materials corrosion, discussing measurement, prevention, secondary interactions, R and D, etc

04 p0613 A71-15776

Corrosion damage relationship to military aircraft accidents, discussing quality control, material selection and manufacturing processes

06 p0911 A71-17415

Wall thickness measurement by ultrasonic tests in presence of corrosion, discussing instruments development

06 p0897 A71-17416

Metal endurance dependence on simultaneous oxygen corrosion and cyclic loading frequency at various temperatures and pressures

06 p1000 A71-17934

Duralumin with anodic film, examining fatigue and corrosion-fatigue rupture

06 p0911 A71-17935

German papers on plasma physics, metal corrosion, organic chemistry, molecular biology, etc

07 p1160 A71-19601

Papers on corrosion science and technology covering electrode processes measurement, surface- and environment-sensitive mechanical behavior, organic inhibitors and aluminum anodic oxidation

11 p1779 A71-25998

Liquid metal elevated temperature time dependent corrosion effects on immersed structural materials, discussing blocked two level factorial experiment design for multiply telescoping sequences

21 p3400 A71-40880

Duralumin fatigue process in air and corrosive medium, showing loading frequency and time dependence effects

23 p3692 A71-44027

Aircraft parts damage by corrosive friction forces, hot gases and intercrystalline attack, noting worn universal joint and blade grain boundary damage

24 p3836 A71-44574

CORROSION PREVENTION

Corrosion processes in and on solids, noting techniques and instrumentation for control

03 p0441 A71-13254

Jet fuel soluble corrosion inhibitors evaluation by potentiostatic polarization methods

03 p0377 A71-14323

Stress corrosion failure prevention in susceptible Al alloys, considering metallurgical structure, environment and stress distribution

09 p1478 A71-23417

Elastomeric seals for aircraft fastener counterlocks, providing corrosion protection to static metal surface treatments and organic coatings

10 p1633 A71-24118

Three greases in oscillatory bearings under various conditions of speed, load and angle of oscillation, determining effects on fretting corrosion prevention [ASLE PREPRINT 71AM 1B-1]

13 p2076 A71-29490

Soviet book on aircraft materials science and treatment covering steel/cast iron processing, metallurgy, heat/thermochemical conditioning, surface protection and corrosion prevention

14 p2256 A71-29529

Metallographic examination of inorganic, metal plated and intermetallic coatings on martensitic stainless steels for pitting and surface corrosion prevention

19 p3081 A71-37902

Condensate removal devices for potassium vapor Rankine space power turbines to prevent blade erosion and efficiency degradation

20 p3262 A71-38918

Corrosive delamination occurrence, reduction and prevention in metal-metal adhesive bonded aircraft structures

22 p3555 A71-42594

CORROSION RESISTANCE

NT OXIDATION RESISTANCE

Al-Si alloys corrosion resistance in humid atmosphere and acid medium, investigating effects of refining process and hydrogen content

01 p0097 A71-10040

Au plated contacts deterioration by pore corrosion, noting resistance relation to basis or underplated metals porosity

01 p0102 A71-10800

Mechanical properties, long term strength and corrosion resistance of low alloy chromium steel with nitrogen

01 p0103 A71-11069

Be mechanical and physical properties, corrosion behavior, toxicity, fabrication and application as aircraft and spacecraft structural material

01 p0104 A71-11539

Corrosion resistant fiberglass reinforced plastic fluid storage vessels, noting structural characteristics, fabrication techniques, etc

02 p0256 A71-12348

Phosphoric acid corrosion resistant alloys for electrolyte fuel cells, discussing materials selection and optimization

03 p0440 A71-13055

High strength stress-corrosion resistant Al alloy forgings fabrication processes, noting chemical composition and physical properties

03 p0441 A71-13255

Erosion resistance characterization and determination - ASTM Conference, Atlantic City, June 1969

03 p0443 A71-14284

Al-Zn-Mg ternary alloys stress corrosion cracking resistance relation to mechanical strength decrease, quenching rate increase and solution treatment temperature

04 p0609 A71-14772

Al-Zn-Mg ternary alloys stress corrosion cracking resistance relation to heat affected zone postannealing aging and cooling rate decrease

04 p0610 A71-14773

Imide-pyrone copolymers preparation by solution polymerization, considering base/acid degradation resistance and thermal stability in air and vacuum

04 p0549 A71-15749

Adhesive/metal interface corrosion resistance tests, discussing salt fog chamber for shear, compression buckling and cleavage stresses

05 p0770 A71-17248

Construction materials characteristic properties significance for design and structural reliability, discussing weldable Al alloys fatigue strength, internal stresses, inhomogeneity and corrosion behavior

06 p0981 A71-17341

High strength Al alloys stress corrosion resistance testing in various heat treatment conditions, using precracked cantilever beam specimens

06 p0912 A71-18012

Mechanical properties, crack formation sensitivity, corrosion resistance and stress cracking behavior of Al-Zr-Mg alloys welded joints

07 p1136 A71-19633

Al-Si and Al-Sn bearing alloys corrosion resistance to lubricating oils, investigating thrust load, operating time and oxidation factor effects

08 p1304 A71-20996

High strength corrosion resistant superalloy structure and mechanical properties

08 p1314 A71-21566

Composition, microstructure, heat treatment and properties of Ni alloy with high rupture strength and hot corrosion resistance for turbine blade applications

08 p1299 A71-21687

Ti-Mo alloys porous materials for work in hot solutions of nonoxidizing acids, discussing production technology and corrosion resistance

08 p1317 A71-21857

High chromium Ni-Cr alloys use and improvement, discussing refractoriness in oxidizing atmospheres and chemical corrosion in combustion products deposits

09 p1470 A71-23043

Metals and welded joints corrosion resistance at high temperatures and pressures, describing tests in autoclave with pneumatic loading

09 p1429 A71-23050

High temperature corrosion in aircraft engine components and gas turbines by sulfur in fuels, vanadium pentoxide and NaCl

09 p1474 A71-23288

Corrosion resistance of adhesive bonded airframe structure components under outdoor weather and salt spray conditions, discussing test results with Al alloy specimens

09 p1459 A71-23690

Metal-metal bonded structures corrosion resistance improvement by use of primers or Al alloy honeycomb core

10 p1626 A71-24110

Corrosion resistant adhesive bonding tested by exposing sandwich structure to outdoor weathering and salt spray environments

10 p1616 A71-24111

Al anodizing processes, stressing modern theory of anodic oxidation and anodized Al corrosion

11 p1779 A71-26000

High chromium hot corrosion resistant superalloys in sheet form, noting precipitation hardening and creep resistance equivalent to Nimonic alloys

12 p1916 A71-26922

Carbon fiber cladding paper for corrosion resistant asbestos laminates, discussing short fibers orientation and acid solutions effects on flexural strength and weight

12 p1921 A71-27014

Fatigue life, fail-safe capability and corrosion resistance of commercial aircraft structures improved through adhesive metal-metal bonding

[ASME PAPER 71-DE-27] 12 p1978 A71-27325

Fatigue corrosion resistance of duralumin anodized at various temperatures

13 p2082 A71-27823

Si, Mo and Cu effects on pitting corrosion of Cr-Ni steel

13 p2082 A71-27831

High strength corrosion resistant multiphase Co-Ni-Cr-Mo alloys with fcc structure hardened to hcp by mechanical deformation

13 p2084 A71-28148

Mechanical properties of composites consisting of Al matrix reinforced by boron fibers, considering high temperature creep, corrosion and thermal shock resistivity

14 p2259 A71-30473

Porous Ti-Mo alloy materials for operation in hot solutions of nonoxidizing acids, discussing production technology and corrosion resistance

14 p2260 A71-30836

Medium strength corrosion resistant weldable Al-Mg alloy for aircraft jettisonable tanks, napalm containers and jet shroud pipes fabrication

15 p2426 A71-31437

Grain size effect on corrosion resistance and mechanical properties of Al alloy sheets between final annealing and quenching

15 p2434 A71-32329

Chemical composition effect on corrosion resistance of Mg-Li system with alloying additions

15 p2435 A71-32339

Mechanical properties, crack formation sensitivity, corrosion resistance and stress cracking behavior of Al-Zr-Mg alloys welded joints after prolonged heating

16 p2593 A71-33629

Electrodeposited Ni-Mo coatings corrosion resistance improvement by heat treatment, showing crystal structure degree of perfection role

16 p2599 A71-34052

Corrosion resistance of Ar TIG welded joints in Ti alloys, discussing chemical and mechanical slag film removal effects

17 p2757 A71-34804

Thermal stability and oxidation and corrosion resistance of lubricating oil based on trimethyl propane ester

[ONERA-TP-930] 18 p2939 A71-36016

Water cooled reactor Zircaloy brazing filler metals, investigating corrosion resistance, joint strength and brazing capability

18 p2928 A71-36856

Electric contact resistance of various conductive metal coatings on aluminum corrosion free joints

19 p3031 A71-38449

Low cost Ti substitutions for Ni and alloys in corrosion resistant applications, prosthetic devices and pollution control equipment

20 p3251 A71-39339

Corrosion resistant materials evaluation for suitability in high strength fasteners, considering mechanical properties, stress corrosion cracking and hydrogen embrittlement problems

20 p3251 A71-39340

Austenitic stainless steels susceptibility to intergranular corrosion under unwelded, welded and heat treated conditions in process environments

20 p3241 A71-39341

Aging conditions effect on stress corrosion resistance in short transverse direction of thick sheet Al alloy, using immersion-emersion tests in air and saline solution

20 p3252 A71-39417

Dislocation arrays effects on heat treated austenitic stainless steel susceptibility to intercrystalline corrosion in sulfuric and nitric acids and cracking in magnesium chloride

21 p3402 A71-41087

Alloying effects on corrosion cracking of Cr-Ni austenitic stainless steels, testing in chloride solutions

21 p3402 A71-41094

Si addition effect on Ni-Cr alloy calorized layer depth, microhardness, phase structure, chemical composition and scaling resistance

21 p3390 A71-41168

Teflon insulated LT type electrical conductors for 203-493 K, including chemical, ozone, UV and fuel resistance tests

22 p3520 A71-41694

Boron addition effects on scaling resistance of Ni-Cr steel at high temperatures

23 p3690 A71-43278

Reduced oxygen effect on structure and mechanical, technological and corrosive properties of stainless steel melted in open and vacuum furnaces

23 p3690 A71-43279

Cavitation damage resistance of Fe, Ni and Co alloys in liquid sodium and mercury 23 p3692 A71-43906

Machining effects on martensitic stainless steels corrosion resistance, showing formation of defects and internal stresses in surface layers 23 p3692 A71-44028

Titanium carbide powder corrosion resistance to sulphuric acid-hydrogen peroxide system at various temperatures 24 p3838 A71-44739

CORROSION TESTS

NT SALT SPRAY TESTS

Boride coatings for Fe-Si alloy, testing corrosion and wear resistances in aqueous salt, acid and alkali solutions 01 p0097 A71-10039

Cyclic fatigue and corrosion test equipment for elastoplastic materials at various temperatures and pressures 01 p0165 A71-10042

Ni maraging steel weldments stress corrosion cracking characteristics in air and pentaborane by electron microscopy 02 p0262 A71-11707

Corrosion rate of Nb in aqueous solutions as function of temperature, using electrochemical potential measurements 03 p0442 A71-13363

Iron corrosion product deposition on pipe wall from aqueous stream dependent on shear rate, using radioactive tracer technique 03 p0442 A71-13368

Ni alloy corrosion tests, evaluating sensitization susceptibility and intergranular attack 06 p0911 A71-17414

High strength Al alloys stress corrosion resistance testing in various heat treatment conditions, using precracked cantilever beam specimens 06 p0912 A71-18012

Cold creep effect on stress corrosion testing of metals under uniaxial bending and constant strain 08 p1306 A71-21439

Multisample test equipment for steels and alloys oxidation resistance at high temperatures in corrosive gaseous atmospheres 08 p1292 A71-21440

Six position machine for fatigue testing in corrosive medium of circular rotating metal specimen with cantilever bending 09 p1426 A71-22327

Underfilm in high humidity environments corrosion of Al alloys coated with paint films, using pH indicating dyes [NACE PAPER 19] 09 p1469 A71-22888

Adhesive primers corrosion resistance test methods, noting aircraft design implications 10 p1633 A71-24112

Hardened and glass reinforced epoxy resin mechanical properties after 180 day hold in water, acid and alkaline solutions 10 p1635 A71-24827

Corrosive contaminants, oxygen, humidity and temperature environment simulation 11 p1746 A71-26496

Corrosion mechanism in Ta-Li high temperature heat pipes by ion analysis, demonstrating oxygen and yttrium diffusion into heating zone 12 p1916 A71-26974

High temperature heat pipes material corrosion problems, considering mass transfer from cooling zone into heating zone 12 p1917 A71-26975

Fiber composites monofilament and strand tests, considering fracture, fatigue, stress, corrosion and microstructure 12 p1921 A71-27635

Artificial corrosion pits effect on fatigue durability of smooth samples and aircraft duraluminum skin elements 13 p1995 A71-27819

Heat resisting Ni base alloy stress rupture strength and fatigue life, observing corrosive high temperature environment effect 13 p2084 A71-28111

High temperature gas turbine alloys corrosion tests, describing laboratory facilities for preliminary screening 13 p2086 A71-28752

Machine for corrosion testing materials under various static and dynamic axial tension, torsion and bending loads 13 p2045 A71-29374

Ti-Al binary alloy embrittlement in sea water by notched cantilever beam stress corrosion test, investigating alpha 2 particle precipitation effect on cracking susceptibility 14 p2256 A71-29522

Metal coated superalloys evaluation for gas turbine engine components, including corrosion, impact and fatigue tests 14 p2256 A71-29635

Fincap communication antennas design and environmental tests for vibration, acceleration, water-

proofing, salt corrosion, ice formation and compass safe distance 14 p2216 A71-31047

Metal and alloys condensates corrosion tests based on recording changes in electrical resistance 15 p2427 A71-31651

Steel joint weld decay mechanism, observing intergranular corrosion initiation and development in nitric acid solutions 15 p2417 A71-32665

Automatic testing machine for materials corrosive strength under varying and combined complex static or dynamic stresses 16 p2580 A71-33687

Preliminary corrosion effect on fatigue strength of Al joints, noting insufficient anticorrosive anodic film and additional protection by paint and varnish 16 p2584 A71-33688

Secondary damage in corrosion fatigue of Al alloy tested to failure 17 p2757 A71-34497

Vibration and corrosion-erosion damage effects on material behavior during short term creep in high speed air flows 17 p2760 A71-35659

Crevice effect at stress corrosion crack apex during cathodic polarization of Ti-Al-Mo-V alloy in sulfuric acid, potassium bromide and iodide and methanol solutions 17 p2761 A71-35733

Salt solution treated and quenched Mg-Al alloy rods tests in distilled water, investigating transgranular stress corrosion cracking and deformation twinning 19 p3083 A71-38722

Corrosion fatigue crack propagation in Ni-Cr-Mo maraging steel in room temperature NaCl solution at various stress intensity ranges 20 p3248 A71-38778

Aging conditions effect on stress corrosion resistance in short transverse direction of thick sheet Al alloy, using immersion-emersion tests in air and saline solution 20 p3252 A71-39417

Stress corrosion testing of Al alloy in NaCl bath under tensile stress, using Weibull distributions 22 p3560 A71-41627

Accelerated intergranular corrosion tests under high humidity on Zn-Al alloy with lamellar eutectoid microstructure due to postforming heat treatment 22 p3564 A71-42534

Prestraining effect on D16 duraluminum corrosion fatigue and tensile strengths 24 p3838 A71-44856

Nondestructive detection of hot corrosion-sulfidation in U.S. Navy aircraft turbine engines 24 p3865 A71-45280

CORRUGATED PLATES

Corrugated membrane of nonuniform profile calculated as variable thickness orthotropic plate, considering corrugations deformation due to bending 02 p0329 A71-12640

Corrugated blank cross section distortion under bending on three roller mill 08 p1295 A71-20795

Deformations and stress concentration on corrugated plate under uniformly distributed load, considering cross section as combination of two cylindrical shells 17 p2818 A71-34401

Three layer trapezoidally corrugated panels with skin under longitudinal compression, determining local stability and stress-strain diagrams 17 p2830 A71-35320

CORRUGATING

Near field radiation characteristics of corrugated feed by spherical mode expansion method 19 p3018 A71-38218

CORSAIR AIRCRAFT

U A-7 AIRCRAFT

CORTICES

Cerebral speech mechanisms division into cortical centers and basal ganglia centers 10 p1563 A71-24229

M-cholinergic and adrenergic subcortical structures blockage effects on blood flow rate in dog pulmonary circulation system 16 p2534 A71-34113

Prefrontal cortex lesions effect on trained anticipatory visual target fixation in cats, noting performance impairment in voluntary eye movement control 21 p3329 A71-40174

CORTI ORGAN

Cochlear sensory epithelium and Corti organ degeneration after noise exposure in guinea pigs and cats, using scanning electron microscopy 02 p0199 A71-12364

CORTICOSTEROIDS

NT ALDOSTERONE

NT HYDROXYCORTICOSTEROID

Glucocorticoid metabolite excretion with urine in healthy people as function of age and sex 06 p0858 A71-18727

Seasonal factors effect on white rat hypophysis-adrenal cortex system functioning by fluorimetric

determination of peripheral blood corticosterone content 07 p1041 A71-19282

Control and prolonged exercised rats adrenal and plasma catecholamine, corticosterone and epinephrine level comparisons using fluorometric analysis 07 p1044 A71-20330

CORUNDUM

U ALUMINUM OXIDES

COSINE

U TRIGONOMETRIC FUNCTIONS

COSMIC DUST

NT INTERPLANETARY DUST

NT METEOROID DUST CLOUDS

NT ZODIACAL DUST

Wide angle far UV photography of Barnard Loop Nebula in Orion suggesting nebular emission intensity difference with near UV region due to interstellar dust 01 p0148 A71-10001

Interstellar dust grains temperature as intracloud position function under assumed radiative heating and cooling, discussing hydrogen formation 01 p0157 A71-10759

Galactic soft X rays role in interstellar dust grains alignment producing starlight polarization 01 p0145 A71-11344

Luminescence of optically reflecting nebulas related to shape of light scattering indicatrix of interstellar dust particles 02 p0311 A71-12355

Interstellar dust, examining diffuse line and band origin, absorption spectra and silicate grains 02 p0312 A71-12466

Cosmic dust in mesosphere and upper atmosphere during weak noctilucent cloud from rocket collecting flight 02 p0246 A71-12703

Zero moments surface in problem of two immovable centers taking into account cosmic dust accumulation before binary apex moving forward with periastron of bright component 03 p0484 A71-13220

Cosmic dust size distribution measurement by electron microscopic examination of in-flight shadowed substrates during particle collection on ESRO rocket 03 p0491 A71-14015

Cosmic dust detection equipment onboard Centaur and Nike-Apache rockets, using recoverable metallic collector and telemetered tungsten target plasma emission detector 03 p0491 A71-14016

Cosmic dust fluxes determination by rocket-borne micrometeorite experiments, using piezoelectric acoustic type impact detectors 03 p0492 A71-14017

Thermal emission from IR star shells calculated from circumstellar graphite dust model 03 p0495 A71-14267

Micrometeorites orbital elements, evaluating cosmic dust experiment data from Pioneer 8 03 p0496 A71-14505

Light propagation in spherically symmetric cosmic dust distribution, obtaining conditions for escape from region of gravitational collapse to one of expansion 04 p0642 A71-14813

Physical and geometrical properties of dust filled universes, using left invariant metrics compatible with Einstein equations 05 p0773 A71-15925

Planetary nebulae and H II region dust density perturbation e-folding time, examining Lyman continuum radiation 05 p0812 A71-16689

Cosmic gas dynamics, discussing galactic mass balance, dark matter and interstellar gas kinetic energy, temperature and density 06 p0971 A71-18327

Interstellar grain formation relation with stellar evolution in terms of density wave theory of spiral structure origin 06 p0973 A71-18339

Visible brightness of Milky Way for various galactic structure models, discussing star and dust distribution effects 06 p0975 A71-18444

Planetary nebulae upper distance limits by photometry, including mean nebular parameters and extinction coefficients in galaxy dust model 07 p1191 A71-18999

Dust history and physical environment near hot stars associated with nebulosity, discussing optical depths and IR energy 07 p1198 A71-19819

Continuous optical conversion to IR and directional stellar radiation flow conversion to diffused radiation fields in circumstellar dust envelopes 07 p1187 A71-19821

Interstellar dust density, constructing cosmological model with gravitational equations 08 p1366 A71-21785

Silica minerals in interstellar dust as source of 2200 A interstellar absorption band from comparisons to 2250 A band in Fe or Al bearing quartz spectra 09 p1522 A71-22936

Interstellar medium molecular composition from ground based and spaceborne UV, visible light, IR, far IR and radio spectroscopy, discussing stellar formation

10 p1669 A71-24170

Ionized gas and dust distribution in Orion nebula from Balmer line intensities photoelectric measurements

11 p1818 A71-25202

Protosun and primordial solar nebula evolution based on dust particles behavior

11 p1819 A71-25221

Dust grain condensation and primordial elements transport into interplanetary space during early stage solar evolution

11 p1819 A71-25222

Star formation angular momentum and magnetic flux problem, investigating collapsing dust cloud theory

11 p1830 A71-26108

Dust particle angular momentum orientation in comet tails through bombardment by solar wind protons, noting role in scattered light polarization

11 p1832 A71-26182

Planetary system formation, examining particulate matter aggregation within dust cloud and gas around sun by computer simulation

11 p1835 A71-26459

Visible brightness of Milky Way for various galactic structure models, discussing star and dust distribution effects

12 p1955 A71-26594

Taurus dust cloud magnetic field line of sight component observations and M17 and Cyg A absorption spectra data noting Zeeman splitting at 21 cm H lines

12 p1957 A71-26623

Interstellar dust, investigating starlight reddening by extinction, galactic light, IR star observations and polarization

12 p1959 A71-26775

Interstellar matter, emphasizing H I and H II regions temperatures, dust, magnetic fields, intermediate and high velocity clouds

12 p1959 A71-26779

Cosmic IR sources model based on assumption of cosmic ray particles emitting galactic sources surrounded by dust shells absorbing and reemitting energy

12 p1947 A71-26933

Earth outward winding by cosmic particle gravitational accretion, examining individual meteor counts crossing celestial meridian in WE and EW directions

12 p1966 A71-27232

Interstellar grain temperatures, considering radiant energy distribution and optical properties effects

14 p2305 A71-29679

Interstellar grain temperatures, determining shape effects on emissivities

14 p2305 A71-29680

Mesospheric extraterrestrial dust and trapped water model of noctilucent cloud formation in high latitude summer conditions, using meridional trajectories

14 p2231 A71-29721

Hypersonic flow of dust containing gases at low density for distribution accuracy of cosmic dust collection by sounding rockets

15 p2387 A71-31171

Dust grain orientation in interstellar space from Fokker-Planck equation, taking into account collisions with gas atoms and magnetic interactions

15 p2485 A71-31715

Numerical analysis of accretion growing grains segregation in gravitational field with resisting gas, discussing motion equation, evaporation rate and planetary evolution

15 p2489 A71-32397

Dust disk around secondary component of Epsilon Aurigae, noting role in system eclipse

15 p2494 A71-32550

Galactic nucleus thermal emission due to dirty ice or silicate grains, explaining far IR radiation power output and spectral dependence

15 p2498 A71-32773

Interstellar gas absorption correlation with dust extinction, obtaining gas to dust density ratio

16 p2632 A71-33323

Hydrogen condensation in interstellar gas clouds onto solid dust grains from vapor pressure measurements of solid hydrogen at low temperatures

16 p2634 A71-33392

Nonlinear correction in Lagrangian density of gravitational field, deriving dusty cosmological model with no singularity

16 p2638 A71-33546

Noctilucent cloud nature from cosmic dust particles collection and detection, discussing mass, absolute falling velocity and model theories

16 p2641 A71-33765

Interplanetary hydrogen and helium from cosmic dust deionizing effect on solar wind, calculating gas density and flux

16 p2628 A71-33940

Circumstellar dust clouds and Bok globules examined for gaseous emission lines, emphasizing forced diffusion process

16 p2643 A71-34077

Star formation at interstellar gas cloud stage, discussing gravitational collapse, Bok dust globules, spectroscopic and IR peculiarities and models

17 p2801 A71-34696

Lyman alpha resonant radiation in regions distant from cometary tails due to additional atomic hydrogen production from dust particles

17 p2809 A71-35595

Nonstatic model of universe based on Newtonian cosmology, considering central body effects on interstellar dust motion

17 p2809 A71-35600

Circumterrestrial cosmic dust clouds properties determination by optical methods, using twilight observations at solar vertical symmetric points

17 p2810 A71-35725

Cosmic dust separation from terrestrial material, using vibrating tray to roll spherical particles from bulk of demagnetized and dried material

17 p2811 A71-35729

Thin layer silica gel chromatography applied to cosmic dust chemical composition

17 p2811 A71-35730

Interstellar dust clouds physical and chemical constitution, discussing molecular gas chemical composition and abundances

18 p2968 A71-37037

Galactic clusters evolution in universe with zero rest mass particles, showing size dependence on cosmic dust energy density

18 p2969 A71-37040

Earth outward winding by cosmic particle gravitational accretion, examining individual meteor counts crossing celestial meridian in WE and EW directions

19 p3132 A71-37384

Laser radar observation of comet Bennett dust at 40-90 km, deducing particle size from rate of descent

19 p3142 A71-38041

Italian soil particles of cosmic origin, noting space research activities relation to micrometeorites and dust studies

20 p3298 A71-39644

Sounding rockets sampling of cosmic dust in upper atmosphere during and after Zeta Perseid and Arietid meteor showers

20 p3299 A71-39651

Electron microprobe analysis of cavity surface and lip of cosmic dust impact craters in stainless steel plates exposed at 400 km altitude in Gemini S-010 experiment

20 p3299 A71-39652

High altitude balloon cosmic dust collection, considering individual particle chemical composition and ablation

20 p3299 A71-39653

Direct measurements of cosmic dust particles in near earth environment and interplanetary space, noting reliability and calibration

20 p3300 A71-39655

Optical properties of graphite-iron-silicate grain mixtures from Mie theory for spherical particles, noting models consistency with interstellar extinction and backscattering observations

21 p3444 A71-40242

Intergalactic dust density limits using absorption magnitude and red shift of distant galaxies

22 p3599 A71-41924

Collapsing dust cloud with small differential rotation described in normal Gaussian coordinate system

22 p3605 A71-42499

Cosmic dust particles impact craters searched for in lunar samples by binocular and electron scanning microscopes, relating to early solar system meteoroid flux

23 p3765 A71-43807

COSMIC GASES

NT INTERPLANETARY GAS

NT INTERSTELLAR GAS

Magnetic field generation during radiation era, discussing generating mechanism by angular momentum transfer between ion and electron-photon gases in expanding plasma

01 p0148 A71-10024

Intergalactic gas photoionization by quasars UV radiation, using Friedman cosmological model

05 p0805 A71-16111

Cosmic gas dynamics, discussing galactic mass balance, dark matter and interstellar gas kinetic energy, temperature and density

06 p0971 A71-18327

Cosmic accretion gas dynamics, discussing star, galaxies and galactic cluster effects

06 p0972 A71-18333

Intergalactic gas ionization and heating by UV radiation

06 p0974 A71-18429

Nonspherical finite amplitude pulsations of uniform gas cloud in smooth gravitational contraction

08 p1364 A71-21413

Intergalactic gas ionization and heating by UV radiation

12 p1955 A71-26579

Atomic and molecular spin in cosmic medium, discussing static/dynamic orientation, resonance mechanism, hyperfine structure and magnetic sublevels

12 p1933 A71-27420

Spatial variations in cosmic He abundance attributed to primordial temperature fluctuations at early epochs in Friedmann universe

14 p2303 A71-29587

Mass transfer in close binaries, determining gaseous ring formation conditions and properties from ejected particle trajectories computation

17 p2809 A71-35594

Mass spectrometric studies of origin of light elements Li, Be and B in universe, considering spallation of stellar and galactic gases by high energy particles

18 p2959 A71-35914

Chondrite classification, primordial matter composition and early solar system chemical processes, discussing cosmic gas condensation and refractory element fractionation

18 p2967 A71-37027

Coma cluster X ray observations implying limits on gas density in intergalactic space and Friedmann models

22 p3599 A71-41926

Current-optical effects of anisotropic absorption of polarized and unpolarized light in rarefied cosmic media

24 p3860 A71-45106

COSMIC NOISE

Polar aurora pulsations of 4-12 sec intensity with associated cosmic radio noise absorption, using photometric measurements

02 p0242 A71-11761

Auroral absorption classification of cosmic noise at 32 MHz, plotting time and amplitude distribution diagrams

02 p0243 A71-11769

Diurnal and seasonal variations of cosmic noise absorption at critical frequency of F2 region

03 p0379 A71-13815

Lower ionospheric cosmic noise absorption at 28.6 MHz, examining diurnal variations

05 p0740 A71-16430

F region cosmic noise absorption at 20-30 MHz over Delhi, examining diurnal, seasonal and solar cycle variations

05 p0808 A71-16431

OGO radio astronomy instrument for cosmic noise sky brightness distribution mapping by electrically short antenna ionospheric focusing

11 p1763 A71-26144

Cosmic microwave background measurements at 8 mm wavelength, examining isotropy

12 p1956 A71-26614

Cosmic radio noise absorption measurements at subauroral latitude for ionospheric absorption, discussing ionization regions spatial nonuniformity and horizontal extension

14 p2196 A71-30561

Electron flux rigidities in polar aurora region, using stratospheric nighttime X ray and cosmic radio noise absorption measurements

14 p2302 A71-30595

Earth velocity vector right ascension, declination and magnitude determination from cosmic 3 K background radiation anisotropy

16 p2563 A71-33402

Auroral zone proton measurements during slowly varying cosmic noise absorption, obtaining energy spectrum by rocket soundings

19 p3125 A71-37418

Auroral pulsations physical correlation with cosmic noise absorption, using statistical correlation analysis

20 p3215 A71-38734

COSMIC PLASMA

Fully ionized hydrogen cosmic plasma interaction with surrounding neutral gas, noting minimum temperature and power input

05 p0810 A71-16637

Cosmic plasma dynamics collective phenomena, investigating models, instabilities, nonlinear interactions, wave transformations, turbulence, cosmic rays and radiative acceleration

06 p0972 A71-18330

Solar wind observations, accounting for cosmic plasma and stellar wind properties

06 p0973 A71-18336

Heliosphere boundary interactions with interstellar medium, considering galactic plasma shock front and boundary radius as function of solar activity level [AIAA PAPER 71-33]

06 p0977 A71-18495

Cosmic plasma stream capture by magnetic dipole of neutron star in binary system

07 p1192 A71-19287

Cosmological plasma physics, considering matter, antimatter, electrodynamics, ambiplasma, annihilation and heavy nuclei

07 p1196 A71-19649

- Interplanetary plasma electron density inhomogeneities formation explained by instability due to electron stream curvilinearly obtained from spacecraft data
09 p1518 A71-22435
- Compton scattering of relativistic electrons in cosmic plasma waves as source of HF radio emission from metagalactic objects
09 p1521 A71-22926
- Nonuniform density cosmic plasma heating allowing energy losses by radiation and heat conduction, using filament-structured high temperature plasma region model
11 p1828 A71-25765
- Neutral hydrogen interstellar wind parameters from Lyman alpha sky background measurements outside geocorona by photometers onOGO 5
16 p2643 A71-33834
- Soviet report to COSPAR on upper atmosphere and cosmic space including Soyuz spacecraft, lunar soil sample recovery and surface vehicle delivery
16 p2666 A71-33865
- Plasma in dayside polar magnetosphere, analyzing Imp 5 and other earth satellites measurements data
19 p3047 A71-37357
- Crab Nebula pulsar timing measurement leading to model involving inflation of closed magnetosphere with explosively released plasma
19 p3142 A71-38007
- Electromagnetic absorption in adiabatically expanding fully ionized cosmic plasma, using Einstein-De Sitter cosmology
21 p3442 A71-40161
- Cosmic plasma electron thermal motions effects on cosmic electromagnetic absorption, taking into account electron-electron collision effects in electromagnetic waves dispersion relationships
21 p3442 A71-40162
- Nonuniform density cosmic plasma heating allowing for energy losses by radiation and heat conduction, using filament-structured high temperature plasma region model
22 p3598 A71-41533
- Magnetospheric substorms relationship to interplanetary magnetic field and solar wind plasma parameters, noting dominant effect of interplanetary southward component
23 p3734 A71-43183
- COSMIC RADIATION**
U COSMIC RAYS
COSMIC RADIO WAVES
U EXTRATERRESTRIAL RADIO WAVES
COSMIC RAY ALBEDO
- High energy albedo neutron production by cosmic ray collisions, investigating balloon altitude flux variations near atmospheric top
06 p0962 A71-18179
- Galactic and albedo X rays measurement by balloon-borne instruments and sounding rockets
12 p1949 A71-27371
- COSMIC RAY SHOWERS**
High energy inelastic interactions in cosmic ray showers, using Wilson chamber
01 p0145 A71-13665
- Extensive atmospheric showers and energy transfer from interacting nucleons to electron photon cascades at high energy levels
01 p0146 A71-13666
- Radiation measuring instruments assembly for extensive air showers and cosmic ray particle nuclear interactions at high energies
01 p0084 A71-13667
- Extensive air shower experiments, considering origin, particle interactions and detectors
03 p0475 A71-13838
- Electron-photon showers, discussing cascade theory equilibrium spectra, avalanches and radio emission
03 p0475 A71-13840
- Pion-nucleon interactions, determining energetically precipitated particle effects in air showers
03 p0461 A71-13841
- Asymmetrical cosmic ray showers kinematic interpretation by heuristic model, discussing particle dispersion angular distribution
03 p0476 A71-13843
- Negative pi-N NN interactions in emulsion at high energies, plotting angular distributions of secondary particles in cosmic ray showers
03 p0476 A71-13847
- Monte Carlo model of muon and active component distribution in nuclear cascade in extensive cosmic ray shower
03 p0476 A71-13849
- Muons spatial distribution function in mountain level extensive air showers
03 p0476 A71-13855
- Extensive air shower muons at mountain levels, describing experimental procedure for fluctuation distribution
03 p0476 A71-13856
- Extensive air shower muon fluctuations at mountain level, determining interaction coordinates distribution, production and energy by Monte Carlo method
03 p0477 A71-13857
- Extensive air shower electron photon and muon components energy spectrum at various depths
03 p0477 A71-13859
- High energy muons in extensive air showers, studying spatial distribution, spectrum and electron showers by photon spark chamber telescope underground
03 p0477 A71-13860
- Extensive air shower electron and muon components at mountain levels, calculating distribution functions by Monte Carlo technique
03 p0477 A71-13861
- Spatial distribution and polarization of radio emission from extensive air showers, using Geiger and scintillation counters, muon detectors and antennae
03 p0477 A71-13865
- Extensive air showers at sea level, plotting mean numbers of muons and electrons
03 p0477 A71-13866
- Cosmic ray shower particles spatial and angular distribution structure near electron-photon cascade core
03 p0478 A71-13867
- Electromagnetic cascade-material boundary crossing transition effect analysis by perturbation theory in terms of differential shower particle flux
03 p0478 A71-13871
- Air shower cores high transverse momenta, discussing primary particle role in core structure
04 p0640 A71-14814
- Underground cosmic ray showers muon pairs lateral distribution measurement
04 p0640 A71-14815
- Supernovae high energy gamma rays detection by extensive air shower arrays
04 p0641 A71-15830
- Type one fluctuations sustained by large air showers at sea level, describing simulation method for influence of first nuclear interaction altitude on shower morphology
10 p1660 A71-23853
- Type I fluctuations experienced by extensive air showers generated by protons or heavy nuclei, discussing effect on primary cosmic ray energy determination
10 p1661 A71-23858
- Extensive air showers and multiple muons frequencies, considering parent pions mean transverse momentum, multiplicity law form and primary cosmic ray intensity
10 p1664 A71-25046
- Angular, spectral and temporal properties of Cerenkov radiation in cosmic ray extensive air showers
11 p1815 A71-25594
- Radio pulses at 2 MHz from cosmic ray air showers, using high speed digital techniques in statistical data analysis
12 p1948 A71-26936
- Nucleon-nucleon interactions produced energetic penetrating particles /muons/ in cosmic ray showers, studying neon flash tube technique
12 p1948 A71-27186
- Cosmic ray storm analysis, showing enhanced daily/shortlived variations, radiation intensity increase and solar flare observations
12 p1949 A71-27375
- Large air shower Cerenkov detectors system, discussing energy spectra from vertical arrays, delayed muons and radio pulse detection rates
12 p1950 A71-27384
- Zenith angular air shower distribution by Monte Carlo method, discussing muons horizontal component separation from background events
12 p1951 A71-27385
- TeV hadrons lateral energy distributions in air shower cores from Ne hodoscope measurements for fluctuations between primary energy and shower size, discussing French alpine scintillators array
12 p1951 A71-27386
- Three dimensional Monte Carlo simulation of extensive air shower development, comparing fireball and mathematical models for mean total hadronic energy spectra
12 p1951 A71-27388
- Coincident radio pulse effects on triggering antenna arrays, considering air shower mechanism
12 p1967 A71-27389
- Geomagnetic effects on radio signals mechanism in extensive air showers, discussing scintillators array for east-west to north-south ratio polarization measurements
12 p1967 A71-27390
- Shower size distributions of accompanying energetic protons at mountain altitude as function of released energy
12 p1951 A71-27392
- High energy interactions at 10 to 12 power eV, discussing muon-poor showers, incoherent muons and horizontal air showers
12 p1933 A71-27395
- Penetrating particle observations on showers produced at 70 mwe underground, revealing weakly ionized group in quark flux contradiction
12 p1951 A71-27396
- Two temperature model of cosmic ray high energy jets, predicting one particle accelerator momentum spectra
12 p1951 A71-27397
- Muon showers underground, considering primary cosmic ray energies greater than 10 TeV
12 p1952 A71-27401
- Cosmic ray muon flux at sea level, allowing for showers, multiple scattering, straggling, zigzag motion, detector efficiency and electronic equipment dead time
12 p1952 A71-27403
- Cosmic rays - Conference, Budapest, August-September 1969, Volume 3, High energy interactions and extensive air showers
13 p2120 A71-28048
- Quarks search near extensive air shower cores, discussing apparatus and results for detection of long delayed particles
13 p2120 A71-28052
- High energy nuclear bursts without accompanying air showers, considering surviving primary protons without inelastic collision in atmosphere
13 p2121 A71-28054
- Nuclear emulsion produced cosmic ray jets secondaries angular distribution, primary energy and anisotropy
13 p2121 A71-28056
- Power law dependence of lateral distribution function and core location of showers detected by Haverah Park array
13 p2122 A71-28068
- Extensive air shower size measurements, relating energy spectra to primary energies up to 10 million TeV by calorimetric method
13 p2122 A71-28069
- Atmospheric scintillation light detection from air shower, determining interaction mean free path of 1-10 million TeV primary particles
13 p2122 A71-28070
- Arrival time distribution of electrons and Cerenkov light in extensive air showers, showing detector feasibility for age classification
13 p2122 A71-28071
- Angular distribution of muon-poor extensive air showers, considering generation by atmospheric nuclei interaction
13 p2123 A71-28073
- Sidereal distribution of arrival directions of extensive air showers containing high energy hadrons
13 p2123 A71-28074
- Extensive air showers multiple core and transverse momenta observations with Kiel neon hodoscope
13 p2123 A71-28075
- Electron, nuclear active and muon components of extensive air showers, discussing statistical results
13 p2123 A71-28076
- Extensive air showers nuclear active component energy flux lateral distribution and spectrum based on Monte Carlo simulation of elementary interactions
13 p2123 A71-28077
- TeV hadronic component in air shower cores, comparing energy spectra and lateral distributions to Monte Carlo simulations
13 p2123 A71-28078
- High energy hadrons energy flow fluctuations and chemical composition of cosmic rays in air shower cores, comparing to Monte Carlo calculations
13 p2123 A71-28079
- Extensive air showers hadronic component observation by nuclear emulsion chambers combined with scintillation detectors
13 p2124 A71-28080
- Local high energy events in extensive air showers core region, using scintillators and multiplate cloud chambers
13 p2124 A71-28081
- Extensive air showers cores structure observed with plastic scintillators and multiplate cloud chamber at 2770 m
13 p2124 A71-28082
- Density, momentum and electric charge measurement of nuclear interacting particles in extensive air showers, using air gap magnet spectrograph and neutron monitor
13 p2124 A71-28083
- Scintillator array investigation of high transverse momenta occurrence in air showers of primary energy above 1000 TeV
13 p2124 A71-28084
- Air shower properties from Monte Carlo simulations, determining electron and muon numbers at sea level for primary protons and copper nuclei
13 p2124 A71-28085
- Particle densities and muon spectra at 100-1300 m from sea level extensive air showers axes for primary energies to 10 to 20th eV
13 p2124 A71-28086
- Density spectrum of cosmic ray showers, discussing altitude effects, structure function and transition
13 p2125 A71-28087
- Extensive air showers muon and electron components primary energy spectrum, using isobar and CKP formula based models
13 p2125 A71-28088

Monte Carlo simulation of high energy atmospheric extensive air shower nuclear cascade based on Aleph model of nuclear interactions

13 p2125 A71-28089

Air showers nuclear active and muon components simulation in space and time, using different shower models based on isobar-fireball concept

13 p2125 A71-28090

High energy muons measurements in extensive air showers, presenting muon densities, momenta and electric charge data obtained from spectrograph long term continuous operation

13 p2125 A71-28091

Extensive air showers muons momenta and densities from shower core spectrographic recordings

13 p2125 A71-28092

Cerenkov light distribution calculation from gamma ray initiated air shower model obtained from Monte Carlo computer program

13 p2125 A71-28093

Primary cosmic rays mass composition at energy levels above 10 TeV, analyzing muons data from extensive air shower experiments

13 p2125 A71-28094

Muons arrival times distribution in extensive air showers, examining delay as function of particle production heights

13 p2126 A71-28095

Extensive air showers muon component arrival time spread and lateral density distribution

13 p2126 A71-28096

Extensive air showers muons angular distribution, considering high energy nuclear reactions

13 p2126 A71-28097

Muons lateral distribution in extensive air showers, studying density vs core distance

13 p2126 A71-28098

Muon rich showers, discussing muon density spectrum relation to primary energy spectrum

13 p2126 A71-28099

Extensive air showers muon density spectrum, describing measurement apparatus and analysis method with particular emphasis on elimination of falsifying absorber multiplication effects

13 p2126 A71-28100

Radio pulse production by extensive air shower charges geomagnetic separation

13 p2126 A71-28101

Air showers emitted radio pulses polarization, noting inconsistency with geomagnetic origin

13 p2127 A71-28102

Extensive air showers radio wave emission based on cascade theory, determining polarization characteristics

13 p2127 A71-28103

Air shower radio emission properties, presenting electric field strength measurements at various frequencies

13 p2127 A71-28104

Air shower radio pulse amplitude variations with zenith and azimuth angle, distance from shower axis and primary energy, examining frequency spectrum characteristics

13 p2127 A71-28105

Radio emission measurement from extensive air showers by system of half wave dipoles in complex array of Moscow State University

13 p2127 A71-28106

Radio particle correlation of extensive air showers at large zenith angles, using twofold coincident 44 MHz receiver trigger-scintillator system

13 p2127 A71-28108

Extensive air showers radio emission pulse shape, noting amplifying system response to input signal

13 p2128 A71-28109

Average function for lateral distribution of radio emission in extensive air showers

13 p2128 A71-28170

Extensive air showers sidereal-diurnal variation determination, considering atmospheric effects and antisidereal wave vector

14 p2301 A71-30591

Cosmic ray shower evolution model based on passive baryon existence and direct energy transfer to gamma quanta hypotheses

14 p2302 A71-30593

Electromagnetic showers in lead, using 20 GeV primary cosmic ray electrons to calculate spatial evolution

14 p2302 A71-30603

Extensive air showers detection by correlation of optical and radio pulses at 60 deg zenith angle

15 p2472 A71-31199

Tachyons in cosmic ray showers, investigating occurrence frequency relative to electrons

15 p2474 A71-31731

Sea level high energy muon flux determination from underground burst energy spectrum measurements, using Kobayakawa-Miono formula for cascade shower fluctuation

15 p2475 A71-31782

Air showers with zenith angles greater than 65 deg recorded by array comprising six scintillation counters, considering angular distribution, intensity and muon content

15 p2475 A71-31786

Energy spectrum of cosmic ray showers from high energy muon interactions with nuclear emulsion chamber

15 p2476 A71-31789

Zenith angle distribution of extremely high energy muons from bremsstrahlung showers by emulsion chamber, noting consistency with pion/kaon decay

15 p2476 A71-31790

Angular distribution of high energy cosmic ray muons incident at sea level at large zenith angles, investigating cascade showers initiated by muons

15 p2476 A71-31792

Cosmic ray shower size spectrum in atmosphere for muon bremsstrahlung at large zenith angles

15 p2479 A71-31868

Field strength of radio emission from cosmic ray showers at 3.6 MHz, stressing data analysis procedure

17 p2732 A71-34623

Radio emission from cosmic ray showers, discussing detection, particle populations and energy spectra

18 p2957 A71-36211

Controlled photographic emulsion study of cosmic ray showers with electron photon components

19 p3124 A71-37261

Air shower pion/proton and neutral/charged ratios at mountain altitude, using cloud chamber, Cerenkov counter and spectrometer measurements

20 p3279 A71-39323

Extensive air showers attenuation length measurement in Japan /1964-1968/, using scintillator

20 p3284 A71-39863

Crab Nebula cosmic gamma rays from air shower emitted Cerenkov light detection, using synchrotron Compton scattering model

20 p3285 A71-39922

Muon showers underground phenomenology in terms of density spectra, shower size and radial density distributions

22 p3594 A71-42407

Sea level high energy cosmic ray muon spectra calculation based on phenomenological model of nucleon-nucleus collisions

22 p3594 A71-42408

Electromagnetic interactions of high energy cosmic ray muons from combined calorimeter-spectrograph investigation

22 p3594 A71-42409

Extensive air shower experiments, considering origin, particle interactions and detector

22 p3594 A71-42639

Electron-photon showers, discussing cascade theory, equilibrium spectra, avalanches and radio emission

22 p3594 A71-42641

Pion-nucleon interactions, determining energetically precipitated particle effects in air showers

22 p3579 A71-42642

Asymmetrical cosmic ray showers kinematic interpretation by heuristic model, discussing particle dispersion angular distribution

22 p3594 A71-42644

Negative pi minus N and NN interactions in emulsion at high energies, plotting angular distributions of secondary particles in cosmic ray showers

22 p3594 A71-42648

Monte Carlo model of muon and active component distribution in nuclear cascade in extensive cosmic ray shower

22 p3595 A71-42650

Muons lateral distribution function in mountain level extensive air showers

22 p3595 A71-42656

Extensive air shower muons flux density at mountain altitudes, describing experimental procedure for fluctuation distribution

22 p3595 A71-42657

Extensive air shower muon flux density fluctuations at mountain level, determining interaction coordinates distribution, production and energy by Monte Carlo method

22 p3595 A71-42658

Extensive air shower electron-photon and muon components energy spectrum at various depths

22 p3595 A71-42660

High energy muons in extensive air showers, studying spatial distribution, spectrum and electron photon showers by underground photon spark chamber telescope

22 p3595 A71-42661

Extensive air shower electron and muon components at mountain levels, calculating probability distribution functions by Monte Carlo technique

22 p3595 A71-42662

Lateral distribution and polarization of radio emission from extensive air showers, using Geiger and scintillation counters, muon detectors and antennae

22 p3595 A71-42666

Extensive air showers at sea level, plotting mean numbers and distribution functions of muons and electrons

22 p3595 A71-42667

Cosmic ray shower particles lateral and angular distribution structure near electron-photon cascade core

22 p3595 A71-42668

Perturbation method in transition effect theory for electron photon cascades in extensive air showers

22 p3596 A71-42672

Extensive air shower radio pulse emission by geomagnetic charge separation mechanism, using antenna and scintillation counters arrays

23 p3646 A71-44012

COSMIC RAYS

NT COSMIC RAY SHOWERS

NT PRIMARY COSMIC RAYS

NT SECONDARY COSMIC RAYS

NT SOLAR COSMIC RAYS

Radio sources, cosmic rays and X ray background origin, discussing synchrotron mechanism, Compton scattering and red shifts

01 p0144 A71-10770

Supernovae positrons and low energy cosmic rays flux, determining ejected matter plasma properties

01 p0145 A71-11338

Soviet papers on cosmic rays and high energy nuclear interactions

01 p0145 A71-11362

High energy multiple birth inelastic interactions between cosmic ray particles and atomic nucleus targets, using Wilson chamber and ionization calorimeter

01 p0083 A71-11363

Cosmic ray nuclear component during solar activity minimum, using Cerenkov counters onboard Elektron satellites

01 p0146 A71-11371

Solar flare proton propagation, examining interplanetary shock wave effects on cosmic ray scattering

01 p0146 A71-11386

Nuclear interactions induced by cosmic ray and accelerator muons, discussing cloud chamber and nuclear emulsion data

01 p0131 A71-11412

Directional cosmic ray cut-off and loop-cone folding distribution at geomagnetic midlatitude sites

01 p0146 A71-11485

Cosmic ray heavy ion component biological effect, describing histological and radioautographic high altitude balloon experiment with black mice and rabbits

01 p0019 A71-11555

Background emission characteristics, discussing cosmic electrons, X rays and radiation sources

02 p0300 A71-12092

Nonrelativistic cosmic particles spectrum and chemical composition changes, examining ionization and heating energy loss effect

02 p0300 A71-12093

Cosmic ray anisotropy fluctuation and propagation function dimensionality relationship, demonstrating essentially one dimensional propagation

02 p0300 A71-12370

Cosmic radiation origin, discussing inner and extragalactic energy density and elements distribution

02 p0300 A71-12372

Diffuse cosmic X ray spectrum obtained from telescope aboard OSO 3 satellite

02 p0300 A71-12580

Diffuse cosmic X rays observation by telescope aboard OSO 3 satellite, determining isotropy

02 p0301 A71-12581

Diffuse cosmic gamma ray background origin, using simple photon production model

02 p0303 A71-12837

Low energy cosmic ray deuteron flux, examining energy spectral shapes of sources

02 p0303 A71-12871

Radiological risks of cosmic radiation during high altitude supersonic flights, considering galactic, solar and incident particles in aircraft atmosphere

03 p0473 A71-13099

Physical processes in galactic and extragalactic sources of nonthermal radio emission, assuming pulsars as principal magnetic field and cosmic rays sources

03 p0483 A71-13201

Relativistic electron spectra of cosmic rays accelerated by plasma turbulence, examining singularity in solution

03 p0483 A71-13202

Galactic radio corona existence, measuring northern galactic hemisphere sky brightness and cosmic ray distribution

03 p0483 A71-13204

Cosmic photons Planck constant, considering photon absorption dependence on variations of spin angular momentum

03 p0473 A71-13562

Solar proton flares, coronal radio diameter and cosmic radiation intensity relationship

03 p0473 A71-13788

Cosmic ray physics - Conference, Leningrad, October 1969

03 p0473 A71-13832

Proton 4 satellite high and superhigh energy cosmic ray spectrometer, discussing principles of operation and parameters

03 p0426 A71-13833

Strong cosmic ray interactions, considering meson production in accelerators

03 p0475 A71-13835

Nuclear cascade pion energies in heavy material by Monte Carlo method, concerning cosmic ray and particle accelerator interactions

03 p0461 A71-13842

High energy cosmic particle interactions with LiH target, discussing relation between longitudinal and transverse momenta of generated pions

03 p0476 A71-13844

Charged particles momenta and spatial arrangement during cosmic ray particles nuclear interactions, describing recording equipment

03 p0476 A71-13845

Nuclear interactions of neutral cosmic particles with carbon target at mountain altitudes

03 p0476 A71-13848

Energy spectra of ionization bursts, electromagnetic cascades and nuclear active particles at mountain altitude

03 p0476 A71-13850

Cosmic rays intensity measurement in deep ocean with Cerenkov counter, determining Muon energy spectrum and absorption in water

03 p0477 A71-13862

Bremsstrahlung photons produced by cosmic ray muons in Fe and Pb at sea level, calculating energy spectra and angular distributions

03 p0477 A71-13863

Ultrahigh energy electrons and gamma quanta in ground produced by cosmic rays, plotting mean free path vs energy

03 p0478 A71-13868

Carbon/oxygen and nitrogen/oxygen ratios in cosmic rays, considering energy dependence interstellar ionization loss and necessity for two component source model

03 p0480 A71-14051

Cosmic ray nuclei galactic disk confinement determination, considering particle mean age by radioactive Be10 tracer method

03 p0480 A71-14052

Soviet book on cosmic ray physics covering high energy particles interactions, origin, acceleration mechanism, etc

03 p0481 A71-14424

Forbush decreases vertical cutoff rigidity dependence, comparing cosmic ray intensities from Pioneer 8 detector and ground based neutron monitors

03 p0481 A71-14501

Low energy cosmic ray propagation anisotropies in interplanetary medium examined by unidirectional detectors on geostationary satellites

03 p0482 A71-14543

Cosmic ray data, showing perpendicular density gradient to ecliptic plane

03 p0482 A71-14547

Heavy cosmic particle dosage measurement by chemical etching of particle tracks on Apollo astronauts plastic helmets

04 p0543 A71-14822

Intensity correlation functions as parameters for cosmic radiation activity

04 p0640 A71-15086

High energy cosmic ray particle charge and direction detector on Proton 3 satellite

04 p0596 A71-15122

Galactic magnetic field characteristics and cosmic rays origin, discussing gas clumping and star formation

04 p0641 A71-15758

Mn 53 age measurement of galactic cosmic rays

05 p0797 A71-15930

Pulsars relationship to very high energy cosmic ray electron propagation, examining far IR background and radiation sources

05 p0797 A71-15941

Cosmic ray Be 7 equilibrium concentration, examining electron capture and radioactive decay

05 p0798 A71-16114

Geomagnetic field effects on cosmic radiation, determining muon component momentum distribution and charge ratio

05 p0798 A71-16219

Cosmic ray particles diffusion with simultaneous energy transport, using leakage lifetime approximation

05 p0798 A71-16448

Forbush midlatitude microdecreases effects on diurnal cosmic ray intensity, using neutron monitor

05 p0799 A71-16624

Rocket-borne beta ray atmospheric densitometer errors due to cosmic rays

05 p0752 A71-16673

Planetary atmospheres ionosphere formation by cosmic rays, examining ionization of various gases

05 p0799 A71-16817

Collective longitudinal space charge waves in trapped relativistic one dimensional plasma, calculating inhibition/enhancement of cosmic ray Fermi acceleration

05 p0791 A71-16940

Semidiurnal variation of galactic cosmic ray intensity, using neutron and meson monitor data

05 p0800 A71-17008

Spherical harmonic analysis of worldwide cosmic ray variations during geomagnetic storms, using ground station and satellite data

06 p0949 A71-17253

Galactic cosmic ray solar modulation in interplanetary medium, discussing spherically symmetric model

06 p0949 A71-17275

Cosmic ray telescopes geometric factor determination, taking into account particle incidence angle

06 p0898 A71-17705

Power spectra of cosmic ray intensity variations at ground and atmospheric pressure oscillations

06 p0950 A71-17979

Cosmic rays - Conference, Budapest August-September 1969, Volume 2, Solar cosmic rays, modulation of galactic radiation, magnetospheric and atmospheric effects

06 p0950 A71-18101

Galactic cosmic rays nonlinear interactions with solar wind, taking into account autofocusing effect

06 p0951 A71-18103

Models for solar wind modulation of galactic cosmic rays by anisotropic diffusion approximation

06 p0951 A71-18104

Diurnal cosmic ray neutron variations after proton flares, comparing calculated radial and azimuthal gradients to experimental data

06 p0951 A71-18105

Satellite cosmic ray monitors data, examining corotation with sun to obtain interplanetary magnetic field spatial structure

06 p0951 A71-18106

Cosmic rays effective angles of acceptance and energy spectrum diurnal variations, using temporal correlation functions

06 p0951 A71-18107

Statistical reliability tests for cosmic ray intensity records from ground stations, stressing time series aspect

06 p0951 A71-18108

Force field model for galactic cosmic rays modulation by solar cycles, noting agreement with Fokker-Planck equation analytic and numerical solutions

06 p0952 A71-18110

Interplanetary cosmic ray gradients and anisotropies from Pioneer 8 probe

06 p0952 A71-18111

Galactic cosmic ray proton and He spectrum measurements in 1968 compared to electron spectra, explaining solar modulation features by models incorporating energy loss effects

06 p0952 A71-18112

Cosmic rays solar diurnal variation, using underground recordings in Bolivia and New Mexico from multiple two fold coincidence scintillator telescopes

06 p0952 A71-18114

Diurnal intensity variations of high energy galactic cosmic rays, taking into account particle trajectories in sectorial interplanetary magnetic field

06 p0952 A71-18115

Heliocentric cosmic ray particle density gradient production of north-south streaming in interplanetary magnetic sector, using neutron monitor

06 p0953 A71-18116

Isotropic galactic cosmic ray diffusion in interplanetary space from solar wind velocity and diffusion coefficient dependence on heliolatitude and heliointensity

06 p0953 A71-18118

Solar wind asymmetric component on basis of 27-day cosmic ray variations

06 p0953 A71-18121

Twenty-seven day variations in cosmic ray intensity and geomagnetic activity index, using filter and power spectrum methods

06 p0953 A71-18122

Solar activity correlation with cosmic ray intensity and solar wind properties, analyzing hysteresis diagrams for wind modulation characteristics dependence on heliolatitude

06 p0954 A71-18123

Cosmic ray neutron component intensity increases dependence on corpuscular stream velocity before Forbush effects

06 p0954 A71-18124

Cosmic ray mu meson intensity power spectrum frequency dependence, comparing to interplanetary field spectra

06 p0954 A71-18125

Cosmic ray intensity variations from magnetic fields of micrometer streams in interplanetary plasma

06 p0954 A71-18126

Quiet time fluxes and differential energy spectra of protons and alpha particles at 2-20 MeV measured by cosmic ray detectors onOGO-3

06 p0954 A71-18127

Low energy cosmic rays modulation and heliocentric gradient during solar minimum, comparingOGO 1 and 2 ion chamber measurements with other space and ground observations

06 p0954 A71-18128

Heavy cosmic ray nuclei intensity and energy spectra, investigating solar modulation effects

06 p0954 A71-18129

Galactic cosmic ray solar modulation with 20 year periodicity, suggesting nearby galactic magnetic field direction

06 p0955 A71-18130

Residual modulation from 1954-1964 solar cycle, considering 19th cycle hysteresis loop from cosmic ray balloon data

06 p0955 A71-18131

Cosmic rays neutron monitors daily data /July 1957-December 1962/, applying corrections for latitude, altitude, solar cycle phase and station efficiency

06 p0955 A71-18132

Sunspot heliographic latitude role in 11 year galactic cosmic ray modulation

06 p0955 A71-18133

Galactic cosmic ray modulation region dimensions calculated during various solar activity cycles

06 p0955 A71-18134

Forbush decrease rigidity dependence relation to cosmic ray solar modulation, using neutron monitors counting rate variations at different vertical cut-off rigidities

06 p0956 A71-18136

Forbush decreases and long term cosmic ray particle intensity changes, investigating spectral variations

06 p0956 A71-18137

Cosmic ray solar modulation anisotropy during 23 March 1966, 25 May 1967 and 26 January 1968 events in preForbush phase, evaluating multidirectional meson observations

06 p0956 A71-18138

Cosmic rays anomalous diurnal variations, describing proton excess flux from direction outside geomagnetic field

06 p0956 A71-18139

Cosmic rays transient north-south polar asymmetry, confirming time lag between Forbush decrease onsets

06 p0956 A71-18140

Solar and galactic cosmic rays interactions with interplanetary magnetic field 28 January-25 February 1967 based on Explorer 33 and 28 satellite observations

06 p0957 A71-18145

Solar flare induced cosmic ray intensity increases registered by high latitude neutron monitors and Explorer 35 satellite, presenting intensity time profiles analyses

06 p0957 A71-18146

Solar flare associated increases in cosmic ray intensity during November 1968-April 1969, correcting anisotropic peak and decay rates to standard barometric coefficients

06 p0957 A71-18148

Cosmic ray intensity variations, discussing trajectory-derived cut-off rigidities for neutron monitor data analysis

06 p0959 A71-18160

Cosmic ray equator position dependence on solar activity level, discussing shipborne neutron monitor observations during IGY and IQSY

06 p0959 A71-18162

Cosmic ray multiple neutron intensities time variations measurements at Syowa Station /Antarctica/, considering Forbush decrease, diurnal variations, solar protons and storm time increase

06 p0960 A71-18163

Solar proton event energy spectra based on multiplicity measurements of cosmic ray neutron intensity increases

06 p0960 A71-18164

Latitude, mesons and radioactivity effects on planetary distribution of cosmic ray neutron component barometer coefficient during IQSY

06 p0960 A71-18166

Galactic cosmic rays solar modulation effects on fast neutron flux in atmosphere

06 p0962 A71-18182

Cosmic plasma dynamics collective phenomena, investigating models, instabilities, nonlinear interactions, wave transformations, turbulence, cosmic rays and radiative acceleration

06 p0972 A71-18330

Galactic magnetic fields and cosmic ray gas, investigating origin and dynamical effects

06 p0972 A71-18332

Cosmic radiation protection of spacecrews by drugs, extrapolating animal data to humans

06 p0861 A71-18359

Cosmic ray intensity Forbush decrease on 23 September 1966 coincidence with magnetic storm sudden commencement from satellite and ground based monitors data

07 p1184 A71-18750

Interstellar gas acceleration and heating by cosmic rays streaming along uniform magnetic field faster than Alfvén speed

07 p1190 A71-18854

Isotropic diffuse cosmic X rays and gamma radiation background origin

07 p1184 A71-19321

Cosmic rays sidereal diurnal variations, considering interplanetary magnetic field shielding effect

07 p1185 A71-19378

Soviet book on active protection of space vehicles covering measures against penetrating radiation from Van Allen belts, solar flares and galactic cosmic rays
07 p1207 A71-19474

Isotropic component of diffuse gamma ray background, discussing possible dense intergalactic medium coexistence with universal cosmic ray flux
07 p1185 A71-19549

Ionized gas galactic cluster stabilization model construction, considering ionizing radiation enhanced cosmic flux and quasar PKS 1116 plus 12 absorption spectrum
07 p1198 A71-19830

Plastic track detectors calibration for heavy charged particles in cosmic ray experiments, considering track etching rates as function of particle charge and velocity
07 p1113 A71-20042

Low energy cosmic X ray observations, examining diffuse background and absolute flux values
08 p1349 A71-20936

Cosmic ray physics - Conference, Leningrad, November 1969
08 p1350 A71-20951

Proton flux range between solar wind and cosmic radiation protons energy by spacecraft observation
08 p1350 A71-20952

Radio background in universe due to synchrotron radiation, X ray and photon backgrounds due to cosmic electrons inverse Compton effect
08 p1351 A71-20960

Cosmic ray modulation processes, spectrum variation and intensity restoration delay, discussing solar activity indices and wind models
08 p1351 A71-20965

Interplanetary space cosmic ray currents global survey based on neutron component measurements, noting anisotropic diffusion, inhomogeneous solar wind and Forbush effect shell model
08 p1351 A71-20966

Chromosphere-flare and galactic cosmic ray hypotheses of Forbush decrease and strong shock waves in interplanetary medium
08 p1352 A71-20967

Cosmic ray modulation spectrum function properties during Forbush decrease by spectrographic analysis
08 p1352 A71-20968

Second spherical harmonic generation mechanisms in axisymmetric diurnal and semidiurnal cosmic ray spectrum variations
08 p1352 A71-20969

Interplanetary space cosmic ray density gradient from three dimensional anisotropic diffusion model
08 p1352 A71-20970

Diurnal cosmic ray anisotropy, investigating solar wind velocity and interplanetary magnetic field effects
08 p1352 A71-20971

Eleven year galactic cosmic ray amplitude variation, determining modulation by sunspot groups and latitude
08 p1352 A71-20972

Active cosmic ray modulation layer boundaries between sun and earth orbits, studying meteorite isotopes radioactivity
08 p1352 A71-20973

Galactic cosmic ray density space-time variations in interplanetary space with solar wind, using spherically symmetrical model with diffusion approximation
08 p1352 A71-20974

Galactic cosmic ray density modulation by solar wind, assuming heliointitudinal asymmetry
08 p1353 A71-20975

Irregularity levels changes in interplanetary magnetic field during solar activity cycle from cosmic ray neutron component measurement data obtained on azimuthal muon telescopes
08 p1353 A71-20976

Solar activity heliolatitudinal distribution effect on interplanetary space electromagnetic conditions governing galactic cosmic ray intensity
08 p1353 A71-20977

Cosmic ray intensity annual variations relationship to heliolatitudinal solar activity index HL, providing hysteresis curves for effective angular width parameter estimation
08 p1353 A71-20978

Cosmic rays amplitude hysteresis dependence on sunspot mean heliographic latitude and cluster number
08 p1353 A71-20979

Forbush decreases effects on radio wave absorption, cosmic ray variations and ionization in lower ionosphere cosmic layer
08 p1353 A71-20981

Galactic cosmic rays interaction with interplanetary magnetic field from Venera 4 measurements June-October 1967
08 p1354 A71-21015

Galactic cosmic ray propagation earth-source distance determination by observing charge spectrum
08 p1354 A71-21018

Heavy cosmic rays slowing in balloon-borne stack, discussing high resolution measurement and synthesis in rapid neutron capture
08 p1354 A71-21038

Background emission characteristics, discussing cosmic electrons, X rays and radiation sources
08 p1355 A71-21142

Nonrelativistic cosmic particles spectrum and chemical composition changes, examining ionization and heating energy loss effect
08 p1355 A71-21143

Galactic cosmic ray proton and He nuclei spectra measurements aboard Pioneer 8 spacecraft over large energy range, considering solar modulation parameters
08 p1355 A71-21626

Cosmic ray electron intensity and energy spectrum from nuclear emulsion-spark chamber combination detector triggered by scintillation and Cerenkov counters on high altitude balloon
08 p1355 A71-21627

Aircraft altitude cosmic ray intensity measurements in lower atmosphere by neutron monitor, considering long term nucleonic intensity variations
08 p1355 A71-21629

Low energy cosmic ray intensity increase at propagating interplanetary shock wave front, discussing one dimensional model with particles undergoing convection and diffusion
08 p1356 A71-21630

X ray astronomy, discussing measurement methods and equipment, radiation mechanism and cosmic sources, with particular reference to hot rarefied plasma and pulsar types
09 p1516 A71-22058

Low energy cosmic ray H 2 and He 3 nuclei intensities /1967-1968/ from Pioneer 8 and IMP 4 measurements
09 p1512 A71-22336

Interplanetary magnetic field inhomogeneities structure from galactic cosmic rays intensity fluctuations observation
09 p1513 A71-22424

Long wave cosmic radio background emission in circumpolar space by Luna 11 and 12 satellites, observing increase in earth magnetosphere tail
09 p1513 A71-22576

Cosmic ray and radiation belt data from vertical probes, determining radiation in instantaneous cross section of atmosphere
09 p1513 A71-22666

Deceleration of low energy cosmic rays in solar wind involving Fermi acceleration by MHD waves and adiabatic energy change
09 p1514 A71-22802

Heavy cosmic rays identification by charge spectrum analysis of balloon-borne combined plastic detectors and nuclear emulsions, noting astrophysical implications
09 p1514 A71-22804

Cosmic X ray astronomy by upper atmosphere research vehicles, noting collimators, detectors, high resolution crystal spectrometers and X ray telescopes
09 p1450 A71-22892

Diffuse cosmic X ray observations, discussing balloon and OSO-3 data
09 p1514 A71-22934

Cosmic X ray astronomy, discussing supernova, variable and extragalactic radiation sources, diffuse background radiation and Crab Nebula measurements
09 p1522 A71-22976

Cosmic rays propagation in solar wind, presenting statistical theory of interplanetary magnetic field effect on charged particles transport
09 p1515 A71-23461

Cosmic rays observations, using particle interaction with interstellar gas and magnetic fields
09 p1515 A71-23536

Interplanetary shock waves sounding and geomagnetic storm forecasting based on cosmic ray intensity increases from ground observations
09 p1515 A71-23633

Twenty-seven day variation and cosmic ray intensity modulation relationship, examining 11 year variation from superposition of transient decreases
10 p1660 A71-23800

Cosmic particle gradient perpendicular to solar equator plane and semiannual cosmic ray variations, using worldwide neutron monitor network
10 p1660 A71-23839

Polar cap cosmic radiation intensity measurement for deducing electromagnetic conditions near earth and in interplanetary space
10 p1661 A71-24310

Eleven year cycle cosmic ray modulation mechanism, considering solar wind and interplanetary magnetic field parameters
10 p1662 A71-24472

Atomic hydrogen equilibrium abundance in dense dark hydrogen clouds as function of low energy cosmic ray ionization rate
10 p1662 A71-24491

Cosmic rays produced He, Ne and Ar isotope concentrations in iron meteorite separated phases, using Rudstam spallation model
10 p1676 A71-24506

Soviet papers on elementary particle and cosmic ray physics covering elastic and nonelastic collisions at high and superhigh energies
10 p1662 A71-24665

Nuclear interactions superhigh energy measurements in cosmic particles on high mountain large sandwich assembly
10 p1662 A71-24666

Cerenkov detectors and He filled spark chambers with large interelectrode spaces in high energy nuclear interaction studies, noting cosmic ray applications
10 p1612 A71-24667

Large Cerenkov detectors in absorption spectrometers during high mountain cosmic ray measurements
10 p1612 A71-24668

Interplanetary space low energy cosmic ray protons steady state anisotropy based on radial gradient model of outward convection at solar wind speeds
10 p1663 A71-24777

Electric charge of interacting cosmic ray particles at sea level by experimental arrangement of flash tubes, and scintillation and proportional counters
10 p1664 A71-25043

High energy gamma rays in steady state universe assuming primary cosmic ray spectrum in extragalactic space by simple power law
10 p1664 A71-25045

X ray astronomy, including celestial sources emission, discrete cosmic sources, recording techniques, isotropic background and shielding
10 p1681 A71-25117

Heavy cosmic ray nuclei track counts in plastics, examining Apollo mission 8 and 12 helmets
10 p1665 A71-25121

Fe meteorite Grant, measuring radial distribution of cosmogenic nuclides of K, Ca, Ti, V, Cr and Mn produced by cosmic rays
11 p1819 A71-25224

Cosmic rays visual perception by Apollo astronauts during lunar flight, discussing human eye as Cerenkov radiation detector
11 p1716 A71-25237

Cosmic background radiation ground based measurements at two high altitude sites, using radiometric technique
11 p1815 A71-25300

Very high energy cosmic ray muons, discussing recent experiments with mu-meson anomalous couplings, triplets and intermediate vector bosons
11 p1815 A71-25356

Real and observable radius of roughly dispersed liquid aerosols correlated by electrophotographic method, assessing galactic cosmic rays energy
11 p1815 A71-25582

Relativistic quarks in cosmic rays at sea level and at mountain altitude, estimating production cross section vs absorption mean free path and mass
11 p1815 A71-25589

Cosmic ray intensity diurnal data recorded during maximum and minimum solar activity periods, relating to 27 day and shorter variations
11 p1815 A71-25590

Neutral pion decay and galactic gamma radiation from demodulated cosmic ray spectrum, discussing neutral pion meson production
11 p1815 A71-25593

Meteorological, geomagnetic and extraterrestrial variations of cosmic ray layer electron production rate in lower D region
11 p1816 A71-25610

Galactic cosmic rays solar modulation and intensity gradient in interplanetary space from satellite observation data
11 p1817 A71-25766

Yearly cosmic rays intensity variations in meridional plane from 1955-1969 ionization temperature coefficient recordings as function of solar activity levels
11 p1817 A71-25783

Cosmic ray spallation products and radiation age determination from spectral analysis of noble gas components in lunar rocks
11 p1829 A71-25837

Cosmic ray propagation in interplanetary space, deriving steady state transport equation with energy losses
11 p1817 A71-26172

Line emission in diffuse cosmic X ray continuum, discussing probable interstellar or intergalactic matter source
11 p1817 A71-26317

Baryon isobars average mass data in cosmic ray interactions, using particle angular measurements in backward direction of center mass system
11 p1818 A71-26427

Soviet book on earth radiation belts and cosmic rays covering space-borne experiments, Van Allen belt, charged particle motion, origin hypotheses, etc
11 p1818 A71-26525

Universe UV radiation intensity, estimating inverse Compton effect interaction of cosmic relativistic electrons with relict radiation
12 p1948 A71-27079

Cosmic rays - Conference, La Paz, Bolivia, July 1970, Volume I
12 p1948 A71-27364

Cosmic rays origin from pulsar model with particles accelerated by magnetic dipole radiation, producing equal energy spectrum
12 p1948 A71-27365

- Cosmic rays resonant interaction with hydromagnetic waves, determining turbulent source for confining high energy radiation to Galactic disk
12 p1948 A71-27366
- Cosmic ray diffusion from discrete sources in random galactic location, studying chemical constituents anisotropy and age with scattering model
12 p1948 A71-27367
- Energetic violent explosive events nature and regional characteristics in universe from cosmic radiation composition studies
12 p1948 A71-27368
- X ray and gamma ray astronomy, considering intensity monotonic decline in cosmic electromagnetic spectrum
12 p1949 A71-27369
- Cosmic soft X rays diffuse component dependence on galactic latitude related to interstellar absorption
12 p1949 A71-27370
- Diurnal variability of cosmic ray anisotropy calculated from abnormal, ephemeral or nonlinear density gradients
12 p1949 A71-27373
- Rigidity dependence of Forbush decreases and 11 year variation in cosmic ray intensity at Calgary and Sulphur Mountain and other neutron monitor stations
12 p1949 A71-27374
- Anisotropy during cosmic radiation Forbush decreases modulation mechanism onset
12 p1950 A71-27376
- Cosmic ray particles propagation anisotropies in model magnetosphere, suggesting detection interplanetary medium with geostationary satellites
12 p1950 A71-27377
- Cosmic radiation nucleonic component intensity diurnal variations relation to solar activity semiperiod
12 p1950 A71-27378
- Diurnal solar variation of cosmic radiation observed by two Argentine meson telescopes
12 p1950 A71-27379
- Cosmic ray anisotropies perpendicular to ecliptic plane from underground muon telescopes in New Mexico and Bolivia
12 p1967 A71-27380
- Proton-proton interactions at 70-600 GeV in Echo Lake cosmic ray experiment, discussing multiplicity, prongs, hadron flux and ionization calorimeter
12 p1933 A71-27391
- Unaccompanied hadron vs primary proton spectra in atmosphere and proton-air inelastic cross sections above 500 GeV from cosmic ray measurements
12 p1951 A71-27394
- Cosmic ray neutrino results from deep underground detector near Johannesburg
12 p1952 A71-27399
- Zenith angle distribution of atmospheric muons at Mt. Chalcaltaya, considering differential intensity of cosmic ray mesons and horizontally incident cosmic rays
12 p1952 A71-27400
- Momentum spectra of cosmic ray particles at sea level, using magnetic spark chamber spectrograph and ionization calorimeter
12 p1952 A71-27402
- Cosmic ray muon flux at sea level, allowing for showers, multiple scattering, straggling, zigzag motion, detector efficiency and electronic equipment dead time
12 p1952 A71-27403
- Underground cosmic ray particles flux and nuclear interaction properties, determining integral sea level energy spectrum as function of range of particles in rock
12 p1953 A71-27407
- Lunar samples mineralogy, petrology and geochemistry, considering lunar surface processes, cosmic ray flux and solar wind
12 p1967 A71-27414
- Pulsar electrodynamics, considering oblique rotator with dense magnetosphere to supply particles for Gunn-Ostriker mechanism
12 p1968 A71-27539
- Cosmic radio waves scattering in outer solar corona, considering refraction and gradients in electron density fluctuations
12 p1970 A71-27706
- Satellite-borne anisotropy and energy spectra measurement instruments for cosmic ray electrons and protons and solar and galactic X-rays
12 p1954 A71-27711
- Differential energy spectrum of cosmic ray deuterium flux of galactic origin from IMP 5 satellite measurements
13 p2120 A71-27974
- High energy sea level cosmic ray neutrons energy spectra, noting angular distribution about zenith and attenuation length in atmosphere
13 p2120 A71-28050
- High energy cosmic ray components, investigating tracks and trapped magnetic monopoles
13 p2120 A71-28051
- Quarks search in cosmic rays at sea level and mountain altitude, using telescope with plastic scintillation counters and wire spark chambers
13 p2121 A71-28055
- Cosmic ray jet interaction with free or quasi-free nucleons, obtaining kinematic measurement, secondary particle composition and transverse momentum
13 p2121 A71-28058
- Cosmic ray components atmospheric diffusion and production based on H quantum, two fireball and aleph model
13 p2122 A71-28064
- Atmospheric very high energy cosmic ray propagation by three dimensional Monte Carlo simulation, employing H quantum and fireball models for multiple meson production
13 p2122 A71-28065
- Cosmic hadron flux measurements and energy spectra at various altitudes in atmosphere, using calorimeters
13 p2122 A71-28066
- Mass spectrum of stopping heavy cosmic ray particles at sea level observed, interpreting flux as deuteron production by high energy protons and neutrons
13 p2122 A71-28067
- Extensive cosmic rays high and low frequency radio pulses investigation, using plastic scintillator triggered receivers
13 p2127 A71-28107
- Primary component corrections for global cosmic ray variations from latitudinal expeditions, discussing method adaptation to computer
13 p2128 A71-28528
- Cosmic ray density distribution inside modulating spherical cone over long-lived solar wind regions, noting modulation depth quasi-periodic variation
13 p2129 A71-28550
- Cosmic ray energetic spectrum variation from observed latitudinal effects during 1954-1962 solar activity cycle
13 p2129 A71-28551
- Cosmic rays galactic component intensity observed on earth correlated with solar phenomena
13 p2130 A71-29061
- Cosmic ray microvariations during thunderstorm perturbations, considering total ionizing, soft and hard components and local temperature effect
13 p2130 A71-29124
- Astronaut protection from solar flare high energy protons, discussing spacesuit, spacecraft orientation and solid, electrostatic, magnetic and plasma shielding
13 p2021 A71-29252
- Cosmic X ray background observations, using rocket-borne proportional counter
13 p2131 A71-29269
- Galactic IR background emission mechanisms, considering electrons, protons and cosmic rays role
13 p2131 A71-29272
- Pulsar cosmic rays emission mechanisms, noting high energy particle, X and gamma rays direction
13 p2131 A71-29298
- Galactic cosmic ray intensity solar diurnal and semidiurnal variations outside magnetosphere
13 p2131 A71-29437
- Temperature effects on cosmic rays muon component variations during cold fronts passage
13 p2131 A71-29485
- Diurnal correlation between cosmic ray meson intensity and atmospheric ozone content on magnetically undisturbed days
14 p2231 A71-29723
- Magnetic cutoff variations during geomagnetic storm from counting rates of neutron monitors, noting cosmic ray intensity augmentation
14 p2298 A71-29748
- Lattice defect mechanism for high coercive force remanence production in meteorites and lunar samples by cosmic ray exposure
14 p2308 A71-29913
- Cosmic ray neutron diurnal variation phases and amplitudes from harmonic analysis of directional intensity
14 p2299 A71-29987
- Solar equatorial plane interplanetary plasma and magnetic field features from cosmic ray variation anomaly observation
14 p2299 A71-29988
- Galactic cosmic ray transport equation numerical solution for interplanetary region, considering modulation, diffusion, convection and energy loss effects
14 p2301 A71-30387
- Cosmic rays compound diffusion, considering combined effects of one dimensional diffusion along interstellar magnetic field lines and field lines three dimensional random walk
14 p2301 A71-30434
- Cosmic gamma ray background flux for photon energies greater than 100 MeV, considering Compton collisions
14 p2301 A71-30435
- Balloon-borne transistorized stratospheric cosmic ray probe, describing simultaneous gas discharge and dual coincidence telescope counters data transmission
14 p2247 A71-30596
- Cosmic ray telescopes with scintillation and Cerenkov counters for 2 to 8 BeV energy range, describing structural details and operational specifications
14 p2247 A71-30597
- Large volume Cerenkov detector design for cosmic ray energy total absorption spectrometer measurements
14 p2247 A71-30599
- High energy cosmic muons momentum spectrum and charge ratio measurements at large zenith angles, describing magnetic spectrometer
14 p2247 A71-30601
- Cosmic ray nucleon-meson and barometric pressure data continuous recording equipment, comparing system to conventional instruments
14 p2248 A71-30602
- Interstellar gas heating by soft X rays and cosmic rays for electron production, calculating heating rate with Boltzmann equation and Monte Carlo method
14 p2302 A71-30642
- Stellar and interstellar magnetic fields effects on plasma instabilities in Colgate cosmic ray model, using computer simulation
14 p2282 A71-30644
- Cosmic ray modulation by solar wind, developing model with time variations based on magnetic bending power
14 p2302 A71-30647
- Radiometric errors in cosmic background radiation measurement
14 p2204 A71-30970
- Nuclear soft core potential reproduction by isoscalar vector meson in nonlocal field theory of fireball in high energy cosmic ray collisions
15 p2472 A71-31151
- Soviet book on cosmic muons and neutrinos covering anomalous and weak interactions
15 p2472 A71-31287
- Chronic and acute gamma irradiation facilities used in animal experiments simulating steady cosmic radiation and powerful solar flare radiation expected in prolonged space flight
15 p2357 A71-31313
- Cosmic radiation doses measurement on Soyuz 3 spacecraft by nuclear emulsions, giving averaged doses absorbed by various cosmonaut tissues
15 p2362 A71-31314
- Systematic phase variation in second harmonic of daily variation of cosmic ray intensity in one year, recorded by neutron monitor at Deep River
15 p2441 A71-31410
- Cosmic ray particles acceleration in pulsar strong electromagnetic fields, investigating refractive index effects
15 p2473 A71-31717
- Galactic cosmic rays electron density, discussing incompatibility of local data estimates with galactic radio background
15 p2473 A71-31721
- Atmospheric cosmic ray propagation based on phenomenological model of hadron-nucleus collisions, predicting sea level nucleon, pion and muon energy spectra and ionization profile
15 p2474 A71-31732
- Cosmic ray secondary background of balloon-borne X ray scintillation astronomical telescopes for equatorial latitudes with reference to shutter technique and NaI/Tl crystal
15 p2406 A71-31751
- Cosmic rays - Conference, Budapest, August 1969, Volume 4, Muons and neutrinos techniques
15 p2474 A71-31776
- Cosmic ray mean intensity drop observation after Forbush decrease, noting rigidity dependence and daily variation from exponential recovery curve
15 p2474 A71-31777
- Energy dependence of cosmic ray muon charge ratio at large zenith angles, using large aperture and high resolution cosmic ray momentum spectrograph
15 p2475 A71-31779
- High energy muons production by cosmic rays, discussing advantages of moon based experiments over earth surface measurements
15 p2475 A71-31780
- Cosmic ray muon intensity measurements in water at large depths by Cerenkov counter
15 p2475 A71-31781
- Momentum spectrum measurement of cosmic ray muons, recording particle trajectories photographically
15 p2475 A71-31783
- Low energy muon production by neutral components of cosmic radiation at sea level, noting correlation with sidereal time
15 p2475 A71-31785
- High energy penetrating component of cosmic radiation at mountain level recorded in underground ionization calorimeter, showing muon production in vertical and horizontal direction
15 p2476 A71-31787
- Anomalous cosmic ray muon interactions at very high energies, using zenith angle distribution data at sea level and deep underground
15 p2476 A71-31791
- Vertical intensity of cosmic ray muons in Mont Blanc tunnel, describing apparatus and experimental site
15 p2477 A71-31795

Vertical intensity and angular distribution of cosmic ray muons from observations using scintillator neon flash tube telescopes at three depths

15 p2477 A71-31796

Sidereal anisotropy in muon signal observed by cosmic ray telescope above sea level, indicating production by neutral particle and leakage relative to anticoincidence factor

15 p2477 A71-31797

Muonic trident production by cosmic ray muons, using quantum electrodynamics methods

15 p2477 A71-31798

Cosmic ray muon-neutrinos sea level energy spectra at low energies for horizontal and vertical directions, estimating geomagnetic cut-off effects for various geomagnetic latitudes

15 p2477 A71-31799

Cosmic ray muon and neutrino measurements with deep underground scintillation detector array

15 p2477 A71-31800

Cosmic ray rigidities spectra measurements above geomagnetic cutoff using balloon-borne emulsion plates in superconducting magnet field

15 p2407 A71-31805

Cosmic ray intensities investigation by worldwide neutron- and supermonitors network, obtaining density and three dimensional current values

15 p2478 A71-31807

Cosmic ray measurements at various altitudes, describing magnet spectrograph for momentum spectra and particle identification

15 p2408 A71-31813

Proportional counters design for ionizing radiation detection, examining cosmic ray meson component

15 p2408 A71-31814

High energy cosmic gamma ray point sources identification near galactic plane from balloon flights data

15 p2478 A71-31826

Isotropic cosmic gamma ray flux, discussing extragalactic point sources detection by high resolution spectrometers

15 p2478 A71-31837

Cosmic rays neutron spectrum at sea level, using charge exchange reaction

15 p2479 A71-31867

Cosmic ray gradient perpendicular to solar equator plane related to coronal intensity

15 p2479 A71-31906

Cosmic ray high energy pion and nucleon nuclear interaction observations, determining statistical fluctuations in secondary particles angular distribution

15 p2479 A71-32076

Cosmic ray intensity gradient measurement from Lost City meteorite Ar 37/Ar 39 ratio

15 p2479 A71-32361

Lost City meteorite Ar isotopes radioactivity measurements, considering cosmic ray flux radial gradient variations during meteoroid orbit

15 p2479 A71-32364

Cosmic ray flux diurnal variation from radial number density gradient, showing Forbush decrease profiles strong dependence on shock radial approach velocity

15 p2480 A71-32755

Diffuse low energy cosmic X rays rocket measurements, noting excess over extrapolated power law valid for higher energies

15 p2480 A71-32761

Cosmic ray modulation by angle dependent solar wind, detailing adiabatic deceleration and radial anisotropy effects

15 p2481 A71-32777

Cosmic ray annual intensity variations indicating gradient perpendicular to solar equatorial plane

16 p2625 A71-32801

Plasma instabilities effectiveness for high energy cosmic rays confinement in galactic disk

16 p2625 A71-33238

Magnetic stars as cosmic ray generators, considering interstellar gas particle acceleration by EM forces produced by rotating stellar magnetic field

16 p2625 A71-33324

Cosmic ray nuclei propagation through interstellar medium, solving transfer equation for simple model with allowance for boundary conditions

16 p2625 A71-33325

Extragalactic cosmic X ray sources at high galactic latitude from sounding rocket experiments, correlating with galactic clusters

16 p2626 A71-33357

Cosmic rays lifetime in Galaxy in presence of particle acceleration in interstellar space

16 p2626 A71-33463

Cosmic and telluric radiation biological effects on parameria, discussing relationship between dosage and growth rate

16 p2532 A71-33757

Netherlands space research including solar, stellar and cosmic radiation observations, photometry and satellite geodesy

16 p2666 A71-33858

Report to COSPAR on French space program covering ionosphere and magnetosphere physics, meteorology, cosmic rays and earth resources

16 p2666 A71-33861

West German space research activities during 1970 on meteorology, ionospheric physics, solar radiation, cosmic rays and life sciences

16 p2666 A71-33866

Solar modulation origin of sidereal diurnal variation in cosmic ray intensity anisotropies as function of interplanetary field direction, using underground muon telescopes

16 p2628 A71-33931

Solar wind modulation effects on galactic protons and cosmic rays, using radial magnetic field mathematical model and Monte Carlo method

17 p2795 A71-34373

Cosmic radiation and gas retention ages of Chassigny achondrite by measuring Al, K and noble gases contents and production rates in meteorites

17 p2800 A71-34514

Deep underground cosmic ray neutrinos interaction experiments, discussing particle motion, inelastic cross section variation, energy, mass and celestial coordinates

17 p2795 A71-34665

Underground search for cosmic ray neutrino interaction products, observing muon products

17 p2795 A71-34666

Collimated nuclear interactions induced by cosmic ray pions and nucleons in carbon and brass, noting energy dependence of events production frequency

17 p2796 A71-34858

Calculation method for zenith and azimuth directional sensitivity characteristics of cylindrical cosmic ray telescopes with circular recording surfaces

17 p2746 A71-35650

Cosmic ray muons energy loss rate measurement in Fe using Durham magnetic spectrograph

18 p2957 A71-35930

Neutron star cooling behavior models based on neutrino emission theory, explaining galactic steady state cosmic rays and pulsar radiation

18 p2959 A71-35931

Cosmic ray injection by clusters of dense magnetic neutron stars, giving particle number for Galaxy

18 p2957 A71-35962

Papers on elementary particle and cosmic ray physics, covering neutron monitor, fireball models, radio pulses and X ray astronomy

18 p2957 A71-36209

Cosmic X ray astronomy by rocket and balloon soundings and discrete emission source measurements, considering energy spectra

18 p2957 A71-36212

German monograph on evaporation neutrons mean multiplicity for cosmic radiation energy spectrum variations measurement

18 p2958 A71-36670

Excess intensities of diffuse cosmic X rays related to characteristic line spectrum excitation and element abundances in interstellar region and nebulas

18 p2958 A71-36761

Polarization measurement of cosmic ray muons at sea level as function of energy and zenith angle

19 p3124 A71-37284

Heavily ionized particles search at sea level for magnetic monopoles existence evidence in highest energy cosmic rays

19 p3124 A71-37285

Cosmic ray nuclear interactions in 10-300 GeV energy range, using balloon-borne emulsion target, spark chambers and ionization spectrometer

19 p3124 A71-37286

Near sea level cosmic ray high energy interactions from data recorded by interleaved stack of cloud and ionization chambers and carbon and iron plates

19 p3124 A71-37287

Apollo astronauts light flashes observation during lunar flight, discussing interpretation as scintillations in eye lens by multiply charged cosmic rays focusing on retina

19 p3001 A71-37299

Median primary energy of underground muon telescopes response as function of depth, studying sidereal daily variation of cosmic rays

19 p3125 A71-37370

Universe UV radiation intensity, estimating inverse Compton effect interaction of cosmic relativistic electrons with relict radiation

19 p3126 A71-37429

Cosmic rays sidereal diurnal variations, considering interplanetary magnetic field shielding effect

19 p3127 A71-37803

Cosmic rays and solar energetic particles properties near earth and requirements on measurement during outer planets missions

19 p3127 A71-37940

Cosmic ray spectrum at nonrelativistic energy region, noting ionization loss effects

19 p3129 A71-38359

Atmospheric temperature effect on solar diurnal variation of muon component, considering asymptotic characteristics of cosmic ray anisotropy

19 p3129 A71-38378

Atmospheric neutron production by cosmic rays, calculating cadmium-indium ratio

19 p3066 A71-38379

Visual sensations produced by cosmic ray muons passing in different directions through human eyes and head

19 p3005 A71-38677

Forbush decreases comparison with 11 year cosmic ray intensity variation, examining rigidity dependence and modulation functions

20 p3277 A71-38742

Horizontal cosmic ray muon component intensity measurement and time studies for solar and sidereal variations

20 p3277 A71-38839

Milky Way galaxy poloidal magnetic field generation with hydromagnetic dynamos, showing galactic cosmic rays as major driving force

20 p3287 A71-39056

Outer space and earth surface galactic cosmic ray intensity data correlation analysis for studying interplanetary magnetic field structure

20 p3278 A71-39129

Galactic cosmic rays interaction with interplanetary magnetic field from Venera 4 measurements of June-October 1967

20 p3280 A71-39595

Galactic cosmic ray propagation earth-source distance determination by observing charge spectrum

20 p3280 A71-39598

Gamma radiation due to cosmic rays interaction with Mars surface/atmosphere and natural radioactive rocks elements decay, calculating intensity and spectral composition

20 p3280 A71-39630

Galactic cosmic ray effects on interplanetary dust particles erosion and spurious counts in micrometeoroid sensors, microphones and capacitor detectors

20 p3280 A71-39635

Galactic cosmic rays and interplanetary magnetic field flux measurements onboard Venera 4 space probe, noting lack of correspondence with Forbush decrease

20 p3282 A71-39737

Cosmic rays cutoff daily variations at ATS geostationary satellite altitude, noting role of magnetospheric tail in lowering cutoff below calculated value

20 p3282 A71-39739

Cosmic soft X ray detection by proportional counters with thin polypropylene windows onboard sounding rocket, considering galactic emission possibility

20 p3283 A71-39750

Diffuse background 0.1-1 MeV gamma ray component observed by balloon-borne counter system, finding no positive evidence for cosmic component existence

20 p3283 A71-39752

Cosmic ray variations due to atmospheric pressure disturbances and ionizing component variations due to temperature effects, estimating ground observation errors

21 p3437 A71-40074

Book on cosmic gamma rays covering secondary particle decay, electron-positron annihilation, proton-antiproton interactions, galactic radiation and cosmology

21 p3438 A71-40450

Cosmic X and gamma radiation, discussing galactic and extragalactic sources, generation processes and spectrometric characteristics

21 p3438 A71-40522

Absolute measurement of vertical cosmic ray muon intensity at 3-50 GeV/c, using solid iron magnetic spectroscopy

21 p3438 A71-40587

Spectrum and galactic isotropy of diffuse cosmic X rays by balloon-borne detector

21 p3438 A71-40605

Fireball identification method in accelerator and cosmic ray produced jets, considering model improvement for Lorentz factor determination

21 p3439 A71-41396

Galactic cosmic rays solar modulation and particle intensity gradient in interplanetary space from satellite observation data

22 p3591 A71-41534

Yearly cosmic rays intensity variations in meridional plane from 1955-1969 ionization temperature coefficient recordings as function of solar activity levels

22 p3591 A71-41551

Diffuse 0.2-2 keV cosmic X ray flux, discussing energy spectrum and spatial distribution

22 p3591 A71-41914

Cosmic ray transport in random magnetic fields, deriving coupled integrodifferential equations for radiant intensity and flux

22 p3592 A71-41915

Cosmic soft X rays in energy range 0.14-7 keV from rocket soundings with thin polypropylene window proportional counters, covering field of view in Cygnus-Cassiopeia region

22 p3593 A71-42330

Direct observation of cosmic ray kinetic energy losses in interplanetary region by measurements at separated spacecraft

22 p3593 A71-42331

Cosmic ray muons absolute intensity determination, using Durham vertical spectrograph

22 p3593 A71-42353

Cosmic ray muon electromagnetic interactions and energy spectrum measurements at large zenith angles at sea level

22 p3593 A71-42356

Cosmic rays origin, discussing nuclear, electron and electromagnetic components, supernovae, pulsars, white dwarfs and gas motions in Galactic Center

22 p3594 A71-42550

Cosmic ray physics - Conference, Leningrad, October 1969

22 p3594 A71-42633

Proton 4 satellite high and superhigh energy cosmic ray spectrometer, discussing operational principles and parameters

22 p3594 A71-42634

Strong cosmic ray interactions and meson production in accelerators

22 p3594 A71-42636

Nuclear cascade pion energies in heavy material by Monte Carlo method, concerning cosmic ray and particle accelerator interactions

22 p3579 A71-42643

High energy cosmic particle interactions with LiH target, discussing relation between longitudinal and transverse momenta of generated pions

22 p3594 A71-42645

Charged particles momenta and spatial arrangement during cosmic ray particles nuclear interactions, describing recording equipment

22 p3594 A71-42646

Nuclear interactions of neutral cosmic particles with carbon target at mountain altitudes

22 p3595 A71-42649

Energy spectra of ionization bursts, electromagnetic cascades and nuclear active particles at mountain altitude

22 p3595 A71-42651

Cosmic rays intensity measurement in deep ocean with Cerenkov counter, determining muon energy spectrum and absorption in sea water

22 p3595 A71-42663

Bremsstrahlung photons produced by cosmic ray muons in Fe and Pb at sea level, calculating energy spectra and angular distributions

22 p3595 A71-42664

Cosmic radiation heavy nuclei intensity and composition measurement, treating nuclear emulsions in calcium bromide solutions

22 p3596 A71-42733

Large area parallel-plate pulse ionization chamber for high altitude balloon measurements of relativistic cosmic ray heavy nuclei

22 p3550 A71-42887

F, Na and Al origin in galactic cosmic radiation, investigating production as spallation fragments and generation in source

23 p3719 A71-42943

Solar modulation of relativistic cosmic ray particles, noting step-like changes and rigidity dependence

23 p3719 A71-42948

Cosmic ray sidereal time period, using neutron monitors, meson telescope and various ion chambers

23 p3719 A71-43126

Cosmic ray solar diurnal variation anomaly at 1954 minimum, discussing diffusion and scattering in interplanetary medium

23 p3720 A71-43136

Solar soft X-rays scattering in upper atmosphere, providing background against cosmic X rays

23 p3721 A71-43363

Cosmic ray exposure ages and rare gas concentration profiles in Apollo 12 lunar rocks, discussing spallation products and neutron capture effects

23 p3753 A71-43719

Microprobe measurements of rare gas composition for lunar rock 12013, 10, 31 mineral separates, noting cosmic ray bombardment role in K and Ar production

23 p3753 A71-43721

Apollo 11 and 12 lunar samples history of irradiation exposure to galactic cosmic rays and solar wind, using rare gas and Gd isotope measurements

23 p3754 A71-43724

High resolution time averaged energy spectrum and chemical composition of iron group cosmic ray nuclei from fossil tracks in Apollo 12 lunar rocks

23 p3764 A71-43804

Ultraheavy cosmic ray nuclei existence inferred from Apollo 12 lunar rock pigeonite crystal track length distribution

23 p3765 A71-43805

Cosmic X ray astronomy, considering discrete sources and isotropic background X radiation

23 p3768 A71-43863

Absolute vertical intensity measurement of cosmic ray muon energy spectrum at sea level, presenting spark chamber and absorption spectrograph data

23 p3722 A71-43876

Diffuse cosmic X rays small scale structure, comparing Wolfe-Burbridge theoretical autocorrelation functions for galaxies clusters and superclusters with experimental value

23 p3722 A71-44013

Cosmic ray dosimetric monitoring in manned spacecraft, discussing ionization, thermoluminescent and nuclear photoemulsion methods of radiation measurement

24 p3826 A71-44888

Manned spacecraft radiation protection against cosmic rays, considering proton attenuation in shielding materials and dose formation in body tissues

24 p3801 A71-44889

Cosmic ray biological effects and admissible dose level normalization in space flight from prolonged tests on dogs

24 p3798 A71-44890

High energy charged particles angular distribution measurements in equatorial region cosmic radiation above atmosphere, using Proton 2 satellite data

24 p3866 A71-45027

COSMOGONY

U COSMOLOGY

COSMOLOGY

Magnetic field generation during radiation era, discussing generating mechanism by angular momentum transfer between ion and electron-photon gases in expanding plasma

01 p0148 A71-10024

Linear MHD theory of inhomogeneities in axisymmetric models of universe with cosmological magnetic field

01 p0160 A71-11093

Galaxies dynamic parameters formation associated with cosmological turbulence in expanding hot universe

02 p0307 A71-12085

Cosmological models with noninteracting matter and radiation, deriving red shift and luminosity-distance relationship

02 p0312 A71-12464

Mean cosmic density determinations, obtaining field galaxy luminosity function moments with red shift catalogs

02 p0313 A71-12499

Relativistic cosmology with singular point, using oscillatory model for Einstein equations general solution with time related physical singularity

02 p0285 A71-12527

Electron charge dependence on universe age, considering possible gravitational constant dependence on time

02 p0313 A71-12547

Cosmological models with matter and radiation for evolution of universe

03 p0484 A71-13206

Galaxies pairs motions, considering disintegrating, rotational and oscillatory types for comparison with observational data

03 p0484 A71-13207

Galaxy clusters stabilization by cosmological constant, considering clusters mass discrepancy

03 p0489 A71-13561

Stellar origin and evolution, discussing interstellar gas heating and condensation, star cluster formation and superdense body decay

04 p0642 A71-14774

Friedman universe model in centrally symmetric reading system

04 p0644 A71-15123

Galactic magnetic field characteristics and cosmic rays origin, discussing gas clumping and star formation

04 p0641 A71-15758

Galaxies and universe evolution, discussing expansion, isotropic black body radiation, present matter distribution, radio source population density and galactic nuclei instability

04 p0661 A71-15895

Physical and geometrical properties of dust filled universes, using left invariant metrics compatible with Einstein equations

05 p0773 A71-15925

Expanding universe adiabatic density fluctuation evolution, describing photon distribution function collision equation for plasma recombination

05 p0801 A71-15929

Primeval intergalactic magnetic field existence, observing radio sources rotation distribution and red shift

05 p0805 A71-16108

Electromagnetic wave absorption in steady state cosmology, considering particle collision and radiation damping effects in plasma model

05 p0806 A71-16167

Electromagnetic wave absorption in Einstein-de Sitter cosmology, considering collision and radiation damping effects for radiated angular frequencies

05 p0806 A71-16168

Vacuum-like state of physical medium as initial state of Friedmann cosmology, noting fluctuation instability for conversion into ordinary matter

05 p0806 A71-16180

Expanding universe magnetic field origin, examining Batchelor condition for spontaneous appearance in turbulent conducting fluid motion

05 p0809 A71-16470

Galaxy cluster expansion theory, noting dispersion in radial velocities of members

05 p0812 A71-16694

Closed evolving universe by vanishing pressure, considering eight different models including three cyclic models

05 p0813 A71-16811

Black hole model for gravitational collapse of universe according to Einstein theory

05 p0813 A71-16956

World models with antipoles for deriving cosmological density parameter upper bound

05 p0814 A71-17092

Quasi-stellar radio sources similarity to pulsars based on similar characteristics

05 p0814 A71-17235

NonMarkoffian kinetic theory for hierarchical structure of clusters in expanding universe

06 p0964 A71-17314

Elliptical and spiral galactic angular momentum and velocity dispersion relations, considering cosmological turbulence during formation

06 p0971 A71-18244

Interstellar grain formation relation with stellar evolution in terms of density wave theory of spiral structure origin

06 p0973 A71-18339

Perturbation growth in free particle expanding Universe with critical density, considering Newton gravitation theory

06 p0974 A71-18427

Light propagation in mixmaster universe model based on Einstein equations solution

06 p0974 A71-18428

Time variable physical singularity in general relativistic cosmological solution of gravitation equations, constructing simplified models

07 p1191 A71-19173

Particle production near Kasner singularity in anisotropic cosmological model

07 p1162 A71-19217

Vortex perturbations in Friedman cosmological model near zero time, showing perturbation growth associated with increasing Hubble expansion anisotropy

07 p1192 A71-19285

Cosmological plasma physics, considering matter, antimatter, electrodynamics, ambiplasma, annihilation and heavy nuclei

07 p1196 A71-19649

Homogeneous cosmological models evolution theory, considering Einstein equations analytic solution for lengthy era

07 p1204 A71-20536

Homogeneous Newtonian cosmological model, constructing ellipsoidal velocity distributions and kinetic theory

08 p1358 A71-20932

Newtonian big bang hierarchical cosmological model, considering mean mass density dependence on volume position and size dependence on cluster order

08 p1358 A71-20933

Galaxies dynamic parameters formation associated with cosmological turbulence in expanding hot universe

08 p1362 A71-21135

Static cylindrically symmetric universes consisting of Einstein-Maxwell gravitational and electromagnetic fields, discussing central axial mass and charge or current density

08 p1334 A71-21361

Anisotropic homogeneous cosmological model, discussing origin of movement and primordial matter chemical composition

08 p1365 A71-21771

Interstellar dust density, constructing cosmological model with gravitational equations

08 p1366 A71-21785

Universe models topology, examining relation between CT and CP invariance

08 p1366 A71-21786

Linear MHD theory of inhomogeneities in axisymmetric models of universe with cosmological magnetic field

08 p1366 A71-21951

Mean luminous cosmic matter density calculations, using galaxy counts and mass data eliminating luminosity functions

09 p1516 A71-22060

Field galaxy cosmological reddening from red shift data at faint magnitudes

09 p1516 A71-22063

Galaxy chemical evolution, discussing stellar mass loss, supernova explosions, white dwarf formations, nucleosynthesis, cosmochemistry, etc

09 p1521 A71-22869

Cosmological evolution in radio galaxies, discussing stellar populations, optical luminosity, model choice, red shift uncertainties, etc

09 p1522 A71-22974

Critique on Mach principle, discussing incompatibility between system inertia in universe and general relativity theory

09 p1522 A71-22980

Homogeneous isotropic relativistic cosmological model of universe, discussing construction

09 p1523 A71-23020

Gravitational stresses derived for Friedmann-Lobachevskii and Schwarzschild spaces

09 p1495 A71-23270

Hot universe model, discussing small scale entropy, matter distribution, adiabatic density perturbations, energy balance, formation of galactic clusters, galaxies, globular clusters and quasars

09 p1527 A71-23531

Media resistance effects on three body problem three dimensional periodic orbits, discussing implications to solar system formation from surrounding nebula

09 p1527 A71-23534

Matter and antimatter separation mechanism in universe based on thermal radiation thermodynamic properties

10 p1665 A71-23739

Gravitational instability of nonhomogeneous cosmological model, establishing density perturbation growth as function of time for model containing matter and radiation

10 p1667 A71-23851

Nonhomogeneous cosmological model with equations describing universe relative density variation, demonstrating thermal instability role in galaxies formation

10 p1667 A71-23856

General relativity theory applicability limits for strong gravitational fields and near singularities in cosmology

10 p1668 A71-24002

Astronomy contributions to cosmology, considering universe nature, origin and evolution

10 p1668 A71-24004

Entropy-free thermodynamics second law based on universe expansion, using homogeneous nonstatic cosmological models

10 p1674 A71-24468

Radiation and gas-dust interactions, examining dispersion relation and instability for cosmological models

10 p1675 A71-24490

Cosmological enhancement of density perturbations and amplitude variation of acoustic and gravitational waves in anisotropic homogeneous universe

10 p1678 A71-24886

Debye-Huckel gravitational potential in Lemaître universe

10 p1680 A71-25019

High energy gamma rays in steady state universe assuming primary cosmic ray spectrum in extragalactic space by simple power law

10 p1664 A71-25045

Infinite universe compatibility with gravity potential satisfying Poisson equation, avoiding cosmological difficulties by universal gravitational field sources and sinks introduction

10 p1681 A71-25074

Relativity - Conference, Cincinnati, June 1969

11 p1798 A71-25279

Gravitational instability picture for galactic rotation, examining numerical model for protogalaxy separation in expanding universe

11 p1820 A71-25535

Astrophysical states of matter and phenomena at extreme temperatures and densities, discussing stellar evolution, terminal states of stars, superdense stellar matter, neutron stars, etc

11 p1828 A71-25734

Thermodynamic, electrodynamic and cosmological time asymmetry, discussing arrow-of-time concept as fundamental to physical space/time relationships

11 p1828 A71-25735

Cosmic evolution and thermodynamic irreversibility, discussing definitions and relationships of thermodynamic, historical and cosmological arrows of time

11 p1828 A71-25736

Theory of originally cool moon in light of Apollo evidence regarding lunar rocks composition, mascons and lunar topology

11 p1834 A71-26379

Perturbation growth in free particle expanding universe with critical density, considering Newton gravitation theory

12 p1954 A71-26577

Light propagation in mixmaster universe model based on Einstein equations solution

12 p1955 A71-26578

Quasar evolution, considering cosmological red shifts

12 p1958 A71-26695

Venus retrograde rotation, showing consistency with Laplacian theory of cosmology and Fesenko theory

12 p1961 A71-26901

Hercules galaxies cluster rotation, determining radial velocities, axis position angle and center position

12 p1962 A71-26911

Homogeneous isotropic zero-pressure cosmological problem of gravitational field solved in Jordan-Dicke equations framework

12 p1963 A71-27030

Gravitational field quantum fluctuations role in general theory of relativity and cosmological model

12 p1965 A71-27179

Statistical space density and velocity perturbations of galaxies relative to origin of rotation in range of Friedman cosmological model

12 p1966 A71-27235

Universe global structure and quasar frequency distribution based on red shifts and cosmological interpretations

12 p1968 A71-27642

Hydrodynamic model of coalescing meteors substantiating cosmogonic Laplace-Schmidt hypotheses of solar system planetary formation from cosmic dust

13 p2131 A71-27892

Expanding metagalaxy closed model with changing gravitational constant, noting matter motion in moving and central reference systems

13 p2136 A71-28423

Early isotropic universe structure evolution, considering non-Friedmannian cosmic expansion stage, metagalactic turbulence and cosmological models

13 p2141 A71-29101

Galactic structure and spectra, examining universe expansion, Hubble law and quasar distances

13 p2142 A71-29129

Strong gravitational wave bursts in galaxy, suggesting collapsed relativistic body cluster burning gravitational potential energy

13 p2142 A71-29137

Spatial variations in cosmic He abundance attributed to primordial temperature fluctuations at early epochs in Friedmann universe

14 p2303 A71-29587

Cosmological models for creation of hierarchy of clusters within clusters, involving gravitational interactions

14 p2303 A71-29588

Very low mass gravitationally collapsed objects, formed as fluctuation effects in early universe

14 p2307 A71-29865

Space research goals emphasizing solar system formation, and plasma physics and chemistry

14 p2310 A71-30197

Submillimeter background radiation origin possibility from extragalactic discrete sources based on cosmological models

15 p2478 A71-31828

Electron charge dependence on universe age, considering possible gravitational constant dependence on time

15 p2494 A71-32503

Anisotropic homogeneous cosmological model, discussing mass motion origin and primordial matter chemical composition

15 p2495 A71-32676

Galaxy formation in expanding universe, discussing primordial plasma and photon gas turbulent medium for magnetic field amplification by dynamo mechanism

16 p2625 A71-33052

Galaxy formation by weak and strong primeval turbulence in relation to velocity and density perturbation

16 p2631 A71-33232

Lower limit on size of matter and antimatter regions in vanishing baryon number cosmology based on homogeneous intergalactic magnetic field existence

16 p2632 A71-33237

Relativistic cosmological models with nonzero pressure, considering matter as perfect gas-radiation mixture and isotropic/homogeneous three space

16 p2611 A71-33274

Einstein field equations solution for universe filled with perfect fluid of position-dependent density

16 p2611 A71-33277

Cosmological implications of microscopic charge-parity violation, considering redefinition of matter and antimatter in time-inverted expansion

16 p2611 A71-33278

Scientific cosmology principles, considering distant galaxies red shift and galactic evolution

16 p2611 A71-33279

Gravitation phenomena based on uniformly expanding universe cosmological model for acceleration field

16 p2612 A71-33281

Nonlinear correction in Lagrangian density of gravitational field, deriving dusty cosmological model with no singularity

16 p2638 A71-33546

Universe models topology, examining relation between CT and CP invariance

16 p2638 A71-33547

Fourth order differential gravitational field equations for non-Einsteinian cosmological model, considering linearly expanding universe

17 p2801 A71-34634

Cosmological upper limit on gravitational constant time variation, extending Dicke theoretical bound to pressure filled cosmologies in flat space

17 p2801 A71-34651

Cosmological singularity, considering homogeneous Newtonian universes expanding or contracting with shear and rotation

17 p2806 A71-35382

Nonstatic model of universe based on Newtonian cosmology, considering central body effects on interstellar dust motion

17 p2809 A71-35600

Density and luminosity evolution of radio source population, considering counts per unit co-moving volume at cosmological epochs

18 p2961 A71-35966

Polynomial Hamiltonian for type VIII and IX vacuum cosmologies, suggesting quantized versions involving fluctuations of 3-space signature and topology

18 p2946 A71-35983

Space transport systems, discussing spaceship earth survival problem from cosmospic criteria

19 p3149 A71-37304

Bianchi type IX universe homogeneous cosmological model, noting oscillatory evolution near singularity and rotating axes of alternating Kaser epochs

19 p3138 A71-37851

Homogeneous isotropic universe, analyzing cosmological solutions with linear theory of gravitation

19 p3104 A71-38191

Empirical dimensionless ratios between universal physical constants, supporting steady cosmological expanding universe model

19 p3145 A71-38543

Mass of virtual particle responsible for gravitation of vacuum and expansion of universe, considering correspondence to red shift in quasar spectra

19 p3146 A71-38644

Critique of cosmological theories based on spontaneous matter creation in strong gravitational fields, deriving particles discrete number constancy in general relativity

20 p3268 A71-38834

IAU Executive Committee, General Assembly and commissions reports on astronomy, including manuscripts preparation guidelines, handbook, etc

20 p3315 A71-39425

Brans-Dicke cosmologies in arbitrary units, deriving power law solutions in flat Friedmann space

20 p3294 A71-39557

Exact solutions to radiation-filled Brans-Dicke cosmologies, using Robertson-Walker metric

20 p3294 A71-39558

Dust environment estimation in asteroid belt during trans-Martian spacecraft missions, considering cosmological, dynamical and observational evidence

20 p3297 A71-39633

Critical analysis of big bang cosmological theory, discussing evidence insufficiency and steady state universe possibility

20 p3305 A71-39955

Mass and discrepant red shifts theory, discussing time dependent gravitational constant, Friedmann cosmological model and Dirac equation

20 p3305 A71-39956

Hydrodynamic model of adhering meteors substantiating cosmogonic Laplace-Schmidt hypotheses of solar system planetary formation from cosmic dust

21 p3441 A71-40076

Expanding metagalaxy closed model with changing gravitational constant, noting matter motion in moving and central reference systems

21 p3441 A71-40078

Time variable physical singularity in general relativistic cosmological solution of gravitation equations, constructing simplified models

21 p3441 A71-40088

Electromagnetic absorption in adiabatically expanding fully ionized cosmic plasma, using Einstein-De Sitter cosmology

21 p3442 A71-40161

Closed formula for relation between luminosity and red shift in expanding Friedman universe for positive cosmological constant, positive space curvature and vanishing pressure

21 p3443 A71-40186

Book on cosmic gamma rays covering secondary particle decay, electron-positron annihilation, proton-antiproton interactions, galactic radiation and cosmology

21 p3438 A71-40450

Cosmological models of universe based on expansion-gravitational interaction, including red shift, radio sources, quasars and background radiation measurements

21 p3451 A71-40776

Cosmological enhancement of density perturbations and amplitude variation of acoustic and gravitational waves in anisotropic homogeneous universe

21 p3453 A71-41251

Extragalactic radio sources counts for proportional space volume determination, comparing various cosmological models 22 p3596 A71-41445

Gravitational field quantum fluctuations role in general theory of relativity and cosmological models 22 p3605 A71-42453

Radio source counts interpretation by cosmological evolution models, suggesting luminosity role 22 p3606 A71-42600

Book on cosmology covering stars, galaxies, radio galaxies, universe models, quasars, expansion, intergalactic matter and microwave radiation 22 p3607 A71-42773

Cosmical constant role in relativistic cosmology, considering retention for additional freedom in linking relativity theory with other parts of physical theory 22 p3736 A71-42882

Mixed world model with arbitrarily moving matter, using coordinate system with matrix of reference point components of three dimensional metric tensor 23 p3736 A71-43404

Cosmogenic radionuclide concentration and exposure rates of Apollo 12 rock from Ocean of Storms 23 p3754 A71-43730

Radio galaxies cosmological evolution, discussing rate and spectrophotometric data 23 p3766 A71-43823

Dissipative processes role in early universe within chaotic cosmology program 23 p3769 A71-43992

Kinetic theory of collisionless system in closed anisotropic cosmologies including rotation effects 23 p3705 A71-44123

Einstein equations for universes with expansion, rotation, shear and Bianchi type IX spaces, obtaining diagrammatic solutions 23 p3770 A71-44124

Thermal history of universe traced from assumption of photon and plasma turbulence for galactic formations, discussing thermal instability and heating effects 23 p3770 A71-44181

Initial singularity removal in model big bang universe compatible with 3K black body radiation in terms of renormalized gravitational theory 23 p3770 A71-44182

Cometary nucleus outbursts and splitting moments spatial distribution, indicating solar radiation and tidal action effects 24 p3868 A71-44457

Lunar evolution theory, discussing terrestrial cluster dynamics during earth accumulation 24 p3870 A71-44811

Space plasma physics, considering solar system origin 24 p3874 A71-45169

Extragalactic astronomical approximate dependences in cosmology of homogeneous isotropic universe from series expansion, considering Einstein field theory and Hoyle matter creation tensor 24 p3874 A71-45175

Stars origin theories, discussing stellar associations, young stars, galaxies instability and cosmology and cosmogony 24 p3875 A71-45198

COSMONAUTS

Cosmonauts selection with regard to psychological and physical fitness, discussing clinical examination, hospital tests and training 09 p1397 A71-22192

Soyuz 9 spacecraft astronauts space flight effect on digestive system enzyme secretion function based on pre- and post-flight examinations 09 p1389 A71-22206

Soyuz 9 spacecraft astronauts otorhinolaryngological organs response to 18-day orbital flight, observing pathological changes from clinical post flight examination 09 p1389 A71-22207

Soviet book on space biology and medicine covering cosmonaut selection and training, flight safety, normal life support factors, interplanetary space sojourn, etc 17 p2689 A71-34475

Soyuz 9 cosmonaut meteorological experiments, observations and atmospheric formations photographs 18 p2944 A71-36686

Voskhod 2 cosmonauts physiological data, presenting heart beat, respiration rates, oculomotor activity and blood composition 22 p3495 A71-42791

COSMOS SATELLITES

Atmospheric total moisture content from Cosmos 243 satellite, describing onboard equipment calibration 01 p0074 A71-11101

Soviet astronautics with emphasis on Cosmos satellite program, discussing launching bases, booster rocket designs, radio signals and missions 01 p0164 A71-11456

Earth radiation measurement at 10-12 microns by Cosmos 243 satellite-borne radiometer, comparing temperatures for boundary air layers in cloudless conditions 02 p0246 A71-12115

Night airglow spectral components by Cosmos 92 satellite measurements, considering UV region sources and intensity variations 03 p0417 A71-14050

Geography of upper atmospheric IR emission layers from Cosmos 65 observation 05 p0738 A71-16045

Atmospheric total moisture content from Cosmos 243 satellite, describing onboard equipment calibration 07 p1102 A71-19650

Atmospheric moisture measurements, using Cosmos 243 satellite radiothermal atmosphere self radiation 08 p1277 A71-21007

Low geomagnetic latitude night airglow characteristics, using Cosmos 215 measurements in 1225 to 1350 A range 08 p1277 A71-21008

UV airglow in 1304 A line of oxygen from Cosmos 215 satellite observation 12 p1899 A71-26638

Radio source 3C120 gamma quanta with energy above 100 MeV from Cosmos satellites scintillation and Cerenkov counter measurements 12 p1953 A71-27417

Auroral precipitation electron energetic and angular distributions as function of geomagnetic activity from Cosmos 261 measurements 14 p2230 A71-29713

Ionospheric geocoronal L sub alpha emission intensity related to solar activity level from Cosmos 215 satellite data 16 p2564 A71-33667

Cosmos satellites tracking and monitoring, decoding and interpreting radio signals 16 p2643 A71-34080

Extragalactic objects luminosity upper limits in hard gamma ray band, using Cosmos 208 scintillation Cerenkov telescope 17 p2796 A71-35736

Cosmos satellite data on mainland China thermonuclear explosion of 27 December 1968, observing radiation effects on particles in natural radiation belts 20 p3278 A71-39128

Atmospheric moisture from Cosmos 243 satellite measurements of intrinsic atmospheric radiothermal emission 20 p3218 A71-39587

Low geomagnetic latitude night airglow characteristics, using Cosmos 215 measurements at 1225-1350 A in oxygen spectrum 20 p3219 A71-39588

Micrometeoroid flux acoustic measurements by Cosmos 135 and 163, discussing detection of shower activity 20 p3299 A71-39649

Reflected radiation brightness field statistical structure in IR range from Cosmos 121 satellite measurements, calculating correlation functions and spectral densities 20 p3259 A71-39680

Short wave radiation fluxes estimation for earth-atmosphere system from Cosmos satellite data, studying brightness field angle structure 20 p3260 A71-39681

Microwave emission measurement of earth surface from Cosmos 243 satellite, detecting radio brightness temperature dependence on latitude and local features 20 p3260 A71-39685

Solar and terrestrial IR reflected radiation from Cosmos satellites measurements, determining clouds upper boundary height 20 p3261 A71-39688

Diurnal and semiannual variations in upper atmosphere density from Cosmos satellite drag observations, noting calculation systematic errors 20 p3223 A71-39707

Cosmos 142 and 259 experiments on ionospheric VLF propagation, discussing diurnal variations of daytime electron density 20 p3197 A71-39743

Primary cosmic rays high energy gamma ray intensity spectrometric measurements onboard Cosmos 208 satellite, allowing for charged particles effects 20 p3283 A71-39753

Nuclear component analysis of primary cosmic radiation by Cerenkov spectrometer onboard Cosmos 228 satellite 22 p3591 A71-41548

High energy gamma quanta flux measurements in primary cosmic rays, using Cosmos 208 satellite data 24 p3866 A71-45026

Simultaneous ionosphere measurements by incoherent ground radio wave scattering and coherent signals from Intercomos 2 and Cosmos 321 satellites 24 p3824 A71-45323

COSSEARAT SURFACES

Axisymmetric load problems in Cosserat medium, expressing displacement states by mathematical functions 03 p0509 A71-13899

Coupled stresses effect on dynamic stress concentration produced by traveling loads on elastic Cosserat plate 03 p0509 A71-13905

German monograph on field equations solution for Cosserat continua in planar strip type regions covering stress analysis 03 p0515 A71-14370

Semiinfinite isotropic linear Cosserat continuum surface under impulsive loading, calculating displacements with Laplace transformation 04 p0672 A71-15834

Cosserat continuous model of dense elastic lattices of regular structure in plane 04 p0673 A71-15884

Cosserat surfaces and variable thickness elastic plates linear isothermal theory, deriving constitutive equations corresponding to isotropic three dimensional plate bending and stretching 05 p0831 A71-17250

Maxwell theory analogy with Cosserat continuum moving dislocations, studying kinematic and dynamic equations common features 07 p1161 A71-20016

Inextensible elastic Cosserat surfaces finite deformation mechanisms, applying theory to flexure of rectangular plate into closed circular cylinder and helical strip 11 p1849 A71-25681

Cracks in Cosserat continuum, investigating couple-stress effects on stress concentration 13 p2153 A71-28521

Cosserat surface static stability, considering construction of direct theories of thin shells 16 p2649 A71-33001

Thermoelastic Cosserat plate with insulated unstressed circular hole under uniform temperature gradient at infinity 17 p2822 A71-34675

Cosserat-type bodies with linear elasticity, obtaining reciprocity theorem and stress solutions under concentrated load 18 p2984 A71-36949

Cosserat continuum elastic tensor potentials applied to Kirchhoff theory of wave diffraction 20 p3269 A71-39033

COST ANALYSIS

Satellite and earth station parameters effects on SPADE communication systems link budget, considering carrier power statistics, amplitude and phase nonlinearities 02 p0221 A71-12779

Satellite regional broadcasting and telephony/data services cost model 02 p0221 A71-12781

Economic evaluation of automatic support systems for maintainability of low quantity high technology space programs 03 p0396 A71-13091

Computer memory reduction through Fortran higher level language, discussing tradeoff between costs saved and additional logic hardware [AIAA PAPER 69-963] 03 p0382 A71-13450

Solar electric propulsion/SEP/ for automated planetary missions, discussing system characteristics, capabilities and costs [AIAA PAPER 69-1103] 03 p0500 A71-14426

Satellite educational TV for developing nations, using cost benefit approach for system selection 04 p0691 A71-15277

Planetary and interplanetary exploration missions, discussing U.S. planetary space program budgets and costs 04 p0657 A71-15818

American-European space shuttle costs, comparing nonrecoverable Europa 3 with ballistic reusable devices 05 p0816 A71-16402

Cost-optimal zero moment shell geometry, developing digital computer algorithm with dynamic programming 06 p0992 A71-17804

Aircraft midair collision avoidance, discussing Elimination Range Zero system operation procedures and cost 07 p1154 A71-19079

Cost aspects of carbon fiber reinforced composites in aircraft structures, suggesting increased aviation market for carbon fiber [PLASTICS INST. PAPER 46] 08 p1378 A71-20929

Semiconductor integrated circuit fabrication optimization, considering defect density, component number, crystal size and cost analysis 09 p1416 A71-22490

Decoding computational work and time, discussing cost increases related to communication reliability 09 p1407 A71-23102

Service support for hardware engineering models from breadboard to preproduction stages, determining spare parts location, quantity and cost requirements 09 p1430 A71-23477

Soft lunar landing powered descent optimal control for cost functional minimization, considering linear analytic approach with fuel consumption reduction 10 p1682 A71-24330

Research and development project funds allocation, developing mathematical dynamic modeling method for cost management 10 p1699 A71-24539

Thornel graphite fibers modulus of elasticity, mechanical properties, applications and price
10 p1635 A71-24773

Resin matrix composite airfoils in gas turbine engines, considering performance, fabrication and cost [ASME PAPER 71-GT-47]
11 p1770 A71-25980

Low cost short life gas turbine design based on parametric performance and component selection, outlining turbojet production
[ASME PAPER 71-GT-69]
11 p1813 A71-25984

Nonlinear systems optimal control, presenting Hamilton-Jacobi equations analytical solutions for quadratic cost function minimization
11 p1742 A71-26420

Economic formulation in reliability engineering, expressing cost of failure and reliability improvement in comparable terms
12 p1987 A71-26678

Helicopter auxiliary power unit (APU)/ life cycle cost computation
12 p1988 A71-26679

Thrust measurement of aircraft and rocket propulsion systems, comparing cost and characteristics of mechanical, electrical and hydraulic systems
12 p1894 A71-26991

Computer methods for automatic diagnosis program applied to future manned space vehicles, discussing cost relationship to fault isolation techniques and component reliability
13 p2044 A71-27940

Airline operator evaluation of maintainability, considering costs and investment return
[SAE PAPER 71-0432]
13 p2073 A71-28317

Costs-reliability relationships in helicopter development testing and demonstration, emphasizing decision making in program management
[SAE PAPER 71-0452]
13 p2167 A71-28330

Optimal linear feedback for systems governed by differential operational equations, considering stochastic control and cost function
13 p2095 A71-28814

Aircraft capabilities in intraurban transportation for Detroit metropolitan area, considering vehicle design, fleet size, cost and terminal location
[AIAA PAPER 71-504]
14 p2172 A71-29548

Advanced composite vs conventional material components in cost comparison for aircraft parts
14 p2263 A71-29656

Vibration data analysis of analog and digital methods for cost comparisons
14 p2221 A71-30057

Air transport and travel expansion rate, discussing motivations and cost
14 p2340 A71-30159

Circumstances inducing growth in different air transport sectors, discussing transportation cost, aviation capital requirement and business and leisure air travel
14 p2340 A71-30160

Aircraft quantitative maintenance cost requirements translation into design criteria, considering airline operations influence on manufacturer
[SAE PAPER 71-0437]
14 p2341 A71-30529

Cost optimization for solar generator thermobatteries by selecting temperature, contact resistance, material parameters and fabrication technology
15 p2351 A71-31671

Iterative technique for state and control-constrained linear optimal control problems with strictly convex cost functions
15 p2380 A71-31936

Concorde lightweight disk brakes, discussing operating costs, weight and volume factors, design philosophy, structural materials, component life, maintenance and reliability
16 p2522 A71-33226

Reliability and maintainability as concepts in life cycle costs applied to airline operations
16 p2552 A71-33287

Cost distribution theory for various costs of failure, using probability distribution functions for modeling maintainability and reliability
16 p2583 A71-33305

Premature scheduled maintenance, providing model for duplication between repair and overhaul/replacement cost
16 p2552 A71-33313

Surface temperature measurements with contact thermometers, discussing sensor design, cost and efficiency
16 p2579 A71-33474

Space program economics, discussing applications benefits, spending and byproduct effects cost planning, funding and organization
16 p2665 A71-33590

VTOL aircraft gross weight and direct operating costs penalties from additionally installed control power
[AIAA PAPER 71-768]
16 p2524 A71-34005

Venus planetology missions, discussing objectives, experimental packages, payloads, costs and entry/lander configurations
[AIAA PAPER 71-829]
17 p2802 A71-34717

Electronic two axis digitizer, discussing electromagnetic measuring concept, modular design, reliability and economics
17 p2711 A71-35291

Equilibrium strategies for linear games with quadratic costs in Hilbert space, deriving nonlinear equation in allowed operator feedback spaces
17 p2723 A71-35297

Cost-performance tradeoffs of aerospace launch vehicle expandable structural components, investigating program factors, materials and construction technologies
[SAE PAPER 884]
17 p2750 A71-35828

Book on optimum structural design covering single element optimizations, load transmission, slender columns, cost-weight tradeoffs and statically indeterminate structures
18 p2977 A71-36249

Operating costs and runway lengths for V/STOL in city and suburban short haul air transportation
18 p2987 A71-36347

Space shuttle avionics system redundancy, calculating costs for individual line replaceable units
18 p2889 A71-36479

Satellite broadcasting of TV programs, assessing cost for European community
18 p2876 A71-36503

Third London airport planning, discussing site selection, cost analysis and decision making
[CASI PAPER 72/1]
19 p3040 A71-37592

Mercury short range passenger aircraft design conception, analyzing cost
19 p2997 A71-38242

Adaptive algorithm designing minimum expected cost test trees for detection and isolation of single faults in systems
19 p3069 A71-38287

Suboptimal control with nearly isocost surfaces involving plants subject to large set point changes
20 p3207 A71-38996

Central terminal rapid processing and high speed VTOL aircraft effects on airport design, flight time, cost and ATC
20 p3210 A71-39394

Airport noise control regulations enforcement feasibility, noting financial burden
22 p3623 A71-41796

Delta launch vehicle capabilities, constraints and costs for Straight 8 model 2914 series
22 p3610 A71-42009

Defense and aerospace industry demand cyclical variations effect on productivity growth and cost
22 p3624 A71-42525

Nuclear test program management, considering reliability problems, delays and cost
23 p3786 A71-43462

Adaptive guaranteed cost control for systems with parametric variation, demonstrating system stability and airframe pitch control
23 p3659 A71-44111

COST EFFECTIVENESS

European governmental and industrial roles in space programs, discussing cost efficiency requirements
01 p0183 A71-10265

SST program relation to airline operations, comparing production configuration, performance, economics and operation with subsonics
[AIAA PAPER 70-1217]
01 p0005 A71-11248

Composite materials structure cost effectiveness demonstrated in aircraft relief crew compartment panels
01 p0177 A71-11281

Large hybrid simulation and analog section replacement by digital model, considering digital simulation techniques for economical solution of special problems class
02 p0227 A71-11797

Subsonic aircraft size effect in conventional design, discussing increased weight increments and economic gain rate
[AIAA PAPER 70-940]
02 p0189 A71-12676

Sounding rockets motors with integrally molded plastic case and nozzle, discussing cost effectiveness and demonstration tests
[AIAA PAPER 70-1386]
03 p0470 A71-13669

Cost efficiency, management and economics of airport operation, considering facilities relationship to airline operations
04 p0690 A71-14993

German monograph on socioeconomic evaluation of air transportation systems for developing nations, using cost-benefit analysis
04 p0691 A71-15125

Gyroscope reliable performance life testing economic justification, noting cost lowering by deficient gyro rejection
[AGARDOGRAPH-128]
05 p0749 A71-16304

Human factors engineering cost effectiveness, citing inspector and assembler performance improvement and warning system audibility verification
08 p1378 A71-21228

Global meteorological systems, discussing variables information content, measurements frequency and ac-

curacy, horizontal/vertical resolution, sensor bearing platform and cost
08 p1327 A71-21715

Discusses project commercial satellite system for telecommunications, air traffic control and navigation, describing simulation method used in cost effectiveness study
09 p1547 A71-22276

Linear processes optimal sampled data controls, noting effect of sampling on closed loop system and cost asymptotic behavior
09 p1422 A71-22281

Space shuttle ground operations analysis emphasizing cost effectiveness, discussing breakdown into ground support activities, facilities and equipment
[AIAA PAPER 71-317]
09 p1427 A71-22614

Space shuttles thermal-structural cost effective ground testing
[AIAA PAPER 71-307]
09 p1531 A71-22620

Engineering task and computing devices cost effective matching, methodology improvements and cost penalties for less effective device spectrum utilization
09 p1412 A71-23279

Precision forging and pressing of Al alloy and Ti alloy parts of aircraft structures at cost effective prices
09 p1459 A71-23691

Sounding rocket flight accurate trajectory data, determining cost effective radar tracking system
10 p1610 A71-24149

Performance-price relations of carbon, boron and glass fiber reinforced resin matrix composites in commercial and aerospace use
10 p1634 A71-24418

Carbon fiber reinforced plastics industrial engineering applications, noting cost effectiveness, strength and elasticity
11 p1861 A71-25407

Pan American reliability program effect on airline maintenance, considering cost effectiveness, aircraft performance, data collection and analysis
12 p1910 A71-26671

Risk assessment associated with reliability demonstration testing, considering fixed price procurement and cost effectiveness
12 p1910 A71-26677

Cost effectiveness of reliability screening program from parts procurement through system test, using experience with attack radar for F-111 aircraft
12 p1885 A71-26683

Space shuttle thermal protection systems, discussing design requirements and constraints, materials selection, tradeoff and cost effectiveness studies
12 p1971 A71-26984

Polyimide plastics, considering mechanical properties high temperature applications and cost effectiveness
13 p2091 A71-28165

Automatic control systems preventive inspection intervals examined from cost optimization viewpoint for various failure distribution rules
13 p2042 A71-28641

Semiconductor random access memory components, discussing LSI circuits developments for RAM applications cost effectiveness in computer main-frame memories
13 p2035 A71-28772

Cost efficient sound limit expenditures per parameter unit in commercial transport aircraft design
13 p2167 A71-28945

Helicopters as cranes and external load carriers, considering operational costs and investment return
13 p1997 A71-29144

Operations research minimum cost model of aircraft noise abatement in airport communities
[AIAA PAPER 71-525]
14 p2339 A71-29551

Optical interferometer with evacuated light paths, describing operating principles, cost efficiency and compactness
14 p2238 A71-29803

Organization and funding criterion of unsuccessful R and D projects, considering project abandonment or failure
14 p2340 A71-29854

Satellite auxiliary electric propulsion systems survey for program managers and systems engineers, considering cost and component reliability
[AIAA PAPER 71-685]
14 p2292 A71-30747

Criteria for converting aeronautical project operational targets into actual requirements and technical specifications, emphasizing cost effectiveness
14 p2177 A71-30824

Weapons R and D flexible economical response to defense needs by emphasis on component and subsystem experimentation
14 p2341 A71-31130

Optical coupling between two axes of laser light beam deflector, using reflective relay optical system for loss reduction, cost effectiveness and easy alignment
16 p2585 A71-33139

Life cycle cost optimization of STOL aircraft and tracked air cushion vehicles for operating transportation system 16 p2522 A71-33306

Maintenance aids evaluation for government contracting and decision making, including cost model based on life cycle economics 16 p2552 A71-33311

Complex systems with n independently failing subsystems, minimizing expected cost per unit usage by assigning replacement age 16 p2552 A71-33312

Service life/stress testing, failure analysis and corrective action from technical and cost positions 16 p2583 A71-33315

Optimum power parameters and economic efficiency of Soviet communication satellite system, comparing with terrestrial multichannel communication 17 p2696 A71-34231

Communication satellite TV and sound broadcasting system design without unreasonable cost 17 p2697 A71-34237

Large software systems development management, discussing steps including program design before analysis, documentation, testing, monitoring and cost effectiveness 17 p2709 A71-34618

Space shuttle cost effectiveness and economic efficiency analyzed for system-level requirements to maximize economic benefits [AIAA PAPER 71-810] 17 p2813 A71-34730

Strapdown or gimbaled inertial measurement units for space shuttle program, considering reliability, redundancy and cost of ownership 17 p2772 A71-35059

ATC system improvement by area navigation, discussing benefits in services, safety and cost effectiveness 17 p2775 A71-35373

Costs/benefits strategy for investment in STOL fleets reducing delay and airport congestion, using heuristic computer model 19 p3173 A71-38029

Simulation model for optimal cost time-independent component replacement of complex system subject to probabilistic deterioration 19 p3069 A71-38288

Systems oriented components selection optimization technique by reliability/quality levels, considering repair and failure cost, storage time and mission duty cycle 19 p3034 A71-38518

Cost effectiveness screening program for integrated circuits, considering four stages of life cycle 20 p3202 A71-38753

Electronic circuit modules effects on alphanumeric display capabilities and costs over wide applications range 21 p3359 A71-40116

Multilayer printed circuit board development, design and production for high reliability and cost effectiveness, emphasizing multidisciplinary communication 21 p3352 A71-40436

Brazing filler metals as cost effective replacement for Au-Ni in aircraft gas turbine engine component 21 p3387 A71-40621

Redundancy optimization of series-parallel k-out-of-n systems for maximum reliability subject to multiple cost constraints 21 p3388 A71-40878

U.S. Army ATC cost-effective system developments for high density low altitude helicopter tactical operations to avoid enemy radar under near-all weather conditions 22 p3571 A71-42084

Cost based algorithm for allocating availability parameters /repair times and failure rates/ to system components 22 p3566 A71-42115

Cost effective general purpose minicomputer PDP-11/45 design and technology using Schottky TTL/MSI, semiconductor memories, multiple buses, microprogramming and floating point units 22 p3519 A71-42761

Cost effective integrated logistics support documentation system for military contractors 23 p3661 A71-43196

Incentive contract with contractor profit based on achievement in cost, schedule and technical performance 23 p3786 A71-43467

Civil transport aircraft and equipment maintenance and reliability problems solutions with best time, cost and weight compromises 24 p3792 A71-44765

COST ESTIMATES

MOS LSI bipolar random access memory feasible at costs competitive with magnetics 02 p0228 A71-11653

Compact aerodynamic reentry vehicle development problems and costs, discussing lifting body vehicle for wind tunnel, ground and flight tests and reentry trajectories 02 p0320 A71-12066

Software cost estimates for automatic test equipment for avionic support analysis 03 p0396 A71-13086

Remote area voice, teletype and data communication using satellites for providing links with central terminals, considering economic feasibility by cost analysis 04 p0555 A71-15338

Nuclear electric space propulsion size and cost factors, discussing scaling laws use for size-performance relationships [AIAA PAPER 71-193] 06 p0947 A71-18631

Defense industry pricing and contracting for inflation, considering statistical analysis and direct cost estimation 14 p2342 A71-31132

Satellite TV broadcasting development in European community, giving cost estimation procedure and program reception methods 18 p2876 A71-36504

Mixed satellite TV broadcasting system for France, estimating cost 18 p2988 A71-36505

TV broadcasting by satellite to isolated users via cable transmission, estimating cost and satellite optimal radiating power 18 p2877 A71-36507

Replacement problem in stochastic point processes, obtaining cost over given time period and moments and correlations of replacement number 21 p3407 A71-40367

Satellite project cost estimation, evaluating formulae for budget, tender offer and contractual expense 23 p3785 A71-43459

COST INCENTIVES

Response strategies in two-choice reaction task with continuous cost for time, confirming fast-guess model prediction 12 p1873 A71-27008

COST REDUCTION

German monograph on systems analysis of future jet and fan propulsion systems for VTOL commercial aircraft weight and cost reduction 01 p0142 A71-10115

Materials R and D economic considerations, emphasizing processing and assembly costs reduction and user benefits 01 p0183 A71-10279

Hydraulic system axial- and radial-piston pumps design and operation principles, considering cost reduction 01 p0006 A71-10817

Large Al forgings machining cost reduction via stress relief involving mechanical working following quench 01 p0091 A71-11547

Explosive forming using compressed air as power source for safety and lower cost 01 p0091 A71-11549

Optical communication systems cost and weight optimization by COMTRAN program 02 p0214 A71-12028

Cost optimal direct broadcast and redistribution satellite systems 02 p0221 A71-12783

Zinc air battery, evaluating materials capable of peroxide decomposition as low cost oxygen electrodes 03 p0351 A71-13040

Hydrazine-oxygen fuel cells energy costs minimization by optimizing diaphragm thickness, hydrazine concentration and load 03 p0355 A71-14321

Technical resources pooling among airlines for investment and maintenance cost cut of aircraft fleets 04 p0690 A71-14992

Minuteman missile technology application as boosters for near earth spacecraft launching, emphasizing tradeoff between reliability and cost 04 p0663 A71-15313

Space transportation system profitability conditions, discussing optimal cost reduction and launcher/booster characteristics 04 p0692 A71-15821

Low stress integral coverslips deposition by high vacuum ion beam sputtering for solar cell manufacturing cost reduction 05 p0702 A71-16078

Gyroscope reliable performance life testing economic justification, noting cost lowering by deficient gyro rejection [AGARDOGRAPH-128] 05 p0749 A71-16304

Linear programming application to optimum structural design, noting savings in design and price 05 p0825 A71-16610

Two stage space shuttle, discussing NASA reusable spacecraft cost reduction and technological problems 07 p1209 A71-20226

Map preparation techniques and cartographic design for cost reduction and production speeding 08 p1280 A71-21247

Jet propulsion optimization by exergy and energy for minimum total cost flux by varying unit compressor pressure ratio 08 p1348 A71-21300

Composite rocket cum hypersonic airbreathing propulsion reducing space exploration program cost 08 p1348 A71-21301

Space shuttle onboard vs ground checkout systems, considering vehicle autonomy and cost reduction [AIAA PAPER 71-311] 09 p1427 A71-22623

Cost reduction concepts in gas turbine engine design and fabrication for general aviation aircraft 09 p1511 A71-22811

Space shuttle development test program, discussing low cost dynamic structural and flight testing [AIAA PAPER 71-308] 09 p1532 A71-23017

Powder form structural adhesives for cost reduction and increased productivity 10 p1614 A71-24066

Earth-to-orbit space shuttle booster and orbiter unit design considerations including low development cost, risk and time, weight and payloads 11 p1840 A71-26529

Processes involved in obtaining materials required for socialist organization operation, discussing operations, cost reduction by work mechanization and optimum data processing 13 p2167 A71-28492

Low cost metal matrix composite fabrication, discussing plasma spraying and continuous casting 14 p2263 A71-29655

Boeing 747 aircraft integrated data system program for reducing engine maintenance and operating costs [AIAA PAPER 71-648] 14 p2290 A71-30725

Cost control over changes in major weapons systems between letting of contract and final hardware delivery 14 p2342 A71-31134

IMPATT diode oscillator for CW Doppler radar, microwave detection and communications systems, emphasizing cost reduction 15 p2377 A71-32522

Aircraft reliability and maintenance cost reduction via allocation of effort and money, considering R and M optimization in airline support cycle 16 p2551 A71-33286

Numerical integration of quasi-static system of hydrodynamic equations, considering economical production of short range high resolution meteorological forecasts 16 p2604 A71-33532

Low noise TWT amplifiers, performance, reliability and cost reduction 17 p2714 A71-34605

Payload cost and response time reductions for shuttleborne space experiments, examining NASA Ames airborne research program management technique [AIAA PAPER 71-808] 17 p2813 A71-34731

Optimal control systems synthesis with reduced sensitivity to parameter variations by trajectory sensitivity feedback with cost minimization 17 p2719 A71-34744

Low cost navigation equipment selection for space shuttle system updating during orbital coast, rendezvous and atmospheric flight 17 p2774 A71-35069

Reduced cost ground stations for satellite communications system and applicability to small nations, using single channel per carrier FM and companders 17 p2704 A71-35087

Solid state diffusion bonded boron-aluminum composites, discussing mechanical properties, weight and cost reduction and applications 17 p2758 A71-35204

Distributed parameter system measurement optimization devices location for error estimation cost minimization by disturbances statistical characteristics and boundary conditions 17 p2722 A71-35211

Aircraft electric power system design with reliability, simplicity, low cost, weight and size, discussing automatic circuit protection and energy power 17 p2678 A71-35780

Administrative techniques of cost/weight tradeoff program for jet transport airplane [SAWE PAPER 899] 17 p2750 A71-35812

Premium mechanical properties for materials in space shuttle orbiter project, emphasizing cost and weight reductions 18 p2979 A71-36465

Airline operations approach to Cape Kennedy launch processing system for reduced hardware and operational costs of shuttle support 18 p2899 A71-36475

Space shuttle design concerning fault detection and isolation, redundancy and maintenance for cost and downtime minimization by application of airline methods 18 p2900 A71-36480

Dynamic polariscope for birefringent materials stress wave low cost analysis 18 p2923 A71-36611

Carbon fiber reinforced plastics, reviewing properties, performance, development, applications and potential cost reduction 18 p2940 A71-36765

Gas lasers, discussing engineering developments for size and cost reduction, reliability, long life and high power

19 p3074 A71-38227

Economical alternative construction materials selection for partmaking cost reduction while maintaining quality

20 p3251 A71-39338

Low cost Ti substitutions for Ni and alloys in corrosion resistant applications, prosthetic devices and pollution control equipment

20 p3251 A71-39339

Picture processing using general purpose digital computer simulation for reduction of processing time and special purpose hardware investments

21 p3376 A71-40111

Dual variational formulation for rigid plastic structure minimum cost design, applying to sandwich and fiber-reinforced plates

[ASME PAPER 71-VIBR-110] 21 p3462 A71-40333

Complex electronic modules automatic checkout, discussing processing time and cost reduction for large printed circuit logic boards test and diagnostic programs

[ASME PAPER 71-VIBR-115] 21 p3362 A71-40335
Test unit number selection for lowest total life test cost, considering operating test environments and component reliability

21 p3386 A71-40368

Leadless electronic packaging system for MOS LSI for low cost, high reliability and heat transfer advantages

21 p3356 A71-40745

Low cost high performance rate gas bearing gyroscope development, emphasizing large scale production and overall instrument design optimization

22 p3551 A71-41664

Space shuttle impact on cost reduction in NASA space operations, considering operations costs of payloads

22 p3609 A71-41994

Spacecraft and payload design under influence of space shuttle availability, discussing program cost savings

22 p3610 A71-42003

Astronaut teleoperators use for space operations cost reduction and future experiments productivity increase

22 p3503 A71-42033

Aircraft part repair-throwaway decisions for minimizing costs over life cycle by economic graphic screening techniques

23 p3661 A71-43197

Nondestructive pulse technique for quality control of electroexplosive devices, noting cost reduction

24 p3864 A71-45279

COSTS

NT AIRCRAFT PRODUCTION

NT AIRPLANE PRODUCTION COSTS

NT FREIGHT COSTS

NT LOW COST

Technical work evaluation in cost-plus contracts for management control

01 p0184 A71-11190

COTTON FIBERS

Flammability and heat transfer characteristics of flame retardant cotton, Nomex and polybenzimidazole (PBI) protective fabrics

07 p1145 A71-19573

COUETTE FLOW

Viscosity model application to turbulent plane Couette flow velocity profile and shear stress values, obtaining skin friction relation

01 p0071 A71-10954

Spherical particle motion investigation in plane Couette flow, predicting critical Reynolds number for transition to turbulent flow

03 p0398 A71-13112

Plane Couette flow turbulence, discussing wall region shear and core homogeneity

03 p0400 A71-13546

Couette flow stability between coaxial rotating cylinders, calculating eigenvector in first approximation small perturbation equations

03 p0404 A71-14231

MHD generalized Couette flow by splitting linear time dependent flow into simultaneous solution of boundary and initial value problems

04 p0571 A71-15201

Couette flow between rotating cylinders and Taylor vortex formation by Liapunov-Schmidt method and spectrum perturbation theory, discussing secondary flow determination accuracy

04 p0575 A71-15603

Rarefied gas Couette flow between concentric cylinders and heat transfer from wire to external cylinder, applying momentum method

05 p0736 A71-16723

Transpiration cooling heat transfer in incompressible turbulent boundary layer, using Couette flow model, boundary layer model and combinations of both

07 p1219 A71-18758

Hydrodynamic stability of viscous conducting fluid plane Couette-Poiseuille flow in transverse magnetic field by linear theory, considering complete spectrum of small disturbances

07 p1169 A71-19727

Rarefied gas flow and heat transfer in plane Couette flow using Bhatnagar-Gross-Krook model with ellipsoidal distribution

07 p1224 A71-20024

MHD Couette flow at stationary plate under transverse magnetic field, discussing effect on heat transfer between electrically conducting walls

07 p1170 A71-20099

Turbulent pipe, channel and plane Couette flow by Prandtl model equations, comparing with experimental data

07 p1092 A71-20278

Density distribution, heat transfer and drag measurements in rarefied Ar cylindrical Couette flow, comparing results with Navier-Stokes and Burnett equations solutions

07 p1093 A71-20286

Polarographic measurements of secondary Couette flow between coaxial cylinders for diffusion coefficient effects on mean friction factor, using wall flush microelectrodes

10 p1592 A71-23978

MHD effects on transpiration cooled Couette flow through porous wall, considering magnetic drag produced pressure differential and shear recovery rates

10 p1649 A71-24404

Heat transfer in Couette flow with/without injection, taking into account wall conduction effects

11 p1856 A71-26049

Plane parallel Couette flow stability with respect to small perturbations, considering positive wave numbers and Reynolds numbers

12 p1897 A71-27307

Plane Couette flow with suction/injection at stationary plate, obtaining motion and continuity equations, pressure distribution and friction coefficient

13 p2047 A71-28520

Blowing and wall curvature effects on gas flow separation and critical pressure gradient in Couette flow examples

13 p1993 A71-29193

Compressible rarefied gas Couette flow over plane wall, calculating mean free path with Boltzmann equation relaxation model

13 p2051 A71-29357

Couette flow two point boundary value problem solution using Navier-Stokes and Barnett viscous gas equations

14 p2224 A71-30185

Incompressible homogeneous isotropic fluid Couette flow between stationary inner and rotating concentric outer cylinders, examining Weissenberg effect

14 p2226 A71-30445

Nonlinear stability theory, considering velocity and vorticity perturbations in circular Couette plane Poiseuille and shear layer flows

15 p2393 A71-32568

Plane Couette flow with finite disturbances, investigating stability in nonlinear terms

16 p2558 A71-32986

Liapunov functions applications, discussing plane Couette flow and feedback control

16 p2607 A71-32994

Nonlinear heat transfer in plane rarefied isothermal Couette gas flow, using BGK model

16 p2561 A71-34143

Impulsively started time-dependent rotational Couette flow stability analysis by initial value problem and quasi-steady approaches

18 p2902 A71-36038

Smallest Taylor number corresponding to Couette flow stability between two rotating cylinders subjected to rotationally symmetrical perturbation

18 p2902 A71-36093

Plane MHD Couette flow stability with asymmetric velocity profile shaped by transverse magnetic field, considering Hartmann flow

19 p3108 A71-37077

Viscous incompressible conducting fluid at constant flow rate under magnetic field variation, investigating laminar unsteady MHD Couette flow problem with approximate solution

19 p3108 A71-37092

Unsteady approach to nonisothermal flow theory for Couette flow, making general assumptions concerning rheological law and temperature dependence of fluidity

19 p3043 A71-37386

Plane Couette-Poiseuille flow stability between porous walls with fluid injection and suction causing uniform crossflow

19 p3044 A71-37728

Plane parallel Couette flow stability with respect to small perturbations, considering positive wave numbers and Reynolds numbers

19 p3046 A71-38263

Stability problem in hydrodynamics of perturbed heterogeneous shear flow, solving initial value problem for Couette flow

20 p3213 A71-39783

Thermal convection induced perturbations in unstably stratified horizontal shear Couette flow of Boussinesq fluid in rectangular channel heated from below

21 p3475 A71-40641

Plane Couette flow temperature and velocity fields for Newtonian fluid with temperature dependent viscosity under locally and temporally constant wall temperature

22 p3620 A71-41881

Laminar Couette flow between parallel plates with mechanical energy dissipation and temperature dependent viscosity, determining velocity and temperature distribution

22 p3531 A71-42683

COULOMB COLLISIONS

HF oscillations excitation in decaying plasma-electron beam system, noting Coulomb collisions and nonlinear effects role

02 p0288 A71-11632

Two stream electron plasma with Coulomb particle collisions, considering autooscillations and nonlinear friction characteristic

04 p0633 A71-15109

Electromagnetic wave generation by interaction in plasma stream resonator, considering Coulomb friction and boundary reflection coefficients

04 p0633 A71-15110

Atmospheric Coulomb interaction influence on longitudinal dependence of electron intensity in anomaly region

06 p0963 A71-18255

Coulomb collisions effect on instability of cold and warm monoenergetic electron beams in plasma

07 p1166 A71-18885

Coulomb collisions in high density plasma beams, examining relaxation time

08 p1340 A71-21486

Broadened energy distributions in electron beams, discussing energy spread delta E and C prime values relationship for studying weak Coulomb interactions

11 p1802 A71-25631

Coulomb collisions in high density plasma beams from numerical integration of Fokker-Planck equation for three initial distribution functions, studying relaxation time

14 p2283 A71-30674

Spatial relaxation of electron energy distribution with inelastic and Coulomb collisions, integrating Boltzmann equation

18 p2949 A71-36969

Coulomb interaction effect between charged traps in amorphous semiconductor, noting state density reduction at Fermi energy

23 p3715 A71-43472

Coulomb interactions within dense Boltzmann plasma in transition from ideal to nonideal state, proposing effective Coulomb pair cross section concept

23 p3712 A71-43913

COULOMB POTENTIAL

Carrier mobility in noncompensated highly doped semiconductors, presenting derivation from Rogachev expression for scattering Coulomb center screening charge density

07 p1175 A71-19218

Ionized gases quantum transport cross sections and collision integrals, considering energy and temperature ranges for attractive and repulsive screened Coulomb potentials

07 p1224 A71-20283

Coulomb forces detrimental effects on electron bunching in three-resonator klystron, defining buncher optimal parameters for different permeance values

12 p1888 A71-27614

Integrodifferential difference equation for isotropic portion of velocity distribution function resulting from electron excitation and Coulomb interaction

20 p3274 A71-39048

Earth electrostatic potential role in experimental Coulomb law verifications

22 p3536 A71-42455

COULOMETERS

Mercury column electrochemical coulometer as ampere-hour type of state-of-charge indicator for secondary batteries in space power applications

15 p2354 A71-32206

COUNTERFLOW

Electromagnetic instability of counterstreaming electron plasmas with anisotropic temperatures, using Vlasov equation

04 p0633 A71-15032

Two phase heat transfer in thermosyphon counterflow under simulated gravities of 0.1 to 100 earth gravity, measuring critical heat flow rates and convection coefficients

04 p0687 A71-15531

Electromagnetic instability growth in counterstreaming nonrelativistic plasmas, comparing electrostatic rate
05 p0788 A71-16601

Counterflow diffusion flame applied in studies of gaseous and powdered agents in chemically inhibiting fires
07 p1182 A71-19244

Plane jet in counterflow with vortex shedding control, discussing solid boundary and jet momentum effects
10 p1592 A71-23980

Flow theory of steady separation zone near body at high Reynolds numbers, determining vortex parameters counterflow inviscid region
13 p2049 A71-29171

Liquid metal MHD cycles for spacecraft power supply systems, proposing counterflow condensation at nozzle outlet
22 p3574 A71-42431

COUNTERMEASURES
NT CHAFF
NT ELECTRONIC COUNTERMEASURES
NT JAMMING

COUNTERS
NT CERENKOV COUNTERS
NT ELECTRON COUNTERS
NT GEIGER COUNTERS
NT NEUTRON COUNTERS
NT PARTICLE TELESCOPES
NT PROPORTIONAL COUNTERS
NT QUANTUM COUNTERS
NT RADIATION COUNTERS
NT SCINTILLATION COUNTERS
NT SPARK CHAMBERS

Hybrid fluidic binary counter, using commercially available fluidic bistable amplifier in conjunction with free disk steering gate
07 p1026 A71-20572

Digital nonregular pulse counter, determining noise characteristics of photomultipliers in single pulse recording mode
14 p2213 A71-30580

Recorder circuit quick response enhancement in Grey code pulse counter, realizing parallel decoding in binary digits at high speeds
15 p2374 A71-31294

Star counting device, showing stellar fields contribution to total brightness
17 p2742 A71-35004

Sequential control with fluid logic programmers, considering decimal and binary counters, shift registers, gray code generator and integrated devices
24 p3793 A71-45087

COUNTING
Laser optical field intensity correlation function determination from photoelectric counting distribution measurements
03 p0436 A71-13876

Extragalactic radio sources counts for proportional space volume determination, comparing various cosmological models
22 p3596 A71-41445

COUNTING CIRCUITS
NT SCALERS
Laser gyro goniometry for fluctuations and angular measurements at low rotational velocities, noting countup/countdown detection systems
02 p0262 A71-12924

Preliminary circuit-stage alignment procedures in multistable triggers manufacture with counter input based on tunnel diodes and transistors
14 p2213 A71-30632

Multijunction functional devices for operation as decade digital counter, step voltage generator, analog/digital converter, binary counter, neuristor line, etc
22 p3520 A71-41706

COUNTING RATE COMPUTERS
Counting rate source encoding algorithm with orthogonal functions in space experiment data processing before telemetering to ground
08 p1259 A71-21592

COUPLED MODES
Book on numerical method for coupled modes in plasmas, elastic media and parametric amplifiers covering differential equations, recursive functions, wave propagation and iterative calculations
01 p0111 A71-10356

Uniform periodic waveguide mode coupling, obtaining mode transducer design
02 p0216 A71-12342

Modal coupling in thermally stressed plates, obtaining solution for frequencies and stiffness
02 p0329 A71-12685

Micropulsations dynamic properties and resonant cavity modes, obtaining coupled toroidal and poloidal modes solution
06 p0969 A71-17976

Solid propellant rocket chamber unstable motion, discussing pressure and velocity coupling
06 p0946 A71-18297

Radio communication system hypersonic delay lines, investigating coupled resonators matching efficiency in parallel and series connection
07 p1074 A71-19142

Electron and proton whistlers polarization reversal and mode coupling, explaining magnetic latitude dependence
07 p1062 A71-19667

Hydromagnetic wave propagation with coupled isotropic and guided modes, obtaining steady state solution with toroidal, plasma resonance induced period dependent reflecting barrier
07 p1197 A71-19767

Cone roll dynamics-ablation patterns coupling in hypersonic wind tunnels
[AIAA PAPER 70-562] 07 p1208 A71-19868

Modal superpositions for mutual coupling on cylindrical array of waveguide elements
09 p1420 A71-23513

Coupled vibration modes for nonrotating blade-disk system in axial flow turbines and fans calculated by finite element method
[AIAA PAPER 71-375] 11 p1845 A71-25348

Coupled vacuum mode equations modified for cylindrical stratification for calculation of propagation characteristics of earth-ionosphere waveguide
11 p1731 A71-25664

MHD waves incident at density step, calculating reflection, refraction and transmission coefficients and coupling modes
11 p1807 A71-26429

Cracks in Cosserat continuum, investigating couple-stress effects on stress concentration
13 p2153 A71-28521

Extensional vibrations of thin cylindrical shell, discussing longitudinal and radial motions coupling and resonant frequency dependence on length/radius ratio
14 p2327 A71-30209

Matrix solution for wave equation with mode coupling of VLF and ELF radio waves in horizontally stratified layer of anisotropic ionosphere plasma
15 p2373 A71-32444

Circular rings coupled twist bending vibrations, considering rotatory inertia and shearing deformation effects
15 p2510 A71-32517

Coupled longitudinal-transverse wave modifications of electrostatic dispersion relation with ion gyrofrequency instabilities in magnetized plasma
18 p2950 A71-35866

Energy transfer between nonlinearly coupled oscillators described by Hamiltonian system in case of third order resonance
18 p2948 A71-36795

Plasmapause Alfvén, ion-acoustic, electron and ion drift wave modes coupling, calculating instability condition and growth rate
19 p3110 A71-37371

Magnetospheric hydromagnetic resonances, considering resonant poloidal-toroidal coupling
20 p3215 A71-38745

Gas dynamic model for coupled vibrational and radiative nonequilibrium in carbon dioxide, obtaining macroscopic collisional and radiative transfer equations
21 p3418 A71-40233

Dynamic influence of isotropic flat plates on spatial vibratory structures containing rigid bodies, considering compatibility and modal coupling
[ASME PAPER 71-VIBR-3] 21 p3456 A71-40267

Coupled bending-bending vibration of pretwisted tapered cantilever blades, obtaining equations of motion
[ASME PAPER 71-VIBR-78] 21 p3460 A71-40315

Optimal trajectories and controls for dynamic systems modeled by coupled rigid bodies, applying to synthesis of robots and all-terrain vehicles
[ASME PAPER 71-VIBR-82] 21 p3414 A71-40318

Hydroelastic coupled oscillations of partially filled circular cylindrical liquid container with flexible bottom and elastic side wall
21 p3366 A71-40545

Free falling spheres rocking/lateral motions, deriving nonlinear damped pendulum equation with motion coupling expressed as Reynolds number dependent phase shift effect
21 p3416 A71-40953

Kinetic wave equation matrix elements for three resonantly coupled electrostatic plasma waves noting application to electron plasma coupling with ion sound waves
22 p3582 A71-41900

Pulse trains of minimum spectral width generated from rectangular pulses by RC elements coupled without feedback
22 p3521 A71-42248

GaAs lasers filamentary coupling, investigating various mode perturbations in temporal output
22 p3558 A71-42346

Magnetoionic mode coupling of HF radio waves, considering Faraday rotation of satellite signals
23 p3642 A71-42963

Ionospheric HF wave ordinary /O/ and extraordinary /E/ modes coupling effect on satellite signal Faraday rotation
23 p3642 A71-42964

Sound transmission through finite closed shells, considering statistical energy analysis, modal coupling and noise reduction
23 p3704 A71-43213

Solid state lasers, discussing ruby lasers application for welding and drilling, mode coupling of glass lasers and extremely short pulses generation
23 p3685 A71-43953

COUPLERS
NT ANTENNA COUPLERS
NT COUPLING CIRCUITS

COUPLES
Gyroscopes motor couple scale factor measurement [AGARDOGRAPH-128] 05 p0750 A71-16311

COUPLING
NT COUPLES
NT CROSS COUPLING
NT GYROSCOPIC COUPLING
NT MICROWAVE COUPLING
NT OPTICAL COUPLING
NT SPIN-SPIN COUPLING
NT THERMODYNAMIC COUPLING

Long elevated horizontal line sources mutual impedance coupling, using image theory techniques
01 p0041 A71-11615

Soviet book on bolting and coupling elements threads used in aircraft industry covering configurations selection, cutting, tolerance requirements and quality control
02 p0258 A71-12723

Ring laser coupling phenomena, presenting angular measurements for laser-gyro with Langmuir-Fizeau and Faraday effect bias
04 p0607 A71-15022

Coupling loss factor estimation, using wave transmission or natural frequency shift methods in statistical energy analysis
07 p1161 A71-19962

Two link approximation of Chaplygin function by coupling to integral equations, applying to ideal gas jet separation flow past symmetrical arc
07 p1016 A71-20084

Multilink approximation of Chaplygin function in subsonic and supersonic flow regions, deriving coupling conditions relative to modified stream function at approximation nodes
07 p1016 A71-20090

Wing-fuselage-tail interacting low speed flutter, considering mechanical tuning and aerodynamic interference couplings
[AIAA PAPER 71-326] 11 p1842 A71-25306

Spherically symmetric initial solutions for coupled gravitation and massless field system generated by physical particle source
16 p2610 A71-33266

Visible spectrum electromagnetic waves propagation in plasma, emphasizing parametric coupling
16 p2620 A71-34136

Dipole coupling, current distribution and impedance of thick dipolar log periodic antennas by 4-term theory
16 p2544 A71-34172

Remote double resonance coupling of radar energy to ionospheric irregularities by sweeping radar modulation frequency through whole range
18 p2914 A71-36929

Coupling effects between two Permalloy films for different interface treatments, using standing spin wave resonances
18 p2955 A71-36941

Coriolis coupled bending vibrations of hingeless helicopter rotor blades, noting out-of-plane component contribution to aerodynamic coupling
19 p3154 A71-37294

Large stiffness matrices building and manipulation, including structural analysis computer programs input determination, coupling techniques and eigenvalue problems solution
19 p3161 A71-38654

Pressure anisotropy effects on plasma wave coupling and modification for dispersion in collisionless beam-plasma systems
20 p3273 A71-39045

Axially coupled turborotors, calculating coupling characteristics, disk inertia and gyroscopic effects on dynamic response, by transfer matrix techniques [ASME PAPER 71-VIBR-108] 21 p3462 A71-40332

Resonant coupling of two electron plasma waves with ion sound wave at large electron Larmor radii under weak magnetic field
22 p3583 A71-42418

COUPLING CIRCUITS
Impedance measurement and standing wave ratios at microwave frequencies, using directional couplers
03 p0377 A71-13269

Frequency response characteristics of nonlinear oscillatory circuits with inductive and complex capacitance couplings
03 p0379 A71-13812

Photodetector-transistor amplifier coupling for maximum SNR in optical communication systems
06 p0866 A71-17370

Slot transmission line bandpass and bandstop filters and hybrid couplers for microwave IC applications, presenting experimental performance data
08 p1262 A71-20761

Electronic equipment for measuring resonant frequency drift during slow wave structure impedance measurements, considering mean square errors
08 p1264 A71-21073

Emitter coupled integrated transistorized logic elements, improving steady state noise stability by hysteresis in transfer characteristics
09 p1416 A71-22467

Magnetically coupled tunnel diode oscillator with square loop core, calculating leakage and source inductances effect on switching pattern
[IEEE PAPER 11.4]
09 p1416 A71-22593

Transistorized pulsed amplifier stage in common base configuration with transformer coupling
11 p1739 A71-26466

Solid state vs electrical-mechanical relay switching and isolation technology
13 p2001 A71-28845

Microwave meander line /coupled parallel commensurate conductors array/ network analysis and synthesis, using equivalent circuit transformation for computerized design
14 p2219 A71-29565

Two loop parametrically coupled oscillatory amplifier with unlimited degrees of freedom, investigating segment of long line loaded at one end with periodically varying capacitance
14 p2211 A71-30083

Radio frequency power meters comparison, reducing mismatch and directivity errors with directional coupler
14 p2205 A71-30984

Coupling effects between reliability components of integrated circuits by modeling failures in structures
15 p2377 A71-32345

Coupled oscillator circuits simultaneous tuning by plane relationship between circuit currents /volts/
16 p2548 A71-34034

German monograph on filters based on coupled lines covering computerized design, numerical approximation, rounding errors and matrix correction method
20 p3208 A71-39263

Subnanosecond digital computer with emitter-coupled fully integrated circuit packaging concept
21 p3351 A71-40748

Coupled resonator AT cut quartz crystal bandpass filter design in ladder configuration with low sensitivity and simple manufacturing methods
21 p3360 A71-40810

COUPLING COEFFICIENTS

Frequency stability of three-loop oscillator with time lag on coupling coefficient plane used for optimal circuit configuration
02 p0230 A71-11835

Mirror-coupled oscillations of open resonant cavities for arbitrary coupling coefficients
03 p0385 A71-13799

Nonlinear interaction between three longitudinal plasma waves, calculating dissipation effect on coupling coefficients
04 p0635 A71-15902

Mechanized ultrasonic inspection probes with high stable dynamic acoustic coupling coefficient, high sensitivity and wear resistance and low coupling fluid expenditure
09 p1450 A71-22897

Electrostatic waves high order interaction in collisionless plasma, deriving coupling constants from energy conservation and invariance under time reversal
10 p1647 A71-23888

Echo reflections and transition through critical coupling in D and E regions at low and medium frequencies, using nighttime electron density distributions
11 p1754 A71-25601

Nonlinear explosive ion beam-plasma interaction, discussing coupling coefficients and Landau damping
12 p1935 A71-26912

Collisional radiative volume recombination and ionization coefficients for quasi-stationary helium, considering singlet and triplet systems as two coupled individual systems
13 p2106 A71-28452

Time domain solution of coupling to two wire transmission line, determining coefficients by steady state measurements
13 p2001 A71-28868

Correlation coupling matrix elements for one electron transfer and ion-ion recombinations in Landau-Zener calculations
18 p2948 A71-35839

Coupling coefficients in set of connected cavity-type transmission lines, analyzing effects of individual elements, slot geometries and conducting walls
19 p3019 A71-38337

Waveguide systems coupled through slots in lattice partition approximated by anisotropic dielectric layer
19 p3019 A71-38338

Elastic plates radial vibrations excited by piezoelectric elements, investigating electromechanical coupling coefficient and ultrasonic radiation constants
21 p3473 A71-41365

Primary and secondary cosmic ray muon variations in vertical and zenith angles, determining coupling coefficients
22 p3593 A71-42357

Underground meson telescope coupling functions calculations, using effective primary threshold energy
23 p3720 A71-43152

Asymptotic stability domain determination for nonlinear distributed parameter system, deriving coupling coefficients
23 p3699 A71-44079

Electrostatic waves nonlinear interactions in uniform plasma in presence of external constant magnetic field, deriving coupling coefficients by coupled mode theory
24 p3858 A71-45276

COUPLINGS

Quick connect/disconnect dry break couplings for aircraft fueling, describing design and operation
06 p0880 A71-18215

Control of time varying mechanical torque normal to ball bearing pair common spin axis by cross torque control through misalignment coupling
[ASLE PREPRINT 70LC-9]
08 p1298 A71-21156

Inertial-inertial beam stabilization application for image surface mechanical coupling to instrument /photography/ and uncoupled surface /eye/
14 p2242 A71-30146

High precision safety couplings performance, discussing flexible clutches enhancing effects
15 p2413 A71-31481

COVALENT BONDS

High temperature pyrolysis molding, discussing covalent organic bonds breakage and subsequent structural rearrangement of crosslinked polymer network
01 p0107 A71-10459

Refractory oxygenless powder metallurgy products in high temperature technology, considering covalent bond formation
09 p1478 A71-23395

Thermal coefficient of resistivity of carbides and solid solutions of Ti, Zr, Hf, V and Nb, noting inverse dependence of covalent bond in Me-Me band
15 p2430 A71-32154

COVARIANCE

Inconsistency in covariant gravitation theory with scalar field, considering limitation to forces of inertia and contradiction of macroscopic physics deterministic principle
04 p0625 A71-15098

Gaussian probability density functions covariance matrices dimension-reducing mapping using confidence spaces
04 p0619 A71-15331

Increase approximation of estimation errors covariance between discrete measurements due to random forcing function uncertainty
04 p0561 A71-15869

Classical and relativistic forces of inertia based on exact solution of Einstein nonlinear gravitational field equations, using general covariance principle
04 p0628 A71-15903

Nonstationary colored noise linear shaping filter to transform white noise into nonstationary random process with specified covariance function
09 p1424 A71-23100

Complex and envelope covariance for Rician fading communication channel, deriving equation for unsymmetric power spectrum
10 p1574 A71-23767

Covariance matrix of coordinate fluctuations of instantaneous radar center of reflection from set of scatterers
10 p1578 A71-24709

Misconceptions and distortions in n dimensional covariance matrices interpretation regarding probability confidence levels to error ellipsoid and hyperellipsoid
11 p1791 A71-25485

Symmetry properties of equation of motion, considering restrictions on force functions form of particles system due to covariance
12 p1929 A71-26959

Acceleration covariance in turbulent flow of isotropic homogeneous incompressible viscous conducting fluid
13 p2109 A71-29295

Variances and covariances calculation for fluctuating numbers of semiconductor conduction electrons in terms of noise
14 p2211 A71-30292

Kalman-Bucy filter construction as true time varying Wiener filter with covariances independent of signal generation, applying to data smoothing problem
14 p2220 A71-30460

Output probability distributions and covariance functions of nonlinear transformations of Gaussian stochastic processes occurring in signal detection and control theory
15 p2379 A71-31822

Spinning and point particles motion from Einstein equations based on covariance with general coordinate transformations
16 p2610 A71-33270

Discrete Kalman filter computational efficiency improvement by iterative processing technique for covariance matrix updating
17 p2722 A71-35182

Covariant definition of radius vector in Riemann space, studying position operator in general relativity theory
19 p3105 A71-38582

Invariant characteristics of Einstein spaces according to Petrov classification, determining gravitational fields described by covariant equation involving space curvature tensor and arbitrary scalar
19 p3105 A71-38585

Stationary covariance generation of matrix of rational functions of complex variable, solving factorization equation via algebraic Riccati equation
20 p3207 A71-38990

Signal process models choice in Kalman-Bucy filtering, proving smallest error covariance matrix existence
21 p3349 A71-41190

Temporal frequency spectra for spherical wave propagating through atmospheric turbulence, using covariance functions and Taylor hypothesis
22 p3575 A71-41788

Steady state gains and covariance computation for time invariant discretely updated linear systems, demonstrating iterative and algebraic solutions
23 p3660 A71-44116

Discrete parameter covariance stationary stochastic process in rotation sampling, deriving minimum variance unbiased linear population mean estimator by constrained optimization procedure
24 p3844 A71-45132

COWELL METHOD

NUMERICAL INTEGRATION

CRAB NEBULA

Crab pulsar optical pulses time of arrival measurements, discussing various emission mechanisms as cause for pulsar slowdown characteristics
01 p0153 A71-10363

Small angular diameter radio source in central Crab Nebula association with pulsar NP 0532 based on spectra and pulse duration
03 p0483 A71-13203

Pulsar NP 0532 average polarization absence due to Crab Nebula depolarization or unpolarized radiation on emission
04 p0643 A71-15047

Crab Nebula pulsar radio pulses polarization using polarimeter feed in Mark I telescope comparison to analysis by integration and photographic recording
04 p0649 A71-15274

Crab Nebula pulsar NP 0532, examining radio pulse shapes, flux densities and dispersion
05 p0800 A71-15926

Radio pulsars optical counterparts, comparing absolute intensity with Crab Nebula NP 0531
05 p0802 A71-15940

Crab Nebula pulsar NP 0532 light flash arrival times, suggesting oscillations due to growing amplitude instabilities
05 p0806 A71-16201

Crab pulsar magnetic field structure measurements, using optical wavelengths linear polarization
05 p0808 A71-16454

Crab Nebula pulsar PSR 0531 plus 21 at 410-1664 MHz, noting mean pulse profiles and spectral indices
05 p0812 A71-16697

HF modulation of optical, X ray and gamma radiation of Crab pulsar, discussing radiation production mechanisms
06 p0970 A71-18033

Balloon-borne telescopes to detect pulsed gamma rays from Crab Nebula, graphing data and diagramming telescope
06 p0950 A71-18034

Precursor pulse disappearance of Crab Nebula pulsar NP 0532 at 606 MHz
07 p1190 A71-18864

Crab Nebula pulsar characteristics, discussing neutron star hypothesis, optical counterparts, magnetic fields, mass, radius and origin
07 p1201 A71-20214

Crab Nebula and pulsar NP 0532 X ray spectra discussing pulse profile, emission and interstellar absorption
08 p1353 A71-20984

Crab Nebula pulsar NP 0532, discussing possible planetary system existence
09 p1522 A71-22975

Cosmic X ray astronomy, discussing supernova, variable and extragalactic radiation sources, diffuse background radiation and Crab Nebula measurements
09 p1522 A71-22976

Crab Nebula emissions on 4 and 6 November 1970, observing optical circular polarization
09 p1522 A71-22981

Crab Nebula pulsar magnetic field structure, discussing linear polarization modifications and wisps
10 p1668 A71-23870

Crab Nebula pulsar NP0532 radio observations, noting long term slowing down and irregular perturbations in periodicity

Crab Nebula model, discussing electromagnetic field time variation and electron acceleration and synchrotron emission

Radio pulses from Crab Nebula pulsar NP 0532, determining multipath scattering delay distribution function and distortion

Pulsars 0527 and 0531 as remnants of binary star supernova explosion, considering mass exchange and measured proper motion of 0531 and Crab Nebula

Crab pulsar optical time of arrival measurements from four observatories, discussing errors in data reduction to inertial reference frame

Crab pulsar frequency increase associated with nebula activity surge

Radio contour map of Crab nebula at 3.5 mm, giving brightness distribution and flux density

Crab nebula pulsar model, discussing charged particles acceleration to relativistic energies by intense LF electromagnetic wave

Rotation measure and intrinsic angle of Crab pulsar emission, discussing optical and radio radiation origin

Crab Nebula pulsar rotation and magnetic axes disposition from pulse shape and polarization data at optical and radio wavelengths

Supernovae outburst remnant radio emission from Crab Nebula, discussing synchrotron mechanism and connection with pulsars

Exploding universe phenomena, considering supernovae, exploding galaxies, Crab Nebula, pulsars, quasars and radio galaxies

Gamma rays in Crab Nebula pulsar, considering synchrotron radiation and inverse Compton scattering as production mechanisms

Compton synchrotron spectra of gamma rays produced in Crab Nebula by photons scattered by relativistic electrons, assuming magnetic field due to pulsar

Pulsed gamma radiation detection from Crab Nebula by balloon-borne telescope

Pulsed emission of hard X rays from Crab Nebula pulsar NP 0532, using balloon-borne telescope

Crab Nebula pulsar timing measurement leading to model involving inflation of closed magnetosphere with explosively released plasma

Neutron star models based on Nemeth-Sprung equation of state, discussing dynamic stability and Crab pulsar central density

Short term timing stability of Crab pulsar clock from telescope observations at 256 and 405 MHz

Crab pulsar NP 0532 low energy gamma radiation emission data, observing flux ratios and pulsations

Crab pulsar observations analysis by means of nonaligning or stabilized oblique rotator, discussing starquake theory and stressed magnetic field instability as alternative interpretations

Critique of Smith oblique rotator model for Crab pulsar radiation, concerning observation of optical pulse position angle variation and interpulse offset location

Hard X ray pulsations limits in higher energy range from Cyg X-1, comparing with Crab Nebula pulsar

Crab Nebula pulsar NP 0532 pulsed gamma emission from balloon flight measurements with spark chamber equipped gamma ray telescope

Crab Nebula - IAU Conference, Victoria University of Manchester, England, August 1970

Crab Nebula integrated electromagnetic emission spectra, noting flux density spectral index at various frequencies

Crab Nebula and pulsar gamma ray emission from synchrotron or inverse Compton mechanism

X ray observations in Crab Nebula, including angular size, location, energy spectra, time variability, line emission, interstellar absorption and polarization

Crab Nebula cosmic gamma rays from air shower emitted Cerenkov light detection, using synchrotron Compton scattering model

Crab Nebula pulsar radio properties, observing energy release due to increase in period, multipath propagation effects, intensity and time dependence

Identity relation of LF compact source to Crab pulsar NP 0532 with respect to interstellar scattering

Time variable dispersion of Crab Nebula pulsar, showing coincidence with occultation by solar corona

Crab Nebula optical pulse timing, noting neutron star crust rotation speedup and relaxation, eccentric planetary orbits and sinusoidal effects

Crab Nebula pulsar timing observations, correcting arrival times to solar system barycenter and dispersion effect

Time arrival measurements of optical pulses from Crab Nebula pulsar correlated to solar system barycenter

Pulse, nebula and wisp component in photometric and polarimetric observations of Crab pulsar

Comparative properties of pulsars, discussing Crab Nebula pulsar period, outside radio band emission, amplitude variations and interpulse intensity

Crab Nebula pulsar magnetosphere, considering model of rotating magnetized neutron star rate of energy generation and rotation law exponent

Crab Nebula pulsar and extar emission from collapsed star magnetosphere, accounting for physical characteristics with nonthermal plasma mechanism

Balloon obtained Crab pulsar gamma ray emission data searched for pulsation above 50 MeV

Tables of Crab Nebula pulsar radio pulse arrival times at Arecibo observatory

Steady state problem of energy spectrum of variable magnetic field accelerated electrons, considering synchrotron X ray emission of Crab Nebula and pulsar

Optical pulsar NP 0532 circular polarization upper limit from measurements throughout light curve

CRACK FORMATION

U CRACK INITIATION

CRACK INITIATION

Notched metal crack initiation, determining high cyclic loads effects by prior local plastic behavior at stress concentration

Metal fatigue research, examining crack initiation and propagation mechanism, stress-strain relationship and statistical nature

Triple point crack nucleation and growth at zero time by grain boundary sliding, estimating time to fracture

Creep failure model, using wedge crack nucleation in polycrystalline materials due to grain boundary sliding

Ti alloys crack initiation by solid Cd coating under tensile stress with intimate contact, noting time and temperature effects

Anisotropic materials ductile fracture involving crack initiation and propagation, using Dugdale mathematical model

[SESA PAPER 1729] Creep failure in elastoviscoplastic media from time and load-path dependent processes near axisymmetric fissure prior to cracking

Grain size effects on metal fatigue, considering work hardening and crack initiation and propagation

Crack initiation and propagation in fracture of plastic materials

Plastic zone effects on notch effect on crack initiation, analyzing ductile-brittle transition temperature relation to sample size

Metal fatigue crack initiation and propagation by continuum mechanics approach, considering dislocation, stress and deformation conditions and load cycle effects

Cracks nucleation by spark discharge in Mo single crystals, using optical and transmission electron microscopy

Dislocation cracks onset and propagation, considering crystal defect theory

Maraging steel weldability, examining crack origin and fracture toughness

Hard metals and WC-Co alloy stress and heat treatment effect on coercive force, crack formation energy and abrasive resistance

Acoustic emission monitoring system for real time detection of crack initiation and propagation in complex structure during static and fatigue tests

High temperature ductility of low alloy ferritic steels, correlating tensile elongation values to crack nucleation resistance

Stress wave emission from subcritical crack growth in thin walled Al-V titanium alloy

Crack opening mechanism for high temperature creep of polycrystalline graphite

Inertia effect in failure mechanics for steadily developing equilibrium cracks in dynamic system with time dependent periodically variable load

Ductile metals fatigue crack propagation model applications to brittle metals, discussing crack initiation effects on high strength steels failure modes

Fatigue crack formation and growth rate relationship, examining variance in cycle number in formation to final failure

Ti-6Al-4V and solution treated and aged Ti-6Al-6V-2Sn alloys, investigating relationship between alpha grain size and crack initiation fatigue strength

High temperature turbine parts protective coatings, discussing aluminum diffusion prevention and crack and oxidation resistance

Arc weld metal carbon content effects on welded joints mechanical properties in Ni at low and high temperatures, noting crack reduction

Welded steel structures fracture safe design, considering continuity conditions responsible for catastrophes resulting from crack initiation

Linear elastic fracture mechanics in presence of notch stress concentration, considering crack formation and propagation under cyclic stresses

Stable cracks initiation by piled up dislocations groups or by impeded strong shear bands

Microcrack formation in carbon fiber-resin matrix composites under thermal stress

Fractographic analysis of failure kinetics and crack formation in Al alloys, showing microfatigue intrusions and extrusions for various initial stress levels

Gas turbine blades fatigue crack development and failure analysis under thermal cycling tests, considering chemical processes and thermal and mechanical stresses

Thermally activated crystal microcrack initiation by fusion of leading and following dislocations

Stress relief cracking in Cr-Mo steel, considering correlation with embrittlement of water quenched base metal tempered at low temperature

Crack initiation in Ti-refined Fe-Ni alloys, using slow bending tests of notched bar samples with various notch angles

Fatigue process analysis through crack initiation and propagation and final fracture, considering ductility, tensile strength and fracture toughness roles

Thermal fatigue cracking of gas turbine blades in fuel combustion product flow, investigating surface composition, microhardness and structure under simulated loads

Precipitation hardenable Ni-base alloys embrittlement in high temperature oxygen atmosphere, considering intergranular crack initiation

Stress rupture ductility of electron beam, gas tungsten arc and gas metal arc welds, considering creep crack initiation

Ferritic steels weldability, establishing relations between transition points and cold crack formation

Alternative approach to fracture mechanics, discussing thickness dependence of residual strength, crack initiation and crack propagation stability 15 p2510 A71-32725

Fatigue failure of polyamide filaments from optical and electron microscopic observations, describing crack initiation and propagation 16 p2600 A71-32817

Mechanical properties, crack formation sensitivity, corrosion resistance and stress cracking behavior of Al-Zr-Mg alloys welded joints after prolonged heating 16 p2593 A71-33629

Cracked metals brittle fracture statistical analysis, discussing plastic deformation under loading 16 p2658 A71-33636

Surface effects of transverse slip screw dislocations in metal fatigue crack nucleation, relating stacking fault energy and number of cycles to failure 16 p2593 A71-33681

Al-Mg alloy with Ti, Zr, Mo and B additions under tensile and impact loads, investigating mechanical properties, strength and crack formation 16 p2594 A71-33712

High strength structural stainless steels with good toughness and little crack sensitivity, noting brittleness due to oxidation, precipitation and carbide network 16 p2597 A71-33916

Ti influence on ductility of normalized low alloy steel, considering crack initiation and propagation 16 p2598 A71-33991

Solution chemistry at stress corrosion crack tips in Al alloys, considering factors affecting pH change with time of initially acidic NaCl solutions 17 p2755 A71-34439

Simulated turbine blade thermal fatigue testing under transient and steady state heating and spanwise loading, obtaining crack initiation and propagation data [SAE PAPER 710459] 17 p2792 A71-34500

Image distortion technique for viewing surface deformation zones at precracked specimens under monotonic loading during fracture test [SESA PAPER 1799] 17 p2738 A71-34547

Toughness testing for low ductility fracture due to crack development in elastic stress field 17 p2757 A71-34557

Fatigue crack initiation and growth and residual strength of F-100 wing, comparing service failure data with full scale fatigue test results 17 p2827 A71-35159

Refractory alloys fatigue cracks formation kinetics based on endurance characteristics during symmetrical and asymmetrical load cycles 17 p2760 A71-35652

Fracture kinetics, emphasizing plastic deformation, dislocation and diffusion micromechanics, point defects effects, microcrack formation and interstitial mechanisms 17 p2834 A71-35667

Notch effect on metallographic characteristics of fatigue crack initiation and propagation in Al-Mg alloy 18 p2933 A71-35877

Metal structure, crack nucleation and propagation during fatigue under cyclic stress 18 p2936 A71-36693

Small holes effect on Ni base superalloy wrought thin sheets fatigue strength under pulsating tension load, analyzing crack initiation, propagation and critical length 18 p2938 A71-36850

Surface properties and environmental effects on fatigue striations development and crack initiation in Cu single crystals 19 p3077 A71-37412

Linear elastic fracture mechanics for design against high cycle fatigue failure, considering stress intensification, crack initiation and propagation 20 p3307 A71-38813

Stress concentration and defects effect on crack initiation and propagation in austenitic steels thermal fatigue 20 p3307 A71-39022

Dislocation arrays effects on heat treated austenitic stainless steel susceptibility to intercrystalline corrosion in sulfuric and nitric acids and cracking in magnesium chloride 21 p3402 A71-41087

Shatter crack incubated nucleation in relation to heat treatment effects on hydrogen elimination in steels, comparing with thermal explosion mechanism 21 p3402 A71-41090

Asymmetrical metal fatigue cracks development under infrequent compression cycles alternating with fundamental cycles of tension 23 p3774 A71-42896

Steel with various intensity stress risers under bending loads, showing difference in crack nucleation and propagation resistance 23 p3778 A71-44036

Failure and crack formation in gas turbine engine compressor disks under variable stresses from fatigue tests, considering safety factors 23 p3779 A71-44210

Grain boundary orientation effect on intergranular cracking, discussing crack introduction in purified iron by cathodic charging with hydrogen 23 p3695 A71-44285

Fatigue lifetime of overlapping joint spot welds of Al alloys, investigating shrinkage crack initiation and propagation 24 p3830 A71-44786

CRACK PROPAGATION

Steel cylinders with circumferential cracks under repeated impact tensile loads, investigating plain strain fracture toughness index temperature dependence 01 p0166 A71-10079

Mechanical properties effect on steels fatigue crack growth rate as function of stress intensity factor 01 p0099 A71-10167

Cleavage fracture equations of motion solved for constant moment, force and deflection, discussing plate crack propagation 01 p0167 A71-10291

Crack opening in infinite isotropic elastic solid via displacements applied to crack surface 01 p0167 A71-10292

Mathematical model for laser-induced supersonic crack propagation in crystals with weak cleavage planes 01 p0092 A71-10293

Photoelastic analysis using stress freezing to evaluate closure and precatastrophic crack extension in plates under cylindrical bending 01 p0167 A71-10295

Cracked rectangular plate bending under uniform transverse load, discussing crack geometry and propagation 02 p0321 A71-11681

Gaseous atmospheres environmental effects on metal mechanical properties at high temperatures, discussing failure mode with crack growth rate dependence on pressure 02 p0263 A71-11864

Metal fatigue research, examining crack initiation and propagation mechanism, stress-strain relationship and statistical nature 02 p0325 A71-12074

Triple point crack nucleation and growth at zero time by grain boundary sliding, estimating time to fracture 02 p0329 A71-12715

Si-Fe fatigue crack growth in vacuum at various temperatures, discussing stress intensity, cleavage and ductility effects 02 p0267 A71-12882

Ni base superalloy single crystal fatigue crack propagation 02 p0268 A71-12886

Ti-Al-V hydrogen induced fatigue crack growth at room temperature under sustained load 02 p0268 A71-12891

Anisotropic materials ductile fracture involving crack initiation and propagation, using Dugdale mathematical model [SESA PAPER 1729] 03 p0507 A71-13760

Through-thickness fatigue crack growth in polymethyl methacrylate sheets, observing stress intensity factor range, frequency and mean effects [SESA PAPER 1727] 03 p0448 A71-13771

Temperature effect on slip- and spark-induced crack propagation in polycrystalline Mo 03 p0444 A71-14317

Soviet book on fracture physics /crack growth in solid bodies/ covering glasses, polymers, single crystals and polycrystalline metals, etc 03 p0515 A71-14398

Grain size effects on metal fatigue, considering work hardening and crack initiation and propagation 03 p0447 A71-14495

Crack growth relation to grain boundaries, considering transgranular cleavage in plain carbon steels and ductile intergranular fracture in Al-Zn alloy 03 p0447 A71-14497

Brittle fracture mechanics, discussing shape, stress and dynamic toughness factors, crack-defect interaction and crack barriers 03 p0516 A71-14578

Crack initiation and propagation in fracture of plastic materials 03 p0516 A71-14580

Energy accumulation effects on pressure vessels strength and failure mode, examining crack propagation and arrest 03 p0517 A71-14586

Carbon steel and heat treated duraluminum fatigue fracture microstructure observation using electron microscope, determining crack propagation relationships to loading sequence 04 p0610 A71-14880

Metal fatigue crack initiation and propagation by continuum mechanics approach, considering dislocation, stress and deformation conditions and load cycle effects 04 p0666 A71-14888

Steels brittle fracture susceptibility by notch impact bending test, considering plastic deformation zone and crack propagation 04 p0610 A71-14889

Ti alloys stress corrosion crack propagation in salt water, investigating existence of threshold stress from electrochemical data 04 p0610 A71-14891

Crack opening displacement concept in fracture mechanics, considering crack tip radius as measure of extension potential 04 p0670 A71-15392

Fatigue crack propagation in aluminum alloy sheet, determining relationship between propagation rate and stress intensity factor and crack initiation conditions 05 p0766 A71-16296

Subgrain volume and orientation effects at tip of fatigue crack on propagation rate 05 p0821 A71-16348

Crack extension by incident elastic wave diffraction for specific shear stress character at wave front 05 p0825 A71-16709

Metal stress corrosion crack propagation rate relationship to electrochemical parameters, considering active and passive regions of potentials 05 p0827 A71-16814

Dislocation cracks onset and propagation, considering crystal defect theory 05 p0827 A71-16853

Brittle fracture propagation velocity and branching, using high speed photography, electrical and ultrasonic methods 06 p0981 A71-17296

Body weakening due to symmetrically expanding crack, discussing internal pressure, elastic equilibrium and stress-strain state 06 p0896 A71-17326

Crack propagation as unstable stress relaxation process, using viscoelastic dislocation model 06 p0984 A71-17557

Acoustic emission monitoring system for real time detection of crack initiation and propagation in complex structure during static and fatigue tests 06 p0906 A71-18461

High and low cycle fatigue crack growth rate in various materials under variable loads 07 p1211 A71-19193

Antiplane stress distribution around single or collinear cracks in nonwork hardening elastoplastic material under uniform load 07 p1212 A71-19350

Residual stress effects on Al alloys stress corrosion crack growth rates as function of plane strain stress intensity, discussing residual stress elimination methods 07 p1137 A71-19974

Stainless steel fatigue crack growth characteristics at liquid metal fast breeder type nuclear reactors elevated temperatures 07 p1138 A71-19983

Steels fatigue tests, observing crack propagation through weld heat affected zones at two orientations to stress axis 07 p1139 A71-19989

Precracked double cantilever beam specimens, measuring resistance to stress corrosion crack propagation as function of overaging in Al alloys 07 p1142 A71-20363

Carbon fiber reinforced epoxy resin fatigue and crack propagation behavior in air, moisture and oil environments, using tensile, bending and torsion test methods [PLASTICS INST. PAPER 49] 08 p1318 A71-20892

Ductile metals fatigue crack propagation model applications to brittle metals, discussing crack initiation effects on high strength steels failure modes 09 p1467 A71-22285

Materials fatigue disintegration process visual examination for crack development kinetics, using fiber optics 09 p1454 A71-22316

Metal sheet failure kinetics, investigating tensile stress and cycle frequency during fatigue crack growth and extension rate effects 09 p1468 A71-22508

Fatigue crack propagation rate in sheet alloys with holes as stress concentrators related to duration of various development phases 09 p1538 A71-22597

Fast brittle crack slowing by mechanical twins in transformer steel and by slip bands in LiF and NaCl crystals 09 p1468 A71-22625

Fatigue life and crack propagation of sheet, plate, extrusions and forgings in annealed and solution treated aged Ti-Al-V-Sn alloy [ASM PAPER W71-22.5] 09 p1471 A71-23096

Fracture toughness relationship to microstructure in alpha-beta Ti alloy heat treated to constant yield strength, considering crack propagation 09 p1472 A71-23126

Fracture models of stress field produced by accelerating crack under shear loading, using pulse diffraction method 10 p1684 A71-23932

Fracture mechanics application to structural adhesives test methods, considering joints crack extension resistance and plane strain fracture toughness 10 p1615 A71-24088

- Processing variables effects on epoxy adhesive joints fracture toughness and crack extension resistance
10 p1632 A71-24089
- Stress corrosion crack extension in adhesive epoxy joints under combined long term static loads and aggressive action of water
10 p1632 A71-24090
- Macroscopic and microscopic plastic zones ahead of propagating fatigue crack on surface and inside of specimen as function of load cycles
10 p1626 A71-24306
- Kinetic crack propagation theory of fatigue fracture toughness for notched and unnotched asurfomed high strength and heat treated ball bearing steels
10 p1687 A71-24307
- Quasi-static problem of stress-strain distributions in elastic medium with moving crack, calculating arbitrary external force effect on crack
10 p1687 A71-24349
- High strength steel fracture toughness, investigating stress wave emission during crack growth
10 p1627 A71-24534
- Linear elastic fracture mechanics in presence of notch stress concentration, considering crack formation and propagation under cyclic stresses
10 p1628 A71-24686
- Epoxy bond strength, cracking and failure of lapped joints as function of composition and mechanical properties
10 p1618 A71-24826
- Crack dislocations nature and significance, density equations, instability conditions, fracture mechanics, including cohesive forces and plastic zone equilibrium
10 p1628 A71-25026
- Fatigue crack propagation rates in Al under constant low stress, discussing data processing methods
10 p1629 A71-25053
- Stress threshold for crack growth in rotating shaft bending fatigue
10 p1693 A71-25058
- Compression, creep, stress relaxation and overload effects on delay in fatigue crack growth and structural life predictions
10 p1694 A71-25059
- Penny shaped crack in elastic layer bonded to two dissimilar half spaces, investigating stress intensity factors and fracture propagation direction
11 p1841 A71-25301
- Elastic-plastic fracture behavior engineering model based on surface flaw severity by crack length dimensions measurements
11 p1845 A71-25345
- Epoxy resin fatigue behavior from double torsion technique, considering stable crack movement in brittle materials
11 p1785 A71-25401
- Semiinfinite crack perpendicular to elastic half plane surface under pressure distribution on faces or remote loading, obtaining fracture mechanics solution with Wiener-Hopf method
11 p1847 A71-25444
- Computer simulation of stress corrosion cracking, considering electrochemical oxidation mechanism for crack propagation
11 p1847 A71-25449
- Crack propagation in chromium steel butt weld sheets, discussing dendrite microstructural effects on brittle resistance and toughness
11 p1770 A71-25945
- Al alloys and steel, determining potential and pH changes during stress corrosion crack propagation by microelectrode technique
11 p1783 A71-26497
- Crack extension criterion for time dependent spallation, correlating simple mechanistic model with Al alloys data
12 p1919 A71-27774
- Critical equilibrium of two component composite material with crack propagating along diameter of round inclusion
13 p2090 A71-27824
- Fatigue crack growth rate in plates of anisotropic materials, considering Al and Ti alloys under cyclic loads
13 p2082 A71-27826
- Modified heat conductivity solutions for region with moving boundary, applying to crystallization front or crack propagation
13 p2159 A71-28037
- Fiberglass reinforced plastics under constant strain rate, deriving failure models as random process for microscopic crack propagation
13 p2148 A71-28115
- Solid bodies crack development theory, emphasizing crack tip fine and hyperfine structures concepts and time dependent effects
13 p2149 A71-28121
- Papers on fracture mechanics covering engineering fundamentals, environment effects, crack growth, photoelastic analysis, nondestructive testing, etc
13 p2151 A71-28212
- Notch analysis of fracture, discussing elasticity theory of stress concentration and applications to brittle inhomogeneous materials and fatigue crack propagation
13 p2151 A71-28215
- High strength alloys fatigue in terms of irreversible microplastic deformations accumulations, discussing fatigue crack mechanisms and cyclic straining effects on bulk properties
13 p2152 A71-28219
- Fatigue crack propagation in thermoplastics, investigating stress intensity effect on factor mean value
13 p2091 A71-28465
- Two stage creep cavity growth by grain boundary sliding as shear crack and Griffith-Orowan fracture, using energy balance argument
13 p2085 A71-28504
- High strength steel delayed fracture, applying Yokobori stochastic-kinetic theory of fatigue crack propagation for time to fracture calculation
13 p2155 A71-28790
- Fatigue crack propagation kinetic theory, investigating microcrack nucleation mechanism based on vacancy condensation near crack tip
13 p2155 A71-28791
- Stress concentration for fatigue crack propagation in smooth and notched samples under symmetrical loading
13 p2157 A71-29373
- Structural fatigue in aircraft design, discussing twin engine transport tests, crack propagation rate, residual strength, etc
13 p2158 A71-29434
- Mechanical properties of fiberglass-epoxy cross-ply laminates, considering tensile strength, crack propagation and ultimate stress and strain
14 p2264 A71-29837
- Fatigue process analysis through crack initiation and propagation and final fracture, considering ductility, tensile strength and fracture toughness roles
14 p2258 A71-29896
- Metal specific work breakdown during crack propagation, investigating thermal effect of plastic deformation with thermocouples
15 p2413 A71-31479
- Crack propagation model in linearly viscoelastic solid strip based on thermodynamics first law
15 p2506 A71-32011
- Fatigue crack propagation anisotropy in hot rolled steel plate, demonstrating crack growth rate sensitivity to microconstituents orientation
15 p2508 A71-32255
- Low alloy high strength steels undetected fabrication originated anomalies, causing brittle behavior and crack propagation susceptibility
15 p2435 A71-32435
- Plastic strain range-fatigue life behavior as two slope relationship, considering low cycle fatigue laws in terms of crack propagation mode change
15 p2436 A71-32508
- Alternative approach to fracture mechanics, discussing thickness dependence of residual strength, crack initiation and crack propagation stability
15 p2510 A71-32725
- Fatigue failure of polyamide filaments from optical and electron microscopic observations, describing crack initiation and propagation
16 p2600 A71-32817
- Linearly viscoelastic strip with slowly propagating central crack, calculating stress intensity factor and crack opening size
16 p2590 A71-32939
- Crack propagation in brittle solids under constant deformation or thermal shock, verifying behavior by results with polycrystalline aluminum oxides
16 p2590 A71-32941
- Stress corrosion fatigue crack growth in Ni-Cr-Mo maraging steel, using controlled-potential techniques, pH measurements and fractographic analysis
16 p2590 A71-32942
- Elastic energy release rates and stress intensity from nonlinear load deflection curves as function of crack length to specimen width ratio
16 p2590 A71-32945
- Strain rate effect on crack growth within subcritical load range, deriving expressions for rate-independent and rate-dependent quasi-brittle solids
16 p2590 A71-32946
- Stress intensity history effect on metal fatigue crack growth rate, using closed loop hydraulic testing machine with stepwise increments in sinusoidal tension-tension load cycles
16 p2591 A71-32948
- Fatigue S-N curves discontinuities associated with plastic yield and crack path tested on mild steel notched specimens
16 p2591 A71-33346
- Crack propagation resistance-cyclic fracture strength relation for austenitic and Mn-Cr-V steels, considering thermomechanical working effects
16 p2592 A71-33408
- Steel cylinders with circumferential cracks under repeated impact tensile loads, investigating plane strain fracture toughness index temperature dependence
16 p2658 A71-33635
- Ti influence on ductility of normalized low alloy steel, considering crack initiation and propagation
16 p2598 A71-33991
- Fractographic investigation of fatigue crack propagation in pure monocrystalline and polycrystalline Al
16 p2599 A71-34095
- Fatigue crack propagation model for explosion bonded titanium-steel system under constant load amplitude conditions
16 p2600 A71-34096
- Simulated turbine blade thermal fatigue testing under transient and steady state heating and spanwise loading, obtaining crack initiation and propagation data
17 p2792 A71-34500
- Propagating crack arrest capability of circular hole in plate, studying dynamic stress intensity and concentration factors changes
17 p2820 A71-34546
- Precatastrophic extension effects on local stresses in cracked plates under bending fields, using stress freezing and slicing for photoelastic experiments
17 p2820 A71-34549
- Fatigue crack propagation dependence on strain energy release rate and crack opening displacement, analyzing data on high yield strength steels, Ti and Al alloys
17 p2826 A71-35152
- Thickness effect on fracture toughness and crack propagation of Al alloy sheets used for aircraft skins
17 p2758 A71-35153
- Fatigue crack propagation in Al alloy panels stiffened with bolted and integral stringers, determining stress intensity factor/crack growth rate relationship
17 p2827 A71-35156
- Metal fatigue crack failure prediction for arbitrary uniaxial cyclic loading, discussing method based on treatment of crack growth as continuous stochastic process
17 p2758 A71-35158
- Fatigue crack initiation and growth and residual strength of F-100 wing, comparing service failure data with full scale fatigue test results
17 p2827 A71-35159
- Al alloy sheet fatigue crack closure under cyclic tensile loading, deriving expression for crack propagation rate in terms of effective stress amplitude
17 p2828 A71-35162
- Helicopter rotor blades fail-safe design, presenting criteria for fatigue loaded structures residual strength and life based on crack propagation rate methods
17 p2828 A71-35163
- Notch effect on metallographic characteristics of fatigue crack initiation and propagation in Al-Mg alloy
18 p2933 A71-35877
- Dynamic yield and absorptivity of steel during brittle fracture propagation under neutron irradiation
18 p2934 A71-35987
- Abbreviated testing for material constants determination of equation of fatigue crack propagation from one specimen at different stress amplitudes
18 p2976 A71-35988
- Metal structure, crack nucleation and propagation during fatigue under cyclic stress
18 p2936 A71-36693
- Fatigue crack propagation in thin aluminum plates under fluctuating tensile loads, concerning Forman model
18 p2938 A71-36851
- Plastic zones and stable crack growth at notches in thin high strength sheet alloys, using replication technique
18 p2938 A71-36853
- Two parallel noncoplanar cracks extension in elastically isotropic solid by applied shear stress with deformation in antiplane strain mode
19 p3157 A71-37797
- Ni-Mo-V, Ni-Cr-Mo-V and Cr-Mo-V high strength rotor forging steels fatigue crack growth characteristics tests at room temperature
20 p3247 A71-38768
- Fatigue crack propagation in high yield strength steels at room temperature in air environments, considering primary influence of applied stress intensity range
20 p3248 A71-38769
- Acoustic emission technique for nondestructive cracking rate determination in hydrogen embrittled steel, using crack-tip stress intensity factor as critical parameter
20 p3241 A71-38773
- Stress corrosion crack branching in high strength steels, considering constant crack velocity and critical stress intensity
20 p3248 A71-38777
- Corrosion fatigue crack propagation in Ni-Cr-Mo maraging steel in room temperature NaCl solution at various stress intensity ranges
20 p3248 A71-38778
- Linear elastic fracture mechanics for design against high cycle fatigue failure, considering stress intensification, crack initiation and propagation
20 p3307 A71-38813

Ultrasonic technique for crack and craze velocity measurement in material subjected to stress in liquid environment

20 p3233 A71-38817

Stress concentration and defects effect on crack initiation and propagation in austenitic steels thermal fatigue

20 p3307 A71-39022

Fracture testing, discussing fracture toughness, proof testing assemblies, crack identification, growth, catastrophic failure probability, etc

21 p3463 A71-40673

Vacancy absorption model for fatigue crack propagation in Al based on X ray inspection and transmission electron microscopy

21 p3399 A71-40698

Computer simulation of crack propagation in plane strain and plane stress geometries, solving continuum mechanics equations in two space dimensions and time

21 p3351 A71-40797

Macroscopic residual stress and strain measurement and crack tip substructure, discussing crystal plastic deformation effect on fatigue crack propagation

21 p3466 A71-40831

Crack shapes and stress intensity factors for deep edge crack in plate under tension or bending

21 p3467 A71-40907

Alloying effects on crack propagation resistance of precipitation hardening austenitic steel

21 p3402 A71-41091

Weldable Al-Zn-Mg alloys with cathodic polarization protection, noting decrease in stress corrosion crack propagation rate

22 p3560 A71-41625

Ductile crack growth detection in crack opening displacement specimens by electrical potential method

22 p3550 A71-41640

Fracture mechanics analysis of metal fatigue crack growth as function of stress intensity factor

22 p3560 A71-41641

Surface strain cyclic flaw growth rates for Al and Ti plates, using end point, flaw opening and striation measurements

22 p3560 A71-41643

Thick Al alloy sheet with central slot under cyclic loads, examining striation spacings and fatigue crack propagation rates with electron fractography

22 p3561 A71-41708

Fracture mode transition under varied mean stress levels in metal fatigue at constant crack growth rate

22 p3561 A71-41711

Crack model with strain rate dependent yield stress, calculating stress intensity factor variation with fracture propagation velocity

23 p3774 A71-43145

Hertzian fracture test for strong solid surface properties measurement based on crack growth in nonuniform stress field due to contact loading

23 p3777 A71-43934

Steel with various intensity stress risers under bending loads, showing difference in crack nucleation and propagation resistance

23 p3778 A71-44036

Fine structure at crack tip expanding in ideally elastoplastic material in plane deformation state and plane stressed state

23 p3778 A71-44061

Fatigue lifetime of overlapping joint spot welds of Al alloys, investigating shrinkage crack initiation and propagation

24 p3830 A71-44786

Crack propagation kinetics in organic glass subjected to monotonically increasing tension perpendicular to crack plane, examining crack contour prior to spontaneous rupture

24 p3883 A71-44858

Polymethyl methacrylate samples resistance to crack propagation, detailing modulus of cohesion effects

24 p3841 A71-45050

Aerospace materials and structures shock sensitivity from derivation of dynamic fracture propagation relationship to stress wave

24 p3886 A71-45370

CRACKING [FRACTURING]

Vapor phase interaction of methanol and carbon tetrachloride with Ti thin films, discussing Ti stress corrosion cracking implications

01 p0102 A71-10812

Ni maraging steel weldments stress corrosion cracking characteristics in air and pentaborane by electron microscopy

02 p0262 A71-11707

Ti-Al alloy hot salt stress corrosion cracking due to hydrogen production and absorption

02 p0267 A71-12880

Ni maraging steel cantilever beams intergranular stress corrosion cracking in aqueous solutions, noting heat treatment effects

02 p0267 A71-12881

Superalloy turbine engine guide vane thermal fatigue cracks repair by plasma arc fusion method

03 p0432 A71-13257

Al-Zn-Mg alloys intergranular failure due to aqueous stress corrosion cracking, fatigue and exfoliation, analyzing mud-crack pattern

03 p0441 A71-13319

Al-Zn-Mg ternary alloys stress corrosion cracking resistance relation to mechanical strength decrease, quenching rate increase and solution treatment temperature

04 p0609 A71-14772

Al-Zn-Mg ternary alloys stress corrosion cracking resistance relation to heat affected zone postannealing aging and cooling rate decrease

04 p0610 A71-14773

Stress corrosion cracking mechanism, considering anodic dissolution, local surface enrichment and hydrogen embrittlement in noble metal species

04 p0610 A71-14892

Polyester resin model fatigue crack closure, determining residual stress distribution and crack opening and closing force by photoelastic research

04 p0670 A71-15390

Microstructure effect on metastable beta Ti alloy strength, toughness, stress corrosion cracking susceptibility

04 p0614 A71-15780

Hot ductility curves for cracking sensitivity prediction during welding

04 p0617 A71-15907

Age hardened Ni base material strain-age cracking phenomenon measurements, using constant strain Gleeble technique

04 p0617 A71-15912

Stress distribution in infinite strip weakened by transverse crack under loading at infinity

05 p0825 A71-16612

High strength Al alloys stress corrosion resistance testing in various heat treatment conditions, using precracked cantilever beam specimens

06 p0912 A71-18012

Refractory metal alloys hot crack sensitivity testing by Vrestraint method, using ultrahigh purity inert atmosphere

06 p0912 A71-18042

Refractory alloys fatigue cracks kinetics based on endurance characteristics reflecting resistance to variable loads

07 p1129 A71-19153

Physical analogy treating low cycle metal fatigue relation to stress growth in plastic region, discussing cracking mechanisms

07 p1211 A71-19166

Lattice defect and grain boundary influence on metal dissolution in electrolyte and stress corrosion cracking

07 p1134 A71-19604

Mechanical properties, crack formation sensitivity, corrosion resistance and stress cracking behavior of Al-Zr-Mg alloys welded joints

07 p1136 A71-19633

High yield strength steel stress corrosion crack tip electrochemical and pH potential conditions, using AgCl reference electrode

07 p1137 A71-19973

Cyclic thermal cracking and fatigue analysis in large steam turbine rotors with three dimensional temperature and triaxial stress computation [ASME PAPER 70-PWR-1]

07 p1216 A71-20198

Methanol stress corrosion cracking of Ti-Al-V foil inhibited by pretreatment in aqueous solutions of electrolytes, discussing colloidal character of microcrystallites

07 p1142 A71-20362

Stress concentration analysis at arbitrarily oriented cracks in shell, noting curvature influence by single integral equations with Cauchy kernel

07 p1217 A71-20458

Stationary temperature field and stresses in infinite body with thermally insulated penny shaped crack, assuming heat source and sink symmetrical distribution

07 p1217 A71-20462

Anisotropy and weldability, considering through-thickness tension decohesion cracking under static nonload conditions in corner and tee joints

09 p1459 A71-23454

Aluminum-epoxy joints stress corrosion cracking inhibition and crack tip plastic deformation by scanning electron microscopy

10 p1615 A71-24091

Metal plates and sheets stress corrosion cracking velocities, using torsion crack propagation specimen at constant load or deflection

10 p1627 A71-24474

Ti-Al-Mo-V alloy stress corrosion cracking, using controlled potential technique in aqueous and methanol environments with and without halogen ions

11 p1777 A71-25448

Heat affected zone crack filling and weld metal-base metal interactions of high strength alloys in dissimilar gas arc welding

11 p1769 A71-25749

Crack kinematics for bodies with time dependent deformation and strength characteristics in brittle fracture, discussing tip region, crack models and energy equation

13 p2149 A71-28123

High strength Al alloy forgings processing for stress corrosion cracking prevention, including plane relocation and compressive relief techniques

13 p2073 A71-28146

Crack growth and fracture mechanics, discussing linear stress field and plasticity analyses for three dimensional and dynamic problems

13 p2151 A71-28213

Stress corrosion cracking, discussing stress effect environmental and metallurgical factors and electrochemical and sorption theories

13 p2085 A71-28221

High strength alloys, discussing fracture mechanics concepts applicability to environmental cracking under static load and combined effects of cyclic stress and aggressive environment

13 p2152 A71-28222

Carbon steel fatigue crack tip plastic zone substructure by X ray microbeam technique, determining dislocation density, stress intensity and crack propagation rate interrelationships

13 p2155 A71-28789

Postweld heat treatment cracking of high Ni alloys using mechanical testing and metallography

13 p2087 A71-29092

Ti-Al binary alloy embrittlement in sea water by notched cantilever beam stress corrosion test, investigating alpha 2 particle precipitation effect on cracking susceptibility

16 p2256 A71-29522

Wells COD /crack opening displacement/ criterion for notch root deformation and fracture measurements

16 p2591 A71-32949

Crack interaction effect along straight line on critical equilibrium and fracture of plate relative to cross-piece length

16 p2658 A71-33685

Surface cracking resistance of polymethyl methacrylate glass in vacuum, air and nitrogen, noting humidity effect

16 p2601 A71-33690

Stress corrosion cracking in high strength steels, showing occurrence along zero isoclinic surfaces

17 p2755 A71-34440

Ti-Al alloys surface film growth and stress corrosion cracking as function of applied potential and environmental pH, presenting results of ellipsometric examination

17 p2756 A71-34489

Anisotropic composite materials failure surface criteria in three dimensional space, using graphical representation

17 p2824 A71-34817

Center cracked tension panels residual strength evaluation and prediction, deriving analysis technique based on stress intensity factor

17 p2827 A71-35155

Fatigue cracks in tempered and aged Al alloy, using scanning electron microscopy

17 p2760 A71-35474

Physical analogy treating low cycle metal fatigue relation to stress growth in plastic region, discussing cracking mechanisms

17 p2834 A71-35662

Stress corrosion cracking in Ni maraging steel in NaCl solution, using electrochemical polarization and potential analysis

18 p2934 A71-35989

Molecular bond rupture and strain energy release rates correlation during ozone cracking of rubber from electron paramagnetic resonance and stress elongation measurements

18 p2939 A71-36244

Nickel maraging steel in NaCl solution, investigating susceptibility to stress corrosion cracking

18 p2935 A71-36595

Aircraft parts testing by NDT methods, considering ultrasonic system for valve defects and fluorescent particle system for crack detection

18 p2929 A71-37056

Salt solution treated and quenched Mg-Al alloy rods tests in distilled water, investigating transgranular stress corrosion cracking and deformation twinning

19 p3083 A71-38722

Partial thickness cracks of preselected depths and shapes by axial and flexural fatigue methods, yielding preferred propagation path

20 p3248 A71-38780

Corrosion resistant materials evaluation for suitability in high strength fasteners, considering mechanical properties, stress corrosion cracking and hydrogen embrittlement problems

20 p3251 A71-39340

Ta-W polycrystals and single crystals oxidation at 850-1100 C, noting anisotropic scale-fracture morphologies

20 p3252 A71-39373

Arutunian method application to crack problems in power law elastic materials and contact problems in nonlinear creep, noting error for crack tip singularity

20 p3310 A71-39868

Alloying effects on corrosion cracking of Cr-Ni austenitic stainless steels, testing in chloride solutions

21 p3402 A71-41094

Koiter theory for structural snap-through buckling behavior, using discretized matrix procedure based on finite element idealization

22 p3613 A71-41436

Preheating effects on crystal lattice orientation, tensile strength and stress corrosion cracking of Al-Zn-Mg alloy thick plates

22 p3559 A71-41516

Ductile crack growth detection in crack opening displacement specimens by electrical potential method

22 p3550 A71-41640

Stress intensity factors analysis of strip with longitudinal crack subject to tension and bending along edges and tension of rectangular plates with central crack

22 p3614 A71-41709

Elastic cracks and screw dislocation pile-ups crossing bimaterial interface, deriving dual singular integral equations

22 p3615 A71-41710

Metal embrittlement by gaseous hydrogen, discussing countermeasures against hydrogen metal interaction and cracking

22 p3562 A71-41999

Inconel superalloy microscopic observation of local melting and hot ductility behavior during weld thermal cycles to clarify cracking cause in heat affected zone

22 p3564 A71-42494

Dynamic three dimensional stress distribution near crack tip in finite plate, using finite difference scheme

23 p3776 A71-43376

Scanning electron microscopic observation of fracture surface of austenitic stainless steels for stress corrosion cracking in magnesium chloride and calcium chloride solution

23 p3693 A71-44073

Loading modes effect on stress corrosion cracking of Ni maraging steel in NaCl solution

23 p3693 A71-44074

Grain boundary orientation effect on intergranular cracking, discussing crack introduction in purified iron by cathodic charging with hydrogen

23 p3695 A71-44285

Ni-base superalloys metallography, investigating catastrophic cracking in weld heat affected zones by electron microscopy

24 p3839 A71-45139

CRACKS

NT MICROCRACKS

NT SURFACE CRACKS

Cracked metals brittle fracture statistical analysis, discussing plastic deformation under load

01 p0166 A71-10080

Two concentric circular arc parallel cracks interaction in infinite plate under tension, calculating crack tip stress intensity factor based on elastostatics theory

01 p0167 A71-10174

Orthotropic cylindrical shell stress distribution near axial line crack, formulating problem as system of singular integral equations

01 p0167 A71-10175

Horizontal shear wave diffraction by finite crack and rigid ribbon in elastic medium

01 p0173 A71-10845

Thermoelastic axisymmetric problem for half space applied to steady temperature field and stress concentration in infinite body with heat conducting plane circular crack

02 p0322 A71-11733

Coupled Riemann-Hilbert boundary value problems for thermoelastic state near thermally insulated crack in inhomogeneous elastic medium

02 p0322 A71-11734

Stress development in elastic plate with crack under edge loads, estimating plastic zone size at crack ends

03 p0514 A71-14361

Plastic zone near crack end under forces causing plane deformation, calculating stress-strain state by finite element method

03 p0515 A71-14363

Crack perpendicular to planar interface between isotropic half spaces, noting elastic constants effect on stress components distribution and relative magnitudes

04 p0670 A71-15384

Stress distribution in infinite cracked elastic plate subjected to constant twisting on basis of Reissner thin plates theory

04 p0670 A71-15385

Fatigue and fracture in elastic cylindrical shells with circumferential crack under axial tension, noting precracked specimens

04 p0670 A71-15386

Stress intensity factors for infinite sheet rectangular cut-out with symmetrical edge internal cracks under axial tension

04 p0670 A71-15387

Thermal fatigue cracks in gas turbine blade models under simultaneous thermal cycling and static tensile loads simulating pulsed regimes

04 p0671 A71-15638

Elastic plate with heat conducting rectilinear crack, determining steady state temperature field and stresses

05 p0827 A71-16889

Stress distribution at cracks in solid bodies, discussing crack models, plasticity and elasticity theories and continuum mechanical basis of fracture theory

06 p0911 A71-17413

Matrix and round inclusion two component composite equilibrium, considering crack effect on strength

06 p1000 A71-17938

Infinite elastic plate with rectilinear crack, determining heat exchange effect on thermoelastic stresses

06 p1000 A71-17939

Brittle plates with statistically distributed cracks, examining limiting equilibrium under tension and compression

06 p1000 A71-17941

Triple integral equations solution based on analytic functions theory, applying to stress-strain state in plate with two equal collinear cracks

06 p1002 A71-18346

Strain field measurement near crack tip in polymethyl methacrylate by holographic interferometry

07 p1209 A71-19043

Unbounded isotropic elastic plate traversed by two parallel cracks, obtaining limiting equilibrium state

07 p1211 A71-19192

Infinite isotropic plate weakened by cracks along circular arcs, calculating stress-strain state and critical loads

09 p1538 A71-22524

Strength characteristics of machine parts with cracks calculated by graphoanalytic procedure

10 p1686 A71-24192

Spherical shell containing through crack, calculating in-plane and Kirchhoff bending stresses under periodic transverse vibrations

10 p1693 A71-25054

Plate thickness effect on stress distribution around crack, using three dimensional elasticity equations

10 p1693 A71-25055

Strain energy calculation of V notched crack in elastic continuum from finite element computer programs applied to fractures in solid propellant rocket motor cartridges or grains

10 p1693 A71-25056

Stress intensity factor of flat toroidal crack under internal pressure, using approximate solution of axisymmetric problems in fracture mechanics

10 p1693 A71-25057

Dissimilar bonded anisotropic half spaces with flat crack under arbitrary loads, determining stress distribution

11 p1842 A71-25303

Stress and displacement fields in elastic half plane containing edge crack normal to free surface, using integral equations

11 p1847 A71-25440

Residual stress at plate crack determined from elastic stress intensity factor measurements [ASME PAPER 71-MET-A]

12 p1977 A71-27311

Equilibrium of elastic body weakened by system of circular planform cracks in single plane

13 p2148 A71-27807

Attitude measurements of fracture bounding lunar rilles from systematic increase with height

13 p2134 A71-28289

Cracks in Cosserat continuum, investigating couple-stress effects on stress concentration

13 p2153 A71-28521

Unbounded orthotropic body with two internal coaxial elliptical cuts, calculating elastic equilibrium

13 p2156 A71-29068

Stress-strain state of thin walled ellipsoidal shell of revolution with arbitrarily oriented crack

13 p2156 A71-29069

Longitudinal and transverse rib reinforced plates with parallel cracks extending to edge, obtaining flexural rigidity and stress-strain state

13 p2156 A71-29070

Stress intensity factors for deep cracks in single edge cracked bend and compact tension specimens

14 p2322 A71-29739

Plastic strain development at fatigue crack tip in mild carbon and stainless austenitic steels from electron and optical microscopy

14 p2257 A71-29841

Elastic sphere equilibrium with penny shaped crack under inner surface pressure, observing stress distribution

14 p2326 A71-30096

Torsion of circular composite rods of sectors with different shear moduli and radial cracks

14 p2326 A71-30193

Monograph on crack problems in mathematical theory of thermoelasticity covering crack effects on stress distribution in circular cylinders, thick plates and infinite solid bodies

14 p2329 A71-30501

Crack tip strain problem in elastic body, relating fracture energy criterion with mathematical models

14 p2334 A71-31002

Brittle plates with stochastic distribution of cracks under biaxial tensile-compressive stresses, obtaining critical load

15 p2504 A71-31853

Elastic-plastic mechanics of steady crack growth under antiplane shear, discussing residual stress effect, plastic zones shape and strain distribution

15 p2428 A71-31974

Elastic-plastic finite element analysis of near crack tip stress and strain field structure

16 p2590 A71-32940

Finite element method application to stress distribution analysis at crack tip of rectangular plate under tension, obtaining elastoplastic response to cyclic loading

16 p2653 A71-33086

Axially symmetric thermal stress distributions in infinite elastic solid containing flat circular external crack

16 p2654 A71-33169

Thermoelastic critical equilibrium of plate with rectilinear crack under heat transfer from edge surface and tensile stress

16 p2658 A71-33686

Thermal stresses distribution in wedge shaped solids with cracks, solving elastic equilibrium equations

16 p2661 A71-34158

Stress distribution in isotropic and anisotropic half spaces with crack in interface bonding, reducing boundary value problem to Hilbert problem

17 p2819 A71-34509

Photoelastic determination of crack tip stress intensity factors for various specimen geometries and loading conditions

17 p2819 A71-34535

Crack wave loading, investigating dynamic stress intensity factor and time response with photoelastic technique

17 p2820 A71-34550

Vibration response NDT for fatigue crack damage in laminated filament-reinforced epoxy composites

17 p2824 A71-34815

Circular symmetry stressed state for flat disk with flat circular crack, detailing potential and elasticity theories

17 p2824 A71-34844

Curvature effect on cylindrical shell circumferential crack tip stress intensity, using fatigue crack growth tests

17 p2827 A71-35154

Crevice effect at stress corrosion crack apex during cathodic polarization of Ti-Al-Mo-V alloy in sulfuric acid, potassium bromide and iodide and methanol solutions

17 p2761 A71-35733

Loaded crack ending at bimaterial composite interface, analyzing crack tip stress field singularity order dependence on material elastic constants

18 p2978 A71-36258

Stress redistribution in laminate composite due to crack normal to interfaces, noting dependence on crack size, layer height and material properties

18 p2982 A71-36841

Stress intensity factors and strain energy rate for bonded layered composites with interface flaw/crack

18 p2983 A71-36846

Edge cracked metal sheet elastoplastic strain distribution determination, using optical interference, moire technique and plane stress model finite element method

18 p2983 A71-36848

Stress wave interaction with macrocrack in elastoplastic and quasi-brittle materials, measuring stress field by optical polarization method and motion picture photography

19 p3154 A71-37086

Deformation and stress distribution three dimensional state around flat parabolic cracks in elastic solids

20 p3307 A71-38772

Experimental stress intensity coefficients for contoured double cantilever beams, using Irwin-Kies method based on compliance with respect to crack length

20 p3307 A71-38779

Harmonic stress function and stress intensity factor for elliptical crack embedded in elastic solid and subjected to arbitrary internal pressure

20 p3307 A71-38782

Internal pressure deformed star shaped crack, calculating stress intensity factor, crack energy and normal displacement

20 p3310 A71-39866

Penny shaped crack under time dependent impact wave loads, investigating transient response with integral transformations

21 p3468 A71-41002

Finite element method for stress intensity factors calculation in cracked plates under bending

22 p3614 A71-41639

Eddy current field formation of defect on extended surface crack in ferromagnetic and nonferromagnetic metals, investigating superposed transformer detector inductor coil effects

22 p3529 A71-41770

Reflected shadow method for constrained zone photoelastic observation around cracks in birefringent transparent plate under plane stress

22 p3549 A71-42555

Longitudinal shear induced stress field around rigid circular cylindrical inclusion and parallel crack, using Jacobi elliptic function in conformal mapping procedure 23 p3777 A71-43495

Lagrangian equation of motion for crack wall driven by square tension impulse, obtaining deflection in terms of crack length and particle velocity 23 p3777 A71-43496

Interaction between two rectilinear cracks, noting angle and disorientation effects 23 p3777 A71-44034

Crack theory application to problems with circular boundaries, solving singular integral equations by Aleksandrov-Libatskii approximation method 24 p3880 A71-44721

Stress-strain state of isotropic elastic plate weakened by cracks, using Fredholm integrals 24 p3881 A71-44832

Automatic eddy current system to detect fastener hole cracks consisting of scanner unit, control box, recorder and mounting hardware 24 p3831 A71-45281

CRANES

Telecontrolled Rotomobile flying crane with jet powered lifting rotor for carrying heavy loads over short distances 10 p1556 A71-24420

Helicopter operation as cranes and for external load transportation, discussing operational and economic aspects 12 p1867 A71-27142

Helicopter design for use as crane and for carrying external loads 13 p1996 A71-28489

Helicopters as cranes and external load carriers, considering operational costs and investment return 13 p1997 A71-29144

CRANIUM

Cancellous bones mechanical properties from compression testing of human femora, vertebrae and cranial bones [AIAA PAPER 71-111] 06 p0863 A71-18561

Tolerance tests including EEG, glucose test, thermal stress and G stress for aircrew fitness assessment after cranio-cerebral incidents 12 p1871 A71-27633

Averaged potentials in vertex and occipital region of human cranium evoked by emotional visual stimuli 24 p3798 A71-45057

CRASH INJURIES

Aircrew radiological examination of spinal anatomical state, emphasizing traumatism due to vibration, acceleration, ejection and crashes 05 p0715 A71-16936

General aviation aircraft accidents involving seat belt and shoulder harness restrained occupants, discussing vertical force effects on survivability and injuries in severe crashes [SAE PAPER 710399] 10 p1555 A71-24261

CRASH LANDING

NT DITCHING (LANDING)

Aircraft galley design safety criteria, considering injuries from routine use, normal, crash or ditching conditions component dislodgment, equipment malfunctions and defects 01 p0004 A71-10029

Aircraft accident trends and preventive practices, considering fatal landing statistics 04 p0529 A71-14995

Bent structure failure under pulse floor acceleration shocks, concerning aircraft seat damage during crash landing 08 p1367 A71-20747

Crashworthy personnel restraint systems for general aviation including upper torso restraint [SAE PAPER 710396] 10 p1569 A71-24260

Airport crash fire fighting equipment requirements and rescue operations 23 p3629 A71-43389

Organophosphate pesticide poisoning implication in aircraft crash of duster pilot from cholinesterase activity drop evidence 23 p3641 A71-44249

CRASHES

NT CRASH LANDING

NT DITCHING (LANDING)

CRATERING

NT PROJECTILE CRATERING

Large lunar craters and circular maria origin problem, disputing formation by meteorite impacts 01 p0149 A71-10047

Lunar crater origin determination by terrestrial volcanic and meteoritic craters and maars geological criteria application to Lunar Orbiter 5 photographs 02 p0313 A71-12549

Apollo lunar rock sample solidification and impact rates, deriving cratering time behavior 04 p0660 A71-15863

Craters on lunar crater Copernicus inner walls, discussing origin based on size distribution frequency comparison with terrestrial basalt flow collapse craters 07 p1196 A71-19542

Large lunar craters and circular maria origin problem, disputing formation by meteorite impacts 08 p1361 A71-21041

Meteorite craters in U.S.S.R., discussing impact, explosive and complex craters 09 p1520 A71-22842

Campo del Cielo, Argentina meteorite crater structural analysis, discussing dimensions, energy of formation, mass, impact velocity, etc 15 p2488 A71-32352

Lunar surface and soil mechanical properties statistical analysis covering Alphonsus event, cratering and erosion 17 p2805 A71-35179

Impact craters and depressions on earth, examining meteoritic origin, characteristic features, energy release and cryptovolcanism 17 p2805 A71-35376

Meteoritics, covering impact on earth, craters, astrometres, tektites, carbonaceous chondrites properties, collisions, fragmentation, etc 17 p2809 A71-35714

Sikhote-Alin meteorite shower expedition, describing craters and pits identification 17 p2809 A71-35716

Sikhote-Alin expedition geological survey, examining crater and pit structural characteristics 17 p2810 A71-35717

Impact and explosive craters production in same target material under controlled laboratory conditions, determining depth of burst simulating impingement 19 p3156 A71-37682

Pueblito de Allende meteorite craters, discussing crater formation and impact direction in comparison with experimental airdrop craters 19 p3052 A71-37684

Lunar mechanical and magnetic properties, discussing impact craters, rocks, soil iron abundance, mascons and convection processes 19 p3142 A71-38020

Lunar glass spheres cratering origin hypothesis from target temperature effects on crater morphology in targets impacted by high velocity Al projectiles 23 p3765 A71-43808

X ray probe, scanning electron microscopy and spectral reflectance analysis of lunar environment effects on Apollo 12 returned Surveyor 3 materials surface cratering 23 p3766 A71-43818

CRATERS

NT LUNAR CRATERS

NT METEORITE CRATERS

Mars surface TV pictures from Mariner 6 and 7, including cratered and uncratered terrains, light and dark markings and south polar cap 06 p0965 A71-17628

Microcraters on Apollo 12 crystalline rocks and breccia surfaces attributed to primary cosmic particles 10 p1673 A71-24427

Lunar and Martian cratering possibility by cometary icy blocks based on sonic impact fluidation experiments 16 p2636 A71-33508

Igneous rocks origin associated with shock metamorphism, considering geochemical investigations of Canadian craters 19 p3051 A71-37668

Impact craters crustal thickness and forms relationship to changing physical state of planetary surface during once-molten cooling 19 p3051 A71-37669

Small lunar and terrestrial craters, determining impact or volcanic origin by depth-diameter ratio 19 p3137 A71-37677

Mariner 6 and 7 Mars color TV recording of craters, chaotic terrain and canals, using wide and narrow angle cameras 20 p3297 A71-39628

Cosmic dust particles impact craters searched for in lunar samples by binocular and electron scanning microscopes, relating to early solar system meteoroid flux 23 p3765 A71-43807

CRAZING

U SURFACE CRACKS

CREATINE

Fatigue factor of lactate, ATP and creatine phosphate /CP/ accumulation in working muscles during short exhaustive exercise in man 02 p0202 A71-11666

Anoxia induced ECG lesion current in conjunction with myocardial phosphorylcreatine collapse, discussing results with air and nitrogen ventilated guinea pigs 13 p2008 A71-28506

Muscle adenosine triphosphate, creatine phosphate, adenosine diphosphate, glycogen, and lactate concentrations during intermittent exercise 15 p2358 A71-31726

Lactic and succinic acids and creatine phosphates content in rat hind leg muscles during swimming and at rest 16 p2532 A71-33897

Physical training effects on human plasma glutamic-oxalacetic transaminase, creatine phosphokinase and lactic dehydrogenase enzyme levels 17 p2683 A71-35143

Anoxia effect on laboratory animals cardiac action, discussing ECG injury current relation to myocardium phosphorylcreatine content 22 p3484 A71-41568

Rat plasma creatine phosphokinase activity, hypothermia and stress, considering cold restraint 22 p3486 A71-41938

CREATININE

Urinary protein excretion rates in high altitude inhabitants, showing polycythemia effect on creatinine clearances levels 19 p3009 A71-38561

CREATION

U CREATIVITY

CREATIVITY

Excitability, reactivity, adequacy, creativity and guidance at molecular, cellular, systemic and psychic levels in human biophysical neurodynamics, plotting stimulus magnitude vs response duration 21 p3344 A71-41063

CREEP ANALYSIS

Anisotropic nonhardenable materials steady creep deformation potential as function of mixed invariant of stress and anisotropy tensor 01 p0172 A71-10797

Unsteady creep calculation based on modified hereditary influence theory relating creep rate to three stage loading history, comparing to experimental results 02 p0323 A71-11740

Creep effect on cooled blades elastoplastic stress-strain relationship using computer programs 02 p0323 A71-11741

Transient creep propagation velocity in dead annealed thin walled Al alloy tubes, using constitutive equation for mean stress-strain-time relationship 03 p0508 A71-13761

Creep failure in elastoviscoplastic media from time and load-path dependent processes near axisymmetric fissure prior to cracking 03 p0509 A71-13874

Al alloy biaxial shear creep under abrupt temperature and stress changes, noting surface size, shape and location [ASME PAPER 70-WA/APM-41] 03 p0443 A71-14164

Circular cylinder creep deformation under complex varying loading, comparing computation and test results [ONERA-TP-846] 04 p0669 A71-15353

Nonlinear creep problems numerical time integration solution, applying to rectangular plate 04 p0672 A71-15755

Doubly symmetric oval ring under lateral load, investigating creep behavior from equilibrium equations 05 p0820 A71-15984

Al single crystals creep deformation, noting thermally activated mechanism at cryogenic temperatures 05 p0769 A71-16879

High temperature diffusion controlled transient creep, considering unimolecular reaction kinetics stress and temperature dependence 05 p0830 A71-17239

Short term creep effect on high speed air flows, investigating material behavior under vibration loads, corrosion and erosion 07 p1130 A71-19163

Cold creep effect on stress corrosion testing of metals under uniaxial bending and constant strain 08 p1306 A71-21439

Short term creep and rupture model, considering strain hardening effect 08 p1371 A71-21610

Finite length rotating cylinder, calculating axisymmetric creep under thermal effects in power series from theory of small elastoplastic deformation 09 p1537 A71-22516

Reference stress parameters for structure creep behavior, using dimensionless stationary state, strain rate and time function 09 p1543 A71-23660

Creep analysis for thermoplastic beams under bending and struts under buckling 10 p1685 A71-23942

Arbitrary plates and axisymmetric bodies creep analysis by finite element method 10 p1691 A71-24820

General dislocation model for high temperature creep of pure metals, discussing strain rate effects 11 p1782 A71-26476

Creep rate intensity approximate solution as invariant function of stress intensity, determining equivalent stresses under creep 12 p1974 A71-26947

Creep of hereditarily aging body, using Rabotnov fractional exponential function for elastic theory solution 12 p1984 A71-27696

Successive approximations method for solving nonlinear elastic problems in transient creep theory, describing stress redistribution

13 p2157 A71-29197

Transient creep of thin walled composite beam under bending and tensile loads in nonuniform temperature field by increment method

14 p2321 A71-29538

Creep-fatigue analysis by strain range partitioning, considering metals inelastic deformation at high temperature due to plastic flow

14 p2325 A71-29923

Closed membrane shell of revolution finite creep due to uniform pressure, applying large deformation incremental theory

14 p2328 A71-30396

Extremum principle for structures in creep under cyclic loading for time dependent stable dissipative material

15 p2505 A71-31944

High temperature creep in Al-Zn solid solution, using isothermal tests

15 p2429 A71-31997

Tensile stress and compressive effects on grain boundary precipitate morphology in Ni-base superalloy during creep

15 p2433 A71-32179

Creep deformation during intermittent loading, obtaining strain rate as function of applied stress and stress cycle time

15 p2508 A71-32254

Compressive creep of aluminum oxide single crystals deformed by dislocation glide and rhombohedral twinning, investigating activation energy and rate controlling mechanism

15 p2439 A71-32439

Polycrystalline graphite total creep time dependent effects based on mathematical model of nonlinear hereditary theory

16 p2600 A71-32799

Single crystal Ni-base superalloy anisotropic hollow cylinder creep under biaxial loading, studying rate dependence on crystallographic axis orientation and stresses ratio

16 p2591 A71-33222

Square cross section prismatic bars transient creep analysis based on strain, time and combined hardening theories

17 p2815 A71-34188

Nonlinear creep analysis of clamped pressurized circular cylindrical sandwich shells representing stress, membrane force and bending moment as displacement based on Mises criterion

17 p2816 A71-34297

Nonlinear creep equation of elastoplastic medium under three dimensional stress, assuming elastic, viscoelastic and irreversible plastic deformation

17 p2817 A71-34337

Stress and temperature dependence of diffusional creep, discussing activation energy, grain boundary effects vacancy diffusion and dislocations motion

17 p2758 A71-35220

Simple gas thermal creep/velocity slip and temperature jump coefficients by applying variational technique to linearized Boltzmann equation with boundary conditions

17 p2785 A71-35446

Saint Venant principle generalization for transient creep and stress relaxation analysis in rectilinear thin walled multiply connected beam under torsion

17 p2833 A71-35612

Creep strain separation theory generalization, describing viscous flow strain division into two components

17 p2833 A71-35617

Vibration and corrosion-erosion damage effects on material behavior during short term creep in high speed air flows

17 p2760 A71-35659

Plastic deformation of circular plates and shells of material with different yield and hardening moduli in tension and compression from creep theory relationships

17 p2834 A71-35660

Composite failure model tested for short term creep and rupture in Mo alloy at constant loads and 785-1400 C, considering strain hardening

17 p2834 A71-35670

High temperature creep of niobium alloy, obtaining creep limit, microhardness and gas analysis data

18 p2936 A71-36715

Shear envelope of thin walled beam with semicircular cross section under creep

19 p3159 A71-38186

Arutunian method application to crack problems in power law elastic materials and contact problems in nonlinear creep, noting error for crack tip singularity

20 p3310 A71-39868

Creep stress and strain analysis in double edged V-shaped notched plates and circumferential V-shaped notched round bars by finite element method

21 p3400 A71-40840

Design and technological calculations in machine building, analyzing flow, creep and elastoplastic deformation theories

21 p3472 A71-41144

Material random temperature and imperfection density effects on 3-bar truss nonlinear steady creep solutions for stress and velocity

22 p3615 A71-42211

Rotating disk creep analysis by Van Fo Fi-Ozerov nonlinear equation, obtaining numerical solution for total creep equation and time to failure for two angular velocities

24 p3882 A71-44839

CREEP BUCKLING

Thin walled circular cylindrical shells creep buckling under radial pressure and thermal gradients [ASME PAPER 70-WA/APM-8] 03 p0512 A71-14152

Circular cylindrical shells creep buckling in pure bending, deriving formula for critical time

18 p2980 A71-36674

German monograph on creep buckling tests of finned and unfinned thin walled pipes of heat resistant breeder reactor cladding materials

21 p3464 A71-40781

Rod buckling under creep conditions, evaluating stability with Shenley model

24 p3877 A71-44405

CREEP DIAGRAMS

Long time strength and creep rectilinear diagrams constructed for heat resistant alloys to obtain extrapolation values

08 p1306 A71-21113

Stress-time superposition creep data for unfilled and coupled glass reinforced polypropylene at 23-80 C

14 p2264 A71-29835

Heat resistant metals long time creep prediction at low stresses or temperatures

15 p2428 A71-31859

Nickel base alloy under axisymmetric tension compression tests, obtaining breaking load diagrams and fatigue and creep curves

18 p2937 A71-36716

CREEP PROPERTIES

NT SHEAR CREEP

NT STEADY STATE CREEP

NT TENSILE CREEP

Linear isotropic viscoelastic media, determining stress relaxation and creep properties

01 p0170 A71-10640

Weight allowance in optimal design of plastic structures under creep

01 p0170 A71-10641

Circular shallow cylindrical panel stability and creep buckling under hydrostatic pressure

01 p0171 A71-10649

Austenitic Cr-Ni-Nb stabilized steel, evaluating high temperature oxidation and creep process interaction

01 p0104 A71-11603

Unsteady creep calculation based on modified hereditary influence theory relating creep rate to three stage loading history, comparing to experimental results

02 p0323 A71-11740

Fiberglass reinforced plastic materials in steady temperature fields, determining creep and load carrying capacity

02 p0272 A71-11753

Free lateral vibration of viscoelastic metallic beam under axial creep, considering elastic deformation

02 p0324 A71-11996

W and W-Mo alloy creep properties during interaction with low pressure oxygen, simulating cladding-oxide fuel interaction in thermionic device

02 p0264 A71-12257

Creep failure model, using wedge crack nucleation in polycrystalline materials due to grain boundary sliding

02 p0329 A71-12716

Finite element program for structural design and stress analysis, introducing creep and plasticity into strain equations

[ASME PAPER 70-WA/DE-4] 03 p0511 A71-14140

Polymer materials linear photocreep characteristics description in terms of differential and integral equations, discussing relationship between optical and mechanical properties

03 p0514 A71-14357

Steel-concrete composite beam creep numerical analysis by reduction to elastic problem with initial strains

04 p0669 A71-15198

Ti-Al and Al alloys and Ni maraging steel creep behavior during high stress, elevated temperatures and rapid heating

04 p0617 A71-15909

Gas turbine engine Ni alloys heat resistance, examining fatigue life and creep properties at various temperatures and test durations

05 p0767 A71-16754

Overload and underload effects on Al-Mg-Si creep deformation and damage accumulation under single load change

05 p0768 A71-16800

High temperature creep comparison of single phase Fe and Ni alloys subjected to constant load tensile tests, measuring strain as function of time

06 p0911 A71-17345

Soviet book on short time creep for designing structural and machine parts operating at high temperatures, analyzing stress-strain state

06 p0983 A71-17432

Cylindrical shell compression stability in presence of creep, determining initial surface dent effects

06 p0992 A71-17805

Thin orthotropic shells thermocreep in variable temperature field reduced to integration of linear partial differential equation system

06 p0997 A71-17852

Stress-strain state of three-layer polymer plate having different thicknesses, Poisson coefficients and creep functions

06 p1005 A71-18707

Thermal creep velocity in rarefied gas over infinite plane wall, using linearized Boltzmann-Krook equation

07 p1084 A71-18746

Annealed Mo creep properties and long term strength, observing temperature and stress effects

07 p1130 A71-19165

Tubular Mg and Ti alloy samples under tension and compression load, observing creep properties

07 p1211 A71-19195

High temperature creep behavior of nickel base alloys with L12 and B2 type lattices, discussing single crystals of beta-NiAl

07 p1133 A71-19446

Low Reynolds number incompressible transmissible creep flow calculation by Marker-Cell numerical solution extension

07 p1094 A71-20613

Hardened plasticity zone around circular hole in creep deformed plane under normal forces, determining stress-strain relation and time dependent variations

07 p1219 A71-20647

Ordered states effects on mechanical properties of Va-Co-Ni ternary alloys, considering creep behavior difference between ordered and disordered structures

08 p1309 A71-21526

Crystalline solids strain rate effects due to simultaneous operation of plastic deformation mechanisms including diffusion controlled creep and dislocation-drag processes

08 p1371 A71-21560

Stoichiometric beta NiAl alloy high temperature creep behavior, presenting electron microscopic observations of deformed single crystals dislocation structures

08 p1314 A71-21571

Tilt boundary intersections during creep in Mo single crystals

08 p1315 A71-21577

Crack opening mechanism for high temperature creep of polycrystalline graphite

08 p1323 A71-21584

Unidirectionally aligned fiber phase solidified eutectic composites model, discussing high temperature rupture and creep properties

08 p1323 A71-21585

Alloy equivalent susceptibility to damage at intermediary service periods and different stress levels under creep conditions at 750 C

08 p1317 A71-21709

Plasticity zone changes near circular hole, examining material structure inhomogeneity effects in presence of creep

09 p1535 A71-22183

Thermal fatigue testing of materials under static load with allowance for creep

09 p1426 A71-22497

Rarefied gas thermal creep flow between parallel plates, using Boltzmann equation relaxation model for all Knudsen numbers

09 p1433 A71-23055

Aerodynamic heating effects on fatigue and creep properties of supersonic aircraft alloys at high temperatures, considering deformation mechanisms interaction

09 p1472 A71-23204

Ni-Al alloy strain hardening, observing high intensity ultrasonic irradiation effect on high temperature creep

09 p1475 A71-23315

Loading rate effect on Ni creep characteristics and substructure

09 p1477 A71-23330

Stress and structure effects on creep rate of two austenitic steels in quenched state, considering decorated stacking faults

09 p1479 A71-23624

Compressive creep behavior of yttria rare earth stabilized zirconia storage heater refractories, determining stress time to failure

09 p1484 A71-23686

Steel sheet specimens under temperature and stress cycles, studying creep, plastic deformation and service life

10 p1686 A71-24189

Compression, creep, stress relaxation and overload effects on delay in fatigue crack growth and structural life predictions

10 p1694 A71-25059

Stress cycling effect on creep deformation rate, using recovery creep model
[ASME PAPER 71-MET-F]

12 p1977 A71-27315

Variable elasticity algorithm for axial flow turbine disks with allowance for plasticity, creep and loading history

12 p1979 A71-27351

Nonisothermal plasticity and creep models, stressing real materials deformation micromechanism theories

12 p1979 A71-27354

Thin walled stiffened Duralumin box spars bending stress-strain states under unsteady creep

12 p1981 A71-27496

Inclusions diffusive motion effects on heterogeneous systems creep properties, determining creep rate as function of stress and temperature

13 p2148 A71-27960

Metallic materials static to dynamic transition in creep noting temperature and purity effects

13 p2084 A71-28110

Refractory steels plastic deformation characteristics under isothermal creep

13 p2084 A71-28125

Fracture under hot creep rupture, discussing grain boundary structure, high temperature region, creep deformation and recovery, void formation and intercrystalline failure

13 p2152 A71-28220

Two stage creep cavity growth by grain boundary sliding as shear crack and Griffith-Orowan fracture, using energy balance argument

13 p2085 A71-28504

Temperature variations of effective fracture surface energy of metals and alloys and relation to crack growth in high temperature creep

13 p2085 A71-28505

Load capacity and transient creep of thin walled rod under free torsion, using successive approximations

13 p2157 A71-29212

High temperature creep in alpha-Fe, Fe-Mo and Fe-Co alloys, investigating stress dependence and alloying effects in ferromagnetic and paramagnetic temperature ranges

13 p2089 A71-29409

Al matrix-stainless steel composites under tensile loading parallel to reinforcement direction, noting creep behavior at ambient temperature

13 p2089 A71-29413

Working fluid /Ar/ purity and stability effects on fatigue life and creep of Nb and Mo alloys using gas analysis, microstructure and microhardness data

14 p2256 A71-29622

Cyclic strain effects on creep for steel at elevated temperatures, discussing overload frequency effects on plastic strain buildup

14 p2256 A71-29626

Thermally activated plastic deformation of metals at low temperatures, determining stress flow, creep properties and upper yield limit

14 p2258 A71-30007

Bloch-wall Permalloy films coercive force effects on low frequency creep, using high resolution Bitter pattern observation technique

15 p2461 A71-32003

Thin walled rod of strain hardenable material, developing constrained torsion approximation for creep and relaxation

16 p2651 A71-33060

Aging theory application to anisotropic strain hardenable metals creep processes description

16 p2659 A71-33984

Al-Mg-Si alloy vibration creep endurance under single step loading, emphasizing strain and defect accumulation

17 p2757 A71-34593

Soviet monograph on plasticity and strength of solid bodies at low temperatures covering solidifying gases, static tests, dynamic properties and creep

17 p2724 A71-35186

Gas turbine engine steels and Ni alloys heat resistance, examining fatigue life and creep properties at various temperatures and test durations

17 p2759 A71-35453

Total inelastic energy dissipation in structure of creeping plastic material under variable repeated loading and shakedown

[ASME PAPER 71-APM-C]

18 p2977 A71-36252

Bending tests of beam with different creep characteristics in tension and compression

18 p2981 A71-36717

Plastic nonlinear creep behavior theory reformulation, obtaining constitutive relations based on experimental data

19 p3084 A71-37524

Rapid thermal fluctuations effect on Inconel 718 creep rate, noting strain rate decrease under cycling conditions

19 p3080 A71-37716

Matrix stacking fault energy effect on tensile creep deformation modes in gamma prime precipitation hardened nickel-base alloys

19 p3080 A71-37721

Thermal creep slip velocity expression in power series for arbitrary fraction of modulus diffusely reflected from surface by Bhatnagar-Gross-Krook model solution

19 p3163 A71-37734

Structural stability and creep properties of heat resistant steel weld joints, considering substitutional and precipitation hardening and dislocation effects

20 p3249 A71-39015

Recovery creep properties and intercrystalline fracture in precipitation hardened alloys heat treated on relative stable conditions

20 p3250 A71-39024

Solution temperature and Ti/C ratio effects on Cr-Ni-Ti austenitic steels creep properties, including precipitation, deformation, rupture and coalescence

20 p3250 A71-39025

Metallic polycrystal deformation equations, obtaining creep, Norton law dependences and thermally dissipated energy

22 p3560 A71-41606

Al-Zn solid solution mean effective and internal stresses and activation area during high temperature creep

23 p3691 A71-43900

Rotating disks optimal design allowing for creep from additional coupling imposition and contour displacement

23 p3780 A71-44220

CREEP RESISTANCE

U CREEP STRENGTH

CREEP RUPTURE STRENGTH

Fiberglass-reinforced plastics loading conditions effects on tensile strength, determining creep rupture strength from test data

01 p0107 A71-10413

Tensile and stress rupture tests of Co base alloy bars extruded from prealloyed powders made by Ar gas atomization

01 p0100 A71-10480

W, W-Re and Re-Mo creep rupture properties investigation for selection of optimum materials for isotope containment for thermionic capsules

02 p0195 A71-12254

Heat resistant materials long term strength characteristics, determining optimum parameters from creep data statistical analysis by least squares method

03 p0440 A71-13194

Solidified Ni-Mo-Al gas turbine guide vane alloy with improved melting point, creep rupture strength and structural stability

03 p0431 A71-13256

Accelerated creep rupture tests on metals and solder alloys, comparing constant stretch rate and load methods

03 p0508 A71-13762

Titanium alloy turbine disks creep rupture strength and service life, considering pressing and forming manufacturing technology

04 p0664 A71-14604

Nb-W-Hf-Y creep rupture properties in thermal vacuum, achieving strength improvement by pretest annealing

05 p0766 A71-16242

Metallic construction materials creep rupture behavior, discussing primary, secondary and tertiary creep metallurgical and physical processes

06 p0911 A71-17346

Stress rupture properties at elevated temperature of nickel base superalloys with varying Ti and Al additions, investigating microstructural and age hardening effects

06 p0913 A71-18676

He embrittled stainless steel stress-rupture behavior under vacuum and elevated temperature conditions, discussing microstructural characteristics

06 p0914 A71-18685

Notch geometry and temperature effects on Ti-Al-Mo-V alloy creep rupture behavior

07 p1134 A71-19470

Bainite structure effects on Cr-Mo-V steels creep and rupture strength

07 p1134 A71-19520

Stress rupture properties of S glass/epoxy single end strands at various load levels, considering distribution functions

07 p1145 A71-20126

Long term creep strengthening by molybdenum in untempered iron and steel

08 p1315 A71-21579

Isotropic material structures under static external loads, considering stress rupture strength models

08 p1371 A71-21608

High temperature precipitation hardening of Ni-Cr alloys, discussing effect on creep rupture strength

09 p1470 A71-23044

High temperature Fe, Co and Ni alloys for gas turbine components, considering tensile and creep rupture strength increase by thermal mechanical processing

09 p1475 A71-23298

Stress rupture behavior of S glass/epoxy multifilament strands, developing tensile and creep test apparatus installed in controlled environment building

11 p1784 A71-25397

Creep rupture data analysis model based on minimum commitment station function approach, generalizing hypothesized time temperature stress relation

11 p1848 A71-25561

Low alloy steels and superalloys inertia welding in gas turbine field, discussing microstructure tensile strength and stress rupture

[ASME PAPER 71-GT-21]

11 p1770 A71-25963

Air- and vacuum-melted Hastelloy-N/Ni-based alloy/ creep-rupture properties dependence on irradiation temperature

11 p1781 A71-26077

High temperature tensile strength, creep rupture behavior and high temperature exposure effects on subsequent room temperature properties of maraging steel plates and welds

[ASME PAPER 71-MET-E]

12 p1918 A71-27314

Heat resisting Ni base alloy stress rupture strength and fatigue life, observing corrosive high temperature environment effect

13 p2084 A71-28111

Fracture under hot creep rupture, discussing grain boundary structure, high temperature region, creep deformation and recovery, void formation and intercrystalline failure

13 p2152 A71-28220

Critical aspect ratio of W fibers in metal matrix composites for stress rupture applications

14 p2258 A71-29921

Creep rupture strength and durability of Al, Ni and Cu irradiated by neutron flux

14 p2258 A71-30004

Comparative creep rupture properties of tungsten-rhenium consolidated by arc melting and powder metallurgy, considering rupture life and rupture ductility

15 p2427 A71-31818

Creep rupture properties of W-Re arc melted and powder metallurgy materials at 1650 and 2200 C as function of time, void and grain size

15 p2428 A71-31819

Power and exponential time dependences of long term creep strength for wide stress range, assuming linear thermal resistance

15 p2433 A71-32228

Creep rupture behavior and high temperature exposure effects on room temperature properties of Ni-Cr-Mo maraging steel plates and welds

15 p2434 A71-32256

Stress rupture ductility of electron beam, gas tungsten arc and gas metal arc welds, considering creep crack initiation

15 p2437 A71-32617

Flight mission severity in cumulative damage/low cycle fatigue and creep stress rupture/ not detected by usual nondestructive testing in aircraft gas turbine industry

16 p2624 A71-33298

Plastic deformation, creep rupture strength, endurance limit and service life of prestressed strain hardenable material

16 p2659 A71-33985

Annealed Mo creep and stress rupture at high temperatures for typical deformation

17 p2760 A71-35661

Fe-Ni base alloy heat treatment for optimum high temperature stress-rupture properties, noting Ni-Nb/Ni-Ti intermetallics precipitation at grain boundaries

19 p3080 A71-37712

Stainless steel and Al alloy creep rupture life apparent reduction by frequent beam leveling

19 p3082 A71-38135

Thermocouple drift effect on creep and tension rupture life at high temperature

19 p3065 A71-38137

Characteristic smooth test bar ductility correlation and prediction in high temperature creep rupture tests, noting application to material quality control

19 p3082 A71-38138

Creep fracture of Cr-Mo-V steel after operational heat treatment and power plant operation, noting intercrystalline and transcrystalline fracture

20 p3249 A71-39016

Creep tests on heat resistant steels, studying elongation/rupture strength and temper hardening

20 p3251 A71-39026

Creep rupture behavior of electron beam melted polycrystalline sheet and powdered rhodium

21 p3397 A71-40454

Microstructure, yield point and creep rupture strength of Nb-Ti alloy, investigating oxygen concentration and temperature effects

22 p3563 A71-42365

Fiber reinforced metallic matrix composite under creep, discussing rigidity, stress distribution, rupture strength and failure time

23 p3697 A71-44201

Tensile and creep rupture strength and microstructure of Co-Fe-Ta alloys at elevated temperatures

24 p3836 A71-44442

CREEP STRENGTH

Refractory Nb alloys with high creep strength, good ductility and moderate density, heat treatment and workability

02 p0271 A71-12937

Creep strength of Nb alloys with Mo at high temperatures in vacuum, noting Zr-C complex alloying effect

04 p0613 A71-15642

German monograph on Co-free heat resistant austenitic steel alloys precipitation hardening and creep strength properties as function of chemical composition

05 p0764 A71-15973

Creep and long term strength of unidirectionally reinforced plastics under compression

05 p0771 A71-16361

Cr alloys endurance and dynamic creep under HF tension-compression loads at room temperature

07 p1129 A71-19154

Ni base superalloys mechanical properties relationship to microstructure, considering precipitate dispersion and phase state effects on flow stress and creep strength

07 p1133 A71-19445

W-Re alloy microstructure creep, long term strength and plastic properties as function of temperature, using electron microscopy

07 p1141 A71-20241

Creep strain effect on cyclic fatigue life of duralumin at room temperature

07 p1143 A71-20486

Creep enhancement by additional microplastic deformation in refractory alloys during thermal cycling

08 p1317 A71-21618

Nb alloy high temperature creep and long term strength, determining exponential relations between stress, strain rate and durability

09 p1468 A71-22628

Cold prestraining effect on steady state creep strength and rate of precipitation hardened heat resistant steel

09 p1477 A71-23331

High chromium hot corrosion resistant superalloys in sheet form, noting precipitation hardening and creep resistance equivalent to Nimonic alloys

12 p1916 A71-26922

Statistical analysis of durability data of heat resistant alloys for gas turbine engines, using long term mass creep strength tests on industrial melts

16 p2592 A71-33413

Columnar grained Ni superalloy lifetimes and transverse creep ductilities enhancement and microstructural alterations due to Hf additions

17 p2759 A71-35394

High temperature creep of niobium alloy, obtaining creep limit, microhardness and gas analysis data

18 p2936 A71-36715

Creep strength tests planning, discussing minimum necessary tests number and samples distribution to obtain characteristics with accuracy and reliability

19 p3082 A71-38346

Ni-base heat resistant alloys loading frequency effect on fatigue resistance, noting linear relationship between creep strain and cycles to failure in logarithmic coordinates

19 p3082 A71-38348

Creep strength extrapolation for high temperature steels, suggesting combined numerical and graphic methods

20 p3249 A71-39017

Cr-Mo-V steel creep strength tests extrapolation by parametric approach, discussing optimum regression dependence

20 p3250 A71-39019

Creep test and long time strength results extrapolation, determining accumulation of plastic deformation and creep fracture effects

20 p3250 A71-39020

High temperature creep characteristics and strain curves of heat resistant Fe and Ni alloys in turbine components

21 p3403 A71-41158

CREEP TESTS

Quenched Al-Mg alloys, investigating dislocation mechanisms for plastic flow by creep tests at various temperatures

01 p0105 A71-11605

W, W-Re and Re-Mo creep rupture properties investigation for selection of optimum materials for isotope containment for thermionic capsules

02 p0195 A71-12254

W and W-Mo alloy creep properties during interaction with low pressure oxygen, simulating cladding-oxide fuel interaction in thermionic device

02 p0264 A71-12257

Single crystal creep strain rate measurement under cryogenic temperatures by hybrid photoelectric servo system with optical extensometer avoiding physical contact with specimen

03 p0426 A71-13759

Recovery rate measurement during creep test by stress drop method

03 p0444 A71-14316

Al-Mg alloys secondary creep relationship to mechanical instability during tension

03 p0445 A71-14340

Circular cylinder creep deformation under complex varying loading, comparing computation and test results [ONERA-TP-846]

04 p0669 A71-15353

Test stand for endurance and creep testing of plastics, glazed ceramics and other brittle materials

04 p0567 A71-15645

Nb-Mo alloy creep test, determining relationships between steady state creep rate, stress and Mo content

04 p0616 A71-15803

Creep testing machine for plastics and composites

05 p0772 A71-16929

Cyclic creep and relaxation of heat resistant alloys at high temperatures, showing inapplicability of static load conditions

07 p1142 A71-20480

Low temperature creep testing apparatus providing for microstructural examination of materials without distortions due to specimen temperature change to room temperature

09 p1426 A71-22318

Comparative tensile and creep tests of reinforced thermoplastics for performance/cost selection [PLASTICS INST. PAPER 4]

09 p1481 A71-22340

Directionally solidified Ni base superalloys, determining stress and temperature effect on primary creep strain

09 p1472 A71-23130

Ni plastic properties and creep measurement under deformation by tension at room temperature, noting effect of impurities content

09 p1473 A71-23231

Cyclic creep test for simulating helicopter rotor blades start-stop cycles effect on adhesive bonded joints, using fixed load-unload cycle

10 p1631 A71-24076

Cylindrical Duralloy shells critical strain measurement in axial compression under creep conditions

10 p1690 A71-24575

Air- and vacuum-melted Hastelloy-N/Ni-based alloy/ creep-rupture properties dependence on irradiation temperature

11 p1781 A71-26077

Long duration high temperatures rated stress effects on Ti beta alloy IVT-1, correlating creep with beta granular boundaries migration

11 p1782 A71-26471

Statistical scatter approximation of creep characteristics using relation to accumulated static damage and time to failure

12 p1979 A71-27352

Torsion creep tests of Al, deriving expression for steady state creep rate as function of temperature and stress

13 p2083 A71-27963

Grain boundary precipitation in austenitic steels during creep deformation and ordinary aging treatment

13 p2086 A71-28623

Creep and failure tests for Ti alloys at 500 C and high stresses, discussing work dissipation during creep process

14 p2256 A71-29621

Equilibrium stability of rods, shells and plates during creep due to applied load

14 p2333 A71-30893

Dilatometric measurement for crazing rate in rubber-toughened plastics during tensile creep tests

15 p2438 A71-31369

Low temperature creep deformation recorder with liquid He coolant, discussing Al and Pb single crystal tests

15 p2385 A71-32239

Creep tests of admissible stress states in viscoelastic isotropic compressible or incompressible linear and nonlinear solids

16 p2591 A71-33206

Constant load tensile creep tests on polycrystalline ceramics, determining high density alumina applied stress and strain rate

16 p2553 A71-33384

Thermal strain hardening influence on structural changes in coarse grain Ni under creep tests during heat treatment

16 p2598 A71-33990

Time dependent bending of circular cross sectioned rod under constant load compression and creep

17 p2821 A71-34564

Creep rate enhancement by additional microplastic deformation in refractory alloys during thermal cycling

17 p2761 A71-35678

Bending tests of beam with different creep characteristics in tension and compression

18 p2981 A71-36717

High temperature creep testing facilities and techniques, evaluating statistically interlaboratory variability and significance of testing and material variables affecting creep results

19 p3081 A71-38132

Creep testing machines load axiality, investigating bending strains allowable limits excess as function of tensile stress and temperature

19 p3082 A71-38134

Thermocouple drift effect on creep and tension rupture life at high temperature

19 p3065 A71-38137

Creep strength tests planning, discussing minimum necessary tests number and samples distribution to obtain characteristics with accuracy and reliability

19 p3082 A71-38346

Al, Cu and Ni high temperature creep noting diffusive, shear and dislocation deformation mechanisms

19 p3083 A71-38525

Creep fracture of Cr-Mo-V steel after operational heat treatment and power plant operation, noting intercrystalline and transcrystalline fracture

20 p3249 A71-39016

Creep tests evaluation for stress and temperature effects on apparent activation energy

20 p3250 A71-39018

Cr-Mo-V steel creep strength tests extrapolation by parametric approach, discussing optimum regression dependence

20 p3250 A71-39019

Creep test and long time strength results extrapolation, determining accumulation of plastic deformation and creep fracture effects

20 p3250 A71-39020

Creep test results scatter, considering non-homogeneity of specimen properties and deviation from test conditions

20 p3250 A71-39021

Creep tests effect on Cr-Mo-V steels mechanical properties during alternating stress fatigue testing, considering preliminary static prestressing

20 p3250 A71-39023

Creep tests on heat resistant steels, studying elongation/rupture strength and temper hardening

20 p3251 A71-39026

Intermittent stress creep tests on low carbon steel, commercially pure iron, Cr-Mo steel and commercially pure tantalum, noting static-to-dynamic transition

21 p3400 A71-40835

Superhigh vacuum apparatus for creep and long term strength tests on metals at high temperatures, giving results for niobium alloys

22 p3538 A71-41699

Fiber reinforced metallic matrix composite under creep, discussing rigidity, stress distribution, rupture strength and failure time

23 p3697 A71-44201

CRESTATRONS

U TRAVELING WAVE TUBES

CRESTS

U WAVES

CREVICES

U CRACKS

CREWS

NT FLIGHT CREWS

CRICKETS

NT BEETLES

CRITERIA

Structural dynamics test simulation technology, discussing criteria, techniques, equipment, combined environments and relationship between testing and analysis

11 p1745 A71-26493

CRITICAL FLICKER FUSION

Summation coefficient determination inside and outside fovea by critical flicker frequency measurement, showing inverse relation to test surface size

01 p0010 A71-10275

Ambient temperature effects on flicker fusion threshold, using constant stimuli and forced choice methods for determination of test subjects sensory sensitivity to heat and cold exposure

10 p1568 A71-24184

Human visual mental imagery for oscillation rate estimation of subfussional light, using critical flicker frequency test

18 p2863 A71-37020

CRITICAL FLOW

One component two phase mixtures critical flow in nozzles, orifices and short tubes, considering interphase heat, mass and momentum transfer

03 p0520 A71-14095

One component two phase flow in tubes with increasing pressure gradient, investigating flow choking and correlating measurements with analytical results

09 p1434 A71-23464

Two phase critical flow of one component mixtures in nozzles, orifices and short tubes, considering interphase heat, mass and momentum transfer rates

13 p2049 A71-28980

Critical overexpanded jet conditions of gas ejector at large pressure gradients based on supersonic compressed layer theory

13 p1993 A71-29213

Critical and near critical two phase flow in venturi tube, applying one dimensional flow equations [ASME PAPER 71-FE-4]

13 p2051 A71-29447

- Methane and natural gas flow through critical flow nozzles, calculating real gas effects on mass flow rate
14 p2224 A71-29937
- Two phase critical flow of saturated and subcooled high pressure liquid nitrogen through convergent-divergent nozzle, comparing with water
21 p3369 A71-40894
- Critical streamline length in axisymmetric and plane ideal gas flows past conical bodies as function of Mach number and form parameter
24 p3790 A71-45058
- Mach number distribution along critical streamline in compressed layer in front of cylinder in supersonic flow
24 p3790 A71-45101

CRITICAL FREQUENCIES

- Upper frequency limit to mechanical tuning range of waveguide-mounted transferred electron oscillators due to transverse resonance
01 p0055 A71-11173
- F 2 layer anomalies association with equatorial electrojet from F 2 and sporadic E critical frequencies analysis
02 p0245 A71-11963
- Wintertime Arctic F region critical frequency secondary maxima, discussing UT control hypothesis
03 p0408 A71-13386
- Diurnal and seasonal variations of cosmic noise absorption at critical frequency of F 2 region
03 p0379 A71-13815
- F 2 region critical frequency ionospheric tidal spectrum during solar minimum and maximum at various global locations and solar and lunar day periods
04 p0583 A71-15214
- Lunar semimonthly oscillations in solar daily H range related to midday F 2 critical frequency at equatorial stations, analyzing lunar tides in ionosphere
05 p0740 A71-16432
- Magnetic disturbances effect on F 2 critical frequencies in Australasian zone during IGY-IGC, correlating to equatorial electrojet
05 p0741 A71-16438
- Sporadic E layer effect on F 2 region critical frequencies
05 p0745 A71-17201
- F 2 region critical frequency diurnal variation forecasting, using series expansion of natural orthogonal components
06 p0895 A71-18276
- Sporadic E layer and critical frequency relationship to traveling ionospheric disturbances, suggesting role of atmospheric internal gravity waves
07 p1100 A71-19402
- Ionospheric characteristics recording concerning critical frequencies and minimum heights above Sverdrlovsk during solar eclipse of 22 September 1968
07 p1101 A71-19407
- Seasonal variations in F 2 region, using critical frequencies during descending solar activity phase
07 p1102 A71-19672
- Lunar tides in sporadic E layer critical frequency, considering wind shears and electrostatic fields associated with lunar current system
08 p1363 A71-21202
- Monthly median F 1 layer critical frequency prediction at arbitrary location and time as function of ionospheric index, geomagnetic latitude and solar zenith angle
08 p1257 A71-21882
- F 2 layer critical frequency and maximum electron concentration statistical characteristics for predicting SW propagation conditions
09 p1435 A71-22427
- Short radio wave propagation over single jump lines in F 2 critical frequency gradient presence, examining maximum usable frequency increase
09 p1405 A71-22439
- Ionospheric layers critical frequencies recording, using automatic interplanetary station type probe
09 p1436 A71-22450
- E layer critical frequencies and sporadic E layer boundary frequencies interrelationship, assuming equal electron production rates
10 p1599 A71-23876
- Solar cycle effects on diurnal variations of F 2 region critical frequency and maximum ionization height
10 p1600 A71-23884
- Maximum usable frequency to critical frequency ratio for whispering gallery propagation in HF and VHF E region
10 p1577 A71-24291
- Trapped waveguide mode frequency of whispering gallery propagation in F region explaining round world echoes and long distance satellite observations
10 p1577 A71-24292
- Microbarometric oscillations enhancement due to atmospheric pressure waves generation and cold fronts passage, considering relationship to sporadic E critical frequency
10 p1606 A71-24918
- Midlatitude F2 region diurnal variations in peak electron density critical frequency and height, noting electric field and ion drag effects
10 p1606 A71-24921

- Storm time variations of F 2 layer electron concentration and critical frequency at Australasian stations
11 p1754 A71-25606
- Distribution curves of F 2 critical frequency variations, considering probability density functions interpretation via asymmetric model
11 p1757 A71-25771
- Universal time effect on E region critical frequency at large solar zenith angles, considering ionization source at midlatitude range
11 p1757 A71-25785
- F 2 layer critical frequency abnormal latitudinal distributions, using Alouette 1 satellite data
12 p1900 A71-26935
- Sporadic E layer effect on F 2 region critical frequencies
13 p2059 A71-28256
- Cross correlation characteristics of deviations in critical frequencies of F 2 region
13 p2030 A71-28538
- Radio communication accuracy characteristics in calculation of maximum frequency, skip distance and emission angle by transmission curves for midlatitude ionosphere
13 p2030 A71-28544
- F 2 layer critical frequency variations relation to solar radio flux intensity, using mathematical approximations
13 p2062 A71-28557
- Time between noontime and evening maxima in F2 layer critical frequency compared with evening maximum period, showing dependence on noontime solar zenith angle
13 p2062 A71-28559
- Epitaxial film thickness and resistivity effect on transistor cut-off frequency, discussing collector junction space charge region boundary location
14 p2213 A71-30626
- Harmonic analysis of F 2 region critical frequency in antarctic region, emphasizing solar activity effects
17 p2731 A71-34317
- Antarctic F 2 layer height and critical frequency diurnal variations due to ionospheric neutral winds, ionization maxima and solar effects
17 p2731 A71-34318
- Sporadic E layer and critical frequency relationship to traveling ionospheric disturbances, suggesting role of atmospheric internal gravity waves
19 p3053 A71-37826
- Ionospheric characteristics recording concerning critical frequencies and minimum heights above Sverdrlovsk during solar eclipse of 22 September 1968
19 p3053 A71-37831
- Computer demonstration of ionospheric F region storm causes, noting critical frequency relationship to ionization shift
19 p3055 A71-38038
- Isoline charts showing F 2 layer critical frequency deviations and negative disturbance zones during solar eclipse of 22 September 1968
19 p3058 A71-38385
- E region electron density and critical frequency seasonal anomaly, allowing for sun zenith angle variations, sunspot activity and earth orbit eccentricity
21 p3371 A71-40034
- Midlatitude ionospheric data comparison to F 2 critical frequency from continuity equation and neutral air winds
21 p3372 A71-40043
- He-Ne lasers noise modulation at DC excitation, confirming existence of critical frequency related to metastable atom lifetime
21 p3392 A71-40373
- Modulation instability of dispersion type NMR stabilizer of resonance conditions, determining critical frequency of self excitation and maximum amplification
22 p3519 A71-41444
- Distribution curves of F 2 critical frequency variations, considering probability density functions interpretation via asymmetric model
22 p3532 A71-41539
- Universal time effect on E region critical frequency at large solar zenith angles, considering ionization source at midlatitude range
22 p3532 A71-41553
- Semiannual variation in F 2 layer peak height and critical frequencies at midlatitudes, considering vertical ionospheric drifts effects
23 p3665 A71-42973
- Earth atmosphere gas composition and electron density variations at F region lower boundary explained by stratospheric explosive and diffusive warmings effect on critical frequency
23 p3671 A71-43578
- Mechanical vibrations effects on mouse embryos growth and development, investigating critical frequencies and accelerations
23 p3637 A71-44246
- Critical frequencies of higher order modes in circular waveguides with arbitrary thick dielectric sleeve
23 p3647 A71-44319

- Approximate calculation of cut-off frequencies of H- and Pi-section waveguides using corrugated plane surface theory
23 p3655 A71-44323
- CRITICAL LOADING**
- Cryogenic pressure vessels carrying capacity, discussing loading types, materials properties, thermal effects, etc
01 p0097 A71-10077
- Buckling of ring stiffened conical shells under axial compression, determining critical loads
01 p0168 A71-10342
- Load deflection relations for rigid plastic cylindrical shells beyond incipient collapse load
01 p0175 A71-11011
- Critical static strength of Duralumin under cyclic impact loads, analyzing statistically load distribution function applicability
01 p0103 A71-11240
- Fiberglass reinforced plastic materials in steady temperature fields, determining creep and load carrying capacity
02 p0272 A71-11753
- Stability loss of cylindrical and spherical shells under heating and external force, determining critical temperature and loads
02 p0325 A71-12286
- Lower bound load carrying capacity of thin walled structures of rods, plates and shells with statistical stable stress field, using plasticity theory
02 p0326 A71-12296
- Infinite MHD journal bearing with electrically conducting fluid lubricant in radial magnetic field, obtaining pressure distribution, load capacity and driving torque
02 p0258 A71-12601
- Skin friction effect on cylindrical shell critical loads at various supersonic gas flow velocities, noting application to flutter analysis
02 p0329 A71-12666
- Polish book on limiting load capacity of structural elements covering notched rods and plates with hole under elastoplastic stress
02 p0330 A71-12750
- Load limit surfaces for composite plates with long elastic plastic fibers site bonded or imbedded in low strength matrix
03 p0504 A71-13429
- Variational methods applied to shells transition into plastic state during cylindrical bending, giving critical load formulas
03 p0509 A71-13873
- MHD conducting lubricant composite slider bearing in transverse magnetic field, calculating conductivity effect on load capacity
04 p0602 A71-14801
- Stability of homogeneous and uniform deformation of isotropic body, using energy criterion
04 p0672 A71-15881
- Internal pressure load carrying capacity of intersecting spherical and cylindrical shells based on limit or plastic design concept
05 p0823 A71-16493
- Critical loads in flat plates under elastic strains
05 p0825 A71-16649
- Bunched parallel reinforcing fibers of equal size and varying strength, deriving critical loads and stresses under gradual failure
05 p0772 A71-16751
- Structural elements carrying capacity increase by strain hardening and nonuniform quenching
05 p0826 A71-16752
- Cylindrical reinforced shells carrying capacity under dynamic external pressure
06 p0982 A71-17354
- Stainless steel shells under uniform external pressure and constrained deformation, noting critical load increase
06 p0986 A71-17760
- Equilibrium stability of orthotropic cylindrical shell under longitudinal compression, discussing critical stresses
06 p0986 A71-17762
- Limiting analysis for upper estimate of carrying capacity of shell of revolution under load concentrated at center, evaluating stability loss
06 p0987 A71-17771
- Cylindrical shells buckling under subcritical loads, considering internal and external hydrostatic pressure and axial compression
06 p0988 A71-17779
- Smooth cylindrical shell stability, considering internal pressure effect on critical axial stresses
06 p0993 A71-17819
- Strain hardened plastic cylindrical shells, investigating load bearing capacity
06 p0994 A71-17822
- Rigid plastic shells carrying capacity by kinematic method based on linear programming
06 p0996 A71-17839
- Viscoelastic rectangular thin plate stability under buckling conditions, showing ratio of long term to instantaneous critical loads as function of hereditary properties
07 p1212 A71-19351

- Optimal structural design for nonconservative elastic stability of cantilever column, obtaining critical load
07 p1212 A71-19473
- Load carrying capacity of finite length self acting gas lubricated journal bearings
[ASME PAPER 70-LUB-23] 07 p1117 A71-19502
- Gallium oxide particles effects on Ag-Ga matrix single crystals critical resolved shear stress
08 p1311 A71-21543
- Stability analysis of cylindrical shells hinged over ends under critical destabilizing axisymmetric radial displacements
08 p1373 A71-21946
- Infinite isotropic plate weakened by cracks along circular arcs, calculating stress-strain state and critical loads
09 p1538 A71-22524
- Reinforced shells of revolution carrying capacity upper limit subjected to internal adiabatic ideal gas flow
09 p1538 A71-22632
- Viscoelastic rectangular sandwich plate bending, stability, deflection and critical load calculation, assuming core stress-strain relation governed by Maxwell-Thompson differential equation
09 p1540 A71-22998
- Cylindrical body stability under axial compression with small elongations and shears, determining critical buckling force
09 p1542 A71-23437
- Thin simply supported polygonal and rhombic plates critical hydrostatic buckling loads and free vibration frequency calculation by conformal mapping and power series expansion
10 p1686 A71-24018
- Multilayer sandwich plates with transverse shear resistant inner layers and bending and twisting moment resistant outer layers, calculating critical buckling loads by finite elements
10 p1686 A71-24020
- Deformability and strength of soft fiber reinforced plastics under biaxial tension, determining low temperature critical tensile stresses and elongation ratios
10 p1634 A71-24194
- Limit load carrying capacity of thin walled tube under combined forces, including pressure effects by variational method of plasticity theory
10 p1688 A71-24384
- Approximate solution for limit load carrying capacity of thin walled tube under combined loadings, deriving formulas describing boundary surface
10 p1688 A71-24385
- Critical load and elastic base one-sided contact effects on cylindrical shell stability under uniform external pressure, using nonlinear programming
10 p1689 A71-24563
- Limiting equilibrium of thin rigid plastic plate with piecewise smooth contour under skew symmetric load
10 p1690 A71-24568
- Cylindrical Duralloy shells critical strain measurement in axial compression under creep conditions
10 p1690 A71-24575
- Environmental effects on laminated anisotropic plates thermoelasticity for critical swelling strains, using Hooke's law extension of Duhamel-Neumann equations
[AIAA PAPER 71-352] 11 p1783 A71-25332
- Fatigue failure probabilistic model under variable amplitude loading, considering relation between safety factor and fatigue failure probability
11 p1848 A71-25492
- Plastic spherical shell containing cylindrical section under Tresca yield conditions, obtaining upper critical load limits
11 p1850 A71-25943
- Piston engine crankshafts load and strength specification, treating axial force as resultant of gas force and inertial force
11 p1851 A71-26200
- Maximum shear and hoop stress gradients in graphite-epoxy angle-ply laminated composite cylinders for axial and internal pressure loading
11 p1852 A71-26391
- Three dimensional nonlinear elastic anisotropic body formulating stability at finite subcritical strains with variational principle
12 p1978 A71-27333
- Plastic conical shell with variable thickness, calculating load carrying capacity under cyclic mechanical and thermal loads
12 p1979 A71-27333
- Jet fuels deoxygenation effects on steels antiwear properties and critical loading under vibrational and gliding friction
12 p1945 A71-27662
- Approximate limiting loads with minimum yield stress for axisymmetric rigid-plastic body of arbitrary shape, using computerized static equilibrium method
13 p2150 A71-28137
- Load bearing capacity of thin walled box shaped rod of strain hardening material during bending beyond elastic limit
13 p2153 A71-28294
- Approximate critical stresses during longitudinal compression of nonmetallic rods of medium flexibility, using stability loss curve tangent to Euler hyperbola
13 p2091 A71-28295
- C-5A airplane Be brakes, considering critical design weight environment for optimum load carrying capacity
[SAE PAPER 710427] 13 p1996 A71-28313
- Stability loss, critical load and wave numbers for smooth conical and cylindrical shells of fiberglass reinforced plastics under uniform axial compression
13 p2157 A71-29181
- Load capacity and transient creep of thin walled rod under free torsion, using successive approximations
13 p2157 A71-29212
- Elastic stability of compressed beams, giving method for evaluating neutral axis form and critical load in buckling
13 p2157 A71-29321
- Instability limit curves for twisted square metal plates under vertical loads with transition from antistatic to synclastic deformation
13 p2158 A71-29431
- Steel bar under longitudinal impact, deriving flexural half waves length formulas for critical force
13 p2158 A71-29435
- Critical stress and stability analysis of cylindrical shell with initial indentation of length comparable to radius under axial compression
14 p2321 A71-29536
- Stress analysis of thin walled framed cylindrical beams under deformation beyond proportionality limit by iteration method
14 p2321 A71-29540
- Critical load of shallow shell of revolution as function of geometric and material parameters
14 p2321 A71-29624
- Heavy hinged nonshallow circular arches stability during buckling sideways with bifurcations in critical load deflection curves
14 p2324 A71-29885
- Critical loads and stability loss equations near edge of thin convex clamped elliptical shell of revolution under uniform external compression loads
14 p2325 A71-30024
- Geometrical parameters and load carrying capacity of fiberglass reinforced plastic composites with elastoplastic adhesive bonding, deriving relations for stress distribution
14 p2264 A71-30270
- In-plane boundary effects on buckling and critical stress of axially loaded cylindrical panels
14 p2331 A71-30697
- Reinforced toroidal shells stability under critical local loads, edge moment and heating, using finite difference method
14 p2332 A71-30847
- Load carrying capacity of edge clamped spherical shells of revolution with Tresca yield condition under uniform internal pressure
14 p2332 A71-30848
- Brittle plates with stochastic distribution of cracks under biaxial tensile-compressive stresses, obtaining critical load
15 p2504 A71-31853
- Thin walled tubes under external and internal pressures axial loads and torques, showing load capacity limit dependence
15 p2428 A71-31860
- Soviet book on structural bearing capacity under thermal cycling conditions covering rotating disks, plates and shells calculations
15 p2505 A71-32002
- Stability loss of circular cylindrical shell with stepped wall thickness of central reinforcing sleeve under annular loading, determining critical load by thin shell theory
16 p2657 A71-33600
- Stability and critical load of constant thickness cylindrical sandwich hinge supported shell under annular loading, using variational method
16 p2657 A71-33601
- Critical loads and stability of longitudinally compressed circular cylindrical shells with eccentric ring and stringer reinforcement
16 p2657 A71-33603
- Variable gap and chamber width effect on load bearing capacity of radial hydrostatic bearing with capillary throttling
16 p2584 A71-33616
- Cryogenic pressure vessels carrying capacity, discussing loading types, materials properties, thermal effects, etc
16 p2593 A71-33633
- Crack interaction effect along straight line on critical equilibrium and fracture of plate relative to cross-piece length
16 p2658 A71-33685
- Thermoelastic critical equilibrium of plate with rectilinear crack under heat transfer from edge surface and tensile stress
16 p2658 A71-33686
- Snap-through buckling of three hinged deep trusses and wire restrained column under critical quasi-static loading based on elastica theory of prismatic bars
17 p2815 A71-34294
- Orthotropic bar under compression loads, calculating Eulerian values for critical force
17 p2817 A71-34335
- Thin walled structure design for critical loading by external force variation, determining carrying capacity loss by digital computer matrix methods
17 p2818 A71-34351
- Rupturing rotations estimates for turbine disks, considering failure modes and load bearing capacity
17 p2829 A71-35305
- Isotropic circular cylindrical shell stability with longitudinal hinges under uniform external pressure, determining critical load
17 p2831 A71-35322
- Bunched parallel reinforcing fibers of equal size and varying tensile strength, deriving critical loads and stresses under gradual failure
17 p2763 A71-35451
- Turbine disks failure under radial temperature drop, studying effects on load bearing capacity for thermal stresses
17 p2832 A71-35454
- Herringbone grooved gas lubricated journal bearing load capacity, attitude angle and power loss measurements
17 p2749 A71-35487
- Free edge effect on critical loading of rectangular sandwich plate with asymmetrical structure and rigid filler
17 p2833 A71-35622
- Cantilever column critical dynamic instability load under nonconservative follower force including thermomechanical coupling effect from boundary value problem formulation
[ASME PAPER 71-APM-L] 18 p2977 A71-36255
- Axisymmetric plastic deformation of imperfection sensitive spherical shell after elastic buckling, considering load carrying capacity
[ASME PAPER 71-APM-FF] 18 p2978 A71-36266
- Clamped rectangular plate buckling under uniaxial and biaxial compression, obtaining critical loads for various aspect ratios
18 p2979 A71-36360
- Nickel base alloy under axisymmetric tension compression tests, obtaining breaking load diagrams and fatigue and creep curves
18 p2937 A71-36716
- Elastic stability and buckling modes of cylindrical shell under critical gravity load, using double Fourier series and linear theory
18 p2983 A71-36847
- Destabilization phenomenon in nonconservative systems, considering simultaneous operation of damping mechanisms and critical load calculation
20 p269 A71-39036
- Nonlinear behavior of compressed elastic and elastoplastic rods in presence of large deformations, determining bearing capacity by step method
20 p269 A71-39164
- Critical coefficients of axial compressive forces with variable intensity for approximate stability analysis of vertical bars
21 p3472 A71-41151
- One dimensional structure failure calculation, using mathematical programming static method for load limit approximation
22 p3613 A71-41430
- Orthotropic shells of revolution limit analysis, considering yield conditions and flow rules
22 p3614 A71-41605
- Radiation dose effects on polymer strain magnitude under critical cyclic loading
23 p3697 A71-44033
- Critical compression loads and stability equations for clamped and hinged circular three layer plates with light filler, using Bessel functions
23 p3778 A71-44043
- Power series analysis of circular cylindrical shells stability under biaxial compression, expressing critical loadings
24 p3878 A71-44612
- Asymptotic design formulas for thermoelastic supercritical strains in thin elastic shallow spherical shells under external pressure
24 p3881 A71-44827
- Stability and critical loads of reinforced geometrically nonlinear cylindrical shells, using strain energy method
24 p3882 A71-44842
- Buckling stability and critical loads of thin elastic cylindrical shells with hollow core in axial compression
24 p3882 A71-44844
- Critical bending moments for elastic beam weakened by elliptical crack in tensile stress region
24 p3882 A71-44847
- Pressure distribution in narrow porous metal bearings solved with Bessel functions in cylindrical coordinates, finding lower load capacity
24 p3830 A71-44950

CRITICAL MACH NUMBER

U CRITICAL VELOCITY

U MACH NUMBER

CRITICAL MASS

Polytropic gas spheres gravitational instability under external pressure, obtaining critical masses and densities

05 p0813 A71-17091

Critical mass calculation for open cycle gas core rocket reactors, considering cavity size, fuel radius, reflector thickness and hydrogen bypass flow

22 p3573 A71-41637

CRITICAL PATH METHOD

Skyнет project UK and U.S. cooperation, discussing system scope, coordination, contract placing and PERT critical path analysis in management planning

02 p0337 A71-12427

Aerospace systems project management using graphic networking critical path method for planning and control

04 p0691 A71-15293

CRITICAL POINT

Bipropellant droplet supercritical steady combustion temperature measurements in zero gravity near critical point, comparing high and low pressures models for ambient gas solubility

01 p0141 A71-11309

Free convection in compressible viscous heat conducting liquid near critical point, discussing temperature gradients, layer heights, density distribution and inhomogeneity effect

02 p0331 A71-12190

Fermion system phase transition model thermodynamic behavior near critical point region for various interactions

03 p0456 A71-13350

Fluorine liquid-vapor coexistence boundary and critical point parameters, considering thermodynamic and transport properties

05 p0831 A71-16409

Density and compressibility of oxygen in critical region, using capacitance measurements

05 p0781 A71-16703

Thin shallow elastic shells boundary value problem, deriving existence and multiplicity of equilibrium state critical points for bending and buckling

07 p1213 A71-19639

Asymptotic stability trajectories and entering theorem of third order real nonlinear autonomous differential equations near critical point

10 p1636 A71-24131

Axisymmetric incompressible boundary layer flow, temperature distribution and heat exchange near critical point of rotating body with varying surface temperature

11 p1854 A71-25239

Temperature gradients effect on density distribution in material near critical point, using classical and scaling-law theories and Ising model

12 p1929 A71-27031

Heat transfer near critical point, examining continuity, momentum and energy equations for variable thermodynamic and transport properties effects

14 p2336 A71-30241

Free convection in compressible viscous heat conducting liquid near critical point, discussing temperature gradients, layer heights, density distribution and inhomogeneity effect

15 p2512 A71-31497

Liquid Zr drops combustion in oxygen-nitrogen atmospheres, examining critical conditions for sac formation with homogeneous bubble nucleation theory

17 p2837 A71-34511

Critical point anomaly in saturation curves of reduced temperature-compressibility planes of pure substances, using metric differential geometry and thermodynamics

18 p2985 A71-36452

Velocity and temperature profiles at near-critical point of nitrogen turbulent boundary layer flow over heated flat plate by thermocouple/pitot-static probe [ASME PAPER 71-HT-23]

19 p3165 A71-37994

Hydrogen near-critical point flow in heated cylindrical tube, measuring flow parameters radial profiles by combination pitot tube/thermopile/hot-wire sensor probe

19 p3165 A71-37995

Thermal conductivity anomalous behavior prediction for carbon dioxide, argon, nitrogen, oxygen and methane in critical region

19 p3165 A71-37998

Binary fluid mixtures density gradients near critical point due to gravity effect, deriving expression as linear function of height with thermodynamic equilibrium as starting point

21 p3345 A71-40236

Degenerate critical points Morse index type characteristics, considering maximum points of functional on surface of another

24 p3843 A71-44707

Slip, surface permeability and temperature gradient effects on surface friction and heat transfer in boundary layer near cylinder critical point

24 p3887 A71-44743

CRITICAL PRESSURE

Critical nozzle pressure ratio and geometry effects on free exhaust gas jets of jet engine models

[DGLR-70-055] 05 p0831 A71-15966

End face frame stiffness effects on cylindrical shell critical pressure

06 p0982 A71-17352

Thin orthotropic shallow elastic shells with initial defects, analyzing critical pressure states

06 p0982 A71-17355

Cylindrical shell stability under critical dynamic radial pressure, discussing geometrical and mechanical parameters and loading law

06 p0997 A71-17847

Free convection turbulent flow under supercritical conditions, investigating convection heat transfer and flow patterns

07 p1220 A71-18780

Rotary inertia effect on critical dynamic pressure parameters and supersonic flutter of in-plane loaded sandwich plates

07 p1213 A71-19887

Eccentricity and clamping effects on stability and critical pressure of ring-reinforced cylindrical shells under internal pressure

08 p1369 A71-21122

Cs thermoelectric power near critical temperature and pressure, determining dense plasma electron-neutral elements interaction effects

11 p1715 A71-26153

Blowing and wall curvature effects on gas flow separation and critical pressure gradient in Couette flow examples

13 p1993 A71-29193

Clamped and hinged spherical and paraboloidal shell caps elastic stability tests under external pressure loading, determining critical pressure

14 p2323 A71-29846

Toroidal shell stability analysis for asymmetric buckling based on small deflection theory linearized relations, deriving upper critical pressure by Bubnov-Galerkin method

17 p2831 A71-35323

Stability formula for critical pressure in cylindrical shells orthotropically reinforced by closely spaced eccentric ribs

22 p3616 A71-42487

Cylindrical and weakly concave shells, testing critical pressure relationship to axial tension load with cellular models

24 p3884 A71-44898

CRITICAL REYNOLDS NUMBER

U CRITICAL VELOCITY

U REYNOLDS NUMBER

CRITICAL SPEED

U CRITICAL VELOCITY

CRITICAL STRESS

U CRITICAL LOADING

CRITICAL TEMPERATURE

Physical properties of Nb-Al-Ge alloys with maximum superconducting transition temperature close to boiling hydrogen

01 p0103 A71-11070

Cu-Ni-Mn alloys hardening by heat treatment, describing various critical temperature measurement methods and micrographic analysis

01 p0105 A71-11622

Plasma generation and nuclear fusion by lasers, investigating critical parameter values for heating

01 p0137 A71-11625

Oxygen and homologous hydrocarbon mixtures detonation limits, discussing propagation, fuel molecule structure, critical temperature, initial cracking mechanism and carbonaceous solids condensation

02 p0331 A71-11957

Stability loss of cylindrical and spherical shells under heating and external force, determining critical temperature and loads

02 p0325 A71-12286

Critical ductile-brittle transition temperature and microstructure under deep drawing of sintered and vacuum melted Mo

02 p0257 A71-12519

Tissue cooling with liquid nitrogen, determining film boiling transition temperature and heat transfer rates [ASME PAPER 70-WA/HT-16]

03 p0372 A71-14096

Faraday rotation near ferromagnetic critical temperature of chromium bromide, discussing scaling laws validity and experimental confirmation

04 p0637 A71-15796

Critical temperature short to long range ordering mechanism theories, discussing lattice type, transition continuity and spinodal decomposition factors

07 p1131 A71-19432

Scattered light depolarization measurement near carbon dioxide critical temperature, using He-Ne laser

07 p1127 A71-20379

Cs thermoelectric power near critical temperature and pressure, determining dense plasma electron-neutral elements interaction effects

11 p1715 A71-26153

Superconducting alloys order parameter spatial variation and resonance scattering near nonmagnetic

impurity at critical temperature, using Heinrich perturbation theory expansion solutions

12 p1942 A71-26744

Superconductive Nb-Al alloy critical temperature as function of chemical composition and heat treatment

13 p2085 A71-28576

Liquid and gaseous Hg thermoelectric power measurements at sub and supercritical temperatures and various pressures

13 p2000 A71-28676

Computerized least squares fit of second virial coefficients vs critical temperature to Lennard-Jones potential function for hydrocarbons, halides, alcohols and cyclic compounds

13 p2103 A71-29005

Nb and Nb alloys coating by hot-dipping in molten Al, investigating critical temperature and growth kinetics

13 p2087 A71-29121

Dipolar charge density of electret formed by polar polymers above critical temperature under dielectric polarization with quenching

14 p2181 A71-29747

Convection stability in arbitrarily shaped fluid containers heated from below with temperature gradient above critical value

14 p2337 A71-30408

Steel structural elements resistance reserve to brittle fracture, considering critical temperatures and breaking stresses

15 p2504 A71-31852

Superconducting microjunctions I-V characteristic at critical temperature, investigating voltage fluctuations effects in external circuit

19 p3119 A71-37860

German monograph on thermal equation of state for nitrogen vapor-liquid phase equilibrium covering vapor pressure and density, phase diagrams, critical temperature, etc

22 p3574 A71-41716

CRITICAL VELOCITY

Critical velocity and elastic panel flutter stabilization in magnetohydrodynamic flow by distributed magnetic field control

02 p0293 A71-12628

Rotor and rotor-disk system response to constant and pulsating torque, experimentally examining critical whirling speed and lateral vibration

[ASME PAPER 70-WA/DE-14] 03 p0511 A71-14146

Superfluid flow through parallel channel, obtaining critical velocity measurements by phase coupling

03 p0404 A71-14199

Cylindrical shell with elastic core under annular sliding load, solving for critical velocity via Fourier transformation

07 p1212 A71-19353

Critical speeds for inviscid compressible potential flow past thin elastic cylindrical shells, using long wave approximation

10 p1689 A71-24565

Critical velocity of fluid flow in cantilever tube, applying Galerkin method to modal type analysis

11 p1748 A71-25163

Surface evaporation and condensation effects on stability of thin liquid film flowing down heated inclined plane at critical Reynolds number

13 p2160 A71-28596

Nonlinear asymptotic stability of motion in critical case involving characteristic equation in first approximation with pair of imaginary roots

15 p2449 A71-31699

Flutter of thin walled cylindrical shells conveying fluid above critical flow velocity

15 p2508 A71-32135

Critical induced acceleration for shock propagation as function of strain in polymethyl methacrylate [ASME PAPER 71-VIBR-53]

16 p2600 A71-33213

Critical forward speed effects on two dimensional peripheral jet ground effect support systems, comparing theoretical analysis with wind tunnel model data

[AIAA PAPER 71-908] 19 p2995 A71-37159

Dimensionless products associated with scale factor effects of parachute critical opening /squidding/ velocity

19 p2996 A71-37293

Rotating shaft critical speed determination as root of polynomial from frequency equation /characteristic determinant/ without iterative search

[ASME PAPER 71-VIBR-53] 21 p3385 A71-40300

Shock wave diffraction at symmetric lenticular wing profile with free stream critical Mach number of 0.87, using Godunov difference scheme

21 p3322 A71-40679

Liquid transition through critical value, considering self oscillation mode frequency

24 p3821 A71-45340

CROCCO METHOD

Conducting fluid in transverse magnetic field at low Reynolds numbers, deriving laminar boundary layer universal equations in Crocco or Mises variables

10 p1648 A71-24028

Inviscid swirling nozzle flow equations from Crocco relation

19 p2993 A71-37890

CROP GROWTH

Airborne surveillance for environmental management, discussing earth resources program, aerial sensors for thermal water pollution, crop disease, salinity and geological structure
07 p1018 A71-19080

Crop species and soil condition computerized identification from film optical density differences, using multibase and multiemulsion photography
08 p1282 A71-21436

Optimization of time intervals of conveyor harvestings and harvested age of oxygen producing plants for life support system
13 p2017 A71-28406

CROPS

Seasonal and year-to-year crop radar sensing in agriculture for socioeconomic applications
07 p1095 A71-18825

World crop areas, yield, production and land use data, using remote sensing devices
09 p1439 A71-23211

CROSS CORRELATION

Instrument for measuring cross and autocorrelation functions with capability of extracting signal masked by noise by averaging operations
01 p0079 A71-10313

Auto and cross correlation function computation from waveform polarity by flexible one bit digital correlator for frequencies to 25 MHz
02 p0211 A71-11644

Signal cross correlation processing in unstable and turbulent plasmas, comparing correlational and spectral analyses of plasma dispersion and transfer function measurements
06 p0938 A71-18456

Linear delay input effects on analog cross correlator mean performance, plotting output SNR vs integration time
07 p1059 A71-18851

Automatic procedure for determining cloud motion from geosynchronous satellite pictures based on cross correlation, discussing real time operational system
08 p1327 A71-21454

Weakly ionized plasma density fluctuations and diffusion from kinetic equations for electron-space density cross correlation, assuming BGK model
09 p1503 A71-22863

Thermal fluctuations in earth upper atmosphere, related to satellite deceleration and X ray solar radiation changes by autocorrelation and cross correlation analyses
11 p1817 A71-25822

Lower extremities interlink angles correlation and cross correlation functions during walking for locomotor functions analysis in man
13 p2006 A71-28382

Cross correlation characteristics of deviations in critical frequencies of F 2 region
13 p2030 A71-28538

Combined heterodyning, beam forming and cross correlation of broadband multichannel signal from multidimensional phased array, using coherent optical system
14 p2241 A71-30142

Statistical methods for calculating cross correlation function integrals of input and output coordinates of automatic control system in presence of random noise at input
22 p3525 A71-41437

Kinetic equations for phase space cross correlation functions of electron density fluctuations in magnetized weakly ionized plasma, using relaxation model
22 p3581 A71-41895

Trace reflex formation in response to acoustic stimulus with verbal reinforcement, determining cross correlation connections between induced activity of auditory and motor areas
24 p3796 A71-44547

CROSS COUPLING

Double balanced cross coupled transistor mixer, predicting conversion gain and inter and cross modulation distortion performances
02 p0233 A71-12345

Systems analysis application to stability of aerodynamic cross coupling in flight vehicle motions with steady sideslip, using feedback and root locus techniques
02 p0190 A71-12687

Nike-Apache sounding rocket vehicle with canted fins, examining pitch-roll coupling characteristics by equilibrium and dynamic simulation methods
03 p0497 A71-13659 [AIAA PAPER 70-1376]

Forward and reverse cross coupling compensation in infinite straight row of radiating elements of antenna array
07 p1078 A71-20071

Antenna feed waveguides interconnection for compensation of cross coupling between elements of two dimensional array
07 p1079 A71-20072

Cross couplings in wideband antenna arrays, determining scattering coefficients, self/mutual impedances and admittances of two radiating elements
11 p1738 A71-26344

Two-shaker single input sinusoidal and random vibration tests, considering Hunter-Helmuth solution with constant cross coupling compensation in frequency band
11 p1745 A71-26491

Soviet book on multiloop automatic control systems covering matrix notation, stability and accuracy, invariance principle, compensating cross couplings, etc
14 p2218 A71-29527

Stability criterion for cross coupled symmetrical two dimensional nonlinear control systems allowing different slopes for Popov lines
15 p2380 A71-31938

Digital systems synthesis for stabilization of triaxial gyrostabilizer consisting of three uniaxial gyrostabilizers with cross couplings
17 p2738 A71-34559

Fail operational control moment gyro configuration of four single gimbal gyros, eliminating cross coupling by simple analog steering law [AIAA PAPER 71-936]
19 p3097 A71-37181

CROSS FLOW

Boundary layer theory extended to cross vorticity transport in outer flow approaching two dimensional stagnation point
03 p0398 A71-13103

Uniform flow stability near two dimensional stagnation region formed by blunt body immersion in cross flow
03 p0400 A71-13728

Jet plume in subsonic cross flow, calculating counter-rotating vortices as function of distance along trajectory from semiempirical model
07 p1090 A71-19901

Cross flow profiles for compressible turbulent boundary layers with and without flow reversal via hodograph models family
08 p1229 A71-22033

Pressure drag and cross flow force coefficients of inclined circular cylinder in supercritical flow
09 p1382 A71-22098

High velocity airstream interaction with multiple gas jets from single row multihole wall injectors, discussing jet penetration and mixing in cross flow
11 p1750 A71-25478

Cross flowing air stream effects on heat transfer characteristics of single lines of air jets impinging on plane surfaces [ASME PAPER 71-GT-1]
11 p1854 A71-25947

Three dimensional turbine end wall boundary layer with shear term, using momentum integral analysis and cross flow velocity profiles [ASME PAPER 71-GT-6]
11 p1751 A71-25952

Forced convection effects on characteristics of steady state cross flow arc in presence of applied transverse magnetic field
12 p1938 A71-27265

Momentum thickness of boundary layer of circular cylinder in cross flow at high Reynolds numbers from static pressure and skin friction measurements
12 p1867 A71-27738

Wing-jet interference effects in cross wind on thrust and aerodynamic characteristics at large distance from and near ground
13 p1993 A71-29207

Hodograph models family for cross flow velocity component of three dimensional turbulent boundary layers, applying integral method to curved rectangular channels data [ASME PAPER 71-FE-1]
13 p2051 A71-29445

Flowfield production by fluid injection into supersonic crossflow, occurring with liquid/gas jet control of vehicle with combustion ramjets [AIAA PAPER 71-728]
14 p2295 A71-30775

Turbulent compressible underexpanded two dimensional jet interaction with crossflowing free stream, analyzing flow field by numerical solution of Navier-Stokes equations [AIAA PAPER 71-611]
15 p2514 A71-32277

Wing installed VTOL coaxial drive lift fan model in wind tunnel test, investigating performance in crosswind environment [AIAA PAPER 71-742]
15 p2469 A71-32284

Heat transfer and hydraulic resistance in cross flow heat exchanger with slitlike channels
17 p2836 A71-34212

Flow visualization and hot-wire measurements, showing vortex shedding association with turbulent air jet issuing from flat plate into cross wind
17 p2670 A71-34659

Transverse magnetic field effects on Ar cross flow arc in constant velocity mainstream
17 p2788 A71-34868

Three dimensional boundary layers on axisymmetric bodies with large positive and negative crossflows, using finite difference method
17 p2727 A71-34875

Heat transfer coefficients calculation for human body in cold water from heat balance equations, comparing with free convection coefficients in cross-flowing water
18 p2862 A71-36900

Plane Couette-Poiseuille flow stability between porous walls with fluid injection and suction causing uniform crossflow
19 p3044 A71-37728

Nonablating inelastic deformable material surface interaction with external supersonic turbulent boundary layer, observing crosshatch patterns
21 p3323 A71-40941

Conical ablation surface models in hypersonic wind tunnel tests, describing Mach number and nose tip bluntness effects on cross hatching
21 p3476 A71-40965

Jet mixing in cross flow at different velocity ratios and incidence angles, calculating momentum and mass flow
23 p3664 A71-43831

Volume-weight characteristics of cross flow heat exchangers for heat regenerating gas turbine engines
24 p3389 A71-45007

CROSS RELAXATION

Collision induced spectral cross relaxation radiative saturation and Lamb dip formation in carbon dioxide molecular lasers, using rate equations
10 p1620 A71-24151

CROSS SECTIONS

Atomic H excitation by electron impact, deriving cross sections for anomalous recombination lines in H II regions radio frequency spectrum
02 p0317 A71-12873

Oscillatory combustion mechanism variations with geometrical configuration changes, considering variable cross sectional area and straight tube combustors
03 p0517 A71-13354

Nozzle system elements size relation to passage cross section in full size two cascade and miniaturized gas turbine engine power plant
03 p0472 A71-14258

Gas turbine engines nozzles flow passage cross sections area measurement, using gas flowmeter, pipes system and vacuum pump
03 p0472 A71-14260

Resonance charge exchange effect on gaseous ions mobility, noting cross sections structure due to resonance and wave interference
04 p0629 A71-14998

Ti-Zr-O alloys cross sections investigation by neutron and X ray diffraction, discussing stoichiometry deviation
06 p0911 A71-17382

Transition curve equation for end cross section of slant-toothed wheel cut by rack type instrument with protuberance and rounded edge
07 p1117 A71-19360

Rectangular, square and circular cross section blanks dynamic metal cutting process by method of characteristics
08 p1295 A71-20794

Contained cross sectional deformation effects on turbine blades natural torsional vibration frequencies
08 p1372 A71-21617

Curved beams bending stress concentration approximate equations for elliptical, circular and rectangular cross sections, providing behavior prediction superior to exact methods
08 p1373 A71-21749

Concentrated elongation dependence on cross sectional area reduction in industrial Ti alloys undergoing thermomechanical treatment
09 p1468 A71-22324

Electron emission from He ion by proton bombardment, calculating double differential cross sections relative to ejection energy and angle
09 p1497 A71-22415

Small cross section viscous vortex ring velocity in ideal fluid with arbitrary vorticity distribution in core
11 p1749 A71-25357

Relativistic quarks in cosmic rays at sea level and at mountain altitude, estimating production cross section vs absorption mean free path and mass
11 p1815 A71-25589

Cavity cross sections deformation in heavy ideal liquid, deriving nonlinear system of equations for time dependence within framework of small perturbation theory
13 p2047 A71-28279

Center of rigidity position determination in cross section of thin walled beam under nonuniform temperature due to creep
13 p2154 A71-28642

Magnetic shielding of various shaped enclosures such as rectangular or cylindrical cross sections in terms of normalized parameters
13 p2039 A71-28870

Modified method of cross sections applied to scalar Helmholtz equation solution in infinite symmetrical waveguides
15 p2449 A71-31711

Nb-Re-C system, investigating polythermal NbC-Re cross section structure by metallographic chemical and X ray analyses and microhardness and melting point measurements
15 p2430 A71-32148

Shock wave interaction with duct cross section changes, discussing experimental apparatus and shadowgraph results

15 p2393 A71-32265

Deformations and stress concentration on corrugated plate under uniformly distributed load, considering cross section as combination of two cylindrical shells

17 p2818 A71-34401

Optimal cross section of minimum volume rotating shaft with complex fatigue strength, accounting for tension and shear effects

17 p2822 A71-34595

Stress-strain state of thin walled curvilinear frame-type rods of variable cross section with variable elastic moduli along length and contour

17 p2829 A71-35309

Cross sectional warpage effects on turbine blades natural torsional vibration frequencies

17 p2834 A71-35677

Commercial Ti alloys homogeneity as function of ingot diameter, noting mechanical properties of semifinished products

20 p3252 A71-39544

Statistical phase space cross sections for helium ion-nitrogen molecule reactions, including dispersion and short range forces in intramolecular potential energy function

23 p3706 A71-43119

Cavity cross sections perturbed motion equations

24 p3819 A71-44840

Curvilinear elasticity solutions to stress concentrations at fine necks in cylindrical shaft under torsion, considering semicircle, semiellipse, rectangle, triangle and arc shapes

24 p3882 A71-44846

Cross section behavior of tube under plastic bending based on hollow rod treatment

24 p3883 A71-44848

CROSSED FIELD AMPLIFIERS

Design concepts providing high plate efficiency in high power injected beam crossed field amplifier capable of CW operation with conduction or liquid cooling

01 p0054 A71-10975

Continuous cold cathode forward wave reentrant beam crossed field amplifiers with cut-off electrode, investigating AM and PM noises and phase coherence

11 p1739 A71-26434

High efficiency and power long life cross field amplifier generator for solar energy conversion in space into microwave, discussing magnetron and amplitron

13 p2000 A71-28668

Output characteristics of three different segmented M-type crossed field TWT amplifiers in large signal operation from field amplitude distribution along interaction space

15 p2378 A71-32628

Magnetron crossed field amplifier multistage frequency multiplier HF field properties, obtaining numerical solutions for nonlinear governing equations

22 p3522 A71-42315

CROSSED FIELDS

Nonequilibrium plasma from pulsed discharge in crossed electric and magnetic fields

02 p0288 A71-11882

Dynamic cross-field photomultiplier sampling function characteristics measurement using self-modelocked He-Ne pulsed laser

02 p0248 A71-12006

Laser light frequency mixing and doubling in isotropic bodies in crossed magnetic and electric fields, examining magneto-electro-optical processes

02 p0261 A71-12171

Electron density fluctuations in nonstationary plasma under crossed electric and magnetic fields, relating times of instability development and background relaxation

02 p0289 A71-12179

Electromagnetic repulsion of conducting and dielectric bodies within liquid metal and electrolyte in crossed field under gravitational acceleration

02 p0293 A71-12630

Electron velocity distribution in fully ionized plasma under crossed electric and magnetic fields, assuming Fokker-Planck expression for Lorentz gas

02 p0293 A71-12743

Nonstationary rotating MHD viscoplastic medium between coaxial cylinders in crossed electric and magnetic fields, determining zone interface position and stress distribution

03 p0464 A71-13601

Cross field instability effect on weakly ionized plasmas with ionization density gradients under crossed electric and magnetic fields, using linear analysis

08 p1339 A71-21207

MHD accelerator in pulsed mode with crossed fields, studying one dimensional steady inviscid flow

09 p1501 A71-22407

Equatorial E region cross field instability and ionization irregularities from Nike-Apache rocket measurements

12 p1900 A71-26934

Hybrid M-type microwave oscillators including backward and traveling wave tubes with crossed fields in large amplitude mode, considering power efficiency and frequency control

12 p1888 A71-27620

Magnetic corrections to Boltzmann distribution function by power expansion, determining current density in system of free electrons accelerated by crossed electric and magnetic fields

13 p2109 A71-29288

Horizontal conducting fluid cylinder ultrasonic oscillations in crossed electric and magnetic fields, obtaining boundary value problem

14 p2278 A71-29614

Two lens high current plasma accelerator with closed electron drift, using crossed electric and magnetic fields

14 p2282 A71-30664

Electron density fluctuations in nonequilibrium plasma under crossed electric and magnetic fields, relating ionization instability development and background relaxation times

15 p2454 A71-31488

Matched/mismatched crossed beam interference field combination with sinusoidal holographic diffraction grating, studying metric properties and moiré-obtured bands

15 p2410 A71-32404

Homogeneous infinite weakly ionized plasma dielectric permittivity tensor in crossed electric and magnetic field

17 p2790 A71-35444

Weakly ionized gas plasma confined by cylindrical electrodes and dielectric fronts, calculating rotational movement behavior in transverse electric and longitudinal magnetic fields

18 p2952 A71-36943

Nighttime equatorial E region ionization and electron density gradient irregularities, noting cross field instability with rocket-borne Langmuir probes

20 p3225 A71-39727

Electron gas in constant crossed E and H fields, deriving nonlinear conductivity theory

21 p3424 A71-41260

Mott exciton differential absorption spectrum in parallel and crossed electric and strong magnetic fields

23 p3716 A71-43479

Strong magnetic field effects on acoustic oscillations and instability in stationary inhomogeneous low temperature plasma flow in crossed fields

23 p3712 A71-43917

Spectroscopic analysis of pulsed gas discharge in crossed electric and magnetic fields of gas magnetron diode in 3100-4660 Å wavelength range

23 p3712 A71-43933

Stratified nonequilibrium plasma ionization instability in crossed fields investigated by physical model without diffusion processes and boundary effects, considering space-time behavior of perturbation

23 p3713 A71-44152

Relativistic electron beam propagation in decelerating medium in crossed electric and magnetic fields, noting nonrelativistic instability condition

24 p3856 A71-44669

Hot electrons in semiconductors within crossed and parallel electric and quantizing magnetic fields, examining collision frequencies and energy relaxation

24 p3861 A71-45165

CROSSLINKING

High temperature pyrrones molding, discussing covalent organic bonds breakage and subsequent structural rearrangement of crosslinked polymer network

01 p0107 A71-10459

Silyl peroxides as promotion agents for polymeric materials adhesion to solid substrates and for crosslinking polyethylene to other polymers

10 p1633 A71-24109

CROSSOVERS

Single metal system Al beam leaded chips, substrates and crossovers for multilead packaging, describing fabrication techniques

09 p1509 A71-23119

CROSSTALK

NT IONOSPHERIC CROSS MODULATION

Two cavity ring-type channel dropping filters for millimeter wave guided communication system, calculating pulse response and interchannel crosstalk characteristics

14 p2210 A71-29569

Optical coupling of degenerative modes in two parallel dielectric waveguides, applying to slab guides and fibers crosstalk problem

19 p3014 A71-37214

Optical dielectric slab waveguides with core thickness variations, computing crosstalk due to light scattering in terms of guided mode radiation loss

19 p3014 A71-37215

AM crosstalk in unified carrier telemetry system, studying implications for carrier false lock and tracking

22 p3514 A71-42390

CRUCIFORM WINGS

Aerodynamic forces and hinge moments of delta cruciform control surface in blunt-nosed canard configuration for subsonic, transonic and supersonic flows

11 p1701 A71-25161

CRUDE OIL

Foamy properties at various temperatures of nonaqueous hydroliquids based on petroleum fractions and organic silicon and phosphorus oligomers

01 p0088 A71-11107

Petroleum mechanical engineering and pressure vessels and piping - ASME Conference, Denver, September 1970

04 p0665 A71-14767

Soviet book on hydrodynamics of nonstationary motions of viscoplastic media covering mechanical properties of clay, mortar, cement, lubricating oil, petroleum and disperse media, etc

21 p3369 A71-40872

CRUISING FLIGHT

Hypersonic cruise aircraft configuration reliable Reynolds numbers extrapolation from laminar boundary to turbulent layer

06 p0883 A71-18576

Cruising flight range as function of supersonic/subsonic transport fuselage geometrical parameters

12 p1868 A71-27494

Minimum drag surface shape of thick lifting delta wing integrated with conical fuselage for supersonic cruising speed

12 p1866 A71-27716

Rotor performance and design for hover and cruise VTOL flights

22 p3482 A71-42238

CRUSADER AIRCRAFT

U F-8 AIRCRAFT

CRUSHING

Rushing effects on fractional composition and quality of sponge titanium, including optimum end size of pieces

04 p0616 A71-15825

CRUSTS

NT EARTH CRUST

NT LUNAR CRUST

CRYODEPOSITS

Equilibrium adsorption isotherms correlation for low temperature cryodeposits, using Dybinin-Ladushevich equilibrium equation to estimate hydrogen capacity of cryosorption pumping system

10 p1643 A71-25011

Spectral reflectance of water cryodeposits on liquid nitrogen cooled surfaces in vacuum IR integrating sphere

11 p1858 A71-26232

Hydrogen sorption capacity by sulfur dioxide frost from cryodeposit formation on stainless steel sphere in vacuum chamber and equilibrium isotherms measurement

17 p2695 A71-35142

CRYOGENIC COMPUTER STORAGE

Cryotron elementary storage cells work region determination by phase transition characteristic form, discussing component reliability

03 p0382 A71-13520

Superconductivity based cryogenic electronics, considering thin film IC, miniaturization, microwave circuits, memory elements, etc

08 p1263 A71-21067

CRYOGENIC EQUIPMENT

Cryogenic pressure vessels carrying capacity, discussing loading types, materials properties, thermal effects, etc

01 p0097 A71-10077

Cryogenic austenitic steels embrittlement dependence on nitrogen content, noting second phase precipitation role

01 p0098 A71-10086

Cryogenic L band three port stripline circulator, discussing design, construction and applications

01 p0056 A71-11200

Aerobee 150 sounding rocket cryogenic air sampler, discussing design, operation and air constituents reaction to cooling

01 p0084 A71-11442

Miniature centrifugal pump for circulating liquid He in flow loop, testing performance

02 p0255 A71-12129

Cryogenic heat pipes with parallel capillary channel wicks

[ASME PAPER 70-WA/ENER-1]

03 p0520 A71-14106

Spacecraft cryogenic cooling systems, discussing passive, phase change and closed cycle coolers and refrigerators

04 p0535 A71-15343

Boiling cryogenic gas-liquid cross-current heat exchanger unit surface power transmission optimization

04 p0626 A71-15463

AC superconducting cables design for utilities underground power transmission lines, discussing superconductor and cryogenic envelope configuration and characteristics

07 p1024 A71-20159

- K band cryogenically cooled wideband /600 MHz/ low noise parametric amplifier for millimeter wave satellite communication earth terminals, discussing design
08 p1263 A71-20770
- Tilting pad hydrodynamic and porous hydrostatic gas lubricated journal bearings for miniature cryogenic turbomachinery
[ASLE PREPRINT 70LC-10] 08 p1298 A71-21158
- Carbon dioxide flow vacuum condensation on cryogenic pump surface, noting flow temperature and directivity effects on condensation rate
09 p1544 A71-22268
- Miniature cryogenic systems for cooling IR detectors in upper atmosphere involving earth surface, air-glow and OH emission measurements
09 p1545 A71-23004
- Terrestrial spectroscopy by cryogenic gravity meter with hollow superconducting niobium sphere in cylindrically symmetric magnetic field, detecting earth spheroidal oscillations
10 p1598 A71-23737
- Receiver systems for 100 meter Effelsberg radio telescope using cryogenically cooled parametric amplifiers for receiver system noise minimization
10 p1578 A71-24510
- Superfluid-helium-cooled rocket-borne far-IR radiometer for night sky radiation measurement, discussing cryogenic, optical detection and electronic systems design features and performance
12 p1903 A71-26791
- Cryogenic propellant tank thermal insulation system based on polypropylene oxide, polyurethane polyvinylchloride and polymethacrylimide foams, discussing design, technology and model tests
12 p1985 A71-26834
- Cryogenic pressure vessels carrying capacity, discussing loading types, materials properties, thermal effects, etc
16 p2593 A71-33633
- Cryogenic austenitic steels embrittlement dependence on nitrogen content, noting second phase precipitation role
16 p2593 A71-33642
- Low thermal flux lightweight glass fiber composite tubing for cryogenic propulsion plumbing systems
17 p2762 A71-35206
- Astigmatic image distortion in low temperature multiple reflection White cell with aluminum dewar assembly for Martian IR interpretation
18 p2914 A71-35844
- Thermal control using nitrogen, circuit board, switching, flexible, transformer and segmented evaporator heat pipes
[ASME PAPER 71-AV-29] 18 p2868 A71-36396
- Multilayer insulation systems development and selection for cryogenics thermal protection on space vehicles, considering mechanical properties, radiation shielding, components, evacuation rate and outgassing
19 p3171 A71-38547
- Heat transfer, fluid flow and pressure loss, noting application to cryogenic heat exchangers and process plants
20 p3312 A71-39245
- Cryogenic refrigeration requirements of low noise microwave amplifiers in satellite communications, discussing solid state masers and liquid helium parametric amplifiers
20 p3204 A71-39251
- Closed cycle refrigeration system for cryogenic cooling of IR illuminator in helicopter mounted U.S. Army NVASS Night Vision System for night reconnaissance
20 p3184 A71-39275
- Vacuum covered gage measurements in sorption and cryogenic systems with activated pumping surfaces, concerning molecular gas flux leaving specimen
21 p3417 A71-41298
- High vacuum mass spectrometric hazardous gas detection system used during cryogenic loading of Saturn vehicles, discussing application to environmental pollution detection
22 p3542 A71-41988
- CRYOGENIC FLUID STORAGE**
Expandable rigidizable solar shields operational, structural and thermal performance tests conducted with spherical models for cryogenically fueled space vehicles
03 p0500 A71-14432
- Outgassing of multilayer insulation materials for use in cryogenic fuel tanks
03 p0522 A71-14441
- Carbon fiber reinforced composite cryogenic fuel tanks development for post-Apollo programs, discussing fiber and resin physical properties
05 p0819 A71-15946
- Hydrogen slush storage and transfer density and flow measuring instrumentation, emphasizing capacitance measurement
[NAS PAPER M-2] 08 p1292 A71-21695
- Superinsulation for long term storage of cryogenic propellants in space tanks using double aluminized Mylar with Dacron needles
09 p1546 A71-23009
- Metallic diaphragms design, fabrication and testing for cryogenic fluid and positive expulsion systems
[AIAA PAPER 70-683] 11 p1768 A71-25518
- Mixed ullage heating, convection and conduction models of thermal stratification of cryogenic propellants stored in low gravity environment
11 p1810 A71-26507
- Jet mixing control of thermodynamic state of space stored cryogenic fluids, minimizing mass penalties resulting from equilibrium departures
[AIAA PAPER 71-646] 14 p2285 A71-30723
- Filament wound glass-reinforced plastic struts for cryogenic tank supports in long term planetary missions, testing thermal and mechanical properties
17 p2762 A71-35205
- Cryogenic fluids, considering refrigerants storage vessels, liquid surface detection devices, transfer lines, level gauges
20 p3270 A71-39241
- Liquid He containment in space zero-g environment, proposing use of high thermal conductivity porous plug operating in superfluid regime
20 p3184 A71-39280
- CRYOGENIC FLUIDS**
NT LIQUID HELIUM
NT LIQUID HYDROGEN
NT LIQUID NITROGEN
NT LIQUID OXYGEN
NT SOLIDIFIED GASES
- Cryogenic fluids nucleate boiling dependence on solid surface characteristics, considering hysteresis, boiling site spreading and radiation effects
01 p0178 A71-10005
- Microwave systems for cryogenic liquid and slush density and flow velocity measurements
04 p0586 A71-14659
- Cryogenic liquids boiling peculiarities concerning heated surface material thermophysical properties effects on cavity stability, density and heat transfer rate
04 p0688 A71-15537
- Variable density turbulent jets, discussing compressible, high temperature gas, cryogenic and supersonic jets, Reynolds equations, etc
04 p0577 A71-15620
- Viscosity measurements for saturated liquid state of Ne, Ar, H, N, O, CO and methane
06 p0929 A71-17315
- Microwave methods for nitrogen or hydrogen densities and flow rate measurement in single phase liquid and slush state
[NAS PAPER M-1] 08 p1292 A71-21696
- Hydrogen fluid phase and temperature measurement by single sensor with fluid phase discrimination circuit for transient response sampling
[NAS PAPER M-3] 08 p1293 A71-21697
- Multilayer insulation systems for cryogenics protection aboard spacecraft, considering mechanical properties, radiation shielding, component evacuation rate and outgassing
08 p1375 A71-21748
- Free molecular flow on cryosurface in cylindrical space simulation chamber with spherical test object
09 p1433 A71-23005
- Thermodynamic properties prediction for liquefied natural gas and other cryogenic fluids, using two fluid method
13 p2100 A71-28603
- Shock wave caused chemical reactions between solids and cryogenic liquids, discussing shock sensitivity tester for liquid propellant- structural material systems
14 p2222 A71-30546
- Cryogenic fluids flow measurement, discussing various fluids, pressures, temperatures and flow rates
15 p2412 A71-32701
- Liquid rocket propellants pressurization by injected cryogenic liquids evaporation, using water and liquefied air for experimental investigation
[DFVLR-SONDDR-117] 15 p2466 A71-32721
- Boiling heat transfer to cryogenic fluids, considering pool convective, nucleate, film and forced convective subcooled boiling
19 p3162 A71-37463
- Microwave instrumentation for measuring cryogenic fluids density and flow rate, noting slush
20 p3237 A71-39277
- Liquid-liquid or solid-liquid interface Leidenfrost film boiling, deriving heat transfer coefficient for liquid drop floating on cryogenic fluid
20 p3313 A71-39288
- Film condensation heat transfer coefficients measurements on vertical heat pipes for cryogenic nitrogen, hydrogen and deuterium
20 p3313 A71-39290
- Variable thickness ice film water-to-cryogen heat exchanger design, presenting mathematical model for performance calculation by modified integration digital analog simulator computer program
20 p3314 A71-39291
- Free convective heat transfer in cryogenic liquid filled enclosure, studying effects of vibration near resonant frequency
20 p3314 A71-39292
- Flow induced vibrations of metal bellows with internal cryogenic fluid flow, noting effects of heat transfer, liquid state properties, external damping and condensation
[ASME PAPER 71-VIBR-14] 21 p3457 A71-40276
- CRYOGENIC GYROSCOPES**
Superfluid gyroscope for general relativity tests, using resonant phonon force field for drift reduction
02 p0248 A71-11943
- CRYOGENIC MAGNETS**
Cu clad Nb-Ti wire wound superconducting solenoids with large fields at 1.6-5.2 K
24 p3809 A71-45105
- CRYOGENIC ROCKET PROPELLANTS**
Thermodynamic similarity laws for rocket fuel tanks with cryogenic propellants, using dimensional analysis for unsteady temperature distributions
02 p0332 A71-12526
- Structural materials criteria for cryogenic propellant tanks, discussing chosen alloy composition, heat treatment and general properties
07 p1118 A71-19802
- Total and vapor pressure sensing and hybrid analog/digital electronic controller for multiburn cryogenic spacecraft propulsion pressurization
[AIAA PAPER 71-647] 14 p2290 A71-30724
- Throttleable bipropellant rocket engine, discussing cryogenic and space storable propellants and injection system optimization based on combustion mechanism photographic observation
[AIAA PAPER 71-740] 14 p2296 A71-30783
- Low thermal flux lightweight glass fiber composite tubing for cryogenic propulsion plumbing systems
17 p2762 A71-35206
- Zero-g propellant tank quantity gaging methods, suggesting large cryogenic propellant tanks for space shuttle orbiter stage
18 p2922 A71-36455
- Cryogenic rocket propulsion technology covering propellant selection, pumping, cavitation, starting, tank stratification, instrumentation, hydrogen uses, nuclear propulsion, cost, availability, toxicity and storability
20 p3306 A71-39250
- Cryogenic liquids thermal behavior under operational conditions, discussing Europa 3 second stage liquid hydrogen and oxygen engine
22 p3588 A71-41502
- Valves and regulators development and testing for liquid hydrogen propellant tank pressurization system
22 p3588 A71-41503
- Cryogenic propellant control system, discussing hot wire sensors, fuel state in fueling and tank pressurizing and feed stage
22 p3588 A71-41504
- CRYOGENIC STORAGE**
Fiber reinforced cryogenic pressure vessels design, manufacture and testing for space and terrestrial applications, comparing glass fibers to carbon fibers
04 p0618 A71-15650
- Cryogenic tanks manufacture from Al alloys
07 p1118 A71-19801
- IR radiation role in limiting central heater maximum temperature and heat transfer to high density oxygen in cryogenic storage systems
13 p2166 A71-29505
- Cryogenics applications to cryosurgery and long term low temperature storage of living cells and tissues
20 p3189 A71-39252
- CRYOGENICS**
Noise temperature measurement of mismatched cryogenic generator, using compensation method
01 p0056 A71-11198
- Nonsupporting aerodynamic foam material thermal insulation system with reliability for cryogenic rocket propellant tank, considering polyurethane and polyvinylchloride
01 p0164 A71-11541
- Apollo 11 lunar rocks excess heat capacity and thermal conductivity at liquid He temperatures due to peaks in vibrational frequency distribution
02 p0306 A71-11989
- Strain free insulated mounting technique for semiconductors onto cold finger at liquid He 3 temperatures
02 p0294 A71-12142
- Optimal gain tuning elements of cryogenically cooled parametric amplifiers
02 p0235 A71-12833
- Vacuum deposited Bi thin films on glass substrates at liquid He temperature, investigating characteristics of critical thickness
03 p0466 A71-13291
- Maintenance free cryogenic noise temperature standard for continuous microwave antenna operation independent of elevation angle
04 p0550 A71-14658
- Thin metallic films thermal radiation properties at cryogenic temperatures, calculating spectral normal emissivity as temperature wavelength and thickness function
04 p0684 A71-15510

Quantitative acoustic vibration effects on cooldown rate of bodies from room temperature to liquid nitrogen or helium temperature

04 p0686 A71-15525

Al single crystals creep deformation, noting thermally activated mechanism at cryogenic temperatures

05 p0769 A71-16879

High vacuum calibration of cryogenic quartz crystal for atmospheric density

07 p1113 A71-19852

Stainless steel coatings vacuum deposition on Ti alloy plates, considering product cryogenic and mechanical properties

07 p1118 A71-19853

Far IR cryogenic black paints absorptive throughout IR with surface stability at liquid He temperature and resistance to abrasion and flaking

08 p1335 A71-21383

Apparatus for rolling and stretching metals at cryogenic temperatures, describing structural features

08 p1300 A71-21810

Materials mechanical properties measurement methods and equipment at cryogenic temperatures including microscopes, X ray cameras, microhardness tester, fatigue and impact strength testing machines

09 p1468 A71-22329

Multicomponent Ti alloys mechanical properties for cryogenics applications, describing alloying advantages with tantalum

09 p1468 A71-22601

Resistance thermometer using amorphous Pd-Si-Cr alloy for enhancing sensitivity at cryogenic temperatures

09 p1444 A71-22714

Fatigue life gages performance test using calibration program for cryogenic temperature applications

09 p1444 A71-22716

Cryogenic engineering - Conference, West Berlin, May 1970

09 p1545 A71-23002

Spatial-temporal emission of n-GaAs laser pumped by electron beam at liquid nitrogen temperatures

10 p1622 A71-24889

Pressure vessel flaw detection at high stress and cryogenic temperatures, noting Lunar Module fuel tanks experience

[AJAA PAPER 71-336]

11 p1777 A71-25315

Graphite fiber resin composites physical and mechanical properties at ambient and cryogenic temperatures, discussing unidirectional ring and bar specimens and filament wound pressure vessels

11 p1785 A71-25409

Stress raisers effect on mechanical properties of fcc materials at cryogenic temperatures

13 p2083 A71-27871

Low temperature test facility for cryogenic and rocket materials under combined tension and torsion

18 p2900 A71-36726

Papers on cryogenics covering materials behavior, heat transfer, fluid flow, superconductive magnets, cryosorption pumping, rocket propulsion and low temperature measurement

20 p3269 A71-39239

Cryogenics applications to cryosurgery and long term low temperature storage of living cells and tissues

20 p3189 A71-39252

Cryogenic engineering - Conference, Boulder, Colorado, June 1970

20 p3312 A71-39265

Glass transition temperature and specific heat of Apiezon N and T greases used as thermal bonding agent at cryogenic temperatures

20 p3253 A71-39267

Lateral heat transfer measurements in cryogenic multilayer insulation, considering effective thermal conductivity

20 p3312 A71-39272

Capacitive thermometry characteristics of dielectric crystallized titanate-containing glass ceramic at cryogenic temperatures

20 p3253 A71-39279

Cryogenic steels, Al and Ti alloys plane strain fracture toughness at room and subzero temperatures, discussing tensile and notch bend results

21 p3401 A71-40915

High strength Al alloys at cryogenic temperatures, presenting plane strain fracture toughness tests results

21 p3401 A71-40916

Pure and doped Ge dumbbell p and n type samples at liquid helium temperatures, investigating electric breakdown

21 p3430 A71-41224

Spatial-temporal emission of n-GaAs laser pumped by electron beam at liquid nitrogen temperatures

21 p3394 A71-41258

Cryogenic temperature cooling systems for IR detectors, describing Joule-Thomson liquefier and liquid transfer devices

22 p3544 A71-42139

CRYOLITE

Lithium tetrafluoro-aluminate equilibrium vapor pressure over solid aluminum fluoride plus solid lithium cryolite examined by weight-loss effusion method

07 p1055 A71-19624

CRYOPUMPING

Clean cryogenic vacuum high speed gas pumping system for calibrating spectrometers for use on Apollo telescope mount

07 p1160 A71-19854

Thermal conductivity measurement of cryopumped solid gas deposits in thin walled stainless steel cylinder with temperature gradients

09 p1546 A71-23007

Hydrogen condensation and evaporation on liquid helium cooled surfaces in cryopump with reduced thermal radiation loading

09 p1546 A71-23008

Equilibrium adsorption isotherms correlation for low temperature cryodeposits, using Dybinn-Raduschkevich equilibrium equation to estimate hydrogen capacity of cryosorption pumping system

10 p1643 A71-25011

Molecular hydrogen sorption pumping by cold carbon dioxide cryodeposits, showing absorbed molecules surface diffusion into disordered frost structure

17 p2695 A71-35138

Adsorption cryopumped He 3 cooled IR detector without encumbrance of external diffusion or mechanical pump

18 p2922 A71-36588

Self regulating steady state cryopump system for simulated altitude testing during rocket engine firings

20 p3184 A71-39198

Gas removal from system by condensation onto cold surface/cryopumping, noting pumping speed, ultimate pressure and applications

20 p3270 A71-39248

Cryosorption vacuum pumping, discussing physical and chemical adsorption, adsorbents, surface migration and diffusion, reactivation, deposits, cryopanel adhesion, pump design, etc.

20 p3270 A71-39249

Paramagnetic cycles for low temperature superconducting magnet cooling, discussing refrigerator, cryogenic pumps, regenerators and adjustable heat source and sink

21 p3476 A71-40898

CRYOSORPTION

U SORPTION

CRYOSTATS

Automatic temperature control for cryostats operating at 1-300 K, describing mechanical, electrical and combined devices

03 p0429 A71-14302

Design curve for estimating conduction heat transfer liquid He cryostats with vapor-cooled vent tubes

07 p1115 A71-20359

Cryostat design and operation for investigating solids mechanical properties and structure at liquid He temperature

09 p1426 A71-22321

Optical cryostat suitable for Raman spectroscopy, using quartz tube optical cell and He evaporation by metal film resistor

20 p3268 A71-38833

Miniature self regulating rapid cooling Joule-Thomson cryostat, noting purging of accumulated contaminants

20 p3184 A71-39274

CRYOTRAPPING

Molecular flux distributions and capture by cryopanel in space simulation chamber using homogeneously emitting spherical gas source

09 p1428 A71-23006

CRYOTRONS

Cryotron elementary storage cells work region determination by phase transition characteristic form, discussing component reliability

03 p0382 A71-13520

CRYSTAL DEFECTS

NT CRYSTAL DISLOCATIONS

NT EDGE DISLOCATIONS

NT FRENKEL DEFECTS

NT POINT DEFECTS

NT SCREW DISLOCATIONS

NT VACANCIES [CRYSTAL DEFECTS]

Hall constant and resistivity of impurity centers in seminsulating n-type GaAs during illumination and heating

01 p0138 A71-10776

Austenitic stainless steels point defect migration sensitivity, measuring dislocation damping during recovery after quenching

02 p0267 A71-12883

Polycrystalline Ni single and overlapping stacking faults production by tensile deformation in premicroyield region, noting stress concentration effects

02 p0268 A71-12888

Deformed metals stage I recovery, considering plastic deformation microscopic description, defect creation, interstitials and experimental methods

03 p0441 A71-13348

CdS thin film grain boundaries and stacking faults effects on electrical resistivity

05 p0791 A71-16055

Production and annealing of defects in lithium diffused bulk silicon after irradiation with 30 MeV electrons and fission neutrons at 300 K

05 p0703 A71-16091

Anomalous Cu concentration profile due to migrating Cu ions-GaAs crystal defects interaction

05 p0794 A71-16877

Niobium oxide defect structure, correlating electrical conductivity and oxygen diffusional properties with nonstoichiometry degree

05 p0770 A71-17097

EPR line width in ruby under charged dislocations and electric fields of lattice defects, using statistical method

06 p0942 A71-18348

Dimensional resonances of standing helicon waves in two layer and multilayer semiconductor structures and crystals with growth inhomogeneities

07 p1176 A71-19273

Lattice defect and grain boundary influence on metal dissolution in electrolyte and stress corrosion cracking

07 p1134 A71-19604

Loop patterns of secondary defect structures in quenched Al based alloys interpreted in terms of internal stress and stacking fault energy

08 p310 A71-21531

Bcc metals single and multilayer stacking faults, twin boundaries and screw dislocations observations, using central force atomic model

08 p310 A71-21537

Fcc crystal strengthening, examining short range core defect dislocations

08 p310 A71-21538

Stacking fault formation and mechanical twinning in Ni base superalloy during tensile deformation at high temperature

08 p315 A71-21581

Stacking faults and fcc precipitation of Ti beta alloys after high temperature heating

09 p1469 A71-22850

Soviet papers on crystalline structure imperfections covering dislocations, structural changes, heating and ultrasound effects, plasticity and substructure disorientation

09 p1475 A71-23311

Stress and structure effects on creep rate of two austenitic steels in quenched state, considering decorated stacking faults

09 p1479 A71-23624

Soviet papers on radiation physics of nonmetallic crystals covering effects of neutron, proton, electron, gamma and X ray irradiation on physical properties

10 p1655 A71-24137

Carrier concentration, radiation dose and temperature effects on radiation defect formation in Si and Ge during gamma irradiation

10 p1655 A71-24138

Radiation defects distribution in Si irradiated by protons, deuterons and alpha particles

10 p1655 A71-24140

Formation kinetics of radiation defects produced by gamma rays in Sb doped n-type Ge single crystals at 77 K

10 p1656 A71-24142

Multiplication, diffusion and vanishing of dislocations, slip band formation mechanism and lattice defects interactions during metal fatigue

10 p1626 A71-24386

Crystal imperfections effect on MC carbide precipitation on coherent twin boundaries and regions close to grain boundaries in austenitic steels, using electron microscopy

11 p1780 A71-26027

Electron structure of transition metals defects, using self consistent method to match resonance and drift integrals to cohesion energy

11 p1808 A71-26342

Magnetization discontinuities in cobalt-rare earth particles at discrete imperfection levels as function of chemical, mechanical and heat treatment, noting Co-Y rectangular loop

12 p1943 A71-26861

Predeformation effects on metastable Ni base Ti alloys precipitation aging at extrinsic stacking faults, using thin foil microscopy

12 p1916 A71-26894

Stacking fault formation in Nb deformed by filing, determining coherent scattering regions with X ray diffraction

12 p1917 A71-27299

P-type gallium selenide crystals impurity photoconductivity measurements by Cr switched ruby laser

13 p2077 A71-27959

Doping dependent mobility analysis of junction FET, calculating drain current and transconductance

13 p2037 A71-28474

Thermal suppression of photoconductivity in crystals with two impurity types, showing carrier concentration decrease in conduction band in narrow temperature range

13 p2112 A71-28924

- Kinetics of Ti single crystals tensile deformation by prismatic gliding, studying moving dislocations interactions with metal impurities 14 p2257 A71-29844
- Lattice defect mechanism for high coercive force remanence production in meteorites and lunar samples by cosmic ray exposure 14 p2308 A71-29913
- Microdefects of lattice structure of molybdenum plasma coatings dependent on spray gun nozzle-surface distance 15 p2437 A71-32671
- GaAs single crystals defects formation during low temperature gamma photons and electron irradiation, considering electrical properties 16 p2620 A71-33185
- Crystal defects and electrical and optical properties changes due to electron bombardment of semiconductors 16 p2622 A71-33622
- Tungsten single crystals under deuteron bombardment, noting structural defects formation as function of irradiation energy 16 p2595 A71-33883
- Crystal structure defects of W samples containing small and large angle grain boundaries, using field ion emission microscopes 16 p2580 A71-33927
- Equiatomic TiNi martensite crystal structure and internal defects investigation by electron microscopy and electron and X ray diffractions 16 p2598 A71-34045
- Surface/volume damage induced by Nd-YAG laser irradiation to LiNbO₃ and KDP crystals in frequency doublers and Pockels cells, using scanning electron micrographs 17 p2790 A71-34376
- Ni-Co alloy fine structure under plastic deformations, determining stacking fault energy effects with X ray diffraction lines 19 p3076 A71-37119
- Electrical resistivity of structural metal crystal defects in terms of Ziman-Harrison pseudopotential theory 21 p3395 A71-40023
- External and internal absorption spectra of silicon crystal doubly doped with boron and indium acceptors, interpreting line broadening and cross section decrease 21 p3426 A71-40071
- Deep level impurity compensation of high resistivity epitaxial films of GaAs by chromium, complex lattice defects and copper acceptors, using cathodo-luminescence spectra 21 p3430 A71-41220
- Semiconductor radiation-induced electrical conductivity changes correlation to forbidden band from theoretical model, considering radiation defects as conductivity compensators 21 p3431 A71-41230
- CdS crystals faces damage caused by picosecond light pulses from free oscillating Nd-glass laser 21 p3432 A71-41305
- Thermal suppression of photoconductivity in crystals with two impurity types, showing carrier concentration decrease in conduction band in narrow temperature range 21 p3434 A71-41320
- Complex TiC-WC carbides under homogenizing annealing, noting defects, solubility, lattice constant and grain growth 23 p3689 A71-43253
- Space charge density and carrier mobility in disordered regions of p-n microjunctions 23 p3717 A71-43486
- Zone refined Be crystals under room temperature compression, examining lattice defects with X ray synergy method 23 p3695 A71-44287
- Phase composition and defect structure of thin film CdTe islet compensates on NaCl and KBr cleavage faces 23 p3718 A71-44316
- Dielectric and semiconductor crystals surface defects, considering electric polarization structures 24 p3860 A71-45098
- Irradiation defects and electrical quality of ion implanted silicon, using minority carrier lifetime measurements 24 p3863 A71-45357
- Diffusion acceleration in bcc Ti due to imperfections of fine structure created during polymorphous transformation 24 p3840 A71-45379
- Zinc single crystals plastic deformation and dislocations movement enhancement under pulsating direct current, noting stress peaks-voltage relationship 02 p0296 A71-12297
- Nb alloys hardening due to interstitial atoms interactions with dislocations, obtaining stress-strain relationship for various impurities, precipitates, strain rates and temperature 02 p0270 A71-12929
- Transport mechanism for holes in polycrystalline Ge films based on Matthiessen rule, considering surface scattering and dislocation 03 p0468 A71-14464
- Silicon single crystal dislocation free growth by Czochralski and Dash methods 05 p0792 A71-16292
- Dislocation cracks onset and propagation, considering crystal defect theory 05 p0827 A71-16853
- Differential equations derivation for metal fatigue point defect colonies concentration changes, discussing diffusion and dislocation interactions 06 p1002 A71-18418
- Crystal dislocations and vacancy colonies complexes generation, discussing metal fatigue microcracks mechanism 06 p1002 A71-18419
- Mg-Cd single crystals deformation by prismatic slip as function of testing temperature and state of order 07 p1132 A71-19437
- Austenitic stainless steel dislocation structures during fatigue deformation under cyclic loading, observing slip lines and lattice strain morphology 07 p1136 A71-19699
- Superconducting Nb experimental tests for hypothesis concerning relations between anisotropic critical field and dislocation cell structure 07 p1138 A71-19988
- Crystal dislocation core analytical model, examining short range interactions 07 p1180 A71-20163
- Deformation amplitude effects on dislocation structure and strengthening mechanism of fcc aluminum under cyclic loading 07 p1142 A71-20482
- High density DC effects on displacement of solid GaAs-liquid metal interface, considering Peltier effect and dislocation density 08 p1344 A71-21444
- Nb single crystals dislocation substructure correlation with strength properties 08 p1307 A71-21508
- Mo single crystals dislocation velocity, discussing slip systems and stress and temperature effects 08 p1307 A71-21509
- Stoichiometric NiAl single crystals plastic deformation study by transmission electron microscopy, determining dislocations by image matching technique 08 p1308 A71-21511
- Segmented slip theory of hardening application to bcc metals, discussing dislocation locking and virtual athermal dislocation model 08 p1308 A71-21516
- Titanium single crystal prism slip dislocation dynamics, examining temperature and strain rate effects on shear stress 08 p1309 A71-21521
- Dilute Al alloys single crystals amplitude dependent internal frictions measurement, obtaining binding energies between substitutional alloying atoms and dislocations 08 p1310 A71-21535
- Dislocation pinning point flow stress decrease in superconducting-normal transition 08 p1345 A71-21536
- Bcc metals single and multilayer stacking faults, twin boundaries and screw dislocations observations, using central force atomic model 08 p1310 A71-21537
- Fcc crystal strengthening, examining short range core defect dislocations 08 p1310 A71-21538
- Aged Al alloys dislocation substructure effect on mechanical properties at elevated temperatures 08 p1313 A71-21559
- Crystalline solids strain rate effects due to simultaneous operation of plastic deformation mechanisms including diffusion controlled creep and dislocation-drag processes 08 p1371 A71-21560
- Crystal dislocation dynamics at high strain rates, investigating viscous phonon drag 08 p1371 A71-21563
- Al dislocation mobility at high strain rates, plotting true stress vs true strain 08 p1313 A71-21564
- Grain boundary sliding and shear deformation in bicrystal Al and Al-Co solid solutions 08 p1345 A71-21576
- Tilt boundary intersections during creep in Mo single crystals 08 p1315 A71-21577
- Paired dislocations after high temperature deformation in precipitation hardened Co-Ti alloy 08 p1315 A71-21582
- Polycrystalline Nb under plastic deformation and annealing, examining dislocation structure and mechanical properties 08 p1316 A71-21611
- Ultrasonic effects on dislocations and grain boundaries in vacuum annealed polycrystalline Al specimens 09 p1467 A71-22288
- Nonelastic unloading microstrains in Cu crystals after stage II macroscopic prestraining, discussing stresses action on dislocations 09 p1468 A71-22700
- Electron microscope investigation of packing defect energy effect on structure of crystal dislocations in hardened metals during annealing and deformation 09 p1473 A71-23226
- Cut metal crystal orientation planes and dislocation structure determination, using Bragg reflection of monochromatic X ray beam 09 p1452 A71-23319
- Yield strength theories of heterophase systems with precipitates surrounded by elastic strain fields, considering dislocation precipitation interaction mechanism 09 p1510 A71-23321
- Ultrasonic irradiation effect on single tungsten crystals deformation characteristics and structure 09 p1477 A71-23327
- Coarse grained recrystallized Mo ductile brittle transition temperature due to dislocation substructure and grain boundary state, noting low temperature annealing and critical straining 10 p1629 A71-25029
- Stress-strain curve and single crystal dislocation structure of Al alloys with coherent precipitates, noting screw dislocations predominance 10 p1629 A71-25033
- High strain rate effects on Al single crystals deformation, presenting overall and local strain and lattice rotation measurements in impact tested specimens 11 p1779 A71-26014
- Niobium alloys single crystals deformations, studying microyielding to macroflow transitions by dynamic microstrain technique 11 p1780 A71-26019
- Solid solution hardening in Nb alloys single crystals, explaining in terms of elastic interaction of dislocations with substitutional atoms 12 p1916 A71-26927
- Aged beta Ti alloy microstructure and mechanical properties, examining initial dislocation structure and interstitial concentration effects 12 p1917 A71-27297
- Activation energy anisotropy for Mo and Nb single crystals dislocation relaxation, noting temperature dependence 12 p1917 A71-27300
- Titanium nitride sintering in vacuum, noting strain by grain sliding to pore center under surface tension force effects 12 p1918 A71-27527
- Coarse grain Al sheet deformation, determining dislocations distribution with etching defects method 12 p1919 A71-27691
- Thermally activated crystal microcrack initiation by fusion of leading and following dislocations 13 p2149 A71-28118
- Stress effects on superconductivity and dislocation cell structure in deformed niobium for compression and tension 13 p2090 A71-29416
- Stable eta phase precipitation at dislocations in Al-Zn alloy, using X ray diffraction and electron microscopy 14 p2260 A71-30477
- Neutron irradiated Mo single crystals polygonization after cold rolling, using X ray topology methods 16 p2596 A71-33886
- Niobium dislocation and electronic structure and mechanical properties after plastic deformation and annealing from electron beam studies 17 p2760 A71-35671
- Semiconductor defects, including stoichiometric vacancies in sphalerite lattices, epitaxial interfaces and dislocations in Ge 18 p2953 A71-35870
- Radiation induced etch-pit dislocations and thermal decomposition kinetics in ammonium perchlorate crystals 18 p2955 A71-35967
- Dezincification of Al-Zn alloys, creating loops and dislocations due to vacancies from Zn evaporation 18 p2935 A71-36199
- Crystal elastic twinning dislocation theory, discussing twins origin and growth, hysteresis effects, crystal development and stability loss 19 p3156 A71-37758
- Formation and interdependence of quenched induced defect structure in Al-Zn, discussing nucleated loops and screw dislocation developed helical dislocations 20 p3249 A71-39001
- Grain boundary dislocations generation and motion in deformed Nb steel in relation to sliding, using electron microscope analysis 21 p3395 A71-40021

CRYSTAL DISLOCATIONS

NT EDGE DISLOCATIONS

NT SCREW DISLOCATIONS

Cu addition effects in solid solution on grain boundary sliding in Al at constant shear stress, considering accompanying crystal dislocations 01 p0102 A71-10739

Intermetallic Ni-Al volume fraction dependent deformation of single crystals of binary Ni-Al system, using X ray and transmission electron microscopy 01 p0102 A71-10740

Strain hardened zirconium alpha tensile stress analysis, explaining inelastic phenomena by dislocation motion blocking with oxygen in lattice structure 21 p3397 A71-40432

Dislocation arrays effects on heat treated austenitic stainless steel susceptibility to intercrystalline corrosion in sulfuric and nitric acids and cracking in magnesium chloride 21 p3402 A71-41087

Crystal dislocations and impurity atmospheres role in kinetics of accumulation of radiation defects in Ge under fast electron bombardment 21 p3429 A71-41209

Transition metal /particularly Ti/ carbide hardness temperature dependence explained from dislocation theory viewpoint, relating hardness to electronic structure 22 p3565 A71-41657

Pure Al annealed polycrystal electron microscopic observation for fatigue deformation at room and elevated temperatures, noting dislocation loop role in crack initiation and propagation 22 p3564 A71-42497

Fine structure dislocation and phase composition of Cr-Mo steel at elevated temperature in steam pipe applications, noting recrystallization stability 23 p3690 A71-43277

Neutron bombardment effect on dislocation mobility in Ge single crystals investigated by bending and etching techniques 23 p3715 A71-43309

Load stress pulse shape and frequency effects on macroscopic dislocations during plastic deformation of crystalline materials 23 p3777 A71-43875

Vacuum annealing and residual gas effects on Mo single crystal dislocation structure and microhardness 23 p3692 A71-44060

Polycrystalline Ni preloading rate effects on dislocation structure, electrical resistance and flow stress, noting strain hardening mechanism 24 p3837 A71-44675

Polycrystalline beta silicon nitride foils containing glide dislocations from room temperature fracture, determining Burgers vectors and slip planes 24 p3842 A71-45194

Mo sheet anisotropic dynamic strain aging at high temperatures, noting plastic strain contribution to texture formation and dislocation consolidation 24 p3840 A71-45378

CRYSTAL GROWTH

NT CZOCHRALSKI METHOD

NT EPITAXY

NT HYDROTHERMAL CRYSTAL GROWTH

T-doped In Sb single crystal growth in transverse magnetic fields, using Czochralski crystal puller 01 p0100 A71-10281

Gd-As direct synthesis from components elements and single crystal growth using chemical transport reactions 01 p0138 A71-10404

IR absorption edge measurement in cadmium antimonide crystals grown with various perfection degrees, considering forbidden band and phonon spectrum anisotropy 01 p0138 A71-10432

Kinetic, morphological and crystallographic effects of Nb crystals oxidation during growth at various temperatures and pressures 02 p0272 A71-12948

Grain size refinement by alloy solute additions inhibition effect on growth and recrystallization, reducing boundary migration 03 p0446 A71-14489

Whisker growth by vapor phase reactions, detailing thermodynamics, kinetics and supersaturation in aluminum oxide whisker formation 04 p0635 A71-14942

Crystal growth mechanism involving vapor, liquid and solid phases, discussing Si whiskers and impurities effects 04 p0636 A71-14943

Sapphire whiskers production by melt growth technique, describing process and whiskers mechanical properties 04 p0636 A71-14944

Liquid drop role in aluminum nitride whisker growth by aluminum oxide reduction in nitrogen or by direct nitriding 05 p0768 A71-16820

Ti microcrystals on single crystal tungsten substrate, discussing phase transformations 05 p0768 A71-16854

Intermetallic compounds structural component applications, considering crystal growth, alloy constitution and development, mechanical properties and processing technology 07 p1131 A71-19427

Fcc metals film growth on air- and vacuum-cleaved PbS, using electron diffraction and conventional electron microscopy 07 p1178 A71-19848

Epitaxial boron phosphides single crystals growth, using thermal decomposition and reduction for deposi-

tion on hexagonal silicon carbide substrates basal plane 07 p1180 A71-20174

High purity Ge crystals growth, studying Hall effect and resistivity for semiconductor detector fabrication 08 p1345 A71-21841

Artificially grown corundum homogeneous single crystals structure relationship to thermodynamic and kinetic growth conditions 09 p1481 A71-22164

Subgrain growth kinetics for tungsten deformed by rolling and polygonizing annealing, using metallography, X ray microradiography and crystal spectroscopy 09 p1476 A71-23324

Macroscopic working model for CVD tungsten assuming change of substrate work function and preferential crystal orientation by impurity adsorbed molecules 11 p1808 A71-25861

Al coating of Nb and Nb alloys by pack cementation, discussing coating structural states, heating cycle temperatures and growth kinetics 11 p1781 A71-26295

Pure W single crystals grown by electron beam zone melting technique, noting rolling workability 12 p1919 A71-27761

Nucleation, growth and spinodal decomposition during aging in Fe-Cr alloys, using Mossbauer spectroscopy 13 p2089 A71-29414

Tantalum disilicide kinetic interaction with Ta, investigating formation rate at various temperatures 13 p2089 A71-29415

Recrystallization nuclei linear growth rate activation energy relationship to Ni plastic deformation magnitude, temperature and purity 15 p2429 A71-31995

Manufacturing processes in orbital workshop, considering metal and optical lenses casting crystal growth and gravity lack effects 16 p2606 A71-32856

Polyhedral Nb single crystals production from niobium pentachloride and hydrogen reaction, determining growth rate 16 p2594 A71-33877

Mo single crystal growth by vacuum melting without oil vapors, noting reduced carbon content and increased ductility 16 p2595 A71-33880

Statistical microstructural analysis for nucleation and growth kinetics of recrystallization nuclei of metal single crystals 17 p2755 A71-34414

Critical growth work hardening germination and recrystallization of oriented compression deformed Nb, Mo and W refractory cubic centered crystals 18 p2935 A71-36200

EuO, YIG, GdIG and ferrite magnetic oxide thin films growth techniques and magnetic properties comparison with bulk materials 18 p2954 A71-36937

Carbon impurity effects on molybdenum ingot formation, detailing crystal growth, size reduction and length 19 p3077 A71-37277

Crystal growth method based on controlled power reduction under stabilizing thermal gradients, eliminating chemical heterogeneities 19 p3077 A71-37416

Stimulated emission in double heterojunction Al-GaAsP quaternary lasers, considering solution grown crystals advantages 19 p3071 A71-37476

Cooling history of magma containing spherulite growth forms on basis of morphological variations in glassy and crystalline rocks 19 p3051 A71-37673

Al-Cu-Mg monovariant alloys directional solidification, considering criterion for plane front growth breakdown based on constitutional supercooling 19 p3078 A71-37701

Cloud elements evolution, investigating electrical charges effects on ice crystal growth rate in water vapor by laboratory experiment 19 p3092 A71-38688

Spherical indium crystal manufacture in space, suspending and positioning weightless containerless melt in air and vacuum by adhesion and cohesion for crystal growth 20 p3247 A71-38767

MnSe-CdSe mixed crystals growth investigation by elements, binary compounds and solid solutions vapor transport properties 21 p3427 A71-40214

Crystal growth of III-V compound semiconductors from vapor phase, studying deposition processes chemistry by mass spectrometry 21 p3427 A71-40216

Aluminum nitride crystals production by sublimation in resistance furnace with graphite heater 22 p3585 A71-41701

Quadratic and linear electro-optical effect dispersion in flux grown crystals of barium titanate 22 p3585 A71-41729

Beta rhombohedral boron whiskers production from hydrogen reduction of boron bromide and chloride by vapor-liquid-solid mechanism 22 p3564 A71-42533

In-Bi whisker growth by squeeze technique, measuring crystal structure by X ray analysis and melting point method 23 p3689 A71-42956

WC and TiC-Co solid solution phase after sintering inhomogeneous structure, investigating grain growth and phase decomposition behavior at various temperatures 23 p3689 A71-43103

Complex TiC-WC carbides under homogenizing annealing, noting defects, solubility, lattice constant and grain growth 23 p3689 A71-43253

Lithium iodate hexagonal and tetragonal form crystal growth conditions from aqueous solution and recorded refractivity 23 p3717 A71-43935

Cast heterophase Mo and alloys fracture strength and plastic characteristics, investigating crystal growth texture, orientation and substructure 23 p3693 A71-44215

Niobium carbide film formation in pseudoliquidified layer on graphite at 3000 C in argon metal vapor mixtures with/without hydrogen 23 p3696 A71-44317

Semiconductor applications of alpha SiC single crystals, showing mechanical separation of polytypes from druses 24 p3841 A71-44742

CRYSTAL LATTICES

NT BODY CENTERED CUBIC LATTICES

NT CUBIC LATTICES

NT FACE CENTERED CUBIC LATTICES

Thermodynamic distribution of amphoteric Ge impurities in sublattices of GaAs semiconductor for compensation by acceptor vacancies 01 p0139 A71-10778

Shock structure in crystalline solids, including dissipative processes, discontinuities, continuum mechanics and lattice dynamics 04 p0664 A71-14662

Pure metal structure effect on friction and lubrication under steady slip in ultrahigh vacuum at low temperatures 05 p0757 A71-16185

Ferrimagnetic vanadate garnet IR Faraday rotation as function of wavelengths and temperature, considering ions multivalence and multilattice site modifications 06 p0941 A71-18040

Vanadium and niobium carbonylhydrides as function of C content, studying lattice constants, microhardness and electrical resistivity 06 p0912 A71-18086

Ion implantation lattice damage effects in crystalline silicon with allowance for optical reflectivity, considering annealing temperature and amorphous layer formation 07 p1175 A71-19062

High temperature creep behavior of nickel base alloys with L12 and B2 type lattices, discussing single crystals of beta-NiAl 07 p1133 A71-19446

IR lattice spectra of rare earth stannate and titanate pyrochlores 07 p1054 A71-19484

Crystal lattice disordered systems, calculating electronic density of states by overlap integral transformation 08 p1344 A71-21364

Fe-Si alloy with pronounced texture and large grain size, determining lattice period from X ray diffractogram obtained by reverse response method 09 p1467 A71-22308

Crystal lattice type influence on volume and boundary diffusion mobility of iron group metals atoms 09 p1510 A71-23325

Thin film compound Au-Al intermetallic structure of CsCl type with lattice period of 3.140 plus or minus 0.003 A from electronographic measurement 12 p1917 A71-27308

Ultrahigh magnesium based alloys classification by Li content, noting lattices, structural composition, specific weight, plastic properties and impact strength 15 p2435 A71-32336

Solid solution hardening in Ta alloy single crystals, investigating temperature effects on interstitial impurities scavenging and lattice mechanism 21 p3395 A71-40027

Strain hardened zirconium alpha tensile stress analysis, explaining inelastic phenomena by dislocation motion blocking with oxygen in lattice structure 21 p3397 A71-40432

Lattice and grain boundary diffusion of Ce and Nd in Ni using radioactive tracer sectioning technique 21 p3398 A71-40468

Crystal lattice drag by conduction electrons and Onsager relationship between electroacoustic coefficients valid for arbitrary topology of Fermi surface 21 p3428 A71-41127

- Nb nitriding kinetics and external effects observations, noting nitrogen diffusion through crystal lattices 21 p3404 A71-41163
- Preheating effects on crystal lattice orientation, tensile strength and stress corrosion cracking of Al-Zn-Mg alloy thick plates 22 p3559 A71-41516
- Crystal lattice energies of solvation of alkali metal perchlorate in water 22 p3508 A71-42530
- Abrikosov vortex lattice in superconductors, calculating resonance linewidth and vacancy formation energy 24 p3860 A71-45119
- Pressure effects on Fermi surface of metals, examining crystal lattice parameters influence on electrons energy spectrum 24 p3839 A71-45168
- CRYSTAL OPTICS**
- He-Ne laser beam diffraction patterns produced by nematic liquid crystal subject to electric field, noting threshold effect 01 p0096 A71-11375
- Laser emission nonchromaticity effect on second harmonic generation in ADP, KDP, RDP and lithium niobate crystals 02 p0259 A71-11935
- Inverted combination light scattering in liquid and solid crystals, showing polarization effects on absorption coefficient 13 p2101 A71-29020
- Fine crystalline substances forced combination scattering at liquid nitrogen temperature, using ultrashort ruby laser pulses for excitation spectra 13 p2080 A71-29022
- Crystalline media impurity light absorption spectral band shape, noting laser resonance emission effects 13 p2080 A71-29023
- Phase holographic data storage in doped barium sodium niobate crystal, detailing decay times, energy density and diffraction efficiency 15 p2412 A71-32586
- Minimum voltages and limiting frequencies for oblique cut longitudinal octahedral crystal modulators with large electro-optic coefficients, including lithium niobates and tantalates 15 p2461 A71-32606
- Electro-optical Fabry-Perot modulator with KDP and ADP crystals as optical resonators, determining modulation and frequency response characteristics 16 p2587 A71-33493
- Laser light pulses in liquid crystal, investigating nonlinear thermal rotation of polarization plane 16 p2587 A71-33570
- Nonlinear optics of combination scattering of IR laser radiation in crystals and statistical frequency mixing-multiplication of polarons and longitudinal phonons 16 p2588 A71-33997
- Savart plate Francon modification at arbitrary angles to optic axis, examining view field limiting factors and fringe patterns 22 p3549 A71-42554
- Second harmonic aperture in ultrashort pulses length measurement by mixing two AM light beams in nonlinear crystals 23 p3683 A71-43397
- Temperature effects on long wavelength photon frequency and linewidth in diamond, using Raman scattering techniques 23 p3715 A71-43471
- SbSI crystal reflection spectra anisotropy and band structure at 90, 273 and 300 K, comparing experimental data with group analysis 23 p3717 A71-43947
- CRYSTAL OSCILLATORS**
- NT PIEZOELECTRIC CRYSTALS**
- Quartz crystal HF resonator unit for high g environments, discussing tradeoff between stiff support and stress-induced frequency instability 01 p0054 A71-10913
- Q switched Nd laser pulse duration control as function of KDP crystal orientation and pumping power 07 p1122 A71-19138
- Crystal oscillator temperature compensation using hyperabrupt junction varactor diode as reactance modulator and thermistor for temperature sensitive voltage control 14 p2215 A71-30902
- CRYSTAL RECTIFIERS**
- Cadmium doped silicon diodes I-V curve sinusoidal relaxation oscillations frequency and amplitude dependence on temperature 16 p2548 A71-34026
- Cd doped thin polycrystalline CdTe films rectification mechanism and DC conductivity, discussing light, electric field and temperature effects 24 p3861 A71-45248
- CRYSTAL STRUCTURE**
- NT WIDMANSTATTEN STRUCTURE**
- High temperature annealing effect on sapphire single whiskers structure, using electron microscopy 01 p0106 A71-10276
- Perovskite crystals phase transition with unit cells atom displacement, considering permittivity anomalies, structure and free energy expansion coefficients 01 p0138 A71-10430
- Crystalline structural changes during decomposition of supersaturated solid solution of Ta in Co 01 p0101 A71-10608
- Fine structure and lattice constants of Al-W, Al-Mo and Al-Mn alloys at high cooling rates 01 p0101 A71-10675
- Vapor deposited W impurities effect on crystal structure and preferred orientation, considering work function increase 02 p0296 A71-12241
- Thermally induced helical inversion absence in single component cholesteric liquid crystals indicating impurity compensation 02 p0296 A71-12571
- Nb single crystals, examining structure in initial deformed and annealed states at various low temperatures 02 p0266 A71-12654
- Rare earth element concentrations in zircons and apatites separated from dacites and granites, explaining partition coefficients between phenocrysts and groundmass by crystal structure 03 p0407 A71-13338
- Semiconductor cadmium sulfide crystal structure changes during high power electron beam and optical pumping, using stimulated emission spectra measurements 03 p0439 A71-13984
- Hexanitroethane /HNE/ crystal transformation, using differential spectroscopy and X ray analysis 04 p0638 A71-15679
- Cosserat continuous model of dense elastic lattices of regular structure in plane 04 p0673 A71-15884
- Heat conduction three dimensional problem in radiation heated thin crystalline plates with temperature dependent thermophysical characteristics 05 p0831 A71-16184
- Te doped InAs single crystals structural characteristics investigation by X ray diffraction, noting laminar growth with alloying impurity varying concentrations 06 p0940 A71-17388
- Loss resistance and dissipated power dependence on crystal configuration of microwave semiconductor junction diode 06 p0873 A71-17544
- Anisotropic tubular Ti alloy samples, noting yield strength and crystal structure dependence on stress-strain state 06 p0912 A71-17937
- Potassium niobate single crystals domain structures by interferometry, discussing surface deformations, dipole couplings and temperature dependent angles 06 p0941 A71-18039
- Structure changes of Al single and polycrystals with initial cube orientation under cold rolling 06 p0913 A71-18420
- Manganese, iron and vanadium ion ordering in orthorhombic zoisite structure by electron paramagnetic resonance technique 07 p1053 A71-18741
- Quadrupole interaction in crystals of diamond-like semiconductors gallium telluride and indium telluride 07 p1177 A71-19275
- Calcite and aragonite high pressure Raman line spectra comparisons, testing structural identification theory 07 p1054 A71-19369
- NiMo alloy fcc disordered structure and mechanical properties correlation to domain size and orientations from thin film transmission electron microscopy 07 p1132 A71-19435
- Binary Ti-Al and ternary Ti-Al-X alloys precipitation strengthening, investigating structure, mechanical properties and deformation behavior 07 p1133 A71-19444
- Biaxial crystals utilization in polarized interferometers, noting Wollaston prisms useful beam aperture and Savart polariscopes streak linearity domain 07 p1109 A71-19453
- Transition metals effect on Ti alloys grain size, suggesting La, Y, Ni, Pd and Pt effectiveness in crystal structure refinement 07 p1136 A71-19632
- Iron-iron carbide structure dissolution behavior from electron transmission microscopy, observing carbide, matrix, general and interface attack modes 07 p1056 A71-20361
- High strength high Ni maraging steels crystal structure, alloying elements effects on mechanical properties, applications, etc 08 p1305 A71-21028
- Silver oxides crystal structures and physical and electrochemical properties 08 p1234 A71-21084
- Artificially grown corundum homogeneous single crystals structure relationship to thermodynamic and kinetic growth conditions 09 p1481 A71-22164
- Soviet papers on alloys crystal structure and properties covering electron microscopy, X ray analysis, heat treatment and pressure effects on phase transformations 09 p1473 A71-23223
- Soviet papers on crystalline structure imperfections covering dislocations, structural changes, heating and ultrasound effects, plasticity and substructure disorientation 09 p1475 A71-23311
- Ultrasonic irradiation effect on single tungsten crystals deformation characteristics and structure 09 p1477 A71-23327
- Crystal structure alterations in work hardened surface layers of W, Nb and Mo during thermocyclic treatment, using X ray micrography 09 p1477 A71-23329
- Intracrystal liquefaction in Ni alloys containing Nb studied with microanalyser 09 p1480 A71-23702
- Air sintered oxides stabilized hafnia body compositions and phases from X ray diffraction and electron microprobe correlation, noting monoclinic and cubic grains 10 p1630 A71-23976
- Gas rich Kapoeta howardite composition, evolution, high particle fossil track densities and normal track rich crystals spatial relations 10 p1672 A71-24392
- Apollo 11 igneous rock vug clinopyroxene composite crystal with tabular pigeonite nucleus and subcalcic augite precipitation 10 p1673 A71-24412
- Electrical conduction in cholesteryl acetate, propionate and stearate in solid, liquid crystal and isotropic liquid states characterized by I-V measurements 11 p1807 A71-25564
- Chemical vapor deposition process for preparing W-Re alloys having uniform Re content and dense coherent grain structure 11 p1797 A71-25862
- Thermionic emitter CVD W layer on Mo, investigating work function change due to Mo diffusion and crystal structure dependence on heat treatment 11 p1808 A71-25863
- Surface structure and environment effects on mechanical behavior of crystalline inorganic solids, giving stress-strain diagrams 11 p1808 A71-25999
- Orientation dependent impact toughness and crack resistance of brittle fiber-ductile matrix composite of solidified carbide reinforced Co-Cr eutectic 11 p1782 A71-26386
- Eighteen layer hexagonal ferrite magnetic properties in various fields and temperatures, noting magnetization and crystal structure 12 p1943 A71-26862
- Accuracy requirements on crystal orientation for p-n junction laser with tilted mirrors and various resonator lengths concerning output vs current characteristics 12 p1914 A71-27095
- Structural characteristics of Ti subjected to high speed deformation rates, examining formation of crystallographic glide lines and twins as function of deformation degree and rate 13 p2085 A71-28226
- Nb single crystals structure and properties after cold rolling and annealing, determining crystallographic parameters of plastic deformation 13 p2086 A71-28579
- Morphological structural changes during firing from scanning electron microscopy of unfired and fired kaolinite 13 p2092 A71-28659
- Structural disorientation dependent recrystallization of cold rolled and annealed Mo single crystals 14 p2258 A71-30006
- Face shear and thickness twist waves in bcc crystal plates, presenting numerical computation results for Fe and W 15 p2426 A71-31418
- Gaseous, liquid and polycrystalline biacetyl vibrational spectra and structure, noting mutual exclusion between IR and Raman radiation 16 p2538 A71-32874
- Transition metals effect on Ti alloys grain size, suggesting La, Y, Ni, Pd and Pt effectiveness in crystal structure refinement 16 p2593 A71-33628
- Oriented Mo single crystals substructure during growth, showing crystallographic orientation 16 p2595 A71-33879
- Thermal polymorphous metals and alloys crystal structure, discussing plastic deformation due to formation of cubic lattice and metallic bonds 16 p2597 A71-33915
- Binary and ternary metal compounds superconductivity parameters comparison, considering crystal structure, valence electron concentration, component position and processing techniques 16 p2622 A71-33925

Crystal structure defects of W samples containing small and large angle grain boundaries, using field ion emission microscopes

16 p2580 A71-33927

Equiatomic TiNi martensite crystal structure and internal defects investigation by electron microscopy and electron and X ray diffractions

16 p2598 A71-34045

Electrodeposited Ni-Mo coatings corrosion resistance improvement by heat treatment, showing crystal structure degree of perfection role

16 p2599 A71-34052

Microcrystal orientation in recrystallized tungsten structure by charged particles channelography

18 p2954 A71-36804

Carbon impurity effects on molybdenum ingot formation, detailing crystal growth, size reduction and length

19 p3077 A71-37277

Ni-Mo single crystals under isothermal aging, observing long range order parameter, domain size and microstrains

19 p3077 A71-37411

Computer program for generation and automatic plotting of perfect and twinned electron diffraction patterns for cubic crystal structures

19 p3118 A71-37719

Cell structure development during room temperature tensile deformation of beryllium after prism slip by combined X ray diffraction-transmission electron microscopy

20 p3249 A71-39002

Microfriction anisotropy of graphite at small loads for sliding on basal and edge planes, using scanning electron microscope

20 p3253 A71-39410

Trigonal crystal field and spin-orbit interaction matrices for ion energy levels in vanadium corundum in strong g scheme, using symmetry group tensor operators

21 p3427 A71-40075

Intermetallic compound Ti-Ni phase transformations, relating martensite crystal structure with pre-martensitic instability

21 p3397 A71-40433

Crystallographic habit plane and martensite plate orientation in Fe-Ni and Fe-Ni-C dilute alloys

21 p3397 A71-40452

Orientation dependent microhardness and columnar and feather crystal structures of directionally cast Al alloys in tensile test bars

21 p3399 A71-40471

Magneto-optical oscillatory absorption spectrum of tin oxide crystal at 1.3 K observed beyond band-absorption edge with peaks as function of magnetic field

21 p3431 A71-41235

Beta eutectoid and solid solution Ti binary alloys omega phase morphology observation by transmission electron microscopy, noting elliptical and cubic types hexagonal crystal structure

22 p3562 A71-41946

Crystal microstructure of strengthening precipitates in Ni maraging steel, giving electron diffraction patterns

22 p3562 A71-41949

Single crystal silicon films deposited on sapphire substrates, determining disorientation angles, block dimensions, dislocation density, orientation and structure

22 p3586 A71-42061

High temperature Ti-Ni alloy stacking variation stability, studying size, shear and valence electron concentration effects

22 p3586 A71-42367

Tungsten and molybdenum oxide crystals shape and size during annealing in various gas atmospheres and vacuum conditions

23 p3690 A71-43255

Pyroxferroite crystal structure from Apollo lunar Mare Tranquillitatis sample, using X ray counter-diffractometer measurements

23 p3737 A71-43606

Exsolution lamellae structure of Lunar pyroxenes from Apollo 12 samples, using electron microscopy and diffraction

23 p3738 A71-43610

Lunar plagioclases, tridymite and cristobalite feldspar crystal structure and chemical analyses from Apollo igneous rocks by X ray and electron diffraction

23 p3738 A71-43611

Tridymite structure in lunar pigeonite porphyry 12021 by single crystal X ray diffraction, comparing with meteorite and silica brick

23 p3738 A71-43613

Single crystal structure of shocked terrestrial and lunar ilmenite from X ray precession and Laue analyses

23 p3740 A71-43623

Apollo 11 and 12 crystalline rocks petrographical analysis and textural-mineralogical-chemical group classification, considering local stratigraphy reconstruction

23 p3742 A71-43638

Lithium iodate hexagonal and tetragonal form crystal growth conditions from aqueous solution and recorded refractivity

23 p3717 A71-43935

MnAlGe crystal domain structure observed for behavior with smaller crystal dimensions and changes in applied magnetic field orientation and strength

23 p3717 A71-43949

Liquid crystals structural, elastic and optical properties, noting application to measurements of temperatures, pressures and electric and magnetic fields

23 p3717 A71-43958

Cast heterophase Mo and alloys fracture strength and plastic characteristics, investigating crystal growth texture, orientation and substructure

23 p3693 A71-44215

W and Mo single and polycrystals structural changes by ion bombardment in Li vapor atmosphere at 1500 C, using mass spectrometer

24 p3838 A71-44862

Hardened cast Al alloys with Cu additions, investigating correlation between mechanical properties and structure at room temperature

24 p3840 A71-45377

CRYSTAL SURFACES

High efficiency epitaxial growth of GaAs by system using substrates oriented along 111/ Ga face

01 p0137 A71-10314

Thermoelectric theory of stressed crystals and higher order elastic constants covering surface electronic and mass transport properties

02 p0294 A71-11799

Crystal surface orientation of chemical vapor deposited W thermionic emitter by hydrogen reduction of hexafluoride, using etch pits and X ray diffraction

02 p0295 A71-12211

Hydrogen and carbon monoxide coadsorption on platinum single crystal surface, examining interactions and species formation by thermal flash and electron impact techniques in ultrahigh vacuum

07 p1055 A71-19844

Rolled metals crystallographic texture and pole figure determination using X ray diffractometer

09 p1467 A71-22307

Microcraters on Apollo 12 crystalline rocks and breccia surfaces attributed to primary cosmic particles

10 p1673 A71-24427

Molecular collisional analysis of normal momentum transfer from flowing rarefied gas to monocrystalline surface

12 p1934 A71-27588

GaAs single crystals real surface electrical characteristics, using pulsed field effect techniques

14 p2284 A71-30403

Surface conductivity and current carrier mobility vs surface potential in CdSe single crystal films deposited on mica base by vacuum vaporization

15 p2461 A71-31511

Oxygen adsorption kinetics at Nb single crystal surface at high temperatures and low pressures

15 p2436 A71-32547

Nucleate boiling of liquid helium I on gallium single crystal surfaces

20 p3312 A71-39282

Germanium single crystal surface conductivity, observing carbon monoxide adsorption effects at various pressures

21 p3435 A71-41341

LEED studies of oxygen adsorption on 111/ and 110/ surfaces of Al single crystals

22 p3561 A71-41730

Room temperature visible surface laser action in praseodymium chloride and bromide, obtaining optical pumping into upper laser level by wavelength tunable dye laser

22 p3556 A71-41802

CRYSTALLINITY

Bond rupture and fracture in semicrystalline polymers, noting agreement with random length molecular tie chain scission model

04 p0670 A71-15388

Gas phase composition effect on CdS deposits crystalline perfection by Knudsen effusion apparatus and mass spectrometry

06 p0942 A71-18084

Crystalline materials plastic deformation and dynamic yield stress based on elastic shock wave damping

07 p1210 A71-19151

Cellulose application as zinc silver oxide battery separator, considering chemical stability, cellophane properties, polymerization and crystallinity

08 p1234 A71-21093

Glassy state beta transition temperatures in cured epoxy resins, showing diglycidyl ether of bisphenol A /DGEBA/ dependence

08 p1323 A71-21475

Alumina and titania codeposition from acid copper electrolyte as function of oxide crystalline form, discussing addition agents effects

11 p1779 A71-26011

Lead borosilicate glass with crystalline opacifiers, observing microstructure and reflectance

13 p2093 A71-28990

Fine crystalline substances forced combination scattering at liquid nitrogen temperature, using ultrashort ruby laser pulses for excitation spectra

13 p2080 A71-29022

Crystalline media impurity light absorption spectral band shape, noting laser resonance emission effects

13 p2080 A71-29023

Fluorescence spectra of anthracene ethyl alcohol solution and powdery crystalline anthracene by single and two photon ruby laser excitation

19 p3071 A71-37263

Coesite-stishovite content in Ries crater nonporous crystalline rocks of variable composition and degree of shock metamorphism

19 p3050 A71-37660

Progressive metamorphism and classification of shocked and brecciated crystalline rocks at impact craters

19 p3050 A71-37665

Apollo 11 lunar crystalline igneous rock samples electrical conductivity temperature dependence, noting age of moon

20 p3295 A71-39619

CRYSTALLINITES

NT SPHERULITES

Microstructure crystallites and voids of polyacrylonitrile based carbon fibers, using X ray diffraction and electron microscopy measurements [PLASTICS INST. PAPER 8]

08 p1320 A71-20901

Crystallites in hydrogenated hydroxy terminated polybutadiene from polarized light examination, viscosity-temperature curve discontinuity and elastomer modulus-temperature curve [JPL-TR-32-1512]

10 p1573 A71-25126

CRYSTALLIZATION

NT RECRYSTALLIZATION

Sintered or cast Re refining in vacuum electron beam furnace using water-cooled crystallizer, discussing metal losses during melting

06 p0904 A71-17948

Apollo 11 flight glass basalt, determining crystallization sequence and phase assemblage of high Ti specimens as oxygen fugacity function

06 p0970 A71-18235

GaAs epitaxial layers growth in open system, noting spontaneous crystallization on reactor walls at high temperatures

09 p1506 A71-22161

Soviet book on metal alloys plasticity gaps covering crystallization, thermomechanical treatment, heat induced brittleness zones formation, etc

09 p1472 A71-23161

Laser pulse induced rapid reversible crystallization of amorphous chalcogenide semiconductor films using photon flux model

10 p1655 A71-24044

Metals crystallization in ultrasonic field, investigating structural change as function of energy and impedance factors and cavitation effects in fine grain formation

10 p1626 A71-24136

Cu-Ti-Al system intermediate phases crystallization from melt in large concentration areas, discussing four-phase reactions

10 p1627 A71-24597

Nickel alloys crystallization at superhigh cooling rates by dropping liquid metals on rotating copper cylinders to obtain films

12 p1917 A71-27301

Modified heat conductivity solutions for region with moving boundary, applying to crystallization front or crack propagation

13 p2159 A71-28037

Steatites replicas electron microscopy for microstructure variations with composition and firing conditions differences, discussing protoenstatite crystallization and glass phase formation

13 p2093 A71-28664

Crystallization temperatures of lunar gabbroid rocks from Tranquillity base, comparing with dry silicate melts

15 p2401 A71-32498

Crystallization behavior and chemical compositions of Apollo 11 lunar basalts including olivine and silica normative varieties

16 p2637 A71-33512

Superhigh cooling rate effects during crystallization of solidified binary alloys, achieving superconductive properties

16 p2598 A71-33998

Artificial crystallization and dispersion in supercooled stratus clouds, observing growth, stabilization and disintegration stages in crystallization zones expansion

19 p3093 A71-38691

Lithium magnesium zinc silicates crystallization phase equilibria, noting temperature effects, structure, melting and solubility

20 p3253 A71-38818

Glass particles crystallization in sintered metal matrix glass materials, examining microcracks and temperature and cyclic heating effects

23 p3696 A71-43251

Apollo 12 crystalline rocks composition from microprobe analyses, indicating undercooled magmatic fractional crystallization 23 p3742 A71-43639

Pyroxenes morphological significance in Apollo 12 lunar igneous rock samples petrogenesis, analyzing crystallization process history 23 p3742 A71-43642

Clinopyroxene crystallization histories of Apollo 12 porphyritic basalt rocks 12021 and 12052 from Oceanus Procellarum 23 p3742 A71-43643

Apollo 12 basalts petrology and petrogenesis, studying crystallization sequences 23 p3743 A71-43646

Petrogenesis and crystallization of protophyres basalt in lunar maria lava lakes, deducing eruption temperatures 23 p3743 A71-43647

Pyroxenes and olivines in lunar rocks from Ocean of Storms, observing plastic deformational processes since crystallization by optical, X ray and electron microprobes 23 p3744 A71-43657

Apollo 11 and 12 devitrified glass fragments temperature histories indicating broad range of subsolidus crystallization temperatures 23 p3746 A71-43667

Condensate particle crystallization retardation effect on energy characteristics of jet engine, calculating nonequilibrium flows of two phase combustion products in nozzle 24 p3864 A71-45004

Ni-Zr alloy crystallization at large cooling rates obtained by melt droplets blowing with compressed He jet onto rotating Cu cylinder surface 24 p3840 A71-45374

CRYSTALLOGRAPHY

Fe-Ni martensite crystals microstructure, using Kossel method and electron microscopes 01 p0106 A71-10278

Self-consistent polycrystalline model for combined stress state time dependent creep, examining flow potential existence 05 p0830 A71-17236

Fast brittle crack slowing by mechanical twins in transformer steel and by slip bands in LiF and NaCl crystals 09 p1468 A71-22625

Cold and hot working effects on Al alloys elastic properties, discussing crystallographic systems reference points 10 p1628 A71-24822

Crystallographic relationships between Ni- and Cr-rich solid solutions, noting preferred interphase interfaces in Ni-Cr eutectic alloy 11 p1778 A71-25532

Thermionic converters surface physics theory, discussing work functions, desorption energy and rates relationship to atomic and crystallographic properties 11 p1711 A71-25878

Mo-Re alloy crystallographic features observation by transmission electron microscopy, noting equivalence of twin-slip and twin-twin interactions 11 p1783 A71-26477

Residual stresses for fused contacts between metals and Si or gallium arsenide from polarization measurements in principal crystallographic planes 15 p2461 A71-31510

Dislocation theory and crystallography in metallurgy, discussing edge and screw dislocation motion and interactions, Burgers vectors and gliding planes 15 p2427 A71-31530

Mechanical and crystallographic structure effect on cold brittleness temperature anisotropy and on exfoliation of Cr alloyed with rare earth elements 17 p2755 A71-34416

Orthorhombic-tetragonal phase transition in barium sodium niobate, investigating expansion curve discontinuities due to crystallographic changes from dilatometric studies 20 p3275 A71-38816

Tantalum and niobium ternary oxides recovery from liquid potassium solution, determining composition and crystallographic modifications by chemical and X ray diffraction analyses 20 p3194 A71-39372

CRYSTALS

NT BICRYSTALS

NT CREATINE

NT CRYSTAL OSCILLATORS

NT CRYSTALLITES

NT DENDRITIC CRYSTALS

NT IONIC CRYSTALS

NT LIQUID CRYSTALS

NT METAL CRYSTALS

NT MICROCRYSTALS

NT MIXED CRYSTALS

NT PIEZOELECTRIC CRYSTALS

NT POLYCRYSTALS

NT QUARTZ CRYSTALS

NT SINGLE CRYSTALS

NT SPHERULITES

NT WHISKERS [SINGLE CRYSTALS]

Crystal time reversal symmetry for macroscopic laws determination, discussing spontaneous electric and magnetic moments and magnetically ordered systems 01 p0138 A71-10348

Atomic collision chains in bcc crystal, determining energy loss relation to temperature by computer model with/without perfect lattice thermal oscillations 04 p0630 A71-15103

Inhomogeneous crystals frequency properties calculation by admittance averaging method, deriving expressions for metal semiconductor contact impedance 07 p1175 A71-19222

Second harmonic generation experiments, considering limited focused laser beam diameter and crystal sample shape 12 p1915 A71-27641

Nonlinear interaction between three weakly coupled waves with well defined phases in dissipative media /fluids, plasmas or crystals/ 13 p2106 A71-28453

Crystal laser elliptic cavity size determination for maximum emission efficiency, using photochemical method for energy transfer measurement 17 p2754 A71-35748

Coupled resonator AT cut quartz crystal bandpass filter design in ladder configuration with low sensitivity and simple manufacturing methods 21 p3360 A71-40810

CSM

U COMMAND SERVICE MODULES

CUBIC EQUATIONS

Cubature formulas for plane triangular domain, giving leading error terms 05 p0726 A71-16958

CUBIC LATTICES

NT BODY CENTERED CUBIC LATTICES

NT FACE CENTERED CUBIC LATTICES

Lamb wave interaction with current carriers in cubic symmetry piezosemiconductors, obtaining amplification factor 06 p0942 A71-18352

Monoclinic, stabilized and metastable tetragonal and cubic zirconias, noting IR and Raman spectra 13 p2093 A71-28991

Absorbed energy spectra and absorption frequencies from elastic constants of vibrating metals with cubic lattice structure, using cold neutron scattering 14 p2190 A71-30149

Critical growth work hardening germination and recrystallization of oriented compression deformed Nb, Mo and W refractory cubic centered crystals 18 p2935 A71-36200

Computer program for generation and automatic plotting of perfect and twinned electron diffraction patterns for cubic crystal structures 19 p3118 A71-37719

Numerical modeling and analysis of homocentrical light beams propagation in cubic and nonlinearity saturation medium, using parabolic equation approximation 21 p3417 A71-41259

Theoretical estimation of tensile strength, elastic modulus and deformation of cubical diamond specimens under tension and compression 22 p3565 A71-42873

CUES

Flight simulation in various degrees of environmental realism by visual and other physiological cues, discussing available devices and techniques relative to specific training tasks 01 p0066 A71-10020

Hybrid real time computer simulation of external visual display cues for Apollo Command and Service Modules 02 p0237 A71-11791

Rotation direction perception by three cue system for polar projection of dotted line, considering differential retinal velocity relative to axis of rotation 05 p0713 A71-16550

Pilot physiological responses as indicators of pitch motion cues effect on flight simulator fidelity 07 p1047 A71-19465

Relevant cue placement effects in concept identification tasks employing enforced verbal encoding 07 p1048 A71-19514

Isolated lower case letters visual recognition, investigating perceptual similarities and common properties serving as cues 17 p2680 A71-34655

Peripheral visual field and perceptual factors effect on accommodation under conflicting cues, using laser scintillation measurement 21 p3338 A71-41198

Perceived distance effect on induced movement from stereoscopic cues 21 p3344 A71-41199

Relative size cue for facilitating stereoscopic depth perception in ambiguous disparity stereograms 23 p3638 A71-43110

CULTIVATION

Mammalian cells cultivation at suboptimal temperatures, considering reproduction and cytophysiological changes 20 p3188 A71-39220

Hydroponic plant cultivation with keramzit substrate, investigating replacement time effect and regenerative power of nutrient solution 22 p3506 A71-42816

CULTURE TECHNIQUES

Soil microorganisms multiplication under simulated Martian conditions in limonite and garden soil mixture 01 p0019 A71-11558

Algae physiology, discussing culture techniques, pure species production, past errors and achievements 03 p0365 A71-14332

Blue green algae activity in Kratz-Myers medium, noting C 14 uptake changes for monocultures and mixed cultures of Anacystis nidulans and Synechocystis aquatilis 06 p0858 A71-17392

Thiol and disulphide compounds radiation protection capacity at cellular level in tissue culture, using reproductive integrity as protection criteria 07 p1034 A71-18948

Optimum mineral medium for algae Chlorella and Scenedesmus cultivation in closed ecological system 09 p1393 A71-22923

Chromosome mapping of Pasteurella pseudotuberculosis by interrupted mating, indicating chromosome transfer in more than one linkage group 09 p1396 A71-23474

Activated charcoal effects moss development alterations on artificial agar substrate 11 p1721 A71-26319

Autotrophic cultivation of cereals with high photosynthetic activity under intensive illumination as biological components in life support systems 13 p2017 A71-28405

Stearothermophilus spore germination stimulation, investigating effects of preheating and amino acid and carbohydrate concentration 13 p2010 A71-28695

Mineral composition optimization of nutrient medium for Hydrogenomonas, using steepest ascent method for mathematical planning of experiments 20 p3193 A71-39236

Bicarbonate requirement for elimination of lag period of chemoautotrophically grown Hydrogenomonas eutropha 21 p3329 A71-40213

Space conditions exposure of lysogenic strains of Escherichia coli and monolayer cultures of human cells aboard Zond 5 and 7 flights 21 p3333 A71-40565

Extraterrestrial life detection methods, discussing bacterial cultures growth dynamics in nutrient media and iron porphyrin proteins and ATP content increase 21 p3334 A71-40570

Chlorella biomass chemical composition stability during prolonged cultivation with nitrates recycling medium 22 p3507 A71-42819

Biologically mineralized human waste products utilization in nutrient solutions for higher and lower autotrophs cultivation 22 p3507 A71-42819

CUMULONIMBUS CLOUDS

Updraft vault dynamic in hailstorms using one dimensional cumulonimbus entraining jet model, observing initial conditions steady state 01 p0119 A71-10744

Turbulence energy spectra in thick convective cumulonimbus cloud zone, using aircraft measurements 04 p0622 A71-15633

Thunderstorms environment analysis from radar and aircraft scanings, determining cumulonimbus cloud air kinematic properties for three dimensional circulation model 09 p1488 A71-23252

Hail precipitation process from cumulonimbus clouds based on aircraft and ground observations 19 p3093 A71-38692

Cumulonimbus cloud hail danger, precipitation and water content measurements with scattering and attenuation of centimeter radar waves, including automated echo subtraction device 19 p3094 A71-38700

CUMULUS CLOUDS

Radar reflectivity pattern calculation from cumulus cloud growth numerical model, noting similarity with radar data from on-line computer system 01 p0118 A71-10584

Solar radiation fluxes at earth surface in presence of cumulus clouds, relating fluxes to cloud magnitude and sunshine duration by regression relations 06 p0889 A71-17648

Relative humidity augmentation for triggering convection in two dimensional numerical cumulus cloud model 06 p0924 A71-18412

Spatial correlations between inside cumulus cloud conditions and precipitation onset and intensity for modification experiments from aircraft penetration measurements 08 p1326 A71-21450

Jet stream axis position from cumuloniform cloud structural differentiation observed over Central Eu-

- rope on 22 May 1970, noting coincidence with high pressure near ground 12 p1924 A71-26575
- Cumulus entrainment and steady state one dimensional convection model 12 p1925 A71-27201
- Steady state one dimensional cloud model for cumulus convection, discussing validity range limits 17 p2770 A71-35125
- Backscattered laser radar pulses and downward IR flux enhancements in clear air around small cumulus clouds, discussing hygroscopic aerosols for increased radiance 17 p2707 A71-35381
- Cumulus clouds macro- and microstructural parameters measurements including convective flow, temperature, water content, droplet concentration and size 19 p3091 A71-38681
- Stationary ascending and descending jets velocities in nonstationary cloud layer, discussing cumulus clouds breakup rate 19 p3093 A71-38695
- Radar measurements of vertical structure and motion trajectories of cumulus-rain clouds, studying vertical flows velocities and radar echo characteristics 19 p3094 A71-38701
- Numerical model of turbulence effect on cumulus cloud mesoscale convective motion 21 p3411 A71-41386
- Cumulus clouds photographs above Northern Hemisphere by meteorological satellite during active periods of earth atmospheric circulation 23 p3701 A71-44047
- CUPOLAS**
- Vestibular physiology, discussing endolymph chemical composition, cupola structure and function and hair cells 04 p0536 A71-14752
- CURIE TEMPERATURE**
- Spontaneous polarization measurement of ferroelectric Rochelle salt near Curie point, using nuclear magnetic resonance for phase transitions 04 p0637 A71-15548
- Autocorrelation functions of anomalous gravitational and magnetic fields for ocean lines, relating Mohorovici boundary and Curie isotherm 06 p0894 A71-18268
- Barium titanate-fluorine substitutional solid solutions production and X ray analysis, examining Curie point behavior 09 p1506 A71-22166
- Coulomb impurity centers in paramagnetics and ferromagnetics at Curie temperature with spin-electron exchange interaction 09 p1508 A71-22881
- Heisenberg ferromagnet with applied external magnetic field, investigating thermodynamic properties near Curie point 11 p1807 A71-25558
- Curie point of solid solutions in ternary system of zirconate-titanate and lead metaniobate, using maxima on temperature dependence curve of permittivity 13 p2111 A71-28152
- Laser Curie point writing characteristics and diffraction efficiencies of MnBi thin films for holographic recording 19 p3062 A71-37143
- High density redundant information storage in magnetic holography with Curie point writing on thin films and magneto-optic readout 19 p3065 A71-38237
- Curie point region automatic thermal stabilization effectiveness of cylindrical/disk shaped segnetoceramic elements in electrostrictive constant magnetic field converters 24 p3828 A71-45164
- CURING**
- Volatile adhesive curing effect on metal-metal bond fatigue strength 05 p0772 A71-16955
- Cured epoxy polymer, determining diffusion coefficients, solubility, permeability and equilibrium water absorption as function of curing agent and temperature 06 p0915 A71-17943
- Single ply sandwich composite prepreps for use with honeycomb reinforcement, noting one step curing for light weight structural panels 10 p1630 A71-24065
- Low temperature curing nylon epoxy adhesive, discussing high peel strengths 10 p1630 A71-24070
- Low temperature curing long open time epoxy adhesives evaluation for 3500 psi shear strength 10 p1631 A71-24072
- Structural film adhesives peel-thickness correlation and cure rate study by torsion pendulum 10 p1614 A71-24074
- Structural adhesive bonding of plastics and metals, emphasizing fast curing, high bond strength, environmental resistance and bonding ability 11 p1768 A71-25393

- Thermosetting acryl modified epoxy resin, stressing adhesive bonding strength, workability and curing characteristics 11 p1787 A71-25423
- Polyphenylene thermal degradation and curing, discussing pyrolytic effects of chlorine and polynuclear structure 11 p1855 A71-26035
- CURL [VECTORS]**
- NT VORTICITY**
- Eigenfunctions of curl operator, rotationally invariant Helmholtz theorem and applications to electromagnetic theory and fluid mechanics 20 p3255 A71-39575
- CURRENT AMPLIFIERS**
- NT PHOTOMULTIPLIER TUBES**
- Two transistor emitter follower DC amplifier, using simplified equivalent circuit 13 p1999 A71-28628
- Modulator-demodulator type push-pull DC amplifier input noise reduction, using electromechanical vibrators 15 p2355 A71-32451
- Transistor current gain as function of emitter current for low injection levels 24 p3807 A71-44381
- Current amplification in CdS and CdSe single crystals and thin films by fast electron bombardment 24 p3859 A71-44386
- CURRENT DENSITY**
- Dense plasma high current density effects on low voltage arc in thermionic converter 01 p0005 A71-10159
- Sunspots surface layers azimuthal electric current density, assuming specific magnetic force distribution 03 p0484 A71-13209
- High efficiency LF operating modes in avalanche diodes under low current density 04 p0558 A71-15147
- Single pulse relativistic electron beam passage through plasma, calculating induced current density in axial direction 04 p0635 A71-15371
- Plasma jet radial velocity distribution measurement by probe technique, calculating current density from azimuthal magnetic field via Maxwell equation [DFVLR-SONDDR-88] 05 p0788 A71-16643
- Quasi-steady MPD accelerators current conduction and power loss mechanism investigation through local anode fall voltage and current density measurements at different arc current levels 06 p0939 A71-18636
- [AIAA PAPER 71-198] 06 p0939 A71-18636
- Packaged microwave avalanche diodes negative resistance properties three-parameter characterization at low current densities 07 p1074 A71-19125
- Time linear increase of magnetic flux flow through superconducting Nb-Zr wall, inferring empirical critical current density model agreement with measured flow rate 07 p1179 A71-20156
- Zinc electrodes performance improvement, discussing electrochemical corrosion rate, current density and temperature effects 08 p1233 A71-21082
- Three dimensional scattering and surface current density measurements on circular tube illuminated by electromagnetic wave 08 p1256 A71-21689
- Surface current density and electromagnetic scattering from finite tubular cylinder solved numerically by approximate product integration method 08 p1256 A71-21691
- Electron radiation bulk damage effects on Si surface barrier detectors, determining reverse leakage current density and alpha particle response changes 08 p1345 A71-21842
- Current spectral noise density in nonlinear element transmitter stage, examining vacuum tube frequency multiplier phase and amplitude fluctuations 09 p1405 A71-22469
- Josephson maximum DC current plot for linear overlap junctions, discussing junction area geometry to current perimetric proportionality 09 p1423 A71-22693
- Electron beam current density measurement using neutral Ar atoms electron impact excitation to metastable states 09 p1497 A71-22731
- Arc melted ingot high field superconductor, combining critical density and resistive critical field 10 p1655 A71-24042
- Pseudo-stationary shock wave in plane MHD flow of conducting gases, deriving existence theorem for linear relations between vorticity and current density 10 p1648 A71-24281
- Ti-V alloys electrolytic deposition, discussing electrolyte composition, current density, temperature and coating thickness 10 p1627 A71-24646
- Ionization wave varieties in nitrogen glow discharge at various pressures and current densities from phase and group velocity measurements 10 p1654 A71-24973

- Flush mounted electrostatic probes behavior under different flow regimes, studying bias, area, geometry and position effects on collected current density 11 p1743 A71-25148
- HF electromagnetic waves absorption as function of discharge current intensity in ionized H, using gas pressure or uniform magnetic field as parameters 11 p1805 A71-25598
- Vacuum arc welding stability in vaporized Mo cathode material as function of current and arc length, describing burner design for material replenishment 11 p1770 A71-25946
- Equations system describing parametric distribution of ionized plasma in thermionic converter gap, discussing current density effects on low voltage arc discharge 12 p1938 A71-27210
- Low voltage arc discharge effects on ionized Cs plasma characteristics under high density current conditions 12 p1938 A71-27213
- Semiconductors high carrier densities at low temperatures, showing possible soft plasma branch and electron sound 12 p1944 A71-27770
- Electric potential and current density in rotor of thin disk unipolar engine with zonal removal, formulating Neumann problem 13 p2002 A71-28930
- Magnetic corrections to Boltzmann distribution function by power expansion, determining current density in system of free electrons accelerated by crossed electric and magnetic fields 13 p2109 A71-29288
- Ion thruster ion beam current density profiles mathematical representation by two parameter equation [AIAA PAPER 71-693] 14 p2293 A71-30752
- Electric arc burning in contracted Ar plasma between two plates, calculating normal current density and I-V characteristic 15 p2457 A71-32271
- Missile circumferential current density for plane wave electromagnetic field illumination, using Kao shadowing theory 15 p2372 A71-32367
- Laboratory simulation of satellite motion in ionospheric plasma, specifying maximum current density, electron velocity distribution and temperature range [AIAA PAPER 71-608] 15 p2385 A71-32545
- Switching on p-n-p-n structure under high injection level in both bases, noting current concentration and voltage steady state buildup 16 p2546 A71-33496
- Critical current density in niobium alloy with disperse superconducting phase as function of transverse magnetic field strength 16 p2593 A71-33653
- Plasma jet formation within high pressure discharges in air at atmospheric pressure, discussing electrode configuration, current density and accelerating magnetic field strength 17 p2787 A71-34285
- Power gain distribution in Ne-He laser cuvettes at 0.63 and 3.39 microns wavelength, noting current density dependent laser power gain shifts 17 p2752 A71-34405
- Static feed water electrolysis system of life support system, discussing current density, operating time and temperature effects on voltage for various electrochemical cell sizes [ASME PAPER 71-AV-25] 18 p2868 A71-36392
- Aerodynamic probes for determining flow state of high enthalpy hypersonic flow fields, considering pitot pressure, total enthalpy and current density 18 p2921 A71-36414
- Area measurement on steady, fluctuating, turbulent and expanding premixed flames, using saturation current method 19 p3168 A71-38103
- Mass transport at high current densities in Al and Mo thin film conducting stripes, noting effect on IC life 19 p3119 A71-38511
- Equations system describing parametric distribution of ionized plasma in thermionic converter gap, discussing current density effects on low voltage arc discharge 19 p3000 A71-38622
- Low voltage arc discharge effects on ionized Cs plasma characteristics under high density current conditions 19 p3117 A71-38625
- Axial and radial components of magnetic induction of steady plane meridional field from rectangular region with azimuthal current density 19 p3000 A71-38638
- Electric discharge carbon dioxide laser gas temperature, electron and current densities radial distribution from mathematical model 20 p3242 A71-38844
- Rechargeable cylindrical hydrogen-oxygen fuel cell for synchronous satellites, determining energy density

- as function of current, pressure and electrolytes with computer model
20 p3182 A71-38947
- Electron beams formation and focusing, including current density distributions, electronic potentiometer recording, parameters and comparison with simulation data
20 p3204 A71-39160
- High perveance three electrode electron gun with longitudinal compression, examining beam profiles and radial current density distributions
20 p3204 A71-39161
- Critical current of ideally homogeneous second class superconducting film, noting lattice resistance to small displacements
23 p3715 A71-43414
- Dynamic carrier density instabilities for semiconductor-metal electronic phase transition by Frenkel-Poole effect in seminsulator with donors
23 p3716 A71-43478
- Nonlinear sum and difference frequency and second harmonic generations of current density in homogeneous magnetoplasma by nonuniform microwave electric fields
23 p3712 A71-44002
- Heterostructure /multisemiconductor junctions/injection laser with reduced current density requirement for continuous operation at room temperature
24 p3833 A71-44974
- Magnetic induction by HF current passing over conducting torus enclosed by larger torus, obtaining vector potential, current density and inductance expressions
24 p3857 A71-45232
- ## CURRENT DISTRIBUTION
- Plane curvilinear radiators synthesis for horizontal or vertical radiation patterns, obtaining current phase amplitude distributions by symmetrical striplines
01 p0056 A71-11205
- Tungsten cathode current partitioning in dense Ar plasma, noting electron emitter work function reduction due to ion space charge field
02 p0289 A71-11940
- Current profile monitor for scanning electron beam irradiations from accelerator, using storage oscilloscope or X-Y recorder for display
02 p0249 A71-12127
- Transverse current leakage effect on energy conversion and Hall characteristics of MHD generator
02 p0290 A71-12195
- Noise-induced current fluctuations on S-shaped I-V curve in Cr-doped GaAs diodes
03 p0387 A71-13982
- Multielectrode MHD channels, investigating relaxation effects on two dimensional current distribution and plasma properties
03 p0466 A71-14319
- Polynomial current analysis of imperfectly conducting thin cylindrical dipoles with arbitrary internal impedance
04 p0558 A71-15144
- Variable properties effects on MHD flow in ducts with finite aspect ratio and electrically insulating walls, noting current distribution
04 p0634 A71-15179
- Nonuniformly rotating Hg fluid, noting hydromagnetic stability and velocity control by imposed radial current distribution between coaxial ring shaped electrodes
05 p0788 A71-16608
- Zigzag antennas current distribution by integral equation analysis
06 p0874 A71-17709
- Collinear and planar arrays of arbitrarily located parallel elements, determining current and charge distribution, admittances and field patterns
06 p0875 A71-17715
- Surface illuminated semiconductor excess current carriers nonstationary distribution and space charge, solving equation system by operational technique
06 p0942 A71-18185
- Terrestrial electrical current distribution diagram based on solar quiet variation hodographs
07 p1104 A71-20048
- N-type InSb microwave noise radiation and attendant RF current oscillations under magnetic field
07 p1180 A71-20177
- Input impedance of cylindrical and helical antennas in cold lossy magnetoplasma, discussing sensitivity to current distribution
07 p1065 A71-20323
- Interplanetary space cosmic ray currents global survey based on neutron component measurements, noting anisotropic diffusion, inhomogeneous solar wind and Forbush effect shell model
08 p1351 A71-20966
- Loop antenna with finite gap at driving point, deriving admittance, current distribution, radiation pattern and directive gain from variational and Fourier series methods
08 p1265 A71-21296
- Intersecting dipoles with sinusoidal current distribution, determining input impedance
08 p1266 A71-21469
- Integral transform methods for analytic solutions to current and potential distribution on disk in infinite plane for four limiting cases
08 p1237 A71-21471
- Load currents and preionization of large nonequilibrium segmented Faraday MHD generator
09 p1386 A71-22072
- Three dimensional model of semiconductor diode current dependence on charge carrier diffusion length and surface recombination rate
09 p1414 A71-22189
- Nondegenerate and degenerate semiconductor current flow equilibrium at low temperatures based on Boltzmann transport equation
09 p1414 A71-22251
- Scattering structures of two parallel elliptical cylinders, tapes or combinations, deriving surface current density distribution under plane TM wave excitation
09 p1407 A71-23107
- Carbon dioxide production laser for automatic resistors trimming without current carrying capability reduction, noting accuracy, flexibility and speed
09 p1465 A71-23405
- Realizable method of pattern synthesis for broadside array antenna giving arbitrary current distribution
09 p1418 A71-23489
- Polynomial approximation of current along thin isolated asymmetrical cylindrical dipoles
09 p1419 A71-23506
- Dipole antenna array exact design for prescribed radiation patterns in magnetic plane, using current distribution integral
09 p1420 A71-23511
- Parabolic antenna instantaneous phase center calculations, using radiation patterns from aperture field and current distribution methods
10 p1582 A71-23807
- Time dependent current flow measurements and energy losses in capacitor discharge of electrodeless MHD motor
11 p1716 A71-26290
- Single element antenna radiation pattern effect on equidistant linear directional gain, current distribution and array shape
11 p1738 A71-26343
- One dimensional charged particle continuity equation solution in low energy neutral plasma with current flows
11 p1804 A71-26374
- Current distribution effect on stability of exploding and collapsing accelerated cylindrical plasma shell in axial and azimuthal magnetic field
12 p1935 A71-26765
- Electric and magnetic surface current coefficients of antenna radiating elements in metallic waveguides and resonators by harmonics expansion applied to circular-cylindrical array
12 p1885 A71-26839
- Transient characteristics of MOS channel transistors, solving nonlinear differential equations describing current and potential distribution
12 p1886 A71-26850
- Electron hole n-p plasma conductivity in cylindrical germanium specimens as function of current produced azimuthal magnetic field
12 p1936 A71-27036
- Antenna analysis method based on transmission line theory, yielding current distribution and input impedance of finite conical antenna
12 p1880 A71-27154
- Nonlinear planar transistor model, analyzing majority carrier current flow fields in base due to injection of emitter and collector p-n junctions
12 p1888 A71-27612
- Uniformly spaced linear arrays directivity as function of spacing, scan angle and current distribution, approximating element radiation intensity
13 p2028 A71-28000
- Numerical solution of current distribution, wave propagation constant and propagation mode cut-off frequencies on periodic linear array
13 p2028 A71-28001
- Current oscillations and switching effect in amorphous chalcogenide compound films sputtered thermally on unheated glass and pyroceram substrates
13 p2111 A71-28173
- Electrode nonlinear current distribution in plasma with anisotropic conductivity, noting Hall parameter effect on electric field structure
13 p2107 A71-28566
- Near periodic current fluctuation stability of single phase parametric electric motor in steady operation
13 p2002 A71-28931
- Metallic body motion in strongly rarefied plasma, determining compensating surface current distribution
13 p1991 A71-29158
- Two dimensional electromagnetic scattering by conducting corrugated circular cylinders, determining surface current by matrix and integral equation methods
14 p2195 A71-30248
- Electromagnetic wave propagation on Yagi-Uda structure, obtaining current distribution, free space vs guided wavenumbers diagram and cutoff frequencies
14 p2196 A71-30514
- Current constriction-resistance variations relations in transistors, discussing current redistribution
14 p2213 A71-30629
- Sputtered tantalum films oxygen content determination by anodization current efficiency measurements
16 p2621 A71-33187
- Plane diode electrode gap differential capacitance for operation with anode negative voltage, current saturation and space charge limitation
16 p2548 A71-33709
- Dipole coupling, current distribution and impedance of thick dipolar log periodic antennas by 4-term theory
16 p2544 A71-34172
- Plane curvilinear radiators synthesis from horizontal or vertical radiation patterns, obtaining current phase amplitude distributions by symmetrical striplines
17 p2697 A71-34257
- Current distribution on grid type dipole antenna in warm isotropic plasma, using direct source approach and boundary value analysis
17 p2698 A71-34430
- Rigorous solution for multiple arm conical log spiral antenna by numerical solution of integral equations, considering current distribution, half power beam-width, etc
17 p2715 A71-34752
- Scattering obstacle with surface currents and radiating fields, determining characteristic current distributions and values of elliptical loops, straight wires and circular arcs
17 p2700 A71-34753
- General media electrical properties from current and charge distributions and impedance characteristics of electrically thin cylindrical antennas
17 p2715 A71-34759
- Electric current distributions measurement along monopole antenna in isotropic and anisotropic plasmas generated in large space chamber
17 p2716 A71-35048
- Current distribution and driving point admittances computation in curtain antenna array with delta function generator driven electrically long elements
17 p2716 A71-35094
- Reynolds magnetic number effect on MHD channel conducting gas flow current distribution, taking into account Hall effect
17 p2790 A71-35642
- Common mode choke for reduction of current unbalance in cable to improve electromagnetic interference performance
19 p3000 A71-38432
- Parasitic wire elements effects on radiation, impedance and current distribution of antennas, using method of moments
19 p3031 A71-38444
- Radiation resistance of small filamentary loop antenna in cold collisionless uniform multicomponent magnetoplasma, assuming uniform current distribution along loop
19 p3023 A71-38594
- Excitation asymmetry effects on current distribution and far field of thin dipole radiators
19 p3036 A71-38604
- Current variation effect on pulsed psn diodes forward characteristics, calculating peak inductive transient voltage value and time position
20 p3205 A71-39430
- Equivalent current systems at 115 km parallel to earth surface profile based on ground observations of geomagnetic field, comparing with auroral electrojet
20 p3218 A71-39525
- Iterative solution of Hallen integral equation for current distribution on lossless cylindrical transmitting dipole antenna
21 p3348 A71-40578
- Current and potential distributions in lossless nonequilibrium MHD plasmas at high magnetic field strengths, using method of characteristics
21 p3423 A71-40946
- Dead ended compartments concentration and current distributions calculation in space hydrogen-oxygen fuel cells, using mathematical model with convective diffusion equation
21 p3326 A71-41249
- Sn-N-GaAs semiconductor surface barrier structure electrical properties measurement over wide electron density range, determining energy band diagram and current flow mechanism
21 p3433 A71-41313
- Narrow strongly radiating slot voltage distribution, investigating cavity coupling with integral equation
22 p3522 A71-42305
- Spheroid with two dielectric separated halves and mixed boundary conditions, determining spreading currents Lf electromagnetic field
22 p3484 A71-42879
- Electric field induced current distribution on cylindrical antenna, considering delta generator and electromagnetic waves excitations
23 p3643 A71-43122
- Polar electrojet development during polar magnetic substorms, considering current intensification at northern and/or southern borders
23 p3668 A71-43167

Acoustoelectrical current oscillations in GaAs films at low temperature under ultrasonic Rayleigh wave amplification

23 p3716 A71-43477

Shunt driven circular loop antenna effective length, current distribution and input admittance, comparing to transmission lines

23 p3655 A71-44169

Current carrier mobility and concentration measurements in inversion metal dielectric semiconductor channels by Hall method

24 p3808 A71-44384

Cylindrical antennas with arbitrary distributed resistive and reactive loading, presenting method based on dipole antennas with constant resistance loading per unit length

24 p3803 A71-44466

Ram current effect in sounding rockets for plasma ion density measurement

24 p3822 A71-44793

Transients determined for Cs vapor discharge phases, observing current fluctuations between steady states in negative resistance zone above 0.2 torr

24 p3858 A71-45246

Current and charge saturation effects on channel electron multipliers in continuous and pulse operation

24 p3811 A71-45330

CURRENT REGULATORS

Pulse width controlled, regulated DC-DC converter with passive low pass filtering, discussing open loop transfer functions, stability analysis and linear models

07 p1024 A71-20413

Electrochemical cell interelectrode planar spacing regulator system, discussing electrode constant vibration amplitude to current ratio

08 p1296 A71-20855

Transistorized gas laser discharge current stabilizer using double feedback circuit, discussing schematic diagram and operation principles

08 p1303 A71-21807

Defectoscopes with current regulation by magnetic amplifiers, describing circuitry and remanent magnetization of components with AC and rectified half wave currents

08 p1273 A71-21894

Current controlled unstable pulse oscillator, discussing depletion layer transistors and upper frequency limit as function of thermal loads and switching times

12 p1887 A71-27043

Current controlled diodes used as voltage variable capacitors in oscillators

23 p3652 A71-43832

CURRENT SHEETS

Stationary waves produced by earth bow shock, calculating cyclotron radiation amplitude and polarization characteristics by thin current sheet model

01 p0075 A71-11490

Shock tube current sheet speed variations, describing discharge voltage, pressure and test gas effects

04 p0632 A71-14689

Current sheet collapse phase in dense deuterium plasma focus gun heating, using streak photography and X ray and neutron measuring techniques

07 p1165 A71-18877

Ionospheric inhomogeneities effect on dipole current system produced magnetic field, deriving analytical expressions as function of distance from current carrying layer and inhomogeneity center

07 p1099 A71-19385

Dungey model generated by interplanetary magnetic field addition to closed magnetospheric model, discussing adiabatic theory breakdown for model current sheet

08 p1280 A71-21217

Micropulsations power spectrum from magnetospheric model based on transient current sheets, approximating background frequency dependence and daytime/nighttime spectral line widths

09 p1441 A71-23638

Turbulent plasma heating in current sheet between opposed magnetic fields

10 p1653 A71-24891

Inductive impulsive plasma accelerator current sheet electron density determination by electron probe and laser light scattering

15 p2455 A71-31545

Radiation from electrostatic waves in thin current sheet in geomagnetic tail into cold magnetized plasma, noting wave damping for wide frequency range

16 p2562 A71-32805

Neutral current sheets in slow moving plasma with frozen-in magnetic field with null force line

16 p2638 A71-33651

Magnetopause current layer equilibrium based on numerical solution of uniform magnetic field confinement by warm plasma with net parallel velocity

19 p3132 A71-37355

Ionospheric inhomogeneities effect on dipole current system produced magnetic field, deriving analytical expressions as function of distance from current carrying layer and inhomogeneity center

19 p3052 A71-37810

Pulsar radiation from oscillating interface with steady current sheet between rotating radiating magnetic dipole and external plasma

20 p3285 A71-39952

Turbulent plasma heating in current sheet between opposed magnetic fields

21 p3424 A71-41270

Solar corona current sheet magnetic model, computing polar plume orientations and radial and nonradial streamers

21 p3453 A71-41359

Spherical wave technique adaptation to antenna radiation determination by equivalent current sheets

22 p3509 A71-42200

Explorer 12 magnetic field observations of magnetopause current layer during magnetic storm, interpreting data by magnetosphere model

23 p3668 A71-43160

Magnetopause current layer deflection duringOGO 5 crossings, noting independence on sun-earth-satellite angle

23 p3668 A71-43161

Plasma current driven sheet at neutral point of cusp and quadrupole magnetic field for space physical simulation of solar flare and geomagnetic tail

23 p3714 A71-44277

CURRENT STABILIZERS

U CURRENT REGULATORS

CURTAINS

Heat and gas curtain efficiency in turbulent boundary layer on flat plate, including heat transfer data

02 p0331 A71-11886

Annular free jets application as air curtains, formulating relations for plane and conical jets to calculate deflection of particles

10 p1596 A71-24938

CURVATURE

Curvature matching method for two dimensional flexible plate nozzle contour of trisonic wind tunnel, obtaining overdetermined simultaneous equations

01 p0068 A71-10970

Level ampoule inner surface curvature nonuniformity, noting correction determination in level scale division

04 p0592 A71-14857

Curved shock reflection from straight rigid boundary, calculating relationship between incident and reflected wave curvatures

09 p1433 A71-22855

Compressible laminar boundary layer flow including second order longitudinal surface curvature effects, deriving flow equations from Navier-Stokes equations

11 p1750 A71-25473

Constant space curvature perturbations, considering density, rotational and propagation of gravitational waves with Lipschitz method

13 p2137 A71-28479

Test particle uniform acceleration motion in curved space-time, requiring torsion free and constant curvature particle world line

14 p2274 A71-29575

Curvature effects on shallow shell free vibration frequencies, solving linear eigenvalue problem

14 p2325 A71-30062

Curved porous wall channels for noise suppression in power plants, ventilation systems, etc

15 p2449 A71-31705

Classification of curvature tensor of relativistic Riemann space-time gravitational metric field

16 p2611 A71-33276

Elementary particle geometrical-group model assuming negative curvature de Sitter space inside and flat space outside

17 p2778 A71-34627

Curvature effect on cylindrical shell circumferential crack tip stress intensity, using fatigue crack growth tests

17 p2827 A71-35154

Conformal integrability for symplectic and cosymplectic structures, studying torsion and curvature tensor fields

18 p2976 A71-36126

Transverse curvature effect on singularity at separation for laminar boundary layer from analogy with flat-plate compressible boundary layer

19 p3044 A71-37726

Curvature effect on heat and mass transfer from isothermal sphere in potential flow

19 p3164 A71-37984

Strongly curved wall jets development in thin boundary layer upstream of blowing slot, discussing calculation method, correction for shear stresses and comparison with experimental results

24 p3819 A71-44952

Slit tube flat-to-circular transition during extension, considering mathematical model for curvature change, modulus of elasticity and Poisson ratio effects

24 p3884 A71-44959

CURVE FITTING

Straight line approximation of random two dimensional discrete set containing large measurement errors, comparing to least squares results

02 p0304 A71-11902

Exact formulas and graphs for RMS error in object position and velocity prediction for long time intervals based on least squares polynomial smoothing

12 p1881 A71-27425

Straight line approximation of random two dimensional discrete set containing large measurement errors, comparing to least squares results

13 p2133 A71-28189

Peak shifts evaluation errors in X ray stress analysis using diffractometer and three point parabola fitting method

14 p2260 A71-30479

Polynomial fitting for information compression of Wild BC-4 satellite photographs, comparing short arc with geometric compensation methods

16 p2581 A71-34041

Dynamic system impulse response model for goodness of fit and linearity hypothesis tests by computer simulation

17 p2722 A71-35181

Book on fitting equations to data by computer analysis of multifactor data for scientists and engineers, covering independent variables selection and least squares method

21 p3406 A71-40166

CURVED BEAMS

Thin rod deformation by gyrostat motion analysis, deriving anisotropic curved rods equilibrium shapes

03 p0458 A71-13600

Elastic straightening of slightly curved shell and significantly curved beam, considering prestressed structural stiffness

04 p0672 A71-15771

Curved beams bending stress concentration approximate equations for elliptical, circular and rectangular cross sections, providing behavior prediction superior to exact methods

08 p1373 A71-21749

Curved beams deformation with open thin walled cross section, using equilibrium and energy methods

11 p1848 A71-25579

Free radial vibrations of curved beams by finite element method, using model to investigate variation with subtended angle of six lowest natural frequencies

21 p3462 A71-40529

Curved sandwich beams free flexural vibration by finite element method, noting parameters effects on natural frequencies

21 p3462 A71-40533

Flexural vibration of transversely isotropic composite material curved beams, deriving curvature effects on natural frequency

24 p3878 A71-44616

CURVED PANELS

Circular shallow cylindrical panel stability and creep buckling under hydrostatic pressure

01 p0171 A71-10649

Singly curved rectangular plate free vibration characteristics obtained by partial differential equations of motion

05 p0825 A71-16605

Cylindrical shell panels with free supported curved edges and arbitrary boundary conditions, investigating natural frequencies and mode shapes

07 p1213 A71-19886

Natural frequencies approximation for vibration modes of stiffened and singly curved panel structures

08 p1369 A71-20810

Initially curved thin elastic plates, predicting large deflection and postbuckling behavior with finite element procedure

11 p1844 A71-25336

Locating neutral layer and critical curvature radius in aircraft components waffle panels under elastoplastic bending

13 p2074 A71-28940

Thin shallow initially curved sheets fracture theory, extending Griffith analysis

14 p2322 A71-29738

In-plane boundary effects on buckling and critical stress of axially loaded cylindrical panels

14 p2331 A71-30697

Structural and inertial nonlinearities influence on flat or curved panel flutter

14 p2331 A71-30825

Eccentrically stiffened thin cylindrical panels instability under uniform axial compression, uniform hoop compression and uniform shear

16 p2661 A71-34150

Long laminar plate and cylindrical panels with hinged lateral edges under buckling by normal uniformly distributed load, calculating deflection as monotonic pressure functions

17 p2823 A71-34781

German monograph on plane, arbitrarily curved and bending resistant trusses calculations allowing for elastic and plastic deformation

17 p2823 A71-34800

Static characteristics and free vibration of doubly curved honeycomb sandwich plates, using finite element method

21 p3462 A71-40534

Edge supported cylindrically curved panels flutter, investigating in-plane boundary conditions and geometry effects on natural frequency
22 p3616 A71-42216

CURVED SURFACES

U CONTOURS
U SHAPES
U SURFACES

CURVES

Supersonic flight path curvature effects on local shock wave production, considering no boom zone and ground rules
11 p1708 A71-26310

CURVES [GEOMETRY]

NT S CURVES

Transition curve equation for end cross section of slant-toothed wheel cut by rack type instrument with protuberance and rounded edge
07 p1117 A71-19360

Rigid body motion implicit representation in curved finite elements
07 p1214 A71-19910

Transient matrix heat transfer test data reduction, discussing direct curve matching methods implementation by distance function minimization
17 p2835 A71-34178

One and two dimensional function values calculation for curve systems by continued fraction interpolation from point grids, using computer program
22 p3518 A71-42394

Computerized screen construction for surfaces with net characterized by singularity-free and curve-edges properties
22 p3518 A71-42395

CUSPS

OGO 5 polar cusp observations showing dayside magnetosheath plasma penetration during magnetic storm
23 p3668 A71-43162

CUT-OFF

Directional cosmic ray cut-off and loop-convex folding distribution at geomagnetic midlatitude sites
01 p0146 A71-11485

Cosmic rays cutoff daily variations at ATS geostationary satellite altitude, noting role of magnetospheric tail in lowering cutoff below calculated value
20 p3282 A71-39739

Approximate calculation of cut-off frequencies of H- and Pi-section waveguides using corrugated plane surface theory
23 p3655 A71-44323

CUT-OUTS

U OPENINGS

CUTANEOUS PERCEPTION

U TOUCH

CUTTERS

NT BLADES [CUTTERS]

NT DRILLS

Ni and Ti cutting, examining wear for various microcutter refractory materials
05 p0759 A71-16862

High melting compound tools wear resistance during Ti and Ni continuous microcutting
08 p1297 A71-21065

Plasma flame temperature and flow characteristics in plasma jet transfer-type metal cutters from spectroscopic measurement and high speed streak camera photography
09 p1454 A71-23032

CUTTING

NT BLANKING [CUTTING]

NT METAL CUTTING

NT MILLING [MACHINING]

NT SLICING

NT SPARK MACHINING

Lasers applications to materials working including welding, cutting, machining, etc
06 p0908 A71-18069

Flow velocity field in main plastic deformation zone during orthogonal cutting from continuity equation
15 p2415 A71-31986

Ion machining techniques for cutting accurate and repeatable pumping grooves in gas bearing component materials typified by boron carbide
22 p3551 A71-41665

CV-2 AIRCRAFT

U DHC 4 AIRCRAFT

CW RADAR

U CONTINUOUS WAVE RADAR

CYANIDES

NT CYANOGEN

NT HYDROGEN CYANIDES

NT IRON CYANIDES

N stars Y CVn, RY Dra and 19 Psc IR synthetic cyanide radical spectrum analysis, determining C 12/C 13 ratio
18 p2969 A71-37044

CN radical red system molecular constants, considering degenerate perturbation effects in shifts between electronic states
19 p3106 A71-37405

Millimeter emission lines from interstellar methyl cyanide transitions, noting kinetic temperature and hydrogen density
21 p3447 A71-40446

CYANOGEN

Shock tube investigation of cyanogen and CN molecule dissociation at high temperatures, considering kinetics of CN decomposition
16 p2538 A71-32891

Chemical-ionization induced by cyanogen in stoichiometric atmospheric pressure carbon monoxide-oxygen-nitrogen flames
19 p3013 A71-38089

Carbon monoxide laser emission from helium-air-cyanogen mixture
21 p3393 A71-41043

CYANOPHYTA

U BLUE GREEN ALGAE

CYANOSIS

Myocardial blood flow and oxidative metabolism in cyanotic congenital heart disease patients, using lactate/pyruvate ratios and coronary sinus catheterization
22 p3484 A71-41521

CYANURATES

Modified low density polyisocyanurate foams for low heating rate thermal protection, considering high char yield with reduced surface recession
13 p2091 A71-28178

CYBERNETICS

Biocybernetic model of vestibular control system for spatial orientation, considering semicircular canals fluid motion angular velocity sensors and linear displacement perception
03 p0367 A71-12982

Biological and medical cybernetics approach to closed systems construction for continuous automatic monitoring and control of human physiological processes under harmful conditions
03 p0368 A71-13000

Biological heuristic programming in cybernetics, discussing solid state logic elements limiting factors in modeling
03 p0383 A71-14394

Complex human memory processes large scale simulation /cybernetic modeling/ based on information handling probability and retrieval
07 p1050 A71-20105

Human operator psychophysiological characteristics as cybernetic man machine system components, emphasizing human memory activity
07 p1050 A71-20117

Soviet papers on cybernetics problems covering control and communication for information handling machines and biological nervous systems
10 p1585 A71-24155

Nervous system modeling, considering cybernetic brain functions, neuroheuristic programming and modes of distributed information processing pertinent to neuropsychological experiments
10 p1568 A71-24222

Discrete control input system oscillations, resembling eye pupil diameter changes, hand tremors and aiming fluctuations during rifle sighting experiments
11 p1723 A71-25166

Automaton concept in cybernetics, emphasizing synchronous switching circuit operation with asynchronous input data
12 p1884 A71-27045

Soviet papers on biological and medical cybernetics covering control principles in living organisms, heuristic programming, higher nervous activity models, learning problems, etc
17 p2691 A71-35164

Hot wire and tubes nondestructive eddy current testing as cybernetic process, noting high speeds with high on-line data flow
17 p2749 A71-35494

Extraterrestrial civilizations, discussing cybernetic approach and development of languages for interstellar communications
19 p3134 A71-37521

Cybernetics and automatic control of space systems with pursuit process, using trajectory approximation with mathematical model graphs
21 p3452 A71-40857

CYCLES

NT ACTIVITY CYCLES [BIOLOGY]

NT BRAYTON CYCLE

NT CARNOT CYCLE

NT RANKINE CYCLE

NT SOLAR CYCLES

NT STRESS CYCLES

NT SUNSPOT CYCLE

NT THERMODYNAMIC CYCLES

NT WORK-REST CYCLE

Linear feedback function for r-stage feedback shift register resulting in equal length branchless cycles [JPL-TR-32-1511]
03 p0388 A71-13282

Damped vibrations logarithmic decrement determination during automatic recording of number of cycles, emphasizing error analysis
09 p1443 A71-22630

Cyclic and multiresidue AN codes, determining single error correcting range
09 p1412 A71-23103

CYCLIC ACCELERATORS

NT BETATONS

NT SYNCHROTRONS

CYCLIC HYDROCARBONS

NT ANTHRACENE

NT CYCLOBUTANE

NT CYCLOPROPANE

NT NAPHTHENE

Ionization potentials of cyclobutadiene, using photoelectron spectrum measurement
03 p0377 A71-14373

Organic compounds oxidation inhibition by polycyclic aromatic hydrocarbons, analyzing peroxide radicals charge transfer complex stability
05 p0716 A71-16382

Esters synthesis from cyclic trimethylolpropane butyral and monobasic saturated acids mixtures
15 p2438 A71-31679

CYCLIC LOADS

Cyclic fatigue and corrosion test equipment for elastoplastic materials at various temperatures and pressures
01 p0165 A71-10042

Metal fatigue relationship to cyclic plastic deformation resistance, considering fracture behavior, stress-strain curve, hardening and ductility
01 p0098 A71-10162

Notched metal crack initiation, determining high cyclic loads effects by prior local plastic behavior at stress concentration
01 p0166 A71-10163

Ductile Ni deformation and fracture, examining simultaneous cyclic and monotonic strain effects
01 p0098 A71-10164

Fiber reinforced plastics fatigue strength investigation by cyclic tension-compression, bending and torsion tests, noting matrix-fiber interface shear stress capacity
01 p0108 A71-10693

Critical static strength of Duralumin under cyclic impact loads, analyzing statistically load distribution function applicability
01 p0103 A71-11240

Al fatigue testing by cyclic uniaxial tensile load, examining deformation, internal friction ductility and plastic strain
02 p0262 A71-11683

Turbine disks under unsteady and cyclic loads and temperature variations, determining stress and strain by flow theory computer calculation
02 p0323 A71-11745

Turbine disks cyclic nonisothermal deformation with allowance for Bauschinger effect, determining stress-strain state and residual microstresses
02 p0323 A71-11747

Structural design for component low cycle fatigue resistance, emphasizing material cyclic stress-strain behavior
03 p0501 A71-13252

Transverse oscillations determination in cyclically deformed thin plate under plane stress by energy dissipation calculation using Hooke law
03 p0502 A71-13401

Test equipment with axial mode closed loop machine for cyclic deformation and fatigue in pure bending [SESA PAPER 1726]
03 p0507 A71-13756

Heat treated low carbon steel fatigue tests at low cycle tension compression loads, determining durability relationships to load and total work to fracture
04 p0666 A71-14878

High strength steel butt welds surface geometry effect on fatigue durability under cyclic loads, using photoelastic analysis
04 p0602 A71-14881

Metallic components strain localization and concentration factors under high pressures or temperatures involving plastic strain, noting static and cyclic load effects
04 p0666 A71-14882

Central hole effect on flat metal sheet fatigue under tension-compression load cycles, noting application to aircraft materials
04 p0670 A71-15389

Metal endurance dependence on simultaneous oxygen corrosion and cyclic loading frequency at various temperatures and pressures
06 p1000 A71-17934

Geometries and technical specifications deviations effects on service life and fatigue characteristics of thin walled structural components under cyclic loads
06 p1005 A71-18710

Refractory alloys elastoplastic deformation under cyclic loading, deriving thermal fatigue equations
07 p1129 A71-19155

Large inhomogeneous bodies of revolution three dimensional strain state under symmetrical cyclic loads
07 p1210 A71-19159

High and low cycle fatigue crack growth rate in various materials under variable loads
07 p1211 A71-19193

Steel under cyclic loads, observing relationship between changes in microstructure and temperature curve shape in fatigue failure process
07 p1211 A71-19194

Minimum squeeze film thickness in journal bearing under reversed periodic loading of double loop form [ASME PAPER 70-LUB-12] 07 p1117 A71-19505

Austenitic stainless steel dislocation structures during fatigue deformation under cyclic loading, observing slip lines and lattice strain morphology 07 p1136 A71-19699

Cyclic thermal cracking and fatigue analysis in large steam turbine rotors with three dimensional temperature and triaxial stress computation [ASME PAPER 70-PWR-1] 07 p1216 A71-20198

Energy dissipation in heat resistant Ni steels under cyclic tension and compression at room temperature 07 p1142 A71-20479

Cyclic creep and relaxation of heat resistant alloys at high temperatures, showing inapplicability of static load conditions 07 p1142 A71-20480

Deformation amplitude effects on dislocation structure and strengthening mechanism of fcc aluminum under cyclic loading 07 p1142 A71-20482

Electronic recording of cyclic strain diagrams of metals in wide loading frequency range using dynamic hysteresis method 07 p1218 A71-20485

Creep strain effect on cyclic fatigue life of duralumin at room temperature 07 p1143 A71-20486

Low carbon steel welds, investigating low cycle deformation and rupture resistance as function of weld zones 08 p1316 A71-21609

Refractory materials at normal and high temperatures, describing cyclic shear test methods 08 p1372 A71-21612

Inertia effect in failure mechanics for steadily developing equilibrium cracks in dynamic system with time dependent periodically variable load 08 p1372 A71-21705

Electromagnetic testing machine for torsion fatigue characteristics under steady and programmed cyclic loading conditions 09 p1426 A71-22498

Tensile-compressive testing apparatus for low cycle load at high temperatures 09 p1426 A71-22499

Low-cycle fatigue curve determination for plane elastoplastic bending with flexible loading, deriving rated fatigue life 09 p1536 A71-22502

Fatigue crack formation and growth rate relationship, examining variance in cycle number in formation to final failure 09 p1536 A71-22507

Metal sheet failure kinetics, investigating tensile stress and cycle frequency during fatigue crack growth and extension rate effects 09 p1468 A71-22508

Measuring apparatus for cyclic plastic strains at high temperatures, discussing data processing techniques 09 p1443 A71-22636

Relaxation analysis of strain range, hold time and cycle number in low cycle fatigue testing of annealed stainless steel at 1200 F [ASM PAPER W71-24.1] 09 p1471 A71-23093

Structural design for low cycle fatigue resistance, considering cyclic stress-strain properties, critical strain and overloads [ASM PAPER W71-22.3] 09 p1541 A71-23097

Macroscopic and microscopic plastic zones ahead of propagating fatigue crack on surface and inside of specimen as function of load cycles 10 p1626 A71-24306

Annealed and cold-worked polycrystalline Fe specimens steady state cyclic stress-strain curves and thin films observation by electron microscopy 11 p1780 A71-26024

Plastic deformation and aging effects on fatigue characteristics of steels until rupture under cyclic loads 12 p1916 A71-26945

Stress cycling effect on creep deformation rate, using recovery creep model [ASME PAPER 71-MET-F] 12 p1977 A71-27315

Heat generation in hinged orthotropic viscoelastic cylindrical shells under transverse vibrations and cyclic surface load 12 p1978 A71-27343

Plastic conical shell with variable thickness, calculating load carrying capacity under cyclic mechanical and thermal loads 12 p1979 A71-27353

Cyclic loading failure criteria based on deformation energy concepts 12 p1984 A71-27679

Deformation fatigue theory extended to tests at stresses below elastic limit, explaining cyclic loading frequency effect on fatigue life 12 p1984 A71-27681

Fatigue crack growth rate in plates of anisotropic materials, considering Al and Ti alloys under cyclic loads 13 p2082 A71-27826

Failure analysis of plastic materials susceptible to cyclic strain hardening under thermal load 13 p2148 A71-28114

Refractory and structural steels and Al alloys, obtaining low cyclic plastic deformation and breaking stress curves 13 p2148 A71-28116

Low cyclic failure resistance at elevated temperatures and static defects calculation, based on fatigue and empirical endurance curves 13 p2149 A71-28122

Distributed inertial forces due to cyclic loading in minimum volume beams cross sectional stress calculations 13 p2154 A71-28643

Energy dissipation measurement in materials during cyclic fatigue testing by dynamic hysteresis loop method 14 p2238 A71-29619

Cyclic strain effects on creep for steel at elevated temperatures, discussing overload frequency effects on plastic strain buildup 14 p2256 A71-29626

Low cycle fatigue strength of high speed rotating aluminum and brass disks, comparing with uniaxial push-pull fatigue test 14 p2328 A71-30418

Fretting fatigue test apparatus with load monitoring as function of cycles for relating quantitatively damage to life 14 p2248 A71-30883

Titanium alloy durability under cyclic torsion in vacuum at various temperatures, investigating fatigue life and tensile strength 15 p2428 A71-31856

Extremum principle for structures in creep under cyclic loading for time dependent stable dissipative material 15 p2505 A71-31944

Creep deformation during intermittent loading, obtaining strain rate as function of applied stress and stress cycle time 15 p2508 A71-32254

Plastic strain range-fatigue life behavior as two slope relationship, considering low cycle fatigue laws in terms of crack propagation mode change 15 p2436 A71-32508

Structural instability due to cyclic strain accumulation, using plastic deformation constitutive relation with stress tensor and elastic effects 16 p2650 A71-33016

Finite element method application to stress distribution analysis at crack tip of rectangular plate under tension, obtaining elastoplastic response to cyclic loading 16 p2653 A71-33086

Stress, slip and damping of clamped elastic plate with finite friction under alternating axial load, using finite element method 16 p2581 A71-33174

Program parameters effects on fatigue life of turbine blade heat resistant alloys at high temperatures under cyclic loading 16 p2592 A71-33407

Crack propagation resistance-cyclic fracture strength relation for austenitic and Mn-Cr-V steels, considering thermomechanical working effects 16 p2592 A71-33408

Recrystallized and unrecrystallized deformed semifinished Al base alloy under cyclic and static loads, investigating macrofracture kinetics 16 p2594 A71-33713

Thermostable and heat resistant steels and alloys vibration loading frequency effects on fatigue at high temperatures 16 p2598 A71-33992

Computer controlled durability and low cycle fatigue testing, using digital random sequencing technique 17 p2821 A71-34555

Fatigue strength anisotropy in glass fiber materials with epoxy-phenol binders under symmetric and pulsed compression-tension cyclic loads 17 p2762 A71-34783

Transverse oscillations determination in cyclically deformed thin plate under plane stress by energy dissipation calculation using Hookes law 17 p2825 A71-35012

Metal fatigue crack failure prediction for arbitrary uniaxial cyclic loading, discussing method based on treatment of crack growth as continuous stochastic process 17 p2758 A71-35158

Al alloy sheet fatigue crack closure under cyclic tensile loading, deriving expression for crack propagation rate in terms of effective stress amplitude 17 p2828 A71-35162

Aircraft structural panels under cyclic static loads, examining fatigue life with probability theory, statistics and regression analysis 17 p2829 A71-35312

Refractory alloys elastoplastic deformation under cyclic loading, deriving thermal fatigue equations 17 p2760 A71-35653

Cyclic torsional shear testing of refractory materials at normal and high temperatures, describing test equipment 17 p2834 A71-35677

Cr-Ni austenitic steels thermomechanical destabilization using cyclic strain hardening 18 p2934 A71-36177

Total inelastic energy dissipation in structure or creeping plastic material under variable repeated loading and shakedown [ASME PAPER 71-APM-C] 18 p2977 A71-36253

Cyclic bending stress distribution in fir tree turbine blade root for arbitrary loading phase 18 p2980 A71-36707

Deformation kinetics and failure of high melting Ni and Mo base alloys in plastic state under low cyclic fatigue 18 p2936 A71-36710

Nb and Nb-Zr alloy tubular and sheet samples cyclic loading tests, determining heat treatment effects on notch sensitivity and fatigue strength 18 p2937 A71-36720

Two-mirror optical system to study energy dissipation in elastic systems subjected to cyclic straining 18 p2924 A71-36722

Ni-base heat resistant alloys loading frequency effect on fatigue resistance, noting linear relationship between creep strain and cycles to failure in logarithmic coordinates 19 p3082 A71-38348

Al-Zn-Mg alloy welded joints under repeated static loads, determining shape, filler wire composition and aging effects on fatigue strength 19 p3083 A71-38425

Computer-aided study of journal bearing performance under cyclic loads, determining bearing loads for circular, linear and elliptical orbits of journal center [ASME PAPER 71-VIBR-87] 21 p3386 A71-40323

Mechanical properties of various polymeric solids under compressive loading cycles of 100 microsec duration and under steady state compressive loads 21 p3406 A71-41427

Thick Al alloy sheet with central slot under cyclic loads, examining striation spacings and fatigue crack propagation rates with electron fractography 22 p3561 A71-41708

Hold time effects on plastic deformation and fracture in high temperature low cycle metal fatigue 22 p3561 A71-41942

Silicon resistance strain gages sensitivity as function of variable signed load cycles 22 p3550 A71-42880

Asymmetrical metal fatigue cracks development under infrequent compression cycles alternating with fundamental cycles of tension 23 p3774 A71-42896

Loading cycles dependence of energy dissipation and plastic deformation during fatigue tests, using Fourier series 23 p3774 A71-42897

Load stress pulse shape and frequency effects on macroscopic dislocations during plastic deformation of crystalline materials 23 p3777 A71-43875

Radiation dose effects on polymer strain magnitude under critical cyclic loading 23 p3697 A71-44033

Dynamic model for microinhomogeneous elastoplastic medium under cyclic loads with varying amplitude 23 p3779 A71-44203

Fatigue test equipment for 293-233 K and 50-100 ton static or 25-50 ton cyclic loads, using Freon 22 as coolant 23 p3661 A71-44234

High cycle fatigue resistance improvement of age hardened Al-Zn-Mg-Cu alloys through thermomechanical treatments 23 p3695 A71-44290

Nonhomogeneous plate under pulsating and uniformly distributed loads, considering dynamic elasticity problem 24 p3880 A71-44712

Cyclic symmetrical deformation of thin elastic conical shells of revolution of variable thickness with meridional ribs under physical and thermal loads 24 p3882 A71-44843

Stress wave propagation in rod consisting of viscoelastic finite and semiinfinite elastic parts during pulsed sinusoidal load at end 24 p3885 A71-45223

CYCLING
U CYCLES
CYCLOBUTANE
IR and Raman vibrational spectra and structure of tetrafluorocyclobutane 17 p2695 A71-35520

CYCLOHEXANE
Remote group interactions after electron impact in 4-substituted cyclohexanones, investigating mass spectrometry in structural and stereochemical problems 02 p0209 A71-12548

Toluene and aniline-methylcyclohexane and toluene-aniline nonideal liquid systems, measuring molecular diffusion coefficients as function of concentration by Savart plate birefringent interferometer 24 p3820 A71-45074

CYCLONES
NT HURRICANES
 Tropical storms and cyclones development numerical simulation with ten-level model, considering radiational cooling and physical parameters effects 03 p0453 A71-14202
 Nongeostrophic wind behavior in free atmosphere during cyclogenesis, noting maximum development during cyclone lifetime middle stage 15 p2400 A71-31969
 Spring and autumn cyclonic circulation in stratosphere and mesosphere up to 95 km, using ionospheric radiosonde and rocket data 17 p2730 A71-34301
 Earth atmosphere wind field motion calculation from displacement of longitudinally elongated cyclones 20 p3277 A71-38736

CYCLOPROPANE
 Shock tube isomerization of cyclopropane to propylene as model system for small ring compounds, noting rate constants 19 p3010 A71-37272

CYCLOTETRAMETHYLENE TETRANITRAMINE
U HMX
CYCLOTRON FREQUENCY
 Electron cyclotron drift instability shown by numerical simulation as cause for anomalous plasma diffusion and heating 01 p0132 A71-10147
 Magnetospheric VLF electric field emissions above electron cyclotron frequency from OGO 5 observation at magnetic equator 01 p0076 A71-11500
 Nonuniform magnetic field cyclotron heating, presenting stochastic criteria in terms of Larmor rotation phase randomization 03 p0462 A71-13928
 Proton whistlers damping compared to predictions by cyclotron damping theory, discussing proton density 06 p0949 A71-17262
 Plasma frequency resonance time duration-local electron cyclotron frequency relationship by oblique echo model 07 p1168 A71-19681
 Cyclotron wave rectifier for S band and X band microwave conversion to DC or LF AC power 07 p1080 A71-20451
 Efficiency deterioration of M type backward wave oscillators /M-BWO/ from cyclotron wave interactions 07 p1080 A71-20453
 Cyclotron instability of high energy protons in magnetosphere with refraction of growing Alfvén waves 09 p1435 A71-22437
 Bounce effects in negative mass instability of plasma in short mirror magnetic bottle with ion cyclotron frequency dispersion 10 p1652 A71-24652
 Short wave ion-cyclotron plasma oscillations excitation by electrons drifting in magnetic field for wavelength much less than ion Larmor radius 12 p1936 A71-27033
 Magnetic field effect on emission spectrum and intensity at electron cyclotron frequency harmonics from PIG Reflex discharge, discussing electron oscillations excitation in plasma 12 p1938 A71-27214
 Resonant plasma heating at electron cyclotron frequency second harmonic, studying interactions with microwave electromagnetic radiation in adiabatic trap 15 p2455 A71-31736
 Radio wave propagation in ionosphere, measuring plasma frequency, cyclotron cut-off and noise level 15 p2373 A71-32443
 Linear and nonlinear whistler mode cyclotron instability, discussing VLF emissions generation mechanism in magnetosphere 16 p2615 A71-32803
 Anisotropy instabilities of hydromagnetic wave propagation at small angle perpendicular to magnetic field above ion cyclotron frequency, calculating dispersion relation 17 p2788 A71-34664
 Finite beta microinstabilities inherent in magnetic mirror confined plasmas, considering wave propagation across magnetic field at multiples of ion cyclotron frequency 18 p2950 A71-35861
 Plasma drift cyclotron instability feedback stabilization, using immersed modulated electron sources 19 p3111 A71-37636
 Electromagnetic radiation from beam-plasma system in strong magnetic field, noting maximum microwave emission near electron cyclotron frequency 19 p3116 A71-38252

Magnetic field effect on emission spectrum and intensity at electron cyclotron frequency harmonics from PIG Reflex discharge, discussing electron oscillations excitation in plasma 19 p3117 A71-38626
 Plasma ordinary wave mode electromagnetic cyclotron instability, discussing Dory-Guest-Harris type loss cone distributions 21 p3421 A71-40627
 Microwave plasma generation in magnetic field, detecting expansion related to electron cyclotron frequency harmonics 21 p3426 A71-41287
 Dense plasma heating by electron beam in magnetic trap as function of cyclotron frequency and field strength, noting strong microwave emission 22 p3583 A71-42064
 Magnetic drift waves near proton cyclotron frequency, noting magnetic field gradient role in plasma instability 23 p3709 A71-43181

CYCLOTRON RADIATION
 Radiation frequency control in cyclotron resonance maser via TEM wavelength oscillations in Fabry-Perot resonator produced by screw electron beam 01 p0095 A71-11212
 Stationary waves produced by earth bow shock, calculating cyclotron radiation amplitude and polarization characteristics by thin current sheet model 01 p0075 A71-11490
 Cyclotron radiation emission and absorption in nonequilibrium plasma, deriving radiative transfer equation 03 p0465 A71-14268
 Rotating electron beam cyclotron and space charge waves interaction with fast electromagnetic waves 05 p0719 A71-16002
 Plasma electron cyclotron heating, observing wave excitation at 100 MHz and decay after initial wave 06 p0930 A71-17396
 Nonlinear Landau damping of circularly polarized electromagnetic cyclotron waves, calculating interaction matrix for particular electron velocity distribution functions 10 p1652 A71-24656
 Charged particles magnetic scattering on cyclotron instability waves of radiation belt plasma, estimating proton relaxation time 13 p2129 A71-28552
 Geomagnetic Pc-1 type micropulsations appearance and development due to proton belt cyclotron instability 14 p2301 A71-30350
 Ion cyclotron harmonic waves development in simulated low density and temperature space plasma, determining propagation upper and lower bounds 15 p2491 A71-32448
 Plasma cyclotron wave excitation with charged particle beam, determining unstable oscillations frequency range and spatial and time development with nonlinear analysis 19 p3111 A71-37633
 Large amplitude monochromatic electron cyclotron wave broadening in plasma, producing shifted phases in finite frequency range 19 p3114 A71-37855
 Spatial dispersion effect on circular polarized cyclotron radiation spontaneous emission coefficient in nonequilibrium plasma 22 p3583 A71-42326
 Rotating electron beam cyclotron and space charge waves interaction with fast electromagnetic waves 22 p3515 A71-42751
 Cyclotron magnetoacoustic wave generation by planets and binary stars in circular orbits, deriving interstellar gas density variations 24 p3869 A71-44804

CYCLOTRON RESONANCE
 Radiation frequency control in cyclotron resonance maser via TEM wavelength oscillations in Fabry-Perot resonator produced by screw electron beam 01 p0095 A71-11212
 Hot electron plasma confinement in cusped magnetic field, considering production in electron cyclotron resonance region by pulsed microwaves 06 p0935 A71-17491
 Fine structure of geomagnetic Pc 1 micropulsations by cyclotron instability due to anisotropic energetic proton velocity 06 p0895 A71-18283
 Ion-molecule collision charge transfer and momentum transfer relaxation rates, using ion cyclotron resonance heterodyning method 07 p1054 A71-19371
 Ion cyclotron resonance application to propanol ion structure formed in double McLafferty rearrangement, demonstrating direct enol ion formation instead of by isomerization or ketonization 07 p1055 A71-19598
 Plasma heated by cyclotron resonance using waveguide method, considering properties, confinement conditions and instabilities 07 p1170 A71-20182

Observation range determination numerically for cyclotron resonances of effective scattering cross section of light wave by collisionless plasma in magnetic field 10 p1646 A71-23848
 Cold Hg plasma in composite HF and magnetostatic field near electron cyclotron resonance, obtaining electron and ion energy spectra 10 p1650 A71-24527
 Negative ions photodetachment by continuously tunable laser and ion cyclotron resonance spectrometer 11 p1772 A71-25371
 Ionospheric VLF and ELF wave observations, noting ion cyclotron resonance and harmonics effects on propagation 14 p2202 A71-30946
 Large signal saturation effects in cyclotron resonance oscillators, using helical electron beam-cavity interaction model 16 p2545 A71-33394
 Relativistic electron precipitation during magnetic storms, showing cyclotron resonances with electromagnetic ion cyclotron waves 16 p2629 A71-33948
 Centimeter TEM waves excitation in Fabry-Perot cavity of cyclotron resonance maser by helical electron beam 17 p2750 A71-34263
 Ion cyclotron resonance power absorption theory application to reactive and nonreactive ions line shapes, using Wobshall-Graham-Malone phenomenological equation of motion 17 p2695 A71-34947
 Ion cyclotron resonance spectroscopy, discussing fundamentals, instrumentation and ion-molecule chemistry applications 17 p2695 A71-35522
 Swept Langmuir probe with sweep speeds greater than 150 V/microsec, considering electron cyclotron resonance heated hydrogen plasma confined in toroidal quadrupole 18 p2952 A71-36582
 Cyclotron resonance energization of trapped electrons in magnetosphere from plasma pseudopotential shape calculation, noting geophysical effect 19 p3117 A71-38724
 Ion cyclotron resonance power absorption, deriving expression for average ion kinetic energy at saturation in steady state limit 21 p3418 A71-40231
 Cyclotron absorption and resonance spectra of hot electrons in p-type InSb samples cut from single crystals containing different amounts of impurities 21 p3430 A71-41226
 Cyclotron resonance measurement for holes in uniaxially compressed Si, determining pressure and temperature effects on relative half width of hole line by relaxation time 21 p3433 A71-41309
 Semiconductors submillimeter and far IR reflection spectra and cyclotron resonance measurements 22 p3586 A71-42140
 Electron periodic energization by magnetospheric RF wave propagation, examining cyclotron resonant interaction 23 p3644 A71-43321

CYCLOTRONS
 Trapping of neutrals from fast atom beam impinging on molecular hydrogen influx fed electron-cyclotron plasma target 21 p3422 A71-40761

CYGNUS CONSTELLATION
 Spectral temporal variations and atmosphere conditions of P Cygnus, including atomic hydrogen densities, electron concentrations, microturbulent velocity and Balmer decrement 07 p1204 A71-20631
 Intensity variations of Cygnus X ray sources, analyzing high resolution results of Adelaide and Tasmania universities 10 p1661 A71-23882
 Cygnus A two component radio source scintillations power spectrum observation by dipole array 10 p1678 A71-24804
 Cygnus X-1 and X-2 X ray source location from Uhuru satellite measurements 11 p1814 A71-25213
 X ray pulsations from Cygnus X-1 observed from Uhuru satellite, suggesting exstar discovery 13 p2120 A71-28004
 Multiple periodicity of Cygnus X-1 X ray emission from rocket sounding 14 p2302 A71-30653
 Cygnus X-1 distance estimate based on low energy X ray spectrum obtained by sounding rocket 15 p2497 A71-32763
 Cygnus-X region radio photography, presenting radio brightness intensity modulated display supplementing contour map 16 p2630 A71-33124
 Cyg X-1 X ray intensity and energy spectrum variation data, using balloon-borne telescope 16 p2629 A71-34076

- Cyg X-1 X ray pulsar age determination and emission model speculations based on observation data for supernova remnant and radio counterpart absence explanation
18 p2962 A71-36151
- X ray source Cygnus X-1 location measurement by balloon, noting agreement with Uhuru data
18 p2959 A71-37052
- X ray source Cygnus X-1 position determination by Aerobee rocket-borne rotating modulation collimator
18 p2970 A71-37053
- Cygnus X-1 X ray data with temporal resolution, examining pulsations and flare activity
20 p3278 A71-39110
- Cygnus XR-1 X ray intensity fluctuations, discussing time scales and periodicities
20 p3278 A71-39111
- Hard X ray pulsations limits in higher energy range from Cyg X-1, comparing with Crab Nebula pulsar
20 p3279 A71-39407
- Negative search for radio pulsar near Cyg X-1 or associated variable radio source, using fast holding algorithm
20 p3292 A71-39408
- Photoelectric telescope observations of red stars in Cygnus at IR wavelength with threshold brightness detection
20 p3293 A71-39537
- Bright star at radio source and X ray observations evaluation from optical identification of Cygnus X-1, taking into account spectrum and energy distribution characteristics
21 p3447 A71-40444
- Cosmic soft X rays in energy range 0.14-7 keV from rocket soundings with thin polypropylene window proportional counters, covering field of view in Cygnus-Cassiopeia region
22 p3593 A71-42330
- Interstellar silicate absorption search using VI Cyg No 12 spectrum observations
22 p3605 A71-42349
- Cygnus X1 short term X ray flux pulsation variability from Southern Hemisphere sounding rocket flight
24 p3865 A71-44445
- ### CYLINDERS
- Steel cylinders with circumferential cracks under repeated impact tensile loads, investigating plain strain fracture toughness index temperature dependence
01 p0166 A71-10079
- Elastic field of cylindrical inclusion, using continuum dislocation theory
02 p0330 A71-12741
- Optimal relaxation time existence for Maxwell solid cylinder bonded to thin casing during forced vibration of rocket assembly, discussing Voigt solid
03 p0497 A71-13469
- Mean velocity profile measurements in turbulent wake behind single or parallel arbitrarily spaced and sized cylinders with adverse pressure gradient
[ASME PAPER 70-WA/FE-10] 03 p0403 A71-14131
- Fracture strength of helical wound glass-epoxy composite cylinder under axial tension, determining tensile strength
05 p0826 A71-16741
- Stiffened long cylinder with time variable thickness and strengthening thin shell system elastic displacements due to nonstationary vibrations and nonuniform pressure distribution
07 p1217 A71-20459
- Electric field equations of plane EM wave diffraction at lattice of conducting cylinders, using Hankel function
09 p1408 A71-23113
- Flow in vicinity of stagnation point of sphere and cylinder during pulsating motion in nonuniform stream
12 p1897 A71-27448
- Steel cylinders with circumferential cracks under repeated impact tensile loads, investigating plane strain fracture toughness index temperature dependence
16 p2658 A71-33635
- Laplace equation solution for double cylinder electrostatic lenses for large range voltage ratios and separations, obtaining focal and aberration coefficients
21 p3377 A71-40178
- Integral and pointwise estimates of insulated cylinder temperature field spatial decay for semilinear parabolic equations
21 p3473 A71-41186
- Slip, surface permeability and temperature gradient effects on surface friction and heat transfer in boundary layer near cylinder critical point
24 p3887 A71-44743
- ### CYLINDRICAL AFTERBODIES
- ### U AFTERBODIES
- ### U CYLINDRICAL BODIES
- ### CYLINDRICAL ANTENNAS
- Cylindrical electric dipole antenna in magnetoactive ionospheric plasma, noting ion sheath effect on input impedance and active length
02 p0212 A71-11873
- Electromagnetic wave propagation along conducting wire in magnetoplasma
03 p0381 A71-14472
- Polynomial current analysis of imperfectly conducting thin cylindrical dipoles with arbitrary internal impedance
04 p0558 A71-15144
- Input impedance of cylindrical and helical antennas in cold lossy magnetoplasma, discussing sensitivity to current distribution
07 p1065 A71-20323
- Cylindrical slot antennas radiation patterns in plane perpendicular to axis, discussing field emission and angular position of each slot for phase multiplier
09 p1415 A71-22458
- Axial slits circular array pattern in large conducting cylinders fed by waveguides
09 p1419 A71-23497
- Pulse excited finite length cylindrical monopole antenna mounted vertically on perfectly conducting ground plane, calculating near point electromagnetic fields
09 p1420 A71-23512
- Modal superpositions for mutual coupling on cylindrical array of waveguide elements
09 p1420 A71-23513
- Single- and two-turn cylindrical spiral antenna, calculating end reflection, current damping and in-phase excitation component effects of radiation characteristics distortion
11 p1741 A71-26553
- Electric and magnetic surface current coefficients of antenna radiating elements in metallic waveguides and resonators by harmonics expansion applied to circular-cylindrical array
12 p1885 A71-26839
- Isolated symmetrical cylindrical dipole antennas in homogeneous conducting media
12 p1880 A71-27153
- Heat transfer on cylindrical antenna in supersonic high temperature gas flow, noting electromagnetic wave damping due to ablation
13 p1990 A71-28296
- Aerospace antenna design, calculating one-wavelength circular slot aperture radiation from circular cylindrical surface
14 p2206 A71-31075
- Radiation pattern of linear radiator mounted at quarter-wavelength in front of cylindrical parabolic reflector, discussing calculation procedure based on half-wavelength dipole near field
15 p2369 A71-31415
- General media electrical properties from current and charge distributions and impedance characteristics of electrically thin cylindrical antennas
17 p2715 A71-34759
- Driving point admittances of resistive cylindrical dipole antennas by variational method using two term trial function for current
17 p2701 A71-34762
- Gravitational radiation antenna consisting of disk cylinder in radial mode of circular symmetry
19 p3104 A71-38190
- Singular integral equation theory application to design of cylindrical antennas with small length-to-radius ratio
19 p3035 A71-38597
- Book on antenna characteristics covering tabulated data for cylindrical dipoles and monopoles, imperfectly conducting dipoles, circular loop antennas and broadside and endfire arrays
20 p3196 A71-39200
- Iterative solution of Hallen integral equation for current distribution on lossless cylindrical transmitting dipole antenna
21 p3348 A71-40578
- Electric field induced current distribution on cylindrical antenna, considering delta generator and electromagnetic waves excitations
23 p3643 A71-43122
- Cylindrical antennas with arbitrary distributed resistive and reactive loading, presenting method based on dipole antennas with constant resistance loading per unit length
24 p3803 A71-44646
- ### CYLINDRICAL BODIES
- ### NT ROTATING CYLINDERS
- Secondary currents on conducting cylinder near dipole antenna manifested as radio frequency interference, considering effect on radiation pattern
01 p0037 A71-11167
- EM wave propagation along radially inhomogeneous dielectric cylinders, considering permittivity variation
01 p0037 A71-11170
- Unsteady axisymmetric temperature and stress distribution in multilayer cylinder in convective heat transfer with temperature-varying medium
02 p0322 A71-11729
- Cylindrical wall with variable heat conductivity coefficient, solving temperature distribution by asymptotic method
02 p0333 A71-12540
- Rectangular parallelepiped and solid cylinder temperature distributions under time dependent ambient heating or cooling, solving thermal conductivity equation
02 p0333 A71-12647
- Light scattering geometry from infinite cylinder shown consistent with Rayleigh-Gans formalism
03 p0425 A71-13647
- Continuous filament composite materials fabrication and tests for dynamic deformation, fracture and wave propagation properties, considering axially reinforced cylindrical body compression
03 p0508 A71-13768
- Cylindrical sample longitudinally isothermal zone unsteady temperature field calculation from heat conduction equation with allowance for temperature dependence of thermodynamic properties
03 p0520 A71-13960
- Unsteady flow about solid cylinder falling through viscous fluid in vertical tube, obtaining velocity profiles via solution of Navier-Stokes equation
[ASME PAPER 70-WA/FE-9] 03 p0403 A71-14130
- Two-member composite cylinders, predicting residual stress and axial loading behavior by elastoplastic analysis for comparison with experiment
04 p0666 A71-14893
- Supersonic compressible turbulent boundary layer on porous cylinder with air injected through wall, investigating heat transfer
04 p0571 A71-15498
- Thick walled noncircular cylinders shape showing full plasticization at collapse
04 p0673 A71-15885
- Cylindrical steel samples with screw type threads, comparing pressed and ground threads effects on tensile strength at low temperatures
05 p0827 A71-16763
- Dilatometric thermal expansion method for determining cylindrical solid body thermal conductivity coefficient
05 p0838 A71-16790
- Elastic deformation of strip, rectangular annulus and cylinder with homogeneous displacement boundary conditions, deriving orthogonality relations for expanded eigenvectors
05 p0828 A71-16993
- Blunt cylinder with small thread in anomalous seeded flow in hypersonic wind tunnels, observing separated shock wave distortion
07 p1013 A71-18924
- Potential flow past cylinder with sources and sinks singularities, deriving formulas for aerodynamic characteristics of infinite span wings with boundary layer control
08 p1227 A71-20777
- Electromagnetic wave scattering by perfectly conducting cylinder in anisotropic plasma with external magnetic field, deriving radiation pattern from asymptotic expression
08 p1253 A71-21295
- Electromagnetic wave diffraction by variable curvature and surface impedance cylindrical structure
08 p1254 A71-21356
- Cylindrical steel specimens bearing strength under cyclic elastoplastic deformation, investigating stress redistribution effects
08 p1316 A71-21607
- Real time and double exposure holographic interferometry measurements of strain on aluminum cylinder under internal pressure, noting discrepancy with strain gage values
09 p1444 A71-22711
- Cylindrical body stability under axial compression with small elongations and shears, determining critical buckling force
09 p1542 A71-23437
- Variational formula for input impedance of thin axisymmetrical cylindrical dipole antenna
09 p1408 A71-23490
- Asymptotic expression for mutual admittance between axial rectangular slots on large conducting cylinder
09 p1419 A71-23507
- Backscatter from nonuniform dielectric coated cylinders in terms of inner surface admittance, using transmission line approach
09 p1410 A71-23515
- Cylindrical spacecraft reentry body self-sustained pitching oscillations due to separation on downstream portion, examining stability derivatives
09 p1533 A71-23604
- Radiation patterns of radar antennas with single near field cylindrical obstructions, considering directional S band antenna
09 p1420 A71-23678
- Cylinder roller bearing for heavy axial and radial loads, determining carrying capacity by sliding surfaces
10 p1617 A71-24683
- German monograph on steady toroidal discharges and cylindrical vortex arcs, using electromagnetic gas dynamics equations
10 p1654 A71-25025
- Plastic spherical shell containing cylindrical section under Tresca yield conditions, obtaining upper critical load limits
11 p1850 A71-25943
- Refraction correction in photometer with cylindrical light scattering cell and detectors, describing experi-

mental testing by mathematical and geometrical analysis

11 p1799 A71-26063

Nondestructive magnetic method for measuring longitudinal residual stress in outer portions of ferromagnetic cylindrical bars

12 p1974 A71-26948

Uniform asymptotic diffraction of plane wave from ideally reflecting cylinder, using parabolic equation method

13 p2027 A71-27900

Steady state scattering of cylindrical magnetoacoustic waves traveling along axis of rigid ideally conducting static cylinder

13 p2105 A71-28281

Motion equation of electron in cylindrical diode subjected to varied voltages

13 p2036 A71-28372

Flow direction effect on combined forced and free convective heat transfer from cylinders to air

13 p2164 A71-28985

Forced and free convective equations combination to represent combined heat transfer coefficients for horizontal cylinder

13 p2164 A71-28986

Thermal transients in composite cylinders, solving diffusion equation by Laplace transform technique

13 p2164 A71-28987

Boundary value problems solution for composite cylinder consisting of three different layers with nonideal thermal contacts

13 p2165 A71-29086

Base pressure measurement behind wedge-parallelepipeds and cone-cylinder models of variable geometry

13 p2049 A71-29199

Finite difference scheme for calculating three dimensional incompressible turbulent boundary layer development on infinite yawed cylinder
[ASME PAPER 71-FE-19]

13 p2052 A71-29457

Bounded flow incident on cylindrical body in transverse magnetic field, determining constraints effects on dynamic and structural characteristics

14 p2278 A71-29609

Horizontal conducting fluid cylinder ultrasonic oscillations in crossed electric and magnetic fields, obtaining boundary value problem

14 p2278 A71-29614

Elastic displacement stress computation in cylindrical systems of isotropic homogeneous material by finite difference method

14 p2323 A71-29744

Electromagnetic field action on living organism simulated with infinite homogeneous cylinder in infinite cylindrical solenoid EM media

14 p2182 A71-30026

Hypersonic shockless gas flow past circular cone and cylindrical surfaces, reducing Vallander equations to nonlinear integral

14 p2169 A71-30183

Differential equation describing nonstationary reflection of symmetrical shock front from spherical and cylindrical blunt bodies

14 p2170 A71-30216

Aerodynamic characteristics of low-aspect-ratio wing mounted on cylindrical body, simulating by system of horseshoe vortices

14 p2170 A71-30264

Surface curvature effects in nonsimilar second order boundary layer solutions for subsonic plane flow over cylinder with separation

14 p2170 A71-30442

Internal frictionless contact stress determination for two telescoped cylinders with different diameters, using integrodifferential equation

14 p2331 A71-30845

Finned solid cylinders surface layers, determining residual axial stresses distribution and amount with induction sensor

15 p2503 A71-31480

Side forces on ogive cylinder bodies at large incidence as function of Mach number, nose fineness and bluntness ratios for laminar and turbulent boundary layers
[AIAA PAPER 71-570]

15 p2345 A71-31563

Ring and cylindrical structures comparative stress relaxation at room temperature

15 p2508 A71-32229

Thermal stability test assembly for refractory materials cylindrical specimens, using argon plasma jet

15 p2385 A71-32238

Contact problems of inflated cylindrical membranes with quadrature reduction under normal stress applied to loaded floating and submerged life raft
[ASME PAPER 71-APM-11]

16 p2656 A71-33215

Stress-strain state of homogeneous and inhomogeneous cylinders and disks with central axial curvilinear hole under internal pressure and thermal loads

17 p2816 A71-34331

Plastic deformation and embrittlement due to stress raisers in steel cylinders from high speed tensile tests at low temperatures

17 p2832 A71-35462

Cylindrical steel and Ni alloy specimens bearing strength in inhomogeneous stress states under cyclic elastoplastic bending and loading to failure

17 p2760 A71-35668

Cone-cylinder-cone missile type body in transonic buffeting environment determining static and fluctuating wall pressure distribution

[ONERA-TP-942]

18 p2843 A71-36020

Vlasov-Poisson equations of collisionless plasma flow around conducting cylinder without magnetic effects, using nonrestrictive hybrid simulation techniques

[ONERA-TP-958]

18 p2951 A71-36025

Transient thermal stresses in infinite cylinder of rectangular cross section with heat sources, using integral transforms

18 p2976 A71-36127

Long small bore metal tube internal diameters calculation from capacitances comparison with cylindrical coaxial probes

18 p2922 A71-36581

Nonheat treated extruded Mo alloy under tension and vacuum conditions at various temperatures, investigating cylindrical samples dimensions effects

18 p2936 A71-36714

Elastic deformation of strip, rectangular annulus and cylinder with homogeneous displacement boundary conditions, deriving orthogonality relations for expanded eigenvectors

18 p2982 A71-36793

Stress distribution in cylindrical bodies in internal contact, considering thick elastic plate with elastic disk fitted tightly into hole

19 p3160 A71-38482

Rayleigh scattering by obliquely oriented uniform thin cylindrical particles /needles/, using dielectric needle approximation

20 p3196 A71-39406

Double frustum phenomenon in mushrooming of cylindrical Al projectiles upon high speed impact with hardened steel anvil

21 p3474 A71-41424

Algorithms for calculating temperature fields of electronic devices on computers, considering solid body in shape of bounded cylinder

22 p3519 A71-41442

Two dimensional cylindrical stress propagation over viscoelastoplastic body arbitrary cylindrical surface under instantaneous compression load, using finite difference method

22 p3613 A71-41564

Laminar free convective heat transfer on vertical cylinder with concentration gradients, considering mass transfer effects prediction

22 p3620 A71-41882

Electromagnetic scattering by imperfectly conducting circular and square cylinders, using matrix technique based on conformal transformation from polygonal to circular cross section

22 p3512 A71-42361

Plane MHD boundary layer growth and separation in viscous incompressible flow past cylinder under abrupt motion and transverse magnetic field

22 p3584 A71-42685

Approximate nonlinear theory of steady incompressible fluid flow about cylindrical bodies from vortex method for thin lifting surfaces

22 p3481 A71-42867

Two-component composite cylindrical body thermoelastic stresses near junction-surface edge under plane deformation conditions

23 p3776 A71-43420

Radiant flux from finite cylindrical volume to coaxial screen calculated under quasi-homogeneous medium and arbitrary optical thickness assumptions

23 p3782 A71-43920

Nonstationary radiative heat transfer between cylindrical body and ambient medium, determining regular heating condition region

23 p3782 A71-43921

Rough spheres, cylinders and annuli in contact, determining surface roughness and waviness effects on surface geometry under elastic and plastic deformations

23 p3682 A71-43928

Temperature distribution in current carrying cylindrical conductor with nonlinear boundary condition of emission by Stefan-Boltzmann law

23 p3783 A71-44070

Stress and displacement solutions to deformation of homogeneous and composite anisotropic near cylindrical bodies, using Almansi algorithm

24 p3885 A71-45061

Flat face cylinders in rarefied supersonic gas flow, investigating perturbed region evolution

24 p3790 A71-45096

Mach number distribution along critical streamline in compressed layer in front of cylinder in supersonic flow

24 p3790 A71-45101

CYLINDRICAL CHAMBERS

Cylindrical cavities in infinite series, examining shear wave diffraction

12 p1975 A71-27109

HF stability and combustion product flow characteristics of laminar burning in cylindrical tube, considering longitudinal and radial instabilities

14 p2338 A71-30856

Molecular incidence rate and emission over surface of cold wall and spherical test object in cylindrical space simulation chamber

15 p2393 A71-32703

Time dependent rotating laminar flow of viscous incompressible fluid in closed cylindrical container, presenting numerical solutions to Navier-Stokes equations

18 p2908 A71-36343

Two phase gas-liquid ejectors with cylindrical mixing chamber, discussing ejection equations, jet flow parameters, operation modes and diffuser substitution

22 p3479 A71-41851

Vacuum water-air ejector with cylindrical mixing chamber and multiball nozzle feed, showing increased efficiency by supersonic diffuser substitution

22 p3480 A71-41852

CYLINDRICAL SHELLS

Orthotropic cylindrical shell stress distribution near axial line crack, formulating problem as system of singular integral equations

01 p0167 A71-10175

Hollow circular cylinder with variable inner radius, solving nonlinear viscoelasticity dynamic load problem

01 p0168 A71-10422

Cylindrical shells and circular plates optimal limiting and adaptable loads calculation by Pontryagin maximum principle

01 p0170 A71-10639

Stability of longitudinally hinged isotropic cylindrical shells under external pressure, using finite difference method

01 p0170 A71-10645

Cylindrical shell stability under combined axial compression and heating, using finite difference method

01 p0170 A71-10646

Finite length elastic cylindrical shell deformation approximate solution by Legendre polynomials

01 p0173 A71-10942

Discrete search method for stiffened cylindrical shell stability under combined uniform axial compression and lateral pressure loads

01 p0174 A71-10963

Load deflection relations for rigid plastic cylindrical shells beyond incipient collapse load

01 p0175 A71-11011

Reinforced cylindrical shells under external pressure, investigating longitudinal tensile stresses effect on stability

01 p0175 A71-11040

Diffraction of cylindrical wave on thin infinite weakly reflecting cylindrical shell

01 p0128 A71-11121

Homogeneous isotropic cylindrical shell stability, considering reinforcement by nonlinear dense symmetrical system of elastic threads under tension

01 p0176 A71-11124

Arbitrary shape and variable thickness cylindrical shell bending numerical solution by replacement of circular cylindrical strip elements

01 p0177 A71-11324

Cylindrical shells finite element analysis by rectangular circular cylindrical elements replacement of actual structure

01 p0177 A71-11325

Simply supported cylindrical shell buckling under linearly varying lateral pressure

01 p0178 A71-11399

Laminar orthotropic circular cylindrical shell stress state under inversely symmetrical loading

02 p0322 A71-11737

Thermal prestress effect on natural vibrations of hinge supported isotropic cylindrical shell, integrating equations of motion by Bubnov-Galerkin method

02 p0322 A71-11738

Highly flexible nonlinearly elastic two layer cylinder reinforced by transversely isotropic shell, examining stressed state in axisymmetric temperature field

02 p0323 A71-11742

Thin cylindrical work hardening shell under nonuniform heating and external stresses, determining elastoplastic deformation by flow theory

02 p0323 A71-11744

Fiberglass reinforced plastic cylindrical shells, investigating rheological effects during heating and concentrated radial loads

02 p0324 A71-11754

Closed cylindrical shell response to random sound in contained fluid, investigating cylinder end acoustic boundary conditions with coupled oscillator theory

02 p0239 A71-11998

Axisymmetric and unsymmetric free vibrations of orthotropic sandwich cylindrical or conical shells under various boundary conditions

02 p0325 A71-11999

Stability loss of cylindrical and spherical shells under heating and external force, determining critical temperature and loads

02 p0325 A71-12286

Stability loss of circular cylindrical shells under bending beyond elastic limit 02 p0325 A71-12287

Cylindrical shell deflection under concentrated radial force expressed in terms of algebraic polynomials 02 p0326 A71-12295

Thin circular cylindrical perforated shell, analyzing stress distribution around circular hole by coordinate transformation and partial differential equations 02 p0326 A71-12346

Matrix algorithm using difference-differential method for thin wall moments of varied thickness anisotropic cylindrical shell 02 p0328 A71-12561

General solution to three dimensional problem in elasticity theory for cylindrical transverse isotropic medium, applying results to thick walled shells stress-strain 02 p0329 A71-12563

Prebuckling deformations influence on circular cylindrical shell buckling under external pressure, applying Galerkin method to Donnell equations 02 p0329 A71-12602

Continuous elastic filler effects on axisymmetric stability loss in cylindrical shell under subcritical compression loads, using three dimensional linearized equations 02 p0329 A71-12665

Skin friction effect on cylindrical shell critical loads at various supersonic gas flow velocities, noting application to flutter analysis 02 p0329 A71-12666

Incompressible fluid filled circular cylindrical shells loaded by pressure ring at center, obtaining yield point load 03 p0500 A71-13022

Laminated cylindrical shells of orthotropic layers, deriving linear theory and equations of motion 03 p0504 A71-13430

Postbuckling behavior of open cylindrical shells under uniform axial compression loads, solving finite difference equations by Newton-Raphson method 03 p0505 A71-13539

Open cylindrical shells with end eccentricity or initial deflection imperfections, investigating buckling under axial compression by Newton-Raphson method 03 p0505 A71-13544

Ring reinforced circular holes in cylindrical shells examining stress concentrations due to internal pressure 03 p0507 A71-13740

Bending of cylindrical shells with and without intermediate supports under arbitrarily distributed and discontinuous loads, using initial parameter method [ASME PAPER 70-WA/PVP-2] 03 p0510 A71-14100

Cylindrical shell spacecraft thermal control coating system optimization, using truncated series representation [ASME PAPER 70-WA/AUT-13] 03 p0499 A71-14151

Thin walled circular cylindrical shells creep buckling under radial pressure and thermal gradients [ASME PAPER 70-WA/APM-8] 03 p0512 A71-14152

Laminated circular cylindrical shells under axisymmetric mechanical and thermal loads, including transverse isotropy and shear deformation effects in stress analysis theory [ASME PAPER 70-WA/APM-53] 03 p0513 A71-14170

Cord reinforced elastic homogeneous isotropic cylindrical membrane axisymmetric deformation, using strain energy function 03 p0514 A71-14348

Circular cylindrical shell with trapezoidal stringers reinforcement system along length, calculating strain during oscillation 03 p0514 A71-14359

Thin walled cylindrical shells with filler, determining stability under axial compression by computer calculation 03 p0514 A71-14360

Cylindrical shells axisymmetric nonlinear strain discontinuities propagation, using Timoshenko equations 03 p0515 A71-14380

Vibration effects on free convection heat transfer from fluid filled horizontal cylinder 04 p0675 A71-14784

Cylindrical cantilever shells (silos) under wind loads by semimembrane analysis, discussing cross section distortion and stress prediction [ASME PAPER 70-WA/APM-7] 04 p0667 A71-15182

Thermomechanical coupling in axially symmetric viscoelasticity of cylindrical cavity under shear stress, determining stress concentration from temperature distribution 04 p0669 A71-15203

Nondestructive test with high resolution instrumentation for observing long thin walled cylinder lateral displacements prior to buckling under axial compression 04 p0669 A71-15297

Fatigue and fracture in elastic cylindrical shells with circumferential crack under axial tension, noting precracked specimens 04 p0670 A71-15386

Circular cylindrical shell reinforced by ring ribs, investigating dynamic characteristics under impulsive loading 04 p0672 A71-15756

Thin elastic orthotropic oval cylindrical shells nonlinear flexural vibration based on assumed modes, using Galerkin method 05 p0819 A71-15979

Multilayered anisotropic cylindrical shells free vibration modes 05 p0819 A71-15982

German monograph on stress distribution around cutouts in disks, plates and cylindrical shells 05 p0820 A71-16121

Thin circular cylindrical shell stability subjected to axisymmetric thermal pulse, describing buckling process by mathematical model 05 p0820 A71-16186

Orthotropic cylindrical shell stability under variable compression loads, considering glass fiber reinforced plastic tube 05 p0822 A71-16368

Low shear rigidity effect on stability of glass fiber reinforced plastic cylindrical shells under loads and elevated temperature 05 p0822 A71-16369

Orthotropic sandwich and homogeneous single layer circular cylindrical shells optimal design 05 p0822 A71-16419

Internal pressure load carrying capacity of intersecting spherical and cylindrical shells based on limit or plastic design concept 05 p0823 A71-16493

Semiinfinite simply supported cylindrical shell transient response due to axisymmetrically engulfing step pressure wave, investigating moving load critical velocity [AIAA PAPER 70-18] 05 p0823 A71-16556

Local axisymmetric dimple imperfection effects on buckling load of circular cylindrical shell under axial compression [AIAA PAPER 70-103] 05 p0823 A71-16557

Circular cylindrical shells buckling with different elastic moduli in tension and compression under arbitrary axial and lateral pressure 05 p0823 A71-16558

Axial buckling tests on machined integrally ring stiffened cylindrical shells 05 p0823 A71-16559

Axisymmetric stability of fluid filled cylindrical shells under rapid axial compression 05 p0824 A71-16592

Rib reinforced circular cylindrical shells, analyzing elementary and zero bending stress states 06 p0982 A71-17351

End face frame stiffness effects on cylindrical shell critical pressure 06 p0982 A71-17352

Cylindrical shells with large arbitrary defects, deriving stability equations from shell theory 06 p0982 A71-17353

Cylindrical reinforced shells carrying capacity under dynamic external pressure 06 p0982 A71-17354

Weight-optimal cylindrical shells of revolution with uniform strength edge reinforcement, discussing pressure vessel design 06 p0982 A71-17356

Reinforced cylindrical minimum weight shells under combined axial compression and internal pressure, examining strength and buckling modes 06 p0982 A71-17357

Short elastic sine waves propagation in cylindrical shells, applying nonclassical equations 06 p0982 A71-17359

Stability loss of cylindrical shell at upper bound of buckling load under axial compression 06 p0983 A71-17365

Long thin circular cylindrical shell circumferential wave functions reduction to beam type transverse vibration equation, including rotatory inertia 06 p0984 A71-17618

Composite hollow cylinders of heteromodulus materials, discussing stress-strain state 06 p0984 A71-17650

Circular cylindrical orthotropic fiberglass-reinforced shell buckling under longitudinal impact, assuming initial surface imperfections 06 p0985 A71-17684

Local distributed load effects on bending of fiberglass reinforced plastic laminar orthotropic cylindrical shell 06 p0986 A71-17761

Equilibrium stability of orthotropic cylindrical shell under longitudinal compression, discussing critical stresses 06 p0986 A71-17762

Compressive contact interaction problem for elastic circular cylindrical shell lying in circular cylindrical cavity of elastic body 06 p0987 A71-17764

Axisymmetric stability loss of thin long cylindrical shell with elastic filler under uniformly distributed compressive forces over shell ends 06 p0987 A71-17770

Cylindrical shell reinforced by transverse ribs under hydrostatic pressure, determining elastoplastic deformation 06 p0988 A71-17777

Closed cylindrical shells behavior under static loads, determining stability 06 p0988 A71-17777

Cylindrical shells buckling under subcritical loads considering internal and external hydrostatic pressure and axial compression 06 p0988 A71-17777

Structural behavior of rods and cylindrical shells under dynamic impact loads 06 p0989 A71-17777

Elastic cylindrical shells stability under dynamic load consisting of conservative forces and normal compression 06 p0990 A71-17780

Cylindrical shell stability under nonuniform loading solving infinite homogeneous algebraic equations system by Bunnov-Galerkin method 06 p0990 A71-17791

Circular cylindrical sandwich shell natural vibrations reduced to shell and filler contact problem, using two and three dimensional models 06 p0990 A71-17793

Cylindrical sandwich shells with multiple isotropic load carrying and transversely compressible filler layers, deriving local stability equations 06 p0990 A71-17793

Circular cylindrical shell stability under uniform tension, taking into account support flexibility and temperature difference 06 p0990 A71-17794

Cylindrical structure longitudinal stress wave propagation characteristics, analyzing wave induced structural instability and destruction process 06 p0991 A71-17800

Local imperfection and stress effects on cylindrical shell stability under various single and combined loads 06 p0991 A71-17803

Cylindrical shell compression stability in presence of creep, determining initial surface dent effects 06 p0992 A71-17800

Eccentrically reinforced cylindrical shells stability equations under axisymmetric loading 06 p0993 A71-17811

Thin imperfect cylindrical shell stability, considering statistical analysis of initial irregularities 06 p0993 A71-17811

Rib reinforced cylindrical shell stability under annular and axial stresses, determining eigenvalue of homogeneous integral equation 06 p0993 A71-17816

Eccentrically reinforced cylindrical shell stability considering numerical analysis of structurally orthotropic shell parameters 06 p0993 A71-17817

Smooth cylindrical shell stability, considering internal pressure effect on critical axial stresses 06 p0993 A71-17819

Elliptical cylindrical shell under internal pressure, investigating stress concentration near surface hole 06 p0994 A71-17821

Strain hardened plastic cylindrical shells, investigating load bearing capacity 06 p0994 A71-17823

Closed circular cylindrical shell stability and buckling during axial compression, using energy method in geometrically nonlinear formulation 06 p0994 A71-17824

Cylindrical anisotropic shells transient deformation processes under external pressure, discussing equations of motion integration 06 p0996 A71-17838

Thin circular cylindrical shell thermoelastic vibrations, deriving differential equations of motion with allowance for shear, rotatory and translational inertia 06 p0996 A71-17840

Elastic and viscoelastic multilayer reinforced circular cylindrical shells stability, determining transverse shear stress role 06 p0996 A71-17841

Dynamic stability of cylindrical shell with freely supported edges partly filled with ideal compressible fluid and undergoing steady longitudinal vibrations 06 p0997 A71-17846

Cylindrical shell stability under critical dynamic radial pressure, discussing geometrical and mechanical parameters and loading law 06 p0997 A71-17847

Cylindrical shell stability under arbitrary external pressure, discussing forces and displacements of precritical stressed state 06 p0997 A71-17848

Circular cylindrical shell stability with ribs of variable cross sections, using method based on semiinvariant theory 06 p0997 A71-17850

Stress nonuniformity and initial imperfection influence on cylindrical shell stability 06 p0999 A71-17868

Nonlinear statics of thin walled cylindrical and spherical shells, including buckling under various end conditions

06 p0999 A71-17869

Three dimensional bending vibration analysis of homogeneous elastic circular cylindrical shell with both ends restrained

06 p1001 A71-18230

Design criteria for buckling prediction of elliptical and circular cylindrical shells under axial compression from asymmetric and axisymmetric shape imperfections distribution

[AIAA PAPER 71-145] 06 p1003 A71-18588

Axially compressed ring and stringer stiffened cylindrical shells minimum weight design, considering configuration instability

[AIAA PAPER 71-147] 06 p1003 A71-18590

Dynamic response of pressurized thin circular cylindrical shells under moving loads

[AIAA PAPER 71-175] 06 p1004 A71-18614

Cylindrical shell with elastic core under annular sliding load, solving for critical velocity via Fourier transformation

07 p1212 A71-19353

Cylindrical, conical and spherical shells natural frequencies and vibration modes determination using matrix series

07 p1212 A71-19365

Cylindrical shell panels with free supported curved edges and arbitrary boundary conditions, investigating natural frequencies and mode shapes

07 p1213 A71-19886

Imperfect elliptical cylindrical shells buckling under axial compression, demonstrating imperfection sensitivity

07 p1213 A71-19888

Infinite circular cylindrical shell with elastic stiffener ring, calculating transient axisymmetric bending stress under radial impulse

07 p1213 A71-19907

Axisymmetric wave propagation in semiinfinite hollow elastic circular cylinders subjected to pressure step loading, obtaining asymptotic solutions for strains by double integral transforms

07 p1214 A71-19954

Steady state thermal stresses and deformations in infinite hollow circular cylinder by sinusoidal internal heat source and Newtonian radiation boundary condition outer surface cooling

07 p1214 A71-20026

Thin single layer orthotropic circular cylindrical shell shear coupled traveling wave reflections, determining stresses in terms of particle velocities

07 p1216 A71-20134

Thin cylindrical shell of revolution delaminations detection model, using free vibration natural frequency parameter under clamped-clamped conditions

07 p1216 A71-20135

Asymmetric three layer cylindrical shells with orthotropic layers under deflection due to high temperature, deriving differential bending equations

07 p1217 A71-20456

Shallow orthotropic cylindrical shells with weak anisotropy, deriving equations for stress concentration at circular hole

07 p1217 A71-20457

Unsteady temperature field determination in infinite cylindrically anisotropic plate with circular hole, calculating stress by Volterra equations

07 p1218 A71-20463

Viscous incompressible fluid partly filling rotating cylindrical cavity, considering motion under centrifugal forces in adjoining unperturbed free surface region

07 p1093 A71-20467

Stress-strain state of anisotropic circular cylindrical shell with constant thickness, using stepwise linear approximation technique for solving mixed system of partial differential equations

08 p1368 A71-20789

Cylindrical shells with arbitrary cross sectional contour, thickness and longitudinal stiffener spacing under tension or compression, presenting computer algorithm for determining stress-strain state

08 p1368 A71-20790

Heterogeneity effects on thin composite cylindrical shells axisymmetric vibration characteristic, considering material and geometric symmetry deviations influence on frequency spectra

08 p1368 A71-20805

First passage time for snap-through of shallow cylindrical shell subject to stationary random loading, considering numerical solution by Pontryagin-Vitt equation

08 p1369 A71-20809

Eccentricity and clamping effects on stability and critical pressure of ring-reinforced cylindrical shells under internal pressure

08 p1369 A71-21122

Book of tables and graphs for circular cylindrical shells free vibrations

08 p1370 A71-21234

Clamped-free and clamped-ring-stiffened cylindrical shells free vibrations analysis for digital computer

programming, using Rayleigh-Ritz technique for approximate solution

08 p1371 A71-21427

Stability analysis of cylindrical shells hinged over ends under critical destabilizing axisymmetric radial displacements

08 p1373 A71-21946

Circular cylindrical shells on coaxial rings coupled by finite number of spokes as structural analytical models for engine casings, deriving formulas for arbitrary loads

08 p1374 A71-22040

Nomograms for normal stresses and bending moments in thin circular cylindrical shell under uniformly distributed local load

08 p1374 A71-22054

First and second frequency harmonics and form shapes of liquid filled cylindrical shell axisymmetric vibrations, analyzing effect of pressure and shell dry portion on vibration frequencies

08 p1374 A71-22055

Flutter analysis of rotating thin cylindrical shell with outer surface exposed to inviscid helical air flowfield

09 p1533 A71-22078

Cylindrical shell dynamic response to random acoustic excitation within narrow frequency band of low modal density

09 p1534 A71-22082

Shallow shell triangular finite element method application to cylindrical shell theory

09 p1534 A71-22106

Circular cylindrical shell initial geometrical imperfections effect on stability under nonuniform composite loading

09 p1537 A71-22518

Two dimensional stress-strain fields under elastic and elastic-plastic strains and steady state creep, calculating stress distribution around hole in cylindrical shell

09 p1538 A71-22631

Circular cylindrical shell under radial local load, determining maximum stresses in center and boundary

09 p1538 A71-22651

Stress concentration near hole in transversely isotropic cylindrical and spherical shells made of oriented glass fiber reinforced plastics

09 p1539 A71-22820

Stability characteristics of glass fiber reinforced plastic orthotropic cylindrical shell with elastic filler under torsion

09 p1539 A71-22821

Optimal design parameters in minimization of reinforcement elements weight in cylindrical glass fiber reinforced orthotropic plastic shells under axial compression

09 p1539 A71-22826

Torsional oscillation of hollow isotropic elastic cylinder encased in thin elastic shell, deriving representation satisfying equation of motion and initial and boundary conditions

09 p1539 A71-22918

Vibrating cylindrical shell with circular plate, discussing bending moments, deflections and frequencies from Lagrangian

09 p1540 A71-23056

Imperfect thin walled circular cylindrical shells under axial compression with relaxed boundary conditions, determining deformations with differential equations

09 p1541 A71-23089

Steady one dimensional temperature field of cylindrical shell spacecraft, allowing for heat conduction and convective and radiative heat transfer within shell

09 p1546 A71-23148

Thin cylindrical shell deformation under concentrated transverse loads applied through rigid boss, determining displacement variations as function of applied loads and edge constraints

09 p1543 A71-23659

Heat resistance, thermal stability, thermal conductivity coefficient and specific heat measured in cylindrical hollow specimens of corundum materials

10 p1634 A71-24200

Circular cylindrical shells stress-strain state in elastic medium, obtaining criteria for boundary conditions limiting values for linear theory applicability

10 p1688 A71-24356

Elastic cylindrical shells oscillations and stability in inviscid incompressible liquid flow, reducing problem to integro-differential equation by Fourier integral transformation

10 p1688 A71-24357

Dynamic deformation of cylindrical shells by elastic body impact, using sequence boundary value solutions in plate theory

10 p1689 A71-24561

Critical load and elastic base one-sided contact effects on cylindrical shell stability under uniform external pressure, using nonlinear programming

10 p1689 A71-24563

Critical speeds for inviscid compressible potential flow past thin elastic cylindrical shells, using long wave approximation

10 p1689 A71-24565

Bidirectional stress-strain analysis of hinged cylindrical shells crosswise reinforced by rigid ribs using equilibrium equations

10 p1690 A71-24566

Cylindrical panel vibration in supersonic flow under random effects, calculating stress-strain statistical properties as function of incident flow velocity

10 p1690 A71-24572

Cylindrical Duralloy shells critical strain measurement in axial compression under creep conditions

10 p1690 A71-24575

Rectangular plate and circular cylindrical shell segment under rotating moment and dynamic loads evaluated by Green function

10 p1691 A71-24812

German monograph on circular cylindrical shells theory comparative studies covering energy and equilibrium methods, tensor representation, reinforced shells, etc

10 p1692 A71-24912

Heterogeneous orthotropic cylindrical shells, calculating free natural vibration frequency spectra from refined equations of motion in Love and Donnell type theories

11 p1841 A71-25184

Thin circular cylindrical shells thermoelastic behavior under one directional radiant heating, comparing measured displacements and strains with calculated values based on measured temperature distributions

11 p1841 A71-25187

Cylindrical shells panel flutter analysis for internal stress and supersonic flow, considering still air buckling data useful for determining buckling loads

[AIAA PAPER 71-328] 11 p1842 A71-25308

Closed cylindrical shell response to randomly time distributed broadband acoustic excitations, using statistical energy method to compute displacement and interior pressure

[AIAA PAPER 71-331] 11 p1842 A71-25311

Linearly elastic cylindrical shells dynamic stability under combined axial and radial stochastic excitations, using Liapunov analysis

[AIAA PAPER 71-333] 11 p1842 A71-25312

Elastic boundary conditions effect on natural frequencies and resonant displacement of thin isotropic circular cylindrical shell under concentrated load with harmonic time history

[AIAA PAPER 71-335] 11 p1843 A71-25314

Buckling of axially compressed imperfect isotropic cylindrical shells with edge constraints, deriving two point boundary value problem numerical solution by shooting method

[AIAA PAPER 71-358] 11 p1844 A71-25337

Digital computerization for cylindrical shells post-buckling stability analysis, discussing FORMAC and REDUCE formula manipulation systems

[AIAA PAPER 71-363] 11 p1845 A71-25341

Flutter analysis of long thin cylindrical shells rotating in circular helical air flow field

[AIAA PAPER 71-373] 11 p1845 A71-25346

Frequency equation for harmonic waves with circumferential nodes traveling in composite traction free circular cylindrical shells, using IBM 7094 computer

11 p1847 A71-25461

Optimum buckling load of cylindrical shells under lateral pressure using Rayleigh-Ritz method

11 p1848 A71-25484

Radial load effects along length of hinged cylindrical shell for maximum displacement positions, using trigonometric Fourier series

11 p1850 A71-25942

Thermal stability of cylindrical laminated fiberglass reinforced plastic shells, solving by linear shell stability theory

11 p1790 A71-26175

Natural vibration analysis method for circular cylindrical shell based on three dimensional theory of elasticity and energy principle, discussing boundary conditions effect

11 p1852 A71-26405

Current distribution effect on stability of exploding and collapsing accelerated cylindrical plasma shell in axial and azimuthal magnetic field

12 p1935 A71-26765

Frequency equation of flexural vibration of fluid filled circular cylindrical shells, using linear elasticity

12 p1974 A71-26928

Rotation effects on vibration traveling waves in rotating cylindrical shells, considering Coriolis, centrifugal and torque loads

[ASME PAPER 71-DE-A] 12 p1977 A71-27316

Heat generation in hinged orthotropic viscoelastic cylindrical shells under transverse vibrations and cyclic surface load

12 p1978 A71-27343

Thermal stress analysis of hinged thin circular cylindrical shells of variable thickness by computerized discrete orthogonalization method

12 p1979 A71-27357

Initial thermal stresses effect on natural vibrations of orthotropic cylindrical shells

12 p1979 A71-27360

Nonlinear equations of motion for cylindrical elastoplastic shell under axial impact

12 p1980 A71-27452

Long circular cylindrical shell stability under action of bending moments at end face, deriving neutral equilibrium equations

12 p1981 A71-27495

Frequencies and modes of natural vibrations of closed cylindrical shell with elastic filler

12 p1981 A71-27508

Buckling of eccentrically stiffened multilayered circular cylindrical shells with different orthotropic moduli in tension and compression

12 p1982 A71-27572

Buckling of circular cylindrical shells with axisymmetric imperfection distributions under axial compression

12 p1983 A71-27573

Influence coefficients for thin walled finite length cylindrical shells subjected to uniform internal pressure and edge loads

12 p1983 A71-27586

Axisymmetric stressed-state problem of finite length hollow circular cylinder in Fourier and Fourier-Dini series form

12 p1984 A71-27692

Dynamic snapthrough of shallow circular cylindrical shell undergoing plane motion in response to nearly symmetric impulsive pressure

13 p2146 A71-27781

Shear strength effect on axisymmetrical stress-strain state of orthotropic cylindrical shell subjected to nonuniform surface heating

13 p2148 A71-27825

Axial compression buckling of elastic core filled circular cylindrical shells with transverse shear flexibility, noting solid propellant rocket cases design application

13 p2148 A71-27984

Strain gage method for residual stress determination in thin walled brass cylindrical shells produced by deep drawing

13 p2066 A71-28034

Stress-strain state of closed circular cylindrical shells stiffened by longitudinal ribs, analyzing general solution of homogeneous equilibrium equations system

13 p2150 A71-28133

Stress-strain state of circular cylindrical shells in elastic medium, reducing linear problem to solution of single eighth order partial differential equation

13 p2150 A71-28134

Acoustically induced cylindrical shell vibrations, solving differential equation derived for expression of system axisymmetric forced vibrations

13 p2150 A71-28136

Forced vibrations of circular cylindrical shell under random normal load and internal pressure, noting stability of transversely pressurized flexible vs rigid structures

13 p2150 A71-28140

Forced axisymmetric vibrations of composite cylindrical shell with spherical bottom, obtaining influence coefficients and inhomogeneous boundary conditions

13 p2150 A71-28141

Approximate determination of first characteristic root of equation for plate, hollow sphere and hollow cylinder, using variational method for heat conduction problem

13 p2159 A71-28184

Minimum weight design of circular cylindrical shell hinged at ends under axial compression, using random search method with self learning

13 p2152 A71-28280

Deformation substructures, strain rates and terminal properties of explosively-formed thin walled stainless steel cylinders, using transmission electron microscopy

13 p2153 A71-28501

Suspended hollow cylinder under force of gravity, calculating stresses and displacements by linear elastic theory differential equations

13 p2153 A71-28518

Cylindrical shell laminar plastic structure effect on stability under hydrostatic pressure, applying Kirchhoff-Love hypothesis

13 p2155 A71-28654

Magnetic shielding of various shaped enclosures such as rectangular or cylindrical cross sections in terms of normalized parameters

13 p2039 A71-28870

Cylindrical shells of revolution with various boundary conditions, calculating free vibrations with differential equations

13 p2156 A71-29067

Cylindrical liquid filled shells under rapid axial compression along generatrix, examining dynamic deformation characteristics

13 p2156 A71-29072

Biaxial plastic extension stability of anisotropic sheets and cylindrical shells, using Hill plasticity theory of orthotropic materials

13 p2156 A71-29074

Variable curvature cylindrical shells elastic post-buckling configurations, showing buckle pattern tessellation discontinuity

13 p2157 A71-29126

Circular cylindrical thin walled shells buckling, determining postbuckling patterns development by high speed cinematography

[DFVLR-SONDDR-99] 13 p2157 A71-29305

Critical stress and stability analysis of cylindrical shell with initial indentation of length comparable to radius under axial compression

14 p2321 A71-29536

Thin shell isotropic clamped free elliptical cylindrical shells with various cross sectional eccentricities, measuring frequencies and mode shapes by vibration analysis

14 p2324 A71-29869

Thin walled cylindrical elastic shell with rectangular holes at equal intervals along straight line, deriving boundary conditions expression by R-functions

14 p2326 A71-30190

HF response of point excited cylindrical shell, converting normal-mode series to integral representation with Watson transformation

14 p2327 A71-30201

Frequency equations for trains of axisymmetric harmonic waves traveling in infinitely long three layered elastic circular cylindrical shells and rods

14 p2327 A71-30202

Extensional vibrations of thin cylindrical shell, discussing longitudinal and radial motions coupling and resonant frequency dependence on length/radius ratio

14 p2327 A71-30209

Free convection in horizontally positioned, water filled circular cylindrical cavity

14 p2336 A71-30228

Transient and steady state creep of circular cylindrical shells loaded by internal pressure, using strain hardening hypotheses and finite difference method

14 p2328 A71-30379

Simply supported nearly circular cylindrical shell, calculating nonlinear damped dynamic response due to exponentially decaying radial pressure

14 p2330 A71-30688

Viscoplastic cylindrical shell dynamic buckling during axial impact of rigid mass, discussing constitutive equations

14 p2331 A71-30841

Nonuniform rotation of nonhomogeneous isotropic elastic cylindrical shell, obtaining steady state axisymmetric vibrations

14 p2331 A71-30842

Stability and stress analysis of elastic finned circular cylindrical shells reinforced by stringers

14 p2332 A71-30852

Closed circular cylindrical shell nonlinear problem solvability extended to anisotropic sandwich shell, using mean deflection theory

14 p2332 A71-30866

Stability of structurally orthotropic stringer reinforced cylindrical shell closed by spherical or plane bottoms under uniform external pressure

14 p2333 A71-30892

Cylindrical shell under internal pressure, detailing axial thermal stresses relaxation

15 p2505 A71-31861

Circular cylindrical shell with elliptic hole, calculating stress concentration around hole under torsion

15 p2506 A71-32014

Short open noncircular cylindrical shells supported at curvilinear ends, obtaining total values of moments

15 p2507 A71-32103

Flutter of thin walled cylindrical shells conveying fluid above critical flow velocity

15 p2508 A71-32135

Orthotropic layered cylindrical shells, deriving equations of motion for rotationally symmetric vibration

15 p2509 A71-32513

Rectangular cylindrical shell finite element, deriving stiffness matrix with stress distribution

15 p2510 A71-32516

Vibrationally loaded hollow cylinder with slanted notch, considering fatigue strength behavior as function of rated stress state

15 p2510 A71-32738

Buckling and postbuckling loads of initially imperfect orthotropic cylindrical shells under axial compression and internal pressure, using potential energy principle

16 p2651 A71-33025

Elements movement and stability loss of circular cylindrical shells during snap, using Gauss least constraint principle

16 p2651 A71-33027

Imperfect circular cylindrical shell under external hydrostatic pressure loads, determining free and resonant vibration modes

16 p2651 A71-33062

Buckling of axially compressed circular cylindrical shells with localized or random axisymmetric imperfections, deriving asymptotic approximation formulas for stress calculation

[ASME PAPER 71-APM-29] 16 p2655 A71-33200

Dynamic midsurface displacements of thin circular cylindrical shell under uniform membrane stress state and three dimensional surface loads

[ASME PAPER 71-APM-12] 16 p2656 A71-33214

Single crystal Ni-base superalloy anisotropic hollow cylinder creep under biaxial loading, studying rate dependence on crystallographic axis orientation and stresses ratio

[ASME PAPER 71-APM-1] 16 p2591 A71-33222

Prestressing of two layer fiberglass-reinforced plastic cylindrical shell under internal pressure

16 p2657 A71-334100

Stability and critical load of constant thickness cylindrical sandwich hinge supported shell under anular loading, using variational method

16 p2657 A71-33601

Critical loads and stability of longitudinally compressed circular cylindrical shells with eccentric ring and stringer reinforcement

16 p2657 A71-33603

Closed circular cylindrical shell stability under dynamic axial compressive loading with static internal pressure

16 p2658 A71-33719

Moment state stability of elastic hinged cylindrical shell and closed ring under pressure and concentrated load, using nonlinear equilibrium theory

16 p2660 A71-34114

Stress distribution in cylindrical shell with two unequal diametrically opposite reinforced circular holes under internal pressure

16 p2661 A71-34159

Nonlinear creep analysis of clamped pressurized circular cylindrical sandwich shells representing stress, membrane force and bending moment as displacement based on Mises criterion

17 p2816 A71-34297

Rotating cylindrical shell symmetrical deformation under external load, obtaining three dimensional axisymmetric problem solution in elastic theory

17 p2816 A71-34330

Equivalent reinforcement of contact area between spherical shell and radial outlet cylindrical pipe under internal pressure and axial force

17 p2817 A71-34332

Cylindrical shells partially filled with liquid, calculating forced vibration under random loads and deterministic internal pressure

17 p2817 A71-34333

Circular cylindrical shell stability under combined axial tensile /compressive/ loads and torque, verifying theory by experiments on stainless steel shell

17 p2817 A71-34336

Stress-strain state of circular cylindrical shell hinged at edges under local radial loads

17 p2817 A71-34340

Deformations and stress concentration on corrugated plate under uniformly distributed load, considering cross section as combination of two cylindrical shells

17 p2818 A71-34401

Finite oval cylindrical shells with clamped boundaries, investigating stability and elastic buckling under axial compression for comparison with circular cylindrical shells

[SESA PAPER 1832] 17 p2819 A71-34536

Impulsively loaded expanding cylindrical shell transient elastic-plastic response, using linearized assumption on plastic flow behavior

17 p2821 A71-34577

Sloshing liquid natural frequencies change in cylindrical shell by movable devices, considering immersed thin elastic plate effect

17 p2726 A71-34579

Finite length thin circular cylindrical shells with clamped or simply supported edges, calculating flexural free vibration natural frequencies

17 p2822 A71-34643

Long laminar plate and cylindrical panels with hinged lateral edges under buckling by normal uniformly distributed load, calculating deflection as monotonic pressure functions

17 p2823 A71-34781

Anisotropic laminated cylinders under combined axial load, torsion and internal pressure, calculating stresses with Vlasov-Ambartsunyan shell theory

17 p2823 A71-34811

Freely vibrating supported elastic isotropic oval cylindrical shells natural frequencies and mode shapes

17 p2825 A71-34873

Thermal buckling prediction for ring-stiffened cylinders, taking into account ring out-of-plane bending stiffness

17 p2825 A71-34896

Finite length heterogeneous thin layered cylindrical shell axisymmetric free vibration frequency spectrum analysis

17 p2826 A71-35035

Analytical model for molecular flow of reactive gaseous species through cylindrical reactors with apertures at either end, evaluating surviving flux magnitude

17 p2695 A71-35137

- Curvature effect on cylindrical shell circumferential crack tip stress intensity, using fatigue crack growth tests 17 p2827 A71-35154
- Stresses in smooth circular cylindrical shell under radial local load applied on small area 17 p2828 A71-35303
- Pure and transverse bending of orthotropic cylindrical shell wound with elastic glass plastic filaments, presenting stress-strain diagrams under tension and compression 17 p2830 A71-35318
- Thin multilayer pressurized glass fiber-plastic cylindrical shells, calculating stress redistribution due to crack initiation and prestressing effects 17 p2830 A71-35319
- Cylindrical shell with continuous filler, calculating stability and axisymmetric buckling in axial compression 17 p2830 A71-35321
- Isotropic circular cylindrical shell stability with longitudinal hinges under uniform external pressure, determining critical load 17 p2831 A71-35322
- Equilibrium bifurcation for nonlinearly elastic incompressible body during finite subcritical homogeneous deformation, obtaining characteristic equations for cylindrical shell, circular and rectangular plates, etc 17 p2832 A71-35609
- Partially liquid filled cylindrical shells with elastically supported end rims, deriving algorithm for nonaxisymmetric natural vibration frequency calculations 17 p2833 A71-35614
- Cantilevered elastic cylindrical shell stability during bending by transverse load uniformly distributed over entire surface or applied at end 17 p2833 A71-35615
- Optimal design of axisymmetrical annular plate and cylindrical and spherical shells by maximum principle 17 p2833 A71-35621
- Superconducting phase transition temperature measurements as function of magnetic field in thin film hollow Al and In cylinders 17 p2791 A71-35742
- Stress-strain behavior of tapered circular cylindrical shell, applying equalization calculation to boundary value problem 18 p2976 A71-36179
- Dynamic response of oddly stiffened circular cylindrical shells, using modified variational method 18 p2980 A71-36495
- Circular cylindrical shells creep buckling in pure bending, deriving formula for critical time 18 p2980 A71-36674
- Photoelastic analysis of cylindrical shells of revolution with one hemispheric closed end and reinforcing flanges at opposite end rim, examining boundary conditions effects 18 p2981 A71-36718
- Rib reinforced cylindrical shells deformation under local load, examining stress-strain distribution 18 p2981 A71-36719
- Elastic buckling load of cylindrical shells with dimple imperfections under external pressure, applying perturbation expansion to Karman-Donnell equations 18 p2982 A71-36839
- Elastic stability and buckling modes of cylindrical shell under critical gravity load, using double Fourier series and linear theory 18 p2983 A71-36847
- Cylindrical shells under uniform external pressure loads, determining boundary conditions effects on natural frequencies and vibration mode shapes 19 p3155 A71-37529
- Variable thickness and rigidity cylindrical shells, determining natural frequencies and vibration mode shapes with algorithm based on Ritz method 19 p3155 A71-37531
- Longitudinal edge stiffness and internal pressure effects on buckling and initial postbuckling behavior of axially compressed stringer reinforced cylindrical panels, discussing imperfection sensitivity 19 p3157 A71-37873
- Hydrostatically loaded noncircular pressurized cylindrical shells with nonuniform rings, using asymptotic expansion procedure 19 p3157 A71-37875
- Clamped oval cylindrical thin walled shells elastic buckling under axial loads, solving stability equations by Fourier method and higher order difference technique 19 p3157 A71-37876
- Inelastic buckling process of axially compressed cylindrical shells with edge constraints, using variational principle and Rayleigh-Ritz method 19 p3158 A71-38182
- Transient response of Euler-Bernoulli and Timoshenko beams and cylindrical shells with moving loads 19 p3158 A71-38183
- In-plane boundary conditions effect on buckling loads of axially compressed simply supported ring stiffened cylindrical shells 19 p3159 A71-38270
- Cylindrical shell stability under radial pressure or axial compression from load-distributing filler model solution 20 p3308 A71-39166
- Membrane and bending stresses analysis around elliptic hole in long thin circular cylindrical shell, using perturbation technique 20 p3309 A71-39776
- Forced and free vibrations of shallow cylindrical shell in rectangular duct filled with ideal fluid 20 p3310 A71-39785
- Transversely vibrating hollow cylindrical beam sound radiation and response to acoustic excitation, predicting resonant frequencies [ASME PAPER 71-VIBR-84] 21 p3461 A71-40320
- Hydroelastic coupled oscillations of partially filled circular cylindrical liquid container with flexible bottom and elastic side wall 21 p3366 A71-40545
- Numerical analysis of steady state creep of simply supported circular cylindrical shells by combined Newton and finite difference methods 21 p3463 A71-40752
- Dynamic response of elastic cylindrical shell-solid core composite under time dependent loading from Laplace transform 21 p3467 A71-40949
- Cylindrical shell under opposing concentrated outwardly directed radial loads applied to reinforcing ring, presenting stress distributions and displacements 21 p3468 A71-40971
- Circular cylindrical shells analysis by Koiter strain energy method for small finite deflections, considering simplifying modifications of energy functionals 21 p3468 A71-40976
- Buckling load reduction for axially compression loaded geometrically perfect cylindrical shells by wall temperature gradients induced partial yielding 21 p3469 A71-41006
- Shear deformation theory of axisymmetric cylindrical shells in contact with smooth rigid surfaces 21 p3470 A71-41017
- Interlaminar shear stress and midsurface displacement of thin orthotropic laminated cylindrical shells, using linear deformation theory 21 p3470 A71-41018
- Circular cylindrical shell under longitudinal parametric load, obtaining nonstationary responses with deformation theory 21 p3471 A71-41029
- Stress-strain state of rotating viscoelastic hollow cylinder with mobile inner boundary under internal pressure and temperature effects 21 p3472 A71-41145
- Zero moment theory application to stability analysis of rib-reinforced cylindrical shell under external pressure 21 p3472 A71-41149
- Natural vibrations of closed reinforced cylindrical shell clamped at end faces 21 p3473 A71-41153
- Nonlinear flutter of hinged closed cylindrical shells in supersonic gas flow, comparing with wind tunnel tests on panels 21 p3473 A71-41155
- Open simply supported cylindrical shell internal stresses due to initial deformation based on thin elastic shell linear theory 22 p3613 A71-41563
- Computer program for nonuniform thickness ring structure stress distribution under uniform radial line load based on reinforced circular cylindrical shell interaction under hydrostatic pressure 22 p3516 A71-41866
- Frequency and buckling stability eigenvalue evaluation for anisotropic circular cylindrical shells under nonuniform lateral prestress 22 p3615 A71-42210
- Stability formula for critical pressure in cylindrical shells orthotropically reinforced by closely spaced eccentric ribs 22 p3616 A71-42487
- Natural frequencies and vibration modes of perforated cylindrical, conical and spherical shells of revolution, using Ritz method 22 p3617 A71-42488
- Three dimensional transient interaction of spherical acoustic waves with cylindrical elastic shell, using integral transform techniques 23 p3775 A71-43207
- Time dependence of radial mechanical driving point impedance of Al cylindrical shell immersed in two anechoic tanks related to chemical reaction 23 p3662 A71-43215
- Oval cross sectioned cylindrical shells, deriving free oscillation solution 23 p3775 A71-43310
- Thin closed circular cylindrical shell under arbitrary loading 23 p3778 A71-44039
- Nonsteady heat conduction of multilayer cylindrical and conical shells in periodic radiation flux, calculating temperature distribution 23 p3783 A71-44067
- Soviet book on elastoplastic deformations of plates and cylindrical shells made of low strain hardening materials, covering strength and stability calculations 23 p3779 A71-44186
- Refractory materials heat resistance criteria, taking into account hollow cylinder thermal stress distribution 23 p3698 A71-44212
- Ribbed cylindrical shells modeling method for stress-strain state and stability 23 p3780 A71-44219
- Longitudinal rib reinforced cylindrical shell under axial compression loads, determining equilibrium stability with approximation of transcendental equations 23 p3780 A71-44222
- Cylindrical shell weakened with large circular hole, deriving nonlinear equilibrium equations in semi-geodesic polar coordinates 24 p3877 A71-44479
- Radial edge displacement effect on circular cylindrical shells compressive buckling stress, noting opposite effects for different length/radius ratio ranges [AIAA PAPER 71-984] 24 p3878 A71-44580
- Metal cored cylindrical plastic shells response to transient external pressures, considering failure modes 24 p3878 A71-44610
- Power series analysis of circular cylindrical shells stability under biaxial compression, expressing critical loadings 24 p3878 A71-44612
- Noncircular cylindrical shells stress and displacement under hydrostatic loads, applying Donnell equations 24 p3879 A71-44618
- Cylindrical shell with elliptical hole, calculating elastic stress concentration due to axial tension based on shallow shell theory 24 p3879 A71-44625
- Stress-strain state of hinged thin multilayer orthotropic cylindrical shells with parameters variable with respect to directrix 24 p3881 A71-44828
- Stability and critical loads of reinforced geometrically nonlinear cylindrical shells, using strain energy method 24 p3882 A71-44842
- Buckling stability and critical loads of thin elastic cylindrical shells with hollow core in axial compression 24 p3882 A71-44844
- Metal cylindrical shells plastic collapse under axial compression, deriving theoretical load/deflection relationship 24 p3883 A71-44875
- Circular cylindrical shell critical stress level leading to stability loss during high speed cogging process based on kinetic energy method 24 p3884 A71-44897
- Cylindrical and weakly concave shells, testing critical pressure relationship to axial tension load with celluloid models 24 p3884 A71-44898
- Finite plane strain inflation of compressible hollow circular cylinder, using perturbation method for nonlinear boundary value problem 24 p3884 A71-44955
- Circular cylindrical laminated anisotropic shells with axisymmetric shape imperfections, investigating upper bound buckling loads 24 p3841 A71-44958
- Cylindrical shell under longitudinal load, examining stress-strain state with semimoment theory 24 p3884 A71-45017
- Conical and cylindrical shell deformation with nonlinear one dimensional wave processes, describing algorithm for method of characteristics application 24 p3885 A71-45341

CYLINDRICAL TANKS

- Optimal viscous damping effect of cylindrical filled fuel tanks on satellite nutations 06 p0979 A71-17417
- Vertical circular cylindrical tank with shallow spherical shell bottom filled partially by ideal incompressible liquid, calculating joint oscillations 06 p0994 A71-17826
- Quasi-stationary one dimensional thermoplastic stress strain state in cylindrical fuel tank during emptying process, allowing for Bauschinger effect 13 p2157 A71-29196
- Dynamic characteristics of fluid oscillations in cylindrical vessel divided by annular diaphragm 13 p2050 A71-29236
- Rotating liquid flow impulsive spin-up and spin-down in finite cylindrical containers, deriving simplified mathematical model at Reynolds number 1002 18 p2901 A71-35853
- Gas heating and energy balance of HF ring discharge in rare gases within cylindrical vessel, discussing electron energy distribution functions 20 p3273 A71-39044

Buoyancy and surface-tension induced fluid instabilities in open and closed vertical cylindrical containers from series solution by Jeffreys-Goldstein method

21 p3367 A71-40667

Cylindrical space simulation chamber with spherical test subject, deriving molecular incidence rate from integral equations with probability matrix for finite partial surfaces

24 p3816 A71-45138

CYLINDRICAL WAVES

Diffraction of cylindrical wave on thin infinite weakly reflecting cylindrical shell

01 p0128 A71-11212

Cylindrical shock waves generation from instantaneous energy release along line in quiescent atmosphere studied by numerical integration of flow equations

01 p0072 A71-11471

Radiation effects on cylindrical magneto-hydrodynamic shock propagation in plasma, deriving jump conditions in terms of Mach number and pressure ratios

02 p0294 A71-12847

Cylindrical electromagnetic wave amplification in TWT with radial line and diverging electron flux

05 p0727 A71-16003

Cylindrical blast waves analytical solutions by combined parameter, coordinate and matched asymptotic expansions

05 p0833 A71-16504

Cylindrical shock wave propagation in inhomogeneous exponential atmosphere from extension of method for spherical wave

07 p1089 A71-19742

Polynomial approximation of current along thin isolated asymmetrical cylindrical dipoles

09 p1419 A71-23506

Cylindrical shock wave in solid body rotating gas for angular variation effects on shock velocity, using similarity method

10 p1593 A71-24405

Strong cylindrical and spherical electromagnetic wave propagation in plasmas, calculating amplitude and electron temperature

11 p1805 A71-25768

Algorithm for numerical analysis of cylindrical shock wave propagation in stationary ideal gas

13 p2046 A71-27903

Steady state scattering of cylindrical magnetoacoustic waves traveling along axis of rigid ideally conducting static cylinder

13 p2105 A71-28281

Plane and cylindrical waves three dimensional propagation, investigating finite electrical fluid conductivity and radiation effects in MGD

16 p2618 A71-33172

Plasma energy cumulation by concentric spherical and cylindrical waves, calculating stability limit by integral solution

16 p2619 A71-33355

Nonuniform self propagation of cylindrical imploding shock waves in electrically conducting gas

18 p2951 A71-36005

Strong cylindrical and spherical electromagnetic wave propagation in plasmas, calculating amplitude and electron temperature

22 p3579 A71-41536

Cylindrical electromagnetic wave amplification in TWT with radial line and diverging electron flux

22 p3524 A71-42752

CYLINDROIDS

U CYLINDRICAL BODIES

CYSTEAMINE

Cysteamine and penicillamine effects on copper ion charge transfer, using electron spin resonance and optical absorption measurements

07 p1033 A71-18935

Sulphydryl cysteamine and disulfide cysteamine effect on bacteriophage survival rate at high anaerobic doses

07 p1033 A71-18938

Cysteamine protection of hydroxyurea sensitized Chinese hamster lung cells during X ray exposure

07 p1034 A71-18947

Cysteamine AET, serotonin and mexamine anti-radiation drugs, investigating protective effect against fractionated lethal gamma irradiation

07 p1037 A71-18969

Rats and mice blood redox potentials injected with cysteamine, investigating increased radioprotection

07 p1039 A71-18980

Metabolic effects of sulphur containing cysteamine, cysteamine and cysteine radioprotective drugs on oxygen uptake in rats

07 p1039 A71-18982

Cystamine effects on lymphocytes chromosomal aberrations in human peripheral blood during local fractionated gamma irradiation

08 p1240 A71-21797

Pathomorphological and histochemical changes in rat lungs, liver, heart, diaphragm and adrenal glands from acceleration and cysteamine caused tissue oxygen deficiency

22 p3491 A71-42703

Death rates, median life span and weight in mice exposed to gamma radiation after intra-abdominal injections of cysteamine

22 p3505 A71-42712

Cystamine elimination rates in rats, extending radiation protective action by reinjection of eliminated portions

22 p3492 A71-42714

Gamma emission effect on cystamine toxicity elimination in rats organism

22 p3492 A71-42715

Cystamine hydrochloride or vitamin B complex with vitamin C for radiation sickness prevention and therapy

22 p3493 A71-42723

Mice acceleration before and after gamma irradiation, determining protective effect of cystamine in adrenaline and amphetamine mixture

22 p3494 A71-42726

Radioprotective effectiveness of cystamine and S beta-aminoethylisothiuronium in mice under combined gamma irradiation and transverse acceleration loads

22 p3494 A71-42730

CYSTEINE

Radioprotective effect of cysteine on lysozyme in dilute aqueous solution, discussing scavenging water radicals

07 p1032 A71-18932

Cysteine incorporation in *Escherichia coli* B, noting X ray sensitivity and radioprotection

07 p1034 A71-18942

Metabolic effects of sulphur containing cysteamine, cystamine and cysteine radioprotective drugs on oxygen uptake in rats

07 p1039 A71-18982

Cysteine prevention of fatty liver induced by carbon tetrachloride and ethionine

07 p1040 A71-18987

CYSTS

Internal short chain alkane populations of paraffinic hydrocarbons in tobacco teratoma and habituated tissue cultures

21 p3345 A71-40204

CYTOCHROMES

Halophilic bacteria electron transport chain, studying protein, phospholipids, flavoproteins and cytochromes sedimentation properties by electron microscopy and light scattering technique

21 p3334 A71-40593

CYTOGENESIS

Space flight effects on survival, mutation and cell development of *Chlorella* cells suspensions onboard Zond 5 spacecraft

01 p0019 A71-11554

Astronaut chromosome aberrations, presenting peripheral blood leukocytes cytogenetic tests for pre and post space flight

20 p3188 A71-39227

CYTOLOGY

Vestibular sensory epithelial cells form and organization, discussing morphological polarization

04 p0536 A71-14760

Automatic cytophotometric techniques including microphotometer, ultramicrospectrophotograph, radiographic analyzer, microinterferometers, cytofluorometer and differential microfluorometer

06 p0864 A71-18693

Cytophotometric method using digital computer program and scanning microscope

06 p0864 A71-18694

Cytotoxic and radiosensitizing effect of thiol binding agents iodoacetamide /IAA/, N-ethylmaleimide /NEM/ and iodoacetic acid /IA/ on crypt cells of mice duodenum

07 p1038 A71-18975

Model experiment for purposeful motor behavior in cells or elements medium, assuming cell to cell system movement, adjacent cell visibility and different reaction to nearby cells

07 p1051 A71-20124

Mammalian cells cultivation at suboptimal temperatures, considering reproduction and cytophysiological changes

20 p3188 A71-39220

Specific banding patterns for identification and structural detection of human chromosomes, using differential staining method

21 p3336 A71-40853

DNA synthesis in human aorta endothelium reproduction, reporting intact nuclei and dyed cell membrane samples cytophotometric studies results

23 p3635 A71-44053

Morphological and cytochemical changes in red and mixed skeletal muscles of animals exposed to hypokinesia

23 p3636 A71-44237

CYTOPLASM

Cytophotometric study of DNA content in fibroblasts from human blood vessel walls, discussing cell proliferation and ploidy

09 p1392 A71-22609

Protein content in cytoplasm of neurons and glial satellite cells in supraoptical and red nuclei of white

rat brains during natural and paradoxical phase deprived sleep

19 p3005 A71-38545

CZOCCHRALSKI METHOD

Silicon single crystal dislocation free growth by Czochralski and Dash methods

05 p0792 A71-16292

D

D LAYER

U D REGION

D LINES

Sodium D line flare emission on solar surface via comet scattering, using photoelectric observation in undisturbed center disk region

10 p1660 A71-23791

Solar Na D lines Doppler width, describing limb darkening data, assuming source function frequency dependent

12 p1970 A71-27748

Solar atmosphere center limb observations, describing line intensity fluctuations in Na D and Na 5688 doublets and Mg 4571 line

13 p2140 A71-29044

Solar spicules H alpha and beta, D3 and K line profiles, considering radial and turbulent velocities, optical thickness, atomic density and He emission

13 p2140 A71-29049

Interstellar 21 cm and Na D lines comparison in directions of 30 stars at intermediate and high galactic latitudes

14 p2304 A71-29595

Na D lines broadening by atomic H, discussing interatomic forces between Na and H atoms in terms of NaH molecular potentials

16 p2614 A71-33101

Single plate interferometer tested by Na vapor anomalous dispersion near D lines, considering application to hook interferometry

16 p2578 A71-33158

Solar limb D3 He line intensity distribution measurements during eclipse of 22 September 1968

19 p3147 A71-38666

High resolution spectroscopy of Na D resonance lines in saturated absorption with repetitively pulsed tunable dye laser

21 p3391 A71-40199

D REGION

Solar hard X ray absorption in D region, calculating integral flux radiation

01 p0145 A71-11076

Quiet D region structure exponential model based on E layer reflection measurements

01 p0074 A71-11079

Ionospheric stability in nighttime and daytime auroral zone with E layer corpuscular stream disturbances

02 p0243 A71-11762

Energetic electron precipitation effects on upper D region wave cluster ion population at various vapor mixing ratios

02 p0245 A71-11961

Ozone screening heights from sunrise effects on D region VLF wave reflection

02 p0212 A71-11968

Hydrogen Lyman alpha radiation intensity and atmospheric absorption before and during solar eclipse of 20 May 1966, considering D region ion production

03 p0407 A71-13376

Solar X-rays role in D region ionization from ion probe sounding during eclipse of 20 May 1966

03 p0407 A71-13377

D region electron density time variations, using partial radio reflection technique during solar eclipse of 20 May 1966

03 p0407 A71-13379

Rocket experiments during 1964 solar eclipse, obtaining D region parameters from parachute-borne blunt probe measurements of atmospheric positive and negative conductivities

03 p0416 A71-14033

Midlatitude nighttime D region ionization source, considering precipitating energetic electrons

03 p0420 A71-14527

Hydrated hydronium ions in D region, discussing sources and production mechanisms

03 p0421 A71-14546

D region exponential model application to high solar activity conditions, using absorption measurement data

05 p0742 A71-16813

D region aeronomy characteristics and ionizing radiation energy spectra during solar flare of 22 October 1969

05 p0799 A71-16818

Diurnal variations of loss factor in D region during polar cap absorption, verifying nighttime D region model by forward propagation data

05 p0744 A71-17185

D region electron density profile relation to radio wave absorption frequency dependence

05 p0746 A71-17204

Ionization in ionosphere E and upper D regions, considering solar short wave radiation, small components, atmospheric dynamics and vertical mass transport

06 p0894 A71-18251

Quasi-exponential model of electron vertical profile in D region for aeronic and ionizing radiation characteristics during solar flare of 30 October 1969

07 p1195 A71-19393

Natural aerosols effects on atmospheric electron content, comparing theoretical prediction with experiments on artificial aerosols in D region

07 p1100 A71-19404

D region oxygen photoionization rates decrease due to carbon dioxide absorption

07 p1103 A71-19673

Night D region ion kinetics data during thermonuclear detonation, discussing formation and conversion rates, electron concentration and recombination

08 p1278 A71-21009

Midlatitude D region considering electron concentration height distribution, ionization process and solar activity effects

10 p1606 A71-24916

D and E region electron density height distribution profiles, using multifrequency absorption data

10 p1606 A71-24920

Solar corpuscular radiation differential and integral spectrum, assessing energetic electron flux in D region at sunrise

11 p1815 A71-25587

Echo reflections and transition through critical coupling in D and E regions at low and medium frequencies, using nighttime electron density distributions

11 p1754 A71-25601

Meteorological, geomagnetic and extraterrestrial variations of cosmic ray layer electron production rate in lower D region

11 p1816 A71-25610

International coordinated solar chromospheric flare effects on D region lower boundary and ionospheric propagation by Cosmos 261 satellite and ground based observatories

11 p1816 A71-25763

D region atomic oxygen measurement via Nike Cajun sounding rocket flight

13 p2056 A71-27932

Diurnal variations of loss coefficient in D region during polar cap absorption, verifying nighttime D region model by forward propagation data

13 p2059 A71-28242

D region electron density profile relation to radio wave absorption frequency dependence

13 p2059 A71-28259

Electron density profile determination in D region based on frequency dependence of radio waves absorption, discussing lower ionosphere anomalous ionization

13 p2061 A71-28539

Electron concentration profiles in D region from radio wave partial reflection coefficients

13 p2030 A71-28558

D region negative ion densities in chemical equilibrium based on electron density observation, noting role of ozone and carbon dioxide

14 p2228 A71-29533

Midlatitude D region electron density winter variability causes consideration based on enhancements, absorption and ionization changes data during stratospheric warming

14 p2237 A71-30944

Ionospheric propagation, considering traveling disturbances, sporadic E phenomena, plasma frequency distributions and D region parameters

14 p2202 A71-30950

Cluster ions concentration and nitric oxide in mesosphere D region, considering electron density profiles

15 p2394 A71-31430

Solar UV radiation data during 7 March 1970 eclipse from photometers sensitive to narrow bands, discussing sources, atmospheric absorption and D region ionosphere

16 p2627 A71-33773

Day and nighttime effective electron loss rate measurement in D region during polar cap absorption events, using rocket-borne spectrometers and Faraday rotation

16 p2573 A71-33961

D region winter anomaly causes from coordinated rocket measurements, discussing electron density profiles and electron-ion recombination

17 p2731 A71-34315

D and E regions advances during 1967-1971 covering ionic composition, electron density profile at various latitudes, hours and seasons during eclipses and winter anomalies

17 p2732 A71-34464

D region electron densities from HF radio waves ionospheric backscatter based on hypothesis of refractive index stochastic fluctuations

19 p3048 A71-37372

Quasi-exponential model of electron vertical profile in D region for aeronic and ionizing radiation characteristics during solar flare of 30 October 1969

19 p3127 A71-37817

Natural aerosols effects on atmospheric electron content, comparing theoretical prediction with experiments on artificial aerosols in D region

19 p3053 A71-37828

Nighttime D region behavior under ionization by X ray spectrum of Scorpius source

19 p3017 A71-37864

Mass spectrometric measurements of negative ion concentration in D and lower E regions

19 p3127 A71-38031

Mass spectrometric measurement of negative ion concentration in nighttime D region

19 p3128 A71-38033

Electron concentration and collisions number fluctuations effect on D region profiles based on radio waves partial reflection data

19 p3057 A71-38365

D region ionization by electron fluxes as explanation for latitudinal radio wave absorption

19 p3057 A71-38370

D region ionization by solar corpuscular streams, considering formation of charged particle concentration profiles

20 p3216 A71-39141

Night D region ion kinetics data during thermonuclear detonation, discussing formation and conversion rates, electron concentration and recombination

20 p3219 A71-39589

D region electron density profiles and ionization models in terms of XUV radiation and minor constituents NO and oxygen, using ground and space measurements

20 p3224 A71-39713

D region night airglow OH emissions and IR atmospheric diatomic oxygen bands excitation mechanism with aid of model involving solar photodissociation

20 p3226 A71-39831

F 2 and D regions disturbances associated with magnetic storms, emphasizing airglow effects

20 p3227 A71-39836

International coordinated measurements of solar chromospheric flare effects on D region lower boundary and ionospheric propagation by Cosmos 261 satellite and ground based observatories

22 p3591 A71-41531

Sporadic E layer observation by reference electrode of electron temperature probe on sounding rocket, determining electron density below 85 km in D region

23 p3671 A71-43367

DAEMO [DATA ANALYSIS]

U DATA PROCESSING

U DATA REDUCTION

U DATA TRANSMISSION

DAMAGE

NT IMPACT DAMAGE

NT METEORITIC DAMAGE

NT PROTON DAMAGE

NT RADIATION DAMAGE

NT RAIN IMPACT DAMAGE

Overload and underload effects on Al-Mg-Si creep deformation and damage accumulation under single load change

05 p0768 A71-16800

High intensity electric current damage in boron and graphite filament reinforced epoxy resin composites

07 p1145 A71-19945

Alloy equivalent susceptibility to damage at intermediary service periods and different stress levels under creep conditions at 750 C

08 p1317 A71-21709

Structures dynamic loading and damage by sonic booms, discussing structural response prediction by boom pressure wave model

10 p1693 A71-25052

Wire connection damage due to high vibration, examining termination and joining techniques

18 p2852 A71-36837

Peak optical flux density for catastrophic damage in close confined and double heterojunction injection Al-GaAs-GaAs lasers

19 p3075 A71-38507

DAMPERS

Steady state motion equations of multiple unit impact damper attached to periodically excited primary system, developing solution for mathematical model

03 p0505 A71-13547

DAMPING

NT ELASTIC DAMPING

NT LANDAU DAMPING

NT VIBRATION DAMPING

NT VISCOUS DAMPING

Mechanical characteristics of generalized Rayleigh waves in piezosemiconductors of cubic symmetry, deriving amplification and damping factors for zero diffusion coefficient

02 p0294 A71-11894

Photosphere and facula turbulent velocities and damping constants from Ni and Fe IR lines analysis

02 p0306 A71-12079

Rectangular waveguide with T junction, deriving characteristic impedance, maximum power and damping constant

05 p0719 A71-15997

Proton whistlers damping compared to predictions by cyclotron damping theory, discussing proton density

06 p0949 A71-17262

Dynamic damping coefficient extracted from flight test lateral rate data telemetering ablative reentry vehicle

[AIAA PAPER 71-49]

06 p0980 A71-18510

Two-body satellite of axisymmetric rigid bodies interconnected by lossy universal joint, calculating transient oscillation damping of forced precession under external torque

07 p1205 A71-18895

Temperature effects on energy dissipation during vibration in ferromagnetic and nonferromagnetic metals, comparing damping capabilities for homologous temperatures

08 p1306 A71-21119

Static tensile stresses effect on magnetized ferromagnetic materials damping properties explained by anisotropic micropartial strains dissipating energy during bending vibration

08 p1306 A71-21120

Photosphere and facula turbulent velocities and damping constants from Ni and Fe IR lines analysis

08 p1361 A71-21129

Ribbed aluminum panels airborne sound transmission loss, evaluating structural damping effects

08 p1231 A71-21431

Damping effects in three frame rotary gyroscope due to force originated by static joint housing design

09 p1449 A71-22794

Asymmetric missile nonlinear angular motion, describing quasi-linear relations for frequencies, damping rates and swerving motion amplitude

09 p1532 A71-22906

Liquid sloshing in liquid propellant containing orbiting vehicle stabilized by active control system, examining expression for ring baffle slosh damping under reduced gravity

09 p1532 A71-22913

Strain effect on ultrasound damping in single W crystals, considering microhardness

09 p1477 A71-23328

Weak damping of free gyro motion in static coordinate system under dry friction in gimbal joint, deriving equations of motion by Lagrange method

13 p2069 A71-28932

Elastic stability of compressed beams, giving method for evaluating neutral axis form and critical load in buckling

13 p2157 A71-29321

Elastic stability and buckling behavior of transversely isotropic rectangular Mindlin plate under initial stress and displacement

14 p2324 A71-29871

Second order stresses and elastic stability analysis for structures, using supplementary load method

16 p2648 A71-32981

Damping disturbances structure in unbounded laminar flow stability at large Reynolds numbers, demonstrating damping modes eigensolutions in form of concentrated wave packets

16 p2559 A71-33022

Heating by thermoelastic damping through sudden removal of stresses on homogeneously strained elastic body, comparing elastic deformation of rubber and steels

17 p2821 A71-34584

Neutral atoms and ions collision damping constants estimation for spectrum synthesis, using approximate formula based on Stark broadening effect

21 p3442 A71-40160

Rectangular waveguide with T shaped pedestal, deriving characteristic impedance, maximum power and damping constant

22 p3515 A71-42746

Gyroscopic systems dynamic drift reduction by inertial damping, using astatic and static stabilizers

23 p3675 A71-43295

Three dimensional incompressible anisotropic body with small deformations, calculating elastic stability theory with variational principle

24 p3880 A71-44708

DAMPING FACTOR

U DAMPING

DAMPING IN PITCH

U DAMPING

U PITCH [INCLINATION]

DAMPING IN ROLL

U DAMPING

U ROLL

DAMPING IN YAW

U DAMPING

U YAW

DAMPING TESTS

Damping in gravity graded satellite passive stabilization systems under eddy currents and dry friction induced by magnet motion

02 p0319 A71-11908

Support systems relative efficiency in external damping free-free configuration production for flexing beam
05 p0828 A71-16967

Damping in gravity gradient satellite passive stabilization systems under eddy currents and dry friction induced by magnet motion
13 p2144 A71-28195

On-line digital dampometer for free oscillation wind tunnel model study under varying Mach number and stagnation pressure avoiding flutter destruction
21 p3363 A71-40391

DAMPNESS

U MOISTURE CONTENT

DANGER

U HAZARDS

DARK ADAPTATION

Background nonequivalence during long term photopic dark adaptation
01 p0008 A71-10143

Cats photopic and scotopic spectral sensitivity functions from dark adaptation curves, using behavioral tracking procedure
01 p0009 A71-10232

Eye movements in dark during attempt to maintain ocular position defined by prior viewing of fixation target
01 p0016 A71-11388

Optic analyzer dark adaptation dynamics during spatial body position changes, observing restoration speed dependence on physical training
03 p0364 A71-13523

Retinal threshold along horizontal meridian for dark and light adapted eyes for stray light from small foveally fixated high luminance target
08 p1247 A71-21000

Electroluminescent aircraft instrument lighting effects on pilots dark adaptation taking into account color, panel legibility, scotopic sensitivity and acuity
08 p1248 A71-21229

Dark adaptation in humans under Arctic conditions, noting role of physiological disorders
08 p1242 A71-21958

Darkness adapted human eye, investigating absolute light perception threshold dependence on light stimulus gradient
09 p1391 A71-22487

Electroretinogram b-wave slope reduction by cooling of dark adapted frogs during serial flash stimulation
10 p1564 A71-24442

Spatial and temporal patterned light flashes effects on dark adapted subjects, discussing cortical response changes in contrast depth
10 p1565 A71-24680

Human rods dark adaptation, investigating rhodopsin resynthesis and bright light flash effects
11 p1718 A71-25635

Light flashes in eyes of dark adapted Apollo astronauts, considering Cerenkov radiation effects from primary cosmic ray single charged particles on retinal elements
12 p1933 A71-27383

Night vision and dark adaptation of eye, noting sunlight effects on visual acuity
13 p2017 A71-28392

Dark adapted albino rats behavioral assessment, measuring absolute visual thresholds to white and colored light
13 p2008 A71-28457

Acuity-dark adaptation in strabismic amblyopia, discussing mechanisms for defects
13 p2012 A71-28833

Pupil size effect on dynamics of pupillary movements, considering reactions to light and darkness
13 p2013 A71-29032

Human electroretinographic dark adaptation recovery curves rod-cone break time dependence on bleach intensity
14 p2185 A71-30503

Beta inflection in darkness adaptation curve, postulating stimulus thresholds in mono and binocular examinations for perception time and sensitivity
16 p2527 A71-32866

Subjects with strabismic amblyopia, investigating defects in cone or rod mechanisms of dark adaptation by using colored filters
18 p2854 A71-36011

Threshold electrical phosphene dependence on impulse duration and stimulation frequency in subjects adapted to darkness
19 p3002 A71-37444

Receptive fields of dark adapted cats striate cortex neurons as function of barbiturate anesthetic level
23 p3634 A71-43871

Quantitative variation in anesthetized cats striate cortex receptive fields as function of light and dark adaptation
23 p3634 A71-43872

Light brightness and duration effect on central vision response time during dark adaptation
24 p3795 A71-44535

DARKENING

Photoelectric photometer with mechanical chopper for extreme limb darkening measurement at total eclipse
03 p0424 A71-13635

DARKNESS

Bright-dark asymmetry testing in solar granulation photography by objective method
19 p3146 A71-38663

DART TURBOPROP ENGINES

U TURBOPROP ENGINES

DASSAULT AIRCRAFT

NT MIRAGE 3 AIRCRAFT

Dassault Mercure short range twin jet aircraft capable of using powerful engine
13 p1997 A71-29276

DASSAULT MIRAGE 3 AIRCRAFT

U MIRAGE 3 AIRCRAFT

DATA ACQUISITION

CAMAC computer guided data acquisition system design and operation
01 p0049 A71-10260

Computerized acquisition and processing of radar precipitation signals and lightning data
01 p0050 A71-10595

Remote sea state information acquisition system using video attachment to radar for sea return spectrum recording and analysis
01 p0031 A71-10600

Apollo integrated shell static and dynamic testing, describing data acquisition system techniques
01 p0067 A71-10863

Instrumentation System Margin Analysis Program /ISMAP/ for ICBM telemetry data acquisition systems performance tests
01 p0032 A71-10882

Data transmission/acquisition/processing systems engineering project management using digital simulation models
01 p0184 A71-10885

Projectile P band FM/FM telemetry system for in-barrel data acquisition
01 p0034 A71-10912

Data acquisition system using associative processor for redundancy removal algorithm
01 p0050 A71-10983

Information collection from ocean data stations networks by satellite and HF digital data communications, noting feasibility of VHF telemetry communications
01 p0037 A71-10991

Science studies, prediction and information procurement - Conference, Kiev, December 1967
02 p0334 A71-11851

Medical data acquisition - Conference, Nancy, France, June, 1969
02 p0206 A71-12106

Thermionic converter with oriented W electrodes, discussing computerized data acquisition system for mapping I-V performance
02 p0193 A71-12215

Open cluster NGC 7789 blue stragglers data acquisition from image tube spectrograms and four color and H beta photometry, obtaining location along main sequence
02 p0314 A71-12583

Biotelemetry data acquisition and electrode technology, discussing physiological measurements and pickup techniques for conversion into electrical signals
03 p0369 A71-13060

Sounding rocket Solar Eclipse Sensor for 7 March 1970 event, discussing mission, capabilities, data acquisition and design [ALAA PAPER 70-1406]
03 p0455 A71-13685

NASA Office of Tracking and Data Acquisition mission support and ground and spacecraft communication networks
04 p0551 A71-14936

Satellites interrogation, recording and location system for data acquisition from deployed remote instrumented platforms
05 p0743 A71-17134

Synchronous meteorological satellite mission goals and system design, describing imaging, data collection, facsimile, space environment, trilateration, ranging and transmission
07 p1067 A71-18807

Central station of German ground system for satellite data acquisition, tracking and telecommand
07 p1082 A71-19021

Multiple sensor heart rate telemetry using automatic data acquisition and management in squirrel ecology
07 p1049 A71-19626

Engineering data integrated test system with sensor based digital computer for data collection and test control
07 p1069 A71-20202

Computer controlled ground based command and data acquisition software system for OAO-A2 spacecraft remote control stations, discussing interface with monitor and interrupt capabilities
08 p1259 A71-21658

Operational uniformity requirements for large meteorological station networks, emphasizing data acquisition and processing
08 p1327 A71-21717

Satellite laser tracking for geodetic data acquisition
08 p1285 A71-21800

Time shared digital computer-based data acquisition and control system for multiple remote laboratories using modular programming, multiprocessing and language processors
08 p1260 A71-21858

Combustion research laboratory at Purdue University consisting of buildings, housing test cells, data acquisition system, propellant storage and instrument service area
09 p1427 A71-22727

Special purpose analog and digital data acquisition systems for test and instrumentation requirements
09 p1449 A71-22788

World crop areas, yield, production and land use data, using remote sensing devices
09 p1439 A71-23218

Urban housing environment data acquisition from remote sensor imagery, stressing rapid surveys and data timeless attribute
09 p1439 A71-23218

Digital synthesizers design and operation for radio communications, discussing reception and transmission noise performance, frequency stability and data acquisition time
10 p1579 A71-24757

Real time high resolution mass spectroscopy using digital computer techniques for data acquisition, processing and presentation
11 p1761 A71-25220

Computer acquired performance mapping of fixed spaced planar diode with etched Re emitter and Nb collector over wide operating temperature range
11 p1737 A71-25907

Pan American reliability program effect on airline maintenance, considering cost effectiveness, aircraft performance, data collection and analysis
12 p1910 A71-26671

Airborne remote sensing for oceanographic data acquisition in UV, visible, IR and microwave spectrum using reflected and emitted radiation instruments
12 p1902 A71-27260

Four dimensional space-time meteorological observation data assimilation schemes and problems
13 p2096 A71-28014

Acquisition system consisting of positioning of local station burst signal in time slot for PCM-TDMA satellite communication system, discussing design and performance tests
13 p2034 A71-29393

Noctilucent clouds observations and data acquisition, considering cloud amount and thickness calculations
14 p2233 A71-29969

Self contained lightweight airborne data acquisition system for atmospheric and meteorological research, using analog recorder and telemetry system
14 p2243 A71-30311

Computer controlled acoustic data acquisition system with real time control of 16 high intensity acoustic generators
14 p2208 A71-30315

Direct digital control and data acquisition system for propulsion research testing, transmitting data over differential signal pairs to remote test cell
14 p2208 A71-30316

Fluctuating pressure measurements in jet engine testing, using miniature transducers with calibration and data acquisition equipment
14 p2244 A71-30325

Automated modal data acquisition and processing system /MODAPS/ for real-time modal vibration testing of complex aerospace vehicle structures, describing features, capabilities and utilization
14 p2245 A71-30341

Synchronous meteorological satellite data collection and transmission system error control, considering design tradeoffs for radio sets and coding techniques
14 p2198 A71-30899

Performance and cost design tradeoff between HF and synchronous meteorological satellite data collection systems, considering platform transmitting power and SNR
14 p2198 A71-30900

Random multiple access technique for satellite data collection, taking advantage of frequency instability associated with oscillator circuits
14 p2199 A71-30908

ERTS telecommunication system for space tracking and high resolution multispectral image data acquisition and commanding
14 p2199 A71-30912

Book on sources and availability of IQSY data, Volume 7, covering stations, sounding rockets, satellites, space probes and World Data Centers catalog
15 p2395 A71-31518

Canadian program of remote sensing for gathering information on earth resources and environment
16 p2566 A71-33749

ERTS system, considering multispectral data acquisition, relay devices and spacecraft and ground information processing 17 p2812 A71-34611

ATC system improvement, presenting data acquisition upgrading and ground automation-aircraft navigation systems interface 17 p2771 A71-34614

ATC avionics equipment, discussing inertial area navigation, autopilots, airborne data acquisition, altitude reporting, collision avoidance, CAT, satellite communications, etc 17 p2771 A71-34615

Telescope automation using servocontrolled drive with spur gearing and dual opposed motors for data acquisition separation and minimum program interaction 17 p2740 A71-34982

Raw remote sensor data acquisition relationship to economic activity and interpretation for earth resource/environmental information 18 p2912 A71-36067

Computer-disk interface system photooptical instrumentation for weather data acquisition, analysis and display 18 p2884 A71-36078

Fluidics analog to digital signal techniques, discussing data transmission, acquisition and processing 18 p2851 A71-36206

Computer simulation model for experimental data in post-Skylab space station design 18 p2973 A71-36458

Ground acquisition of digital rate synchronization during experiments in French Disources project 18 p2946 A71-36512

Worldwide data acquisition and tracking of meteorological balloon stations by flyby gravity stabilized satellite 18 p2878 A71-36528

Numerical methods for noise elimination from ERTS pictorial data, describing data acquisition system 18 p2886 A71-36542

Telecommunications satellite data acquisition from automatic beacons, discussing Eole program 18 p2988 A71-36543

Papers on communication satellites for 1970s covering various national domestic systems, aeronautical service, ERTS data transmission and collection problems, etc 21 p3347 A71-40473

Satellite observations for earth resources management, discussing operational ground-based remote sensor system and information extraction techniques 22 p3534 A71-41973

Computer controlled multichannel high speed data acquisition and processing system featuring redundant data deletion, arbitrary number of predeterminations and printing output in full English statements 22 p3517 A71-42108

TV data acquisition system for auroral and ionospheric research, noting visual and subvisual detection sensitivity 23 p3677 A71-43515

DATA ADAPTIVE EVALUATOR/MONITOR

U DATA PROCESSING

U DATA REDUCTION

U DATA TRANSMISSION

DATA ANALYSIS

U DATA PROCESSING

U DATA REDUCTION

DATA COMPRESSORS

U DATA REDUCTION

U DATA TRANSMISSION

DATA CONTROL SYSTEMS

U DATA SYSTEMS

DATA CONVERSION ROUTINES

NT SUBROUTINES

DATA CONVERTERS

NT ANALOG TO DIGITAL CONVERTERS

NT DIGITAL TO ANALOG CONVERTERS

Logarithmic signal converter with parallel circuits arrangement for large dynamic range operation 02 p0231 A71-12040

Eight channel physiological data scanning and timing control, sequential conversion, printing and punching 05 p0714 A71-16923

Converter-indicator direct digital readout design, using photodiodes for LSI VOR area navigation display systems low power operation 09 p1491 A71-22610

Design principles of complex value converters with selfbalancing circuits based on generalized graph of essential information transformations 12 p1892 A71-27024

Magnetic mirror system measured axial energy distribution of electron beams conversion to equivalent electrostatic analyzer 14 p2249 A71-30886

Electro-pneumatic transducer for conversion of electrical into fluidic signals, using temperature depen-

dence of laminar gas jet deflection angle in flow along heated curved wall 15 p2353 A71-32072

Logic devices of adaptive scale-time converters of single pulsed processes on electron beam memory tubes, proposing polynomial methods of data reduction 18 p2887 A71-35881

Static converters of computer graphic information using photoreceivers with linearly decreasing and increasing spatial sensitivity 18 p2884 A71-35882

Tridea ALTAPE /automatic line tracing and programming/ system for drawing data conversion to tape for machining surfaces in direct numerical control applications 19 p3068 A71-37244

Return beam vidicon characteristics and applications for reconnaissance, optical storage and scan conversion, data and signal processing 22 p3548 A71-42509

Wideband solid state converter circuit for quantization of signals from semiconductor nuclear radiation detectors, noting cost reduction 23 p3677 A71-43527

Data transmitting and receiving instruments and systems development problems covering signal shaping and converters and information channel and data reception theories 24 p3806 A71-44375

DATA CORRELATION

NT SIGNAL ANALYSIS

Radar precipitation measurement accuracy improvement, using various Z-R relationships for correlation of radar data and rainfall rates 01 p0117 A71-10581

Meteorological radar rainfall estimates comparison with dispersed tipping bucket gage measurements during storms 01 p0118 A71-10582

Storm reflectivity models using weather radar and surface rainfall data correlations 01 p0118 A71-10585

Thermionic emitter work function extrapolation and interpolation, noting correlation to surface temperature and Cs pressure 02 p0294 A71-12202

Spectraspectroheliograph observations, noting correlations between contour maps of solar continuum intensity and magnetic fields [AIAA PAPER 70-1360] 02 p0315 A71-12693

Solar mm bursts impulsive component correlation with associated soft X ray burst 03 p0473 A71-13184

High pressure arc heater data correlation for laminar and turbulent flows, examining radiation and thermal and electrical conduction effects 03 p0517 A71-13443

Correlation measurements by laser in turbulent gas flow, determining phase structure velocity distributions and coherence lengths 03 p0435 A71-13529

Earth and planetary surface soil dielectric constants and conductivity determination based on p-wave velocity data correlation 05 p0743 A71-17142

Solar 3.3 mm bursts observation, showing temporal correlation with soft X ray bursts 06 p0968 A71-17915

Cosmic rays neutron monitors daily data /July 1957-December 1962/, applying corrections for latitude, altitude, solar cycle phase and station efficiency 06 p0955 A71-18132

Parachute weight, configuration and strength correlations for tradeoffs and design 07 p1017 A71-18900

Correlation and spectrum analysis of simultaneous EEG data in mono and dizygotic twins using computer and FFT algorithm 08 p1246 A71-20746

Pressure conditions across distant magnetopause from interplanetary magnetic field measurements, comparing Pioneer 7 plasma data with Explorer 33 distant geomagnetic tail field magnitudes 08 p1285 A71-21692

Static aerodynamic data correlation for high subsonic speed transport aircraft model in transonic wind tunnels, including relative buoyancy and turbulence effects 09 p1429 A71-23423

[AIAA PAPER 71-291] Auroral zone magnetic substorm correlation to magnetospheric plasma drift 09 p1441 A71-23640

Organic adhesives performance evaluation based on correlations between accelerated laboratory aging tests and underground exposure in adverse environments 10 p1633 A71-24113

Real and observable radius of roughly dispersed liquid aerosols correlated by electrophotographic method, assessing galactic cosmic rays energy 11 p1815 A71-25582

Correlation, transfer and coherence functions in measurements, using digital signal analysis 11 p1731 A71-25597

Outer radiation belt energetic electron flux intensity correlation with auroral activity and Kp index 11 p1816 A71-25760

ATM for manned solar observation, discussing thermal design, thermal vacuum test philosophy, mathematical models and analytical and test data correlation [AIAA PAPER 71-433] 11 p1838 A71-26222

Computer simulation of fading records in spaced antenna ionospheric drift experiment, detecting mean direction and diffraction pattern velocity with correlation analysis 13 p2054 A71-27800

Hysteresis loop measurements and functional measurements correlation on periodic permanent magnet stacks of TWT ring magnets of Sm-Co alloy 14 p2285 A71-30705

Binary pulse sequences correlation and synchronization, developing effectiveness criteria with two stage measures 14 p2201 A71-30927

Pc-type micropulsation amplitude variation correlation at separate places up to 10,000 km distances, suggesting pi-type as cause 15 p2395 A71-31435

Telemetry polarization diversity combiners for data dropout elimination, considering input signal characteristics and propagation 15 p2370 A71-31642

Supersonic flow base pressure correlation based on reduced Reynolds number in mixing region 15 p2346 A71-32121

Pulse compression and optical data correlation in side-looking radar, considering Doppler effect 15 p2374 A71-32650

German monograph on correlation of Vickers and Rockwell C hardness testing methods covering indentation form measurements, deformation work, etc 17 p2739 A71-34797

Intermittency signals correlation, determining lateral motion of two dimensional jet boundaries 18 p2901 A71-35854

Space-time correlation measurements in grid-generated isotropic turbulence, determining full- and narrow-band velocity signals Eulerian time correlation 18 p2902 A71-36035

In-flight noise radiation by wing-mounted jet engines on aircraft fuselage based on correlation with turbulent boundary layer pressure fluctuations 19 p2997 A71-37846

Surface layer humidity correlation to height of atmosphere emitting in IR spectral region, determining water vapor content by recording earth radiation angular distribution 19 p3054 A71-37974

Dynamic tear fracture toughness test and fracture mechanics parameter correlation for high strength Al alloys 20 p3248 A71-38771

Three phase code transformation task reliability and correlation, representing general/factor analytic intellectual abilities and personality characteristics 20 p3192 A71-39073

Higher order noisy optical pulse intensity correlations interpretation by statistical model, estimating spike amplitude 20 p3196 A71-39103

Outer space and earth surface galactic cosmic ray intensity data correlation analysis for studying interplanetary magnetic field structure 20 p3278 A71-39129

Heat transfer rate correlation with local surface pressure for blunt cones at angle of attack 20 p3176 A71-39355

Total lift data correlation for thin sharp edged low aspect ratio delta wings at low speeds, noting trailing edge effects in incompressible flow 20 p3176 A71-39398

Qualitative micrometeoroid model for predicting results of in situ experiments, considering correlation to Pioneer 8 and 9 results 20 p3300 A71-39654

ELF and VLF emissions during PCA, correlating data with particle and photometer recordings from ground based, satellite and rocket-borne observations 20 p3229 A71-39856

Visible optical pulsars search with Fourier and correlation techniques in X ray sources, supernova remnants, white dwarfs, IR stars, planetary nebulae, etc 20 p3304 A71-39939

Outer radiation belt energetic electron flux intensity correlation with auroral activity and Kp index 22 p3591 A71-41528

Optical information processing holographic techniques, describing random masks correlation method for pattern classification 22 p3539 A71-41747

Mean ratio of mass to three-halves power of luminosity for elliptical and lenticular galaxies based on catalog mass data emphasizing uncertainties 22 p3599 A71-41935

Ocean surface condition correlation to radar backscattering cross sections and wind velocity from scatterometer data 22 p3569 A71-42545

Psychological screening of pilot trainees, showing neurosis noncorrelation with learning ability to fly 23 p6339 A71-43221

Psychological screening of pilot trainees, investigating Minnesota Multiphasic Personality Inventory test data correlation with learning ability to fly 23 p6339 A71-43222

OSO satellite observed soft solar X-ray data correlation to solar activity 23 p3721 A71-43840

Planetary tidal forces correlation with solar activity distribution, observing Ca II H&K spectrum 23 p3768 A71-43851

Tables for aurora correlation with solar radio bursts at 185 MHz 23 p3769 A71-43908

Continued flight training correlation with general aviation aircraft accident rates reduction 23 p3641 A71-44252

Trace reflex formation in response to acoustic stimulus with verbal reinforcement, determining cross correlation connections between induced activity of auditory and motor areas 24 p3796 A71-44547

Hardened cast Al alloys with Cu additions, investigating correlation between mechanical properties and structure at room temperature 24 p3840 A71-45377

DATA HANDLING SYSTEMS

U DATA SYSTEMS

DATA LINKS

Centralized inquiry-response systems for information retrieval, analyzing voice-data communications interaction 01 p0048 A71-10220

Physiological data telemetry link using time division multiplex method 01 p0024 A71-10981

Antenna and telemetry system for spherical shell ICBM reentry vehicles data link to ground 01 p0036 A71-10986

Ultrawide bandwidth optical data link between earth satellites, discussing system design concept 02 p0214 A71-12024

Ultrawide bandwidth laboratory laser communication link for high fidelity signal transmission, discussing system configuration, components and preliminary test results 02 p0214 A71-12025

Skylink communication systems, describing long distance strategic communication links between ground and mobile air/helicopter stations via wide and narrow band pathways 02 p0218 A71-12439

Satellite regional broadcasting and telephony/data services cost model 02 p0221 A71-12781

Radio link diversity reception improvements by multiple baseband combinations in one or several stages 03 p0380 A71-14333

High altitude rocket-borne radiosonde communication, examining transmission link characteristics, signal losses and antenna radiation patterns 04 p0551 A71-15012

Remote area voice, teletype and data communication using satellites for providing links with central terminals, considering economic feasibility by cost analysis 04 p0555 A71-15338

Synchronous orbit satellite links in tandem for government and military telephone communications, discussing subjective evaluation for acceptability 05 p0725 A71-17070

Coherent communication link pseudonoise synchronization error due to white Gaussian noise and amplitude jitter produced by reference carrier phase error, discussing digital simulation 05 p0725 A71-17072

Error free SATCOM computer to computer data communication via satellite link 07 p1058 A71-18822

Multichannel laser telephone communication link experimental operation results in U.S.S.R. 07 p1058 A71-18838

Multipath distortion and wavenumber spectrum of refractive index in radio links 07 p1060 A71-19258

Combined data compression and error control by digital sequential decoding for space to earth data links using digital computers 14 p2193 A71-30023

L band aircraft antenna array consisting of circularly polarized elements and static electronic steering circuits for synchronous satellites radio links 14 p2273 A71-31074

Simulation equipment installation with link to Concorde flight simulator, discussing functional and operational features 15 p2384 A71-31885

Atmospheric laser link with automatic sensitivity control during reception, measuring detector output signal fluctuation reduction characteristics 15 p2372 A71-32319

Space radio communications, considering radio links reliability between multistage launcher rocket and ground stations 17 p2696 A71-34228

Satellite-to-aircraft links propagation characteristics, considering specular reflected signals, diffuse scattering and scattering function 17 p2705 A71-35097

Hadamard transform source encoding application to Apollo unified S-band telemetry links, considering possible system performance improvement 18 p2876 A71-36470

Satellite to aircraft radio link simulation, evaluating electronic scanning antenna operation, intelligibility, data transmission rate and distance measurement accuracy 18 p2945 A71-36511

Optical wideband digital communication system performing operational space-ground link functions 18 p2878 A71-36520

Intercontinental point to point radio communication, discussing Hertzian beam /radio relay links/ and satellite communication comparison with underground and submarine cables 19 p3016 A71-37343

RF noise surveys in urban areas for effective space to earth communication link design at UHF 19 p3021 A71-38443

Narrow beam acquisition and angle tracking for spaceborne laser communication links between low earth orbiting and synchronous satellite 21 p3348 A71-40805

Signal processing circuits for 1000 MS/S optical communication link using multiplier/signal switch, bit synchronizer and data regenerator 21 p3357 A71-40807

Carrier aircraft inertial navigation system /CAINS/ design, noting thermal modeling, statistically filtered alignment modes and digital data links 21 p3571 A71-42081

Bit error rate detector for testing digital data links, using analog network mathematical model 22 p3519 A71-42764

Relay data link and trajectory design integration for Viking orbiter 1975 mission [AAS PAPER 71-320] 23 p3726 A71-42994

Jupiter atmospheric probe using relay-link communications geometry between probe and flyby spacecraft for 3.5 hr intervals [AAS PAPER 71-321] 23 p3726 A71-42995

Real time interactive simulation of multifunction phased array radar, using digital computer links 23 p3648 A71-44272

DATA MANAGEMENT

ESRO/ELDO space documentation service involving NASA file remote processing and data bank for space component selection 07 p1225 A71-20001

Maastricht automatic data processing and display system concept for automatic management of reception and data transmission and information visualization 15 p2384 A71-31888

European meteorological satellite system, discussing measurement program, data management, orbital parameters and stability, satellite positioning and instrumentation 16 p2644 A71-32844

Satellite systems for educational TV program distribution, discussing orbit utilization, ground stations and ATS program 16 p2645 A71-33588

Airborne display and electric management system, discussing weight reduction, protective function coordination, power quality, onboard maintenance, data processing and reliability 17 p2739 A71-34617

Information organizer system of symbolic manipulation on model data structures, providing row and column creation, sorting and indexing 22 p3516 A71-41865

Two stage reusable manned space shuttle computerized onboard data management system hardware and software [IBM-712000405] 22 p3517 A71-41977

Skylink program data management systems, discussing onboard data collection, transmission and ground facilities 22 p3610 A71-42007

ERTS remote sensing for ground system data management, emphasizing processing, reception, reproduction, storage, retrieval and distribution [AIAA PAPER 71-976] 24 p3817 A71-45294

DATA PROCESSING

NT BATCH PROCESSING
NT DATA CORRELATION
NT DATA REDUCTION
NT DATA RETRIEVAL
NT DATA SMOOTHING
NT DATA STORAGE
NT OPTICAL DATA PROCESSING
NT PARALLEL PROCESSING [COMPUTERS]
NT SIGNAL ANALYSIS
NT SIGNAL PROCESSING
NT VOICE DATA PROCESSING

Information processing - Conference, Las Vegas November 1969 01 p0041 A71-10141

Cryptographic techniques applications to data processing systems, considering digital substitution and digital route transposition matrix 01 p0044 A71-10141

SYMPLE /Syntax Macro Preprocessor for Language Evaluations/ for processing higher level language texts 01 p0045 A71-10141

Time shared input/output /I/O/ processor with hybrid I/O separation from hybrid computation 01 p0048 A71-10220

Contour-mapped and digital data field processing and analysis for National Severe Storms Laboratory /NSSL/ radar signal processing and recoding system 1 01 p0118 A71-10555

Weather radar echoes quantization following detection, discussing subsequent digital processing 01 p0049 A71-10555

Radar weather echo data processing by digital computer, providing economical means for analyzing large quantities of data 01 p0050 A71-10555

Computerized data management program for Minuteman radio telemetry instrumentation systems 01 p0050 A71-10881

Data transmission/acquisition/processing systems engineering project management using digital simulation models 01 p0184 A71-10881

Semiautomatic stereophotographic processing of particle interaction data from Wilson chamber 01 p0083 A71-11364

Acquisition and processing of aircraft search radar data obtained by track-while-scan technique, using off-line digital computer 01 p0040 A71-11393

Linear algorithms for determining spacecraft relative orbital state using angle data with digital computer 01 p0163 A71-11588

Left ventricular volume determination by high speed cineangiography, using optical scanning and automatic data processing 02 p0203 A71-11709

French book on numerical filtering, data smoothing, parameter prediction and process identification, considering expansion, transform, least squares and Kalman methods 02 p0236 A71-11726

Fourier transform chart showing interrelationships between data block length, frequency resolution sampling rate, fast Fourier transform /FFT/ stages and other related variables 02 p0215 A71-12045

Medical data processing techniques in electrocardiography and effort vectorcardiography facilitating clinical observations 02 p0207 A71-12110

Computer program for processing elliptical polarization observations of nebulae and comets 02 p0251 A71-12360

Ground based data derivation and transmission system for multicontrol satellite communication system 02 p0225 A71-12834

Digital filtration and processing of electrocardiograms on computers using linear difference equations 03 p0367 A71-12992

ECG telemetric data computerized processing, describing cardiac data acquisition, long distance telephone transmission, analog to digital converter, central processor and output devices 03 p0370 A71-13066

Neural activities during simultaneous contrast and information processing in visual system 03 p0364 A71-14188

FM data recording system with transducers for converting varying parameters into frequency and tape recorder capable of playback for computer analysis 03 p0383 A71-14344

NASA program concerning determination of RF spectrum sharing criteria and automatic data processing in aerospace systems 03 p0381 A71-14588

NASA Office of Technology Utilization, examining publications, information sources, data processing and dissemination facilities 04 p0690 A71-14938

Space station information management, examining data processing and distribution to space and ground users 04 p0661 A71-15001

MITOL problem-oriented compiler language for real time and postflight telemetry data processing 04 p0556 A71-15295

Geodetic survey adjustment and accuracy improvement using satellite radar range and ballistic camera data 04 p0583 A71-15302

Soviet book on radio measurement methods and mathematical data processing in space trajectory measurements 04 p0555 A71-15375

- Eight channel physiological data scanning and timing control, sequential conversion, printing and punching 05 p0714 A71-16923
- Multicomputer system with preparatory and processing subsystems, discussing algorithm for distributing problems flow among processors 05 p0726 A71-17018
- OAQ for observations of stars, galaxies, planets and nebulae, discussing ground system and men and data systems integration 05 p0734 A71-17130
- Nimbus 4 satellite telemetry information processor with data sampling and formatting flexibility 05 p0726 A71-17135
- NASA Data Processing Facility for earth resources technology satellite telemetry 05 p0818 A71-17146
- USAF space missions information processing requirements relative to space transportation system, emphasizing real time image processing 05 p0727 A71-17229
- Soviet papers on mechanical processing methods for aerological observations covering weather forecasting, dew point deficit computer control, etc 06 p0921 A71-17501
- Global computer processing scheme for aerological radiosonde observation, using coded telegrams as primary information data 06 p0922 A71-17502
- Meteorological satellite data interpretation, including atmospheric layers thermal balance and global absorbed and outgoing radiation distribution mapping 06 p0923 A71-17508
- Astronomical-geodetic networks processing in three dimensional rectangular coordinates, considering advantages and accuracy 06 p0889 A71-17674
- Complex supply system large quantity data handling and cost savings through optimum planning of storage points and transport using linear separable programming 06 p1010 A71-17746
- Pole path deconvolution by optimum Wiener filter for acausal and causal cases, considering earthquake excitation 06 p0890 A71-17884
- Direction finding problems involving several waves of same frequency, discussing nonlinear computation methods with hybrid computers 06 p0927 A71-18205
- Worldwide remote sensing with satellites, high flying aircraft and computer data processing, discussing application in less developed countries 06 p0896 A71-18409
- Earth based orbit determination for Mars orbiting spacecraft, comparing batch and sequential tracking filter data processing methods [AIAA PAPER 71-119] 06 p0978 A71-18657
- NASA ground based digital data processing facility for Earth Resources Technology Satellite system 07 p1067 A71-18804
- Environmental satellite data on-line processing and extraction procedures, including visible and IR imagery mapping and cloud pictures analysis 07 p1067 A71-18806
- Ionospheric columnar electron content, describing data processing and analysis programs 07 p1096 A71-19008
- Computer aided automatic fault data logging, classification, analysis and reporting methods in integrated ATC system 07 p1155 A71-19556
- Space-time interactions and associated input-output mismatches from overprinting, sequential blanking and displacement visual perceptual information processing 07 p1049 A71-19695
- Space shuttle integrated information management system, emphasizing software element requirements and data processor hardware [AIAA PAPER 71-222] 07 p1155 A71-19703
- Statistical methods for inventory boundary determination and data compression in automatic processing of multispectral scanner remote sensor earth observations from aircraft and spacecraft [AIAA PAPER 71-234] 07 p1068 A71-19711
- Associative digital processor with associative memory for high speed ATC data processing, discussing design and operation 07 p1068 A71-19997
- Complex human memory processes large scale simulation/cybernetic modeling/ based on information handling probability and retrieval 07 p1050 A71-20105
- Human eye information processing algorithms mathematical model technological materialization 07 p1051 A71-20119
- Data handling system with digital computer and multichannel scanning, processing and recording for simultaneously conducting two environmental tests of satellites 07 p1069 A71-20403
- Soviet book on spacecraft motion parameters measurements accuracy covering electronic systems error sources and reduction in design and data processing 08 p1251 A71-20675
- Earth resources survey remote sensor system with human for spatial and machine for spectral data processing 08 p1257 A71-20691
- Spacecraft orbital elements determination, using statistical analysis in processing observed motion data 08 p1360 A71-21005
- Integrated data processing of stereotriangulation system providing automatic map plotting 08 p1281 A71-21249
- Computer processing in communications - Conference, Polytechnic Institute of Brooklyn, April 1969 08 p1255 A71-21590
- Counting rate source encoding algorithm with orthogonal functions in space experiment data processing before telemetering to ground 08 p1259 A71-21592
- Operational uniformity requirements for large meteorological station networks, emphasizing data acquisition and processing 08 p1327 A71-21716
- Observational data characteristics analysis as contributor to knowledge and utilization of all atmospheric physical occurrences 08 p1328 A71-21722
- Numerical weather prediction models, discussing automatic data processing meteorological parameter requirements 08 p1328 A71-21723
- Guiana Space Center facilities and equipment, describing computerized and automated real time telemetering and data processing systems for spacecraft tracking 09 p1425 A71-22274
- Measuring apparatus for cyclic plastic strains at high temperatures, discussing data processing techniques 09 p1443 A71-22636
- Decoding computational work and time, discussing cost increases related to communication reliability 09 p1407 A71-23102
- Cophase ad hoc statistic for data processing of detectors array sensing signal propagating in uncorrelated noise 09 p1408 A71-23452
- Experimental flight mechanics in terms of data processing quality, discussing subsystems control 10 p1581 A71-23928
- Wind velocity data processing technique for azimuthal radar observations in meteor zone, using least squares method 10 p1600 A71-24035
- Nervous system modeling, considering cybernetic brain functions, neuroheuristic programming and modes of distributed information processing pertinent to neuropsychological experiments 10 p1568 A71-24222
- Information processing by living systems, considering nervous system and brain operation with emphasis on neuron structure, message coding, programming and information storage 10 p1562 A71-24223
- Information processing in biological and artificial brains, analyzing visual perceptual system 10 p1568 A71-24224
- Neurophysiological auditory information processing, considering mechanical transformation of two dimensional pressure-time signal and three dimensions for presentation to nervous system 10 p1562 A71-24228
- Fatigue crack propagation rates in Al under constant low stress, discussing data processing methods 10 p1629 A71-25053
- Real time high resolution mass spectroscopy using digital computer techniques for data acquisition, processing and presentation 11 p1761 A71-25220
- Information support system for physiological studies of human performance, including indexing approach for references categorization, microfiche file and data bank 11 p1860 A71-25253
- Model of retinal information in cats from physiological and anatomical evidence, considering processing of contrast and eye movement information 11 p1723 A71-25254
- Computer controlled source data preparation Keycheck system, discussing real-time software support for documents audio/visual error detection 11 p1734 A71-25638
- Aircraft gas turbine condition analysis instrumentation used for status diagnosis of naval turbine engines, discussing sensor and electronic data interpretation progress [ASME PAPER 71-GT-86] 11 p1813 A71-25994
- Real time modal purity and data quality assessment techniques 11 p1853 A71-26501
- Wind structure in boundary layer pilot-balloon observation, discussing baseline data processing for digital computer 11 p1796 A71-26560
- Alouette 2 satellite housekeeping data processing, obtaining selected satellite temperatures, solar cell current, geomagnetic field, direction of sun and satellite attitude 12 p1883 A71-26607
- Reliability experience acquired in collecting, processing and analyzing U.S. Army test and field data, stressing field data reduction work 12 p1909 A71-26662
- Experimental plan group characteristics, describing main goals, construction methods, mathematical models and data analysis procedures 12 p1988 A71-26706
- Automaton concept in cybernetics, emphasizing synchronous switching circuit operation with asynchronous input data 12 p1884 A71-27045
- Solar type 3 radio bursts polarization measurement by recording and subsequent digital processing 12 p1969 A71-27653
- Processes involved in obtaining materials required for socialist organization operation, discussing operations, cost reduction by work mechanization and optimum data processing 13 p2167 A71-28492
- Automated data acquisition and analysis during cardiac catheterization, using photokymographic and analog magnetic tape recording system in conjunction with digital computer 13 p2020 A71-29003
- Normal accelerations experienced by transport aircraft fleet from fatigue load meter data analysis, discussing counting rates seasonal variations 14 p2174 A71-29788
- Vibration data analysis of analog and digital methods for cost comparisons 14 p2221 A71-30057
- Harmonic vibration analysis methods, discussing mathematical model, ground tests, structure suspension exciter and pickup location eigenvalue measurement and mode research 14 p2175 A71-30058
- Special purpose computer mechanization of inertial attitude reference computation and transformation of body axis information into desired reference frame 14 p2271 A71-30317
- Real time radar instrumentation data processing and control system, discussing computer selection, software requirements and configuration, etc 14 p2196 A71-30338
- Computer real time data monitoring and control software in satellite integration support and test operations, noting test oriented language 14 p2208 A71-30339
- Automated modal data acquisition and processing system/ MODAPS/ for real-time modal vibration testing of complex aerospace vehicle structures, describing features, capabilities and utilization 14 p2245 A71-30341
- French ATC, discussing automatic coordinator systems, computer utilization and flight plan data processing 14 p2272 A71-30382
- Maastricht Automatic Data Processing and Display ATC system with digital computers for aiding controllers in issuing instructions and making decisions 14 p2272 A71-30383
- Errors in spectral estimates by single-mode filters using analog computer for geoscientific data processing 14 p2246 A71-30482
- Field testing for radio telemetry receiving systems calibration, including tape recorder degradation effects during data processing 14 p2198 A71-30903
- Computer program for processing of UHF radiation patterns of ESRO 4 scientific satellite omnidirectional antenna systems 14 p2217 A71-31051
- IQSY night airflow from multistation photometric observation network, discussing data processing, instruments, publications and catalogs 15 p2396 A71-31609
- Polygraphic sleep recordings automatic analysis, presenting numerical results for rapid and slow eye movements, muscle tone, heart and respiratory rates 15 p2363 A71-31958
- Solar image correction in high resolution radio interferometer by digital data processing technique maintaining required phase relations in antenna elements 15 p2373 A71-32446
- Data processing technique for radio mapping of sun, discussing unwanted harmonics elimination and noise reduction 15 p2491 A71-32447
- ATC data automation, discussing flight plant processing system /FPPS/, radar data processing system /RDPS/ and signal automatic control system /SATCO/ 15 p2446 A71-32523

Small scale solid state digital computer for experimental medical data statistical processing
15 p2365 A71-32534

Goddard trajectory determination system, discussing attitude dynamics, data preparation, differential correction and orbit information
15 p2495 A71-32645

European space research center, discussing satellite scientific and engineering data transmission and processing
16 p2553 A71-33422

ONR human engineering research program concerning information input, display and processing concepts, decision making and motor output and control
16 p2536 A71-33529

Redundancy information effect on human performance in forced pace cognitive tasks under overload stimulus presentation rates
16 p2536 A71-33679

Optimal inertialess transformation of output signals from several devices, noting method application to analog data processing systems
16 p2550 A71-33892

DC 10 flight test program improvement using data acquisition/processing with real time monitoring, instrument landing and laser tracking
[AIAA PAPER 71-788] 16 p2553 A71-34018

Space tractography radars for measurements on military firing ranges and civil space centers, using microelectronics for data processing
16 p2544 A71-34098

Digital computer techniques for transient data processing and test control
17 p2709 A71-34544

ERTS system, considering multispectral data acquisition, relay devices and spacecraft and ground information processing
17 p2812 A71-34611

Microphotometer digital data processing at Canadian astrophysical observatory
17 p2743 A71-35007

Integrated vehicular information management systems consisting of computers, multiprocessors, multiplexers, dedicated subsystem processors, sensors and effectors
17 p2743 A71-35057

Redundant strapdown Inertial Measurement Unit processor recovery requirements, investigating IMU information loss effects during recovery on spacecraft mission
17 p2772 A71-35058

Neurobionics, considering data processing in brain and central nervous system
17 p2691 A71-35165

Variables affecting processing mode /serial or parallel/ of complex stimuli information
17 p2684 A71-35255

NASA ERTS program, discussing system concept automatic data processing capability, compatibility with tracking ground stations and international cooperation
17 p2805 A71-35329

X 4 satellite of British National Space Program, discussing design features, orbit, configuration, power subsystem, data handling and attitude control
17 p2814 A71-35429

ERTS remote sensor data processing, describing space and ground equipment and techniques
[AIAA PAPER 71-839] 17 p2814 A71-35429

Astronomical data correction for smearing effects applying Fast Fourier Transform algorithm
18 p2960 A71-35933

Infrared Michelson interferometer system digital data processing by computer, developing spectral density plots
18 p2920 A71-36092

Digital data acquisition and processing systems for large quantity rapidly generated measurements using reduction computer
18 p2885 A71-36160

Fluidics analog to digital signal techniques, discussing data transmission, acquisition and processing
18 p2851 A71-36206

Perturbation free delay time measurement in digital data processing system, using Schmitt triggers or tunnel diode discriminators
18 p2885 A71-36225

Computer interpretation of Mossbauer effect spectra with iterative, integration and comparison procedure
18 p2887 A71-36858

Computer aided digital transform natural image processing, using Fourier, Hadamard and Haar matrix algebra
19 p3026 A71-38404

Computer automated systems development for electromagnetic compatibility analysis, noting interactive processing in near real time mode
19 p3030 A71-38439

Spacecraft orbital elements determination, using statistical analysis in processing observed motion data
20 p3294 A71-39585

Computer implementation for Hansen theory of general perturbations, constructing program based on automatic Poisson series processor
21 p3445 A71-40257

Europa 3 electrical system as integrated vehicle control system using central processor and data bus
22 p3608 A71-41957

Space technology applications to earth environment and resources management, discussing satellite-borne remote sensor systems and data processing techniques [SD-71-734] 22 p3535 A71-42047

Computerized bacterial identification system to process Apollo spacecraft sample laboratory test results in NASA Planetary Quarantine Lunar Information System
22 p3504 A71-42233

Injection laser range finder with avalanche photodiode for Mars rover obstacle sensing, discussing range data processing methods
22 p3529 A71-42772

Earth rotational and deformational motion equations in extended Kalman-Schmidt filter for geodetic data processing
[AAS PAPER 71-339] 23 p3666 A71-43012

Fourier series approach to gravity anomaly data representation
[AAS PAPER 71-342] 23 p3666 A71-43015

Batch and sequential consider filters data processing methods for Mars orbiting spacecraft state estimation, investigating error sources
[AAS PAPER 71-385] 23 p3731 A71-43055

Primary sensor transfer function selection to minimize rms error in information transmission over telemetry channel for subsequent digital processing
23 p3648 A71-43294

Muscular bioelectric potential input processing into digital computer, describing amplitude, frequency and time domain analysis of electromyogram signals
24 p3801 A71-44542

Microchannel plate /compact array of channel electron multipliers/ amplifying electron beam containing spatial information, discussing material and technological considerations in plate construction
24 p3811 A71-45334

DATA PROCESSING EQUIPMENT

NT AIRBORNE/SPACEBORNE COMPUTERS

NT ANALOG COMPUTERS

NT AUXILIARY EQUIPMENT [COMPUTERS]

NT COMPUTERS

NT COUNTING RATE COMPUTERS

NT DIGITAL COMPUTERS

NT HYBRID COMPUTERS

NT IBM COMPUTERS

NT IBM 360 COMPUTER

NT ILLIAC 4 COMPUTER

NT PDP 8 COMPUTER

NT PRINTERS [DATA PROCESSING]

NT RCA SPECTRA 70 COMPUTER

NT SEQUENTIAL COMPUTERS

NT SITE DATA PROCESSORS

ADEPT-50 resource sharing system for classified data processing, describing time sharing security control model
01 p0044 A71-10188

Central data processing unit based on short-rod memories of coated Be-Cu alloy, discussing arithmetic-logic unit operation
01 p0049 A71-10263

Automatic aerological ground station with processing and transmission facilities for radio probe and radar data
01 p0029 A71-10360

Weather radar automatic data processing system for digitizing echo reflectivity by Video Integrator and Processor
01 p0050 A71-10594

Ground operations computer system for German Aeros, Symphonie and Helios satellite projects, discussing communication and data processing systems integration
[DGLR-70-079] 05 p0733 A71-15962

Dynamic data processing systems with feedback and internal noise, evaluating carrying capacities, limiting parameters and optimal transfer function
05 p0732 A71-17164

Teleautomatic data processing systems with computer control, synthesizing optimal structure
06 p0871 A71-17495

Manned space flight data processing system data storage, describing data base structure, direct access display and batch processing
[AIAA PAPER 71-237] 07 p1068 A71-19713

Department of Defense data processing equipment for all weather airborne terrain imaging radar mapping sensor
08 p1288 A71-21250

Data reading function synchronized digital mass spectrometer with incremental scan by magnetic field sweeping, describing method for polynomial fitting of data
11 p1762 A71-25663

Analog, digital and special data processing equipment interface for aerospace computer system
11 p1735 A71-25844

MODAPS real time data processing system modal vibration testing consisting of analog subsystems, digital interfaces and on-line minicomputer
11 p1746 A71-2615

Dynamic data processing systems with feedback and internal noise, evaluating carrying capacities, limiting parameters and optimal transfer function
12 p1893 A71-2747

Associative processor for ATC with fast arithmetic processing, equality search and input/output operations
15 p2374 A71-3119

Simulation equipment installation with link to C-130 flight simulator, discussing functional and operational features
15 p2384 A71-3181

Maastricht automatic data processing and display system concept for automatic management of reception and data transmission and information visualization
15 p2384 A71-3181

Avionic and missile computer control systems describing universal function unit design and digital processing requirements
17 p2711 A71-3577

Data display units as man machine interface elements in data processing operations, discussing combined alphanumeric/graphic CRT units
20 p3202 A71-3888

Real time coherent optical data processing, describing spatial filtering and reactive processor and image converter designs
22 p3540 A71-4177

Information organizer system of symbolic manipulation on model data structures, providing row and column creation, sorting and indexing
22 p3516 A71-4186

Operations and equipment of NASA ground data handling system for earth resources technology satellites
22 p3509 A71-4201

Computer controlled multichannel high speed data acquisition and processing system featuring redundant data deletion, arbitrary number of predeterminations and printing output in full English statements
22 p3517 A71-4210

DATA PROCESSORS

U DATA PROCESSING EQUIPMENT

DATA READOUT SYSTEMS

U DATA SYSTEMS

U DISPLAY DEVICES

DATA RECORDERS

Computer microfilm data recorder for output speed increase and information retrieval, discussing cost reduction
01 p0048 A71-10214

Metabolic rate and ergometric data recording by analog and digital systems
01 p0026 A71-11406

Photoelectric automatic logger with perforated tape recorder, discussing block diagram
04 p0589 A71-14837

Automatic coordinate measuring and recording devices for photogrammetric restitution equipment
06 p0901 A71-18293

Automatic frequency spectrum recorder to monitor radio emissions in space service allocated bands
10 p1578 A71-24587

Wired monitoring system for continuous interference-free twelve-lead ECG recording before, during and after exercise
12 p1876 A71-27636

DATA RECORDING

Flight simulators pilot performance monitoring and recording, discussing multichannel data acquisition and use in specific training tasks performance evaluation
01 p0066 A71-10021

System logic and usage recorder for storage area monitoring and data reduction
01 p0045 A71-10197

Magnetic disk storage media for recording and reproducing wideband instrumentation data
01 p0082 A71-10893

Notch power ratio noise tests on magnetic tape recorder/reproducer using direct recording in baseband
01 p0034 A71-10910

Standardized EEG data recordings in Air Force neurological evaluations
02 p0208 A71-12393

Photoelectric measurements of four comets, discussing instrumental data transformations to international UVB system
03 p0490 A71-13943

FM data recording system with transducers for converting varying parameters into frequency and tape recorder capable of playback for computer analysis
03 p0383 A71-14344

Solar spectrum line digital recording, discussing design and operation principles
04 p0590 A71-14842

- Prewhitening technique for acoustic turbulent flow data recording and analysis 04 p0600 A71-15598
- EEG topography continuous recording for signal analysis based on regression theory 05 p0713 A71-16321
- Coded recording technique for microfilming daily aerological data, decoding by computer in rapid and compact search and recognition procedure 06 p0922 A71-17503
- Pc 3-4 period range geomagnetic micropulsations simultaneous recordings at Canadian stations spanning auroral and polar regions 07 p1102 A71-19665
- Wideband photographic signal recording by modulated laser beams, discussing performance characteristics in terms of signal to noise ratio and laser power 09 p1460 A71-22355
- Ionospheric layers critical frequencies recording, using automatic interplanetary station type probe 09 p1436 A71-22450
- Damped vibrations logarithmic decrement determination during automatic recording of number of cycles, emphasizing error analysis 09 p1443 A71-22630
- Physical model describing mechanism of recording through surface corrugation of thermoplastic viscofluid layer by electron beam 10 p1613 A71-24873
- Midlatitude whistlers occurrence rates, dispersion and structural features sampled recording over North Italy 10 p1579 A71-25002
- Solar type 3 radio bursts polarization measurement by recording and subsequent digital processing 12 p1969 A71-27653
- Nimbus 4 Interrogation Recording and Location System meteorological experiment for tropical region upper atmosphere information 14 p2200 A71-30917
- Polygraphic sleep recordings automatic analysis, presenting numerical results for rapid and slow eye movements, muscle tone, heart and respiratory rates 15 p2363 A71-31958
- Airflow surveys using extended field large aperture interferometer-spectrometer with optical wedge compensators and digital recording 18 p2914 A71-35842
- Solid state light emitting diodes in aerial camera data recording system for enhanced spectral matching, increased photo conversion efficiency and lower power drive 18 p2920 A71-36089
- Hologram recording materials within and outside visible spectrum, considering sensitivity, reconstruction efficiency, resolution limitations, nonlinear and noise effects 21 p3380 A71-40920
- Three-receiver radio wave dispersion analysis application to ionospheric drift records to assess effects of velocity variation with time 22 p3515 A71-42599

DATA REDUCTION

NT DATA SMOOTHING

- System logic and usage recorder for storage area monitoring and data reduction 01 p0045 A71-10197
- Data reduction accuracy estimation via simulation technique, using method of least squares 01 p0073 A71-10357
- Bits round-off and approximate division error effects in data compressor design, suggesting best maximum error criteria 01 p0050 A71-10878
- Output format coding for telemetry data compressor channel and frame identification 01 p0036 A71-10984
- Tactical missile flight test planning using digital simulation data reduction techniques for fast cost effective trajectory synthesis 02 p0226 A71-11784
- Continuous signal discretization for communication channels maximum information compression rates 02 p0211 A71-11826
- Time vector method for aircraft flight test data evaluation, discussing control deflections effects on phugoid motion, lateral stability derivatives and error estimation 03 p0347 A71-13341
- Nighttime F layer true height profiles reduction from routine ionograms, discussing error corrections 03 p0408 A71-13387
- Ballistic data reduction for drag coefficient of spherical projectiles, using time distance relation for constant coefficient 03 p0341 A71-13467
- Nonhomogeneous strain fields analysis by moiré fringe multiplication with full field data reduction by mechanical differentiation 03 p0425 A71-13753
- UH-1B helicopter flight test noise measurements data reduction and analysis, presenting sound pressure vs frequency and time plots 04 p0531 A71-15405

- Data reduction for badly conditioned systems, describing general classical and modified linear statistical models for parameter determination from erroneous measurements data [DGLR-70-084] 05 p0726 A71-15950
- Fourier data decomposition technique for recovering Doppler temperature, emission line intensity and Doppler shift of central frequency of Fabry-Perot fringes in presence of statistical noise 05 p0748 A71-16265
- Satellite ion energy analyzer with onboard data reduction for ionospheric ion temperature and concentration measurement with high temporal resolution 05 p0755 A71-17139
- Soviet papers on mechanical processing methods for aerological observations covering weather forecasting, dew point deficit computer control, etc 06 p0921 A71-17501
- Meteorological satellite data interpretation, including atmospheric layers thermal balance and global absorbed and outgoing radiation distribution mapping 06 p0923 A71-17508
- Data reduction for information retrieval, considering electron beams application for electronic circuit ultraminiaturization 06 p0871 A71-17525
- Eclipse observations interpretation for transition region between extreme limb and low chromosphere 06 p0967 A71-17905
- Follow-up scanning systems and reading volume reduction in biological image descriptions facilitating computer aided microstructure analysis 06 p0871 A71-18697
- Rotating modulation collimator as astronomical X ray camera, discussing data reduction techniques for image synthesis 07 p1109 A71-19455
- Onboard self adaptive multichannel data reduction for redundancy by oversampling [ALAA PAPER 71-232] 07 p1063 A71-19709
- Landmark navigation improvement by redundant measurements and statistical data reduction measurement for lunar roving vehicles 07 p1156 A71-20339
- Laboratory test set for integration of data compression and error correction encoding of digital communications system 07 p1065 A71-20424
- Deep space probes telemetry system a priori data compression ratio evaluation using channel activities under unknown output signals cross correlation [ALAA PAPER 71-231] 08 p1258 A71-20799
- PCM TV photographic data communication for grand tour of outer planets, emphasizing adaptive information-preserving data compression system for optimal performance 08 p1254 A71-21346
- Observational data characteristics analysis as contributor to knowledge and utilization of all atmospheric physical occurrences 08 p1328 A71-21722
- Observational data statistical evaluation, considering meteorological instrument bias, corresponding instrument fluctuations and noise/signal separation by linear algebraic filter 08 p1329 A71-21726
- Meteorological data quality control, discussing inconsistencies, data interrelationships and frequency distribution 08 p1329 A71-21729
- Organic impurities effects on carbon dioxide dissociation activation energy, considering magnitude dependence on experimental conditions and data reduction techniques 08 p1251 A71-21783
- Satellite geodetic data interpretation of geoid undulations and gravity anomalies 08 p1285 A71-21803
- Electroencephalogram analysis, using analog computers for biopotential data reduction 09 p1398 A71-22489
- Lunar Mapping Camera ground support operations, describing pre and post mission assistance, stellar field calibration and data reduction 09 p1429 A71-23221
- Biosatellite 3 neurophysiological data analysis by digital computer presenting maps of parietal cortex spectra, responsive states transient changes, circadian rhythms and EEG activity 09 p1395 A71-23243
- Redundancy reduction method based on least squares approximation for recording solar radio burst emissions 10 p1661 A71-23926
- Speech processing and recognition, considering progressive data reduction by ear and physiological limitations imposed information rate time variation 10 p1568 A71-24230
- Real time spectrum analyzer, discussing data sampling rates, statistical uncertainties, waveform and bandwidth 10 p1612 A71-24832
- Nonlinear dynamic systems phase coordinate variations statistical characteristics, describing data reduction method 11 p1798 A71-25662

- Mineral and water resources remote sensing, discussing sensor systems and data interpretation techniques with special reference to Colorado Bonanza project 11 p1760 A71-26531
- Reliability experience acquired in collecting, processing and analyzing U.S. Army test and field data, stressing field data reduction work 12 p1909 A71-26662
- Experimental plan group characteristics, describing main goals, construction methods, mathematical models and data analysis procedures 12 p1988 A71-26706
- Data transmission with redundancy, discussing optimum data compressing encoding of correlated source signals through linear transformation 12 p1883 A71-27009
- Minimum error pre- and post-filtered sampled signals for pulse modulation and data compression optimization 12 p1879 A71-27070
- Radar cross section data analysis, considering economical approximation techniques in HF and LF ranges 12 p1882 A71-27440
- Redundant information reduction during electrocardiograms analysis by Legendre polynomials, considering equivalent model in dipole and quadrupole form 13 p2017 A71-28376
- OGO 4 satellite micrometeoroid flux detection, emphasizing noise control procedures for data correlation 13 p2145 A71-28700
- Information reduction for three dimensional image projection holography, using horizontally direction selective stereoscreen 13 p2068 A71-28710
- Binary data compression for satellite-borne instrumentation for space physics measurements, discussing redundancy reduction technique 13 p2033 A71-29274
- Hybrid computer program for data reduction or on-line analysis of nystagmus during closed loop experiment involving visual and/or vestibular function 13 p2022 A71-29359
- Heat transfer within resonant cavities at subsonic and supersonic flow, discussing wind tunnels, test procedures and data reduction [ASME PAPER 71-FE-9] 13 p2166 A71-29450
- Circumferential traversing probe technique for intrastage analysis of axial flow compressors, considering mass flow averaging data reduction technique [ASME PAPER 71-FE-33] 13 p2118 A71-29468
- Accelerometer precision centrifuge test data reduction by inversion method, extracting odd second order coefficients 13 p2072 A71-29506
- Aircraft instrumentation and data analysis for clear air turbulence, including orthogonal components and temperature and wind distributions 14 p2267 A71-29753
- Atmospheric turbulence space-time relationships measurements, discussing computerized time series, spatial and phase spectral analysis for sensors data 14 p2267 A71-29754
- Combined data compression and error control by digital sequential decoding for space to earth data links using digital computers 14 p2193 A71-30023
- Vibration data analysis of analog and digital methods for cost comparisons 14 p2221 A71-30057
- Absorbent materials test methods and acoustic data reduction with simulation principle 14 p2275 A71-30525
- Classification changes in IQSY Auroral Atlas, considering symbolism, synoptic map plotting and data reduction 15 p2396 A71-31608
- IQSY data analysis of pulse reflection measurements from midlatitude station, determining polar cap and auroral absorption 15 p2396 A71-31611
- Materials ultrasonic structural analysis, describing statistical methods for damping data processing 16 p2584 A71-33561
- Polynomial fitting for information compression of Wild BC-4 satellite photographs, comparing short arc with geometric compensation methods 16 p2581 A71-34041
- Transient matrix heat transfer test data reduction, discussing direct curve matching methods implementation by distance function minimization 17 p2835 A71-34178
- Field strength of radio emission from cosmic ray showers at 3.6 MHz, stressing data analysis procedure 17 p2732 A71-34623
- Distributed Fetch sequencing computer technique, discussing system speeds, throughput rates, bus requirement and arithmetic processor demand reduction and task performing capability 17 p2712 A71-35779
- Pattern recognition techniques application to metallurgical data analysis, discussing spatial filtering and classification process 17 p2749 A71-35791

Logic devices of adaptive scale-time converters of single pulsed processes on electron beam memory tubes, proposing polynomial methods of data reduction
18 p2887 A71-35881

Computer-disk interface system photooptical instrumentation for weather data acquisition, analysis and display
18 p2884 A71-36078

Step-change single blow transient temperature response synthesis by data reduction with aid of operational calculus and half-line convolution integral equation theory
20 p3314 A71-39488

Automated diurnal variation analysis program applied to IGY observed solar quiet day geomagnetic variations
20 p3218 A71-39520

Geodetic satellite observational data condensation by substitution for all measurements of pass above station with pseudomeasurement expressed by vector with almost six components
20 p3220 A71-39663

Atmospheric thermal sounding radiation data interpretation, determining integral Fredholm equation solution, absorption characteristics and temperature profiles
20 p3258 A71-39670

Book on fitting equations to data by computer analysis of multifactor data for scientists and engineers, covering independent variables selection and least squares method
21 p3406 A71-40166

Turbulent jet flow concentration, velocity and direction measurements, describing cold and hot wire techniques and data reduction system
21 p3378 A71-40401

Unified international scaling for annual and seasonal precipitations measured by national gages, comparing U.S.S.R. and U.S. reduction coefficients
21 p3383 A71-41377

Atmospheric background radiation measurements with balloon-borne Michelson interferometer, noting data reduction and calibration methods
22 p3549 A71-42563

Least squares and sequential estimation techniques application to Mariner 6 and 7 tracking data analysis, verifying Einstein relativity theory on electromagnetic radiation propagation
23 p3731 A71-43054

Corporate aircraft 1970 accident statistics analysis stressing pilot selection, training and supervision
23 p3628 A71-43227

Mariner S-band occultation experimental data compared with theory for accuracy of physical characteristics of Mars and Venus atmosphere, reviewing data reduction and error analysis
23 p3735 A71-43331

Lunar gravity estimate from low degree spherical harmonic coefficients in potential model and Lunar Orbiter 4 radio tracking data reduction
23 p3768 A71-43882

Binary nonconsecutive one code for time-tag data compression in digital communication, noting transmission power and bandwidth requirements reduction
24 p3803 A71-44651

Geophysical data analysis for high latitude negative geomagnetic disturbances revealing geomagnetic pulsations during auroral arcs passage
24 p3823 A71-45037

DATA RETRIEVAL

Quantization in data transmission and extraction, considering analog signals transmission in digital form and radar echoes recognition by digital integration systems
01 p0029 A71-10307

Strain data retrieval from moiré or photoelastic patterns by numerical technique based on light intensity distribution phase angle
02 p0225 A71-11703

Geographic urban information and change detection systems with remote sensing inputs, discussing data storage and retrieval
09 p1439 A71-23214

NASA Scientific and Technical Information System, illustrating advantages of machine retrieval systems for legal profession
18 p2986 A71-35868

Aircraft industry license norms and standards, describing indexing procedures, storage techniques and data recovery operations with computer
18 p2886 A71-36810

DATA SAMPLING

Automatic pattern recognition in photographic transparencies, using diffraction pattern sampling
02 p0225 A71-11704

Mathematical model for optimizing observational data sampling and working time losses by scientific research personnel
02 p0336 A71-11859

Fourier transform chart showing interrelationships between data block length, frequency resolution sampling rate, fast Fourier transform /FFT/ stages and other related variables
02 p0215 A71-12045

ECG signal analog to digital conversion at sampling rate and quantizing accuracy for minimal losses and/or distortion
02 p0208 A71-12949

Sampling and averaging techniques in fast random signal analysis using oscilloscope and memory unit
03 p0379 A71-13911

Sampled data feedback control system analysis and synthesis by state variable method, discussing computer algorithms for optimal pulse control
03 p0392 A71-14409

Nimbus 4 satellite telemetry information processor with data sampling and formatting flexibility
05 p0726 A71-17135

Sampling efficiency of total power balanced Dicke type radiometers using digital integration
08 p1267 A71-21879

Linear processes optimal sampled data controls, noting effect of sampling on closed loop system and cost asymptotic behavior
09 p1422 A71-22281

Nonlinear sampled data feedback control systems periodic mode of oscillations, using state variable approach
09 p1423 A71-23033

Sampled data feedback control systems with neural pulse frequency modulation, deriving periodic oscillations existence conditions
09 p1424 A71-23387

Independently sampled indirect and direct magnitude measurements, noting linear system effects in astrometry
10 p1575 A71-23845

Real time spectrum analyzer, discussing data sampling rates, statistical uncertainties, waveform and bandwidth
10 p1612 A71-24832

French monograph on nonlinear recurrences solutions and applications to sampled data systems
12 p1928 A71-26567

Electrical waveform sampling circuits without switched feedback amplifiers, discussing advantages of open loop configuration with circuit diagrams
12 p1891 A71-26997

Nonlinear sampled data control systems stabilization, eliminating intersample ripples by zero-order hold
13 p2042 A71-28702

Nonlinear multivariable sampled data systems synthesis and analysis in first harmonic approximation, introducing function arbitrary order difference
13 p2042 A71-28704

Auto- and cross-spectral estimation from irregularly sampled data by extending complex demodulation
14 p2246 A71-30483

Gated phase locked loop system characteristics based on sampled data model, comparing with continuous loop operation
14 p2214 A71-30795

Sampled data delay-lock loop for tracking biphas modulated pulsed-envelope RF signal arrival time
14 p2197 A71-30796

Gaussian input signal nonlinear sampled data systems analysis using linear components and transfer function
14 p2220 A71-30800

Approximate root locus method in S plane for sampled data systems, mapping constant frequency and constant damping ratio loci onto W plane
15 p2381 A71-31942

Pulse detection equipment by peak voltage and current value sampling, using avalanche transistors
15 p2377 A71-32324

N-order continuous linear automatic control system compensation method, using model of sampled systems with duration modulation
16 p2549 A71-33377

Linear single loop sampled data time delay feedback systems stability analysis
16 p2550 A71-34168

Optimal control synthesis for saturating time-varying and stationary sampled data systems, using integral performance index and extended maximum principle
16 p2551 A71-34169

Human motor control behavior sampling hypothesis of open loop system at voluntary effort initiation, discussing validity based on ankle rotation physiological test
17 p2690 A71-34741

Error sampled discrete continuous feedback control system performance, comparing adaptive and periodic sampling methods
17 p2722 A71-35184

Nonuniform sampling procedure for linear transversal filters synthesis, obtaining phase-sampled impulse response filters suitable for AM and FM waveforms generation and matched filtering
20 p3203 A71-38859

Digital sequential detector based on range sampling technique, comparing performance to digital sequential probability test /SPRT/ detector
20 p3206 A71-39906

Linear multivariate sampled-data control system optimal design based on deadbeat performance
21 p3360 A71-4061

Soviet book on nonlinear sampled-data control systems with PFM and PDM covering mathematical description, transient analysis and system stability problems
22 p3526 A71-4181

Sampled data control systems with pulse frequency modulation and time lag element, determining error response
22 p3527 A71-4240

Sampled video data technique with informational redundancy for processing and narrow-band transmission, discussing TV display, noting applications in corporate communications and teaching
22 p3547 A71-4259

Computer generation of sensitivity functions for nonlinear sampled data control systems, discussing simulator components and computational time economy problems
23 p3648 A71-4388

Multivariable regression equations validity from dispersion analysis and limiting complexity with allowance for data sample volume
24 p3842 A71-4439

Optimum design of linear multivariate sampled data systems, using deadbeat and integral performance criteria and output response error
24 p3812 A71-4445

Nonlinear and multivariate optimal sampled data control systems design with bounded control and state variables, using dynamic programming and divisional technique
24 p3812 A71-4445

Discrete parameter covariance stationary stochastic process in rotation sampling, deriving minimum variance unbiased linear population mean estimator by constrained optimization procedure
24 p3844 A71-45133

DATA SMOOTHING

French book on numerical filtering, data smoothing, parameter prediction and process identification, considering expansion, transform, least squares and Kalman methods
02 p0236 A71-11728

Successive approximation procedure for discretized time nonlinear systems data smoothing, developing Newton method algorithm for two point boundary value problem
02 p0277 A71-12726

Exact formulas and graphs for RMS error in object position and velocity prediction for long time intervals based on least squares polynomial smoothing
12 p1881 A71-27425

Transition probabilities of random processes with rapid variability, using continuous Markov smoothing under Fokker-Planck equation
16 p2612 A71-33520

Global numerical weather prediction model, using finite difference grid and operators with smoothing techniques
22 p3568 A71-42413

Anisotropically weighted smoothing theoretical interpretation based on numerical variational analysis for upstream and downstream observations in weather forecasting
22 p3569 A71-42415

Suboptimal fixed point data smoothing algorithm for parameter and initial state estimation of nonlinear dynamic systems
23 p3659 A71-44113

DATA STORAGE

Single and multiple exposure storage holograms with comparable diffraction efficiency
05 p0748 A71-16261

Manned space flight data processing system data storage, describing data base structure, direct access display and batch processing
07 p1068 A71-19713

Phototechnology for phase holograms recording and information storage in hardened gelatin
07 p1116 A71-20620

Analog surveillance radar signal analysis by digital storage and evaluation methods
08 p1252 A71-20745

Optical data storage photodetector output signal to noise and signal to background ratios, using Fourier transform amplitude and phase holograms
08 p1287 A71-21186

TV and silver halide emulsion application to planetary photography from space orbit, providing film system immediate information storage and high resolution
09 p1447 A71-22746

Geographic urban information and change detection systems with remote sensing inputs, discussing data storage and retrieval
09 p1439 A71-23214

Large capacity ferrite core buffer memory for spacecraft telemetry temporary data storage, using access circuitry with multichip and thin film circuits
09 p1421 A71-23735

Memory behavior in floating gate avalanche injection MOS structure, considering long term charge storage in insulated gate field effect device
13 p2036 A71-28045

EDITOR program for writing, reading, copying or altering data on file disk via display station
13 p2035 A71-29015

Holography background, classification and application to microscopy, particle size analysis, interferometry, optical elements and data storage
13 p2071 A71-29349

Phase holographic data storage in doped barium sodium niobate crystal, detailing decay times, energy density and diffraction efficiency
15 p2412 A71-32586

Binary intensity holographic information storage system, investigating nonlinear effects
15 p2412 A71-32591

Holographic lens magnification aberrations in various Fourier transform optical data storage geometries
15 p2412 A71-32592

Linear filtering algorithms computational efficiency, deriving formulas for arithmetic operation count and storage requirements
16 p2602 A71-33352

Recording device with Fourier hologram memory based on optical spatial filtration principle for identifying chemical compounds by IR absorption spectra
19 p3064 A71-37773

Deformographic storage display tube system, describing construction, development, design, performance and operating principles
21 p3352 A71-40135

Glass switching elements with storage properties for electronically controlled flip-flop circuitry, noting composition and fabrication
21 p3355 A71-40742

Holographic optical memory breadboard development system based on CW Ar ion laser, discussing component operating, power requirement and cost problems
21 p3380 A71-40922

High capacity holographic storage system including frequency doubled Nd-YAG laser, Si integrated photodetector array and digital light deflector
22 p3540 A71-41754

Hologram storage in evaporated thin films of arsenic trisulfides, considering simple diffraction gratings and complex data masks
22 p3542 A71-41811

Two dimensional holography application to fault-tolerant high density mass data storage design for digital information retrieval system
22 p3548 A71-42517

Laser use in computer technology, reporting lithium and barium sodium niobate single crystals capacity for data storage
23 p3686 A71-43959

DATA SYSTEMS

Scientific data transmission systems signal design considerations for Apollo lunar exploration missions
01 p0035 A71-10915

Telemetry and communications roles in Apollo flight operations, describing data system management
01 p0035 A71-10918

Data acquisition system using associative processor for redundancy removal algorithm
01 p0050 A71-10983

Onboard monitoring sensor trends for airborne computer automatic data systems, noting digital transducers, LSI logic and solid state devices
03 p0395 A71-13081

Air traffic control using collision risk equations, noting data handling automation, airborne collision avoidance devices and geostationary satellites
04 p0624 A71-15646

Flexibly programmable spacecraft data handling system, considering computer aided telemetry system for data acquisition and transmission
08 p1258 A71-21317

MOSFET data systems evolution for IMP, discussing effects on system design and reliability approach
08 p1267 A71-21844

Spacecraft computer centered data systems with standby redundancy, automated flexibility and LSI devices for grand tour mission
08 p1260 A71-21846

Integrated flight test data system combining digital airborne data acquisition/recording system with telemetry/microwave link to computerized ground station
14 p2243 A71-30318

Airborne integrated data system capabilities based on flight tests with commercial aircraft
14 p2208 A71-30319

Boeing 747 aircraft integrated data system program for reducing engine maintenance and operating costs [AIAA PAPER 71-648]
14 p2290 A71-30725

Approximate root locus method in S plane for sampled data systems, mapping constant frequency and constant damping ratio loci onto W plane
15 p2381 A71-31942

Computer controlled data handling system for quadrupole mass spectrometer performing on-line chemical analysis of rocket chamber combustion gases [JPL-TR-32-1518]
16 p2578 A71-33182

Human performance reliability data system using taxonomic structure for classifying behavioral studies and predicting man-machine performance
16 p2536 A71-33318

F-15 aircraft integrated data system for flight test program information, discussing development and major elements
16 p2524 A71-34010

Reliability in key project decision making, including failure mode/effect analyses, design tradeoff, baseline meetings, hardware storage and data bases
18 p2926 A71-36491

Grand Tour missions centralized data handling, describing computer aided telemetry system and self testing and repairing control computer
19 p3025 A71-37954

Two stage reusable manned space shuttle computerized onboard data management system hardware and software
22 p3517 A71-41977

VOR/DME air navigation equipment using Kalman-Bucy filter and airborne air data system [ADS/ [AAS PAPER 71-152]
22 p3573 A71-42289

Earth observation system design decision making, considering data needs, technology readiness, man role in earth resources programs and space program schedule
24 p3892 A71-44867

Mariner 9 spacecraft mission, discussing configuration, data handling and TV surface mapping of Mars
24 p3876 A71-45267

DATA TRANSMISSION

NT AUTOMATIC PICTURE TRANSMISSION
NT CHANNELS [DATA TRANSMISSION]

Quantization in data transmission and extraction, considering analog signals transmission in digital form and radar echoes recognition by digital integration systems
01 p0029 A71-10307

PCM telemetry data transmission bit error probability confidence intervals upper bounds based on Markov chain model analysis
01 p0032 A71-10877

Bits round-off and approximate division error effects in data compressor design, suggesting best maximum error criteria
01 p0050 A71-10878

Data transmission/acquisition/processing systems engineering project management using digital simulation models
01 p0184 A71-10885

Radio telemetry data transmission, investigating multipath propagation effects on signal to noise ratio and distortion
01 p0033 A71-10889

Data transmission systems using information feedback techniques to achieve high bit rates /channel capacity/
01 p0064 A71-10902

Block code for retransmission of information damaged by noise bursts for feedback digital communication systems
01 p0034 A71-10905

Noiseless linear feedback limitation over bandlimited channel capacity in analog data transmission
01 p0064 A71-10906

Scientific data transmission systems signal design considerations for Apollo lunar exploration missions
01 p0035 A71-10915

Gaussian message optimal transmission through channel with white Gaussian noise in presence of total feedback
01 p0064 A71-11152

Soviet papers on digital information transmission via channels with memory
01 p0039 A71-11314

Binary error correcting codes in asynchronous systems for separate message transmission, discussing decoding and spacing
01 p0039 A71-11315

Two-directional digital data transmission system, determining probability of not obtaining message for arbitrary interrogation signals number
01 p0039 A71-11319

Medium speed data transmission systems tested for quality and functional characteristics
02 p0228 A71-11819

Radio signal reception error in cadence synchronization of binary data transmission systems with indeterminate signal arrival time
02 p0212 A71-11834

Ground based data derivation and transmission system for multicontrol satellite communication system
02 p0225 A71-12834

Neuromuscular spindles sensory information processing, determining fibers selective data transmission functions by frequency meter and model for electrical and mechanical properties
03 p0366 A71-12977

Statistical analysis of digital data transmission time error distributions in Polish post office and railroad communications network
03 p0380 A71-14375

Signal optimization for binary data transmission system with noiseless feedback channel, considering receiver signal energy and structure
04 p0560 A71-14743

Digital network data communication system advantages, characteristics and configuration
04 p0550 A71-14747

Solar spectrograph data transmission to digital computer, discussing intermediate magnetic tape storage
04 p0590 A71-14841

CW sounding for HF adaptive control for data transmission with ionospheric phase error
04 p0552 A71-15145

Real time missile radio telemetry data transmission to ground station, using instrumented aircraft
04 p0554 A71-15321

Deception repeaters for erroneous information transmission to radar, considering echo signal level, burnthrough, target size, sensitivity, gain and bandwidth
04 p0555 A71-15359

Carbon dioxide lasers for wideband data transmission in space
04 p0556 A71-15648

Data transmission via FDM/FM troposcatter channels, predicting system performance in error rate terms
05 p0723 A71-17052

Path intermodulation data distortion derivation from noise power ratio measurements over five tropospheric scatter paths during system acceptance tests
05 p0723 A71-17055

Digital asynchronous information transmission, describing schemes for coding binary into ternary signals
05 p0724 A71-17058

Phase-coherent communication systems with phase locked loops for data detector synchronization, calculating noisy timing effects on detection efficiency
05 p0724 A71-17059

All-digital multichannel narrow band FSK data receiver with time-shared arithmetic processor, discussing prototype design and performance [IEEE PAPER 70-TP-49-COM]
05 p0724 A71-17064

Decision-directed digital adaptive signal equalizer for high speed data transmission, discussing design and advantages
05 p0725 A71-17065

Real time processor design for sequential control of all-digital multiline data set [IEEE PAPER 70-TP-375-COM]
05 p0725 A71-17067

Multichannel on-line data terminals using minicomputer for communication control, error detection and data buffering [IEEE PAPER 68-TP-448-COM]
05 p0727 A71-17068

Optimality criteria for communication systems, considering data transmission rate
06 p0867 A71-17496

Synchronous meteorological satellite mission goals and system design, describing imaging, data collection, facsimile, space environment, trilateration, ranging and transmission
07 p1067 A71-18807

Information rates attainable in optical communication channel
07 p1110 A71-19481

Low data rate m-ray frequency shift keyed /MFSK/ modulation system design
07 p1061 A71-19534

Jet engine rotor strain and temperature data transmission, examining special purpose telemeters design
07 p1062 A71-19628

Data communication role in National Airspace System, concerning radar and flight data acquisition, intersystem transfer and voice control [AIAA PAPER 71-248]
07 p1063 A71-19722

Optimum transmitted data volume, orientation accuracy and size of narrow beam parabolic spacecraft antennas, defining optimum parabola for approximate radiation pattern
07 p1078 A71-19871

Digital transmission in Defense Communications System, discussing data requirements, converter and TDM involving terrestrial and satellite links
07 p1066 A71-20432

Information transmission rate and error probability in analog feedback systems, showing normalized maximum transmission speed dependence on signal to noise ratio
08 p1268 A71-21283

Flexibly programmable spacecraft data handling system, considering computer aided telemetry system for data acquisition and transmission
08 p1258 A71-21317

PCM TV photographic data communication for grand tour of outer planets, emphasizing adaptive in-

formation-preserving data compression system for optimal performance
08 p1254 A71-21346

Optimal error correcting code structure selection for binary data transmission systems synchronization, using criterion of minimum false detection probability
08 p1260 A71-21979

Frequency signal structure selection to ensure maximum information capacity for given SNR at receiver output in discrete information transmission
08 p1257 A71-21980

Mission objectives and orbit parameters of Azur satellite, considering satellite control and data transmission as function of ground support system
10 p1589 A71-23927

Solid state pulse modulated radioonde for meteorological data transmission in digital form, using MOS integrated circuits
10 p1583 A71-24052

Diversified frequency radio data transmission and reception by linear modulation, considering error rate in white noise and selective/flat fading
10 p1580 A71-25109

Data transmission with redundancy, discussing optimum data compressing encoding of correlated source signals through linear transformation
12 p1883 A71-27009

Multiplexer concentrators for data telecommunication systems with erratic information flow, concerning statistical assumptions, transient response, queuing tails and message clustering
12 p1880 A71-27072

Communication satellites telephone, telex and high speed data transmission systems engineering, discussing intercontinental TV, synchronous orbit injection and solar panel deployment
12 p1973 A71-27610

Signals single set synthesis for simultaneous target information transmission and range and velocity measurement
12 p1883 A71-27617

Book on nonlinear modulation based on optimum estimation theory covering phase synchronization, analog data transmission, digital and analog systems performance, Markov processes, etc
13 p2029 A71-28041

Telemetry system for control data transmission, noting pulse comparison with feedback signal
13 p2031 A71-28633

Error detection and/or correction coding techniques for digital data transmission, comparing efficiency
13 p2036 A71-29279

Direct digital control and data acquisition system for propulsion research testing, transmitting data over differential signal pairs to remote test cell
14 p2208 A71-30316

Sensing and communications technologies for short wayside headways, considering applicable equipment for personal rapid transit systems, modulation, coding and data transmission techniques
14 p2195 A71-30337

Balloon-borne transistorized stratospheric cosmic ray probe, describing simultaneous gas discharge and dual coincidence telescope counters data transmission
14 p2247 A71-30596

Synchronous meteorological satellite data collection and transmission system error control, considering design tradeoffs for radio sets and coding techniques
14 p2198 A71-30899

Digital wire line system data bus design, calculating transmission performance of noise environment shielded twisted pair cable by linear filter model
14 p2198 A71-30904

Walsh orthogonal functions application in signal processing and as carrier waves in telemetry data transfer systems
14 p2199 A71-30909

Satellite telemetry systems for data transmission to developing nations ground stations decoding equipment
14 p2199 A71-30910

ERTS telecommunication system for space tracking and high resolution multispectral image data acquisition and commanding
14 p2199 A71-30912

Asynchronous digital node combination into synchronous multiplex with data traffic routing functions through switch from remote terminals
14 p2201 A71-30928

Air transport accident research in night approach simulators, noting visual information null in descent path and delay in relative motion supplemented data
15 p2363 A71-31602

PAM data transmission systems timing recovery, discussing maximum likelihood estimation method for timing parameter from random data
15 p2377 A71-32314

Synchronous data transmission system digital signal harmonic analysis based on stochastic process theory, applying to amplitude and phase modulation
15 p2372 A71-32321

Random images transmission rates, comparing line-by-line and two dimensional encoding
16 p2541 A71-32819

Apollo 14 communications support by USAF, discussing voice and data relay between spacecraft and control center, global weather support, cartographic and geodetic services, etc
16 p2541 A71-33178

European space research center, discussing satellite scientific and engineering data transmission and processing
16 p2553 A71-33422

European telecommunication and TV distribution satellite system, including telephony, telegraphy, telex and wideband data transmission
17 p2696 A71-34232

Communication satellite systems integration into general telecommunication network, considering telephone circuit data transmission characteristics, routing and signal processing
17 p2696 A71-34235

Space station communications systems, discussing data relay satellites transmission paths to ground, multiple voice channels, two way color TV and onboard telephones
17 p2699 A71-34610

Synchronous meteorological satellite programs, noting earth imaging, data transmission, collection and relay and space environment monitoring
17 p2812 A71-34612

Time division multiplexing system for ATS, discussing surveillance geostationary satellite feasibility, delta modulation for data transmission and aircraft equipment
17 p2772 A71-34680

Decoding at high transmission rates, describing algorithm for mean number of operations and error probabilities
17 p2702 A71-34971

Additional redundancy in information transmission systems with feedback to reduce error probability due to incorrect addressing
17 p2702 A71-34975

SPADE system digital channel unit applicability to services other than voice transmission, discussing narrow- and wide-band data transmissions and bit-error-rate performance
17 p2706 A71-35104

Information transfer in all-weather aircraft operation, discussing pilot role in overall reliability based on man machine system information process
17 p2693 A71-35209

Tuned loop antenna for missile telemetric data transmission, discussing design, implementation and impedance and radiation measurements
17 p2718 A71-35749

High speed BPSK communication components and system aspects with V band propagating medium, considering carrier modulation and transmitted digital data reception with minimum errors
17 p2709 A71-35759

Synchronization of high-speed digital data communication systems with continentwide interconnected switching centers, discussing elastic storage buffering to compensate for transmission time delay variations
17 p2712 A71-35784

Aerospace data bus for multiplexed transmission within vehicles, considering control and sequencing methods terminal concepts, capability noise reduction and reliability
17 p2712 A71-35785

BITSIM computer simulation technique for application to real time airborne photoreconnaissance imagery data transmission system design and performance analysis
18 p2917 A71-36070

Fluidics analog to digital signal techniques, discussing data transmission, acquisition and processing
18 p2851 A71-36206

ESRO part of joint ATC communication experiment for L band satellite use, giving voice and data transmission and distance measurement techniques tests results
18 p2945 A71-36510

Earth-spacecraft radio communication requirements for future unmanned planetary missions, emphasizing imaging experiments and sensors
18 p2877 A71-36518

Data transmission system of Franco-German Symphonie communication satellite
18 p2889 A71-36523

Jovian probe and spacecraft mission feasibility, discussing launch opportunities, targeting, objectives and data transmission
19 p3141 A71-37944

Hybrid thin film radioonde transmitter design for atmospheric temperature and humidity data transmission from meteorological sounding balloon to ground station
19 p3035 A71-38539

Transmission characteristics of communication systems with incoherent carriers through fading and nonfading media, showing advantage of PFM-AM with clipped noise carrier
20 p3201 A71-39913

Papers on communication satellites for 1970s covering various national domestic systems, aeronautical service, ERTS data transmission and collection problems, etc
21 p3347 A71-40444

High data rate optical communication system error rate determination from models for noncoherent digital baseband and subcarrier modulation formats
21 p3348 A71-40449

Combined AM/PM digital data transmission, using error rate and communication efficiency in bits per cycle of bandwidth vs average SNR as performance criteria
21 p3349 A71-41191

Swept frequency or chirp signals for data transmission and pulse compression, considering long range ground communication in HF band
22 p3510 A71-42272

Sampled video data technique with information redundancy for processing and narrow-band transmission, discussing TV display, noting applications in corporate communications and teaching
22 p3547 A71-42500

Pulse duration of atmospheric radio noise bursts at 1 MHz from lightning flashes, considering effect on data communication
23 p3643 A71-42970

TV multiplexing and broadband multichannel real-time telemetry data transmission without loss between Kennedy Space Center and ground station for computer operation
23 p3645 A71-43519

Data transmitting and receiving instruments and systems development problems covering signal shaping and converters and information channel and data reception theories
24 p3806 A71-44375

DATING

U CHRONOLOGY U TIME MEASUREMENT DAWN CHORUS

Polar chorus background hiss generation, investigating VLF wave characteristics responsible for harder electron precipitation from magnetosphere
05 p0743 A71-17004

Dawn chorus western drift and relationship to magnetic disturbances on night side
05 p0745 A71-17189

Midlatitude VLF hiss distinction from discrete emissions /chorus/ based on event tape recording and spectrum analysis
12 p1878 A71-26892

Dawn chorus westward drift and relationship to polar substorm and magnetic disturbances on night side
13 p2059 A71-28246

Auroral ELF and VLF emission at high latitudes, discussing chorus and hiss generation regions and noise mechanism
20 p3229 A71-39854

DAYGLOW

Photoionization coefficients and photoelectron impact excitation efficiencies in daytime ionosphere, noting role in dayglow
01 p0077 A71-11515

Sodium dayglow rocket measurements, comparing emission intensities with ground based measurements
03 p0407 A71-13312

Solar activity effects on day airglow atomic oxygen red line, calculating production rates for photodissociation, dissociative recombination and electron impact excitation
03 p0418 A71-14265

Martian dayglow spectrum, examining excitation processes for carbon monoxide Cameron bands
03 p0497 A71-14544

He I 584 A dayglow radiation measurement by retarding potential photoelectron analyzer on Javelin sounding rocket
06 p0887 A71-17267

Oxygen and nitrogen metastable constituents in daytime atmosphere airglow, obtaining altitude density distributions
07 p1103 A71-19764

Daytime near horizon atmospheric luminescence measurement by Cosmos 224 satellite, discussing contributions of nitrogen and aerosol and Rayleigh scatterings
09 p1435 A71-22432

Carbon dioxide cations emission bands in Mars and Venus dayglows, suggesting fluorescent scattering and photoionization as main excitation sources
11 p1827 A71-25724

Jupiter upper atmosphere extreme UV dayglow, involving resonant scattering and fluorescence of incident solar flux
12 p1961 A71-26888

Photodissociative excitation of atomic oxygen dayglow emission, considering electron impact and dissociative recombination
13 p2056 A71-27933

Nitrogen molecular excitation by photoelectron impacts in dayglow, investigating 1 PG band emission intensity variation with solar activity
14 p2235 A71-30349

Ionized magnesium dayglow measurement in sporadic E layer by rocket-borne UV spectrometer, determining ion to atom ratio

15 p2398 A71-31765

Atomic oxygen 1304-A day airglow observed from OGO-D spacecraft, attributing subsolar emission rates to photoelectron impact excitation

16 p2574 A71-33964

Dayglow emissions for OH, molecular oxygen, sodium, lithium, potassium, atomic oxygen and nitrogen, considering height profiles and diurnal variations

20 p3226 A71-39828

Dayglow neutral and ionized diatomic nitrogen band system emission excitation mechanism from vibrational and rotational intensity distributions observations

20 p3226 A71-39829

Earth UV dayglow observation by Aerobee rocket-borne scanning spectrometer, noting features due to atomic oxygen and nitrogen and nitrogen oxide gamma band

20 p3226 A71-39830

Dayglow and twilight emission data, discussing atomic excitation mechanisms, particle production rates, height profiles and temporal variations

20 p3227 A71-39835

Day airglow columnar emission rates for Lyman-Birge-Hopfield system of molecular nitrogen as function of solar zenith angle, using OGO 4 observations

20 p3231 A71-39892

Atomic hydrogen dayglow Lyman alpha structure of Mars exosphere from Mariner 6 and 7 UV spectrometric observations

23 p3734 A71-43156

DAYTIME

Daytime stratospheric X ray bursts, examining occurrence time, duration, cosmic radio noise and magnetic activity relationship

02 p0299 A71-11775

Differential radiometer with ultranarrow interference filter for daytime tracking of high altitude chemical vapor trails

03 p0424 A71-13636

Cloudless day sky brightness expressions, discussing singular points

05 p0778 A71-16842

Daytime ionosphere rocket observations at Antarctica, examining electron density profiles

05 p0743 A71-17006

Daytime pulsed optical communication within line-of-sight using GaAs IR laser

06 p0907 A71-17570

Equatorial zone daytime F 2 maximum height diurnal variation latitude change with decreasing solar activity from vertical sounding

07 p1100 A71-19401

Daytime lower ionosphere electron density profiles over equator, using rocket-borne Langmuir and plasma noise probes

10 p1606 A71-24913

Earth surface nighttime, twilight and daytime horizons visual observations by Soyuz 9 spacecraft

13 p2060 A71-28426

Daytime and nighttime sporadic F layer regularities correlation with other ionospheric phenomena based on vertical sounding data

13 p2062 A71-28555

Midlatitude daytime ionospheric electron density profile during low solar activity based on rocket sounding data

14 p2228 A71-29535

Day sky brightness and polarization observation during total solar eclipse of 7 March 1970

14 p2309 A71-30120

Electric field, atmospheric wave and other factors effects on F region storms by day and night in tables

14 p2236 A71-30941

Daytime electron density profiles above 90 km from Doppler radio measurements by rockets launched from Southern Hemisphere site

16 p2567 A71-33779

Equatorial zone daytime F 2 maximum height diurnal variation latitude change with decreasing solar activity from vertical sounding

19 p3053 A71-37825

Brightness profiles of earth daytime horizon from Soyuz spacecraft photographic photometry, deriving atmospheric scattering coefficient relation to optical thickness vertical distribution

19 p3054 A71-37967

Latitudinal distribution of electron temperature in F 2 layer during summer daytime period of low solar activity from electron density profile geometrical parameters

19 p3057 A71-38369

Daylight photometric flux derivation from filtered measurements of global sun and sky radiant energy, using natural illumination and short wave radiation relationship

20 p3234 A71-39175

Cosmos 142 and 259 experiments on ionospheric VLF propagation, discussing diurnal variations of daytime electron density

20 p3197 A71-39743

DC [CURRENT]

U DIRECT CURRENT

DC 10 AIRCRAFT

Laboratory facilities for DC-10 structural test program using fatigue test machines and computer controlled servo loading systems

[SAE PAPER 700829] 03 p0397 A71-13724

DC-10 aircraft test program effectiveness, discussing performance, operational envelope, airworthiness, noise measurements, etc

[SAE PAPER 700830] 03 p0348 A71-13726

Stress analysis of DC 10 nose landing gear unit, using photoelastic coating technique

04 p0534 A71-15669

DC-10 flight test program, discussing handling, takeoff and landing, and flutter, stall and stability characteristics

07 p0108 A71-19085

DC 10 specifications for airport planning, including ground clearances, payload-range characteristics and jet engine exhaust velocities

14 p2175 A71-30239

DC 10 flight crew individualized ground training program, emphasizing hands-on equipment and instruction hardware

[SAE PAPER 710472] 14 p2176 A71-30538

DC-10 design dispatch and component reliability through flight test and follow-up fault isolation programs

16 p2522 A71-33297

DC 10 flight test program improvement using data acquisition/processing with real time monitoring, instrument landing and laser tracking

[AIAA PAPER 71-788] 16 p2553 A71-34018

DC-10 wide body tri-jet aircraft design and development, considering sizing, number of engines and thrust optimization and selection of cruise, approach and stall speeds

[AIAA PAPER 71-780] 17 p2674 A71-34525

DC-10 fuselage pressure shell fail-safe design, presenting analysis methods for residual strength prediction of damaged stiffened panels

17 p2827 A71-35160

Low noise levels of DC-10 aircraft with CF6-6D turbofan engines, discussing design, flyover tests and FAA requirements

[CASI PAPER 72/5] 20 p3178 A71-39424

Computer controlled modular automatic test equipment for DC-10 aircraft maintenance, discussing system block diagram

22 p3519 A71-41518

On-condition monitoring of aircraft hydraulic systems for component deterioration, applying to Boeing 747, L-1011 and DC 10 aircraft

22 p3483 A71-42075

DE HAVILLAND AIRCRAFT

NT COMET 4 AIRCRAFT

NT DH 121 AIRCRAFT

NT DHC 4 AIRCRAFT

DE HAVILLAND DH 106 AIRCRAFT

U COMET 4 AIRCRAFT

DE HAVILLAND DH 121 AIRCRAFT

U DH 121 AIRCRAFT

DE HAVILLAND DHC 4 AIRCRAFT

U DHC 4 AIRCRAFT

DE LAVAL NOZZLES

U CONVERGENT-DIVERGENT NOZZLES

DEACCLIMATIZATION

U ACCLIMATIZATION

DEACTIVATION

Free radicals role in photodynamic inactivation of Rhodotorula glutinis subjected to high intensity light irradiation

01 p0019 A71-11560

Vibrationally excited carbon dioxide deactivation by collisions with CO, determining rate constants by laser fluorescence method

08 p1250 A71-20665

Deactivation and radiative lifetime of CO Cameron forbidden transition spectral bands produced by photon absorption

21 p3418 A71-40232

DEAD RECKONING

Lunar surface vehicle navigation system, describing dead reckoning and sun aspect compass for initial gyro alignment

01 p0124 A71-10514

DEADWEIGHT

U STATIC LOADS

DEAFNESS

U AUDITORY DEFECTS

DEATH

Sudden death and syncope mechanism in aortic valve stenosis, noting presence of baroreceptors in left ventricular wall

13 p2014 A71-29301

Papers on exercise and cardiac death covering coronary athero- and arteriosclerosis, congenital anomalies, myocarditis, tumors and physical exertion

18 p2855 A71-36213

Acute fatal nontraumatic collapse during physical work and sports due to pathological processes

18 p2855 A71-36214

Unconsciousness, confusion, amnesia, syncope and sudden death of pilots in flight due to silent ischemic heart diseases

18 p2855 A71-36216

Sudden death during physical exertion due to congenital anomalies of coronary arteries

18 p2855 A71-36217

DEBRIS

NT SPACE DEBRIS

DEBRUING

U CHECKOUT

DEBYE LENGTH

Poisson-Boltzmann equation solution for potential of charged sphere with radius not larger than Debye radius

05 p0781 A71-16383

Correction factors for small values of logarithm of Debye length ratio to mean impact parameter in electrical conductivity of fully ionized plasma

12 p1936 A71-26950

Niobium-zirconium system alloys Debye-Waller factor temperature and concentration dependence, noting nonmonotonicities due to phonon spectra

15 p2437 A71-32625

Debye potential well formation in collisionless current carrying plasma, noting wave-particle resonant interaction role

19 p3115 A71-38216

DEBYE TEMPERATURE

U SPECIFIC HEAT

DEBYE-HUCKEL THEORY

Debye-Huckel gravitational potential in Lemaitre universe

10 p1680 A71-25019

DECAMETRIC WAVES

Very long baseline interferometry /VLBI/ of Jupiter decametric bursts at HF

02 p0310 A71-12326

Frequency and phase analyses of cross correlated signals from very long baseline interferometry of decametric radiation from Jupiter

02 p0310 A71-12333

Solar bursts position and motion measurements at decameter wavelengths, using sweep frequency grating interferometer

02 p0302 A71-12764

Jupiter decametric radiation source A position variation, considering radiation controlling influence of Jovian satellite Io

09 p1521 A71-22935

High sensitivity radiospectrography, obtaining solar emission spectra on decametric waves by radio telescope, focal antenna and receivers

10 p1667 A71-23826

Jupiter rotation from Jovian decametric emission data

13 p2135 A71-28347

Forward/reverse drift pair bursts relation to decameter type 3 solar radio emission, postulating existence of electron acceleration sources in upper corona

15 p2485 A71-31714

Scattering effects on decameter wavelength quiet sun emissions flux densities, frequencies and brightness temperatures

15 p2485 A71-31716

Decameter solar radio bursts time splitting data, presenting high time and frequency resolution on double bursts

15 p2473 A71-31720

Solar wind velocity and Io phase relationship during decametric radio bursts from Jupiter, indicating plasmasphere existence

15 p2474 A71-31723

Jupiter radio spectrum decametric component observations, emphasizing core and mantle rotation under coupled torsional oscillations

16 p2637 A71-33514

Jupiter decametric radio emission relation to solar wind, geomagnetic activity and shock waves causing Forbush decreases

20 p3291 A71-39312

Rocket-borne explosive charge initiated detonation wave effects on decameter wavelength radio waves in lower E layer

20 p3199 A71-39894

DECARBONATION

Decarbonization monitoring of ball bearing steel bars, describing defectoscope based on eddy current higher harmonics method

22 p3553 A71-41768

DECARBURIZATION

Welded joint structural stability determination by measuring decarburized steel layer thickness after carbon diffusion into lower activity region

03 p0432 A71-13690

DECAY

NT BIOLUMINESCENCE

NT CHEMILUMINESCENCE

NT ELECTROLUMINESCENCE

NT ELECTRON EMISSION

NT FIELD EMISSION

NT FLUORESCENCE

NT HALF LIFE

NT ION EMISSION

NT LIGHT EMISSION

NT LUMINESCENCE

NT LUNAR LUMINESCENCE

NT NEUTRON DECAY

NT NEUTRON EMISSION
 NT NUCLEAR FISSION
 NT OPTICAL RESONANCE
 NT PARTICLE EMISSION
 NT PHOTOELECTRIC EFFECT
 NT PHOTOELECTRIC EMISSION
 NT PHOTOIONIZATION
 NT PHOTOLUMINESCENCE
 NT PHOTOPRODUCTION
 NT PLASMA DECAY
 NT RADIO EMISSION
 NT RADIOACTIVE DECAY
 NT SECONDARY EMISSION
 NT SOLAR RADIO BURSTS
 NT SOLAR RADIO EMISSION
 NT SPECTRAL EMISSION
 NT STIMULATED EMISSION
 NT THERMAL EMISSION
 NT THERMIONIC EMISSION
 NT THERMOLUMINESCENCE
 NT TYPE 2 BURSTS
 NT TYPE 3 BURSTS
 NT TYPE 4 BURSTS
 NT X RAY FLUORESCENCE

Self preserving solutions of Stewart-Townsend and Ogura-Meakoda equations for isotropic turbulence decay, discussing asymptotic nature for small and large wavenumbers

07 p1091 A71-20027

Ultrafast laser pulses, revealing fluorescence decay, stimulated Raman scattering and plasma formation transient details

16 p2588 A71-33873

DECAY RATES

NT ELECTRON DECAY RATE

Decay time of low Reynolds number weak turbulence generated by single and multistage grids, considering three dimensional energy spectrum

04 p0569 A71-15026

Solar flare associated increases in cosmic ray intensity during November 1968-April 1969, correcting anisotropic peak and decay rates to standard barometric coefficients

06 p0957 A71-18148

Fokker-Planck equation for convection dominated transport of solar cosmic rays solved for exponential decay phase of solar particle events

07 p1185 A71-19651

Metastable radiative lifetimes of molecular states of nitrogen and CO, using time of flight and high resolution electron gun techniques

09 p1497 A71-22417

Night glow emission post twilight decay rates at different seasons by Chamberlain relation, discussing F layer ionization

09 p1441 A71-23644

Soft solar X-ray bursts characteristics, discussing temporal and intensity differential distributions, flux measurements and decay time

12 p1953 A71-27654

Combustion chambers unstable acoustic oscillations, calculating equations for nonlinear growth and decay rate and limiting amplitude

13 p2160 A71-28613

Type 3 solar emission bursts, investigating time profiles and quasi-oscillatory decay

15 p2480 A71-32750

Solar flare radiation data from Pioneer spacecraft, detailing anisotropy, heliocentric longitude gradients, decay time constants and energy spectra

15 p2480 A71-32752

Cosmic rays lifetime in Galaxy in presence of particle acceleration in interstellar space

16 p2626 A71-33463

Homogeneous turbulence decay calculation from multipoint velocity correlations or spectral equivalents at initial time

19 p3044 A71-37730

Surface energy absorption coefficient determination from decaying sound fields, deriving reverberation time and decay rate equations

23 p3703 A71-43201

Luminescence time decay in optically excited thin direct gap semiconductor with surface losses, establishing phase shift method for carrier lifetime and semiconductor surface properties

24 p3863 A71-45360

DECELERATION

NT SPIN REDUCTION

Computer simulation of human body kinematics under rapid decelerations

04 p0542 A71-14786

Magnetic stars models on possibility of rotational deceleration by hydromagnetic waves radiation without mass loss

07 p1190 A71-18857

Parachute decelerator towline energy absorber shock attenuation characteristics, discussing drop test results

11 p1708 A71-25527

Civil aircraft arresting on runway overshoots, describing safe deceleration method by use of soft ground arresters

17 p2674 A71-35210

Karman vortex street breakdown under deceleration, noting vortices distortion and annihilation followed by vortex street formation of different frequency

19 p3046 A71-38202

Spacecraft entry into planetary atmosphere, considering heating, deceleration and landing

20 p3305 A71-38814

Impulsive retrofire deboost of rocket vehicles initially moving in elliptical orbits for maximum and minimum atmospheric entry angles

22 p3608 A71-41697

DECELERATORS

U BRAKES [FOR ARRESTING MOTION]

DECEPTION

Deception repeaters for erroneous information transmission to radar, considering echo signal level, burnthrough, target size, sensitivity, gain and bandwidth

04 p0555 A71-15359

DECIMETER WAVES

Jupiter decimetric emission circular polarization, observing equatorial magnetic field strength in radiation belt

02 p0317 A71-12868

Solar radio astronomy decimeter wave multichannel spectrograph for solar bursts fine structure spectrum analysis

03 p0488 A71-13530

Decimeter radio wave propagation in Venusian atmosphere, determining refraction and absorption coefficients height dependence based on Venera spacecraft data

05 p0718 A71-15993

Microwave semiconductor limiter diode for decimeter operation using spark gap analog

06 p0873 A71-17540

Superhigh multiplicity wideband tunable parametric diode frequency multipliers for decimeter range

06 p0873 A71-17542

Meter and decimeter wavelength periodic filters with bent row arranged posts, deriving dispersion equations

09 p1415 A71-22460

Jupiter magnetic field geometry related to Io modulated Jovian decametric radio emission

12 p1956 A71-26620

Transistorized microwave amplifier/limiter for upper part of decimeter wave range, suggesting limitation in automatic gain control transistors

16 p2547 A71-33499

Decimeter wave multichannel spectrograph design for radar astronomy, stressing HF section

17 p2739 A71-34600

Venus atmosphere decimeter wave field intensity fluctuations and refraction coefficient variations

20 p3297 A71-39627

Decimeter radio wave propagation in Venusian atmosphere, determining refraction and absorption coefficients height dependence based on Venera spacecraft data

22 p3515 A71-42742

Two stage decimeter wavelength quantum paramagnetic amplifier, noting noise temperature and gain

23 p3652 A71-43529

DECISION ELEMENTS

U LOGICAL ELEMENTS

DECISION MAKING

Flight simulator ancillary features using computer data storing and processing capabilities for flight instructor decision making process improvement

01 p0066 A71-10018

Modified integrate and dump detector using FM click mechanism for improving bit decision and reducing error rates in FSK system

01 p0032 A71-10879

Mission requirements in decision processes for guidance and control system design of aerospace vehicles

[AIAA PAPER 70-1231]

01 p0126 A71-11301

Human operator thinking and decision making model for man-machine interaction

03 p0368 A71-12999

Decision making heuristic program reflecting human brain function in problems with listed requirements and unspecified goal

03 p0369 A71-13002

Design management, discussing organization, planning and control

03 p0524 A71-13743

Decision and control /adaptive processes/ - IEEE Conference, Pennsylvania State University, November 1969

03 p0393 A71-14478

Optimal space experiments selection for satellites and space probes, discussing criteria and techniques for guidance in program management decision making

05 p0816 A71-16138

R and D management decision making process structural model, discussing technological forecasting based on organized technical information, quantized judgments, optimum resource allocation and hybrid technique

05 p0840 A71-16744

Operational research for decision making in weapons procurement and deployment, considering military effectiveness, weapon assessment criteria, local conflict conditions, cost and operational environment

07 p1206 A71-19418

Interactive computer graphics in cartography, considering on-line updating of digital topographic map file by human decision making

08 p1281 A71-21248

Clustering and decision making with interactive a priori problem knowledge insertion in subcategory mean vectors and covariance matrices form for pattern recognition and learning

08 p1260 A71-21664

Man machine systems classification, suggesting machine-only system for decision making

10 p1567 A71-23998

Pattern recognition systems, considering receptor, preprocessing and decision making stages

10 p1568 A71-24225

Uncertainty factors in management decisions and operations optimization in international air transportation industry

10 p1698 A71-24265

ATC automation system design, considering controllers decision time savings

10 p1640 A71-24271

Deferred state sampling plans using accept/reject decisions dependent on future lot disposition according to quality drift

12 p1909 A71-26661

Costs-reliability relationships in helicopter development testing and demonstration, emphasizing decision making in program management

[SAE PAPER 710452]

13 p2167 A71-28330

Mathematical programming models for resource allocation and project selection decision in R and D

14 p2340 A71-29855

Aviation within total transport system, discussing decision making and management planning

14 p2341 A71-30165

Quandary recognition and referee strategy in digitally controlled modal survey system, noting decision making sources

14 p2208 A71-30314

Book on dynamic probabilistic systems, Volume 2, covering semi-Markov and decision processes

15 p2440 A71-31197

Aircraft/environment compatibility, emphasizing decision making process for airport planning, site location, development and operation

15 p2516 A71-32248

Community actions for jet aircraft noise reduction, discussing noise environments, nationwide goals, decision making and economic incentives

15 p2516 A71-32249

Stability conditions approximation for assessment of single parameters effect and in making choices

16 p2607 A71-33003

Monte Carlo Bayesian analysis technique applied to decision problem concerning population of single-use item in state of operational readiness

16 p2582 A71-33288

Redundancy verification of parallel systems related to element MTBF and decision maker perspective involving acceptance risk of system failure

16 p2582 A71-33292

Airline fleet equipment planning, discussing management decision making based on aircraft and ground equipment life cycle costs

16 p2522 A71-33307

Maintenance aids evaluation for government contracting and decision making, including cost model based on life cycle economics

16 p2552 A71-33311

ONR human engineering research program concerning information input, display and processing concepts, decision making and motor output and control

16 p2536 A71-33529

Mental load physiological parameters determination by binary choice task, noting changes in heart and respiratory rates and systolic and diastolic pressure

17 p2688 A71-34364

Optimum and suboptimum decision rules for two-channel deep space telemetry system with modulation consisting of PM with two orthogonal phase functions

17 p2704 A71-35088

Reliability in key project decision making, including failure mode/effect analyses, design tradeoff, baseline meetings, hardware storage and data bases

18 p2926 A71-36491

Human psychomotor performance measurements in rotating environments, using Langley complex coordinator and decision response time devices

[AIAA PAPER 71-887]

19 p3006 A71-37275

Third London airport planning, discussing site selection, cost analysis and decision making

[CASI PAPER 72/1]

19 p3040 A71-37592

Parallel strategies effectiveness in R and D projects, discussing learning rate as critical parameter in project management decision making process

19 p3173 A71-37629

Simulator for operating decision rules for control of airborne IR forest fire detection system
19 p3066 A71-38409

Aircraft part repair-throwsaway decisions for minimizing costs over life cycle by economic graphic screening techniques
23 p3661 A71-43197

International HEOS project organization, discussing communication, task delegation, decision making and structure
23 p3785 A71-43455

Management information techniques, discussing project reports, meetings, decision process, work breakdown, planning schedules and computerization
23 p3785 A71-43457

Computer-aided decision algorithm for ATC problem in near terminal area, emphasizing scheduling and holding strategies
23 p3703 A71-44105

Earth observation system design decision making, considering data needs, technology readiness, man role in earth resources programs and space program schedule
24 p3892 A71-44867

DECISION THEORY

NT STATISTICAL DECISION THEORY

Three element model for choice behavior binary prediction consisting of logical, experiential and error components
07 p1048 A71-19595

Decision logic table application, utilizing valid response sets development maximum number and biparameter conditions
09 p1412 A71-23283

Large system performance test resources allocation priorities determination methodology using decision theory, discussing extensive and diminutive forms
12 p1895 A71-27438

Bayesian decision theory, discussing choice of possible systems to convert wind into electrical energy
16 p2582 A71-33291

Linear dynamic systems state estimation, using empirical Bayes decision theory to develop filter set
17 p2825 A71-34897

German monograph on nonlinear distortion correction of binary bipolar signals in Gaussian noise covering receiver, decision theory and error probabilities
18 p2874 A71-35959

Linear programming problems with multidimensional decisions, proposing solution method based on utility theory
18 p2940 A71-36040

Optimal design procedure as experimental design finite decision problem, using Bayes and minimax techniques
21 p3408 A71-40879

German book on adaptive control systems covering decision processes and application examples
23 p3660 A71-44188

Potential function, permissible transformations, geometrical, linguistic, optimal statistical and heuristic methods for pattern recognition, discussing unifying approach based on invariant decision functions
24 p3812 A71-44391

DECKS (FLOORS)

U FLOORS

DECLINATION

Discrete radio sources precise declinations and optical identifications, using prototype space frequency interferometer
04 p0641 A71-14735

Quartz magnetometer design and operation for simultaneous geomagnetic field declination and horizontal component measurements
05 p0756 A71-17216

Cyclic variations in geomagnetic field from 1550 through 1960 using spherical harmonic analysis of magnetic declination
07 p1099 A71-19395

Radiotelescopic observations of period and declination of pulsar Mp 0450 in South India
07 p1201 A71-20499

Quartz magnetometer design and operation for simultaneous geomagnetic field declination and horizontal component measurements
13 p2067 A71-28270

Right ascension and declination accuracy for Sirio satellite attitude determination in transfer orbit, describing computer program
19 p3150 A71-37312

Cyclic variations in geomagnetic field from 1550 through 1960, using spherical harmonic analysis of magnetic declinations
19 p3053 A71-37819

Goloseyev latitude star catalog, considering observation error distribution and stellar declination estimations
23 p3771 A71-44258

DECODERS

Differential PSK signal detection, using decoding circuit with uncontrolled oscillator
01 p0031 A71-10822

Decoding n-bit Johnson code to decimal numbers using n 2-input 2-output comparator circuits
01 p0037 A71-11175

Satellite telemetry systems for data transmission to developing nations ground stations decoding equipment
14 p2199 A71-30910

Reed-Solomon erasure-correcting sequential decoder implementation for hybrid coding scheme, using digital circuitry
22 p3513 A71-42387

DECODING

Decoding n-bit Johnson code to decimal numbers using n 2-input 2-output comparator circuits
01 p0037 A71-11175

Majority decoding schemes for cyclic and decyclic codes, using successive application of separate checks
01 p0039 A71-11318

Coded recording technique for microfilming daily aerological data, decoding by computer in rapid and compact search and recognition procedure
06 p0922 A71-17503

Error correction coding/decoding techniques integration, discussing convolutional and block coding and Viterbi, Sequential and Threshold decoding algorithms
07 p1066 A71-20425

Two algorithms for decoding beyond Bose-Chaudhuri-Hocquenhem bound
08 p1258 A71-21314

Decoding computational work and time, discussing cost increases related to communication reliability
09 p1407 A71-23102

Hybrid decoding technique for symmetrical binary input channels, using bootstrap algorithm across convolutionally encoded information streams
11 p1730 A71-25375

Binary periodic convolutional codes with lower bound everywhere stronger than Wagner on definite decoding minimum distance
11 p1731 A71-25758

Holographic method for coding and decoding three dimensional information
13 p2067 A71-28443

Majority logic decoding for primitive polynomial and dual codes, discussing nonorthogonal parity-check sums formation methods and Euclidean geometry maximality
14 p2207 A71-30011

Combined data compression and error control by digital sequential decoding for space to earth data links using digital computers
14 p2193 A71-30023

Performance predictions for Viterbi decoding algorithm by simulation on UNIVAC 1108
14 p2200 A71-30922

Analog error correcting redundancy codes, examining coding and decoding procedures
17 p2701 A71-34967

Majority decoding of cyclic codes, determining number of checks upper bound for various decoding schemes
17 p2702 A71-34969

Successive block decoding procedure for reduction of operations required for single information symbol decoding, noting substantial gains at equal error probabilities
17 p2702 A71-34970

Decoding at high transmission rates, describing algorithm for mean number of operations and error probabilities
17 p2702 A71-34971

Decoding of linear codes combinations for nonidentical domains of correct reception, noting dependence on signal structure
17 p2702 A71-34973

Fano and stack algorithms comparison by computer simulation of two sequential decoding algorithms
22 p3512 A71-42379

Decoding of correlative level coding or partial response signaling systems with ambiguity zone detection, discussing error correction algorithm
22 p3513 A71-42382

Error correcting binary block code decoding on Q-ary output channels/weighted erasure decoding/, considering applications
24 p3806 A71-44936

DECOMMUTATORS

NRZ PCM signal conditioning, bit and group synchronization and decommutation techniques
01 p0034 A71-10901

Telemetry decommutation system using linguistic and statistical methods in pattern recognition
01 p0036 A71-10989

DECOMPOSITION

NT AMMONOLYSIS
NT GLYCOLYSIS
NT HYDROGENOLYSIS
NT PHOTODECOMPOSITION
NT PHOTODISSOCIATION
NT PHOTOLYSIS
NT PROPELLANT DECOMPOSITION
NT RADIOLYSIS

Periodically modulated phase structure transformations in decomposition of Cu-Ti and Cu-Ti-Al alloys during aging at different temperatures
01 p0101 A71-10670

Decomposition structure of supersaturated solid solution in Co-Nb alloy, showing beta phase transformation inhibition
01 p0101 A71-10671

Decomposition of unstable beta solid solution of Ti-V alloy, using X ray and microscopic analyses
02 p0263 A71-11929

Hydrogen-sensitized decomposition of hydrogen peroxide, taking oxygen inhibiting effect into account
03 p0376 A71-14277

Hydrogen peroxide decomposition acceleration by carbon monoxide, discussing reaction mechanisms and rate coefficients
03 p0376 A71-14280

Catalytic decomposition of sodium chlorate using cobalt oxide catalysts
04 p0549 A71-15750

Ignition and nondetonating decomposition of liquid nitromethane explosive at 10 kbar pressure
05 p0795 A71-16517

Beryllium hydride pyrolytic decomposition kinetics noting temperature range, time distribution, linear growth rate and X ray irradiation
07 p1182 A71-19241

Metastable beta phase Ti-Mo and Ti-V alloys ternary additions effect on decomposition
07 p1138 A71-19982

Mossbauer effect study of 475 C decomposition of binary Fe-Cr alloys, considering fluctuations about average composition
07 p1138 A71-19985

Block decomposition of linear time invariant multivariable control systems
08 p1269 A71-21328

Discontinuous decomposition and aging kinetics of supersaturated solid solutions of tungsten in cobalt, comparing to precipitation theories
09 p1469 A71-22848

Rhenium tellurides phase transformation during decomposition in Ar
16 p2621 A71-33566

Eutectoidal decomposition of tantalum dicarbide, noting X ray phase identification during carburization of tantalum ribbons
20 p3252 A71-39961

Co-Ni-Ti alloy intermittent decomposition kinetics observation by light and electron microscopy, noting finely divided phase coagulation
24 p3836 A71-44670

DECOMPRESSION

U PRESSURE REDUCTION

DECOMPRESSION SICKNESS

Neurological altitude decompression sickness clinical manifestations, pathophysiology, treatment by compression therapy and subsequent grand mal seizures
06 p0859 A71-17614

Spacecraft cabin rare gas-oxygen atmosphere decompression effects on animal metabolic rates
06 p0853 A71-17956

Gas bubble statics in physical systems and organism tissues during decompression
06 p0855 A71-18374

Decompression urticaria response in subjects after inert gas breathing at constant ambient pressure, noting osmosis mechanism
08 p1246 A71-20813

Pressure and gas composition effects on sodium acetate-C 14 incorporation into liver lipids, indicating metabolic relationships to decompression sickness
08 p1238 A71-20814

Oxygen vs air in treatment of divers with decompression sickness
08 p1242 A71-21957

Decompression sickness physical and physiological aspects, discussing gas transport quantification, inert gas elimination and metabolic gas exchange in recompression therapy, work performance, etc
09 p1394 A71-23236

Pressure effects on human ventilation and gas exchange, determining stratified inhomogeneity during deep diving
12 p1873 A71-27126

Body fat influence with and without denitrogenation on decompression sickness in men exercising after abrupt exposure to altitude
13 p2022 A71-29361

Emergency surface decompression and treatment procedures for project Teklite aquanauts, determining safe interval and schedules for return to habitat on ocean floor
16 p2535 A71-33110

Advantages and drawbacks of pure oxygen and oxygen-nitrogen space breathing, considering decompression sickness in Apollo missions
18 p2863 A71-35907

Decompression sickness, investigating surface excursion diving and selection of limb bends vs CNS symptoms by tests on goats
21 p3330 A71-40344

Humoral smooth muscle acting factor and phenylpiperazinylmethyl cyclohexanone effects on decompression sickness production and prevention in thin mice

21 p3331 A71-40352

Scanning ultrasonic imaging technique for in vivo monitoring of microscopic bubble formation in decompression sickness, presenting image displays

22 p3504 A71-42250

High altitude decompression disorders prevention in humans by increasing pressure level in oxygen equipment assembly

24 p3795 A71-44474

DECONTAMINATION

NT SPACECRAFT STERILIZATION

Glow discharge cleaning for surface contaminants removal from hydrodynamic gas bearing components, discussing equipment application to thin film lubricant vapor deposition

02 p0256 A71-12461

Hydraulic system and fluid cleanliness maintenance, discussing contamination sources and prevention techniques including filtration, dehydration and degasification

19 p2999 A71-38319

Hydraulic components and equipment contamination control and effects on system efficiency, discussing filter ratings and location

19 p2999 A71-38321

Hydraulic equipment fluid contamination control, discussing sample bottle cleaning, fluid sampling, component tolerance profiles and filtration performance specifications

19 p2999 A71-38322

Hydraulic fluids contribution to system contamination, discussing precipitate formation due to reaction with water, filtration inability and contaminant elimination

19 p2999 A71-38323

Vacuum package with Ti bulk sublimation/ion pump combination for 150 kv neutron generator tritium decontamination

21 p3414 A71-40900

Mathematical models for microorganism exponential die-off rate and variance estimation from decontamination data

22 p3504 A71-42231

DECOUPLING

Aircraft longitudinal motion decoupling through direct lift control, investigating flight control for landing

03 p0347 A71-13339

Generalized Watson sums calculation with application to magnetization of anisotropic ferromagnet for Callen type decoupling schemes

09 p1506 A71-22149

Flight path optimization with multiple time scales, discussing decoupling of high order three dimensional aircraft flight problem into several low order problems

10 p1556 A71-24858

Multivariable control system state variable feedback decoupling theory generalization to include output subset, using matrices

17 p2718 A71-34736

DEDUCTION

Syntactical characterization of tautologies for deductive systems and theories based on formalized algorithmic languages

18 p2942 A71-36822

Generalized computing machines deductive systems, introducing sequence of partial functions

18 p2886 A71-36823

DEEP DRAWING

Plastic deformation rate effect on deep drawing of sintered and vacuum melted thin sheet Mo

02 p0256 A71-12516

Temperature effect on ductility of thin sheet sintered or vacuum melted Mo during deep drawing

02 p0257 A71-12517

Longitudinal and cross rolling effects on anisotropy of mechanical properties and deep drawability of sintered thin sheet Mo

02 p0257 A71-12518

Critical ductile-brittle transition temperature and microstructure under deep drawing of sintered and vacuum melted Mo

02 p0257 A71-12519

Titanium, Inconel and stainless steel alloys deep drawing press loads under various lubrication and temperature conditions, considering work hardening, friction and anisotropic coefficients

[ASME PAPER 70-WA/PROD-26]

03 p0433 A71-14114

DEEP SPACE

NT INTERPLANETARY SPACE

NT INTERSTELLAR SPACE

Pioneer spacecraft flight missions, discussing interplanetary, solar-earth and deep space observations

01 p0160 A71-10990

Deep space shuttles operating modes and vehicle types, considering chemical vs nuclear propulsion, direct vs near-orbit rendezvous, refueling, etc

01 p0165 A71-11593

Drag free spacecraft performance in deep space, examining inner residual disturbance forces for motion control systems

[ONERA-TP-887] 06 p0900 A71-18022

Deep space probes telemetry system a priori data compression ratio evaluation using channel activities under unknown output signals cross correlation

[AIAA PAPER 71-231] 08 p1258 A71-20799

Pioneer 9 interplanetary observations, presenting deep space data for solar rotations and radial gradient in VLF electric field behavior

13 p2064 A71-29163

Missions beyond solar system for studying origin and evolution of life, planets and stars

[AAS PAPER 71-163] 19 p3141 A71-37960

Deep space plasma measurement techniques by instruments on earth satellites

19 p3116 A71-38245

Geodetic parameters describing earth gravity field and satellite tracking stations positions in geocentric reference frame, using satellite observation and deep space probes

20 p3220 A71-39659

Onboard optical tracking effectiveness for Grand Tour deep space navigation, considering star-planet angles, plane diameter angles and natural satellite observations

[AAS PAPER 71-394] 23 p3732 A71-43062

DEEP SPACE INSTRUMENTATION FACILITY

Electrical performance of Cassegrain antenna reflector for space communication via ATS and deep space research

17 p2700 A71-34747

Optimum and suboptimum decision rules for two-channel deep space telemetry system with modulation consisting of PM with two orthogonal phase functions

17 p2704 A71-35088

DEEP SPACE NETWORK

Wideband subcarrier frequencies demodulation technique for uncoded or coded PSK telemetry over large input SNR range for deep space interplanetary communication

08 p1254 A71-21316

Solar wind motion irregularities near sun from interplanetary scintillation observations, using receivers at Goldstone deep space tracking station

10 p1674 A71-24435

Deep Space Communications System low noise microwave receiver, discussing operating noise temperature calibration, error analysis and programming

15 p2372 A71-32311

DEFECTS

NT AUDITORY DEFECTS

NT CRYSTAL DEFECTS

NT CRYSTAL DISLOCATIONS

NT EDGE DISLOCATIONS

NT FRENKEL DEFECTS

NT INCLUSIONS

NT POINT DEFECTS

NT SCREW DISLOCATIONS

NT SPEECH DEFECTS

NT SURFACE DEFECTS

NT VACANCIES [CRYSTAL DEFECTS]

Metal flaw size measurement, discussing ultrasonic echo amplitude and defect scanning methods

01 p0086 A71-10304

Electroinductive defectoscopy using eddy currents as nondestructive materials testing method

01 p0079 A71-10335

Open cylindrical shells with end eccentricity or initial deflection imperfections, investigating buckling under axial compression by Newton-Raphson method

03 p0505 A71-13544

Stress analysis of multilayered composite structures with flaws, emphasizing application to fracture studies

04 p0671 A71-15753

High voltage electron microscopy of internal defects in carbon fibers, considering fiber strength

[PLASTICS INST. PAPER 10]

08 p1297 A71-20921

Electronic digital automatic defect indicator attachment to industrial echo defectoscope

08 p1300 A71-21897

Buckling of circular cylindrical shells with axisymmetric imperfection distributions under axial compression

12 p1983 A71-27573

Computer methods for automatic diagnosis program applied to future manned space vehicles, discussing cost relationship to fault isolation techniques and component reliability

13 p2044 A71-27940

Low cyclic failure resistance at elevated temperatures and static defects calculation, based on fatigue and empirical endurance curves

13 p2149 A71-28122

Al-Zn-Mg alloy plates welded with Al-Mg filler metals, observing ghost defects in radiographs

13 p2074 A71-28524

Al alloy spot welding, investigating defects effects on welded joint fatigue strength under dynamic tests by metallographic and X ray examinations

15 p2436 A71-32467

Ultrasonic reflection from defects, using method of similarity and approximation of ray acoustics

16 p2584 A71-33560

Two frequency ultrasonic flaw detector for determination of defects opening widths, examining ultrasonic pulse transmission through thin air layers

16 p2580 A71-33562

Aluminum alloy gas tungsten arc welds, determining defect size and distribution effects on fracture strength

18 p2929 A71-36857

Radiation flaw detection by fast neutrons, monitoring thick lead plates and three-layer articles

22 p3528 A71-41761

Ultrasonic inspection apparatus for defects detection in metal pipes, using immersion echo mode with two piezoelectric scanning heads rotating about pipe

22 p3529 A71-41774

Hydrogen dissolution in fused silica, investigating temperature effects during impregnation on reactive defect sites number

24 p3841 A71-44869

DEFENSE COMMUNICATIONS SATELLITE

SYSTEM

Defense Satellite Communications System Phase II design and implementation, considering earth, space and control subsystems

07 p1057 A71-18818

Time division multiple access techniques for Defense Satellite Communications System

07 p1057 A71-18819

Time division multiple access (TDMA)/hardware for military communication satellite systems

07 p1057 A71-18821

DCS TDM/DSCS TDMA synchronous operation, examining rate buffering, slaved clocks and constant feedback approaches

07 p1058 A71-18823

DEFENSE COMMUNICATIONS SYSTEMS [DCS]

DCS TDM/DSCS TDMA synchronous operation, examining rate buffering, slaved clocks and constant feedback approaches

07 p1058 A71-18823

Digital transmission in Defense Communications System, discussing data requirements, converter and TDM involving terrestrial and satellite links

07 p1066 A71-20432

DEFENSE INDUSTRY

Weapons R and D flexible economical response to defense needs by emphasis on component and subsystem experimentation

14 p2341 A71-31130

Defense industry pricing and contracting for inflation, considering statistical analysis and direct cost estimation

14 p2342 A71-31132

Cost control over changes in major weapons systems between letting of contract and final hardware delivery

14 p2342 A71-31134

Defense and aerospace industry demand cyclical variations effect on productivity growth and cost

22 p3624 A71-42525

DEFENSE PROGRAM

Defense and space programs management systems, discussing structured activities planning for efficient resources use

[ASME PAPER 70-WA/MGT-5] 03 p0524 A71-14097

Space station program characteristics, discussing technology, sciences, exploration, public services, foreign relations and national defense

04 p0689 A71-14930

Human role in Aerospace Defense Command navigation, discussing Airborne Warning And Control System and navigational aspects of ADC mission

07 p1157 A71-20346

Space transportation system of two stage reusable space shuttle and orbit-to-orbit shuttle, supporting NASA and DOD missions

08 p1367 A71-21890

Defense management efficiency improvement concepts for weapon systems programs, discussing elimination of bureaucracy, communication between organizational levels, mission instead of function orientation, etc

12 p1988 A71-27246

DEFINITION

State definition international standardization for cold rolled Al sheets, examining yield curves and strain energy

05 p0764 A71-15923

DEFLAGRATION

Thermal radiation effects on M-2 double base solid propellant ignition, deflagration and burning rate

02 p0298 A71-12851

Solid propellant oxidizers hydroxylammonium perchlorate and hydrazine nitroform self deflagration, determining combustion temperatures and burning rate pressure relationships

06 p0944 A71-18299

Gas phase model for ammonium perchlorate deflagration at 20-100 atmospheres

[AIAA PAPER 71-171] 06 p0944 A71-18611

- Ammonium perchlorate deflagrations, determining intrinsic stability of one dimensional burning configuration based on flame structure modeling
[AIAA PAPER 70-123] 11 p1809 A71-25455
- Experimental method for determining condensed phase heat of reaction of deflagrating double-base propellant, defining minimum surface temperature at solid surface without heat feedback
11 p1809 A71-25493
- Space propulsion by plasma deflagration gun, measuring specific impulse by piezoelectric probe and pendulum methods
19 p3122 A71-37871
- Deflagration behavior of pure and isomorphously doped ammonium perchlorate, using cinephotomicrography of burning samples and scanning electron microscopy of quenched samples
19 p3120 A71-38118
- DEFLATING**
U INFLATABLE STRUCTURES
U PRESSURE REDUCTION
- DEFLECTION**
Cylindrical shell deflection under concentrated radial force expressed in terms of algebraic polynomials
02 p0326 A71-12295
- Instantaneous deflection and velocity distribution curves of cantilever beam with uniformly varying length in constant gravity field by numerical methods
03 p0504 A71-13465
- Deflection-optimal elastic beams design for distributed dynamic loading
05 p0825 A71-16717
- Maximal deflection of square and rectangular thin plates with small initial concavities, using dynamic relaxation method for lateral and postbuckling in-plane edge loads
05 p0830 A71-17225
- Rectangular plates and shallow shells large asymmetric deflection, using computerized finite difference technique
06 p0991 A71-17802
- Tapered cantilevered beams design, determining end deflection and bending stress magnitude by graphical method
07 p1213 A71-19693
- Dynamic response of beams to transverse impact, considering deflection curve
09 p1541 A71-23205
- Initially curved thin elastic plates, predicting large deflection and postbuckling behavior with finite element procedure
[AIAA PAPER 71-357] 11 p1844 A71-25336
- Geometrically nonlinear large deflection and structural stability problems, using finite element method
16 p2653 A71-33087
- Circular plate deflection weakened by hole and under constant external pressure, obtaining successive approximation method solution convergence
17 p2816 A71-34329
- Conical shell with circular hole, determining stress function and normal deflection in torsion
17 p2817 A71-34338
- Multilayer asymmetrical shallow shells with transverse shear strains, deriving finite deflection nonlinear equations
17 p2833 A71-35613
- Deflection equations and bending stress for forced vibration of beam with time dependent boundary condition
[ASME PAPER 71-VIBR-32] 21 p3458 A71-40286
- Lagrangean equation of motion for crack wall driven by square tension impulse, obtaining deflection in terms of crack length and particle velocity
23 p3777 A71-43496
- Discrete element finite deflection analysis of shallow arches using numerical method of potential energy minimization
24 p3879 A71-44636
- Rigidly plastic shell theory Lagrangian formulation for moderately large deflections, defining kinematic and dynamic tensors for field equations
24 p3880 A71-44640
- DEFLECTORS**
Optico-acoustical deflector with high resolving capability, using Bragg light diffraction by ultrasonic waves
04 p0604 A71-14627
- Acoustooptic deflector modulation transfer function calculated from autocorrelation theorem
14 p2241 A71-30141
- Optico-acoustical deflector with high resolving capability, using Bragg light diffraction by ultrasonic waves
22 p3558 A71-42267
- DEFOCUSING**
Nonlinear effects of IR beam passage from continuous neodymium-yttrium garnet laser through defocusing media
09 p1460 A71-22231
- Carbon dioxide laser, measuring focal length of gas defocusing lens in active medium as function of gas pressure and discharge tube diameter
19 p3073 A71-37771
- Nonlinear effects in high power Nd-YAG CW IR laser beam transmission through defocusing media
21 p3394 A71-41110
- Defocused optical system imaging properties and optical transfer function improvement by shaded aperture, discussing necessary conditions and light absorption effect
22 p3548 A71-42551
- Turbulent defocusing and displacement fluctuations of focused He-Ne laser beam in atmosphere over paths near ground
23 p3688 A71-44329
- DEFORMATION**
NT AXIAL STRAIN
NT ELASTIC BENDING
NT ELASTIC BUCKLING
NT ELASTIC DEFORMATION
NT NUCLEAR DEFORMATION
NT PLASTIC DEFORMATION
NT STATIC DEFORMATION
NT TENSILE DEFORMATION
NT WAVE FRONT DEFORMATION
- Ductile Ni deformation and fracture, examining simultaneous cyclic and monotonic strain effects
01 p0098 A71-10164
- Reinforced polymers strength and deformation under tensile loads applied across fibers
01 p0107 A71-10496
- Thick walled slowly rotating viscoelastic cylinder under varying gravitational loads, using theory of elasticity
01 p0169 A71-10500
- Glass fiber reinforced durometer and hard foam sandwich structures deformation characteristics under static loads, presenting theoretical and experimental results
01 p0172 A71-10700
- Nonconservative generalized nodal forces on finitely deformed finite elements
01 p0174 A71-10960
- Turbine disks cyclic nonisothermal deformation with allowance for Bauschinger effect, determining stress-strain state and residual microstresses
02 p0323 A71-11747
- Fiber reinforced thermoplastics deformation characteristics, using uniaxial tensile test
02 p0274 A71-12480
- Mo single crystals polygonization and recrystallization, examining strain rate and deformation conditions effects
02 p0266 A71-12652
- Nb single crystals, examining structure in initial deformed and annealed states at various low temperatures
02 p0266 A71-12654
- Spherical shells deformation subjected at elevated temperature to high velocity impact on planar rigid target
03 p0503 A71-13427
- Stresses and deformation in circular matrix subject to internal pressure gradients, assuming cylindrical anisotropy on macroscopic scale
03 p0504 A71-13463
- Shell of revolution bending deformation, assessing Trefftz approximation error
03 p0506 A71-13597
- Anisotropic thin rods deformation, extending Nikolai constraints condition on Kirchhoff analogy for isotropic rods
03 p0506 A71-13598
- Plane nonhomogeneous strain fields deformation tensor determination by moire equations for fringe pitch and angle measurement, considering rectangular block bending
03 p0508 A71-13772
- Flat products skin milling work determination from microgrid deformation graphs, using continuum mechanics equations
04 p0602 A71-14607
- Circular cylinder creep deformation under complex varying loading, comparing computation and test results
04 p0669 A71-15353
- [ONERA-TP-846] Stability of homogeneous and uniform deformation of isotropic body, using energy criterion
04 p0672 A71-15881
- Deformation stability of three dimensional body with rheological properties under compression
05 p0824 A71-16591
- Liquid droplet elliptical deformation in gas flow upon external flow force application, presenting solution as ellipsoid semiaxes plot of dimensionless time functions at various Weber numbers
05 p0736 A71-16749
- Solid deformable body combined brittle and plastic elements model for strain analysis
05 p0827 A71-16758
- Optical systems aberrations, discussing possible deformations transfer from reflecting or refracting elements
05 p0783 A71-17032
- Combined deformation of reinforcing elements and polymer binder in monodirectional composite structure, determining stress distribution
06 p0915 A71-17380
- Axisymmetric deformed state of three layer circular conical shell with rigidly clamped edges, obtaining equilibrium equations by Bubnov-Galerkin method
06 p0997 A71-17851
- Nb-W single crystal deformation, discussing athermal solid solution strengthening
06 p0914 A71-18683
- Deformation-thermal diffusion processes relation for thin coated composite materials under variable thermal stresses
07 p1210 A71-19156
- Stress-strain state of large inhomogeneous bodies of revolution, considering deformation due to arbitrary surface and mass forces in temperature field
07 p1210 A71-19158
- Technical equations of shells of slowly varying curvature with transverse shear deformation and normal stress
07 p1211 A71-19252
- Heat treatment and deformation effects on blended metal powder compacts homogenization, using mathematical model
07 p1137 A71-19976
- Steady state thermal stresses and deformations in infinite hollow circular cylinder by sinusoidal internal heat source and Newtonian radiation boundary condition outer surface cooling
07 p1214 A71-20026
- Stress wave propagation in plates from explosive loading, discussing wave front interaction and scab formation
07 p1215 A71-20091
- Deformation amplitude effects on dislocation structure and strengthening mechanism of fcc aluminum under cyclic loading
07 p1142 A71-20482
- Fastener group behavior under combination of direct shear and moment, obtaining load deformation response of individual connections
08 p1370 A71-21410
- Bcc Ti-V single crystals deformation modes and resolved shear stresses as function of temperature and composition
08 p1307 A71-21510
- Bcc metals slip band formation, investigating deformation and fraction behavior
08 p1308 A71-21515
- Single crystal TiC-VC alloys mechanical properties, considering room temperature hardness, high temperature deformation and brittle to ductile transition temperature
08 p1316 A71-21589
- Cylindrical steel specimens bearing strength under cyclic elastoplastic deformation, investigating stress redistribution effects
08 p1316 A71-21607
- Low carbon steel welds, investigating low cycle deformation and rupture resistance as function of weld zones
08 p1316 A71-21609
- Contained cross sectional deformation effects on turbine blades natural torsional vibration frequencies
08 p1372 A71-21617
- Nonshallow spherical shells of small shear modulus materials, examining boundary conditions and axisymmetric deformation
09 p1535 A71-22184
- Imperfect thin walled circular cylindrical shells under axial compression with relaxed boundary conditions, determining deformations with differential equations
09 p1541 A71-23089
- Steels, Ni alloys and Ti alloys deformation resistance and deformability, discussing temperature effects on forging rate
09 p1475 A71-23305
- Thin cylindrical shell deformation under concentrated transverse loads applied through rigid boss, determining displacement variations as function of applied loads and edge constraints
09 p1543 A71-23659
- Soviet book on vibrations of deformable systems and computer solutions covering ponderable rods, beams, plane frames, lattice structures, plates, bars, blades, shafts, etc
11 p1852 A71-26402
- Strain rate and temperature effects on flow stress of Ni-Al in polycrystalline and single crystal for activation energies and deformation volumes evaluation
11 p1782 A71-26440
- Iterative solution of semidefinite eigenvalue problems, identifying rigid body and deformation coordinates
12 p1974 A71-26873
- Spherical shell stressed state weakened by holes, investigating shear deformation effect
12 p1975 A71-27107
- Asymmetrical three layer plate with filler under impact loading, examining material and layer thickness effects on deformation
12 p1975 A71-27111
- Combined deformation of reinforcing elements and polymer binder in monodirectional composite structure, determining stress distribution
12 p1921 A71-27462

Deformation fatigue theory extended to tests at stresses below elastic limit, explaining cyclic loading frequency effect on fatigue life

12 p1984 A71-27681

Structural characteristics of Ti subjected to high speed deformation rates, examining formation of crystallographic glide lines and twins as function of deformation degree and rate

13 p2085 A71-28226

Cavity cross sections deformation in heavy ideal liquid, deriving nonlinear system of equations for time dependence within framework of small perturbation theory

13 p2047 A71-28279

Laser interference patterns recorded on photosensitive surface of test sample before and after deformation, considering irregularly shaped objects with rough surfaces

13 p2067 A71-28441

Cylindrical liquid filled shells under rapid axial compression along generatrix, examining dynamic deformation characteristics

13 p2156 A71-29072

Optimization algorithm for multielement support structure exhibiting minimum deformation energy, comparing Lagrange conditional search method

13 p2101 A71-22186

Ni-Ni Nb eutectic composite, investigating monotonic mechanical response, deformation and fracture mechanisms

13 p2088 A71-29401

Compression rolled and hot upset Be sheet stress-strain behavior and deformation dynamics, emphasizing temperature and strain rate effects on polycrystalline flow stress

13 p2088 A71-29404

Polycrystalline Hf under tension at various temperatures, determining H effects on fracture, operative deformation modes and hydride habit planes

13 p2090 A71-29417

Three dimensional elastic plastic solid, calculating stress and deformation with finite difference procedure

14 p2322 A71-29737

Complex media and plasticity theory deformation models based on central friction mechanism, discussing elastic spring analog

14 p2332 A71-30879

Shear deformations effect on circular plates from Reissner theory, expressing bending moments and shear forces as functions of lateral deflection and stress function

15 p2507 A71-32112

Cold worked pure Mo recrystallization kinetics, indicating dependence on deformation mode and techniques

15 p2433 A71-32177

Low temperature creep deformation recorder with liquid He coolant, discussing Al and Pb single crystal tests

15 p2385 A71-32239

Creep deformation during intermittent loading, obtaining strain rate as function of applied stress and stress cycle time

15 p2508 A71-32254

Deformable magnesium alloys, discussing applications and semifinished products manufacturing equipment

15 p2435 A71-32337

Crack propagation in brittle solids under constant deformation or thermal shock, verifying behavior by results with polycrystalline aluminum oxides

16 p2590 A71-32941

Wells COD /crack opening displacement/ criterion for notch root deformation and fracture measurements

16 p2591 A71-32949

Thermoelastic stability of finitely deformed solids under nonconservative surface tractions without body force

16 p2649 A71-33009

Continuous media nonlinear thermomechanical behavior, presenting finite element formulation of deformation and irreversible thermodynamics problems

16 p2654 A71-33095

Two massive arbitrarily shaped hard bodies spatial collision, determining kinetic energy loss, motion and deformation of impact point

17 p2818 A71-34347

Deformations and stress concentration on corrugated plate under uniformly distributed load, considering cross section as combination of two cylindrical shells

17 p2818 A71-34401

Image distortion technique for viewing surface deformation zones at precracked specimens under monotonic loading during fracture test [SESA PAPER 1799]

17 p2738 A71-34547

Oxygen metabolic rate in isolated canine lungs at various static inflation levels and cyclic ventilation, examining mechanical deformation effects

17 p2683 A71-35145

Combined brittle and plastic elements model for strain analysis of nonelastic deformed solid

17 p2832 A71-35457

Strain hardening energy curves in generalized coordinates, discussing deformable body state, stress-strain relation, etc

17 p2832 A71-35459

Fluid jets and droplets deformation in transverse supersonic two phase gas flow

17 p2673 A71-35638

Deformation-thermal diffusion processes relation for thin coated composite materials under variable thermal stresses

17 p2834 A71-35654

Difficulties in using Richter and Noll symbolism in theory of nonlinear deformation, involving representation of tensors as double fields

18 p2976 A71-36095

Deformation field of continuous medium in Minkowski space-time, defining tensor in Euclidean space of initial configuration

18 p2947 A71-36191

Single crystal Ni-Al solid solutions deformations, examining temperature and concentration dependence of critical cleavage stresses

19 p3076 A71-37120

Deformation rate and temperature effects on optimum strength and ductility of die forged and extruded Mo-Ti alloys

19 p3077 A71-37269

Localized deformation effect on common-emitter transistor current gain, giving equations system defining band diagram configuration of p-n junction in thermal equilibrium

19 p3027 A71-37490

Anisotropic material circular rotating disks of various thickness, calculating stress and deformation

19 p3160 A71-38473

Al, Cu and Ni high temperature creep noting diffusive, shear and dislocation deformation mechanisms

19 p3083 A71-38525

Deformation and stress distribution three dimensional state around flat parabolic cracks in elastic solids

20 p3307 A71-38772

Acoustic emission test facility with constant strain rate compressive sample deformation

20 p3208 A71-38823

Holographic interferometry equipment design for NDT and vibrational and deformation analysis, discussing apparatus construction, optical quality and industrial applications

20 p3238 A71-39344

Holographic interferometry for structure and material deformation measurement, presenting static loading and resonant vibration surveys

20 p3238 A71-39346

Mo and high temperature Mo alloys thermally activated deformation mechanisms from flow stress thermal component and effective stress temperature dependence observation

21 p3396 A71-40030

Deformographic storage display tube system, describing construction, development, design, performance and operating principles

21 p3352 A71-40135

Shear deformation and rotary inertia effects on flexural vibration frequencies of pretwisted, nonpretwisted and tapered cantilever beams [ASME PAPER 71-VIBR-79]

21 p3461 A71-40316

Strain rate and temperature effects on polycrystalline Al-Mg alloy strength, considering deformation mechanism

21 p3400 A71-40834

Deformation and translation measurements with holographic interferometry, considering flat surface moved with precision differential screw micrometer

21 p3381 A71-40933

Circular cylindrical shell under longitudinal parametric load, obtaining nonstationary responses with deformation theory

21 p3471 A71-41029

Shallow two pinned sinusoidal arches stability under random symmetrically distributed lateral loads, observing deformation, buckling and critical value

22 p3612 A71-41429

Metallic polycrystal deformation equations, obtaining creep, Norton law dependences and thermally dissipated energy

22 p3560 A71-41606

Duralumin rods deformation and stress propagation study under dynamic pulse loads, using photosensitive epoxy coatings and high speed photography

22 p3537 A71-41612

Isotropic parabolic elastic cylinder deformation, determining displacements and stresses with Fourier integral and Weber functions

24 p3880 A71-44713

Conical and cylindrical shell deformation with nonlinear one dimensional wave processes, describing algorithm for method of characteristics application

24 p3885 A71-45341

DEFORMETERS

TSH-2 hardness test gage, investigating deformation of steel under increasing loads

07 p1106 A71-19141

DEGASSING

NT DEOXYGENATION

High melting point metal systems with nitrogen or oxygen, discussing degassing and degassing reactions kinetics and thermodynamic equilibrium

03 p0442 A71-13362

Mo wire annealing with degassing, investigating temperature effect on mechanical properties

04 p0616 A71-15802

Small scale vacuum stream degassing of molten aluminum for hydrogen removal

05 p0758 A71-16247

Simultaneous degassing and thermal diffusion phenomena in annealed tantalum-oxygen mixed crystals, investigating maximum temperature effect

16 p2599 A71-34094

Photoelectric tubes microchannel plates degassing during bake-out or during operation by electron bombardment, discussing desorption elimination by multiplier treatment before tube sealing

24 p3811 A71-45337

DEGENERATIVE FEEDBACK

U NEGATIVE FEEDBACK

DEGRADATION

Copper sulfide-cadmium disulfide thin film solar cells degradation under simulated orbital conditions, determining electrochemically induced copper filament growth as electric shorts causes

05 p0699 A71-16057

Ti-Ag and Ti-Pd-Ag solar cell contacts structure and degradation dependence on high temperature and humidity environmental exposure

05 p0699 A71-16060

Solderless Ag-Ti solar cell contacts humidity degradation mechanism

05 p0699 A71-16061

Solar cell and coverslide degradations measurement from telemetry data on satellites at near-synchronous altitudes

05 p0702 A71-16086

Metal microfinishing technique, evaluating surface integrity degrading effects and total time requirements

05 p0759 A71-16464

Planar transistors operating conditions effects on current gain degradation following emitter-base reverse biasing

07 p1076 A71-19560

Degradation rate tests on adhesive bonded sandwich panels of temperature resistant composite structural materials at varying atmospheric pressures

10 p1614 A71-24073

Nondestructive testing method obtaining relaxation modulus and accelerated degradation/stress corrosion of reinforced plastics

11 p1768 A71-25404

Structural stability degradation mechanisms in welded joint of plain and low alloy steels, deriving equation for carbon diffusing

11 p1771 A71-26158

Vacuum UV phototube module for degradation measurement of optical components, including mirrors, windows, lenses and thermal control surfaces [AIAA PAPER 71-461]

11 p1800 A71-26243

Physical model of Zn diffused GaAs electroluminescent diodes gradual degradation, establishing formation of new recombination centers through injected carrier lifetime measurement

15 p2377 A71-32607

DEGREES OF FREEDOM

Poincare hydrodynamic analogy in celestial mechanics, relating differential equations for dynamic systems with two degrees of freedom and two and three dimensional flow

01 p0154 A71-10383

Real time six degree of freedom aircraft flight digital simulation using SL-1 continuous system simulation language

02 p0226 A71-11786

Six degree of freedom flight vehicle kinematics digital simulation using CSSL-II language

02 p0227 A71-11789

Missile six degree of freedom simulation by hybrid computer, discussing roll and pitch dynamics

02 p0227 A71-11798

Lagrange theorem inversion for two degrees of freedom systems, emphasizing Liapunov assumption regarding mechanical systems stability

03 p0449 A71-13114

Nonlinear system with one degree of freedom under HF and velocity dependent force, determining quasi-periodic vibrations with two frequencies by averaging method

03 p0502 A71-13406

Postflight analysis including six degree of freedom trajectory digital simulation of Aerobee 350 sounding rocket behavior under large thrust misalignment [AIAA PAPER 70-1380]

03 p0498 A71-13663

Single degree of freedom vibration isolation systems, examining nonlinear damping range [ASME PAPER 70-DE-8]

03 p0432 A71-13711

First passage failure probabilities for single degree of freedom systems under random vibration [ASME PAPER 70-WA/APM-14]

03 p0512 A71-14155

Cochlear auditory patterns degrees of freedom along spatial axis, considering displacement of basilar membrane and mechanical coupling

05 p0706 A71-16281

Numerical and graphic drive shaft motion trajectories in dynamic gyroscopic system with four degrees of freedom

06 p0928 A71-18232

Discrete structure continuous medium model with internal degrees of freedom, studying physicochemical properties in elastic materials

07 p1217 A71-20455

Spatial resolution improvement by utilizing temporal degree of freedom of transmitted signal, discussing hologram plate recording during exposition intervals

08 p1287 A71-21191

Matrix multiplication algorithm based on degrees of freedom analysis for various transformations and spectral analysis

08 p1260 A71-21662

Equilibrium position stability of Hamiltonian systems with one and two degrees of freedom in resonance

08 p1336 A71-21859

Motion synchronization of objects with single degree of freedom and weak coupling interactions, using small parameter method

08 p1336 A71-21862

Kinetic coefficients calculation for gas with internal degrees of freedom during free energy exchange between translational and internal motion

08 p1338 A71-21918

Linear one dimensional systems with infinite degrees of freedom, examining optimal constrained control

09 p1421 A71-22118

Subharmonic forced vibrations of one degree of freedom nonlinear mechanical systems, deriving formulas for oscillation amplitude, phase shift and shape factor

09 p1536 A71-22410

Conservative systems of differential equations with single degree of freedom, considering periodic solutions existence, determination and stability

09 p1495 A71-23436

Linear one dimensional system with infinite degrees of freedom, discussing optimal control by Fredholm integral equation

09 p1424 A71-23457

Two-degree of freedom Hamiltonian system stability and motion about equilibrium point for two-to-one commensurability

10 p1679 A71-24936

Buckled rectangular panels response to random excitation via single degree of freedom nonlinear vibration equation

11 p1841 A71-25196

Nonlinear aerodynamic stability coefficients from free angular motion of rigid bodies, using three degrees of freedom subsonic wind tunnel tests on Apache model

11 p1837 A71-25515

Six degree of freedom hybrid digital computer program for complex flight control and associated mode logic design and training

11 p1736 A71-25852

Three degrees of freedom gyrocompass with common drive and gimbal bearing, exhibiting westerly deviation from drive axis

11 p1763 A71-26188

Equations of motion for variable mass system of bodies, developing mathematical model of flight vehicle as six degrees of freedom control plant

12 p1926 A71-26728

Stationary motions of holonomous five degree of freedom mechanical system of rod suspended homogeneous symmetrical body in central gravitational field

13 p2100 A71-28730

Kinetic theory of nonspherical multiatomic molecules with electrons having rotational and oscillatory degrees of freedom, giving expressions for oscillatory relaxation times calculation

13 p2103 A71-29150

Vibration absorbers optimization for multiple degree of freedom systems with random excitations, applying optimal control theory in frequency domain

13 p2158 A71-29427

Nonlinear differential equations system for one degree of freedom isochronous and anisochronous conservative oscillators resonance behavior during natural perturbation solved by coordinate transformations

14 p2265 A71-29687

Linear one dimensional systems with infinite degrees of freedom, examining optimal constrained control

14 p2219 A71-29996

Two loop parametrically coupled oscillatory amplifier with unlimited degrees of freedom, investigating segment of long line loaded at one end with periodically varying capacitance

14 p2211 A71-30083

Deterministic and random nonlinear forced vibrations of one degree of freedom system with broken line elastic response

14 p2328 A71-30378

Quantum-theoretical transport equation for dilute gases with internal degrees of freedom, generalizing for arbitrary spacing between internal energy levels

14 p2275 A71-30449

Nonstationary perturbation propagation in gaseous medium with irreversible internal process /chemical reactions or excitations with one degree of freedom of molecules/

14 p2338 A71-30823

Similar solution of strong shock wave propagation with nonequal heat coefficients, approximating dissociation, ionization and excitation energy of molecules vibrational degrees of freedom

14 p2228 A71-30996

Motion characteristics of elastically supported gyroscope, presenting linearized equation of motion for eight degrees of freedom system

15 p2401 A71-31180

Kinetic equation for gases with rotational degrees of freedom under equality of probabilities of direct and inverse transitions and stereoisomerism of molecules

15 p2387 A71-31192

Equilibrium state instability in system with two degrees of freedom, using Liapunov method

16 p2608 A71-33026

Weakly nonlinear single degree of freedom cubic system under simultaneous time varying force and parametric excitation, presenting resonance frequencies classification

[ASME PAPER 71-APM-24] 16 p2655 A71-33205

Approximate method for solution of nonlinear equations with certain degree of freedom subjected to recall and small hereditary forces

17 p2780 A71-34916

Functional analytical iteration methods for calculating nonlinear vibrations of several degrees of freedom and error estimation improvement, considering uniformly converging Fourier series expansion

17 p2782 A71-34939

Nonlinear system with one degree of freedom under HF and velocity dependent forces, determining two-frequency quasi-periodic vibrations by averaging method

17 p2826 A71-35016

ST-224 redundant inertial measurement system, using conventional gimbaled platforms, each with three skewed single-degree-of-freedom control gyro and one caged gyro

17 p2773 A71-35060

Kinetic coefficients calculation for gas with free energy exchange between translational and internal degrees of freedom

17 p2785 A71-35263

Rotor asymmetry effect on errors of two degrees of freedom gyro mounted on dynamic platform

17 p2746 A71-35608

French book on linear vibrations covering systems with one or more degrees of freedom in free and forced vibration, propagation in discontinuous and continuous media, etc

17 p2784 A71-35737

Link 747 simulator with six degrees of motion system for engineers and pilot training

18 p2900 A71-36970

Boeing 747 digital computer type flight simulator with four degrees of movement for engineer and pilot training

18 p2901 A71-36971

Vertically statically unbalanced rotating shaft with two degrees of freedom, investigating internal damping, flexural vibrations and equation of motion

19 p3154 A71-37348

Parametric resonance of single degree of freedom system with double bilinear hysteresis

20 p3267 A71-38793

Higher order approximation for normal vibration modes in nonlinear two degree of freedom systems

20 p3267 A71-38799

Equilibrium position stability of Hamiltonian systems with one and two degrees of freedom in resonance

20 p3270 A71-39358

Motion synchronization of objects with one degree of freedom and weak coupling interactions, using small parameter method

20 p3270 A71-39361

Existence theorem of quasi-periodic solutions with two degrees of freedom for planar three body problem

21 p3441 A71-40093

Steady state performance of two degrees of freedom system consisting of main linear spring mass system under periodic forcing

[ASME PAPER 71-VIBR-49] 21 p3459 A71-40298

Transient torsional vibration due to suddenly applied torque, deriving transfer function for systems with four degrees of freedom

[ASME PAPER 71-VIBR-99] 21 p3461 A71-40326

Dynamic problems for molecular gases with rotational degrees of freedom, deriving hydrodynamic equations from kinetic equations integration

21 p3420 A71-41121

Molecular gas mixtures inelastic collision integral spectra, describing internal degrees of freedom with correlation functions

21 p3420 A71-41271

Attitude stability of dual spin spacecraft with energy dissipation in flexible momentum wheel having two degrees of freedom

23 p3772 A71-43020

First order variational equations of Hamiltonian systems with two degrees of freedom for symmetric periodic orbit

23 p3699 A71-43240

Chebyshev polynomials computation of nonlinear oscillations of conservative autonomous system with single degree of freedom

23 p3777 A71-43493

Parameter sensitivity reduction in linear optimal feedback control systems based on two degree of freedom structure

23 p3658 A71-44080

Optical system superresolution by reduction of temporal degrees of freedom using holography

24 p3824 A71-44453

Motion equations of statically unbalanced two degree of freedom gyroscope excited by base linear vibrations, determining instrument errors as function of casing/body coupling

24 p3828 A71-45159

DEHYDRATION

Prolonged water deprivation effects on hypothalamic self stimulation of rats with electrodes chronically implanted in posterior lateral hypothalamus

05 p0711 A71-17087

Amidoximes dehydration with and without rearrangement, suggesting carbodiimide formation from O-benzenesulfonyl ester

06 p0865 A71-17550

Immunological reactivity of human body during 120 day feeding on dehydrated diet

06 p0861 A71-18368

Human body temperature regulation, investigating mild exercise dehydration effects

07 p1044 A71-20349

Dehydration effects on blood parameters in Somali donkeys and zebu steers, observing increases in plasma osmolality, sodium chloride, hemoglobin, packed cell volume, etc

17 p2681 A71-34940

Manned spacecraft life support system dehydrated food ration effects on human organisms health, metabolism and immunoreactivity during long space flight

22 p3507 A71-42823

DEHYDROGENATION

Binary Ti alloys hydrogenation-dehydrogenation treatment effect on alloying element activity

04 p0615 A71-15801

DEICING

Runway deicing methods, discussing spreading of chemicals by ground vehicles and aircraft

07 p1083 A71-19425

Ground deicing system for transport aircraft, discussing antifreeze liquid spray application after mechanical snow removal

09 p1428 A71-22948

Aircraft ice protection problems, considering one dimensional Stefan method for cyclic deicing system

17 p2838 A71-34850

DEIMOS

Phobos and Deimos missions, examining lander and lander/orbiter configurations and Titan-Centaur and space shuttle-Centaur launch systems

[AIAA PAPER 71-830] 17 p2802 A71-34716

DEIONIZATION

Air and oxygen electron-ion recombination coefficients, considering plasma deionization rate

05 p0756 A71-17208

Air and oxygen electron-ion recombination coefficients, considering plasma deionization rate

13 p2067 A71-28263

Interplanetary hydrogen and helium from cosmic dust deionizing effect on solar wind, calculating gas density and flux

16 p2628 A71-33940

DEKATRONS

U COUNTERS

DELAMINATING

Multilayered composite mathematical model, studying interfacial delamination under airplane shear load

07 p1215 A71-20127

Stacking sequence effect on laminate strength, considering specific layer orientations for optimal protection against delamination under uniaxial static and fatigue loadings

07 p1216 A71-20130

Thin cylindrical shell of revolution delaminations detection model, using free vibration natural frequency parameter under clamped-clamped conditions

07 p1216 A71-20135

Corrosive delamination occurrence, reduction and prevention in metal-metal adhesive bonded aircraft structures

22 p3555 A71-42594

DELAY CIRCUITS

NT PHANTASTRONS

Varicap loop circuits for controllable IF phase corrector with independent delay suitable for automatic control
01 p0054 A71-11083

Resonators sequence delay system with external capacitance link, calculating dispersion characteristic and coupling resistance
03 p0386 A71-13802

Noise rejection of two channel asynchronous storage circuit with internal detection for weak signal reception
08 p1252 A71-20734

Delay compensation in flip-flop element of optimal relay system with self oscillations, using optimal control algorithm constructed by phase space method
11 p1742 A71-26095

Tunnel diode switching forward and reverse non-regenerative delay, examining external load resistance and diode characteristic nonlinearity effects on non-regenerative delay
13 p2038 A71-28717

Avalanche transistors circuits, generating rectangular and sawtooth pulses for use in time delay devices
14 p2213 A71-30582

High speed pulse response and power-delay product of planar Gunn diodes, noting delay time and power delay product
14 p2215 A71-30834

Transistorized long time delay relay for power supply circuits with constant function on reenergization after interruption
15 p2376 A71-32021

DELAY LINES

NT ACOUSTIC DELAY LINES

NT DELAY LINES [COMPUTER STORAGE]

Spectral properties of solid state laser with cavity lengthened by optical delay line
01 p0095 A71-11096

Surface wave filters, tapped delay line pulse compression networks and amplifiers, discussing design and applications
05 p0728 A71-16915

Radio communication system hypersonic delay lines, investigating coupled resonators matching efficiency in parallel and series connection
07 p1074 A71-19142

Spectral properties of solid state laser with cavity lengthened by optical delay line
08 p1303 A71-21954

Emission dynamics of pulsed laser with optical delay line in resonator
10 p1622 A71-24885

TEM mode delay line microwave filters, deriving relationships between risetime, settling time, bandwidth and Q
14 p2219 A71-29601

Quasi-optimum frequency measurement with linearly dispersive delay line, introducing variance factor for real-ideal systems comparison
14 p2192 A71-29806

Dispersionless delay line design producing signal frequency shifts for calibration tests of wideband Doppler shift measuring equipment
15 p2373 A71-32632

Varactor tuned FM pulsed Gunn oscillator for testing X band delay lines for pulse compression radar
16 p2546 A71-33415

Fuel cell system steam/hydrogen mixture mass ratio detector using fluidic delay line oscillator
17 p2745 A71-35294

Slow wideband excitation of ultrasonic waves with piezoelectric crystal delay line subject to microwave radiation
19 p3015 A71-37251

Piezoelectric transducer materials and techniques for ultrasonic devices, covering delay lines, light deflectors and modulator operating above 100 MHz
20 p3237 A71-39256

Distributed RC network application as microelectronic delay line, discussing delay response improvement by compensating network
21 p3353 A71-40589

Surface wave delay lines with near octave bandwidth using lithium niobate interdigital ultrasonic transducer with lumped element impedance inverter network
22 p3521 A71-42202

Error correction by tapped delay line coded equalizer and channel introduced redundancy, deriving upper bound for error probability
22 p3512 A71-42377

Trigonometric synthesizers with nonuniformly sectioned tapped delay line and summation circuit for signal distortion correction in telephone channel
23 p3650 A71-43288

Low loss microwave iris-loaded circular TE mode waveguide delay line for pulse compression at X band
23 p3653 A71-43963

DELAY LINES [COMPUTER STORAGE]

Plant and compensator parameters deviations effect on accuracy of complex unitary-code programmed automatic control system with delay line digital compensator
12 p1893 A71-27342

DELTA FUNCTION

Electron gun diode design for beam-collisionless plasma interaction nonlinear evolution, studying delta function beam velocity distribution
09 p1502 A71-22754

Integral containing Heaviside and Dirac delta function in integrand with minus and plus infinity limits, computing value using thin spherical shells in general relativity
16 p2656 A71-33263

DELTA LAUNCH VEHICLE

Delta booster second stage packaged attitude control three-axis system, discussing electronic implementation for gyroscopic action control
05 p0818 A71-17138

Delta launch vehicle capabilities, constraints and costs for Straight 8 model 2914 series
22 p3610 A71-42009

DELTA MODULATION

Time division multiplexing system for ATS, discussing surveillance geostationary satellite feasibility, delta modulation for data transmission and aircraft equipment
17 p2772 A71-34680

Transmission performance of thin route satellite communication system for northern Canada, comparing FM, PCM and delta modulation techniques
17 p2703 A71-35081

Ternary delta modulation evolution from binary system by addition of encoder-analyzer, calculating SNR
20 p3202 A71-39468

Mathematical model for pulse waveform identical with single integrator delta modulator, using analog techniques of angle modulation and sampling
22 p3522 A71-42276

Nonlinear and syllabic companded digital delta modulation systems, discussing SNR measurement and computer simulation for optimum design
22 p3514 A71-42392

DELTA WINGS

Thin delta wing with leading edge separation, obtaining drag lift and rolling moment coefficients and pressure distribution
02 p0185 A71-12408

Optimal cross sectional dimensions of thin walled longeron beams and ribs of skin reinforced delta wings minimizing weight
02 p0329 A71-12562

Hypersonic conical flow with attached shock waves over delta wings
03 p0344 A71-14243

Hypersonic aerodynamic characteristics of flat delta and caret wing models at high incidence angles for space shuttles
03 p0344 A71-14445

Viscous gas flow interaction on delta wing and oblique airfoil at Mach number of infinity
07 p1014 A71-19739

Vortex breakdown on slender sharp edged and modified delta wings with varying sweep angles investigated in wind tunnel using schlieren system for flow visualization
[AIAA PAPER 69-778]
08 p1229 A71-22028

Delta wing of symmetrical thickness and optimum variable geometry for two supersonic cruising speeds
09 p1384 A71-23617

Leading edge suction analogy for predicting low speed lift and drag-due-to-lift characteristics of sharp edge delta and related wing planforms
[AIAA PAPER 69-1133]
10 p1553 A71-24851

Aerodynamic forces and hinge moments of delta cruciform control surface in blunt-nosed canard configuration for subsonic, transonic and supersonic flows
11 p1701 A71-25161

Thin delta wing in hypersonic inviscid flow at small angles of attack, calculating motion equations and boundary conditions at small perturbations
12 p1863 A71-27330

Shock interaction effects on flapped delta wing at hypersonic speed, presenting method for estimating reflected expansion wave impingement boundaries and resulting aerodynamic coefficients
12 p1868 A71-27598

Minimum drag surface shape of thick lifting delta wing integrated with conical fuselage for supersonic cruising speed
[ONERA-TP-947]
12 p1866 A71-27716

Air flow about low aspect ratio delta wing at large angles of attack, deriving lift coefficient
13 p1990 A71-28282

Hypersonic flow around delta wing at small angles of attack, using pressure sources method and Fredholm integral equation
13 p1992 A71-29189

Hypersonic flow pattern past windward side of delta wing with supersonic leading edges, joining potential and vortex regions behind shock wave
14 p2171 A71-30874

Inviscid supersonic flow field structure over blunt delta wing, determining attack angle effects on shock layer surface pressure distributions and streamline patterns
[AIAA PAPER 71-596]
15 p2512 A71-31576

Flat delta and caret wings aerodynamic performance over incidence angle and Mach number range suitable for lifting reentry
16 p2519 A71-32877

Rarefaction and angle of attack effects on delta wing in hypersonic flow in wind tunnel
16 p2520 A71-33376

Two vortex model for downwash variations in supersonic flow past thin delta wing with separation at leading edges
17 p2669 A71-34190

Pressures, velocities and aerodynamic characteristics of supersonic flow around slender delta wings with forced asymmetry and separation at leading edges
18 p2843 A71-36134

Supersonic flow past thin delta wings with finite velocities at leading edges, noting wing deformation to avoid corner vortices appearance
18 p2843 A71-36181

V shaped conical wing in supersonic and hypersonic flow with shock attached to leading edge, investigating complex wave system with time dependent and analytical methods
18 p2845 A71-36339

Space shuttle booster configuration design, comparing stowed, fixed straight and delta wing approaches, discussing air breathing engines, stage mating, fins, etc
18 p2972 A71-36444

Hypersonic lee surface vortex heating alleviation on delta wing by apex alignment with free stream
19 p2993 A71-37895

Total lift data correlation for thin sharp edged low aspect ratio delta wings at low speeds, noting trailing edge effects in incompressible flow
20 p3176 A71-39398

Delta wing problem reduction to Laplace equation solution, using perturbation technique to solve Lame equation resulting from elliptic conal coordinates transformation
20 p3177 A71-39498

Delta wing shock envelope visualization at hypersonic speed, obtaining flow field photographs by vapor screen technique
21 p3324 A71-40973

Optimal ascent trajectories for delta wing space shuttle flight, using accelerated gradient methods [AAS PAPER 71-328]
23 p3726 A71-43001

Slender two dimensional wedge wings aerodynamic characteristics in hypersonic strong interaction flow, determining wall shear stress and lift drag ratio effects
24 p3789 A71-44621

DEMAGNETIZATION

Permanent magnet optimal size selection from initial operating point on demagnetization curve
05 p0705 A71-17173

Lunar magnetic field demagnetization effect hypothesis for explaining Apollo 11 lunar rock samples remanent magnetization
07 p1200 A71-20055

DEMAND [ECONOMICS]

Cost aspects of carbon fiber reinforced composites in aircraft structures, suggesting increased aviation market for carbon fiber [PLASTICS INST. PAPER 46]
08 p1378 A71-20929

Long term prospects of air traffic development in competition with other modes, estimating VTOL service demand
14 p2340 A71-30164

Defense and aerospace industry demand cyclical variations effect on productivity growth and cost
22 p3624 A71-42525

DEMODULATION

Digital FM discriminator for demodulating FM signals with high deviation percentage
01 p0033 A71-10899

Optical systems using photoelectron counter system for optical signal detection and demodulation
02 p0214 A71-12031

Wideband subcarrier frequencies demodulation technique for uncoded or coded PSK telemetry over large input SNR range for deep space interplanetary communication
08 p1254 A71-21316

Neutral pion decay and galactic gamma radiation from demodulated cosmic ray spectrum, discussing neutral pion meson production
11 p1815 A71-25593

Auto- and cross-spectral estimation from irregularly sampled data by extending complex demodulation
14 p2246 A71-30483

Lock-lock loop technique with pulled oscillator for feedback frequency demodulation and tracking filter operation
14 p2220 A71-30920

Digital phase locked loop for FM signals demodulation, considering system nonlinear difference equation
17 p2704 A71-35084

Harmonically modulated reflected light signals phase shift and demodulation, assuming single scattering
19 p3018 A71-37975

DEMODULATORS

NT FREQUENCY COMPRESSION DEMODULATORS

NT PHASE DEMODULATORS

NT PHASE LOCK DEMODULATORS

Ground station integrated receiver cabinet formed by down-converter, demodulator and baseband equipment packaging

02 p0224 A71-12817
Narrow band FM modems with high carrier frequency stability for satellite communication terminals with small dish antennas

02 p0234 A71-12820
Dynamic FM demodulator with tracking filter for threshold extension

02 p0235 A71-12821
Earth station equipment for Intelsat 4, discussing thermal noise, transmitters, wideband receivers and demodulators

02 p0224 A71-12829
Chopper amplifier modulator and demodulator circuits analysis, discussing SNR performance

03 p0387 A71-13821
FM radio relay system modulation-demodulation equipment for multichannel FDM or TV signal transmission

05 p0728 A71-16146
FM demodulator system with parametric tracking filters for threshold improvement, discussing reception performance

08 p1265 A71-21279
CW X band frequency-locked Gunn oscillators as frequency demodulator with millivolt range detection sensitivity

09 p1421 A71-23720
Threshold-extension phase-lock demodulator design for optimizing satellite communication ground station systems, using FM carriers

10 p1580 A71-25106
PSK modem for multiple access communication system with time distribution, discussing performance tests on INTELSAT 3

17 p2700 A71-34688
Quadruphase modem development in time division multiple access system

18 p2880 A71-36546
Intelsat 3 and 4 RF demodulator design with tracking filters, using varactor for frequency control and discriminator for frequency drift compensation

18 p2890 A71-36558
Demodulator interference noise in FM modulation radio relay system as function of ratio between interfered and interfering carrier powers and AM sensitivity

24 p3804 A71-44988

DENDRITIC CRYSTALS

Solute core redistribution and dendritic refinement in highly undercooled Fe-Ni alloy, using metallographic and electron microprobe analyses

03 p0442 A71-13365
Crack propagation in chromium steel butt weld sheets, discussing dendritic macrostructural effects on brittle resistance and toughness

11 p1770 A71-25945
Quantitative description of solidification structures of Al-Cu, Al-Cu-Ti, Al-Si, Al-Mg and Al-Si-Cu, discussing dendritization index, cooling rate and tensile strength

14 p2257 A71-29842
AlCu alloy cellular dendritic substructure segregation observation by electron microprobes

23 p3689 A71-42931

DENITROGENATION

Body fat influence with and without denitrogenation on decompression sickness in men exercising after abrupt exposure to altitude

13 p2022 A71-29361

DENSIFICATION

Pressure histories from densification and relaxation measurements on lunar glass and synthetic samples, investigating refractive index changes after annealing

23 p3758 A71-43760

DENSITOMETERS

NT MICRODENSITOMETERS

Rocket-borne beta ray atmospheric densitometer errors due to cosmic rays

05 p0752 A71-16673
Photoemulsions densitometric characteristics for protonogram analysis, during fast charged particle interaction with single crystals

05 p0754 A71-17031
High vacuum calibration of cryogenic quartz crystal for atmospheric density

07 p1113 A71-19852
Alpha particle gas densitometric response to planet atmospheric density profiles in terms of radioactive source energy distribution, considering contoured baffles models

11 p1763 A71-26079
Scanning densitometer for spectral transmission density continuous recording at low image contrast, discussing design and performance tests

19 p3063 A71-37248

Stellar proper motion measurement by densitometer automatic scanning of star plates pairs, assessing accuracy

20 p3239 A71-39529
Vesicular photographic film mechanics, sensitometry and densitometry

22 p3548 A71-42513

DENSITY [MASS/VOLUME]

NT ATMOSPHERIC DENSITY

NT GAS DENSITY

NT SPACE DENSITY

Earth surface density distribution, using earth gravity field representation as potential of simple layer determined from combined satellite and gravity anomalies observations

02 p0246 A71-12463
Australian tektites population polygons of bulk specific gravity and refractive index, indicating variations in chemical composition

04 p0582 A71-15133
Liquid silicate systems density calculation from partial molar volumes of oxide components

05 p0716 A71-16407
Density and temperature dependences of viscosity and thermal conductivity of dense fluids

05 p0831 A71-16408
Sintered Al-Ni-Co alloys, investigating magnetic properties and density after heat treatment

06 p0913 A71-18099
Forged superhigh density sintered steels strength and fracture mechanism

08 p1304 A71-20995
Mean luminous cosmic matter density calculations, using galaxy counts and mass data eliminating luminosity functions

09 p1516 A71-22060
Local mean cosmic density from double galaxy data

09 p1516 A71-22061
Mean cosmic density based on galactic clusters masses

09 p1516 A71-22062
Nonhomogeneous cosmological model with equations describing universe relative density variation, demonstrating thermal instability role in galaxies formation

10 p1667 A71-23856
Body of revolution potential expanded in spherical function series, showing analytical density limited by surface

10 p1679 A71-24934
General relativistic von Zeipel theorem providing necessary and sufficient condition for equidensity surfaces coincidence in stationary star axisymmetric rotating mass fluid

11 p1833 A71-26327
Dense liquid thermodynamic model, using approximate equation of state

13 p2160 A71-28571
Disperse systems dynamic behavior, considering density ratio, discontinuity diameter, viscosity and shear modulus

14 p2256 A71-29518
High density polyethylene composition oxidation rates and photodegradation resistance data, using IR spectroscopy

14 p2261 A71-29641
Prealloyed Al powder liquid phase sintering without precompacting, discussing oxidation and density control

18 p2928 A71-36667
Equilibrium rotating superdense configurations in general relativity theory, determining integral parameters in low angular velocity approximation

20 p3289 A71-39297
Globular clusters with inhomogeneous composition, deriving partial densities of masses

20 p3291 A71-39318
Total mass density in neighborhood of sun and Galactic force law from stellar motions perpendicular to Galactic plane, using King pseudomoments method

21 p3440 A71-40061
Macaca nemestrina monkey bone density change during Biosatellite 3 mission

21 p3330 A71-40343
Frequency, density, thickness and structural factors (stiffness) influence on sound insulation of uncoated and foil coated absorbers

22 p3575 A71-42401
Spectral directional reflectance of Apollo 11 and 12 fines as function of bulk density

23 p3760 A71-43771
Carbon fiber reinforced plastics featuring high strength and Young modulus and low density for engineering applications

24 p3840 A71-44363
Total-to-open porosity ratio for carbide-iron type materials sintering, noting relative density and chemical composition effects

24 p3838 A71-44736

DENSITY [NUMBER/VOLUME]

NT ELECTRON DENSITY [CONCENTRATION]

NT ELECTRON DENSITY PROFILES

NT ELECTRON DISTRIBUTION

NT ION DENSITY [CONCENTRATION]

NT IONOSPHERIC ELECTRON DENSITY

NT IONOSPHERIC ION DENSITY

NT MAGNETOSPHERIC ELECTRON DENSITY

NT MAGNETOSPHERIC ION DENSITY

NT MAGNETOSPHERIC PROTON DENSITY

NT METEOROID CONCENTRATION

NT PACKING DENSITY

NT PARTICLE DENSITY [CONCENTRATION]

NT PLASMA DENSITY

NT PROTON DENSITY [CONCENTRATION]

NT SPACE DENSITY

Fibrous body optimum material distribution, considering arbitrary density continuous three dimensional bar network

01 p0177 A71-11285
Mean cosmic density determinations, obtaining field galaxy luminosity function moments with red shift catalogs

02 p0313 A71-12499
Double galaxies relative number determination, taking into account differences of components absolute magnitudes

17 p2808 A71-35578

DENSITY [RATE/AREA]

U FLUX DENSITY

DENSITY DISTRIBUTION

Real vortices velocity, density and temperature distribution determination, discussing flow measurements by hot-wire anemometer, multiple spark camera interferography and smoke visualization techniques

01 p0069 A71-10107
Lunar moments of inertia and density distributions, using gravitational potential and physical librations

01 p0158 A71-10772
Wolf-Rayet star atmospheres, discussing matter density distribution, light pressure effects on particle motion and H and He ionization levels

01 p0158 A71-10803
Electron density variations in ionospheric layers of different recombination types

01 p0074 A71-11080
Quasi-transverse extraordinary wave interaction with density fluctuations in inhomogeneous magnetized plasma, using modulation measurement for instability diagnosis

01 p0136 A71-11440
Lifting oscillatory reentry trajectories, developing equation method to consider density and velocity distributions

02 p0320 A71-12403
Galactic spiral structure model, examining nonlinear stellar density waves in plasma cylinder

03 p0484 A71-13205
Galaxy clusters stabilization by cosmological constant, considering clusters mass discrepancy

03 p0489 A71-13561
Turbulent mixing of two parallel similar and dissimilar fluid streams, comparing velocity and density profiles measurements with similarity solution [ASME PAPER 70-WA/APM-38]

03 p0404 A71-14163
Cosmic ray data, showing perpendicular density gradient to ecliptic plane

03 p0482 A71-14547
Finite maximum and minimum angular zero densities of integral functions, noting relationship to angular additive measure

04 p0618 A71-14647
Hypersonic rarefied nitrogen flow over wedge, investigating density field

04 p0570 A71-15033
Two dimensional hypersonic flow field density gradient distribution measurement by space-time resolved laser schlieren system

04 p0600 A71-15592
German monograph on open turbulent methane-oxygen flame temperature and concentration distribution determination from jet density measurements, using radiometric method

05 p0831 A71-16123
Perturbations effect on tube flow and density variations due to noninstantaneous shock wave formation

05 p0836 A71-16529
Jupiter rotating inner magnetosphere plasma density distribution, using Lorentz term in force balance equation

05 p0810 A71-16631
Electron concentration vertical profile in ionosphere as function of altitude of radio wave reflection and group refraction and velocity characteristics

06 p0895 A71-18278
Interstellar grain formation relation with stellar evolution in terms of density wave theory of spiral structure origin

06 p0973 A71-18339
Neutral condensations and protostars in H II regions noting original density distributions

06 p0973 A71-18340
Density spatial and temporal fluctuations correlation in stars

06 p0974 A71-18431
Turbulent boundary layer in incompressible fluid with vanishing viscosity, analyzing degeneration of isothermal boundary layer, viscous sublayer and density pulsations

07 p1085 A71-18753

Atmospheric turbulence steady random process correlation function, spectral density and probability distribution based on aircraft measurements

07 p1150 A71-18797

Self similar shock wave propagation in exponentially varying density at constant pressure, solving by method of successive approximation

07 p1089 A71-19731

Oxygen and nitrogen metastable constituents in daytime atmosphere airglow, obtaining altitude density distributions

07 p1103 A71-19764

Semiconductor injection lasers, discussing energy characteristics of state density distribution, coherent emission, etc

07 p1126 A71-20252

Density distribution, heat transfer and drag measurements in rarefied Ar cylindrical Couette flow, comparing results with Navier-Stokes and Burnett equations solutions

07 p1093 A71-20286

Rock forming monomineralic aggregates thermal conductivity at ordinary temperature and pressure in relation to density, crystal structure and chemical composition

07 p1105 A71-20448

Low density plasma flow past bodies, measuring disturbed zone velocity, density and temperature distributions by Langmuir probes

07 p1173 A71-20528

Stagnation point flow flame sheet model, showing density-viscosity product variation for injection rate effect on velocity profile

08 p1375 A71-20865

Cross field instability effect on weakly ionized plasmas with ionization density gradients under crossed electric and magnetic fields, using linear analysis

08 p1339 A71-21207

Planet density distributions, deriving successive approximations for equilibrium figure equations

08 p1365 A71-21775

Low latitude atmospheric vertical density variations, comparing solar and geomagnetic activities effects

09 p1436 A71-22578

Rarefied gases heat transfer and density distribution between parallel plates at different temperatures

09 p1432 A71-22854

Weakly ionized plasma density fluctuations and diffusion from kinetic equations for electron-space density cross correlation, assuming BGK model

09 p1503 A71-22863

Midlatitude stratosphere and lower ionosphere density model, discussing vertical, diurnal and seasonal variations effects on spacecraft trajectories

09 p1438 A71-23137

Motion effects on atmospheric density altitude distribution, discussing vertical waves, gravity, temperature and winds

09 p1441 A71-23645

Gravitational instability of nonhomogeneous cosmological model, establishing density perturbation growth as function of time for model containing matter and radiation

10 p1667 A71-23851

Supersonic turbulent boundary layer density profile over flat plate at single Reynolds number, using Mach-Zehnder interferometer

10 p1593 A71-24270

Large angle Rayleigh light scattering for density fluctuations determination in dilute gases with wavelength comparable to mean free path

10 p1642 A71-24835

Cosmological enhancement of density perturbations and amplitude variation of acoustic and gravitational waves in anisotropic homogeneous universe

10 p1678 A71-24886

Velocity, temperature and concentration profiles correlation for compressible turbulent boundary layer along porous flat plate, with carbon dioxide injection, discussing cooling applications

10 p1598 A71-25095

Edge waves on sloping beach in exponentially stratified fluid, finding lowest mode/Stoke edge wave/insensitivity to density field

11 p1749 A71-25358

Thermosphere diurnal variations two dimensional model atmosphere characteristic waves, separating density and temperature variations

11 p1756 A71-25649

Lunar geometrical and dynamical properties, deriving force function from density distribution and surface equation

11 p1822 A71-25687

Asymmetric three dimensional aerodynamic density fields from holographic interferograms, applying to supersonic flow from free jet

11 p1762 A71-25802

Atmospheric density semiannual variations from satellite observation, comparing with atmospheric models

11 p1760 A71-25824

Density matrix components for multiconfiguration wave functions, constructing N electron /spin free/ Hamiltonian configuration interaction matrix

11 p1802 A71-26056

Restricted set of correlated measurements with inductive theta pinch in MHD plasma accelerators, determining electromagnetic field structure and electron density distribution

11 p1766 A71-26288

Spatial and temporal density fluctuations correlation in stars

12 p1955 A71-26581

Spherically symmetric galactic and star clusters at Hubble expansion, deriving spatial density

12 p1962 A71-26909

Temperature gradients effect on density distribution in material near critical point, using classical and scaling-law theories and Ising model

12 p1929 A71-27031

Potential theory mixed inverse problem and uniqueness theorem concerning body shape and density determination from external potential of bulk masses

12 p1931 A71-27510

Extensive air showers muon component arrival time spread and lateral density distribution

13 p2126 A71-28096

Extensive air showers muon density spectrum, describing measurement apparatus and analysis method with particular emphasis on elimination of falsifying absorber multiplication effects

13 p2126 A71-28100

Interferometric studies of focused Nd laser radiation interaction with thin graphite absorbing surface layer, discussing time behavior of plasma expansion and density distribution

13 p2078 A71-28446

Diffusion measurement of highly ionized thermal Cs plasma in magnetic field by Langmuir probe, determining density profile

13 p2106 A71-28450

German monograph on drift waves in plasma with density gradient covering LF electrostatic disturbances in low density plasma

14 p2277 A71-29581

Internal potential of heterogeneous ellipsoids for even and odd power variation of density with coordinates, using depolarization factors

14 p2304 A71-29600

Matter density in universe, comparing delayed galactic growth with observed radio sources and quasars

14 p2305 A71-29675

Freestream density field in nonequilibrium dissociating nitrogen flow over circular cylinder, using free piston shock tunnel and optical interferometry measurements

14 p2169 A71-29884

Supersonic plasma flow effects on neutral hydrogen, helium and charged particle density and velocity profiles in polar ionosphere

14 p2234 A71-30040

Jupiter and Saturn gravitational moments calculation procedure based on planetary density angular distribution

14 p2310 A71-30167

Atmospheric neutron data at various altitudes, relating densities, fluxes and spectra to solar activity

14 p2301 A71-30589

Hydrogen plasma transport in linear magnetic quadrupole field, studying polarization potential and density distribution

14 p2282 A71-30669

Upper atmosphere exploration by San Marco 2 satellite, studying diurnal density variations and effects of large geomagnetic storms

14 p2236 A71-30817

Density and velocity profiles of transonic flow past wavy wall at various channel heights, using Mach-Zehnder interferometer

15 p2386 A71-31165

Austenite and carbide chromium manganese steel boron distribution obtained by tracing elements

15 p2425 A71-31397

Test equipment for radiometric analysis of impurities concentration distribution in semiconductors, using thin plane-parallel layers continuous removal method

15 p2383 A71-31657

Density distribution of neutral matter in cometary atmosphere in transition region between hydrodynamic and free molecular flow

15 p2484 A71-31662

Radio sources 3C 48, 3C 144, 3C 161, 3C 273 and 3C 298 scintillations by interplanetary plasma at 60 MHz, determining electron density fluctuations

15 p2487 A71-32033

Electromagnetic wave propagation along homogeneous and inhomogeneous plasma columns, establishing density distribution functions and dispersion curves

15 p2459 A71-32641

Gravitating continuous medium instability in presence of delta shaped point density perturbations,

discussing cloud structure development in interstellar gas

15 p2495 A71-32642

Planet density distribution, deriving successive approximations for equilibrium figure equations for gravitational potential and level surfaces

15 p2495 A71-32680

Solar atmosphere vertical temperature and density distribution measurements, using spatially averaged H_α and K resonance line profiles central reversals

15 p2496 A71-32742

Spiral density wave structure in computer simulations of evolution of galaxies, showing azimuthal dependence on gravitational and radial forces

15 p2497 A71-32766

Density distribution of plasmaspheric particles in equatorial plane via model of plasmasphere streaming, noting current system production in lower ionosphere

16 p2562 A71-32806

Holographic interferometry measurements of mean and localized fluctuating wake density field of cones fired at Mach 6 at ballistic range, using pulsed laser [AIAA PAPER 71-564]

16 p2520 A71-33105

Interstellar medium dispersion and rotation measurements, calculating electron concentration fluctuation effects

16 p2608 A71-33227

Quasi-neutral inhomogeneity /particle cloud/ in collisionless hot or cold plasmas without magnetic field

16 p2619 A71-33521

Upper atmosphere density fluctuations associated with solar activity and local time values, using Cosmos 14 satellite drag data

16 p2564 A71-33666

Seasonal temperature and density models for stratosphere and mesosphere from observations by resistance thermometers at Heiss Island Soviet rocket station

16 p2566 A71-33743

Neutral lower thermosphere density variations at high and middle latitude in Southern Hemisphere from OVI-15 /SPADES/ satellite accelerometer measurements

16 p2570 A71-33824

Neutral atmosphere density profile data from satellite-borne accelerometer experiment, observing gravity waves propagating in north-south direction at high latitudes

16 p2570 A71-33825

Atmospheric density variation response time measurement to geomagnetic activity by satellites-borne low-G accelerometer calibration system, considering atmospheric heating mechanism

16 p2571 A71-33839

Heterosphere semiannual density variation with amplitude as function of height, noting dependence on temperature distribution and sunspot cycle

16 p2574 A71-33963

Density perturbation effect on transient spin down of incompressible dissipative rotating stratified fluid in cylindrical container

16 p2561 A71-34164

Cylindrical nonuniform plasma with radial temperature and emitter density gradients, analyzing molecular rotational levels intensity distribution and Doppler widths

17 p2787 A71-34587

Continuously stratified fluid flow into contraction, assuming constant upstream dynamic pressure and density gradient /Long model/

17 p2726 A71-34661

Two dimensional compressible turbulent boundary layer with time dependent mean velocity and density fields, deriving momentum and kinetic energy integral equations

17 p2727 A71-34876

Flight test results for CACTUS accelerometer launched by rocket probe at Guiana Space Center, considering atmospheric density profile in 120-150 km altitude zone

18 p2924 A71-36755

Thin walled shell free linear vibrations frequency density calculation using asymptotic method

18 p2982 A71-36794

Plasma confinement in injector-diverter system of stellarator, measuring radial density distribution

19 p3109 A71-37131

Variable density effect on inviscid free shear layer instability at small Mach numbers, deriving difference equation for inviscid disturbance

19 p3043 A71-37300

Second order MHD equations for density fluctuations driven by Alfvén waves with relation to solar wind

19 p3110 A71-37352

Ion-exosphere in open magnetic field, calculating number density, particle, moment and energy flux distribution from simple mathematical model

19 p3138 A71-37737

Electron beams formation and focusing, including current density distributions, electronic potentiometer recording, parameters and comparison with simulation data

20 p3204 A71-39160

Gravitational fields of giant planets in hydrostatic equilibrium, solving equations for linear and quadratic density distributions

20 p3290 A71-39310

Nonhomogeneous flow stratification in fluid region under thermal and gravitational forces, considering steady state and time dependent density fields

20 p3212 A71-39502

Sloping flat plate impulsively started constant velocity motion through slightly diffusive viscous density-stratified fluid, investigating transient and oscillatory viscous boundary layer flow

20 p3212 A71-39503

Mesosphere and stratosphere ozone vertical density distribution from sounding rocket data, considering photochemical theory and hydrogenic reductions

20 p3221 A71-39694

Partially thermalized model of stellar system, considering potential and density distribution

21 p3439 A71-40052

Binary fluid mixtures density gradients near critical point due to gravity effect, deriving expression as linear function of height with thermodynamic equilibrium as starting point

21 p3345 A71-40236

Steady propagation of plane laminar flame through uniform mixture of hydrogen and bromine gases, obtaining temperature and concentration profiles

21 p3474 A71-40524

Cosmological enhancement of density perturbations and amplitude variation of acoustic and gravitational waves in anisotropic homogeneous universe

21 p3453 A71-41251

Semiconducting plasma carrier density gradient instability, investigating threshold curve for n-type germanium

21 p3434 A71-41330

Exposing light and resulting density distribution and granularity in lower photographic emulsion layer, investigating modulation transfer function and power spectrum

22 p3538 A71-41733

Material random temperature and imperfection density effects on 3-bar truss nonlinear steady creep solutions for stress and velocity

22 p3615 A71-42211

Muon showers underground phenomenon in terms of density spectra, shower size and radial density distributions

22 p3594 A71-42407

Translational and rotational temperature and density variations through shock waves in oxygen and nitrogen, using Monte Carlo scheme

23 p3781 A71-43444

Primary cosmic ray and spallation track density distribution in Apollo 12 deep core soil samples

23 p3764 A71-43801

Oxygen dissociation in He, Ar, Kr and Xe gas mixtures behind incident shock waves, calculating density gradients and vibrational relaxation time

24 p3802 A71-44924

Liquid droplet vaporization under exposure to hot gas, obtaining time dependent temperature and concentration profiles in vicinity from coupled diffusion equations

24 p3888 A71-44963

Steady acceleration sensor system with two electrode chambers in closed circuit, producing convective flow by electrolyte density gradients

24 p3828 A71-45099

DENSITY MEASUREMENT

NT X RAY DENSITY MEASUREMENT

Rotational temperature and density measurements in rarefied flow over sharp leading edge flat plate, obtaining shock layer static pressure

01 p0082 A71-10955

Hydrocarbon fuels high temperature oxidation behind shock waves, investigating reaction process by combustion products IR emissions and density gradient

02 p0298 A71-12860

Modified Ashby-Jephcott laser interferometer schlieren system for HF gas density measurements

03 p0427 A71-13922

Microwave systems for cryogenic liquid and slush density and flow velocity measurements

04 p0586 A71-14659

Compressible flow density measurement using optical polarization interferometry with birefringent devices

04 p0601 A71-15918

Atmospheric density variations determination from Proton 2 braking data for aerodynamic drag coefficient, constructing model for rarefied gas flow-satellite interaction

05 p0804 A71-16043

Atmospheric density and rotation measurements below 195 km from high resolution drag analysis of satellite OV1-15 using least squares fitting

06 p0887 A71-17272

Upper atmosphere nitric oxide density measurement by scanning UV spectrometers on Nike-Apache rockets, noting ionization consequences for D region

06 p0888 A71-17273

Collisionless plasma density determination valid for probe/Debye radii finite ratio, using positive ion current-voltage characteristics

06 p0936 A71-17680

Ionospheric electron content from Faraday rotation measurements of earth satellite and deep space probe

07 p1098 A71-19029

Stratospheric small ion density measurements by level flight balloons

07 p1103 A71-19768

Velocity and density measurements in hypervelocity ballistic projectile turbulent wakes, using hot film anemometers

[AIAA PAPER 68-701]

07 p1015 A71-19891

Annihilation quanta detector and positron source for gas density measurement, noting sensitivity, counting interval and Be covering thickness

07 p1164 A71-20178

Radio galaxies flux density measurements at 8000 MHz

08 p1357 A71-20869

Inner and outer planets groups mass and mean density, considering terrestrial seismic data and lunar, Venus, Mars and Mercury structural models

08 p1358 A71-20888

Hydrogen slush storage and transfer density and flow measuring instrumentation, emphasizing capacitance measurement

[NAS PAPER M-2]

08 p1292 A71-21695

Microwave methods for nitrogen or hydrogen densities and flow rate measurement in single phase liquid and slush state

[NAS PAPER M-1]

08 p1292 A71-21696

Velocity components, species densities and temperature local measurements, using laser Doppler velocimeters, Raman scattering and tunable lasers

[AIAA PAPER 71-283]

08 p1303 A71-22008

Laser Doppler velocimetric technique for supersonic flow particle trajectory and density measurements, noting particle lag

[AIAA PAPER 71-287]

08 p1303 A71-22010

Density gradient visualization with schlieren optical system, discussing propeller aerodynamics

10 p1616 A71-24103

Thermospheric gas density determined from solar UV absorption measurement at grazing ray and near vertical incidence

10 p1676 A71-24551

Ultrasonic energy density measurement over various frequencies in liquids, using instrument unperturbed by standing acoustic waves

10 p1612 A71-24682

Light scattering from gas thermal fluctuations, deriving density-density correlation function over various pressures

10 p1642 A71-24836

Pulsed ion laser electron density measurement by cavity method in S band, evaluating relaxation time

10 p1623 A71-25021

Crack dislocations nature and significance, density equations, instability conditions, fracture mechanics, including cohesive forces and plastic zone equilibrium

10 p1628 A71-25026

Mean and fluctuating forces on flat plates normal to turbulent flow, giving power spectral density measurements of drag fluctuating component

10 p1598 A71-25085

Excited atom density determination for two-photon light absorption in one-dimensional medium, obtaining energy balance equation asymptotic solution and secondary radiation intensity

12 p1914 A71-27028

Optical properties and relative density of lunar surface layer, deriving light reflection and scattering formulas

12 p1964 A71-27089

Local electron density measurements in low beta plasmas, using nonlinear electromagnetic wave mixing under synchronism condition

13 p2104 A71-27849

Temperature and radical concentration measurements for high temperature flowing gas streams in rig simulating conditions in ramjet combustion chamber and nozzle

13 p2162 A71-28758

Planet Mercury density, discussing optical and radar measurements and theory comparison with observation

14 p2306 A71-29728

Electron temperature and density measurement apparatus using Thomson scattering of laser light for collisionless MHD shock waves

14 p2280 A71-30424

Pigeon vestibular apparatus fluids and structures physical properties, detailing specific gravity and viscosity of endolymph, perilymph and cupula

14 p2185 A71-30467

Satellite measurements of cold plasma density and plasmapause in magnetosphere, comparing Whistler, Langmuir probe and ion trap data

14 p2237 A71-30951

Electron intensities measurement in pulsating aurora on ESRO Skylark rocket launched from Sweden

15 p2394 A71-31424

Rotational temperature and density measurements in high speed gas flow by electron beam fluorescence technique

[AIAA PAPER 71-605]

15 p2406 A71-31544

Solution concentration, solid content, specific gravity and bulk modulus measurements by sound velocity measurement

15 p2409 A71-32197

Atmospheric density measurements at 70 to 115 km altitude range from rocket soundings with accelerometer instrumented inflatable spheres

16 p2562 A71-33066

Atmospheric density variations determination from Proton 2 braking data for aerodynamic drag coefficient, constructing model for rarefied gas flow-satellite interaction

16 p2635 A71-33447

Semiannual atmospheric density variation measurements by OV3-6 satellite

16 p2570 A71-33821

Upper atmosphere density determination from Cosmos satellite deceleration data, allowing for diurnal and semiannual variations and solar radio emission intensity effects

16 p2571 A71-33837

OH emission column density upper limit from rocket-borne UV spectrometer measurement of resonantly scattered sunlight intensity in electronic transition vibrational band

16 p2574 A71-33967

Microfield double probe for plasma density and electron temperature determination, studying random signals crossed spectrum

17 p2789 A71-35350

Gum Nebula size, density and electron temperature data from RAE-1 and OGO-5 satellites and ground based telescopes observations, correlating with Vela X supernova outburst

17 p2806 A71-35409

MIS structure voltage-farad characteristics, determining surface state densities for silicon compound dielectric films

18 p2954 A71-35875

Unsteady multispecies gas mixture concentration flow measurement, using Raman scattering of pulsed nitrogen laser light

18 p2930 A71-36060

Optical properties and relative density of lunar surface layer, deriving light reflection and scattering formulas

19 p3133 A71-37439

First and second order density matrices calculation of pure state N fermion systems, using higher random phase approximation

19 p3107 A71-38054

Porous material slab pyrolysis, studying density and thermal conductivity changes and reaction kinetics

19 p3170 A71-38117

Flow around obstacle in plasma with ions cold relative to electrons and with directed subsonic, considering relative density measurement

19 p3115 A71-38207

Hamster body fat, water and density measurements by dilution method and air displacement technique, comparing to determination by direct chemical analysis upon sacrificing

19 p3005 A71-38555

Ionospheric electron concentration and temperature measurements, describing rocket-borne asymmetrical Langmuir probe

19 p3067 A71-38631

Capacitance measurement technique for density and mass flow measurements for hydrogen slush storage and transfer

20 p3237 A71-39276

Microwave instrumentation for measuring cryogenic fluids density and flow rate, noting slush

20 p3237 A71-39277

Electron density measurement in microwave cavity resonator as function of plasma parameter or time, using digital control system

20 p3274 A71-39428

Lunar surface layer density and dielectric permeability from radio wave scattering data from automatic spacecraft radar measurements

20 p3295 A71-39616

Atmospheric density variations calculation, using aerodynamic drag coefficient data from gas flow-satellite surface interactions

20 p3223 A71-39706

Equatorial ionospheric density measurements on quiet and perturbed days, using San Marco 2 satellite balance

21 p3373 A71-40047

Hypersonic turbulent wake density measurements in free flight hyperballistic ranges by electron beam fluorescence probe technique

21 p3363 A71-40389

Direct local density gradient measurement in rarefied free jet flow using electron beam deflection signal processed with lock-in amplifier

21 p3364 A71-40394

- Gas density measurement and flow visualization in hypersonic wind tunnel by electron beam probe, noting isobaric boundary layer application 21 p3364 A71-40395
- Turbulent hypersonic wake density and temperature measurement for slender cone model in shock tunnel, using dual electron beam excitation technique 21 p3364 A71-40396
- Transient pressure, temperature and density measurement of dense hot gas 21 p3364 A71-40402
- Solar flux density measurements at 2980 MHz, noting integration with spectral curve 22 p3590 A71-41463
- Electron beam fluorescence probe with modulation technique for measuring density disturbance near sharp wedge in rarefied hypersonic flow 22 p3529 A71-42052
- Unbounded turbulent jet transducer element fluidic sensors, measuring ambient velocity and density from pressure data 22 p3531 A71-42768
- Zirconium hydride phases density determination from lattice parameters, comparing results with direct measurement 23 p3689 A71-42930
- Interplanetary magnetic shock front location and geometry determination, using interstellar hydrogen density measurements 23 p3720 A71-43133
- Upper atmospheric temperature and density measurements from artificial cloud observations 23 p3667 A71-43139
- Apollo 12 lunar glass spherules chemical composition, homogeneity, densities and thermal histories, using electron probe analysis 23 p3758 A71-43758
- Transverse instability of charged particle beam in segmented linear accelerators due to beam encounter with wall 24 p3855 A71-44522
- Isodensity mapping with digital computer symbol selection and cathode ray X-Y plotter, showing photographic image display and enhancement of density or height information 24 p3826 A71-44787
- Gas concentration measurement at wall with argon and helium injection at pipe entrance, investigating protecting film cooling efficiency 24 p3819 A71-44929
- Radio-optical dispersometer for atmospheric water vapor density measurement with increased sensitivity 24 p3809 A71-44985
- Lunar topsoil density variations from Lunik and Surveyor radio wave, alpha and gamma scattering data, discussing Lunik 13 and Surveyor 7 landing sites 24 p3875 A71-45314
- DEOXIDIZING**
- Stainless steel deoxidation by carbon in laboratory scale vacuum induction melting, explaining reaction kinetics 05 p0758 A71-16246
- DEOXYGENATION**
- Jet fuels deoxygenation effects on steels antiwear properties and critical loading under vibrational and gliding friction 12 p1945 A71-27662
- DEOXYRIBONUCLEIC ACID**
- Mumie preparation effect on DNA and RNA contents in hemopoietic organs during acute radiation sickness due to low power radiation 01 p0013 A71-11118
- In vitro lymphocyte antigen response measurements in cellular immunity evaluation under adverse logistical conditions, emphasizing RNA and DNA synthesis rates 02 p0199 A71-12390
- Radiosensitizer and radioprotector action mode in altering X ray effects on DNA in biological systems of different complexity 07 p1032 A71-18928
- DNA modification in *Escherichia coli* exposed to X rays and sensitized by triacetoneamine N-oxyl and oxygen 07 p1033 A71-18939
- Lethal radiation in *Escherichia coli* B/r, investigating post irradiation DNA breakdown inhibitors 07 p1033 A71-18940
- Polycation effect on tumor cells, describing growth rate inhibitions, X ray sensitivity and DNA interference 07 p1035 A71-18951
- SH containing radioprotectors action on nucleic acid metabolism, discussing DNA synthesis inhibitory effects 07 p1039 A71-18983
- Tumor DNA increase of halogenated pyrimidines incorporation compared to normal tissue DNA, discussing intraarterial infusion of radiosensitizing agents 07 p1040 A71-18989
- Dinitrophenol inhibition of rejoining of X ray induced DNA breaks by L cells 07 p1045 A71-20447
- Cytophotometric study of DNA content in fibroblasts from human blood vessel walls, discussing cell proliferation and ploidy 09 p1392 A71-22609
- Tritiated thymidine effects on splenic lymphocytes regeneration, discussing DNA synthesis, cycle completion and resident populations 11 p1719 A71-26055
- Acidic and alkaline deoxyribonucleases activity by spectrophotometer and horizontal viscosimeter in normal states and pathology 12 p1872 A71-27743
- DNA synthesis rhythm in aorta endothelial cells nuclei during direct division, noting effects of amitosis by autoradiography 12 p1872 A71-27752
- Deleterious mutations and neutral substitutions, discussing molecular evolution model for DNA and proteins 13 p2013 A71-29096
- Ultrasonic vibration effects on DNA and RNA content in skin and kidneys of albino rats 15 p2356 A71-31288
- DNA replication in intercostal artery muscle cells during vascular wall physiological regeneration, noting cytophotometric study of polyploidization 16 p2531 A71-33467
- DNA synthesis in human aorta endothelium reproduction, reporting intact nuclei and dyed cell membrane samples cytophotometric studies results 23 p3635 A71-44053
- DEPENDENCE**
- NT SPATIAL DEPENDENCIES
- NT TIME DEPENDENCE
- DEPENDENT VARIABLES**
- Unknowns elimination from partial linear equations system with constant coefficients, applying to differential equations for bending transversely isotropic plate under normal external load 09 p1535 A71-22257
- System of $n+1$ differential equations with right members in coordinate origin neighborhood represented by holomorphic functions of dependent variables 16 p2603 A71-33530
- DEPLOYMENT**
- Bare base shelter/hangar expandable structures for rapid worldwide Tactical Fighter Organization deployment, noting foam and honeycomb fabrication [AIAA PAPER 71-398] 11 p1744 A71-25274
- DEPOLARIZATION**
- Manganese dioxide depolarizer for biomedical electrodes, discussing electrochemical and toxicological characteristics 01 p0021 A71-10239
- Pulsar NP 0532 average polarization absence due to Crab Nebula depolarization or unpolarized radiation on emission 04 p0643 A71-15047
- Gas laser radiation depolarization coefficient as function of radiation energy, cavity anisotropy and operating transition type 06 p0907 A71-17595
- High power light beams attenuator usable as polarizing and depolarizing device, describing design for efficiency and elimination of beam shifting 06 p0908 A71-18081
- Scattered light depolarization measurement near carbon dioxide critical temperature, using He-Ne laser 07 p1127 A71-20379
- Internal potential of heterogeneous ellipsoids for even and odd power variation of density with coordinates, using depolarization factors 14 p2304 A71-29600
- Linearly polarized lidar light scattering in spherically symmetrical uniformly distributed cloud water drops, investigating multiple backscattering effects on depolarization 17 p2770 A71-35807
- Hydrogen depolarized fuel cell for space station prototype carbon dioxide concentrator, describing modular design concept and operation [ASME PAPER 71-AV-37] 18 p2870 A71-36404
- Electromagnetic waves depolarization by rough terrain backscatter, applying theory of surface currents perturbation due to surface irregularities 19 p3021 A71-38447
- Spectral resolution of matrix Raman spectroscopy and depolarization measurements of isotope splitting, comparing with complementary IR data 20 p3194 A71-39404
- DEPOLARIZERS**
- U DEPOLARIZATION
- DEPOSITION**
- NT ANODIZING
- NT ELECTRODEPOSITION
- NT VACUUM DEPOSITION
- NT VAPOR DEPOSITION
- Ionosphere artificial Joule heating by RF energy, deriving expressions for deposition function frequency dependence 01 p0040 A71-11538
- Stellar wind effect on accretion, showing critical intensity of particle ejection replacement 03 p0484 A71-13221
- Iron corrosion product deposition on pipe wall from aqueous stream dependent on shear rate, using radioactive tracer technique 03 p0442 A71-13368
- Na and Mn homogeneity in chondritic meteorites, discussing accretion processes, metamorphisms, weathering effects and specimens size 04 p0659 A71-15855
- Cu and Ni electroless deposition on carbon fibers for composites 05 p0759 A71-16927
- Tungsten or molybdenum disulfide formation discussing tribolytic deposition process 10 p1635 A71-25010
- Earth outward winding by cosmic particle gravitational accretion, examining individual meteor counts crossing celestial meridian in WE and EW directions 12 p1966 A71-27232
- Carbon deposition rates in gas turbine engine combustion chambers with airstream-mechanical propellant atomization 13 p2118 A71-28970
- Planetary mass distribution, considering accretional theory of gas condensation into particles and particle accretion by growing embryo 14 p2312 A71-30389
- Heat and mass transfer during deposition on heated surfaces in nonisothermal gas flow with suspended solid particles, using motion of continuous Newtonian medium 17 p2836 A71-34305
- Earth outward winding by cosmic particle gravitational accretion, examining individual meteor counts crossing celestial meridian in WE and EW directions 19 p3132 A71-37584
- DEPOSITS**
- NT CRYODEPOSITS
- Soviet monograph on carbon deposits in jet engines covering distribution, formation, fuel properties, reduction and removal and harmful effects in gas turbines 21 p3437 A71-40871
- DEPRESSANTS**
- Cardiac impulse conduction measurements noting delay, block and one way block in excised canine Purkinje fibers with depressed responsiveness 07 p1041 A71-19637
- Cardiac impulse conduction in depressed canine Purkinje fibers, discussing experimental results in connection with reentrant arrhythmias 07 p1041 A71-19638
- Myocardial depressant factor purified preparation effect on isolated perfused cat heart, studying coronary vascular, dromotropic and inotropic actions 08 p1239 A71-21176
- DEPRESSION**
- Critique of Ethiopian Afar depression formation as oceanic crust resulting from Arabia drift, considering plate tectonics analysis for bifurcated spreading zones 04 p0582 A71-15126
- DEPRESSURIZATION**
- U PRESSURE REDUCTION
- DEPRIVATION**
- NT SENSORY DEPRIVATION
- NT SLEEP DEPRIVATION
- NT WATER DEPRIVATION
- DEPTH MEASUREMENT**
- Groove depth /residual deformation/ in vibrational rolling of Ti cylindrical samples, considering impression force, cylinder and steel spheres diameters 02 p0258 A71-12641
- Electron beam welding, calculating penetration depth from mathematical model [ASME PAPER 70-WA/HT-2] 13 p2075 A71-28978
- DEPTH PERCEPTION**
- U SPACE PERCEPTION
- DERIVATION CALCULUS**
- U DIFFERENTIAL CALCULUS
- DESALINIZATION**
- Soil and ground rock amino acids preparation and analysis by desalting method 08 p1251 A71-21891
- DESCENT**
- NT PARACHUTE DESCENT
- DESCENT PROPULSION SYSTEMS**
- Soft lunar landing powered descent optimal control for cost functional minimization, considering linear analytic approach with fuel consumption reduction 10 p1682 A71-24330
- DESCENT TRAJECTORIES**
- NT REENTRY TRAJECTORIES
- Apollo 12 Lunar Module high landing accuracy, discussing control actions, trajectory error sources and power descent 07 p1206 A71-19086
- Soviet book on dynamics of spacecraft descent to earth covering reentry vehicles trajectory optimization, with allowance for atmospheric perturbation effects 11 p1840 A71-26375
- Vibration amplitudes and transverse acceleration of reentry vehicle during uncontrolled atmospheric descent trajectory 13 p2146 A71-29208

Optimal control algorithm for spacecraft descent in atmosphere at speed near escape velocity, using game theory 16 p2646 A71-33702

Atmospheric entry probe from flyby mission to Jupiter, considering descent trajectory feasibility and instrument package [AAS PAPER 71-142] 19 p3153 A71-37945

Jupiter probe design and communication for deep penetration into atmosphere, concerning mission phases through entry and descent to sample altitudes [AAS PAPER 71-143] 19 p3153 A71-37946

Analytic solution to range deviations along descending branch of free flight trajectory of ballistic vehicle in planetary atmosphere 24 p3872 A71-45015

DESIGN

Design management, discussing organization, planning and control 03 p0524 A71-13743

Reliability engineering techniques for design control of electromagnetic compatibility, employing statistical theory 19 p3030 A71-38437

DESIGN OF EXPERIMENTS

U EXPERIMENTAL DESIGN

DESORPTION

Desorption and migration of Cs adsorbed on W surface under electric field, using field emission microscope 02 p0296 A71-12340

Hydrogen and nitrogen binding states and desorption kinetics on /100/ plane of Mo, using flash mass spectrometry 06 p0865 A71-18302

Thermionic converters surface physics theory, discussing work functions, desorption energy and rates relationship to atomic and crystallographic properties 11 p1711 A71-25878

Binding states, adsorbate densities and desorption kinetics of hydrogen on crystal planes of tungsten 15 p2367 A71-31676

Lower thermosphere and ionosphere upper limits of positively ionized water molecules number density, considering desorption and recombination processes 16 p2571 A71-33842

Oxygen interaction with polycrystalline W, calculating sticking probabilities and desorption spectra at various temperatures 23 p3641 A71-42906

Corrosive oxide layer formation kinetics during interaction of oxygen with polycrystalline W at 500-1000 K, using desorption mass spectrometry 23 p3641 A71-42907

DESPOINING

U SPIN REDUCTION

DESTABILIZATION

Destabilization phenomenon in nonconservative systems, considering simultaneous operation of damping mechanisms and critical load calculation 20 p3269 A71-39036

DESTRUCTIVE TESTS

Destructive and nondestructive material testing techniques, discussing equipment design and procedures standardization 13 p2074 A71-28493

Carbon-carbon spacecraft reentry heatshields evaluation and selection by nondestructive and destructive tests on flight cones 14 p2262 A71-29647

Test unit number selection for lowest total life test cost, considering operating test environments and component reliability 21 p3386 A71-40368

Apollo 12 returned Surveyor 3 component materials analysis for lunar exposure effects by nondestructive and destructive tests 23 p3765 A71-43811

DESYNCHRONIZED SLEEP

U RAPID EYE MOVEMENT STATE

DETACHMENT

Detachment prediction in turbulent incompressible plane flows on thick bodies applied to wall with disconnections and flat plate normal to wind 17 p2669 A71-34189

DETECTION

NT AIRCRAFT DETECTION

NT CORRELATION DETECTION

NT FOREST FIRE DETECTION

NT HIGH ALTITUDE NUCLEAR DETECTION

NT RADAR DETECTION

NT SIGNAL DETECTION

NT TARGET RECOGNITION

Dynamic fault detection, using mathematical condition between measurement taken, difference equation theoretical coefficients and bounds of each 03 p0449 A71-13092

Total radiative interchange kernel measurements, describing remote excitation/detection 04 p0684 A71-15511

DETECTORS

Small mass spectrometers as substance specific detectors for gas chromatography, differential thermal analysis and thermogravimetry 04 p0601 A71-15916

He-Ne laser as detectors in mine boring, quality/compensational control, data collection/reduction and positioning accuracies 09 p1458 A71-23409

Output pulse amplitude from lithium-drifted detector-amplifier combination under conditions of carrier diffusion and bulk and surface recombination 11 p1802 A71-25804

Gas chromatography techniques, discussing carrier tank, flow control, injector, reactor, column, detector, recorder, flowmeter, etc 11 p1729 A71-26291

Junction conversion and fabrication of Hg-Cd-Te n-p photovoltaic detectors by proton bombardment 13 p2066 A71-28043

Galactic cosmic ray effects on interplanetary dust particles erosion and spurious counts in micrometeoroid sensors, microphones and capacitor detectors 20 p3280 A71-39635

DETERGENTS

Antiarrhythmic effects of detergents on digitalis induced arrhythmia in dogs 01 p0010 A71-10392

DETERIORATION

Book on electrical equipment deterioration in adverse environments covering climatic action, excessive heat, atmospheric temperature variations, water vapor adsorption and condensation, etc 10 p1583 A71-24478

DETERMINANTS

Factorial determinants in solving space contours, considering bending and torsional moments in structural analysis 24 p3881 A71-44800

DETERMINATION

U MEASUREMENT

DETONABLE GAS MIXTURES

Oxygen and homologous hydrocarbon mixtures detonation limits, discussing propagation, fuel molecule structure, critical temperature, initial cracking mechanism and carbonaceous solids condensation 02 p0331 A71-11957

Double diaphragm shock tube with detonable buffer hydrogen-oxygen mixture 04 p0564 A71-14676

Implosion driven shock tube using hydrogen-oxygen mixtures detonated by short exploding wire 04 p0673 A71-14679

IR radiation measurement of chain branching rates in hydrogen-oxygen mixtures ignited by reflected shock waves 04 p0548 A71-14695

Gaseous explosives free detonation waves for hydrogen-oxygen, noting propagation velocity deficit and detonability limit 05 p0834 A71-16512

Spark ignited hydrogen-oxygen detonations in supersonic wind tunnel, using schlieren photographs 05 p0835 A71-16520

Steady state supersonic flow of combustible gas mixture around solid blunt bodies 05 p0836 A71-16530

Far field sonic boom pressure profiles simulation by methane-oxygen mixture detonation in balloons [AIAA PAPER 71-186] 06 p0886 A71-18625

Flame propagation dynamics of layered methane-air mixtures in vertical tubes, using interferometric techniques 08 p1346 A71-20864

Gas dynamic effects of reaction center in explosive gas mixture, using model and numerical computation [AIAA PAPER 70-147] 11 p1854 A71-25452

Shock induced combustion by firing spheres or cone cylinders into air- or oxygen-hydrogen mixtures, taking shadow photographs of resulting disturbances 11 p1860 A71-26268

Multiple port baffles tests using stoichiometric propane-air mixtures 13 p2116 A71-28746

German monograph on gaseous detonations stability covering carbon dioxide thermal decomposition, initial temperature/pressure, reflected shock waves and water adsorption 13 p2049 A71-28878

Blast wave propagation in explosive gaseous mixtures, presenting analysis based on detonation decay to Chapman-Jouget state 16 p2556 A71-32920

Cold combustible gas mixture ignition temperature at flat plate forward stagnation point, investigating inert gas concentration, activation energy and first Damkohler number effects 17 p2837 A71-34436

Flash photolysis initiated gaseous explosions detonation effects, observing ionization and radical emission spectra, absorption intensities and induction periods 19 p3169 A71-38110

Shock induced ignition in explosive homogeneous hydrogen-oxygen gaseous mixtures 19 p3171 A71-38130

DETONATION

Gas dynamic equations of arbitrary materials detonation without allowance for transport phenomena, deriving stability criteria from boundary value problem steady solution 01 p0070 A71-10490

Detonation propagation velocity through tubes with walls coated with thin fuel film, using turbulent boundary layer theory 01 p0181 A71-11305

Two-phase detonations, discussing importance of stripping mechanism and droplets deformation in reaction zone fuel consumption 05 p0834 A71-16515

Monopropellant /isopropyl nitrate/ detonation limits, characteristics and properties 05 p0795 A71-16516

One dimensional detonation hydrodynamics of condensed high explosives and small inert particles mixtures on basis of mathematical flow model 05 p0834 A71-16518

Nitrogen tetroxide/hydrazine pulse mode rocket engines structural failure due to chemically reactive gaseous hot spots causing high pressure spiking and detonation initiation 06 p0944 A71-17663

Liquid fuel droplets in heterogeneous detonation of dilute sprays, noting deformation and fragmentation in reaction zone 07 p1222 A71-19189

Nitromethane detonation initiation by long duration low amplitude shock waves 07 p1182 A71-19242

Shock formation and chemical activation in solid secondary explosives detonation, considering propagation acceleration by pressure rise in terms of reaction products thermodynamic properties 07 p1223 A71-19246

Steady planar detonation with direct first order one-step irreversible exothermic unimolecular reaction, examining structure by limit process expansions analysis 08 p1375 A71-20857

Gaseous nitromethane-oxygen mixtures detonation characteristics, determining reaction time by schlieren technique 08 p1346 A71-20862

Detonation sensitivity of ammonium nitrate containing fertilizers, compared with metadinitrobenzene in powder form 10 p1658 A71-25070

Piezoelectric transducer/oscilloscope technique for simultaneously rating fuels knock properties and detonation intensity 13 p2113 A71-28228

Shock compressed tetranitromethane mixtures with various benzene ethyl iodide proportions, investigating lateral discharge wave effects on detonation process structure 15 p2511 A71-31382

Heterogeneous detonations literature review, indicating need for research on heat transfer processes in subsonic and supersonic flows 15 p2511 A71-31387

Casing material effects on velocity of low speed phase prior to detonation onset of high density PETN, testing steel, Plexiglas, Duralumin and brass 15 p2511 A71-31390

Evolved stellar cores thermonuclear explosion products state, investigating Chapman-Jouget detonation propagation effects with carbon 12 and oxygen 16 burning under high electron degeneracy 17 p2806 A71-35407

Detonation processes in gases, considering Zeldovich-Doering-Neumann model and reaction kinetics 19 p3162 A71-37457

Gas dynamic laser, obtaining initial high temperature gas mixture by detonating solid 22 p3556 A71-41813

DETONATION WAVES

Annealed steels strengthening and structural changes under explosive shock wave 01 p0085 A71-10037

Nonequilibrium effects of vibrational relaxation on diatomic gas flow behind blast waves 03 p0342 A71-13785

Detonation waves in gases and two phase systems with nonideal wave front, calculating acetylene explosion parameters for different initial pressures 03 p0520 A71-13991

Radiation absorbing detonation waves calculation by finite difference techniques based on pseudoviscosities 03 p0439 A71-14064

Ionizing shock waves and high speed gas flow generation in tubes using high explosives 04 p0674 A71-14683

Strong shock wave generation by detonation with simultaneous working gas heating and compression 05 p0735 A71-16381

One dimensional unsteady flows of combustible gas mixtures with detonation waves generation, noting electromagnetic effects

05 p0833 A71-16502

Gas dynamic conditions resulting in reacting gases detonation waves at high initial temperatures, simulating internal combustion engine knock

05 p0833 A71-16506

Detonation waves Mach configuration, noting frontal structure similarity, lead shock velocity and non-reactive blast wave model

05 p0833 A71-16507

Multiple wave intersections at marginal detonation front, determining dynamic behavior by soot technique

05 p0833 A71-16508

Multidimensional detonation wave structure, presenting spacing prediction by transverse wave strength

05 p0834 A71-16509

Detonation front at Chapman-Jouguet velocity demonstration by numerical transient flow calculations

05 p0834 A71-16510

Detonation wave with finite reaction velocity interaction with rarefaction wave from behind, noting oscillations development associated with attenuation

05 p0834 A71-16511

Gaseous explosives free detonation waves for hydrogen-oxygen, noting propagation velocity deficit and detonability limit

05 p0834 A71-16512

Shock initiated detonation wave propagation in combustible hydrogen oxygen flow in constant area duct, considering wave initiation Mach number and ignition temperature

05 p0834 A71-16519

Shock formation and chemical activation in solid secondary explosives detonation, considering propagation acceleration by pressure rise in terms of reaction products thermodynamic properties

07 p1223 A71-19246

Detonation products expansion in vacuum, measuring gas flow speeds and pressure profiles far from charge

09 p1545 A71-22690

Sonic boom and explosion shock wave propagation over long distances through turbulence modeled by sound speed fluctuation, including acoustic scattering effect

09 p1433 A71-22858

Heterogeneous detonation propagation in mixture of liquid fuel droplets suspended in gaseous oxidizer, discussing droplets disintegration time and shock wave parameters

10 p1698 A71-25124

Detonation wave of gas in circular cylinder with nonsimultaneous axisymmetric initiation at plane boundary, obtaining solution for small perturbation flow behind detonation front

11 p1853 A71-25152

Strong shock wave generation by detonation with simultaneous working gas heating and compression

12 p1898 A71-27460

Explosive shock loading effect on materials properties, describing test equipment

12 p1895 A71-27689

Soviet book on detonation waves in condensed media covering excitation and propagation in compacted explosives, liquid/solid explosives and pulsations

13 p2161 A71-28737

Monograph on shock and detonation waves ionization and structure covering diagnostic techniques, heat transfer, particle flow, pressure measurements, etc

14 p2335 A71-29933

Stoichiometric hydrogen-oxygen mixture spinning detonation fine structure determination by trace technique and high speed space-time photography

15 p2465 A71-32083

Stoichiometric hydrogen-carbon monoxide-oxygen mixtures detonation wave propagation at critical Mach number, noting explosion limit chemical kinetics role

15 p2465 A71-32088

Ionization measurement in detonation and shock waves in reactive gas mixtures by microwave cavity techniques

15 p2411 A71-32556

Blast wave propagation in explosive gaseous mixtures, presenting analysis based on detonation decay to Chapman-Jouguet state

16 p2556 A71-32920

Collapsing white dwarf stars, investigating detonation wave formation for thermonuclear explosion

16 p2631 A71-33228

Boundary effects on gaseous detonation velocity deficit and limit using approximation into boundary layer equations, comparing to experimental data

17 p2837 A71-34437

Detonation wave with dual front structure, calculating attenuation in Chapman-Jouguet regime by boundary shock layer method

17 p2839 A71-35635

Transverse wave structure of two-dimensional detonation waves propagating in narrow channel, considering longitudinal instabilities

17 p2841 A71-35708

Shock layer reattachment initiated by point explosion and driven continuously outward by inner contact surface

18 p2985 A71-36034

MHD detonation waves in relativistic perfect fluid of magnetic permeability μ immersed in electromagnetic field

18 p2951 A71-36189

Two dimensional steady state detonation waves, obtaining generalized Rankine-Hugoniot equations

19 p3045 A71-38126

One dimensional nonsteady combustion processes accompanying self sustained detonation waves initiated by merger of two weak shock waves, using Lax finite difference method

19 p3170 A71-38127

Decane and hexadecane fog detonation propagation in gaseous oxygen

19 p3170 A71-38128

Detonation propagation through tubes with thin fuel film coated walls, obtaining heat transfer coefficients, friction, evaporation rate, reaction zone length and propagation velocity

19 p3171 A71-38129

Rocket-borne explosive charge initiated detonation wave effects on decimeter wavelength radio waves in lower E layer

20 p3199 A71-39894

Approximate motion equations of gas flow behind detonation front in flat explosive plate covered by inert coating

23 p3781 A71-43358

Pressure and mass velocity profiles behind two dimensional shock wave generation on Al flat plates explosive surface

24 p3839 A71-45228

DEUTERIDES

Boron and carbon hydrides and carbon deuteride molecular ions radiative lifetime measurements, computing absolute oscillator strengths

08 p1250 A71-20671

Rayleigh-Brillouin light scattering in compressed hydrogen, hydrogen deuteride and deuterium, noting discrepancy between observed and theoretical spectra

08 p1301 A71-20743

DEUTERIUM

Solar photospheric spectrum, investigating deuterium abundance relative to hydrogen

01 p0157 A71-10762

Deuterium formation in early solar system by examining autogenetic spallogenic model

01 p0157 A71-10763

Free radical effect on exchange reaction between ammonia and deuterium in high diluted argon shock tube

04 p0548 A71-14698

Hydrogen and deuterium oscillator strengths and transition probabilities for Lyman and Werner system individual bands by electronic dipole moment functions

07 p1164 A71-20019

Rayleigh-Brillouin light scattering in compressed hydrogen, hydrogen deuteride and deuterium, noting discrepancy between observed and theoretical spectra

08 p1301 A71-20743

Reaction dynamics for CO ion plus deuterium to yield COD ion plus D, noting polarization forces role

09 p1497 A71-22702

Net fusion energy from laser heated deuterium-tritium particles dependent on plasma temperature, electrical energy and electron-ion thermalization through collisions

11 p1805 A71-25799

Isotope effects in Lyman and Werner systems of molecular hydrogen, HD and molecular deuterium, calculating band strengths, oscillator strengths and Franck-Condon factors

11 p1803 A71-26072

Deuterium gas breakdown by ruby laser, using quantum kinetic equation for electron interactions with molecules and photon field

12 p1915 A71-27284

Differential energy spectrum of cosmic ray deuterium flux of galactic origin from IMP 5 satellite measurements

13 p2120 A71-27974

Inert gases, hydrogen, deuterium and carbon dioxide flow in plane parallel glass slots over various Knudsen numbers, calculating slippage constants and volumetric discharge

14 p2227 A71-30673

Physical conditions leading to deuterium enhancement in earth upper atmosphere as function of thermopause temperature and eddy diffusion

16 p2569 A71-33809

Venus L alpha emission, negating deuterium origin

18 p2970 A71-37055

Deuterium Balmer line intensities and overpopulations measurements relationship to thermal equilibrium in pinch discharges

21 p3421 A71-40142

HD rotational relaxation collision number temperature dependence calculation from excitation probability, comparing with experiment

21 p3419 A71-40911

Apollo 11 and 12 lunar samples O 18/O 16, Si 30/Si 28, D/H and C 13/C 12 ratio determination, examining whole rocks, breccias, soils, plagioclases and fines

23 p3751 A71-43705

Velocity dependent HD beam scattering by inert gases, measuring total effective cross section in thermal energy range

23 p3707 A71-43879

He, HD and deuterium scattering by various gas molecules, measuring total effective cross sections for comparison with calculation

23 p3707 A71-43880

Thermal conductivities of pure and mixed ortho- and parahydrogen and/or deuterium at temperatures with no molecular internal energy exchange

24 p3850 A71-44553

DEUTERIUM COMPOUNDS

NT DEUTERIDES

NT HEAVY WATER

Intense superradiant emission in HF and DF molecules high gain IR transitions, examining spectral distributions with pneumatically tuned Fabry-Perot interferometer

09 p1498 A71-23478

Transverse gas flow effects on deuterium fluoride-carbon dioxide chemical laser output, discussing amplifier medium homogeneity factor

10 p1619 A71-23834

Autoionic mass spectroscopy, discussing emitters, ion sources and mass spectra of deuterized benzene, chlorobenzene and chloroform molecules during electron ionization and autoionization

10 p1611 A71-24383

Line shifts in first overtone band of DF perturbed by HF, studying pressure induced transitions and partial pressures

11 p1729 A71-26139

Methane and deuteromethane released from Apollo 11 and 12 lunar fines by deuterated acid etch, using gas chromatography for carbon compounds separation

13 p2136 A71-28427

Exponential approximation of rotational relaxation of polar HCl and DCl at 300 and 500 K by molecular dynamics, comparing with perturbation calculations

15 p2451 A71-31673

Comparative IR and Raman spectra of gaseous, liquid and polycrystalline symmetrical dimethylhydrazine and deuterium analogs

19 p3013 A71-38345

Transient photoconductivity measurements of room temperature electron mobility in deuterated anthracene single crystals, discussing isotope effect

20 p3194 A71-39348

Gain and spectral characteristics of transverse flow CW chemical laser with hydrogen and deuterium fluorides active medium

21 p3393 A71-41041

Prebiotic organic matter in solar system, investigating contamination free amino acid catalytic synthesis from deuterated reactants

23 p3633 A71-43245

Lithium deuteride nuclear fuel autocatalytic burning via proton and beryllium isotope resonance in fusion chain reactions

24 p3847 A71-44497

DEUTERIUM OXIDES

U HEAVY WATER

DEUTERIUM PLASMA

Current sheet collapse phase in dense deuterium plasma focus gun heating, using streak photography and X ray and neutron measuring techniques

07 p1165 A71-18877

Theta pinch deuterium plasma heating by carbon dioxide laser as function of pulse duration and energy

16 p2587 A71-33188

D-T plasma cumulation laser heating problem, considering similarity theory for electron conductivity and bremsstrahlung

21 p3395 A71-41360

Expanding D-T plasma laser heating equations derivation, allowing for heat produced by associated thermonuclear fusion

23 p3710 A71-43320

Q values, costs, efficiencies and radioactive evaluation of D-D, D-T and D-He 3 mirror fusion plasma power systems

24 p3847 A71-44493

DEUTERON IRRADIATION

Radiation defects distribution in Si irradiated by protons, deuterons and alpha particles

10 p1655 A71-24140

Tungsten single crystals under deuterium bombardment, noting structural defects formation as function of irradiation energy

16 p2595 A71-33883

DEUTERONS

Low energy cosmic ray deuteron flux, examining energy spectral shapes of sources

02 p0303 A71-12871

- DEVIATION**
Harmonic residuum of solar quiet, considering mean deviation and correlation coefficients
20 p3217 A71-39514
- DEVITRIFICATION**
U CRYSTALLIZATION
- DEW**
Cold front zone meteorological elements, calculating temperature gradients, dew point deficit, and wind vector vertical distribution
11 p1795 A71-26558
- DEWAR SYSTEMS**
U CRYOGENIC EQUIPMENT
- DH 106 AIRCRAFT**
U COMET 4 AIRCRAFT
- DH 121 AIRCRAFT**
Hawker Siddeley Trident 3B flight test program, booster engine, structural features, power plants, systems and landing gear
09 p1385 A71-22890
Trident aircraft autopilot for automatic landings in blind conditions, discussing operational problems
13 p2098 A71-29261
European automatic flight control systems for landing in category IIIA conditions, discussing triplex system in Trident and simplex in Caravelle
24 p3846 A71-44456
- DHC 4 AIRCRAFT**
Strut pressure and axle strain gage systems testing for balance and weighing onboard De Havilland C-7A aircraft
[SAWE PAPER 881]
17 p2676 A71-35827
- DIABATIC PROCESSES**
U HEAT TRANSFER
- DIABETES MELLITUS**
Photoplethysmographic analysis of pulse wave velocity in healthy subjects and in patients with hypertension, heart disease, diabetes and anemia
22 p3490 A71-42518
- DIAGNOSIS**
Ultrasonics applications in surgery, therapy and diagnosis, discussing physical principles, piezoelectric transducers, tissue acoustic properties and measurement methods
03 p0372 A71-13351
Autopsies compared to ECG for diagnosis accuracy for acute recurrent myocardial infarction
05 p0711 A71-16951
Aircrews coronary insufficiency diagnosis via electrocardiographic modifications after exertion, observing ischemia
06 p0860 A71-18192
Stochastic identification method for transforming ECG and VCG data to approximate diagnosis, using computerized dipole models
13 p2020 A71-29002
Polygraphic sleep recordings automatic analysis, presenting numerical results for rapid and slow eye movements, muscle tone, heart and respiratory rates
15 p2363 A71-31958
Medical screening techniques, discussing sensitive, specific, reliable, fail-safe and self calibrating instrumentation systems
17 p2689 A71-34609
Frequency power and resolution effects on ultrasonic holography for medical diagnosis involving information processing on computer
19 p3066 A71-38240
Radiation damage diagnosis in humans, investigating free amino acid excretion with urine by paper chromatography method
22 p3495 A71-42736
Anatomic examinations and diagnostic techniques in ophthalmologic aviation medicine, discussing electronic time interval and storage measurements, cortical response, etc
23 p3631 A71-42928
- DIAGRAMS**
NT BENDING DIAGRAMS
NT CIRCUIT DIAGRAMS
NT CREEP DIAGRAMS
NT FEYNMAN DIAGRAMS
NT HERTZSPRUNG-RUSSELL DIAGRAM
NT MOLLIER DIAGRAM
NT NYQUIST DIAGRAM
NT PHASE DIAGRAMS
NT S-N DIAGRAMS
NT STRESS-STRAIN DIAGRAMS
Wyld diagram method extended to turbulence decay, considering operators expressed as integrals with kernels
04 p0575 A71-15604
Terrestrial electrical current distribution diagram based on solar quiet variation hodographs
07 p1104 A71-20048
- DIAL SATELLITE**
Scientific goals and mission behavior of Dial aeronomy satellite for spatial distribution determination of atmospheric hydrogen concentration
[DGLR-71-004]
15 p2501 A71-32781
Condition equations for zonal harmonics using low inclination DIAL satellite interferometric measurements over perigee revolution
20 p3300 A71-39664
- DIALYSIS**
NT ELECTRODIALYSIS
Parabiotic dialysis, examining uses as in vivo diffusible substances test and alternative for conventional chronic hemodialysis
09 p1401 A71-23370
Coronary dilating substances of low molecular weight separated through dialysis from hypothalamus protein carriers
21 p3338 A71-41072
- DIAMAGNETISM**
Diamagnetic moment of strong shock waves from high temperature light spark explosion in gases
06 p0930 A71-17399
Ferrite microstrip microwave phase shifters with transverse and longitudinal magnetization, calculating diamagnetic and permeability tensor effects
08 p1263 A71-20768
Low pressure paramagnetic regime axially symmetric hydromagnetic equilibria with spherical plasma-vacuum interfaces, extending solution to high pressure diamagnetic regime
13 p2104 A71-27843
Lunar diamagnetic cavity signatures from Ames magnetometer experiment on Explorer 35 orbiter, indicating solar wind interaction
13 p2132 A71-27909
Energy transport mechanisms of rapid diamagnetism decay in plasma stream collisions, using two fluid shock front model
13 p2110 A71-29371
Hydrogen plasma HF heating boundaries by magnetic traps, noting diamagnetic effects due to ion and electron heating
14 p2282 A71-30667
Finite-beta stabilization of collisionless trapped particle mode in toroidal plasma confinement devices, using magnetic well dug by plasma diamagnetism
19 p3112 A71-37742
Superconductivity, reviewing critical current/field concepts, Meissner effect, negative surface tension, zero resistance and applications
20 p3276 A71-39247
- DIAMANT LAUNCH VEHICLE**
Diamant launch vehicle multistage development for placing satellites in low perigee and high eccentricity and high and low circular orbits
22 p3610 A71-42020
Project management quality control factors learned from Diamant A satellite launching vehicle and French military programs
23 p3786 A71-43469
- DIAMETERS**
Planets and satellites diameter determination, reviewing double image technique
02 p0309 A71-12153
Precise Brorfelde transit circle reading by photoelectric scanning, determining diameter and group corrections
06 p0899 A71-17967
Long small bore metal tube internal diameters calculation from capacitances comparison with cylindrical coaxial probes
18 p2922 A71-36581
- DIAMOND WINGS**
U LOW ASPECT RATIO WINGS
U SWEPT WINGS
- DIAMONDS**
NT METEORITIC DIAMONDS
Theoretical estimation of tensile strength, elastic modulus and deformation of cubical diamond specimens under tension and compression
22 p3565 A71-42873
Temperature effects on long wavelength photon frequency and linewidth in diamond, using Raman scattering techniques
23 p3715 A71-43471
- DIAPHRAGM [ANATOMY]**
Respiratory diaphragmatic center, investigating motor-neuron system integral activity by recording and analyzing phrenic-nerve signals in rabbits
10 p1562 A71-24164
Reduced diaphragmatic muscle tissue resistance in rats during prolonged hypokinesia, showing sorption of basic vital neutral red stain
13 p2007 A71-28417
Diaphragm mechanics, discussing thoracic pressure-lung volume and air flow relationships of respiratory system during electrophrenic stimulation in men and cats
16 p2530 A71-33239
- DIAPHRAGMS [MECHANICS]**
Laser beam trajectory changes due to asymmetrical shading with circular absorbing diaphragm, noting characterization by energy distribution over cross section
01 p0095 A71-11216
Shock wave dynamic behavior in shock tube under variable diaphragm opening time for high pressure gas flow into lower pressure section
03 p0472 A71-14261
Double diaphragm shock tube with detonable buffer hydrogen-oxygen mixture
04 p0564 A71-14676
- Shock tube diaphragm bursting by passing heavy current through overlapping heated wire under pressure
05 p0734 A71-16583
Metallic diaphragms design, fabrication and testing for cryogenic fluid and positive expulsion systems [AIAA PAPER 70-683]
11 p1768 A71-25518
Diaphragm opening time influence on gas flow in shock tubes
12 p1897 A71-27451
Dynamic characteristics of fluid oscillations in cylindrical vessel divided by annular diaphragm
13 p2050 A71-29236
Altimeter-airspeed and Mach number pressure transducer with diaphragm free of temperature and vibration effects
14 p2243 A71-30322
Scattering coefficients of thick inductive diaphragm in rectangular waveguide, using ray-optical method
15 p2376 A71-32023
Ruby watch jewels as pinhole diaphragms in laser beam broadening systems, determining optimal size
16 p2588 A71-34102
Laser beam trajectory changes due to asymmetrical shading with circular absorbing diaphragm, noting characterization by energy distribution over cross section
17 p2750 A71-34267
Double-diaphragm shock tube optimal parameters with allowance for boundary layer effect behind shock wave propagating in central chamber
17 p2730 A71-35634
Cascade displacements and stresses in nozzle ring guide vanes with sectional diaphragm under axial and circumferential flow
18 p2980 A71-36706
Wave diffraction at step junction of two rectangular waveguides and symmetrical diaphragm with dielectric fillers
19 p3019 A71-38332
Room temperature and heated driver gas low attenuation electric shock tube, investigating diaphragm opening process and effect on shock wave motion
20 p3209 A71-38837
High performance solar prominence telescope components design, considering lenses and diaphragms with special attention to image degrading influences
21 p3378 A71-40523
- DIASTOLE**
Left ventricular function analysis by atrial pacing in subjects with normal and elevated left ventricular filling pressure, relating stroke volume to end diastolic pressure
07 p1044 A71-20352
Heart rate and diastolic inflow coronary resistance extravascular component, discussing heart artificial stimulation and pharmacological maximal dilation effects
10 p1565 A71-24679
Diastolic and mean blood pressure responses to exercise after beta-adrenergic blockade in normal and labile hypertensive subjects, using Trascior
13 p2014 A71-29320
Left ventricular power as product of pressure and volume change rate, relating peak values to end diastolic mass
14 p2187 A71-37079
Diastolic heart sounds and filling waves in coronary artery disease, relating graphic abnormalities and clinical, arteriographic and hemodynamic findings
19 p3002 A71-37550
Pulmonary diastolic pressure relation to left ventricle and atrium of patient with diagnostic heart catheterization at rest
19 p3004 A71-38296
Cardiac automatic rhythms, discussing diastolic depolarization in Purkinje fibers and factor controlling automaticity
21 p3330 A71-40250
- DIATOMIC GASES**
Nonequilibrium effects of vibrational relaxation on diatomic gas flow behind blast waves
03 p0342 A71-13785
Time measurements of vibration relaxation in diatomic gases excited by shock waves
04 p0568 A71-14795
Dissociated diatomic gas nonequilibrium boundary layer flow over catalytic flat plate, examining velocity profiles, temperature and concentration
05 p0735 A71-16389
Boundary condition effects on thermomagnetic torque from moment method solution for Boltzmann equation for diatomic molecular gas in magnetic field and cylindrical geometry
09 p1502 A71-22853
Laser designs with thermal pumping, obtaining electron states phototransition probability, cooling rates for population inversion and laser action threshold for diatomic gas molecules
12 p1914 A71-27029
High temperature singly and doubly ionized monatomic gas and partially dissociated and singly ionized diatomic gas, showing adiabatic and isentropic exponents relationship
16 p2662 A71-32837

Diatomic gas molecules three body recombination and dissociation rate coefficients from modified phase-space theory of reaction rates

19 p3107 A71-38078

Relaxation equations for dilute diatomic gas dissociation-recombination reactions, transforming kinetic equations to normal modes

19 p3107 A71-38079

Gas nature effect on wall temperature and heat transfer in Hartmann-Sprenger tube

21 p3366 A71-40102

Translational and rotational temperature and density variations through shock waves in oxygen and nitrogen, using Monte Carlo scheme

23 p3781 A71-43444

DIATOMIC MOLECULES

Collision induced homonuclear diatomic molecules vibrational excitation using three dimensional model, obtaining transition cross sections and relaxation rates as function of temperature

01 p0129 A71-10367

Vibrational transition matrix elements for diatomic molecules, using semiempirical Cashion method for potential functions

03 p0460 A71-13497

Anharmonic oscillator diatomic molecule system, examining vibrational relaxation in expanding gas flow

03 p0460 A71-13499

Diatomic molecules dissociation and recombination in presence of third body, considering quantum mechanical scattering theory

05 p0785 A71-16728

Diatomic molecular autoionization model, calculating limit of high vibrational and electronic principal quantum numbers

07 p1164 A71-19687

Diatomic molecules nonsigma states rotational excitation adiabatic theory

07 p1164 A71-19691

Rotating nonvibrating diatomic low density gas molecules rotational relaxation time and viscosity, based on quantum mechanics

08 p1336 A71-20659

Born-Oppenheimer approximation for elastic and inelastic electron scattering by diatomic molecules

08 p1337 A71-20886

Solar diatomic molecules vibrational degree of freedom model, applying Boltzmann distribution

08 p1365 A71-21773

Inelastic collision effects on vibrational excitation of diatomic molecules with conserved energy

08 p1338 A71-21781

Positive diatomic nitrogen ions dissociation during collisions with inert gas atoms, measuring mass and energy distributions from focusing parabolic spectrograph

11 p1801 A71-25227

Franck-Condon factors, densities and r-centroids for diatomic molecules, computing vibrational wave functions by FORTRAN V

14 p2276 A71-30297

Carbon monoxide gas dynamic laser oscillation generation, observing maximum power and vibrational exchange among single diatomic species states

15 p2422 A71-32583

Solar diatomic molecules vibrational degree of freedom model, applying Boltzmann distribution

15 p2495 A71-32678

Anharmonic effects in time dependent vibrational relaxation of diatomic molecules in rapidly expanding flows, considering N-CO-Ar mixtures

18 p2948 A71-35837

Integrated absorption coefficient of pressure induced pure rotational and vibrational transitions in binary collisions of homonuclear diatomic molecules at high temperatures

19 p3108 A71-38719

Reversible electron transitions selection rule in diatomic molecules excitation by electron impact, obtaining differential cross sections

21 p3417 A71-40198

Transport properties of low density gas of rotating diatomic molecules, deriving quantum mechanical expression for relaxation time via restricted distorted wave approximation method

23 p3706 A71-42908

Total and momentum transfer cross sections for low energy electron scattering by atomic and diatomic molecules

23 p3707 A71-43898

Chemical lasers diatomic and multiatomic molecules dissociation in nonequilibrium conditions, discussing vibrational energy exceeding gas temperature

24 p3834 A71-45112

Magnesium diatomic metal static and dynamic properties, using multiple electron and ion analysis system

24 p3839 A71-45118

DIBORANE

Oxygen difluoride/diborane propellant thrust chamber and injector technology, discussing engine duty cycles and performance

07 p1183 A71-18890

Initial reaction rates of oxygen difluoride with diborane related to reactant concentration and temperature

09 p1510 A71-22071

Diborane release into upper atmosphere, considering effectiveness as atmospheric tracer

09 p1489 A71-23450

DICHLORIDES

Photolysis of HCl photosensitized evolution from dichlorobutane in solution by aliphatic ketones

11 p1728 A71-25937

DICHOTOMIES

Extremals optimal endpoints, obtaining necessary and sufficient conditions by method based on dichotomy concept

05 p0774 A71-16645

DICHOISM

Visual perceptual masking under binocular and dichoptic conditions separating peripheral and central interference effects

21 p3342 A71-40225

DICHROMATES

U CHROMATES

DICKE RADIOMETERS

Dicke type radiometer sensitivity and spectrum, recommending antenna gain improvement, intrinsic receiver noise reduction and large averaging times

04 p0596 A71-15065

Sampling efficiency of total power balanced Dicke type radiometers using digital integration

08 p1267 A71-21879

HF amplifier statistical gain fluctuations effect on Dicke radiometer sensitivity, using Davenport-Root theory of random processes

16 p2548 A71-34132

Microwave amplifiers gain fluctuations effect on Dicke radiometers minimum detectable temperature difference, considering traveling wave tubes and tunnel diode and mixer IF amplifiers

16 p2548 A71-34133

Comparative detection performance of Siebert and Dicke-fix constant false alarm rate (CFAR) radar detectors for signals in Gaussian noise

20 p3195 A71-38866

DICKE TYPE RADIOMETERS

U DICKE RADIOMETERS

DICTIONARIES

German glossary of commercial air traffic with English equivalents

18 p2989 A71-36962

DIELECTRIC CONSTANT

U DIELECTRIC PROPERTIES

DIELECTRIC MATERIALS

U DIELECTRICS

DIELECTRIC PERMEABILITY

Lunar surface layer density and dielectric permeability from radio wave scattering data from automatic spacecraft radar measurements

20 p3295 A71-39616

Dielectric permeability tensor of relativistic plasma stream, considering collisionless damping of surface waves in seminfinit isotropic plasma

23 p3713 A71-44148

DIELECTRIC POLARIZATION

Dipolar charge density of electret formed by polar polymers above critical temperature under dielectric polarization with quenching

14 p2181 A71-29747

Weldable Al-Zn-Mg alloys with cathodic polarization protection, noting decrease in stress corrosion crack propagation rate

22 p3560 A71-41625

Dielectric and semiconductor crystals surface defects, considering electric polarization structures

24 p3860 A71-45098

DIELECTRIC PROPERTIES

NT PERMITTIVITY

Perovskite crystals phase transition with unit cells atom displacement, considering permittivity anomalies, structure and free energy expansion coefficients

01 p0138 A71-10430

Microwave permittivity dispersion in segnetoelectrics as function of single crystal domains size, considering barium titanate dielectric spectrum resonance

01 p0138 A71-10433

Electromagnetic wave reflection from ferrite moving domain wall, considering wave separation and permittivity and magnetic susceptibility tensors

01 p0138 A71-10435

Microwave receiving and transmitting antennas proximity effects on permittivity measurements of dielectric layer

01 p0057 A71-11206

Complex permittivity and impedance of dielectric samples in coaxial lines and rectangular waveguides by moving probe and resonant Q factor measurements

02 p0229 A71-11713

Apollo 11 lunar samples dielectric constants, losses and electrical conductivities as function of temperature and frequency, comparing with terrestrial and simulated lunar rocks

02 p0305 A71-11985

Earth and planetary surface soil dielectric constant and conductivity determination based on p-wave velocity data correlation

05 p0743 A71-171423

Microwave measurements of semiconductors and semiconductor films including resistivity, permittivity and carrier mobility

06 p0873 A71-17530

Antarctic terrain dielectric and loss properties effects on VLF attenuation and phase constants of earth-ionosphere waveguide paths over ice covered regions

06 p0868 A71-17733

Nonequilibrium plasma HF conductivity, introducing dressed ion expression in terms of dielectric permittivity

07 p1165 A71-18743

Light effect on dielectric constant of thin hardened dichromated gelatin films for holographic recordings

07 p1110 A71-19480

Vector solution for electromagnetic wave scattering from rough surface of arbitrary dielectric constant

07 p1064 A71-20316

Free-space focused microwave system for determining materials complex permittivity to temperatures over 2000 C

07 p1115 A71-20357

Plane electromagnetic wave propagation and reflection in presence of substances with arbitrary complex permittivity

07 p1066 A71-20543

Varactor capacitance variations compensation for temperature dependent diffusion potentials and dielectric constants changes

08 p1265 A71-21299

Two center bound polaron in rutile single crystal, studying dielectric behavior in applied magnetic field

08 p1345 A71-21690

Fabry-Perot interferometer for dielectrics permittivity and loss measurements in millimeter and submillimeter ranges, discussing design, tests and accuracy

08 p1294 A71-21806

Quasi-stationary permittivity tensor corrections for smoothly nonuniform electron plasma in absence of magnetic field, using geometrical optics methods

09 p1500 A71-22240

Ground wave propagation over nonuniform overburden with arbitrarily varying complex dielectric coefficient and depth, discussing application to water table mapping

09 p1436 A71-22644

Pyrolytic aluminum oxide thin films on Si substrate by thermodecomposition, measuring vapor deposition parameters and Si surface preparation effects on dielectric and interface properties

09 p1509 A71-23117

Dielectric constant and loss tangent measurements at 60 and 90 GHz for Teflon, polystyrene and Lucite sheets, using Fabry-Perot interferometer

09 p1418 A71-23415

Effective dielectric constant of macroscopically homogeneous and isotropic two phase composites in terms of sample geometry

10 p1655 A71-23922

Reflectance measurements of dielectric coating on metallic substrate, comparing with analytical model

11 p1799 A71-26233

Bounds for effective dielectric constant of fiber reinforced materials, using Miller geometry of matrix and inclusion

11 p1782 A71-26388

Semiconductor or gas-discharge two-component plasmas, calculating permittivity variation due to carrier heating and diffusion during strong plane monochromatic, electromagnetic wave propagation

12 p1937 A71-27184

Dielectric properties of barium titanate with Nb, noting metal oxide additives effects on conductivity

13 p2092 A71-28661

Longitudinal waves correlation damping in high temperature plasma under magnetic field, calculating dielectric constant by quantum statistical method

14 p2280 A71-30450

HF modulated transverse electromagnetic wave penetration into plasma with negative dielectric constant, noting plasma density fluctuations and electroacoustic wave formation

14 p2281 A71-30542

Apparatus for measuring polar liquids dielectric permittivity and losses at microwave frequencies over wide temperature and pressure ranges

14 p2222 A71-30583

Dielectric relaxation time in Debye binary liquid, comparing liquid filled coaxial transmission line step response measurements with Debye model

14 p2215 A71-30985

Homogeneous infinite weakly ionized plasma dielectric permittivity tensor in crossed electric and magnetic field

17 p2790 A71-35444

Fabrication technology limitations effect on use of dielectric interference filters in wide angle optical receivers

18 p2946 A71-35847

Continuously variable microwave stripline phase shifter with linear shift vs frequency by dielectric constant variation

18 p2889 A71-36272

Bulk semiconductor microwave control components, considering dielectric and conductive properties of plasma state

18 p2894 A71-36980

Photographic observations of plasma eruptions from metal and opaque dielectric targets subjected to neodymium laser pulses, discussing successive shock wave formation

19 p3070 A71-37085

Isotropic materials with memory, discussing induced birefringence theory to account for memory and nonlinearity effects in dielectric properties dependence on deformation history

19 p3118 A71-37525

Double refracting dielectric microwave lenses design for horn antennas in SHF applications

19 p3036 A71-38643

Rayleigh scattering by obliquely oriented uniform thin cylindrical particles /needles/, using dielectric needle approximation

20 p3196 A71-39406

Antiferromagnetic semiconductors and metals in magnetic field, obtaining Fourier components of electromagnetic fluctuation correlators for dielectric permittivity and magnetic permeability tensors

22 p3586 A71-42062

Semiconductor or gas-discharge two-component plasmas, calculating permittivity variation due to carrier heating and diffusion during strong plane monochromatic electromagnetic wave propagation

22 p3584 A71-42461

Normal wave scattering on random permittivity inhomogeneities of stratified waveguide dielectric layer, calculating beam width and energy loss by perturbation procedure

23 p3645 A71-43567

Apollo 11 and 12 rocks dielectric constants, discussing far IR absorption spectrum of fines

23 p3760 A71-43772

Dielectric conductivity, relative permittivity and loss tangent of Apollo 11 and 12 rock samples

23 p3762 A71-43787

Dielectric properties of Apollo 12 samples and lunar interior as function of frequency and temperature

23 p3762 A71-43788

Antenna radome noise temperature under aerodynamic heating as function of losses in material, interface reflection and dielectric surfaces

23 p3647 A71-44324

Temperature and frequency effects on permittivity and dielectric loss angle tangent in glasses and pyroceramics

24 p3859 A71-44379

DIELECTRICS

NT RADOME MATERIALS

Electric potential and field distribution in dielectric plate insert of rectangular waveguide calculated by net point method using computer program

01 p0051 A71-10149

Complex dielectric structure simulation for microwave scattering purposes using rotating target and zone technique

01 p0051 A71-10255

Round dielectric waveguides dominant mode radiation losses calculation

01 p0052 A71-10467

EM wave propagation along radially inhomogeneous dielectric cylinders, considering permittivity variation

01 p0037 A71-11170

Wave dispersion and evanescent modes in rectangular waveguides filled with transversely inhomogeneous dielectric rod

01 p0056 A71-11196

Variational bounds on phase shifts for electromagnetic wave scattering by dielectric obstacles in waveguides

01 p0056 A71-11199

Trapped LF ion wave propagation along warm plasma cylinder imbedded in dielectric, obtaining dispersion relation

01 p0136 A71-11476

Transparent dielectrics sheet radiation absorbance, emittance and transmittance determination by Monte Carlo method

01 p0183 A71-11591

Surface destruction of glass dielectric by pulsed laser beam, considering plasma clouds, shock waves, ablation and crack formation

02 p0258 A71-11640

Complex permittivity and impedance of dielectric samples: in coaxial lines and rectangular waveguides by moving probe and resonant Q factor measurements

02 p0229 A71-11713

Metallized capacitors types and properties, considering extra thin dielectric films and high field strength

02 p0230 A71-11817

Integrated optical communication circuit technology adaptable to batch processing, considering encapsu-

lated planar arrays of rectangular dielectric waveguides

02 p0231 A71-12008

Heat pipe improvement of capacitor energy storage and I-V, analyzing in terms of heat loss vs conducted heat

03 p0352 A71-13045

Characteristic energy absorption spectra of dielectric solids from direct IR measurements for single crystal and thin film specimens

03 p0385 A71-13645

Semitransparent spherical dielectric shell under diffuse incident radiation, determining absorbance and reflectance by Monte Carlo method

03 p0518 A71-13648

EM oscillations of open elliptic profile cylindrical mirrors resonator with dielectric elliptic cylinder

03 p0386 A71-13800

Dielectrics erosion under pulsed electric discharge in conical plasma accelerator, varying capacitance and inductance for evaporated mass relation to current strength

04 p0631 A71-14597

Radiation patterns of dielectric rod antennas with axial emission in near field

04 p0557 A71-14630

Input resistance and effective height of gap excited metallic and dielectric antennas in conductive environment

04 p0558 A71-15220

Ferromagnetic dielectric composites physicochemical properties, considering thermal conductivity, density, linear expansion, resistivity, thermal stability and magnetic permeability

04 p0618 A71-15570

Directional dielectric loaded waveguide antenna for probing electromagnetic field oscillations, discussing design and performance tests

04 p0560 A71-15880

Beam splitter prisms with dielectric multilayer coatings

06 p0907 A71-17534

Radiation pattern of narrow beam antenna using artificial dielectric medium with permittivity less than unity

06 p0868 A71-17741

Dielectric thin optical film waveguides excitation for integrated optical circuitry by Gaussian laser beams

07 p1123 A71-19213

Microwave noise generation by triboelectric charging of dielectric surfaces

07 p1063 A71-19932

Lightning protection for dielectric composites, analyzing damage from shock waves, vaporization pressure, magnetic forces and burning

07 p1021 A71-19942

Gain and radiation properties of phased array antenna with dielectric, using integral method

07 p1078 A71-20070

Heavy ion track registration in nonconductor minerals, discussing radiation damage and atomic species along trajectory

07 p1158 A71-20270

Infinitely long dielectric rod waveguide HE sub 11 surface wave mode launching efficiency, using Fourier integral

08 p1262 A71-20754

Dielectric loaded waveguide electromagnetic field and coupling matrix derivation by finite element computer program, presenting dispersion curves and field plots

08 p1262 A71-20765

Plane light wave interactions with moving dispersive dielectric medium, considering electron UV or ion IR resonant oscillation in regions of anomalous dispersion

08 p1253 A71-21278

Wideband microwave absorbing wall using dielectric material of foamed polystyrol powder coated with graphite, discussing design procedure and thickness reduction

08 p1253 A71-21297

Wide beam lens antenna synthesis from non-homogeneous dielectric with specified refractive index, using conformal mapping for lens and beam conversion

08 p1266 A71-21466

High Q factor rotor systems applications in dielectrics electromagnetic viscosity measurement and radio transmitters with low oscillation phase drift

09 p1492 A71-22363

High temperature ultraminiature pressure transducers, reviewing p-n junctions thermal limitations and thermal properties of dielectric oxides used with solid state epitaxially grown sensors

09 p1448 A71-22772

Artificial dielectric refractive index with diffraction allowance as function of multilayer geometry, wave frequency, polarization and propagation direction

09 p1406 A71-22884

Optical-electrical analogy of thermal radiation impedance of thin dielectric films in low temperature insulation

09 p1494 A71-23003

Electromagnetic wave propagation in circular waveguide loaded with coaxial dielectric cylinders, calculating band pass characteristics

09 p1406 A71-23039

Backscatter from nonuniform dielectric coated cylinders in terms of inner surface admittance, using transmission line approach

09 p1410 A71-23515

Cerenkov energy losses of rigid cylindrical uniformly charged bunch moving at constant speed through homogeneous isotropic dispersive dielectric

09 p1498 A71-23574

Lateral heat transfer along parallel conducting and radiating plates spaced by absorbing and isotropically scattering dielectric

[AIAA PAPER 70-849]

11 p1788 A71-25524

Variance and correlation radius of distortions from transparent dielectric plate, using statistical theory of antennas

11 p1738 A71-26348

Dielectric layer surface electric charge movement determination by measuring metal-insulator-semiconductor (MIS) capacity response at very low frequency

12 p1942 A71-26829

Microwave dielectric measurement system sensitivity to electric field energy in dielectric non-magnetic specimen

12 p1889 A71-27621

Electromagnetic backscatter cross section for HF irradiated turbulent dielectric media by rigorous and heuristic derivations

13 p2028 A71-27998

Circular waveguides containing pure dielectrics, examining propagation mode inversion criteria via TE and TM characteristic equations

13 p2037 A71-28606

Complex permittivity of spherical conducting particles in dielectric host medium, showing dependence of real and imaginary parts

13 p2038 A71-28611

Nonuniform trap distribution effect on I-V characteristics of dielectric diodes, allowing for field ionization

13 p2040 A71-28927

Dielectric loaded waveguides electromagnetic fields solution by finite element method for cutoff modes determination

14 p2212 A71-30509

Arbitrarily dimensioned microwave dielectric modules complex permittivity calculation

14 p2212 A71-30511

Plasma display panel with rectangular gas discharge cells array separated by thin dielectric sheets, discussing operation principles

14 p2249 A71-31030

Microwave wideband and multiband radome design for strength, environmental and electrical requirements, achieving transmission efficiencies with dielectric and wall thickness selection

14 p2216 A71-31037

Resonant excitation of thin film dielectric optical waveguide through supercritical layer by limited light beam with arbitrary amplitude-phase distribution

15 p2375 A71-31227

Electrical insulation failure in dielectric fluid layer due to electrocapillary instability, presenting critical potential difference approximate and exact calculation

15 p2376 A71-31932

Single mode ruby laser emission on transparent dielectrics, observing surface luminescence, free electrons production and adsorbed gases heating

16 p2585 A71-32797

Optimum pulse width and information carrying capacity for dielectric single mode glass optical waveguides under distortion due to attenuation and phase velocity dispersion

16 p2541 A71-33127

Optical filter characteristics obtainable with periodic stacks of two dielectric materials having commensurate optical thicknesses

16 p2577 A71-33128

Microwave IC bandpass filters, utilizing dielectric resonators for high Q values

16 p2548 A71-33559

Transparent polymer dielectric luminescence and destruction under Q switched laser radiation with subthreshold power and picosecond pulses

16 p2588 A71-33652

Microwave receiving and transmitting antennas proximity effects on permittivity measurements of dielectric layer

17 p2697 A71-34258

Low loss surface oriented waveguide for millimeter IC, using high permittivity rectangular dielectric image line

17 p2714 A71-34603

Radiation pattern of dielectric disk antenna, using computerized analysis of electromagnetic scattering and spherical volume cell

17 p2715 A71-34765

TE modes propagation in rectangular guide partially filled with dielectric slab, considering two waveguides junction equivalent circuit

17 p2708 A71-35481

Densely packaged microelectronics thermal control, using immersion cooling in dielectric fluids

17 p2718 A71-35786

Dielectric potential operator as arbitrary bounded Lebesgue measurable set, obtaining eigenvalues and eigenfunctions spectrum

18 p2942 A71-36820

Optical coupling of degenerative modes in two parallel dielectric waveguides, applying to slab guides and fibers crosstalk problem

19 p3014 A71-37214

Microwave reflection from semiconductor wafers with dielectric film, presenting electromagnetic field parameters as function of electrophysical properties

19 p3117 A71-37264

Dielectrophoresis force measurements and wedge shaped capacitor separation properties in satellite zero gravity conditions

19 p3103 A71-37278

Wave diffraction at step junction of two rectangular waveguides and symmetrical diaphragm with dielectric fillers

19 p3019 A71-38332

Nonreflecting dielectric support washers design in coaxial-stripline junctions, calculating VSWR as function of dimensions and frequency

19 p3019 A71-38335

Linear antenna in anisotropic plasma, calculating reactance change with surrounding dielectric layer thickness with allowance for ion depletion

20 p3204 A71-39142

Capacitive thermometry characteristics of dielectric crystallized titanate-containing glass ceramic at cryogenic temperatures

20 p3253 A71-39279

Narrow flare angle low permittivity conical dielectric waveguide antenna, examining radiation patterns and propagation characteristics by approximate theory

20 p3196 A71-39380

Thin dielectric films on germanium substrates, using oxygen diffusion through silicon dioxide

20 p3205 A71-39435

Normal emission factors of dielectric materials at 1000-1500 C, using black bodies in study of thermal radiation of refractory materials

20 p3254 A71-39960

Electromagnetic stress gage for wave propagation study in nonconducting materials, discussing calibration, design and accuracy

21 p3379 A71-40793

Hollow dielectric waveguide gas laser with He-Ne mixtures at 6328 A

21 p3393 A71-41040

Nonuniform trap distribution effect on I-V characteristics of dielectric diodes, allowing for field ionization

21 p3358 A71-41325

Dielectric articles thickness and flow control by microwave magic tee junction waveguide, describing instrument design and operating characteristics

22 p3521 A71-41772

Pyroelectric IR detectors performance, investigating strontium barium nitrate, lithium sulphate and triglycine sulfate materials effects on frequency range and sensitivity

22 p3542 A71-42122

Radiation patterns of dielectric rod antennas with axial emission in near field

22 p3521 A71-42270

Wave diffraction by air gap multilayered dielectric coated sphere with azimuthal slot for low loss transmission, obtaining radiation pattern

22 p3522 A71-42283

Ideally conducting and dielectric coaxial bodies of revolution, investigating joint excitation by TM wave

22 p3522 A71-42304

Ferrite and dielectric element waveguide phase shifters with rectangular hysteresis loop, deriving differential phase and attenuation constants for wave propagation

22 p3512 A71-42308

Spheroid with two dielectric separated halves and mixed boundary conditions, determining spreading currents Lf electromagnetic field

22 p3484 A71-42879

Laser radiation destruction of transparent dielectrics, proposing electronic excitations conversion to heat and thermal explosion

23 p3682 A71-42891

Heating dynamics of transparent dielectrics exposed to pulsed laser beam operating in free laser mode

23 p3683 A71-43270

Thin film oxide, ferroelectric and bismuth titanate dielectrics for high capacitance microwave IC technology

23 p3651 A71-43429

Quasi-optical waveguide system for measuring electrical properties of dielectric and magnetic materials in submillimeter band

23 p3677 A71-43530

Far field radiation patterns of axially oriented point current sources in presence of dielectric circular cylinders, developing solutions via plane wave scattering

23 p3654 A71-44160

Numerical solution for plane wave scattering by dielectric sheet with imbedded periodic array of conducting strips

23 p3654 A71-44164

Critical frequencies of higher order modes in circular waveguides with arbitrary thick dielectric sleeve

23 p3647 A71-44319

Nonmagnetic dielectric artificial birefringence determination, using permittivity additivity with bivalent symmetrical tensor

24 p3877 A71-44408

Electromagnetic scattering solutions for inhomogeneous dielectrics as power series, using multipoles for far field determination

24 p3847 A71-44427

Electromagnetic wave propagation in radially and axially nonuniform dielectric media, using geometric optics approximation

24 p3848 A71-44976

Reflection coefficient of multimode laser beam from dielectrics interface

24 p3833 A71-45044

Plane TEM wave propagation in free space using rectangular waveguide partially filled with two dielectric slabs

24 p3809 A71-45093

Dielectrics breakdown under ultrashort neodymium laser pulses at fundamental and second harmonic frequencies

24 p3834 A71-45120

DIENES

NT BUTADIENE

DIES

Ti alloys isothermal forging, using precision-cast superalloy dies

[SME PAPER MF-70-122] 01 p0089 A71-11255

Hot forming/die quenching of aluminum and titanium alloy integrally stiffened panels

[SME PAPER EM-70-178] 01 p0089 A71-11259

Ni and Fe alloys for tooling materials, examining die life and wear at elevated temperatures

[SME PAPER MF-70-121] 01 p0090 A71-11266

Closed die forgings for aircraft industry, discussing technology, tolerances, materials and costs

07 p1119 A71-20075

Extrusion tools development since 1930, emphasizing economic aspects

14 p2253 A71-30470

Unsteady press forging process in dies with material extrusion through plane strained slot, describing deformation stages, slip line patterns and hodographs

16 p2581 A71-32818

Aluminum bronze alloy forming dies fabrication and repair, discussing surfacing, hot working grinding, machining and welding methods

18 p2928 A71-36855

DIESEL ENGINES

Turbocharged diesel engine precompressed inlet air cooling by evaporation cooling, considering water injection effects on centrifugal compressor

08 p1347 A71-20781

Performance test facility for pulsed axial flow gas turbine of turbocharger unit on large diesel engines

15 p2469 A71-31943

Optimal design for noise attenuation by diesel engine exhaust mufflers using linearized acoustic models

20 p3268 A71-38961

DIETHYL ETHER

Dog cardiac output measurement by using ethyl ether dissolved in saline solution as indicator, comparing to Fick method results

06 p0856 A71-18389

Manometric apparatus determining solubility of inert gases in water, blood and other liquids, establishing partition coefficients of ethyl ether

06 p0862 A71-18390

DIETS

Diet effects on hepatic fatty acid synthesis in rats and mice, noting linoleate content role

01 p0011 A71-10848

Mortality of myocardial infarction patients on diet low in saturated fats and cholesterol

01 p0015 A71-11299

Immunological reactivity of human body during 120 day feeding on dehydrated diet

06 p0861 A71-18368

Soyuz 9 spacecraft crew food diet description including products and packaging

09 p1397 A71-22205

Solid and liquid diets during thiamine deficiency, noting hunger dependence on novelty

13 p2011 A71-28808

Soviet book on aviation medicine covering human anatomy and physiology, atmospheric physics, flight effects, respiratory systems, crew diets, etc

14 p2188 A71-29943

Mitotic response to various diets in normal and regenerating rat liver

14 p2182 A71-30069

Human adaptation to high altitude, considering effects of physical preconditioning, exercise, high carbohydrate diets and normal food intake maintenance

18 p2859 A71-36867

Dietary effects of formose sugars ingestion, investigating toxic mechanisms involved

19 p3011 A71-37573

Food utility calculation for various formose sugar treatments as valid qualitative measure of relative effects of dietary materials

19 p3007 A71-37575

Humans under constant diet feeding in closed ecological system, demonstrating instability in elimination process of various elements

22 p3506 A71-42817

DIFFERENCE EQUATIONS

Dynamic fault detection, using mathematical condition between measurement taken, difference equation theoretical coefficients and bounds of each

03 p0449 A71-13092

Numerical solution of Laplace difference equations for circular and irregular annulus

04 p0619 A71-14811

Round cylinder in viscous fluid asymmetrically disturbed flow, calculating dynamic and temperature conditions with difference method

04 p0571 A71-15492

Turbine machine elements approximation by difference equations of axisymmetrical elasticity theory problem

04 p0671 A71-15644

Error estimation for algorithms identifying linear systems described by higher order scalar difference equation

06 p0877 A71-17329

Convection schemes finite difference formulation for nonlinear instability prevention by absolute spatial conservation rather than flux form

06 p0917 A71-17552

Difference scheme for solution of static boundary value problem differential equations of elasticity theory

07 p1211 A71-19181

Identification algorithm for linear discrete time systems difference equations with input-output measurements coefficients

10 p1586 A71-24737

Multistage two player zero-sum games with state determined by difference equations, deriving optimal strategy pair satisfying saddle point condition

10 p1637 A71-24842

Difference equations derivation for flat plates plane stress extension as localized Ritz process, providing common classification of finite difference and finite element methods

13 p2147 A71-27784

Numerical solution of Stefan type partial differential equations with phase variations, using nonlinear homogeneous implicit difference scheme

13 p2100 A71-27898

Second order difference approximations with large viscosity coefficient for primitive barotropic model over spherical geodesic grid, comparing with first order approximations

13 p2097 A71-28231

Two dimensional contact problem for isotropic body in triangle form on half plane, calculating elastic constants with difference Green function

13 p2156 A71-29071

Differential equations analytic theory - Conference, Kalamazoo, April-May 1970

13 p2096 A71-29422

Difference equations system trivial solution stability condition existence and uniqueness theorems

14 p2265 A71-29628

A priori bounds on linear and nonlinear quotients of Neumann boundary value problem for uniformly elliptic difference equations over rectangular regions

14 p2265 A71-30291

Sufficient stability of difference approximations for initial boundary value problems

15 p2441 A71-31354

Bogoliubov averaging method application to nonlinear stochastic systems described by ordinary and partial differential equations and differential-difference equations

15 p2449 A71-31829

Light beam diffraction by supersonic waves, calculating amplitudes with difference-differential equations

15 p2450 A71-32075

Difference analogs of Dirichlet problem for second order quasi-linear elliptic operators with mixed derivatives, using discretization method

15 p2442 A71-32312

Linear equations general form including difference, differential, deviating argument, aftereffect and integrodifferential equations

16 p2603 A71-33531

Invariant imbedding for two point boundary value problems for difference equations, noting conversion to initial value problem

17 p2764 A71-34519

Stress difference elasticity equations from photoelastic data and first stress invariant

[SESA PAPER 1780] 17 p2819 A71-34530

Laplace transform application to linear system of partial differential, integrodifferential and difference equations with periodic and quasi-periodic coefficients

17 p2780 A71-34911

Smooth solutions of functional and differential-difference equations in neighborhood of singular points with deviation of argument tending to zero
17 p2767 A71-34938

Digital phase locked loop for FM signals demodulation, considering system nonlinear difference equation
17 p2704 A71-35084

Difference analog of nonlinear hydrodynamic boundary value problem from Navier-Stokes steady state theory
17 p2728 A71-35241

Difference schemes for approximating system of one dimensional gas dynamics equations in Eulerian coordinates, taking into account mass conservation law and viscosity
17 p2729 A71-35370

Roundoff error reduction in numerical solution of second-order differential equation by splitting into two difference equations
17 p2769 A71-35691

Difference methods for hyperbolic flow equations, using third order accuracy space and time split difference operators
18 p2844 A71-36305

Laminar boundary layer flow analysis from nonlinear difference equations solution by Newton method, using block-tridiagonal factorization
18 p2905 A71-36313

Shock wave profile nonlinear one dimensional problems in gas dynamics, using monotonic difference scheme
18 p2907 A71-36333

Singularities of Euler equations in turbulent flow problems, studying design of difference schemes
18 p2907 A71-36335

Difference equations derivation for meteorological turbulent flow prediction, considering errors due to finite difference approximations
19 p3087 A71-38306

Error analysis for stable implicit difference methods for heat equation with derivative boundary condition
20 p3254 A71-38758

Neutral functional equation including scalar differential-difference equation, determining sufficient conditions for zero solution
20 p3254 A71-38899

Integrodifferential difference equation for isotropic portion of velocity distribution function resulting from electron excitation and Coulomb interaction
20 p3274 A71-39048

Thin elastic shell of revolution under asymmetric loads, calculating time dependent transient response with implicit backward and explicit central differencing schemes
21 p3467 A71-40960

Optimal control of time delay systems described by linear differential difference equations
23 p3658 A71-44087

Minimal order linear time-invariant systems description by smallest possible number of parameters, deriving differential or difference equations based on input/output parameters
24 p3816 A71-45122

Spatial characteristics based difference scheme application to axisymmetric problems of elastic wave propagation, allowing for solid or hollow circular cylinder boundary conditions
24 p3885 A71-45221

DIFFERENTIAL ALGEBRA
U DIFFERENTIAL CALCULUS
U MATRICES [MATHEMATICS]

DIFFERENTIAL AMPLIFIERS
Differential charge amplifier design using ferromagnetic high signal bandwidth isolation with grounded input transducer and output load
09 p1417 A71-22782

Low cost directly coupled differential amplifier with thermodynamic drift stabilization for biological studies
10 p1570 A71-24444

DIFFERENTIAL ANALYZERS
U ANALOG COMPUTERS

DIFFERENTIAL CALCULUS
Q approach to problem solving applied to partial derivatives determination on digital computer, discussing approach structure and characteristics
01 p0048 A71-10221

Fractional derivatives of Navier-Stokes equations weak solutions
10 p1636 A71-23913

Differentiation of maxmin function with respect to direction, analyzing theorems on differentiability
14 p2265 A71-29563

Differentiable random processes, deriving approximate determination of correlation functions
17 p2777 A71-34348

Nonlinear operators differentiation and integration, considering Gateaux and Frechet derivatives and Riemann integral
18 p2943 A71-36953

Nonlinear operators properties, considering differentials role in nonlinear functional analysis
18 p2943 A71-36954

Linear programs optimality conditions, using differential calculus approach to classical optimization theory in Danzig simplex algorithm development
19 p3086 A71-37548

Fundamental derivative γ and other thermodynamic variables in gas dynamics, considering transonic passage variation, Prandtl-Meyer wave, adiabatic flow and nonlinear wave propagation
22 p3530 A71-41887

DIFFERENTIAL EQUATIONS
NT BIHARMONIC EQUATIONS
NT BLASIUS EQUATION
NT BURGER EQUATION
NT CAUCHY-RIEMANN EQUATIONS
NT DUFFING DIFFERENTIAL EQUATION
NT ELLIPTIC DIFFERENTIAL EQUATIONS
NT FALKNER-SKAN EQUATION
NT FOKKER-PLANCK EQUATION
NT GAUSS EQUATION
NT HELMHOLTZ VORTICITY EQUATION
NT LIOUVILLE EQUATIONS
NT PARABOLIC DIFFERENTIAL EQUATIONS
NT PARTIAL DIFFERENTIAL EQUATIONS
NT POISSON EQUATION
NT VLASOV EQUATIONS

Gravitating particle system phase density, finding differential and integral equations for Fourier transform
01 p0150 A71-10064

Optimal prediction of stochastic differential equation solution with Gaussian member and small nonlinearity
01 p0110 A71-10098

Hybrid computers solution of linear differential equations, analyzing Taylor series /derivatives/ use for compensation
01 p0048 A71-10224

Medium length journal bearing pressure profiles, deriving ordinary differential equation for load capacity
01 p0086 A71-10300

Linear homogeneous nth order ordinary differential equations reduction to equations with constant coefficients by transformation of independent variables
01 p0110 A71-10317

Numerical integration finite difference methods stabilization for perturbed Keplerian motion differential equations
01 p0154 A71-10378

Poincare hydrodynamic analogy in celestial mechanics, relating differential equations for dynamic systems with two degrees of freedom and two and three dimensional flow
01 p0154 A71-10383

Space navigation variation problem, examining perturbation differential equation for semimajor axis and eccentricity and momentum and eccentric anomaly relationship
01 p0122 A71-10389

Lipschitz functional differential equations systems uniform asymptotic stability under diminishing perturbations
01 p0111 A71-10470

Differential equations systems construction from given integral manifold, deriving steady state functionals and stability conditions
01 p0111 A71-10487

Canonical transformations for method of variations applied to differential equations describing satellite orbit perturbations
01 p0156 A71-10544

Liapunov method applied to nonlinear differential equations for distant satellite orbit secular perturbations
01 p0156 A71-10546

Liapunov stability of neutral first order nonlinear differential equations solutions with time lag
01 p0112 A71-10655

Invariance in automatic control systems nonlinear differential equations of motion
01 p0064 A71-10730

Critique of Chapman-Kirk iterative method for differential equations yielding aerodynamic coefficients from free flight data
01 p0002 A71-10971

Nuclear reactor kinetic differential equations, ascertaining positive bounded solutions existence
01 p0126 A71-11290

Stability conditions of Liapunov function for system of ordinary differential equations with prescribed phase flow
01 p0113 A71-11294

Neutral and superneutral equations properties analysis and existence theorems, using successive approximation procedures
02 p0275 A71-11723

Nonlinear differential equations description in functional product form structure for digital simulation
02 p0226 A71-11781

Thermodynamic calculations simplification, using identical transformation of differential expressions
02 p0332 A71-12320

German monograph on polygonal thin plates calculation by differential equations method for two dimensional boundary value problems solution
02 p0327 A71-12399

Gravitation theory equations with higher order derivatives based on two point geometry, using differential equations systems
02 p0285 A71-12664

Initial value problems differential equations discontinuities, describing step-size adjustment for fourth order Runge-Kutta methods
02 p0277 A71-12728

Gradient /steepest ascent/ methods for differential equation systems optimization, discussing convergence acceleration and nonlinear programming
02 p0277 A71-12729

Linear ordinary differential equations system with random coefficients, proving mean stability theorem
03 p0450 A71-13119

Thermodynamical theories and differential equations of thermoelasticity, generalizing energy and variational theorems
03 p0501 A71-13127

Differential equations of thermodynamics presentation to engineering students in form suitable for programmed study
03 p0518 A71-13526

Differential equations of spherical motion of heavy solid body with ellipsoidal cavity filled with liquid, deriving stationary solutions
03 p0457 A71-13586

Two-point boundary value problems for linear differential equation systems, describing adjoints and complementary functions methods
03 p0451 A71-13624

Inhomogeneous elasticity theory under spherical symmetry, using linear differential equations transformation into constant coefficient equations
03 p0507 A71-13714

Characteristic exponents for linear differential equations with periodic coefficients, using recurrence multipliers suitable for computer
03 p0451 A71-13786

Nonlinear systems near steady state oscillation transient behavior analysis by linear differential equations with periodic coefficients
03 p0451 A71-13817

First order nonlinear nonautonomous systems equivalence to second order linear autonomous systems through governing differential equations variables integral transformation
03 p0390 A71-14076

Three dimensional mixed boundary value problems, obtaining solutions for elastic body differential equilibrium equations
03 p0513 A71-14235

Single axis gyroscopic stabilizer with floating type integrating gyro, describing natural oscillations by differential equations of motion
03 p0429 A71-14237

Polymer materials linear photo creep characteristics description in terms of differential and integral equations, discussing relationship between optical and mechanical properties
03 p0514 A71-14357

Time optimal control for system described by linear differential equations, discussing two-step sequential synthesis
03 p0392 A71-14407

Nystrom formula error estimation for numerical integration of first order differential equation, tabulating results
04 p0619 A71-15448

Heat transfer differential equations numerical solution, using latin square experimental design plans for reducing repetitions
04 p0678 A71-15461

Semiempirical differential equation derived for turbulence scale behavior and turbulent boundary layer on flat plate
04 p0575 A71-15606

Closed system of differential equations derived for kinematic characteristics of turbulent flow in pressurized smooth pipe
04 p0575 A71-15608

N person nonzero sum differential games with linear dynamics, proving existence of equilibrium strategies
04 p0620 A71-15864

Linear functional differential equations trajectory optimization, proving maximal principle
04 p0620 A71-15866

Neutral functional differential equation solution operator properties
05 p0773 A71-15972

Arbitrary surface gravitational potential function normal derivative determination, using Tikhonov regularization method for obtaining integrodifferential equation
05 p0739 A71-16421

Variational principle for generalized theory of heat conduction with finite wave speed, reducing nonlinear boundary value problem to ordinary differential equation
05 p0837 A71-16567

Schwarz differential invariant in Kepler problem, describing point motion under Newtonian force effect
05 p0811 A71-16640

Finite difference and initial value solutions of nonlinear boundary problems for ordinary differential equations, generating algorithms by quasi-linearization method
05 p0775 A71-16646

Differential equations system continuability theorem for specific initial conditions
05 p0775 A71-16885

Two-point boundary value problems approximation for differential equation systems with discontinuity in right-side derivatives
05 p0775 A71-16886

Sufficient conditions for differential game encounter
05 p0782 A71-16976

Differential games with information lag, considering pursuit problems and capture conditions
05 p0782 A71-16980

Differential game of convergence, constructing extremal strategy for ensuring motion encounter with given set
05 p0783 A71-17011

Differential descent method modifications, comparing convergence rates and insensitivity to computer computational errors
05 p0775 A71-17012

Dynamic relaxation method for solving simultaneous linear differential equations, comparing asymptotic rate of convergence with degenerate Chebyshev approximation
05 p0776 A71-17122

Initial value problems involving linear ordinary differential equations, deriving theorems for Runge-Kutta and Adams methods effectiveness
06 p0917 A71-17566

Differential operator determination in spectral analysis of inverse problem stability
06 p0865 A71-17582

Advances in differential and integral equations - Conference, University of Wisconsin, August 1968
06 p0918 A71-17637

Equilibrium points and periodic orbits, using qualitative theory of autonomous functional differential equations
06 p0927 A71-17639

Branching of periodic solutions of second order nonlinear ordinary differential equations similar to Duffing equation
06 p0918 A71-17643

Iteration method application to shell design nonlinear differential equations solution
06 p0988 A71-17777

Axissymmetric isotropic shells of revolution, using matrix-operator notation for differential equations systems solution
06 p0995 A71-17835

Two countable systems of differential inequalities, applying to stability of feedback controls synthesizing equilibrium solutions to linear quadratic differential games
06 p0919 A71-18198

Approximation theory applications to differential and integral equations, considering nonlinear Chebyshev method in connection with hyperbolic and heat transfer equations
06 p0919 A71-18207

Neutral functional differential equations, discussing forward and backward continuation
06 p0921 A71-18239

Differential equations derivation for metal fatigue point defect colonies concentration changes, discussing diffusion and dislocation interactions
06 p1002 A71-18418

Optimal vacuum rocket trajectories over spherical earth, deriving nonlinear differential equations for position and velocity
06 p0976 A71-18487

Computer graphic search for stiffly stable methods of high orders for ordinary differential equations
07 p1067 A71-18738

Orientation vector differential equation formulation for strapdown inertial navigation, applying to rigid body rotation problem
07 p1154 A71-18832

Soviet papers on special problems of differential equations and functions theory covering approximation, complex variables, integral operators, etc
07 p1146 A71-19038

Trajectory optimization, using Pontryagin maximum principle for differential inclusions
07 p1146 A71-19178

Difference scheme for solution of static boundary value problem differential equations of elasticity theory
07 p1211 A71-19181

Linear ordinary differential equation systems first order output sensitivity coefficients generation and application to second order cross sensitivities
07 p1148 A71-20416

Two nonlinear coupled second order differential equations finite difference solution, using nonsquare and nonuniform grids for minimum error
07 p1149 A71-20612

Boundary value problem solution of nonlinear differential equation system with delayed arguments
07 p1149 A71-20644

Book on numerical solution of ordinary differential equations covering integration algorithms, Runge-Kutta, single-step, multistep, predictor-corrector and extrapolation methods
08 p1324 A71-21233

Self oscillatory system behavior under sinusoidal external force, using nonlinear differential equations transformation
08 p1334 A71-21292

Complex hydrodynamic systems nonlinear differential motion equations integration, taking friction forces into account
08 p1299 A71-21620

Surface station pressure reduction to sea level, determining differential expression by least squares method
08 p1329 A71-21727

Boundary value problems solution, using Runge-Kutta method with computer for eigenfunctions of ordinary differential equations
09 p1484 A71-22177

Nontrivial expansion of rigid surface infinitesimal motions into analytical bendings, deriving differential equations system for n-order bendings of singly connected continuously differentiable surface
09 p1535 A71-22211

Unknowns elimination from partial linear equations system with constant coefficients, applying to differential equations for bending transversely isotropic plate under normal external load
09 p1535 A71-22257

Mode conversion in inhomogeneous plasma, discussing conservation laws relationships to differential equation invariants
09 p1501 A71-22535

Lie group differential equation application to gravitation theory, rejecting Riemann geometry in favor of Klein geometry
09 p1495 A71-23073

Asymmetric buckling of spherical caps with asymmetrical imperfections, using nonlinear relaxation technique for treatment of finite difference representation of differential equations
09 p1541 A71-23090

Celestial mechanics, discussing fourth order linear differential equation for Hansen coefficients
09 p1486 A71-23340

Soviet papers on differential equations and application covering control and system stability, elastic theory, boundary value problems, etc
09 p1495 A71-23428

Differential equations system theorems for conditions of solution stability in presence of large initial perturbation
09 p1495 A71-23429

Two-differential equations system in critical case of double zero root, deriving motion stability criteria with aid of Liapunov functions
09 p1495 A71-23430

Differential equations construction for controlled systems and controller starting from programmed motion stability requirement
09 p1495 A71-23432

Conformally variable body, formulating differential equations of motion in moving coordinate system using Hamilton-Ostrogradskii form of least action principle
09 p1495 A71-23434

Heat conduction differential equation boundary value problem, obtaining closed solution to Cauchy problem in integral form with finite limits by reflection method
09 p1547 A71-23435

Conservative systems of differential equations with single degree of freedom, considering periodic solutions existence, determination and stability
09 p1495 A71-23436

Ordinary differential equations invariance properties, considering applications to stability problems
09 p1486 A71-23470

Linear differential equations stability analysis by implicit functions applied to resonance phenomena, using Weierstrass theorem
09 p1640 A71-23803

Small parameter method in gyrocompass theory, deriving differential equations for motion of sensitive element of two rotor gyrocompass
09 p1608 A71-23804

Numerical integration of perturbed linear systems of differential equations by step method comparing power series
09 p1636 A71-23960

Proof theorem for Chaplygin successive approximations method, presenting lemma for convergence of solutions to differential equations system
09 p1636 A71-24021

Nonlinear second order differential system two point boundary problems, establishing eigenvalues and associated solutions boundedness and oscillations
10 p1636 A71-24130

Asymptotic stability trajectories and entering theorem of third order real nonlinear autonomous differential equations near critical point
10 p1636 A71-24131

One dimensional linear stationary systems described by linear differential equations, discussing identification procedure with transformation into integral equations
10 p1585 A71-24157

Ionospheric irregularities two fluid model, using nonlinear differential equations for longitudinal waves propagating in hot collisional magnetoplasma
10 p1648 A71-24294

Necessary and sufficient controllability conditions for linear nonstationary system with deterministic inputs described by two differential equations
10 p1586 A71-24387

German book on optimization for variational problems with ordinary differential equations as secondary conditions
10 p1636 A71-24480

Spherical harmonics differential approximation generalized from one dimensional radiation specific intensity angular dependence Jacobi polynomial expansion
10 p1696 A71-24536

Reducible parametric systems of second order linear differential equations with variable coefficients for FM or AM-FM oscillations and Riccati equations
10 p1586 A71-24712

Nonstationary linear systems analysis over finite time interval and graphical method for differential equation, comparing exact and approximate solutions for free oscillations
10 p1643 A71-24908

Radiative transfer in nongray gas with local molecular and slightly disturbed radiative equilibrium, deriving linearized differential equation with application to radiatively driven acoustic waves
10 p1697 A71-25065

Weber differential hydrodynamic equations with earth rotation allowance related to Bjerknes circulation theorem and Ertel variational principle of atmospheric dynamics
10 p1607 A71-25111

Magnetic field effects on plane wave propagation in plasma, reducing motion data problem to vectorial differential equation with mean electronic velocity as only unknown
11 p1804 A71-25174

Numerical methods solutions of implicit differential equations systems, discussing first order implicit to second order explicit systems transformation
11 p1791 A71-25640

Comet orbits correction, including differential coefficients perturbations based on Kuiklov equation for difference between computed and true radius vector
11 p1833 A71-26328

Asymptotic solution of second order nonlinear differential equation for autonomous nonlinear resonance system
11 p1743 A71-26536

Statistical estimation in monitoring and control systems analysis, discussing algorithm construction for computer solution of nonlinear differential equations system
12 p1891 A71-26724

Transient characteristics of MOS channel transistors, solving nonlinear differential equations describing current and potential distribution
12 p1886 A71-26850

Equivalence relationship between state space defined parameter and difference order of time-variable scalar differential equation
12 p1922 A71-27006

Asymptotic solutions for system of nonlinear quasilinear type differential equations for gyroscopic couplings
12 p1923 A71-27170

Critical stability solutions to ordinary second order differential equations including holomorphic functions with series expansions
12 p1930 A71-27238

Theorems of instability for differential equation in linear normalized spaces, using Liapunov second method
12 p1930 A71-27239

Elastic laminated plates with various thickness layers, deriving independent differential equations for displacement
12 p1978 A71-27334

EM wave scattering in waveguide by active regular shape bodies, using integrodifferential equations
12 p1881 A71-27337

Natural frequencies of finite circular cylinders in axially symmetric longitudinal vibration, using Rayleigh-Ritz method to derive differential equations for expansion functions coefficients
12 p1981 A71-27482

- Kane-Mindlin differential equations solved by perturbation techniques for free extensional vibrations in elastic plates 12 p1981 A71-27483
- Optimally controlled boundary layer equations reduction to ordinary differential equations 12 p1898 A71-27490
- Saddle point type differential game problem structure, determining optimal player strategies for fixed point termination 12 p1931 A71-27521
- Differential guidance game with aftereffects, investigating extremal strategies 12 p1931 A71-27522
- Contact stress between half plane and elastic cover plate, reducing problem to Prandtl type integrodifferential equation with Hilbert kernel 12 p1982 A71-27526
- Differential equations for wave propagation in irregular electromagnetic waveguides 12 p1888 A71-27530
- Numerical solution of implicit first order ordinary differential equations with initial conditions 12 p1923 A71-27731
- Inhomogeneous plasma, describing linear wave transformation with fourth order differential equation with variable coefficients 12 p1942 A71-27768
- Optimal control systems with discontinuities in right members of differential equations, considering solution to Cauchy problem 13 p2040 A71-27896
- Hill-Brown differential equations for satellite coordinates transformed for integration with analytical programming language 13 p2135 A71-28352
- Analytic theories in celestial mechanics, checking by exact differential equations form based on Von Zeipel method 13 p2135 A71-28353
- Adaptive automatic control systems, determining damping coefficient and natural oscillation frequencies with second order differential equations 13 p2041 A71-28639
- Optimal linear feedback for systems governed by differential operational equations, considering stochastic control and cost function 13 p2095 A71-28814
- Optimal control problems solution using linear vector space of continuous operators with constraints in Volterra integral and functional differential equations 13 p2043 A71-28829
- Cylindrical shells of revolution with various boundary conditions, calculating free vibrations with differential equations 13 p2156 A71-29067
- General adjoint relation between linear functional differential equations and Volterra integral equations 13 p2096 A71-29381
- Differential equations analytic theory - Conference, Kalamazoo, April-May 1970 13 p2096 A71-29422
- Fluctuations in numerical computations of discontinuous solutions of differential equations 14 p2265 A71-29556
- Group-invariant properties of boundary layer flow differential equation for electrically conducting liquid in magnetic field 14 p2279 A71-29629
- Nonlinear differential equations system for one degree of freedom isochronous and anisochronous conservative oscillators resonance behavior during natural perturbation solved by coordinate transformations 14 p2265 A71-29687
- Dynamic systems conservative by bits and governed by differential equation with discontinuous second member, obtaining limiting cycle existence condition 14 p2265 A71-29691
- Celestial mechanics relationship to astronomy, establishing differential equations of earth rotation in relation to terrestrial mantle 14 p2306 A71-29703
- Approximate method for nonlinear ordinary differential equations with variable coefficients applied to cylinder oscillation and flexible ring deformation 14 p2324 A71-29881
- Differential rotational equations of motion for triaxial rigid body about center of mass under arbitrary torque 14 p2307 A71-29882
- Hybrid binary floating point digital differential analyzer technology, noting speed, cost and utility 14 p2207 A71-30021
- Differential equation describing nonstationary reflection of symmetrical shock front from spherical and cylindrical blunt bodies 14 p2170 A71-30216
- Two spheroid rigid bodies rotational and translational motion, using linear and Hill type differential equations for angular variables and coordinates 14 p2312 A71-30384
- Parametric differentiation technique for axisymmetric stability of spherical shells, using Reissner nonlinear differential equations 14 p2329 A71-30506
- Nonlinear ordinary first order differential equation solution for mechanical system motion, constructing asymptotic representation 14 p2266 A71-30838
- Liapunov stability of neutral first order nonlinear differential equations solutions with time lag 14 p2266 A71-30989
- Differential equation systems optimal scaling for analog computer, proposing amplitude and time scaling factors and disposition parameters with linear programming 15 p2440 A71-31155
- Pulsating follower loads implementation by pulsating gas or liquid jets, using Mettler differential equations for forced vibrations of elastic bodies 15 p2502 A71-31172
- Asymptotic error expansions of differential equations approximate solutions by finite difference schemes for use as technical devices in theoretical numerical analysis 15 p2440 A71-31347
- Averaging of nonlinear integrodifferential equations, demonstrating uniform convergence of sequence by successive approximations 15 p2442 A71-31521
- Degree of closeness estimates for initial and averaged systems of differential and integrodifferential equations with conditions on right members 15 p2442 A71-31523
- Bogoliubov averaging method application to nonlinear stochastic systems described by ordinary and partial differential equations and differential-difference equations 15 p2449 A71-31829
- Zero solution stability of nonlinear system of differential equations with constantly acting perturbations 15 p2449 A71-31830
- Collocation method application to linear boundary value problems for system of differential equations 15 p2442 A71-31831
- Existence and uniqueness theorem for n-point boundary value problems of nonlinear ordinary differential equations, using Polya condition 15 p2442 A71-31871
- Light beam diffraction by supersonic waves, calculating amplitudes with difference-differential equations 15 p2450 A71-32075
- General solution of cylindrical fourth order differential equation with zero index representing circular disk and ring plate problems in elasticity theory 16 p2602 A71-33400
- System of n plus 1 differential equations with right members in coordinate origin neighborhood represented by holomorphic functions of dependent variables 16 p2603 A71-33530
- Linear equations general form including difference, differential, deviating argument, aftereffect and integrodifferential equations 16 p2603 A71-33531
- Matrix trace method for identities relating eigenvalues of singular ordinary differential operators and zero Bessel functions 16 p2603 A71-33593
- Uniqueness theorem for second order differential equation associated with inverse problem of spectral analysis, developing operator transformation procedure 16 p2603 A71-33890
- Kolmogoroff differential equations for probabilities of system states, showing validity for Markovian random processes and processes with aftereffects 16 p2603 A71-33891
- Nonhomogeneous media electrodynamics, solving nonstationary equations by differential operators dependent on permittivity and permeability 17 p2776 A71-34277
- Limit cycle of nonlinear oscillations of third order differential equations dependent on Euclidean phase space with central restoring control force 17 p2763 A71-34293
- Fourth order differential gravitational field equations for non-Einsteinian cosmological model, considering linearly expanding universe 17 p2801 A71-34634
- Generalized ordinary nonlinear differential equations, considering systems with impulses acting on surfaces 17 p2764 A71-34639
- Differential equations optimization method based on auxiliary functional and minimization at simple structure manifold 17 p2765 A71-34849
- Optimal extrapolation and filtration for class of random processes, considering functionals of solutions of stochastic differential equations 17 p2765 A71-34863
- Asymptotic formulas for two point boundary value problem of differential equations system, using averaging method 17 p2765 A71-34905
- Integration method for second order nonlinear differential equation describing vibrational processes in mechanics, physics and engineering 17 p2766 A71-34913
- Statistical theory of nonlinear differential equation system with discontinuous trajectory solution, deriving motion stability to first approximation using Liapunov functions 17 p2780 A71-34915
- Free and forced nonlinear oscillations differential equations approximate solution by orthogonal polynomial linearization, applying method to systems analysis near singular points 17 p2780 A71-34917
- Periodic solutions of singularly perturbed hereditary systems of ordinary nonlinear integrodifferential equations 17 p2780 A71-34920
- Functional analytic methods for periodic and quasiperiodic solution of differential equations in nonlinear oscillation theory 17 p2780 A71-34921
- Linear differential equations solutions stability in Banach space for finite and infinite dimensional cases, generalizing Liapunov theorems 17 p2781 A71-34922
- Averaging methods of nonlinear differential and integrodifferential equations with fast and slow variables over finite and infinite segments 17 p2766 A71-34923
- Oscillatory systems motion by nonlinear differential equations with variable coefficients 17 p2781 A71-34924
- Periodic solutions for strongly nonlinear differential system of n-coupled nonautonomous equations of Lienard and Rayleigh types 17 p2766 A71-34925
- Nonlinear differential equation system periodic solutions in terms of uniformly converging periodic functions sequence 17 p2781 A71-34927
- Stroboscopic method of differential equations transformation, considering application to linear and nonlinear Mathieu equations 17 p2781 A71-34928
- Steady oscillation frequencies in systems described by nonlinear differential equations, including external perturbations 17 p2782 A71-34931
- Linear differential equations system with periodic coefficients, determining solutions by stationary components matrix location on complex plane 17 p2766 A71-34933
- Periodic solutions existence for autonomous system of ordinary differential equations, modifying parameter functionalization of vector fields in phase spaces 17 p2766 A71-34934
- Smooth solutions of functional and differential-difference equations in neighborhood of singular points with deviation of argument tending to zero 17 p2767 A71-34938
- Linear neutral differential equation uniform asymptotic stability relation to perturbed differential equation containing bounded linear operators 17 p2767 A71-35523
- Soviet book on ordinary differential equations covering basic concepts, existence and uniqueness theorems, linear homogeneous and nonhomogeneous equations with constant coefficients, etc 17 p2768 A71-35626
- Reynolds differential equations for three dimensional gas lubrication flows, noting linear velocity at rotating cylinder surface 17 p2749 A71-35639
- Friction forces in complex hydrodynamic systems nonlinear differential motion equations integration 17 p2749 A71-35680
- Roundoff error reduction in numerical solution of second-order differential equation by splitting into two difference equations 17 p2769 A71-35691
- Bounded integral manifolds existence for perturbed system of nonlinear differential equations near critical point, periodic orbit or periodic surface 17 p2769 A71-35795
- Monograph on nonlinear first order differential equations adjunction fields and solutions asymptotic behavior, seeking adjoinable solutions 18 p2940 A71-36098
- Digital computers for analytic solution of second order nonlinear ordinary differential equations 18 p2884 A71-36142
- Unstable two point boundary value problems solution by decomposition into lower order differential equations sequence for computer integration, giving illustrative examples 18 p2940 A71-36143
- Time ordering operators applications to nonlinear unsteady systems, covering stochastic differential

equations solution and phase locked loop phase error probability density calculation

18 p2940 A71-36222

Asymptotic approximations to Emden nonlinear differential equations of astrophysics for polytropic gas spheres, using multiple scale technique

18 p2941 A71-36226

Lower bound on distance between vertical asymptotes of second order differential equations solutions involving integral inequality

18 p2941 A71-36227

Book on stability theory covering Liapunov functions, variable structure automatic control systems and differential equations solutions in Banach space

18 p2947 A71-36250

Two dimensional flow of non-Newtonian fluids with rigid spherical substructure, solving linear coupled ordinary differential equations for spin and velocity field [ASME PAPER 71-APM-N]

18 p2926 A71-36257

Numerical solution of time dependent incompressible flow differential transport equations including turbulence effects

18 p2905 A71-36312

Stefan problem reduction to order n differential flow equation solution using Runge-Kutta method

18 p2947 A71-36314

Generalized relaxation methods application to transonic flow problems, combining with numerical integration theory for ordinary differential equations

18 p2906 A71-36324

Local error estimators comparison for Runge-Kutta method in production code design for ordinary differential equations numerical solution

18 p2941 A71-36353

Finite difference approximation application to linear two-point boundary value problem differential equation for testing finite point suitability for infinity before computation

18 p2941 A71-36354

Frictionless hypersonic flows by transforming partial differential equations into ordinary, noting detonation wave analogy

18 p2846 A71-36424

Sufficient conditions for differential game encounter, considering conflict controlled motion guidance onto given set

18 p2947 A71-36776

Differential games with information lag, considering pursuit problems and capture conditions

18 p2948 A71-36780

Swirling flow problem in boundary layer theory, proving existence theorem and asymptotic formula for differential equations solution

18 p2910 A71-36815

Complementary variational principles, noting application to differential, integral and matrix equations

18 p2943 A71-36957

Differential games with deviation from encounter, considering strategies for continuous, programmed and discontinuous control classes to bring motion to given set

19 p3103 A71-37093

Longitudinal instability of bunch interacting with passive resonator, considering Landau damping influence by linear differential equations of motion solution

19 p3110 A71-37141

Optimal control of linear time varying neutral system, solving differential equations set

19 p3037 A71-37238

Closed loop control of nonlinear systems in potentially large neighborhood of nominal trajectory, reducing nonlinear differential equations to related canonical linear form

19 p3037 A71-37239

Autonomous two dimensional system with given trajectory and singular points, describing differential equations construction

19 p3085 A71-37350

Time averaging with variable period for ordinary differential equations, proving existence of unified analytical solutions

19 p3085 A71-37385

Stability theorem for predictor-corrector methods for differential equations systems solution using computer

19 p3085 A71-37421

Optimization problems for control processes described by ordinary differential equations, solving by variational methods

19 p3086 A71-37555

Noniterative scheme for treating two-point boundary value problems for single and multipoint linear constant systems, requiring solution of 2n differential equations

19 p3086 A71-37559

Plasma potential differential measuring method, using emitting and cold probes for simultaneous current data

19 p3112 A71-37638

Nonlinear differential equations and boundary conditions describing behavior of electrically polarizable finitely deformable heat conducting continuum interacting with electric field

19 p3118 A71-37793

Transient simultaneous conductive and radiative heat transfer in plane gray layer bounded by black walls, yielding nonlinear integrodifferential equation [ASME PAPER 71-HT-22]

19 p3165 A71-37993

Signal propagation in model neuron network in terms of differential equations system, representing retina major cell types in planar model

19 p3003 A71-38276

Latin square factorial design plans for reducing number of repetitions solutions of theoretical problems, noting application to differential equations numerical solution

19 p3087 A71-38290

Constant coefficient linear systems sensitivity functions computational procedure using nth order differential equations linear transformations

19 p3039 A71-38714

Compiler program generation for ordinary differential equations system automatic numerical solution by Taylor series method

20 p3254 A71-38754

Critical time calculation for singularity in solutions of homogeneous nonlinear hyperbolic differential equations with smooth initial data, discussing application examples

20 p3254 A71-38790

Free and forced nonlinear vibrations of rigidly clamped thin circular plate, deriving ordinary differential equations

20 p3307 A71-38795

Vibrational behavior of nonlinear systems subjected to finite duration pulse excitation, transforming original differential equation into Lighthill method solvable form

20 p3267 A71-38798

Van der Pol equation periodic solutions using approximation scheme for all Fourier amplitudes

20 p3254 A71-38800

Neutral functional equation including scalar differential-difference equation, determining sufficient conditions for zero solution

20 p3254 A71-38899

Linearized unsteady gas dynamic differential equation, obtaining parameter characteristics from boundary values

20 p3211 A71-39032

Integrodifferential difference equation for isotropic portion of velocity distribution function resulting from electron excitation and Coulomb interaction

20 p3274 A71-39048

Nonlinear second order differential equations periodic solutions in terms of Fourier series, applying method to calculation of charged particle orbit in radial electric field

20 p3255 A71-39081

Error bounds and variational principles for nonlinear differential and integral equations, exemplifying by Liouville and Poisson-Boltzmann equations

20 p3255 A71-39496

Liapunov functions application to Stability of systems described by nonlinear second-order ordinary differential equations, considering feedback control loops construction

20 p3255 A71-39499

Generalized Riccati equation reduction to integral equation, leading to asymptotic solution of second order linear differential equations

20 p3255 A71-39574

Asymptotic geometric optics methods application to thin shell theory, reducing transport equation to ordinary differential equation

20 p3310 A71-39865

Lagrange-Dirichlet and Routh systems stability theorems inversion, proving motion instability in case of potential energy maximum in solutions to differential equations

21 p3414 A71-40092

Time optimal control synthesis for linear integration-type system described by n-order differential equations, using operational calculus

21 p3359 A71-40165

Solutions near equilibrium point of finitely retarded autonomous functional differential equation, noting bifurcation

21 p3407 A71-40208

Frequency response optimization of one dimensional damped linear continuous systems, requiring initial value numerical integration of state and adjoint differential equations

[ASME PAPER 71-VIBR-1]

21 p3456 A71-40265

Temperature distribution along short heated wire cooled by flowing liquid with parabolic velocity distribution, using power series for differential equation solution

21 p3378 A71-40581

Numerical power series integration of differential equations of special three body problem with truncation errors elimination to fifth order

21 p3450 A71-40654

Book on classical theory of structures based on differential equations, covering shear wall behavior and maximum-minimum theorem for frameworks

21 p3466 A71-40890

Extracting coefficients of nonlinear differential equations from data on oscillating systems, using time derivative methods

21 p3409 A71-41015

Asymptotics for nonanalytic second order differential equations solutions

21 p3409 A71-41076

Asymptotic behavior of nonlinear Volterra integrodifferential equation solution, noting application to nuclear reactor dynamics

21 p3409 A71-41077

Real symmetric matrix eigenvectors calculation with differential equation, using Liapunov function

21 p3409 A71-41080

Holomorphic matrix valued function on connected open subset of complex plane, obtaining conditions for satisfying homogeneous linear differential equation

21 p3410 A71-41185

Disconjugacy criterion for self adjoint linear differential equations containing nonnegative continuous function in interval under study

21 p3410 A71-41187

Ascoli theorem generalization and application to functional differential equations, proving existence theorem

21 p3410 A71-41188

Complex solutions blocking in sectoral second order differential equations with polynomials, involving conformal mapping

21 p3410 A71-41191

Numerical model of three dimensional convection in atmosphere with vertical wind shear, solving system of differential equations

21 p3411 A71-41385

Linear time-varying system state space representation determination based on scalar differential equation, considering advantages

22 p3566 A71-41853

Cosmic ray transport in random magnetic fields, deriving coupled integrodifferential equations for radiant intensity and flux

22 p3592 A71-41915

Differential equations system numerical integration solution global discretization error local estimation by Runge-Kutta and multistep methods

22 p3567 A71-42293

Semilinear hyperbolic systems analogous to differential-integral Boltzmann equations of gas dynamics, developing solutions existence for nonnegative initial data

22 p3531 A71-42690

Nonautonomous nonlinear functional differential equations periodic solutions, reducing problem to existence proof of fixed point for operator in suitable space of periodic functions

22 p3567 A71-42691

Nonlinear differential equations with retarded argument, proving asymptotic and oscillatory solutions theorems

22 p3568 A71-42692

Controllability conditions for linear differential equations of dynamic system

22 p3568 A71-42696

Variable structure digital control servomechanism flutter mode analysis, using nonlinear differential equation

22 p3528 A71-42878

Piecewise polynomial Taylor methods to numerically solve first order ordinary differential equations

23 p3698 A71-42901

Integrable linear differential equations application to Riccati equation and Bessel, Legendre and other functions relations in celestial mechanics [AAS PAPER 71-333]

23 p3727 A71-43006

Differential equations system for convective incompressible fluid flow boundary layer temperature profile description, analyzing solution existence and uniqueness

23 p3781 A71-43306

Differential equation solution for plane self focusing and one dimensional self modulation of waves interacting in nonlinear media

23 p3704 A71-43408

Small autooscillations of high order differential equations system, investigating bifurcation occurrence relationship to zero equilibrium position stability change

23 p3699 A71-43572

Optimal control of time delay systems described by linear differential difference equations

23 p3658 A71-44087

Zero sum differential game solution for aerial combat problem, applying direct gradient methods

23 p3699 A71-44103

Exact solutions of elasticity theory nonlinear differential equations by Lie group theory methods

24 p3877 A71-44480

Unified electrical machine theory with allowance for space harmonics effects, transforming time-dependent linear differential equations into linear time-invariant equations

24 p3793 A71-44657

Boundary value problems eigenvalues determination with differential equations for lifting surfaces vibration theory 24 p3818 A71-44706

Computer systems design for complex process control, constructing models with differential equations and Boolean functions 24 p3806 A71-44714

Composite materials thermal diffusivity at high temperatures by quasi-stationary and monotonic methods, determining validity domain of differential heat conduction equation without heat sources 24 p3889 A71-44967

Unstable systems dynamic stabilization, deriving conditions from second order linear differential equations with variable coefficients 24 p3849 A71-45048

Minimal order linear time-invariant systems description by smallest possible number of parameters, deriving differential or difference equations based on input/output parameters [DPV/LR-SONDDR-135] 24 p3816 A71-45122

Algorithm for preparation of nonlinear differential equations for simulation by analog computer in linear form 24 p3807 A71-45156

Second order differential guidance game, formulating strategy for optimal feedback control 24 p3849 A71-45338

Shell of revolution natural vibration spectrum, investigating moment and momentless type systems of differential equations 24 p3886 A71-45342

DIFFERENTIAL GEOMETRY

NT LIE GROUPS
NT RIEMANN MANIFOLD
NT SPINOR GROUPS
NT TENSOR ANALYSIS

Solid body motion about fixed point on pseudoeuclidean Lobachevskii plane under external forces, using Euler angle analogy 03 p0457 A71-13423

Nonlinear systems bang-bang controllability by differential geometry approach 04 p0562 A71-15872

Continuum mechanics in differential forms, discussing material and spatial coordinates, compatibility conditions energy balance, entropy inequality and invariance principles 16 p2613 A71-34146

G structure tensors integrability and fiber extensions, using differential geometry 18 p2976 A71-36097

Critical point anomaly in saturation curves of reduced temperature-compressibility planes of pure substances, using metric differential geometry and thermodynamics 18 p2985 A71-36452

DIFFERENTIAL INTERFEROMETRY

Differential radiometer with ultranarrow interference filter for daytime tracking of high altitude chemical vapor trails 03 p0424 A71-13636

Single mode polarization in simple gas laser for long path difference Michelson interferometry 03 p0436 A71-13653

Shock wave propagation in bent and branched ducts, discussing schlieren method flow visualization, diffraction measurement with differential interferometer and interaction between shock and vortex 03 p0400 A71-13696

Radial direction shearing interferometry, considering wave front radial phase derivative display by axicon or circular grating arrangements 07 p1110 A71-19477

Modified double point source differential shear interferometer for neutral reference light beam, using pinhole stop 07 p1110 A71-19478

In situ double exposure differential interferometry, using photoconductive thermoplastic sandwich in place of film, allowing second hologram inscription 14 p2242 A71-30153

Wave reconstruction from gaseous flow hologram analysis with differential interferometry in polarized light and schlieren techniques with phase filter defocusing 20 p3239 A71-39461

DIFFERENTIAL OPERATORS

U DIFFERENTIAL EQUATIONS
U OPERATORS [MATHEMATICS]

DIFFERENTIAL PRESSURE

Book on fluid meter theory and applications covering quantity and rate measurements and differential pressure meters 10 p1610 A71-24148

MHD effects on transpiration cooled Couette flow through porous wall, considering magnetic drag produced pressure differential and shear recovery rates 10 p1649 A71-24404

Maximum velocity position in turbulent shear flow for differential pressure effect between double pitot tubes, using inductance type transducer 11 p1767 A71-26313

Parallel pressure multiplexer and encoder for aerodynamic testing, employing zero pressure detectors coupled with IC digital electronics and reference pressure signal 14 p2222 A71-30342

Vortex type pneumatic angular rate sensor with vanes and hydrodynamic viscous coupling, determining differential pressure outputs 15 p2352 A71-32063

DIFFERENTIAL THERMAL ANALYSIS

High purity hafnium titanate, discussing preparation and DTA, electron microscopy wet chemical and X ray analyses 02 p0275 A71-12595

Calorimeter for quantitative differential thermal analysis at high temperatures 04 p0595 A71-14958

Temperature uncertainties determination in spacecraft thermal analysis, using influence coefficients obtained from steady state heat balance equation [AIAA PAPER 71-430] 11 p1858 A71-26219

Ammonium perchlorate sublimation using simultaneous differential thermal analysis and thermogravimetry 23 p3641 A71-43116

DIFFERENTIATION

Q approach to problem solving applied to partial derivatives determination on digital computer, discussing approach structure and characteristics 01 p0048 A71-10221

Differentiability of nonlinear Volterra integral equations of second kind with convolutional weakly singular kernels 15 p2442 A71-31870

Differential method of ultrasonic inspection and binary comparative search heads for implementation, combining mirror shadow and echo methods features 22 p3553 A71-41760

DIFFERENTIATORS

Discrete and analog electrical differentiators accuracy for input functions time derivatives determination, considering systematic errors and application suitability 04 p0599 A71-15567

Electronic double differentiator for producing spectroscopic absorption curves second derivatives, considering application to polymers IR examination 22 p3545 A71-42154

DIFFRACTION

NT ELECTRON DIFFRACTION
NT FRESNEL DIFFRACTION
NT NEUTRON DIFFRACTION
NT PULSE DIFFRACTION
NT WAVE DIFFRACTION
NT X RAY DIFFRACTION

Self reproduction of diffraction and reconstructed images of finite aperture in coherent radiation field by periodic transverse and longitudinal alternation 01 p0092 A71-10032

Microwave ultrasonic beam visualization techniques via Bragg diffraction of laser beam, investigating resolution capability 03 p0436 A71-13717

Monograph on optical imaging of ultrasonic fields by acoustic Bragg diffraction covering heuristic plane wave and ray approach scattered fields 07 p1111 A71-19575

Vertical electric dipole field diffraction by circular aperture in flat conducting screen between two electromagnetically different half spaces 09 p1406 A71-22877

Field correlation diffraction theory of symmetrical microwave Cassegrain antenna, calculating main reflector focused field by spherical wave expansion 13 p2028 A71-27992

Shock front detection by Fraunhofer diffraction of narrow parallel Gaussian laser beam 13 p2067 A71-28162

Cosserat continuum elastic tensor potentials applied to Kirchhoff theory of wave diffraction 20 p3269 A71-39033

Constrained-impedance eigenfunctions, using projection method for field expansion in diffraction problems 22 p3512 A71-42307

Diffraction phenomena numerical modeling by Monte Carlo statistical analysis, using Heisenberg uncertainty principle 22 p3576 A71-42556

DIFFRACTION GRATINGS

U GRATINGS [SPECTRA]

DIFFRACTION PATHS

Midlatitude VLF discrete emissions generation regions location by dispersion analysis of ground station observations, determining plasma density along path for events 08 p1282 A71-21634

DIFFRACTION PATTERNS

NT KOSSEL PATTERN

He-Ne laser beam diffraction patterns produced by nematic liquid crystal subject to electric field, noting threshold effect 01 p0096 A71-11375

Shadow current method for asymptotic solution to two dimensional problem of electromagnetic wave far diffraction field on ideally conducting plane with infinite rectangular slot 02 p0210 A71-11629

Automatic pattern recognition in photographic transparencies, using diffraction pattern sampling 02 p0225 A71-11704

Truncated periodic targets modulation in partially coherent light, deriving diffraction image formulas 02 p0260 A71-12146

Optimum frequency channels and delay estimates in very long baseline interferometry with large bandwidth for fringe and phase measurements 02 p0216 A71-12329

Strain analysis by moire-rosette method, using fringe patterns from pair of crossed gratings through optical spatial filtering 03 p0423 A71-13549

Strain-optical constants determination by ultrasonic technique, using Raman-Nath theory for optical diffraction produced by standing ultrasonic wave 03 p0425 A71-13716

Nonhomogeneous strain fields analysis by moire fringe multiplication with full field data reduction by mechanical differentiation 03 p0425 A71-13753

Holographic interferometry application to photoelasticity, discussing absolute retardation in terms of plane or circularly polarized light fringe pattern interpretation [SESA PAPER 1719] 03 p0426 A71-13767

Scattered light method application to two dimensional plane stress problems, considering fringe spacing and gradient relationship [SESA PAPER 1718] 03 p0426 A71-13779

Tropospheric diffraction fields computation in atmospheres with modified refractive index increasing monotonically with height, discussing IF and LF ground wave propagation 04 p0552 A71-15020

Laser produced schlieren interferometry diffraction pattern determination, using Doppler frequency shift law 04 p0596 A71-15222

Classical and hologram interferometry, considering fringe localization and visibility 05 p0747 A71-16190

Circular apertures with Besinc correlated illumination, examining far field diffraction properties and intensity distribution 05 p0781 A71-16193

Fatigue damage detection by X ray diffraction method, testing different steel specimens with Co-K-alpha radiation to obtain characteristic diffraction patterns 05 p0749 A71-16295

Principal stresses separation method combining conventional isocline parameter and isochromatic fringe order measurements and scattered light method 05 p0822 A71-16373

Photoelectric photometer measurements of stellar interferometer fringes strength by light modulation 05 p0752 A71-16681

Plane electromagnetic wave inhomogeneous diffraction field from multilayer metal band gratings 05 p0722 A71-16829

Holographic interferometry application to gas dynamics, analyzing interferential patterns in monochromatic and achromatic light 05 p0695 A71-17166

Electron thermal diffusion effects during light interference patterns exposure, generating strong electric fields and holographic storage in electro-optic materials 06 p0940 A71-17309

Photoelastic fringe patterns in double exposure holography interferometric technique for stress wave analysis 07 p1209 A71-19044

Axisymmetric phase object holographic interferometry, showing light beam refraction effect on interference pattern 07 p1108 A71-19237

Nickel molybdenide disorder to order early transition mechanism diffraction model, using transmission electron and field ion microscopy studies 07 p1132 A71-19436

Fringe interferogram variable visibility control, eliminating vibration effects 07 p1109 A71-19467

Holographic multiple beam interferometry, considering phase retardation role in hologram diffracted waves for fringes irradiance distribution definition 07 p1110 A71-19479

Magnetic hologram reconstruction process, discussing diffracted field, polarization properties and efficiency [IEEE PAPER 8.2] 07 p1112 A71-19610

Coherent optical data processing techniques, discussing diffraction phenomena, spectral analysis and holography 07 p1067 A71-19629

Holograph interferometer methods classification according to diffuse elements in objects and illumination sources, considering effect on interference fringe interpretation 07 p1114 A71-20144

Aperture concentric diffraction ring differential effects on focal irradiance, using perfect lens half-wave filter model 08 p1333 A71-21178

Radiant flux diffraction effectiveness of amplitude holograms with allowance for nonlinearity of photomaterial 09 p1442 A71-22400

Mirror reflection coefficients effect on fringe characteristics of multibeam series interferometer, showing improvement by Fabry-Perot etalon system 09 p1451 A71-23174

Locally illuminated diffracting edge near field calculation in terms of Hankel function asymptotic solution 09 p1409 A71-23514

Fringe interpretation in stress-holo-interferometry, emphasizing isopachic-isochromatic interaction effects in photoelastic analysis [SESA PAPER 1642] 09 p1542 A71-23538

Iterative technique using continuous gas laser for alignment of Mach-Zehnder interferometer for monochromatic and white light fringes 09 p1453 A71-23692

Classical vs holographic interferometry comparing same fringe profiles 10 p1608 A71-23844

Far field diffraction pattern of corner reflector for normally incident monochromatic light, considering polarization characteristics 10 p1640 A71-23947

Isolated ionospheric irregularities, describing refraction and diffraction pattern calculations for satellite signals 10 p1578 A71-24463

Variable shear interferometer for infinite fringe operation and velocity measurement, discussing refractive index distributions in stationary and moving media 10 p1613 A71-24994

Array spacing dependence of ionospheric irregularities horizontal drift and anisotropy, using statistical properties of ground diffraction patterns 11 p1731 A71-25614

Surface strain measurements in turbine blades by time average holographic interferometry, reviewing resonant modes and holographic fringe patterns [ASME PAPER 71-GT-84] 11 p1762 A71-25992

Light diffraction by superposed parallel ultrasonic waves for diffraction pattern symmetry, using n-th order approximation method 12 p1928 A71-26650

Axisymmetric phase object holographic interferometry, showing light beam refraction effect on interference pattern 12 p1903 A71-26755

Digital data recording system based on multiple beam interference pattern photography, using optical phase modulation 12 p1905 A71-26807

Parallel light beam triangular path interferometer with linear compressive shear effect for flow measurement applications, describing prism system and interference patterns 12 p1905 A71-26816

Holographic interferometry application to gas dynamics, analyzing interferential patterns in monochromatic and achromatic light 12 p1864 A71-27458

Computer simulation of fading records in spaced antenna ionospheric drift experiment, detecting mean direction and diffraction pattern velocity with correlation analysis 13 p2054 A71-27800

Laser interference patterns recorded on photosensitive surface of test sample before and after deformation, considering irregularly shaped objects with rough surfaces 13 p2067 A71-28441

Interference spectroscopy and spectrometry techniques, describing transverse achromatic light source beam splitting and frequency analysis of photogenerated fringes 14 p2238 A71-29804

Electromagnetic wave diffraction at multilayer wire grating, discussing computer program for diffraction field calculation 14 p2194 A71-30086

Reference/object wave temporal modulation effect on fringe formation in holographic interferometry 14 p2241 A71-30133

Cartesian shear and rigid rotation moiré patterns by spatial filtering of superposed diffraction gratings 14 p2329 A71-30464

Atmospheric turbulence effect on far field diffraction pattern of annular aperture 14 p2275 A71-30465

Parabolic two-mirror antenna design with one small mirror for diffraction fringe effects correction 14 p2196 A71-30637

Imagery of periodic objects through interposed turbulent medium, investigating diffraction images irradiance distribution and contrast 14 p2275 A71-30827

Holographic interferometry, discussing deformation second derivatives mapping and fringes formation and visibility 15 p2403 A71-31262

Diffusely reflecting object element three dimensional displacement measurement from single hologram nonlocalized patterns 15 p2403 A71-31263

Three dimensional deformation surface displacement measurement by holographic interferometry, using equal inclination fringes 15 p2403 A71-31264

Fringe order determination in holographic interferometry, discussing zero motion object region identification 15 p2403 A71-31266

Radio sources interplanetary scintillations observation, discussing solar wind velocity and diffraction pattern scale 15 p2480 A71-32445

Fabry-Perot interferometer laser beam diffraction effects on fringe pattern formation, deriving field distributions in near and far zones 15 p2421 A71-32459

Time average holographic interferometric fringes of circular plate vibrating in two rationally related modes 15 p2412 A71-32593

Short length strain interferometric measurement from interference patterns of laser light diffracted from adjacent small reflecting surfaces 16 p2576 A71-32864

Shock wave diffraction patterns on plane walled convex corners in air, nitrogen and carbon dioxide at various Mach numbers 16 p2556 A71-32918

Diffraction limited circular holographic determination of Airy radius by photoelectric scanning of image irradiance 16 p2577 A71-33143

Light diffraction by holographic gratings in pink ruby due to absorption coefficient spatial variations 16 p2578 A71-33149

Orthogonal bicolored moiré fringes in mechanical interferometry, considering interpolation type determination of fractional fringe orders [SESA PAPER 1817A] 17 p2738 A71-34548

Holographic interferometry fringe patterns interpretation for small displacements measurement, considering precision gyro stability 17 p2744 A71-35286

Holographic diffraction gratings on plane or concave spherical surface photographic plate, investigating interference fringes and aberration properties 17 p2745 A71-35588

Interference holography, discussing precision displacement measurement, fringe localization, multiple beam techniques, contour generation and flow visualization 18 p2920 A71-36148

Laser velocimeter for wide range velocity measurement, using photodetector to observe light scattering by particles flowing across fringe pattern 18 p2932 A71-36618

Adhesively bonded structures inspection by laser holography, producing diffraction pattern recording of amplitude and phase shift 18 p2925 A71-37057

Thermospheric winds measurement during geomagnetic storms with Fabry-Perot interferometer from Doppler shift of two 6300 Å fringe profiles 19 p3047 A71-37366

High efficiency inline multiple imaging by means of multiple phase holograms, giving diffraction patterns 19 p3063 A71-37482

Computer program for generation and automatic plotting of perfect and twinned electron diffraction patterns for cubic crystal structures 19 p3118 A71-37719

Moiré equivalence device for simulating fringe patterns in hologram interferometry, using loci of constant pathlength 20 p3235 A71-39188

Holographic interferometry application to photoelasticity, interpreting fringe patterns for two dimensional stress analysis 20 p3238 A71-39345

Holographic interferometry application to photoelasticity, discussing relationship between isochromatic and isopachic fringes and fringe families separation method 21 p3456 A71-40228

Low speed wind tunnel air velocity measurement with laser velocimeter, using dark background illumination detection of particles scattering across fringe pattern 21 p3378 A71-40398

Interference rings formation mechanism near main beam emitted by ruby laser with plane and reflecting terminal faces 21 p3392 A71-40515

Kinoform diffuser technique based on speckle pattern formation by ground glass illumination with undiverged laser beam 21 p3381 A71-40928

Hologram interference fringes formation and location using grating model of diffusely reflecting surface 22 p3539 A71-41739

Beam electrons correlations effect on interference fringes visibility 22 p3546 A71-42243

Savart plate Francon modification at arbitrary angles to optic axis, examining view field limiting factors and fringe patterns 22 p3549 A71-42554

Large path difference laser interferometry, discussing test tower instrumentation problems of interference fringe flicker and loss of contrast due to laser mode instability 23 p3683 A71-43356

Interferometric fringes from study of gas plasma produced by ruby laser pulses, using Nd glass laser for heating 23 p3710 A71-43409

Holographic evaluation of low power ruby laser emitted wave spatial coherence factor via fringe visibility measurements 23 p3679 A71-43894

Fraunhofer diffraction apparatus design based on He-Ne laser, testing performance in distorted point lattices photography 23 p3686 A71-43956

Boundary retardation with respect to fringes in scattered light photoelasticity, using quarter wave plate 24 p3881 A71-44776

Interference patterns from hologram interferometer related to aberration theory 24 p3826 A71-44980

Culgoora radiotelescope electronic imaging system for diffraction pattern generation 24 p3828 A71-45205

Leed rotation diagrams for aluminum, obtaining low energy electron diffraction intensity profiles by band structure matching approach 24 p3862 A71-45349

DIFFRACTION PROPAGATION

Two dimensional diffraction of plane wave by perfectly conducting wedge using straightforward scattering approach 03 p0456 A71-13347

Plane wave holographic recording and reconstruction, investigating effects of photosensitive medium as three dimensional diffractive pupil 13 p2068 A71-28711

Shock wave diffraction propagation through nonuniform fluid, noting application to two dimensional unsteady flows 18 p2907 A71-36332

DIFFRACTION TELESCOPES

U SPECTROSCOPIC TELESCOPES

DIFFRACTOMETERS

High accuracy deflector and diffraction sensors for optical tracking systems, noting dependence on ultrasonic frequency 10 p1610 A71-24169

Peak shifts evaluation errors in X ray stress analysis using diffractometer and three point parabola fitting method 14 p2260 A71-30479

DIFFUSE RADIATION

Plant leaves mean effective optical constants from diffuse UV reflectance and transmittance measurements 01 p0073 A71-10834

Diffuse galactic X ray background intensity as function of galactic scattering and discrete sources 01 p0145 A71-11345

Interstellar dust, examining diffuse line and band origin, absorption spectra and silicate grains 02 p0312 A71-12466

Diffuse cosmic X ray spectrum obtained from telescope aboard OSO 3 satellite 02 p0300 A71-12580

Diffuse cosmic X rays observation by telescope aboard OSO 3 satellite, determining isotropy 02 p0301 A71-12581

Laser image speckle interferometer design for observing vibrational modes on diffusely reflecting surfaces as alternative to holographic methods 02 p0254 A71-12718

Diffuse cosmic gamma ray background origin, using simple photon production model 02 p0303 A71-12837

Semitransparent spherical dielectric shell under diffuse incident radiation, determining absorptance and reflectance by Monte Carlo method 03 p0518 A71-13648

Diffusely reflected radiation from semiinfinite atmosphere, deriving asymptotic formula including high order scattering terms 04 p0643 A71-14905

Radiation diffusion in one dimensional isothermal medium moving with constant velocity gradient, assuming complete frequency redistribution and arbitrary absorption coefficient profile 07 p1192 A71-19290

Backscattered radiation energy during laser beam scanning of diffusely scattering surface
07 p1123 A71-19309

Isotropic diffuse cosmic X rays and gamma radiation background origin
07 p1184 A71-19321

Solid state laser with different diffuse coatings on external reflector of pumping source, measuring energy output
07 p1125 A71-19812

Holograph interferometer methods classification according to diffuse elements in objects and illumination sources, considering effect on interference fringe interpretation
07 p1114 A71-20144

Low energy cosmic X ray observations, examining diffuse background and absolute flux values
08 p1349 A71-20936

Diffuse cosmic X ray observations, discussing balloon and OSO-3 data
09 p1514 A71-22934

Lunar surface specific effective radio signal scattering area measured by Luna 9 and 13, describing signal fluctuations
09 p1523 A71-23145

Diffuse interstellar bands polarization and extinction based on silicate and graphite grain composition and sizes
10 p1675 A71-24469

Diffuse interstellar absorption centered at 4430 Å observed in reflection nebulae, using narrow band filters
11 p1831 A71-26135

Line emission in diffuse cosmic X ray continuum, discussing probable interstellar or intergalactic matter source
11 p1817 A71-26317

Monodispersed particle semiinfinite atmosphere, calculating invariance principles of diffused radiation based on Mie theory
12 p1960 A71-26823

Cosmic soft X rays diffuse component dependence on galactic latitude related to interstellar absorption
12 p1949 A71-27370

Diffuse reflection from clouds with horizontal surface striations, using Monte Carlo method to follow photons through simplified models
13 p2056 A71-27975

Tables of scattering functions and albedo for semiinfinite atmospheres according to nonconservative Rayleigh phase matrix for diffuse radiation computation
14 p2274 A71-30059

Night sky submillimeter wave diffuse background radiation telescopic measurements above 120 km
15 p2399 A71-31827

Line emission in diffuse X ray background at high galactic latitudes, interpreting rocket observations
15 p2480 A71-32760

Diffuse low energy cosmic X rays rocket measurements, noting excess over extrapolated power law valid for higher energies
15 p2480 A71-32761

Absorption spectra formation by diffuse reflection from semiinfinite plane parallel scattering planetary atmosphere, using asymptotic expressions for higher order scattering
17 p2736 A71-35568

Extragalactic background soft X ray diffuse flux consistent with absorption by Small Magellanic Cloud
20 p3278 A71-39108

Interplanetary medium thermal emission detection, presenting diffuse background radiation upper limits in intermediate IR from sounding rocket data
20 p3288 A71-39114

Diffuse background 0.1-1 MeV gamma ray component observed by balloon-borne counter system, finding no positive evidence for cosmic component existence
20 p3283 A71-39752

Spectrum and galactic isotropy of diffuse cosmic X rays by balloon-borne detector
21 p3438 A71-40605

Diffuse radiation field inside homogeneous spherically symmetric dust nebula from radiative transfer equation solution as expansion after Legendre polynomials
21 p3451 A71-40716

Quasi-binary InAs-GaP single crystals absorption and diffuse reflection spectra, determining forbidden bandwidth as function of compound composition
21 p3434 A71-41332

Diffuse 0.2-2 keV cosmic X ray flux, discussing energy spectrum and spatial distribution
22 p3591 A71-41914

Galactic diffuse radiation in far UV, discussing consistency of findings on optical properties of interstellar grains
22 p3593 A71-42337

Diffuse object scanned illumination hologram recording, discussing intermodulation flare light elimination for speed and reconstruction efficiency
22 p3549 A71-42561

Nongray radiative heat transfer in finite slab with discrete absorption coefficient and specularly and dif-

fusely reflecting boundary surfaces of uniform temperature
24 p3886 A71-44372

DIFFUSERS

Plane diffuser cascade losses at low main stream pressures, discussing Reynolds number role
01 p0003 A71-11062

Optimum two fluid mixing chamber length for energy efficiency of conical diffusers in straight pipe jet pump systems
03 p0399 A71-13369

Diverging flow structure in conical diffuser using two Townsend turbulent parameters
03 p0399 A71-13456

Noise generation increase with unchanged mass flow rate by cone angle diffusers in jet nozzles, considering far field sound pressure level
[ASME PAPER 70-WA/GT-5] 03 p0402 A71-14117

Cone shaped diffusers effectiveness, noting inlet conditions effect on pressure recovery coefficient
05 p0694 A71-16750

Conical diffusers swirling inlet flow effects on pressure recovery and outlet flow profile
[AIAA PAPER 71-84] 06 p0883 A71-18541

Positive pressure gradient turbulent boundary layer local characteristics in plane diffuser, using Reynolds stress change equations
07 p1086 A71-18770

Truncated conical diffusers with various geometrical configurations and incompressible inlet flow conditions, noting reduced pressure recovery
13 p2047 A71-28468

Pressure recovery performance of straight-wall two dimensional diffusers with subsonic air-water mixtures, studying gas volume flow ratio and diffuser geometry effects
[ASME PAPER 71-FE-20] 13 p2052 A71-29458

Spatial MHD flow in diffuser bounded by two diverging and two parallel walls, showing solutions with axial symmetry in cylindrical and spherical coordinate systems
14 p2278 A71-29605

Short conical diffusers with radial splitters for flow stabilization with high pressure recovery performance
14 p2225 A71-30304

Holographic interferometry for flow visualization within aerodynamic wind tunnels with retrodiffuser apparatus
15 p2405 A71-31276

Laser output speckle removal with slowly moving and motionless diffusers system, reducing integration time for obtaining SNR
15 p2451 A71-32590

Aperture angle effect on flow separation in inlet section of diffuser with cylindrical to conical channel transition
16 p2521 A71-33611

Plasma wind tunnels for high enthalpy flows of low density, considering plasma arc heaters and expansion nozzles with diffusers
19 p3040 A71-37461

Highly uniform inlet velocity profile influence on conical diffuser characteristics
20 p3177 A71-39798

Circular conical diffuser inlet velocity profile effect on efficiency, presenting experimental results for different cone angles and expansion ratios
20 p3177 A71-39799

Uniform inlet flow inside centrifugal turbomachinery diffusers with flat parallel side walls, measuring pressure distribution and boundary layer velocity profiles
21 p3323 A71-40757

Kinoform diffuser technique based on speckle pattern formation by ground glass illumination with undiverged laser beam
21 p3381 A71-40928

Conical diffusers outlet flow profile and performance, investigating swirling inlet flow effects on pressure recovery
21 p3323 A71-40950

Medium compressibility effect on gas dynamic characteristics and aerodynamic forces and moments in centrifugal compressor end stage bladed diffuser
23 p3626 A71-43552

DIFFUSION

NT AMBIPOLAR DIFFUSION

NT ATMOSPHERIC DIFFUSION

NT ELECTRON DIFFUSION

NT GASEOUS DIFFUSION

NT IONIC DIFFUSION

NT MAGNETIC DIFFUSION

NT MOLECULAR DIFFUSION

NT PARTICLE DIFFUSION

NT PLASMA DIFFUSION

NT SPECIES DIFFUSION

NT SURFACE DIFFUSION

NT THERMAL DIFFUSION

NT TURBULENT DIFFUSION

Diffusion with convection in flow between parallel walls, using Von Mises transformation
02 p0332 A71-12410

DIFFUSION COEFFICIENT

Welded joint structural stability determination by measuring decarburized steel layer thickness after carbon diffusion into lower activity region
03 p0432 A71-13690

Diffusion controlled combustion of liquid fuel droplet in oxygen-steam oxidizer mixture
03 p0468 A71-13996

Submicron sectioning apparatus for studying slow carbon self diffusion in dense polycrystalline tungsten carbide
03 p0429 A71-14187

Volume diffusion role in Ni-Cr eutectic and cast alloys cellular structure growth
04 p0615 A71-15793

Multicomponent gas laminar boundary layer equations, deriving asymptotic formulas for friction coefficient, concentration, temperature and diffusion flows
07 p1089 A71-19734

Composite material dynamic processes based on diffusing mixtures continuum theory
09 p1540 A71-23085

Parabolic dialysis, examining uses as in vivo diffusible substances test and alternative for conventional chronic hemodialysis
09 p1401 A71-23370

Cavitation in liquids with dissolved gases by acoustic wave induced oscillating pressure, discussing gas bubble formation through rectified diffusion process
10 p1597 A71-24942

Carbon monoxide methods for studying diffusing capacity of human lungs
12 p1869 A71-26654

Diffusion component of alveolar-arterial oxygen pressure differences in man at rest and during exercise
19 p3009 A71-38556

Excited states drift and diffusion effects on spatial hole burning and laser oscillation, solving rate equation for population inversion
20 p3242 A71-38842

Dispensing devices and error sources in radial immunodiffusion and electroimmunodiffusion techniques
22 p3508 A71-42888

DIFFUSION BONDING

U DIFFUSION WELDING

DIFFUSION COEFFICIENT

Oxygen diffusion coefficient during metal /Ti/ oxidation in unsteady high temperature region, allowing for interfacial phase boundary shift
01 p0101 A71-10673

Ambipolar diffusion coefficients application to analysis of laminar multicomponent ionized boundary layer flow in channel
01 p0070 A71-10795

Nb-impurity binary solid solutions, calculating interdiffusion and heterodiffusion coefficients
02 p0270 A71-12930

Discrete values of inverse diffusion length occurring in solutions of anisotropic transfer equations
04 p0642 A71-14904

Galaxy gaseous disk as low mode dynamo, calculating turbulent diffusion coefficient for passive magnetic fields
05 p0811 A71-16688

Diffusion coefficient and thermal conductivity dependence on plasma parameters in Tokamak installation
06 p0930 A71-17397

Cured epoxy polymer, determining diffusion coefficients, solubility, permeability and equilibrium water absorption as function of curing agent and temperature
06 p0915 A71-17943

Mesosphere and lower thermosphere heat input rates and circulation, calculating worldwide average eddy diffusion coefficient
06 p0892 A71-17978

Ambipolar diffusion coefficient noting vertical variations
06 p0893 A71-17993

Onsager relations for Soret-Dufour and diffusion coefficients in moderately dense gas mixtures based on kinetic theory, considering symmetry relations for transport properties
06 p0929 A71-18036

Low density monatomic gases mixtures multicomponent thermal diffusion coefficients, demonstrating for heat conductivity and dissociated air equations
06 p0929 A71-18072

Turbulent diffusion coefficients in isothermal and nonisothermal pipe flow, comparing with Bory and Taylor theories
07 p1222 A71-18994

Diffusion coefficient estimation for energetic charged particles across magnetic fields from mathematical model
07 p1186 A71-19662

Nickel ion diffusion coefficients in high purity magnesium oxide single crystals in high temperature argon atmosphere
08 p1343 A71-20664

Electron diffusion in trap with magnetic mirrors under pulsed field perturbations, determining coefficients by numerical integration of drift equation
09 p1513 A71-22551

Fe-Ni alloys, determining hydrogen permeability, diffusion coefficient and solubility as function of composition by electrochemical method
09 p1472 A71-23127

Unstable electron plasma oscillations quasi-linear theory, discussing improper treatment of perturbed electron distribution for damped waves leading to negative diffusion coefficient
10 p1647 A71-23893

Polarographic measurements of secondary Couette flow between coaxial cylinders for diffusion coefficient effects on mean friction factor, using wall flush microelectrodes
10 p1592 A71-23978

Electrical and thermal conductivity coefficients and energy diffusion coefficient in lower ionosphere, assuming weak ionization of ionospheric plasma
10 p1607 A71-24998

Nb-Pd system concentration profiles and thermal diffusion coefficients, investigating phase formations by electron probe microanalysis
10 p1629 A71-25035

Nb-V, V-Pd and Pd-Nb systems diffusion coefficient as function of concentration for equilibrium diagrams, using method of diffusion layers
11 p1782 A71-26475

Orionid and Leonid meteor trains, determining diffusion coefficient from isophotes variation
12 p1965 A71-27230

Anisotropy of solar cosmic ray electrons, considering parallel diffusion coefficients for ions and electrons
12 p1954 A71-27712

Fe/Ti pair diffusion coefficients at various temperatures, showing thin central and two single phase zone formation
13 p2087 A71-29263

Transverse spatial diffusion of phase-dispersed pulses, showing effects on dechirped pulse duration, output beam cross section and two-photon fluorescence display
13 p2081 A71-29332

Diffusion coefficient as function of height in turbulent atmospheric boundary layer, considering similarity laws between wind tunnel and field data
13 p2051 A71-29432

Temperature dependent diffusion coefficient of yttrium in refractory metal single crystals of Mo, W, Nb and Ta, using radiometric analysis
14 p2258 A71-30005

Galactic cosmic ray transport equation numerical solution for interplanetary region, considering modulation, diffusion, convection and energy loss effects
14 p2301 A71-30387

Chemical trimethyl aluminum releases in lower thermosphere for temperature, density, winds, turbulence, diffusion coefficients and atomic oxygen content measurements
16 p2568 A71-33792

Physical conditions leading to deuterium enhancement in earth upper atmosphere as function of thermopause temperature and eddy diffusion
16 p2569 A71-33809

Aluminum effect on nickel diffusion in iron from stainless and aluminum steels study
16 p2599 A71-34053

Richardson number relationship to vertical heat diffusion coefficients in boundary layer
16 p2605 A71-34070

Photoresonance cesium plasma development and decay, determining density spatial-temporal behavior and recombination and polar diffusion coefficients by probe measurements
17 p2787 A71-34287

Concentration profiles around burning droplet, assuming constant binary diffusion coefficients for all species
17 p2840 A71-35705

Diffusion coefficients determination in planetary boundary layer with radon and ThB, using vertical distribution profile of concentration
18 p2912 A71-36193

Integral operating mode of nerve paths representation by linear diffusion channel with electrochemically active synapses, deriving complementary partial differential equations
19 p3001 A71-37250

Orionid and Leonid meteor trains, determining diffusion coefficient from isophotes variation
19 p3132 A71-37382

Galactic and solar cosmic rays diffusion coefficient as function of solar activity and interstellar medium properties, considering particle velocity and proton scattering transport
19 p3127 A71-37804

Ionospheric wind velocity, direction and diffusion coefficient measurements using artificial aluminum oxide luminescent clouds
19 p3091 A71-38629

Charged particle motion in constant magnetic field under random electric field, deriving maximum energy and diffusion coefficient
20 p3269 A71-39163

Eddy viscosity in barotropic planetary boundary layer, finding turbulent diffusion coefficient dependence on turbulent kinetic energy
20 p3257 A71-39437

Morphological change of spherical G.P. zones and solute diffusion coefficient in binary Al-Zn alloy during dissolution, using X ray small angle scattering
21 p3395 A71-40022

Lower thermosphere eddy diffusion coefficient effects on height variations in ionospheric composition
21 p3372 A71-40044

Co-Ni alloy interdiffusion coefficient determination as function of concentration by magnetic transformation effect
21 p3399 A71-40700

Oxygen diffusion coefficient during metal/titanium oxidation in unsteady high temperature region, allowing for interfacial phase boundary shift
21 p3401 A71-41054

Mathematical description by Gaussian error function for metals diffusive saturation and diffusion constants determination
21 p3403 A71-41160

Au diffusion parameters in CdS determined under Cd and sulfur vapor atmospheres at 540-1000 C, explaining profile difference by dissociative mechanism
21 p3433 A71-41315

Quantum fluctuations in gas laser radiation, obtaining photon diffusion coefficients for traveling and standing waves
22 p3558 A71-42456

Apparatus for optical diagnostics of helioelectrochemical conversion reaction phototransformation kinetics including diffusion coefficient measurement in liquid phase
22 p3484 A71-42845

Delta-zirconium hydride hydrogen engassing experiment, investigating hydrogen absorption rate and diffusion constant temperature dependence
23 p3688 A71-42929

Mars atmospheric carbon dioxide dissociation, solving and comparing diffusion equations to Mariner oxygen and carbon dioxide observations
23 p3735 A71-43332

Neutron irradiation effects on dissociative high temperature zinc diffusion in indium and gallium arsenides
23 p3716 A71-43480

Solute diffusion coefficients dependence on proteins concentrations in human plasma from experiment, presenting equation for prediction
23 p3637 A71-44253

Mo-W, Ta-W and Nb-W alloys X ray analysis at high temperatures, calculating interdiffusion coefficients and temperature effects on W concentration
24 p3836 A71-44671

Toluene and aniline-methylcyclohexane and toluene-aniline nonideal liquid systems, measuring molecular diffusion coefficients as function of concentration by Savart plate birefringent interferometer
24 p3820 A71-45074

Hydrogen plasma generation by microwave field in magnetic-mirror device due to electron cyclotron resonance, measuring transverse diffusion coefficient dependence on magnetic field
24 p3858 A71-45235

Diffusion acceleration in bcc Ti due to imperfections of fine structure created during polymorphous transformation
24 p3840 A71-45379

DIFFUSION EFFECT

U DIFFUSION

DIFFUSION FLAMES

Enclosed diffusively turbulent flames, determining area of maximum ion concentration
01 p0178 A71-10338

Maximum ion concentration zone in diffusively turbulent flames in fuel gas free jets, using mass exchange processes analysis
01 p0178 A71-10341

Extended Spline Fit Technique for determining refractivity from interferograms of axisymmetric laminar diffusion flames
01 p0180 A71-10946

Spherical hydrogen-oxygen diffusion flame structure, discussing combustion processes chemical kinetics
02 p0210 A71-12856

Hydrogen fuel injection into hot oncoming air flow, investigating boundary layer chemical behavior at stagnation point of diffusion flame
02 p0334 A71-12857

Diffusion flame stability, investigating critical dependencies for ignition point coordinates for fuel gas burning
07 p1220 A71-18779

Counterflow diffusion flame applied in studies of gaseous and powdered agents in chemically inhibiting fires
07 p1182 A71-19244

Ethylene diffusion flame radiation measurements, determining pressure effects and contributory ratio of carbon particles and gaseous radiation
08 p1346 A71-20855

Axisymmetric wake diffusion flame response to HF periodic velocity oscillations at combustor boundaries
08 p1375 A71-20863

Turbulent diffusion flame laminarization by superimposed rotating flow field, discussing boundary layer stabilizing effect of external centrifugal force field
10 p1695 A71-24048

Single boundary layer flame sheet model for continuous diffusion chemical lasers, obtaining integrated zero power gain, laser power and efficiency
11 p1774 A71-25928

Unenclosed laminar jet diffusion flame phenomenological analysis predicting flame height relationship to fuel flow rate and atmospheric density and oxygen concentration
15 p2513 A71-31622

Grid induced turbulence effects on air flow around enclosed diffusion flame
15 p2463 A71-31623

Magnesium vapor-oxygen low pressure diffusion flames temperature profile measurement, using subminiature thermocouple
15 p2464 A71-31631

Radiative heat transfer effects on small fires in zero gravity spacecraft and free falling chamber environments from diffusion flame models
15 p2514 A71-32084

Nonpremixed and premixed combustion theory in laminar flows, considering diffusion flame- reaction time ratio and activation energy effects
15 p2515 A71-32564

Supersonic hydrogen diffusion flames ignition aids at near-thermal self ignition point, discussing catalytically induced preractions
15 p2466 A71-32718

Diffusion flame theoretical model characterization as singular perturbation problem
16 p2664 A71-34073

Combustion products and temperature distributions along axis of hexane/air diffusion flame
18 p2984 A71-35867

Air-methane supersonic diffusion flame in duct, comparing pressure measurement and gas sampling data with two dimensional combustion analysis
18 p2984 A71-36027

Tollmien-Schlichting waves in flow field of mixed coaxial laminar air diffusion flames, using flow visualization and hot-wire anemometry
19 p3167 A71-38094

Counterflow methane diffusion flames structure in forward stagnation region of porous cylinder, measuring velocity, temperature, concentration, reaction rate and heat release rate profiles
19 p3168 A71-38108

Radial temperature profiles in low pressure oxygen-calcium wire diffusion flames from optical measurements based on radiative transfer equation
19 p3170 A71-38115

Low pressure trimethylaluminum vapor and oxygen flat diffusion flame structure, observing separation, formation and growth
19 p3121 A71-38299

Soot emission suppression from propane diffusion flame by metallic additives
22 p3588 A71-42101

Aerodynamic combustion noise generation from premixed or diffusion open turbulent flames, using fluid mechanics and Lighthill method
23 p3781 A71-43448

Flat diffusion flame structure experimental investigation on Parker-Wolfhard burner, comparing results with perturbation solutions theoretical predictions
24 p3888 A71-44939

DIFFUSION PUMPS

Liquid nitrogen cold trap for oil diffusion pump
05 p0757 A71-16232

Oil diffusion pumped space simulation vacuum chamber performance improvement methods including water vapor and carbon dioxide desorption, Ti sublimation pumping and 20 K cryopumping
06 p0881 A71-18462

DIFFUSION THEORY

Solar corona and wind composition, accounting for He flux and heavy elements from diffusion equations solution
02 p0303 A71-12770

Dispersion model of turbulent mixing of isothermal and nonisothermal slipstreams of air-gasoline combustion products in nozzles
04 p0577 A71-15622

Turbulent jet diffusion and vortex models, noting velocity profile in mixing and turbulent boundary layers
04 p0577 A71-15625

Refractory metals coating of various substrates by gaseous phase chemical deposition, discussing diffusion process theoretical analysis, experimental ap-

paratus and coatings mechanical and physical properties
11 p1768 A71-25391

Dutch monograph on Cr-W interdiffusion in solid state concerning Kirkendall effect and relation between chemical and self diffusion
11 p1783 A71-26488

Diffusion and thermal mechanism ignition theories, applying to altitude relighting of gas turbine engine combustors
13 p2116 A71-28745

Thermal transients in composite cylinders, solving diffusion equation by Laplace transform technique
13 p2164 A71-28987

Reactor shielding problems solutions involving removal-diffusion theory, two dimensional transport theory and Monte Carlo method
13 p2099 A71-29255

Lecher waves, line waves and TEM waves, demonstrating advantage of solving diffusion equation within transversal plane for determination of line parameters
19 p3014 A71-37075

Intermetallic formation in Au-Al systems via diffusion couples, determining activation energy, silicon effect and tensile strength
19 p3119 A71-38513

Diffusion controlled order-disorder transformations kinetics, considering internal strain and gradient energy
21 p3397 A71-40431

Impurity diffusion self aligned MOS and lateral transistors used in IC
21 p3354 A71-40730

Dead ended compartments concentration and current distributions calculation in space hydrogen-oxygen fuel cells, using mathematical model with convective diffusion equation
21 p3326 A71-41249

Multicomponent diffusion process calculation using eigenvalues of Onsager diffusion matrix
22 p3575 A71-42371

One dimensional diffusion model for on state propagation along p-n-p-n structure, determining propagation velocity as function of structural parameters and current density
24 p3859 A71-44462

Radiation diffusion in finite thickness medium with variable optical properties, giving equations for illumination levels and excited atom density in steady state medium
24 p3833 A71-44660

DIFFUSION WAVES
Experimental dispersion curve for LF drift waves in inhomogeneous magnetoplasma
01 p0134 A71-11003

Mass transfer and Biot diffusion in MHD flows with mixed boundary reaction kinetics, considering Hartmann and plate problems
02 p0293 A71-12632

Thermal and bleaching waves as diffusion phenomena in opposite limits, discussing laser heating [AIAA PAPER 71-109]
06 p0928 A71-18559

Dynamic stress and strain concentration in flat plate at sharp change of section, assuming diffuse bending wave field
12 p1973 A71-26703

Dispersion and boundary equation concerning space-charge wave propagation under diffusion effect in Gunn semiconductors with anisotropic conductivity and finite thickness
14 p2283 A71-29793

Ray acoustic treatment, estimating diffusion of radiation patterns due to scattering by random inhomogeneities
17 p2783 A71-35036

DIFFUSION WELDING
Metal matrix composites formation methods, emphasizing diffusion bonding and plasma spray deposition
[SME PAPER EM-70-124]
01 p0090 A71-11265

Metallurgical and structural production of diffusion bonded titanium honeycomb sandwich panels for aerospace hardware weight saving
01 p0090 A71-11270

Diffusion bonding cycles for Al-B composite materials fabrication, relating strength enhancement to residual stress relief
01 p0104 A71-11284

Combined vacuum furnace brazing with diffusion welding for joining high strength Ni base superalloys
02 p0255 A71-11708

Mechanical and interface reaction properties of alumina reinforced Ti-Al-V alloy composites fabricated by vacuum diffusion bonding
07 p1137 A71-19965

Continuous seam diffusion bonding of Ti alloy thin gage and sandwich structures in air, considering joint types
[ASM PAPER W71-23.4]
09 p1455 A71-23094

Diffusion bonding for vacuum tight heat resistant and oscillation proof large area joints
09 p1459 A71-23584

Metal matrix composite fabrication procedures for gas turbine engine fan blades, stressing diffusion

bonding process susceptibility to blades volume producibility
[ASME PAPER 71-GT-46]
11 p1770 A71-25979

Grade 15 steel vacuum diffusion welding to AlMn alloy or AD1 aluminum, using nickel interlayer in joints
15 p2418 A71-32667

Ti alloys diffusion bonding and forging, discussing joints testing and material utilization improvement through die forging process
[SME PAPER AD-71-244]
18 p2927 A71-36656

Diffusion bonding in production of shuttle type vehicles, considering fluxless brazing of refractory superalloys for heat shielding
[SME PAPER AD-71-246]
18 p2927 A71-36660

Diffusion bonding as economical fabrication process for aerospace applications involving Ti alloys, emphasizing mechanical properties and structural reliability improvement
[SME PAPER AD-71-245]
18 p2927 A71-36661

Metallurgical and mechanical properties of Ti-Al-V joints produced by thin film diffusion brazing with copper
19 p3070 A71-38316

DIFFUSIVITY
Damkohler analysis of nitrogen-silica gel absorption isotherm in multimolecular range, noting vapor phase transport and absorbed phase diffusivities
03 p0517 A71-13175

Al alloy rapidly crystallized film structure, studying atomic diffusion mobility effects on formation of supersaturated solid solutions
07 p1130 A71-19299

Simultaneous partial differential equations, applying to one directional diffusion in finite porous slab accompanied by chemical reaction
13 p2025 A71-29011

Lung diffusing capacity for oxygen during exercise and alveolar hypoxia measured without blood samples by ear oximeter
13 p2023 A71-29492

Diffusive p-type Si valve photocells, investigating barrier capacitance
17 p2713 A71-34565

Mass diffusivity effects in film boiling of water droplets vaporizing in air, Ar, N, He and steam
23 p3782 A71-43907

Thermal conductivity, diffusivity and specific heat of lunar soil and basalt analogs, using Luna 16 samples
24 p3873 A71-45103

DIFLUORIDES
NT CALCIUM FLUORIDES
Atomic bond strength of solid solution hardening as function of composition for calcium/strontium difluorides, using vibrational IR and laser Raman spectra
12 p1877 A71-26804

Calcium difluoride powder under sintering, examining optical transparency and morphological features
19 p3069 A71-38049

Flash photolysis produced gaseous carbon difluoride IR spectrum analysis by rapid scan IR spectroscopy
19 p3011 A71-38053

DIFLUORO COMPOUNDS
NT POLYTETRAFLUOROETHYLENE
DIGESTING
Eating and digestion effects on conscious dog coronary and visceral vasoactivity
01 p0015 A71-11183

DIGESTIVE SYSTEM
NT ESOPHAGUS
NT GASTROINTESTINAL SYSTEM
NT INTESTINES
NT MOUTH
NT PANCREAS
NT RECTUM
NT STOMACH
NT TONGUE
Soyuz 9 spacecraft astronauts space flight effect on digestive system enzyme secretion function based on pre- and post-flight examinations
09 p1389 A71-22206

Secretory function intensity of salivary glands, liver and stomach of animals and humans with different water-salt metabolism conditions
11 p1719 A71-25669

Microflora simplification effects on immunocompetent organism systems, observing shifts in guinea pigs lymphoid tissue with limited flora
21 p3332 A71-40555

DIGITAL COMMAND SYSTEMS
Fluid logic random input, irregularly activated or stochastic control network analysis, using digital control network synthesis technique [DICONESYN III]
15 p2351 A71-31685

Direct digital control technology for optical tracking systems, discussing advantage and deficiencies
18 p2883 A71-36913

Photogrammetric instruments digital servo, using printed disk DC motor drive, incremental measurement, nonlinear feedback and digital integrated circuit logic
20 p3233 A71-38829

Variable structure digital control servomechanism flutter mode analysis, using nonlinear differential equation
22 p3528 A71-42878

Digital servo system with signal quantization by level and time, evaluating oscillating motion in steady state mode
23 p3655 A71-43292

DIGITAL COMMUNICATION
U PULSE COMMUNICATION
DIGITAL COMPUTERS
NT IBM 360 COMPUTER
NT ILLIAC 4 COMPUTER
NT PDP COMPUTERS
NT PDP 8 COMPUTER
NT RCA SPECTRA 70 COMPUTER
NT SEQUENTIAL COMPUTERS
Batch/Time-Sharing Monitor for achieving balance of digital computer systems efficiency and responsiveness, discussing performance modeling and empirical measurements
01 p0043 A71-10178

Multiprogrammed and time shared multiaccess digital computers operating systems design, discussing dynamic memory protection structures
01 p0043 A71-10179

Time sharing executive component of general purpose operating system for digital computers, discussing architecture and construction
01 p0043 A71-10180

Operational memory share supervisor program with storage protection feature for real time multitask digital process control and teleprocessing of electrical power utility system
01 p0043 A71-10181

LSI device standardized set for implementing digital computer systems of varying functional complexities
01 p0044 A71-10183

Computerized acquisition and processing of radar precipitation signals and lightning data
01 p0050 A71-10595

Digital control system for azimuthal optical telescope, using invariance techniques and photoelectric system to compensate for position and program errors
01 p0081 A71-10727

Basic digital circuits with integrated TTL and MOS structural elements, giving diagrams for dual counters, frequency dividers, adders and shift registers
02 p0231 A71-11862

Automatic test equipment with digital computer for control, discussing software schemes and tradeoff analysis
03 p0381 A71-13079

ELDO inertial guidance system digital computer, explaining guidance law subsystem formulation and programming
03 p0454 A71-13247

Aerospace digital computer partitioning based on MOS MSI technology using functional building blocks /FBB/
03 p0384 A71-13281

Digital computers in aviation electronics, discussing automatic control loop in automatic pilot
03 p0382 A71-13687

High speed magnetic printing apparatus for digital computers, discussing ferrographic process
03 p0382 A71-13819

ESCA /Electron Spectroscopy for Chemical Analysis/ spectrometer using small digital computer as process regulator
03 p0428 A71-13925

Solar spectrograph data transmission to digital computer, discussing intermediate magnetic tape storage
04 p0590 A71-14841

Automatic excitation forces generation for aircraft structure ground vibration tests using digital computer [ONERA-TP-870]
04 p0669 A71-15352

Linear digital computer simulation and process control, considering state space method
05 p0730 A71-16126

Multicomputer system with preparatory and processing subsystems, discussing algorithm for distributing problems flow among processors
05 p0726 A71-17018

Kalman linear multidimensional filters stability, examining digital computer algorithms
05 p0732 A71-17024

All-digital multichannel narrow band FSK data receiver with time-shared arithmetic processor, discussing prototype design and performance [IEEE PAPER 70-TP-49-COM]
05 p0724 A71-17064

Real time processor design for sequential control of all-digital multiline data set [IEEE PAPER 70-TP-375-COM]
05 p0725 A71-17067

Multichannel on-line data terminals using minicomputer for communication control, error detection and data buffering [IEEE PAPER 68-TP-448-COM]
05 p0727 A71-17068

Digital computer operated from remote terminal for signal analysis including Fourier transform, complex multiplication and conjugation

05 p0727 A71-17144

Digital computer components reliability determination, using bypass algorithm

06 p0870 A71-17492

Field distribution in multiple-opening ferromagnetic digital computer elements, using linear approximation integral method

06 p0872 A71-17497

Digital computer techniques for Mars surface imagery systematic video data distortions quantification and correction onboard Mariner 6 and 7

06 p0871 A71-17631

Stored-programmed special purpose computer for double precision arithmetic realization of digital filters, discussing design, implementation and testing

07 p1067 A71-18733

NASA ground based digital data processing facility for Earth Resources Technology Satellite system

07 p1067 A71-18804

Navy avionics modular multiprocessing digital computer operating system reliability, comparing totally software and partly hardware approaches

07 p1067 A71-18833

Complex digital computer systems effectiveness measurement, using simulation program with programming language SIMSCRIPT

[AIAA PAPER 71-229] 07 p1068 A71-19707

ECG beat-to-beat variation reduction using digital computer wave recognition

07 p1049 A71-19839

Associative digital processor with associative memory for high speed ATC data processing, discussing design and operation

07 p1068 A71-19997

Universal materials testing system control using digital computer and changeable programs

07 p1069 A71-20201

Engineering data integrated test system with sensor based digital computer for data collection and test control

07 p1069 A71-20202

Data handling system with digital computer and multichannel scanning, processing and recording for simultaneously conducting two environmental tests of satellites

07 p1069 A71-20403

Microprogramming by Computer Design Language for describing digital computer functional configuration and sequential operation

07 p1069 A71-20404

Multiradar tracking system with monoradar units interconnected by central digital computers for wide airspace surveillance

08 p1255 A71-21598

Optimum antenna array processing design for target detection in nonuniform clutter background, using decision-theoretic processor with digital computer

08 p1256 A71-21604

Digital computer modular LSI control logic design using multifunctional binary decoder with transistor array read-only memory for odd and even parity error detection

08 p1260 A71-21663

Harmonic analysis of metals and alloys fine structure X ray photographs via digital computers

08 p1293 A71-21765

Time shared digital computer-based data acquisition and control system for multiple remote laboratories, using modular programming, multiprocessing and language processors

08 p1260 A71-21851

Multiple reflections method for complex reflection and transmission coefficients of microwave transmission line permitting use of digital computers

09 p1413 A71-22151

Integrated dynamic digital computer elements, examining regenerative information storage, internal duration determination by clock pulse frequency and switching

09 p1411 A71-22494

Biosatellite 3 neurophysiological data analysis by digital computer presenting maps of parietal cortex spectra, responsive states transient changes, circadian rhythms and EEG activity

09 p1395 A71-23243

British Aircraft Corporation Numerical Master Geometry system using parameter surface mathematics and digital computer

10 p1580 A71-23759

Man-machine interactive scanned-display computer graphics system implemented on Honeywell DDP-224 computer

10 p1581 A71-23967

Book on digital computers in engineering covering systems, man machine communication, numerical analysis, network analysis program, circuits, devices, control, etc

10 p1581 A71-24476

Six degree of freedom hybrid digital computer program for complex flight control and associated mode logic design and training

11 p1736 A71-25852

Wind structure in boundary layer pilot-balloon observation, discussing baseline data processing for digital computer

11 p1796 A71-26560

Experiment planning, using digital computer in real time with programmed algorithm

12 p1883 A71-26713

Analog recursive computer with serial digital program for arithmetic unit and storage system control

12 p1884 A71-27150

Floating point arithmetic units design for large high speed digital computer

12 p1884 A71-27151

Plant and compensator parameters deviations effect on accuracy of complex unitary-code programmed automatic control system with delay line digital compensator

12 p1893 A71-27342

Multistage axial flow compressors on digital computer, testing gas dynamic design in final adjustment phase

13 p2115 A71-28584

Time sharing digital computers busy period task completions modeling as semi-Markov process

13 p2035 A71-28974

Combined data compression and error control by digital sequential decoding for space to earth data links using digital computers

14 p2193 A71-30023

Wind tunnel model trajectory simulation system with closed loop control by digital computer, describing instrumentation, system servoamplifiers and testing procedures

14 p2208 A71-30334

Maastricht Automatic Data Processing and Display ATC system with digital computers for aiding controllers in issuing instructions and making decisions

14 p2272 A71-30383

Inertial navigation systems improvements for commercial air transportation, noting digital computer program revision and increased functional capability

[SAE PAPER 710458] 14 p2272 A71-30534

AN/ASN-86 inertial navigation system consisting of inertial platform, digital computer and control indicator

[AHS PREPRINT 533] 14 p2273 A71-31094

EEG phase relations measurement technique, using small digital computer for frequency components separation and EEG activity phases comparison between electrodes

15 p2363 A71-31959

Small scale solid state digital computer for experimental medical data statistical processing

15 p2365 A71-32534

Digital computer techniques for transient data processing and test control

17 p2709 A71-34544

Interactive digital computing systems survey, describing one language AMTRAN system as example

17 p2710 A71-34621

Mathematically oriented digital computer system implemented on IBM 360 with graphic remote consoles for engineering problems

17 p2710 A71-34622

Digital computer process controller for telescope with driving system consisting of single worm wheels for tracking and slewing

17 p2740 A71-34985

Small digital computers applications to astronomical electronic instrumentation systems of microphotometry and spectroscopy

17 p2743 A71-35010

Hardware executive control with associative memory for avionics digital computer system, comparing computation speed, cost and reliability with software method

17 p2712 A71-35778

Computer-disk interface system phototactical instrumentation for weather data acquisition, analysis and display

18 p2884 A71-36078

Digital computers for analytic solution of second order nonlinear ordinary differential equations

18 p2884 A71-36142

Ferrite core memories for information storage of digital computer onboard Eole satellite, discussing design and reliability measures

18 p2891 A71-36560

Low power nonpulsating arithmetic unit of 16 bit integer numbers for spaceborne applications, using module printed circuit cards

18 p2886 A71-36570

Integrated digital emitter coupled logic (ECL) circuits with transistors in nonsaturated mode

18 p2896 A71-36799

Minerva digital computing system with learning cells and electronic microcircuit elements capable of self organizing similar to human intelligence

19 p3025 A71-37420

Computer aided digital transform natural image processing, using Fourier, Hadamard and Haar matrix algebra

19 p3026 A71-38404

Random vibration testing digital computer control system and experiment design, considering discrete Fourier transform techniques application

[ASME PAPER 71-VIBR-30] 21 p3360 A71-40283

Subnanosecond digital computer with emitter-coupled fully integrated circuit packaging concept

21 p3351 A71-40744

Coherent optical processing system coupled to electronic readout system incorporating image orthicon TV camera, small digital computer and cell generator

21 p3381 A71-40929

Ternary code and three value logic in digital computers, considering economic advantages, signal distinguishability and numerical interpretation of p digit abstract alphabet

22 p3516 A71-41856

Fast Fourier transform calculating discrete Fourier transform, considering optimized algorithm for digital computers

22 p3566 A71-42249

Digital computer holography, discussing generation, reconstruction, applications in optical spatial filtering and surface testing and sampling and quantization effects

22 p3546 A71-42479

Australian National Radio Astronomy Observatory integrated time and frequency system with cesium beam frequency standard and digital computer for real time operation

22 p3547 A71-42498

Digital computer applications to physics problems, giving examples of plasma research and methane molecule properties determination based on quantum mechanics

24 p3847 A71-44355

Design method for high speed economical arithmetic units of digital computers, describing functional logic circuits

24 p3806 A71-44396

Muscular bioelectric potential input processing into digital computer, describing amplitude, frequency and time domain analysis of electromyogram signals

24 p3801 A71-44542

DIGITAL DATA

Contour-mapped and digital data field processing and analysis for National Severe Storms Laboratory /NSSL/ radar signal processing and recoding system

01 p0118 A71-10590

Information collection from ocean data stations networks by satellite and HF digital data communications, noting feasibility of VHF telemetry communications

01 p0037 A71-10991

Soviet papers on digital information transmission via channels with memory

01 p0039 A71-11314

Two-directional digital data transmission system, determining probability of not obtaining message for arbitrary interrogation signals number

01 p0039 A71-11319

Astronomical objects light polarization recording on magnetic video tape, providing digitized data for computer input

03 p0424 A71-13631

Statistical analysis of digital data transmission time error distributions in Polish post office and railroad communications network

03 p0380 A71-14375

Solar spectrum line digital recording, discussing design and operation principles

04 p0590 A71-14842

Digital asynchronous information transmission, describing schemes for coding binary into ternary signals

05 p0724 A71-17058

Automatic cartography, using plotting machine digital output via attached shaft encoders

06 p0895 A71-18292

TV monitoring and digital data recording of human corneal reflection during voluntary eye movements, considering visual perception studies application

07 p1051 A71-20210

Fluidic pneumatic control system compensator for digital signal processing

07 p1026 A71-20567

Special purpose analog and digital data acquisition systems for test and instrumentation requirements

09 p1449 A71-22789

Solid state pulse modulated radiodecade for meteorological data transmission in digital form, using MOS integrated circuits

10 p1583 A71-24052

Analog, digital and special data processing equipment interface for aerospace computer system

11 p1735 A71-25844

Error detection and/or correction coding techniques for digital data transmission, comparing efficiency

13 p2036 A71-29279

Vibration data analysis of analog and digital methods for cost comparisons

14 p2221 A71-30057

Asynchronous digital node combination into synchronous multiplex with data traffic routing functions through switch from remote terminals

14 p2201 A71-30928

- Low voltage signal conversion to digital code, emphasizing SNR improvement 15 p2382 A71-32452
- Microphotometer digital data processing at Canadian astrophysical observatory 17 p2743 A71-35007
- Upper bound on error probability due to intersymbol interference for correlated and uncorrelated digital signals, presenting examples for data communication systems 17 p2703 A71-35077
- Multiple access satellite digital communication system with onboard distribution center, discussing time frame synchronization methods 17 p2706 A71-35105
- High speed BPSK communication components and system aspects with V band propagating medium, considering carrier modulation and transmitted digital data reception with minimum errors 17 p2709 A71-35759
- Synchronization of high-speed digital data communication systems with continentwide interconnected switching centers, discussing elastic storage buffering to compensate for transmission time delay variations 17 p2712 A71-35784
- Airglow surveys using extended field large aperture interferometer-spectrometer with optical wedge compensators and digital recording 18 p2914 A71-35842
- Infrared Michelson interferometer system digital data processing by computer, developing spectral density plots 18 p2920 A71-36092
- Digital data acquisition and processing systems for large quantity rapidly generated measurements using reduction computer 18 p2885 A71-36160
- Perturbation free delay time measurement in digital data processing system, using Schmitt triggers or tunnel diode discriminators 18 p2885 A71-36225
- Ground acquisition of digital rate synchronization during experiments in French Dioscures project 18 p2946 A71-36512
- Error occurrence due to perturbations in space communication channels for digital data transmission, describing binary channels models based on Markov chains 18 p2881 A71-36567
- Star sensor telescope, employing digitally coded silicon photocell detector for precise optical image location 18 p2925 A71-36910
- Flying spot digitizer angle encoding system, describing multispeed transducer output conversion to digital format 18 p2925 A71-36914
- National Aviation System stage A ATC displaying digitized radar data positions together with automatic track positions 22 p3570 A71-41634
- Signal to quantizing noise ratios for differential PCM systems used to encode analog signals from Markov processes into digital form 22 p3514 A71-42391
- Binary coding and phase displacement modulation of digital data in radio transmission 22 p3514 A71-42471
- Bit error rate detector for testing digital data links, using analog network mathematical model 22 p3519 A71-42764
- DIGITAL FILTERS**
- Digital delta filter for quantifying sleep EEG slow wave activity 01 p0011 A71-10767
- Digital filtration and processing of electrocardiograms on computers using linear difference equations 03 p0367 A71-12992
- Book on electrical, microwave and digital filter systems and design covering approximations, phase shift, ladder networks, frequency transformation, time domain, etc 04 p0560 A71-15075
- Time shared FSK FM modulator using second order digital filter with one variable multiplier 05 p0725 A71-17066
- Soviet book on radar signal processing optimization covering detection and measurement, electronic analog and discrete digital filters design, etc 06 p0867 A71-17445
- Stored-programmed special purpose computer for double precision arithmetic realization of digital filters, discussing design, implementation and testing 07 p1067 A71-18733
- Power spectrum analysis of ELDO Europa 1 third stage thrust phase vibrations, using digital filters 07 p1208 A71-19804
- Digital adaptive spectral filtering canceling undesired power spectra based on measured mean square values ratio and stochastic approximation methods 07 p1082 A71-20408
- Strapdown inertial navigator alignment by digital filtering techniques, discussing application to aircraft and spacecraft 08 p1331 A71-21170
- Adaptation algorithm for real time minimum mean square error array processing, using with multidimensional digital filter 08 p1256 A71-21605
- Arterial circulatory system parameter identification from diastolic blood pressure curves by digital filter techniques 09 p1398 A71-22254
- Amplitude characteristic polynomial Chebyshev approximation by linear phase nonrecursive digital filter transfer function 09 p1417 A71-23037
- Pulse radar moving target indication and stationary targets reflection suppression, using recursive type digital filter and quadrature channels for improving signal detectability 10 p1579 A71-25068
- Gram-Charlier error probabilities of digital satellite communication systems due to intersymbol interference and additive noise applied to Chebyshev, Gaussian and cutoff filters 12 p1879 A71-27069
- Two theorems on minimax transversal filter equalization at receiver for digital communication systems distortion reduction 14 p2193 A71-30012
- Digital filters, describing transfer function, frequency response, stability and design 16 p2546 A71-33478
- Stellar spectrograms digital filtering for SNR improvement for photographic plate with line widths larger than granulation noise mean period 17 p2743 A71-35008
- Digital filtering in PCM communication systems with active repeater satellites and space vehicle telemetry 18 p2881 A71-36569
- Probability error calculation for digital signals contaminated by intersymbol interference and additive Gaussian noise 19 p3015 A71-37222
- Modular component computational algorithm for sequential least squares estimation /filtering/ with process noise for straightforward computer code conversion 20 p3201 A71-38757
- Surface wave digital and analog signal processing filters for time delayed, frequency or phase coded transmission and reception applications 21 p3357 A71-40811
- Digital programmable matched filter for LSI technology, considering signal/noise discrimination 22 p3519 A71-41511
- Automatic control systems optimal nonlinear digital filter design, using theoretical numerical grid 24 p3813 A71-44680
- Respiratory sinus arrhythmia by spectral analysis and digital filtering, using linear model to approximate lung volume relationship to heart rate during normal breathing 24 p3802 A71-45067
- DIGITAL INTEGRATORS**
- Digital range-bin integrator for precipitation echoes, using static shift registers as memory element 01 p0049 A71-10592
- Solid state digital integrator for weather radar signals, using recursive integration scheme 01 p0050 A71-10593
- Decoding n-bit Johnson code to decimal numbers using n 2-input 2-output comparator circuits 01 p0037 A71-11175
- Sampling efficiency of total power balanced Dicke type radiometers using digital integration 08 p1267 A71-21879
- P channel enhanced MOS transistors, logic elements and digital integrated circuits in silicon films on sapphire substrates 13 p2038 A71-28716
- Hybrid binary floating point digital differential analyzer technology, noting speed, cost and utility 14 p2207 A71-30021
- Binary moving-window integrator radar target azimuth measurement error determination, presenting target detection probability curves obtained by digital simulation 21 p3348 A71-40725
- DIGITAL NAVIGATION**
- Converter-indicator direct digital readout design, using photodiodes for LSI VOR area navigation display systems low power operation 09 p1491 A71-22610
- Carrier aircraft inertial navigation system /CAINS/ design, noting thermal modeling, statistically filtered alignment modes and digital data links 22 p3571 A71-42081
- DIGITAL SIMULATION**
- Project DARE /Differential Analyzer Replacement/ providing all-digital on-line digital simulation of dynamical systems 01 p0046 A71-10199
- MOBSSL-UAF block structured simulation language for digital and hybrid computers 01 p0046 A71-10200
- Hybrid computer programming for continuous systems simulation 01 p0046 A71-10201
- Digital structures simulation system as computer systems design aid, discussing basic building blocks, flow charts, task assignments, cost and performance constraints, etc 01 p0048 A71-10222
- Digital simulation of steam boiler by process control computer using coefficients directly calculable from transfer function of continuous system 01 p0049 A71-10324
- Speech signals digital encoding with adaptive linear predictor for reducing redundancy, discussing digital simulation results and subjective comparison with log-PCM encoder 01 p0030 A71-10472
- Error model and digital computer simulation programs for technical management of missile development and testing 01 p0068 A71-10883
- Data transmission/acquisition/processing systems engineering project management using digital simulation models 01 p0184 A71-10885
- Digital simulation for translational and rotational equilibrium breakdown in gaseous molecules expansions by Monte Carlo method 01 p0130 A71-10936
- Three dimensional dynamic CRT display for simulation, using VECTRAN /Vector Transformer/ digital computing device for control 01 p0084 A71-11394
- Computer source code generation for symbolic partial differentiation program for continuous system digital simulation 02 p0226 A71-11778
- Fast on-line block-diagram-based DARE II digital simulation program for use on PDP-9 computer with CRT display console 02 p0226 A71-11779
- Nonlinear differential equations description in functional product form structure for digital simulation 02 p0226 A71-11781
- Satellite system design digital simulation model in GPSS language for performance interrelationships between subsystems and reliability gain in orbit from redundancy 02 p0318 A71-11782
- Mathematical model and digital simulation for nonlinear characteristics of prototype integrated actuator package for fighter aircraft control 02 p0190 A71-11783
- Tactical missile flight test planning using digital simulation data reduction techniques for fast cost effective trajectory synthesis 02 p0226 A71-11784
- Real time six degree of freedom aircraft flight digital simulation using SL-1 continuous system simulation language 02 p0226 A71-11786
- Aircraft manual flight control analysis using continuous mathematical pilot model for closed loop digital simulation 02 p0188 A71-11787
- Six degree of freedom flight vehicle kinematics digital simulation using CSSL-II language 02 p0227 A71-11789
- Digital simulation computer program in FORTRAN IV for radar systems performance evaluation in various environments 02 p0211 A71-11796
- Large hybrid simulation and analog section replacement by digital model, considering digital simulation techniques for economical solution of special problems class 02 p0227 A71-11797
- Human body temperature regulation feedback control system model by electric circuit analog, discussing digital simulation for static and dynamic responses 02 p0203 A71-11805
- Digital simulation mathematical model describing simultaneous energy and mass transfer process in clothing-airspace-skin system 02 p0203 A71-11806
- Atmospheric general circulation model for numerical climate digital simulation and weather forecasting, using fluid flow equations 02 p0277 A71-11808
- Digital simulation program in GPSS language for airline operations including aircraft maintenance, flight scheduling, terminal space, equipment, work forces utilization, etc 02 p0227 A71-11809
- Thermionic system transient behavior analysis by digital simulation using one diode model 02 p0196 A71-12261
- Hydride thermionic reactor system transient behavior dynamic mathematical model and digital simulation 02 p0281 A71-12262
- Communication satellite ground station steerable antenna autotracking, evaluating on-line optimal search techniques by digital simulation 02 p0222 A71-12791
- Sounding rocket-moving target spatial relationship trajectory modeling by digital simulation, applying to vehicle launching during solar eclipse of March 1970 [AIAA PAPER 70-1374] 03 p0497 A71-13657

Postflight analysis including six degree of freedom trajectory digital simulation of Aerobee 350 sounding rocket behavior under large thrust misalignment [AIAA PAPER 70-1380] 03 p0498 A71-13663

Wind compensation method for launching sounding rockets susceptible to nonlinear wind effects, using data generated by six degree of freedom trajectory digital simulation program 03 p0498 A71-13672 [AIAA PAPER 70-1390]

Finite difference simulation of high energy Mach 120 to 40 air shock experiment 04 p0565 A71-14678

German monograph on digital simulation system for ergonomic investigation of radar observation problems covering flight plan data with density variation 04 p0551 A71-14900

MF, LF and VLF ionospheric radio wave propagation theory using spherical wave functions for computer simulation 04 p0552 A71-15215

Time sharing program for digital logic circuits simulation 05 p0726 A71-16959

Coherent communication link pseudonoise synchronization error due to white Gaussian noise and amplitude jitter produced by reference carrier phase error, discussing digital simulation 05 p0725 A71-17072

OAQ simulation system including prototype spacecraft and digital computer for verifying ground system performance 05 p0734 A71-17131

Stratified statistical filtering algorithm for numerical simulation of nonlinear systems behavior 07 p1081 A71-18836

Computer generated motion pictures to simulate real events, discussing design problems and airfield simulation with GPSS software package 07 p1111 A71-19511

Selection index estimation from partial multivariate normal data for precision improvement, discussing procedure and Monte Carlo simulation results 07 p1147 A71-19599

Satellite carrier tracking and phase lock carrier loops, evaluating lock and reacquisition performance loss by linear model and Monte Carlo digital simulation 08 p1270 A71-21352

Linear antenna radiation patterns digital computer simulation, applying algorithm based on Kotelnikov to antenna synthesis 08 p1266 A71-21467

Unique word detection in digital burst communication, determining effects on voice quality from analytic study and digital simulation 08 p1255 A71-21595

Electromechanical systems digital simulation, discussing reticulation, bignaph reduction, mathematical modeling, etc 09 p1428 A71-22774

Analytical nonlinear landing gear model of flexible aircraft and strut lockup-breakout interaction using digital simulation language /DSL/ [SAE PAPER 71-0401] 10 p1555 A71-24263

Digital simulation facility for airborne collision avoidance system effects on ATC terminal automation, discussing operation, hardware and software equipment 10 p1590 A71-24774

Josephson junction I-V characteristics self resonant current peaks calculation by finite difference scheme simulation, comparing results with perturbation technique and experiment 11 p1742 A71-25800

German book on simulation systems for digital computers covering programming language requirements, program structures and comparative analysis 14 p2207 A71-30263

Autonomous unknown landmark tracking space shuttle navigation system performance assessment by digital computer program providing error analysis and Monte Carlo simulation 17 p2773 A71-35067

BITSIM computer simulation technique for application to real time airborne photoreconnaissance imagery data transmission system design and performance analysis 18 p2917 A71-36070

Nonlinear time varying systems digital integration simulation techniques by variational equations approach, discussing accuracy, execution time and limitations 18 p2884 A71-36141

Dynamic formulation for number of communicative civilizations in Milky Way galaxy suitable for digital simulation 18 p2965 A71-36295

Free-Lagrange method for two dimensional flow numerical simulation, covering mesh optimization and equations of motion 18 p2905 A71-36304

Prototype space station environmental thermal control and life support system digital simulation for transient design and performance prediction [ASME PAPER 71-AV-34] 18 p2869 A71-36401

Flow simulation with digital computer by Monte Carlo computation methods based on interacting molecular gas kinetics, noting application to gas flow 18 p2941 A71-36427

Boeing 747 digital computer type flight simulator with four degrees of movement for engineer and pilot training 18 p2901 A71-36971

Digital simulation for predicting static directional aerodynamic forces and moments characteristics of air cushion vehicle configuration through 180 degrees of sideslip 19 p2995 A71-37158 [AIAA PAPER 71-907]

Kalman filter for computerized optimal SRAM air to surface missile alignment, discussing design, digital simulation and flight tests 19 p3098 A71-37189 [AIAA PAPER 71-948]

Collisionless plasma Vlasov and Poisson equations numerical solution based on Fourier-Fourier transform, comparing with particle motion simulation 19 p3113 A71-37748

Digital simulation of pseudowaves and plasma sheath formation about grid by computer solution of ion Vlasov equation for ion distribution function time evolution 19 p3113 A71-37749

Airfield surface system digital simulation model application to airport planning for airline operations 19 p3041 A71-38022

Air traffic congestion and delay Monte Carlo digital simulation in FORTRAN, exemplifying two-runway airport operation under instrument flight rules 19 p3041 A71-38024

Picture processing using general purpose digital computer simulation for reduction of processing time and special purpose hardware investments 21 p3376 A71-40111

Fast time digital computer simulation model for evaluation of man-machine interface /display/ problem of ATC system including personnel and equipment 21 p3412 A71-40112

Information producing capabilities of various combinations of SNR, bandwidth and contrast in simulated digital encoding TV systems 21 p3347 A71-40130

Graphical display of digital computer simulated steady state unbalanced turborotor response for lumped and distributed parameter models, using GATRAN language [ASME PAPER 71-VIBR-42] 21 p3459 A71-40292

Digital picture processing and holography, considering spatial filtering computer simulation and image synthesis 22 p3539 A71-41745

Digital computer simulation of random disturbances with uniform distribution, determining generated sequence correlation coefficient mean and variance 22 p3518 A71-42492

Thermal radiation hemi-ellipsoidal and hemispherical collectors efficiency characteristics from Monte Carlo simulation for focusing photon bundle trajectories 23 p3783 A71-44191

Error evaluation of digital real time simulation of nonlinear systems 24 p3813 A71-44571

Digital computer simulation for extremal finite network synthesis 24 p3806 A71-44715

DIGITAL SYSTEMS

NT DIGITAL NAVIGATION

Digital systems intermittent failures effects and detection, using system simulation 01 p0046 A71-10204

Quantization in data transmission and extraction, considering analog signals transmission in digital form and radar echoes recognition by digital integration systems 01 p0029 A71-10307

Fluidic systems as digital devices, considering stream interaction, vortex and turbulence amplifiers 01 p0006 A71-10801

Digital FM discriminator for demodulating FM signals with high deviation percentage 01 p0033 A71-10899

Reliability test for fluidic digital comparison device 01 p0006 A71-10925

Auto and cross correlation function computation from waveform polarity by flexible one bit digital correlator for frequencies to 25 MHz 02 p0211 A71-11644

Digital hybrid systems simulator /DIHYSYS/ program, examining subsystems sampling and execution time and applications 02 p0226 A71-11780

Time division multiplexing methods for optical communications systems, considering error performance of digital formats used with mode-locked laser sources 02 p0214 A71-12021

Digital network data communication system advantages, characteristics and configuration 04 p0550 A71-14747

MOS transistor and circuits in digital applications presenting current-voltage characteristics, conduction resistance, transconductance, etc 04 p0557 A71-15083

Solid state circuit digital frequency discrimination with low pass filter in ESRO stations telemetry receivers AFC and antisideband system 05 p0720 A71-16323

Digital tachystoscope functions, operating principles and designs, discussing tests of visual perception related functions 05 p0714 A71-16924

Dynamic digital predictive compensation learning control systems with time delay transform identification by template matching technique 06 p0878 A71-17334

Coded control circuit for digital frequency synthesizer 06 p0870 A71-17494

Relay type pulsed control systems performance, determining noise effects by statistical analysis 06 p0879 A71-17927

Digital attitude reference systems for three axis stabilized earth oriented satellites using sun sensor measurements [AIAA PAPER 71-61] 06 p0926 A71-18520

Long life spacecraft tape recorders, considering digital and analog equipment and life and reliability testing of components and complete units 07 p1106 A71-18812

Binary sequences with relaxed Barker criterion, examining correlation coefficients 07 p1149 A71-20418

Digital transmission in Defense Communications System, discussing data requirements, converter and TDM involving terrestrial and satellite links 07 p1066 A71-20432

Digital turbulence amplifiers, investigating dynamic switching response 07 p1024 A71-20552

Digital active fluid amplifiers static and dynamic behavior, defining complex parameters for system engineering 07 p1026 A71-20564

Moving part digital pneumatic logic system, using elements molded into rubber sheet between two rigid flat plates 07 p1027 A71-20575

N-channel PSK/PM digital telemetry system modulation scheme for space exploration 08 p1254 A71-21315

First order digital phase locked loops analysis for single channel command system, using random walk techniques 08 p1270 A71-21351

Areal precipitation quantitative radar measurements, describing signal processing and digital system for contour mapped displays and numerical summaries 08 p1257 A71-21738

Electronic digital automatic defect indicator attachment to industrial echo defectoscope 08 p1300 A71-21897

Digital synthesizers design and operation for radio communications, discussing reception and transmission noise performance, frequency stability and acquisition time 10 p1579 A71-24757

Respiration parameters digital recording system, describing analog signal recording and processing, analog to digital conversion and digital readout equipment and techniques 11 p1724 A71-25595

Accuracy requirements determination method for digital controller coefficients, discussing bits needed 11 p1792 A71-26415

Frequency phase multistable elements, discussing automatic control, telemechanics and digital measurement applications 11 p1739 A71-26465

Computer programs for random noise vibration test digital control, describing data base and logic programs 11 p1736 A71-26499

Direct digital control system for random excitation environmental testing, discussing interfacing of TIME/DATA time series processor and minicomputer 11 p1736 A71-26500

Digital control systems for electrodynamic vibration exciters, discussing computer ranged instrumentation amplifier, digitally controlled sine wave oscillator and FFT processor 11 p1746 A71-26503

Synthesis of high speed digital computer non-searching adaptive control program to ensure closed system required dynamic characteristics for complex linear unsteady control plant 12 p1926 A71-26731

Testistorized multichannel registers for optical oscillograph records, discussing frame storage and digital processing circuitry 12 p1889 A71-27755

Book on nonlinear modulation based on optimum estimation theory covering phase synchronization,

analog data transmission, digital and analog systems performance, Markov processes, etc
13 p2029 A71-28041

Digital multiplier based on cellular logic iterative arrays for complex numbers processing
13 p2037 A71-28470

Power line and signal line transients in digital systems
13 p2032 A71-28863

Quantization by levels effect on steady state processes in digital automatic control systems
13 p2044 A71-28918

Failures detection in combinational digital switching circuits due to component malfunction
13 p2036 A71-29291

Metal oxide semiconductor digital circuit supply voltage, load capacitance and standby power drain
14 p2206 A71-29547

Quandary recognition and referee strategy in digitally controlled modal survey system, noting decision making sources
14 p2208 A71-30314

Direct digital control and data acquisition system for propulsion research testing, transmitting data over differential signal pairs to remote test cell
14 p2208 A71-30316

Integrated flight test data system combining digital airborne data acquisition/recording system with telemetry/microwave link to computerized ground station
14 p2243 A71-30318

Parallel pressure multiplexer and encoder for aerodynamic testing, employing zero pressure detectors coupled with IC digital electronics and reference pressure signal
14 p2222 A71-30342

Low-power long-life high-accuracy digital inertial reference assembly, using dual voltage spinmotor operated pulse rebalanced temperature compensated gas bearing gyroscopes
14 p2272 A71-30803

Digital wire line system data bus design, calculating transmission performance of noise environment shielded twisted pair cable by linear filter model
14 p2198 A71-30904

Microstrip p-n diode controlled L band digital phase shifter for aircraft-satellite communication
14 p2217 A71-31055

Digital on-off follow-up system dynamics under signal time and amplitude quantization effects on transient and steady state processes, using phase-plane analysis
15 p2382 A71-32453

Digital systems synthesis for stabilization of triaxial gyrostabilizer consisting of three uniaxial gyrostabilizers with cross couplings
17 p2738 A71-34559

Digital phase locked loop for FM signals demodulation, considering system nonlinear difference equation
17 p2704 A71-35084

Computer simulation of error probability performances of binary coherent PSK system under thermal noise and intersymbol and interchannel radio interferences effects
17 p2707 A71-35476

Binary differentially coherent PSK modulated PCM radio link performance under noise and intersymbol and interchannel interferences effects, deriving error probability
17 p2707 A71-35477

Binary and quaternary PSK systems performance with intersymbol, interchannel and cochannel interferences and fading
17 p2707 A71-35478

Automatic system for follow-up balancing of digital bridge, noting fast response rate
17 p2723 A71-35711

Rapid response multiple phase detector for balancing of AC digital bridge networks
17 p2718 A71-35712

Avionic and missile computer control systems, describing universal function unit design and digital processing requirements
17 p2711 A71-35775

Fluid amplifier digital elements dynamic switching, noting back pressure effects
18 p2851 A71-36207

Optical wideband digital communication system performing operational space-ground link functions
18 p2878 A71-36520

Discrete time digital flight control systems design resulting in closed loop aircraft response characteristics approximation to prescribed flying quality specifications
19 p3024 A71-37196 [AIAA PAPER 71-955]

Automated test capability for digital modules, describing test generation, circuit analysis and simulation programs
19 p3030 A71-38406

Ternary delta modulation evolution from binary system by addition of encoder-analyzer, calculating SNR
20 p3202 A71-39468

Digital sequential detector based on range sampling technique, comparing performance to digital sequential probability test /SPRT/ detector
20 p3206 A71-39906

Signal quantization induced low amplitude oscillations in digital control systems, discussing relationship to digital controller programming form
21 p3361 A71-40980

Statistical analysis of digital automatic control system with unreliable communication channel, determining system mean square error
22 p3525 A71-41439

Multijunction functional devices for operation as decade digital counter, step voltage generator, analog/digital converter, binary counter, neuristor line, etc
22 p3520 A71-41706

Semiconductor diode image tube system as digital multichannel photometer, noting cost, weight and size advantages over photomultiplier tube array with pulse counting electronics
22 p3541 A71-41793

Soviet book on digital servomechanisms dynamics covering logarithmic frequency characteristics and pulsed and hybrid control systems
22 p3526 A71-41800

Reed-Solomon erasure-correcting sequential decoder implementation for hybrid coding scheme, using digital circuitry
22 p3513 A71-42387

Two dimensional holography application to fault-tolerant high density mass data storage design for digital information retrieval system
22 p3548 A71-42517

Active digital and proportional fluidic devices design and manufacture including turbulence, wall-attachment, focused jet, beam deflection and vortex amplifiers
22 p3483 A71-42783

German monograph on analysis and design of digital microwave phase shifters for phase controlled antennas covering admittance loaded lines, transmission and reflection behavior
23 p3649 A71-42999

DIGITAL TECHNIQUES

Cryptographic techniques applications to data processing systems, considering digital substitution and digital route transposition matrix
01 p0044 A71-10187

Digital simulation of steam boiler by process control computer using coefficients directly calculable from transfer function of continuous system
01 p0049 A71-10324

Inertial navigation system augmented by digital distance measuring equipment in FAA flight inspection aircraft for performance evaluation
01 p0124 A71-10507

Weather radar echoes quantization following detection, discussing subsequent digital processing
01 p0049 A71-10591

Block code for retransmission of information damaged by noise bursts for feedback digital communication systems
01 p0034 A71-10905

Multioctave microwave frequency synthesizer by subharmonic synthesis and frequency multiplication under digital programmed commands
01 p0054 A71-10972

Weak magnetic field measurement using magnetometer with digital technique time coding
02 p0247 A71-11722

Optimal quantum receiver mathematical specification derivation for M-ary digital signal detection
02 p0215 A71-12036

Digital optimal feedback control device, discussing design requirements, algorithm, block diagram, flow chart and measurement results
02 p0236 A71-12150

Very long baseline interferometry /VLBI/ one-bit instrumentation using videotape recorders in geodetic and geophysical measurements
02 p0251 A71-12332

Versatile Avionic Shop Test /VAST/ general purpose digital tester, discussing hardware and software
03 p0395 A71-13084

Automatic digital test unit for avionics systems
03 p0396 A71-13085

Radar information digital extractors for processing signals from airborne transponder
03 p0382 A71-13570

Microwave phase measuring system using programmable digital dividing circuits, considering application to plasma diagnostics
04 p0586 A71-14655

Analog and digital methods for interactions between aircraft lifting elements in steady or unsteady supersonic flow
04 p0527 A71-15358 [ONERA-TP-850]

Digital measurement equipment production and circuit design principles, considering decimal memory elements in adder and divider circuits, miniaturization, reliability and integration
04 p0599 A71-15566

Decision-directed digital adaptive signal equalizer for high speed data transmission, discussing design and advantages
05 p0725 A71-17065

On-off keying system digital detection using random sampling for achieving high bit rates
05 p0725 A71-17073

Multispectral and multitemporal digital imagery spatial registration using fast Fourier transform techniques, applying to earth resources satellite imagery preprocessing
05 p0756 A71-17147

Phase shift measurement by digital encoding via time interval, angle of rotation and voltage conversions
06 p0876 A71-18076

Turbulent He jet measurements using hot-wire anemometry and digital recording techniques, assessing accuracy
06 p0886 A71-18639 [AIAA PAPER 71-201]

Lunar module digital autopilot design, considering attitude state estimator, reaction control system and thrust vector control
07 p1154 A71-18897 [AIAA PAPER 70-991]

Digital on-off predictive adaptive control system feasibility analysis
07 p1082 A71-20407

Digital fluidic metering system for composition control of liquid batch mixing from circuit design to final product
07 p1028 A71-20581

Weather radar plan position indicator automatic film reading for digital mapping of rainfall intensity, discussing raindrop sizing
08 p1286 A71-20690

Analog surveillance radar signal analysis by digital storage and evaluation methods
08 p1252 A71-20745

Interdigital capacitors frequency response and application to lumped element microwave integrated circuits
08 p1261 A71-20753

Papers on modern practice in servo design covering digital techniques, applications of analog and hybrid computers and thyristors, reliability engineering, etc
08 p1268 A71-21195

Natural image computer for terrain pattern recognition and delineation from aerial photographic inputs
08 p1281 A71-21255

Manual vs automatic contouring, comparing accuracy and economy
08 p1281 A71-21256

EEG analyzer voltage peaks recording on computer, using digital readout for simultaneous initial and terminal stage markings
08 p1248 A71-21446

Transform coding techniques using orthogonal matrices to implement bandwidth or dimensionality reduction for image processing in digital communication systems
08 p1259 A71-21591

Digital simulator for training ATC officers, considering authenticity and working and geographical environments
09 p1428 A71-22954

Hall MHD generator duct optimization, using digital calculation for Carter integral minimum for size under required power output
09 p1512 A71-23441

Correlation, transfer and coherence functions in measurements, using digital signal analysis
11 p1731 A71-25597

Data reading function synchronized digital mass spectrometer with incremental scan by magnetic field sweeping, describing method for polynomial fitting of data
11 p1762 A71-25663

User-oriented conversational language computer program for Jet Propulsion Laboratory digital control random excitation environmental test system for spacecraft
11 p1736 A71-26498

Digital data recording system based on multiple beam interference pattern photography, using optical phase modulation
12 p1905 A71-26807

Phase controlled linear FM pulse generation by digital square wave carrier phase modulation, using parabolic function generator
12 p1879 A71-26995

Modular digital TDM switch for radially distributed clock synchronization, discussing design and control
13 p2034 A71-29318

Digital FM techniques for combined time and frequency division multiplexing, improving telemetry sampling channel bandwidth utilization
14 p2193 A71-30020

Digital nonregular pulse counter, determining noise characteristics of photomultipliers in single pulse recording mode
14 p2213 A71-30580

Soviet book on discrete control systems covering linear and nonlinear systems synthesis and analysis,

digital computer techniques, one and multidimensional pulsed systems optimization, etc

15 p2381 A71-31976

Coincidence adders with digit by digit alteration of direct and inverse signals, discussing synthesis and reliability

15 p2376 A71-32183

Synchronous data transmission system digital signal harmonic analysis based on stochastic process theory, applying to amplitude and phase modulation

15 p2372 A71-32321

Nonlinear filters synthesis by digital computer technique, discussing density storage and Bayes law computation problems

16 p2549 A71-33351

Digital generation algorithm for random number sequences with specified autocorrelation and probability density function, illustrating computation accuracy and versatility

17 p2719 A71-34745

Optical grating measuring systems high resolution interpolation using phase analog and digital counter techniques

17 p2745 A71-35293

Digital processing for automatic extraction of information from reconnaissance images, discussing target and terrain configurations pattern recognition technique

17 p2747 A71-35774

Computerized digital techniques for image motion compensation as function of additive noise level, using Fourier transform image filtering and half-tone display

18 p2919 A71-36083

Digital speech interpolation technique application to PCM-TDMA demand assignment system, noting traffic handling capacity and cost reduction

18 p2880 A71-36549

Digital integrated circuits technology with MOS transistors packed on crystal wafer without isolation diffusions

19 p3028 A71-37566

Panels and cassettes mechanical design for Camac modular construction of electronic analog and digital measuring instruments based on integrated circuits

19 p3029 A71-38065

Free flight model accelerations, forces and trajectory measurements in short duration facilities, using optical methods and digital recording

21 p3362 A71-40383

On-line digital dampometer for free oscillation wind tunnel model study under varying Mach number and stagnation pressure avoiding flutter destruction

21 p3363 A71-40391

Digital techniques for tactical radar signal processing functions, discussing low cost integrated circuitry, moving target indicators, and analog to digital converters

21 p3348 A71-40588

Nonlinear and syllabic companded digital delta modulation systems, discussing SNR measurement and computer simulation for optimum design

22 p3514 A71-42392

Telemetry systems with discrete compression-expansion function, calculating noise stability improvement as compared to linear and nonlinear signal conversion operations

22 p3515 A71-42859

Linear digital interpolator in program controlled metal cutting tool circuit, determining transfer function with z transforms

22 p3525 A71-42876

Digital algorithm for automatic aircraft engine monitoring system, using Boolean algebra and events/states theory

23 p3679 A71-43897

Reduced error spectral power density calculations for random processes with digital spectral analyzers

23 p3681 A71-44320

Automatic reseau detection and reference ground control points for computing and correcting geometric and radiometric image for earth resource data, noting correlation with reference system

[ALAA PAPER 71-978]

24 p3806 A71-44576

Crop surveys from multiband and multibase satellite photography during Apollo 9 mission, using statistical multispectral pattern recognition digital techniques

24 p3827 A71-44987

Digital computer numerical procedure to solve dynamo theory MHD equations for earth nucleus, using combination of Fourier and finite difference methods for integration

24 p3823 A71-45038

DIGITAL TO ANALOG CONVERTERS

Switched binary-weighted resistor network combined with operational amplifier to construct current-summing digital to analog converter

07 p1070 A71-18850

Current-switching digital to analog converters based on resistance ladder networks, discussing operation principles, problems and error sources

08 p1258 A71-20988

German monograph on PHENO hybrid computing elements for nonlinear operations covering ADC and

DAC, level and time quantization effects on computational accuracy, etc

14 p2207 A71-30238

DIGITAL TO VOICE TRANSLATORS

Problem Oriented Languages for consulting and construction engineering problem solving by translator-generator for time shared system

09 p1412 A71-23278

DIGITAL TRANSDUCERS

Onboard monitoring sensor trends for airborne computer automatic data systems, noting digital transducers, LSI logic and solid state devices

03 p0395 A71-13081

Interdigital converter for excitation and reception of acoustic surface waves on piezoelectric materials in bandpass filter design

03 p0388 A71-14574

Interdigital broadband hybrid junction transducer terminated in negative resistances for acoustic surface waves amplification

13 p2037 A71-28476

Piezoelectric substrate dependent differences between in-line and crossed field three port circuit models for interdigital surface wave transducers

13 p2038 A71-28612

Surface wave delay lines with near octave bandwidth using lithium niobate interdigital ultrasonic transducer with lumped element impedance inverter network

22 p3521 A71-42202

DIGITALIS

Antiarrhythmic effects of detergents on digitalis induced arrhythmia in dogs

01 p0010 A71-10392

Digitalis-induced bundle branch ventricular tachycardia from electrode catheter recordings of dogs specialized conducting tissues

06 p0852 A71-17873

DIGITIZERS

U ANALOG TO DIGITAL CONVERTERS

DIGITS

NT BINARY DIGITS

DIHEDRAL ANGLE

Tungsten boride sintering bonds with molten Ni as function of wettability low dihedral angle, discussing cermet porosity range

07 p1130 A71-19297

Plane unsteady gas flow under action of dihedral angle shaped piston traveling at constant velocity

19 p3042 A71-37080

Sweep and dihedral geometry effects on blade to blade and meridional flows in turbomachinery blade rows, using actuator disk theory

19 p2994 A71-38274

DIHEDRAL EFFECT

U LATERAL STABILITY

DILATION

U STRETCHING

DILATATIONAL WAVES

Geometric dispersion of dilatational stress wave propagating in laminated plate composite, comparing transmitted wave forms to code calculations

09 p1538 A71-22687

Seismic wave velocity measurements in pahoehoe basalt flows in lava beds, comparing with laboratory dilatational velocities

19 p3052 A71-37685

DILATOMETERS

U EXTENSOMETERS

DILATOMETRY

Ti alloy research, describing transparent atmosphere chamber design and dilatometer control modifications

04 p0604 A71-15908

Low carbon Mn-Mo-Ni steel dilatometric measurements with RPI Gleeble machine, examining bainitic transformation

04 p0617 A71-15913

Dilatometric thermal expansion method for determining cylindrical solid body thermal conductivity coefficient

05 p0838 A71-16790

Volume spectra during heat treatment in metallic systems, using automatic dilatometry

07 p1112 A71-19613

Dilatometric measurement for crazing rate in rubber-toughened plastics during tensile creep tests

15 p2438 A71-31369

DILUENTS

Water diluent effect on molten hydrazine mononitrate critical diameter and condensed explosive detonation stability

15 p2463 A71-31383

DILUTION

Human renal diluting capacity, examining prolonged absolute bed rest effects

09 p1401 A71-23365

Thermomodulation and indocyanine green dye technique comparison for cardiac output measurement in man

11 p1724 A71-25435

Evaporative injector system for capillary column gas chromatography for solutes in dilute solution

20 p3194 A71-39257

DIMENSIONAL ANALYSIS

Scale lengths in atmospheric turbulence from spectra and autocorrelation of vertical air velocity component measured in low flying aircraft

01 p0120 A71-10859

Thermodynamic similarity laws for rocket fuel tanks with cryogenic propellants, using dimensional analysis for unsteady temperature distributions

02 p0332 A71-12526

Parallel incompressible gas jets mixing of variable densities based on dimensional analysis

04 p0577 A71-15623

Atrial and ventricular dimensional analysis in animals and man, discussing angiocardigraphic, biplane, X ray, indicator dilution, radioisotopic and noninvasive methods

05 p0715 A71-16925

Auroral phenomena, using dimensional analysis to examine MHD equations for fields and plasmas in magnetosphere

06 p0888 A71-17286

Lorentz group infinite dimensional representation, establishing forms for all irreducible unitary representations

08 p1324 A71-21359

Solar wind heat conduction evaluation by electron energy equation dimensional analysis

10 p1663 A71-24778

Laser heating induced turbulence in fluid medium, using dimensional analysis for effective Reynolds number

10 p1622 A71-24960

Dynamics of planetary atmospheres large scale motions, using similarity theory and dimensional analysis methods for atmospheric circulation characteristics calculation

11 p1826 A71-25720

Minimum dimensionality determination for control process stabilizing linear mechanical system, obtaining necessary and sufficient conditions for stabilization

16 p2607 A71-32933

Time dependent multidimensional axisymmetric computations for extended extragalactic radio sources propagation into intergalactic media having different densities and temperatures

17 p2806 A71-35411

NASA-SRI Round Robin Ablation Program summary, discussing dimensional analysis, Teflon, nylon and surface temperature

18 p2985 A71-36279

Dimensional analysis of wear by solid particle impact in fluid flows in pumps and ducts

19 p3046 A71-38273

Elastic shell strain energy calculation, using dimensional analysis and invariance properties for inversion of normal to middle surface

22 p3616 A71-42217

Dimensions in physical science, discussing fundamentals and constants in dimensional analysis, operational measurements and numerical quantities

22 p3577 A71-42677

DIMENSIONAL MEASUREMENT

Planimetric aerial photographic block adjustment to ground control

08 p1288 A71-21257

Metallic polycrystalline materials volume changes in plastic deformation from measurements on steel elongation and cross section diameter reduction

09 p1540 A71-22997

Campo del Cielo, Argentina meteorite crater structural analysis, discussing dimensions, energy of formation, mass, impact velocity, etc

15 p2488 A71-32352

Modified Young interferometer for measuring separation between centers of two nearly coincident slits with high resolution

16 p2577 A71-33132

Galactic clusters characteristics tabulation and statistical analysis, calculating dimensions, luminosity and radial velocities dispersion

17 p2804 A71-34841

Photogrammetric three dimensional digitizer for automatically measuring and recording automotive models dimensions

17 p2744 A71-35288

Ultrasonic immersion echo pulse thickness meter for single side access measurement in Al and Zr alloys

22 p3528 A71-41759

Photoelectric polarization curve, reflectivity and absolute diameter of Vesta, comparing with Lyot curve

22 p3602 A71-42177

Dimensions in physical science, discussing fundamentals and constants in dimensional analysis, operational measurements and numerical quantities

22 p3577 A71-42677

Radiation field profiles and applications of broadband ultrasonic transducers, including thickness and viscosity measurements

23 p3674 A71-42919

Static and dynamic measurement errors in contact and contactless sensors of automatic dimensional control of finished product sorting

23 p3679 A71-43866

Gas lasers application to length measurement technology, discussing temperature, air pressure and vibration effects on laser frequency stabilization
24 p3833 A71-44449

DIMENSIONAL STABILITY

NT SHELL STABILITY

NT STRUCTURAL STABILITY

Be mirrors thermal dimensional instabilities dependence on crystalline anisotropy, discussing X ray quality control technique
03 p0424 A71-13637

Stress relaxation as source of dimensional instability in precision devices, discussing thermal cycling role in residual stress relief
15 p2436 A71-32507

DIMENSIONLESS NUMBERS

NT FROUDE NUMBER

NT GRASHOF NUMBER

NT HARTMANN NUMBER

NT MACH NUMBER

NT NUSSELT NUMBER

NT PECLET NUMBER

NT PRANDTL NUMBER

NT RAYLEIGH NUMBER

NT REYNOLDS NUMBER

NT RICHARDSON NUMBER

NT SCHMIDT NUMBER

NT SIMILARITY NUMBERS

NT STANTON NUMBER

NT STROUHAL NUMBER

Empirical dimensionless ratios between universal physical constants, supporting steady cosmological expanding universe model
19 p3145 A71-38543

Dimensionless parameters effect on divided blood flow characteristics in large arterial bifurcation
24 p3801 A71-44622

DIMENSIONS

NT DIAMETERS

NT FILM THICKNESS

NT HEIGHT

NT LENGTH

NT RADII

NT SCALE HEIGHT

NT TARGET THICKNESS

NT THICKNESS

DIMERS

Atmospheric water vapor dimers absorption of microwaves, computing total absorption coefficient
03 p0378 A71-13295

Atmospheric water vapor dimers microwave absorption, computing total absorption coefficient
09 p1408 A71-23268

Water vapor dimer effects on atmospheric brightness temperature in cm and mm radiometric investigations from satellites above ocean areas
12 p1901 A71-27099

Water vapor dimer effects on atmospheric brightness temperature in cm and mm radiometric investigations from satellites above oceans
22 p3533 A71-41654

DIMETHYLHYDRAZINES

Unsymmetrical dimethylhydrazine (UDMH)/effect on canine blood coagulation, blood-aqueous barrier and cornea
02 p0199 A71-12383

Vitamin B6 protection against asymmetrical dimethylhydrazine poisoning, administering B6 alone and with cortical phospholipids in mice
10 p1572 A71-24979

High density nitric acid oxidizer and unsymmetrical dimethyl hydrazine with silicone fluid additive application to Agena rocket engine for higher performance [AIAA PAPER 71-736]
14 p2287 A71-30781

Comparative IR and Raman spectra of gaseous, liquid and polycrystalline symmetrical dimethylhydrazine and deuterium analogs
19 p3013 A71-38345

DIMPLING

Local axisymmetric dimple imperfection effects on buckling load of circular cylindrical shell under axial compression [AIAA PAPER 70-103]
05 p0823 A71-16557

Elastic buckling load of cylindrical shells with dimple imperfections under external pressure, applying perturbation expansion to Karman-Donnell equations
18 p2982 A71-36839

DINITRATES

Engine pressure spiking restart preignition products, determining hydrazine nitrate and dinitrate presence by spectrum analysis
06 p0945 A71-18296

DIODES

NT AVALANCHE DIODES

NT CESIUM DIODES

NT CRYSTAL RECTIFIERS

NT GERMANIUM DIODES

NT JUNCTION DIODES

NT PARAMETRIC DIODES

NT PHOTODIODES

NT PLASMA DIODES

NT THERMIONIC DIODES

NT TUNNEL DIODES

NT VARACTOR DIODES

Frequency multipliers and dividers with step-recovery diodes, calculating steady state behavior as function of circuit parameters and input frequency
01 p0052 A71-10322

Shift register based on coplanar Gunn diodes for pulse processing, considering diodes application to logic circuits of digital instrumentation and communication systems
01 p0052 A71-10323

GaAs S diodes with negative differential resistance, examining selectivity and oscillation characteristics
01 p0057 A71-11460

Semiconductor laser diodes structural and operational characteristics, discussing applications in aircraft and construction machines guidance systems
05 p0761 A71-16328

Solid state single injection diodes with shallow traps, calculating trapping noise
06 p0872 A71-17313

Microwave semiconductor limiter diode for decimeter operation using spark gap analog
06 p0873 A71-17540

Microwave Gunn diodes made from GaAs single crystals, describing fabrication by diffusion process
06 p0876 A71-18082

Neutron irradiation induced degradation in epitaxial Gunn diode performance
07 p1071 A71-19069

Light emitting diodes performance comparison under electron irradiation effect in space environment
07 p1071 A71-19070

Gunn diodes impedance measurement at bias voltage above threshold, using broadband equivalent circuit model for mount and package
07 p1072 A71-19103

Self pumped parametric amplification and oscillation of Gunn effect diodes
07 p1075 A71-19262

Negative resistance diodes characteristics under laser radiation, investigating switching properties, temperature effects and noise characteristics
07 p1076 A71-19373

YAG-Nd laser rods CW pumping by cooled and room temperature GaAsP diodes, determining threshold temperature dependence
07 p1129 A71-20621

Limited space charge accumulation layer diodes operating characteristics, using GaAs devices with uniform doping for microwave peak power
08 p1266 A71-21624

Gunn diode with capacitive probe on side surface for signaling strong field domain passage, calculating maximum permissible microwave coupling
10 p1584 A71-24721

Gunn diodes and heterojunction laser applications in optical pulse communication systems synthesis
11 p1772 A71-25235

Electroluminescent semiconductor diodes based on GaP and GaAlAs, discussing design, properties, uses and production
11 p1737 A71-25569

Single and double balanced diode mixers characteristics comparisons for spurious response suppression, considering RF third order intercept technique
11 p1737 A71-25674

Decimeter range diode commutation devices, calculating speed, wideband capability, noise level and maximum power
11 p1741 A71-26555

Annular solid state microwave diodes temperature distribution at diode/heat sink interface, presenting closed form solution for calculation of absolute temperature rise
12 p1889 A71-27699

Gunn diode operation at below threshold bias voltage, investigating microwave oscillations amplification
13 p2036 A71-27953

Sb and As base chalcogenide diode structures, determining switching and memory characteristics
13 p2110 A71-27956

Fluidic diodes designs with and without fluid discharge
13 p1998 A71-28010

Microwave phase discriminators sensitivity and linearity performance improvement, noting diode detectors nonideal nature
13 p2038 A71-28779

Nonuniform trap distribution effect on I-V characteristics of dielectric diodes, allowing for field ionization
13 p2040 A71-28927

Gunn effect diode in portable Doppler radar, describing electron transfer, negative resistance and domains formation and propagation
13 p2040 A71-29238

Electron beam interaction with external harmonic microwave field in planar diode gap, calculating electric field current and voltage distribution functions
14 p2211 A71-30084

Thermal noise in space charge limited solid state diodes with field dependent mobility and hot carriers
14 p2284 A71-30502

Triangular pulse shaper using transistors and dynistors, obtaining pulse duration, rise time and maximum repetition frequency
14 p2213 A71-30581

High speed pulse response and power-delay product of planar Gunn diodes, noting delay time and power delay product
14 p2215 A71-30834

Microstrip p-i-n diode controlled L band digital phase shifter for aircraft-satellite communication
14 p2217 A71-31055

Knudsen arc firing potential in plane gas filled diode with hot cathode as function of electrode gap and atom concentration
15 p2455 A71-31739

Physical model of Zn diffused GaAs electroluminescent diodes gradual degradation, establishing formation of new recombination centers through injected carrier lifetime measurement
15 p2377 A71-32607

Computer algorithm for diode detector static and dynamic I-V characteristics calculation by trial and error process with piecewise linear approximation
16 p2546 A71-33399

Plane diode electrode gap differential capacitance for operation with anode negative voltage, current saturation and space charge limitation
16 p2548 A71-33709

Cadmium doped silicon diodes I-V curve sinusoidal relaxation oscillations frequency and amplitude dependence on temperature
16 p2548 A71-34026

Sensitive mm wave receivers, using local oscillator and mixer functions in single Gunn diode for large dynamic signal input range and wide IF bandwidth capability
17 p2717 A71-35111

Solid state light emitting diodes in aerial camera data recording system for enhanced spectral matching, increased photo conversion efficiency and lower power drive
18 p2920 A71-36089

Overcritically doped Gunn diode I-V characteristics stability under constant voltage, discussing use as subnanosecond switching element
18 p2895 A71-36989

Gunn diodes stable high field domains parameters and behavior, considering hole effects in various carriers
19 p3028 A71-37861

Foiless diode for production of high power relativistic electron beams, using multilathode system
20 p3202 A71-38831

Fluidic diodes designs with and without fluid discharge into atmosphere
21 p3326 A71-41140

Ge and Si point contact semiconductor diodes anisotropic deformation, investigating pressure effects on current and negative resistance in forward branch of I-V characteristics
21 p3430 A71-41222

Nonuniform trap distribution effect on I-V characteristics of dielectric diodes, allowing for field ionization
21 p3358 A71-41325

Copper gallium diselenide point contact diodes I-V characteristics temperature and illumination dependence, considering high temperature and photoelectric devices applications
21 p3434 A71-41327

Gunn diode operation at below threshold bias voltage, investigating microwave oscillations amplification
21 p3358 A71-41339

Glassy antimony and arsenic chalcogenide diode structures, determining switching and memory characteristics
21 p3435 A71-41343

Dummy S4 diode packages mounted in coaxial line, deriving mount-independent equivalent circuit parameters from broadband admittance measurements
22 p3521 A71-42206

Current controlled diodes used as voltage variable capacitors in oscillators
23 p3652 A71-43832

GaP diodes with metal-semiconductor potential barriers manufactured by chemical deposition of metal on n-GaP surface
23 p3653 A71-43960

DIOXIDES

NT CARBON DIOXIDE

NT COESITE

NT ENSTATITE

NT HYDROGEN PEROXIDE

NT PYROXENES

NT QUARTZ

NT SILICON DIOXIDE

DIPHOSPHATES

NT ADENOSINE DIPHOSPHATE [ADP]

Erythrocytes diposphoglycerate increase mechanisms during hypoxia and anemia, studying hemoglobin oxygenation state effects
17 p2685 A71-35368

DIPOLE ANTENNAS

Stacked dipole antenna arrays with modulated phase velocity, comparing measured and calculated radiation patterns
01 p0052 A71-10474

Secondary currents on conducting cylinder near dipole antenna manifested as radio frequency interference, considering effect on radiation pattern
01 p0037 A71-11167

Electrical stability of double sphere dipole antennas for FR-1 satellite ionospheric plasma electric fields measurements
02 p0229 A71-11714

Cylindrical electric dipole antenna in magnetoactive ionospheric plasma, noting ion sheath effect on input impedance and active length
02 p0212 A71-11873

Dipole antennas mutual influence near conducting intersecting circular cylinders, using geometrical diffraction theory
03 p0384 A71-13395

Vertical dipole electromagnetic field diffraction by circular aperture in opaque screen with coaxial concentric conducting disk
03 p0379 A71-13963

Polynomial current analysis of imperfectly conducting thin cylindrical dipoles with arbitrary internal impedance
04 p0558 A71-15144

Vertical and horizontal VLF fields excited by dipoles of arbitrary orientation and elevation for nighttime ionosphere
04 p0552 A71-15216

Short dipole antenna impedance in warm isotropic plasma using Vlasov theory
04 p0553 A71-15221

Dipole antenna array coupling for circularly polarized radio waves amplitude fluctuations reflected from ionosphere at vertical incidence
05 p0738 A71-16216

Log periodic dipole antennas Maxwell equations solution in cylindrical coordinates for all boundary conditions
06 p0874 A71-17706

Log periodic dipole array transient radiation, obtaining radiated pulse envelope time dependence as function of antenna admittance and input pulse frequency spectrum
06 p0875 A71-17720

Radiation resistance of center fed dipole antenna with transversely displaced feed points, using Schelkunoff moment method
07 p1075 A71-19267

Center fed dipole antenna with displaced feed points in warm plasma medium, calculating radiation patterns
08 p1264 A71-21221

Conducting disk with slot dipole at center, determining asymptotic expressions for radiation field far zone
08 p1266 A71-21465

Intersecting dipoles with sinusoidal current distribution, determining input impedance
08 p1266 A71-21469

Phase velocity modulated backward wave antenna with slow wave structure, consisting of dipoles spaced along antenna length
09 p1415 A71-22295

Beam compression technique for log periodic dipole antenna array using axial displacement of antenna dipoles feed points
09 p1406 A71-23035

Variational formula for input impedance of thin asymmetrical cylindrical dipole antenna
09 p1408 A71-23490

Polynomial approximation of current along thin isolated asymmetrical cylindrical dipoles
09 p1419 A71-23506

Dipole antenna array exact design for prescribed radiation patterns in magnetic plane, using current distribution integral
09 p1420 A71-23511

Ground metallic plate effect on electric dipole antenna radiation characteristics as function of aperture field
09 p1420 A71-23572

Input resistance of electric dipole above metallic disk lying on homogeneous conducting half space at HF, using compensation theorem
09 p1495 A71-23573

Earth-ionosphere waveguide model of VLF signals propagation with perturbed ionosphere, considering magnetic dipole transmitting antenna array
09 p1410 A71-23575

Signal fluctuation effect on directional properties of multipole receiving antenna, calculating radiation pattern
10 p1583 A71-24708

Phase sector direction finder for VHF range, using log periodic dipole arrays
11 p1738 A71-26338

Dipole elements input impedance of wideband linear antenna arrays, using coupled circuits and induced emf
11 p1738 A71-26345

Isolated symmetrical cylindrical dipole antennas in homogeneous conducting media
12 p1880 A71-27153

Radio emission measurement from extensive air showers by system of half wave dipoles in complex array of Moscow State University
13 p2127 A71-28106

Three dimensional fields excited by arbitrarily oriented dipole in cylindrically inhomogeneous isotropic plasma, deriving closed form solution
13 p2107 A71-28786

Dipole antenna with displaced feed points, deriving radiation pattern expression with spherical coordinate system
13 p2033 A71-28898

Resonant dipole antenna with feed points immersed in weakly ionized plasma, investigating performance under electro-acoustic and electromagnetic wave excitation
14 p2193 A71-29858

Earth-ionosphere waveguide excitation by satellite-borne horizontal dipole antenna, deriving fields at earth surface based on idealized model
14 p2196 A71-30562

Thick unsymmetrically fed dipole antenna radiation pattern measurements and impedance matching
15 p2377 A71-32318

Oscillations excited by pulsed dipole antenna at upper hybrid resonance in weakly inhomogeneous plasma investigated by Wentzel-Krammer-Brillouin approximation
15 p2460 A71-32656

Dipole antenna near electric field, basing calculation method on integral equation for antenna surface charge distribution function
16 p2546 A71-33487

Dipole coupling, current distribution and impedance of thick dipolar log periodic antennas by 4-term theory
16 p2544 A71-34172

Current distribution on grid type dipole antenna in warm isotropic plasma, using direct source approach and boundary value analysis
17 p2698 A71-34430

Driving point admittances of resistive cylindrical dipole antennas by variational method using two term trial function for current
17 p2701 A71-34762

Radiation pattern of dielectric disk antenna, using computerized analysis of electromagnetic scattering and spherical volume cell
17 p2715 A71-34765

Nonplanar dipole antenna with transversely displaced feed points, considering effects on far field radiation patterns, radiation resistance, power gain, effective aperture and efficiency
18 p2887 A71-35970

Feed point axial displacement effects on radiation resistance and patterns of dipole antenna in weakly ionized plasma
18 p2875 A71-35971

Nonplanar dipole antenna with arbitrarily displaced feedpoints, considering far field radiation patterns, radiation resistance, power gain, effective aperture and efficiency
18 p2887 A71-36014

Corner reflector excitation by vertical or horizontal log-periodic dipole antenna for unidirectional wideband radiation, deriving far field expression
18 p2895 A71-36994

VLF fields of horizontal dipole in waveguide formed between ice covered ground and anisotropic ionosphere of Antarctica
19 p3024 A71-38595

Dipole antenna with parallel parasitic element, investigating resonant length variation as function of spacing with matrix inversion method
19 p3035 A71-38599

Dipole antenna bandwidth extension by conjugate reactance loading based on periodically loaded transmission line theory
19 p3036 A71-38602

Excitation asymmetry effects on current distribution and far field of thin dipole radiators
19 p3036 A71-38604

Active region and truncation point of log periodic dipole antenna as function of length and design parameters
20 p3203 A71-39091

Book on antenna characteristics covering tabulated data for cylindrical dipoles and monopoles, imperfectly conducting dipoles, circular loop antennas and broadside and endfire arrays
20 p3196 A71-39200

Radiation resistance, power gain, effective aperture and efficiency of modified log periodic dipole antenna
21 p3352 A71-40378

Iterative solution of Hallen integral equation for current distribution on lossless cylindrical transmitting dipole antenna
21 p3348 A71-40578

Reflection and scattering properties of two dimensional periodic arrays of loaded dipoles with bandpass filter characteristics as function of frequency
23 p3654 A71-44159

Wideband transistorized active dipole antenna for reception at 100-1000 MHz, calculating impedance and effective height by linear theory
24 p3807 A71-44360

Cylindrical antennas with arbitrary distributed resistive and reactive loading, presenting method based on dipole antennas with constant resistance loading per unit length
24 p3803 A71-44646

DIPOLE MOMENTS

NT ELECTRIC MOMENTS

NT MAGNETIC MOMENTS

Vibrational degrees of freedom effects on capture cross sections and ion-molecule complexes formation in ion-dipole collisions
01 p0130 A71-10477

Interatomic electric dipole moment coefficient derivation by approximation involving accessible atomic properties, noting application to H atoms
02 p0287 A71-12708

Satellite altitude dipole source effectiveness in lower ionosphere, comparing to ground based source with same dipole moment
07 p1064 A71-20319

Vibrational effects on capture cross sections and ion-molecule complexes formation based on ion-dipole collisions, noting multiple reflection probabilities and collision lifetimes
09 p1498 A71-23662

Heart electric generator system simulation by dipolar or multidipolar generators
10 p1569 A71-24238

Low frequency electromagnetic wave scattering by metallic cone, noting dipole moment contribution
12 p1879 A71-27054

Coherent electromagnetic excitation of optical transition levels by fluorescence measurement, obtaining dipole moment and relaxation times
18 p2929 A71-35903

IR auroral/airglow study covering hydroxyl emission and dipole moment function determination and atmospheric nitrogen vibrational temperature measurement
20 p3240 A71-39843

Potassium photoionization cross section, including spin-orbit interaction, orientation of photoejected electrons and dipole transition moment correction due to core polarization
21 p3417 A71-40197

Rotational and vibrational effects in ion dipole collisions
21 p3419 A71-40905

DIPOL

Dipole, quadrupole and octapole measurements in isolated beating hearts
13 p2016 A71-28150

Mutual impedance of interacting dipoles at wedge tip, determining errors for short spacing distances
13 p2036 A71-28370

Reflection and refraction patterns of various wave number media vertical electromagnetic dipole fields at even and uneven interfaces
14 p2192 A71-29805

DIRAC EQUATION

Integral containing Heaviside and Dirac delta function in integrand with minus and plus infinity limits, computing value using thin spherical shells in general relativity
16 p2656 A71-33263

Vacuum symmetry and asymmetry, analyzing physical meaning of Dirac vacuum in quantum field theory
22 p3577 A71-42853

DIRECT CURRENT

Zinc single crystals plastic deformation and dislocations movement enhancement under pulsating direct current, noting stress peaks-voltage relationship
02 p0296 A71-12297

Nondissipatively-regulated DC to DC converter design, describing circuit technique and magnetic-semiconductor combinations
03 p0352 A71-13046

Spacecraft electric power transformation and control techniques enhancement, using DC to DC converter, voltage converter/regulator and solar array reorientation system
03 p0352 A71-13049

High voltage DC power supplies for aerospace detectors operation, considering different resonant configurations for performance
03 p0352 A71-13051

FET chopper amplifier for low level DC signals from thermocouples, strain gauge bridge circuits and weak transducer sources
03 p0384 A71-13275

AC signal amplitude measurements, describing circuit design with DC voltage generation proportional to input AC voltage
06 p0899 A71-17926

Low gain microwave amplifier cascade DC to RF conversion efficiency analysis
07 p1073 A71-19115

Transistorized DC amplifiers operational characteristics, discussing principal electrical parameters and application in phase lock AFC loops
08 p1263 A71-20786

Correlation detection systems, calculating DC component effects on output signal to noise ratio
08 p1253 A71-21281

High density DC effects on displacement of solid GaAs-liquid metal interface, considering Peltier effect and dislocation density
08 p1344 A71-21444

Oscillation frequency shift and gas discharge tube design relation in He-Ne DC lasers
09 p1462 A71-22402

Josephson maximum DC current plot for linear overlap junctions, discussing junction area geometry to current perimetric proportionality
09 p1423 A71-22693

Second harmonic voltage effects on quenched domain mode Gunn effect oscillator for DC to RF conversion efficiency, discussing negative device conductance at multiharmonic frequencies
09 p1417 A71-22696

DC vacuum arc ion currents between copper electrodes, discussing wall geometry, plasma ionization, starvation phenomena and anode spot formation
12 p1939 A71-27269

Two transistor emitter follower DC amplifier, using simplified equivalent circuit
13 p1999 A71-28628

Pulse width modulation controlled DC motors, deriving formulas for speed and torque characteristics
13 p1999 A71-28630

Ion migration direction in thin Ag, Cu and Au films under direct current effect from resistance radioactive tracer measurements and scanning electron micrographs
13 p2112 A71-29333

Gyrator circuit design with two antiparallel transistor amplifier stages for minimal DC current reception
18 p2888 A71-36223

MOS field effect transistors operation and DC characteristics including threshold voltage and substrate doping effects
19 p3027 A71-37562

He-Ne lasers noise modulation at DC excitation, confirming existence of critical frequency related to metastable atom lifetime
21 p3392 A71-40373

Brushless DC motor as power source for meteorological, communications and geological satellites, describing electromechanical design features and operating characteristics
21 p3326 A71-40724

Adjustable speed drive with brushless DC synchronous motor using rotor position sensor and three phase bridge inverter
23 p3630 A71-43499

Current harmonics in passively nonlinear resistance subject to simultaneous DC and AC fields
24 p3860 A71-44872

DIRECT LIFT CONTROLS

Aircraft direct lift control based on flight and simulator experiments, discussing effect on design
01 p0005 A71-10754

Aircraft longitudinal motion decoupling through direct lift control, investigating flight control for landing
03 p0347 A71-13339

L-1011 aircraft automatic landing safety and performance improvement through direct lift control, discussing flight control system integration [AIAA PAPER 71-906]
19 p3095 A71-37157

DIRECT POWER GENERATORS

NT ALKALINE BATTERIES

NT FUEL CELLS

NT HYDROGEN OXYGEN FUEL CELLS

NT MAGNESIUM CELLS

NT MAGNETOHYDRODYNAMIC GENERATORS

NT METAL AIR BATTERIES

NT NICKEL ZINC BATTERIES

NT PHOTOELECTRIC GENERATORS

NT RADIOISOTOPE BATTERIES

NT REGENERATIVE FUEL CELLS

NT SNAP 15

NT SNAP 19

NT SNAP 21

NT SNAP 23

NT SNAP 27

NT SOLAR CELLS

NT THERMAL BATTERIES

NT THERMIONIC CONVERTERS

NT THERMOELECTRIC GENERATORS

NT ZINC-OXYGEN BATTERIES

Book on fuel cells covering types, applications, thermodynamics, chemical reactions, direct electrical generation, etc
01 p0006 A71-11192

Electrofluid dynamic direct energy conversion, discussing working media, duct geometry, unipolar charges, and fluidic switches [ASME PAPER 70-ENER-A]
03 p0353 A71-13704

Electrofluiddynamic colloid generator performance characteristics, considering power output limitation due to electric breakdown [ASME PAPER 70-WA/ENER-5]
03 p0355 A71-14108

Thick film microcircuit DC-TO-DC converter electronics design for TOPS spacecraft power subsystem
14 p2214 A71-30801

Test facility and performance predictions for Rankine cycle power system components, including lithium heater, potassium boiler, condenser and preheater [GESP-451]
15 p2448 A71-32223

DIRECTION FINDERS (RADIO)

U RADIO DIRECTION FINDERS

DIRECTIONAL ANTENNAS

NT DIPOLE ANTENNAS

NT HELICAL ANTENNAS

NT HORN ANTENNAS

NT LENS ANTENNAS

NT LOG PERIODIC ANTENNAS

NT LOOP ANTENNAS

NT PARABOLIC ANTENNAS

NT RADAR ANTENNAS

NT RHOMBIC ANTENNAS

NT SLOT ANTENNAS

NT STEERABLE ANTENNAS

NT TWO REFLECTOR ANTENNAS

NT YAGI ANTENNAS

L and S band paraboloidal dish antenna stellar calibration technique using absolute flux density from Cassiopeia A or Cygnus A
01 p0032 A71-10888

Skyнет ground stations design, equipment and operations, discussing antennas movement control, Cassegrain reflectors, receiving system amplifier noise temperature and tracking demodulator
02 p0233 A71-12432

Antenna gain of Space Communications and Tracking terminal from feedhorn radiation pattern and reflector geometry
02 p0219 A71-12448

High efficiency spherical reflector antennas with scanning and multiple feed properties for communication satellite portable earth stations
02 p0233 A71-12792

Gain/temperature measurement test set for earth station receiving system by radio sources program tracking unit, noting antenna power ratios determination by attenuator
02 p0222 A71-12797

Gain/temperature measurement for earth station antenna and receiving subsystem by FM method, determining Y-factor [noise power proportional increase]
02 p0222 A71-12798

Earth station antennas structural parameters and performance prediction, considering autotrack loop stability optimization by multiple lag compensation using single axis model
02 p0223 A71-12803

High efficiency feeds for large satellite autotracking earth station antennas, using focal plane distribution
02 p0223 A71-12808

Frequency selective conical scanning for direction finding earth station antennas for communication satellite automatic tracking, using waveguide mode conversion
02 p0223 A71-12809

Satellite ground station autotracking receivers, discussing antenna position control systems
02 p0239 A71-12816

Large antenna electrical and mechanical requirements, considering gain/temperature ratio, steerability, housing, design life and erection
02 p0235 A71-12831

Antenna steering systems for satellite communications, discussing tracking, mechanical drives and subreflector servo
02 p0235 A71-12832

Directional dielectric loaded waveguide antenna for probing electromagnetic field oscillations, discussing design and performance tests
04 p0560 A71-15880

Radiation pattern of narrow beam antenna using artificial dielectric medium with permittivity less than unity
06 p0868 A71-17741

Buitrago /Spain/ earth station for Intelsat operation, discussing tracking antenna design and performance
06 p0880 A71-18396

Directional antenna with parabolic reflector for missile tracking in telemetry band, considering radiation diagrams and design approach
07 p1078 A71-20012

Highly directive radio telescope antenna parameters in near zone, using focusing at minimum distance
09 p1414 A71-22218

Statistical directivity, radiation pattern, drift dispersion of segmented traveling wave antennas
09 p1414 A71-22226

Linear and circular apertures sum and difference radiation patterns for minimum sidelobe power
09 p1407 A71-23108

Double curved reflectors assembly methods for rotating search radar antennas, considering parabolic

and elliptic strip shapes for sidelobe suppression modification
09 p1409 A71-23495

Waves arrival directional fluctuations effect on power gain of horizontal rhombic antennas for high frequencies and various antenna and wave parameters
09 p1420 A71-23676

Radiation patterns of radar antennas with single near field cylindrical obstructions, considering directional S band antenna
09 p1420 A71-23678

Iterative synthesis of dipole antenna array for maximum directivity radiation pattern, considering amplitude-phase distributions
10 p1583 A71-24707

Signal fluctuation effect on directional properties of multipole receiving antenna, calculating radiation pattern
10 p1583 A71-24708

Space communications antennas main reflecting surface accuracy determination by statistical evaluation of efficiency degradation due to mechanical inaccuracies and structural flexibility
12 p1887 A71-27003

High directivity antennas lateral radiation level, showing field in sidelobe segment approximation by logarithmically normal law
13 p2040 A71-28994

Parabolic two-mirror antenna design with one small mirror for diffraction fringe effects correction
14 p2196 A71-30637

Radar target direction variation /glint/ sensed by amplitude monopulse tracking antenna receiving nonuniform waves
14 p2214 A71-30807

Quasi-isotropic directional, omnidirectional and auxiliary antennas of Helios Solar Probe S band system, discussing design, radiation patterns, adaptability and X band measurements
14 p2217 A71-31052

High directional microwave antennas optical simulation, design and measurement based on coherent optics and holography
15 p2375 A71-31282

Far field minimum radiation over angular sector for directional broadside array with optimum interelement spacing, considering sidelobe reduction
18 p2875 A71-35972

Antenna tracking, RF and bore sight alignment on ships and ground stations using Apollo lunar surface experiments package /ALSEP/
18 p2876 A71-36473

Beam direction weight center of signal spectrum and effective antenna centers of airborne Doppler velocimeter in horizontal flight
19 p3033 A71-38496

Pattern space factor and aperture distribution of continuous line source for maximum directivity
19 p3023 A71-38590

Satellite tracking ground antenna servocontrol, discussing system requirements and automatic and programmed operating modes [DFVLR-SONDDR-125]
22 p3483 A71-41520

Algorithms for directional antenna boresight orientation estimation errors relative to spacecraft attitude sensor, based on measurement of received signal strength
22 p3525 A71-42775

Receiving and transmitting antennas directional gain effect on microwave long range tropospheric propagation
23 p3644 A71-43289

DIRECTIONAL CONTROL

NT THRUST VECTOR CONTROL

Single rotor helicopter directional stability in rectilinear flight with constant angle of side slip
06 p0847 A71-18307

Subsonic tactical missile hydraulic and fluidic autopilot systems for directional control, considering costs, reliability, vulnerability, maintainability, weight and mobility [SME PAPER MS-70-524]
07 p1024 A71-20547

Electronically tunable compact X band triplexer, consisting of four port nonreciprocal directional YIG filters in cascade
09 p1418 A71-23416

Inertial navigation system consisting of gyro horizon compass, directional gyro and computer, considering errors due to compass vibrations
12 p1927 A71-27169

DIRECTIONAL STABILITY

NT GYROSCOPIC STABILITY

Executive jet landing approach lateral-directional handling under IFR ILS simulated conditions, investigating Dutch roll control power effect on crosswind component [SAE PAPER 710374]
10 p1554 A71-24243

Subsonic flight characteristics of LB 21 reentry vehicle, discussing lateral directional stability and lifting fuselage
18 p2972 A71-36436

Variable stability aircraft lateral directional flying qualities, investigating turbulence effects
22 p3483 A71-42833

DIRECTIVITY

- Long range troposcatter, evaluating antenna directivity effects on signal fading rate and fluctuation 01 p0037 A71-11087
- Ultrasonic Doppler techniques in medical diagnosis, measuring ultrasonic probes directivities by echo amplitudes from various target configurations 03 p0373 A71-14422
- Reflector antenna under wideband noise radiation, determining directivity characteristics by solution for angle range homologous to region of irregular lobes 05 p0728 A71-16008
- Chebyshev array directivity for various element spacings and sidelobe ratios, presenting formulas for computer calculations 06 p0875 A71-17725
- Doubly shunt loaded short slot antenna, determining optimum capacitive loadings for enhanced radiation or improved directivity 06 p0876 A71-17740
- Algorithmic threshold directivity pattern for adaptive array processors in quasi-stationary signal and noise fields 08 p1256 A71-21603
- Meteor-reflected radio wave propagation directivity and diurnal and annual variations, comparing experimental and theoretical calculation results 10 p1576 A71-24033
- Uniformly spaced linear arrays directivity as function of spacing, scan angle and current distribution, approximating element radiation intensity 13 p2028 A71-28000
- Radio frequency power meters comparison, reducing mismatch and directivity errors with directional coupler 14 p2205 A71-30984
- Retinal directional effect measurements confirming mathematical model based on Gaussian distribution of retinal cone orientation, explaining brightness stimuli effectiveness and hue shift 21 p3335 A71-40670
- Perturbation procedure application to linear and circular antenna array directivity optimization by phase adjustments under uniform amplitude excitation 21 p3359 A71-41412
- Reflector antenna under wideband noise radiation, determining directivity characteristics by solution for angle range homologous to region of irregular sidelobes 22 p3524 A71-42757

DIRECTORIES

U INDEXES (DOCUMENTATION)

DIRECTORS (ANTENNA ELEMENTS)

- Passive two-terminal networks in rod antenna for bandwidth increase, investigating equivalent circuit on digital computer 12 p1886 A71-26987

DIRICHLET PROBLEM

- Schwarz-Neumann method for Dirichlet problem of elliptic differential equations describing regions intersection in n-dimensional Euclidean space 01 p0109 A71-10031
- Two dimensional mixed boundary value problems solution in elasticity theory by linear differential operators, applying to Dirichlet and Neumann problems 02 p0326 A71-12293
- Initial Dirichlet boundary value problem parabolic and elliptic equations of order 2b, discussing existence and uniqueness proofs 02 p0276 A71-12532
- Dirichlet problem for elliptic equations with unbounded lowest coefficients, proving Gordin inequality 03 p0451 A71-13966
- Soviet monograph on universal program for finite difference solution of Dirichlet problem of Poisson equation with enhanced accuracy formulas 04 p0619 A71-15450
- Diffraction on strip, investigating for Dirichlet boundary conditions, deriving excited current density and scattered pattern 05 p0722 A71-16869
- Dirichlet problem associated with elliptic partial differential equation, discussing integral operator methods for approximating numerical solution 06 p0920 A71-18208
- Uniqueness theorem for Dirichlet series bounded on real axis 07 p1146 A71-19040
- Analytic function steady approximation with aid of polynomials in given region, considering Dirichlet series 07 p1146 A71-19042
- Two dimensional Laplace equation solution by Fredholm integral equation method for Dirichlet problem 07 p1148 A71-20096
- Geomagnetic field calculation for intermediate ionosphere altitudes, applying Dirichlet sphere problem to rectangular magnetic field components 11 p1757 A71-25778

Single circuit parametric oscillator with balance modulated pumping voltage envelope as periodic function satisfying Dirichlet condition 11 p1740 A71-26539

Dirichlet problem for elliptic differential equations with lowest derivatives coefficients and leading term in Bitsadze operator, discussing reduction to singular integral equation 12 p1923 A71-27511

Dirichlet problem for degenerate elliptic differential equations, discussing existence and uniqueness of solution by Schwarz alternating method 12 p1923 A71-27512

Inverse diffraction of plane wave by periodic and doubly periodic arrays, calculating velocity potential and pressure distributions for Neumann and Dirichlet problems 13 p2027 A71-27905

Existence and uniqueness of solution to Dirichlet boundary value problem of invariant in nonclassical theory of elasticity concerning behavior of media with memory 13 p2154 A71-28651

Dirichlet, neumann and mixed boundary value problems relative to wave equation for rectangle, discussing solution based on singularity theorem 14 p2266 A71-30810

Dirichlet problem for second order linear elliptic differential equations, considering convergence theory results for finite difference approximations 15 p2440 A71-31349

Uniqueness of positive solutions to self adjoint elliptic partial differential equations with nonlinear forcing terms under Dirichlet and Neumann boundary conditions 15 p2442 A71-31872

Difference analogs of Dirichlet problem for second order quasi-linear elliptic operators with mixed derivatives, using discretization method 15 p2442 A71-32312

Direct variational methods for solving parabolic boundary value problems of arbitrary order in space variables, considering Dirichlet problem solution 17 p2764 A71-34640

Dirichlet problem in hodograph plane of compressible fluid flow from aircraft, helicopter blades or turbine blade airfoils 17 p2672 A71-35470

Divergence structure nonlinear elliptic equations, demonstrating smooth solutions uniqueness of Dirichlet problem 18 p2942 A71-36816

Plane electromagnetic wave diffraction by dense periodic array with Dirichlet and mixed boundary conditions, determining solution asymptotic behavior 19 p3104 A71-38416

Geomagnetic field calculation for intermediate ionosphere altitudes, applying Dirichlet sphere problem to rectangular magnetic field components 22 p3532 A71-41546

DIRIGIBLES

U AIRSHIPS

DISCHARGE COEFFICIENT

- Small gas discharge coefficient of venturi tubes 02 p0253 A71-12557
- Proportional fluidic elements jet nozzle discharge coefficients as function of control pressure and geometrical parameters 03 p0354 A71-13959
- Discharge coefficient correction factor for curvature effect on mass flow rate measurement by sonic throat for axisymmetric nozzles [ONERA-TP-956] 18 p2915 A71-36024
- Discharge coefficient formula for supersonic nozzles at low throat Reynolds numbers, investigating boundary layer thickness for various nozzle geometries 19 p2993 A71-37896

DISCHARGE TUBES

U GAS DISCHARGE TUBES

DISCHARGERS

NT STATIC DISCHARGERS

- Controllable overhead arc spark gap discharger system design and characteristics for high power research, communication or industrial electrical installations 19 p3000 A71-38642
- Nanosecond solid dielectric discharger fired by Q switched ruby laser for commutation of coaxial line forming high amplitude voltage pulses 24 p3835 A71-45238

DISCIPLINING

Air traffic controllers legal responsibility and disciplinary procedure, considering clearances, flight crew instructions and aircraft accidents 09 p1548 A71-22891

DISCOLORATION

- Surveyor 3 spacecraft TV camera surface discoloration patterns caused by lunar soil blown by Apollo 12 exhaust 08 p1363 A71-21219
- Kinematic method for determining interstellar extinction/discoloration ratio 20 p3293 A71-39533

Surveyor 3 surfaces discoloration and lunar dust contamination, noting Apollo 12 lunar module caused disturbances by on-site observation 23 p3766 A71-43816

DISCONTINUITY

NT SHOCK DISCONTINUITY

- Initial value problems differential equations discontinuities, describing step-size adjustment for fourth order Runge-Kutta methods 02 p0277 A71-12728
- Anisotropic plasma discontinuities in solar wind, noting shock misidentification 03 p0463 A71-13307
- Cylindrical shells axisymmetric nonlinear strain discontinuities propagation, using Timoshenko equations 03 p0515 A71-14380
- Hydrodynamic equations for discontinuity problems of origin and disruption of vortices, transonic gas flow and shock wave formation, using Lagrange equations 04 p0579 A71-15813
- Transient heat flow mean and first moments prediction by discontinuous linear or quadratic trial functions and variations 05 p0831 A71-16491
- Two component hydromagnetic system Kelvin instability due to tangential velocities discontinuity, using normal mode analysis 05 p0788 A71-16626
- Two-point boundary value problems approximation for differential equation systems with discontinuity in right-side derivatives 05 p0775 A71-16886
- Boundary value problem for second order elliptic equation with discontinuous coefficients, discussing solvability conditions and boundary characteristics 05 p0775 A71-16887
- Weak discontinuities propagation and growth in MGD with finite electrical and thermal conductivity, calculating shock wave generation critical time 07 p1170 A71-20094
- Preferred orientations of rotational and tangential discontinuities in solar wind from Mariner 5 data 08 p1356 A71-21642
- Temperature and pressure discontinuity stresses in compact heat exchangers, considering tubes as elastic foundation underneath tube plate 08 p1374 A71-22034
- Fourth order boundary problems with discontinuous boundary conditions, considering circular plate transverse vibrations 09 p1543 A71-23614
- Disperse systems dynamic behavior, considering density ratio, discontinuity diameter, viscosity and shear modulus 14 p2256 A71-29518
- Electromagnetic wave diffraction coefficients for discontinuity in curvature from surface field asymptotic description near singularity 14 p2192 A71-29794
- Iris-type discontinuity problems in waveguides and periodic structures, investigating numerical solutions convergence 14 p2212 A71-30513
- Solar wind rotational to tangential discontinuities ratio determination and hypothesis concerning origin in interplanetary magnetic field 16 p2628 A71-33942
- Weak discontinuities propagation speeds, equations and eigenvectors in uniform collisionless plasma 21 p3421 A71-40209
- Three ideal incompressible fluid jets collision induced flow, reducing discontinuity region analytic functions to nonlinear system with two numerical parameters and singular integrals 21 p3367 A71-40684
- Jump type behavioral uncertainties in stochastic optimal control problems, considering control of spinning spacecraft 23 p3659 A71-44112

DISCRETE FUNCTIONS

- Optimal control discrete time matrix Riccati equation, establishing convergence, uniqueness and stability properties 02 p0275 A71-11673
- Stability of linear time invariant discrete systems including multiple poles 03 p0393 A71-14471
- Discrete Fourier transform associated with discrete function theory 07 p1147 A71-19324
- Linear discrete time stochastic system with unknown gain parameters, interpreting open loop feedback optimal control identifier and controller equations 11 p1741 A71-25361
- Closed-loop control of discrete time systems with uncertainty, discussing minimax reachability of target sets and tubes 14 p2219 A71-29698
- Influence coefficient matrix method for discretized Poisson equation solution 18 p2905 A71-36306

Boundary conditions discretization on fluid flow moving discontinuities for analytical or numerical integration 18 p2906 A71-36315

Quasar red shifts distribution, indicating discretization in form of geometrical series 19 p3142 A71-38154

Exponential continually discrete analytic functions of complex variable in explicit form, obtaining addition theorem for trigonometric functions 19 p3089 A71-38479

Discrete renewal processes applied to mathematical modeling of physical processes, using statistics of complicated events in reliability analysis 21 p3407 A71-40361

High order finite element solution roundoff error reduction, using discretization of elliptic equations 21 p3409 A71-40962

Koiter theory for structural snap-through buckling behavior, using discretized matrix procedure based on finite element idealization 22 p3613 A71-41436

Differential equations system numerical integration solution global discretization error local estimation by Runge-Kutta and multistep methods 22 p3567 A71-42293

DISCRIMINATION

NT BRIGHTNESS DISCRIMINATION

NT SENSORY DISCRIMINATION

NT TACTILE DISCRIMINATION

NT VISUAL DISCRIMINATION

Motor learning error performance with discrimination reaction timer, discussing commitment to wrong response, group observations and specific error repetition 07 p1047 A71-19462

DISCRIMINATORS

Digital FM discriminator for demodulating FM signals with high deviation percentage 01 p0033 A71-10899

Solid state circuit digital frequency discriminator with low pass filter in ESRO stations telemetry receivers AFC and antiseband system 05 p0720 A71-16326

FM discriminator with nonideal limiting, calculating signal to noise ratio under white Gaussian noise input 05 p0730 A71-17071

Injection phase locked oscillator as input microwave limiting amplifier for noise measuring microwave discriminator 07 p1074 A71-19126

FM discriminator detection, calculating false click probability and effect on output signal to noise ratio 07 p1061 A71-19535

Hydrogen fluid phase and temperature measurement by single sensor with fluid phase discrimination circuit for transient response sampling [NAS PAPER M-3] 08 p1293 A71-21697

Mutual coherence effects in time varying radiation fields on two beam interferometric optical discriminator response 11 p1800 A71-26306

Microwave phase discriminators sensitivity and linearity performance improvement, noting diode detectors nonideal nature 13 p2038 A71-28779

FM threshold extension bounds during click elimination, considering pulse-averaging type discriminator 14 p2198 A71-30906

Space flight sleep pattern data with EEG, using three descriptors and regression and linear discriminant analysis 16 p2528 A71-33108

Solid state voltage regulator with hybrid tunnel-diode/transistor circuit discriminator for overload protection, discussing operation, circuit diagram and performance 17 p2716 A71-34786

FSK L-level or duobinary system performance evaluation under intersymbol interference, using limiter-discriminator without postdetection filter as detector 17 p2707 A71-35479

Microwave acoustic delay device incorporated in phase discriminator for AFC, FM noise meters and pseudo-superheterodyne receivers 18 p2893 A71-36599

Fokker-Planck-Kolmogoroff equation for radar tracking meter with nonlinear discriminator and second-order smoothing loops, obtaining steady solution by separated variables method 24 p3815 A71-44702

DISEASES

NT AIRBORNE INFECTION

NT ANEMIAS

NT ARTERIOSCLEROSIS

NT ASTHMA

NT CANCER

NT CARBON MONOXIDE POISONING

NT CYANOSIS

NT DIABETES MELLITUS

NT EDEMA

NT EPILEPSY

NT HEART DISEASES

NT INFARCTION

NT INFECTIOUS DISEASES

NT KIDNEY DISEASES

NT LEUKEMIAS

NT LITHIASIS

NT NARCOLEPSY

NT PARALYSIS

NT PARKINSON DISEASE

NT PNEUMONIA

NT PULMONARY LESIONS

NT RADIATION SICKNESS

NT RESPIRATORY DISEASES

NT SCHIZOPHRENIA

NT TACHYCARDIA

NT THROMBOSIS

NT TOXIC DISEASES

NT TUBERCULOSIS

NT TUMORS

Diseased plants and crop loss per field from aerial IR-color photography 14 p2236 A71-30576

USAF aeromedical consultation service experience on vertigo cases covering symptoms and related diseases 21 p3331 A71-40358

DISTES

U PARABOLIC REFLECTORS

DISILICIDES

Tantalum and niobium disilicides enthalpy and heat capacity temperature dependences 02 p0263 A71-12198

Tantalum disilicide kinetic interaction with Ta, investigating formation rate at various temperatures 13 p2089 A71-29415

Silicidization on Nb-Ta alloys, considering formation of niobium disilicide phase with hexagonal lattice 15 p2425 A71-31401

Tantalum and niobium disilicides enthalpy and specific heat temperature dependences in 1200-2100 K range 15 p2426 A71-31504

High temperature oxidation protection of niobium by molybdenum disilicide coatings applied by hot pressing powder metallurgy method 18 p2934 A71-35952

Molybdenum hemicarbid layer as diffusion barrier between metal and disilicide, investigating system thermal stability 21 p3399 A71-40526

DISINTEGRATION

Uniform matter fragmentation under gravitational influence, examining approximate solution for density perturbations 01 p0150 A71-10062

Fluid jets disintegration into uniform droplets with and without satellite formation, using stroboscopic photography 03 p0399 A71-13292

Fluid jets disintegration into uniform droplets with and without satellite formation, using stroboscopic photography 09 p1434 A71-23267

Disintegration energy of hard compounds /carbides, nitrides and borides/ related to wear resistance and microhardness of alloys 13 p2072 A71-27818

Melting body disintegration in hypersonic gas flow under radiation influence from shock layer, assuming optically thin boundary layer and intense vaporization 14 p2336 A71-30222

Photoconductive CdS disintegration effect on heterophase electrophotographic layer electric and photoelectric properties, noting optimal properties relationship to grain diameter 22 p3586 A71-42406

Cometary nucleus disintegration rate as function of orbital elements, calculating lifetimes for Encke and Halley type comets 23 p3772 A71-44313

DISKS

German monograph on stress distribution around cutouts in disks, plates and cylindrical shells 05 p0820 A71-16121

Static thin shells and disks gravitational fields in general relativity 05 p0781 A71-16447

DISKS (SHAPES)

NT ROTATING DISKS

German monograph on stress strain state calculation in strengthening material disks 01 p0176 A71-11221

Disk elongation plastic deformation, determining elastoplastic stressed state for inhomogeneous thermal cycles 02 p0323 A71-11748

Stress distribution in gelatin disk and rectangular plate compressed between horizontal slabs, using tangential difference method 02 p0328 A71-12512

Optimal design with geometric constraints for simply supported Tresca plastic disk and cantilever plate under concentrated force 05 p0830 A71-17223

Axissymmetrical potential theory for two spherical circular disks system, using X-analytic functions for reducing to Fredholm equation 06 p0928 A71-18345

Elliptic ring shaped disk with external and internal loading, determining stresses due to uniformly distributed loads 06 p1002 A71-18416

Particle motion in gravitational field for disk-like configurations, solving kinetic equation for quadratic potential 07 p1192 A71-19286

Thermal diffusivity in disks and rods irradiated by sinusoidally modulated thermal radiation beam, measuring temperature phase difference across front and back faces 07 p1223 A71-19622

Sphere and disk drag measurements for Reynolds numbers from 5 to 100,000, examining forces, moments, flow visualization, unsteady modes and constant acceleration 07 p1015 A71-19893

Steel conical disks two dimensional stressed state determined with deformations at elastic and elastoplastic strains using digital computers 08 p1369 A71-21116

Gas dynamic test stand analyzing elastoplastic strains in aircraft gas turbine disks and liquid propellant rocket engines turbopumps under alternating nonisothermal loads 09 p1427 A71-22603

Thin metallic disk radar cross sections for near resonance frequencies backscatter, comparing experimental and computer results 09 p1410 A71-23518

Unsteady inward and outward velocities of subsonic radial air flow between two disks, using hot-wire anemometer and cylindrical wave equation 10 p1550 A71-24000

Nodal points stresses determination from finite element solved elastic problems, discussing thin disk stresses as function of mesh pattern regularity 11 p1851 A71-26312

Monograph on heat transfer from rotating heated surface with induced turbulent boundary layers covering disk, cone and sphere geometries 13 p2162 A71-28882

German monograph on spline functions interpolation for solving integral equations and stress calculation in curvilinear edged disks 13 p2157 A71-29420

Stress values at arbitrary point of infinite disk loaded by concentrated force acting through rigid slit of circular arc segment 14 p2323 A71-29814

Imperfect circular disks large amplitude free transverse vibration calculation by Galerkin procedure 14 p2326 A71-30064

Nondimensional entrance loss equation for radial turbulent flows without swirl between parallel disks 14 p2226 A71-30415

Torsionally oscillating disk in steadily rotating incompressible second order fluid, calculating transverse and radial shear stress 15 p2387 A71-31185

Incompressible viscous fluid flow between disks oscillating about state of rigid rotation, studying spin-up time effects 16 p2607 A71-32861

Solid disk supported above flat plate by thin layer of gas flowing from central orifice, studying vertical motion equilibrium and dynamic data [ASME PAPER 71-APM-3] 16 p2559 A71-33220

Stress-strain state of homogeneous and inhomogeneous cylinders and disks with central axial curvilinear hole under internal pressure and thermal loads 17 p2816 A71-34331

Rotating inertia effects on step-type MHD hydrostatic thrust bearing characteristics, discussing disk shape and operating conditions for improvement 17 p2748 A71-34641

Radiation pattern of dielectric disk antenna, using computerized analysis of electromagnetic scattering and spherical volume cell 17 p2715 A71-34765

Electromagnetic plane wave monostatic scattering incident to thin circular metallic disk, calculating spectral and transient response from far field amplitude and phase data 19 p3036 A71-38608

Potential flow and laminar boundary layer separation about profiled circular disks, calculating streamlines 20 p3175 A71-39029

Disk fillets stressed state, determining concentration coefficient and bearing capacity effect 23 p3780 A71-44221

Stress field due to two rigid circular disk inclusions in isotropic homogeneous infinite plate 24 p3879 A71-44627

DISLOCATIONS [MATERIALS]

NT CRYSTAL DISLOCATIONS

NT EDGE DISLOCATIONS

NT SCREW DISLOCATIONS

Quenched Al-Mg alloys, investigating dislocation mechanisms for plastic flow by creep tests at various temperatures

01 p0105 A71-11605

Dislocation pinning by interstitial atoms during Cr and Cr-Ce strain aging, using amplitude dependent internal friction technique

02 p0263 A71-11897

Temperature fields without induced stress, considering relation between thermal and dislocation stresses in shells of revolution

02 p0325 A71-12283

Austenitic stainless steels point defect migration sensitivity, measuring dislocation damping during recovery after quenching

02 p0267 A71-12883

Displacement and stress distribution in infinite elastic medium weakened by Griffith crack

03 p0509 A71-13909

Work hardening model for grain size effects on metals flow stress, discussing dislocation density as stress-strain function

03 p0447 A71-14494

Physical-metallurgical nature of brittle fracture of steels from phenomenological and atomic /dislocation/ approach

03 p0516 A71-14576

Yield point in metals, using Cottrell theory of atmospheres of foreign atoms near dislocations

04 p0612 A71-15062

Carbide particles mean interparticle spacing and low alloyed steels dislocation density determination by planar and volume methods for metal matrix

04 p0612 A71-15076

Reversible hydrogen brittleness of steels in terms of dislocation theory

04 p0612 A71-15550

Crack propagation as unstable stress relaxation process, using viscoelastic dislocation model

06 p0984 A71-17557

Intrinsic stacking fault energy temperature dependence in austenitic Fe-Cr-Ni alloys determination from dislocation mode measurements by high temperature transmission electron microscopy

07 p1138 A71-19984

Maxwell theory analogy with Cosserat continuum moving dislocations, studying kinematic and dynamic equations common features

07 p1161 A71-20016

Luders bands motion in steel and iron, studying plastic zone velocity dependence on stress, composition, grain size, dislocation substructure and temperature

08 p1308 A71-21517

Portevin-Le-Chatelier effect and sharp yield point in zone refined Ni, discussing internal friction and pinning effect on dislocations by hydrogen atoms at low temperatures

08 p1310 A71-21533

Bubble raft model for atomic configurations in ordered grain boundary and grain boundary dislocation at high temperatures, discussing Al-Mg alloys

08 p1345 A71-21575

Fracture kinetics, emphasizing plastic deformation, dislocation and diffusion micromechanics, point defects effects and microcrack formation

08 p1371 A71-21606

Prior deformation and subsequent annealing influence on fatigue response of coarse grained alpha Ti, evaluating relative effects of dislocation locking and mechanical twinning

10 p1626 A71-24445

Crack dislocations nature and significance, density equations, instability conditions, fracture mechanics, including cohesive forces and plastic zone equilibrium

10 p1628 A71-25026

High strength stainless steel dislocation structure and mechanical properties, discussing tempering, tensile strength, precipitation hardening and temperature effects

11 p1776 A71-25167

General dislocation model for high temperature creep of pure metals, discussing strain rate effects

11 p1782 A71-26476

Al and Al-Mg alloys average interdislocation internal stress measurement during steady state creep

12 p1916 A71-26895

Suspended hollow cylinder under force of gravity, calculating stresses and displacements by linear elastic theory differential equations

13 p2153 A71-28518

Cr and Cr-Y alloy interstitial residual content and dynamic dislocation-interstitial interactions at various temperatures and strain rates

13 p2085 A71-28578

Mechanical properties, hardness and dislocation structure of Ti bearing maraging steels, considering Mo role in strength and plastic properties improvement

13 p2086 A71-28581

Kinetics of Ti single crystals tensile deformation by prismatic gliding, studying moving dislocations interactions with metal impurities

14 p2257 A71-29844

Dislocation stress analysis in infinite elastic plate with two circular holes under arbitrary steady temperature field

14 p2332 A71-30850

Dislocation theory and crystallography in metallurgy, discussing edge and screw dislocation motion and interactions, Burgers vectors and gliding planes

15 p2427 A71-31530

Stress-microstrain relationship for metal crystals prestrained in easy glide, obtaining mobile inelastic dislocation density and internal stress

16 p2654 A71-33102

Incompressible materials weak compressibility effect in elastic theory, deriving displacement equation with average pressure function for any Poisson coefficient values

17 p2818 A71-34350

Fracture kinetics, emphasizing plastic deformation, dislocation and diffusion micromechanics, point defects effects, microcrack formation and interstitial mechanisms

17 p2834 A71-35667

High purity metals residual electrical resistivity, observing impurities, vacancies, dislocations, plastic strain and polyisotropy effects

19 p3076 A71-37115

Iron precipitation rate from supersaturated Al alloy solid solution in structures with low and high dislocation densities

19 p3079 A71-37702

Continuum mechanical approach to velocity dispersion of longitudinal plane waves in elastic solid containing dislocations

19 p3118 A71-37794

Field induced changes in W specimens during field ion microscope operation, considering behavior of dislocations and grain boundaries

21 p3395 A71-40024

Dislocation structures of polycrystalline tungsten after deformation and recovery annealing, observing temperature dependence of critical strain for recrystallization

21 p3399 A71-40472

Transition layer structure formation of epitaxial semiconducting films, discussing model for dislocations origin

21 p3427 A71-40727

Dislocation structures in austenitic steel fatigued at various stress cycles and tensioned at various strains, using transmission electron microscopy

21 p3400 A71-40833

Continuum dislocation theory, discussing initial stress couple problem, slip motion and dislocation rate tensor

21 p3468 A71-41000

High strength stainless steel dislocation structure and mechanical properties, discussing tempering, tensile strength, precipitation hardening and temperature effects

21 p3402 A71-41088

Temperature and velocity dependence of electronic dislocation stopping power in superconductor due to scattering of normal electrons

21 p3432 A71-41268

DISORDERS

Sound and vibration disorder measure for choosing statistical or deterministic models for system/response situation

[ASME PAPER 70-WA/DE-1] 03 p0459 A71-14138

Human ocular control system supranuclear disorder syndromes and signs in terms of physiological concepts

22 p3488 A71-42438

DISORIENTATION

NT DISORDERS

Disorientation response of survived chicks hatched from eggs injected with radioprotective 2-beta-aminoethylisothiuronium-Br-HBr after incubation

07 p1040 A71-18988

Labyrinths and proprioceptors from aerospace medicine viewpoint, discussing motion sickness, spatial disorientation, manned space flight and rotation in space

08 p1244 A71-20711

Modeling human disorientation and motion sickness in rotating spacecraft, stressing sensors dynamic response

[AIAA PAPER 71-870] 18 p2872 A71-36654

Epidemiology statistics of USAF spatial disorientation aircraft accidents, noting pilot training, flight environment and indoctrination remedy programs

21 p3342 A71-40359

DISPENSERS

Dispensing devices and error sources in radial immunodiffusion and electroimmunodiffusion techniques

22 p3508 A71-42888

DISPERSION

Transparent solids unpolished samples refractive index and dispersion measurement using Abbe refractometer

01 p0128 A71-10837

Calculated dispersion in decaying grid turbulence, showing agreement with test results for diffusion of heat from line source

01 p0072 A71-11484

Sounding rocket dispersion analysis, discussing roll rate errors, earth rotation and wind effects and improved computational techniques

[AIAA PAPER 70-1379] 03 p0498 A71-13662

Dispersion equations for complex transmission coefficients of submillimeter EM waves in solid state InSb plasma, applying plasma effects to control elements

03 p0467 A71-13797

Galaxy cluster expansion theory, noting dispersion in radial velocities of members

05 p0812 A71-16694

Condensed water vapor in supersonic nozzle flow, describing dispersion coefficient measurement

08 p1275 A71-21269

Time dependent dispersion simulation by random number generator, introducing horizontal and vertical shear, buoyancy and anisotropic turbulence

09 p1488 A71-23027

Radiation and gas-dust interactions, examining dispersion relation and instability for cosmological models

10 p1675 A71-24490

Critique on pulsar distance estimates based on dispersion measure, introducing period luminosity function

13 p2137 A71-28592

Asymptotic theory of wave propagation extended to slightly inhomogeneous and slowly varying anisotropic media exhibiting spatial and temporal dispersion

15 p2449 A71-31476

Interstellar medium dispersion and rotation measurements, calculating electron concentration fluctuation effects

16 p2608 A71-33227

Crab Nebula pulsar timing observations, correcting arrival times to solar system barycenter and dispersion effect

20 p3302 A71-39929

Quadratic and linear electro-optical effect dispersion in flux grown crystals of barium titanate

22 p3585 A71-41729

Dispersion equation for electromagnetic surface wave propagation along plane boundary of adjacent hot plasma streams

23 p3713 A71-44149

Fluid elements streamwise dispersion in two dimensional turbulent shear open channel flow, using Markovian model for numerical simulation

24 p3817 A71-44421

DISPERSION PRECIPITATION HARDENING

U PRECIPITATION HARDENING

DISPERSIONS

NT AEROSOLS

NT COLLOIDAL PROPELLANTS

NT COLLOIDS

NT EMULSIONS

NT FOG

NT LIQUID-GAS MIXTURES

NT NUCLEAR EMULSIONS

NT PHOTOGRAPHIC EMULSIONS

NT SMOKE

Dispersion medium effects on thermal hardening of lubricating oils with Na or Li additives

05 p0772 A71-16385

TD NiCr nickel based alloy high temperature oxidation control, discussing thoria dispersion effect on Ni-Cr oxidation properties

11 p1779 A71-26015

High temperature gas dispersed Al particle flow, investigating electrical conductivity and radiation properties

19 p3161 A71-37265

Electric fields for solid and liquid fuels dispersion and trajectory manipulation of charged particles to control mixing with air, vaporization and burning

19 p3171 A71-38193

Soviet book on hydrodynamics of nonstationary motions of viscoplastic media covering mechanical properties of clay, mortar, cement, lubricating oil, petroleum and disperse media, etc

21 p3369 A71-40872

DISPLACEMENT

Crack opening in infinite isotropic elastic solid via displacements applied to crack surface

01 p0167 A71-10292

Maraging steel welded plates edge displacements under linear multiflame burner heating, determining temporal deformations by heat distribution from additional source

01 p0088 A71-11098

German monograph on displacement elimination method in viscoelastic shell theory covering shearing loads derivation from stress functions

02 p0327 A71-12398

Axisymmetric load problems in Cosserat medium, expressing displacement states by mathematical functions

03 p0509 A71-13899

Spherical shell segments stresses and displacement due to arbitrary axisymmetric surface tractions and edge boundary conditions, using axisymmetric elasticity solutions
[ASME PAPER 70-WA/APM-27] 03 p0512 A71-14159

Translational vs deformation displacement motion in sensitivity of double exposure holographic interferometry 03 p0429 A71-14181

Semiinfinite isotropic linear Cosserat continuum surface under impulsive loading, calculating displacements with Laplace transformation 04 p0672 A71-15834

Piezoelectric ceramic transducer vibration measurement under mechanical loading, noting displacement as function of thickness and time 04 p0601 A71-15835

Flat plate wake displacement sources in potential flow, considering high Reynolds numbers outside boundary layer 05 p0695 A71-16960

Rolling contact body displacement effect on bearings rigidity with allowance for inner ring transverse vibration 08 p1295 A71-20689

Stress distribution in infinite elastic solid containing spherical cavity and external crack, discussing displacement components for axisymmetric loading 12 p1974 A71-26740

Elastic body displacement equilibrium equations, using variable direction iteration methods for boundary value problems 12 p1978 A71-27329

Elastic laminated plates with various thickness layers, deriving independent differential equations for displacement 12 p1978 A71-27334

Optimal design of minimum volume beams of variable height under bilateral restrictions on stresses and displacements 13 p2154 A71-28645

Local slip theory in elastic contact region with dry friction, assuming Amontons-Coulomb law for displacement, rolling and sticking 17 p2747 A71-34327

Displacement field of constant thickness elastic disk with stress boundary conditions, using finite difference technique 17 p2818 A71-34505

Continuous stress distributions across interelement boundaries, using finite element approximations based on displacement assumptions 17 p2831 A71-35352

Displacement in circular plate with radial slit under transverse forces 19 p3156 A71-37796

High precision displacement functions for finite element models of rotational shell and plate bending problems 21 p3470 A71-41019

Displacement fields for two dimensional minimum weight frames for load dispositions analogous to perfectly plastic plane flow in metal working 21 p3391 A71-41428

Rotating disks optimal design allowing for creep from additional coupling imposition and contour displacement 23 p3780 A71-44220

Noncircular cylindrical shells stress and displacement under hydrostatic loads, applying Donnell equations 24 p3879 A71-44618

Critique of variational formulation approach in finite displacement analysis, considering applicability requirements and limitations 24 p3880 A71-44639

Approximate periodic Green matrix solution to equilibrium equations in displacements for shell of revolution under linear loads 24 p3881 A71-44826

DISPLACEMENT MEASUREMENT

Inner ear basilar membrane motions estimation for lower hearing threshold, using nonlinear model 02 p0201 A71-12474

Solar general magnetic field determination by measuring visually small displacements on photographic plate 02 p0316 A71-12752

Beams and plates deflection optical measurement using moire gap effect generalized to include linear and rotational mismatches [SESA PAPER 1703] 03 p0507 A71-13754

Transistorized displacement meter with variable frequency oscillator and inductive transducer as sensing element 03 p0387 A71-13816

Stereophotogrammetric measurement of plastic deformations of circular Al membrane loaded by pressure pulse, using high speed cameras 03 p0428 A71-13948

Thick strips widening by rolling, deriving formula for maximum widening from plastic deformation process description by displacement-rate fields 04 p0602 A71-14608

Nondestructive test with high resolution instrumentation for observing long thin walled cylinder lateral displacements prior to buckling under axial compression 04 p0669 A71-15297

In-plane surface displacement measurement by double exposure speckle photography 05 p0747 A71-16191

Anisotropic shells theory, discussing displacement components 06 p0986 A71-17759

Dynamic characteristics of two degree of freedom gyroscopes with positional and integral negative feedback for simultaneous angular velocity and displacement measurement 09 p1451 A71-23171

Thin cylindrical shell deformation under concentrated transverse loads applied through rigid boss, determining displacement variations as function of applied loads and edge constraints 09 p1543 A71-23659

Stress and displacement fields in elastic half plane containing edge crack normal to free surface, using integral equations 11 p1847 A71-25440

Radial load effects along length of hinged cylindrical shell for maximum displacement positions, using trigonometric Fourier series 11 p1850 A71-25942

Inertial instruments with outputs indicative of time integral and time double integral of vehicle acceleration for velocity and distance determination 14 p2245 A71-30343

High sensitivity three beam holographic interferometry using Zernike method, applying to small deformation measurement 15 p2402 A71-31258

Diffusely reflecting object element three dimensional displacement measurement from single hologram nonlocalized patterns 15 p2403 A71-31263

Three dimensional deformation surface displacement measurement by holographic interferometry, using equal inclination fringes 15 p2403 A71-31264

Diffusely reflecting in-plane surface displacement measurement by holographic interferometry, comparing static and dynamic methods for accuracy 15 p2403 A71-31265

Fringe order determination in holographic interferometry, discussing zero motion object region identification 15 p2403 A71-31266

Pin connected beam under axial loading, discussing resultant constraint forces, bending moments and lateral displacements 16 p2661 A71-34116

Holographic interferometry fringe patterns interpretation for small displacements measurement, considering precision gyro stability 17 p2744 A71-35286

Autokinetic motion of luminous target, relating apparent visual movement to experienced displacement 17 p2694 A71-35739

Interference holography, discussing precision displacement measurement, fringe localization, multiple beam techniques, contour generation and flow visualization 18 p2920 A71-36148

Holography as nondestructive testing tool, considering application in vibration analysis, stress/strain measurement, bond inspection, internal flaw detection and displacement measurement 18 p2927 A71-36657

[SME PAPER IQ-71-121] Three dimensional surface displacement measurement by hologram interferometry, applying to cantilever 20 p3235 A71-39187

Holographic interferometry application to two step static displacement measurement of diffusely reflecting surface of rigid body in motion 21 p3377 A71-40227

Moire fringe method for direct determination of displacement and strain fields in two and three dimensional surfaces 21 p3377 A71-40230

Deformation and translation measurements with holographic interferometry, considering flat surface moved with precision differential screw micrometer 21 p3381 A71-40933

Elastic shells of revolution displacement analysis, using incremental variational theory with finite element method 22 p3613 A71-41434

Stress and displacement analysis in linear elastic half space consisting of one or two layers bonded to another homogeneous half space 23 p3779 A71-44178

Stereophotogrammetric measurements of displacements and strains in Al membrane during explosive forming 24 p3825 A71-44755

DISPLAY DEVICES

NT ANEMOMETERS

NT APPROACH INDICATORS

NT FLOW DIRECTION INDICATORS

NT GYRO HORIZONS

NT HEAD-UP DISPLAYS

NT HOT-FILM ANEMOMETERS

NT HOT-WIRE ANEMOMETERS

NT KINOFORM

NT PLAN POSITION INDICATORS

NT POSITION INDICATORS

NT RADARSCOPE

NT RADIO DIRECTION FINDERS

NT SONIC ANEMOMETERS

NT SPACECRAFT POSITION INDICATORS

NT SPEED INDICATORS

Flight simulator visual systems, discussing improvement objectives in terms of current technology, image quality, system reliability and maintainability 01 p0066 A71-10016

Time shared computer display system design with analog drive signal generator and digital information channeling processor 01 p0045 A71-10196

Real time graphic display monitoring of time sharing computer systems operational state 01 p0046 A71-10207

Alphanumeric character generation from resistive storage of time derivatives for CRT displays 01 p0047 A71-10216

Computer output microfilm /COM/ technology, describing recorders and applications 01 p0047 A71-10218

Analog computers seven segment numeral display, describing code converters 01 p0049 A71-10261

Man machine considerations in all-weather low level navigation system design, noting off-course error reduction by command information display to pilot 01 p0125 A71-10515

Electronic control indicator for human pilot capability enhancement using color coded cathode ray display, presenting information from seven different instruments 01 p0081 A71-10750

Steepest approach to landing for jet transport aircraft noise abatement, using ground based equipment and onboard TV display 01 p0126 A71-11311

Three dimensional dynamic CRT display for simulation, using VECTRA /Vector Transformer/ digital computing device for control 01 p0084 A71-11394

Manual tracking systems identification and real time display, developing software system 01 p0027 A71-11437

Fast on-line block-diagram-based DARE II digital simulation program for use on PDP-9 computer with CRT display console 02 p0226 A71-11779

Hybrid real time computer simulation of external visual display cues for Apollo Command and Service Modules 02 p0237 A71-11791

Real time large scale display system with information image projection on reversible photochromic emulsion via IR laser 02 p0249 A71-12072

Filter effect on CRT display resolution and relation to photometric and color contrast 02 p0249 A71-12073

Current profile monitor for scanning electron beam irradiations from accelerator, using storage oscilloscope or X-Y recorder for display 02 p0249 A71-12127

Real time contourgram for monitoring ECG waveform data, describing cardiac measurement and data display 02 p0199 A71-12384

Holographic display applications in portraiture, data storage and retrieval, motion pictures, TV, etc 02 p0253 A71-12597

Aircraft information display simulation and flight tests of experimental display systems, discussing man machine communication systems development [DFVLR-SONDDR-81] 03 p0396 A71-13344

Real time analysis and display of pulsed laser propagation data in rectangular X-Y field 03 p0427 A71-13920

Matrix addressed polarization rotating or retarding light valve arrays for optical selectors, composers and displays from nonswitching threshold materials 03 p0430 A71-14468

Laser display technology, discussing recent systems, light beam deflectors and modulators 04 p0607 A71-14723

Holography developments concerning interferometry, microscopy, display systems, data storage and ultrasonic tests 04 p0587 A71-14724

Beam-combining prism/magnifier eyepiece configuration with miniature CRT for superimposing magnified virtual image upon user visual field 04 p0597 A71-15362

V/STOL aircraft visual aids flight evaluation concerning minimum landing area operations 04 p0534 A71-15445

Organic and inorganic phosphors for monochromatic laser illuminated black and white color displays 05 p0760 A71-16258

Black and white and multicolor laser display systems with monochromatic or bichromatic source, using photoluminescent materials and acousto-optic deflectors and modulators 05 p0760 A71-16259

LF oscilloscope display of periodic subnanosecond optical pulses from mode locked lasers 05 p0761 A71-16334

Cathode ray tubes as real time display device in various types of professional equipment, describing functional performance and related tube design aspects 06 p0872 A71-17319

Electron tubes for radars, discussing history and development of magnetrons, Thomson-CSF display tube and power amplifiers 06 p0874 A71-17568

Aircraft cockpit instrumentation display media research, discussing brightness and contrast ratio requirements for gray scale displays 07 p1046 A71-18736

Light emitting film /LEF/ displays, discussing physical principles, construction and applications of electroluminescent thin film devices 07 p1105 A71-18737

Fiber optic faceplates for contrast enhancement under high ambient light conditions for commercial and military cockpits, eliminating ghost, halo and direct sunlight problems 07 p1107 A71-19175

Radial direction shearing interferometry, considering wave front radial phase derivative display by axicon or circular grating arrangements 07 p1110 A71-19477

Computer generated motion pictures to simulate real events, discussing design problems and airfield simulation with GPSS software package 07 p1111 A71-19511

Aircraft visual warning indicating system, outlining design criteria, color and brightness recommendations [SAE-ARP-1088] 07 p1019 A71-19644

Manned space flight data processing system data storage, describing data base structure, direct access display and batch processing [AIAA PAPER 71-237] 07 p1068 A71-19713

Three-phase time-ordered functional organization for ground based collision avoidance, discussing information flow, display capability and dynamic simulation model [AIAA PAPER 71-240] 07 p1155 A71-19716

Computer display channel for en route air traffic control flexible real time data processing and display subsystem [AIAA PAPER 71-247] 07 p1156 A71-19721

Aircraft navigation system requiring computer and display for approach guidance to circular orbit over fixed ground area [AIAA PAPER 69-986] 07 p1156 A71-20305

Manned aircraft crew long range navigation, discussing sensor, information processing and display systems for future commercial and military missions 07 p1157 A71-20343

Star maps for recognition and attitude orientation aids as function of stereographic display realism in manned space flight 07 p1157 A71-20348

TV display eye movement monitor with automatic coordinate digital printout for permanent record 07 p1053 A71-20402

Signal fluctuation noise reduction with input screen inertia by lagging component introduction to introsopic system 08 p1294 A71-21903

Converter-indicator direct digital readout design, using photodiodes for LSI VOR area navigation display systems low power operation 09 p1491 A71-22610

Real time remote test site computation and display of complex engine inlet distortion parameters from dynamic pressure signal, using analog computer 09 p1446 A71-22726

Aircraft display designs, emphasizing man machine problems 09 p1402 A71-23621

Computer controlled electromechanical system for luminous projection on world map of satellite orbits, using Ne-He laser beam 09 p1430 A71-23627

Navy pilots performance improvement through symbolic flight displays 09 p1453 A71-23675

V/STOL aircraft automatic flight controls and electronic head down displays, discussing handling qualities, lift effectiveness and autostabilization 10 p1554 A71-23944

Terminal area control, discussing geographically grouped visual information displays, controllers coordination, plan position indicators and telecommunication 10 p1639 A71-23945

Man-machine interactive scanned-display computer graphics system implemented on Honeywell DDP-224 computer 10 p1581 A71-23967

Papers on photoelectronic imaging devices covering radiometry, photometry, vision, electro-optical system evaluation, etc 10 p1609 A71-24055

Photoelectric imaging devices resolution performance, considering modulation transfer function and measurement methods 10 p1610 A71-24060

Electro-optical devices evaluation search model, considering imagery and image transmission 10 p1610 A71-24062

Area navigation facility, discussing control and display and navigation standards 12 p1927 A71-26879

Concorde economic flight testing methods, discussing Blagnac flight simulator mobile cabin visualization and color TV terrain model 12 p1868 A71-27608

Vibration mode patterns of acoustoelectric oscillators, describing detecting apparatus 13 p2036 A71-28469

EDITOR program for writing, reading, copying or altering data on file disk via display station 13 p2035 A71-29015

V/STOL aircraft instruments, deck display and automatic flight controls for takeoff and landing operation 13 p2098 A71-29132

ATC radar display systems mapping techniques using vectors and optical projections 14 p2271 A71-30014

Concorde SST flight test equipment installation with PCM recording and visual instruments 14 p2174 A71-30055

Image spatial frequency content of speckle patterns on illuminated diffuse screen and photographic film by optical Fourier analysis 14 p2242 A71-30152

Maastricht Automatic Data Processing and Display ATC system with digital computers for aiding controllers in issuing instructions and making decisions 14 p2272 A71-30383

Area navigation system based on radio aids by airborne receivers and sensors for aircraft movement improvement, noting advantages of pilot displays [SAE PAPER 71-0457] 14 p2272 A71-30533

Display devices - IEEE Conference, New York, December 1970 14 p2249 A71-31028

Alphanumeric display devices with liquid crystal and dynamic light scattering for low voltage, power, cost and fabrication advantages, testing performance 14 p2249 A71-31029

Plasma display panel with rectangular gas discharge cells array separated by thin dielectric sheets, discussing operation principles 14 p2249 A71-31030

Light line and dark photochromic film large scale display devices, using neodymium and UV lasers for film bleaching and darkening respectively 14 p2249 A71-31031

Current-sensitive single-gun polychromatic CRT phosphor screen operational characteristics 14 p2215 A71-31032

Electrical fiber plates as high resolution conductive arrays for storage and display in electron beam addressed systems 14 p2250 A71-31033

Head- or helmet-mounted display/control system in V/STOL aircraft for pilot workload and training reduction [AHS PREPRINT 532] 14 p2189 A71-31093

Optimum configuration/cost design of computer graphics systems, using mathematical model involving response time prediction by queueing analysis 15 p2374 A71-31181

Maastricht automatic data processing and display system concept for automatic management of reception and data transmission and information visualization 15 p2384 A71-31888

Visual devices for training simulators, discussing film and closed circuit TV systems and components 15 p2385 A71-31889

Laser interferometer application in machine tool calibration, digital readout and feedback system, discussing advantages and limitations [SME PAPER IQ-71-745] 15 p2421 A71-32433

ONR human engineering research program concerning information input, display and processing concepts, decision making and motor output and control 16 p2536 A71-33529

Aircraft instrumentation deficiencies from pilot viewpoint, proposing pilot designed display [AIAA PAPER 71-787] 16 p2537 A71-34017

Airborne display and electric management system, discussing weight reduction, protective function coordination, power quality, onboard maintenance, data processing and reliability 17 p2739 A71-34617

Cockpit display, discussing aircraft operators delay in use of head-up displays, area map navigation, CRT and electroluminescent readouts 17 p2691 A71-35110

Soviet book on air transportation covering ATC, automatic landing and information display systems 17 p2774 A71-35194

Real time reconnaissance cockpit display system for airborne sensor systems, providing night combat imagery 17 p2747 A71-35772

Operator-computer communication devices with graphic data display, discussing construction and operation 18 p2884 A71-35879

Information display device with electro-optical system for discrete deviation of monochromatic linearly polarized light beam, analyzing electronic control circuits energy characteristics 18 p2884 A71-35880

Holographic display for blind landing system with variable image perspective over wide field of view, using collimated or cylindrical laser beam 18 p2945 A71-36061

Dynamic display of abstract visual perspective using fiber optic material as discrete lines of light-emitting elements 18 p2918 A71-36075

Computer-disk interface system photooptical instrumentation for weather data acquisition, analysis and display 18 p2884 A71-36078

Computerized digital techniques for image motion compensation as function of additive noise level, using Fourier transform image filtering and halftone display 18 p2919 A71-36083

Eye-point-of-regard system including eye and head movements devices and analog computer for pilot scanning and display research 18 p2864 A71-36091

Electronic processing of coherent optical data for measurement and display using holography, speckle patterns, interferograms, image intensifiers and TV systems 18 p2923 A71-36608

Visual displays preview, noting miniature eight-character alphanumeric, tabular, video, telephone and graphical displays 18 p2924 A71-36619

Human performance in optical high inertia tracking system interface, considering proprioceptive feedback, display magnification, control dynamics view field and anticipatory processes effects 18 p2873 A71-36912

Airborne traffic situation display for use with national airspace/automatic radar control terminal system, using computer selected message, map and heading data [AIAA PAPER 71-929] 19 p3097 A71-37175

Airfield performance evaluation by simulation, providing statistical measures and computer generated motion picture for visual display of simulated future activity 19 p3041 A71-38027

Automatic ATC display systems, discussing electronic flight progress strip for telemetry reproduction 19 p3102 A71-38300

Nematic and cholesteric mixtures liquid crystals electro-optic properties and applications to display devices 19 p3120 A71-38537

Data display units as man machine interface elements in data processing operations, discussing combined alphanumeric/graphic CRT units 20 p3202 A71-38885

Display devices components in highly interactive man machine systems, noting drawbacks of CRT 20 p2333 A71-39059

Stability conditions for square wave sustaining voltage, including complex rectangular waveforms with pulsed discharges in plasma display 20 p2333 A71-39060

High resolution gas discharge plasma display panel, discussing design, capabilities and performance 20 p2333 A71-39061

Three dimensional display with multicolor capability, continuously variable intensity and random accessed flying spot, exhibiting fixed or moving objects 20 p2324 A71-39063

Cholophor /passive polarization switched liquid crystal screen/ for laser power enhancement in multicolor displays 20 p3234 A71-39064

Displays - IEE Conference, Loughborough University of Technology, England, September 1971 21 p3376 A71-40107

Monolithic alphanumeric array of planar light-emitting GaAsP diode matrix on common chip for programmed function keyboard use in display devices 21 p3349 A71-40108

Bicolor cathode ray display tubes with triple-layer bombarding electron beam energy-dependent red-green fluorescent screen 21 p3347 A71-40109

Red and green light emitting GaP junction diodes and monolithic arrays for display devices, discussing fabrication and properties
21 p3352 A71-40110

Picture processing using general purpose digital computer simulation for reduction of processing time and special purpose hardware investments
21 p3376 A71-40111

Fast time digital computer simulation model for evaluation of man-machine interface [display/problem of ATC system including personnel and equipment
21 p3412 A71-40112

Display devices in aircraft cockpit providing pilots with information from various sources, considering head-up display and CRT
21 p3376 A71-40113

Computerized touch display for ATC tasks compared to conventional keyboard tabular display performance
21 p3413 A71-40114

Computerized tabular data display with cross-bar addressed glow discharge panel, discussing system details
21 p3350 A71-40115

Electronic circuit modules effects on alphanumeric display capabilities and costs over wide applications range
21 p3359 A71-40116

Low voltage IR image converter display system using scanned line array of GaAsP light-emitting junction diodes
21 p3352 A71-40117

ATC display devices with computer-derived alphanumeric labels on radar screen, examining feasibility and effectiveness
21 p3413 A71-40118

ATC display device man-computer interaction faults and delays effects on operator performance
21 p3413 A71-40119

AC plasma panel /gas discharge matrix/ display, discussing operation principles, static and switching characteristics and driving circuitry
21 p3352 A71-40120

Alphanumeric fonts for 5-by-7 matrix display, comparing legibility with USAF font
21 p3350 A71-40121

Computerized multiparametric data three dimensional CRT graphic display involving isometric viewing and intensity modulation
21 p3350 A71-40123

Stereo viewing transmission/reflection display by producing stereopair image on CRT screen with polarizing polaroid sheets
21 p3376 A71-40126

Contrast level reading tests of CRT and self luminous display devices with optical filters at high ambient light for cockpit applications
21 p3376 A71-40127

ATC height and plan position indicator composite picture display system design and operation, combining functions of primary and secondary surveillance radars
21 p3413 A71-40128

Large character set display terminal for public information service system, describing design, construction, components and operating characteristics for nonalpha languages
21 p3350 A71-40129

Aircraft head-up display systems for providing pilot information focused at infinity within pilot normal field of view
21 p3413 A71-40131

Three dimensional graphics software package for CRT and storage tube displays and plotters, describing coordinate transformation
21 p3347 A71-40133

Deformographic storage display tube system, describing construction, development, design, performance and operating principles
21 p3352 A71-40135

Computer generated buffered displays for psychological experiments involving interception, tracking, steering, memory and calculation tasks
21 p3341 A71-40136

Avionics combined display system for area navigation, discussing design, color map projection, overlays, CRT unit and viewability
21 p3413 A71-40137

Graphical display of digital computer simulated steady state unbalanced turborotor response for lumped and distributed parameter models, using GATRAN language
[ASME PAPER 71-VIBR-42] 21 p3459 A71-40292

Oscilloscope and automatically tuned super-heterodyne receiver panoramic display units for 10 kHz-60 MHz, considering design, circuits, performance and mechanical arrangement
21 p3353 A71-40518

Canadian Forces experiments on aircraft flashing lights covering warning signals, navigation and anti-collision displays and autokinetic phenomenon
22 p3499 A71-41491

Strobe lighting for aircraft midair collision hazard reduction, comparing Collision Avoidance System and Pilot Warning Indicator effectiveness
22 p3499 A71-41493

National Aviation System stage A ATC displaying digitized radar data positions together with automatic track positions
22 p3570 A71-41634

Operator performance improvement in monitoring automated processes by alternating displays, discussing simulated radar and sonar CRT display laboratory tests
22 p3501 A71-41636

Display system for scanning medical thermometer covering temperature range 28.0-37.4 C with 0.2 C accuracy, using liquid nitrogen cooled indium antimonide photoresistive detector
22 p3545 A71-42149

Character size, case and symbol generation effects on CRT display search time
22 p3503 A71-42195

Scanning ultrasonic imaging technique for in vivo monitoring of microscopic bubble formation in decompression sickness, presenting image displays
22 p3504 A71-42250

IR linescan technique for airborne terrain mapping, discussing choice of waveband, system parameters and display techniques with emphasis on film recording
22 p3546 A71-42425

Visual information discernibility measurement for suprathreshold transfer in display to observer system, noting use for color contrast scaling and disturbance evaluation
22 p3547 A71-42504

Sampled video data technique with information redundancy for processing and narrow-band transmission, discussing TV display, noting applications in corporate communications and teaching
22 p3547 A71-42508

Low light level TV system using Plumbicon tube and 3-stage image intensifiers
22 p3548 A71-42511

Large display direct view low light level system with objective lens, image intensifiers and eyepiece
22 p3548 A71-42512

Solid state charge controlled electroluminescent display panel with image memory capability, describing negative oxygen ions and photoconductive charge control methods
22 p3548 A71-42514

Projection type 3-D display lenticular lens sheet optimum design and depth resolution
22 p3549 A71-42560

Central panel luminance effect on peripheral visual detection time in search tasks
23 p3638 A71-42899

Observer psychological response to air defense oriented visual information displays
23 p3640 A71-43904

Integrated system for aircraft control and operation with visualization and manual regulation techniques, emphasizing interconnections with onboard electronic equipment
24 p3791 A71-44353

Cathode ray tube graphical display system as digital computer output terminal, using analog memory for flickerfree image
24 p3806 A71-44652

Isodensity mapping with digital computer symbol selection and cathode ray X-Y plotter, showing photographic image display and enhancement of density or height information
24 p3826 A71-44787

DISPLAY SYSTEMS
U DISPLAY DEVICES
DISPOSAL
NT WASTE DISPOSAL
DISSIPATION
NT ENERGY DISSIPATION
NT OHMIC DISSIPATION
Dissipative gyroscopic system with servo link, obtaining steady motion stability
02 p0252 A71-12402

Nondissipatively-regulated DC to DC converter design, describing circuit technique and magnetic-semiconductor combinations
03 p0352 A71-13046

Lunar physical libration in longitude, considering nonlinear and dissipation terms
09 p1530 A71-23715

Parametric dissipative plasma instability in HF electric field, showing plateau formation in velocity distribution function causes Cerenkov dissipation decrease
12 p1941 A71-27765

Constant profile solutions stability for nonlinear wave equations with convection and dissipation
16 p2608 A71-33023

Supercooled fog dissipation by liquid propane, determining effectiveness in providing operational support to aircraft landing and takeoff
16 p2604 A71-33536

DISSIPATORS
U DISSIPATION

DISSOCIATION
NT AUTOIONIZATION
NT GAS DISSOCIATION
NT PHOTODISSOCIATION
NT THERMAL DISSOCIATION
Chronic hypercapnic oxygen dissociation curves and red cell cation exchange in rats, considering compensated/uncompensated phases of respiratory acidosis
03 p0360 A71-13181

Diatomic molecules dissociation and recombination in presence of third body, considering quantum mechanical scattering theory
05 p0785 A71-16728

Dissociative electron attachment excess energy correlation with fragment ion translational energies, determining radical affinity
08 p1338 A71-21782

Ionization mechanisms for deviation of experimental altitude vs velocity curves of meteor trails, considering various electron and ion emissions and dissociation effects
10 p1669 A71-24032

Ground state dissociation energies and long range internuclear potentials of diatomic molecules of halogens from spectroscopic vibrational spacings
11 p1728 A71-26065

Dissociative recombination rates in partially ionized gases at elevated gas temperatures, using shock tube for limited ionization introduction
11 p1765 A71-26283

HBr positive ion formation by Ar ion beam collision with HBr, using predissociation to establish dissociation limit
13 p2026 A71-29039

Chemical lasers diatomic and multiatomic molecules dissociation in nonequilibrium conditions, discussing vibrational energy exceeding gas temperature
24 p3834 A71-45112

DISSOLUTION
U DISSOLVING
DISSOLVING
Anomalous anodic Be dissolution in anhydrous environment, considering chunk effect and multivalent ions production mechanisms
07 p1118 A71-19568

Iron-iron carbide structure dissolution behavior from electron transmission microscopy, observing carbide, matrix, general and interface attack modes
07 p1056 A71-20361

Dissolution rate of vertical nickel cylinder in liquid aluminum under free convection, showing fluid boundary layer mass transfer role
19 p3079 A71-37709

Morphological change of spherical G.P. zones and solute diffusion coefficient in binary Al-Zn alloy during dissolution, using X ray small angle scattering
21 p3395 A71-40022

Hydrogen dissolution in fused silica, investigating temperature effects during impregnation on reactive defect sites number
24 p3841 A71-44869

DISSYMMETRY
U ASYMMETRY
DISTANCE
NT DEBYE LENGTH
NT MISS DISTANCE
NT MISSILE RANGES
NT RADAR RANGE
NT RADIO RANGE
Pulsar distances tabulation, discussing possible IR emission
01 p0153 A71-10365

Planetary nebulae upper distance limits by photometry, including mean nebular parameters and extinction coefficients in galaxy dust model
07 p1191 A71-18999

Cygnus X-1 distance estimate based on low energy X ray spectrum obtained by sounding rocket
15 p2497 A71-32763

DISTANCE MEASURING EQUIPMENT
NT ALTIMETERS
NT GEODIMETERS
NT LASER RANGE FINDERS
NT OPTICAL RANGE FINDERS
NT RADIO ALTIMETERS
NT RANGE FINDERS
Inertial navigation system augmented by digital distance measuring equipment in FAA flight inspection aircraft for performance evaluation
01 p0124 A71-10507

Design principles for sensitive elements of capacitive sensors for distance measurement via electrostatic induction effects
01 p0079 A71-10527

L band DME and TACAN improvements, emphasizing use of static broadband amplifiers
02 p0235 A71-12905

Radiometric determination of diametrical distance between rotor and stator of turbomachines
03 p0421 A71-13003

Laser metrology, discussing precise distance measurement techniques based on modulated CW and pulse sources, laser systems for constructional angular alignment and materials spectrography
04 p0606 A71-14719

Supernova remnant kinematic distance estimates, using molecular absorption line velocities with Schmidt model
05 p0805 A71-16107

Geometrical and physical distance measurement by laser telemetry, involving time and speed factors of emission and receiver beams
06 p0869 A71-18065

Ionospheric error correction in distance measurements involving satellites, noting simultaneous differential Doppler and Faraday signal measurements
07 p1097 A71-19023

Holography and interferometry industrial applications, considering three dimensional imaging, precision distance measurement, nondestructive testing and structural strains and failures detection
07 p1113 A71-19784

U.S. domestic ATC airspace enroute and terminal area navigation system effects on pilot workload, projecting future FAA requirements
07 p1157 A71-20347

Reflected jet proximity detector dynamic and static characteristics, considering response speed and separation distance
07 p1030 A71-20600

Galactic cosmic ray propagation earth-source distance determination by observing charge spectrum
08 p1354 A71-21018

VOR/DME ground station oriented aircraft area navigation horizontal guidance capability, discussing digital input/output flight control
08 p1331 A71-21166

Trilateration evaluated as replacement for triangulation, considering electronic distance measuring equipment
08 p1280 A71-21244

Optical distance correction for fluctuating atmospheric index of refraction in long base line measurements using Lidar with Q switched ruby laser
09 p1495 A71-23451

Meteor trails distance determination by radar pulses reflection observation, estimating reflected signal delay dispersion and plotting mean square errors
10 p1576 A71-24037

Earth-moon distance perturbations from anisotropic gravitational mass effect
11 p1819 A71-25209

Geodetic geographic coordinate transformations and ellipsoid heights, azimuth and length determination from synchronous photographic observations and distance measurements of artificial satellites
11 p1759 A71-25313

Dual laser ranging for distance measurements superimposing beams modulated at different frequencies
11 p1774 A71-25936

Artificial earth satellites equatorial topocentric coordinate determination, using photographic distance observations and least squares method
12 p1961 A71-26902

Critique on pulsar distance estimates based on dispersion measure, introducing period luminosity function
13 p2137 A71-28592

Photographic and laser observations during passage of satellite for determination of distance between observer and earth rotational axis
14 p2250 A71-31123

McDonald Observatory lunar ranging station including telescope matching optics, guiding, timing equipment, pulsed ruby laser system and calibration procedures
16 p2553 A71-33780

Laser radar system using retroreflector on lunar surface for measurement of distance between earth and moon
16 p2543 A71-33811

Novas distance determination from estimates of envelope ejection during outburst at maximum brightness, calculating absolute magnitudes
17 p2803 A71-34838

Satellite distance measurement by laser, describing energy calculation, equipment parameters, ground tests, cloud echo and Geos B satellite experiments
17 p2709 A71-35598

Galactic star cluster K 4 and Ba 10 observations with RGU photographic photometry, noting distances and types
18 p2960 A71-35938

Distance measurement system with onboard transponder, discussing subcarrier and pseudorandom code signal techniques synthesis
18 p2879 A71-36532

Navigational accuracy improvement by combining VOR/DME information with airspeed and heading data via maximum likelihood filter, using small airborne computer
19 p3097 A71-37174

[AIAA PAPER 71-928]
Global cluster NGC 6541 UVB photometric investigation, determining distance from sun and galactic plane
19 p3143 A71-38164

Galactic cosmic ray propagation earth-source distance determination by observing charge spectrum
20 p3280 A71-39598

Open stellar clusters Tr 14, 15, 16 and eta Carinae Nebula distance determination, using photoelectric and photographic photometry
21 p3441 A71-40064

Total to selective extinction ratio determination, obtaining distance to galactic center
21 p3445 A71-40245

Combined inertial navigation and VOR/DME systems contribution to area navigation accuracy and efficiency
22 p3571 A71-42080

VOR/DME air navigation equipment using Kalman-Bucy filter and airborne air data system (ADS)
22 p3573 A71-42289

Light velocity measurements by optical and microwave techniques, noting electromagnetic constant error and role in distance measurement and physical theories development
24 p3827 A71-44996

Pulsar JP 1933 distance lower limit from 21 cm absorption and galactic rotation model, noting scintillation parameters consistency with observations in thin screen model
24 p3873 A71-45141

Atomic hydrogen cloud distances determined by interstellar absorption lines of early stars
24 p3874 A71-45145

Optimum signal processing for distance measurement with lasers, considering propagation, detection and measure process statistical properties, optical radar and sine wave modulation
24 p3834 A71-45206

DISTANCE PERCEPTION

U SPACE PERCEPTION

DISTILLATION

NT STRIPPING [DISTILLATION]

DISTILLATION EQUIPMENT

Space station life support prototype vapor diffusion water reclamation system for pure and sterile water distillation from urine process stream
18 p2869 A71-36398

DISTORTION

NT FLOW DISTORTION

NT SIGNAL DISTORTION

NT SURFACE DISTORTION

Pressure wave distortion effects on combustor acoustic mode instability based on model with burning rate related to Reynolds number
07 p1224 A71-19906

Internal friction from hydrogen dissolved in Ti-Mn alloys, considering solute interstitial atoms caused asymmetrical distortion decrease with increased Mn concentration
10 p1625 A71-24008

DISTRIBUTED AMPLIFIERS

Amplifier stability with distributed feedback by root locus trajectories
01 p0059 A71-10605

Neuristor pulse propagation analysis for nonlinear distributed circuit of superconductive tunnel junction stripline
03 p0393 A71-14470

Liapunov stability prediction of minimum length for distributed oscillators of superconductive tunnel junction strip line
03 p0388 A71-14475

Distributed gain amplifiers synthesis technique permitting use of filter and transmission line design tables
09 p1413 A71-22158

DISTRIBUTION [PROPERTY]

NT ANGULAR DISTRIBUTION

NT ANTENNA RADIATION PATTERNS

NT BOLTZMANN DISTRIBUTION

NT CHARGE DISTRIBUTION

NT CURRENT DISTRIBUTION

NT DIFFRACTION PATTERNS

NT ELECTRON DENSITY PROFILES

NT ELECTRON DISTRIBUTION

NT ENERGY DISTRIBUTION

NT FLOW DISTRIBUTION

NT FORCE DISTRIBUTION

NT FREQUENCY DISTRIBUTION

NT HOLE DISTRIBUTION [ELECTRONICS]

NT HOLE DISTRIBUTION [MECHANICS]

NT INTERFERENCE LIFT

NT ION DISTRIBUTION

NT KOSSEL PATTERN

NT LOAD DISTRIBUTION [FORCES]

NT MASS DISTRIBUTION

NT MOMENT DISTRIBUTION

NT NEUTRON DISTRIBUTION

NT PRESSURE DISTRIBUTION

NT RADIAL DISTRIBUTION

NT RADIATION DISTRIBUTION

NT SIDELOBES

NT SPATIAL DISTRIBUTION

NT SPECTRAL ENERGY DISTRIBUTION

NT STAR DISTRIBUTION

NT STRESS CONCENTRATION

NT TEMPERATURE DISTRIBUTION

NT VELOCITY DISTRIBUTION

NT VERTICAL DISTRIBUTION

Germanium distribution coefficient in GaAs epitaxial crystals by radiotracer, mass spectroscopy and

electron probe analysis noting total impurity concentration from Hall mobility
07 p1180 A71-201767

Distributed parameter systems under load disturbances regulatory control by feedforward feedback and state measures
09 p1422 A71-22284

Distribution laws of statistical Q characteristics and of junction capacitance of varicaps
11 p1740 A71-26542

Rumanian book on distribution theory applications in mechanics covering physical point motions, variable mass, concentrated and distributed loads, elasticity theory equilibrium, motion equations, etc
15 p2501 A71-31147

Bayes theorem tests based on experimental observations, considering binomial, exponential and normal sampling distribution of priors as family of natural conjugates
16 p2582 A71-33290

DISTRIBUTION FUNCTIONS

Time distribution of first passage through fixed level for nondecreasing whole number regeneration process with step trajectories
01 p0110 A71-10094

Time distribution of first passage through fixed level for regeneration vector Markov process with step trajectories
01 p0110 A71-10095

Dwell time of semiMarkov system in given state with mixed Erlang and exponential distribution functions
01 p0110 A71-10096

Weibull density functions applied to fracture location distribution in brittle solids
01 p0167 A71-10294

Distribution function for two circularly polarized modes in laser with axial magnetic field derived by master equation transformation to Fokker-Planck equation
01 p0094 A71-10745

Area distributed incidental radio noise voltage envelope distribution functions conversion to Rayleigh distribution with range frequency relationships
01 p0037 A71-11163

Low pressure Cs vapor discharge in positive column, determining electron energy distribution function
02 p0289 A71-11956

Multicomponent gaseous mixtures and plasmas transport analysis improved formalism consisting of moment Boltzmann equation and N parameter distribution function representation
02 p0290 A71-12229

Nonlinear stabilization of beam instability during electron beam interaction with decay plasma, determining distribution function in damping dynamics of HF vibrations
02 p0292 A71-12610

Muons spatial distribution function in mountain level extensive air showers
03 p0476 A71-13855

Extensive air shower electron and muon components at mountain levels, calculating distribution functions by Monte Carlo technique
03 p0477 A71-13861

Resonance phenomena in spiral galaxies, determining stellar orbits, potential and distribution functions
04 p0655 A71-15725

Electronic components failure rate distribution
04 p0559 A71-15875

Soviet monograph on meromorphic functions covering behavior variables, asymptotic properties and defects and Riemann surfaces application for values distribution analysis
05 p0773 A71-16249

In vivo green soybean and corn leaves bidirectional IR reflection and transmission distribution functions
05 p0739 A71-16253

Phonon distribution function kinetic equation solution, determining two dimensional lattice heat conductivity
05 p0794 A71-16876

Computer algorithm for distribution functions of meteorological element on isobaric surface
06 p0922 A71-17506

Photoelectron counting distribution for random medium passage scintillated stochastic light, considering low level amplitude stabilized and chaotic radiation transmission through turbulent atmosphere
07 p1159 A71-19513

Stress rupture properties of S glass/epoxy single end strands at various load levels, considering distribution functions
07 p1145 A71-20126

Nonlinear Fokker-Planck equation solution by Mott-Smith bimodal distribution function method, investigating fully ionized nonequilibrium plasma relaxation time
07 p1171 A71-20295

Charged particles acceleration in pulsed magnetic field, deriving distribution function by diffusion coefficient and turbulence spectrum determination
08 p1351 A71-20963

Fluctuations effect on MHD shock wave propagating in plasma perpendicular to external magnetic field, obtaining field amplitude distribution function

09 p1500 A71-22242

Low temperature plasma electron velocity distribution function perturbation due to exothermal chemical reactions

09 p1501 A71-22289

Normal shock wave in He, comparing measured and predicted molecular velocity distribution functions

09 p1433 A71-22857

Distribution functions of initial and established intervals of stochastic and Poisson sequences in automatic control, reliability and communications theories

10 p1588 A71-24902

Weighted distribution functions of normal processes, calculating stochastic mixture components in Borel sets

10 p1637 A71-24903

Pair correlation function for gaseous hydrogen at low density and temperature from quantum mechanical calculation, using Lennard-Jones potential

11 p1801 A71-25367

Transverse EM field in plasma, deriving closed equation for distribution function

11 p1804 A71-25500

Lunar geometrical and dynamical properties, deriving force function from density distribution and surface equation

11 p1822 A71-25687

Thermionic converter electrostatic sheath analysis, using discontinuous distribution functions for emitted, plasma and trapped particles, and computer program

11 p1713 A71-25891

Normality-independence characterization of stochastic integrals in linear processes

11 p1792 A71-26102

Maximum entropy principle for prior distribution determination in Bayesian reliability estimation, comparing with statistical decision theory

11 p1772 A71-26164

Multicomponent exponential curves analysis by Post-Widder equation, providing continuous distribution function of time constants in inhomogeneous systems

12 p1870 A71-27129

Electron energy distribution functions in carbon dioxide laser plasmas, using Langmuir probes

12 p1940 A71-27280

Parametric dissipative plasma instability in HF electric field, showing plateau formation in velocity distribution function causes Cerenkov dissipation decrease

12 p1941 A71-27765

Random radio signals distributions properties with parameters subject to random variation

13 p2029 A71-28371

Electron energy distribution function in weakly ionized monatomic gas with inelastic collisions, using differential equation asymptotic resolution techniques

13 p2106 A71-28398

Electron avalanche processes in gas discharges, deriving electron energy distribution function and similarity laws

13 p2103 A71-29079

Integral kinetic equation for flow distribution past body and surface heat flow, noting representation in form for computer solution

13 p1991 A71-29156

Boltzmann equation applicability to rarefied multiatomic gases if distribution function is identical with integral of free molecular motion

14 p2276 A71-29561

Coulomb collisions in high density plasma beams from numerical integration of Fokker-Planck equation for three initial distribution functions, studying relaxation time

14 p2283 A71-30674

Nonlinear Fokker-Planck equation numerical tests for collision effects on self consistent field first order component and plasma electron distribution function perturbation

15 p2453 A71-31146

Boltzmann equation approximate solution for molecular velocity distribution function perturbations by inelastic collisions

15 p2386 A71-31158

Structural dynamic responses as nonstationary narrow band random process, establishing peak values distribution functions with frequency interpretation

15 p2510 A71-32515

Electromagnetic wave propagation along homogeneous and inhomogeneous plasma columns, establishing density distribution functions and dispersion curves

15 p2459 A71-32641

Plasma oscillations growth rates for symmetrical double-humped velocity distributions, comparing with distribution functions without infinite tails

15 p2460 A71-32657

German book on problems, mathematical foundations and investigation methods of technical reliability covering Boole model, random variables, distribution functions, failure rates, etc

16 p2583 A71-33524

Plane uniform waves reflected from layer with random permittivity inhomogeneities, determining distribution function and scattered wave propagation direction

16 p2543 A71-33568

Weibull distribution analysis of saccadic eye movements interval during visual task

17 p2688 A71-34366

Distribution functions of observed and true spherulites/axis ratios of Sculptor-type dwarf galaxies

17 p2804 A71-34842

Explosive instability effect on plasma distribution function, field energy level and time response

18 p2950 A71-35863

Kinetic models for gas-surface interactions, considering distribution functions of molecules at solid wall

18 p2874 A71-35900

Optimal solutions for antenna synthesis problem for bounded norm of source distribution function and limited error in realization of given directional pattern

18 p2893 A71-36620

Finite radius rotating cylinder stability analysis, using equilibrium functions of distribution with trajectory integration method

19 p3134 A71-37512

Bounded nonthermal plasma radiation temperature variations relationship to electron velocity distribution functions

19 p3113 A71-37747

Digital simulation of pseudowaves and plasma sheath formation about grid by computer solution of ion Vlasov equation for ion distribution function time evolution

19 p3113 A71-37749

Two dimensional objects three dimensional image possibility based on self-reproduction effect for arbitrary periodic distribution function of transparency, using coherent light source

19 p3064 A71-37770

Homogeneous collisionless plasma in external electric field, considering evolution in time of charged particles distribution functions

19 p3114 A71-37858

Plasma ion and electron distribution functions measurement on outer planet missions [AAS PAPER 71-124]

19 p3114 A71-37938

Radiation energy density and radiation heat flux in small rectangular cavity, assuming modes excitation spectrum according to Planck distribution function [ASME PAPER 71-HT-16]

19 p3164 A71-37987

Electron distribution functions construction from spectrum of laser light Thomson scattering by rarefied plasma

19 p3074 A71-38215

Meteor bodies mass distribution function for Geminid stream, determining parameter S from radio echoes

19 p3145 A71-38528

Cloud particles coagulation kinetics, using integral equation for distribution function

19 p3095 A71-38704

Nonlinear Faraday effect in nonparabolic semiconductors subjected to strong electromagnetic field and steady magnetic field, deriving distribution function of charge carriers

20 p3276 A71-39010

Approximations to regular solutions by finding distribution function for bonds between unlike molecules, deriving Gibbs energy, enthalpy and entropy

21 p3474 A71-40234

Conditional failure density evaluation from hazard rate, considering failure time distribution function, reliability function and conditional failure distribution

21 p3408 A71-40370

Steady slow free molecule flow past sphere, obtaining distribution function and surface boundary conditions

21 p3370 A71-40987

Fluctuations effect on MHD shock wave propagating in plasma perpendicular to external magnetic field, obtaining field amplitude distribution function

21 p3424 A71-41131

Superradiant laser stationary characteristics description by Fokker-Planck equation for classical distribution function, taking into account phase destroying effects

21 p3421 A71-41398

Muons lateral distribution function in mountain level extensive air showers

22 p3595 A71-42656

Extensive air showers at sea level, plotting mean numbers and distribution functions of muons and electrons

22 p3595 A71-42667

Distribution function integral representation application to steady motion of monocomponent rarefied gas containing amorphous particles, using successive approximation for kinetic equation solution

22 p3482 A71-42868

Strong current z discharge collisionless plasma, investigating ions distribution functions fine structure

23 p3708 A71-42890

Plasma conductivity dependence on electron velocity distribution function in distorted Maxwellian form

23 p3709 A71-43259

Free electron distribution function, atomic level population and ionization rate in low voltage arc near electrodes

23 p3709 A71-43266

Langmuir paradox problem concerning electron energy distribution function and anisotropy in low pressure DC Hg vapor discharge positive column plasma

23 p3710 A71-43402

Fine structure of energy distribution function for electron beam interacting with plasma

23 p3711 A71-43411

Latitudinal observation errors by two zenith telescopes concurrent data, showing distribution function in long term measurement

23 p3771 A71-44255

Knudsen effusion problem in thermal molecular gas jet mixing, using moment method based on velocity distribution function

24 p3817 A71-44354

Electron motion in plasma under stochastic electric field, emphasizing distribution function dependence on velocity and time

24 p3853 A71-44510

Wave field pulsations induced electron scattering as factor modifying excited plasma electron distribution function

24 p3855 A71-44668

Linear systems with randomly varying parameters, deriving stability conditions from one dimensional distribution functions

24 p3815 A71-44699

Boundary conditions determined for hydrodynamic equations from solution of Boltzmann kinetic equation in Knudsen layer, obtaining distribution function in Enskog function superposition form

24 p3821 A71-45226

DISTRIBUTION MOMENTS

NT MEAN

NT STANDARD DEVIATION

NT VARIANCE (STATISTICS)

Laser oscillation buildup from quantum noise, deriving equations of motion for moments of photon distribution and time dependence

01 p0094 A71-10826

Subsequences of pseudorandom sequences for correlation detection, discussing algorithms for weight distribution moments determination

05 p0724 A71-17062

Two dimensional distribution moments of harmonic signal and normal narrow band noise mixture envelope, deriving expressions by power series expansion

09 p1404 A71-22293

Spatial coherence measurement for two points of pseudothermal light source by comparing photocathode luminous intensity probability density and photoelectron distribution moments

17 p2754 A71-35585

Spectral distribution moments of light scattering due to polarizability changes in colliding molecule pair

18 p2947 A71-36196

Spatially distributed systems with random parameters, determining random output signals statistical moments

24 p3813 A71-44678

DISTURBANCE THEORY

U PERTURBATION THEORY

DISTURBANCES

Disturbances within hypersonic transitional boundary layer in Mach 7 gun tunnel observed with hot-wire anemometer, comparing results with surface heat transfer measurement

06 p0886 A71-18637

Vibrational systems stability in presence of time dependent random parametric disturbances, using frequency analysis methods

24 p3848 A71-44851

DISTURBING FUNCTIONS

Planetary motion mutual perturbation, presenting method for expansion of disturbing function

09 p1525 A71-23334

Artificial lunar satellites orbits, examining disturbing functions expansions due to nonsphericity of primary body and disturbing point mass body actions

10 p1679 A71-24931

DISULFIDES

NT CARBON DISULFIDE

Chemical protection against ionizing radiation by thiols and disulfides, discussing hydrogen transfer

07 p1032 A71-18930

Thiol and disulphide compounds radiation protection capacity at cellular level in tissue culture, using reproductive integrity as protection criteria

07 p1034 A71-18948

Tungsten or molybdenum disulfide formation discussing tribolytic deposition process

10 p1635 A71-25010

DITCHING [LANDING]

Aircraft galley design safety criteria, considering injuries from routine use, normal, crash or ditching conditions component dislodgment, equipment malfunctions and defects

01 p0004 A71-10029

Aircraft ditching and flying personnel survival, stressing passenger briefing and crew jacket equipment with VHF transceiver for rescue operations coordination

23 p3628 A71-43229

DITHIOLS

U THIOLS

DIURNAL RHYTHMS

U CIRCADIAN RHYTHMS

DIURNAL VARIATIONS

Diurnal variations of polar aurora-magnetic activities correlation at high latitudes

02 p0242 A71-11758

Martian exospheric temperatures diurnal variations during Mariner 4, 6 and 7 observations by solving time dependent heat balance equations

02 p0305 A71-11972

Atmospheric refractive index average structural characteristics measurement over 25 km light propagation path, noting diurnal variation

02 p0245 A71-12011

Neutral atmospheric wind measurements at 75-110 km by radar observation of meteor trail drift, discussing diurnal variations

03 p0407 A71-13308

Ionospheric nondeviative absorption diurnal variation describing function suitable for computer methods

03 p0378 A71-13315

F region diurnal behavior, comparing neutral winds and electric field effects

03 p0408 A71-13383

Diurnal variations and waves in ionospheric electron and ion temperatures and concentrations from Thomson scatter measurements

03 p0408 A71-13384

Midlatitude topside ionosphere electron density diurnal variations, discussing F 2 layer seasonal anomaly altitudinal extension

03 p0409 A71-13390

Thermospheric neutral particle molecular nitrogen density and temperature measurements by rockets, noting correlations with diurnal, solar cycle and other variations

03 p0414 A71-14020

Diurnal minimum and geomagnetic storms effect on equatorial air density from San Marco 2 satellite drag experiment

03 p0415 A71-14024

Night airglow, discussing spectrum, latitudinal dependency, diurnal variation, time and space correlations and sunspot cycle and solar activity effects

03 p0417 A71-14071

Diurnal variations due to actual heat output, oxygen consumption and carbon dioxide production in rats undergoing eating habit changes

04 p0539 A71-15157

Noctilucent cloud observations and research covering geographic distribution, annual and diurnal variations, kinematics, volcanic connections, cosmic dust eruptions, etc

04 p0584 A71-15677

Ionospheric absorption measurements noting diurnal, seasonal and solar cycle variations

05 p0740 A71-16429

Lower ionospheric cosmic noise absorption at 28.6 MHz, examining diurnal variations

05 p0740 A71-16430

Lunar semimonthly oscillations in solar daily H range related to midday F 2 critical frequency at equatorial stations, analyzing lunar tides in ionosphere

05 p0740 A71-16432

Forbush midlatitude microdecreases effects on diurnal cosmic ray intensity, using neutron monitor

05 p0799 A71-16624

Semidiurnal variation of galactic cosmic ray intensity, using neutron and meson monitor data

05 p0800 A71-17008

Annual and diurnal variations of temperature inversion over antarctic plateau, discussing wind field structure and ice crystal precipitation

05 p0778 A71-17043

Light and drugs effect on diurnal body temperature from radio telemetry of adult male rats

05 p0715 A71-17111

Atmospheric ion concentration at 100-200 km related to solar zenith angle, describing diurnal and vertical behavior by photochemical theory

05 p0744 A71-17182

Diurnal variations of loss factor in D region during polar cap absorption, verifying nighttime D region model by forward propagation data

05 p0744 A71-17185

Auroral absorption latitudinal distribution diurnal variations, showing existence of two zone model

05 p0746 A71-17205

Polar auroras emission bursts at 6300 and 5577 Å, noting diurnal variation with electrophotometer

05 p0746 A71-17209

Geomagnetic activity diurnal variation dependence on latitude and longitude during IGY

05 p0746 A71-17210

Neutral ionospheric temperature profile diurnal variation at Arecibo from incoherent scatter measurements, considering relevance to 1400 hour density maximum

06 p0887 A71-17271

Automatic computer verification of diurnal temperature and geopotential observations on principal isobaric surfaces by statistical data analysis, describing computer algorithm

06 p0922 A71-17504

Ionospheric absorption winter anomaly observation based on Loran-A pulse signals during IQSY, noting diurnal variation

06 p0889 A71-17685

Geomagnetic field daily variation, discussing ambient field weakening on night side

06 p0893 A71-17992

Diurnal cosmic ray neutron variations after proton flares, comparing calculated radial and azimuthal gradients to experimental data

06 p0951 A71-18105

Cosmic rays effective angles of acceptance and energy spectrum diurnal variations, using temporal correlation functions

06 p0951 A71-18107

Solar cosmic ray diurnal variations latitude effect explained by two way anisotropy model

06 p0952 A71-18109

Cosmic rays solar diurnal variation, using underground recordings in Bolivia and New Mexico from multiple two fold coincidence scintillator telescopes

06 p0952 A71-18114

Diurnal intensity variations of high energy galactic cosmic rays, taking into account particle trajectories in sectorial interplanetary magnetic field

06 p0952 A71-18115

Primary cosmic ray solar modulation calculations using Trilling formula for response functions and upper limiting rigidity to diurnal variation

06 p0953 A71-18119

Cosmic rays anomalous diurnal variations, describing proton excess flux from direction outside geomagnetic field

06 p0956 A71-18139

Primary cosmic ray electrons energy spectrum measurement at Fort Churchill, examining geomagnetic cut-off rigidity daily variations

06 p0959 A71-18159

High energy muon flux diurnal variations related to lunar time

06 p0960 A71-18169

F 2 region critical frequency diurnal variation forecasting, using series expansion of natural orthogonal components

06 p0895 A71-18276

Diurnal variations in polarization axis direction of Pc 1 pulsations

06 p0895 A71-18282

Tranquility Base lunar soil diurnal temperature calculation from one dimensional energy equation, using temperature dependent thermodynamic properties [AIAA PAPER 71-79]

06 p0977 A71-18536

Midlatitude scintillation diurnal and seasonal variations, using satellite communications data

07 p1095 A71-19003

Ionosphere and magnetosphere daily electron content change measurement, describing satellite beacon experiment

07 p1096 A71-19017

Solar half cycle total ionospheric electron content and slab thickness diurnal and seasonal variations from Syncom 3 beacon signal

07 p1097 A71-19020

Upper atmosphere semidiurnal pressure variations from wind data obtained by radar observation of meteors, discussing seasonal and planetary changes

07 p1151 A71-19147

Semiannual nutation term determination from diurnal latitudinal observation with zenith telescope over 6 year period

07 p1194 A71-19319

Cosmic rays sidereal diurnal variations, considering interplanetary magnetic field shielding effect

07 p1185 A71-19378

Lower ionosphere electron density profile diurnal, seasonal and 11 year variations, tabulating calculated numerical values for 45-70 km altitudes

07 p1099 A71-19383

Twilight helium emission diurnal and seasonal variations relationship to geomagnetic activity and solar depression, using Abastumani observations

07 p1099 A71-19389

Time-altitude diurnal variations in molecular and atomic oxygen concentrations at 65-200 km from continuity equations

07 p1099 A71-19391

Equatorial zone daytime F 2 maximum height diurnal variation latitude change with decreasing solar activity from vertical sounding

07 p1100 A71-19401

Cosmic ray intensity mean diurnal variation, taking into account angle between solar corotational velocity and earth equatorial plane

07 p1187 A71-19683

Geomagnetic field quiet solar diurnal variations, examining dynamo theory in lower ionosphere at middle latitudes

07 p1104 A71-20044

Geomagnetic solar quiet field and terrestrial currents diurnal variations, discussing interrelations and vector polarization

07 p1104 A71-20041

Planetary diurnal rotation, discussing motion of small particle in solar and planet gravitational fields

07 p1201 A71-20437

Second spherical harmonic generation mechanisms in axisymmetric diurnal and semidiurnal cosmic ray spectrum variations

08 p1352 A71-20969

Diurnal cosmic ray anisotropy, investigating solar wind velocity and interplanetary magnetic field effects

08 p1352 A71-20971

Geomagnetic activity indices-overall diurnal interplanetary magnetic field strength correlation by satellite magnetometer data

08 p1360 A71-21016

Earth free diurnal nutation frequency, examining latitude variation power spectrum

08 p1285 A71-21780

Diurnal variation symmetry of upper atmosphere molecular oxygen concentration in terms of ozone photodissociation

09 p1435 A71-22446

Diurnal variations of meridional winds by dynamo electric field in troposphere, comparing with Thomson scattering

09 p1490 A71-23646

Solar cycle effects on diurnal variations of F 2 region critical frequency and maximum ionization height

10 p1600 A71-23884

Meteor-reflected radio wave propagation directivity and diurnal and annual variations, comparing experimental and theoretical calculation results

10 p1576 A71-24033

Upper atmosphere semidiurnal pressure variation calculation from hydrodynamic equations similar to atmospheric tides theory

10 p1600 A71-24038

Geomagnetic disturbance field asymmetry Fourier analysis for amplitude G and local time phase of first diurnal harmonic for IGY

10 p1600 A71-24295

Seasonal effect on daily periodicity of microwave radioisotropy related to changes in bright/dark daytime proportion and feeding

10 p1565 A71-24654

Nitric oxide diurnal variation model in upper atmosphere incorporating solar flux, absorption cross sections and chemical rate constants

10 p1605 A71-24795

Midlatitude F2 region diurnal variations in peak electron density critical frequency and height, noting electric field and ion drag effects

10 p1606 A71-24921

Electric field, neutral air winds and atmospheric composition changes effects on electron concentration diurnal variation in midlatitude F layer

10 p1607 A71-24922

Vibrational and rotational temperature diurnal variations of upper atmospheric OH emissions from IR spectroscopic measurements, discussing earth shadow effects on mean intensity

11 p1753 A71-25541

Thermosphere diurnal variations two dimensional model atmosphere characteristic waves, separating density and temperature variations

11 p1756 A71-25649

Upper atmospheric molecular and atomic N and O diurnal variations correlated to atmospheric heating as function of solar UV radiation from sounding rocket data

11 p1757 A71-25775

Midlatitude topside ionospheric electron density mean diurnal and seasonal variations from Alouette 1 satellite observation

11 p1757 A71-25784

Obliquely incident radio wave absorptions measurements from January-October 1968 vertical ionospheric soundings, correlating diurnal variations with solar zenith angular changes

11 p1732 A71-25787

Sudden commencements occurrence frequency diurnal and seasonal variations from worldwide magnetic storms data

11 p1758 A71-25793

Diurnal temperature variations in middle ionosphere by rocket probes, noting solar activity changes influence

11 p1759 A71-25823

Diurnal variations in catecholamine excretion, alertness and performance of subjects with different working habits

11 p1722 A71-26356

- Diurnal and seasonal variations of scintillations in short wave radio signals transmitted from earth satellites and spacecraft, noting relationship to ionospheric inhomogeneities 12 p1898 A71-26635
- Mars regolith carbon dioxide, water and Kr adsorption, explaining diurnal brightness phenomena 12 p1961 A71-26875
- Surges and drops in sunspot cycle from 1832 to 1964, considering minima and maxima of diurnal relative numbers 12 p1962 A71-26957
- Diurnal variability of cosmic ray anisotropy calculated from abnormal, ephemeral or nonlinear density gradients 12 p1949 A71-27373
- Cosmic ray storm analysis, showing enhanced daily/shortlived variations, radiation intensity increase and solar flare observations 12 p1949 A71-27375
- Cosmic radiation nucleonic component intensity diurnal variations relation to solar activity semiperiod 12 p1950 A71-27378
- Diurnal solar variation of cosmic radiation observed by two Argentine meson telescopes 12 p1950 A71-27379
- Thermosphere daily variations consisting of diurnal oscillations excited by ozone and EUV heating 12 p1925 A71-27729
- E and F region irregularities random movements over Waltair, India, during IQSY, obtaining diurnal and seasonal variations 13 p2056 A71-27931
- Atmospheric ion concentration at 100-200 km related to solar zenith angle, describing vertical and diurnal density pattern by photochemical theory 13 p2059 A71-28239
- Diurnal variations of loss coefficient in D region during polar cap absorption, verifying nighttime D region model by forward propagation data 13 p2059 A71-28242
- Auroral absorption latitudinal distribution diurnal variations, showing existence of two zone model 13 p2060 A71-28260
- Polar auroras emission bursts at 6300 and 5577 Å, noting diurnal variation with electrophotometer 13 p2060 A71-28264
- Geomagnetic activity diurnal variation dependence on latitude and longitude during IGY 13 p2060 A71-28265
- Daytime and nighttime sporadic F layer regularities correlation with other ionospheric phenomena based on vertical sounding data 13 p2062 A71-28555
- Midlatitude ionospheric signatures from narrow beam HF radar backscatter sounder, discussing diurnal and seasonal occurrences 13 p2031 A71-28782
- Geomagnetic field horizontal component daily variation due to ionospheric E region dynamo, magnetopause surface and magnetospheric tail/partial ring currents 13 p2064 A71-29161
- Galactic cosmic ray intensity solar diurnal and semidiurnal variations outside magnetosphere 13 p2131 A71-29437
- Pulsating aurora observations, noting light intensity, diurnal variations and power spectra 14 p2229 A71-29671
- Seasonal variations in semidiurnal tidal wind velocities in upper atmosphere for Northern Hemisphere radio meteor observations 14 p2231 A71-29720
- Diurnal correlation between cosmic ray meson intensity and atmospheric ozone content on magnetically undisturbed days 14 p2231 A71-29723
- Cosmic ray neutron diurnal variation phases and amplitudes from harmonic analysis of directional intensity 14 p2299 A71-29987
- Diurnal variations of electron number density against height in lower ionosphere over Resolute Bay, relating to solar proton events 14 p2300 A71-30044
- Magnetospheric tail regions, investigating McIntosh effect in AE and Dst indices daily variations 14 p2236 A71-30354
- Extensive air showers sidereal-diurnal variation determination, considering atmospheric effects and antisidereal wave vector 14 p2301 A71-30591
- Upper atmosphere exploration by San Marco 2 satellite, studying diurnal density variations and effects of large geomagnetic storms 14 p2236 A71-30817
- VLF and LF time and frequency international comparison, noting diurnal shifts and SID constant magnitude ratio 14 p2204 A71-30972
- VLF signal propagation during low and high solar activity, discussing equipment precision, diurnal and seasonal phase variations and phase anomalies correlation 14 p2204 A71-30973
- Systematic phase variation in second harmonic of daily variation of cosmic ray intensity in one year, recorded by neutron monitor at Deep River 15 p2441 A71-31410
- Pc micropulsations spectra fine structure and diurnal variations, analyzing rubidium magnetometer recordings by power spectral density method 15 p2394 A71-31425
- F 2 layer peak electron density diurnal and seasonal variations, noting geomagnetic latitude and solar activity effects 15 p2394 A71-31427
- Local time variations of power spectra of magnetospheric electric field from balloon flight data 15 p2397 A71-31758
- Cosmic ray mean intensity drop observation after Forbush decrease, noting rigidity dependence and daily variation from exponential recovery curve 15 p2474 A71-31777
- Semiannual nutation term determination from diurnal latitudinal observation with zenith telescope over 6 year period for earth axis 15 p2486 A71-31899
- Summertime meridional wind component profile construction and hydrodynamic model for semidiurnal fluctuations in upper atmosphere 15 p2399 A71-31962
- Jupiter exospheric temperature diurnal variations for various solar activities and latitudes, using time dependent heat balance equations 15 p2491 A71-32423
- Earth free diurnal nutation frequency, examining latitude variation power spectrum 15 p2401 A71-32685
- Cosmic ray flux diurnal variation from radial number density gradient, showing Forbush decrease profiles strong dependence on shock radial approach velocity 15 p2480 A71-32755
- Diurnal variation of atmospheric parameters in thermosphere deduced from incoherent scatter and satellite drag, discussing atmospheric model correspondence to observed data 16 p2566 A71-33742
- Ionospheric density diurnal variations and atmospheric rotation data from OV1-15 satellite drag measurements, noting geomagnetic activity effects 16 p2566 A71-33746
- Northern high latitude electron trapping boundary position diurnal, seasonal and geomagnetic Kp variations based on ESRO 1/Aurora polar satellite observations 16 p2627 A71-33753
- Geomagnetic field daily variation amplitude increase under equatorial electrojet during 7 July 1966 solar proton flare 16 p2567 A71-33768
- Diurnal variation of Venus and Mars exospheric temperatures, using neutral heating efficiency calculation based on molecular theory 16 p2641 A71-33769
- Upper atmospheric neutral composition diurnal variations as function of altitude, local time and solar activity 16 p2570 A71-33829
- Solar modulation origin of sidereal diurnal variation in cosmic ray intensity anisotropies as function of interplanetary field direction, using underground muon telescopes 16 p2628 A71-33931
- Antarctic F 2 layer height and critical frequency diurnal variations due to ionospheric neutral winds, ionization maxima and solar effects 17 p2731 A71-34318
- Factor analysis of phase discrimination in mental fatigue during diurnal variation of cortical functions in railroad traffic control center operators 17 p2688 A71-34362
- Neutral thermosphere and exosphere structure, discussing density, temperature, composition and diurnal and seasonal variations 17 p2732 A71-34461
- Sq day to day variability relation to interplanetary plasma parameters including magnetic field and solar wind velocity and kinetic energy 17 p2801 A71-34625
- Polar auroras visual observations, plotting diurnal changes in height and occurrence frequency 17 p2803 A71-34837
- VHF wave transhorizonal propagation correlation with daytime E layers in temperature zone, noting height dependence and seasonal and diurnal variations 17 p2707 A71-35445
- Omega navigation application to general aviation aircraft, presenting diurnal course shift to overcome deficiencies 17 p2776 A71-35767
- Cross power spectral analysis of atmospheric electric potential gradient relation to meteorological parameters, noting diurnal variations 18 p2944 A71-36010
- Geomagnetic diurnal variations near Sq current vortex focus, indicating existence of ionospheric diverging or converging currents 18 p2912 A71-36298
- Composition and daily fluctuations of trace contaminants during 90-day space station simulator test [ASME PAPER 71-AV-17] 18 p2867 A71-36384
- Sunspot cycle effect on solar and lunar daily geomagnetic variations 18 p2966 A71-36745
- Mean dry bulb temperature estimation during daylight hours by subtracting proportion of average daily range from daily maxima average 18 p2944 A71-36961
- Diurnal variations in equatorial and precipitating low energy solar proton-produced gamma rays in magnetosphere 19 p3125 A71-37359
- Diurnal distribution, latitudinal occurrence and intensity patterns of ELF, VLF and LF whistler-mode noise emissions from Alouette 2 satellite observation 19 p3016 A71-37364
- Median primary energy of underground muon telescopes response as function of depth, studying sidereal daily variation of cosmic rays 19 p3125 A71-37370
- Cosmic rays sidereal diurnal variations, considering interplanetary magnetic field shielding effect 19 p3127 A71-37803
- Lower ionosphere electron density profile diurnal, seasonal and 11 year variations, tabulating calculated numerical values for 45-70 km altitudes 19 p3052 A71-37808
- Twilight helium emission diurnal and seasonal variations relationship to geomagnetic activity and solar depression, using Abastumani observations 19 p3053 A71-37814
- Time-altitude diurnal variations in molecular and atomic oxygen concentrations at 65-200 km from continuity equations 19 p3053 A71-37815
- Equatorial zone daytime F 2 maximum height diurnal variation latitude change with decreasing solar activity from vertical sounding 19 p3053 A71-37825
- Quiet sun diurnal variations of intertropical F 2 ionization in true heights over Tamanrasset meridian 19 p3054 A71-37863
- Solar semidiurnal atmospheric tide theory based on gravitational action only, taking into account atmospheric stratification 19 p3055 A71-38044
- Atmospheric temperature effect on solar diurnal variation of muon component, considering asymptotic characteristics of cosmic ray anisotropy 19 p3129 A71-38378
- Daytime ionogram corrections for underlying ionization in absence of x-trace of sporadic E layer 19 p3058 A71-38386
- Magnetic perturbations in near polar region and morning-night sectors of auroral oval as function of current sources and modulation by universal time 19 p3059 A71-38397
- Arctic polar region geomagnetic perturbations during IQSY, noting diurnal variations 19 p3059 A71-38399
- Seasonal, latitudinal and diurnal variations of upper atmospheric structural parameters including density and temperature 19 p3061 A71-38656
- Earth thermosphere models, discussing shortwave solar radiation as major energy source during quiet conditions, diurnal variations of structure, neutral-charged components interconnection, etc 20 p3216 A71-39117
- Solar regular daily geomagnetic variations - Conference, Potsdam, East Germany, April 1970 20 p3216 A71-39508
- Magnetospheric interactions with ionosphere for solar regular daily geomagnetic variations, discussing dynamo region electric fields effects 20 p3217 A71-39509
- Midlatitude solar quiet geomagnetic field dynamics morphology, emphasizing regular diurnal and annual changes and irregular fluctuations 20 p3217 A71-39510
- Daily geomagnetic variations ionospheric current systems calculation from total magnetic field data obtained at ground stations during IGY 20 p3217 A71-39511
- Geomagnetic activity daily variability index statistical dependence on geomagnetic latitude, noting maximum below equatorial electrojet 20 p3217 A71-39513
- Lunar and solar daily geomagnetic variation morphology correlation based on atmospheric dynamo model 20 p3217 A71-39515
- Diurnal variations of Sq currents in terms of electroconductivity model of ionosphere and geomagnetic field, using two dimensional dynamo theory 20 p3217 A71-39517
- Automated diurnal variation analysis program applied to IGY observed solar quiet day geomagnetic variations 20 p3218 A71-39520

Dynamo theory for ionospheric thin shell model, considering wind fields determination from diurnal geomagnetic variations

20 p3218 A71-39522

Equatorial electrojet region ionospheric currents during magnetically quiet day and nighttime from rocket measurements

20 p3218 A71-39524

Geomagnetic activity indices—overall diurnal interplanetary magnetic field strength correlation by satellite magnetometer data

20 p3294 A71-39596

Neutral upper atmosphere observations, discussing lower thermospheric density and composition diurnal, seasonal and latitudinal variations and solar activity effects

20 p3220 A71-39690

Diurnal and semiannual variations in upper atmosphere density from Cosmos satellite drag observations, noting calculation systematic errors

20 p3223 A71-39707

Ionospheric effective recombination coefficient and reaction rate models for various solar activity periods and day and night conditions

20 p3224 A71-39714

Midlatitude ionospheric electron density and electron temperature measurements by rocket experiments, noting diurnal and seasonal variations

20 p3224 A71-39718

Ionospheric electron and neutral particle temperature average diurnal behavior from bottomside vertical soundings

20 p3225 A71-39723

Solar radiation effects on upper atmosphere soft electron flux and energy spectrum during day and night

20 p3281 A71-39724

Cosmic rays cutoff daily variations at ATS geostationary satellite altitude, noting role of magnetospheric tail in lowering cutoff below calculated value

20 p3282 A71-39739

Cosmos 142 and 259 experiments on ionospheric VLF propagation, discussing diurnal variations of daytime electron density

20 p3197 A71-39743

Dayglow emissions for OH, molecular oxygen, sodium, lithium, potassium, atomic oxygen and nitrogen, considering height profiles and diurnal variations

20 p3226 A71-39828

Nighttime hydroxyl airglow emission intensity and excitation temperature measurements, noting seasonal and nocturnal variations

20 p3227 A71-39834

Night and daytime auroral zone ionospheric electric field measurement by rocket-borne Langmuir probe, noting components parallel and perpendicular to magnetic field

20 p3231 A71-39884

Lunar tidal effects on semidiurnal periodicity in ionospheric absorption, showing time of maximum amplitude variation with geographic latitude

20 p3232 A71-39900

E region wind and temperature measurements from Nancy incoherent scatter experiments, observing prevailing semidiurnal oscillation with phase propagating downwards

21 p3372 A71-40041

Geomagnetic field horizontal component H daily variation nature, using graphs to show increases above or decreases below given level

21 p3373 A71-40050

Solar radioelectric activity in 1966, tabulating mean daily density and variability of solar flux

21 p3442 A71-40152

E region irregularities drift and anisotropy at Wal-tair during IQSY, inferring trends of diurnal and seasonal variation

21 p3374 A71-40379

Upper atmospheric molecular and atomic nitrogen and oxygen diurnal variations correlated to atmospheric heating as function of solar UV radiation from sounding rocket data

22 p3532 A71-41543

Midlatitude topside ionospheric electron density mean diurnal and seasonal variations from Alouette 1 satellite observation

22 p3532 A71-41552

Obliquely incident radio wave absorptions measurements from January-October 1968 vertical ionospheric soundings, correlating diurnal variations with solar zenith angular changes

22 p3509 A71-41555

Sudden commencements occurrence frequency diurnal and seasonal variations from worldwide magnetic storms data

22 p3533 A71-41561

Diurnal water and food intake and body weight changes pattern in rats with hypothalamic lesions

22 p3486 A71-41936

Nearly diurnal nutation observations from Danjon astrolabe data, comparing theoretical earth models

22 p3602 A71-42172

Interplanetary magnetic sector polarity effects on polar geomagnetic field diurnal variation

22 p3604 A71-42221

Astronomical radio sources from Parkes catalog, calculating daily and hourly variations in flux density

23 p3722 A71-42937

Quiet and stormy day diurnal variations of geomagnetic field, investigating ionospheric contribution

23 p3665 A71-42968

Day to day fluctuations of winter anomaly in ionospheric absorption, showing regular and irregular trends

23 p3666 A71-42974

Noon-midnight high latitude proton trapping and precipitation boundary variations associated with polar magnetic substorms observed by ESRO 1A satellite

23 p3719 A71-43127

Blanketing sporadic E layer diurnal and seasonal variations from equatorial stations ionosonde data obtained during IGY, discussing wind shear mechanism

23 p3667 A71-43134

Cosmic ray solar diurnal variation anomaly at 1954 minimum, discussing diffusion and scattering in interplanetary medium

23 p3720 A71-43136

Lunar daily geomagnetic variations separation into oceanic and ionospheric origin in Indian region

23 p3667 A71-43149

Dynamo theory of solar and lunar magnetic fields diurnal variations, determining ionospheric wind velocities and pressure changes

23 p3669 A71-43174

Periodic and isolated /nonperiodic/ ionospheric electron content fluctuations showing noon and midnight peaks and winter increase at high latitudes

23 p3670 A71-43180

Least geomagnetic diurnal variation effects period determination by statistical method

23 p3673 A71-43984

Large geomagnetic diurnal variations effects period determination by statistical method, considering partial ring currents in night magnetosphere

23 p3673 A71-43985

Astrometrical HF range latitudinal observation error spectrum estimation, showing random dispersion and Chebyshev polynomial expansion parameters for nightly variation

23 p3771 A71-44256

Human skin cold receptor diurnal activity rhythm

24 p3795 A71-44499

Diurnal fluctuations in radio echo producing ionospheric region horizontal scale and height, discussing dependence on solar position

24 p3804 A71-45042

DIVERGENCE

Point matching techniques, discussing effects of metal boundary on divergence of series and error from numerical examples of rectangular waveguide and scattering

08 p1252 A71-20755

Simple algorithms for accelerating convergence and averting divergence in Kalman filters, using feedback from measurement residuals

08 p1324 A71-21333

Solid state laser emission divergence, calculating far zone fields for arbitrary amplitude and phase distributions

15 p2418 A71-31243

Divergence structure nonlinear elliptic equations, demonstrating smooth solutions uniqueness of Dirichlet problem

18 p2942 A71-36816

Direct solution for divergence speed of lifting surface using matrices of structural and static aerodynamic influence coefficients

21 p3456 A71-40171

Divergence behavior of flat rectangular panel at subsonic speeds, discussing boundary conditions, natural vibration modes and temperature effects

24 p3878 A71-44611

DIVERGENT NOZZLES

Gas density distributions in argon and carbon dioxide supersonic jets with low angular divergence in vacuum, using Laval supersonic nozzle

24 p3858 A71-45241

DIVERTERS

Plasma guns hot and cold plasma separation, describing diverter operation principles

19 p3112 A71-37639

DIVIDERS

Iterative graphical method for broadband N way TEM mode power divider design, using Smith chart

01 p0055 A71-11194

DIVING (UNDERWATER)

Cardiovascular, respiratory and thermoregulatory mechanisms in aqualung diver drillers

06 p0864 A71-18721

Oxygen vs air in treatment of divers with decompression sickness

08 p1242 A71-21957

Blood plasma volume decrease, red cell mass and survival measurements in aquanauts of Teklite I at prolonged habitation

11 p1720 A71-26123

Pressure effects on human ventilation and gas exchange, determining stratified inhomogeneity during deep diving

12 p1873 A71-27126

Convective and conductive heat loss analysis of underwater swimmers and divers exercising in cold water

18 p2861 A71-36892

Decompression sickness, investigating surface excursion diving and selection of limb bends vs CNS symptoms by tests on goats

21 p3330 A71-40344

Aquanauts tremor response measurement by muscle force transducer during compression and decompression in 520-foot saturation dive, noting differences among individuals

21 p3331 A71-40350

Biochemical measurements of human urine and blood changes during simulated oxygen-helium dives to 1500 feet

21 p3331 A71-40353

DIVISION

Algorithms for multiplication and division by different bases in residual class system

17 p2711 A71-34977

Cellular array for multiplication and division of two binary numbers, discussing implementation with transistor-transistor logic integrated circuits

18 p2894 A71-36833

DIVOT (VOICE TRANSLATORS)

U DIGITAL TO VOICE TRANSLATORS

DME-A SATELLITE

U EXPLORER 31 SATELLITE

DNA

U DEOXYRIBONUCLEIC ACID

DO-31 AIRCRAFT

Commercial V/STOL and jet VTOL transport, discussing Do-31 test results, landing approach, air traffic control automation and electronic control

13 p1997 A71-29131

DOCKING

U SPACECRAFT DOCKING

DOCUMENTATION

NASA Space Documentation Service on-line information retrieval system using direct access remote consoles

01 p0183 A71-10397

Computerized system evaluation and feedback data for assurance at hardware level, including reject and failure report documentation

12 p1890 A71-26673

Large software systems development management, discussing steps including program design before analysis, documentation, testing, monitoring and cost effectiveness

17 p2709 A71-34618

Cost effective integrated logistics support documentation system for military contractors

23 p3661 A71-43196

DOCUMENTS

NT BIBLIOGRAPHIES

NT DRAWINGS

NT ENGINEERING DRAWINGS

NT PAPERS

NT TEXTBOOKS

NT TEXTS

Laser document scanner for computer entry and communications systems

05 p0762 A71-16480

DOGS

Dog blood leucocyte composition relation to alimentary satiation and adrenocorticotrophic and reticuloendothelial systems, considering effect of ACTH and india ink injections

01 p0008 A71-10092

Dog cardiac output measurement by using ethyl ether dissolved in saline solution as indicator, comparing to Fick method results

06 p0856 A71-18389

Carbon dioxide absorption of dog blood and plasma under anoxia at simulated high altitudes, deriving equations for protein concentration rated buffer values

07 p1043 A71-20327

Dynamic respiratory and circulatory responses to hypoxia in anesthetized dogs, recording oxygen partial pressures, heart rate, blood pressure, blood flows, respiratory rate, etc

09 p1396 A71-23358

Helium and nitrogen breathing effects upon intraocular pressure during and after near vacuum exposure in anesthetized and unanesthetized dogs

09 p1400 A71-23359

Canine heart rate Frank-Starling mechanism effects on ventricular volumes during natural and artificial cardiac pacing

10 p1565 A71-24681

DOMAIN WALL

Electromagnetic wave reflection from ferrite moving domain wall, considering wave separation and permittivity and magnetic susceptibility tensors

01 p0138 A71-10435

Magnetic thin film domain wall velocity dependence on magnetic field intensity as function of film thickness, discussing nonlinearity causes

18 p2955 A71-36938

Electromagnetic wave reflection from ferrite plate in external alternating magnetic field, showing frequency change due to moving domain wall

23 p3645 A71-43568

DOMAINS

NT MAGNETIC DOMAINS

Microwave permittivity dispersion in segnetoelectrics as function of single crystal domains size, considering barium titanate dielectric spectrum resonance 01 p0138 A71-10433

GaAs high resistivity n-type Cr doped samples, examining field domains shape and motion by visual observation 01 p0141 A71-11467

Barium titanate single crystals domain structure and electrical properties at room temperature under uniaxial tensile stresses, measuring dielectric hysteresis loops 04 p0637 A71-15104

Potassium niobate single crystals domain structures by interferometry, discussing surface deformations, dipole couplings and temperature dependent angles 06 p0941 A71-18039

Frequency domain and time domain methods analysis of signal from laser velocimeter 06 p0900 A71-18053

Boundary value problems in noncylindrical domains investigated by Green matrix 09 p1484 A71-22176

Hysteresis effects during retuning of n-type GaAs Gunn oscillator with bias source and RLC circuit, showing range of domain damping by low field 09 p1414 A71-22228

Second harmonic voltage effects on quenched domain mode Gunn effect oscillator for DC to RF conversion efficiency, discussing negative device conductance at multiharmonic frequencies 09 p1417 A71-22696

Current induced flow of superconducting domains in superconductor intermediate state, presenting theoretical analysis of motion of domains of arbitrary topology 12 p1942 A71-26745

Randomly distributed domain structure of ordered Ni-Cr alloy, using electron microscopy and neutron diffraction 17 p2755 A71-34413

Nonlinear frequency shift in GaAs electroacoustic domains, using Bommel-Dransfeld analysis technique 17 p2791 A71-35447

Conformal transformation of multiply connected plane domain of Poincare standardization 17 p2672 A71-35469

Eigenvalues lower bounds determination for arbitrary shape region, presenting domain constriction method 21 p3416 A71-41014

DOMES [STRUCTURAL FORMS]

NT RADOMES

Shallow shell theory boundary value problems, calculating stress concentration for domes and shells with holes 03 p0513 A71-14230

Thin elastic shallow spherical dome nonlinear motion under uniformly distributed external pressure 06 p0982 A71-17360

Thin spherical roller supported domes stability and axisymmetric deformation under apex point loads, investigating plastic buckling and inelastic strain effects 07 p1216 A71-20222

Flexible spherical domes elastic-plastic deformation, using variational equation and iterative algorithm 14 p2331 A71-30840

Rigid framed dome structure stiffness analysis using multiglobal axes and joint equilibrium equations 15 p2507 A71-32105

DOMINANCE

NT EYE DOMINANCE

DONNELL EQUATIONS

In-plane boundary conditions influence on clamped conical shells buckling under external pressure, using displacement method based on Donnell stability equations 11 p1841 A71-25158

Noncircular cylindrical shells stress and displacement under hydrostatic loads, applying Donnell equations 24 p3879 A71-44618

DONOR MATERIALS

Carrier scattering related to orbiting and resonance states in screening impurity donor center of weakly doped homeopolar n-type semiconductor under injection 13 p2112 A71-28928

Hall effect measurements utilization for simultaneous determination of donors and acceptors concentration in semiconductors, applying to n-type silicon 19 p3118 A71-37487

Carrier scattering related to orbiting and resonance states in screened field of impurity donor center in weakly doped homeopolar n-type semiconductor under injection 21 p3434 A71-41331

Electron transitions between excited states of donors in Ge, investigating photoconductivity in 500-1300 micron band 22 p3585 A71-41817

Dynamic carrier density instabilities for semiconductor-metal electronic phase transition by Frenkel-Poole effect in semiconductor with donors 23 p3716 A71-43478

DOPES

Sasaki effect in doped semiconductors at low temperatures concerning conduction anisotropy and intervalley impurity electron scattering 01 p0139 A71-10777

DOPING [ADDITIVES]

U ADDITIVES

DOPPLER EFFECT

HF radio wave Doppler shift by ionosphere effect in retransmitted and backscatter signals 01 p0040 A71-11524

Projectile velocity measurement by laser and Fabry-Perot interferometer using Doppler effect 02 p0258 A71-11657

Ultrasonic Doppler techniques in medical diagnosis, measuring ultrasonic probes directivities by echo amplitudes from various target configurations 03 p0373 A71-14422

Radar scattering from turbulent underdense ionized wakes, showing relationship between Doppler spectrum and wake characteristics 04 p0551 A71-15011

Matched filter output response computation for combined Barker codes, considering Doppler mismatch 04 p0551 A71-15013

Doppler effect in laser beam probe of scattering objects, using interferometer for scattered light intensity angular distribution relation to hologram sizes 04 p0608 A71-15117

Laser produced schlieren interferometry diffraction pattern determination, using Doppler frequency shift 04 p0596 A71-15222

Stellar radial velocity measurements using Doppler shifted absorption lines, discussing cluster stars 04 p0646 A71-15227

Geodetic position rapid determination accuracy by Doppler satellite observation 04 p0583 A71-15304

Fourier data decomposition technique for recovering Doppler temperature, emission line intensity and Doppler shift of central frequency of Fabry-Perot fringes in presence of statistical noise 05 p0748 A71-16265

Gas and liquid flows local velocity measurements, using Doppler frequency shifts due to wave scattering at solid microparticles suspended in flow 05 p0753 A71-16786

Laser Doppler heterodyning system for bidirectional pulsatile fluid flow velocity magnitude and direction measurement 05 p0756 A71-17233

Laser Doppler velocimeter, describing simplified stable optical arrangement 06 p0900 A71-18054

Ionospheric refraction during radio wave propagation using space diversity recordings of Faraday and Doppler effects for coherent signals from geophysical rockets 06 p0894 A71-18256

Total electron content from ionospheric Doppler shift data, discussing usable frequencies 07 p1096 A71-19005

Receiving equipment for direct differential Doppler frequency measurement via beacon satellites observation 07 p1059 A71-19012

Second order phase path differences for Faraday rotation and dispersive Doppler shift in transionospheric propagation 07 p1097 A71-19027

Ionospheric electron mean content by polar satellites, using combination of Doppler differential and Faraday rotation hybrid methods 07 p1206 A71-19032

Annular gas laser beat frequency as function of Doppler shift emission, examining mirrors feedback, cavity Q and pumping variational effects 07 p1122 A71-19137

Laser dynamic theory with uniformly broadened and Doppler spectral lines based on nonlinear interactions between harmonic oscillations 07 p1127 A71-20255

Doppler effect mechanism for laser Q switching with rotating mirror, noting pulse width dependence on wavelength 08 p1302 A71-21434

Recombination frequency spectrum asymmetry in interaction between high and low frequency plasma oscillations, noting role of Doppler effect 08 p1340 A71-21495

Velocity components, species densities and temperature local measurements, using laser Doppler velocimeters, Raman scattering and tunable lasers [AIAA PAPER 71-283] 08 p1303 A71-22008

Laser Doppler system for subsonic and supersonic jet flow velocity measurements, discussing calibration and measurement errors [AIAA PAPER 71-285] 08 p1303 A71-22009

Laser Doppler velocimetric technique for supersonic flow particle trajectory and density measurements, noting particle lag [AIAA PAPER 71-287] 08 p1303 A71-22010

Laser Doppler velocimeter, determining basic operational parameters including required particle density, number, type, size, output signal to noise ratio, etc [AIAA PAPER 71-288] 08 p1304 A71-22011

Spectral analysis of laser Doppler flowmeter signals, considering time independent systems 09 p1463 A71-22691

Doppler jitter stabilization of carbon dioxide laser without internal modulation to inverted Lamb dip in extracavity absorption cell 09 p1463 A71-22759

Solar prominence spectra, presenting equivalent line widths, central line intensities and Doppler half widths 09 p1524 A71-23190

Tropospheric temperature and aerosol/molecule ratio determination by optical radar measurements, using Doppler broadening in spectral analysis of laser radar echoes 09 p1466 A71-23628

Velocity measurements for slowly moving pendulum bob with incandescent filament lamp, detecting Doppler shifted beam interference beat frequency with photomultiplier 10 p1574 A71-23738

Vertical velocities in atmosphere measured by acoustic Doppler during diurnal thermal plumes and breaking wave occurrence within nocturnal inversion 10 p1574 A71-23746

Solar granular or convective motion velocities vs photospheric oscillations for Doppler shifts in line spectra 10 p1665 A71-23776

Solar Doppler widths from spectral line profiles by Goldberg profile intercomparison method, determining solar microturbulence depth dependence 10 p1665 A71-23777

Air jet velocity and turbulence measurements by modified Doppler technique, using CW lasers 10 p1609 A71-23874

Analytic approximations in closed form for curves of growth of Doppler-Lorentz broadened lines, considering radiative transport in nonisotropic gases 10 p1646 A71-24991

Doppler geodetic measurements, discussing ionospheric wave diffraction errors, refractive index and electromagnetic wave propagation 11 p1732 A71-25831

Relativistic effects and optimization in Doppler geodetic measurements, using model computations for satellite azimuth-elevation relation 11 p1732 A71-25832

Directional laser Doppler velocimeter measurements in perturbed circular flow, noting use in cardiovascular research 11 p1766 A71-26303

Constant Doppler wide-angle laser beam scanning, presenting expressions for Doppler shift, spread in spectral width of scanned laser beam and scan angle 12 p1913 A71-26814

Blood pressure measurement with Doppler ultrasonic flowmeter, providing sensitive and accurate noninvasive approach for continuous measurement of systemic arterial pressure 12 p1874 A71-27139

Error introduced into coherent two-way Doppler tracking measurements on spinning satellite, using turnstile antenna 12 p1882 A71-27431

Solar Na D lines Doppler width, describing limb darkening data, assuming source function frequency dependence 12 p1970 A71-27748

Boundary layers velocity distribution measurements, using scattered laser radiation Doppler shift 13 p2078 A71-28574

Spectrometer slit-width cancellation by Doppler shift of light emission by fast ion beams, resulting in spectral lines increased intensities 13 p2071 A71-29331

Laser Doppler velocimetry accuracy degrading factors, considering light beam focus phase anomaly and distortions due to density fluctuations 14 p2245 A71-30331

Ionospheric electromagnetic wave path calculation by Haselgrove ray method, applying to Faraday and Doppler effects 14 p2235 A71-30348

Doppler effect satellite location of crystal controlled CW transmitters on earth surface for animal tracking 14 p2200 A71-30924

Spectral lines Doppler broadening reduction in spectroscopy using foil and gas excited accelerator beams as light sources 15 p2412 A71-32579

Laser Doppler turbulent and laminar flow velocity measurement model, using optical mixing spectroscopy theory 15 p2423 A71-32589

Dispersionless delay line design producing signal frequency shifts for calibration tests of wideband Doppler shift measuring equipment

15 p2373 A71-32632

Pulse compression and optical data correlation in side-looking radar, considering Doppler effect

15 p2374 A71-32650

Gas and liquid flows local velocity measurements, using Doppler frequency shifts due to wave scattering at solid microparticles suspended in flow

16 p2576 A71-33038

Combination frequency spectrum asymmetry in interaction between high and low frequency plasma oscillations, noting Doppler effect role

16 p2618 A71-33045

Daytime electron density profiles above 90 km from Doppler radio measurements by rockets launched from Southern Hemisphere site

16 p2567 A71-33779

Refraction effects of moving inhomogeneous media in electromagnetic Doppler measurements, using Maxwell equations or relativistic ray tracing method for frequency variations

16 p2544 A71-33850

He-Ne laser emission spectra with AM by reflected Doppler shifted signal and matched/mismatched three-mirror resonator/mobile outer mirror

17 p2750 A71-34289

Optimal parameters of Fabry-Perot etalon for error minimization in Doppler and dispersion portions determination of Voigt profile width

17 p2737 A71-34410

Electromagnetic wave diffraction by moving wedge with surface impedance, evaluating Doppler shifts and scattered field in shadow region

17 p2698 A71-34429

Statistical evaluation of Doppler ultrasonic blood flowmeter, determining correlation between Doppler signal zero crossing density and fluid flow velocity

17 p2689 A71-34448

Laser Doppler anemometer, defining signal transmission region and spectrum bandwidth/amplitude from photocurrent and single moving scattering particle emission

17 p2745 A71-35328

Vortex laser Doppler velocimeter system for aircraft wake turbulence velocity profile mapping, describing optical arrangements, back and forward scattering modes and prototype design

17 p2754 A71-35756

Flow velocity measurement by laser differential Doppler heterodyning, obtaining SNR from frequency difference between shifted beams

18 p2914 A71-35848

Random noise effects on oscillator short term frequency stability and velocity measurement by Doppler effect

18 p2879 A71-36531

Optical readout system for analysis of laser Doppler velocimeter signals displayed on TV screen and recorded photographically

18 p2931 A71-36587

Spectroheliogram Doppler movies of solar velocity fields showing oscillatory and slowly varying components

18 p2965 A71-36728

Doppler velocity field recording method over two dimensional solar active region image, using narrow band filter with video photographic subtraction technique

18 p2924 A71-36730

Thermospheric winds measurement during geomagnetic storms with Fabry-Perot interferometer from Doppler shift of two 6300 A fringe profiles

19 p3047 A71-37366

Backscattering laser Doppler velocimeter for water flow and moving opaque object measurements, discussing velocity resolution and optical geometry

19 p3072 A71-37552

Beam direction weight center of signal spectrum and effective antenna centers of airborne Doppler velocimeter in horizontal flight

19 p3033 A71-38496

Doppler distortions of clutter and resolution performance of pulse trains with large time bandwidth products

20 p3195 A71-38861

Laser Doppler holographic technique for fluid velocity field visualization and quantitative two dimensional vector velocity measurement

20 p3235 A71-39183

Monograph on blood flow rates instantaneous measurement from ultrasound signals of Doppler flowmeter, discussing steady laminar flow test results

20 p3193 A71-39262

Acoustic signal pressure mode propagation velocity in infinite rectangular hard-walled duct with steady flow, noting Doppler effect

20 p3271 A71-39765

Doppler carrier frequency shift measurement accuracy

20 p3198 A71-39808

Real time multitrack half tone recorder for displaying three dimensional information on instantaneous blood velocity measurement by Doppler effect

21 p3377 A71-40132

Dual scatter laser Doppler velocimeters for transonic wind tunnel measurements and calibration applied to simulated helicopter downwash, high lift wing and jet crossflow

21 p3364 A71-40399

Scattering atom recoil effect in resonance line transfer with Doppler redistribution, discussing neglect from microscopic point of view

21 p3447 A71-40429

Laser system for atmospheric wind velocity and turbulence, using Doppler frequency shift undergone by radiation beam scattered by particles suspended in flows

21 p3319 A71-40490

Streamline pattern deduction for sun large scale flow from Doppler line of sight velocities

22 p3596 A71-41454

Ionospheric electron density measurements by differential Doppler and Faraday effects, using coherent radio signals of artificial earth satellites

22 p3508 A71-41526

Fluid velocity gradient measurement by laser-Doppler techniques based on signal spectrum bandwidth or frequency shift corresponding to position shift near wall

22 p3541 A71-41792

Atmospheric self-aligning dual-scatter laser Doppler velocimeter, calculating backscattered power, range, wavelength and scatter centers number relationships

22 p3559 A71-42564

Geodetic locations of Doppler satellite observing stations consistent with CIO pole and astronomical determinations

[AAS PAPER 71-341]

23 p3666 A71-43014

Ionospheric electron density measurement by K-9M rocket, comparing VLF Doppler with Langmuir probe methods

23 p3671 A71-43366

Light modulator based on Doppler effect and diffraction, providing spatially separated beams with different wavelengths

23 p3678 A71-43535

Two dimensional velocity field observations in and around sunspots from Doppler spectroheliograms

23 p3767 A71-43838

DOPPLER NAVIGATION

Ships and aircraft position finding method based on satellite radio signals Doppler measurements, analyzing ionospheric influences

07 p1154 A71-19036

Air navigation techniques history, considering radio, radar, loran Doppler and inertial navigation

14 p2272 A71-30712

Doppler satellite/airborne inertial navigation system integration with delayed state Kalman filter

17 p2776 A71-35766

Radio and radar air navigation for civil aviation, discussing Doppler effect, inertia and satellite systems

19 p3100 A71-37344

Doppler scanning landing microwave system for air-derived azimuth and elevation angle aircraft guidance by frequency coding and reference carrier transmission

22 p3572 A71-42089

DOPPLER RADAR

CAT wind structure and velocity dynamics, using Doppler radar techniques

01 p0116 A71-10564

Convective thunderstorm propagation from Doppler radar velocities at leading edges

01 p0117 A71-10571

Wind flow patterns in severe thunderstorms structures, using Doppler radar

01 p0117 A71-10573

Dual Doppler radar method of convective storms observation, noting optimization via COPLAN scanning

01 p0117 A71-10574

Doppler radar techniques for turbulent kinetic energy budget in boundary layer, discussing wind profile and turbulence in snow conditions

01 p0117 A71-10577

Lower atmosphere turbulence model derivation from data obtained by Doppler radar windfield measurements in snowfall environment

01 p0117 A71-10578

Doppler radar velocity sensors and altimeters for lunar and planetary spacecraft instruments soft landing

04 p0597 A71-15324

Thunderstorms anvil cloud high level outflow mapping by Doppler radar at various heights and elevation angles

05 p0721 A71-16669

Doppler pulse radar signal reception, calculating noise signal optimal relationship for comparison with adapted filtration technique

05 p0722 A71-16707

Vertical air motions velocity in rainfall from Doppler spectrum total radar reflectivity and median velocity

07 p1150 A71-18798

Video MTI pulse radar Doppler filter optimum symmetrical weighting factors in clutter-plus-noise environment

07 p1059 A71-18847

Two-frequency moving target indicator Doppler radar system, predicting efficiency to clutter drift under stochastic echo and clutter signals

10 p1578 A71-24591

Airborne Doppler radar receiver transmitter failure testing by Versatile Avionics Shop Test computer controlled system

13 p2031 A71-28778

Gunn effect diode in portable Doppler radar, describing electron transfer, negative resistance and domains formation and propagation

13 p2040 A71-29238

Pulse-burst radar design optimization and performance comparison with low and high pulse repetition frequency Doppler radar

14 p2197 A71-30797

Slotted waveguide arrays in precision Doppler radar antennas, correlating predicted and actual performance

14 p2206 A71-31073

IMPATT diode oscillator for CW Doppler radar, microwave detection and communications systems, emphasizing cost reduction

15 p2377 A71-32522

Flight test of hybrid strapdown inertial navigator with Doppler radar and occasional position fixes through Kalman filter mechanized in small computer

17 p2776 A71-35765

Airborne Doppler velocity sensors, considering hydrometeors effects on HF signal attenuation and reflection

17 p2747 A71-35768

Resolution and clutter performance of simultaneous Doppler and acceleration measurement with coherent pulse trains

20 p3195 A71-38855

Doppler tracking radar systems, obtaining probability density function of Doppler signal amplitude

20 p3200 A71-39907

Aircraft wing tip vortex air motion measurements, utilizing Doppler radar techniques

21 p3318 A71-40489

Book on pulse, CW, Doppler, pulse Doppler and space radar theory, operation and maintenance, describing equipment, tracking and siting

22 p3509 A71-41621

Microwave quasi-holographic techniques, discussing synthetic aperture, chirp radar, rotating target imaging system and beam forming method

22 p3546 A71-42477

Upwind/downwind differential Doppler spectra of radar sea echo for P, L and C bands

23 p3646 A71-44173

DORNIER AIRCRAFT

NT DO-31 AIRCRAFT

Do-132 light five seat tip drive turbine helicopter, discussing applications, flight testing, design and major components

01 p0004 A71-10465

Do 132 turbine powered helicopter, discussing icing problems solution

06 p0847 A71-17745

Alpha jet trainer, describing design, configuration, power plants, landing gear maintainability and mission duration

15 p2347 A71-31209

DORNIER DO-31 AIRCRAFT

U DO-31 AIRCRAFT

DORSAL SECTIONS

Visual projection, magnification and retina overlap on dorsal lateral geniculate nucleus in cats measured by random scatter in receptive field

21 p3335 A71-40668

Inhibitory binocular receptive fields in dorsal nucleus of lateral geniculate body for dominant and nondominant eye in cats, using moving slit and flash spot stimulation

21 p3335 A71-40669

DOSAGE

NT RADIATION DOSAGE

Erythropoietic activity dosage in polycythemic mice after intermittent hypobaric hypoxia

23 p3632 A71-43216

DOSE

U DOSAGE

DOSIMETERS

NT THRESHOLD DETECTORS [DOSIMETERS]

Small tissue equivalent ionization chamber quartz fiber electrometer dosimeter system, for use as space qualified radiation detection instruments

02 p0250 A71-12136

Heavy cosmic particle dosage measurement by chemical etching of particle tracks on Apollo astronauts plastic helmets

04 p0543 A71-14822

Soviet papers on dosimetry of ionizing radiation intense fluxes covering electron collision, neutron spectra and gamma radiation
04 p0593 A71-14913

Ionization chamber for high intensity isotopic gamma radiation dose measurement, discussing saturation current and Compton interaction process
04 p0594 A71-14917

Nuclear photoemulsions for fast neutron dosimetry, recording recoil proton tracks during elastic scattering by hydrogen nuclei
04 p0594 A71-14919

Unified approach to dosimetry in radiological protection, discussing practical application and instrument calibration to existent standards
06 p0859 A71-18030

Soviet book on radiation dosimetry and spectrometry of ionizing radiations covering chemical, electrochemical, thermoluminescence, scintillation and diffuse reflection methods
11 p1797 A71-26450

Neutron radiography and dosimetry as clinical diagnostic tool, calculating resolution through tissues for simulated human arm
17 p2693 A71-35449

Thermoluminescent dosimeter for skin basal layer dose measurement in mixed beta and gamma radiation fields
17 p2693 A71-35450

Pion beam dosimetry with silicon detectors and plastic scintillators, presenting depth dose and isodose distributions and differential range curves
24 p3799 A71-44359

Cosmic ray dosimetric monitoring in manned spacecraft, discussing ionization, thermoluminescent and nuclear photoemulsion methods of radiation measurement
24 p3826 A71-44888

DOSIMETRY
U DOSIMETERS

DOUBLE BASE PROPELLANTS
Thermal radiation effects on M-2 double base solid propellant ignition, deflagration and burning rate
02 p0298 A71-12851

Reaction heat for flameless combustion of double-base propellant using differential scanning calorimetry and thermogravimetric analysis, noting pressure effects
07 p1183 A71-19898

Ballistic modification of nitric ester based propellant combustion by lead compounds, concerning burning rate-pressure relation
08 p1346 A71-20860

Experimental method for determining condensed phase heat of reaction of deflagrating double-base propellant, defining minimum surface temperature at solid surface without heat feedback
11 p1809 A71-25493

DOUBLE PRECISION ARITHMETIC
Stored-programmed special purpose computer for double precision arithmetic realization of digital filters, discussing design, implementation and testing
07 p1067 A71-18733

N-step conjugate gradient minimization algorithm for nonquadratic functions, giving numerical example of application to double precision arithmetic
24 p3842 A71-44623

DOUBLE SIDEBAND TRANSMISSION
Harmonic and independent subcarrier DSB/FM telemetry systems implementation and utilization
01 p0033 A71-10898

Baseband recorder flutter, pilot and AGC noise effects on quadrature double sideband/QDSB/FM systems
07 p1066 A71-20430

DOUGLAS AIRCRAFT
NT DC 10 AIRCRAFT

DOVAP
U DOPPLER EFFECT

DOWN-CONVERTERS
Ground station integrated receiver cabinet formed by down-converter, demodulator and baseband equipment packaging
02 p0224 A71-12817

Microstrip double down-converter receiver for satellite earth stations, describing thin film integrated circuits and carrier selection
02 p0235 A71-12835

DOWNWASH
Helicopter and V/STOL aircraft external noise and downwash measurements during simulated jungle rescue mission
04 p0531 A71-15409

Helicopter downwash velocities, noise and airloads, examining rotor tip modification effects
04 p0527 A71-15410

Adverse physiological effects of downwash on man, considering tissue damage, hypothermia, dust and sound pressure effects
04 p0546 A71-15411

Turbulent and laminar jet propagation and mixing in rotor downwash field
05 p0795 A71-15961

Unsteady flow downwash behind finite span slender wing during supersonic motion at finite Strouhal numbers
12 p1866 A71-27697

Two vortex model for downwash variations in supersonic flow past thin delta wing with separation at leading edges
17 p2669 A71-34190

Critique of paper on spanwise distribution of induced drag in subsonic flow by vortex lattice method, noting infinities in downwash across all vortex lines
19 p2991 A71-37297

Helicopter experimental fog clearing by downwash mixing at Greenbrier Valley Airport, Lewisburg, West Virginia
20 p3256 A71-39206

Numerical calculation of trailing vortex sheet pattern behind unstalled swept wing at low speed, obtaining downwash field
20 p3176 A71-39397

Two dimensional flow over two dimensional finite wing without correction for downwash, assuming known pressure distribution
21 p3318 A71-40173

Subsonic force effect calculations on rectangular wings, using downwash velocity potential method
24 p3789 A71-44613

DRAG
NT AERODYNAMIC DRAG
NT FRICTION DRAG
NT INTERFERENCE DRAG
NT MINIMUM DRAG
NT PRESSURE DRAG
NT SATELLITE DRAG
NT VISCOUS DRAG
NT WAVE DRAG

Spheres drag coefficient at hypersonic Mach numbers for near free molecular flow
01 p0002 A71-10969

Spheres Oseen drag, extending Goldstein expansion for Navier-Stokes equation in powers of Reynolds number
02 p0185 A71-12380

Ballistic data reduction for drag coefficient of spherical projectiles, using time distance relation for constant coefficient
03 p0341 A71-13467

Nozzle performance prediction inaccuracy due to invalid drag laws, considering unresolved problem of condensed phase particle size
03 p0344 A71-14453

Boundary layer higher order effects on zero-lift drag of short slender bodies, emphasizing shock generated vorticity
04 p0569 A71-15029

Liquid metals vapor drag and electromagnetic fields effects on laminar film condensation, using finite difference method
04 p0688 A71-15539

Equations of motions solution for variable mass point, taking into account drag and velocity
06 p0979 A71-17498

Drag free spacecraft performance in deep space, examining inner residual disturbance forces for motion control systems
06 p0900 A71-18022

Two dimensional laminar boundary layer equation local drag coefficient from one and two term Merk expansion in regions upstream of stagnation point
12 p1896 A71-27051

Land-sea drag, Ekman parameterization and Monin-Obukhov transfer process in surface boundary layer of atmospheric circulation model
13 p2097 A71-28725

Unsteady hypersonic self similar gas flow and drag on circular cone accelerated according to power law, using small perturbation theory
13 p1993 A71-29205

Supercavitating flow past straight cascade with arbitrary blade shapes, considering lift and drag coefficients, cavitation number, cavity shape and exit flow conditions
13 p1995 A71-29448

Pressure distribution and drag prediction over slender axisymmetric fuselages and afterbodies and exhaust nozzles at transonic Mach numbers
14 p2170 A71-30771

Drag coefficients of bodies of revolution from wind tunnel shock induced steady flow data, considering blast loading experiments in shock tube
16 p2519 A71-32878

Lift and drag coefficients for arbitrary body form in hypersonic flow calculated for cylindrical surface with reference to space shuttle reentry
19 p2992 A71-37320

V shaped notches drag coefficients behavior in transonic regime, observing inviscid-viscid interaction controlling flow separation and reattachment
21 p3323 A71-40954

Fluctuating lift and drag forces on accelerating free falling sphere, discussing relation to asymmetrical wake vortex shedding
21 p3324 A71-40970

Crystal lattice drag by conduction electrons and Onsager relationship between electroacoustic coefficients valid for arbitrary topology of Fermi surface
21 p3428 A71-41127

Aerodynamic aspect ratio effects on drag and aircraft performance, noting span loading as major force on wing lifting function
21 p3325 A71-41246

Magnetosphere aerodynamic parameters, discussing lift and drag coefficient, shape, magnetic field gradients and tail
21 p3374 A71-41333

Wall effects and correction rules for cavitation flow past wedge in closed water tunnel, deriving drag coefficient from various theoretical models
23 p3663 A71-43442

DRAG BALANCE
U AERODYNAMIC BALANCE
U LIFT DRAG RATIO

DRAG CHUTES
Parachute decelerator towline energy absorber shock attenuation characteristics, discussing drop test results
[AIAA PAPER 70-1202] 11 p1708 A71-25527

DRAG COEFFICIENT
U AERODYNAMIC COEFFICIENTS
U DRAG

DRAG DEVICES
NT AERODYNAMIC BRAKES
NT BALLUTES
NT DRAG CHUTES
NT LEADING EDGE SLATS
NT SPOILERS
NT TRAILING-EDGE FLAPS
NT WING FLAPS

DRAG EFFECT
U DRAG

DRAG MEASUREMENT
Jet interference effects on aircraft static stability with ejector afterbody, noting wind tunnel methods of drag minimization and measurement
[DGLR-70-048] 05 p0696 A71-15953

High accuracy hypersonic low density cone drag measurements, using method with advantages of free jet and wind tunnel electromagnetic balance
[AIAA PAPER 71-133] 06 p0845 A71-18577

Sphere and disk drag measurements for Reynolds numbers from 5 to 100,000, examining forces, moments, flow visualization, unsteady modes and constant acceleration
07 p1015 A71-19893

Density distribution, heat transfer and drag measurements in rarefied Ar cylindrical Couette flow, comparing results with Navier-Stokes and Burnett equations solutions
07 p1093 A71-20286

Low speed wind tunnel stability tests of small glide surface, slotted solid, ring slot, cross and streamer decelerators, considering parachutes and drag measurement
07 p1022 A71-20310

Airfoil profile drag measurements, correlating full scale flight tests and scale model tests in transonic and high Reynolds number wind tunnels
[AIAA PAPER 71-289] 08 p1229 A71-22012

In-flight profile drag measurement of gliders with total and static pressure sensors in boundary layer wake, using moments method
09 p1384 A71-23667

Numerical calculation of Oseen hydrodynamic fields around sphere in unbounded fluid for various Reynolds numbers, obtaining flow velocity and drag
10 p1592 A71-23935

Aerodynamic characteristics and flow pattern in wake behind star-shaped body at supersonic speed, determining drag and shock waves location
10 p1551 A71-24371

MHD effects on transpiration cooled Couette flow through porous wall, considering magnetic drag produced pressure differential and shear recovery rates
10 p1649 A71-24404

Wake flow behind two dimensional perforated plates normal to air stream, measuring drag, shedding, velocity and turbulence at Reynolds number 25,000-90,000
11 p1705 A71-26449

Ballistic wind tunnel for drag measurement on models during free flight at supersonic speeds
13 p2045 A71-29201

Sphere drag in hypersonic jet transition flow near free molecule limit, using magnetic suspension method
15 p2347 A71-32124

Liquid flow about oscillating flat plates, determining drag coefficient relationships to low Reynolds number and period parameter from graphical representation
18 p2902 A71-36033

Sting-free aerodynamic drag measurement on ellipsoidal cylinders in subsonic wind tunnel at transition Reynolds numbers
18 p2843 A71-36037

Shock tunnel drag measurements on sharp slender cones in near free molecule hypersonic flow in air and He
19 p2993 A71-37897

Momentum transfer between gas and condensed phase in metallized solid propellant rocket motors, measuring noncontinuum and turbulence effects on sphere drag

21 p13437 A71-40861

DRAG REDUCTION

Variable geometry external fuel tanks for high performance aircraft with drag reduction upon fuel transfer

[AIAA PAPER 71-395] Elastic boundary interaction with viscous sublayer of turbulent boundary layer for Reynolds stresses and drag reduction possibility

19 p3042 A71-37082

Submerged vehicle drag reduction and turbulence transition damping by MHD boundary layer control, using Lorentz force and optimum magnetic field

20 p3214 A71-39963

Sword shaped tip on plastic sphere front portion, detailing hydrodynamic drag reduction at various Reynolds numbers

24 p3818 A71-44711

DRAGULATORS

U BRAKES [FOR ARRESTING MOTION]

DRAINAGE

Nonlinear free surface effects in low gravity tank draining, finding domains of validity for linearized and nonlinear analysis

[AIAA PAPER 69-680] Atlanta airport instant runway construction using concrete pavement, compacted subbase and longitudinal/herringbone underdrain

18 p2897 A71-36349

DRAINING

U DRAINAGE

DRAWING

Polymer neck autooscillatory expansion under drawing as result of interaction between elastic deformation and heat release during orientational transformation

03 p0448 A71-14362

DRAWINGS

NT ENGINEERING DRAWINGS

Tridea ALTAPE /automatic line tracing and programming/ system for drawing data conversion to tape for machining surfaces in direct numerical control applications

19 p3068 A71-37244

DREAMS

Brain subcortical structure neuronal assemblies impulse activity during sleeping and dreaming in patients treated with implanted electrodes

13 p2005 A71-28378

DRIFT

Launch vehicle attitude control system for lateral drift minimization and prevention of structural load limit exceeding maneuvers, presenting stability analysis

06 p0979 A71-17338

Earth rotation polar motion dynamics, discussing wobble, drift, nutation, precession and sway

06 p0890 A71-17877

Gyroscopic integrating accelerometer dynamics on high frequency angular vibrating base, determining self oscillations and drift motions

13 p2065 A71-27946

Unstable collisional drift waves in high density ionized Li arc plasma, possibly causing anomalous losses and fluctuations

14 p2281 A71-30544

Forward/reverse drift pair bursts relation to decimeter type 3 solar radio emission, postulating existence of electron acceleration sources in upper corona

15 p2485 A71-31714

Excited states drift and diffusion effects on spatial hole burning and laser oscillation, solving rate equation for population inversion

20 p3242 A71-38842

DRIFT [INSTRUMENTATION]

Drift causes in floated-rotor integrating gyros used as accelerometers, discussing gyromotor magnetic field effects

01 p0080 A71-10535

Astatic gyroscope with gimbal system on rocking base, discussing effects of Cardan joint adjustment to insensitivity zone on instrument drift

01 p0080 A71-10631

Gyroscopic drift tests, using sinusoidal linear VLF acceleration

[AGARDOGRAPH-128]

05 p0750 A71-16312

Onboard air navigation computers drift correction by mapping radar, calculating position by region overflown image/measured geographic features comparison

06 p0925 A71-17952

Observational data statistical evaluation, considering meteorological instrument bias, corresponding instrument fluctuations and noise/signal separation by linear algebraic filter

08 p1329 A71-21726

Gate voltage drift in enhanced p-channel MIS transistors having either pure silicon dioxide insulation or silicon dioxide with silicon nitride

09 p1413 A71-22156

NBS traceable nonferrous conductivity standards for eddy current testing, discussing error analysis, long term drift, grain direction and stratification effects

09 p1469 A71-22710

Low cost directly coupled differential amplifier with thermodynamic drift stabilization for biological studies

10 p1570 A71-24444

Rocketsonde instrumentation noise separation from stratospheric variability, discussing paired soundings based large scale discrepancies in temperature and wind observations

11 p1794 A71-25386

Heterodyne oscillator instability free frequency drift measurement of mixed FM signals in circuits with supplementary conversion

12 p1885 A71-26842

Gravity center effect on drift of gyro linear acceleration integrator on vibrating base, showing errors at frequencies near nutations

13 p2069 A71-28933

Systematic drift of astatic gyroscope in gimbal suspension during rundown

13 p2070 A71-29076

Neutron irradiated and unirradiated Ta sheathed BeO insulated grounded junction thermocouples drift measurement

18 p2916 A71-36046

Thermal emf changes for noble and refractory metal thermocouples, determining drift in high temperature air, Ar and vacuum environments for long time periods

18 p2916 A71-36049

Experimental comparison between double drift and single drift region mm wave IMPATT diodes on room temperature metal heat sinks

18 p2895 A71-36984

Thermocouple drift effect on creep and tension rupture life at high temperature

19 p3065 A71-38137

Gyroscopic systems dynamic drift reduction by inertial damping, using astatic and static stabilizers

23 p3675 A71-43295

Two rotor gyrocompass with random parameter excitation, calculating angular velocity random variation effects on drift

24 p3825 A71-44700

DRIFT RATE

Ionospheric vertical drift velocities and east-west electric fields at magnetic equator from incoherent scatter observations

01 p0076 A71-11505

Type 3 solar radio bursts observed at low frequencies for half rotation, discussing occurrence, drift rates, propagation time and emission

05 p0804 A71-16031

Resonant proton drift in axisymmetric rotating magnetosphere, discussing flow from boundary or tail to auroral region

05 p0800 A71-17178

Dawn chorus western drift and relationship to magnetic disturbances on night side

05 p0745 A71-17189

Sporadic E layer formation based on wind shift theory with drift data

05 p0746 A71-17202

Western frequency drift effects on spectrum time evolution azimuthal asymmetry in diminishing period geomagnetic pulsation intervals

05 p0747 A71-17214

Periodic drift echoes in magnetospheric energetic proton fluxes from satellite observation

06 p0950 A71-17283

Drift type plasma instabilities, discussing feedback stabilization and remote sensing

06 p0932 A71-17465

Ionospheric drift velocity fluctuations by similar fading method, discussing applicability and errors

06 p0894 A71-18262

Geomagnetic secular variation as main field drift superposition and strength changes, reflecting drift and convection in earth fluid core

07 p1103 A71-19763

Wakes in Ar plasma beam, discussing obstacle geometry effects and plasma drift velocity

07 p1169 A71-19805

Plasma with oriented charged particle fluxes macroscopic parameter measurement by multigrid probes facing and reversed to drift, noting graphical data processing

07 p1171 A71-20183

Plasma instabilities and mode stabilization, discussing density-gradient-driven drift waves in collision-dominated regime

07 p1173 A71-20510

Meridional solar magnetic field shape determination, discussing latitude drift of spot forming zones, coronal penetrations and 80 year sunspot periodicity

08 p1358 A71-20887

Confined plasma drift instability universal eigenmode stabilization by magnetic field shear

09 p1500 A71-22246

Satellite-borne sensor for ionospheric ions velocity measurement, describing design and operation principles

09 p1438 A71-23141

Ionospheric ions drift velocity horizontal and vertical components distribution, using satellite-borne sensor

09 p1438 A71-23142

Atmospheric wind velocity radial components measurements for meteor drift as function of wind direction, using transmitter and receiver antennas synchronized orientation method

11 p1758 A71-25791

Short wave ion-cyclotron plasma oscillations excitation by electrons drifting in magnetic field for wavelength much less than ion Larmor radius

12 p1936 A71-27033

Plasma jet drift stabilization in toroidal magnetic field with diverter producing 180 degree field line rotation

12 p1941 A71-27548

Magnetic dipole field second invariant and drift frequency in terms of pitch angle and energy from analytical approximation to trapped charged particle bounce period

13 p2055 A71-27925

Resonant proton drift in asymmetric rotating magnetosphere, discussing flow from boundary or tail to auroral zone

13 p2128 A71-28235

Dawn chorus westward drift and relationship to polar substorm and magnetic disturbances on night side

13 p2059 A71-28246

Sporadic E layer formation, using wind shear theory and drift data

13 p2059 A71-28257

Western frequency drift effects on spectrum time evolution azimuthal asymmetry in decreasing period geomagnetic pulsation intervals

13 p2060 A71-28269

Quasi-unsteady approximation of mutual hydrodynamic drift velocity of aerosol particles in high power sound field

13 p2101 A71-28849

F region vertical drift velocities at Millstone Hill, deriving ion velocity along magnetic field lines in upper part of F2 region from continuity equation

17 p2732 A71-34427

Microwave avalanche diodes, considering drift velocity and power efficiency limitations of IMPATT mode

18 p2894 A71-36976

Gyro drift rate acceptance test design to reflect system performance, using Bayes philosophy for derivation of test cost, product yield and quality

[AIAA PAPER 71-968]

19 p3068 A71-37209

Optimal Kalman filter gyro drift rate mathematical models for limiting inertial navigation errors

19 p3100 A71-37212

Altitude dependent vertical drift velocity of small scale ionospheric inhomogeneities, using correlation of signal time lag scanning in frequency domain

19 p3058 A71-38391

Monograph on electron drift rate measurement in low pressure arc discharge using microwave dragging technique

19 p3116 A71-38549

Confined plasma drift instability universal eigenmode stabilization by magnetic field shear

21 p3424 A71-41135

Atmospheric wind velocity radial components measurements for meteor drift as function of wind direction, using transmitter and receiver antennas synchronized orientation method

22 p3533 A71-41559

Velocity and frequency drifting measurement apparatus developed for rotating machinery study

22 p3523 A71-42474

DRILLING

Electron beam drilled workpieces, investigating residual stresses origin and character with photoelastic measurement

06 p0905 A71-18092

Optically pumped pulsed ruby laser welding unit, noting joining and hole drilling problems

07 p1119 A71-19968

Long pulse glass laser welder-driller, determining mean energy densities and spot sizes

09 p1464 A71-23404

Automated orifice drilling optimal treatment routines, including proper timing and adequate total depth allowance

13 p2074 A71-28941

Minimum output power required for CW carbon dioxide laser drilling of thin stainless steel sheets in vacuum and air, using cylindrical source model

17 p2750 A71-34369

Laser drilled holes in alumina substrates, studying structure by scanning electron microscopy and X ray diffraction patterns analysis

17 p2763 A71-35738

Laser-drilled transparent material hole geometry dependence on beam focus and intensity, computing laser power, mode and work positioning
20 p3246 A71-39492

Laser beam applications in drilling, shaping and surface finishing of miniature journal and step-type friction bearings, deriving regression equations for optimal process parameters
24 p3834 A71-45162

DRILLS
Lunar drilling equipment design from probe data, describing powered hand drill, 3 meter coring device and Apollo lunar surface drill
15 p2385 A71-32497

DRINKING
Incentive goal and extensive stimulation experience effects on proportion increase of hypothalamic electrode sites yielding elicited eating and drinking behavior
21 p3336 A71-40706

DRIVES
High performance shock tube driving techniques, determining effectiveness and flow properties predictability
04 p0564 A71-14669

DROGUE PARACHUTES
U DRAG CHUTES

DROGUES
U TOWED BODIES

DRONE AIRCRAFT
Tethered, ground supplied, rotor-borne, self stabilized surveillance platform (Kiebitz) system, discussing reconnaissance tasks, fire and communication control and data acquisition transmission and evaluation
15 p2347 A71-31212

DRONE HELICOPTERS
U DRONE AIRCRAFT
U HELICOPTERS

DRONE VEHICLES
NT DRONE AIRCRAFT

DROP SIZE
Surface roughness and contamination, drop volume and liquid subcooling effects on Leidenfrost temperature
04 p0675 A71-14783

Holographic measurement of moving cloud droplets size distribution from aircraft using Q switched ruby laser
04 p0596 A71-14968

Cloud drop size distribution from spectral transmission measurements, using spectroradiometer
04 p0621 A71-15073

Liquid hydrogen, oxygen and water droplets released in space, examining size and temperature histories
06 p0964 A71-17277

Warm fog modification by condensation nucleus seeding, discussing droplet concentrations, cloud height and aerosol content effects on salt seeding material optimal size and dosage
09 p1488 A71-23253

Two phase mixture nonequilibrium flow mathematical model with allowance for colliding droplets coagulation and atomization based on high speed photographic studies
10 p1551 A71-24380

Transient nature of fuel droplet combustion, discussing burning rates and flame to drop diameter ratio
13 p2161 A71-28614

Optical measurement of sprays mean droplet size, assessing operating variables effect on air-blast atomizer characteristics
13 p2117 A71-28756

Atomization drop size distributions in sprays from convergent pneumatic nozzles for molten wax and polyethylene mixtures
13 p2049 A71-29007

Fog evolution and droplet radii spectrum determination by scattered laser beam angular distribution measurement
13 p2082 A71-29484

Single and multibeam holography application to size, trajectory, distribution, population density and velocity measurements of water and electric arc welding sprays droplets
14 p2243 A71-30299

Nitric oxide formation analytical model for gas turbine combustion chamber, considering influence of primary zone equivalence ratio, combustor residence time and initial fuel droplet size
14 p2191 A71-30767 [AIAA PAPER 71-715]

Be droplet burning rate in oxygen-argon mixtures, using laser ignition technique
15 p2464 A71-31632 [WSS/CI PAPER 71-23]

Frequency response of rainfall attenuation for various drops size distributions, plotting measured values at 890 and 110 GHz
15 p2374 A71-32696

Droplet size and concentration in gas stream, discussing measurement error analysis and recording medium calibration procedure
16 p2663 A71-33363

Fog drop size distribution measurement with laser hologram camera
16 p2604 A71-33535

Convective mass or heat transfer to or from uniform or size distributed drops, bubbles or solid particles at high Peclet and low particle Reynolds numbers
17 p2837 A71-34690

Automatic analyzer for rapid counting and sizing of raindrops, using collimated flashlamp source for illumination
18 p2918 A71-36076

Monosized oil droplet streams combustion in stationary free flames, examining burning times and constants
19 p3169 A71-38112

Fog droplet size spectral distribution from artificial fog induced He-Ne laser beam scatter, using five photometers for angular distribution measurements
19 p3091 A71-38657

Burning rates of single laser ignited beryllium droplets, considering particle size effect
21 p3475 A71-40862

Solid particle or droplet admixture effect on turbulent gas jet structure
22 p3530 A71-41872

Electrification induced instabilities, breakup and drop size of charged cylindrical liquid jets, using small perturbation method
23 p3663 A71-43445

Electrooptical measurement of high altitude rain cloud droplets size, shape and distribution
23 p3676 A71-43507

Spherical hydrocarbon fuel droplet combustion in air, considering mass burning rates and flame zone locations as function of drop size
24 p3887 A71-44584 [AIAA PAPER 71-989]

Two phase nonequilibrium flow mathematical model with allowance for colliding droplets coagulation and atomization based on high speed photographic studies
24 p3790 A71-44927

DROP TESTS
External stores separation induced aerodynamic interactions, using high speed cinematographic recording of drop trajectories and/or store loads weighing in aircraft flow field
04 p0527 A71-15357 [ONERA-TP-849]

Alumina, boron carbide and silicon carbide notched and unnotched impact strength tests, using drop weight technique
22 p3565 A71-42542

DROP WEIGHT TESTS
U DROP TESTS

DROPS [LIQUIDS]
NT RAINDROPS
Spherical alcohol droplet vaporization in acoustically disturbed medium, considering convective heat and mass transfer
01 p0179 A71-10798

Liquid droplet diameter effect on solid surface erosive wear
01 p0072 A71-11242

Bipropellant droplet supercritical steady combustion temperature measurements in zero gravity near critical point, comparing high and low pressures models for ambient gas solubility
01 p0141 A71-11309

Combustion velocity of burning liquid fuel droplets as function of number and distance
01 p0182 A71-11445

Vaporization and combustion kinetics of condensed single drop kerosene and gasoline thickened by polyisobutylene
01 p0142 A71-11446

Capillary ball game phenomenon under weightlessness, showing photographs of mercury droplet reflection from fluid boundary
02 p0239 A71-11925

Mercury droplet dynamics in conducting liquid within electromagnetic field under reduced gravitation
02 p0293 A71-12631

Fluid jets disintegration into uniform droplets with and without satellite formation, using stroboscopic photography
03 p0399 A71-13292

Diffusion controlled combustion of liquid fuel droplet in oxygen-steam oxidizer mixture
03 p0468 A71-13996

Axially symmetrical two phase turbulent air jet, examining small liquid droplets effect on flow structure [ASME PAPER 70-WA/APM-45]
03 p0404 A71-14166

Hydrodynamic and thermal measurements in turbulent boundary layer of liquid drop flow past plate for mineral oil-water mixtures
04 p0576 A71-15617

Liquid fuel drop evaporation under pressure on hot surface, measuring lifetime and transient interface temperature at subcritical and supercritical conditions
04 p0689 A71-15919

Two-phase detonations, discussing importance of stripping mechanism and droplets deformation in reaction zone fuel consumption
05 p0834 A71-16515

Liquid droplet elliptical deformation in gas flow upon external flow force application, presenting solution as ellipsoid semiaxes plot of dimensionless time functions at various Weber numbers
05 p0736 A71-16749

Liquid drop role in aluminum nitride whisker growth by aluminum oxide reduction in nitrogen or by direct nitriding
05 p0768 A71-16820

Hafnium droplets burning in ultrapur oxygen at various pressures, considering combustion induced natural mode periodic oscillations [WSS/CI PAPER 70-14]
06 p0942 A71-17654

Liquid fuel droplet transient evaporation in high temperature environment, examining vaporization process with coupled heat and mass transfer [AIAA PAPER 71-126]
06 p1008 A71-18570

Incident shock wave interaction with liquid hydrocarbon fuel drops in oxidizing and inert atmospheres, considering combustion characteristics and ignition mechanism [AIAA PAPER 71-206]
06 p0886 A71-18642

Liquid fuel droplets in heterogeneous detonation of dilute sprays, noting deformation and fragmentation in reaction zone
07 p1222 A71-19189

Cloud droplet growth by condensation, deriving equation solution computational stability
07 p1152 A71-19756

Ion diffusion and conduction to cloud droplets, determining resulting mean charge distribution for polar conductivities fixed ratio
07 p1152 A71-19757

Evaporation rate of droplet with internal heat source from Maxwell-Langmuir theory extension
08 p1377 A71-21926

Fluid jets disintegration into uniform droplets with and without satellite formation, using stroboscopic photography
09 p1434 A71-23267

Electromagnetic wave diffraction on arbitrary spheres, including scattering and attenuation by four water droplets
10 p1579 A71-24877

Heterogeneous detonation propagation in mixture of liquid fuel droplets suspended in gaseous oxidizer, discussing droplets disintegration time and shock wave parameters
10 p1698 A71-25124

Cavitation microstreaming near spherical drop or bubble performing translational harmonic oscillations in liquid at rest
11 p1749 A71-25183

Normal shock wave acceleration of water droplets by external pressure, observing distortion and breakup through shadowgraph techniques [AIAA PAPER 71-325]
11 p1749 A71-25305

Water drops deformation and fragmentation due to shock wave impact in high velocity air stream [AIAA PAPER 71-392]
11 p1749 A71-25354

Initially spherical liquid droplet transient response under surface tension accelerated by external gas flow [AIAA PAPER 71-393]
11 p1749 A71-25355

Metal droplet motion in mercury weld pool in tungsten arc, noting cause by Lorentz force and surface arc plasma jet
11 p1769 A71-25748

Shock wave ignition of liquid fuel drop in oxidizing atmosphere, discussing combustion process [AIAA PAPER 70-9]
12 p1986 A71-27566

Laser light scattering by fuel droplets in flame combustion zone, measuring intensity distribution with contactless optical probe
13 p2065 A71-27886

Phase changes /droplet solidification/ effect on two phase nozzle flow, considering perturbation treatment [ASME PAPER 71-FE-11]
13 p2052 A71-29452

Ethyl and methyl alcohol droplets vaporization rate variation with respective distance from photographic observations
14 p2285 A71-30612

Liquid phase evaporation rates in free turbulent air-liquid droplet jet, giving droplet dynamic characteristics determination criterion
14 p2227 A71-30613

Individual liquid fuel droplets ignition factors, introducing heating-up and evaporation delay
15 p2516 A71-32709

Unified raindrop breakup theory, examining spherical liquid drop transient response under surface tension accelerated by uniform external gas flow
16 p2557 A71-32924

Transient response of water drops to shock wave induced accelerations at near critical Weber numbers
16 p2557 A71-32925

Fluid droplet collapse in two phase system gas flows, noting time dependence
16 p2663 A71-33893

Gas and liquid drop laminar, transition and turbulent flows heat transfer intensification in circular tubes, applying to hydraulic resistance design
17 p2835 A71-34205

Liquid hydrocarbon fuel drop interaction with incident shock wave in oxidizing and inert atmospheres, investigating aerodynamic shattering and combustion
17 p2836 A71-34435

Evaporation rate of droplet with internal heat source from Maxwell-Langmuir theory extension
17 p2838 A71-35270

Fluid jets and droplets deformation in transverse supersonic two phase gas flow
17 p2673 A71-35638

Concentration profiles around burning droplet, assuming constant binary diffusion coefficients for all species
17 p2840 A71-35705

Droplet pairs collision efficiencies and coalescence parameters, computing flow fields from nonlinear time dependent Navier-Stokes equations
17 p2770 A71-35805

Linearly polarized lidar light scattering in spherically symmetrical uniformly distributed cloud water drops, investigating multiple backscattering effects on depolarization
17 p2770 A71-35807

Two phase flow model of water droplets velocity in air stream, using Fresnel biprism and laser differential scheme
19 p3072 A71-37587

Wakes of freely falling water drops, discussing flow patterns, kinetic energy, vorticity decay and velocity profiles
19 p3089 A71-37733

Mean curvature of deformed spherical surface in study of equilibrium configuration of water drops under surface tension, using differential geometry
19 p3045 A71-37899

Droplet clouds microstructure and phase state occurrence as function of temperature, size distribution and water content based on experimental data
19 p3091 A71-38680

Water aerosol flux interaction and drop capture with particles of solid reagent, considering agaroid films and precipitation on thin wires
19 p3094 A71-38699

Liquid nitrogen drops anomalous behavior in Leidenfrost film boiling, investigating vapor instabilities effect on total vaporization time
20 p3313 A71-39287

Burning rates of single laser ignited beryllium droplets, considering particle size effect
21 p3475 A71-40862

Room temperature evaporating water drop shape history on cooper, lucite, stainless steel and Teflon, observing wetting dynamics effects
21 p3476 A71-40903

Incompressible inviscid fluid free droplet surface layer tension determination as function of curvature from mechanical moment model
22 p3613 A71-41565

Liquid drop deformation and mass loss in high speed gas flow at high Weber numbers due to capillary surface waves
23 p3662 A71-43371

Mass diffusivity effects in film boiling of water droplets vaporizing in air, Ar, N, He and steam
23 p3782 A71-43907

Fuel droplet burning rate variation with ambient temperature and oxygen concentration in combustion gas environment
24 p3887 A71-44606

Liquid droplet vaporization under exposure to hot gas, obtaining time dependent temperature and concentration profiles in vicinity from coupled diffusion equations
24 p3888 A71-44963

N-heptane, carbon dioxide and Freon 13 droplet vaporization measurements at supercritical pressure, comparing with film theory calculation
24 p3890 A71-45072

DROSOPHILA

Lethal recessive point mutation in *Drosophila melanogaster* eggs on Zond 5 spacecraft
01 p0018 A71-11552

Low and high linear energy transfer /LET/ cyclotron-accelerated alpha particles effects on *Drosophila melanogaster* longevity
06 p0853 A71-18028

Carotenoid depleted *Drosophila* circadian rhythm and visual receptors photosensitivity, discussing photopigment effects
09 p1394 A71-23160

DROWSINESS

U SLEEP

DRUG THERAPY

U CHEMOTHERAPY

DRUGS

NT ADRENERGICS
NT ANESTHETICS
NT ANTIBIOTICS
NT ANTICONVULSANTS
NT ANTIDIURETICS
NT ANTIDOTES
NT ANTIHISTAMINICS
NT ANTIIRADIATION DRUGS
NT ATROPINE

NT CENTRAL NERVOUS SYSTEM STIMULANTS

NT CHLOROFORM
NT CHOLINERGICS
NT CYCLOPROPANE
NT CYSTEINE
NT DIGITALIS
NT EPINEPHRINE
NT HISTAMINES
NT INSULIN
NT MOTION SICKNESS DRUGS
NT MUSCLE RELAXANTS
NT NORADRENALINE
NT NOREPINEPHRINE
NT PENICILLIN
NT PENTOBARBITAL SODIUM
NT TRANQUILIZERS
NT VASOCONSTRICTOR DRUGS

Temperature telemetry for pyrogenic drugs testing on dogs
01 p0023 A71-10977

Antithrombotic agent search, finding anticoagulants useful for Venous system
02 p0200 A71-12418

Antiarrhythmic drugs choice based on excitable tissues biophysics, considering contrast between cardiac muscle and nerve
02 p0201 A71-12419

Anticonvulsant drugs for counteracting noise effects on central nervous system, discussing audiogenic seizure in mice
03 p0360 A71-13163

Alpha and beta receptor blocking drugs effects on oxygen consumption of methemoglobin-containing erythrocytes and hemolysates
03 p0363 A71-13483

Angiotensin I infusion effect on intrarenal blood flow distribution, using krypton 85 method and autoradiography
04 p0538 A71-15088

Light and drugs effect on diurnal body temperature from radio telemetry of adult male rats
05 p0715 A71-17111

Drug-radiation damage interaction relationship to radiosensitization in mammalian cells
07 p1034 A71-18946

Mitomycin C radiosensitizing effect on hematopoietic colony forming cells, using technique based on bone marrow cells spleen colonies forming ability
07 p1036 A71-18958

Central nervous system role in body metabolism effects on cardiac output, measuring 2,4-dinitrophenol /DNP/ dosage effect on arterial pressure and oxygen consumption in dogs
09 p1396 A71-23541

Arterial tonometry for atraumatic measurement of arterial blood pressure, considering transient effects of drugs or physiological interventions
12 p1874 A71-27140

Human subjects REM sleep characteristics under 5-hydroxytryptophan influence, analyzing continuous polygraphic recordings of parietal EEG, horizontal eye movement and submental electromyographic activity
15 p2359 A71-31952

Hemodynamic evaluation of glucagon in symptomatic heart disease, comparing to isoproterenol
17 p2682 A71-35040

EEG study of hyperoxic convulsions in Macacus nemestrinus and Papio primates, considering preventive effect of Diazepam and derivatives
21 p3339 A71-41418

Pilot EEG, behavioral and subjective correlates of natural and drug induced sleep at atypical hours, using calculation and vigilance tests
22 p3502 A71-41835

Beta-aminoethylthiophosphoric acid monosodium salt effect on mice stability to lateral accelerations
22 p3491 A71-42701

Medical preparations use and avoidance by spacecraft and aircraft crew members, discussing aftereffects, allergies and health requirements
22 p3491 A71-42705

Caffeine, ephyllin, cordiamin, morphine, calcium chloride, adrenaline and mesaton effects on organism physiology during hypothermia
22 p3492 A71-42709

DRUMS [CONTAINERS]

Material point motion in conveyor horizontal pipe drums with screw surface on inner walls, using law of addition
13 p1998 A71-28297

DRY CELLS

NT MAGNESIUM CELLS
NT NICKEL ZINC BATTERIES

DRY FRICTION

Hipp pendulum controller electromechanical clock, considering dry and viscous friction dynamic models
12 p1932 A71-27525

Damping in gravity gradient satellite passive stabilization systems under eddy currents and dry friction induced by magnet motion
13 p2144 A71-28195

Weak damping of free gyro motion in static coordinate system under dry friction in gimbal joint, deriving equations of motion by Lagrange method
13 p2069 A71-28932

Local slip theory in elastic contact region with dry friction, assuming Amontons-Coulomb law for displacement, rolling and sticking
17 p2747 A71-34327

Uniaxial gyroscopic stabilizer errors in presence of base random vibration, taking into account dry friction forces in bearings
17 p2738 A71-34560

Friction force moment in ball bearing without lubrication in presence of angular vibrations of one race
17 p2748 A71-34563

Thin layers shear strength and friction under high pressure, describing rotating-anvil shear press with high sensitivity strain gage equipped load and torque cells
20 p3241 A71-38878

Diboride-nitride system dry friction and wear resistance at room temperature
23 p3681 A71-43254

DRY HEAT

Dry heat spacecraft sterilization-compatibility tests of reagents and growth media for planetary biological exploration
01 p0027 A71-11563

Dry heat destruction rates for microorganisms encapsulated in and on spacecraft hardware, concluding temperature and water conditions in spore as major factors
01 p0027 A71-11564

Spacecraft sterilization by microbial inactivation, comparing thermoradiation and dry heat methods
06 p0853 A71-17959

Dry heat and Co 60 gamma radiation combined effects on spacecraft sterilization, discussing kinetic analysis of spore inactivation
10 p1565 A71-24613

Combined dry heat and ionizing radiation for spacecraft sterilization process, detailing synergistic effect on microbes
16 p2537 A71-33770

Bacterial spore distribution and dry heat resistance on Mariner-Mars 1969 spacecraft, using randomly selected aerobic mesophilic isolates
19 p3002 A71-37646

DRYING

NT DEHYDRATION

DSIF [INSTRUMENTATION FACILITY]

U DEEP SPACE INSTRUMENTATION FACILITY

DTA [ANALYSIS]

U DIFFERENTIAL THERMAL ANALYSIS

DTMB-111 GROUND EFFECT MACHINE

U GROUND EFFECT MACHINES

DTMB-430 GROUND EFFECT MACHINE

U GROUND EFFECT MACHINES

DUAL SPIN SPACECRAFT

Semipassive and active nutation dampers in orbiting dual spin spacecraft, using single axis control moment gyro
13 p2144 A71-27976

Preflight balance analysis of dual spin satellites, discussing error sources
17 p2815 A71-35821

Nutation damping and vibration isolation in dual spin spacecraft, using flexible dissipative coupling between platform and rotor
18 p2971 A71-36276

Bearing axis wobble for dual spin vehicle in terms of rotor static and dynamic unbalance and platform mass geometry and inertias
20 p3306 A71-39351

Spinning and dual spin spacecraft angular momentum and axis control, investigating optimal fuel and small angle reorientation techniques
22 p3611 A71-42045

Dynamic unbalances effects for axially symmetrical dual spin space station with rigid or low coupling interconnections, considering control moment gyros use
22 p3612 A71-42770

Attitude stability of dual spin spacecraft with energy dissipation in flexible momentum wheel having two degrees of freedom
23 p3772 A71-43020

DUCTED BODIES

MHD generator duct external loop electric current maximization by working material resistivity tensor optimal distribution
19 p3108 A71-37102

DUCTED FAN ENGINES

Blade bound vortex system mathematical model for optimum heavily loaded ducted fans, including thrust, power and efficiency design parameters
02 p0299 A71-12677

Turbofan engine noise reduction, using acoustic liners in inlet and exhaust ducts
06 p0947 A71-18622

DUCTED FANS

Helicopters safe antitorque control, describing Fenestron ducted fan design
04 p0532 A71-15417

- Subsonic fan noise, using helicopter rotor noise theory for analysis of phase related and randomly time varying flow distortions 05 p0796 A71-17161
- Fan noise random propagation and sound power in cylindrical air ducts from modal spectra and pressure measurements 10 p1596 A71-24834
- Acoustic linings for attenuation of fan generated noise in turbofan engines, considering interaction between analytical lining performance prediction and flow duct testing [AIAA PAPER 71-731] 14 p2295 A71-30778
- Low speed wind tunnel measurements correction for acoustic effects due to fan noise propagation 24 p3790 A71-44763
- ### DUCTED FLOW
- #### NT KNUDSEN FLOW
- Natural convective heat transfer from fin-flat in vertical rectangular arrays, comparing duct and open channel coefficients 02 p0333 A71-12605
- Variable viscosity effect on laminar forced convective heat transfer in rectangular duct, using ethylene glycol and aqueous solutions 03 p0518 A71-13616
- Shock wave propagation in bent and branched ducts, discussing schlieren method flow visualization, diffraction measurement with differential interferometer and interaction between shock and vortex 03 p0400 A71-13696
- Laminar flow of liquid in duct with zero heat resistance of walls, calculating temperature distribution during radiative convective heating 03 p0519 A71-13745
- One dimensional ionized gas flow behind shock wave propagating in MGD duct 03 p0466 A71-14569
- Heat transfer correlations for turbulent flow in ducts with rough surfaces 04 p0674 A71-14778
- German monograph on loss estimation for nonsteady gasdynamic duct-drum pressure exchangers, discussing design and optimization problems 04 p0568 A71-14925
- Variable properties effects on MHD flow in ducts with finite aspect ratio and electrically insulating walls, noting current distribution 04 p0634 A71-15179
- Frictional resistance reduction in hydrodynamics, considering critical shear stress in ducted flow 04 p0571 A71-15209
- Wall stability of parallel elastic plate duct in contact with inviscid compressible fluid flow 04 p0573 A71-15563
- Semicircular canal ducts dynamic behavior, using mathematical model for wave transmission of elastic fluid-filled toroidal shell in rigid channel 04 p0547 A71-15772
- Axial and swirling mean flow effects on sound transmission and generation in hard walled ducts 06 p0945 A71-17620
- Laminar pulsating ducted flow heat transfer, taking into account velocity distribution time dependence 06 p1005 A71-17682
- Large aspect ratio rectangular duct with nonuniform surface texture, investigating turbulent flow, maximum velocity positions and zero shear stress 07 p1086 A71-18772
- Turbulent velocity field in noncircular cross section rectilinear duct, determining relation between viscosity ratio and dimensionless velocity by integral transformation 07 p1087 A71-18992
- Acoustic propagation through variable area duct with steady compressible flow, transforming governing equations into two decoupled linear ordinary differential equations 07 p1160 A71-19952
- Local turbulent friction factors and heat transfer coefficients for fluid flows through ducts of arbitrary cross section with prescribed wall heat flux distribution 07 p1224 A71-20654
- Stored gas retrorocket total impulse expression, deriving from flow continuity equation in closed duct 08 p1366 A71-21308
- Optimal lining impedance for jet engine inlet duct, yielding discrete frequency, flow velocity and geometry on basis of minimum radiated power 08 p1349 A71-21661
- Arc heated duct facilities providing high temperature supersonic turbulent boundary layer flows over large samples for orbital logistic vehicle thermal protection tests 09 p1429 A71-23060
- Supersonic and subsonic jets coexistence in rectilinear constant section duct, characterizing flow boundaries by pressure readings and Schlieren flow visualization 09 p1384 A71-23605
- Three dimensional unsteady irrotational flow in variable cross section duct, reducing Navier-Stokes equation to Euler equation 10 p1591 A71-23850
- Duct thermal entrance region with axial conduction, evaluating laminar heat transfer rate with finite difference technique 10 p1696 A71-24409
- Wall conductivity effects in MHD rectangular duct flow at high Hartmann numbers with uniform magnetic field applied parallel to one pair of duct sides 10 p1649 A71-24419
- Traveling shock waves interaction with orifice inside ducts, noting anomalous phenomena probably due to unsteady boundary layer growth or time lag 10 p1596 A71-24923
- Velocity profiles for flows with laminar heat transfer in circular tube and rectangular duct inlet region with wall suction and injection 10 p1597 A71-25064
- Acoustic and shock waves propagation in quasi-steady supersonic flow in duct with varying cross section 10 p1598 A71-25083
- Three dimensional MHD flows with strong transverse magnetic fields variable area rectangular ducts with conducting sides 12 p1938 A71-27216
- Cylindrical duct stationary uniform axial flow effects on propagation of acoustic vibration modes of wavelength smaller than damping length [ONERA-TP-969] 12 p1981 A71-27479
- Wall shear stress and static pressure of developing turbulent flow in square ducts with convective accelerating core for various Reynolds numbers 13 p2048 A71-28595
- Turbulent gas flow through duct with alternating pressure gradient, considering heat transfer and frictional resistance 13 p2166 A71-29370
- Friction factor for low Reynolds number turbulent flow in large aspect ratio rectangular ducts, comparing Blasius and Prandtl relations [ASME PAPER 71-FE-A] 13 p2051 A71-29378
- Soviet book on liquid metals nonstationary flow in ducts of MHD devices covering laminar flow at constant and variable flow rates 14 p2277 A71-29526
- Turbulent flow and high sound level effects on acoustic attenuation in narrow rectangular duct 14 p2224 A71-30207
- Acoustic linings for attenuation of fan generated noise in turbofan engines, considering interaction between analytical lining performance prediction and flow duct testing 14 p2295 A71-30778
- [AIAA PAPER 71-731] Eddy diffusivity of mass in air measurement discrepancies in circular duct, considering axial concentration and radial distributions 14 p2339 A71-30934
- Book on pressure losses in ducted flows covering subsonic flow in straight or curved ducts, constrictions flow characteristics, etc 15 p2386 A71-31149
- End wall sampling of high pressure shock tube, using abrupt pressure rise to drive test gas flow through duct to sample bottle [WSS/CI PAPER 71-18] 15 p2383 A71-31627
- Tube or duct confined submerged turbulent jet exit cone angle calculation for various expansion area ratios 15 p2390 A71-32016
- Annular ducts finite amplitude spinning acoustic modes propagation and subsonic choking, allowing for nonlinear effects in perturbation procedure 15 p2450 A71-32133
- Acoustic propagation in rigid wall rectangular duct with uniform flow, calculating higher mode energy transmission properties 15 p2392 A71-32195
- Ducted axisymmetric jet mixing flow, investigating flow separation and reattachment as function of diameter and velocity 15 p2392 A71-32252
- Low Reynolds number turbulent flow in large aspect ratio rectangular ducts, investigating Blasius and Prandtl circular tube friction factor relations 15 p2392 A71-32261
- Shock wave interaction with duct cross section changes, discussing experimental apparatus and shadowgraph results 15 p2393 A71-32265
- Metal particle nonequilibrium effects in mixing and combustion of ducted particle laden flow in air breathing engines [AIAA PAPER 71-722] 15 p2466 A71-32573
- Turbulent flow in circular duct, determining asymptotic temperature profiles and Nusselt number values from Prandtl numbers and velocity distribution 16 p2554 A71-32836
- Shock wave attenuation in perforated duct, using pressure transducers and schlieren photography 16 p2554 A71-32884
- Hypersonic viscid-inviscid internal flow field interaction with laminar boundary layer in circular ducts, using method of characteristics and implicit finite difference scheme 17 p2671 A71-35281
- Air-methane supersonic diffusion flame in duct, comparing pressure measurement and gas sampling data with two dimensional combustion analysis [ONERA-TP-961] 18 p2984 A71-36027
- Space time structure of acoustic waves propagating in cylindrical duct with weakly absorbing walls and axial inviscid time dependent fluid flow [ONERA-TP-965] 18 p2946 A71-36030
- Adverse pressure gradient effects on compressible turbulent boundary layer flow in parallel duct at Mach 4 and high Reynolds number 18 p2904 A71-36297
- Pressure wave interaction with orifices inside ducts, calculating reflection and transmission characteristics relationship to orifice geometry and initial steady flow conditions 19 p3044 A71-37642
- Viscous electrically conducting laminar fluid steady flow through insulated MHD duct under uniform external magnetic field by extended Kantorovich method 20 p3275 A71-39561
- Acoustic signal pressure mode propagation velocity in infinite rectangular hard-walled duct with steady flow, noting Doppler effect 20 p3271 A71-39765
- Lined ducts design for flow with intense sound, discussing analysis methods, testing procedures, liner materials development and acoustic attenuation 21 p3361 A71-40212
- Aerodynamic approximations for unsteady supersonic flow of perfect inviscid gas through flexible duct of revolution [ASME PAPER 71-VIBR-23] 21 p3458 A71-40280
- Sound propagation in sheared fluid in duct, determining energy flux from linearized gas dynamic equations 21 p3366 A71-40536
- Unsteady laminar flow in polygonal ducts, calculating velocity profiles, friction factors and energy dissipation 21 p3371 A71-40994
- Two phase flow in asymmetrically roughened ducts, investigating secondary flow effects on heat transfer characteristics 21 p3477 A71-40995
- Obstruction effects in rarefied gas flow through cylindrical ducts by numerical analysis, considering specular reflection, adsorption, absorption and finite molecular mean free path 22 p3531 A71-42343
- Approximate analytic solution for nonstationary heat transfer for viscous incompressible laminar fluid flow in annular cylindrical ducts 22 p3622 A71-42679
- Symmetrical and unilateral sticking flow modes of nozzle air jets expelled into plane-parallel and parabolic ducts 22 p3480 A71-42681
- Shear flow effects on sound propagation in rigid rectangular ducts, taking into account boundary layer thickness 23 p3704 A71-43212
- Perturbation and projection operator algorithms for Navier-Stokes equations for incompressible flow in rectangular cavities and injection into cylindrical ducts 23 p3662 A71-43238
- Laminar incompressible flow velocities and heat transfer by radiation and convection in inlet section of parallel plate duct 23 p3781 A71-43313
- Mass flow function diagram for axisymmetric isentropic compressible swirling flow in annular duct 24 p3820 A71-44960
- Interaction between two incompressible fluid flows in plane duct, deriving parametric equations for free stream line and flow interface 24 p3820 A71-45005
- ### DUCTED PROPELLERS
- #### U SHROUDED PROPELLERS
- #### DUCTILITY
- Ductile Ni deformation and fracture, examining simultaneous cyclic and monotonic strain effects 01 p0098 A71-10164
- Metal sheet plate and bar fabrication, calculating minimum bend radii from ductility ratings 01 p0087 A71-10457
- Temperature effect on ductility of thin sheet sintered or vacuum melted Mo during deep drawing 02 p0257 A71-12517
- Critical ductile-brittle transition temperature and microstructure under deep drawing of sintered and vacuum melted Mo 02 p0257 A71-12519
- Refractory Nb alloys with high creep strength, good ductility and moderate density, heat treatment and workability 02 p0271 A71-12937
- Niobium alloys for gas turbine blades, examining working temperatures, protective coatings and ductility 02 p0271 A71-12939
- Notched tensile plate steel specimens, investigating temperature and stress state effects on nil ductility transition and fracture strength [SESA PAPER 1735] 03 p0443 A71-13752

Anisotropic materials ductile fracture involving crack initiation and propagation, using Dugdale mathematical model
[SESA PAPER 1729] 03 p0507 A71-13760

Ultrafine grain alloys ductility from tensile tests, discussing grain size, temperature and strain rate effects
03 p0446 A71-14493

Notched tensile tests for measuring metal ductile-brittle transition temperature, deriving proportionality law
04 p0666 A71-14877

Hot ductility curves for cracking sensitivity prediction during welding
04 p0617 A71-15907

Ductility of simulated weld fusion zones in Inconel 718
04 p0617 A71-15911

Plastic deformation and ductility of Mo alloys under various stress concentrations at room and high temperatures
05 p0765 A71-16175

Metals and alloys with bcc structure, investigating ductile-to-brittle transition by ultrasonic MHz technique
05 p0770 A71-17251

High temperature ductility of low alloy ferritic steels, correlating tensile elongation values to crack nucleation resistance
07 p1134 A71-19517

High strength martensite beta Ti alloy microstructure, discussing ductility and age hardening
08 p1312 A71-21552

Ductile metals fatigue crack propagation model applications to brittle metals, discussing crack initiation effects on high strength steels failure modes
09 p1467 A71-22285

Macroscopically ductile and brittle fracture via electron microscope photographs, considering brittle fracture and embrittlement temperature under uniaxial and multiaxial stress
10 p1627 A71-24595

Mo-Fe-C ternary system, investigating various concentrations, microhardness measurements, solid state solubility and ductility
10 p1628 A71-24648

Hydrogen effects on low temperature solution strengthening and ductility of Nb-H single crystals, noting effects of normal and strain induced hydride precipitation
11 p1780 A71-26020

Ductility and susceptibility to brittle fracture of alloys under stress at low temperatures
12 p1919 A71-27685

Multiaxial stress state effects on materials fracture strength, ductility and structural design
13 p2151 A71-28216

Notch effect on ductile fracture, considering plastic stress and strain concentration in stainless steel, brass, copper and mild steel
13 p2088 A71-29343

Be sheet plastic bend ductility and yield strength, considering purity and processing effects
13 p2088 A71-29403

Hot ductility correlation with microstructure from nickel softening and fracture mechanisms interaction
13 p2089 A71-29410

Low ductility materials, considering applications to stress analysis, failure criteria, fatigue, physical metallurgy and polymer mechanics
14 p2251 A71-29893

Cast Nb-W-Mo-Zr-C alloys heat treatment effect on microstructure and phase composition, noting ductility improvement
15 p2426 A71-31406

Monograph on ductile fracture covering electron microscopy of fracture surfaces and microstructures of Al alloys
15 p2434 A71-32301

Fabrication, texture, alloying, substructure and fracture effects on bend ductility and toughness of beryllium sheet
15 p2436 A71-32509

Stress rupture ductility of electron beam, gas tungsten arc and gas metal arc welds, considering creep crack initiation
15 p2437 A71-32617

Ti alloys argon TIG welding to Nb alloys, detailing joint impact strength, fusion zone ductility and bending tests
15 p2418 A71-32668

Notch effect on stainless steel and alpha brass rods and plates ductility and fracture strength
16 p2591 A71-32947

Mo single crystal growth by vacuum melting without oil vapors, noting reduced carbon content and increased ductility
16 p2595 A71-33880

Ti influence on ductility of normalized low alloy steel, considering crack initiation and propagation
16 p2598 A71-33991

Hot pressed W-Cu pseudoalloys strength and ductility under tension and compression
17 p2760 A71-35674

Carbon effects on strength, ductility, brittle transition and plastic strains of tungsten at high temperatures
18 p2936 A71-36713

Beryllium impurities effects on ductile-brittle transition temperature, investigating fracture characteristics deformation mechanism
19 p3076 A71-37121

Static ductile deformation in quartz, olivine, pyroxenes and plagioclase, noting plastic deformation and recovery
19 p3050 A71-37664

High strength Cr-Mo-Co stainless steels with improved toughness and ductility by austenitizing temperature selection
19 p3079 A71-37707

Characteristic smooth test bar ductility correlation and prediction in high temperature creep rupture tests, noting application to material quality control
19 p3082 A71-38138

AMg6M alloy hot rolling butt joints, showing ductility and strength of welds
19 p3070 A71-38424

Soviet book on steels high temperature elastic stiffness and ductility covering carbon, alloyed and special steels at different temperatures and strain rates
21 p3404 A71-41375

Inconel superalloy microscopic observation of local melting and hot ductility behavior during weld thermal cycles to clarify cracking cause in heat affected zone
22 p3564 A71-42494

Mo additions to Co rich ductile permanent magnet alloys, obtaining higher coercive forces and energy products
23 p3694 A71-44283

DUCTS

NT ACOUSTIC DUCTS
NT AIR DUCTS

Ducting materials and joints technology fallout from aerospace projects, discussing reliability in terms of corrosion resistance, fatigue strength and thrust compensating duct design
01 p0007 A71-11431

Bellows for aerospace feed line ducting, discussing liquid propellant rocket engines, cryogenic valves, etc
01 p0007 A71-11433

Whistler ducts as enhanced ionization from OGO 3 satellite observations near magnetic equator, noting magnetospheric ionization hydrostatic model and predicted cut-off
01 p0076 A71-11499

Enhanced ionization density duct propagation of VLF radio waves in magnetosphere
07 p1062 A71-19578

Hall MHD generator duct optimization, using digital calculation for Carter integral minimum for size under required power output
09 p1512 A71-23441

Sound attenuation in lined duct, using Newton-Raphson method for complex roots of equations
18 p2947 A71-36499

Lined ducts design for flow with intense sound, discussing analysis methods, testing procedures, liner materials development and acoustic attenuation
21 p3361 A71-40212

DUFFING DIFFERENTIAL EQUATION

Partial differential equation solution for aircraft hydraulic lines flexural vibration by Bubnov-Galerkin method, reducing to Duffing equation analysis
08 p1286 A71-20783

DUMMIES

Dummy S4 diode packages mounted in coaxial line, deriving mount-independent equivalent circuit parameters from broadband admittance measurements
22 p3521 A71-42206

DUMMY LOADS
U IMPEDANCE
U OUTPUT

DUNGEYS WIND SHEAR MECHANISM
U WIND SHEAR

DUPLEXERS

Microwave transmitting and receiving duplexers for Intelsat 3 satellite, discussing design, operation and performance
06 p0877 A71-18402

Wideband gas discharge duplexer as transmitter receiver microwave antenna switch in H/01 mode circular waveguide
10 p1584 A71-24720

DUPPLICATING

U REPRODUCTION [COPYING]

DURABILITY

Heat treated low carbon steel fatigue tests at low cycle tension compression loads, determining durability relationships to load and total work to fracture
04 p0666 A71-14878

Metal endurance dependence on simultaneous oxygen corrosion and cyclic loading frequency at various temperatures and pressures
06 p1000 A71-17934

Cyclic heating and thermal stresses effect on fatigue strength and durability of turbine blade alloys and structural elements
08 p1372 A71-21702

Materials durability in presence of stress concentration under biharmonic loading
09 p1538 A71-22626

Specimen sample mounting stress effects on fatigue durability scatter in axial load tests
12 p1976 A71-27116

Titanium alloy durability under cyclic torsion in vacuum at various temperatures, investigating fatigue life and tensile strength
15 p2428 A71-31856

Machine structural elements endurance margin prediction from limited tests, proposing statistical method of integral estimates and tolerance factors
16 p2651 A71-33064

Statistical analysis of durability data of heat resistant alloys for gas turbine engines, using long term mass creep strength tests on industrial melts
16 p2592 A71-33413

Glass fibers durability in air and vacuum conditions, showing stress concentration coefficients at various tensile stresses
23 p3697 A71-44031

DURATION

U TIME

DUST

NT COSMIC DUST
NT INTERPLANETARY DUST
NT LUNAR DUST
NT METEOROID DUST CLOUDS
NT TERRESTRIAL DUST BELT
NT ZODIACAL DUST

Static charged dust distributions, investigating general relativity field equations with electromagnetic stress tensor
04 p0625 A71-14732

Sand and dust effects on military helicopter flight controls and equipment service life, discussing relief program
04 p0533 A71-15430

Molecular hydrogen formation on dust grain surfaces, discussing recombination efficiency as function of surface temperature
05 p0784 A71-16205

Combustion kinetics of premixed laminar graphite dust-oxygen-nitrogen flames with/without hydrocarbon
08 p1346 A71-20866

Mars yellow clouds extent during near perihelion apparitions since 1877, considering dust storm origin in Southern Hemisphere
09 p1520 A71-22698

Diffuse skylight measurement for atmospheric dust particle concentration, considering sunlight scattering by air molecules and aerosol layers
16 p2567 A71-33767

Sunlight scattering by dust in upper atmosphere from primary twilight intensities investigations
20 p3219 A71-39647

Martian dust storm observation by telescope on New Mexico, noting brilliant yellow cloud cover
24 p3872 A71-45000

DUST COLLECTORS

VTOL aircraft engine air particle separator development, examining airflow and engine design
04 p0533 A71-15433

Hypersonic flow of dust containing gases at low density for distribution accuracy of cosmic dust collection by sounding rockets
15 p2387 A71-31171

Cosmic dust separation from terrestrial material, using vibrating tray to roll spherical particles from bulk of demagnetized and dried material
17 p2811 A71-35729

High altitude balloon cosmic dust collection, considering individual particle chemical composition and ablation
20 p3299 A71-39653

DWARF STARS

NT WHITE DWARF STARS

RR Lyr type dwarf stars, discussing brightness curves, color indices, effective temperatures, line of sight velocities and spectral classes
03 p0485 A71-13265

MHD parameters in photospheric plasmas of giant and dwarf stars, noting electric conductivity, Joule dissipation, Reynold and Lundquist numbers
03 p0490 A71-13938

UV dwarfs observational lifetime, considering progenitor main sequence, red giants and planetary nebulae central stars evolutionary sequence
04 p0648 A71-15249

UV dwarf star evolution, using central and gap star models emphasizing photoneutrino emission
04 p0648 A71-15250

High galactic latitude faint blue stars from Tonantzintla and Asiago catalogs, finding quasars and subdwarfs by spectroscopy and UVB photoelectric photometry
04 p0651 A71-15659

Book on dwarf novae covering light variations, spectra, binary systems, absolute magnitude, mass, gas streams, outburst, etc
08 p1363 A71-21165

Subluminous star spectroscopic data, determining temperature and surface gravity 14 p2317 A71-31011

Subdwarf star data, reviewing spectra, kinematics, nucleosynthesis, interiors, atmospheres, angular momentum, formation, abundances and distribution 16 p2633 A71-33126

B and O hot dwarf stars ionic UV line spectra, observing electron and ion damping constants with impact and semiclassical approximations 16 p2633 A71-33338

Solar-type dwarf star rotation effect on stellar wind structure and thermal regime, obtaining time independent solutions with heat conduction 17 p2796 A71-35577

Degenerate dwarfs theory, discussing stellar structure, stability, evolution and thermal properties 18 p2969 A71-37039

Radio stars classes, discussing red dwarf flare, red supergiants, blue dwarf companion, novae, pulsars and X ray stars 21 p3448 A71-40582

Red dwarf flare stars sporadic outbursts, considering light and radio emission curves, outburst energy and galactic emission 22 p3607 A71-42881

DWELL

Dwell or dark pause measurements of shock tube driver high pressure arc discharge for various gases 05 p0788 A71-16578

DYES

Nonlinear light absorption in organic dyes liquid solutions 01 p0095 A71-11028

Flash light excited dye solutions in liquid lasers, investigating wavelength and energy dependence of forced emission 02 p0261 A71-12322

Organic dye laser output and service life enhancement, using filters for absorption of UV pumping radiation photodecomposition of rhodamine 6G alcohol solution 03 p0435 A71-13509

Tuned nitrogen laser pumped dye lasers, investigating bandwidth influence on output power 03 p0436 A71-13643

Long pulse rhodamine 6G flash lamp-pumped circulating dye laser with cyclooctatetraene cycloheptatriene as triplet state quenchers, testing performance 03 p0437 A71-13884

Organic lasers using fluorescent dye in liquid solution or polymer, discussing gain and output performance, tuning, mode locking and CW operation 04 p0605 A71-14710

Near UV dye lasers, using various organic compounds as scintillators with excitation through nitrogen gas UV laser transverse pumping 04 p0606 A71-14717

Spectroscopic hole burning in coupled saturable dye-robby lasers with frequency locking 04 p0607 A71-14725

Dye lasers operational principles and characteristics, considering dyes molecular structure, optical pumping, continuous operation, wavelength selection and applications 05 p0761 A71-16330

IR difference frequency generation using tunable dye laser 06 p0910 A71-18663

Organic dye lasers flash lamp pumped system for tunable coherent light production in visible and near IR spectrum 07 p1125 A71-19796

Organic dye lasers lasing conditions calculation for constant emission frequency from nonstationary emission kinetics analysis 07 p1125 A71-19807

Harmful induced stimulated emission losses in rhodamine unpumped ethyl alcohol and heavy water solutions of various excitation energies 09 p1461 A71-22383

Wide angle high gain image amplification by organic dye solution lasers using rhodamine or fluorescein disodium salt 09 p1463 A71-22752

Organic lasers with xanthene dyes solutions, investigating triplet states molecular population effect on output energy characteristics in pumping 10 p1620 A71-24344

Nitrogen laser pumped cresyl violet dye laser output increase through excitation transfer from added intermediary dye 11 p1773 A71-25926

Dye emission frequency variation during quasi-stationary emission process 11 p1774 A71-26002

Light combination scattering in organic liquids, measuring frequency dependence with dye laser technique 13 p2080 A71-29021

Broadly tunable liquid dye laser action with narrow line output through use of distributed feedback obtained by spatial modulation of gain and refractive index 13 p2081 A71-29339

Absorption spectra enhancement by organic dye laser quenching, considering applications for absorbing species spectroscopic detection 13 p2082 A71-29439

Flashtube pumped rhodamine 6G dye laser with four prism tuner, giving reflection losses equations and performance characteristics 14 p2254 A71-30135

Pulsed nitrogen-pumped dye laser output spectral narrowing by injection of argon laser monochromatic radiation into cavity 15 p2420 A71-32382

Hexamethylindotricarbocyanine iodide ethanol dye solution stimulated fluorescence during excitation by ruby laser radiation in spike generation quasi-continuous monopulse modes 15 p2421 A71-32406

Rhodamine 6 G in ethanol partial mode locked dye laser picosecond pulses, using pulsed nitrogen laser pumping 15 p2422 A71-32580

Ruby laser pumped tunable organic dye laser to excite atomic flame fluorescence of 5535.5 A barium resonance line, obtaining intensity vs concentration 15 p2422 A71-32582

Compact monochromatic rhodamine doped polymethyl methacrylate dye laser with internal diffraction grating resonator, describing frequency selection from emission spectrum 15 p2422 A71-32585

Rhodamine, sodium fluorescein and cryptocyanamine dyes for liquid lasers, investigating electroluminescence by polarography 16 p2587 A71-33382

Flash lamp pumped pulsed dye lasers using triplet quenchers cycloheptatriene and cyclooctatetraene with 600 microsec emission times in rhodamine 16 p2589 A71-34122

Energy balance and emission power of organic dye laser under nonmonochromatic excitation 17 p2751 A71-34381

Organic dye laser properties analysis using universal relation between absorption and emission spectra for solvent molecules reorientation after excitation 17 p2752 A71-34388

Dynamic rate equation model of single wavelength flash lamp pumped rhodamine dye laser accounting for short molecular triplet state lifetimes 18 p2929 A71-35958

Dye lasers developments and applications, including flash lamp pumps, frequency narrowing and tuning and picosecond pulse mode locking 18 p2931 A71-36602

Organic dyes pulse emission spectra shifts during pumping by ruby and neodymium-glass lasers, discussing vibrational relaxations role in mechanism 19 p3072 A71-37766

Papers on semiconductor, carbon dioxide and dye lasers 20 p3243 A71-39065

Dye laser physics and technology development, discussing dye selection for frequency and cavity parameter variation tuning of lasing wavelength 20 p3243 A71-39068

Laser dye cell optical quality dependence on light pumping and liquid dye flow velocity, using schlieren method 20 p3246 A71-39489

Repetitively pulsed flashlamp pumped dye laser, noting high average outputs in red end of spectrum with rhodamine B 20 p3246 A71-39760

High power tunable second harmonic and UV sum frequency generation from rhodamine 6G dye laser and ADP crystal 22 p3556 A71-41803

Nonstationary laser generation of organic dyes in picosecond optical pumping, considering kinetic and spectrum nonstationarity 22 p3557 A71-41815

UV absorber dyes in fluorescent tracers, discussing theory of dimensional sensitivity and use in liquid-film developers to quench background fluorescence 23 p3681 A71-43194

Liquid laser output wavelength dependence on rhodamine dye concentration, comparing experimental data with Stepanov theory 23 p3684 A71-43417

Mode locked CW dye laser operation, describing output stability and pulse rate and widths 23 p3687 A71-44133

CW dye laser mode locking with lithium niobate phase modulator, observing 500 psec pulse generation 23 p3687 A71-44134

Dye laser electronic tuning by inserting calcium-molybdenum oxide acousto-optic filter into cavity 23 p3687 A71-44137

DYNAMIC CHARACTERISTICS

NT AERODYNAMIC DRAG

NT AERODYNAMIC STABILITY

NT AIRCRAFT STABILITY

NT ATTITUDE STABILITY

NT BOUNDARY LAYER STABILITY

NT COMBUSTION STABILITY

NT CONTROL STABILITY

NT DIRECTIONAL STABILITY

NT DRAG

NT DYNAMIC PRESSURE

NT DYNAMIC STABILITY

NT FLAME STABILITY

NT FLOW CHARACTERISTICS

NT FLOW DISTRIBUTION

NT FLOW STABILITY

NT FLOW VELOCITY

NT FREQUENCY STABILITY

NT FRICTION DRAG

NT GYROSCOPIC STABILITY

NT HOVERING STABILITY

NT INTERFERENCE DRAG

NT INTERFERENCE LIFT

NT JET LIFT

NT LATERAL STABILITY

NT LIFT

NT LONGITUDINAL STABILITY

NT LOW SPEED STABILITY

NT MAGNETOHYDRODYNAMIC STABILITY

NT MINIMUM DRAG

NT MOTION STABILITY

NT PRESSURE DRAG

NT ROTARY STABILITY

NT ROTOR LIFT

NT SATELLITE DRAG

NT SPACECRAFT STABILITY

NT TRANSIENT RESPONSE

NT VISCOUS DRAG

NT WAVE DRAG

NT ZERO LIFT

Dynamic behavior of liquids in partially filled mobile tanks under almost centrifugal force fields 01 p0069 A71-10396

Rotary hydraulic motors dynamic behavior during pressure and fluid flow control 01 p0066 A71-10823

Dynamics of tropical disturbances on Interpolar Convergence Zone (ITCZ), using model covering entire hemisphere 01 p0120 A71-10856

Semiconductor quantum amplifier dynamic range in steady operation mode, analyzing monochromatic signal gain 01 p0096 A71-11219

Ferritic steel with 17 percent Cr, examining dynamic behavior under high speed tension test regarding heterogeneity of plastic deformation, stress peak, etc 01 p0105 A71-11616

MOS transistor inverters static and dynamic characteristics in IC assemblies 02 p0228 A71-11656

Uniaxial satellite rotational motion, examining magnetic and gravitational torque effects on gyro dynamic properties 02 p0320 A71-11975

Rotating accelerometer with magnetic amplifier for angular acceleration detection, investigating static, dynamic and frequency response characteristics 02 p0252 A71-12421

Servoamplifier dynamic response effects on dynamic characteristics of fluid-filled pendulous accelerometers 02 p0252 A71-12455

Radially deforming sphere dynamic behavior during translational motion in infinite incompressible static medium 02 p0241 A71-12669

Transition metal carbides and nitrides, observing metallic and nonmetallic sublattice dynamic characteristics by X ray diffraction 02 p0266 A71-12672

Soviet book on flight vehicle instruments and sensors static and dynamic characteristics, instrument errors and reliability 02 p0254 A71-12720

Ball bearing dynamics, considering motion equations for four degree of freedom balls and six degree of freedom separator [ASME PAPER 70-LUB-H] 03 p0432 A71-13708

Jupiter details rotational periods variations, characterizing dynamic properties of atmosphere upper layers 03 p0490 A71-13940

Cauchy problem solution for elasticity theory dynamic system in Euclidean space arbitrary region 03 p0510 A71-13962

Single rotor gyrocompass with electromagnetism correction during random interactions involving intercardinal deviation, constructing correcting device to obtain optimal dynamic characteristics 03 p0430 A71-14353

Multilayer structures dynamic phenomena during switching, examining similarity theory with simple p-n junctions 03 p0388 A71-14387

Hugoniot elastic limit and dynamic compression strength for brittle bodies, considering hydrostatic stress and porous specimens 04 p0617 A71-14750

Body position effect on dynamic characteristics of human operator under random vibration, considering pelvis-head amplitude-frequency characteristics 04 p0543 A71-14791

Ettingshausen refrigerator dynamic behavior mathematical models, using current density and potential gradient as controlling variables

04 p0678 A71-15465

Dynamic characteristics of submerged twisted jet flow of incompressible viscous fluid

04 p0573 A71-15560

Circular cylindrical shell reinforced by ring ribs, investigating dynamic characteristics under impulsive loading

04 p0672 A71-15756

Semicircular canal ducts dynamic behavior, using mathematical model for wave transmission of elastic fluid-filled toroidal shell in rigid channel

04 p0547 A71-15772

Dynamic objects optimal linear model existence and uniqueness conditions, considering gradient technique and stochastic approximation algorithms convergence

05 p0731 A71-16794

Dynamic systems oscillation period doubling in presence of C bifurcations

05 p0782 A71-16985

Electro-hydraulic servomechanisms dynamic performance variation probabilistic model, presenting sixth order system variable parameters for Monte Carlo simulation

06 p0848 A71-17318

Industrial and biological polymer compounds active surface layers, discussing thermodynamic aspects, molecular dynamics, energy conversion and boundary layer entropy

06 p0915 A71-17585

Qualitative behavior for classical dynamical systems, discussing various theorems

06 p0918 A71-17641

Pulsating liquid filled hemispherical shell dynamic characteristics, determining hydrodynamic pressure and shell displacements

06 p0882 A71-17837

Micropulsations dynamic properties and resonant cavity modes, obtaining coupled toroidal and poloidal modes solution

06 p0969 A71-17976

Dynamic strength of elastic elements from wire and tapes of Mo-Re alloy

07 p1120 A71-20249

Laser dynamic theory with uniformly broadened and Doppler spectral lines based on nonlinear interactions between harmonic oscillations

07 p1127 A71-20255

Multimass system oscillations due to viscous friction factor and kinematic random disturbances, considering dynamic behavior of wheeled vehicle on rough roadbed

07 p1162 A71-20469

Digital active fluid amplifiers static and dynamic behavior, defining complex parameters for system engineering

07 p1026 A71-20564

Moving part pneumatic logic element static and dynamic characteristics, determining air flow rate and output pressure

07 p1027 A71-20574

Reflected jet proximity detector dynamic and static characteristics, considering response speed and separation distance

07 p1030 A71-20600

Oscillatory systems with nonlinear elastic arresting devices, calculating dynamic characteristics and motion stability

08 p1332 A71-20687

Self adaptive systems with dynamic characteristics stabilization, obtaining algorithm for adaptive loop optimization

09 p1422 A71-22120

Book on dynamic characteristics of aerosol particles in terms of classical mechanics covering continuum approximation, single particles heat and mass transfer, diffusion, dispersion, etc

09 p1431 A71-22284

Structurally similar models, investigating space vehicles dynamic characteristics

09 p1532 A71-22658

Composite material dynamic processes based on diffusing mixtures continuum theory

09 p1540 A71-23085

Dynamic characteristics of two degree of freedom gyroscopes with positional and integral negative feedback for simultaneous angular velocity and displacement measurement

09 p1451 A71-23171

Second order dynamic relay system with unstable linear part, investigating constant disturbance effects with point mapping and bifurcation theory

09 p1424 A71-23458

Wave propagation in elastoviscoplastic medium in temperature field under complex dynamic and thermal conditions, considering mathematical models and mechanical properties changes

09 p1543 A71-23611

Dynamic behavior of circular and rectangular membrane panels with time and space dependent boundary conditions for aerospace structures

09 p1544 A71-23736

Hydrogen isotopes around terrestrial planets, discussing H and deuterium dynamic behavior in Venus and Mars coronas

10 p1668 A71-24001

Stationary and dynamic characteristics of integrators with dosage capacitor for analog frequency measurements, analyzing dynamic response at large modulation depth via analog computer simulation

10 p1589 A71-24502

Soviet book on liquid propellant rocket engines non-stationary operation covering dynamic processes, transient conditions, component elements, fuel delivery, etc

10 p1659 A71-24649

Dynamics of focusing electric discharges generated by coaxial plasma gun illuminated by ruby laser beam, using schlieren photography

10 p1653 A71-24758

Dynamic analysis of vibrating beams on viscoelastic supports, using Galerkin approximate method

10 p1694 A71-25088

Nonlinear dynamic systems phase coordinate variations statistical characteristics, describing data reduction method

11 p1798 A71-25662

Earth-moon system, examining kinematical and dynamical relationships, tidal deformation, earth rotation, secular variations, inclination and eccentricity

11 p1822 A71-25686

Lunar geometrical and dynamical properties, deriving force function from density distribution and surface equation

11 p1822 A71-25687

Small fast spectrum thermionic reactor experiment open loop dynamics and control, discussing nonlinear transient simulation studies on closed loop plant

11 p1712 A71-25886

Open loop transient analysis of thermionic diode kinetics experiment with analog computer nuclear reactor simulator

11 p1797 A71-25904

Equation error approach to parameter identification in third order pitch plane dynamics for high performance aerodynamically controlled aerospace vehicle

11 p1742 A71-26418

Heat pipes steady state and dynamic behavior, noting pressure balance, vapor flow, transport capability and applications

12 p1987 A71-27741

Variable structure automatic control system dynamic properties, using frequency response method

13 p2041 A71-27943

Dynamic characteristics of fluid oscillations in cylindrical vessel divided by annular diaphragm

13 p2050 A71-29236

Disperse systems dynamic behavior, considering density ratio, discontinuity diameter, viscosity and shear modulus

14 p2256 A71-29518

Dynamic characteristics of hydraulic fatigue testing machines, using hydraulic activation efficiency factor

14 p2221 A71-29625

Uniaxially reinforced W-Cu matrix composite material dynamic compressive load properties, considering strain rates and yield stress

14 p2257 A71-29643

Dynamic systems conservative by bits and governed by differential equation with discontinuous second member, obtaining limiting cycle existence condition

14 p2265 A71-29691

Automatic amplitude control dynamic performance of system with oscillating frequency determination by ring gain bandpass behavior

14 p2210 A71-29809

Self adaptive systems with dynamic characteristics stabilization, obtaining algorithm for adaptive loop optimization

14 p2220 A71-29998

Liquid phase evaporation rates in free turbulent air-liquid droplet jet, giving droplet dynamic characteristics determination criterion

14 p2227 A71-30613

Nonlinear mathematical model for dynamical behavior of extensible towing cable subjected to aerodynamic forces generated by uniform flow field, discussing system stability

14 p2171 A71-31026

Dynamic nonshock properties of large amplitude microscale Alfvén waves in interplanetary medium, using plasma and magnetic field data from Mariner 5

15 p2456 A71-31752

Independent noise driven nonlinear dynamic systems identification, performing linear discrete-time scalar measurements

15 p2380 A71-31934

Liapunov approach to nonlinear dynamic systems controllability, deriving conditions for linear dynamic systems

15 p2380 A71-31935

Materials dynamic characteristics determination by acoustic input signal impedance measurement, presenting expressions as functions of reflection factor and signal propagation phase shift

15 p2409 A71-32186

Digital on-off follow-up system dynamics under signal time and amplitude quantization effects on transient and steady state processes, using phase-plane analysis

15 p2382 A71-32453

Square cross section rectangular rotating grains dynamic behavior in magnetic fields, obtaining orientation data with Monte Carlo method

15 p2498 A71-32772

Dynamic characteristics of weakly damped elastic body, considering complex natural modes generation for vibration tests in aircraft design

16 p2657 A71-33403

M 13 spherical star cluster, determining spatial distribution, center coordinates, radius and dynamic behavior

16 p2634 A71-33428

Traveling ionospheric disturbances dynamic properties, calculating horizontal phase velocity from triangulation data

16 p2568 A71-33783

Gas turbine blades dynamic characteristics determination, investigating vibrational stresses, thermal cycles, alloy physicochemical properties and coatings effects

16 p2659 A71-33987

Elastic static and dynamic physicochemical characteristics of resin type amorphous materials under pulsed loads, using electromagnetic excitation of torsional vibrations

16 p2659 A71-33996

Dynamic amplification ranges of monochromatic signal by semiconductor, solid state and gas lasers in steady operation mode

17 p2750 A71-34270

Hydraulic system self acting valves natural vibration dynamic characteristics, showing energy transfer by phase shift of variable hydrostatic compression component

17 p2677 A71-34349

Dynamic compressive strength and failure of steel reinforced epoxy composites, discussing strain rate sensitivity

17 p2762 A71-34813

Linear dynamic systems state estimation, using empirical Bayes decision theory to develop filter set

17 p2825 A71-34897

Superharmonic resonance in piecewise linear systems with unsymmetrical characteristics, investigating stability properties by Fourier series method

17 p2781 A71-34926

Redundancy utilization in automatic control systems synthesis, considering dynamic characteristics sensitivity

17 p2721 A71-34965

Dynamic properties of modulating and mixing nonlinear systems consisting of time dependent impedance controlled by pumping source

18 p2875 A71-35975

Dynamic characteristics of arterial oxygen tension response to supine submaximal leg exercise in man from harmonic analysis

18 p2856 A71-36239

Dynamic characteristics of arterial blood pressure responses to sinusoidal work load in man from harmonic analysis

18 p2856 A71-36240

Dynamic properties of turbine wheels under bending vibrations, classifying resonant frequencies on basis of vibration modes

18 p2981 A71-36722

Dynamic piecewise-continuous linear systems oscillation period doubling in presence of C bifurcations

18 p2948 A71-36785

Nonspherical nose bluntness effects on slender vehicle dynamics, considering conical geometry as approximate nose shape after ablation due to turbulent heating

[AIAA PAPER 71-931]

19 p3148 A71-37176

Automatic flight control accommodation to dynamic characteristics variations of airframe, providing uniform response for all flight conditions

19 p2996 A71-37296

Sound reflection by dense doubly periodic lattice parallel to rigid screen, describing asymptotic characteristics by double lattice virtual mass including mirror image

20 p3268 A71-38807

Variational methods application to high order dynamic systems resonance boundary value problem

20 p3309 A71-39487

Composites and mechanical systems dynamic behavior prediction, calculating Hugoniot with effective modulus

21 p3465 A71-40792

Envelope process transfer function calculation for self adaptive systems parametric control dynamic characteristics

21 p3361 A71-41138

Soviet book on digital servomechanisms dynamics covering logarithmic frequency characteristics and pulsed and hybrid control systems

22 p3526 A71-41800

- Local dynamical system behavior in perturbed Tikhonov space, showing fundamental cycle periods continuous variations 22 p3568 A71-42695
- Terrestrial, lunar and planetary dynamical properties and internal constitution, considering data obtained from artificial satellites, lunar and planetary dynamics 22 p3607 A71-42883
- Dynamic characteristics of human respiratory and circulatory adaptation to muscular exercise, using systems analysis approach 23 p3634 A71-43905
- Suboptimal fixed point data smoothing algorithm for parameter and initial state estimation of nonlinear dynamic systems 23 p3659 A71-44113
- Unknown parameter identification in nonlinear dynamic systems from state variable time history measurement 23 p3660 A71-44114
- Parameters steady random variations effect on linear and nonlinear systems steady motion characteristics, using integral equation and averaging methods 24 p3815 A71-44696
- Dynamic characteristics of self oscillating systems from response to sinusoidal test signals, using Abel integral equations 24 p3881 A71-44835
- Transient dynamic characteristics of aircraft under unsteady flight, using Laplace-Carson integral transforms 24 p3792 A71-45016
- Magnesium diatomic metal static and dynamic properties, using multiple electron and ion analysis system 24 p3839 A71-45118
- Nonlinear controlled plant dynamic behavior sensitivity in parameter perturbation derived from mathematical model, applying to satellite attitude control [ASME PAPER 70-WA/AUT-5] 24 p3816 A71-45136
- DYNAMIC CONTROL**
- Polynomial finite difference description of first order nonlinear dynamic control plants with incomplete information 01 p0058 A71-10405
- Model performance index $/P_i/$ providing criterion for approximating one dynamic flight control system by another based on geometrical representation of linear autonomous systems 02 p0189 A71-12682
- Maximum likelihood identification of stochastic linear dynamic systems using Kalman filter 05 p0731 A71-16554
- Dynamic digital predictive compensation learning control systems with time delay transform identification by template matching technique 06 p0878 A71-17336
- Feedback and dynamic control of plasmas - Conference, Princeton, June 1970, Volume 1 06 p0931 A71-17451
- Magnetically confined plasma dynamic stabilization, using HF potential 06 p0933 A71-17473
- Inhomogeneous collisionless low beta plasma drift wave instability dynamic stabilization, considering AC electric field parallel to confining field 06 p0933 A71-17474
- Dynamic stabilization of instability in bumpy theta pinch by generalization of energy principle 06 p0934 A71-17480
- Dynamic stabilization of magnetoplasma drift dissipative instability by HF oscillating magnetic field, discussing helium and hydrogen afterglow plasmas 06 p0934 A71-17481
- Dynamic stabilization of two stream ion instability in collisionless plasma 06 p0934 A71-17483
- Dynamic stabilization of MHD instability of low current z-pinch by HF quadrupole and oscillating magnetic fields 06 p0935 A71-17486
- Dynamic stabilization of MHD instabilities in high beta plasma column, using superposed fluids parametric resonance model 06 p0935 A71-17488
- Dynamic stabilization of helical and sausage instabilities of p-indium antimonide electron-hole plasmas, using Ioffe type RF energized magnetic quadrupoles 06 p0935 A71-17489
- Dynamic control of steady state plasma loss in cusped magnetic field, considering density and electron and ion temperatures 06 p0935 A71-17490
- Finite difference description for dynamic control plants with unknown disturbances based on integral transformation and extrapolation, applying to automatic control systems synthesis 08 p1270 A71-21975
- Optimal variational control with frequency and time coupling concerning dynamic precision of linear systems 08 p1271 A71-22023
- Dynamical nonlinear systems observability definition and necessary and sufficient criterion for checking 10 p1587 A71-24743
- Control parameter optimization of dynamic system for single and series maneuvers 10 p1637 A71-24846
- Soviet papers on automatic control for flight vehicles, Part 1, covering dynamics of linearized systems, deterministic and random inputs, stability, oscillations, thrust control, etc 10 p1588 A71-24897
- Stability and coordinate bounds of motion of linear dynamic systems over finite time intervals by solutions of differential equations 10 p1643 A71-24900
- Dynamic frequency and phase characteristics of oscillatory circuit dependent linearly on time variable capacitance 10 p1643 A71-24907
- Optimal characteristics for single-input single-output memoryless time invariant nonlinear dynamic systems 11 p1742 A71-25751
- Dynamic optimization with constrained state and control vectors, solving problems by hybrid method with partial derivatives 11 p1735 A71-25842
- Optimal fixed dimensionality dynamic compensator design for linear time-invariant closed-loop system based on quadratic cost and gain criteria 11 p1742 A71-26414
- Logical dynamic control systems, interpreting structural properties in categories of logic-operator matrices and predicate systems 12 p1893 A71-27338
- Gyro platform orientation control system, using inertial flywheels 13 p2068 A71-28634
- Soviet book on long range rocket ballistics covering control system, dynamics, firing distance, motion equations, stage separation and nominal trajectories 13 p2146 A71-29438
- Infimum principle for dynamic optimal control with nonscalar valued cost criteria, rederiving Kalman-Bucy filter 14 p2219 A71-29627
- Unsteady controlled object dynamic characteristics evaluation for search-free self adjusting systems and telemetric information processing improvements 14 p2220 A71-30814
- Suboptimal control of nonlinear autonomous dynamical systems via linear approximation by hyperplanes 15 p2379 A71-31823
- On-line identification of stochastic linear dynamic control systems with applications to Kalman filtering based on statistical correlation technique 15 p2380 A71-31933
- Input signal preservation in nonlinear dynamic system described by finite difference equation in presence of noise, deriving algorithms for discrete time computers 15 p2381 A71-31982
- Dynamic stability and reliability analysis of pulse width modulated control systems by point-to-point mapping method 15 p2382 A71-32621
- Synthesis algorithms for model reference adaptive control systems using Liapunov second and Popov hyperstability methods 15 p2382 A71-32623
- Infinite-time linear dynamic system suboptimal control derivation from lower dimension models, exemplifying by flexible-bodied rocket vehicle pitch plane dynamics 17 p2720 A71-34871
- Computer algorithm for simulating dynamic systems by functional graphs, noting extension to complex systems 18 p2884 A71-35917
- German monograph on field effect transistors as controllable resistors with applications in adjustable amplifiers and dampers, covering nonlinear harmonic distortion and control dynamics 18 p2887 A71-35961
- Vibration control methods, discussing oscillation and acoustic noise reduction 19 p3069 A71-37518
- Minimal time function of optimal feedback controls for normal and semidynamical systems 21 p3359 A71-40252
- Damped isolation and undamped vibration absorber model for dynamic control, discussing frequency response and tuning and damping performance [ASME PAPER 71-VIBR-45] 21 p3459 A71-40294
- Free vortices from slender wings, controlling strength, position, core stability and thickness on basis of one dimensional flow model 21 p3319 A71-40492
- Relative motion interaction dynamics in rocket biaxial control with azimuth and elevation servos, using Mathieu equation and stability criterion 22 p3526 A71-41971
- Compensator design for linear controllers for time varying nonlinear systems, using digital computer oriented approach 22 p3577 A71-42676
- Controllability conditions for linear differential equations of dynamic system 22 p3568 A71-42696
- Cost functional gradient optimization of pulse width modulated control inputs for nonlinear dynamic systems 23 p3658 A71-44088
- Generalized matrix inverses application to estimation of state vector in dynamic control system, determining covariance matrix of estimator 23 p3700 A71-44117
- Pole placement design of dynamic compensators for linear time invariant multivariable systems, using transfer function matrices 23 p3660 A71-44119
- Accuracy analysis of statistically optimal dynamic system with modulus bounded control for discrete and continuous information input, using Fokker-Planck-Kolmogoroff equation 24 p3814 A71-44689
- Optimal linear final parameter control synthesis for dynamic systems with given accuracy, using multivariate statistical analysis 24 p3814 A71-44690
- Optimal dynamic accuracy of control systems with random signals and parameter oscillations, using sensitivity theory 24 p3815 A71-44697
- DYNAMIC LOADS**
- NT AERODYNAMIC LOADS
- NT BLAST LOADS
- NT CYCLIC LOADS
- NT GUST LOADS
- NT IMPACT LOADS
- NT LANDING LOADS
- NT ROLLING CONTACT LOADS
- NT SHOCK LOADS
- NT THRUST LOADS
- NT TRANSIENT LOADS
- NT VIBRATORY LOADS
- NT WING LOADING
- Hollow circular cylinder with variable inner radius, solving nonlinear viscoelasticity dynamic load problem 01 p0168 A71-10422
- Impulsively loaded rigid plastic continua deformation lower bounds calculation, considering beams and plates 01 p0173 A71-10943
- Clamped rectangular metal plates dynamic plastic behavior under uniformly distributed impulsive velocities 02 p0321 A71-11678
- Clamped shallow spherical and conical shells axisymmetric dynamic buckling under step loads of infinite duration, showing similarity with static buckling 03 p0504 A71-13455
- Photoelastic study of stress wave propagation in composites under fiber matrix strip directed impulsive loading with exploding wire [SESA PAPER 1708] 03 p0507 A71-13758
- Coupled stresses effect on dynamic stress concentration produced by traveling loads on elastic Cosserat plate 03 p0509 A71-13905
- Brittle fracture mechanics, discussing shape, stress and dynamic toughness factors, crack-defect interaction and crack barriers 03 p0516 A71-14578
- Circular cylinder creep deformation under complex varying loading, comparing computation and test results [ONERA-TP-846] 04 p0669 A71-15353
- Semiinfinite isotropic linear Cosserat continuum surface under impulsive loading, calculating displacements with Laplace transformation 04 p0672 A71-15834
- Deformation time and displacement bound theorems for impulsive loading of plastic and viscoplastic materials 04 p0673 A71-15883
- Semiinfinite simply supported cylindrical shell transient response due to axisymmetrically engulfing step pressure wave, investigating moving load critical velocity [ATAA PAPER 70-18] 05 p0823 A71-16556
- Deflection-optimal elastic beams design for distributed dynamic loading 05 p0825 A71-16717
- Elastic cylindrical shells stability under dynamic load consisting of conservative forces and normal compression 06 p0990 A71-17789
- Acceleration inequalities of dynamically loaded elastoplastic shells, using permissible stress and displacement velocity fields 06 p0990 A71-17790
- Elastic rectangular and thin plates design under dynamic loading, using Bubnov-Galerkin method for computer solutions 06 p0992 A71-17808

Dynamic response of pressurized thin circular cylindrical shells under moving loads
[AIAA PAPER 71-175] 06 p1004 A71-18614

Dynamic stress measurement of cantilever beams, frame structures and rings under impulsive loads
07 p1210 A71-19046

Cylindrical shell with elastic core under annular sliding load, solving for critical velocity via Fourier transformation
07 p1212 A71-19353

Free vibration of spherical sandwich shell under axisymmetric static and dynamic loading
07 p1212 A71-19350

Bonded rod of two semiinfinite elastic bars subjected to end impulse, formulating motion equations and initial and boundary conditions
07 p1217 A71-20367

Conical shell stability under dynamic longitudinal compression
07 p1218 A71-20472

Viscoelastic plates forced motion under dynamic loads by Valani method, considering elastic and layered elastic-viscoelastic circular plates
08 p1368 A71-20801

Rectangular plate and circular cylindrical shell segment under rotating moment and dynamic loads evaluated by Green function
10 p1691 A71-24812

Circular plates with radially symmetric membrane stresses and thickness, investigating stability under peripheral-moving load excitations
10 p1692 A71-24995

Structures dynamic loading and damage by sonic booms, discussing structural response prediction by boom pressure wave model
10 p1693 A71-25052

Dynamically loaded rigid plastic bodies, solving limiting equilibrium problems by extremal principles
13 p2156 A71-29065

Machine for corrosion testing materials under various static and dynamic axial tension, torsion and bending loads
13 p2045 A71-29374

Arbitrary dynamic load problem for elastic infinite bodies, solving with Lamé equations and Fourier and Laplace transforms in distribution space
14 p2323 A71-29817

Impedance testing techniques based on ratio of mechanical input force to velocity response for structures and systems behavior evaluation under dynamic loads
14 p2252 A71-30054

Stability and longitudinal vibrations of elastic beam under rapid monotonously increasing and impulsive loading assuming free end
14 p2326 A71-30194

Pulsating follower loads implementation by pulsating gas or liquid jets, using Mettler differential equations for forced vibrations of elastic bodies
15 p2502 A71-31172

Plates analysis under static and dynamic loads based on finite difference, lattice analogs, mathematically consistent lumped parameters and finite element models
15 p2503 A71-31438

Al and Cu dynamic plastic deformation at elevated temperatures, discussing relationship between strain rate sensitivity and activation energy
15 p2428 A71-31972

Time dependent fracture and failure criteria for aluminum under stress pulse loading in uniaxial strain, using exploding foil spallation tests in air and vacuum
16 p2590 A71-32943

Circular plates finite amplitude response under pulse loading, presenting nonlinear equations finite difference solution
16 p2650 A71-33014

Stiffened rectangular plates parametric instability under in-plane sinusoidal dynamic forces, using mathematical model with stiffeners as discrete elements
[ASME PAPER 71-APM-26] 16 p2655 A71-33203

Dynamic stress on rotor blades of aircraft engine axial compressor stages with low hub/diameter ratio
16 p2624 A71-33345

Automatic testing machine for materials corrosive strength under varying and combined complex static or dynamic stresses
16 p2580 A71-33687

Snap-through buckling of three hinged deep trusses and wire restrained column under critical quasi-static loading based on elastica theory of prismatic bars
17 p2815 A71-34294

Crack wave loading, investigating dynamic stress intensity factor and time response with photoelastic technique
[SESA PAPER 1835] 17 p2820 A71-34550

Nonlinear elastic bending of nonhomogeneous cantilever beam under stepwise and triangular pulse loads of finite duration
17 p2821 A71-34578

Weightless elastoplastic beam dynamic bending under moving concentrated load, calculating deformation by reduction to Cauchy problem
17 p2822 A71-34780

Finite element analysis codes for complex two layered linear elastic shells of revolution under static and dynamic loads
17 p2831 A71-35351

Convergent approximations of impulsively loaded stable structures with account of geometry changes and discontinuity interfaces
[ASME PAPER 71-APM-KK] 18 p2978 A71-36267

Dynamic loading of cantilever beams by magnetomotive and explosive loads and high bullet speed impact, noting elastic and plastic deformation modes
18 p2981 A71-36770

High frequency modal response of elastic plates to impulsive line load, using Rayleigh-Lamb branch equation
18 p2983 A71-36844

Transient response of Euler-Bernoulli and Timoshenko beams and cylindrical shells with moving loads
19 p3158 A71-38183

Nonassociated constitutive equations for rigid viscoplastic plates and thin rotationally symmetric shells under dynamic loading with Huber-Mises yield condition
20 p3310 A71-39777

Computerized analysis of fluid film behavior, load capacity and center locus of journal bearing under dynamic load
[ASME PAPER 71-VIBR-86] 21 p3386 A71-40322

Iron response to dynamic loads, discussing pressure induced phase changes, constitutive equation relationship to dislocation processes and dynamic fracture criteria
21 p3399 A71-40789

Hypersonic flat plate under impulsive loads, calculating time dependent transient wall shear stress and boundary layer induced pressure
21 p3369 A71-40964

Thin elastic plate under dynamic loading, applying asymptotic expansion techniques to three dimensional dynamic elasticity theory
22 p3613 A71-41435

Lower bound deformation theorem for rigid plastic continua and structures under impulsive loading, using kinematically admissible velocity field
22 p3614 A71-41608

Optically sensitive epoxy resin based high polymers under pulsed loads, observing deformation and mechanical displacement with high speed photography
22 p3614 A71-41610

Dynamic three dimensional stress distribution near crack tip in finite plate, using finite difference scheme
23 p3776 A71-43376

Dynamic flexures in beam during massive extended load motion with allowance for inertial forces, using Bubnov-Galerkin method
23 p3778 A71-44046

Longitudinal stability of plate-like load towed beneath helicopter in horizontal forward flight
23 p3630 A71-44346

DYNAMIC MODELS

Andromeda galaxy M31 hydrodynamic model, examining kinematical and dynamical functions
01 p0150 A71-10057

Clear air convective process, examining dynamic model with radar patterns
01 p0116 A71-10562

Switching bipolar transistor dynamic model equivalent circuit diagram characterization by parameters
02 p0228 A71-11655

Dynamic systems synthesis by exponential power input packet
02 p0285 A71-12670

Dynamic polysystems stability and optimization, discussing minimality and recurrence in state space set
03 p0450 A71-13120

Fermion system phase transition model thermodynamic behavior near critical point region for various interactions
03 p0456 A71-13350

Mechanical model for orthotropic elastoplastic plates with clamped torsion susceptible ribs
03 p0504 A71-13528

Optimal adaptive estimation, considering Gaussian process and linear dynamic models and partition theorem for structure and parameter adaptation
03 p0394 A71-14484

Computation scheme for hinged plate systems subject to arbitrarily oriented loads based on two layer flexible base model
04 p0664 A71-14601

Dynamic model of flow separation of plane fluid past body in channel with eddy wake formation
04 p0578 A71-15630

Dynamic problems of two dimensions with semisurface of section, examining charged particles motion in axisymmetric magnetic field
04 p0627 A71-15706

Metal powders sintering computer simulated dynamic volume diffusion model based on Laplace equation, comparing calculated growth rates with electron microscope data
06 p0903 A71-17344

Macroscale atmospheric vorticity model, using nonlinear system hydrodynamic and addends free motion equations
06 p0923 A71-17513

Geomagnetic field modeling facility based on nine-dipole model parameters
07 p1100 A71-19406

Three-phase time-ordered functional organization for ground based collision avoidance, discussing information flow, display capability and dynamic simulation model
[AIAA PAPER 71-240] 07 p1155 A71-19716

Alternate reduced order particle dynamics model in aircraft mission analysis featuring instantaneously variable speed by time scale separation
07 p1019 A71-19913

Space shuttle vibrational characteristics, investigating dynamic models, aeroelasticity, reentry, wing stall flutter and buffet boundaries
07 p1209 A71-20229

Linearized Boltzmann equation analytic solutions for rarefied gas dynamic problems, using ellipsoid model
07 p1093 A71-20285

Two dimensional adaptive pattern-recognizing model of human operator in visual-manual compensatory tracking task
07 p1053 A71-20406

Model and glass tank furnaces for earth upper mantle convection movements simulation, studying fluid dynamics and geodynamic processes
07 p1105 A71-20449

Discrete structure continuous medium model with internal degrees of freedom, studying physicomechanical properties in elastic materials
07 p1217 A71-20455

Wall attachment jet control volume model, examining flow momentum with restrictive force
07 p1031 A71-20609

Carbon fibers structural features, confirming model of slowly undulating ribbons of sp 2 carbons as basic structural elements by high resolution dark field micrographs
[PLASTICS INST. PAPER 9] 08 p1319 A71-20895

Globular cluster star velocities distribution, examining dynamic evolution models and gravitational effects
08 p1362 A71-21153

Centrifugal compressor vaneless diffuser, estimating energy losses with hydrodynamic model
08 p1348 A71-21266

Aircraft collision avoidance dynamical system, determining barriers between possible capture regions by optimal control problem solution
08 p1331 A71-21322

Bubble raft model for atomic configurations in ordered grain boundary and grain boundary dislocation at high temperatures, discussing Al-Mg alloys
08 p1345 A71-21575

Earth and sun magnetic field production models as function of dynamo states, discussing solar field effects on terrestrial space environment
09 p1517 A71-22334

Machine tool friction slides dynamics simulation for phase diagrams analysis, using Szoke model
10 p1614 A71-23994

Laboratory simulation of solid primordial condensation from low density partially excited gas for solar system origin
10 p1673 A71-24413

Research and development project funds allocation, developing mathematical dynamic modeling method for cost management
10 p1699 A71-24539

Hydrodynamic model for heating of pulsed laser produced plasma generated at plane solid target, deriving electron temperature and ion expansion energy
10 p1621 A71-24673

Physical model describing mechanism of recording through surface corrugation of thermoplastic viscofluid layer by electron beam
10 p1613 A71-24873

Anisotropic homogeneous two-point double-velocity correlation tensor model for turbulent flow field, deriving relation between micro and macro scale
11 p1748 A71-25153

Inviscid model for flow field within plumes of two-dimensional underexpanded jets calculated by time dependent finite difference method
11 p1853 A71-25160

Thermal louver models in space simulation chambers, determining heat dissipation, optical efficiencies, blade geometry and solar radiation effects
11 p1854 A71-25191

Large space structures zero backlash deployment mechanism, discussing dynamically scaled model for mechanical and structural design and dynamic analysis
[AIAA PAPER 71-400] 11 p1836 A71-25276

Multilayered spherical model induced fields and static bending patterns, approximating primate cranial structure EM plane wave irradiation
11 p1717 A71-25287

Elastic-plastic fracture behavior engineering model based on surface flaw severity by crack length dimensions measurements
[AIAA PAPER 71-371] 11 p1845 A71-25345

- Dust devil vortex model, considering boundary layer velocity profiles and thickness and integrated radial and vertical mass flows
11 p1794 A71-25470
- Turbulent vortex rings motion empirical model, deriving equations valid at large distances from discharging orifice
11 p1751 A71-25498
- Iodine photodissociation laser kinetic model for pumping, radiative and collisional processes, predicting reactant pressure and flashlamp parameters
11 p1773 A71-25795
- Single boundary layer flame sheet model for continuous diffusion chemical lasers, obtaining integrated zero power gain, laser power and efficiency
[AIAA PAPER 71-28] 11 p1774 A71-25928
- Gas turbine engine combustor stability dynamic model, representing premixing and combustion chambers as Helmholtz resonators for stability criteria derivation
[ASME PAPER 71-GT-73] 11 p1813 A71-25987
- Gas dynamics models for plasma production by irradiating solids with laser beams, taking into account spatial inhomogeneity of absorption process
11 p1775 A71-26090
- Viscous model for stress wave propagation perpendicular to plates of bilaminate composite material
11 p1851 A71-26381
- General dislocation model for high temperature creep of pure metals, discussing strain rate effects
11 p1782 A71-26476
- Stress cycling effect on creep deformation rate, using recovery creep model
[ASME PAPER 71-MET-F] 12 p1977 A71-27315
- Nonisothermal plasticity and creep models, stressing real materials deformation micromechanism theories
12 p1979 A71-27354
- Kalman filtering for complex systems, deriving algorithms for dynamic modeling and bias errors effects in discrete-time state optimum estimation
12 p1893 A71-27435
- Rigid plastic media dynamic model, showing yielding time delay effect on residual deflection as function of load duration
12 p1982 A71-27515
- Hereditary elastic body model with various tensile and compressive strengths, using elasticity theory with differing moduli
12 p1982 A71-27518
- Hipp pendulum controller electromechanical clock, considering dry and viscous friction dynamic models
12 p1932 A71-27525
- Flow field model for steady asymmetric vortex system shed from slender body of revolution in coning motion
[AIAA PAPER 70-52] 12 p1865 A71-27552
- Stability of first order gain model reference adaptive control system with sinusoidal input
12 p1973 A71-27580
- Forced dynamic regimes of machines and mechanisms, evaluating role of second order acceleration
13 p2099 A71-27806
- Mathematical and mechanical models of human thermal system thermodynamic/transport processes and external regulation devices for single elements and entire body
13 p2023 A71-29400
- Hodograph models family for cross flow velocity component of three dimensional turbulent boundary layers, applying integral method to curved rectangular channels data
[ASME PAPER 71-FE-1] 13 p2051 A71-29445
- Space charge delay angle, RF induced current and mode instability interrelated for actual high power heavy duty magnetrons, using electron bunch model
14 p2211 A71-29831
- Human body attitude control in space, using ten body complex geometry system, noting astronaut training jig
14 p2188 A71-29832
- Spherical stellar system dynamical evolution model, applying constant point mass technique
14 p2314 A71-30640
- Analytical model of compressor sensitivity to transient and distorted transient flows, considering inlet duct, compressor stages and combustor up to turbine nozzles
[AIAA PAPER 71-670] 14 p2291 A71-30734
- Analytical model for performance and pollutant emissions of gas turbine combustors, predicting gas composition and temperature
[AIAA PAPER 71-711] 14 p2294 A71-30765
- Nitric oxide formation analytical model for gas turbine combustion chamber, considering influence of primary zone equivalence ratio, combustor residence time and initial fuel droplet size
[AIAA PAPER 71-715] 14 p2191 A71-30767
- Book on dynamic probabilistic systems, Volume 1, covering Markov models, linear processes, systems analysis, statistics, recurrent events, population models, time variations, etc
15 p2440 A71-31196
- Metals dynamic fracture model, discussing critical incubation time and temperature dependence
15 p2503 A71-31446
- Room with windows and open doors under sonic boom, determining cavity resonance model for impulsive loading conditions
15 p2450 A71-32514
- Physical model of Zn diffused GaAs electroluminescent diodes gradual degradation, establishing formation of new recombination centers through injected carrier lifetime measurement
15 p2377 A71-32607
- Man machine system dynamic properties and biomechanical model concepts, determining random vibration effects on sitting and working human body
15 p2366 A71-32728
- Free flight static and dynamic stability tests on lightweight cone shaped models in longshot tunnel at hypersonic speeds, using spark recording
16 p2519 A71-32879
- Hybrid computer use for dynamic system probabilistic modeling, determining hydraulic actuator output statistics
16 p2549 A71-33295
- Fatigue crack propagation model for explosion bonded titanium-steel system under constant load amplitude conditions
16 p2600 A71-34096
- Stress analysis through physical modeling, discussing transducing techniques and fabrication-loading analysis
17 p2819 A71-34533
- Linear time-invariant dynamic feedback system suboptimal control by lower order generalized aggregated model for reducing computational complexity
17 p2719 A71-34740
- Monograph on parametric errors estimation for dynamic models of linear time invariant control systems
17 p2720 A71-34793
- Eddy viscosity model for turbulent pipe flow, yielding velocity distribution, shear, energy production and viscous dissipation rate
17 p2728 A71-34881
- Torsion problem of inhomogeneous anisotropic viscoelastic rod transformation, using area variation coefficient for modeling
17 p2828 A71-35240
- Combined brittle and plastic elements model for strain analysis of nonelastic deformed solid
17 p2832 A71-35457
- Rarefied gas dynamic models with velocity dependent collision frequencies, investigating linearized Boltzmann equations
17 p2729 A71-35573
- Kinetic models for gas-surface interactions, considering distribution functions of molecules at solid wall
18 p2874 A71-35900
- Energy momentum stress tensors for harmonic oscillator model, calculating energetic interaction with plane gravitational wave of same frequency
18 p2946 A71-35982
- Nondeveloping synoptic weather systems description by isentropic structural analysis, studying particle motion and dynamic behavior using models
18 p2944 A71-36219
- High temperature gas dynamics, including hypersonic wind tunnel nozzles, air-breathing/chemical rocket propulsion systems, thermodynamic models and relaxation boundary layers
18 p2846 A71-36425
- Geodetic satellite data utilization for test range specific point positioning, control densification, earth gravitational model determination and tracking station locations
18 p2913 A71-36492
- Activation impulse blocking in nerve, using inhomogeneous Lillie electrochemical model
19 p3006 A71-37282
- Force equations for static and dynamic friction under external forced vibration, determining mean values from mechanical model
19 p3068 A71-37346
- Geomagnetic field modeling facility based on nine-dipole model parameters
19 p3053 A71-37830
- Photographic study of acceleration and pressure effects on Al agglomerates and combustion processes on solid propellant surface, describing pit growth by combustion model
19 p3120 A71-38121
- Stable earth core geomagnetic dynamo model consisting of disk oscillating about symmetry axis with coil connected to brushes on axle and at disk edge
19 p3061 A71-38676
- Pulmonary nitrogen washout and carbon monoxide uptake, developing dynamic mathematical models for volume and distensibility distributions in airways and alveoli
20 p3193 A71-39441
- Lumped parameter simulation model for flexible turbine rotor dynamics in nonspinning coordinate system, discussing bearing constraints modeling methods and eigenanalysis applicability
[ASME PAPER 71-VIBR-71] 21 p3385 A71-40309
- Optimal trajectories and controls for dynamic systems modeled by coupled rigid bodies, applying to synthesis of robots and all-terrain vehicles
[ASME PAPER 71-VIBR-82] 21 p3414 A71-40318
- Nonlinear flight dynamic simulation using wind tunnel and aircraft model as analog function generator and computer for motion equation processing and command orientation
21 p3363 A71-40392
- Fog formation and dispersal by velocity field induced by helicopter trailing vortices, presenting dynamic model with droplet depletion, evaporation and condensation
21 p3321 A71-40510
- Porous Cu and W shock loading properties, discussing principal Hugoniot data for P alpha dynamic response model
21 p3466 A71-40796
- Physical model for electric current carrying shock discontinuity driven through nonconducting gas by Lorentz force, investigating uniqueness and stability
22 p3581 A71-41889
- Dynamic formation and structure of plasma focus, using two dimensional numerical fluid model
22 p3581 A71-41892
- Dynamic analysis of ATS 5 heat pipe fluid energy dissipation, confirming estimated stability of planned rescue approach configuration
22 p3611 A71-42038
- Dynamic model for Saturn rings radial structure, considering outside composition material, Titan perturbation effect and particle space density
22 p3603 A71-42186
- Linear dynamic system sensitivity models simplification conditions application to adaptive nonsearching system synthesis algorithms
22 p3527 A71-42857
- Orbital spacecraft trajectory and attitude dynamics, using computerized state model for mission planning, orbit determination, satellite geodesy and reentry analysis
[AAS PAPER 71-344] 23 p3727 A71-43017
- Crack model with strain rate dependent yield stress, calculating stress intensity factor variation with fracture propagation velocity
23 p3774 A71-43145
- Man machine system dynamic properties and biomechanical model concepts, determining random vibration effects on sitting and working human body
23 p3639 A71-43299
- Reproduction accuracy of holographic model, discussing coordinates origin and X-Y-Z errors
23 p3675 A71-43303
- Underthrusting mechanism during southwest Japan earthquakes, presenting model of convergent plate interactions
23 p3672 A71-43885
- Dynamic model for microinhomogeneous elastoplastic medium under cyclic loads with varying amplitude
23 p3779 A71-44203
- Dynamic active element model of electroluminescent image converter with positive optical feedback, using voltage-brightness approximation
24 p3808 A71-44389
- Dynamic system optimal weighting function determination, using variational methods for statistical criteria
24 p3813 A71-44677
- Galactic stochastic magnetic field lines, deriving dynamic equation for probability density function
24 p3871 A71-44902

DYNAMIC PRESSURE

- Accelerometers and dynamic pressure transducers calibration, using laser interferometer system
01 p0082 A71-10862
- Temperature compensated semiconductor transducers for dynamic pressure measurements, using Si Zener diodes
01 p0057 A71-11289
- Dynamic pressure reduction method errors in vacuum gages calibration
05 p0754 A71-16949
- Cylindrical reinforced shells carrying capacity under dynamic external pressure
06 p0982 A71-17354
- Cylindrical shell stability under critical dynamic radial pressure, discussing geometrical and mechanical parameters and loading law
06 p0997 A71-17847
- Rotary inertia effect on critical dynamic pressure parameters and supersonic flutter of in-plane loaded sandwich plates
07 p1213 A71-19887
- Large model fluid proportional amplifier, investigating optimum static and dynamic pressure gain by methodological and transmission line approach
07 p1025 A71-20558
- Real time remote test site computation and display of complex engine inlet distortion parameters from dynamic pressure signal, using analog computer
09 p1446 A71-22726

Dynamic pressure primary standard in terms of mass, time, length and temperature, describing phenomenon selection, error analysis and physical and mathematical models

09 p1448 A71-22769

Solar wind static and dynamic pressures on earth magnetosphere, using geomagnetic parameters

09 p1514 A71-23152

Plane normal shock wave reflection in relaxing gas for shock tube endwall upstream and downstream dynamic pressures, using method of characteristics

09 p1546 A71-23166

Cold cathode ionization gages dynamic pressure response as function of gas pulse mean speed and gas type, using magnetron test measurements

10 p1610 A71-24182

Continuously stratified fluid flow into contraction, assuming constant upstream dynamic pressure and density gradient / Long model/

17 p2726 A71-34661

Nonlinear motion of asymmetric rolling reentry vehicle with variable roll rate, dynamic pressure and stability derivatives

[AIAA PAPER 71-932]

19 p3148 A71-37177

Dynamic pressure measurement method and apparatus for anode center of heavy current electric arcs in plasmas, applying to plasma welding arcs

20 p3274 A71-39047

Hydraulic resistance and heat transfer in annular channel with rotating flow, comparing to axial flow

24 p3888 A71-44747

DYNAMIC PROGRAMMING

Book on optimal control theory covering dynamic programming, calculus of variations, Pontryagin maximum principle and iterative techniques

02 p0236 A71-12773

Dynamic programming and Bayes algorithm for self organizing and self adjusting Markovian systems

03 p0389 A71-13515

Optimal controller analytical design procedures using dynamic programming and Liapunov function

03 p0392 A71-14404

Optimal on-off control systems with structural constraints, discussing synthesis by dynamic programming and phase plane methods

03 p0392 A71-14408

Continuous time stochastic optimal control systems necessary and sufficient dynamic programming conditions for optimality

04 p0562 A71-15871

Elastic plates and members deformation with constraints on deflections, determining strain state with dynamic programming

06 p0984 A71-17651

System with aftereffect along programmed trajectory, studying controlled motion stability and accuracy

07 p1161 A71-20269

Atmospheric reentry trajectories optimization by differential dynamic programming

08 p1363 A71-21347

Integrated dynamic digital computer elements, examining regenerative information storage, internal duration determination by clock pulse frequency and switching

09 p1411 A71-22494

Book on mathematical theory nonlinear control processes covering dynamic programming, calculus of variations, etc

09 p1486 A71-23724

Optimal stochastic orbit transfer strategy solution by dynamic programming algorithm

10 p1678 A71-24844

Dynamic programming for designing beams and plates under steady creep with minimum weight, discussing cantilever beam optimization

11 p1853 A71-26564

Stochastic discrete time control systems optimization by dynamic programming

13 p2095 A71-28812

Book on dynamic probabilistic systems, Volume 2, covering semi-Markov and decision processes

15 p2440 A71-31197

Suboptimization of closed loop adaptive systems by simple dual control method, using dynamic programming

16 p2549 A71-33353

High order optimality conditions of singular controls, considering Pontryagin maximum principle, Bellman dynamic programming and functional analysis

16 p2550 A71-33701

Accelerated procedures for Markov chain model optimal control problems solution with computation time advantage over usual dynamic programming

17 p2719 A71-34737

Linear system optimal stochastic control and observation strategies simultaneous determination with quadratic cost by dynamic programming

17 p2719 A71-34742

Dynamic programming to design beams and plates under steady creep with minimum weight, applying to cantilever beam

17 p2832 A71-35505

Optimal design for system reliability and maintainability, using dynamic programming model

21 p3407 A71-40363

Optimal numerical solutions of linear control systems with quadratic integral form, using dynamic programming, successive optimization and algorithm-aided dynamic programming

21 p3360 A71-40617

Book on dynamic programming application to optimal control covering discrete random processes, continuous deterministic and stochastic processes, etc

22 p3567 A71-42428

Nonlinear discrete system optimal feedback controller synthesis for low sensitivity to parameter variations by difference equations quasilinearization and dynamic programming

23 p3656 A71-43855

Stochastic optimal control theory application to air-plane rescheduling model, obtaining dynamic programming algorithm for optimal landing and takeoff rules

23 p3702 A71-44104

Nonlinear and multivariate optimal sampled data control systems design with bounded control and state variables, using dynamic programming and divisional technique

24 p3812 A71-44452

DYNAMIC RESPONSE

U DYNAMIC CHARACTERISTICS

DYNAMIC RESPONSE

NT TRANSIENT RESPONSE

Piezoelectric transducer voltage-displacement response characteristics under connection with interferometric device, considering linearity and repeatability

01 p0079 A71-10311

Aircraft response to atmospheric gust, discussing spectral analysis procedures and calculation results on T-tail aircraft design

01 p0005 A71-10752

Machine for measuring inertial and structural responses to shock in single degree of freedom and more complex systems having dominant resonant frequency

01 p0068 A71-11548

Hybrid computer structural response simulation for helicopter fuselage, using matrix displacement method

02 p0227 A71-11790

Closed cylindrical shell response to random sound in contained fluid, investigating cylinder end acoustic boundary conditions with coupled oscillator theory

02 p0239 A71-11998

Human operator adaptive response characteristics to step changes in compensatory tracking system dynamics

02 p0207 A71-12349

Servoamplifier dynamic response effects on dynamic characteristics of fluid-filled pendulous accelerometers

02 p0252 A71-12455

Gyro dynamic errors in strapdown inertial guidance system due to body rate

02 p0279 A71-12457

Covering plate steady state response to acoustic vibrations in viscoelastic half space, calculating interface displacement frequency spectra under zero shear stress assumption

03 p0459 A71-13719

Periodic beam structure vibration response, using formulation for flexural wave propagation groups

[ASME PAPER 70-WA/DE-3]

Structural vibration response to nonhomogeneous random pressure fields based on homogeneous field theory

[ASME PAPER 70-WA/DE-11]

Rotor and rotor-disk system response to constant and pulsating torque, experimentally examining critical whirling speed and lateral vibration

[ASME PAPER 70-WA/DE-14]

Dynamic response of hydraulic hoses, considering tests with closed loop electrohydraulic position servo

03 p0356 A71-14443

Dynamic response of linear systems with parameters subjected to step perturbations, obtaining quasi-linear mathematical model describing parameter-perturbation transmission path

03 p0394 A71-14483

Biomechanical systems dynamic response - ASME Conference, New York, November-December 1970

04 p0542 A71-14785

Semicircular canal ducts dynamic response characteristics, using suspended liquid filled inner tube for endolymph simulation

04 p0542 A71-14789

Circular arches static equilibrium path and dynamic response due to concentrated static and step loading using energy approach

04 p0668 A71-15184

Dynamic response with feedback characterization of human musculoskeletal frameworks by linegraph-flow graph procedure

05 p0713 A71-16485

Dynamic thermoelastic response of rapidly heated plate elements, developing variational principle

05 p0824 A71-16560

Automatic control systems with parametric invariance, describing method for quick response increase

05 p0731 A71-16797

Linear dynamic object output reaction prediction by Kalman method constructed model

06 p0879 A71-17673

HF dynamic elastic deformation observation and measurement, including photoelastic method for transient phenomena

06 p1003 A71-18422

Dynamic response of pressurized thin circular cylindrical shells under moving loads

[AIAA PAPER 71-175]

06 p1004 A71-18614

Monte Carlo technique for time domain response analysis of nonlinear structure in random pressure field with large deflection

[AIAA PAPER 71-213]

06 p1004 A71-18649

Crystalline materials plastic deformation and dynamic yield stress based on elastic shock wave damping

07 p1210 A71-19151

Ring structure with nonlinear stress-strain law and linear strain-displacement relationship, deriving dynamic response to impulse

07 p1213 A71-19904

AL particle size and filler volume optimization effects on epoxy composite dynamic response

07 p1139 A71-20136

Digital turbulence amplifiers, investigating dynamic switching response

07 p1024 A71-20552

Fastener group behavior under combination of direct shear and moment, obtaining load deformation response of individual connections

08 p1370 A71-21410

Three degree of freedom gas bearing for wind tunnel dynamic measurements, allowing models simultaneous spin, pitch and yaw motions

[AIAA PAPER 71-279]

08 p1275 A71-22004

Cylindrical shell dynamic response to random acoustic excitation within narrow frequency band of low modal density

09 p1534 A71-22082

Dynamic systems current state estimate, using Kalman filter with exponential aging

09 p1421 A71-22110

Dynamic response of beams to transverse impact, considering deflection curve

09 p1541 A71-23205

Dynamic respiratory and circulatory responses to hypoxia in anesthetized dogs, recording oxygen partial pressures, heart rate, blood pressure, blood flows, respiratory rate, etc

09 p1396 A71-23358

Two dimensional rigid wings, investigating response characteristics to gust loads

09 p1383 A71-23440

Perfectly plastic and viscoplastic materials relation between permanent deflection and response time in boundary value problems

10 p1684 A71-23931

Nonperiodic orbit behavior in highly perturbed dynamic systems, examining invariant curve evolution

10 p1669 A71-24178

Stationary and dynamic characteristics of integrators with dosage capacitor for analog frequency measurements, analyzing dynamic response at large modulation depth via analog computer simulation

10 p1589 A71-24502

Systems approximation by incontinuous orthogonal Harre functions, discussing dynamic properties and input signal synthesis with minimal errors in estimating parameters

10 p1587 A71-24741

Random response of stationary linear system to pulse noise in time with independent amplitudes

10 p1588 A71-24901

Structures dynamic loading and damage by sonic booms, discussing structural response prediction by boom pressure wave model

10 p1693 A71-25052

Closed cylindrical shell response to randomly time distributed broadband acoustic excitations, using statistical energy method to compute displacement and interior pressure

[AIAA PAPER 71-331]

Nonstationary random analysis of flight vehicle response to atmospheric turbulence, using Priestley evolutionary spectral method

[AIAA PAPER 71-341]

Dynamic response of rotationally symmetric open-ended thin shells of revolution under transient impulsive and thermal loadings, using FORTRAN 4 finite difference program

11 p1847 A71-25466

Direct impulse response method application to function optimization, using high speed hybrid computer

11 p1735 A71-25841

Liquid metal cooled, fast spectrum thermionic reactor experiment design based on Fast Reactor Core Test Facility use for dynamic and steady state characteristics determination

11 p1710 A71-25867

Twin spool turbojet engine dynamic response, discussing simulator predictions, digital computer control, nozzle area variations and operating trajectories

[ASME PAPER 71-GT-14]

11 p1812 A71-25960

All-beta Ti alloy Ti-V-Cr-Al, testing dynamic behavior of strain aging during stress relaxation period 11 p1780 A71-26026

Sailplanes tail load static derivation for instantaneous unchecked longitudinal maneuver, considering aperiodic response 11 p1708 A71-26486

Dynamic snapthrough of shallow circular cylindrical shell undergoing plane motion in response to nearly symmetric impulsive pressure 13 p2146 A71-27781

Aircraft with T tail configuration, examining dynamic response to lateral gusts 14 p2174 A71-29786

Discrete gust and power spectrum models of atmospheric turbulence, considering energy distribution effect on aircraft dynamic response 14 p2174 A71-29790

Nonlinear /mixed/ damping forces on forced vibration system response, developing recursion procedure for equation of motion coefficients 14 p2327 A71-30203

Damped gravity orientated satellite linearized analysis for vibrational response to large amplitude motion 14 p2320 A71-30307

Simply supported nearly circular cylindrical shell, calculating nonlinear damped dynamic response due to exponentially decaying radial pressure 14 p2330 A71-30688

High thrust throttleable monopropellant hydrazine catalytic reactors for planetary landing vehicles, considering engine designs, dynamic characteristics and response to commanded duty cycles [ALAA PAPER 71-705] 14 p2294 A71-30762

Stable plasma resonance behavior, calculating small signal and nonlinear responses for theory verification and diagnostic techniques 14 p2283 A71-30948

Recorder circuit quick response enhancement in Grey code pulse counter, realizing parallel decoding in binary digits at high speeds 15 p2374 A71-31294

Dynamic response and perforation of thin plates subjected to projectile impact, measuring plastic deformation, dynamic strain and displacement with high speed camera 15 p2503 A71-31422

Phase locked AFC system, calculating phase detector response effects on dynamic properties 15 p2370 A71-31592

Bridge-feedback amplifier constant-temperature hot-wire anemometer static and dynamic response determination 15 p2408 A71-31931

Constant speed vortex rate sensor, calculating angular momentum dissipation due to shear stresses and response to step signal input 15 p2352 A71-32064

Nonlinear coupled parametric response of crooked thin walled columns under harmonic longitudinal load 15 p2507 A71-32095

Structural dynamic responses as nonstationary narrow band random processes, establishing peak values distribution functions with frequency interpretation 15 p2510 A71-32515

Age hardenable Inconel X-750 superalloy mechanical response to tensile loads for identifying microstructural changes due to deformation 15 p2437 A71-32616

Near field dynamic response of semifinite elastic plate to lateral impact, comparing displacement field observations to numerical results 15 p2510 A71-32792

Circular plates finite amplitude response under pulse loading, presenting nonlinear equations finite difference solution 16 p2650 A71-33014

Structural vibration and dynamic response analysis, applying finite element motion equations 16 p2653 A71-33090

Unloading boundary in longitudinal elastic-plastic stress wave propagation, describing response in semifinite rods [ASME PAPER 71-APM-15] 16 p2655 A71-33212

Dynamic midsurface displacements of thin circular cylindrical shell under uniform membrane stress state and three dimensional surface loads [ASME PAPER 71-APM-12] 16 p2656 A71-33214

Dynamic cryptodeterministic linear systems with random initial state, calculating stochastic response by perturbation scheme 16 p2660 A71-34072

Slender elastic column dynamic buckling under constant compressive axial end displacement, considering damping effects 17 p2818 A71-34506

Steady wave propagation in laminated media, developing mechanical theory for composite response with hydrodynamic, thermodynamic and strength effects 17 p2823 A71-34808

Orthotropic laminated plates dynamic response to impulse loads, detailing flexural wave propagation 17 p2823 A71-34809

Cat pupillary system static and dynamic response determination under light and electrical stimulation, using TV pupillometer and on-line computer 17 p2691 A71-35044

Dynamic response as function of time of nonlinear nonautonomous second order control system to external disturbances, using moving phase plane method 17 p2721 A71-35135

Dynamic system impulse response model for goodness of fit and linearity hypothesis tests by computer simulation 17 p2722 A71-35181

Fast response anemometer for measuring atmospheric wind speeds and turbulence components 17 p2745 A71-35327

Dynamic response of oddly stiffened circular cylindrical shells, using modified variational method 18 p2980 A71-36495

Aircraft random heave-pitch response to taxiing on rough runways, analyzing dynamic loads and fatigue damage by power spectral techniques 18 p2850 A71-36675

Frequency domain approach for analysis of linear variable networks demonstrated by calculating system response to input 19 p3036 A71-37147

Nonlinear mechanical system stationary random forcing input and output response data, determining statistical linearization coefficients in Kazakov-Bootton method 19 p3037 A71-37347

Peak resonant response of thin rectangular plate with elastic edge restraint under concentrated load [ASME PAPER 71-VIBR-6] 21 p3456 A71-40269

Linear second order multidegree of freedom vibrational system with singular mass matrix, determining response to excitation [ASME PAPER 71-VIBR-10] 21 p3457 A71-40272

Beams with multiple constrained viscoelastic layer coatings, presenting damped vibrational response prediction for various materials, geometries, wavelengths and temperatures [ASME PAPER 71-VIBR-40] 21 p3459 A71-40290

Graphical display of digital computer simulated steady state unbalanced turborotor response for lumped and distributed parameter models, using GATRAN language [ASME PAPER 71-VIBR-42] 21 p3459 A71-40292

Gradient search procedures application for nonlinear system unknown parameters identification from system dynamic response observations [ASME PAPER 71-VIBR-50] 21 p3460 A71-40299

Single mass flexible rotor in elastic bearings mounted on damped flexible supports, analyzing dynamic unbalance response and transient motions [ASME PAPER 71-VIBR-72] 21 p3460 A71-40310

Axially coupled turborotors, calculating coupling characteristics, disk inertia and gyroscopic effects on dynamic response, by transfer matrix techniques [ASME PAPER 71-VIBR-108] 21 p3462 A71-40332

Small deformation dynamic response of vibrating isotropic linearly elastic spherical shell to radial and time dependent body force field 21 p3464 A71-40769

Porous Cu and W shock loading properties, discussing principal Hugoniot data for P alpha dynamic response model 21 p3466 A71-40796

Quasi-fluid mechanical formulation generation for ionized gases dispersive transport coefficients by linear dynamic response function technique 21 p3423 A71-40800

Dynamic response of elastic cylindrical shell-solid core composite under time dependent loading from Laplace transform 21 p3467 A71-40949

Axially loaded slender beam mass and deformation effect on constrained bending motion system stability and dynamic response 21 p3469 A71-41010

Circular cylindrical shell under longitudinal parametric load, obtaining nonstationary responses with deformation theory 21 p3471 A71-41029

Dynamic frequency and phase response of digital communications system of synchronized oscillators from time-incremental computer simulation 22 p3523 A71-42376

Computer operated RF automatic test system for HF radio receiver spurious response measurements, giving test results 22 p3514 A71-42389

Sampled data control systems with pulse frequency modulation and time lag element, determining error response 22 p3527 A71-42493

Coupled plate-cavity acoustic system response at LF and spatially uniform pressure, using plate finite elements and acoustic volume-displacement theory 22 p3617 A71-42540

Stepping electromotor in self commutation mode with local feedback, examining dynamics with phase plane method 23 p3655 A71-43293

Dynamic coupling response between convectively controlled burning process and nonsteady flow field with pressure, density and gas velocity periodic variations 23 p3782 A71-43593

Boundary value problems solution for reaction pressure to elastic base circular plate bending under uniformly distributed load 23 p3777 A71-43910

Minimal partial realizations of linear input/output map, discussing significance in regard to adaptive dynamics identification procedures 23 p3661 A71-44190

Dynamic response of thin walled structures natural frequency analyzed for formulating potential and kinetic energy for stiffness and mass matrices by minimization principle 24 p3878 A71-44555

Lifting rotors aerodynamic damping in forward flight, describing methods for blade response variance matrix computation 24 p3789 A71-44559

Nonhomogeneous plate under pulsating and uniformly distributed loads, considering dynamic elasticity problem 24 p3880 A71-44712

Validity proof of asymptotic methods in one dimensional dynamic systems described by hyperbolic and parabolic differential equations 24 p3844 A71-45063

DYNAMIC STABILITY

NT AERODYNAMIC STABILITY

NT AIRCRAFT STABILITY

NT ATTITUDE STABILITY

NT BOUNDARY LAYER STABILITY

NT COMBUSTION STABILITY

NT CONTROL STABILITY

NT DIRECTIONAL STABILITY

NT FLAME STABILITY

NT FLOW STABILITY

NT FREQUENCY STABILITY

NT GYROSCOPIC STABILITY

NT HOVERING STABILITY

NT LATERAL STABILITY

NT LONGITUDINAL STABILITY

NT LOW SPEED STABILITY

NT MAGNETOHYDRODYNAMIC STABILITY

NT MOTION STABILITY

NT ROTARY STABILITY

NT SPACECRAFT STABILITY

Object constant speed motion in terrestrial orthodromy, examining Shuler vertical small oscillations stability 01 p0125 A71-10628

Dissipative mechanical filter for rocket self excited vibrations to eliminate oscillatory instability, describing transfer function and modal characteristics 01 p0164 A71-11021

Elastic shell filled with ideal fluid, analyzing dynamic stability under periodic impulses 01 p0176 A71-11049

Shock wave front propagation instability in decreasing density medium, applying to stellar structure 02 p0241 A71-12510

Edge jet Hovercraft dynamic stability in heaving motion, deriving two dimensional mathematical model [ASME PAPER 70-APM-QQQ] 03 p0348 A71-13712

Synchronous digital communication system with each station clock rate established by phase locked oscillator input average, calculating two-station network dynamic stability 05 p0729 A71-17051

Dynamic plasma stabilization, discussing closed and open loop approaches 06 p0933 A71-17472

Dynamic stabilization of drift dissipative instability by inhomogeneous RF electric field parallel to magnetic field 06 p0934 A71-17475

Dynamic stabilization of high-beta plasmas with sharp boundary, illustrating model effect on stability by numerical calculation 06 p0934 A71-17478

MHD dynamic stabilization, deriving stability conditions from periodic solutions of time dependent equations in Eulerian form 06 p0934 A71-17479

Dynamic stability of cylindrical shell with freely supported edges partly filled with ideal compressible fluid and undergoing steady longitudinal vibrations 06 p0997 A71-17846

Dynamic damping coefficient extracted from flight test lateral rate data telemetering ablative reentry vehicle [ALAA PAPER 71-49] 06 p0980 A71-18510

Elastic, inertial and aerodynamic forces aeroelastic triangle, examining lift changes due to aircraft structure deformation, dynamic flight stability and space shuttle development problems 07 p1215 A71-20063

Dynamic system stability criterion under constantly acting perturbations over finite time interval 07 p1161 A71-20267

Dynamic stability of cantilever under pulsating scanning load

07 p1218 A71-20474

Variational principle application to stability in failure mechanics of arbitrary linearly elastic bodies, discussing inertia effect on steady state vibrations of cracked bodies

08 p1372 A71-21704

Wind tunnel dynamic stability testing of unconventional aircraft configurations without sting support [AIAA PAPER 71-276]

08 p1274 A71-22001

Dynamic instability of finned missiles occurring as angle of attack undamping and caused by differential lift from windward and leeward fins [AIAA PAPER 70-206]

09 p1530 A71-22075

Transferred electron bulk negative differential conductivity devices, analyzing combined doping and geometry effects on space charge and domain dynamics

09 p1507 A71-22250

Book on stability theory of dynamical systems covering invariant sets and trajectories, limit sets, minimal sets, Liapunov functions, asymptotic stability of closed sets, etc

09 p1492 A71-22347

Coupled control of space vehicle orientation with reference to three celestial bodies, reducing plane vibrations to dynamic third order system

09 p1491 A71-22547

Surface geometry effect of polycentric gas bearing on rotor stability in dynamic equilibrium without radial load

09 p1454 A71-22799

Dense /relativistic/ stars structural stability with respect to centrally symmetrical perturbations

09 p1523 A71-23019

Thin spherical shell under uniform normal pressure using dynamic stability criterion and energy method for asymptotic nonlinear shell equations

10 p1685 A71-23937

Stability conditions of three body problem constant libration solutions by Routh, presenting geometrical interpretation for locus of mass centers

10 p1679 A71-24932

Linearly elastic cylindrical shells dynamic stability under combined axial and radial stochastic excitations, using Liapunov analysis [AIAA PAPER 71-333]

11 p1842 A71-25312

Aerodynamic characteristics of slender body of revolution traveling in long tube with circular cross section, deriving static and dynamic stability derivatives formulas

11 p1702 A71-25477

Dynamic systems with singular trajectories, analyzing orbital stability in locally compact space

11 p1799 A71-26157

Drift waves dynamic stabilization in collisionless plasma, considering AC electric field effects on low frequency instabilities

12 p1935 A71-26914

Gimbal suspended gyroscope in elastically damped frame with dynamically unbalanced rotor, noting oscillations and drifts

13 p2065 A71-27945

Blue edge of RR Lyrae instability strip, examining convection, radiation and surface boundary conditions effects

13 p2133 A71-27969

Metallic materials static to dynamic transition in creep noting temperature and purity effects

13 p2084 A71-28110

Support conditions influence on dynamic stability of hinged elastic rod

13 p2151 A71-28143

Necessary and sufficient global stability criteria for axisymmetric perturbations of stellar dynamic disk models of galaxies

13 p2138 A71-28775

Propulsion, guidance and stability of ground effect vehicle with perimetric Coanda fluid boundary

13 p1997 A71-29308

Dynamic stabilization of plasma column drift dissipative instability by inhomogeneous RF electric field, using two fluid macroscopic equations

14 p2196 A71-30560

High rotor advance ratio from multiblade general coordinates method in linear analysis of lifting rotor dynamic stability and gust ratio [AHS PREPRINT 512]

14 p2178 A71-31083

Globular star clusters and spherical galaxies stability, proposing rotating gravitating masses spherically symmetrical system model

15 p2482 A71-31331

Bounded-input bounded-output stability of systems with multiplicative nonlinearity, presenting sufficient conditions in frequency domain

15 p2381 A71-31939

Nonlinear system design based on generalized Popov stability criterion

15 p2381 A71-31940

Elastic structure dynamic stability problem, determining optimum inequality relating energy functional to displacement, and considering beam column with various boundary conditions

15 p2506 A71-32015

Spherical caps under step pressure loading, noting elastic damping effects on dynamic stability

15 p2506 A71-32093

Gas dynamic elastically mounted bearing, describing stability analysis of unloaded rotor central equilibrium position

15 p2417 A71-32457

Hydrodynamic instability generation by stable layer tilting at high altitude, considering clear air turbulence

15 p2445 A71-32712

Static stability criterion dynamic extension for nonlinear continua under conservative loads, using Liapunov functions

16 p2607 A71-32980

Stability conditions approximation for assessment of single parameters effect and in making choices

16 p2607 A71-33003

Dynamic stability of controlled spacecraft with liquid propellant rocket engines, considering acceleration and braking sections of trajectory

16 p2646 A71-33656

Component assembly effect on dynamic stability of liquid propellant rocket engine spacecraft during thrust sections of trajectory

16 p2646 A71-33657

Thin elastic shallow cylindrical panel in steady conducting supersonic gas flow, detailing magnetic field effects on static and dynamic stability and flutter

17 p2816 A71-34326

Nonlinear elastic incompressible bodies with small deformations, obtaining three dimensional static and dynamic stability variational equation

17 p2816 A71-34328

Multiple mass rheonomic vibrational systems dynamic stability, presenting approximate solution and critical dissipation level for damping parametric resonances

17 p2777 A71-34346

Periodic surface concept application to restricted three body problem of dynamical systems through averaging method, presenting stability theorem

17 p2804 A71-34918

Nonlinear automatic control systems stability during large modulus-limited deviations based on method of sections and direct Liapunov method

17 p2783 A71-35131

Soviet book on self adjusting systems dynamics with frequency stabilization characteristics, covering linearized motion equations, narrow band processes, etc

17 p2722 A71-35175

Dynamic stabilization of undamped gyrosystems with elastically pliable structural elements by inertial damper mounted on gimbal suspension

17 p2746 A71-35602

High resolution 16mm pulse mode cine reconnaissance camera design features, discussing dynamic balance and reaction forces cancellation

17 p2746 A71-35761

Dynamic positioning stationkeeping and stability criteria for formation flight systems extended to helicopter and V/STOL transports

18 p2849 A71-35923

Type II supernovae observations and models, considering photographic light curves and dynamic instabilities in star development, outbursts and ejected matter composition and amounts

18 p2961 A71-35976

Cantilever column critical dynamic instability load under nonconservative follower force including thermomechanical coupling effect from boundary value problem formulation [ASME PAPER 71-APM-L]

18 p2977 A71-36255

Simply supported Bernoulli-Euler beam resting on elastic foundation and carrying equally spaced moving mass particles, calculating lateral response dynamic stability by Galerkin method [ASME PAPER 71-APM-M]

18 p2978 A71-36256

Static and dynamic stability characteristics of X-15 aircraft, lifting body and trapezoidal and delta wing reentry body

18 p2971 A71-36434

Elastic beam dynamic buckling stability under transverse follower force, considering force direction dependence on cross sectional twist angle [DEVL-R-SONDDR-137]

18 p2980 A71-36679

Fuel slosh energy dissipation and dynamic stability of Intelsat 4, discussing spacecraft and tank selection [AIAA PAPER 71-954]

19 p3148 A71-37195

Longitudinal dynamic stability of space shuttle during atmospheric entry, noting magnetic storms effects

19 p3151 A71-37322

Finite radius rotating cylinder stability analysis, using equilibrium functions of distribution with trajectory integration method

19 p3134 A71-37512

Wave growth for distributed parameter dynamic system independent of time and coordinates, investigating stability with linear approximation

19 p3103 A71-37757

Neutron star models based on Nemeth-Sprung equation of state, discussing dynamic stability and Crab pulsar central density

19 p3143 A71-38161

Cyclic discrete holonomic mechanical systems Liapunov stability analysis, developing matrix formalism for kinetic energy, Routhian, Hamiltonian and dynamic potential energy quadratic approximation

21 p3454 A71-40097

Stability of rotating unsymmetrically mass distributed cantilever shaft with unsymmetrical rotor, determining unstable region boundaries by theoretical analysis and experiment [ASME PAPER 71-VIBR-58]

21 p3385 A71-40303

Lightweight free oscillating cone shaped model design for intermittent wind tunnel facilities, discussing dynamic stability derivatives measuring techniques

21 p3363 A71-40390

Liapunov-type analysis of linear systems dynamic stability under stochastic parametric excitation, noting application to rectangular flat plates

21 p3469 A71-41008

Solid propellant rocket motor stable operation region, describing propellant response function to pressure and velocity fluctuations [ONERA-TP-1016]

22 p3588 A71-41956

Dynamic stability analysis, ground testing and corrective accumulator devices for POGO oscillations in space booster structure

22 p3609 A71-41992

Structure and stability of rapidly uniformly rotating supermassive star, using post-Newtonian hydrodynamic equations and standard model

22 p3604 A71-42328

Globular star clusters and spherical galaxies stability, modeling as rotating gravitating masses in spherically symmetrical system

22 p3606 A71-42606

Dynamics of pipelines with nonstationary fluid flow, deriving equations for dynamic instability regions and for resonant vibration amplitudes

24 p3884 A71-45014

Unstable systems dynamic stabilization, deriving conditions from second order linear differential equations with variable coefficients

24 p3849 A71-45048

DYNAMIC STRUCTURAL ANALYSIS

Apollo integrated shell static and dynamic testing, describing data acquisition system techniques

01 p0067 A71-10863

Impulsively loaded rigid plastic continua deformation lower bounds calculation, considering beams and plates

01 p0173 A71-10943

Short beams vibrational analysis extended to stability analysis, using Timoshenko theory

01 p0174 A71-10966

Hybrid computer structural response simulation for helicopter fuselage, using matrix displacement method

02 p0227 A71-11790

Projectile impacts into laminated targets consisting of plastic layers backed by Al substrates using SHAPE code with hydrodynamic elastoplastic distortional model

03 p0504 A71-13431

Streak interferometry providing single impact test data for calculating dynamic stress-strain curve [SESA PAPER 1717]

03 p0509 A71-13777

Polish book on impact in discrete mechanical systems covering beams, curved rods, plates, nonlinear damping, numerical analysis, subjected to shock loading

03 p0513 A71-14297

Redundant structure dynamic analysis for forced and free vibrations, using finite element rank force method

05 p0829 A71-17120

Maximal deflection of square and rectangular thin plates with small initial concavities, using dynamic relaxation method for lateral and postbuckling in-plane edge loads

05 p0830 A71-17225

Elastic shell dynamics under initial and boundary conditions, developing variational principle algorithm

06 p0986 A71-17756

Structural behavior of rods and cylindrical shells under dynamic impact loads

06 p0989 A71-17783

Vibration and wave analysis in dynamic deformation of elastic shells and plates with environmental allowance

06 p1000 A71-17870

Critical dynamic snap-through of shallow clamped arches under concentrated loads, using finite difference method [AIAA PAPER 71-176]

06 p1004 A71-18615

Apollo lunar module structural integrity for lunar landing verified by Monte Carlo dynamic analysis

07 p1205 A71-18896

Resistive network computation in plate and shell dynamics, exemplifying skew plate under central concentrated load

08 p1370 A71-21303

Inertia effect in failure mechanics for steadily developing equilibrium cracks in dynamic system with time dependent periodically variable load

08 p1372 A71-21705

Space shuttle development test program, discussing low cost dynamic structural and flight testing [AIAA PAPER 71-308] 09 p1532 A71-23017

Optimal prestressing against buckling of structures with reserve capacity, using energy methods of structural analysis 10 p1689 A71-24514

Dynamic deformation of cylindrical shells by elastic body impact, using sequence boundary value solutions in plate theory 10 p1689 A71-24561

Variational principle for continua dynamic analysis by hybrid finite element method, considering consistent inertia properties of elements obtainable from assumed stress functions 10 p1692 A71-25047

Structural dynamics motion matrix Newmark generalized acceleration operator, Wilson averaging variant and Gurtin variational principle investigations for stability and approximation viscosity 10 p1693 A71-25050

Transform method application to structural dynamic analysis for engineering structure transient response to various vibration modes 11 p1841 A71-25150

Dynamic frequency characteristics of built-up structures by transient rapid sweep testing 11 p1841 A71-25178

Transient mean square response of simple structural systems to forcing function representing rocket engine noise, comparing with stationary mean square response for each launch stage [AIAA PAPER 71-348] 11 p1837 A71-25327

Structural materials dynamic analysis, considering viscous, hysteresis and viscoelastic damping [AIAA PAPER 71-349] 11 p1843 A71-25328

Nonlinear dynamic analysis of shells of revolution under symmetric and asymmetric loads, obtaining solutions for shallow cap buckling 11 p1847 A71-25465

Structural dynamics test simulation technology, discussing criteria, techniques, equipment, combined environments and relationship between testing and analysis 11 p1745 A71-26493

Cylindrical liquid filled shells under rapid axial compression along generatrix, examining dynamic deformation characteristics 13 p2156 A71-29072

Nonconservative dynamic instability of columns under distributed tangential force, using analog computer 13 p2158 A71-29430

Arbitrary periodic composite structure system with local interactions, obtaining macroscopic properties from unit cell boundary value problems 14 p2323 A71-29812

Hyperelastic continuous bodies with periodic structure, developing macroscopic model based on boundary value problem for unit cell 14 p2323 A71-29813

Symmetric and asymmetric dynamic buckling of shallow elastic arches under uniform loads, using nonlinear finite difference method 14 p2331 A71-30695

Convergent finite element equations for dynamic stability of plates dependent on vibration and buckling modes 14 p2331 A71-30696

Viscoplastic cylindrical shell dynamic buckling during axial impact of rigid mass, discussing constitutive equations 14 p2331 A71-30841

Extremum principle for structures in creep under cyclic loading for time dependent stable dissipative material 15 p2505 A71-31944

Structural vibration and dynamic response analysis, applying finite element motion equations 16 p2653 A71-33090

Dynamic vibration analysis of mechanical structures, considering transfer and stiffness matrix methods 16 p2653 A71-33091

Hydrodynamic and plate structural analysis by finite element method, discussing diffusion, oil films and element couplings 16 p2654 A71-33096

Arterioles and corneo-scleral shell structural response under various loading conditions, using finite element method for mechanical and hydrostatic stress distribution 16 p2528 A71-33099

Dynamic uncoupled thermoelasticity analysis using integration by Goodier method in five dimensional space 16 p2662 A71-33171

Structural changes and phases nucleation and growth in metal alloys during prolonged loading at high temperatures, examining steel strengthening precipitates coagulation kinetics 16 p2597 A71-33918

Propagating crack arrest capability of circular hole in plate, studying dynamic stress intensity and concentration factors changes [SESA PAPER 1827A] 17 p2820 A71-34546

Dynamic flexibility method based on Green resolvent, presenting applications to linear damped/undamped forced/free harmonic/periodic vibration 18 p2947 A71-36177

Total inelastic energy dissipation in structure of creeping plastic material under variable repeated loading and shakedown [ASME PAPER 71-APM-C] 18 p2977 A71-36252

Two dimensional dynamic thermal stresses in Al plate, allowing for Newtonian surface heat exchange 18 p2981 A71-36720

Simple structures large elastic-plastic transient deformations, using finite element method 19 p3157 A71-37874

Structural analysis trends, considering strain and force methods, flutter, dynamic response, atmospheric turbulence and random phenomena problems 20 p3308 A71-39400

Maximum yielding tensile stress envelope curves as function of structural load index based on compression tests of Al alloy stiffened plane panels 20 p3309 A71-39570

Broadband random vibration simulation of force environment action on multimode structure [ASME PAPER 71-VIBR-2] 21 p3362 A71-40266

Deflection equations and bending stress for forced vibration of beam with time dependent boundary condition [ASME PAPER 71-VIBR-32] 21 p3458 A71-40286

Complex structural systems response characteristics under steady state sinusoidal, transients and random loadings, developing hybrid elastodynamic equations 21 p3470 A71-41011

Dynamic photoelasticity for stress wave propagation in anisotropic fiber reinforced composites, using birefringent models and pulsed ruby laser beam 21 p3471 A71-41027

Asymptotic solution to dynamic buckling of thin slowly compressed eccentric elastic columns, using two time scheme 23 p3776 A71-43373

Nonlinear structural frame analysis by dynamic relaxation for use with computers 24 p3879 A71-44632

Unsteady random processes structural analysis application to nonlinear dynamic systems, evaluating algorithms effectiveness and improvement by self adaptive operators with finite memory 24 p3815 A71-44705

DYNAMIC TESTS

Elastic parameter dynamic measurements using resonance methods with electrostatic attraction 02 p0328 A71-12406

Dynamic fault detection, using mathematical condition between measurement taken, difference equation theoretical coefficients and bounds of each 03 p0449 A71-13092

Launching intermediate velocity thin plastic sheets for short duration pressure pulse studies of dynamic materials properties 03 p0427 A71-13916

Static and dynamic testing of fluidic elements as function of geometrical and operating parameters 03 p0355 A71-14296

Stiffened flat panel dynamic analysis, using finite element method 08 p1374 A71-22027

Discrete fluidic element dynamic tests, using magnified models with similarity criteria 09 p1386 A71-22653

All-beta Ti alloy Ti-V-Cr-Al, testing dynamic behavior of strain aging during stress relaxation period 11 p1780 A71-26026

Dynamic Test Chamber for sounding rocket or spacecraft functional testing in simulated flight environment 11 p1746 A71-26508

Gas dynamic test assemblies experiments for demonstrating theoretical basis of supersonic nozzle design with radial flow section 13 p1992 A71-29173

Dynamic testing - Conference, London, January 1971 14 p2251 A71-30053

Impedance testing techniques based on ratio of mechanical input force to velocity response for structures and systems behavior evaluation under dynamic loads 14 p2252 A71-30054

Diffusely reflecting in-plane surface displacement measurement by holographic interferometry, comparing static and dynamic methods for accuracy 15 p2403 A71-31265

Dynamic tear fracture toughness test and fracture mechanics parameter correlation for high strength Al alloys 20 p3248 A71-38771

Flexible rotor multiplane field balancing analysis, investigating test validity and accuracy and sensing instruments effects [ASME PAPER 71-VIBR-74] 21 p3460 A71-40312

DYNAMICS

Soviet book on continuous medium covering dynamic, thermodynamic and electrodynamic equations mechanic problems, three dimensional space, internal degrees of freedom, etc 04 p0626 A71-15373

Air lubricated mechanical oscillator dynamics and modes of operation as function of system parameters, using analog computer 05 p0758 A71-16352

Second order dynamic relay system with unstable linear part, investigating constant disturbance effects with point mapping and bifurcation theory 06 p0927 A71-17672

Celestial mechanics and nonlinear dynamics in Poisson series, discussing Echelon Series Processor for computer programming 13 p2034 A71-28355

Viscometric motions of continuous bodies, studying kinematics and dynamics of d'Alembert, homogeneous and circulation preserving groups 20 p3309 A71-39567

Three dimensional solution for statics and dynamics of homogeneous plates, laminates and orthotropic materials in series form, noting Mindlin analysis 21 p3456 A71-40262

DYNAMO THEORY

Solar activity cycles mechanism, deriving nonlinear equations from quasisymmetric magnetic dynamo models 02 p0307 A71-12081

Astrophysical bodies dynamo equations describing large scale magnetic fields generation by small scale cyclonic turbulence in rotating fluid body 02 p0314 A71-12588

Galactic magnetic field generation by dynamo process with nonuniform rotation and turbulence in gaseous disk 05 p0811 A71-16687

Galaxy gaseous disk as low mode dynamo, calculating turbulent diffusion coefficient for passive magnetic fields 05 p0811 A71-16688

Equatorial electric field generation by ionosphere dynamo region neutral wind meridional component 07 p1101 A71-19409

Geomagnetic field quiet solar diurnal variations, examining dynamo theory in lower ionosphere at middle latitudes 07 p1104 A71-20045

Solar activity cycles mechanism, deriving nonlinear equations from quasi-symmetric magnetic dynamo models 08 p1362 A71-21131

Solar flare EUV radiation and ionospheric currents dynamo region ground based detection by geomagnetic crochets time structure analysis 08 p1355 A71-21198

Dynamo theory for electric current variations in magnetosphere-ionosphere interactions, discussing electrostatic fields mapping and plasma particle drift motion production 08 p1279 A71-21213

Solar activity cycle model, considering dynamo equations with only radial rotation differentiability 08 p1365 A71-21774

Earth and sun magnetic field production models as function of dynamo states, discussing solar field effects on terrestrial space environment 09 p1517 A71-22334

Dynamo role in magnetospheric disturbances and ionospheric inhomogeneities, allowing for charged particle concentration height dependence 09 p1435 A71-22430

Diurnal variations of meridional winds by dynamo electric field in troposphere, comparing with Thomson scattering 09 p1490 A71-23646

Astrophysical objects magnetic field generation, examining behavior at large dynamo numbers 10 p1676 A71-24494

Terrestrial, solar and galactic magnetic fields, discussing generation by combined nonuniform rotation and cyclonic turbulence based on dynamo equation 12 p1961 A71-26859

Krause-Steenbeck solar dynamo eigenvalue evaluation assuming step function differential rotation and delta function alpha-effect for approximation 12 p1971 A71-27749

Oscillatory hydromagnetic dynamo model of large scale solar magnetic field of variable sign, using Bénard convective cell with Coriolis velocity disturbance 13 p2137 A71-28529

Galactic dynamo generated magnetic field periodic modes based on mathematical model involving cyclonic turbulence and nonuniform rotation of gaseous disk 14 p2303 A71-29591

Large scale kinematic dynamo theory for magnetic field generation in turbulent fluids based on Lorentz force helicity

14 p2314 A71-30646

Rapidly rotating early stars and quasars, determining magnetic field generation by turbulent dynamo mechanism

15 p2485 A71-31725

Solar activity cycle model, considering magnetic dynamo equations with radial rotation differentiability

15 p2495 A71-32679

Solar alpha effect dynamo effect model, determining nonaxisymmetric magnetic field generation

18 p2960 A71-35936

Kinematic dynamo theory application to infinite stationary media with large scale magnetic field components and isotropic turbulence

18 p2967 A71-37025

Kinematic-dynamo theory with turbulent diffusivity effect, discussing resistivity as random function of position

18 p2969 A71-37045

Kinematic-dynamo equations for stationary unsharpened conducting nonrotating sphere dynamo action in isotropic velocity turbulence

18 p2969 A71-37046

Equatorial electric field generation by ionosphere dynamo region neutral wind meridional component

19 p3053 A71-37833

Large scale alternating solar magnetic field generation by outer shell convective flow, constructing oscillator hydromagnetic dynamo model

19 p3145 A71-38353

Electrical conduction in orthogonal coordinates from nondipole nature of geomagnetic field on conductivity tensor of ionospheric dynamo region

19 p3057 A71-38381

Stable earth core geomagnetic dynamo model consisting of disk oscillating about symmetry axis with coil connected to brushes on axle and at disk edge

19 p3061 A71-38676

Milky Way galaxy internal small scale magnetic field generation, relating strength to cyclonic turbulence properties and large scale shear

20 p3287 A71-39055

Milky Way galaxy poloidal magnetic field generation with hydromagnetic dynamos, showing galactic cosmic rays as major driving force

20 p3287 A71-39056

Three dimensional atmospheric dynamo models in quasi-stationary and stationary approximation for ionospheric and magnetospheric electric fields and currents production during quiet conditions

20 p3217 A71-39512

Lunar and solar daily geomagnetic variation morphology correlation based on atmospheric dynamo model

20 p3217 A71-39515

Emf dynamo nonuniformities effect on magnetospheric field aligned electric currents associated with solar quiet geomagnetic variations, calculating ionospheric electrostatic fields

20 p3217 A71-39516

Diurnal variations of S_q currents in terms of electroconductivity model of ionosphere and geomagnetic field, using two dimensional dynamo theory

20 p3217 A71-39517

Atmospheric dynamo equations derivation based on Maxwell equations and Ohm law with anisotropic and asymmetric electric conductivity tensor for quiet geomagnetic variations explanation

20 p3217 A71-39518

Dynamo equations solution for electrostatic potential, discussing three dimensional model for ionospheric equatorial conditions and Northern-Southern Hemispheres coupling

20 p3218 A71-39519

Dynamo theory for ionospheric thin shell model, considering wind fields determination from diurnal geomagnetic variations

20 p3218 A71-39522

Regenerative kinematic-dynamo action under incompressible isotropic velocity turbulence, noting turbulent Lorentz force role

21 p3447 A71-40422

Kinematic dynamo equations for turbulent generation of large scale magnetic and small scale turbulent fields, presenting exact treatment of fluctuation and ordered field equations

21 p3416 A71-41194

Dynamo theory of solar and lunar magnetic fields diurnal variations, determining ionospheric wind velocities and pressure changes

23 p3669 A71-43174

Digital computer numerical procedure to solve dynamo theory MHD equations for earth nucleus, using combination of Fourier and finite difference methods for integration

24 p3823 A71-45038

DYNAMOMETERS

Dynamic hysteresis loop measurement of energy dissipation in materials, showing deformation effects on accuracy

15 p2508 A71-32233

DYNAMOS

U ROTATING GENERATORS

DYSPROSIUM

Dy-ion-doped calcium fluoride laser with monochromatic pumping, examining mode selection and coupling

08 p1303 A71-21791

E

E LAYERS

U E REGION

E REGION

NT SPORADIC E LAYER

Atomic and molecular collisions in gases, considering E and F regions processes, auroras and applications

01 p0129 A71-10133

E layer meteor ionization, considering ablation processes effects of meteoroids evaporation and micrometeorites sputtering

03 p0486 A71-13310

E layer atmospheric densities from decaying satellites observation, discussing solar activity and geomagnetic correlations

03 p0414 A71-14022

Electric field strength measurement at rocket surface in ionosphere by electrostatic fluxmeter, obtaining E and F region ion drift velocities

03 p0417 A71-14035

Solar soft X ray and extreme UV relative contribution to E layer ion production rates during solar eclipse of 12 November 1966

03 p0481 A71-14511

Ionospheric current system in polar E region, using earth surface equivalence model

04 p0584 A71-15547

Top side ionosphere electromagnetic probing techniques, noting F and E regions

05 p0740 A71-16428

Magnetic disturbances effect on drift behavior and anisotropy parameters of E and F region irregularities

05 p0740 A71-16433

Ionization in ionosphere E and upper D regions, considering solar short wave radiation, small components, atmospheric dynamics and vertical mass transport

06 p0894 A71-18251

E layer electron concentrations, effective recombination coefficient and ionization sources during solar eclipse, noting soft X radiation intensity

06 p0894 A71-18260

Ionization rate experimental profiles during maximum solar activity compared with calculations, showing additional source of ionization in E region

06 p0895 A71-18272

Vertical profile of electron collisions effective frequencies in auroral ionosphere E region

06 p0895 A71-18279

High latitude E region plasma irregularities based on wind velocity shear fields

07 p1153 A71-19760

Polar E region equivalent current system, determining height direction and width

08 p1279 A71-21209

Middle latitude night E region ionization, describing solar EM and corpuscular radiation absorption effects

08 p1286 A71-21853

Nighttime E layer behavior during geomagnetic storms in quiet sun years, investigating corpuscular flux effects

08 p1356 A71-21854

E layer near solar culmination relaxation, determining ion and electron concentration variations

08 p1286 A71-21855

E region ion composition nighttime variations, examining nitrogen monoxide and oxygen ion nonequilibrium concentrations by ionic-molecular reactions

09 p1435 A71-22438

E region additional ionization source during solar activity maximum, analyzing ion production function and electron concentration

09 p1435 A71-22440

E region electron concentration profiles, using ground sounding equipment allowing accurate signal reflection altitude measurements

09 p1435 A71-22441

E layer critical frequencies and sporadic E layer boundary frequencies interrelationship, assuming equal electron production rates

10 p1599 A71-23876

Maximum usable frequency to critical frequency ratio for whispering gallery propagation in HF and VHF E region

10 p1577 A71-24291

E and F region positive ion composition, electron concentration and thermal balance vertical profile, discussing ionizing radiation spectrum, plasma cooling, primary chemical reaction rates and ionospheric formation

10 p1573 A71-24550

D and E region electron density height distribution profiles, using multifrequency absorption data

10 p1606 A71-24920

Ionospheric drift mechanism in midlatitude F region, discussing ground level magnetic field, E region side effects, horizontal winds and polarization fields

11 p1753 A71-25550

Electron precipitation in nocturnal E region from radiowave and rocket data, calculating ionization rates and midlatitude morphology

11 p1815 A71-25552

Echo reflections and transition through critical coupling in D and E regions at low and medium frequencies, using nighttime electron density distributions

11 p1754 A71-25601

Neutral wind effects on redistribution of E region ionization and recombination, comparing electron density profiles to vertical ion drift velocities

11 p1755 A71-25613

Universal time effect on E region critical frequency at large solar zenith angles, considering ionization source at midlatitude range

11 p1757 A71-25785

Neutral winds produced vertical ion drift toward electric polarization in equatorial F region, discussing field discharge through E region and atmospheric superrotation effects

12 p1900 A71-26890

Equatorial E region cross field instability and ionization irregularities from Nike-Apache rocket measurements

12 p1900 A71-26934

E and F region irregularities random movements over Waltair, India, during IQSY, obtaining diurnal and seasonal variations

13 p2056 A71-27931

E layer phase height measurements with spaced receivers without ultra stable oscillators, calculating scale height

14 p2230 A71-29712

F 2 and E layers peak electron densities semiannual variations, suggesting association with solar activity and charged particles penetration

16 p2568 A71-33785

Midlatitude E region electron density profile data for various solar activity levels, investigating formation theory and atmospheric models

16 p2570 A71-33822

Lower E region drift data, noting wave-like nature of inhomogeneities

17 p2731 A71-34314

D and E regions advances during 1967-1971 covering ionic composition, electron density profile at various latitudes, hours and seasons during eclipses and winter anomalies

17 p2732 A71-34464

VHF wave transhorizonal propagation correlation with daytime E layers in temperate zone, noting height dependence and seasonal and diurnal variations

17 p2707 A71-35445

Magnetically conjugate range-time observations of E region radio aurora by pulsed VHF radar echoes

18 p2875 A71-35963

Dissipative plasma instability in lower E region investigation by alkali plasma clouds injection, observing irregular echo behavior by coherent pulse Doppler radar

19 p3110 A71-37365

Mass spectrometric measurements of negative ion concentration in D and lower E regions

19 p3127 A71-38031

Ionospheric E region nighttime model from rocket soundings, obtaining electron density profiles by Langmuir probe and wind measurements by glowing vapor release

19 p3055 A71-38036

Radio wave scattering from ionosphere, considering plasma experiments in E and F region

19 p3018 A71-38247

Nighttime E region ion composition and concentration profiles, using rocket sounding

19 p3061 A71-38628

Nighttime equatorial E region ionization and electron density gradient irregularities, noting cross field instability with rocket-borne Langmuir probes

20 p3225 A71-39727

Plasma transport processes role in E region from midlatitude nocturnal and auroral ionospheric models in terms of transport equations

20 p3232 A71-39893

Rocket-borne explosive charge initiated detonation wave effects on decimeter wavelength radio waves in lower E layer

20 p3199 A71-39894

E region electron density and critical frequency seasonal anomaly, allowing for sun zenith angle variations, sunspot activity and earth orbit eccentricity

21 p3371 A71-40034

Sun-earth distance and earth orbital eccentricity effect on E region peak electron density, discussing Chapman-like model

21 p3372 A71-40035

- Solar cycle effects on E region peak electron density, correlating sunspot number by regression analysis
21 p3372 A71-40036
- E region electron density isopleths height correlation with atmospheric pressure variations, noting sympathetic isobaric surface movements in upper stratosphere
21 p3372 A71-40038
- E region wind and temperature measurements from Nancy incoherent scatter experiments, observing prevailing semidiurnal oscillation with phase propagating downwards
21 p3372 A71-40041
- E region irregularities drift and anisotropy at Walair during IQSY, inferring trends of diurnal and seasonal variation
21 p3374 A71-40379
- Universal time effect on E region critical frequency at large solar zenith angles, considering ionization source at midlatitude range
22 p3532 A71-41553
- Solar flare induced E and F regions electron density enhancement observation by Thomson scatter, noting relationship to EUV ionizing radiation
23 p3721 A71-43173
- Steady nonlinear waves propagation along ring electron beam axis analogous to ionospheric E layer
23 p3711 A71-43412
- Small scale electrostatic field penetration from E into F region of ionosphere based on plane stratified model
23 p3671 A71-43577
- E layer vertical velocity fluctuations from scattered signal phase and amplitude correlation measurements, using perturbation technique
23 p3647 A71-44334
- Hysteresis effect at solar cycle maximum for midlatitude E layer electron density response to solar activity
24 p3824 A71-45125
- EAR**
NT COCHLEA
NT CORTI ORGAN
NT LABYRINTH
NT MASTOIDS
NT MIDDLE EAR
NT SEMICIRCULAR CANALS
NT VESTIBULES
Arterioles, arteriovenous anastomoses and efferent veins functional behavior in anesthetized white mice ears
01 p0007 A71-10035
- Auditory meatus sound pressure levels measurements in subjects with fabricated human earmolds with canal modifications, considering frequency responses and resonance
05 p0712 A71-16279
- Endolymph and perilymph fluid systems pathophysiology from induced and spontaneous disorders changes observed in inner ear
14 p2183 A71-30254
- Ear inherent channel capacity estimation by applying Shannon equations for binary signal transmission
20 p3191 A71-39769
- EAR PROTECTORS**
Flight helmet sound attenuation test, using Manikin method
01 p0026 A71-11189
- Jet fighter-bomber aircraft noise survey, discussing sound pressure levels and frequency analysis during ground running, speech interference levels and ear protectors requirements
12 p1875 A71-27629
- Earmuff hearing protectors evaluation for attenuation of narrow band noise on experienced subjects
14 p2188 A71-30196
- Gundefender earplug evaluation tests, using temporary threshold shift reduction and modified rhyme techniques for speech intelligibility measurement in noise
15 p2364 A71-32196
- EARLY BIRD SATELLITES**
Low elevation polarimetric recordings of 136.44 MHz transmission from Early Bird geostationary satellite
07 p1206 A71-19022
- EARLY STARS**
NT PROTOSTARS
NT T TAURI STARS
Planetesimal growth in nebulae around young stars, examining accretion and physical chemistry of solar types
01 p0157 A71-10761
- IR stars, discussing very young stars, circumstellar clouds and IR excesses
04 p0648 A71-15251
- Early type stars radiant flux observation from OGO 6 satellite
06 p0969 A71-17975
- AB Aur light variations in three colors, estimating visual absolute magnitudes free of interstellar absorption and B-V
07 p1201 A71-20433
- Evaporation of dirty ice particles surrounding early type stars, using dust grains model for explanation of anomalous reddening of Orion Nebulae
08 p1364 A71-21415
- Early stars Vilnius intermediate band and UVB systems comparison for color excess ratios and magnitudes, obtaining reddening line slopes by spectral energy distributions
10 p1682 A71-25131
- Young cluster NGC 2264 main sequence A and F stars four color and H beta observation, suggesting evidence of circumstellar gas shells
12 p1956 A71-26615
- Early type stars, open clusters, associations and stellar rings space distribution and state of motion
12 p1959 A71-26776
- Perseus early stars photometry and far UV spectra from Aerobee rocket flight observations
14 p2304 A71-29596
- Early type close binary systems AO Cas, HD 47129, HD 190918 and HD 193793 spectral observations
14 p2311 A71-30369
- Rapidly rotating early stars and quasars, determining magnetic field generation by turbulent dynamo mechanism
15 p2485 A71-31725
- Main sequence A and early F stars with shallow convective envelopes, investigating particle diffusion effects on element abundance data
18 p2960 A71-35939
- IR radiation sources, discussing intermediate and early stars, galactic nucleus and extragalactic sources
18 p2958 A71-37029
- Early stars UV continuum brightness from rocket-borne photoelectric spectrophotometer, estimating total interstellar flux density
21 p3444 A71-40244
- Early stars with extended atmospheres, discussing long term observational programs
24 p3873 A71-45126
- Atomic hydrogen cloud distances determined by interstellar absorption lines of early stars
24 p3874 A71-45145
- Stars origin theories, discussing stellar associations, young stars, galaxies instability and cosmology and cosmogony
24 p3875 A71-45198
- EARTH (PLANET)**
Brightness field spatial structure of solar radiation reflected from earth by Cosmos 149 satellite, discussing homogeneity and isotropy
02 p0246 A71-12114
- Orbital space stations for earth studies, considering atmospheric, hydrological and meteorological observations, astronomy, medico-biological and technological experiments and interplanetary spacecraft bases construction
03 p0497 A71-13418
- Earth ellipsoid physical constants using satellite measurements of geocentric gravitational constant, earth-moon mass ratio and geopotential harmonic coefficients
04 p0581 A71-15066
- Earth variable electromagnetic field spatial harmonics asymptotic properties
05 p0746 A71-17212
- Earth international compartmentalization into equal area elements on reference sphere for spherical functions utilization
10 p1601 A71-24460
- Orbital space stations for earth studies, considering atmospheric, hydrological and meteorological observations, astronomy, medico-biological and technological experiments and interplanetary spacecraft bases construction
14 p2319 A71-29695
- Normal terrestrial gravitational field potential, taking into account second order variables and distances from earth ellipsoid
16 p2563 A71-33466
- General relativistic time delay and moon-earth masses and Mars mass-ephemeris ratios from S-band range and Doppler tracking
20 p3296 A71-39623
- Differential correction for redetermination of satellite observation stations geodetic coordinates as related to earth center of gravity and terrestrial potential coefficients
22 p3534 A71-42023
- Earth electrostatic potential role in experimental Coulomb law verifications
22 p3536 A71-42455
- Terrestrial, lunar and planetary dynamical properties and internal constitution, considering data obtained from artificial satellites, lunar and planetary dynamics
22 p3607 A71-42883
- Earth ellipsoid gravitational potential selection influence on geoid height determination, using near-geoid model
23 p3674 A71-44051
- Lunar evolution theory, discussing terrestrial cluster dynamics during earth accumulation
24 p3870 A71-44811
- EARTH ALBEDO**
Earth optical radiation environment observation from satellites, reviewing solar spectra, near IR cloud spectra and vacuum UV radiometer scans
09 p1437 A71-22739
- Angular discretization effect on calculations of emerging radiation and integrated albedo from model cloudy atmosphere, using multiple scattering with terrestrial particle phase functions
10 p1643 A71-24972
- Rotating spacecraft attitude control system, using sun-earth albedo sensor for attitude determination [DFVLR-SONDDR-113]
12 p1972 A71-26986
- Autocorrelation functions of quasi-uniform solar radiation field reflected from earth with scattering allowance, using stationary random theory
12 p1901 A71-27097
- Earth radiation budget measurements, noting planetary albedo, IR radiant emittance and net balance
12 p1901 A71-27191
- Atmospheric optics and radiative transfer, including earth albedo, sky brightness, heat balance, cloud/terrain reflectance, molecular spectroscopy and multiple scattering
14 p2275 A71-30497
- Earth atmosphere radiation fields analysis from Nimbus 3 five-channel scanning radiometer measurements, determining mean planetary albedo and temperature
20 p3259 A71-39679
- Earth surface characteristics measurements with remote sensors, proposing overland albedo measurements for clues as to ground type /clouds, vegetation, sand and snow/
20 p3260 A71-39684
- High altitude aerosol layer effects on atmospheric UV albedo, correcting ozone scale height spaceborne measurements
20 p3221 A71-39695
- Autocorrelation functions of quasi-uniform solar radiation field reflected from earth, using stationary random theory and allowing for scattering
22 p3533 A71-41652
- EARTH ATMOSPHERE**
NT D REGION
NT E REGION
NT EXOSPHERE
NT F REGION
NT F 1 REGION
NT F 2 REGION
NT FREE ATMOSPHERE
NT HETEROSPHERE
NT INNER RADIATION BELT
NT IONOSPHERE
NT LOWER ATMOSPHERE
NT LOWER IONOSPHERE
NT MAGNETOPAUSE
NT MAGNETOSPHERE
NT MESOPAUSE
NT MESOSPHERE
NT MIDLATITUDE ATMOSPHERE
NT OUTER RADIATION BELT
NT OZONOSPHERE
NT PROTON BELTS
NT RADIATION BELTS
NT SPORADIC E LAYER
Extra-atmospheric submillimeter astronomy, discussing emission observations between IR and RF region and astrophysical-cosmological applications
01 p0151 A71-10146
- Earth atmosphere origin, discussing oxygen and carbon dioxide balance
03 p0409 A71-13697
- Layer boundaries and critical concentrations of anomalous increase of radiation in earth and Venus atmospheres along tangential directions
05 p0738 A71-16044
- Soviet monograph on thermal sounding of atmosphere by satellite covering moisture content, cloud surfaces and stratosphere temperatures and thermal radiation distribution
05 p0738 A71-16197
- Earth bow shock configuration model from dual satellite observation
05 p0742 A71-16632
- Earth atmosphere thermal sounding problems, considering indirect temperature profile determination, various degrees of cloudiness and Planck function dependence on pressure
07 p1151 A71-18909
- Earth atmosphere polytropic equilibrium model density distribution and effective size and mass, taking into account gravitational interactions
07 p1152 A71-19375
- Atmospheric oxygen evolution and stability, discussing effects of photosynthesis inhibition, hydrogen passage and burial carbon
07 p1102 A71-19540
- Earth twilight aureole and cloud spectra from satellite photometry
08 p1285 A71-21792
- Satellite studies of geoscientific particles and photoelectrons, including interactions with earth atmosphere
09 p1436 A71-22552

- Differential rotation in sun, giant planets and upper atmospheres of earth and Venus, attributing solar rotation to tides caused by planets
09 p1522 A71-22961
- Vertical velocities in atmosphere measured by acoustic Doppler during diurnal thermal plumes and breaking wave occurrence within nocturnal inversion
10 p1574 A71-23746
- Laboratory model for radio star scintillation and other diffraction phenomena by thin weak random phase changing screen including earth atmosphere or solar wind
10 p1678 A71-24797
- Linear vector differential Fridman equations for cosmic and telluric effects on earth atmosphere facilitating dynamic climate forecasts
10 p1639 A71-25115
- Planetary distribution of primary cosmic rays and residual charged particles over atmosphere from Cosmos 208 and 228 satellite data
11 p1816 A71-25761
- Atmospheric modeling for earth and Venus heterosphere structure using multicomponent radiative hydrodynamic equations, determining atmospheric temperature and constituents height variation
11 p1828 A71-25764
- Thermal fluctuations in earth upper atmosphere, related to satellite deceleration and X ray solar radiation changes by autocorrelation and cross correlation analyses
11 p1817 A71-25822
- Solar wind effects on space around earth, discussing dipole image of magnetic field, radiation belt feeding and atmospheric phenomena based on artificial satellite observations
11 p1817 A71-26337
- Solar system space physics review covering earth atmospheric temperature, density and models, solar wind, auroras, and moon, Venus and Mars data from space missions
13 p2131 A71-27877
- Global environmental monitoring system for atmosphere, oceans, land and biology, considering international cooperation
14 p2198 A71-30897
- World Weather Watch global telemetry system including observing stations, and rockets, balloons and satellite-borne sensors, determining atmospheric states on ground and sea
14 p2199 A71-30913
- Radiative heat transfer equilibrium in earth, Venus and Mars atmospheres, taking into account interaction with ground
15 p2395 A71-31448
- Layer boundaries and critical concentrations of anomalous increase of radiation in earth and Venus atmospheres along tangential directions
16 p2635 A71-33448
- Mars, Venus and earth atmospheres, considering abundance of volatiles such as carbon dioxide, water, oxygen, nitrogen, argon, carbon monoxide, chlorine and fluorine
18 p2968 A71-37032
- Atmosphere meteorological sounding, measuring geodetic quadrangle sides and diagonals by aircraft radio direction finder
19 p3065 A71-38175
- Solar effects contradictory relationships with earth atmosphere, discussing geomagnetic disturbance, annual variations, stratospheric transport and high energy particles
19 p3128 A71-38354
- Earth atmosphere wind field motion calculation from displacement of longitudinally elongated cyclones
20 p3277 A71-38736
- Planetary distribution of primary cosmic rays and residual charged particles over atmosphere from Cosmos 208 and 228 satellite data
22 p3591 A71-41529
- Atmospheric modeling for earth and Venus heterosphere structure using multicomponent radiative hydrodynamic equations for atmospheric temperature and constituents height variation determination
22 p3598 A71-41532
- Methane atmosphere polymerization by solar UV to form primordial oil slick, discussing importance to life development
22 p3535 A71-42074
- EARTH AXIS**
- Earth rotation axis and mass center position determination, using earth-moon laser ranging data
01 p0161 A71-11383
- Earth poles motion harmonic analysis, using observational data
03 p0406 A71-13245
- Earth rotation polar motion dynamics, discussing wobble, drift, nutation, precession and sway
06 p0890 A71-17877
- Earth rotation pole coordinates from International Latitude Service stations and International Polar Motion Service data
06 p0890 A71-17878
- International Polar Motion Service stations residual latitudes variation by other than polar motion, considering dependence on earth figure deformation
06 p0890 A71-17880
- Earth mantle-inner core nutational dynamic coupling and rotation pole 24 year libration
06 p0890 A71-17883
- Pole path deconvolution by optimum Wiener filter for acausal and causal cases, considering earthquake excitation
06 p0890 A71-17884
- Earthquakes association with Chandler wobble from ILS-IPMS polar data
06 p0891 A71-17888
- Major earthquakes effects on earth rotation pole disturbances from latitude and time data, considering Chandler nutation excitation
06 p0891 A71-17889
- Kimura annual Z term in latitude variations, noting agreement with semiannual solar nutation and earth tide observations
08 p1364 A71-21422
- Force moment method estimation of atmospheric circulation effect on earth polar movement
08 p1284 A71-21674
- Earth poles motion, measurement methods and possible causes due to earth core and mantle effects on earth rotation
09 p1434 A71-22057
- Newcomb precession constant accuracy, noting stellar motion analogies and analytic effects on earth polar secular motion
12 p1901 A71-27092
- Satellite paralactical mounted camera installation for adjusting axis parallel to earth rotation axis
13 p2070 A71-29120
- Photographic and laser observations during passage of satellite for determination of distance between observer and earth rotational axis
14 p2250 A71-31123
- Semiannual nutation term determination from diurnal latitudinal observation with zenith telescope over 6 year period for earth axis
15 p2486 A71-31899
- Falling body problem solution, considering curvilinear motion effects of earth rotation axis
15 p2450 A71-32039
- Newcomb precession constant accuracy, noting stellar motion analogies and analytic effects on earth polar secular motion
19 p3049 A71-37442
- EARTH CORE**
- Lunar tides and precession effects on model earth fluid core dynamics
02 p0245 A71-11994
- Meteorites and earth core composition and models for terrestrial planets internal constitution
02 p0310 A71-12159
- Earth and Jupiter magnetic fields relationship to core motional induction
02 p0310 A71-12160
- Earth gravitational and magnetic field correlation, determining undulations on core-mantle interface
02 p0247 A71-12953
- Spherical superconducting geomagnetic field generating layer under ultrahigh pressure in earth center
06 p0889 A71-17734
- Earth mantle-inner core nutational dynamic coupling and rotation pole 24 year libration
06 p0890 A71-17883
- Geophysical and astronomical consequences of core-mantle interactions, considering earth rotation changes
06 p0891 A71-17887
- Earth core-mantle coupling as energy source for mantle wobble, taking into account precession cross coupling
06 p0891 A71-17890
- Geomagnetic secular variation as main field drift superposition and strength changes, reflecting drift and convection in earth fluid core
07 p1103 A71-19763
- Adiabatic and melting point gradients in earth core, discussing temperature distribution inhibition to convection radial components
09 p1436 A71-22642
- Earth interior structure, composition and evolution, using seismic, ultrasonic, shock wave and petrological data
09 p1438 A71-23159
- Geomagnetic quadrupole field secular oscillation causing earth rotation change, discussing earth core induced velocity field and field attenuation
10 p1603 A71-24599
- Lighter-than-iron elements in earth iron core, assuming formation timed chemical equilibrium with mantle
10 p1607 A71-24986
- Critique of paper on earth core-mantle chemical equilibrium, considering upper mantle element abundance, oxidation state and volatiles nature
10 p1607 A71-24987
- Atomic scale elastic structure equations of state for Thomas-Fermi model extension to high pressures, considering earth core iron-silicates composition
11 p1802 A71-25572
- Lower earth mantle shear velocity models derivation and core radius estimation based on S travel times observation
11 p1760 A71-26060
- Earth tide and nutation correlation, examining internal structure based on model with liquid center and solid inner core
15 p2401 A71-32684
- Stable earth core geomagnetic dynamo model consisting of disk oscillating about symmetry axis with coil connected to brushes on axle and at disk edge
19 p3061 A71-38676
- Earth mantle material chemical differentiation from structural model, considering gravitational instability relationship to low density layer formation at core boundary
23 p3671 A71-43579
- Digital computer numerical procedure to solve dynamo theory MHD equations for earth nucleus, using combination of Fourier and finite difference methods for integration
24 p3823 A71-45038
- EARTH CRUST**
- Astronomically determined latitude, longitude and azimuth reduction to common epoch, discussing secular nonperiodic pole motion due to crust drift
03 p0484 A71-13217
- K-U abundance systematics in Apollo 11 and 12 lunar rock suites and earth crust
06 p0968 A71-17961
- Earth rotation, crust deformation and solar activity related, noting variations in longitude difference between Europe and America
08 p1284 A71-21671
- Earth and meteorites evolution, discussing material transport between lower and upper mantles and crust based on model of trace elements
11 p1820 A71-25226
- Crustal and meteoritic abundances of elements and water, considering chondritic and achondritic composition
19 p3055 A71-38145
- EARTH ENVIRONMENT**
- Commercial SST environmental effects on stratospheric air, water vapor content and earth surface temperature
01 p0074 A71-11178
- Near earth solar wind Fe, Si and O ions, using electrostatic analyzer on Vela 5A satellite
01 p0148 A71-11520
- Conference report on impact of man on global environment, assessing actions covering climatic and ecological effects, pollution monitoring, etc
02 p0246 A71-12350
- Micrometeorites composition and mass distribution in earth orbit vicinity, describing spaceborne and ground based data acquisition
02 p0313 A71-12470
- Vestibular function on earth and in space - Conference, Uppsala, May 1968
04 p0536 A71-14751
- Gravity gradient torque and near earth environment effects on rotationally damped dual spin satellite attitude motion
06 p0980 A71-18546
- Earth environment from aviation viewpoint, discussing atmospheric physics and chemistry, flight physiology, radiation, etc
08 p1243 A71-20702
- Extraterrestrial and earth life genesis, discussing carbon foundation, planetary conditions, water prerequisite and space exploration
13 p2009 A71-28679
- Global environmental monitoring system for atmosphere, oceans, land and biology, considering international cooperation
14 p2198 A71-30897
- Urban environmental quality analysis using color IR aerial photography, considering film sensitivity and haze penetration
18 p2911 A71-36062
- Raw remote sensor data acquisition relationship to economic activity and interpretation for earth resource/environmental information
18 p2912 A71-36067
- Space technology applications to earth environment and resources management, discussing satellite-borne remote sensor systems and data processing techniques [SD-71-734]
22 p3535 A71-42047
- EARTH FIGURE**
- U GEODESY**
- EARTH HYDROSPHERE**
- Biosphere contamination, discussing sterilization and quarantine experiments at Lunar Receiving Laboratory, flight crew testing and microbiological studies
21 p3448 A71-40569
- Solar activity effects on biosphere, examining solar-geomagnetic and medico-biological indexes relation-

ships and clinico-statistical evidence of human organ-
ism effects 24 p3799 A71-45197

EARTH MANTLE

Kamchatka volcanic mantles and lunar surface
radiation polarization characteristics similarities
01 p0149 A71-10049

Earth gravitational and magnetic field correlation,
determining undulations on core-mantle interface
02 p0247 A71-12953

Mineralogy and chemistry of earth upper mantle,
using partial fusion-partial crystallization model
04 p0583 A71-15266

Critique of paper on lithosphere thermal regime
descending into mantle 06 p0889 A71-17636

Earth mantle-inner core nutational dynamic
coupling and rotation pole 24 year libration
06 p0890 A71-17883

Geophysical and astronomical consequences of
core-mantle interactions, considering earth rotation
changes 06 p0891 A71-17887

Earth core-mantle coupling as energy source for
mantle wobble, taking into account precession cross
coupling 06 p0891 A71-17890

Earthquake correlation to polar motions explained
by local stress distribution in lower mantle
06 p0891 A71-17891

Model and glass tank furnaces for earth upper man-
tle convection movements simulation, studying fluid
dynamics and geodynamic processes 07 p1105 A71-20449

Rayleigh and phase change instability for olivine-
spinel mantle convection 07 p1105 A71-20450

Kamchatka volcanic mantles and lunar surface
radiation polarization characteristics similarities
08 p1361 A71-21043

Lighter-than-iron elements in earth iron core, as-
suming formation timed chemical equilibrium with
mantle 10 p1607 A71-24986

Critique of paper on earth core-mantle chemical
equilibrium, considering upper mantle element
abundance, oxidation state and volatiles nature
10 p1607 A71-24987

Earth and meteorites evolution, discussing material
transport between lower and upper mantles and crust
based on model of trace elements 11 p1820 A71-25226

Lower earth mantle shear velocity models deriva-
tion and core radius estimation based on S travel times
observation 11 p1760 A71-26060

Canary Islands volcanic rocks, investigating lead
isotope compositions for upper mantle multistage his-
tory 13 p2062 A71-28698

Celestial mechanics relationship to astronomy,
establishing differential equations of earth rotation in
relation to terrestrial mantle 14 p2306 A71-29703

Low degree gravity harmonics source, discussing
upper mantle hypothesis of mass anomalies location
16 p2563 A71-33150

Earth upper mantle electrical conductivity as func-
tion of depth based on geomagnetic variation field spa-
tial distribution data 16 p2572 A71-33907

Elastic seismic waves attenuation in polycrystalline
ceramics and rocks by grain boundary relaxation, not-
ing strong frequency dependence of earth mantle in-
ternal friction 17 p2735 A71-35390

Earth mantle material chemical differentiation from
structural model, considering gravitational instability
relationship to low density layer formation at core
boundary 23 p3671 A71-43579

EARTH MOTION

Earth poles motion harmonic analysis, using obser-
vational data 03 p0406 A71-13245

Earth free diurnal nutation frequency, examining
latitude variation power spectrum 08 p1285 A71-21780

Earth poles motion, measurement methods and
possible causes due to earth core and mantle effects
on earth rotation 09 p1434 A71-22057

Earth free diurnal nutation frequency, examining
latitude variation power spectrum 15 p2401 A71-32685

Earth velocity vector right ascension, declination
and magnitude determination from cosmic 3 K
background radiation anisotropy 16 p2563 A71-33402

Sun-earth distance and earth orbital eccentricity ef-
fect on E region peak electron density, discussing
Chapman-like model 21 p3372 A71-40035

Nearly diurnal nutation observations from Danjon
astrolabe data, comparing theoretical earth models
22 p3602 A71-42172

EARTH MOVEMENTS

NT EARTHQUAKES

Earth eigen vibrations excitation by gravity waves,
tabulating energy content of even and odd harmonics
overtones 10 p1607 A71-25005

Transient ground motion velocity measurement
system, using piezoresistive acceleration transducers,
electronic integrator and digital zeroing circuit
14 p2245 A71-30340

Spheroidal oscillations attenuation, considering dis-
crepancy between theory and experiment due to earth
interior dissipation 17 p2735 A71-35244

Satellite data techniques and instrumentation in
earth geometry and kinetics, reviewing geopotential
models, pole positions, tides, ocean physics and inter-
national cooperation 20 p3219 A71-39656

EARTH ORBITAL RENDEZVOUS

Reusable space shuttle optimization, discussing
earth-to-orbit transportation, economic aspects,
booster vehicles design, propellant cryogenic tanks
and thermal protection 17 p2814 A71-35430

[AIAA PAPER 71-805]

Large synchronous communication satellite
launching by propulsion stages assembling in orbit
through automatic rendezvous maneuvers 18 p2975 A71-36526

EARTH ORBITING SPACE STATIONS

U EOSS

EARTH ORBITS

NT APOGEES

NT PERIGEEES

Krylov-Bogoliubov integration theory for first-
order perturbation analysis of multidimensional har-
monic oscillator applied to body motion in earth gravi-
ty 01 p0151 A71-10113

Computerized simulation of disturbance torques of
spin stabilized spacecraft in near earth orbit
03 p0500 A71-14433

Pulse gated binary modulation /PGBM/ visible laser
communications for earth orbital missions
07 p1056 A71-18810

Active cosmic ray modulation layer boundaries
between sun and earth orbits, studying meteorite
isotopes radioactivity 08 p1352 A71-20973

Optimal acceleration from earth orbit to hyperbolic
velocities of low thrust space vehicle, constructing
asymptotic expansions near and far from central field
09 p1519 A71-22545

Orbital space stations and spacecraft courses, deter-
mining orbit precession and perturbation 12 p1968 A71-27628

Earth orbital radiation variations effect on climate,
noting minor temperature, wind and hydrological
changes 16 p2562 A71-33069

Space station assembly in earth orbit, providing low
transportation costs, modular elements return and in-
cremental growth 18 p2974 A71-36485

Saliut 1/Soyuz 10 mission, discussing configuration,
size orbits and docking procedure 18 p2975 A71-36685

Artificial earth satellite orbital decay rate mea-
surement for upper atmosphere density data, using com-
bined directional observations and orbit data
19 p3048 A71-37394

Sporadic and cometary meteor particles concentra-
tion along earth orbit, using optical and radiant mea-
surements 20 p3299 A71-39650

Earth orbital photography for geologic applications,
discussing advantages over aerial photography
22 p3534 A71-41962

Earth-orbiting space vehicle attitude motion under
constantly acting disturbances based on mathematical
total stability of equilibrium 22 p3608 A71-41968

Mission analysis aspects of space shuttle operations
between earth orbit station and lunar orbit station
[AAS PAPER 71-301] 23 p3724 A71-42977

Earth orbit shuttle payload increase, discussing
refueling and auxiliary hydrogen tank concept
[AAS PAPER 71-302] 23 p3772 A71-42978

EARTH PLANETARY STRUCTURE

Earth rotation axis and mass center position deter-
mination, using earth-moon laser ranging data
01 p0161 A71-11383

Regionalized models for earth with oceanic, shield
or tectonic crust and upper mantle, taking phase
velocities into consideration 02 p0245 A71-11992

Annular structures on earth, moon and Mars, ex-
plaining cosmic origin on basis of lens-shaped subsur-
face breccia 02 p0310 A71-12298

Earth, moon and planets sizes, masses and moments
of inertia determination by artificial satellites, space
probes and radar observation 05 p0815 A71-17241

Critique of paper on lithosphere thermal regime
descending into mantle 06 p0889 A71-17636

Inner and outer planets groups mass and mean den-
sity, considering terrestrial seismic data and lunar,
Venus, Mars and Mercury structural models
08 p1358 A71-20888

Earth tide and nutation correlation, examining inter-
nal structure 08 p1285 A71-21779

Earth interior structure, composition and evolution,
using seismic, ultrasonic, shock wave and petrological
data 09 p1438 A71-23159

Stokes earth shape formula derivation without
removing continental masses for regularization
requirement 09 p1438 A71-23181

Apollo 11 sample basalts lunar interior origin as-
sumption from comparison with terrestrial massif
anorthosite series, using chemical and petrographic
analyses 11 p1834 A71-26452

Earth-moon tectonic relationships and structural
similarity, analyzing earthquake frequency depen-
dence on lunar phase and distance based on Mid-
dlehurst catalogs 15 p2492 A71-32478

Earth tide and nutation correlation, examining inter-
nal structure based on model with liquid center and
solid inner core 15 p2401 A71-32684

Earth mantle material chemical differentiation from
structural model, considering gravitational instability
relationship to low density layer formation at core
boundary 23 p3671 A71-43579

EARTH RADIATION

U TERRESTRIAL RADIATION

EARTH RESOURCES

NT COAL

NT CRUDE OIL

NT FARM CROPS

NT FORESTS

NT GRAINS [FOOD]

NT GRANITE

NT LAKES

NT LAVA

NT LIMESTONE

NT ROCKS

NT SANDS

NT SANDSTONES

NT VEGETATION

Remote sensing systems for vegetation analysis,
discussing machine-aided photointerpretation
methods for data analysis [AIAA PAPER 70-308] 01 p0084 A71-11590

Earth resources survey remote sensor system with
human for spatial and machine for spectral data
processing 08 p1257 A71-20691

Image specifications and data interpretation
techniques for regional resource survey using small
scale aerial and space photography 08 p1288 A71-21245

Space photography for earth resource assessment,
discussing multi-band, -date and -stage techniques ad-
vantages, image analysis and conference systems
11 p1767 A71-26530

Mineral and water resources remote sensing,
discussing sensor systems and data interpretation
techniques with special reference to Colorado Bonan-
za project 11 p1760 A71-26531

Canadian program of remote sensing for gathering
information on earth resources and environment
16 p2566 A71-33749

Report to COSPAR on French space program
covering ionosphere and magnetosphere physics,
meteorology, cosmic rays and earth resources
16 p2666 A71-33861

Manned orbital research modules design for at-
mospheric physics, weather and earth resources ob-
servations and stellar astronomy [AIAA PAPER 71-815] 17 p2814 A71-35426

Monograph on satellite-borne orbital photographic
imaging techniques application to natural resources
survey, discussing remote areas geomorphological and
geological reconnaissance maps preparation
18 p2915 A71-35905

Raw remote sensor data acquisition relationship to
economic activity and interpretation for earth
resource/environmental information 18 p2912 A71-36067

French space programs, discussing European and
international activities, telecommunication,
meteorology, data collecting, natural resources and air
and sea traffic control 18 p2975 A71-36753

- Space technology applications to earth environment and resources management, discussing satellite-borne remote sensor systems and data processing techniques [SD-71-734] 22 p3535 A71-42047
- Astronomical and earth resources observations accommodation by space shuttle orbital sortie missions, obtaining sensor use rate estimate from worldwide cloud cover statistical distribution [AAS PAPER 71-303] 23 p3724 A71-42979
- Automatic rescan detection and reference ground control points for computing and correcting geometric and radiometric image for earth resource data, noting correlation with reference system [AIAA PAPER 71-978] 24 p3806 A71-44576
- ### EARTH RESOURCES PROGRAM
- Satellite monitoring impacts on global ecological and natural resource public policy issues 04 p0689 A71-14820
- Earth resources coverage capabilities of manned orbital space station, comparing to remote measurement requirements [AIAA PAPER 71-75] 06 p0980 A71-18532
- Airborne surveillance for environmental management, discussing earth resources program, aerial sensors for thermal water pollution, crop disease, salinity and geological structure 07 p1018 A71-19080
- NASA Earth Resources Survey Program as basis for future earth survey system combining spaceborne, airborne and ground observations 10 p1600 A71-24171
- ERTS A and B projects, describing satellite communications, data handling, telemetry, tracking and command, thermal control, orbit-adjust, image processing and ground equipment 10 p1682 A71-24172
- Orbital Earth Resources Experiment Package sensor components, functions and crew tasks for operation 15 p2500 A71-31459
- Earth Resources Remote Sensing Systems effectiveness, discussing sensor and satellite development, spectral and spatial recognition, data management and ecological and resource relationship 16 p2645 A71-33582
- Space applications to world needs, emphasizing potential major agricultural production improvements 16 p2665 A71-33589
- Skylab earth resources experimental equipment, describing sensing and recording instrumentation for electromagnetic spectral pattern recognition studies [AIAA PAPER 71-841] 17 p2739 A71-34712
- Earth resources experiments package electromagnetic compatibility with Apollo Applications Program 19 p3032 A71-38453
- Skylab manned scientific space laboratory for medical, solar astronomy, earth resources, technology and engineering experiments 22 p3608 A71-41950
- Satellite observations for earth resources management, discussing operational ground-based remote sensor system and information extraction techniques 22 p3534 A71-41973
- Earth observation system design decision making, considering data needs, technology readiness, man role in earth resources programs and space program schedule 24 p3892 A71-44867
- ERTS remote sensing for ground system data management, emphasizing processing, correction, reproduction, storage, retrieval and distribution [AIAA PAPER 71-976] 24 p3817 A71-45294
- ### EARTH RESOURCES SURVEY AIRCRAFT
- Multispectral scanner and data system with 24 channels for NASA C-130 earth resources survey aircraft 18 p2920 A71-36361
- ### EARTH RESOURCES TECHNOLOGY SATELLITES
- Manned space flight network technology system modification for Skylab, ERTS and Apollo J missions, giving data flow diagrams and equipment electrical characteristics 01 p0035 A71-10917
- Earth Resources Technology Satellites (ERTS) A and B providing one year high resolution multispectral imagery, noting data processing and distribution functions 01 p0164 A71-11436
- Space applications international programs in 1970s, discussing political, legal, economic and management aspects of earth resources survey (ERS) satellite program 04 p0691 A71-15348
- TV systems for earth resources survey satellites, discussing high resolution return beam vidicon tubes, laser beam image reproducer and electron beam recorder systems 05 p0816 A71-16143
- Earth resources satellite systems R and D planning, using case study approach in economic benefit analysis for parametric requirements determination [AIAA PAPER 68-1077] 05 p0840 A71-17050
- NASA Data Processing Facility for earth resources technology satellite telemetry 05 p0818 A71-17146
- Multispectral and multitemporal digital imagery spatial registration using fast Fourier transform techniques, applying to earth resources satellite imagery preprocessing 05 p0756 A71-17147
- Photographic and IR multiband spectral discrimination for rock and soil mapping from orbiting ERTS satellites [AIAA PAPER 70-303] 06 p0898 A71-17562
- User requirements for Earth Resources Satellite data, considering information dissemination and forest inventory application 07 p1106 A71-18802
- NASA ground based digital data processing facility for Earth Resources Technology Satellite system 07 p1067 A71-18804
- ERTS-A imagery, Apollo 9 and high altitude aircraft photography applications to Land Management Bureau, Indian Affairs and Reclamation 09 p1451 A71-23208
- ERTS A and B projects, describing satellite communications, data handling, telemetry, tracking and command, thermal control, orbit-adjust, image processing and ground equipment 10 p1682 A71-24172
- Video tape recorder (VTR) for onboard storage of wideband analog and high rate digital sensor outputs of ERTS 14 p2249 A71-30901
- ERTS telecommunication system for space tracking and high resolution multispectral image data acquisition and commanding 14 p2199 A71-30912
- NASA earth resources technology satellites system, discussing ERTS A and B development, payloads and ground support systems and international aspects 16 p2630 A71-32854
- Earth remote sensing in Brazil, discussing program organization and data acquisition related to NASA environmental resources technology satellites 16 p2570 A71-33826
- Electronic multiimage processor for enhancement and interpretation of ERTS multiband remote sensor imagery data 17 p2737 A71-34273
- ERTS system, considering multispectral data acquisition, relay devices and spacecraft and ground information processing 17 p2812 A71-34611
- NASA ERTS program, discussing system concept automatic data processing capability, compatibility with tracking ground stations and international cooperation 17 p2805 A71-35329
- ERTS remote sensor data processing, describing space and ground equipment and techniques [AIAA PAPER 71-839] 17 p2814 A71-35429
- Two dimensional optical Fourier approach diagnosing interpretation-limiting pictorial noise patterns in ERTS image output 18 p2919 A71-36082
- Aerospace imagery enhancement for visual interpretation, considering ERTS applications 18 p2919 A71-36084
- ERTS satellite-based laser communication system, calculating cloud cover effect on clear line-of-sight light transmission probability through atmosphere to ground station 18 p2876 A71-36472
- Rectilinear correction of geometric errors of images transmitted from earth resources satellites, using digital computer 18 p2886 A71-36540
- ERTS-A and B pictorial data processing center, describing image processing system and available user services in terms of international participation 18 p2900 A71-36541
- Numerical methods for noise elimination from ERTS pictorial data, describing data acquisition system 18 p2886 A71-36542
- Systems planning and operation of European applications satellites, noting Sirio and Symphonie programs 19 p3172 A71-37329
- Papers on communication satellites for 1970s covering various national domestic systems, aeronautical service, ERTS data transmission and collection problems, etc 21 p3347 A71-40473
- Earth resources survey satellites, discussing natural sources/radiation, matter-energy interactions and perturbing media/, remote sensors, space applications and reconnaissance 21 p3455 A71-40910
- ERTS remote sensing techniques, discussing objectives for southeastern U.S. in terms of agriculture, forestry, strip mine land reclamation and thermal pollution 22 p3534 A71-41967
- Radio regulation planning and frequency assignments for operational earth exploration satellite service 22 p3623 A71-41974
- Operations and equipment of NASA ground data handling system for earth resources technology satellites 22 p3509 A71-42018
- Earth resources technology satellites image processing system including electron beam recorder, image corrector, electro-optical systems and digital processors as design features [AIAA PAPER 71-977] 24 p3825 A71-44575
- ERTS remote sensing for ground system data management, emphasizing processing, correction, reproduction, storage, retrieval and distribution [AIAA PAPER 71-976] 24 p3817 A71-45294
- ### EARTH ROTATION
- Compressible corotation of model magnetosphere, considering electric field induced by earth rotation 01 p0077 A71-11514
- Atmospheric circulation and earth rotational energy contribution to energy release by intense polar auroras, noting ionospheric current subsonic heating and oxygen emission 02 p0244 A71-11909
- Astronomical-geodetic observations of direction of instantaneous earth rotation vector at South Pole 03 p0406 A71-13007
- High drag satellite 1968-59A orbits from optical and radar observations, obtaining rotational speed of upper atmosphere 03 p0407 A71-13305
- Earth instantaneous rotation pole coordinates, calculating yearly and Chandler motions 03 p0492 A71-14192
- Photoelectric reflector zenith telescope for determination of earth rotation and latitude variations, noting recording by photon counts 04 p0598 A71-15381
- Earthquake displacement fields and earth rotation-Conference, London, Canada, June 1969 06 p0889 A71-17876
- Earth rotational acceleration and polar secular motion changes, considering correlation with earthquakes 06 p0890 A71-17881
- Secular changes in cooperative stations mean latitudes related to mean pole drift 06 p0890 A71-17882
- Solar wind torque on earth magnetic dipole based on magnetosphere model analytic solution in rotating reference frame 06 p0891 A71-17885
- Geophysical and astronomical consequences of core-mantle interactions, considering earth rotation changes 06 p0891 A71-17887
- Earthquake correlation to polar motions explained by local stress distribution in lower mantle 06 p0891 A71-17891
- Long base line radio interferometry role in earth rotation rate measurement 06 p0891 A71-17892
- Spectral analysis of five-day pulsations in earth rotational velocity, estimating amplitudes of suspected velocity fluctuations 06 p0896 A71-18452
- Navigational precision timing from earth rotation based pendulum to atomic second based quartz oscillator clocks 07 p1156 A71-20341
- Earth rotation, crust deformation and solar activity related, noting variations in longitude difference between Europe and America 08 p1284 A71-21671
- Earth rotation velocity studies (1956-1966), noting slowing 08 p1284 A71-21672
- Ephemeride and atomic uniform time scales comparison for earth rotation velocity changes, estimating diurnal and semidiurnal tides effect 08 p1284 A71-21673
- Earth poles motion, measurement methods and possible causes due to earth core and mantle effects on earth rotation 09 p1434 A71-22057
- Flow equations of vertical shear modes in inertial waves on rotating earth, comparing chemical release ionospheric wind profiles 09 p1489 A71-23449
- Frequency domain spectral energy equations for large scale atmospheric motions, discussing earth rotation effects on kinetic energy spectrum 10 p1638 A71-23963
- Geomagnetic quadrupole field secular oscillation causing earth rotation change, discussing earth core induced velocity field and field attenuation 10 p1603 A71-24599
- Earth rotation slowing, discussing observations of earth and lunar time variations and methods of computing tidal effects 10 p1603 A71-24691
- Weber differential hydrodynamic equations with earth rotation allowance related to Bjerknes circulation theorem and Ertel variational principle of atmospheric dynamics 10 p1607 A71-25111

Spectral analysis of five day pulsations in earth rotational velocity, estimating periods and amplitudes of suspected velocity fluctuations 12 p1898 A71-26602

Newcomb precession constant accuracy, noting stellar motion anomalies and analytic effects on earth polar secular motion 12 p1901 A71-27092

Earth outward winding by cosmic particle gravitational accretion, examining individual meteor counts crossing celestial meridian in WE and EW directions 12 p1966 A71-27232

Atmospheric circulation and earth rotational energy contribution to energy release by intense polar auroras, noting ionospheric current subsonic heating and oxygen emission 13 p2058 A71-28196

Scott effect observation of superrotation of upper atmosphere, relating temperature gradient, magnetic field and gas rotation 13 p2063 A71-29095

Celestial mechanics relationship to astronomy, establishing differential equations of earth rotation in relation to terrestrial mantle 14 p2306 A71-29703

Seasonal, irregular and long term earth rotation rate variations 14 p2310 A71-30198

Falling body problem solution, considering curvilinear motion effects of earth rotation axis 15 p2450 A71-32039

Earth gravitational and magnetic field correlations, considering nondipole geomagnetic potential latitudinal rotation effects 17 p2735 A71-35383

Earth outward winding by cosmic particle gravitational accretion, examining individual meteor counts crossing celestial meridian in WE and EW directions 19 p3132 A71-37384

Newcomb precession constant accuracy, noting stellar motion anomalies and analytic effects on earth polar secular motion 19 p3049 A71-37442

Earth clock precision and rotation retardation effects on ephemeris time, comparing with atomic clock 19 p3060 A71-38529

Universal time and atomic clock earth rotation irregularities measurements checked for Chandler period 20 p3216 A71-39479

Earth rotation effect on mesoscale wave characteristics, considering Coriolis force influence in homogeneous inertly stratified jet stream 21 p3375 A71-41393

Earth rotational and deformational motion equations in extended Kalman-Schmidt filter for geodetic data processing [AAS PAPER 71-339] 23 p3666 A71-43012

Upper atmosphere rotation rate decrease at altitudes above 350 km, determining zonal wind variations by satellite orbits analysis from Hewitt camera observations 23 p3667 A71-43140

Earth angular velocity of rotation vector, discussing rotation rate and polar motion variations 23 p3674 A71-44260

EARTH SATELLITES

NT AEROS SATELLITE

NT ALOUETTE SATELLITES

NT ALOUETTE 1 SATELLITE

NT ALOUETTE 2 SATELLITE

NT APPLICATIONS TECHNOLOGY SATELLITES

NT ARIEL 1 SATELLITE

NT ARIEL 2 SATELLITE

NT ARIEL 3 SATELLITE

NT ATS 1

NT ATS 5

NT ATS 6

NT ATS 7

NT BEACON SATELLITES

NT BIOSATELLITE 2

NT BIOSATELLITE 3

NT BIOSATELLITES

NT COMMUNICATION SATELLITES

NT COSMOS SATELLITES

NT EARLY BIRD SATELLITES

NT EARTH RESOURCES TECHNOLOGY SATELLITES

NT ECHO 1 SATELLITE

NT ECHO 2 SATELLITE

NT ELEKTRON SATELLITES

NT ELEKTRON 2 SATELLITE

NT ELEKTRON 4 SATELLITE

NT ENVIRONMENTAL RESEARCH SATELLITES

NT BOSS

NT ESRO SATELLITES

NT ESRO 1 SATELLITE

NT ESRO 2 SATELLITE

NT EXPLORER SATELLITES

NT EXPLORER 12 SATELLITE

NT EXPLORER 22 SATELLITE

NT EXPLORER 26 SATELLITE

NT EXPLORER 28 SATELLITE

NT EXPLORER 31 SATELLITE

NT EXPLORER 33 SATELLITE

NT EXPLORER 35 SATELLITE

NT EXPLORER 37 SATELLITE

NT EXPLORER 38 SATELLITE

NT EXPLORER 40 SATELLITE

NT GEODETIC SATELLITES

NT GEOPHYSICAL SATELLITES

NT GEOS 1 SATELLITE

NT GEOS 2 SATELLITE

NT GEOS-C SATELLITE

NT HEOS A SATELLITE

NT HEOS SATELLITES

NT INJUN SATELLITES

NT INTLSAT SATELLITES

NT LINCOLN EXPERIMENTAL SATELLITES

NT METEOROLOGICAL SATELLITES

NT MOLNIYA SATELLITES

NT MOON

NT NAVIGATION SATELLITES

NT NIMBUS SATELLITES

NT NIMBUS 2 SATELLITE

NT NIMBUS 3 SATELLITE

NT NIMBUS 4 SATELLITE

NT OAO

NT OGO

NT OGO-B

NT OGO-C

NT OGO-D

NT OGO-E

NT OSO

NT OSO-F

NT OSO-G

NT OUTER PLANETS EXPLORERS

NT PAGEOS SATELLITE

NT PROTON 1 SATELLITE

NT PROTON 4 SATELLITE

NT RADIO ASTRONOMY EXPLORER SATELLITE

NT RELAY SATELLITES

NT SAN MARCO SATELLITE

NT SAN MARCO 2 SATELLITE

NT SPUTNIK SATELLITES

NT SYNCHRONOUS METEOROLOGICAL SATELLITE

NT SYNCOM SATELLITES

NT TELSTAR SATELLITES

NT TIROS SATELLITES

NT VELA SATELLITES

NT VENERA SATELLITES

NT VENERA 4 SATELLITE

NT VENERA 6 SATELLITE

Higher geodesy problems, determining earth dimensions and figure, gravitational field and absolute and relative point positions with artificial earth satellites 01 p0159 A71-10809

Gyroscopic precession effects in earth polar orbital satellite experiments for Einstein general relativity tests 02 p0312 A71-12369

Earth satellites ferrite core buffer storage replacement by magnetic tape unit noting design, performance, volume and operation [DGLR-70-082] 05 p0726 A71-15952

Book on earth satellite telecommunications systems and international law covering historical, scientific, economic, legal and political background 06 p1010 A71-18020

Astronautical TV camera and photogrammetric systems use on manned and unmanned lunar probes, discussing applications to earth surface surveys 06 p0901 A71-18287

Angular motion of deformable earth satellite as solid-elastic system with distributed masses, applying automatic control transfer function 09 p1491 A71-22548

Artificial earth satellites orientation determined by onboard telemetric measurements, constructing model for rotational motion around center of mass 09 p1531 A71-22569

Satellite path geometry along Keplerian elliptical orbit, taking earth flattening into consideration 09 p1520 A71-22664

Artificial earth satellite circular orbit determination from topocentric directions measurement by optical and electronic observations 09 p1408 A71-23176

Launch time selection for meteorological earth satellites, discussing launching sites, orbital altitude variations and orbit inclination 11 p1793 A71-25172

Algorithms for close earth satellite orbit calculation developed by numerical integration methods, discussing solution efficiency [AIAA PAPER 69-948] 11 p1820 A71-25463

Polish papers on artificial earth satellite observation covering celestial mechanics and orbit determination, geodetic applications, upper atmosphere and instruments 11 p1758 A71-25806

NonKeplerian intermediate orbit of artificial earth satellite motion with account of zonal harmonics, using fixed centers 11 p1829 A71-25807

Quasi-draconic and draconic orbital periods of earth satellites, showing ascending and descending passage variations 11 p1829 A71-25811

Eccentric satellite observation, considering geodesic determination of coordinate difference between observation station and reference point 11 p1732 A71-25818

Artificial earth satellite observation by Soviet universal and semiautomatic cameras with quartz clocks and four component mirror lens optical system 11 p1762 A71-25829

Lunar gravitational field application for placing spacecraft into static earth satellite orbit with standing position with respect to rotating earth 12 p1957 A71-26627

Artificial earth satellites equatorial topocentric coordinate determination, using photographic distance observations and least squares method 12 p1961 A71-26902

Artificial earth satellite orientation determination from single vector measurements, discussing coordinate systems transition 13 p2145 A71-28204

Oscillating artificial earth satellite orientation determination from geomagnetic field strength vector, using least squares method 13 p2145 A71-28205

Artificial earth satellites initial elliptical orbit calculation, discussing function minimization for optical radar and laser observation 15 p2481 A71-31301

Circular orbit patterns for continuous whole earth surface coverage with five satellites 16 p2630 A71-32840

Earth satellite plane periodic oscillations damping with respect to center of mass in orbital plane during motion on elliptical Kepler orbit 16 p2646 A71-33659

Angular position of sun nonoriented artificial earth satellites with angular velocities not exceeding 0.5 deg/sec, using harmonic analysis of magnetometric data 16 p2543 A71-33662

French monograph on satellite stabilization by ion propulsion and attitude control logic element design covering geostationary and geocentric satellites, mass and power balances 17 p2814 A71-35500

Deep space plasma measurement techniques by instruments on earth satellites 19 p3116 A71-38245

German monograph on locking process in earth satellites with passive magnetic attitude control covering satellite rotational motion mathematical model, stability analysis, etc 21 p3455 A71-40773

Narrow beam acquisition and angle tracking for spaceborne laser communication links between low earth orbiting and synchronous satellite 21 p3348 A71-40805

Circular sun synchronous earth satellites, investigating swathing patterns control by orbit selection and modification [AAS PAPER 71-353] 23 p3728 A71-43025

Satellite project cost estimation, evaluating formulae for budget, tender offer and contractual expense 23 p3785 A71-43459

Physical and radiobiological studies on earth satellites covering radiation hazards and effects on animals, plants, unicellular organisms and biochemical systems 24 p3798 A71-44886

EARTH SHAPE
U GEODESY
EARTH SURFACE

Autocorrelation function for gravity anomaly stochastic field outside earth spherical surface 01 p0127 A71-10358

Global atmospheric circulation, discussing surface irregularities and variable heating role in disturbances 01 p0121 A71-11352

Earth surface density distribution, using earth gravity field representation as potential of simple layer determined from combined satellite and gravity anomalies observations 02 p0246 A71-12463

Earth surface and atmosphere thermal radio emission measurement by radio telescope on Cosmos 243 satellite 03 p0409 A71-13420

Sudden impulses in geomagnetic field, discussing synchronous equatorial orbit-satellite magnetometer observations 03 p0421 A71-14537

Solar radiation fluxes at earth surface in presence of cumulus clouds, relating fluxes to cloud magnitude and sunshine duration by regression relations 06 p0889 A71-17648

Astronautical TV camera and photogrammetric systems use on manned and unmanned lunar probes, discussing applications to earth surface surveys 06 p0901 A71-18287

Satellite-borne long wave transmitting antenna excitation, calculating electromagnetic field near earth surface by earth-ionosphere waveguide model

08 p1252 A71-20744

World Weather Watch plan, discussing upper air, surface and satellite observations, telecommunication and data processing

08 p1328 A71-21719

Atmospheric pressure pulsation time spectra on earth surface as function of stratification conditions

08 p1286 A71-21876

Ionospheric current flow past circular inhomogeneous spot with Pederson and Hall conductivities, calculating earth surface magnetic field by Lipshitz-Hankel integral

09 p1436 A71-22549

Meteorite craters in U.S.S.R., discussing impact, explosive and complex craters

09 p1520 A71-22842

Distribution functions of errors in earth and moon horizon sighting due to planetary surface unevenness

09 p1523 A71-23147

Geodetic azimuth between two remote points on earth surface based on synchronous satellites positions and photographs

11 p1759 A71-25817

Earth surface thermal radio emission measurements by UHF radiometry onboard Cosmos 243 satellite, showing brightness profiles of water, ice and land areas

12 p1899 A71-26639

Recursion formulas for mapping entire earth ellipsoid on plane in single zone of Gauss-Kruger projection

12 p1900 A71-26970

Earth surface formations and clouds angular brightness distribution based on reflected solar radiation intensity

12 p1901 A71-27102

Satellite antenna power density contours on earth, using pattern operator for coordinate transformation

12 p1881 A71-27423

Earth surface nighttime, twilight and daytime horizons visual observations by Soyuz 9 spacecraft

13 p2060 A71-28426

Magnetosphere transmittance for fast magnetosonic waves, considering refraction, reflection and earth surface intersection

13 p2060 A71-28531

Earth surface temperature measurement by airborne IR radiometers, discussing accuracy provided by narrow and wideband filters

14 p2240 A71-30126

Jet aircraft sound spectrum on ground and in air, comparing calculation with experiment

14 p2289 A71-30524

Circular orbit patterns for continuous whole earth surface coverage with five satellites

16 p2630 A71-32840

Satellite view of earth surface, deriving expressions for cone-sphere intersections in terms of geographic coordinates

16 p2638 A71-33539

Earth and ocean surface state and cloud height determination using airborne laser radar observations

16 p2568 A71-33786

Global temperature effects on atmospheric carbon dioxide and aerosols density based on atmospheric model, noting earth surface temperature decrease

16 p2575 A71-34047

Polar asymmetry between distribution of surface features on earth, moon, Mars and Mercury

17 p2801 A71-34670

Impact craters and depressions on earth, examining meteoritic origin, characteristic features, energy release and cryptovolcanism

17 p2805 A71-35376

Meteoritics, covering impact on earth, craters, astrometites, tektites, carbonaceous chondrites properties, collisions, fragmentation, etc

17 p2809 A71-35714

Australian Liverpool and Strang way craters as probable meteoritic impact origin from topographic and petrographic data

19 p3049 A71-37653

Wideband spectrum utilization above 10 GHz for high rate digital communications and ecology monitoring of sea state, earth surface contour and atmospheric pollutants

19 p3020 A71-38407

Atmospheric pressure pulsation time spectra on earth surface as function of stratification conditions

19 p3060 A71-38469

Outer space and earth surface galactic cosmic ray intensity data correlation analysis for studying interplanetary magnetic field structure

20 p3278 A71-39129

Global, regional and local earth IR imagery for earth sciences from space TV, photography and spectrophotometry

20 p3220 A71-39665

Microwave sounding of ocean and earth surface thermal emission and atmospheric water vapor content by Cosmos 243 satellite-borne radiometers

20 p3259 A71-39672

Spectrophotometry and photography of earth twilight aureole, clouds and underlying surface from manned Soyuz 5 and 7 spacecraft

20 p3240 A71-39675

Earth surface characteristics measurements with remote sensors, proposing overland albedo measurements for clues as to ground type /clouds, vegetation, sand and snow/

20 p3260 A71-39684

Microwave emission measurement of earth surface from Cosmos 243 satellite, detecting radio brightness temperature dependence on latitude and local features

20 p3260 A71-39685

Earth surface effective temperature map from meteorological satellites IR imagery interpretation

20 p3260 A71-39686

Earth surface characteristics relationship to meteorological elements based on interpretation of color space photographs from automated Zond 7 station

20 p3260 A71-39687

Airborne measurement of directional variation in reflected solar radiation over soil surface and vegetation, using scanning radiometer

24 p3826 A71-44984

EARTH-MARS TRAJECTORIES

Free-fall periodic orbits /interplanetary trajectories/ connecting earth and Mars, using patched conic analysis

[ALAA PAPER 71-92] 06 p0977 A71-18547

Trans-Mars launch window problem, discussing minimum delta-V three-impulse noncoplanar transfer from circular parking orbit onto asymptotic velocity vector

10 p1671 A71-24331

Actual navigation dispersions, estimation uncertainties and resultant Mars orbit insertion statistical delta V requirements for six Mars approach angles in 1977 Mars window

[AAS PAPER 71-323] 23 p3726 A71-42997

Midcourse and planetary approach guidance by on-board optical measurements, noting application to earth-Mars trajectories and Grand Tour missions

[AAS PAPER 71-393] 23 p3702 A71-43061

EARTH-MOON SYSTEM

Earth rotation axis and mass center position determination, using earth-moon laser ranging data

01 p0161 A71-11383

Lunar origin by earth-moon fission, deriving parent planet characteristics from geochemical considerations

02 p0306 A71-11991

Earth-moon mass ratio correction, observing artificial satellite motion near triangular libration point

02 p0308 A71-12100

Accretion theory of planet and satellite formation in solar system, including earth-moon model

03 p0495 A71-14262

Precambrian and Cambrian stromatolites used for determination of nearest lunar approach to earth

04 p0583 A71-15141

Earth-moon test range for testing earth environmental characteristics in cislunar space, discussing administrative benefits

04 p0649 A71-15296

Two dimensional motion stability near sun-perturbed earth-moon triangular libration points, using computerized high order treatment

04 p0653 A71-15708

Orbit evolution of small mass near earth-moon system, noting solar perturbations and equations of motion

04 p0653 A71-15709

Three body stellar problem libration calculation using nonlinear mechanics methods, and application to lunar satellite perturbation by earth and lunar gravitational effects

04 p0655 A71-15728

Earth-moon mass ratio correction, observing artificial satellite motion near triangular libration point

08 p1362 A71-21150

Earth-moon libration point space station optimal control, considering restricted four body problem

08 p1363 A71-21233

Distribution functions of errors in earth and moon horizon sighting due to planetary surface unevenness

09 p1523 A71-23147

Collinear libration centers of spacecraft motion in sun perturbed three dimensional earth-moon system

10 p1671 A71-24329

Tumor theory of crust formation and moon-earth consolidation, showing fractional crystallization of basaltoid silicate melts

10 p1681 A71-25112

Earth-moon distance perturbations from anisotropic gravitational mass effect

11 p1819 A71-25209

Earth-moon system, examining kinematical and dynamical relationships, tidal deformation, earth rotation, secular variations, inclination and eccentricity

11 p1822 A71-25686

Earth-moon tectonic relationships and structural similarity, analyzing earthquake frequency dependence on lunar phase and distance based on Middlehurst catalogs

15 p2492 A71-32478

Apollo lunar expeditions assessment, discussing rock samples composition, origin, age and relation to earth system

21 p3442 A71-40148

EARTH-MOON TRAJECTORIES

Earth-moon mission fuel cells, discussing development of direct, indirect and redox cells

04 p0535 A71-15082

Reusable Nuclear Shuttle using NERVA nuclear engine for low cost transportation to lunar and geosynchronous orbit, discussing design, operation, tests and problems

11 p1840 A71-26516

Lunar orbiter earth-moon-earth optimal trajectories geocentric section calculations from low circumlunar flight procedures

13 p2142 A71-29178

Papers on mathematical methods in astrodynamics and celestial mechanics for earth-moon trajectories computation, satellite orbit determination and three body problem

16 p2630 A71-33056

Space shuttle operations analysis for cislunar space, including transfer trajectory inclination and long term effects

[AAS PAPER 71-300] 23 p3724 A71-42976

Mission analysis aspects of space shuttle operations between earth orbit station and lunar orbit station

[AAS PAPER 71-301] 23 p3724 A71-42977

Earth-moon and other trajectories calculation in planar elliptic restricted three body problem by slowly varying Jacobi function

[AAS PAPER 71-381] 23 p3731 A71-43051

EARTHQUAKES

Earthquakes correlation with lunar orbital motions, analyzing lunar perigee and new moon coincidences

05 p0809 A71-16457

Earthquake displacement fields and earth rotation - Conference, London, Canada, June 1969

06 p0889 A71-17876

Earth rotational acceleration and polar secular motion changes, considering correlation with earthquakes

06 p0890 A71-17881

Pole path deconvolution by optimum Wiener filter for acausal and causal cases, considering earthquake excitation

06 p0890 A71-17884

Chandler wobble seismic excitation by dislocations elasticity theory, discussing pole path changes-earthquake correlation

06 p0891 A71-17886

Earthquakes association with Chandler wobble from ILS-IPMS polar data

06 p0891 A71-17888

Major earthquakes effects on earth rotation pole disturbances from latitude and time data, considering Chandler nutation excitation

06 p0891 A71-17889

Earthquake correlation to polar motions explained by local stress distribution in lower mantle

06 p0891 A71-17891

Infrasonic shock wave generation in troposphere by powerful earthquakes, causing upper atmosphere density rise due to heating

08 p1278 A71-21019

Earth-moon tectonic relationships and structural similarity, analyzing earthquake frequency dependence on lunar phase and distance based on Middlehurst catalogs

15 p2492 A71-32478

Infrasonic shock wave generation in troposphere by powerful earthquakes, causing upper atmosphere density rise due to heating

20 p3219 A71-39599

P times least squares analysis complications by systematic earthquake location errors and azimuthal station anomalies variation

23 p3672 A71-43884

Underthrusting mechanism during southwest Japan earthquakes, presenting model of convergent plate interactions

23 p3672 A71-43885

EATING

Optimal preflight feeding for pilots, discussing protein content and vitamin enrichment

01 p0024 A71-11109

Eating and digestion effects on conscious dog coronary and visceral vasoactivity

01 p0015 A71-11183

Diurnal variations due to actual heat output, oxygen consumption and carbon dioxide production in rats undergoing eating habit changes

04 p0539 A71-15157

Incentive goal and extensive stimulation experience effects on proportion increase of hypothalamic electrode sites yielding elicited eating and drinking behavior

21 p3336 A71-40706

EBULLITION

U BOILING

ECCENTRIC ORBITS

Highly eccentric satellite orbit, determining analytical solution for HEOS 1 launch window

01 p0154 A71-10386

Stroboscopic and analytical studies of oscillations and stability regions of gravity gradient satellite in eccentric orbit 18 p2963 A71-36282

Sun-earth distance and earth orbital eccentricity effect on E region peak electron density, discussing Chapman-like model 21 p3372 A71-40035

Apollo type asteroid with high orbital eccentricity and inclination and rough elongated shape, noting ephemerides 21 p3443 A71-40188

HEOS-A2 eccentric orbit satellite for interplanetary space and high latitude magnetosphere data, discussing onboard experiments, major subsystems and design philosophy 22 p3607 A71-41505

Diamant launch vehicle multistage development for placing satellites in low perigee and high eccentricity and high and low circular orbits 22 p3610 A71-42020

ECCENTRICITY

Eccentricity and clamping effects on stability and critical pressure of ring-reinforced cylindrical shells under internal pressure 08 p1369 A71-21122

Rotor elements eccentricity effect on rotor dynamic deflection, discussing rotor unbalance determination 24 p3884 A71-45010

ECCHELETTE GRATINGS

Echelle grating and transmission optics spectrographs using image intensifier tubes for increased sensitivity 02 p0250 A71-12138

UV solar spectrum rocket-borne high resolution spectroscopy by Fabry-Perot interferometer and echelle grating, discussing design parameters and recorded data 06 p0903 A71-18718

Echelle gratings in single pass spectrometers, discussing properties, instrument profiles quality and accuracy 22 p3537 A71-41473

Astronomical Cassegrain echelle spectrograph, discussing optical and mechanical design and aberration effects 22 p3542 A71-41933

ECHO SATELLITES

NT ECHO 1 SATELLITE

NT ECHO 2 SATELLITE

ECHO 1 CARRIER ROCKET

U THOR DELTA LAUNCH VEHICLE

ECHO 1 SATELLITE

Light pressure measurement acting on Echo 1 satellite, considering integral reflection coefficient 20 p3306 A71-39132

ECHO 2 SATELLITE

Trace length analysis of Pageos and Echo 2 satellites by camera observations 14 p2318 A71-31119

ECHOES

NT AURORAL ECHOES

NT CLUTTER

NT LUNAR ECHOES

NT LUNAR RADAR ECHOES

NT RADAR ECHOES

NT RADIO ECHOES

NT SIGNAL REFLECTION

NT VENUS RADAR ECHOES

HF and LF spatial echo plasma oscillations associated with wave transformations produced by external perturbations 01 p0135 A71-11033

Light echo obtained via giant laser pulse peak overlapping in space and time 01 p0095 A71-11034

Plasma echo oscillations superposition of consecutive perturbations separated by intervals greater than characteristic decay time 02 p0291 A71-12508

Electron line density determination by relative aerial power pattern effect on observed meteor echo amplitude 03 p0490 A71-13935

Satellite topside sounders oblique echoes, investigating upper hybrid resonance with WKB technique 03 p0420 A71-14531

Collision effects on temporal plasma wave echoes, using free particle model 05 p0790 A71-16661

Periodic drift echoes in magnetospheric energetic proton fluxes from satellite observation 06 p0950 A71-17283

Plasma waves and echoes characteristics and diagnostics, emphasizing longitudinal waves 07 p1172 A71-20502

Pulse echo ultrasonic measurement of thin film layer between thick media, using real time computation 09 p1458 A71-23439

Time and space variable echo waves in electron plasma by wave packets interaction, considering spectral line width finiteness influence 12 p1937 A71-27038

Magnetospheric electron echo probe experiment, using sounding rocket and injecting gun for controlled particle trapping investigation 12 p1953 A71-27674

Echo location systems theorem concerning ambiguity density relationship to signal bandwidth 14 p2194 A71-30063

Pulse type ultrasonic flaw detecting apparatus based on reflected echo size estimation 15 p2409 A71-32194

Temporal echo oscillations in collisionless relativistic electron plasma 17 p2786 A71-34198

Collisions or weak turbulence caused noise effects on broadening of echo pulses in magnetically trapped particles, using propagator formalism 19 p3113 A71-37746

Differential method of ultrasonic inspection and binary comparative search heads for implementation, combining mirror shadow and echo methods features 22 p3553 A71-41760

Exact test particle propagator of Lenard-Bernstein equation for magnetoplasma, applying to transverse plasma echoes 22 p3584 A71-42466

ECLIPSES

NT LUNAR ECLIPSES

NT SOLAR ECLIPSES

Geostationary communication satellites system with timed orbital motions for avoiding serial sun transit outages and eclipses 01 p0030 A71-10471

Jovian atmosphere physical properties inferred from eclipses of Galilean satellites, using color photoelectric photometry 13 p2134 A71-28284

Four eclipse reappearances observations of Jovian satellite Io by area scanning photometer, considering anomalous brightening 13 p2134 A71-28285

Io brightness anomaly after eclipse by Jupiter 15 p2491 A71-32421

Ganymede thermal inertia data from simultaneous visual photometry and IR radiometry observations during 17 March 1971 eclipse 17 p2807 A71-35418

Jovian satellite eclipse observations, reviewing simultaneous narrow band multichannel visual and near IR studies [AAS PAPER 71-107] 19 p3139 A71-37908

ECLIPSING BINARY STARS

Multicolor polarimetry of Beta Lyrae system, discussing observations instrumentation and reduction 01 p0153 A71-10354

Semidetached eclipsing binary stars mass exchange, examining stellar evolution, luminosity, mass loss and exchange and Roche limit 02 p0313 A71-12497

Algol type variables, investigating gradient Balmer discontinuity and diameter variations 04 p0651 A71-15662

AG Vir /HD 104350/ orbital element variations and light curve distortions, using least squares method 04 p0651 A71-15665

Black hole model accounting for epsilon Aur eclipsing binary secondary component observations 06 p0970 A71-18031

Epsilon Aur eclipsing binary primary star mass and evolutionary stage considered to interpret secondary 06 p0970 A71-18032

Eclipsing variable binary stars spectral and luminosity classes determination 07 p1200 A71-20035

Light and radial velocity curves of binary HD 175514, obtaining spectroscopic and photometric orbital elements 07 p1204 A71-20633

Eclipsing variable V701 Cen photoelectric observations in UVB tabulated, fitting Russell model solutions to data 08 p1357 A71-20874

Eclipsing variable binary system RR Centauri observed photoelectrically in yellow and blue light 08 p1357 A71-20875

WX Cep eclipsing system photoelectric components computed in standard UVB colors, obtaining orbital elements 09 p1527 A71-23526

Eclipsing system GG Cas, presenting photoelectric data 09 p1527 A71-23527

Eclipsing binary IZ Persei, examining photoelectric light elements 09 p1527 A71-23528

Algol secondary component gravity darkening observations, examining IR light curve 09 p1527 A71-23530

Orbital elements and corrected light curve of eclipsing variable star Z Vulpeculae, using FORTRAN 4 program 13 p2137 A71-28513

Dust disk around secondary component of Epsilon Aurigae, noting role in system eclipse 15 p2494 A71-32550

AO Algol-type variables W Del, T L Mi, RZ Cas, and delta Lib gradient variation and Balmer discontinuity, detailing luminosity and radius ratio effects 16 p2634 A71-33427

Computer model of eclipsing binary stars tested with photometric B and V observations and orbital elements of RU Ursae Minoris 16 p2635 A71-33436

Algol type star AW Peg, determining gradient, temperature, absolute visual magnitudes, equivalent absorption line widths, atmospheric parameters and spectral class 17 p2800 A71-34567

Luminosity curves for eclipsing Algol-type systems with extended atmospheres based on stellar models 17 p2803 A71-34840

Papers on astronomy covering eclipsing binaries, eclipse functions computations, silicon in sun, Magellanic clouds and stellar kinematics 20 p3300 A71-39819

Orbital elements of W Ursae Majoris systems, considering radial velocity curves, spectroscopic orbital solution, spectral peculiarities and spectrophotometry 20 p3300 A71-39820

Eclipsing binaries among Wolf-Rayet AO Cassiopeia and U Geminorum stars from photometric observations 20 p3300 A71-39821

Light curve and orbital elements of eclipsing binary star V 539 Arae 21 p3440 A71-40058

Spectroscopic radial velocity study of Algol eclipsing variable stars, deriving masses and apsidal motion evidence in short period orbit 21 p3446 A71-40418

Nonlinear photometric effects of limb darkening and gravity darkening dominance in eclipsing variables from light minima observations 22 p3604 A71-42332

Analytical model of eclipsing binary star systems, testing validity through numerical integration error analysis 24 p3867 A71-44437

Eclipsing variables period change dependence on spherical coordinate of stellar position in sky from O-C diagrams 24 p3873 A71-45080

ECLIPTIC

Zodiacal light polarized component observation at ecliptic longitudes and latitudes compared to zodiacal cloud model 01 p0158 A71-10773

Cosmic ray data, showing perpendicular density gradient to ecliptic plane 03 p0482 A71-14547

Interplanetary magnetic field in plane perpendicular to ecliptic, investigating force lines configuration by solar proton events 07 p1189 A71-20640

Two-parametric models of interplanetary dust distribution predictions involving zodiacal light scattering measurements from space probes for in- and out-of-ecliptic missions 20 p3219 A71-39637

ECOLOGICAL SYSTEMS

U ECOLOGY

ECOLOGY

Circadian rhythm in dermestid beetles *Trogoderma glabrum* Herbst as response to compulsory constant light and temperature conditions 01 p0020 A71-11567

Conference report on impact of man on global environment, assessing actions covering climatic and ecological effects, pollution monitoring, etc 02 p0246 A71-12350

Satellite monitoring impacts on global ecological and natural resource public policy issues 04 p0689 A71-14820

Ecological interpretation of daytime data from Nimbus 3 high resolution IR radiometer for hydrologic and plant distribution mapping 08 p1277 A71-20884

Airport environmental protection, discussing area-wide agency, FAA planning grant program and legal aspects 15 p2385 A71-32247

Earth Resources Remote Sensing Systems effectiveness, discussing sensor and satellite development, spectral and spatial recognition, data management and ecological and resource relationship 16 p2645 A71-33582

Space transport systems, discussing spaceship earth survival problem from cosmospic criteria 19 p3149 A71-37304

Wideband spectrum utilization above 10 GHz for high rate digital communications and ecology monitoring of sea state, earth surface contour and atmospheric pollutants 19 p3020 A71-38407

Remote sensing aerospace system for agriculture, considering soil mapping, forest fire reconnaissance, productivity evaluation and environmental and ecological conditions assessment 21 p3373 A71-40263

Earth-like ecology for habitation in space, considering hollow sunlit rotating space chamber for life cycles in controlled weather environment 21 p3343 A71-40360

ECONOMIC ANALYSIS

Book on aviation technology and market structure covering technological and scientific effects on industry innovative behavior, R and D programs, operating costs, etc 10 p1698 A71-23982

Model concepts and mathematical methods for planned economy conditions and goals representation, considering prediction reliability 11 p1860 A71-25257

Economic formulation in reliability engineering, expressing cost of failure and reliability improvement in comparable terms 12 p1987 A71-26678

Airport terminal building design and construction, noting economy and expansibility corequirements [SAE PAPER 710418] 13 p2044 A71-28307

Economic analysis of subsonic transport airplane design, evaluation and operation [SAE PAPER 710423] 13 p1995 A71-28310

Extrusion tools development since 1930, emphasizing economic aspects 14 p2253 A71-30470

Communication satellites electric propulsion economic tradeoff studies, considering propellant requirements for north-south stationkeeping, and near-synchronous orbit maneuvers [AIAA PAPER 71-683] 14 p2292 A71-30746

Air transport propulsion systems economics, considering first cost, specific weight, fuel consumption and maintenance effect on direct operating cost 16 p2523 A71-33469

Communication satellite systems vs conventional terrestrial methods, emphasizing economic comparison 17 p2697 A71-34236

Space shuttle cost effectiveness and utilization analyzed for system-level requirements to maximize economic benefits [AIAA PAPER 71-810] 17 p2813 A71-34730

Space shuttle economic and design impact on satellite payloads, noting variations in flight frequency and cost, hardware and performance [AIAA PAPER 71-807] 17 p2813 A71-34732

NASA space transportation system economics, discussing cost analytic considerations in comparing reusable vs expendable launch systems [AIAA PAPER 71-806] 17 p2841 A71-34733

Economic acceptability, structure and decomposition of multilevel optimal control for complex systems 18 p2896 A71-35916

Civil aircraft market analysis, examining replacement cycle and used aircraft market based on aircraft histories 18 p2989 A71-36676

Hypersonic air transportation based on supersonic combustion ramjet development, discussing economic feasibility 19 p2995 A71-37124

Economically optimal operation of circuits protecting object subject to stationary random process, determining object malfunction intensity 19 p3025 A71-37572

Satellite navigation system for aviation and marine use, examining operational requirements, economic viability and technical solutions 22 p3570 A71-41509

Air freight economics and growth forecast, discussing rates, cost and technological aspects 22 p3623 A71-41840

Ternary code and three value logic in digital computers, considering economic advantages, signal distinguishability and numerical interpretation of p digit abstract alphabet 22 p3516 A71-41856

Economic analysis effect on R and D projects choice, assessing Space Shuttle system 22 p3624 A71-42526

Aircraft part repair-throwsaway decisions for minimizing costs over life cycle by economic graphic screening techniques 23 p3661 A71-43197

ECONOMIC FACTORS

Socioeconomic changes in aeronautics, discussing faster long range aircraft, airport access problems, technological advances, short haul transportation and industry/government relations 12 p1868 A71-27601

Raw remote sensor data acquisition relationship to economic activity and interpretation for earth resource/environmental information 18 p2912 A71-36067

Space transportation system design concept based on reusable engines and partially external expendable tankage [REPEET], discussing economic factors 19 p3147 A71-37125

Satellite systems contributions to transmission technology, considering economic factors, satellite antennas and receiver noise figures 19 p3017 A71-37519

Plastic encapsulation for microcircuits including packaging, failure mechanisms, military qualifications and economic factors 19 p3033 A71-38508

Third London airport, discussing interface problems, economic factors, airspace utilization and compatibility with other countries 20 p3209 A71-39389

Airport operation costs affected by runway utilization, parking bays alignment, baggage handling and aircraft noise 20 p3209 A71-39390

Air traffic control delays, airport airspace congestion, flyover noise reduction and performance requirements effect on airline operations economics 20 p3209 A71-39391

Book on space technology for developing countries covering economic, social and educational reform, solar system exploration and extraterrestrial civilizations 22 p3623 A71-42066

Weather interruption effects on air transportation operations and economics, considering fog, snow, freezing rain, thunderstorms, winds, CAT and runway conditions 24 p3845 A71-44983

ECONOMICS

NT DEMAND [ECONOMICS]

Flight training simulator use in airline operations, discussing economics of various simulator types with projection toward ultimate simulator 01 p0183 A71-10023

Materials R and D economic considerations, emphasizing processing and assembly costs reduction and user benefits 01 p0183 A71-10279

Economic contributions of U.S. domestic airline industry in 1970s regarding air transportation constraints and impact on short haul [AIAA PAPER 70-1309] 01 p0004 A71-10486

Aeronautical projects development and planning in European Economic Community, discussing aerospace industry organizational problems and role in economy 02 p0334 A71-11676

Niobium processing methods from economic standpoint, describing pyrochlore metallothermic reduction 02 p0271 A71-12938

Economic trends of international air transport in 1970s 04 p0690 A71-14991

German monograph on socioeconomic evaluation of air transportation systems for developing nations, using cost-benefit analysis 04 p0691 A71-15125

Remote area voice, teletype and data communication using satellites for providing links with central terminals, considering economic feasibility by cost analysis 04 p0555 A71-15338

Satellite communication system parameters optimization based on economical and technical constraints, applying to Intelsat 3 07 p1063 A71-20040

Air cushion vehicle technology, considering economics, propulsion, structures, controllability, flexible skirt systems and R and D [SAE PAPER 710183] 08 p1231 A71-21713

International telephone transmission, comparing technical and economic characteristics between submarine cable and satellite systems 10 p1577 A71-24267

Radar cross section data analysis, considering economical approximation techniques in HF and LF ranges 12 p1882 A71-27440

Aircraft jet engines technological progress review over past 25 years, emphasizing industry economics considerations 14 p2341 A71-30303

Aircraft-simulating cockpit procedure trainer statistical data and development problems concerning safety, economy and efficiency performance 15 p2384 A71-31883

Community actions for jet aircraft noise reduction, discussing noise environments, nationwide goals, decision making and economic incentives 15 p2516 A71-32249

Space program economics, discussing applications benefits, spending and byproduct effects cost planning, funding and organization 16 p2665 A71-33590

Radio communication system optimization from viewpoints of global synthesis including economics and partial synthesis based on noise stability, precision and reliability 17 p2698 A71-34392

Satellite communication system selection vs underground cable or hybrid systems, based on power requirements and economics 17 p2700 A71-34678

Economical alternative construction materials selection for partmaking cost reduction while maintaining quality 20 p3251 A71-39338

Broadband point-to-point communication satellite systems for 1970s, discussing R and D effort, economics and international and domestic applications 20 p3197 A71-39606

Government and public agencies procurement policy evolution from legal obligations to economic impact consideration 23 p3786 A71-43464

Incentive contract with contractor profit based on achievement in cost, schedule and technical performance 23 p3786 A71-43467

ECONOMY

German monograph on airport role in national economy and growth and location determination for enterprises maintaining connections with foreign countries 17 p2841 A71-34482

Manned orbital operations economy for space station utilization, discussing laboratory equipment, on-orbit supervision, maintenance and remote communications limitations [MDAC-WD-1746] 22 p3611 A71-42030

KODIES

U VORTICES

EDDINGTON APPROXIMATION

Spherically symmetric systems radiative transfer problems using iteration on Eddington factor 14 p2307 A71-29864

EDDY CURRENTS

Electroinductive defectoscopy using eddy currents as nondestructive materials testing method 01 p0079 A71-10335

Flaw detection system for wide Al sheets, using eddy current equipment with modulation analysis principle 01 p0087 A71-10458

Damping in gravity graded satellite passive stabilization systems under eddy currents and dry friction induced by magnet motion 02 p0319 A71-11908

Metal parts fatigue life prediction by eddy current method, using experimental relationship between disbalance voltage and stress cycle number 08 p1300 A71-21893

Eddy current nondestructive tests for surface defects detection, determining optimum test parameters based on calculation 09 p1454 A71-22213

Mechanical characteristics of extruded thermally hardened aluminum alloys determined by eddy current method 09 p1468 A71-22326

NBS traceable nonferrous conductivity standards for eddy current testing, discussing error analysis, long term drift, grain direction and stratification effects 09 p1469 A71-22710

Damping in gravity gradient satellite passive stabilization systems under eddy currents and dry friction induced by magnet motion 13 p2144 A71-28195

Book on electromagnetic nondestructive test methods covering eddy current test, EM field theory, operation and design of sensing coils, etc 15 p2418 A71-32768

Electric field in flow of medium with tensor conductivity due to Hall effect, studying eddy currents structure in magnetic field variation region 16 p2616 A71-32929

Hot wire and tubes nondestructive eddy current testing as cybernetic process, noting high speeds with high on-line data flow 17 p2749 A71-35494

Characterization of high purity metals by residual resistivity ratio, using nondestructive eddy current decay method 18 p2938 A71-36992

Decarbonization monitoring of ball bearing steel bars, describing defectoscope based on eddy current higher harmonics method 22 p3553 A71-41768

Varying magnetic field disturbance by eddy currents in conductive elliptical cylinder, obtaining field vector potential and magnetic induction vector 22 p3528 A71-41769

Eddy current field formation of defect on extended surface crack in ferromagnetic and nonferromagnetic metals, investigating superposed transformer detector inductor coil effects 22 p3529 A71-41770

LF eddy current bridge to measure small magnetic permeability changes in weakly ferromagnetic materials, applying to nondestructive tests of austenitic stainless steels 23 p3681 A71-43193

Automatic eddy current system to detect fastener hole cracks consisting of scanner unit, control box, recorder and mounting hardware 24 p3831 A71-45281

EDDY DIFFUSION

U TURBULENT DIFFUSION

EDDY VISCOSITY

Adiabatic compressible turbulent boundary layer equations for two dimensional and axisymmetric flow,

- discussing methods of solution based on eddy viscosity formulation
[AIAA PAPER 69-687] 01 p0071 A71-10933
- Separated turbulent eddy viscosity models incompressible similar reverse flow velocity profiles from Falkner-Skan equations
[AIAA PAPER 71-203] 06 p0886 A71-18641
- Nonlinear subgrid scale eddy viscosity formulation for turbulence generated by mean shear or thermal instability at large Reynolds number
07 p1094 A71-20615
- Turbulent wakes from subsonic-hypersonic bodies for downstream mean flow predictions analysis, considering eddy viscosity function
10 p1550 A71-24338
- Thermosphere heating due to auroral electrojets, discussing thermospheric variations and eddy viscosity
10 p1602 A71-24554
- Circular turbulent liquid jet in external stream, considering Reichardt theory, jet expansion law, asymptotic similarity and constant eddy viscosity hypotheses
10 p1597 A71-24940
- Shear stress and eddy viscosity distribution in Mach 20 compressible turbulent boundary layer, using mixing length flow theory
11 p1751 A71-25499
- Boundary layer equations based on eddy viscosity model for turbulent free shear flow, solving numerically in Crocco coordinate plane
[ASME PAPER 71-FE-17] 13 p2052 A71-29456
- Shear stress, eddy viscosity and mixing length distributions in compressible turbulent boundary layers with air and carbon dioxide injection
14 p2228 A71-31025
- Eddy viscosity model for turbulent pipe flow, yielding velocity distribution, shear, energy production and viscous dissipation rate
17 p2728 A71-34881
- Incompressible turbulent boundary layers at low Reynolds numbers, using eddy viscosity and mixing length concepts for computation
17 p2728 A71-34884
- Eddy viscosity in barotropic planetary boundary layer, finding turbulent diffusion coefficient dependence on turbulent kinetic energy
20 p3257 A71-39437
- Mercury perihelion advance due to solar mass distribution departure from spherical symmetry because of negative eddy viscosity
21 p3439 A71-41422
- Generalized eddy viscosity model application to quiescent and coflowing axisymmetric turbulent jets mixing
24 p3818 A71-44626
- ## EDEMA
- Pulmonary oxygen toxicity, considering composition of endobronchial saline extracts of rats and edema development
13 p2015 A71-29362
- Rabbit tolerance to pulmonary edema by lung exposure to low ozone dosage
19 p3009 A71-38558
- ## EDGE DISLOCATIONS
- Edge dislocations in deformed single crystals of Nb-Mo and Nb-Re alloys at various temperatures
01 p0101 A71-10738
- Stationary edge dislocation interaction with partially bonded bimetallic interface, noting isotropic elastic continuum approximation
04 p0670 A71-15383
- Bcc metals slip band formation, investigating deformation and fraction behavior
08 p1308 A71-21515
- Li and temperature effects on mechanical properties of Mg base single crystals in basal and prismatic slip
08 p1309 A71-21525
- Fcc binary alloys cross slip difficulty due to solute atoms and small short range order regions
08 p1309 A71-21527
- Fast brittle crack slowing by mechanical twins in transformer steel and by slip bands in LiF and NaCl crystals
09 p1468 A71-22625
- Multiplication, diffusion and vanishing of dislocations, slip band formation mechanism and lattice defects interactions during metal fatigue
10 p1626 A71-24386
- Linear isotropic and centro-symmetric second-grade elastic material and special case with coupling stress, calculating stress field of long straight screw and edge dislocations
14 p2327 A71-30290
- Surface deformation in polycrystalline Al samples produced by ultrasound generated cyclic stresses, examining slip bands formation by electron microscope
16 p2591 A71-33224
- Electro-optic He-Ne laser microscope for high-speed high-precision edge detection for IC masks
19 p3075 A71-38236
- Microfriction anisotropy of graphite at small loads for sliding on basal and edge planes, using scanning electron microscope
20 p3253 A71-39410
- Inconel-600 under heat treatment and tension tests, examining grain boundaries slip interaction
21 p3397 A71-40458
- Edge dislocations mobility in zone refined alpha Ti single crystals in bending, using etch pit techniques at 77, 200 and 300 K
21 p3404 A71-41415
- Plastic deformation of solid body in terms of slip dislocations displacement rate
24 p3885 A71-45052
- ## EDGE LOADING
- Thermoplasticity plane problems with complex edge loading, deriving algorithm based on theory of flow with translational hardening
02 p0323 A71-11746
- Biorthogonal relation for bending of uniformly loaded clamped sector plates with boundary functions along curved edge
02 p0327 A71-12397
- Stress development in elastic plate with crack under edge loads, estimating plastic zone size at crack ends
03 p0514 A71-14361
- Photographic study of early vortex formation in flow started by shock diffracting over edge
04 p0586 A71-14702
- Stress state analysis in rigidly clamped circular plate bent by edge loads, using three dimensional elasticity theory
06 p0989 A71-17786
- Semiinfinite solid elastic cylinder under self equilibrium end loading, obtaining elastostatic solution
06 p1000 A71-18027
- Thin elastic toroidal shells under nonsymmetric harmonic loadings, reducing problem to membrane and edge effect linear solutions
06 p1002 A71-18415
- Stress-strain state of rectangular transversely isotropic plate with clamped edge under uniformly distributed load, considering bending moments
07 p1218 A71-20473
- Edge loading effects on shallow hyperbolic parabolic shell elastic damping, discussing flat plate theory analog solution
10 p1686 A71-23995
- Interlaminar plane shear stress in fibrous composites under elastic deformation with edge effect, using membrane finite element analysis
11 p1852 A71-26394
- Plane stress distribution solution for rectangular elastic plastic plate under partial edge loading, using incremental theory
12 p1976 A71-27122
- Sharp circular edged orifice dynamic characteristics under high amplitude periodic fluid flow conditions, discussing hydraulic resistance coefficients
12 p1898 A71-27506
- Influence coefficients for thin walled finite length cylindrical shells subjected to uniform internal pressure and edge loads
12 p1983 A71-27586
- Edge restraint effects on postbuckling behavior of thin flat plates under uniformly distributed compressive loads, noting buckling load and stiffness increase
13 p2153 A71-28466
- Reinforced toroidal shells stability under critical local loads, edge moment and heating, using finite difference method
14 p2332 A71-30847
- Free edge effect on critical loading of rectangular sandwich plate with asymmetrical structure and rigid filler
17 p2833 A71-35622
- Axisymmetric buckling of annular plate subjected to unequal uniform radial compression along inner and outer edges
22 p3615 A71-42036
- Radial edge displacement effect on circular cylindrical shells compressive buckling stress, noting opposite effects for different length/radius ratio ranges
[AIAA PAPER 71-984] 24 p3878 A71-44580
- Edge supported anisotropic elliptic plate with hole under bending by constant lateral edge load, presenting stress-strain state
24 p3882 A71-44837
- ## EDGES
- ### NT LEADING EDGES
- ### NT SHARP LEADING EDGES
- ### NT TRAILING EDGES
- Rectilinear edge aperture filtration, examining mismatch angle effects on video signal amplitude
02 p0248 A71-11828
- Locally illuminated diffracting edge near field calculation in terms of Hankel function asymptotic solution
09 p1409 A71-23514
- Stress analysis near free surfaces in thin composite plates with unidirectionally oriented elastic isotropic fibers, applying boundary point least squares technique
11 p1851 A71-26382
- Thermal stresses in circular plate with cylindrical orthotropy and reinforced edge, determining temperature and stress distributions
12 p1979 A71-27356
- Edge effect in elastic lattice shells generalized from lattice plates and disks
19 p3158 A71-38152
- Edge effects in finite linear arrays of uniform slits fed by parallel plate waveguides terminated on ground plane
23 p3653 A71-44156
- ## EDUCATION
- ### NT ASTRONAUT TRAINING
- ### NT FLIGHT TRAINING
- ### NT PILOT TRAINING
- ### NT SPACE FLIGHT TRAINING
- Entropy-disorder concepts relation in teaching thermodynamics, urging treatment as macroscopic theory
01 p0126 A71-10134
- Airline experience with dual inertial systems as sole means of navigation, considering equipment reliability, cockpit design, training, etc
01 p0124 A71-10509
- Planetaria as celestial navigation instruction aids, discussing astronomical simulation capabilities, celestial coordinate systems, special effect projectors, etc
01 p0022 A71-10519
- USAF navigator training, discussing operational demands, philosophy, present and future training capabilities, etc
01 p0022 A71-10520
- Complex navigation systems training philosophy emphasizing functional approach to system and components
01 p0023 A71-10523
- Flight crew training process oriented systems approach through multimedia instruction
01 p0023 A71-10524
- Microelectronics technology effects on electronics engineer education, considering data processing applications and circuit types
03 p0388 A71-13005
- Multidisciplinary design courses in engineering education for professionals appreciating inputs from outside fields
04 p0691 A71-15278
- NASA and Army Research Office /ARO/ instruction monographs applications for classroom and self study use
04 p0691 A71-15279
- Beam foil spectroscopy using van de Graaff accelerator, considering applications to atomic physics research and teaching
08 p1272 A71-21667
- ATC services training and operations methods adopted by International Aeradio Ltd
09 p1491 A71-22952
- Digital simulator for training ATC officers, considering authenticity and working and geographical environments
09 p1428 A71-22954
- Human position in socialist productive system, examining pedagogical aspects of leadership
13 p2019 A71-28491
- Communication satellites use as educational medium, discussing program organization, student and faculty involvement, course contents and methods
14 p2341 A71-30829
- Education in creative engineering - Conference, MIT, April 1970
15 p2348 A71-31593
- Characteristics study of technical entrepreneurs, considering family background, education and motivation
19 p3173 A71-37631
- Psychological training for personality development of aircraft stewaresses for conscious passenger relation establishment
19 p3008 A71-38224
- ## EDUCATIONAL TELEVISION
- Satellite educational TV for developing nations, using cost benefit approach for system selection
04 p0691 A71-15277
- Education satellite technology, discussing transmission levels, low cost high sensitivity receiver design and TV broadcasting
16 p2638 A71-33581
- Satellite systems for educational TV program distribution, discussing orbit utilization, ground stations and ATS program
16 p2645 A71-33588
- Satellite broadcasting defined by UN, discussing community and home direct reception modes and educational TV potentialities and problems
17 p2697 A71-34238
- Satellite TV educational applications, outlining joint Indian Atomic Energy Department and NASA project
17 p2841 A71-34239
- UN leadership in space communications international cooperation, emphasizing communication satellite systems application to educational TV
17 p2841 A71-34249
- Satellite instructional TV experiment for direct community broadcasting to Indian villages
[AIAA PAPER 71-844] 17 p2700 A71-34709

Joint India-U.S. satellite instructional television experiment for national development using ATS-F spacecraft 18 p2988 A71-36502

Pilot system of satellite transmitted educational TV involving lines reduction on TV screen 18 p2988 A71-36506

EEG [ELECTROENCEPHALOGRAMS]

U ELECTROENCEPHALOGRAPHY

EFFECTIVENESS

NT COST EFFECTIVENESS

NT SYSTEM EFFECTIVENESS

EFFECTORS

U CONTROL EQUIPMENT

EFFERENT NERVOUS SYSTEMS

Interhemispherical synthesis of conditioned reflex motor reactions at different running angles in mice 01 p0011 A71-11051

Circadian work-rest cycles in isolated humans 01 p0017 A71-11411

Muscle simulation by information theory for statistical analysis of behavior based on gas thermodynamics methods, showing stress relation to motor units excitation 03 p0366 A71-12979

Adaptation mechanism of human movement control as motor neuron reaction to external stimuli, considering peripheral arch, cerebrospinal canal and feedback 03 p0356 A71-12986

Movement coordination in animals during walking and running, revealing neurophysiological mechanisms of locomotion control 03 p0356 A71-12987

Human motor reactions sequential systems control characteristics, considering effects of external stimulus and repetition time interval 03 p0357 A71-12988

Electroencephalographic and motor effects of electrically stimulated reinforcing and negative subcortical structures in sleeping cats 06 p0852 A71-17669

Venomotor responses of forearm veins to local and remote thermal stimuli to skin in exercising man 06 p0862 A71-18383

Antagonistic descending characteristics of medial and lateral hypothalamic nuclei on excitation of spinal cord motoneurons 06 p0856 A71-18465

Cerebellum efferent visceral field functional organization in cats 08 p1240 A71-21794

Motor analyzer role in animal orientation to external conditions 08 p1243 A71-21969

Signal transformation laws of central nervous system motor command patterns construction from sensory impulse streams 10 p1569 A71-24236

Globus pallidus damage in cats, investigating effects on conditioned motor reflexes, learning and memory 10 p1564 A71-24466

Muscular fibers analysis for motoneuron split potentials, using needle electrode 10 p1564 A71-24484

High motor stresses effects on muscle acetylcholine content, cholinesterase activity and localization, solitary contractions fusion and pessimal weakening 14 p2186 A71-30553

Pulse frequency behavior during acquisition of perceptual and motor skills with particular attention to rest periods 15 p2362 A71-31195

Human skeletal muscle reflex and motor reactions in response to tibial nerve stimulation 15 p2360 A71-32532

Efferent vagal activity increase prior to intermittent cardiac block due to rise in blood pressure 16 p2529 A71-33192

Human motor control behavior sampling hypothesis of open loop system at voluntary effort initiation, discussing validity based on ankle rotation physiological test 17 p2690 A71-34741

Rat brain acetylcholine levels circadian rhythm correlated to spontaneous motor activity and sleep-awake cycle 17 p2684 A71-35326

Reaction times distributions in visual or auditory mode single and multiple motor response units 17 p2686 A71-35433

Extraocular muscle structure and function, defining slow and fast motor system based on slow and fast fibers 17 p2687 A71-35801

Cats preoptic and skin temperature change effects on posterior hypothalamic neurons 18 p2861 A71-36888

Circadian rhythm maturation of brain norepinephrine and serotonin in rat, relating spontaneous motor activity and sleep-wakefulness mechanism 19 p3003 A71-38071

Book on noise effects on man covering audiometry, aural reflex, hearing damage risk, physiological

responses, motor performance and speech communication 20 p3193 A71-39874

Alpha activity parameters during human performance of motor tasks with open and closed eyes 23 p3631 A71-43108

Human motor system control mechanism for stretch reflex loop gain with simplified central nervous system computation 23 p3639 A71-43354

Trace reflex formation in response to acoustic stimulus with verbal reinforcement, determining cross correlation connections between induced activity of auditory and motor areas 24 p3796 A71-44547

EFFERVESCENCE

Sulfur effervescing molten slag/gas systems causing planetary vulcanism, examining patterns on earth, moon and Mars 15 p2496 A71-32708

EFFICIENCY

NT COMBUSTION EFFICIENCY

NT COMPRESSOR EFFICIENCY

NT ENERGY CONVERSION EFFICIENCY

NT NOZZLE EFFICIENCY

NT POWER EFFICIENCY

NT PROPELLER EFFICIENCY

NT PROPULSIVE EFFICIENCY

NT THERMODYNAMIC EFFICIENCY

NT TRANSMISSION EFFICIENCY

Efficiency improvement of holograms with very high reference beam to object beam intensity ratio by constructing copy from first hologram 08 p1291 A71-21399

EFFORT

Mental reactive exertion increase phenomenon, investigating achievement under various degrees of carefulness and fatigue 18 p2862 A71-36945

EFFUSIVES

Lithium tetrafluoroaluminate equilibrium vapor pressure over solid aluminum fluoride plus solid lithium cryolite examined by weight-loss effusion method 07 p1055 A71-19624

EGGS

Lethal recessive point mutation in *Drosophila melanogaster* eggs on Zond 5 spacecraft 01 p0018 A71-11552

EIGENFUNCTIONS

U EIGENVECTORS

EIGENSTATES

U EIGENVECTORS

EIGENVALUES

Variable thickness circular plate uniformly clamped along edge, calculating critical force from eigenfunctions and eigenvalues of equation with one independent variable 01 p0171 A71-10650

Eigenvalue errors in applying method of weighted residuals to linear nonself adjoint problems of structural analysis 01 p0174 A71-10944

Undamped structural vibration problems solution for eigenvalues and eigenvectors using simultaneous iteration method 05 p0829 A71-17113

Large linear systems smallest eigenvalues determination, examining various algorithms 05 p0829 A71-17114

Integral equation eigenvalues extension from single to multiple interface Neumann problem 05 p0776 A71-17222

Nonrecursive solution for discrete Riccati equation by finding eigenvalues and eigenvectors of canonical state-costate equations 06 p0878 A71-17335

Control systems root contours boundary lines, dividing a plane into realizability regions for system characteristic equation complex conjugate roots 06 p0878 A71-17337

Rib reinforced cylindrical shell stability under annular and axial stresses, determining eigenvalue of homogeneous integral equation 06 p0993 A71-17816

Laminar flow heat transfer in circular pipes, solving for Graetz equation eigenvalues and eigenfunctions 06 p1007 A71-18304

Matrix eigenvalue problem solution by reducing to nonlinear algebraic equations for iterative solution or integration by Runge-Kutta method 06 p0921 A71-18342

Spring supported beam-column n th vibration and buckling eigenvalues, discussing Monte Carlo simulation for evaluating perturbation method accuracy for variance calculation [AIAA PAPER 71-149] 06 p1004 A71-18591

Discrete linear vibration systems viscous damping local modifications effect on eigenvalues and vectors, using Weissenburgers procedure in matrix form [AIAA PAPER 71-215] 06 p0928 A71-18651

Kato upper and lower bounds formula applications to Hermitian operator eigenvalues 07 p1146 A71-18748

Ground state energy approximate eigenvalues calculation for electron in stationary finite electric dipole field by variational approach 07 p1163 A71-19684

Surface pressure field sampled natural functions, statistical stability, taking into account eigenvalues magnitudes and rate of decrease 09 p1487 A71-23240

Complex zeros of complex polynomials, matrix inequalities and nonlinear programming, constructing areas intersection in complex plane defined by inequality bounds on eigenvalues of companion matrix 09 p1485 A71-22970

Comparative study of consistent and simplified finite element analyses of eigenvalue problems 09 p1541 A71-23220

Asymptotic solution for conical horn modes, comparing with exact solution for eigenfunctions and eigenvalues 09 p1420 A71-23677

Nonlinear second order differential system two-point boundary problems, establishing eigenvalues and associated solutions boundedness and oscillations 10 p1636 A71-241308

Nonconservative force system eigenvalues and eigenvectors reproduction by related conservative system 10 p1689 A71-24513

Linearized relativistic transport equation for mixture of isobaric Maxwellian molecules, solving in terms of eigenfunctions and eigenvalues of collision operators 10 p1645 A71-24609

Retroversion from preferred eigenvalues to determine compatible structural characteristics, deducing design changes in model configurations from perturbations imposed [AIAA PAPER 71-345] 11 p1843 A71-25324

Eigenvalues of axially uniform fluid waveguide with eccentric annulus cross section and acoustically hard boundaries 12 p1928 A71-26700

Iterative solution of semidefinite eigenvalue problems, identifying rigid body and deformation coordinates 12 p1974 A71-26873

Krause-Steenbeck solar dynamo eigenvalue evaluation assuming step function differential rotation and delta function alpha-effect for approximation 12 p1971 A71-27749

Conditions for obtaining analytical expressions for eigenvalues and eigenfunctions of homogeneous Fredholm equation 13 p2096 A71-28015

Equilibrium of three dimensional elastic body under finite uniform deformation, deriving characteristic equations for cylindrical shells, circular and rectangular plates and circular rods 13 p2149 A71-28126

Eigenvalue, shooting and parallel shooting methods for solving Falkner-Skan boundary layer equation with positive or negative wall shear 13 p2047 A71-28397

Characteristic equation of respiration vibrations of cylindrical ring in incompressible viscous fluid at rest, obtaining damping coefficient for large induced flow Reynolds numbers 13 p2047 A71-28397

Laser resonator with selector for Hermite-Gaussian TEM₂₂ mode, obtaining integral equation solutions for eigenmodes and eigenvalues on digital computer 13 p2078 A71-28608

Eigenvalue problem for transfer matrix of two dimensional Ising lattice with free boundaries perpendicular to transfer direction, calculating correlation function between spins 13 p2094 A71-28777

Existence theorems for eigenvalues of integral equations with continuous kernels 13 p2096 A71-28907

Spherical waveguide eigenvalues calculation from two layer model of earth with radially inhomogeneous atmosphere, using Airy functions 14 p2209 A71-29515

Eigenvalue problems in theory of sandwich plates with rigid cores, obtaining solutions by Galerkin method 14 p2322 A71-29734

Numerical study of three dimensional structure and energetics of unstable disturbances in pure baroclinic and barotropic zonal currents, using eigenvalue technique 14 p2269 A71-29949

Harmonic vibration analysis methods, discussing mathematical model, ground tests, structure suspension exciter and pickup location eigenvalue measurement and mode research 14 p2175 A71-30058

Curvature effects on shallow shell free vibration frequencies, solving linear eigenvalue problem 14 p2325 A71-30062

Ridged waveguide complete eigenvalue solution by integral equation formulation and Ritz-Galerkin method 14 p2212 A71-30516

Simplified characteristic equation for plane piezoelectric vibrations of lithium niobate and lithium tantalate crystals, using perturbation methods 15 p2461 A71-31701

Asymptotic eigenvalue density estimates for edge-hinged thin elastic rectangular shell, determining shell stability linear equation solution conditions 16 p2647 A71-32937

Matrix trace method for identities relating eigenvalues of singular ordinary differential operators and zero Bessel functions 16 p2603 A71-33593

Convergence and error estimates for finite difference methods for approximately positive solutions of mildly nonlinear eigenvalue problems 17 p2768 A71-35683

Eigenvalues of band matrices with nonzero elements below main diagonal or differing from Toeplitz matrix in first row 17 p2768 A71-35687

Jacobi algorithm for computation of eigenvalues and eigenvectors of skew symmetric matrix by real arithmetic 18 p2942 A71-36698

Finite difference approximation for discrete eigenvalues of clamped plate, using operator and perturbation technique 18 p2980 A71-36701

Nonlinear eigenvalue problem solution in real Banach space, investigating continua existence and elliptic equations application 18 p2942 A71-36818

Dielectric potential operator as arbitrary bounded Lebesgue measurable set, obtaining eigenvalues and eigenfunctions spectrum 18 p2942 A71-36820

Natural axisymmetric vibration of thin elastic shell of revolution, deriving eigenvalues convergence to spectrum lower bound by asymptotic method 19 p3154 A71-37097

Large stiffness matrices building and manipulation, including structural analysis computer programs input determination, coupling techniques and eigenvalue problems solution 19 p3161 A71-38654

Iterative finite difference solution of Laplace operator interior eigenvalues and eigenfunctions, noting convergence in application to Helmholtz equation 20 p3201 A71-38755

Sequence convergence of similarity transformations in matrix balancing for accurate eigenvalues computation 20 p3254 A71-38756

Rapidly converging second order optimal tracking algorithms for adaptive equalization on basis of estimated bounds for eigenvalues of signal plus noise correlation matrix 20 p3201 A71-38872

Eigenvalues lower bounds determination for arbitrary shape region, presenting domain constriction method 21 p3416 A71-41014

Extreme eigenvalues of Toeplitz matrices associated with Laguerre and Jacobi polynomials, using finite difference operators 21 p3410 A71-41084

Frequency and buckling stability eigenvalue evaluation for anisotropic circular cylindrical shells under nonuniform lateral prestress 22 p3615 A71-42210

Multicomponent diffusion process calculation using eigenvalues of Onsager diffusion matrix 22 p3575 A71-42371

Eigenvalues and eigenvectors error estimation in vibration and stability finite element analysis as function of mesh size, using Birkhoff perturbation method 22 p3617 A71-42541

Ax equals lambda Bx eigenvalue problem, presenting Perron and Frobenius results and dual characteristics 22 p3567 A71-42627

Sturm-Liouville type nonlinear problems solution by Prufer polar coordinate technique, proving equivalency theorem for eigenvalues infinite sequence conversion 22 p3567 A71-42689

Simultaneous iterative solution for obtaining dominant subset of unsymmetric matrix eigenvalues and eigenvectors 23 p3698 A71-43098

Iterative solution of eigenvalue problems for positive real symmetric matrices without first approximation of eigenvalues and eigenvectors, constructing by powers of spectral decomposition 23 p3699 A71-43488

Characteristic modes theory for radiation and scattering by conducting bodies, considering electric and magnetic fields 23 p3660 A71-44161

Characteristic modes computation for conducting bodies of revolution, discussing radiation and scattering patterns convergence 23 p3654 A71-44162

Biharmonic operator eigenvalues for rectangular domain, presenting bilateral a posteriori estimation

methods based on discrete analysis and approximate separation of variables 24 p3842 A71-44476

Boundary value problems eigenvalues determination with differential equations for lifting surfaces vibration theory 24 p3818 A71-44706

Elasticity and acoustic theory eigenvalues determination in spherical coordinates using transcendental equation 24 p3882 A71-44836

EIGENVECTORS

Variable thickness circular plate uniformly clamped along edge, calculating critical force from eigenfunctions and eigenvalues of equation with one independent variable 01 p0171 A71-10650

Elastic body problems, determining eigenfunctions homogeneous geometrical and static boundary conditions 02 p0328 A71-12405

Couette flow stability between coaxial rotating cylinders, calculating eigenvector in first approximation small perturbation equations 03 p0404 A71-14231

Antenna aperture random radiation field representation in expansion in eigenfunctions, comparing results with linear antenna statistical theory 05 p0727 A71-15994

Elastic deformation of strip, rectangular annulus and cylinder with homogeneous displacement boundary conditions, deriving orthogonality relations for expanded eigenvectors 05 p0828 A71-16993

Undamped structural vibration problems solution for eigenvalues and eigenvectors using simultaneous iteration method 05 p0829 A71-17113

Nonrecursive solution for discrete Riccati equation by finding eigenvalues and eigenvectors of canonical state-costate equations 06 p0878 A71-17335

Control systems root contours boundary lines, dividing a plane into realizability regions for system characteristic equation complex conjugate roots 06 p0878 A71-17337

Laminar flow heat transfer in circular pipes, solving for Graetz equation eigenvalues and eigenvectors 06 p1007 A71-18304

Discrete linear vibration systems viscous damping local modifications effect on eigenvalues and vectors, using Weissenburgers procedure in matrix form [AIAA PAPER 71-215] 06 p0928 A71-18651

Rucker multidevice symmetrical microwave oscillator analysis, overcoming nonlinearity difficulties in eigenvector approach 07 p1073 A71-19118

Eigenvectors spectral structure analysis of monotonic and completely continuous nonlinear operator equations in separable real reflexive Banach space 07 p1149 A71-20646

Arbitrarily shaped waveguide analysis computer program EHPOL for polynomial approximation to eigenfunctions of Helmholtz equation, considering homogeneous Neumann and Dirichlet boundary conditions 08 p1261 A71-20752

Eigenfunction expansions of reduced nonGaussian phase error transition probability density function for first order tracking loop, analyzing spectral properties of Fokker-Planck equation 08 p1324 A71-21341

Boundary value problems solution, using Runge-Kutta method with computer for eigenfunctions of ordinary differential equations 09 p1484 A71-22177

Pc and Pi micropulsations, correlating magnetospheric cavity eigenmodes with sunspot activity 09 p1440 A71-23637

Asymptotic solution for conical horn modes, comparing with exact solution for eigenfunctions and eigenvalues 09 p1420 A71-23677

Anisotropy tensor and figurative vector components relation with eigenvector correspondence to eigenstate and eigenmodulus in similitude ratio 10 p1688 A71-24451

Nonconservative force system eigenvalues and eigenvectors reproduction by related conservative system 10 p1689 A71-24513

Linearized relativistic transport equation for mixture of isobaric Maxwellian molecules, solving in terms of eigenfunctions and eigenvalues of collision operators 10 p1645 A71-24609

Conditions for obtaining analytical expressions for eigenvalues and eigenfunctions of homogeneous Fredholm equation 13 p2096 A71-28015

Equilibrium of three dimensional elastic body under finite uniform deformation, deriving characteristic

equations for cylindrical shells, circular and rectangular plates and circular rods 13 p2149 A71-28129

Periodic disturbances propagation in radiating gray gas, using singular eigenfunction expansions 13 p2165 A71-29356

Simplified characteristic equation for plane piezoelectric vibrations of lithium niobate and lithium tantalate crystals, using perturbation methods 15 p2461 A71-31701

Equilibrium bifurcation for nonlinearly elastic incompressible body during finite subcritical homogeneous deformation, obtaining characteristic equations for cylindrical shell, circular and rectangular plates, etc 17 p2832 A71-35609

Jacobi algorithm for computation of eigenvalues and eigenvectors of skew symmetric matrix by real arithmetic 18 p2942 A71-36698

Elastic deformation of strip, rectangular annulus and cylinder with homogeneous displacement boundary conditions, deriving orthogonality relations for expanded eigenvectors 18 p2982 A71-36793

Iterative finite difference solution of Laplace operator interior eigenvalues and eigenfunctions, noting convergence in application to Helmholtz equation 20 p3201 A71-38755

German monograph on comparison between quantum mechanical approximate methods through projection of approximated eigenfunctions covering Schroedinger equation, wave functions, Born-Oppenheimer approximation, etc 20 p3271 A71-39042

Eigenfunctions of curl operator, rotationally invariant Helmholtz theorem and applications to electromagnetic theory and fluid mechanics 20 p3255 A71-39575

Walsh function imagery analysis by Hadamard-Walsh transform and eigenvector expansion technique 20 p3197 A71-39610

Weak discontinuities propagation speeds, equations and eigenvectors in uniform collisionless plasma 21 p3421 A71-40209

Real symmetric matrix eigenvectors calculation with differential equation, using Liapunov function 21 p3409 A71-41080

Constrained-impedance eigenfunctions, using projection method for field expansion in diffraction problems 22 p3512 A71-42307

Eigenvalues and eigenvectors error estimation in vibration and stability finite element analysis as function of mesh size, using Birkhoff perturbation method 22 p3617 A71-42541

Antenna aperture random radiation field representation in expansion in eigenfunctions, comparing results with linear antenna statistical theory 22 p3524 A71-42743

Simultaneous iterative solution for obtaining dominant subset of unsymmetric matrix eigenvalues and eigenvectors 23 p3698 A71-43098

EIKONAL EQUATION

EM field and wave propagation in static and spherical gravitation, obtaining modified Debye potentials and amplitude and eikonal equations 13 p2139 A71-28999

EINSTEIN EQUATIONS

Relativistic cosmology with singular point, using oscillatory model for Einstein equations general solution with time related physical singularity 02 p0285 A71-12527

General relativity and gravitational collapse, discussing experimental tests, waves, use of Riemann geometry and Einstein field equations 03 p0482 A71-12972

Einstein universe fictitious forces in noninertial frames, deriving equations from classical formulas by general covariance 03 p0490 A71-13942

Classical and relativistic forces of inertia based on exact solution of Einstein nonlinear gravitational field equations, using general covariance principle 04 p0628 A71-15903

Light propagation in mixmaster universe model based on Einstein equations solution 06 p0974 A71-18428

Equivalence principle in Einstein general relativity, discussing gravitation and inertial forces, cosmological postulate and metagalactic evolution 07 p1189 A71-18739

Einstein equations of gravitational field for universe filled with radiation, obtaining spherical symmetrical inhomogeneous solutions 07 p1203 A71-20530

Homogeneous cosmological models evolution theory, considering Einstein equations analytic solution for lengthy era 07 p1204 A71-20536

Conformally flat universe class with short ranged scalar gravity, satisfying Einstein field equations 08 p1334 A71-21360

- Static cylindrically symmetric universes consisting of Einstein-Maxwell gravitational and electromagnetic fields, discussing central axial mass and charge or current density 08 p1334 A71-21361
- Coordinate conditions necessary for Einstein gravitation equations system completion 08 p1336 A71-21796
- Weak gravitational field negative energy possibility from energy momentum leakages consideration for asymptotically flat solutions of Einstein equations 09 p1494 A71-22807
- Scalar theory for nonstatic gravitational fields, using tensor and linearized equations 10 p1641 A71-23975
- Light propagation in mixmaster universe model based on Einstein equations solution 12 p1955 A71-26578
- Einstein relations for stimulated luminescence, and application to high pressure chemical laser power gain and population inversion calculation 12 p1913 A71-26966
- Energy-radiation problems in relativity theory, considering electromagnetic waves, Einstein equations, momentum tensors and moving charged particles 16 p2609 A71-33259
- Wave fronts in Einstein-Maxwell theory, showing perturbation propagation along background spacetime metric field 16 p2609 A71-33261
- Angular momentum of rotating Einstein-Rosen bridge, comparing neutron star models 16 p2609 A71-33262
- Spinning and point particles motion from Einstein equations based on covariance with general coordinate transformations 16 p2610 A71-33270
- Einstein equations solution as hypersurface of four dimensions in Euclidean space, investigating imbedded manifold deformations 16 p2610 A71-33272
- Einstein field equations solution for universe filled with perfect fluid of position-dependent density 16 p2611 A71-33277
- Gravitational fields invariant evolution, noting Einstein equations constraints effects on initial values of variables 16 p2611 A71-33280
- Stability analysis of nonradial oscillations of cold nonrotating relativistic neutron stars by linearized Einstein equations with coupled gravitational waves 16 p2635 A71-33482
- Coordinate conditions necessary for Einstein gravitation equations system 16 p2612 A71-33548
- Real turbulent fluctuations superimposed on metric and satisfying free space Einstein equations, basing model on oscillating gravitation and elementary particles as excitons 17 p2777 A71-34586
- Simultaneous solution of Einstein and elementary particle motion equations for space-time curvature within particle resulting from self gravitation 17 p2778 A71-34628
- Quasi-closed Einstein universe model, showing orbits rotation similar to perihelions in Schwarzschild field 17 p2778 A71-34630
- Jordan theory of gravitational constant variation, showing nonreducibility to Einstein model 17 p2778 A71-34633
- Uniformly rotating thin relativistic disks structure, stability and gravitational fields within general relativity framework 17 p2806 A71-35405
- Einstein relations for stimulated luminescence, and application to high pressure chemical laser power gain and population inversion calculation 19 p3075 A71-38265
- Tensors in relativistic asymmetric field theory, generalizing Einstein gravitation and Maxwell electromagnetic equations for electrogravitational fields 19 p3105 A71-38580
- Invariant characteristics of Einstein spaces according to Petrov classification, determining gravitational fields described by covariant equation involving space curvature tensor and arbitrary scalar 19 p3105 A71-38585
- Generalized Einstein field equations in general relativity based on ennuple or tetrad variation, comparing with Schwarzschild solution 22 p3575 A71-42354
- Gravitational shock waves study by tensor distribution technique including Einstein equations solution 23 p3770 A71-44006
- Einstein equations for universes with expansion, rotation, shear and Bianchi type IX spaces, obtaining diagrammatic solutions 23 p3770 A71-44124
- EJECTION**
- NT STELLAR MASS EJECTION**
- High acceleration resistant electronic trigger fuse for in-flight gun launched projectile payloads ignition and ejection [AIAA PAPER 70-1389] 03 p0468 A71-13671

EJECTION INJURIES

- Aircrew radiological examination of spinal anatomical state, emphasizing traumas due to vibration, acceleration, ejection and crashes 05 p0715 A71-16936
- Spinal column radiographic examination after pilot ejection, discussing vertebral injuries detection 13 p2019 A71-28510
- Inertial properties of segmented cadaver trunk for mathematical model of spinal response to impact in seat ejection acceleration injuries in high speed aircraft 16 p2528 A71-33117
- EJECTION SEATS**
- Stowable aircraft vehicle escape rotoseat autogyro, providing controllable flight for pilot after ejection 04 p0532 A71-15418
- Tractor rocket actuated Yankee escape system, discussing advantages of pulling action over conventional pushed ejection seat under low speed low altitude conditions 13 p1998 A71-29383
- Ejection system performance in relation to aircraft performance dependent extreme flight conditions, examining ejection seat design features and trajectories 13 p1998 A71-29385
- EJECTORS**
- High secondary/primary mass ratio multinozzle jet pump/ejector/operation feasibility [AIAA PAPER 70-579] 03 p0344 A71-14452
- Ejector pump with gas-air jet, deriving momentum conservation equation 06 p0882 A71-18010
- Structural design effects on air driven two stage ejector supersonic propelling nozzle with conical mixing chamber 13 p2115 A71-28585
- Critical overexpanded jet conditions of gas ejector at large pressure gradients based on supersonic compressed layer theory 13 p1993 A71-29213
- Supersonic gas ejector characteristics of mixing gases with different adiabatic exponents, heat capacities and stagnation temperatures 13 p1994 A71-29233
- Liquid-vapor interactions in constant area steam-water condensing ejector mixing section, measuring axial static and stagnation pressure profiles [ASME PAPER 71-FE-21] 13 p2052 A71-29459
- High entrainment constant area multiple nozzle ejectors with two mixing tube lengths for boundary layer control, estimating performance with analytical model [ASME PAPER 71-FE-34] 13 p2053 A71-29469
- Low area ratio ejectors internal flow phenomena synthesis, increasing thrust augmentation by mixing and diffusion 15 p2468 A71-31566
- Geometrical parameters effect on operation of high pressure two-stage nozzle ejector with conical mixing chamber, measuring gas flow rates, total pressures and stagnation temperatures 16 p2521 A71-33612
- Two phase gas-liquid ejectors with cylindrical mixing chamber, discussing ejection equations, jet flow parameters, operation modes and diffusor substitution 22 p3479 A71-41851
- Vacuum water-air ejector with cylindrical mixing chamber and multiball nozzle feed, showing increased efficiency by supersonic diffusor substitution 22 p3480 A71-41852

EKMAN LAYER**U BOUNDARY LAYER TRANSITION****ELASTIC ANISOTROPY**

- Variable elasticity algorithm for axial flow turbine disks with allowance for plasticity, creep and loading history 12 p1979 A71-27351

ELASTIC BARS

- Bar impact against rigid obstacle, using method of characteristics for elastoplastic waves propagation and interaction 01 p0171 A71-10651
- Thin nonlinear elastic bar small longitudinal oscillations, solving boundary value problem for disturbances propagation 01 p0176 A71-11050
- Flexural-torsional vibration stability of thin walled elastic bars under longitudinal periodic force, using parametric resonance theory 02 p0321 A71-11687
- Elastic bar buckling load nondestructive determination using actual boundary conditions 03 p0504 A71-13454
- Elastic metal thin beams transverse resonant free vibrations, analyzing viscoelastic coatings damping effects [ASME PAPER 70-DE-D] 03 p0507 A71-13710
- Infinite elastic beam normal impact by semiinfinite elastic rod, using Timoshenko beam and one dimensional bar theory to describe elastic waves [ASME PAPER 70-W/APM-54] 03 p0513 A71-14171

- Direct pointwise stress determination in twisted cracked elastic bars under torsion and longitudinal shear by numerical methods 04 p0667 A71-15180

- Deflection-optimal elastic beams design for distributed dynamic loading 05 p0825 A71-16717
- Circular and elliptical holes and inclusions effects on stress concentration in elastic beams under uniform compression 06 p1002 A71-18414
- Bonded rod of two semiinfinite elastic bars subjected to end impulse, formulating motion equations and initial and boundary conditions 07 p1217 A71-20367
- Buckling by torsion of straight circular cylindrical elastically supported bars, using initial parameters method based on matrix calculus 09 p1536 A71-22412
- C-5A cargo box side wall deformations, examining square plates center deflections with elastic beams 10 p1557 A71-24871
- Support conditions influence on dynamic stability of hinged elastic rod 13 p2151 A71-28143
- Longitudinal wave propagation in ideal elastic bar with viscous stress, calculating approximation to nonlinear wave equations 13 p2153 A71-28483
- Optimized thin walled elements in elastic planar frame structures minimum weight design 14 p2324 A71-29872
- Stress-strain state of finite length elastic rod free of bending moments and coupled to semiinfinite plate 14 p2332 A71-30868
- Elastic rods and rings stability under compression beyond elasticity limit, determining equilibrium branching characteristics near bifurcation point 16 p2647 A71-32927
- Optimal structural design for nonconservative systems under buckling, noting application to minimal weight nonprismatic elastic bar shape determination 16 p2649 A71-33012
- Potential energy minimization for elastic elements with integral loads applied to bending of bar and wedge, using variational method 16 p2659 A71-33995
- Large deflections of thin piecewise prismatic elastic bars by electronic analog computer simulation 16 p2661 A71-34117
- Elastic bar boundary conditions, noting bending stiffness 17 p2825 A71-34886
- Hinged bar dynamic buckling under harmonic axial load, using Timoshenko beam theory with longitudinal vibration effects 17 p2832 A71-35400
- Rigid body longitudinal impact against free end of variable cross sectioned viscoelastic cantilever beam, obtaining solution as rapidly converging Fourier series 19 p3160 A71-38485
- Numerical analysis for flexural stress pulse propagation in nonuniform elastic bars by geometric acoustics 22 p3616 A71-42213
- ELASTIC BENDING**
- Bending of thin elastic orthotropic shallow shells, taking into account large deflections, temperature distribution and material nonuniformities 02 p0325 A71-12288
- Stress-strain state of thin circular plate with variable thickness along circumference under bending due to uniformly distributed load, using small p 02 p0326 A71-12289
- Bending of plate of nonuniform elasticity over thickness due to gas surface layer saturation during heating prior to rolling 02 p0328 A71-12513
- Thin reinforced viscoelastic isotropic multiconnected plate stress-strain state under bending due to concentrated loads and distributed normal forces 02 p0329 A71-12668
- Naturally twisted and orthotropic cylindrical beam bending by transverse load 04 p0673 A71-15886
- Bending stress around elliptic elastic inclusions in thin anisotropic plate 05 p0824 A71-16590
- Symmetrical elastic bending of anisotropic annular circular plates of variable thickness, solving for line and uniform pressure loads with different boundary conditions 05 p0830 A71-17224
- Stress state analysis in rigidly clamped circular plate bent by edge loads, using three dimensional elasticity theory 06 p0989 A71-17786
- Thin shallow elastic shells boundary value problem, deriving existence and multiplicity of equilibrium state critical points for bending and buckling 07 p1213 A71-19639
- Nontrivial expansion of rigid surface infinitesimal motions into analytical bendings, deriving differential

- equations system for n -order bendings of singly connected continuously differentiable surface
09 p1535 A71-22211
- Low-cycle fatigue curve determination for plane elastoplastic bending with flexible loading, deriving rated fatigue life
09 p1536 A71-22502
- Asymmetric structure elastic transversely isotropic sandwich panels bending equations, taking into account transverse shear strain and stability
12 p1981 A71-27497
- Bending stress of thick laminated plates of isotropic material with variable elasticity modulus
14 p2333 A71-30890
- Matrix force analysis, discussing methods for expressing elastic behavior of semimonocoque polygon membrane and isotropic polygon bending elements
16 p2652 A71-33082
- Small deflection analysis within Cartesian coordinate system applicable to elastic-plastic rectangular plates bending under Tresca yield criterion
16 p2654 A71-33122
- Potential energy minimization for elastic elements with integral loads applied to bending of bar and wedge, using variational method
16 p2659 A71-33995
- Strain energy and stability of nonlinear plate and shell bending under Love-Kirchhoff hypothesis, using three dimensional elasticity theory
17 p2815 A71-34296
- Infinite length rectangular thin plate bent by uniform load, presenting exact solutions for stresses and displacements from couple-stresses plane strain elasticity theory
17 p2818 A71-34441
- Nonlinear elastic bending of nonhomogeneous cantilever beam under stepwise and triangular pulse loads of finite duration
17 p2821 A71-34578
- Elastic bar boundary conditions, noting bending stiffness
17 p2825 A71-34886
- Pure and transverse bending of orthotropic cylindrical shell wound with elastic glass plastic filaments, presenting stress-strain diagrams under tension and compression
17 p2830 A71-35318
- Cantilevered elastic cylindrical shell stability during bending by transverse load uniformly distributed over entire surface or applied at end
17 p2833 A71-35615
- Maximum vector values for stability and rigidity of elastic systems under modulo limited disturbances, applying to beam deflection and second derivative
21 p3473 A71-41154
- Boundary value problems solution for reaction pressure to elastic base circular plate bending under uniformly distributed load
23 p3777 A71-43910
- Variational stress-strain equation for flexible shallow orthotropic multilayer shells with large deflections under normal pressure and contour loading
23 p3778 A71-44040
- Critical bending moments for elastic beam weakened by elliptical crack in tensile stress region
24 p3882 A71-44847
- ELASTIC BODIES**
- Euler method applicability for finite subcritical deformation stability of isotropically nonlinear elastic body
01 p0165 A71-10065
- Shock absorber selection for reducing one dimensional oscillations of elastic linearly damped body on supporting base
01 p0127 A71-10633
- Nonlinear magnetoelasticity theory applied to deformation of elastic bodies by magnetic field, considering ferromagnetic membrane deflection and flexible conductor equilibrium
01 p0171 A71-10661
- Plane micropolar static strain in homogeneous isotropic elastic solid, deriving existence theorems for interior and exterior problems
01 p0172 A71-10841
- Partially closed Griffith crack shape and stress intensity factor in infinite elastic solid
01 p0172 A71-10842
- Micropolar elastic body with spherical inclusion, investigating thermal and couple stresses
01 p0181 A71-11286
- Elastic half space transient response to normal impulsive surface line load
02 p0321 A71-11677
- Elastic elliptic inclusion stress state in plane elastostatics
02 p0321 A71-11680
- Boundary value problems solution in elasticity theory of isotropic homogeneous body configurations close to ellipsoid of revolution, obtaining stress-strain state by approximate method
02 p0325 A71-12285
- Elastic body problems, determining eigenfunctions homogeneous geometrical and static boundary conditions
02 p0328 A71-12405
- Elastic column optimization, examining material distribution for minimum volume without buckling
03 p0501 A71-13023
- Axisymmetric mixed boundary problem for elastic infinite cone, obtaining solution by assuming zero shearing stresses
03 p0513 A71-14234
- Three dimensional mixed boundary value problems, obtaining solutions for elastic body differential equilibrium equations
03 p0513 A71-14235
- Surface tension effect on dispersion of Rayleigh waves in elastic body
04 p0673 A71-15882
- Elastic isotropic body finite plane deformations, considering displacement and stress functions relationship
05 p0822 A71-16378
- Three dimensional elastic body fracture analysis, considering lateral constraint factor contour plots
05 p0822 A71-16412
- Linear elastic structure statistical response characteristics relation to natural environment random pressures, considering flexural vibrations of thin cylinder for modal density
05 p0826 A71-16732
- Body weakening due to symmetrically expanding crack, discussing internal pressure, elastic equilibrium and stress-strain state
06 p0896 A71-17326
- Elastic systems vibrations calculated with allowance for amplitude and frequency dependent energy dissipation, using hysteresis loop contour expression
07 p1218 A71-20476
- Variational principle application to stability in failure mechanics of arbitrary linearly elastic bodies, discussing inertia effect on steady state vibrations of cracked bodies
08 p1372 A71-21704
- Boundary problem for displacement equilibrium equations of elastic body using iterative methods, demonstrating convergence of difference equation solution
08 p1372 A71-21706
- Bifurcation of equilibrium of three dimensional elastic isotropic body with arbitrary elastic potential under large subcritical strains
08 p1373 A71-21866
- Nonlinear elastic incompressible transversely isotropic body with finite initial deformations, considering linearized problems of static and dynamic equations
09 p1534 A71-22178
- Angular motion of deformable earth satellite as solid-elastic system with distributed masses, applying automatic control transfer function
09 p1491 A71-22548
- Elastic deformable satellite motion stability in central Newtonian force field
09 p1532 A71-23134
- Euler method applicability for finite subcritical deformation stability of isotropically nonlinear elastic body
09 p1541 A71-23272
- Isotropic homogeneous incompressible elastic body under surface tensions and conservative forces, showing six families of equilibrated deformations
10 p1687 A71-24347
- Normal shock wave interaction with deformable solid walls, determining explosion or sonic booms effects on elastic structures and protection devices
10 p1556 A71-24483
- Homogeneous isotropic elastic body stresses after imposing small deformation on strain configuration obtained from initial small deformation of original configuration
10 p1689 A71-24503
- Critical load and elastic base one-sided contact effects on cylindrical shell stability under uniform external pressure, using nonlinear programming
10 p1689 A71-24563
- Random vibrations of statistically inhomogeneous elastic systems, using perturbation method
10 p1691 A71-24644
- Surface layer-bulk body interaction and Rayleigh wave propagation in elastic solid, using two dimensional continuum theory
10 p1691 A71-24645
- Forced rotational oscillations of plane-convex glass lens pressed against brass plate, determining contact frictional and elastic characteristics from resonance and hysteresis
11 p1849 A71-25621
- Stress distribution in infinite elastic solid containing spherical cavity and external crack, discussing displacement components for axisymmetric loading
12 p1974 A71-26740
- Elastic body displacement equilibrium equations, using variable direction iteration methods for boundary value problems
12 p1978 A71-27329
- Three dimensional nonlinear elastic anisotropic body formulating stability at finite subcritical strains with variational principle
12 p1978 A71-27333
- Two dimensional periodic and doubly periodic boundary value problems solution in theory for stable oscillations of elastic and viscoelastic bodies perforated by circular holes
12 p1980 A71-27447
- Elastic isotropic body finite plane deformations, considering displacement and stress functions relationship
12 p1981 A71-27464
- Hereditary elastic body model with various tensile and compressive strengths, using elasticity theory with differing moduli
12 p1982 A71-27518
- Semielastic body rotational stability, investigating elastic coupling effects on controllability of rotating space stations in earth orbit
12 p1973 A71-27590
- Large deformation of incompressible elastic body reinforced by unidirectional system of elastic fibers
12 p1922 A71-27695
- Equilibrium of elastic body weakened by system of circular planform cracks in single plane
13 p2148 A71-27807
- Equilibrium of three dimensional elastic body under finite uniform deformation, deriving characteristic equations for cylindrical shells, circular and rectangular plates and circular rods
13 p2149 A71-28129
- Surface waves propagation in initially deformed elastic body, using elastic potential to define half space mechanical properties
13 p2150 A71-28131
- Solid propellant combustion stability theory for two dimensional disturbances, considering process as elastic body transformation into gaseous combustion products
13 p2159 A71-28138
- Uniform torsion of elastic body weakened by spherical cut in form of rigid inclusion
13 p2150 A71-28139
- Green tensor for large initial deformations of isotropic elastic body
13 p2152 A71-28277
- Relativistic thermo-magnetoelastic wave propagation, considering elastic solid under magnetic and thermal fields
13 p2101 A71-29105
- Thin hyperelastic tube forced large amplitude radial oscillations, deriving exact solution for general forcing function
14 p2322 A71-29690
- Three dimensional elastic plastic solid, calculating stress and deformation with finite difference procedure
14 p2322 A71-29737
- Hyperelastic continuous bodies with periodic structure, developing macroscopic model based on boundary value problem for unit cell
14 p2323 A71-29813
- Arbitrary dynamic load problem for elastic infinite bodies, solving with Lamé equations and Fourier and Laplace transforms in distribution space
14 p2323 A71-29817
- Elastic sphere equilibrium with penny shaped crack under inner surface pressure, observing stress distribution
14 p2326 A71-30096
- Stability and longitudinal vibrations of elastic beam under rapid monotonously increasing and impulsive loading assuming free end
14 p2326 A71-30194
- Axisymmetric bodies torsion problems solution by superimposing elasticity equations, using point matching technique
14 p2329 A71-30463
- Circular stresses and concentration coefficient variations in star shaped elastic surface projected onto ring under internal pressure
14 p2287 A71-30853
- Three dimensional elasticity theory solutions for isotropic axisymmetric bodies of revolution by p -analytic and generalized analytic functions
14 p2333 A71-30889
- Crack tip strain problem in elastic body, relating fracture energy criterion with mathematical models
14 p2334 A71-31002
- Pulsating follower loads implementation by pulsating gas or liquid jets, using Mettler differential equations for forced vibrations of elastic bodies
15 p2502 A71-31172
- Thermodynamic properties effects on transverse acceleration wave propagation in inhomogeneous isotropic elastic bodies with internal state variables
15 p2504 A71-31729
- Thermoelastic stability as function of thermodynamic properties of elastic materials, applying invariance principle to dynamical systems on Banach space
16 p2649 A71-33004
- Finite element analytical technique for calculating stress distribution in elastic body, using minimum potential energy principle
16 p2652 A71-33079

Axially symmetric thermal stress distributions in finite elastic solid containing flat circular external crack

16 p2654 A71-33169

Stress field in elastic strip of finite width under pressure applied to faces of symmetrically situated Griffith crack

16 p2654 A71-33170

Linear elastic body stress field singularities, investigating local geometry and boundary condition effects

16 p2654 A71-33175

Orthotropic semiinfinite elastic solid under plane strain, calculating thermal stresses in terms of Green functions

[ASME PAPER 71-APM-18] 16 p2655 A71-33211

Dynamic characteristics of weakly damped elastic body, considering complex natural modes generation for vibration tests in aircraft design

16 p2657 A71-33403

Isotropic elastic body steady vibrations with moment stresses, solving two dimensional boundary value problem

16 p2658 A71-33716

Nonlinear elastic incompressible bodies with small deformations, obtaining three dimensional static and dynamic stability variational equation

17 p2816 A71-34328

Thermal stresses in plane strain of isotropic micropolar elastic solids without heat sources, reducing thermoelastic to isothermal problem

17 p2821 A71-34583

Heating by thermoelastic damping through sudden removal of stresses on homogeneously strained elastic body, comparing elastic deformation of rubber and steels

17 p2821 A71-34584

Equilibrium bifurcation for nonlinearly elastic incompressible body during finite subcritical homogeneous deformation, obtaining characteristic equations for cylindrical shell, circular and rectangular plates, etc

17 p2832 A71-35609

Circular contact area in theory of elasticity with allowance for surface structure of bodies in contact, solving Hertz axisymmetrical problem of elastic bodies

17 p2833 A71-35610

Optimal design of locally orthotropic elastic flat bodies of fiber reinforced plastics or metals

17 p2763 A71-35620

Oblique shock wave incident on plane boundary of nonlinear homogeneous elastic solid, proving wave reflection pattern uniqueness

18 p2982 A71-36813

Cosserat-type bodies with linear elasticity, obtaining reciprocity theorem and stress solutions under concentrated load

18 p2984 A71-36949

Wave motions in viscous fluid layer in presence of surfactant elastic substances adjoining solid surface or gas, using Navier-Stokes equations

19 p3042 A71-37084

Nonlinear elasticity theory variational principles modification for finite deformation of elastic body

19 p3154 A71-37095

Energy and variational principles, studying local stability of equilibrium of elastic body subjected to conservative and gyroscopic forces

20 p3232 A71-38797

Bifurcation of equilibrium of three dimensional elastic isotropic body with arbitrary elastic potential under large subcritical strains

20 p3308 A71-39365

Thermal stresses and couples in micropolar elastic solid cavity and rigid inclusion during uniform heat flow

20 p3309 A71-39560

Thermoelastic plane harmonic and Rayleigh surface waves in elastic solids with thermal relaxation, using Maxwell heat conduction equation

20 p3310 A71-39779

Algorithm for linearly elastic structures vibration natural undamped frequency computation, assuming known dynamic stiffness matrix

20 p3311 A71-39964

Iterative method for linearly elastic structure undamped vibration natural frequency determination with fast convergence

20 p3311 A71-39965

Parametric instability in first spatial and temporal modes of cantilevered elastic columns with longitudinal inertia and end mass

21 p3462 A71-40531

ELASTIC BUCKLING

Prebuckling deformations influence on circular cylindrical shell buckling under external pressure, applying Galerkin method to Donnell equations

02 p0329 A71-12602

Elastic instability of transversely isotropic Timoshenko beam, deriving buckling coefficients curves vs parameter measuring shear deformation effect

03 p0504 A71-13452

Elastic bar buckling load nondestructive determination using actual boundary conditions

03 p0504 A71-13454

Maximal deflection of square and rectangular thin plates with small initial concavities, using dynamic relaxation method for lateral and postbuckling in-plane edge loads

05 p0830 A71-17225

Deformation theory of dynamic bending, buckling and stability of plates and shells beyond elastic limit

06 p0999 A71-17865

Thin shallow elastic shells boundary value problem, deriving existence and multiplicity of equilibrium state critical points for bending and buckling

07 p1213 A71-19639

Buckling loads prediction for conservative elastic systems from vibration data by stochastic and deterministic models, providing nondestructive testing procedure

08 p1368 A71-20804

Buckling by torsion of straight circular cylindrical elastically supported bars, using initial parameters method based on matrix calculus

09 p1536 A71-22412

Rings elastic buckling problems under various loading conditions, using rate equations

11 p1840 A71-25138

Elastic collapse analysis of shell structures with variable rectangular grid spacing based on modified finite difference computer program

[ALAA PAPER 71-359] 11 p1844 A71-25338

Digital computerization for cylindrical shells postbuckling stability analysis, discussing FORMAC and REDUCE formula manipulation systems

[ALAA PAPER 71-363] 11 p1845 A71-25341

Buckling loads of square laminated anisotropic composite plates under compression, including bending-membrane coupling effects

11 p1847 A71-25462

Optimum buckling load of cylindrical shells under lateral pressure using Rayleigh-Ritz method

11 p1848 A71-25484

Axial compression buckling of elastic core filled circular cylindrical shells with transverse shear flexibility, noting solid propellant rocket cases design application

13 p2148 A71-27984

Elastoplastic plates and shallow shells with rigid orthotropic filler, bending and buckling beyond elastic limit

13 p2156 A71-29066

Variable curvature cylindrical shells elastic postbuckling configurations, showing buckle pattern tessellation discontinuity

13 p2157 A71-29126

Axissymmetrical snap buckling of clamped shallow spherical shell with initial deformation under external pressure, using energy method

14 p2322 A71-29689

Elastic stability and buckling behavior of transversely isotropic rectangular Mindlin plate under initial stress and displacement

14 p2324 A71-29871

Heavy hinged nonshallow circular arches stability during buckling sideways with bifurcations in critical load deflection curves

14 p2324 A71-29885

Symmetric and asymmetric dynamic buckling of shallow elastic arches under uniform loads, using nonlinear finite difference method

14 p2331 A71-30695

Thin infinite isotropic elastic plate on nonlinear elastic foundation under uniform two dimensional hydrostatic pressure, detailing imperfection effects on initial postbuckling behavior

16 p2648 A71-32979

Coupled elastic buckling in continuous systems, determining postbuckling paths for strut, spherical shell and flat plate

16 p2650 A71-33017

Snap-through buckling of three hinged deep trusses and wire restrained column under critical quasi-static loading based on elastica theory of prismatic bars

17 p2815 A71-34294

Slender elastic column dynamic buckling under constant compressive axial end displacement, considering damping effects

17 p2818 A71-34506

Finite oval cylindrical shells with clamped boundaries, investigating stability and elastic buckling under axial compression for comparison with circular cylindrical shells

[SESA PAPER 1832] 17 p2819 A71-34536

Axissymmetric nonlinear buckling equations for composite thin circular elastic plates of isotropic or orthotropic layers under radial compression

17 p2821 A71-34580

Axissymmetric plastic deformation of imperfection sensitive spherical shell after elastic buckling, considering load carrying capacity

[ASME PAPER 71-APM-FF] 18 p2978 A71-36266

Elastic beam dynamic buckling stability under transverse follower force, considering force direction dependence on cross section twist angle

[DFVLR-SONDDR-137] 18 p2980 A71-36679

Elastic buckling load of cylindrical shells with dimple imperfections under external pressure, applying perturbation expansion to Karman-Donnell equations

18 p2962 A71-36839

Elastic stability and buckling modes of cylindrical shell under critical gravity load, using double Fourier series and linear theory

18 p2983 A71-36847

Clamped oval cylindrical thin walled shells elastic buckling under axial loads, solving stability equations by Fourier method and higher order difference technique

19 p3157 A71-37876

Flow induced flutter and buckling instability of elastic tube with displacement spring support

[ASME PAPER 71-VIBR-39] 21 p3459 A71-40289

Elastic buckling and initial postbuckling behavior of clamped shallow spherical sandwich shells under axisymmetrical load

21 p3469 A71-41007

Micropolar continuum, potential energy, stresses and constitutive relations for buckling of large rectangular grid frameworks under axial load

21 p3469 A71-41009

Buckling for thin stress walled open sections on elastic foundation with constrained direction reinforcement

22 p3614 A71-41693

Local elastic buckling of component plate elements of single-cell simply supported folded plate structures under uniform transverse loads

22 p3618 A71-42585

Nonlinear finite element analysis of sandwich arches elastic buckling, using straight beam-column type model

22 p3618 A71-42586

Asymptotic solution to dynamic buckling of thin slowly compressed eccentric elastic columns, using two time scheme

23 p3776 A71-43373

Buckling stability and critical loads of thin elastic cylindrical shells with hollow core in axial compression

24 p3882 A71-44844

Numerical evaluation of structures buckling loads, considering matrix equation application to elastic stability problems

24 p3883 A71-44870

ELASTIC COLLISIONS

U ELASTIC SCATTERING

ELASTIC CONSTANTS

U ELASTIC PROPERTIES

ELASTIC CYLINDERS

Stress concentration and free surface shape at sliding contact for elastic semiinfinite cylinder, discussing mixed boundary value problem

01 p0171 A71-10658

Homogeneous isotropic cylindrical shell stability, considering reinforcement by nonlinear dense symmetrical system of elastic threads under tension

01 p0176 A71-11124

Highly flexible nonlinearly elastic two layer cylinder reinforced by transversely isotropic shell, examining stressed state in axisymmetric temperature field

02 p0323 A71-11742

Optimal design of one end-clamped elastic column subject to conservative concentrated compressive loads

03 p0501 A71-13110

Elastic columns under transient loading, ascertaining stability by Liapunov function direct method

03 p0505 A71-13540

Stiff rings attached to elastic cylinders, analyzing stresses and deformations under concentrated loads and bending moments about radial and tangential axes

[ASME PAPER 70-WA/PVP-1] 03 p0510 A71-14099

Axissymmetric normal loading of lateral surface of finite length elastic solid cylinder

05 p0824 A71-16595

Stress wave scattering in fiber reinforced composite material, using model of parallel elastic cylinders embedded in unbounded elastic medium

05 p0826 A71-16719

Structural stability of incompressible elastic rod of variable rigidity flattened along axis, reducing boundary value problem to equation with continuous operator

05 p0828 A71-16987

Compressive contact interaction problem for elastic circular cylindrical shell lying in circular cylindrical cavity of elastic body

06 p0987 A71-17764

Elastic and viscoelastic multilayer reinforced circular cylindrical shells stability, determining transverse shear stress role

06 p0996 A71-17841

Semiinfinite solid elastic cylinder under self equilibrium end loading, obtaining elastostatic solution

06 p1000 A71-18027

Axissymmetric wave propagation in semiinfinite hollow elastic circular cylinders subjected to pressure step loading, obtaining asymptotic solutions for strains by double integral transforms

07 p1214 A71-19954

- Torsional wave propagation in elastic circular composite cylinders, introducing correction factors for approximate theory 07 p1214 A71-19955
- Elastic harmonic waves propagation in composite circular elastic cylinder 07 p1214 A71-19956
- Stress distribution boundary value problem for long isotropic elastic cylinder with strip cracks due to internal pressure 07 p1215 A71-20100
- Torsional oscillation of hollow isotropic elastic cylinder encased in thin elastic shell, deriving representation satisfying equation of motion and initial and boundary conditions 09 p1539 A71-22918
- Thick walled anisotropic nonhomogeneous elastic cylinder or plate under axial symmetric time dependent pressure, investigating transient response 09 p1540 A71-23087
- Infinitely small flexural oscillations of initially stretched incompressible elastic circular cylinder, showing stretch effect on wave propagation velocity 10 p1689 A71-24521
- Infinitely slender cylinder elastic equilibrium, deriving Saint Venant problem solution in power series form 10 p1692 A71-25022
- Two dimensional effects of cylinders rolling on elastic half space, investigating inflated tire shear stress and slip region 11 p1850 A71-26101
- Stress concentration and free surface shape at sliding contact for elastic semiinfinite cylinder, discussing mixed boundary value problem 14 p2333 A71-30992
- Boundary conditions of elastic deformations of constrained circular cylinders under axial load, discussing modulus dependence on Poisson ratio 15 p2505 A71-32007
- Thermal stresses in anisotropic infinite elastic orthotropic laminated cylinder with arbitrary number of layers under axisymmetric heating 16 p2657 A71-33599
- Isotropic elastic circular cylinders longitudinal stress waves, presenting dispersion relation [Pochhammer equation] numerical solutions 16 p2658 A71-33625
- Thin elastic shallow cylindrical panel in steady conducting supersonic gas flow, detailing magnetic field effects on static and dynamic stability and flutter 17 p2816 A71-34326
- Hyperelastic compressible isotropic elliptical and circular cylinders simple bending, studying second order effects 18 p2977 A71-36195
- Structural stability of incompressible elastic rod of variable rigidity flattened along axis, reducing boundary value problem to equation with continuous operator 18 p2982 A71-36787
- Three dimensional orthotropic elastic cylinders symmetric deformations under external loads, calculating stress-strain state with approximate method 19 p3155 A71-37528
- Stress analysis of rotating orthotropic disks mounted on elastic shafts, obtaining closed form solution for governing differential equations 20 p3308 A71-39088
- Stress-strain state of rotating viscoelastic hollow cylinder with mobile inner boundary under internal pressure and temperature effects 21 p3472 A71-41145
- Sliding contact between closed annulus and elastic cylinder, deriving integral expressions 21 p3472 A71-41147
- Acoustic waves transmitted through solid elastic cylinders, calculating wavefront loci and waves amplitudes 23 p3704 A71-43210
- Isotropic parabolic elastic cylinder deformation, determining displacements and stresses with Fourier integral and Weber functions 24 p3880 A71-44713
- ELASTIC DAMPING**
- Oscillatory systems with nonlinear elastic arresting devices, calculating dynamic characteristics and motion stability 08 p1332 A71-20687
- Elastoplastic arresting device, predicting mass impact effect for optimal design in terms of deformation or contact time 08 p1367 A71-20688
- Edge loading effects on shallow hyperbolic parabolic shell elastic damping, discussing flat plate theory analog solution 10 p1686 A71-23995
- Structural materials dynamic analysis, considering viscous, hysteresis and viscoelastic damping [AIAA PAPER 71-349] 11 p1843 A71-25328
- Power spectral density analysis of aircraft structural response to taxiing produced random vibrations involving landing gear orifice damping and Coulomb friction 11 p1708 A71-26311
- Vibration damping of simply supported sandwich beam with viscoelastic core, using energy method [ASME PAPER 71-DE-C] 12 p1977 A71-27318
- Gimbal suspended gyroscope in elastically damped frame with dynamically unbalanced rotor, noting oscillations and drifts 13 p2065 A71-27945
- Dynamic damping of plane one dimensional unsteady stress wave passing through viscoelastic layer separating linearly elastic half spaces 13 p2155 A71-28848
- Nonconservative elastic system involving standard double pendulum model under retarded follower load, calculating damping, time delay and parameter variations effects on stability 15 p2449 A71-32012
- Spherical caps under step pressure loading, noting elastic damping effects on dynamic stability 15 p2506 A71-32093
- Stress, slip and damping of clamped elastic plate with finite friction under alternating axial load, using finite element method 16 p2581 A71-33174
- Dynamic characteristics of weakly damped elastic body, considering complex natural modes generation for vibration tests in aircraft design 16 p2657 A71-33403
- Rotary inertia and shear deformation effects on three dimensional flexural vibrations of circular ring on elastic foundation 16 p2657 A71-33421
- Forced transverse vibration damping of end loaded elastic cantilever beam, determining hysteresis loop contour from resonance curves 16 p2658 A71-33977
- Von Karman equations analogs solution for nonlinear large amplitude vibrations of circular plate on uniform elastic foundation [ASME PAPER 71-VIBR-9] 21 p3457 A71-40271
- Four layer sandwich damping with viscoelastic material, noting frequency dependent effectiveness [ASME PAPER 71-VIBR-20] 21 p3458 A71-40278
- Lumped parameter modeling of fluid elastic vibration response of nonlinear piston driven pneumatic-mechanical system, using finite element control volumes [ASME PAPER 71-VIBR-41] 21 p3459 A71-40291
- Distributed mass and elastic damping finite element model for turborotor system on fluid film bearings [ASME PAPER 71-VIBR-56] 21 p3385 A71-40301
- Optimum geometry and vibration damping ability of laminated three layer elastic-viscoelastic-elastic beam at resonance [ASME PAPER 71-VIBR-102] 21 p3461 A71-40328
- ELASTIC DEFORMATION**
- NT ELASTIC BENDING**
- NT ELASTIC BUCKLING**
- Euler method applicability for finite subcritical deformation stability of isotropically nonlinear elastic body 01 p0165 A71-10065
- Nonlinear magnetoelasticity theory applied to deformation of elastic bodies by magnetic field, considering ferromagnetic membrane deflection and flexible conductor equilibrium 01 p0171 A71-10661
- Finite length elastic cylindrical shell deformation approximate solution by Legendre polynomials 01 p0173 A71-10942
- Thin cylindrical work hardening shell under nonuniform heating and external stresses, determining elastoplastic deformation by flow theory 02 p0323 A71-11744
- Free lateral vibration of viscoelastic metallic beam under axial creep, considering elastic deformation 02 p0324 A71-11996
- Nonlinear quadratic elasticity theory of isotropic tube and hollow sphere under small linear deformations, obtaining stress-strain relation 02 p0326 A71-12294
- Equivalence theory applications in three dimensional elasticity, plane deformation and stresses 02 p0328 A71-12534
- Prebuckling deformations influence on circular cylindrical shell buckling under external pressure, applying Galerkin method to Donnell equations 02 p0329 A71-12602
- Finite elastic deformation differential operator strong ellipticity conditions, discussing dependence on material elastic moduli 03 p0501 A71-13071
- Thin rod deformation by gyrostat motion analysis, deriving anisotropic curved rods equilibrium shapes 03 p0458 A71-13600
- Displacement type equilibrium equations for small deformation imposed on initial finite deformation, estimating elastic energy function based on strong ellipticity condition 03 p0510 A71-13945
- Stiff rings attached to elastic cylinders, analyzing stresses and deformations under concentrated loads and bending moments about radial and tangential axes [ASME PAPER 70-WA/PVP-1] 03 p0510 A71-14099
- Intraluminal pressure effect on stress concentration and deformation of arterial wall in relation to atherosclerosis, using finite element method [ASME PAPER 70-WA/BHF-15] 03 p0373 A71-14113
- Cord reinforced elastic homogeneous isotropic cylindrical membrane axisymmetric deformation, using strain energy function 03 p0514 A71-14348
- Thermoelastic deformation of elastic media with stochastically inhomogeneous microstructure, characterizing physical properties as steady random variables 03 p0514 A71-14358
- Polymer neck autooscillatory expansion under drawing as result of interaction between elastic deformation and heat release during orientational transformation 03 p0448 A71-14362
- Elastic straightening of slightly curved shell and significantly curved beam, considering prestressed structural stiffness 04 p0672 A71-15771
- Cosserat continuous model of dense elastic lattices of regular structure in plane 04 p0673 A71-15884
- Elastic isotropic body finite plane deformations, considering displacement and stress functions relationship 05 p0822 A71-16378
- Elastic deformation of strip, rectangular annulus and cylinder with homogeneous displacement boundary conditions, deriving orthogonality relations for expanded eigenvectors 05 p0828 A71-16993
- Fibrous composite materials stress and deformation analysis, using point matching numerical method and boundary point least squares method 05 p0829 A71-17119
- Elastic plates and members deformation with constraints on deflections, determining strain state with dynamic programming 06 p0984 A71-17651
- Cylindrical shell reinforced by transverse ribs under hydrostatic pressure, determining elastoplastic deformation 06 p0988 A71-17774
- Geometrically nonlinear thin nonshallow shells of revolution, deriving axisymmetrical elastic deformation equations 06 p0988 A71-17780
- Multilayer conical and spherical shells of revolution axisymmetric elastic deformation, deriving stress-strain state equations with allowance for transverse shear 06 p0990 A71-17795
- Flexible plates and shallow shells supercritical deformation in high temperature field, taking into account modulus of elasticity and thermal expansion coefficient temperature dependence 06 p0990 A71-17796
- Elastic shells under pressure wave loads, examining front discontinuities induced by plane and axisymmetrical wave deformation 06 p0992 A71-17807
- Thin walled flexible shell theory and equilibrium under large deformation 06 p0999 A71-17862
- Thermoelasticity, mechanical and thermal processes in deformation of elastic plates and shells 06 p0999 A71-17866
- Vibration and wave analysis in dynamic deformation of elastic shells and plates with environmental allowance 06 p1000 A71-17870
- Plane or axisymmetric revolution geometry elasticity problems using finite element method and Fourier series 06 p1002 A71-18421
- HF dynamic elastic deformation observation and measurement, including photoelastic method for transient phenomena 06 p1003 A71-18422
- Refractory alloys elastoplastic deformation under cyclic loading, deriving thermal fatigue equations 07 p1129 A71-19155
- Elastic, inertial and aerodynamic forces aeroelastic triangle, examining lift changes due to aircraft structure deformation, dynamic flight stability and space shuttle development problems 07 p1215 A71-20063
- Stiffened long cylinder with time variable thickness and strengthening thin shell system elastic displacements due to nonstationary vibrations and nonuniform pressure distribution 07 p1217 A71-20459
- Steady state thermoelastic mixed boundary value problem for elastic layer, obtaining temperature, stresses and displacements in finite integrals through Hankel transforms 08 p1370 A71-21238
- Cylindrical steel specimens bearing strength under cyclic elastoplastic deformation, investigating stress redistribution effects 08 p1316 A71-21607

Displacement function and principal stress differences in transverse plane of symmetry of axially symmetric photoelastic body

08 p1372 A71-21653

Boundary problem for displacement equilibrium equations of elastic body using iterative methods, demonstrating convergence of difference equation solution

08 p1372 A71-21706

Elastic swept wing subsonic aerodynamic characteristics, taking into account aerodynamic load redistribution due to aeroelastic deformations

08 p1229 A71-22035

Unsteady interaction of compressible fluid and flat circular deforming elastic membrane analyzed coupled computer program method

[AIAA PAPER 70-75]

09 p1430 A71-22085

Nonlinear elastic incompressible transversally isotropic body with finite initial deformations, considering linearized problems of static and dynamic equations

09 p1534 A71-22178

Nontrivial expansion of rigid surface infinitesimal motions into analytical bendings, deriving differential equations system for n -order bendings of singly connected continuously differentiable surface

09 p1535 A71-22211

Elastic and plastic plane deformation photoelastic measurement at room and elevated temperatures by moiré patterns, comparing performance with other methods

09 p1536 A71-22328

General nonlinear elasticity theory including applications, deformation laws, complex nonlinear equations solutions, equilibrium and stability problems, experimental methods and mathematical models

09 p1536 A71-22512

Elastic waves in isotropic body, calculating initial deformation effect on propagation rate based on finite deformation theory

09 p1537 A71-22515

Theory of plates under finite initial elastic deformation, applying to rectangular plate stability under compressions in two mutually perpendicular directions

09 p1537 A71-22521

Symmetric three-layer girder with contact deformations and transverse compression of filler, calculating vibration under elastic impact by numerical analysis

09 p1538 A71-22522

Euler method applicability for finite subcritical deformation stability of isotropically nonlinear elastic body

09 p1541 A71-23272

Dispersion hardened Ni and Co alloys production by powder metallurgy, noting elastic distortion due to particle strengthened base material

09 p1474 A71-23294

Hot deformation of superrefractory austenitic Ni alloy, considering elastic and plastic limits

09 p1479 A71-23625

Operational research methods application to beam theory, deriving general deformation equation for beams with constant or variable moments of inertia and isostatic or hyperstatic systems

10 p1687 A71-24289

Isotropic homogeneous incompressible elastic body under surface tensions and conservative forces, showing six families of equilibrated deformations

10 p1687 A71-24347

Homogeneous isotropic elastic body stresses after imposing small deformation on strain configuration obtained from initial small deformation of original configuration

10 p1689 A71-24503

Elastic-plastic fracture behavior engineering model based on surface flaw severity by crack length dimensions measurements

[AIAA PAPER 71-371]

11 p1845 A71-25345

Axisymmetric deformation differential equations system for nonlinearly elastic shells under vertical loadings, considering various Euler buckling boundary problems

11 p1848 A71-25567

Curved beams deformation with open thin walled cross section, using equilibrium and energy methods

11 p1848 A71-25579

Shear deformation effect on optimal design of elastic beams, considering rectangular cross section circular ring by Timoshenko beam theory

11 p1849 A71-25677

Optimal elastic beam structural design for given deflection in presence of body forces, considering rod under centrifugal loads

11 p1849 A71-25680

Inextensible elastic Cosserat surfaces finite deformation mechanisms, applying theory to flexure of rectangular plate into closed circular cylinder and helical strip

11 p1849 A71-25681

Ultrasonic wave propagation in deformed isotropic elastic materials based on second order theory, examining principal stress axis rotation effect

11 p1849 A71-25682

Monograph on turbine blade fir tree roots, calculating stress-strain state of long term static strength

under elastic and elastoplastic deformation and unsteady creep

11 p1852 A71-26400

Large elastic deformations of incompressible materials shells with inclusion of transverse normal strain, considering thickness change at boundaries

12 p1976 A71-27159

Soviet book on spherical bottoms weakened by openings covering shell stress/strain, elastic-plastic deformations, reinforcing elements and composite materials

12 p1977 A71-27293

Axisymmetric deformation of thin elastic shell of revolution under combined effect of static surface load and nonuniform heating

12 p1979 A71-27359

Elastic isotropic body finite plane deformations, considering displacement and stress functions relationship

12 p1981 A71-27464

Large deformation of incompressible elastic body reinforced by unidirectional system of elastic fibers

12 p1922 A71-27695

Morera and Maxwell stress functions determination by integrodifferential equations of deformation continuity for bending of thin plates

13 p2148 A71-27891

Equilibrium of three dimensional elastic body under finite uniform deformation, deriving characteristic equations for cylindrical shells, circular and rectangular plates and circular rods

13 p2149 A71-28129

Nonlinear elasticity displacement equations, presenting three dimensional boundary value problem formulation and solution by small parameter method

13 p2150 A71-28130

Elastic stresses during local deformation in Nb-Mo, Ni-Cr, Cu-Al and pure bcc metals, using X ray analysis

13 p2085 A71-28225

Green tensor for large initial deformations of isotropic elastic body

13 p2152 A71-28277

Integral transformations application to approximate elastic solutions for nonlinear hereditary media, considering elastoplastic deformations under active loads

13 p2154 A71-28649

Complex loading history effect on elastoplastic deformation trajectories delay trail characteristic angles and length variation, determining plastic strain vector components in Euclidean space

13 p2155 A71-28652

Elastic deformation and plastic buckling of rectangular column with initial deflection under axial compression

13 p2157 A71-29287

Nonconservative dynamic instability of columns under distributed tangential force, using analog computer

13 p2158 A71-29430

Static load and stress distribution in rolling element bearings, using elastic contact area analysis method

[ASLE PREPRINT 71AM 1D-1]

13 p2076 A71-29487

Elastic displacement stress computation in cylindrical systems of isotropic homogeneous material by finite difference method

14 p2323 A71-29744

Image distortion technique for viewing deformation zones at crack tips on highly polished surface

14 p2323 A71-29849

Numerical incremental solution of large deformation elasticity problems at finite rotations and strains

14 p2324 A71-29862

Optical method for elastic deformations measurement of radio telescope reflector at various elevations

14 p2211 A71-29991

Weight effect on large elastic deflection of thin arches, studying stability via nonlinear differential equation using elastical approach

14 p2330 A71-30686

Flexible spherical domes elastic-plastic deformation, using variational equation and iterative algorithm

14 p2331 A71-30840

Elastic deformation of double cavity hyperboloid of revolution under variable loads applied to boundaries

14 p2332 A71-30846

Elastic properties relativistic theory, defining deformation tensor and constitutive laws

15 p2442 A71-31904

Elastic interaction between specimen and testing machine in mechanical property tests, considering drawbacks to machine stiffness calculation methods

15 p2414 A71-31947

Boundary conditions of elastic deformations of constrained circular cylinders under axial load, discussing modulus dependence on Poisson ratio

15 p2505 A71-32007

Arbitrarily shaped thin shell elastic-plastic deformation transient response prediction, using improved finite difference method

15 p2505 A71-32008

Elastic structure dynamic stability problem, determining optimum inequality relating energy functional

to displacement, and considering beam column with various boundary conditions

15 p2506 A71-32015

Interfiber stress model for elastic matrix-fiber reinforced composites under inplane shear and transverse normal loading

15 p2507 A71-32096

Elastic energy release rates and stress intensity from nonlinear load deflection curves as function of crack length to specimen width ratio

16 p2590 A71-32945

Yield condition and stability of elastoplastic bodies with large deformations, using Gibbs method of thermodynamics

16 p2650 A71-33015

Finite elasticity theory for isotropic incompressible solids, formulating Ericksen problem for requirements of statically possible radially symmetric deformations in equilibrium

16 p2661 A71-34147

Nonlinear elastic incompressible bodies with small deformations, obtaining three dimensional static and dynamic stability variational equation

17 p2816 A71-34328

Rotating cylindrical shell symmetrical deformation under external load, obtaining three dimensional axisymmetric problem solution in elastic theory

17 p2816 A71-34330

Toughness testing for low ductility fracture due to crack development in elastic stress field

17 p2757 A71-34557

Heating by thermoelastic damping through sudden removal of stresses on homogeneously strained elastic body, comparing elastic deformation of rubber and steels

17 p2821 A71-34584

Axisymmetrical elasticity theory for vertical finite length cylinder with mixed boundary conditions on top and bottom end surfaces, obtaining stress and displacement expressions

17 p2822 A71-34779

Isotropic compressible homogeneous body with small deformations superposed on finite elastic deformation, deriving equations of motion and boundary conditions

17 p2823 A71-34788

German monograph on plane, arbitrarily curved and bending resistant trusses calculations allowing for elastic and plastic deformation

17 p2823 A71-34800

Transverse oscillations determination in cyclically deformed thin plate under plane stress by energy dissipation calculation using Hookes law

17 p2825 A71-35012

Stresses and deformation in solid propellants charges under gravitational load, assuming homogeneous isotropic and linearly viscoelastic charge material

17 p2829 A71-35307

Axisymmetric dynamic deformation of elastic solid, obtaining characteristic properties and solutions of mixed initial and boundary value problems

17 p2831 A71-35353

Equilibrium bifurcation for nonlinearly elastic incompressible body during finite subcritical homogeneous deformation, obtaining characteristic equations for cylindrical shell, circular and rectangular plates, etc

17 p2832 A71-35609

Refractory alloys elastoplastic deformation under cyclic loading, deriving thermal fatigue equations

17 p2760 A71-35653

Viscoplastic elastic medium behavior, breaking down elastoplastic deformation into plastic and elastic deformations

18 p2977 A71-36187

Incompressible fiber reinforced composite materials finite plane deformation continuum theory and stress analysis without restriction concerning elasticity, plasticity or viscoelasticity behavior

[ASME PAPER 71-APM-V]

18 p2978 A71-36264

Dynamic loading of cantilever beams by magnetomotive and explosive loads and high bullet speed impact, noting elastic and plastic deformation modes

18 p2981 A71-36770

Finiteness of deformations and convective terms effect on medium velocity in terms of displacements on shock wave propagation in three dimensional elastic medium

18 p2982 A71-36788

Elastic deformation of strip, rectangular annulus and cylinder with homogeneous displacement boundary conditions, deriving orthogonality relations for expanded eigenvectors

18 p2982 A71-36793

Minimum weight design of statically determinate elastic truss under multiple stress and displacement constraints, using virtual work of dummy loads

18 p2982 A71-36842

Stress field singularities at interface corners in bonded dissimilar isotropic elastic materials under plane force field applied to wedge subregion

18 p2983 A71-36843

Prestressed thin shells elastic deformation, using Kirchhoff hypothesis of shell theory

19 p3154 A71-37072

Nonlinear elasticity theory variational principles modification for finite deformation of elastic body 19 p3154 A71-37095

Three dimensional orthotropic elastic cylinders symmetric deformations under external loads, calculating stress-strain state with approximate method 19 p3155 A71-37528

Linearly deformable beams with distributed parameters and lumped inclusions, determining natural transverse vibration frequencies and mode shapes 19 p3155 A71-37535

Contact problem for elasticity theory taking hereditarity in deformation into account, proving existence and uniqueness theorems 19 p3156 A71-37538

Two dimensional stress tensor invariants for finite elastic deformations of thin plate using initial complex coordinates 19 p3156 A71-37541

Simple structures large elastic-plastic transient deformations, using finite element method 19 p3157 A71-37874

Finite strain theory for elastic-plastic deformation, considering isothermal shear of neo-Hookean material before yielding and during elastic unloading 20 p3267 A71-38794

Heat stresses in elastic compressible material plate strip subjected to finite deformation 20 p3308 A71-39038

Nonlinear behavior of compressed elastic and elastoplastic rods in presence of large deformations, determining bearing capacity by step method 20 p3269 A71-39164

Finite elastoplastic deformation thermodynamic theory based on isotropic work hardening, excluding Bauschinger effect or localized modification of yield surface due to plastic flow 20 p3308 A71-39486

Fiber reinforced tube under lateral compression between two flat dies, determining finite deformation from nonlinear elastic and elastoplastic shearing response analysis 20 p3311 A71-39966

Morera and Maxwell stress functions determination by integrodifferential equations of deformation continuity for bending of thin plates 21 p3455 A71-40085

Axisymmetric stress and strain states calculation for linear elastic fit in cylindrical tight fits between hub and shaft 21 p3463 A71-40656

Plastic wave propagation along rods and through slabs, describing finite deformation elastic-plastic theory 21 p3464 A71-40785

Nonlinear elastic deflection analysis of beams in space, deriving geometric curvature, free center line torsion and cross section twist angle 21 p3471 A71-41022

Design and technological calculations in machine building, analyzing flow, creep and elastoplastic deformation theories 21 p3472 A71-41144

Elastic cracks and screw dislocation pile-ups crossing bimaterial interface, deriving dual singular integral equations 22 p3615 A71-41710

Inertia-loaded elastic thin circular ring in rigid cavity with small initial clearance, calculating deformation by nonlinear bending theory 22 p3616 A71-42215

Theoretical estimation of tensile strength, elastic modulus and deformation of cubical diamond specimens under tension and compression 22 p3563 A71-42873

Boundary displacement conditions in linear elasticity with friction, using minimization of nondifferentiable convex functional and variational inequalities 23 p3775 A71-43239

Micropolar elasticity plane problems equilibrium equations system solution, considering elastic half space deformation and steady thermoelasticity 23 p3775 A71-43316

Two-component composite cylindrical body thermoelastic stresses near junction-surface edge under plane deformation conditions 23 p3776 A71-43420

Rough spheres, cylinders and annuli in contact, determining surface roughness and waviness effects on surface geometry under elastic and plastic deformations 23 p3682 A71-43928

Axisymmetrical elastic deformation of thin helical shell with rectilinear profile, deriving equilibrium equations and stress-strain relationships 23 p3778 A71-44038

Stresses and displacements in elastic half space with variable modulus of elasticity under axisymmetrical shifting load distributed along ring 23 p3778 A71-44045

Fine structure at crack tip expanding in ideally elastoplastic material in plane deformation state and plane stressed state 23 p3778 A71-44061

Soviet book on elastoplastic deformations of plates and cylindrical shells made of low strain hardening materials, covering strength and stability calculations 23 p3779 A71-44186

Fiber reinforced viscoelastic rectangular beam, deriving asymptotic values of stress, curvature and position of neutral axis under constant moment 24 p3879 A71-44630

Deformations and stresses in elastoplastic half space indented by rigid sphere, using finite element method 24 p3879 A71-44631

Convergence and strain accuracy of finite element solutions for nodal displacements in plane elastic mesh 24 p3842 A71-44633

Axisymmetric elastic deformation of layered thin anisotropic shells of revolution, using computer integration for arbitrary loads and boundary conditions 24 p3882 A71-44841

Cyclic symmetrical deformation of thin elastic conical shells of revolution of variable thickness with meridional ribs under physical and thermal loads 24 p3882 A71-44843

Curvilinear elasticity solutions to stress concentrations at fine necks in cylindrical shaft under torsion, considering semicircle, semiellipse, rectangle, triangle and arc shapes 24 p3882 A71-44846

Circular conical shell initial deformation under impulsive load, using Timoshenko theory 24 p3883 A71-44852

Elastoplastic deformation of Zn single crystals under uniaxial tensile loads, noting critical stresses relationship to current pulses 24 p3838 A71-45100

Residual resistance measurements for studying recovery of high purity potassium wires deformed at/below 4.2 K, discussing anomalous difference with sodium 24 p3861 A71-45195

ELASTIC MEDIA

Crack opening in infinite isotropic elastic solid via displacements applied to crack surface 01 p0167 A71-10292

Book on numerical method for coupled modes in plasmas, elastic media and parametric amplifiers covering differential equations, recursive functions, wave propagation and iterative calculations 01 p0111 A71-10356

Rayleigh wave propagation in stochastically inhomogeneous elastic medium 01 p0169 A71-10637

Horizontal shear wave diffraction by finite crack and rigid ribbon in elastic medium 01 p0173 A71-10845

Elastic waves excitation by pressure wave in shells of revolution, investigating acoustic medium effects on frontal discontinuities intensity 01 p0176 A71-11148

Thermal stress concentration around hole in edge-heated elastic strip, using quasi-static formulation 02 p0322 A71-11732

Coupled Riemann-Hilbert boundary value problems for thermoelastic state near thermally insulated crack in inhomogeneous elastic medium 02 p0322 A71-11734

Elastoplastic, viscoelastic and directed elastic continuous media kinematic and thermodynamic description based on intermediate state of reference concept 02 p0326 A71-12335

Piecewise linear elastic material three dimensional stress-strain analysis for limiting surfaces between regions with different moduli 03 p0451 A71-13901

Displacement and stress distribution in infinite elastic medium weakened by Griffith crack 03 p0509 A71-13909

Stationarity of complementary energy in nonlinear elasticity theory, using Piola stress tensor representation for isotropic elastic media 03 p0513 A71-14228

Thermoelastic deformation of elastic media with stochastically inhomogeneous microstructure, characterizing physical properties as steady random variables 03 p0514 A71-14358

Elastic solids mechanical characterization using finite element formulation of minimum potential energy theorem 04 p0671 A71-15751

Shock heating effects due to compression and plastic dissipation on basis of finite one dimensional waves in strain rate sensitive elastic viscoplastic solids 05 p0830 A71-17238

Stress wave propagation from spherical cavity in isotropic nonhomogeneous elastic medium in contact with vacuum at infinity, obtaining closed form solution 06 p1001 A71-18228

Elastic medium residual microstresses probability distribution, noting microdistortion tensor linear and transverse components and tangential and normal stresses relation 06 p1002 A71-18417

Spheroidal cavity effects on elastic medium under axisymmetric stress field, using Legendre potential functions 07 p1212 A71-19253

Elastic solids fourth order anharmonic equation of state from finite strain theory, resolving ambiguities by Mie-Grüneisen equation 07 p1178 A71-19800

Three-part mixed boundary problem concerning equilibrium of semiinfinite two dimensional elastic medium containing Griffith cracks parallel to free boundary 07 p1214 A71-20021

Discrete structure continuous medium model with internal degrees of freedom, studying physicomaterial properties in elastic materials 07 p1217 A71-20455

Pulse propagation from time-step point force at surface of transversely isotropic elastic half space, obtaining solutions by integral transforms 08 p1371 A71-21428

Theoretical model of elastic medium with diverse tensile and compression resistances under finite deformation 08 p1373 A71-21944

Elastic half space two dimensional unsteady temperature and stress fields under induction heating and convective heat transfer 09 p1537 A71-22519

Elastic media damping effects on rigid bodies HF vertical and rotational vibrations, considering approximate solution for structural amplitude response 09 p1541 A71-23088

Binary phase systems stress analytical method for water saturated elastic porous medium 10 p1685 A71-23993

Adhesive fracture blister tests, using energy balance for treating stress singularities in brittle elastic materials 10 p1631 A71-24077

Adhesive bonded joints mechanical behavior relation to materials, processes and experimental techniques, developing statistical analysis and formulas for orthotropic-elastic joints 10 p1614 A71-24087

Quasi-static problem of stress-strain distributions in elastic medium with moving crack, calculating arbitrary external force effect on crack 10 p1687 A71-24349

Elastic half space with plane boundary subjected to transient temperature field, calculating temperature distribution and thermoelastic strain through Laplace transform 10 p1688 A71-24351

Strain energy calculation of V notched crack in elastic continuum from finite element computer programs applied to fractures in solid propellant rocket motor cartridges or grains 10 p1693 A71-25056

Penny shaped crack in elastic layer bonded to two dissimilar half spaces, investigating stress intensity factors and fracture propagation direction 11 p1841 A71-25301

Semiinfinite crack perpendicular to elastic half plane surface under pressure distribution on faces or remote loading, obtaining fracture mechanics solution with Wiener-Hopf method 11 p1847 A71-25444

Equilibrium thermodynamics of ideal elastic solids under stress, using Cauchy stress tensor 11 p1799 A71-25740

Soviet book on elasticity theory covering stress and strain tensors, linear closed systems of equations and methods of solution, Saint Venant problem, etc 11 p1850 A71-26097

Traveling wave propagation, modal vibrations and elastic transmission medium studies from theoretical seismograms for realistic gravitating heterogeneous spherical earth model 11 p1760 A71-26148

Mechanical waves propagation in elastic viscoplastic medium in presence of temperature field, using mechanical and mathematical models 11 p1850 A71-26177

Heat conduction effects on small amplitude plane harmonic wave propagation in transversely isotropic elastic Zn single crystals 12 p1985 A71-26925

High altitude balloon gore meridional stresses effects on film response by analyzing cylindrical elastic membrane under uniform hydrostatic pressure and axial loads 12 p1976 A71-27121

Stress-strain state of circular cylindrical shells in elastic medium, reducing linear problem to solution of single eighth order partial differential equation 13 p2150 A71-28134

Free elastically joined composite rod under tracking forces, calculating stability and oscillations by numerical method 13 p2154 A71-28644

Elastic wave propagation in infinite elastic medium due to explosion at spherical cavity center, consider-

ing material properties thermal change as function of radial distance

13 p2165 A71-29104

Linear isotropic and centro-symmetric second-grade elastic material and special case with coupling stress, calculating stress field of long straight screw and edge dislocations

14 p2327 A71-30290

Dissimilar elastic half spaces joined over circular region, calculating interfacial traction stresses induced by arbitrary loading from coupled integral equations

14 p2328 A71-30293

External field perturbations by local inhomogeneities in elastic medium, deriving expressions for interaction energy and forces between defects

14 p2332 A71-30869

Dispersion and attenuation of plane longitudinal waves in laminated medium of elastic and viscoelastic layers, showing effect of composite parameters variations

[ASME PAPER 70-WA/APM-40]

15 p2505 A71-32009

Soviet book on multilayered media elasticity theory three dimensional problems covering Fourier and Hankel integral transformations, compression, bending, normal and tangential loads, etc

15 p2506 A71-32020

Elastic materials Poisson ratio measurement by moire method in coherent and incoherent light

16 p2575 A71-32825

Displacements produced by impulsive torsional body force situated within elastic half space bonded to half space of different material properties

16 p2647 A71-32859

Elastic stability theory for perfectly elastic materials with couple stresses, deriving exact functional for overall conservative systems of forces and couples

16 p2648 A71-32989

Periodically laminated elastic half plane response to rapid internal heating, obtaining far field composite stress waves variation due to dispersion

[ASME PAPER 71-APM-28]

16 p2663 A71-33201

Viscoplastic elastic medium behavioral relations, considering instantaneous and nonretarded plastic deformation

16 p2660 A71-34066

Normal stress discontinuity propagation over expanding circular region below free surface of semi-infinite isotropic elastic media

17 p2815 A71-34179

Axisymmetric dynamic deformation of elastic solid, obtaining characteristic properties and solutions of mixed initial and boundary value problems

17 p2831 A71-35353

Mechanical interactions of point defects in homogeneous isotropic continuous elastic media, deriving interaction energy from Siemens multipole forces analysis

17 p2831 A71-35395

Viscoplastic elastic medium behavior, breaking down elastoplastic deformation into plastic and elastic deformations

18 p2977 A71-36187

Two parallel noncoplanar cracks extension in elastically isotropic solid by applied shear stress with deformation in antiplane strain mode

19 p3157 A71-37797

Temperature effects in incompressible elastic materials, adapting Adkins-Green isothermal successive approximation technique to thermoelasticity problems

19 p3157 A71-37800

Circular planform punch pressure on elastic half space, solving system of two dimensional dual integral equations

19 p3160 A71-38478

Deformation and stress distribution three dimensional state around flat parabolic cracks in elastic solids

20 p3307 A71-38772

Harmonic stress function and stress intensity factor for elliptical crack embedded in elastic solid and subjected to arbitrary internal pressure

20 p3307 A71-38782

Arutiunian method application to crack problems in power law elastic materials and contact problems in nonlinear creep, noting error for crack tip singularity

20 p3310 A71-39868

Stress state determination in birefringent elastic material for plane dynamic problems by photoelasticimetric and interferometric techniques

21 p3376 A71-40103

Rayleigh wave reflection from crack tip after propagation along open crack faces in elastic solid, determining surface wave energy loss

21 p3468 A71-41003

Elastic continuous medium with nonlocal interactions, calculating surface waves dispersion equations with boundary solutions

21 p3417 A71-41366

Coupled thermoelastic problem of homogeneous isotropic elastic half space with embedded spherical cavity

22 p3613 A71-41566

Effective shear modulus of multilayered rectangular elastic isotropic member in uniform torsion

22 p3618 A71-42587

Stress and displacement analysis in linear elastic half space consisting of one or two layers bonded to another homogeneous half space

23 p3779 A71-44178

Elasticity theory for rectangular region with thin-walled inclusion under symmetrical external forces, reducing to three quasi-regular infinite systems of linear algebraic equations

24 p3880 A71-44722

Three dimensional unbounded anisotropic elastic medium with ellipsoidal inhomogeneity and modulus tensor of piecewise-constant form

24 p3885 A71-45062

Axisymmetric contact problem of elastic half space stress-strain state, seeking displacements in Hankel integral expansion form

24 p3885 A71-45222

Micrononhomogeneous elastic media with moduli as coordinate random function, investigating stress and strain tensors

24 p3849 A71-45345

ELASTIC MODULUS

U MODULUS OF ELASTICITY ELASTIC PLATES

Thin elastic plates generalized variational equations derivation from virtual displacements and forces principles for arbitrary subdomains, observing node displacement continuity condition

01 p0166 A71-10124

Thin elastic orthotropic plate in finite difference formulation, determining natural vibration mode and instability by summary representation method

01 p0168 A71-10410

Isotropic nonlinearly elastic plate weakened by doubly periodic reinforced curvilinear holes, calculating stress-strain state by Cauchy integrals

01 p0168 A71-10412

Elastic plane with hypocycloid hole under axial tension, determining stress concentration at hole boundary due to irregularities

01 p0168 A71-10424

Stress fields statistical characteristics in randomly inhomogeneous elastic plate, considering Lomakin solution

01 p0170 A71-10642

Stability theory of plates beyond elastic limit, discussing elimination of stress variations discontinuity at interface between plastic loading and unloading zones

01 p0170 A71-10648

Circular elastoplastic plates, solving adaptation theory kinematic equations by linear programming procedures

02 p0324 A71-11751

German monograph on arbitrarily distributed internal stresses effect on elastic stability of plates, considering variational problem solution as matrix eigenvalue problem

02 p0327 A71-12375

Critical velocity and elastic panel flutter stabilization in magnetohydrodynamic flow by distributed magnetic field control

02 p0293 A71-12628

Elastic plate plane stress analysis by Euler variational method for arbitrary geometric shapes and loading, obtaining isotropic and orthotropic solutions

02 p0330 A71-12747

Book on laminated plate theory covering anisotropic continua, bending, orthotropic plates, energy equations, etc

02 p0330 A71-12844

Stress-strain state of plate made from highly elastic polymer containing circular and elliptical holes

03 p0506 A71-13602

Stress distribution around elliptical hole in thin flat rectangular elastic plate under axial in-plane edge loads

[ASME PAPER 70-DE-M]

03 p0506 A71-13705

Coupled stresses effect on dynamic stress concentration produced by traveling loads on elastic Cosserat plate

03 p0509 A71-13905

Plane acoustic wave diffraction at thin semiinfinite elastic plate, reducing to Riemann boundary problems for Helmholtz equation in half space

03 p0459 A71-14061

Stress development in elastic plate with crack under edge loads, estimating plastic zone size at crack ends

03 p0514 A71-14361

Monograph on bounds for vibration frequencies and buckling loads of clamped uniform thin elastic plates covering stability, harmonic and biharmonic functions

04 p0667 A71-14899

Stress distribution in infinite cracked elastic plate subjected to constant twisting on basis of Reissner thin plates theory

04 p0670 A71-15385

Wall stability of parallel elastic plate duct in contact with inviscid compressible liquid flow

04 p0573 A71-15563

Rectangular thin elastic plate with circular holes under heat flow, solving thermoelastic problem by point matching

05 p0823 A71-16492

Elastic plate with heat conducting rectilinear crack, determining steady state temperature field and stresses

05 p0827 A71-16889

Cosserat surfaces and variable thickness elastic plates linear isothermal theory, deriving constitutive equations corresponding to isotropic three dimensional plate bending and stretching

05 p0831 A71-17250

Mixed boundary value problem in elasticity theory for piecewise homogeneous isotropic plate with slits, reducing to integral equations

06 p0983 A71-17361

Elastic plates and members deformation with constraints on deflections, determining strain state with dynamic programming

06 p0984 A71-17651

Flexible plates and shallow shells supercritical deformation in high temperature field, taking into account modulus of elasticity and thermal expansion coefficient temperature dependence

06 p0990 A71-17796

Elastic plates and shells stability and vibration problems asymptotic solution methods, considering edge effect

06 p0991 A71-17800

Elastic rectangular and thin plates design under dynamic loading, using Bubnov-Galerkin method for computer solutions

06 p0992 A71-17808

Circular and angular elastic plates elastoplastic bending theory, using Saint Venant conditions and equations of equilibrium and deformation

06 p0993 A71-17812

Infinite elastic plate with rectilinear crack, determining heat exchange effect on thermoelastic stresses

06 p1000 A71-17939

Soviet book on computer calculation of three-layer elastic plates and shells covering programs, initial equations, input number language, numerical solution, etc

07 p1210 A71-19047

Unbounded isotropic elastic plate traversed by two parallel cracks, obtaining limiting equilibrium state

07 p1211 A71-19192

Forced thickness-stretch vibrations of plated elastic plate, involving time derivatives in boundary conditions

07 p1212 A71-19589

Viscoelastic plates forced motion under dynamic loads by Valani method, considering elastic and layered elastic-viscoelastic circular plates

08 p1368 A71-20801

Energy dissipation in free oscillations of multilayer shells consisting of alternating rigid elastic layers and soft fillers, deriving equations of motion

08 p1369 A71-21123

Buckling of thin elastic circular plates under steady state asymmetric temperature distribution

08 p1370 A71-21304

Stress analysis of elastic bending plates by holographic interferometry, comparing results to theory

08 p1373 A71-21752

Thermoelastic stress and temperature distribution in doubly connected isotropic plate

08 p1374 A71-21948

Unsteady interaction of compressible fluid and flat circular deforming elastic membrane analyzed coupled computer program method

[AIAA PAPER 70-75]

09 p1430 A71-22085

Elastic plate with circular hole, solving contact problem in elasticity theory with integrodifferential equation

09 p1535 A71-22181

Thick walled anisotropic nonhomogeneous elastic cylinder or plate under axial symmetric time dependent pressure, investigating transient response

09 p1540 A71-23087

Physically nonlinear theory of isotropic elastic shells and plates eliminating Love-Kirchhoff hypothesis

09 p1543 A71-23613

Book on elastic plate theory covering bending and transverse shear effects, boundary problems, rectangular isotropic, structurally orthotropic, circular and annular plates under various loads

09 p1544 A71-23701

Flexural vibration analysis of rectangular isotropic and orthotropic polygonal elastic plates with constant or variable thickness, considering mass distribution and boundary conditions

10 p1625 A71-24019

Stress state elastic equilibrium of ponderable anisotropic half plane with free and ring reinforced elliptic hole near rectilinear boundary

10 p1690 A71-24567

Polygonal elastic plates natural frequencies investigation by conformal mapping and variational method, transforming holomorphic function into equivalent problem of circular boundary plate

10 p1691 A71-24813

- Plate thickness effect on stress distribution around crack, using three dimensional elasticity equations 10 p1693 A71-25055
- Initially curved thin elastic plates, predicting large deflection and postbuckling behavior with finite element procedure [ALAA PAPER 71-357] 11 p1844 A71-25336
- Plane stress distribution solution for rectangular elastic plastic plate under partial edge loading, using incremental theory 12 p1976 A71-27122
- Elastic laminated plates with various thickness layers, deriving independent differential equations for displacement 12 p1978 A71-27334
- Kane-Mindlin differential equations solved by perturbation techniques for free extensional vibrations in elastic plates 12 p1981 A71-27483
- Asymmetric structure elastic transversely isotropic sandwich panels bending equations, taking into account transverse shear strain and stability 12 p1981 A71-27497
- Contact stress between half plane and elastic cover plate, reducing problem to Prandtl type integrodifferential equation with Hilbert kernel 12 p1982 A71-27526
- Stretching, twisting, pure bending and flexure of pretwisted elastic rectangular plates of rectangular cross section 13 p2147 A71-27783
- Stress concentration in variable-modulus perforated plate of isotropic elastic material under hydrostatic pressure 13 p2151 A71-28142
- Elastoplastic plates and shallow shells with rigid orthotropic filler, bending and buckling beyond elastic limit 13 p2156 A71-29066
- Circular elastic ideally plastic plate deformation due to circumferentially distributed rectangular pulse loading 13 p2156 A71-29075
- Multiple Fourier method for plate bending compared with least squares and boundary collocation solutions 14 p2325 A71-29888
- Thermoelastic shells and plates approximate linear theory, detailing uniqueness theorem for initial mixed boundary value problem 14 p2329 A71-30446
- Dislocation stress analysis in infinite elastic plate with two circular holes under arbitrary steady temperature field 14 p2332 A71-30850
- Stress analysis of nonlinearly elastic plate with ring reinforced circular hole 14 p2332 A71-30854
- Bending stress of thick laminated plates of isotropic material with variable elasticity modulus 14 p2333 A71-30890
- Thermal buckling of elastic plates exposed to random temperature field producing biaxial stress concentration 15 p2504 A71-31834
- Monograph on rectangular shear elastic plates stability covering Cosserat plane, stress functions, buckling conditions, compressive forces and two dimensional equations 15 p2509 A71-32302
- Near field dynamic response of semiinfinite elastic plate to lateral impact, comparing displacement field observations to numerical results 15 p2510 A71-32792
- Thin infinite isotropic elastic plate on nonlinear elastic foundation under uniform two dimensional hydrostatic pressure, detailing imperfection effects on initial postbuckling behavior 16 p2648 A71-32979
- Combined finite element method and Rayleigh-Ritz procedure for geometrically nonlinear problems solution of elastic plates with arbitrary shape, boundary and load distribution 16 p2653 A71-33088
- Stress, slip and damping of clamped elastic plate with finite friction under alternating axial load, using finite element method 16 p2581 A71-33174
- Elastic plate with part-through surface crack, determining stress intensity factor for remote tensile and bending loads [ASME PAPER 71-APM-20] 16 p2655 A71-33209
- General solution of cylindrical fourth order differential equation with zero index representing circular disk and ring plate problems in elasticity theory 16 p2602 A71-33400
- Uniformly extended elastic circular plate with rectilinear slot under normal tensile loads at boundary 16 p2660 A71-34115
- Multicomponent system of elastic plate with hole and built-in viscous-fluid-filled syphon bellows, calculating oscillation by asymptotic methods 17 p2777 A71-34423
- Displacement field of constant thickness elastic disk with stress boundary conditions, using finite difference technique 17 p2818 A71-34505
- Sloshing liquid natural frequencies change in cylindrical shell by movable devices, considering immersed thin elastic plate effect 17 p2726 A71-34579
- Axisymmetric nonlinear buckling equations for composite thin circular elastic plates of isotropic or orthotropic layers under radial compression 17 p2821 A71-34580
- Thermoelastic Cosserat plate with insulated unstressed circular hole under uniform temperature gradient at infinity 17 p2822 A71-34675
- Stressed state of nonuniformly heated thermoelastic flexible plates with variable elastic parameters, using integral principle of minimum total potential energy 17 p2829 A71-35310
- Thin circular disk rotating at constant angular velocity, solving three dimensional elasticity problem with formal power series of thickness-diameter ratio [ASME PAPER 71-APM-Q] 18 p2978 A71-36260
- Fundamental frequency of large amplitude bending vibration of elastic and isotropic rectangular plates, considering effects of transverse shear and rotatory inertia 18 p2980 A71-36496
- High frequency modal response of elastic plates to impulsive line load, using Rayleigh-Lamb branch equation 18 p2983 A71-36844
- Free vibrations frequencies and mode shapes of anisotropic elastic thin plates, using Galerkin method 18 p2983 A71-36931
- Elastic boundary interaction with viscous sublayer of turbulent boundary layer for Reynolds stresses and drag reduction possibility 19 p3042 A71-37082
- Elastic circular plate with hole traversed by tube filled with viscous fluid, studying system motion 19 p3043 A71-37539
- Circular inclusion effects in infinite viscoelastic plate under monotonically increasing uniaxial tension, considering stress distribution 19 p3157 A71-37798
- Thermoelastic axisymmetric equilibrium of elastic semiinfinite two dimensional medium with Griffith crack under prescribed heat flux 19 p3159 A71-38189
- Isotropic viscoelastic plates of variable thickness subjected to mechanical and thermal stress, considering circular and rectangular plates vibration by external thermal shock 19 p3160 A71-38480
- Stress distribution in cylindrical bodies in internal contact, considering thick elastic plate with elastic disk fitted tightly into hole 19 p3160 A71-38482
- Heat stresses in elastic compressible material plate strip subjected to finite deformation 20 p3308 A71-39038
- Infinite elastic plate forcing by time varying radial pressure in circular hole at center 20 p3309 A71-39563
- Approximate theory for vibration of nonhomogeneous anisotropic layered plates using asymptotic integration of elasticity equations 20 p3310 A71-39782
- Numerical analysis of natural frequency spectrum of elastic plate free vibrations in compressible inviscid fluid 20 p3310 A71-39784
- Thermal stresses in infinite elastic plate with circular hole and single heat source, considering steady state heat conduction 21 p3464 A71-40753
- Stress intensity factors of periodically spaced elastic cover plates bonded to elastic half plane, solving contact problem by Fredholm integral equation 21 p3470 A71-41020
- Clamped circular elastic plate nonlinear free vibrations, obtaining mode shapes and amplitude-frequency relationships 21 p3471 A71-41025
- Free and forced finite amplitude nonlinear oscillations of thin elastic annular plate with free inner and clamped immovable boundaries 21 p3471 A71-41026
- Stress and contact time calculation for impact of spheres on finite thickness elastic plate overlying rigid foundation 21 p3472 A71-41031
- Elastic plates radial vibrations excited by piezoelectric elements, investigating electromechanical coupling coefficient and ultrasonic radiation constants 21 p3473 A71-41365
- Thin elastic plate under dynamic loading, applying asymptotic expansion techniques to three dimensional dynamic elasticity theory 22 p3613 A71-41435
- Plane wave propagation following thin elastic rectangular plate impact against smooth rigid obstacle, using difference scheme 22 p3531 A71-41910
- One dimensional propagation and multiple reflection of plane thermoelastic wave in Lamé elastic isotropic plate with finite heat transmission 22 p3615 A71-41911
- Thin elastic elliptic plate stress analysis by approximate solution for rectangular plate and parallelepiped equilibrium problems 22 p3616 A71-42212
- Elastic plates transverse vibrations fundamental frequency from constant deflection lines method 22 p3617 A71-42537
- Finite plates coincidence effect occurrence with sound waves, examining backing cavity and incidence angle influence 22 p3576 A71-42538
- Coupled plate-cavity acoustic system response at L.F. and spatially uniform pressure, using plate finite elements and acoustic volume-displacement theory 22 p3617 A71-42540
- Equilibrium equations of elastic plates, reducing to Cauchy problem by use of invariant imbedding 22 p3618 A71-42584
- Irregularly shaped thin elastic plates under uniform transverse or point loads with singularities resulting from loading or corner conditions 22 p3618 A71-42591
- Singly and nonsingly connected thin elastic rectangular plate stability analysis under arbitrary compression load on surface 23 p3777 A71-43423
- Nonlinear geometry effects on stress concentration in elastic plates weakened by two circular holes, using complex potential approximations 23 p3778 A71-44041
- Stress-strain state of isotropic elastic plate weakened by cracks, using Fredholm integrals 24 p3881 A71-44832
- Stress-strain state of nonlinearly elastic reinforced polymer plate with circular hole, deriving stress tensor components and first approximation solution for pure bending 24 p3882 A71-44838
- Three dimensional stress field error estimates in linear plate bending, using Prager-Syngue hypercircle elasticity theorem 24 p3884 A71-44964
- Mixed boundary elasticity solutions for plane with cut on real axis, using Riemann surface 24 p3885 A71-45102

ELASTIC PROPERTIES

- NT AEROELASTICITY
- NT ANELASTICITY
- NT ELASTOPLASTICITY
- NT HYDROELASTICITY
- NT HYPOELASTICITY
- NT MAGNETOSTRICTION
- NT MODULUS OF ELASTICITY
- NT PHOTOELASTICITY
- NT PHOTOVISCOELASTICITY
- NT PROPORTIONAL LIMIT
- NT THERMOELASTICITY
- NT THERMOVISCOELASTICITY
- NT VISCOELASTICITY
- Cr-Ni steel elastic properties under intercrystalline corrosion, examining temperature effects on internal friction, electric resistivity and vibration frequency 01 p0096 A71-10038
- Artery wall elasticity relation to Korotkoff sound wave frequency by upper arm blood pressure model, using cylindrical rubber tubes and canine specimens 01 p0009 A71-10240
- Ta alloys single crystals elastic compliance constants over temperature range, deriving bulk and shear moduli and anisotropy factor 01 p0100 A71-10373
- Elastic boundary value problem of viscoelastic cylindrical body with temperature and time variations and relaxation kernel 01 p0169 A71-10492
- Boundary value problem of elasticity theory for reinforced plastics with internal stresses due to shrinkage 01 p0107 A71-10495
- Linear integral equations with difference and summation kernels in elasticity theory, developing approximate solution method 01 p0171 A71-10657
- Orthogonal polynomials method for integral equations solution in two dimensional mixed boundary value problems of elasticity theory 01 p0171 A71-10660
- Plane micropolar static strain in homogeneous isotropic elastic solid, deriving existence theorems for interior and exterior problems 01 p0172 A71-10841
- Fatigue effects on metallic materials elastoviscoplasticity properties 01 p0175 A71-11025

Thermoelastic theory of stressed crystals and higher order elastic constants covering surface electronic and mass transport properties

02 p0294 A71-11799

Nonlinearly elastic rings and arches under hydrostatic pressure, examining equilibrium with sixth order differential equations

02 p0325 A71-12125

Rigid and flexible pavement design and construction in Europe, discussing unreinforced and crack reinforced slabs and CBR method

02 p0238 A71-12167

Two dimensional mixed boundary value problems solution in elasticity theory by linear differential operators, applying to Dirichlet and Neumann problems

02 p0326 A71-12293

Elastic parameter dynamic measurements using resonance methods with electrostatic attraction

02 p0328 A71-12406

Equivalence theory applications in three dimensional elasticity, plane deformation and stresses

02 p0328 A71-12534

Boundary value problems solution of Helmholtz and Poisson equations for parallelepiped, applying to elasticity theory

02 p0328 A71-12542

Elastic field of cylindrical inclusion, using continuum dislocation theory

02 p0330 A71-12741

Cyclic deformations and internal energy dissipation effect on hysteresis loop shape equations derivation in terms of three components including nonlinear and inelastic materials properties

03 p0502 A71-13407

Vibration dampers optimization, considering viscous and inelastic resistance effect on sensitivity of harmonically moving system response

03 p0503 A71-13409

Nonlinear elastic effect on stress concentration of incased tubular solid propellant grain

03 p0504 A71-13462

Thin reinforced laminates configurations with elastic behavior of homogeneous orthotropic or isotropic material, considering flat plates and thin shells constitutive equations

03 p0505 A71-13537

Elastic and perfectly plastic plane stress problems yield point load lower bounds by finite element method, considering weakened slabs

03 p0505 A71-13541

Anisotropic rod elastic curve equilibrium shape for rigidity conditions, considering Goriachev solution to heavy solid body motion about fixed point

03 p0458 A71-13599

Inhomogeneous elasticity theory under spherical symmetry, using linear differential equations transformation into constant coefficient equations

03 p0507 A71-13714

Rigid-perfectly plastic model for real materials behavior, considering modification for strain hardening and elastic effects under various load conditions

03 p0509 A71-13780

Cauchy problem solution for elasticity theory dynamic system in Euclidean space arbitrary region

03 p0510 A71-13962

Elastic behavior of bone as two phase composite material, using ultrasonically measured hydroxyapatite moduli

[ASME PAPER 70-WA/BHF-3] 03 p0373 A71-14110

Spherical shell segments stresses and displacement due to arbitrary axisymmetric surface tractions and edge boundary conditions, using axisymmetric elasticity solutions

[ASME PAPER 70-WA/APM-27]

03 p0512 A71-14159

Elasticity theory two dimensional contact problems, examining cohesion or friction in contact area

03 p0513 A71-14229

Hugoniot elastic limit and dynamic compression strength for brittle bodies, considering hydrostatic stress and porous specimens

04 p0617 A71-14750

Elastic properties of lunar surface material from Surveyor spacecraft strain gage data

04 p0644 A71-15129

Free boundary value problems in elasticity, applying plane linear theory to electroelasticity

04 p0667 A71-15175

Pressure-temperature equivalences in elasticity problems, considering applications to case bonded solid propellant rocket grains

04 p0638 A71-15197

Crack perpendicular to planar interface between isotropic half spaces, noting elastic constants effect on stress components distribution and relative magnitudes

04 p0670 A71-15384

Turbine machine elements approximation by difference equations of axisymmetrical elasticity theory problem

04 p0671 A71-15644

Homogeneous integral equations of asymmetrical elasticity in steady state, using compound layer volume potentials

04 p0620 A71-15887

Elastic and compression strength characteristics of fiberglass-reinforced plastics prepared by cold solidification

05 p0771 A71-16364

Elasticity and strength anisotropy changes of unidirectional fiberglass reinforced plastics during winding

05 p0759 A71-16372

Soviet monograph on refractory materials elasticity at high temperatures covering elastic and shear moduli, Poisson coefficient and resonance methods

05 p0766 A71-16400

Algorithm for stress functions in elastic region, using variational difference method

05 p0827 A71-16759

Stress-strain state in elasticity theory of three layer symmetrical plate

05 p0828 A71-16986

Isotropic and slightly anisotropic materials elastic constants evaluation from ultrasonic reflection measurement

05 p0771 A71-17252

Axisymmetric problem solution method for ring shaped body of revolution in elasticity theory

06 p0983 A71-17366

Variable thickness truncated hollow cone elastic equilibrium, considering asymptotic analysis of axisymmetric problem

06 p0994 A71-17820

Chandler wobble seismic excitation by dislocations elasticity theory, discussing pole path changes-earthquake correlation

06 p0891 A71-17886

Linear elastic fracture mechanics based on elasticity theory, discussing Griffith theory for crack behavior

06 p1001 A71-18091

Unidirectional fiber reinforced orthotropic composite materials elastic constants calculation as function of two isotropic components characteristics

06 p1001 A71-18309

Main mixed axisymmetric stress for elastic half space with single line separation between boundary conditions, using p-analytic functions

06 p1001 A71-18341

Elastic and thermodynamic properties of transition metal carbides, comparing Debye temperatures obtained from elastic constant to those obtained from specific heat data

06 p0915 A71-18687

Elasticity theory axisymmetrical problem, applying finite element method

07 p1210 A71-19161

Difference scheme for solution of static boundary value problem differential equations of elasticity theory

07 p1211 A71-19181

Elasticity theory equations for homogeneous boundary value problem, deriving solution existence conditions by Fourier method validity demonstration

07 p1213 A71-19799

Boundary value problems of analytic functions and singular integral equations, considering hydromechanics and elasticity theory applications

07 p1148 A71-20077

Riemann surfaces use in plane boundary value problems and singular integral equations, considering plane elasticity and filtration theories

07 p1148 A71-20079

Laminate analogy predicting elastic and thermal expansion properties of short fiber reinforced composites, extending to two and three dimensional woven fabric composites

07 p1215 A71-20129

Equilibrium diagrams of Re with W, Mo, Co, Ni, discussing high strength system elastic components with torsional support applications

07 p1140 A71-20232

W-Mo-Re high temperature alloys, discussing high strength, elastic properties, creep, thermal resistivity and expansion coefficient

07 p1141 A71-20243

Dynamic strength of elastic elements from wire and tapes of Mo-Re alloy

07 p1120 A71-20249

Aircraft elastic mode control for turbulence gust alleviation, noting riding quality, structural fatigue life and peak loads

07 p1022 A71-20301

Homogeneous isotropic layers stack on rigid base with periodically varying elasticity parameters, calculating equilibrium under normal distributed load

07 p1217 A71-20460

Elastic solutions convergence in nonlinear problems of viscoelastic incompressible media, formulating and proving uniqueness theorem for certain conditions

08 p1369 A71-21053

Cast Mo alloy at low temperatures, investigating elasticity, plasticity and tensile strength characteristics

08 p1316 A71-21615

Mixed plane elasticity theory of narrow rectangle imbedded in static walls under normal loads

08 p1373 A71-21943

Nonlinear elastoplastic ring buckling under compression

09 p1534 A71-22145

True torsional stress at plastic strain onset determination in terms of elasticity theory

09 p1536 A71-22323

Anisotropic medium theory of elasticity boundary value problem, considering plane with two closed Liapunov curves without common point

09 p1485 A71-22637

Mechanical strength and elastic properties under tension and bending of boron fibers, noting dependence on surface defects

09 p1482 A71-22823

Elastic characteristics of graphite plastics and graphite materials impregnated with synthetic resins, considering aging effect on elastic modulus

09 p1483 A71-22824

Cr alloys alloying elements Os, Re, Fe, Co and Mn effect on lattice constant and elastic properties, using acoustic measurements

09 p1473 A71-23229

Elastic ultrasonic vibrations effects on metals and alloys microstructure and elastic and nonelastic properties

09 p1477 A71-23326

Soviet book on problems in anisotropic body elasticity theory, covering orthotropic beams and plates torsion, bending, vibration, stability and boundary value problems, etc

09 p1542 A71-23438

Macroheterogeneous carbon materials elastic characteristics during heat treatment process

10 p1634 A71-24203

Soviet book on mechanical systems oscillations with allowance for imperfect elasticity covering energy dissipation, linear asymptotic methods, etc

10 p1691 A71-24729

Reissner variational theorem for boundary values in linear anisotropic and nonhomogeneous elasticity

10 p1691 A71-24809

Cold and hot working effects on Al alloys elastic properties, discussing crystallographic systems reference points

10 p1628 A71-24822

Aircraft continuous elastomechanical system parameters determination by ground vibration tests, using integral equation, phase resonance and separation technique

10 p1692 A71-24946

Stress and displacement fields in elastic half plane containing edge crack normal to free surface, using integral equations

11 p1847 A71-25440

Rat heart muscle series elasticity compliance, showing hypoxia effects

11 p1719 A71-25930

Soviet book on elasticity theory covering stress and strain tensors, linear closed systems of equations and methods of solution, Saint Venant problem, etc

11 p1850 A71-26097

Elastic properties of bonded orthotropic layer plates, finding good agreement with fiberglass reinforced plastic laminates

11 p1851 A71-26199

Elastic stress-strain law and internal structure symmetry for three dimensional fibrous composites, including caltrop reinforcement

11 p1852 A71-26396

Igneous and metamorphic rocks as simulated lunar rocks, determining elastic and attenuation symmetry by quasi-longitudinal pulse velocity and amplitude measurements on spherical specimens

11 p1834 A71-26454

Error estimate for solution of approximately linear elastic boundary value problems of shells with no strain energy functional, discussing stress-strain relations

12 p1974 A71-26943

Natural frequencies and elastic stability of simply supported rectangular plate under linearly varying compressive loads

12 p1976 A71-27162

Axisymmetric problem solution in theory of elasticity and thermoelasticity for semiinfinite circular cones truncated along spherical surface

12 p1980 A71-27361

Elastic characteristics of multilayer structures with honeycomb fillers, discussing deflection, tensile and compression tests

12 p1980 A71-27362

Frequencies and modes of natural vibrations of closed cylindrical shell with elastic filler

12 p1981 A71-27508

Creep of hereditarily aging body, using Rabotnov fractional exponential function for elastic theory solution

12 p1984 A71-27696

Solids continuum mechanics and fracture criteria, emphasizing intermixed elastic, plastic or viscoelastic types materials behavior idealization

13 p2151 A71-28214

Homogeneous anisotropic body elasticity theory, calculating boundary value problem for arbitrary conditions

13 p2153 A71-28422

Suspended hollow cylinder under force of gravity, calculating stresses and displacements by linear elastic theory differential equations

13 p2153 A71-28518

Integral transformations application to approximate elastic solutions for nonlinear hereditary material, considering elastoplastic deformations under active loads

13 p2154 A71-28649

Existence and uniqueness of solution to Dirichlet boundary value problem of invariant in nonclassical theory of elasticity concerning behavior of media with memory

13 p2154 A71-28651

Unbounded orthotropic body with two internal coaxial elliptical cuts, calculating elastic equilibrium

13 p2156 A71-29068

Two dimensional contact problem for isotropic body in triangle form on half plane, calculating elastic constants with difference Green function

13 p2156 A71-29071

Cascading turbomachine blade row coupled flutter, correlating camber angle, cascade condition and elasticity

13 p2157 A71-29128

Successive approximations method for solving nonlinear elastic problems in transient creep theory, describing stress redistribution

13 p2157 A71-29197

Cold rolled recrystallized Ni-Fe alloy, considering short range order structure effect on elastic limit

13 p2087 A71-29264

Composite materials elastic-plastic behavior under uniaxial loading, determining stress-strain relationships by dislocation theory

14 p2321 A71-29688

Deterministic and random nonlinear forced vibrations of one degree of freedom system with broken line elastic response

14 p2328 A71-30378

Elastic properties of orthotropic composite disks of fiber-reinforced materials, comparing actual stress in composite with permissible stress of fiber and matrix

14 p2329 A71-30472

Linear integral equations with difference and summation kernels in elasticity theory, developing approximate solution method

14 p2333 A71-30991

Orthogonal polynomials method for integral equations solution in two dimensional mixed boundary value problems of elasticity theory

14 p2333 A71-30994

Rumanian book on distribution theory applications in mechanics covering physical point motions, variable mass, concentrated and distributed loads, elasticity theory equilibrium, motion equations, etc

15 p2501 A71-31147

Elastic properties relativistic theory, defining deformation tensor and constitutive laws

15 p2442 A71-31904

Soviet book on plane elasticity theory boundary value problems solution on digital and analog computers

15 p2508 A71-32276

German monograph on spatial elasticity problems solution by multidimensional Fourier transformation covering stress concentration on hollow and solid cones for given load distribution

15 p2509 A71-32300

German monograph on orthotropic plate equations derivation by kinematics and statics in general coordinates and elasticity relation

15 p2509 A71-32304

Displacements produced by impulsive torsional body force situated within elastic half space bonded to half space of different material properties

16 p2647 A71-32859

Maximum stress concentration in two dimensional elasticity theory for half plane and circle as function of contour distribution, using Cauchy-Buniakovskii inequality in Banach space

16 p2648 A71-32938

Structural instability due to cyclic strain accumulation, using plastic deformation constitutive relation with stress tensor and elastic effects

16 p2650 A71-33016

Unified finite element theory of geometrically nonlinear elasticity problems, noting restrictions applicable to different displacement formulations

16 p2653 A71-33089

Elastic static and dynamic physicomaterial characteristics of resin type amorphous materials under pulsed loads, using electromagnetic excitation of torsional vibrations

16 p2659 A71-33996

Incompressible materials weak compressibility effect in elastic theory, deriving displacement equation with average pressure function for any Poisson coefficient values

17 p2818 A71-34350

Mixed boundary value problem of hereditary elasticity theory, discussing existence and uniqueness of solution

17 p2818 A71-34425

Stress difference elasticity equations from photoelastic data and first stress invariant [SESA PAPER 1780]

17 p2819 A71-34530

Gross static material elastic constants for layered composite materials, using photoelastic models [SESA PAPER 1845A]

17 p2761 A71-34531

Circular symmetry stressed state for flat disk with flat circular crack, detailing potential and elasticity theories

17 p2824 A71-34844

Vibration dampers optimization, considering viscous and inelastic resistance effect and sensitivity of harmonically moving system response

17 p2826 A71-35018

Postbuckling elastic characteristics of structures under combined loading near special critical point

17 p2832 A71-35420

Algorithm for stress functions in elastic region, using variational difference method based on differentiation of strain energy

17 p2832 A71-35458

Circular contact area in theory of elasticity with allowance for surface structure of bodies in contact, solving Hertz axisymmetrical problem of elastic bodies

17 p2833 A71-35610

Elasticity theory axisymmetrical problem, applying finite element method

17 p2834 A71-35657

Vacuum melted Mo alloy low temperatures elasticity, plasticity and tensile strength characteristics

17 p2760 A71-35675

Elastic adhesive interlayer effect on bond fracture strength, considering propellant-liner-steel combination in solid rocket motors

18 p2977 A71-36245

Loaded crack ending at bimaterial composite interface, analyzing crack tip stress field singularity order dependence on material elastic constants

18 p2978 A71-36258

Hysteresis loop analysis with allowance for material imperfect elasticity in mechanical vibration problems, using strain amplitude decrement relation

18 p2981 A71-36707

Mathematical model of hemispherical inclusion in elastic half space for estimating plastic deformation

18 p2937 A71-36772

Stress-strain state in elasticity theory of three layer symmetrical plate

18 p2982 A71-36786

Torsion of hollow beam consisting of two homogeneous isotropic rods with different elastic properties and simply connected cross sections, solving by conformal mapping

19 p3155 A71-37387

Shock wave data for Bamlé enstatite in 60-480 kb range, considering Hugoniot elastic limit and phase transition produced shock front

19 p3050 A71-37663

Elastic field and stress distribution in composite circular rotating disk under constant normal pressure

19 p3159 A71-38187

Stress determination by vibration measurement in cantilever specimens fatigue tests with audio frequency loading, taking into account end restraint elasticity

19 p3160 A71-38347

Third basic problem solution in elasticity theory satisfying boundary condition and Lamé equation system with two arbitrary vectors

19 p3160 A71-38484

Bi-harmonic problems solution in elasticity theory for piecewise homogeneous doubly connected media with interface in conformal mapping of ring onto doubly connected region

19 p3160 A71-38486

Deep lunar interior elastic properties, seismic speeds and Debye temperature determination from equations of equilibrium and state and measured moment of inertia

20 p3286 A71-38738

Error independence and elasticity allowance for moon librations and satellite perturbations

20 p3286 A71-38759

Steady state thermoelastic mixed boundary value problem for elastic layer with one face stress free and other face resting on rigid frictionless foundation

20 p3309 A71-39495

Homogeneous anisotropic body elasticity theory, calculating boundary value problem for arbitrary conditions

21 p3455 A71-40086

Book on complex variable methods in elasticity, covering boundary value problems for half planes and circular regions

21 p3456 A71-40264

Perturbation study of subharmonic rotor instability due to elastic symmetry, obtaining equations of motion

[ASME PAPER 71-VIBR-57] 21 p3385 A71-40302

Harmonic excitation response of masses on elastic half space, considering Poisson ratio effect, vibration amplitudes and resonant frequencies

[ASME PAPER 71-VIBR-59] 21 p3460 A71-40304

Macroscopically isotropic and homogeneous two phase composite materials elastic constants determination, discussing approximate formulas and validity

21 p3463 A71-40583

German book on static elasticity and theoretical mechanics covering materials stresses and deformations, virtual work principle, linear isotropic elasticity and thermoelasticity

21 p3464 A71-40782

Soviet book on steels high temperature elastic stiffness and ductility covering carbon, alloyed and special steels at different temperatures and strain rates

21 p3404 A71-41375

Elastic field generation in two bonded isotropic half planes with circular or rectangular inclusion

23 p3774 A71-43146

Thin nickel films elastoresistance properties, examining magnetic state effects

23 p3691 A71-43361

Validity theorems derived for complex parameter elasticity theory equations by vector functions expansion

23 p3777 A71-43583

Apollo 11 and 12 rocks specific heat and thermal conductivity at 2-5 K, comparing elastic properties

23 p3761 A71-43785

Liquid crystals structural, elastic and optical properties, noting application to measurements of temperatures, pressures and electric and magnetic fields

23 p3717 A71-43958

Exact solutions of elasticity theory nonlinear differential equations by Lie group theory methods

24 p3877 A71-44480

Couple-stress theory application to body model with constrained rotations, discussing elasticity theory modifications in relation to real physical phenomena

24 p3848 A71-44643

Nonhomogeneous plate under pulsating and uniformly distributed loads, considering dynamic elasticity problem

24 p3880 A71-44712

Finite difference scheme for elasticity theory boundary value problem in curvilinear region, estimating solution convergence rates

24 p3881 A71-44771

Elasticity and acoustic theory eigenvalues determination in spherical coordinates using transcendental equation

24 p3882 A71-44836

Stress wave propagation in rod consisting of viscoelastic finite and semi-infinite elastic parts during pulsed sinusoidal load at end

24 p3885 A71-45223

Orthogonal experiment plans application to metal elastic stiffness description as function of temperature and strain rate

24 p3840 A71-45375

ELASTIC SCATTERING

Negative pion elastic scattering differential cross section measurements from 1.71 to 5.53 GeV/c, using zero gradient synchrotron beam on liquid hydrogen target

02 p0286 A71-11647

DWBA optical model coupled channels comparison in 2s-1d shell for predicting proton scattering elastic cross sections

06 p0929 A71-17579

Fast neutron energy spectrum from free proton elastic scattering in emulsion plates, studying upper atmospheric altitude and latitude factors

06 p0962 A71-18180

Born-Oppenheimer approximation for elastic and inelastic electron scattering by diatomic molecules

08 p1337 A71-20886

Partial wave method for nonspiral quantum scatterer, applying to electron elastic scattering by molecules

09 p1496 A71-22237

Nitrogen molecules vibrational excitation effect on elastic collisions frequency in nitrogen plasma

10 p1646 A71-23819

Two phase supersonic barotropic flow with solid particles around thin profile with allowance for elastic particle collisions

12 p1864 A71-27450

LF hot-electron noise during quasi-elastic scattering in semiconductor with simple band structure, evaluating convective fluctuations contribution to noise temperature

13 p2112 A71-29082

Three particle elastic scattering amplitudes calculation using local Yukawa potentials

14 p2277 A71-30862

Plasma mobility, diffusion, electron energy distribution, surface phenomena, elastic collisions, charge transfer, etc

16 p2617 A71-32954

- S-wave elastic positron-hydrogen scattering in ionization region, estimating error in extrapolated 1 matrix from complex energy 19 p3106 A71-37375
- Binary elastic collision integral between particles of disparate mass, determining angular momentum form of Boltzmann equation for Lorentz mixtures 19 p3115 A71-38210
- Glauber approximations for elastic and inelastic scattering of protons by ground state hydrogen atoms, comparing with measurements 20 p3272 A71-39578
- Close coupling calculation for low energy hydrogen atom-molecule collision, discussing cross section, transition probabilities and elastic scattering 20 p3272 A71-39579
- Partial wave method for nonspherical quantum scatterer, applying to electron elastic scattering by molecules 21 p3420 A71-41119
- Electron elastic scattering in thin films by impurities, noting conductivity dependence on film thickness 21 p3428 A71-41126
- Wave interference phenomena associated with elastic scattering of atoms, considering differential inelastic scattering cross sections anomalies 24 p3851 A71-45166
- ELASTIC SHEETS**
- Axially loaded finite stringer bonded to infinite elastic sheet, considering adhesive shear flow 03 p0514 A71-14350
- Nonlinear elastic membranes large axisymmetric deformation, deriving initial value problem with differential equations 04 p0667 A71-15183
- Temperature and pressure discontinuity stresses in compact heat exchangers, considering tubes as elastic foundation underneath tube plate 08 p1374 A71-22034
- ELASTIC SHELLS**
- Nonlinear viscoelastic material with stress dependent properties, solving for thick walled shells deformation under internal pressure 01 p0168 A71-10423
- Elastoplastic zero moment shells weight minimization for given middle surface geometry 01 p0170 A71-10647
- Finite length elastic cylindrical shell deformation approximate solution by Legendre polynomials 01 p0173 A71-10942
- Elastic thin walled shells of variable thickness with zero Gaussian curvature, deriving stress strain state with allowance for elastoplasticity 01 p0176 A71-11041
- Spherical elastic shell axisymmetric vibrations in compressible fluid with free surface 01 p0071 A71-11046
- Elastic shell filled with ideal fluid, analyzing dynamic stability under periodic impulses 01 p0176 A71-11049
- Bending of thin elastic orthotropic shallow shells, taking into account large deflections, temperature distribution and material nonuniformities 02 p0325 A71-12288
- Acoustic plane waves transient interaction with cylindrical elastic shell, using Volterra integral equations 04 p0668 A71-15189
- Fatigue and fracture in elastic cylindrical shells with circumferential crack under axial tension, noting precracked specimens 04 p0670 A71-15386
- Elastic straightening of slightly curved shell and significantly curved beam, considering prestressed structural stiffness 04 p0672 A71-15771
- Thin elastic orthotropic oval cylindrical shells nonlinear flexural vibration based on assumed modes, using Galerkin method 05 p0819 A71-15979
- Novozhilov complex transformation method extended to Timoshenko theory of elastic shells constructed with allowance for transverse shear deformation 05 p0820 A71-16187
- Isotropic elastic spherical shells stability under combined axial compression and local loads 05 p0824 A71-16593
- Thin orthotropic shallow elastic shells with initial defects, analyzing critical pressure states 06 p0982 A71-17355
- Thin elastic shallow spherical dome nonlinear motion under uniformly distributed external pressure 06 p0982 A71-17360
- Elastic rib-reinforced flexible shallow shells theory, deriving variational equations for multicontact problem 06 p0985 A71-17752
- Elastic shell dynamics under initial and boundary conditions, developing variational principle algorithm 06 p0986 A71-17756
- Variational methods application to optimal heating of thin elastic shells, using elastic-energy functional minimization as optimality criterion 06 p1006 A71-17767

- Elastic cylindrical shells stability under dynamic load consisting of conservative forces and normal compression 06 p0990 A71-17879
- Elastic plates and shells stability and vibration problems asymptotic solution methods, considering edge effect 06 p0991 A71-17800
- Elastic shells under pressure wave loads, examining front discontinuities induced by plane and axisymmetric wave deformation 06 p0992 A71-17807
- Elastic composite liquid filled shell containers, calculating natural vibration with Ritz method 06 p0992 A71-17809
- Thin elastic shell of revolution with negative Gaussian curvature, discussing free nonaxisymmetric oscillations 06 p0992 A71-17811
- Relation uniaxial stressed state relationship to internal geometry of flexible shell 06 p0993 A71-17814
- Elastic momentless conical tank with spherical bottom partially filled by liquid, calculating axisymmetric oscillation 06 p0995 A71-17828
- Elastic spherical shell three dimensional stress-strain state asymptotic behavior near concentrated force as function of parameter characterizing relative thickness and curvature 06 p0995 A71-17830
- Thin elastic partially liquid filled shells of revolution, applying asymptotic integration method to free vibrations case 06 p0995 A71-17834
- General linear shell theory, considering elastic processes in structural design 06 p0998 A71-17860
- Numerical algorithms of elastic stability solutions for thin walled axisymmetrically loaded shells of revolution with finite difference schemes 06 p0999 A71-17864
- Vibration and wave analysis in dynamic deformation of elastic shells and plates with environmental allowance 06 p1000 A71-17870
- Three dimensional bending vibration analysis of homogeneous elastic circular cylindrical shell with both ends restrained 06 p1001 A71-18230
- Thin elastic toroidal shells under nonsymmetric harmonic loadings, reducing problem to membrane and edge effect linear solutions 06 p1002 A71-18415
- Soviet book on computer calculation of three-layer elastic plates and shells covering programs, initial equations, input number language, numerical solution, etc 07 p1210 A71-19047
- Stress waves in elastic spherical shell due to external pressure pulse, approximating near field by saddle point technique 07 p1215 A71-20097
- Momentless theory of anisotropic shells, using three dimensional elasticity theory 08 p1373 A71-21867
- Tensor elasticity relations in linear theory of thin elastic shells in Kirchhoff-Love range 08 p1373 A71-21868
- Physically nonlinear theory of isotropic elastic shells and plates eliminating Love-Kirchhoff hypothesis 09 p1543 A71-23613
- Elastic cylindrical shells oscillations and stability in inviscid incompressible liquid flow, reducing problem to integro-differential equation by Fourier integral transformation 10 p1688 A71-24357
- Critical speeds for inviscid compressible potential flow past thin elastic cylindrical shells, using long wave approximation 10 p1689 A71-24565
- German monograph on basic equations for isotropic elastic homogeneous thin shell subjected to infinitesimal displacements, determining work of form change 10 p1692 A71-25037
- Linearly elastic cylindrical shells dynamic stability under combined axial and radial stochastic excitations, using Liapunov analysis 11 p1842 A71-25312
- [AIAA PAPER 71-333] Elastic boundary conditions effect on natural frequencies and resonant displacement of thin isotropic circular cylindrical shell under concentrated load with harmonic time history 11 p1843 A71-25314
- [AIAA PAPER 71-335] High precision finite element for static analysis of loaded thin elastic shells of revolution including shear deformations 11 p1844 A71-25339
- [AIAA PAPER 71-360] Axisymmetric deformation differential equations system for nonlinearly elastic shells under vertical loadings, considering various Euler buckling boundary problems 11 p1848 A71-25567

- Nonlinear elastic shells free vibrations, obtaining phase trajectories with finite bending within Hooke's law 12 p1975 A71-27106
- Axisymmetrically strained thin elastic shells of revolution with temperature dependent random elastic characteristics 12 p1979 A71-27358
- Axisymmetric deformation of thin elastic shell of revolution under combined effect of static surface load and nonuniform heating 12 p1979 A71-27359
- Thin walled elastic isotropic shallow shell with thermal boundary conditions, obtaining thermoelastic solution in series form 12 p1984 A71-27687
- Axial wave propagation in linearly elastic membrane shells of revolution, using dynamic finite element technique 13 p2147 A71-27786
- Viscoelastic and elastic shells boundary value problems relation, studying natural and forced oscillations of isotropic viscoelastic shells 13 p2155 A71-28656
- Clamped and hinged spherical and paraboloidal shell caps elastic stability tests under external pressure loading, determining critical pressure 14 p2323 A71-29846
- Elastic plastic shells of revolution deflection analysis by numerical integration with computer program 14 p2324 A71-29870
- Thin walled cylindrical elastic shell with rectangular holes at equal intervals along straight line, deriving boundary conditions expression by R-functions 14 p2326 A71-30190
- Frequency equations for trains of axisymmetric harmonic waves traveling in infinitely long three layered elastic circular cylindrical shells and rods 14 p2327 A71-30202
- Thermoelastic shells and plates approximate linear theory, detailing uniqueness theorem for initial mixed boundary value problem 14 p2329 A71-30446
- Generalized elastic thin shell nonlinear theory, deriving equilibrium equations and boundary conditions from shape dependent energy considerations 14 p2329 A71-30448
- Nonuniform rotation of nonhomogeneous isotropic elastic cylindrical shell, obtaining steady state axisymmetric vibrations 14 p2331 A71-30842
- Stability and stress analysis of elastic finned circular cylindrical shells reinforced by stringers 14 p2332 A71-30852
- Perturbed motion linear equations of body rigidly coupled to thin walled elastic shell partially filled with heavy compressible fluid 14 p2227 A71-30867
- Stress-strain state of unclamped thin elastic zero curvature shell under three component surface load and tangential boundary forces 16 p2647 A71-32926
- Asymptotic eigenvalue density estimates for edge-hinged thin elastic rectangular shell, determining shell stability linear equation solution conditions 16 p2647 A71-32937
- Thin elastic shells Koiter-Sanders mathematical model finite element analysis using Ritz method [ASME PAPER 71-APM-32] 16 p2655 A71-33197
- Moment state stability of elastic hinged cylindrical shell and closed ring under pressure and concentrated load, using nonlinear equilibrium theory 16 p2660 A71-34114
- Error estimates in thin elastic shell linear theory, modifying three dimensional displacement field 17 p2815 A71-34224
- Elastic spherical shell coupled to rigid body, calculating asymmetric free vibration natural frequencies and mode shapes from boundary conditions 17 p2817 A71-34339
- Book on asymptotic approximation in three dimensional thin and thick elastic shell theory including interior and Kirchhoff edge zone equations 17 p2822 A71-34770
- Freely vibrating supported elastic isotropic oval cylindrical shells natural frequencies and mode shapes 17 p2825 A71-34873
- Thin elastic spherical shells reinforced by stringers and frames and loaded by internal or external uniform pressure, calculating by energy method 17 p2829 A71-35311
- Pure and transverse bending of orthotropic cylindrical shell wound with elastic glass plastic filaments, presenting stress-strain diagrams under tension and compression 17 p2830 A71-35318
- Finite element analysis codes for complex two layered linear elastic shells of revolution under static and dynamic loads 17 p2831 A71-35351
- Elastic lattice shells linear theory, deriving stress functions and equations from static-geometric analogy 17 p2831 A71-35396

Cantilevered elastic cylindrical shell stability during bending by transverse load uniformly distributed over entire surface or applied at end
17 p2833 A71-35615

Traveling waves propagation in elastic shell of revolution subjected to bending moment
17 p2833 A71-35618

Natural axisymmetric vibration of thin elastic shell of revolution, deriving eigenvalues convergence to spectrum lower bound by asymptotic method
19 p3154 A71-37097

Externally pressurized thin walled elastic spherical shells influence coefficients singularity
19 p3158 A71-37886

Edge effect in elastic lattice shells generalized from lattice plates and disks
19 p3158 A71-38152

Acoustic field HF asymptotic characteristics after sound passage through elastic shell, expressing sound fields inside and outside by integro-differential equations system
20 p3268 A71-38810

Membrane theory of anisotropic shells, using three dimensional elasticity theory
20 p3308 A71-39366

Tensor elasticity relations in linear theory of thin elastic shells in Kirchhoff-Love range
20 p3308 A71-39367

Hydroelastic coupled oscillations of partially filled circular cylindrical liquid container with flexible bottom and elastic side wall
21 p3366 A71-40545

Small deformation dynamic response of vibrating isotropic linearly elastic spherical shell to radial and time dependent body force field
21 p3464 A71-40769

Fluid dynamics in elastic complex geometry tanks, obtaining liquid mass and stiffness matrices for gravitational effects
21 p3467 A71-40948

Dynamic response of elastic cylindrical shell-solid core composite under time dependent loading from Laplace transform
21 p3467 A71-40949

Thin elastic shell of revolution under asymmetric loads, calculating time dependent transient response with implicit backward and explicit central differencing schemes
21 p3467 A71-40960

Elastic shells of revolution displacement analysis, using incremental variational theory with finite element method
22 p3613 A71-41434

Open simply supported cylindrical shell internal stresses due to initial deformation based on thin elastic shell linear theory
22 p3613 A71-41563

Elastic shell strain energy calculation, using dimensional analysis and invariance properties for inversion of normal to middle surface
22 p3616 A71-42217

Three dimensional transient interaction of spherical acoustic waves with cylindrical elastic shell, using integral transform techniques
23 p3775 A71-43207

Elastic and inelastic thin shell nonlinear theory derivation by integrating material continuity equations of motion over shell thickness
23 p3775 A71-43318

Thin elastic shell of revolution with waves along parallel, considering small free nonaxisymmetric vibrations
24 p3877 A71-44406

Cylindrical shell with elliptical hole, calculating elastic stress concentration due to axial tension based on shallow shell theory
24 p3879 A71-44625

Two layer anisotropic spherical shell of elastohereditary material under uniform pressure, investigating stress-strain state
24 p3880 A71-44710

Asymptotic design formulas for thermoelastic supercritical strains in thin elastic shallow spherical shells under external pressure
24 p3881 A71-44827

Elastic momentless shell completely filled with ideal incompressible liquid, detailing small steady natural vibrations
24 p3821 A71-45344

ELASTIC STABILITY
U DAMPING
ELASTIC STRENGTH
U PROPORTIONAL LIMIT
ELASTIC SYSTEMS
Elastic theory problems, deriving continuum spectral models in Cartesian coordinate system
02 p0327 A71-12404

Vibrationally stressed elastic system stability, considering vibration rate amplitude as criterion
03 p0503 A71-13408

Elastoplastic impact, optimizing system with respect to mass kinetic energy with elastic and dry friction properties taken into account
05 p0821 A71-16354

Buckling loads prediction for conservative elastic systems from vibration data by stochastic and deterministic models, providing nondestructive testing procedure
08 p1368 A71-20804

Friction role in impact dampers for elastic systems out of static equilibrium
08 p1372 A71-21619

Atomic scale elastic structure equations of state for Thomas-Fermi model extension to high pressures, considering earth core iron-silicates composition
11 p1802 A71-25572

Nodal points stresses determination from finite element solved elastic problems, discussing thin disk stresses as function of mesh pattern regularity
11 p1851 A71-26312

Perpendicularly woven fiberglass reinforced plastics stability, elasticity and viscoelasticity as function of temperature
12 p1921 A71-27347

Elastically mounted gyroscope stability under parameter excited vertical vibrations, using vector differential equation and multichannel oscillograph
15 p2502 A71-31173

Motion characteristics of elastically supported gyroscope, presenting linearized equation of motion for eight degrees of freedom system
15 p2401 A71-31180

Nonconservative elastic system involving standard double pendulum model under retarded follower load, calculating damping, time delay and parameter variations effects on stability
15 p2449 A71-32012

Elastically suspended gyroscope dynamics, using Euler equations of motion allowing for casting rotation
15 p2410 A71-32455

Gas dynamic elastically mounted bearing, describing stability analysis of unloaded rotor central equilibrium position
15 p2417 A71-32457

Elastic structures stability under randomly fluctuating external loads based on statistical methods
16 p2648 A71-32988

Mathematical techniques of equilibrium states and periodic vibrations in nonlinear elastic systems illustrated by thin plate and shallow cap buckling under uniform pressure
16 p2649 A71-32998

Holder stability and logarithmic convexity as special case of Liapunov function applied to linear elastic systems without body force
16 p2608 A71-33008

Vibration simulation of elastohysteretic systems on analog computers using photocurrent-voltage relationship of polycrystalline photoresistors
16 p2658 A71-33978

Nonlinear elastic suspension springs with symmetrically hardened behavior for shock and vibration isolation of aerospace instruments and controls
17 p2825 A71-34890

Vibrationally stressed elastic system stability, considering vibration rate amplitude as criterion
17 p2826 A71-35017

Dynamic stabilization of undamped gyrosystems with elastically pliable structural elements by inertial damper mounted on gimbal suspension
17 p2746 A71-35602

Friction role in impact shock absorbers for elastic systems out of static equilibrium and resonance excitation in vibrations, noting harmful effects
17 p2834 A71-35679

Two-mirror optical system to study energy dissipation in elastic systems subjected to cyclic straining
18 p2924 A71-36727

Elastic beam-columns with initial curvature and pinned or clamped ends under transient axial and distributed lateral loads, deriving upper displacement bounds
19 p3159 A71-38184

Single mass flexible rotor in elastic bearings mounted on damped flexible supports, analyzing dynamic unbalance response and transient motions
21 p3460 A71-40310

Linear elastic structures analysis by quadratic programming, considering equilibrium equations for forces at joints
22 p3618 A71-42589

Boundary value problems of forced vibration of nonconservatively loaded dynamic elastic system, using William method
24 p3878 A71-44554

ELASTIC WAVES
NT AERODYNAMIC NOISE
NT AIRCRAFT NOISE
NT BAROCLINIC WAVES
NT CAPILLARY WAVES
NT COHERENT ACOUSTIC RADIATION
NT COMPRESSION WAVES
NT DETONATION WAVES
NT DILATATIONAL WAVES
NT ELECTROSTATIC WAVES
NT ENGINE NOISE
NT GRAVITY WAVES
NT IONIC WAVES
NT JET AIRCRAFT NOISE

NT LAMB WAVES
NT MACH CONES
NT MAGNETOACOUSTIC WAVES
NT MAGNETOELASTIC WAVES
NT MAGNETOHYDRODYNAMIC STABILITY
NT MAGNETOHYDRODYNAMIC WAVES
NT NOISE [SOUND]
NT NORMAL SHOCK WAVES
NT OBLIQUE SHOCK WAVES
NT P WAVES
NT PHONONS
NT PLASMA WAVES
NT RAYLEIGH WAVES
NT RIEMANN WAVES
NT RIPPLES
NT ROCKET ENGINE NOISE
NT S WAVES
NT SEISMIC WAVES
NT SHOCK WAVES
NT SONIC BOOMS
NT SOUND WAVES
NT STRESS WAVES
NT THERMAL NOISE
NT TOLLEMIN-SCHLICHTING WAVES
NT ULTRASONIC RADIATION
NT UNLOADING WAVES

Elastic waves excitation by pressure wave in shells of revolution, investigating acoustic medium effects on frontal discontinuities intensity
01 p0176 A71-11148

Longitudinal elastic wave propagation equations of motion in cone with small apex angle, using perturbation theory
03 p0456 A71-12974

Sonic boom wave pressure history prediction on arbitrarily oriented plane walls by explicit fixed mesh time dependent numerical method
03 p0349 A71-14153

Infinite elastic beam normal impact by semiinfinite elastic rod, using Timoshenko beam and one dimensional bar theory to describe elastic waves
03 p0513 A71-14171

Unsteady one dimensional isentropic gas flows, discussing nonlinear pressure waves geometry
03 p0405 A71-14345

Pressure wave propagation through annular and mist flow patterns, noting virtual mass effects in interphase momentum transport of rarefaction and compression waves
03 p0405 A71-14418

Boundary value problems solution by partial absorption method for elastic oscillations in inhomogeneous media, discussing Hilbert space methods
04 p0665 A71-14809

Semiinfinite simply supported cylindrical shell transient response due to axisymmetrically engulfing step pressure wave, investigating moving load critical velocity
05 p0823 A71-16556

Crack extension by incident elastic wave diffraction for specific shear stress character at wave front
05 p0825 A71-16709

Elastic wave properties and technological applications, discussing acoustic delay, compression and filtering electric signals
05 p0722 A71-16745

Short elastic sine waves propagation in cylindrical shells, applying nonclassical equations
06 p0982 A71-17359

Elastic shells under pressure wave loads, examining front discontinuities induced by plane and axisymmetrical wave deformation
06 p0992 A71-17807

Short rotor blade span supersonic fan for pressure wave forward propagation elimination, obtaining acoustic and aerodynamic characteristics
06 p0885 A71-18621

Pressure wave distortion effects on combustor acoustic mode instability based on model with burning rate related to Reynolds number
07 p1224 A71-19906

Elastic harmonic waves propagation in composite circular elastic cylinder
07 p1214 A71-19956

Pressure shocks propagation through electrically and thermally conducting viscous gas in presence of uniform magnetic field
07 p1169 A71-20025

Acoustic wattmeter with piezometric electric signal sensor and amplifier for measuring elastic wave intensity in liquids
07 p1114 A71-20059

Elastoplastic loading or unloading wave complex in solids, analyzing stability by breakdown into elastic and plastic components
07 p1217 A71-20461

Flow lines construction in two dimensional supersonic flow region with rarefaction waves interaction from several disturbance sources
08 p1230 A71-22052

Elastic waves in isotropic body, calculating initial deformation effect on propagation rate based on finite deformation theory
09 p1537 A71-22515

Microbarometric oscillations enhancement due to atmospheric pressure waves generation and cold fronts passage, considering relationship to sporadic E critical frequency

10 p1606 A71-24918

Longitudinal, flexural and elastic waves propagation in infinite orthotropic circular cylinders

11 p1850 A71-26176

Elastic plane shear wave diffraction on elliptical cylinders in half space, using elliptical wave function series and linear algebraic equations

12 p1978 A71-27332

Elastoplastic and elastic-viscoplastic waves propagation, considering longitudinal wave resonance, plane load waves and loading and unloading criteria

12 p1980 A71-27446

Asymptotic solutions of improved equations for elastic and elastoplastic waves in rods, considering longitudinal waves propagation

12 p1980 A71-27449

Composite propellant flame temperature and emission spectra during depressurization by rarefaction waves, using rapid scanning spectrometer [AIAA PAPER 70-663]

12 p1945 A71-27564

Elastic wave diffraction in infinite series of spherical cavities with centers on straight line

13 p2100 A71-28275

Conical bar with yield point lag, investigating elastoplastic wave propagation with Rabotnov model

13 p2155 A71-29064

Elastic wave propagation in infinite elastic medium due to explosion at spherical cavity center, considering material properties thermal change as function of radial distance

13 p2165 A71-29104

Steel bar under longitudinal impact, deriving flexural half waves length formulas for critical force

13 p2158 A71-29435

Linear elastokinetics dynamic problems, emphasizing elastic wave propagation in infinite micropolar medium

15 p2502 A71-31153

Helmholtz, half and full mode standing pressure waves for separated flow induced acoustic resonance in open cavities

15 p2391 A71-32106

Temporal and spatial flow velocity profiles produced by shock tube generated pressure wave propagation in open-end pipe

16 p2556 A71-32921

Initial strains effect on propagation rate of elastic waves, applying finite deformation theory

16 p2658 A71-33902

Orthotropic laminated plates dynamic response to impulse loads, detailing flexural wave propagation

17 p2823 A71-34809

Elastic seismic waves attenuation in polycrystalline ceramics and rocks by grain boundary relaxation, noting strong frequency dependence of earth mantle internal friction

17 p2735 A71-35390

Pressure wave interaction with orifices inside ducts, calculating reflection and transmission characteristics relationship to geometry and initial steady flow conditions

19 p3044 A71-37642

Continuum mechanical approach to velocity dispersion of longitudinal plane waves in elastic solid containing dislocations

19 p3118 A71-37794

Pressure wave propagation through one and two component annular and mist flows, showing importance of inertial interphase momentum transfer

19 p3171 A71-38293

Small pressure wave transmission in abdominal venae cavae of dogs in mathematical model development for viscoelastic behavior of large veins

20 p3187 A71-38987

Galaxies spiral structure interpretation in terms of gravitation theory of pressure and density waves

20 p3293 A71-39528

CO relaxation measurement in unsteady expansion wave, removing metal carbonyls by passing gas through liquid oxygen cooled trap

21 p3418 A71-40237

Stress concentration near holes in high modulus epoxy resin polymer thin plates under pressure wave loads

22 p3614 A71-41611

Finite plates coincidence effect occurrence with sound waves, examining backing cavity and incidence angle influence

22 p3576 A71-42538

Flexural wave propagation in thin curved rod oscillating in plane, calculating frequency and velocity from boundary conditions according to Saint Venant

22 p3617 A71-42574

Plastic work hardening produced by pressure application to spherical cavity surface in infinite elastoplastic medium, considering spherical elastic wave attenuation

23 p3775 A71-43147

Infinite plane elastic wave reflection and refraction coefficients at fluid-solid interface, noting reflected beam lateral displacement at critical angles

23 p3703 A71-43202

Equations of elastic wave propagation in isotropic materials in presence of static surface stresses and body forces

23 p3775 A71-43205

Elastic surface waves bi-phase modulated encoding and decoding at 10 Mbit/sec using Y-cut quartz

23 p3645 A71-43436

Elastic wave velocities in Apollo 12 rocks 12052 and 12065 at high pressures, noting basalt-like composition and crystal structure

23 p3761 A71-43783

Elastic surface wave amplitude and propagation velocity in lunar rocks, calculating Poisson ratio

23 p3761 A71-43784

Free elastic vibrations and waves in laminated orthotropic circular cylinders

24 p3878 A71-44561

Spatial characteristics based difference scheme application to axisymmetric problems of elastic wave propagation, allowing for solid or hollow circular cylinder boundary conditions

24 p3885 A71-45221

Ultrasonic flaw detection analytical and experimental wave propagation procedure including dynamic photoelasticity and elastic wave computer codes in nondestructive testing

24 p3831 A71-45282

ELASTICITY

U ELASTIC PROPERTIES

ELASTIN

Collagen and elastin transmedial gradients in human aortas as function of age, discussing relationship to atherogenesis

18 p2858 A71-36751

ELASTODYNAMICS

NT ELASTIC DAMPING

NT ELASTOHYDRODYNAMICS

Turbine blades coupled bending vibrations in centrifugal field, deriving vibration equations including previously neglected centrifugal coupling terms

01 p0166 A71-10120

Finite element method approximations outside variational principle in elasticity problems, examining convergence to exact solution [ASME PAPER 70-WA/APM-34]

03 p0512 A71-14160

Viscoelastic plates forced motion under dynamic loads by Valani method, considering elastic and layered elastic-viscoelastic circular plates

08 p1368 A71-20801

Linear elastokinetics tensorial field integral representation derivation from reciprocal dynamic theorem for equations of motion

10 p1687 A71-24350

Cascaded inertial vibration isolation systems, using rigid masses interconnected by air spring type isolator elements

11 p1853 A71-26492

Oscillation and stability of free composite body with elastically suspended masses, simulating liquid sloshing in cavity by equivalent mechanical model

14 p2321 A71-29537

Linear elastokinetics dynamic problems, emphasizing elastic wave propagation in infinite micropolar medium

15 p2502 A71-31153

Elastically suspended gyroscope dynamics, using Euler equations of motion allowing for casting rotation

15 p2410 A71-32455

German monograph on upper and lower bounds in elastomechanics covering elastostatic, natural vibration and stability problems, elastic states Hilbert space, numerical methods, etc

17 p2818 A71-34480

Elastodynamics three dimensional mixed initial and boundary value problems, presenting infinite series solution

18 p2979 A71-36359

Complex structural systems response characteristics under steady state sinusoidal, transients and random loadings, developing hybrid elastodynamic equations

21 p3470 A71-41011

Generalized tensorial equation of motion for stresses in linear elastodynamics, proving limit existence in Sobolev functional space

22 p3614 A71-41607

ELASTOHYDRODYNAMICS

Optical point elastohydrodynamic contact, describing optical interference system consisting of chromium plated glass plate and steel ball

01 p0087 A71-10463

Elastohydrodynamic oil film measurements for rolling point contact of ball bearing under starvation using optical interferometry

01 p0087 A71-10481

Lubricating oil thin films interfacial Newtonian flow elastohydrodynamics, studying transient effects on contact load damping parameters

10 p1614 A71-23981

EHD lubricant film thickness and friction forces effects on ball and roller bearings selection and design [ASME PAPER 71-DE-3]

12 p1911 A71-27322

ELASTOMERS

Stillman rubber elastomers tests by cyclic exposure to hydrazine and air, water vapor or carbon dioxide, considering suitability as valve seat

05 p0772 A71-16466

High pressure and temperature seals and sealing in aircraft and spacecraft, including O rings and elastomers use

06 p0905 A71-18056

Aerospace adhesives and elastomers - Conference, Dallas, Texas, October 1970, Volume 2

10 p1630 A71-24063

Elastomers for aerospace vehicles extreme environments, discussing fuel tank integral high temperature sealants

10 p1631 A71-24078

Nonflammable self extinguishing nontoxic fluorocarbon elastomers as adhesives and coatings for Apollo program

10 p1632 A71-24097

Nonflammable elastomeric materials and coatings for oxygen enriched atmospheres

10 p1632 A71-24098

Elastomeric seals for aircraft fastener countersinks, providing corrosion protection to static metal surface treatments and organic coatings

10 p1633 A71-24118

Ablation residue, including silicone elastomer foam heat shield material ablative degradation

11 p1855 A71-26040

Flame retardant silicone elastomers for use as aircraft construction materials, describing fabrication techniques, mechanical, aging and weathering properties

12 p1921 A71-27412

Fluid sealing capabilities of silicone, fluorosilicone and fluorocarbon elastomers above 250 F [ASLE PREPRINT 71AM 3B-1]

13 p2093 A71-29488

Synthetic elastomers, including polymer chain growth, monomer sequence distribution, structural compatibility effects and commercial products development

18 p2939 A71-35886

Carbon and noncarbon polymers based high temperature elastomeric materials chemical structure and physical properties

19 p3085 A71-38068

Elastomeric rocket motor thermal insulants ablation, considering composite properties, heat transfer, compounding and tests

21 p3406 A71-40603

ELASTOPLASTICITY

Cyclic fatigue and corrosion test equipment for elastoplastic materials at various temperatures and pressures

01 p0165 A71-10042

Elastoplastic zero moment shells weight minimization for given middle surface geometry

01 p0170 A71-10647

Bar impact against rigid obstacle, using method of characteristics for elastoplastic waves propagation and interaction

01 p0171 A71-10651

Acceleration waves propagation in elastoplastic materials based on nonlinear thermodynamic theory

01 p0173 A71-10873

Elastoplastic constitutive laws with nonassociated flow laws and work hardening, nonhardening and softening behavior

01 p0174 A71-10999

Elastic thin walled shells of variable thickness with zero Gaussian curvature, deriving stress strain state with allowance for elastoplasticity

01 p0176 A71-11041

Simple variable loading and unloading in theory of small elastoplastic deformation under nonuniform heating for residual stress-strain determination

02 p0323 A71-11739

Creep effect on cooled blades elastoplastic stress-strain relationship using computer programs

02 p0323 A71-11741

Disk elongation plastic deformation, determining elastoplastic stressed state for inhomogeneous thermal cycles

02 p0323 A71-11748

Circular elastoplastic plates, solving adaptation theory kinematic equations by linear programming procedures

02 p0324 A71-11751

Elastoplastic, viscoelastic and directed elastic continuous media kinematic and thermodynamic description based on intermediate state of reference concept

02 p0326 A71-12335

Polish book on limiting load capacity of structural elements covering notched rods and plates with hole under elastoplastic stress

02 p0330 A71-12750

Small forced flexural elastoplastic vibrations of structural beam, deriving approximate partial differential equation based on stress-strain relation

03 p0502 A71-13403

Load limit surfaces for composite plates with long elastic plastic fibers site bonded or imbedded in low strength matrix

03 p0504 A71-13429

Mechanical model for orthotropic elastoplastic plates with clamped torsion susceptible ribs

03 p0504 A71-13528

Photoelastoplastic analysis of creep and stress of aluminum notched bars and cracked plates under thermal cycle using epoxy resin simulation

03 p0507 A71-13757

Creep failure in elastoviscoplastic media from time and load-path dependent processes near axisymmetric fissure prior to cracking

03 p0509 A71-13874

Truss systems optimal structural design, noting elastic-plastic stability conditions

03 p0509 A71-13897

Shells and plate disk structures elastoplasticity analysis problems, considering limit loads, large deflections, boundary state theory, optical design, etc

03 p0510 A71-13944

Elastoviscoplastic materials infinitesimal theory extension to thermodynamic processes by limit tension, deriving constitutive equations

03 p0510 A71-13946

Elastoplastic stress analysis for samples with notches and holes under tension, discussing boundary condition calculation by finite element method

03 p0510 A71-13949

Stress analysis of thin elastoplastic shells with large displacements loaded into strain hardening range, assuming plastic strain incompressibility

[ASME PAPER 70-WA/PVP-3] 03 p0511 A71-14101

Constant/variable thickness isotropic elastoplastic shallow shells stress analysis and limiting load determination, using numerical method based on successive approximation technique

04 p0664 A71-14603

Service life of pin jointed connections with elastoplastic strains in bore walls

04 p0602 A71-14606

Two-member composite cylinders, predicting residual stress and axial loading behavior by elastoplastic analysis for comparison with experiment

04 p0666 A71-14893

Elastoplastic impact, optimizing system with respect to mass kinetic energy with elastic and dry friction properties taken into account

05 p0821 A71-16354

Acceleration inequalities of dynamically loaded elastoplastic shells, using permissible stress and displacement velocity fields

06 p0990 A71-17790

Circular and annular elastic plates elastoplastic bending theory, using Saint Venant conditions and equations of equilibrium and deformation

06 p0993 A71-17812

Elastoplastic conical shells strain under longitudinal impact by large rigid body, analyzing plastic bending

06 p0996 A71-17842

Deformation theory of dynamic bending, buckling and stability of plates and shells beyond elastic limit

06 p0999 A71-17865

Dynamic elastic-plastic buckling of rectangular plates in sustained flow involving mass impact

07 p1211 A71-19251

Antiplane stress distribution around single or collinear cracks in nonwork hardening elastoplastic material under uniform load

07 p1212 A71-19350

Elastoplastic tubular rods rotation under constant bending moments, solving for large rotational angles

07 p1212 A71-19352

Elastoplastic loading or unloading wave complex in solids, analyzing stability by breakdown into elastic and plastic components

07 p1217 A71-20461

Tensile tests of elastoplastic notched plate in plane stress

07 p1218 A71-20500

Elastoplastic arresting device, predicting mass impact effect for optimal design in terms of deformation or contact time

08 p1367 A71-20688

Flexible elastoplastic shallow shell theory, using mixed variational principle for flexure velocity and stress function

09 p1535 A71-22179

Low-cycle fatigue curve determination for plane elastoplastic bending with flexible loading, deriving rated fatigue life

09 p1536 A71-22502

Finite length rotating cylinder, calculating axisymmetric creep under thermal effects in power series from theory of small elastoplastic deformation

09 p1537 A71-22516

Two dimensional stress-strain fields under elastic and elastic-plastic strains and steady state creep, calculating stress distribution around hole in cylindrical shell

09 p1538 A71-22631

Wave propagation in elastoviscoplastic medium in temperature field under complex dynamic and thermal

conditions, considering mathematical models and mechanical properties changes

09 p1543 A71-23611

Limiting equilibrium of thin rigid plastic plate with piecewise smooth contour under skew symmetric load

10 p1690 A71-24568

Solid circular Ti shaft torsion boundary value problem solution, using elastic-viscoplastic materials thermodynamics and constitutive relations

11 p1849 A71-25801

Bending problems of elastoplastic plate rigidly clamped over edges, deriving theorems on existence, uniqueness and convergence of approximate solutions

12 p1974 A71-26962

Soviet papers on wave propagation in viscoelastic and elastoplastic media covering shock wave interaction, magnetoelastic waves, etc

12 p1980 A71-27444

Elastoplastic and elastic-viscoplastic waves propagation, considering longitudinal wave resonance, plane load waves and loading and unloading criteria

12 p1980 A71-27446

Asymptotic solutions of improved equations for elastic and elastoplastic waves in rods, considering longitudinal waves propagation

12 p1980 A71-27449

Nonlinear equations of motion for cylindrical elastoplastic shell under axial impact

12 p1980 A71-27452

Inhomogeneous microstructure elastoplastic medium, examining strain and work in plastic deformation

12 p1982 A71-27516

Elastoplastic problem of stress concentration in orthotropic plate with circular notch under tension

12 p1982 A71-27517

Conical bar with yield point lag, investigating elastoplastic wave propagation with Rabotnov model

13 p2155 A71-29064

Elastoplastic plates and shallow shells with rigid orthotropic filler, bending and buckling beyond elastic limit

13 p2156 A71-29066

Unloading effects on elastoplastic stability of shells, using method based on successive approximations

13 p2156 A71-29073

Principal stresses separation in nitrocellulose transparent material with photoelastoplastic properties, using scattered light method

14 p2322 A71-29700

Arbitrarily shaped thin shell elastic-plastic deformation transient response prediction, using improved finite difference method

15 p2505 A71-32008

Elastic-plastic finite element analysis of near crack tip stress and strain field structure

16 p2590 A71-32940

Yield condition and stability of elastoplastic bodies with large deformations, using Gibbs method of thermodynamics

16 p2650 A71-33015

Elastoplastic buckling of structures, considering strain hardening materials, slip and Bauschinger effect

16 p2650 A71-33024

Finite element analysis with material nonlinearities, obtaining linear incremental elastoplastic stress-strain relation

16 p2652 A71-33084

Elastoplastic analysis by matrix displacement method, discussing perforated plate under tension and bar thermal stress due to rapid heating

16 p2652 A71-33085

Finite element method application to stress distribution analysis at crack tip of rectangular plate under tension, obtaining elastoplastic response to cyclic loading

16 p2653 A71-33086

Elastic-plastic stiffness matrix methods, applying linear and nonlinear programming techniques to framed structures analysis

16 p2653 A71-33094

Small deflection analysis within Cartesian coordinate system applicable to elastic-plastic rectangular plates bending under Tresca yield criterion

16 p2654 A71-33122

Unloading boundary in longitudinal elastic-plastic stress wave propagation, describing response in semiinfinite rods

16 p2655 A71-33212

Weak discontinuity unloading wave propagation in semiinfinite slender prismatic bar of elastoplastic material

16 p2656 A71-33356

Approximate elastoplastic problems solutions by method analogous to antiplane deformation of circular incompressible region in flow theory

16 p2657 A71-33594

Stationary small elastoplastic longitudinal forced vibrations of rods with internal resonance, obtaining asymptotic solution of nonlinear partial differential equations

16 p2659 A71-33980

Small elastoplastic cyclic strain effects on internal friction and energy dissipation in metals during vibrations

16 p2598 A71-33983

Neuber elastoplastic analysis of residual notch stresses for improved cumulative damage predictions applied to aluminum alloy under overload

[AIAA PAPER 71-776] 16 p2659 A71-34012

Elastoplasticity shell theory, demonstrating analogy between stresses and strains in three dimensional medium

16 p2660 A71-34067

Nonlinear creep equation of elastoplastic medium under three dimensional stress, assuming elastic, viscoelastic and irreversible plastic deformation

17 p2817 A71-34337

Dynamical thermal expansion effect on plane elastic-plastic stress wave propagation, using classical heat conduction equation

17 p2819 A71-34507

Elastoplastic strain distribution in bent circular Al plate with central hole under concentrated load, giving moire patterns and stress-strain diagram

[SESA PAPER 1822] 17 p2820 A71-34542

Impulsively loaded expanding cylindrical shell transient elastic-plastic response, using linearized assumption on plastic flow behavior

17 p2821 A71-34577

Weightless elastoplastic beam dynamic bending under moving concentrated load, calculating deformation by reduction to Cauchy problem

17 p2822 A71-34780

Small forced flexural elastoplastic vibration of structural beam, deriving approximate partial differential equation based on stress-strain relation

17 p2825 A71-35013

Cylindrical steel and Ni alloy specimens bearing strength in inhomogeneous stress states under cyclic elastoplastic bending and loading to failure

17 p2760 A71-35668

Viscoplastic elastic medium behavior, breaking down elastoplastic deformation into plastic and elastic deformations

18 p2977 A71-36187

Elastoviscoplastic system with components undergoing effects of external, resistance and attraction forces, determining motion

18 p2977 A71-36194

Nonstationary resonance analysis of forced flexural elastoplastic vibrations of beam of hardening/softening material under cyclic strain

18 p2981 A71-36709

Mathematical model for continuous elastoplastic transition stress-strain response of steels and nonferrous metals

18 p2937 A71-36835

Edge cracked metal sheet elastoplastic strain distribution determination, using optical interference, moire technique and plane stress model finite element method

18 p2983 A71-36848

Stress wave interaction with macrocrack in elastoplastic and quasi-brittle materials, measuring stress field by optical polarization method and motion picture photography

19 p3154 A71-37086

Work hardening materials yield criterion derivation from mathematical model for inclusions embedded in elastoplastic matrix

19 p3078 A71-37644

Linear-elastic fracture mechanics limits concerning toughness based on elastic-plastic rupture model for yielding materials

19 p3161 A71-38726

Nonlinear behavior of compressed elastic and elastoplastic rods in presence of large deformations, determining bearing capacity by step method

20 p3269 A71-39164

Finite elastoplastic deformation thermodynamic theory based on isotropic work hardening, excluding Bauschinger effect or localized modification of yield surface due to plastic flow

20 p3308 A71-39486

Superposed plastic deformation and plane wave propagation in elastic-plastic media applied to circular bar twisting

20 p3310 A71-39780

Fiber reinforced tube under lateral compression between two flat dies, determining finite deformation from nonlinear elastic and elastoplastic shearing response analysis

20 p3311 A71-39966

Elastic-plastic stress wave attenuation, applying theory of wave propagation in single crystals to flow field numerical solution

21 p3465 A71-40786

Elastic viscous plastic effects calculation in materials, describing method permitting constitutive equations introduction into computer programs for continuum mechanics equations solution

21 p3465 A71-40787

Elastic viscous plastic waves profiles of finite uniaxial strain, obtaining constitutive equations

21 p3465 A71-40788

Numerical analysis for transient elastoplastic thermal stresses on turbine disks at variable rotation speeds

21 p3466 A71-40836

Elastoplastic thermal stress analysis in axisymmetric bodies by finite element method, calculating residual stresses 21 p3466 A71-40841

Elastoplastic work hardening material characteristics, using microhardness analysis 21 p3468 A71-41001

Elastoplastic indentation of half space by infinitely long rigid circular cylinder, using finite element method 21 p3474 A71-41426

GWU-FAP computer program for rigid frame elastic-inelastic analysis based on finite element method and plastic initial strain concept 22 p3516 A71-41867

Thermal conductivity of elastic, elastoplastic and plastic contact area between two compressed rough surfaces 22 p3622 A71-42686

Plastic work hardening produced by pressure application to spherical cavity surface in infinite elastoplastic medium, considering spherical elastic wave attenuation 23 p3775 A71-43147

Fine structure at crack tip expanding in ideally elastoplastic material in plane deformation state and plane stressed state 23 p3778 A71-44061

Dynamic model for microinhomogeneous elastoplastic medium under cyclic loads with varying amplitude 23 p3779 A71-44203

Deformations and stresses in elastoplastic half space indented by rigid sphere, using finite element method 24 p3879 A71-44631

Curved finite element for elastic-plastic analysis of thin toroidal shells of revolution with discontinuous meridional slope under axisymmetric loadings 24 p3879 A71-44634

Geometrically nonlinear elastoplastic bending of rectangular flexible plates with various side ratios, using finite difference and strain theory 24 p3883 A71-44849

ELASTOSTATICS

Elastic elliptic inclusion stress state in plane elastostatics 02 p0321 A71-11680

Semiinfinite solid elastic cylinder under self equilibrium end loading, obtaining elastostatic solution 06 p1000 A71-18027

Plane and spatial load transfer and diffusion in linear elastostatics, noting application to aircraft and civil engineering structures and fiber reinforced materials 06 p1001 A71-18222

Plane stress state determination in laminated locally isotropic elastic solid based on stress functions 11 p1788 A71-25438

Existence theorems in micropolar elastostatics three dimensional boundary value problems relating to isotropic and homogeneous bodies equilibrium 11 p1847 A71-25442

Finite elasticity theory for isotropic incompressible solids, formulating Ericksen problem for requirements of statically possible radially symmetric deformations in equilibrium 16 p2661 A71-34147

German monograph on upper and lower bounds in elastomechanics covering elastostatic, natural vibration and stability problems, elastic states Hilbert space, numerical methods, etc 17 p2818 A71-34480

German book on static elasticity and theoretical mechanics covering materials stresses and deformations, virtual work principle, linear isotropic elasticity and thermoelasticity 21 p3464 A71-40782

ELDO LAUNCH VEHICLE

ELDO inertial guidance system digital computer, explaining guidance law subsystem formulation and programming 03 p0454 A71-13247

ELDO test firings failure analysis program, considering self destruction charges and vibration environmental load [DGLR-70-060] 05 p0815 A71-15964

Europa project ELDO multistage launchers electrical mockup tests for interface and coordination problems 06 p0979 A71-18000

Power spectrum analysis of ELDO Europa 1 third stage thrust phase vibrations, using digital filters 07 p1208 A71-19804

Equatorial CECELES/ELDO base management and conduct of launch operations, discussing installations, facilities, equipment and personnel 12 p1894 A71-26696

ELDO space tug development, discussing uses for earth orbital space stations and applications satellites logistics and interplanetary injection 22 p3609 A71-41978

Project management by contractual procedures for ELDO space research 23 p3786 A71-43466

ELECTRETS

Photoelectret effects in semiconductor materials containing deep lying impurity centers, discussing inhomogeneity regions and noise and reverse current levels 11 p1808 A71-25915

Dipolar charge density of electret formed by polar polymers above critical temperature under dielectric polarization with quenching 14 p2181 A71-29747

Photoelectret effects in semiconductor materials containing deep lying impurity centers, discussing inhomogeneity regions and noise and reverse current levels 21 p3429 A71-41205

ELECTRIC ANALOGIES

U ANALOGIES

ELECTRIC APPLIANCES

U ELECTRIC EQUIPMENT

ELECTRIC ARCS

NT CARBON ARCS

NT MERCURY ARCS

Imploding wire trigger technique for high shock velocity electric arc drivers in shock tubes 04 p0564 A71-14671

High current free-burning arc characteristics in air at various pressures, examining dimensions from photographs 04 p0676 A71-15031

Electric arc column in laminar gas flow, using integral method for stabilization conditions 09 p1544 A71-22266

German monograph on steady toroidal discharges and cylindrical vortex arcs, using electromagnetic gas dynamics equations 10 p1654 A71-25025

Electric arc motion division into relative velocity of arc phenomenon with respect to mass flow and mass motion 12 p1938 A71-27264

Forced convection effects on characteristics of steady state cross flow arc in presence of applied transverse magnetic field 12 p1938 A71-27265

Thermal boundary layer equation for sulfur hexafluoride steady arc constriction effects in nozzle throat 12 p1939 A71-27268

Thermal load capacity and nozzle shape for guiding and constricting high current plasmas from electric arc data, using Ar as discharge gas 14 p2279 A71-29851

Nonlinear and linear plasma properties influence on nonstationary processes in channeling arc core 15 p2455 A71-31740

Cathode damage of nanosecond atmospheric arcs on silver, gold, tungsten and palladium contacts, using scanning electron microscope 15 p2376 A71-32022

Steady and unsteady modes of electric arc combustion in Ar and Ar-Cs flows produced by plasma accelerator in closed glass contour 15 p2457 A71-32269

Resonance radiation field of positive column of low current electric arc burning in nonequilibrium Ar plasma with admixture of K, using optical probe 15 p2457 A71-32270

Electric arc burning in contracted Ar plasma between two plates, calculating normal current density and I-V characteristic 15 p2457 A71-32271

Transverse magnetic field effects on Ar cross flow arc in constant velocity mainstream 17 p2788 A71-34868

Dynamic pressure measurement method and apparatus for anode center of heavy current electric arcs in plasmas, applying to plasma welding arcs 20 p3274 A71-39047

High performance electric arc driven shock tube for shock velocities to 45 km/sec and test times over 4 microseconds, using 80/20 helium-hydrogen mixture 21 p3365 A71-40975

German monograph on experimental determination of noble gas plasma conductivity under normal pressure in high temperature range, covering measurements under electric arc conditions 23 p3711 A71-43475

ELECTRIC BATTERIES

NT ALKALINE BATTERIES

NT MAGNESIUM CELLS

NT METAL AIR BATTERIES

NT NICKEL CADMIUM BATTERIES

NT NICKEL ZINC BATTERIES

NT SILVER ZINC BATTERIES

NT STORAGE BATTERIES

NT THERMAL BATTERIES

NT ZINC-OXYGEN BATTERIES

Electric properties of solid modified AgI electrolyte batteries 03 p0351 A71-13032

Mercuric oxide-cadmium batteries optimum cell design for low temperature operating conditions and elevated temperature storage life 03 p0351 A71-13038

Zinc-mercuric oxide cells with self supporting anodes of controlled porosity for improving low temperature performance 03 p0351 A71-13039

High energy long shelf life lithium-nickel sulfide batteries performance tests 03 p0351 A71-13041

High energy batteries electronic discharge mechanisms, examining use of semiconductor cathodes 03 p0352 A71-13042

Oxide bronzes as oxygen reduction catalysts in batteries and fuel cells, considering effects of varying compositions and crystal faces 03 p0374 A71-13054

Solid electrolyte batteries development, considering design, performance, advantages and applications 03 p0355 A71-14322

Integrated high voltage CdS solar batteries with interconnected cells in series without grid 05 p0699 A71-16058

Failure modes and mechanisms for electric battery diagnostic tests 08 p1236 A71-21107

Spacecraft power system batteries performance, specifications, development, reliability and manufacture 08 p1236 A71-21108

Ten-year old missile battery reliability programs based on two aspects of remotely activated one-shot battery 08 p1236 A71-21110

Porous structure effects in oxygen consuming cathode, discussing electrode thickness, effective pore diameter, pressure difference and electrode performance 11 p1709 A71-25553

Mercury column electrochemical coulometer as amper-hour type of state-of-charge indicator for secondary batteries in space power applications 15 p2354 A71-32206

Orbital electric power system performance simulation for analysis of solar array/battery lock-up, comparing graphical and computer techniques 20 p3183 A71-38957

ELECTRIC BRIDGES

NT WHEATSTONE BRIDGES

NT WIRE BRIDGE CIRCUITS

Thermistor bridges for temperature measurement, discussing linearity conditions 01 p0079 A71-10250

Frequency division multiplexing of antenna feeder ducts without resonators using bridge circuits 01 p0054 A71-11084

Magnetic thermometry below 3 K using stable AC mutual inductance bridge 03 p0427 A71-13915

Two-wire IC pressure transducer bridge circuit performance features based on circuit analysis 04 p0561 A71-15594

Superconducting thin film bridges by vacuum deposition of tin, measuring current-voltage and resistance at SHF and critical temperatures 05 p0793 A71-16828

NbN Dayem bridge characteristics, discussing negative resistance region, self induced subharmonic current steps, temperature dependence and microwave radiation effects 07 p1079 A71-20161

Materials microstrain determination using automatic capacitance bridge gage and analog or hybrid computer for measurement signal processing 10 p1609 A71-23916

Bridge circuit for minimizing parasitic electrical disturbances in resistance strain gage measurement of dynamic stresses in impact tests 15 p2408 A71-31865

Bridge-feedback amplifier constant-temperature hot-wire anemometer static and dynamic response determination 15 p2408 A71-31931

IR transducer with detector for space applications, measuring capacitance on electronic bridge circuit based on temperature and pressure effects [ONERA-TP-963] 16 p2576 A71-32845

Automatic system for follow-up balancing of digital bridge, noting fast response rate 17 p2723 A71-35711

Rapid response multiple phase detector for balancing of AC digital bridge networks 17 p2718 A71-35712

Inductive voltage divider bridge network for ferrite coils inductance and Q measurements 17 p2723 A71-35713

Energy requirement measurements for bridge wire igniters at low voltage, using capacitor discharge 22 p3587 A71-41448

Hot-wire anemometer remote operation, discussing coaxial cable length, terminal connection and bridge current 22 p3541 A71-41794

Q band relative phase measurement using single sideband suppressed carrier ferrite modulator in serrodyne phase bridge 24 p3803 A71-44649

ELECTRIC CELLS

- Silver zinc batteries and cells case cover materials and sealing techniques for space missions 08 p1235 A71-21097
- Zinc-silver oxide batteries underwater and aerial applications, designing medium high rate long life cells 08 p1236 A71-21102
- Sealed secondary Ag cells, controlling H and O recombination by auxiliary electrode 08 p1236 A71-21106
- Parametric performance of quasi-vacuum mode thermionic multilevel space power generator, discussing surface parameters, fuel form, emitter geometry, helium management and generator reliability 11 p1714 A71-25900
- Semiconductor thermoelectric battery p-n cell elements joining with mercury amalgam for commutating 14 p2181 A71-29953

ELECTRIC CHARGE

- NT ELECTRIC DIPOLES
- NT ELECTROSTATIC CHARGE
- NT ION CHARGE
- NT SPACE CHARGE
- Physical changes at lithium electrodes during charge-discharge cycling in propylene carbonate electrolyte 03 p0350 A71-13030
- Nonraining clouds electric fields and charge distribution, calculating convection influence by numerical means 05 p0777 A71-16675
- Microwave noise generation by triboelectric charging of dielectric surfaces 07 p1063 A71-19932
- Helicopter charging mechanisms, considering engine and rain precipitation charging 07 p1020 A71-19933
- Supersonic aircraft electrification measurements using projectile frictional charging in ice-fog cloud 07 p1020 A71-19934
- Electric charge of interacting cosmic ray particles at sea level by experimental arrangement of flash tubes, and scintillation and proportional counters 10 p1664 A71-25043
- Stellar electric charges, determining sign and magnitude by exchange processes between stars and surroundings 12 p1971 A71-27763
- Density, momentum and electric charge measurement of nuclear interacting particles in extensive air showers, using air gap magnet spectrograph and neutron monitor 13 p2124 A71-28083
- Reversible and irreversible processes and arrow of time concept, considering direct interaction of two charges without field 13 p2101 A71-28766
- Dipolar charge density of electret formed by polar polymers above critical temperature under dielectric polarization with quenching 14 p2181 A71-29747
- Vertical muon spectra and charge ratio in energy range 30-800 GeV at sea level from Kiel cosmic ray spectrometry 15 p2474 A71-31778
- Mercury column electrochemical coulometer as ampere-hour type of state-of-charge indicator for secondary batteries in space power applications 15 p2354 A71-32206
- Analog computer application for determination of charge centers in multilayer gate structure of variable threshold FET, deriving equations yielding position of internally stored charge 15 p2462 A71-32639
- Cloud elements evolution, investigating electrical charges effects on ice crystal growth rate in water vapor by laboratory experiment 19 p3092 A71-38688
- Electric charge generation in storm clouds, considering water droplets, ice crystals and air movements role in precipitation and charge separation mechanism 20 p3256 A71-39071

- FET chopper amplifier for low level DC signals from thermocouples, strain gauge bridge circuits and weak transducer sources 03 p0384 A71-13275
- Chopper amplifier modulator and demodulator circuits analysis, discussing SNR performance 03 p0387 A71-13821
- Modulator-demodulator type push-pull DC amplifier input noise reduction, using electromechanical vibrators 15 p2355 A71-32451

ELECTRIC CHOPPERS

- FET chopper amplifier for low level DC signals from thermocouples, strain gauge bridge circuits and weak transducer sources 03 p0384 A71-13275
- Chopper amplifier modulator and demodulator circuits analysis, discussing SNR performance 03 p0387 A71-13821
- Modulator-demodulator type push-pull DC amplifier input noise reduction, using electromechanical vibrators 15 p2355 A71-32451

ELECTRIC CIRCUITS

- U CIRCUITS
- ELECTRIC COILS
- NT MAGNETIC COILS
- Weakly damped Alfvén ion-cyclotron waves and fast magnetoacoustic waves in infinite plasma cylinder inserted into current bearing finite coil 24 p3858 A71-45245

ELECTRIC CONDUCTORS

- Secondary currents on conducting cylinder near dipole antenna manifested as radio frequency interference, considering effect on radiation pattern 01 p0037 A71-11167
- General relativistic formulation of massive magnetized rotating conductor, showing electrodynamic properties of surrounding empty space for explanation of stellar structure 01 p0160 A71-11273
- Cylindrical post shunt impedance in rectangular waveguide, evaluating approximate theory for free space thin wire conductor 03 p0378 A71-13808
- Integrated circuit conductors short pulse high current rating, identifying three failure regimes 04 p0559 A71-15874
- Symmetrical wave excitation by electric dipole of conical surface ideally conducting along hyperbolic spirals, obtaining solution by integral transformation 05 p0727 A71-15996
- Chromium oxide electric conductivity activation energy and active oxygen, discussing perchloric acid and ammonium perchlorate vapors effect 07 p1182 A71-19247
- Electromagnetic wave scattering by perfectly conducting sphere, using integral equation formulation 08 p1253 A71-1294
- Electromagnetic wave scattering by perfectly conducting cylinder in anisotropic plasma with external magnetic field, deriving radiation pattern from asymptotic expression 08 p1253 A71-1295
- Electrodynamic forces distribution in conducting bodies in two traveling magnetic fields with different frequencies and pole spacings 09 p1499 A71-22137
- Electromagnetic effects in infinite conducting layer situated in field of inductors with mutually opposed traveling magnetic fields 09 p1499 A71-22138
- Average radar backscattering cross section calculation for conducting obstacles for arbitrary transmitter and receiver antenna polarizations, obtaining results for straight wires, circular loops and helices 09 p1410 A71-23516
- Plane electromagnetic wave reflection from conducting convex cylinder in radially inhomogeneous absorbing medium, deriving equations for beam trajectories calculation 10 p1574 A71-23805
- Induced electrostatic field in forced Hg vortex of ideal viscous electrically conducting fluid under axial magnetic field 10 p1649 A71-24456
- Scattering matrix of stripline segment with random change in width of inner strip conductor 11 p1733 A71-26350
- Two dimensional electromagnetic scattering by conducting corrugated circular cylinders, determining surface current by matrix and integral equation methods 14 p2195 A71-30248
- Plane electromagnetic wave diffraction on ideally conducting convex body of large electrical dimensions, obtaining Maxwell equations asymptotic solution 16 p2542 A71-33485
- High speed system for thermophysical properties measurement of electrical conductors above 2000 K in subsecond experiments 19 p3062 A71-37246
- Frequency dependent conductor coating matrices for lossy cylindrical conductors with circular section, using diffusion equation 20 p3197 A71-39450
- Electrodynamics of turbulently moving electrically conducting medium, allowing for Hall effect 21 p3453 A71-41356
- Teflon insulated LT type electrical conductors for 203-493 K, including chemical, ozone, UV and fuel resistance tests 22 p3520 A71-41694
- Point-matching method application to electromagnetic scattering from quadrilateral conducting cylinders in resonance range, using computer programs 22 p3510 A71-42205
- Symmetrical wave excitation by electric dipole of conical surface ideally conducting along hyperbolic spirals, obtaining solution by integral transformation 22 p3524 A71-42745
- Bulk metal electromigration and crack failure in Al thin film conductors, considering purity, glassing and hole nucleation 23 p3651 A71-43426
- Temperature distribution in current carrying cylindrical conductor with nonlinear boundary condition of emission by Stefan-Boltzmann law 23 p3783 A71-44070
- Characteristic modes theory for radiation and scattering by conducting bodies, considering electric and magnetic fields 23 p3660 A71-44161

- Characteristic modes computation for conducting bodies of revolution, discussing radiation and scattering patterns convergence 23 p3654 A71-44162
- Point source average signal reflection from conductive plane in random oscillation 23 p3654 A71-44163
- Electromagnetic pulses scattering by conducting wedge in uniaxially anisotropic plasma, obtaining electric dipole radiation fields transient time for various plasma frequencies 23 p3646 A71-44171

ELECTRIC CONNECTORS

- Reliability evaluation for electrical connectors used in electronic equipment based on probability and environment considerations 07 p1076 A71-19555
- Filter connectors for conducted electromagnetic interference suppression ensuring system electromagnetic compatibility, considering ceramic capacitors, pi-section and distributed feedthrough filters 21 p3353 A71-40442
- Printed circuit board components and connections survival under severe vibration and G forces, considering resonant frequency, mounting methods and lead wire strain relief 23 p3652 A71-43538

ELECTRIC CONTACTS

- Irreversible processes during formation of contact between indium telluride thin film and metal in vacuum at high temperature 01 p0137 A71-10150
- Au plated contacts deterioration by pore corrosion, noting resistance relation to basis or underplated metals porosity 01 p0102 A71-10800
- Gold and Aquadag contacts with single crystal nickel oxide surfaces, determining I-V characteristics 04 p0637 A71-15588
- Ti-Ag and Ti-Pd-Ag solar cell contacts structure and degradation dependence on high temperature and humidity environmental exposure 05 p0699 A71-16060
- Solderless Ag-Ti solar cell contacts humidity degradation mechanism 05 p0699 A71-16061
- Electroformed Al contact solar cells without soldering, investigating process parameters effects on performance 05 p0699 A71-16062
- Ti-Ag contact N-P and P-N single crystal Si solar cells electrical and mechanical performance characteristics 05 p0700 A71-16069
- N-p Si solar cells, investigating mechanism of low energy proton irradiation damage to back contacts 05 p0702 A71-16084
- Molybdenum disulfide treated graphite brushes in electric contact with copper slip rings at high rates in dry pure inert gas atmospheres 07 p1120 A71-20275
- Gold sliding electric contacts friction behavior, studying adsorbed gas lubrication in ultrahigh purity environments 12 p1912 A71-27637
- Self adhesion in relay contacts, discussing cold weld conditions and prevention by dry oxygen addition 13 p2074 A71-28835
- High-strength low-cost moderate-conductivity cobalt modified aluminum brass for electrical contacts, terminals and relay springs 13 p2086 A71-28836
- Base metal impurity effects on coercive force and contact properties of miniature multilayered diffused reed switches 13 p2038 A71-28837
- Dry reed sealer transfer contact design, operation and embodiment, noting Au diffused and Rh contacts with hydrogen gas 13 p2038 A71-28838
- Miniature dry reed switch for latching and speech path, using semihard magnetic material, sealing glass and electroplated rhodium contact 13 p2001 A71-28842
- Cathode damage of nanosecond atmospheric arcs on silver, gold, tungsten and palladium contacts, using scanning electron microscope 15 p2376 A71-32022
- Contact materials effects on X band FM noise and current fluctuations of Gunn elements 19 p3029 A71-38073
- Contactless piston resonator ensuring one parallel resonance in tuning range, using quadrupole theory 19 p3030 A71-38341
- Electric contact resistance of various conductive metal coatings on aluminum corrosion free joints 19 p3031 A71-38449
- Failure prediction for metal film semiconductor contacts on silicon substrate by electromigration, considering current density and temperature gradients 19 p3119 A71-38510
- Failure analysis of vacuum deposited Al film interconnections at contact windows, considering grain size effect and reliability improvement techniques 19 p3119 A71-38512

Metal film ohmic contacts to n-type GaP devices operating at high ambient temperatures

22 p3520 A71-41687

GaAs contacts fabrication by successive metals or alloy evaporation, examining surface distribution by X ray microprobe

22 p3585 A71-41703

Plated through holes interconnection in nine layer phased array antenna printed circuit board, using numerically controlled drilling and plastic encased preform solder system

22 p3525 A71-42765

Emitter-base W metallized contacts RF power transistors for improved hot spotting and breakdown reliability, comparing with Al

23 p3651 A71-43441

ELECTRIC CONTROL

Electrohydraulic thrust control system for supersonic transport aircraft engines, considering reliability, performance and weight

[SAE PAPER 700819]

01 p0143 A71-11546

Aircraft electric systems control by solid state switching, discussing reliability, service life, versatility and compatibility

01 p0007 A71-11627

High resistance single crystal light sensitive n-type GaAs wafer for obtaining long wave photographic images via electric photosensitivity control

03 p0428 A71-13986

Electro-hydraulic servomechanisms dynamic performance variation probabilistic model, presenting sixth order system variable parameters for Monte Carlo simulation

06 p0848 A71-17318

Electrodynamics transducer design for structural vibration testing system, using low power steering signal converter to generate large scale electromechanical loads

09 p1386 A71-22606

Optokinetic nystagmus device, combining TV set and bar generator with controllable frame desynchronization for moving image and electrical control of stimulus parameters

09 p1399 A71-22973

Electric fields for solid and liquid fuels dispersion and trajectory manipulation of charged particles to control mixing with air, vaporization and burning

19 p3171 A71-38193

Electrohydraulic stand for vibration strength testing, discussing system design, specifications, frequency-amplitude characteristics and applications

23 p3662 A71-44235

ELECTRIC CORONA

Tunable filter reflecting telescope and accessory optics for H alpha monochromatic photography of electron corona during total eclipse

03 p0424 A71-13626

Calibration and operation of corona discharge anemometer involving highly stressed anode and large plate cathode

13 p2066 A71-28156

Insulating materials breakdown by surface discharge, determining corona lifetimes by hemisphere-plane configuration and cylinder-plane electrode

21 p3358 A71-41193

Organic synthesis in simulated Jovian atmosphere by passing semicorona discharge through methanecorona mixture

22 p3602 A71-42180

ELECTRIC CURRENT

NT ALTERNATING CURRENT

NT ARC DISCHARGES

NT AURORAL ELECTROJETS

NT BEAM CURRENTS

NT CARBON ARCS

NT DIRECT CURRENT

NT EDDY CURRENTS

NT ELECTRIC ARCS

NT ELECTRIC CORONA

NT ELECTRIC DISCHARGES

NT ELECTRIC SPARKS

NT ELECTRODELESS DISCHARGES

NT ELECTROJETS

NT EQUATORIAL ELECTROJET

NT GAS DISCHARGES

NT GLOW DISCHARGES

NT HIGH CURRENT

NT IONOSPHERIC CURRENTS

NT LIGHTNING

NT LOW CURRENTS

NT MERCURY ARCS

NT PENNING DISCHARGE

NT RADIO FREQUENCY DISCHARGE

NT RING CURRENTS

NT RING DISCHARGE

NT THRESHOLD CURRENTS

NT TOROIDAL DISCHARGE

NT TOWNSEND DISCHARGE

Electric current carrying plasma with finite and anisotropic conductivity in longitudinal magnetic field, determining equilibrium and stability

01 p0132 A71-10173

Phase and amplitude fluctuations in oscillator circuits, determining power spectrum, disturbing voltage and current sources and step and impulse functions

03 p0383 A71-13168

Corrugated theta pinch stabilization, considering variable axial HF current and quadrupole magnetic field

03 p0464 A71-13930

Auroral oval transverse magnetic disturbance, examined as field aligned current models

03 p0419 A71-14523

High current free-burning arc characteristics in air at various pressures, examining dimensions from photographs

04 p0676 A71-15031

Current/voltage converter for measurements at floating potential with respect to ground, using Wheatstone bridge type circuit

04 p0560 A71-15894

Temperature effects on Si solar cell short circuit currents, considering solar spectrum, photon absorption coefficient and diffusion length

05 p0700 A71-16067

Field effect transistors with nonuniform doping profiles along channel, calculating carrier accumulation and space charge limited current flow by two dimensional model analysis

05 p0791 A71-16166

Shock tube diaphragm bursting by passing heavy current through overlapping heated wire under pressure

05 p0734 A71-16583

Dry reed switches service life relation to crossing or switching current, considering contact degradation and operational conditions

05 p0728 A71-16747

Oscillation application to steady current in MHD generator to stabilize electrothermal instability

05 p0791 A71-16938

Current-interchange instability in plasma turbulent heating by current

06 p0930 A71-17395

Oscillatory magnetic field superimposition effects on flux flow properties of superconducting metal foils

07 p1177 A71-19596

Avalanche transistor emitter current voltage characteristics, using Kirchhoff equations for equivalent circuit

07 p1077 A71-19798

Lightning current transfer tests of p-static discharger for aircraft installations

07 p1020 A71-19935

Surge voltages produced by transient currents on signal conductors in shielded cables

07 p1022 A71-19946

Blowout characteristics prediction analysis for safety fuses with current limiting feature

08 p1233 A71-21075

Polar substorms electric current systems and magnetic effect below and above ionosphere

08 p1279 A71-21211

Electric currents in undisturbed magnetospheric tail, discussing interplanetary magnetic field polarity effect and neutral sheet characteristics

08 p1280 A71-21214

Current carrying plasma in toroidal trap, studying instability and equilibrium due to captured and escaping particles

08 p1339 A71-21476

Integrated circuits semiconductor components, determining effects of heat energy production/withdrawal and strong field on electric current carriers mobility and concentration

09 p1416 A71-22496

Soviet book on large pulsed currents and magnetic fields technology covering condenser bank discharge systems and components design, electrical characteristics and structural details

10 p1557 A71-24014

Geomagnetic and interplanetary magnetic fields, considering inverse direction of electric currents in Northern and Southern Hemispheres

11 p1757 A71-25776

Spontaneous magnetic fields in laser produced plasmas explained as thermoelectric currents

11 p1807 A71-26406

Cavity controlled Gunn effect oscillators FM-current noise ratio, studying device current and domain capacitance as functions of carrier concentration and GaAs layer internal field

11 p1739 A71-26437

Thyristors junction area current rise time extension, discussing emitter field regional delay times as function of p-n-p structural properties

12 p1886 A71-26849

Electric current heated thin resistance film thermoelectric transducer, measuring temperature rise with thermocouple

12 p1888 A71-27158

Comparison of lightning and long laboratory spark, considering luminous processes, current, voltage, power, energy inputs, radiated visible spectra, electron density, etc

12 p1939 A71-27266

Pulsed MPD arc experiment, determining voltage characteristics and rotating current spokes occurrence and behavior

12 p1941 A71-27567

Acoustic instability of plasma with current under ionization equilibrium and moderate neutral gas pressures

13 p2105 A71-27878

Hydrodynamic instabilities of MHD plasma with current, using two fluid model in crossed magnetic-electric fields

13 p2105 A71-27879

Lightning problem from electrodynamic viewpoint, considering vertical discharge channel, charge distribution, current and nonuniform inducing fields

13 p2097 A71-28394

Helicon and magnetoacoustic waves instability during passage through hot collisionless plasma with current transverse to weak external magnetic field

13 p2107 A71-28851

Superconducting thin films nonlinear excess current near transition temperature, deriving expression from Tsuzuki microscopic basic equations

13 p2112 A71-29012

Electromagnetic flowmeters readings for boundary effects of current equalization

14 p2279 A71-29616

Space charge delay angle, RF induced current and mode instability interrelated for actual high power heavy duty magnetrons, using electron bunch model

14 p2211 A71-29831

Unipolar sunspot magnetic field and electric currents, comparing chromosphere and photosphere total field vector

14 p2298 A71-29978

Silicon planar transistors at low injection levels, showing current transfer function temperature dependence

14 p2213 A71-30624

Collector current delay and rise times in transistor common emitter configuration for linear, sine and exponential input signals

14 p2213 A71-30630

Channel width effect on FET transconductance in low current operation

14 p2214 A71-30634

Radio frequency measurements below 30 GHz, considering power, impedance, phase shift, voltage and current data

14 p2205 A71-30981

Particle collision effects on electrostatic probe electron or ion current collection in transition regime as function of relative thermal energy

15 p2409 A71-32107

Steady state analysis of phase controlled parasitic current, discussing reduction of alternator apparent power requirements and harmonic distortion

15 p2355 A71-32218

Magnetic field perturbation and electric current injection techniques for characterizing high strength alloys fatigue microcracks

16 p2581 A71-32865

Electrical plasma probes, discussing ion-surface effects, geometry, cleaning procedures, collisionless regime and electron/ion current

16 p2617 A71-32961

Fluidic ammeter for measuring electric current in uninsulated wire, using fluoric oscillator sensor

16 p2576 A71-32974

Closed circuit electrical, mass and heat flow stability analysis, showing capacities or inductances trace effects

16 p2607 A71-32991

Bayesian decision theory, discussing choice of possible systems to convert wind into electrical energy

16 p2582 A71-33291

Intense pulsed electron beam formation during current flow through plasma

17 p2786 A71-34279

Composite piezoelectric transducer subjected to current flow in semiconducting boundary layer under polarization gradient, determining mechanical response by Laplace transform

17 p2739 A71-34669

Electrical medical apparatus with electrodes and intracardiac catheters, considering electric current danger threshold, electrocution hazards and safety precautions

17 p2693 A71-35486

Quadrupole probe for measuring magnetospheric electric currents, noting transfer impedance dependence on probe motion relative to ambient plasma

18 p2912 A71-36198

Rogowski belts application to pulsed discharges current measurements, describing measuring circuits and calibration

18 p2924 A71-36758

MHD generator duct external loop electric current maximization by working material resistivity tensor optimal distribution

19 p3108 A71-37102

Stationary plasma flow interaction with axisymmetric spatially periodic magnetic field in presence of Hall effect, determining electric currents structure

19 p3109 A71-37139

Localized deformation effect on common-emitter transistor current gain, giving equations system defining band diagram configuration of p-n junction in thermal equilibrium 19 p3027 A71-37490

Magnetospheric current effects on geomagnetic field structure, noting electron and proton precipitation into auroral zone 19 p3059 A71-38396

Plasma sheath formation near absorbing wall, calculating electric potential and current variations in space and time 19 p3117 A71-38723

Emf dynamo nonuniformities effect on magnetospheric field aligned electric currents associated with solar quiet geomagnetic variations, calculating ionospheric electrostatic fields 20 p3217 A71-39516

Tellurium concentrations and photocurrent spectra in Te-doped InSb single crystal samples, determining Te diffusion after annealing 21 p3430 A71-41225

Nonelectrostatic helicon and magnetoacoustic waves instability during passage through hot collisionless plasma with current transverse to weak external magnetic field 21 p3425 A71-41280

Photocurrent for two stage transition in space charge layer in p-n junctions of germanium with radiation defects 21 p3435 A71-41333

Geomagnetic and interplanetary magnetic fields, considering inverse direction of electric currents in Northern and Southern Hemispheres 22 p3532 A71-41544

Physical model for electric current carrying shock discontinuity driven through nonconducting gas by Lorentz force, investigating uniqueness and stability 22 p3581 A71-41889

Lumped model for two dimensional current flow in grown junction transistor base, predicting small signal common emitter short circuit input impedance 22 p3523 A71-42359

Illumination effects on drain current for p channel enhancement type MOS transistor, attributing photoresponse to electron excitation in conduction band 22 p3523 A71-42481

Asymptotic expressions for electromagnetic field and currents induced in unbounded dense plasma by relativistic electron beam passage 23 p3711 A71-43410

Critical current of ideally homogeneous second class superconducting film, noting lattice resistance to small displacements 23 p3715 A71-43414

Harmonic analysis applicability to amplitude-frequency characteristics of plasma current fluctuations, governing spectral characteristics determination accuracy by passband filter delineation precision 24 p3851 A71-44394

Current harmonics in passively nonlinear resistance subject to simultaneous DC and AC fields 24 p3860 A71-44872

Magnetic induction by HF current passing over conducting torus enclosed by larger torus, obtaining vector potential, current density and inductance expressions 24 p3857 A71-45232

ELECTRIC DIPOLES

Cylindrical electric dipole antenna in magnetoactive ionospheric plasma, noting ion sheath effect on input impedance and active length 02 p0212 A71-11873

Interatomic electric dipole moment coefficient derivation by approximation involving accessible atomic properties, noting application to H atoms 02 p0287 A71-12708

Symmetrical wave excitation by electric dipole of conical surface ideally conducting along hyperbolic spirals, obtaining solution by integral transformation 05 p0727 A71-15996

Dipole conversion to equivalent quadrupoles and multipoles, replacing resistances by corresponding h matrices 06 p0872 A71-17373

Ground state energy approximate eigenvalues calculation for electron in stationary finite electric dipole field by variational approach 07 p1163 A71-19684

Satellite altitude dipole source effectiveness in lower ionosphere, comparing to ground based source with same dipole moment 07 p1064 A71-20319

Vertical electric dipole field diffraction by circular aperture in flat conducting screen between two electromagnetically different half spaces 09 p1406 A71-22877

Input resistance of electric dipole above metallic disk lying on homogeneous conducting half space at HF, using compensation theorem 09 p1495 A71-23573

Horizontal electric dipole gain dependence on height above plane lossy earth, deriving radiation intensity expression from Hertzian potential integral representation 11 p1730 A71-25249

Electromagnetic radiation from stationary electric dipole imbedded in plasma column moving in axial direction 13 p2110 A71-29389

Radio waves tropospheric refraction based on far field of vertical electrical dipole on impedance sphere 14 p2191 A71-29510

Dipole coupling, current distribution and impedance of thick dipolar log periodic antennas by 4-term theory 16 p2544 A71-34172

Symmetrical wave excitation by electric dipole of conical surface ideally conducting along hyperbolic spirals, obtaining solution by integral transformation 22 p3524 A71-42745

Electromagnetic pulses scattering by conducting wedge in uniaxially anisotropic plasma, obtaining electric dipole radiation fields transient time for various plasma frequencies 23 p3646 A71-44171

ELECTRIC DISCHARGES

NT ARC DISCHARGES

NT CARBON ARCS

NT ELECTRIC ARCS

NT ELECTRIC CORONA

NT ELECTRIC SPARKS

NT ELECTRODELESS DISCHARGES

NT GAS DISCHARGES

NT GLOW DISCHARGES

NT LIGHTNING

NT MERCURY ARCS

NT PENNING DISCHARGE

NT RADIO FREQUENCY DISCHARGE

NT TOROIDAL DISCHARGE

NT TOWNSEND DISCHARGE

Shock tube generated Ar plasma electric conductivity augmentation by electrical discharge through supersonic plasma flow in Faraday tube 01 p0134 A71-10998

Atmospheric pressure pulsed carbon dioxide lasers electrical excitation using double transverse discharge technique 02 p0260 A71-12130

Beam current instability and plasma heating by electron beam generated in linear discharge, discussing electron beam-cold plasma interactions 02 p0291 A71-12501

High energy batteries electronic discharge mechanisms, examining use of semiconductor cathodes 03 p0352 A71-13042

CW chemical laser operation with HF and DF in subsonic electric discharge mixing device, obtaining 5.5 w output 03 p0434 A71-13479

High power carbon dioxide electric discharge mixing laser with vibrationally excited nitrogen providing population inversion 03 p0434 A71-13480

Dielectrics erosion under pulsed electric discharge in conical plasma accelerator, varying capacitance and inductance for evaporated mass relation to current strength 04 p0631 A71-14597

Plasma ring vortex formation in atmospheric crossed electric discharges, analyzing photographs of vortex onset and development 04 p0631 A71-14600

Shock tube current sheet speed variations, describing discharge voltage, pressure and test gas effects 04 p0632 A71-14689

Hypersonic shock wave production into air at one atmosphere in tube with electrical discharge gas heating 04 p0566 A71-14970

Si solar cell test for electrical discharge effect on series resistance, curve power factor, conversion efficiency and spectral response 05 p0705 A71-16169

Electric discharge carbon dioxide lasers, obtaining increased power output with convective cooling process [AIAA PAPER 71-63] 06 p0909 A71-18522

Carbon dioxide electric discharge lasers physics, discussing electron energy distributions and excitations, gain and saturation intensity [AIAA PAPER 71-64] 06 p0909 A71-18523

Electric discharge carbon dioxide mixing laser, presenting model with chemical, vibrational and thermal nonequilibrium effects [AIAA PAPER 71-66] 06 p0909 A71-18525

CW electric discharge mixing chemical lasers, identifying molecular transitions responsible for radiations from output spectral distribution measurements [AIAA PAPER 71-216] 06 p0909 A71-18652

Plasma ring vortices in crossed electrical discharges attributed to shock wave induced plasma flow across lines of force of azimuthal magnetic field 08 p1338 A71-20785

Zn-Ag oxide cell discharge, determining heat generation rate and voltage production model 08 p1235 A71-21099

Cathode material ions acceleration during pulsed discharge in vacuum, discussing experimental investigation results 08 p1341 A71-21496

ELECTRIC ENERGY STORAGE

Pulsed discharge path in He at 100 atm and air atmosphere pressures, determining electrical conductivity dependence on discharge time by high speed photography 08 p1341 A71-21497

Electrodischarge machining operational principles, discussing spark energy, gap, discharge time, liquid dielectric, spark generator and electrode 09 p1455 A71-23251

Carbon dioxide laser performance quantitative analysis, considering electron to optical energy conversion via electric discharge in carbon dioxide-nitrogen-helium mixture 09 p1465 A71-23481

Dynamics of focusing electric discharges generated by coaxial plasma gun illuminated by ruby laser beam, using schlieren photography 10 p1653 A71-24758

Linear sawtooth generator, using MOS unijunction transistors to switch and maintain constant discharge current from timing capacitor 11 p1740 A71-26549

Cross field magnetic discharge stabilization of plasma column in flowing CW electrically initiated chemical laser 12 p1940 A71-27278

Superpressurization mechanism in hollow cathode active zone, calculating upstream pressure variation as function of discharge current 13 p2106 A71-28399

VLF noise spectra in earth-ionosphere cavity due to thunderstorm discharges, noting resonance level splitting by geomagnetic field 13 p2030 A71-28542

Electric discharge machining process for hard and brittle materials, based on metal erosion by interrupted electric spark 13 p2075 A71-28946

Metal removal rate optimization in electrodischarge machining process, considering governing parameters of relaxation circuit 13 p2075 A71-28947

Convectively cooled carbon dioxide-nitrogen-helium electric discharge laser theory based on excitation and relaxation processes, comparing with experiment [AIAA PAPER 71-588] 15 p2419 A71-31574

Closed path recycling shock tubes, presenting numerical simulation of circular path continuous shock wave driven by successive electrical discharges in presence of perpendicular magnetic field 16 p2551 A71-32917

Electrical discharge plasmas, investigating electron multiplication, secondary processes, Paschen law, pressure effects and formation time lag 16 p2617 A71-32957

Chemical reactions in electrical discharges, discussing H, O, N, halogens and free radicals, hydrides, halides and fluorinated compound synthesis and ion-molecule reactions 16 p2540 A71-32966

Plasma jet formation within high pressure discharges in air at atmospheric pressure, discussing electrode configuration, current density and accelerating magnetic field strength 17 p2787 A71-34285

Rogowski belts application to pulsed discharges current measurements, describing measuring circuits and calibration 18 p2924 A71-36758

VLF plasma oscillations in spherical magnetized cold cathode DC discharge, determining frequency relationship to current/voltage, gas pressure, magnetic field strength and cathode diameter 20 p3273 A71-38880

Crossbeam electric discharge convection laser, reviewing uniform and stable discharges in rectangular channel and laser optical properties 20 p3246 A71-39758

Plasma losses in high current plasma configuration due to inverse skin effect by observation for discharge regimes in theta pinch, zeta and Tokamak systems 21 p3422 A71-40763

Semiconductor materials compensated trapping levels analysis, applying thermally simulated capacitor discharge technique 21 p3431 A71-41231

Electrical breakdown initiation in high vacuum by electron beam, investigating discharge delay time dependence on beam parameters 21 p3420 A71-41292

Energy requirement measurements for bridge wire igniters at low voltage, using capacitor discharge 22 p3587 A71-41448

Superconductors application to electric energy storage and discharge 23 p3630 A71-43106

Transients determined for Cs vapor discharge phases, observing current fluctuations between steady states in negative resistance zone above 0.2 torr 24 p3858 A71-45246

ELECTRIC ENERGY STORAGE

Solid state electrochemical energy storage device using rubidium silver iodide electrolyte 03 p0350 A71-13031

Heat pipe improvement of capacitor energy storage and IOV, analyzing in terms of heat loss vs conducted heat

03 p0352 A71-13045

AlN insulating films electrical characteristics for use in charge storage devices, presenting Al-AlN-Au capacitor current-voltage-insulator thickness relationships

09 p1509 A71-23118

Superconductors application to electric energy storage and discharge

23 p3630 A71-43106

ELECTRIC EQUIPMENT

Electrical measuring device error caused by longitudinal instability of frame held in tensile suspension during casing transverse vibration

02 p0253 A71-12635

Thermoconductometric portable hydrogen analyzer for air around industrial centers, using bridge tungsten sensor network

04 p0601 A71-15675

Electrical potting compounds reversion problems on Air Force aircraft, discussing inherent properties and environmental effects on polyester urethane and polyacrylate compounds deterioration

10 p1633 A71-24116

Book on electrical equipment deterioration in adverse environments covering climatic action, excessive heat, atmospheric temperature variations, water vapor adsorption and condensation, etc

10 p1583 A71-24478

Various configuration thermal contacts, examining conductance with electric analog

[AIAA PAPER 71-437]

Force springs flexural pivots and miniature incandescent lamp tests failure distribution analysis for comparing mechanical vs electrical components

[ASME PAPER 71-DE-34]

12 p1911 A71-27326

Soviet handbook of aircraft electrical equipment covering DC and turbine powered generators, lubrication materials, electromagnetic interference countermeasures, etc

14 p2181 A71-29530

Undesirable electromagnetic interference minimization in electrical equipment by filtering, shielding, balancing lines, hot/neutral lines twisting and coaxial cables

15 p2369 A71-31506

Brayton power system electrical subsystem and component performance tests, discussing engine control package, DC supply, inverters and instrumentation

15 p2354 A71-32204

Electronic and electrical systems optimization effectiveness through generation of statistical priorities

22 p3525 A71-41438

ELECTRIC EQUIPMENT TESTS

Chemical test method for composition analysis of Ni-Cd electrodes

03 p0374 A71-13028

High voltage power supply for NASA orbital gravity substitute electrostatic workbench, including abnormal load and oxygen environment tests

03 p0394 A71-13050

Europa project ELDO multistage launchers electrical mockup tests for interface and coordination problems

06 p0979 A71-18000

Service performance and tests of zinc silver oxide batteries on Explorers 17 and 32

08 p1236 A71-21105

Failure modes and mechanisms for electric battery diagnostic tests

08 p1236 A71-21107

Startup testing of SNAP 8 power conversion system coupled with nuclear reactor simulator

15 p2447 A71-32217

ELECTRIC FIELD STRENGTH

Electrostatic vibrations from turbulent plasma heating on basis of Stark broadening of hydrogen spectral lines, obtaining electric field strength

01 p0131 A71-10069

Solar wind injection into magnetosphere, noting effects of magnetopause outward velocity and electric field strength

01 p0146 A71-11452

Magnetic field effects on electron heating by strong electric field in n-Ge single crystals

01 p0140 A71-11459

Metallized capacitors types and properties, considering extra thin dielectric films and high field strength

02 p0230 A71-11817

Langmuir probe DC detector for rocket quasi-static and AC electric field measurements in auroral zone ionosphere

03 p0406 A71-13302

Si diffusion p-n junctions at high injection levels in strong electric fields, discussing I-V characteristics, minority carrier lifetime, barrier capacitance, etc

03 p0384 A71-13374

Pontyagin maximum principle applied to optimal control of standing TE wave electric field strength in microwave gyrotron

03 p0386 A71-13813

Polarization of spontaneous emission in Zn-doped GaAs p-n junctions as function of electric field strength

03 p0467 A71-13985

Electric field strength measurement at rocket surface in ionosphere by electrostatic fluxmeter, obtaining E and F region ion drift velocities

03 p0417 A71-14035

Electron-hole plasma in current carrying wire azimuthal magnetic field, noting electric field intensity by hydrodynamic approximation

05 p0790 A71-16880

Electric field strength in earth ionosphere and magnetosphere during irregular motion of fast ions and electrons

06 p0894 A71-18253

Ionizing radiation induced surface damage dependence in matched oxide passivated silicon planar epitaxial transistors on junction fringing electric field strength during exposure

07 p1174 A71-19052

Roughrider F-100F aircraft flights in thunderstorms and Apollo 12 launch electric field measurements, comparing patterns and magnitudes of lightning strikes to vehicles

07 p1208 A71-19927

Nonlinear collisionless magnetoplasma waves and ionospheric irregularities electric field intensity, defining nonlinear oscillations domain by pseudopotential well

08 p1339 A71-21206

Electrostatic vibrations from turbulent plasma heating on basis of Stark broadening of hydrogen spectral lines, obtaining electric field strength

09 p1504 A71-23264

Lightning return stroke electric field intensity exact expression derivation, obtaining charge moment equation approximation

09 p1488 A71-23443

Inferring ionospheric electric fields at stratospheric levels with tropospheric penetration, using balloon measurements and model atmosphere

10 p1603 A71-24700

Dielectrophoresis force measurements and wedge shaped capacitor separation properties in satellite zero gravity conditions

19 p3103 A71-37278

Excitation and ionization cross sections of atmospheric molecular species by low energy ions in strong auroral and man-made electric fields

19 p3055 A71-38039

Ionospheric electric field strength at equatorial and medium geomagnetic latitudes during twilight from barium-ion cloud drift measurements

20 p3218 A71-39523

Electromagnetic wave propagation in gas with interdependent electron density and electric field strength, calculating transmitted power limit value

24 p3851 A71-44428

ELECTRIC FIELDS

Semiconductors optical properties, measuring Franz-Keldysh effect in specimen under strong sinusoid electric field perpendicular to light beam direction

01 p0137 A71-10089

Electric potential and field distribution in dielectric plate insert of rectangular waveguide calculated by net point method using computer program

01 p0051 A71-10149

Nonlinear resonance excitation of ion acoustic plasma waves by weak external electric field, using partial differential equations

01 p0134 A71-11027

Electrons motion across gas plasma magnetic field under stochastic electric field, noting accelerating effect

01 p0135 A71-11032

Auroral electrojet electric fields from plasma electron density and collision frequency profiles measurements via Black Brant rockets variable frequency impedance probes

01 p0075 A71-11332

Plasma electric field effects on atomic spectral line shape by plasma kinetic theory

01 p0130 A71-11349

Magnetospheric VLF electric field emissions above electron cyclotron frequency fromOGO 5 observation at magnetic equator

01 p0076 A71-11500

Ionospheric vertical drift velocities and east-west electric fields at magnetic equator from incoherent scatter observations

01 p0076 A71-11505

Compressible corotation of model magnetosphere, considering electric field induced by earth rotation

01 p0077 A71-11514

Electrical stability of double sphere dipole antennas for FR-1 satellite ionospheric plasma electric fields measurements

02 p0229 A71-11714

Carrier mobility dependence on channel transverse electric field in MOS transistor

02 p0231 A71-11841

Desorption and migration of Cs adsorbed on W surface under electric field, using field emission microscope

02 p0296 A71-12340

Parallel and perpendicular electric fields in auroral arcs from rocket-borne experiment

03 p0406 A71-13303

F region diurnal behavior, comparing neutral winds and electric field effects

03 p0408 A71-13383

Atmospheric electrical properties derivation from continuity equation, considering ion concentration, conductivity, space charge density and electric field

03 p0409 A71-13610

Carbon dioxide laser induced thermal lensing /focusing/ reduction in liquid carbon disulfide with DC electric field

03 p0436 A71-13877

Atmospheric air breakdown by mode-locked Q switched laser pulse train, investigating threshold electric field dependence on characteristic diffusion length

03 p0440 A71-14178

Rare earth alloys spin disorder resistivity in crystalline electric field absence and presence

04 p0637 A71-15797

Troposphere and stratosphere electric field above Atlantic Ocean, investigating electrode effect role in atmospheric circuit

05 p0738 A71-16220

Gravitationally induced electric field shielding using whisker model with conducting metal surface for reducing strain dependence on altitude

05 p0792 A71-16315

Electrostatic wave perturbation current using accelerated particles orbits in neutral sheet with electric field in plane

05 p0788 A71-16633

Coherent light propagation guidance by helicoidal guide, calculating transverse electric field distribution for luminous beam variations

05 p0722 A71-16705

Radioelectric /Hall/ effect due to electromagnetic wave propagation in semiconductors, noting longitudinal electric field generation by thermoelectric forces

05 p0794 A71-16882

Ionization disturbances caused by gravity waves in neutral air propagating through ionosphere in electrostatic field and background wind

06 p0888 A71-17278

Electron thermal diffusion effects during light interference patterns exposure, generating strong electric fields and holographic storage in electro-optic materials

06 p0940 A71-17309

Electron plasma in strong HF electric field, investigating possibility of parametric resonance

06 p0930 A71-17403

Plasma confinement in Tokamak, calculating particle and heat fluxes due to conductivity current and electric field

06 p0930 A71-17405

Dynamic stabilization of drift dissipative instability by inhomogeneous RF electric field parallel to magnetic field

06 p0934 A71-17475

Drift wave instability suppression by homogeneous RF electric field in DC discharge diffused plasma

06 p0934 A71-17482

Double probe technique for electric field measurements in magnetoplasma

06 p0936 A71-17703

Electrostatic fields parallel to geomagnetic field role in charged particles acceleration mechanism to auroral energies, considering electron and proton precipitation

06 p0893 A71-17989

Classical many component plasma dynamics with collective particle interactions in self consistent longitudinal electric field, deriving complex wave equations

06 p0937 A71-18062

EPR line width in ruby under charged dislocations and electric fields of lattice defects, using statistical method

06 p0942 A71-18348

Electric field effects on burning rates of composite metallized solid propellant containing ammonium perchlorate

06 p0947 A71-18613

Magnetospheric Debye radius, critical electric field voltage and normal and anomalous conductivities from low energy plasma concentration and temperature measurements

07 p1098 A71-19377

Rarefied plasma disturbances produced by large slowly moving charged spherical body, deriving electric field, ion and electron concentrations in body vicinity

07 p1195 A71-19380

Equatorial electric field generation by ionosphere dynamo region neutral wind meridional component

07 p1101 A71-19409

SHF electric fields effects on free carrier redistribution in semiconductors and surface effect influence on sample conductivity

07 p1177 A71-19496

- VLF electric field data in interplanetary medium from Pioneer 8 space probe observation
07 p1196 A71-19655
- Magnetopause electric field accounting for ATS 5 energetic proton and electron flux measurements, comparing to various models
07 p1186 A71-19660
- Ground state energy approximate eigenvalues calculation for electron in stationary finite electric dipole field by variational approach
07 p1163 A71-19684
- Effective electric field formulation of kinetic theory of classical Coulomb plasmas, computing wavevectors
07 p1169 A71-19994
- N and p junction field effect transistor /JFET/ gate current measurement leading to understanding of impact ionization mechanism and field distribution
07 p1081 A71-20542
- Thin shallow shells under surface loads with allowance for electric field induced body forces and moments, deriving four equations system
08 p1368 A71-20788
- Simultaneous auroral ionospheric electric field measurements by Skylark rockets, deriving plasma drift direction
08 p1279 A71-21208
- Dynamo theory for electric current variations in magnetosphere-ionosphere interactions, discussing electrostatic fields mapping and plasma particle drift motion production
08 p1279 A71-21213
- Electric field formation of field aligned electron density irregularities in magnetosphere
08 p1280 A71-21215
- Solid state laser oscillation transient features analysis by dynamic rate equations, taking into account electric field phase variations in mode locking
08 p1301 A71-21277
- Electron fluxes hydrodynamic stability in vacuum confined by external electric and magnetic fields and inertia forces, noting electron oscillations possibility
08 p1340 A71-21494
- Magnetospheric electric fields properties via simultaneous balloon flights between plasmopause and polar cap, indicating fields and bulk plasma flow turbulence
08 p1282 A71-21632
- Turbulent plasmas nonequilibrium electric fields determination from hydrogen spectral lines Stark broadening
08 p1341 A71-21790
- Cs ions surface diffusion /migration/ in presence of blocking electric field on emitter surface, examining contact-ionization ion sources
08 p1342 A71-21914
- Hot Cs plasma parametric resonance in variable electric field related to plasma heating
09 p1499 A71-22229
- Solar wind electric field relation to ground magnetic disturbances during magnetic storm from Explorer 28 and ground data
09 p1435 A71-22433
- Spatially uniform dense partially ionized plasmas asymptotic thermochemical relaxation processes due to heavy particle density, temperature or superimposed electric field changes
09 p1502 A71-22859
- Conductivity measurement of hot ion hydrogen plasma for runaway electric field, comparing Spitzer and Buneman formulas
09 p1502 A71-22860
- Electric field equations of plane EM wave diffraction at lattice of conducting cylinders, using Hankel function
09 p1408 A71-23113
- Solar wind simulation for interaction with lunar magnetic field, discussing particle shadowing effects generation of electric fields
09 p1514 A71-23310
- Electric field bounds over phased array antenna aperture, discussing use in predicting array power handling capability
09 p1419 A71-23646
- Magnetospheric electric field diagnosis, using geomagnetic disturbances in equatorial plane and pulsations in middle and high latitudes
09 p1441 A71-23639
- Diurnal variations of meridional winds by dynamo electric field in ionosphere, comparing with Thomson scattering
09 p1490 A71-23646
- Geomagnetic solar quiet day horizontal current and electrostatic potential field model in ionosphere, using dynamo equations
09 p1442 A71-23708
- Pioneer 9 space probe electric field experiment and near earth observations of noise spectra variations related to diffusive plasma layer
09 p1529 A71-23711
- Charged conductors in homogeneous collisionless magnetoactive plasma at hybrid frequencies, investigating antenna array quasi-electrostatic field one dimensional structure
10 p1582 A71-23809
- Nonlinear electrostatic theory Lagrangian analogous to gravitational Lagrangian from correspondence between Maxwell electromagnetism and Einstein gravitation
10 p1667 A71-23815
- Electrostatic field second order penetration into Vlasov warm electron plasma, using electron velocity distribution models
10 p1647 A71-23890
- Induced electrostatic field in forced Hg vortex of ideal viscous electrically conducting fluid under axial magnetic field
10 p1649 A71-24456
- Electric field, neutral wind velocities and ion collision frequency from artificial ionic clouds motion and deformation in ionospheric E and F regions
10 p1602 A71-24549
- Vertical and horizontal atmospheric electric fields measurements at balloon altitudes, considering magnetospheric processes effect and potential differences
10 p1603 A71-24699
- Magnetic field aligned currents during 18 March 1969 substorms, observing electric field by Ba plasma cloud motion for magnetic perturbation field
10 p1677 A71-24789
- Photoelectron sheath and electric field around spacecraft in interplanetary space, considering typical sheath profiles and tenuous ambient plasma effects
10 p1678 A71-24799
- Midlatitude F2 region diurnal variations in peak electron density critical frequency and height, noting electric field and ion drag effects
10 p1606 A71-24921
- Electric field, neutral air winds and atmospheric composition changes effects on electron concentration diurnal variation in midlatitude F layer
10 p1607 A71-24922
- First order EM discontinuities propagation in nonlinear centrosymmetric isotropic material with displacement field dependent on electric field and induction field dependent on magnetic intensity
11 p1798 A71-25568
- Hydrogen plasma simulation of solar wind-planetary body interaction, showing electric fields behind moon and Venus
11 p1816 A71-25755
- Single isolated solid particle irradiation in vacuum, using electrical suspension system with electric field produced by six electrodes on solid cube surface
11 p1806 A71-26087
- Anisotropic instability in velocity distribution of ions in plasmas under external RF electric field
12 p1934 A71-26572
- Solar flare two stage particle acceleration from X-ray burst observations, discussing induced electric field and Fermi mechanism
12 p1946 A71-26624
- Drift waves dynamic stabilization in collisionless plasma, considering AC electric field effects on low frequency instabilities
12 p1935 A71-26914
- Similarity laws for gas discharges in carbon dioxide lasers verified by longitudinal electric field measurements
12 p1914 A71-27209
- Soviet book on MHD flows in channels covering one dimensional theory, viscous fluids, boundary layers, electric fields, laminar flow, etc
12 p1940 A71-27294
- Electrohydrodynamic ideal incompressible fluid flow in flat and circular channels, determining electric potential and field distribution
12 p1941 A71-27520
- Electric and magnetic fields of fundamental modes in cylindrical and rectangular dielectric microwave resonators, classifying transmission lines connections
12 p1888 A71-27613
- Microwave dielectric measurement system sensitivity to electric field energy in dielectric non-magnetic specimen
12 p1889 A71-27621
- Parametric dissipative plasma instability in HF electric field, showing plateau formation in velocity distribution function causes Cerenkov dissipation decrease
12 p1941 A71-27765
- Electric field angular distribution of short radio frequency probe in warm anisotropic plasma under magnetic field
13 p2104 A71-27852
- Color frequency-time spectrograms of VLF electric and magnetic field Poynting flux data from Injun 5 satellite
13 p2054 A71-27914
- Vacuum merging speed and magnetospheric cross tail electric field inverse proportionality to plasma sheet particle concentration
13 p2056 A71-27934
- Air shower radio emission properties, presenting electric field strength measurements at various frequencies
13 p2127 A71-28104
- Constant emf in bulk age and Si N-type semiconductors under multifrequency microwave electric field
13 p2111 A71-28368
- Electrode nonlinear current distribution in plasma with anisotropic conductivity, noting Hall parameter effect on electric field structure
13 p2107 A71-28566
- Plane one dimensional steady compressible ideally charged gas flow characteristics in electric field
13 p2107 A71-28567
- Phase measurement at millimeter wavelengths in free space, using reference signal and interference pattern of slowly varying electric field
13 p2030 A71-28609
- States stabilization in low density plasma layer in ion-accelerating constant external electric field
13 p2108 A71-28857
- Pioneer 9 interplanetary observations, presenting deep space data for solar rotations and radial gradient in VLF electric field behavior
13 p2064 A71-29163
- Infinite radially nonuniform thin plasma cylinder wave scattering with electrical field component along inhomogeneity gradient
14 p2191 A71-29512
- Motor using electric field interactions with lossy dielectric rotor induced surface charge as force mechanism
14 p2181 A71-29543
- German monograph on drift waves in plasma with density gradient covering LF electrostatic disturbances in low density plasma
14 p2277 A71-29581
- Rectangular cross section MHD channel spatial electrical field distribution, obtaining electrostatic potential, boundary conditions and efficiency
14 p2278 A71-29612
- Conjugate duct irregularities in magnetosphere involving interchange of plasma tubes by spatially varying electric fields, applying to spread F formation
14 p2230 A71-29714
- Ionospheric currents due to electric polarization field transfer from magnetosphere under quiet and disturbed conditions, using Ba ion cloud and geomagnetic measurements
14 p2230 A71-29715
- Physical processes and variations in polar F region, discussing solar photoionization, particle ionization, thermal expansion, electric fields, neutral air winds, ion drag, etc
14 p2234 A71-30038
- Electron beam interaction with external harmonic microwave field in planar diode gap, calculating electric field current and voltage distribution functions
14 p2211 A71-30084
- Thermal boundary layer instability near heated vertical flat plate in poorly conducting liquid under horizontal DC electric field
14 p2337 A71-30407
- Afterglow plasma drift-dissipative instability stabilization by RF magnetic and electric fields
14 p2280 A71-30504
- Schwarz-Christoffel conformal transformation inversion for electrostatic field integral equation formulation, applying to stepped-guide junction
14 p2212 A71-30515
- Dynamic stabilization of plasma column drift dissipative instability by inhomogeneous RF electric field, using two fluid macroscopic equations
14 p2196 A71-30560
- F region drift velocity, wind, electric field, current and atmospheric composition variation measurements and related theoretical topics
14 p2201 A71-30940
- Electric field, atmospheric wave and other factors effects on F region storms by day and night in tables
14 p2236 A71-30941
- F region ionization drift and electric field observation by incoherent scatter techniques and data interpretation
14 p2236 A71-30942
- DC electric fields measurements in magnetosphere at equator, midlatitudes and close to or inside auroral arcs
14 p2237 A71-30955
- Atmospheric spectral and structural characteristics, reviewing studies of source phenomena and related electric, magnetic and electromagnetic fields
14 p2237 A71-30965
- Local time variations of power spectra of magnetospheric electric field from balloon flight data
15 p2397 A71-31758
- Random walk theory applied to electron motion in early stage of He breakdown in electric field, based on integral and differential cross section data
15 p2452 A71-31921
- Steady state of nonequilibrium Ar-Cs plasma in electric field, attributing instability to plasma radiation effect
15 p2457 A71-32273
- Electric field effect of epitaxial thin silver films on mica in vacuum as function of temperature, thickness and surface secularity
15 p2461 A71-32377
- Electric field in flow of medium with tensor conductivity due to Hall effect, studying eddy currents structure in magnetic field variation region
16 p2616 A71-32929

Atmospheric space charge and distribution measurement through oscillating electric field modulation by sound waves

16 p2562 A71-33067

Dipole antenna near electric field, basing calculation method on integral equation for antenna surface charge distribution function

16 p2546 A71-33487

Collisionless turbulent plasmas nonequilibrium electric fields determination from hydrogen spectral lines Stark broadening

16 p2619 A71-33549

Cs ions surface diffusion/migration in presence of retarding electric field on emitter surface, showing temperature effects

17 p2789 A71-35258

Electric field effects on town gas and hydrocarbon flame reaction rate, burning velocity and propagation speed due to free electrons in flame front

17 p2840 A71-35704

Earth upper atmosphere superrotation due to zonally averaged magnetospheric electric fields

18 p2911 A71-35992

Electric and magnetic fields effect on turbulent boundary layer of conducting gas near electrode in MHD channel with insulated walls

18 p2951 A71-36113

Weakly ionized gas plasma confined by cylindrical electrodes and dielectric fronts, calculating rotational movement behavior in transverse electric and longitudinal magnetic fields

18 p2952 A71-36943

Electric fields effects on ionization and recombination rate in non-LTE Cs plasma

18 p2852 A71-36967

Parametric plasma instability in HF electric field and constant magnetic field, noting longitudinal plasma oscillations growth

19 p3108 A71-37130

Balloon-measured magnetospheric electric fields comparison with all sky camera pictures of large scale visible auroral form motions, noting relationship

19 p3047 A71-37363

Electric field fluctuations in magnetospheric plasma at multiples of local electron gyrofrequency due to plasma instability

19 p3048 A71-37368

Magnetic field aligned electric field production by hot magnetospheric plasma interaction with cold ionosphere

19 p3048 A71-37401

Polar auroras production by electric fields and electron precipitation from magnetospheric magnetic storms

19 p3052 A71-37761

Magnetospheric Debye radius, critical electric field voltage and normal and anomalous conductivities from low energy plasma concentration and temperature measurements

19 p3052 A71-37802

Rarefied plasma disturbances produced by large slowly moving charged spherical body, deriving electric field, ion and electron concentrations in body vicinity

19 p3138 A71-37805

Equatorial electric field generation by ionosphere dynamo region neutral wind meridional component

19 p3053 A71-37833

Homogeneous collisionless plasma in external electric field, considering evolution in time of charged particles distribution functions

19 p3114 A71-37858

Solar and lunar hydromagnetic tides in earth magnetosphere obtained from electrostatic fields in dynamo region

19 p3142 A71-38030

Numerical integration of Schrodinger equation for spontaneous ionization of hydrogen atom in electric field

19 p3107 A71-38056

Electric fields for solid and liquid fuels dispersion and trajectory manipulation of charged particles to control mixing with air, vaporization and burning

19 p3171 A71-38193

Electromagnetic wave scattering on single ellipsoidal inhomogeneity in cylindrical waveguide, obtaining relationship for electric and magnetic waves reflection coefficient

19 p3019 A71-38330

H wave propagation in waveguide consisting of two parallel plates with longitudinal rectangular grooves, determining electric and magnetic fields by reduction method

19 p3019 A71-38331

Asymmetrical single ring resonator with electric and magnetic waves, determining intrinsic fields

19 p3019 A71-38340

Transverse electric field in ionosphere and magnetosphere during inhomogeneities consisting of fast electrons

19 p3057 A71-38367

Charged particle acceleration by nonstationary sinusoidal electric fields in earth magnetosphere based on mathematical model

19 p3129 A71-38377

Ionospheric currents fields, determining Hall conductivity and geomagnetic lines of force slope effects

19 p3058 A71-38387

Accuracy modeling guidelines for analyzing thin wire scattering structures using electric field integral equation

19 p3035 A71-38598

Similarity laws for gas discharges in carbon dioxide lasers verified by longitudinal electric field measurements

19 p3075 A71-38621

Thermospheric wind induction by auroral electrojet heating, considering effects of Joule dissipation of magnetospheric electric fields

20 p3215 A71-38744

High electric field Gunn effect in n-type InAs under hydrostatic pressure due to transferred carrier mechanism

20 p3275 A71-38786

Charged particle motion in constant magnetic field under random electric field, deriving maximum energy and diffusion coefficient

20 p3269 A71-39163

Magnetospheric interactions with ionosphere for solar regular daily geomagnetic variations, discussing dynamo region electric fields effects

20 p3217 A71-39509

Three dimensional atmospheric dynamo models in quasi-stationary and stationary approximation for ionospheric and magnetospheric electric fields and currents production during quiet conditions

20 p3217 A71-39512

Electric fields effects on ions temperature and electron densities of auroral ionosphere

20 p3228 A71-39844

Polar cap magnetic variation mechanism based on electric field aligned continuity of Hall current auroral electrojets, noting ionospheric electron density gradients effects

20 p3230 A71-39862

Magnetospheric plasma convection electric field double-probe measurement at high latitude by Injun-5 satellite, noting east-west velocity reversals or discontinuities at auroral zone

20 p3230 A71-39882

Polar cap electric field and relationship to magnetic disturbances from measurements on Ba ion clouds released by rockets

20 p3230 A71-39883

Night and daytime auroral zone ionospheric electric field measurement by rocket-borne Langmuir probe, noting components parallel and perpendicular to magnetic field

20 p3231 A71-39884

Projective numerical solution of integral equations arising in boundary value problems of electric and magnetic field theory

21 p3416 A71-40846

Experimental analysis of information content of aural electric field of human body, considering electrotonic and triboelectric components

21 p3338 A71-41066

Highly ionized hot Cs plasma parametric resonance in alternating electric field related to plasma heating

21 p3424 A71-41107

N-type negative resistance, photoconductivity and I-V characteristics of sulfur-doped p-type Si, showing hole capture cross section dependence on electric field

21 p3429 A71-41204

HF electric field influence on collisionless electron gas acoustoelectric effect, emphasizing electron scattering mechanism

21 p3431 A71-41232

Electron gas in constant crossed E and H fields, deriving nonlinear conductivity theory

21 p3424 A71-41260

Sound waves excitation and amplification in weakly ionized plasma within alternating electric field

21 p3425 A71-41282

Weak three dimensional plasma inhomogeneity effect on average force acting on plasma in HF electric field

21 p3425 A71-41284

Low density collisionless plasma stabilization in ion-accelerating external DC electric field

21 p3426 A71-41293

Au-n-GaAs surface barrier diode space charge layer strong electric field effects on photoconductivity quantum efficiency

21 p3432 A71-41302

Magnetosphere-ionosphere electric coupling for polar magnetic disturbances and auroral break-up origin, discussing thermal particles precipitation due to transient electric field

21 p3375 A71-41354

Electron acceleration and solar flare triggering due to quasi-static electric field caused by gas motion near photosphere

22 p3590 A71-41466

Spectra and correlation functions for ion sound turbulence, calculating anomalous resistivity for plasma in external electric field

22 p3579 A71-41582

Threshold AC electric field calculation for inhomogeneous plasma parametric instability excitation,

noting role of electron plasma wave energy propagation from unstable region

22 p3582 A71-41901

Radial electric field and electrostatic potential in solar wind from two fluid model

22 p3592 A71-41921

Field ion current angular distribution for large point emitter potentials as function of emitter geometry

22 p3578 A71-42057

Multivalley semiconductors scale effect due to nonuniform electron heating by electric field, determining effective conductivity as function of plate thickness and surface characteristics

22 p3585 A71-42058

Computerized electrostatic field model of biological cell membrane

22 p3487 A71-42119

Photoactivated electric field effects in nematic liquid crystals for recording real time transparent phase holograms

23 p3674 A71-42955

Subequatorial ionospheric upward moving irregularities during high sunspot activity, explaining phenomenon at F 2 region level by Hall drift from daytime west-east electric field

23 p3665 A71-42971

Electric field induced current distribution on cylindrical antenna, considering delta generator and electromagnetic waves excitations

23 p3643 A71-43122

Electron velocity distribution relaxation in time dependent weakly ionized plasma within electric field, solving Boltzmann equation

23 p3708 A71-43151

Low energy particle plasma sheet and convection electric field distributions over auroral zones and polar caps from satellite Injun 5 observation

23 p3669 A71-43168

Model prediction for magnetospheric electric field dependence on solar wind velocity, comparing results with plasmaspheric measurements for different Kps

23 p3721 A71-43177

Electric parameters of cold hollow cathode discharge and effect, controlling electron free paths by electric or magnetic field

23 p3710 A71-43276

Small scale electrostatic field penetration from E into F region of ionosphere based on plane stratified model

23 p3671 A71-43577

Nonlinear sum and difference frequency and second harmonic generations of current density in homogeneous magnetoplasma by nonuniform microwave electric fields

23 p3712 A71-44002

Characteristic modes theory for radiation and scattering by conducting bodies, considering electric and magnetic fields

23 p3660 A71-44161

Log spiral antenna with selectable polarization, showing electric field radiation patterns

23 p3654 A71-44165

Ohmic discharge plasma resistance, temperature and oscillations in weak electric fields under electron beam excitation in Sirius stellarator

24 p3854 A71-44518

Hot electrons in semiconductors within crossed and parallel electric and quantizing magnetic fields, examining collision frequencies and energy relaxation

24 p3861 A71-45165

Quasi-stationary electric field in toroidal metallic ionization chamber with meridional and equatorial slots, deriving formulas for components as function of coordinates

24 p3857 A71-45231

Experimental verification for electrostatic field gradient effects on charge carrier concentration in diffused regions of semiconductors

24 p3863 A71-45359

High DC field induced ionic wind, deriving electric and pneumatic parameters for various electrode configurations

24 p3849 A71-45369

ELECTRIC FILTERS

NT BANDPASS FILTERS

NT DIGITAL FILTERS

NT ELECTROMAGNETIC WAVE FILTERS

NT INFRARED FILTERS

NT LINEAR FILTERS

NT LOW PASS FILTERS

NT MICROWAVE FILTERS

NT OPTICAL FILTERS

NT RADAR FILTERS

NT RADIO FILTERS

NT TRACKING FILTERS

NT WAVEGUIDE FILTERS

Active RC filters synthesis, using expanded denominator of given transfer function

02 p0230 A71-11839

German monograph on frequency filter behavior of human retina regarding electric pulses, using ganglion model

03 p0373 A71-14372

- RC active filter with lumped-distributed components, discussing system stability at transition region between extreme electrical lengths
04 p0560 A71-14744
- Book on electrical, microwave and digital filter systems and design covering approximations, phase shift, ladder networks, frequency transformation, time domain, etc
04 p0560 A71-15075
- Automatic phase control system with separating capacitance containing low and high frequency electric filters
06 p0866 A71-17375
- Insertion loss approach to doubly resistor terminated filters approximation-synthesis problem
14 p2209 A71-29544
- Errors in spectral estimates by single-mode filters using analog computer for geoscientific data processing
14 p2246 A71-30482
- Undesirable electromagnetic interference minimization in electrical equipment by filtering, shielding, balancing lines, hot/neutral lines twisting and coaxial cables
15 p2369 A71-31506
- Automatic equalizer with fast startup time for digital communication systems including partial response and single sideband Nyquist systems
19 p3026 A71-37220
- Filter connectors for conducted electromagnetic interference suppression ensuring system electromagnetic compatibility, considering ceramic capacitors, pi-section and distributed feedthrough filters
21 p3353 A71-40442
- High Q micropower filters for VHF applications based on conditionally stable negative resistance operation, describing computer-aided design, construction and performance
21 p3361 A71-40822
- Error correction by tapped delay line coded equalizer and channel introduced redundancy, deriving upper bound for error probability
22 p3512 A71-42377
- ## ELECTRIC FUSES
- Blowout characteristics prediction analysis for safety fuses with current limiting feature
08 p1233 A71-21075
- Scaled and vented fusing devices, testing vacuum effects on performance at high and low temperatures
19 p3035 A71-38536
- ## ELECTRIC GENERATORS
- NT AC GENERATORS
- NT ALKALINE BATTERIES
- NT DIRECT POWER GENERATORS
- NT DYNAMOMETERS
- NT FUEL CELLS
- NT HYDROGEN OXYGEN FUEL CELLS
- NT MAGNESIUM CELLS
- NT MAGNETOHYDRODYNAMIC GENERATORS
- NT METAL AIR BATTERIES
- NT NICKEL ZINC BATTERIES
- NT PHOTOELECTRIC GENERATORS
- NT RADIOISOTOPE BATTERIES
- NT REGENERATIVE FUEL CELLS
- NT ROTATING GENERATORS
- NT SNAP 15
- NT SNAP 19
- NT SNAP 21
- NT SNAP 23
- NT SNAP 27
- NT SOLAR AUXILIARY POWER UNITS
- NT SOLAR CELLS
- NT SOLAR GENERATORS
- NT THERMAL BATTERIES
- NT THERMIONIC CONVERTERS
- NT THERMOELECTRIC GENERATORS
- NT TURBOGENERATORS
- NT ZINC-OXYGEN BATTERIES
- Laser produced plasmas for electrical power generation and space propulsion using fusion of deuterium-tritium pellet
01 p0135 A71-11179
- Nuclear electric space power plant rejecting waste heat by heat pipes
01 p0126 A71-11576
- Electric power supplies for communication satellite earth stations, considering methods for power availability and stability
02 p0222 A71-12788
- Aircraft variable frequency electrical generating systems, discussing weight and size reduction in motors and static inverters by gate controlled switches
02 p0197 A71-12908
- Natural gas organic Rankine cycle system for commercial on site electrical power generation and heating-cooling purposes
03 p0351 A71-13035
- Electrodynamical plasma accelerator with single phase salient pole magnetoelectric generator and storage condenser, giving component characteristics and transient processes equations systems
04 p0535 A71-15812
- Aircraft generator service life improvement and weight minimization by close coupling with drive and heat producing components cooling with oil spray and mist
06 p0849 A71-18463
- Soviet book on asynchronous generators for aircraft covering design and operation
09 p1387 A71-23420
- Heart electric generator system simulation by dipolar or multipolar generators
10 p1569 A71-24238
- Design optimization of aircraft starting and generating systems, identifying information required and system analysis methods
[SAE PAPER 710392] 10 p1558 A71-24256
- Parametric performance of quasi-vacuum mode thermionic multicell space power generator, discussing surface parameters, fuel form, emitter geometry, helium management and generator reliability
11 p1714 A71-25900
- STOL aircraft electric power variable frequency generation and high voltage DC distribution with secondary square wave AC distribution
[SAE PAPER 710444] 13 p1998 A71-28325
- Soviet book on airplane and helicopter electrical power supply systems covering storage batteries, DC generators, alternators, voltage regulators, current and frequency control, etc
14 p2180 A71-29525
- Electrically-heated Brayton power conversion system, comparing performance tests with prediction
15 p2354 A71-32212
- Three stage potassium vapor turbine for space systems electric power generation, discussing erosion and endurance tests
15 p2415 A71-32214
- Startup testing of SNAP 8 power conversion system coupled with nuclear reactor simulator
15 p2447 A71-32217
- Materials evaluation of SNAP 8 power conversion system breadboard assembly after 8700 hour test, extrapolating service life for space flight application
15 p2448 A71-32222
- NERVA nuclear rocket engine for space propulsion and long duration auxiliary power generation
[AIAA PAPER 71-639] 15 p2448 A71-32285
- Incore thermionic reactor as low cost power supply for direct-to-home TV satellite, converting thermal power to electrical without moving masses
16 p2526 A71-32853
- NASA space station electrical power systems discussing configurations, growth capacity, volume reliability and long term effects
[AIAA PAPER 71-825] 17 p2677 A71-34720
- Communication satellite ground station electric power generation and distribution equipment characteristics, emphasizing reliability
17 p2724 A71-35517
- Integrated drive generator for aircraft electrical power systems, improving weight, life and reliability
17 p2678 A71-35781
- Asynchronous generators classification based on primary distinction by independent or self operated excitation and stabilized or controlled frequency
19 p3000 A71-38639
- Automated endurance testing of 2-15 kW Brayton power conversion system, using rotating unit, heat exchanger, electronic voltage regulator, parasitic speed control
20 p3180 A71-38907
- Brayton cycle power conversion system using He-Xe gas mixture, discussing compressor net engine and turbine static efficiencies
20 p3180 A71-38908
- Post test inspection of Brayton Rotating Unit for closed Brayton cycle electric power conversion system for long space missions
20 p3180 A71-38909
- Electrical subsystem of 2-15 kW Brayton power conversion system consisting of speed controller, alternator voltage regulator, DC power supply, etc
20 p3180 A71-38910
- Motor starting techniques for 2-15 kW Brayton space power system with turbine driven radial flow compressor and Lundell type alternator
20 p3180 A71-38911
- Windage data for inert gas in high speed generators rotor-stator gap, investigating turbulent velocity profiles
20 p3181 A71-38915
- Reactor power systems for earth orbital space station, considering thermoelectric and Brayton cycle power conversion modules
20 p3262 A71-38919
- Brayton cycle electric space power supply systems, describing shielded reactor and heat exchanger design
20 p3263 A71-38924
- Unified electrical machine theory with allowance for space harmonics effects, transforming time-dependent linear differential equations into linear time-invariant equations
24 p3793 A71-44657
- ## ELECTRIC IGNITION
- Dual magneto ignition system for business and small military aircraft, describing development, design and test program
[SAE PAPER 710382] 10 p1659 A71-24247
- ## ELECTRIC IMPULSES
- U ELECTRIC PULSES
- ## ELECTRIC LEADS
- U ELECTRIC WIRE
- ## ELECTRIC MOMENTS
- Crystal time reversal symmetry for macroscopic laws determination, discussing spontaneous electric and magnetic moments and magnetically ordered systems
01 p0138 A71-10348
- Lightning return stroke electric field intensity exact expression derivation, obtaining charge moment equation approximation
09 p1488 A71-23443
- ## ELECTRIC MOTORS
- NT MICROMOTORS
- NT SYNCHRONOUS MOTORS
- NT TORQUE MOTORS
- Aircraft variable frequency electrical generating systems, discussing weight and size reduction in motors and static inverters by gate controlled switches
02 p0197 A71-12908
- Mathematical model for fields and currents calculation for asynchronous linear motors and MHD converters by Fourier transformation
09 p1387 A71-23650
- Pulse width modulation controlled DC motors, deriving formulas for speed and torque characteristics
13 p1999 A71-28630
- Basket wound and printed circuit moving coil electric and servomotors design characteristics
13 p2000 A71-28794
- Electric potential and current density in rotor of thin disk unipolar engine with zonal removal, formulating Neumann problem
13 p2002 A71-28930
- Near periodic current fluctuation stability of single phase parametric electric motor in steady operation
13 p2002 A71-28931
- Motor using electric field interactions with lossy dielectric rotor induced surface charge as force mechanism
14 p2181 A71-29543
- Soviet book on synchronous reluctance motors covering operation principles, design features and starting characteristics
15 p2354 A71-32200
- Nickel-zinc batteries for use in hybrid heat engine/electric systems of low pollutant passenger cars, increasing service life by aerospace technology
20 p3181 A71-38936
- Brushless DC motor as power source for meteorological, communications and geological satellites, describing electromechanical design features and operating characteristics
21 p3326 A71-40724
- Stepping electromotor in self commutation mode with local feedback, examining dynamics with phase plane method
23 p3655 A71-43293
- Unified electrical machine theory with allowance for space harmonics effects, transforming time-dependent linear differential equations into linear time-invariant equations
24 p3793 A71-44657
- ## ELECTRIC NETWORKS
- Torsion computation for bar with rectangular cross section by analogy with electrical networks, comparing with Saint Venant results
01 p0167 A71-10340
- Maximum power transfer theorem generalization for n-terminal pair network containing sources
02 p0236 A71-12043
- Current-switching digital to analog converters based on resistance ladder networks, discussing operation principles, problems and error sources
08 p1258 A71-20988
- Passive two-terminal networks in rod antenna for bandwidth increase, investigating equivalent circuit on digital computer
12 p1886 A71-26987
- Europa 3 two stage vehicle characteristics, outlining electrical system configuration and payload capacity
18 p2971 A71-35927
- R and C parameters determination for electric circuit simulating heat transfer in rod by amplitude-frequency characteristics
18 p2985 A71-36125
- Skylab electrical power system located on Orbital Workshop and Airlock Module and on ATM, discussing capabilities, characteristics and limitations
20 p3179 A71-38903
- ## ELECTRIC POTENTIAL
- NT BIOELECTRIC POTENTIAL
- NT CONTACT POTENTIALS
- NT COULOMB POTENTIAL
- NT LOW VOLTAGE
- NT PHOTOVOLTAGES
- NT SPIKE POTENTIALS

Anode sheath width for collisionless thermionic converter with Ba plus Cs filler, assuming linear potential variation

01 p0005 A71-10157

Piezoelectric transducer voltage-displacement response characteristics under connection with interferometric device, considering linearity and repeatability

01 p0079 A71-10311

Output properties of electrically pulsed carbon dioxide laser as functions of partial gas pressure and discharge voltage

01 p0092 A71-10372

Voltage distribution measurements between electrodes of MHD Faraday nozzle across ionized Ar plasma supersonic flow

01 p0136 A71-11373

Zn deposition on Zn single crystals in KOH solution, examining time and potential effects on deposit morphology

02 p0210 A71-12956

Variable voltage and frequency thyristor inverter, describing series commutation power stage

03 p0352 A71-13047

Nonlinear vector potential analysis of aerospace homopolar inductor alternators, considering fully armature currents

03 p0353 A71-13053

Phase and amplitude fluctuations in oscillator circuits, determining power spectrum, disturbing voltage and current sources and step and impulse functions

03 p0383 A71-13168

Filter output voltage in pseudorandom signals correlation processing, using Duhamel integral

03 p0378 A71-13392

Interelectrode focusing voltage effect on electron beam and tube efficiency in TW and backward wave tubes with electrostatic focusing systems

03 p0385 A71-13793

Gunn oscillator frequency characteristics vs displacement voltage in low Q factor resonance circuits

04 p0557 A71-14634

Current/voltage converter for measurements at floating potential with respect to ground, using Wheatstone bridge type circuit

04 p0560 A71-15894

Voltage distribution in transistor base for forward and reverse biases, discussing nonuniform potential distribution

05 p0728 A71-16007

Molten glass inclusion and stress concentrator/empty hole/ effects on Armo iron electrode potential

05 p0766 A71-16384

Carbonic acid effect on isolated skeletal muscle, discussing membrane potential and ion content measurements

05 p0710 A71-16941

Gunn diode generated signal frequency jumps as function of voltage variations, basing explanation on high field domain formation and decay

05 p0729 A71-16999

Lightning induced voltages in aircraft wing structures, examining induced voltage across load impedances in electric circuits

06 p0874 A71-17581

X irradiation induced currents across aluminum oxide films sandwiched between thin metal electrodes as function of voltage and time

07 p1174 A71-19056

Avalanche transistor emitter current voltage characteristics, using Kirchhoff equations for equivalent circuit

07 p1077 A71-19798

Surge voltages produced by transient currents on signal conductors in shielded cables

07 p1022 A71-19946

Voltage induction in superconductors by superimposed AC and DC magnetic fields

08 p1343 A71-20881

Zn-Ag oxide cell discharge, determining heat generation rate and voltage production model

08 p1235 A71-21099

Integral transform methods for analytic solutions to current and potential distribution on disk in infinite plane for four limiting cases

08 p1237 A71-21471

Space charge sign distribution sounding in atmosphere by electrode potential difference measurement

09 p1437 A71-22677

Potential and ion charge distribution in proximity to conducting sphere moving in low density collisionless ion-electron plasma

12 p1958 A71-26647

Electrohydrodynamic ideal incompressible fluid flow in flat and circular channels, determining electric potential and field distribution

12 p1941 A71-27520

Pulsed MPD arc experiment, determining voltage characteristics and rotating current spokes occurrence and behavior

12 p1941 A71-27567

Traveling wave tube magnetic field focusing and accelerating voltage effects on power output

12 p1889 A71-27627

Radial distribution of electric potential in Penning discharge based on relation between sulfur hexafluoride negative ions transit time and initial energy

13 p2107 A71-28852

Electric potential and current density in rotor of thin disk unipolar engine with zonal removal, formulating Neumann problem

13 p2002 A71-28930

Electric field potential near sphere moving through rarefied collisionless plasma in condensation zone, determining ion and electron concentrations

13 p1991 A71-29159

Electrode voltage of rectangular cross section MHD channel in conductive flowmeter, investigating magnetic field inhomogeneity and velocity profile effects

14 p2279 A71-29617

Capacitance/voltage characteristics of MOS capacitors before/after 25 MeV proton irradiation

14 p2210 A71-29797

Near anode surface electrode potential region width measurement in Knudsen thermionic converter with Ba-Cs interelectrode medium

14 p2181 A71-29954

Surface conductivity and current carrier mobility vs surface potential in CdSe single crystal films deposited on mica base by vacuum vaporization

15 p2461 A71-31511

Satellite skin potential and errors in electron density and temperature determinations by Langmuir probe measurements, using model ionosphere

15 p2398 A71-31768

Electrical insulation failure in dielectric fluid layer due to electrocapillary instability, presenting critical potential difference approximate and exact calculation

15 p2376 A71-31932

Switching on p-n-p-n structure under high injection level in both bases, noting current concentration and voltage steady state buildup

16 p2546 A71-33496

Continuous automatic recording of semiconductor diodes integral conductivity components, using circuit with controlled steady voltage bias

17 p2713 A71-34569

MIS structure voltage-farad characteristics, determining surface state densities for silicon compound dielectric films

18 p2954 A71-35875

Somatic cell mitosis control by simulated changes in electrical transmembrane potential difference

18 p2853 A71-35892

Cross power spectral analysis of atmospheric electric potential gradient relation to meteorological parameters, noting diurnal variations

18 p2944 A71-36010

Transistors life testing for temperature and voltage dependence of failure rates

18 p2893 A71-36805

Superconducting microjunctions I-V characteristic at critical temperature, investigating voltage fluctuations effects in external circuit

19 p3119 A71-37860

Calculation method for standard potentials and enthalpies of metals during oxidation and chlorination, representing molar functions dependence on temperature

19 p3082 A71-38153

Collisionless momentum transfer between interstreaming ions in laser produced plasma, using fast photography, shadowgraphy and electric potential probes

19 p3114 A71-38177

Interference voltage prediction model of induced noise in reference ground of electronic systems

19 p3031 A71-38448

Single point grounding of electronic system providing personnel safety and voltage reference potential

19 p3032 A71-38451

Plasma sheath formation near absorbing wall, calculating electric potential and current variations in space and time

19 p3117 A71-38723

Thermistor bolometer characteristics, considering resistance-performance relationship, radiation and Wheatstone bridge potentials

20 p3233 A71-38969

Stability conditions for square wave sustaining voltage, including complex rectangular waveforms with pulsed discharges in plasma display

20 p3233 A71-39060

Dynamo equations solution for electrostatic potential, discussing three dimensional model for ionospheric equatorial conditions and Northern-Southern Hemispheres coupling

20 p3218 A71-39519

Lunar dust potential as function of solar wind flux and particle photoefficiency

20 p3298 A71-39639

Intracochlear electric potential of anesthetized cats recorded with potassium filled glass micropipets, determining magnitude and phase of responses

20 p3191 A71-39768

Current and potential distributions in lossless nonequilibrium MHD plasmas at high magnetic field strengths, using method of characteristics

21 p3423 A71-40946

Voltage-polarization induced optical waveguide using electrooptical lithium niobate crystal

21 p3393 A71-41039

Spacecraft-borne high voltage system breakdown prevention by avoiding high electric field and critical gas pressure

21 p3358 A71-41192

Radial distribution of electric potential in Penning discharge based on relation between sulfur hexafluoride negative ions transit time and initial energy

21 p3425 A71-41281

Ductile crack growth detection in crack opening displacement specimens by electrical potential method

22 p3550 A71-41640

Radial electric field and electrostatic potential in solar wind from two fluid model

22 p3592 A71-41921

Field ion current angular distribution for large point emitter potentials as function of emitter geometry

22 p3578 A71-42057

Gunn oscillator frequency characteristics vs displacement voltage in low Q factor resonance circuits

22 p3521 A71-42274

Narrow strongly radiating slot voltage distribution, investigating cavity coupling with integral equation

22 p3522 A71-42305

Earth electrostatic potential role in experimental Coulomb law verifications

22 p3536 A71-42455

Early effect incorporation in Ebers-Moll simulation model for junction transistor large signal behavior to obtain current gain and conductance dependence on voltage

22 p3523 A71-42484

Voltage distribution in transistor base for forward and reverse biases, discussing nonuniform potential distribution

22 p3524 A71-42756

Impurity redistribution errors in C-V characteristics of MOS capacitors due to Si thermal oxidation

24 p3809 A71-44993

ELECTRIC POWER

Electric power source requirements of USAF aircraft, missile and spacecraft electrical systems

03 p0351 A71-13036

Spacecraft electric power transformation and control techniques enhancement, using DC to DC converter, voltage converter/regulator and solar array reorientation system

03 p0352 A71-13049

Ferrite resonator coupled to microwave transmission line, deriving instability effects threshold power level for comparison with measurement

10 p1584 A71-24725

In-core thermionic reactor flight system for space base applications, providing electric power and thermal shielding

11 p1710 A71-25870

In-pile tests of multiclement thermionic converter with Mo- and W-based alloy cathodes, noting output electric power dependence on internal heat release

11 p1711 A71-25877

Switched power limitation in p-n-p-n devices turned off by control current pulse, discussing thermal signal level

11 p1808 A71-25916

STOL aircraft electric power variable frequency generation and high voltage DC distribution with secondary square wave AC distribution

[SAE PAPER 710444]

13 p1998 A71-28325

Symmetrical hysteretic micromotors stator structure with windings around unilateral crowned teeth, calculating maximum EM power in starting mode

13 p1999 A71-28631

Satellite solar power station for microwave generation, transmission and energy conversion to electrical power on earth

13 p1999 A71-28665

Microwave power transmission for supplying electric power to space station complex for performing scientific experiments over long periods in earth orbits

13 p2000 A71-28667

High power linear beam tube devices for space power generation station, considering use of klystron with heat pipes for low weight and high efficiency

13 p2000 A71-28669

Mobility capability of lunar roving vehicles relative to terrain roughness, computing power requirements

15 p2494 A71-32496

Thyristor power conditioning application to high voltage DC electric power system, presenting SST aircraft sample load profiles

17 p2678 A71-35770

Aircraft electric power system design with reliability, simplicity, low cost, weight and size, discussing automatic circuit protection and energy power

17 p2678 A71-35780

Remote power controller as static circuit protection device for aircraft and spacecraft automatically controlled electrical wiring system, discussing performance improvement

17 p2678 A71-35782

- Electric power and efficiency of thermoelements with temperature dependent thermoelectric properties by heat balance technique 18 p2852 A71-36965
- Electrical power systems for spacecraft, reviewing solar cells, batteries, fuel cells and radioisotope thermoelectric generators 19 p3121 A71-37122
- Recoverable usable energy maximization from solar oriented spacecraft electrical power system, using silicon cell array and nickel cadmium batteries 20 p3182 A71-38956
- MHD power generator for converting heat into electricity by interacting magnetic field with flowing electrically conducting fluid 21 p3436 A71-40020
- Switched power limitation due to thermal processes in p-n-p devices turned off by gate current pulse 21 p3430 A71-41219
- High power hydrogen thyratron grid-anode structure without gradient grids, discussing design and performance tests 23 p3649 A71-42916
- ## ELECTRIC POWER CONVERSION
- ### U ELECTRIC GENERATORS
- ### NT NUCLEAR POWER PLANTS
- Electrical power generation from sunlight without pollution, using solar cell elevated rug technology 05 p0704 A71-16100
- Nuclear reactor design as heat source for electric power generation in space 16 p2606 A71-33249
- ## ELECTRIC POWER TRANSMISSION
- Cyclotron wave rectifier for S band and X band microwave conversion to DC or LF AC power 07 p1080 A71-20451
- Soviet book on airplane and helicopter electrical power supply systems covering storage batteries, DC generators, alternators, voltage regulators, current and frequency control, etc 14 p2180 A71-29525
- High voltage DC electric power transmission systems with ground return, reducing aircraft wiring weight and energy dissipation 17 p2678 A71-35771
- Multiple scattering of VHF and UHF radio waves from bundle conductor high voltage power transmission lines 19 p3021 A71-38446
- ## ELECTRIC PROPULSION
- ### NT ARC JET ENGINES
- ### NT ELECTROMAGNETIC PROPULSION
- ### NT ELECTROSTATIC PROPULSION
- ### NT ION PROPULSION
- ### NT PLASMA PROPULSION
- Spacecraft onboard power supply problem, discussing relative merits of electric and nuclear thermal propulsion systems 01 p0143 A71-11434
- Hall ion thruster using electron neutralized positive space charge in acceleration zone 02 p0283 A71-12312
- Electric propulsion in space, emphasizing rocket performance relation to exhaust velocity, propellant consumption, thrust duration and payload capability 03 p0469 A71-13285
- Solar electric propulsion /SEP/ for automated planetary missions, discussing system characteristics, capabilities and costs [AIAA PAPER 69-1103] 03 p0500 A71-14426
- Oxide hollow cathode ion thruster power conditioner, evaluating electrical efficiency, weight, reliability integration and testing [AIAA PAPER 71-159] 06 p0947 A71-18601
- Electric propulsion spacecraft mission performance scaling laws for invariant trajectory, obtaining optimum gross payload over wide range of system input parameters [AIAA PAPER 71-160] 06 p0981 A71-18602
- Soviet book on interplanetary electric spacecraft covering chemical and nuclear jet engines and rockets, electrothermal engines, plasma thrusters, etc 06 p0981 A71-18732
- Electric propulsion systems integration into SERT 2 spacecraft, discussing launch imposed environment, thrust vector control, thruster breakdown, power conditioning, etc [AIAA PAPER 70-1123] 09 p1511 A71-22898
- Hollow cathode ion thruster and lightweight power conditioner of solar-electric propulsion system for unmanned deep space probes [AIAA PAPER 70-648] 09 p1511 A71-22904
- Thermionic reactor electric propulsion for unmanned outer planets exploration, discussing spacecraft design, launch vehicle, weight factors, etc [AIAA PAPER 70-1122] 09 p1492 A71-22914
- Soviet monograph on electric space propulsion systems theory covering ion and plasma engines, gas turbine engines, nuclear energy sources, solar cells, etc 10 p1658 A71-24011
- Kaufman ion thruster providing electric propulsion for satellite spiraling from parking to synchronous orbit [AIAA PAPER 70-1101] 11 p1810 A71-25501
- Low specific impulse hollow cathode mercury thruster for deep space electric propulsion, using SERT 2 configuration [AIAA PAPER 70-1099] 11 p1811 A71-25526
- Radioisotope thermionic power supply for unmanned electric propulsion missions to outer planets, using 69 modules consisting of thermionic converter and emitter heat pipe 11 p1811 A71-25897
- Soviet book on space electric rocket engines design and stress analysis covering nuclear reactors, radioactive isotope energy sources and energy converters 13 p2118 A71-29421
- Communication satellites electric propulsion economic tradeoff studies, considering propellant requirements for north-south stationkeeping, and near-synchronous orbit maneuvers [AIAA PAPER 71-683] 14 p2292 A71-30746
- Satellite auxiliary electric propulsion systems survey for program managers and systems engineers, considering cost and component reliability [AIAA PAPER 71-685] 14 p2292 A71-30747
- European electric propulsion systems for flight trajectories within low gravity fields and orbital parameter attitude control and correction 15 p2469 A71-31730
- Shortest transfer time interstellar propulsion systems, considering nuclear pulse and electric rockets, fusion and photon rockets, and ramjets 15 p2469 A71-31748
- Solar electric propulsion and transfer system for higher payloads of SECOM communication satellites, using Europa 2 launcher 16 p2644 A71-32855
- ESRO activity in low thrust electric propulsion systems development for attitude stabilization and stationkeeping, using colloid and field emission thruster concepts [DGLR 71-035] 17 p2794 A71-35541
- Electrical propulsion systems research at Braunschweig installation covering plasma generation, ion sources, plasma accelerators, etc [DGLR 71-024] 17 p2794 A71-35544
- Solar electric propulsion system design for interplanetary spacecraft, describing Hg bombardment ion engine 17 p2794 A71-35546
- Electrical or electromagnetic acceleration of ionized gas to obtain high velocity rocket exhaust for deep space manned flight 19 p3123 A71-38249
- Solar electric multimission spacecraft design, discussing off-optimum propulsion parameters effects on low thrust performance by characteristic surface representation [AAS PAPER 71-324] 23 p3772 A71-42998
- Solar electric propulsion application to Halley Comet flythrough and rendezvous missions, describing trajectory characteristics and payload capabilities [AAS PAPER 71-363] 23 p3729 A71-43033
- ## ELECTRIC PULSES
- Zinc single crystals plastic deformation and dislocations movement enhancement under pulsating direct current, noting stress peaks-voltage relationship 02 p0296 A71-12297
- German monograph on frequency filter behavior of human retina regarding electric pulses, using ganglion model 03 p0373 A71-14372
- Laser Q-branch emission near 8 microns from flowing hydrogen-acetylene-helium mixture under pulsed electrical excitation 04 p0607 A71-15038
- Elastic wave properties and technological applications, discussing acoustic delay, compression and filtering electric signals 05 p0722 A71-16745
- MOSFET inverter pulse response analysis using hyperbolic functional dependence 05 p0726 A71-17086
- Organic thin film layer semiconductors photoconductivity, developing semiempirical theory of pulse formation 06 p0941 A71-17735
- Si step-junction avalanche diodes conduction current pulse waveforms during large signal operation, using numerical calculation 08 p1265 A71-21290
- Pulsed discharge path in He at 100 atm and air atmosphere pressures, determining electrical conductivity dependence on discharge time by high speed photography 08 p1341 A71-21497
- Pulsed signal amplitude and delay time measurement in presence of interfering /reverberated/ signals and steady noise 09 p1407 A71-23111
- Pulse excited finite length cylindrical monopole antenna mounted vertically on perfectly conducting ground plane, calculating near point electromagnetic fields 09 p1420 A71-23512
- Soviet book on large pulsed currents and magnetic fields technology covering condenser bank discharge systems and components design, electrical characteristics and structural details 10 p1557 A71-24014
- Flow visualization by cathodic hydrogen bubble technique, using electric pulsing for regular pattern formation for flow distortion tracing [ASME PAPER 71-FE-36] 13 p2053 A71-29471
- Triangular pulse shaper using transistors and dynistors, obtaining pulse duration, rise time and maximum repetition frequency 14 p2213 A71-30581
- Avalanche transistors circuits, generating rectangular and sawtooth pulses for use in time delay devices 14 p2213 A71-30582
- Rectangular pulse formation in nonlinear homogeneously distributed systems, discussing energy conversion efficiency 15 p2382 A71-32626
- Radio telemetry stimulator for conditioning large animals by applying high voltage short duration pulses to skin surface 16 p2534 A71-33050
- Numerical identification of linear automatic control system, starting from pulse response 16 p2549 A71-33378
- Temperature effects on photoelectric photometry, considering photomultiplier tube and electronics as black box with photons and electric pulses 16 p2548 A71-34097
- Rogowski belts application to pulsed discharges current measurements, describing measuring circuits and calibration 18 p2924 A71-36758
- Carbon dioxide laser triggered pressurized spark gap producing high voltage fast risetime pulses for use in IR radiation control by electro-optic shutters 20 p3244 A71-39106
- Current variation effect on pulsed p-n diodes forward characteristics, calculating peak inductive transient voltage value and time position 20 p3205 A71-39430
- Periodic current pulse and superradiant radiation pulsing in DC excited xenon plasma with increased cathode-anode capacitance 21 p3424 A71-41046
- Circuit generating short rectangular current pulses for pumping semiconductor lasers 23 p3685 A71-43528
- Nanosecond solid dielectric discharger fired by Q switched ruby laser for commutation of coaxial line forming high amplitude voltage pulses 24 p3835 A71-45238
- ## ELECTRIC RELAYS
- Canonic synthesis of electronic relays, considering cascade connected isolation box, analog to digital converter and switch 03 p0393 A71-14469
- Second order dynamic relay system with unstable linear part, investigating constant disturbance effects with point mapping and bifurcation theory 06 p0927 A71-17672
- Relay type pulsed control systems performance, determining noise effects by statistical analysis 06 p0879 A71-17927
- Second order dynamic relay system with unstable linear part, investigating constant disturbance effects with point mapping and bifurcation theory 09 p1424 A71-23458
- Self adhesion in relay contacts, discussing cold weld conditions and prevention by dry oxygen addition 13 p2074 A71-28835
- High-strength low-cost moderate-conductivity cobalt modified aluminum brass for electrical contacts, terminals and relay springs 13 p2086 A71-28836
- Analog computer power relay analysis simulating flux, coil current, moving mass motion and magnetic and spring forces as function of time 13 p2001 A71-28839
- Miss/stick oscilloscope techniques in signal and switching relay testing with automated human-interactive time-and-level-measurement machine 13 p2001 A71-28840
- Plug-in relay hazards and minimization for aircraft flight safety applications 13 p2001 A71-28841
- Solid state vs electrical-mechanical relay switching and isolation technology 13 p2001 A71-28845
- Transistorized long time delay relay for power supply circuits with constant function on reenergization after interruption 15 p2376 A71-32021
- ## ELECTRIC ROCKET ENGINES
- ### NT ARC JET ENGINES
- ### NT CESIUM ENGINES
- ### NT ELECTROSTATIC ENGINES
- ### NT ELECTROTHERMAL ENGINES

Electric propulsion in space, emphasizing rocket performance relation to exhaust velocity, propellant consumption, thrust duration and payload capability
03 p0469 A71-13285

Electric microthrusters for geostationary satellites orbit corrections, discussing orbital perturbations and operational characteristics of ammonia electrothermal and ion thrusters
07 p1207 A71-19528

Soviet book on space electric rocket engines design and stress analysis covering nuclear reactors, radioactive isotope energy sources and energy converters
13 p2118 A71-29421

ELECTRIC SPARKS

Multiple spark camera for unsteady compressible flow investigations, considering geometrical optical design, parallax, spark producing electric circuitry, etc
01 p0078 A71-10106

Spark discharge ignition in air by Q switched ruby laser
01 p0093 A71-10684

Spectrochemical analysis of alloy steels using microspark method
03 p0375 A71-13974

Quantitative spectrographic microanalysis using laser pulse vaporization and spark discharge
03 p0438 A71-13975

Cracks nucleation by spark discharge in Mo single crystals, using optical and transmission electron microscopy
05 p0766 A71-16323

Spark discharge ignition in air by Q switched ruby laser
07 p1125 A71-20146

Refractory metals and carbides and borides, investigating laws governing electrodes erosion during electric spark breakdown
07 p1139 A71-20205

Spark discharge enhancement of heavy ion track etching in Lexan polycarbonate
07 p1114 A71-20271

Sparks induced in gases by transversely excited atmospheric pressure carbon dioxide IR pulsed lasers, observing plasma filament forward propagation
07 p1129 A71-20619

Electrodischarge machining operational principles, discussing spark energy, gap, discharge time, liquid dielectric, spark generator and electrode
09 p1455 A71-23251

Spark sintering powder metallurgy using alternating and direct current plus pressure, discussing use in Be components production for aerospace applications
10 p1618 A71-24765

Comparison of lightning and long laboratory spark, considering luminous processes, current, voltage, power, energy inputs, radiated visible spectra, electron density, etc
12 p1939 A71-27266

Subnanosecond interferograms with high spatial resolution of plasma filaments in ruby laser produced spark
13 p2077 A71-28047

Electric discharge machining process for hard and brittle materials, based on metal erosion by interrupted electric spark
13 p2075 A71-28946

Titanium alloys analysis by dissolution in sulfuric acid and aerosol injection into spark discharge, discussing standard solution preparation
15 p2367 A71-31650

German monograph on spark discharges behavior in nitrogen, carbon dioxide and argon at excess pressure covering Toepfer, Weizel-Rompe and Braginskii laws applicability
17 p2779 A71-34799

Streamer discharges effects on integrated aircraft antenna and associated avionics, emphasizing RF interference and component damage
19 p3033 A71-38462

Sequential electric spark technique for hypervelocity projectiles turbulent wake velocity measurements at ballistic ranges in free flight regime
21 p3362 A71-40385

High voltage spark generating circuit design for studying electrostatic sensitivity of electroexplosive devices, considering pyrotechnic flash charges, bridgewire detonators and electric blasting caps
22 p3587 A71-41449

Chemical laser action at atmospheric pressure from vibrational rotational transitions of HF produced by multiple transverse spark discharges in propane-helium-sulfur fluoride mixtures
22 p3556 A71-41727

ELECTRIC STIMULI

Midbrain reticular neurons discharges in response to electrical stimulation of posterior ventral nucleus of thalamus
01 p0008 A71-10072

Dorsomedial nucleus electric impulse stimulation in anesthetized cats with oscillogram recorded response potentials of cortex proral gyrus, indicating relay transmission function
01 p0008 A71-10091

Feedback circuit for constant current stimulation through intracellular microelectrode
01 p0021 A71-10245

Matrix switch amplitude analyzer for EEG signals providing feedback stimuli to subject
01 p0021 A71-10246

Rabbit hypothalamic neuron stimulation by changes in ambient temperature
03 p0361 A71-13225

Bilateral and single median nerve electrical stimulation, observing summated cortical responses from homologous scalp derivations
05 p0706 A71-16322

Hippocampal, neocortical and somatic effects of HF electrical stimulation of mesencephalic reticular formation during different stages of sleep in cats
05 p0707 A71-16424

Oxygen respiration effect on self stimulation and emotional reactions in rabbits during hypothalamus electrical stimulation
06 p0855 A71-18376

Left ventricular function analysis by atrial pacing in subjects with normal and elevated left ventricular filling pressure, relating stroke volume to end diastolic pressure
07 p1044 A71-20352

Ventral controllers automatism suppression by HF electric stimulation, examining energy metabolism inhibitors effects
08 p1240 A71-21793

Monocular vision field structural color in violet and yellow region under increasing light frequency and periodic electric stimulation
10 p1560 A71-23990

Direct electrical stimulation of musculus tensor tympani on click elicited responses in cochlea and cochlear nucleus
13 p2003 A71-27832

Behavioral arousal and EEG thresholds changes during sleep due to electrical and audio stimulation
13 p2005 A71-28379

Behavioral effects of electrically induced EEG abnormalities in intertemporal and occipital cortex in monkeys on visual pattern discrimination and successive spatial reversals
13 p2011 A71-28806

Respiratory wave basic pattern during cat diaphragm artificial activation by electric rectangular stimulus to phrenic nerves
14 p2185 A71-30412

Cerebral ischemia effects on sensorimotor cortex function in cats, recording spontaneous EEG and pyramidal response to cortex electrical stimulation
15 p2359 A71-31956

Cardiovascular responses to hypothalamic, spinal cord and stellate ganglion stimulation as function of intensity, pulse duration and frequency in cats
16 p2531 A71-33367

Tympanic-cavity nerve plexus electric stimulation effects on cerebral blood circulation and overall arterial pressure in dogs and cats
16 p2533 A71-34108

Hypothalamus and cerebral cortex electric stimulation effects on temperature homeostasis under hyperoxia
17 p2680 A71-34645

Human visual perception response to brightness under sinusoidal current, suggesting interaction with retinal neural structures
17 p2680 A71-34656

Differentiation of hypothalamic drive and reward centers, applying electric stimulation via chronically implanted electrodes
17 p2681 A71-34944

Cat pupillary system static and dynamic response determination under light and electrical stimulation, using TV pupillometer and on-line computer
17 p2691 A71-35044

Long term exposure to electric shock and associated stimuli on squirrel monkeys, considering aggressive and manual responses
20 p3187 A71-39070

Incentive goal and extensive stimulation experience effects on proportion increase of hypothalamic electrode sites yielding elicited eating and drinking behavior
21 p3336 A71-40706

Heart excitation and membrane permeability effects on two component action potentials in human atrial muscle strips, using microelectrodes
21 p3336 A71-40865

Orthodromic and antidromic impulsion role in functional state changes of contralateral cerebrosplinal center during mixed nerve prolonged stimulation by rectangular pulses
21 p3337 A71-41059

Excitability, reactivity, adequacy, creativity and guidance at molecular, cellular, systemic and psychic levels in human biophysical neurodynamics, plotting stimulus magnitude vs response duration
21 p3344 A71-41063

Stabilographic indices and excitability curves of vestibular response to galvanic currents, using van Egmond cupulometry method
24 p3796 A71-44544

Postsynaptic de- and hyperpolarization potential development mechanisms in wafekal cats cortical neurons during LF thalamic structure stimulation
24 p3797 A71-44720

ELECTRIC STRAIN GAGES

U STRAIN GAGES

ELECTRIC SWITCHES

NT CRYOTRONS

NT THERMOSTATS

Dry reed switches service life relation to crossing or switching current, considering contact degradation and operational conditions
05 p0728 A71-16747

Base metal impurity effects on coercive force and contact properties of miniature multilayered diffused reed switches
13 p2038 A71-28837

Miss/stick oscilloscope techniques in signal and switching relay testing with automated human-interactive time-and-level-measurement machine
13 p2001 A71-28840

Miniature dry reed switch for latching and speech path, using semihard magnetic material, sealing glass and electroplated rhodium contact
13 p2001 A71-28842

Permeance and magnetic pull curves for miniature reed switch with wire pressed blades in sealed glass, using computer program
13 p2001 A71-28843

Driving modes and operation characteristics of reed switches with permanent magnets
13 p2001 A71-28844

ELECTRIC TERMINALS

N-port networks interconnection by NASAP-70 transfer function capability for large scale circuit problems, considering Laemmel and Cascade Parameter methods
03 p0390 A71-14309

Three-pole theory of amplifiers, deriving operational resistances as function of wave resistance and control parameters by current-voltage matrices
20 p3205 A71-39467

Hot-wire anemometer remote operation, discussing coaxial cable length, terminal connection and bridge current
22 p3541 A71-41794

Two-terminal negative resistance circuit analysis for parameters effect on linearity by parabolic relation
22 p3521 A71-42203

ELECTRIC WELDING

NT ARC WELDING

NT ELECTRON BEAM WELDING

NT ELECTROSLAG WELDING

NT GAS TUNGSTEN ARC WELDING

NT PLASMA ARC WELDING

Gas tungsten arc, manual, machine and resistance welding in assembly of gas turbine parts
[SME PAPER AD-70-147] 01 p0089 A71-11258

Solar cell module joints welding technology development under ESRO sponsorship, emphasizing resistance welding and process optimization
05 p0704 A71-16095

Ti alloys inert gas shielded welding, determining relationship between welding current, electrode feed rate and electrode wire protruding length and diameter
15 p2413 A71-31219

ELECTRIC WIRE

NT EXPLODING WIRES

Resistively heated W-Re wire sublimation characteristics between 1550-1950 C in low pressure oxygen
02 p0264 A71-12255

Lunar Module Ag coated stranded Cu wire, analyzing fluorine contamination with proton microprobe
02 p0209 A71-12592

Doped W wire core porosity and anomalous recrystallization behavior microstructural observation by electron microscopy
02 p0268 A71-12890

Electromagnetic wave propagation along conducting wire in magnetoplasma
03 p0381 A71-14472

Shock tube diaphragm bursting by passing heavy current through overlapping heated wire under pressure
05 p0734 A71-16583

Permeance and magnetic pull curves for miniature reed switch with wire pressed blades in sealed glass, using computer program
13 p2001 A71-28843

Scattering obstacle with surface currents and radiating fields, determining characteristic current distributions and values of elliptical loops, straight wires and circular arcs
17 p2700 A71-34753

Laboratory method assessing homogeneity and interchangeability of thermocouple wires, considering thermoelectric properties of widely separated wire from same spool
18 p2852 A71-36990

Parasitic wire elements effects on radiation, impedance and current distribution of antennas, using method of moments
19 p3031 A71-38444

- Long wire electromagnetic scattered field modification by multiple impedance loading, deriving calculation formulas
19 p3024 A71-38607
- Automated electrical wire harness manufacturing for Boeing 747 aircraft, discussing development of numerical control program
21 p3386 A71-40441
- ELECTRIC WIRING**
U ELECTRIC WIRE
U WIRING
- ELECTRICAL BREAKDOWN**
U ELECTRICAL FAULTS
U ELECTRICAL CONDUCTIVITY
U ELECTRICAL RESISTIVITY
U ELECTRICAL ENERGY
U ELECTRIC POWER
U ELECTRICAL ENGINEERING
- AGC system with transfluxor as gain control element and output-level memory device
01 p0054 A71-11086
- Integrated circuits electrical parameters and design joint optimization, describing technological analysis, physical component characteristics, operating conditions and design factors
09 p1422 A71-22493
- ELECTRICAL FAULTS**
Electrical fault location and detection techniques for cellular logic circuit arrays fabricated with LSI procedures
01 p0044 A71-10184
- Cylindrical Xe filled thermionic diodes breakdown and low voltage arcs at various pressures and interelectrode distances
02 p0190 A71-11942
- Breakdown voltage measurement for Cs vapor in cracks in Alumina insulator of pressure bonded sheath tube assemblies
02 p0232 A71-12252
- N-type Ge semiconductor low temperature breakdown potential dependence on neutral impurity concentration
05 p0793 A71-16420
- Avalanche diodes as solid state noise sources, observing planar silicon junctions breakdown voltages
06 p0940 A71-17324
- Refractory metals and carbides and borides, investigating laws governing electrodes erosion during electric spark breakdown
07 p1139 A71-20205
- Electric breakdown in supersonic Ar or air flow behind shock wave, determining threshold discharge currents
08 p1276 A71-21485
- Breakdown voltage and high power tests for pressure bonded collector sheath tubes with cracked alumina insulators and flowing liquid metal coolant
11 p1709 A71-25859
- Laser triggered switching, considering theory of laser induced voltage breakdown of gas filled spark
12 p1915 A71-27283
- Voltage breakdown in scientific spacecraft systems during test and flight, discussing factors affecting gas discharges
14 p2181 A71-29863
- Electrical breakdown of supersonic Ar and air stream behind shock wave, determining threshold discharge currents
14 p2227 A71-30672
- Electrical breakdown in transverse magnetic field and Ar plasma flow in pressure range 0.2-1400 mm Hg and velocity range 0-50,000 cm/sec
15 p2457 A71-32272
- German monograph on electron production effect on channel breakdown in nitrogen, showing positive space charge accumulation near anode in gas discharge
17 p2788 A71-34775
- Equipment survival in natural and nuclear explosion electromagnetic and particle radiation environment
19 p3027 A71-37450
- Hot spots and voltage breakdowns due to open or shadowed solar cells, studying effect in orbital workshop array
20 p3182 A71-38945
- Spacecraft-borne high voltage system breakdown prevention by avoiding high electric field and critical gas pressure
21 p3358 A71-41192
- Insulating materials breakdown by surface discharge, determining corona lifetimes by hemisphere-plane configuration and cylinder-plane electrode
21 p3358 A71-41193
- Pure and doped Ge dumbbell p and n type samples at liquid helium temperatures, investigating electric breakdown
21 p3430 A71-41224
- Electrical breakdown initiation in high vacuum by electron beam, investigating discharge delay time dependence on beam parameters
21 p3420 A71-41292
- Emitter-base junction degradation by avalanche breakdown in planar transistors with low doped /epitaxial/ base region
22 p3520 A71-41682
- Bulk metal electromigration and crack failure in Al thin film conductors, considering purity, glassing and hole nucleation
23 p3651 A71-43426
- Dielectrics breakdown under ultrashort neodymium laser pulses at fundamental and second harmonic frequencies
24 p3834 A71-45120
- ELECTRICAL GROUNDING**
Differential charge amplifier design using ferromagnetic high signal bandwidth isolation with grounded input transducer and output load
09 p1417 A71-22782
- Ground metallic plate effect on electric dipole antenna radiation characteristics as function of aperture field
09 p1420 A71-23572
- ELECTRICAL IMPEDANCE**
NT CONTACT RESISTANCE
NT ELECTRICAL RESISTANCE
NT LC CIRCUITS
NT REACTANCE
NT SKIN RESISTANCE
- Long elevated horizontal line sources mutual impedance coupling, using image theory techniques
01 p0041 A71-11615
- Cylindrical electric dipole antenna in magnetoactive ionospheric plasma, noting ion sheath effect on input impedance and active length
02 p0212 A71-11873
- Wellenweber antennas characteristics, calculating input and mutual impedances, total field radiated and power gain
02 p0232 A71-12343
- Cylindrical post shunt impedance in rectangular waveguide, evaluating approximate theory for free space thin wire conductor
03 p0378 A71-13808
- Admittance first derivative interpretation in flux sounding by electromagnetic field stabilization
04 p0581 A71-15068
- Polynomial current analysis of imperfectly conducting thin cylindrical dipoles with arbitrary internal impedance
04 p0558 A71-15144
- Rectangular waveguide with T junction, deriving characteristic impedance, maximum power and damping constant
05 p0719 A71-15997
- Lightning induced voltages in aircraft wing structures, examining induced voltage across load impedances in electric circuits
06 p0874 A71-17581
- Collinear and planar arrays of arbitrarily located parallel elements, determining current and charge distribution, admittances and field patterns
06 p0875 A71-17715
- Ge diodes double injection experiments, measuring I-V characteristics, AC small signal admittance and noise
06 p0876 A71-18037
- Avalanche diodes Evans circuit /low pass filter located one half wavelength from diode/ analytic theory, developing expressions for efficiency and diode impedance
07 p1074 A71-19121
- Electromagnetic pulse propagation over flat impedance surface, determining similarity parameters
07 p1060 A71-19187
- Series impedance elements in RF immittance measurements
07 p1112 A71-19772
- Input impedance of cylindrical and helical antennas in cold lossy magnetoplasma, discussing sensitivity to current distribution
07 p1065 A71-20323
- Reflex klystron electron beam admittance calculation, comparing results with measurement
08 p1264 A71-21275
- Loop antenna with finite gap at driving point, deriving admittance, current distribution, radiation pattern and directive gain from variational and Fourier series methods
08 p1265 A71-21296
- Intersecting dipoles with sinusoidal current distribution, determining input impedance
08 p1266 A71-21469
- Self and mutual admittance, isolation and radiation pattern of slots on infinite cylinder covered by inhomogeneous lossy plasma
08 p1341 A71-21886
- Laminar geoelectromagnetic field excited by coaxial ring current, determining impedance and magnetic field ratios of spherical harmonics
09 p1435 A71-22434
- Variational formula for input impedance of thin asymmetrical cylindrical dipole antenna
09 p1408 A71-23490
- Asymptotic expression for mutual admittance between axial rectangular slots on large conducting cylinder
09 p1419 A71-23507
- Rudimentary broadband linearly polarized horn antenna design, impedance and radiation characteristics
09 p1419 A71-23509
- Backscatter from nonuniform dielectric coated cylinders in terms of inner surface admittance, using transmission line approach
09 p1410 A71-23515
- Admittance of aperture antenna radiating into lossy warm overdense plasma half space, considering electron energy
09 p1505 A71-23521
- Azimuthal surface waves launching on cylindrical impedance boundary using waveguide open end as excitation aperture
09 p1410 A71-23571
- Transient ion sheath effects on spherical metallic plasma probe complex admittance at different frequencies, comparing numerical results with experiment
11 p1805 A71-25803
- RF discharge quasi-homogeneous plasma device for measuring antenna impedance and sheath effects
13 p2105 A71-27996
- Self- and mutual admittances for axial rectangular slots in inhomogeneous cylindrical plasma layer, giving coupled radial transmission line model for propagation
13 p2105 A71-28002
- Radio waves tropospheric refraction based on far field of vertical electrical dipole on impedance sphere
14 p2191 A71-29510
- Surface impedance of sphere based on received electromagnetic field amplitude-frequency characteristics
14 p2191 A71-29511
- Book on antenna admittance problem covering iterative solution of integral equations, Fourier series solution, Wiener Hopf methods, transmission line theory, etc
14 p2193 A71-29932
- Phase velocity for three dimensional structures of impedance elements, using approximate solution methods and dispersion equation
14 p2194 A71-30080
- Warm plasmas impedances and power transfer near lower hybrid resonance, including electron pressure effects in full electromagnetic treatment
15 p2456 A71-31923
- Electromagnetic wave diffraction by moving wedge with surface impedance, evaluating Doppler shifts and scattered field in shadow region
17 p2698 A71-34429
- Driving point admittances of resistive cylindrical dipole antennas by variational method using two term trial function for current
17 p2701 A71-34762
- Wall impedance method application to long distance transmission elliptical, parabolic and circular waveguides
17 p2707 A71-35480
- Laminar semiconductor and metallic structures electromagnetic impedance dependence on layers thickness, resistances and permittivities
18 p2953 A71-35873
- Impedance variations vs electrophysical properties of epitaxial and diffusive semiconductor structures for electronic equipment, applying microwave fields for parameter control
18 p2954 A71-35874
- Dynamic properties of modulating and mixing nonlinear systems consisting of time dependent impedance controlled by pumping source
18 p2875 A71-35975
- Waveguide mounted X band CW Gunn effect oscillators load impedance characteristics, proposing lumped equivalent circuit
18 p2894 A71-36830
- Impedance determination for symmetrical spherical probes and spacecraft housing with flat screen separation, using partial capacitance formula
19 p3066 A71-38389
- Parasitic wire elements effects on radiation, impedance and current distribution of antennas, using method of moments
19 p3031 A71-38444
- Transistor circuit driven hydrogen-oxygen fuel cell, testing internal impedance effect on power supply noise for comparison with lumped parameter model
19 p3000 A71-38463
- Conversion losses as function of signal power and circuit impedance in narrow band triode frequency converter
19 p3022 A71-38499
- Dipole antenna bandwidth extension by conjugate reactance loading based on periodically loaded transmission line theory
19 p3036 A71-38602
- Long wire electromagnetic scattered field modification by multiple impedance loading, deriving calculation formulas
19 p3024 A71-38607

- Linear antenna in anisotropic plasma, calculating reactance change with surrounding dielectric layer thickness with allowance for ion depletion 20 p3204 A71-39142
- Transistorized high power telemetry amplifier design, describing test equipment for input and collector load impedance 22 p3519 A71-41632
- Four electrodes Hall effect isolator equivalent circuit, describing impedance matrix elements frequency dependence 22 p3520 A71-41705
- Constrained-impedance eigenfunctions, using projection method for field expansion in diffraction problems 22 p3512 A71-42307
- Thin circular frame antenna input admittance computation formulas numerical results comparison, noting insignificant discrepancies 22 p3523 A71-42319
- Lumped model for two dimensional current flow in grown junction transistor base, predicting small signal common emitter short circuit input impedance 22 p3523 A71-42359
- Rectangular waveguide with T shaped pedestal, deriving characteristic impedance, maximum power and damping constant 22 p3515 A71-42746
- Impedance and capacitance frequency dependence of p-n junction diodes at microwave frequencies with high injection levels 23 p3650 A71-43308
- Shunt driven circular loop antenna effective length, current distribution and input admittance, comparing to transmission lines 23 p3655 A71-44169
- Wideband transistorized active dipole antenna for reception at 100-1000 MHz, calculating impedance and effective height by linear theory 24 p3807 A71-44360
- Two sided error estimates for electrodynamic impedance, admittance and scattering matrices in diffraction theory 24 p3805 A71-45256
- Input admittance, drain noise and induced gate noise measurements in search for excess gate noise in large geometry MOSFET 24 p3863 A71-45355
- ELECTRICAL INSULATION**
- High voltage solar cell array operation for satellite in ionosphere, discussing plasma leakage current minimization by electrical insulation 05 p0703 A71-16094
- MHD generator with Ar-K plasma, examining electrical insulation behavior 08 p1237 A71-21930
- Electrical potting compounds reversion problems on Air Force aircraft, discussing inherent properties and environmental effects on polyester urethane and polyacrylate compounds deterioration 10 p1633 A71-24116
- Electrical insulation failure in dielectric fluid layer due to electrocapillary instability, presenting critical potential difference approximate and exact calculation 15 p2376 A71-31932
- Electrical insulation behavior of MHD generator channel having Ar-K plasma, noting temperature dependence of surface conductivity 17 p2789 A71-35274
- Thermionic reactor technology, including insulator seal, nuclear fuel, emitter, tri-layer structure and interelectrode plasma 20 p3265 A71-38949
- Substrate influence on circuit board conformal coatings electrical insulation resistance, discussing test results with epoxy/glass and ceramic substrates and various coating materials 21 p3353 A71-40438
- Spacecraft-borne high voltage system breakdown prevention by avoiding high electric field and critical gas pressure 21 p3358 A71-41192
- Insulating materials breakdown by surface discharge, determining corona lifetimes by hemisphere-plane configuration and cylinder-plane electrode 21 p3358 A71-41193
- Teflon insulated LT type electrical conductors for 203-493 K, including chemical, ozone, UV and fuel resistance tests 22 p3520 A71-41694

ELECTRICAL LEADS**U ELECTRIC CONDUCTORS****ELECTRICAL MEASUREMENT****NT POLAROGRAPHY**

- Breakdown voltage measurement for Cs vapor in cracks in Alumina insulator of pressure bonded sheath tube assemblies 02 p0232 A71-12252
- Ballistic projectile velocity measurement using condenser charged thin wire circuit 03 p0422 A71-13273
- Langmuir probe DC detector for rocket quasi-static and AC electric field measurements in auroral zone ionosphere 03 p0406 A71-13302

- GaAs injection lasers phenomenological theory and internal parameters physical meanings, giving maximum optical gain dependence on current density 03 p0434 A71-13349
- Gap in atrioventricular conduction in humans by catheter technique for recording electrical activity of His bundle 03 p0363 A71-13488
- High impedance source with shunt capacitance, discussing periodic output measurement using operational amplifier 03 p0427 A71-13923
- Current/voltage converter for measurements at floating potential with respect to ground, using Wheatstone bridge type circuit 04 p0560 A71-15894
- Solar cells lumped series resistance determination, comparing dark forward characteristics method and two light level approach 05 p0000 A71-16068
- Double probe technique for electric field measurements in magnetoplasma 06 p0936 A71-17703
- Automatic test equipment for sorting large quantity resistors based on nonlinearity measurement 07 p1076 A71-19554
- Thin oxide films on solution grown single crystals of cubic beta-silicon carbide, discussing physical and electronic properties measurements 07 p1177 A71-19571
- Hydrogen solubility in alpha Ti, using electrical resistivity measurement at liquid nitrogen temperature 07 p1139 A71-19991
- Free-space focused microwave system for determining materials complex permittivity to temperatures over 2000 C 07 p1115 A71-20357
- N and p junction field effect transistor (JFET) gate current measurement leading to understanding of impact ionization mechanism and field distribution 07 p1081 A71-20542
- Electrochemical detection of hydrogen, carbon monoxide and hydrocarbons in inert or oxygen atmospheres, using electrical biasing technique 08 p1250 A71-21473
- Capacitance voltage measurements on interface of pyrolytically deposited n-type silicon dioxide-InAs MOS diodes as function of admittance at room and 77 K temperatures 10 p1582 A71-23774
- MHD Hg flow between concentric cylinders with nonconductive walls, comparing pressure loss and voltage measurements with theoretical predictions for large Hartmann numbers 10 p1647 A71-23862
- AC power meters using electronic multiplier for overcoming limitations concerning frequency ranges, response times, power factor and distortion 10 p1609 A71-23918
- Microwave resonator Q factor and coupling and matching characteristics measurement using line probe with AM and FM signals 10 p1584 A71-24724
- Hydrazine feed control in hydrazine-oxygen fuel cells, discussing continuous measurement of limiting diffusion current for determining fuel concentration in electrolyte 11 p1708 A71-25241
- Zero point fluctuations measurement standards for thermal and quantum noise, considering microwave network analytic application 11 p1733 A71-26366
- Left ventricular enlargements, comparing vectorcardiographic spatial magnitude and electrocardiographic precordial QRS voltage measurements 11 p1725 A71-26428
- Microwave dielectrometer measurement system sensitivity to electric field energy in dielectric non-magnetic specimen 12 p1889 A71-27621
- ECG measuring locations number and positions for determination of time varying total body QRS surface potential distribution 13 p2016 A71-28149
- Nondestructive testing, discussing visual, liquid penetrant, thermal, X and gamma rays, ultrasonics, magnetic, electrical and eddy currents methods 13 p2073 A71-28218
- Hall effect measurements and electron microscope examination of Te-doped gallium arsenide crystals annealed at various temperatures 13 p2111 A71-28503
- Monograph on oscillographic high accuracy technique for phase angle measurement covering applications for harmonic generator phase control 14 p2243 A71-30237
- Apparatus for measuring polar liquids dielectric permittivity and losses at microwave frequencies over wide temperature and pressure ranges 14 p2222 A71-30583
- Radio signals fine structure examination by instantaneous pulsed voltage measurements, describing fast response digital voltmeter circuit with memory element 15 p2409 A71-32188

- IR transducer with detector for space applications, measuring capacitance on electronic bridge circuit based on temperature and pressure effects [ONERA-TP-963] 16 p2576 A71-32845
- Atmospheric potential gradient measurements during solar eclipse of 7 March 1970, using airborne and ground observations 17 p2731 A71-34321
- Inductive voltage divider bridge network for ferrite coils inductance and Q measurements 17 p2723 A71-35713
- Rogowski belts application to pulsed discharges current measurements, describing measuring circuits and calibration 18 p2924 A71-36758
- Metals and alloys thermal conductivity prediction using Lorentz ratio and electrical resistivity measurements 18 p2938 A71-36991
- Plasma wave instrument for measuring AC electrical and magnetic field levels in outer planets missions [AAS PAPER 71-125] 19 p3064 A71-37939
- German monograph on experimental determination of noble gas plasma conductivity under normal pressure in high temperature range, covering measurements under electric arc conditions 23 p3711 A71-43475
- Pulse code modulation systems measurement techniques, deriving diagrams with preset limit patterns incorporated 23 p3652 A71-43925
- NaI-glycerol solution resistivity values, determining measurement frequency, temperature, outgas procedures, purity and doping level effects 24 p3802 A71-44614
- MOS transistors operating in unsaturated region, discussing source and drain series resistance measurement techniques 24 p3808 A71-44656

ELECTRICAL PROPERTIES

- NT CAPACITANCE
- NT CARRIER MOBILITY
- NT CHARGE DISTRIBUTION
- NT CONTACT RESISTANCE
- NT DIELECTRIC PROPERTIES
- NT ELECTRIC MOMENTS
- NT ELECTRICAL IMPEDANCE
- NT ELECTRICAL RESISTANCE
- NT ELECTRICAL RESISTIVITY
- NT ELECTRON MOBILITY
- NT ELECTROSTRICTION
- NT FERROELECTRICITY
- NT HOLE MOBILITY
- NT INDUCTANCE
- NT IONOSPHERIC CONDUCTIVITY
- NT LC CIRCUITS
- NT MAGNETORESISTIVITY
- NT PERMITTIVITY
- NT PHOTOCONDUCTIVITY
- NT PHOTOVOLTAIC EFFECT
- NT PIEZOELECTRICITY
- NT PLASMA CONDUCTIVITY
- NT POLARIZATION CHARACTERISTICS
- NT PYROELECTRICITY
- NT REACTANCE
- NT SKIN RESISTANCE
- NT SUPERCONDUCTIVITY
- Nondestructive high reliability rapid comparison and identification of metals by electrical interpretation method for product variation control and laboratory unknowns determination 01 p0085 A71-10258
- Synthetic plastic materials mechanical and electrical properties for electronics industry use, emphasizing injection molded polymers, pressed molding compounds and casting resins 01 p0051 A71-10285
- Molybdenum borocarbide synthesis and properties, discussing melting temperature, electrical and heat conductivity, thermal emf, microhardness, etc 01 p0100 A71-10402
- Porous Ti thermal and electrical properties from room to high temperatures 01 p0102 A71-10785
- Book on radome engineering covering electromagnetic and thermal-mechanical design, organic and inorganic radomes, electrical evaluation and rain erosion 01 p0055 A71-11191
- Electrical stability of double sphere dipole antennas for FR-1 satellite ionospheric plasma electric fields measurements 02 p0229 A71-11714
- FET insulating layer electrical properties requirements, considering threshold voltage, dielectric constant, breakdown voltage and insulated gate FET instabilities 02 p0229 A71-11813
- Life, efficiency and electrical stability tests of cylindrical thermionic converters with various emitter and collector materials 02 p0193 A71-12216
- Surface thermal and electrical stresses effect on bipolar transistors electrical properties, using NDT criteria for components selection 02 p0236 A71-12921

- Electric properties of solid modified AgI electrolyte batteries
03 p0351 A71-13032
- Si diffusion p-n junctions at high injection levels in strong electric fields, discussing I-V characteristics, minority carrier lifetime, barrier capacitance, etc
03 p0384 A71-13374
- Single crystal indium gallium phosphide solid solution synthesis, discussing crystallophysical and electrophysical properties
03 p0467 A71-13424
- Physical, chemical and electrical properties of silicon nitride thin films deposited pyrolytically on Si substrates, analyzing deposition process effects
03 p0468 A71-14001
- Automatic electric network topological and electrical characteristic analysis, using mixed method for computational accuracy and speed
04 p0560 A71-14746
- Barium titanate single crystals domain structure and electrical properties at room temperature under uniaxial tensile stresses, measuring dielectric hysteresis loops
04 p0637 A71-15104
- Air/Ar with ionizable lithium oxide plasma stream electric properties determination by shock tube wall electrode pair, using ambipolar diffusion theory
04 p0634 A71-15113
- N-P Si solar cells controlled lifetime doping effects on electrical performance
05 p0700 A71-16063
- Ti-Ag contact N-P and P-N single crystal Si solar cells electrical and mechanical performance characteristics
05 p0700 A71-16069
- Magnetoplasma electric and magnetic resonances by Voigt configuration, noting similarity to single particle scattering and particle size dependence
05 p0787 A71-16497
- Photoelectrical and thermoelectrical properties of CdS, CdS-CdSe and CdSe single crystals epitaxial films
05 p0793 A71-16823
- Electrical, photoelectrical and optical properties of crystalline cadmium telluride-indium telluride alloys, discussing temperature dependence, spectral characteristics and photoconductivity
05 p0793 A71-16824
- Single chamber plasmatron with rising arc I-V characteristics, obtaining electrical and thermal properties in dimensionless form
05 p0790 A71-16844
- Plasma feedback system boundary conditions, describing electrical properties, dispersion relation and mode interaction
06 p0931 A71-17455
- Pulkovo radio telescope antenna surface precision and electrical characteristics at eight mm, using ground oscillators and solar, lunar and Venusian observations for radiation pattern
07 p1075 A71-19342
- Amorphous semiconductors theories and models, considering structural, optical and electrical characteristics
07 p1178 A71-19847
- Josephson superconducting devices electrical characteristics
07 p1079 A71-20153
- Mo-Re alloys thermal and electrical properties from X ray analysis of two phase structure
07 p1141 A71-20246
- Amorphous semiconducting thin films quenching fabrication techniques and electrical properties
07 p1181 A71-20410
- High temperature nitrogen plasma, calculating thermodynamic and electrical parameters dependence on pressure and temperature
08 p1342 A71-21917
- AIN insulating films electrical characteristics for use in charge storage devices, presenting Al-AIN-Au capacitor current-voltage-insulator thickness relationships
09 p1509 A71-23118
- Electrochemical properties of Na-W bronzes for use as electrocatalysts in acid electrolyte fuel cells
09 p1387 A71-23648
- Gamma radiation effect on electrical properties of n-type GaAs single crystals with doping impurities, calculating defect introduction rate and forbidden zone energy levels
10 p1656 A71-24141
- Fiber reinforced plastics/epoxy resins/ electrical effects association with deformation and failure
10 p1635 A71-25013
- Electrical properties, chemical resistance and reinforced plastics applications of telechelic ultrahigh vinyl polybutadiene resins
11 p1786 A71-25422
- Quantitative analysis of secondary harmonic generation in DC polarized isotropic laser beam, emphasizing molecular mechanisms and symmetrical effects
11 p1773 A71-25566
- Incore thermionic cell power output limitation and thermal/electrical data determination at steady state operation, considering temperature distribution
11 p1713 A71-25894
- Unijunction transistors operation principles, electrical parameters, structural features and circuit applications
11 p1740 A71-26548
- Thermal oxidation and metal evaporation effects on electrical properties of silicon-silicon dioxide wafer interface in MOS structures
12 p1944 A71-27096
- I-V characteristics and electrical properties of n-p silicon solar cells at low temperature and low illumination intensities
12 p1869 A71-27434
- Electrical conductivity, thermal emf, expansion and Hall coefficient of hot compressed powdered diborides of group IV and V transition metals
13 p2084 A71-28036
- Electrical and physical nature of microbial membranes implicated in aircraft fuel quantity probe malfunction
13 p2113 A71-28321
- [SAE PAPER 710439] Electrode size effects on voltage loss and boundary layer conductivity of combustion driven MHD generator
14 p2287 A71-29880
- GaAs single crystals real surface electrical characteristics, using pulsed field effect techniques
14 p2284 A71-30403
- Optical, mechanical, thermal and electrical properties of IR sensor materials at low operating temperatures
14 p2284 A71-30545
- Heat balance and 8.22 mm radio emission of Mars, evaluating surface thermal and electrical parameters including brightness temperature
15 p2490 A71-32411
- Neutron and gamma radiation effects on electrophysical properties of high resistivity Si single crystals grown in hydrogen atmosphere
16 p2621 A71-33186
- GaAs epitaxial layer growth process parameters relationship to electrical properties
16 p2621 A71-33563
- Crystal defects and electrical and optical properties changes due to electron bombardment of semiconductors
16 p2622 A71-33622
- Electrical performance of Cassegrain antenna reflector for space communication via ATS and deep space research
17 p2700 A71-34747
- General media electrical properties from current and charge distributions and impedance characteristics of electrically thin cylindrical antennas
17 p2715 A71-34759
- High temperature nitrogen plasma, calculating thermodynamic and electrical parameters dependence on pressure and temperature
17 p2789 A71-35262
- MIS structure voltage-farad characteristics, determining surface state densities for silicon compound dielectric films
18 p2954 A71-35875
- Hybrid circuits thick film technology, discussing printed circuits fabrication processes and electrical and mechanical properties
18 p2888 A71-36224
- Photolithographic fabrication and electrical characteristics of GaAs Schottky barrier diodes for pulse operation
19 p3027 A71-37259
- Heavily Ge doped p-InSb photoelectric and electric properties, showing impurity concentration effects
19 p3120 A71-38526
- Soviet book on cloud electricity covering space charge and electrical characteristics
19 p3091 A71-38533
- Rainfall, aerosols and cloud water samples analyzed for chlorides and sulfates content and electrical properties
19 p3092 A71-38687
- Al electrolytic capacitors characteristics as function of temperature, time and frequency of operation, noting improvement by organic solvents use as electrolyte component
20 p3203 A71-38884
- Ni-Cd battery cell with third electrode for charge control, testing thermal and electrical performance as function of charge and discharge rate
20 p3179 A71-38905
- Thermal protection and electrophysical and mechanical evaluation of SNAP 19 radioisotope thermoelectric generator for integration with Viking Mars lander
20 p3267 A71-38964
- Structural support system for large long-periodic antenna, discussing asbestos-cement pressure pipes and fiberglass rods as construction materials for antenna critical electrical characteristic needs
20 p3210 A71-39871
- Polarized plane electromagnetic waves oblique specular reflection from discretely layered lunar models based on Apollo 11 and 12 data, determining near-surface layers electrical properties
21 p3450 A71-40644
- Junction structures and electrical properties of silicon n-p-n transistors fabricated by various combinations of diffusion and ion implantation
21 p3354 A71-40728
- Metals and systems for semiconductor devices metallization, evaluating conductivity, adhesion, contact resistance, deposition ease, electrochemical corrosion, reliability and stability
21 p3356 A71-40802
- Electrical, photoelectric and electroluminescent properties of reverse biased GaP n-p structures at room temperature, considering isolated microplasmas
21 p3430 A71-41217
- Monte Carlo method computer simulation for displacement cascades energy and space structure in Ge, Si and PbS, interpreting semiconductor electrical properties under hard radiation
21 p3432 A71-41304
- Electrical properties and electroluminescent measurements for p-n junctions in Au- and Ag-doped GaP, noting negative resistance in I-V characteristics
21 p3433 A71-41312
- Oxygen effects on SiC electrical properties by comparison of photoluminescence spectra of alpha-SiC crystals grown by sublimation in Ar atmosphere
21 p3436 A71-41348
- Intense ionizing radiation and thermal treatment effects on electrical parameters of Si semiconductor devices
22 p3584 A71-41619
- Gold doping effect on minority carrier lifetime and other electrical properties of epilayer Si transistors
22 p3520 A71-41702
- Mica selection quality criteria for capacitors, outlining electrical, physical and optical properties standards
22 p3520 A71-41712
- Photoconductive CdS disintegration effect on heterophase electrophotographic layer electric and photoelectric properties, noting optimal properties relationship to grain diameter
22 p3586 A71-42406
- Evaporated tellurium thin films electric properties, discussing fabrication techniques, temperature dependence, field effect and Hall mobilities, threshold voltage and stability
23 p3715 A71-43435
- Quasi-optical waveguide system for measuring electrical properties of dielectric and magnetic materials in submillimeter band
23 p3677 A71-43530
- Waveguide system for measuring semiconductors electrical and photoelectric properties at SHF, observing temperature effects
23 p3652 A71-43531
- Grain size distribution and optical and RF electrical properties of Apollo 12 lunar fines and core samples
23 p3759 A71-43769
- Solar to electric energy conversion efficiency and electrical properties of photoconverters using compressed sintered CdS
24 p3808 A71-44390
- CNES hypotheses and methods determining current delivered by solar generator of FR 1 satellite, discussing electrical performance due to electron and proton irradiation
24 p3793 A71-44760
- Germanium extrinsic photoconductive IR detectors with Au, Hg and Cu doping, discussing preparation and electrical and optical characteristics
24 p3860 A71-45070
- Doping profile effects on performance properties of hypersensitive capacity variation junction diodes, describing basic interrelation between capacity and potential
24 p3812 A71-45351
- ELECTRICAL RESISTANCE**
NT CONTACT RESISTANCE
NT LC CIRCUITS
NT SKIN RESISTANCE
- Space charge hypersurface layer conductance in semiconductors, allowing for three dimensional surface impurity fields
03 p0467 A71-13976
- Field effect transistors internal source and drain resistances measurement, using characteristic tracer
04 p0558 A71-15084
- Solar cells lumped series resistance determination, comparing dark forward characteristics method and two light level approach
05 p0000 A71-16068
- Differential drain resistance calculation for junction field effect transistors
07 p1070 A71-18869
- Finite wall conductance effect on performance/pressure and load capacity/ of MHD hydrostatic thrust bearings
07 p1117 A71-19503
- [ASME PAPER 70-LUB-1] Transistorized ultrasonic oscillator active conductances and other circuit parameters effects on self oscillation frequency stability
07 p1078 A71-20060

ELECTRICAL RESISTIVITY

Transition metals hydrides electrical resistance calculation based on theory of hydrogen electrodiffusion /occlusion/ into incomplete d-states

09 p1473 A71-23232

Traveling wave antenna arrays of mismatched elements, calculating element resistances and spacings

09 p1408 A71-23488

Input resistance of electric dipole above metallic disk lying on homogeneous conducting half space at HF, using compensation theorem

09 p1495 A71-23573

Negative differential conductance of homogeneous nonequilibrium electronic solid-body plasma in electromagnetic field upon Cherenkov interaction

11 p1807 A71-25584

Resistance increases in thin film Evanohm resistors due to hydrogen gas absorption and desorption

11 p1738 A71-26162

Anomalous resistance and turbulent heating of strongly nonisothermal plasma in strong magnetic field due to electron scattering by ion-acoustic turbulent pulsations beats

12 p1936 A71-27032

MOS transistor saturation range transconductance, internal resistance and gain factor calculation, allowing for field effect on space charge near drain

12 p1889 A71-27626

Potentiometric measurement of temperature effects on electrical resistance and Hall effect in Ni-Co alloys

14 p2259 A71-30188

NiGa intermetallic compound electrical transport and resistance, Hall coefficient and optical adsorption, discussing defect structure and electron scattering

14 p2260 A71-30478

Current constriction-resistance variations relations in transistors, discussing current redistribution

14 p2213 A71-30629

Transistor resistances difference measurement under reversed polarities during quality control testing

14 p2214 A71-30635

Metal and alloys condensates corrosion tests based on recording changes in electrical resistance

15 p2427 A71-31651

Nonlinear dependence of resistance in metals on impurity concentration and temperature due to unklapp electron phonon interaction and anisotropy of phonon spectrum

16 p2593 A71-33654

Low noise microwave transistor, describing geometry and diffusions optimization, power gain, reliability and base resistance

18 p2892 A71-36564

Temperature dependence of electrical resistance in mixed superconducting-normal systems, solving transport equation

18 p2954 A71-36746

Thermistor bolometer characteristics, considering resistance-performance relationship, radiation and Wheatstone bridge potentials

20 p3233 A71-38969

Thermodynamic measurement of cryogenic temperatures based on gases at low pressures or platinum electrical resistance

20 p3270 A71-39243

Superconductivity, reviewing critical current/field concepts, Meissner effect, negative surface tension, zero resistance and applications

20 p3276 A71-39247

Three-pole theory of amplifiers, deriving operational resistances as function of wave resistance and control parameters by current-voltage matrices

20 p3205 A71-39467

Refractory diborides in oxidizing environments, considering mechanical strength, thermal stability, oxidation resistance, heat conductivity, thermal expansion, specific heat and electrical resistance

21 p3405 A71-40138

Distributed gate multielectrode MOS transistor, presenting negative resistance operation mode

22 p3520 A71-41685

Mean value theorem for broadband matching of source with known resistance and parasitic capacitance matched to load resistance

22 p3510 A71-42247

Macromolecular binding agent effect on electrophotographic properties of high resistance layers containing photoconductive CdS

22 p3586 A71-42405

Early effect incorporation in Ebers-Moll simulation model for junction transistor large signal behavior to obtain current gain and conductance dependence on voltage

22 p3523 A71-42484

Electromechanical converters mathematical model, calculating conductivity behavior and derivative

22 p3484 A71-42877

Silicon resistance strain gages sensitivity as function of variable signed load cycles

22 p3550 A71-42880

Structure, hardness, density and electrical resistance of binary alloys V-Ti, V-Cr, V-Al and V-Sn

23 p3691 A71-43283

Cylindrical antennas with arbitrary distributed resistive and reactive loading, presenting method based

on dipole antennas with constant resistance loading per unit length

24 p3803 A71-44646

MOS transistors operating in unsaturated region, discussing source and drain series resistance measurement techniques

24 p3808 A71-44656

Polycrystalline Ni preloading rate effects on dislocation structure, electrical resistance and flow stress, noting strain hardening mechanism

24 p3837 A71-44675

Current harmonics in passively nonlinear resistance subject to simultaneous DC and AC fields

24 p3860 A71-44872

ELECTRICAL RESISTIVITY

NT IONOSPHERIC CONDUCTIVITY

NT MAGNETORESISTIVITY

NT PHOTOCONDUCTIVITY

NT PLASMA CONDUCTIVITY

NT SUPERCONDUCTIVITY

Electrical resistivity and structure of thin films of W, Mo and Cr evaporated in vacuum by neodymium laser

01 p0101 A71-10674

Hall constant and resistivity of impurity centers in seminsulating n-type GaAs during illumination and heating

01 p0138 A71-10776

Electric conductivity dependence on optical depth in photospheres of spectral type F, G and K stars for different gravitational acceleration values on surface

01 p0159 A71-10866

Sunspot and photosphere electric conductivity relationships based on Michard, Mattig and Fricke-El-sasser models

01 p0159 A71-10867

In-Bi alloys electrical conductivity measurement for compositions covering characteristic points of phase diagram at temperatures from liquidus line to 850 K

02 p0294 A71-11895

Apollo 11 lunar samples dielectric constants, losses and electrical conductivities as function of temperature and frequency, comparing with terrestrial and simulated lunar rocks

02 p0305 A71-11985

LF EM wave absorption in disordered semiconductors, calculating frequency dependence of conductivity due to electron transitions between discrete local levels

02 p0297 A71-12618

Varying electrical resistivity incompressible fluid flow with Hall effect in presence of thin airfoil

03 p0343 A71-13903

Hole effect on residual resistivity of crystalline binary ordered substitution alloy with bcc lattice

03 p0467 A71-13952

MHD conducting lubricant composite slider bearing in transverse magnetic field, calculating conductivity effect on load capacity

04 p0602 A71-14801

Al-Zn-Mg alloys hardness and conductivity behavior as function of aging time and temperature

04 p0610 A71-14884

Air/Ar with ionizable lithium oxide plasma stream electric properties determination by shock tube wall electrode pair, using ambipolar diffusion theory

04 p0634 A71-15113

Rare earth alloys spin disorder resistivity in crystalline electric field absence and presence

04 p0637 A71-15797

CdS thin film grain boundaries and stacking faults effects on electrical resistivity

05 p0791 A71-16055

Partially ionized Hg plasma electrical conductivity at various pressures and temperatures

05 p0790 A71-16787

CdS single crystals treatment in salt melts to obtain given conductivity and photosensitivity, discussing LiCl, Ag, Cu, Na, Cd and In concentration effects

05 p0793 A71-16822

Low electrical conductivity semiconductor melts thermal conductivity, discussing energy quasi-gap existence

05 p0794 A71-16881

Earth and planetary surface soil dielectric constants and conductivity determination based on p-wave velocity data correlation

05 p0743 A71-17142

Porphyrins optical and semiconductor properties concerning absorption, electrical conductivity and photoconductivity spectra

06 p0941 A71-17526

Microwave measurements of semiconductors and semiconductor films including resistivity, permittivity and carrier mobility

06 p0873 A71-17538

Low energy magnetoacoustic wave with finite conductivity, determining gas parameters near singular points

06 p0936 A71-17652

Nonstoichiometric VC, studying thermal and electrical conductivities, thermoelectric properties and Hall coefficient

06 p0912 A71-18085

Vanadium and niobium carbohydrides as function of C content, studying lattice constants, microhardness and electrical resistivity

06 p0912 A71-18086

Polycrystalline semiconductors grain boundaries effect on conductivity, Hall mobility and current carriers concentration

06 p0942 A71-18187

Electromagnetic induction in plate with two dimensional conductivity distribution for case of E polarization, representing field by Green functions

06 p0928 A71-18264

Thin film cermet resistive elements physical controls electrical properties, physical controls, thermal and radiation stability

07 p1071 A71-19075

Conductivity of films with surface roughness dimensions large in proportion to screening radius and carrier free path length, presenting refined analysis

07 p1175 A71-19223

SHF electric fields effects on free carrier redistribution in semiconductors and surface effect influence on sample conductivity

07 p1177 A71-19496

Electrical conductivity measurement for thorium oxide at 1000-1600 K and at low oxygen partial pressures, discussing Seebeck coefficient behavior

07 p1177 A71-19569

Polarization of thunderstorm IF electromagnetic noise, taking into account earth electrical conductivity under detector

07 p1063 A71-19758

Hydrogen solubility in alpha Ti, using electrical resistivity measurement at liquid nitrogen temperature

07 p1139 A71-19991

MHD Couette flow at stationary plate under transverse magnetic field, discussing effect on heat transfer between electrically conducting walls

07 p1170 A71-20099

Fast neutron irradiation effects on Mo recovery stages 1 to 3 in bcc metals using electrical resistivity measurements

07 p1143 A71-20491

Thermal recovery effects on electrical resistivity in deformed polycrystalline Nb samples tested at varying strain rates and 263-509 R temperatures

07 p1144 A71-20496

High purity Ge crystals growth, studying Hall effect and resistivity for semiconductor detector fabrication

08 p1345 A71-21844

Electrical conductivity of strontium zirconate and hafnate at 1400-2600 K measured by two-probe method with alternating and direct currents, calculating activation energy

08 p1323 A71-21934

Semiconductor thermoelectric materials intercrystalline boundaries porosity effects on electrical and thermal conductivity

09 p1506 A71-22162

Anomalous electrical resistivity during decomposition of supersaturated solid solution of Fe-Co-Mo alloy

09 p1468 A71-22359

NBS traceable nonferrous conductivity standards for eddy current testing, discussing error analysis, long term drift, grain direction and stratification effects

09 p1469 A71-22710

Measuring instrument for amorphous and polycrystalline materials resistivity and Seebeck coefficient as function of temperature and pressure

09 p1446 A71-22737

Phase diagram of Ti-Ta-Mo alloy system, obtaining solubility and electrical conductivity for various cross sections

09 p1480 A71-23706

Pyrolytic graphite microcalorimeter for X ray absorbed dose measurement, exploiting for calibration self heating

10 p1608 A71-23742

Electron collision frequency energy dependence influence on electrical conductivity of weakly ionized plasmas, considering Taylor series expansion around probable plasma electron velocity

10 p1623 A71-23875

Thermal conductivity, electrical resistivity and specific heat of hot pressed beryllium

10 p1624 A71-23908

Ti thermal conductivity, electrical resistivity and total emittance at high temperatures in ultrahigh vacuum, discussing phase transformation effect

10 p1624 A71-23910

Mo high temperature melting point and electrical resistivity measurement by pulse heating method

10 p1624 A71-23912

Electrical resistive incompressible fluid motion past thin airfoils in oblique field, showing inverse dependence of lift on magnetic Reynolds number

10 p1648 A71-23956

Arc melted ingot high field superconductor, combining critical density and resistive critical field

10 p1655 A71-24042

Wall conductivity effects in MHD rectangular duct flow at high Hartmann numbers with uniform magnetic field applied parallel to one pair of duct sides
10 p1649 A71-24419

Waves generated by obstacle steady motion along axis of uniformly rotating electrically conducting homogeneous fluid, using Lighthill technique
10 p1593 A71-24624

Electrical and thermal conductivity coefficients and energy diffusion coefficient in lower ionosphere, assuming weak ionization of ionospheric plasma
10 p1607 A71-24998

Carbon fiber-epoxy resin composites Young modulus, thermal and electrical conductivities as function of fiber alignment and porosity
11 p1784 A71-25399

Electrical conduction in cholesteryl acetate, propionate and stearate in solid, liquid crystal and isotropic liquid states characterized by I-V measurements
11 p1807 A71-25564

Lunar electrical conductivity profile measurements, providing mantle-core stratification near surface thermal gradient, heat flux and composition data
11 p1822 A71-25632

Interplanetary magnetic field measurements from lunar surface and lunar orbit, discussing solar wind effects on bulk electrical conductivity of lunar crust
12 p1947 A71-26691

Gamma irradiation effect on conductivity of varistors made of p-type black SiC
12 p1886 A71-26897

Correction factors for small values of logarithm of Debye length ratio to mean impact parameter in electrical conductivity of fully ionized plasma
12 p1936 A71-26950

Hypersonic wakes conductivity measurements behind models in argon and air, using electrodynamic technique
12 p1863 A71-27208

Amorphous semiconductors, including electrical conductivity, temperature dependence, germanium/silicon structural model and mobility energy
12 p1944 A71-27244

Nb-N and Ta-N alloys, calculating electrical resistivity and solid solutions lattice constants at various temperatures
12 p1917 A71-27295

Anomalous resistivity due to weak electrostatic turbulence in plasma, discussing applications to perpendicular collisionless shock experiments
12 p1940 A71-27418

Thin solid films on ball bearing surfaces, measuring electrical conductivity
13 p2072 A71-27817

Dissimilar metals welding, emphasizing melting point, linear expansion coefficient, thermal conductivity, electrical resistivity and polymorphic transformation
13 p2072 A71-27887

Fast neutron irradiation effect on Ni-Cr alloy electrical resistivity as function of temperature and initial composition
13 p2083 A71-27964

Steady state scattering of cylindrical magnetoacoustic waves traveling along axis of rigid ideally conducting static cylinder
13 p2105 A71-28281

Dielectric properties of barium titanate with Nb, noting metal oxide additives effects on conductivity
13 p2092 A71-28661

Vertical distribution of small ion density and of electric polar conductivity and ion temperature profiles in atmosphere at 1.5-19 km from balloon measurements
13 p2065 A71-29425

High moisture content rock samples electrical conductivity and permittivity by VLF electrospectroscopic investigations based on signal phase shift
14 p2238 A71-29514

Electron and ion concentrations, electron temperature and electrical conductivity of ionized air before shock wave, using shock tube with He driver gas
14 p2225 A71-30225

Theorem proving impossibility of stabilizing unstable MHD configuration with nondissipative plasma in vacuum surrounded by superconducting wall by means of finite electrical conductivity wall
14 p2282 A71-30557

Epitaxial film thickness and resistivity effect on transistor cut-off frequency, discussing collector junction space charge region boundary location
14 p2213 A71-30626

Channel width effect on FET transconductance in low current operation
14 p2214 A71-30634

Electrical conductivity measurement of Apollo 11 and 12 lunar surface rocks, using two-probe technique in vacuum furnace
14 p2315 A71-30864

Transition metals addition effects on cast Zr grain size, microhardness and electrical resistivity, explaining results in terms of solid state electron theory
15 p2424 A71-31239

Molybdenum doped zirconium monocarbide, investigating Hall coefficient, thermal emf and resistivity measurements
15 p2460 A71-31284

Surface conductivity and current carrier mobility vs surface potential in CdSe single crystal films deposited on mica base by vacuum vaporization
15 p2461 A71-31511

Resonant charge transfer cross sections in inert rarefied gases from atomic screening parameters, considering positive charge conductivity of ionized dense gases
15 p2452 A71-31825

Ni-Co alloys electrical resistivity dependence on temperature after mechanical and thermal treatments
15 p2429 A71-31994

Strength, plastic properties, electrical conductivity and fine structure associated with decomposition kinetics of Al alloy supersaturated solid solution
15 p2435 A71-32333

Epitaxial Ag thin film with controlled surface roughness on mica, measuring electrical resistivity as function of temperature, thickness and surface specularly in vacuum
15 p2461 A71-32376

Partially ionized Hg plasma electrical conductivity at various pressures and temperatures
16 p2618 A71-33039

Plasma flow wave propagation, investigating compressibility, radiation and finite electrical conductivity effects with plane asymptotic solution combinations
16 p2618 A71-33173

Electrical conductivity of lunar rock, considering radial variation of bulk composition with oxygen loss in outer layers due to thermal cycles and vacuum
16 p2634 A71-33388

Anomalous electrical resistivity variation during decomposition of supersaturated solid solution of Fe-Co-Mo alloy
16 p2593 A71-33632

Molybdenum single crystals isotropic thermal conductivity, electrical resistivity and total hemispheric degree of blackness at high temperatures
16 p2595 A71-33882

Microwave reflection factor analytical and graphical dependences on resistivity of variable thickness semiconductor layers
16 p2544 A71-34032

Electrical conductivities of Apollo 11 and 12 lunar rocks and chondritic meteorites at 300-1100 K
17 p2796 A71-34182

Curve power factors and radiation induced changes in silicon photovoltaic solar cells, considering junction depth, bulk resistivity, temperature and illuminating light intensity
17 p2677 A71-35049

Hall coefficient and electrical resistivity increase during aging of Al-Zn alloys, suggesting free electron energy reduction due to solute atoms clustering
17 p2759 A71-35227

Metals and alloys thermal conductivity prediction using Lorentz ratio and electrical resistivity measurements
18 p2938 A71-36991

Characterization of high purity metals by residual resistivity ratio, using nondestructive eddy current decay method
18 p2938 A71-36992

MHD generator duct external loop electric current maximization by working material resistivity tensor optimal distribution
19 p3108 A71-37102

High purity metals residual electrical resistivity, observing impurities, vacancies, dislocations, plastic strain and polyisotropy effects
19 p3076 A71-37115

High temperature gas dispersed Al particle flow, investigating electrical conductivity and radiation properties
19 p3161 A71-37265

Structure, superconductivity transition temperature, microhardness and electrical resistivity of V-Ta-Ti cast alloys
19 p3078 A71-37468

Specific contact resistance at zero bias as measure of ohmic or rectifying behavior of metal-semiconductor barrier under operating conditions
19 p3117 A71-37485

Hypersonic wakes conductivity measurements behind models in argon and air, using electrodynamic technique
19 p2994 A71-38620

Hall coefficient and resistivity in undoped heteroepitaxial GaAs on aluminum oxide films grown by trimethylgallium arsine process
20 p3276 A71-38881

Heat treated thallium bismuth sulfide, selenide and telluride amorphous and polycrystalline thin films electrical conductivity, differential thermal emf and forbidden bandwidth
20 p3276 A71-39076

Lunar interior electrical conductivity and temperature three-layer model from magnetic transient response measurement in solar wind
20 p3301 A71-39877

Electrical resistivity of structural metal crystal defects in terms of Ziman-Harrison pseudopotential theory
21 p3395 A71-40023

Electron elastic scattering in thin films by impurities, noting conductivity dependence on film thickness
21 p3428 A71-41126

Deep level impurity compensation of high resistivity epitaxial films of GaAs by chromium, complex lattice defects and copper acceptors, using cathodoluminescence spectra
21 p3430 A71-41220

Semiconductor radiation-induced electrical conductivity changes correlation to forbidden band from theoretical model, considering radiation defects as conductivity compensators
21 p3431 A71-41230

High resistivity Fe-doped GaAs, investigating carrier lifetime dependence on Fe atoms concentration
21 p3431 A71-41234

Electron gas in constant crossed E and H fields, deriving nonlinear conductivity theory
21 p3424 A71-41260

Electrical conductivity and thermoelectric power measurements for polycrystalline beta-SiC heavily doped with nitrogen, estimating electron effective mass and carrier mobility at high temperatures
21 p3433 A71-41307

Optical investigation of metal-semiconductor interface blocking layer and photo-Hall effect in high resistivity crystals
21 p3433 A71-41316

Thin bismuth films thermal and electrical conductivities and thermoelectric power measurements, examining preparation methods
21 p3435 A71-41338

GeTe alloyed with Zn, Cd or Hg, measuring electrical conductivity and thermoelectric power temperature dependence
21 p3435 A71-41345

Electron scattering magnetic impurities effect in insulator layer of tunnel junction on superconductor current
22 p3585 A71-41818

Low temperature aging behavior of maraging stainless steels from electrical resistivity measurements
22 p3562 A71-41948

Multivalley semiconductors scale effect due to nonuniform electron heating by electric field, determining effective conductivity as function of plate thickness and surface characteristics
22 p3585 A71-42058

Electrical resistivity and thermoelectric power sensitivity for simple liquid metals near melting temperature, determining temperature effects from pseudopotential models
22 p3586 A71-42370

Irradiation dose effect on alpha particle irradiated Al foil electrical resistivity recovery, using Wheatstone bridge measurement
23 p3689 A71-42934

Lunar electrical conductivity profile from joint power spectral density analysis of Apollo 12 and Explorer 35 magnetometer data
23 p3762 A71-43790

Zirconium monocarbide electrical conductivity, Hall coefficient, thermal emf and magnetic susceptibility measurements for temperature dependence at 500-1000 K in homogeneity region
23 p3692 A71-44021

Nd-Bi phase diagrams from thermal differential, metallographic and X ray analyses, discussing carrier concentration and mobilities, Hall coefficients, conductivity and thermal emf
23 p3692 A71-44022

Vacuum fusion sintered rhodium borides melting point, microhardness and conductivity and thermal emf temperature dependences determination by thermal metallographic and X ray analyses
23 p3717 A71-44024

Electric conductivity correlation between solar faculae and Bilderberg model of photosphere and chromosphere
24 p3868 A71-44458

NaI-glycerol solution resistivity values, determining measurement frequency, temperature, outgas procedures, purity and doping level effects
24 p3802 A71-44614

Homogenizing annealed TiC-WC carbides properties at room temperature, investigating microhardness, microbrittleness and resistivity
24 p3838 A71-44740

Transition from metallic to activation conductivity in doped semiconductors, noting activation energy dependence on compensation degree
24 p3860 A71-45121

ELECTRICITY

NT ALTERNATING CURRENT
NT ATMOSPHERIC ELECTRICITY
NT AURORAL ELECTROJETS
NT ELECTROJETS
NT EQUATORIAL ELECTROJET
NT GEOELECTRICITY
NT IONOSPHERIC CURRENTS
NT STATIC ELECTRICITY

ELECTRIFICATION

ELECTRIFICATION

- Supersonic aircraft electrification measurements using projectile frictional charging in ice-fog cloud 07 p1020 A71-19934
- Charge generating mechanism based on charge separation from falling precipitation particles effect on thunderstorm electrification 14 p2269 A71-29951
- Cloud particle electrification mechanism with allowance for secondary collisions between particles 19 p3092 A71-38685

ELECTRO-OPTICAL EFFECT

- High speed small aperture electro-optic, acousto-optic and magneto-optic modulators for optical communications, considering capabilities and limitations 02 p0231 A71-12003
- High rate electro-optical modulator for 10.6 micron IR laser beam consisting of GaAs crystal multitraversed by beam 02 p0262 A71-12923
- Carbon dioxide laser stable mode locking with resonated internal electro-optic phase modulator driven at frequencies near axial mode interval 03 p0434 A71-13481
- Heterojunctions with II-VI compound semiconductors, evaluating electro-optical performance 07 p1181 A71-20409
- Noncrystalline amorphous solids electro-optical effects, studying semiconductor energy band models 07 p1181 A71-20422
- Lossless KDP Pockels cell modulator for high power laser Q switching based on tuned face electro-optical crystal 12 p1905 A71-26813
- Electro-optical Fabry-Perot modulator with KDP and ADP crystals as optical resonators, determining modulation and frequency response characteristics 16 p2587 A71-33493
- Nematic and cholesteric mixtures liquid crystals electro-optic properties and applications to display devices 19 p3120 A71-38537
- Electro-optic mode locking of dual polarization carbon dioxide laser using intracavity birefringence modulation 20 p3244 A71-39096
- Single and double pass traveling wave electro-optic light modulator phase retardation transient response calculation 20 p3235 A71-39180
- Nanosecond ruby laser pulse generation using electro-optic shutter switching circuit external to Q-spilled cavity 21 p3391 A71-40179
- Voltage-polarization induced optical waveguide using electro-optical lithium niobate crystal 21 p3393 A71-41039
- Quadratic and linear electro-optical effect dispersion in flux grown crystals of barium titanate 22 p3585 A71-41729
- Barium titanate single crystal solid solution electro-optic characteristics at 6328 Å and temperatures above Curie point, determining temperature dependences 24 p3860 A71-44667
- Current-optical effects of anisotropic absorption of polarized and unpolarized light in rarefied cosmic media 24 p3860 A71-45106
- Low loss mode selection and wavelength regulation of gas lasers with electro-optical intracavity resonator 24 p3834 A71-45163

ELECTRO-OPTICAL PHOTOGRAPHY

- Transverse conductivity and temperature dependence of storage time during photographic scanning of astronomical objects with superorthicon camera 03 p0422 A71-13008
- Intercept Ground Optical Recording telescope and Mobile Optical Tracking System for electro-optical photography, discussing measurement and system errors and CAMDAT computer program 04 p0554 A71-15320
- Electro-optical shutter with low control voltage /3 kV/ for ruby laser consisting of Pockels cell and Porro prism 07 p1125 A71-19808
- Electron-optical system with electro- and magneto-static lenses, ensuring large image reduction for producing printed microcircuits 16 p2579 A71-33500
- Quantitative schlieren system for shock wave velocity, density ratio and relaxation time measurements, discussing electro-optical modification and calibration technique 21 p3364 A71-40404
- Mars Viking Lander camera system with solid state focus switching, radiometry and solar imaging survivability 23 p3677 A71-43517

ELECTRO-OPTICS

- Electro-optic monitoring method for single isolated heart cell activity 02 p0202 A71-11672

Free generation regime of ruby laser studied by electro-optical method of smoothing spatial inhomogeneities 02 p0261 A71-12502

Automatic testing of electro-optical systems including TV, IR and laser applications 03 p0395 A71-13082

Electro-optical solar simulator, describing system design, performance and applications for spacecraft testing 04 p0567 A71-15366

Divergent laser light beams continuous electro-optical deflection using prism with single crystal at Curie temperature in cryostat 05 p0763 A71-16834

Laser cavity standing wave field electro-optic modulation for uniform population inversion, producing spontaneous single frequency output 05 p0764 A71-17232

Electron thermal diffusion effects during light interference patterns exposure, generating strong electric fields and holographic storage in electro-optic materials 06 p0940 A71-17309

Contact electro-optic KDP crystal shutters for Q switching ruby laser 06 p0907 A71-17530

Ruby Q switched lasers with modular electro-optic shutters for low insertion loss and high optical radiation resistance 06 p0908 A71-18303

Electro-optical method for energy dissipation characteristics of mechanical systems subject to attenuating vibration 07 p1107 A71-19170

Mode locked He-Ne laser pulse compression and expansion by electro-optic internal modulator 10 p1619 A71-23873

Electro-optical systems in photoelectronic imaging devices, discussing electron gun, electrostatic focusing lens, spherical aberration, magnetic field computation and ray tracing 10 p1609 A71-24058

Electro-optical devices evaluation search model, considering imagery and image transmission 10 p1610 A71-24062

Electro-optical and high contrast properties of structurally stabilized anil-type nematic liquid crystals in display devices 11 p1729 A71-26070

Semiconductor materials technologies, discussing optoelectronic and microwave components, photodiode arrays, HF diodes and transistors and IC Doppler radar units 13 p2111 A71-28908

Atmospheric turbulence effects on stellar irradiance and phase, discussing electro-optical recording technique and computer generated statistical data 14 p2270 A71-30016

Image classification by optical and electro-optic processing methods for spatial signal perception and treatment in natural form 14 p2248 A71-30816

Phase holographic data storage in doped barium sodium niobate crystal, detailing decay times, energy density and diffraction efficiency 15 p2412 A71-32586

Minimum voltages and limiting frequencies for oblique cut longitudinal octahedral crystal modulators with large electro-optic coefficients, including lithium niobates and tantalates 15 p2461 A71-32606

Parametric microwave amplifier feasibility with laser pumped electro-optical crystal as nonlinear element 16 p2589 A71-34135

Optoelectronic elements for information system applications, discussing photomultipliers, photodiodes, photoresistors, avalanche and photoparametric diodes response and bandwidth characteristics 17 p2752 A71-34391

Electro-optical method for energy dissipation characteristics determination for mechanical systems subject to attenuating vibration 17 p2746 A71-35666

Electro-optics - Conference, Brighton, England, March 1971 18 p2923 A71-36601

Electronic processing of coherent optical data for measurement and display using holography, speckle patterns, interferograms, image intensifiers and TV systems 18 p2923 A71-36608

Electro-optic direction sensor, discussing single axis star tracking application [AIAA PAPER 71-966] 19 p3100 A71-37207

Electro-optic He-Ne laser microscope for high-speed high-precision edge detection for IC masks 19 p3075 A71-38236

Carbon dioxide laser triggered pressurized spark gap producing high voltage fast risetime pulses for use in IR radiation control by electro-optic shutters 20 p3244 A71-39106

Numerical calculation of electron guns with converging spherical beams near cathode and electron optic systems decelerating at collector 20 p3204 A71-39106

High power continuous electron-optical beam formation in electron gun, determining cathode emission current and I-V characteristics as function of pressure 20 p3204 A71-39106

Raman tensor, scattering efficiency and line width in semiconductors due to optical phonons, discussing electro-optical coefficients 21 p3427 A71-40606

Electro-optical systems design - Conference, Anaheim, May 1971 23 p3684 A71-43517

Electrooptical measurement of high altitude rain cloud droplets size, shape and distribution 23 p3676 A71-43517

Electro-optical techniques for particle size measurements from aircraft, noting imaging techniques superiority for nonaerosol and large particles 23 p3677 A71-43517

Radio-optics prospects in signal and information processing, image reconstruction, data transmission, computer storage, display and holographic movies and TV 23 p3681 A71-44313

Dynamic active element model of electroluminescent image converter with positive optical feedback, using voltage-brightness approximation 24 p3808 A71-44313

ELECTROACOUSTIC TRANSDUCERS

NT MICROPHONES

Electroacoustic properties of GaAs diffusion layers, transducers as function of resistivity and charge carrier concentration in single crystals 01 p0140 A71-11112

Electroacoustical device for recording gas and vapor cavitation resistance in liquids 04 p0617 A71-14559

FET transistors on epitaxial GaAs as input and output transducers for acoustic surface waves 09 p1417 A71-22770

Fluid velocity measurements by electroacoustic transducers using phase difference relation 13 p2069 A71-28909

Electroacoustic circuit of ultrasonic resonant thickness gage based on frequency dependence of piezoelectric transducer conductance in multilayered acoustic system 22 p3528 A71-41729

Electromagnetoacoustic ultrasonic vibrations radiation and reception angular orientation as function of transducer design parameter, frequency and propagation velocity 22 p3528 A71-41729

Transient response of electroacoustic transducer arrays, computing time dependent velocities for prescribed electrical inputs 23 p3704 A71-43216

ELECTROACOUSTIC WAVES

Linear theory of acoustoelectric oscillator with sandwiched piezoelectric plate accounting for mode enhancement and quenching 04 p0558 A71-15141

Plasma coated spherical antenna radiation discussing hot and cold plasmas frequency and electroacoustic wave effects 06 p0875 A71-17770

Coupled electroacoustic and electromagnet wave propagation in inhomogeneous compressible and lossy plasma 07 p1065 A71-20333

HF modulated transverse electromagnetic wave penetration into plasma with negative dielectric constant, noting plasma density fluctuations and electroacoustic wave formation 14 p2281 A71-30505

Nonlinear frequency shift in GaAs electroacoustic domains, using Bommel-Dransfeld analysis technique 17 p2791 A71-35441

Acoustoelectrical current oscillations in GaAs film at low temperature under ultrasonic Rayleigh wave amplification 23 p3716 A71-43476

ELECTROCARDIOGRAMS

U ELECTROCARDIOGRAPHY

ELECTROCARDIOGRAPHY

Heart rhythm coordinate curves for continuous EKG analysis using digital computer 01 p0025 A71-11111

Computer differential analysis of cardiac rhythm regularities involving comparison of EKG RR intervals 01 p0025 A71-11111

Electrocardiograph recording fidelity relative specification recommendations 01 p0026 A71-11212

Abnormal left ventricular contour with late systolic murmur at apex preceded by click and with abnormal T waves in electrocardiogram 02 p0197 A71-11616

Medical data processing techniques in electrocardiography and effort vectorcardiography facilitating clinical observations

02 p0207 A71-12110

Real time contourgram for monitoring ECG waveform data, describing cardiac measurement and data display

02 p0199 A71-12384

ECG signal analog to digital conversion at sampling rate and quantizing accuracy for minimal losses and/or distortion

02 p0208 A71-12949

Digital filtration and processing of electrocardiograms on computers using linear difference equations

03 p0367 A71-12992

Long term day and night ECG recordings of healthy human subjects, analyzing heart rate and amplitude variations during normal wakefulness and sleep periods

03 p0370 A71-13061

In-flight ECG telemetry for aircraft pilots diagnostics, discussing characteristic recordings and measuring probes development for simultaneous parameters transmission

03 p0370 A71-13062

In-flight telemetric ECG recordings of aircraft pilots during normal, abnormal and aerobatic flight, analyzing heart rate variations as function of stresses

03 p0370 A71-13064

Telemetric ECG recordings of workers under high and strongly varying temperature conditions, discussing heart rate variations under heat stress

03 p0370 A71-13065

ECG telemetric data computerized processing, describing cardiac data acquisition, long distance telephone transmission, analog to digital converter, central processor and output devices

03 p0370 A71-13066

ECG changes and coronary risk of acquired bundle branch block in healthy population

03 p0363 A71-13490

Submaximal exercise ECG test in screening high risk populations for occult ischemic heart disease

03 p0372 A71-13491

Autopsies compared to ECG for diagnosis accuracy for acute recurrent myocardial infarction

05 p0711 A71-16951

Aircrews coronary insufficiency diagnosis via electrocardiographic modifications after exertion, observing ischemia

06 p0860 A71-18192

ECG beat-to-beat variation reduction using digital computer wave recognition

07 p1049 A71-19839

Primary T wave derived from ECG waveform dependent intrinsic ventricular recovery properties

07 p1050 A71-19840

ECG signals on-line and real time monitoring mathematical, statistical and bioengineering considerations

08 p1248 A71-21330

Book on clinical physiology techniques and anesthesiology measurements covering electronics, ECG analysis, blood pressure measurement, cardiac function, respiratory mechanics, etc

09 p1398 A71-22459

Jet pilots flight stresses assessment via biotelemetric transmission of pulse rate, respiratory rate, electrocardiographic data, flight altitude and velocity

10 p1567 A71-23880

ECG miniaturized single channel biotelemetry transmitter, discussing lightweight design and power supply

10 p1570 A71-24487

Left ventricular enlargements, comparing vectorcardiographic spatial magnitude and electrocardiographic precordial QRS voltage measurements

11 p1725 A71-26428

Digital computer analysis of orthogonal ECG and VCG from patients with myocardial infarction

12 p1875 A71-27287

Heart size estimated from chest X rays related to corrected orthogonal ECG findings in patients with congestive heart failure symptoms

12 p1875 A71-27288

Ectopic right atrial rhythms in ECG vectorial analysis

12 p1870 A71-27289

Wired monitoring system for continuous interference-free twelve-lead ECG recording before, during and after exercise

12 p1876 A71-27630

Computer analysis for normal ranges of orthogonal lead ECG parameters derived from modified axial lead systems

13 p2016 A71-27812

Three vs 12 lead electrocardiogram input for computer assisted interpretation

13 p2016 A71-27813

ECG measuring locations number and positions for determination of time varying total body QRS surface potential distribution

13 p2016 A71-28149

Redundant information reduction during electrocardiograms analysis by Legendre polynomials, considering equivalent model in dipole and quadrupole form

13 p2017 A71-28376

Anoxia induced ECG lesion current in conjunction with myocardial phosphorylcreatine collapse, discussing results with air and nitrogen ventilated guinea pigs

13 p2008 A71-28506

Isolation technique for recording low level ECG and deep body temperature signals in animals exposed to large amplitude RF fields

13 p2020 A71-28864

Stochastic identification method for transforming ECG and VCG data to approximate diagnosis, using computerized dipole models

13 p2020 A71-29002

Ventricular mass estimation using electrocardiographic parameters

13 p2021 A71-29302

Electrocardiography from unprepared skin without paste, using integrated stainless steel electrode-buffer amplifiers

13 p2023 A71-29399

T wave abnormalities in electrocardiograms of athletes without organic heart diseases

14 p2187 A71-30708

Early diagnosis of atherosclerosis in civil aviation pilots by lipid metabolism and electrocardiographic examinations

15 p2357 A71-31318

Computer quantitation of ST segment response to graded exercise in untrained and trained subjects, continuously recording amplitude of selected points on ECG waveform

15 p2358 A71-31452

Maximal treadmill stress test correlation with postexercise phonocardiogram, ECG and double master test in normal subjects, discussing third and fourth heart sound incidence

15 p2361 A71-32538

Concealed and supernal atrioventricular conduction data, using His bundle electrogram recordings

15 p2366 A71-32539

Computer analysis of ECG compared to cardiologist conclusions, noting discordance in rhythm analysis

15 p2366 A71-32543

Spatial ECG ventricular gradient ECG morphology, noting use in stimulus intraventricular conduction disturbances recording

17 p2690 A71-34823

Monophasic action potential recording of intact human heart, using bipolar electrode catheter for explanation of ECG abnormalities

18 p2853 A71-35910

Sagittal path of moving electrical center of human heart from measurements of surface ECG potentials

18 p2853 A71-35911

Electrocardiographic evidence of false complete bilateral bundle branch block with impaired atrioventricular conduction in patient with hypertensive heart disease

18 p2853 A71-35912

Correlative ECG survey of surgically proven constrictive pericarditis involving left ventricle with T wave inversion

18 p2853 A71-35913

Left ventricular aneurysm electrocardiographic features and postresection changes based on ECG statistical analysis

18 p2854 A71-36138

Human blood pressure in brachial artery during spontaneous night sleep, recording EEG, EKG and horizontal eye movements

21 p3329 A71-40185

Mathematical model of electrocardiographic QT-RR relationship, showing agreement with membrane theories

21 p3343 A71-40586

Electrical heart activity and ECG mathematical model with nonlinear oscillator system construction for normal and abnormal rhythms

21 p3336 A71-40986

Heart rate and systolic pressure variability control through visual feedback of physiological information, obtaining respiratory measurements and ECG

21 p3344 A71-41037

Anoxia effect on laboratory animals cardiac action, discussing ECG injury current relation to myocardium phosphorylcreatine content

22 p3484 A71-41568

Miniaturized multichannel FM/AM biological telemetry system for simultaneous transmission of EEGs, EMGs, EOGs and EKGs

22 p3500 A71-41574

ST segment elevation spectrum in ECG of healthy male USAF flying personnel

22 p3504 A71-42417

Vectorcardiographic analysis of patients with ECG diagnosed inferior atrial rhythm

22 p3490 A71-42519

Mid systolic clicks and papillary muscle dysfunction evidence in arteriosclerotic heart disease from ECG, carotid pulse tracing and phonocardiography

23 p3635 A71-44126

ELECTROCHEMICAL MACHINING

Preclinical coronary heart disease detection by near maximal treadmill exercise ECG

23 p3636 A71-44129

Transistorized AGC circuit for use with ultrasonic Doppler-cardiogram recording system to retain signal characteristics under strong fluctuations

24 p3801 A71-44543

ELECTROCATALYSTS

Ni-Ti system electrocatalysts for fuel cell and accumulator electrodes

03 p0355 A71-14318

Electrochemical properties of Na-W bronzes for use as electrocatalysts in acid electrolyte fuel cells

09 p1387 A71-23648

Bronsted relationship between adsorption heat and activation energy in electrocatalysis of purified orthophosphoric acid and phase-oxide-free noble metals

21 p3345 A71-40540

ELECTROCHEMICAL CELLS

NT ALKALINE BATTERIES

NT ELECTRIC BATTERIES

NT FUEL CELLS

NT HYDROGEN OXYGEN FUEL CELLS

NT MAGNESIUM CELLS

NT METAL AIR BATTERIES

NT NICKEL CADMIUM BATTERIES

NT NICKEL ZINC BATTERIES

NT REGENERATIVE FUEL CELLS

NT SILVER ZINC BATTERIES

NT STORAGE BATTERIES

NT THERMAL BATTERIES

NT ZINC-OXYGEN BATTERIES

Radionuclide batteries for energy supply in space, comparing with electrochemical sources

02 p0282 A71-12303

Electrochemical cell interelectrode planar spacing regulator system, discussing electrode constant vibration amplitude to current ratio

08 p1296 A71-20855

Electrochemical plasma production based on cathodic hydrogen combustion using giant condenser batteries for energy storage and quick release, applying to space propulsion technology

15 p2456 A71-31833

Self contained one man module cell design and tests of electrochemical carbon dioxide concentrating system for space applications

18 p2867 A71-36388

Static feed water electrolysis system of life support system, discussing current density, operating time and temperature effects on voltage for various electrochemical cell sizes

18 p2868 A71-36392

Integral operating mode of nerve paths representation by linear diffusion channel with electrochemically active synapses, deriving complementary partial differential equations

19 p3001 A71-37250

ELECTROCHEMICAL CORROSION

Phosphoric acid corrosion resistant alloys for electrolyte fuel cells, discussing materials selection and optimization

03 p0440 A71-13055

Ti alloys stress corrosion crack propagation in salt water, investigating existence of threshold stress from electrochemical data

04 p0610 A71-14891

Metal stress corrosion crack propagation rate relationship to electrochemical parameters, considering active and passive regions of potentials

05 p0827 A71-16814

High yield strength steel stress corrosion crack tip electrochemical and pH potential conditions, using AgCl reference electrode

07 p1137 A71-19973

Zinc electrodes performance improvement, discussing electrochemical corrosion rate, current density and temperature effects

08 p1233 A71-21082

Stress corrosion cracking, discussing stress effect, environmental and metallurgical factors and electrochemical and sorption theories

13 p2085 A71-28221

Welded, bearing and interlocking joints and adhesive bonding in carbon fiber reinforced plastics, discussing anisotropy, thermal expansion and electrochemical corrosion problems

17 p2748 A71-34344

Stress corrosion cracking in Ni maraging steel in NaCl solution, using electrochemical polarization and potential analysis

18 p2934 A71-35989

ELECTROCHEMICAL MACHINING

Electrochemical machining for aircraft engine metal components, discussing cost, time comparisons, tooling techniques and applications

01 p0089 A71-11252

Electrochemical machining role in jet engine industry, discussing drilling, contouring, electrolyte handling, etc

01 p0089 A71-11253

Electrochemical machining accuracy, discussing gap geometry, optimal conditions, electrolyte types, etc

01 p0089 A71-11257

ELECTROCHEMICAL OXIDATION

- Electrochemical machining package consisting of machine tool, electrolyte system and power supply [SME PAPER MR-70-512] 01 p0090 A71-1268
- Electrolytic saw for slicing strain-free metal crystals without damage, noting improved surface flatness 02 p0255 A71-12141
- Hard alloys electrolyte selection for electrochemical dimensional machining 07 p1120 A71-20206
- Electroerosion and electrochemical combined effects on machining surface removal, discussing optimal anodic removal rates and electrolyte concentrations 08 p1296 A71-20852
- Electrochemical metal machining tool profile two dimensional steady state problem, solving for cathode surface changes as function of interelectrode potential 08 p1296 A71-20854
- Electrochemical machining based on Faraday laws of electrolysis 13 p2075 A71-28948
- Carbon-graphite bound electrochemical grinding wheel, describing composition formulation, fabrication techniques, mechanical and electrical properties and performance criteria 14 p2263 A71-29654
- Photochemical machining, describing parts design, line width and corner radii relation to metal thickness and base materials 15 p2416 A71-32428
- Complex variable solutions to electrochemical machining with two dimensional straight sided tool 23 p3682 A71-44142
- ELECTROCHEMICAL OXIDATION**
- Oxidation potential criterion for metal sticking to rolls during rolling in vacuum, considering Ta, Zr, Mo, W, Ni, Cu, Nb and V 02 p0256 A71-12515
- Computer simulation of stress corrosion cracking, considering electrochemical oxidation mechanism for crack propagation 11 p1847 A71-25449
- Electron beam vapor deposited CoCrAlY coating composition optimization with ballistic impact and furnace/long term burner rig oxidation tests 14 p2257 A71-29636
- ELECTROCHEMISTRY**
- NT ELECTROLYSIS**
- Fick diffusion model for Haxo-Blinks electrochemical determination of photosynthetic oxygen evolution 04 p0546 A71-15169
- Copper sulfide-cadmium disulfide thin film solar cells degradation under simulated orbital conditions, determining electrochemically induced copper filament growth as electric shorts causes 05 p0699 A71-16057
- Silver-silver oxide electrode chemistry in alkaline solutions, describing oxide structure, solubility and stability 08 p1234 A71-21083
- Silver oxides crystal structures and physical and electrochemical properties 08 p1234 A71-21084
- Silver oxide electrodes electrochemical reaction kinetics, examining oxidation, anodic formation and cathodic reduction 08 p1234 A71-21086
- Concorde aircraft components electrochemical marking, considering stamping and engraving acceptability for highly stressed thin material parts 09 p1459 A71-23582
- Heat treatment effect on electrochemical behavior of Ni-Co-Mo maraging steel in sulfuric acid aqueous solution, studying anodic polarization 14 p2257 A71-29840
- Papers on heat transfer covering theoretical and experimental heat transfer in liquids, gases and liquid-solid interfaces, transport phenomena, heat pipes, electrochemical method, etc 14 p2336 A71-30240
- Diffusion electrochemical linear and angular accelerations sensors, noting lack of friction surfaces 15 p2409 A71-32184
- Carbon dioxide traces effects on composition, volume and electrochemical characteristics of trapped electrolyte hydrogen oxygen alkaline fuel cells 15 p2354 A71-32205
- Electrosensing liquid level gage using electrochemical charge transfer through fluid 17 p2744 A71-35290
- Activation impulse blocking in nerve, using inhomogeneous Lillie electrochemical model 19 p3006 A71-37282
- Calculation method for standard potentials and enthalpies of metals during oxidation and chlorination, representing molar functions dependence on temperature 19 p3082 A71-38153
- Apparatus for optical diagnostics of helioelectrochemical conversion reaction phototransformation kinetics including diffusion coefficient measurement in liquid phase 22 p3484 A71-42845

ELECTROCONDUCTIVITY

- Multicomponent plasma electrical and thermal conductivities from quantum mechanical scattering cross sections 02 p0289 A71-12176
- Finite electrical conductivity effects on solar flare-induced interplanetary shock waves, discussing solar wind time dependent bulk flow characteristics 05 p0810 A71-16634
- Finite electrical conductivity role in interplanetary piston driven shock waves propagation in solar wind 05 p0810 A71-16635
- Niobium oxide defect structure, correlating electrical conductivity and oxygen diffusional properties with nonstoichiometry degree 05 p0770 A71-17097
- Lunar interior electrical conductivity and temperature from various conductivity models, considering interplanetary magnetic source field 06 p0964 A71-17281
- Electrophysical properties of Ga-In-As single crystals in varying mixture ratios at 78-380 K, determining electrical conductivity, Hall coefficient and electron mobility 07 p1176 A71-19224
- EM induction in flat plates with two dimensional conductivity distribution, describing approximation method 09 p1492 A71-22425
- Black SiC varistors IV characteristics and conductivity, investigating fast neutron irradiation and isochronal annealing effects 12 p1886 A71-26898
- Atmospheric pressure electrical and thermal conductivities on nitrogen and hydrogen up to 26,000 K from argon arc measurements 12 p1939 A71-27271
- Fluctuation enhanced conductivity of superconductor, considering Maki graph evaluation 13 p2111 A71-28454
- Analog simulation of cardiac malfunctions associated with A-V conduction block and Wenckebach phenomenon, using P and R wave and internal function generators 13 p2020 A71-29001
- Multicomponent plasma electrical and thermal conductivities from Debye potential quantum mechanical scattering cross sections 15 p2454 A71-31485
- Magnetoelastic oscillations of thin conducting plate in magnetic field, solving electrodynamic equations 16 p2647 A71-32928
- Earth upper mantle electrical conductivity as function of depth based on geomagnetic variation field spatial distribution data 16 p2572 A71-33907
- Thermoelectric and thermomagnetic phenomena in semiconductors with impurity ions, solving electric conductivity and diffusion and Poisson equations for weak magnetic fields 16 p2622 A71-34027
- Electroconductivity and Hall effect in doped GaAs at low temperatures, studying temperature dependence of electron concentration, mobility and localization 16 p2623 A71-34030
- High porosity carbon-graphite materials thermal and electrical conductivities at high temperatures by potentiometric method 17 p2761 A71-34208
- Electrical conductivity of pyrographite at high temperatures along and across deposition plane, using optical pyrometer measurements 17 p2761 A71-34304
- Continuous automatic recording of semiconductor diodes integral conductivity components, using circuit with controlled steady voltage bias 17 p2713 A71-34569
- Electrical insulation behavior of MHD generator channel having Ar-K plasma, noting temperature dependence of surface conductivity 17 p2789 A71-35274
- German monograph on high temperature measurement of thermal and electrical conductivity of W and Mo single crystals 18 p2915 A71-35960
- Lunar stratified composition based on electrical conductivity profile from magnetic field fluctuations measurement in terms of two layer model 18 p2961 A71-35993
- Tunnelling conductance anomaly in metal-insulator-metal junctions containing paramagnetic impurities, analyzing I-V characteristics during switching effect 18 p2954 A71-36802
- Electrolytic behavior of yttria-bafnia solid solutions from X ray analysis and electroconductivity measurements 18 p2874 A71-37001
- MHD channels end effects at finite magnetic Reynolds numbers, discussing wall conductivity and external magnetic field geometry effects 19 p3108 A71-37078
- Aerosol layers in stratosphere, determining vertical distribution of electrical conductivity 19 p3047 A71-37335

- Lunar electroconductivity, examining moon response to large discontinuity in interplanetary magnetic field 19 p3131 A71-37354
- Free carrier surface density and mobility in large MOS transistors from conductivity and Hall measurements 19 p3028 A71-37564
- Electroconductivity, thermal conductivity and diffusivity, specific heat and emissivities of Ti at 1000-1700 K 19 p3078 A71-37582
- Electrical conduction in orthogonal coordinates from nondipole nature of geomagnetic field on conductivity tensor of ionospheric dynamo region 19 p3057 A71-38384
- Stratospheric dust effect on electrical conductivity measurements, noting proportionality to ion concentration 20 p3216 A71-38792
- Moon surface electrical conductivity, seismic transmission properties, dust components, chemical analysis and comparison to earth 20 p3295 A71-39615
- Apollo 11 lunar crystalline igneous rock samples electrical conductivity temperature dependence, noting age of moon 20 p3295 A71-39619
- Temperature, magnetic field and pressure dependence of electrical conductivity, thermal emf, Hall effect and transverse Nernst-Ettingshausen effect in indium-doped lead telluride 21 p3429 A71-41210
- High resistance undoped GaAs samples at different temperatures, investigating energy spectra, Hall effect and electron conductivity 21 p3431 A71-41227
- Germanium single crystal surface conductivity, observing carbon monoxide adsorption effects at various pressures 21 p3435 A71-41341
- Dielectric conductivity, relative permittivity and loss tangent of Apollo 11 and 12 rock samples 23 p3762 A71-43787
- Apollo 12 magnetic measurements of lunar interior electroconductivity simultaneously on lunar surface and in circumlunar orbit 23 p3762 A71-43789
- Symbiotic shifts of conductivity compensation effect in glassy chalcogenide semiconductors unaffected by heat treatment of blanks or impurities 23 p3717 A71-44315
- Capacitance and conductivity in metal dielectric semiconductor during majority current carrier population depletion by pulsed voltage, discussing concentration and mobility determination 24 p3859 A71-44376
- Cd doped thin polycrystalline CdTe films rectification mechanism and DC conductivity, discussing light, electric field and temperature effects 24 p3861 A71-45248
- Surface electronic conductivity in oxide glasses for microchannel electron multipliers, noting heat treatment and chemical composition effects 24 p3862 A71-45327
- ELECTRODELESS DISCHARGES**
- Microwave signal scattering by LF oscillations in electrodeless induction discharge plasma 01 p0135 A71-11031
- Radio frequency electrostatic ion thruster using mercury ion source electrodeless self sustaining discharge 02 p0283 A71-12311
- German monograph on helicon resonances in low pressure plasmas, examining HF discharge with applied external static cross magnetic field 04 p0633 A71-14975
- Time dependent current flow measurements and energy losses in capacitor discharge of electrodeless MHD motor 11 p1716 A71-26290
- High pressure electrodeless HF gas discharge plasmas, investigating effects of external magnetic field, gas and pressure on discharge rotation frequency 17 p2789 A71-35260
- Gas and electron temperature and thermal nonequilibrium in argon plasma jet from electrodeless induction discharge 19 p3111 A71-37578
- ELECTRODEPOSITION**
- Zn deposition on Zn single crystals in KOH solution, examining time and potential effects on deposit morphology 02 p0210 A71-12956
- Electrodeposition of coherent coatings of zirconium diboride from solution of zirconium tetrafluoride and boron oxide in molten eutectic mixture of NaF-KF-LiF 07 p1118 A71-19567
- Zinc morphology electrodeposited from alkaline electrolyte, investigating charging and cell failure 08 p1233 A71-21081

- Ti-V alloys electrolytic deposition, discussing electrolyte composition, current density, temperature and coating thickness 10 p1627 A71-24646
- Alumina and titania codeposition from acid copper electrolyte as function of oxide crystalline form, discussing addition agents effects 11 p1779 A71-26011
- Electrodeposited Ni-Mo coatings corrosion resistance improvement by heat treatment, showing crystal structure degree of perfection role 16 p2599 A71-34052
- Carbon fiber/metal matrix composites fabrication by electrodeposition, discussing aluminum warp sheet lamination and filament wound techniques 21 p3387 A71-40599
- Chromium and Ni-Cr electrodeposition from amide solvent system, describing water and sulfur ligands effects on plating efficiency 22 p3554 A71-42528
- ELECTRODERMAL RESPONSE**
U GALVANIC SKIN RESPONSE
ELECTRODES
 NT ANODES
 NT CATHODES
 NT CELL ANODES
 NT COLD CATHODE TUBES
 NT COLD CATHODES
 NT GLASS ELECTRODES
 NT HOLLOW CATHODES
 NT HOT CATHODES
 NT PHOTOCATHODES
 NT PHOTOMULTIPLIER TUBES
 NT PLASMA ELECTRODES
 NT THERMIONIC CATHODES
 NT TUBE ANODES
 NT TUBE GRIDS
 Pt electrode oxygen diffusion and consumption systematic errors effect on oxygen partial pressure measurement in perfused tissues 01 p0021 A71-10073
- Percutaneous vitreous carbon electrodes long term effects, considering mechanical stability, bioelectrical signal receptivity, low interface impedance and surrounding epidermis growth 01 p0021 A71-10238
- Manganese dioxide depolarizer for biomedical electrodes, discussing electrochemical and toxicological characteristics 01 p0021 A71-10239
- Feedback circuit for constant current stimulation through intracellular microelectrode 01 p0021 A71-10245
- Open and closed eyes electroretinogram, discussing lamellar electrode placed on lower eyelid 01 p0024 A71-11077
- Cylindrical Xe filled thermionic diodes breakdown and low voltage arcs at various pressures and interelectrode distances 02 p0190 A71-11942
- Thermionic converter tests, discussing W emitter with Nb and Mo-on-Nb collectors, surface and electrode combinations 02 p0193 A71-12214
- Volt-ampere characteristics dependence on collector temperature in thermionic converters compared with collector work function 02 p0195 A71-12235
- Oxygen reduction on Teflon bonded Pt electrodes, eliminating concentrated overvoltage 02 p0210 A71-12955
- Rapid mass transport to Pt electrodes in foamed electrolytes, examining current density-anode overpotential relationship 02 p0210 A71-12957
- Chemical test method for composition analysis of Ni-Cd electrodes 03 p0374 A71-13028
- Physical changes at lithium electrodes during charge-discharge cycling in propylene carbonate electrolyte 03 p0350 A71-13030
- Zinc air battery, evaluating materials capable of peroxide decomposition as low cost oxygen electrodes 03 p0351 A71-13040
- Fuel cell electrodes preparation by sputtering thin Ta and Pt layers on porous Vycor 03 p0353 A71-13056
- Biotelemetry data acquisition and electrode technology, discussing physiological measurements and pickup techniques for conversion into electrical signals 03 p0369 A71-13060
- Vectorcardiograms comparison recorded with different electrode leads or amplification systems based on spatial points coordinates correlation coefficients 03 p0371 A71-13115
- Interelectrode focusing voltage effect on electron beam and tube efficiency in TW and backward wave tubes with electrostatic focusing systems 03 p0385 A71-13793
- Small-tipped microelectrode minimizing capacitance artifacts during current passage through bath in membrane potential measurement 03 p0372 A71-13912
- Brain electrodes rapid implantation method, using preassembled, stereotactically loaded, preconnected and pretested electrode and pedestal assemblies 04 p0538 A71-15059
- Pt electrode response time during unsteady oxygen partial pressures measurement 06 p0860 A71-18323
- Machining electrode materials, investigating high melting transition metals electroerosive stability and bending strength on basis of electronic theory 08 p1296 A71-20853
- Electrochemical metal machining tool profile two dimensional steady state problem, solving for cathode surface changes as function of interelectrode potential 08 p1296 A71-20854
- Electrochemical cell interelectrode planar spacing regulator system, discussing electrode constant vibration amplitude to current ratio 08 p1296 A71-20855
- Zinc-silver oxide batteries thermodynamic characteristics obtained from silver-silver oxide and zinc-zinc hydroxide electrodes data 08 p1233 A71-21077
- Zinc-zinc oxide electrode chemistry, describing interaction with strongly alkaline solution of alkaline battery system 08 p1233 A71-21078
- Zinc electrode kinetics noting exchange reactions, anodic behavior in alkaline solutions and capacitance 08 p1233 A71-21080
- Zinc electrodes performance improvement, discussing electrochemical corrosion rate, current density and temperature effects 08 p1233 A71-21082
- Silver-silver oxide electrode chemistry in alkaline solutions, describing oxide structure, solubility and stability 08 p1234 A71-21083
- Silver oxide electrodes electrochemical reaction kinetics, examining oxidation, anodic formation and cathodic reduction 08 p1234 A71-21086
- Zinc electrodes manufacturing processes, describing materials used in electrodeposition and pressed powder methods, quality control procedures and Zn-Ag batteries electrical characteristics 08 p1297 A71-21088
- Manufacture and mechanical properties of sintered silver electrodes involving oxide, powder and resin bonding methods 08 p1297 A71-21089
- Chemically prepared silver oxide for silver zinc batteries bivalent electrode fabrication 08 p1298 A71-21090
- Integral transform methods for analytic solutions to current and potential distribution on disk in infinite plane for four limiting cases 08 p1237 A71-21471
- Conical metal core electrode erosion rates in pulsed plasma accelerators with refractory dielectric chamber 08 p1340 A71-21484
- Boundary value problem of end effect in MHD channel with semiinfinite electrodes for arbitrary Reynolds numbers 09 p1499 A71-22130
- Ion currents to cylindrical electrodes in mobility dominated plasma flow from thin sheath theory involving convection currents 09 p1505 A71-23374
- Muscular fibers analysis for motoneuron split potentials, using needle electrode 10 p1564 A71-24484
- Atmospheric pressure carbon dioxide laser electrode design for uniform pulse excitation discharge 10 p1621 A71-24508
- Percutaneous access to implanted electrodes, discussing metal plaque-needle system and connection to instruments 11 p1724 A71-25436
- Porous structure effects in oxygen consuming cathode, discussing electrode thickness, effective pore diameter, pressure difference and electrode performance 11 p1709 A71-25553
- Design, fabrication and testing of electrically heated externally configured thermionic diodes with emitter using mandrel side of CVD fluoride tungsten for electrode surface 11 p1715 A71-25911
- Single isolated solid particle irradiation in vacuum, using electrical suspension system with electric field produced by six electrodes on solid cube surface 11 p1806 A71-26087
- DC vacuum arc ion currents between copper electrodes, discussing wall geometry, plasma ionization, starvation phenomena and anode spot formation 12 p1939 A71-27269
- Electrocardiography from unprepared skin without paste, using integrated stainless steel electrode-buffer amplifiers 13 p2023 A71-29399
- Electrode voltage of rectangular cross section MHD channel in conductive flowmeter, investigating magnetic field inhomogeneity and velocity profile effects 14 p2279 A71-29617
- Electrode size effects on voltage loss and boundary layer conductivity of combustion driven MHD generator 14 p2287 A71-29880
- Conical metal core electrode erosion rates in pulsed plasma accelerators with refractory dielectric chamber 14 p2282 A71-30671
- Plane diode electrode gap differential capacitance for operation with anode negative voltage, current saturation and space charge limitation 16 p2548 A71-33709
- Plasma jet formation within high pressure discharges in air at atmospheric pressure, discussing electrode configuration, current density and accelerating magnetic field strength 17 p2787 A71-34285
- Ti alloys electrosag welding with consumable and nonconsumable electrode combinations, presenting W electrode consumption and weld mechanical properties 17 p2748 A71-34805
- Electrosag welding of large pressed Al-Mg alloys sections, using electrodes to reduce weld grain size and obtain high mechanical properties 17 p2748 A71-34807
- Electric and magnetic fields effect on turbulent boundary layer of conducting gas near electrode in MHD channel with insulated walls 18 p2951 A71-36113
- Plasma wind tunnels for high enthalpy flows of low density, considering plasma arc heaters and expansion nozzles with diffusers 19 p3040 A71-37461
- NiCd battery and third electrode characteristics for different charge and discharge rates, considering end-of-charge control system optimized for satellites and manned spacecraft applications 20 p3179 A71-38904
- Ni-Cd battery cell with third electrode for charge control, testing thermal and electrical performance as function of charge and discharge rate 20 p3179 A71-38905
- High temperature properties of weld metals formed by electrodes for welding of low alloy heat resistant Cr-Mo and Cr-Mo-V steels 20 p3249 A71-39014
- Electrode configuration and power output for transverse flow carbon dioxide laser consisting of two parallel water cooled copper tubes perpendicular to gas flow 21 p3391 A71-40182
- Sporadic E layer observation by reference electrode of electron temperature probe on sounding rocket, determining electron density below 85 km in D region 23 p3671 A71-43367
- High DC field induced ionic wind, deriving electric and pneumatic parameters for various electrode configurations 24 p3849 A71-45369
- ELECTRODIALYSIS**
 Automated self sterilizing breadboard unit for potable water reclamation from urine by electrolysis-electrodialysis for long term space missions [ASME PAPER 71-AV-11] 18 p2866 A71-36378
- ELECTRODYNAMICS**
 NT ELECTROHYDRODYNAMICS
 NT ELECTROMECHANICS
 NT QUANTUM ELECTRODYNAMICS
 Quantum dynamics boundary value problems numerical solutions, explaining algorithms used 01 p0052 A71-10419
- Threshold emission and self excitation of spatially inhomogeneous laser, considering active element gain and refractive index by electrodynamic model 01 p0094 A71-10687
- General relativistic formulation of massive magnetized rotating conductor, showing electrodynamic properties of surrounding empty space for explanation of stellar structure 01 p0160 A71-11273
- Ionospheric research covering electron and ion distributions, ion chemistry, neutral atmosphere interactions, thermal structure, electrodynamics, etc 03 p0416 A71-14031
- Electrical polarization of vacuum around rotating magnetic Newtonian star, evaluating electrostatic potential 04 p0643 A71-14912
- Soviet book on continuous medium covering dynamic, thermodynamic and electrodynamic equations mechanic problems, three dimensional space, internal degrees of freedom, etc 04 p0626 A71-15373
- Numerical solution of nonself adjoint boundary value problems of electrodynamics using finite difference scheme and iterative processes 07 p1159 A71-19179
- Physics laws and simplifications, discussing Newtonian mechanics, electrodynamics, relativity, atomic physics and quantum theory 07 p1163 A71-19603
- Cosmological plasma physics, considering matter, antimatter, electrodynamics, ambiplasma, annihilation and heavy nuclei 07 p1196 A71-19649

- Threshold emission and self excitation of spatially inhomogeneous laser, considering active element gain and refractive index by electrodynamic model
07 p1125 A71-20148
- Electrodynamics forces distribution in conducting bodies in two traveling magnetic fields with different frequencies and pole spacings
09 p1499 A71-22137
- Electrodynamics transducer design for structural vibration testing system, using low power steering signal converter to generate large scale electromechanical loads
09 p1386 A71-22606
- Helmholtz and relativistic electrodynamics, discussing kinetic interaction potential using Lorentz invariance
10 p1644 A71-25110
- Digital control systems for electrodynamic vibration exciters, discussing computer ranged instrumentation amplifier, digitally controlled sine wave oscillator and FFT processor
11 p1746 A71-26503
- Hypersonic wakes conductivity measurements behind models in argon and air, using electrodynamic technique
12 p1863 A71-27208
- Pulsar electrodynamics, considering oblique rotator with dense magnetosphere to supply particles for Gunn-Ostriker mechanism
12 p1968 A71-27539
- Lightning problem from electrodynamic viewpoint, considering vertical discharge channel, charge distribution, current and nonuniform inducing fields
13 p2097 A71-28394
- Electromagnetic radiation from stationary electric dipole imbedded in plasma column moving in axial direction
13 p2110 A71-29389
- Electric circuits calculation in MHD problems such as MHD channel flow, electrodynamic plasma, etc
14 p2277 A71-29558
- Optimal phase trajectories of coordinates of electrodynamic vibration test stand, analyzing motion of moving part and optimal control signal along coil
15 p2353 A71-32190
- Magnetoelastic oscillations of thin conducting plate in magnetic field, solving electrodynamic equations
16 p2647 A71-32928
- Electrodynamics Lagrangian with gauge invariant electron operator, obtaining free field nonequilibrium commutators and photon propagator for perturbation theory
16 p2610 A71-33269
- Nonhomogeneous media electrodynamics, solving nonstationary equations by differential operators dependent on permittivity and permeability
17 p2776 A71-34277
- Coaxial electrodynamic plasma acceleration, investigating tripler electron and ion recombinations effects
19 p3108 A71-37129
- Electromagnetic wave propagation in comb type waveguides, obtaining boundary value electrodynamic problem rigorous solution
19 p3020 A71-38342
- Hypersonic wakes conductivity measurements behind models in argon and air, using electrodynamic technique
19 p2994 A71-38620
- Peak electron density variations during midlatitude F region storm, investigating electrodynamic drift effects
21 p3372 A71-40037
- Superconductors intermediate state interrelated electrodynamic and thermal effects, calculating resistivity, heat conduction and thermoelectricity tensors
21 p3432 A71-41267
- Electrodynamics of turbulently moving electrically conducting medium, allowing for Hall effect
21 p3453 A71-41356
- Two sided error estimates for electrodynamic impedance, admittance and scattering matrices in diffraction theory
24 p3805 A71-45256
- ELECTRODYNAMOMETERS**
U DYNAMOMETERS
ELECTROENCEPHALOGRAM
U ELECTROENCEPHALOGRAPHY
ELECTROENCEPHALOGRAPHY
Matrix switch amplitude analyzer for EEG signals providing feedback stimuli to subject
01 p0021 A71-10246
- Digital delta filter for quantifying sleep EEG slow wave activity
01 p0011 A71-10767
- EEG dynamics and visual cortex neuron responses in cats to conditioned optical stimulus during defensive reflex formation
01 p0011 A71-11052
- Standardized EEG data recordings in Air Force neurological evaluations
02 p0208 A71-12393
- In-flight EEG recordings telemetry for pilot aptitude testing, showing pilot error relationship to brain oversteering
03 p0370 A71-13067
- Sound duration effect on brain activity of cats, studying EEG and behavioral responses
03 p0361 A71-13189
- EEG topography continuous recording for signal analysis based on regression theory
05 p0713 A71-16321
- EEG wave phase durations over human brain surface, examining asymmetry distribution level
05 p0709 A71-16801
- Topography of acoustically evoked potentials triggered by alpha activity in man
05 p0710 A71-16942
- Multichannel EEG radio telemetry for remote recording of biological activity from subjects in motion and within human body
05 p0715 A71-17110
- Surface negative slow EEG potential (CNV) in human brain after total sleep loss
06 p0850 A71-17428
- Mean period spontaneous EEG as psychophysiological characteristics of higher nervous activity in human individuals
06 p0858 A71-17600
- Photostimulation at South Pole by EEG, showing no brain stress, undue tension nor anxiety during hypobaric hypoxia acclimatization
06 p0851 A71-17608
- Electroencephalographic and motor effects of electrically stimulated reinforcing and negative subcortical structures in sleeping cats
06 p0852 A71-17669
- Bioelectric activity of cerebral cortex in man under neuroemotional stress, using multicannel radioelectroencephalography
06 p0856 A71-18464
- Correlation and spectrum analysis of simultaneous EEG data in mono and dizygotic twins using computer and FFT algorithm
08 p1246 A71-20746
- EEG analyzer voltage peaks recording on computer, using digital readout for simultaneous initial and terminal stage markings
08 p1248 A71-21446
- Human conditioned reflexes to time and EEG responses under acute hypoxia
08 p1243 A71-21970
- Humans and animals acute hypoxia effects on EEG pattern and behavioral reactions
09 p1390 A71-22210
- Electroencephalophone for stereophonic display of four channel EEG physiological signals from skull quadrants
09 p1397 A71-22252
- Computer aided statistical model of visual evoked potential in man as normality criterion for pathological indicator
09 p1397 A71-22253
- Electroencephalogram alterations in dogs and monkeys during bromotrifluoromethane exposure, correlating brain wave patterns with CNS depression [AMRL-TR-69-14]
09 p1398 A71-22475
- Electroencephalogram analysis, using analog computers for biopotential data reduction
09 p1398 A71-22489
- W-formed summated evoked potential to light stimulus in healthy subjects significant to Wilcoxon test
09 p1393 A71-23012
- Clinical value of electroencephalogram following sleep deprivation in detecting abnormalities in neurological patients
09 p1395 A71-23248
- Biological learning, considering EEG wave activity association with structural change underlying information storage in cerebral tissue
10 p1562 A71-24226
- Astronaut electrode-amplifier helmet harness for cable and radiotelemetry acquisition of EEG, EGO, EMG and blood pressure data on noninterference basis
10 p1570 A71-24475
- Central nervous system responsiveness changes after exhausting physical exercise, giving electroencephalogram and sensorimotor reaction records
11 p1719 A71-25668
- Waking and sleeping EEG signals bispectrum analysis, correlating component waves interactions with alpha activity, lead placement and state of consciousness
11 p1722 A71-26378
- Cortico- and subcorticograms rhythm dynamics in sleeping and awake cats by spectral analysis and EEG integration
12 p1871 A71-27486
- Rabbits and humans behavioral reactions and EEG changes relation to hypoxia in pressure chamber
12 p1871 A71-27488
- EEG examination of healthy aircrew for high performance aircraft flying fitness evaluation, stressing hyperventilation factor importance
12 p1876 A71-27631
- Somatosensory cortical and cuneate evoked responses and EEG amplitude/frequency changes due to hypovolemic shock
13 p2003 A71-27836
- Behavioral arousal and EEG thresholds changes during sleep due to electrical and audio stimulation
13 p2005 A71-28379
- Behavioral effects of electrically induced EEG abnormalities in inferotemporal and occipital cortex in monkeys on visual pattern discrimination and successive spatial reversals
13 p2011 A71-28806
- Evoked cortical responses to taste solutions of acid and salt applied to human tongue surface, using averaging technique
13 p2012 A71-28887
- Visual evoked cortical response in man related to rate, spatial frequency and wavelength of alternating barred pattern with background illumination
13 p2012 A71-28888
- Compact head mounted six channel IC telemeter for artifact free EEG recording during laughter
13 p2020 A71-28889
- Electroencephalographic and evoked cortical potential correlates of reaction time and visual discrimination in humans
13 p2022 A71-29345
- Psychobiological effects of prolonged bed rest in young healthy volunteers from EEG recording, psychological testing and psychomotor performance
13 p2022 A71-29363
- Alpha rhythm activity, periodicity and mean frequency in cortex regions of healthy humans based on EEG frequency and correlation analyses
14 p2186 A71-30551
- EEG and derivative spectral characteristics evaluation in determining pilot mental activity during flight
15 p2362 A71-31250
- Subcortical-cortical EEG recording of unrestrained chimpanzees sleep cycles, using computer analysis and bioelectricity techniques
15 p2359 A71-31951
- Human subjects REM sleep characteristics under 5-hydroxytryptophan influence, analyzing continuous polygraphic recordings of parietal EEG, horizontal eye movement and submental electromyographic activity
15 p2359 A71-31952
- Human vigilance performance and personality traits characterization by EEG alpha frequencies, correlating rest and task period recordings
15 p2359 A71-31954
- Cerebral ischemia effects on sensorimotor cortex function in cats, recording spontaneous EEG and pyramidal response to cortex electrical stimulation
15 p2359 A71-31956
- EEG phase relations measurement technique, using small digital computer for frequency components separation and EEG activity phases comparison between electrodes
15 p2363 A71-31959
- Simplified EEG time domain procedure, using method of period analytic estimates of power spectrum moments
15 p2364 A71-31960
- Computerized assistance in EEG analysis and interpretation, describing computer program for time and effort reduction in EEG reporting
15 p2365 A71-32449
- Human operator work quality evaluation with EEG data based on brain electrical activity as function of central nervous system
15 p2365 A71-32530
- Cortical neurodynamics during vestibular afferent activity and associated cardiovascular and respiratory reactions, noting EEG correlation to hemodynamics
16 p2527 A71-32828
- Space flight sleep pattern data with EEG, using three descriptors and regression and linear discriminant analysis
16 p2528 A71-33108
- Adrenalectomy influence on electrical activity of cortex and subcortical areas in rats under hyperbaric oxygen, using implanted electrode electroencephalographic recordings
16 p2528 A71-33118
- Objective monitoring of human operator, using statistical analysis of EEG based on numerical characteristics of energy spectrum
17 p2692 A71-35168
- Rhesus monkeys electrocortical events recorded during foreperiod of reaction time tasks
18 p2853 A71-35895
- Bispectral analysis of EEG frequency bands interrelations
18 p2863 A71-35896
- Human EEG changes and motor analyzer activity during mental visualization of motions
19 p3002 A71-37445
- Electroencephalographic evaluation of brain functions disturbances in response to stress in flying personnel, relating fatigue and rest periods allocation
19 p3008 A71-38223
- Regional cerebral blood flow, tissue oxygen, EEG activity and behavioral reaction at high pressure
19 p3009 A71-38557

- Medical, zoological and biological effects of ELF signals in atmosphere, comparing with EEG alpha and gamma rhythm
20 p1393 A71-39478
- Corned-retinal potential as generator of occipital alpha rhythm in human electroencephalogram modulated at 10 Hz by tremor in extraocular muscles
21 p3329 A71-40176
- Miniature biopotential transmitter suitable for telemetry, giving EEG and circuit and performance characteristics
21 p3342 A71-40184
- Human blood pressure in brachial artery during spontaneous night sleep, recording EEG, EKG and horizontal eye movements
21 p3329 A71-40185
- Hyperbaric normoxic breathing helium, nitrogen and neon gas mixture effects on EEG and reaction time in man
21 p3342 A71-40347
- Potential epilepsy determination in flight personnel, suggesting systematic EEG with hyperventilation and photic stimulation tests and personal history data of head trauma and unconsciousness
21 p3331 A71-40357
- Analog statistical analyzer for measuring one dimensional EEG amplitude distribution functions, illustrating reaction response to threshold acoustic stimuli
21 p3344 A71-41067
- Analog computer analysis of EEG wave asymmetry for organism functional state detection illustrated on human reaction response to threshold acoustic stimuli
21 p3344 A71-41068
- EEG study of hyperoxic convulsions in Macacus nemestrinus and Papio primates, considering preventive effect of Diazepam and derivatives
21 p3339 A71-41418
- Miniaturized multichannel FM/AM biological telemetry system for simultaneous transmission of EEGs, EMGs, EOGs and EKGs
22 p3500 A71-41574
- Pilot EEG, behavioral and subjective correlates of natural and drug induced sleep at atypical hours, using calculation and vigilance tests
22 p3502 A71-41835
- EEG characteristics of cadets and flying personnel, noting spike wave paroxysmal screening and epilepsy detection
22 p3502 A71-41836
- Human cerebral EEG phenomena and evoked potential relationships to eye and retinal image movements
22 p3488 A71-42437
- Hypothalamus anterior and hippocampus limbic system relation and oxytocin effect in rabbits, using EEG analysis
22 p3490 A71-42577
- Prolonged bed rest effects on EEG sleep patterns in young healthy subjects with and without exercise
23 p3631 A71-43109
- ELECTROEROSION**
U SPARK MACHINING
ELECTROEXPLOSIVE DEVICES
U INITIATORS [EXPLOSIVES]
ELECTROFORMING
Electroformed Al contact solar cells without soldering, investigating process parameters effects on performance
05 p0699 A71-16062
- ELECTROGENERATORS**
U ELECTRIC GENERATORS
ELECTROHYDRAULIC CONTROL
U ELECTRIC CONTROL
U HYDRAULIC CONTROL
ELECTROHYDRODYNAMICS
Electrofluid dynamic direct energy conversion, discussing working media, duct geometry, unipolar charges, and fluidic switches
[ASME PAPER 70-ENER-A] 03 p0353 A71-13704
- Electrofluiddynamic colloid generator performance characteristics, considering power output limitation due to electric breakdown
[ASME PAPER 70-WA/ENER-5] 03 p0355 A71-14108
- Electrohydrodynamic flow in plane channel with conducting walls and axial emitter electrode, determining velocity and pressure profiles distortion
09 p1502 A71-22538
- Quasi-one dimensional approximation equations derivation for electrohydrodynamic channel flows with small interaction parameter, obtaining I-V characteristics
10 p1649 A71-24365
- Electrohydrodynamic ideal incompressible fluid flow in flat and circular channels, determining electric potential and field distribution
12 p1941 A71-27520
- Quasi-one dimensional nonlinear model of electrohydrodynamic stability and control of current carrying seminsulating jets at supercritical and subcritical regimes
13 p2118 A71-29249
- Jet streams simulation method by electrohydrodynamic analog, using principle of mapping free lines of flow
19 p3043 A71-37542
- ELECTROJETS**
NT AURORAL ELECTROJETS
NT EQUATORIAL ELECTROJET
SD geomagnetic variations and electron jet spread over polar cap stream during solar cycle
02 p0243 A71-11763
- Polar magnetic disturbances in electrojet, studying Hall conductivity, electric field behavior and auroral ionosphere ionization
07 p1101 A71-19415
- Sq ionospheric current systems longitude and seasonal variations, observing focus positions and electrojet characteristics
08 p1278 A71-21197
- German monograph on three component magnetometer for position determination of polar electrojet by sounding rocket
18 p2915 A71-35921
- Polar magnetic disturbances in electrojet, studying Hall conductivity, electric field behavior and auroral ionosphere ionization
19 p3054 A71-37839
- Radio and optical aurora correlation and control by polar electrojet, using VHF backscatter and geomagnetic recordings
20 p3229 A71-39853
- Ionospheric small scale electron content irregularities and electrostatic plasma instabilities correlated with electrojet current intensity
22 p3535 A71-42223
- Polar electrojet development during polar magnetic substorms, considering current intensification at northern and/or southern borders
23 p3668 A71-43167
- ELECTROKINETICS**
Capillary and electro-osmotic flow pumping in heat pipes, discussing capacity increase
[AIAA PAPER 71-423] 11 p1857 A71-26214
- ELECTROLUMINESCENCE**
Light emitting film /LEF/ displays, discussing physical principles, construction and applications of electroluminescent thin film devices
07 p1105 A71-18737
- Electroluminescent aircraft instrument lighting effects on pilots dark adaptation taking into account color, panel legibility, scotopic sensitivity and acuity
08 p1248 A71-21229
- Electroluminescent semiconductor diodes based on GaP and GaAlAs, discussing design, properties, uses and production
11 p1737 A71-25569
- Physical model of Zn diffused GaAs electroluminescent diodes gradual degradation, establishing formation of new recombination centers through injected carrier lifetime measurement
15 p2377 A71-32607
- Rhodamine, sodium fluorescein and cyanocyanine dyes for liquid lasers, investigating electroluminescence by polarography
16 p2587 A71-33382
- Long duration brightness change in electroluminescent panel detection during monitoring task, discussing role of payoffs and signal ratios
17 p2690 A71-34705
- Oxygen contamination effect on GaP solar cell electroluminescence and photoluminescence characteristics from electrical and mass spectroscopic analysis data
19 p2998 A71-38143
- Electrical, photoelectric and electroluminescent properties of reverse biased GaP p-n structures at room temperature, considering isolated microplasmas
21 p3430 A71-41217
- Electrical properties and electroluminescence measurements for p-n junctions in Au- and Ag-doped GaP, noting negative resistance in I-V characteristics
21 p3433 A71-41312
- Solid state charge controlled electroluminescent display panel with image memory capability, describing negative oxygen ions and photoconductive charge control methods
22 p3548 A71-42514
- Dynamic active element model of electroluminescent image converter with positive optical feedback, using voltage-brightness approximation
24 p3808 A71-44389
- ELECTROLUMINESCENT LAMPS**
U ELECTROLUMINESCENCE
U LUMINAIRES
ELECTROLYSIS
Anomalous anodic Be dissolution in anhydrous environment, considering chunk effect and multivalent ions production mechanisms
07 p1118 A71-19568
- Al electrodes in molten salt electrolytes, investigating electrochemical kinetics by polarization measurements
[ECS PAPER 200] 08 p1250 A71-21470
- Electrochemical machining based on Faraday laws of electrolysis
13 p2075 A71-28948
- Closed cycle life support water electrolysis system using solid plastic sheet electrolyte /ion exchange membrane/ of sulfonated perfluoro polymer
[ASME PAPER 71-AV-9] 18 p2866 A71-36376
- Automated self sterilizing breadboard unit for potable water reclamation from urine by electrolysis-electrodialysis for long term space missions
[ASME PAPER 71-AV-11] 18 p2866 A71-36378
- Oxygen generation system for 90-day space station simulator, considering carbon dioxide removal and reduction and water electrolysis
[ASME PAPER 71-AV-18] 18 p2867 A71-36385
- Zero-gravity circulating water electrolysis system prototype design for metabolic and leakage makeup oxygen supply in 12-man space station regenerative life support system
[ASME PAPER 71-AV-20] 18 p2867 A71-36387
- Water vapor electrolysis for oxygen generation and humidity control in long term manned space flight
[ASME PAPER 71-AV-24] 18 p2868 A71-36391
- Static feed water electrolysis system of life support system, discussing current density, operating time and temperature effects on voltage for various electrochemical cell sizes
[ASME PAPER 71-AV-25] 18 p2868 A71-36392
- Electrolytic production of metal powder in continuously operating facility, using vibrating cathodes with chambers filled with granulated anode metal
19 p3068 A71-37105
- ELECTROLYTE METABOLISM**
Sound effects on endocrine function and electrolyte excretion in animals and man, considering adenylohypophyseal, neurohypophyseal and thyroid functions, diuresis and natriuresis
03 p0359 A71-13153
- Carbohydrate metabolism and electrolyte changes in human muscle tissue during heavy exercise
06 p0856 A71-18387
- Biosatellite postflight experiment evaluating effects of forced electrolyte imbalance in Macaca nemestrina
08 p1239 A71-20821
- In-flight monkey cardiovascular observations, discussing central venous pressure, urine volume, electrolyte imbalances and heart rate
09 p1395 A71-23244
- Urinary metabolites relationship to fatigue, considering excretion of proteins, electrolytes, simple organic compounds and hormones
17 p2679 A71-34357
- Ouabain insensitive effects of metabolism on ion and water content of red blood cells
17 p2681 A71-34943
- High altitude exposure effects on concentration and total quantity of electrolytes in human serum and extracellular space
19 p3009 A71-38562
- Hibernation effects on hedgehog electrolyte distributions and renal function, determining Na, K, Mg and Cl concentrations in muscles, liver, kidney, plasma red blood cells and bladder urine
22 p3488 A71-42416
- ELECTROLYTES**
NT ION EXCHANGE MEMBRANE ELECTROLYTES
Electrochemical machining package consisting of machine tool, electrolyte system and power supply
[SME PAPER MR-70-512] 01 p0090 A71-11268
- Electromagnetic repulsion of conducting and dielectric bodies within liquid metal and electrolyte in crossed field under gravitational acceleration
02 p0293 A71-12630
- Rapid mass transport to Pt electrodes in foamed electrolytes, examining current density-anode overpotential relationship
02 p0210 A71-12957
- Physical changes at lithium electrodes during charge-discharge cycling in propylene carbonate electrolyte
03 p0350 A71-13030
- Electric properties of solid modified AgI electrolyte batteries
03 p0351 A71-13032
- Alkaline fuel cells electrochemical regeneration for controlling carbonate concentration in electrolyte for performance improvement
03 p0353 A71-13057
- Solid electrolyte batteries development, considering design, performance, advantages and applications
03 p0355 A71-14322
- K, Na, Ca and I electrolytes content in thyroid gland and blood during experimental hypothyroidism in rabbits
06 p0852 A71-17668
- Hard alloys electrolyte selection for electrochemical dimensional machining
07 p1120 A71-20206
- Electroerosion and electrochemical combined effects on machining surface removal, discussing optimal anodic removal rates and electrolyte concentrations
08 p1296 A71-20852
- Zinc morphology electrodeposited from alkaline electrolyte, investigating charging and cell failure
08 p1233 A71-21081

Temperature dependent ionic domain for yttrium oxide doped thoria as solid electrolytes at low oxygen activities

09 p1480 A71-22114

Ti-V alloys electrolytic deposition, discussing electrolyte composition, current density, temperature and coating thickness

10 p1627 A71-24646

Alumina and titania codelposition from acid copper electrolyte as function of oxide crystalline form, discussing addition agents effects

11 p1779 A71-26011

Solid electrolyte oxygen generator electrolysis test module with improved ceramic to ceramic and metal seals, electrode and grid design, discussing performance tests

[ASME PAPER 71-AV-8]

18 p2866 A71-36375

Closed-loop solid electrolyte oxygen regeneration life support system, discussing 180-day life test

[ASME PAPER 71-AV-32]

18 p2869 A71-36399

Electrolytic behavior of yttria-hafnia solid solutions from X ray analysis and electroconductivity measurements

18 p2874 A71-37001

Al electrolytic capacitors characteristics as function of temperature, time and frequency of operation, noting improvement by organic solvents use as electrolyte component

20 p3203 A71-38884

Negative differential conductance of anthracene single crystals in electrolytes, observing N-shaped I-V characteristics

21 p3430 A71-41221

Maximum bubble pressure automatic capillary electrometer for salt solutions and organic compounds electroosorption, comparing with Lippmann instrument and capacitance bridge

22 p3548 A71-42529

Crystal Al powder electrolytic production in inert atmosphere, discussing fractional composition, current efficiency, gravimetric density and particle morphology

24 p3837 A71-44734

Steady acceleration sensor system with two electrode chambers in closed circuit, producing convective flow by electrolyte density gradients

24 p3828 A71-45099

ELECTROLYTIC CELLS

Copper oxide-magnesium thermal cells open circuit voltage drop in latter discharge stages, discussing cuprous ion activity at cathode

02 p0197 A71-12959

Solid state electrochemical energy storage device using rubidium silver iodide electrolyte

03 p0350 A71-13031

High energy density solid state electrolyte cell with lithium anode

03 p0351 A71-13033

Zinc-mercuric oxide cells with self supporting anodes of controlled porosity for improving low temperature performance

03 p0351 A71-13039

Phosphoric acid corrosion resistant alloys for electrolyte fuel cells, discussing materials selection and optimization

03 p0440 A71-13055

Solid electrolyte batteries development, considering design, performance, advantages and applications

03 p0355 A71-14322

Primary and secondary silver oxide-zinc cells performance capability

08 p1235 A71-21098

Electrochemical properties of Na-W bronzes for use as electrocatalysts in acid electrolyte fuel cells

09 p1387 A71-23648

Carbon dioxide traces effects on composition, volume and electrochemical characteristics of trapped electrolyte hydrogen oxygen alkaline fuel cells

15 p2354 A71-32205

Energy transfer to MPD quasi-steady accelerator having electrolytic capacitors with large series resistance, integrating transmission line equations with Ruge-Kutta method

[DGLR-71-037]

17 p2794 A71-35539

High voltage solid state electrolytic cell battery with Li anodes, testing storage and discharge characteristics

20 p3181 A71-38935

Ni-Cd cells thermal conductivity measurements for heat balance and dissipation calculations for space vehicle power supply systems, describing experimental apparatus

[ECS PAPER 170]

20 p3184 A71-39556

Development and performance characteristic of batteries including Zn and Mg dry cells, metal air, organic electrolytic, organic cathode and secondary systems

24 p3793 A71-45133

ELECTROLYTIC GRINDING

U ELECTROCHEMICAL MACHINING

ELECTROLYTIC POLARIZATION

Heat resistant Ni alloys intermetallic gamma prime phase analysis by electrolytic separation

09 p1467 A71-22322

ELECTROLYTIC POLISHING

U ELECTROPOLISHING

ELECTROMAGNETIC ABSORPTION

NT AUROREAL ABSORPTION

NT MOLECULAR ABSORPTION

NT PHOTOABSORPTION

NT POLAR CAP ABSORPTION

NT ULTRAVIOLET ABSORPTION

NT X RAY ABSORPTION

Nonlinear light absorption in organic dyes liquid solutions

01 p0095 A71-11028

Ionospheric absorption of radio waves reflected from sporadic E layer, noting attenuation frequency dependence

02 p0211 A71-11768

Riometers accuracy and stability, considering measurement error of ionospheric radio wave absorption

02 p0247 A71-11774

Ionospheric absorption at solar maximum and minimum, comparing riometer measurements with ray tracing calculations and electron density, collision frequency or temperature profiles

02 p0245 A71-11962

Structural characteristics of light absorbing matter near sun from optical observations

02 p0308 A71-12096

LF EM wave absorption in disordered semiconductors, calculating frequency dependence of conductivity due to electron transitions between discrete local levels

02 p0297 A71-12618

IR radiation effect on gas molecular dissociation, showing dissociation temperature decrease due to IR photon absorption

02 p0288 A71-12850

Ionospheric nondeviative absorption diurnal variation describing function suitable for computer methods

03 p0378 A71-13315

Weak nonlinear absorption effects shown by passive optical elements placed in laser resonator cavity with large angular emission divergence

03 p0435 A71-13511

Cosmic photons Planck constant, considering photon absorption dependence on variations of spin angular momentum

03 p0473 A71-13562

CW carbon dioxide laser beam IR absorption by sulfur hexafluoride, investigating saturation parameter relationship to pressure, temperature and relaxation time

03 p0437 A71-13879

Conjugate observations of ionospheric absorption associated with electron precipitation during sudden commencement of magnetic storm

03 p0419 A71-14520

Absorption coefficient of plane wave scattering by thin spherical resistive shell for broadband RF radiation monitoring

04 p0558 A71-15149

Electromagnetic wave absorption in steady state cosmology, considering particle collision and radiation damping effects in plasma model

05 p0806 A71-16167

Electromagnetic wave absorption in Einstein-de Sitter cosmology, considering collision and radiation damping effects for radiated angular frequencies

05 p0806 A71-16168

Ionospheric absorption measurements noting diurnal, seasonal and solar cycle variations

05 p0740 A71-16429

Lower ionospheric cosmic noise absorption at 28.6 MHz, examining diurnal variations

05 p0740 A71-16430

F region cosmic noise absorption at 20-30 MHz over Delhi, examining diurnal, seasonal and solar cycle variations

05 p0808 A71-16431

Lunar oscillations in ionospheric absorption measurements, noting tides in f-min during high sunspot years

05 p0740 A71-16434

Radio wave ionospheric heating effect on absorption of probing waves of different polarization

06 p0888 A71-17289

Ionospheric absorption winter anomaly observation based on Loran-A pulse signals during IQSY, noting diurnal variation

06 p0889 A71-17685

Solar X-ray control of lower ionospheric radio wave absorption determined from Solrad 9 and Panska Ves Observatory data

06 p0892 A71-17921

Oblique incidence effect on reflection and absorption of laser light by solid surrounded by plasma in vacuum

07 p1166 A71-18886

Nighttime ionospheric absorption frequency dependence during solar activity cycle

07 p1100 A71-19400

Signal reflection from sporadic E layer, investigating multiplicity relationship to earth surface, ionization level, D region and nighttime absorption

07 p1100 A71-19403

Radio wave absorption measurement at constant solar zenith angle of 65 deg, discussing seasonal variation

07 p1101 A71-19400

Optical absorption spectra in Cu-doped p-type GaAs samples

07 p1177 A71-19400

Ionospheric absorption relation to solar X-ray flux enhancement during short wave fade-outs from OGO 4 and Solrad 9 satellites

07 p1064 A71-20100

Forbush decreases effects on radio wave absorption, cosmic ray variations and ionization in lower ionosphere cosmic layer

08 p1353 A71-20900

Structural characteristics of light absorbing matter near sun from optical observations

08 p1362 A71-21140

Wideband microwave absorbing wall using dielectric material of foamed polystyrol powder coated with graphite, discussing design procedure and thickness reduction

08 p1253 A71-21290

HF wave absorption in Ar plasma, observing production in open magnetic trap

08 p1339 A71-21480

Hydrogen-like centers in semiconductors, investigating secondary optical absorption

09 p1506 A71-22140

Electron entrainment by photons during intraband light absorption by free carriers in Ge semiconductors

09 p1507 A71-22230

Plane electromagnetic wave reflection from conducting convex cylinder in radially inhomogeneous absorbing medium, deriving equations for beam trajectories calculation

10 p1574 A71-23800

Balloon sonde for auroral luminosity measurement and comparison of auroral emissions, X rays and ionospheric absorptions

10 p1602 A71-24530

Thermospheric gas density determined from solar UV absorption measurement at grazing ray and near vertical incidence

10 p1676 A71-24550

Anomalous winter ionospheric radio wave absorption related to amplitude increases of microbarometric oscillations at ground level

10 p1606 A71-24910

Excited atom density determination for two-photon light absorption in one-dimensional medium, obtaining energy balance equation asymptotic solution and secondary radiation intensity

12 p1914 A71-27020

F region ion and temperature effects on VLF and ELF wave absorption in whistler mode propagation at midlatitudes during solar minimum

12 p1879 A71-27040

Photon emission-absorption probabilities relation in thermodynamically quasi-equilibrium state as function of photo transition excitation frequency, temperature and chemical potential

12 p1931 A71-27300

Simultaneous equatorial ionospheric absorption measurements at different longitudinal locations, using pulse reflection technique at 2.0-7.5 MHz

12 p1902 A71-27670

Winter day absorption variability of HF radio waves reflected at oblique incidence from ionosphere, using ray tracing method

13 p2027 A71-27790

Nondeviative absorption of RF signal at 2.2 MHz in presence of cusp type sporadic E layer

13 p2055 A71-27920

Semiconductor zinc selenide and zinc cadmium selenide crystals two photon absorption coefficients, noting forbidden bandwidth relation

13 p2077 A71-27950

Laser emission absorption in surface layer of optically glass, determining surface temperature dependence on emission energy density

13 p2079 A71-28850

Carrier mobility, conductivity and optical absorption in strong electric fields of chalcogenide glasses for switching and memory effect amorphous semiconductors

13 p2112 A71-28920

Inverted combination light scattering in liquid and solid crystals, showing polarization effects on absorption coefficient

13 p2101 A71-29020

Crystalline media impurity light absorption spectral band shape, noting laser resonance emission effects

13 p2080 A71-29023

Absorption, divergence and scattering attenuations and scintillation of microwaves from space sources, calculating frequency and distance dependence characteristics

13 p2034 A71-29390

Concentration and transport from auroral zone of minor constituents in mesosphere and lower thermosphere during anomalous midlatitude radio absorption periods

14 p2230 A71-29711

Limiting frequency for Ar plasma absorption of HF waves, observing plasma production in open magnetic mirror configuration

14 p2282 A71-30668

Ionospheric absorption winter anomaly including temporal and local variations and frequency dependence, examining possible correlations with stratospheric and mesospheric phenomena

14 p2237 A71-30943

Ionospheric propagation prediction accuracy problems, considering numerical mapping, horizontal gradients, absorption, scatter, maximum usable frequency and transequatorial propagation

14 p2202 A71-30949

Height variations of ionospheric absorption of downgoing whistler waves during nighttime at moderate and low latitudes

15 p2369 A71-31426

Superhigh frequency microwave absorption region localization in collisionless plasmas by plasma parameters measurement in toroidal magnetic field

15 p2370 A71-31737

Refraction and absorption length of coherent laser radiation propagating in high temperature cylindrical plasma column

15 p2458 A71-32390

Photon dwell time in one dimensionally isotropically scattering medium, assuming absorbed state as arbitrary function of optical thickness

15 p2492 A71-32460

Ionospheric absorption of 20 MHz radio waves as function of solar activity level, using electron density and temperature profiles

15 p2401 A71-32686

Continuous light absorption, emission and ionization relaxation behind shock front in xenon

16 p2613 A71-32890

Ionospheric absorption measurements at 272 kHz, using surface wave attenuation factor as calibration technique

16 p2562 A71-33072

Highly ionized plasma column anomalous microwave absorption near critical density as function of plasma frequency

16 p2619 A71-33176

Electromagnetic absorption cross sections from wave function of free carriers in semiconductors with point defects

16 p2623 A71-34031

HF radio absorption in antarctic night ionosphere, discussing solar activity effects

17 p2733 A71-34776

Mirror-contained collisional plasmas, deriving wave reflection and absorption from equilibrium density and temperature profile equations

18 p2950 A71-35860

Laser light beam attenuation, considering turbulent pulsation effects in closed channel fluid flow axial region

19 p3071 A71-37279

Nighttime ionospheric absorption frequency dependence during solar activity cycle

19 p3053 A71-37824

Signal reflection from sporadic E layer, investigating multiplicity relationship to earth surface, ionization level, D region and nighttime absorption

19 p3053 A71-37827

Radio wave absorption measurement at constant solar zenith angle of 65 deg, discussing seasonal variation

19 p3053 A71-37832

Solar activity effects on equatorial ionospheric absorption of radio waves, deriving solar cycle constant

19 p3055 A71-38042

F region radio wave absorption dependence on electron-ion temperature difference from energy balance considerations, testing by radar backscatter measurements

19 p3055 A71-38045

D region ionization by electron fluxes as explanation for latitudinal radio wave absorption

19 p3057 A71-38370

Recalculated radio wave absorption during oblique transit through ionosphere from vertical measurements using rhombic antenna at 25 MHz

19 p3058 A71-38388

Photometric measurements of light attenuation on baffles in visible, considering sensor location and surface coating

20 p3234 A71-39174

Mars ionosphere radio wave absorption integral coefficients, studying electron concentration and electron/gas molecular collisions frequency vertical profiles

20 p3297 A71-39629

Physical interpretation of electromagnetic waves attenuation function HF singularity during diffraction over spherical surface, applying to short wave diffraction in tropospheric model

20 p3198 A71-39802

Lunar tidal effects on semidiurnal periodicity in ionospheric absorption, showing time of maximum amplitude variation with geographic latitude

20 p3232 A71-39900

Ionospheric radio wave absorption winter anomaly concerning seasonal variations of D and lower E region collision frequencies and F region oxygen concentrations

21 p3373 A71-40048

Optical absorption and electron spin resonance in KCl with and without KOH, noting F band existence

21 p3414 A71-40070

Electromagnetic absorption in adiabatically expanding fully ionized cosmic plasma, using Einstein-De Sitter cosmology

21 p3442 A71-40161

Cosmic plasma electron thermal motions effects on cosmic electromagnetic absorption, taking into account electron-electron collision effects in electromagnetic waves dispersion relationships

21 p3442 A71-40162

Deactivation and radiative lifetime of CO Cameron forbidden transition spectral bands produced by photon absorption

21 p3418 A71-40232

Electron drag by photons during intraband light absorption by free carriers in n-Ge semiconductors

21 p3428 A71-41111

Nonisothermal turbulent plasma ion acoustic oscillations spectral energy density in electromagnetic wave field, calculating HF conductivity and absorption coefficient

21 p3424 A71-41132

Spectral dependence of photon capture cross section of negative Zn center in Zn-doped n-type silicon during electron excitation to conduction band

21 p3429 A71-41206

Nonlinear absorption in transparent semiconductors of picosecond light pulses from Nd laser with locked modes

21 p3431 A71-41256

Laser emission absorption in surface layer of optical glass, determining surface temperature dependence on emission energy density

21 p3394 A71-41297

Carrier mobility, conductivity and optical absorption in strong electric fields of chalcogenide glasses for switching and memory effect amorphous semiconductors

21 p3434 A71-41323

Two photon absorption coefficients of ZnSe and zinc cadmium selenide crystals for ruby laser radiation, showing energy gap reduction effect

21 p3395 A71-41340

Obliquely incident radio wave absorption measurements from January-October 1968 vertical ionospheric soundings, correlating diurnal variations with solar zenith angular changes

22 p3509 A71-41555

Air pressure effects on absorption dependence at IR wavelengths, using water vapor transmittance windows

22 p3511 A71-42303

Ambient medium, reabsorption and Faraday rotation effects on circular polarization degree of synchrotron radiation, using transfer equation

22 p3593 A71-42335

Day to day fluctuations of winter anomaly in ionospheric absorption, showing regular and irregular trends

23 p3666 A71-42974

Urbach absorption-photon energy law for excitons in AII-BVI semiconductors

23 p3716 A71-43481

Stratospheric warmings effect on F 2 region parameters and ionospheric radio wave absorption, assessing time lag

23 p3673 A71-44049

Absorption cross section for plane electromagnetic wave in circular plasma cylinder in constant magnetic field, assuming small Larmor radius

23 p3714 A71-44328

Microwave upper hybrid resonance absorption, emission and heating of nonuniform axially magnetized afterglow plasma column in waveguide geometry

24 p3851 A71-44430

Lower hybrid frequency heating and wave absorption efficiency in inhomogeneous HF cylindrical plasma

24 p3852 A71-44492

RF power absorption by magnetized uniform hot electron-ion plasma column submitted to TE and TM waves

24 p3852 A71-44498

Riometer measurement of ionospheric absorption, comparing with IQSY method

24 p3822 A71-44525

Radio absorption in lower ionosphere, determining vertical distribution of electron density and production rates from solar protons energy spectrum

24 p3867 A71-45041

Linear transformation and absorption of electromagnetic waves in plasma

24 p3857 A71-45167

Laser IR radiation attenuation in natural and artificial fogs, noting dependence on particle size distribution

24 p3835 A71-45254

ELECTROMAGNETIC COMPATIBILITY

Electromagnetic compatibility in space age, discussing effects of spectrum crowding, wider bandwidths, coding forms and growing use of microelectronics and solid state devices

04 p0555 A71-15342

Electromagnetic compatibility - IEEE Conference, San Antonio, October 1970

13 p2031 A71-28860

Electromagnetic compatibility program for aerospace systems, considering EM shielding and emission

13 p2001 A71-28866

MACE (management aid to compatibility engineering), consisting of analysis routines for IBM 7030 and Univac 1108 computers

13 p2032 A71-28871

EMC susceptibility test equipment consisting of portable buzzing relay noise generator

13 p2045 A71-28874

Communication electronic equipment electromagnetic compatibility characteristics derived from spectrum signature data, discussing application to systems design

13 p2032 A71-28876

Electromagnetic compatibility, measuring microwave antennas characteristics, including frequency range, gain, beamwidth, voltage standing wave ratio, impedance and radiation patterns

13 p2039 A71-28877

Broadband radiated interference measurement of nonhyperbolic propellant rocket engine spark gap ignition for electromagnetic compatibility

15 p2471 A71-32372

Electromagnetic compatibility - IEEE Conference, Anaheim, California, July 1970

19 p3030 A71-38426

RF communications spectrum pollution, discussing corrective and preventive electromagnetic compatibility measures

19 p3020 A71-38427

Electromagnetic compatibility performance of pulse Doppler radar receivers, considering CW or synchronous pulse interference

19 p3020 A71-38430

Everyday antipollution policy in electromagnetic compatibility, concerning social, medical, commercial, industrial, scientific and national defense aspects

19 p3021 A71-38431

Baluns as electromagnetic compatibility control devices for signal and common mode currents, providing basic parameters and equivalent circuits

19 p3030 A71-38433

Performance prediction model for electromagnetic compatibility of ATC radar beacon system, testing in interrogator-transponder links along air route

19 p3102 A71-38435

Reliability engineering techniques for design control of electromagnetic compatibility, employing statistical theory

19 p3030 A71-38437

Automated information systems for electromagnetic compatibility analysis using computer

19 p3030 A71-38438

Computer automated systems development for electromagnetic compatibility analysis, noting interactive processing in near real time mode

19 p3030 A71-38439

Environment, coupling and electronic equipment modeling for electromagnetic compatibility analysis

19 p3031 A71-38440

Earth resources experiments package electromagnetic compatibility with Apollo Applications Program

19 p3032 A71-38453

Electromagnetic compatibility in radio astronomy, discussing frequency spectrum pollution and national radio quiet zone

19 p3032 A71-38454

Power density prediction based on electromagnetic compatibility analysis of radar environments, comparing predicted propagation losses with measurements

19 p3021 A71-38455

Electromagnetic compatibility problems solution, discussing moment analysis methods

19 p3032 A71-38456

Co-site analysis model automated for evaluation EM compatibility of single site employing large number of transmitting and receiving equipments

19 p3032 A71-38457

Interference of transferred electron device operation involving harmonic tuning, considering EMC aspects

19 p3032 A71-38461

Complex airborne electronic system design for interference minimization, considering electromagnetic compatibility

19 p3033 A71-38464

Electromagnetic compatibility characteristics in terms of receiver susceptibility to interference effects on selectivity and nonlinearity parameters

19 p3033 A71-38465

Filter connectors for conducted electromagnetic interference suppression ensuring system electromagnetic compatibility, considering ceramic capacitors, pi-section and distributed feedthrough filters

21 p3353 A71-40442

- Book on practical design for electromagnetic compatibility covering interference control, reduction, analysis, prediction and measurement, shielding problems, etc 21 p3356 A71-40779
- ELECTROMAGNETIC CONTROL**
 U ELECTROMAGNETS
 U REMOTE CONTROL
ELECTROMAGNETIC DEDUCTION
 U MAGNETIC INDUCTION
ELECTROMAGNETIC FIELDS
 NT FAR FIELDS
 Electromagnetic wave fields in outer space during gravitational collapse of aspherical mass 01 p0160 A71-11064
 Semiconductor with charged impurities in strong electromagnetic field, investigating scattering effects on electron energy spectrum 01 p0140 A71-11463
 Electromagnetic potentials and Lorentz relation in anisotropic medium, considering Bromwich function and plane wave propagation 02 p0211 A71-11719
 Mercury droplet dynamics in conducting liquid within electromagnetic field under reduced gravitation 02 p0293 A71-12631
 Warm continuously stratified electron plasma fields behavior in coupling region excited by incident electron-acoustic wave 02 p0293 A71-12742
 Relativistic kinetic theory of particles with magnetic dipole moment in external EM field, deriving transport equations for distribution function 03 p0463 A71-13425
 Optical plate induced helicoidal steady light field in laser cavity, imparting structure to isotropic transparent material medium 03 p0436 A71-13787
 Vertical dipole electromagnetic field diffraction by circular aperture in opaque screen with coaxial concentric conducting disk 03 p0379 A71-13963
 Servosystems errors of indicator-receiver for recording electromagnetic field pattern extremes in amplitude radio interferometers 04 p0557 A71-14635
 Perturbation method in microwave electromagnetic field pattern determination and resonator design 04 p0586 A71-14657
 Shock tube flow interaction with EM field, using two step Lax-Wendroff finite difference method for partial differential equations 04 p0631 A71-14686
 Surface impedance of thin metal plate excited by RF electromagnetic field as function of external DC magnetic field 04 p0636 A71-14972
 Liquid metals vapor drag and electromagnetic fields effects on laminar film condensation, using finite difference method 04 p0688 A71-15539
 Relativistic electromagnetic field analysis, using fluid dynamic approach 04 p0628 A71-15917
 Plane wave diffraction by double grating of thin cylindrical cylinders, determining field polarization in directions parallel and perpendicular to axis 05 p0718 A71-15995
 SCL nomenclature denoting solar flare effect on long wave field intensity 05 p0804 A71-16033
 Complex rays for electromagnetic field construction, considering application to Gaussian laser beams 05 p0763 A71-16905
 Electromagnetic induction by plates with nonuniform conductivity distribution, applying results to North German anomaly 05 p0745 A71-17190
 Earth variable electromagnetic field spatial harmonics asymptotic properties 05 p0746 A71-17212
 Uniqueness theorem for sources of electromagnetic fields expressible as magnitude integrable functions of time, considering implications for antenna aperture limitations on radar resolution 06 p0868 A71-17729
 Electromagnetic induction in plate with two dimensional conductivity distribution for case of E polarization, representing field by Green functions 06 p0928 A71-18264
 Macroscopic dynamics of many-component plasmas in electromagnetic fields, discussing formulation in scalar complex wave equations containing pressure and electromagnetic potentials 07 p1168 A71-19688
 Supersonic wind tunnel electromagnetic balance with superconducting coils 07 p1084 A71-20151
 Self consistent Darwin model for slow wave electromagnetic plasma simulation 07 p1172 A71-20297
 Nonlinear effects in superconductors in electromagnetic field with constant and alternating components 07 p1181 A71-20535

- Bessel equation solutions for electromagnetic and acoustic wave equations in form of Hankel functions 08 p1333 A71-20740
 Satellite-borne long wave transmitting antenna excitation, calculating electromagnetic field near earth surface by earth-ionosphere waveguide model 08 p1252 A71-20744
 Dielectric loaded waveguide electromagnetic field and coupling matrix derivation by finite element computer program, presenting dispersion curves and field plots 08 p1262 A71-20765
 Static cylindrically symmetric universes consisting of Einstein-Maxwell gravitational and electromagnetic fields, discussing central axial mass and charge or current density 08 p1334 A71-21361
 Book on electromagnetic fields and waves covering vectors, current density, flux integral, Coulomb law, Laplace equation, magnetomotive force, waveguides, etc 08 p1335 A71-21459
 Book on plasma physics, Volume 1, covering electromagnetic fields, fluid mechanics and theory, mathematical analysis and thermodynamics 08 p1341 A71-21892
 Ring laser active medium polarization characteristics in strong field, taking into account spatial modulation of population 09 p1461 A71-22365
 Laminar geoelectromagnetic field excited by coaxial ring current, determining impedance and magnetic field ratios of spherical harmonics 09 p1435 A71-22434
 Lower ionosphere electromagnetic induction effect on geomagnetic field guided MHD wave propagation, considering Hall effect 09 p1435 A71-22436
 Microwaves anomalous skin effect in high density gaseous magnetoplasma, comparing experimental electromagnetic field penetration increase due to thermal electron motion with theoretical prediction 09 p1502 A71-22800
 Near field approximation for strong gravitational fields, noting close similarities to electromagnetic fields 09 p1493 A71-22803
 Steady electromagnetic oscillation amplitude calculation from solution kernel to Maxwell equations boundary value problems through orthogonal coordinate transformation to Fredholm integral equations 09 p1495 A71-23431
 Synthesis of primary electromagnetic fields of transmitting feed antenna for two dimensional circular cylindrical reflector 09 p1418 A71-23492
 Pulse excited finite length cylindrical monopole antenna mounted vertically on perfectly conducting ground plane, calculating near point electromagnetic fields 09 p1420 A71-23512
 Locally illuminated diffracting edge near field calculation in terms of Hankel function asymptotic solution 09 p1409 A71-23514
 Electromagnetic field measurements for continuous noise sources and traversed ionospheric region parameters, using ground, rocket and satellite techniques 09 p1440 A71-23629
 Polar cap cosmic radiation intensity measurement for deducing electromagnetic conditions near earth and in interplanetary space 10 p1661 A71-24310
 Soviet book on lasers with large angular divergence covering single mode generation, free electromagnetic fields equations, emission spectra, etc 10 p1621 A71-24728
 Stochastic particle acceleration in random electromagnetic field determination by turbulent plasma motion in external homogeneous magnetic field 10 p1655 A71-25075
 Source-subject coupling, reactive near field, multipath components and arbitrary polarization in hazardous EM fields quantification, discussing measuring techniques and instruments 11 p1717 A71-25286
 Electromagnetic fields induction in biological tissues, recording energy absorption temperature distribution in phantom models with thermograph camera 11 p1717 A71-25289
 Transverse EM field in plasma, deriving closed equation for distribution function 11 p1804 A71-25500
 Negative differential conductance of homogeneous nonequilibrium electronic solid-body plasma in electromagnetic field upon Cherenkov interaction 11 p1807 A71-25584
 Restricted set of correlated measurements with inductive theta pinch in MHD plasma accelerators, determining electromagnetic field structure and electron density distribution 11 p1766 A71-26288

- High velocity plasma jet accelerator operation, plotting heat and electromagnetic forces vs air current, mass flow rate and nozzle diameter 11 p1807 A71-26289
 Radiation mechanism of line sources array above finite ground plane, studying maximum field intensity variation and angle 13 p2028 A71-27991
 Local and sequential propagation characteristics of electromagnetic fields and waves in inhomogeneous lossy medium 13 p2028 A71-27995
 Earth variable electromagnetic field spatial harmonics asymptotic properties 13 p2060 A71-28267
 Three dimensional fields excited by arbitrarily oriented dipole in cylindrically inhomogeneous isotropic plasma, deriving closed form solution 13 p2107 A71-28786
 Isolation technique for recording low level ECG and deep body temperature signals in animals exposed to large amplitude RF fields 13 p2020 A71-28864
 EM field and wave propagation in static and spherical gravitation, obtaining modified Debye potentials and amplitude and eikonal equations 13 p2139 A71-28999
 Computer phase hologram synthesis simplified modification, using EM field vector transformation for points 13 p2070 A71-29029
 Gravitational radiation theory, discussing mechanisms, wave properties and analogies with EM fields 13 p2130 A71-29117
 Ion wave frequency shift and instability suppression by RF electric field, examining wave-field coupling 13 p2110 A71-29334
 Surface impedance of sphere based on received electromagnetic field amplitude-frequency characteristics 14 p2191 A71-29511
 Crab Nebula model, discussing electromagnetic field time variation and electron acceleration and synchrotron emission 14 p2304 A71-29632
 Reflection and refraction patterns of various wave number media vertical electromagnetic dipole fields at even and uneven interfaces 14 p2192 A71-29805
 Quasi-point type radar target angular motion simulation by controlling electromagnetic wave phase front in receiving field 14 p2193 A71-29825
 Electromagnetic field action on living organism simulated with infinite homogeneous cylinder in infinite cylindrical solenoid EM media 14 p2182 A71-30026
 Dielectric loaded waveguides electromagnetic fields solution by finite element method for cutoff modes determination 14 p2212 A71-30509
 Ion-acoustic oscillations excitation in rarefied plasma layers confined by external high frequency TE wave electromagnetic field 14 p2281 A71-30555
 Earth-ionosphere waveguide excitation by satellite-borne horizontal dipole antenna, deriving fields at earth surface based on idealized model 14 p2196 A71-30562
 Atmospheric spectral and structural characteristics, reviewing studies of source phenomena and related electric, magnetic and electromagnetic fields 14 p2237 A71-30965
 Cosmic ray particles acceleration in pulsar strong electromagnetic fields, investigating refractive index effects 15 p2473 A71-31717
 Fluid jet control by acting on thin guiding filament, noting electromagnetic deflections by ferromagnetic wire 15 p2353 A71-32073
 Gas dynamics of explosions, considering electromagnetic fields and chemical reactions effects on blast wave propagation in unbounded media 15 p2515 A71-32567
 Aperture field distribution for excitation of surface waves with high efficiency and gain 15 p2378 A71-32627
 Book on electromagnetic nondestructive test methods covering eddy current test, EM field theory, operation and design of sensing coils, etc 15 p2418 A71-32768
 Static electromagnetic fields in general relativity obtained for space-time metrics of group G automorphisms, considering Rainich unified field theory equations 16 p2610 A71-33265
 Harmonic electromagnetic field outside closed surface perfectly conducting antenna, using Kirchhoff formula 16 p2544 A71-34171
 Gravitational field equations derivation from least action principle, interpreting additional vector field in

generalization as vector potential of electromagnetic field

17 p2778 A71-34632

Book on microwave fields and circuits covering waveguides, transmission lines, impedance matching, sources, resonators, antennas, etc

17 p2716 A71-34772

MHD detonation waves in relativistic perfect fluid of magnetic permeability μ immersed in electromagnetic field

18 p2951 A71-36189

MHD equations of motion solved for conducting fluid interaction with electromagnetic field in porous media in range of Darcy law

18 p2953 A71-36948

Microwave reflection from semiconductor wafers with dielectric film, presenting electromagnetic field parameters as function of electrophysical properties

19 p3117 A71-37264

Computerized calculation of field configurations in automated design of electromagnetic transducers

19 p3038 A71-37774

Five component electromagnetic field station to record geomagnetic field magnetic and electric components variations

19 p3042 A71-38374

Electromagnetic and gravitational fields geometry, using compensating fields concept

19 p3105 A71-38581

Electromagnetic fields of finite linear antennas in dissipative half space, obtaining antenna patterns from computer results

19 p3023 A71-38589

Wide angle paraboloid reflector electromagnetic field intensity distribution measurements in focal region

19 p3035 A71-38601

Long wire electromagnetic scattered field modification by multiple impedance loading, deriving calculation formulas

19 p3024 A71-38607

Numerical procedure for electromagnetic field penetration through inhomogeneous cold plasma slab with collisions, using Riccati type differential equation

20 p3273 A71-39004

Nonlinear Faraday effect in nonparabolic semiconductors subjected to strong electromagnetic field and steady magnetic field, deriving distribution function of charge carriers

20 p3276 A71-39010

Electromagnetically driven shock tube with precursor effect due to ionization of impurities by UV radiation from discharge, using gages to tag gas flow

20 p3239 A71-39431

Thermodynamics second law restrictions on constitutive equations of electromagnetic theory for nonlinear materials with long-range gradually fading memory, considering dissipation principle consequences

20 p3270 A71-39485

$E \times B$ plasma instability in auroral arcs, deriving dispersion relation

21 p3373 A71-40045

Electromagnetic HF wave field pressure effects on slow transverse magnetic wave propagation along plasma layer, noting dispersion equations difference from linear theory

21 p3426 A71-41400

Plasma confinement in bounded systems, considering externally induced field HF pressure effect on plasma density distribution

22 p3580 A71-41600

Electromagnetic field distributions and far field radiation patterns of three layer waveguide GaAs heterostructure injection lasers, using Maxwell equations

22 p3555 A71-41688

Tracking servosystems errors of indicator-receiver of amplitude radio interferometers for recording electromagnetic field pattern extremes

22 p3521 A71-42275

Field configuration of TM mode in elliptical waveguide, showing inaccuracy of microwave theory

22 p3522 A71-42279

Magnetron crossed field amplifier multistage frequency multiplier HF field properties, obtaining numerical solutions for nonlinear governing equations

22 p3522 A71-42315

Plane wave diffraction by double grating of thin circular cylinders, determining field polarization in directions parallel and perpendicular to axis

22 p3515 A71-42744

Spheroid with two dielectric separated halves and mixed boundary conditions, determining spreading currents Lf electromagnetic field

22 p3484 A71-42879

Linearly and circularly polarized electromagnetic field effective scattering surfaces relationships determination as value proportional to reflected and transmitted rms flux density ratio

23 p3644 A71-43285

Asymptotic expressions for electromagnetic field and currents induced in unbounded dense plasma by relativistic electron beam passage

23 p3711 A71-43410

Mott exciton differential absorption spectrum in parallel and crossed electric and strong magnetic fields

23 p3716 A71-43479

Laser resonator natural field amplitude fluctuation calculation based on two- and four- level models for photon number dispersion

23 p3685 A71-43560

Electromagnetic field theory formulation, using Maxwell equations for spinors

23 p3705 A71-43827

Asymptotic expansion of axisymmetric electromagnetic beams with azimuthal dependence near internal caustic /focal line/

23 p3647 A71-44330

Open waveguide field expansion in orthogonal wave system with proper and improper modes

23 p3647 A71-44332

Microwave structures symmetry analysis based on group theoretic concepts application to vector electromagnetic fields, investigating single wire helix

24 p3809 A71-45090

Electromagnetic fields in moving anisotropic medium, using network formulation based on radial transmission line representation

24 p3805 A71-45092

TEM mode hybrid networks analysis extension to tapered transmission lines, indicating design limitations on VSWR and isolation characteristics

24 p3816 A71-45094

ELECTROMAGNETIC INTERACTIONS

NT PLASMA-ELECTROMAGNETIC INTERACTION

Electromagnetic mechanism of direct muon and gamma quanta production by collision of strongly interacting particles

03 p0462 A71-13864

Particle diffusion modulation by simultaneous VLF and ULF electromagnetic waves during rocket experiment

07 p1062 A71-19680

High microwave power for studying interactions in high concentration linear Ar discharge plasma waveguide in magnetic field

08 p1339 A71-21479

Electromagnetic effects in infinite conducting layer situated in field of inductors with mutually opposed traveling magnetic fields

09 p1499 A71-22138

Linear phased antenna arrays, calculating influence of interaction between radiating elements on radiation pattern

09 p1404 A71-22225

Photon emission from electron moving in field of two plane electromagnetic waves with different frequencies and propagating in same direction

09 p1460 A71-22364

Electron loss by resonant interaction with whistlers in nonuniform magnetic field, taking Fokker-Planck equation as distribution function

09 p1513 A71-22423

Pulsed radio wave interactions with various lower ionosphere models, estimating cross modulation by computer calculation for comparison with measurements

09 p1405 A71-22443

Models for nonferromagnetic solid body mechanics allowing for relationships among mechanical, thermal and electromagnetic processes

09 p1509 A71-23076

Neutrino magnetic moment spin precession effects on solar magnetic fields, discussing electromagnetic field-charged particles interaction

09 p1528 A71-23593

Astrophysics - Conference, University of Nice, France, April 1969

10 p1670 A71-24186

Intense light pulses interaction with solid materials, using laser techniques

11 p1775 A71-26088

Second harmonic generation in magnetized ferrite, considering nonlinear interaction between electromagnetic field and medium

12 p1879 A71-26996

Electromagnetic wave propagation on uniform transmission line network, discussing passivity and stability notions concerning energy exchange between waves and material

12 p1879 A71-27039

Reversible and irreversible processes and arrow of time concept, considering direct interaction of two charges without field

13 p2101 A71-28766

Linear nonequilibrium shock tunnel driven supersonic MHD generator operation under large scale power extraction and strong electromagnetic- rare gas interactions

14 p2287 A71-29879

Electron beam interaction with external harmonic microwave field in planar diode gap, calculating electric field current and voltage distribution functions

14 p2211 A71-30084

High microwave power for studying interactions in high density linear Ar discharge plasma waveguide in magnetic field

14 p2282 A71-30666

ELECTROMAGNETIC INTERFERENCE

Nonlinear interaction between three resonant modified ordinary electromagnetic waves propagating perpendicular to static magnetic field in homogeneous electron plasma, studying relativistic effects

15 p2460 A71-32655

Production cross section of Lee-Wick hypothetical massive electromagnetic bosons by muons at high energy, giving Feynman diagrams

17 p2785 A71-34750

Dynamic loading of cantilever beams by magnetomotive and explosive loads and high bullet speed impact, noting elastic and plastic deformation modes

18 p2981 A71-36770

Electrostatic oscillations excitation in magnetized homogeneous plasma by electromagnetic waves nonlinear interactions, deriving expression for induced fluctuations spectral density

20 p3273 A71-38966

Parametric excitation of ionic waves in ionosphere by irradiation with electromagnetic wave at characteristic electron frequency

20 p3218 A71-39546

Cosmic ray muon electromagnetic interactions and energy spectrum measurements at large zenith angles at sea level

22 p3593 A71-42356

Electromagnetic interactions of high energy cosmic ray muons from combined calorimeter-spectrograph investigation

22 p3594 A71-42409

Electromagnetic mechanism of direct muon and photon production by collision of strongly interacting particles

22 p3579 A71-42665

Microwave emission from plasmas in InSb with and without magnetic fields, deriving pseudolongitudinal wave interaction theory for explanation

23 p3714 A71-42914

Interplanetary time delay and light deflection measurements anomalies, investigating gravitational and electromagnetic fields interaction

23 p3766 A71-43824

Nonlinear theory for synchrotron emission of tubular electron flux in cylindrical waveguide, discussing wave-electron interactions optimization

23 p3653 A71-44058

ELECTROMAGNETIC INTERFERENCE

NT ATMOSPHERICS

NT BLACKOUT (PROPAGATION)

NT COSMIC NOISE

NT CROSSTALK

NT DAWN CHORUS

NT ELECTROMAGNETIC NOISE

NT HISS

NT IONOSPHERIC CROSS MODULATION

NT IONOSPHERIC NOISE

NT IONOSPHERICS

NT JAMMING

NT RADIO FREQUENCY INTERFERENCE

NT SHOT NOISE

NT SUDDEN ENHANCEMENT OF ATMOSPHERICS

NT THERMAL NOISE

NT WHISTLERS

NT WHITE NOISE

Noise interference problems solution by electrical and physical design action, discussing contact arc and ringing suppression

03 p0388 A71-13243

Electromagnetic compatibility in space age, discussing effects of spectrum crowding, wider bandwidths, coding forms and growing use of microelectronics and solid state devices

04 p0555 A71-15342

Interference reduction in logic circuits using combined signal amplitude-pulse duration discrimination

04 p0562 A71-15893

Optimal discrete signal filters with finite duration transient process, describing approximation procedure to restore noise distorted signals

06 p0876 A71-17928

Ground space facilities protection from lightning and electromagnetic interference

07 p1084 A71-19947

He-Ne laser coherence measurement by Young interference method, noting dependence on resonator mirror alignment

07 p1127 A71-20378

Pulsed signal amplitude and delay time measurement in presence of interfering /reverberated/ signals and steady noise

09 p1407 A71-23111

Inferring ionospheric electric fields at stratospheric levels with tropospheric penetration, using balloon measurements and model atmosphere

10 p1603 A71-24700

Handbook on electrical noise and electromagnetic interference specifications, Volume 1, covering noise pollution, industrial electronic equipment operation control, test plans and military standards

11 p1731 A71-25744

Electromagnetic interference, discussing man-made, inherent and natural types including atmospheric

ic electrical disturbance, precipitation static, sunspots, etc

12 p1879 A71-27059

Soviet handbook of aircraft electrical equipment covering DC and turbine powered generators, lubrication materials, electromagnetic interference counter-measures, etc

14 p2181 A71-29530

Electromagnetic interference measurements, considering direct reading with RI-FI receiver, impulse generators and spectrum analysis

14 p2193 A71-29915

Undesirable electromagnetic interference minimization in electrical equipment by filtering, shielding, balancing lines, hot/neutral lines twisting and coaxial cables

15 p2369 A71-31506

Matched/mismatched crossed beam interference field combination with sinusoidal holographic diffraction grating, studying metric properties and moiré/obtured bands

15 p2410 A71-32404

Space-time correlating antenna array forming matched filter for modulated signal reception with interference ejection

17 p2716 A71-34767

Cochannel interference reduction in FSK system by applying Hilbert transform techniques

17 p2703 A71-35079

High intensity continuous gas discharge line source for extreme UV with low electromagnetic interference

18 p2914 A71-35845

Phase locked loop models with off-tuned binary PSK interfering signal and angle modulated signal and noise at input, noting performance degradation

19 p3020 A71-38429

Electromagnetic compatibility performance of pulse Doppler radar receivers, considering CW or synchronous pulse interference

19 p3020 A71-38430

Common mode choke for reduction of current unbalance in cable to improve electromagnetic interference performance

19 p3000 A71-38432

Interference voltage prediction model of induced noise in reference ground of electronic systems

19 p3031 A71-38448

Radar antenna interference determination based on model using electrical and physical characteristics of reflector type antenna for statistical gain distribution prediction

19 p3021 A71-38458

Interference of transferred electron device operation involving harmonic tuning, considering EMC aspects

19 p3032 A71-38461

Complex airborne electronic system design for interference minimization, considering electromagnetic compatibility

19 p3033 A71-38464

Electromagnetic compatibility characteristics in terms of receiver susceptibility to interference effects on selectivity and nonlinearity parameters

19 p3033 A71-38465

Envelope limiting in control loops of adaptive array antennas, reducing varying noise interference

20 p3195 A71-38863

Pseudotransfer function for interference contrast of coherent illuminated phase edge object

20 p3245 A71-39427

Filter connectors for conducted electromagnetic interference suppression ensuring system electromagnetic compatibility, considering ceramic capacitors, pi-section and distributed feedthrough filters

21 p3353 A71-40442

Book on practical design for electromagnetic compatibility covering interference control, reduction, analysis, prediction and measurement, shielding problems, etc

21 p3356 A71-40779

Interfering beams amplitude modulation, applying optical heterodyne techniques

22 p3512 A71-42321

Book on interference of electromagnetic waves covering Michelson-Fizeau and Fabry-Perot interferometers, Fourier transform spectroscopy, etc

22 p3576 A71-42429

ELECTROMAGNETIC MEASUREMENT

L and S band paraboloidal dish antenna stellar calibration technique using absolute flux density from Cassiopeia A or Cygnus A

01 p0032 A71-10888

Radio telemetry transmitter receiver systems notch noise testing for relationships between spectral power density, video and IF bandwidths and peak deviation

01 p0034 A71-10908

Precision electromagnetic measurements - Conference, Boulder, June 1970

04 p0585 A71-14651

Submillimeter wave attenuation measurement over 1 km path during summer rainstorms, comparing results with millimeter waves

05 p0718 A71-15989

Upper atmosphere electromagnetic probing - Conference, Calcutta, July 1969

05 p0739 A71-16426

Top side ionosphere electromagnetic probing techniques, noting F and E regions

05 p0740 A71-16428

VLF electric field data in interplanetary medium from Pioneer 8 space probe observation

07 p1196 A71-19655

High Q factor rotor systems applications in dielectrics electromagnetic viscosity measurement and radio transmitters with low oscillation phase drift

09 p1492 A71-22363

Electromagnetic field measurements for continuous noise sources and traversed ionospheric region parameters, using ground, rocket and satellite techniques

09 p1440 A71-23629

Lunar surface electromagnetic sounding, presenting analysis of radiation fields and polarization characteristics for magnetic dipole situated on layered half space

10 p1576 A71-24054

Antenna effective area and radiation pattern measurement using emission characteristics of extraterrestrial radio sources, sun and moon

12 p1967 A71-27422

Refractive errors in spaced antenna radio angle-of-elevation measurements based on comparison with use of single directional antenna

12 p1881 A71-27424

Solar type 3 radio bursts polarization measurement by recording and subsequent digital processing

12 p1969 A71-27653

Local electron density measurements in low beta plasmas, using nonlinear electromagnetic wave mixing under synchronism condition

13 p2104 A71-27849

Narrow band atmospheric radio noise burst average and rms field strength measurement

13 p2033 A71-28900

Electromagnetic flowmeters readings for boundary effects of current equalization

14 p2279 A71-29616

F region drift velocity, wind, electric field, current and atmospheric composition variation measurements and related theoretical topics

14 p2201 A71-30940

Primary and secondary standardization and precision measurement of thermal noise power at various radio frequencies and temperatures

14 p2204 A71-30977

Atmospheric and man-made noise measurement techniques, using signal generator as reference standard for absolute amplitudes

14 p2204 A71-30978

Low frequency noise spectra measurement in varicaps by frequency modulation of harmonic oscillator, noting application to diode and p-n transistors

15 p2369 A71-31232

Shock wave splitting in KBr, determining shock profiles and velocities by electromagnetic method

15 p2463 A71-31385

Subsurface water detection on lunar traverse by tilt angle electromagnetic depth sounding

15 p2492 A71-32475

Lunar subsurface water detection from satellite in polar orbit around moon by electromagnetic measurement

15 p2492 A71-32476

Statistical analysis of radiometer measurement data of solar emission atmospheric attenuation at 19 GHz

15 p2496 A71-32710

Book on electromagnetic nondestructive test methods covering eddy current test, EM field theory, operation and design of sensing coils, etc

15 p2418 A71-32768

Electromagnetic coupling measurement between two antennas in cluttered communications system, emphasizing scale model prediction technique

17 p2703 A71-35078

Electronic two axis digitizer, discussing electromagnetic measuring concept, modular design, reliability and economics

17 p2711 A71-35291

Force and heat transfer measurement in hypersonic flows of low gas density, using electromagnetic balances for horizontal and vertical forces and pendulum method for measuring resistance

18 p2921 A71-36416

Inhomogeneous plasma sounding with electromagnetic waves

18 p2953 A71-37000

Gas flow velocity measurements in channel, using electromagnetic technique

19 p3061 A71-37090

Five component electromagnetic field station to record geomagnetic field magnetic and electric components variations

19 p3042 A71-38374

Impedance determination for symmetrical spherical probes and spacecraft housing with flat screen separation, using partial capacitance formula

19 p3066 A71-38389

Physical nature and measurement of broadband noise, considering rms value directly proportional to square root of frequency bandwidth

19 p3020 A71-38426

Coercive force and specimen thickness effects on outputs of meters with attached electromagnets

22 p3553 A71-41767

Microwave antenna near field apparent image area phase-amplitude distribution measurement with photocontrolled semiconductor panel

22 p3523 A71-42132

Vertically polarized millimeter and submillimeter wave attenuation measurement in rain

23 p3646 A71-43525

Miniature battery operated electromagnetic flowmeter for data acquisition from unrestrained animals

24 p3801 A71-44787

ELECTROMAGNETIC NOISE

NT ATMOSPHERICS

NT COSMIC NOISE

NT DAWN CHORUS

NT HISS

NT IONOSPHERIC NOISE

NT IONOSPHERICS

NT SHOT NOISE

NT SUDDEN ENHANCEMENT OF ATMOSPHERICS

NT WHISTLERS

NT WHITE NOISE

Area distributed incidental radio noise voltage envelope distribution functions conversion to Rayleigh distribution with range frequency relationships

01 p0037 A71-11161

Phase meter channels correlation effect on measurement phase difference measurements accuracy in heterodyne oscillators

02 p0212 A71-11837

Illiac 4 and Spectra 70 computers comparison in terms of logic circuit noise immunity and system noise sources

03 p0388 A71-13177

Noise-induced current fluctuations on S-shaped I-V curve in Cr-doped GaAs diodes

03 p0387 A71-13987

Automatic transistor noise factor measurement equipment consisting of noise source, signal amplifier, synchronizing oscillator, controllable attenuator and automatic control circuits

04 p0557 A71-15078

Reflector antenna under wideband noise radiation: determining directivity characteristics by solution for angle range homologous to region of irregular lobes

05 p0728 A71-16008

Microwave transistor circuit simplified noise figure expression including feedback and parasitics effects

05 p0719 A71-16164

Broadband radiated man-made electromagnetic noise measurement for communication systems performance determination, noting instrumentation problems

05 p0721 A71-16466

Singly tuned IMPATT diodes, examining noise and power saturation

05 p0729 A71-16915

Temperature compensated Zener diodes noise voltage measurements in ELF domain

05 p0729 A71-17004

Dynamic data processing systems with feedback and internal noise, evaluating carrying capacities limiting parameters and optimal transfer function

05 p0732 A71-17164

Solid state single injection diodes with shallow traps, calculating trapping noise

06 p0872 A71-17313

Avalanche diodes as solid state noise sources, observing planar silicon junctions breakdown voltages

06 p0940 A71-17324

Relay type pulsed control systems performance determining noise effects by statistical analysis

06 p0879 A71-17927

Ge diodes double injection experiments, measuring I-V characteristics, AC small signal admittance and noise

06 p0876 A71-18037

Injection phase locked oscillator as input microwave limiting amplifier for noise measuring microwave discriminator

07 p1074 A71-19126

Coherent noise elimination in coherent light imaging systems by time averaging noise concentration through lens rotation about optical axis

07 p1107 A71-19208

Real noise stability of coherent FM receiver for case of spectrum limited signals due to passage through channel and selective networks

07 p1061 A71-19508

Polarization of thunderstorm IF electromagnetic noise, taking into account earth electrical conductivity under detector

07 p1063 A71-19755

Microwave noise generation by triboelectric charging of dielectric surfaces

07 p1063 A71-19933

Electrostatic charging noise measurement, reduction and flight test verification 07 p1021 A71-19937

Current-voltage characteristics of Josephson junction, discussing noise effect at near transition temperature of superconductor and external signal driving 07 p1079 A71-20170

N-type InSb microwave noise radiation and attendant RF current oscillations under magnetic field 07 p1180 A71-20177

Fading microwave radio channel baseband gain and noise stability, assuming nonuniform frequency selective fading effects 07 p1066 A71-20426

Noise behavior of Schottky barrier gate FET at microwave frequencies, discussing effects of carrier velocity saturation and parasitic resistances on noise parameters and measurement method 08 p1261 A71-20741

FM type system for measurement of wear narrow band noise power based on phase components processing 08 p1253 A71-21289

Noise stability of synchronous phase demodulator in satellite and tropospheric communications, considering threshold characteristics 09 p1413 A71-22146

Integrated circuit components equivalent circuits, considering transistor logic circuits and admissible noise 09 p1416 A71-22491

Nonstationary colored noise linear shaping filter to transform white noise into nonstationary random process with specified covariance function 09 p1424 A71-23100

X band Schottky barrier diodes RF impedance mismatch and noise factor, calculating dependence on microwave oscillator voltage-standing wave ratio 09 p1421 A71-23723

Noise analysis of microelectronic active RC filters by cascade of passive and active networks, considering low pass filter 10 p1582 A71-23915

Spurious spikes in microwave circulators due to hybrid resonant modes of ferrite post open-resonator structure 10 p1583 A71-24212

Positive signal optimal detection system in unsteady non-Gaussian noise 10 p1577 A71-24282

IMPATT diode oscillators noise and injection phase locking, discussing theoretical refinements of original simple model by Read 10 p1584 A71-24818

Handbook on electrical noise and electromagnetic interference specifications, Volume 1, covering noise pollution, industrial electronic equipment operation control, test plans and military standards 11 p1731 A71-25744

IMPATT oscillators noise properties at large RF amplitudes, deriving expression for noise current as function of threshold current 11 p1733 A71-26369

TWT amplifiers in radar and communication systems, investigating AM and FM noise theory and reduction 11 p1734 A71-26435

Microwave radiometers transfer calibrations by noise injection through avalanche diode directional coupler similar to plasma tube 11 p1739 A71-26438

Sky noise temperature measurements for ATS-5 millimeter wave radiometers, taking into account variations due to atmospheric temperature and humidity conditions 12 p1877 A71-26608

Man-made HF noise interference with satellite broadcasting, giving special consideration to automotive ignition systems 12 p1878 A71-26994

Electromagnetic noise pulses generated by convective storms in Iowa during 1970 12 p1881 A71-27200

Dynamic data processing systems with feedback and internal noise, evaluating carrying capacities, limiting parameters and optimal transfer function 12 p1893 A71-27455

Energetic electrons generating solar flares position relation with active regions associated with type 1 radio noise storms 12 p1953 A71-27656

Transient ELF electromagnetic disturbances propagation in earth-ionosphere cavity, determining waveguide source-observer separation and attenuation constant 13 p2027 A71-27796

Industrial helium-neon laser emission noise characteristics, defining amplitude fluctuations by variable proportional to photoelectric multiplier current random modulation factor 13 p2077 A71-27937

Verification, control and forecasting information characteristics for random process mixed with additive noise 13 p2041 A71-27942

Radio noise amplitude probability distribution, considering RMS voltage, average voltage and average logarithm of voltage 13 p2031 A71-28861

RF noise measurement instrumentation using statistical analysis for better interference characterization 13 p2035 A71-28865

LF whistler mode radio noise emissions observations in polar regions with Alouette 2, noting association with energetic particles influx into ionosphere 14 p2300 A71-30036

Noise effect on signal parameter control in linear measurement devices 14 p2194 A71-30082

Transfer function optimization for linear tracking filter model with controlled resonant frequency, analyzing noise band performance 14 p2194 A71-30089

Digital nonregular pulse counter, determining noise characteristics of photomultipliers in single pulse recording mode 14 p2213 A71-30580

Noisy image visual discrimination and detection, investigating Bayes criterion ideal statistical method validity for pattern recognition 14 p2197 A71-30815

Radio science - Conference, Ottawa, August 1969, Volume 1, Ionosphere, magnetosphere, radio noise 14 p2201 A71-30939

Thunderstorms and lightning flashes location determination by ground based and satellite measurements of disturbance induced RF noise, using atmospheric spectral characteristics for range estimating methods 14 p2203 A71-30958

Man made radio noise sources frequency-distance dependence and location, noting vehicular ignition, power transmission and electrical pulsing 14 p2203 A71-30962

Noise measurements on discrete radio sources spectra, studying Cas A and Cyg A flux density ratio 14 p2316 A71-30975

Independent noise driven nonlinear dynamic systems identification, performing linear discrete-time scalar measurements 15 p2380 A71-31934

Noise stability and false response probabilities of receivers in circular remote control systems under harmonic interference for signal transmitted over power distribution grids 15 p2353 A71-32081

Modulator-demodulator type push-pull DC amplifier input noise reduction, using electromechanical vibrators 15 p2355 A71-32451

Noise equivalent resistance of thermionic tubes as stability and reliability criterion 16 p2545 A71-33073

Compact Q band magic tee with matched loads to check noise performance of two-input switched radiometer 16 p2579 A71-33385

Short light pulse evolution from noise, considering time dependence of pulse duration and peak intensity 16 p2589 A71-34137

Laser longitudinal oscillation modes and maximum radiation envelope formation from noise at start of emission, using electric field strength recurrent relations 17 p2751 A71-34386

German book on noise covering electrical fluctuation phenomena, thermodynamic equilibrium, electromechanical systems, semiconductors and ferromagnetic fields, diodes, etc 17 p2713 A71-34478

Ground noise reduction with balancing units, discussing transmission line driving and receiving end applications 17 p2716 A71-34859

Error correcting codes in binary symmetrical communication channel with additive white noise at large SNR 17 p2702 A71-34972

X-band Gunn oscillator equivalent circuit parameters determination for baseband and RF noise contribution to AM and FM noise 18 p2888 A71-36270

Low noise microwave transistor, describing geometry and diffusions optimization, power gain, reliability and base resistance 18 p2892 A71-36564

Adaptive frequency selection for reduction of effects of noise differing irregularly from useful pulse signals, estimating error probabilities 18 p2882 A71-36622

Fabrication and noise performance of high power Schottky barrier GaAs IMPATT diodes with double epitaxial layer structure on low-etch-pit density substrates 18 p2895 A71-36982

HF radio communication receiver performance requirements and realization, considering gain, noise, interference, filtering, reciprocal mixing, intermodulation and frequency stability 18 p2895 A71-36998

Stark contours of hydrogen spectral lines in turbulent plasma with high noise level due to HF Langmuir oscillations 19 p3110 A71-37388

Gas discharge-current modulation noise of He-Ne laser, using sinusoidal signal at various frequencies 19 p3072 A71-37698

Equivalent circuit parameters determination for baseband and microwave noise from Gunn oscillator, using AM-FM correlation coefficient 19 p3028 A71-37699

Collisions or weak turbulence caused noise effects on broadening of echo pulses in magnetically trapped particles, using propagator formalism 19 p3113 A71-37746

Auroral radio noise from electrostatic oscillations excited by fast proton beams 19 p3018 A71-38046

Contact materials effects on X band FM noise and current fluctuations of Gunn elements 19 p3029 A71-38073

X band output power and FM noise of parallel multicontact Gunn oscillators 19 p3029 A71-38074

Noise, admittance and I-V characteristics of hot holes in space charge limited Ge diodes at high voltage and frequencies to 22 MHz 19 p3029 A71-38141

Physical nature and measurement of broadband noise, considering rms value directly proportional to square root of frequency bandwidth 19 p3020 A71-38428

RF noise surveys in urban areas for effective space to earth communication link design at UHF 19 p3021 A71-38443

Transistor circuit driven hydrogen-oxygen fuel cell, testing internal impedance effect on power supply noise for comparison with lumped parameter model 19 p3000 A71-38463

Noise stability and rejection probability of code sequence in real multifrequency communications systems with multipositional frequency shift keying 19 p3022 A71-38495

Narrow band magnetospheric radio noise between electron plasma and upper hybrid resonance frequencies from satellite observations 20 p3285 A71-38728

Liquid nitrogen cooled microwave low temperature noise standard in WR-51 waveguide 20 p3202 A71-38832

He-Ne laser output noise due to mode competition, predicting behavior by Lamb three mode laser equation numerical solution 20 p3242 A71-38883

Auroral electron and proton precipitation patterns, noting LF radio noise emissions relationship to low energy electron flux through Cerenkov process 20 p3228 A71-39846

He-Ne lasers noise modulation at DC excitation, confirming existence of critical frequency related to metastable atom lifetime 21 p3392 A71-40373

Semiconductor surface layer noise generation physical model with allowance for relaxation effects due to traps in space charge region 21 p3432 A71-41301

Incoherent receiver noise stability in multichannel system with channel frequency separation, deriving formula for receiver error probability 22 p3522 A71-42314

Signal design and error rate of impulse noise channel, analyzing error probability of smear-desmear and standard data channels through Rice integral evaluation 22 p3513 A71-42381

IMPATT diodes noise performance lower limits, deriving optimization theorem for GaAs diodes under assumption of equal ionization coefficients for electrons and holes 22 p3524 A71-42632

Reflector antenna under wideband noise radiation, determining directivity characteristics by solution for angle range homologous to region of irregular sidelobes 22 p3524 A71-42757

Laser pumped solid state masers operational characteristics, describing spontaneous emission noise 23 p3683 A71-43084

Two component 1/f noise measurements in p-channel MOS transistors 24 p3812 A71-45352

Substrate effect on MOSFET noise and y-parameters using wave equation 24 p3862 A71-45354

ELECTROMAGNETIC PROPAGATION
U ELECTROMAGNETIC WAVE TRANSMISSION
ELECTROMAGNETIC PROPERTIES
NT ABSORPTANCE
NT ABSORPTIVITY
NT BIREFRINGENCE
NT BRIGHTNESS
NT COLOR
NT DICHROISM
NT FARADAY EFFECT

- Electromagnetic repulsion of conducting and dielectric bodies within liquid metal and electrolyte in crossed field under gravitational acceleration
02 p0293 A71-12630
- Finite antenna arrays excitation patterns, yielding electromagnetic parameters approaching preselected optimal values
14 p2192 A71-29807
- Radome lightning protection systems involving electrostatic shielding, considering effect on electromagnetic characteristics and radiation patterns of nearby antennas
19 p3031 A71-38450
- Computer algorithms for gamma algebra of electromagnetic form factors in terms of Chebyshev polynomials with photon 4-momentum
21 p3415 A71-40842
- CdS single crystal acoustoelectric domain determination, using light diffraction method
21 p3436 A71-41364
- ELECTROMAGNETIC PROPULSION**
- Electric rocket propulsion systems using nuclear or solar energy and electrothermal, electromagnetic or electrostatic principle
02 p0283 A71-12309
- Electrical or electromagnetic acceleration of ionized gas to obtain high velocity rocket exhaust for deep space manned flight
19 p3123 A71-38249
- ELECTROMAGNETIC PULSES**
- LF spiral monochromatic wave pulse propagation from vacuum into semifinite semiconductor, considering bandwidth relation to electron heating
01 p0138 A71-10431
- EM pulse distortion in resonant and nonresonant gases, discussing applications to homogeneous tropospheric propagation
01 p0040 A71-11608
- EM oscillations of open elliptic profile cylindrical mirrors resonator with dielectric elliptic cylinder
03 p0386 A71-13800
- Crab Nebula pulsar radio pulses polarization using polarimeter feed in Mark I telescope comparison to analysis by integration and photographic recording
04 p0649 A71-15274
- Solar wind parameters-terrestrial electromagnetic field micropulsations relation based on interplanetary probes and time correlated ground observations
05 p0800 A71-17170
- Energy balance during ring blanks widening by electromagnetic pulses, establishing theoretical limit of mechanical efficiency
06 p0906 A71-18712
- Electromagnetic pulse propagation over flat impedance surface, determining similarity parameters
07 p1060 A71-19187
- Electromagnetic pulse propagation through inhomogeneous plasma, discussing electron collision frequency effects
09 p1504 A71-22987
- Ionospheric dispersion of FM electromagnetic pulse, examining distortion of amplitude, pulse length and modulation in terms of integrated electron density along transmission path
09 p1410 A71-23523
- Amplitude distribution of nuclear burst electromagnetic pulse propagated through atmosphere, deriving two probability distribution functions by central limit theorem
09 p1410 A71-23524
- Flush mounted annular slot missile antenna theory application to near zone field strength instrumentation calibration and plane wave electromagnetic field pulse response determination
10 p1580 A71-25071
- Gravitational radiation events-galactic microwave emission pulses relation, comparing with Weber gravitational wave experiment
11 p1820 A71-25298
- Electromagnetic noise pulses generated by convective storms in Iowa during 1970
12 p1881 A71-27200
- Coincident radio pulse effects on triggering antenna arrays, considering air shower mechanism
12 p1967 A71-27389
- Air showers emitted radio pulses polarization, noting inconsistency with geomagnetic origin
13 p2127 A71-28102
- Extensive air showers radio emission pulse shape, noting amplifying system response to input signal
13 p2128 A71-28109
- Ultrashort optical pulse propagation through two level attenuating or amplifying atomic medium
13 p2080 A71-29136
- Transverse spatial diffusion of phase-dispersed pulses, showing effects on dechirped pulse duration, output beam cross section and two-photon fluorescence display
13 p2081 A71-29332
- Extensive air showers detection by correlation of optical and radio pulses at 60 deg zenith angle
15 p2472 A71-31199
- Inductor winding dependent magnetic pulse deformation of cylindrical blanks allowing for mutual electromagnetic and mechanical coupling
15 p2417 A71-32525

- Measuring apparatus for envelope distortion of transmitted high-energy transversely polarized pulses through ionizable or partially ionized gas
18 p2952 A71-36589
- Radio pulses from pulsars, noting relativistic energy of particles from volume emissivity and surface flux density
20 p3305 A71-39950
- Radio pulses from pulsars based on model of coherent synchrotron radiation from magnetosphere trapped charged particles
20 p3285 A71-39951
- Pulse trains of minimum spectral width generated from rectangular pulses by RC elements coupled without feedback
22 p3521 A71-42248
- Electromagnetic pulses scattering by conducting wedge in uniaxially anisotropic plasma, obtaining electric dipole radiation fields transient time for various plasma frequencies
23 p3646 A71-44171
- Tables of Crab Nebula pulsar radio pulse arrival times at Arecibo observatory
24 p3867 A71-44435
- ELECTROMAGNETIC PUMPS**
- Helical induction boiler feed electromagnetic pump design, fabrication and testing for potassium Rankine cycle space power system [GESP-455]
15 p2415 A71-32202
- Radioisotope testing methods for dissolution and mass transfer of alloying additives in Pb-Sb alloys during preparation in electromagnetic pumps
22 p3553 A71-41765
- ELECTROMAGNETIC RADIATION**
- NT AIRGLOW
NT BLACK BODY RADIATION
NT BREMSSTRAHLUNG
NT CERENKOV RADIATION
NT COHERENT ELECTROMAGNETIC RADIATION
NT COHERENT LIGHT
NT CYCLOTRON RADIATION
NT DAYGLOW
NT DECA-METRIC WAVES
NT DECIMETER WAVES
NT ELECTROMAGNETIC PULSES
NT EXTRATERRESTRIAL RADIO WAVES
NT FAR INFRARED RADIATION
NT FAR ULTRAVIOLET RADIATION
NT GALACTIC RADIO WAVES
NT GAMMA RAYS
NT GEGENSCHNEIN
NT GEORCONAL EMISSIONS
NT H WAVES
NT INFRARED RADIATION
NT LIGHT [VISIBLE RADIATION]
NT LIGHT BEAMS
NT LONG WAVE RADIATION
NT LYMAN ALPHA RADIATION
NT LYMAN BETA RADIATION
NT MICROWAVES
NT MILLIMETER WAVES
NT MODULATED CONTINUOUS RADIATION
NT MONOCHROMATIC RADIATION
NT NEAR INFRARED RADIATION
NT NEAR ULTRAVIOLET RADIATION
NT NIGHTGLOW
NT NONEQUILIBRIUM RADIATION
NT PHOTON BEAMS
NT PLANETARY RADIATION
NT POLARIZED ELECTROMAGNETIC RADIATION
NT POLARIZED LIGHT
NT RADIO EMISSION
NT RADIO WAVES
NT SHORT WAVE RADIATION
NT SKY RADIATION
NT SKY WAVES
NT SOLAR RADIO BURSTS
NT SOLAR RADIO EMISSION
NT SOLAR X-RAYS
NT SUBMILLIMETER WAVES
NT SUNLIGHT
NT SYNCHROTRON RADIATION
NT TERRESTRIAL RADIATION
NT THERMAL RADIATION
NT TWILIGHT GLOW
NT TYPE 2 BURSTS
NT TYPE 3 BURSTS
NT TYPE 4 BURSTS
NT ULTRAVIOLET RADIATION
NT X RAYS
NT ZODIACAL LIGHT
- Galactic EM energy radiation, discussing flux upper limits in Low model
01 p0153 A71-10364
- Electromagnetic wave reflection from ferrite moving domain wall, considering wave separation and permittivity and magnetic susceptibility tensors
01 p0138 A71-10435
- Round dielectric waveguides dominant mode radiation losses calculation
01 p0052 A71-10467

- Threshold currents of injection lasers with heterojunctions providing correction for optical thickness in terms of electromagnetic theory
01 p0094 A71-10777
- EM wave propagation along radially inhomogeneous dielectric cylinders, considering permittivity variation
01 p0037 A71-11177
- Transient effects due to electromagnetic cascades of lead during copper wall passage in ionization chamber
01 p0084 A71-11376
- Shadow current method for asymptotic solution to two dimensional problem of electromagnetic wave field diffraction field on ideally conducting plane with finite rectilinear slot
02 p0210 A71-11617
- Collisionless damping of electromagnetic waves in regions with strong homogeneity of cold plasma
02 p0291 A71-12509
- Electrode material function of electromagnetic radiation from heterogeneous plasma
03 p0466 A71-14477
- Plane electromagnetic wave diffraction on infinite system of parallel metallic strips, determining natural frequencies
04 p0549 A71-14611
- Reflected electromagnetic wave polarization parameters, obtaining correlation functions for radar echoes
04 p0557 A71-14632
- Electromagnetic wave glancing incidence on ideally conducting screen of infinitely thin strips by geometrical optics approximation
04 p0625 A71-14646
- Electromagnetic wave generation by interaction in plasma stream resonator, considering Coulomb friction and boundary reflection coefficients
04 p0633 A71-15110
- Amino acid content alteration in internal organs in rabbits under HF electromagnetic and ultrasound oscillations
04 p0547 A71-15573
- Cylindrical electromagnetic wave amplification in TWT with radial line and diverging electron flux
05 p0727 A71-16007
- Far field characteristics for diffraction of plane harmonic electromagnetic wave obliquely incident on rectangular wedge in uniaxially anisotropic medium
05 p0781 A71-16414
- Broadband radiated man-made electromagnetic noise measurement for communication systems performance determination, noting instrumentation problems
05 p0721 A71-16468
- Electromagnetic waves energy flow and dissipation in frequency dispersive absorbing medium, exemplifying by oscillating particle system and electric circuit
05 p0781 A71-16702
- Electromagnetic waves phase velocity in helical waveguides in magnetodielectric medium with cylindrical void interspace
05 p0722 A71-16827
- Plane electromagnetic wave inhomogeneous diffraction field from multilayer metal band gratings
05 p0722 A71-16829
- Plane EM waves at two dimensional periodic media boundary, obtaining reflection and refraction for harmonics
05 p0723 A71-17025
- Ion-acoustic waves generation mechanism in outer space by strong electromagnetic radiation, considering quasars, supernovae shells, pulsars and solar supercorona
05 p0800 A71-17196
- Electromagnetic wave trapping by nonlinear resonant interactions involving ion sound wave and two electromagnetic waves in isotropic plasma
06 p0869 A71-17988
- Fourier resonance associated with electromagnetic wave diffraction from multilayer gratings
06 p0870 A71-18349
- Electromagnetic wave diffraction by multielement and multilayer arrays, discussing asymptotic solution, error estimate and convergence
07 p1060 A71-19180
- Electromagnetic radiation pumping by stimulated Compton scattering near pulsars, determining secondary emission frequencies from energy and momentum conservation laws
07 p1192 A71-19292
- Evanescent electromagnetic waves quantization by treating transverse triplet wave modes as noninteracting harmonic oscillator, discussing atomic excitation
07 p1159 A71-19548
- Superconducting tunnel junctions radiation emission, discussing superconductivity theory
07 p1178 A71-19777
- Field intensity of plane electromagnetic wave diffracted at conducting sphere
08 p1252 A71-20735
- Energy conversion efficiency from microwave into magnetostatic waves propagation inside cylindrical ferromagnetic substance
08 p1265 A71-21276

Electromagnetic wave diffraction by variable curvature and surface impedance cylindrical structure
08 p1254 A71-21356

Book on electromagnetic fields and waves covering vectors, current density, flux integral, Coulomb law, Laplace equation, magnetomotive force, waveguides, etc
08 p1335 A71-21459

HF wave absorption in Ar plasma, observing production in open magnetic trap
08 p1339 A71-21481

Tropospheric height integral of refractivity for predicting atmospheric electromagnetic wave field, calculating HF conductivity and absorption coefficient
08 p1257 A71-21881

Nonisothermal plasma ion acoustic oscillations spectral energy density in electromagnetic wave field, calculating HF conductivity and absorption coefficient
09 p1500 A71-22243

Naturally generated electromagnetic waves interaction with electron flux in magnetoplasma, noting gyroresonance
09 p1501 A71-22304

Electric field equations of plane EM wave diffraction at lattice of conducting cylinders, using Hankel function
09 p1408 A71-23113

Electromagnetic and electrostatic waves direct nonlinear coupling in plasma, describing experimental measurements of interacting waves frequency, wavelength, field configuration and power levels
09 p1504 A71-23254

Kinetic theory of electromagnetic waves obliquely incident upon plasma slab considered as boundary value problem
09 p1409 A71-23499

Lossless radiating antenna element efficiency in circular cylindrical arrays of identical elements, relating to reflection coefficient
09 p1419 A71-23505

Electromagnetic transient signal nonlinear dispersion in homogeneous isotropic partially ionized plasma medium
09 p1505 A71-23520

Near field electromagnetic radiation probe for microwave measurements in proximity of hazard source
09 p1453 A71-23626

Near field asymptotic solution for electromagnetic wave diffraction by perfectly conducting wedge, using steepest descent method
09 p1411 A71-23679

Plane electromagnetic wave reflection from conducting convex cylinder in radially inhomogeneous absorbing medium, deriving equations for beam trajectories calculation
10 p1574 A71-23805

Ferromagnetic and antiferromagnetic characteristics relation to electromagnetic and spin waves coupling in nonresonant and resonant regions
10 p1656 A71-24317

EM wave excitation in plane parallel waveguide by rotating relativistic electron flux, deriving dispersion relation and interaction solutions
10 p1577 A71-24323

Rough circular rod effective surface impedance and propagation constant, discussing guided electromagnetic wave attenuation on structure
10 p1578 A71-24399

Nonlinear Landau damping of circularly polarized electromagnetic cyclotron waves, calculating interaction matrix for particular electron velocity distribution functions
10 p1652 A71-24656

Electromagnetic wave conversion into plasma waves in cold anisotropic plasma with two dimensional inhomogeneity
10 p1654 A71-24893

Pulsar oblique magnetic rotator model, noting large amplitude EM traveling wave effects on electron motion
10 p1679 A71-24956

HF electromagnetic waves absorption as function of discharge current intensity in ionized H, using gas pressure or uniform magnetic field as parameters
11 p1805 A71-25598

Italian book on microwave propagation covering electromagnetic wave attenuation, rainfall space-time structure and radioelectrical/meteorological data recording
11 p1731 A71-25650

Homogeneous Gaussian beam propagation in inhomogeneous negative absorption media, noting amplification of plane wave
11 p1798 A71-25665

Fast shock waves electromagnetic production in light gases, discussing interferometric measurements at optical and microwave frequencies in H
11 p1764 A71-26272

Charge particle motion and radiation in strong plane and spherical electromagnetic waves with nonthermal astrophysical applications
12 p1877 A71-26616

Book on electromagnetic fields and life environment covering biological effects of radio waves, protection, radiation sources, permissible intensities, working conditions
12 p1873 A71-26868

Nonlinear waves in weakly dispersing media, discussing packet self-focusing and -compression, electromagnetic radiation with acoustic oscillations, geometric optics and HF-LF interactions
12 p1929 A71-27166

High temperature aerodynamics with electromagnetic radiation, considering thermally radiating shock layers, electric arc driven wind tunnels and gas dynamic lasers
12 p1940 A71-27277

Electromagnetic longitudinal cascades development numerical treatment based on Boltzmann equation, discussing Monte Carlo computing times for primary energy total electron counts
12 p1933 A71-27387

Ion-acoustic waves generation in outer space by strong electromagnetic radiation, considering quasars, supernovae shells, pulsars and solar supercorona
13 p2128 A71-28251

HF diffraction of plane electromagnetic waves by ideally conducting iris diaphragm, developing boundary value problem asymptotic solution
13 p2029 A71-28448

Electromagnetic wave reflection from interface between moving and stationary electron plasma, giving boundary conditions at velocity discontinuity surface
13 p2108 A71-28855

Soviet monograph on EM waves in solid state plasma covering propagation, amplification, generation and penetration
13 p2112 A71-29078

Electromagnetic wave reflection by rough surfaces based on geometrical optics, discussing reflected power density reflection coefficient and frequency limit
13 p2033 A71-29240

Electromagnetic radiation from stationary electric dipole imbedded in plasma column moving in axial direction
13 p2110 A71-29389

Electromagnetic wave diffraction coefficients for discontinuity in curvature from surface field asymptotic description near singularity
14 p2192 A71-29794

German book on radiation climate of earth covering EM, corpuscular IR radiation sources, spectral composition, biological effects, etc
14 p2298 A71-29941

Beamguides with inhomogeneities regulated for constant radiation losses of waves-analogs of modes
14 p2211 A71-30077

Radiation patterns and scattering cross sections of plane black disks excited by electromagnetic and acoustic waves
14 p2194 A71-30079

Electromagnetic wave diffraction at multilayer wire grating, discussing computer program for diffraction field calculation
14 p2194 A71-30086

Electromagnetic wave scattering on inhomogeneities by Born approximation, estimating maximum error for small correlation radius
14 p2194 A71-30100

Plastic scintillators anomalous pulse spectra in sea level transition region attributed to EM cascades single particles /muons/ production
14 p2301 A71-30425

Hot jet aerodynamic parameters from emissions of electromagnetic and acoustic energies by crossed beam IR probing
14 p2288 A71-30520

RF power absorption of uniform hot ion-electron plasma column, considering collision effects and EM radiation
14 p2281 A71-30556

Electromagnetic showers triggered in lead by 6 GeV primary cosmic ray electrons, calculating spatial distribution with Monte Carlo method
14 p2302 A71-30594

Electromagnetic showers in lead, using 20 GeV primary cosmic ray electrons to calculate spatial evolution
14 p2302 A71-30603

Azimuthal current growth and microwave radiation in theta pinch hydrogen plasma discharge from sensitive superheterodyne receivers
14 p2282 A71-30663

Electromagnetic and gravitational waves scattering by static gravitational field, comparing classical general relativistic and quantum field theoretic results
14 p2275 A71-30861

Atmospheric VLF electromagnetic emissions and electron instabilities data from satellite observation, detailing source regions, large amplitude electrostatic waves and wave-particle correlation
14 p2202 A71-30952

Electromagnetic waves in interplanetary space and effects on magnetosphere, considering solar wind characteristics due to wave interactions
14 p2202 A71-30956

Binary optical detour phase holograms formation in measurements with centimeter electromagnetic waves, describing dielectric diffusers for microwaves
15 p2405 A71-31280

Electromagnetic wave energy absorption in inhomogeneous cold magnetoactive plasma cylindrical columns
15 p2455 A71-31735

Lateral spread of nuclear-electromagnetic cascades in iron absorber from three-dimensional Monte Carlo simulation
15 p2452 A71-31810

Green function or Huygens principle for radiation and diffraction of electromagnetic or acoustic waves in anisotropic media
15 p2449 A71-31869

Thin metallic body of revolution under electromagnetic pulse, predicting transient induced currents with radiation condition in finite difference solution
15 p2372 A71-32368

External off-axis TEM wave transformation into natural oscillation modes in Fabry-Perot resonator under axiality disturbance and impinging-excited wave mismatch
15 p2410 A71-32401

Arbitrary gravitational field effects on natural frequencies of rotating ring laser with traveling electromagnetic wave
15 p2421 A71-32408

Energy-radiation problems in relativity theory, considering electromagnetic waves, Einstein equations, momentum tensors and moving charged particles
16 p2609 A71-33259

Plane electromagnetic wave diffraction on ideally conducting convex body of large electrical dimensions, obtaining Maxwell equations asymptotic solution
16 p2542 A71-33485

Refraction effects of moving inhomogeneous media in electromagnetic Doppler measurements, using Maxwell equations or relativistic ray tracing method for frequency variations
16 p2544 A71-33850

Ionospheric electric and electromagnetic waves broadband characteristics, investigating auroral hiss and LHR noise
16 p2572 A71-33951

Arbitrary cross sectional semiinfinite conductor, investigating electromagnetic wave diffraction
17 p2701 A71-34754

Astronomical telescopes design and characteristics, reviewing electromagnetic radiation properties
18 p2925 A71-36769

Polarization direction finder determining electromagnetic waves azimuth on basis of field intensity vectors
19 p3014 A71-37074

Lecher waves, line waves and TEM waves, demonstrating advantage of solving diffusion equation within transversal plane for determination of line parameters
19 p3014 A71-37075

High temperature gas dispersed Al particle flow, investigating electrical conductivity and radiation properties
19 p3161 A71-37265

Equipment survival in natural and nuclear explosion electromagnetic and particle radiation environment
19 p3027 A71-37450

Pulsars electromagnetic radiation, considering bunch of relativistic charged particles
19 p3134 A71-37513

Electromagnetic radiation from beam-plasma system in strong magnetic field, noting maximum microwave emission near electron cyclotron frequency
19 p3116 A71-38252

Electromagnetic phenomena extraneous to established scientific and engineering disciplines, considering eptotics, dowsing, hydronics, radionics, radiesthesia, orgone, backster phenomena, etc
19 p3031 A71-38441

Thermal or chemical energy conversion to electromagnetic radiation by laser, discussing atomic or molecular processes and thermodynamic limitations
20 p3242 A71-38939

Uniformly moving homogeneous isotropic non-dispersive conducting medium with arbitrarily distributed electromagnetic radiation sources, deriving solution in four dimensional covariant form
20 p3196 A71-39083

Light ponderability in gravitation theory, discussing hypothetical Freundlich effect of light velocity dependence on radiation field intensity, based on Maxwell electrodynamics nonlinear generalization
20 p3270 A71-39457

Monochromatic plane electromagnetic wave reflection by electrically perfectly conducting diffraction grating
21 p3415 A71-40665

Electromagnetic wave conversion into plasma waves in cold anisotropic plasma with two dimensional inhomogeneity

21 p3425 A71-41273

Surface waves at Fermi electron plasma boundary, using kinetic theory of plasma electromagnetic oscillations

21 p3425 A71-41278

Electromagnetic wave reflection from interface between moving and stationary electron plasmas, giving boundary conditions at velocity discontinuity surface

21 p3426 A71-41288

HF electric signal detection, using acoustoelectric surface wave field in piezo semiconducting crystal

21 p3436 A71-41363

Gravitational wave impingement upon static magnetic field, noting EM waves excitation

21 p3417 A71-41397

Electromagnetic radiation active gravitational mass relationship to particle mass from decay of particle into two radiation pulses

21 p3417 A71-41402

Plane electromagnetic wave diffraction by infinite system of parallel metallic strips, determining natural frequencies and eigenfunctions

22 p3510 A71-42251

Reflected electromagnetic wave polarization parameters, obtaining correlation functions for radar echoes

22 p3510 A71-42272

Narrow strongly radiating slot voltage distribution, investigating cavity coupling with integral equation

22 p3522 A71-42305

Book on interference of electromagnetic waves covering Michelson-Fizeau and Fabry-Perot interferometers, Fourier transform spectroscopy, etc

22 p3576 A71-42429

Nonlinear waves in weakly dispersing media, discussing packet self-focusing and -compression, electromagnetic radiation with acoustic oscillations, geometric optics and HF-LF interactions

22 p3576 A71-42621

Cylindrical electromagnetic wave amplification in TWT with radial line and diverging electron flux

22 p3524 A71-42752

Electric field induced current distribution on cylindrical antenna, considering delta generator and electromagnetic waves excitations

23 p3643 A71-43122

Dual integral equations solutions to electromagnetic wave diffraction at plane conducting slotted screen

23 p3644 A71-43258

Conversion effectiveness of oscillations induced by electron beam in bounded anisotropic plasma into electromagnetic emission

23 p3710 A71-43275

Dispersion equation for electromagnetic surface wave propagation along plane boundary of adjacent hot plasma streams

23 p3713 A71-44149

Plane electromagnetic wave diffraction by infinitely conductive grating at nonorthogonal incidence angles, using conformal mapping technique

24 p3847 A71-44357

Electromagnetic wave amplification using coaxial line matching with plasma waveguide by charged particle beam

24 p3853 A71-44508

Electromagnetic waves excitation in coaxial resonator by relativistic electron beam, assuming presence of steady longitudinal magnetic field

24 p3833 A71-44663

ELECTROMAGNETIC SCATTERING

NT HALOS

NT IONOSPHERIC F-SCATTER PROPAGATION

NT LIGHT SCATTERING

NT MICROWAVE SCATTERING

NT MIE SCATTERING

NT RAMAN SPECTRA

NT RAYLEIGH SCATTERING

NT THOMSON SCATTERING

NT X RAY SCATTERING

Variational bounds on phase shifts for electromagnetic wave scattering by dielectric obstacles in waveguides

01 p0056 A71-11199

Classification of electromagnetic wave scattering fluctuating objects from statistical scattering matrices, obtaining incident wave polarization

01 p0038 A71-11208

Multiple scattering boundary value problem for two parallel circular cylinders

01 p0041 A71-11613

Electromagnetic scattering by oblique circular cylinder, deriving field equations

02 p0215 A71-12145

Quantum diffusion in scattering medium with absorption as sequence of random events

02 p0311 A71-12354

Two dimensional diffraction of plane wave by perfectly conducting wedge using straightforward scattering approach

03 p0456 A71-13347

Plane monochromatic electromagnetic wave scattering by moving and rotating cylinder

04 p0549 A71-14612

Arbitrary lossless antennas radiative, scattering and coupling properties interrelations

06 p0874 A71-17707

Structures electromagnetic scattering and multipath transmission effects on aircraft instrument landing system localizer signals, using computer program

07 p1153 A71-18831

Vector solution for electromagnetic wave scattering from rough surface of arbitrary dielectric constant

07 p1064 A71-20316

Electromagnetic wave scattering by perfectly conducting sphere, using integral equation formulation

08 p1253 A71-21294

Electromagnetic wave scattering by perfectly conducting cylinder in anisotropic plasma with external magnetic field, deriving radiation pattern from asymptotic expression

08 p1253 A71-21295

Three dimensional scattering and surface current density measurements on circular tube illuminated by electromagnetic wave

08 p1256 A71-21689

Surface current density and electromagnetic scattering from finite tubular cylinder solved numerically by approximate product integration method

08 p1256 A71-21691

HF backscattering by plane electromagnetic wave at oblique incidence from perfectly conducting right circular cone, applying geometrical theory of diffraction

08 p1257 A71-21884

Electromagnetic scattering matrix formulation, considering volume and surface type scattering for objects of arbitrary shape, comparing numerical results with experimental measurements

09 p1493 A71-22806

Lunar rocks permittivity and density and surface roughness from radio wave scattering data

09 p1523 A71-23105

Plane TM wave scattering by systems of two parallel conducting elliptical cylinders, metal tapes and combinations

09 p1407 A71-23106

Scattering structures of two parallel elliptical cylinders, tapes or combinations, deriving surface current density distribution under plane TM wave excitation

09 p1407 A71-23107

Extraterrestrial Lyman alpha radiation source attributed to solar Lyman alpha scattering on cold interplanetary hydrogen penetrating to inner solar system

09 p1526 A71-23462

Plane electromagnetic wave scattering, arbitrarily polarized and normally impinging on wedge tapered absorbing structure

09 p1409 A71-23501

Electromagnetic transient signal nonlinear dispersion in homogeneous isotropic partially ionized plasma medium

09 p1505 A71-23520

Ionospheric dispersion of FM electromagnetic pulse, examining distortion of amplitude, pulse length and modulation in terms of integrated electron density along transmission path

09 p1410 A71-23523

Scalar wave equation of mutual coherence propagation in turbulent medium with stochastic permittivity using local independence approximation

10 p1641 A71-24398

Water and ice cloud discrimination by angular distribution measurement of various polarization parameters of scattered laser beam radiation, using Mie theory

11 p1776 A71-26298

Low frequency electromagnetic wave scattering by metallic cone, noting dipole moment contribution

12 p1879 A71-27054

EM wave scattering in waveguide by active regular shape bodies, using integrodifferential equations

12 p1881 A71-27337

Electromagnetic backscatter cross section for HF irradiated turbulent dielectric media by rigorous and heuristic derivations

13 p2028 A71-27998

Electromagnetic wave diffraction by ideally conducting wedge of finite radius, deriving asymptotic formula for plane wave scattering

13 p2029 A71-28360

Electromagnetic field amplitude and phase scattering diagrams analysis for shape information capacity

13 p2029 A71-28369

Radiation field description with spatial complex variables, considering application to scattering and waveguide problems

14 p2209 A71-29567

Two dimensional electromagnetic scattering by conducting corrugated circular cylinders, determining surface current by matrix and integral equation methods

14 p2195 A71-30248

Electromagnetic inverse scattering model of electrical radius of conducting spherical radar target employing expansion of scattered field in vector wave functions

14 p2196 A71-30564

Electromagnetic radiation scattering detection limits for plasma diagnostics, considering plasma properties effect on satellites aperture broadening in spectrum

14 p2283 A71-30677

Electromagnetic wave scattering from rough surfaces, discussing radar return differences for different polarizations

14 p2203 A71-30968

Missile circumferential current density for plane wave electromagnetic field illumination, using Kao shadowing theory

15 p2372 A71-32367

Classification reliability of electromagnetic wave scattering fluctuating objects from statistical scattering matrices, obtaining incident wave polarization

17 p2698 A71-34260

Electromagnetic wave diffraction by moving wedge with surface impedance, evaluating Doppler shifts and scattered field in shadow region

17 p2698 A71-34429

Scattering obstacle with surface currents and radiating fields, determining characteristic current distributions and values of elliptical loops, straight wires and circular arcs

17 p2700 A71-34753

Multiple EM scattering by two spheres, using multipole expansion and ray optics

17 p2701 A71-34756

Electromagnetic wave multiple scattering by collinear spheres, computing radar cross sections with recursion relation for computer solution

17 p2701 A71-34757

Radiation pattern of dielectric disk antenna, using computerized analysis of electromagnetic scattering and spherical volume cell

17 p2715 A71-34765

Critique of Vela 4 scattered Lyman alpha experiment, discussing maximum flux region and radiation intensity

17 p2805 A71-35380

Pulsar radiation generation by charged particles nonlinear Thomson scattering of strong LF electromagnetic wave and nonthermal radio emission

18 p2960 A71-35940

Electromagnetic wave scattering on single ellipsoidal inhomogeneity in cylindrical waveguide, obtaining relationship for electric and magnetic waves reflection coefficient

19 p3019 A71-38330

Ray statistics of electromagnetic wave scattering in homogeneous isotropic turbulent medium with ellipsoidal inhomogeneities of refractive index, using Fokker-Planck equation

19 p3020 A71-38364

Plane electromagnetic wave diffraction by circular cylinder with longitudinal slot, determining scattered field by Riemann-Hilbert method

19 p3020 A71-38417

Accuracy modeling guidelines for analyzing thin wire scattering structures using electric field integral equation

19 p3035 A71-38598

Long wire electromagnetic scattered field modification by multiple impedance loading, deriving calculation formulas

19 p3024 A71-38607

Electromagnetic plane wave monostatic scattering incident to thin circular metallic disk, calculating spectral and transient response from far field amplitude and phase data

19 p3036 A71-38608

Electromagnetic wave arbitrary incidence on conducting circular disk for polarization parallel and perpendicular to incidence plane, calculating backscatter cross section for comparison with measurement

20 p3194 A71-38840

Point-matching method application to electromagnetic scattering from quadrilateral conducting cylinders in resonance range, using computer programs

22 p3510 A71-42205

Plane monochromatic electromagnetic wave scattering by moving and rotating cylinder

22 p3510 A71-42252

Electromagnetic scattering by imperfectly conducting circular and square cylinders, using matrix technique based on conformal transformation from polygonal to circular cross section

22 p3512 A71-42361

Transfer equation formulation for radiation field determination in anisotropically scattering medium

22 p3621 A71-42598

Linearly and circularly polarized electromagnetic field effective scattering surfaces relationships determination as value proportional to reflected and transmitted rms flux density ratio

23 p3644 A71-43285

Large scale electron-neutral and neutral-neutral correlation effects on turbulent weakly ionized plasma electromagnetic scattering cross section

23 p3711 A71-43524

PAM signal transmission through statistically rough waveguide, calculating wall roughness effects on transient response by multiple scattering theory

23 p3645 A71-43566

Normal wave scattering on random permittivity inhomogeneities of stratified waveguide dielectric layer, calculating beam width and energy loss by perturbation procedure 23 p3645 A71-43567

Electromagnetic scattering solutions for inhomogeneous dielectrics as power series, using multipoles for far field determination 24 p3847 A71-44427

Pulsar 0833-45 LF radiation spectrum decrease explained by pulse broadening due to interstellar scattering 24 p3868 A71-44565

Electromagnetic wave diffraction properties by ribbon metallic lattice in optically active media using Riemann-Hilbert method 24 p3804 A71-44716

Multiple scattering theory of radiative transfer boundary value problems, showing Neumann intensity expansion coefficients relation to singular normal modes 24 p3848 A71-44788

Radiative transfer in linearly anisotropic-scattering conservative and nonconservative slabs with reflective boundaries, obtaining angular radiation distribution by normal mode expansion technique 24 p3888 A71-44966

Electromagnetic scattering of plane wave obliquely incident on infinitely long circular cylinder with radially varying permittivity and permeability 24 p3805 A71-45179

Linearly polarized plane electromagnetic wave scattering by radially inhomogeneous spherical shell, presenting boundary value problems solutions and approximations 24 p3805 A71-45184

Circularly polarized ultrashort radio wave reflection from lunar and planetary surfaces, determining angular scattering spectrum 24 p3805 A71-45313

ELECTROMAGNETIC SHIELDING

NT RADIO FREQUENCY SHIELDING

Surge voltages produced by transient currents on signal conductors in shielded cables 07 p1022 A71-19946

Metallic spherical shell shielding of electromagnetic waves, deriving approximation for first n terms for EM fields inside due to impinging plane monochromatic wave 09 p1405 A71-22683

Concentric shield for surface wave propagation loss at bend in open waveguide, using Airy function 09 p1410 A71-23570

Electromagnetic compatibility program for aerospace systems, considering EM shielding and emission 13 p2001 A71-28866

Undesirable electromagnetic interference minimization in electrical equipment by filtering, shielding, balancing lines, hot/neutral lines twisting and coaxial cables 15 p2369 A71-31506

Coaxial cable antenna lead with shield or external conductor in form of slotted corrugated metal foil, testing performance 20 p3197 A71-39469

Book on practical design for electromagnetic compatibility covering interference control, reduction, analysis, prediction and measurement, shielding problems, etc 21 p3356 A71-40779

ELECTROMAGNETIC SHOCK TUBES

U SHOCK TUBES

ELECTROMAGNETIC SPECTRA

NT BALMER SERIES

NT D LINES

NT ELECTRONIC SPECTRA

NT FRAUNHOFER LINES

NT H ALPHA LINE

NT H BETA LINE

NT H GAMMA LINE

NT H LINES

NT INFRARED SPECTRA

NT K LINES

NT LINE SPECTRA

NT LYMAN SPECTRA

NT MICROWAVE SPECTRA

NT RADIO SPECTRA

NT RAMAN SPECTRA

NT RYDBERG SERIES

NT SOLAR SPECTRA

NT STELLAR SPECTRA

NT TELLURIC LINES

NT UV SPECTRA

NT ULTRAVIOLET SPECTRA

NT VIBRATIONAL SPECTRA

Thermal DC noise generated in plasma at electron-ion collisions, using quantum mechanics for noise frequencies in EM radiation RF spectra 03 p0463 A71-13345

Solar corona emissions, discussing very high temperatures origin, eclipses and electromagnetic radiation spectrum 06 p0970 A71-18058

Agronomic research by remote sensing, discussing spatial, spectral and temporal measurements from electromagnetic multispectral response 06 p0896 A71-18407

X ray and gamma ray astronomy, considering intensity monotonic decline in cosmic electromagnetic spectrum 12 p1949 A71-27369

Atmospherics sources spectral amplitude ratios and group delay times correlation, obtaining VLF ionospheric propagation characteristics from single station observations 14 p2237 A71-30957

Skylab earth resources experimental equipment, describing sensing and recording instrumentation for electromagnetic spectral pattern recognition studies [AIAA PAPER 71-841] 17 p2739 A71-34712

Crab Nebula integrated electromagnetic emission spectra, noting flux density spectral index at various frequencies 20 p3301 A71-39918

ELECTROMAGNETIC WAVE FILTERS

NT INFRARED FILTERS

NT MICROWAVE FILTERS

NT OPTICAL FILTERS

NT RADAR FILTERS

NT WAVEGUIDE FILTERS

Holographic filters for optical automatic pattern recognition systems, discussing reconnaissance target and fingerprint 02 p0247 A71-11702

Solar magnetic field polarity mapping from H-alpha filtergrams, using magnetic configurations in flare location and time forecasting [AIAA PAPER 70-1369] 02 p0316 A71-12696

Optimal discrete signal filters with finite duration transient process, describing approximation procedure to restore noise distorted signals 06 p0876 A71-17928

Computer synthesis of nondegenerate parametric amplifiers with single mesh filter for maximum flat or Chebyshev frequency response applicable to quantum devices 12 p1886 A71-26844

Discretization interval in discrete analog filters for optimal processing of complex radar signals, estimating systematic errors 14 p2194 A71-30081

Detectors for deterministic signals in noise with rational spectral density, considering analog filter for continuous input sampling and discrete filter for point sampling 14 p2195 A71-30108

Undesirable electromagnetic interference minimization in electrical equipment by filtering, shielding, balancing lines, hot/neutral lines twisting and coaxial cables 15 p2369 A71-31506

Be star theta Corona Borealis UVBY H alpha filter observations, noting spectroscopic changes of light variation due to particles in stellar atmosphere 21 p3443 A71-40193

ELECTROMAGNETIC WAVE TRANSMISSION

NT DOUBLE SIDEBAND TRANSMISSION

NT HALOS

NT IONOSPHERIC F-SCATTER PROPAGATION

NT IONOSPHERIC PROPAGATION

NT LIGHT SCATTERING

NT LIGHT TRANSMISSION

NT MICROWAVE TRANSMISSION

NT MULTIPATH TRANSMISSION

NT RADAR TRANSMISSION

NT RADIO TRANSMISSION

NT SCATTER PROPAGATION

NT SHORT WAVE RADIO TRANSMISSION

NT SINGLE SIDEBAND TRANSMISSION

NT TELEVISION TRANSMISSION

NT TRANSEQUATORIAL PROPAGATION

LF spiral monochromatic wave pulse propagation from vacuum into semimetallic semiconductor, considering bandwidth relation to electron heating 01 p0138 A71-10431

Electromagnetic wave nonlinear propagation in semiconductors, considering field amplitude and electron temperature for strong electron phonon interaction and degenerate semimetals 01 p0138 A71-10434

Weakly divergent electromagnetic wave beam propagation in optically nonlinear laminarily inhomogeneous medium, considering absorption coefficient and self focusing 01 p0037 A71-11201

Electromagnetic wave Poynting vector trajectories in absorbing inhomogeneous media, discussing reversibility and energy propagation of spherical and plane structures 02 p0210 A71-11631

Optimum VLF electromagnetic link between underground terminals with emitter-receiver horizontal antennas, calculating radiation pattern 02 p0211 A71-11717

Dispersion equations for complex transmission coefficients of submillimeter EM waves in solid state

InSb plasma, applying plasma effects to control elements 03 p0467 A71-13797

Soviet book on electromagnetic waves diffraction and propagation covering numerical analysis, media and asymptotic theory based on local field principle 03 p0380 A71-14400

Electromagnetic wave propagation along conducting wire in magnetoplasma 03 p0381 A71-14472

Monochromatic wave propagation along cylindrical helical line, showing tubular waveguide formation from wave field and collisionless plasma interaction 04 p0633 A71-15107

Slow electromagnetic wave propagation in plasma waveguide with inhomogeneous electron concentration, considering interaction with electron beam 04 p0634 A71-15112

Magnetospheric whistlers, deriving group refractive index and velocity, propagation time and various L values 05 p0721 A71-16443

Radioelectric /Hall/ effect due to electromagnetic wave propagation in semiconductors, noting longitudinal electric field generation by thermoelectric forces 05 p0794 A71-16882

Electromagnetic pulse propagation over flat impedance surface, determining similarity parameters 07 p1060 A71-19187

Optimal nonreciprocal waveguide phase shifters using ferrites with rectangular hysteresis loop, considering electromagnetic wave propagation 07 p1079 A71-20074

Plane electromagnetic wave propagation and reflection in presence of substances with arbitrary complex permittivity 07 p1066 A71-20543

Galactic cosmic ray propagation earth-source distance determination by observing charge spectrum 08 p1354 A71-21018

Compressible isotropic plasma slab effect on magnetic dipole radiation pattern, using reciprocity theorem 08 p1253 A71-21274

Nonlinear theory of intrinsic semiconductors electromagnetic wave transmission under skin effect conditions, determining reflectance and carrier temperature 08 p1344 A71-21442

Electromagnetic propagation errors in radar tracking, photogrammetric cameras and laser range finders due to atmospheric refraction, discussing error compensation techniques 09 p1405 A71-22356

Photon emission from electron moving in field of two plane electromagnetic waves with different frequencies and propagating in same direction 09 p1460 A71-22364

Electromagnetic wave propagation through bounded time-space periodic cold plasma under plane wave incidence, calculating transmitted and reflected components 09 p1503 A71-22986

Electromagnetic pulse propagation through inhomogeneous plasma, discussing electron collision frequency effects 09 p1504 A71-22987

Electromagnetic wave propagation in circular waveguide loaded with coaxial dielectric cylinders, calculating band pass characteristics 09 p1406 A71-23039

Bounded electromagnetic wave propagation in randomly inhomogeneous medium, calculating correlation in amplitude and phase fluctuations 09 p1407 A71-23109

Electromagnetic waves reflection and transmission from weakly ionized moving plasma, noting dependence on medium velocity and nonlinearity effect 09 p1505 A71-23519

Electromagnetic wave propagation - Conference, Graz, Austria, June 1970 09 p1410 A71-23569

Azimuthal surface waves launching on cylindrical impedance boundary using waveguide open end as excitation aperture 09 p1410 A71-23571

VLF electromagnetic propagation, calculating mode conversion efficiency at solar terminator on angle based on flat model with finite wall conductivities 09 p1411 A71-23576

Electromagnetic wave propagation in anisotropic ionospheric plasma with time-varying random electron density irregularities 09 p1506 A71-23586

Phase and frequency instabilities in electromagnetic wave propagation - NATO/AGARD Conference, Ankara, Turkey, October 1967 10 p1576 A71-24185

Transient electromagnetic wave propagation in lossy directionally anisotropic time varying stratified plasma, using characteristics method 10 p1648 A71-24296

Electromagnetic extraordinary wave propagation in toroidal plasma with sheared magnetic field,

discussing ordinary component generation at upper hybrid frequency

10 p1650 A71-24629

Electromagnetic wave diffraction on arbitrary spheres, including scattering and attenuation by four water droplets

10 p1579 A71-24877

First order EM discontinuities propagation in nonlinear centrosymmetric isotropic material with displacement field dependent on electric field and induction field dependent on magnetic intensity

11 p1798 A71-25568

Strong cylindrical and spherical electromagnetic wave propagation in plasmas, calculating amplitude and electron temperature

11 p1805 A71-25768

Electromagnetic wave propagation on uniform transmission line network, discussing passivity and stability notions concerning energy exchange between waves and material

12 p1879 A71-27039

Semiconductor or gas-discharge two-component plasmas, calculating permittivity variation due to carrier heating and diffusion during strong plane monochromatic, electromagnetic wave propagation

12 p1937 A71-27184

Differential equations for wave propagation in irregular electromagnetic waveguides

12 p1888 A71-27530

Plane traveling electromagnetic wave existence, propagation and refraction in nonlinear dispersive nonmagnetic isotropic lossless medium

13 p2027 A71-27899

Local and sequential propagation characteristics of electromagnetic fields and waves in inhomogeneous lossy medium

13 p2028 A71-27995

Circular thin glass tube waveguide containing cold cylindrically stratified plasma, calculating electromagnetic wave propagation

13 p2029 A71-28499

Self modulation of amplitude modulated electromagnetic wave propagation in magnetoplasmas, considering interaction effects for ordinary and extraordinary propagation modes

13 p2107 A71-28787

EM field and wave propagation in static and spherical gravitation, obtaining modified Debye potentials and amplitude and eikonal equations

13 p2139 A71-28999

Nonlinear skin effects in gas discharge plasma during electromagnetic wave propagation with dissipation, obtaining wave amplitude and carrier temperature dependence on reflection parameters

13 p2108 A71-29042

Normally incident electromagnetic wave propagation in inhomogeneous gyration medium, obtaining reflection and transmission coefficients and discussing resonance

13 p2108 A71-29088

Diffraction-limited electromagnetic theory of image formation for point reference arbitrary shape hologram

13 p2072 A71-29440

Plane electromagnetic waves diffraction by moving periodic metal strip grating, taking into account relativistic effects

14 p0000 A71-30076

Electromagnetic wave propagation on Yagi-Uda structure, obtaining current distribution, free space vs guided wavenumbers diagram and cutoff frequencies

14 p2196 A71-30514

HF modulated transverse electromagnetic wave penetration into plasma with negative dielectric constant, noting plasma density fluctuations and electroacoustic wave formation

14 p2281 A71-30542

Magnetized plasma and vacuum plane interface, deriving dispersion equation for electromagnetic surface waves propagating at arbitrary angles

15 p2456 A71-31744

Electromagnetic wave propagation along homogeneous and inhomogeneous plasma columns, establishing density distribution functions and dispersion curves

15 p2459 A71-32641

General relativistic time delay of electromagnetic radiation propagation due to solar gravitational field measured from Mariner 6 and 7 range and Doppler data

16 p2640 A71-33737

Tropospheric range error in EM signal arriving at earth zenith, measuring integral of refractivity through atmosphere from height, pressure, temperature and humidity

16 p2569 A71-33800

Visible spectrum electromagnetic waves propagation in plasma, emphasizing parametric coupling

16 p2620 A71-34136

Weakly divergent electromagnetic wave beam propagation in optically nonlinear laminarly inhomogeneous medium, considering absorption coefficient and self focusing

17 p2697 A71-34253

Plasma conductivity frequencies, including electromagnetic wave propagation in alternating field and scattered light intensities

17 p2786 A71-34276

Electromagnetic wave diffraction by moving wedge with surface impedance, evaluating Doppler shifts and scattered field in shadow region

17 p2698 A71-34429

Electromagnetic wave propagation in uniform simple medium, demonstrating drag effects relative to inertial and accelerated frame

17 p2699 A71-34431

Electromagnetic waves propagation in inhomogeneous medium, using simulation chamber with NaCl and ethyl alcohol diffused agar-agar

17 p2724 A71-34755

Optimum pulse transmission through thin exponentially inhomogeneous plasma region for maximum amplitude signal reception, using matched filter theory

17 p2788 A71-34768

Uniform inhomogeneous waveguides with linear time invariant passive medium, determining functional behavior in frequency domain of electromagnetic waves propagation constant

17 p2708 A71-35492

Reflection and transmission coefficients for electromagnetic propagation across magnetic field in parabolic plasma layer, determining EM-plasma wave conversion efficiency

19 p3014 A71-37079

Electromagnetic wave propagation through magnetoplasma disturbed by acoustic wave, calculating transmitted and reflected waves amplitude modulation

19 p3110 A71-37480

Transmitted and reflected waves dispersion and structure in waveguide loaded by semiinfinite series of equidistant homogeneous scattering bodies

19 p3019 A71-38329

Electromagnetic wave propagation in comb type waveguides, obtaining boundary value electrodynamic problem rigorous solution

19 p3020 A71-38342

Plane electromagnetic wave diffraction by dense periodic array with Dirichlet and mixed boundary conditions, determining solution asymptotic behavior

19 p3104 A71-38416

Electromagnetic waves depolarization by rough terrain backscatter, applying theory of surface currents perturbation due to surface irregularities

19 p3021 A71-38447

Free space diffraction of E-polarized plane electromagnetic wave by slit in thick conducting screen, deriving approximate solution from Wiener Hopf equation by matrix techniques

19 p3023 A71-38592

Anisotropic plasma half space moving normal to interface, investigating incident H waves reflection and transmission coefficients

19 p3024 A71-38610

Electromagnetic wave transmission through conducting plasma slab, reducing nonlocal wave interaction two point boundary value problem to Cauchy system

20 p3274 A71-39080

Galactic cosmic ray propagation earth-source distance determination by observing charge spectrum

20 p3280 A71-39598

Strong cylindrical and spherical electromagnetic wave propagation in plasmas, calculating amplitude and electron temperature

22 p3579 A71-41536

Electromagnetic wave dispersion in interstellar plasma, noting indistinguishable form from natural dispersion of photons with nonzero rest mass

22 p3574 A71-41598

Electromagnetic wave propagation and radiation pattern of circular corrugated waveguide antenna feeds, considering unity azimuthally dependent modes

22 p3511 A71-42278

Plane electromagnetic wave diffraction on periodic arbitrary profile array, presenting near and far field asymptotic characteristics

22 p3511 A71-42306

Semiconductor or gas-discharge two-component plasmas, calculating permittivity variation due to carrier heating and diffusion during strong plane monochromatic electromagnetic wave propagation

22 p3584 A71-42461

Plane electromagnetic waves reflection and transmission at boundary of semiinfinite magnetolectric medium

23 p3642 A71-42918

Least squares and sequential estimation techniques application to Mariner 6 and 7 tracking data analysis, verifying Einstein relativity theory on electromagnetic radiation propagation

[AAS PAPER 71-384]

23 p3731 A71-43054

Particle collisions and relativistic effects on electromagnetic wave propagation within plasma in direction normal to external magnetic field near gyrofrequencies

23 p3645 A71-43559

Electromagnetic wave reflection from ferrite plates in external alternating magnetic field, showing frequency change due to moving domain wall

23 p3645 A71-43560

Plane electromagnetic wave diffraction on dense periodic array at conducting screen, showing far field asymptotic behavior for E and H polarization

23 p3647 A71-44331

Electromagnetic wave propagation in gas with independent electron density and electric field strength, calculating transmitted power limit value

24 p3851 A71-44420

Numerical analysis of electromagnetic wave diffraction on inhomogeneous transmitting bodies, reducing Maxwell equations boundary value problem to differential equations solution

24 p3804 A71-44722

Electromagnetic wave propagation in radially and axially nonuniform dielectric media, using geometrical optics approximation

24 p3848 A71-44970

Plane TEM wave propagation in free space using rectangular waveguide partially filled with two dielectric slabs

24 p3809 A71-45093

Inhomogeneous rarefied plasma, investigating nonlocal, linear and nonlinear effects on electromagnetic wave reflection and transmission

24 p3857 A71-45117

Refraction of electromagnetic wave with electric field perpendicular to applied magnetic field in anisotropic plasma cylinder cross section

24 p3858 A71-45236

ELECTROMAGNETIC WAVES

U ELECTROMAGNETIC RADIATION

ELECTROMAGNETICS

U ELECTROMAGNETISM

ELECTROMAGNETISM

NT MAGNETOSTATICS

Electromagnetic cascade-material boundary crossing transition effect analysis by perturbation theory in terms of differential shower particle flux

03 p0478 A71-13871

Gravitational waves properties and detection, discussing relationship between electromagnetism and special relativity theory

03 p0459 A71-13950

Magnetoresistance of coil surrounded electromagnetic mechanisms air gaps, noting potential distribution at pole aperture axis

05 p0705 A71-17175

Linearized gravitation theory in macroscopic media, deriving refraction of gravitational waves based on classical electromagnetism

17 p2777 A71-34585

Eigenfunctions of curl operator, rotationally invariant Helmholtz theorem and applications to electromagnetic theory and fluid mechanics

20 p3255 A71-39575

Antiferromagnetic semiconductors and metals in magnetic field, obtaining Fourier components of electromagnetic fluctuation correlators for dielectric permittivity and magnetic permeability tensors

22 p3586 A71-42062

ELECTROMAGNETS

NT HIGH FIELD MAGNETS

NT SUPERCONDUCTING MAGNETS

Electropneumatic transducer system linearization, matching nonlinearities in EM and pneumatic subsystems

13 p1999 A71-28638

Stability control of magnetic suspension with stabilizer allowing for energy dissipation in electromagnet using Lagrange-Maxwell electromechanical equations

15 p2353 A71-32080

Coercive force and specimen thickness effects on outputs of meters with attached electromagnets

22 p3553 A71-41766

Ferrite corecimeter with attached electromagnet and compensation winding, deriving analytical expressions for demagnetization and compensation currents

22 p3521 A71-41767

ELECTROMECHANICAL DEVICES

Null shift errors of compensated electromechanical pendulum accelerometers during random vibration of base

07 p1108 A71-19308

Inertial sensors, considering electromagnetic mechanical devices, single and two degrees of freedom floated gyros and electromagnetic rebalance pendulous accelerometers

09 p1443 A71-22594

Electromechanical systems digital simulation, discussing reticulation, bigraph reduction, mathematical modeling, etc

09 p1428 A71-22774

Computer controlled electromechanical system for luminous projection on world map of satellite orbits, using Ne-He laser beam

09 p1430 A71-23627

Electronic communication system critical design evaluation, concerning electromechanical components and packaging impact on overall reliability and cost

12 p1878 A71-26688

- Hipp pendulum controller electromechanical clock, considering dry and viscous friction dynamic models 12 p1932 A71-27525
- Solid state vs electrical-mechanical relay switching and isolation technique 13 p2001 A71-28845
- Modulator-demodulator type push-pull DC amplifier input noise reduction, using electromechanical vibrators 15 p2355 A71-32451
- Automatic regulation of volumetric blood flow rate during artificial blood circulation, using electromechanical system for controlling arterial pump of cardiopulmonary machine 19 p3010 A71-38641
- Hybrid electromechanical analog computer real time simulation technique for optimizing vibration response of two degree of freedom system with impact damper [ASME PAPER 71-VIBR-119] 21 p3350 A71-40338
- Brushless DC motor as power source for meteorological, communications and geological satellites, describing electromechanical design features and operating characteristics 21 p3326 A71-40724
- Electromechanical converters mathematical model, calculating conductivity behavior and derivative 22 p3484 A71-42877
- Transient response of electroacoustic transducer arrays, computing time dependent velocities for prescribed electrical inputs 23 p3704 A71-43211
- ELECTROMECHANICS**
- Videotape sampling in electromechanical equilibria feedback stabilization of hydromagnetically contained plasmas 06 p0932 A71-17460
- German book on noise covering electrical fluctuation phenomena, thermodynamic equilibrium, electromechanical systems, semiconductors and ferromagnetic fields, diodes, etc 17 p2713 A71-34478
- Composite piezoelectric transducer subjected to current flow in semiconducting boundary layer under polarization gradient, determining mechanical response by Laplace transform 17 p2739 A71-34669
- German monograph on similarity principle as design method in electromechanics covering similarity laws in mechanics, thermodynamics and electricity 17 p2748 A71-34791
- Elastic plates radial vibrations excited by piezoelectric elements, investigating electromechanical coupling coefficient and ultrasonic radiation constants 21 p3473 A71-41365
- ELECTROMETERS**
- Small tissue equivalent ionization chamber quartz fiber electrometer dosimeter system, for use as space qualified radiation detection instruments 02 p0250 A71-12136
- Microwave dielectrometer measurement system sensitivity to electric field energy in dielectric non-magnetic specimen 12 p1889 A71-27621
- Simultaneous measurement of transverse and longitudinal bioelectric potential differences in plants without direct contact with tissues, using vibrating reed electrometer 21 p3375 A71-39985
- Maximum bubble pressure automatic capillary electrometer for salt solutions and organic compounds electrosorption, comparing with Lippmann instrument and capacitance bridge 22 p3548 A71-42529
- ELECTROMIGRATION**
- MOS large scale IC phosphosilicate glass substrate vapor deposits effects, including hardness, pinhole density and electromigration 07 p1070 A71-18868
- Failure prediction for metal film semiconductor contacts on silicon substrate by electromigration, considering current density and temperature gradients 19 p3119 A71-38510
- Ni-Cr thin film resistors reliability, describing deposits on silicon dioxide, intermetallic formation and electromigration 19 p3034 A71-38515
- Bulk metal electromigration and crack failure in Al thin film conductors, considering purity, glassing and hole nucleation 23 p3651 A71-43426
- ELECTROMOTIVE FORCES**
- NT PONDEROMOTIVE FORCES**
- Fusibility and thermal emf of ternary intermetallic TiFe-TiCo-TiNi system 01 p0103 A71-11090
- Electron mobility and thermal emf in nondegenerate ferromagnetic semiconductors, considering entrainment of electrons by magnons at temperatures below Curie point 04 p0636 A71-15102
- Constant emf in bulk age and Si N-type semiconductors under multifrequency microwave electric field 13 p2111 A71-28368
- Time dependence of signal emf induced in toroidal proton precession magnetometer sensor with elliptical cross section 14 p2246 A71-30481
- Thermal emf changes for noble and refractory metal thermocouples, determining drift in high temperature air, Ar and vacuum environments for long time periods 18 p2916 A71-36049
- Emf dynamo nonuniformities effect on magnetospheric field aligned electric currents associated with solar quiet geomagnetic variations, calculating ionospheric electrostatic fields 20 p3217 A71-39516
- Dispersion equation determining periodic structures natural modes propagation constants, using induced electromotive and magnetomotive forces method 20 p3198 A71-39806
- Liquid flow rate measurement by determining fall time of emf generated in sensor coil by fluid nuclei precessing freely in magnetic field 23 p3678 A71-43536
- Differential magnetic circuit sensor with movable screen, analyzing neutral point lag for calculation of emf distributed output winding and neutral point displacement 24 p3810 A71-45153
- ELECTROMYOGRAMS**
- U ELECTROMYOGRAPHY**
- ELECTROMYOGRAPHS**
- U ELECTROMYOGRAPHY**
- ELECTROMYOGRAPHY**
- On-line parameter tracking algorithm, obtaining parameters in mathematical relation between full wave rectified EMG and human triceps muscle force during isometric task 03 p0374 A71-14423
- Subjective and electromyographic estimation of fatigue and muscle activity physiological levels, considering isometric muscle contraction task endurance 07 p1047 A71-19458
- Human electromyogram and isometric muscle tension dynamic relationship 09 p1400 A71-23363
- Surface electromyographic recordings on biceps and peripheral muscles during sustained isometric contractions 13 p2024 A71-29499
- Operator mental performance reliability prediction from heart beat rate and electromyogram 16 p2534 A71-32826
- Human respiratory muscles electrical activity, discussing correlation analysis of interferential electromyograms from external intercostal muscles during breathing exercises 19 p3003 A71-38198
- Shin muscle electrical activity during standing after 120 day bed rest hypokinesia from EMG measurement 20 p3188 A71-39230
- Miniaturized multichannel FM/AM biological telemetry system for simultaneous transmission of EEGs, EMGs, EOGs and EKGs 22 p3500 A71-41574
- Prior muscle exertions effect on reaction time and duration of simple discrete movements, considering electromyogram frequency changes 22 p3503 A71-42194
- Muscular work level shifts effectiveness during pedaling activity from oxygen requirement measurement, electromyograms and stress dynamograms 24 p3794 A71-44412
- Muscular bioelectric potential input processing into digital computer, describing amplitude, frequency and time domain analysis of electromyogram signals 24 p3801 A71-44542
- ELECTRON ACCELERATORS**
- NT BETATRONS**
- Electron accelerator with broad stable beam for calibration of spectrometers and channel electron multipliers 04 p0599 A71-15587
- Relativistic electrons acceleration in solar proton flares, taking into account plasma density and magnetic field intensity 09 p1512 A71-22059
- Linear and nonlinear laser induced ion emission from solid targets with and without magnetic field, considering electron space charge accelerator 11 p1775 A71-26085
- Power amplifier klystron self excitation in linear electron accelerators, describing tunable driver circuit with quartz reference oscillator 12 p1889 A71-27754
- Accelerator with electron pregrouping for exciting semiconductor lasers based on amplifying klystrons 13 p2079 A71-28858
- Crab Nebula model, discussing electromagnetic field time variation and electron acceleration and synchrotron emission 14 p2304 A71-29632
- Linear electron accelerator using shaping system debunching properties for minimizing electron energy differences in bunched beam 15 p2376 A71-31743
- Prebunching electron accelerator for exciting semiconductor lasers based on amplifying klystrons 21 p3394 A71-41296
- Steady state problem of energy spectrum of variable magnetic field accelerated electrons, considering synchrotron X ray emission of Crab Nebula and pulsar 24 p3869 A71-44802
- ELECTRON ATTACHMENT**
- Dissociative electron attachment excess energy correlation with fragment ion translational energies, determining radical affinity 08 p1338 A71-21782
- Halogen molecules electron affinities by measuring negative ion average translational energy and appearance potentials, noting free radicals heat of formation 09 p1498 A71-23376
- Rate constant measurements of hot plasma electron attachment from ion current collection plots for communication during atmospheric entry 12 p1939 A71-27272
- Electron attachment rate determination by combined photographic and radar observation of meteors 13 p2137 A71-28545
- ELECTRON AVALANCHE**
- Polarization influence on transition effect behavior in avalanche transition between media, discussing critical energies 03 p0478 A71-13869
- Memory behavior in floating gate avalanche injection MOS structure, considering long term charge storage in insulated gate field effect device 13 p2036 A71-28045
- Electron avalanche processes in gas discharges, deriving electron energy distribution function and similarity laws 13 p2103 A71-29079
- Average energy of electron avalanches in gases for linear inelastic collision cross sections, including ionization coefficient and Stoletov constant for atomic hydrogen 13 p2103 A71-29080
- Stoletov constant for gas mixture, discussing average avalanche energy at reduced electric field with maximum ionization coefficient and Penning effect for Ne-Ar 13 p2103 A71-29081
- Avalanche transistors circuits, generating rectangular and sawtooth pulses for use in time delay devices 14 p2213 A71-30582
- Pulse detection equipment by peak voltage and current value sampling, using avalanche transistors 15 p2377 A71-32324
- One- and two-sided abrupt junction IMPATT diodes, investigating Si junction type effects on avalanche region and diode design 18 p2895 A71-36987
- Emitter avalanche stress on gated silicon planar n-p-n transistors, investigating degradation phenomena 19 p3034 A71-38523
- Emitter-base junction degradation by avalanche breakdown in planar transistors with low doped /epitaxial/ base region 22 p3520 A71-41682
- Polarization influence on transition effect behavior in avalanche transition between media, discussing critical energies 22 p3595 A71-42670
- CW avalanche microwave oscillator frequency modulation /pulling/ by injected RF signal, discussing theory and experiment 23 p3646 A71-43903
- ELECTRON BEAM WELDING**
- Electron beam welding system, discussing solid state controls, programmed operation and type and thickness of welded materials 01 p0087 A71-10451
- Carbon dioxide laser vs electron beam welding, examining weldability of high thermal conductivity metals 01 p0087 A71-10452
- Laser vs electron beam welding, examining high and partial vacuum and atmospheric pressure environments, penetration and ionization and dissociation processes [SME PAPER MR-70-523] 01 p0090 A71-11269
- Electron beam welding penetration depth, using constant melt temperature boundary interface [ASME PAPER 70-WA/HT-2] 03 p0432 A71-14094
- Electron beam welding and boring, considering temperature distribution relation to pulse duration 03 p0433 A71-14271
- Liquid Na heat exchanger fabrication, using electron beam welding technique for stainless steel components assembly 11 p1768 A71-25390
- Bi-metallic refractory metal joints electron beam welding and aging for applications to in-pile thermionic converters 11 p1769 A71-25857
- Electron beam welding of tungsten to tungsten/rhenium and tungsten/rhenium to niobium, discussing techniques for assembly of thermionic converter fuel elements 11 p1769 A71-25858

- Electron beam welding machine reducing number of fabrication variables during final assembly procedure in thermionic converters fabrication, discussing UHV systems 11 p1709 A71-25866
- Pulsed laser holographic applications to aerospace components nondestructive testing, inspecting electron beam welds and internal structural flaws [ASME PAPER 71-GT-74] 11 p1770 A71-25988
- Electron beam welding of metal-metal and metal-ceramic joints and sapphire sealing under vacuum 11 p1745 A71-26399
- Book on electron beam welding covering generation and control, thermal effects, techniques and equipment, metallurgical and mechanical properties, etc 13 p2074 A71-28736
- Electron beam welding, calculating penetration depth from mathematical model [ASME PAPER 70-WA/HT-2] 13 p2075 A71-28978
- Optimal electron beam welding of Nb alloy to bronze, showing high mechanical properties due to deep Cu diffusion 14 p2253 A71-30491
- Residual stress determination from stress intensity factor measurements, describing application to electron beam welded aluminum plate 15 p2508 A71-32259
- Mo sheet electron beam penetration during welding, calculating heat-affected zone temperature distribution 15 p2435 A71-32466
- Stress rupture ductility of electron beam, gas tungsten arc and gas metal arc welds, considering creep crack initiation 15 p2437 A71-32617
- Electron beam welding of martensitic turbine grade steel thick sections, showing accelerating voltage and focus coil current effect on weld profile 19 p3070 A71-38314
- Tungsten and tungsten alloys weldability by gas tungsten arc, electron beam and chemical vapor deposition techniques 21 p3388 A71-40624
- Flash X ray technique for imaging of cavities formation during electron beam welding of Al alloy 23 p3681 A71-43195
- ### ELECTRON BEAMS
- Plasma beam systems dispersion equation with allowance for electron collisions with heavy particles 01 p0132 A71-10154
- VHF radiation from plasma during electron beam interaction with fast magnetoacoustic wave stimulated by external spatially periodic currents 01 p0132 A71-10155
- Wave propagation in plane neutral electron beam near interface with semiconductor 01 p0139 A71-10782
- Electron beam nonlinear interaction with plasma, considering electrostatic wave propagation, instability and dispersion equation 01 p0135 A71-11209
- HF oscillations excitation in decaying plasma-electron beam system, noting Coulomb collisions and nonlinear effects role 02 p0288 A71-11632
- Inhomogeneous plasma oscillations excitation by high intensity electron beam, causing instability greater than hydrodynamic beam mode 02 p0288 A71-11890
- Relativistic self confined electron beam produced plasmas, measuring electron density profile by multiple pass Mach-Zehnder laser illuminated interferometer 02 p0289 A71-11946
- Current profile monitor for scanning electron beam irradiations from accelerator, using storage oscilloscope or X-Y recorder for display 02 p0249 A71-12127
- Beam current instability and plasma heating by electron beam generated in linear discharge, discussing electron beam-cold plasma interactions 02 p0291 A71-12501
- Quasi-neutral electron beam instabilities in plasmas within longitudinal magnetic field with ion compensated space charge 02 p0291 A71-12546
- Nonlinear stabilization of beam instability during electron beam interaction with decay plasma, determining distribution function in damping dynamics of HF vibrations 02 p0292 A71-12610
- TWT microwave amplifier parameters effect on power threshold for electron beam signal control loss 03 p0385 A71-13790
- Interelectron focusing voltage effect on electron beam and tube efficiency in TW and backward wave tubes with electrostatic focusing systems 03 p0385 A71-13793
- Swept electron beam scanning in microwave beam-wave interaction devices via periodic magnetic fields 03 p0385 A71-13794
- Cyclotron electron beam transverse waves interaction in microwave amplifier resonant coupling element with double spiral 03 p0385 A71-13795

Current interception in TWT electron beam affecting minimum noise factor level 03 p0386 A71-13803

Semiconductor cadmium sulfide crystal structure changes during high power electron beam and optical pumping, using stimulated emission spectra measurements 03 p0439 A71-13984

Photoelasticity application for stress-strain state determination around bores made by electron beam, using epoxy models for internal stress distribution 03 p0429 A71-14272

Phase fluctuations in nonautonomous reflex klystron oscillators due to shot noise in electron beams 04 p0557 A71-14624

Thermal diffusivity measurements over 40 to 1400 C range using pulsed electron beam 04 p0595 A71-14963

Slow electromagnetic wave propagation in plasma waveguide with inhomogeneous electron concentration, considering interaction with electron beam 04 p0634 A71-15112

Plasma oscillations excitation in ion sheath by electron beam, presenting frequency and amplitude variations as functions of discharge current and target bias voltage 04 p0634 A71-15259

Single pulse relativistic electron beam passage through plasma, calculating induced current density in axial direction 04 p0635 A71-15371

Rotating electron beam cyclotron and space charge waves interaction with fast electromagnetic waves 05 p0719 A71-16002

Ti-Al-V foils by electron beam vapor deposition, discussing metallurgical characteristics 05 p0765 A71-16237

High energy electron penetration and scattering in solids, obtaining beam density profiles by polymethyl methacrylate resist exposure 06 p0940 A71-17305

Longitudinal electron oscillation suppression by beam density modulation in axially and transversely finite beam-plasma system 06 p0934 A71-17484

Electron scattering out of electron beam in beam plasma, presenting evidence for nonlinear effective inverse mean free path 06 p0935 A71-17485

Data reduction for information retrieval, considering electron beams application for electronic circuit ultraminiaturization 06 p0871 A71-17525

Three electrode image translator with electrostatic electron beam focusing, rendering high uniform resolution over entire viewfield 06 p0897 A71-17531

Monochromatic plasma waves excitation by electron beams, discussing nonlinear theory 06 p0936 A71-17688

Sintered or cast Re refining in vacuum electron beam furnace using water-cooled crystallizer, discussing metal losses during melting 06 p0904 A71-17948

High power pulsed electron beam generator, using distilled water as dielectric and multiblade cathode electron gun 06 p0876 A71-18077

Electron beam drilled workpieces, investigating residual stresses origin and character with photoelastic measurement 06 p0905 A71-18092

Multiple speed flow onset and energy distribution in nonlinear electron beam-plasma interaction 06 p0937 A71-18354

Coulomb collisions effect on instability of cold and warm monoenergetic electron beams in plasma 07 p1166 A71-18885

Plasma produced by pulsating fast electron beam, observing electron temperature and charged particle concentration 07 p1167 A71-19232

Ion source for double focusing magnetic mass spectrometer for use with gas chromatograph on Mars mission, requiring electron beam stabilization in space 07 p1113 A71-19851

Ion source emitter plasma column generated by electron beam injection through gas filled chamber, compensating ion space charge with fast discharge electrons 07 p1170 A71-20180

Plasma-electron beam interaction instability transition from absolute to convective in hydrogen tube system at various pressures, considering electron collision effects 07 p1170 A71-20181

Stimulated emission wavelength tuning from GaAs and CdSe electron beam pumping laser crystals as function of time and current 07 p1128 A71-20393

Reflex klystron electron beam admittance calculation, comparing results with measurement 08 p1264 A71-21275

Electron beam pumped CdS laser, investigating output pulse time duration based on laser oscillation quenching model 08 p1302 A71-21435

Longitudinal electron plasma waves generated by electron beam-plasma interactions, discussing simultaneous radiation and incoherent microwave scattering measurements in relation to theory 08 p1341 A71-21746

Molecular and atomic oxygen properties in nonequilibrium flows, determining vibrational temperature and number density by electron beam fluorescence technique [AIAA PAPER 71-271] 08 p1338 A71-21997

Single gap klystron output resonator optimization showing maximum electronic efficiency during bunched beam excitation 09 p1414 A71-22220

Relativistic electron beam instability and mean free path in dense plasma target, using Vlasov equation 09 p1500 A71-22328

Electron gun synthesis by nonparaxial method, calculating beam potential distribution, trajectories and cathode geometry for cylindrical diode 09 p1415 A71-22461

Electron beam shaping by inverted coaxial magnetron gun with steady oscillatory energy exceeding analogous value 09 p1415 A71-22462

Electron beam current density measurement using neutral Ar atoms electron impact excitation to metastable states 09 p1497 A71-22731

Electron gun diode design for beam-collisionless plasma interaction nonlinear evolution, studying delta function beam velocity distribution 09 p1502 A71-22754

Electron beam relaxation in plasma, discussing experimental studies of oscillation amplitude and beam electrons energy distribution relationships during predominantly longitudinal plasma oscillation excitation 10 p1650 A71-24627

Strong interaction between plasma forward wave and electron beam slow wave at equal densities, causing double stream instability nonlinear limitations 10 p1651 A71-24636

Microwave devices with transmission lines excited by curvilinear electron beams, deriving dispersion equations for TWT with allowance for space charge effect 10 p1584 A71-24717

Physical model describing mechanism of recording through surface corrugation of thermoplastic viscofluid layer by electron beam 10 p1613 A71-24873

Spatial-temporal emission of n-GaAs laser pumped by electron beam at liquid nitrogen temperatures 10 p1622 A71-24889

Quasi-linear relaxation of ultrarelativistic electron beam in homogeneous and inhomogeneous plasmas, noting initial divergence angle threshold 10 p1654 A71-24895

Broadened energy distributions in electron beams, discussing energy spread delta E and C prime values relationship for studying weak Coulomb interactions 11 p1802 A71-25631

Plasma production by pulsating fast electron beam, observing electron temperature and charged particle concentration 12 p1934 A71-26750

Design and operation of scanning laser based on exciting electron beam directional variation, discussing laser characteristics for various operating modes 12 p1913 A71-26851

Small amplitude oscillations in system of relativistic electron beam penetrated plasma, calculating dispersion curves 12 p1936 A71-26919

Electron beam high frequency modulation effects on hot ions production in cold plasma 12 p1938 A71-27207

Ion sources designs involving high energy electron beam injections, discussing input power continuous and pulsed modes optimal efficiencies 12 p1940 A71-27507

Optical losses and quantum efficiencies of electron beam pumped CdS lasers, determining extinction coefficient from dependence of threshold current on resonator length 12 p1915 A71-27639

Ionospheric wave/particle interactions under controlled electron beam energy and flux conditions, using Aerobee rocket for experimental investigation 12 p1902 A71-27668

Statistical analysis of random oscillations excited in electron beam-plasma system based on signal recording data 13 p2106 A71-28364

Electron and laser pulse plumes, using thermomechanical shock wave theory 13 p2079 A71-28768

Electron beam vapor deposited CoCrAlY coating composition optimization with ballistic impact and furnace/long term burner rig oxidation tests
14 p2257 A71-29636

Electron beam interaction with external harmonic microwave field in planar diode gap, calculating electric field current and voltage distribution functions
14 p2211 A71-30084

Electron beam instability in cylindrical magnetically confined plasma column, calculating quasi-static oscillations spatial growth increments
14 p2279 A71-30090

Semiconductor lasers with fast electron pencil beam excitation for high capacity computer storage application
14 p2207 A71-30110

Ion and electron beams technology application to microelectronics, discussing limitations imposed by electron/ion optical effects
14 p2277 A71-30701

Magnetic mirror system measured axial energy distribution of electron beams conversion to equivalent electrostatic analyzer
14 p2249 A71-30886

Electrical fiber plates as high resolution conductive arrays for storage and display in electron beam addressed systems
14 p2250 A71-31033

Relativistic electron beams in plasma, considering electrostatic instability conditions and critical currents
15 p2453 A71-31235

Nb alloy ingots electron beam melting, investigating reverse zone liquation intensity and behavior dependence on melting parameters
15 p2424 A71-31241

Rotational temperature and density measurements in high speed gas flow by electron beam fluorescence technique
[AIAA PAPER 71-605] 15 p2406 A71-31544

Linear electron accelerator using shaping system debunching properties for minimizing electron energy differences in bunched beam
15 p2376 A71-31743

Surface melting, spallation and stress response prediction for metals under pulsed electron beam heating, using one dimensional finite difference computer program
15 p2390 A71-32005

Pulsed electron beam heating of metals, determining surface melting, spallation and induced stresses with one dimensional computer programs
15 p2429 A71-32006

Quasi-neutral electron beam instabilities in plasmas within longitudinal magnetic field with ion compensated space charge
15 p2459 A71-32502

Gain improvement in TWT parametric amplifiers based on slow space charge waves interaction with slow wave structure field by electron beam modulation
15 p2378 A71-32629

Plasma-electron beam system relaxation oscillations due to threshold excitation of transverse ionic oscillations by HF vibrations
15 p2460 A71-32706

Modulated relativistic electron beams interaction with plasma, investigating coherent energy loss
15 p2460 A71-32789

Large signal saturation effects in cyclotron resonance oscillators, using helical electron beam-cavity interaction model
16 p2545 A71-33394

Pulsating auroral patches with sudden intensity dependent spatial expansion, noting relation to triggering instabilities of precipitating electron beam
16 p2573 A71-33954

Stimulated emission of ZnO laser by electron beam excitation at 82-250 K near A-LO line, considering exciton interactions
16 p2589 A71-34121

Electron beam nonlinear interaction with plasma, considering electrostatic wave propagation, instability and dispersion equation
17 p2786 A71-34261

Centimeter TEM waves excitation in Fabry-Perot cavity of cyclotron resonance maser by helical electron beam
17 p2750 A71-34263

Intense pulsed electron beam formation during current flow through plasma
17 p2786 A71-34279

Velocity determination in hypersonic low density wind tunnel based on high energy electron beam produced nitrogen ions time of flight
17 p2670 A71-34887

Electron beam modulation by laser light, considering quantum mechanical theory
17 p2753 A71-35024

Logic devices of adaptive scale-time converters of single pulsed processes on electron beam memory tubes, proposing polynomial methods of data reduction
18 p2887 A71-35881

Temperature measurement by electron beam, using rarefied gas probing for determination of molecule distribution at various vibrational and rotational levels [ONERA-TP-960] 18 p2915 A71-36026

Rarefied hypersonic flow density, velocity and temperature determination by electron beam technology, including ion production, calibration curves, collisions and spectroscopic analysis
18 p2949 A71-36419

Ion charge composition in plasma-electron beam system in strong longitudinal magnetic field, noting multiply charged ions production under high temperature conditions
19 p3109 A71-37132

X ray flare regions structure, temperature and density, showing directed electron beams presence
19 p3126 A71-37622

Periodic electrostatic focusing of high permeance electron beams for high power klystrons
19 p3028 A71-37696

Modulated electron beam interaction with plasma, showing amplitude growth and traveling wave profile distortion
19 p3114 A71-37856

Electromagnetic radiation from beam-plasma system in strong magnetic field, noting maximum microwave emission near electron cyclotron frequency
19 p3116 A71-38252

Electron beam HF modulation effects on hot ions production in cold plasma
19 p3117 A71-38619

Intense relativistic electron beam propagation in drift tube with neutral gas and plasma background, determining front velocity and energy transport
20 p3272 A71-38784

Foillless diode for production of high power relativistic electron beams, using multicathode system
20 p3202 A71-38831

Nonlinear equations for traveling wave amplifiers using transverse wave interaction modes (cyclotron and synchronous electron beam waves), calculating saturation characteristics
20 p3203 A71-39003

Electron beam for determining plasma potential and charge density as function of radius of inertially confined tenuous plasma cylinder
20 p3273 A71-39009

Cathode ray tube, including electron beam peak power, resolution elements, luminescent materials, fabrication techniques, contrast preservation and reliability
20 p3234 A71-39062

High current pulsed electron beams formation in bounded plasma due to changes in current, ohmic resistance and potential difference in electrode gap
20 p3274 A71-39159

Electron beams formation and focusing, including current density distributions, electronic potentiometer recording, parameters and comparison with simulation data
20 p3204 A71-39160

High permeance three electrode electron gun with longitudinal compression, examining beam profiles and radial current density distributions
20 p3204 A71-39161

Hybrid circuit methods for aligning resistors manufactured by different technologies, considering mechanical methods, electric erosion, electron and laser beam alignment, etc
20 p3208 A71-39434

Electron oscillation induced longitudinal standing wave excitation and suppression in beam-plasma system by passing electron beam through axially bounded plasma
20 p3275 A71-39864

Artificial auroral experiment by Aerobee rocket-borne electron accelerator generated monoenergetic electron beam injection onto magnetospheric field
20 p3231 A71-39885

Ground based optical observation of raylike artificial auroras produced by rocket-borne accelerator generated electron beams, using image orthicon TV system
20 p3231 A71-39886

Direct local density gradient measurement in rarefied free jet flow using electron beam deflection signal processed with lock-in amplifier
21 p3364 A71-40394

Turbulent hypersonic wake density and temperature measurement for slender cone model in shock tunnel, using dual electron beam excitation technique
21 p3364 A71-40396

Creep rupture behavior of electron beam melted polycrystalline sheet and powdered rhenium
21 p3397 A71-40454

Electron beam modulation by laser (Schwarz-Hora effect), investigating failure factors
21 p3394 A71-41045

Relativistic electron beam instability and mean free path in dense plasma target, using Vlasov equation
21 p3424 A71-41124

Waveguide structure effect on electron beam pumped GaAs laser characteristics, considering diffraction losses and laser threshold reduction
21 p3394 A71-41233

Electron beam modulation at optical frequencies, calculating excited radiation characteristics with quantum theory
21 p3420 A71-41254

Spatial-temporal emission of n-GaAs laser pumped by electron beam at liquid nitrogen temperatures
21 p3394 A71-41258

Quasi-linear relaxation of ultrarelativistic electron beam in homogeneous and inhomogeneous plasmas, noting initial divergence angle threshold
21 p3425 A71-41275

Electron beam heating of cold plasma in magnetic trap as function of plasma density, showing two stream instability due to Cerenkov effect
21 p3425 A71-41285

Relativistic neutralized cylindrical electron beam paraxial motion through uniform longitudinal magnetic field
21 p3426 A71-41289

Electrical breakdown initiation in high vacuum by electron beam, investigating discharge delay time dependence on beam parameters
21 p3420 A71-41292

Electron beam interaction with plasma in ion sources with oscillating electrons, noting increased ion current
22 p3580 A71-41645

Rotational energy electron beam-plasma interactions in static magnetic field, showing exponential saturated intensity variation
22 p3582 A71-41906

Dense plasma heating by electron beam in magnetic trap as function of cyclotron frequency and field strength, noting strong microwave emission
22 p3583 A71-42064

Stochastic ion acceleration by relativistic electron beam in plasma traveling waves with different phase velocities
22 p3578 A71-42065

Beam electrons correlations effect on interference fringes visibility
22 p3546 A71-42243

Fluctuation in synchronized reflex klystron oscillators due to shot noise in electron beams
22 p3521 A71-42264

TWT off-transmission band area exponentially fading wave effects on electron beam modulation and amplification
22 p3522 A71-42316

Electron beam-plasma system oscillation spectrum control through modulation by external HF signal, discussing theory and experimental verification
22 p3583 A71-42317

Bulk quantum efficiency in electron beam pumped n-type GaAs lasers at 300 K as function of impurity concentration
22 p3558 A71-42362

Electron beam image recorder applications, discussing superior resolution, dynamic range width and high precision controllability advantages over laser or CRT techniques
22 p3548 A71-42516

Nonlinear effects on spatial growth of cesium plasma wave excited by electron beam of varying density and velocity
22 p3584 A71-42535

Rotating electron beam cyclotron and space charge waves interaction with fast electromagnetic waves
22 p3515 A71-42751

Suprathermal electron beam induced HF wave instability in solar wind upstream from earth bow shock, interpreting OGO 5 observations
23 p3720 A71-43158

Nonlinear stabilization of beam instability in plasma with comparable phase velocity, electron capture and decay effects
23 p3709 A71-43264

Conversion effectiveness of oscillations induced by electron beam in bounded anisotropic plasma into electromagnetic emission
23 p3710 A71-43275

Asymptotic expressions for electromagnetic field and currents induced in unbounded dense plasma by relativistic electron beam passage
23 p3711 A71-43410

Fine structure of energy distribution function for electron beam interacting with plasma
23 p3711 A71-43411

Steady nonlinear waves propagation along ring electron beam axis analogous to ionospheric E layer
23 p3711 A71-43412

Intercavity scanning for mode selection of carbon dioxide laser in transversely degenerate resonator by localized electron-beam-trigger excitation
23 p3687 A71-44132

Relativistic electron beam propagation entering vacuum or neutral gas filled region through grounded conducting wall, using one dimensional model
23 p3713 A71-44146

Ohmic discharge plasma resistance, temperature and oscillations in weak electric fields under electron beam excitation in Sirius stellarator
24 p3854 A71-44518

Electromagnetic waves excitation in coaxial resonator by relativistic electron beam, assuming presence of steady longitudinal magnetic field
24 p3833 A71-44663

Relativistic electron beam propagation in decelerating medium in crossed electric and magnetic fields, noting nonrelativistic instability condition
24 p3856 A71-44669

Electron beam and plasma nonlinear interactions, noting scattering zone, amplitude oscillation maximum, longitudinal velocity and relaxation patterns
24 p3856 A71-45097

Spark source generated electron beam interaction with plasma in uniform magnetic field, estimating HF longitudinal oscillation power
24 p3857 A71-45233

Microchannel plate /compact array of channel electron multipliers/ amplifying electron beam containing spatial information, discussing material and technological considerations in plate construction
24 p3811 A71-45334

ELECTRON BOMBARDMENT

GaAs strongly doped p-n junctions, examining I-V characteristics changes under electron bombardment and mixed reactor field irradiation
01 p0140 A71-11458

Submillipound mercury electron bombardment ion thruster efficiency, noting cathode pole piece, baffle position and geometry influence on ion chamber performance
[AIAA PAPER 70-616] 01 p0143 A71-11577

Kaufman electrostatic ion thruster using electron bombardment ionized mercury vapor in cylindrical vessel and acceleration by electrostatic field
02 p0283 A71-12310

Angular distribution of atomic oxygen ions produced by electron bombardment of oxygen, showing electron energy dependence
04 p0631 A71-15657

Electron, proton and UV irradiation effects on CdS solar cell protective plastic films with or without adhesive coatings, measuring transmission changes
05 p0771 A71-16087

SERT II electron bombardment thruster operation with Ar and Hg propellants
[AIAA PAPER 71-157] 06 p0947 A71-18599

Electron bombardment ion thruster using hollow cathode and two-grid ion accelerating geometry, discussing performance tests
[AIAA PAPER 71-158] 06 p0947 A71-18600

Electron trapping in dielectrics, providing effective light and inexpensive spacecraft bremsstrahlung shield and lower average radiation energy at synchronous altitudes
07 p1164 A71-20625

Performance tests of electron bombardment ion thruster, using xenon, krypton, argon, neon, nitrogen, helium and carbon dioxide
14 p2287 A71-29922

NASA Lewis Research Center Hg electron bombardment ion thrusters research programs
14 p2288 A71-29931

Energy necessary to produce beam ion in plasma discharge of Hg electron bombardment ion source
16 p2623 A71-32841

Crystal defects and electrical and optical properties changes due to electron bombardment of semiconductors
16 p2622 A71-33622

Electron bombardment mercury ion rocket engine, considering mass flow rate and magnetic field strength effect on performance
17 p2794 A71-35540

Si solar cells transparent radiation protective coatings stability and degree of blackness, discussing UV irradiation and proton and electron bombardment
20 p3240 A71-39604

Bicolor cathode ray display tubes with triple-layer bombarding electron beam energy-dependent red-green fluorescent screen
21 p3347 A71-40109

Crystal dislocations and impurity atmospheres role in kinetics of accumulation of radiation defects in Ge under fast electron bombardment
21 p3429 A71-41209

Stimulated and spontaneous emission from InSe single crystal under focused fast electron beam bombardment
21 p3434 A71-41326

Ion engine development at Farnborough (England), considering 10 mN mercury electron bombardment thruster system with hollow cathode
22 p3588 A71-41508

Electron bombardment effects on shot noise of silicon junction transistors, noting generation-recombination current increase in emitter junction
22 p3586 A71-42298

Current amplification in CdS and CdSe single crystals and thin films by fast electron bombardment
24 p3859 A71-44386

ELECTRON BUNCHING

Nonlinear electron beam bunching in zero temperature plasma during modulation by two frequencies, using klystron model
04 p0631 A71-14625

Type 2 and 3 solar radio burst model, examining exciting agent as electron bunch emitting electron plasma waves
08 p1356 A71-21756

Single gap klystron output resonator optimization, showing maximum electronic efficiency during bunched beam excitation
09 p1414 A71-22220

Coulomb forces detrimental effects on electron bunching in three-resonator klystron, defining buncher optimal parameters for different perveance values
12 p1888 A71-27614

Accelerator with electron pregrouping for exciting semiconductor lasers based on amplifying klystrons
13 p2079 A71-28858

Space charge delay angle, RF induced current and mode instability interrelated for actual high power heavy duty magnetrons, using electron bunch model
14 p2211 A71-29831

Electron cluster formation in klystron buncher, calculating focusing longitudinal magnetic field variation for maximum electron radial stability
15 p2376 A71-31742

Longitudinal instability of bunch interacting with passive resonator, considering Landau damping influence by linear differential equations of motion solution
19 p3110 A71-37141

Prebunching electron accelerator for exciting semiconductor lasers based on amplifying klystrons
21 p3394 A71-41296

Nonlinear electron beam bunching in zero temperature plasma during modulation by two frequencies, using klystron model
22 p3583 A71-42265

ELECTRON CAPTURE

Cross sections for single-electron capture by C/4 plus/ from He, Ne and Ar target gases
04 p0630 A71-15656

Cosmic ray Be 7 equilibrium concentration, examining electron capture and radioactive decay
05 p0798 A71-16114

Cs ion beam space charge and current neutralization by electron capture for partially ionized plasma formation, investigating longitudinal electrostatic wave excitation
07 p1171 A71-20193

Symmetric excited state electron capture cross sections in ion-atom inelastic scattering, using two state approximation formalism
08 p1338 A71-21235

Electron loss and capture by hydrogen atoms, protons and negative ions during collisions between atoms and molecules in gases, interpreting cross section data
08 p1338 A71-21491

Quasi-captured and escaped electron flux angular dependence and latitudinal variations observations at low altitudes by Cosmos 228 satellite
09 p1512 A71-22362

Strongly magnetized relativistic degenerate electron gas proton-proton reaction rates and electron capture over various temperatures, densities and magnetic field strengths
10 p1661 A71-24305

Cu doped GaAs electron radiative capture mechanisms based on photoconductivity and photoluminescence dependence on temperature and excitation intensity
10 p1657 A71-24324

Average energy electron capture coefficient dependence on air density, temperature and altitude under gamma radiation
13 p2061 A71-28543

Electron loss and capture by hydrogen atoms, protons and negative ions during collisions between atoms and molecules in gases, interpreting cross section data
16 p2614 A71-33042

Nonlinear stabilization of beam instability in plasma with comparable phase velocity, electron capture and decay effects
23 p3709 A71-43264

ELECTRON CLOUDS

Thermalization and diffusion of electron cloud injected into afterglow cylindrical plasma, calculating steady state distribution as function of position and velocity
14 p2280 A71-30175

ELECTRON COLLISIONS

U ELECTRON SCATTERING

ELECTRON COUNTERS

Sensitive fast response scintillation electron detector for use with signal energy analyzer
07 p1115 A71-20358

Satellite-borne scintillation spectrometers for medium and high energy electron and proton measurements
09 p1513 A71-22555

Electromagnetic longitudinal cascades development numerical treatment based on Boltzmann equation discussing Monte Carlo computing times for primary energy total electron counts
12 p1933 A71-27383

Laser beam ionization of gold investigated by pre-perturbational electron counter
21 p3392 A71-40516

ELECTRON DECAY RATE

Inner radiation zone electrons loss and replenishment observation by Pegasus satellite during magnetically quiet and active periods
06 p0949 A71-17264

Solar flare high energy electrons, examining rise time and decay
06 p0961 A71-18171

Decay lifetimes of Starfish electrons in trapped radiation belt inner zone
08 p1356 A71-21646

Nitrogen beam foil spectrum analysis, calculating transitions and decay times
15 p2452 A71-32598

Day and nighttime effective electron loss rate measurement in D region during polar cap absorption events, using rocket-borne spectrometers and Faraday rotation
16 p2573 A71-33961

ELECTRON DENSITY (CONCENTRATION)

NT ELECTRON DENSITY PROFILES

NT IONOSPHERIC ELECTRON DENSITY

NT MAGNETOSPHERIC ELECTRON DENSITY

Sulfur hexafluoride effects on equilibrium electron concentrations in air and argon plasmas, discussing earth reentry simulation applications
01 p0133 A71-10957

Shock tube generated Xe plasma electron density measurements by spectroscopy and laser interferometry, deriving ionization relaxation time
01 p0134 A71-10995

Pulsed Ar ion laser plasma electron density and temperature, discussing Tonks-Langmuir free fall model validity
01 p0096 A71-11623

Gunn diodes I-V characteristics width as function of carrier concentration/mobility and diode length, noting role of impact ionization in strong electric field
02 p0231 A71-11877

Electron concentration and temperature data from Langmuir probe on Explorer 22, discussing magnetic storms effects
02 p0244 A71-11910

Thin exploding wire restrike channels, examining temperature, electron density and thermal conductivity temporal behavior
02 p0284 A71-11941

Thermionic converter Cs plasmas electron temperature and density gradients spectroscopic measurements compared with prediction from energy transport analysis and ionization coefficients
02 p0194 A71-12226

Quasi-stationary coronal magnetic field and electron density from Faraday rotation experiment, using theoretical model
02 p0302 A71-12769

Planetary nebula NGC 7027 mapping at 11.1 cm, examining structure, ionized H mass and electron density
02 p0317 A71-12869

Collisionless electrostatic single and double probe measurements for electron temperature and number density, making algebraic fit for numerical analysis results
03 p0423 A71-13442

Extensive air showers at sea level, plotting mean numbers of muons and electrons
03 p0477 A71-13866

Electron line density determination by relative aerial power pattern effect on observed meteor echo amplitude
03 p0490 A71-13935

Electron density measurement behind shock waves in air/argon mixture by free molecular Langmuir probes
04 p0629 A71-14705

Argon plasma jet local thermodynamic equilibrium at various electron densities, examining Boltzmann excitation and ionization temperatures
04 p0633 A71-14902

Locally slowly varying magnetoplasma, determining electron concentration and collision frequency by wave propagation experiment
04 p0633 A71-15034

High temperature plasma electron density and ion signal intensity measuring apparatus for reaction rate evaluation
04 p0600 A71-15591

Solar corona magnetic fields and structure during 12 November 1966 eclipse, determining electron densities and temperatures
05 p0802 A71-16013

Interstellar gas small scale irregularities in electron density, considering nonlinear processes in plasmas causing turbulence in spectrum
05 p0805 A71-16113

Electron density and collision frequency in plasma under RF modulation, solving energy balance equation 05 p0787 A71-16290

Plasma diagnostics with focussed laser beams, discussing localized electron density determination 05 p0787 A71-16331

Density thresholds for anisotropy and loss-cone instabilities onset in hot electron plasmas as function of frequency, wavelength and propagation direction of oscillations 05 p0790 A71-16937

Diurnal variations of loss factor in D region during polar cap absorption, verifying nighttime D region model by forward propagation data 05 p0744 A71-17185

Inner radiation zone electrons loss and replenishment observation by Pegasus satellite during magnetically quiet and active periods 06 p0949 A71-17264

Plasma physics, obtaining very high temperatures and electron/ion densities by power laser heating 06 p0908 A71-18066

Rarefied plasma disturbances produced by large slowly moving charged spherical body, deriving electric field, ion and electron concentrations in body vicinity 07 p1195 A71-19380

Plasma refractive index effects in pulsed HCN lasers, calculating stable cavity mirror curvatures constriction as function of electron density by ray matrix approach 07 p1124 A71-19795

Corotating solar wind electron number density from sun orbiting Pioneer spacecraft radio propagation measurements 07 p1189 A71-20320

High dispersion spectrograms of manganese Ap stars alpha And and pi Boo A, estimating electron concentration 07 p1204 A71-20632

Crystal lattice disordered systems, calculating electronic density of states by overlap integral transformation 08 p1344 A71-21364

GaAs epitaxial layers inhomogeneous doping in continuous chloride system, discussing electron concentration with respect to gas flow direction 09 p1506 A71-22167

Electron concentration and superconducting characteristics of Nb-Sn alloys from optical measurements 09 p1507 A71-22234

H beta, H gamma and H delta Stark broadened profiles, investigating perturbing electron-radiating atom inelastic collisions, Gaunt factors and half widths 09 p1496 A71-22413

Interplanetary plasma electron density inhomogeneities formation explained by instability due to electron stream curvilinearly obtained from spacecraft data 09 p1518 A71-22435

Microwave noise emission in He negative glow plasma frequency range, discussing high energy electron densities near cathode 09 p1502 A71-22694

Bright quiescent solar prominences metastable He excitation, studying electron temperatures and densities in interfilament areas 09 p1525 A71-23197

Ionospheric dispersion of FM electromagnetic pulse, examining distortion of amplitude, pulse length and modulation in terms of integrated electron density along transmission path 09 p1410 A71-23523

Two-wavelength interferometry of plasmas generated by Nd laser beam focalization, deriving electron and neutral particle densities 10 p1646 A71-23818

Hollow cathode arc discharge parameters at active zone level, examining gas pressure and electron density 10 p1646 A71-23843

Pulsar dispersion measures for spatial distributions above galactic plane, determining mean interstellar electron density of local spiral arm 10 p1671 A71-24304

Polar cap atomic processes stimulated by photons, electrons and protons, considering particle morphology 10 p1661 A71-24311

Interplanetary medium small scale plasma irregularities by scintillation techniques, considering electron density deviations 10 p1674 A71-24434

E and F region positive ion composition, electron concentration and thermal balance vertical profile, discussing ionizing radiation spectrum, plasma cooling, primary chemical reaction rates and ionospheric formation 10 p1573 A71-24550

Plasma immersed photoemitting plate surface potential distribution, discussing electron/photoelectron temperatures and number densities 10 p1653 A71-24800

Pulsed ion laser electron density measurement by cavity method in S band, evaluating relaxation time 10 p1623 A71-25021

Thermionic converters performance in ignited mode from transport equations for diffusion region, determining electron concentration, potential and temperature 11 p1711 A71-25879

Restricted set of correlated measurements with inductive theta pinch in MHD plasma accelerators, determining electromagnetic field structure and electron density distribution 11 p1766 A71-26288

Plasma electron density measurements by carbon dioxide laser as function of discharge current, using interferometry and scattering methods 12 p1912 A71-26573

Planetary nebulae continuous UV spectrum, discussing glow process, electron temperature and density and Balmer discontinuity 12 p1955 A71-26584

Wire grid simulation of electron density, transmission and reflection of lossless and lossy reentry plasma sheath under microwave radiation at X and K bands 12 p1935 A71-26767

Solar limb flocculus on 15 June 1967, noting electron temperature and concentration, effective length, emission and luminescence 12 p1964 A71-27083

Holographic interferometry method application to plasma electron concentration measurements 12 p1906 A71-27211

Comparison of lightning and long laboratory spark, considering luminous processes, current, voltage, power, energy inputs, radiated visible spectra, electron density, etc 12 p1939 A71-27266

Low temperature plasma collisional-radiative ionization and recombination coefficients, discussing nonequilibrium factors affecting electron density change rate 12 p1939 A71-27270

V groove cathode discharge produced He plasma parameters studied for reentry electron density and temperature simulation, correlating energy flux and microwave noise emission 12 p1895 A71-27273

Plasma refractive index and electron density measurements by He-Ne vernier interferometric laser 12 p1940 A71-27282

Cosmic radio waves scattering in outer solar corona, considering refraction and gradients in electron density fluctuations 12 p1970 A71-27706

Equatorial electrojet model instability to gradient instability and electron density irregularities 13 p2055 A71-27922

Electric field potential near sphere moving through rarefied collisionless plasma in condensation zone, determining ion and electron concentrations 13 p1991 A71-29159

Electron and ion concentrations, electron temperature and electrical conductivity of ionized air before shock wave, using shock tube with He driver gas 14 p2225 A71-30225

Electron temperature and density measurement apparatus using Thomson scattering of laser light for collisionless MHD shock waves 14 p2280 A71-30424

Flat plate electrostatic probe for ionization rate measurements behind reflected shock waves, monitoring time evolution of electron production 14 p2248 A71-30884

Electron hole plasma in plate shaped semiconductor under rapidly increasing external magnetic field, examining density 15 p2453 A71-31247

Holographic interferograms for determining spatial configuration and absolute electron density of fully ionized transient plasmas 15 p2405 A71-31278

Electron density fluctuations in nonequilibrium plasma under crossed electric and magnetic fields, relating ionization instability development and background relaxation times 15 p2454 A71-31488

Inductive impulsive plasma accelerator current sheet electron density determination by electron probe and laser light scattering 15 p2455 A71-31545

Galactic cosmic rays electron density, discussing incompatibility of local data estimates with galactic radio background 15 p2473 A71-31721

Holographic investigation of laser sparks in hydrogen and helium, determining electron concentration spatial distribution and plasma dispersion dynamics 15 p2419 A71-31738

Carbon dioxide laser flow-through discharge, measuring electron density and collision rates with heavy particles as function of tube parameters 15 p2419 A71-31741

Microwave probing of electron number density and collision frequency in slightly ionized plasmas 15 p2458 A71-32395

Electron density gradient and radial compression waves in pulsed IR laser gas discharge tube 16 p2585 A71-32795

Free piston double diaphragm shock tube for hypersonic speeds without attenuation in argon, discussing time resolved channeled spectra measurements of electron density 16 p2551 A71-32916

Forbidden O II spectra brightness ratio measurements across Orion nebula, determining electron density variations 16 p2631 A71-33229

Electron-ion recombination and ambipolar diffusion disruption of electron density in cryogenic helium plasma, using cavity resonator measurements 16 p2619 A71-33648

Total electron content throughout solar cycle maximum, discussing annual variations 16 p2571 A71-33833

Energy spectrum parameters from Burstein-Moss effect observation in thin CdO layers, explaining absorption edge shape at various electron concentrations 16 p2622 A71-34029

Electroconductivity and Hall effect in doped GaAs at low temperatures, studying temperature dependence of electron concentration, mobility and localization 16 p2623 A71-34030

Time variation of electron density and temperature in pulsed lasers operating on nitrogen band transitions, using charged particle balance equation 17 p2751 A71-34382

Combined differential Faraday and absorption measurements, extracting total electron content, ratio to density squared integral and irregularity sensitive parameter 17 p2698 A71-34428

Electron density and temperature distribution in boundary layer flow of reflected shock tunnel conical nozzle 17 p2727 A71-34877

Ionospheric storms morphology, analyzing F2 layer maximum relative electron concentration worldwide propagation 17 p2734 A71-35192

Water vapor effects on shock compressed air in thermodynamic equilibrium by computer program, noting temperature and electron concentration reduction 18 p2984 A71-35857

Multipass laser interferometry sensitivity improvement for He plasma electron density determination by increasing effective path length of laser beam in medium 18 p2931 A71-36584

Solar activity and intensity ratios of O VII X-ray coronal emission lines, giving upper bound on electron density 18 p2965 A71-36734

Electron concentration and mobility of heavily doped n-type InSb single crystals at high temperatures, investigating temperature dependence of Hall coefficient 18 p2954 A71-36803

Argon plasma electron temperature by laser absorption and electron density measurements 19 p3110 A71-37406

Solar limb flocculus on 15 June 1967, noting electron temperature and concentration, effective length, emission and luminescence 19 p3133 A71-37433

Helium plasma interaction with inhomogeneous transverse magnetic field, noting plasma electron temperature and density increase 19 p3112 A71-37743

Diagnostic He-Ne laser interferometer for measuring electron concentration in cross section of argon plasma jet 19 p3073 A71-37786

Rarefied plasma disturbances produced by large slowly moving charged spherical body, deriving electric field, ion and electron concentrations in body vicinity 19 p3138 A71-37805

Electron density inhomogeneity behavior, examining thermal electron motion and collisionless plasma initial condition effects 19 p3114 A71-37857

Electromagnetic wave scattering from turbulent plasma at 31 GHz, determining cross section dependence on bistatic angle and electron density 19 p3017 A71-37868

Synchronous satellite transmission Faraday rotation conversion into total electron content, removing n pi ambiguity 19 p3128 A71-38032

Stable auroral red arc excitation observations by HF radar scattering, scanning photometers and Alouette 1 satellite, noting local electron concentration increase 19 p3054 A71-38034

Holographic interferometry method application to plasma electron concentration measurements
19 p3067 A71-38623

Electric discharge carbon dioxide laser gas temperature, electron and current densities radial distribution from mathematical model
20 p3242 A71-38844

Electron density measurement in microwave cavity resonator as function of plasma parameter or time, using digital control system
20 p3274 A71-39428

H II regions near O and R stars effect on interstellar electron density in solar vicinity
20 p3294 A71-39542

Ion and electron production rate during PCA event, computing electron/ion density, differential proton flux spectrum and ion production rate
20 p3225 A71-39729

Optical constants of beta-phase NiIn, PdAl and nickel gallium aluminate, noting chemical composition and electron density effects on photon energy absorption
21 p3426 A71-40033

Electron temperature and density vs ionization potential in bright planetary gaseous nebulae, using forbidden emission line intensity ratios and level populations
21 p3440 A71-40059

Electron density and temperature in diffuse interstellar medium from H alpha and beta radio recombination lines near galactic plane
21 p3445 A71-40411

Photoelectric and photographic spectrophotometric observations of relatively bright moderate excitation planetary nebula NGC 6826, obtaining electron density and ion concentration
21 p3446 A71-40415

Electron concentration and superconducting characteristics of Nb-Sn alloys from optical measurements
21 p3428 A71-41114

Electron concentration and degeneracy effect on threshold photon energy for optical transitions onset from splitoff valence band to conduction band in n-type GaAs
21 p3429 A71-41211

Soviet monograph on radio wave propagation in fluctuating parameters media covering ionosphere /fluctuating electron concentration/ and troposphere /fluctuating inhomogeneities and refractive index values/
21 p3349 A71-41372

Kinetic equations for phase space cross correlation functions of electron density fluctuations in magnetized weakly ionized plasma, using relaxation model
22 p3581 A71-41895

High temperature Ti-Ni alloy stacking variation stability, studying size, shear and valence electron concentration effects
22 p3586 A71-42367

Extensive air showers at sea level, plotting mean numbers and distribution functions of muons and electrons
22 p3595 A71-42667

Millimeter transverse electric wave diffraction by spherical plasma, interpreting interferometric measurements of electron density
23 p3708 A71-43085

Carbon dioxide absorption temperature dependence in 1750-1200 A region, calculating electron densities and transition moments
23 p3641 A71-43326

Kinetic equations for electron density matrix of superconductors, describing two phase relaxation process
23 p3715 A71-43413

Neon red lines Stark widths and shifts in function of electron and neutral Ne densities in shock tube
23 p3707 A71-43585

Solar atmosphere electron densities from ion emission line intensities in Be isoelectronic sequence
23 p3721 A71-43839

Supersonic Ar, He and molecular nitrogen jets, determining electron temperature and concentration and atomic state population in shock waves region by spectroscopic measurement
23 p3712 A71-43916

Temperature and electron density measurements for free jet of ionized nitrogen at atmospheric pressure by plasma spectroscopy, estimating Prandtl numbers
23 p3664 A71-44197

Electromagnetic wave propagation in gas with interdependent electron density and electric field strength, calculating transmitted power limit value
24 p3851 A71-44428

Plasma diffusion lifetime and electron concentration measurements in Tokamak-3 by pulsed neutral hydrogen injection and microwave multichord probing
24 p3852 A71-44488

Electron temperature and density oscillations in beam plasma discharge, using light intensity spectroscopic observations
24 p3854 A71-44516

Transverse instability of charged particle beam in segmented linear accelerators due to beam encounter with wall
24 p3855 A71-44522

Electron temperature and density of HF inductive discharge in hydrogen plasma
24 p3855 A71-44524

ELECTRON DENSITY PROFILES

Electron density profiles in ruby laser generated Xe plasma, using differential interferometry
01 p0134 A71-10996

Electron density variations in ionospheric layers of different recombination types
01 p0074 A71-11080

Auroral electrojet electric fields from plasma electron density and collision frequency profiles measurements via Black Brant rockets variable frequency impedance probes
01 p0075 A71-11332

Electron density maps of human deoxyhemoglobin revealing C-terminal residues configurations of beta chain by three dimensional Fourier synthesis
01 p0015 A71-11343

Ionospheric columnar electron content perturbation by plane atmospheric waves
01 p0077 A71-11509

Spatial-temporal distribution of laser spark plasma electron density and temperature based on holographic interferometry
02 p0258 A71-11639

F region electron density profile changes during negative magnetic bays, deriving ionization drift from continuity equation
02 p0243 A71-11771

F 2 layer transmission coefficient, describing altitude linear dependence of electron density maximum
02 p0244 A71-11773

Electron concentration distribution over plasma discharge cross section, using interferometry
02 p0288 A71-11887

Relativistic self confined electron beam produced plasmas, measuring electron density profile by multiple pass Mach-Zehnder laser illuminated interferometer
02 p0289 A71-11946

Ionospheric electron content at mid to high latitudes from satellite and station data, discussing possible solar control
02 p0244 A71-11960

ELF and VLF radio attenuation for propagation below inhomogeneous isotropic ionosphere with realistic vertical variation models for electron density and collision frequency
02 p0212 A71-11964

Ionospheric electron content distribution from satellite transmission data, discussing ionospheric irregularities and electron production rates
02 p0245 A71-11966

Electron density fluctuations in nonstationary plasma under crossed electric and magnetic fields, relating times of instability development and background relaxation
02 p0289 A71-12179

Ionospheric electron concentration enhancement at different heights during solar flare, using incoherent scatter radar technique
02 p0300 A71-12471

Shock-reflection interferometry of electron and mass density profiles of ionized argon end wall thermal layer
04 p0674 A71-14701

Lower ionosphere electron density changes with solar zenith angle during active sun year
04 p0583 A71-15213

Average electron density profiles for quiet and disturbed topside ionosphere at high latitudes, tabulating profile numbers
05 p0743 A71-17005

Daytime ionosphere rocket observations at Antarctica, examining electron density profiles
05 p0743 A71-17006

D region electron density profile relation to radio wave absorption frequency dependence
05 p0746 A71-17204

Electron density profiles correction allowing for ionospheric interlayer ionization
05 p0746 A71-17206

Vertical electron density profiles correction coefficients, noting computational work decrease and F region frequency discrepancy due to ionization
05 p0746 A71-17207

High energy electron penetration and scattering in solids, obtaining beam density profiles by polymethyl methacrylate resist exposure
06 p0940 A71-17305

Electron temperature and concentration profiles behind shock front from IR emission and absorption simultaneous measurement, applying method to xenon ionization and recombination processes
06 p0936 A71-17594

F 1 region unsteady model, examining vertical distribution profile of electron concentration on summer day
06 p0895 A71-18273

Vertical electron density profile variations during ionospheric perturbations in years of solar activity: maximum and minimum
06 p0895 A71-18277

Sporadic ionization occurrences nighttime observation in auroral E region, describing vertical electron concentration profile
06 p0895 A71-18280

Quasi-exponential model of electron vertical profile in D region for aeronomic and ionizing radiation characteristics during solar flare of 30 October 1969
07 p1195 A71-19393

Altitudinal storm effect in electron concentration in outer atmosphere during nighttime hours
07 p1100 A71-19398

Nonequilibrium electron temperature, concentration and reflection in reentry boundary layers discussing heat transfer and ionization energy diffusion
07 p1015 A71-19879

[AIAA PAPER 69-82] Single Born scattering theory applicability to critical electron density fluctuations
07 p1171 A71-20293

Rocket-borne HF capacitance probe for measuring ionospheric electron density profile
07 p1116 A71-20498

Electron density profiles in supersonic plasma jet, using immersed microwave probe [AIAA PAPER 71-272]
08 p1342 A71-21998

E region electron concentration profiles, using ground sounding equipment allowing accurate signal reflection altitude measurements
09 p1435 A71-22441

Ionospheric electron density profiles at various altitudes determined by HF impedance probe method
09 p1436 A71-22575

Average electron density profiles for forecasting MF sky waves field strengths, using nocturnal ionospheric measurements
10 p1575 A71-23866

Radar incoherent scatter technique for ionospheric propagation forecasting, using nocturnal and diurnal electron density profiles measurements
10 p1575 A71-23867

Magnetic mirror confined plasma diagnostics, considering hot electron density, X ray pulse height and synchrotron radiation measurement techniques
10 p1651 A71-24651

Daytime lower ionosphere electron density profiles over equator, using rocket-borne Langmuir and plasma noise probes
10 p1606 A71-24913

D and E region electron density height distribution profiles, using multifrequency absorption data
10 p1606 A71-24920

Midlatitude whistlers propagation paths during minimum solar activity for estimating magnetospheric electron density profile
10 p1580 A71-25135

Midlatitude ionosphere electron production rates during quiet solar activity, deriving seasonally varying electron density profiles
11 p1755 A71-25609

VLF propagation in low latitude ionosphere from FR-1 satellite observations, obtaining electron density model of equatorial anomaly
11 p1755 A71-25642

Integral equations inversion in geophysics, discussing ionospheric profile from electron content and Faraday rotation measurements
11 p1756 A71-25645

Measured and calculated comparison of thermionic converter cesium plasma electron densities, using rate equations taking into account collision, diffusion and photoabsorption processes
11 p1712 A71-25889

Green line intensity and electron/ion density contours as function of height over solar limb for March 1970 coronal enhancement
12 p1969 A71-27651

Electron density distribution determination from microwave resonant frequencies of parallel plate cavity containing cold, collisionless, isotropic plasma
13 p2105 A71-27994

D region electron density profile relation to radio wave absorption frequency dependence
13 p2059 A71-28259

Electron density profiles correction, taking into account ionospheric interlayer ionization
13 p2060 A71-28261

Vertical electron density profiles correction coefficients, noting computational work decrease and F region frequency discrepancy due to ionization
13 p2060 A71-28262

Electron density profile determination in D region based on frequency dependence of radio waves absorption, discussing lower ionosphere anomalous ionization
13 p2061 A71-28539

Radio model of brightness temperature and electron density in transition layer of solar active regions, using Laplace transformation and hydrostatic equilibrium equation
13 p2141 A71-29050

- Midlatitude daytime ionospheric electron density profile during low solar activity based on rocket sounding data 14 p2228 A71-29535
- Diurnal variations of electron number density against height in lower ionosphere over Resolute Bay, relating to solar proton events 14 p2300 A71-30044
- Cluster ions concentration and nitric oxide in mesosphere D region, considering electron density profiles 15 p2394 A71-31430
- Supersonic arc-heated Ar flow, measuring heavy particle temperature and velocity and electron density profiles by pressure scanned Fabry-Perot interferometer [AIAA PAPER 71-589] 15 p2454 A71-31534
- Traveling ionospheric disturbances at magnetic equator, determining electron concentration profiles by incoherent scatter radar 15 p2398 A71-31771
- Radio sources 3C 48, 3C 144, 3C 161, 3C 273 and 3C 298 scintillations by interplanetary plasma at 60 MHz, determining electron density fluctuations 15 p2487 A71-32033
- Shock front electron number density profile due to ground state precursor atoms photoionization, assuming LTE in heated gas 15 p2392 A71-32120
- Thermal electron density fluctuations in weakly ionized gas from viewpoint of particle diffusion in single charged particle phase space, considering incoherent scattering 15 p2458 A71-32392
- Interstellar medium dispersion and rotation measurements, calculating electron concentration fluctuation effects 16 p2608 A71-33227
- Total electron content and F region plasma frequencies height during magnetic storm of 8 March 1970 16 p2563 A71-33393
- Daytime electron density profiles above 90 km from Doppler radio measurements by rockets launched from Southern Hemisphere site 16 p2567 A71-33779
- Orbiting satellites VHF radio signal transmissions enhancement, considering focusing effect of electron density contours resulting from gravity or acoustic wave in ionosphere 16 p2543 A71-33817
- Midlatitude E region electron density profile data for various solar activity levels, investigating formation theory and atmospheric models 16 p2570 A71-33822
- Atmospheric electron density irregularities observations, using Alouette 2 satellite electrostatic probe 16 p2574 A71-33973
- D region winter anomaly causes from coordinated rocket measurements, discussing electron density profiles and electron-ion recombination 17 p2731 A71-34315
- D and E regions advances during 1967-1971 covering ionic composition, electron density profile at various latitudes, hours and seasons during eclipses and winter anomalies 17 p2732 A71-34464
- Charged particles transport in thermionic converter near-emitter plasma, determining potential and electron density profiles 18 p2953 A71-36968
- Light elements thermodynamic state variables at high pressure, calculating electron density distribution as function of ion configuration with linear response theory 18 p2970 A71-37047
- Nonspherical axisymmetric model of minimum type solar corona, investigating light scattering electrons density distribution relation to brightness and polarization 19 p3131 A71-37240
- Mean ionospheric height selection effect on total electron content latitudinal variation determination 19 p3047 A71-37367
- Rotating magnetic field plasma pinch, discussing streak and framing photography, electron line density profiles, magnetic probes and ion and electron temperature measurements 19 p3111 A71-37632
- Quasi-exponential model of electron vertical profile in D region for aeronomic and ionizing radiation characteristics during solar flare of 30 October 1969 19 p3127 A71-37817
- Altitudinal storm effect in electron concentration in outer atmosphere during nighttime hours 19 p3053 A71-37822
- Short path VLF phase and amplitude measurements during stratospheric warming in February 1969, discussing D region electron density changes 19 p3018 A71-38040
- Whistlers as diagnostic tools in space plasma, measuring electron densities at large distances in earth outer atmosphere within magnetosphere 19 p3116 A71-38246
- Electron concentration and collisions number fluctuations effect on D region profiles based on radio waves partial reflection data 19 p3057 A71-38365
- Martian lower ionospheric models during solar proton event, determining electron density profiles 20 p3286 A71-38741
- D region electron density profiles and ionization models in terms of XUV radiation and minor constituents NO and oxygen, using ground and space measurements 20 p3224 A71-39713
- Upper ionospheric plasma measurements by gyro plasma probe equipped Lambda rocket, deducing electron density profile from plasma resonance effects 20 p3224 A71-39721
- Equilibrium neutral gas and plasma electron number density fluctuation determination, deriving correlation functions from Liouville equation 22 p3530 A71-41894
- Positive column He-Cd/plus/ laser discharge, determining electron temperature and density 22 p3558 A71-42345
- Solar corona O VII and Ne IX helium line triplets observations, examining electron density limits 22 p3605 A71-42352
- Premidnight asymmetry in directional 40 keV ionospheric electron flux profiles in magnetic local time observed on Azur satellite 23 p3721 A71-43185
- Carbon dioxide additions effect on electron temperature relaxation and electron concentration distribution in expanding supersonic flow of low temperature Ar plasma 23 p3713 A71-44065
- Multicomponent meteoritic composition effects on meteor trails radio wave reflections, obtaining ionospheric electron concentration distribution 24 p3804 A71-45033
- Radio absorption in lower ionosphere, determining vertical distribution of electron density and production rates from solar protons energy spectrum 24 p3867 A71-45041
- Microwave radio signals refraction angles and group delay times for biexponential model of ionospheric electron density profile 24 p3805 A71-45253
- Vertical electron concentration and temperature profiles at 80-170 km measured by rocket launched on 10 July 1969 at Volgograd 24 p3824 A71-45322
- ELECTRON DETECTORS**
- U ELECTRON COUNTERS**
- ELECTRON DIFFRACTION**
- Alloy matrix short range ordered particle microstructures and properties, correlating electron diffraction and field ion microscopy studies 07 p1132 A71-19439
- Polygonization and recrystallization processes in Fe-Cr alloy, using electron diffraction and microscopy 09 p1476 A71-23322
- Thin gallium films metastable gamma and delta phase ring diagrams using electron diffraction techniques 12 p1942 A71-26821
- Computer program for generation and automatic plotting of perfect and twinned electron diffraction patterns for cubic crystal structures 19 p3118 A71-37719
- Silicon reactions with aluminum surfaces, using low energy electron diffraction technique 20 p3194 A71-38882
- Thin single crystalline film deposition by molecular beam epitaxy of GaAs, describing surface structure observation with high energy electron diffraction 21 p3427 A71-40217
- LEED studies of oxygen adsorption on /111/ and /110/ surfaces of Al single crystals 22 p3561 A71-41730
- Free surface equilibrium segregation in solid solutions of Cu-Al alloys single crystals by Auger electron spectroscopy and low energy electron diffraction 24 p3839 A71-45123
- Leed rotation diagrams for aluminum, obtaining low energy electron diffraction intensity profiles by band structure matching approach 24 p3862 A71-45349
- ELECTRON DIFFUSION**
- Electroacoustic properties of GaAs diffusion layer transducers as function of resistivity and charge carrier concentration in single crystals 01 p0140 A71-11122
- High resistance semiconductors minority carriers mean diffusion length based on induced charge dependence on applied voltage during illumination by absorbable light 02 p0294 A71-11898
- Gold plated Ge surfaces, investigating LEED patterns and electronic properties 04 p0636 A71-15016
- Electron thermal diffusion effects during light interference patterns exposure, generating strong electric fields and holographic storage in electro-optic materials 06 p0940 A71-17309
- Varactor capacitance variations compensation for temperature dependent diffusion potentials and dielectric constants changes 08 p1265 A71-21299
- Three dimensional model of semiconductor diode current dependence on charge carrier diffusion length and surface recombination rate 09 p1414 A71-22189
- Electron diffusion in trap with magnetic mirrors under pulsed field perturbations, determining coefficients by numerical integration of drift equation 09 p1513 A71-22551
- Unstable electron plasma oscillations quasi-linear theory, discussing improper treatment of perturbed electron distribution for damped waves leading to negative diffusion coefficient 10 p1647 A71-23893
- Earth outer radiation belt electrons intensity, differential energy spectra and radial diffusion during maximum solar activity 10 p1663 A71-24783
- Model for relativistic electrons diffusion from IR sources, determining injected electron spectrum distortion due to inverse Compton losses and X ray spectrum 11 p1814 A71-25294
- MgO single crystals dominant coloration in solar spectral region by electron hole pair diffusion, trapping and recombination [AIAA PAPER 71-450] 11 p1808 A71-26234
- Anisotropy of solar cosmic ray electrons, considering parallel diffusion coefficients for ions and electrons 12 p1954 A71-27712
- Semiconductor radiation detectors, discussing minority charge carrier diffusion length measurements by nuclear method 13 p2065 A71-27957
- F 2 ion velocity and electron density perturbations in terms of gravity waves, comparing incoherent scatter techniques 14 p2230 A71-29716
- Thermalization and diffusion of electron cloud injected into afterglow cylindrical plasma, calculating steady state distribution as function of position and velocity 14 p2280 A71-30175
- Auroral electrons interaction with atmosphere from Fokker-Planck equation, considering angular diffusion, energy loss and geomagnetic field convergence effects 14 p2235 A71-30345
- Pitch angle diffusion of electrons in postbreakup auroral glow, measuring electron intensities by Petrel sounding rocket 15 p2394 A71-31423
- Sagittarius A model involving relativistic electron diffusion from point source due to Compton scattering for observed radio spectra explanation 18 p2957 A71-36155
- Diffusion processes electron mechanism in metal-metal and metal-nonmetal systems, using configurational model for valence electrons localization 21 p3403 A71-41159
- Semiconductor radiation detectors, discussing minority charge carrier diffusion length measurements by nuclear method 21 p3383 A71-41346
- Excess minority carrier diffusion length measurement in thin silicon wafers, using light-spot and dark-spot methods 24 p3861 A71-45202
- ELECTRON DISTRIBUTION**
- NT ELECTRON DENSITY PROFILES**
- F region electron concentration distribution during global magnetic storm, latitude and diurnal variation effects and radio wave reflections diffusion 02 p0243 A71-11770
- Plasma jet electron temperature and distribution behind pulsed coaxial accelerator exit section 02 p0290 A71-12182
- MOS junction transistor operation governing equations and electron distribution, using numerical analysis 02 p0233 A71-12423
- Electron velocity distribution in fully ionized plasma under crossed electric and magnetic fields, assuming Fokker-Planck expression for Lorentz gas 02 p0293 A71-12743
- Low temperature weakly ionized molecular plasma kinetic equation in electric field, considering free electron distribution function for molecule-electron inelastic collisions 04 p0634 A71-15114
- Energetic electrons distribution in magnetotail plasma sheet from Explorer 35 satellite observation data 07 p1186 A71-19657
- Equatorial proton belt radial profile analysis by satellite electron distribution data 08 p1351 A71-20962
- Highly ordered pressure-annealed pyrolytic graphite majority carrier electrons and holes locations in Brillouin zone from measurements in magnetic fields 08 p1344 A71-21363

- Trapezoidal and Killian distributions profile parameters at S band in plasma column, noting electron density 09 p1501 A71-22306
- Magnetron devices with anode voltage as independent variable, calculating output characteristics based on electron cluster model 09 p1415 A71-22463
- Macroscopic model of impurity electron centers for strong exchange interactions in ferromagnetic and paramagnetic semiconductors 09 p1508 A71-22880
- Solar flare produced hard X-ray bursts, examining thermal processes and nonthermal electron distribution 10 p1660 A71-23796
- Unstable electron plasma oscillations quasi-linear theory, discussing improper treatment of perturbed electron distribution for damped waves leading to negative diffusion coefficient 10 p1647 A71-23893
- Higher order laser light coherence effects on photoelectron distribution detected by third order photoeffect 12 p1913 A71-26961
- Arrival time distribution of electrons and Cerenkov light in extensive air showers, showing detector feasibility for age classification 13 p2122 A71-28071
- TM, TE and combination cavity modes choice for plasma column electron density distribution determination by perturbation methods 14 p2279 A71-29859
- Thermalization and diffusion of electron cloud injected into afterglow cylindrical plasma, calculating steady state distribution as function of position and velocity 14 p2280 A71-30175
- Ionospheric electron density variation at neutral acoustic gravity wave passage from continuity equation, noting ionization in wake 14 p2236 A71-30355
- Nonlinear Fokker-Planck equation numerical tests for collision effects on self consistent field first order component and plasma electron distribution function perturbation 15 p2453 A71-31146
- Plasma jet electron temperature and distribution behind pulsed coaxial electromagnetic accelerator exit section, studying time variation 15 p2454 A71-31490
- Northern high latitude electron trapping boundary position diurnal, seasonal and geomagnetic Kp variations based on ESRO 1/Aurora polar satellite observations 16 p2627 A71-33753
- Spatial coherence measurement for two points of pseudothermal light source by comparing photocathode luminous intensity probability density and photoelectron distribution moments 17 p2754 A71-35585
- Plasma ion and electron distribution functions measurement on outer planet missions [AAS PAPER 71-124] 19 p3114 A71-37938
- Electron distribution functions construction from spectrum of laser light Thomson scattering by rarefied plasma 19 p3074 A71-38215
- Gravity waves effects on ionospheric columnar electron content data, using Faraday rotation and differential Doppler measurements of geostationary satellite radio signals 20 p3224 A71-39717
- Auroral electrons temporal and spatial structure from ground based optical observations and rocket-borne electron detector measurements 20 p3228 A71-39849
- Field produced by equilibrium electron distributions on analytic Jordan curve 21 p3419 A71-41082
- Electron distributions in afterglow of hot electron mirror contained plasma as function of time, using bremsstrahlung spectra measurement 22 p3582 A71-41903
- Equatorial proton and electron pitch angle distributions in loss cone and at large angles from geostationary ATS 5 satellite observation 23 p3720 A71-43165
- Mars and Venus upper atmospheric electron distribution compared with theoretical ionospheric models, considering solar wind as ionization source 23 p3736 A71-43342
- Wave field pulsations induced electron scattering as factor modifying excited plasma electron distribution function 24 p3855 A71-44668
- Electron multiplier pulse height distribution for single electron input, investigating relative variance correlation with statistical fluctuations of gain 24 p3811 A71-45329
- Tungsten exploding wires electron emission during vacuum melting 02 p0284 A71-11881
- Titanium and niobium monocarbides electron work function relation to homogeneity region composition, considering electron structure and thermal emission 02 p0263 A71-12199
- Electron emission formulation for cesiated metal surfaces in thermionic converter in terms of work function, using Swanson-Strayer correlation 02 p0295 A71-12210
- Solar X-ray flare activity statistical prediction based on correlation to coronal electron temperature and emission measure [AIAA PAPER 70-1371] 02 p0301 A71-12698
- Photoelectron emission of organic semiconductors, considering molecular and defect photoionization and exciton collisions 03 p0467 A71-13399
- Electron plasma waves one dimensional quasi-linear instability with allowance for spontaneous emission 03 p0464 A71-13929
- Emission structure of large electron active region McMath plage 8905 mapped by 40 keV solar flare electrons 06 p0950 A71-17918
- Energetic solar electron emission and cone propagation by IMP satellites, noting relation to proton and relativistic energy events 06 p0961 A71-18174
- Radial microdistribution of absorbed dose in heavy charged particle track, allowing for delta electron emission 06 p0963 A71-18365
- Be films evaporated in vacuum on W single crystals, investigating adsorption and electron emission by field emission microscopy 07 p1178 A71-19918
- Laser operation instability with nonlinear filter, deriving electrons differential velocity distribution functions on inhomogeneous emitter 07 p1126 A71-20197
- Book on gaseous ionization and plasma electronics covering atomic structure, electron emission, charged particle behavior, self sustaining discharge and breakdown mechanisms 08 p1341 A71-21700
- Electron emission from He ion by proton bombardment, calculating double differential cross sections relative to ejection energy and angle 09 p1497 A71-22415
- Solid metals and alloys electron emission, considering applications in surface phenomena observation 09 p1473 A71-23224
- Ionization mechanisms for deviation of experimental altitude vs velocity curves of meteor trails, considering various electron and ion emissions and dissociation effects 10 p1669 A71-24032
- Plasma anode tube in metal-ceramic envelope with improved capabilities for electron emission studies, considering movable Langmuir probe 11 p1806 A71-25902
- Frequency vs time spectral shapes of magnetospheric VLF discrete emissions for field line and electron stream parameters 13 p2027 A71-27916
- Nonthermal X rays and 10-100 KeV electron acceleration and emission from solar flares, using spacecraft observations 13 p2129 A71-29056
- Point defects relation to thermoelectric emission at high temperatures in yttrium oxide 15 p2462 A71-32714
- Molybdenum-niobium alloys single crystals electron work function in vacuum from emission patterns and anisotropy 16 p2595 A71-33881
- Metals and alloys surface deformation stages by exoelectron emission method, discussing mechanical energy absorption and dissipation 16 p2580 A71-33930
- Copper on copper friction coefficient dependence on oxygen pressure, investigating exoelectron emission from differently oxidized copper surface layers 18 p2928 A71-36750
- Radioisotopic power applications of beta and gamma emitting Co 60, noting powder ceramic fabrication of dense wafers for irradiation to convert natural Cn 59 20 p3265 A71-38938
- Electron removal from neutralizing emitter in cylindrical ion beam, determining I-V characteristics of plane diode with positive charge distribution 20 p3272 A71-39152
- VLF emissions and low energy electrons relation to other auroral phenomena from satellite-borne data associating midnight maximum with particles from plasma sheet 20 p3229 A71-39855
- Pulsar radio emission via maser amplification, presenting model based on electrons behavior in intense magnetic field 20 p3285 A71-39949
- Potassium photoionization cross section, including spin-orbit interaction, orientation of photoejected electrons and dipole transition moment correction due to core polarization 21 p3417 A71-40197
- Electron-electron correlation effects in photoabsorption induced double electron ejection process, using many body perturbation theory 22 p3577 A71-41628
- Electron emitter photomultipliers and photocathodes for low light level and scintillation counter applications, using negative electron affinity 23 p3651 A71-43432
- Thermally stimulated exoelectron emission and surface properties of lunar rocks and soil 23 p3758 A71-43759
- Nonlinear theory for synchrotron emission of tubular electron flux in cylindrical waveguide, discussing wave-electron interactions optimization 23 p3653 A71-44058
- Channel electron multiplier principles and characteristics, discussing secondary electron production probability during electron irradiation of surface in vacuum 24 p3811 A71-45326
- ELECTRON ENERGY**
- NT ELECTRON STATES**
- Total free electron energy disparity with energy radiated in forbidden O I lines in supernova spectra explained by nova luminescence formation 01 p0151 A71-10067
- Collisionless shock waves in magnetized plasma as function of Alfvén-Mach number, measuring electron temperature jump on wave front spectroscopically 01 p0132 A71-10153
- Electromagnetic wave nonlinear propagation in semiconductors, considering field amplitude and electron temperature for strong electron phonon interaction and degenerate semimetals 01 p0138 A71-10434
- High electron temperature H and He I and II, calculating partition functions 01 p0158 A71-10806
- Electron temperature determination in low density helium plasma 01 p0134 A71-11005
- Magnetic field effects on electron heating by strong electric field in n-Ge single crystals 01 p0140 A71-11459
- Semiconductor with charged impurities in strong electromagnetic field, investigating scattering effects on electron energy spectrum 01 p0140 A71-11463
- F region reflected radio wave heating effect, considering electron temperature, collision frequency and heat conductivity 01 p0040 A71-11531
- F region electrons heating by RF energy at or near ionospheric plasma frequency, detecting temperature changes via optical nightglow intensity variations 01 p0040 A71-11533
- Ionospheric modification by electrons radiant heating, discussing effects on 1.27 micron radiation 01 p0078 A71-11534
- Ionospheric F layer modification by artificial heating, using radio echo detection of electron temperature changes 01 p0040 A71-11537
- Pulsed Ar ion laser plasma electron density and temperature, discussing Tonks-Langmuir free fall model validity 01 p0096 A71-11623
- Magnetic probes effectiveness study of electron heating behind shock wave front in plasma, measuring electron temperature 02 p0288 A71-11636
- Electron concentration and temperature data from Langmuir probe on Explorer 22, discussing magnetic storms effects 02 p0244 A71-11910
- Charged particle temperature distribution in outer ionosphere, disregarding collisional energy exchange 02 p0244 A71-11920
- Low pressure Cs vapor discharge in positive column, determining electron energy distribution function 02 p0289 A71-11956
- Plasma jet electron temperature and distribution behind pulsed coaxial accelerator exit section 02 p0290 A71-12182
- Thermionic converter Cs plasmas electron temperature and density gradients spectroscopic measurements compared with prediction from energy transport analysis and ionization coefficients 02 p0194 A71-12226
- Carbon dioxide molecules dissociative excitation processes by low energy electrons, examining light emission mechanism in VUV 02 p0261 A71-12318
- Electrons longitudinal and transverse energy distribution in beam during cyclotron interaction with magnetoactive plasma waveguide 02 p0292 A71-12611

ELECTRON EMISSION
 NT FIELD EMISSION
 NT PHOTOELECTRIC EMISSION
 NT SECONDARY EMISSION

- Solar X-ray flare activity statistical prediction based on correlation to coronal electron temperature and emission measure
[AIAA PAPER 70-1371] 02 p0301 A71-12698
- Radio sources LF spectra distortions at critical value brightness temperature, noting induced Compton scattering effect on ambient gas thermal electrons
02 p0317 A71-12865
- Diurnal variations and waves in ionospheric electron and ion temperatures and concentrations from Thomson scatter measurements
03 p0408 A71-13384
- Collisionless electrostatic single and double probe measurements for electron temperature and number density, making algebraic fit for numerical analysis results
03 p0423 A71-13442
- Ultrahigh energy electrons and gamma quanta in ground produced by cosmic rays, plotting mean free path vs energy
03 p0478 A71-13868
- Knocked out atomic electron energy during impact ionization, comparing Thomson and Drawin formulas
03 p0465 A71-13954
- Injection breakdown in Fe and Cr-doped high resistance GaAs laser due to increased electron-hole plasma during electron heating
03 p0467 A71-13979
- Sodium atom excitation by high energy particle collisions behind shock waves, measuring electron and vibrational temperatures
03 p0376 A71-13992
- Ionospheric electron temperature global pattern from satellite observations
03 p0415 A71-14029
- Electron and proton energy measurements by near-polar orbit ESRO 1 satellite, noting anisotropy and isotropy near and in proton zones
03 p0479 A71-14040
- Ionospheric electron production, slowing down and disappearance processes, considering collisions with atmospheric constituents
03 p0417 A71-14072
- Auroral oval electrojet poleward expansion correlation to energetic electron enhancement in magnetotail during substorm from satellite observation
03 p0419 A71-14518
- Auroral zone electron and proton energy spectra measurements, using sounding rockets with electrostatic analyzers
03 p0419 A71-14524
- Topside ionosphere plasma resonance due to electrostatic wave echoes, comparing electron temperature dependent beat pattern with ray tracing calculations
03 p0421 A71-14540
- Primary cosmic ray electrons intensity energy spectrum data, suggesting plots based on electron energy to positive gamma power
03 p0482 A71-14542
- Magnetotail energetic electron event simultaneous observations by Vela 3A and Imp 3 satellites, evaluating plasma sheet boundary motion hypotheses
03 p0421 A71-14545
- High Mach number collisionless shock waves in low density argon plasma, measuring electron heating and shock thickness
04 p0631 A71-14685
- Electron temperature measurement in electromagnetic shock tube by spectroscopy and ruby laser light scattering in plasma, examining validity of local thermal equilibrium assumption
04 p0632 A71-14688
- Ionospheric electron and ion temperatures and charged particle concentration from satellite and space probe observations
04 p0640 A71-14775
- Gold plated Ge surfaces, investigating LEED patterns and electronic properties
04 p0636 A71-15016
- Impulsive solar flare X rays spectral characteristics, examining electron energy, bremsstrahlung, microwave bursts and particle escape, collisions and injection
05 p0797 A71-15937
- Solar corona magnetic fields and structure during 12 November 1966 eclipse, determining electron densities and temperatures
05 p0802 A71-16013
- Electron heating in weakly ionized plasma by magnetic perturbation
05 p0787 A71-16291
- Zinc chalcogenides core electron energy levels measurement by X ray induced photoemission, noting agreement with observed auger transitions
05 p0792 A71-16318
- Flat HF radio spectra from optically thin sources with low electron energy distribution indexes
05 p0808 A71-16399
- Quasars spectrophotometry data, obtaining physical conditions, abundances and electron temperature
05 p0811 A71-16685
- Two fluid model solar wind, predicting electron temperature and heat flow
05 p0799 A71-16692
- Electron temperature anisotropy in lower ionosphere, discussing effects of solar UV radiation propagating along geomagnetic field during daytime
05 p0744 A71-17183
- Magnetotail plasma sheet electron and proton energy spectra and angular distribution over auroral zone, comparing Vela satellite and rocket measurements
06 p0887 A71-17260
- Electron temperature and concentration profiles behind shock front from IR emission and absorption simultaneous measurement, applying method to xenon ionization and recombination processes
06 p0936 A71-17594
- Primary cosmic ray electrons energy spectrum measurement at Fort Churchill, examining geomagnetic cut-off rigidity daily variations
06 p0959 A71-18159
- Thomson scattering role in solar corona electrons cooling
06 p0976 A71-18454
- Carbon dioxide electric discharge lasers physics, discussing electron energy distributions and excitations, gain and saturation intensity
06 p0909 A71-18523
- Kinetic theory calculation of partially ionized plasma near-electrode electron temperature profiles
[AIAA PAPER 71-140] 06 p0939 A71-18583
- Fully ionized quasi-one dimensional magnetic nozzle flow analysis, including effects of unequal electron and ion temperatures and electron thermal conductivity
[AIAA PAPER 71-141] 06 p0939 A71-18584
- Plasma produced by pulsating fast electron beam, observing electron temperature and charged particle concentration
07 p1167 A71-19232
- Electron temperature in hydrocarbon air flame, discussing extra equilibrium excitation, energy relaxation rate and chemiluminescent emission
07 p1182 A71-19250
- Electron and ion temperature in ionosphere, discussing measurements, solar heating, F and E region, variability over solar cycle, etc
07 p1098 A71-19320
- Magnetospheric convection and polar wind influence on outer radiation belt energetic electron loss, subjecting previously large fluxes of lower energy electrons to trapping limit
07 p1186 A71-19661
- Plasma electron temperature probes, investigating electron heating effects
07 p1112 A71-19765
- Nonequilibrium electron temperature, concentration and reflection in reentry boundary layers, discussing heat transfer and ionization energy diffusion
[AIAA PAPER 69-82] 07 p1015 A71-19879
- Flow-through carbon dioxide lasers population inversion relation to individual gas components and electron velocity distribution functions
07 p1126 A71-20187
- Atmospheric high energy gamma rays, pion production and electron energy spectra over Hyderabad, using stack nuclear emulsions
07 p1189 A71-20497
- Crystal lattice disordered systems, calculating electronic density of states by overlap integral transformation
08 p1344 A71-21364
- Cosmic ray electron intensity and energy spectrum from nuclear emulsion-spark chamber combination detector triggered by scintillation and Cerenkov counters on high altitude balloon
08 p1355 A71-21627
- Dissociative electron attachment excess energy correlation with fragment ion translational energies, determining radical affinity
08 p1338 A71-21782
- ATS-5 satellite-borne auroral electron and proton energy spectrum measuring instrument using cylindrical coordinate electrostatic analyzer
08 p1294 A71-21845
- Nonequilibrium plasma molecular impurities effect on electron energy balance, considering importance in closed cycle MHD generators
08 p1342 A71-21916
- Ionospheric wake spacecraft potential, electron current and temperature observations, using Agena/Gemini manned two body system sensors
09 p1517 A71-22175
- Plasma electrons heating by interaction with ultrashort laser pulses, considering hard bremsstrahlung generation
09 p1460 A71-22245
- Superthermal electrons continuous stream release into interplanetary medium during hectometric solar noise storm activities
09 p1518 A71-22353
- Carbon dioxide lasers gas discharges positive column, studying electron energy distribution by probe method
09 p1461 A71-22381
- Low temperature plasma electron velocity distribution function perturbation due to exothermal chemical reactions
09 p1501 A71-22389
- Plasma electron temperature measurement from scattering indicatrix of laser radiation
09 p1501 A71-22394
- Satellite-borne spectrometer for low energy electrons measurement, describing virgin photoelectrons equilibrium energy spectrum for different latitudes and pitch angles
09 p1436 A71-22553
- Electron energy spectra construction from Al, Sn and Au target layers transmission angular distribution measurements, using computer calculated spectra for comparison
09 p1497 A71-22688
- Bright quiescent solar prominences metastable He excitation, studying electron temperatures and densities in interfilament areas
09 p1525 A71-23197
- Total free electron energy disparity with energy radiated in forbidden O I lines in supernova spectra explained by nova luminescence formation
09 p1525 A71-23260
- Admittance of aperture antenna radiating into lossy warm overdense plasma half space, considering electron energy
09 p1505 A71-23521
- Auroral zone electron energy spectra local time dependence from polar satellite observations
09 p1515 A71-23632
- Heat conductivity anomalies of thin metallic plates at very low temperatures, discussing secondary phonons angular distribution and electron energy flux
10 p1640 A71-23816
- Electron collision frequency energy dependence influence on electrical conductivity of weakly ionized plasmas, considering Taylor series expansion around probable plasma electron velocity
10 p1623 A71-23875
- Thin metal foils total energy flux, electron/phonon temperatures and thermal conductivity anomalies at liquid He temperatures
10 p1657 A71-24457
- Cold Hg plasma in composite HF and magnetostatic field near electron cyclotron resonance, obtaining electron and ion energy spectra
10 p1650 A71-24527
- Photoelectron energy loss rate to ambient electrons in thermal plasma, noting geomagnetic field influence
10 p1662 A71-24558
- Asymptotic expression for low energy photoelectron energy loss to ambient thermal electrons
10 p1662 A71-24559
- Electron beam relaxation in plasma, discussing experimental studies of oscillation amplitude and beam electrons energy distribution relationships during predominantly longitudinal plasma oscillation excitation
10 p1650 A71-24627
- Solar wind heat conduction evaluation by electron energy equation dimensional analysis
10 p1663 A71-24778
- Plasma immersed photoemitting plate surface potential distribution, discussing electron/photoelectron temperatures and number densities
10 p1653 A71-24800
- Fully ionized gas under electric and magnetic fields, calculating electron velocity distribution and runaway rate as function of time from Boltzmann equation
10 p1654 A71-24975
- Solar corpuscular radiation differential and integral spectrum, assessing energetic electron flux in D region at sunrise
11 p1815 A71-25587
- Shot noise effect on ambient plasma magnetosphere electric field measurements with Langmuir and double probes for electron density and temperature
11 p1756 A71-25644
- Earth radiation belts high energy electron flux intensity monotonic decrease during magnetically quiet periods from satellite data analysis
11 p1816 A71-25759
- Energy transfer during charged particles passage through material media as function of spatial distribution, discussing electron production rates
11 p1802 A71-25769
- Planetary nebulae continuous UV spectrum, discussing glow process, electron temperature and density and Balmer discontinuity
12 p1955 A71-26584
- Solar corona electrons cooling by Thomson scattering, calculating electron energy loss
12 p1955 A71-26604
- Plasma production by pulsating fast electron beam, observing electron temperature and charged particle concentration
12 p1934 A71-26750
- Auroral electron temperature, noting field aligned energy transport current effects
12 p1899 A71-26887
- Electron energy distribution for spectroscopic determination in hollow cathode discharge helium-mercury plasma based on Drayvesteyn function
12 p1937 A71-27050
- Solar limb flocculus on 15 June 1967, noting electron temperature and concentration, effective length, emission and luminescence
12 p1964 A71-27083

Electron energy distribution functions in carbon dioxide laser plasmas, using Langmuir probes 12 p1940 A71-27280

Energetic electrons generating solar flares position relation with active regions associated with type 1 radio noise storms 12 p1953 A71-27656

Long term storage of relativistic energetic electrons and protons in solar corona from IMP 4 and Pioneer 8 observations related to delayed emission from flares 12 p1969 A71-27657

Type 2 and 3 solar radio burst generation, proposing coherent synchrotron electron deceleration mechanism 12 p1954 A71-27710

Helliwell VLF discrete emission theory application to determination of electron stream energy spectrum and structure 13 p2027 A71-27915

Cadmium mercury telluride solid solutions electron energy spectrum at low temperatures, calculating electron mobility in crystals with zero forbidden band 13 p2110 A71-27955

Electron energy distribution in plasma discharge of Hg electron bombardment ion engines, using Langmuir probe 13 p2114 A71-27985

Extensive air showers muon and electron components primary energy spectrum, using isobar and CKP formula based models 13 p2125 A71-28088

Ionospheric electron concentration and temperature data from Langmuir probe on Explorer 22, discussing magnetic storms effects 13 p2058 A71-28197

Charged particle temperature distribution in outer ionosphere, disregarding collisional energy exchange 13 p2058 A71-28207

Electron temperature anisotropy in lower ionosphere, discussing effects of solar UV radiation propagating along geomagnetic field during daytime at middle latitudes 13 p2059 A71-28240

Electron energy distribution function in weakly ionized monatomic gas with inelastic collisions, using differential equation asymptotic resolution techniques 13 p2106 A71-28398

Average energy electron capture coefficient dependence on air density, temperature and altitude under gamma radiation 13 p2061 A71-28543

Electron energy spectra of amorphous semiconductors by cell method, replacing conditions for splicing wave functions by extremum integral 13 p2112 A71-28925

Electron avalanche processes in gas discharges, deriving electron energy distribution function and similarity laws 13 p2103 A71-29079

Electron velocity, spin, energy and mass derivation based on consideration as negative component of photon 13 p2103 A71-29277

Improved accuracy electron temperature Langmuir probe by eliminating geomagnetic field, rocket velocity and random noise effects 14 p2238 A71-29532

Energetic electron power spectrum effect on synchrotron radiation from magnetosphere 14 p2298 A71-29722

Low energy electron precipitation effects on upper atmosphere based on polar cap and auroral oval electron spectrum comparison 14 p2300 A71-30035

Suprathermal electron temperature and ion composition as function of geomagnetic latitude in polar ionosphere, using Explorer 31 mass spectrometer measurements 14 p2234 A71-30037

Planetary nebulae observations in radio spectrum, determining interstellar extinction, electron temperature recombination theory and models 14 p2312 A71-30388

Electron temperature and density measurement apparatus using Thomson scattering of laser light for collisionless MHD shock waves 14 p2280 A71-30424

Anomalous microwave energy dissipation and electron heating in collisionless plasma without decay at high collision frequencies 14 p2281 A71-30539

Nitrogen inductive low pressure discharge, determining vibrational and rotational temperatures, ionization degree, electron temperature and energy balance by spectroscopic technique 15 p2451 A71-31487

Plasma jet electron temperature and distribution behind pulsed coaxial electromagnetic accelerator exit section, studying time variation 15 p2454 A71-31490

Nonequilibrium effects in Ar free jet plasma, using cooled Langmuir probe for electron temperature and ion density measurements through shock wave in front of blunt body [AIAA PAPER 71-591] 15 p2454 A71-31536

Linear electron accelerator using shaping system debunching properties for minimizing electron energy differences in bunched beam 15 p2376 A71-31743

Carbon dioxide electron impact energy loss spectrum and molecular orbit calculations, discussing fourth positive bands production in Mars upper atmosphere UV dayglow 15 p2398 A71-31766

Satellite skin potential and errors in electron density and temperature determinations by Langmuir probe measurements, using model ionosphere 15 p2398 A71-31768

Synchronous and oscillatory energy gain with electron-wave resonance time in collision magnetospheric plasma 15 p2371 A71-32024

Laboratory simulation of satellite motion in ionospheric plasma, specifying maximum current density, electron velocity distribution and temperature range [AIAA PAPER 71-608] 15 p2385 A71-32545

Thermal properties of solar wind plasma, determining electron and proton temperature distributions, proton heating rate, electron thermal conductivity and energy exchange rates 15 p2480 A71-32754

Electron energy distribution function and ionization rate constant of atoms by electron impact as function of heavy particle temperature 16 p2615 A71-32796

Plasma mobility, diffusion, electron energy distribution, surface phenomena, elastic collisions, charge transfer, etc 16 p2617 A71-32954

Combustion flame plasma reactions, considering collisional and chemical ionization, ion decay, electron temperatures and additives 16 p2540 A71-32969

Extragalactic radio sources millimeter wavelength spectra measurements, investigating electron energy loss mechanism, magnetic field strengths and dynamics 16 p2631 A71-33234

Upper atmosphere He, Ne, Na and K atoms collisions with molecular oxygen, determining ejected electron energy during fast Na, K, Rb and Cs ionization for meteor phenomena modeling 16 p2639 A71-33695

Low energy solar X-ray emission spectra observations, discussing nonthermal electron spectrum relation to acceleration by electric fields 16 p2626 A71-33725

Thermospheric electron heating rate and ion chemistry above Wallops Island during 7 March 1970 solar eclipse, measuring ion composition and concentration 16 p2565 A71-33732

Electron temperature profiles in ionosphere from rocket probes, noting correlation with geomagnetic activity indexes 16 p2569 A71-33798

Rocket-borne electron spectrometer measurements of low energy electrons during auroral events, noting influx sudden enhancement 16 p2570 A71-33820

Secondary electrons and photons energy spectra and depth dependence in upper atmosphere from numerical solution of one dimensional transport equations 16 p2628 A71-33937

Time variations of magnetotail plasma sheet from electron energy spectral measurements on Vela satellites 16 p2629 A71-33945

Low energy auroral thermal electrons flux after geomagnetic substorm, entering magnetosphere from solar wind 16 p2629 A71-33953

Ionospheric atomic oxygen concentration estimates from radar backscatter and rocket probe measurements of electron and ion temperatures and concentration 16 p2574 A71-33965

Nonthermal electron population of energy levels in cool dense helium afterglow for small principal quantum number, using Saha equation and optical spectroscopy techniques 16 p2620 A71-34044

Nonisothermal collisionless low beta plasma with electron temperature greater than ion, investigating low frequency potential modes for Kelvin-Helmholtz instability 16 p2620 A71-34167

Time variation of electron density and temperature in pulsed lasers operating on nitrogen band transitions, using charged particle balance equation 17 p2751 A71-34382

German monograph on electron motion in cesium plasma covering Boltzmann equation, radiative transfer, mathematical model, electron velocity distribution, etc 17 p2787 A71-34485

Electron density and temperature distribution in boundary layer flow of reflected shock tunnel conical nozzle 17 p2727 A71-34877

Hall coefficient and electrical resistivity increase during aging of Al-Zn alloys, suggesting free electron energy reduction due to solute atoms clustering 17 p2759 A71-35227

Nonequilibrium plasma molecular impurities effect on electron energy balance, noting importance in closed cycle MHD generators 17 p2789 A71-35261

Microfield double probe for plasma density and electron temperature determination, studying random signals crossed spectrum 17 p2789 A71-35350

Gum Nebula size, density and electron temperature data from RAE-1 and OGO-5 satellites and ground based telescopes observations, correlating with Vela X supernova outburst 17 p2806 A71-35409

Anomalous microwave heating of electrons in magnetized plasma, showing resonances dependence on magnetic fields and charged particles concentration 17 p2790 A71-35735

Medium energy electrons action on photographic emulsions, assuming volume element behavior not totally opaque 18 p2916 A71-36044

Spatial relaxation of electron energy distribution with inelastic and Coulomb collisions, integrating Boltzmann equation 18 p2949 A71-36969

Ribbed surface electrode effects in plasma accelerator producing high speed monoenergetic blobs 19 p3108 A71-37091

Undisturbed ionospheric ion and electron temperature warming, investigating frictional heating effect by neutral winds 19 p3048 A71-37399

Argon plasma electron temperature by laser absorption and electron density measurements 19 p3110 A71-37406

Solar limb flocculus on 15 June 1967, noting electron temperature and concentration, effective length, emission and luminescence 19 p3133 A71-37433

Relaxation time model of solid state diodes based on equations for electrons of given energy, including p-n junction and tunnel diodes 19 p3027 A71-37495

Gas and electron temperature and thermal nonequilibrium in argon plasma jet from electrodeless induction discharge 19 p3111 A71-37578

Electron temperatures for lithium-like ions O VI, Ne VIII and Mg X formation in solar chromosphere and corona, using rocket spectrometric measurements 19 p3136 A71-37618

Low density plasma electron velocity distribution deviation due to Maxwellian photon radiation resulting from inelastic collisions with atoms 19 p3112 A71-37739

Helium plasma interaction with inhomogeneous transverse magnetic field, noting plasma electron temperature and density increase 19 p3112 A71-37743

Bounded nonthermal plasma radiation temperature variations relationship to electron velocity distribution functions 19 p3113 A71-37747

Tokamak T-3A device plasma electron temperature measurements, using Thomson scattering with electric, microwave, laser and diamagnetic data 19 p3113 A71-37854

Outer planets Grand Tour X ray investigation of planetary magnetospheres to obtain flux and energy spectrum of electrons precipitated from Jovian magnetosphere [AAS PAPER 71-130] 19 p3127 A71-37941

F region radio wave absorption dependence on electron-ion temperature difference from energy balance considerations, testing by radar backscatter measurements 19 p3055 A71-38045

Transverse waves and electromagnetic instabilities propagating along magnetic field in homogeneous plasma, discussing ions and electrons energy losses and plasma dispersion 19 p3114 A71-38206

Nighttime polar atmospheric structure and temperature variations due to gas kinetic and electron energy changes 19 p3056 A71-38361

Latitudinal distribution of electron temperature in F 2 layer during summer daytime period of low solar activity from electron density profile geometrical parameters 19 p3057 A71-38369

Magnetic activity effect on pitch angle distribution of low energy auroral electrons from ESR0 1A measurements 19 p3060 A71-38575

ESRO-1A /Aurora/ observations of variations in low energy electron spectrum, noting relationship to magnetic activity

19 p3060 A71-38576

Ionospheric electron concentration and temperature measurements, describing rocket-borne asymmetrical Langmuir probe

19 p3067 A71-38631

Cyclotron resonance energization of trapped electrons in magnetosphere from plasma pseudopotential shape calculation, noting geophysical effect

19 p3117 A71-38724

Performance measurement of electrostatic spectrometers as monochromators by calculation of electron energy distribution

20 p3233 A71-38821

Gas heating and energy balance of HF ring discharge in rare gases within cylindrical vessel, discussing electron energy distribution functions

20 p3273 A71-39044

Scintillation spectrometers sensitivity evaluation for low energy electrons in various regions of magnetosphere

20 p3234 A71-39127

Materials behavior at low temperatures, investigating lattice vibrational spectra relation to specific heat, conducting electron energies, thermal expansion, etc

20 p3270 A71-39242

Midlatitude ionospheric irregularities, electron density vertical distribution and electron and ion temperature variation measurements, during solar eclipse of 22 September 1968

20 p3224 A71-39716

Midlatitude ionospheric electron density and electron temperature measurements by rocket experiments, noting diurnal and seasonal variations

20 p3224 A71-39718

Ionospheric electron and neutral particle temperature average diurnal behavior from bottomside vertical soundings

20 p3225 A71-39723

Photoelectron flux and energy spectra effects on ionospheric phenomena, examining sunlit and predawn atmospheric models

20 p3225 A71-39726

PCA due to solar proton event, measuring electron/ion densities and temperatures, proton/electron energy flux spectrum, Lyman alpha radiation and X rays

20 p3281 A71-39730

Suprathermal electrons energy spectra and pitch angle distribution, presenting photoelectron flux recordings by Cosmos 261 satellite

20 p3282 A71-39740

Electron temperature and density vs ionization potential in bright planetary gaseous nebulae, using forbidden emission line intensity ratios and level populations

21 p3440 A71-40059

Electron density and temperature in diffuse interstellar medium from H alpha and beta radio recombination lines near galactic plane

21 p3445 A71-40411

Temperature control bracket energy equation as measure of temperature distribution in pure hydrogen stellar atmosphere, considering electron energy and radiation field

21 p3446 A71-40419

Electrons heating by matter interaction with ultrashort laser pulses, considering hard bremsstrahlung generation

21 p3394 A71-41134

Quasi-static surface waves in Fermi electron plasma with Maxwellian electron velocity distribution

21 p3425 A71-41277

Electron energy spectra of amorphous semiconductors by cell method, replacing wave functions condition extremum integral

21 p3434 A71-41321

Solid solution electron energy spectrum at low temperatures, considering electron mobility in cadmium-mercury telluride crystals with zero forbidden band

21 p3435 A71-41342

Electron acceleration and solar flare triggering due to quasi-static electric field caused by gas motion near photosphere

22 p3590 A71-41466

Strong cylindrical and spherical electromagnetic wave propagation in plasmas, calculating amplitude and electron temperature

22 p3579 A71-41536

Energy transfer during charged particles passage through material media as function of spatial distribution, discussing electron production rates

22 p3577 A71-41537

Spectral line intensity measurement errors due to electron-temperature fluctuations averaging in continuous plasma sources

22 p3581 A71-41790

Rotational energy electron beam-plasma interactions in static magnetic field, showing exponential saturated intensity variation

22 p3582 A71-41906

Multivalley semiconductors scale effect due to nonuniform electron heating by electric field, determining effective conductivity as function of plate thickness and surface characteristics

22 p3585 A71-42058

Jovian ionospheric electron and ion densities and temperatures, considering radiative association role

22 p3603 A71-42181

Positive column He-Cd/laser discharge, determining electron temperature and density

22 p3558 A71-42345

Electron velocity distribution relaxation in time dependent weakly ionized plasma within electric field, solving Boltzmann equation

23 p3708 A71-43151

Plasma conductivity dependence on electron velocity distribution function in distorted Maxwellian form

23 p3709 A71-43259

Electron periodic energization by magnetospheric RF wave propagation, examining cyclotron resonant interaction

23 p3644 A71-43321

Langmuir paradox problem concerning electron energy distribution function and anisotropy in low pressure DC Hg vapor discharge positive column plasma

23 p3710 A71-43402

Electron energy spectrum in periodic semiconductor structures of super thin p-n junction layers

23 p3716 A71-43485

Total and momentum transfer cross sections for low energy electron scattering by atomic and diatomic molecules

23 p3707 A71-43898

Experimental techniques for differential, total and momentum transfer electron-molecule scattering cross sections at low electron energies, discussing rotational excitation

23 p3707 A71-43899

Supersonic Ar, He and molecular nitrogen jets, determining electron temperature and concentration and atomic state population in shock waves region by spectroscopic measurement

23 p3712 A71-43916

Bounded plasma ionization instability inhomogeneity scale evaluation, assuming negligible electron energy losses due to heat conduction as compared to elastic losses

23 p3712 A71-43923

F region ion and electron temperature relationship to electron density, examining incoherent scatter data and physical processes

23 p3672 A71-43977

Carbon dioxide additions effect on electron temperature relaxation and electron concentration distribution in expanding supersonic flow of low temperature Ar plasma

23 p3713 A71-44065

Laser pulse produced plasma in freely expanding high density nitrogen gas jets, measuring electron temperature and light-plasma interaction time

23 p3687 A71-44140

Local thermodynamic equilibrium deviation theory and application in low density Ar plasma, noting difference in Langmuir probe and spectroscopic electron temperature measurements

23 p3714 A71-44154

Off-resonance electron heating by microwaves in mirror contained high beta plasmas

24 p3852 A71-44486

Magnetosonic wave excitation and electron heating in magnetically confined hydrogen plasma hybrid resonance region

24 p3853 A71-44502

Temporal electron and ion temperature behavior for pulsed beam-plasma discharge interaction in probkotron mirror-like device

24 p3854 A71-44515

Electron temperature and density oscillations in beam plasma discharge, using light intensity spectroscopic observations

24 p3854 A71-44516

Electron temperature and density of HF inductive discharge in hydrogen plasma

24 p3855 A71-44524

Steady state problem of energy spectrum of variable magnetic field accelerated electrons, considering synchrotron X ray emission of Crab Nebula and pulsar

24 p3869 A71-44802

Pressure effects on Fermi surface of metals, examining crystal lattice parameters influence on electrons energy spectrum

24 p3839 A71-45168

Ionospheric and neutral atmospheric temperature profile, composition and electron density and energy measurements by MR-12 rocket

24 p3824 A71-45310

Vertical electron concentration and temperature profiles at 80-170 km measured by rocket launched on 10 July 1969 at Volgograd

24 p3824 A71-45322

ELECTRON FLUX
U ELECTRONS
U FLUX [RATE]

ELECTRON FLUX DENSITY

Photoelectron fluxes and energy spectra in ionosphere for predawn and sunlit atmospheres, taking into account elastic and inelastic collisions

01 p0147 A71-11506

Polar ionospheric auroral zone ionization, obtaining ion production function for single electron and proton flux

02 p0244 A71-11772

Inner belt electron flux variations following geomagnetic storms from satellite instrument data

03 p0418 A71-14212

Suprathermal electron flux and temperature in 5-200 eV range at high latitude with Explorer 31 potential analyzer

03 p0420 A71-14528

Primary cosmic ray electrons intensity energy spectrum data, suggesting plots based on electron energy to positive gamma power

03 p0482 A71-14542

Primary auroral electron flux angular distribution measurement by rocket probe, showing particle precipitation and trapping by electrostatic double layers in ionosphere

04 p0584 A71-15896

Atmospheric Coulomb interaction influence on longitude dependence of electron intensity in anomaly region

06 p0963 A71-18255

Penetrating electron flux relation to magnetic perturbations and auroral substorms development

07 p1185 A71-19392

Low energy electron and proton fluxes observation by Isis 1 satellite, concluding solar wind penetration to low altitudes through magnetopause cusp

07 p1186 A71-19659

Magnetopause electric field accounting for ATS 5 energetic proton and electron flux measurements, comparing to various models

07 p1186 A71-19660

Upper atmosphere balloon altitudes electron flux dependence on magnetosphere magnetic perturbation

08 p1351 A71-20957

High energy electron background flux in F 2 layer, discussing grouped particle acceleration

08 p1354 A71-21012

Plasma sheet convection velocities from electron flux measurements at synchronous altitude, noting flux increase time dependence on energy

08 p1339 A71-21216

Cosmic ray electron intensity and energy spectrum from nuclear emulsion-spark chamber combination detector triggered by scintillation and Cerenkov counters on high altitude balloon

08 p1355 A71-21627

Differential secondary electron flux measurement in aurora with Aerobee rocket spectrometer

08 p1282 A71-21635

Naturally generated electromagnetic waves interaction with electron flux in magnetoplasma, noting gyroresonance

09 p1501 A71-22304

Soft electron fluxes spatial distribution and temporal variations in magnetosphere based on Elektron 2 charged particle trap data

09 p1513 A71-22573

Charge source density during interaction between atmosphere and electron/proton fluxes at prescribed boundary parameters

09 p1513 A71-22675

Polar caps energetic particle environment involving solar flare proton and electron fluxes

10 p1600 A71-24309

EM wave excitation in plane parallel waveguide by rotating relativistic electron flux, deriving dispersion relation and interaction solutions

10 p1577 A71-24323

Satellite instruments to measure intensity and energy spectrum of high energy electrons and protons

10 p1683 A71-24464

Earth outer radiation belt electrons intensity, differential energy spectra and radial diffusion during maximum solar activity

10 p1663 A71-24783

Solar corpuscular radiation differential and integral spectrum, assessing energetic electron flux in D region at sunrise

11 p1815 A71-25587

Integral electron flux and current in retarding-potential plasma probes, considering application to nonconcave geometry and spacecraft probes

11 p1805 A71-25615

Earth radiation belts high energy electron flux intensity monotonic decrease during magnetically quiet periods from satellite data analysis

11 p1816 A71-25759

Outer radiation belt energetic electron flux intensity correlation with auroral activity and Kp index

11 p1816 A71-25760

Low energy electron and proton fluxes in geomagnetic tail of equatorial magnetosphere forming plasma sheet related to auroral oval

14 p2299 A71-30029

Electron flux rigidities in polar aurora region, using stratospheric nighttime X ray and cosmic radio noise absorption measurements

14 p2302 A71-30595

Primary cosmic ray electron energy and intensity measuring equipment, using Cerenkov and scintillation counters, spark chamber, lead absorber and photorecorder

14 p2247 A71-30598

Pitch angle diffusion of electrons in postbreakup auroral glow, measuring electron intensities by Petrel sounding rocket

15 p2394 A71-31423

Electron intensities measurement in pulsating aurora on ESRO Skylark rocket launched from Sweden

15 p2394 A71-31424

Rocket-borne electron spectrometer measurements of low energy electrons during auroral events, noting influx sudden enhancement

16 p2570 A71-33820

Low energy auroral thermal electrons flux after geomagnetic substorm, entering magnetosphere from solar wind

16 p2629 A71-33953

Coherent periodic compressional micropulsations of geomagnetic field intensity and energetic electron fluxes at synchronous altitude during quiet day

19 p3016 A71-37361

Electron and proton fluxes intercorrelation in recovery phase of auroral substorm

19 p3125 A71-37362

Penetrating electron flux relation to magnetic perturbations and auroral substorms development

19 p3127 A71-37816

Outer planets Grand Tour X ray investigation of planetary magnetospheres to obtain flux and energy spectrum of electrons precipitated from Jovian magnetosphere

[AAS PAPER 71-130] Upper atmosphere supplementary electron flux data following geomagnetic disturbance from high altitude balloon experiments

19 p3129 A71-38357

D region ionization by electron fluxes as explanation for latitudinal radio wave absorption

19 p3057 A71-38370

Electron flux and energy spectra measurements at 200-600 km altitude by Cerenkov counters onboard Proton 1 and 2

19 p3129 A71-38375

German monograph on electron flux properties in polar atmosphere, discussing pitch angle distribution, energy spectrum and relation to geomagnetic field disturbances

19 p3130 A71-38646

High energy electron background flux in F₂ layer, discussing grouped particle acceleration

20 p3280 A71-39592

Solar radiation effects on upper atmosphere soft electron flux and energy spectrum during day and night

20 p3281 A71-39724

Photoelectron flux and energy spectra effects on ionospheric phenomena, examining sunlit and predawn atmospheric models

20 p3225 A71-39726

Electron flux time dependence, observing flare increases, Forbush decreases, counting rate changes and intensity variations

20 p3281 A71-39733

Auroral electron and proton precipitation patterns, noting LF radio noise emissions relationship to low energy electron flux through Cerenkov process

20 p3228 A71-39846

Earth radiation belts high energy electron flux intensity monotonic decrease during magnetically quiet periods from satellite data analysis

22 p3591 A71-41527

Outer radiation belt energetic electron flux intensity correlation with auroral activity and Kp index

22 p3591 A71-41528

Cylindrical electromagnetic wave amplification in TWT with radial line and diverging electron flux

22 p3524 A71-42752

Magnetospheric substorms observations by satellite and balloon-borne X ray detectors, considering auroral arc brightening and energetic electron flux enhancement in magnetotail

23 p3668 A71-43163

Precipitation measurements in polar cap electron aurora, discussing neutral point entry, acceleration mechanisms, flux, pitch angle and magnetospheric models

23 p3669 A71-43169

Vela 4A and 4B satellite observation of impulsive energetic electron fluxes in distant magnetotail associated with magnetospheric polar substorms

23 p3670 A71-43184

ELECTRON GAS

Electron gas column rotating about axis parallel to uniform external magnetic field, considering equilibria within Vlasov-Maxwell model

01 p0136 A71-1478

Hot electron gas on metal surface under strong heat flux as function of crystal lattice temperature at Fermi level

02 p0332 A71-12196

Thermoelectric transport properties of ionospheric electron gas above 100 km

03 p0406 A71-13301

Electron gas problem in metal physics by self consistent Green function formalism, presenting momentum-space Feynman rules and integral equations derivation

04 p0631 A71-15795

Photoresonant cesium plasma ionization, discussing pumping spectra, electron gas, molecular-atomic ion ratio and dynamics

06 p0936 A71-17591

Quantum mechanical relation for magnetized electron gas in constant magnetic field and thermal equilibrium

08 p1337 A71-21192

Strongly magnetized relativistic degenerate electron gas proton-proton reaction rates and electron capture over various temperatures, densities and magnetic field strengths

10 p1661 A71-24305

Excess Knight shift due to spin polarization in electron gas by magnetic impurity Fermi contact coupling as function of distance from nucleus

11 p1801 A71-25373

Monatomic mercury gas excitation and ionization mechanisms ahead of and behind shock front, establishing electron gas heating kinetics in relaxation zone

16 p2616 A71-32902

Two-stream instability for magnetically confined pure electron gas column resulting from surface wave interaction

18 p2950 A71-35864

Relativistic and/or degenerate electron gas equation of state formulae for density, temperature, entropy and internal energy

18 p2960 A71-35937

Ionospheric heating Q calculation of electron gas, evaluating heat inflow at various altitudes

20 p3281 A71-39725

HF electric field influence on collisionless electron gas acoustoelectric effect, emphasizing electron scattering mechanism

21 p3431 A71-41232

Electron gas in constant crossed E and H fields, deriving nonlinear conductivity theory

21 p3424 A71-41260

Spectral line broadening due to radiating atom-electron gas interaction in nonequilibrium partially ionized plasma

23 p3710 A71-43392

Daytime photoelectron energy distribution and electron gas heating in F region as function of height and solar cycle variations

23 p3673 A71-44003

ELECTRON GUNS

Computer design of magnetron gun forming electron beam of specific pervance and oscillatory energy in converging magnetic field

03 p0385 A71-13796

High power pulsed electron beam generator, using distilled water as dielectric and multiblade cathode electron gun

06 p0876 A71-18077

Electron gun synthesis by nonparaxial method, calculating beam potential distribution, trajectories and cathode geometry for cylindrical diode

09 p1415 A71-22461

Electron beam shaping by inverted coaxial magnetron gun with steady oscillatory energy exceeding analogous value

09 p1415 A71-22462

Electron gun diode design for beam-collisionless plasma interaction nonlinear evolution, studying delta function beam velocity distribution

09 p1502 A71-22754

Electro-optical systems in photoelectronic imaging devices, discussing electron gun, electrostatic focusing lens, spherical aberration, magnetic field computation and ray tracing

10 p1609 A71-24058

Electron guns pervance increase by transverse and longitudinal charge compression, reviewing beam formation theory

20 p3204 A71-39154

Electron guns with band shaped flow, improving klystron performance and increasing pervance by anodic aperture action

20 p3204 A71-39155

Pulsed high pervance electron gun with hot lanthanum boride cathode

20 p3204 A71-39156

Numerical calculation of electron guns with converging spherical beams near cathode and electron-optical systems decelerating at collector

20 p3204 A71-39157

High power continuous electron-optical beam formation in electron gun, determining cathode and

leakage current and I-V characteristics as function of pressure

20 p3204 A71-39158

High pervance three electrode electron gun with longitudinal compression, examining beam profiles and radial current density distributions

20 p3204 A71-39161

ELECTRON IMPACT

Photoionization coefficients and photoelectron impact excitation efficiencies in daytime ionosphere, noting role in dayglow

01 p0077 A71-11515

Remote group interactions after electron impact in 4-substituted cyclohexanones, investigating mass spectrometry in structural and stereochemical problems

02 p0209 A71-12548

Atomic H excitation by electron impact, deriving cross sections for anomalous recombination lines in H II regions radio frequency spectrum

02 p0317 A71-12873

Ionospheric photoelectron exchange at magnetic conjugates, considering electron density and impact ionization by inelastic collisions

03 p0408 A71-13381

Knocked out atomic electron energy during impact ionization, comparing Thomson and Drawin formulas

03 p0465 A71-13954

Magnetic field effect on mean electron impact ionization probability in valent semiconductors with ellipsoidal equienergetic surfaces

03 p0467 A71-13978

Oxygen molecule vibrational excitation by electron impact, measuring elastic and inelastic processes

04 p0630 A71-15653

Lambda 6300 A/OI airglow excitation by soft electron fluxes

07 p1103 A71-20006

Resonance line radiation polarization of potassium and cesium isotopes excited by electron impact

09 p1490 A71-22187

Electron beam current density measurement using neutral Ar atoms electron impact excitation to metastable states

09 p1497 A71-22731

Single to triplet transitions of water vapor as function of scattering angle in electron impact detection

09 p1498 A71-23381

Electron impact excitation rates of bound electronic states of hydrogen, helium and alkali atoms

10 p1645 A71-24543

Atomic nitrogen far UV emission excitation in auroral ionosphere due to electron impact dissociations

10 p1605 A71-24792

Nitrogen excitation by fast protons and electrons impact, obtaining primary collision cross sections by measurements extrapolation to zero pressure

10 p1664 A71-24793

Atmospheric molecular species, calculating electron impact ionization cross sections and recombination coefficients

10 p1645 A71-24970

Lithium-like and sodium-like positive ions electron impact ionization, calculating cross sections and reaction rates with binary encounter model

11 p1801 A71-25211

CO Fourth Positive band system excitation cross sections by electron impact on carbon monoxide and carbon dioxide

11 p1727 A71-25366

Radiation from long lived ionic excited states, studying emission spectra, electron impact cross sections and positive nitric oxide ions band system

11 p1727 A71-25368

IMPATT oscillators noise properties at large RF amplitudes, deriving expression for noise current as function of threshold current

11 p1733 A71-26369

Photodissociative excitation of atomic oxygen dayglow emission, considering electron impact and dissociative recombination

13 p2056 A71-27933

Carbon dioxide electron impact energy loss spectrum and molecular orbit calculations, discussing fourth positive bands production in Mars upper atmosphere UV dayglow

15 p2398 A71-31766

Electron energy distribution function and ionization rate constant of atoms by electron impact as function of heavy particle temperature

16 p2615 A71-32796

Low temperature plasma reactions, discussing electron impact and collisions, ion formation, molecular excitation and thermal dissociation, vibrational relaxation, recombination, etc

16 p2539 A71-32964

Relative excitation functions for electron impact with Mg in crossed beam experiment, considering simultaneous ionization of neutral Mg

16 p2614 A71-33331

Atomic oxygen 1304-A day airglow observed fromOGO-D spacecraft, attributing subsolar emission rates to photoelectron impact excitation

16 p2574 A71-33964

Time of flight energy spectra of high lying and Rydberg metastable atoms by electron impact dissociation of molecular oxygen, noting atmospheric applications 16 p2614 A71-34043

Ionization and excitation kinetics of Hg in relaxation flow zone behind shock wave front, considering electron impact role in ground state atoms ionization 18 p2951 A71-35980

Medium energy electrons action on photographic emulsions, assuming volume element behavior not totally opaque 18 p2916 A71-36044

Excitation cross sections for resonance states by electron impact on atomic nitrogen and oxygen over aeronautical energy range 18 p2949 A71-36350

Vacuum UV emission features dissociative excitation by electron impact on molecular hydrogen and oxygen, measuring excitation cross sections from threshold to 350 eV 19 p3107 A71-38344

Glauber and Vainshtein approximations for cross sections of 1s-2p excitation during inelastic electron-atomic hydrogen scattering 20 p3272 A71-39470

Reversible electron transitions selection rule in diatomic molecules excitation by electron impact, obtaining differential cross sections 21 p3417 A71-40198

GaAs and silicon IMPATT diodes applications and performance, discussing power levels, amplifier applications, injection locked oscillators and microwave signal source 21 p3357 A71-40818

Glauber scattering amplitudes for atomic hydrogen excitation by electrons or protons, presenting closed form expressions requiring no numerical integration 21 p3420 A71-41195

Impact ionization cross section measurements for multielectron-oxygen ion reaction, using crossed beams 22 p3578 A71-42421

Molecular oxygen dissociative excitation in vacuum UV by electron impact, discussing resonance triplet atomic emission cross section 23 p3706 A71-42903

Electron impact excited carbon monoxide and dioxide 1260-5000 A spectral emission, discussing cross sections of Cameron and fourth positive bands 23 p3706 A71-42904

Carbon dioxide spectral emission at 1260-4500 A from electron impact excitation, discussing cross sections and Mars atmosphere application 23 p3706 A71-42905

Photoelectron impact vs dissociative excitation cross sections of atomic oxygen resonance radiation in terrestrial airglow 23 p3669 A71-43171

Absolute transition probabilities derivation for excitation of atmospheric nitrogen molecules and positive ion systems by electrons impact from optical measurement 24 p3850 A71-44371

Werner band system and Lyman alpha radiation emission from molecular hydrogen excitation by electron impact 24 p3850 A71-44923

Atomic and molecular gases electron impact ionization, measuring secondary particle energy distribution and angular dependence 24 p3850 A71-44925

ELECTRON INTENSITY
U ELECTRON FLUX DENSITY

ELECTRON INTERACTIONS
U ELECTRON SCATTERING

ELECTRON IONIZATION
U IONIZATION

ELECTRON IRRADIATION
Current profile monitor for scanning electron beam irradiations from accelerator, using storage oscilloscope or X-Y recorder for display 02 p0249 A71-12127

Si solar cells under low temperature electron irradiation, noting damage rate dependence on measurement temperature 05 p0701 A71-16076

Si solar cells electrical performance tests, considering 1 MeV electron irradiation effect on efficiency 05 p0702 A71-16082

Si solar cells electron spectrum irradiation, simulating space environment synchronous altitude trapped electrons omnidirectional and flux/energy characteristics 05 p0702 A71-16083

Lithium concentration and defects in doped radiation resistant silicon solar cells during electron irradiation 05 p0703 A71-16089

Production and annealing of defects in lithium diffused bulk silicon after irradiation with 30 MeV electrons and fission neutrons at 300 K 05 p0703 A71-16091

Defects and annealing in electron irradiated lithium diffused silicon solar cells 05 p0703 A71-16092

Permanent IR electron radiation effects on hardened MOS integrated inverter circuits, using units with plasma grown and vapor deposited aluminum oxide 07 p1174 A71-19053

Electron-proton radiation effects on scintillating materials in space environment chamber, evaluating background light degradation of active source monitoring 07 p1175 A71-19066

Light emitting diodes performance comparison under electron irradiation effect in space environment 07 p1071 A71-19070

Electron bombardment mercury ion thruster plasma properties and performance, computing ion beam current, discharge losses and propellant utilization efficiency [ALAA PAPER 69-256] 07 p1184 A71-19881

EPR study of electron irradiated LIF surface defects, emphasizing F-centers generation possibility 11 p1807 A71-25557

Thermoluminescent phosphorus films irradiation by electrons with energies up to 15 keV in vacuum chamber 12 p1942 A71-26648

Preferential pairing detection in CdS at 4.2 K through electron radiation damage of donor-acceptor pair green edge emission, discussing resulting wavelength shift 14 p2284 A71-29818

GaAs single crystals defects formation during low temperature gamma photons and electron irradiation, considering electrical properties 16 p2620 A71-33185

Lunar fines luminescence emission spectra in visible and near IR region under proton and electron excitations, discussing cause and plagioclase distribution 23 p3760 A71-43777

CNES hypotheses and methods determining current delivered by solar generator of FR 1 satellite, discussing electrical performance due to electron and proton irradiation 24 p3793 A71-44760

Artificial magnetosphere interaction with 8 keV electrons in hydrogen plasma beam simulating solar wind, noting penetration caused by boundary instability 24 p3823 A71-45043

Channel electron multiplier principles and characteristics, discussing secondary electron production probability during electron irradiation of surface in vacuum 24 p3811 A71-45326

Photoelectric tubes microchannel plates degassing during bake-out or during operation by electron bombardment, discussing desorption elimination by multiplier treatment before tube sealing 24 p3811 A71-45337

ELECTRON MASS
Electron mass and photon wave renormalizations functional relationships, studying perturbation theory based electrodynamic divergences 07 p1162 A71-20550

Electron velocity, spin, energy and mass derivation based on consideration as negative component of photon 13 p2103 A71-29277

Electrical conductivity and thermoelectric power measurements for polycrystalline beta-SiC heavily doped with nitrogen, estimating electron effective mass and carrier mobility at high temperatures 21 p3433 A71-41307

N-type cadmium germanium arsenide single crystal semiconductor electron and hole effective mass determination from thermoelectric power measurement 21 p3436 A71-41350

ELECTRON MICROSCOPES
High purity hafnium titanate, discussing preparation and DTA, electron microscopy wet chemical and X ray analyses 02 p0275 A71-12595

Cu and Al bronze civil transformation kinetics, using electron photoemission microscopy 03 p0444 A71-14337

Electron microscope micrographs enhancement by holographic image deblurring 04 p0596 A71-15135

Limitations of electron and X ray microscopy concerning damage of biological molecules by observation 04 p0596 A71-15140

Isolated tobacco chloroplasts disintegration, measuring simultaneous particle size and photochemical reduction rate changes by electron microscopy 04 p0539 A71-15269

Lunar dust samples 10084 and 12070 texture studies with electron microscope, noting difference from meteoritic or lunar rock matter 05 p0807 A71-16299

Electron microscopic studies of nerve membrane fine structure, discussing cell membrane multienzyme and macromolecular energy and information transduction, protein synthesis and nucleic acids interrelations 06 p0850 A71-17500

Scanning electron microscopy for microstructures of various eutectic Ni alloys, discussing rod-plate transition 06 p0914 A71-18681

TiNi antiphase boundaries direct observation using transmission electron dark field imaging technique 07 p1131 A71-19431

Scanning electron microscope for surface morphological investigations of materials after laser irradiation 07 p1113 A71-19793

High voltage electron microscopy of internal defects in carbon fibers, considering fiber strength [PLASTICS INST. PAPER 10] 08 p1297 A71-20921

Shock reheated chondrites metal phases, discussing postshock cooling thermal histories by metallographic and electron microprobe studies 09 p1519 A71-22643

Electron microscope investigation of packing defect energy effect on structure of crystal dislocations in hardened metals during annealing and deformation 09 p1473 A71-23226

Polygonization and recrystallization processes in Fe-Cr alloy, using electron diffraction and microscopy 09 p1476 A71-23522

Aluminum-epoxy joints stress corrosion cracking inhibition and crack tip plastic deformation by scanning electron microscopy 10 p1615 A71-24091

Macroscopically ductile and brittle fracture via electron microscope photographs, considering brittle fracture and embrittlement temperature under uniaxial and multiaxial stress 10 p1627 A71-24595

Hall effect measurements and electron microscope examination of Te-doped gallium arsenide crystals annealed at various temperatures 13 p2111 A71-28503

Morphological structural changes during firing from scanning electron microscopy of unfired and fired kaolinite 13 p2092 A71-28659

Petrographic study of Allende carbonaceous chondrite by high voltage transmission electron microscopy, comparing substructure with terrestrial rocks 14 p2308 A71-29912

Scanning electron microscope in nondestructive testing, reviewing signal mode produced topographical data, image recording and inspection procedures 16 p2581 A71-32862

Metal matrix composites fractured and cut surfaces analysis using scanning electron microscopy [ASM PAPER W71-3.4] 16 p2579 A71-33541

Laser drilled holes in alumina substrates, studying structure by scanning electron microscopy and X ray diffraction patterns analysis 17 p2763 A71-35738

Scanning electron microscope examination of components and materials quality and reliability in satellite onboard equipment 18 p2890 A71-36537

Electro-optic He-Ne laser microscope for high-speed high-precision edge detection for IC masks 19 p3075 A71-38236

Scanning electron microscope for poor metallization detection in manufacturing cycle of semiconductor devices 19 p3034 A71-38519

Recrystallization behavior of thorium dispersion hardened W-Re alloy compared to pure W by X ray diffraction, hardness tests, metallographic and electron microscopy methods 20 p3247 A71-38763

Ion bombardment thinning apparatus for preparing electron microscope foils of inorganic nonmetallic samples including ceramics, minerals and rocks 20 p3233 A71-38826

Cell structure development during room temperature tensile deformation of beryllium after prism slip by combined X ray diffraction-transmission electron microscopy 20 p3249 A71-39002

Holographic electron microscopy, discussing speckle-free illuminated plane object reconstruction from holograms 22 p3538 A71-41732

Low loss images from smooth solid specimens in surface scanning electron microscope by collecting backscattered electrons 23 p3674 A71-42959

Particle size and shape distributions of Apollo 12 lunar fines by computer evaluation of scanning electron microscope images 23 p3758 A71-43755

Objective lens with superconductive winding for high voltage electron microscope, describing optical properties and vibration reduction system 23 p3679 A71-44008

Electron microscopic study of antiphase domains size and shape in Ni-Mn alloy after annealing 23 p3692 A71-44009

Scanning electron microscopic observation of fracture surface of austenitic stainless steels for stress cor-

rosion cracking in magnesium chloride and calcium chloride solution

23 p3693 A71-44073

Electron transmission microscopy of Mo single crystals irradiated with fission neutrons and defect structures prior/after postirradiation anneal

24 p3839 A71-45192

ELECTRON MICROSCOPY

U ELECTRON MICROSCOPES

ELECTRON MOBILITY

Electrons motion across gas plasma magnetic field under stochastic electric field, noting accelerating effect

01 p0135 A71-11032

Disordered materials electronic structure band states localization, examining mobility edges

01 p0140 A71-11441

Electron mobility in gallium arsenide phosphide solid solutions, discussing temperature effects

01 p0141 A71-11465

Hall electron mobility in cadmium arsenide as function of concentration and temperature

01 p0141 A71-11466

Cs doped Mg vapor arc discharge, determining electron mobility and diffusion cross section

02 p0286 A71-12180

Energetic electron magnetospheric motion and acceleration during substorms, examining fault line existence at near local midnight

03 p0419 A71-14519

Field aligned currents and high potential drop space charge regions above aurora associated with electron acceleration

03 p0419 A71-14525

Electron mobility and thermal emf in nondegenerate ferromagnetic semiconductors, considering entrapment of electrons by magnons at temperatures below Curie point

04 p0636 A71-15102

Electrophysical properties of Ga-In-As single crystals in varying mixture ratios at 78-380 K, determining electrical conductivity, Hall coefficient and electron mobility

07 p1176 A71-19224

Degenerate n-type GaSb, calculating electron mobility dependence on impurities concentration for comparison with experiment

09 p1507 A71-22361

Microwaves anomalous skin effect in high density gaseous magnetoplasma, comparing experimental electromagnetic field penetration increase due to thermal electron motion with theoretical prediction

09 p1502 A71-22800

Pulsar oblique magnetic rotator model, noting large amplitude EM traveling wave effects on electron motion

10 p1679 A71-24956

Laser radiation and plasma nonlinear interaction, using particle description of electron motion

11 p1806 A71-26093

Cadmium mercury telluride solid solutions electron energy spectrum at low temperatures, calculating electron mobility in crystals with zero forbidden band

13 p2110 A71-27955

Motion equation of electron in cylindrical diode subjected to varied voltages

13 p2036 A71-28372

Doping dependent mobility analysis of junction FET, calculating drain current and transconductance

13 p2037 A71-28474

Thermal noise in space charge limited solid state diodes with field dependent mobility and hot carriers

14 p2284 A71-30502

Two lens high current plasma accelerator with closed electron drift, using crossed electric and magnetic fields

14 p2282 A71-30664

Random walk theory applied to electron motion in early stage of He breakdown in electric field, based on integral and differential cross section data

15 p2452 A71-31921

Electroconductivity and Hall effect in doped GaAs at low temperatures, studying temperature dependence of electron concentration, mobility and localization

16 p2623 A71-34030

Electron concentration and mobility of heavily doped n-type InSb single crystals at high temperatures, investigating temperature dependence of Hall coefficient

18 p2954 A71-36803

Monograph on electron drift rate measurement in low pressure arc discharge using microwave dragging technique

19 p3116 A71-38549

Transient photoconductivity measurements of room temperature electron mobility in deuterated anthracene single crystals, discussing isotope effect

20 p3194 A71-39348

Cosmic plasma electron thermal motions effects on cosmic electromagnetic absorption, taking into account electron-electron collision effects in electromagnetic waves dispersion relationships

21 p3442 A71-40162

Solid solution electron energy spectrum at low temperatures, considering electron mobility in cadmium-mercury telluride crystals with zero forbidden band

21 p3435 A71-41342

Low frequency phase method application to fast electron processes and characteristic relaxation times in quick response Ge and Si junction diodes

23 p3650 A71-43307

Electron motion in plasma under stochastic electric field, emphasizing distribution function dependence on velocity and time

24 p3853 A71-44510

ELECTRON MULTIPLIERS

U PHOTOMULTIPLIER TUBES

ELECTRON OPTICS

Electron spectrophotometry in molecular and solid state physics, comparing to X ray analysis

10 p1645 A71-24695

Flying spot scanner electron optical systems for reading data from photographic film for studies of recognition algorithms, image simulation and automatic particle track measurements

15 p2409 A71-32191

Book on electron optics covering image formation principles, field plotting and ray tracing analog and computational methods, electrostatic and magnetic lenses, etc

19 p3103 A71-37522

Laplace equation solution for double cylinder electrostatic lenses for large range voltage ratios and separations, obtaining focal and aberration coefficients

21 p3377 A71-40178

Electronic techniques in optoelectronics/, discussing CRT, image tubes, semiconductor and lasers

22 p3559 A71-42467

ELECTRON ORBITALS

Metals and nonmetals orbital atomic radii and lattice parameters

08 p1345 A71-21762

Condensed state Ni and Pd atoms X ray emission spectra and electron structure

09 p1474 A71-23233

Electron exchange and nuclear symmetry for 2s and 2p collisional excitations of hydrogen by H atom based on symmetrized atomic orbitals set

10 p1644 A71-23925

Spherical shell potential extension to shells of differing diameters for intermolecular forces in globular molecules, considering binary gaseous mixtures

11 p1801 A71-25369

D-transition metal carbides properties based on electron configuration localization model

15 p2429 A71-32138

Structure and properties of beryllium compounds from solid state stable electron configuration formation viewpoint, discussing classification based on chemical bond

16 p2597 A71-33920

Transition metals monocarbides and mononitrides electronic structure, investigating electrical, thermoelectrical and galvanomagnetic properties

16 p2597 A71-33922

ELECTRON OSCILLATIONS

Longitudinal electron oscillation suppression by beam density modulation in axially and transversely finite beam-plasma system

06 p0934 A71-17484

Spontaneous oscillations in semiconductors with deep traps, deriving conditions for soft or hard excitation

07 p1176 A71-19226

Plane light wave interactions with moving dispersive dielectric medium, considering electron UV or ion IR resonant oscillation in regions of anomalous dispersion

08 p1253 A71-21278

Submillimeter wave oscillations possibility by Bloch oscillation of conduction electrons in ideal crystal with periodic energy band structure

08 p1343 A71-21280

Electron fluxes hydrodynamic stability in vacuum confined by external electric and magnetic fields and inertia forces, noting electron oscillations possibility

08 p1340 A71-21494

Ion sources with oscillating electrons, discussing operating principles and characteristics of sources with cold and incandescent cathodes and Penning ionization chamber

08 p1343 A71-22043

Natural potential and nonpotential electron oscillations excitation in plasma by transverse wave field, determining wave amplitude threshold and excitation instability

09 p1500 A71-22239

Book on lasers and masers covering electric and magnetic dipole transitions, electron oscillator, collision broadening, optical resonators, waveguides, etc

09 p1466 A71-23725

Magnetic field effect on emission spectrum and intensity at electron cyclotron frequency harmonics from PIG Reflex discharge, discussing electron oscillations excitation in plasma

12 p1938 A71-27214

Semiconductors high carrier densities at low temperatures, showing possible soft plasma branch and electron sound

12 p1944 A71-27774

Electron electrostatic or space charge oscillations in nonneutral plasma columns with cylindrical symmetry around axial magnetic field

13 p2104 A71-27844

Kinetic theory of nonspherical multimode molecules with electrons having rotational and oscillatory degrees of freedom, giving expressions for oscillatory relaxation times calculation

13 p2103 A71-29150

Electron gyro and synchrotron radiation from vacuum and isotropic plasma, deriving approximate general formula for power spectrum and polarization

14 p2282 A71-30666

Ionospheric electron resonance observation by sounders aboard rocket and satellites

14 p2202 A71-30947

Na and K transition oscillator strengths, noting core polarization effects on mathematical model

16 p2615 A71-34088

Magnetic field effect on emission spectrum and intensity at electron cyclotron frequency harmonics from PIG Reflex discharge, discussing electron oscillations excitation in plasma

19 p3117 A71-38262

Electron oscillation induced longitudinal standing wave excitation and suppression in beam-plasma system by passing electron beam through axially bounded plasma

20 p3275 A71-39864

Natural potential and nonpotential electron oscillations excitation in plasma by transverse wave field, determining wave amplitude threshold and excitation instability

21 p3424 A71-41125

High voltage source model for fast neutral particles, showing energy and yield as function of potential, pressure and magnetic field

21 p3421 A71-41295

Electron beam interaction with plasma in ion sources with oscillating electrons, noting increased ion current

22 p3580 A71-41645

Longitudinal electron oscillations damping in ionized plasma, obtaining wave dispersion relation from BGK model

22 p3583 A71-42372

B stars spectra, calculating C III ions spontaneous electric dipole transitions and oscillator strengths in vacuum UV region

23 p3767 A71-43829

Langmuir electron oscillation excitation by ion beam at velocity exceeding average electron thermal velocity in plasma formed by residual gas ionization

24 p3858 A71-45234

ELECTRON PARAMAGNETIC RESONANCE

Zinc reduced di(4-pyridyl) ketone methiodides, examining electronic and electron spin resonance spectrum

03 p0377 A71-14301

EPR spectrum of tetravalent vanadium ions in gamma irradiated corundum at liquid He temperatures, showing equidistant lines width temperature dependence

04 p0637 A71-15105

EPR line width in ruby under charged dislocations and electric fields of lattice defects, using statistical method

06 p0942 A71-18348

Manganese, iron and vanadium ion ordering in orthorhombic zoisite structure by electron paramagnetic resonance technique

07 p1053 A71-18744

Electron paramagnetic resonance and optical absorption spectra of transition metal ions in zoisite crystal

08 p1343 A71-20658

Smectic C liquid crystal molecules electron paramagnetic resonance study, determining tilt angle

09 p1508 A71-22753

EPR study of electron irradiated LiF surface defects, emphasizing F-centers generation possibility

11 p1807 A71-25557

Reacting gases atom concentration quantitative measurements with electron spin resonance, discussing microwave power, saturation and modulation amplitude effects

11 p1765 A71-26284

Electron paramagnetic resonance spectral investigation of dynamic Jahn-Teller effect in La doped strontium chloride, discussing structural variations as function of temperature

12 p1942 A71-26743

Electron paramagnetic resonance atomic scale stress analysis of high polymer fibers and rubber, measuring chain scission and bond rupture for different loading histories

13 p2091 A71-28440

Hydrogen atoms trapped in gamma irradiated calcium phosphates, studying radiation yields, electron paramagnetic resonance line widths, dose saturation and relaxation

16 p2538 A71-32873

Atomic bond rupture and molecular mechanisms of polymer fracture, using EPR spectroscopy 16 p2600 A71-32944

EPR spectra and spin-lattice relaxation time in coal pitch and polyvinyl chloride during low temperature carbonization 17 p2763 A71-35245

Molecular bond rupture and strain energy release rates correlation during ozone cracking of rubber from electron paramagnetic resonance and stress elongation measurements 18 p2939 A71-36244

Double electron-nuclear resonance spectrometer using HF modulation of magnetic field for observation of electron paramagnetic resonance signal 18 p2924 A71-36626

Optical absorption and electron spin resonance in KCl with and without KOH, noting F band existence 21 p3414 A71-40070

Ion pairing study in unresolved metal hyperfine splitting spectral region, using electron spin resonance line shape analysis 21 p3345 A71-40372

Electron spin resonance studies of Apollo 11 and 12 lunar soil samples, determining ferromagnetism due to Fe particles 23 p3763 A71-43797

ELECTRON PATHS

U ELECTRON TRAJECTORIES

ELECTRON PHONON INTERACTIONS

Microwave emission from InSb due to sound amplification by piezoelectric electron-phonon coupling at low magnetic fields 01 p0052 A71-10321

Electromagnetic wave nonlinear propagation in semiconductors, considering field amplitude and electron temperature for strong electron phonon interaction and degenerate semimetals 01 p0138 A71-10434

Thermal conductivity anomalies in thin superconducting metal foils in contact with two superfluid He basins at low temperatures, examining surface electron phonon interactions 10 p1640 A71-23832

Nonlinear dependence of resistance in metals on impurity concentration and temperature due to umklapp electron phonon interaction and anisotropy of phonon spectrum 16 p2593 A71-33654

Electrons interaction with impurities and longitudinal optical phonon in metal-insulator-semiconductor tunnel junctions 19 p3119 A71-37869

Temperature and frequency dependence of electron phonon interaction maxima in rhenium, explaining transverse and longitudinal waves ultrasonic attenuation by two band theory 22 p3578 A71-42597

ELECTRON PHOTOGRAPHY

Condensed metal particle size distribution measurement at ambient conditions by photography using electron microscope 02 p0333 A71-12854

Visual binary star observations by Lallemand electronic camera and photo-electronic image devices 14 p2311 A71-30363

Stratospheric extraterrestrial particles identification from balloon-collected electron microscope photographs, suggesting cometary origin 16 p2644 A71-34127

ELECTRON PHOTON CASCADES

Extensive atmospheric showers and energy transfer from interacting nucleons to electron photon cascades at high energy levels 01 p0146 A71-11366

Electron photon cascade energy measurement by photomonitoring blackened spots on X ray films 01 p0084 A71-11369

X ray films in emulsion chambers, discussing electron-photon cascades 03 p0426 A71-13839

Electron-photon showers, discussing cascade theory equilibrium spectra, avalanches and radio emission 03 p0475 A71-13840

Extensive air shower electron photon and muon components energy spectrum at various depths 03 p0477 A71-13859

High energy muons in extensive air showers, studying spatial distribution, spectrum and electron showers by photon spark chamber telescope underground 03 p0477 A71-13860

Cosmic ray shower particles spatial and angular distribution structure near electron-photon cascade core 03 p0478 A71-13867

Electron photon cascades in multilayer substrate-free nuclear emulsion chamber with X ray films under lead plate 03 p0427 A71-13872

Controlled photographic emulsion study of cosmic ray showers with electron photon components 19 p3124 A71-37261

X ray films in emulsion chambers, discussing electron-photon cascades 22 p3550 A71-42640

Electron-photon showers, discussing cascade theory, equilibrium spectra, avalanches and radio emission 22 p3594 A71-42641

Extensive air shower electron-photon and muon components energy spectrum at various depths 22 p3595 A71-42660

High energy muons in extensive air showers, studying spatial distribution, spectrum and electron photon showers by underground photon spark chamber telescope 22 p3595 A71-42661

Cosmic ray shower particles lateral and angular distribution structure near electron-photon cascade core 22 p3595 A71-42668

Perturbation method in transition effect theory for electron photon cascades in extensive air showers 22 p3596 A71-42672

Electron photon cascades in multilayer substrate-free nuclear emulsion chamber with X ray films under lead plate 22 p3550 A71-42673

ELECTRON PLASMA

Analog device for harmonic functions modeling and electron plasma dispersion function computation 01 p0135 A71-11078

Electron-positron pair production during focusing of laser radiation in dense plasma 01 p0135 A71-11094

Surface oscillations energy and attenuation in damped spectral region of semibounded degenerate electron plasma 02 p0288 A71-11630

Warm continuously stratified electron plasma fields behavior in coupling region excited by incident electron-acoustic wave 02 p0293 A71-12742

Microwave interferometer for low density electron laboratory plasmas 03 p0428 A71-13926

Electron plasma waves one dimensional quasi-linear instability with allowance for spontaneous emission 03 p0464 A71-13929

Electromagnetic instability of counterstreaming electron plasmas with anisotropic temperatures, using Vlasov equation 04 p0633 A71-15032

Two stream electron plasma with Coulomb particle collisions, considering autooscillations and nonlinear friction characteristic 04 p0633 A71-15109

Refractive index equation for oblique wave propagation in inhomogeneous compressible electron plasmas 05 p0786 A71-16287

Quasi-linear equations consequences in discrete spectra and damped electron plasma waves, discussing conservation laws relation to resonance approximation 05 p0789 A71-16652

Electrostatic waves linear dispersion relation in Maxwellian unmagnetized ions and magnetized electrons Vlasov plasma 05 p0789 A71-16656

Electron-hole plasma in current carrying wire azimuthal magnetic field, noting electric field intensity by hydrodynamic approximation 05 p0790 A71-16880

Density thresholds for anisotropy and loss-cone instabilities onset in hot electron plasmas as function of frequency, wavelength and propagation direction of oscillations 05 p0790 A71-16937

Electron plasma in strong HF electric field, investigating possibility of parametric resonance 06 p0930 A71-17403

Electron-hole plasmas feedback stabilization, considering instability coefficients measurement 06 p0933 A71-17470

Hot electron plasma, observing flute instabilities with feedback 06 p0933 A71-17471

Dynamic stabilization of helical and sausage instabilities of p-indium antimonide electron-hole plasmas, using Ioffe type RF energized magnetic quadrupoles 06 p0935 A71-17489

Hot electron plasma confinement in cusped magnetic field, considering production in electron cyclotron resonance region by pulsed microwaves 06 p0935 A71-17491

Extraordinary waves propagating perpendicularly to uniform magnetic field in hot electron plasma, discussing wave interaction 07 p1166 A71-18884

Plasma frequency resonance time duration-long electron cyclotron frequency relationship by oblique echo model 07 p1168 A71-19681

Plasma electron temperature probes, investigating electron heating effects 07 p1112 A71-19765

Effective electric field formulation of kinetic theory of classical Coulomb plasmas, computing wavevectors 07 p1169 A71-19994

Type 2 and 3 solar radio burst model, examining exciting agent as electron bunch emitting electron plasma waves 08 p1356 A71-21756

Electron-positron pair production during focusing of laser radiation in dense plasma 08 p1342 A71-21952

Quasi-stationary permittivity tensor corrections for smoothly nonuniform electron plasma in absence of magnetic field, using geometrical optics methods 09 p1500 A71-22240

Electron-electron interaction effects on electronic states density in electron gas impurity bands, using matrix method 10 p1644 A71-23772

Electrostatic field second order penetration into Vlasov warm electron plasma, using electron velocity distribution models 10 p1647 A71-23890

Parametric excitation of transverse waves in inhomogeneous electron plasma driven by oscillating electric field, using multimode perturbation method 10 p1647 A71-23891

Unstable electron plasma oscillations quasi-linear theory, discussing improper treatment of perturbed electron distribution for damped waves leading to negative diffusion coefficient 10 p1647 A71-23893

Neutrino luminosity in strongly magnetized degenerate relativistic electron gas plasma from URCA energy loss rate calculations 10 p1671 A71-24303

Pseudoacoustic energy flux influence on accessibility of ground emitted wave to plasma resonance in F region, using adiabatic approximation with scalar pressure 10 p1602 A71-24465

Spatially uniform external periodic magnetic field effect on wave propagation perpendicular to hot electron plasma, obtaining dispersion relation from hydrodynamic equations 10 p1578 A71-24655

Negative differential conductance of homogeneous nonequilibrium electronic solid-body plasma in electro-magnetic field upon Cherenkov interaction 11 p1807 A71-25584

Magnetoactive cold electron plasma wave interaction theory, investigating energy transfer 12 p1934 A71-26748

Electron hole n-p plasma conductivity in cylindrical germanium specimens as function of current produced azimuthal magnetic field 12 p1936 A71-27036

Time and space variable echo waves in electron plasma by wave packets interaction, considering spectral line width finiteness influence 12 p1937 A71-27038

Electromagnetic wave reflection from interface between moving and stationary electron plasma, giving boundary conditions at velocity discontinuity surface 13 p2108 A71-28855

Soviet monograph on EM waves in solid state plasma covering propagation, amplification, generation and peneration 13 p2112 A71-29078

Electron thermal anisotropy effect on oblique whistlers preceding strong collisionless shock waves, using linear Vlasov theory 13 p2064 A71-29168

Wave propagation near upper hybrid frequency in mirror-confined hot electron unstable plasma 13 p2109 A71-29242

Nonlinear Fokker-Planck equation numerical tests for collision effects on self consistent field first order component and plasma electron distribution function perturbation 15 p2453 A71-31146

Ion beam collisionless relaxation in hot electron plasma, observing oscillation spectra and velocity distributions 15 p2453 A71-31245

Magnetic field and electron plasma observations near dawn magnetopause by triaxial spectrometer and fluxgate magnetometer on satellite OGO 5 15 p2485 A71-31754

Nonlinear interaction between three resonant modified ordinary electromagnetic waves propagating perpendicular to static magnetic field in homogeneous electron plasma, studying relativistic effects 15 p2460 A71-32655

Collision integral for classical electron plasma, concerning Born-Bogoliubov-Green-Kirkwood-Yvon equations for long range interaction potential and motions of multiple particles 16 p2619 A71-33650

Temporal echo oscillations in collisionless relativistic electron plasma 17 p2786 A71-34198

Free-free bremsstrahlung emission in anisotropic hot electron plasma in magnetic mirror, measuring polarization by Compton scattering 17 p2788 A71-34853

Nonthermal electrons interaction with electron plasma oscillations and HF transverse waves in upstream solar wind 19 p3125 A71-37353

Electron wave coupling in plasma column, determining exact resonance and field configurations of frequencies 19 p3111 A71-37635

Narrow band magnetospheric radio noise between electron plasma and upper hybrid resonance frequencies from satellite observations 20 p3285 A71-38728

Nonlinear Landau damping proposed as explanation for electron plasma oscillations amplification by plasma wave amplitude increase 20 p3274 A71-39349

Trapping of neutrals from fast atom beam impinging on molecular hydrogen influx fed electron-cyclotron plasma target 21 p3422 A71-40761

Stochastic model for electron-cyclotron plasma heating by high power microwaves in magnetic mirror 21 p3422 A71-40762

Quasi-stationary permittivity tensor corrections for smoothly nonuniform electron plasma in absence of magnetic field, using geometrical optics methods 21 p3424 A71-41129

Quasi-static surface waves in Fermi electron plasma with Maxwellian electron velocity distribution 21 p3425 A71-41277

Surface waves at Fermi electron plasma boundary, using kinetic theory of plasma electromagnetic oscillations 21 p3425 A71-41278

Microwave plasma generation in magnetic field, detecting expansion related to electron cyclotron frequency harmonics 21 p3426 A71-41287

Electromagnetic wave reflection from interface between moving and stationary electron plasmas, giving boundary conditions at velocity discontinuity surface 21 p3426 A71-41288

Piezosemiconductors nonequilibrium electron plasma current oscillations under strong electric and magnetic field interactions 22 p3584 A71-41644

Electron plasma waves and free streaming bursts response to fast rising voltage step in low density cylindrical plasma in strong magnetic field 22 p3582 A71-41899

Electron distributions in afterglow of hot electron mirror contained plasma as function of time, using bremsstrahlung spectra measurement 22 p3582 A71-41903

Resonant coupling of two electron plasma waves with ion sound wave at large electron Larmor radii under weak magnetic field 22 p3583 A71-42418

Statistical HF electron heating at oscillating plasma boundary with acceleration of double Langmuir layer 23 p3709 A71-43260

Acoustic instability of Joule heated nonisothermal electron plasma 23 p3709 A71-43261

Sound waves propagation in fully ionized gas, considering electron plasma frequency 23 p3705 A71-44001

External, HF, traveling wave field interactions with homogeneous electron plasma longitudinal oscillations under magnetic field 24 p3853 A71-44503

Relativistic electron beam propagation in decelerating medium in crossed electric and magnetic fields, noting nonrelativistic instability condition 24 p3856 A71-44669

ELECTRON PRECIPITATION

Auroral ionization relationship to incident magnetospheric electrons based on atmospheric model 01 p0073 A71-10253

Energetic electron precipitation effects on upper D region water cluster ion population at various vapor mixing ratios 02 p0245 A71-11961

Bremsstrahlung X rays-radar echoes relation in southern auroral zone, discussing electron precipitation role 03 p0408 A71-13388

Conjugate observations of ionospheric absorption associated with electron precipitation during sudden commencement of magnetic storm 03 p0419 A71-14520

Midlatitude nighttime D region ionization source, considering precipitating energetic electrons 03 p0420 A71-14527

Nonlinear M-type traveling wave tube equations for large signal mode, discussing electron precipitation 04 p0556 A71-14623

Polar chorus background hiss generation, investigating VLF wave characteristics responsible for harder electron precipitation from magnetosphere 05 p0743 A71-17004

Electrostatic fields parallel to geomagnetic field role in charged particles acceleration mechanism to auroral energies, considering electron and proton precipitation 06 p0893 A71-17989

Energetic electron and proton precipitation measurements by sounding rocket-borne particle detectors in pulsating aurora 07 p1186 A71-19669

Auroral electron and proton precipitation patterns observed at Fort Churchill, discussing particle energies 08 p1282 A71-21636

Lower ionospheric region parameters during 24 and 30 March 1968 substorms, determining auroral electron precipitation effects 09 p1440 A71-23630

Morphology, dynamics and time variations of auroral zone electron precipitation events from balloon measurements of bremsstrahlung X rays 10 p1662 A71-24535

Electron precipitation in nocturnal E region from radiowave and rocket data, calculating ionization rates and midlatitude morphology 11 p1815 A71-25552

Particle precipitation at auroral heights, examining ground based observations evidence for existence of protons, neutrons and electrons 12 p1947 A71-26864

Auroral zone X ray events due to electron precipitation, considering relationship to polar magnetic substorms 13 p1219 A71-27798

Midnight sector balloon measurements of X ray bremsstrahlung from electrons precipitating in auroral zone during polar magnetic substorms 13 p1219 A71-27798

Precipitation energy flux of continuous noontime aurora, using airborne ionospheric and optical measurements 13 p2054 A71-27801

Insufficient auroral electron spectra and pitch angle distributions from ground based altitude luminosity profiles 13 p2054 A71-27802

Properties of higher latitude region of structured low energy electron precipitation in noon hemisphere, relating radiation with optical emissions in dayside auroral oval 13 p2119 A71-27911

Auroral precipitation electron energetic and angular distributions as function of geomagnetic activity from Cosmos 261 measurements 14 p2230 A71-29713

Low energy precipitating auroral particle fluxes over magnetic poles delineating polar cap, noting electron precipitated flux 14 p2299 A71-30030

High latitude measurements of low energy electron precipitation by Auroral 1 satellite, explaining anomalous high level F region ionization near dark pole 14 p2299 A71-30031

High latitude regions of low energy electron precipitation from OGO 4 satellite auroral particle experiment 14 p2300 A71-30032

Geomagnetic tail influence on polar ionosphere proton and electron precipitation, considering ionospheric ionization and polar cap absorption 14 p2300 A71-30034

Low energy electron precipitation effects on upper atmosphere based on polar cap and auroral oval electron spectrum comparison 14 p2300 A71-30035

Atmospheric VLF electromagnetic emissions and electron instabilities data from satellite observation, detailing source regions, large amplitude electrostatic waves and wave-particle correlation 14 p2202 A71-30952

Electron and proton precipitation observations in auroral, polar cap and outer radiation zones by electrostatic analyzers on earth satellite Injun 5 15 p2397 A71-31756

Auroral 4278 A positive nitrogen ions emission relation to low energy electron precipitation, using polar orbiting Aurorae satellite photometer and particle detector data 16 p2568 A71-33794

Electron and proton precipitation, studying effects at high latitudes on 2 February 1969 magnetic storm 16 p2627 A71-33795

Relativistic electron precipitation during magnetic storms, showing cyclotron resonances with electromagnetic ion cyclotron waves 16 p2629 A71-33948

Local time dependence of auroral zone electron precipitation X ray events from balloon measurements of bremsstrahlung 18 p2911 A71-35894

Polar auroras production by electric fields and electron precipitation from magnetospheric magnetic storms 19 p3052 A71-37761

Outer planets Grand Tour X ray investigation of planetary magnetospheres to obtain flux and energy spectrum of electrons precipitated from Jovian magnetosphere [AAS PAPER 71-130] 19 p3127 A71-37995

Magnetospheric current effects on geomagnetic field structure, noting electron and proton precipitation into auroral zone 19 p3059 A71-38390

Auroral luminosity patterns over northern Scandinavia based on ESRO all-sky camera recordings, noting relationship to electron and proton precipitation 19 p3060 A71-38375

Auroral electrons and protons precipitation patterns from ESRO 1A northern polar cap observations identifying electron energy zones 19 p3060 A71-38375

Low energy electron and proton precipitation pattern in northern polar region, using low orbit satellite borne spectrometer 20 p3281 A71-39727

Auroral morphology, covering static and dynamic ovals, polar cap and dayside auroras, auroral zone substorms and electron precipitation 20 p3227 A71-39813

Auroral electron and proton precipitation patterns, noting LF radio noise emissions relationship to low energy electron flux through Cerenkov process 20 p3228 A71-39840

Low energy auroral particle measurements from polar satellites, obtaining electron and proton precipitations location, and angular and energy distributions 20 p3228 A71-39847

Auroral electron and proton precipitation patterns, measuring airglow emissions 20 p3284 A71-39847

Auroral zone X ray events in midnight sector associated with substorm and electron precipitation following electrojet, using balloon-borne detector measurements 20 p3284 A71-39855

Large and small scale auroral formation dynamics, covering precipitating electron and proton acceleration and plasma instabilities role 20 p3229 A71-39864

Polar ionospheric ion density enhancement correlation to low energy electron precipitation from observations by polar satellite 20 p3231 A71-39889

Magnetospheric plasma observation by Sirio 1 satellite, measuring protons, electrons and magnetic fields with sensors 20 p3307 A71-39954

High latitude auroral particle precipitation patterns and connections to plasma sheet, ring current, cusps and radiation belt sources, using rocket and satellite observations 21 p3439 A71-41175

Electric current shear at auroral arcs due to electron precipitation into lower ionosphere 22 p3536 A71-42622

Precipitation measurements in polar cap electron aurora, discussing neutral point entry, acceleration mechanisms, flux, pitch angle and magnetospheric models 23 p3669 A71-43163

Night enhancements in 6300 A line at Sanae related to diurnal excursion of auroral oval, observing ionospheric blackout and high energy electrons precipitation 23 p3672 A71-43987

Electron production cross sections in inelastic atomic collisions, evaluating classical scaling law and quantum mechanical statistical methods against experimental results [AIAA PAPER 71-995] 24 p3850 A71-44587

ELECTRON PRESSURE

Hot stellar atmospheres, calculating mean radiation absorption coefficients as function of temperature and electron pressure 01 p0158 A71-10805

Warm plasmas impedances and power transfer near lower hybrid resonance, including electron pressure effects in full electromagnetic treatment 15 p2456 A71-31923

ELECTRON PROBES

Elongation characteristics of modulation type charged particle traps and analyzers, discussing ions and electrons trapping 09 p1513 A71-22668

Nb-Pd system concentration profiles and thermal diffusion coefficients, investigating phase formations by electron probe microanalysis 10 p1629 A71-25033

Magnetospheric electron echo probe experiment using sounding rocket and injecting gun for controlled particle trapping investigation 12 p1953 A71-27674

Local electron density measurements in low beta plasmas, using nonlinear electromagnetic wave mixing under synchronism condition 13 p2104 A71-27844

Ion and electron probe currents correlation for justification of electrostatic probes use for turbulent plasma diagnostics 14 p2280 A71-30171

- X ray absorption and atomic number corrections in quantitative microprobe analysis of metals 14 p2277 A71-30476
- Plasma drift cyclotron instability feedback stabilization, using immersed modulated electron sources 19 p3111 A71-37636
- Variable Nb composition of meteoritic rutile grains from quantitative electron microprobe analysis 20 p3292 A71-39384
- Sn-Pb alloy solidification point analysis around liquid-solid front with interface visualization by electron microprobe 20 p3238 A71-39416
- Electron microprobe analysis of cavity surface and lip of cosmic dust impact craters in stainless steel plates exposed at 400 km altitude in Gemini S-010 experiment 20 p3299 A71-39652
- Hypersonic turbulent wake density measurements in free flight hyperballistic ranges by electron beam fluorescence probe technique 21 p3363 A71-40389
- Gas density measurement and flow visualization in hypersonic wind tunnel by electron beam probe, noting isobaric boundary layer application 21 p3364 A71-40395
- Electron beam fluorescence probe with modulation technique for measuring density disturbance near sharp wedge in rarefied hypersonic flow 22 p3529 A71-42052
- ELECTRON RADIATION**
NT BETA PARTICLES
NT ELECTRON BEAMS
- Solar radio waves varying component local sources relationship with sunspots development, describing characteristics based on thermal bremsstrahlung and cyclotron/synchrotron fast electrons radiation 07 p1195 A71-19339
- Electron trapping in MIS transistor, discussing thermal annealing process activation energy and trap production by radiation 07 p1076 A71-19499
- Electron radiation bulk damage effects on Si surface barrier detectors, determining reverse leakage current density and alpha particle response changes 08 p1345 A71-21842
- Spectral studies on radiation from molecules, atoms and electrons, demonstrating shock tube applications in opacity measurements 11 p1764 A71-26265
- Thermal control coating materials, measuring separate and combined electron and UV radiation effects on reflectance and emittance in vacuum 11 p1800 A71-26519
- Magnetic shield design for protecting cylindrical space vehicle from space electron radiation, using simulator for engineering data 15 p2500 A71-32042
- ELECTRON RECOMBINATION**
NT RADIATIVE RECOMBINATION
- Coaxial electrodynamic plasma acceleration, investigating triple electron and ion recombinations effects 19 p3108 A71-37129
- Adhesion, recombination and electron-band curvature nomograms for space charge region in photosensitive CdS single crystals 24 p3859 A71-44388
- He ionization and excitation in optically thick solar prominences, considering recombination excitation for observed triplet-level populations at 5000-10,000 K electron temperature 24 p3869 A71-44805
- Microwave detection of anomalous interstellar electron recombination line emission toward W49 A, using radio telescopes 24 p3871 A71-44904
- ELECTRON SCATTERING**
- Plasma beam systems dispersion equation with allowance for electron collisions with heavy particles 01 p0132 A71-10154
- Sasaki effect in doped semiconductors at low temperatures concerning conduction anisotropy and intervalley impurity electron scattering 01 p0139 A71-10777
- Semiconductor with charged impurities in strong electromagnetic field, investigating scattering effects on electron energy spectrum 01 p0140 A71-11463
- Thermionic converter electron-cesium atom momentum transfer collision probability, considering scattering cross sections 02 p0287 A71-12227
- Cs vapor filled cracks breakdown in thermionic triayer insulators, calculating electron reflection and ion recombination kinetics on surfaces 02 p0232 A71-12239
- Fast electron elastic and inelastic scattering Ar plasma at large Rutherford cross section, obtaining charged particle density 02 p0291 A71-12317
- Effective electron collision frequency and RF conductivity along geomagnetic lines in magnetosphere 03 p0377 A71-13272
- Ionospheric electron collision frequency and concentration height distribution during annular solar eclipse of 20 May 1966 03 p0407 A71-13378
- Ionospheric electron production, slowing down and disappearance processes, considering collisions with atmospheric constituents 03 p0417 A71-14072
- Electron collision cascades in braking medium, deriving integral equations for energy structure, displacement and ionization yield 04 p0629 A71-14914
- Locally slowly varying magnetoplasma, determining electron concentration and collision frequency by wave propagation experiment 04 p0633 A71-15034
- Extragalactic radio sources relativistic electrons interaction with cosmic black body radiation, noting effect on sources lifetime and X ray background 04 p0641 A71-15838
- Perturbation theory diagrammatic version for describing lattice vibrations effect on scattering cross sections of low energy electrons from single crystal solid surfaces 05 p0792 A71-16316
- Weakly ionized magnetoplasma waves and instabilities due to effects of electrons parallel, Hall and diamagnetic drifts relative to ions 05 p0789 A71-16653
- High energy electron penetration and scattering in solids, obtaining beam density profiles by polymethyl methacrylate resist exposure 06 p0940 A71-17305
- Electron-ion collision effects on parametric instability growth rate in plasma dynamic stabilization 06 p0934 A71-17477
- Electron scattering out of electron beam in beam plasma, presenting evidence for nonlinear effective inverse mean free path 06 p0935 A71-17485
- Hydrogen-slow electron collision cross sections, calculating Jovian upper atmosphere Lyman alpha and Balmer H alpha emission 06 p0929 A71-17679
- Relaxation time for nitrogen molecule vibration temperature in ionosphere due to thermal electron collisions 06 p0895 A71-18274
- Vertical profile of electron collisions effective frequencies in auroral ionosphere E region 06 p0895 A71-18279
- Coulomb collisions effect on instability of cold and warm monoenergetic electron beams in plasma 07 p1166 A71-18885
- Electron scattering effect on emission and absorption lines in stellar atmosphere, considering primary radiation sources uniform distribution and photosphere radiation transmission through electron atmosphere 07 p1192 A71-19291
- Plasma-electron beam interaction instability transition from absolute to convective in hydrogen tube system at various pressures, considering electron collision effects 07 p1170 A71-20181
- Plasma concentration and heavy particle-electron collision frequency in open cylindrical cutoff resonator based on frequency shift and passband broadening data 07 p1171 A71-20184
- Bogoliubov electronic excitations anomalous scattering and tunneling in superconductor intermediate state, noting pair production one direction step function changes 07 p1181 A71-20207
- Electron-nuclear interactions in ruby by magnetoacoustic double resonance, comparing experimental and theoretical data 07 p1181 A71-20526
- Born-Oppenheimer approximation for elastic and inelastic electron scattering by diatomic molecules 08 p1337 A71-20886
- Two fluid continuum theory of Thomson scattering extended to uniform DC magnetic field and electron drift, finding backscattered power dependent on magnetism 08 p1283 A71-21640
- Quantum mechanical theory of nonrelativistic fast electron backscattering from continuous media, considering scattering cross sections 09 p1496 A71-22236
- Partial wave method for nonspherical quantum scatterer, applying to electron elastic scattering by molecules 09 p1496 A71-22237
- X ray spectrum measurement of Scorpius X-1 by Bragg spectrometer, explaining emission or absorption absence by source model with line weakened by electron scattering 09 p1518 A71-22349
- Electron loss by resonant interaction with whistlers in nonuniform magnetic field, taking Fokker-Planck equation as distribution function 09 p1513 A71-22423
- Compton scattering of relativistic electrons in cosmic plasma waves as source of HF radio emission from metagalactic objects 09 p1521 A71-22926
- Electromagnetic pulse propagation through inhomogeneous plasma, discussing electron collision frequency effects 09 p1504 A71-22987
- Complex alloying of structural steels, stressing structural changes, electron interactions and phase transition changes 09 p1470 A71-23075
- High altitude low latitude aurora, observing intense spectral bands and lines and excitation due to optical resonance, atom- and molecule-electron collisions 09 p1441 A71-23643
- Angular dependence of specularly parameter /probability of specular scattering of electron incident upon surface/ via magnetic field dependence of magnetomorph harmonic oscillations 10 p1655 A71-23771
- Electron-electron interaction effects on electronic states density in electron gas impurity bands, using matrix method 10 p1644 A71-23772
- Electron collision frequency energy dependence influence on electrical conductivity of weakly ionized plasmas, considering Taylor series expansion around probable plasma electron velocity 10 p1623 A71-23875
- Strong interaction between plasma forward wave and electron beam slow wave at equal densities, causing double stream instability nonlinear limitations 10 p1651 A71-24636
- Electron collisional-radiative ionization and recombination rate coefficients, using hydrogenic plasma model with resonance radiation trapping 10 p1653 A71-24672
- German monograph on absorbed anions effect on Ni and Ni-Mo alloys anodic behavior covering temperature dependence, electrons interaction, sulfide ions activation and magnetic properties 10 p1628 A71-24874
- Broadened energy distributions in electron beams, discussing energy spread delta E and C prime values relationship for studying weak Coulomb interactions 11 p1802 A71-25631
- Impurity lifetime broadening due to scattering at Fermi surfaces, calculating Dingle temperature in noble metals 11 p1808 A71-26145
- Transverse electromagnetic wave penetration in semibounded plasma with specular electron reflection 12 p1878 A71-26958
- Anomalous resistance and turbulent heating of strongly nonisothermal plasma in strong magnetic field due to electron scattering by ion-acoustic turbulent pulsations beats 12 p1936 A71-27032
- Proton form factors and radius determination from experimental data analysis of cross sections of electron scattering by protons over wide transferred-momentum range 12 p1901 A71-27180
- Plasma in strong electric and magnetic field with allowance for inelastic electron collisions with neutral particles, showing resonant oscillations from Born approximation 12 p1937 A71-27183
- Weakly ionized plasma instabilities in high frequency field exceeding electron collision frequency, considering waves parametric excitations 12 p1937 A71-27204
- Deuterium gas breakdown by ruby laser, using quantum kinetic equation for electron interactions with molecules and photon field 12 p1915 A71-27284
- Pitch angle distribution effects of auroral electrojet on scattering and absorption of fast precipitated electrons in upper atmosphere, using computerized Monte Carlo technique 13 p2119 A71-27794
- N-type germanium Seitz coefficients relationship based on anisotropic electron scattering theory 13 p2110 A71-27958
- Electron-hole scattering effect on carrier heating and I-V characteristics in semiconductors, using relaxation time and self consistent analysis 13 p2111 A71-28921
- Carrier scattering related to orbiting and resonance states in screening impurity donor center of weakly doped homeopolar n-type semiconductor under injection 13 p2112 A71-28928
- Electron scattering effects on spectral emission at optical and X ray wavelengths for homogeneous spherical ionized hydrogen plasma cloud, discussing radiation transfer 14 p2297 A71-29592
- Electron production by proton impact on nitrogen, oxygen, neon and argon, measuring cross sections angular and energy distribution by electrostatic analysis and electron counting 14 p2277 A71-30660

Dispersive effect on bremsstrahlung radiation from electron atom collisions in weakly ionized plasma, using Boltzmann transport equation
15 p2456 A71-31850

Microwave probing of electron number density and collision frequency in slightly ionized plasmas
15 p2458 A71-32395

Conductivity measurement of shock generated nitrogen plasma in transverse magnetic field, considering vibrationally excited molecules role in electron collision frequency
16 p2616 A71-32899

Electron lifetime in earth radiation belt due to resonant scattering with hiss VLF radiation
16 p2626 A71-33674

Energetic electrons pitch angle scattering during magnetic storms due to resonant interaction with proton generated Doppler shifted ion cyclotron waves
16 p2574 A71-33972

Inelastic electron scattering cross sections and energy spectra from Al and Au targets, using magnetic analyzer with high resolution detector
16 p2614 A71-34042

Homogeneous spherical hot hydrogen plasma cloud at various temperatures and optical depths, presenting electron scattering effects on optical and X ray spectral emission
18 p2951 A71-36012

Electron concentration and collisions number fluctuations effect on D region profiles based on radio waves partial reflection data
19 p3057 A71-38365

Weakly ionized plasma instabilities in high frequency field exceeding electron collision frequency, considering waves parametric excitations
19 p3117 A71-38616

Atmospheric gases effective electron collision frequency calculations, using momentum transfer cross sections
20 p3271 A71-38743

Integrodifferential difference equation for isotropic portion of velocity distribution function resulting from electron excitation and Coulomb interaction
20 p3274 A71-39048

Schottky barrier diodes as photodetectors in hot electron mode, deriving ballistic transport model for scattering mechanisms effects
20 p3236 A71-39191

Mars ionosphere radio wave absorption integral coefficients, studying electron concentration and electron/gas molecular collisions frequency vertical profiles
20 p3297 A71-39629

Vela pulsar interstellar scattering, studying pulse broadening, rotation measure and radiation origin near magnetic pole
20 p3303 A71-39937

Cosmic plasma electron thermal motions effects on cosmic electromagnetic absorption, taking into account electron-electron collision effects in electromagnetic waves dispersion relationships
21 p3442 A71-40162

Quantum mechanical theory of nonrelativistic fast electron backscattering from continuous media, considering scattering cross sections
21 p3419 A71-41118

Partial wave method for nonspherical quantum scatterer, applying to electron elastic scattering by molecules
21 p3420 A71-41119

Electron elastic scattering in thin films by impurities, noting conductivity dependence on film thickness
21 p3428 A71-41126

HF electric field influence on collisionless electron gas acoustoelectric effect, emphasizing electron scattering mechanism
21 p3431 A71-41232

Temperature and velocity dependence of electronic dislocation stopping power in superconductor due to scattering of normal electrons
21 p3432 A71-41268

Electron-hole scattering effect on carrier heating and I-V characteristics in semiconductors, using relaxation time and self consistent analysis
21 p3433 A71-41308

Carrier scattering related to orbiting and resonance states in screened field of impurity donor center in weakly doped homeopolar n-type semiconductor under injection
21 p3434 A71-41331

N-type germanium Seitz coefficient relationship based on anisotropic electron scattering theory
21 p3436 A71-41347

Electron scattering magnetic impurities effect in insulator layer of tunnel junction on superconductor current
22 p3585 A71-41818

Beam electrons correlations effect on interference fringes visibility
22 p3546 A71-42243

Proton form factors and radius determination from experimental data analysis of cross sections of electron scattering by protons over wide momentum transfer range
22 p3578 A71-42454

Plasma in strong electric and magnetic field with allowance for inelastic electron collisions with neutral particles, showing resonant oscillations from Born approximation
22 p3584 A71-42460

Interplanetary electron associations with type 3 solar bursts, using decametric OGO 3 and solar geophysical observations
23 p3721 A71-43176

Boltzmann kinetic equation with electron-electron collision coefficients for isothermal weakly ionized cesium-argon plasma, using nodal point method
23 p3709 A71-43267

Total and momentum transfer cross sections for low energy electron scattering by atomic and diatomic molecules
23 p3707 A71-43898

Experimental techniques for differential, total and momentum transfer electron-molecule scattering cross sections at low electron energies, discussing rotational excitation
23 p3707 A71-43899

Metagalactic X ray and cosmic electrons power spectra explanation by electron acceleration and scattering in turbulent plasma with frozen-in magnetic field
24 p3865 A71-44568

Wave field pulsations induced electron scattering as factor modifying excited plasma electron distribution function
24 p3855 A71-44668

Electron beam and plasma nonlinear interactions, noting scattering zone, amplitude oscillation maximum, longitudinal velocity and relaxation patterns
24 p3856 A71-45097

Magnesium diatomic metal static and dynamic properties, using multiple electron and ion analysis system
24 p3839 A71-45118

ELECTRON SOURCES

Solar proton and electron events from viewpoint of particle acceleration and magnetic field configuration in active region
03 p0478 A71-14036

Forward/reverse drift pair bursts relation to decameter type 3 solar radio emission, postulating existence of electron acceleration sources in upper corona
15 p2485 A71-31714

Hydrazine formation from ammonia in constricted plasma discharge using electron source in selected high energy range
18 p2955 A71-35968

Solar prompt and delayed discrete particle events, discussing proton and electron sources, distribution and flare association
19 p3126 A71-37624

Microchannel plates detection efficiency for 2-150 keV electrons from C 14 pellet and electron gun
24 p3829 A71-45336

ELECTRON SPIN

Rare earth alloys spin disorder resistivity in crystalline electric field absence and presence
04 p0637 A71-15797

Plasma echo and spin echo holoforms for electrical signals temporal sequence recording and cued playback, noting human brain memory function analogy
05 p0787 A71-16451

Coulomb impurity centers in paramagnetics and ferromagnetics at Curie temperature with spin-electron exchange interaction
09 p1508 A71-22881

Electron velocity, spin, energy and mass derivation based on consideration as negative component of photon
13 p2103 A71-29277

Optical pumping and detection of spin polarized electrons created in p-type GaSb conduction band by excitation with light
17 p2791 A71-35583

Tunable spin-flip magneto-Raman IR laser, describing indium antimonide scattering, tuning range and applications
22 p3557 A71-42133

Ferromagnetic electron spin resonance spectra of Apollo 11 lunar samples, using model for polycrystalline spectra simulation
23 p3734 A71-43242

ELECTRON SPIN RESONANCE

U ELECTRON PARAMAGNETIC RESONANCE

ELECTRON STATES

Electron states in highly doped semiconductors, describing energies in conduction and forbidden bands
02 p0297 A71-12616

Semiconductors isoelectronic impurity states, using semiempirical delta-potential method to calculate bonding energy for GaP containing nitrogen as impurity
07 p1175 A71-19220

Ground state energy approximate eigenvalues calculation for electron in stationary finite electric dipole field by variational approach
07 p1163 A71-19684

Diatomic molecules nonsigma states rotational excitation adiabatic theory
07 p1164 A71-19695

Rayleigh-Schrodinger perturbation energies for ground state of two electron atomic Hookes law model through tenth order
11 p1803 A71-26150

UV photoemission measurements on hexagonal ZnO cleaved in vacuum, determining Zn 3d states ionization
17 p2791 A71-34805

Hydrated electrons photoexcitation by giant pulses Q-switched ruby laser, investigating absorbency over wide range of light intensities
17 p2753 A71-34950

Lande g factors measurement of excited electronic states in Ne 20 II and III, using alignment of radiating particles in beam foil light source
18 p2949 A71-35970

CN radical red system molecular constants, considering degenerate perturbation effects in shifts between electronic states
19 p3106 A71-37405

Unpaired electrons and oxygen adsorptive capacity of clean lunar rock and soil surfaces, noting decrease of uptake rate at one monolayer coverage
23 p3764 A71-43798

Supersonic Ar, He and molecular nitrogen jets, determining electron temperature and concentration and atomic state population in shock waves region by spectroscopic measurement
23 p3712 A71-43916

ELECTRON SWEEPING

U SWEEP FREQUENCY

ELECTRON TELESCOPES

U PARTICLE TELESCOPES

ELECTRON TEMPERATURE

U ELECTRON ENERGY

ELECTRON TRAJECTORIES

Interplanetary plasma electron density inhomogeneities formation explained by instability due to electron stream curvilinearity obtained from spacecraft data
09 p1518 A71-22435

Parallel plate electrostatic analyzer design, discussing second order focusing, angular aberrations and magnification
12 p1903 A71-26570

Low density plasma-double gridded antenna system for ion and electron signal propagation studies, observing multiple reflections of acoustic and ballistic pulses and bulk phenomenon
12 p1935 A71-26913

Quasi-classical ionization model under assumption of straight-line electron trajectories, presenting Hamilton-Jacobi equations solution
12 p1932 A71-27241

Reflex klystron repeller space analysis of potential distribution, electron trajectories, transit time and admittance, taking into account space charge effect
17 p2713 A71-34432

Nonlinear M-type traveling wave tube equations for large signal mode, discussing electron trajectories
22 p3521 A71-42263

ELECTRON TRANSFER

Electron transfer in ion microscope field ionization, analyzing band and periodic surface structure effects, ionization probability and collision formalism
02 p0288 A71-12734

Ionospheric photoelectron exchange at magnetic conjugates, considering electron density and impact ionization by inelastic collisions
03 p0408 A71-13381

Hall effect, conductivity, thermal emf and Nernst-Ettingshausen transfer in n-type highly doped compensated GaAs
03 p0466 A71-13398

Solid state transferred electron broadband amplifiers in electronic countermeasure memory systems for radar pulse replica retransmission, comparing with low noise traveling wave tubes
04 p0558 A71-15361

Transferred electron devices (TED), reviewing physics of transferred electron effect, theory and design of amplifiers and oscillators
07 p1072 A71-19102

Compact microwave circuits for high efficiency operation of high power transferred electron oscillators
07 p1072 A71-19107

Nonadiabatic H-H collisions cross sections in two state time dependent impact parameter approximation, including electron exchange
08 p1337 A71-21193

Transferred electron bulk negative differential conductivity devices, analyzing combined doping and geometry effects on space charge and domain dynamics
09 p1507 A71-22250

Electron transfer bulk oscillators negative conductivity as function of geometry, field and doping nonuniformities, using computerized simulation for device frequency-voltage characteristics
09 p1417 A71-22689

- Ni-Mo alloys electron transfer and ion diffusion at high temperatures 09 p1471 A71-23077
- Electron exchange and nuclear symmetry for 2s and 2p collisional excitations of hydrogen by H atom based on symmetrized atomic orbitals set 10 p1644 A71-23925
- Transferred electron microwave oscillators high efficiency operation mode with more severe limitation than limited space charge accumulation mode 14 p2215 A71-30826
- Correlation coupling matrix elements for one electron transfer and ion-ion recombinations in Landau-Zener calculations 18 p2948 A71-35839
- Transferred electron /Gunn/ amplifiers and oscillators for microwave applications, considering electronic and mechanical tuning over large frequency ranges 18 p2894 A71-36977
- Semiconductor device with stable negative conductance over wide range of microwave frequencies and power levels, using transferred electron effect in epitaxial GaAs 18 p2895 A71-36985
- Interference of transferred electron device operation involving harmonic tuning, considering EMC aspects 19 p3032 A71-38461
- Electron drag by photons during intraband light absorption by free carriers in n-Ge semiconductors 21 p3428 A71-41111
- Multilayer epitaxial InP transferred electron microwave oscillator I-V characteristics and frequency dependence on layer thickness 23 p3649 A71-42912
- Electron transport chain of extremely halophilic bacteria, investigating cytochrome oxidase activity dependence on pH 23 p3633 A71-43525
- Electron transfer cross sections for low energy negative oxygen ion collisions with oxygen molecules measured by single-collision beam technique 23 p3707 A71-43930
- ## ELECTRON TRANSITIONS
- Collision induced homonuclear diatomic molecules vibrational excitation using three dimensional model, obtaining transition cross sections and relaxation rates as function of temperature 01 p0129 A71-10367
- LF EM wave absorption in disordered semiconductors, calculating frequency dependence of conductivity due to electron transitions between discrete local levels 02 p0297 A71-12618
- Wall shift measurement of unperturbed hydrogen hyperfine transition frequency against cesium reference 04 p0585 A71-14652
- Ne, Ar, Kr and Xe ionized states transition and level lifetimes from photographically recorded beam foil spectra, discussing particle energies 04 p0629 A71-14805
- Laser action in visible and near IR on atomic fluorine transitions based on collisional dissociation of hydrogen fluoride 04 p0608 A71-15040
- Transition radiation generation zones, determining physical cause 05 p0786 A71-17030
- Halogens atomic transition probabilities spectroscopic measurements in visible and near IR spectra, using gas driven shock tube 07 p1163 A71-19685
- Atomic processes in plasmas including excitation, deexcitation, ionization, recombination, charge transfer, free-free transitions and spectral line broadening for theta pinch parameters determination 07 p1172 A71-20505
- Multiple valued Sasaki effect concerning electron transitions in multivalley Ge semiconductors 07 p1181 A71-20537
- O I and II resonance transitions radiative lifetimes in vacuum UV, using beam foil method 10 p1676 A71-24501
- Sunspots forbidden Fe I lines, calculating magnetic dipole and electric quadrupole transition probabilities 11 p1830 A71-26112
- Solar X-ray and radio fluxes at earth for high order temperatures by free-free transitions and Maxwell electron velocities in corona 12 p1947 A71-26770
- Laser designs with thermal pumping, obtaining electron states phototransition probability, cooling rates for population inversion and laser action threshold for diatomic gas molecules 12 p1914 A71-27029
- Nitrogen dioxide ground and excited state self consistent fields energy calculations, discussing electron transitions probable assignments in spectrum 12 p1934 A71-27759
- Monograph on carbon dioxide laser gain observations covering spectroscopy, energy levels, radiative transitions, molecular collisions, power efficiency, etc 13 p2078 A71-28494
- Interstellar SH search for ground state main line transitions at 111 MHz 14 p2313 A71-30433
- Benzene, benzene-d sub 6 and sulfur dioxide radiative lifetime measurement comparison, investigating internal conversion behavior 14 p2190 A71-30570
- Solar corona visible lines, indentifying V VI to Fe IX electron transitions with variable inductance three electrode spark source 14 p2314 A71-30650
- CW laser transitions in Se II, investigating current saturation behavior and output power and structure 15 p2422 A71-32581
- Ca, Mg, B and Al prominent resonance transitions radiative lifetimes and absolute oscillator strengths 15 p2452 A71-32596
- Nitrogen beam foil spectrum analysis, calculating transitions and decay times 15 p2452 A71-32598
- Multiply ionized Ar excited valency and inner shell transitions, investigating emission spectrum and energy levels 15 p2368 A71-32747
- OH emission column density upper limit from rocket-borne UV spectrometer measurement of resonantly scattered sunlight intensity in electronic transition vibrational band 16 p2574 A71-33967
- Na and K transition oscillator strengths, noting core polarization effects on mathematical model 16 p2615 A71-34088
- Population inversion damping on vibrational-rotational transitions of carbon dioxide molecule during interaction with monochromatic radiation pulse, using two level model 17 p2752 A71-34387
- Ab initio calculations on trajectories and nonadiabatic transitions in reactions of hydrogen atomic ions with hydrogen molecules 18 p2949 A71-35897
- Wavelength prediction for coronal transitions at various atomic configurations, deriving semiempirical expressions from observed data for energy level intervals determination 18 p2965 A71-36733
- Mode selection of transition frequencies in carbon dioxide laser with Fabry-Perot interferometer in resonator 19 p3073 A71-37790
- Integrated absorption coefficient of pressure induced pure rotational and vibrational transitions in binary collisions of homonuclear diatomic molecules at high temperatures 19 p3108 A71-38719
- Carbon dioxide lasers, covering molecular structure, IR spectra and laser transitions, population inversion mechanisms, gas discharge and longitudinal flow 20 p3243 A71-39067
- Low vibrational level CO transitions of flowing electrochemically excited liquid nitrogen cooled helium-air-methane-carbon monoxide laser in Q switched operation 20 p3244 A71-39100
- Reversible electron transitions selection rule in diatomic molecules excitation by electron impact, obtaining differential cross sections 21 p3417 A71-40198
- Methyl alcohol transitions in Orion at 1 cm noting emission source coincidence with IR nebula 21 p3447 A71-40445
- Millimeter emission lines from interstellar methyl cyanide transitions, noting kinetic temperature and hydrogen density 21 p3447 A71-40446
- Interstellar carbonyl sulfide transition at 109.5 GHz, noting column density 21 p3447 A71-40447
- Electronic transitions in oxygen molecule due to ion impact from kinetic energy loss spectrum 21 p3418 A71-40886
- He-Cd CW laser transitions, describing charge exchange and Penning ionization-excitation processes 21 p3393 A71-41038
- Electron transitions between excited states of donors in Ge, investigating photoconductivity in 500-1300 micron band 22 p3585 A71-41817
- Formaldehyde transitions in ground and excited states at 6 cm, attaining line widths and hyperfine structure at 1-3 kHz 23 p3723 A71-42953
- H transition excitation during atomic hydrogen collision with alkali elements and inert gases, discussing inner electron excitement 23 p3707 A71-43268
- Carbon dioxide absorption temperature dependence in 1750-1200 A region, calculating electron densities and transition moments 23 p3641 A71-43326
- Time dependent progress of vibrational rotational transitions in chemical laser using hydrogen-fluorine mixture investigated by oscillography with IKM-1 monochromator 23 p3684 A71-43405
- Dynamic carrier density instabilities for semiconductor-metal electronic phase transition by Frenkel-Poole effect in seminsulator with donors 23 p3716 A71-43478
- B stars spectra, calculating C III ions spontaneous electric dipole transitions and oscillator strengths in vacuum UV region 23 p3767 A71-43829
- Sgr B2 region interstellar gas microwave emission spectrum, observing inversion transitions in metastable rotational levels of ammonia 24 p3872 A71-44916
- ## ELECTRON TUBES
- NT CAMERA TUBES
- NT CATHODE RAY TUBES
- NT IMAGE DISSECTOR TUBES
- NT IMAGE ORTHICONS
- NT MICROWAVE OSCILLATORS
- NT ORTHICONS
- NT RETURN BEAM VIDICONS
- NT VACUUM TUBE OSCILLATORS
- NT VACUUM TUBES
- NT VIDICONS
- Electron tubes for radars, discussing history and development of magnetrons, Thomson-CSF display tube and power amplifiers 06 p0874 A71-17568
- Re based W alloys for electronic tube hot cathodes, discussing reduction and annealing effects on mechanical and plastic properties 07 p1140 A71-20238
- Plasma anode tube in metal-ceramic envelope with improved capabilities for electron emission studies, considering movable Langmuir probe 11 p1806 A71-25902
- High power microwave CW tubes and power amplifier requirements for communication satellites 18 p2892 A71-36571
- Electronic component products improvement history, discussing electron tubes, future trends and reliability 19 p3027 A71-37345
- ## ELECTRON TUNNELING
- Electron tunneling through interfaces of MIS structures, calculating conductance and current characteristics 01 p0140 A71-11413
- Tunneling in boron doped p-type silicon metal-semiconductor and MIS tunnel junctions 04 p0636 A71-14973
- CaAs Schottky tunnel junctions properties and bias independent structure evaluation by excess noise generation 06 p0940 A71-17312
- Bogoliubov electronic excitations anomalous scattering and tunneling in superconductor intermediate state, noting pair production one direction step function changes 07 p1181 A71-20207
- Numerical method for computing exact permeability /tunneling probability/ of one dimensional potential barrier 11 p1728 A71-26059
- Josephson and IC type superconducting tunneling junction neuristor devices performance tests, presenting bibliography 15 p2377 A71-32317
- Tunnelling conductance anomaly in metal-insulator-metal junctions containing paramagnetic impurities, analyzing I-V characteristics during switching effect 18 p2954 A71-36802
- Electrons interaction with impurities and longitudinal optical phonon in metal-insulator- semiconductor tunnel junctions 19 p3119 A71-37869
- Avalanche Si photodiode current pulse formation frequency governing mechanism, considering roles of free carriers and electron tunneling 21 p3358 A71-41344
- Nonequilibrium negative bias effects on n-type metal oxide semiconductor tunnel currents 24 p3812 A71-45356
- ## ELECTRON-ION RECOMBINATION
- NT RADIATIVE RECOMBINATION
- Nonequilibrium Ar-Cs plasma under rectangular pulse overvoltage, analyzing ionization and recombination kinetics 02 p0289 A71-12177
- Electron-ion recombination in dense molecular gas, presenting semiquantitative method for hydrogen, nitrogen, carbon dioxide and damp gas mixtures 05 p0785 A71-16726
- Air and oxygen electron-ion recombination coefficients, considering plasma deionization rate 05 p0756 A71-17208
- Ion-electron recombination coefficient measurement for ionized trails left by rocket exhausts in high atmosphere using radio observation 06 p0895 A71-18314
- Electron collisional-radiative ionization and recombination rate coefficients, using hydrogenic plasma model with resonance radiation trapping 10 p1653 A71-24672
- Li photoionization cross sections determined from spectral intensity measurements as function of

threshold wavelength, discussing radiative electron-ion recombination into first excited state

10 p1646 A71-24992

Numerical integration of unsteady continuity equation for electron-ion gas concentration distribution in F2 region

11 p1757 A71-25770

Air and oxygen electron-ion recombination coefficients, considering plasma deionization rate

13 p2067 A71-28263

Nonequilibrium Ar-Cs plasma under rectangular pulse overvoltage, analyzing ionization and recombination kinetics

15 p2454 A71-31486

Plasma decay due to charged particles recombination, linearizing nonlinear equations describing diffusion of singly ionized two-component gas undergoing recombination

15 p2456 A71-31999

Steady state partially ionized monatomic gas expansion from sonic orifice, investigating electron-ion recombination effects on flow properties

15 p2457 A71-32101

Electron-ion recombination and ambipolar diffusion disruption of electron density in cryogenic helium plasma, using cavity resonator measurements

16 p2619 A71-33648

D region winter anomaly causes from coordinated rocket measurements, discussing electron density profiles and electron-ion recombination

17 p2731 A71-34315

Langmuir probe measurement of ionization density of Ar plasma jet, suggesting electron-ion recombination in probe vicinity

17 p2789 A71-35338

Numerical integration of unsteady continuity equation for electron-ion gas concentration distribution in F2 region

22 p3532 A71-41538

Carbon ion and free electrons three body recombination rate coefficient measurement in carbon monoxide flows

24 p3802 A71-44607

ELECTRONIC AMPLIFIERS

U AMPLIFIERS

ELECTRONIC CONTROL

Aircraft flaps and ailerons actuators electronic fly by wire control as alternative to mechanical linkages for maneuverability and reliability in flight

01 p0006 A71-10825

Relay type pulsed control systems performance, determining noise effects by statistical analysis

06 p0879 A71-17927

Aircraft electronic control systems, considering hydraulic servocontrol, force simulation and reliability models

07 p1156 A71-20064

Equatorially mounted parabolic reflector radio telescope, discussing structural design, mechanical drives and electronic control system

08 p1271 A71-21152

Automatic control circuits for millimeter wave backward wave tube frequency tuning and supply voltage regulation

08 p1267 A71-21804

High temperature thermal null strain gage with sensing unit and electronic control unit to measure mechanical strain in terms of induced thermal strain

09 p1445 A71-22721

ATC electronic automation systems development for air safety improvements

09 p1491 A71-22953

Quasi-point type radar target angular motion simulation by controlling electromagnetic wave phase front in receiving field

14 p2193 A71-29825

Total and vapor pressure sensing and hybrid analog/digital electronic controller for multiburn cryogenic spacecraft propulsion pressurization [AIAA PAPER 71-647]

14 p2290 A71-30724

Multiple planar Luneberg lens circular array for airborne electronically scanned X band narrow beam antenna mounted under aircraft nose or fuselage

14 p2216 A71-31038

High speed electronic phase and frequency scanned linear, static fed and monopulse arrays element and angular error analysis

14 p2205 A71-31049

Steady state and transient performance of Brayton cycle alternator and electronic controls for space power

15 p2355 A71-32215

Discreet communication satellite system for air traffic control and navigation, discussing aircraft antenna beam electronic scanning by computerized control

17 p2714 A71-34681

Optical telescopes automatic electronic control by positioning mechanical axis to specified coordinates and tracking guide star

17 p2740 A71-34983

Integrated telescope computer system, including magnetic disk storage, digital encoding, drive control and automatic guiding

17 p2711 A71-34984

Information display device with electro-optical system for discrete deviation of monochromatic linearly polarized light beam, analyzing electronic control circuits energy characteristics

18 p2884 A71-35880

Aircraft electronic or fly by wire control systems, discussing aircraft design fuel-structure weight reduction cycle and control system redundancy requirements

[AIAA PAPER 71-959]

19 p3099 A71-37200

Glass switching elements with storage properties for electronically controlled flip-flop circuitry, noting composition and fabrication

21 p3355 A71-40742

Dye laser electronic tuning by inserting calcium-molybdenum oxide acousto-optic filter into cavity

23 p3687 A71-44137

ELECTRONIC COUNTERMEASURES

NT CHAFF

Electronic warfare technology, discussing airborne platforms, battlefield surveillance, jamming devices, homing and warning systems

04 p0557 A71-15019

Deception repeaters for erroneous information transmission to radar, considering echo signal level, burnthrough, target size, sensitivity, gain and bandwidth

04 p0555 A71-15359

Solid state transferred electron broadband amplifiers in electronic countermeasure memory systems for radar pulse replica retransmission, comparing with low noise traveling wave tubes

04 p0558 A71-15361

Emitter location techniques for airborne passive ECM, discussing accuracies in terms of geometry, sample number, random and bias errors

15 p2375 A71-31205

Airborne ECM receiver, determining conditions for detecting victim radar signal before signal reflection from aircraft

15 p2368 A71-31207

ELECTRONIC EQUIPMENT

NT AVALANCHE DIODES

NT CRYOTRONS

NT CRYSTAL RECTIFIERS

NT ELECTRONIC FILTERS

NT ELECTRONIC MODULES

NT ELECTRONIC PACKAGING

NT ELECTRONIC RECORDING SYSTEMS

NT ELECTRONIC TRANSDUCERS

NT FIELD EFFECT TRANSISTORS

NT GALLIUM ARSENIDE LASERS

NT GERMANIUM DIODES

NT JUNCTION DIODES

NT JUNCTION TRANSISTORS

NT METAL OXIDE SEMICONDUCTORS

NT MICROMODULES

NT MIS [SEMICONDUCTORS]

NT NEURISTORS

NT PARAMETRIC DIODES

NT PHOTODIODES

NT PHOTOVOLTAGE CELLS

NT RUBY LASERS

NT SEMICONDUCTOR DEVICES

NT SEMICONDUCTOR LASERS

NT SILICON TRANSISTORS

NT SOLID STATE DEVICES

NT SOLID STATE LASERS

NT THERMISTORS

NT THYRISTORS

NT TRANSISTOR AMPLIFIERS

NT TRANSISTORS

NT VARACTOR DIODES

NT VARISTORS

Algorithm for nonstationary thermal regime of electronic equipment using heat balance method for variation in thermal coefficients and source power

01 p0052 A71-10536

Electronic components - IEEE-EIA Conference, Washington, D.C., May 1970

01 p0053 A71-10731

Electronic circuit analysis using parametric reliability criteria based on progressive failures, applying statistical computerized simulation method

02 p0230 A71-11840

Aeronautical electronic equipment, discussing static transformer, radiotelephone sets, angle of approach meter, etc

03 p0383 A71-13018

Electronic equipment shielding against spurious signals, determining minimum metal thickness for desired effectiveness based on transmission line theory

03 p0383 A71-13178

Computer algorithm for state variables equations used in linear and nonlinear, active and passive electronic circuits analysis

03 p0389 A71-13807

Electronic time scale converters for frequency synthesizers

04 p0592 A71-14861

Optoelectronic signal transfer from rotating shafts to stationary equipment without rubbing contacts

05 p0723 A71-16973

Delta booster second stage packaged attitude control three-axis system, discussing electronic implementation for gyroscopic action control

05 p0818 A71-17138

Reliability evaluation for electrical connectors used in electronic equipment based on probability and environment considerations

07 p1076 A71-19555

Satellite electronic equipment reliability engineering, considering circuit and system design, components screening, assembly and test procedures and quality assurance plans

07 p1207 A71-19563

Electronic equipment reliability prediction, considering confidence limits

07 p1077 A71-19566

Power station electronic control equipment and integrated circuit computer reliability data analysis, emphasizing combined mathematical prediction and observation

07 p1077 A71-19565

Fluidic/electronic pressure ratio computer prototype, using two free jets interaction for instrument error reduction

07 p1031 A71-20603

Soviet book on spacecraft motion parameters measurements accuracy covering electronic systems error sources and reduction in design and data processing

08 p1251 A71-20675

Avionics for gliders and touring aircraft, considering safety and VHF radio equipment

08 p1261 A71-20684

Electronic equipment for measuring resonant frequency drift during slow wave structure impedance measurements, considering mean square errors

08 p1264 A71-21073

Avionics for gliders and touring aircraft, surveying available electronic equipment for 1971

08 p1294 A71-21768

Electronic digital automatic defect indicator attachment to industrial echo defectoscope

08 p1300 A71-21897

Thermal field calculation theory for complex shape electronic devices

09 p1414 A71-22185

IC quality control by temperature fields contactless measurement, using microthermographs

09 p1450 A71-22894

Cartographic characteristics and applications of airborne radar sensors, stressing synthetic aperture radar and electronic techniques and equipment

09 p1452 A71-23211

Electronic ergometer calibration equipment and errors at high work loads

09 p1401 A71-23373

Electronic apparatus isolating temporal segments from spoken syllable for speech analysis

09 p1408 A71-23383

Electronic imaging devices specifications, emphasizing real time reconnaissance systems performance requirements

10 p1609 A71-24059

Pressure vessel method improvement by electronic equipment application in determining data characteristics for propellant powders ballistic properties

10 p1696 A71-24447

Airborne electronics reliability testing in temperature controlled chamber

10 p1589 A71-24604

Life tests and properties of organic working fluids heat pipes for electronic component cooling [AIAA PAPER 71-408]

11 p1856 A71-26203

Automated facility for electronic equipment production reliability environmental testing, discussing human engineering and test and failure mode designs

11 p1746 A71-26512

Particle impact noise detection of loose particles in electronic component cavities, discussing implementation, cost savings and reliability improvement

12 p1884 A71-26659

Equivalent circuit concepts in diagnostic metrology as converging logical-physical process, stressing electronic failure analysis

12 p1890 A71-26666

Electronic communication system critical design evaluation, concerning electromechanical components and packaging impact on overall reliability and cost

12 p1878 A71-26688

Experiment planning in electronic component design and microelectronics, using mathematical theory for optimal strategies

12 p1885 A71-26712

Avionics growth, discussing use of digital computers, solid state transducers, integrated circuits, electronic flight instruments, area navigation and collision avoidance systems

12 p1906 A71-26878

Waveform and spectral analysis program for electronic system designs, discussing fast Fourier transform modular staging and noise control applications

12 p1884 A71-27148

Cosmic ray muon flux at sea level, allowing for showers, multiple scattering, straggling, zigzag motion

- tion, detector efficiency and electronic equipment dead time 12 p1952 A71-27403
- Communication electronic equipment electromagnetic compatibility characteristics derived from spectrum signature data, discussing application to systems design 13 p2032 A71-28876
- Electron device techniques - IEEE Conference, New York, September 1970 14 p2214 A71-30700
- Electronically scanned circular array elements number in receiver design, discussing gain distribution 14 p2206 A71-31072
- Sounding rockets, outlining experimental missions, design and payload varieties, auxiliary systems and electronic equipment 15 p2499 A71-31213
- Small digital computers applications to astronomical electronic instrumentation systems of microphotometry and spectroscopy 17 p2743 A71-35010
- Soviet book on algorithms for electronic circuit analysis covering linear and nonlinear transistor or tube circuits matrix-topological description and frequency-time domain solutions 17 p2717 A71-35219
- Electronic circuit system for IR astronomy, describing noise figure, linearity and frequency response 17 p2744 A71-35229
- Electronic and hydraulic devices for communication satellite ground station steerable antenna servocontrol, driving and pointing, discussing tracking error signals 17 p2724 A71-35511
- Communication satellite ground station equipment modifications for second station compatible with Intelsat 3 17 p2709 A71-35519
- Impedance variations vs electrophysical properties of epitaxial and diffusive semiconductor structures for electronic equipment, applying microwave fields for parameter control 18 p2954 A71-35874
- Computer program formulation of equations of state of electronic circuits, using state variable method with mixed coordinate basis 18 p2896 A71-35883
- Computer algorithm determining transfer function of linear electronic circuit in autonomous quadrupole form with zero initial conditions 18 p2887 A71-35884
- Electronic time delay fuses with high-g components for gun launched projectiles for placing payloads at high altitudes 18 p2851 A71-36281
- Electronic component products improvement history, discussing electron tubes, future trends and reliability 19 p3027 A71-37345
- Automatic ATC display systems, discussing electronic flight progress strip for telemetry reproduction 19 p3102 A71-38300
- Environment, coupling and electronic equipment modeling for electromagnetic compatibility analysis 19 p3031 A71-38440
- Interference voltage prediction model of induced noise in reference ground of electronic systems 19 p3031 A71-38448
- Single point grounding of electronic system providing personnel safety and voltage reference potential 19 p3032 A71-38451
- Criterion selection and minimum margin search for optimization of complex electronic circuit parameters described by mathematical models 19 p3039 A71-38503
- Electronic components - Conference, Washington, D.C., May 1970 19 p3035 A71-38535
- Power conditioning electronics for integrally regulated and controlled high voltage solar array spacecraft power system, increasing reliability and reducing weight 20 p3181 A71-38942
- Book on electronic components covering radio, cathode ray and microwave tubes, telecommunication, ceramic materials, light conversion to electricity, integrated circuits, etc 20 p3205 A71-39775
- Gunn effect devices properties and applications, discussing microwave energy sources tunable and local oscillators, parametric amplifier pumps and radar transmitters 21 p3357 A71-40819
- Electronic and electrical systems optimization effectiveness through generation of statistical priorities 22 p3525 A71-41438
- Algorithms for calculating temperature fields of electronic devices on computers, considering solid body in shape of bounded cylinder 22 p3519 A71-41442
- Computer-aided statistical analysis correlation method for prediction of electronic circuit component part variability effects on performance and reliability 22 p3517 A71-42102
- Computerized reliability optimization system program for electronic equipment design and management methods to achieve high reliability and low cost 22 p3517 A71-42105
- Validity study of mathematical models representing failure rate variations of electronic components, considering thermal and electrical stresses 22 p3517 A71-42109
- Electronic imaging systems - Conference, Palo Alto, California, April 1970 22 p3547 A71-42502
- Book on electronic aids for navigation systems for marine and aerospace transport operation covering measuring and display instruments, radio wave properties, etc 23 p3702 A71-43225
- Conventional components in hybrid circuits, using leadless inverted device, SOT-23 transistor and multilayer ceramic capacitors 23 p3655 A71-43349
- Electronic optical astronomy, describing image detectors and computer controlled microphotometers and telescope setting systems 23 p3678 A71-43542
- Integrated system for aircraft control and operation with visualization and manual regulation techniques, emphasizing interconnections with onboard electronic equipment 24 p3791 A71-44353
- All-electronic synchro-digital converter design using hybrid tracking mode circuit 24 p3811 A71-45298
- ELECTRONIC EQUIPMENT TESTS**
- Hybrid microcircuits reliability, discussing test data regarding receiving and sample inspection, environmental and performance testing, etc 01 p0053 A71-10733
- Field tests for telemetry receiving systems solar calibration, describing antenna pointing 01 p0033 A71-10891
- Test laboratory for Skynet spacecraft communications subsystems at microwave frequencies 02 p0238 A71-12443
- Nondestructive testing for reliability and lifetime of mass produced radio equipment under maximum load 02 p0257 A71-12530
- Multiple dialect automatic test language for avionics industry, considering software design 03 p0381 A71-13077
- Automatic RF and microwave test equipment for communication, navigation, radar and tactical systems 03 p0395 A71-13083
- Versatile Avionic Shop Test /VAST/ general purpose digital tester, discussing hardware and software 03 p0395 A71-13084
- Automatic digital test unit for avionics systems 03 p0396 A71-13085
- Software cost estimates for automatic test equipment for avionic support analysis 03 p0396 A71-13086
- User requirements of Versatile Avionic Shop Test /VAST/ computer controlled automatic test equipment, including documentation, compatibility, assurance plan, etc 03 p0396 A71-13087
- STOL navigation equipment and microwave landing instruments test programs, noting data recording and flight operations 03 p0454 A71-13286
- Radio electronic equipment components reliability, using image recognition theory 03 p0384 A71-13422
- VC-10 aircraft ILS electronic equipment reliability tests 04 p0559 A71-15873
- Electronic components failure rate distribution 04 p0559 A71-15875
- Transistors and Zener diodes temperature dependence and normal and accelerated life tests 05 p0728 A71-16289
- Digital electronic equipment logic networks computer controlled tester, describing method for test patterns synthesis 06 p0879 A71-17322
- Long life spacecraft tape recorders, considering digital and analog equipment and life and reliability testing of components and complete units 07 p1106 A71-18812
- Phase locked automatic direction finder /ADF/ flight test results, indicating signal to noise threshold reduction by coherent detection 07 p1057 A71-18815
- Radiation hardened semiconductor device technique by irradiating silicon wafers on lot to lot basis 07 p1071 A71-19065
- Broadband IMPATT diode multistage transmission amplifiers computer aided design and X band performance 07 p1073 A71-19114
- Microwave oscillator circuit with cap structures for testing millimeter wave IMPATT diodes 07 p1073 A71-19119
- Statistical scatter of pulse duration in relaxation oscillator with common-emitter coupling concerning mass production 08 p1261 A71-20739
- Microelectronic circuits reliability in aircraft engine control applications, discussing testing and selection for severe temperature and vibration environments [SAE PAPER 700822] 08 p1265 A71-21369
- Soviet book on reliability and efficiency prediction of radio electronic devices covering a priori and posteriori random quality indices, mathematical and physical models and applications 10 p1582 A71-23900
- Measurement system for communication satellite ground station equipment including parametric amplifier, wideband receiver, power oscillators, and radio transmitters and receivers 10 p1590 A71-25103
- Intelsat system ground station equipment testing including antenna radiometric gain, noise temperature, energy dissipation, telephone and TV performance measurements 10 p1580 A71-25104
- Computer aided reliability assurance system /CARAS/ for integrated circuits, correlating process and failure data 12 p1890 A71-26658
- Airborne Doppler radar receiver transmitter failure testing by Versatile Avionics Shop Test computer controlled system 13 p2031 A71-28778
- Miss/stick oscilloscope techniques in signal and switching relay testing with automated human-interactive time-and-level-measurement machine 13 p2001 A71-28840
- EMC susceptibility test equipment consisting of portable buzzing relay noise generator 13 p2045 A71-28874
- Failures detection in combinational digital switching circuits due to component malfunction 13 p2036 A71-29291
- Heuristic algorithm for computation of failures detection tests in asynchronous sequential logic circuits 14 p2218 A71-29520
- Transistor resistances difference measurement under reversed polarities during quality control testing 14 p2214 A71-30635
- Computer program for prediction of repair time elements for versatile avionic ship test 16 p2545 A71-33314
- Electronic equipment maintenance simplification by proceduralized troubleshooting method for malfunction isolation and tests and checks selection and sequencing, noting technician training cost reduction 17 p2689 A71-34702
- Aircraft onboard equipment tests in air navigation aid satellite project, estimating tracking random errors 18 p2877 A71-36509
- Transistors life testing for temperature and voltage dependence of failure rates 18 p2893 A71-36805
- Strapdown guidance systems computerized test system consisting of minicomputer and cathode ray display tube with keyboard control over all system elements [AIAA PAPER 71-967] 19 p3040 A71-37208
- Life tested thermoelements postoperative diagnostic analysis, using thermoelectric techniques 20 p3182 A71-38952
- Complex electronic modules automatic checkout, discussing processing time and cost reduction for large printed circuit logic boards test and diagnostic programs [ASME PAPER 71-VIBR-115] 21 p3362 A71-40335
- Independent sideband transmitter checkout and maintenance for maximum communication circuit performance 21 p3353 A71-40519
- LSI logic arrays testing problems minimization by test procedures based on circuit design characteristics and MOS structure properties 21 p3356 A71-40803
- ELECTRONIC FILTERS**
- Active filters of triple layer rectangular-shaped distributed RC elements, calculating components geometric variation effect on frequency response 01 p0058 A71-10312
- Filter output voltage in pseudorandom signals correlation processing, using Duhamel integral 03 p0378 A71-13392
- Matched filter output response computation for combined Barker codes, considering Doppler mismatch 04 p0551 A71-15013
- Active directional nanosecond pulse filter design based on hybrid technique, using metal semiconductor field effect transistors /MESFET/ 04 p0559 A71-15698
- Surface wave filters, tapped delay line pulse compression networks and amplifiers, discussing design and applications 05 p0728 A71-16915

Squaring loops for establishing coherent carrier reference for bi-phase PSK modulation, deriving optimal presquaring filter

05 p0730 A71-17075

Soviet book on radar signal processing optimization covering detection and measurement, electronic analog and discrete digital filters design, etc

06 p0867 A71-17445

Distributed gain amplifiers synthesis technique permitting use of filter and transmission line design tables

09 p1413 A71-22158

Electronically tunable compact X band triplexer, consisting of four port nonreciprocal directional YIG filters in cascade

09 p1418 A71-23416

Optimum synthesis and design of distributed RC filter for oscillator feedback circuit, using calculus of variations

09 p1425 A71-23652

Noise analysis of microelectronic active RC filters by cascade of passive and active networks, considering low pass filter

10 p1582 A71-23915

Thick film flat spiral inductor filter design for television signals, using linear analysis computer program

13 p2039 A71-28913

Optimum L shaped quadrupole filter for controlled valve voltage inverters

15 p2353 A71-32079

Filter design for optimal transient performance, comparing with steady state frequency response

19 p3038 A71-38487

Radar resolution performance for targets with range acceleration, determining matched filter or correlation radar effects

20 p3195 A71-38868

Real operational amplifier analysis application to state variable filter design emphasizing high-Q HF phenomena, noting undesirable behavior by heuristic argument

21 p3360 A71-40808

Distributed active RC filters design for low pass, bandpass and biquadratic network functions, including charts for element values determination

21 p3360 A71-40809

Batch and sequential considering filters data processing methods for Mars orbiting spacecraft state estimation, investigating error sources

23 p3731 A71-43055

Signal filtration algorithms and parameter estimation in additive non-Gaussian noise background by conditional Markov process theory

23 p3644 A71-43290

ELECTRONIC LEVELS

U ELECTRON ENERGY

U ENERGY LEVELS

ELECTRONIC MODULES

NT MICROMODULES

Binary cellular logic circuit array multiplication unit based on functional module concept adaptable to LSI implementation, discussing design methodology

01 p0044 A71-10185

NASA modular aerospace computer for attitude control high speed computation, describing implementation with LSI functional characters

01 p0045 A71-10198

High performance LSI main frame MOS flip-flops memory module for digital computers

01 p0047 A71-10210

Remote modules for spacecraft analog/digital telemetry distributing multiplexer input gates

01 p0036 A71-10988

Single phase static inverter module with voltage waveform synthesis by time optimal response /bang-bang/ closed loop technique

04 p0535 A71-15287

Solar cell array for probe mission, using optimized high temperature low resistance modules combined with mirrors of high thermal emissivity

05 p0704 A71-16096

Multichannel modular tropospheric scatter equipment as economic solution for medium range HF communication

13 p2034 A71-29317

Modular digital TDM switch for radially distributed clock synchronization, discussing design and control

13 p2034 A71-29318

Arbitrarily dimensioned microwave dielectric modules complex permittivity calculation

14 p2212 A71-30511

Low carrier power aircraft antenna module for airborne UHF communications system, considering range/field strength measurements

14 p2216 A71-31046

Reliability analysis of solar thermoelectric generator module as function of individual photocells, circuit design and redundancy

15 p2351 A71-31672

S-band hybrid microwave IC module for phased arrays, presenting mechanical and electrical design details and performance test data

16 p2547 A71-33554

Redundant modules introduction in microelectronic systems for increased reliability

17 p2716 A71-34954

Electronic two axis digitizer, discussing electromagnetic measuring concept, modular design, reliability and economics

17 p2711 A71-35291

Pulse bursts phase regulation subassembly modules, noting use for time division multiple access system control

18 p2879 A71-36545

Low power nonpulsating arithmetic unit of 16 bit integer numbers for spaceborne applications, using module printed circuit cards

18 p2886 A71-36570

High power GaAs injection laser diodes characteristics and array module design for pulsed operation, using confinement junction formation and reflective end coating

18 p2931 A71-36604

Combinational possibilities of special application modules based on thin-film hybrid integrated circuits in standardized encapsulations

18 p2893 A71-36625

Panels and cassettes mechanical design for Camac modular construction of electronic analog and digital measuring instruments based on integrated circuits

19 p3029 A71-38065

Automated test capability for digital modules, describing test generation, circuit analysis and simulation programs

19 p3030 A71-38406

Electronic circuit modules effects on alphanumeric display capabilities and costs over wide applications range

21 p3359 A71-40116

Complex electronic modules automatic checkout, discussing processing time and cost reduction for large printed circuit logic boards test and diagnostic programs

[ASME PAPER 71-VIBR-115]

21 p3362 A71-40335

Microcomputer design using standard interfacing module for balanced electronic logic amounts in central processor and peripheral controllers

22 p3518 A71-42207

Conventional components in hybrid circuits, using leadless inverted device, SOT-23 transistor and multilayer ceramic capacitors

23 p3655 A71-43349

ELECTRONIC PACKAGING

Sequential environmental testing effects on large hybrid microcircuit packages, reviewing solder sealing processes and repair methods

01 p0053 A71-10732

Ground station integrated receiver cabinet formed by down-converter, demodulator and baseband equipment packaging

02 p0224 A71-12817

Reciprocal thermal influence, temperature areas and conduction distance of electronic components in compact circuits

03 p0387 A71-14325

Parasitic reactances in Gunn effect device packages from microwave equivalent circuit parameters

07 p1072 A71-19104

Electronic encapsulated assemblies thermal stresses due to components expansion coefficients mismatch

07 p1213 A71-19774

Large aperture telescope in-orbit maintainability packaging, examining optical systems replacement tolerances and astronauts EVA mode accessibility

09 p1446 A71-22742

Single metal system Al beam leaded chips, substrates and crossovers for multilead packaging, describing fabrication techniques

09 p1509 A71-23119

Spacecraft systems radiation hardening design, discussing Tiros satellite mission hazards and space exposure prediction for electronic parts, using flow chart rationale

11 p1839 A71-26333

HF microcircuits packaging inside magnetic cores, discussing inherent advantages of RF interference and radiation shielding and heat transfer properties

12 p1888 A71-27433

Batch fabricated three dimensional planar coaxial microelectronic interconnection and packaging technique for semiconductor chips

12 p1890 A71-27771

Microwave transistor case design, considering RF parasitics, thermal dissipation, environmental mechanical factors, ceramic technology and sealing

15 p2377 A71-32500

Subminiature TV camera with hybrid electronic packaging, providing EIA composite video output format and 450 TVL/RH resolution capability

17 p2747 A71-35788

Plastic encapsulation for microcircuits including packaging, failure mechanisms, military qualifications and economic factors

19 p3033 A71-38508

Electronic packaging and production - Conference, Anaheim and New York, February and June 1971

21 p3352 A71-40435

High density packaging effects on multilayer interconnection board reliability tested in thermal environments

21 p3352 A71-40437

Integrated circuits failures due to plastic or ceramic packaging methods, describing failure analysis technique

21 p3353 A71-40438

Microelectronics high power hybrid circuit design, discussing application of packaging techniques to 100W Amp series regulator

21 p3353 A71-40440

Leadless electronic packaging system for MOS LSI's for low cost, high reliability and heat transfer advantages

21 p3356 A71-40748

Subnanosecond digital computer with emitter-coupled fully integrated circuit packaging concept

21 p3351 A71-40748

Beam-lead nitride-passivated IC seal junction chip reliability evaluation by life tests for optimum packaging into functional modules

21 p3357 A71-40811

Dummy S4 diode packages mounted in coaxial line, deriving mount-independent equivalent circuit parameters from broadband admittance measurements

22 p3521 A71-42206

Plated through holes interconnection in nine layer phased array antenna printed circuit board, using numerically controlled drilling and plastic encased preform solder system

22 p3525 A71-42765

Book on thick film microelectronics covering microcircuit design, fabrication, packaging and applications

23 p3650 A71-43224

Thick film technology and tests for hybrid microcircuits and semiconductor packaging

23 p3651 A71-43430

Interconnection Ta thin films and silicon encapsulation for solid state components in hybrid IC under high humidity

23 p3656 A71-43431

Semiconductor package designs for high performance miniature IR sensors, including flat packs, TO, custom metal and glass dewar configurations

23 p3676 A71-43509

ELECTRONIC PHOTOGRAPHY

U ELECTRO-OPTICAL PHOTOGRAPHY

ELECTRONIC RECORDING SYSTEMS

Electronic instrumentation for monitoring intragastric pH, temperature, motility and electrical activity

01 p0023 A71-10887

Electronic contour line recorder with intermittent line setting capacity and interpolation frequency regulation

01 p0083 A71-11329

Analog to digital converters employing subharmonic oscillator phase as recording medium, discussing parametron application as phase comparator

11 p1743 A71-26541

Electron beams formation and focusing, including current density distributions, electronic potentiometer recording, parameters and comparison with simulation data

20 p3204 A71-39160

Coherent optical processing system coupled to electronic readout system incorporating image orthicon TV camera, small digital computer and cell generator

21 p3381 A71-40929

ELECTRONIC SIGNAL MEASUREMENT

U SIGNAL MEASUREMENT

ELECTRONIC SPECTRA

Solar flare electron spectra in interplanetary space and within earth magnetosphere, investigating simultaneous observations by satellite-borne magnetic electron spectrometers

08 p1354 A71-21037

Radiative mean lives and transition probabilities of electronic states in beam foil excited atomic and ionic carbon

11 p1803 A71-26061

Secondary emission analog for improved Auger spectroscopy to eliminate objectionable feature of electron spectra taken with retarding potential analyzer

18 p2922 A71-36579

Wavelength prediction for coronal transitions at various atomic configurations, deriving semiempirical expressions from observed data for energy level intervals determination

18 p2965 A71-36733

Core binding energy difference between bridging and nonbridging oxygen atoms in silicate chain of pyroxenes, using X ray photoelectron spectra

19 p3011 A71-37415

ELECTRONIC STRUCTURE

U ATOMIC STRUCTURE

ELECTRONIC SWITCHES

U SWITCHING CIRCUITS

ELECTRONIC TRANSDUCERS

Analog transducers and tape recorders measurement sensitivity and conversion factor stabilization using push-pull signals

05 p0747 A71-16144

Electromagnetic transducer DC rotor magnetic state diagram, describing simulation procedure for moment pickup

06 p0899 A71-17933

- Design, construction and performance of photoelectric isometric force transducer for muscle mechanics
06 p0862 A71-18392
- Missile fluidic attitude control system, discussing integrator, transducer amplifiers and circuits
07 p1028 A71-20583
- Chain reversible functional transducer design, obtaining reversibility by additional resistances without changing operating voltage level
13 p2041 A71-27950
- IR transducer with detector for space applications, measuring capacitance on electronic bridge circuit based on temperature and pressure effects
[ONERA-TP-963] 16 p2576 A71-32845
- Computerized calculation of field configurations in automated design of electromagnetic transducers
19 p3038 A71-37774
- Electromagnetic stress gage for wave propagation study in nonconducting materials, discussing calibration, design and accuracy
21 p3379 A71-40793
- Electromechanical converters mathematical model, calculating conductivity behavior and derivative
22 p3484 A71-42877
- Phase shift and attenuation measurements in high power microwave ferrite tetrodes circuits, using semiconductor transducers/digadectors/
24 p3809 A71-44871
- Photon noise limited interferometer transducer for gravitational radiation antenna, using piezoelectric driver to generate subangstrom vibrations
24 p3835 A71-45209

ELECTRONICS

- Gold plated Ge surfaces, investigating LEED patterns and electronic properties
04 p0636 A71-15016
- Geoscience electronics - IEEE Conference, Washington, D.C., April 1970
05 p0754 A71-17126
- Electronics and aerospace systems - IEEE Conference, Washington, D.C., October 1970
07 p1056 A71-18801
- Reliability in electronics - IEE Conference, London, December 1969
07 p1076 A71-19551
- Laser microbeam welding, drilling and trimming of electronic devices
07 p1118 A71-19787
- Electronics - Conference, Chicago, December 1970
07 p1080 A71-20401
- Electronic computation - Conference, Purdue University, Lafayette, Indiana, August 1970
09 p1412 A71-23273
- Papers on electronics and electron physics, Volume 29, covering plasma-RF field interactions, cluster ions formation and electron beams energy distribution
11 p1802 A71-25628
- Averaging method for nonlinear oscillations in celestial mechanics, radio engineering and electronics and for time lag, random forces and integrodifferential equations
17 p2779 A71-34904
- Aerospace electronics - IEEE Conference, Dayton, Ohio, May 1971
17 p2746 A71-35752
- Automatic electronics design, analyzing visual and graphic devices for initial data preparation, introduction, operator computer interaction and results extractions
18 p2887 A71-35878
- Book on active and nonlinear wave propagation in electronics covering transmission lines, wave systems stability, quasi-harmonic active propagation, equivalent circuits, etc
19 p3029 A71-38018
- Electronics - Conference, San Francisco, August 1971
21 p3356 A71-40801
- Soviet book on rational, irrational and transcendental transfer functions electronic modeling covering mathematical theory and applications to control plants
23 p3648 A71-44185

ELECTRONICS

- NT CONDUCTION ELECTRONS
NT FREE ELECTRONS
NT HIGH ENERGY ELECTRONS
NT HOT ELECTRONS
NT N ELECTRONS
NT PHOTOELECTRONS
NT POLARONS
- Stability analysis of magnetosphere whistler amplification, discussing energetic electron interaction with background plasma
01 p0038 A71-11308
- Electron charge dependence on universe age, considering possible gravitational constant dependence on time
02 p0313 A71-12547
- Extensive air shower electron and muon components at mountain levels, calculating distribution functions by Monte Carlo technique
03 p0477 A71-13861
- Eddington theory validity based on formulas connecting light velocity, Planck and gravitational constants and electron, proton and neutron masses
04 p0626 A71-15136

Type 3 solar radio bursts, examining proton and electron stream excitors
05 p0804 A71-16030

Solar electrons access to closed field lines in geomagnetosphere quasi-trapping region from satellite observation
06 p0949 A71-17257

Solar protons and electrons latitude profiles, discussing dependence on magnetic rigidity
06 p0964 A71-17276

Electron and proton whistlers polarization reversal and mode coupling, explaining magnetic latitude dependence
07 p1062 A71-19667

Photon emission from electron moving in field of two plane electromagnetic waves with different frequencies and propagating in same direction
09 p1460 A71-22364

Electron, nuclear active and muon components of extensive air showers, discussing statistical results
13 p2123 A71-28076

Ion production rates during electron flux-atmosphere interactions based on atmospheric models with different energy and angular distributions
13 p2061 A71-28541

Electron charge dependence on universe age, considering possible gravitational constant dependence on time
15 p2494 A71-32503

Earth bow shock internal structure based on correlated observations of magnetic field, ELF magnetic fluctuations and suprathermal electrons by OGO 5 satellite
16 p2628 A71-33943

Extensive air shower electron and muon components at mountain levels, calculating probability distribution functions by Monte Carlo technique
22 p3595 A71-42662

Transition metal physicochemical properties explanation by many-electron effects in Hubbard model
23 p3714 A71-42932

ELECTROPHORESIS

He-Cd laser stable long life CW excitation by DC cataphoresis to maintain spatially uniform and optimum DC vapor concentration
01 p0091 A71-10007

Ehrlich ascites tumor cell membrane potassium and electrophoretic mobility loss, investigating radiation effects under radiosensitizing and radioprotecting drugs
07 p1036 A71-18956

Human lens fluorescent pigment O-beta-D-glucoside of L-3-hydroxykynurenic, discussing preparation, electrophoresis and paper chromatograms
11 p1718 A71-25634

Electrophoretic mobility of tear lysozyme in human subjects, noting applicability to genetics
13 p2013 A71-29033

Dielectrophoresis force measurements and wedge shaped capacitor separation properties in satellite zero gravity conditions
19 p3103 A71-37278

ELECTROPHOTOMETERS

Fesenkov photometer for aureole flux observations eliminating solar diffraction
01 p0080 A71-10542

Semiautomatic electrophotometer with interference light filters for atmospheric ozone, aerosol and solar radiation recording
01 p0080 A71-10602

Photographic and photoelectric photometry of asteroids, discussing luminescence, reflectivities, light curves, colors and phase variations observations
02 p0310 A71-12157

Vela pulsar optical emission identification by photoelectric measurements
02 p0315 A71-12659

Photoelectric photometer with mechanical chopper for extreme limb darkening measurement at total eclipse
03 p0424 A71-13635

Photoelectric automatic logger with perforated tape recorder, discussing block diagram
04 p0589 A71-14837

Portable photoelectric recorder for solar limb vibration frequency spectrum and amplitude measurements
04 p0590 A71-14844

Semiautomatic photoelectric apparatus for limb graduations using pivoted optical arrangement, discussing accuracy, measurement rate and reliability improvement methods for similar instruments
04 p0591 A71-14852

Photoelectric device for recording stellar passages, discussing photocascade structure
04 p0592 A71-14858

Photoelectric recording devices for star passages, describing automatic compensation for signal delay instability
04 p0592 A71-14864

H II region high velocity observations by two etalon, propane scanned photoelectric Fabry-Perot spectrometer with reflecting telescope
04 p0581 A71-15044

Photoelectric photometer measurements of stellar interferometer fringes strength by light modulation
05 p0752 A71-16681

TV spectrophotometer with photographic and photoelectric measurement techniques advantages for measuring astronomical telescope spectral passbands
07 p1109 A71-19349

Photoelectric stellar image analyzer for measuring close binary stars separation, collecting data by image coherent superposition
08 p1290 A71-21393

Photoelectric servosystem for three dimensional positioning of slit image, discussing system applications and accuracy
08 p1291 A71-21395

Variable stars, quasars and X ray source ScoX-1 UVB light photoelectric data, examining optical emissions and brightness variations
09 p1524 A71-23186

Eclipsing system GG Cas, presenting photoelectric data
09 p1527 A71-23527

Eclipsing binary IZ Persei, examining photoelectric light elements
09 p1527 A71-23528

Multicolor photographic photometry of flare stars in Orion aggregate based on two UVBR photoelectric sequences
10 p1680 A71-25061

Jupiter color variations observation by multicolor photoelectric photometry, noting consistency with activity in Jovian atmosphere
11 p1827 A71-25725

Astronomical photoelectric photometer design features, operation modes and efficiency
13 p2067 A71-28391

Rocket-borne twin-channel photoelectric stellar photometer for use in 1400-3000 A region, describing nondispersive wavelength isolation methods
14 p2240 A71-30124

Photoelectric scanning photometer for visual binaries measurement, using on-line computer for data sampling and acquisition from three photon counters
14 p2246 A71-30357

Luxmeters and photoelectric receptors for illumination measurement of light beams in limited solid angle in image systems, considering automatic polar photogoniometer
14 p2246 A71-30417

Three color photoelectric photometer improvements by introducing synchronous signal detection and electronic gates by field effect transistors
16 p2579 A71-33434

Temperature effects on photoelectric photometry, considering photomultiplier tube and electronics as black box with photons and electric pulses
16 p2548 A71-34097

Computer controlled pulse counting technique application to astronomical photoelectric photometry for improved telescope efficiency
17 p2740 A71-34989

Rapid photoelectric spectrum scanning techniques using multichannel analyzer and triggering mechanism
17 p2741 A71-34991

Narrow band and UVB photoelectric photometry of Uranus geometric albedo and magnitude at unit distance as functions of wavelength
21 p3443 A71-40191

H beta and UVB photoelectric photometry of southern galactic cluster, deriving absolute magnitude calibrations and intrinsic color relations
21 p3443 A71-40194

Early stars UV continuum brightness from rocket-borne photoelectric spectrophotometer, estimating total interstellar flux density
21 p3444 A71-40244

Photoelectric polarization curve, reflectivity and absolute diameter of Vesta, comparing with Lyot curve
22 p3602 A71-42177

ELECTROPHOTOMETRY

Mira Ceti type long period variable giant stars emission spectra, emphasizing UVB photometry and IR electrophotometry
03 p0486 A71-13267

Error allowance of photoelectric sighting grating with incline slits in stellar observations at Pulkovo
07 p1108 A71-19330

Electrophotometric and spectral observations of continuous airglow spectrum
07 p1105 A71-20438

Photomultiplier tube operation in terms of photoelectron counting photometry, examining emitted signal statistical properties
15 p2408 A71-31832

H beta fluxes of planetary nebulae along southern Milky Way from photoelectric telescope
17 p2809 A71-35593

Photoelectric telescope observations of red stars in Cygnus at IR wavelength with threshold brightness detection
20 p3293 A71-39537

SV Cephei variable photoelectric UVB observation showing existence of quasi-periodic minima with changing characteristics
21 p3451 A71-40715

ELECTROPHYSICS

- NT ELECTRO-OPTICS
NT MOLECULAR ELECTRONICS

ELECTROPHYSIOLOGY

- Papers on electronics and electron physics, Volume 29, covering plasma-RF field interactions, cluster ion formation and electron beams energy distribution
11 p1802 A71-25628
- Impedance variations vs electrophysical properties of epitaxial and diffusive semiconductor structures for electronic equipment, applying microwave fields for parameter control
18 p2954 A71-35874
- Microwave reflection from semiconductor wafers with dielectric film, presenting electromagnetic field parameters as function of electrophysical properties
19 p3117 A71-37264

ELECTROPHYSIOLOGY

- Automatic temperature monitor and proportional solid state DC controller for electrophysiological use
01 p0022 A71-10247
- Soviet book on spinal cord conducting paths electrophysiology covering anatomical and clinical data and neuron theory
03 p0364 A71-13691
- Vagal sensitive neurons unitary activity, applying microelectrode technique to nodose ganglion ventral part
05 p0707 A71-16342
- Electrophysiological audiometry noting average brain response in man
06 p0858 A71-17295
- Electrophysiological studies of olfaction in vertebrates, describing role in orientation, sexual behavior and population control
08 p1241 A71-21942
- Line fed microelectrode amplifier for electrophysiology, discussing noise reduction
08 p1249 A71-21974
- Biophysical nature of human memory, investigating electrosensibility phase modulators and variations by suprainvasive light stimulus to eye and adjustment reflex
09 p1391 A71-22484
- Human auditory signal detection related to averaged evoked potential in scalp by electrophysiological measurements
16 p2534 A71-32951
- Calcium ions effects on electrophysiological properties of portal vein muscle cells in rats
16 p2533 A71-34109
- Temperature effects on spontaneous electrical and contractile activity of smooth muscle cells of portal vein in rats
16 p2533 A71-34110
- Higher nervous activity physiology, discussing induction, protective and conditioned inhibition mechanisms in cerebrum and electrophysiological indices
17 p2684 A71-35359
- Direct and reverse conditioned connections including defense reflexes, response to indifferent stimuli and electrophysiological manifestations
17 p2685 A71-35360
- Normal females electrophysiological changes during sensory isolation of water tank variety from EEG, EMG, EOG, EKG and electrodermal measurements, considering cortical activities reduction
21 p3330 A71-40346
- ELECTROPOLISHING**
Anodic dissolution of aluminum bicrystals in electrolytes containing perchloric acid during electropolishing, showing anisotropic layer existence
16 p2592 A71-33371
- Epitaxial metal film formation on Al-Ni fibers in Al matrix during electropolishing
21 p3387 A71-40456
- ELECTROREFINING**
High purity Sb, In and Ag by vacuum distillation, zone melting and electrolytic refining for semiconductor electronics
24 p3861 A71-45201
- ELECTRORETINOGRAPHY**
Open and closed eyes electroretinogram, discussing lamellar electrode placed on lower eyelid
01 p0024 A71-11077
- Acoustic stimulation effect on electroretinogram of man
03 p0361 A71-13191
- Frog eye response to UV light stimulation, investigating sensitivity from electroretinogram
03 p0363 A71-13484
- Illumination level effect on corneo-retinal potential and electro-oculography (EOG) recording
08 p1246 A71-20812
- Delayed e-wave like electrical response to light and inhibition in developing frog retina
09 p1393 A71-23011
- Vitamin A deficiency effect on rhodopsin loss dependent on illumination level in rat eye using electroretinography
10 p1563 A71-24326
- Electroretinogram b-wave slope reduction by cooling of dark adapted frogs during serial flash stimulation
10 p1564 A71-24442

Postexcitatory inhibition of monochromatic flickering potentials on electroretinogram in man under intensive dazzling stimuli
10 p1564 A71-24443

Human electroretinographic dark adaptation recovery curves rod-cone break time dependence on bleach intensity
14 p2185 A71-30503

Visual latencies at photopic levels as function of binocular differences in retinal illuminance, using Limulus adaptation model and ERG correspondence
16 p2527 A71-32867

Multiple positive off effects in human electroretinogram, recording rhythmic wavelets due to intense stimuli with averaging computer and short time constant amplifier
17 p2687 A71-35802

Positive and negative deflections in human electroretinogram off response to stimuli
19 p3007 A71-38058

Anatomic examinations and diagnostic techniques in ophthalmologic aviation medicine, discussing electronic time interval and storage measurements, cortical response, etc
23 p3631 A71-42928

Simultaneous recordings of ERG and visually evoked cortical potential to stimuli of differing luminance and pattern, comparing spatial frequency characteristics
24 p3801 A71-44977

ELECTROSEISMIC EFFECT

U ELECTRIC CURRENT

U SEISMIC WAVES

ELECTROSLAG REFINING

Steel structural transformations under arc melting, cooling and electroslog remelting, noting delta ferrite precipitation with hot stage microscope
11 p1776 A71-25168

Binary alloy solidification in electroslog remelting process, determining temperature distribution and solidus, mushy and liquidus zones by heat transfer analysis
19 p3079 A71-37706

ELECTROSLAG WELDING

Complex alloyed steel under electroslog welding, investigating heat treatment effect on heat affected zone phase composition
15 p2437 A71-32661

Ti alloys electroslog welding with consumable and nonconsumable electrode combinations, presenting W electrode consumption and weld mechanical properties
17 p2748 A71-34805

Electroslog welding of large pressed Al-Mg alloys sections, using electrodes to reduce weld grain size and obtain high mechanical properties
17 p2748 A71-34807

ELECTROSTATIC CHARGE

Static dissipator additives in aviation fuels for eliminating electrostatic charging hazards
02 p0297 A71-12300

Electron charge dependence on universe age, considering possible gravitational constant dependence on time
02 p0313 A71-12547

Static discharge hazards for aircraft, discussing causes for static charge build-up, dangers and precautionary methods during refueling operations
07 p1019 A71-19424

Electrostatic charging noise measurement, reduction and flight test verification
07 p1021 A71-19937

Thermionic converter electrostatic sheath analysis, using discontinuous distribution functions for emitted, plasma and trapped particles, and computer program
11 p1713 A71-25891

Electron electrostatic or space charge oscillations in nonneutral plasma columns with cylindrical symmetry around axial magnetic field
13 p2104 A71-27848

Electrostatic spray generated charged colloids adaptation to thruster with metal capillary needles under AC voltage, evolving low thrust propellants
13 p2118 A71-29503

Motor using electric field interactions with lossy dielectric rotor induced surface charge as force mechanism
14 p2181 A71-29543

Electron charge dependence on universe age, considering possible gravitational constant dependence on time
15 p2494 A71-32503

Performance measurement of electrostatic spectrometers as monochromators by calculation of electron energy distribution
20 p3233 A71-38821

Laplace equation solution for double cylinder electrostatic lenses for large range voltage ratios and separations, obtaining focal and aberration coefficients
21 p3377 A71-40178

High voltage spark generating circuit design for studying electrostatic sensitivity of electroexplosive

devices, considering pyrotechnic flash charges, bridgewire detonators and electric blasting caps
22 p3587 A71-41449

ELECTROSTATIC ENGINES

Kaufman electrostatic ion thruster using electron bombardment ionized mercury vapor in cylindrical vessel and acceleration by electrostatic field
02 p0283 A71-12310

Radio frequency electrostatic ion thruster using mercury ion source electrodeless self sustaining discharge
02 p0283 A71-12313

Electrostatic ion propulsion systems for interplanetary missions, using experimental engine characteristics as basis for flight studies [DFVLR-SONDDR-121]
15 p2496 A71-32722

Direct thrust measurement on electrostatic ion engine ESKA 18 P, comparing with values calculated from applied voltage and ionic current [DGLR-71-043]
17 p2793 A71-35538

ELECTROSTATIC EROSION

U SPARK MACHINING

ELECTROSTATIC FIELDS

U ELECTRIC FIELDS

ELECTROSTATIC PLASMA

U PLASMAS [PHYSICS]

ELECTROSTATIC PROBES

Boundary layer thickness measurement behind shock wave front using oscillogram of electrostatic probe current
01 p0078 A71-10160

Plasma potential measurement in closed magnetic trap /stellarator/ by electron emitting electrostatic probe
01 p0133 A71-10679

Tungsten cathode current partitioning in dense Ar plasma, noting electron emitter work function reduction due to ion space charge field
02 p0289 A71-11940

Langmuir probe DC detector for rocket quasi-static and AC electric field measurements in auroral zone ionosphere
03 p0406 A71-13302

Spherical and cylindrical electrostatic probes for point ion density measurements in continuum flowing plasmas in hypersonic wake, discussing shock tube program for calibration
03 p0423 A71-13441

Collisionless electrostatic single and double probe measurements for electron temperature and number density, making algebraic fit for numerical analysis results
03 p0423 A71-13442

Capacitive and floating Langmuir probes paired comparison measurements of electrostatic potential fluctuations spectrum in steady state turbulent magnetically confined plasma
03 p0430 A71-14416

High density atmospheric pressure plasma ionization measurement by negatively pulsed Langmuir probe, showing agreement with space charge controlled sheath expansion model
04 p0586 A71-14660

Electron density measurement behind shock waves in air/argon mixture by free molecular Langmuir probes
04 p0629 A71-14705

Cylindrical Langmuir probe LF transient response characteristics in transition regime [AIAA PAPER 71-142]
06 p0902 A71-18585

Negatively charged conical electrostatic probe characteristics determination in supersonic plasma stream, using shock tube [AIAA PAPER 71-143]
06 p0939 A71-18586

Plasma potential measurement in closed magnetic trap /stellarator/ by electron emitting electrostatic probe
07 p1170 A71-20140

ATS-5 satellite-borne auroral electron and proton energy spectrum measuring instrument using cylindrical coordinate electrostatic analyzer
08 p1294 A71-21845

Flush-mounted electrostatic probe for plasma properties measurement, calculating negative ions effect on I-V characteristics
09 p1442 A71-22073

Flush mounted electrostatic probes behavior under different flow regimes, studying bias, area, geometry and position effects on collected current density
11 p1743 A71-25148

Shot noise effect on ambient plasma magnetosphere electric field measurements with Langmuir and double probes for electron density and temperature
11 p1756 A71-25644

Plasma anode tube in metal-ceramic envelope with improved capabilities for electron emission studies, considering movable Langmuir probe
11 p1806 A71-25902

Electrostatic probe measurements of charged particles and thermal ionization relaxation in shock heated low density supersonic monatomic gas flows
11 p1766 A71-26286

- Parallel plate electrostatic analyzer design, discussing second order focusing, angular aberrations and magnification 12 p1903 A71-26570
- Paired comparison tests of relative signal detected by capacitive and floating Langmuir probes in steady state turbulent plasma confined in magnetic mirror geometry 13 p2066 A71-28155
- Improved accuracy electron temperature Langmuir probe by eliminating geomagnetic field, rocket velocity and random noise effects 14 p2238 A71-29532
- Ion and electron probe currents correlation for justification of electrostatic probes use for turbulent plasma diagnostics 14 p2280 A71-30174
- Flat plate electrostatic probe for ionization rate measurements behind reflected shock waves, monitoring time evolution of electron production 14 p2248 A71-30884
- Satellite skin potential and errors in electron density and temperature determinations by Langmuir probe measurements, using model ionosphere 15 p2398 A71-31768
- Spherical free-molecular electrostatic probe surrounded by finite sheath, calculating I-V characteristic saturation current regimes 15 p2409 A71-32100
- Particle collision effects on electrostatic probe electron or ion current collection in transition regime as function of relative thermal energy 15 p2409 A71-32107
- Potential measurements in collisionless plasma sheath of conducting plate, evaluating electrostatic vs emissive and floating emissive probes 15 p2458 A71-32391
- Langmuir probe measurement of ionization density of Ar plasma jet, suggesting electron-ion recombination in probe vicinity 17 p2789 A71-35338
- Continuous flush electrostatic probe for weakly ionized flowing gas surface density gradient and charged particle free stream density determination, obtaining I-V characteristics 18 p2950 A71-35858
- Swept Langmuir probe with sweep speeds greater than 150 V/microsec, considering electron cyclotron resonance heated hydrogen plasma confined in toroidal quadrupole 18 p2952 A71-36582
- Mathematical model of arc Pioneer 6/7 plasma probe electrostatic analyzer responding to monoenergetic unidirectional charged particle beam 18 p2952 A71-36583
- Langmuir probe and microwave measurements of density, velocity and electron and ion temperatures in streaming plasmas generated by focused laser pulse 19 p3112 A71-37740
- Ionospheric electron density irregularities measurement, comparing scintillation, spread F and electrostatic probe methods 19 p3128 A71-38035
- Ionospheric electron concentration and temperature measurements, describing rocket-borne asymmetrical Langmuir probe 19 p3067 A71-38631
- Charge density fluctuation measurements in ionized turbulent hypersonic sphere wakes, using Langmuir and continuum electrostatic probes and microwave interferometric and scattering equipment 21 p3363 A71-40388
- Cooled spherical electrostatic probe idealized theory in quiescent continuum slightly ionized chemically frozen gas, interpreting plasma measurements 21 p3423 A71-40947
- Probe size and orientation effects in turbulent plasma flow diagnostics, considering electrostatic probes frequency filtering and wake effects 21 p3423 A71-40979
- Acoustic wave detection in K-seeded methane-oxygen flame plasma, using I-V characteristic modulation of fixed electrostatic probe 22 p3580 A71-41622
- Spacecraft communication cut-off during atmospheric reentry due to thermal ionization of gas boundary layer, discussing sulfur hexafluoride injection alleviation and electrostatic probe 22 p3583 A71-41998
- Ionospheric electron density measurement by K-9M rocket, comparing VLF Doppler with Langmuir probe methods 23 p3671 A71-43366
- Raman microwave scattering on Langmuir oscillations, showing suprathermal emission origin in theta pinch plasma 24 p3853 A71-44505
- Ion current sheath-convection effects with flush mounted electrostatic probes in high pressure flowing plasmas 24 p3826 A71-44792
- Electric rocket propulsion systems using nuclear or solar energy and electrothermal, electromagnetic or electrostatic principle 02 p0283 A71-12309
- High thrust density colloid emitting source development as basic microthruster for electrostatic propulsion systems [AIAA PAPER 71-694] 14 p2293 A71-30753
- Hollow cathodes as main and neutralizer cathodes in Kaufman electrostatic propulsion system, discussing test installation and results [DGLR-71-045] 17 p2794 A71-35542
- ESKA-18P electrostatic ion propulsion system control characteristics and power conditioning, describing pulse width modulated power supply unit [DGLR-71-029] 17 p2794 A71-35543
- Propulsion systems evaluation for Mars and Jupiter missions, using bundled ESKA 28 electrostatic ion thrusters and incore thermionic reactors [DGLR-71-046] 17 p2794 A71-35545
- ELECTROSTATIC SHIELDING**
- Gravitationally induced electric field shielding using whisker model with conducting metal surface for reducing strain dependence on altitude 05 p0792 A71-16315
- Astronaut protection from solar flare high energy protons, discussing spacesuit, spacecraft orientation and solid, electrostatic, magnetic and plasma shielding 13 p2021 A71-29252
- Radome lightning protection systems involving electrostatic shield, considering effect on electromagnetic characteristics and radiation patterns of nearby antennas 19 p3031 A71-38450
- ELECTROSTATIC WAVES**
- Electrostatic vibrations from turbulent plasma heating on basis of Stark broadening of hydrogen spectral lines, obtaining electric field strength 01 p0131 A71-10069
- Electron beam nonlinear interaction with plasma, considering electrostatic wave propagation, instability and dispersion equation 01 p0135 A71-11209
- Particle acceleration by coherent electrostatic wave propagation through plasma, producing monoenergetic particle beam 01 p0131 A71-11513
- Nonlinear electrostatic vibrations in colliding antiparallel flows of rarefied plasmas 02 p0289 A71-11928
- Electrostatic wave growth rates in anisotropic medium with or without cold plasma 03 p0464 A71-13532
- Topside ionosphere plasma resonance due to electrostatic wave echoes, comparing electron temperature dependent beat pattern with ray tracing calculations 03 p0421 A71-14540
- Collisionless electrostatic shock formation and structure, using one dimensional two species numerical simulation code 04 p0634 A71-15174
- Inhomogeneous magnetoplasma electrostatic LF oscillations, discussing wave modes and instability conditions 04 p0634 A71-15257
- Electrostatic wave perturbation current using accelerated particles orbits in neutral sheet with electric field in plane 05 p0788 A71-16633
- Electrostatic waves linear dispersion relation in Maxwellian unmagnetized ions and magnetized electrons Vlasov plasma 05 p0789 A71-16656
- Charged particle beam interaction with electrostatic surface waves in plasma layer 06 p0929 A71-17317
- Unstable electrostatic waves propagating in uniform infinite plasma with weak beam, Fourier transforming space dependent variables 07 p1166 A71-18881
- Cs ion beam space charge and current neutralization by electron capture for partially ionized plasma formation, investigating longitudinal electrostatic wave excitation 07 p1171 A71-20193
- LF electrostatic waves axisymmetric and nonaxisymmetric propagation modes in weakly ionized plasma column under weak magnetic field 09 p1504 A71-23051
- Electromagnetic and electrostatic waves direct nonlinear coupling in plasma, describing experimental measurements of interacting waves frequency, wavelength, field configuration and power levels 09 p1504 A71-23254
- Electrostatic vibrations from turbulent plasma heating on basis of Stark broadening of hydrogen spectral lines, obtaining electric field strength 09 p1504 A71-23264
- Electrostatic waves high order interaction in collisionless plasma, deriving coupling constants from energy conservation and invariance under time reversal 10 p1647 A71-23888
- One dimensional Gaussian electrostatic wave packet nonlinear time development due to weak resonant broad beam introduction into cold uniform plasma 10 p1652 A71-24658
- Linear longitudinal ion wave instabilities in electrostatic shock in plasma by double humped/bump in tail/velocity distribution 12 p1935 A71-26916
- Topside ionospheric instabilities of electrostatic ion acoustic and ion cyclotron waves to field aligned currents in single and multion plasmas 13 p2054 A71-27917
- Isomagnetic potential discontinuity of electrostatic character in collisionless plasma shock waves, studying Mach number effect 13 p2105 A71-28169
- Atmospheric VLF electromagnetic emissions and electron instabilities data from satellite observation, detailing source regions, large amplitude electrostatic waves and wave-particle correlation 14 p2202 A71-30952
- Radiation from electrostatic waves in thin current sheet in geomagnetic tail into cold magnetized plasma, noting wave damping for wide frequency range 16 p2562 A71-32805
- Electron beam nonlinear interaction with plasma, considering electrostatic wave propagation, instability and dispersion equation 17 p2786 A71-34261
- Particle gyration in homogeneous magnetic field and perpendicularly propagating electrostatic wave, calculating wave-particle energy transfer and wave-amplitude limiting effects 18 p2950 A71-35862
- Coupled longitudinal-transverse wave modifications of electrostatic dispersion relation with ion gyrofrequency instabilities in magnetized plasma 18 p2950 A71-35866
- Auroral radio noise from electrostatic oscillations excited by fast proton beams 19 p3018 A71-38046
- Electrostatic oscillations excitation in magnetized homogeneous plasma by electromagnetic waves nonlinear interactions, deriving expression for induced fluctuations spectral density 20 p3273 A71-38966
- Broadband electrostatic VLF wave observation in polar magnetosphere by OV3-3 satellite, noting emission power spectra density relationship to frequency 20 p3199 A71-39889
- VLF ion wave instabilities in polar wind based on plasma kinetic theory, comparing with electrostatic wave observation by OV3-3 satellite 20 p2321 A71-39890
- Enhanced scattering signal observation at electrostatic plasma wave frequency by focusing Q switched laser beam on hydrogen plasma 22 p3580 A71-41596
- Kinetic wave equation matrix elements for three resonantly coupled electrostatic plasma waves noting application to electron plasma coupling with ion sound waves 22 p3582 A71-41900
- Electrostatic plasma instabilities under HF alternating electric field oscillating at plasma frequency 22 p3584 A71-42465
- Turbulent low Mach number electrostatic ion shocks evolution, correlating turbulence spatial growth with reflected ions distribution 23 p3708 A71-42892
- Electrostatic waves nonlinear interactions in uniform plasma in presence of external constant magnetic field, deriving coupling coefficients by coupled mode theory 24 p3858 A71-45276
- ELECTROSTATICS**
- Elastic parameter dynamic measurements using resonance methods with electrostatic attraction 02 p0328 A71-12406
- Minimum image size in parallel plate electrostatic spectrograph under focusing with small angular aberrations 04 p0600 A71-15593
- Power spectra and electrostatic mechanism of thunder from intercloud and cloud to ground lightning using analog and digital methods 09 p1489 A71-23444
- Nonlinear electrostatic theory Lagrangian analogous to gravitational Lagrangian from correspondence between Maxwell electromagnetism and Einstein gravitation 10 p1667 A71-23815
- Electro-optical systems in photoelectronic imaging devices, discussing electron gun, electrostatic focusing lens, spherical aberration, magnetic field computation and ray tracing 10 p1609 A71-24058
- Induced electrostatic field in forced Hg vortex of ideal viscous electrically conducting fluid under axial magnetic field 10 p1649 A71-24456

Magnetoelectrostatic containment ion thruster, considering adaptation for Hg operation based on discharge chamber loss comparison with Cs [AIAA PAPER 71-692] 15 p2470 A71-32288
Periodic electrostatic focusing of high permeance electron beams for high power klystrons 19 p3028 A71-37696

Dynamo equations solution for electrostatic potential, discussing three dimensional model for ionospheric equatorial conditions and Northern-Southern Hemispheres coupling 20 p3218 A71-39519

Lunar lines transportation process in mare surface evolution, suggesting electrostatics role from photographic and seismic evidence 23 p3765 A71-43810

ELECTROSTRICTION

Curie point region automatic thermal stabilization effectiveness of cylindrical/disk shaped segnetoelectric elements in electrostrictive constant magnetic field converters 24 p3828 A71-45164

ELECTROTHERMAL ENGINES

NT ARC JET ENGINES

Electric rocket propulsion systems using nuclear or solar energy and electrothermal, electromagnetic or electrostatic principle 02 p0283 A71-12309

Aerodynamic probe measurements for plasma jets produced by electrothermal and Hall current accelerators 11 p1764 A71-26275

ELEKTRON SATELLITES

NT ELEKTRON 2 SATELLITE

NT ELEKTRON 4 SATELLITE

Elektron 2 and 4 satellites rotary motion with orbital variance of precession parameters and kinetic moment vector, considering gravitational and magnetic forces 05 p0815 A71-16034

Elektron 2 and 4 satellites rotary motion with orbital variance of precession parameters and kinetic angular momentum vector, considering gravitational and magnetic effects 16 p2645 A71-33438

ELEKTRON 2 SATELLITE

Elektron 2 and 4 satellites orientation based on on-board solar and magnetic sensors 09 p1531 A71-22570

Soft electron fluxes spatial distribution and temporal variations in magnetosphere based on Elektron 2 charged particle trap data 09 p1513 A71-22573

ELEKTRON 4 SATELLITE

Elektron 2 and 4 satellites orientation based on on-board solar and magnetic sensors 09 p1531 A71-22570

Positive H, He and O ions in exosphere from mass spectrometers mounted on Elektron 4 satellite 12 p1899 A71-26644

ELEMENT ABUNDANCE

U ABUNDANCE

ELEMENTARY EXCITATIONS

NT EXCITONS

NT MAGNONS

NT PHONONS

NT PLASMONS

NT POLARONS

ELEMENTARY PARTICLE INTERACTIONS

NT ELECTRON CAPTURE

Proton form factors and radius determination from experimental data analysis of cross sections of electron scattering by protons over wide transferred-momentum range 12 p1901 A71-27180

Soviet book on cosmic muons and neutrinos covering anomalous and weak interactions 15 p2472 A71-31287

Proton form factors and radius determination from experimental data analysis of cross sections of electron scattering by protons over wide momentum transfer range 22 p3578 A71-42454

PN interactions, using emulsion technique in strong magnetic field 22 p3579 A71-42647

Negative pi minus N and NN interactions in emulsion at high energies, plotting angular distributions of secondary particles in cosmic ray showers 22 p3594 A71-42648

Momenta measurements of particles produced by high energy quasi-nucleon interactions of pions on photoemulsion layers, using primary particle tracks scanning 22 p3579 A71-42655

Nonlinear theory for synchrotron emission of tubular electron flux in cylindrical waveguide, discussing wave-electron interactions optimization 23 p3653 A71-44058

ELEMENTARY PARTICLES

NT ALPHA PARTICLES

NT ANTINEUTRINOS

NT ANTIPARTICLES

NT BARYONS

NT BETA PARTICLES

NT BOSONS

NT CONDUCTION ELECTRONS

NT DEUTERONS

NT ELECTRONS

NT FAST NEUTRONS

NT FERMIONS

NT FREE ELECTRONS

NT GRAVITONS

NT HADRONES

NT HIGH ENERGY ELECTRONS

NT HOT ELECTRONS

NT HYPERONS

NT MESONS

NT N ELECTRONS

NT NEUTRINOS

NT NEUTRON BEAMS

NT NEUTRONS

NT NUCLEONS

NT PHOTOELECTRONS

NT PHOTONS

NT PIONS

NT POLARONS

NT POSITRONS

NT PROTONS

NT QUARKS

NT RECOIL PROTONS

NT SOLAR PROTONS

NT TACHYONS

NT THERMAL NEUTRONS

Soviet papers on elementary particle and cosmic ray physics covering elastic and nonelastic collisions at high and superhigh energies 10 p1662 A71-24665

Particle precipitation at auroral heights, examining ground based observations evidence for existence of protons, neutrons and electrons 12 p1947 A71-26864

Elementary particle recombination probabilities on solid body surface, using reactive gas model in form of quantum mechanics three body problem 12 p1934 A71-27546

Elementary particle geometrical-group model assuming negative curvature de Sitter space inside and flat space outside 17 p2778 A71-34627

Simultaneous solution of Einstein and elementary particle motion equations for space-time curvature within particle resulting from self gravitation 17 p2778 A71-34628

Papers on elementary particle and cosmic ray physics, covering neutron monitor, fireball models, radio pulses and X ray astronomy 18 p2957 A71-36209

Soviet papers on geometrical and group methods in gravitational and elementary particles theory, covering relativity and electromagnetic and quantum fields 19 p3104 A71-38578

Wave and elementary particles equations invariance properties relationship with respect to Lie group and conservation laws 19 p3105 A71-38579

Critique of cosmological theories based on spontaneous matter creation in strong gravitational fields, deriving particles discrete number constancy in general relativity 20 p3268 A71-38834

ELEVATION

Elevation determination methods for unmanned lunar roving vehicle, considering instruments, orbiter tracking, etc 08 p1272 A71-21324

ELEVATION ANGLE

Circumzenithal micrometric recording of almucantar passages of stars 03 p0422 A71-13011

Thunderstorms anvil cloud high level outflow mapping by Doppler radar at various heights and elevation angles 05 p0721 A71-16669

High target geodetic coordinates determination by measuring vertical angles without using azimuth 06 p0889 A71-17675

Monopole radiation on ground screens, deriving modified elevation angle to transform quasi-far zone measurements 06 p0868 A71-17716

Refractive errors in spaced antenna radio angle-of-elevation measurements based on comparison with use of single directional antenna 12 p1881 A71-27424

Low elevation angle tropospheric fading relationship to satellite communications and broadcasting at frequencies between 1 and 20 GHz 17 p2703 A71-35083

ELEVATIONS [DRAWINGS]

U DRAWINGS

ELEVATORS [CONTROL SURFACES]

Automatic gust alleviation system employing inertial sensors and feedback devices with wing flaps and elevators, considering linkage control, noninteracting control and split control 11 p1706 A71-25195

Sailplane elevator induced maneuvering and horizontal tail surface loads, discussing airworthiness requirements 13 p1997 A71-29256

ELEVONS

Elevons as longitudinal and lateral control elements on low aspect ratio wings, calculating subsonic and supersonic aerodynamic characteristics 13 p1993 A71-29198

ELLIPSOIDS

Boundary value problems solution in elasticity theory of isotropic homogeneous body configurations close to ellipsoid of revolution, obtaining stress-strain state by approximate method 02 p0325 A71-12288

Ellipsoidal pressure vessel heads failure mode analysis, considering buckling under internal pressure and design formula with safety factors [ASME PAPER 70-PVP-26] 04 p0665 A71-14766

Earth ellipsoid physical constants using satellite measurements of geocentric gravitational constant earth-moon mass ratio and geopotential harmonic coefficients 04 p0581 A71-15066

Orthotropic shell with hollow elliptical paraboloid form, discussing numerical solution for normal concentrated load action 06 p0998 A71-17855

Influence coefficients closed forms for one and two sheet hyperboloids and ellipsoidal and paraboloidal shells under axisymmetrical edge loads 06 p1002 A71-18413

Stable ellipsoidal plasma configurations in alternating electrode annular system, considering longitudinal magnetic field strength, electrode voltage and gas discharge chamber pressure 07 p1171 A71-20185

Linearized Boltzmann equation analytic solutions for rarefied gas dynamic problems, using ellipsoid model 07 p1093 A71-20285

Gyrostator with center of gravity on ellipsoid axis, determining motion by two invariant algebraic equations 07 p1209 A71-20645

Composite elongated ellipsoid of revolution under torsion, determining stress-strain state, boundary conditions and elastic displacements 08 p1368 A71-20800

Incompressible equilibrium plasma ellipsoid stability in electromagnetic traveling wave field 08 p1341 A71-21500

Generalization of restricted three body problem in formulation with principal gravitating body constituting flattened ellipsoid 12 p1964 A71-27177

Rotating Jacobi ellipsoid evolution by gravitational waves emission, discussing triaxial nonaxisymmetrical configurations for rapidly rotating pulsars 13 p2140 A71-29000

Stress-strain state of thin walled ellipsoidal shell of revolution with arbitrarily oriented crack 13 p2156 A71-29069

Internal potential of heterogeneous ellipsoids for even and odd power variation of density with coordinates, using depolarization factors 14 p2304 A71-29600

Triaxial ellipsoid asteroid models, determining light curves and variations 14 p2312 A71-30385

Incompressible equilibrium plasma ellipsoid stability in electromagnetic traveling wave field 16 p2618 A71-33048

Sun as flattened ellipsoid of revolution, showing flatness effects on planet motion in relativity theory framework 16 p2612 A71-33356

Earth ellipsoid gravitational potential selection influence on geoid height determination, using near-geoid model 23 p3674 A71-44051

Thermal radiation hemi-ellipsoidal and hemispherical collectors efficiency characteristics from Monte Carlo simulation for focusing photon bundle trajectories 23 p3783 A71-44191

ELLIPSOIDOMETERS

Ellipsometric determination of optical constants for weakly and strongly absorbing specimen 22 p3576 A71-42572

ELLIPTIC DIFFERENTIAL EQUATIONS

Schwarz-Neumann method for Dirichlet problem of elliptic differential equations describing regions intersection in n-dimensional Euclidean space 01 p0109 A71-10031

Initial Dirichlet boundary value problem parabolic and elliptic equations of order 2n, discussing existence and uniqueness proofs 02 p0276 A71-12532

Finite elastic deformation differential operator strong ellipticity conditions, discussing dependence on material elastic moduli 03 p0501 A71-13071

Atmospheric models integration, discussing elliptic partial differential equation solution 03 p0453 A71-13326

- Dirichlet problem for elliptic equations with unbounded lowest coefficients, proving Gordin inequality 03 p0451 A71-13966
- Boundary value problem for second order elliptic equation with discontinuous coefficients, discussing solvability conditions and boundary characteristics 05 p0775 A71-16887
- Algorithm for solving parabolic and elliptic partial differential equations with computing time, storage requirement and programming ease advantages 05 p0776 A71-17221
- Boundary value problems for singular elliptic partial differential operators, with application to region bounded by smooth manifold 06 p0916 A71-17386
- Dirichlet problem associated with elliptic partial differential equation, discussing integral operator methods for approximating numerical solution 06 p0920 A71-18208
- Singular perturbation problems for linear second order elliptic equation, obtaining asymptotic approximations for simple unbounded regions with free boundary layer terms 10 p1636 A71-23934
- Sturm oscillation theorems for second order elliptic equation nonlinear partial derivatives, using linear Picone identity 11 p1791 A71-25176
- Elliptic equation boundary value problems solution, using finite difference representation 11 p1792 A71-26156
- Plastic deformation of elliptic inclusion in plane strain of infinite plate, using viscoelastic analogy 11 p1852 A71-26395
- Dirichlet problem for elliptic differential equations with lowest derivatives coefficients and leading term in Bitsadze operator, discussing reduction to singular integral equation 12 p1923 A71-27511
- Dirichlet problem for degenerate elliptic differential equations, discussing existence and uniqueness of solution by Schwarz alternating method 12 p1923 A71-27512
- Error estimates for class of least squares methods for 2nd order elliptic boundary value problems solution approximation 13 p2093 A71-27803
- A priori bounds on linear and nonlinear quotients of Neumann boundary value problem for uniformly elliptic difference equations over rectangular regions 14 p2265 A71-30291
- Cauchy problem solution for elliptic equations of fourth order in two independent variables, improving Henrici, Pucci and Colton results 14 p2266 A71-30811
- Singularities in linear elliptic partial differential equations, considering Cartesian and cylindrical polar coordinate problems 15 p2440 A71-31348
- Dirichlet problem for second order linear elliptic differential equations, considering convergence theory results for finite difference approximations 15 p2440 A71-31349
- Monograph on elliptic differential equations numerical solution covering approximations, relaxation, iterative, integral equation and variational methods, and applications to boundary value problems 15 p2441 A71-31508
- Uniqueness of positive solutions to self adjoint elliptic partial differential equations with nonlinear forcing terms under Dirichlet and Neumann boundary conditions 15 p2442 A71-31872
- Difference analogs of Dirichlet problem for second order quasi-linear elliptic operators with mixed derivatives, using discretization method 15 p2442 A71-32312
- Hilbert space valued systems and elliptic boundary value problems stability, employing circle criterion 16 p2549 A71-32978
- Convergence rate for finite element method, considering Neumann problem for second-order elliptic differential equations with constant coefficients in m dimensional Euclidean space 17 p2769 A71-35688
- Global convergence of iterative schemes by Newton-Gauss-Seidel method, considering discrete approximations of elliptic partial differential equations 17 p2769 A71-35689
- Linear functional equations bounded solutions stability by reflexive Banach space mapping, applying to elliptical and parabolic differential equations ill-posed problems 18 p2941 A71-36351
- Divergence structure nonlinear elliptic equations, demonstrating smooth solutions uniqueness of Dirichlet problem 18 p2942 A71-36816
- Approximation solution for elliptic boundary value problem with nondifferentiable parameters, considering second order linear partial differential equations in two independent variables 18 p2942 A71-36817
- Regular boundary value problems singularities for linear second order analytic elliptic equations solutions in two independent variables 18 p2942 A71-36925
- Finite element method for elliptic differential equations solution, avoiding incidental technical difficulties 19 p3087 A71-38303
- Error behavior in numerical solution of elliptic differential equations boundary value problems by least squares approximation 19 p3087 A71-38304
- Numerical solutions of boundary value problems for linear elliptic partial differential equations by function theoretic methods 19 p3087 A71-38308
- Pointwise bounds in Cauchy problem for fourth order quasi-linear equation using a priori inequality, applying Rayleigh-Ritz technique to elliptic partial differential equations 20 p3255 A71-39573
- Positive solutions for nonlinear elliptic boundary value problems with convex nonlinearities 21 p3407 A71-40211
- Theorems on parabolic and hyperbolic differential equations solutions continuous dependence on elliptic operator coefficients, deriving proof by hypothesis of existence and uniqueness 21 p3408 A71-40651
- Constructive existence theorem for nonlinear elliptic equation with restricted bounded domain 21 p3409 A71-41078
- Finite difference methods application to Euler nonlinear elliptic differential equations, using symmetric and positive Jacobian 22 p3567 A71-42375
- Viscous hydrodynamic equations functional type boundary value problem, investigating uniqueness theorem for elliptic equations 22 p3531 A71-42629
- Three dimensional unbounded anisotropic elastic medium with ellipsoidal inhomogeneity and modulus tensor of piecewise-constant form 24 p3885 A71-45062
- ELLIPTIC FUNCTIONS**
- Elliptic integrals for gravitational potential in symmetry plane of Milky Way galaxy 01 p0148 A71-10033
- Elliptic boundary value methods applied to parabolic initial boundary problems 01 p0111 A71-10320
- Earth spherical and ellipsoidal gravity potential coefficients association using Lamé orthogonal function properties 01 p0155 A71-10388
- Quasi-linear elliptic boundary point solutions, deriving modulus of continuity estimates 04 p0619 A71-15552
- Elliptical boundary value problems with conditions not in direction normal to boundary, deriving theorems on homomorphisms and Green formula 05 p0774 A71-16418
- Elliptic-function low pass microwave filters and other C sections applications including broadband impedance transformers 08 p1262 A71-20766
- Homogeneous Newtonian cosmological model, constructing ellipsoidal velocity distributions and kinetic theory 08 p1358 A71-20932
- Tricomi problem for elliptic-hyperbolic Chaplygin equation extended to mixed Lavrentev-Bitsadze equation 10 p1635 A71-23802
- Spherical and ellipsoidal functions relationship for terrestrial gravitational field anomalies 16 p2564 A71-33571
- Soviet book on theory of elliptic functions covering analytic functions, Jacobi and Liouville theorems, modular functions, Weierstrass functions, theta and Jacobi functions 17 p2767 A71-35200
- Nonlinear eigenvalue problem solution in real Banach space, investigating continua existence and elliptic equations application 18 p2942 A71-36818
- High order finite element solution roundoff error reduction, using discretization of elliptic equations 21 p3409 A71-40962
- Out-of-plane motion about libration points within framework of elliptic restricted three body problem, using Mathieu and Hill equation [AAS PAPER 71-336] 23 p3727 A71-43009
- ELLIPTIC INTEGRALS**
- U ELLIPTIC FUNCTIONS**
- ELLIPTICAL CYLINDERS**
- EM oscillations of open elliptic profile cylindrical mirrors resonator with dielectric elliptic cylinder 03 p0386 A71-13800
- Computerized nonlinear collapse analysis of elliptical cylinders and cones under axial compression 05 p0823 A71-16555
- Elliptical cylindrical shell under internal pressure, investigating stress concentration near surface hole 06 p0994 A71-17821
- Design criteria for buckling prediction of elliptical and circular cylindrical shells under axial compression from asymmetric and axisymmetric shape imperfections distribution 06 p1003 A71-18588
- Nonlinear finite difference computer program applied to elliptic cylinder collapse under uniform external pressure, comparing with theoretical bifurcation buckling [AIAA PAPER 71-146] 06 p1003 A71-18589
- Equilibrium positions of multiple pairs of vortices in wakes of circular and elliptic bodies 07 p1087 A71-18901
- Imperfect elliptical cylindrical shells buckling under axial compression, demonstrating imperfection sensitivity 07 p1213 A71-19888
- Viscous incompressible fluid flow between two cofocal elliptic cylinders, discussing temperature distribution and heat transfer in annuli 07 p1224 A71-20029
- Plane TM wave scattering by systems of two parallel conducting elliptical cylinders, metal tapes and combinations 09 p1407 A71-23106
- Scattering structures of two parallel elliptical cylinders, tapes or combinations, deriving surface current density distribution under plane TM wave excitation 09 p1407 A71-23107
- Numerical analysis of steady symmetric incompressible flow past elliptical cylinders for Reynolds numbers up to 90 12 p1895 A71-26739
- Newtonian limit of hypersonic flow over elliptic cylinder, finding standoff distance by Freeman result 12 p1863 A71-27055
- Elastic plane shear wave diffraction on elliptical cylinders in half space, using elliptical wave function series and linear algebraic equations 12 p1978 A71-27332
- Thin shell isotropic clamped free elliptical cylindrical shells with various cross sectional eccentricities, measuring frequencies and mode shapes by vibration analysis 14 p2324 A71-29869
- Sting-free aerodynamic drag measurement on ellipsoidal cylinders in subsonic wind tunnel at transition Reynolds numbers 18 p2843 A71-36037
- Hyperelastic compressible isotropic elliptical and circular cylinders simple bending, studying second order effects 18 p2977 A71-36195
- Elliptical cylinder pump cavity design for solid state laser with ideal beam geometry 20 p3246 A71-39493
- Varying magnetic field disturbance by eddy currents in conductive elliptical cylinder, obtaining field vector potential and magnetic induction vector 22 p3528 A71-41769
- ELLIPTICAL ORBITS**
- NT APOGEES**
- NT INTERPLANETARY TRANSFER ORBITS**
- NT PERIGEEES**
- NT PERIHELIONS**
- NT TRANSFER ORBITS**
- Monograph on visibility of satellite in elliptic orbit covering probabilistic aspects, communication, navigation, weather, reconnaissance and scientific satellites 02 p0319 A71-11970
- Hyperbolic, elliptical and parabolic heliocentric motion, determining location of body in orbit with unitary method 03 p0493 A71-14194
- Artificial satellites rendezvous, describing common Kepler ellipse in central body field with positioning after time delay 03 p0500 A71-14389
- Elliptic restricted problem periodic Trojan librations about equatorial points, analyzing stability 04 p0652 A71-15704
- Resonance in planar elliptic restricted three body problem, noting primaries eccentricity and long term effects 04 p0653 A71-15710
- General elliptic three body problem, discussing triangular Lagrangian point stability 05 p0809 A71-16472
- Exact expression for minimum range sensitivity deorbit from elliptical orbits for ballistic atmospheric entry vehicle, considering retrovelocity 07 p1199 A71-19873
- Spacecraft minimum impulse /or fuel/ ellipse-ellipse transfer, discussing computer survey results of 650 trajectories 07 p1199 A71-19899
- Minimal characteristic velocity of single impulse transfer between coplanar elliptical orbits with allowance for thrust action finite time 09 p1519 A71-22544
- Satellite path geometry along Keplerian elliptical orbit, taking earth flattening into consideration 09 p1520 A71-22664

Intermediate elliptical orbits for planetary satellites with small inclination to equatorial plane
09 p1520 A71-22671

Elliptical motion series representation, presenting methods for estimating values of Bessel functions, Fourier and Hansen coefficients
09 p1486 A71-23336

Minimum N-impulse time free transfers between elliptic orbits for Lawden primer vector, using state and adjoint variables during firing
11 p1820 A71-25460

Weierstrass condition for optimality in coplanar elliptic orbit transfer involving velocity impulse control variables, discussing switching relations at corner of optimal trajectory
12 p1963 A71-27061

Tumbling triaxial satellite in elliptical orbit about spherical planet, determining resonant and nonresonant gravity gradient perturbations
13 p2145 A71-28356

Minimum time low thrust rocket transfer between elliptic orbits in strong gravity field, using averaging method
13 p2139 A71-28816

Gravity stabilized satellite in elliptic orbit, examining rotational motion equations stability
15 p2499 A71-31159

Forced vibration damping of satellites in elliptical orbits by variable cantilevers and rotor
15 p2499 A71-31177

Artificial earth satellites initial elliptical orbit calculation, discussing function minimization for optical radar and laser observation
15 p2481 A71-31301

Plane librational motion of axially symmetric satellite in elliptic orbit, developing periodic solution
15 p2488 A71-32092

Elliptical and circular orbit satellite injection capabilities of Europa 2 launch vehicle, considering geostationary orbit and launcher performance
16 p2645 A71-33364

Earth satellite plane periodic oscillations damping with respect to center of mass in orbital plane during motion on elliptical Kepler orbit
16 p2646 A71-33659

Approximate multi-impulse large amplitude optimal rendezvous between neighboring elliptical orbits
17 p2807 A71-35472

Martian satellites motion along arbitrary elliptical orbits, expressing planet gravitational potential
18 p2962 A71-36108

Spectroscopic binary star system with orbital eccentricities less than 5 percent, discussing elliptical or circular orbit possibility
18 p2971 A71-37068

Elliptic parameters of osculating orbits in two body problem with variable mass
20 p3267 A71-38791

Two dimensional elliptic restricted three body problem, considering regularization mechanism and periodic collision orbits
21 p3441 A71-40095

Impulsive retrofire boost of rocket vehicles initially moving in elliptical orbits for maximum and minimum atmospheric entry angles
22 p3608 A71-41697

High and low propulsion for optimal transfers between coplanar coaxial elliptic orbits, determining impulse number and timing
23 p3729 A71-43038

ELLIPTICAL POLARIZATION

Computer program for processing elliptical polarization observations of nebulas and comets
02 p0251 A71-12360

Modified Fesenkov method for calculating Stokes polarization parameters applied to elliptical polarization observations of nebulae
02 p0251 A71-12361

Coherence matrix of elliptically polarized radio signal scattered by statistically rough conductive surface
04 p0550 A71-14619

Handedness formula for elliptical polarization after specular metallic reflection of linearly polarized light
07 p1111 A71-19485

Magnetoionic component with fluctuating elliptical polarization during wave reflection from F 2 layer, discussing suppression mechanism
13 p2030 A71-28537

Jupiter reflected light, examining model having elliptical polarization by surface layer scattering
14 p2306 A71-29730

Polarization ellipse and depolarization coefficients for monochromatic radio waves reflected from F 2 ionosphere using Stokes parameters
19 p3056 A71-38362

Coherence matrix of elliptically polarized radio signal scattered by statistically rough conductive surface
22 p3510 A71-42259

ELLIPTICITY

Displacement type equilibrium equations for small deformation imposed on initial finite deformation,

estimating elastic energy function based on strong ellipticity condition
03 p0510 A71-13945

Principal homogeneous spaces above elliptical curves over discretely normalized local field
06 p0918 A71-17572

Elliptic ring shaped disk with external and internal loading, determining stresses due to uniformly distributed loads
06 p1002 A71-18416

Elliptical cones at large angle of attack, calculating three-component real gas properties effects on aerodynamic characteristics
13 p1993 A71-29191

Galactic brightness, color distribution and ellipticity data from photometry and colorimetry observations
15 p2486 A71-32028

Hypercircle method application to elliptic variational problems, obtaining bounds for error in boundary value problems approximation
19 p3087 A71-38302

Conical ablation surface models in hypersonic wind tunnel tests, describing Mach number and nosetip bluntness effects on cross hatching
21 p3476 A71-40965

Lifting line equation inversion for twisted wings of elliptic planform with arbitrary spanwise upwash
22 p3481 A71-42838

Ellipticity of weakly rotating configurations, determining 5m/4 delta ratio for white dwarfs
23 p3770 A71-44063

ELONGATION

Disk elongation plastic deformation, determining elastoplastic stressed state for inhomogeneous thermal cycles
02 p0323 A71-11748

Reduction-elongation relation in plastic deformation of tensile test samples of Ti alloys subject to thermomechanical treatment
02 p0265 A71-12523

Strengthening curve determination by tensile tests for plastic yield limit, strength and elongation at rupture
04 p0673 A71-15898

Concentrated elongation dependence on cross sectional area reduction in industrial Ti alloys undergoing thermomechanical treatment
09 p1468 A71-22324

Ferrous and nonferrous sheet metals neck formation prevention for increasing elongation in tensile tests, using continuous plastic bending method
09 p1479 A71-23697

Tensile yield and ultimate strength and elongation of Al after unidirectional and reversed torsional prestrain
10 p1624 A71-23940

Ta nitriding temperature and duration effects on tensile strength, elongation and surface hardness
15 p2424 A71-31240

Al alloy tensile tests at high temperature and constant elongation and loading rates, noting creep strain
20 p3251 A71-39167

Graphite high modulus fiber material tensile strength, modulus of elasticity and elongation measurement method and equipment
23 p3696 A71-42898

ELUTION

Dipeptides separation and identification by column and paper chromatography for elution times prediction and sequence studies
08 p1251 A71-21688

ELUTRIATION

U ELUTION

EMBEDDING

Embedded electrical resistance strain gages for three dimensional stress measurement, describing modifications for internal stresses reduction
05 p0830 A71-17242

EMBOLISMS

NT AEROEMBOLISM

Acute pulmonary embolism diagnoses, using vasculature angiography
07 p1042 A71-19838

Pulmonary dissipation of gas emboli produced by oxygen, nitrogen and carbon dioxide intravenous injection in unanesthetized sheep with chronically implanted ultrasonic Doppler flow probes
21 p3330 A71-40342

EMBRITTELEMENT

Cryogenic austenitic steels embrittlement dependence on nitrogen content, noting second phase precipitation role
01 p0098 A71-10086

Stress intensity factors of hollow notched bars and hydrogen embrittled solid specimens
03 p0443 A71-13751

Stress corrosion cracking mechanism, considering anodic dissolution, local surface enrichment and hydrogen embrittlement in noble metal species
04 p0610 A71-14892

High strength steel reversible hydrogen embrittlement mechanisms, noting role of hydrogen diffusion
04 p0615 A71-15790

He embrittled stainless steel stress-rupture behavior under vacuum and elevated temperature conditions, discussing microstructural characteristics
06 p0914 A71-18688

Ti alloy embrittlement by prolonged high temperature exposure, using substandard fracture mechanics test for time-temperature dependence
06 p0915 A71-18688

Ultrasound effects on Ti alloys Hg embrittlement and stress corrosion cracking by methanol-water-hydrochloric acid mixture
07 p1137 A71-19978

Hydrogen embrittlement in hot salt stress corrosion of Ti alloy
07 p1142 A71-20373

Maraging steels thermal embrittlement, discussing austenite grain boundaries inclusions, carbide network precipitation and carbon concentration
08 p1305 A71-21027

Phosphorus segregation to prior austenite grain boundaries in ferrite, considering effect on Ni-Cr-C-P steel temper embrittlement
09 p1471 A71-23123

Steel alloys solid Cd embrittlement, discussing crack propagation rate temperature dependence and Cd surface diffusion as controlling effect
11 p1777 A71-25447

Quenched and tempered steel, investigating embrittlement as function of temperature in partially dissociated atomic hydrogen environment
11 p1779 A71-26013

Ni-base alloys hardened by gamma prime precipitation, investigating embrittlement by oxygen
12 p1917 A71-27313

Stress relief cracking in Cr-Mo steel, considering correlation with embrittlement of water quenched base metal tempered at low temperature
13 p2086 A71-29091

Ti-Al binary alloy embrittlement in sea water by notched cantilever beam stress corrosion test, investigating alpha 2 particle precipitation effect on cracking susceptibility
14 p2256 A71-29522

Precipitation hardenable Ni-base alloys embrittlement in high temperature oxygen atmosphere, considering intergranular crack initiation
15 p2434 A71-32257

Cryogenic austenitic steels embrittlement dependence on nitrogen content, noting second phase precipitation role
16 p2593 A71-33642

Refining and hardening reactive additions effect on slow cooling grain boundary embrittlement response of maraging steel
17 p2756 A71-34490

Reversible hydrogen embrittlement mechanism in hydrogenated steels
17 p2757 A71-34496

Plastic deformation and embrittlement due to stress raisers in steel cylinders from high speed tensile tests at low temperatures
17 p2832 A71-35462

Omega phase embrittlement in aged Ti-Mo alloy, giving tensile properties and load-elongation diagrams
19 p3082 A71-38176

Stress relief, temper and creep embrittlement effects on ferrous alloy welds
19 p3082 A71-38317

Acoustic emission technique for nondestructive cracking rate determination in hydrogen embrittled steel, using crack-tip stress intensity factor as critical parameter
20 p3241 A71-38773

Corrosion resistant materials evaluation for suitability in high strength fasteners, considering mechanical properties, stress corrosion cracking and hydrogen embrittlement problems
20 p3251 A71-39340

Charpy impact test measurement of maraging steel thermal embrittlement, observing fracture mode and toughness changes with heat treatment
21 p3398 A71-40467

Metal embrittlement by gaseous hydrogen, discussing countermeasures against hydrogen metal interaction and cracking
22 p3562 A71-41999

EMBRYOS

Embryo chemical sensitization to low radiation doses damage by radiosensitizer iodoacetamide
07 p1037 A71-18963

Prenatal exposure to hypoxia, showing prolonged suppression of labeled amino acid incorporation into developing submandibular gland and pancreas in neonatal period
07 p1042 A71-19698

Mechanical vibrations effects on mouse embryos growth and development, investigating critical frequencies and accelerations
23 p3637 A71-44246

EMERGENCY BREATHING TECHNIQUES

Emergency surface decompression and treatment procedures for project Tektite aquanauts, determining safe interval and schedules for return to habitat on ocean floor
16 p2535 A71-33110

EMERGENCY LIFE SUSTAINING SYSTEMS

Aircraft emergency evacuation illumination standards, considering independent power source, crash survivable installation, operation initiation and exit visibility

01 p0004 A71-10030

Altitude range for supplemental aircraft continuous flow, diluter and pressure demand oxygen systems, discussing regulations and pressure breathing

08 p1244 A71-20714

Emergency backup /secondary pressurization/ devices for aerospace crew and passenger safety and comfort, considering high altitude pressure suits

08 p1244 A71-20716

Aerospace emergency escape systems and procedures, discussing physical, biophysical and physiological aspects related to increased flight speeds and altitudes

08 p1245 A71-20717

Reevaluation of emergency pressurization requirements for brief flights over 50,000 feet, considering pressure suit requirement

08 p1247 A71-20822

Biomedical requirements and emergency planning for aerodromes, surveying U.S. airports

18 p2864 A71-35999

Recovery, launch and landing operations of earth orbital shuttle vehicles, discussing space rescue capabilities

22 p3609 A71-41989

EMISSION

NT BIOLUMINESCENCE
NT CHEMILUMINESCENCE
NT ELECTROLUMINESCENCE
NT ELECTRON EMISSION
NT FIELD EMISSION
NT FLUORESCENCE
NT HYDROXYL EMISSION
NT ION EMISSION
NT LIGHT EMISSION
NT LUMINESCENCE
NT LUNAR LUMINESCENCE
NT NEUTRON EMISSION
NT OPTICAL RESONANCE
NT PARTICLE EMISSION
NT PHOTOELECTRIC EFFECT
NT PHOTOELECTRIC EMISSION
NT PHOTOIONIZATION
NT PHOTOLUMINESCENCE
NT RADIO EMISSION
NT SECONDARY EMISSION
NT SOLAR RADIO BURSTS
NT SOLAR RADIO EMISSION
NT SPECTRAL EMISSION
NT SPONTANEOUS EMISSION
NT STIMULATED EMISSION
NT THERMAL EMISSION
NT THERMIONIC EMISSION
NT THERMOLUMINESCENCE
NT TYPE 2 BURSTS
NT TYPE 3 BURSTS
NT TYPE 4 BURSTS
NT X RAY FLUORESCENCE

EMISSION SPECTRA

Wide angle far UV photography of Barnard Loop Nebula in Orion suggesting nebular emission intensity difference with near UV region due to interstellar dust

01 p0148 A71-10001

Mg I and II vacuum UV emission series, presenting quantum defect plot

01 p0129 A71-10137

Extra-atmospheric submillimeter astronomy, discussing emission observations between IR and RF region and astrophysical-cosmological applications

01 p0151 A71-10146

Solar emission line spectra second observation outside total eclipse, noting big coronal condensation above eastern limb

01 p0159 A71-10869

Shock generated Ar plasma emission spectrum intensity measurements, describing fast-response spectrometer sensitivity calibration method

01 p0134 A71-10997

Multifrequency gas laser spectrum structural changes caused by small external light signals

01 p0095 A71-11115

Visual, photographic and photoelectric observations of polar auroras and hydrogen emission at conjugate points

02 p0242 A71-11757

Multiatomic molecules emission spectra excitation by superhigh frequency short duration pulsed gas discharges

02 p0286 A71-11889

K-beta and L-alpha X ray spectral emission bands of high melting vanadium compounds, considering chemical bonds

02 p0263 A71-11892

Particulate silicates IR emission spectra under simulated lunar conditions, noting existence of nearly optimum conditions on moon surface

02 p0305 A71-11987

Extragalactic radio source 3CR catalog, analyzing emission spectra

02 p0300 A71-12087

Hydroxyl and water vapor emission properties in interstellar medium attributed to maser action

02 p0313 A71-12498

Wolf-Rayet WN6 stars emission line spectral profiles observation by spectrograms and photoelectric scanning

02 p0314 A71-12584

Potassium vapor emission spectrum fine structure in high power ruby laser field, noting dependence on vapor pressure

02 p0262 A71-12612

Jupiter decimetric emission circular polarization, observing equatorial magnetic field strength in radiation belt

02 p0317 A71-12868

Organic compounds carbon K emission spectra, using light element X ray spectrometer for aliphatic, aromatic and partly ionic substances spectral analysis

03 p0375 A71-13200

Mira Ceti type long period variable giant stars emission spectra, emphasizing UVB photometry and IR electrophotometry

03 p0486 A71-13267

Sodium dayglow rocket measurements, comparing emission intensities with ground based measurements

03 p0407 A71-13312

Optically coupled GaAs injection lasers emission spectra, determining maximum frequency difference in gain bandwidths for mode synchronization

03 p0435 A71-13506

Emission kinetics for linearly polarized waves from composite ruby laser, describing pumping power effects

03 p0435 A71-13513

Fabry-Perot spectrometer systems for solar corona emission spectra and temperature measurements during eclipses

03 p0489 A71-13629

Nd glass laser radiation time and spectral structure

03 p0437 A71-13885

Emission threshold current in semiconductor heterojunction p-p-n laser

03 p0439 A71-13977

Solar X-ray emissions dynamic spectra at flare times by E-T tracing

03 p0479 A71-14045

CdS single crystals green edge emission and optical flash spectra, discussing wavelength, UV excitation intensity and temperature effects

03 p0468 A71-14384

Parametric laser with single mode pumping, investigating emission spectra fine structure

04 p0608 A71-15120

URCA neutrino emission processes explaining anomalous isotopic heavy element abundance in solar system

04 p0651 A71-15660

High pressure rare gas UV emission spectra, examining wavelength cut-offs and flux ratios

04 p0549 A71-15691

Galactic sources 18 cm OH emission and/or absorption observation

04 p0657 A71-15759

CO laser emission lines and nitrogen oxides absorption lines spectral coincidences observations

05 p0762 A71-16339

VLF emissions at low latitudes by transverse and longitudinal resonance electron energies calculations

05 p0721 A71-16441

Lunar microwave emission effects and local surface temperature variations due to outward heat flow and low thermal conductivity

05 p0809 A71-16459

Ionic meteor emission spectra calculation using two-step ionization and excitation model, accounting for atmospheric molecules and vapor atoms collisions

05 p0812 A71-16693

IR object IRC plus 10216 carbon monoxide emission at 2.6 mm, noting spectral line width, thermal emission and mass

05 p0812 A71-16695

W, Nb, Mo and Ta spectral radiative power at wavelengths from 0.66 to 5.12 mu at various high temperatures

05 p0768 A71-16780

Arsenic first spark line spectra using high resolution grating spectrograph and Fabry-Perot interferometer

05 p0717 A71-16910

Emission line spectra of halogens Cl I, Br I and I I in 4-micron region

05 p0717 A71-16911

Cross sections for fluorescence production in carbon dioxide photoionization by 58.4 nm radiation, deriving emission spectra

06 p0963 A71-17255

Laser emission from helium-air-methane mixture identification by comparing with vibrational rotational transition

06 p0906 A71-17307

Atlas of 21 cm H I emission line profiles of outer part of Galaxy in Galactic anticenter region, plotting brightness temperature vs radial velocity

06 p0964 A71-17348

Solar corona emissions, discussing very high temperatures origin, eclipses and electromagnetic radiation spectrum

06 p0970 A71-18058

Markarian galaxies spectra, analyzing emission line characteristics

07 p1191 A71-19283

Electron scattering effect on emission and absorption lines in stellar atmosphere, considering primary radiation sources uniform distribution and photosphere radiation transmission through electron atmosphere

07 p1192 A71-19291

Geomagnetic activity effects on atomic oxygen emissions in green and red light, noting radiant intensity, strong dispersion, local and planetary Kp indices

07 p1101 A71-19413

Laser microprobe emission spectroscopy of biological matrix elements, investigating bovine albumine effect on spectrum analysis

07 p1113 A71-19785

Organic dye lasers lasing conditions calculation for constant emission frequency from nonstationary emission kinetics analysis

07 p1125 A71-19807

Chlorine dioxide induced fluorescence spectra, using argon ion laser

08 p1300 A71-20667

Crab Nebula and pulsar NP 0532 X ray spectra discussing pulse profile, emission and interstellar absorption

08 p1353 A71-20984

Solar X-ray flare region structure and emission flux density and spectral composition, using satellite-borne photometers and spectroheliographs

08 p1354 A71-21014

Extragalactic radio source 3CR catalog, analyzing emission spectra

08 p1362 A71-21137

Book on nonresonant feedback in lasers covering multimode cavity, emission spectra, generation in cloud, quasi-concentric resonator, etc

08 p1301 A71-21226

Microwave electromagnetic emission in theta pinch hydrogen plasma by sensitive superheterodyne receivers, noting discharge azimuthal current

08 p1339 A71-21477

Twilight helium 10,830 A emission observations and calculations, using grille spectrometer

08 p1283 A71-21638

Radio source OZ-252 radiant flux density spectrographic observation, noting quasi-stellar object emission spectra

09 p1516 A71-22065

Holographic spectrum analyzer for plasma diagnostics in microwave band, deriving formulas for emission spectrum based on interference patterns intensities in waveguide

09 p1499 A71-22150

Balmer emission lines in hydrogen cloud in bright galactic nucleus

09 p1518 A71-22351

Organic scintillators as active laser materials, discussing absorption, oscillation and emission spectra and luminescence quantum yield

09 p1461 A71-22386

Crab Nebula emissions on 4 and 6 November 1970, observing optical circular polarization

09 p1522 A71-22981

Emission line profile and source function in finite optical thickness plane layer, using matrix equation

09 p1525 A71-23195

Condensed state Ni and Pd atoms X ray emission spectra and electron structure

09 p1474 A71-23233

Al-Co alloys, investigating Al and Co intermediate phases formation effect on X ray emission K spectra

09 p1474 A71-23234

Lunar equatorial region IR emission directional characteristics from brightness temperature measurements, developing cratered soil thermal model for negative surface relief studies

09 p1530 A71-23713

Solar simplified geometrical model, observing emission peak center to limb variation of Mg II, H and K lines and optical thickness

10 p1666 A71-23782

Sodium D line flare emission on solar surface vs comet scattering, using photoelectric observation in undisturbed center disk region

10 p1660 A71-23791

High sensitivity radiospectrography, obtaining solar emission spectra on decametric waves by radio telescope, focal antenna and receivers

10 p1667 A71-23826

NGC 2655 galaxy nucleus emissive gas/absorption line widths and stellar population, using network spectrographs

10 p1667 A71-23827

Isotropic emission features at 11.7/cm, discussing high resolution ground based spectrum measurement

10 p1599 A71-23869

Book on stellar spectroscopy for peculiar stars covering hot star spectra emission lines, novae, magnetic, metallic line and related stars

10 p1675 A71-24477

Soviet book on lasers with large angular divergence covering single mode generation, free electromagnetic fields equations, emission spectra, etc

10 p1621 A71-24728

Upper Martian atmosphere UV emission spectrum observation noting carbon dioxide photoionization, ion fluorescent scattering and photon/electron dissociative excitation

10 p1604 A71-24776

Magnetospheric VLF banded emissions spectral analysis, investigating OGO-5 data by high time resolution spectral techniques

10 p1579 A71-24788

Pulse rate and pumping power effects on emission spectra and I-V characteristics of multielement GaAs injection lasers

10 p1622 A71-24884

Emission dynamics of pulsed laser with optical delay line in resonator

10 p1622 A71-24885

Emission spectra, wavelengths and photoelectric intensities of triply-ionized gadolinium, using hollow cathode source with Czerny-Turner vacuum spectrograph

11 p1801 A71-25137

Gravitational radiation events-galactic microwave emission pulses relation, comparing with Weber gravitational wave experiment

11 p1820 A71-25298

Radiation from long lived ionic excited states, studying emission spectra, electron impact cross sections and positive nitric oxide ions band system

11 p1727 A71-25368

Jupiter far IR emission spectra models, examining atmospheric composition, temperature and structure

11 p1821 A71-25538

Carbon dioxide cations emission bands in Mars and Venus dayglows, suggesting fluorescent scattering and photoionization as main excitation sources

11 p1827 A71-25724

Emission spectra of solutions of oxazole and axadiazole derivatives and of tetraphenylbutadiene as effective active media for liquid phase lasers

11 p1774 A71-26001

Star Arcturus chromospheric Lyman alpha emission observation by rocket-borne precision pointing telescope and UV spectrometer

12 p1957 A71-26625

Measuring methods for internal velocities of stars and gas within spiral galaxy, considering emission lines and Fabry-Perot interferometer

12 p1960 A71-26786

Sidelight emission spectrum of He-Ne laser with/without oscillations, determining line intensity change and laser power dependence on discharge current

12 p1913 A71-26896

Magnetic field effect on emission spectrum and intensity at electron cyclotron frequency harmonics from PIG Reflex discharge, discussing electron oscillations excitation in plasma

12 p1938 A71-27214

Composite propellant flame temperature and emission spectra during depressurization by rarefaction waves, using rapid scanning spectrometer [AIAA PAPER 70-663]

12 p1945 A71-27564

Solar inner corona forbidden emission lines and continuum enhancement during 30 May 1965 eclipse as function of heliocentric position angle

12 p1969 A71-27650

Barium titanate pyroelectric receivers for giant pulse laser emission measurements

12 p1915 A71-27756

Gadolinium molybdate neodymium ions stimulated emission, noting luminescence, absorption and spectroscopic properties

13 p2111 A71-28424

Mathematical model for harmonic emission spectrum in FM and PM communication transmitters modulated by random signal

13 p2032 A71-28875

Crystalline media impurity light absorption spectral band shape, noting laser resonance emission effects

13 p2080 A71-29023

Kar quiet region chromosphere K emission line behavior, identifying surface characteristics for width absolute magnitude relation

13 p2140 A71-29046

Solar corona soft X ray emission, investigating temperature and flare activity effects

13 p2129 A71-29051

Continuous emission in solar flare spectra from spectroheliographic data, suggesting photospheric origin

13 p2129 A71-29052

Galactic H II regions 35 cm water source emission line profile observation, noting frequency and intensity variations

14 p2304 A71-29594

Michelson interferometer onboard Nimbus 4 satellite for recording earth IR emission spectrum

14 p2241 A71-30140

Neodymium glass laser free generation power with inert gas filled emission sources

14 p2254 A71-30274

Planetary nebula NGC 7009 narrow band filter photographs and spectra, detailing emission lines, intensity and velocity variations and model

14 p2313 A71-30430

Complex noise emission spectra from superposition of continuous component and peaks, calculating level separations due to perfectly reflecting plane

14 p2289 A71-30523

Lyman alpha emission cross sections for collisions of hydrogen ion and atom beams with thin target nitrogen and oxygen relevant to proton auroral analysis

15 p2397 A71-31763

Carbon monoxide-helium-oxygen laser emission continuous self mode locking and temporal structure for various optical cavity lengths

15 p2420 A71-32379

Uranus and Neptune microwave emission spectra and atmospheric temperatures, comparing with Jupiter and Mars

15 p2490 A71-32410

Multiply ionized Ar excited valency and inner shell transitions, investigating emission spectrum and energy levels

15 p2368 A71-32747

High temperature nitrogen plasma emission spectrum in 2500-5000 A range, estimating negative ion photoionization cross sections

16 p2613 A71-32900

Low energy solar X-ray emission spectra observations, discussing nonthermal electron spectrum relation to acceleration by electric fields

16 p2626 A71-33725

Coronal IR emission lines during solar eclipse of 7 March 1970, using high altitude aircraft-borne Fourier transform spectrometer

16 p2640 A71-33751

Circumstellar dust clouds and Bok globules examined for gaseous emission lines, emphasizing forced diffusion process

16 p2643 A71-34077

Periodic solar flare X-ray emission, presenting time separation from Vela 5 and 6 scintillation detectors

16 p2629 A71-34078

He-Ne laser emission spectra with AM by reflected Doppler shifted signal and matched/mismatched three-mirror resonator/mobile outer mirror

17 p2750 A71-34289

Organic dye laser properties analysis using universal relation between absorption and emission spectra for solvent molecules reorientation after excitation

17 p2752 A71-34388

NGC 2024 direction H I region H 137 alpha recombination line emission detection, determining ionized hydrogen fraction

17 p2807 A71-35415

Interstellar silicon monoxide discovery from 130,246 MHz frequency line emission of galactic radio source Sag B2

17 p2807 A71-35416

Solar activity and intensity ratios of O VII X-ray coronal emission lines, giving upper bound on electron density

18 p2965 A71-36734

Type 3 solar radio burst instantaneous emission frequency relationship to local plasma frequency in region with subrelativistic particles

18 p2958 A71-36742

Interstellar molecular hydrogen gas near IR emission detection in dark clouds

18 p2969 A71-37042

H alpha emission photometry for galactic H II region, obtaining contour diagrams

19 p3130 A71-37227

Nitrogen X ray emission K alpha band behavior in zirconium mononitride in entire range of Zn homogeneity

19 p3083 A71-37280

Vibrational energy distribution and emission lines of fluorine atoms plus chloroform reactions in chemical laser, using equal gain measurements

19 p3071 A71-37331

Spectral composition of emitted radiation, emissivity and absorptivity of Venus atmosphere at high temperatures

19 p3135 A71-37580

Solar flare X ray spectrum analysis for lower corona physical conditions, discussing continuum and line emission

19 p3126 A71-37623

Stellar chromosphere characteristics from OAO observation of magnesium II emission in late type stars

19 p3137 A71-37628

Gas concentration, field frequency and applied power level for control over electron temperature and emission spectra in microwave gas discharge plasma

19 p3113 A71-37764

Plasma diagnostics based on IR continuum intensity due to bremsstrahlung emission from plasma

19 p3113 A71-37765

Organic dyes pulse emission spectra shifts during pumping by ruby and neodymium-glass lasers, discussing vibrational relaxations role in mechanism

19 p3072 A71-37766

Geomagnetic activity effects on atomic oxygen emissions in green and red light, noting radiant intensity, strong dispersion, local and planetary Kp indices

19 p3054 A71-37833

Surface layer humidity correlation to height of atmosphere emitting in IR spectral region, determining water vapor content by recording earth radiation angular distribution

19 p3054 A71-37977

NO, CO and Ar mixtures IR spectral emission radiant intensities behind shock tube generated reflected shock waves

19 p3012 A71-38087

Ion formation in photochemically initiated combustion of acetylene-oxygen-nitric oxide mixtures, measuring carbon, CH and OH emission spectra and ion current time change

19 p3013 A71-38091

Flash photolysis initiated gaseous explosions detonation effects, observing ionization and radical emission spectra, absorption intensities and induction periods

19 p3169 A71-38110

Emission lines of star S22 in Large Magellanic Cloud, identifying H, Fe II and forbidden Fe II and Ni II lines

19 p3144 A71-38167

Spurious emissions from CW and pulsed GaAs solid state oscillators as function of material active layer thickness and contacting procedure

19 p3032 A71-38460

Magnetic field effect on emission spectrum and intensity at electron cyclotron frequency harmonics from PIG Reflex discharge, discussing electron oscillations excitation in plasma

19 p3117 A71-38626

Emission characteristics above solar limb in four EUV lines, comparing with K-coronameter measurements to estimate element abundances

19 p3130 A71-38671

Low temperature phonon assisted edge emission bands in pure cadmium sulfide crystals

20 p2376 A71-39008

Crab pulsar NP 0532 low energy gamma radiation emission data, observing flux ratios and pulsations

20 p2378 A71-39100

Formaldehyde absorption and emission lines in Orion IR nebula, indicating pumping suppression by neutral particle collisions

20 p3288 A71-39113

Solar X-ray flare region structure and emission flux density and spectral composition, using satellite-borne photometers and spectroheliographs

20 p3280 A71-39594

Dayglow neutral and ionized diatomic nitrogen band system emission excitation mechanism from vibrational and rotational intensity distributions observations

20 p3226 A71-39829

F region nightglow emission mechanism in terms of oxygen cations reactions with diatomic nitrogen and subsequent recombination

20 p3226 A71-39832

Nighttime hydroxyl airglow emission intensity and excitation temperature measurements, noting seasonal and nocturnal variations

20 p3227 A71-39834

Dayglow and twilight emission data, discussing atomic excitation mechanisms, particle production rates, height profiles and temporal variations

20 p3227 A71-39835

Emissive molecular beam masers, discussing cavity resonators, spectroscopy, amplifiers characteristics, oscillators behavior and electrostatics

20 p3247 A71-39873

Broadband electrostatic VLF wave observation in polar magnetosphere by OV3-3 satellite, noting emission power spectra density relationship to frequency

20 p3199 A71-39889

Crab Nebula integrated electromagnetic emission spectra, noting flux density spectral index at various frequencies

20 p3301 A71-39918

Crab Nebula and pulsar gamma ray emission from synchrotron or inverse Compton mechanism

20 p3301 A71-39919

Hydrogen molecule Lyman band continuous emission spectrum with fluctuations due to wave functions maxima, corresponding to transitions from vibrational levels

20 p3305 A71-39968

OH emission sources associated with long period variable IR stars emitting in 1665-1667 MHz lines

21 p3441 A71-40067

Gadolinium molybdate-neodymium ions stimulated emission, noting luminescence, absorption and spectroscopic properties

21 p3427 A71-40082

- Spectral analysis of Markarian galaxies, observing emission and absorption lines and hydrogen reversal 21 p3441 A71-40105
- Plasmaron coupling and laser emission in optically excited Ag-doped cadmium tin diphosphide 21 p3391 A71-40200
- Arc driven hypersonic wind tunnels total enthalpy measurement from blunt body gas cap emission, using rapid scan spectrometer for gray gas continua 21 p3364 A71-40403
- Solar low energy X-ray spectra observation during impulsive bursts, discussing thermal and nonthermal emission properties 21 p3438 A71-40425
- Millimeter emission lines from interstellar methyl cyanide transitions, noting kinetic temperature and hydrogen density 21 p3447 A71-40446
- Mathematical model of emission spectrum for PKZ radiosonde and radiosondes using superregenerative transceivers 21 p3383 A71-41243
- Stratospheric submillimeter wave emission and water vapor mixing ratios measurements, using Michelson interferometer with phase modulation and Fourier spectroscopy methods 22 p3545 A71-42145
- Quasars emission line red shifts distribution observations, evaluating selection effects 22 p3605 A71-42351
- Hydrogen plasma Balmer spectrum measurement for emission coefficients, comparing results with theories 22 p3583 A71-42373
- Molecular oxygen dissociative excitation in vacuum UV by electron impact, discussing resonance triplet atomic emission cross section 23 p3706 A71-42903
- H II regions kinematic properties in Large Magellanic Cloud, presenting emission line profiles and radial velocities 23 p3723 A71-42939
- Interstellar medium recombination line emission origin from discrete distribution of cold and dense clouds 23 p3723 A71-42942
- Lunar fines luminescence emission spectra in visible and near IR region under proton and electron excitations, discussing cause and plagioclase distribution 23 p3760 A71-43777
- Solar atmosphere electron densities from ion emission line intensities in Be isoelectronic sequence 23 p3721 A71-43839
- Plasma generation with transversely excited high pressure carbon dioxide laser and solid targets, describing optical emission spectral characteristics 23 p3712 A71-43932
- Seyfert galaxy NGC 5548 H alpha profile spectroscopic observations, discussing broad emission lines 24 p3870 A71-44901
- Galactic nucleus X ray source observations by Uhuru satellite, discussing emission and absorption spectra 24 p3866 A71-44915
- EMISSIVITY**
- Emissivity and temperature measurement of assembled microscopic particles in black body cavity 04 p0676 A71-14954
- Thermal diffusivity and total emissivity measurements of solids between 1500 K and melting point, using arc image furnace 04 p0595 A71-14966
- Thin metallic films thermal radiation properties at cryogenic temperatures, calculating spectral normal emissivity as temperature wavelength and thickness function 04 p0684 A71-15510
- Tungsten, molybdenum and rhenium single crystals hemispherical emissivity at high temperatures by electron beam heating, considering grain boundary contribution 04 p0613 A71-15581
- Pure W monochromatic emissivity measurements at 0.4 to 4 microns and at high temperatures 05 p0767 A71-16600
- Thin gas optical limit isothermal curves, discussing Planck mean emission coefficients 07 p1222 A71-18993
- Pyrolytic graphite hemispherical emissivity measurement on surface parallel and perpendicular to deposition surface at 1200-2300 K 08 p1323 A71-21921
- Industrial polycrystalline graphite monochromatic emissivity in visible and IR spectral regions at high temperatures 13 p2090 A71-27882
- Pyrolytic graphite hemispherical emissivity measurement on surface parallel and perpendicular to deposition surface at 1200-2300 K 17 p2763 A71-35265
- Hot water vapor total emissivity charts at various temperatures, using band model parameters with spectroscopic data 18 p2985 A71-36592
- Spectral composition of emitted radiation, emissivity and absorptivity of Venus atmosphere at high temperatures 19 p3135 A71-37580
- Emissivity calculation for radiant heat flux from isothermal gas mixture of hydrocarbon fuel combustion products 23 p3718 A71-43918
- Materials thermal accommodation coefficient and emissivity dependence on surface roughness, noting correlation 24 p3888 A71-44934
- EMISSOGRAPHS**
- U ACTINOMETERS**
- U RECORDING INSTRUMENTS**
- EMITTANCE**
- Transparent dielectrics sheet radiation absorbance, emittance and transmittance determination by Monte Carlo method 01 p0183 A71-11591
- Calorimetric measurements determining total hemispheric emittance of thin gold films as function of temperature, demonstrating film thickness effect [AIAA PAPER 70-63] 03 p0522 A71-14456
- Local radiative heat transfer and equilibrium temperature between identical uniform surface geometry planes, discussing directional dependent emittance and absorbance effects [AIAA PAPER 71-76] 06 p1008 A71-18533
- Thermal conductivity, electrical resistivity and total emittance at high temperatures in ultrahigh vacuum, discussing phase transformation effect 10 p1624 A71-23910
- Total normal emittance under simulated reentry conditions, using emissometer with aluminum oxide reference cavity integral within sample 11 p1764 A71-26249
- Total emittance measurements by portable IR reflectometer, tabulating nongray error effects 13 p2159 A71-27979
- Thermal conductivity and coating emittance measurements by stationary substrate heater method suitable for materials applied by flame vaporization 15 p2512 A71-31501
- Spectral emittance ranges of Apollo 12 lunar fines dependent on density for 2.5-14 micron wavelengths [ASME PAPER 71-HT-21] 19 p3142 A71-37992
- EMITTERS**
- NT THERMIONIC EMITTERS**
- Space charge problem for thermionic converter emitter sheath for electrons and ions with half-Maxwellian distribution 02 p0291 A71-12234
- AlAs-GaAs heterojunction laser threshold currents and CW operation at room temperature as function of p- and n-type emitter regions 03 p0439 A71-13987
- Minimum core storage forms for radiant heat transfer doubly subscripted nonsymmetric equations, giving simple modifications for interchange between emitting and reflecting surfaces 03 p0522 A71-14454
- Avalanche transistor emitter current voltage characteristics, using Kirchhoff equations for equivalent circuit 07 p1077 A71-19798
- Emitter coupled integrated transistorized logic elements, improving steady state noise stability by hysteresis in transfer characteristics 09 p1416 A71-22467
- Thyristors junction area current rise time extension, discussing emitter field regional delay times as function of p-n-p-n structural properties 12 p1886 A71-26849
- Two transistor emitter follower DC amplifier, using simplified equivalent circuit 13 p1999 A71-28628
- Field ion current angular distribution for large point emitter potentials as function of emitter geometry 22 p3578 A71-42057
- Minimum elements number on discrete two dimensional hologram with constant distance between emitters, considering reduction of matrix elements 22 p3546 A71-42311
- Bipolar junction transistor doping effects on bandgap decrease and emitter efficiency, explaining current gain temperature dependence 23 p3648 A71-42911
- Plane collisionless plasma diode between two hot emitters, considering potential distributions 24 p3808 A71-44551
- EMOTIONAL FACTORS**
- Emotionally induced osmotic pressure and thirst increase of rats during stress, noting eating behavior 02 p0201 A71-12875
- Short haul STOL aircraft transport system, discussing neighborhood stolport ownership, technical feasibility and economic, emotional, ecological and sociological viability 03 p0523 A71-13618
- Personnel selection for emotionally and physically taxing situations by studying physiological responses to anticipated stressors and stress recovery 06 p0851 A71-17607
- Oxygen respiration effect on self stimulation and emotional reactions in rabbits during hypothalamus electrical stimulation 06 p0855 A71-18376
- Young pilot performance in emergency situations including communication system failure and other equipment breakdowns, noting emotional reactions 16 p2534 A71-32831
- Literature survey of nervous-emotional stress effects on pilot during flight, discussing premature fatigue, cardiovascular disorders, psychic disturbances and circadian rhythms 19 p3002 A71-37763
- Psychophysiological and conversion mechanisms as unconscious expression of student pilot motivation decrease for further flight training, presenting case histories 22 p3502 A71-41837
- Serotonin metabolism of helicopter pilots, showing effects of emotional factors due to flight inexperience 23 p6332 A71-43220
- Hematological characteristics of emotional stresses during parachute jump, studying leucocyte, erythrocyte and eosinophil populations changes 24 p3800 A71-44413
- Emotional stress of pilots in difficult flight conditions, noting pulse rate increase and biopotentials amplitude changes 24 p3800 A71-44473
- EMOTIONS**
- Arousal and activation in nonspecific reticulothalamo-cortical systems due to underlying emotion expressed through cortical, visceral and somatomotor channels 21 p3330 A71-40247
- EMPLOYMENT**
- Nationwide man machine remote employment/personal services system including synchronous communication satellite, information and control network and remote terminals 14 p2199 A71-30914
- Aerospace industry unemployment and future development prospects, reviewing NASA, DOD, AEC and other aerospace agencies R and D and procurement budgets decline [AIAA PAPER 71-1023] 24 p3892 A71-44601
- EMPTYING**
- Transient thermodynamic processes of two phase vapor-liquid emulsion emptying at subcritical temperature in heat engines 12 p1944 A71-27500
- Quasi-stationary one dimensional thermoplastic stress strain state in cylindrical fuel tank during emptying process, allowing for Bauschinger effect 13 p2157 A71-29196
- Transient thermodynamic processes of two phase vapor-liquid emulsion draining at subcritical temperature in heat engines 24 p3819 A71-44928
- EMULSIONS**
- NT NUCLEAR EMULSIONS**
- NT PHOTOGRAPHIC EMULSIONS**
- Book on fluid mechanics covering rotating fluids, flow between concentric cylinders, emulsions, standing waves on water, etc 14 p2226 A71-30554
- ENAMELS**
- Ti dioxide-opacified porcelain enamel reflectance spectra analysis, deriving scattering cross sections and dispersed particle sizes and distribution 09 p1480 A71-22116
- ENCAPSULATING**
- Helical channel multipliers encapsulation for space flight applications 04 p0600 A71-15597
- Plastics for long life microcircuit encapsulation, investigating materials properties and failure mechanisms for device reliability assessment 07 p1077 A71-19561
- Plastics for long life microcircuit encapsulation, investigating water absorption and resin-to-lead adhesion effects on reliability 07 p1077 A71-19562
- Electronic encapsulated assemblies thermal stresses due to components expansion coefficients mismatch 07 p1213 A71-19774
- Microencapsulation of bonded reactive resins in packaging, logistics and adhesive applications at room and elevated temperatures 10 p1634 A71-24120
- Space radiation environmental effects on reactively encapsulated zinc orthophosphates and paints [AIAA PAPER 71-449] 12 p1920 A71-26762
- Preencapsulated strain gage measurement during water pressure tests on site built vessels 17 p2744 A71-35238
- Combinational possibilities of special application modules based on thin-film hybrid integrated circuits in standardized encapsulations 18 p2893 A71-36625
- Reliable plastic encapsulated semiconductor devices design, production and evaluation, noting application to IC 19 p3033 A71-38509

Plastic encapsulated IC reliability tests, relating results to failure mechanism 21 p3356 A71-40747

ENCLOSURE

Streptococcal flora in pharynx of men during prolonged enclosure noting concomitant hemolytic microbes 06 p0854 A71-18369

Radiation condenser computer program generalization to include effective radiative steady state node multiple enclosure simplification shield for thermal analysis optimization 20 p3314 A71-39357

ENCLOSURES

Sound field in multiple source enclosures, discussing noise and vibration control, acoustic modes excitation and environment simulation [ASME PAPER 70-WA/DE-8] 03 p0511 A71-14142
Steady state node simplification technique for thermal radiation in gray enclosures, including computer program 03 p0522 A71-14446

Magnetic shielding of various shaped enclosures such as rectangular or cylindrical cross sections in terms of normalized parameters 13 p2039 A71-28870

ENCODERS

U CODERS

ENCODING

U CODING

ENCOUNTERS

Visual pattern perception learning, recognition upon subsequent encountering and unfavorable conditions 05 p0716 A71-17243

Binary systems formation probability during triple encounters, considering random initial conditions 20 p3290 A71-39301

END PLATES

Thin walled lipped-channel and trapezoidal section beams under end moment loading, deriving differential equations and strain energy for end plates 02 p0330 A71-12950

ENDFIRE ARRAYS

NT YAGI ANTENNAS

Synthetic endfire hologram radar for small target and clear air turbulence detection 03 p0381 A71-14476

ENDOCRINE GLANDS

NT ADRENAL GLAND

NT PANCREAS

NT PINEAL GLAND

NT PITUITARY GLAND

NT THYROID GLAND

Sound effects on endocrine function and electrolyte excretion in animals and man, considering adenohipophyseal, neurohipophyseal and thyroid functions, diuresis and natriuresis 03 p0359 A71-13153

Mammalian neurons, neuroendocrine transducer /pinealocytes and adrenomedullary chromaffin and endocrine cells communication properties, noting signal transmission 14 p2182 A71-30180

ENDOCRINE SECRETIONS

NT ALDOSTERONE

NT HORMONES

NT INSULIN

Endocrine and metabolic effects of noise in normal, hypertensive and psychotic subjects, considering increased corticoadrenal and adrenergic activity 03 p0359 A71-13154

Pineal gland endocrine functions, discussing melanin synthesis and secretion in response to environmental illumination 05 p0712 A71-17108

Adrenocortical function in garden dormouse during autumnal preparation for hibernation, considering environmental temperature factors 13 p2014 A71-29315

ENDOCRINE SYSTEMS

Brain monoamines localization and metabolism and endocrine function, discussing pituitary secretion and neurotransmitter input 23 p3637 A71-44274

ENDOGENOUS CONDITIONS

U PHYSIOLOGY

ENDOLYMPH

Vestibular physiology, discussing endolymph chemical composition, cupula structure and function and hair cells 04 p0536 A71-14752

Semicircular canal ducts dynamic response characteristics, using suspended liquid filled inner tube for endolymph simulation 04 p0542 A71-14789

Coriolis effects on endolymph shift direction in semicircular canals of man under rotation with head movements in sagittal plane, involving nystagmus and illusory sensations 09 p1392 A71-22640

Endolymph and perilymph fluid systems pathophysiology from induced and spontaneous disorders changes observed in inner ear 14 p2183 A71-30254

Pigeon vestibular apparatus fluids and structures physical properties, detailing specific gravity and viscosity of endolymph, perilymph and cupula 14 p2185 A71-30467

ENDOTHELIUM

DNA synthesis rhythm in aorta endothelial cells nuclei during direct division, noting effects of amiotosis by autoradiography 12 p1872 A71-27752

DNA synthesis in human aorta endothelium reproduction, reporting intact nuclei and dyed cell membrane samples cytophotometric studies results 23 p3635 A71-44053

ENDOTHERMIC REACTIONS

Atomic oxygen-nitrogen shock tube endothermic reaction under high translational and low vibrational energy, noting ozone loss 03 p0375 A71-13493

Hydrocarbon fuel for hypersonic vehicle cooling, discussing use of endothermic reactions to achieve maximum heat sinks [AIAA PAPER 68-997] 10 p1658 A71-24852

Plasma jet chemical reactions, discussing temperature and quenching effects, molecular and gas decomposition and endothermic compounds formation 16 p2540 A71-32967

ENDOTOXINS

Irradiation protection in mice, dogs and sheep by bacterial endotoxin injection, discussing hematopoietic system stimulation and leukocyte counts 07 p1038 A71-18974

ENDURANCE

Universal endurance test machine for tubular samples torsion testing under hydrostatic pressure 04 p0673 A71-15899

Capillary density relationship to maximal oxygen uptake, indicating endurance training effects on human skeletal muscle 16 p2530 A71-33245

Plastic deformation, creep rupture strength, endurance limit and service life of prestressed strain hardenable material 16 p2659 A71-33985

Endurance limit of construction materials under fast and thermal neutron irradiation in reactor channel 16 p2598 A71-33986

ENERGETIC PARTICLE EXPLORER A

U EXPLORER 12 SATELLITE

ENERGETIC PARTICLE EXPLORER D

U EXPLORER 26 SATELLITE

ENERGY

Energy relations in physical space of general relativity theory and inertia space of Newtonian classical mechanics 03 p0458 A71-13605

Stationarity of complementary energy in nonlinear elasticity theory, using Piola stress tensor representation for isotropic elastic media 03 p0513 A71-14228

Weak gravitational field negative energy possibility from energy momentum leakages consideration for asymptotically flat solutions of Einstein equations 09 p1494 A71-22807

Experimental techniques in propulsion and energetics research - NATO/AGARD Conference, Munich, September 1967 11 p1764 A71-26263

First law of thermodynamics implications to general theory of work and energy for material systems 18 p2986 A71-36811

ENERGY ABSORPTION

NT AURORAL ABSORPTION

NT ELECTROMAGNETIC ABSORPTION

NT MOLECULAR ABSORPTION

NT PHOTOABSORPTION

NT POLAR CAP ABSORPTION

NT SELF ABSORPTION

NT THERMAL ABSORPTION

NT THERMALIZATION [ENERGY ABSORPTION]

NT ULTRAVIOLET ABSORPTION

NT X RAY ABSORPTION

Point source acoustic radiation field in presence of absorbing plane, presenting solutions and approximations based on plane wave reflection and modified image method 03 p0456 A71-13276

Characteristic energy absorption spectra of dielectric solids from direct IR measurements for single crystal and thin film specimens 03 p0385 A71-13645

Thermal conductivity determination for materials by pulsed laser or flash lamp energy absorption 04 p0595 A71-14961

Electromagnetic fields induction in biological tissues, recording energy absorption temperature distribution in phantom models with thermograph camera 11 p1717 A71-25289

Elastic plastic wave cancellation in energy absorbing materials, considering polymer group efficiency for shock mitigation from weight and volume standpoint [AIAA PAPER 71-350] 11 p1843 A71-25329

Energy flux of tropospheric mesoscale waves and heat influx into upper mesosphere caused by energy absorption, discussing wavelength and latitude effects 12 p1924 A71-26771

Solar energy absorptance changes in spacecraft thermal control surfaces exposed to particulate radiation at simulated synchronous altitude, using computerized model [AIAA PAPER 71-453] 12 p1928 A71-26767

RF power absorption of uniform hot ion-electron plasma column, considering collision effects and EM radiation 14 p2281 A71-30559

Electromagnetic wave energy absorption in homogeneous cold magnetoactive plasma cylindrical columns 15 p2455 A71-31730

Metals and alloys surface deformation stages by electron emission method, discussing mechanical energy absorption and dissipation 16 p2580 A71-33934

Ion cyclotron resonance power absorption theory application to reactive and nonreactive ions line shapes, using Wobbschall-Graham-Malone phenomenological equation of motion 17 p2695 A71-34944

Optical constants of beta-phase NiIn, PdAl and nickel gallium aluminide, noting chemical composition and electron density effects on photon energy absorption 21 p3426 A71-40031

Ion cyclotron resonance power absorption, deriving expression for average ion kinetic energy at saturation in steady state limit 21 p3418 A71-40023

Absorption variation with solar activity in seasons, reexamining vertical incidence absorption measurements at 5.65 MHz /1958 and 1959/ at Waitaiti 21 p3373 A71-40377

HF plasma heating in Tokamak torus device by magnetosonic wave energy absorption in high density region via Buchsbaum hybrid resonance 21 p3422 A71-40766

Surface energy absorption coefficient determination from decaying sound fields, deriving reverberation time and decay rate equations 23 p3703 A71-43200

Radiation flux induced material dispersion of solid surface, taking into account radiation energy absorption by discontinuity introduction 24 p3835 A71-45221

ENERGY BANDS

NT CONDUCTION BANDS

NT FORBIDDEN BANDS

L-alpha X ray spectral band and K absorption edge in vanadium silicides and high temperature superconductors, obtaining energy bands electron distribution 02 p0294 A71-11899

Noncrystalline amorphous solids electro-optical effects, studying semiconductor energy band models 07 p1181 A71-20421

Single crystal indium gallium phosphide p-n junction preparation by epitaxial vapor phase growth technique, determining energy gap dependence on alloy composition 09 p1510 A71-23121

Alkali and rare earth metal hexaborides energetics, discussing semiconducting, semimetallic and metallic compounds on basis of energy bands and effective valence 12 p1944 A71-27099

Surface state energy positions determination in high-energy gap semiconductors by photovoltaic spectral distribution 14 p2284 A71-30400

Vertical muon spectra and charge ratio in energy range 30-800 GeV at sea level from Kiel cosmic ray spectrometry 15 p2474 A71-31777

Semiconductor heterostructure junction diode lasers for operation at room temperature, discussing energy band structure and mass communications application 16 p2587 A71-33447

Anisotropic carrier redistribution near semiconductor charged surface with energy band bending discussing relaxation rate 17 p2790 A71-34119

Characteristic energies of exponential band tails in GaAs junction lasers from wavelength shift with cavity Q and spontaneous emission line width 22 p3558 A71-42366

ENERGY BUDGETS

NT ATMOSPHERIC HEAT BUDGET

Dissipating instability in plasma by variational method, using relation between energy balance of wave and medium 01 p0132 A71-10155

Doppler radar techniques for turbulent kinetic energy budget in boundary layer, discussing wind profile and turbulence in snow conditions 01 p0117 A71-10577

Free convection in turbulent Ekman layer discussing kinetic energy budget above surface layer 01 p0119 A71-10744

Kinetic energy and available potential energy balance in atmospheric stationary disturbances (standing waves), using atmospheric flow statistics
01 p0119 A71-10853

Turbulent energy balance equation terms for atmospheric boundary layer
05 p0778 A71-16837

Energy balance during ring blanks widening by electromagnetic pulses, establishing theoretical limit of mechanical efficiency
06 p0906 A71-18712

Incompressible turbulent circulatory fluid flow in plane curvilinear channel, deriving energy balance equations
07 p1088 A71-19199

Pulsed plasma accelerator energy balance determination by spectroscopic measurement
09 p1498 A71-22100

Atmospheric surface layer shear/buoyant production, flux divergence and dissipation in terms of turbulent kinetic energy and transport in temperature variance budget
09 p1490 A71-23555

Excited atom density determination for two-photon light absorption in one-dimensional medium, obtaining energy balance equation asymptotic solution and secondary radiation intensity
12 p1914 A71-27028

Earth radiation budget measurements, noting planetary albedo, IR radiant emittance and net balance
12 p1901 A71-27191

Consistent discrete models of continuous bodies electrothermoelastic behavior, using finite element formulations for general energy balance equations derivation
13 p2099 A71-27785

Jupiter atmosphere nonequilibrium radiative processes, considering energy balance and pressure and temperature conditions
16 p2637 A71-33516

Energy balance and emission power of organic dye laser under nonmonochromatic excitation
17 p2751 A71-34381

Nonequilibrium plasma molecular impurities effect on electron energy balance, noting importance in closed cycle MHD generators
17 p2789 A71-35261

Recoverable usable energy maximization from solar oriented spacecraft electrical power system, using silicon cell array and nickel cadmium batteries
20 p3182 A71-38956

Seasonal variations of kinetic energy balance of mean meridional circulation in Northern Hemisphere
20 p3257 A71-39436

Mars and Venus atmospheres, considering energetics, mean winds, temperature differences, circulations and climates
20 p3296 A71-39624

Energy in universe from stellar and galactic evolution, discussing flow mechanisms, entropy, arresting factors and catastrophic phenomena
20 p3301 A71-39916

CAT energy budget and physical mechanisms in relation to aviation and atmospheric processes incorporating long range numerical prediction model
21 p3411 A71-41178

Turbulence energy balance and temperature pulsations in free atmosphere in presence of water phase transformation in clouds of given microstructure
21 p3412 A71-41394

Turbulent energy budget and velocity dissipation spectrum near grass surface as function of atmospheric stability
22 p3569 A71-42546

Ion cloud expansion perpendicular to initially homogeneous magnetic field, estimating maximum radius with energy balance and expansion process
23 p3667 A71-43132

Energy balance in cool quiescent solar prominences, using 6000 K isothermal slab model
23 p3767 A71-43843

Nonlocal thermodynamics constitutive theory of continuous systems with global energy balance in terms of classical thermostatics
23 p3782 A71-43868

Nonlinear theory of nonlocal continuum mechanics, considering global energy balance, constitutive equations and Clausius-Duhem inequality
23 p3705 A71-43869

ENERGY CONVERSION

Book on direct energy conversion principles and methods covering fusion, fuel cells, MHD, thermoelectric, thermionic, photovoltaic, electrohydrodynamic, piezoelectric and ferroelectric power generation
01 p0006 A71-11193

Electrofluid dynamic direct energy conversion, discussing working media, duct geometry, unipolar charges, and fluidic switches
[ASME PAPER 70-ENER-A] 03 p0353 A71-13704

Chemical energy conversion in mechanical work, examining irreversible mixing, Van Hoff box and Carnot cycle
05 p0717 A71-16785

Chemical energy conversion in lasers, discussing vibrational inversions in diatomic and multiautomic molecules and chain reactions
07 p1121 A71-19098

Subdomain magnetic particles ferrofluid colloidal dispersions, for energy conversion devices, viscous dampers, accelerometers, gyroscope supports and specific gravity meters
[IEEE PAPER 27.2] 07 p1178 A71-19611

Metal pipes coaxial welding by detonation, estimating energy conversion
08 p1300 A71-21910

Soviet book on thermionic and MHD energy conversion covering gas ionization, converter operation and low temperature plasma physics
11 p1715 A71-26099

Aerodynamic noise scattering near Lighthill multiples, considering intense near-field energy conversion into sound waves
11 p1705 A71-26448

Heat rejection radiator influence on space nuclear power system as function of mass/area for Brayton, Rankine, thermoelectric and thermionic conversion schemes
13 p1999 A71-28597

Satellite solar power station for microwave generation, transmission and energy conversion to electrical power on earth
13 p1999 A71-28665

Microwave receiving antenna with solid state power rectifier for converting energy from space solar cell array into DC power on earth
13 p2000 A71-28671

Thick film microcircuit DC-TO-DC converter electronics design for TOPS spacecraft power subsystem
14 p2214 A71-30801

Fusion reactor applications to space propulsion and power generation, considering conversion of thermal energy of reacting plasma to electrical power and exhaust jet
15 p2447 A71-32207

Radioactive decay energy conversion of beta particle emitting cerium 144 into high voltage electricity in coaxial cylinder cell
15 p2447 A71-32211

German monograph on conversion of human muscular work into flywheel mechanical kinetic energy covering testing and analysis of biomechanical relationships
15 p2364 A71-32308

German textbook on fundamentals of thermodynamics covering energy conversion, reversible/irreversible processes, chemical/molecular thermodynamics, statistical analysis, probability theory, etc.
15 p2516 A71-32767

Chemical energy conversion into mechanical work, examining irreversible mixing, vant Hoff box and Carnot cycle
16 p2540 A71-33037

Bayesian decision theory, discussing choice of possible systems to convert wind into electrical energy
16 p2582 A71-33291

Electric power system for satellites, considering energy conversion, storage and processing from chemical, solar and nuclear sources
17 p2676 A71-34227

Hydrostatic power transmission systems classifications, considering transformation, transport and accumulation of energies /mass, heat, optical, chemical, pneumatic, hydraulic, etc/
18 p2850 A71-36202

Combustion oscillator for MHD energy conversion, using products flow modulation by traveling pressure wave
19 p2998 A71-38099

Energy conversion engineering - Conference, Boston, August 1971
20 p3261 A71-38901

Electrical subsystem of 2-15 kW Brayton power conversion system consisting of speed controller, alternator voltage regulator, DC power supply, etc
20 p3180 A71-38910

Reactor powered Brayton cycle power conversion system, evaluating performance at different turbine inlet temperatures and power levels by computer simulation
20 p3262 A71-38914

Thermal or chemical energy conversion to electromagnetic radiation by laser, discussing atomic or molecular processes and thermodynamic limitations
20 p3242 A71-38939

Radioisotopes as energy source for power conversion systems, discussing future availability of fission products and transuranium elements from commercial nuclear power reactors
20 p3265 A71-38948

SNAP 19 Radioisotope Thermoelectric Generator (RTG) for advanced space missions, using lead telluride and silver antimony germanium telluride as conversion materials
20 p3267 A71-38965

Solar wind velocity increase by magnetic field energy conversion to kinetic energy, constructing steady state MHD one fluid model
23 p3719 A71-42949

Mathematical model for solar flares formation based on magnetic/kinetic energy conversion, investigating plasma instability
23 p3719 A71-42950

French R and D Directorate exhibits at 29th Le Bourget air show, discussing laser applications, telecommunication, navigation-guidance, energy conversion, test facilities and environmental studies
24 p3816 A71-44764

Response nonlinearity of multiple turn transformer type transducer for angular displacement magnitudes conversion to electrical signals, noting relationship to turning angle and instrument dimensions
24 p3810 A71-45152

Structural materials ability for irreversible conversion of mechanical to thermal energy from free longitudinal vibrations attenuation measurements in rod
24 p3817 A71-45200

ENERGY CONVERSION EFFICIENCY

Jet pump optimization for incompressible flow, considering friction losses, nonuniform densities and diffuser losses for overall energy conversion efficiency
01 p0085 A71-10105

Optical heterodyne mixing efficiency invariance to thin detector position for small frequency difference between signal and local oscillator
02 p0249 A71-12033

Transverse current leakage effect on energy conversion and Hall characteristics of MHD generator
02 p0290 A71-12195

Thermionic dispenser cathodes with emitter surfaces covered and replenished from inside by high work function material
02 p0295 A71-12213

Life, efficiency and electrical stability tests of cylindrical thermionic converters with various emitter and collector materials
02 p0193 A71-12216

Long term stability and post test analysis of vapor deposited W emitters in high performance cylindrical thermionic converters
02 p0193 A71-12218

Maximum efficiency of cylindrical thermionic converters with Mo emitter and collector over temperature range
02 p0194 A71-12224

Electrofluiddynamic colloid generator performance characteristics, considering power output limitation due to electric breakdown
[ASME PAPER 70-WA/ENER-5] 03 p0355 A71-14108

Si solar cells low temperature and solar intensity performance optimization by identifying and eliminating low output problems
05 p0701 A71-16071

Si solar cells electrical performance tests, considering 1 MeV electron irradiation effect on efficiency
05 p0702 A71-16082

Si solar cells with high electrical output in space sunlight, discussing device limitations
05 p0704 A71-16102

Si solar cell technology, discussing contacts, low temperature performance and conversion efficiency
05 p0757 A71-16103

Power loss processes in Si solar cells, noting improvement in collection, voltage and curve factors
05 p0704 A71-16104

Si solar cell test for electrical discharge effect on series resistance, curve power factor, conversion efficiency and spectral response
05 p0705 A71-16169

Second harmonic generation with focused pump beams of optimum phase mismatch and confocal parameters values for obtaining high conversion efficiency
05 p0762 A71-16337

Energy balance during ring blanks widening by electromagnetic pulses, establishing theoretical limit of mechanical efficiency
06 p0906 A71-18712

Low gain microwave amplifier cascade DC to RF conversion efficiency analysis
07 p1073 A71-19115

Energy conversion efficiency from microwave into magnetostatic waves propagation inside cylindrical ferromagnetic substance
08 p1265 A71-21276

Thermionic converter output improvement by Ar injection at low Cs pressures, noting electron space charge neutralization
08 p1340 A71-21490

Carbon dioxide laser performance quantitative analysis, considering electron to optical energy conversion via electric discharge in carbon dioxide-nitrogen-helium mixture
09 p1465 A71-23481

VLF electromagnetic propagation, calculating mode conversion efficiency at solar terminator on angle based on flat model with finite wall conductivities
09 p1411 A71-23576

Excitation schemes, fluid velocity and power of jet MHD induction generator
11 p1709 A71-25456

Chemically vapor deposited deep etched tungsten emitter for high performance cylindrical thermionic converter

11 p1714 A71-25906

Time dependent current flow measurements and energy losses in capacitor discharge of electrodeless MHD motor

11 p1716 A71-26290

High efficiency and power long life cross field amplifier generator for solar energy conversion in space into microwave, discussing magnetron and amplifier

13 p2000 A71-28668

High power linear beam tube devices for space power generation station, considering use of klystron with heat pipes for low weight and high efficiency

13 p2000 A71-28669

Energy conversion efficiency improvement of silicon solar cells, noting power loss effects

14 p2181 A71-29702

Electrode size effects on voltage loss and boundary layer conductivity of combustion driven MHD generator

14 p2287 A71-29880

Nuclear fusion powered pulsed space propulsion systems with laser initiation, discussing energy conversion to momentum, limitations, vehicle configuration and mission performance

14 p2288 A71-30095

Thermionic converter output improvement by Ar injection at low Cs pressures

14 p2182 A71-30679

Electrically-heated Brayton power conversion system, comparing performance tests with prediction

15 p2354 A71-32212

Test facility and performance predictions for Rankine cycle power system components, including lithium heater, potassium boiler, condenser and preheater [GESP-451]

15 p2448 A71-32223

Rectangular pulse formation in nonlinear homogeneously distributed systems, discussing energy conversion efficiency

15 p2382 A71-32626

Krypton arc lamps of high conversion efficiency for optical pumping of neodymium lasers, setting lamp and Nd-YAG rod in prolate ellipsoidal cavity

16 p2585 A71-33140

High power efficiency solid state UHF sources, comparing Gunn and avalanche diodes performance

17 p2715 A71-34685

Crystal laser elliptic cavity size determination for maximum emission efficiency, using photochemical method for energy transfer measurement

17 p2754 A71-35748

High efficiency avalanche diode microwave oscillator design guidelines based on oscillation mode theory, covering CW and pulsed operations

18 p2888 A71-36131

Electric power and efficiency of thermoelements with temperature dependent thermoelectric properties by heat balance technique

18 p2852 A71-36965

Elliptical laser illuminator pumping efficiency dependence on light source focal displacement, using optical systems image forming theory

20 p3243 A71-39075

Turbomolecular vacuum pump impeller theoretical efficiency with allowance for diffuse flow of interaction between gas molecules and interblade channel walls

20 p3183 A71-39170

Bulk quantum efficiency in electron beam pumped n-type GaAs lasers at 300 K as function of impurity concentration

22 p3558 A71-42362

Photoeffect efficiency of solar energy converters based on semiconductor cadmium sulfide-copper sulfide heterojunctions

22 p3483 A71-42536

Conversion effectiveness of oscillations induced by electron beam in bounded anisotropic plasma into electromagnetic emission

23 p3710 A71-43275

Solar to electric energy conversion efficiency and electrical properties of photoconverters using compressed sintered CdS

24 p3808 A71-44390

Plasma microwave harmonic generation conversion efficiency, applying field gradient theory to case of positive column placed through rectangular waveguide

24 p3803 A71-44648

Gaseous media parameters in wave energy exchanger, examining compression cycles, temperature ratios and flow velocities for maximum conversion efficiency

24 p3891 A71-45199

ENERGY CONVERTERS

U DIRECT POWER GENERATORS

ENERGY DENSITY

U FLUX DENSITY

ENERGY DISSIPATION

Dissipating instability in plasma by variational method, using relation between energy balance of wave and medium

01 p0132 A71-10152

Round dielectric waveguides dominant mode radiation losses calculation

01 p0052 A71-10467

Resonance tube heat losses, discussing thermal exchange mechanism and wall temperature limits

01 p0180 A71-10993

Locally isotropic hydrodynamic turbulent fields statistical properties for kinetic energy and temperature dissipation fluctuations

01 p0120 A71-11106

Output increase through waste energy dissipation improvement by forced convection via high speed flow for thermally pumped gas dynamic laser

01 p0096 A71-11626

Radar energy loss estimate over space targets, considering various energy distributions in given search volume, target acquisition probability, signal to noise ratio, etc

02 p0212 A71-11879

Nonrelativistic cosmic particles spectrum and chemical composition changes, examining ionization and heating energy loss effect

02 p0300 A71-12093

Turbulent energy dissipation in lower atmospheric layer on meteorological mast during various temperature stratifications

02 p0246 A71-12112

Coherent light wave propagation in two level system, discussing wave periodicity, deviation from sinusoidal form, interaction with medium and energy loss and gain effects

02 p0215 A71-12319

Pulsars as rotating neutron stars with frozen-in magnetic field, accounting for energy and angular momentum losses due to gravitational radiation

02 p0300 A71-12473

Turbulence level effects on aerodynamic losses of axial flow turbomachines, discussing boundary layer of blades

03 p0340 A71-13143

Finite amplitude sound interaction with Helmholtz resonator, attributing losses to viscous damping and orifice jet flow kinetic energy dissipation

03 p0456 A71-13279

Transverse oscillations determination in cyclically deformed thin plate under plane stress by energy dissipation calculation using Hooke law

03 p0502 A71-13401

Hysteresis loop parameters for energy dissipation in material, considering relation to calculated values for oscillations of system

03 p0502 A71-13402

Equations of motion for free vibrations of three layer plate, considering energy dissipation in soft low modulus of elasticity middle layer

03 p0502 A71-13404

Carbon steel specimens size effect on energy dissipation and damping characteristics under transverse flexural vibrations

03 p0503 A71-13412

Neodymium glass laser with intracavity emission polarization, determining thermally induced double refraction effect on energy characteristics

03 p0435 A71-13505

Two-terminal pair broadband matching circuits losses from method for LF series-shunt coupler with uniform scattering

03 p0386 A71-13810

Differential energy losses of alpha particles traversing materials in superconducting and normal states

03 p0468 A71-14414

Simple two fluid solar wind speed and proton temperature model, discussing nonthermal energy dissipation

03 p0481 A71-14504

Dissipative structures in thermodynamics of irreversible processes of hydrodynamics and chemical kinetics

04 p0675 A71-14792

Atomic collision chains in bcc crystal, determining energy loss relation to temperature by computer model with/without perfect lattice thermal oscillations

04 p0630 A71-15103

Fluctuation-dissipation thermodynamics with variables changing sign during time reversal

04 p0676 A71-15118

Viscous heating effects on laminar combined free and forced convection through vertical circular tubes

04 p0676 A71-15177

Shock induced exothermic reactions on boundary layer transition in shock tube, investigating free stream thermal energy release effects

04 p0572 A71-15503

Energy dissipation patterns of metal fatigue failure during static and cyclic loading applied to untreated and heat treated steel samples

04 p0671 A71-15637

Energy dissipation during torsional and flexural vibrations of steel and duralumin specimens subjected to plastic deformation, accounting for discrepancies due to methodical errors

04 p0671 A71-15640

Pressure effects on calibration characteristics of hot-film anemometers, discussing heat loss from sensing element

04 p0601 A71-15765

Nonlinear interaction between three longitudinal plasma waves, calculating dissipation effect on coupling coefficients

04 p0635 A71-15902

Coronal condensations emission changes after microwave solar bursts, discussing circular polarization and flare mechanism based on collisionless dissipation of magnetic energy

05 p0804 A71-16029

Concentric layer model for estimating energy expenditure of left ventricle

05 p0713 A71-16488

Electromagnetic waves energy flow and dissipation in frequency dispersive absorbing medium, exemplifying by oscillating particle system and electric circuit

05 p0781 A71-16702

Atmospheric diffusion parameters investigated by smoke plumes in atmospheric boundary layer, evaluating turbulent energy dissipation

05 p0778 A71-16838

Variable viscosity fluid laminar flow, measuring tube resistance at critical Reynolds numbers as function of energy dissipation

05 p0737 A71-17037

Soviet book on air driven microturbines covering design, operation, energy losses, efficiency, economy and applications

06 p0848 A71-17446

Loss resistance and dissipated power dependence on crystal configuration of microwave semiconductor junction diode

06 p0873 A71-17544

Defense of damping theory applications in flutter analysis, discussing energy dissipation

06 p0984 A71-17623

Flare stars in solar neighborhood, obtaining time averaged energy radiation upper bounds

06 p0976 A71-18474

Nitrogen-carbon dioxide thermally pumped gas dynamic lasers, using high speed flow for waste energy removal

06 p0908 A71-18490

Quarter wave tube in off- and near-resonance regimes, dissipating energy by jet formation during flow emergence from cavity into duct

06 p0881 A71-18543

Quasi-steady MPD accelerators current conduction and power loss mechanism investigation through local anode fall voltage and current density measurements at different arc current levels

06 p0939 A71-18636

Secondary losses in plane compressor grid with low aspect vanes, discussing flow characteristics dependence on fins, protruding elements and smoothed junctions

06 p0846 A71-18705

Electro-optical method for energy dissipation characteristics of mechanical systems subject to attenuating vibration

07 p1107 A71-19170

Thermally induced modifications of high power CW laser beam, considering heat losses by forced and free convection

07 p1122 A71-19207

Elastic suspension energy dissipation effect on three degrees of freedom gyroscope drift

07 p1108 A71-19307

Clear air turbulence role in general atmosphere circulation, considering energy dissipation, momentum transfer and shear layer producing mesoscale processes

07 p1153 A71-20221

Elastic systems vibrations calculated with allowance for amplitude and frequency dependent energy dissipation, using hysteresis loop contour expression

07 p1218 A71-20476

Martensitic stainless steels structure related to energy dissipation capability, obtaining damping mechanism as magnetomechanical hysteresis

07 p1142 A71-20477

Loading frequency effect on carbon steel energy dissipation at large stress amplitudes, deriving strain rate relations

07 p1142 A71-20478

Energy dissipation in heat resistant Ni steels under cyclic tension and compression at room temperature

07 p1142 A71-20479

Locally isotropic hydrodynamic turbulent fields statistical properties for kinetic energy and temperature dissipation fluctuations

08 p1325 A71-20850

Energy dissipation-fatigue strength relationships during vibrations for prestrained metals and alloys

08 p1369 A71-21118

Temperature effects on energy dissipation during vibration in ferromagnetic and nonferromagnetic metals, comparing damping capabilities for homologous temperatures

08 p1306 A71-21119

Static tensile stresses effect on magnetized ferromagnetic materials damping properties explained by anisotropic microplastic strains dissipating energy during bending vibration

08 p1306 A71-21120

Energy dissipation in free oscillations of multilayer shells consisting of alternating rigid elastic layers and soft fillers, deriving equations of motion

08 p1369 A71-21123

Nonrelativistic cosmic particles spectrum and chemical composition changes, examining ionization and heating energy loss effect

08 p1355 A71-21143

Dissipative effects on tidal winds at ionospheric heights concerning Lorentz force, molecular viscosity and heat conductivity

08 p1278 A71-21201

Centrifugal compressor vaneless diffuser, estimating energy losses with hydrodynamic model

08 p1348 A71-21266

Free and forced vibrations of three layer freely suspended plate with allowance for energy dissipation

08 p1372 A71-21707

Soviet papers on physics of metals and metallography covering residual stresses, energy dissipation after plastic deformation, heat treatment, etc

08 p1317 A71-21759

Vibration decrement amplitude dependence study using internal friction method of freely attenuated transverse vibrations, considering energy dissipation

08 p1317 A71-21761

Radial flow energy losses in rotating cylindrical cascade of inward-flow turbine wheel, determining profile losses and exit blade angle

08 p1349 A71-22044

Gunn diodes temperature, calculating power density dissipation by simple domain mode models and accumulation mode operation

09 p1414 A71-22249

Turbulent hot gas motion in round pipes from semiempirical turbulence theory, accounting for energy dissipation and thermodynamic parameter variability

09 p1431 A71-22370

Homogeneous equilibrium low temperature dense helium plasma ionization composition and radiative energy losses, calculating ionization potential

09 p1501 A71-22380

Multilayer plate vibrations calculated with allowance for energy dissipation in material, deriving equations of motion

09 p1538 A71-22602

Energy dissipation during independent flexural-torsional vibrations of rods, noting alternating shear stress superposition effect on damping

09 p1538 A71-22629

Ray transformation after passing through optical resonator with Brewster prism, calculating spectral energy losses dependence by geometrical optics method

09 p1464 A71-23072

Cerenkov energy losses of rigid cylindrical uniformly charged bunch moving at constant speed through homogeneous isotropic dispersive dielectric

09 p1498 A71-23574

Edge losses effects on thermal conductivity of thermal insulations at high temperature measured by guarded hot plate method

10 p1694 A71-23907

Neutrino luminosity in strongly magnetized degenerate relativistic electron gas plasma from URCA energy loss rate calculations

10 p1671 A71-24303

Friction drag and energy losses of steady plane incompressible boundary layer flow of viscous liquid on nonconducting wall in MHD channel

10 p1649 A71-24377

Photoelectron energy loss rate to ambient electrons in thermal plasma, noting geomagnetic field influence

10 p1662 A71-24558

Asymptotic expression for low energy photoelectron energy loss to ambient thermal electrons

10 p1662 A71-24559

Soviet book on mechanical systems oscillations with allowance for imperfect elasticity covering energy dissipation, linear asymptotic methods, etc

10 p1691 A71-24729

Microwave energy dissipation as heat in eye, using agar for eye model construction

10 p1572 A71-25078

Thermoelastic heat release in muscular twitch final phase, discussing energy storage as function of active or passive muscular tension

11 p1718 A71-25626

Nonuniform density cosmic plasma heating allowing energy losses by radiation and heat conduction, using filament-structured high temperature plasma region model

11 p1828 A71-25765

Reynolds number effects on centrifugal compressor performance characteristics, discussing power losses in compressor, impeller and diffuser stages and compressor adiabatic efficiency

11 p1703 A71-25967

Cosmic ray propagation in interplanetary space, deriving steady state transport equation with energy losses

11 p1817 A71-26172

Junction thermal behavior and energy losses in active contactless bipolar transistor switch loaded by capacitive impedance

11 p1739 A71-26377

Solar corona electrons cooling by Thomson scattering, calculating electron energy loss

12 p1955 A71-26604

Atmospheric viscous dissipation energy relationships, calculating Martian atmosphere thermal structure

12 p1965 A71-27192

Satellite rotation about center of mass, allowing for energy dissipation due to magnetic hysteresis

13 p2144 A71-28194

Regular beamguides of second kind consisting of nonidentical nonequidistant correctors, calculating energy losses

13 p2029 A71-28362

Air bypass behind compressor into variable area exhaust nozzle, obtaining energy losses from gas turbine jet engine indices

13 p2115 A71-28586

Viscous dissipation effects on Nusselt number in combined free and forced convection through vertical concentric annuli

13 p2160 A71-28601

Gas flow heat loss through porous metals, deriving hydraulic resistance and heat release coefficients

13 p2165 A71-29218

Numerical method for two dimensional or axisymmetric heated flows allowing for dissipation extended to viscous flow, using Navier-Stokes equations in streamwise coordinates

13 p2118 A71-29280

Damping characteristics [absorption coefficient] of dissipative systems, defining authentic value of energy dissipation characteristic determination from forced and free vibrations

14 p2321 A71-29618

Energy dissipation measurement in materials during cyclic fatigue testing by dynamic hysteresis loop method

14 p2238 A71-29619

Creep and failure tests for Ti alloys at 500 C and high stresses, discussing work dissipation during creep process

14 p2256 A71-29621

Beamguides with inhomogeneities regulated for constant radiation losses of waves-analogs of modes

14 p2211 A71-30077

Planar Fabry-Perot optical resonator mirror rims effect on modes and losses

14 p2254 A71-30138

Incompressible plastic shells behavior, discussing deformation, energy dissipation rate, equilibrium equations and boundary conditions

14 p2328 A71-30380

Anomalous microwave energy dissipation and electron heating in collisionless plasma without decay at high collision frequencies

14 p2281 A71-30539

Apparatus for measuring polar liquids dielectric permittivity and losses at microwave frequencies over wide temperature and pressure ranges

14 p2222 A71-30583

Nonresonant noise from turbulent nonpremixed flames, discussing burner diameter, impingement angle and equivalence ratio effects on acoustic power radiated

14 p2295 A71-30779

Cloud energy dissipation coefficient determination by ruby laser device, applying to water content and liquid particle concentration, vapor cloud and aerosol concentration

15 p2445 A71-31449

Carbon dioxide electron impact energy loss spectrum and molecular orbit calculations, discussing fourth positive bands production in Mars upper atmosphere UV dayglow

15 p2398 A71-31766

Mean and standard deviation of fraction of total primary cosmic ray energy losses not measurable by ionization spectrometers

15 p2407 A71-31809

Constant speed vortex rate sensor, calculating angular momentum dissipation due to shear stresses and response to step signal input

15 p2352 A71-32064

Stability control of magnetic suspension with stabilizer allowing for energy dissipation in electromagnet, using Lagrange-Maxwell electromechanical equations

15 p2353 A71-32080

Energy dissipation in harmonically oscillating spherical annulus filled with viscous fluid

15 p2391 A71-32104

Dynamic hysteresis loop measurement of energy dissipation in materials, showing deformation effects on accuracy

15 p2508 A71-32233

Energy dissipation in material under complex vibrations, noting role of summary shear stress

15 p2508 A71-32234

Modulated relativistic electron beams interaction with plasma, investigating coherent energy loss

15 p2460 A71-32789

Elastic energy release rates and stress intensity from nonlinear load deflection curves as function of crack length to specimen width ratio

16 p2590 A71-32945

Energy dissipation measurement in liquid filled spinning precessing spherical cavity by gimbaled mechanism

16 p2644 A71-33219

Extragalactic radio sources millimeter wavelength spectra measurements, investigating electron energy loss mechanism, magnetic field strengths and dynamics

16 p2631 A71-33234

Rotating dumbbell shaped satellites orientation optimization by system of jets, calculating energy losses

16 p2646 A71-33672

Upper atmospheric winds viscous damping energy deposition calculation for midlatitude profiles

16 p2568 A71-33789

Metals and alloys surface deformation stages by exoelectron emission method, discussing mechanical energy absorption and dissipation

16 p2580 A71-33930

Stable auroral red arcs generation at plasmopause from ion cyclotron wave turbulent dissipation of ring current proton energy

16 p2572 A71-33947

Van Allen radiation belts and plasma sheet energy loss control, using cold plasma injection

16 p2629 A71-33976

Logarithmic decrement of flexural, longitudinal and torsional vibration damping of various size rods, taking into account surface layer energy loss

16 p2659 A71-33979

Energy dissipation of vibrating structures in complex stress state, using generalized stresses and strains as coordinates

16 p2659 A71-33981

Polymers mechanical losses temperature-frequency dependence, using nonlinear viscoelastic theory

16 p2602 A71-33982

Small elastoplastic cyclic strain effects on internal friction and energy dissipation in metals during vibrations

16 p2598 A71-33983

Limit analysis of dissipation power and collapse load of rigid perfectly plastic continua with piecewise linear yield surface, using linear programming

17 p2816 A71-34324

Two massive arbitrarily shaped hard bodies spatial collision, determining kinetic energy loss, motion and deformation of impact point

17 p2818 A71-34347

HF anodic oscillation tube tripler circuit optimization under constraints due to heat losses in grid electrode

17 p2714 A71-34572

Channel P MOS memory elements, discussing factors governing electrical energy dissipation and consumption

17 p2715 A71-34684

Antenna radiation resistance and efficiency in dissipative medium, using concept of modified power density

17 p2701 A71-34764

Transverse oscillations determination in cyclically deformed thin plate under plane stress by energy dissipation calculation using Hookes law

17 p2825 A71-35012

Equations of motion for free vibrations of three layer plate, considering energy dissipation in soft low modulus of elasticity middle layer

17 p2825 A71-35014

Spheroidal oscillations attenuation, considering discrepancy between theory and experiment due to earth interior dissipation

17 p2735 A71-35244

Batch unit for investigation of injectors in vapor-liquid flows, discussing measurement system and energy dissipation

17 p2724 A71-35275

Herringbone grooved gas lubricated journal bearing load capacity, attitude angle and power loss measurements

17 p2749 A71-35487

Electro-optical method for energy dissipation characteristics determination for mechanical systems subject to attenuating vibration

17 p2746 A71-35666

High voltage DC electric power transmission systems with ground return, reducing aircraft wiring weight and energy dissipation

17 p2678 A71-35771

Cosmic ray muons energy loss rate measurement in Fe using Durham magnetic spectrograph

18 p2957 A71-35930

Total inelastic energy dissipation in structure of creeping plastic material under variable repeated loading and shakedown
[ASME PAPER 71-APM-C] 18 p2977 A71-36252
Channel F doped MOS memory elements, discussing factors governing electrical energy dissipation and consumption 18 p2891 A71-36561

Two-mirror optical system to study energy dissipation in elastic systems subjected to cyclic straining 18 p2924 A71-36727
Reflection, material and resonator losses correlation in solid state lasers, investigating pulse power in Q switched operation 18 p2932 A71-36801

Temperature variations effect on TRAPATT microwave oscillator parameters, considering upper temperature limit dependence on heat dissipated in diode and heat sink thermal resistance 18 p2895 A71-36988

Active precession control devices for spin stabilized spacecraft, noting energy dissipation effect [AIAA PAPER 71-952] 19 p3148 A71-37193
Attitude dynamics and control of apogee motor assembly with paired satellites, discussing energy dissipation and spin axis reorientation time 19 p3099 A71-37194
Fuel slosh energy dissipation and dynamic stability of Intelsat 4, discussing spacecraft and tank selection [AIAA PAPER 71-954] 19 p3148 A71-37195
Temperature limit determination of rotating neutron stars based on heat dissipation due to slowing by frictional forces, noting Crab and Vela pulsars 19 p3131 A71-37337

Dissipative fluid motion, discussing approaches to analysis of real fluids time dependent complex flow equations 19 p3089 A71-37499

Turbulent pipe flow dissipation rate, presenting turbulence energy diffusion and stress components spectral distribution measurements 19 p3045 A71-38201

Transverse waves and electromagnetic instabilities propagating along magnetic field in homogeneous plasma, discussing ions and electrons energy losses and plasma dispersion 19 p3114 A71-38206

On-design performance characteristics of radial gas turbines, investigating blade geometry, rotor losses and pressure ratio effects 19 p3123 A71-38269

Simultaneous radar and instrumented aircraft observations in clear air turbulent layer for eddy dissipation rates calculation 20 p3256 A71-39207

Thermodynamics second law restrictions on constitutive equations of electromagnetic theory for nonlinear materials with long-range gradually fading memory, considering dissipation principle consequences 20 p3270 A71-39485

Transistorized microwave amplifiers with dissipative equalizing networks, describing transistor equivalent circuit 20 p3205 A71-39810

Crab Nebula pulsar radio properties, observing energy release due to increase in period, multipath propagation effects, intensity and time dependence 20 p3302 A71-39923

Multiple pulsar ejection in supernova core collapse and neutron star formation energy loss 20 p3305 A71-39947

Turbulent viscosity, energy dissipation and diffusion parameters of steady plane boundary layer flows of incompressible fluids with transverse shift in closed system of differential equations 21 p3368 A71-40691

Electronic transitions in oxygen molecule due to ion impact from kinetic energy loss spectrum 21 p3418 A71-40886

Unsteady laminar flow in polygonal ducts, calculating velocity profiles, friction factors and energy dissipation 21 p3371 A71-40994

Rayleigh wave reflection from crack tip after propagation along open crack faces in elastic solid, determining surface wave energy loss 21 p3468 A71-41003

Plasma shock wave propagation along weak magnetic field, considering energy dissipation 21 p3425 A71-41279

Nonuniform density cosmic plasma heating allowing for energy losses by radiation and heat conduction, using filament-structured high temperature plasma region model 22 p3598 A71-41533

Threshold AC electric field calculation for inhomogeneous plasma parametric instability excitation, noting role of electron plasma wave energy propagation from unstable region 22 p3582 A71-41901

ATS power supply concepts, considering growth capability, control, reliability, thermal dissipation and weight minimization 22 p3588 A71-41958

Dynamic analysis of ATS 5 heat pipe fluid energy dissipation, confirming estimated stability of planned rescue approach configuration 22 p3611 A71-42038

Dynamic sampling calorimeter for continuous measurement of human radiative, convective and evaporative heat loss, enabling closed loop control system analysis 22 p3503 A71-42155

Direct observation of cosmic ray kinetic energy losses in interplanetary region by measurements at separated spacecraft 22 p3593 A71-42331

Laminar Couette flow between parallel plates with mechanical energy dissipation and temperature dependent viscosity, determining velocity and temperature distribution 22 p3531 A71-42683

Solar energy degradation heat trapping-dissipating walls for inhabited living space on lunar surface 22 p3529 A71-42844

Loading cycles dependence of energy dissipation and plastic deformation during fatigue tests, using Fourier series 23 p3774 A71-42897

Attitude stability of dual spin spacecraft with energy dissipation in flexible momentum wheel having two degrees of freedom 23 p3772 A71-43020

Centrifugal compressor bladeless diffuser parameters, flow kinematics and energy losses, noting effects of friction coefficient and expansion angle 23 p3626 A71-43551

Normal wave scattering on random permittivity inhomogeneities of stratified waveguide dielectric layer, calculating beam width and energy loss by perturbation procedure 23 p3645 A71-43567

Bounded plasma ionization instability inhomogeneity scale evaluation, assuming negligible electron energy losses due to heat conduction as compared to elastic losses 23 p3712 A71-43923

Dissipative processes role in early universe within chaotic cosmology program 23 p3769 A71-43992

Filler quantity and type effects on mechanical energy losses in polymers, discussing molecular interaction and chemical bond influences 23 p3697 A71-44205

Laminar heat transfer losses effects on piston gas heater performance, computing heat transfer rate and thermal boundary layer thickness 24 p3887 A71-44603

Energy losses of collisional He plasma with ohmic heating in Uragan stellarator with large shear, comparing plasma lifetime to Bohm confinement time 24 p3855 A71-44664

Heat transfer with dissipation from longitudinal surface curvature, numerically integrating all equations for parameters 24 p3889 A71-44968

Evolved Cepheid-type stars vibrational stability against nonradial perturbations from quasi-adiabatic approximation of radiative dissipation 24 p3872 A71-45077

Thermal resistance, junction temperature and maximum power meter for semiconductor transistors and diodes with/without heat sinks 24 p3810 A71-45203

Nonadiabatic and atmosphere induced energy losses as causes of proton capture in geomagnetic field 24 p3867 A71-45320

Predawn effect on hot and cold electrons at magnetoconjugate point in F2 layer, discussing electron shock wave speed and thermal collisionless wave energy dissipation 24 p3824 A71-45321

ENERGY DISTRIBUTION

NT SPECTRAL ENERGY DISTRIBUTION

Energy distribution of laser spark spectrum in air, He and Ar, determining transmission coefficients of spark plasmas by self absorption method 02 p0258 A71-11638

Earth atmosphere X ray absorption, determining photon flux, energy and angular distribution as function of altitude by Monte Carlo method 02 p0299 A71-11776

Low pressure Cs vapor discharge in positive column, determining electron energy distribution function 02 p0289 A71-11956

Electrons longitudinal and transverse energy distribution in beam during cyclotron interaction with magnetoactive plasma waveguide 02 p0292 A71-12611

Polyatomic organic adsorbates effect on field emission total energy distribution from W and Mo surfaces, discussing electronic and phononic spectra 02 p0297 A71-12733

Huffman /impulse-equivalent/ pulse sequence design, examining energy distribution form control of signal in time-frequency plane 04 p0551 A71-15005

White dwarf data, examining continuous energy distribution, degenerate star theory, mass-radius relation, spectra, radial velocities and Einstein shift 04 p0648 A71-15244

MOSFET transistors instabilities due to charge exchange near oxide-silicon interface states, determining energy levels distribution and time constants 05 p0791 A71-16165

Radiation energy deposition profiles in transparent liquids, using holographic interferometer 05 p0748 A71-16265

Flat HF radio spectra from optically thin sources with low electron energy distribution indexes 05 p0808 A71-16399

Multiple speed flow onset and energy distribution in nonlinear electron beam-plasma interaction 06 p0937 A71-18354

Carbon dioxide electric discharge lasers physics discussing electron energy distributions and excitations, gain and saturation intensity [AIAA PAPER 71-64] 06 p0909 A71-18523

High subsonic jet near-field acoustic energy flux distribution calculation from pressure gradient measurements [AIAA PAPER 71-155] 06 p0884 A71-18597

Silicon detector measurements of energy deposition in aluminum by monoenergetic electrons 07 p1106 A71-19073

Continuity and balance equations of acoustic energy in nonuniform fluid flows 07 p1160 A71-19588

Solar burst theories, considering type 3 radiation source model for determination of lower corona plasma waves energy densities 08 p1358 A71-20889

Holographic recording media low signal energy densities comparison, determining peak values of diffraction efficiency and normal contrast ratio divided by signal beam exposure 08 p1290 A71-21389

Continuous energy distribution around light maximum of Nova Serpentis 1970 represented by yellow supergiant model, correcting observations for interstellar reddening 08 p1364 A71-21416

Carbon dioxide lasers gas discharges positive column, studying electron energy distribution by probe method 09 p1461 A71-22381

Electron emission from He ion by proton bombardment, calculating double differential cross sections relative to ejection energy and angle 09 p1497 A71-22415

Solar radiation energy distribution simulated by vacuum monochromator, discussing Ar-Kr-Xe-methane mixture 09 p1513 A71-22557

Long pulse glass laser welder-driller, determining mean energy densities and spot sizes 09 p1464 A71-23404

Thin metal foils total energy flux, electron/phonon temperatures and thermal conductivity anomalies at liquid He temperatures 10 p1657 A71-24457

Optimal control law for regulating energy distribution of emitted radar signals in multichannel system for minimizing target search duration 10 p1579 A71-24722

Solar wind blast wave dependence on initial disturbance energy and angular extent by time dependent two dimensional hydrodynamic flow simulation 10 p1663 A71-24779

Polar substorm energy from auroral region size and brightness photographic observations, discussing total flux dependence on magnetic field disturbance intensity 10 p1606 A71-24917

Hydrodynamics of matter-antimatter in contact, discussing coalescence, particles annihilation pressure and energy balance 11 p1821 A71-25539

Broadened energy distributions in electron beams, discussing energy spread delta E and C prime values relationship for studying weak Coulomb interactions 11 p1802 A71-25631

Alpha particle gas densitometric response to planet atmospheric density profiles in terms of radioactive source energy distribution, considering contoured baffle models 11 p1763 A71-26079

Thermally stratified turbulent shear flow, calculating turbulent energy balance and temperature inhomogeneity spectral equations 12 p1895 A71-26899

Electron energy distribution for spectroscopic determination in hollow cathode discharge helium-mercury plasma based on Druryesteyn function 12 p1937 A71-27050

Equilibrium energy distribution in system of nonlinearly coupled oscillators 12 p1930 A71-27168

Electron energy distribution functions in carbon dioxide laser plasmas, using Langmuir probes 12 p1940 A71-27280

TeV hadrons lateral energy distributions in air shower cores from Ne hodoscope measurements for fluctuations between primary energy and shower size, discussing French alpine scintillators array 12 p1951 A71-27386

Ground and mountain level measurements of energy and angular distribution of high energy neutrons in lower atmosphere, using double elastic scattering with hydrogen nuclei 13 p2119 A71-27906

Electron energy distribution in plasma discharge of Hg electron bombardment ion engines, using Langmuir probe 13 p2114 A71-27985

Electron energy distribution function in weakly ionized monatomic gas with inelastic collisions, using differential equation asymptotic resolution techniques 13 p2106 A71-28398

Fast plasma ions energy distributions in toroidal accelerators with quasi-stationary discharge 13 p2108 A71-28854

Electron avalanche processes in gas discharges, deriving electron energy distribution function and similarity laws 13 p2103 A71-29079

Interstellar grain temperatures, considering radiant energy distribution and optical properties effects 14 p2305 A71-29679

Discrete gust and power spectrum models of atmospheric turbulence, considering energy distribution effect on aircraft dynamic response 14 p2174 A71-29790

Proton flux measuring spectrometer with automatic tracking of distribution maxima over energy range from 0.15 to 4 keV 14 p2247 A71-30578

Energy state approximation and supersonic aircraft minimum fuel fixed range trajectory optimization, noting not convex velocity set 14 p2177 A71-30609

Electron production by proton impact on nitrogen, oxygen, neon and argon, measuring cross sections angular and energy distribution by electrostatic analysis and electron counting 14 p2277 A71-30660

Magnetic mirror system measured axial energy distribution of electron beams conversion to equivalent electrostatic analyzer 14 p2249 A71-30886

Low energy gamma ray measurements by balloon flights, detecting peak energy due to electron-positron annihilation 15 p2479 A71-32077

Electron energy distribution function and ionization rate constant of atoms by electron impact as function of heavy particle temperature 16 p2615 A71-32796

Continuum mechanics in differential forms, discussing material and spatial coordinates, compatibility conditions energy balance, entropy inequality and invariance principles 16 p2613 A71-34146

Electron density and temperature distribution in boundary layer flow of reflected shock tunnel conical nozzle 17 p2727 A71-34877

Heliocentric energy per mass changes in close planetary encounters, noting relation to cometary and asteroidal material evolution 17 p2811 A71-35744

IR chemiluminescence from HCl formed in atomic hydrogen reaction with sulfur dichloride, noting energy distribution among reaction products 18 p2874 A71-35832

Spatial relaxation of electron energy distribution with inelastic and Coulomb collisions, integrating Boltzmann equation 18 p2949 A71-36969

Ion-exosphere in open magnetic field, calculating number density, particle, moment and energy flux distribution from simple mathematical model 19 p3138 A71-37737

Latitudinal distribution of electron temperature in F2 layer during summer daytime period of low solar activity from electron density profile geometrical parameters 19 p3057 A71-38369

Performance measurement of electrostatic spectrometers as monochromators by calculation of electron energy distribution 20 p3233 A71-38821

Gas heating and energy balance of HF ring discharge in rare gases within cylindrical vessel, discussing electron energy distribution functions 20 p3273 A71-39044

Diffusion controlled order-disorder transformations kinetics, considering internal strain and gradient energy 21 p3397 A71-40431

Sound propagation in sheared fluid in duct, determining energy flux from linearized gas dynamic equations 21 p3366 A71-40536

Hot plasma fast ions energy distributions in toroidal accelerators with quasi-stationary discharge 21 p3426 A71-41286

Pulsar radio emission from expanding charge sheets moving relativistically along dipolar magnetic field near neutron star polar caps, calculating energy distribution 22 p3604 A71-42336

Fine structure of energy distribution function for electron beam interacting with plasma 23 p3711 A71-43411

Daytime photoelectron energy distribution and electron gas heating in F region as function of height and solar cycle variations 23 p3673 A71-44003

Uniform signal energy distribution in wideband synchronous data transmission channels using linear sequential filters with scramblers 23 p3647 A71-44345

Atomic and molecular gases electron impact ionization, measuring secondary particle energy distribution and angular dependence 24 p3850 A71-44925

ENERGY EXCHANGE

U ENERGY TRANSFER

ENERGY LEVELS

NT ATOMIC ENERGY LEVELS

NT ELECTRON STATES

NT GROUND STATE

NT INTERMOLECULAR FORCES

NT MOLECULAR ENERGY LEVELS

Gas laser output allowing for energy exchange between levels using population balance method 01 p0093 A71-10603

Inelastic scattering by impurities and phonons in metals, determining energy level structure from nonlinear corrections to Ohm law 02 p0297 A71-12615

Ne, Ar, Kr and Xe ionized states transition and level lifetimes from photographically recorded beam foil spectra, discussing particle energies 04 p0629 A71-14805

Average energies of ground and excited configurations in highly ionized atoms, using orthogonalized screened hydrogenic radial functions 04 p0630 A71-14999

Statistical equilibrium equations solved for atom/ion with complex energy level structure and weak spectral lines, discussing deviations from LTE 06 p0969 A71-17969

Low energy cosmic rays modulation and heliocentric gradient during solar minimum, comparing OGO 1 and 2 ion chamber measurements with other space and ground observations 06 p0954 A71-18128

Primary cosmic rays mass composition at energy levels above 10 TeV, analyzing muons data from extensive air shower experiments 13 p2125 A71-28094

Energy level threshold gradients for steady and unsteady lasing in four-level lasers, obtaining power output and pulse duration 13 p2077 A71-28153

Monograph on carbon dioxide laser gain observations covering spectroscopy, energy levels, radiative transitions, molecular collisions, power efficiency, etc 13 p2078 A71-28494

Quantum-theoretical transport equation for dilute gases with internal degrees of freedom, generalizing for arbitrary spacing between internal energy levels 14 p2275 A71-30449

Multiply ionized Ar excited valency and inner shell transitions, investigating emission spectrum and energy levels 15 p2368 A71-32747

Wavelength prediction for coronal transitions at various atomic configurations, deriving semiempirical expressions from observed data for energy level intervals determination 18 p2965 A71-36733

Trigonal crystal field and spin-orbit interaction matrices for ion energy levels in vanadium corundum in strong g scheme, using symmetry group tensor operators 21 p3427 A71-40075

Energy levels and vacancy association of defects in annealed GaAs at 600-1100 C under controlled vapor pressures, using cathodoluminescence measurements 21 p3428 A71-41044

Electroabsorption spectra of cadmium telluride at photon energies smaller than forbidden band width, observing energy levels 21 p3429 A71-41212

Traveling wave par interaction with three energy level medium at resonance frequencies, deriving coupled differential equations for amplitude variations 24 p3833 A71-44662

Charged particles effect on plasma negative ions, examining Stark effect in energy level 24 p3857 A71-45114

ENERGY LOSSES

U ENERGY DISSIPATION

ENERGY METHODS

NT STRAIN ENERGY METHODS

Book on laminated plate theory covering anisotropic continua, bending, orthotropic plates, energy equations, etc 02 p0330 A71-12844

Approximate minimum energy control for time variable linear system, using mathematical model 03 p0389 A71-13447

Composite viscoelastic materials fracture energy determination using equations for line crack in linear materials from spherical flaw theory and Griffith concept [SESA PAPER 1647] 03 p0508 A71-13764

Displacement type equilibrium equations for small deformation imposed on initial finite deformation, estimating elastic energy function based on strong ellipticity condition 03 p0510 A71-13945

Energy conservation in linear atmospheric models using first order kinetic equations 04 p0581 A71-15067

Circular arches static equilibrium path and dynamic response due to concentrated static and step loading using energy approach 04 p0668 A71-15184

Elastic solids mechanical characterization using finite element formulation of minimum potential energy theorem 04 p0671 A71-15751

Incomplete energy equilibration in short lived activated complexes, measuring translational energy of unimolecular ion decomposition fragments 05 p0716 A71-15924

Incompressible inviscid perfectly conducting cylindrical plasma stability against azimuthal disturbance in monotonic decreasing magnetic field with constant pitch, using energy principle 05 p0787 A71-16478

Dynamic stabilization of instability in bumpy theta pinch by generalization of energy principle 06 p0934 A71-17480

Shells with arbitrary moment initial stressed state, calculating stability by energy method 06 p0986 A71-17758

Circular cylindrical shell stability with ribs of variable cross sections, using method based on semimomentless theory 06 p0997 A71-17850

Metal fretting corrosion energy analysis in terms of thermodynamics of irreversible process 06 p0904 A71-17942

Coupling loss factor estimation, using wave transmission or natural frequency shift methods in statistical energy analysis 07 p1161 A71-19962

Cassini second and third laws generalization to energy extremes, discussing Mercury shape 07 p1203 A71-20523

Optimal prestressing against buckling of structures with reserve capacity, using energy methods of structural analysis 10 p1689 A71-24514

Composites under transverse normal tensile loading micromechanics failure criteria based on distortion energy theory, taking into account multiaxial stress concentration [AIAA PAPER 71-355] 11 p1784 A71-25334

Energy calculation for oscillatory systems with nonlinear, hysteretic and parametric elements 11 p1743 A71-26537

Soviet book on variational methods in mathematical physics covering energy method, Ritz process, Bubnov-Galerkin method and least squares method 12 p1931 A71-27292

Global hydrodynamic stability theory, discussing energy methods and nonlinear Boussinesq equations for disturbed motion 16 p2558 A71-32995

Cauchy problem for nonlinear Boltzmann equation in general relativity, utilizing energy inequalities 16 p2612 A71-34059

Moller gravitational field energy-momentum pseudotensor comparison with Einstein canonical and Landau-Lipschitz pseudotensors and Minkewitsch quasitensor, noting chronometric invariance 17 p2778 A71-34638

Mechanical interactions of point defects in homogeneous isotropic continuous elastic media, deriving interaction energy from Siems multipole forces analysis 17 p2831 A71-35395

Three dimensional minimum fuel turns for supersonic aircraft by energy state approximation [AIAA PAPER 71-913] 19 p3096 A71-37163

Energy and variational principles, studying local stability of equilibrium of elastic body subjected to conservative and gyroscopic forces 20 p3232 A71-38797

Power balance and statistical analysis of energy flow and response in lightly damped resonant structures 20 p3268 A71-38960

Steady and unsteady flow work and energy loss relationships expressed in integral form representing

perturbation kinetic energy, internal energy and pressure work

21 p3317 A71-40011

Ionization amplitude calculation method, using extrapolation from complex energies approach

21 p3418 A71-40249

Semiinfinite rods in maximal plastic deformation, observing impulse and energy constraint distinction

21 p3467 A71-40961

Energy method application to inhomogeneous turbulent flow with large eddies as recurrent velocity field structures, considering longitudinal rolls in boundary layer wall region

21 p3370 A71-40985

Neutron star matter equation of state and models from energy computations, discussing maximum stable mass

21 p3452 A71-41034

Invariance theory for nonlocal variational principles, covering energy forms and identities, weak coordinate invariance, integral balance and conservation laws

23 p3700 A71-44179

Compressible viscous flow calculation, deriving finite element analog of Navier-Stokes and energy equations

24 p3818 A71-44617

ENERGY OF FORMATION

Nonpairwise van der Waal interactions effects on vacancy formation energies in monatomic solids, using Lorentz oscillator and two body models for comparison

08 p1344 A71-21367

Campo del Cielo, Argentina meteorite crater structural analysis, discussing dimensions, energy of formation, mass, impact velocity, etc

15 p2488 A71-32352

ENERGY REQUIREMENTS

Human work level adjustment to specific energy expenditures during hard work on servocontrolled treadmill

02 p0202 A71-11665

Nonlinear stabilization systems time and energy optimal control syntheses using Pontryagin maximum principle

03 p0393 A71-14411

Space vehicles dimensions effects on working fluid mass and power required for orientation

09 p1532 A71-23133

Metabolic energy cost prediction equation for level or grade walking with/without loads

09 p1401 A71-23372

Mobility capability of lunar roving vehicles relative to terrain roughness, computing power requirements

15 p2494 A71-32496

Energy necessary to produce beam ion in plasma discharge of Hg electron bombardment ion source

16 p2623 A71-32841

Human energy requirements in weightless environments, correlating metabolic data from Gemini and Apollo missions with food consumption and energy balance measurements

16 p2532 A71-33778

Satellite communication system selection vs underground cable or hybrid systems, based on power requirements and economics

17 p2700 A71-34678

Channel P MOS memory elements, discussing factors governing electrical energy dissipation and consumption

17 p2715 A71-34684

Channel P doped MOS memory elements, discussing factors governing electrical energy dissipation and consumption

18 p2891 A71-36561

Future space flight energy requirements for onboard power supplies and propulsion, considering high temperature reactors with nuclear fuel in plasma state

19 p3122 A71-37319

Energy requirement measurements for bridge wire igniters at low voltage, using capacitor discharge

22 p3587 A71-41448

ENERGY SOURCES

Cylindrical shock waves generation from instantaneous energy release along line in quiescent atmosphere studied by numerical integration of flow equations

01 p0072 A71-11471

Capillary plasma heating source processes, using textolite and fiberglass-reinforced textolite dielectric discharge chambers

02 p0292 A71-12556

IR astronomy, considering basic principles, instrumentation energy production and radiation, spectroscopy, detectors and atmospheric absorption and emission

04 p0649 A71-15254

Tropospheric and stratospheric turbulence, discussing energy sources and sinks and energy spectra pattern at different atmospheric conditions

05 p0741 A71-16625

Earth core-mantle coupling as energy source for mantle wobble, taking into account precession cross coupling

06 p0891 A71-17890

Bulk effect microwave oscillators energy source design, considering operation mode and circuit tuning control parameters

08 p1266 A71-21623

Pulsar association with supernova remnants as energy source for supernova explosions, considering Crab Nebula, Vel X, Cas A and eta Car observations

09 p1518 A71-22350

Extragalactic violent events energy from collapsing stars or pulsar bodies rotational energy, producing extended radio sources

09 p1522 A71-22977

Atmospheric jet stream reinforcement by cold pseudofronts and convective energy from local source

12 p1924 A71-26824

Solar coronal heating homopolar generator model, proposing neutrons as energy source

12 p1961 A71-26877

Energetic violent explosive events nature and regional characteristics in universe from cosmic radiation composition studies

12 p1948 A71-27368

Meteorological research on upper atmosphere energy sinks/sources, composition, density, turbulence, winds and thermal structure

14 p2236 A71-30494

Hot jet aerodynamic parameters from emissions of electromagnetic and acoustic energies by crossed beam IR probing

14 p2288 A71-30520

Complex form plates with energy sources in combined cooling system, calculating temperature field

17 p2836 A71-34422

Coherent neutral sheet radiation from pulsars, examining relationship between pulsation-driving energy source and mechanisms for pulsed emission

18 p2958 A71-36928

Radioisotopes as energy source for power conversion systems, discussing future availability of fission products and transuranium elements from commercial nuclear power reactors

20 p3265 A71-38948

Earth thermosphere models, discussing shortwave solar radiation as major energy source during quiet conditions, diurnal variations of structure, neutral-charged components interconnection, etc

20 p3216 A71-39117

Power derived from aerobic, lactic acid and alactacid energy sources during human muscular work under normoxic and hypoxic conditions, noting oxygen consumption

22 p3485 A71-41721

ENERGY SPECTRA

NT ELECTRONIC SPECTRA

NT NEUTRON SPECTRA

Semiconductor with charged impurities in strong electromagnetic field, investigating scattering effects on electron energy spectrum

01 p0140 A71-11463

Photoelectron fluxes and energy spectra in ionosphere for predawn and sunlit atmospheres, taking into account elastic and inelastic collisions

01 p0147 A71-11506

High energy albedo neutrons energy and angular distributions, determining solar neutron flux upper limit

01 p0147 A71-11517

Solar wind ion abundances from satellite observation, discussing energy spectra, particle distributions, etc

01 p0147 A71-11518

Miniature multigrid probes for measuring energy spectra of charged particles and absolute plasma densities, comparing results to microwave measurements

02 p0247 A71-11637

Energy spectra of expanding relativistic particle clouds producing quasar and Seyfert galaxy nuclei outbursts

02 p0307 A71-12082

Low energy cosmic ray deuteron flux, examining energy spectral shapes of sources

02 p0303 A71-12871

Omnidirectional intensity of atmospheric gamma rays at balloon altitudes at various energy thresholds, noting integral spectrum flattening at lower energies

03 p0473 A71-13306

Energy spectra of ionization bursts, electromagnetic cascades and nuclear active particles at mountain altitude

03 p0476 A71-13850

Extensive air shower electron photon and muon components energy spectrum at various depths

03 p0477 A71-13859

Cosmic rays intensity measurement in deep ocean with Cerenkov counter, determining Muon energy spectrum and absorption in water

03 p0477 A71-13862

Bremsstrahlung photons produced by cosmic ray muons in Fe and Pb at sea level, calculating energy spectra and angular distributions

03 p0477 A71-13863

Inelastic alpha particle scattering experiment for studying energy spectrum and angular distribution of Sc-45 excited states

03 p0462 A71-14417

Auroral zone electron and proton energy spectra measurements, using sounding rockets with electrostatic analyzers

03 p0419 A71-14524

Primary cosmic ray electrons intensity energy spectrum data, suggesting plots based on electron energy to positive gamma power

03 p0482 A71-14542

Turbulence energy spectra in thick convective cumulonimbus cloud zone, using aircraft measurements

04 p0622 A71-15632

Solar flare relative abundance and energy spectra of He 3 and He 4, using charged particle telescope on IMP 4

05 p0797 A71-15944

Interplanetary space He 3 differential energy spectrum in 10-30 MeV range from IMP 4 satellite observations, noting solar contributions

05 p0802 A71-15944

Time interval maximum transmittable energy under spectral limitation, deriving time limited pulse functions for minimum energy loss

05 p0720 A71-16393

Novae-like X ray source near or in Centaurus constellation, presenting energy spectra measured by sounding rockets in Japan during August 1969

05 p0808 A71-16452

Internal combustion engine exhaust system sound radiation, discussing pressure wave effects, energy flux and boundary conditions

05 p0796 A71-16604

Tropospheric and stratospheric turbulence, discussing energy sources and sinks and energy spectra pattern at different atmospheric conditions

05 p0741 A71-16625

D region aeronomy characteristics and ionizing radiation energy spectra during solar flare of 22 October 1969

05 p0799 A71-16818

Magnetotail plasma sheet electron and proton energy spectra and angular distribution over auroral zone, comparing Vela satellite and rocket measurements

06 p0887 A71-17260

Directional differential energy spectra for proton intensities in outer radiation zone near magnetic equator from satellite observations

06 p0949 A71-17261

Projected Hartree-Fock energy spectra using basis wave functions with harmonic oscillator and Woods-Saxon radial dependence

06 p0929 A71-17577

Nucleus energy spectra projection from Hartree-Fock intrinsic wave functions model space, using coupled orbital matrix elements

06 p0929 A71-17578

Solar protons energy spectrum upper cut-off based on worldwide neutron monitors recordings of 28 January 1967 solar event

06 p0950 A71-17998

Cosmic rays effective angles of acceptance and energy spectrum diurnal variations, using temporal correlation functions

06 p0951 A71-18107

Galactic cosmic ray proton and He spectrum measurements in 1968 compared to electron spectra, explaining solar modulation features by models incorporating energy loss effects

06 p0952 A71-18112

Quiet time fluxes and differential energy spectra of protons and alpha particles at 2-20 MeV measured by cosmic ray detectors on OGO-3

06 p0954 A71-18127

Heavy cosmic ray nuclei intensity and energy spectra, investigating solar modulation effects

06 p0954 A71-18129

Solar modulation variation of secondary cosmic ray energy spectra, noting dependence on atmospheric depth and geomagnetic cut-off

06 p0955 A71-18135

Protons and alpha particles energy spectra during 25 February 1969 solar event from Centaur rocket observations as part of ESRO PCA campaign

06 p0957 A71-18144

Solar flare on 9 June 1968, observing proton energy spectra and flux variation with time profiles

06 p0958 A71-18155

Particle flux energy spectra and time dependence of 25 February 1969 solar proton event

06 p0959 A71-18156

Primary cosmic ray electrons energy spectrum measurement at Fort Churchill, examining geomagnetic cut-off rigidity daily variations

06 p0959 A71-18159

Solar proton event energy spectra based on multiplicity measurements of cosmic ray neutron intensity increases

06 p0960 A71-18164

Secondary cosmic ray spectrum latitude knee based on nucleon, proton and muon energy spectra

06 p0960 A71-18167

Solar flare electrons at 10-200 MeV region, discussing energy spectra and time history

06 p0961 A71-18170

- Muon momentum spectra and charge ratio at 60 deg in east-west plane 06 p0961 A71-18176
- Extraterrestrial gamma ray and neutron flux and energy spectrum at balloon altitudes over equatorial latitudes, using pulse shape discriminator during solar flare 06 p0962 A71-18177
- Fast neutron energy spectrum and flux, using balloon flight neutron detector with charged particle rejection scheme and pulse shape discriminator for gamma rays separation 06 p0962 A71-18178
- Atmospheric gamma rays energy spectrum and implication on high energy interactions characteristics 06 p0962 A71-18181
- Solar vicinity particle storage implication from flare proton energy spectrum observation by Injun 5 satellite 07 p1186 A71-19653
- Ionospheric low energy electron and proton fluxes near equator from Isis 1 satellite soft particle spectrometer observations, considering energy spectra and pitch angle distribution 07 p1187 A71-19679
- Atmospheric high energy gamma rays, pion production and electron energy spectra over Hyderabad, using stack nuclear emulsions 07 p1189 A71-20497
- Multicharge nuclei fluxes from satellite observation, plotting energy and rigidity spectra from latitudinal dependences 08 p1350 A71-20955
- Primary cosmic ray variations energy spectra on rising and declining solar activity arm, analyzing stratospheric particle intensities 08 p1353 A71-20980
- Energy spectra of expanding relativistic particle clouds producing quasar and Seyfert galaxy nuclei outbursts 08 p1362 A71-21132
- Plasma ions lifetime and energy spectra in quadrupole magnetic trap as function of energy and time 08 p1340 A71-21483
- Galactic cosmic ray proton and He nuclei spectra measurements aboard Pioneer 8 spacecraft over large energy range, considering solar modulation parameters 08 p1355 A71-21626
- Cosmic ray electron intensity and energy spectrum from nuclear emulsion-spark chamber combination detector triggered by scintillation and Cerenkov counters on high altitude balloon 08 p1355 A71-21627
- Satellite-borne spectrometer for low energy electrons measurement, describing virgin photoelectrons equilibrium energy spectrum for different latitudes and pitch angles 09 p1436 A71-22553
- Electron energy spectra construction from Al, Sn and Au target layers transmission angular distribution measurements, using computer calculated spectra for comparison 09 p1497 A71-22688
- Planetary scale atmospheric motion energy spectra and error prediction from numerical model, using eddy-damped Markovian approximation for two dimensional turbulence 09 p1489 A71-23551
- Auroral zone electron energy spectra local time dependence from polar satellite observations 09 p1515 A71-23632
- Energy spectrum of iron group solar cosmic ray particles determined from glass removed from Surveyor 3 spacecraft, considering lunar erosion implications 09 p1515 A71-23656
- Frequency domain spectral energy equations for large scale atmospheric motions, discussing earth rotation effects on kinetic energy spectrum 10 p1638 A71-23963
- Satellite instruments to measure intensity and energy spectrum of high energy electrons and protons 10 p1683 A71-24464
- Negative pion capture in nuclei, examining charged particle emission energy spectra 10 p1644 A71-24538
- Earth outer radiation belt electrons intensity, differential energy spectra and radial diffusion during maximum solar activity 10 p1663 A71-24783
- Geomagnetically trapped protons differential energy spectrum in Van Allen inner and outer radiation belts over various energies, using thin solid state detector 10 p1663 A71-24784
- Muon bundles frequencies from model for propagation of various atmospheric components in combination with theoretical pion spectra 10 p1664 A71-25044
- Energy spectrum minimization of intrinsic phase fluctuations in multistage vacuum tube frequency multiplier, using graphic analysis 11 p1738 A71-25940
- FORTAN 4 computer program for gamma ray energy spectra, determining peak locations, peak areas and elemental abundances 11 p1729 A71-26069
- Criticism of paper on synchrotron sources energy spectra formation, examining time dependent spectrum on boundary conditions 11 p1832 A71-26170
- Large air shower Cerenkov detectors system, discussing energy spectra from vertical arrays, delayed muons and radio pulse detection rates 12 p1950 A71-27384
- Three dimensional Monte Carlo simulation of extensive air shower development, comparing fireball and mathematical models for mean total hadronic energy spectra 12 p1951 A71-27388
- Two temperature model of cosmic ray high energy jets, predicting one particle accelerator momentum spectra 12 p1951 A71-27397
- Momentum spectra of cosmic ray particles at sea level, using magnetic spark chamber spectrograph and ionization calorimeter 12 p1952 A71-27402
- Sea level muon spectra at 83 degrees zenith angle up to 1 TeV, using Kiel spectrometer 12 p1952 A71-27404
- Sea level muon spectrum measurements at 80 degrees to vertical up to 1 TeV, using Nottingham spectrometer 12 p1953 A71-27405
- Muon spectra and charge ratios at sea level, analyzing by collision model and one dimensional diffusion equations 12 p1933 A71-27406
- Underground cosmic ray particles flux and nuclear interaction properties, determining integral sea level energy spectrum as function of range of particles in rock 12 p1953 A71-27407
- Helliwell VLF discrete emission theory application to determination of electron stream energy spectrum and structure 13 p2027 A71-27915
- Cadmium mercury telluride solid solutions electron energy spectrum at low temperatures, calculating electron mobility in crystals with zero forbidden band 13 p2110 A71-27955
- Differential energy spectrum of cosmic ray deuteron flux of galactic origin from IMP 5 satellite measurements 13 p2120 A71-27974
- High energy sea level cosmic ray neutrons energy spectra, noting angular distribution about zenith and attenuation length in atmosphere 13 p2120 A71-28050
- Nucleon-nucleon and meson-nucleon collisions, determining secondary cosmic ray multiplicity dependence on primary particles energy spectra 13 p2121 A71-28057
- Cosmic hadron flux measurements and energy spectra at various altitudes in atmosphere, using calorimeters 13 p2122 A71-28066
- Extensive air shower size measurements, relating energy spectra to primary energies up to 10 million TeV by calorimetric method 13 p2122 A71-28069
- Atmospheric scintillation light detection from air shower, determining interaction mean free path of .1-10 million TeV primary particles 13 p2122 A71-28070
- Extensive air showers nuclear active component energy flux lateral distribution and spectrum based on Monte Carlo simulation of elementary interactions 13 p2123 A71-28077
- TeV hadronic component in air shower cores, comparing energy spectra and lateral distributions to Monte Carlo simulations 13 p2123 A71-28078
- Particle densities and muon spectra at 100-1300 m from sea level extensive air showers axes for primary energies to 10 to 20th eV 13 p2124 A71-28086
- Extensive air showers muon and electron components primary energy spectrum, using isobar and CKP formula based models 13 p2125 A71-28088
- Muon rich showers, discussing muon density spectrum relation to primary energy spectrum 13 p2126 A71-28099
- Electron energy spectra of amorphous semiconductors by cell method, replacing conditions for splicing wave functions by extremum integral 13 p2112 A71-28925
- Pulsar CP 0834 pulse energy fluctuations spectra secondary periodicities fluctuations from radioheliographic observation 13 p2141 A71-29099
- Particle energy spectrum function effect on fluid energy spectrum in turbulent gas-solid suspension flow [ASME PAPER 71-FE-15] 13 p2052 A71-29454
- Energetic electron power spectrum effect on synchrotron radiation from magnetosphere 14 p2298 A71-29722
- Proton recoil measurements of PuBe neutron source spectra, using pressurized hydrogen spherical proportional counter and liquid scintillator measurements 14 p2276 A71-29918
- Low energy electron precipitation effects on upper atmosphere based on polar cap and auroral oval electron spectrum comparison 14 p2300 A71-30035
- Absorbed energy spectra and absorption frequencies from elastic constants of vibrating metals with cubic lattice structure, using cold neutron scattering 14 p2190 A71-30149
- Circular air jet velocity, turbulence intensity and energy spectra distributions, investigating longitudinal acoustic field influence 14 p2225 A71-30226
- Cosmic ray telescopes with scintillation and Cerenkov counters for 2 to 8 BeV energy range, describing structural details and operational specifications 14 p2247 A71-30597
- High energy cosmic muons momentum spectrum and charge ratio measurements at large zenith angles, describing magnetic spectrometer 14 p2247 A71-30601
- Plasma ions lifetime and energy spectra in quadrupole magnetic trap as function of energy and time 14 p2282 A71-30670
- Atmospheric cosmic ray propagation based on phenomenological model of hadron-nucleus collisions, predicting sea level nucleon, pion and muon energy spectra and ionization profile 15 p2474 A71-31732
- Energy dependence of cosmic ray muon charge ratio at large zenith angles, using large aperture and high resolution cosmic ray momentum spectrograph 15 p2475 A71-31779
- Momentum spectrum measurement of cosmic ray muons, recording particle trajectories photographically 15 p2475 A71-31783
- Muon sea level differential energy spectrum at 80 deg to vertical up to 1 TeV, using Nottingham spectrometer 15 p2475 A71-31784
- Energy spectrum of cosmic ray showers from high energy muon interactions with nuclear emulsion chamber 15 p2476 A71-31789
- Cosmic ray muon-neutrinos sea level energy spectra at low energies for horizontal and vertical directions, estimating geomagnetic cut-off effects for various geomagnetic latitudes 15 p2477 A71-31799
- High energy primary cosmic ray program of Goddard Space Flight Center involving charge composition and energy spectra studies in balloon and satellite experiments 15 p2478 A71-31804
- Cosmic ray measurements at various altitudes, describing magnet spectrograph for momentum spectra and particle identification 15 p2408 A71-31813
- Cosmic ray shower size spectrum in atmosphere for muon bremsstrahlung at large zenith angles 15 p2479 A71-31868
- Extragalactic nebulae, considering galactic formation stages and energy supply problems 15 p2486 A71-31925
- High resolution energy spectra and valence band structure vs carbon content in homogeneous titanium carbides 15 p2430 A71-32150
- Solar flare radiation data from Pioneer spacecraft, detailing anisotropy, heliocentric longitude gradients, decay time constants and energy spectra 15 p2480 A71-32752
- Energy-radiation problems in relativity theory, considering electromagnetic waves, Einstein equations, momentum tensors and moving charge particles 16 p2609 A71-33259
- Pulsating gamma ray flux from pulsar NP 0532 in energy range from 250 keV to 2.3 MeV 16 p2626 A71-33389
- Low energy solar X-ray emission spectra observations, discussing nonthermal electron spectrum relation to acceleration by electric fields 16 p2626 A71-33725
- Secondary electrons and photons energy spectra and depth dependence in upper atmosphere from numerical solution of one dimensional transport equations 16 p2628 A71-33937
- Time variations of magnetotail plasma sheet from electron energy spectral measurements on Vela satellites 16 p2629 A71-33945
- Energy spectrum parameters from Burstein-Moss effect observation in thin CdO layers, explaining absorption edge shape at various electron concentrations 16 p2622 A71-34029

Inelastic electron scattering cross sections and energy spectra from Al and Au targets, using magnetic analyzer with high resolution detector

16 p2614 A71-34042

Time of flight energy spectra of high lying and Rydberg metastable atoms by electron impact dissociation of molecular oxygen, noting atmospheric applications

16 p2614 A71-34043

Cyg X-1 X ray intensity and energy spectrum variation data, using balloon-borne telescope

16 p2629 A71-34076

Objective monitoring of human operator, using statistical analysis of EEG based on numerical characteristics of energy spectrum

17 p2692 A71-35168

Galactic weak X ray sources observation in Southern Hemisphere for flux and energy spectrum

17 p2796 A71-35408

Radio emission from cosmic ray showers, discussing detection, particle populations and energy spectra

18 p2957 A71-36211

Cosmic X ray astronomy by rocket and balloon soundings and discrete emission source measurements, considering energy spectra

18 p2957 A71-36212

German monograph on evaporation neutrons mean multiplicity for cosmic radiation energy spectrum variations measurement

18 p2958 A71-36670

Balloon observations of solar protons on 29-30 September 1968 over Iceland with GM telescopes and scintillation detectors, considering energy spectrum and time behavior

18 p2958 A71-36744

Radiation belt proton intensities and energy spectra measurements by Azur satellite solid state detector telescope with energy level discrimination electronics

19 p3125 A71-37417

Auroral zone proton measurements during slowly varying cosmic noise absorption, obtaining energy spectrum by rocket soundings

19 p3125 A71-37418

Primary cosmic ray proton energy spectrum in 50 GeV to 300 TeV range, using Proton 1, 2 and 3 satellite-borne counters

19 p3128 A71-38352

Cosmic ray spectrum at nonrelativistic energy region, noting ionization loss effects

19 p3129 A71-38359

Electron flux and energy spectra measurements at 200-600 km altitude by Cerenkov counters onboard Proton 1 and 2

19 p3129 A71-38375

ESRO-1A /Aurorae/ observations of variations in low energy electron spectrum, noting relationship to magnetic activity

19 p3060 A71-38576

German monograph on electron flux properties in polar atmosphere, discussing pitch angle distribution, energy spectrum and relation to geomagnetic field disturbances

19 p3130 A71-38646

Dynamic energy spectra of nonthermal electrons in solar flares from balloon-borne high resolution hard X ray observations

19 p3130 A71-38673

Chemical composition of atmospheric aerosols from Tokyo region, measuring energy spectrum of neutron irradiated specimens by gamma spectrometer

19 p3094 A71-38698

Thermodynamics and statistical mechanics of low temperature physics, including entropy, probability, energy spectra and gas liquefaction

20 p3270 A71-39240

Energy spectrum minimization of intrinsic phase fluctuations in multistage vacuum tube frequency multiplier, using graphic analysis

20 p3205 A71-39260

Solar radiation effects on upper atmosphere soft electron flux and energy spectrum during day and night

20 p3281 A71-39724

Photoelectron flux and energy spectra effects on ionospheric phenomena, examining sunlit and pre dawn atmospheric models

20 p3225 A71-39726

PCA due to solar proton event, measuring electron/ion densities and temperatures, proton/electron energy flux spectrum, Lyman alpha radiation and X rays

20 p3281 A71-39730

Superthermal electrons energy spectra and pitch angle distribution, presenting photoelectron flux recordings by Cosmos 261 satellite

20 p3282 A71-39740

Turbulent energy variations in unsteadily moving flow with structural shift, emphasizing formation of vortices with various inertia scales

20 p3214 A71-39796

X ray observations in Crab Nebula, including angular size, location, energy spectra, time variability, line emission, interstellar absorption and polarization

20 p3302 A71-39920

High resistance undoped GaAs samples at different temperatures, investigating energy spectra, Hall effect and electron conductivity

21 p3431 A71-41227

Electron energy spectra of amorphous semiconductors by cell method, replacing wave functions condition extremum integral

21 p3434 A71-41321

Solid solution electron energy spectrum at low temperatures, considering electron mobility in cadmium-mercury telluride crystals with zero forbidden band

21 p3435 A71-41342

Diffuse 0.2-2 keV cosmic X ray flux, discussing energy spectrum and spatial distribution

22 p3591 A71-41914

UK 5 spacecraft experiments in X ray astronomy, investigating spatial distribution and energy spectra of emissions in space, polarization and pulsar periodicities

22 p3610 A71-42015

Lunik 14 spacecraft radio signal reflection from lunar surface, showing energy spectrum dependence on surface roughness

22 p3511 A71-42301

Cosmic ray muon electromagnetic interactions and energy spectrum measurements at large zenith angles at sea level

22 p3593 A71-42356

Energy spectra of ionization bursts, electromagnetic cascades and nuclear active particles at mountain altitude

22 p3595 A71-42651

Extensive air shower electron-photon and muon components energy spectrum at various depths

22 p3595 A71-42660

Cosmic rays intensity measurement in deep ocean with Cerenkov counter, determining muon energy spectrum and absorption in sea water

22 p3595 A71-42663

Bremsstrahlung photons produced by cosmic ray muons in Fe and Pb at sea level, calculating energy spectra and angular distributions

22 p3595 A71-42664

Superheavy elements search in lunar fine grains from Apollo 12 mission by measuring kinetic energy spectrum of nuclear fission fragments

23 p3761 A71-43718

High resolution time averaged energy spectrum and chemical composition of iron group cosmic ray nuclei from fossil tracks in Apollo 12 lunar rocks

23 p3764 A71-43804

Interplanetary energy spectrum of solar flare Fe nuclei from tracks in Surveyor 3 glass filter and rock 12022

23 p3765 A71-43813

Absolute vertical intensity measurement of cosmic ray muon energy spectrum at sea level, presenting spark chamber and absorption spectrograph data

23 p3722 A71-43876

Steady state problem of energy spectrum of variable magnetic field accelerated electrons, considering synchrotron X ray emission of Crab Nebula and pulsar

24 p3869 A71-44802

ENERGY STORAGE

NT ELECTRIC ENERGY STORAGE

Inertial and semiinertial propulsion systems output power and efficiency, taking into account continuous kinetic and potential energy buildup and fuel release

06 p0979 A71-17583

Thermoelastic heat release in muscular twitch final phase, discussing energy storage as function of active or passive muscular tension

11 p1718 A71-25626

Atmospheric energy storage and meridional transport, calculating annual cycle in Northern Hemisphere

12 p1925 A71-27193

Equations system describing plasmoid acceleration process in coaxial injector with inductive energy storage

12 p1938 A71-27205

Plasma acceleration in injector with inductive energy storage, discussing arc discharge circuit opening time effect

13 p2108 A71-28856

Plasma energy cumulation by concentric spherical and cylindrical waves, calculating stability limit by integral solution

16 p2619 A71-33355

Particle flux, energy storage and beam loading effects on superconducting traveling and standing wave resonators in linear accelerators

16 p2587 A71-33494

Electric power system for satellites, considering energy conversion, storage and processing from chemical, solar and nuclear sources

17 p2676 A71-34227

Hydrostatic power transmission systems classifications, considering transformation, transport and accumulation of energies /mass, heat, optical, chemical, pneumatic, hydraulic, etc/

18 p2850 A71-36202

Equations system describing plasmoid acceleration process in coaxial injector with inductive energy storage

19 p3117 A71-38617

Flight mechanics of point with limited power propulsion system and energy storage unit, investigating variational maximum payload problem with singular control optimization

20 p3288 A71-39125

Plasma acceleration in inductive energy storage injector, discussing arc discharge circuit opening time effect

21 p3426 A71-41291

Pulsed atmospheric pressure carbon dioxide laser, studying pulse power and shape as functions of energy storage capacitor value, charging voltage and gas composition

22 p3557 A71-42159

HF dispersion, power and energy storage in periodic slow wave waveguides of resonator chains coupled through openings

24 p3805 A71-45257

ENERGY STORAGE DEVICES

U ENERGY STORAGE

ENERGY TRANSFER

NT COUPLING CIRCUITS

NT LINEAR ENERGY TRANSFER [LET]

Er lasing efficiency dependence on dopants in Li-Ca-silicate glass host, determining energy transfer rates for optimum concentration

01 p0092 A71-10010

Extensive atmospheric showers and energy transfer from interacting nucleons to electron photon cascades at high energy levels

01 p0146 A71-11366

Power transfer in plasma heating with combined RF and steady magnetic fields

01 p0137 A71-11481

Digital simulation mathematical model describing simultaneous energy and mass transfer process in clothing-airspace-skin system

02 p0203 A71-11806

Atmospheric circulation and earth rotational energy contribution to energy release by intense polar auroras, noting ionospheric current subsonic heating and oxygen emission

02 p0244 A71-11909

Maximum power transfer theorem generalization for n-terminal pair network containing sources

02 p0236 A71-12043

Heat transfer to walls of quartz discharge tube in Ne, Ar and Xe, measuring integral energy flux

02 p0290 A71-12191

Thermionic converter Cs plasmas electron temperature and density gradients spectroscopic measurements compared with prediction from energy transport analysis and ionization coefficients

02 p0194 A71-12226

Solar core to surface energy transfer mechanism, discussing chromosphere spectrographic, photoelectric and telescopic observations

02 p0312 A71-12373

CO chemical laser power output augmentation by selective depopulation of CO lower vibrational levels by energy transfer to added gases

02 p0262 A71-12709

High power regulated energy transfer by inductor-transformers with single and multiple stages using trapezoidal current waveshapes

03 p0352 A71-13048

Active nitrogen afterglow complex spectrum analysis from vacuum UV to IR, proposing energy transfer mechanism

03 p0460 A71-13352

Plasma column ohmic and collisional heating by RF electromagnetic field, deriving energy transfer expressions

03 p0464 A71-13550

CW laser output in carbon dioxide and nitrous oxide induced by vibrational energy transfer from excited carbon monoxide

03 p0438 A71-13893

Severe storm mass and energy convective transport characteristics, using ATS-3 cloud photographs and three layer model

03 p0454 A71-14204

Shock tube measurements of vibrational energy transfer in molecular carbon dioxide-nitrogen-water system

04 p0629 A71-14693

Energy transport over turbulence spectrum of free atmosphere, using aircraft experiments

04 p0622 A71-15634

Soviet papers on energy transfer in channels covering aerothermoptics, hydrodynamics, light propagation, free convection and thermoconvective waves

04 p0628 A71-15807

Cosmic ray particles diffusion with simultaneous energy transport, using leakage lifetime approximation

05 p0798 A71-16448

Energy transfer in general relativity, discussing time sequences restriction of static deformable configurations in near field

05 p0781 A71-16729

Energy transfer between nonlinearly coupled oscillators described by Hamiltonian system in case of third order resonance

05 p0783 A71-16995

Interplanetary medium during magnetic storm periods, noting pressure and density increases of various energy flows of media and static pressure/magnetic pressure ratio

05 p0744 A71-17179

F region photoionization heating, investigating energy transfer from ionizing photon to neutral gas atoms and molecules

06 p0893 A71-17982

Parallel plate plasma accelerator energy deposition, considering kinetic and thermal modes based on flow velocity, temperature and Mach number measurements

[AIAA PAPER 71-197]

06 p0939 A71-18635

Magnetoelectric cold plasma wave interaction theory, investigating energy transfer

07 p1167 A71-19230

First exchange energy inhomogeneity term numerical coefficient approximate derivation

07 p1164 A71-19690

Energy transfer at colliding streams in solar wind from Explorer 34 and Vela 4B measurements of proton, alpha particle, electron and magnetic field parameters

07 p1188 A71-19824

Triatomic molecules relaxation process, considering translational-vibrational energy exchange in atomic collisions and transition probabilities for carbon dioxide-helium system

08 p1337 A71-20669

Nitrogen molecule collision with metastable inert gas atoms and ions, investigating energy exchange mechanism

08 p1337 A71-20670

Fluoro-alkyl s-triazines as high temperature lubricants and energy transfer fluids for aerospace systems [ASLE PREPRINT 70LC-5]

08 p1322 A71-21155

Tropical hurricane central pressure drop to maximal wind velocity ratio, discussing thermal to mechanical energy transfer as function of ocean surface temperature

08 p1330 A71-21873

Wave interference effects and energy transfer in coupled thin film optical waveguides

09 p1460 A71-22159

Energy transmission mechanism in calcium fluoride-europium ion plus holmium ion system, investigating luminescence and absorption spectra

09 p1461 A71-22388

Coupled fiber lasers maximum energy transfer between passive conductors, determining minimum pulse duration

09 p1464 A71-23112

Optimization of slot angle, slot positioning and flow quantity affecting boundary layer control in energy transfer over airfoil profiles

09 p1383 A71-23201

Nonhomogeneous plane parallel cold plasma flows in external magnetic field, deriving energy transfer between two sliding plasmas

10 p1651 A71-24634

Ion beam deceleration and effective energy transfer to plasma at nonisothermal acoustic velocities in presence of ion acoustic instability

10 p1653 A71-24892

Vibrational nonequilibrium influence on IR radiative energy transfer in nongray nonisothermal gases

10 p1643 A71-24967

Electrical and thermal conductivity coefficients and energy diffusion coefficient in lower ionosphere, assuming weak ionization of ionospheric plasma

10 p1607 A71-24998

Energy transfer during charged particles passage through material media as function of spatial distribution, discussing electron production rates

11 p1802 A71-25769

Net fusion energy from laser heated deuterium-tritium particles dependent on plasma temperature, electrical energy and electron-ion thermalization through collisions

11 p1805 A71-25799

Stimulated Compton effect in compact radio sources, giving formulas for energy flow between relativistic electron and radiation field

11 p1831 A71-26169

Elemental maximum energy transport formula for wick heat pipe evaporators under artificial gravity and external acceleration, testing by laboratory centrifuge [AIAA PAPER 71-419]

11 p1857 A71-26210

Magnetoelectric cold electron plasma wave interaction theory, investigating energy transfer

12 p1934 A71-26748

Auroral electron temperature, noting field aligned energy transport current effects

12 p1899 A71-26887

Electromagnetic wave propagation on uniform transmission line network, discussing passivity and stability notions concerning energy exchange between waves and material

12 p1879 A71-27039

Impulsive energy deposition generated stress waves in composite media formed by two plane layers with interfacial molecular bond joining

12 p1983 A71-27575

Rotation-convection model of solar equatorial acceleration and temperature, assuming inhomogeneous isotropic latitude dependent turbulent energy transport

12 p1968 A71-27644

Vibrational energy transfer from excited nitrogen to CO and NO, describing flow tube measurements

12 p1934 A71-27760

High energy hadrons energy flow fluctuations and chemical composition of cosmic rays in air shower cores, comparing to Monte Carlo calculations

13 p2123 A71-28079

Atmospheric circulation and earth rotational energy contribution to energy release by intense polar auroras, noting ionospheric current subsonic heating and oxygen emission

13 p2058 A71-28196

Interplanetary medium characteristics during geomagnetic storms, discussing changes in pressures, energy flux densities, acoustic velocities and static/magnetic pressure ratio

13 p2058 A71-28236

Rotating solar wind nonradial oscillations and energy transport, showing internal solar gravity waves effects

13 p2130 A71-29118

Boundary conditions formulation for energy and mass transfer in weakly rarefied gas flows past bodies

13 p1991 A71-29149

Solar wind-magnetosphere interaction based on electric fields and currents, discussing energy transfer and magnetic field reversal at magnetopause

13 p2064 A71-29165

Energy transport mechanisms of rapid diamagnetism decay in plasma stream collisions, using two fluid shock front model

13 p2110 A71-29371

Stellar wind flow models associating energy transport with propagation and dissipation of hydrodynamic waves and heat conduction

14 p2297 A71-29586

German monograph on network method application for conductive and radiative energy transfer coupling problems

14 p2336 A71-30231

Nitrogen-carbon dioxide system molecular resonant energy exchange vibration-vibration probability measurement by shock tube and IR emission monitoring, noting temperature effects

14 p2276 A71-30399

Cosmic ray shower evolution model based on passive baryon existence and direct energy transfer to gamma quanta hypotheses

14 p2302 A71-30593

Equations for radiative contribution to energy and mass transfer in monatomic and ionized gas flow in local thermodynamic nonequilibrium

14 p2338 A71-30819

Fokker-Planck equation for Compton scattering in hot plasma, considering energy exchange rates for scattering in relativistic Maxwellian plasma

14 p2283 A71-30859

Ejection explosion energy transfer to ambient media, examining effect of orifice distance from explosive charge center

15 p2511 A71-31386

Calorimetrically measured energy feedback heat of reaction dependence from laminar diffusion flames above water cooler

15 p2463 A71-31621

Inertial range transfer in two and three dimensional turbulence, using almost-Markovian Galilean-invariant model

15 p2445 A71-31928

Acoustic propagation in rigid wall rectangular duct with uniform flow, calculating higher mode energy transmission properties

15 p2392 A71-32195

Bondi condition gravity waves, investigating radiation and energy transfer in given coordinate system

15 p2451 A71-32726

Radiative energy transfer equations solution in magnetic field, facilitating magnetograph calibration

15 p2496 A71-32740

Thermal properties of solar wind plasma, determining electron and proton temperature distributions, proton heating rate, electron thermal conductivity and energy exchange rates

15 p2480 A71-32754

Shock tube measurements of vibration-vibration energy exchange probability in nitrogen-carbon monoxide-argon mixtures

16 p2613 A71-32896

Plasma heat transport associated with matter, momentum, energy and electrical charges transfer

16 p2617 A71-32956

Resonant energy exchanges between gaseous media and externally applied radiation fields from wavelength-tunable lasers

16 p2586 A71-33164

Hydraulic system self acting valves natural vibration dynamic characteristics, showing energy transfer by phase shift of variable hydrostatic compression component

17 p2677 A71-34349

Vibrational population inversions due to molecular energy exchanges from rapid heating behind normal shock wave in carbon dioxide-nitrogen-helium mixtures

17 p2728 A71-34883

Radiation field inhomogeneity effect on radiation gas jet flow, taking into account radiative energy transfer by differential approximation

17 p2728 A71-35117

Kinetic coefficients calculation for gas with free energy exchange between translational and internal degrees of freedom

17 p2785 A71-35263

Energy transfer to MPD quasi-steady accelerator having electrolytic capacitors with large series resistance, integrating transmission line equations with Runge-Kutta method [DGLR-71-037]

17 p2794 A71-35539

Electronic to vibrational energy transfer in mercury vapor reaction with hydrogen fluoride, studying IR emission and scattering cross section

18 p2874 A71-35834

Operating characteristics of Q switched CO-He laser, discussing energy transfer processes leading to population inversion

18 p2929 A71-35835

Atmospheric energy balance and transfer in lower atmosphere in terms of population temperatures and degrees of freedom [translational, rotational, vibrational, electronic, chemical, etc/]

18 p2910 A71-35841

Particle gyration in homogeneous magnetic field and perpendicularly propagating electrostatic wave, calculating wave-particle energy transfer and wave-amplitude limiting effects

18 p2950 A71-35862

Gas flow energy transport, discussing thermal radiation, radiant flux density, planetary atmosphere entry, thermodynamic equilibrium and differential approximations

18 p2847 A71-36426

Energy transfer between nonlinearly coupled oscillators described by Hamiltonian system in case of third order resonance

18 p2948 A71-36795

IR pumped stimulated light emission in semiconductor, noting upconversion due to energy transfer between impurity ions

19 p3071 A71-37479

Beam pointing and tracking requirements for optical space communication system, from energy transfer considerations

19 p3018 A71-38235

Longitudinal wave interaction and excitation by current instability in equatorial jet, considering energy transfer mechanism

19 p3057 A71-38363

Intense relativistic electron beam propagation in drift tube with neutral gas and plasma background, determining front velocity and energy transport

20 p3272 A71-38784

High efficiency room temperature lasing operation assisted by energy transfer in holmium doped yttrium lithium fluoride

20 p3247 A71-39761

Solar wind theory, discussing thermal conduction and MHD wave energy supply mechanisms of large scale solar corona expansion

21 p3439 A71-41183

Ion beam deceleration and effective energy transfer to plasma at nonisothermal acoustic velocities in presence of ion acoustic instability

21 p3425 A71-41272

Temperature field of thermochemical sensor in automatic control systems, developing thermal energy transport models for circular disk with energy source at center

22 p3537 A71-41443

Energy transfer during charged particles passage through material media as function of spatial distribution, discussing electron production rates

22 p3577 A71-41537

Optimal power transfer through atmospheric turbulence by adaptive laser transmitter using beacon waveform to probe channel state

22 p3512 A71-42378

Electrical CO laser performance prediction from pumping mechanism based on vibrational energy exchange under thermal nonequilibrium conditions

23 p3683 A71-42954

Energy transfer between in-plane and out-of-plane motions in L4 neighborhood for restricted three body problem

23 p3725 A71-42989

Macroscopic values of energy exchange between polyatomic gas and solid wall, considering heat transfer rate and wall temperature change

23 p3781 A71-43105

Bondi condition gravitational waves, investigating radiation and energy transfer in given coordinate system

23 p3704 A71-43300

Nonisothermal plasma longitudinal ion acoustic and Langmuir oscillations phase and amplitude interaction

tions, estimating energy transfer and turbulence criteria

24 p3853 A71-44509

Atmosphere hydrodynamic simulation model for cascade engine transfer in turbulent flow, using Euler gyro equations

24 p3844 A71-44818

Gaseous media parameters in wave energy exchanger, examining compression cycles, temperature ratios and flow velocities for maximum conversion efficiency

24 p3891 A71-45199

ENGINE ANALYZERS

Phase-plane motion of engine assembly, using graphoanalytic delta method

01 p0128 A71-11241

ENGINE CONTROL

NT ROCKET ENGINE CONTROL

NT TURBOJET ENGINE CONTROL

Electrohydraulic thrust control system for supersonic transport aircraft engines, considering reliability, performance and weight

[SAE PAPER 700819] 01 p0143 A71-11546

Thrust equation, control volume and propulsive efficiency for rockets and air breathing jets from energy conservation principle

02 p0299 A71-12681

Concorde aircraft Olympus 593 two-spool turbojet engine, discussing variable nozzle and intake assembly, afterburner and control system

07 p1183 A71-19081

Aerospace Recommended Practice for gas turbine engine steady state performance presentation for digital computer programs, describing engine type, operating and control characteristics

[SAE-ARP-681B] 07 p1183 A71-19647

Experimental arrangement for delay times in propeller/rpm controller system

08 p1271 A71-20832

Microelectronic circuits reliability in aircraft engine control applications, discussing testing and selection for severe temperature and vibration environments

[SAE PAPER 700822] 08 p1265 A71-21369

Control and instrumentation fluidics, describing equipment, circuits and applications to jet engine controls, missile guidance, flight control, ordnance and machine tool control

09 p1386 A71-22775

D-30 bypass engine hydraulic control system for Tu-134 aircraft, discussing fuel flow regulator assembly and operation

09 p1511 A71-22947

Turboprop and turboshaft engine control requirements, showing torque and power dependence on engine speed and control block diagrams

10 p1659 A71-24755

Small fast spectrum thermionic reactor experiment open loop dynamics and control, discussing nonlinear transient simulation studies on closed loop plant

11 p1712 A71-25886

Twin spool turbojet engine dynamic response, discussing simulator predictions, digital computer control, nozzle area variations and operating trajectories

[ASME PAPER 71-GT-14] 11 p1812 A71-25960

Soviet book on liquid rocket engines covering combustion chambers, fuel supply systems, static and dynamic characteristics, control and reliability

15 p2466 A71-31296

Brayton power system electrical subsystem and component performance tests, discussing engine control package, DC supply, inverters and instrumentation

15 p2354 A71-32204

Linear two shaft turbojet model development and conditions for stability, observability, controllability and feedback loop parameters

15 p2383 A71-32711

ESKA-18P electrostatic ion propulsion system control characteristics and power conditioning, describing pulse width modulated power supply unit

[DGLR-71-029] 17 p2794 A71-35543

Multivariable frequency response methods for feedback control design for aircraft gas turbines, involving digital test bed trials

20 p3277 A71-38989

Hybrid computer control of engine start-up using adaptive logic, adaptive programming and self organizing storage

20 p3208 A71-38998

ENGINE COOLANTS

Fan jet first stage turbine blade air cooling, describing design, heat transfer data, efficiency and temperature distribution

18 p2956 A71-35904

NERVA reactor in-flight cooldown during engine shut-down phase of reusable earth-lunar transportation vehicle, discussing coolant management considerations

23 p3703 A71-44270

ENGINE DESIGN

Jet engine evolution, considering thrust, combustion chamber, fans, high-pressure-ratio compressors and turbine inlet temperature

01 p0143 A71-11181

RB 211 turbofan engine design, emphasizing modular construction, systems integration, maintainability and noise reduction

02 p0298 A71-11682

M49 Larzac turbofan engine, describing design, development, performance data, manufacturing techniques, operation and maintenance

02 p0299 A71-12607

Blade bound vortex system mathematical model for optimum heavily loaded ducted fans, including thrust, power and efficiency design parameters

02 p0299 A71-12677

Soviet book on aircraft power plant systems and devices covering layout, engine attachment, propellers, control, fuel and oil systems, fire fighting, monitoring, etc

02 p0299 A71-12722

Tubular gas turbine engine combustor design by combining turbulent flame speed, microvolume burning and stirred reactor models

02 p0299 A71-12852

Turbomachinery R and D to improve components and engine performance

03 p0470 A71-13824

Axial flow compressor design emphasizing component efficiency

03 p0470 A71-13825

High bypass ratio jet engine noise reduction in relation to mission requirements

[ASME PAPER 70-WA/GT-13] 03 p0471 A71-14121

High bypass ratio fan engine design for low noise, discussing acoustic treatment, turbine noise and modulation tones

[ASME PAPER 70-WA/GT-14] 03 p0471 A71-14122

Composite propulsion systems including Turbo-Ram-Scramjet, Ejector Ramjet, Hyperjet and Biliquid Ramjet Rocket

04 p0638 A71-15285

VTOL aircraft engine air particle separator development, examining airframe and engine design

04 p0533 A71-15433

Helicopter turbine engine protection device design guidelines

04 p0533 A71-15434

Book on fixed and rotary winged aircraft air cooled piston engine design, performance and maintenance in business and military operators manual terminology

05 p0796 A71-17125

Combustion research for air breathing engines, discussing combustion stability in thrust augmentors, aircraft fire detection, MHD and external burning

[AIAA PAPER 71-1] 06 p0946 A71-18476

Resistojet design criteria for performance modeling of ammonia propellant thrusters and manned space stations using biowaste propellants

[AIAA PAPER 70-211] 07 p1183 A71-18898

Colloid microthruster system life test, discussing design and steady state performance

[AIAA PAPER 70-1110] 07 p1184 A71-19864

Soviet book on aircraft gas turbine and internal combustion engines covering structural design schemes, inlet devices, combustion chambers, materials, compressors, etc

08 p1347 A71-20674

Combustor design for minimum exhaust smoke emission from aircraft gas turbine jet engines, considering air pollution

08 p1347 A71-20867

Multistage gas turbine design optimization, using parameter and component analysis with computer calculations

08 p1348 A71-21267

Design point selection on fan characteristic curve of turbofan engines, discussing bypass ratio effect on specific impulse, flight velocity and turbine inlet temperature

08 p1349 A71-22042

Cost reduction concepts in gas turbine engine design and fabrication for general aviation aircraft

09 p1511 A71-22811

Centrifugal compressor fluid dynamics, discussing unresolved problems governing design and performance prediction

10 p1550 A71-24216

High pressure ratio radial outflow compressor analysis, design, construction and testing

10 p1550 A71-24217

Small high pressure ratio single-stage centrifugal compressor design, testing and efficiency

10 p1550 A71-24219

Light aircraft piston engines design and maintenance, discussing engine design features, materials, lubrication, controlled flight operation and maintenance techniques

[SAE PAPER 710381] 10 p1658 A71-24246

Inclined engine cold circular jet effects on tail control surfaces aerodynamic characteristics, considering aircraft longitudinal stability

[DFVLR-SONDDR-104] 10 p1552 A71-24593

Lift/cruise engine design and thrust vector control influence on VTOL transport aircraft transition characteristics and ground acoustic field

[DGLR-70-040] 10 p1556 A71-24749

VTOL lift fan engine design for minimum noise levels, noting silencers application

10 p1659 A71-24750

VTOL heat engine and propulsion system design and performance, citing Pegasus jet lift engine as compromise between takeoff and cruise function

10 p1659 A71-24751

Turbofan VTOL or STOL intercity aircraft, examining high bypass lift engine design

10 p1557 A71-24861

Lightweight high performance regenerative gas turbine designs for aircraft propulsion, comparing various compressor, turbine, combustor and recuperator arrangements

[ASME PAPER 71-GT-67] 11 p1812 A71-25983

Low cost short life gas turbine design based on parametric performance and component selection, outlining turbojet production

[ASME PAPER 71-GT-69] 11 p1813 A71-25984

Vertical straight lift turbojet engine design and development, presenting component materials properties/weights, endurance tests and performance data

[ASME PAPER 71-GT-75] 11 p1813 A71-25989

Supersonic turbine design, presenting performance data for film cooled blunt leading edge rotor blades measured in two dimensional cascade experiments

[ASME PAPER 71-GT-76] 11 p1704 A71-25990

Boron-glass-epoxy lightweight composite gear case for aircraft engine reduction gearbox, describing design, molding, machining and testing

[ASME PAPER 71-GT-85] 11 p1771 A71-25993

Design and fabrication of Borsic aluminum composite fan blades for supersonic turbofan engines, considering 430 F application without severe vibratory stress

[ASME PAPER 71-GT-90] 11 p1771 A71-25997

Convertible fan/shaft engine for V/STOL tactical and transport aircraft, detailing mechanical arrangement, design and performance

11 p1813 A71-26054

Gas field nonuniformity as function of turbine engine combustion chamber design parameters, discussing hot tube circumferential holes total area effect

12 p1945 A71-27501

VTOL propulsion, discussing gas turbine pressure ratio inlet temperature and lifting and high bypass fans

13 p2114 A71-27838

Olympus 593 pure jet twin shaft engine development program for Concorde, discussing engine evolution, design considerations and flight development

[SAE PAPER 710422] 13 p2114 A71-28309

High temperature aircraft gas turbine engine design, discussing developments in manufacturing processes, materials, cooling techniques, aerodynamic and mechanical design improvements

[SAE PAPER 710462] 13 p2115 A71-28335

STOL aircraft/engine integrated systems for medium distance air transportation, discussing tradeoff factors involving performance, noise, weight and cost

[SAE PAPER 710469] 13 p2115 A71-28337

Optimization of mechanical characteristics of asynchronous capacitor microengine designs with asymmetric stator circuit for prolonged continuous operation with negligible steel wear

13 p2002 A71-28929

Subsonic and supersonic turbojet aircraft engines development, discussing design, operation, reliability, weight, fuel consumption and cost

14 p2287 A71-29811

Aircraft jet engines technological progress review over past 25 years, emphasizing industry economics considerations

14 p2341 A71-30303

Transport aircraft JT9D high bypass ratio engine development, noting maintainability and stability improvements

[SAE PAPER 710419] 14 p2289 A71-30527

Aircraft JT9D engine development for airline operation, discussing construction, condition monitoring, maintenance, noise and smoke reduction

[SAE PAPER 710434] 14 p2289 A71-30528

Design interface requirements for optimal aircraft engine condition monitoring system, using parameter, vibration, oil, borescope and radiography analysis

[SAE PAPER 710447] 14 p2289 A71-30531

Space shuttle airbreathing propulsion systems requirements and design studies, considering cruise, landing, go-around and ferry capabilities

[AIAA PAPER 71-662] 14 p2290 A71-30731

STOL commercial aircraft propulsion systems, considering two stream augmentor wing engine and high bypass ratio three stream engine

[AIAA PAPER 71-746] 15 p2467 A71-31325

Space shuttle main engine based on high pressure, staged combustion, reusable, minimum risk and low cost concepts

[AIAA PAPER 71-658] 15 p2470 A71-32290

French SNECMA M56 turbofan engine design for medium capacity airliners, featuring low specific fuel consumption and low noise level

15 p2471 A71-32692

Jet engine combustion chamber design, considering air supply and geometrical criteria

16 p2624 A71-33344

- Gas turbine design advances for helicopter powerplants, illustrating by Turbomeca engines
16 p2624 A71-33416
- VTOL transport optimal airframe/propulsion systems design, discussing thrust requirements, performance, control, cruise functions, fuel consumption and fan characteristics
[AIAA PAPER 71-744] 17 p2792 A71-34225
- Maximum temperature engine concept, definition and application to future aircraft propulsion system performance
[SAE PAPER 710461] 17 p2792 A71-34498
- Propulsion systems trends for 1980s, discussing environmental noise levels, stoichiometric gas turbine engines for military aircraft, high bypass ratio engines for V/STOL aircraft, etc
17 p2795 A71-35625
- Four phase reluctance motor design for electromagnetic torque variation, examining function of commutation frequency and phase time constants
17 p2677 A71-35710
- Hybrid V/STOL jet lift aircraft design, examining wing area-lift engine bypass ratios relation
[AIAA PAPER 71-767] 18 p2850 A71-36273
- Aircraft high temperature turbine engine design, reviewing technological advances coupled with laboratory engine and component tests
20 p3277 A71-39399
- Low thrust long burning solid rocket propellant motor for orbit insertion maneuvers, discussing design, static tests, nozzle composition, igniter and performance
22 p3589 A71-42016
- Small hybrid rocket engine using aromatic amines mixture as fuel and nitric acid as oxidizer, discussing regression rate relations and internal ballistics design
22 p3589 A71-42019
- Hybrid rocket /Barbarella I/ design, tests, engine, feed system oxidizer tank, fairings fins, propellants and launch facilities
22 p3589 A71-42049
- ENGINE FAILURE**
- Equivalent test results, studying damaging factors in aircraft engine compared with regular tests
08 p1348 A71-21115
- VTOL propulsion systems safety requirements, considering single and double breakdowns
10 p1659 A71-24752
- Regeneratively cooled stainless steel thrust chamber failure related to internal carburization by fuel decomposition and propellant combustion
11 p1810 A71-25505
- Optimum weight protective system against uncontained rotor failure with radial fragment passage through turbine engine casing
[ASME PAPER 71-GT-70] 11 p1813 A71-25985
- Aircraft accidents due to engine-out simulation, discussing human factors, minimum control speed certification requirements and pilot flight training procedures
[AIAA PAPER 71-793] 16 p2525 A71-34025
- In-flight monitoring of aircraft turbine engine reliability
23 p3718 A71-43233
- ENGINE INLETS**
- Twin jet aircraft engine installation effects and exhaust nozzle integration, noting closely spaced inlet interference
[ICAS PAPER 70-47] 03 p0469 A71-13148
- Inlet particle separators for engine erosion prevention, discussing tests of various models for separation efficiency, clogging resistance, pressure loss and flow distortion
04 p0639 A71-15435
- Gas turbine aircraft engine compressor blades foreign object ingestion control by inlet vortex flow suppression jets, indicating wind tunnel air intake applications
06 p0945 A71-17696
- Mathematical model of nonstationary intake and exhaust gas motion in two cycle internal combustion engine cylinders
08 p1347 A71-20780
- Turbocharged diesel engine precompressed inlet air cooling by evaporation cooling, considering water injection effects on centrifugal compressor
08 p1347 A71-20781
- Air temperature effects on internal combustion engines intake process, using similarity theory
08 p1347 A71-20782
- Real time remote test site computation and display of complex engine inlet distortion parameters from dynamic pressure signal, using analog computer
09 p1446 A71-22726
- Engine inlet noise prediction from static test and flyover data as function of time at various observer locations, examining suppression effects on total spectra
[SAE PAPER 710386] 10 p1659 A71-24250
- Supersonic transport inlet-engine-airframe compatibility programs, noting exhaust nozzle installation effects, distortions and noise
[AIAA PAPER 68-993] 10 p1659 A71-24854
- Aircraft propulsion system testing, stressing noise reduction and inlet-engine exhaust system compatibility
[SAE PAPER 710450] 13 p2114 A71-28328
- HF rake probes with high temperature integrated sensor for inflight aircraft engine intake air flow distortion measurements
14 p2243 A71-30321
- Engine surge pressure transients in mixed-compression supersonic inlet, describing scale wind tunnel model simulation and measurement techniques
[AIAA PAPER 71-671] 14 p2291 A71-30735
- ENGINE MONITORING INSTRUMENTS**
- Air transportation reliability through turbojet engine performance monitoring
02 p0298 A71-12368
- Soviet book on aircraft power plant systems and devices covering layout, engine attachment, propellers, control, fuel and oil systems, fire fighting, monitoring, etc
02 p0299 A71-12722
- Flight test evaluation of onboard automatic computer controlled jet engine monitoring system with reduced fault detection time
03 p0395 A71-13080
- Onboard monitoring sensor trends for airborne computer automatic data systems, noting digital transducers, LSI logic and solid state devices
03 p0395 A71-13081
- Thrustmeter for direct in-flight measurement of aircraft engine jet thrust
03 p0422 A71-13332
- Flight test completed on onboard real time engine performance monitoring system, discussing thermodynamic analysis technique
[ASME PAPER 71-GT-77] 11 p1813 A71-25991
- Gas turbine auxiliary power unit accessories, discussing high energy igniters, cables and connectors, thermocouples and speed and temperature monitoring equipment
13 p2071 A71-29262
- Design interface requirements for optimal aircraft engine condition monitoring system, using parameter, vibration, oil, borescope and radiography analysis
[SAE PAPER 710447] 14 p2289 A71-30531
- Boeing 747 aircraft integrated data system program for reducing engine maintenance and operating costs
[AIAA PAPER 71-648] 14 p2290 A71-30725
- Engine condition monitoring systems, discussing engineering design requirements with respect to accessibility, accuracy, economics, effectiveness, reliability and maintainability
[AIAA PAPER 71-652] 14 p2290 A71-30728
- Engine performance monitoring for jet engine troubleshooting, noting analyzable malfunctions
15 p2471 A71-32524
- Digital algorithm for automatic aircraft engine monitoring system, using Boolean algebra and events/states theory
23 p3679 A71-43897
- ENGINE NOISE**
- NT ROCKET ENGINE NOISE**
- Aladin 2 interurban Stol transport design with blown wings and jet deflection by wing flaps, emphasizing engine noise reduction
01 p0005 A71-10749
- High bypass ratio jet engine noise reduction in relation to mission requirements
[ASME PAPER 70-WA/GT-13] 03 p0471 A71-14121
- High bypass ratio fan engine design for low noise, discussing acoustic treatment, turbine noise and modulation tones
[ASME PAPER 70-WA/GT-14] 03 p0471 A71-14122
- Low velocity and coaxial jet noise data and correlations for noise prediction of turbofan engines
05 p0796 A71-17155
- Turbofan engine noise reduction, using acoustic liners in inlet and exhaust ducts
[AIAA PAPER 71-183] 06 p0947 A71-18622
- SST noise suppression research, discussing engine noise suppressor conceptual designs and test results with installed devices
07 p1184 A71-20302
- Noise nuisance value index /noise pollution level/, considering aircraft and motor vehicle noise surveys and tradeoff of intensity against duration
08 p1333 A71-20802
- Human panel comparison of aircraft engine noise tape recordings with synthetic broadband noise approximating pure jet
09 p1398 A71-22255
- VTOL lift fan engine design for minimum noise levels, noting silencers application
10 p1659 A71-24750
- One dimensional flow models of internal combustion engine exhaust silencers in noisy systems
11 p1810 A71-25180
- Absorbent materials for sound attenuation in turboreactor ducts, examining flow velocity, absorbent structure and cladding effects
14 p2288 A71-30518
- Fan induced low speed jet noise from turbofan engines, discussing results of far field sound measurements for simulated nacelle configurations with and without acoustic liners
[AIAA PAPER 71-586] 15 p2467 A71-31533
- Commercial SST aircraft engine noise during takeoff, discussing exhaust geometries for suppression
15 p2468 A71-31595
- Quiet turbofan STOL feasibility, discussing structural, propulsive and technical aspects, economy, passenger comfort and performance estimates
15 p2348 A71-31605
- Aircraft powerplant noise test facilities and reduction, emphasizing jet acoustic Mach number, pressure and temperature ratio and exit turbulence effects
15 p2384 A71-31876
- Concorde aircraft engine noise emission and reduction, examining acoustic measurements in takeoff and approach phases, reduced thrust and retractable silencer
15 p2469 A71-31877
- STOL jet aircraft noise reduction by using engines with moderate dilution rate
15 p2349 A71-31882
- Aircraft noise in-flight measurement and analysis, including engine parameters, synchronous recordings, flight paths and coded analog bands
15 p2349 A71-31884
- Aircraft engine noise test methods for acoustic certification, investigating jet and compressor silencing, absorbent materials, rotor and propeller noise and psychoacoustic tests
15 p2385 A71-31890
- Jet aircraft noise generation, transmission and reduction, emphasizing turbofan engine acoustics, operational characteristics and exhaust sound
15 p2349 A71-32241
- French SNECMA M56 turbofan engine design for medium capacity airliners, featuring low specific fuel consumption and low noise level
15 p2471 A71-32692
- French disengageable silencer for jet engine noise attenuation during aircraft takeoff
15 p2471 A71-32695
- Experimental research at Building Research Station on outdoor sound propagation for building design in relation to aircraft and road traffic noise
17 p2674 A71-35237
- Siren wall in turbine axial stage due to nonuniform pressure fields behind blade cascades
18 p2843 A71-36180
- ENGINE PARTS**
- Ni base superalloys fatigue strength improvement for gas turbine engine components, discussing homogeneous deformation distribution, grain size control, etc
01 p0099 A71-10166
- Electrochemical machining for aircraft engine metal components, discussing cost, time comparisons, tooling techniques and applications
[SME PAPER MR-70-206] 01 p0089 A71-11252
- Soviet book on aircraft gas turbine engine assembly covering organization, specified accuracy, automatic systems, mechanization problems, quality control, etc
04 p0639 A71-15449
- Aircraft gas turbine engine components equivalent testing by shortening testing time required to increase service life
05 p0796 A71-16761
- Gas dynamic test stand for cyclic thermal load testing of gas turbine engine materials and components at variable heating and cooling rates and mechanical loads
08 p1271 A71-20839
- Carbon fiber reinforced plastics applications for aero-engine components, considering mechanical and thermal properties and environmental conditions
[PLASTICS INST. PAPER 45] 08 p1347 A71-20905
- Plasma arc welding of jet engine components of Ti and Ni alloys, comparing to gas tungsten arc and electron beam processes
08 p1299 A71-21684
- Composite materials for compressor blades in aircraft engines, considering boron and carbon fiber reinforced materials
09 p1456 A71-23286
- High temperature corrosion in aircraft engine components and gas turbines by sulfur in fuels, vanadium pentoxide and NaCl
09 p1474 A71-23288
- High temperature turbine parts protective coatings, discussing aluminum diffusion prevention and crack and oxidation resistance
09 p1456 A71-23290
- Gas turbine components precision casting, discussing high temperature alloys and casting techniques in manufacture of components subject to high thermal and mechanical stresses
09 p1456 A71-23293
- Chromium and titanium alloyed austenitic steels, examining short and long time application as turbine engine parts
09 p1475 A71-23295

- High temperature Fe, Co and Ni alloys for gas turbine components, considering tensile and creep rupture strength increase by thermal mechanical processing 09 p1475 A71-23298
- Aircraft engines and stationary gas turbines high precision components, discussing die forging and machining combined with joining processes 09 p1456 A71-23299
- High temperature Ni and Co alloys for stationary gas turbines and jet engine parts, considering microstructure and mechanical behavior under stress and temperature 09 p1475 A71-23302
- Metallic and nonmetallic composite materials in jet engine component design, discussing integral blade/disk, reinforcement hoop, rotors and airfoils 09 p1456 A71-23307
- Jet engine components inertia welding, discussing process, equipment, low weight-cost advantage and mechanical properties reproducibility [ASME PAPER 71-GT-33] 11 p1770 A71-25970
- Piston engine crankshafts load and strength specification, treating axial force as resultant of gas force and inertial force 11 p1851 A71-26200
- Vacuum heat treatment of brazed and diffusion bonded jet engine components near melting temperature 13 p2073 A71-28145
- Silicide coated Nb alloys for gas turbine engine components operating at temperatures above 2000 F [SAE PAPER 71-0460] 13 p2115 A71-28334
- Metal coated superalloys evaluation for gas turbine engine components, including corrosion, impact and fatigue tests 14 p2256 A71-29635
- Machine structural elements endurance margin prediction from limited tests, proposing statistical method of integral estimates and tolerance factors 16 p2651 A71-33064
- Gas turbine engines materials and components equivalent service life estimation 17 p2793 A71-35452
- Aircraft gas turbine engine components equivalent testing by shortening testing time required to increase service life 17 p2793 A71-35460
- Supersonic propulsion system inlet, engine and exhaust nozzle in wind tunnel and flight tests, discussing boundary layer effects on performance 23 p3718 A71-43599
- ENGINE STARTERS**
- Aerospace engine starting systems military and industry specifications and standards, considering cartridge pneumatic, electric, gas turbine, hydraulic and mechanical types 01 p0067 A71-10103
- Engine pressure spiking restart preignition products, determining hydrazine nitrate and dinitrate presence by spectrum analysis 06 p0945 A71-18296
- Jet fuel starter, describing small gas turbine for starter, providing sufficient pressurized gas flow to rotate main engine [ASME PAPER 71-GT-43] 11 p1812 A71-25976
- Gas turbine engine startup igniter with modified propellant atomizer enhanced by air injection 13 p2118 A71-28969
- Motor starting techniques for 2-15 kW Brayton space power system with turbine driven radial flow compressor and Lundell type alternator 20 p3180 A71-38911
- ENGINE TESTING LABORATORIES**
- Aircraft powerplant noise test facilities and reduction, emphasizing jet acoustic Mach number, pressure and temperature ratio and exit turbulence effects 15 p2384 A71-31876
- ENGINE TESTS**
- NT COLD FLOW TESTS
- NT PREFIRING TESTS
- NT SPACE ELECTRIC ROCKET TESTS
- Engine/compressor test inlet flow field simulation, considering ramp angle, screen location and diffuser length effects 02 p0299 A71-12909
- RB 211 turbofan engine development testing, describing test program, test facilities, equipment and instrumentation 02 p0299 A71-12912
- High temperature tests of gas turbine engine with transpiration air cooled blades, discussing blade design, fabrication, ductility and oxidation resistance [ASME PAPER 70-WA/GT-1] 03 p0470 A71-14115
- Two shaft turbojet engine parameter plot techniques effectiveness, varying low pressure cascade rpm or nozzle system passage cross sections 03 p0472 A71-14259
- NERVA XE-Prime test series, discussing computer simulation full power and high specific impulse operation and startup under varying initial conditions [ALAA PAPER 70-709] 03 p0456 A71-14428
- Altitude engine test stands evolution in Germany, discussing design 04 p0566 A71-14989

- Aircraft gas turbine engine components equivalent testing by shortening testing time required to increase service life 05 p0796 A71-16761
- Aircraft engine double-reverberant chamber duct lining test facility, discussing noise fields, air flow, layout, performance, insertion and transmission losses, etc 06 p0880 A71-17619
- Equivalent test results, studying damaging factors in aircraft engine compared with regular tests 08 p1348 A71-21115
- Rocket engine thermodynamic characteristics and parameters determination, using extrapolation formulas with initial fuel composition 08 p1346 A71-21264
- Turboprop aircraft engine service life extension, correcting deficiencies via accelerated tests based on relation between failure rate and usage 09 p1511 A71-22633
- High thrust aircraft engines test facility design 09 p1428 A71-22956
- High pressure ratio radial outflow compressor analysis, design, construction and testing 10 p1550 A71-24217
- Small high pressure ratio single-stage centrifugal compressor design, testing and efficiency 10 p1550 A71-24219
- Long term life test and vacuum tests of high temperature resistojets, using ammonia and hydrogen propellants [ALAA PAPER 70-1136] 11 p1811 A71-25523
- Supersonic inlet turbojet engine compatibility tests in wind tunnels, using light panels and Summation Device analysis 13 p2114 A71-28032
- CF6 turbofan engine development, discussing performance and endurance tests and design changes for reliable low cost operation 13 p2114 A71-28308
- Long life labyrinth seal designs based on actual service experience and component or factory engine tests [SAE PAPER 71-0435] 13 p2073 A71-28319
- Commercial aircraft powerplant development, discussing engine and components test programs and techniques [SAE PAPER 71-0449] 13 p2114 A71-28327
- Aircraft propulsion system testing, stressing noise reduction and inlet-engine exhaust system compatibility [SAE PAPER 71-0450] 13 p2114 A71-28328
- Airline engine performance testing from operator perspective, using automated test cell data acquisition system [SAE PAPER 71-0451] 13 p2044 A71-28329
- Performance tests of electron bombardment ion thruster, using xenon, krypton argon, neon, nitrogen, helium and carbon dioxide 14 p2287 A71-29922
- Miniature transducers design and fabrication for fluctuating pressure measurements in jet engine testing, noting frequency response and power dissipation 14 p2244 A71-30324
- Fluctuating pressure measurements in jet engine testing, using miniature transducers with calibration and data acquisition equipment 14 p2244 A71-30325
- Low cost go/no-go portable aircraft engine tester connected to engine mounted sensors 14 p2221 A71-30327
- Gas turbine engine condition analysis by digital computer and fault isolation techniques [SAE PAPER 71-0448] 14 p2289 A71-30532
- Wind tunnel force test program design for jet aircraft configurations, including propulsion system simulation 14 p2176 A71-30605
- Open cycle gas core nuclear rocket engine, considering reactor critical experiments and cold and hot flow tests [ALAA PAPER 71-641] 14 p2273 A71-30718
- Minuteman 2 third stage rocket engine instrumentation performance evaluation for oscillatory combustion characteristics analysis [ALAA PAPER 71-755] 14 p2248 A71-30789
- Axial flow steam and gas turbines performance estimations over ranges of loading, velocity/blade ratio, Reynolds number and aspect ratio 15 p2469 A71-31733
- Hot performance tests of three identical Brayton rotating units on gas bearings 15 p2355 A71-32226
- Aircraft gas turbine engine components equivalent testing by shortening testing time required to increase service life 17 p2793 A71-35460
- Heater and nozzle design of ONERA/S4MA hypersonic wind tunnel for supersonic combustion ramjet tests [ONERA-TP-924] 18 p2956 A71-36017
- Multivariable frequency response methods for feedback control design for aircraft gas turbines, involving digital test bed trials 20 p3277 A71-38989

- Aircraft high temperature turbine engine design, reviewing technological advances coupled with laboratory engine and component tests 20 p3277 A71-39399
- Hydrazine-hydrazine azide blending for propellant performance improvement and freezing point reduction, presenting engine test data 22 p3588 A71-42778
- Mixed and unmixed turbofan engines transient and steady state off-design characteristics, investigating effects of fuel flow rate, nozzle area, inlet pressure, ambient temperature and air bleed 22 p3590 A71-42836
- Condensate particle crystallization retardation effect on energy characteristics of jet engine, calculating nonequilibrium flows of two phase combustion products in nozzle 24 p3864 A71-45004
- Test bed engine studies of overall excess air ratio permissible deviation, obtaining diagram for constraints calculation 24 p3864 A71-45022
- ENGINEERING**
- Multidisciplinary design courses in engineering education for professionals appreciating inputs from outside fields 04 p0691 A71-15278
- Problem Oriented Languages for consulting and construction engineering problem solving by translator-generator for time shared system 09 p1412 A71-23278
- Education in creative engineering - Conference, MIT, April 1970 15 p2348 A71-31593
- Interactive graphical computer system with remote on-line consoles for engineering problem modeling and analysis, giving illustrative examples 22 p3516 A71-41868
- ENGINEERING DEVELOPMENT**
- U PRODUCT DEVELOPMENT**
- ENGINEERING DRAWINGS**
- Interactive computer graphics technology industrial applications, emphasizing structural analysis and engineering master drawings 10 p1580 A71-23758
- ENGINEERING MANAGEMENT**
- Engineers time and intellectual utilization in industry dependence on local company attitudes, suggesting better management application of motivation factor [ASME PAPER 70-WA/MGT-12] 07 p1225 A71-19501
- Engineering management, discussing technical men work effort, time/intellectual changes, performance measurements, motivational factors and relationship to company 13 p2167 A71-28799
- Organizational climate inventories in R and D establishments, comparing obstacles and incentives to creativity in government and industrial laboratories 14 p2339 A71-29852
- Organization and funding criterion of unsuccessful R and D projects, considering project abandonment or failure 14 p2340 A71-29854
- Safety engineers integration into overall system through basic development programs, involving management, manufacturing, testing and integrated logistic support 16 p2664 A71-33309
- ENGINES**
- NT AIR BREATHING ENGINES
- NT ARC JET ENGINES
- NT BOOSTER ROCKET ENGINES
- NT BRISTOL-SIDDELEY OLYMPUS 593 ENGINE
- NT CESIUM ENGINES
- NT DIESEL ENGINES
- NT DUCTED FAN ENGINES
- NT ELECTRIC ROCKET ENGINES
- NT ELECTROSTATIC ENGINES
- NT ELECTROTHERMAL ENGINES
- NT GAS TURBINE ENGINES
- NT HYBRID PROPELLANT ROCKET ENGINES
- NT HYDRAZINE ENGINES
- NT HYDROGEN OXYGEN ENGINES
- NT INTERNAL COMBUSTION ENGINES
- NT ION ENGINES
- NT J-2 ENGINE
- NT J-57 ENGINE
- NT J-85 ENGINE
- NT JET ENGINES
- NT LIQUID PROPELLANT ROCKET ENGINES
- NT MICROROCKET ENGINES
- NT NUCLEAR ENGINE FOR ROCKET VEHICLES
- NT NUCLEAR ROCKET ENGINES
- NT PISTON ENGINES
- NT PLASMA ENGINES
- NT PULSED JET ENGINES
- NT RAMJET ENGINES
- NT RESTARTABLE ROCKET ENGINES
- NT RETROCKET ENGINES
- NT ROCKET ENGINES
- NT SOLID PROPELLANT ROCKET ENGINES

NT SUPERSONIC COMBUSTION RAMJET ENGINES
 NT TURBINE ENGINES
 NT TURBOFAN ENGINES
 NT TURBOJET ENGINES
 NT TURBOPROP ENGINES
 NT TURBORAMJET ENGINES
 NT ULLAGE ROCKET ENGINES
 NT WANKEL ENGINES

ENGLISH LANGUAGE

Computer program for compiling interpreter coded test instructions from high order pseudoEnglish language
 03 p0381 A71-13078

ENHANCEMENT

U AUGMENTATION

ENLARGING

U EXPANSION

ENSKOG-CHAPMAN THEORY

U CHAPMAN-ENSKOG THEORY

ENSTATITE

Stearites replicas electron microscopy for microstructure variations with composition and firing conditions differences, discussing protoenstatite crystallization and glass phase formation
 13 p2093 A71-28664

Horse Creek, Mount Egerton and Norton County enstatite meteorites metal phases and perovskite inclusions from electron microprobe data
 13 p2144 A71-29474

Shock wave data for Bamle enstatite in 60-480 kb range, considering Hugoniot elastic limit and phase transition produced shock front
 19 p3050 A71-37663

ENTHALPY

Small size calorimetric probe for measuring enthalpy, temperature and pressure in high velocity dense plasma flow
 02 p0290 A71-12194

Tantalum and niobium disilicides enthalpy and heat capacity temperature dependences
 02 p0263 A71-12198

Laminar shock induced boundary layers, examining velocity, pressure gradients and enthalpy
 03 p0400 A71-13739

Two dimensional and axisymmetric flow film cooling effectiveness in supersonic turbulent boundary layer, using Eckert reference enthalpy method
 04 p0571 A71-15496

W-Mo alloy enthalpy and specific heat measurement at high temperatures by drop calorimetry
 04 p0613 A71-15580

High temperature apparatus for enthalpy and specific heat measurements of refractory metals
 08 p1273 A71-21936

Continuous flow arc air heater for reentry vehicle components ground testing, achieving combined high pressure and enthalpy
 09 p1429 A71-23061

Prediction analysis of downstream effectiveness in high speed laminar boundary layer for reentry vehicular surfaces film cooling, using reference enthalpy method
 11 p1752 A71-26216

Shock tunnel extremely high enthalpy and pressure for scramjet engine combustion research
 11 p1860 A71-26267

High enthalpy flow temperature probe, determining stagnation temperature of combustion gases by chromel-alumel thermocouple
 11 p1765 A71-26277

Pressure and wall temperature gradients effects on equilibrium enthalpy profiles and heat transfer coefficients of incompressible turbulent boundary layers, using eddy conductivity model
 12 p1986 A71-27553

Small size calorimetric probe for measuring enthalpy, temperature and pressure in high velocity dense plasma flow
 15 p2454 A71-31500

Tantalum and niobium disilicides enthalpy and specific heat temperature dependences in 1200-2100 K range
 15 p2426 A71-31504

Heat content measurement of tantalum carbide in homogeneity range at high temperatures by mixing method using bulk calorimeter
 15 p2431 A71-32155

Niobium and zirconium carbides enthalpy and specific heat dependence on temperature and composition
 15 p2431 A71-32156

Truncated-cone hot-pressed silicon carbide samples, measuring enthalpy and heat capacity as temperature function at high temperatures
 15 p2431 A71-32160

Enthalpy probe heat response dependence on surface thermal load amplitude
 16 p2581 A71-34033

High temperature apparatus for enthalpy and specific heat measurements of refractory metals
 17 p2724 A71-35278

High enthalpy plasma jet wind tunnels, considering arc heaters and simulation range extension to higher

adiabatic static pressures to avoid nonequilibrium expansion in nozzle
 18 p2898 A71-36413

Aerodynamic probes for determining flow state of high enthalpy hypersonic flow fields, considering pitot pressure, total enthalpy and current density
 18 p2921 A71-36414

Carbon activity, free energy entropy and enthalpy in fcc solid solution of Fe-Ni-C alloy
 19 p3080 A71-37714

Calculation method for standard potentials and enthalpies of metals during oxidation and chlorination, representing molar functions dependence on temperature
 19 p3082 A71-38153

Arc driven hypersonic wind tunnels total enthalpy measurement from blunt body gas cap emission, using rapid scan spectrometer for gray gas continua
 21 p3364 A71-40403

Enthalpy change between atmospheric carbon dioxide and Venus surface rocks for damping short term lower atmosphere temperature excursions
 23 p3736 A71-43344

ENTHALPY-ENTROPY DIAGRAMS

U MOLLIER DIAGRAM

ENTIRE FUNCTIONS

Differential equations systems construction from given integral manifold, deriving steady state functional and stability conditions
 01 p0111 A71-10487

Finite maximum and minimum angular zero densities of integral functions, noting relationship to angular additive measure
 04 p0618 A71-14647

Feynman path integration for multiply connected space systems of indistinguishable particles, considering bosons and fermions propagators
 10 p1644 A71-24214

Weakly singular integrals numerical compound quadrature error bound and convergence rate estimate by applying Peano theorem with modification for avoiding singularity
 18 p2941 A71-36355

Convergence theorem for singular integrands numerical quadratures, assuming domination near singularity by monotone integrable function
 18 p2941 A71-36356

Time optimal control for distributed systems with random properties, considering integral relations and flying wing vehicle torsional vibration problems
 19 p2994 A71-37094

Sliding contact between closed annulus and elastic cylinder, deriving integral expressions
 21 p3472 A71-41147

ENTRAINMENT

Forced plume entrainment of turbulent buoyant jet in stratified fluid as function of Reynolds, similarity and Froude numbers
 02 p0278 A71-12704

Turbulent diffusion of impurity from infinite linear source in clouds and fog, allowing for particle entrainment
 05 p0776 A71-16422

Mass transfer net rate /evaporation plus entrainment/ from thin liquid film, using methanol, water, butanol and RP-1 as coolants
 07 p1222 A71-18997

Compressible turbulent boundary layers integral solution based on entrainment theory
 07 p1090 A71-19903

Turbulent shear flows, examining zero and negative entrainment in boundary layers
 10 p1595 A71-24626

Entrainment induced potential flow near free jets, using equivalent sink distribution derived from known boundary layer solutions
 10 p1596 A71-24937

Cumulus entrainment and steady state one dimensional convection model
 12 p1925 A71-27201

Storm clouds tops maximum height and vertical velocity calculation, allowing for entrainment and vertical wind shear
 15 p2444 A71-31362

Turbulent wakes flow entrainment mechanism, investigating turbulence spreading near interface between laminar and turbulent regions
 17 p2671 A71-34899

Solid cylindrical particles interaction under entrainment in pipe by viscous incompressible fluid, obtaining numerical solution by reduction to flow past moving body
 19 p3046 A71-38418

ENTROPY

Entropy-disorder concepts relation in teaching thermodynamics, urging treatment as macroscopic theory
 01 p0126 A71-10134

Centrifugal compressor impeller exit flow velocity distribution distortion based on equations of motion involving entropy gradient terms
 03 p0343 A71-13831

Turbulence properties in supersonic flow, considering modes with vorticity, entropy and acoustic aspects
 09 p1383 A71-23603

Entropy-free thermodynamics second law based on universe expansion, using homogeneous nonstatic cosmological models
 10 p1674 A71-24468

Maximum entropy principle for prior distribution determination in Bayesian reliability estimation, comparing with statistical decision theory
 11 p1772 A71-26164

Turbomachine blade cascades in supersonic flow, noting wave configurations, entropy and counter pressure variations
 12 p1864 A71-27475

Stochastic modification of binary fluid mixtures hydrodynamic dissipative equations, considering nonequilibrium entropy
 13 p2051 A71-29354

Entropy production in adiabatic flow in turbomachines, based on momentum equations for inviscid flow
 13 p1994 A71-29446

High entropy layer in hypersonic flow with arbitrary large freestream Mach number behind shock
 14 p2334 A71-29559

Entropy layer in hypersonic flows, determining body configuration from shock wave shape described by coordinates power function
 14 p2171 A71-30875

Arc-heated nonequilibrium air expansion flow mass spectroscopic analysis, noting reservoir entropy effect [AIAA PAPER 71-621]
 15 p2366 A71-31550

Continuum mechanics in differential forms, discussing material and spatial coordinates, compatibility conditions energy balance, entropy inequality and invariance principles
 16 p2613 A71-34146

Dynamic parameters of supersonic flow incident on conical bodies at large angles of attack, considering flow field and entropy distribution
 18 p2845 A71-36328

Small scale flow and surface effects in multiphase media hydromechanics, obtaining entropy production in mixture for interphase transformations characterization
 19 p3042 A71-37098

Carbon activity, free energy entropy and enthalpy in fcc solid solution of Fe-Ni-C alloy
 19 p3080 A71-37714

Graphite solubility in Co and Ni, discussing solution energies and entropies
 19 p3081 A71-37723

Entropy generation and survival of protogalaxies in expanding universe, deriving bulk/shear viscosity, heat transport and sound waves damping rate in relativistic fluid
 20 p3287 A71-39051

Thermodynamics and statistical mechanics of low temperature physics, including entropy, probability, energy spectra and gas liquefaction
 20 p3270 A71-39240

Finite amplitude entropic waves with propagated acoustic radiation-fluid particle motion energy coupling, using thermodynamic J function methods
 20 p3315 A71-39772

ENVIRONMENTAL MODELS

Primitive centralized quality control program model applicable to Department of Commerce environmental sciences
 08 p1329 A71-21728

Random access signaling system application to aircraft control, discussing signal redundancy requirement for access capability optimization based on radio environment model
 17 p2747 A71-35783

High energy particle environment model at synchronous altitudes during quiet geomagnetic periods from satellite observation, establishing outer radiation belt distribution function
 23 p3722 A71-43978

ENVIRONMENTAL POLLUTION

NT AIR POLLUTION

NT WATER POLLUTION

Commercial SST environmental effects on stratospheric air, water vapor content and earth surface temperature
 01 p0074 A71-11178

Short haul air transportation technological factors for VTOL, STOL, CTOL and light aircraft, considering operating costs, passenger service and environment impact
 02 p0188 A71-11700

Conference report on impact of man on global environment, assessing actions covering climatic and ecological effects, pollution monitoring, etc
 02 p0246 A71-12350

Direct lift V/STOL transport aircraft design, discussing environmental factors in relation to noise, air pollution, jet interference and safety
 04 p0530 A71-15403

Airborne surveillance for environmental management, discussing earth resources program, aerial sensors for thermal water pollution, crop disease, salinity and geological structure
 07 p1018 A71-19080

ENVIRONMENT SIMULATION

Noise nuisance value index /noise pollution level/, considering aircraft and motor vehicle noise surveys and tradeoff of intensity against duration
08 p1333 A71-20802

Nighttime airflow deviations over urban areas from radar tracked tetron flights, discussing effects as function of atmospheric wind and temperature
11 p1793 A71-25377

CO exposure effects on human psychomotor performance for blood carboxyhemoglobin saturation levels, using sleep monitored EEG methods
11 p1726 A71-26509

Aircraft and environment - Conference, Washington, D.C., February 1971, Part 2
15 p2516 A71-32240

Aircraft pollutant emission regulation, discussing low smoke combustors and fuel dumping problem
15 p2516 A71-32246

Remote sensing imaging techniques for oil pollution survey, using airborne UV, IR, color and filtered panchromatic photography
17 p2735 A71-35386

Environmental water pollution observation by remote sensing, discussing aerial photography
19 p3059 A71-38403

High vacuum mass spectrometric hazardous gas detection system used during cryogenic loading of Saturn vehicles, discussing application to environmental pollution detection
22 p3542 A71-41988

Environment degradation relation to technology, discussing priorities
[AIAA PAPER 71-1016] 24 p3892 A71-44597

ENVIRONMENT SIMULATION
NT ACOUSTIC SIMULATION
NT ALTITUDE SIMULATION
NT SPACE ENVIRONMENT SIMULATION
NT THERMAL SIMULATION
NT WEIGHTLESSNESS SIMULATION

Flight simulation in various degrees of environmental realism by visual and other physiological cues, discussing available devices and techniques relative to specific training tasks
01 p0066 A71-10020

ATC communication environment simulation via mathematical model based on ATC statistics
01 p0126 A71-10979

Soil microorganisms multiplication under simulated Martian conditions in limonite and garden soil mixture
01 p0019 A71-11558

Digital simulation computer program in FORTRAN IV for radar systems performance evaluation in various environments
02 p0211 A71-11796

Propellant low temperature preignition reactions during simulated engine shutdown conditions, discussing IR spectroscopic observation method
02 p0298 A71-12861

Engine/compressor test inlet flow field simulation, considering ramp angle, screen location and diffuser length effects
02 p0299 A71-12909

Amino acid synthesis in simulated primitive environments, discussing possible effects of meteoric kinetic energy and lightning-associated shock waves
03 p0358 A71-13015

Simulated sonic booms effects on sleeping humans, considering intensity levels, age factors, sleep stage, adaptability and housing
03 p0371 A71-13165

Water cooled channel flow test device for arc jet material ablation studies, simulating reentry environment of high energy turbulent boundary layer flow
[AIAA PAPER 71-260] 08 p1273 A71-21987

Reentry environment simulation at vehicle stations away from stagnation point, using arc heater with supersonic nozzle duct
[AIAA PAPER 71-261] 08 p1274 A71-21988

Organic compounds biosynthesis in simulated Mars atmosphere, using UV irradiation for photocatalytic production from CO and water mixtures
09 p1403 A71-22647

Time dependent dispersion simulation by random number generator, introducing horizontal and vertical shear, buoyancy and anisotropic turbulence
09 p1488 A71-23027

Terrestrial microorganisms adaptation to simulated methane-ammonia-hydrogen Jupiter atmosphere
10 p1566 A71-24688

Structural dynamics test simulation technology, discussing criteria, techniques, equipment, combined environments and relationship between testing and analysis
11 p1745 A71-26493

Corrosive contaminants, oxygen, humidity and temperature environment simulation
11 p1746 A71-26496

Thermal scale modeling limitations for radiation-conduction system of unmanned spacecraft, discussing material thermal properties, model dimensions, instrumentation effects and environment simulation
13 p2159 A71-27988

Mars physical conditions compared to earth, simulating Martian conditions and low temperature and UV effects on proteins
13 p2009 A71-28688

Film cooling studies in subsonic and supersonic flows, using shock tunnel for gas turbine conditions simulation
16 p2551 A71-32882

Mathematical model for underwater simulation of astronaut extravehicular activities in weightless conditions, using computer program
[AIAA PAPER 71-852] 18 p2872 A71-36644

Integrated test concept for terminal guidance subsystems and components evaluation, laboratory calibration and simulation tests
[AIAA PAPER 71-969] 19 p3040 A71-37210

Jet streams simulation method by electrohydrodynamic analog, using principle of mapping free lines of flow
19 p3043 A71-37542

Environment, coupling and electronic equipment modeling for electromagnetic compatibility analysis
19 p3031 A71-38440

Cystine synthesis in simulated primitive conditions by UV irradiation of methane, ethane, ammonia, water vapor and hydrogen sulfide in spherical vessel
19 p3014 A71-38678

Broadband random vibration simulation of force environment action on multimode structure
[ASME PAPER 71-VIBR-2] 21 p3362 A71-40266

Biochemical measurements of human urine and blood changes during simulated oxygen-helium dives to 1500 feet
21 p3331 A71-40353

Bacterial spores survival under simulated lunar surface conditions, comparing results with vegetable cells experiments
21 p3334 A71-40567

Simulated Martian environment effects on terrestrial microorganisms survival
22 p3487 A71-42227

Blue-green algae survival or growth ability tests under simulated Precambrian atmospheric conditions
22 p3487 A71-42230

Random parietal environment representation by homogeneous distribution of independent sources, using boundary layer model
[ONERA-TP-933] 22 p3576 A71-42500

Infusoria adaptation ability to extreme environmental conditions with emphasis on Mars surface
22 p3496 A71-42825

Microorganisms survival in simulated Martian environment noting culture cells concentration increase
22 p3507 A71-42826

Cone penetration resistance tests on granular lunar soil simulants for in-place shear strength and packing characteristics under various gravity conditions
23 p3757 A71-43751

Rat thyroid gland changes during acclimatization to simulated high altitude environments, observing high hormone stimulation
23 p3637 A71-44300

ENVIRONMENT SIMULATORS
NT SOLAR SIMULATORS
NT SPACE SIMULATORS

Martian environment simulator chamber for pressure, visible light, biological objectives UV irradiation and daily temperature cycle
01 p0068 A71-11559

Toulouse space environment simulator artificial sun assembly consisting of xenon lamp and projection optics for cylindrical light beam production
02 p0239 A71-12748

Data system environment simulator /DASYS/ for real time test bed capability for software development and testing
04 p0556 A71-15294

Simulation chamber for experimental investigation of organisms reactions to Mars environment
22 p3507 A71-42827

ENVIRONMENTAL CHAMBERS
U TEST CHAMBERS
ENVIRONMENTAL CONTROL

Atmospheric pollution long term effects measurement and control using spacecraft-mounted instruments
04 p0581 A71-14821

OART space station development, discussing long term effects, artificial gravity, environmental problems, electric power, life support, protection systems and human factors
04 p0643 A71-14932

Lyons-Satolas /France/ International Airport project, discussing layout, facilities and noise control problem
06 p0880 A71-17590

Analytic functions approximation in complex regions with aid of different systems of functions
07 p1146 A71-19041

Pressure suit assemblies /PSA/ reference for aerospace and environmental control engineers
[SAE-AIR-1103] 07 p1049 A71-19641

Spacecraft cabin atmospheres, discussing controlled atmosphere composition, barometric pressure,

physiological effects, trace constituents, fire hazards, etc
08 p1245 A71-20729

Air pollution emissions at Heathrow Airport, London, from aircraft operations, heating installations and road traffic
08 p1378 A71-21823

National Air Pollution Control Administration control of aircraft engine pollutant emissions covering measurement, test instrumentation, research, standards and regulations
08 p1379 A71-21831

Federal assistance to air transportation, considering airport development-environment conflicts
08 p1380 A71-21834

Airport system planning for natural and urban environment compatibility
08 p1380 A71-21835

Optimal control theory application to environmental control of confined spaces and life support systems, considering algorithm of Pontryagin principle
09 p1423 A71-22588

Piper Cherokee aircraft air conditioning system, discussing various operating principles, design criteria, power drain, effects on aircraft performance and weight, system serviceability and control
[SAE PAPER 710391] 10 p1558 A71-24255

Stress rupture behavior of S glass/epoxy multifilament strands, developing tensile and creep test apparatus installed in controlled environment building
11 p1784 A71-25397

Space station thermal control system design, verifying radiator adequacy by parametric computer analysis with allowance for thermal coating degradation, vehicle attitude and other variables
[AIAA PAPER 71-435] 11 p1858 A71-26223

Circadian rhythm of leaves of Phaseolus angularis plants in controlled carbon dioxide and humidity environment
13 p2015 A71-29475

Aircraft and airports as air pollution sources, stressing industries understanding of applicable control technology
15 p2349 A71-32243

Airport environmental protection, discussing area-wide agency, FAA planning grant program and legal aspects
15 p2385 A71-32247

Environmental controls, health services and safety programs for outdoor range laser applications, considering USAF hazard regulations, public address system, etc
17 p2723 A71-34524

Rain and fog modification concerning natural and artificial nuclei role, warm fog clearing and supercooled cloud experimentation
17 p2769 A71-34545

Environmental thermal control/life support system for manned space station, discussing maintenance, weight, power and volume
[AIAA PAPER 71-827] 17 p2690 A71-34719

Wide heat load range space radiator design for space mission environmental control/life support system, using stagnation control
[ASME PAPER 71-AV-5] 18 p2865 A71-36372

Solar-array space station environmental control and life support system design for 12-man 10-year mission capability with 180-day resupply
[ASME PAPER 71-AV-12] 18 p2866 A71-36379

Environmental control and life support subsystems selection and definition for 12-man space station
[ASME PAPER 71-AV-13] 18 p2866 A71-36380

SkyLab life support systems design and performance prediction covering thermal and humidity control, atmospheric supply, carbon dioxide removal, water and waste management
[ASME PAPER 71-AV-14] 18 p2866 A71-36381

Space Shuttle Orbiter Environmental Control and Life Support Systems, discussing maintenance
[ASME PAPER 71-AV-15] 18 p2866 A71-36382

Space shuttle environmental control and life support system design covering atmospheric pressure, composition, humidity, temperature, water and waste management
[ASME PAPER 71-AV-16] 18 p2867 A71-36383

Long mission duration manned spacecraft contaminant control system design, discussing catalytic, oxidation, chemisorption and charcoal adsorption removal techniques and computerized performance prediction
[ASME PAPER 71-AV-19] 18 p2867 A71-36386

Space station prototype environmental thermal control and life support systems, considering maintainability, reliability, weight penalties and fault detection and isolation
[ASME PAPER 71-AV-22] 18 p2867 A71-36389

Water vapor electrolysis for oxygen generation and humidity control in long term manned space flight
[ASME PAPER 71-AV-24] 18 p2868 A71-36391

Three day mission biosatellite environmental thermal control system design and flight performance
[ASME PAPER 71-AV-33] 18 p2869 A71-36400

- Prototype space station environmental thermal control and life support system digital simulation for transient design and performance prediction
[ASME PAPER 71-AV-34] 18 p2869 A71-36401
- Space station thermal control systems design, discussing pumped loop, air cooled semipassive and heat pipe systems
[ASME PAPER 71-AV-36] 18 p2869 A71-36403
- Architectural and environmental design tools for space system habitability, discussing work and living areas, hygienic facilities, etc
[AIAA PAPER 71-879] 18 p2871 A71-36632
- NASA 12-man 10-year space station program, discussing design, information management, environmental control and life support system
19 p3153 A71-38147
- NASA space station program, discussing design, guidance, navigation, electrical power and environmental control
19 p3154 A71-38150
- Earth-like ecology for habitation in space, considering hollow sunlit rotating space chamber for life cycles in controlled weather environment
21 p3343 A71-40360
- Subscale modeling of aircraft trailing vortices in controllable laboratory environment
21 p3318 A71-40488
- Global environmental monitoring and remote sensing from satellites, considering thermal, air and water pollution
22 p3534 A71-41961
- Skylab life support, habitability and thermal comfort system, discussing ventilation, humidity, carbon dioxide and odor control and water, food and waste management
22 p3609 A71-41976
- Scientific research methods and applications experiments from orbiting Space Shuttle, noting environmental control and life support provision
22 p3611 A71-42039
- Aircraft pilots and astronauts relationship with environment, considering weightlessness, emotional reactions, cabin pressure and temperature control and space survival and rescue
23 p3639 A71-43223
- Environment degradation relation to technology, discussing priorities
[AIAA PAPER 71-1016] 24 p3892 A71-44597
- SST operation climatic impact assessment program, considering carbon dioxide, water vapor, contrails, particulates, nitrogen oxides and carbon monoxide
24 p3823 A71-44982
- ENVIRONMENTAL ENGINEERING**
- Airport system planning from environmental viewpoint, discussing travel market, airport accessibility, airspace utilization and control and land use
02 p0334 A71-11642
- Accelerometer design for nuclear reactor vibration measurements, considering environmental effects
04 p0587 A71-14824
- Reliability and maintenance problems of U.S. Army operational environment, noting inadequate design and test criteria during development
04 p0530 A71-15402
- Sand and dust effects on military helicopter flight controls and equipment service life, discussing relief program
04 p0533 A71-15430
- Colorado Land Use and Environmental Resource Inventory Project /CLARI/ by computer methods, saving information retrieval time and cost
08 p1281 A71-21253
- Primitive centralized quality control program model applicable to Department of Commerce environmental sciences
08 p1329 A71-21728
- Aircraft and environment - Conference, New York, February 1971, Part I
08 p1378 A71-21811
- Elastomers for aerospace vehicles extreme environments, discussing fuel tank integral high temperature sealants
10 p1631 A71-24078
- Corrosion resistant adhesive bonding tested by exposing sandwich structure to outdoor weathering and salt spray environments
10 p1616 A71-24111
- Book on electrical equipment deterioration in adverse environments covering climatic action, excessive heat, atmospheric temperature variations, water vapor adsorption and condensation, etc
10 p1583 A71-24478
- Environment sciences - Conference, Los Angeles, April 1971
11 p1745 A71-26490
- Aircraft and environment - Conference, Washington, D.C., February 1971, Part 2
15 p2516 A71-32240
- Aircraft/environment compatibility, emphasizing decision making process for airport planning, site location, development and operation
15 p2516 A71-32248
- Room with windows and open doors under sonic boom, determining cavity resonance model for impulsive loading conditions
15 p2450 A71-32514
- Materials selection for manned spacecraft, discussing environmental interactions between man, materials and atmosphere
16 p2601 A71-33874
- Engineering for conservation of mankind - IEEE Conference, Sacramento, May 1971
19 p3030 A71-38401
- Human performance as function of task and environmental factors, using psychological and physiological references
22 p3503 A71-42193
- Environmental rationale behind thermal shock testing, discussing approaches for temperature cycle provision
23 p3682 A71-43902
- ENVIRONMENTAL INDEX**
- Humid operative temperature as index for biophysical thermometry and thermal comfort sensation prediction
18 p2861 A71-36887
- Environmental quality indices from spaceborne or airborne remote sensing
22 p3534 A71-41995
- ENVIRONMENTAL LABORATORIES**
- Biosatellite 3 reduced gravity environmental laboratory with subhuman primate on 30 day mission, discussing ground base tests, simulated and actual flight
09 p1400 A71-23238
- ENVIRONMENTAL RESEARCH SATELLITES**
- Environmental satellite data on-line processing and extraction procedures, including visible and IR imagery mapping and cloud pictures analysis
07 p1067 A71-18806
- ENVIRONMENTAL TEMPERATURE**
- U AMBIENT TEMPERATURE**
- ENVIRONMENTAL TESTS**
- NT COLD WEATHER TESTS
- NT CORROSION TESTS
- NT HIGH TEMPERATURE TESTS
- NT LOW TEMPERATURE TESTS
- NT SALT SPRAY TESTS
- Space systems aerospace ground support equipment environmental testing criteria under varying conditions for optimal operation and deterioration reduction in use and storage
01 p0067 A71-10104
- Sequential environmental testing effects on large hybrid microcircuit packages, reviewing solder sealing processes and repair methods
01 p0053 A71-10732
- Medications stability regarding high temperature, humidity, ambient gas composition, increased oxygen content, radiation, vacuum, vibrations and accelerations
01 p0025 A71-11144
- Gaseous atmospheres environmental effects on metal mechanical properties at high temperatures, discussing failure mode with crack growth rate dependence on pressure
02 p0263 A71-11864
- Sirene 311 cylindrical thermionic converter in-pile life testing in Triton swimming pool nuclear reactor
02 p0193 A71-12220
- Out-of-pile experiment for measuring uranium dioxide fuel redistribution rates, determining vent hole plugging time and thermal cycling
02 p0296 A71-12247
- Ti alloy hot salt stress corrosion under simulated engine environmental conditions, presenting threshold data based on residual tensile ductility
02 p0268 A71-12885
- Rugged stable differential Pt resistance thermometer for Lunar Heat Flow Program, discussing construction, calibration and environmental test
03 p0427 A71-13917
- AH-56A Cheyenne compound helicopter icing spray rig tests, discussing ice protection systems design and operating performance
04 p0534 A71-15438
- Environmental development and testing of OH-58A light observation helicopter for close ground support, noting particle separator and injection seals
04 p0534 A71-15439
- Ti-Ag and Ti-Pd-Ag solar cell contacts structure and degradation dependence on high temperature and humidity environmental exposure
05 p0699 A71-16060
- Si solar cells with titanium oxide antireflection coatings, discussing environmental test results
05 p0700 A71-16064
- Si solar cells with and without cover slides performance in severe thermal and light environment /near sun missions/
05 p0701 A71-16070
- Solar cells for Jupiter mission, discussing radiation and environmental tests concerning I-V characteristics
05 p0701 A71-16074
- Si solar cell test for electrical discharge effect on series resistance, curve power factor, conversion efficiency and spectral response
05 p0705 A71-16169
- Inertial instruments system-level tests under final use environment, discussing cost reduction
[AGARDOGRAPH-128] 05 p0750 A71-16308
- Cured thermosetting polymers, investigating water effect on microstructure and mechanical properties
06 p0916 A71-17945
- Algae survival and growth under adverse conditions, considering high and low temperatures, desiccation and halophilism
07 p1048 A71-19522
- Anomalous anodic Be dissolution in anhydrous environment, considering chunk effect and multivalent ions production mechanisms
07 p1118 A71-19568
- Martensitic high strength steels composition effect on environmentally induced delayed failure
07 p1139 A71-19990
- Data handling system with digital computer and multichannel scanning, processing and recording for simultaneously conducting two environmental tests of satellites
07 p1069 A71-20403
- Fluidics application to weapon systems safety and arming devices, investigating reliability and immunity to environmental conditions
07 p1025 A71-20561
- Medical flight information on astronauts response to space flight environment in confined and unconfined state and during intra- and extravehicular activities
08 p1246 A71-20731
- Large space vehicle acoustic environment test facility, investigating combined direct and/or reverberant sound field effects
08 p1272 A71-21430
- Air-to-air, air-to-ground and USN surface-to-air guided weapons operational assessment in military environment
09 p1532 A71-22991
- Thunderstorms environment analysis from radar and aircraft scanings, determining cumulonimbus cloud air kinematic properties for three dimensional circulation model
09 p1488 A71-23252
- Supersonic transport fuel tank environments and sealant requirements, describing Boeing laboratory environment approach
09 p1385 A71-23424
- Concorde environmental testing, considering endurance tests, thermal shock rigs and plant for simulating air supply from compressor stages of aircraft gas turbine engines
09 p1430 A71-23583
- Corrosion resistance of adhesive bonded airframe structure components under outdoor weather and salt spray conditions, discussing test results with Al alloy specimens
09 p1459 A71-23690
- ESRO 1 satellites space simulation chamber tests for residual gas effects, measuring spacecraft outgassing rate
09 p1533 A71-23732
- Organic adhesives performance evaluation based on correlations between accelerated laboratory aging tests and underground exposure in adverse environments
10 p1633 A71-24113
- Plastics as potting compounds in military aircraft electrical systems, investigating resistance to reversion and hydrolytic stability
10 p1633 A71-24115
- Potting compounds service life estimation based on accelerated hydrolytic reversion data at high temperatures and humidities
10 p1633 A71-24117
- Outdoor five year aging tests on polysulfide and silicone adhesive sealants under semiarid, marine and high humidity environments
10 p1634 A71-24119
- Environmental effects on laminated anisotropic plates thermoelasticity for critical swelling strains, using Hookes law extension of Duhamel-Neumann equations
[AIAA PAPER 71-352] 11 p1783 A71-25332
- Ti-Al-Mo-V alloy stress corrosion cracking, using controlled potential technique in aqueous and methanol environments with and without halogen ions
11 p1777 A71-25448
- Quenched and tempered steel, investigating embrittlement as function of temperature in partially dissociated atomic hydrogen environment
11 p1779 A71-26013
- Direct digital control system for random excitation environmental testing, discussing interfacing of TIME/DATA time series processor and minicomputer
11 p1736 A71-26500
- Computer program for interpretation of residual gas analyzer mass spectra, considering vacuum environmental testing of spacecraft
11 p1730 A71-26505

Dynamic Test Chamber for sounding rocket or spacecraft functional testing in simulated flight environment

11 p1746 A71-26508

Automated facility for electronic equipment production reliability environmental testing, discussing human engineering and test and failure mode designs

11 p1746 A71-26512

Solar simulator with wide range irradiation strength variability for laboratory investigation of radiation effects on spacecraft components

12 p1894 A71-26982

Hand/machine sanded surfaces moderate environment exposure time effects on adhesive bonding of glass fiber reinforced plastic joints

12 p1921 A71-27411

Papers on fracture mechanics covering engineering fundamentals, environment effects, crack growth, photoelastic analysis, nondestructive testing, etc

13 p2151 A71-28212

High strength alloys, discussing fracture mechanics concepts applicability to environmental cracking under static load and combined effects of cyclic stress and aggressive environment

13 p2152 A71-28222

Fincap communication antennas design and environmental tests for vibration, acceleration, water-proofing, salt corrosion, ice formation and compass safe distance

14 p2216 A71-31047

Cold environment exposure effect on mouse resistance to infection with *Klebsiella pneumoniae*

16 p2528 A71-33115

Surface cracking resistance of polymethyl methacrylate glass in vacuum, air and nitrogen, noting humidity effect

16 p2601 A71-33690

Life support systems test under weightlessness environment in Nike Tomahawk sounding rockets launched from Wallops Island

16 p2537 A71-33816

Muscular fatigue of healthy Bengali males with increasing work loads under varying environmental conditions, considering ventilation, heart rate and oxygen consumption

17 p2688 A71-34360

Fatigue measurements in hot working conditions on subjects wearing self contained breathing apparatus in heat chamber

17 p2688 A71-34361

Telemetric accelerometer for assessing mental performance under industrial working conditions for work characterized by periodically repeated stereotyped movements

17 p2688 A71-34363

Environmental effects on SST structural materials fatigue, discussing Ti alloys studies involving temperature effects, crack propagation and residual strength

17 p2821 A71-34556

Environment and frequency effects on fatigue properties of age hardening Al-Cu-Mg alloy

18 p2933 A71-35876

Ninety day manned test of regenerative life support system in space station simulator, presenting operational and maintenance data

[ASME PAPER 71-AV-3] 18 p2865 A71-36370

Self contained one man module cell design and tests of electrochemical carbon dioxide concentrating system for space applications

[ASME PAPER 71-AV-21] 18 p2867 A71-36388

Human performance in rotating environment, discussing Stromberg Dexterity, pursuit rotor, mental arithmetic, verbal learning and NAMI Ataxia tests

[AIAA PAPER 71-888] 18 p2871 A71-36637

Dynamic seal development for space base rotating hubs, describing simulated environmental tests for elastomer inflatable seals and lubricants evaluation

[AIAA PAPER 71-863] 18 p2927 A71-36651

Weightless environment effects on fluid behavior and heat transfer in life support systems, obtaining analytical models

[AIAA PAPER 71-864] 18 p2909 A71-36652

Human thermoregulation, discussing experimental determination of equation for mean body temperature calculation in neutral and warm environments

18 p2858 A71-36866

Human psychomotor performance measurements in rotating environments, using Langley complex coordinator and decision response time devices

[AIAA PAPER 71-887] 19 p3006 A71-37275

Surface properties and environmental effects on fatigue striations development and crack initiation in Cu single crystals

19 p3077 A71-37412

K band satellite transmit/receive frequency converters, describing design features and performance tests under simulated environmental conditions

19 p3028 A71-37697

Discrete semiconductor devices test program assessing environmental screening for improved component reliability

19 p3034 A71-38517

Noisy environment effects on circulatory, respiratory and metabolic parameters during physical exercise,

measuring heart rate, systolic blood pressure, oxygen intake and respiratory quotient

20 p3185 A71-38889

Test unit number selection for lowest total life test cost, considering operating test environments and component reliability

21 p3386 A71-40368

High density packaging effects on multilayer interconnection board reliability tested in thermal environments

21 p3352 A71-40437

Spacecraft tape recorder design for five years minimum continuous unattended reliable operation, describing quality control and environmental/life testing procedures

22 p3608 A71-41507

Time sense modifications among human groups isolated in underground environment and deprived of timekeeping means, evaluating average individual behavior

22 p3500 A71-41577

Manned 90 day test of closed chamber regenerative life support system simulator, describing subsystems, crew nutrition, hygiene, maintenance and leisure activities

22 p3503 A71-42043

Simulated Martian environment effects on terrestrial microorganisms survival

22 p3487 A71-42227

Fuel droplet burning rate variation with ambient temperature and oxygen concentration in combustion gas environment

24 p3887 A71-44606

Liquid properties and ambient pressure effects on cavitation erosion in thin film

24 p3819 A71-44946

Nimbus B-2 satellite-borne IR spectrometer lubrication using solid film technique, discussing real time and accelerated vacuum environmental tests

[ASLE PREPRINT 71LC-3] 24 p3831 A71-45286

ENVIRONMENTS

NT AEROSPACE ENVIRONMENTS

NT CHROMOSPHERE

NT CISLUNAR SPACE

NT DEEP SPACE

NT EARTH ENVIRONMENT

NT EXTRATERRESTRIAL ENVIRONMENTS

NT FRICTIONLESS ENVIRONMENTS

NT HIGH ALTITUDE ENVIRONMENTS

NT HIGH TEMPERATURE ENVIRONMENTS

NT INTERPLANETARY SPACE

NT INTERSTELLAR SPACE

NT JUPITER ATMOSPHERE

NT LOW TEMPERATURE ENVIRONMENTS

NT LUNAR ATMOSPHERES

NT LUNAR ENVIRONMENT

NT MARS ATMOSPHERE

NT MARS ENVIRONMENT

NT PLANETARY ATMOSPHERES

NT PLANETARY ENVIRONMENTS

NT ROTATING ENVIRONMENTS

NT SOLAR ATMOSPHERE

NT SPACECRAFT ENVIRONMENTS

NT STELLAR ATMOSPHERES

NT THERMAL ENVIRONMENTS

Linear elastic structure statistical response characteristics relation to natural environment random pressures, considering flexural vibrations of thin cylinder for modal density

05 p0826 A71-16732

Surface structure and environment effects on mechanical behavior of crystalline inorganic solids, giving stress-strain diagrams

11 p1808 A71-25999

Existence of life under extreme environmental conditions, discussing biological temperature limits and adaptability to lack of water

11 p1721 A71-26321

ENZYME ACTIVITY

Renin level in renal venous and peripheral blood in patients with renovascular hypertension

01 p0010 A71-10391

Enzyme activity reduction in thyroid gland tissue of albino rats under deep hypothermia

01 p0012 A71-11057

Aspartic aminotransferase activity relation to clinical and biochemical indices of human tolerance to impact accelerations

01 p0014 A71-11140

Self-sustaining coacervates photochemical formation, discussing enzyme-like properties and abiogenesis

01 p0017 A71-11453

Biological clocks self oscillating mechanism as temperature dependent component of circadian clocks in multicellular organisms, assuming small enzyme concentrations

01 p0020 A71-11566

Healthy subjects physical training effects on blood flow and enzymatic activity in skeletal muscle

02 p0201 A71-12916

Glutaminase isoenzyme activators in mitochondrial brain fractions of rabbits

03 p0361 A71-13235

Gamma-aminobutyric acid /GABA/ effects on brain serotonin following transaminase inhibitor aminooxyacetic acid administration

03 p0362 A71-13236

Decaborane effects on amino acid metabolic patterns of various rat tissues, considering holoenzyme inactivation

05 p0706 A71-16294

Metabolic processes in bone tissues as basis for fighting bone disease, emphasizing enzymes role

05 p0710 A71-16858

Bovine pituitary proteinase I action on oxidized B chain of insulin, noting preference for specific bonds

05 p0718 A71-17108

Myocardial infarction, investigating alpha dehydroxybutyric acid dehydrogenase enzymatic activity

06 p0849 A71-17298

Myocardium enzyme activity after sympathetic denervation of heart in cats and mice

06 p0857 A71-18726

Radiosensitizing effect of iodine compounds in dilute solution on Ehrlich ascites tumor cells and SH enzymes

07 p1036 A71-18957

Sodium fluoroacetate as radiation protective agent, noting dependence on selective blockade of enzyme anionase

07 p1037 A71-18967

Cellular damage to rat mitochondria and endoplasmic reticulum by injection of radioprotectors, discussing intracellular enzymes passage into plasma

07 p1039 A71-18981

Amino-ethyl-S-2-isothiuronium radio protective dose effects on enzyme activity, cardiovascular changes, blood transaminases concentration, bone marrow and peripheral circulation

07 p1040 A71-18986

Oxidative and hydrolytic enzymes localization in rhesus monkey brain, investigating glutaraldehyde fixation effect with histochemistry

07 p1042 A71-20017

Mitochondrial oxidation of substrates coupled with phosphorylation studied using organelles isolated from red and white skeletal muscles of rabbit, noting enzyme activity of fatty acids

08 p1238 A71-20682

Myocardial lysosomal enzymes activity in adaptation to high altitude hypoxia and during cardiac diseases, using albino rats

08 p1239 A71-21058

Soyuz 9 spacecraft astronauts space flight effect on digestive system enzyme secretion function based on pre- and post-flight examinations

09 p1389 A71-22206

Ionizing radiation inhibition of spinal cord neurons ribonucleic acid synthesis and enzyme activity in mice, using autoradiographic method

09 p1393 A71-22925

Rats under various exercise programs, determining cardiac ventricle and gastrocnemius muscles calcium activated adenosine triphosphatase activities

09 p1400 A71-23361

Cell free extracts with high nitrogenase activity from blue green alga *Anabaena cylindrica* by sonic oscillation and French press treatment

09 p1402 A71-23475

Streptomycetes sp chitinase purification and properties by column chromatography, noting calcium component

11 p1728 A71-26064

Succinic dehydrogenase activity inhibition and pentobarbital sodium protection of lung tissue in mouse breathing oxygen at atmospheric pressure

11 p1721 A71-26125

Acidic and alkaline deoxyribonucleases activity by spectrophotometer and horizontal viscosimeter in normal states and pathology

12 p1872 A71-27743

Dipeptidyl aminopeptidase I /cathepsin C/ properties, subcellular localization and polypeptide degradation in rat liver and bovine spleen and pituitary glands

13 p2025 A71-28179

Ionized air exposure effects on acetylcholine content and cholinesterase activity in mice, noting cholinergic and serotonic interaction

13 p2006 A71-28404

Rat liver and lung collagenase activity Circadian rhythm, noting maximum enzyme activity in early morning and minimum during afternoon and early evening

13 p2010 A71-28788

High motor stresses effects on muscle acetylcholine content, cholinesterase activity and localization, solitary contractions fusion and pessimal weakening

14 p2186 A71-30553

Acetyl-coenzyme A synthetase in aerobic yeast cells localization in microsomal fraction by density gradients

14 p2187 A71-31003

Substrate and light dependent fixation of molecular nitrogen in *Rhodospirillum rubrum* tested for nitrogenase activity by manometric measurement

16 p2527 A71-33057

Ion-membrane hydrogen oxygen fuel cell, using microbially or biochemically produced hydrogen by enzymatic reactions

16 p2527 A71-33550

Histochemical investigation of enzymes activity during various cardiac cycle phases in frogs, noting effects of ion concentration

16 p2533 A71-33913

Physical training effects on human plasma glutamic-oxalacetic transaminase, creatine phosphokinase and lactic dehydrogenase enzyme levels

17 p2683 A71-35143

Coagulation and fibrinolysis changes after physical exercise in males with atherosclerosis, noting fibrinolytic response differences with age

18 p2853 A71-35918

Glucose and fructose extraction from formose sugar mixtures by enzymatic methods using hexokinase reaction

19 p3011 A71-37574

Chlorella extracellular metabolites, identifying indole nature biologically active substances

19 p3004 A71-38544

Phosphoenolpyruvate as enzyme inhibitor of phosphoribulokinase in *Pseudomonas facilis* with respect to ribulose-5-phosphate and ATP

20 p3185 A71-38820

Plasma renin activity in hypertonic and normotonic persons exposed to exogenous stress, comparing with measurements at rest and in orthostasis

20 p3185 A71-38893

Space environment simulation for ultrahigh vacuum effects on crystalline enzymes activity, measuring by chemiluminescence techniques

21 p3334 A71-40573

Low temperature effects on succinate oxidase activity of mitochondrial membranes in hibernating squirrels

21 p3336 A71-40854

Soviet monograph on coacervates and protoplasm covering colloidal-chemical properties, enzyme catalysts and multiphase cell and organism simulation

21 p3336 A71-40870

Aminazine and chloral hydrate effects on metabolism intensity of rats brain gangliosides components including N-acetylneuramine acid and N-acetylgalactosamine

21 p3337 A71-41055

Thyroxine effects on brain glutaminase isoenzymes interaction and deamidation in mitochondrial fractions, comparing with sodium phosphate, bicarbonate and aspartate

21 p3338 A71-41069

Water immersion effect on plasma renin activity, urinary aldosterone excretion and renal sodium and potassium handling in normal man

22 p3485 A71-41720

Rat plasma creatine phosphokinase activity, hypothermia and stress, considering cold restraint

22 p3486 A71-41938

Urea hydrolysis reaction rates by urease at low water activity, noting use for Mars surface bioassay

22 p3487 A71-42226

Nonaqueous biosystems unlikelyhood from consideration of enzymatic activity possibility and liquid water unique ability for complexity required by carbonaceous biosystems

22 p3487 A71-42229

Glutamicoaspartic and glutamicoalanine aminotransferases activity in blood serum of dogs under gamma irradiation with shielded abdomen or head, observing hyperfermentemia

22 p3493 A71-42720

Hyperoxia pathological effects on albino rats subcutaneous connective tissue, noting oxidizing enzyme activity depression and cellular metabolism suppression

22 p3496 A71-42802

Physiological effects on mice of air pollution with gaseous toxic substances from urine and feces, noting increased respiration rate and choline esterase activity

22 p3506 A71-42807

Combined and individual effects of UV light, X ray irradiation and freezing-thawing cycles on ribonuclease

22 p3496 A71-42830

Gaseous medium composition and multiple freezing temperature effects on catalase activity

22 p3497 A71-42831

Electron transport chain of extremely halophilic bacteria, investigating cytochrome oxidase activity dependence on pH

23 p3633 A71-43525

Organophosphate pesticide poisoning implication in aircraft crash of duster pilot from cholinesterase activity drop evidence

23 p3641 A71-44249

Allosteric adenosine monophosphate nucleosidase stabilization by inorganic salts, substrate and essential activator, investigating enzyme inactivation mechanism in low ionic strength environments

23 p3642 A71-44268

Cholinesterase activity and acetylcholine level dependence on adrenaline dose injected in heart during rats experimental myocardiodystrophy

24 p3800 A71-44500

Transverse acceleration effect on aspartic aminotransferase activity in humans and rats

24 p3795 A71-44528

Analog modeling of enzyme and biochemical systems with fixed and variable functional properties, using operational amplifier integrator

24 p3802 A71-45109

ENZYMES

NT CATALASE
NT CHOLINESTERASE
NT COENZYMES
NT HEXOKINASE
NT LYSOZYME
NT OXIDASE
NT PEPSIN

Physical determinants of gravity receptor mechanisms, discussing hydrostatic stress effects on membranes and gravity influence on enzymatic transport

21 p3339 A71-39972

ENZYMOMOLOGY

Immunochemical investigation of dogfish pepsinogens A, C and D, determining characteristics in terms of immunodiffusion, immuno-electrophoresis, complement fixation and enzymic activity inhibition

13 p2015 A71-29480

EOR (RENDEZVOUS)

U EARTH ORBITAL RENDEZVOUS

EOSS

Long range near-earth orbit research and applications based on NASA goals, including laboratory/observatory definition

17 p2802 A71-34729

Reactor power systems for earth orbital space station, considering thermoelectric and Brayton cycle power conversion modules

20 p3262 A71-38919

Nuclear safety considerations for ground checkout, launch and in-orbit operations of reactors for earth orbital manned space stations

20 p3262 A71-38920

ELDO space tug development, discussing uses for earth orbital space stations and applications satellites logistics and interplanetary injection

22 p3609 A71-41978

EPE-A

U EXPLORER 12 SATELLITE

EPE-D

U EXPLORER 26 SATELLITE

EPHEMERIDES

NT PLANET EPHEMERIDES

Orbital coordinates for body moving along parabola with small perihelion distance calculated for ephemeride

01 p0157 A71-10607

Planetary dynamics bibliography and review, considering range determination and ephemerides, general relativity, tidal evolution and lunar orbit, solar system commensurabilities, etc

17 p2798 A71-34457

Ephemerides of sun, moon, planets and minor planets for October through December 1971

21 p3442 A71-40153

Automatic multi-satellite ephemeris maintenance by mathematical procedures, describing computer automated scheduling system program

23 p3728 A71-43026

EPHEMERIS TIME

Lunar position on stellar field for ephemeris time determination, discussing planet and satellite positions with respect to astronomical constants

05 p0809 A71-16460

Lunar ephemeris for nanosecond resolution laser ranging systems by literal and numerical integration techniques

05 p0811 A71-16682

Ephemeride and atomic uniform time scales comparison for earth rotation velocity changes, estimating diurnal and semi-diurnal tides effect

08 p1284 A71-21673

Suzuki-Sato-Seki and other 1970 comets, discussing position observation and ephemeris calculation

09 p1516 A71-22069

Asteroids photographic observations for catalog of faint stars positions orientation, correcting observation times to ephemeris time

09 p1525 A71-23338

Gravitational lunar theory high order solution for geophysical relevance, discussing perturbation methods and computer analyzed ephemeris time

12 p1961 A71-26837

Earth clock precision and rotation retardation effects on ephemeris time, comparing with atomic clock

19 p3060 A71-38529

EPIDEMIOLOGY

Preventive medicine for air travelers in flight and at route stops, considering disease dissemination and control, international quarantinable diseases, sanitation, etc

08 p1245 A71-20727

Epidemiological aspects of airport medicine in relation to global public health and international cooperation

11 p1725 A71-26129

Epidemiological statistics for age specific incidence rate of serious in-flight pilot failure, considering fatal and nonfatal causes

16 p2535 A71-33121

EPIDERMIS

Percutaneous vitreous carbon electrodes long term effects, considering mechanical stability, bioelectrical signal receptivity, low interface impedance and surrounding epidermis growth

01 p0021 A71-10238

EPILEPSY

Protective brain function in epileptical convulsive seizures during sonic stimulation in rats

03 p0359 A71-13159

Potential epilepsy determination in flight personnel, suggesting systematic EEG with hyperventilation and photic stimulation tests and personal history data of head trauma and unconsciousness

21 p3331 A71-40357

EEG characteristics of cadets and flying personnel, noting spike wave paroxysmal screening and epilepsy detection

22 p3502 A71-41836

EPINEPHRINE

NT NOREPINEPHRINE

Aortic and sinus nerves afferent electric impulsion under adrenalin and nicotine, considering age peculiarities

03 p0363 A71-13522

Epinephrine infusion in man, examining systolic time intervals and sympathetic stimulation in cardiovascular dynamics

06 p0850 A71-17440

Control and prolonged exercised rats adrenal and plasma catecholamine, corticosterone and epinephrine level comparisons using fluorometric analysis

07 p1044 A71-20330

Adrenal medulla biochemistry and morphology, discussing epinephrine synthesis control by glucocorticoid hormones

14 p2187 A71-30809

Renin, plasma norepinephrine and epinephrine responses to work loads of various intensities, evaluating sympathetic nervous system as stimulus for secretion

19 p3008 A71-38551

Cholinesterase activity and acetylcholine level dependence on adrenaline dose injected in heart during rats experimental myocardiodystrophy

24 p3800 A71-44500

Adrenaline, noradrenaline and catecholamine excretion in railroad men during daytime and nighttime work

24 p3799 A71-45085

EPITAXY

High efficiency epitaxial growth of GaAs by system using substrates oriented along /111/ Ga face

01 p0137 A71-10314

Neutron irradiation induced degradation in epitaxial Gunn diode performance

07 p1071 A71-19069

Cadmium telluride epitaxial films on potassium bromide, investigating external gases effects on photovoltaic properties

07 p1179 A71-19919

CW GaAs semiconductor laser fabrication by liquid epitaxy, noting Ag plating role in output power

07 p1126 A71-20196

GaAs-InAs type single crystals, polycrystals and epitaxial films solid solutions, studying optical, electrical and luminescent properties

08 p1344 A71-21443

GaAs epitaxial layers growth in open system, noting spontaneous crystallization on reactor walls at high temperatures

09 p1506 A71-22161

GaAs epitaxial layers inhomogeneous doping in continuous chloride system, discussing electron concentration with respect to gas flow direction

09 p1506 A71-22167

FET transistors on epitaxial GaAs as input and output transducers for acoustic surface waves

09 p1417 A71-22755

High temperature ultraminiature pressure transducers, reviewing p-n junctions thermal limitations and thermal properties of dielectric oxides used with solid state epitaxially grown sensors

09 p1448 A71-22772

Epitaxial deposition of discrete separated p- and n-type silicon on single sapphire substrate, considering technique for MOS devices fabrication

09 p1509 A71-23116

Single crystal indium gallium phosphide p-n junction preparation by epitaxial vapor phase growth technique, determining energy gap dependence on alloy composition

09 p1510 A71-23121

Multilayer liquid phase epitaxy heterostructures growth with crystalline solid solutions of aluminum gallium arsenide for injection lasers

09 p1464 A71-23122

- Epitaxial InP three level oscillators in K and Q bands /18-40 GHz/, suggesting optimum operating frequency determined by defined transit velocity
09 p1421 A71-23719
- Apollo 12 clinopyroxenes exsolution and epitaxy by electron microprobe and single crystal X ray diffraction
10 p1672 A71-24391
- Epitaxial garnet films magnetic anisotropic models, describing mobile cylindrical domains
12 p1943 A71-26854
- Polycrystalline copper and magnetic films thin intermediate layers, showing prevention of epitaxial growth
12 p1943 A71-26855
- Epitaxial deposition of Au on ultrahigh vacuum cleaved mica during early nucleation and growth
14 p2284 A71-30072
- Epitaxial film thickness and resistivity effect on transistor cut-off frequency, discussing collector junction space charge region boundary location
14 p2213 A71-30626
- Epitaxial Ag thin film with controlled surface roughness on mica, measuring electrical resistivity as function of temperature, thickness and surface specularly in vacuum
15 p2461 A71-32376
- Electric field effect of epitaxial thin silver films on mica in vacuum as function of temperature, thickness and surface specularity
15 p2461 A71-32377
- GaAs epitaxial layer growth process parameters relationship to electrical properties
16 p2621 A71-33563
- Semiconductor defects, including stoichiometric vacancies in sphalerite lattices, epitaxial interfaces and dislocations in Ge
18 p2953 A71-35870
- Al distribution in gallium aluminum arsenide films obtained by epitaxial growth from liquid phase, showing temperature variation dependence during deposition
18 p2954 A71-36161
- Fabrication and noise performance of high power Schottky barrier GaAs IMPATT diodes with double epitaxial layer structure on low-etch-pit density substrates
18 p2895 A71-36982
- MOS transistors thin monocrystalline silicon layers formation by epitaxial growth and substrate selective electrochemical etching
19 p3028 A71-37565
- Neutron irradiation effects on radiative, nonradiative and threshold currents in epitaxial GaAs laser diodes at room temperature
20 p3275 A71-38785
- Hall coefficient and resistivity in undoped heteroepitaxial GaAs on aluminum oxide films grown by trimethylgallium arsine process
20 p3276 A71-38881
- Transition layer structure formation of epitaxial semiconducting films, discussing model for dislocations origin
21 p3427 A71-40727
- P-n-p-n quadruple layer semiconductor junction light emitting diode with negative resistance characteristics, discussing epitaxial regrowth process and applications
21 p3355 A71-40739
- Current-voltage characteristics of n-GaAs epitaxial structures at various temperatures, indicating use in memory devices and high power switches
21 p3430 A71-41223
- Emitter-base junction degradation by avalanche breakdown in planar transistors with low doped /epitaxial/ base region
22 p3520 A71-41682
- Multiple layer liquid epitaxial growth of lead tin tellurides from Pb-Sn solution, determining low carrier concentrations by Hall effect and capacitance measurements
22 p3585 A71-41810
- Kinetic parameters and conditions for optimal epitaxial growth of GaAs from liquid phase, observing solution cooling rate effect on p-n junction quality
24 p3808 A71-44724
- EPITHELIUM**
- Cochlear sensory epithelium and Corti organ degeneration after noise exposure in guinea pigs and cats, using scanning electron microscopy
02 p0199 A71-12364
- Vestibular sensory epithelial cells form and organization, discussing morphological polarization
04 p0536 A71-14760
- EPOCHS**
- U TIME MEASUREMENT**
- EPOXIDES**
- U EPOXY COMPOUNDS**
- EPOXY COMPOUNDS**
- NT ETHYLENE OXIDE
- Graphite/epoxy composite structural spacecraft panels, discussing design analysis and fabrication procedure
04 p0618 A71-15344

- Low temperature curing nylon epoxy adhesive, discussing high peel strengths
10 p1630 A71-24070
- Graphite epoxy composites fiber microstructure and surface condition, noting tensile fracture, crack propagation and brittleness
13 p2092 A71-28594
- Substrate influence on circuit board conformal coatings electrical insulation resistance, discussing test results with epoxy/glass and ceramic substrates and various coating materials
21 p3353 A71-40438
- Solid lubricant-epoxy compounds shear modulus measurement by cantilever beam specimens dynamic testing, calculating wear life coefficients for molybdenum disulfide in epoxy resin
24 p3842 A71-45284
- EPOXY RESINS**
- Glass fiber-epoxy resin composites shear strength, considering fiber length and interfacial bond effects
01 p0106 A71-10277
- Viscoelastic behavior of boron fiber-epoxy resin composites at high temperature from torsion pendulum study, proposing linear model for damping peak effect
01 p0107 A71-10460
- Epoxy resin reinforcement by various fiberglass types, discussing effects of bond-enhancing agents, fatigue strength properties, etc
01 p0108 A71-10691
- Nonmetallic aircraft construction materials, discussing wood epoxy and polyester resins
02 p0273 A71-12299
- Carbon fiber reinforced epoxy composites, evaluating application as helicopter tail rotor blade material
02 p0273 A71-12477
- Carbon fiber composites, examining epoxy resin matrix effects on mechanical performance and heat tolerance
02 p0274 A71-12486
- Carbon fiber-epoxy resin composites in aircraft industry, examining fatigue life, cost, specific moduli and mechanical properties
02 p0275 A71-12488
- Three phase particulate epoxy composite compressive yield strength, considering strain rate filler content, porosity and voids effect
03 p0442 A71-13538
- Thermal cycle stresses at interface of composite glass tape-epoxy casting resin cylinder, using strain gages
03 p0508 A71-13763
- Thermal expansion of unidirectional, angle-ply and complex laminated graphite-epoxy composites, considering fiber orientation, hysteresis and interlayer stress relaxation
03 p0449 A71-14459
- Aluminum reinforced epoxy model making, testing and stress analysis for aircraft structures, including creep, photoelastic coating and strain gage effects
05 p0821 A71-16346
- Unidirectional glass-epoxy filament wound composite material fracture strength based on three dimensional stress components of fiber-containing plane
05 p0826 A71-16740
- Fracture strength of helical wound glass-epoxy composite cylinder under axial tension, determining tensile strength
05 p0826 A71-16741
- Cured epoxy polymer, determining diffusion coefficients, solubility, permeability and equilibrium water absorption as function of curing agent and temperature
06 p0915 A71-17943
- High intensity electric current damage in boron and graphite filament reinforced epoxy resin composites
07 p1145 A71-19945
- Stress rupture properties of S glass/epoxy single end strands at various load levels, considering distribution functions
07 p1145 A71-20126
- AL particle size and filler volume optimization effects on epoxy composite dynamic response
07 p1139 A71-20136
- Strain rate effect on fiber reinforced unidirectional epoxy composites tensile stress, noting steel, boron, beryllium and graphite/epoxy strands
07 p1139 A71-20137
- Charpy notched impact strength of carbon fiber reinforced epoxy resin composites over temperature range
[PLASTICS INST. PAPER 20]
- Carbon fiber reinforced epoxy resin fatigue and crack propagation behavior in air, moisture and oil environments, using tensile, bending and torsion test methods
08 p1318 A71-20891
- Epoxy resin matrix properties influence on carbon fiber composites performance, discussing test methods for measuring mechanical and fatigue properties over temperature and frequency range
[PLASTICS INST. PAPER 22]
- 08 p1320 A71-20908

- Tensile, flexural and compressive shear, impact and fatigue characteristics of carbon fiber-epoxy resin composites
[PLASTICS INST. PAPER 26]
- 08 p1322 A71-20923
- Glass state beta transition temperatures in cured epoxy resins, showing diglycidyl ether of bisphenol A /DGEBA/ dependence
[JPL-TR-32-1509]
- 08 p1323 A71-21475
- Epoxy resins - ACS Conference, San Francisco, April 1968
09 p1482 A71-22404
- Ultrasonic modulus vs strength of high modulus fiber reinforced epoxy matrix composites in non-destructive testing
09 p1484 A71-23687
- High peel strength epoxy and urethane adhesives for aircraft bonding, discussing high temperature curing and honeycomb panel repair
10 p1630 A71-24064
- Low temperature curing long open time epoxy adhesives evaluation for 3500 psi shear strength
10 p1631 A71-24072
- Surface chemical characteristics of monomeric liquid epoxy resins
10 p1632 A71-24085
- Bulk properties effect on adhesive properties of seven epoxy resins, considering stress-strain properties and statistical analysis for tensile shear evaluation
10 p1632 A71-24086
- Processing variables effects on epoxy adhesive joints fracture toughness and crack extension resistance
10 p1632 A71-24089
- Stress corrosion crack extension in adhesive epoxy joints under combined long term static loads and aggressive action of water
10 p1632 A71-24090
- Aluminum-epoxy joints stress corrosion cracking inhibition and crack tip plastic deformation by scanning electron microscopy
10 p1615 A71-24091
- Al alloys and ferrous metals adhesive bonding, discussing surface preparation and surface exposure time influence on bonded joint strength for various epoxy adhesive types
10 p1615 A71-24095
- Coupling agents in urethane and epoxy adhesives, discussing lap shear and T-peel tests on mild and stainless steels, Al and glass cloth substrates
10 p1616 A71-24108
- Filamentary composites for primary aircraft structural applications, emphasizing boron-epoxy material
10 p1618 A71-24770
- Time and temperature effects on epoxy composites mechanical behavior, changing from brittle to ductile to rubbery failure mode
10 p1635 A71-24805
- Epoxy bond strength, cracking and failure of lapped joints as function of composition and mechanical properties
10 p1618 A71-24826
- Hardened and glass reinforced epoxy resin mechanical properties after 180 day hold in water, acid and alkaline solutions
10 p1635 A71-24827
- Fiber reinforced plastics /epoxy resins/ electrical effects association with deformation and failure
10 p1635 A71-25013
- Simultaneous determination of first and second mode photoelastic maximum shear stress intensity patterns of epoxy model, using computer plotted ellipses
10 p1694 A71-25060
- Stress rupture behavior of S glass/epoxy multifilament strands, developing tensile and creep test apparatus installed in controlled environment building
11 p1784 A71-25397
- Carbon fiber-epoxy resin composites Young modulus, thermal and electrical conductivities as function of fiber alignment and porosity
11 p1784 A71-25399
- Epoxy resin fatigue behavior from double torsion technique, considering stable crack movement in brittle materials
11 p1785 A71-25401
- Graphite epoxy composites fatigue testing, including loaded and unloaded shear, hardness and tensile strength in wet and dry environments
11 p1785 A71-25402
- Carboxyl terminated butadiene-acrylonitrile/epoxy carbon fiber composites fracture energy, noting fracture strength, short beam shear strength and tensile strength at cryogenic temperatures
11 p1785 A71-25403
- Longitudinal tensile strength of unidirectional fibrous glass/polymeric matrix composites under high loading rates
11 p1785 A71-25405
- Epoxy resin in fiber reinforced composite preregs, characterizing by thermomechanical analysis and gel permeation chromatography
11 p1786 A71-25411

Interfacial bonding effect on fracture toughness of glass sphere filled epoxy and polyester resins, using tapered cleavage specimen

11 p1846 A71-25413

Strength transfer at glass-epoxy laminates interface in reference to critical surface tension of coupling agent on fabrics

11 p1786 A71-25414

Boron-epoxy structural skins design for F-14 honeycomb horizontal stabilizer, using computer program

11 p1786 A71-25420

Thermosetting acryl modified epoxy resin, stressing adhesive bonding strength, workability and curing characteristics

11 p1787 A71-25423

Difunctional epoxy resins from dihydroxydiphenyl sulfone /bisphenol S/, obtaining increased heat resistance and thermal stability

11 p1787 A71-25424

Research bibliography on resins and additives covering polyesters, epoxies and new polymers with improved corrosion, fire and heat resistance

11 p1788 A71-25431

Epoxy novolac resin-cured alicyclic anhydride amine-catalyzed ablative polymers molecular structure from computer correlation of analytical data

11 p1789 A71-26033

Epoxy resin heat shield performance prediction based on chemical structure relation to ablative properties, discussing thermal degradation mechanism and char forming reactions

11 p1855 A71-26038

Unidirectional glass fiber epoxy composite material nonlinear viscoelastic behavior, using isothermal uniaxial creep and recovery tests with thermodynamic constitutive equations

11 p1851 A71-26385

Graphite-epoxy composite skins for commercial aircraft flight spoiler, discussing multiangle ply design and fabrication

12 p1921 A71-27413

Probability characteristics of glass/epoxy plastics mechanical properties, considering tangential and axial tensile and bending strength, modulus of elasticity, buckling and compression strength

13 p2092 A71-28653

Hybrid boron-graphite filaments in epoxy matrix composite, describing increased tensile strength and modulus of elasticity

14 p2261 A71-29638

Advanced plastic composites fabrication and processing techniques, using resins, reinforcements and fillers

14 p2263 A71-29653

Radiation effects on epoxy adhesive mechanical properties including compressive shear stress, modulus of elasticity and tensile strength

15 p2439 A71-32510

Radiation effects on bonding characteristics of epoxy-metal and epoxy-glass adhesive joints

15 p2439 A71-32511

Epoxy and unsaturated polyester resin compounds for embedding glass fibers in fiberglass-reinforced plastics

15 p2439 A71-32737

Monograph on fiber-resin composites covering glass, boron and carbon fibers and epoxy matrix materials tensile and thermoelastic properties

17 p2761 A71-34469

Aluminum powder filled epoxy composites, investigating particle size and filler percent effects on damping properties and elastic modulus

17 p2762 A71-34819

Boron-epoxy composite wing box beam design, describing preliminary weight estimation from layouts [SAWE PAPER 891]

17 p2834 A71-35815

Radiative ignition of polymeric fuels /polystyrene and epoxy/ in oxygen/nitrogen mixtures

19 p3121 A71-38125

Optically sensitive epoxy resin based high polymers under pulsed loads, observing deformation and mechanical displacement with high speed photography

22 p3614 A71-41610

Stress concentration near holes in high modulus epoxy resin polymer thin plates under pressure wave loads

22 p3614 A71-41611

Epoxy resin plate mechanical stress measurement under impact load, using laser light source three beam interferometric assembly with photographic recorder

22 p3555 A71-41613

Photosensitive epoxy resin coating light path propagation variation measurements, using continuous radiation gas laser and Fabry-Perot interferometer

22 p3555 A71-41615

Nondestructive testing evaluation of graphite epoxy composites and adhesive bonded Al composite structures using acoustical holography

22 p3554 A71-41781

Epoxy-alumina trihydrate composite system fracture energy data, noting interdependence of surface

topography, phase dispersion volume fraction, particle size and spacing

23 p3696 A71-43102

Linear viscoelastic stress-strain-time relations for polymethyl methacrylate and epoxy resin

23 p3696 A71-43375

Solid lubricant-epoxy compounds shear modulus measurement by cantilever beam specimens dynamic testing, calculating wear life coefficients for molybdenum disulfide in epoxy resin [ASLE PREPRINT 71LC-1]

24 p3842 A71-45284

EQUATIONS OF MOTION

NT EULER EQUATIONS OF MOTION

NT HELMHOLTZ VORTICITY EQUATION

NT HYDRODYNAMIC EQUATIONS

NT KINEMATIC EQUATIONS

NT KINETIC EQUATIONS

NT NAVIER-STOKES EQUATION

NT REYNOLDS EQUATION

NonNewtonian /second order/ fluids motion equation derivation based on statistical nonequilibrium distribution

01 p0068 A71-10026

Cleavage fracture equations of motion solved for constant moment, force and deflection, discussing plate crack propagation

01 p0167 A71-10291

Atmospheric boundary layer nonlinear equations of motion numerical integration for eddies structure and wind direction and latitude effects on turbulence intensities

01 p0113 A71-10351

Numerical integration finite difference methods stabilization for perturbed Keplerian motion differential equations

01 p0154 A71-10378

Matrix perturbation methods for nonlinear perturbed systems, involving variational equations solution of regularized Keplerian motion

01 p0154 A71-10380

Dynamic problems linear variation equations associated with one and two particle motion in force field

01 p0111 A71-10385

Object constant speed motion in terrestrial orthodromy, examining Shuler vertical small oscillations stability

01 p0125 A71-10628

Gyrosystems motion equations, obtaining nutation, precession and drift components as asymptotic expansions by small parameter technique

01 p0080 A71-10632

Invariance in automatic control systems nonlinear differential equations of motion

01 p0064 A71-10730

Laser oscillation buildup from quantum noise, deriving equations of motion for moments of photon distribution and time dependence

01 p0094 A71-10826

Generalized Hamilton-Jacobi theorem extension to dynamic equations of motion for holonomic mechanical systems of variable mass with impulse connection multiplier

01 p0128 A71-11151

Perturbed motion stabilization in nonlinear control system with applicable equation containing zero root and imaginary roots

01 p0128 A71-11158

Phase-plane motion of engine assembly, using graphoanalytic delta method

01 p0128 A71-11241

Motion equations of spherical gyroscope in gravitational field of larger mass derived from Gupta quantum theory of gravitation

01 p0161 A71-11274

Cable-connected spinning and orbiting satellite spring-mass system, deriving in-plane motion equations by Hamilton principle for numerical analysis

01 p0165 A71-11587

Reference trajectory and additional phase variable methods for motion equations integration applied to vehicle in atmosphere

02 p0304 A71-11904

Motion components about center of mass of body using flywheel attitude control by small parameter method

02 p0279 A71-11906

Law of motion for two degrees of freedom integrating gyro mounted on oscillating base, using averaging method

02 p0253 A71-12637

Atmospheric air columns centers of gravity, determining height from vertically integrated equations of motion

02 p0278 A71-12745

Longitudinal elastic wave propagation equations of motion in cone with small apex angle, using perturbation theory

03 p0456 A71-12974

Nonstationary automatic control system asymptotic series solution for equations of perturbed motion, deriving unperturbed motion local stability criteria

03 p0388 A71-13287

Machine assemblies forced vibrations equations of motion determination, considering elastic dissipative qualities, structural hysteresis and damping

03 p0503 A71-13410

Solid body motion about fixed point on pseudoeuclidean Lobachevskii plane under external forces, using Euler angle analogy

03 p0457 A71-13423

Laminated cylindrical shells of orthotropic layers, deriving linear theory and equations of motion

03 p0504 A71-13430

Steady state motion equations of multiple unit impact damper attached to periodically excited primary system, developing solution for mathematical model

03 p0505 A71-13547

Centrifugal and Coriolis force in general relativity, discussing paradox associated with terms in mass shell test particles equations of motion

03 p0489 A71-13564

Equations of motion of heavy gyrost at with fixed point in uniform force field

03 p0457 A71-13580

Equations of motion of gyroscope body having fixed point, determining conditions for existence of quadratic invariant correlation

03 p0457 A71-13583

Heavy gyroscope equations of motion solution, assuming center of mass on major axis

03 p0457 A71-13584

Heavy gyrost at equations of motion having fixed point and zero momentum integral constant, obtaining polynomial solutions

03 p0457 A71-13585

Differential equations of spherical motion of heavy solid body with ellipsoidal cavity filled with liquid, deriving stationary solutions

03 p0457 A71-13586

Integrodifferential equations of motion of body with fixed point, obtaining solution and geometrical interpretation

03 p0457 A71-13587

Traveling angular velocity hodograph equations in solution to gyrost at motion problem

03 p0457 A71-13588

Kinematic interpretation of body motion about fixed point for case of traveling angular velocity hodograph integrable in closed form

03 p0457 A71-13589

Hess solution for motion of heavy solid body with fixed point, surveying various methods

03 p0458 A71-13590

Spinning rocket vehicle with aerodynamic asymmetry, deriving equations of motion and steady aerostatic behavior

03 p0499 A71-13678

Ball bearing dynamics, considering motion equations for four degree of freedom balls and six degree of freedom separator

03 p0432 A71-13708

Variational equation of motion for thin walled open section bars coupled flexure and torsion, considering thermal effects

[ASME PAPER 70-WA/APM-51]

03 p0513 A71-14169

Single axis gyroscopic stabilizer with floating type integrating gyro, describing natural oscillations by differential equations of motion

03 p0429 A71-14237

Geometrically nonlinear shell dynamics, basing equations of motion and compatibility on variational principles

03 p0514 A71-14346

Two-rotor gyrocompass equations of motion under perturbation, demonstrating reducibility to canonical form

03 p0430 A71-14354

Perturbed motion equations of body with liquid filled cylindrical cavity reinforced by elastically clamped ribs, solving boundary value problems

03 p0460 A71-14356

Gyrostatic system with center of mass in uniform circular motion, deriving rotary motion equations invariant

03 p0460 A71-14386

Orbit evolution of small mass near earth-moon system, noting solar perturbations and equations of motion

04 p0653 A71-15709

Equations of motion of restricted four body problem numerically integrated for positions of three primaries

04 p0653 A71-15711

Absolute orbit construction for Jovian great satellites, obtaining linear equations of motion

04 p0654 A71-15714

Von Zeipel procedure convergence for proving theorem pertaining to conditionally periodic motion equations with small change in Hamiltonian

04 p0661 A71-15892

Liquid-solid viscoelastic motion equations derived from conservation laws and nonequilibrium processes phenomenological theory

05 p0821 A71-16359

Singly curved rectangular plate free vibration characteristics obtained by partial differential equations of motion

05 p0825 A71-16605

Lagrangian methods yielding relativistically covariant formalism for wave packets in weakly inhomogeneous and time dependent plasma dynamics, obtaining motion equations from Euler-Lagrange equations

05 p0789 A71-16657

Equations of motion solution of heavy solid body about stationary point applied to Hess gyroscope

05 p0754 A71-16998

Equations of motions solution for variable mass point, taking into account drag and velocity

06 p0979 A71-17498

Time vector method extension to equations of motion with real roots, noting applications to aircraft flight control problems

06 p0925 A71-18049

Optimal vacuum rocket trajectories over spherical earth, deriving nonlinear differential equations for position and velocity

[AIAA PAPER 71-20]

06 p0976 A71-18487

Magnetically confined laser produced plasma radial oscillations, deriving equation of motion for expanding boundary

[AIAA PAPER 71-108]

06 p0938 A71-18558

Cavitation flow of fluid with free surface past underwater wing with jet flap, solving equations of motion for thin foil with jet emergent from trailing edge

07 p1092 A71-20086

Spherical sandwich shells free vibration motion equations, taking into account transverse shear deformation and rotary inertia effects

07 p1215 A71-20095

Bonded rod of two semiinfinite elastic bars subjected to end impulse, formulating motion equations and initial and boundary conditions

07 p1217 A71-20367

Gyrostats with center of gravity on ellipsoid axis, determining motion by two invariant algebraic equations

07 p1209 A71-20645

Aircraft optimum minimum noise takeoff profile, solving by equations of motion system for jet aircraft

08 p1331 A71-20779

Periodic comets Giacobini-Zinner and Borrelly motions, determining orbits with nonNewtonian motion equations and three orthogonal nongravitational terms

08 p1358 A71-20877

Complex hydrodynamic systems nonlinear differential motion equations integration, taking friction forces into account

08 p1299 A71-21620

Equations of motion for Poiseuille flow in circular tubes, solving Gromeko problem with integral Laplace transforms and Bubnov-Galerkin method

08 p1277 A71-21935

Nonlinear aerodynamic moment system for nonaxisymmetric bodies free flight motion analysis, taking into account interactions excluded in classical treatment

[AIAA PAPER 71-275]

08 p1228 A71-22000

Linear coupling between orbital and attitude motions of rigid body, deriving 12th order six degrees of freedom linearized motion equation

09 p1516 A71-22173

Series inverse in powers of time and radius of convergence for universal form of Kepler equation, discussing recursion formulas for coefficients

09 p1516 A71-22174

Motion perturbation equations for guided space vehicles, allowing for sloshing liquid propellant viscosity effects

09 p1532 A71-22657

Three stage astatic gyrocompass design with pendulum correction, considering equations of motion

09 p1449 A71-22795

Rendezvous equations near second lunar libration point, using Halo orbiting relay satellite for communication with spacecraft behind moon

09 p1521 A71-22912

Nonstationary automatic control system asymptotic series solution for equations of perturbed motion, deriving unperturbed motion local stability criteria

09 p1424 A71-23262

Celestial mechanics n body equations simultaneous integration, using Taylor-Steffensen numerical method

09 p1525 A71-23335

Conformally variable body, formulating differential equations of motion in moving coordinate system using Hamilton-Ostrogradskii form of least action principle

09 p1495 A71-23434

Small parameter method in gyrocompass theory, deriving differential equations for motion of sensitive element of two rotor gyrocompass

10 p1608 A71-23804

Translation-rotation motion of elongated body in Vinti potential field

10 p1667 A71-23814

Restricted three body problem involving two spherical bodies and elongated artificial satellite, considering equations of motion and positions stability

10 p1667 A71-23830

Numerical integration of motion equations for two layer atmospheric fronts model with baroclinicity along frontal surface separating two incompressible fluids in stable stratification

10 p1638 A71-23965

Minimum propellant optimal rendezvous maneuver of two cosmic vehicles on circular orbits, considering tracking vehicle motion equations

10 p1672 A71-24335

Wing aperiodic motion during change from one frequency to another, using Laplace and Fourier transforms to reduce partial to ordinary differential equation

10 p1688 A71-24353

Precessional equation of gyroscopic systems with rigid structural elements connected by single degree of freedom axial hinges

10 p1611 A71-24577

Ionospheric dynamic behavior, describing time dependent continuity and ion, electron and neutral particle motion equations

10 p1606 A71-24914

Infinitesimal body motion near triangular points of elliptic restricted three body problem, dividing equations of motion into two independent components by transformation

10 p1679 A71-24930

German monograph on basic equations for isotropic elastic homogeneous thin shell subjected to infinitesimal displacements, determining work of form change

10 p1692 A71-25037

Structural dynamics motion matrix Newmark generalized acceleration operator, Wilson averaging variant and Gurtin variational principle investigations for stability and approximation viscosity

10 p1693 A71-25050

Magnetic field effects on plane wave propagation in plasma, reducing motion data problem to vectorial differential equation with mean electronic velocity as only unknown

11 p1804 A71-25174

Linearized equations of motion for stability of dual spin satellite composed of platform, rotor, platform mounted damper and rotor mounted damper

11 p1837 A71-25514

Equations of motion for variable mass system of bodies, developing mathematical model of flight vehicle as six degrees of freedom control plant

12 p1926 A71-26728

Stellar cluster evolution equations in terms of free particle physics based on Boltzmann equation, describing computerized integrations

12 p1960 A71-26785

Symmetry properties of equation of motion, considering restrictions on force functions form of particles system due to covariance

12 p1929 A71-26959

Gas relaxation process equations of motion based on reversibility of time, considering application to particle systems with magnetic field moments

12 p1932 A71-27206

Equations of motion for single trajectory model of nonspherical stationary rotating stellar systems, assuming phase density dependence on motion integrals

12 p1966 A71-27234

Thin delta wing in hypersonic inviscid flow at small angles of attack, calculating motion equations and boundary conditions at small perturbations

12 p1863 A71-27330

Nonlinear equations of motion for cylindrical elastoplastic shell under axial impact

12 p1980 A71-27452

Plate and acoustic finite elements simulation of window-room system coupled transient response to sonic booms, discussing equations of motion and cavity depth effect

12 p1981 A71-27481

Liquid propellant rockets with rotating reactive force vectors, improving equations of motion

12 p1972 A71-27492

Hamilton-Jacobi type theorem on equations of motion with factors of constraints, giving proof for stationary mechanical systems

12 p1923 A71-27529

Gyroscopic systems equations of motion solution by Bogoliubov averaging method, considering free gyroscope on rotating base

13 p2065 A71-27952

Reference trajectory and additional phase variable methods for motion equations integration applied to vehicle in atmosphere

13 p2133 A71-28191

Motion components about center of mass of body using flywheel attitude control by small parameter method

13 p2098 A71-28193

Motion equation of electron in cylindrical diode subjected to varied voltages

13 p2036 A71-28372

Weak damping of free gyro motion in static coordinate system under dry friction in gimbal joint, deriving equations of motion by Lagrange method

13 p2069 A71-28932

Variable structure control system synthesis with roots of equation of perturbed motion of characteristic point in dead zone

13 p2096 A71-28934

Equations of motion of infinitesimal particles attracted by Newtonian gravitation of two mutual revolving masses in circular orbits

13 p2101 A71-29114

Weakly rarefied gas flow past bodies of various geometry, deriving equations of motion with approximate macroscopic integrodifferential equations

13 p1991 A71-29148

Shimmying wheel with elastic tire, investigating motion equations for wobble and forces exerted by ground

13 p1997 A71-29230

Soviet book on long range rocket ballistics covering control system, dynamics, firing distance, motion equations, stage separation and nominal trajectories

13 p2146 A71-29438

Differential rotational equations of motion for triaxial rigid body about center of mass under arbitrary torque

14 p2307 A71-29882

Approximate analytical method for nonlinear coupled equations of axisymmetric satellite librations in circular orbit, using constant Hamiltonian

14 p2319 A71-29892

Flight vehicle equations of motion for computer simulation, calculating optimal servosystem parameters and optimal range control by hybrid computer scheme

14 p2319 A71-30001

Nonlinear /mixed/ damping forces on forced vibration system response, developing recursion procedure for equation of motion coefficients

14 p2327 A71-30203

Nonlinear vibrations of clamped and edge supported laminated orthotropic plates, obtaining nonlinear equations of motion solutions by Ritz-Galerkin method

14 p2327 A71-30206

Flowfields calculation in inlet design, using flow variable gradients from equations of motion

14 p2170 A71-30608

Perturbed motion linear equations of body rigidly coupled to thin walled elastic shell partially filled with heavy compressible fluid

14 p2227 A71-30867

Kinematic interpretation of body motion in Hess solution, discussing axoid vector rolling without slip

14 p2275 A71-30881

Rumanian book on distribution theory applications in mechanics covering physical point motions, variable mass, concentrated and distributed loads, elasticity theory equilibrium, motion equations, etc

15 p2501 A71-31147

Gravity stabilized satellite in elliptic orbit, examining rotational motion equations stability

15 p2499 A71-31159

Motion characteristics of elastically supported gyroscope, presenting linearized equation of motion for eight degrees of freedom system

15 p2401 A71-31180

Gravitational potential tensor and equations of motion of relativistic mechanics for isolated system of masses

15 p2481 A71-31187

Free vibrations of beam-like structures, deducing equations of motion

15 p2502 A71-31419

Equation for motion of buoyant free vortices in inviscid fluid subjected to gravity

[AIAA PAPER 71-604]

15 p2388 A71-31543

Hingeless rotor stability characteristics at high advance ratios, examining equations of motion and time variant aerodynamic coefficients

[AIAA PAPER 71-580]

15 p2345 A71-31569

Motion equations for neutral matter in head atmosphere of bright comet with high density spherical source and molecular collisions

15 p2484 A71-31661

Numerical analysis of accretion growing grains segregation in gravitational field with resisting gas, discussing motion equation, evaporation rate and planetary evolution

15 p2489 A71-32397

Orthotropic layered cylindrical shells, deriving equations of motion for rotationally symmetric vibration

15 p2509 A71-32513

Field theoretic approach of Jordan-Brans-Dicke theory within Lorentz invariant gravitation theories framework, solving linear motion equations inconsistency

15 p2451 A71-32646

Structural vibration and dynamic response analysis, applying finite element motion equations

16 p2653 A71-33090

Spinning and point particles motion from Einstein equations based on covariance with general coordinate transformations

16 p2610 A71-33270

Spacecraft banking control during reentry, deriving dynamic equations of angular motion

16 p2646 A71-33655

Velocity and magnetic field equations of electroconductive fluid vortex motion due to annular receptacle insulating walls rotation

16 p2620 A71-34057

Simultaneous solution of Einstein and elementary particle motion equations for space-time curvature within particle resulting from self gravitation

17 p2778 A71-34628

Isotropic compressible homogeneous body with small deformations superposed on finite elastic deformation, deriving equations of motion and boundary conditions

17 p2823 A71-34788

Oscillatory systems motion by nonlinear differential equations with variable coefficients

17 p2781 A71-34924

Equations of motion for free vibrations of three layer plate, considering energy dissipation in soft low modulus of elasticity middle layer

17 p2825 A71-35014

Asymptotic solution to nonlinear motion of heavy gyro in gimbal suspension, noting convergence within finite time interval

17 p2746 A71-35606

Friction forces in complex hydrodynamic systems nonlinear differential motion equations integration

17 p2749 A71-35680

Book on astrodynamics covering n body equations of motion, orbital elements, differential corrections, time of flight, ballistic missiles and interplanetary transport

18 p2963 A71-36248

Generalized vectorial equation of motion for vibrating nonprismatic thin space beams, discussing boundary conditions, rotary inertia and shear deformation [ASME PAPER 71-APM-P]

18 p2978 A71-36259

Free-Lagrange method for two dimensional flow numerical simulation, covering mesh optimization and equations of motion

18 p2905 A71-36304

Equations of motion solution of heavy solid body about stationary point applied to Hess gyroscope

18 p2925 A71-36798

Computerized solutions of gas turbine engines motion equations, considering Euler, fourth order and fifth order Runge-Kutta, Adams, Bashforth and implicit methods

18 p2957 A71-36809

Equations of multiple periodic motions, considering quantification of parameters with Hamilton-Jacobi equation

18 p2948 A71-36947

Inertial effects induced by rotating thin walled shell of finite thickness, considering general relativity equations of motion for test particle

18 p2970 A71-37059

Longitudinal instability of bunch interacting with passive resonator, considering Landau damping influence by linear differential equations of motion solution

19 p3110 A71-37141

On-line radar tracking of six orbital elements of thrust maneuvering spacecraft, obtaining discrete nonlinear measurement and dynamical equations [AIAA PAPER 71-902]

19 p3095 A71-37153

Nonlinear motion of asymmetric rolling reentry vehicle with variable roll rate, dynamic pressure and stability derivatives

19 p3148 A71-37177

Vertical statically unbalanced rotating shaft with two degrees of freedom, investigating internal damping, flexural vibrations and equation of motion

19 p3154 A71-37348

Nonautonomous system equations of motion solution, determining conditions for nonlinearities conversion to linear equations

19 p3037 A71-37349

Natural vibrations of two coaxial rotors with unbalanced disk and different angular velocities, solving equations of motion by energy balance method

19 p3156 A71-37536

Motion stability for critical case of characteristic equation with purely imaginary roots, deriving solution by nonlinear mechanics asymptotic method

19 p3104 A71-38013

Three degree of freedom perturbed two body problem, applying theory of redundant variables to Lagrangian equations of motion

19 p3143 A71-38163

Fully ionized plasma expansion from spherical source into vacuum, deriving equations of motion and collision integrals

19 p3115 A71-38212

Partially ionized plasma expansion from spherical source into vacuum, obtaining equations of motion, collision integrals and recombination rate coefficient

19 p3115 A71-38213

Self adaptive controlled robot velocipedist, discussing speed control and equations of motion

19 p3039 A71-38540

Gas relaxation process equations of motion based on reversibility of time, considering application to particle systems with magnetic field moments

19 p3108 A71-38618

Partially nonlinear theory of anisotropic shells of uniform thickness, obtaining variational integrals of stress equations of motion

20 p3307 A71-38796

Charged particles interaction with geomagnetic field, discussing plasma equations of motion, ionospheric current induction, transition layer and magnetotail rotation

20 p3216 A71-39118

Stellar systems existence with positive total energy, using numerical integration of equations of motion for components of Trapezium in Orion

20 p3290 A71-39300

Mass changes in restricted quasi-circular variable mass three body problem with particle equations of motion having Jacobi integral

20 p3291 A71-39320

Heavy gyroscope motion in gimbal suspension for arbitrary housing gravity center, showing steady solutions with respect to nutation angle

20 p3238 A71-39369

Generalized continuum of interleaved microstructures coupled by forces, investigating equations of motion, tensor indices and asymmetrical effects

20 p3309 A71-39566

Nearby high velocity stars energy and momentum data, determining orbital properties and integrals of motion

21 p3440 A71-40062

Lagrange-Dirichlet and Routh systems stability theorems inversion, proving motion instability in case of potential energy maximum in solutions to differential equations

21 p3414 A71-40092

Vibration isolation system performance under transient conditions, deriving equations of motion with and without inertia torque effect [ASME PAPER 71-VIBR-33]

21 p3458 A71-40287

Perturbation study of subharmonic rotor instability due to elastic symmetry, obtaining equations of motion

21 p3385 A71-40302

Coupled bending-bending vibration of pretwisted tapered cantilever blades, obtaining equations of motion [ASME PAPER 71-VIBR-78]

21 p3460 A71-40315

Relativistic equation derivation for dynamics of point with varying rest mass from Newtonian principle

21 p3415 A71-40659

Book on turbulence covering measurement techniques, equations of motion, Newtonian viscous fluids, Reynolds stresses, flow visualization, random processes, turbulent energy, boundary layers, etc

21 p3371 A71-41248

Relativistic neutralized cylindrical electron beam paraxial motion through uniform longitudinal magnetic field

21 p3426 A71-41289

Generalized tensorial equation of motion for stresses in linear elastodynamics, proving limit existence in Sobolev functional space

22 p3614 A71-41607

Lorentz invariant theory for relativistic gravity testing, deriving conservation laws and parameter constraints from parametrized post-Newtonian equations of motion

22 p3575 A71-41919

Automatic methods for equations of motion solution for artificial satellites orbits

22 p3600 A71-41951

Motion equations derived for slender beam transverse vibrations on continuous viscoelastic foundation, considering nonlinearities from external couplings, longitudinal displacements and curvature

22 p3617 A71-42539

Energy transfer between in-plane and out-of-plane motions in L4 neighborhood for restricted three body problem

[AAS PAPER 71-313]

23 p3725 A71-42989

Grand Tour interplanetary trajectories regularization, removing singularities in equations of motion of space vehicles

[AAS PAPER 71-315]

23 p3725 A71-42990

Equations of motion averaging method, constructing series representation of function [AAS PAPER 71-334]

23 p3727 A71-43007

Out-of-plane motion about libration points within framework of elliptic restricted three body problem, using Mathieu and Hill equation [AAS PAPER 71-336]

23 p3727 A71-43009

Earth rotational and deformational motion equations in extended Kalman-Schmidt filter for geodetic data processing

[AAS PAPER 71-339]

23 p3666 A71-43012

Lagrange equations for variable mass systems with rotational transport and relative motions

23 p3773 A71-43093

Wave equations for motion in stochastic medium, using linear random operator theory

23 p3699 A71-43115

Equations of elastic wave propagation in isotropic materials in presence of static surface stresses and body forces

23 p3775 A71-43205

Elastic and inelastic thin shell nonlinear theory derivation by integrating material continuity equations of motion over shell thickness

23 p3775 A71-43318

Approximate motion equations of gas flow behind detonation front in flat explosive plate covered by inert coating

23 p3781 A71-43358

Objects motion analysis by dynamical photogrammetric methods, integrating optical image points differential motion for trajectory equations

23 p3678 A71-43589

Ideal gas and liquid droplets two phase flow continuity and motion one dimensional equations, describing relations between velocity, density, pressure and bulk component concentrations

24 p3818 A71-44709

Motion equations numerical integration step as function of celestial object location and velocity in interplanetary probe orbit computation

24 p3869 A71-44799

Cavity cross sections perturbed motion equations

24 p3819 A71-44840

Geckeler-Anschutz gyrohorizon compass element motion with uncoupled gyrocompasses, obtaining equations of motion with quadratures solution

24 p3827 A71-45049

Motion equations of statically unbalanced two degree of freedom gyroscope excited by base linear vibrations, determining instrument errors as function of casing/body coupling

24 p3828 A71-45159

Motion integrals conservation under Hamiltonian function variations, examining gyroscope equations of motion with parameter disturbances

24 p3849 A71-45343

Nonlinear equations of compressible medium motion near point of contact between shock and diffraction waves

24 p3821 A71-45365

EQUATIONS OF STATE

NT HUGONOT EQUATION OF STATE

Equations of state for materials with memory, discussing derivation methods based on nonlinear functional analysis and applications

01 p0175 A71-11037

Thermodynamic equations of state for dissociating and ionizing high temperature air applied to vertical and oblique compression shocks

02 p0331 A71-12067

Simple gases and liquids thermodynamic properties, calculating isotopic effects by corresponding states law with quantum corrections

02 p0331 A71-12187

Jupiter model construction from improved state equation, considering chemical composition, contraction and rotation

02 p0314 A71-12589

Linear feedback function for r-stage feedback shift register resulting in equal length branchless cycles [JPL-TR-32-1511]

03 p0388 A71-13282

Computer algorithm for state variables equations used in linear and nonlinear, active and passive electronic circuits analysis

03 p0389 A71-13807

Approximate optimal control law formulation by harmonic linearization for nonlinear time invariant state regulator problem with high performance index

03 p0390 A71-14299

Molecular gas vibrational and rotational state equations, discussing relaxation times, sound propagation and transport processes

03 p0462 A71-14557

Stellar structure theory, examining particle aggregates gravitational and pressure forces, energy flow, generation and opacity and equations of state

04 p0648 A71-15246

Combined continuity and force equations for sound attenuation as function of thermal and viscous losses in liquid gases, taking into account fcc and bcc packing

06 p0927 A71-17569

Optimal control sufficient conditions with state and control constraints

07 p1082 A71-19771

Elastic solids fourth order anharmonic equation of state from finite strain theory, resolving ambiguities by Mie-Grüneisen equation

07 p1178 A71-19800

Nonideal plasma thermodynamically complete equation of state based on shock wave experiments

07 p1173 A71-20533

Ionizing plasmas partition functions, determining opacities and equations of state

08 p1359 A71-20943

Compressed nitrogen thermodynamic calculations, determining virial equation of state applicability 08 p1376 A71-21905

Dynamic systems current state estimate, using Kalman filter with exponential aging 09 p1421 A71-22110

Phase transitions possibility in nonideal multiply ionized plasma, analyzing equation of state and ionization equilibrium equation for various ionization multiplicities 09 p1500 A71-22244

Rotating self gravitating axisymmetric fluid mass structure steady state equations, examining Clairaut theory asymptotic nature 09 p1527 A71-23532

Neutron star matter equations of state involving hyperon formation effects for maximal stable mass models, tabulating moments of inertia 10 p1671 A71-24302

Penalty method and decomposition of state equations applied to nonlinear systems 10 p1637 A71-24840

Atomic scale elastic structure equations of state for Thomas-Fermi model extension to high pressures, considering earth core iron-silicates composition 11 p1802 A71-25572

Hyperon stars thermodynamics, deriving hot neutron stars equation of state with particular reference to center singularities 11 p1828 A71-25737

Theoretical equations of state in geophysics, considering systematics approach to laboratory data, seismic velocity profiles, finite strain and atomistic approach 12 p1931 A71-27415

Dense liquid thermodynamic model, using approximate equation of state 13 p2160 A71-28571

Optimization of nonclassical equations of state systems, considering concepts of adjoint and Hamiltonian states 13 p2043 A71-28830

Solidification pressure of nuclear and neutron star matter, suggesting modifications to equation of state 15 p2452 A71-32548

High pressure pneumatic lines dynamics, considering equation of state for real gas with given compressibility function 16 p2527 A71-33618

Two level Kalman filter for high order interconnected systems states estimation, deriving coordination algorithm with one step convergence by multilevel systems theory 17 p2718 A71-34735

Computer program formulation of equations of state of electronic circuits, using state variable method with mixed coordinate basis 18 p2896 A71-35937

Relativistic and/or degenerate electron gas equation of state formulae for density, temperature, entropy and internal energy 18 p2960 A71-35937

Normal and oblique shock thermodynamic equilibrium state variables calculation, taking into account air dissociation and ionization 18 p2970 A71-37047

Light elements thermodynamic state variables at high pressure, calculating electron density distribution as function of ion configuration with linear response theory 18 p2970 A71-37047

Neutron star models based on Nemeth-Sprung equation of state, discussing dynamic stability and Crab pulsar central density 19 p3143 A71-38161

Optimal control with minimax cost for systems of n first-order state equations with performance measured by Chebyshev type functional over state trajectory 19 p3039 A71-38716

Relativistic and Newtonian neutron star models with nuclear forces in equation of state, using unitary transformations for hard core and soft core potential 21 p3442 A71-40143

Computationally convenient equation of state describing porous materials shock response 21 p3466 A71-40795

Neutron star matter equation of state and models from energy computations, discussing maximum stable mass 21 p3452 A71-41034

Phase transitions possibility in nonideal multiply ionized plasma, analyzing equations of state and ionization equilibrium equation for various ionization multiplicities 21 p3424 A71-41133

Superconductors intermediate state interrelated electrodynamic and thermal effects, calculating resistivity, heat conduction and thermoelectricity tensors 21 p3432 A71-41267

German monograph on thermal equation of state for nitrogen vapor-liquid phase equilibrium covering vapor pressure and density, phase diagrams, critical temperature, etc 22 p3574 A71-41716

Linear time-varying system state space representation determination based on scalar differential equation, considering advantages 22 p3566 A71-41853

Plane steady rotational flow of inviscid gas with arbitrary state equation for straight or circular streamlines 23 p3662 A71-43236

Unknown parameter identification in nonlinear dynamic systems from state variable time history measurement 23 p3660 A71-44114

EQUATORIAL ELECTROJET

Ionospheric vertical wind role in anomaly of quiet sun diurnal geomagnetic variation at magnetic equator 02 p0243 A71-11764

F 2 layer anomalies association with equatorial electrojet from F 2 and sporadic E critical frequencies analysis 02 p0245 A71-11963

HF Hall current instability, discussing short wavelength backscatter for equatorial and auroral electrojets in disturbed ionosphere 08 p1279 A71-21205

Quasi-linear theory of inhomogeneities generation in equatorial jet, considering space charge waves excitation by electric current perpendicular to geomagnetic field 11 p1757 A71-25772

Equatorial electrojet model instability to gradient instability and electron density irregularities 13 p2055 A71-27922

Quasi-biennial oscillation in low latitude geomagnetic Sq field, showing larger amplitude under equatorial electrojet by harmonic analysis 14 p2231 A71-29719

Electron density irregularities and frequency deviation patterns role in equatorial electrojet 14 p2235 A71-30352

Equatorial electrojet as supplementary heat source for tropical region upper atmosphere based on thermal energy release calculation 15 p2399 A71-31964

Geomagnetic field daily variation amplitude increase under equatorial electrojet during 7 July 1966 solar proton flare 16 p2567 A71-33768

Longitudinal wave interaction and excitation by current instability in equatorial jet, considering energy transfer mechanism 19 p3057 A71-38363

Geomagnetic activity daily variability index statistical dependence on geomagnetic latitude, noting maximum below equatorial electrojet 20 p3217 A71-39513

Equatorial electrojet region ionospheric currents during magnetically quiet day and nighttime from rocket measurements 20 p3218 A71-39524

Quasi-linear theory of inhomogeneities generation in equatorial jet, considering space charge waves excitation by electric current perpendicular to geomagnetic field 22 p3532 A71-41540

EQUATORIAL ORBITS

NT STATIONARY ORBITS

C, N and O nuclei abundances in radiation belt near geometric equator, using data obtained byOGO-5 satellite in 1968 03 p0473 A71-13475

Diurnal minimum and geomagnetic storms effect on equatorial air density from San Marco 2 satellite drag experiment 03 p0415 A71-14024

Intermediate elliptical orbits for planetary satellites with small inclination to equatorial plane 09 p1520 A71-22671

Dynamic derivation of surface layer representation of lunar gravitational field from Doppler observations on polar and equatorial lunar orbiters 21 p3449 A71-40643

EQUATORS

NT MAGNETIC EQUATOR

Far UV equatorial airglow and aurora intensities and occurrence frequencies from satellite observation 01 p0076 A71-11504

Planet Mars polar and equatorial radii optical measurements comparison with radar and Mariner probes occultations results, determining optical ellipticity 03 p0493 A71-14200

Atmospheric excess radiation flux azimuthal asymmetry in equatorial region, discussing angular intensity distribution data from Proton 2 Cerenkov counter 08 p1354 A71-21011

Ionization crests of equatorial anomaly at magnetic L values from Ariel 2 satellite electron probe measurements 11 p1754 A71-25603

Jupiter equatorial belt effective temperature during 1965 apparition from limb darkening profile observation 11 p1827 A71-25726

PERLO program for analysis of satellite orbital period changes to determine celestial equator crossings from sequence of positions 11 p1829 A71-25825

Equatorial airglow enhancement data, observing 6300 and 5577 Å intensity variations 16 p2562 A71-32809

Atmospheric excess radiation flux azimuthal asymmetry in equatorial region, discussing angular intensity distribution data from Proton 2 Cerenkov counter 20 p3279 A71-39591

Nighttime equatorial E region ionization and electron density gradient irregularities, noting cross field instability with rocket-borne Langmuir probes 20 p3225 A71-39727

Equatorial proton and electron pitch angle distributions in loss cone and at large angles from geostationary ATS 5 satellite observation 23 p3720 A71-43165

Longitudinal dependence of solar quiet geomagnetic field horizontal component at equator, discussing discrepancy between theory and observation 23 p3673 A71-43986

Vertical equatorial ozone distribution, incorporating oxygen hydrogen reactions and diffuse and advective transport in time dependent meridional model 23 p3673 A71-43987

EQUILIBRIUM

Human equilibrium maintenance system analogy to multiinput/multioutput controller, considering motion of projection of center of gravity onto horizontal plane 03 p0356 A71-12981

Heavy liquid shells of revolution, determining equilibrium form in gravitational and surface tension forces from condition of minimal functional of total free energy 06 p0994 A71-17827

Bifurcation of equilibrium of three dimensional elastic isotropic body with arbitrary elastic potential under large subcritical strains 08 p1373 A71-21866

Sudden step changes in parameters of nonlinear resonance systems having several stable steady state solutions 09 p1543 A71-23612

Equilibrium energy distribution in system of nonlinearly coupled oscillators 12 p1930 A71-27168

Equilibrium of elastic body weakened by system of circular planform cracks in single plane 13 p2148 A71-27807

Stability of trapped particle equilibrium, considering contribution to plasma wave dispersion 13 p2104 A71-27847

Steady state and transient performance of Brayton cycle alternator and electronic controls for space power 15 p2355 A71-32215

Bifurcation of equilibrium of three dimensional elastic isotropic body with arbitrary elastic potential under large subcritical strains 20 p3308 A71-39365

Gravitational and other forces involved in equilibrium of growing plants, showing gravity sensing ability lower limit existence 21 p3339 A71-39971

Integrative action of central nervous system in converting gravity sensation into crustacean equilibrium reactions 21 p3327 A71-39993

Solutions near equilibrium point of finitely retarded autonomous functional differential equation, noting bifurcation 21 p3407 A71-40208

EQUILIBRIUM DIAGRAMS

U PHASE DIAGRAMS

EQUILIBRIUM EQUATIONS

Rib reinforced shells linear theory, deriving equilibrium equations with allowance for temperature terms 01 p0170 A71-10644

Nonlinearly elastic rings and arches under hydrostatic pressure, examining equilibrium with sixth order differential equations 02 p0325 A71-12125

Planetary boundary layer flow three dimensional steady state equations applied to air motions over horizontally varying surface roughness, temperature and moisture 03 p0453 A71-13230

Displacement type equilibrium equations for small deformation imposed on initial finite deformation, estimating elastic energy function based on strong ellipticity condition 03 p0510 A71-13945

Three dimensional mixed boundary value problems, obtaining solutions for elastic body differential equilibrium equations 03 p0513 A71-14235

Consistent finite element model for two dimensional continuum problems on basis of virtual work principle 04 p0672 A71-15770

Homogeneous integral equations of asymmetrical elasticity in steady state, using compound layer volume potentials 04 p0620 A71-15887

Doubly symmetric oval ring under lateral load, investigating creep behavior from equilibrium equations 05 p0820 A71-15984

Hunt process equilibrium potentials /special supermartingales processes/, obtaining additive functionals
05 p0773 A71-16158

Restricted three body problem, discussing secular variations equilibrium solutions stability
05 p0814 A71-17093

Equilibrium equations for flexible plates and shells with nonlinear terms in one dimensional case
06 p0989 A71-17782

Axisymmetric deformed state of three layer circular conical shell with rigidly clamped edges, obtaining equilibrium equations by Bubnov-Galerkin method
06 p0997 A71-17851

Statistical equilibrium equations solved for atom/ion with complex energy level structure and weak spectral lines, discussing deviations from LTE
06 p0969 A71-17969

Boundary problem for displacement equilibrium equations of elastic body using iterative methods, demonstrating convergence of difference equation solution
08 p1372 A71-21706

Planet density distributions, deriving successive approximations for equilibrium figure equations
08 p1365 A71-21775

Phase transitions possibility in nonideal multiply ionized plasma, analyzing equation of state and ionization equilibrium equation for various ionization multiplicities
09 p1500 A71-22244

Sulfide formation process from solar composition cooling gas, examining constrained equilibrium theory
10 p1676 A71-24505

Boundary value problem concerning stability and oscillations of shells of revolution through reduction to Cauchy problem based on direct integration of equilibrium equations
10 p1690 A71-24569

Transversally isotropic spherical shell with constant thickness, calculating equation system for equilibrium
12 p1975 A71-27105

Elastic body displacement equilibrium equations, using variable direction iteration methods for boundary value problems
12 p1978 A71-27329

Low pressure paramagnetic regime axially symmetric hydromagnetic equilibria with spherical plasma-vacuum interfaces, extending solution to high pressure diamagnetic regime
13 p2104 A71-27843

Structural properties of equilibrium solutions of quadratic matrix equation, using variational interpretation of associated Riccati equation, transform techniques and Parseval formula
13 p2095 A71-28815

Incompressible plastic shells behavior, discussing deformation, energy dissipation rate, equilibrium equations and boundary conditions
14 p2328 A71-30380

Planet density distribution, deriving successive approximations for equilibrium figure equations for gravitational potential and level surfaces
15 p2495 A71-32680

Mathematical techniques of equilibrium states and periodic vibrations in nonlinear elastic systems illustrated by thin plate and shallow cap buckling under uniform pressure
16 p2649 A71-32998

Magnetic properties of contained plasma, discussing equilibrium equations and pressure profiles
17 p2788 A71-35025

Small strain theory of shells derived from three dimensional equations of equilibrium and compatibility by asymptotic approach
18 p2982 A71-36840

Vibration characteristics of cantilever beam about nonlinear equilibrium state, showing flexibility and prestressed state effect
21 p3468 A71-40968

Phase transitions possibility in nonideal multiply ionized plasma, analyzing equations of state and ionization equilibrium equation for various ionization multiplicities
21 p3424 A71-41133

Equilibrium equations of elastic plates, reducing to Cauchy problem by use of invariant imbedding
22 p3618 A71-42584

Linear elastic structures analysis by quadratic programming, considering equilibrium equations for forces at joints
22 p3618 A71-42589

Low thrust interplanetary spacecraft tracking, using spectral factorization for Kalman filtering equations steady state solution
23 p3732 A71-43063

Micropolar elasticity plane problems equilibrium equations system solution, considering elastic half space deformation and steady thermoelasticity
23 p3775 A71-43316

Axisymmetrical elastic deformation of thin helicoidal shell with rectilinear profile, deriving equilibrium equations and stress-strain relationships
23 p3778 A71-44038

Equilibrium equations solutions for ideal gas composition, pressure, volume and temperature based on Newton-Raphson method, outlining programming method
24 p3887 A71-44635

Approximate periodic Green matrix solution to equilibrium equations in displacements for shell of revolution under linear loads
24 p3881 A71-44826

Geometrically nonlinear integral solutions to equilibrium equations of curvilinear beam under uniform pressure, using Weierstrass functions
24 p3883 A71-44850

EQUILIBRIUM FLOW

Steady state supersonic flow of combustible gas mixture around solid blunt bodies
05 p0836 A71-16530

Near equilibrium shock layers nonequilibrium radiant emission calculation, noting application to Mars entry conditions
07 p1091 A71-19914

Reactive equilibrium hypersonic gas flow over slender pointed body, neglecting rate chemistry
09 p1383 A71-23054

MHD oscillations of homogeneous compressible self gravitating fluid spheroid in static equilibrium with poloidal magnetic field inside and dipole field outside
11 p1831 A71-26167

Equilibrium air boundary layer flows at three dimensional stagnation points, discussing flow characteristics and real gas heat transfer parameters
12 p1866 A71-27582

Multicomponent ionized gas mixtures chemically equilibrated flows over nonporous and ablating surfaces, using Navier-Stokes and Prandtl equations for asymptotically thin boundary layer
13 p2048 A71-28570

Incompressible equilibrium plasma ellipsoid stability in electromagnetic traveling wave field
16 p2618 A71-33048

Ideally conducting magnetostatic equilibria and associated time dependent resistive flows from two dimensional solution for MHD equations
19 p3115 A71-38211

Plane equilibrium turbulent boundary layer with longitudinal pressure gradient
20 p3214 A71-39791

Trailing vortex pair behind aircraft, presenting equilibrium characteristics and effects on safety
21 p3321 A71-40504

Molecular beam extraction from equilibrium gas flows, describing shock beam formation model with associated escape probability
21 p3419 A71-40956

EQUILIBRIUM METHODS

Complex shells strength analysis using limiting equilibrium theory and mathematical programming
06 p0998 A71-17859

General nonlinear elasticity theory including applications, deformation laws, complex nonlinear equations solutions, equilibrium and stability problems, experimental methods and mathematical models
09 p1536 A71-22512

Coaxial shells of revolution connected by meridional ribs, deriving elastic equilibrium conditions, stress-strain components and contact forces under thermal and mechanical loads
10 p1688 A71-24358

Infinitely slender cylinder elastic equilibrium, deriving Saint Venant problem solution in power series form
10 p1692 A71-25022

Stress-strain state of closed circular cylindrical shells stiffened by longitudinal ribs, analyzing general solution of homogeneous equilibrium equations system
13 p2150 A71-28133

Equilibrium temperatures, pressures and oxygen fugacities of equilibrated chondrites in meteorites
13 p2141 A71-29098

Equilibrium strategies for linear games with quadratic costs in Hilbert space, deriving nonlinear equation in allowed operator feedback spaces
17 p2723 A71-35297

Finite radius rotating cylinder stability analysis, using equilibrium functions of distribution with trajectory integration method
19 p3134 A71-37512

Cylindrical shell weakened with large circular hole, deriving nonlinear equilibrium equations in semigeodesic polar coordinates
24 p3877 A71-44479

EQUINOXES

Ionospheric electron mean content 1964-1969 from density, ionization, slab thickness and solar flux diurnal and equinoctial peaks
07 p1097 A71-19025

Cosmic ray sidereal time period, using neutron monitors, meson telescope and various ion chambers
23 p3719 A71-43126

EQUIPMENT SPECIFICATIONS

Flight simulators procurement and commissioning, discussing difficulties due to different aircraft configura-

tions, advantages of equipment and procedures standardization, etc
01 p0066 A71-10015

Aerospace engine starting systems military and industry specifications and standards, considering cartridge pneumatic, electric, gas turbine, hydraulic and mechanical types
01 p0067 A71-10103

Electrocardiograph recording fidelity relative to specification recommendations
01 p0026 A71-1298

Laser data on coherence and radiance, deriving from manufacturer specifications for application selection
02 p0261 A71-12325

Skyнет system shipborne earth station design and specifications, discussing size and weight restrictions, radar proximity, gun shocks, antenna stabilization and power budgets
02 p0217 A71-12435

Collision avoidance system flight test and evaluation program for airline industry CAS specification
02 p0280 A71-12896

IFR design requirements for STOL navigation equipment from flight tests
04 p0623 A71-15424

Europa 1 multistage booster rocket interstage electric circuit connection, discussing specifications and compatibility tests
05 p0697 A71-15955

Indonesian Intelsat 3 earth station equipment, operation and performance
06 p0880 A71-18397

Continuous flow oxygen regulators construction, performance and testing SAE standard, covering automatic, adjustable and preset types
07 p1049 A71-19648

Multicomponent microwave equipment, discussing design automation by matrix notation with computer calculations
09 p1416 A71-22468

Traveling wave antenna arrays of mismatched elements, calculating element resistances and spacings
09 p1408 A71-23488

Realizable method of pattern synthesis for broadside array antenna giving arbitrary current distribution
09 p1418 A71-23489

Geometry optimization of error-free distributed nondirectional aperture array receivers, using signal detectability technique
09 p1408 A71-23491

Synthesis of primary electromagnetic fields of transmitting feed antenna for two dimensional circular cylindrical reflector
09 p1418 A71-23492

Efficiency evaluation of large parabolic antenna reflector by frequency scaling
09 p1409 A71-23496

Linear antenna arrays synthesis with Z transforms permitting sidelobe reduction and nulls in antenna radiation patterns
09 p1419 A71-23498

Waves arrival directional fluctuations effect on power gain of horizontal rhombic antennas for high frequencies and various antenna and wave parameters
09 p1420 A71-23676

Main mirror shape in three mirror telescopes permitting spherical aberration suppression
10 p1608 A71-23820

Electronic imaging devices specifications, emphasizing real time reconnaissance systems performance requirements
10 p1609 A71-24059

Light aircraft engine lubricating oil filter types and model specification, noting dirt holding ratings
10 p1617 A71-24248

Expandable structures for midair pilot rescue device with hot air filled BALLUTE, discussing BALLUTE material development
11 p1707 A71-25278

Aircraft industry materials development, discussing innovations in governmental programs management, procurement specifications and Department of Defense contracting procedures
12 p1918 A71-27677

Destructive and nondestructive material testing techniques, discussing equipment design and procedures standardization
13 p2074 A71-28493

Vertical intensity of cosmic ray muons in Mont Blanc tunnel, describing apparatus and experimental site
15 p2477 A71-31795

Second Pleumeur-Bodou /France/ ground station for Telstar satellite communication, discussing equipment specifications, Cassegrain antenna and parabolic reflector
17 p2708 A71-35509

Pleumeur-Bodou /France/ ground station steerable parabolic reflector Cassegrain antenna for communication satellites, discussing specifications and radioelectric and mechanical characteristics
17 p2717 A71-35510

Hydraulic equipment fluid contamination control, discussing sample bottle cleaning, fluid sampling, component tolerance profiles and filtration performance specifications
19 p2999 A71-38322

Electrohydraulic stand for vibration strength testing, discussing system design, specifications, frequency-amplitude characteristics and applications
23 p3662 A71-44235

EQUIVALENCE

Equivalence theory applications in three dimensional elasticity, plane deformation and stresses
02 p0328 A71-12534

First order nonlinear nonautonomous systems equivalence to second order linear autonomous systems through governing differential equations variables integral transformation
03 p0390 A71-14076

Hori and Deprit perturbation theories comparison based on Poisson brackets, giving computer program determining functions through sixth order for equivalence proof
04 p0660 A71-15889

Lenslike media with parabolic index profiles, deriving equivalent transformation theorem for distributed optical systems design
12 p1928 A71-26810

Higher order linear and nonlinear systems equivalence from partial/ordinary differential equations
15 p2443 A71-32521

Nonlinear optimal closed loop system control problems equivalence relations as one-to-one correspondences between Hamilton-Jacobi equations solutions
17 p2719 A71-34743

Necessary and sufficient conditions for optimal control problems equivalence, considering time functions for disturbing influence of external forces
23 p3656 A71-43861

EQUIVALENT CIRCUITS

Planar diffused transistor characterization by equivalent circuit model using input impedance and amplification measurements
01 p0051 A71-10310

Switching bipolar transistor dynamic model equivalent circuit diagram characterization by parameters
02 p0228 A71-11655

Thevenin and Norton equivalent circuits determination using sequential method of network analysis
02 p0236 A71-12041

Permanent magnet system as nonlinear computer problem, using Newton method and equivalent circuits with lumped parameters
05 p0705 A71-17174

Dipole conversion to equivalent quadrupoles and multipoles, replacing resistances by corresponding h matrices
06 p0872 A71-17373

Modified Ebers-Moll equivalent circuit model for saturation characteristics of high voltage transistors
07 p1174 A71-19058

Gunn diodes impedance measurement at bias voltage above threshold, using broadband equivalent circuit model for mount and package
07 p1072 A71-19103

Parasitic reactances in Gunn effect device packages from microwave equivalent circuit parameters
07 p1072 A71-19104

Postcoupled waveguide cavity Gunn effect microwave oscillator equivalent circuit analysis, using lumped constant elements
07 p1072 A71-19106

Large signal microwave equivalent circuits analysis of IMPATT diodes, allowing carrier multiplication by impact ionization at every point in diode
07 p1072 A71-19108

Avalanche transistor emitter current voltage characteristics, using Kirchhoff equations for equivalent circuit
07 p1077 A71-19798

Internally ported vortex amplifier, presenting dynamic equivalent circuit with transfer functions
07 p1025 A71-20555

Integrated circuit components equivalent circuits, considering transistor logic circuits and admissible noise
09 p1416 A71-22491

Equivalent electrical circuits of interdigital transducers for piezoelectric generation and detection of ultrasonic Rayleigh waves
09 p1420 A71-23680

Equivalent circuit concepts in diagnostic metrology as converging logical-physical process, stressing electronic failure analysis
12 p1890 A71-26666

Passive two-terminal networks in rod antenna for bandwidth increase, investigating equivalent circuit on digital computer
12 p1886 A71-26987

Equivalent circuit for interdigital piezoelectric Rayleigh wave transducer
13 p2037 A71-28472

Piezoelectric substrate dependent differences between in-line and crossed field three port circuit models for interdigital surface wave transducers
13 p2038 A71-28612

Two transistor emitter follower DC amplifier, using simplified equivalent circuit
13 p1999 A71-28628

Analog computer power relay analysis simulating flux, coil current, moving mass motion and magnetic and spring forces as function of time
13 p2001 A71-28839

Microwave meander line/coupled parallel commensurate conductors array/network analysis and synthesis, using equivalent circuit transformation for computerized design
14 p2219 A71-29565

Equivalent circuit parameters of microwave planar power transistors at high injection levels, indicating parameters frequency dependence determination
14 p2213 A71-30627

FLE-251 fluidic NOR gate impact modulator developing equivalent circuit model for pressure gain recovery and cut-off, output capacitance and step response
15 p2351 A71-31684

DC equivalent circuit, describing pressure and flow distribution at input ports of fluidic line branchings
15 p2352 A71-32067

Book on fluidic systems design covering analog and digital control, application to aircraft, spacecraft, computers, tracking devices and equivalent circuits
16 p2526 A71-33475

French monograph on DC/DC transformers with controllable output voltage covering ion beam electrostatic deviation during attitude control, equivalent transformer circuits, etc
17 p2677 A71-35234

TE modes propagation in rectangular guide partially filled with dielectric slab, considering two waveguides junction equivalent circuit
17 p2708 A71-35481

Ultrasonic surface wave generation by infinite interdigital electrode array on piezoelectric material, predicting behavior from equivalent circuit by variational principle
17 p2717 A71-35491

X-band Gunn oscillator equivalent circuit parameters determination for baseband and RF noise contribution to AM and FM noise
18 p2888 A71-36270

Waveguide mounted X band CW Gunn effect oscillators load impedance characteristics, proposing lumped equivalent circuit
18 p2894 A71-36830

Tunnel diode oscillator equivalent circuits with frequency variance by changing load susceptibility
19 p3026 A71-37145

Equivalent circuit parameters determination for baseband and microwave noise from Gunn oscillator, using AM-FM correlation coefficient
19 p3028 A71-37699

Book on active and nonlinear wave propagation in electronics covering transmission lines, wave systems stability, quasi-harmonic active propagation, equivalent circuits, etc
19 p3029 A71-38018

Baluns as electromagnetic compatibility control devices for signal and common mode currents, providing basic parameters and equivalent circuits
19 p3030 A71-38433

Equivalent circuits for planar devices behavior under ionizing radiation, considering bipolar and MOS transistors
19 p3034 A71-38521

Transistorized microwave amplifiers with dissipative equalizing networks, describing transistor equivalent circuit
20 p3205 A71-39810

Four electrodes Hall effect isolator equivalent circuit, describing impedance matrix elements frequency dependence
22 p3520 A71-41715

Design parameters optimization for flat spiral coils printed on dielectric substrates based on equivalent circuit analysis, emphasizing coil shape effects on Q and inductance
22 p3520 A71-41715

Dummy S4 diode packages mounted in coaxial line, deriving mount-independent equivalent circuit parameters from broadband admittance measurements
22 p3521 A71-42206

Pneumatic passive lead networks for fluidic systems, presenting transfer functions, equivalent circuits and design information
23 p3631 A71-44096

ERBIUM

Er laser efficiency dependence on dopants in Li-Ca-silicate glass host, determining energy transfer rates for optimum concentration
01 p0092 A71-10010

Erbium ions stimulated emission, spectroscopic properties, pulsed laser action and absorption spectra in yttrium orthoaluminate
07 p1126 A71-20165

Cavity loss dependent erbium glass laser line oscillations in lower threshold region under Q switch and long pulse conditions
15 p2424 A71-32612

ERECTION

U CONSTRUCTION

ERGODIC PROCESS

Quasi-stationary spherical various mass star system, applying ergodic theory in stellar dynamics
01 p0150 A71-10058

Shear-invariant mean value of positive-definite operator on bicomplex group in form function of integral sequence, considering ergodic theorem
01 p0110 A71-10097

Random ergodic process extremal behavior, determining mean time to reach original maximum or minimum
14 p2194 A71-30087

Ergodic boundary in time evolution of two dimensional incompressible Navier-Stokes equations solution at large Reynolds numbers
19 p3045 A71-37841

ERGOMETERS

Metabolic rate and ergometric data recording by analog and digital systems
01 p0026 A71-11409

Electronic ergometer calibration equipment and errors at high work loads
09 p1401 A71-23373

ERGONOMICS

U HUMAN FACTORS ENGINEERING

EROS PROJECT

U EXPERIMENTAL REFLECTOR ORBITAL SHOT PROJ

EROSION

NT WATER EROSION

Liquid droplet diameter effect on solid surface erosive wear
01 p0072 A71-11242

Erosion resistance characterization and determination - ASTM Conference, Atlantic City, June 1969
03 p0443 A71-14284

Cavitation and jet impingement erosion, discussing materials response and exposure time effects
03 p0404 A71-14285

Dielectrics erosion under pulsed electric discharge in conical plasma accelerator, varying capacitance and inductance for evaporated mass relation to current strength
04 p0631 A71-14597

Inlet particle separators for engine erosion prevention, discussing tests of various models for separation efficiency, clogging resistance, pressure loss and flow distortion
04 p0639 A71-15435

Sand and dust erosion on small VTOL gas turbine engines, discussing effects on inlets, compressor housing and blades
04 p0639 A71-15436

Refractory metals and carbides and borides, investigating laws governing electrodes erosion during electric spark breakdown
07 p1139 A71-20205

Electroerosion and electrochemical combined effects on machining surface removal, discussing optimal anodic removal rates and electrolyte concentrations
08 p1296 A71-20852

Conical metal core electrode erosion rates in pulsed plasma accelerators with refractory dielectric chamber
08 p1340 A71-21484

Energy spectrum of iron group solar cosmic ray particles determined from glass removed from Surveyor 3 spacecraft, considering lunar erosion implications
09 p1515 A71-23656

Lunar soil particle production, noting radiation erosion effects
10 p1673 A71-24414

Plasma accelerator central electrode erosion and heat flux, describing measurement techniques and results
14 p2280 A71-30266

Conical metal core electrode erosion rates in pulsed plasma accelerators with refractory dielectric chamber
14 p2282 A71-30671

Porous refractory materials for thermochemical protection against high temperature plasma flow, discussing effectiveness in erosive wear reduction
15 p2432 A71-32164

Three stage potassium vapor turbine for space systems electric power generation, discussing erosion and endurance tests
15 p2415 A71-32214

Solid metal plates erosion mechanism at high temperatures under supersonic plasma jet action, noting dependence on specific heat and latent heat of fusion
16 p2591 A71-33030

Spores released from solids interiors by aeolian erosion on planetary surface, noting application to microbes in planetary quarantine
16 p2537 A71-33796

Lunar, meteoroid and asteroid surface erosion, investigating hypervelocity impact, solar wind flux and ion sputtering effect
16 p2642 A71-33818

Lunar surface and soil mechanical properties statistical analysis covering Alphonsus event, cratering and erosion

17 p2805 A71-35179

Vibration and corrosion-erosion damage effects on material behavior during short term creep in high speed air flows

17 p2760 A71-35659

Cavitation erosion of aluminum at high hydrostatic pressure, using chamber focusing acoustic system

18 p2910 A71-36932

Laser optical system for hyperballistic range hypervelocity models surface erosion measurement, describing instrumentation of front-lighted, silhouette and stereo stations

23 p3677 A71-43513

Alkali metals vaporization from heated lunar samples, suggesting lunar rock erosion by localized heating due to volcanism or meteorite impact

23 p3741 A71-43636

Lunar surface erosion and mixing from cosmogenic and primordial radionuclide measurement in Apollo 12 lunar rock and soil samples

23 p3755 A71-43731

Nuclear track densities in lunar core and fine samples, relating erosion history, solar activity and surface stirring

23 p3764 A71-43799

ERROR ANALYSIS

Pt electrode oxygen diffusion and consumption systematic errors effect on oxygen partial pressure measurement in perfused tissues

01 p0021 A71-10073

Error bounds for inverted nonsingular matrices using interval arithmetic in ALGOL-60

01 p0049 A71-10325

Computer program for orbital elements of spectroscopic binaries and probable error computation

01 p0152 A71-10352

Spacecraft navigation, guidance and control for manual rendezvous with orbiting target, examining error sources perturbing effects

01 p0022 A71-10513

Themis project automatic navigation program, examining optimum stochastic feedback error analysis and sensitivity algorithms

01 p0125 A71-10525

Probability method for gyroscope instrumental errors associated with inaccurate fabrication and components assembly, classifying external moments

01 p0080 A71-10534

Drift causes in floated-rotor integrating gyros used as accelerometers, discussing gyromotor magnetic field effects

01 p0080 A71-10535

Dynamic errors estimation for nearly invariant automatic control systems, discussing parameter-change sensitivity

01 p0061 A71-10715

Automatic control systems without disturbance feedback, examining invariance under positive-zero-negative error transition

01 p0062 A71-10720

Automatic feedback control systems steady dynamic error reduction by introducing control action forward loop, determining transfer function

01 p0062 A71-10721

PCM telemetry data transmission bit error probability confidence intervals upper bounds based on Markov chain model analysis

01 p0032 A71-10877

Bits round-off and approximate division error effects in data compressor design, suggesting best maximum error criteria

01 p0050 A71-10878

PCM telemetry signal encoding, investigating aliasing and pulse width errors dependence on frequency band occupied by bandpass signal

01 p0032 A71-10881

Error model and digital computer simulation programs for technical management of missile development and testing

01 p0068 A71-10883

PCM telemetry bit synchronizer/signal conditioner, discussing bit acquisition, error and slippage rates

01 p0053 A71-10907

Eigenvalue errors in applying method of weighted residuals to linear nonself adjoint problems of structural analysis

01 p0174 A71-10944

Lunar surface thermal characteristics revised from analysis of error sources in daytime lunar surface temperatures derived from Surveyor 5 compartment data [ALAA PAPER 69-594]

01 p0163 A71-11582

Radio signal reception error in cadence synchronization of binary data transmission systems with indeterminate signal arrival time

02 p0212 A71-11834

Signal sources output impedance matching effect on phase difference measurement accuracy

02 p0212 A71-11842

Straight line approximation of random two dimensional discrete set containing large measurement errors, comparing to least squares results

02 p0304 A71-11902

Earth radiation latitude nonuniformity effect on error in onboard satellite local vertical determinations, using Cosmos satellite data

02 p0304 A71-11915

Free space optical channel analog and digital communication theory, considering SNR, M-ary signaling, error probabilities and information rates, etc

02 p0213 A71-12018

Time division multiplexing methods for optical communications systems, considering error performance of digital formats used with mode-locked laser sources

02 p0214 A71-12021

Short pulse optical tracking systems ranging error, analyzing effects of tracker, target and propagating medium characteristics

02 p0214 A71-12029

Skyнет and SCAT ground stations system noise temperature, considering receiver, antenna and sky sources, measurement techniques and error analysis

02 p0217 A71-12434

Gyro dynamic errors in strapdown inertial guidance system due to body rate

02 p0279 A71-12457

Kinematic error equations application to real inertial navigation systems analysis

02 p0253 A71-12636

Monograph on corrections to Holtsmark continuum model for plasma fluctuations covering probability distributions, quantum mechanical corrections for hot plasmas, etc

02 p0293 A71-12843

Nighttime F layer true height profiles reduction from routine ionograms, discussing error corrections

03 p0408 A71-13387

Shell of revolution bending deformation, assessing Trefftz approximation error

03 p0506 A71-13597

Sounding rocket dispersion analysis, discussing roll rate errors, earth rotation and wind effects and improved computational techniques

[ALAA PAPER 70-1379]

03 p0498 A71-13662

Satellite triangulation network adjustment based on simultaneous errors observations, using filtering equations for matrix manipulations reduction

03 p0413 A71-14009

Statistical analysis of digital data transmission time error distributions in Polish post office and railroad communications network

03 p0380 A71-14375

Group and form classification of production errors and tolerances in aircraft construction

04 p0602 A71-14610

Error probability during diversity reception under random radio noise

04 p0549 A71-14613

Stellar distances inaccuracy effects on kinematical parameters estimation from radial velocities

04 p0643 A71-14907

Computer simulation of thermal diffusivity measurements by flash method, considering errors due to boundary conditions

04 p0607 A71-14964

PCM telemetry bit error probability confidence intervals and Bayesian posterior distributions derivation, using statistical method

04 p0554 A71-15327

Kalman filtering sequential estimates convergence theorems for identifying modeling errors

04 p0561 A71-15328

Nystrom formula error estimation for numerical integration of first order differential equation, tabulating results

04 p0619 A71-15448

Error estimates for turbulent flow characteristics determination by visualization and solid particle photography

04 p0573 A71-15562

Pseudo-problem method for errors accumulated in numerical integration computation of orbits

04 p0654 A71-15718

Satellite motion in orbits with semilatus rectum of 1/6 equatorial radius of oblate planet, discussing errors outside planetary radius

04 p0656 A71-15735

Increase approximation of estimation errors covariance between discrete measurements due to random forcing function uncertainty

04 p0561 A71-15869

Statistical method in geodetic surveying including equilibration calculations, error theory, estimation, verification, distributionless tests, etc

04 p0584 A71-15900

Inertial quality accelerometer tests, including mathematical models and error analysis [AGARDOGRAPH-128]

05 p0750 A71-16307

Neptune orbital motion prediction, determining effect of variations in time and mean distance on accuracy

05 p0810 A71-16542

Dynamic pressure reduction method errors in vacuum gages calibration

05 p0754 A71-16949

Cubature formulas for plane triangular domain, giving leading error terms

05 p0726 A71-16958

Differential descent method modifications, comparing convergence rates and insensitivity to computer computational errors

05 p0775 A71-17012

Automatic systems multipositional elements reliability, analyzing output errors and transition states stability

05 p0729 A71-17039

Coordinatograph control system transfer function and interpolation error calculation

05 p0732 A71-17040

Universal testing machines dynamic load errors due to testing speed

05 p0734 A71-17247

Error estimation for algorithms identifying linear systems described by higher order scalar difference equation

06 p0877 A71-17329

Computer estimation of correctness of tropopause determination from singular points based on criteria from global meteorological network

06 p0922 A71-17505

Optimum line source approximation to desired radiation pattern, deriving least mean squared error expression

06 p0868 A71-17721

Planetary atmosphere Mariner spacecraft occultation experiments, showing neglect of latitudinal and longitudinal variations introduce serious errors

06 p0970 A71-17984

Parabolic equation for plate unsteady thermal conductivity during nonuniform heating, analyzing finite difference solution accuracy

06 p1006 A71-18007

Numerical approximation of continuous real function in interval by polynomials using appropriate nets, estimating error

06 p0920 A71-18209

Unsteady supersonic aerodynamic coefficients evaluation to desired kinematic consistency level using finite element method [ALAA PAPER 71-177]

06 p0845 A71-18616

Wideband microwave monopulse radar direction finding techniques, discussing concept, operation theory, characteristic equations and error analysis

07 p1059 A71-18846

Solid particle impurity effects on hypersonic shock tube flow, determining error in blunt body measurements

07 p1013 A71-18916

Apollo 12 Lunar Module high landing accuracy, discussing control actions, trajectory error sources and power descent

07 p1206 A71-19086

Electromagnetic wave diffraction by multielement and multilayer arrays, discussing asymptotic solution, error estimate and convergence

07 p1060 A71-19180

Latitude observation program at Pulkovo from 1968 through 1987 with zenith telescope, noting faint star declination and motion errors in General Catalog

07 p1194 A71-19328

Error allowance of photoelectric sighting grating with incline slits in stellar observations at Pulkovo

07 p1108 A71-19330

Altazimuthal telescope mounting with computer controlled guidance, discussing instrumental and methodical error effects on positioning and tracking accuracy

07 p1083 A71-19348

Motor learning error performance with discrimination reaction timer, discussing commitment to wrong response, group observations and specific error repetition

07 p1047 A71-19462

Bit error probability estimation from sync word error rate data

07 p1062 A71-19538

Light scattering and attenuation coefficients calculation by small particle approximation, determining applicability limits from comparison with use of exact Mie formulas

07 p1160 A71-19809

Algorithm for simultaneous estimate of spacecraft state and covariance matrix with observation error vector

07 p1148 A71-19882

Laser thermally generated stress waves measurement errors by comparison with time response predicted from strain theory

07 p1214 A71-19912

Signal detection payoff in symmetrical auditory task, studying effect on rates and error analysis

07 p1045 A71-20384

Two nonlinear coupled second order differential equations finite difference solution, using nonsquare and nonuniform grids for minimum error

07 p1149 A71-20612

Soviet book on spacecraft motion parameters measurements accuracy covering electronic systems error sources and reduction in design and data processing

08 p1251 A71-20675

Point matching techniques, discussing effects of metal boundary on divergence of series and error from numerical examples of rectangular waveguide and scattering

06 p1252 A71-20755

Aircraft systems assembly methods, discussing rigidity effects on error redistribution in external and internal force field application

08 p1295 A71-20792

Current-switching digital to analog converters based on resistance ladder networks, discussing operation principles, problems and error sources

08 p1258 A71-20988

Electronic equipment for measuring resonant frequency drift during slow wave structure impedance measurements, considering mean square errors

08 p1264 A71-21073

U.S. Navy Satellite Navigation System error study, considering dead reckoning accuracy, random instrument errors, mathematical error model and statistical analysis procedure

08 p1331 A71-21168

Aerial photographic block aerotriangulation error analysis, discussing block configuration, perimeter and vertical controls, premarking, overlapping, etc

08 p1288 A71-21260

Information transmission rate and error probability in analog feedback systems, showing normalized maximum transmission speed dependence on signal to noise ratio

08 p1268 A71-21283

Error analysis of adaptive estimators and gradient following algorithms for engineering regression equations, comparing stochastic approximation

08 p1269 A71-21332

Surface navigation system and error analysis for Martian roving vehicle, using continuous tracking of pole star and local vertical

08 p1332 A71-21350

Adaptation algorithm for real time minimum mean square error array processing, using with multidimensional digital filter

08 p1256 A71-21605

Meteorological network design, analysis and forecast errors, optimum interpolation and station density and distance

08 p1327 A71-21717

Radiosonde with radiation sensor, minimizing temperature measurement errors in free atmosphere

08 p1293 A71-21745

Favorable construction of elementary figures of cosmic triangulation in three dimensional Cartesian coordinates, determining errors

09 p1404 A71-22272

Quasi-static problems in nonlinear viscoelasticity theory, comparing integral operator and variable moduli methods for convergence and accuracy of successive approximations

09 p1537 A71-22513

Damped vibrations logarithmic decrement determination during automatic recording of number of cycles, emphasizing error analysis

09 p1443 A71-22630

Angular estimation precision in amplitude monopulse off-boresight radar, using linear approximation to error curve

09 p1405 A71-22695

NBS traceable nonferrous conductivity standards for eddy current testing, discussing error analysis, long term drift, grain direction and stratification effects

09 p1469 A71-22710

Error analysis of random and system degradation between calibrations for complex instrumentation by digital computer models

09 p1449 A71-22790

Blood pressure measurement by catheter gages, analyzing error due to wave reflection at catheter tip

09 p1399 A71-22972

Error reduction in reconstructions of time concentrated band limited signals from given set of linear measurements

09 p1407 A71-23101

Screw run and period error stability of eyepiece micrometer of universal astronomical instruments showing dependence on attitudes in space

09 p1451 A71-23179

Umkehr inversion system for vertical ozone distribution observation, calculating error due to ignorance of temperature dependence of ozone absorption

09 p1489 A71-23447

State regulator optimal control problem error bounds, using finite dimensional piecewise polynomial approximations

09 p1424 A71-23466

Planetary scale atmospheric motion energy spectra and error prediction from numerical model, using eddy-damped Markovian approximation for two dimensional turbulence

09 p1489 A71-23551

Unstable electron plasma oscillations quasi-linear theory, discussing improper treatment of perturbed electron distribution for damped waves leading to negative diffusion coefficient

10 p1647 A71-23893

Meteor-reflected radio wave propagation diurnal and annual variations prognosis, discussing indispensability of incident meteor particle velocity and density distributions

10 p1669 A71-24034

Atmospheric turbulence parameters determination from radar meteor observation, calculating antenna radiation patterns effect on error

10 p1583 A71-24036

Star catalogue systematic error corrections from minor planet photographic observations and orbital elements determination

10 p1670 A71-24180

Boltzmann equation for shock wave structure, comparing errors of variational principles and moment methods of approximation

10 p1593 A71-24279

Planetary mass system as pulsar timing error sources, noting change in barycenter of solar system

10 p1675 A71-24493

Systems approximation by incontinuous orthogonal Harre functions, discussing dynamic properties and input signal synthesis with minimal errors in estimating parameters

10 p1587 A71-24741

Numerical errors in computer programmed structural analysis calculations, using finite element displacement method for exact solutions and error sources identification

10 p1693 A71-25051

Cloud base height estimation methods involving vertical radar, laser, stereotelemeter and ceilograph measurements with instrument error analyses

10 p1639 A71-25100

Diversified frequency radio data transmission and reception by linear modulation, considering error rate in white noise and selective/flat fading

10 p1580 A71-25109

Binary on-off laser communication channels, calculating atmospheric turbulence effect on Poisson detection error probability

11 p1730 A71-25198

Misconceptions and distortions in n dimensional covariance matrices interpretation regarding probability confidence levels to error ellipsoid and hyperellipsoid

11 p1791 A71-25485

Thermionic collector work function measurements, considering error sources and I-V characteristics

11 p1711 A71-25881

Green corona corrections of position-angle errors, east-west asymmetry, photometric scale instability and threshold measurements

11 p1832 A71-26181

Equation error approach to parameter identification in third order pitch plane dynamics for high performance aerodynamically controlled aerospace vehicle

11 p1742 A71-26418

Sparse antenna arrays with small sidelobe level, estimating error due to radiation pattern substitution by statistical method

11 p1741 A71-26556

Maximum likelihood method for accuracy of spacecraft trajectory determination by complex expressions in multidimensional geometric representation

12 p1957 A71-26629

Errors due to air flow pulsation in orifice meters, discussing various diameter ratios

12 p1906 A71-26872

Error estimate for solution of approximately linear elastic boundary value problems of shells with no strain energy functional, discussing stress-strain relations

12 p1974 A71-26943

Al alloys endurance limit determination by accelerated methods, evaluating errors by comparison with conventional tests

12 p1916 A71-26944

Space communications antennas main reflecting surface accuracy determination by statistical evaluation of efficiency degradation due to mechanical inaccuracies and structural flexibility

12 p1887 A71-27003

Statistical estimation techniques for error probability of digital communication systems

12 p1880 A71-27145

Amplitude-quantized random noise contaminated unknown signal sample, deriving conditional probability density function of combined output error and signal confidence interval

12 p1880 A71-27157

Plant and compensator parameters deviations effect on accuracy of complex unitary-code programmed automatic control system with delay line digital compensator

12 p1893 A71-27342

Refractive errors in spaced antenna radio angle-of-elevation measurements based on comparison with use of single directional antenna

12 p1881 A71-27424

Error introduced into coherent two-way Doppler tracking measurements on spinning satellite, using turnstile antenna

12 p1882 A71-27431

Kalman filtering for complex systems, deriving algorithms for dynamic modeling and bias errors effects in discrete-time state optimum estimation

12 p1893 A71-27435

Modulation cancellation altimeter error analysis and performance optimization

12 p1908 A71-27437

High stability frequency standard distribution system involving use of geostationary satellites and two-way microwave transmission, discussing errors

12 p1882 A71-27439

Error estimates for class of least squares methods for 2mth order elliptic boundary value problems solution approximation

13 p2093 A71-27803

Physical pendulum normalized error variance as irregularity function in excitation with narrow band frequency spectrum

13 p2065 A71-27947

Total emittance measurements by portable IR reflectometer, tabulating nongray error effects

13 p1519 A71-27979

Straight line approximation of random two dimensional discrete set containing large measurement errors, comparing to least squares results

13 p1333 A71-28189

Earth radiation latitude nonuniformity effect on error in onboard satellite local vertical determinations, using Cosmos satellite data

13 p1333 A71-28202

Analytic theories in celestial mechanics, checking by exact differential equations form based on Von Zeipel method

13 p1335 A71-28353

Mutual impedance of interacting dipoles at wedge tip, determining errors for short spacing distances

13 p2036 A71-28370

Primary component corrections for global cosmic ray variations from latitudinal expeditions, discussing method adaptation to computer

13 p1218 A71-28528

Smith method for radio wave propagation time lag calculation, assessing maximum error by comparing calculated with measured distance/frequency characteristics

13 p2030 A71-28561

Measurement errors in testing single stage air driven axial flow compressors and turbines

13 p1215 A71-28582

Aerial and block triangulation error analysis accuracy dependence on reference point number, introducing camera internal orientation improvement

13 p2062 A71-28903

Anblock method adjusted photogrammetric strips and blocks accuracy, examining errors by model coordinates covariance matrix

13 p2062 A71-28904

Parallax errors in drawing contour lines on universal stereograph due to aerial photographic images brightness difference

13 p2070 A71-29083

Complex geometry surface light pressure momenta determination by body image projection onto photometric wedge and linear edge sliding screen procedure respectively, considering errors

13 p2071 A71-29154

Error in determining pressure and loading distribution on surface of slender bodies of revolution

13 p1994 A71-29323

Algorithm determining sequential machine error partition representing inessential errors

14 p2206 A71-29521

Point and large sources acoustic free field measurement, predicting reflecting ground surface effects on accuracy

14 p2274 A71-30066

Discretization interval in discrete analog filters for optimal processing of complex radar signals, estimating systematic errors

14 p2194 A71-30081

Electromagnetic wave scattering on inhomogeneities by Born approximation, estimating maximum error for small correlation radius

14 p2194 A71-30100

Temperature and thermal flux measurement with calorimetric heat receivers during gas dynamic processes, determining physical properties and geometry effects on errors

14 p2335 A71-30184

German monograph on error analysis in strapdown inertial navigation system covering gimbaled platforms, error propagation, Kalman filtering technique and mathematical equations

14 p2271 A71-30236

Laser Doppler velocimetry accuracy degrading factors, considering light beam focus phase anomaly and distortions due to density fluctuations

14 p2245 A71-30331

Observational errors respecting orbital visual binaries periods, major axes and total mass, considering random and systematic errors

14 p2312 A71-30371

Errors in spectral estimates by single-mode filters using analog computer for geoscientific data processing

14 p2246 A71-30482

Tape recorder equalization techniques effects on attainable bit error probability in digital communication, considering asymptotic prediction recording PCM/FM case

14 p2249 A71-30918

Ionospheric propagation prediction accuracy problems, considering numerical mapping, horizontal gradients, absorption, scatter, maximum usable frequency and transequatorial propagation

14 p2202 A71-30949

Radiometric errors in cosmic background radiation measurement

14 p2204 A71-30970

Error reduction in automatic systems using computers and measuring network parameters over broad frequency ranges

14 p2205 A71-30983

High speed electronic phase and frequency scanned linear, static fed and monopulse arrays element and angular error analysis

14 p2205 A71-31049

Asymptotic error expansions of differential equations approximate solutions by finite difference schemes for use as technical devices in theoretical numerical analysis

15 p2440 A71-31347

Radio direction finding with discrete antenna scanning and multilevel beacon signal quantization, investigating accuracy

15 p2370 A71-31591

Error analysis of Corcos hypothesis concerning cross spectra of pseudocoustic LF turbulent pressure pulsations on flat plate

15 p2389 A71-31708

Optimal tracking of goal seeking vehicles, evaluating Luenberger formulation for tracking error sensitivity

15 p2380 A71-31937

Linearly increasing input signal tracking in nonlinear control systems with pulse frequency modulation, discussing error determination, asymptotic stability and equations of motion

15 p2381 A71-31980

Linear stationary lumped-constant relaxation systems with real and positive eigenvalues and impulsive response characterizable by exponentials, evaluating error in identification

15 p2450 A71-32322

Nonparametric Bayes risk estimation for measurement classification, using nearest neighbor error rate and Parzen probability density function estimators

16 p2602 A71-32822

Manipulation errors in structural systems finite element analyses, examining sources, magnitudes and characteristics

16 p2654 A71-33100

Critique on photomultiplier tube for photon counting, considering pulse height distribution, SNR and electron collection efficiency errors

16 p2578 A71-33146

Plasma temperature determination errors from relative gf-values, noting effects on absolute transition probabilities

16 p2618 A71-33154

Droplet size and concentration in gas stream, discussing measurement error analysis and recording medium calibration procedure

16 p2663 A71-33363

Numerical integration of Poisson kinematic equations for direction cosines, using Runge principle for accuracy values proportional to third power of integration step

16 p2605 A71-33455

Least squares method effectiveness in nonnormally distributed observation errors compensation

16 p2602 A71-33477

Error probability and reception stability in synchronous detection of phase manipulated signals with additive Gaussian noise at multiplied carrier frequency

16 p2542 A71-33498

Vertical acceleration effect on gas-hydraulic analogy for turbulent flows with and without jumps with error dependence on Froude number and length to depth ratio

16 p2560 A71-33598

Error estimates in transmission of pulse code telemetering signals by nonredundant binary code through asymmetric channel

16 p2543 A71-33706

Ionospheric refraction errors in satellite tracking, computing elevation, range and range rate corrections

16 p2640 A71-33734

Tropospheric range error in EM signal arriving at earth zenith, measuring integral of refractivity through atmosphere from height, pressure, temperature and humidity

16 p2569 A71-33800

Nonlinear equations solution with error estimate, using iteration convergence method

16 p2604 A71-34083

Error estimates in thin elastic shell linear theory, modifying three dimensional displacement field

17 p2815 A71-34224

Monograph on parametric errors estimation for dynamic models of linear time invariant control systems

17 p2720 A71-34793

Functional analytical iteration methods for calculating nonlinear vibrations of several degrees of freedom and error estimation improvement, considering uniformly converging Fourier series expansion

17 p2782 A71-34939

Decoding at high transmission rates, describing algorithm for mean number of operations and error probabilities

17 p2702 A71-34971

Additional redundancy in information transmission systems with feedback to reduce error probability due to incorrect addressing

17 p2702 A71-34975

Autonomous unknown landmark tracking space shuttle navigation system performance assessment by digital computer program providing error analysis and Monte Carlo simulation

17 p2773 A71-35067

Upper bound on error probability due to intersymbol interference for correlated and uncorrelated digital signals, presenting examples for data communication systems

17 p2703 A71-35077

Linear, affine and projective coordinate transformation from one mapping plane to another with quick maximum error estimation

17 p2734 A71-35187

Distributed parameter system measurement optimization devices location for error estimation cost minimization by disturbances statistical characteristics and boundary conditions

17 p2722 A71-35211

Computer simulation of error probability performances of binary coherent PSK system under thermal noise and intersymbol and interchannel radio interferences effects

17 p2707 A71-35476

Binary differentially coherent PSK modulated PCM radio link performance under noise and intersymbol and interchannel interferences effects, deriving error probability

17 p2707 A71-35477

Gyroscope errors with gimbal suspension mounted on slowly moving base, discussing base steady rotation

17 p2746 A71-35605

Convergence and error estimates for finite difference methods for approximately positive solutions of mildly nonlinear eigenvalue problems

17 p2768 A71-35683

Roundoff error reduction in numerical solution of second-order differential equation by splitting into two difference equations

17 p2769 A71-35691

Statistical analysis of error sources and magnitudes in Boeing 747 weight values obtained by onboard aircraft weighing system and by manual calculations [SAWE PAPER 897]

17 p2676 A71-35813

Preflight balance analysis of dual spin satellites, discussing error sources

17 p2815 A71-35821

Stellar catalogs errors assessment from Ceres and Vesta asteroids observations

18 p2962 A71-36109

Numerical fluid dynamics problems in Hele-Shaw cell secondary flow, blast wave and plane jet electrostatic pinching, presenting algorithms and error estimates

18 p2905 A71-36310

Planar supersonic near wake flow field problem with variable viscosity and base injection, investigating boundary errors spatial decay rate

18 p2906 A71-36321

Two dimensional steady laminar boundary layer theory for incompressible medium, presenting error bounds for Prandtl equation solution

18 p2906 A71-36322

Local error estimators comparison for Runge-Kutta method in production code design for ordinary differential equations numerical solution

18 p2941 A71-36353

Weakly singular integrals numerical compound quadrature error bound and convergence rate estimate by applying Peano theorem with modification for avoiding singularity

18 p2941 A71-36355

Radio tracking of aircraft by two geostationary satellites, discussing measurement, navigation and position errors

18 p2945 A71-36508

Commutation and combined transmission free access system, discussing error probability

18 p2880 A71-36552

Error occurrence due to perturbations in space communication channels for digital data transmission, describing binary channels models based on Markov chains

18 p2881 A71-36567

Optimal solutions for antenna synthesis problem for bounded norm of source distribution function and limited error in realization of given directional pattern

18 p2893 A71-36620

Adaptive frequency selection for reduction of effects of noise differing irregularly from useful pulse signals, estimating error probabilities

18 p2882 A71-36622

Convergence theory for Newton-like iterative methods to solve nonlinear equations in abstract spaces, presenting error analysis

18 p2943 A71-36955

Operating principles of spacelift simulators, considering star coordinates errors in collimator simulator of stellar sky

19 p3062 A71-37150

Unified error analysis application to altimeter-aided terrestrial inertial navigation systems [AIAA PAPER 71-901]

19 p3095 A71-37152

Aircraft position errors computation for ATC mathematical surveillance models, estimating collision risk [AIAA PAPER 71-927]

19 p3097 A71-37173

Reentry vehicles trajectory reconstruction by computer program and Kalman filter estimation theory, analyzing instrument errors [AIAA PAPER 71-933]

19 p3097 A71-37178

Gyro and star tracker precision attitude determination system, assessing computational and other error effects on system performance [AIAA PAPER 71-964]

19 p2996 A71-37205

Optimal Kalman filter gyro drift rate mathematical models for limiting inertial navigation errors [AIAA PAPER 71-971]

19 p3100 A71-37212

Probability error calculation for digital signals contaminated by intersymbol interference and additive Gaussian noise

19 p3015 A71-37222

Signal detection on Gaussian noise background, deriving error probabilities and optimal processing algorithms

19 p3015 A71-37224

Image parameters identification and estimation problems in learning without teacher, deriving error variance lower bounds and spurious solution probabilities

19 p3024 A71-37225

Sunspot relative number observation accuracy test by least squares method for solar observatories

19 p3130 A71-37226

S-wave elastic positron-hydrogen scattering in ionization region, estimating error in extrapolated matrix from complex energy

19 p3106 A71-37375

Small parameter method application to quasi-linear problems solution in nonstationary heat conduction with substantial nonlinearities and weak perturbation, analyzing error

19 p3162 A71-37584

Space and missile guidance performance analysis based on error sources, using Monte Carlo simulation

19 p3101 A71-37754

Planets masses based on observational or analytical methods, discussing systematic errors effects [AAS PAPER 71-106]

19 p3139 A71-37907

Navigation error sources and orbit determination accuracies for Jupiter planetary encounter, using earth based radio tracking data [AAS PAPER 71-118]

19 p3101 A71-37937

Radio sources position data table based on high accuracy telescope observation including calibration uncertainties and measurement random errors

19 p3142 A71-38008

One layer midlatitude beta plane channel model of incompressible fluid for study of systematic error propagation on nearly stationary synoptic scale wave

19 p3090 A71-38268

Hypercircle method application to elliptic variational problems, obtaining bounds for error in boundary value problems approximation

19 p3087 A71-38302

Error behavior in numerical solution of elliptic differential equations boundary value problems by least squares approximation

19 p3087 A71-38304

Difference equations derivation for meteorological turbulent flow prediction, considering errors due to finite difference approximations

19 p3087 A71-38306

Error analysis for stable implicit difference methods for heat equation with derivative boundary condition

20 p3254 A71-38758

Error independence and elasticity allowance for moon librations and satellite perturbations

20 p3286 A71-38759

Errors equations for space stable inertial navigation systems, considering rotating platforms and velocity and altitude damping

20 p3261 A71-38854

German monograph on filters based on coupled lines covering computerized design, numerical approximation, rounding errors and matrix correction method

20 p3208 A71-39263

Action reproduction accuracy of nonlinear controlled systems with constraints and delays, estimating maximum error and stability degree

20 p3208 A71-39360

Error bounds and variational principles for nonlinear differential and integral equations, exemplifying by Liouville and Poisson-Boltzmann equations

20 p3255 A71-39496

Accuracy in maximum likelihood estimate for correlation function parameter of random process in signal reception on normal noise background

20 p3199 A71-39816

Cosmic ray variations due to atmospheric pressure disturbances and ionizing component variations due to temperature effects, estimating ground observation errors

21 p3437 A71-40074

Multivariate statistical analysis of parameters measuring reference stars effects on parallax and error estimates

21 p3444 A71-40195

Precision relaxation oscillators design and error sources, discussing miniaturization by microelectronic approaches

21 p3355 A71-40736

High data rate optical communication system bit error rate determination from models for noncoherent digital baseband and subcarrier modulation formats

21 p3348 A71-40804

Critical evaluation of Schur-Cohn condition test for stability of multilevel finite difference schemes

21 p3408 A71-40851

Elastic trusses optimal design under multiple mechanical constraint conditions, describing steepest descent method with constraint error compensation

21 p3470 A71-41021

Photoimpact strain measurement errors in tensile tests due to deformation dynamics and quantization in time reduced by scanning along Archimedes spiral

21 p3473 A71-41157

Combined AM/PM digital data transmission, using error rate and communication efficiency in bits per cycle of bandwidth vs average SNR as performance criteria

21 p3349 A71-41197

Air temperature measurement errors, comparing thermometers with and without meteorological screening

21 p3383 A71-41240

Nonrandom measurement error analysis in vector form for mutually dependent and independent errors

21 p3383 A71-41241

Flashing lights radiation characteristics photometric measurement, discussing measuring apparatus sensitivity and errors analysis

22 p3499 A71-41496

Loran-C pulse hyperbolic navigation system application to time and frequency measurements, evaluating errors

22 p3570 A71-41524

Spectral line intensity measurement errors due to electron-temperature fluctuations averaging in continuous plasma sources

22 p3581 A71-41790

Errors resulting from linear interpolation use in opacity tables for stellar interior calculations

22 p3599 A71-41923

Inertial navigation impact on aircraft safety, discussing error sources and midair collision risks

22 p3571 A71-42079

Combined inertial navigation and VOR/DME systems contribution to area navigation accuracy and efficiency

22 p3571 A71-42080

Pattern recognition technique for system error analysis, applying to inertial guidance system test

22 p3566 A71-42110

Error probability during diversity reception under random radio noise

22 p3510 A71-42253

Differential equations system numerical integration solution global discretization error local estimation by Runge-Kutta and multistep methods

22 p3567 A71-42293

Error correction by tapped delay line coded equalizer and channel introduced redundancy, deriving upper bound for error probability

22 p3512 A71-42377

Signal design and error rate of impulse noise channel, analyzing error probability of smear-desmer and standard data channels through Rice integral evaluation

22 p3513 A71-42381

Gaussian errors effect in maximal ratio diversity combiner weighting factors on probability distribution of output SNR

22 p3513 A71-42384

Sampled data control systems with pulse frequency modulation and time lag element, determining error response

22 p3527 A71-42493

Eigenvalues and eigenvectors error estimation in vibration and stability finite element analysis as function of mesh size, using Birkhoff perturbation method

22 p3617 A71-42541

Algorithms for directional antenna boresight orientation estimation errors relative to spacecraft attitude sensor, based on measurement of received signal strength

22 p3525 A71-42775

Visual stimulus control removal and restoration in rhesus monkeys, analyzing test errors

22 p3497 A71-42860

Dispensing devices and error sources in radial immunodiffusion and electroimmunodiffusion techniques

22 p3508 A71-42888

Quadrature errors in satellite geodesy via geopotential simple layer model, investigating different size surface elements and methods of subdivision

[AAS PAPER 71-340] 23 p3666 A71-43013

Sequential processor performance prediction error with linear method from Monte Carlo cycle analysis of Apollo 14 early rendezvous profile

[AAS PAPER 71-386] 23 p3731 A71-43056

Polynomial equation roots determination, analyzing floating point arithmetic errors

23 p3698 A71-43097

Reproduction accuracy of holographic model, discussing coordinates origin and X-Y-Z errors

23 p3675 A71-43303

Mariner S-band occultation experimental data compared with theory for accuracy of physical characteristics of Mars and Venus atmosphere, reviewing data reduction and error analysis

23 p3735 A71-43331

Static and dynamic measurement errors in contact and contactless sensors of automatic dimensional control of finished product sorting

23 p3679 A71-43866

Exact and approximate algorithms for computation of modeling and bias errors in linear minimum error variance estimation

23 p3656 A71-43940

Longitudinal dependence of solar quiet geomagnetic field horizontal component at equator, discussing discrepancy between theory and observation

23 p3673 A71-43986

Estimation error covariance matrices of linearized Kalman tracker for ballistic reentering missiles, observing strong coupling of range and range rate with ballistic coefficient

23 p3646 A71-44083

Onboard computation of Mars atmospheric density and temperature, evaluating error covariance

23 p3774 A71-44095

Maximally achievable accuracy of linear optimal regulators and filters

23 p3659 A71-44099

State estimation errors in quadratic optimal control feedback gain design of stochastic linear regulator

23 p3659 A71-44100

Latitudinal observation errors by two zenith telescopes concurrent data, showing distribution function in long term measurement

23 p3771 A71-44255

Astrometrical HF range latitudinal observation error spectrum estimation, showing random dispersion and Chebyshev polynomial expansion parameters for nightly variation

23 p3771 A71-44256

Goloseyev latitude star catalog, considering observation error distribution and stellar declination estimations

23 p3771 A71-44258

Reduced error spectral power density calculations for random processes with digital spectral analyzers

23 p3681 A71-44320

Servosystems consisting of command and single executive elements error estimation based on mathematical planning of experiment for time loss reduction, deriving regression equation

24 p3808 A71-44395

Analytical model of eclipsing binary star systems, testing validity through numerical integration error analysis

24 p3867 A71-44437

Optimum design of linear multivariate sampled data systems, using deadbeat and integral performance criteria and output response error

24 p3812 A71-44451

Error evaluation of digital real time simulation of nonlinear systems

24 p3813 A71-44571

Convergence and strain accuracy of finite element solutions for nodal displacements in plane elastic mesh

24 p3842 A71-44633

Statistically optimal linear systems characteristics under unsteady input signal, noting relation between error components

24 p3813 A71-44679

Linear control system optimal weighting function determination from maximum probability for system error

24 p3814 A71-44687

Correlation system of equations for mathematical expectations and phase coordinate correlation moments for accuracy analysis in flight vehicle dynamics problems

24 p3792 A71-44692

Unsteady nonlinear multidimensional feedback control systems characterized by equations in normal form for phase coordinates, investigating solutions accuracy by statistical linearization

24 p3814 A71-44694

Nonlinear stochastic systems approximate analysis based on multidimensional nonlinear transforms and distribution functions in Chebyshev-Hermite polynomials, determining dynamic accuracy

24 p3814 A71-44695

Geodetic grid points coordinates accuracy estimate based on normal equations system cracovian matrix, determining arbitrary elements by numerical process without error equations linearization

24 p3822 A71-44768

Radio echo average power measurement errors due to clouds

24 p3845 A71-44882

Three dimensional stress field error estimates in linear plate bending, using Prager-Syng hypercircle elasticity theorem

24 p3884 A71-44964

Multiple mismatch reflection and mode conversion echo effect on error rate in guided millimeter wave phase shift keying systems

24 p3804 A71-44989

Weakly damped nonstationary linear systems analysis by modified sensitivity function method, evaluating solution error

24 p3816 A71-45001

Two sided error estimates for electrodynamic impedance, admittance and scattering matrices in diffraction theory

24 p3805 A71-45256

ERROR BAND

U ACCURACY

ERROR CORRECTING DEVICES

Inertial navigation system error reduction by gyroplatform rapid rotation

01 p0122 A71-10421

Modulo value influence on computer operation reliability, allowing for supplementary verification equipment reliability

01 p0049 A71-10531

Automatic feedback control systems performance correction for errors due to weakly damped components effects

01 p0061 A71-10712

Threshold currents of injection lasers with heterojunctions providing correction for optical thickness in terms of electromagnetic theory

01 p0094 A71-10779

Modified integrate and dump detector using FM click mechanism for improving bit decision and reducing error rates in FSK system

01 p0032 A71-10879

Low cost error control technique for bulk data transmission over channels with noisy feedback link

01 p0034 A71-10903

Relay corrector for widening automatic control systems stability via jump-change in signal amplification factor

01 p0065 A71-11236

Binary error correcting codes in asynchronous systems for separate message transmission, discussing decoding and spacing

01 p0039 A71-11315

Error localization codes with deletion correction

01 p0039 A71-11316

Supporting fluid effects in floated inertial instruments, examining cause, frequency, extent and solution

02 p0253 A71-12462

TWT and klystron intermodulation reduction by amplitude and phase correction device

02 p0223 A71-12811

Clock corrections determinations by stars pairs situated symmetrically around zenith, obtaining formulas by various methods

03 p0484 A71-13219

Cassiopee attitude control device for sounding rocket impulse trajectory correction, discussing spinning nose cones, corrective algorithm and final impact accuracy

03 p0498 A71-13661

Single rotor gyrocompass with electromagnetism correction during random interactions involving intercardinal deviation, constructing correcting device to obtain optimal dynamic characteristics

03 p0430 A71-14353

Linear pattern classifiers design, using error correction and least mean square adaptive algorithms

03 p0383 A71-14480

Electronic frequency divider with discrete correction of negative quartz clock rate

04 p0592 A71-14859

Lense-Thirring effect in test masses approaching in same orbit around rotating body, noting correction dependence on central body geometry and angular velocity

05 p0806 A71-16183

Analog to digital converter optimal algorithm for detecting and correcting errors caused by pulsed noise at input

06 p0871 A71-17524

Transionospheric ranging error correction by second difference of phase shift method
06 p0867 A71-17714

Onboard air navigation computers drift correction by mapping radar, calculating position by region overflow image/measured geographic features comparison
06 p0925 A71-17952

Ionospheric error correction in distance measurements involving satellites, noting simultaneous differential Doppler and Faraday signal measurements
07 p1097 A71-19023

System phase errors subtraction in interferometry, using modified laser unequal path interferometer and technique eliminating data reduction problem
07 p1107 A71-19210

Equipment and procedures for group servicing of parallel data transmission channels with error correcting codes and automatic interrogation of erroneous sequences
07 p1061 A71-19510

Laboratory test set for integration of data compression and error correction encoding of digital communications system
07 p1065 A71-20424

Reproduction quality of information transmitted by error correcting codes for stationary symmetrical channel without storage
08 p1251 A71-20732

Information loss in transmission by group error correcting codes in stationary symmetric channel without storage
08 p1252 A71-20733

Clock correction for Danjon prism astrolabe determination method description and verification
08 p1284 A71-21678

Optimal error correcting code structure selection for binary data transmission systems synchronization, using criterion of minimum false detection probability
08 p1260 A71-21979

Three stage astatic gyrocompass design with pendulum correction, considering equations of motion
09 p1449 A71-22795

Cyclic and multiresidue AN codes, determining single error correcting range
09 p1412 A71-23103

Optical distance correction for fluctuating atmospheric index of refraction in long base line measurements using Lidar with Q switched ruby laser
09 p1495 A71-23451

Stress concentration correcting factors for fillets in landed aircraft structures
09 p1542 A71-23539

Astrometric instruments optimal spatial sampler with parallel slits grill in focal plane, studying error minimization
10 p1608 A71-23825

Lift correction in perforated two dimensional transonic wind tunnels, considering incidence angle and streamline curvature effects on airfoil models
10 p1590 A71-24953

Single loop fixed adjustment system with adaptation similar properties, discussing special correcting devices
12 p1891 A71-26733

Gram-Charlier error probabilities of digital satellite communication systems due to intersymbol interference and additive noise applied to Chebyshev, Gaussian and cutoff filters
12 p1879 A71-27069

Minimum error pre- and post-filtered sampled signals for pulse modulation and data compression optimization
12 p1879 A71-27070

Error detection coding limitations at high error rates, discussing forward error correcting codes and multiple frequency shift keying techniques
12 p1880 A71-27146

Engineering method for synthesizing and calculating AC correcting devices with synchronous switches, deriving equivalent transfer function
13 p2041 A71-27949

Methods for reducing integrating gyroscope errors caused by angular oscillations of base, considering use of two identical gyros with opposite kinetic moment vectors
13 p2065 A71-27951

Error detection and/or correction coding techniques for digital data transmission, comparing efficiency
13 p2036 A71-29279

Majority logic decoding for primitive polynomial and dual codes, discussing nonorthogonal parity-check sums formation methods and Euclidean geometry maximality
14 p2207 A71-30011

Combined data compression and error control by digital sequential decoding for space to earth data links using digital computers
14 p2193 A71-30023

Synchronous meteorological satellite data collection and transmission system error control, considering design tradeoffs for radio sets and coding techniques
14 p2198 A71-30899

Block code construction for binary single, double and triple error correction, including cyclic BCH, circulant and nonlinear codes
14 p2200 A71-30919

Solar image correction in high resolution radio interferometer by digital data processing technique maintaining required phase relations in antenna elements
15 p2373 A71-32446

Astronomical mirror mass balancing system, discussing counterweights and levers arrangement and error and temperature compensation
15 p2411 A71-32526

Ionospheric refraction errors in satellite tracking, computing elevation, range and range rate corrections
16 p2640 A71-33734

Correction method for satellite radio tracking errors due to VHF refraction in atmosphere
16 p2543 A71-33832

Optimal parameters of Fabry-Perot etalon for error minimization in Doppler and dispersion portions determination of Voigt profile width
17 p2737 A71-34410

Redundant variables method as solution to problem of functional coding and algorithm synthesis, examining error control and correcting properties
17 p2710 A71-34963

Analog error correcting redundancy codes, examining coding and decoding procedures
17 p2701 A71-34967

Error correcting codes in binary symmetrical communication channel with additive white noise at large SNR
17 p2702 A71-34972

Redundancy encoding with error correcting codes for controlling results of rational operations series in residual classes system
17 p2710 A71-34976

Circuit synthesis from unreliable functional elements through probabilistic logic, correcting codes and logic algebra functions
17 p2721 A71-34978

Error correction in autonomous linear finite automata with correcting codes
17 p2711 A71-34979

Predictor-corrector algorithms with identical regions of absolute or relative stability
17 p2769 A71-35690

Astronomical data correction for smearing effects applying Fast Fourier Transform algorithm
18 p2960 A71-35933

Discharge coefficient correction factor for curvature effect on mass flow rate measurement by sonic throat for axisymmetric nozzles
[ONERA-TP-956] 18 p2915 A71-36024

Lens test facility calibrating Mipir radar boresight lenses by measuring deviations due to gravitational effects
18 p2897 A71-36072

Stellar proper motions in photographic zenith tubes programs for time service clocks correction, examining catalogs used for astronomical data processing
18 p2962 A71-36110

Automatic argon ion laser tracking system for high speed rocket sleds, describing apparatus configuration and error correcting devices
18 p2883 A71-36908

Correction values to centennial precession, using stellar proper motions
18 p2970 A71-37063

Synchronous satellite transmission Faraday rotation conversion into total electron content, removing n pi ambiguity
19 p3128 A71-38032

Majority-logic decodable block codes construction by combining shorter length codes, obtaining correctable error bounds
20 p3201 A71-38873

Backscattering patterns in atmospheric opacity measurements, minimizing errors due to atmospheric inhomogeneities and different stratifications
20 p3257 A71-39334

Computer programming for on-line correction of microwave measurements of loss and reflection effects between network analyzer and device/circuit under test
20 p3205 A71-39377

Probability functional formulas for quasi-determinate signal on unsteady normal noise background for use in false alarm and correct detection
20 p3199 A71-39815

Self referencing holographic system for image compensation in fluctuating random medium, describing homodyning procedure
21 p3382 A71-40935

Memory cell fault tolerant sequential machine synthesis, considering masking feasibility and lower bounds on minimum redundancy
21 p3351 A71-41036

Holographic correction of lens aberration in optical system, considering turbulence effect correction
22 p3358 A71-41737

Differential correction for redetermination of satellite observation stations geodetic coordinates as related to earth center of gravity and terrestrial potential coefficients
22 p3534 A71-42023

Decoding of correlative level coding or partial response signaling systems with ambiguity zone detection, discussing error correction algorithm
22 p3513 A71-42382

Reed-Solomon erasure-correcting sequential decoder implementation for hybrid coding scheme, using digital circuitry
22 p3513 A71-42387

Bit error rate detector for testing digital data links, using analog network mathematical model
22 p3519 A71-42764

Gyrocompass with optimal error correction under rapid acceleration change
23 p3675 A71-43297

Automatic resau detection and reference ground control points for computing and correcting geometric and radiometric image for earth resource data, noting correlation with reference system
[AIAA PAPER 71-978] 24 p3806 A71-44576

Large random access computer store based on redundancy in form of error correcting codes, discussing use for manufacturing yield improvements
24 p3806 A71-44655

Error correcting binary block code decoding on Q-ary output channels/weighted erasure decoding/, considering applications
24 p3806 A71-44936

Rate 1/2 convolutional error correcting binary codes with complementary generators, discussing synthesis and search procedure for largest free distance
24 p3807 A71-44937

ERROR DETECTING CODES

NT BCH CODES

ERROR DETECTION CODES

Block code for retrasmmission of information damaged by noise bursts for feedback digital communication systems
01 p0034 A71-10905

Error localization codes with deletion correction
01 p0039 A71-11316

Iterative and cascaded codes for single and grouped error detection
01 p0039 A71-11317

Equipment and procedures for group servicing of parallel data transmission channels with error correcting codes and automatic interrogation of erroneous sequences
07 p1061 A71-19510

Catastrophic error propagation and minimum weight codewords in convolutional codes
07 p1069 A71-20417

Error correction coding/decoding techniques integration, discussing convolutional and block coding and Viterbi, Sequential and Threshold decoding algorithms
07 p1066 A71-20425

Reproduction quality of information transmitted by error correcting codes for stationary symmetrical channel without storage
08 p1251 A71-20732

Information loss in transmission by group error correcting codes in stationary symmetric channel without storage
08 p1252 A71-20733

Digital computer modular LSI control logic design using multifunctional binary decoder with transistor array read-only memory for odd and even parity error detection
08 p1260 A71-21663

Optimal error correcting code structure selection for binary data transmission systems synchronization, using criterion of minimum false detection probability
08 p1260 A71-21979

Cyclic block code structures for generating binary sequences with good autocorrelation properties
09 p1407 A71-23110

Binary periodic convolutional codes with lower bound everywhere stronger than Wagner on definite decoding minimum distance
11 p1731 A71-25758

Error detection coding limitations at high error rates, discussing forward error correcting codes and multiple frequency shift keying techniques
12 p1880 A71-27146

Error detection and/or correction coding techniques for digital data transmission, comparing efficiency
13 p2036 A71-29279

Majority logic decoding for primitive polynomial and dual codes, discussing nonorthogonal parity-check sums formation methods and Euclidean geometry maximality
14 p2207 A71-30011

Synchronous meteorological satellite data collection and transmission system error control, considering design tradeoffs for radio sets and coding techniques
14 p2198 A71-30899

Analog error correcting redundancy codes, examining coding and decoding procedures
17 p2701 A71-34967

Information effectiveness of redundant error detecting coding systems
17 p2702 A71-34968

ERROR FUNCTIONS

- Majority decoding of cyclic codes, determining number of checks upper bound for various decoding schemes 17 p2702 A71-34969
- Redundancy encoding with error correcting codes for controlling results of rational operations series in residual classes system 17 p2710 A71-34976
- Circuit synthesis from unreliable functional elements through probabilistic logic, correcting codes and logic algebra functions 17 p2721 A71-34978
- Error correction in autonomous linear finite automata with correcting codes 17 p2711 A71-34979
- Optical target detection and position error signal system for boost phase missiles, using TV with digital computer controlled dual tracking electronics 18 p2883 A71-36911
- Majority-logic decodable block codes construction by combining shorter length codes, obtaining correctable error bounds 20 p3201 A71-38873
- Noise variance maximum likelihood estimate based on order statistics for first order Reed-Muller code transmission over zero-mean white Gaussian noise channel 20 p3202 A71-38875
- Error correction by tapped delay line coded equalizer and channel introduced redundancy, deriving upper bound for error probability 22 p3512 A71-42377
- Bit error rate detector for testing digital data links, using analog network mathematical model 22 p3519 A71-42764
- Large random access computer store based on redundancy in form of error correcting codes, discussing use for manufacturing yield improvements 24 p3806 A71-44655
- Error correcting binary block code decoding on Q-ary output channels/weighted erasure decoding/considering applications 24 p3806 A71-44936
- Rate 1/2 convolutional error correcting binary codes with complementary generators, discussing synthesis and search procedure for largest free distance 24 p3807 A71-44937
- ERROR FUNCTIONS**
- Distribution functions of errors in earth and moon horizon sighting due to planetary surface unevenness 09 p1523 A71-23147
- Zoellner illusion as function of inducing and test lines intersect angle and lines density, deriving error functions 18 p2863 A71-37019
- High order finite element solution roundoff error reduction, using discretization of elliptic equations 21 p3409 A71-40962
- Mathematical description by Gaussian error function for metals diffusive saturation and diffusion constants determination 21 p3403 A71-41160
- ERROR SIGNALS**
- Complex control systems using self adjustment compensation of error signals according to input derivative 01 p0063 A71-10723
- Coherent communication link pseudonoise synchronization error due to white Gaussian noise and amplitude jitter produced by reference carrier phase error, discussing digital simulation 05 p0725 A71-17072
- Microwave discriminators with IF error signal ensuring high stabilization of master oscillator frequency without complex tuning operations 11 p1737 A71-25939
- Linear estimation with stochastic feedback control to cancel out disturbances or error signals effect, applying to integrated navigation systems involving inertial measurement 12 p1893 A71-27436
- Algol 60 object time error messages detection with test run in-core load-and-go compiler 13 p2035 A71-29014
- Shock wave propagation in ducts and cavities of different shapes and cross sections, compensating errors in recorded signals for shock tube pressure measuring equipment development 16 p2555 A71-32885
- Electronic and hydraulic devices for communication satellite ground station steerable antenna servocontrol, driving and pointing, discussing tracking error signals 17 p2724 A71-35511
- Radar glint reduction by diversity techniques, indicating tracking improvement by error signal choice 19 p3022 A71-38587
- Microwave discriminators with IF error signal ensuring high stabilization of master oscillator frequency without complex tuning operations 20 p3205 A71-39259
- Single frequency He-Ne laser stabilization by Lorentz absorption contour in external gas cell, obtaining error signal based on absorption line scanning 23 p3683 A71-43396

- Comparative qualitative simulation of pulse frequency modulation control with/without error signal derivatives 23 p3656 A71-43867
- Fault detection, diagnosis and prognosis in linear dynamic systems based on statistical decision theory, considering error signal generation and statistics 23 p3682 A71-43945
- ERRORS**
- NT INSTRUMENT ERRORS
- NT PHASE ERROR
- NT PILOT ERROR
- NT POSITION ERRORS
- NT RANDOM ERRORS
- NT RANGE ERRORS
- NT ROOT-MEAN-SQUARE ERRORS
- NT TRUNCATION ERRORS
- NT VELOCITY ERRORS
- ERTS**
- E EARTH RESOURCES TECHNOLOGY
- SATELLITES

ERYTHROCYTES

- NT RETICULOCYTES
- Chronic hypercapnia oxygen dissociation curves and red cell cation exchange in rats, considering compensated/uncompensated phases of respiratory acidosis 03 p0360 A71-13181
- Human erythrocytes phosphate metabolism in hyperthermia 05 p0711 A71-16944
- Erythrocytometric curve analysis by conductometric granulometric method 06 p0863 A71-18692
- Vitamin K3 effect on redox equilibria in red cell, discussing radiosensitizer mechanism 07 p1039 A71-18985
- Hydrodynamic model of human red blood cell rotation in flow toward sizing orifice, predicting volume distribution 07 p1045 A71-20446
- Heart, lungs and erythropoiesis optimum functional parameters mathematical model based on oxygen transport minimum losses 09 p1388 A71-22126
- Altitude acclimatization of albino rats and guinea pigs, measuring chronic and acute hypoxia effect on oxygen affinity and red cell 2,3 diphosphoglycerate concentration 10 p1558 A71-23894
- Prolonged hypoxia, hypercapnia and combination effects on rats circulating red cell volume 10 p1559 A71-23970
- Rapid erythroblast multiplication in vitro by incubation of rabbit blood buffy coat and marrow cells, giving autoradiographic results 10 p1566 A71-25014
- Blood plasma volume decrease, red cell mass and survival measurements in aquanauts of Teklite I at prolonged habitation 11 p1720 A71-26123
- Spleen role as erythrocytic depot in reticulocytic reaction to acute hypoxia in splenectomized dogs inhaling air with reduced partial oxygen pressure 13 p2007 A71-28418
- Erythrocytes life span and bone marrow production in dogs subjected to gamma irradiation in doses simulating prolonged space flight conditions 15 p2356 A71-31307
- Human erythrocyte 2, 3-diphosphoglycerate concentration elevation effects on glycolytic metabolism and intracellular pH 16 p2533 A71-34090
- Erythrocyte disintegration products role in blood regeneration, showing erythropoiesis link to erythrodiuresis for different forms of hypoxia 17 p2679 A71-34219
- Ouabain insensitive effects of metabolism on ion and water content of red blood cells 17 p2681 A71-34943
- Erythrocytes diphosphoglycerate increase mechanisms during hypoxia and anemia, studying hemoglobin oxygenation state effects 17 p2685 A71-35368
- Red blood cell image hologram reconstruction and superresolution based on coherent physical optics, using computer program 17 p2693 A71-35586
- Organic phosphate compounds effects on oxygen affinity and intracellular pH of human erythrocytes 18 p2857 A71-36691
- Physiological responses of burro Equus asinus to oxygen lack in mountain altitudes, studying red blood cell and plasma volumes 19 p3005 A71-38560
- Chronic hypercapnia effects on oxygen affinity and 2,3-diphosphoglycerate in red cell from tests on guinea pigs 20 p3189 A71-39440
- Erythropoietic activity dosage in polycythemic mice after intermittent hypobaric hypoxia 23 p3632 A71-43216

- Hypobaric hypoxia effect on polycythemic mice erythropoietic hyperactivity, evaluating iron content in peripheral erythrocytes 23 p3632 A71-43217
- Extrarenal production of erythropoietin in binephrectomized rats after hypobaric hypoxia 23 p3632 A71-43218
- Age effects on plasma aldosterone levels, red cell, plasma and total blood volume at sea level and high altitude 24 p3797 A71-44781
- ESAKI DIODES**
- U TUNNEL DIODES
- ESCAPE [ABANDONMENT]**
- Safe escape from toxic combustion products environment, discussing time of environmental difference dependence on consolidated biokinetic forces 04 p0543 A71-15055
- ESCAPE CAPSULES**
- Stowable aircrew vehicle escape rotoseat autogyro, providing controllable flight for pilot after ejection 04 p0532 A71-15418
- ESCAPE ROCKETS**
- Tractor rocket actuated Yankee escape system, discussing advantages of pulling action over conventional pushed ejection seat under low speed low altitude conditions 13 p1998 A71-29383
- ESCAPE SYSTEMS**
- Manned space flight escape systems evolution, examining requirements and devices from X-15 to Apollo program 02 p0320 A71-11977
- Piloted lunar escape to orbit systems simulation using simplified manual guidance and attitude control [AIAA PAPER 71-60] 06 p0977 A71-18519
- Manned aerospace vehicular escape systems, discussing human vertebral column structural limits under vertical gravity acceleration 06 p0863 A71-18587
- Aerospace Recommended Practice criteria for flight deck crew escape systems applicable to all commercial aircraft propulsion systems, design speeds and payloads [SAE-ARP-808A] 07 p1019 A71-19646
- Aerospace emergency escape systems and procedures, discussing physical, biophysical and physiological aspects related to increased flight speeds and altitudes 08 p1245 A71-20717
- German book on rescue systems for space emergencies covering mission failure, biological problems, escape vehicles, orbital operations safety and spacecraft transfer 12 p1972 A71-27185
- Tractor rocket actuated Yankee escape system, discussing advantages of pulling action over conventional pushed ejection seat under low speed low altitude conditions 13 p1998 A71-29383
- Ejection system performance in relation to aircraft performance dependent extreme flight conditions, examining ejection seat design features and trajectories 13 p1998 A71-29385
- Space flight safety, discussing escape, rescue and survival design approaches for astronauts 22 p3611 A71-42037
- ESCAPE VELOCITY**
- Control programs realizability for optimal escape trajectories of low thrust vehicles with motion about mass of center and with or without artificial gravity 02 p0319 A71-11905
- Microthrust powered spacecraft earth escape, using lunar attraction by orbiting spacecraft with vector opposite to moon 12 p1968 A71-27579
- Control programs reliability for optimal escape trajectories of low thrust vehicles with motion about mass of center and with or without artificial gravity 13 p2144 A71-28192
- Optimal control algorithm for spacecraft descent in atmosphere at speed near escape velocity, using game theory 16 p2646 A71-33702
- Radiation role in nonequilibrium boundary layer during atmospheric reentries at speeds exceeding escape velocity 21 p3368 A71-40694
- Space tug optimal round trip trajectories for payload earth escape injection missions, obtaining boundary value problem solution by Newton-Raphson iteration technique 21 p3452 A71-40908
- Space tug assist to escape branched trajectories optimization [AAS PAPER 71-330] 23 p3727 A71-43003
- Reusable space tug payload injection missions, determining optimal round trip trajectories at earth escape energy levels [AAS PAPER 71-370] 23 p3730 A71-43040
- Solar system escape trajectory analysis for Jupiter-Saturn-Pluto and Jupiter-Uranus-Neptune Grand Tour missions, presenting flyby characteristics and heliocentric postencounter directions [AAS PAPER 71-383] 23 p3731 A71-43053

Spacecraft motion control algorithm for reentry at escape velocity based on object motion model
24 p3846 A71-45305

ESCHERICHIA

Biosynthesis of inosinic acid in transfer RNA in *Escherichia coli* by polynucleotide modification
03 p0375 A71-13173

Structure and function of 50 S ribosomes of *Escherichia coli* based on determination of role of 5 S ribosomal RNA
04 p0548 A71-14733

DNA modification in *Escherichia coli* exposed to X rays and sensitized by triacetoneamine N-oxyl and oxygen
07 p1033 A71-18939

Lethal radiation in *Escherichia coli* B/r, investigating post irradiation DNA breakdown inhibitors
07 p1033 A71-18940

Cysteine incorporation in *Escherichia coli* B, noting X ray sensitivity and radioprotection
07 p1034 A71-18942

Composition and colicinogenic and hemolytic activities changes of *Escherichia* isolated from man during long term confinement
21 p3333 A71-40558

Space conditions exposure of lysogenic strains of *Escherichia coli* and monolayer cultures of human cells aboard Zond 5 and 7 flights
21 p3333 A71-40565

ESOPHAGUS

Mediastinum effect on human esophageal pressure and lung compliance measurements
10 p1565 A71-24678

Dogs intrapleural and intraesophageal pressures dependence on head positions
19 p3010 A71-38564

ESRO SATELLITES

NT AZUR SATELLITE
NT ESRO 1 SATELLITE
NT ESRO 2 SATELLITE
NT HEOS A SATELLITE
NT HEOS SATELLITES

European satellite projects chronological survey covering ESRO and national projects
09 p1547 A71-22419

ESRO preoperational aeronautical satellite system for Atlantic and Pacific coverage, noting position determination for reduced aircraft separation, frequency selection and performance trade-offs
16 p2644 A71-32850

ESRO report to COSPAR on sounding rockets and geostationary satellites development, orbits and decay during extraterrestrial gamma radiation
16 p2667 A71-33867

Technical parameters and performance tradeoffs of ESRO preoperational aeronautical satellite program
19 p3153 A71-38067

ESRO-1A /Aurora/ observations of variations in low energy electron spectrum, noting relationship to magnetic activity
19 p3060 A71-38576

Equatorial modulation in pulsating aurora, discussing electron measurements with channel multipliers and electrostatic analyzers aboard ESRO Skylark S29/2
20 p3228 A71-39841

Noon-midnight high latitude proton trapping and precipitation boundary variations associated with polar magnetic substorms observed by ESRO 1A satellite
23 p3719 A71-43127

Multinational consortiums of industrial firms from member states for ESRO satellite programs
23 p3786 A71-43463

ESRO 1 SATELLITE

ESRO 1 satellite hydrogen and ionized nitrogen auroral emissions photometric measurements, discussing electron/proton phenomena relation to geomagnetic activity
03 p0406 A71-13248

U.S.-Europe cooperative space programs survey and experience from project management with ESRO-1 satellite
04 p0692 A71-15349

ESRO 1 small scientific satellite attitude measurement system, discussing design and flight test results
07 p1154 A71-18840

ESRO 1 satellites space simulation chamber tests for residual gas effects, measuring spacecraft outgassing rate
09 p1533 A71-23732

Magnetic activity effect on pitch angle distribution of low energy auroral electrons from ESRO 1A measurements
19 p3060 A71-38575

ESRO 2 SATELLITE

Solar proton event on 9 June 1968 observed at polar caps by ESRO 2 satellite, noting flux profile structure
06 p0958 A71-18154

ESRO 2 satellite program reliability prediction and procedures in design and manufacture, defects during development and tests and performance in orbit
07 p1207 A71-19552

Solar proton enhancement over auroral zone observed aboard near earth polar orbiting ESRO 2 satellite
20 p3282 A71-39735

ESTERS

NT ACRYLATES
NT ASPARTATES
NT CELLULOSE NITRATE
NT CYANURATES
NT GLUTAMATES
NT GLYCERIDES
NT HYDRAZINE NITROFORM
NT ISOPROPYL NITRATE
NT LACTATES
NT LEXAN [TRADEMARK]
NT NITROGLYCERIN
NT PETN
NT PHTHALATES
NT POLYCARBONATES
NT POLYESTERS
NT URETHANES

Synthesized amino esters and ketones with varying distance between functionalities, examining mass spectral fragmentation
02 p0209 A71-12574

Ethyl esters of long chain fatty acids as biological products from gas chromatographic and mass spectrometric analyses on lipid fractions
13 p2015 A71-29352

Esters synthesis from cyclic trimethylolpropane butyral and monobasic saturated acids mixtures
15 p2438 A71-31679

Thermal stability and oxidation and corrosion resistance of lubricating oil based on trimethyl propane ester
18 p2939 A71-36016

Low temperature viscous lubricants from mixed pentaerythritol esters for precision inertial guidance gyroscope bearings and instrument applications
20 p3254 A71-39800

ESTIMATES

NT COST ESTIMATES

Degree of closeness estimates for initial and averaged systems of differential and integrodifferential equations with conditions on right members
15 p2442 A71-31523

Linear unbiased estimates of mathematical expectation of random process optimal in sense of norm of symmetrical Banach space
17 p2765 A71-34861

Second approximation estimates of spatial-temporal signals parameters
19 p3015 A71-37260

Bayesian estimates in nonlinear filtration of nonstationary non-Gaussian radio signals, deriving second central moments and parameter estimate errors
20 p3198 A71-39807

Integral and pointwise estimates of insulated cylinder temperature field spatial decay for semilinear parabolic equations
21 p3473 A71-41186

ESTIMATING

NT ORBITAL POSITION ESTIMATION

Dynamic errors estimation for nearly invariant automatic control systems, discussing parameter- change sensitivity
01 p0061 A71-10715

Frame structures linear-mode failure probability estimation by reliability analysis
02 p0327 A71-12347

Optimal adaptive estimation, considering Gaussian process and linear dynamic models and partition theorem for structure and parameter adaptation
03 p0394 A71-14484

Stellar distances inaccuracy effects on kinematical parameters estimation from radial velocities
04 p0643 A71-14907

Increase approximation of estimation errors covariance between discrete measurements due to random forcing function uncertainty
04 p0561 A71-15869

Parameter estimation of mixed autoregressive moving-average /ARMA/ time series using output data
06 p0878 A71-17332

Computer estimation of correctness of tropopause determination from singular points based on criteria from global meteorological network
06 p0922 A71-17505

Weighted least squares nonlinear estimation problem, presenting partial step algorithm for convergence region enlargement
06 p0921 A71-18658

Bit error probability estimation from sync word error rate data
07 p1062 A71-19538

Selection index estimation from partial multivariate normal data for precision improvement, discussing procedure and Monte Carlo simulation results
07 p1147 A71-19599

Algorithm for simultaneous estimate of spacecraft state and covariance matrix with observation error vector
07 p1148 A71-19882

Design curve for estimating conduction heat transfer liquid He cryostats with vapor-cooled vent tubes
07 p1115 A71-20359

Force moment method estimation of atmospheric circulation effect on earth polar movement
08 p1284 A71-21674

Identification algorithm for estimating parameters in constant coefficient linear system independent of prior estimates
09 p1484 A71-22074

[AIAA PAPER 70-34] Parameter estimation - Conference, Prague, June 1970
10 p1586 A71-24735

Deterministic parameter estimation in nonlinear system near optimum feedback control by power series expansion
10 p1586 A71-24738

Sensitivity algorithms and application to attitude estimation of rigid body satellite in circular earth orbit
10 p1587 A71-24747

Suboptimal estimation of remaining flight distance of aircraft at each radar range measurement by limited state recursive estimators
11 p1741 A71-25489

Algorithm for nonparametric estimation of random parameters of general exponential family of unknown density distributions, investigating empirical estimates convergence to Bayes optimal estimates
12 p1892 A71-27022

Book on detection, estimation and modulation theory, Part 3, Gaussian and radar-sonar signals in noise, covering point targets, random process and scatter channels
15 p2371 A71-31841

French monograph on algorithms for parameters estimation for adaptive identification in real time of linear processes perturbed by related noise
17 p2767 A71-35232

Image parameters identification and estimation problems /in learning without teacher/, deriving error variance lower bounds and spurious solution probabilities
19 p3024 A71-37225

Specific optimal techniques in control and estimation, emphasizing fixed configuration optimization with time variant parameters and two point boundary value problem
19 p3036 A71-37237

Algorithm for nonparametric estimation of random parameters of general exponential family of unknown density distributions, investigating empirical estimates convergence to Bayes optimal estimates
19 p3038 A71-37691

Location and scale parameters estimation from ordered statistical samples with numerical applications to Gumbel and Weibull distributions
19 p3088 A71-38471

Best linear unbiased estimates for location and scale parameters of extreme value distribution based on given order statistics
21 p3407 A71-40366

Astronomical observations weighted estimation based on smoothing Pearson curves empirical distribution
23 p3771 A71-44257

Goloseyev latitude star catalog, considering observation error distribution and stellar declination estimations
23 p3771 A71-44258

Pseudomoments estimation of convergence rate in central limit theorem for random variables series
24 p3843 A71-44874

ESTIMATORS

Frequency-wavenumber power spectrum estimators probability distribution, using Gaussian distribution probability density function
02 p0215 A71-12046

Nonparametric Bayes risk estimation for measurement classification, using nearest neighbor error rate and Parzen probability density function estimators
16 p2602 A71-32822

Local error estimators comparison for Runge-Kutta method in production code design for ordinary differential equations numerical solution
18 p2941 A71-36353

Analog mass center estimator for spinning drag-free orbiting satellite, using free-falling proof mass shielded from external forces inside satellite cavity as reference
19 p3148 A71-37188

[AIAA PAPER 71-947] Reduced state estimator for satellite orbital heading reference, describing decoupled single-skewed-gyro gyrocompass design for attitude control
19 p3148 A71-37206

[AIAA PAPER 71-965] Feedback system estimation algorithm, comparing performance to algorithm based on stochastic control separation principle
19 p3039 A71-38715

Generalized matrix inverses application to estimation of state vector in dynamic control system, determining covariance matrix of estimator
23 p3700 A71-44117

ETCHANTS

ETCHANTS

Aqueous etchant for charged particle tracks revelation in olivines

23 p3737 A71-43544

ETCHING

High work function stable faceted W thermionic emitter surface preparation by electroetching and vapor deposition

02 p0295 A71-12209

Metallographic specimens etching by cavitation damage, testing performance by ultrasonic vibration technique

03 p0445 A71-14420

Plastic track detectors calibration for heavy charged particles in cosmic ray experiments, considering track etching rates as function of particle charge and velocity

07 p1113 A71-20042

Etchant type, concentration and temperature effect on various plastics track etching ratio and sensitivity

07 p1145 A71-20272

Coarse grain Al sheet deformation, determining dislocations distribution with etching defects method

12 p1919 A71-27691

MOS transistors thin monocrystalline silicon layers formation by epitaxial growth and substrate selective electrochemical etching

19 p3028 A71-37565

Holographic methods for etching masks of IC and other semiconductor components

21 p3354 A71-40731

ETHANE

Methane and ethane binary mixtures with chlorine, determining main combustion products under flame propagation

07 p1054 A71-19280

Inhibiting mechanism of ethane in hydrogen-oxygen mixtures ignition, discussing lower limits, carbon monoxide effect and chain lengthening reactions

11 p1730 A71-26566

Perchloric acid reactivity with respect to hydrogen, methane, ethane and ethylene by flow method, using twin concentric jet reactor of Pyrex glass

17 p2792 A71-35709

ETHERS

NT DIETHYL ETHER

NT POLYPHENYL ETHER

Mass spectral properties of alkoxy-cyclohexanol trimethylsilyl ethers and alkoxy-cyclohexyl trimethylsilyl ethers, using deuterium labeling

02 p0209 A71-12575

Ablative polymers synthesis from formaldehyde, phenols and ethers reaction products, discussing char yield, thermally stable fillers incorporation and thermogravimetric analysis

11 p1855 A71-26034

ETHYL ALCOHOL

Alcohol effects on complex task performance including monitoring, compensatory tracking and mental arithmetic

04 p0547 A71-15850

Harmful induced stimulated emission losses in rhodamine unpumped ethyl alcohol and heavy water solutions of various excitation energies

09 p1461 A71-22383

Ethyl and methyl alcohol droplets vaporization rate variation with respective distance from photographic observations

14 p2285 A71-30612

Psychological and neurophysiological definitions of vigilance, considering alcohol and tranquilizers effects

16 p2533 A71-34040

Electromagnetic waves propagation in inhomogeneous medium, using simulation chamber with NaCl and ethyl alcohol diffused agar-agar

17 p2724 A71-34755

Fluorescence spectra of anthracene ethyl alcohol solution and powdery crystalline anthracene by single and two photon ruby laser excitation

19 p3071 A71-37263

Ethyl alcohol combustion effect on laminar boundary layer structure near flat plate, assuming thermal cracking of fuel

19 p3169 A71-38113

ETHYL COMPOUNDS

Ethyl esters of long chain fatty acids as biological products from gas chromatographic and mass spectrometric analyses on lipid fractions

13 p2015 A71-29352

Shock compressed tetranitromethane mixtures with various benzene ethyl iodide proportions, investigating lateral discharge wave effects on detonation process structure

15 p2511 A71-31382

ETHYLENE

Ethylene diffusion flame radiation measurements, determining pressure effects and contributory ratio of carbon particles and gaseous radiation

08 p1346 A71-20859

Surface roughness of 304 stainless steel by Brunauer-Emmett-Teller measurements, using ethylene as adsorbate

14 p2284 A71-30073

Perchloric acid reactivity with respect to hydrogen, methane, ethane and ethylene by flow method, using twin concentric jet reactor of Pyrex glass

17 p2792 A71-35709

Fluorinated ethylene propylene covers for silicon solar cells, describing processing parameters effects on optical and electrical characteristics

20 p3182 A71-38944

Critical atomic carbon to oxygen ratio measurement for incipient soot formation in shock heated acetylene, ethylene and ethane/oxygen/argon mixtures

21 p3436 A71-40859

ETHYLENE COMPOUNDS

NT CHLOROETHYLENE

ETHYLENE OXIDE

Ethylene oxide and methyl bromide sporadic activity compared for spacecraft sterilization of *B. subtilis* var niger spores

01 p0027 A71-11565

Space objects sterilization techniques in Soviet Union and United States, covering hot air, ionizing radiation, UV light, ethylene oxide with or without Freon, etc

13 p2019 A71-28694

ETIOLOGY

High altitude pulmonary edema in unacclimatized humans, discussing symptoms, etiology incidence and prevention

14 p2183 A71-30277

ETTINGSHAUSEN COOLERS

U ETTINGSHAUSEN EFFECT

U THERMOELECTRIC COOLING

ETTINGSHAUSEN EFFECT

Ettinghausen refrigerator dynamic behavior mathematical models, using current density and potential gradient as controlling variables

04 p0678 A71-15465

EUCLIDEAN GEOMETRY

NT ANALYTIC GEOMETRY

NT ANGLES [GEOMETRY]

NT BRAGG ANGLE

NT BREWSTER ANGLE

NT CARTESIAN COORDINATES

NT CHORDS [GEOMETRY]

NT CIRCLES [GEOMETRY]

NT GREAT CIRCLES

NT HEXAGONS

NT HYPERBOLAS

NT LINES [GEOMETRY]

NT LOCI

NT MERCATOR PROJECTION

NT OBLATE SPHEROIDS

NT PARALLELEPIPEDS

NT POINTS [MATHEMATICS]

NT POLYGONS

NT POLYHEDRONS

NT PROJECTIVE GEOMETRY

NT PROLATE SPHEROIDS

NT RADII

NT RECTANGLES

NT RHOMBOHEDRONS

NT S CURVES

NT SPHEROIDS

NT TETRAHEDRONS

NT TORUSES

NT TRAPEZOIDS

NT TRIANGLES

Cauchy problem solution for elasticity theory

dynamic system in Euclidean space arbitrary region

03 p0510 A71-13962

Complex loading history effect on elastoplastic deformation trajectories delay trail characteristic angles and length variation, determining plastic strain vector components in Euclidean space

13 p2155 A71-28652

Majority logic decoding for primitive polynomial and dual codes, discussing nonorthogonal parity-check sums formation methods and Euclidean geometry maximality

14 p2207 A71-30011

Explicit formulas for Euclidean geometry and Berlekamp subcodes weight enumerators for second order binary Reed-Muller codes

14 p2209 A71-30828

Einstein equations solution as hypersurface of four dimensions in Euclidean space, investigating imbedded manifold deformations

16 p2610 A71-33272

Normal mode vibrations of system with trajectories of unit mass in Euclidean space, determining modal subspaces by potential function

17 p2776 A71-34295

Approximate self contained numerical integration formulas for compact symmetrical regions in n-dimensional Euclidean space

17 p2768 A71-35684

Convergence rate for finite element method, considering Neumann problem for second-order elliptic differential equations with constant coefficients in m dimensional Euclidean space

17 p2769 A71-35688

Deformation field of continuous medium in Minkowski space-time, defining tensor in Euclidean space of initial configuration

18 p2947 A71-36191

EUCLIDEAN SPACE

U EUCLIDEAN GEOMETRY

EULER BUCKLING

Euler method applicability for finite subcritical deformation stability of isotropically nonlinear elastic body

01 p0165 A71-10065

Euler method applicability for finite subcritical deformation stability of isotropically nonlinear elastic body

09 p1541 A71-23272

Euler buckling of hinged slender prismatic bars of rectangular and elliptic cross sections with shear and transverse stress allowance

10 p1685 A71-23959

Axisymmetric deformation differential equations system for nonlinearly elastic shells under vertical loadings, considering various Euler buckling boundary problems

11 p1848 A71-25567

Orthotropic bar under compression loads, calculating Eulerian values for critical force

17 p2817 A71-34335

EULER EQUATIONS OF MOTION

Lunar arbitrary and free librations and Euler motion of poles, considering hard and elastic models

01 p0158 A71-10807

One dimensional unsteady barotropic fluid flow based on Euler equations, describing rarefied plasma nonlinear motions

03 p0462 A71-13289

Euler-Poisson equations for heavy solid body motion about fixed point, deriving particular solution

03 p0457 A71-13581

Euler problem on permanent axes of rotation with extension to spinning gyrostat

04 p0662 A71-15195

One dimensional unsteady barotropic fluid flow based on Euler equations, describing rarefied plasma nonlinear motions

09 p1504 A71-23265

Three dimensional unsteady irrotational flow in variable cross section duct, reducing Navier-Stokes equation to Euler equation

10 p1591 A71-23850

Elastically suspended gyroscope dynamics, using Euler equations of motion allowing for casting rotation

15 p2410 A71-32455

Numerical integration of Euler equations for three dimensional time dependent unsteady flow by extension of method of characteristics

18 p2904 A71-36302

Singularities of Euler equations in turbulent flow problems, studying design of difference schemes

18 p2907 A71-36335

Finite difference methods application to Euler nonlinear elliptic differential equations, using symmetric and positive Jacobian

22 p3567 A71-42375

EULER-LAGRANGE EQUATION

Lagrange equations of motion of gyroscope having fixed point in presence of constant gyrostatic moment, obtaining particular solution

03 p0457 A71-13582

Lagrangian methods yielding relativistically covariant formalism for wave packets in weakly inhomogeneous and time dependent plasma dynamics, obtaining motion equations from Euler-Lagrange equations

05 p0789 A71-16657

Criterion on types of extrema of singular solutions of conditional equations in calculus of variations from Euler function behavior with respect to integration path

13 p2096 A71-29322

Ekman boundary layer energy stability, determining effective Reynolds number critical value by Euler-Lagrange equations numerical integration

14 p2226 A71-30410

Hamilton-Jacobi equation application to forces selection for mechanical systems asymptotic stabilization, minimizing functional by Euler-Lagrange equations

16 p2602 A71-32814

Electrodynamics Lagrangian with gauge invariant electron operator, obtaining free field nonequal time commutators and photon propagator for perturbation theory

16 p2610 A71-33269

Free-Lagrange method for two dimensional flow numerical simulation, covering mesh optimization and equations of motion

18 p2905 A71-36304

Lagrange equations for variable mass systems with rotational transport and relative motions

23 p3773 A71-43093

Lagrangian equation of motion for crack wall driven by square tension impulse, obtaining deflection in terms of crack length and particle velocity

23 p3777 A71-43496

EUROPA LAUNCH VEHICLES

NT EUROPA 1 LAUNCH VEHICLE

NT EUROPA 2 LAUNCH VEHICLE

NT EUROPA 3 LAUNCH VEHICLE

- Europa I/II third stage integration and systems testing, discussing checkout hardware and software [DGLR-70-058] 05 p0815 A71-15971
- Europa project ELDO multistage launchers electrical mockup tests for interface and coordination problems 06 p0979 A71-18000
- Qualification tests for equatorial ELDO Europa Launch Site with MSRV, discussing checkout system and performance 23 p3661 A71-43474
- EUROPA 1 LAUNCH VEHICLE**
- Europa 1 multistage booster rocket interstage electric circuit connection, discussing specifications and compatibility tests [DGLR-70-059] 05 p0697 A71-15955
- Europa 1 third stage flight testing for onboard control system performance parameters [DGLR-70-061] 05 p0815 A71-15963
- Power spectrum analysis of ELDO Europa 1 third stage thrust phase vibrations, using digital filters 07 p1208 A71-19804
- EUROPA 2 LAUNCH VEHICLE**
- Europa 2 booster payload increase by using beryllium-containing solid fuels in perigee and apogee stages 05 p0815 A71-15969
- Europa 2 booster rocket third stage attitude control system, describing measuring, controlling and actuating functions dynamic integration and checkout 05 p0815 A71-16134
- Solar electric propulsion and transfer system for higher payloads of SECOM communication satellites, using Europa 2 launcher 16 p2644 A71-32855
- Elliptical and circular orbit satellite injection capabilities of Europa 2 launch vehicle, considering geostationary orbit and launcher performance 16 p2645 A71-33364
- High energy solid propellants use in Europa 2 launch vehicle perigee-apogee motor, considering synchronous satellite payload increase 16 p2645 A71-33365
- Scientific objectives and satellite design of ESRO sponsored geostationary space mission, describing Europa II launcher design and operation 22 p3608 A71-41952
- EUROPA 3 LAUNCH VEHICLE**
- Europa 3 experimental preparatory program, discussing hardware development and project management planning and control [DGLR-70-064] 05 p0839 A71-15949
- Europa 3B launcher first stage, discussing design concept with emphasis on reliability and low cost 05 p0816 A71-16401
- Europa 3 two stage vehicle characteristics, outlining electrical system configuration and payload capacity 18 p2971 A71-35927
- Europa 3 launch vehicle, considering background history, mission requirements and performance profile 21 p3454 A71-40157
- Cryogenic liquids thermal behavior under operational conditions, discussing Europa 3 second stage liquid hydrogen and oxygen engine 22 p3588 A71-41502
- Europa 3 electrical system as integrated vehicle control system using central processor and data bus 22 p3608 A71-41957
- EUROPE**
- Aeronautical projects development and planning in European Economic Community, discussing aerospace industry organizational problems and role in economy 02 p0334 A71-11676
- Synoptic climatology of Euroatlantic blocking situations, investigating geographic location and duration 14 p2271 A71-30937
- Synoptic climatology of blocking situations over European-Atlantic region, obtaining middle troposphere circulation patterns by statistical analysis 21 p3411 A71-40826
- EUROPEAN AIRBUS**
- French contribution to air transportation, discussing international cooperation on supersonic Concorde, medium range airbus and short range Mercure 15 p2350 A71-32688
- European airbus development, discussing basic, long range and stretched capacity versions and aerodynamic and structural design features 20 p3177 A71-38749
- European airbus design and performance, covering electrical system, air conditioning, engines and flying control circuits 22 p3482 A71-42236
- EUROPEAN SPACE PROGRAMS**
- European governmental and industrial roles in space programs, discussing cost efficiency requirements 01 p0183 A71-10265
- Air traffic control by satellite, discussing CNES-SGAC and ESRO experiments within Dioscours project test program 01 p0125 A71-10748
- Position finding for auroral electrojet using magnetometer measurements onboard Black Brant 3 rockets 01 p0075 A71-11331
- French book on European space program covering past decade events and future prospects 02 p0337 A71-12594
- Regional European communications satellite system operation, discussing coverage area, performance requirements, meteorological aspects of propagation, etc 02 p0221 A71-12782
- European X ray astronomy lunar occultation satellite, providing high resolution cosmic X ray source observation 02 p0303 A71-12952
- U.S.-Europe cooperative space programs survey and experience from project management with ESRO-1 satellite 04 p0692 A71-15349
- DIAL satellite project, discussing geocoronal hydrogen concentration, upper atmosphere electron density, magnetic field measurement, etc 04 p0664 A71-15649
- Europa 3 experimental preparatory program, discussing hardware development and project management planning and control [DGLR-70-064] 05 p0839 A71-15949
- Post-Apollo space programs European collaboration, discussing space shuttle and space tug projects [DGLR-70-067] 05 p0839 A71-15957
- Ground operations computer system for German Aeros, Symphonie and Helios satellite projects, discussing communication and data processing systems integration [DGLR-70-079] 05 p0733 A71-15962
- UK space program, discussing international cooperation, sounding rocket development and performance and military communication satellites 05 p0806 A71-16148
- American-European space shuttle costs, comparing nonrecoverable Europa 3 with ballistic reusable devices 05 p0816 A71-16402
- Europa 3C light alloy space booster powered by Rolls-Royce engines using kerosene and LOX 05 p0816 A71-16403
- European telecommunications satellite project, discussing INTELSAT and telephony-telegraphy-telex system 06 p1010 A71-17999
- Thermal control surfaces experiment onboard Black Arrow X3 satellite 06 p0981 A71-18675
- Central station of German ground system for satellite data acquisition, tracking and telecommand 07 p1082 A71-19021
- ESRO/ELDO space documentation service involving NASA file remote processing and data bank for space component selection 07 p1225 A71-20001
- European satellite projects chronological survey covering ESRO and national projects 09 p1547 A71-22419
- SIRIO project mission analysis, discussing space communication and magnetospheric investigations by scientific satellite in geostationary orbit 10 p1670 A71-24268
- SIRIO satellite project, discussing orbital dynamics, propulsion system, attitude control, onboard and ground electronic equipment 10 p1682 A71-24272
- European research on reentry vehicle configurations, noting French concentration on flow fields and German emphasis on overall shape and control surfaces 10 p1684 A71-24848
- Post Apollo program European participation in space tug design and orbiter model flight tests, considering mini shuttle support applications 11 p1839 A71-26331
- Symphonie Franco-German satellite telecommunication system, describing orbital launching operations 11 p1840 A71-26523
- Project Symphonie status in January 1971, discussing booster stages, ground stations, thermal control, stabilization, power supply system, telecommunication equipment and telecontrol system 11 p1840 A71-26524
- Equatorial CECELES/ELDO base management and conduct of launch operations, discussing installations, facilities, equipment and personnel 12 p1894 A71-26696
- Sirio B European communication satellite, discussing electronic equipment for simultaneous multichannel telephony and color TV transmission 14 p2319 A71-29820
- German-French Symphony synchronous communication satellites, discussing frequency and time division multiple access subsystems characteristics 14 p2193 A71-29824
- Post-Apollo program European participation, discussing need for multilateral international agreements on space shuttle, space tug and space station projects 14 p2341 A71-30262
- European electric propulsion systems for flight trajectories within low gravity fields and orbital parameter attitude control and correction 15 p2469 A71-31730
- French space programs review with emphasis on compatibility with European and international programs 15 p2495 A71-32689
- European scientific experiments satellite, describing design features and mission capabilities 15 p2501 A71-32693
- Azur satellite mission report, discussing major anomalies, energy supply, position control, temperature behavior and orbit [DGLR-71-008] 15 p2501 A71-32779
- Scientific goals and mission behavior of Dial aeronomy satellite for spatial distribution determination of atmospheric hydrogen concentration [DGLR-71-004] 15 p2501 A71-32781
- European meteorological satellite system, discussing measurement program, data management, orbital parameters and stability, satellite positioning and instrumentation 16 p2644 A71-32844
- European satellite telecommunications network design, discussing shuttle-tug launcher use and economy 16 p2644 A71-32848
- European geostationary telecommunication satellite stabilization using ion thrusters 16 p2623 A71-32851
- European space research center, discussing satellite scientific and engineering data transmission and processing 16 p2553 A71-33422
- Symphonie communication satellite subsystem, discussing geostationary positions, launchers, frequency ranges and transmission zones 16 p2543 A71-33583
- German space operations center for performing ground operations for Azur research satellite 16 p2553 A71-33747
- Swiss space research, surveying international cooperative scientific activity relative to upper atmosphere satellite geodesy, solar wind, lunar samples analysis, IR and UV astronomy and celestial mechanics 16 p2665 A71-33852
- Swedish space research activity covering upper atmospheric physics, ionosphere, magnetosphere and solar phenomena 16 p2665 A71-33853
- Rumanian space research, reviewing participation in socialist nations programs in physics, meteorology, communications and biology 16 p2665 A71-33854
- Polish space research covering satellite tracking, solar physics interplanetary gas dynamics, meteorological rockets and aerospace medicine 16 p2666 A71-33856
- Netherlands space research including solar, stellar and cosmic radiation observations, photometry and satellite geodesy 16 p2666 A71-33858
- UK space research programs, discussing ground based, satellite and rocket-borne experiments 16 p2666 A71-33859
- Italian report to COSPAR on 1970 space research, discussing 1971-72 programs for cosmic radiation, space plasma, meteorology, communications and international cooperation 16 p2666 A71-33862
- German Democratic Republic space research, reviewing meteorological, ionospheric, geomagnetic and solar physics studies 16 p2666 A71-33864
- West German space research activities during 1970 on meteorology, ionospheric physics, solar radiation, cosmic rays and life sciences 16 p2666 A71-33866
- ESRO report to COSPAR on sounding rockets and geostationary satellites development, orbits and decay during extraterrestrial gamma radiation 16 p2667 A71-33867
- Belgian report to COSPAR, reviewing experiments with gas release at high altitudes and stratospheric balloons 16 p2667 A71-33870
- European regional satellite communication system, discussing TV coverage, spot beam antennas, frequency reuse, speech interpolation and circuits allocation 17 p2700 A71-34679
- X 4 satellite of British National Space Program, discussing design features, orbit, configuration, power subsystem, data handling and attitude control 17 p2814 A71-35330
- Direct thrust measurement on electrostatic ion engine ESKA 18 P, comparing with values calculated from applied voltage and ionic current [DGLR-71-043] 17 p2793 A71-35538
- ESRO activity in low thrust electric propulsion systems development for attitude stabilization and stationkeeping, using colloid and field emission thruster concepts [DGLR-71-035] 17 p2794 A71-35541
- Electrical propulsion systems research at Braunschweig installation covering plasma generation, ion sources, plasma accelerators, etc [DGLR-71-024] 17 p2794 A71-35544

ESRO sounding rocket program covering atmospheric and ionospheric physics and solar and auroral phenomena

18 p2896 A71-35926

European space tug orbit to orbit autonomous shuttle system, discussing participation in post-Apollo programs

18 p2988 A71-36489

European space programs, presenting post-Apollo utilization views [ALAA PAPER 71-817]

18 p2988 A71-36500

Satellite broadcasting of TV programs, assessing cost for European community

18 p2876 A71-36503

Satellite TV broadcasting development in European community, giving cost estimation procedure and program reception methods

18 p2876 A71-36504

ESRO part of joint ATC communication experiment for L band satellite use, giving voice and data transmission and distance measurement techniques tests results

18 p2945 A71-36510

European regional satellite communication system, discussing TV coverage, spot beam antennas, frequency reuse, speech interpolation and circuits allocation

18 p2877 A71-36516

European 12 GHz regional satellite telecommunications systems, discussing band assignment limitation and frequency reuse

18 p2877 A71-36517

Italian SIRIO experimental SHF telecommunications satellite, noting trapped radiation and high energy electron experiments

18 p2974 A71-36521

Franco-German Symphonic communication satellite, discussing missions and subsystems design features

18 p2974 A71-36522

Data transmission system of Franco-German Symphonic communication satellite

18 p2889 A71-36523

Franco-German Symphonic communication satellite reliability measures, describing component selection methods

18 p2889 A71-36524

Propagation model type effect on modulation and multiple access techniques choice for regional European communication satellite system

18 p2880 A71-36550

Italian SIRIO synchronous satellite for SHF communication, analyzing thermoelastic deformations effect on antenna radiation patterns

18 p2882 A71-36575

U.S. and U.S.S.R. space stations with European participation, discussing design, international cooperation and legal and political problems

19 p3149 A71-37305

European unmanned interorbital tug, investigating configurations, structure, hookup system, docking and propellant supply

19 p3150 A71-37309

European contribution to space shuttle and tug reusable space transportation systems, discussing post-Apollo programs cost analysis and hardware

19 p3150 A71-37310

Right ascension and declination accuracy for Sirio satellite attitude determination in transfer orbit, describing computer program

19 p3150 A71-37312

Italian weather satellite system for Mediterranean meteorology, noting social and economic aspects

19 p3150 A71-37313

Technical prospects of European aerospace industries participation in post-Apollo program, noting space shuttle development role

19 p3151 A71-37324

European contributions to post-Apollo space program, considering space station, space shuttle and space tug

19 p3151 A71-37325

ELDO studies of interorbital space tug for transfer of satellites in geosynchronous orbits

19 p3151 A71-37327

Systems planning and operation of European applications satellites, noting Sirio and Symphonic programs

19 p3172 A71-37329

European launcher programs and participation in post-Apollo shuttles and orbital stations development in partnership with U.S.

19 p3151 A71-37330

Technical parameters and performance tradeoffs of ESRO preoperational aeronautical satellite program

19 p3153 A71-38067

Mission tasks and design problems of European space tug, considering geostationary transfer missions and cargo bay geometry

21 p3454 A71-40158

Scientific objectives and satellite design of ESRO sponsored geostationary space mission, describing Europa II launcher design and operation

22 p3608 A71-41952

International cooperation in astronautics, reviewing European satellites launching and world distribution of lunar rock and soil samples

22 p3623 A71-42012

Space project management techniques under European conditions, covering requirements, style, motivations, concepts and rules

23 p3785 A71-43458

Project management by contractual procedures for ELDO space research

23 p3786 A71-43466

Quality control organization in British spacecraft projects, discussing material selection system and subsystem tests, process engineering and inspector training

23 p3681 A71-43470

EUROPEAN SPACE RESEARCH ORGANIZATION SAT

NT AZUR SATELLITE

NT ESRO 1 SATELLITE

NT ESRO 2 SATELLITE

EUROPIUM

Redox estimation from natural phase Eu ion concentrations in rocks

01 p0029 A71-11428

Eu II and La II line profiles in sunspots and undisturbed photosphere

05 p0803 A71-16022

Energy transmission mechanism in calcium fluoride-europium ion plus holmium ion system, investigating luminescence and absorption spectra

09 p1461 A71-22388

EUROPIUM COMPOUNDS

Europlum hexaboride-high melting point metals reaction for intermetallic compounds production, noting evaporation kinetics

06 p0913 A71-18087

EUTECTIC ALLOYS

Splat cooled hypoeutectic Al-Cu alloy superplasticity, using tensile tests and electron microscopy

01 p0100 A71-10280

Cu compatibility with refractory Ta-W alloy interface at high temperature, noting eutectic formation

01 p0100 A71-10374

Cadmium-copper fibrous eutectic alloy morphology, describing sample preparation and crystallographic examinations by optical and electron microscopes

01 p0103 A71-11018

Cr-chromium nitride fusion phase diagram analysis, establishing nonvariant eutectic and dissociative transformations

02 p0266 A71-12673

Metal whisker composite technology based on unidirectionally solidified eutectics, discussing mechanical behavior of whisker phase isolated from matrix

04 p0611 A71-14950

Zr-Ga phase diagram eutectoid region metallographic analysis, discussing solubility, reactions and compound formation

04 p0614 A71-15779

Volume diffusion role in Ni-Cr eutectic and cast alloys cellular structure growth

04 p0615 A71-15793

Scanning electron microscopy for microstructures of various eutectic Ni alloys, discussing rod-plate transition

06 p0914 A71-18681

Ni-W eutectic alloy unidirectional solidification to obtain composite structure in Ni-W solid solution

06 p0915 A71-18689

Unidirectionally aligned fiber phase solidified eutectic composites model, discussing high temperature rupture and creep properties

08 p1323 A71-21585

Co-Cr and Ni-Cr eutectic alloys with single crystal TaC fiber reinforcement, discussing unidirectional solidification

09 p1479 A71-23623

Ti-Ti5Si3 eutectic oriented solidification structures, showing unidirectional growth faceted silicide fibers and disorientation

10 p1626 A71-24402

Crystallographic relationships between Ni- and Cr-rich solid solutions, noting preferred interphase interfaces in Ni-Cr eutectic alloy

11 p1778 A71-25532

Mg-Al eutectic alloy and commercial-purity Zr stress relaxation tests and mechanical behavior

11 p1780 A71-26022

Monovariant eutectic Co-Cr-C ternary systems, determining pseudobinary and near-pseudobinary phases by differential thermal and microprobe analyses and optical microscopy

11 p1780 A71-26025

Orientation dependent impact toughness and crack resistance of brittle fiber-ductile matrix composite of solidified carbide reinforced Co-Cr eutectic

11 p1782 A71-26386

Strain and strain rate effect on flow stress and microstructure of Al-Cu eutectic alloy during superplastic deformation, deriving stress-strain diagrams

13 p2086 A71-28624

Ni-Ni Nb eutectic composite, investigating monotonic mechanical response, deformation and fracture mechanisms

13 p2088 A71-29401

Shape instabilities for eutectic alloys composite microstructure at elevated temperatures

14 p2259 A71-30413

Al and Cu-Al alloys eutectic composites with small interlamellar spacing, characterizing ambient temperature compressive stress strain behavior to failure

15 p2432 A71-32168

Nickel and cobalt pseudobinary eutectic alloys reinforced by refractory metal monocarbides whiskers, studying mechanical properties, solidification and phase equilibria

15 p2432 A71-32169

Unidirectionally solidified Ti-base eutectic composites and alloys strength and microstructural stability under heat treatment

15 p2432 A71-32170

Thermally induced residual stresses effect on yield behavior of unidirectionally solidified eutectic composites

15 p2432 A71-32171

Mechanical properties of carburized cermet steel with hypereutectic structure after water quenching and tempering at 300 C

19 p3076 A71-37113

Intermediary eutectic delta phase in Ti-Os equilibrium diagram based on microstructural, X ray and differential thermal analyses

19 p3078 A71-37467

Eutectic Al alloys parallel alignment formation by stable isothermal boundary surface, investigating microstructure

21 p3396 A71-40029

Aluminum-aluminum nickelide rod eutectic composite elevated temperature stability, presenting coarsening kinetic analysis

21 p3398 A71-40469

Resistance NOR Ti BOND joining of Ti shapes, forming Ti-Cu eutectic at Cu plated Ti joint interface

21 p3387 A71-40620

Beta eutectoid and solid solution Ti binary alloys omega phase morphology observation by transmission electron microscopy, noting elliptical and cubic types hexagonal crystal structure

22 p3562 A71-41946

Al-Co and Al-Ni alloy rods unidirectionally solidified, discussing compositional range in eutectic structures at high solidification rates

23 p3689 A71-43101

Zirconium carbide eutectic and supraeutectic alloys preparation with graphite addition, determining heat resistance under thermal cycling tests

23 p3697 A71-44025

Mechanical properties of Al-aluminum intermetallic eutectic alloys after rapid solidification in semicontinuous casting technique, noting flow stress and tensile strength increase

23 p3695 A71-44286

EUTECTIC DIAGRAMS

U PHASE DIAGRAMS

EUTECTICS

NT EUTECTIC ALLOYS

Eutectoidal decomposition of tantalum dicarbide, noting X ray phase identification during carburization of tantalum ribbons

20 p3252 A71-39961

Heat resistant and refractory materials contact eutectic melting for surface coating production

21 p3390 A71-41175

EVACUATING (TRANSPORTATION)

Aircraft emergency evacuation illumination standards, considering independent power source, crash survivable installation, operation initiation and exit visibility

01 p0004 A71-10030

EVACUATING (VACUUM)

Hydrogen evacuation with He condensation pump in ultrahigh vacuum region

23 p3661 A71-43272

EVAPORATION

NT PROPELLANT EVAPORATION

NT TRANSPARATION

Interstellar gas cloud equilibrium and gravitational stability, examining evaporation, condensation, thermal balance and pressure

04 p0658 A71-15837

Liquid fuel drop evaporation under pressure on hot surface, measuring lifetime and transient interface temperature at subcritical and supercritical conditions

04 p0689 A71-15919

Mass transfer net rate /evaporation plus entrainment/ from thin liquid film, using methanol, water, butanol and RP-1 as coolants

07 p1222 A71-18997

Laser beam evaporation of dense substances, examining luminous flux densities with gas dynamic equations

07 p1127 A71-20253

Evaporation of dirty ice particles surrounding early type stars, using dust grains model for explanation of anomalous reddening of Orion Nebulae

08 p1364 A71-21415

Kinetic theory of transient condensation and evaporation at plane surface, using Maxwell moment formulation 09 p1545 A71-22852

Plane stationary shock wave propagation through one component vapor-liquid mixture, calculating profile and mixture parameters under evaporation and condensation 10 p1593 A71-24348

Solids evaporation into vacuum, considering interconnected problems of heat conduction and evaporation front boundary conditions 10 p1697 A71-25063

Mo evaporation in vacuum, oxygen and water vapor atmospheres at high temperatures 11 p1709 A71-25865

Heat and mass transfer in triple interline region of stationary evaporating meniscus on flat plate immersed in liquid pool 13 p2164 A71-29006

Room temperature evaporating water drop shape history on cooper, lucite, stainless steel and Teflon, observing wetting dynamics effects 21 p3476 A71-40903

EVAPORATION RATE

Pure hydrocarbon droplets heating, expansion, vapor phase fuel storage and gasification in oxidizing gas at elevated pressures, using high speed cinematography 06 p1007 A71-18300

Evaporation rate of droplet with internal heat source from Maxwell-Langmuir theory extension 08 p1377 A71-21926

Shock wave interaction with evaporating aerosol for diffusive and ablative models taking into account thermal conductivity 09 p1433 A71-22856

Ethyl and methyl alcohol droplets vaporization rate variation with respective distance from photographic observations 14 p2285 A71-30612

Liquid phase evaporation rates in free turbulent air-liquid droplet jet, giving droplet dynamic characteristics determination criterion 14 p2227 A71-30613

Thermal emission analysis method for studying phase transformations and chemical conversion kinetics in multicomponent systems, applying to liquid evaporation rate measurement 14 p2338 A71-30618

Zirconium monocarbide congruent vaporization rate and temperature dependence for nonstoichiometric compositions 15 p2431 A71-32157

Numerical analysis of accretion growing grains segregation in gravitational field with resisting gas, discussing motion equation, evaporation rate and planetary evolution 15 p2489 A71-32397

Liquid spray steady evaporation and mixing in gaseous swirl, using continuum mechanics 17 p2727 A71-34693

Evaporation rate of droplet with internal heat source from Maxwell-Langmuir theory extension 17 p2838 A71-35270

Detonation propagation through tubes with thin fuel film coated walls, obtaining heat transfer coefficients, friction, evaporation rate, reaction zone length and propagation velocity 19 p3171 A71-38129

Laser pulse heated target with thermal plasma production, obtaining target surface temperature as function of time and vaporization rate 20 p3242 A71-38845

EVAPORATIVE COOLING

NT FILM COOLING

NT SWEAT COOLING

Transpiration cooling heat transfer in incompressible turbulent boundary layer, using Couette flow model, boundary layer model and combinations of both 07 p1219 A71-18758

Turbocharged diesel engine precompressed inlet air cooling by evaporation cooling, considering water injection effects on centrifugal compressor 08 p1347 A71-20781

Single phase and evaporative systems for liquid cooling high temperature gas turbine rotor blades, reviewing heat transfer performance evaluation 15 p2469 A71-31734

Thermal control using nitrogen, circuit board, switching, flexible, transformer and segmented evaporator heat pipes [ASME PAPER 71-AV-29] 18 p2868 A71-36396

Maximal sweat evaporative heat loss and permitted work load measurements as function of temperature and clothing insulation 18 p2872 A71-36861

Heat acclimatization by evaporative cooling prevention in men wearing vapor barrier suits, considering body temperature and heart and sweat rates 21 p3331 A71-40355

EVAPORATORS

Elemental maximum energy transport formula for wick heat pipe evaporators under artificial gravity and external acceleration, testing by laboratory centrifuge [AIAA PAPER 71-419] 11 p1857 A71-26210

EVAPOROGRAPHY

Light ion flow from polar caps in hydrodynamic and evaporative forms, noting pressure gradient force, exospheric electric field and realistic boundary conditions 09 p1440 A71-23459

EVASIVE ACTIONS

Efficient evasion strategies for vehicle pursuit-evasion games with imperfect information, using computer solution 06 p0846 A71-17331

Soviet monograph on differential games of encounter of motions covering optimal control, rendezvous, pursuit, evasion, extremal guidance, etc 06 p0926 A71-17438

Optimal control epsilon technique solution for capture conditions in pursuit and evasion problems 06 p0918 A71-17597

Pursuit and evasion games, proving existence and approximation theorems 06 p0921 A71-18238

Unmanned spacecraft pursuit of evading manned vehicle by game theory, assuming full information availability to both players 19 p3038 A71-38014

EJECTION

U LUNAR ORBITS

U ORBIT PERTURBATION

U SOLAR GRAVITATION

EVENTS

NT CONSECUTIVE EVENTS

EVOLUTION [DEVELOPMENT]

NT ABIOTIC EVOLUTION

NT BIOLOGICAL EVOLUTION

NT GALACTIC EVOLUTION

NT LUNAR EVOLUTION

NT PLANETARY EVOLUTION

NT STELLAR EVOLUTION

Precision gyro and accelerometer testing evolution, noting instrument performance and electrical and mechanical equipment [AGARDOGRAPH-128] 05 p0749 A71-16303

Solar system evolutionary problems - Conferences, University of Rome, November 1968 and February 1969 07 p1202 A71-20512

Resonances stability and development in restricted three body problem with two degrees of freedom 07 p1202 A71-20514

N body system variables evolution, discussing complete scattering based on mean quadratic and harmonic distances 10 p1642 A71-24432

Lost City meteorite secular and encounter perturbation effects on orbital evolution, interpreting short lived cosmic radiogenic isotopes formation 15 p2489 A71-32359

Density and luminosity evolution of radio source population, considering counts per unit co-moving volume at cosmological epochs 18 p2961 A71-35966

Radio source counts interpretation by cosmological evolution models, suggesting luminosity role 22 p3606 A71-42600

EVOLUTION [LIBERATION]

NT GAS EVOLUTION

EXACTNESS

U PRECISION

EXAMINATION

NT EYE EXAMINATIONS

EXCHANGING

NT CHARGE EXCHANGE

NT GAS EXCHANGE

NT ION EXCHANGING

NT RESONANCE CHARGE EXCHANGE

EXCITATION

NT ACOUSTIC EXCITATION

NT ATOMIC EXCITATIONS

NT HARMONIC EXCITATION

NT MOLECULAR EXCITATION

NT SELF EXCITATION

NT WAVE EXCITATION

Fluorine ions excited levels mean lives from beam-foil line spectrum analysis 01 p0129 A71-10138

Inhomogeneous plasma oscillations excitation by high intensity electron beam, causing instability greater than hydrodynamic beam mode 02 p0288 A71-11890

Carbon dioxide molecules dissociative excitation processes by low energy electrons, examining light emission mechanism in VUV 02 p0261 A71-12318

CW carbon dioxide lasers low voltage excitation, using cold cathode transverse glow discharges 03 p0436 A71-13642

Total radiative interchange kernel measurements, describing remote excitation/detection 04 p0684 A71-15511

Arrhenius activation energy in relation to excitation functions for various reaction types 05 p0716 A71-15976

Lasers operating on rotation vibration of chemically formed carbon monoxide, discussing excitation methods 06 p0908 A71-18312

Ce 138 excited states identification in beta decay spectra of Pr 138m and Pr 138 sources, using proton target bombardment 07 p1163 A71-19547

Diatomic molecules nonsigma states rotational excitation adiabatic theory 07 p1164 A71-19691

Vibrationally excited ground state hydroxyl in fast flow system, considering mean radiative lifetime and reaction rate with ozone 08 p1250 A71-20662

Symmetric excited state electron capture cross sections in ion-atom inelastic scattering, using two state approximation formulas 08 p1338 A71-21235

Inelastic collision effects on vibrational excitation of diatomic molecules with conserved energy 08 p1338 A71-21781

Nitrogen excitation by fast protons and electrons impact, obtaining primary collision cross sections by measurements extrapolation to zero pressure 10 p1664 A71-24793

Strip array excitation by field with large phase shift per period, deriving approximate solution from averaged boundary conditions 13 p2029 A71-28361

Hydrated electrons photoexcitation by giant pulse Q-switched ruby laser, investigating absorptivity over wide range of light intensities 17 p2753 A71-34950

Ionization and excitation kinetics of Hg in relaxation flow zone behind shock wave front, considering electron impact role in ground state atoms ionization 18 p2951 A71-35980

Cd ion laser with He-Ne, suggesting Cd ion excitation by Penning process 18 p2929 A71-35981

Bifurcation/branch point/ theorems and limit cycles for integral curves of hard excitation nonlinear systems 22 p3527 A71-42675

EXCITED STATES

U EXCITATION

EXCITONS

Photoelectron emission of organic semiconductors, considering molecular and defect photoionization and exciton collisions 03 p0467 A71-13399

KCl films exciton-induced photoemission, discussing mechanism of photoelectron emission rise with time under steady UV radiation 09 p1508 A71-22685

Stimulated emission of ZnO laser by electron beam excitation at 82-250 K near A-L-O line, considering exciton interactions 16 p2589 A71-34121

Exchange interaction in excitons for arbitrary band structure of semiconductors in effective mass approximation allowing correction 21 p3431 A71-41262

Mott exciton differential absorption spectrum in parallel and crossed electric and strong magnetic fields 23 p3716 A71-43479

Urbach absorption-photon energy law for excitons in AII-BVI semiconductors 23 p3716 A71-43481

EXCRETION

Toxic substances absorption, metabolism and excretion by man, discussing role of solubility, transfer through membrane tissue, liver and kidney as metabolizing and excreting organs 07 p1042 A71-19700

Dog uropepsin excretion dynamics under extremal flight conditions, detailing hypoxia, high temperature radical accelerations and impact G forces effects 15 p2358 A71-31322

Antidiuretic action of chlorpromazine in mammalian kidney, considering intrarenal infusions effect on urinary concentration, free water clearance, glomerular filtration and sodium excretion 22 p3486 A71-41939

EXERCISE AIRCRAFT

U GENERAL AVIATION AIRCRAFT

U PASSENGER AIRCRAFT

EXERCISE [PHYSIOLOGY]

Vasodilator, oxygen, potassium and osmolality effects on exercise hyperemia in dog gracilis muscle 01 p0015 A71-11184

Cardiovascular and ventilatory responses to room air and pure oxygen breathing under various exercise work load conditions 01 p0016 A71-11407

CO pulmonary diffusing capacity rebreathing measurements at rest and while exercising, noting relationship to oxygen consumption 04 p0545 A71-15162

Blood lactate levels in human males after bicycle rides, considering altitude effects on oxygen consumption and glycolytic and aerobic activity
05 p0709 A71-16623

Carbohydrate metabolism and electrolyte changes in human muscle tissue during heavy exercise
06 p0856 A71-18387

Walking effects on body composition and cardiovascular function of middle aged men
06 p0862 A71-18388

Rats under various exercise programs, determining cardiac ventricle and gastrocnemius muscles calcium activated adenosine triphosphatase activities
09 p1400 A71-23361

Coronary blood flow measurements during strenuous upright exercise, using nitrous oxide method
09 p1400 A71-23362

Human electromyogram and isometric muscle tension dynamic relationship
09 p1400 A71-23363

Skin cooling effect on awake exercising dog ventilation, noting carbon dioxide response curve, arterial partial pressure and hypernea
09 p1396 A71-23366

Human steady and unsteady state treadmill exercise, comparing cardiac output, heart rate and oxygen uptake interrelationships
09 p1401 A71-23367

On-line computer technique for pulmonary ventilation continuous/automatic measurement of cardiac patients exercise and work tolerances
11 p1734 A71-25255

Body temperature regulation and heat dissipation responses during continuous and intermittent exercise in man
11 p1721 A71-26354

High oxygen tension during severe exercise, studying effects on humoral and nervous ventilation changes
11 p1722 A71-26363

Wired monitoring system for continuous interference-free twelve-lead ECG recording before, during and after exercise
12 p1876 A71-27630

Baroreflex regulation of pulse interval during bicycling exercise, using systolic pressure-pulse relation to express reflex sensitivity
13 p2012 A71-28951

Body fat influence with and without denitrogenation on decompression sickness in men exercising after abrupt exposure to altitude
13 p2022 A71-29361

Maximal human anaerobic power, discussing unsplit phosphagen concentration in muscles during steady state exercise
16 p2530 A71-33247

Papers on exercise and cardiac death covering coronary athero- and arteriosclerosis, congenital anomalies, myocarditis, tumors and physical exertion
18 p2855 A71-36213

Convective and conductive heat loss analysis of underwater swimmers and divers exercising in cold water
18 p2861 A71-36892

Daily endurance exercise influence on key tissues resting aerobic metabolism, using Warburg technique to determine rats heart, skeletal muscle and liver tissue oxygen consumption
20 p3185 A71-38886

Alkalosis effect on human maximal performance and lactic acid formation in blood under supramaximal exercise conditions
20 p3185 A71-38888

Postexercise elevated tissue temperatures contributions to oxygen consumption in rats, suggesting hypothalamic adjustment
20 p3186 A71-38981

EXERTION

U PHYSICAL WORK

EXHALATION

Exhaled air microimpurities composition of humans exposed to stress effects including bed rest, starvation, lyophilized diet feeding, high temperature and humidity
13 p2007 A71-28412

EXHAUST DIFFUSERS

Inlet circulation and swirl effect and optimum vane angle for maximum efficiency of subsonic straight conical diffusers
20 p3177 A71-39875

EXHAUST FLOW SIMULATION

NT ATMOSPHERIC ENTRY SIMULATION

NT FLIGHT SIMULATION

One dimensional flow models of internal combustion engine exhaust silencers in noisy systems
11 p1810 A71-25180

Rocket engine exhaust jet simulation in wind tunnel tests, discussing principles derived from aerodynamic geometrical and physical similarity laws
12 p1945 A71-27466

Transient pressure measurement in plasma exhaust flow of 500 microsec duration, discussing discharge temporal behavior and cold gas pressure front existence
23 p3711 A71-43598

EXHAUST GASES

Gas turbines air pollution control, discussing exhaust composition, combustion chamber design, engine efficiency, etc
01 p0142 A71-10820

Heat transfer boundary conditions determination in studying heat protective coatings effectiveness, discussing measurement methods for stagnation temperatures and heat fluxes from exhaust gases
04 p0600 A71-15643

Critical nozzle pressure ratio and geometry effects on free exhaust gas jets of jet engine models [DGLR-70-055]
05 p0831 A71-15966

Aircraft gas turbine engines nitric oxide emission model, describing flow behavior and chemical processes
06 p0948 A71-18659

Lanthanum cobalt oxide as potential auto exhaust catalyst from studies of activity in gas phase
07 p1055 A71-19545

Mathematical model of nonstationary intake and exhaust gas motion in two cycle internal combustion engine cylinders
08 p1347 A71-20780

Gas turbine engines emission characteristics, discussing methods for pollutants reduction
08 p1349 A71-21820

Commercial supersonic flight, investigating air pollution and alleged climate and weather modification effects due to principal exhaust products
08 p1232 A71-21821

National Air Pollution Control Administration control of aircraft engine pollutant emissions covering measurement, test instrumentation, research, standards and regulations
08 p1379 A71-21831

Aircraft engine smoke emission control, discussing Ringelmann chart assessment for various commercial jet aircraft and airport gaseous pollutants
08 p1380 A71-21832

Aircraft smoke emission control, outlining legal action by New Jersey State Department of Health
08 p1380 A71-21833

Standard equipment and procedures for aircraft gas turbine engine exhaust smoke measurement [ASME PAPER 71-GT-88]
11 p1813 A71-25995

Aircraft piston and turbine engine soot extracts cancerogenic activity in hybrid mice
12 p1872 A71-27724

Visible exhaust smoke trails from aircraft jet engines, measuring optical density by photographic photometry [SAE PAPER 710428]
13 p2114 A71-28314

Air pollution study of jet aircraft emissions in airport vicinity, involving exhaust gas testing, ground operations and passenger cabin measurements [SAE PAPER 710429]
13 p2005 A71-28315

Chemical kinetic calculation of nitric oxide formation in spark ignition automobile engines and gas turbine combustors
14 p2190 A71-30454

Dispersion of jet aircraft exhaust emissions near airports and of smoke trails in upper atmosphere, assessing pollutant levels near large urban airports
15 p2349 A71-32244

Aircraft pollutant emission regulation, discussing low smoke combustors and fuel dumping problem
15 p2516 A71-32246

Rotating arc plasma jet exhaust flow pattern visualization, using bifocal lens system and photographic flash technique in particle track photography
16 p2579 A71-33339

Gas turbine engine combustion chamber outlet gas temperature field peripheral nonuniformity, detailing jets disruptive capacity effects in mixing zone
16 p2625 A71-33609

Spectral scanning method for determining temperature profile of jet- or rocket-engine exhaust stream by gas radiation and transmittance measurements, discussing radiometric errors effects
18 p2916 A71-36048

Stratospheric ozone reduction through catalytic action of nitrogen oxides from SST exhaust, discussing degrading effect on atmospheric radiation shield
18 p2874 A71-36922

Turbine propulsion system smoking and exhaust gas emission, discussing aircraft and automobile pollution emission
20 p3277 A71-39452

Operating variables effect on pollutant exhaust from jet aircraft turbine engines, discussing combustor design techniques for emissions reduction
23 p3718 A71-43600

EXHAUST JETS

U EXHAUST GASES

EXHAUST NOZZLES

NT CONVERGENT-DIVERGENT NOZZLES

NT PLUG NOZZLES

NT TURBINE EXHAUST NOZZLES

Flow field of two dimensional nozzle exhausting to vacuum, describing computer program based on BGK equation and plotting exhaust region density, temperature and velocity [AIAA PAPER 69-658]
01 p0002 A71-10932

Approximate calculation for far field flow distribution of nozzle exhausting into vacuum
01 p0072 A71-11595

Twin jet aircraft engine installation effects and exhaust nozzle integration, noting closely spaced inlet interference [ICAS PAPER 70-47]
03 p0469 A71-13148

Exhaust nozzles configurations effect on shear jet noise based on Ribner theoretical model
05 p0735 A71-16278

Supersonic transport inlet-engine-airframe compatibility programs, noting exhaust nozzle installation effects, distortions and noise [AIAA PAPER 68-993]
10 p1659 A71-24854

Air bypass behind compressor into variable area exhaust nozzle, obtaining energy losses from gas turbine jet engine indices
13 p2115 A71-28586

Optimal penetration effect on peripheral gas flow temperature field at outlet of turbine combustion chamber with circular flame tubes
13 p2118 A71-28971

High entrainment constant area multiple nozzle ejectors with two mixing tube lengths for boundary layer control, estimating performance with analytical model [ASME PAPER 71-FE-34]
13 p2053 A71-29469

Airframe installation effects on underwing nacelle nozzle performance, using calibrated engines and load cells on F-106 for measurements [AIAA PAPER 71-681]
14 p2292 A71-30745

Isolated axisymmetric jet engine exhaust nozzles thrust and drag predictions in sub-, trans- and supersonic flight regimes [AIAA PAPER 71-719]
14 p2295 A71-30770

Pressure distribution and drag prediction over slender axisymmetric fuselages and afterbodies and exhaust nozzles at transonic Mach numbers [AIAA PAPER 71-720]
14 p2170 A71-30771

Optimum conical mixing chambers configuration in supersonic ejectors, showing cylindrical exhaust channel requirement
18 p2903 A71-36121

Jet engines with afterburners, describing exhaust nozzle control, takeoff and landing advantages and thrust variations
21 p3437 A71-40858

Symmetrical and unilateral sticking flow modes of nozzle air jets expelled into plane-parallel and parabolic ducts
22 p3480 A71-42681

Supersonic propulsion system inlet, engine and exhaust nozzle in wind tunnel and flight tests, discussing boundary layer effects on performance
23 p3718 A71-43599

Plane cascades efficiency and exit blade angles dependence on cooling air admitted to air-gas flow area from exhaust nozzle guide vanes
24 p3864 A71-45009

EXHAUST SYSTEMS

Internal combustion engine exhaust system sound radiation, discussing pressure wave effects, energy flux and boundary conditions
05 p0796 A71-16604

Book on aircraft gas turbine engine technology covering combustion chambers, exhaust systems, lubricating oils, thrust augmentation, inlet ducts and overhaul procedures
08 p1348 A71-21625

Flow variation effect on velocity and flow angle distribution at exit of shrouded radial flow impeller with backward swept blades, using streamline curvature method [ASME PAPER 71-GT-15]
11 p1703 A71-25961

Aircraft propulsion system testing, stressing noise reduction and inlet-engine exhaust system compatibility [SAE PAPER 710450]
13 p2114 A71-28328

Commercial SST aircraft engine noise during takeoff, discussing exhaust geometries for suppression
15 p2468 A71-31595

Soundproofing of air inlets and fan exhausts with reference to absorbent systems with resonant cavities, technologies, environmental conditions and material fatigue
15 p2469 A71-31880

Transverse flow in cavity ensurance by air exhaust cooling of trailing edges of gas turbine blades with deflector
16 p2624 A71-33544

Optimal design for noise attenuation by diesel engine exhaust mufflers using linearized acoustic models
20 p3268 A71-38961

EXHAUST VELOCITY

Optimal control of exhaust velocity for plane motion of variable mass point along trajectory under gravitational and resisting forces
02 p0284 A71-12292

Minimum propellant deterministic guidance law for bounded-thrust constant jet exhaust velocity spacecraft, using neighboring extremal theory [AIAA PAPER 71-118]
06 p0978 A71-18568

- Solid Teflon fuel pulsed plasma thruster optical measurements, showing different exhaust velocities for neutral, singly, doubly and triply ionized atoms [AIAA PAPER 71-194] 06 p0948 A71-18632
- Multistep rocket mass ratios optimization, including exhaust gas velocities, structure and efficiency 16 p2644 A71-32843
- Pulsed plasma rail mercury propellant thruster for satellite attitude control, measuring thrust and exhaust velocity with balance and Langmuir probe respectively 18 p2956 A71-36243
- Minimum propellant deterministic guidance law for bounded thrust constant jet exhaust velocity rocket guidance law, comparing to minimum propellant impulsive thrust guidance law [AAS PAPER 71-310] 23 p3725 A71-42986
- EXHAUSTION**
- Respiratory features for conscious or unconscious warning of impending exhaustion, noting work load-performance decrement relation 04 p0545 A71-15159
- EXISTENCE THEOREMS**
- German monograph on invariant curves of annulus differentiable mappings covering existence theorem for closed curve within annulus transformed by mapping 01 p0110 A71-10127
- Plane micropolar static strain in homogeneous isotropic elastic solid, deriving existence theorems for interior and exterior problems 01 p0172 A71-10841
- Neutral and superneutral equations properties analysis and existence theorems, using successive approximation procedures 02 p0275 A71-11723
- Boundary value problem for linear Boltzmann equation in kinetic theory, proving existence and uniqueness theorems [ONERA-TP-820] 02 p0276 A71-12338
- Existence and construction of modified L lag inverses solution method for linear dynamical systems 03 p0393 A71-14482
- Boundary layer equations existence and convergence theorems, using von Mises transformation for conversion into parabolic differential equation boundary value problem 04 p0568 A71-14810
- Halley method of tangential hyperbolas in Banach space, deriving local existence, uniqueness and convergence theorems 04 p0620 A71-15668
- Limiting bounds determination for existence of periodic orbits near known existing periodic orbit, presenting linear perturbation analysis 04 p0654 A71-15717
- N person nonzero sum differential games with linear dynamics, proving existence of equilibrium strategies 04 p0620 A71-15864
- Existence of Lagrangian and Eulerian solutions of generalized three body problem, discussing applications 04 p0660 A71-15888
- Singularity carrier auxiliary curves in airfoil cascade design, formulating and proving existence theorem 05 p0693 A71-16397
- Existence theorems for compressible boundary layer problems, discussing Blasius differential equation and Falkner-Skan class of similarity solutions 06 p0881 A71-17638
- Iterative solution of nonlinear operator equations in Banach spaces, proving existence, uniqueness and convergence theorems 06 p0920 A71-18211
- Linear sequential circuits feedforward inverse transfer function matrix existence condition and construction procedure 07 p1081 A71-18735
- Existence theorem and optimal approximation of functions of many variables by superimposing sums of smaller number of variables in complex region 07 p1146 A71-19039
- Optimal control for distributed parameter system described by linear hyperbolic partial differential equation, deriving existence theorem and cost function 07 p1147 A71-19471
- Optimal solution existence theorem for control system described by linear hyperbolic partial differential equation 07 p1148 A71-19770
- Elasticity theory equations for homogeneous boundary value problem, deriving solution existence conditions by Fourier method validity demonstration 07 p1213 A71-19799
- Free boundary problems for heat equation involving interface coinciding initially with fixed face, proving existence, uniqueness and continuous dependence theorems 08 p1324 A71-20879
- Rectilinear trajectory optimization of second order nonlinear system, formulating existence and uniqueness theorems of optimal control 09 p1424 A71-23433
- Conservative systems of differential equations with single degree of freedom, considering periodic solutions existence, determination and stability 09 p1495 A71-23436
- Existence theorems in micropolar elastostatics three dimensional boundary value problems relating to isotropic and homogeneous bodies equilibrium 11 p1847 A71-25442
- Bending problems of elastoplastic plate rigidly clamped over edges, deriving theorems on existence, uniqueness and convergence of approximate solutions 12 p1974 A71-26962
- Linear complexes in three dimensional space considered with canonical transverse system, discussing nonintegral presentation and existence theorem 12 p1922 A71-27119
- Existence proof of periodic solutions to second order partial differential equations with imaginary roots 12 p1923 A71-27240
- Dirichlet problem for degenerate elliptic differential equations, discussing existence and uniqueness of solution by Schwarz alternating method 12 p1923 A71-27512
- Existence and uniqueness of solution to Dirichlet boundary value problem of invariant in nonclassical theory of elasticity concerning behavior of media with memory 13 p2154 A71-28651
- Existence theorems for eigenvalues of integral equations with continuous kernels 13 p2096 A71-28907
- Existence theorem for nonlinear boundary value problems involving two dimensional incompressible boundary layer equations 14 p2264 A71-29523
- Difference equations system trivial solution stability condition existence and uniqueness theorems 14 p2265 A71-29628
- Dynamic systems conservative by bits and governed by differential equation with discontinuous second member, obtaining limiting cycle existence condition 14 p2265 A71-29691
- Stokes flow equations solutions existence and completeness, considering vector and scalar potentials 14 p2224 A71-30094
- Existence and uniqueness theorem for n-point boundary value problems of nonlinear ordinary differential equations, using Polya condition 15 p2442 A71-31871
- Pontryagin maximum principle application to optimal control problems with phase coordinate constraints, noting existence theorem validity 16 p2550 A71-33592
- Existence and uniqueness of generalized weak solution to problem of coupling unsteady partial differential equations 16 p2603 A71-34000
- Mixed boundary value problem of hereditary elasticity theory, discussing existence and uniqueness of solution 17 p2818 A71-34425
- Periodic solutions existence for autonomous system of ordinary differential equations, modifying parameter functionalization of vector fields in phase spaces 17 p2766 A71-34934
- Soviet book on ordinary differential equations covering basic concepts, existence and uniqueness theorems, linear homogeneous and nonhomogeneous equations with constant coefficients, etc 17 p2768 A71-35626
- Bounded integral manifolds existence for perturbed system of nonlinear differential equations near critical point, periodic orbit or periodic surface 17 p2769 A71-35795
- Existence and uniqueness of weak solution of wave equation with nonlinear boundary condition, using Galerkin method 18 p2940 A71-36094
- Swirling flow problem in boundary layer theory, proving existence theorem and asymptotic formula for differential equations solution 18 p2910 A71-36815
- Nonlinear eigenvalue problem solution in real Banach space, investigating continua existence and elliptic equations application 18 p2942 A71-36818
- Time averaging with variable period for ordinary differential equations, proving existence of unified analytical solutions 19 p3085 A71-37385
- Contact problem for elasticity theory taking heredity in deformation into account, proving existence and uniqueness theorems 19 p3156 A71-37538
- Existence proof for Blasius equation and initial conditions system solution, using Luke results with integrals of incomplete gamma function 20 p3255 A71-39035
- Existence theorem of quasi-periodic solutions with two degrees of freedom for planar three body problem 21 p3441 A71-40093
- Convergence of progressive shock wave solutions for higher order equations of conservation laws with dissipation and dispersion terms, proving shock curves existence 21 p3414 A71-40141
- Optimal control laws existence for stochastic systems with minimized cost functional, considering trajectory information for controller decisions 21 p3360 A71-40254
- Theorems on parabolic and hyperbolic differential equations solutions continuous dependence on elliptic operator coefficients, deriving proof by hypothesis of existence and uniqueness 21 p3408 A71-40651
- Existence theorem derivation for moving surface one dimensional geometrical and kinematic compatibility condition 21 p3415 A71-40658
- Constructive existence theorem for nonlinear elliptic equation with restricted bounded domain 21 p3409 A71-41078
- Generalized radiation cooling of convex solid, demonstrating existence of unique stable positive solution to boundary value problem related to temperature distribution 21 p3477 A71-41184
- Ascoli theorem generalization and application to functional differential equations, proving existence theorem 21 p3410 A71-41188
- Random analogs of boundary value problems class for biharmonic functions, demonstrating unique solution existence 21 p3410 A71-41189
- Signal process models choice in Kalman-Bucy filtering, proving smallest error covariance matrix existence 21 p3349 A71-41190
- Existence and uniqueness of boundary layer equations similarity solution for viscous incompressible fluid flow past paraboloid 22 p3531 A71-42197
- Axially symmetric flow in half space above rotating disk, proving boundary value problem solution existence by fixed point technique 22 p3531 A71-42402
- Nonautonomous nonlinear functional differential equations periodic solutions, reducing problem to existence proof of fixed point for operator in suitable space of periodic functions 22 p3567 A71-42691
- Generalized solutions existence proof for viscous incompressible fluids free convection, investigating smoothness properties dependence on initial values and forces 22 p3622 A71-42863
- Differential equations system for convective incompressible fluid flow boundary layer temperature profile description, analyzing solution existence and uniqueness 23 p3781 A71-43306
- EXOBIOLGY**
- Biological rhythms and space nutrition - COSPAR Conference, Prague, May 1969, Life sciences and space research 01 p0017 A71-11551
- Dry heat spacecraft sterilization-compatibility tests of reagents and growth media for planetary biological exploration 01 p0027 A71-11563
- Martian surface environment from biological viewpoint, considering atmosphere, radiation field, temperature, polar caps, composition, granularity and topography 02 p0310 A71-12161
- Extraterrestrial vestibular research, discussing geocentric and heliocentric otolithic regulation and gravitation theory 04 p0542 A71-14759
- Exobiological survey of solar system beyond Mars, considering asteroids, Jovian planets and moons, Pluto and comets 13 p2133 A71-28040
- Soviet book on space biology and medicine covering cosmonaut selection and training, flight safety, normal life support factors, interplanetary space sojourn, etc 17 p2689 A71-34475
- Exobiology in astronautics, surveying extraterrestrial life possibilities, conditions and forms 17 p2686 A71-35438
- EXOSPHERE**
- Venusian exospheric temperature local time dependence from heat conduction equation for instantaneous heating during Mariner 5 observation 02 p0304 A71-11971
- Martian exospheric temperatures diurnal variations during Mariner 4, 6 and 7 observations by solving time dependent heat balance equations 02 p0305 A71-11972
- Lyman alpha radiation scattering observation by satellites, obtaining geocoronal atomic hydrogen distribution in thermosphere and exosphere 03 p0415 A71-14028
- Ionospheric and exospheric ELF magnetic waves generation by high altitude nuclear explosions, discussing hydromagnetic waves propagation 04 p0581 A71-14981

Collisionless ion exosphere kinetic and hydrodynamic models comparison for polar wind super-sonic flow characteristics 10 p1605 A71-24796

Mariner 5 Venus exospheric Lyman alpha measurements for dayside temperature value, using molecular hydrogen photodissociation model 11 p1823 A71-25692

Positive H, He and O ions in exosphere from mass spectrometers mounted on Elektron 4 satellite 12 p1899 A71-26644

Radar based values of neutral night exospheric temperature, discussing dominant effect of annual variation 13 p2055 A71-27921

Jupiter exospheric temperature diurnal variations for various solar activities and latitudes, using time dependent heat balance equations 15 p2491 A71-32423

Thermosphere and exosphere static models with empirical thermal profiles, giving temperature, density and composition as function of height 16 p2564 A71-33722

Thermospheric hydrogen density and temporal variations from Explorer 32 measurements, discussing dependence on exospheric temperature 16 p2565 A71-33731

Diurnal variation of Venus and Mars exospheric temperatures, using neutral heating efficiency calculation based on molecular theory 16 p2641 A71-33769

Seasonal density variations in thermosphere and exosphere, obtaining model from Explorers 19 and 39 drag measurements for comparison with OGO-6 mass spectroscopy 16 p2569 A71-33802

Escaping photoelectrons effect on polar wind exospheric model, suggesting kinetic pressure predominance at very high altitudes 16 p2569 A71-33814

Exospheric density semiannual variations from June 1968 to December 1970 at altitudes of 900 and 1070 km, using satellite drag determination by orbital period rate of change measurement 16 p2643 A71-33848

Neutral thermosphere and exosphere structure, discussing density, temperature, composition and diurnal and seasonal variations 17 p2732 A71-34461

Solar cycle variation of planetary exospheric temperature from heat balance equation solution 19 p3131 A71-37334

Ion-exosphere in open magnetic field, calculating number density, particle, moment and energy flux distribution from simple mathematical model 19 p3138 A71-37737

Exospheric evening temperature behavior data, using Fabry-Perot interferometer measurements of atomic oxygen line Doppler broadening 20 p3222 A71-39703

Exospheric ion composition determination by vertical space probe mass spectrometer measurements, obtaining H, He, N, O and NO ion concentration vertical profiles 20 p3280 A71-39720

H, He and O ion fluxes along exospheric magnetic field lines, determining flux energy and direction from RF mass spectrometer measurements onboard Elektron 4 satellite 20 p3226 A71-39742

Rocket measured exospheric temperatures correlation with global model values based on incoherent scatter measurements 23 p3670 A71-43187

High energy charged particles angular distribution measurements in equatorial region cosmic radiation above atmosphere, using Proton 2 satellite data 24 p3866 A71-45027

EXOTHERMIC REACTIONS

Shock induced exothermic reactions on boundary layer transition in shock tube, investigating free stream thermal energy release effects 04 p0572 A71-15503

Steady planar detonation with direct first order one-step irreversible exothermic unimolecular reaction, examining structure by limit process expansions analysis 08 p1375 A71-20857

Low temperature plasma electron velocity distribution function perturbation due to exothermal chemical reactions 09 p1501 A71-22389

Exothermic hypersonic blunt body flow periodic instability mechanism, using ballistic range with schlieren photographic equipment 14 p2337 A71-30455

Ammonium perchlorates deflagration rate at 20-100 atm, assessing relative roles of exothermic condensed phase and gas phase reactions by mathematical model 15 p2465 A71-32099

Pulsed laser emission chemically pumped by exothermic chain reaction between hydrogen and fluorine mixed with He initiated by flash photolysis 21 p3391 A71-40238

Inverted populations of molecular vibrational states for lasers, using strongly exothermal explosion-accompanied chemical reactions 22 p3557 A71-41819

Exothermic decomposition reaction and sublimation mechanism of ammonium perchlorate burning, showing pressure dependence of burning rate 22 p3587 A71-42100

EXPANDABLE STRUCTURES

NT BALLONS

NT BALLUTES

NT BEACON SATELLITES

NT BELLWS

NT EXPLORER 22 SATELLITE

NT GAS BAGS

NT HIGH ALTITUDE BALLOONS

NT INFLATABLE STRUCTURES

NT METEOROLOGICAL BALLOONS

Flexible Storable Tubular Extendible Member

/STEM/ in-plane bending vibrations under solar heating 01 p0173 A71-10941

Expandable rigidizable solar shields operational, structural and thermal performance tests conducted with spherical models for cryogenically fueled space vehicles 03 p0500 A71-14432

Spacecraft deployable booms, discussing structural design, self loading, weight, stowage volume and thermal stability requirements 11 p1841 A71-25272

Lightweight parabolic antenna model with inflated Mylar tube torus and central mast interconnected by wires, discussing construction, performance tests and tradeoffs 11 p1736 A71-25273

Bare base shelter/hangar expandable structures for rapid worldwide Tactical Fighter Organization deployment, noting foam and honeycomb fabrication 11 p1744 A71-25274

Full scale models, nonflammable materials and tests for manned space expandable structures including airlocks, transfer tunnels, station modules, lunar shelters and flexible windows 11 p1744 A71-25275

Expandable structures for midair pilot rescue device with hot air filled BALLUTE, discussing BALLUTE material development 11 p1707 A71-25278

Impulsively loaded expanding cylindrical shell transient elastic-plastic response, using linearized assumption on plastic flow behavior 17 p2821 A71-34577

Two dimensional steady potential incompressible flow past elastic expandable gas filled envelope fastened to edge of plate normal to flow 17 p2730 A71-35640

Cost-performance tradeoffs of aerospace launch vehicle expandable structural components, investigating program factors, materials and construction technologies 17 p2750 A71-35828

Slit tube flat-to-circular transition during extension, considering mathematical model for curvature change, modulus of elasticity and Poisson ratio effects 24 p3884 A71-44959

EXPANSION

NT GAS EXPANSION

NT PRANDTL-MEYER EXPANSION

NT THERMAL BUCKLING

Polymer neck autooscillatory expansion under drawing as result of interaction between elastic deformation and heat release during orientational transformation 03 p0448 A71-14362

Adhesive bonding of materials with different coefficients of expansion, discussing strength vs stress relief [SAE PAPER 710108] 08 p1372 A71-21712

External geopotential zonal harmonics expansion coefficients estimate 12 p1898 A71-26603

Nonlinear autonomous systems transient response, obtaining approximate solutions by generalized averaging technique based on ultraspherical polynomial expansions 21 p3415 A71-40532

EXPANSION WAVES

U ELASTIC WAVES

EXPECTANCY HYPOTHESIS

Variance estimates and error expectations for satellite coordinates and velocity vectors from star altitude measurements 02 p0278 A71-11903

Q factor of control systems as mathematical expectation of functional on input signal set with prescribed probabilistic measure and random initial conditions 10 p1588 A71-24904

Average risk minimization based on empirical data, showing relationship of problem to uniform convergence of averages toward expectation value 12 p1892 A71-27020

Variance estimates and error expectations for satellite coordinates and velocity vectors from star altitude measurements 13 p2098 A71-28190

Linear unbiased estimates of mathematical expectation of random process optimal in sense of norm of symmetrical Banach space 17 p2765 A71-34861

Average risk minimization based on empirical data, showing relationship of problem to uniform convergence of averages toward expectation value 19 p3037 A71-37689

EXPEDITIONS

Sikhote-Alin 1967 meteoritic expedition, discussing collected fragments and soil samples, crater and hole structures and mapped sites 17 p2809 A71-35715

Sikhote-Alin meteorite shower expedition, describing craters and pits identification 17 p2809 A71-35716

Sikhote-Alin expedition geological survey, examining crater and pit structural characteristics 17 p2810 A71-35717

EXPERIMENTAL DESIGN

NT FACTORIAL DESIGN

Thermal design of space experiment by analytical model for temperature regime acceptable to all experimental elements 01 p0017 A71-11454

Liquid filled gyroscope motion stability, examining experimental data, design and testing procedures 03 p0426 A71-13776

Apollo 12 lunar rock 12013 preliminary examination and preparation for international analysis, noting feldspar content and igneous nature 03 p0493 A71-14213

Heat transfer differential equations numerical solution, using latin square experimental design plans for reducing repetitions 04 p0678 A71-15461

Optimal space experiments selection for satellites and space probes, discussing criteria and techniques for guidance in program management decision making 05 p0816 A71-16138

Space station plasma physics experiments, investigating electron and ion wakes, resonance, VLF electromagnetic energy propagation and magnetospheric phenomena 06 p0938 A71-18529

Thermal control surfaces experiment onboard Black Arrow X3 satellite 06 p0981 A71-18675

Experimental arrangement for delay times in propeller/rpm controller system 08 p1271 A71-20832

Human olfactory analyzer, describing equipment for discrete delivery of successive stimuli 09 p1398 A71-22485

Thirring effect experimental measurements in gravitation theory, magnetic suspension system or torsion balance with two rotating disks generating angular momentum 10 p1642 A71-24467

Liquid metal cooled, fast spectrum thermionic reactor experiment design based on Fast Reactor Core Test Facility use for dynamic and steady state characteristics determination 11 p1710 A71-25867

Thermionic reactor experiment design to evaluate U-235 fueled fast spectrum core dynamic and steady state characteristics, discussing system features 11 p1710 A71-25868

Experimental plan group characteristics, describing main goals, construction methods, mathematical models and data analysis procedures 12 p1988 A71-26706

Second order experimental plans, obtaining regression analysis for matrix elements and regression coefficients variance 12 p1988 A71-26707

Experimental plan construction, describing group divisible partially balanced incomplete blocks, asymmetrical multiple factor construction and symmetrical plan transformation 12 p1988 A71-26708

Extremal experiment planning for optimal search, defining intuitive acceptance of solutions during non-formal stages 12 p1988 A71-26710

Experiment dispersion analysis planning, using solution acceptance procedures block diagrams 12 p1988 A71-26711

Experiment planning in electronic component design and microelectronics, using mathematical theory for optimal strategies 12 p1885 A71-26712

Experiment planning, using digital computer in real time with programmed algorithm 12 p1883 A71-26713

Wind tunnel force test program design for jet aircraft configurations, including propulsion system simulation 14 p2176 A71-30605

Instrument calibration, discussing statistical estimation of relationship and experimental design for precision improvement 17 p2738 A71-34526

Gyro drift rate acceptance test design to reflect system performance, using Bayes philosophy for derivation of test cost, product yield and quality [ALAA PAPER 71-968] 19 p3068 A71-37209

Aerodynamic testing for space transport vehicle design, discussing experimental gas dynamics role in high stagnation enthalpy systems 19 p3161 A71-37315

Creep strength tests planning, discussing minimum necessary tests number and samples distribution to obtain characteristics with accuracy and reliability 19 p3082 A71-38346

Mineral composition optimization of nutrient medium for Hydrogenomonas, using steepest ascent method for mathematical planning of experiments 20 p3193 A71-39236

Artificial auroral experiment by Aerobee rocket-borne electron accelerator generated monoenergetic electron beam injection onto magnetospheric field 20 p3231 A71-39885

Water radiolysis measurement in nuclear reactor tests, discussing experiment design as doubly telescoping sequences of blocks 21 p3345 A71-40202

Random vibration testing digital computer control system and experiment design, considering discrete Fourier transform techniques application [ASME PAPER 71-VIBR-30] 21 p3360 A71-40285

Free flight hypersonic wind tunnel model testing in Ludwig tube, discussing launching device and recording setup 21 p3362 A71-40381

Optimal design procedure as experimental design finite decision problem, using Bayes and minimax techniques 21 p3408 A71-40879

Soviet book on experimental research on human higher nervous activity from growth aspect covering normal and pathological states, cerebral cortex interaction with central nervous system 21 p3339 A71-41374

Material fatigue failure under narrow band random vibration effects, deriving fatigue life prediction equation based on composite experimental design and statistical tests 22 p3615 A71-42002

Apollo 12 multispectral lunar photography experiment using four camera configuration, verifying by ground photoelectric photometry 23 p3761 A71-43780

Servosystems consisting of command and single executive elements error estimation based on mathematical planning of experiment for time loss reduction, deriving regression equation 24 p3808 A71-44395

Orthogonal experiment plans application to metal elastic stiffness description as function of temperature and strain rate 24 p3840 A71-45375

EXPERIMENTAL REFLECTOR ORBITAL SHOT PROJ

EROS program mapping cameras, discussing wide angle, narrow angle and telescopic imaging 08 p1288 A71-21243

EXPIRATION

Airway smooth muscle relaxation mechanical consequences concerning lung volumes, airway conductance, isovolume pressure flow, maximum expiratory flow volume and static lung recoil 13 p2024 A71-29497

EXPIRED AIR

Exhaled air microimpurities composition of humans exposed to stress effects including bed rest, starvation, lyophilized diet feeding, high temperature and humidity 13 p2007 A71-28412

Hot-wire anemometer design for measuring forced expiratory flow and volume, testing dynamic non-linearity on hybrid computer 17 p2738 A71-34449

Human expiratory oxygen and carbon dioxide partial pressure and dissociation curves for intrapulmonary gas mixing, using mass spectrometry 21 p3328 A71-40098

Human expired air toxicity effect on mice neurohumoral changes stimulating inhibitory reactions in central nervous system 22 p3506 A71-42813

EXPLODING CONDUCTOR CIRCUITS

U CIRCUITS

U EXPLODING WIRES

EXPLODING CONDUCTORS

U EXPLODING WIRES

EXPLODING WIRES

Tungsten exploding wires electron emission during vacuum melting 02 p0284 A71-11881

This exploding wire restrike channels, examining temperature, electron density and thermal conductivity temporal behavior 02 p0284 A71-11941

Explosive boiling of water and organic liquids around pulse heated Pt wire, discussing vaporization

process, fluctuating nucleation and temperature behavior 02 p0331 A71-12193

Quasi-spherical divergent shock waves produced by Pt wire explosion in air 02 p0332 A71-12336

Exploding wires in photoelastic specimens, examining axially symmetric cylindrical stress wave front with high speed photographs [SESA PAPER 1656] 03 p0459 A71-13769

Imploding wire trigger technique for high shock velocity electric arc drivers in shock tubes 04 p0564 A71-14671

Implosion driven shock tube using hydrogen-oxygen mixtures detonated by short exploding wire 04 p0673 A71-14679

Volt-ampere characteristics of exploding Cu, Nichrome, Al and Ni wires during explosions induced by pulsed current in air 07 p1161 A71-20194

Explosive boiling of water and organic liquids around pulse heated Pt wire, discussing vaporization process, fluctuating nucleation and temperature behavior 15 p2512 A71-31499

Expanding metal vapor density-radius measurements in wire explosions, using twin tube flash X ray unit 20 p3311 A71-38827

EXPLORATION

NT LUNAR EXPLORATION

NT SPACE EXPLORATION

EXPLORER SATELLITES

NT EXPLORER 12 SATELLITE

NT EXPLORER 22 SATELLITE

NT EXPLORER 26 SATELLITE

NT EXPLORER 28 SATELLITE

NT EXPLORER 31 SATELLITE

NT EXPLORER 33 SATELLITE

NT EXPLORER 35 SATELLITE

NT EXPLORER 37 SATELLITE

NT EXPLORER 38 SATELLITE

NT EXPLORER 40 SATELLITE

NT OUTER PLANETS EXPLORERS

NT RADIO ASTRONOMY EXPLORER SATELLITE

Service performance and tests of zinc silver oxide batteries on Explorers 17 and 32 08 p1236 A71-21105

Theta /north-south/ component in spherical polar coordinates of interplanetary magnetic field from Explorer 33 and 35 measurements 23 p3734 A71-43155

Explorer SAS-D astronomical satellites for UV spectra recording by TV cameras 24 p3876 A71-45275

EXPLORER 12 SATELLITE

Explorer 12 magnetic field observations of magnetopause current layer during magnetic storm, interpreting data by magnetosphere model 23 p3668 A71-43160

EXPLORER 22 SATELLITE

Electron concentration and temperature data from Langmuir probe on Explorer 22, discussing magnetic storms effects 02 p0244 A71-11910

Ionospheric electron concentration and temperature data from Langmuir probe on Explorer 22, discussing magnetic storms effects 13 p2058 A71-28197

EXPLORER 26 SATELLITE

Comparative proton flux and Pc-1 pulsations from Explorer 26 satellite and ground observations 11 p1756 A71-25648

EXPLORER 28 SATELLITE

Polar substorms relation to interplanetary magnetic field from IMP 3 satellite magnetic measurements 19 p3132 A71-37396

EXPLORER 31 SATELLITE

Suprathermal electron flux and temperature in 5-200 eV range at high latitude with Explorer 31 potential analyzer 03 p0420 A71-14528

EXPLORER 33 SATELLITE

Low energy protons radial gradient in interplanetary space measured with intercalibrated solid state detectors on Venus bound Mariner 5 and earth orbiting Explorer 33 06 p0952 A71-18113

Pressure conditions across distant magnetopause from interplanetary magnetic field measurements, comparing Pioneer 7 plasma data with Explorer 33 distant geomagnetic tail field magnitudes 08 p1285 A71-21692

EXPLORER 35 SATELLITE

Fossil lunar magnetism observations, using magnetometer data from orbiter Explorer 35 08 p1365 A71-21747

Lunar diamagnetic cavity signatures from Ames magnetometer experiment on Explorer 35 orbiter, indicating solar wind interaction 13 p2132 A71-27909

Lunar electrical conductivity profile from joint power spectral density analysis of Apollo 12 and Explorer 35 magnetometer data 23 p3762 A71-43790

EXPLOSER 37 SATELLITE

Solar X-ray flares recorded by SOLRAD-9 on Explorer 37 satellite occurring in optical flares-microwave bursts-X-ray flares sequence 17 p2796 A71-35391

EXPLOSER 38 SATELLITE

Space radio astronomy, discussing frequency range in terrestrial atmosphere, RAE-1 satellite, cosmic and solar emissions and magnetopause generation, propagation and absorption processes 17 p2797 A71-34243

EXPLOSER 40 SATELLITE

VLF Poynting flux measurement technique on Injun 5 satellite using one electric and one magnetic antenna, discussing magnetic orientation events effects 07 p1062 A71-19668

Whistlers with harmonic bands caused by multiple stroke lightning, using Injun 5 VLF data 08 p1283 A71-21649

Electron and proton precipitation observations in auroral, polar cap and outer radiation zones by electrostatic analyzers on earth satellite Injun 5 15 p2397 A71-31756

Low energy particle plasma sheet and convection electric field distributions over auroral zones and polar caps from satellite Injun 5 observation 23 p3669 A71-43168

EXPLOSIONS

NT AERIAL EXPLOSIONS

NT CHEMICAL EXPLOSIONS

NT GAS EXPLOSIONS

NT NUCLEAR EXPLOSIONS

NT THERMONUCLEAR EXPLOSIONS

Aircraft crash investigation, deducing in-flight explosion by failure analysis techniques 01 p0087 A71-10456

Explosive boiling of water and organic liquids around pulse heated Pt wire, discussing vaporization process, fluctuating nucleation and temperature behavior 02 p0331 A71-12193

Gas dynamics of explosions - Conference, Novosibirsk, U.S.S.R., August 1969 05 p0832 A71-16501

Blast wave propagation following explosions at center of generalized Roche model, discussing core radius and envelope thickness 09 p1431 A71-22371

Energetic violent explosive events nature and regional characteristics in universe from cosmic radiation composition studies 12 p1948 A71-27368

Source count statistics of radio galaxy lifetimes and intergalactic heating, assuming multiple explosions 12 p1968 A71-27540

Elastic wave propagation in infinite elastic medium due to explosion at spherical cavity center, considering material properties thermal change as function of radial distance 13 p2165 A71-29104

Massive rotating plasma cloud contraction with magnetic field perpendicular to rotation axis, causing magneto-rotational explosions 14 p2312 A71-30386

Impact reaction intensity test, determining fire or explosion hazards of materials exposed to liquid oxygen 14 p2222 A71-30549

Ejection explosion energy transfer to ambient media, examining effect of orifice distance from explosive charge center 15 p2511 A71-31386

Explosive boiling of water and organic liquids around pulse heated Pt wire, discussing vaporization process, fluctuating nucleation and temperature behavior 15 p2512 A71-31499

Gas dynamics of explosions, considering electromagnetic fields and chemical reactions effects on blast wave propagation in unbounded media 15 p2515 A71-32567

Russian /Popigay river basin/ hollow as meteoritic explosion crater 15 p2496 A71-32734

Tunguska explosion of 30 June 1908, determining air waves propagation velocity 16 p2639 A71-33696

Explosively shock strengthened austenitic stainless steel, investigating mechanical properties at elevated temperatures 21 p3398 A71-40462

Inverted populations of molecular vibrational states for lasers, using strongly exothermal explosion-accompanied chemical reactions 22 p3557 A71-41819

EXPLOSIVE DECOMPRESSION

Aeromedical requirements, control limitations and hazards of aircraft pressure cabins and rapid decompression 08 p1244 A71-20715

Arthropoda /Daphnia, crawfish, wood lice, cockroaches, flies and ants/ hypoxia survival time and resistance to explosive decompression
24 p3797 A71-44719

EXPLOSIVE DEVICES

NT BOMBS [ORDNANCE]

NT INITIATORS [EXPLOSIVES]

Shock tubes with linear explosive driver for helium and air, determining performance by high speed camera measurements
04 p0565 A71-14680

Casing material effects on velocity of low speed phase prior to detonation onset of high density PETN, testing steel, Plexiglas, Duralumin and brass
15 p2511 A71-31390

Approximate motion equations of gas flow behind detonation front in flat explosive plate covered by inert coating
23 p3781 A71-43358

EXPLOSIVE FORMING

Explosive forming using compressed air as power source for safety and lower cost
01 p0091 A71-11549

Thermal recovery in stainless steel after explosive shock loading and forming
04 p0614 A71-15781

Deformation substructures, strain rates and terminal properties of explosively-formed thin walled stainless steel cylinders, using transmission electron microscopy
13 p2153 A71-28501

Explosive and isostatic forming effects on commercial precipitation-hardenable Al-Cu alloy microstructure, tensile properties and fatigue life
15 p2433 A71-32180

Bonding conditions effect on wave mode formation at explosive bonded interface in bullet experiments on thin metal targets
22 p3617 A71-42495

Explosive peening effects on weld fatigue in Ni maraging steel, Fortiweld and Al-Zn-Mg alloy
23 p3682 A71-43877

EXPLOSIVE CASES

U FLAMMABLE GASES

EXPLOSIVE WELDING

Explosive metal welding bond interface, investigating heat treatment effect on microstructure
06 p0914 A71-18680

Metal pipes coaxial welding by detonation, estimating energy conversion
08 p1300 A71-21910

Jetting collision effect on structural changes at interface between Ti and steel in explosive bonding, considering plastic deformation and residual stresses
10 p1629 A71-25030

Fatigue crack propagation model for explosion bonded titanium-steel system under constant load amplitude conditions
16 p2600 A71-34096

Metal joint explosive bonding, investigating wavy interface formation mechanism by aerohydrodynamic analogy
17 p2748 A71-34494

Mechanical properties of explosively clad plates, considering stainless steel/mild steel and brass/mild steel composites
17 p2757 A71-34663

Wave formation during metals explosive welding, indicating process of wave freezing by acoustic equations analysis
17 p2749 A71-35369

Hypothetical analogy between wave formation during explosive welding and Karman vortex street arising in liquid flow around cylinder
19 p3068 A71-37083

EXPLOSIVES

NT CELLULOSE NITRATE

NT HYDRAZINE NITROFORM

NT TRINITROTOLUENE

Hexanitroethane /HNE/ crystal transformation, using differential spectroscopy and X ray analysis
04 p0638 A71-15679

Ignition and nondetonating decomposition of liquid nitromethane explosive at 10 kbar pressure
05 p0795 A71-16517

One dimensional detonation hydrodynamics of condensed high explosives and small inert particles mixtures on basis of mathematical flow model
05 p0834 A71-16518

Cellulose, explosives and propellants thermal surface ignition, using heat transport and chemical kinetic equations
06 p0944 A71-18298

Shock formation and chemical activation in solid secondary explosives detonation, considering propagation acceleration by pressure rise in terms of reaction products thermodynamic properties
07 p1223 A71-19246

Water diluent effect on molten hydrazine mononitrate critical diameter and condensed explosive detonation stability
15 p2463 A71-31383

Explosives in porous state under impact loads, obtaining adiabats, compressibility and temperatures
15 p2511 A71-31384

Pressure, time and attenuation measurements of high explosive driven air shock in steel pipe, comparing with numerical simulation
20 p3208 A71-38787

EXPONENTIAL FUNCTIONS

NT LOGARITHMS

Logarithmic signal converter with parallel circuits arrangement for large dynamic range operation
02 p0231 A71-12040

Photoelectron count of logarithmically fading optical signal, discussing noncentral chi square random variable approximation
05 p0726 A71-17085

Fokker-Planck equation for convection dominated transport of solar cosmic rays solved for exponential decay phase of solar particle events
07 p1185 A71-19651

Rate constant for oxygen uptake exponential increase during low intensity exercise by algebraic solution
07 p1052 A71-20336

Mean periodic exponential functions with certain trigonometric properties, proving summation and equivalence theorems
08 p1325 A71-22018

Creep of hereditarily aging body, using Rabotnov fractional exponential function for elastic theory solution
12 p1984 A71-27696

Collector current delay and rise times in transistor common emitter configuration for linear, sine and exponential input signals
14 p2213 A71-30630

Linear stationary lumped-constant relaxation systems with real and positive eigenvalues and impulsive response characterizable by exponentials, evaluating error in identification
15 p2450 A71-32322

Rotationally symmetric quasi-cylindrical viscous incompressible vortex flows at high swirl, discussing numerical integration with exponential functions
18 p2908 A71-36342

Exponential continually discrete analytic functions of complex variable in explicit form, obtaining addition theorem for trigonometric functions
19 p3089 A71-38479

Exponential absolute stability of nonlinear discrete systems of Lure type, deriving modified frequency condition
20 p3255 A71-39028

Rotationally symmetric quasi-cylindrical viscous incompressible vortex flow, using method of weighted residuals approximating axial velocity and circulation profiles by series of exponentials
21 p3369 A71-40951

Mathematical models for microorganism exponential die-off rate and variance estimation from decontamination data
22 p3504 A71-42231

Damped exponential cosine probability distribution function for clipped waveforms of voiced speech signal
23 p3645 A71-43439

Exponential type equation for carbon steel stretched sample necking profile curve
23 p3780 A71-44228

EXPONENTS

Characteristic exponents for linear differential equations with periodic coefficients, using recurrence multipliers suitable for computer
03 p0451 A71-13786

Ideal gas isentropic mean value exponent, calculating state variables
03 p0520 A71-13900

EXPOSERS

U INTERNATIONAL TRADE

EXPOSURE

Aerial photography, discussing optimal exposure selection and control to obtain maximum number of fine details
04 p0585 A71-14642

Pre- and post-exposure recording in holographic measurement of high object velocities for enhanced image reconstruction
22 p3537 A71-41597

Analytical function approximation of photofilms characteristic curves, noting validity for all exposure times
23 p3680 A71-44055

EXPRESSIONS [MATHEMATICS]

U FORMULAS [MATHEMATICS]

EXTARS

X ray pulsations from Cygnus X-1 observed from Uhuru satellite, suggesting extar discovery
13 p2120 A71-28004

Crab Nebula pulsar and extar emission from collapsed star magnetosphere, accounting for physical characteristics with nonthermal plasma mechanism
20 p3285 A71-39954

Radio stars classes, discussing red dwarf flare, red supergiants, blue dwarf companion, novae, pulsars and X ray stars
21 p3448 A71-40582

Scorpius X-1 X ray flux observations, noting high frequency oscillations responsible for radiation production
23 p3733 A71-43078

EXTENSOMETERS

Extensometer for evaluating remote reading strain gage performance at high and rapidly changing temperatures
09 p1445 A71-22720

Inductive extensometers with spherical tips for materials testing, noting Young modulus and Poisson ratio determination
17 p2744 A71-35239

EXTERNAL STORES

NT PODS [EXTERNAL STORES]

External stores separation induced aerodynamic interactions, using high speed cinematographic recording of drop trajectories and/or store loads weighing in aircraft flow field [ONEKA-TP-849]
04 p0527 A71-15357

Captive trajectory techniques for six degree of freedom external store separation wind tunnel testing, noting capability for missile guidance system simulation
08 p1275 A71-22007

High speed aircraft external store separation testing and prediction techniques, considering flow field survey, dynamically similar drop models and captive trajectory methods
08 p1229 A71-22014

External store surface pressure distributions during captive flight aboard F-4B aircraft, considering carrying aircraft effects on flow field about airborne ordnance
08 p1232 A71-22015

Performance evaluation of variable geometry external fuel tank prototypes by static structural tests, wind tunnel tests and flight tests on F-111 aircraft
17 p2675 A71-35533

Active feedback wing/store flutter control for fighter aircraft, using computer programs based on frequency and time domains for linear analysis
23 p3630 A71-44109

EXTINCTION

NT INTERSTELLAR EXTINCTION

Atmospheric extinction coefficients dependence on wavelength, comparing theoretical prediction to observational data
01 p0119 A71-10832

Fluid mechanics of shallow liquid fuel layer near burning wick, deriving continuity, momentum and convective diffusion equations to obtain extinction condition
02 p0334 A71-12855

Planetary nebulae upper distance limits by photometry, including mean nebular parameters and extinction coefficients in galaxy dust model
07 p1191 A71-18999

Interstellar extinction curve accounted for by graphite, iron and silicate grains, presenting refractive index values plotted as functions of wavelength
07 p1199 A71-20009

EXTINGUISHING

Motor design parameters effects on solid propellant extinguishment predicted from mathematical combustion model
03 p0469 A71-14442

Flame quenching device for distances determination by burning premixed laminar propane-air at atmospheric pressures between nonparallel walls
15 p3385 A71-32089

Solid propellants extinguishment by depressurization, using transient flame model
15 p2466 A71-32283

EXTRACTION

Microelement extraction from mineralized biological samples in food rations and human excretions
24 p3800 A71-44540

Serotonin /5-oxytryptamine/ extraction from rat whole blood in series analysis, using acidic butanol instead of ordinary butanol
24 p3801 A71-44541

EXTRAGALACTIC LIGHT

U EXTRATERRESTRIAL RADIATION

U LIGHT [VISIBLE RADIATION]

EXTRAGALACTIC MEDIA

U INTERGALACTIC MEDIA

EXTRAPOLATION

Book on numerical solution of ordinary differential equations covering integration algorithms, Runge-Kutta, single-step, multistep, predictor-corrector and extrapolation methods
08 p1324 A71-21233

Rocket engine thermodynamic characteristics and parameters determination, using extrapolation formulas with initial fuel composition
08 p1346 A71-21264

Finite difference description for dynamic control plants with unknown disturbances based on integral transformation and extrapolation, applying to automatic control systems synthesis
08 p1270 A71-21975

German monograph on extrapolation procedure based on Taylor series expansion and on algorithm for

identification and prediction of eye pursuit movements 17 p2690 A71-34790

Optimal extrapolation and filtration for class of random processes, considering functionals of solutions of stochastic differential equations 17 p2765 A71-34863

Storm models for space-path attenuation calculations using digitized weather radar data for fine structure and surface rainfall data for extrapolation 17 p2704 A71-35090

S-wave elastic positron-hydrogen scattering in ionization region, estimating error in extrapolated t matrix from complex energy 19 p3106 A71-37375

Creep strength extrapolation for high temperature steels, suggesting combined numerical and graphic methods 20 p3249 A71-39017

Cr-Mo-V steel creep strength tests extrapolation by parametric approach, discussing optimum regression dependence 20 p3250 A71-39019

French monograph on extrapolation type extremal control systems speed and stability performance improvement based on Jacob step duration modulation method 22 p3526 A71-42067

Heat resistant steels long time strength determination by graph-analytical time-temperature extrapolation 23 p3693 A71-44213

EXTRATERRESTRIAL ENVIRONMENTS

NT CHROMOSPHERE
NT CISLUNAR SPACE
NT DEEP SPACE
NT INTERPLANETARY SPACE
NT INTERSTELLAR SPACE
NT JUPITER ATMOSPHERE
NT LUNAR ATMOSPHERES
NT LUNAR ENVIRONMENT
NT MARS ATMOSPHERE
NT MARS ENVIRONMENT
NT PLANETARY ATMOSPHERES
NT PLANETARY ENVIRONMENTS
NT SOLAR ATMOSPHERE
NT STELLAR ATMOSPHERES

Direct measurements of cosmic dust particles in near earth environment and interplanetary space, noting reliability and calibration 20 p3300 A71-39655

EXTRATERRESTRIAL LIFE

Life detection for space missions based on detecting optical asymmetry in biogenic molecules by gas chromatography involving diastereomeric esters synthesis 01 p0029 A71-11562

Extraterrestrial civilizations, discussing probability theory and radio communication 06 p0852 A71-17739

Extraterrestrial life hypotheses, citing astronomical considerations, inorganic chemical evolution and prebiotic synthesis with emphasis on Mars exploration for microorganisms 07 p1044 A71-20374

Carbonaceous chondrite and Precambrian chert amino acids detection, using simultaneous optical configuration determination and gas chromatography 09 p1393 A71-22984

Terrestrial microorganisms adaptation to simulated methane-ammonia-hydrogen Jupiter atmosphere 10 p1566 A71-24688

Exobiological survey of solar system beyond Mars, considering asteroids, Jovian planets and moons, Pluto and comets 13 p2133 A71-28040

Soviet papers on extraterrestrial life and detection methods covering biological conditions, extremal environmental factors and spacecraft sterilization 13 p2009 A71-28677

Hydrocarbons as foundation for life development universe, discussing chemical composition of galaxy, antimatter existence, interstellar medium and cosmic age factors 13 p2009 A71-28678

Extraterrestrial and earth life genesis, discussing carbon foundation, planetary conditions, water prerequisite and space exploration 13 p2009 A71-28679

Chemical evolution and extraterrestrial life detection, noting cell proliferation methods, automatic biological stations and Mars microorganisms 13 p2009 A71-28680

Optimal mineral-organic nutrient medium and soil selection for microorganism detection on Mars 13 p2009 A71-28681

Visible and UV photometric recording of microorganism reproduction in liquid medium for application to Mars extraterrestrial life detection 13 p2019 A71-28682

Luciferin fermentative oxidation method for adenosine triphosphate determination in extraterrestrial life detection, using extract of firefly luminescent organs 13 p2009 A71-28683

Biochemical luminescence reaction for ferroprophyrin proteins determination in extraterrestrial life detection 13 p2009 A71-28684

Extraterrestrial life detection by tagged carbon dioxide extraction from substrate in radioactive glucose containing soil nutrient media 13 p2068 A71-28685

Extraterrestrial life detection by measuring microorganism breeding dynamics with photometric, radiometric and bioluminescent methods from chemiluminescent reactions 13 p2068 A71-28686

Extraterrestrial microorganisms penetration into rocks and meteorites under various climate conditions, noting effects of humidity 13 p2010 A71-28693

Exobiology in astronautics, surveying extraterrestrial life possibilities, conditions and forms 17 p2686 A71-35438

Mars surface features observed during opposition in August 1971, discussing canal controversy, life, dark areas shift and Mariner probes results 18 p2959 A71-35908

Dynamic formulation for number of communicative civilizations in Milky Way galaxy suitable for digital simulation 18 p2965 A71-36295

Extraterrestrial amino acids identification in carbonaceous chondrite Murray meteorite by gas chromatographic method 19 p3132 A71-37414

Extraterrestrial civilizations, discussing cybernetic approach and development of languages for interstellar communications 19 p3134 A71-37521

Extraterrestrial life detection methods, discussing bacterial cultures growth dynamics in nutrient media and iron porphyrin proteins and ATP content increase 21 p3334 A71-40570

Diamond radiation counters for C 14 containing carbon dioxide in extraterrestrial life detection, noting radioactivity curves as function of sample microflora 21 p3378 A71-40571

Living organisms life-sustaining possibility under simulated Martian temperature, humidity and atmospheric composition conditions, emphasizing unicellular organisms radiation resistance 21 p3334 A71-40572

Gas exchange between air or gas mixture flows and terrestrial soil in extraterrestrial microorganisms detection, using continuous sampling and gas chromatography 21 p3346 A71-40575

Book on space technology for developing countries covering economic, social and educational reform, solar system exploration and extraterrestrial civilizations 22 p3623 A71-42066

Nonaqueous biosystems unlikelihood from consideration of enzymatic activity possibility and liquid water unique ability for complexity required by carbonaceous biosystems 22 p3487 A71-42229

Soviet papers on cosmic biology, Volume 16, covering man and animal physiology under extremal loads, spacecraft life support systems and extraterrestrial life detection, etc 22 p3505 A71-42789

Early solar system organic matter origin, discussing amino acid synthesis from CO, H and ammonia reaction with N, alumina or clay catalysts 23 p3633 A71-43244

Prebiotic organic matter in solar system, investigating contamination free amino acid catalytic synthesis from deuterated reactants 23 p3633 A71-43245

Unified procedure for detection of life on Mars by Viking program missions, using mass spectrometer for remote biologically oriented experiments 23 p3736 A71-43541

Apollo 12 lunar dust, rocks and microbreccia microsection examined for evidence of biogenic structure 23 p3757 A71-43746

EXTRATERRESTRIAL MATTER

NT COSMIC GASES
NT COSMIC PLASMA
NT INTERPLANETARY GAS
NT INTERSTELLAR GAS

Cosmic objects and phenomena research, considering matter and galaxy compacting and dispersing processes, red shift, quasars, etc 08 p1358 A71-20890

Legal principles and rules governing lunar and other extraterrestrial materials, considering establishment of international code 10 p1698 A71-23861

Solar temperature after formation, using isotopic composition differences in terrestrial and extraterrestrial xenon 10 p1668 A71-23871

Astrophysical states of matter and phenomena at extreme temperatures and densities, discussing stellar

evolution, terminal states of stars, superdense stellar matter, neutron stars, etc 11 p1828 A71-25734

Stratospheric extraterrestrial particles identification from balloon-collected electron microscope photographs, suggesting cometary origin 16 p2644 A71-34127

Spherical microparticles in atmospheric boundary layer and fallout above Pacific Ocean correlated to extraterrestrial origin 17 p2810 A71-35719

EXTRATERRESTRIAL RADIATION

NT EXTRATERRESTRIAL RADIO WAVES
NT GALACTIC RADIATION
NT GALACTIC RADIO WAVES
NT GEGENSCHIEIN
NT INTERSTELLAR RADIATION
NT LUNAR RADIATION
NT PLANETARY RADIATION
NT PRIMARY COSMIC RAYS
NT SOLAR CORPUSCULAR RADIATION
NT SOLAR COSMIC RAYS
NT SOLAR PROTONS
NT SOLAR RADIATION
NT SOLAR RADIO BURSTS
NT SOLAR RADIO EMISSION
NT SOLAR WIND
NT SOLAR X-RAYS
NT STELLAR RADIATION
NT STELLAR WINDS
NT SUNLIGHT
NT TYPE 2 BURSTS
NT TYPE 3 BURSTS
NT TYPE 4 BURSTS
NT ZODIACAL LIGHT

Galactic and extragalactic sources of far IR radiation, discussing spectral distribution and luminosities 02 p0315 A71-12656

Extragalactic LF background radiation spectra, using model for free-free absorption in galactic disk 03 p0473 A71-13563

Extraterrestrial gamma ray and neutron flux and energy spectrum at balloon altitudes over equatorial latitudes, using pulse shape discriminator during solar flare 06 p0962 A71-18177

Nuclear and space radiation effects - NASA/IEEE Conference, University of California at San Diego, July 1970 07 p1070 A71-19051

High energy electrons in near space excess radiation from high altitude balloon and satellite data 09 p1513 A71-22667

Extraterrestrial Lyman alpha radiation source attributed to solar Lyman alpha scattering on cold interplanetary hydrogen penetrating to inner solar system 09 p1526 A71-23462

Extraterrestrial hydrogen Lyman alpha emission source, investigating interstellar wind with OGO 5 satellite 10 p1601 A71-24438

Extraterrestrial ring current under very quiet magnetic conditions from mean long term daily horizontal intensities 11 p1755 A71-25616

Space radiation environmental effects on reactively encapsulated zinc orthotitanates and paints [AIAA PAPER 71-449] 12 p1920 A71-26762

Optical variation and radio spectral index statistics of extragalactic sources, including quasars from photographic monitoring with 30 inch reflector 12 p1962 A71-26932

Universe UV radiation intensity, estimating inverse Compton effect interaction of cosmic relativistic electrons with relic radiation 12 p1948 A71-27079

Extraterrestrial Lyman alpha radiation, showing interplanetary principal anisotropic effects 14 p2307 A71-29731

BL Lac extragalactic source of radio, IR and visual radiation, estimating upper limit to distance based on spectrum model 14 p2313 A71-30452

Extraterrestrial slow neutron flux and decay density, calculating spatial distribution by power function 14 p2302 A71-30592

Extragalactic cosmic X ray sources at high galactic latitude from sounding rocket experiments, correlating with galactic clusters 16 p2626 A71-33357

ESRO report to COSPAR on sounding rockets and geostationary satellites development, orbits and decay during extraterrestrial gamma radiation 16 p2667 A71-33867

Extragalactic gravitational radiation focusing by galactic core acting as lens 17 p2798 A71-34399

Extragalactic objects luminosity upper limits in hard gamma ray band, using Cosmos 208 scintillation Cerenkov telescope 17 p2796 A71-35736

Double extragalactic radio sources luminosities and confinement observations, comparing with ram pressure prediction 18 p2963 A71-36156

- Kinematic illusions in connection with retardation effects involving extragalactic sources with varying microwave output, noting occurrence in quasar 3C 279
18 p2925 A71-36924
- Two dimensional structures of 76 extragalactic radio sources at 1425 MHz in tabular and graphical forms
18 p2970 A71-37064
- Universe UV radiation intensity, estimating inverse Compton effect interaction of cosmic relativistic electrons with relic radiation
19 p3126 A71-37429
- Integral wavelength solar radiation constant measurements by jet and rocket research aircraft, high level balloons and Mariner space probes
20 p3260 A71-39682
- Extragalactic radio sources polarized radiation intensity statistical analysis, calculating magnetic field scale
22 p3602 A71-42175

EXTRATERRESTRIAL RADIO WAVES

- NT GALACTIC RADIO WAVES
NT SOLAR RADIO BURSTS
NT SOLAR RADIO EMISSION
NT TYPE 2 BURSTS
NT TYPE 3 BURSTS
NT TYPE 4 BURSTS
- Extragalactic violent events energy from collapsing stars or pulsar bodies rotational energy, producing extended radio sources
09 p1522 A71-22977
- Antenna effective area and radiation pattern measurement using emission characteristics of extraterrestrial radio sources, sun and moon
12 p1967 A71-27422
- Cosmic radio emission coherent generation mechanism, involving derelativization and relativization of particles in small space
15 p2483 A71-31343
- Time dependent multidimensional axisymmetric computations for extended extragalactic radio sources propagation into intergalactic media having different densities and temperatures
17 p2806 A71-35411
- Extragalactic centimeter radio sources flux density data and spectral distribution, presenting expression for error estimation
18 p2970 A71-37065
- Cosmic radio astronomy, evaluating sensitivity and resolution limitation of ground based radio telescopes
19 p3138 A71-37762
- Radio telescopic search for extraterrestrial oxygen 18 containing water microwave emission, suggesting water vapor maser pumping mechanism dependence on isotopic species
21 p3444 A71-40223
- Cosmic radio emission coherent generation mechanism involving derelativization and relativization of particles in small space
22 p3606 A71-42618

EXTRAVEHICULAR ACTIVITY

- Soyuz 4 and 5 self contained cosmonaut life support system for extravehicular activity, discussing principal components block diagram
01 p0025 A71-11141
- Human foot-balancing reflex as basis for hands-free EVA control system
01 p0068 A71-11306
- Thermal environment loads in lunar ambulation, discussing Apollo EVA suit system and internally produced heat
02 p0207 A71-12386
- Medical flight information on astronauts response to space flight environment in confined and unconfined state and during intra- and extravehicular activities
08 p1246 A71-20731
- Advanced regenerative portable life support system concept analysis for long duration and multiple extravehicular activity
18 p2866 A71-36377
- Orbital maintenance in pressurized environment, incorporating limited habitability, electronic/pneumatic bench access, critical spares storage racks, extravehicular activity manipulators and repair area
18 p2899 A71-36468
- Mathematical model for underwater simulation of astronaut extravehicular activities in weightless conditions, using computer program
18 p2872 A71-36644
- Human response to space environment, discussing prolonged weightlessness, extravehicular work and lunar surface activity
19 p3002 A71-37492
- Extravehicular activity protection systems, discussing resource regeneration, technology, methodology and space station, lunar base and Martian missions schematic configurations
22 p3503 A71-41990

EXTREMA**U RANGE [EXTREMES]****EXTREMELY HIGH FREQUENCIES**

- Terrain backscatter characteristics in EHF band, establishing average radar cross sections for various incidence angles
06 p0867 A71-17713

- K band double-tuned nondegenerative parametric amplifier using single-packaged GaAs varactor diode, discussing design and performance
08 p1262 A71-20763

- K band cryogenically cooled wideband /600 MHz/ low noise parametric amplifier for millimeter wave satellite communication earth terminals, discussing design
08 p1263 A71-20770

- Long distance PCM-AM pulse regenerator for 4 GHz band and millimeter wave communication
08 p1265 A71-21285

- Epitaxial InP three level oscillators in K and Q bands /18-40 GHz/, suggesting optimum operating frequency determined by defined transit velocity
09 p1421 A71-23719

- High speed BPSK communication components and system aspects with V band propagating medium, considering carrier modulation and transmitted digital data reception with minimum errors
17 p2709 A71-37579

- Electromagnetic wave scattering from turbulent plasma at 31 GHz, determining cross section dependence on bistatic angle and electron density
19 p3017 A71-37868

- Interstellar carbonyl sulfide transition at 109.5 GHz, noting column density
21 p3447 A71-40447

- Power spectral density of N-ary orthogonal continuous phase FSK waveforms for ELF/VLF communications
22 p3513 A71-42385

- Q band relative phase measurement using single sideband suppressed carrier ferrite modulator in serrodyne phase bridge
24 p3803 A71-44649

EXTREMELY LOW RADIO FREQUENCIES

- Attenuation and phase velocities of ELF slow tail atmospherics for easterly and westerly nighttime propagation over Pacific Ocean
04 p0552 A71-15217

- Temperature compensated Zener diodes noise voltage measurements in ELF domain
05 p0729 A71-17000

- Particle diffusion modulation by simultaneous VLF and ULF electromagnetic waves during rocket experiment
07 p1062 A71-19680

- F region ion and temperature effects on VLF and ELF wave absorption in whistler mode propagation at midlatitudes during solar minimum
12 p1879 A71-27049

- Ionospheric VLF and ELF wave observations, noting ion cyclotron resonance and harmonics effects on propagation
14 p2202 A71-30946

- Hydromagnetic approximation of ELF propagation modes and emission in magnetosphere, using satellite and ground based observations
14 p2202 A71-30953

- Lower ionosphere effects on ELF noise in Schumann resonances range
14 p2203 A71-30961

- Global distribution and location of large lightning discharges from single station observations of transient ELF disturbances propagated in earth-ionosphere cavity
15 p2394 A71-31429

- Perturbations effects on ELF propagation in inhomogeneous anisotropic ionospheric waveguide
19 p3017 A71-37867

- Medical, zoological and biological effects of ELF signals in atmosphere, comparing with EEG alpha and gamma rhythm
20 p3193 A71-39478

- ELF and VLF emissions during PCA, correlating data with particle and photometer recordings from ground based, satellite and rocket-borne observations
20 p3229 A71-39856

- Power spectral density of N-ary orthogonal continuous phase FSK waveforms for ELF/VLF communications
22 p3513 A71-42385

- Ionospheric geomagnetic field effect on ELF/VLF radio propagation
23 p3643 A71-42967

EXTREMUM VALUES**NT LIMITS [MATHEMATICS]**

- Extremal control systems operation, analyzing search and scanning phases
01 p0064 A71-10840

- Single channel step-type extremal systems with inertial control plants, proposing automatic optimizer
01 p0065 A71-11235

- Book on approximate methods in optimization problems covering nonlinear extremum, functional analysis, algorithms, optimal control theory and finite dimensional spaces
01 p0113 A71-11323

- Combinatorial extremum problem distribution among units of hierarchical control system
02 p0236 A71-12623

- Extremals optimal endpoints, obtaining necessary and sufficient conditions by method based on dichotomy concept
05 p0774 A71-16645

- Constrained function extremization, taking into account modified quasi-linearization algorithm
05 p0776 A71-17088

- Optimal control problems for functional extremization, developing modified quasi-linearization algorithm
05 p0776 A71-17089

- Primary cosmic ray solar modulation calculations using Trilling formula for response functions and upper limiting rigidity to diurnal variation
06 p0953 A71-18119

- Kato upper and lower bounds formula applications to Hermitian operator eigenvalues
07 p1146 A71-18748

- Komkov class of boundary value problems and associated variational principles, discussing necessary conditions for basic functional or potential extremal behavior
08 p1323 A71-20878

- Heuristic search algorithm for highest and lowest values of functions, considering Algol program
09 p1485 A71-22313

- Random ergodic process extremal behavior, determining mean time to reach original maximum or minimum
14 p2194 A71-30087

- FM threshold extension bounds during click elimination, considering pulse-averaging type discriminator
14 p2198 A71-30906

- Best linear unbiased estimates for location and scale parameters of extreme value distribution based on given order statistics
21 p3407 A71-40366

- Amplitude estimates and bounds derivation for nonlinear two parameter oscillators, obtaining iterative solution for computation
21 p3358 A71-41013

- IMPATT diodes noise performance lower limits, deriving optimization theorem for GaAs diodes under assumption of equal ionization coefficients for electrons and holes
22 p3524 A71-42632

- Digital computer simulation for extremal finite network synthesis
24 p3806 A71-44715

EXTRUDING

- Tensile and stress rupture tests of Co base alloy bars extruded from prealloyed powders made by Ar gas atomization
01 p0100 A71-10480

- Ceramic fibers formation by particles mechanical deformation by extrusion in W matrix, describing grain structure of various extruded metal oxides
02 p0273 A71-12149

- Al alloys extrusion and chemical composition relationship to mechanical properties, examining various metallurgical processes
04 p0604 A71-15743

- Thermomechanical treatment effects on microstructure and fracture toughness of extruded Beta III titanium alloy
08 p1313 A71-21558

- Vertical hydraulic press for metal extrusion at temperatures from 4 to 77 K, discussing design
08 p1299 A71-21809

- Hydrodynamic lubrication temporary breakdown during initiation of extrusion process
10 p1618 A71-24924

- Cast cobalt base superalloys extrusion and forging, noting hot deformation effects on tensile properties, stress rupture strength and ductility
11 p1778 A71-25854

- Hydrostatic extrusion, emphasizing prismatic products fabrication from industrial metals and alloys
14 p2252 A71-30469

- Extrusion tools development since 1930, emphasizing economic aspects
14 p2253 A71-30470

- Al-base alloys granules dimension and shape effects on extruded semifinished product mechanical properties and structural stability
15 p2424 A71-31242

- Al alloys rods and sections extrusion process R and D, using lubricant without press residue
15 p2415 A71-32335

- Unsteady press forging process in dies with material extrusion through plane strained slot, describing deformation stages, slip line patterns and hodographs
16 p2581 A71-32818

- Structural shapes extrusion technique with superalloy powders, noting fine grain, chemical homogeneity and elevated temperature mechanical properties
16 p2592 A71-33540

- Production efficiency prerequisites in extruded Al alloy products manufacture, discussing billet material and processing conditions effects
16 p2584 A71-34091

- Extruding complex structural shapes of Ti alloys, considering use of glass as lubricant
18 p2927 A71-36662

Carburizing steels cold forging, investigating pressure requirement relationship to compressive stress from comparison of backward extrusion and laboratory compression tests

18 p2935 A71-36669

Nonheat treated extruded Mo alloy under tension and vacuum conditions at various temperatures, investigating cylindrical samples dimensions effects

18 p2936 A71-36714

Hot extrusion properties of free machining Al alloys with low melting point Pb as chip breakers

21 p3384 A71-40026

EYE [ANATOMY]

NT CHOROID MEMBRANES

NT CORNEA

NT FOVEA

NT NYSTAGMUS

NT OCULOMOTOR NERVES

NT PUPILS

NT RETINA

Monochromatic light glare effect on human eye as function of wavelength, using visual threshold variation as criterion

01 p0016 A71-11389

Eye wavelength /color/ discrimination ability measurements for linear dispersion spectra

01 p0016 A71-11390

Mathematical model for eye crystalline lens accommodation control interaction with pupil, deriving dynamic equations from human/cat experiments with/without neurological control

03 p0356 A71-12984

Pupil neurological control system for reaction to light and accommodation process by statistical eye noise analysis and microelectrode recordings of brain stem neurons

03 p0367 A71-12985

Accommodation model concerning nervous control of ciliary muscle

03 p0373 A71-14378

Human eye optical performance, noting retina anatomy and physiology, visual acuity, resolving power and reflectometry

05 p0713 A71-16482

Book on eye injuries covering mechanical trauma, neuro-ophthalmology, chemical, thermal, radiation, electrical and sonic injuries, etc

05 p0711 A71-17010

Laser ocular effects, discussing corneal /retinal/ lens lesion production, damage thresholds and application to clinical ophthalmological problems

07 p1049 A71-19792

Human eye optimum information reception assessment by Weber-Fechner law, threshold amount constancy and minimum continuous signal energy

07 p1043 A71-20110

Human eye information processing algorithms mathematical model technological materialization

07 p1051 A71-20119

Electronic model of color recognition by human eye using spectral filter-photosensor system

07 p1051 A71-20122

Mathematical model of visual information of edge contrast effects in human eye as functions of image brightness and viewing angle

07 p1051 A71-20123

Human crystalline lens protein and lipid discussing cholesterol accumulation with age

09 p1390 A71-22421

Darkness adapted human eye, investigating absolute light perception threshold dependence on light stimulus gradient

09 p1391 A71-22487

Visual accommodation mechanism, discussing microinterval nerve interaction role

09 p1391 A71-22488

Stabilized image movement control by mounting object in electric synchronous motor and rotating eccentrically

10 p1567 A71-23989

Night vision visual systems with image intensifiers, noting effect on human eye performance at low light levels

10 p1641 A71-24057

Vitamin A deficiency effect on rhodopsin loss dependent on illumination level in rat eye using electroretinography

10 p1563 A71-24326

Irreversible damage effects of visible light on retina in rats as function of irradiation, exposure time and vitamin A deficiency cell adaptation

10 p1563 A71-24327

Exposure time and power effects of CW Ar laser damage to rabbit iris, comparing with pulsed ruby laser effects

10 p1572 A71-25076

Microwave energy dissipation as heat in eye, using agar for eye model construction

10 p1572 A71-25078

Cataract production from microwave radiation exposure by lens nutrition alteration and surface shape changes

11 p1718 A71-25292

Human lens fluorescent pigment O-beta-D- glucoside of L-3-hydroxykynurenine, discussing preparation, electrophoresis and paper chromatograms

11 p1718 A71-25634

Human rods dark adaptation, investigating rhodopsin resynthesis and bright light flash effects

11 p1718 A71-25635

Book on color and pattern vision physiology covering retinal induction, electrical excitation of eye, optical illusion, figural aftereffect, movement sensation, etc

12 p1870 A71-26769

Night vision and dark adaptation of eye, noting sunlight effects on visual acuity

13 p2017 A71-28392

Pupil size influence on surface area and radius of inner /pupillary/ and outer /ciliary/ iris ring

13 p2013 A71-29034

Inertial-inertial beam stabilization application for image surface mechanical coupling to instrument /photography/ and uncoupled surface /eye/

14 p2242 A71-30146

Acoustical wave generation measurement during iris and retina photocoagulation and ruby laser burns, noting intraocular pressure surge simultaneous with ocular tissue explosion

15 p2365 A71-32346

Histopathological and fluorescein angiographic studies of rhesus monkey chorioretinal lesions produced at threshold and suprathreshold power levels of Ar laser

15 p2365 A71-32347

Ultrasonic softening of lens material to facilitate aspiration, using in vivo rabbit lenses for cataracts production

15 p2365 A71-32348

Arterioles and corneo-scleral shell structural response under various loading conditions, using finite element method for mechanical and hydrostatic stress distribution

16 p2528 A71-33099

Optical organs and autonomic nervous system fatigue assessment by blink method associated with eyelids, oculomotor muscles, retina and cerebrum

17 p2687 A71-34356

Meniscus induced thinning of tear films due to fluid film fracture and straining

17 p2687 A71-35803

Subjects with strabismic amblyopia, investigating defects in cone or rod mechanisms of dark adaptation by using colored filters

18 p2854 A71-36011

Refraction and image forming qualities of frog eye using measurement of intensity profile /point spread function/, confirming hyperopia

18 p2857 A71-36690

Visual sensations produced by cosmic ray muons passing in different directions through human eyes and head

19 p3005 A71-38677

Neosynthesized alpha-glycerophosphate and 2,3-diphosphoglycerate role in human extraocular muscle metabolism

21 p3328 A71-40099

Holography applications in ophthalmology to determine optical constants of living eye, including retinal receptors

22 p3540 A71-41753

Mammal extraocular muscle fiber structural and functional properties, discussing histological arrangement, fiber type classification and motor nerve endings

22 p3488 A71-42434

Anatomic examinations and diagnostic techniques in ophthalmologic aviation medicine, discussing electronic time interval and storage measurements, cortical response, etc

23 p3631 A71-42928

Eye pupil response during short term memory task, noting postsignal cycle of dilation-constriction

23 p3638 A71-43112

Human eye theoretical model with aspherical cornea front and lens back surfaces, computing astigmatism, coma, meridional and sagittal focal lengths by ray tracing method

24 p3798 A71-44978

Postsynaptic potentials in adjacent synaptic regions of tonic fiber of rabbit external eye muscle

24 p3798 A71-45066

EYE DISEASES

NT ASTIGMATISM

NT CATARACTS

NT GLAUCOMA

NT HYPEROPIA

Unilateral oscillopsia with vertical retinal nystagmus and internuclear ophthalmoplegia due to multiple sclerosis

06 p0852 A71-17615

Aerospace ophthalmology, discussing flying personnel selection, eye anatomy, presbyopia, macular degeneration, cataracts, corneal dystrophy and glaucoma

08 p1238 A71-20721

Acuity-dark adaptation in strabismic amblyopia, discussing mechanisms for defects

13 p2012 A71-28833

Passive and active extraocular muscle forces in strabismus, giving horizontal binocular alignment during fixation or eye movement

22 p3489 A71-42442

Crossed retinal pathways in Siamese cats due to neuroanatomical defect impairing binocular vision and stereoscopic depth perception

23 p3633 A71-43546

EYE DOMINANCE

Inhibitory binocular receptive fields in dorsal nucleus of lateral geniculate body for dominant and nondominant eye in cats, using moving slit and flash spot stimulation

21 p3335 A71-40669

EYE EXAMINATIONS

Open and closed eyes electroretinogram, discussing lamellar electrode placed on lower eyelid

01 p0024 A71-11077

Q switched and continuous laser collimated radiation exposure limits for eye cornea and skin, discussing environmental contamination

09 p1402 A71-23414

Ultrasonic/radiographic method for intraocular foreign body localization

13 p2013 A71-29031

Holography applications in ophthalmology to determine optical constants of living eye, including retinal receptors

22 p3540 A71-41753

Eye and orbit A and B ultrasonography scanning technique, showing minimal echogram distortions in meridional arc scans

24 p3799 A71-44367

Human eyes macular pigment optical density curves through spectral sensitivity measurements, noting differences due to race, environment, age, skin, eye and hair color

24 p3794 A71-44466

HF signals adaptation dependence from human cornea potential measurements by presenting narrow band chromatic stimuli to subjects under photopic, mesopic and scotopic adaptation conditions

24 p3794 A71-44467

EYE MOVEMENTS

NT NYSTAGMUS

Ocular pursuit movement evocation by visual and proprioceptive stimulation

01 p0009 A71-10235

Stimulus transretinal velocity effects on human torsional eye movements

01 p0009 A71-10236

Guinea pigs head and eye movements produced by vestibular apparatus stimulation via static pressure changes

01 p0010 A71-10347

Eye movements in dark during attempt to maintain ocular position defined by prior viewing of fixation target

01 p0016 A71-11388

Human eye cyclofusional movement response measurement in terms of disparity threshold for diplopia

01 p0016 A71-11391

Eye movements frequency and slow phase displacement in response to optokinetic stimulation of parrots and cats

02 p0199 A71-12385

Heat rotation induced eye movements in cats by neuron level determination, considering vestibular apparatus of signal transmission loop for mathematical model

03 p0356 A71-12983

Ocular counter-rolling as otolith organ function indicator

04 p0542 A71-14761

Labyrinth destruction, Meniere disease, labyrinthectomy and vestibular neuritis effects on eyes counter-rolling, discussing otolith organ damage determination

04 p0537 A71-14762

Binocular synchronization data, suggesting visual coordination dependent on continuous eye movement and retinal feedback timing

05 p0712 A71-16218

Saccadic eye movements scanpaths during pattern perception under poor visibility

06 p0859 A71-17962

TV monitoring and digital data recording of human corneal reflection during voluntary eye movements, considering visual perception studies application

07 p1051 A71-20210

Eye motion phase and amplitude measurement concerning visual acuity during whole body vibration

07 p1053 A71-20338

TV display eye movement monitor with automatic coordinate digital printout for permanent record

07 p1053 A71-20402

Dynamic visual acuity-horizontal eye movements correlation in man and monkeys, discussing fovea, parafovea and oculomotor control

10 p1560 A71-23984

Saccadic and smooth pursuit eye movements modification to visual targets instantaneous velocity changes at varying intervals

10 p1560 A71-23988

Overtraining reversal effect on attention process, using choice response and eye fixations compared to criterion trained group

10 p1562 A71-24204

Eye movement tendencies, investigating rectilinear, horizontal or vertical and center of gravity fixation effects on visual perception

10 p1570 A71-24602

Predictive stochastic optimal control model for saccadic eye movements in visual target tracking based on target motion estimate

11 p1723 A71-25142

Model of retinal information in cats from physiological and anatomical evidence, considering processing of contrast and eye movement information

11 p1723 A71-25254

Visual suppression and intensity threshold changes during voluntary eye saccades with different luminance regions in visual field, discussing inhibition processes

11 p1718 A71-25583

Spatio-temporal patterns in visual contrast sensitivity, noting exaggerated eye movements effects

13 p2018 A71-28462

Pupil size effect on dynamics of pupillary movements, considering reactions to light and darkness

13 p2013 A71-29032

Eye movements and visual perception, describing scan path for memory traces

14 p2188 A71-29801

Weibull distribution analysis of saccadic eye movements interval during visual task

17 p2688 A71-34366

German monograph on extrapolation procedure based on Taylor series expansion and on algorithm for identification and prediction of eye pursuit movements

17 p2690 A71-34790

Conjugate eye movement stimulator and monitor for human experimentation in closed loop, open loop and variable feedback modes of operation

17 p2693 A71-35392

Accommodometer for automatic measurement of eye response to accommodation stimulus

18 p2863 A71-35849

Eye-point-of-regard system including eye and head movements devices and analog computer for pilot scanning and display research

18 p2864 A71-36091

Eye-head coordination in monkeys by recordings from neck and eye muscles, noting central neural command role

18 p2856 A71-36232

Firing frequency of single trochlear nerve fibers during eye movements in alert monkey

19 p3001 A71-37413

Extraretinal correction and memory for target position, suggesting corrective tendency of eye movements in dark

19 p3004 A71-38286

Prefrontal cortex lesions effect on trained anticipatory visual target fixation in cats, noting performance impairment in voluntary eye movement control

21 p3529 A71-40174

Human blood pressure in brachial artery during spontaneous night sleep, recording EEG, EKG and horizontal eye movements

21 p3329 A71-40185

Eye movement control - Conference, University of the Pacific, San Francisco, November 1969

22 p3488 A71-42432

Eye movement neurophysiology, discussing ocular proprioception, oculomotor muscle sensory receptor role, extraocular muscle afferent and efferent innervation and central nervous system control effect

22 p3488 A71-42433

Central pathway connection between vestibular and oculomotor nuclei through pons responsible for horizontal eye movements induced by visual and vestibular stimuli

22 p3488 A71-42436

Human cerebral EEG phenomena and evoked potential relationships to eye and retinal image movements

22 p3488 A71-42437

Human ocular control system supranuclear disorder syndromes and signs in terms of physiological concepts

22 p3488 A71-42438

Extraocular muscle pharmacology, discussing eye twitch and tonic neuromuscular systems structure and function in frogs

22 p3488 A71-42439

Eye movement effect on visual system input and information use in perception

22 p3489 A71-42440

Cat and human eye movement control system measurements, studying isolated oculorotatory muscles and globe restraining tissues dynamics

22 p3489 A71-42441

Passive and active extraocular muscle forces in strabismus, giving horizontal binocular alignment during fixation or eye movement

22 p3489 A71-42442

Saccadic eye movement control system behavior simulation model evaluation, considering oculomotor pathways

22 p3504 A71-42443

Versional eye movement control system models, considering dual mode control, intermittency, plant dynamics and pattern recognition

22 p3489 A71-42444

Rapid saccadic and smooth pursuit tracking eye movement systems characteristics

22 p3489 A71-42445

Vergence eye movements control, discussing transient and frequency responses

22 p3489 A71-42446

Eye vergence movement control, describing effective target configurations and binocular units receptive field disparities

22 p3489 A71-42447

Vestibular and proprioceptive stabilization of eye movements

22 p3489 A71-42448

Human eye-tracking phase lags representation by time delays depending on target motion class

22 p3490 A71-42451

Apparent movement due to closely spaced sequentially flashed dots in human peripheral field of vision, considering eye movement role

23 p3634 A71-43970

Circumscribed eccentric afterimages effect on visual oculomotor control system, examining central transfer functions

23 p3635 A71-43971

Metric characteristics of horizontal saccadic eye movements in normal humans from electrooculographic recordings, discussing dysconjugacies mechanisms

23 p3635 A71-43972

Scanpaths in saccadic eye movements during pattern vision and recognition

23 p3635 A71-43973

Afterimage induced smooth eye movements despite absence of moving visual stimulus, suggesting retinal image stabilization and saccadic behavior inhibiting processes

24 p3794 A71-44469

Eye movements and visual images evoked by verbal stimuli, considering hereditary factors contribution to image formation

24 p3796 A71-44548

EYE PROTECTION

Control of biological laser radiation hazards

07 p1049 A71-19791

Flash blindness recovery with/without protection in simulated flight conditions, using aircraft instrument reading criteria

08 p1246 A71-20815

Biological tests of laser protective filters for eye as function of optical density and wavelength by sensitivity of in vivo ocular tissue response

13 p2020 A71-29035

EYEPIECES

Beam-combining prism/magnifier eyepiece configuration with miniature CRT for superimposing magnified virtual image upon user visual field

04 p0597 A71-15362

Large display direct view low light level system with objective lens, image intensifiers and eyepiece

22 p3548 A71-42512

EYRING THEORY

German monograph on heat transfer in Prandtl-Eyring fluid flows through flat channels with allowance for dissipation and asymmetrical thermal boundary

02 p0241 A71-12675

F

F CENTERS

U COLOR CENTERS

F DISPLAYS

U F REGION

F LAYER

U F REGION

F REGION

NT F1 REGION

NT F2 REGION

Atomic and molecular collisions in gases, considering E and F regions processes, auroras and applications

01 p0129 A71-10133

Ionospheric modification of F region through high power HF transmitter heating

01 p0040 A71-11529

Early phase model of F region heating and hydrodynamic expansion by deviative absorption of radio waves

01 p0040 A71-11530

F region reflected radio wave heating effect, considering electron temperature, collision frequency and heat conductivity

01 p0040 A71-11531

Electron density early time increase after artificial ionospheric heating, discussing F region recombination chemistry temperature dependence

01 p0040 A71-11532

F region electrons heating by RF energy at or near ionospheric plasma frequency, detecting temperature changes via optical nightglow intensity variations

01 p0040 A71-11533

F region ionospheric modification by heating from high power HF ground based transmission, discussing ionosonde observations

01 p0078 A71-11535

Ionospheric F layer modification by artificial heating, using radio echo detection of electron temperature changes

01 p0040 A71-11537

Nighttime F region molecular ion concentrations of oxygen and nobelium and associated nightglow morphology, using numerical method for solving nonlinear equations

01 p0078 A71-11611

F region electron concentration distribution during global magnetic storm, latitude and diurnal variation effects and radio wave reflections diffusion

02 p0243 A71-11770

F region electron density profile changes during negative magnetic bays, deriving ionization drift from continuity equation

02 p0243 A71-11771

Metastable atomic oxygen ion production in F region plasma due to photoionization by solar XUV radiation

03 p0462 A71-13271

F region diurnal behavior, comparing neutral winds and electric field effects

03 p0408 A71-13383

Wintertime Arctic F region critical frequency secondary maxima, discussing UT control hypothesis

03 p0408 A71-13386

Nighttime F layer true height profiles reduction from routine ionograms, discussing error corrections

03 p0408 A71-13387

Electric field strength measurement at rocket surface in ionosphere by electrostatic fluxmeter, obtaining E and F region ion drift velocities

03 p0417 A71-14035

Lower F region ionospheric response to internal gravity waves as function of azimuth of wave propagation, noting anisotropy

03 p0420 A71-14534

Top side ionosphere electromagnetic probing techniques, noting F and E regions

05 p0740 A71-16428

F region cosmic noise absorption at 20-30 MHz over Delhi, examining diurnal, seasonal and solar cycle variations

05 p0808 A71-16431

Magnetic disturbances effect on drift behavior and anisotropy parameters of E and F region irregularities

05 p0740 A71-16433

Reflection point slide velocity of traveling F region ionospheric disturbance by receivers amplitude focusing and echo phase path changes

05 p0741 A71-16440

Vertical electron density profiles correction coefficients, noting computational work decrease and F region frequency discrepancy due to ionization

05 p0746 A71-17207

F region photoionization heating, investigating energy transfer from ionizing photon to neutral gas atoms and molecules

06 p0893 A71-17982

F layer absence and nonuniform horizontal electron concentration of nighttime ionosphere at high latitudes, using Alouette 1 sounding

06 p0894 A71-18258

Thomson scatter measurements of F region ionization drifts vertical velocity at midlatitudes, studying electric field influence

08 p1279 A71-21204

Short radio wave propagation over single jump lines in F2 critical frequency gradient presence, examining maximum usable frequency increase

09 p1405 A71-22439

Ion and electron drift due to F layer wind and associated polarization fields, causing equatorial atmosphere eastward rotation

09 p1438 A71-22979

Night glow emission post twilight decay rates at different seasons by Chamberlain relation, discussing F layer ionization

09 p1441 A71-23644

Pseudoacoustic energy flux influence on accessibility of ground emitted wave to plasma resonance in F region, using adiabatic approximation with scalar pressure

10 p1602 A71-24465

E and F region positive ion composition, electron concentration and thermal balance vertical profile, discussing ionizing radiation spectrum, plasma cool-

ing, primary chemical reaction rates and ionospheric formation

10 p1573 A71-24550

Electric field, neutral air winds and atmospheric composition changes effects on electron concentration diurnal variation in midlatitude F layer

10 p1607 A71-24922

Geomagnetic Pc1 pulsations propagation in F region, deriving hydromagnetic waves equations by ray tracing method and waves refractivity index in extraordinary mode

10 p1607 A71-25118

Ionospheric drift mechanism in midlatitude F region, discussing ground level magnetic field, E region side effects, horizontal winds and polarization fields

11 p1753 A71-25550

Midlatitude F layer electron concentration increase during magnetic storm, assuming auroral zone heating of horizontal winds

11 p1754 A71-25607

Predawn enhancement structure of oxygen red line airglow at 6300 Å from time-latitude isophote diagrams, discussing F region photoelectrons recombination role

11 p1755 A71-25611

High latitude F region electron density irregularity measurements, using rocket-borne impedance probe

11 p1755 A71-25617

F region layers vertical drift from phase paths of radio waves reflected from constant electron density surfaces

11 p1756 A71-25646

Neutral winds produced vertical ion drift toward electric polarization in equatorial F region, discussing field discharge through E region and atmospheric superrotation effects

12 p1900 A71-26890

F region ion and temperature effects on VLF and ELF wave absorption in whistler mode propagation at midlatitudes during solar minimum

12 p1879 A71-27049

F layer vertical drifts due to winds at midlatitudes, computing longitudinal variations

13 p2054 A71-27793

E and F region irregularities random movements over Waltair, India, during IQSY, obtaining diurnal and seasonal variations

13 p2056 A71-27931

Small scale F layer inhomogeneities parameters and motion characteristics from radio echo observations

13 p2056 A71-27935

Vertical electron density profiles correction coefficients, noting computational work decrease and F region frequency discrepancy due to ionization

13 p2060 A71-28262

Log normal random fluctuations of ionospheric electron concentration in F region from vertical sounding and incoherent scatter data

13 p2061 A71-28553

Sizes, shapes and temporal characteristics of small scale inhomogeneities in F region, using vertical sounding, space diversity reception and radio astronomy

13 p2061 A71-28554

Daytime and nighttime sporadic F layer regularities correlation with other ionospheric phenomena based on vertical sounding data

13 p2062 A71-28555

High latitude measurements of low energy electron precipitation by Auroral 1 satellite, explaining anomalous high level F region ionization near dark pole

14 p2299 A71-30031

Physical processes and variations in polar F region, discussing solar photoionization, particle ionization, thermal expansion, electric fields, neutral air winds, ion drag, etc

14 p2234 A71-30038

Upper F region transpolar plasma distribution from Alouette 1 data, relating results to satellite measurements of magnetospheric low energy charged particles

14 p2234 A71-30041

F region drift velocity, wind, electric field, current and atmospheric composition variation measurements and related theoretical topics

14 p2201 A71-30940

Electric field, atmospheric wave and other factors effects on F region storms by day and night in tables

14 p2236 A71-30941

F region ionization drift and electric field observation by incoherent scatter techniques and data interpretation

14 p2236 A71-30942

Incoherent scatter measurements for ionospheric ion bulk velocity, thermospheric dynamics, F region gravity wave, photoelectron flux, ionic collision frequency and magnetic field direction

14 p2202 A71-30945

Total electron content and F region plasma frequencies height during magnetic storm of 8 March 1970

16 p2563 A71-33393

Neutral winds in F region from traveling ionospheric disturbance data, investigating gravity wave hypothesis

16 p2570 A71-33828

Thermospheric circulation and temperature changes due to global scale winds flow through F region ionization anomalies, using time independent dynamic model

16 p2571 A71-33836

Midlatitude nighttime F region electron concentration enhancements as downward diffusion flux from protonosphere induced by ionospheric substorm associated electric fields

16 p2573 A71-33958

F region vertical drift velocities at Millstone Hill, deriving ion velocity along magnetic field lines in upper part of F 2 region from continuity equation

17 p2732 A71-34427

F region plasma phenomena discoveries by U.S. researchers /1967-1970/, considering thermal structure, ion composition, conjugate photoelectrons effects, wind effects, etc

17 p2732 A71-34465

Scintillation fading of signals in SHF band due to electron density irregularities in F region

17 p2699 A71-34624

Computer demonstration of ionospheric F region storm causes, noting critical frequency relationship to ionization shift

19 p3055 A71-38038

F region radio wave absorption dependence on electron-ion temperature difference from energy balance considerations, testing by radar backscatter measurements

19 p3055 A71-38045

Radio wave scattering from ionosphere, considering plasma experiments in E and F region

19 p3018 A71-38247

F region seasonal anomaly relationship with lower atmosphere composition changes, discussing effects of oxygen/nitrogen relative concentration on ionospheric and atmospheric parameters

20 p3215 A71-38746

Day and night E and F region ion composition under solar maximum winter conditions from rocket measurements with RF mass spectrometers

20 p3280 A71-39719

F region nightglow emission mechanism in terms of oxygen cations reactions with diatomic nitrogen and subsequent recombination

20 p3226 A71-39832

Peak electron density variations during midlatitude F region storm, investigating electrodynamic drift effects

21 p3372 A71-40037

Ionospheric propagation hysteresis relationship to secular variation in F region response to sunspot number, noting differences in succeeding solar cycles

22 p3536 A71-42419

Traveling ionospheric disturbances excitation in F 2 layer by passing acoustic gravity waves

23 p3665 A71-42966

Sporadic E layer thickness measurement by Phase Ionosonde, measuring phase advance on F region echoes

23 p3666 A71-42975

Atomic oxygen 6300 and 5577 Å emissions nocturnal covariation from nightglow observation, considering relation to F layer height changes

23 p3667 A71-43131

Comparative north and south polar F layer electron density dependence on universal time and latitude, using ionosonde data

23 p3669 A71-43172

Solar flare induced E and F regions electron density enhancement observation by Thomson scatter, noting relationship to EUV ionizing radiation

23 p3721 A71-43173

F layer perturbations by intense vertically upward radio waves for aeronomy and plasma control studies

23 p3671 A71-43543

Small scale electrostatic field penetration from E into F region of ionosphere based on plane stratified model

23 p3671 A71-43577

Earth atmosphere gas composition and electron density variations at F region lower boundary explained by stratospheric explosive and diffusive warmings effect on critical frequency

23 p3671 A71-43578

F region ion and electron temperature relationship to electron density, examining incoherent scatter data and physical processes

23 p3672 A71-43977

Daytime photoelectron energy distribution and electron gas heating in F region as function of height and solar cycle variations

23 p3673 A71-44003

F 1 REGION

Seasonal altitude variation of atomic ion-electron ratio of oxygen/nitrogen species in F 1 region comparing to radar measurements

01 p0076 A71-11507

F 1 layer development at summer midday midlatitude, noting role of molecular ions composition

05 p0745 A71-17200

F 1 region unsteady model, examining vertical distribution profile of electron concentration on summer day

06 p0895 A71-18273

F 1 layer occurrence frequency probability vs solar elevation

07 p1100 A71-19399

Monthly median F 1 layer critical frequency prediction at arbitrary location and time as function of ionospheric index, geomagnetic latitude and solar zenith angle

08 p1257 A71-21882

F 1 layer development at summer midday midlatitude, analyzing molecular ions composition effect

13 p2059 A71-28255

Flight test results for CACTUS accelerometer launched by rocket probe at Guiana Space Center, considering atmospheric density profile in 120-150 km altitude zone

18 p2924 A71-36755

F 1 layer occurrence frequency probability vs solar elevation

19 p3053 A71-37823

F 1 region ion structure during ionospheric magnetic disturbances by numerical simulation of quiet and disturbed conditions based on electron concentration profiles

19 p3057 A71-38368

Atmospheric composition and temperature effects on F 1 region ion concentration structure from 140 to 220 km for low solar activity conditions

19 p3058 A71-38382

Incoherent scatter observations of ion concentration and plasma line in F 1 region

23 p3670 A71-43188

F 2 REGION

Meridional ionization cross section in ionosphere between Leningrad and Murmansk with local anomaly and diurnal reversing of F 2 probability

02 p0243 A71-11766

F 2 layer transmission coefficient, describing altitude linear dependence of electron density maximum

02 p0244 A71-11773

F 2 layer anomalies association with equatorial electrojet from F 2 and sporadic E critical frequencies analysis

02 p0245 A71-11963

Midlatitude topside ionosphere electron density diurnal variations, discussing F 2 layer seasonal anomaly altitudinal extension

03 p0409 A71-13390

Diurnal and seasonal variations of cosmic noise absorption at critical frequency of F 2 region

03 p0379 A71-13815

F 2 region critical frequency ionospheric tidal spectrum during solar minimum and maximum at various global locations and solar and lunar day periods

04 p0583 A71-15214

Lunar semimonthly oscillations in solar daily H range related to midday F 2 critical frequency at equatorial stations, analyzing lunar tides in ionosphere

05 p0740 A71-16432

Magnetic disturbances effect on F 2 critical frequencies in Australasian zone during IGY-IGC, correlating to equatorial electrojet

05 p0741 A71-16438

Sporadic E layer effect on F 2 region critical frequencies

05 p0745 A71-17201

Midlatitude F 2 layer electromagnetic drift during magnetic storm

06 p0888 A71-17287

Solar wind velocity relationship with F 2 layer electron density

06 p0950 A71-17991

Electron concentration disturbances in outer ionosphere and F 2 maximum on daylight side during magnetic storm

06 p0894 A71-18257

F 2 region critical frequency diurnal variation forecasting, using series expansion of natural orthogonal components

06 p0895 A71-18276

F 2 layer nighttime ionization seasonal fluctuations, considering dependence on geographical longitude and latitude and solar activity levels

07 p1098 A71-19382

Equatorial zone daytime F 2 maximum height diurnal variation latitude change with decreasing solar activity from vertical sounding

07 p1100 A71-19401

Seasonal variations in F 2 region, using critical frequencies during descending solar activity phase

07 p1102 A71-19672

High energy electron background flux in F 2 layer, discussing grouped particle acceleration

08 p1354 A71-21012

Electron continuity equation for lower F 2 layer near dip equator, estimating photoionization and recombination rates

08 p1278 A71-21203

F 2 layer nighttime ionization at midlatitudes, investigating conjugate point effects on observation point

09 p1434 A71-22426

F 2 layer critical frequency and maximum electron concentration statistical characteristics for predicting SW propagation conditions

09 p1435 A71-22427

F2 region ionospheric disturbances association with severe thunderstorms from radio observations

09 p1490 A71-23559

Ionospheric propagation forecasting as function of solar and magnetic activity conditions for maximum usable communications frequencies, using F2 layer peak electron density

10 p1575 A71-23865

Satellite data for ionospheric radio communication forecasting involving maximum usable radio frequencies, discussing F 2 region large scale disturbances

10 p1575 A71-23868

Solar cycle effects on diurnal variations of F 2 region critical frequency and maximum ionization height

10 p1600 A71-23884

Midlatitude F2 region diurnal variations in peak electron density critical frequency and height, noting electric field and ion drag effects

10 p1606 A71-24921

Storm time variations of F 2 layer electron concentration and critical frequency at Australasian stations

11 p1754 A71-25606

A type red aurora in polar region accompanied by sporadic F 2 layer

11 p1754 A71-25608

Numerical integration of unsteady continuity equation for electron-ion gas concentration distribution in F 2 region

11 p1757 A71-25770

Distribution curves of F 2 critical frequency variations, considering probability density functions interpretation via asymmetric model

11 p1757 A71-25771

F 2 layer critical frequency abnormal latitudinal distributions, using Alouette 1 satellite data

12 p1900 A71-26935

Ionospheric continuity in F 2 region during partial solar eclipses, using EUV radiation and additional corpuscular source of ionization

13 p2053 A71-27792

Sporadic E layer effect on F 2 region critical frequencies

13 p2059 A71-28256

Magnetoionic component with fluctuating elliptical polarization during wave reflection from F 2 layer, discussing suppression mechanism

13 p2030 A71-28537

Cross correlation characteristics of deviations in critical frequencies of F 2 region

13 p2030 A71-28538

F 2 layer critical frequency variations relation to solar radio flux intensity, using mathematical approximations

13 p2062 A71-28557

Time between noontime and evening maxima in F2 layer critical frequency compared with evening maximum period, showing dependence on noontime solar zenith angle

13 p2062 A71-28559

F 2 ion velocity and electron density perturbations in terms of gravity waves, comparing incoherent scatter techniques

14 p2230 A71-29716

F 2 layer peak electron density diurnal and seasonal variations, noting geomagnetic latitude and solar activity effects

15 p2394 A71-31427

F 2 and E layers peak electron densities semiannual variations, suggesting association with solar activity and charged particles penetration

16 p2568 A71-33785

Harmonic analysis of F 2 region critical frequency in antarctic region, emphasizing solar activity effects

17 p2731 A71-34317

Antarctic F 2 layer height and critical frequency diurnal variations due to ionospheric neutral winds, ionization maxima and solar effects

17 p2731 A71-34318

Ionospheric storms morphology, analyzing F 2 layer maximum relative electron concentration worldwide propagation

17 p2734 A71-35192

Semiannual amplitude variations in F 2 region for estimating oxygen density dissociation and temperature ratios in lower thermosphere

19 p3048 A71-37398

F 2 layer noontime ionization seasonal fluctuations, considering dependence on geographical longitude and latitude and solar activity levels

19 p3052 A71-37807

Equatorial zone daytime F 2 maximum height diurnal variation latitude change with decreasing solar activity from vertical sounding

19 p3053 A71-37825

Quiet sun diurnal variations of intertropical F 2 ionization in true heights over Tamanrasset meridian

19 p3054 A71-37863

Polarization ellipse and depolarization coefficients for monochromatic radio waves reflected from F 2 ionosphere using Stokes parameters

19 p3056 A71-38362

Latitudinal distribution of electron temperature in F 2 layer during summer daytime period of low solar activity from electron density profile geometrical parameters

19 p3057 A71-38369

Magnetic storm effect on integral electron content in F 2 layer and in outer ionosphere

19 p3058 A71-38383

F 2 region electron density spatial and temporal distribution, investigating plasma vertical drift effects

19 p3058 A71-38384

Isoline charts showing F 2 layer critical frequency deviations and negative disturbance zones during solar eclipse of 22 September 1968

19 p3058 A71-38385

High energy electron background flux in F 2 layer, discussing grouped particle acceleration

20 p3280 A71-39592

F 2 and D regions disturbances associated with magnetic storms, emphasizing airglow effects

20 p3227 A71-39836

Midlatitude ionospheric data comparison to F 2 critical frequency from continuity equation and neutral air winds

21 p3372 A71-40043

Ionospheric properties at geomagnetic equator from ionograms by automatic sounder at Thumba, noting F 2 layer ionization frequencies solar cycle variations altitude dependence

21 p3373 A71-40376

Numerical integration of unsteady continuity equation for electron-ion gas concentration distribution in F 2 region

22 p3532 A71-41538

Distribution curves of F 2 critical frequency variations, considering probability density functions interpretation via asymmetric model

22 p3532 A71-41539

Subequatorial ionospheric upward moving irregularities during high sunspot activity, explaining phenomenon at F 2 region level by Hall drift from daytime west-east electric field

23 p3665 A71-42971

Semiannual variation in F 2 layer peak height and critical frequencies at midlatitudes, considering vertical ionospheric drifts effects

23 p3665 A71-42973

Equatorial F 2 region lattice model with curved field line geometry for plane stratified atmosphere and time dependent problem solution

23 p3667 A71-43137

Stratospheric warmings effect on F 2 region parameters and ionospheric radio wave absorption, assessing time lag

23 p3673 A71-44049

F 2 region magnetic disturbances conjugacy mechanisms, considering vertical ionization profiles

24 p3823 A71-45029

Predawn effect on hot and cold electrons at magnetoconjugate point in F 2 layer, discussing electron shock wave speed and thermal collisionless wave energy dissipation

24 p3824 A71-45321

F-4 AIRCRAFT

USAF F-4E Stall/Near Stall Investigation, discussing testing requirements, fighter aircraft improvement, spin avoidance and high angle of attack limitations

07 p1019 A71-19095

Late model F-4 air superiority aircraft and electronic flight control systems protection against lightning discharges damage to electric and electronic systems

07 p1021 A71-19940

External store surface pressure distributions during captive flight aboard F-4B aircraft, considering carrying aircraft effects on flow field about airborne ordnance

[AIAA PAPER 71-295]

08 p1232 A71-22015

Skin friction, trailing edge boundary profiles and tuft flow patterns on model F-4D aircraft in transonic flow

[AIAA PAPER 71-762]

16 p2521 A71-34001

Potential benefits accruing to air superiority fighters by integrating automatic feedback control system technology into design, using F-4 as baseline configuration

[AIAA PAPER 71-764]

16 p2523 A71-34002

F-4E stall/spin development and flight tests, relating mass distribution and angle of attack aerodynamic design

[AIAA PAPER 71-772]

16 p2524 A71-34008

Numerical method for near field antenna coupling over conducting surface of aerospace vehicles applied to L band slot antennas on F-4 Phantom aircraft

19 p3031 A71-38445

F-8 AIRCRAFT

F-8D aircraft transonic flight and wing tunnel tests for buffet onset prediction, considering effects of g level and fluctuation amplitude and frequency

[AIAA PAPER 70-341]

10 p1557 A71-24863

F-14 AIRCRAFT

F-14A twin engine variable geometry carrier based jet fighter aircraft, discussing design, development program and manufacturing techniques

02 p0188 A71-12050

Boron-epoxy structural skins design for F-14 honeycomb horizontal stabilizer, using computer program

11 p1786 A71-25420

Fighter F-14 podded engine high variable sweep wing design including nozzle, nacelle, fuselage shift, aspect ratio and lift control improvements

16 p2526 A71-34152

Flight test program, facilities and instrumentation for F-14 aircraft structural, powerplant, avionics, performance and carrier suitability evaluation

16 p2526 A71-34153

Integrated logistics support program for F-14 aircraft maximum maintainability, reliability and operational readiness at optimum cost

16 p2553 A71-34154

Avionics systems for weapons control in F-14 fighter aircraft, discussing track multiple targets, sighting aids, radar, computer navigation, communications and built-in self testing

16 p2527 A71-34155

Titanium and composite fabrication for F-14 aircraft, discussing hot forming, chemical milling and electron beam welding

16 p2585 A71-34156

Modular manufacturing for F-14 aircraft at low cost using end product configuration reducing final assembly

16 p2585 A71-34157

F-15 AIRCRAFT

F-15 air superiority fighter, describing military requirements, program management and procedures in terms of speed, maneuverability, acceleration and weaponry

07 p1018 A71-19078

F-15 aircraft integrated data system for flight test program information, discussing development and major elements

16 p2524 A71-34010

F-28 TRANSPORT AIRCRAFT

Experimental and theoretical aeroelastic analysis of Fokker F-28 T tail, using flutter model and flight flutter tests

17 p2676 A71-35649

F-90 AIRCRAFT

U T-33 AIRCRAFT

Roughrider F-100F aircraft flights in thunderstorms and Apollo 12 launch electric field measurements, comparing patterns and magnitudes of lightning strikes to vehicles

07 p1208 A71-19927

F-100 pilots acute HF hearing loss due to noise ground environment and excessive in-flight noise exposure

09 p1400 A71-23249

Fatigue crack initiation and growth and residual strength of F-100 wing, comparing service failure data with full scale fatigue test results

17 p2827 A71-35159

F-104 AIRCRAFT

F-104D aircraft side stick control system design and function, curriculum maneuvers and component reliability

07 p1018 A71-19092

Physical and physiopathological effects of high altitude supersonic flight in TF-104G aircraft told by flight surgeon

10 p1572 A71-24980

Minimum time profiles for F-104 aircraft by Balakrishnan epsilon technique, comparing solutions with energy method

13 p1996 A71-28831

F-110 AIRCRAFT

U F-4 AIRCRAFT

F-111 AIRCRAFT

F-111 airframe static test instrumentation, describing computerized processing of simultaneous inputs from 400 channels of tape recorded strain, load and deflection data

09 p1444 A71-22717

Cost effectiveness of reliability screening program from parts procurement through system test, using experience with attack radar for F-111 aircraft

12 p1885 A71-26683

Performance evaluation of variable geometry external fuel tank prototypes by static structural tests, wind tunnel tests and flight tests on F-111 aircraft

[AIAA PAPER 71-763]

17 p2675 A71-35533

Design, analysis and testing of F-111 complex fuselage full scale section of composite materials, noting weight savings

[SAWE PAPER 889]

17 p2835 A71-35825

FAB (PROGRAMMING LANGUAGE)

U FORTRAN

FABRICATION

U-tube rocket nozzle and fuel element fabrication methods for NERVA space engine, emphasizing coating process

01 p0126 A71-10006

Metal sheet plate and bar fabrication, calculating minimum bend radii from ductility ratings
01 p0087 A71-10457

Composite fiber-reinforced structures fabrication methods
[SME PAPER EM-70-112] 01 p0089 A71-11256

Metal matrix composites fabrication techniques, discussing isostatic hot pressing, explosive processing and in situ fiber
[SME PAPER EM-70-125] 01 p0090 A71-11264

Basic and special field effect transistor design and operation, discussing performance and fabrication
02 p0229 A71-11810

Low temperature cylindrical thermionic converters with CVD Re electrodes, discussing design, fabrication and performance
02 p0193 A71-12219

Whisker reinforced composites fabrication principles and methods, discussing constituents, mechanical, geometrical, physical and chemical requirements
04 p0603 A71-14949

Sandwich metal construction with welded Norsial corrugated core for light weight and strength, discussing fabrication and application to hypersonic research vehicles
04 p0603 A71-15207

Solar cell array fabrication for operation at 173-383 K, discussing honeycomb sandwich substrate using epoxy-novolac-fiberglass facings and Al core
05 p0756 A71-16097

Apparatus for thin film solid state devices fabrication under ultrahigh vacuum
05 p0733 A71-16233

Masking techniques for printed and thin film circuits and semiconductor devices fabrication
05 p0759 A71-16775

Sandwich structures fabrication of foam core and solid polymer skin by automated injection molding
05 p0759 A71-16931

Muscovite mica substrate surface composition as function of preparation and processing, using Auger electron spectroscopy
06 p0941 A71-17408

Intelsat 3 satellite mechanical and electronic components fabrication, emphasizing quality and reliability assurance procedures and assembly techniques
06 p0905 A71-18403

Continuous filament metal matrix composites fabrication from hot pressed composites by diffusion reaction process
06 p0915 A71-18688

Refractory metals and alloys fabrication and mechanical and physical properties at high temperatures
07 p1134 A71-19581

MOS transistors for high digital logic speed and microwave performance, discussing fabrication by double diffusion through mask opening
07 p1078 A71-19998

Amorphous semiconducting thin films quenching fabrication techniques and electrical properties
07 p1181 A71-20410

Filament winding manufacturing methods using unidirectional glass reinforcements for design and fabrication of aircraft wing structure
[SME PAPER EM-70-406] 07 p1120 A71-20546

Fluidic element fabrication techniques, discussing concrete and epoxy molds and stainless steel chemical milling
07 p1121 A71-20562

Titanium-steel bimetal part fabrication using explosive and drop forging
08 p1295 A71-20840

Filament wound carbon fiber reinforced plastics components fabrication and performance tests
[PLASTICS INST. PAPER 47] 08 p1296 A71-20902

Composite materials with metallic matrix and carbon fibers, discussing production techniques and mechanical properties
[PLASTICS INST. PAPER 15] 08 p1320 A71-20907

Carbon fiber/carbon composites produced by moulded carbon technique, discussing mechanical properties and applications in rocket motors
[PLASTICS INST. PAPER 38] 08 p1348 A71-20914

Carbon fiber reinforced Al composites fabrication and evaluation by metallographic examination, considering tensile strength
[PLASTICS INST. PAPER 17] 08 p1322 A71-20930

Bipolar silicon microwave transistors process technology improvements related to extensions of frequency, power handling or low noise performance
08 p1263 A71-20991

Uncooled Si nuclear particle detector charge sensitive and pulse shaping amplifier design, discussing spacecraft instrumentation and fabrication requirements
08 p1267 A71-21848

Semiconductor integrated circuit fabrication optimization, considering defect density, component number, crystal size and cost analysis
09 p1416 A71-22490

Integrated microwave circuits substrate materials, discussing fabrication techniques with attention to mechanical, thermal and electrical characteristics
09 p1418 A71-23059

Epitaxial deposition of discrete separated p- and n-type silicon on single sapphire substrate, considering technique for MOS devices fabrication
09 p1509 A71-23116

TI alloys structural high temperature applications in fighter aircraft, considering fabrication and assembly methods
09 p1458 A71-23427

Opaque ceramic armor materials for lightweight personnel and equipment ballistic protection applications, discussing mechanical properties and fabrication techniques
09 p1484 A71-23689

Composites fabrication techniques, component materials and nature, emphasizing fiber orientation and matrix properties
10 p1618 A71-24769

Fiber reinforced thermoplastics fabrication by fluidized bed techniques, fusing powder matrix to fiber surface for continuous coating
11 p1768 A71-25415

Representative Thorneil fiber aircraft fuselage component nondestructive testing and repair, and Thorneil fiber, polysulfone and polyamide-imide composites fabrication and evaluation
11 p1787 A71-25427

Glass fiber reinforced plastics reinforcement techniques, emphasizing E glass filament manufacture, properties, advantages and products
11 p1788 A71-25653

Double ended full length external fuel thermionic converter, describing component fabrication, assembly sequence, joining methods, vacuum test procedures and converter load control
11 p1715 A71-25910

Design, fabrication and testing of electrically heated externally configured thermionic diodes with emitter using mandrel side of CVD fluoride tungsten for electrode surface
11 p1715 A71-25911

Resin matrix composite airfoils in gas turbine engines, considering performance, fabrication and cost
[ASME PAPER 71-GT-47] 11 p1770 A71-25980

Design and fabrication of Borsic aluminum composite fan blades for supersonic turbofan engines, considering 430 F application without severe vibratory stress
[ASME PAPER 71-GT-90] 11 p1771 A71-25997

Fabrication and properties of carbon reinforced carbon matrix composites
14 p2261 A71-29639

Materials and processing methods for rain erosion resistant ceramic coated plastic structures for supersonic aircraft, considering fiberglass reinforced polyimide radomes with alumina coating
14 p2262 A71-29645

Advanced plastic composites fabrication and processing techniques, using resins, reinforcements and fillers
14 p2263 A71-29653

Low cost metal matrix composite fabrication, discussing plasma spraying and continuous casting
14 p2263 A71-29655

Miniature transducers design and fabrication for fluctuating pressure measurements in jet engine testing, noting frequency response and power dissipation
14 p2244 A71-30324

Hydrostatic extrusion, emphasizing prismatic products fabrication from industrial metals and alloys
14 p2252 A71-30469

Luneberg lens fabrication technique using thin insulated Al slivers embedded in low density polystyrene foam
14 p2205 A71-31059

Composite materials fabrication primary and secondary aerospace and aeropropulsion structural components
[SME PAPER EM-71-710] 15 p2416 A71-32434

Reliability implications of Boeing 747 program, considering problem detection and identification, parts fabrication and installation, airline operating variables, etc
16 p2522 A71-33285

Fabrication technology limitations effect on use of dielectric interference filters in wide angle optical receivers
16 p2946 A71-35847

Hybrid circuits thick film technology, discussing printed circuits fabrication processes and electrical and mechanical properties
18 p2888 A71-36224

Fabrication and noise performance of high power Schottky barrier GaAs IMPATT diodes with double epitaxial layer structure on low-etch-pit density substrates
18 p2895 A71-36982

Hybrid microelectronics IC S band double conversion phase locked receiver, discussing fabrication, process requirements and component selection criteria
19 p3035 A71-38538

Radioisotopic power applications of beta and gamma emitting Co 60, noting powder ceramic fabrication of dense wafers for irradiation to convert natural Co 59
20 p3265 A71-38938

Hybrid circuit methods for aligning resistors manufactured by different technologies, considering mechanical methods, electric erosion, electron and laser beam alignment, etc
20 p3208 A71-39434

Carbon-carbon composites fabrication by electrostatic fiber deposition/flocking, using liquid impregnation-carbonization cycles with coal tar pitch
21 p3384 A71-40140

Ion beam milling techniques for device fabrication involving atomic interactions on solid surfaces
21 p3384 A71-40219

Opposed hemispherical self acting gas bearings fabrication for gyro wheels, using machine lapping and sputter etching
22 p3553 A71-41677

Wireless assembly methods for thin and thick film hybrid and monolithic IC, emphasizing flip-chip elements microelectronic devices fabrication and interconnection
22 p3525 A71-41714

Book on thick film microelectronics covering microcircuit design, fabrication, packaging and applications
23 p3650 A71-43224

Li-filled vacuum-deposited W heat pipes for efficient heat extraction from nuclear reactors, discussing design, fabrication and testing
23 p3682 A71-43595

Transistor compensation stabilizers design and fabrication with enhanced voltages
24 p3807 A71-44382

Glass multichannel perforated plate manufacture technology, discussing drawing and hollow fiber techniques
24 p3832 A71-45335

FABRICS

NT FELTS
NT GAUZE
NT PARACHUTE FABRICS

Flammability and heat transfer characteristics of flame retardant cotton, Nomex and polybenzimidazole (PBI)/ protective fabrics
07 p1145 A71-19573

High strength flexible carbon fabrics from oxidized polyacrylonitrile yarns for reinforced plastic laminates
[PLASTICS INST. PAPER 39] 08 p1319 A71-20900

FABRY-PEROT INTERFEROMETERS

Projectile velocity measurement by laser and Fabry-Perot interferometer using Doppler effect
02 p0258 A71-11657

Limited scanning function of optical system consisting of He-Ne laser and Fabry-Perot interferometers with small effective apertures
03 p0435 A71-13514

Fresnel annular zone objective lens for multichannel Fabry-Perot interferometer
03 p0425 A71-13651

Prismatic absorption type wavemeter consisting of frequency divider and Fabry-Perot interferometer, considering tests in millimeter and submillimeter range
03 p0386 A71-13801

Fabry-Perot etalon and focal reducer parameters for extragalactic radial velocities measurement, comparing optical mountings
04 p0593 A71-14909

Thermal variations of all-glass and air-gap Fabry-Perot etalons for radial velocities measurement, discussing resolution
04 p0593 A71-14910

Ghost images due to reflection between interference filters and Fabry-Perot etalons during measurement of radial velocities
04 p0593 A71-14911

Fourier data decomposition technique for recovering Doppler temperature, emission line intensity and Doppler shift of central frequency of Fabry-Perot fringes in presence of statistical noise
05 p0748 A71-16265

FM optical signals detection using Fabry-Perot interferometer with air gap between mirrors
05 p0753 A71-16875

UV solar spectrum rocket-borne high resolution spectroscopy by Fabry-Perot interferometer and echelle grating, discussing design parameters and recorded data
06 p0903 A71-18718

Oscillation mode selection method applied to Fabry-Perot interferometer using Faraday effect
07 p1109 A71-19454

Fabry-Perot interferograms analysis by Fourier transforms, considering mirror defects, light incident angle spread and spectral lines Lorentzian and Gaussian shapes
08 p1289 A71-21378

Instrumental function of Fabry-Perot interferometer and lamp-emitted line profile determined with hollow cathode thorium lamp
08 p1290 A71-21380

FABRY-PEROT LASERS

- Fabry-Perot interferometer for dielectrics permittivity and loss measurements in millimeter and submillimeter ranges, discussing design, tests and accuracy 08 p1294 A71-21806
- Book on applied diffraction theory covering scalar and vector wave theory, radio wave propagation, linear integral equations, microwave lens, Fabry-Perot interferometers, etc 09 p1494 A71-22959
- Mirror reflection coefficients effect on fringe characteristics of multibeam series interferometer, showing improvement by Fabry-Perot etalon system 09 p1451 A71-23174
- Dielectric constant and loss tangent measurements at 60 and 90 GHz for Teflon, polystyrene and Lucite sheets, using Fabry-Perot interferometer 09 p1418 A71-23415
- Q switched ruby laser time dependent spectrum analysis by high speed camera with Fabry-Perot interferometer, noting holographic interferometry application 10 p1622 A71-24962
- Measuring methods for internal velocities of stars and gas within spiral galaxy, considering emission lines and Fabry-Perot interferometer 12 p1960 A71-26786
- Wide field high resolution birefringent filter based on Fabry-Perot etalon and Lyot-Ohman filter, discussing limitations and applications 12 p1904 A71-26802
- Frequency and temperature variations of active diode region in pulsed GaAs laser, using Fabry-Perot interferometer 13 p2079 A71-28923
- Multiple-beam interference effects in Fabry-Perot interferometer with small wedge between mirrors, deriving expressions for light beams path 14 p2243 A71-30273
- Fabry-Perot interferometer laser beam diffraction effects on fringe pattern formation, deriving field distributions in near and far zones 15 p2421 A71-32459
- Optimal parameters of Fabry-Perot etalon for error minimization in Doppler and dispersion portions determination of Voigt profile width 17 p2737 A71-34410
- Solar Fe XIV 5303 coronal line isolation, using solid Fabry-Perot interferometer as monochromator 18 p2966 A71-36736
- Mode selection of transition frequencies in carbon dioxide laser with Fabry-Perot interferometer in resonator 19 p3073 A71-37790
- Instrument function for central spot distribution of Fabry-Perot etalon with finite aperture, comparing to Airy formula 21 p3379 A71-40636
- Frequency and temperature variation with time in active region of pulsed GaAs laser diode, using Fabry-Perot interferometer 21 p3394 A71-41318
- Photosensitive epoxy resin coating light path propagation variation measurements, using continuous radiation gas laser and Fabry-Perot interferometers 22 p3555 A71-41615
- Book on interference of electromagnetic waves covering Michelson-Fizeau and Fabry-Perot interferometers, Fourier transform spectroscopy, etc 22 p3576 A71-42429
- Monochromatic observations of coronal loop, using isophotal map from coronagraph through Fabry-Perot interferometer 23 p3768 A71-43846
- FABRY-PEROT LASERS**
U LASERS
- FABRY-PEROT SPECTROMETERS**
Fabry-Perot spectrometer systems for solar corona emission spectra and temperature measurements during eclipses 03 p0489 A71-13629
- H II region high velocity observations by two etalon, propane scanned photoelectric Fabry-Perot spectrometer with reflecting telescope 04 p0581 A71-15044
- High resolution Fabry-Perot spectrometer with stepwise automatic scanning, discussing reproducibility, flexibility and stability 12 p1908 A71-27672
- Auroral spectroscopy, considering grating spectrometers, Fabry-Perot and Michelson spectrometers, filter photometers, etc 13 p2058 A71-28039
- Scanning system with hydropneumatic drive for Fabry-Perot spectrometers in IR region, describing He-Ne laser tests 14 p2247 A71-30587
- IR modulator in space equipment, considering Fabry-Perot cavity with variable plate separation 22 p3544 A71-42138
- CH radical 10 cm line frequency determination by photographic Fabry-Perot interferometry 23 p3733 A71-43082

FACE (ANATOMY)
NT NOSE (ANATOMY)

FACE CENTERED CUBIC LATTICES

- Fcc metals cohesion strengths, using fracture technique with subsequent cold welding 02 p0267 A71-12879
- NiMo alloy fcc disordered structure and mechanical properties correlation to domain size and orientations from thin film transmission electron microscopy 07 p1132 A71-19435
- Atomic ordered alloy compressive strengthening for fcc and bcc lattices in terms of yielding, work hardening and no hardening stages 07 p1132 A71-19438
- Fcc metals film growth on air- and vacuum-cleaved PbS, using electron diffraction and conventional electron microscopy 07 p1178 A71-19848
- Deformation amplitude effects on dislocation structure and strengthening mechanism of fcc aluminum under cyclic loading 07 p1142 A71-20482
- Fcc binary alloys cross slip difficulty due to solute atoms and small short range order regions 08 p1309 A71-21527
- Fcc crystal strengthening, examining short range core defect dislocations 08 p1310 A71-21538
- Iron and fcc metal composite wires, determining fiber thickness and strength relationship 08 p1323 A71-21588
- Stacking faults and fcc precipitation of Ti beta alloys after high temperature heating 09 p1469 A71-22850
- Thermodynamic properties of interstitial solid solutions with fcc metals from atomically discrete model by computer simulation 11 p1778 A71-25531
- Stress raisers effect on mechanical properties of fcc materials at cryogenic temperatures 13 p2083 A71-27871
- High strength corrosion resistant multiphase Co-Ni-Cr-Mo alloys with fcc structure hardened to hcp by mechanical deformation 13 p2084 A71-28148
- Elastically and plastically anisotropic single crystals randomly oriented in polycrystalline aggregate, noting initial yield surface in fcc lattice 13 p2155 A71-29063
- Vibration fatigue of metallic materials in vacuum and different gas atmospheres, considering fcc metals, Al alloys and steels 14 p2259 A71-30466
- [DEVL-SONDDR-62] Cobalt and lanthanum with face and body centered lattices, studying plastic deformation during allotropic transformations under sliding friction and gripping 16 p2584 A71-33895
- Carbon activity, free energy entropy and enthalpy in fcc solid solution of Fe-Ni-C alloy 19 p3080 A71-37714
- Titanium dihydride room temperature polymorphic transition from fcc to body centered tetragonal, noting different transition temperatures 22 p3563 A71-42368
- Stable austenitic stainless steels and fcc metals plastic deformation flow curve model, presenting stress-strain relation 23 p3695 A71-44284
- FACETS**
U FLAT SURFACES
- FACSIMILE COMMUNICATION**
NT AUTOMATIC PICTURE TRANSMISSION
Synchronous meteorological satellite mission goals and system design, describing imaging, data collection, facsimile, space environment, trilateration, ranging and transmission 07 p1067 A71-18807
- FACSIMILE TRANSMISSION**
U FACSIMILE COMMUNICATION
- FACTOR ANALYSIS**
Steels mechanical properties factor analysis, considering Brinell hardness, tensile strength, yield point, relative contraction, elongation and impact strength 09 p1467 A71-22312
- Experimental plan construction, describing group divisible partially balanced incomplete blocks, asymmetrical multiple factor construction and symmetrical plan transformation 12 p1988 A71-26708
- Factor analysis in construction of human fatigue rating scale from individual appearance and comportment 17 p2687 A71-34355
- Factor analysis of phase discrimination in mental fatigue during diurnal variation of cortical functions in railroad traffic control center operators 17 p2688 A71-34362
- Project management quality control factors learned from Diamant A satellite launching vehicle and French military programs 23 p3786 A71-43469
- Factor methods convergence for abstract equations with nonlinear entirely continuous operators 23 p3699 A71-43570

FACTORIAL DESIGN

- Latin square factorial design plans for reducing number of repetitions solutions of theoretical problems, noting application to differential equations numerical solution 19 p3087 A71-38290
- Liquid metal elevated temperature time dependent corrosion effects on immersed structural materials, discussing blocked two level factorial experiment design for multiply telescoping sequences 21 p3400 A71-40880
- FACTORIALS**
Factorial determinants in solving space contours, considering bending and torsional moments in structural analysis 24 p3881 A71-44800
- FACTORIES**
U INDUSTRIAL PLANTS
- FACULAE**
Solar magnetic field regions, bright line structures and faculae from Fraunhofer lines analysis, discussing magnetic downward velocities 01 p0152 A71-10328
- Solar magnetic fields configuration and evolution, discussing sunspots and white light faculae 01 p0152 A71-10330
- Photosphere and facula turbulent velocities and damping constants from Ni and Fe IR lines analysis 02 p0306 A71-12079
- Solar faculae semiempirical models, cospatial with strong photospheric magnetic fields constructed from continuum observations 02 p0316 A71-12757
- Quiescent and sunspot prominences line of sight velocity measurements on limb, investigating statistical properties of velocity field 02 p0316 A71-12759
- Plane intensity variations on basis of photometrically analyzed Lyot filtergrams and ionosonde records 05 p0740 A71-16435
- Vertical structure of solar faculae from spectroscopic method for three dimensional information derivation 06 p0967 A71-17908
- Emission structure of large electron active region McMath plage 8905 mapped by 40 keV solar flare electrons 06 p0950 A71-17918
- Photosphere and facula turbulent velocities and damping constants from Ni and Fe IR lines analysis 08 p1361 A71-21129
- Solar photosphere facula, applying Schuster-Schwarzschild model for molecular lines and bedding level of carbon hydride 08 p1365 A71-21772
- Unusual sunspot rotation from 30 September to 8 October 1969 in plage region No. 10344, noting flare activity and rotational motion 10 p1666 A71-23786
- Solar photosphere and faculae temperature, gas/electron pressures, density and turbulence velocity from Schuster-Schwarzschild model 15 p2495 A71-32677
- Profile changes of magnetically non-split lines in faculae, explaining observations by outer layers temperature increase 18 p2965 A71-36731
- Solar chromospheric plage area related to peak K coronal brightness at limb 18 p2966 A71-36738
- Electric conductivity correlation between solar faculae and Bilderberg model of photosphere and chromosphere 24 p3868 A71-44458
- Scattered light effect on measured facula-to-photosphere contrast, leading to hotter average facula model 24 p3868 A71-44460
- FADING**
NT SELECTIVE FADING
NT SIGNAL FADING
Moving type IV solar bursts polarization and rapid fadeout, discussing relativistic electrons synchrotron radiation intensity 01 p0152 A71-10331
- Noise stability during noncoherent reception of frequency shift keyed signal by receiver with finite Q predetector integrators in presence of fading 11 p1733 A71-25938
- TWT off-transmission band area exponentially fading wave effects on electron beam modulation and amplification 22 p3522 A71-42316
- Retinal image stabilization variables, noting whole fade characteristics sensitivity to stimulus pattern variations 24 p3795 A71-44470
- FAHRENHEIT TEMPERATURE SCALE**
U TEMPERATURE SCALES
- FAIL-SAFE SYSTEMS**
Wing structure fatigue substantiation procedures under fail-safe concept for general aviation aircraft [SAE PAPER 710404] 10 p1555 A71-24264

- Fatigue life, fail-safe capability and corrosion resistance of commercial aircraft structures improved through adhesive metal-metal bonding
[ASME PAPER 71-DE-27] 12 p1978 A71-27325
- Fail-safe helicopter rotor control design, discussing damage tolerant components, redundant system, failure warning and maintenance
[AHS PREPRINT 550] 14 p2179 A71-31102
- Integral spar inspection system for making CH-46 rotor blade fail-safe
[AHS PREPRINT 551] 14 p2180 A71-31103
- DC-10 fuselage pressure shell fail-safe design, presenting analysis methods for residual strength prediction of damaged stiffened panels
17 p2827 A71-35160
- Helicopter rotor blades fail-safe design, presenting criteria for fatigue loaded structures residual strength and life based on crack propagation rate methods
17 p2828 A71-35163
- Space shuttle auxiliary propulsion subsystems for attitude control, orbit maneuvering and power supply, discussing design requirements with emphasis on fail-operational and fail-safe criteria
[AIAA PAPER 71-661] 17 p2795 A71-35624
- Thermal design, analysis, testing and flight performance of ITOS-1 spacecraft, noting fail-safe temperature regulation
[ASME PAPER 71-AV-23] 18 p2868 A71-36390
- Fail operational control moment gyro configuration of four single gimbal gyros, eliminating cross coupling by simple analog steering law
[AIAA PAPER 71-936] 19 p3097 A71-37181
- Computerized automatic redundancy management for space shuttle guidance, navigation and control, using fly by wire control technique for in-flight failure detection and correction
[AIAA PAPER 71-946] 19 p3098 A71-37187
- Memory cell fault tolerant sequential machine synthesis, considering masking feasibility and lower bounds on minimum redundancy
21 p3351 A71-41036
- FAILURE**
- NT BURNTHROUGH [FAILURE]
NT ENGINE FAILURE
NT FAILURE ANALYSIS
NT STRUCTURAL FAILURE
NT SYSTEM FAILURES
- FAILURE ANALYSIS**
- Cr-Si steels cold shortness tests, identifying low temperature failure mechanisms
01 p0098 A71-10082
- Two-phase composites stability at various temperatures, noting failure regularities dependence on components mechanical properties relationship
01 p0106 A71-10083
- Digital systems intermittent failures effects and detection, using system simulation
01 p0046 A71-10204
- Metal products structural failure analysis, discussing laboratory equipment and analyst experience and ingenuity
01 p0087 A71-10455
- Aircraft crash investigation, deducing in-flight explosion by failure analysis techniques
01 p0087 A71-10456
- Variant function describing long term fatigue strength under complex loads in determining given material damage point during breakdown
01 p0169 A71-10494
- External actions effect on restorable products failure sequence, extending nonrestorable products reliability theory
01 p0088 A71-11231
- Electronic circuit analysis using parametric reliability criteria based on progressive failures, applying statistical computerized simulation method
02 p0230 A71-11840
- Aircraft multiwheel undercarriage effect on rigid and flexible pavements, examining failure modes
02 p0189 A71-12164
- Reliability prediction for machine parts subjected to cyclic stresses, using statistical analysis of fatigue data for failure rate calculation
02 p0327 A71-12367
- Creep failure model, using wedge crack nucleation in polycrystalline materials due to grain boundary sliding
02 p0329 A71-12716
- Computer simulation for evaluating equipment effect on weapon mission success, considering failure time, repair cycle, operational and maintenance parameters
03 p0431 A71-13090
- Creep failure in elastoviscoplastic media from time and load-path dependent processes near axisymmetric fissure prior to cracking
03 p0509 A71-13874
- First passage failure probabilities for single degree of freedom systems under random vibration
[ASME PAPER 70-WA/AFM-14] 03 p0512 A71-14155
- Ellipsoidal pressure vessel heads failure mode analysis, considering buckling under internal pressure and design formula with safety factors
[ASME PAPER 70-PVP-26] 04 p0665 A71-14769
- Ceramic and metallic whiskers mechanical properties, discussing failure and deformation mechanisms
04 p0611 A71-14946
- Electronic components failure rate distribution
04 p0559 A71-15875
- ELDO test firings failure analysis program, considering self destruction charges and vibration environmental load
[DGLR-70-060] 05 p0815 A71-15964
- Bunched parallel reinforcing fibers of equal size and varying strength, deriving critical loads and stresses under gradual failure
05 p0772 A71-16751
- Macro- and microfractographic methods in failure analysis
06 p0911 A71-17347
- Coplanar n-type GaAs Gunn effect microwave oscillators failure mechanism, suggesting role of current filament formation in thermal breakdown
06 p0874 A71-17665
- Statistical analysis of neutron induced gain degradation of silicon power transistors, determining failures distribution fit to Weibull function
07 p1070 A71-19063
- Failure criteria percentages for bipolar transistors, determining adequacy of Weibull distribution for low gamma ray dose survival probability
07 p1071 A71-19064
- Computer aided automatic fault data logging, classification, analysis and reporting methods in integrated ATC system
07 p1155 A71-19556
- RF distributed transistors for high reliability and power operation, discussing failure physics
07 p1076 A71-19559
- Plastics for long life microcircuit encapsulation, investigating materials properties and failure mechanisms for device reliability assessment
07 p1077 A71-19561
- Power station electronic control equipment and integrated circuit computer reliability data analysis, emphasizing combined mathematical prediction and observation
07 p1077 A71-19565
- Failure theory for anisotropic homogeneous materials, discussing interaction factor, resistance, orthotropism and planar stress
07 p1214 A71-20011
- Failure analysis of unidirectionally reinforced fiberglass composites due to winding, using critical stress distribution function
08 p1323 A71-21701
- Variational principle application to stability in failure mechanics of arbitrary linearly elastic bodies, discussing inertia effect on steady state vibrations of cracked bodies
08 p1372 A71-21704
- Inertia effect in failure mechanics for steadily developing equilibrium cracks in dynamic system with time dependent periodically variable load
08 p1372 A71-21705
- Alloy equivalent susceptibility to damage at intermediary service periods and different stress levels under creep conditions at 750 C
08 p1317 A71-21709
- Miner-Sediakin failure models for element operation without manufacturing process stability restrictions
08 p1300 A71-22019
- Optimal unconditional sequential search for defects, using rejection function
08 p1300 A71-22020
- Components field failure rates assessment methods for ground support equipment
[AIAA PAPER 71-304] 09 p1454 A71-22618
- Constant, programmed and random amplitude spectral analysis and signal averaging correlation with failure statistics, noting laboratory simulation
09 p1444 A71-22709
- Timesaving reliability tests for Si transistors involving failure mechanism acceleration
09 p1418 A71-23042
- Unidirectional fibrous composites brittle and ductile failures prediction under tension and torsion, comparing results with tests on glass-epoxy composites
10 p1686 A71-24017
- Elementary component constant failure rate for systems with prolonged operation without maintenance, determining mathematical model for confidence levels and dependability figures
10 p1617 A71-24266
- Carbon fiber strength/microstructure relationship, examining failure mechanism initiated by graphite crystallites shearing
10 p1634 A71-24446
- Composites under transverse normal tensile loading micromechanics failure criteria based on distortion energy theory, taking into account multiaxial stress concentration
[AIAA PAPER 71-355] 11 p1784 A71-25334
- Failure analysis of notched unidirectional composites under tensile load parallel to fiber, considering Griffith-Irwin-Orowan fracture theory applicability
[AIAA PAPER 71-369] 11 p1784 A71-25343
- Reliability test extent, duration, confidence limits and failure rate computed by nomograms
11 p1737 A71-25623
- Gas turbine wheel design fracture mechanics, discussing buried and surface flaws analysis for rotor failure prediction applications
[ASME PAPER 71-GT-10] 11 p1811 A71-25956
- Random failure definition based on stochastic processes mutual implication, producing unique characteristic events
11 p1771 A71-26160
- Limited reliability mathematical model for radioisotopic thermoelectric generators semiconductor couples based on catastrophic failures
11 p1715 A71-26165
- Failure rate data in reliability analysis, considering material failure phenomena, and maintainability
12 p1909 A71-26665
- Equivalent circuit concepts in diagnostic metrology as converging logical-physical process, stressing electronic failure analysis
12 p1890 A71-26666
- Failure prevention, test discrepancy reporting and circuit analysis workshop techniques for program audits, integrating reliability managers, performers and customers
12 p1910 A71-26670
- Service life testing and reliability estimation, using ordinary and empirical Bayes approach in failure model with gamma probability distribution
12 p1910 A71-26685
- Bayesian time to failure distribution for graphical estimation of component burn-in time and reliability prediction, comparing with Weibull technique failure rates
12 p1911 A71-26686
- Failure prediction from interval data for reliability and inventory problems, considering irregular inspection and manufacture for aging in calendar time
12 p1911 A71-26687
- Force springs flexural pivots and miniature incandescent lamp tests failure distribution analysis for comparing mechanical vs electrical components
[ASME PAPER 71-DE-34] 12 p1911 A71-27326
- Fibrous composite materials experimental failure studies at high temperatures and cyclic loading
12 p1922 A71-27683
- Failure analysis of plastic materials susceptible to cyclic strain hardening under thermal load
13 p2148 A71-28114
- Fiberglass reinforced plastics under constant strain rate, deriving failure models as random process for microscopic crack propagation
13 p2148 A71-28115
- Gas turbine blades fatigue crack development and failure analysis under thermal cycling tests, considering chemical processes and thermal and mechanical stresses
13 p2149 A71-28117
- Low cyclic failure resistance at elevated temperatures and static defects calculation, based on fatigue and empirical endurance curves
13 p2149 A71-28122
- Automatic control systems preventive inspection intervals examined from cost optimization viewpoint for various failure distribution rules
13 p2042 A71-28641
- Airborne Doppler radar receiver transmitter failure testing by Versatile Avionics Shop Test computer controlled system
13 p2031 A71-28778
- Structure service life and storage failure probability calculation with current load measurements and laboratory fatigue testing
13 p2076 A71-29231
- Failures detection in combinational digital switching circuits due to component malfunction
13 p2036 A71-29291
- Heuristic algorithm for computation of failures detection tests in asynchronous sequential logic circuits
14 p2218 A71-29520
- Failure mechanisms and manufacturing improvement of sealed nickel cadmium batteries
14 p2181 A71-29701
- Rolling contact spalling fatigue failure incidence in subsurface defects, using engineering model based on crack growth rate
14 p2251 A71-29828
- Contacting surface rolling spalling fatigue failure incidence prediction using engineering model with preexisting discontinuities and microgeometrical asperities
14 p2251 A71-29829
- Aerospace pressure vessels delayed time failure, discussing flaws growth rate in context of linear elastic crack tip stress intensity factors
14 p2325 A71-29898
- Space systems safety programs, discussing failure mode and single point failure analysis techniques, escape mechanisms and redundancy design
14 p2320 A71-30258
- Accelerated semiempirical method determining metallurgical processing techniques effects on steel

and titanium alloy compressor blades fatigue life, comparing results with experimental data

14 p2252 A71-30269

Gas turbine engine condition analysis by digital computer and fault isolation techniques

[SAE PAPER 710448] 14 p2289 A71-30532

Notched unidirectional composites failure mechanics under tensile load in fiber direction, considering debonding, plasticity and strength

15 p2428 A71-31971

Gradual failure effects on operational reliability of centralized automatic control machine

15 p2374 A71-32192

Markov process models of failure times of repairable systems, using lumping and decomposing techniques

15 p2415 A71-32340

Availability and failure frequency of systems of independent repairable units, using representation by network or reliability block diagram

15 p2415 A71-32341

Mathematical models to optimize successive fault finding programs in complex control systems with/without recovery

15 p2382 A71-32618

Fatigue failure of polyamide filaments from optical and electron microscopic observations, describing crack initiation and propagation

16 p2600 A71-32817

DC-10 design dispatch and component reliability through flight test and follow-up fault isolation programs

16 p2522 A71-32397

Allocation, assessment and demonstration of system mean-time-to-repair in complex multiple failure situations

16 p2583 A71-33300

Service life/stress testing, failure analysis and corrective action from technical and cost positions

16 p2583 A71-33315

Fault tree, failure mode and effect analysis, prediction apportionment and assessment, discussing system effectiveness

16 p2664 A71-33317

Two-phase composites stability at various temperatures, studying mechanical properties dependence on second phase proportion

16 p2593 A71-33639

Service failure prediction by photoelastic methods, discussing failure sources and analysis techniques

17 p2820 A71-34554

Anisotropic composite materials failure surface criteria in three dimensional space, using graphical representation

17 p2824 A71-34817

Anisotropic bolt bearing specimens failure mode and strength prediction, evaluating relative merits of maximum stress, maximum strain and distortional energy as failure criteria

17 p2824 A71-34820

Optimum diagnostics algorithm for complex automatic control system state detection based on Bayesian rule successive application for minimum time requirement

17 p2720 A71-34959

Binary relation algebra application to diagnostics tests for system involving redundant subsystems

17 p2720 A71-34960

DC-10 fuselage pressure shell fail-safe design, presenting analysis methods for residual strength prediction of damaged stiffened panels

17 p2827 A71-35160

Bunched parallel reinforcing fibers of equal size and varying tensile strength, deriving critical loads and stresses under gradual failure

17 p2763 A71-35451

Statistical evaluation of switching elements reliability, considering permanent and temporary failure rates

17 p2718 A71-35627

Hot pressed TiC cylinder thermal shock resistance from tests to failure after heat cycling at 1000-1200 C

17 p2760 A71-35664

Long time failure modeling of real structure behavior in short times by scale and mathematical models, noting nonaccountability of crack propagation time

17 p2834 A71-35669

Composite failure model tested for short term creep and rupture in Mo alloy at constant loads and 785-1400 C, considering strain hardening

17 p2834 A71-35670

Turbine alternating fan failure due to flutter by coupling of vibration modes and effect of mass distribution in blade

18 p2980 A71-36696

Transistors life testing for temperature and voltage dependence of failure rates

18 p2893 A71-36805

Reliability engineering, reviewing MTBF, redundancy, complexity effects on failure rate, reliability prediction, repair and replacement cost and test techniques

18 p2928 A71-36806

Notched fixed-pinned columns under concentric and eccentric compressive loads, presenting failure analysis based on stress intensity concept and methods of limit analysis

18 p2983 A71-36852

Temperature effects on wear and failure of titanium and niobium carbides, using electron microscopy

19 p3076 A71-37114

Aircraft structures sonic fatigue due to high frequency noise from turbofan engines, discussing case histories, failure diagnosis and precautionary design measures

19 p2997 A71-37843

Parts qualification and acceptance for outer planet mission spacecraft, minimizing random and wear-out failures to meet weight and other constraints

19 p3153 A71-37958

Boeing computer simulator for logic design confirmation and failure diagnostic programs, providing for propagation delays and feedback simulation

19 p3025 A71-37959

Adaptive algorithm designing minimum expected cost test trees for detection and isolation of single faults in systems

19 p3069 A71-38287

Failure prediction for metal film semiconductor contacts on silicon substrate by electromigration, considering current density and temperature gradients

19 p3119 A71-38510

Failure analysis of vacuum deposited Al film interconnections at contact windows, considering grain size effect and reliability improvement techniques

19 p3119 A71-38512

Machinery failure prediction under high vibration amplitudes using stochastic excursions principles

[ASME PAPER 71-VIBR-60] 21 p3460 A71-40305

Failure analysis of memory organization in self repair memory system, using various coding and modularization techniques on subsystems

21 p3350 A71-40365

Conditional failure density evaluation from hazard rate, considering failure time distribution function, reliability function and conditional failure distribution

21 p3408 A71-40370

Integrated circuits failures due to plastic or ceramic packaging methods, describing failure analysis technique

21 p3353 A71-40439

Semiconductor components reliability assurance under assumption of failure rate decrease with time for IC quality and performance improvement

21 p3356 A71-40746

Plastic encapsulated IC reliability tests, relating results to failure mechanism

21 p3356 A71-40747

Electron beam modulation by laser /Schwarz-Hora effect/, investigating failure factors

21 p3394 A71-41045

Failure diagnosis and localization algorithm for combinational circuits of functional elements, considering arbitrary combinations and essential fault presence

21 p3361 A71-41141

One dimensional structure failure calculation, using mathematical programming static method for load limit approximation

22 p3613 A71-41430

Bias network analysis computer program for reliability analysis suited to failure mode, criticality, drift and catastrophic failures prediction

22 p3517 A71-42104

Validity study of mathematical models representing failure rate variations of electronic components, considering thermal and electrical stresses

22 p3517 A71-42109

Computerized simulation of maintenance man hour loading for communication system based on repair, failure and availability distributions

22 p3554 A71-42113

System quality analysis by reliability measures /mean time between failures/, using distribution free evaluation models

22 p3566 A71-42114

Cost based algorithm for allocating availability parameters /repair times and failure rates/ to system components

22 p3566 A71-42115

Optimal redundancy and availability allocation for MTBF and time to repair in multistage system, using dynamic programming

22 p3518 A71-42116

Statistical fatigue life models, surveying failure probability distributions in reliability studies

22 p3566 A71-42117

Hazard rate functions of systems with identically distributed subsystem failure times in sequential or simultaneous operation

22 p3566 A71-42118

FAILURE MODES

Gaseous atmospheres environmental effects on metal mechanical properties at high temperatures, discussing failure mode with crack growth rate dependence on pressure

02 p0263 A71-11864

Sailplane fatigue testing determining load spectra fail safe structures and damage calculation

02 p0324 A71-11949

Frame structures linear-mode failure probability estimation by reliability analysis

02 p0327 A71-12347

Intergranular failure modes in polycrystalline metals and alloys, discussing boundary sliding, cracking and structure

03 p0447 A71-14496

Energy accumulation effects on pressure vessels strength and failure mode, examining crack propagation and arrest

03 p0517 A71-14586

Integrated circuit conductors short pulse high current rating, identifying three failure regimes

04 p0559 A71-15874

Turbine disks failure under nonuniform heating, deriving expression for critical rpm

05 p0826 A71-16755

Haunched beam design optimization for lightest weight, analyzing failure modes under assumption of elastically rigid perfectly plastic material

06 p0981 A71-17301

Long term IR X ray irradiation effects on complementary MOS logic networks with several p and n channels on single silicon, determining radiation induced failure modes

07 p1174 A71-19054

Failure modes and mechanisms for electric battery diagnostic tests

08 p1236 A71-21107

Ductile metals fatigue crack propagation model applications to brittle metals, discussing crack initiation effects on high strength steels failure modes

09 p1467 A71-22285

Failure/yield points, stiffness and failure energy from adhesive shear stress elongation curves, using computer assisted thick adherent tests

10 p1631 A71-24071

Anisotropic bolt bearing specimens failure mode and ultimate load, investigating stress concentrations for failure prediction

11 p1844 A71-25333

Thermionic converter 9000 hour endurance test, performing metallographic, spectrographic and chemical analysis on emitter, collector, metal ceramic seal, brazing and alumina spacers

11 p1715 A71-25913

Automated facility for electronic equipment production reliability environmental testing, discussing human engineering and test and failure mode designs

11 p1746 A71-26512

Fiber reinforced composite materials plastic behavior shear stress theory, determining yield criteria and plastic strain rates associated with various failure modes

12 p1984 A71-27773

Helicopter power transmission failure modes, presenting field experiences correlation with conventional design stress analysis and bench test data

13 p2074 A71-28331

Linear viscoelastic materials, investigating failure and bending as function of time in response to load under creep conditions

13 p2154 A71-28522

Book on durability and reliability in engineering design covering materials strength and service longevity concepts, failure modes, fabrication philosophies, etc

15 p2414 A71-31836

Reliability prediction of narrow band structures under random excitations, considering catastrophic and fatigue failure modes

15 p2506 A71-32094

Structural synthesis and analysis concepts, discussing design philosophy, failure modes, load conditions, algorithms and computer aided design

16 p2653 A71-33093

Unmanned spacecraft first day failures, discussing launch environment, duration tests in simulated space and performance improvement

16 p2645 A71-33296

Fault tree, failure mode and effect analysis, prediction apportionment and assessment, discussing system effectiveness

16 p2664 A71-33317

Dynamic compressive strength and failure of steel reinforced epoxy composites, discussing strain rate sensitivity

17 p2762 A71-34813

Rupturing rotations estimates for turbine disks, considering failure modes and load bearing capacity

17 p2829 A71-35305

Turbine disks failure under radial temperature drop, studying effects on load bearing capacity for thermal stresses

17 p2832 A71-35454

Composite materials and structures analysis and design, examining elastic constants, thermal expansion coefficients, viscoelastic moduli, conductivities and failure modes

[AIAA PAPER 71-366] 18 p2979 A71-36274

- Reliability in key project decision making, including failure mode/effect analyses, design tradeoff, baseline meetings, hardware storage and data bases
18 p2926 A71-36491
- Plastic encapsulation for microcircuits including packaging, failure mechanisms, military qualifications and economic factors
19 p3033 A71-38508
- Lightweight solar cell structural failure modes under automatic thermal cycling for prolonged period in wide temperature range and by immersion in liquid nitrogen
20 p3179 A71-38852
- C-MOS integrated circuit technology emphasizing reliability, design, failure mechanisms and performance parameters
[DFVLR-SONDDR-100] 21 p3355 A71-40737
- Aircraft parts lubrication friction and wear problems, discussing failure modes, solid and liquid lubricants, component damage and lubrication systems
21 p3389 A71-40902
- Bias network analysis computer program for reliability analysis suited to failure mode, criticality, drift and catastrophic failures prediction
22 p3517 A71-42104
- Metal cored cylindrical plastic shells response to transient external pressures, considering failure modes
24 p3878 A71-44610
- PAINTING**
U SYNCOPE
- FAIRCHILD-HILLER AIRCRAFT**
NT XC-142 AIRCRAFT
- FALKNER-SKAN EQUATION**
Existence theorems for compressible boundary layer problems, discussing Blasius differential equation and Falkner-Skan class of similarity solutions
06 p0881 A71-17638
- Incompressible fluid plane laminar unsteady boundary layer, obtaining Falkner-Skan equation as special case for similar solutions in steady flow case
10 p1592 A71-24026
- Eigenvalue, shooting and parallel shooting methods for solving Falkner-Skan boundary layer equation with positive or negative wall shear
13 p2047 A71-28230
- Transformed boundary layer equation solution for power law fluid flows of Falkner-Skan type by gamma functions series
[ASME PAPER 71-FE-35] 13 p2053 A71-29470
- FALLING**
Falling body problem solution, considering curvilinear motion effects of earth rotation axis
15 p2450 A71-32039
- FALLING SPHERES**
Construction, operation and in-flight performance of triaxial bridge accelerometer used in falling sphere experiment for atmospheric density, temperature and pressure determination
13 p2066 A71-28160
- FALLOUT**
Radioactive impurities transfer from lower stratosphere into upper troposphere based on vertical air transport data
15 p2400 A71-31970
- FAN IN WING AIRCRAFT**
STOL commercial aircraft propulsion systems, considering two stream augmentor wing engine and high bypass ratio three stream engine
[AIAA PAPER 71-746] 15 p2467 A71-31325
- FANLIFT DEVICES**
U LIFT FANS
- FANS**
Large low-speed fan for low noise production, testing performance on suppression effects of acoustic treatment and exhaust jet noise
[ASME PAPER 70-WA/GT-15] 03 p0471 A71-14123
- Short rotor blade span supersonic fan for pressure wave forward propagation elimination, obtaining acoustic and aerodynamic characteristics
[AIAA PAPER 71-182] 06 p0885 A71-18621
- Fan propulsion power plants with mechanical and gas dynamical energy distribution systems for commercial VTOL aircraft
09 p1511 A71-22964
- Axial flow fan noise, investigating louvers effects on sound field
12 p1945 A71-26704
- Soundproofing of air inlets and fan exhausts with reference to absorbent systems with resonant cavities, technologies, environmental conditions and material fatigue
15 p2469 A71-31880
- FAR FIELDS**
Approximate calculation for far field flow distribution of nozzle exhausting into vacuum
01 p0072 A71-11595
- Shadow current method for asymptotic solution to two dimensional problem of electromagnetic wave far diffraction field on ideally conducting plane with infinite rectilinear slot
02 p0210 A71-11629
- Cassegrain system far field radiation pattern and gain loss prediction for beam steering by subreflector tilting
02 p0222 A71-12793
- Antenna polar diagrams short range measurement, using far field approximation for incident plane waves source and radio star or satellite
02 p0223 A71-12801
- GaAs heterojunction diode injection lasers, predicting high order transverse cavity modes and far field patterns from theoretical model
03 p0434 A71-13482
- Far field diffraction of unidirectional surface wave by conducting rectangular wedge in cold anisotropic plasma, showing frequency dependent transmission coefficient
03 p0465 A71-13953
- Circular apertures with Besinc correlated illumination, examining far field diffraction properties and intensity distribution
05 p0781 A71-16193
- Far field characteristics for diffraction of plane harmonic electromagnetic wave obliquely incident on rectangular wedge in uniaxially anisotropic medium
05 p0781 A71-16414
- Far field sound radiated from steady loading of isolated subsonic rotor, noting dependence on spatial uniformity of flow entering rotor
05 p0697 A71-17160
- Aerodynamic sound radiation from point force in accelerative circular motion, obtaining closed form for overall far field radiation
05 p0784 A71-17162
- Horn antennas phase centers calculation by vector method from far field expressions
06 p0867 A71-17708
- Thermal radiation from finite cylindrical particle cloud, determining far field angular distribution by Monte Carlo method
[AIAA PAPER 71-78] 06 p1008 A71-18535
- Far field sonic boom pressure profiles simulation by methane-oxygen mixture detonation in balloons
[AIAA PAPER 71-186] 06 p0886 A71-18625
- Beam pattern near vibrating piston near sound field, discussing boundary between far field
07 p1113 A71-19953
- Conducting disk with slot dipole at center, determining asymptotic expressions for radiation far zone
08 p1266 A71-21465
- Antenna optimal radiation patterns, discussing antenna synthesis based on desired far field characteristics
10 p1582 A71-23806
- Far field diffraction pattern of corner reflector for normally incident monochromatic light, considering polarization characteristics
10 p1640 A71-23947
- Far field sound radiation pattern from vibrating circular piston set in nonrigid baffle for sonar detectors
11 p1798 A71-25186
- Simulated far field patterns of linear and phased arrays without radiation coupling by hybrid analog computer
11 p1735 A71-25851
- Spherical wave expansion theory application to near field and far field patterns, using analytical, experimental and numerical data
13 p2028 A71-27993
- Radio waves tropospheric refraction based on far field of vertical electrical dipole on impedance sphere
14 p2191 A71-29510
- Reflectors group mean effective scattering cross section measurement by far field criterion
14 p2194 A71-30075
- Laser beam scintillation covariance beyond turbulent atmospheric layer in Fresnel and Fraunhofer zones
14 p2254 A71-30423
- Atmospheric turbulence effect on far field diffraction pattern of annular aperture
14 p2275 A71-30465
- Far zone field and radiated power equations for corner driven traveling wave loop antenna in warm plasma, comparing data for Ariel 3 satellite
14 p2283 A71-31040
- Far field patterns for short active antennas obtained by integration of transistors and passive antennas
14 p2217 A71-31058
- Microwave antenna far field radiation pattern determination from Brown transmission equation solution
15 p2368 A71-31143
- Solid state laser emission divergence, calculating far zone fields for arbitrary amplitude and phase distributions
15 p2418 A71-31243
- Near field flow pattern of inclined slender body of revolution, using Whitham far field theory of super-sonic flow
[AIAA PAPER 71-626] 15 p2344 A71-31554
- Random time variation in sound radiation far field of point sources in subsonic circular rotational motion
15 p2450 A71-32129
- Turbomachinery rotor and stator row aerodynamic interaction, describing discrete tone noise generation from far field measurements
15 p2450 A71-32134
- Numerical analysis of far field gain pattern of shielded acoustic antenna by Kirchhoff integral, assuming circular symmetry and perfectly absorbing walls
15 p2372 A71-32193
- Subsonic turbulent jets acoustic emission, calculating noise intensity in far field for various Mach numbers
17 p2725 A71-34213
- Array design by matrix inversion for specified pattern in far zone field exceeding number of independent excitation volumes
17 p2715 A71-34766
- Linear array antenna far field transient time response formulation, using concise vector field integral equations and generalization
17 p2717 A71-35584
- Far field radiation patterns and optimum design of horizontal rhombic antenna in warm plasma, using linearized hydrodynamic theory
18 p2875 A71-35969
- Nonplanar dipole antenna with transversely displaced feed points, considering effects on far field radiation patterns, radiation resistance, power gain, effective aperture and efficiency
18 p2887 A71-35970
- Far field minimum radiation over angular sector for directional broadside array with optimum interelement spacing, considering sidelobe reduction
18 p2875 A71-35972
- Nonplanar dipole antenna with arbitrarily displaced feedpoints, considering far field radiation patterns, radiation resistance, power gain, effective aperture and efficiency
18 p2887 A71-36014
- VOR antenna system with Alford loops above circular conducting ground plate, investigating radiation fields
18 p2894 A71-36827
- Corner reflector excitation by vertical or horizontal log-periodic dipole antenna for unidirectional wide-band radiation, deriving far field expression
18 p2895 A71-36994
- Sound radiation from subsonically rotating annular disk source, calculating far field pressure and efficiency
19 p2997 A71-37845
- Monostatic plane wave scattering by semiinfinite perfectly conducting wedge with rounded edge for line source excitation in far field
19 p3023 A71-38593
- Excitation asymmetry effects on current distribution and far field of thin dipole radiators
19 p3036 A71-38604
- Far field light diffraction due to circular plane wave apertures rendered partially coherent by atmospheric turbulence
21 p3415 A71-40635
- Electromagnetic field distributions and far field radiation patterns of three layer waveguide GaAs heterostructure injection lasers, using Maxwell equations
22 p3555 A71-41688
- Plane electromagnetic wave diffraction on periodic arbitrary profile array, presenting near and far field asymptotic characteristics
22 p3511 A71-42306
- Far field radiation patterns of axially oriented point current sources in presence of dielectric circular cylinders, developing solutions via plane wave scattering
23 p3654 A71-44160
- Plane electromagnetic wave diffraction on dense periodic array at conducting screen, showing far field asymptotic behavior for E and H polarization
23 p3647 A71-44331
- Electromagnetic scattering solutions for inhomogeneous dielectrics as power series, using multipoles for far field determination
24 p3847 A71-44427
- Transonic flows about two dimensional airfoils, calculating far field boundary conditions with coordinate transformation
24 p3789 A71-44620
- FAR INFRARED RADIATION**
Thermal pattern visualizing and interpretation by imaging in far IR, noting equipment and uses of thermography in medicine, science and technology
01 p0078 A71-10135
- Far IR spectrophotometry improvement with lamellar grating, describing construction, alignment and performance
01 p0082 A71-10836
- Galactic and extragalactic sources of far IR radiation, discussing spectral distribution and luminosities
02 p0315 A71-12656
- Celestial sources far IR radiation detection using balloon-borne telescope
02 p0315 A71-12657
- Rocket observations of far IR radiation from upper atmosphere
03 p0415 A71-14026

FAR ULTRAVIOLET RADIATION

Theta pinch plasma enhanced radiation at far IR wavelengths, observing emission exceeding thermal bremsstrahlung 03 p0465 A71-14189

Planck formula correction for small cavity black body radiation, considering application to far IR standard sources 04 p0676 A71-14955

Pulsars relationship to very high energy cosmic ray electron propagation, examining far IR background and radiation sources 05 p0797 A71-15941

Liquid water far IR absorption spectrum, presenting transmission coefficients table 07 p1158 A71-18911

X ray and far IR measurement inconsistency from Centaurus A, discussing metagalactic submillimeter background 07 p1185 A71-19546

Galactic center region far IR map in 75-125 microns spectral interval with 6 minute resolution 07 p1199 A71-19835

Far IR cryogenic black paints absorptive throughout IR with surface stability at liquid He temperature and resistance to abrasion and flaking 08 p1335 A71-21383

Far IR materials optical constants analysis by channeled spectra, using Fourier spectroscopy single signature in interferogram to yield real and imaginary parts of refractive index 08 p1335 A71-21384

High order harmonic mixing of klystron microwave and far IR laser radiation using Josephson junction 09 p1464 A71-22766

Cirrus ice cloud detection from remote emission measurements in far IR by satellite radiometer 09 p1487 A71-23022

Continuously tunable stimulated far IR emission in lithium niobate with Q switched ruby laser as pumping agent, discussing power-wavelength characteristics determination 09 p1465 A71-23482

Solar spectra of far IR absorption of atmosphere above 4.2 km, using interferometer and cryogenic bolometer measurements 09 p1490 A71-23557

Far IR fluxes from H II regions with solar luminosities at .02-2 times 10 to 7th 10 p1675 A71-24488

Jupiter far IR emission spectra models, examining atmospheric composition, temperature and structure 11 p1821 A71-25538

Variable output coupling far IR gas lasers, using Michelson interferometer with polyethylene or polypropylene beam splitter 11 p1773 A71-25805

Superfluid-helium-cooled rocket-borne far-IR radiometer for night sky radiation measurement, discussing cryogenic, optical detection and electronic systems design features and performance 12 p1903 A71-26791

High resolution far IR interferometer in Michelson configuration for measuring gas optical properties in symmetric or asymmetric operation mode, testing performance 12 p1904 A71-26799

Phase modulation theory for two-beam far IR Michelson interferometers, discussing application to Fourier transform spectrometry 14 p2238 A71-29741

Phase modulation in far IR interferometers applied to Fourier spectrometry and metrology, obtaining modulus, phase, absorption and refraction spectra 14 p2238 A71-29742

Phase modulation in far IR interferometers applied to laser refraction measurements in solids and organic liquids 14 p2238 A71-29743

Far IR coupled cavity HCN laser interferometer for measuring low density transient plasma 15 p2410 A71-32384

Far IR sulfur dioxide laser line prediction from transitions involving irregular Fermi interactions between molecular energy levels 15 p2422 A71-32587

Galactic nucleus thermal emission due to dirty ice or silicate grains, explaining far IR radiation power output and spectral dependence 15 p2498 A71-32773

Far IR collision induced spectrum in carbon dioxide, observing temperature and pressure dependence in gas phase and absorption in liquid 19 p3106 A71-38051

Millimeter wave klystrons phase locking to HCN far IR laser line via harmonic mixing in Si and metal-oxide-metal Josephson point contacts 22 p3555 A71-41599

Josephson junctions for far IR radiation detection, mixing and frequency measurement 22 p3543 A71-42128

Semiconductors submillimeter and far IR reflection spectra and cyclotron resonance measurements 22 p3586 A71-42140

Far IR spectrum analysis using Michelson interferometer with beam splitter 23 p3676 A71-43400

Balloon-borne far IR survey of sky portions in Galactic plane 23 p3736 A71-43539

Apollo 11 and 12 rocks dielectric constants, discussing far IR absorption spectrum of fines 23 p3760 A71-43772

Spectral properties and tunability of far IR from ZnTe and lithium niobate crystals from difference-frequency mixing of mode-locked Nd glass laser pulses 23 p3686 A71-43997

Night sky far IR background radiation measurements by rocket-borne superfluid He cooled radiometer, determining average signal strength equivalency to black body temperature of 3.1 K 24 p3822 A71-44752

Balloon measurement of solar flux and brightness temperature in 12-24 micron range 24 p3873 A71-45142

FAR ULTRAVIOLET RADIATION NT LYMAN ALPHA RADIATION NT LYMAN BETA RADIATION

Wide angle far UV photography of Barnard Loop Nebula in Orion suggesting nebular emission intensity difference with near UV region due to interstellar dust 01 p0148 A71-10001

Mg I and II vacuum UV emission series, presenting quantum defect plot 01 p0129 A71-10137

Carbon disulfide absorption spectrum measurement in far UV region 01 p0129 A71-10251

Auroral vacuum UV spectra and 3914 A emission from sounding rocket data 01 p0076 A71-11502

Far UV equatorial airglow and aurora intensities and occurrence frequencies from satellite observation 01 p0076 A71-11504

Sky radiation background in far UV spectral region, calculating stellar component 02 p0304 A71-11913

Vacuum UV laser emission from molecular hydrogen in Lyman band using short risetime traveling wave discharge 03 p0434 A71-13478

Solar soft X ray and extreme UV relative contribution to E layer ion production rates during solar eclipse of 12 November 1966 03 p0481 A71-14511

Vacuum UV degradation of thermal control coatings on ATS-1 satellite, comparing with laboratory simulation 04 p0618 A71-14896

Charged particles-noble gases interactions with resultant vacuum UV radiation, considering conservation of energy principle and Jesse effect 04 p0630 A71-15652

Vacuum UV monochromators calibration by molecular branching ratio technique based on electron transition probabilities 05 p0717 A71-16907

Intensity calibrated grazing incidence spectrographs on Skylark sounding rockets, recording solar soft X-ray and XUV spectra 06 p0967 A71-17903

Impulsive hard X ray and far UV emission during solar flares 07 p1188 A71-19825

Evaporated Rh films preparation at various substrate temperatures in vacuum UV, determining reflectance and optical constants 08 p1343 A71-21183

Solar flare EUV radiation and ionospheric currents dynamo region ground based detection by geomagnetic crochets time structure analysis 08 p1355 A71-21198

Na I absorption spectrum interpretation between 150 and 900 A in vacuum UV, noting various discrete features 10 p1676 A71-24500

Atomic nitrogen far UV emission excitation in auroral ionosphere due to electron impact dissociations 10 p1605 A71-24792

Atomic N and C photoionization cross sections by shock tube vacuum UV spectrometry 10 p1646 A71-24990

Oxygen and carbon dioxide continua absorption cross sections in Schumann and far UV regions by photoelectric technique with vacuum monochromator 11 p0181 A71-25364

Extreme UV spectra of Sc XIV, Ti XV and V XVI, identifying and classifying lines in 18-25 A range 11 p1729 A71-26140

Quiet sun extreme UV spectrum measurements by OSO-4 Harvard scanning spectrometer, discussing instrument design and experimental results 12 p1956 A71-26618

Flash photolysis produced methyl and methylene radical transitions maximum extinction coefficients and oscillator strength in vacuum UV 12 p1876 A71-26788

Vacuum UV laser emission from molecular hydrogen, discussing theory and experimental verification 12 p1914 A71-27281

Energetic solar X-rays, microwaves and EUV ionizing radiation during periodic bursts of solar flare 12 p1953 A71-27655

Fe XIV intensities in solar EUV spectrum, calculating equilibrium population of energy levels in coronal conditions 12 p1970 A71-27704

Thermosphere daily variations consisting of diurnal oscillations excited by ozone and EUV heating 12 p1925 A71-27729

Ionospheric continuity in F 2 region during partial solar eclipses, using EUV radiation and additional corpuscular source of ionization 13 p2053 A71-27792

Sky radiation background stellar component in far UV spectral region, determining intensity with Venera instruments 13 p2133 A71-28200

Solar vacuum UV spectrum analysis, using echelle grating spectrograph onboard Skylark sounding rockets 13 p2070 A71-29048

Perseus early stars photometry and far UV spectra from Aerobee rocket flight observations 14 p2304 A71-29596

Solar corona XUV resonance line spectrum interpretation, using thermal emission from inhomogeneous regions 14 p2297 A71-29678

Intense vacuum UV atomic line source excited in 2450 MHz microwave discharge cavity with clean spectrum, noting window deterioration and self absorption 14 p2240 A71-30127

Carbon dioxide photodissociation in vacuum UV, using time-of-flight spectroscopy and metastable photofragment detection by electron emission from metal surfaces 14 p2190 A71-30571

Rocket observation for spatial distribution of far UV nightglow at Lyman alpha and shorter wavelengths 15 p2398 A71-31764

Spectroscopic measurement of vacuum UV radiation from shock heated krypton plasma, noting self reversed resonance lines indicating cold boundary layer 17 p2787 A71-34589

Paraterphenyl coated photomultiplier as detector in far UV spectra, detailing efficiency range and sensitivity 17 p2745 A71-35589

High intensity continuous gas discharge line source for extreme UV with low electromagnetic interference 18 p2914 A71-35845

Far UV solar spectra observations, using OSO-2, 4, 5 and 6 spectroheliograms 19 p3136 A71-37614

Quiet sun, active regions and flares far UV space observations interpretation based on models 19 p3136 A71-37615

Solar flare X and gamma rays, radio and far UV emission, discussing model for chromospheric cool plasma heating by flow through magnetic instability 19 p3126 A71-37620

Vacuum UV emission features dissociative excitation by electron impact on molecular hydrogen and oxygen, measuring excitation cross sections from threshold to 350 eV 19 p3107 A71-38344

Emission characteristics above solar limb in four EUV lines, comparing with K-coronameter measurements to estimate element abundances 19 p3130 A71-38671

Vacuum UV reflecting surfaces deterioration by intermetallic formation, recommending separation by dielectric barrier layer 20 p3236 A71-39196

Far UV auroral luminosity profile using calibrated EUV spectrometer, noting nitrogen band emission 20 p3225 A71-39731

Atmospheric neutral and singly ionized He extreme UV emission altitude distribution measurement by sounding rocket-borne thin film photon counters 20 p3231 A71-39891

Auroral far UV spectrum and intensity measurements, discussing atmospheric absorption effects on rocket-borne spectrometer sensitivity 21 p3372 A71-40039

Galactic diffuse radiation in far UV, discussing consistency of findings on optical properties of interstellar grains 22 p3593 A71-42337

Interstellar spherical grains surface roughness model, noting far UV radiation extinction enhancement 22 p3605 A71-42340

Molecular oxygen dissociative excitation in vacuum UV by electron impact, discussing resonance triplet atomic emission cross section 23 p3706 A71-42903

Solar far UV Fe and Ni ion lines 23 p3723 A71-42951

Vacuum UV traveling wave excitation by high voltage pulse and hydrogen laser technology
23 p3684 A71-43502

Photographic far UV solar spectra during eclipse of 7 March 1970, discussing coronal lines, prominences and quiet atmosphere structure
24 p3871 A71-44911

FARADAY DARK SPACE
Plasma anodization of Si in positive column of DC oxygen glow discharge, considering silicon dioxide growth rate in negative glow, Faraday dark space and anode fall
22 p3581 A71-41809

FARADAY EFFECT
Quasi-stationary coronal magnetic field and electron density from Faraday rotation experiment, using theoretical model
02 p0302 A71-12769

Satellite tracking by radio direction finder, noting periodic azimuth deviations related to ionospheric Faraday effect
03 p0377 A71-13169

Ring laser coupling phenomena, presenting angular measurements for laser-gyro with Langmuir-Fizeau and Faraday effect bias
04 p0607 A71-15022

High red shift quasars linear polarization, examining absorption lines and depolarization due to Faraday rotation
04 p0649 A71-15272

Faraday rotation near ferromagnetic critical temperature of chromium bromide, discussing scaling laws validity and experimental confirmation
04 p0637 A71-15796

Large scale ionospheric irregularities from Faraday fading records by satellite observations, studying height, fluctuations, electron contents, horizontal size and orientations
05 p0741 A71-16439

Ionospheric electron content measurement from Faraday fading of Explorer 22 satellite transmissions during low and high solar activity
05 p0741 A71-16444

Ionospheric total electron content determination by Faraday fadings of 40 MHz radio transmissions from Explorer 22 satellite, considering seasonal variations
05 p0741 A71-16445

Ferrimagnetic vanadate garnet IR Faraday rotation as function of wavelengths and temperature, considering ions multivalence and multilattice site modifications
06 p0941 A71-18040

Pulsar 150 MHz radiation linear polarization measurements, correlating interstellar Faraday rotation with determinations from neighboring extragalactic radio sources
06 p0971 A71-18242

Ionospheric refraction during radio wave propagation using space diversity recordings of Faraday and Doppler effects for coherent signals from geophysical rockets
06 p0894 A71-18256

Second order phase path differences for Faraday rotation and dispersive Doppler shift in transionospheric propagation
07 p1097 A71-19027

Ionospheric electron content from Faraday rotation measurements of earth satellite and deep space probe
07 p1098 A71-19029

Linearly polarized CW signal transmission through near solar corona, measuring Faraday rotation
07 p1191 A71-19030

Ionospheric electron mean content by polar satellites, using combination of Doppler differential and Faraday rotation hybrid methods
07 p1206 A71-19032

Doping effect on positive Faraday rotation in n- and p-type GaAs at different impurity concentrations, noting shift of maximum to lower concentrations in p-type samples
07 p1176 A71-19227

Oscillation mode selection method applied to Fabry-Perot interferometer using Faraday effect
07 p1109 A71-19454

Faraday and polar Kerr reconstruction effects in stored magnetic holography
[IEEE PAPER 8.1]
07 p1112 A71-19609

High beta turbulent plasmas radiation scattering due to magnetic field strength and direction fluctuations from optical Faraday rotation observation
10 p1652 A71-24660

Geomagnetic field inclination determination by incoherently scattered signal Faraday rotation calibration and simultaneous ionosonde measurements of ionospheric electron density
10 p1605 A71-24798

Integral equations inversion in geophysics, discussing ionospheric profile from electron content and Faraday rotation measurements
11 p1756 A71-25645

Faraday rotation of satellite signals, deriving relations for second order effects
13 p2031 A71-28784

Faraday rotation of Transit 4A satellite signals recorded at three stations within Southeast Asian equatorial zone, showing latitudinal variation of ionospheric electron content at sunspot minimum
14 p2235 A71-30249

Ionospheric electromagnetic wave path calculation by Haselgrove ray method, applying to Faraday and Doppler effects
14 p2235 A71-30348

Faraday rotation of satellite signals across transverse region, considering sudden jumps at transverse point in lower and topside ionosphere
16 p2544 A71-33959

Ionospheric electron content measurements from satellite signals Faraday rotation, criticizing graphical procedure for ambiguity reduction
17 p2732 A71-34322

Combined differential Faraday and absorption measurements, extracting total electron content, ratio to density squared integral and irregularity sensitive parameter
17 p2698 A71-34428

Extragalactic Faraday rotation models, examining galactic plane and Galaxy supercluster
19 p3142 A71-38005

Synchronous satellite transmission Faraday rotation conversion into total electron content, removing n pi ambiguity
19 p3128 A71-38032

Nonlinear Faraday effect in nonparabolic semiconductors subjected to strong electromagnetic field and steady magnetic field, deriving distribution function of charge carriers
20 p3276 A71-39010

Homogeneous large scale intergalactic magnetic field evidence in terms of Faraday rotation measurements of extragalactic radio sources
20 p3294 A71-39541

Cadmium-tin-arsenide conduction and valence band structure parameter refinement from Faraday effect and absorption spectra of single crystals in polarized light
21 p3433 A71-41319

Ionospheric electron density measurements by differential Doppler and Faraday effects, using coherent radio signals of artificial earth satellites
22 p3508 A71-41526

Ambient medium, reabsorption and Faraday rotation effects on circular polarization degree of synchrotron radiation, using transfer equation
22 p3593 A71-42335

Compact optical Faraday rotation isolator using terbium-aluminum garnet and high field permanent magnets of rare earth alloys
22 p3559 A71-42566

Magnetoionic mode coupling of HF radio waves, considering Faraday rotation of satellite signals
23 p3642 A71-42963

Ionospheric HF wave ordinary (O) and extraordinary (E) modes coupling effect on satellite signal Faraday rotation
23 p3642 A71-42964

Type 3 solar radio bursts polarization characteristics distribution, determining Faraday rotation dispersion effect by trial and error technique
23 p3768 A71-43850

FARADAY ROTATION
U FARADAY EFFECT
FARM CROPS
Automatic pattern recognition, discussing texture as discriminant of crops on radar imagery
05 p0743 A71-17145

Air-photo interpretation to inventory kind of cattle-raising operation practiced on farms of southern Ontario
08 p1282 A71-21437

World crop areas, yield, production and land use data, using remote sensing devices
09 p1439 A71-23211

Diseased plants and crop loss per field from aerial IR-color photography
14 p2236 A71-30576

Multispectral color aerial photography for identification of farm crops and tree species, using broadband camera filters
17 p2737 A71-34274

Crop surveys from multiband and multibase satellite photography during Apollo 9 mission, using statistical multispectral pattern recognition digital techniques
24 p3827 A71-44987

FAST NEUTRONS
Nuclear photoemulsions for fast neutron dosimetry, recording recoil proton tracks during elastic scattering by hydrogen nuclei
04 p0594 A71-14919

Fast neutron energy spectrum and flux, using balloon flight neutron detector with charged particle rejection scheme and pulse shape discriminator for gamma rays separation
06 p0962 A71-18178

Fast neutron energy spectrum from free proton elastic scattering in emulsion plates, studying upper atmospheric altitude and latitude factors
06 p0962 A71-18180

Galactic cosmic rays solar modulation effects on fast neutron flux in atmosphere
06 p0962 A71-18182

Atmospheric fast neutron flux, discussing solar proton events and Forbush decreases effects
06 p0963 A71-18183

O-barenylacetic and methyl-o-barencarboxylic acids effects on mice radiosensitivity to fast neutrons and gamma rays
07 p1038 A71-18976

Superheavy elements formation due to fast neutron capture during supernova outbursts, discussing meteorites fission produced noble gases
08 p1337 A71-20959

Fast neutrons scintillation counters effectiveness, presenting calculation procedure with corrections for double carbon-hydrogen scattering and nuclear reaction effects
11 p1761 A71-25577

Fast neutron irradiation effect on Ni-Cr alloy electrical resistivity as function of temperature and initial composition
13 p2083 A71-27964

Radiation defects isochronal annealing effects on absorption spectral distribution of gallium arsenide irradiated with fast neutron flux
16 p2620 A71-33184

Fast neutron spectra in lead and water shielded reactor, comparing liquid scintillator measurements with discrete ordinates code calculations
16 p2606 A71-33253

Endurance limit of construction materials under fast and thermal neutron irradiation in reactor channel
16 p2598 A71-33986

IR absorption of oxygenated dislocationless phosphorus doped fast neutron irradiated n-type silicon, investigating dominant defects for different radiation dosages
17 p2790 A71-34199

Radiation flaw detection by fast neutrons, monitoring thick lead plates and three-layer articles
22 p3528 A71-41761

Relative biological effectiveness of fast neutrons, allowing for gamma component contribution
22 p3494 A71-42735

FAST NUCLEAR REACTORS
Compact fast reactor design for space power with rotating fuel drums, Mo alloy reflectors and honeycomb support structure
16 p2606 A71-33252

FAST TEST REACTORS
NT FAST NUCLEAR REACTORS
FASTENERS
NT BOLTS
NT NUTS [FASTENERS]
NT PINS
NT SCREWS
NT WASHERS [SPACERS]
Fastener group behavior under combination of direct shear and moment, obtaining load deformation response of individual connections
08 p1370 A71-21410

Elastomeric seals for aircraft fastener countersinks, providing corrosion protection to static metal surface treatments and organic coatings
10 p1633 A71-24118

Corrosion resistant materials evaluation for suitability in high strength fasteners, considering mechanical properties, stress corrosion cracking and hydrogen embrittlement problems
20 p3251 A71-39340

Automatic eddy current system to detect fastener hole cracks consisting of scanner unit, control box, recorder and mounting hardware
24 p3831 A71-45281

FATIGUE [BIOLOGY]
NT FLIGHT FATIGUE
NT MUSCULAR FATIGUE
Subjective and electromyographic estimation of fatigue and muscle activity physiological levels, considering isometric muscle contraction task endurance
07 p1047 A71-19458

Human operators performance under control problem programs, determining training and fatigue effects
09 p1398 A71-22483

Methodology of fatigue assessment - Conference, Kyoto, September 1969
17 p2687 A71-34352

Human fatigue with emphasis on chronic conditions unrelieved by rest or sleep, recommending elimination of conditions resulting in excessive stress, anxiety or boredom
17 p2687 A71-34353

Mathematical fatigue models based on permeability variations in synaptic membranes and feedback regulation due to working organ metabolic changes
17 p2687 A71-34354

Factor analysis in construction of human fatigue rating scale from individual appearance and comportment
17 p2687 A71-34355

Optical organs and autonomic nervous system fatigue assessment by blink method associated with eyelids, oculomotor muscles, retina and cerebrum
17 p2687 A71-34356

Urinary metabolites relationship to fatigue, considering excretion of proteins, electrolytes, simple organic compounds and hormones
17 p2679 A71-34357

Circulatory fatigue during shift work, determining pulse rate/oxygen intake at two different loads on bicycle ergometer
17 p2687 A71-34358

Fatigue measurements in hot working conditions on subjects wearing self contained breathing apparatus in heat chamber
17 p2688 A71-34361

Factor analysis of phase discrimination in mental fatigue during diurnal variation of cortical functions in railroad traffic control center operators
17 p2688 A71-34362

Fatigue and stress measurement on air traffic controllers, using critical fusion frequency methods, tapping tests, self rating and urine catecholamine
17 p2688 A71-34365

Subjective fatigue feeling correlation to symptoms based on bank clerks and broadcasting workers work load assessment ratings
17 p2688 A71-34367

Mental reactive exertion increase phenomenon, investigating achievement under various degrees of carefulness and fatigue
18 p2862 A71-36945

Fatigue effects on standing broad jump and other body movements patterns
18 p2873 A71-36975

In-flight study of work/rest cycle effects on double crew performance and fatigue in flying transport missions
22 p3501 A71-41829

Short term central fatigue as causal factor of delayed psychological refractory period in multiple choice visual signal tasks
23 p3634 A71-43864

FATIGUE [MATERIALS]

NT BENDING FATIGUE

NT METAL FATIGUE

NT THERMAL FATIGUE

Epoxy resin reinforcement by various fiberglass types, discussing effects of bond-enhancing agents, fatigue strength properties, etc
01 p0108 A71-10691

Reliability prediction for machine parts subjected to cyclic stresses, using statistical analysis of fatigue data for failure rate calculation
02 p0327 A71-12367

Book on fatigue design covering load, stress and stability analyses, fail safe design, damage, residual strength, life, load spectra, structural reliability, etc
03 p0506 A71-13695

Through-thickness fatigue crack growth in polymethyl methacrylate sheets, observing stress intensity factor range, frequency and mean effects
[SESA PAPER 1727] 03 p0448 A71-13771

Rain and sand erosion materials tests, considering temperature and atmosphere pressure effects and relation between fatigue behavior and erosion/cavitation strength
03 p0444 A71-14289

Stress-strain function for metal fatigue including mean stress effect
04 p0610 A71-14890

Whisker composites tensile and fatigue properties, fracture toughness and mechanical properties at high temperatures
04 p0611 A71-14951

Fatigue and fracture in elastic cylindrical shells with circumferential crack under axial tension, noting precracked specimens
04 p0670 A71-15386

Polyester resin model fatigue crack closure, determining residual stress distribution and crack opening and closing force by photoelastic research
04 p0670 A71-15390

Soviet book on fundamentals of thermoviscoelasticity mathematical theory covering deformable media mechanics and thermodynamics, fatigue defects, etc
06 p0984 A71-17437

High and low cycle fatigue crack growth rate in various materials under variable loads
07 p1211 A71-19193

Stainless steel fatigue crack growth characteristics at liquid metal fast breeder type nuclear reactors elevated temperatures
07 p1138 A71-19983

Cyclic thermal cracking and fatigue analysis in large steam turbine rotors with three dimensional temperature and triaxial stress computation
[ASME PAPER 70-PWR-1] 07 p1216 A71-20198

Cyclic stress-strain behavior prediction by mathematical model and computer simulation, applying to Al alloy fatigue
07 p1216 A71-20204

Cross-ply carbon fiber reinforced epoxy resin laminates fatigue behavior under axial loading, discussing various failure mechanisms
08 p1321 A71-20912

Fatigue crack formation and growth rate relationship, examining variance in cycle number in formation to final failure
09 p1536 A71-22507

Metal sheet failure kinetics, investigating tensile stress and cycle frequency during fatigue crack growth and extension rate effects
09 p1468 A71-22508

Fatigue crack propagation rate in sheet alloys with holes as stress concentrators related to duration of various development phases
09 p1538 A71-22597

Strain level counter monitoring aircraft structural fatigue, describing system components consisting of sensors in critical structure areas and indicator unit with visual display
09 p1445 A71-22725

Cruciform biaxial fatigue under alternate tensile and compressive forces, using finite element analysis and photoelastic-coating techniques
10 p1685 A71-23941

Wing structure fatigue substantiation procedures under fail-safe concept for general aviation aircraft
[SAE PAPER 710404] 10 p1555 A71-24264

Slip front mechanisms in clamped or bolted double lap joints from photoelastic analysis of stress environments, discussing fretting fatigue
[AIAA PAPER 71-370] 11 p1845 A71-25344

Epoxy resin fatigue behavior from double torsion technique, considering stable crack movement in brittle materials
11 p1785 A71-25401

Metal carbide grain boundary precipitates effect on austenitic stainless steels high temperature fatigue fracture behavior
11 p1782 A71-26439

High strength alloys fatigue in terms of irreversible microplastic deformations accumulations, discussing fatigue crack mechanisms and cyclic straining effects on bulk properties
13 p2152 A71-28219

Fatigue crack propagation in thermoplastics, investigating stress intensity effect on factor mean value
13 p2091 A71-28465

Carbon steel fatigue crack tip plastic zone substructure by X ray microbeam technique, determining dislocation density, stress intensity and crack propagation rate interrelationships
13 p2155 A71-28789

Fatigue crack propagation kinetic theory, investigating microcrack nucleation mechanism based on vacancy condensation near crack tip
13 p2155 A71-28791

Plastic strain development at fatigue crack tip in mild carbon and stainless austenitic steels from electron and optical microscopy
14 p2257 A71-29841

Low ductility materials, considering applications to stress analysis, failure criteria, fatigue, physical metallurgy and polymer mechanics
14 p2251 A71-29893

Fatigue process analysis through crack initiation and propagation and final fracture, considering ductility, tensile strength and fracture toughness roles
14 p2258 A71-29896

Two-parameter statistical theory of material fatigue, considering random and ordered structural nonuniformities in space distributions
16 p2647 A71-32823

Fatigue cracks in tempered and aged Al alloy, using scanning electron microscopy
17 p2760 A71-35474

Mechanical properties in glass fiber optics, measuring tensile strength and modulus, Poisson ratio and fatigue
18 p2939 A71-36074

Partial thickness cracks of preselected depths and shapes by axial and flexural fatigue methods, yielding preferred propagation path
20 p3248 A71-38780

Linear elastic fracture mechanics for design against high cycle fatigue failure, considering stress intensification, crack initiation and propagation
20 p3307 A71-38813

Macroscopic residual stress and strain measurement and crack tip substructure, discussing crystal plastic deformation effect on fatigue crack propagation
21 p3466 A71-40831

Fatigue properties of satin woven fiberglass reinforced plastic cloth under various stress directions
21 p3406 A71-40839

FATIGUE DIAGRAMS

U S-N DIAGRAMS

FATIGUE LIFE

High fatigue resistance in metals and alloys - Conference, Atlantic City, July 1969
01 p0098 A71-10161

High metal fatigue resistance obtained via metallurgical means, discussing plastic deformation, crack initiation and propagation mechanisms, etc
01 p0099 A71-10165

Ni base superalloys fatigue strength improvement for gas turbine engine components, discussing homogeneous deformation distribution, grain size control, etc
01 p0099 A71-10166

Al alloys improved fatigue resistance via thermomechanical processing, considering microstructure and deformation characteristics
01 p0099 A71-10168

Discrete coatings, surface diffusion and thermomechanical surface treatments for metal fatigue strengthening
01 p0099 A71-10169

Aircraft structure fatigue life improvement via material stress coining inside and around holes and slots
01 p0085 A71-10170

High compressive residual stress and high hardness for long life fatigue strength in nonrotating bending of notched machine parts
01 p0167 A71-10171

Notched steel bars fatigue strength improvement via compressive self stresses/residual stresses/
01 p0167 A71-10172

Prealloyed hot formed Cr-Ni-Mo and Ni-Mo steels manufactured from powders, considering toughness, tensile properties, fatigue and impact strength
01 p0100 A71-10464

Variant function describing long term fatigue strength under complex loads in determining given material damage point during breakdown
01 p0169 A71-10494

Fiber reinforced plastics fatigue strength investigation by cyclic tension-compression, bending and torsion tests, noting matrix-fiber interface shear stress capacity
01 p0108 A71-10693

LAMS flight control systems for turbulence induced fatigue damage reduction in B-52 and C-5A aircraft, using mathematical models
02 p0188 A71-11660

Glass reinforced polyester laminates under static and repeated loading, investigating resin flexibility effects on fatigue strength
02 p0274 A71-12479

Structural design for component low cycle fatigue resistance, emphasizing material cyclic stress-strain behavior
03 p0501 A71-13252

Pinned steel lug joints fretting fatigue, examining cumulative damage under constant amplitude and narrow band random loading
03 p0513 A71-14244

Cu-Al alloy, Ti and low carbon steel under LF flexural stress, testing parameters effect on fatigue resistance
03 p0445 A71-14339

Miner theory of fatigue damage mechanism, considering validity and limitations
04 p0666 A71-14879

High strength steel butt welds surface geometry effect on fatigue durability under cyclic loads, using photoelastic analysis
04 p0602 A71-14881

Gas turbine engine Ni alloys heat resistance, examining fatigue life and creep properties at various temperatures and test durations
05 p0767 A71-16754

Volatile adhesive curing effect on metal-metal bond fatigue strength
05 p0772 A71-16955

Construction materials characteristic properties significance for design and structural reliability, discussing weldable Al alloys fatigue strength, internal stresses, inhomogeneity and corrosion behavior
06 p0981 A71-17341

Geometries and technical specifications deviations effects on service life and fatigue characteristics of thin walled structural components under cyclic loads
06 p1005 A71-18710

Industrial Ni alloys and steels fatigue life by short time data extrapolation
07 p1129 A71-19152

Vibration tumbling duration effects on surface quality, fatigue strength and damping properties of titanium alloy structural parts
07 p1130 A71-19169

Lubricant and ball steel effects on fatigue life /pit formation after repeated stress cycles/
[ASME PAPER 70-LUB-16] 07 p1118 A71-19507

Al alloys thermal fatigue resistance measurement using testing apparatus involving HF induction heating
07 p1142 A71-20325

Creep strain effect on cyclic fatigue life of duralumin at room temperature
07 p1143 A71-20486

Al-Cu precipitation hardened alloys, determining microstructure effects on fatigue life and flow stress
08 p1312 A71-21547

Gas turbine blades design and exploitation processes, discussing long time fatigue strength, static durability and heating effects at elevated temperatures
08 p1299 A71-21708

Metal parts fatigue life prediction by eddy current method, using experimental relationship between disbalance voltage and stress cycle number 08 p1300 A71-21893

Low-cycle fatigue curve determination for plane elastoplastic bending with flexible loading, deriving rated fatigue life 09 p1536 A71-22502

Expansion bellows fatigue strength based on load and displacement measurements performed during low cycle model tests 09 p1538 A71-22604

Nb alloy high temperature creep and long term strength, determining exponential relations between stress, strain rate and durability 09 p1468 A71-22628

Fatigue life gages performance test using calibration program for cryogenic temperature applications 09 p1444 A71-22716

Fatigue life and crack propagation of sheet, plate, extrusions and forgings in annealed and solution treated aged Ti-Al-V-Sn alloy [ASM PAPER W71-22.5] 09 p1471 A71-23096

Structural design for low cycle fatigue resistance, considering cyclic stress-strain properties, critical strain and overloads [ASM PAPER W71-22.3] 09 p1541 A71-23097

Ti-6Al-4V and solution treated and aged Ti-6Al-6V-2Sn alloys, investigating relationship between alpha grain size and crack initiation fatigue strength 09 p1472 A71-23131

Aerodynamic heating effects on fatigue and creep properties of superalloy aircraft alloys at high temperatures, considering deformation mechanisms interaction 09 p1472 A71-23204

TiNi martensitic transformations-fatigue strength relation at room temperature, observing hysteresis in tensile compressive loading cycle to maximum stress 09 p1477 A71-23349

Polymer adhesive protective coatings for improving fatigue resistance of butt and lap welded joints in thin Al sheet construction 09 p1478 A71-23355

Aircraft structural fatigue life in-flight monitoring, describing sensor installation on aircraft fin structure and measurement results 10 p1685 A71-23938

Point defects and fine precipitates effects on fatigue strength of high strength alloys, exhibiting higher fatigue strength in isothermally aged samples 10 p1625 A71-24009

Wing structure fatigue substantiation procedures under fail-safe concept for general aviation aircraft [SAE PAPER 710404] 10 p1555 A71-24264

Compression, creep, stress relaxation and overload effects on delay in fatigue crack growth and structural life predictions 10 p1694 A71-25059

Fatigue failure probabilistic model under variable amplitude loading, considering relation between safety factor and fatigue failure probability 11 p1848 A71-25492

Ni-based superalloy stress cycle frequency effect on elevated temperature fatigue life 11 p1779 A71-26012

Al alloys endurance limit determination by accelerated methods, evaluating errors by comparison with conventional tests 12 p1916 A71-26944

Plastic deformation and aging effects on fatigue characteristics of steels until rupture under cyclic loads 12 p1916 A71-26945

Passenger aircraft structures accelerated testing for safety and fatigue durability under operational conditions, describing tests, planning and evaluation 12 p1974 A71-26946

Fatigue life, fail-safe capability and corrosion resistance of commercial aircraft structures improved through adhesive metal-metal bonding [ASME PAPER 71-DE-27] 12 p1978 A71-27325

High speed roller bearing design with long fatigue life and weight reduction for high temperature operation in inert environment 12 p1912 A71-27328

Milling, band grinding, final manual polishing and tumbler polishing effect on fatigue life and surface finish of steel compressor blades 12 p1912 A71-27680

Deformation fatigue theory extended to tests at stresses below elastic limit, explaining cyclic loading frequency effect on fatigue life 12 p1984 A71-27681

Artificial corrosion pits effect on fatigue durability of smooth samples and aircraft duraluminum skin elements 13 p1995 A71-27819

Heat resisting Ni base alloy stress rupture strength and fatigue life, observing corrosive high temperature environment effect 13 p2084 A71-28111

Working fluid /Ar/ purity and stability effects on fatigue life and creep of Nb and Mo alloys using gas analysis, microstructure and microhardness data 14 p2256 A71-29622

Aircraft design and fatigue life monitoring, investigating effects of gust velocity frequency distribution in patches of atmospheric turbulence 14 p2174 A71-29789

Rolling contact spalling fatigue failure incidence in subsurface defects, using engineering model based on crack growth rate 14 p2251 A71-29828

Contacting surface rolling spalling fatigue failure incidence prediction using engineering model with preexistent discontinuities and microgeometrical asperities 14 p2251 A71-29829

Spalling fatigue life prediction in rolling contact, studying ductility, compressive stresses, inclusions, surface imperfections and bearing ring deflections effects with mathematical model 14 p2251 A71-29830

Accelerated semiempirical method determining metallurgical processing techniques effects on steel and titanium alloy compressor blades fatigue life, comparing results with experimental data 14 p2252 A71-30269

Low cycle fatigue strength of high speed rotating aluminum and brass disks, comparing with uniaxial push-pull fatigue test 14 p2328 A71-30418

Fatigue strength of polyester laminates reinforced with glass cloth and mats 14 p2264 A71-30484

Ti-Al-V alloy forgings fatigue strength improvements, discussing surface finish, heat treatments and alpha and beta grain size [AHS PREPRINT 553] 14 p2261 A71-31105

Comparative creep rupture properties of tungsten-rhenium consolidated by arc melting and powder metallurgy, considering rupture life and rupture ductility 15 p2427 A71-31818

Reliability prediction of narrow band structures under random excitations, considering catastrophic and fatigue failure modes 15 p2506 A71-32094

Explosive and isostatic forming effects on commercial precipitation-hardenable Al-Cu alloy microstructure, tensile properties and fatigue life 15 p2433 A71-32180

Structural inhomogeneity effect on fatigue strength of Al alloys, considering microstructure qualitative estimation on basis of microplastic deformation 15 p2434 A71-32330

Al alloy spot welding, investigating defects effects on welded joint fatigue strength under dynamic tests by metallographic and X ray examinations 15 p2436 A71-32467

Plastic strain range-fatigue life behavior as two slope relationship, considering low cycle fatigue laws in terms of crack propagation mode change 15 p2436 A71-32508

Grain size effect on fatigue life during tension and compression tests of alpha brass, copper and aluminum, considering slip character 15 p2437 A71-32578

Vibrationally loaded hollow cylinder with slanted notch, considering fatigue strength behavior as function of rated stress state 15 p2510 A71-32738

Annealed stainless steel and Ti alloy in solution heat treated aged condition, detailing elevated temperature and high strain rate effects on fatigue life and tensile properties 15 p2438 A71-32791

Fatigue failure of polyamide filaments from optical and electron microscopic observations, describing crack initiation and propagation 16 p2600 A71-32817

Aircraft structures fatigue properties, discussing stresses, life estimates, safety factors and descriptive curves 16 p2656 A71-33343

Fatigue limits of Ti alloy by Wohler and Locati loading methods 16 p2592 A71-33406

Program parameters effects on fatigue life of turbine blade heat resistant alloys at high temperatures under cyclic loading 16 p2592 A71-33407

Probabilistic approach to prolonged lifetime design and static strength of structures of monocoque and multispar wings, using fatigue characteristics of individual elements 16 p2657 A71-33604

Preliminary corrosion effect on fatigue strength of Al joints, noting insufficient anticorrosive anodic film and additional protection by paint and varnish 16 p2584 A71-33688

Atmospheric turbulence prediction, discussing gust sensitive aircraft design for structural overload and fatigue failure decreases [AIAA PAPER 71-775] 16 p2524 A71-34011

Computer controlled durability and low cycle fatigue testing, using digital random sequencing technique 17 p2821 A71-34555

Optimal cross section of minimum volume rotating shaft with complex fatigue strength, accounting for tension and shear effects 17 p2822 A71-34595

Fatigue strength anisotropy in glass fiber materials with epoxy-phenol binders under symmetric and pulsed compression-tension cyclic loads 17 p2822 A71-34783

Fatigue crack initiation and growth and residual strength of F-100 wing, comparing service failure data with full scale fatigue test results 17 p2827 A71-35159

Helicopter rotor blades fail-safe design, presenting criteria for fatigue loaded structures residual strength and life based on crack propagation rate methods 17 p2828 A71-35163

Gas turbine engine steels and Ni alloys heat resistance, examining fatigue life and creep properties at various temperatures and test durations 17 p2759 A71-35453

Fatigue life prediction for structure undergoing random steady Gaussian centered process, determining statistics of absolute maximums 17 p2832 A71-35471

Vibrotumbling duration effects on surface quality, fatigue resistance and damping properties of titanium alloy structural parts 17 p2760 A71-35665

Structural steels fatigue resistance, investigating processing technique, chemical composition, plastic and hot working and heat treatment effects 18 p2934 A71-36149

Stochastic character of metal fatigue fracture and fatigue life dependence on stress cycle amplitude, using equiprobability curves 18 p2936 A71-36694

Nb and Nb-Zr alloy tubular and sheet samples cyclic loading tests, determining heat treatment effects on notch sensitivity and fatigue strength 18 p2937 A71-36724

Small holes effect on Ni base superalloy wrought thin sheets fatigue strength under pulsating tension load, analyzing crack initiation, propagation and critical length 18 p2938 A71-36850

Ni-base heat resistant alloys loading frequency effect on fatigue resistance, noting linear relationship between creep strain and cycles to failure in logarithmic coordinates 19 p3082 A71-38348

Statistical analysis of endurance limits for castings and forgings of the forged and cast steel, using rotating beam fatigue tests 21 p3388 A71-40754

Temperature effect on fatigue strength of Ni steel by tension-compression fatigue test at low temperatures 21 p3400 A71-40832

Carbon and stainless steels chemical composition effects on diffusion layer structure and fatigue strength after diffusive boring 21 p3403 A71-41162

Steels fatigue behavior and cumulative damage effect prediction under strain controlled conditions, comparing with experimental data 22 p3559 A71-41593

Material fatigue failure under narrow band random vibration effects, deriving fatigue life prediction equation based on composite experimental design and statistical tests 22 p3615 A71-42002

Statistical fatigue life models, surveying failure probability distributions in reliability studies 22 p3566 A71-42117

Gas turbine blade models of heat resistant Zr56K alloy under operational temperature variations, observing fatigue strength 23 p3779 A71-44209

Heat treatment effect on tensile and bending fatigue strength of Al alloy thin sheet 23 p3693 A71-44217

Fatigue strength of two phase Ti alloys, considering work hardening, electrochemical finishing, electropolishing and protective media 23 p3694 A71-44232

High cycle fatigue resistance improvement of age hardened Al-Zn-Mg-Cu alloys through thermomechanical treatments 23 p3695 A71-44290

Fatigue lifetime of overlapping joint spot welds of Al alloys, investigating shrinkage crack initiation and propagation 24 p3830 A71-44786

Prestraining effect on D16 duraluminum corrosion fatigue and tensile strengths 24 p3838 A71-44856

Polyethylene coated machine steel fatigue strength in air, 3 percent NaCl bath and molecular sulfuric acid solution 24 p3841 A71-44865

- Multiple rig rolling fatigue life tester, evaluating aviation gas turbine lubricants [ASLE PREPRINT 71LC-15] 24 p3832 A71-45292
- Metal fatigue strength evaluation for nonstationary loading and complex stress-amplitude variation 24 p3886 A71-45364
- ### FATIGUE TESTING MACHINES
- Gas flame heater for heat resistant samples under fatigue tests, simulating gas turbine engine operating conditions 01 p0067 A71-10041
- Cyclic fatigue and corrosion test equipment for elastoplastic materials at various temperatures and pressures 01 p0165 A71-10042
- Aircraft structures fatigue testing device using programmed control of electrical inputs to electrodynamic vibration stand, noting load cycle effects and damage accumulation 01 p0168 A71-10409
- Soviet book on machines and instruments for programmed fatigue tests 05 p0734 A71-17025
- Refractory metals and alloys thermal fatigue testing, describing test equipment allowing for variable test specimen constraints and arbitrarily programmed temperature control 09 p1425 A71-22317
- Six position machine for fatigue testing in corrosive medium of circular rotating metal specimen with cantilever bending 09 p1426 A71-22327
- Electromagnetic testing machine for torsion fatigue characteristics under steady and programmed cyclic loading conditions 09 p1426 A71-22498
- Two frequency axial loading fatigue testing machine using torsional/linear vibration transducer 09 p1426 A71-22500
- Apparatus for fatigue testing under tensile stress in vacuum at frequencies of 15-30 Hz with 500 kg maximum load 09 p1426 A71-22505
- Hydropulsation equipment for fatigue tests, presenting schematic diagrams and technical data 09 p1427 A71-22510
- Dynamic characteristics of hydraulic fatigue testing machines, using hydraulic activation efficiency factor 14 p2221 A71-29625
- Fretting fatigue test apparatus with load monitoring as function of cycles for relating quantitatively damage to life 14 p2248 A71-30883
- Elastic interaction between specimen and testing machine in mechanical property tests, considering drawbacks to machine stiffness calculation methods 15 p2414 A71-31947
- Fatigue test equipment for 293-233 K and 50-100 ton static or 25-50 ton cyclic loads, using Freon 22 as coolant 23 p3661 A71-44234
- ### FATIGUE TESTS
- Rolling ball fatigue and lubrication with fluorinated polyethers at cryogenic temperatures compared to superfinned mineral oil 01 p0107 A71-10484
- Airplane materials mechanical properties degradation due to fatigue, discussing breaking strain of Al alloy 01 p0104 A71-11395
- Metallic materials semimicroscopic damage in fatigue of S/N gage under constant strain 01 p0104 A71-11396
- Al alloys low cycle fatigue test under axial load, observing hardening behavior and structure by transmission electron microscopy 01 p0104 A71-11397
- Al fatigue testing by cyclic uniaxial tensile load, examining deformation, internal friction ductility and plastic strain 02 p0262 A71-11683
- Sailplane fatigue testing determining load spectra fail safe structures and damage calculation 02 p0324 A71-11949
- Laboratory facilities for DC-10 structural test program using fatigue test machines and computer controlled servo loading systems [SAE PAPER 700829] 03 p0397 A71-13724
- Test equipment with axial mode closed loop machine for cyclic deformation and fatigue in pure bending [SESA PAPER 1726] 03 p0507 A71-13756
- Thin Al and plexiglass sheets biaxial stress field effect on fatigue and fracture [ASME PAPER 70-PVP-17] 04 p0665 A71-14768
- Heat treated low carbon steel fatigue tests at low cycle tension compression loads, determining durability relationships to load and total work to fracture 04 p0666 A71-14878
- Carbon steel and heat treated duraluminum fatigue fracture microstructure observation using electron microscope, determining crack propagation relationships to loading sequence 04 p0610 A71-14880

- Test stand for endurance and creep testing of plastics, glazed ceramics and other brittle materials 04 p0567 A71-15645
- Fatigue damage detection by X ray diffraction method, testing different steel specimens with Co-K-alpha radiation to obtain characteristic diffraction patterns 05 p0749 A71-16295
- Glass fiber reinforced plastic plates static tensile and low cycle fatigue tests under pulsating tension 05 p0772 A71-16739
- Test facility for fatigue and thermal fatigue of turbine blades in high temperature gas flow 05 p0734 A71-16762
- Fiber reinforced plastics fatigue testing, discussing machines, specimen preparation and design, data analysis and environmental control 05 p0772 A71-16928
- Acoustic emission monitoring system for real time detection of crack initiation and propagation in complex structure during static and fatigue tests 06 p0906 A71-18461
- Austenitic stainless steel dislocation structures during fatigue deformation under cyclic loading, observing slip lines and lattice strain morphology 07 p1136 A71-19699
- Steels fatigue tests, observing crack propagation through weld heat affected zones at two orientations to stress axis 07 p1139 A71-19989
- Materials fatigue testing using analog computer interfaced with closed loop test system 07 p1216 A71-20203
- Al alloys thermal fatigue resistance measurement using testing apparatus involving HF induction heating 07 p1142 A71-20325
- Fatigue limit of titanium alloy machine parts after finishing mechanical treatment under resonance testing 07 p1142 A71-20484
- Titanium-steel continuously reinforced composites strength to weight ratings, describing ausforming process and fatigue tests 08 p1316 A71-21587
- Cyclic heating and thermal stresses effect on fatigue strength and durability of turbine blade alloys and structural elements 08 p1372 A71-21702
- Materials fatigue disintegration process visual examination for crack development kinetics, using fiber optics 09 p1454 A71-22316
- Refractory metals and alloys thermal fatigue testing, describing test equipment allowing for variable test specimen constraints and arbitrarily programmed temperature control 09 p1425 A71-22317
- Thermal fatigue testing of materials under static load with allowance for creep 09 p1426 A71-22497
- High vacuum low temperature fatigue tests, describing design and operation of equipment for microstructural observation 09 p1427 A71-22511
- Materials bending fatigue strength calculations for biaxial tension compared with experiments, showing agreement 09 p1538 A71-22596
- Heat resistant alloys low cycle fatigue tests at 20-800 C, establishing residual strain change patterns as function of stress and temperature 09 p1468 A71-22600
- Thermal fatigue tests of high temperature Ni and Co base alloys by fluidized bed technique 09 p1469 A71-22812
- Al alloys HF accelerated fatigue testing, using magnetostrictive transducer excited mechanical resonance and electronic circuitry 09 p1428 A71-22939
- Relaxation analysis of strain range, hold time and cycle number in low cycle fatigue testing of annealed stainless steel at 1200 F [ASM PAPER W71-24.1] 09 p1471 A71-23093
- 21-6Al-4V and solution treated and aged Ti-6Al-6V-2Sn alloys, investigating relationship between alpha grain size and crack initiation fatigue strength 09 p1472 A71-23131
- Concorde thermal fatigue test installation, controlling temperature by transfer temperature variation in single heat exchanger block 09 p1430 A71-23580
- High temperature fatigue test assembly for symmetric tension compression cycles at 10 kHz 10 p1589 A71-24201
- Wing structure fatigue substantiation procedures under fail-safe concept for general aviation aircraft [SAE PAPER 710404] 10 p1555 A71-24264
- Macroscopic and microscopic plastic zones ahead of propagating fatigue crack on surface and inside of specimen as function of load cycles 10 p1626 A71-24306
- Al alloys one step fatigue tests under combined high temperature and structural vibration conditions 10 p1628 A71-24821

- Nonstationary stress modeling in aircraft structures using random pulse generator applied to jet landing gear break strut fatigue test 10 p1692 A71-24954
- Fatigue crack propagation rates in Al under constant low stress, discussing data processing methods 10 p1629 A71-25053
- Aircraft wing fatigue test procedures for gust, maneuver, ground-air-ground, taxi and landing impact loads [SAE PAPER 710403] 10 p1694 A71-25133
- Carburized steel surface stresses and fatigue behavior, correlating stress distribution measurements and notched bar bending fatigue tests after several heat treatment steps 11 p1777 A71-25388
- Graphite epoxy composites fatigue testing, including loaded and unloaded shear, hardness and tensile strength in wet and dry environments 11 p1785 A71-25402
- Glass fiber reinforced plastics fatigue tests, discussing closed loop hydraulic servomechanism equipment, testing methods and materials and mean stress effects 11 p1789 A71-25658
- Ni-based superalloy stress cycle frequency effect on elevated temperature fatigue life 11 p1779 A71-26012
- Specimen sample mounting stress effects on fatigue durability scatter in axial load tests 12 p1976 A71-27116
- Fiber composites monofilament and strand tests, considering fracture, fatigue, stress, corrosion and microstructure 12 p1921 A71-27635
- Gas turbine blades thermal fatigue test and analysis, investigating static tensile loading effects on heat resistance under thermal cycling 13 p2149 A71-28124
- Structure service life and storage failure probability calculation with current load measurements and laboratory fatigue testing 13 p2076 A71-29231
- Stress concentration for fatigue crack propagation in smooth and notched samples under symmetrical loading 13 p2157 A71-29373
- Structural fatigue in aircraft design, discussing twin engine transport tests, crack propagation rate, residual strength, etc 13 p2158 A71-29434
- Energy dissipation measurement in materials during cyclic fatigue testing by dynamic hysteresis loop method 14 p2238 A71-29619
- Creep and failure tests for Ti alloys at 500 C and high stresses, discussing work dissipation during creep process 14 p2256 A71-29621
- Metal coated superalloys evaluation for gas turbine engine components, including corrosion, impact and fatigue tests 14 p2256 A71-29635
- Notched age hardening Al alloys sheets, obtaining fatigue damage test data and S-N curves 14 p2326 A71-30067
- Refractory metals fatigue testing under nonstationary thermal loads, considering test data reliability improvement 14 p2259 A71-30268
- Pisa University Aeronautical Institute activities /1960-1970/, considering supersonic and subsonic flow research, thin stiffened shells fatigue under compressive or tensile loads, etc 14 p2222 A71-30822
- Fatigue testing machine for axial and torsional loadings at low temperatures in vacuum 15 p2384 A71-31858
- Sheet metal fatigue test method for transverse 100-1000 Hz bending at normal and high temperatures, applying to 1.5 mm Ti alloy sheet 15 p2505 A71-31864
- Stress corrosion fatigue crack growth in Ni-Cr-Mo maraging steel, using controlled-potential techniques, pH measurements and fractographic analysis 16 p2590 A71-32942
- Secondary damage in corrosion fatigue of Al alloy tested to failure 17 p2757 A71-34497
- Simulated turbine blade thermal fatigue testing under transient and steady state heating and spanwise loading, obtaining crack initiation and propagation data [SAE PAPER 710459] 17 p2792 A71-34500
- Computer controlled durability and low cycle fatigue testing, using digital random sequencing technique 17 p2821 A71-34555
- Limited fatigue strength tests for Al-Mg-Si alloy stress amplitude coefficients under continuous loading, defects, strains and creep accumulation 17 p2757 A71-34596
- Vibration response NDT for fatigue crack damage in laminated filament-reinforced epoxy composites 17 p2824 A71-34815

Stiffened panel acoustically induced stress estimation using experimentally determined random S-N curves with various structural parameters

17 p2826 A71-35033

Test apparatus for mechanical/thermal fatigue and vibration strength of turbine blades in high temperature gas flow

17 p2724 A71-35461

Environment and frequency effects on fatigue properties of age hardening Al-Cu-Mg alloy

18 p2933 A71-35876

Abbreviated testing for material constants determination of equation of fatigue crack propagation from one specimen at different stress amplitudes

18 p2976 A71-35988

Thermal ground testing of Concorde and Veras, considering static and fatigue testing in heat environment

18 p2899 A71-36464

Statistical methods for S-N curve and fatigue limit tests, including iterative method, probit analysis, etc

18 p2936 A71-36695

Fatigue crack propagation in thin aluminum plates under fluctuating tensile loads, concerning Forman model

18 p2938 A71-36851

Surface properties and environmental effects on fatigue striations development and crack initiation in Cu single crystals

19 p3077 A71-37412

Stress determination by vibration measurement in cantilever specimens fatigue tests with audio frequency loading, taking into account end restraint elasticity

19 p3160 A71-38347

Ni-base heat resistant alloys loading frequency effect on fatigue resistance, noting linear relationship between creep strain and cycles to failure in logarithmic coordinates

19 p3082 A71-38348

Ni-Mo-V, Ni-Cr-Mo-V and Cr-Mo-V high strength rotor forging steels fatigue crack growth characteristics tests at room temperature

20 p3247 A71-38768

Creep tests effect on Cr-Mo-V steels mechanical properties during alternating stress fatigue testing, considering preliminary static prestressing

20 p3250 A71-39023

Steels fatigue behavior and cumulative damage effect prediction under strain controlled conditions, comparing with experimental data

22 p3559 A71-41593

Random loading parameters adjustment in fatigue tests of welded aircraft structures

22 p3528 A71-41692

Vacuum apparatus for fatigue tests at room and low temperatures, giving results for annealed copper

22 p3538 A71-41700

Microhardness and magnetic permeability and viscosity changes during fatigue loading of steel parts, describing electromagnetic fatigue testing method

22 p3554 A71-41771

Fatigue, necked-out and intermediate fracture types observation in load-controlled low-cycle fatigue tests of rolled steel

22 p3617 A71-42496

Loading cycles dependence of energy dissipation and plastic deformation during fatigue tests, using Fourier series

23 p3774 A71-42897

Gas turbine blades of cast ZhS6K heat resistant alloy, investigating structural strength from fatigue test data

23 p3779 A71-44208

Failure and crack formation in gas turbine engine compressor disks under variable stresses from fatigue tests, considering safety factors

23 p3779 A71-44210

Multiple rig rolling fatigue life tester, evaluating aviation gas turbine lubricants

[ASLE PREPRINT 71LC-15] 24 p3832 A71-45292

Metal fatigue strength evaluation for nonstationary loading and complex stress-amplitude variation

24 p3886 A71-45364

FATS

NT CHOLINE

Space diets for maximum energy consisting of fats and proteins from biological systems and carbohydrates from chemical systems

01 p0027 A71-11573

Hamster body fat, water and density measurements by dilution method and air displacement technique, comparing to determination by direct chemical analysis upon sacrificing

19 p3005 A71-38555

Cholesterol and esterified cholesterol distribution in human skin from analysis on fat, epidermis, corium, subcutaneous tissue and serum by chromatographic/colorimetric methods

20 p3185 A71-38892

FATTY ACIDS

NT IODOACETIC ACID

Diet effects on hepatic fatty acid synthesis in rats and mice, noting linoleate content role

01 p0011 A71-10848

Blood plasma nonesterified fatty acids mobilization in relation to work load severity during and after prolonged exercise in men

04 p0544 A71-15154

Complex calcium-based lubricants preparation based on hydrogenated castor oil or free fatty acids, considering saturation effect on structure and properties

13 p2091 A71-28227

Ethyl esters of long chain fatty acids as biological products from gas chromatographic and mass spectrometric analyses on lipid fractions

13 p2015 A71-29352

Perfluorinated monocarboxylic fatty acids additives for controlling lubricating oils spreading on metals and antifriction properties improvement

15 p2438 A71-31680

Thermophilic, mesophilic and psychrophilic anaerobes fatty acid composition, discussing results obtained by mass spectral analysis

15 p2360 A71-32050

Free fatty acids reduced availability effects on physical working capacity in normal man

22 p3485 A71-41722

FAULT MECHANICS

U FRACTURE MECHANICS

FAULTS

Dynamic fault detection, using mathematical condition between measurement taken, difference equation theoretical coefficients and bounds of each

03 p0449 A71-13092

Permanent logical faults identification in discrete combination devices by practical behavior in response to given input sets, using one of Boolean algebras

19 p3025 A71-37571

FBFM [MODULATION]

U FEEDBACK FREQUENCY MODULATION

FCC LATTICES

U FACE CENTERED CUBIC LATTICES

FEAR

Fear measurement and mastery, investigating relationship between experience and electrodermal arousal in responses to stimulus words of varying relevance

18 p2862 A71-36944

FEED SYSTEMS

Bellows for aerospace feed line ducting, discussing liquid propellant rocket engines, cryogenic valves, etc

01 p0007 A71-11433

Liquid fluorine feed system valves, seals and seats, discussing design criteria for flight weight components [AIAA PAPER 70-705]

11 p1709 A71-25519

Cryogenic propellant control system, discussing hot wire sensors, fuel state in fueling and tank pressurizing and feed stage

22 p3588 A71-41504

Modular slotted fed fluid bearing using jacking gas effects for pumping power conservation under high speed steady state, discussing design and application

22 p3552 A71-41669

Pulsed plasma thrusters, propellants, trigger and feed systems developments for long life secondary spacecraft propulsion

22 p3588 A71-41975

Hybrid rocket /Barbarella I/ design, tests, engine, feed system oxidizer tank, fairings fins, propellants and launch facilities

22 p3589 A71-42049

Film ablative cooled gas pressure feed liquid rocket engine unstationary process analysis with digital computer, detailing engine dynamics, heat transfer and temperature profile

22 p3589 A71-42054

Molins 24 integrated automatic complete-processing system for small light-metal parts, using numerically controlled machine tools integrated with palletized feeder system

23 p3681 A71-43473

Working gas parameter determination for valve supply main system during feed opening, explaining heating effect for second valve by shock wave theory

24 p3793 A71-45021

FEEDBACK

NT NEGATIVE FEEDBACK

NT NONLINEAR FEEDBACK

NT POSITIVE FEEDBACK

NT SENSORY FEEDBACK

Signal optimization for binary data transmission system with noiseless feedback channel, considering receiver signal energy and structure

04 p0560 A71-14743

Flight simulators simulation width and parameter sensitivity analysis by state vector feedback method, using multiparameter control root-locus technique

05 p0733 A71-15970

Dynamic data processing systems with feedback and internal noise, evaluating carrying capacities, limiting parameters and optimal transfer function

05 p0732 A71-17164

Book on nonresonant feedback in lasers covering multimode cavity, emission spectra, generation in cloud, quasi-concentric resonator, etc

08 p1301 A71-21226

Simple algorithms for accelerating convergence and averting divergence in Kalman filters, using feedback from measurement residuals

08 p1324 A71-21333

Dynamic data processing systems with feedback and internal noise, evaluating carrying capacities, limiting parameters and optimal transfer function

12 p1893 A71-27455

Optimal linear filter gain relation to feedback difference, using Riccati matrix differential equation

14 p2220 A71-30808

Naval Air Rework Facility, discussing primary mission, technical disciplines and operational performance feedback

[AIAA PAPER 71-765] 16 p2523 A71-34003

Additional redundancy in information transmission systems with feedback to reduce error probability due to incorrect addressing

17 p2702 A71-34975

Stepping electromotor in self commutation mode with local feedback, examining dynamics with phase plane method

23 p3655 A71-43293

FEEDBACK AMPLIFIERS

Feedback role in mathematical operation amplifiers for analog computers

01 p0049 A71-10361

Amplifier stability with distributed feedback by root locus trajectories

01 p0059 A71-10605

Regenerative feedback amplifier with maximally flat amplitude-frequency response

04 p0556 A71-14621

Transistorized amplifiers synthesis with multiloop feedback

05 p0728 A71-16871

Regenerative transfer amplifiers normalized reactive parameters effects on phase linearity

06 p0872 A71-17376

Combined HF compensation of single stage transistor amplifier with RC feedback in emitter circuit

07 p1079 A71-20262

Frequency characteristics calculation of regenerative two cavity microwave bandpass amplifiers, applying to parametric and quantum amplifiers and underexcited microwave relaxation oscillators

09 p1413 A71-22157

Piezotron accelerometer for vibration measurement, combining quartz sensing element with subminiature solid state electrostatic amplifier

11 p1767 A71-26442

Neural spikes and LF components separation from background noise, describing feedback amplifiers circuit

15 p2356 A71-31251

Bridge-feedback amplifier constant-temperature hot-wire anemometer static and dynamic response determination

15 p2408 A71-31931

Parametric regeneration amplifier with capacitor modulation by signal voltage only

16 p2378 A71-32633

Series and bypass fluidic pressure regulators, discussing component selection, performance details, sensing circuits, feedback amplifier and flow controller

16 p2579 A71-33526

Traveling wave tube for reflex type amplifier on-board space communication satellite, discussing prototype reliability and performance

17 p2714 A71-34682

Differential phase frequency characteristics of low noise or tunnel diode regenerative amplifiers

20 p3205 A71-39261

Regenerative feedback amplifier with maximally flat amplitude-frequency response

22 p3521 A71-42261

Regenerative nonlinear RC amplifier oscillations due to series opposed varicap diode capacitance

24 p3810 A71-45261

FEEDBACK CIRCUITS

Feedback circuit for constant current stimulation through intracellular microelectrode

01 p0021 A71-10245

Data transmission systems using information feedback techniques to achieve high bit rates /channel capacity/

01 p0064 A71-10902

Low cost error control technique for bulk data transmission over channels with noisy feedback link

01 p0034 A71-10903

Block code for retransmission of information damaged by noise bursts for feedback digital communication systems

01 p0034 A71-10905

Noiseless linear feedback limitation over band-limited channel capacity in analog data transmission

01 p0064 A71-10906

Low- and high-pass active filters theory and design, describing positive and negative feedback circuits

02 p0231 A71-11863

Linear feedback function for r-stage feedback shift register resulting in equal length branchless cycles [JPL-TR-32-151]

03 p0388 A71-13282

Monostable fluidic feedback oscillator analysis, using mathematical models describing function, feedback control theory and analog computer simulation to determine oscillation frequency
07 p1027 A71-20577

External feedback fluidic oscillators design and analysis using branched pneumatic transmission line arrangements
07 p1027 A71-20578

Information transmission rate and error probability in analog feedback systems, showing normalized maximum transmission speed dependence on signal to noise ratio
08 p1268 A71-21283

M-ary linear feedback shift register cycle structure determination, relating behavior to p-ary LFSR
08 p1269 A71-21345

Transistorized gas laser discharge current stabilizer using double feedback circuit, discussing schematic diagram and operation principles
08 p1303 A71-21807

Optimum synthesis and design of distributed RC filter for oscillator feedback circuit, using calculus of variations
09 p1425 A71-23652

Return-difference matrix for optimal stationary Kalman-Bucy filter behavior examination in associated feedback system, noting spectral factorization and signal/noise separation
09 p1425 A71-23683

Single loop quartz vacuum tube oscillators, calculating oscillation spectral line width due to thermal and shot noise and circuit parameters fluctuations
12 p1889 A71-27622

Closed loop circuit stability determination based on predetermined area requirement for characteristic equation roots
13 p2043 A71-28793

Coding for feedback communication system with additive white Gaussian noise, using mean-square estimation error
13 p2034 A71-29379

Heading reference system feedback linear control circuits containing fluidic vortex rate sensor applied to turbine drive
15 p2353 A71-32070

Laser interferometer application in machine tool calibration, digital readout and feedback system, discussing advantages and limitations
[SME PAPER IQ-71-745] 15 p2421 A71-32433

Feedback system estimation algorithm, comparing performance to algorithm based on stochastic control separation principle
19 p3039 A71-38715

Dual input null networks application in RC feedback oscillators, examining frequency stability
20 p3206 A71-39915

FEEDBACK CONTROL

NT CASCADE CONTROL

Matrix switch amplitude analyzer for EEG signals providing feedback stimuli to subject
01 p0021 A71-10246

Nonminimal phase feedback control system synthesis by frequency methods, discussing invariance characteristics
01 p0061 A71-10709

Automatic feedback control systems performance correction for errors due to weakly damped components effects
01 p0061 A71-10712

Quasi-invariant automatic feedback control system, deriving basis for determination of perturbation compensating components parameters
01 p0061 A71-10713

Elastic flight vehicles feedback control systems synthesis by invariance theory
01 p0163 A71-10714

Complex servo systems with feedback loop and anticipating path, demonstrating equivalence to systems based on error measurements
01 p0062 A71-10719

Automatic feedback control systems steady dynamic error reduction by introducing control action forward loop, determining transfer function
01 p0062 A71-10721

Nonlinear feedback control systems invariance, investigating coordinate and parametric disturbances compensation
01 p0063 A71-10728

Linear information feedback methods for white Gaussian noise channels
01 p0064 A71-10904

Satellite static inverter for voltage wave form synthesis by time optimal response closed loop technique, providing input insensitive AC output
02 p0190 A71-11675

Aircraft manual flight control analysis using continuous mathematical pilot model for closed loop digital simulation
02 p0188 A71-11787

Book on fluid power circuits and systems covering switching theory, closed loop systems, pneumatic circuits, servo systems and pressure control
02 p0190 A71-11871

Digital optimal feedback control device, discussing design requirements, algorithm, block diagram, flow chart and measurement results
02 p0236 A71-12150

Phased array radar systems accuracy increase, using ferrite core magnetic flux feedback for phase shifter control
02 p0215 A71-12174

Incore thermionic diode reactor stability review and evaluation, discussing reactivity feedback mechanisms, analytical models and results
02 p0280 A71-12260

Nonlinear closed loop-shape characteristics of vibrational mechanical systems, using forced vibration analysis
02 p0284 A71-12284

Balanced modulators and multipliers, using feedback control for suppressing carrier leak
02 p0236 A71-12425

Optimal control synthesis for inertialess plant with feedback based on parameter estimation
02 p0236 A71-12622

C-5 military transport stability augmentation for pitch and yaw inertia at low speed, using pilot evaluation on cockpit simulator
02 p0190 A71-12684

Communication satellite earth station steerable antennas drive train resonance and traction drive wheel slippage control by differential velocity feedback, discussing analog simulation
02 p0222 A71-12790

Muscle activity control mechanism in animals locked into external feedback loop, relating exciting stimulus to muscles stressed state
03 p0367 A71-12980

Control system for resonant mechanical loads with feedback, examining stability conditions and oscillation damping by Coulomb friction
03 p0431 A71-13074

Nonlinear time varying discrete feedback systems input-output properties, deriving stability criteria by generalized small gain and passivity theorems
03 p0389 A71-13327

Neighboring optimum feedback guidance to motivate min-distance lookup parameter determined by minimizing metric function of perturbed state and reference trajectory
[AIAA PAPER 69-888] 03 p0454 A71-13446

Test equipment with axial mode closed loop machine for cyclic deformation and fatigue in pure bending
[SESA PAPER 1726] 03 p0507 A71-13756

Sampled data feedback control system analysis and synthesis by state variable method, discussing computer algorithms for optimal pulse control
03 p0392 A71-14409

Nonlinear time optimal off-on feedback control system synthesis, deriving algorithms
03 p0392 A71-14410

Regulator logic synthesis using state variable feedback for stationary linear plants
03 p0393 A71-14467

Vestibular system semicircular canals mathematical model determination of galvanic stimulation and directional preponderance, considering visual, postural and vehicle orientation feedback loops
04 p0543 A71-14790

Feedback control system parameters optimization by target model method, with automatic pilot example
04 p0560 A71-15205

Feedback control circuits with delay time, examining overshoot diagrams
05 p0730 A71-16127

Aircraft longitudinal control during landing approach, investigating back side operation characteristics by closed loop system analysis regarding pilot and aircraft as elements
05 p0696 A71-16388

Closed control loop system design using direct time domain synthesis
05 p0731 A71-16394

Control system synthesis for asymptotically stable systems, using Liapunov functions for feedback laws
05 p0732 A71-17023

Positive-negative feedback control system optimum switching conditions, deriving simple algebraic formula for nth order system switching equation coefficients
06 p0878 A71-17339

Feedback and dynamic control of plasmas - Conference, Princeton, June 1970, Volume 1
06 p0931 A71-17451

Plasma stabilization, considering feedback loop system with Maxwell-Vlasov equations
06 p0931 A71-17452

Plasma confinement in specified bounded spatial domain by feedback control localized to outer shell
06 p0931 A71-17453

Plasma stability criterion for feedback systems limitations, noting geometrical and electronic effects on phase and amplitude
06 p0931 A71-17454

Plasma feedback system boundary conditions, describing electrical properties, dispersion relation and mode interaction
06 p0931 A71-17455

Plasma stabilization, discussing external feedback system model
06 p0931 A71-17456

Fusion reactor plasma feedback stabilization by nonlinear interaction of two carbon dioxide IR laser beams to produce difference frequency near hybrid resonance
06 p0931 A71-17457

MHD continua z-theta pinch stabilization, discussing analytical models for determining feedback spatial and temporal resolution
06 p0931 A71-17458

Plasma stabilization by nonlinear bang-bang feedback
06 p0932 A71-17459

Videotype sampling in electromechanical equilibria feedback stabilization of hydromagnetically contained plasmas
06 p0932 A71-17460

Cylindrical plasma Kruskal-Shafranov modes, examining active feedback stabilization
06 p0932 A71-17461

Tokamak copper shell as feedback control device for toroidal plasma, considering stabilization of thermal instability
06 p0932 A71-17462

High-beta sharp-boundaried stellarator plasma column feedback stabilization with helical fields
06 p0932 A71-17463

Collisional drift instability remote feedback suppression in Q machine C5 plasma by microwave modulation at upper hybrid frequency
06 p0932 A71-17464

Drift type plasma instabilities, discussing feedback stabilization and remote sensing
06 p0932 A71-17465

Plasma LF instabilities, observing temporal growth and effect on confinement by switching feedback control off
06 p0932 A71-17466

Q-machine with boundary segments to provide passive feedback for reducing Kelvin-Helmholtz instability and plasma losses
06 p0933 A71-17467

Plasma transverse Kelvin-Helmholtz instability, describing stabilization by feedback controlled electron sink
06 p0933 A71-17468

Multimode ionization wave growth and saturation in finite length positive plasma column of gas discharge, investigating feedback and external driving signal effects
06 p0933 A71-17469

Electron-hole plasmas feedback stabilization, considering instability coefficients measurement
06 p0933 A71-17470

Hot electron plasma, observing flute instabilities with feedback
06 p0933 A71-17471

Dynamic plasma stabilization, discussing closed and open loop approaches
06 p0933 A71-17472

Two stage integrating float gyroscopes with reactive moment meters and sensors, examining feedback design for stabilization systems
06 p0899 A71-17930

Two countable systems of differential inequalities, applying to stability of feedback controls synthesizing equilibrium solutions to linear quadratic differential games
06 p0919 A71-18198

Gas proportional counting system gain stabilization, using feedback loop radioactive X ray emitter and correction signal
06 p0901 A71-18225

Steady state current-free magnetized plasma generation by microwave discharge, using feedback control to reduce power fluctuations
06 p0938 A71-18458

Transfer function voltage controlled transistorized amplifier using silicon carbide nonlinear resistance element
07 p1075 A71-19301

Fluidic diverting valve independent of turbulent reattachment, examining large scale model and digital element characteristics in closed loop system
07 p1024 A71-20553

Beam deflection fluidic circuit design by linear static matching method, considering servoamplifier feedback control system
07 p1026 A71-20569

Precision temperature controller using resistive sensor and Wheatstone bridge in heater loop, discussing prototype design for gyroscope application
08 p1287 A71-20986

Stability of model tracking adaptive control systems with reduced state feedback and measurement noise
08 p1269 A71-21336

Satellite carrier tracking and phase lock carrier loops, evaluating lock and reacquisition performance loss by linear model and Monte Carlo digital simulation
08 p1270 A71-21352

Hybrid phase locked loop for deriving phase error estimate from carrier and information components,

discussing system parameters optimization for performance

08 p1270 A71-21353

Liapunov design technique for model reference adaptive control systems with feedback and prefilter adjustable gains

08 p1270 A71-21669

Ionization instabilities feedback suppression in magnetized nonisothermal plasma

08 p1342 A71-21932

Linear processes optimal sampled data controls, noting effect of sampling on closed loop system and cost asymptotic behavior

09 p1422 A71-22281

Distributed parameter systems under load disturbances regulatory control by feedforward feedback and state measures

09 p1422 A71-22282

Linear optimal stochastic regulator control, using system output instantaneous feedback with minimum quadratic performance measure

09 p1422 A71-22283

Closed loop systems with odd-symmetrical nonlinear components and distributed delay, calculating self oscillations

09 p1422 A71-22367

Nonlinear sampled data feedback control systems periodic mode of oscillations, using state variable approach

09 p1423 A71-23033

Sampled data feedback control systems with neural pulse frequency modulation, deriving periodic oscillations existence conditions

09 p1424 A71-23387

Discrete time finite dimensional autonomous linear systems, investigating controllability and pole assignment to closed loop transfer matrix by choice of state variable feedback gain

09 p1424 A71-23465

Plasma feedback stabilization, investigating flute instabilities

10 p1651 A71-24633

Deterministic parameter estimation in nonlinear system near optimum feedback control by power series expansion

10 p1586 A71-24738

On-line closed loop adaptive control for tracking filter with several inputs and outputs

10 p1586 A71-24739

Closed-loop nonlinear systems synthesis, using mapping in Chebyshev series converging everywhere, multidimensional linearization and Volterra singular integral equations

10 p1587 A71-24744

Constrained gain problem optimality conditions, presenting algorithm for optimal gains and application to aircraft control problems

10 p1588 A71-24859

Linear automatic flight control systems synthesis based on transfer functions and logarithmic amplitude characteristics of open systems

10 p1588 A71-24911

Automatic gust alleviation system employing inertial sensors and feedback devices with wing flaps and elevators, considering linkage control, noninteracting control and split control

11 p1706 A71-25195

Linear discrete time stochastic system with unknown gain parameters, interpreting open loop feedback optimal control identifier and controller equations

11 p1741 A71-25361

Variable conductance heat pipes feedback mechanisms for spacecraft electrical temperature control system design, using steady state analysis based performance model

11 p1857 A71-26212

[AIAA PAPER 71-421] Quasi-optimal proportional navigation, deriving feedback guidance laws for interceptor aerodynamically controlled missiles

11 p1796 A71-26409

Optimal fixed dimensionality dynamic compensator design for linear time-invariant closed-loop system based on quadratic cost and gain criteria

11 p1742 A71-26414

Linear continuous time delay feedback systems stability analysis, using root-locus and frequency response techniques

11 p1742 A71-26423

Single loop fixed adjustment system with adaptation similar properties, discussing special correcting devices

12 p1891 A71-26733

Adaptive array antennas with control loop, deriving noise expression for maximizing signal to noise ratio

12 p1881 A71-27426

Linear estimation with stochastic feedback control to cancel out disturbances or error signals effect, applying to integrated navigation systems involving inertial measurement

12 p1893 A71-27436

Nonlinear closed loop control system with PFM and PWM, obtaining asymptotic stability condition by Liapunov and La Salle theorems

12 p1893 A71-27726

Stability of feedback systems with backlash, deriving stability criterion in form of existence theorem for multiplier function

13 p2042 A71-28703

Stability criteria for nonlinear time-varying feedback systems, using passivity theorem

13 p2042 A71-28705

Design charts relating time response characteristics to parameters of closed loop transfer functions possessing conjugate pair of poles

13 p2042 A71-28706

Optimal control systems design with random parameters and initial state, considering open loop and feedback correction terms

13 p2042 A71-28708

Optimal linear feedback for systems governed by differential operational equations, considering stochastic control and cost function

13 p2095 A71-28814

Plasma ion-sound instability feedback stabilization with remote modulated source at electron cyclotron resonance frequency

13 p2109 A71-29245

Distributed parameter systems with transfer function as ratio of output and input multiple transforms, deriving open and closed loop stability criteria

14 p2265 A71-29602

Closed-loop control of discrete time systems with uncertainty, discussing minimax reachability of target sets and tubes

14 p2219 A71-29698

Sinusoidal vibration tests using narrowband tracking filters, considering automatic servocontrols and feedback loop optimum matching

14 p2175 A71-30310

Wind tunnel model trajectory simulation system with closed loop control by digital computer, describing instrumentation, system servoamplifiers and testing procedures

14 p2208 A71-30334

Gated phase locked loop system characteristics based on sampled data model, comparing with continuous loop operation

14 p2214 A71-30795

VTOL aircraft minimum climb-to-cruise time transition optimal open loop and suboptimal closed loop control synthesis

14 p2220 A71-30799

Gunpowder unsteady burning as closed dynamic system, studying frequency characteristics and transient processes

15 p2462 A71-31375

Structural stability for two beam plasma model with proportional controller using distributed feedback

15 p2456 A71-31846

Suboptimal feedback control law for second order nonlinear systems with quadratic performance index, determining power series coefficients

15 p2381 A71-31941

Closed loop system analysis of triangular wave generator consisting of integrator, on-off element with hysteresis and multiplier

15 p2376 A71-32026

Heading reference system feedback linear control circuits containing fluidic vortex rate sensor applied to turbine drive

15 p2353 A71-32070

Linear closed loop optimal intercept guidance law compensating for short range tactical missile time lag, guidance command saturation and target acceleration

15 p2446 A71-32113

Control system stability with nonlinear feedback in steady equilibrium state

16 p2548 A71-32934

Liapunov functions applications, discussing panel flutter, Couette flow and feedback control

16 p2607 A71-32994

Feedback stabilization of linear distributive systems in form of second-order evolutionary equation in Hilbert space, applying to plasma stabilization

16 p2618 A71-33006

Suboptimization of closed loop adaptive systems by simple dual control method, using dynamic programming

16 p2549 A71-33353

Potential benefits accruing to air superiority fighters by integrating automatic feedback control system technology into design, using F-4 as baseline configuration

[AIAA PAPER 71-764]

16 p2523 A71-34002

SST stability augmentation system, discussing performance, operational safety and reliability benefits

16 p2525 A71-34015

[AIAA PAPER 71-785] Linear single loop sampled data time delay feedback systems stability analysis

16 p2550 A71-34168

Optimal respiration mode based on controlled artificial feedback characteristics, making resistance to inhalation dependent on duration

17 p2680 A71-34644

Multivariable control system state variable feedback decoupling theory generalization to include output subset, using matrices

17 p2718 A71-34736

Linear time-invariant dynamic feedback system suboptimal control by lower order generalized aggregated model for reducing computational complexity

17 p2719 A71-34740

Nonlinear optimal closed loop system control problems equivalence relations as one-to-one correspondences between Hamilton-Jacobi equations solutions

17 p2719 A71-34743

Optimal control systems synthesis with reduced sensitivity to parameter variations by trajectory sensitivity feedback with cost minimization

17 p2719 A71-34744

Nonlinear feedback control system with two nonlinear memoryless energyless elements separated by linear device, discussing grapho-analytical method for self sustained oscillation determination

17 p2722 A71-35183

Error sampled discrete continuous feedback control system performance, comparing adaptive and periodic sampling methods

17 p2722 A71-35184

Optimal state regulator approximate design for nonlinear system with quadratic performance index, determining suboptimal feedback law

17 p2722 A71-35212

Optimal control of plant with varying parameters, obtaining suboptimal systems with feedback loops

17 p2722 A71-35214

Ionization instabilities suppression in magnetized nonisothermal plasma by feedback control

17 p2789 A71-35276

Equilibrium strategies for linear games with quadratic costs in Hilbert space, deriving nonlinear equation in allowed operator feedback spaces

17 p2723 A71-35297

Conjugate eye movement stimulator and monitor for human experimentation in closed loop, open loop and variable feedback modes of operation

17 p2693 A71-35392

Soviet book on radio control of various flight vehicles covering closed loop synthesis, missile guidance, spacecraft trajectory correction and air traffic control

17 p2775 A71-35403

Steady state and transient response of heat source with temperature regulated by electrical feedback controlled variable conductance heat pipe

[ASME PAPER 71-AV-27]

18 p2868 A71-36394

Computer designed optimal or suboptimal feedback controllers, considering least-pth and minimax cost functions

18 p2886 A71-36832

Operator solutions of nonlinear equations in linear feedback optimal control

18 p2943 A71-36956

Discrete time digital flight control systems design resulting in closed loop aircraft response characteristics approximation to prescribed flying quality specifications

[AIAA PAPER 71-955]

19 p3024 A71-37196

USAF total in-flight simulator model-following feedback control system, discussing conceptual design and flight test results

[AIAA PAPER 71-961]

19 p2995 A71-37202

Discrete closed loop system stability with Kalman filter by determining z plane poles of special augmented transition matrix

19 p3036 A71-37235

Closed loop control of nonlinear systems in potentially large neighborhood of nominal trajectory, reducing nonlinear differential equations to related canonical linear form

19 p3037 A71-37239

Plasma drift cyclotron instability feedback stabilization, using immersed modulated electron sources

19 p3111 A71-37636

Structural synthesis of on-off servo feedback control system with combined dynamic and counterconnection braking of actuating motor within relay dead zone limits

19 p3038 A71-37776

Model-reference feedback control system, investigating effects of equivalence lack between reference and plant on iterative process convergence by linear transformation

19 p3038 A71-37778

Controller design for linear closed loop system with transport delay, discussing simplified procedure with correction by zero-pole cluster outside bandpass

19 p3040 A71-38717

Envelope limiting in control loops of adaptive array antennas, reducing varying noise interference

20 p3195 A71-38863

Suboptimal design of closed loop least upper bound fuel control for dynamic systems, minimizing fuel consumption on basis of fixed ultimate error

20 p3206 A71-38971

Simultaneous identification and feedback control optimization using predictor updating scheme

20 p3206 A71-38972

Multivariable frequency response methods for feedback control design for aircraft gas turbines, involving digital test bed trials

20 p3277 A71-38989

State feedback decoupling sensitivity of time invariant linear multivariable system, using Liapunov matrix equations

20 p3207 A71-38992

Interaction measure for optimal multivariable feedback control system design for complex blending processes, noting paradoxical solution

20 p3207 A71-38993

Frequency domain computer graphics technique for linear time-invariant multivariable feedback control system design

20 p3207 A71-38997

Liapunov functions application to Stability of systems described by nonlinear second-order ordinary differential equations, considering feedback control loops construction

20 p3255 A71-39499

Frequency response of nonlinear feedback control systems, using modified polar plot of open loop transfer function

20 p3208 A71-39914

Optimal tracking feedback filter for closed loop systems with irrational transfer function, using heuristic method

21 p3359 A71-40251

Minimal time function of optimal feedback controls for normal and semidynamical systems

21 p3359 A71-40252

Feedback control system with combined PFM and PDM, obtaining nonlinear discrete equivalence

21 p3360 A71-40615

Heart rate and systolic pressure variability control through visual feedback of physiological information, obtaining respiratory measurements and ECG

21 p3344 A71-41037

Variable sweep rate frequency response and vibration testing for test time reduction, using closed loop controller for sweep rate modulation

22 p3537 A71-41635

Design technique based on frequency response loci associated with characteristic transfer functions for linear time-invariant multivariable feedback control system

22 p3526 A71-42284

Human motor system control mechanism for stretch reflex loop gain with simplified central nervous system computation

23 p3639 A71-43354

Neodymium glass laser emission kinetics control with positive and negative feedback by introducing nonlinear media into plane-parallel resonator with two positive lenses

23 p3684 A71-43418

Distributed parameter system optimal feedback control with quadratic performance indices dependence on discrete point states, applying to uniform bar temperature control

23 p3656 A71-43853

Nonlinear discrete system optimal feedback controller synthesis for low sensitivity to parameter variations by difference equations quasilinearization and dynamic programming

23 p3656 A71-43855

Closed loop response speed evaluation for model reference adaptive control system, using sinusoidal test signal

23 p3656 A71-43860

Adaptive random search optimization of optical tracking self organizing feedback control system under inherent coupling signals

23 p3657 A71-43942

Stable feedback control of single variable nonlinear plants with arbitrary uncertainties, ensuring system error convergence to guaranteed stability

23 p3657 A71-43943

Stability conditions of linear discrete system with periodic feedback from spectrum location of bounded linear operator acting in Banach space

23 p3657 A71-44078

Parameter sensitivity reduction in linear optimal feedback control systems based on two degree of freedom structure

23 p3658 A71-44080

Synthesis procedure for feedback parameter adaptive control systems, discussing computer simulation data

23 p3658 A71-44081

Optimal inner product angular momentum controllers, analyzing performance criteria and feedback control laws

23 p3658 A71-44090

Analysis and stability of multiloop attitude control systems for flexible spacecraft

23 p3773 A71-44091

Operational amplifier design with fluidic Schmitt trigger and linear resistor feedback network

23 p3631 A71-44098

State estimation errors in quadratic optimal control feedback gain design of stochastic linear regulator

23 p3659 A71-44100

Stability augmentation system for aircraft elastic modes control, discussing active flutter suppression technology

23 p3629 A71-44107

Active feedback wing/store flutter control for fighter aircraft, using computer programs based on frequency and time domains for linear analysis

23 p3630 A71-44109

Analytic synthesis of optimal feedback controller for nonlinear multivariable systems based on reduction to linear control problems

23 p3659 A71-44110

Adaptive guaranteed cost control for systems with parametric variation, demonstrating system stability and airframe pitch control

23 p3659 A71-44111

Suboptimal feedback link estimation algorithms for stochastic control, comparing with separation principle

23 p3660 A71-44118

Sequential zero-pole placement technique for multivariable control systems, developing algorithm for computing closed loop transfer function matrix

23 p3660 A71-44120

Automatic flight control systems, discussing pilot as systems manager or retained in control loop

24 p3845 A71-44454

Feedback controlled computerized queueing system, deriving generating functions for system state probabilities corresponding to different service time types

24 p3806 A71-44653

Unsteady nonlinear multidimensional feedback control systems characterized by equations in normal form for phase coordinates, investigating solutions accuracy by statistical linearization

24 p3814 A71-44694

Fokker-Planck-Kolmogoroff equation for radar tracking meter with nonlinear discriminator and second-order smoothing loops, obtaining steady solution by separated variables method

24 p3815 A71-44702

Code conversion and coincidence circuits design for positional digital control systems with combinatorial code producing feedback elements

24 p3805 A71-45154

Second order differential guidance game, formulating strategy for optimal feedback control

24 p3849 A71-45338

FEEDBACK FREQUENCY MODULATION

Pulse frequency modulation feedback system nonlinear discrete equivalence, investigating stability by Liapunov method

09 p1422 A71-22280

Slip vs static error offset for first and passive second order phase locked loop as function of signal to noise ratio via computer simulation

12 p1892 A71-27073

Phase locked loop model configuration derivation to yield same locking signatures as driven oscillators with FM feedback

13 p2037 A71-28605

Broadly tunable liquid dye laser action with narrow line output through use of distributed feedback obtained by spatial modulation of gain and refractive index

13 p2081 A71-29339

Lock-lock loop technique with pulsed oscillator for feedback frequency demodulation and tracking filter operation

14 p2220 A71-30920

Closed phase lock loop FM demodulator design, determining resonant frequency parameters, attenuation factor and low pass filter elements

23 p3650 A71-43094

FEEDERS

Matched impedance microwave vacuum feedthrough

05 p0757 A71-16234

FEEDFORWARD CONTROL

Automatic feedback control systems steady dynamic error reduction by introducing control action forward loop, determining transfer function

01 p0062 A71-10721

Linear sequential circuits feedforward inverse transfer function matrix existence condition and construction procedure

07 p1081 A71-18735

Nonuniform feed effects on height of electrospray surface machining microasperities, investigating linear elliptical interpolator pulse sequence

08 p1296 A71-20851

Distributed parameter systems under load disturbances regulatory control by feedforward feedback and state measures

09 p1422 A71-22282

FEEDING [SUPPLYING]

Hemispherical and spherical pressurized gas bearing design with narrow circumferential feed slot as laminar flow restrictors, predicting static load performance

22 p3551 A71-41667

FEEDING DEVICES

U ANTENNA FEEDS

FEEL

U SENSORY FEEDBACK

FELDSPARS

Apollo 12 lunar rock 12013 preliminary examination and preparation for instrumental analysis, noting feldspar content and igneous nature

03 p0493 A71-14213

North American feldspathoidal and silica unsaturated rocks progression in space and time

04 p0584 A71-15775

Mg 26 isotopic abundance in meteoritic, lunar and terrestrial feldspar by mass spectrometry, suggesting limits on Al 26 in early solar system

06 p0966 A71-17896

Apollo 12 soils composition and derivation, finding feldspathic orthopyroxene rich rock and chemically comparable glass fragments

10 p1672 A71-24393

Antiperthitic intergrowths from single crystal X ray studies of lunar rock plagioclase

13 p2142 A71-29140

K-Ar isotope ages of whole sample and feldspar concentrate from Apollo 11 lunar rock 10003

16 p2633 A71-33349

Fluorine and other trace elements in lunar plagioclase concentrates from Apollo 11 fines, and anorthosite inclusion from Apollo 12 breccia

20 p2922 A71-39383

Lunar plagioclases, tridymite and cristobalite feldspar crystal structure and chemical analyses from Apollo igneous rocks by X ray and electron diffraction

23 p3738 A71-43611

Minor element concentrations and population sources of Apollo 11 and 12 olivine and plagioclase, using microprobe analyses

23 p3738 A71-43614

Mineralogical and petrographic investigation of olivines, feldspars and pyroxenes in Apollo 12 fines and igneous rocks, using optical and X ray diffraction

23 p3741 A71-43631

Oxygen isotope fractionation in Apollo 12 rocks and soils, noting plagioclase ilmenite isotopic temperature

23 p3751 A71-43704

Natural and X ray excited thermoluminescence in Apollo 12 lunar samples and terrestrial plagioclases

23 p3761 A71-43778

FELLOWSHIP AIRCRAFT

U F-28 TRANSPORT AIRCRAFT

FELSITE

U IGNEOUS ROCKS

FELTS

Three dimensional orthogonally woven reinforced felt-yarn composite for low density thermal insulation and chemical vapor deposition

14 p2262 A71-29651

FEMALES

Normal females electrophysiological changes during sensory isolation of water tank variety from EEG, EMG, EOG, EKG and electrodermal measurements, considering cortical activities reduction

21 p3330 A71-40346

FEMUR

Ischemic deafferentation of transversostriated muscle quadriceps femoris in cats contributing to hypokinesia and psychophysiological disturbances

06 p0854 A71-18362

Cancellous bones mechanical properties from compression testing of human femora, vertebrae and cranial bones

06 p0863 A71-18561

Bending and torsional oscillations in rectangular specimens of femur and tibia, calculating elastic and shear moduli of compact bone tissues

13 p2019 A71-28658

Femoral nerve afferent muscle fibers bioelectric activity in anesthetized cats, determining effect of blood circulation level on receptors functional activity

15 p2358 A71-31323

FERMI STATISTICS

U QUANTUM STATISTICS

FERMI SURFACES

Hot electron gas on metal surface under strong heat flux as function of crystal lattice temperature at Fermi level

02 p0332 A71-12196

Tungsten crystal Fermi surface galvanomagnetic coefficients in scattering process by semimipirical scheme

08 p1344 A71-21366

Excess Knight shift due to spin polarization in electron gas by magnetic impurity Fermi contact coupling as function of distance from nucleus

11 p1801 A71-25373

Impurity lifetime broadening due to scattering at Fermi surfaces, calculating Dingle temperature in noble metals

11 p1808 A71-26145

Crystal lattice drag by conduction electrons and Onsager relationship between electroacoustic coefficients valid for arbitrary topology of Fermi surface

21 p3428 A71-41127

Pressure effects on Fermi surface of metals, examining crystal lattice parameters influence on electrons energy spectrum

24 p3839 A71-45168

FERMI-DIRAC STATISTICS

U QUANTUM STATISTICS

FERMIONS

- NT ANTINEUTRINOS
 NT BARYONS
 NT FAST NEUTRONS
 NT HYPERONS
 NT MESONS
 NT NEUTRONS
 NT PROTONS
 NT RECOIL PROTONS
 NT SOLAR PROTONS
 NT THERMAL NEUTRONS

Fermion system phase transition model thermodynamic behavior near critical point region for various interactions

03 p0456 A71-13350
 Fermi particles /fluid/ oscillations in external gravitational field, discussing hydrodynamic equations, acoustic modes and sonic waves due to turbulent effects

05 p0813 A71-16833
 Quasi-means definition and auxiliary system introduction for models including negative four-fermion interaction, solving limiting expressions problem for free energy

05 p0775 A71-16865
 General relativity theory quantization, admitting kink states with fermion-like properties and spin

08 p1335 A71-21362
 Feynman path integration for multiply connected space systems of indistinguishable particles, considering bosons and fermions propagators

10 p1644 A71-24214
 First and second order density matrices calculation of pure state N fermion systems, using higher random phase approximation

19 p3107 A71-38054

FERRATES

Phase relationships in magnesium ferrate-magnesium chromate systems subjected to annealing in air and hydrogen atmospheres

01 p0107 A71-10403

FERRIC ION

Sunspots forbidden Fe I lines, calculating magnetic dipole and electric quadrupole transition probabilities

11 p1830 A71-26112

FERRIMAGNETIC MATERIALS

Phonon-magnon absorption bands temperature dependences in Ni, Co and Li ferrimagnetic spinels, giving graphical data for Curie points

04 p0637 A71-15106

Ferrimagnetic vanadate garnet IR Faraday rotation as function of wavelengths and temperature, considering ions multivalence and multilattice site modifications

06 p0941 A71-18040

High power magnetically tunable microwave interference filters based on spin waves magnetic field dependent dispersion in ferrimagnetic materials

09 p1421 A71-23721

Microwave scattering by DC magnetized ferrimagnetic circular cylinder in rectangular waveguide

14 p2212 A71-30512

Ferrimagnetic components in microwave IC, considering junction circulators, planar phase shifters, etc

16 p2547 A71-33551

FERRITES

Orthoferrite cylindrical magnetic domains in memory and logic devices, considering conductor, angelfish and in-plane rotating field circuits

01 p0047 A71-10211

Electromagnetic wave reflection from ferrite moving domain wall, considering wave separation and permittivity and magnetic susceptibility tensors

01 p0138 A71-10435

Temperature dependence curves and X ray spectrum analyses of different ferrite compositions, indicating absorption band K-edge shift toward shorter wave region

01 p0139 A71-11111

Stainless steel sputter deposits equilibrium phases, determining deposition temperature ranges for austenite and ferrite formation

02 p0267 A71-12884

Broadband mini ferrite T circulator and isolator for X band

03 p0384 A71-13274

German monograph on polycrystalline ferrites studies with quasi-optical resonators in mm wave range

05 p0791 A71-16125

Ordered phases precipitation in ternary and quaternary ferritic alloys, investigating morphology, structure, distribution, coarsening kinetics and mechanical properties

07 p1133 A71-19443

Uniaxial elastic stresses effect on ferromagnetic resonance parameters in polycrystalline ferrites

07 p1177 A71-19497

Chemical composition effect of low carbon alloys metallic matrix on wear resistance in abrasive medium, showing austenitic manganese alloys superiority to martensitic or ferritic alloys

07 p1136 A71-19630

Optimal nonreciprocal waveguide phase shifters using ferrites with rectangular hysteresis loop, considering electromagnetic wave propagation

07 p1079 A71-20074

Short-slot waveguide latching ferrite switch structure, operation principle, phase constants calculation and isolation characteristics

08 p1262 A71-20756

Microwave dual mode reciprocal ferrite phase shifters, deriving insertion phase variations as function of ambient temperature and high average power heating

08 p1262 A71-20760

Dual mode latching reciprocal ferrite microwave phase shifter, discussing operation principles, design and performance

08 p1262 A71-20764

Ferrite microstrip microwave phase shifters with transverse and longitudinal magnetization, calculating diamagnetic and permeability tensor effects

08 p1263 A71-20768

Polarization of LF oscillation branch of uniaxial ferrites in noncollinear phases analyzed by four column matrix, considering magnetic moments terminal points

09 p1507 A71-22291

Large capacity ferrite core buffer memory for spacecraft telemetry temporary data storage, using access circuitry with multichip and thin film circuits

09 p1421 A71-23735

Ferrite resonator coupled to microwave transmission line, deriving instability effects threshold power level for comparison with measurement

10 p1584 A71-24725

Gain and noise characteristics of reactive phase/amplitude modulation ferrite amplifier as function of pumping power and resonator coupling

12 p1886 A71-26845

Eighteen layer hexagonal ferrite magnetic properties in various fields and temperatures, noting magnetization and crystal structure

12 p1943 A71-26862

Second harmonic generation in magnetized ferrite, considering nonlinear interaction between electromagnetic field and medium

12 p1879 A71-26996

Coplanar-guide and slot-guide junction circulators on ferrite substrate magnetized perpendicular to surface

13 p2037 A71-28473

Cylindrical waveguide with three differential phase shift sections, deriving microwave output magnitude and polarization for comparison with ferrite experiment

13 p2037 A71-28604

Magnetostriction in cobalt and nickel-cobalt ferrites from room temperature to 300 C

15 p2426 A71-31514

Ferritic steels weldability, establishing relations between transition points and cold crack formation

13 p2417 A71-32662

Chemical composition effect of low carbon alloys metallic matrix on abrasive wear resistance, showing austenitic manganese alloys superiority to martensitic or ferritic alloys

16 p2593 A71-33626

High power microwave phase shifter, using beryllium oxide filler ceramic dielectrics to obtain thermal coupling between ferrite element and waveguide wall

17 p2713 A71-34396

Strength and toughness optimization in high strength stainless steels by austenitizing and removing delta ferrite by isothermal transformation

17 p2756 A71-34491

Ferrite core memories for information storage of digital computer onboard Eole satellite, discussing design and reliability measures

18 p2891 A71-36560

Mass spectrometric investigation of plasma created in atomization of Ni and Y ferrites by laser radiation

19 p3110 A71-37142

Design algorithm for gyrotropic waveguide consisting of symmetrical rectangular coaxial with magnetized ferrite rods

19 p3019 A71-38333

Electron beam hearth refined ferritic stainless steel, presenting weldability with gas tungsten arc process

21 p3388 A71-40623

Cr and Cr-Ni ferritic and austenitic steels, investigating high temperature nitriding for intensifying nitrogen diffusion saturation

21 p3389 A71-41098

Ferrite coercimeter with attached electromagnet and compensation winding, deriving analytical expressions for demagnetization and compensation currents

22 p3521 A71-41767

Ferrite and dielectric element waveguide phase shifters with rectangular hysteresis loop, deriving differential phase and attenuation constants for wave propagation

22 p3512 A71-42308

Mn-Zn ferrite for pulse transformers, discussing permeability and temperature range

23 p3650 A71-43348

Electromagnetic wave reflection from ferrite plate in external alternating magnetic field, showing frequency change due to moving domain wall

23 p3645 A71-43568

Opaque mineral compositions in Apollo 12 lunar rocks, noting ilmenite, spinels, native iron and troilite

23 p3739 A71-43620

Phase shift and attenuation measurements in high power microwave ferrite tetrodes circuits, using semiconductor transducers /digadectors/

24 p3809 A71-44871

FERROELECTRICITY

Spontaneous polarization measurement of ferroelectric Rochelle salt near Curie point, using nuclear magnetic resonance for phase transitions

04 p0637 A71-15548

Monolithic optically written and electrically read semiconductor-ferroelectric memory device employing single crystal barium titanate

07 p1067 A71-19261

Ferroelectric barium titanate ceramics technology for capacitor fabrication

09 p1483 A71-23394

Optical phonons and temperature dependent phase transitions in paraelectric antimony and ferroelectric sulfonide semiconductors, using polarized IR and Raman spectra measurements

21 p3428 A71-40775

Thin film oxide, ferroelectric and bismuth titanate dielectrics for high capacitance microwave IC technology

23 p3651 A71-43429

Curie point region automatic thermal stabilization effectiveness of cylindrical/disk shaped segnetoceramic elements in electrostrictive constant magnetic field converters

24 p3828 A71-45164

FERROMAGNETIC FILMS

Thin uniaxial ferromagnetic metal films blocking curve verification using rotational hysteresis and transverse susceptibility measurements

07 p1180 A71-20171

Longitudinal and transverse differential permeabilities of discrete regions in thin ferromagnetic films, accounting for material inhomogeneities

11 p1809 A71-26546

Modified Landau-Lipschitz equation of thin ferromagnetic film for slowly reversing magnetic fields solved by interpolation, discussing magnetization curve subrelaxation segment

11 p1809 A71-26547

Power losses and construction of microwave switch, using orthogonal striplines around thin ferromagnetic film on nonmagnetic substrate

11 p1741 A71-26551

FERROMAGNETIC MATERIALS

NT FERROMAGNETIC FILMS

NT MAGNETITE

NT PERMALLOYS [TRADEMARK]

Magnetoelastic anisotropy and low temperature annealing effects on coercive force of ferromagnetic Fe-Ni foils

01 p0138 A71-10669

Quantum statistical analogy between laser threshold region and second order phase transition of ferromagnets

03 p0440 A71-14197

Electron mobility and thermal emf in nondegenerate ferromagnetic semiconductors, considering entrapment of electrons by magnons at temperatures below Curie point

04 p0636 A71-15102

Ferromagnetic dielectric composites physicochemical properties, considering thermal conductivity, density, linear expansion, resistivity, thermal stability and magnetic permeability

04 p0618 A71-15570

Faraday rotation near ferromagnetic critical temperature of chromium bromide, discussing scaling laws validity and experimental confirmation

04 p0637 A71-15796

Conducting and ferromagnetic liquids thermoconvective waves, considering disturbance propagation process in equilibrium state with constant entropy gradient

04 p0628 A71-15809

Field distribution in multiple-opening ferromagnetic digital computer elements, using linear approximation integral method

06 p0872 A71-17497

Subdomain magnetic particles ferrofluid colloidal dispersions, for energy conversion devices, viscous dampers, accelerometers, gyroscope supports and specific gravity meters

07 p1178 A71-19611

Temperature effects on energy dissipation during vibration in ferromagnetic and nonferromagnetic metals, comparing damping capabilities for homologous temperatures

08 p1306 A71-21119

Static tensile stresses effect on magnetized ferromagnetic materials damping properties explained by anisotropic microplastic strains dissipating energy during bending vibration

08 p1306 A71-21120

Energy conversion efficiency from microwave into magnetostatic waves propagation inside cylindrical ferromagnetic substance

08 p1265 A71-21276

Magnetic recording device for defect field recording by ferromagnetic tape polarization

08 p1273 A71-21900

FERROMAGNETIC RESONANCE

- Macroscopic model of impurity electron centers for strong exchange interactions in ferromagnetic and paramagnetic semiconductors 09 p1508 A71-22880
- Coulomb impurity centers in paramagnetics and ferromagnetics at Curie temperature with spin-electron exchange interaction 09 p1508 A71-22881
- Nondestructive magnetic method for measuring longitudinal residual stress in outer portions of ferromagnetic cylindrical bars 12 p1974 A71-26948
- Ferromagnetic and antiferromagnetic single crystals thermal conductivity at 193-673 K, analyzing anomalies on basis of magnetic and structural characteristics 12 p1944 A71-27661
- Book on materials for magnetic functions covering magnetic materials and devices, magnetic phenomena, parameters and interrelations, ferrites chemistry, microstructure and processing, etc 13 p2112 A71-29443
- Ferromagnetic shields effectiveness against magnetic fields, permitting solutions to nonlinear shielding problems 15 p2377 A71-32369
- Heisenberg ferromagnet magnetic and thermodynamic properties in random phase approximation, determining magnetization and susceptibility with Green function theory 21 p3476 A71-40897
- Eddy current field formation of defect on extended surface crack in ferromagnetic and nonferromagnetic metals, investigating superposed transformer detector inductor coil effects 22 p3529 A71-41770
- Ferromagnetic Co phase nondestructive determination in hard powdered-metal alloys by permanent magnet ponderomotive force measurement based on relationship to ferromagnetic alpha phase 22 p3561 A71-41775
- LF eddy current bridge to measure small magnetic permeability changes in weakly ferromagnetic materials, applying to nondestructive tests of austenitic stainless steels 23 p3681 A71-43193
- Aerospace industry magnetic particle inspection problem identification in complex ferromagnetic structures 24 p3831 A71-45277
- FERROMAGNETIC RESONANCE**
- Fe 57 nuclei longitudinal and transverse relaxation in yttrium iron oxide sublattices at various temperatures and magnetic field strengths 05 p0794 A71-16878
- Uniaxial elastic stresses effect on ferromagnetic resonance parameters in polycrystalline ferrites 07 p1177 A71-19497
- LF ferromagnetic resonance in anisotropic polycrystalline thin magnetic films, noting dependence on magnetization inhomogeneity 18 p2955 A71-36940
- Ferromagnetic electron spin resonance spectra of Apollo 11 lunar samples, using model for polycrystalline spectra simulation 23 p3734 A71-43242

FERROMAGNETISM

- Generalized Watson sums calculation with application to magnetization of anisotropic ferromagnet for Callen type decoupling schemes 09 p1506 A71-22149
- Ferromagnetic and antiferromagnetic characteristics relation to electromagnet and spin waves coupling in nonresonant and resonant regions 10 p1656 A71-24317
- Heisenberg ferromagnet with applied external magnetic field, investigating thermodynamic properties near Curie point 11 p1807 A71-25558
- Temperature gradients effect on density distribution in material near critical point, using classical and scaling-law theories and Ising model 12 p1929 A71-27031
- Electron spin resonance studies of Apollo 11 and 12 lunar soil samples, determining ferromagnetism due to Fe particles 23 p3763 A71-43797

FERROUS METALS

- Bismuth oxide and iron oxide equimolar mixtures solid state reactions, determining rates from integrated X ray diffraction and activation energies 08 p1318 A71-20699

FERTILIZERS

- Detonation sensitivity of ammonium nitrate containing fertilizers, compared with metadinitrobenzene in powder form 10 p1658 A71-25070

FET [TRANSISTORS]

U FIELD EFFECT TRANSISTORS

Feynman Diagrams

- Feynman path integration for multiply connected space systems of indistinguishable particles, considering bosons and fermions propagators 10 p1644 A71-24214

Canonical quantization, discussing Schroedinger equation, Hamilton-Jacobi theory, Feynman integrals and sandwich conjecture 16 p2609 A71-33258

Production cross section of Lee-Wick hypothetical massive electromagnetic bosons by muons at high energy, giving Feynman diagrams 17 p2785 A71-34750

FIBER OPTICS

- Liquefied and solidified gas IR measurements describing versatile optical cell 02 p0250 A71-12133
- Cladded fibers propagation modes launching coefficients evaluation by Gaussian field laser beam 03 p0433 A71-13170
- Fiberoptic indicator-dilution assessment of myocardial function 03 p0362 A71-13329
- Optical fibers scattering loss measurement, describing Si solar cell integrating cube scattering detector 03 p0424 A71-13638
- Light propagation in gas filled pipe with uniform heat flux through wall under forced convection, determining lens efficiency relation to length 04 p0628 A71-15811
- Round multiple fibers for manufacturing vacuum-tight heat-molded fiber-optical plates 06 p0897 A71-17532
- Optical fiber index profiles for long distance light transmission, comparing single and multimode, rectangular and parabolic guides 07 p1159 A71-19174
- Fiber optic faceplates for contrast enhancement under high ambient light conditions for commercial and military cockpits, eliminating ghost, halo and direct sunlight problems 07 p1107 A71-19175
- Light attenuation and depolarization measurements on glass fibers in index matching oil 07 p1159 A71-19212
- Fiber optic laser devices properties and potential applications as amplifiers, logic elements, active mode selectors and intense light sources 07 p1124 A71-19781
- Statistical analysis of fiber optics imagery, considering resolution difference between static and dynamically scanned bundles 08 p1334 A71-21180
- Holography with fiber optics, allowing three dimensional photography of inaccessible objects in biomedical research and other applications 08 p1291 A71-21400
- Materials fatigue disintegration process visual examination for crack development kinetics, using fiber optics 09 p1454 A71-22316
- Coupled fiber lasers maximum energy transfer between passive conductors, determining minimum pulse duration 09 p1464 A71-23112
- Solid propellant burning surface irradiance measurement, using optical lightpipe and radiation detector [AIAA PAPER 71-469] 11 p1859 A71-26250
- Fiber optics for spectroscopic illumination, discussing absolute and angular transmission measurements and optical angular transfer function calculation 12 p1905 A71-26806
- Electrical fiber plates as high resolution conductive arrays for storage and display in electron beam addressed systems 14 p2250 A71-31033
- Applied optics, reviewing homogeneous and inhomogeneous optical conversion elements, fiber and Fresnel optics, lens properties, programmed optical reliefs, holography, etc 15 p2410 A71-32299
- Holographic fiber optics image-guiding structures preparation in sensitized polymethyl methacrylate cast sheet by refractive index gratings pair recording 18 p2946 A71-35852
- Mechanical properties in glass fiber optics, measuring tensile strength and modulus, Poisson ratio and fatigue 18 p2939 A71-36074
- Dynamic display of abstract visual perspective using fiber optic material as discrete lines of light-emitting elements 18 p2918 A71-36075
- Wideband fiber waveguide communication systems for optical frequencies, considering information carrying capacity limitation by components available for repeaters and terminal equipment 18 p2883 A71-36995
- Optical coupling of degenerative modes in two parallel dielectric waveguides, applying to slab guides and fibers crosstalk problem 19 p3014 A71-37214
- Weakly guiding glass fiber parameters design formulas and functions for optical communication, considering propagation constant, mode delay, cladding field depth and power distribution 22 p3576 A71-42557

Pulsed signal secondary forward scattering in optical fiber transmission lines 23 p3646 A71-43968

FIBER STRENGTH

- High modulus graphite fiber composites, considering production, properties, utilization, availability and price/performance [SME PAPER EM-70-114] 01 p0109 A71-11251
- Anisotropic polycrystalline carbon fiber tensile strength and bending behavior, interpreting inelastic characteristics from single filament experiments 02 p0273 A71-11945
- Composite materials with high strength short discontinuous fibers, considering manufacturing processes and mechanical properties 02 p0273 A71-12478
- Carbon base multifiber yarns for metal matrix composites reinforcement, considering fiber strength degradation minimization methods 03 p0449 A71-14419
- High strength metal and ceramic reinforcement fibers, discussing properties and fabrication for plastic composites 06 p0916 A71-18088
- Parachute weight, configuration and strength correlations for tradeoffs and design 07 p1017 A71-18900
- Tensile, shear, bulk density and electrical properties of pitch based strain graphitized glassy carbon fibers [PLASTICS INST. PAPER 13] 08 p1319 A71-20897
- High strength flexible carbon fabrics from oxidized polyacrylonitrile yarns for reinforced plastic laminates [PLASTICS INST. PAPER 39] 08 p1319 A71-20900
- High voltage electron microscopy of internal defects in carbon fibers, considering fiber strength [PLASTICS INST. PAPER 10] 08 p1297 A71-20921
- Iron and fcc metal composite wires, determining fiber thickness and strength relationship 08 p1323 A71-21588
- Thermally stable fibers fabricability and properties relation to polymer chemical structure and tensile strength 09 p1481 A71-22247
- Reinforcement theory fiber filled thermoplastics, considering fiber strength and length [PLASTICS INST. PAPER 2] 09 p1481 A71-22341
- Deformation and strength characteristics of fiber composite thermoplastic resins in terms of stiffness and reinforcement factors [PLASTICS INST. PAPER 3] 09 p1481 A71-22343
- Specimen width effect on ultimate fiberglass tensile strength for specimens cut from tubes and oriented at certain angle to symmetry axes 09 p1482 A71-22504
- Mechanical strength and elastic properties under tension and bending of boron fibers, noting dependence on surface defects 09 p1482 A71-22823
- Microstructural defects responsible for tensile strength reduction in carbon fibers subjected to high temperature graphitization, using transmission electron microscopy 09 p1483 A71-23653
- Ultrasonic modulus vs strength of high modulus fiber reinforced epoxy matrix composites in non-destructive testing 09 p1484 A71-23687
- Carbon fiber strength/microstructure relationship, examining failure mechanism initiated by graphite crystallites shearing 10 p1634 A71-24446
- Transverse impact resistive graphite fiber reinforced plastic (GFRP) lightweight sandwich panels and beam structures, using thin inner core facings 11 p1846 A71-25417
- Boron and carbon fracture and debonding in epoxy matrix, using acoustic emission analysis 11 p1772 A71-26392
- Electron paramagnetic resonance atomic scale stress analysis of high polymer fibers and rubber, measuring chain scission and bond rupture for different loading histories 13 p2091 A71-28440
- Fiber strengthening of Cu-Fe-Cr wire by cold drawing and annealing, discussing age hardening process of chromium ferrite needles in ductile Cu matrix 13 p2088 A71-29402
- High modulus organic fiber for aerospace use, considering fiber-epoxy composite mechanical and physical properties 14 p2263 A71-29658
- Tensile strength of boron, silicon carbide coated boron, silicon carbide, stainless steel and tungsten fibers after exposure to air, argon and aluminum at high temperatures 15 p2435 A71-32440
- Specific strength of unidirectional fiber reinforced metal matrix composites, showing dependence on volume ratio and transmission coefficient 16 p2592 A71-33412

Large plastic strains in fiber in sheet bending for wide angle range, using Hill theory
17 p2816 A71-34298

Fiber to matrix modulus of elasticity ratio for two dimensional plane stress composite by finite element and moire strain analyses
[SESA PAPER 1826A]
17 p2761 A71-34527

Polymer type, temperature, crystallinity and orientation effects on fracture mode, discussing macroload carrying capacity, nylon fiber tie chains and molecular behavior
18 p2939 A71-35889

G structure tensors integrability and fiber extensions, using differential geometry
18 p2976 A71-36097

Microradiographic and acoustic evaluation of fracture in boron filament aluminum matrix composite under tensile stress
19 p3081 A71-37903

FIBERGLASS
U GLASS FIBERS

FIBERS
NT CARBON FIBERS
NT COTTON FIBERS
NT GLASS FIBERS
NT HAIR
NT NYLON [TRADEMARK]
NT RAYON
NT REINFORCING FIBERS
NT SYNTHETIC FIBERS

Porous metal fiber laminar vacuum insulation, calculating steady state heat and mass transfer
01 p0179 A71-10615

Fibrous body optimum material distribution, considering arbitrary density continuous three dimensional bar network
01 p0177 A71-12185

Small tissue equivalent ionization chamber quartz fiber electrometer dosimeter system, for use as space qualified radiation detection instruments
02 p0250 A71-12136

Neuromuscular spindles sensory information processing, determining fibers selective data transmission functions by frequency meter and model for electrical and mechanical properties
03 p0366 A71-12977

Ni coated carbon fibers tensile properties, examining thickness, stress-strain curve, plasticity and grain size
03 p0448 A71-14185

Unidirectionally aligned fiber phase solidified eutectic composites model, discussing high temperature rupture and creep properties
08 p1323 A71-21585

Graphite fiber surfaces atomic composition data, using Auger electron spectroscopy in ultrahigh vacuum low energy electron diffraction system
11 p1788 A71-25633

Fibrous composite structure stress analysis procedures, considering nonisotropy and brittleness effect
[ASME PAPER 71-DE-2]
12 p1977 A71-27321

Unidirectional fiber composites impact resistance, showing matrix modulus, fabrication process, fiber and void volume ratios and microresidual stress effects
14 p2264 A71-29920

Ceramic fibrous materials for high temperature insulation, discussing practical approach to obtain lower thermal conductivity
18 p2939 A71-36668

Spherulitic linear polyethylene rod cold drawing, observing fibrous structure formation by light and electron microscopy and X ray scattering
19 p3084 A71-37650

Epitaxial metal film formation on Al-Ni fibers in Al matrix during electropolishing
21 p3387 A71-40456

Earth pointing satellites gravity gradient stabilization by thin inextensible fibers with end tip masses
22 p3590 A71-42779

FIBRILLATION
Nonactomyosin component differentiation in potassium chloride insoluble myofilaments in vertebrate smooth muscle cells
24 p3794 A71-44424

FIBRIN
Human coronary arteries fibrinolytic activity, considering histochemical and quantitative methods for arteriosclerosis and occlusion investigations
02 p0200 A71-12416

Natural or endogenous fibrinolysis and its pharmacological enhancement as possible approach to prophylaxis of vascular occlusions
02 p0200 A71-12417

Blood liquid state control in sanguiferous canal as function of humoral feedback in coagulation, fibrinolytic and anticoagulation systems
13 p2010 A71-28718

Coagulation and fibrinolysis changes after physical exercise in males with atherosclerosis, noting fibrinolytic response differences with age
18 p2853 A71-35918

FIBROBLASTS
NT COLLAGENS

Cytophotometric study of DNA content in fibroblasts from human blood vessel walls, discussing cell proliferation and ploidy
09 p1392 A71-22609

FIBROUS MATERIALS
U FIBERS

FIDELITY
U ACCURACY

FIELD EFFECT TRANSISTORS
High input impedance wideband frequency measurement probe with bipolar and unipolar transistor circuits
01 p0051 A71-10284

Field effect photocurrent maximum in thin film semiconductors below Debye radius associating hole capture by recombination centers
01 p0139 A71-10781

Basic and special field effect transistor design and operation, discussing performance and fabrication
02 p0229 A71-11810

P-channel MOSFET tetrodes static and dynamic characteristics compared to conventional MOS triode, considering transfer and gate threshold voltage
02 p0229 A71-11811

Inner FET and FET static and dynamic inverters in digital IC, discussing switching characteristics, gates, memory cells, etc
02 p0228 A71-11812

FET insulating layer electrical properties requirements, considering threshold voltage, dielectric constant, breakdown voltage and insulated gate FET instabilities
02 p0229 A71-11813

FET as voltage controlled linear resistors, discussing use in attenuators, automatic gain control, volume compressors and RC networks frequency control elements
02 p0229 A71-11814

Gallium arsenide devices in microwave communications, discussing Gunn oscillators, FET, varactors and radar applications
02 p0231 A71-12049

FET chopper amplifier for low level DC signals from thermocouples, strain gauge bridge circuits and weak transducer sources
03 p0384 A71-13275

Semiconductor developments, discussing field effect transistors, MOS, microwave components, piezoelectric effects, optoelectronics and galvanomagnetism
03 p0384 A71-13534

Field effect transistors internal source and drain resistances measurement, using characteristic tracer
04 p0558 A71-15084

Active directional nanosecond pulse filter design based on hybrid technique, using metal semiconductor field effect transistors [MESFET]
04 p0559 A71-15698

MOSFET transistors instabilities due to charge exchange near oxide-silicon interface states, determining energy levels distribution and time constants
05 p0791 A71-16165

Field effect transistors with nonuniform doping profiles along channel, calculating carrier accumulation and space charge limited current flow by two dimensional model analysis
05 p0791 A71-16166

GaAs FET design and performance, discussing fabrication techniques and scattering and noise parameter measurements
05 p0729 A71-16916

C band field effect transistor amplifiers with stable power gain, discussing circuit analysis, design parameters and test results
05 p0729 A71-16917

MOSFET inverter pulse response analysis using hyperbolic functional description
05 p0726 A71-17086

Differential drain resistance calculation for junction field effect transistors
07 p1070 A71-18869

N and p junction field effect transistor [JFET] gate current measurement leading to understanding of impact ionization mechanism and field distribution
07 p1081 A71-20542

Noise behavior of Schottky barrier gate FET at microwave frequencies, discussing effects of carrier velocity saturation and parasitic resistances on noise parameters and measurement method
08 p1261 A71-20741

MOSFET data systems evolution for IMP, discussing effects on system design and reliability approach
08 p1267 A71-21844

FET transistors on epitaxial GaAs as input and output transducers for acoustic surface waves
09 p1417 A71-22755

Microwave front end designs for low noise operation, discussing FET applications and mixer conversion loss reductions
11 p1731 A71-25673

Memory behavior in floating gate avalanche injection MOS structure, considering long term charge storage in insulated gate field effect device
13 p2036 A71-28045

FIELD EMISSION

Doping dependent mobility analysis of junction FET, calculating drain current and transconductance
13 p2037 A71-28474

Power gain of Q-band GaAs FET with Schottky-barrier gate, giving amplifier and oscillator designs
14 p2210 A71-29800

Characteristics of field effect and surface barrier GaAs transistor [MESFET] operating at 4.2 K, noting very low temperature hyperfrequency amplifier application
14 p2212 A71-30439

Channel width effect on FET transconductance in low current operation
14 p2214 A71-30634

Analog computer application for determination of charge centers in multilayer gate structure of variable threshold FET, deriving equations yielding position of internally stored charge
15 p2462 A71-32639

Three color photoelectric photometer improvements by introducing synchronous signal detection and electronic gates by field effect transistors
16 p2579 A71-33434

Low noise FET amplifiers for earth station radio receivers
17 p2715 A71-34687

German monograph on field effect transistors as controllable resistors with applications in adjustable amplifiers and dampers, covering nonlinear harmonic distortion and control dynamics
18 p2887 A71-35961

Gridistor microwave FET for space communication equipment, combining advantages of FET and bipolar transistors
18 p2892 A71-36565

MOS field effect transistors operation and DC characteristics including threshold voltage and substrate doping effects
19 p3027 A71-37562

Free carrier surface density and mobility in large MOS transistors from conductivity and Hall measurements
19 p3028 A71-37564

Digital integrated circuits technology with MOS transistors packed on crystal wafer without isolation diffusions
19 p3028 A71-37566

Storage arrays of high operational speed with field effect transistors, evaluating contributions to access and cycle times
21 p3354 A71-40734

Microwave MESFET HF circuits, discussing noise factor advantage over bipolar transistors in low noise preamplifiers
21 p3355 A71-40743

Microwave Si MESFET for 15 GHz oscillation with reduced gate metallization resistance and pad parasitics, improving gain and noise figure
22 p3520 A71-41683

Neutron irradiation effects on Si p-n junction field effect transistors I-V characteristics, charge distribution in space charge region and transconductance
22 p3586 A71-42297

FET nonlinear and cross modulation characteristics, basing performance prediction on power series approximation to measured LF transfer characteristics
23 p3649 A71-43068

Field effect devices mathematical modeling for computer aided circuit design, using unified approach
23 p3649 A71-43069

Thermal feedback modification of Si JFETs AC and DC characteristics at low operating temperatures
23 p3649 A71-43070

Silicon thin film on sapphire for bipolar and MOSFET transistors for microwave IC and subnanosecond switching circuits
23 p3715 A71-43434

Frequency and power limits of field effect triodes, noting application to gridistor for millimeter waves
23 p3653 A71-43950

Ion implantation technique utilization for reducing MOSFET devices threshold voltage and gate drain capacitance
24 p3808 A71-44725

Substrate effect on MOSFET noise and y-parameters using wave equation
24 p3862 A71-45354

Input admittance, drain noise and induced gate noise measurements in search for excess gate noise in large geometry MOSFET
24 p3863 A71-45355

FIELD EMISSION
Field-ion, field emission microscopy - Conference, University of Florida, March 1970
02 p0287 A71-12732

Polyatomic organic adsorbates effect on field emission total energy distribution from W and Mo surfaces, discussing electronic and phononic spectra
02 p0297 A71-12733

Thermal characteristics of emission and work functions of spherical Ta single crystal faces by Martin microscope measurements
15 p2453 A71-32644

- Ti adsorption on W and Re, measuring field emission average work function at various Ti layer thicknesses 17 p2791 A71-34855
- MOS sandwich grid diode for gas ionization and field electrons generation at solid-gas phase boundaries 17 p2717 A71-35448
- FIELD IONIZATION SOURCES**
- U BRUSHES**
- FIELD MODE THEORY**
- Solar alpha effect dynamo effect model, determining nonaxisymmetric magnetic field generation 18 p2960 A71-35936
- FIELD STRENGTH**
- NT ELECTRIC FIELD STRENGTH**
- NT MAGNETIC FLUX**
- Radio galaxies emission source, examining Patchy model for prestellar matter magnetic field strength 01 p0150 A71-10063
- Electromagnetic wave nonlinear propagation in semiconductors, considering field amplitude and electron temperature for strong electron phonon interaction and degenerate semimetals 01 p0138 A71-10434
- Radiator systems field calculation based on waveguide and resonator excitation method, noting field amplitudes in two and three dimensional arrays 01 p0038 A71-11202
- Natural fluctuations sources intensity in annular lasers taking into account field strength dependence 02 p0261 A71-12507
- Jupiter decimetric emission circular polarization, observing equatorial magnetic field strength in radiation belt 02 p0317 A71-12868
- Laser optical field intensity correlation function determination from photoelectric counting distribution measurements 03 p0436 A71-13876
- LF radio waves field strength monitoring for study of ionospheric effects due to celestial X rays 05 p0721 A71-16442
- Geomagnetic secular variation as main field drift superposition and strength changes, reflecting drift and convection in earth fluid core 07 p1103 A71-19763
- Field intensity of plane electromagnetic wave diffracted at conducting sphere 08 p1252 A71-20735
- Average electron density profiles for forecasting MF sky waves field strengths, using nocturnal ionospheric measurements 10 p1575 A71-23866
- Flush mounted annular slot missile antenna theory application to near zone field strength instrumentation calibration and plane wave electromagnetic field pulse response determination 10 p1580 A71-25071
- Earth-ionosphere spherical waveguide, calculating mean and differential phase velocities and field amplitude of low frequency waves 11 p1731 A71-25774
- Radio interference suppression rules optimization, using mathematical model to characterize interference voltage, antenna sensitivity and radio transmitter field strength 11 p1733 A71-26339
- Air shower radio emission properties, presenting electric field strength measurements at various frequencies 13 p2127 A71-28104
- Sunset and sunrise vertical displacement rate of lower ionosphere from spectral analysis of field strength at 236, 557 and 1277 kHz 13 p2059 A71-28241
- Narrow band atmospheric radio noise burst average and rms field strength measurement 13 p2033 A71-28900
- Field strength standards and calibrations for frequencies from audio to 1 GHz range, discussing uncertainties 14 p2205 A71-30980
- Radiator system field calculation based on waveguide and resonator excitation method, noting field amplitudes in two and three dimensional arrays 17 p2697 A71-34254
- Plane infinite horn antenna with small aperture angle coupled to waveguide, discussing wave excitation and field strength 17 p2697 A71-34259
- Field strength of radio emission from cosmic ray showers at 3.6 MHz, stressing data analysis procedure 17 p2732 A71-34623
- Lense-Thirring spin-spin gravitational forces measurement between disks and cylinders, using weak field low velocity relativity approximation 20 p3292 A71-39409
- Venus atmosphere decimeter wave field intensity fluctuations and refraction coefficient variations 20 p3297 A71-39627
- Earth-ionosphere spherical waveguide, calculating mean and differential phase velocities and field amplitude of LF waves 22 p3509 A71-41542

- Laser resonator natural field amplitude fluctuation calculation based on two- and four- level models for photon number dispersion 23 p3685 A71-43560
- FIELD THEORY [ALGEBRA]**
- NT CUBIC EQUATIONS**
- NT QUADRATIC EQUATIONS**
- Principal homogeneous spaces above elliptical curves over discretely normalized local field 06 p0918 A71-17572
- FIELD THEORY [PHYSICS]**
- Ellipsoidal plasmod equilibrium in external HF field, calculating rotation rate and potential energy 01 p0132 A71-10151
- Earth gravity anomalies calculation, discussing normal field structure 01 p0074 A71-11060
- Complementary field component of radiation from Cassegrain subreflector 01 p0055 A71-11172
- Nondissipative micromorphic media field equations derivation, applying variational principle to theory of deformable bodies 01 p0177 A71-11372
- Electromagnetic scattering by oblique circular cylinder, deriving field equations 02 p0215 A71-12145
- Equations of motion of heavy gyrostat with fixed point in uniform force field 03 p0457 A71-13580
- Auroral oval transverse magnetic disturbance, examined as field aligned current models 03 p0419 A71-14523
- Static axially symmetric gravitational field equations, presenting Weyl solutions for standard coordinates 04 p0625 A71-14730
- Static charged dust distributions, investigating general relativity field equations with electromagnetic stress tensor 04 p0625 A71-14732
- Book on nonequilibrium /irreversible/ thermodynamics covering field theories, balance equations, continua, variational principles, energy dissipation, entropy, etc 04 p0626 A71-15600
- Relativistic electromagnetic field analysis, using fluid dynamic approach 04 p0628 A71-15917
- Chronometrically invariant formulation of Petrov gravitational fields algebraic classification at space-time fixed point in general relativity 05 p0781 A71-16182
- Expanding universe magnetic field origin, examining Batchelor condition for spontaneous appearance in turbulent conducting fluid motion 05 p0809 A71-16470
- Auroral phenomena, using dimensional analysis to examine MHD equations for fields and plasmas in magnetosphere 06 p0888 A71-17286
- Field distribution in multiple-opening ferromagnetic digital computer elements, using linear approximation integral method 06 p0872 A71-17497
- Complex incident fields analysis by ray diffraction method, using set of simple sources with same amplitude and phase characteristics as actual incident field 06 p0868 A71-17728
- Sun daily mean-interplanetary polarized magnetic fields correlation, using source surface model 06 p0968 A71-17920
- Purely azimuthal magnetic toroidal-meridional component poloidal field conversion by slow precessional motion superimposition on rotating fluid under uniform current distribution 06 p0894 A71-18016
- Nondipole geomagnetic field effect on magnetosphere boundary, presenting graphs for distance dependence on polar angle 06 p0895 A71-18271
- Sonic boom near field behavior, discussing N wave focusing [ALAA PAPER 71-185] 06 p0886 A71-18624
- Action at distance gravitation as alternative to general relativity, discussing gravitational frequency shift and light bending 07 p1189 A71-18747
- Functional method application to ultrarelativistic particles in external fields quantum electrodynamics, discussing electromagnetic field superposition 07 p1162 A71-20549
- Conformally flat universe class with short ranged scalar gravity, satisfying Einstein field equations 08 p1334 A71-21360
- Near field approximation for strong gravitational fields, noting close similarities to electromagnetic fields 09 p1493 A71-22803
- Gravitational field equations in classical Newtonian mechanics within framework of macroscopic gravitation theory 09 p1523 A71-23074

- Nonlinear electrostatic theory Lagrangian analogous to gravitational Lagrangian from correspondence between Maxwell electromagnetism and Einstein gravitation 10 p1667 A71-23815
- Scalar theory for nonstatic gravitational fields, using tensor and linearized equations 10 p1641 A71-23975
- Dynamically symmetrical gyrostat steady state motion stability in force field of two fixed centers, using Raus-Liapunov theorem 10 p1683 A71-24579
- Lunar libration presented as general rotation of solid body in external force field 11 p1822 A71-25685
- Optimal flight of material point in central field of forces subject to controlled small thrust 12 p1957 A71-26632
- Field aligned anisotropy for auroral ionospheric energetic ions, calculating pitchangle distributions 12 p1899 A71-26885
- Auroral electron temperature, noting field aligned energy transport current effects 12 p1899 A71-26887
- Milky Way galaxy radio halo, investigating background brightness distribution and local spiral arm magnetic field structure 12 p1963 A71-27078
- General relativity gravitational field equations, giving composite sphere internal structure for core and shell 12 p1932 A71-27643
- Field correlation diffraction theory of symmetrical microwave Cassegrain antenna, calculating main reflector focused field by spherical wave expansion 13 p2028 A71-27992
- Radiation field description with spatial complex variables, considering application to scattering and waveguide problems 14 p2209 A71-29567
- External field perturbations by local inhomogeneities in elastic medium, deriving expressions for interaction energy and forces between defects 14 p2332 A71-30869
- Variable mass body rotational motion stability in central Newtonian field with gyroscope on symmetry axis 14 p2275 A71-30880
- Ferromagnetic shields effectiveness against magnetic fields, permitting solutions to nonlinear shielding problems 15 p2377 A71-32369
- Field theoretic approach of Jordan-Brans-Dicke theory within Lorentz invariant gravitation theories framework, solving linear motion equations inconsistency 15 p2451 A71-32646
- Kerr-Newman black hole as generic final state of gravitational collapse developed from Schwarzschild geometry and mass, angular momentum and charge parameters 16 p2631 A71-33177
- Physical meaning of fifth coordinate in five dimensional field theory, discussing relationship as parameter metric of de Sitter four dimensional space-time manifold 16 p2608 A71-33223
- Spin weighted field functions for group SU [2] in gravitational radiation problems of general relativity, using Newman-Penrose formalism 16 p2609 A71-33260
- Natural symplectic structure for twistors on cotangent bundle over space-time manifold, considering Lagrange identity for Jacobi fields 16 p2609 A71-33264
- Static electromagnetic fields in general relativity obtained for space-time metrics of group G automorphisms, considering Rainich unified field theory equations 16 p2610 A71-33265
- Spherically symmetric initial solutions for coupled gravitation and massless field system generated by physical particle source 16 p2610 A71-33266
- Classical gravitational field equations modification for virtual quantized matter, taking into account additional mass due to attractive forces 16 p2610 A71-33271
- Einstein field equations solution for universe filled with perfect fluid of position-dependent density 16 p2611 A71-33277
- Gravitational fields invariant evolution, noting Einstein equations constraints effects on initial values of variables 16 p2611 A71-33280
- Gravitational radiation existence from Riemann curvature tensor Fourier transform measurements, giving antenna directivity theory 16 p2612 A71-33283
- Brans-Dicke gravitation theory, applying units transformation to field equations 17 p2777 A71-34398
- Scalar-tensor field self consistent interaction theory eliminating Einstein gravitational model paradox 17 p2801 A71-34629

Gravitational field equations derivation from least action principle, interpreting additional vector field in generalization as vector potential of electromagnetic field 17 p2778 A71-34632

Multidimensional canonical formalism based on field system state description with potentials and momenta 17 p2778 A71-34635

Weyl and Schwarzschild field metric equivalence, showing nonreducibility from one to other by coordinate transformation 17 p2778 A71-34637

Transverse feed design for spherical reflector antennas, noting efficiency and field distribution 17 p2700 A71-34751

Coherent optical fields properties, discussing equivalence of quantum and classical descriptions 18 p2932 A71-36959

Milky Way galaxy radio halo, investigating background brightness distribution and local spiral arm magnetic field structure 19 p3133 A71-37428

Tensors in relativistic asymmetrical field theory, generalizing Einstein gravitation and Maxwell electromagnetic equations for electrogravitational fields 19 p3105 A71-38580

Thermodynamics second law restrictions on constitutive equations of electromagnetic theory for nonlinear materials with long-range gradually fading memory, considering dissipation principle consequences 20 p3270 A71-39485

Small deformation dynamic response of vibrating isotropic linearly elastic spherical shell to radial and time dependent body force field 21 p3464 A71-40769

Projective numerical solution of integral equations arising in boundary value problems of electric and magnetic field theory 21 p3416 A71-40846

Field adsorption of inert gas atoms at metal surface from variational calculation 21 p3419 A71-40887

Field produced by equilibrium electron distributions on analytic Jordan curve 21 p3419 A71-41082

Zero-charge and scale-invariance problems in solvable field theory model, considering Green function and vertex parts behavior under perturbation theory invalidity 21 p3420 A71-41128

Kinematic dynamo equations for turbulent generation of large scale magnetic and small scale turbulent fields, presenting exact treatment of fluctuation and ordered field equations 21 p3416 A71-41194

Discrete approximations for continuous fields in solid body nonlinear theory with differential and nonlinear equations replaced by algebraic and linear equations respectively 22 p3616 A71-42218

Constrained-impedance eigenfunctions, using projection method for field expansion in diffraction problems 22 p3512 A71-42307

Generalized Einstein field equations in general relativity based on ennuple or tetrad variation, comparing with Schwarzschild solution 22 p3575 A71-42354

Vacuum symmetry and asymmetry, analyzing physical meaning of Dirac vacuum in quantum field theory 22 p3577 A71-42853

Electromagnetic field theory formulation, using Maxwell equations for spinors 23 p3705 A71-43827

Plasma microwave harmonic generation conversion efficiency, applying field gradient theory to case of positive column placed through rectangular waveguide 24 p3803 A71-44648

General theory of relativity for symmetric field, discussing De Donder incompressible fluid model and Tolman-Schwarzschild metrics 24 p3849 A71-45064

Point source radiation in stratified waveguide system with magnetoplasma slab, evaluating transverse field by Fourier integral representation 24 p3857 A71-45181

Experimental verification for electrostatic field gradient effects on charge carrier concentration in diffused regions of semiconductors 24 p3863 A71-45359

FIGHTER AIRCRAFT
 NT F-4 AIRCRAFT
 NT F-8 AIRCRAFT
 NT F-14 AIRCRAFT
 NT F-15 AIRCRAFT
 NT F-100 AIRCRAFT
 NT F-104 AIRCRAFT
 NT F-111 AIRCRAFT
 NT HARRIER AIRCRAFT
 NT JAGUAR AIRCRAFT

Navigator role in TACAN of reconnaissance and fighter aircraft, noting Weapon System Officer functions 01 p0123 A71-10503

Mathematical model and digital simulation for nonlinear characteristics of prototype integrated actuator package for fighter aircraft control 02 p0190 A71-11783

Swept wing fighter aircraft transonic buffet onset lift coefficient from camber and trailing edge deflection, considering design variations 02 p0186 A71-12679

Mach 2 Mirage Milan ground attack fighter, noting lift aid moustache, low speed and steep approach handling from short airstrips 02 p0190 A71-12740

F-15 air superiority fighter, describing military requirements, program management and procedures in terms of speed, maneuverability, acceleration and weaponry 07 p1018 A71-19078

High performance fighter aircraft engine pressure ratio and turbine inlet temperature measurement, using fluidic sensors 07 p1028 A71-20586

TI alloys structural high temperature applications in fighter aircraft, considering fabrication and assembly methods 09 p1458 A71-23427

Hydraulically powered duplex input servos for flight control system of VFW-Fokker V-STOL fighter aircraft 12 p1867 A71-26884

Combat aircraft vulnerability to projectile impact predicted by model giving target penetration, damage size and structural response 16 p2660 A71-34013

Interceptor aircraft optimal nonlinear command guidance scheme for reduction of airborne computation load with forward prediction of interceptor and target state vectors 19 p3096 A71-37166

Interference loading linear prediction on aircraft stores at supersonic speeds, considering flow field due to jet fighter bomber 19 p2996 A71-37290

V-STOL developments at Hawker Siddeley Aviation, noting circulation controlled rotor concept and HS-141 aircraft 19 p2997 A71-37605

CASI PAPER 72/18 Aircraft performance and optimal energy flight path control in combat environment 19 p2997 A71-37724

German VAK 191B combat VTOL aircraft development program, describing prototype ground tests, autopilot preoptimization and hover flight tests 22 p3482 A71-41517

Active feedback wing/store flutter control for fighter aircraft, using computer programs based on frequency and time domains for linear analysis 23 p3630 A71-44109

FIGURE OF MERIT

Optical systems with large aberration, deriving merit function expressed as quadratic form of aberration coefficients 08 p1333 A71-21179

Pneumatic membrane logic elements on basis of figure of merit characterizing usability in system engineering 11 p1709 A71-25570

Noise equivalent irradiance evaluation of passive IR scanners for target thermal mapping systems operating in earth atmosphere, determining figure of merit 22 p3545 A71-42150

Guidance system figure of merit determining relative effectiveness of launch vehicle in delivering spacecraft onto interplanetary trajectory 22 p3573 A71-42788

FILAMENT WINDING

Automated machinery for reinforced plastic structural products manufacture by filament winding [SME PAPER EM-70-135] 01 p0089 A71-11261

Orthotropic photoelastic analysis of residual stresses in filament-wound composite ring structures, comparing with boring-out and cut-through methods 03 p0508 A71-13773

Unidirectional glass-epoxy filament wound composite material fracture strength based on three dimensional stress components of fiber-containing plane 05 p0826 A71-16740

Filament winding manufacturing methods using unidirectional glass reinforcements for design and fabrication of aircraft wing structure [SME PAPER EM-70-406] 07 p1120 A71-20546

Filament wound carbon fiber reinforced plastics components fabrication and performance tests [PLASTICS INST. PAPER 47] 08 p1296 A71-20902

Carbon fiber evaluation of structural reinforcement potentialities for rocket motor cases and pressure vessels filament winding [PLASTICS INST. PAPER 48] 08 p1297 A71-20924

Tetra-Core structural composite material, discussing fabrication techniques, test results, potential and applications 08 p1369 A71-21225

Failure analysis of unidirectionally reinforced fiberglass composites due to winding, using critical stress distribution function 08 p1323 A71-21701

Filament winding geodesic characteristics of shells of revolution made of glass fiber reinforced plastics 09 p1482 A71-22815

Numerical analysis of winding and heat treatment effects on residual stress distribution in cylindrical glass fiber reinforced plastic products 09 p1482 A71-22816

Steady multifiber winding process conditions in compact glass fiber packing for glass fiber reinforced plastic tubes 09 p1482 A71-22817

Residual stresses in ring shaped specimens of wound glass fiber plastic products, using radial cutting technique 09 p1482 A71-22822

Winding equipment for continuous production of large diameter cylindrical filaments of reinforcing materials and polyester resins 11 p1768 A71-25418

Sapphire windowed argon filled tungsten ribbon filament lamp in vacuum UV for application in photomultiplier quantum efficiency calibration 12 p1904 A71-26801

Filament winding techniques for glass fiber reinforced plastics, discussing processes, configurations and materials for achieving optimum strength 12 p1920 A71-27011

Filament wound pressure vessels and composites flaw detection nondestructive tests with X rays and thermography 14 p2262 A71-29644

Filament wound glass-reinforced plastic struts for cryogenic tank supports in long term planetary missions, testing thermal and mechanical properties 17 p2762 A71-35205

Filament wound shell of revolution optimum configuration, deriving equations for orthotropic filament axes coincidence with principal stress trajectories 17 p2830 A71-35317

Pure and transverse bending of orthotropic cylindrical shell wound with elastic glass plastic filaments, presenting stress-strain diagrams under tension and compression 17 p2830 A71-35318

Filament wound carbon/carbon composite heat shields, describing fabrication process involving winding, carbonization, pyrolytic carbon infiltration and graphitization [SME PAPER EM-71-204] 18 p2939 A71-36664

FILAMENT WOUND CONSTRUCTION
U FILAMENT WINDING
FILAMENTS
 Filamentary metal matrix composite superconductors for magnet construction 05 p0769 A71-16926

High temperature tensile strength testers for metallic and carbon filaments 09 p1446 A71-22735

Boron filaments and whiskers as reinforcements in high strength composite materials 11 p1790 A71-26336

Boron modifications and carbides formation by vapor deposition on tantalum filaments 12 p1943 A71-27093

Advanced filamentary composite materials behavior, discussing limited ductility, sensitivity to stress concentrations, fatigue and viscoelastic properties 14 p2264 A71-29897

Tension test for filamentary composites, employing hardened Al alloy wedges adhesive bonded to gripping edges 17 p2739 A71-34818

Spiral topology of chromospheric fibrils and filaments in H alpha near sunspots, noting similarity with axisymmetric force free magnetic field configuration 22 p3597 A71-41458

FILLERS

Three-layer spherical shell, determining filler effects on stress-strain state at circular hole 01 p0176 A71-11047

Continuous elastic filler effects on axisymmetric stability loss in cylindrical shell under subcritical compression loads, using three dimensional linearized equations 02 p0329 A71-12665

Soviet book on welding fillers based on high melting point compounds covering alloy selection, surfacing techniques, working machine maintenance, etc 03 p0432 A71-13689

Thin walled cylindrical shells with filler, determining stability under axial compression by computer calculation 03 p0514 A71-14360

FILLETS

Space shuttle systems structural joints thermal control, discussing contact conductance with and without interstitial fillers

04 p0676 A71-15334

Sandwich panels with conical shell or elongated honeycomb fillers, calculating stability and elastic properties

06 p0986 A71-17757

Cylindrical sandwich shells with multiple isotropic load carrying and transversely compressible filler layers, deriving local stability equations

06 p0990 A71-17793

AL particle size and filler volume optimization effects on epoxy composite dynamic response

07 p1139 A71-20136

Energy dissipation in free oscillations of multilayer shells consisting of alternating rigid elastic layers and soft fillers, deriving equations of motion

08 p1369 A71-21123

Filler and reinforcing agent effects on polypropylene rigidity, tensile strength and creep resistance at elevated temperatures [PLASTICS INST. PAPER 11]

09 p1481 A71-22342

Mechanical property modifications of polytetrafluoroethylene by filler additions, noting improved wear resistance [PLASTICS INST. PAPER 13]

09 p1482 A71-22346

Heat resistant plastics, considering thermal endurance characteristics and use of high strength fillers in aerospace industry

10 p1634 A71-24580

Mechanical properties and performance characteristics comparison of syntactic foams fabricated by conventional mixing or vacuum impregnation, including filler packing factors

11 p1784 A71-25394

Asymmetrical three layer plate with filler under impact loading, examining material and layer thickness effects on deformation

12 p1975 A71-27111

Al-Zn-Mg alloy plates welded with Al-Mg filler metals, observing ghost defects in radiographs

13 p2074 A71-28524

Elastoplastic plates and shallow shells with rigid orthotropic filler, bending and buckling beyond elastic limit

13 p2156 A71-29066

Advanced plastic composites fabrication and processing techniques, using resins, reinforcements and fillers

14 p2263 A71-29653

Aluminum powder filled epoxy composites, investigating particle size and filler percent effects on damping properties and elastic modulus

17 p2762 A71-34819

Cylindrical shell with continuous filler, calculating stability and axisymmetric buckling in axial compression

17 p2830 A71-35321

Water cooled reactor Zircaloy brazing filler metals, investigating corrosion resistance, joint strength and brazing capability

18 p2928 A71-36856

Cylindrical shell stability under radial pressure or axial compression from load-distributing filler model solution

20 p3308 A71-39166

Hysteresis to strength relationship and particulate filler effect on reinforcement of rubbers and plastics

21 p3405 A71-40601

Brazing filler metals as cost effective replacement for Au-Ni in aircraft gas turbine engine component

21 p3387 A71-40621

Filler quantity and type effects on mechanical energy losses in polymers, discussing molecular interaction and chemical bond influences

23 p3697 A71-44205

FILLETS

Residual and mean stresses effects on fatigue strength of specimens with longitudinal nonload-carrying fillet welds

04 p0613 A71-15763

Stress concentration correcting factors for fillets in landed aircraft structures

09 p1542 A71-23539

Minimum strength of groove and fillet welded joints in heat treated Al alloy tubular members

11 p1769 A71-25745

Spreading, wettability, diffusion and aggressive properties of nickel base brazing filler metals on stainless steels

11 p1769 A71-25750

Disk fillets stressed state, determining concentration coefficient and bearing capacity effect

23 p3780 A71-44221

FILM BOILING

Flat plate film boiling heat transfer under forced boundary layer convection, examining nonstationary wall temperature effects

02 p0333 A71-12646

Tissue cooling with liquid nitrogen, determining film boiling transition temperature and heat transfer rates [ASME PAPER 70-WA/HT-16]

03 p0372 A71-14096

Turbulent film boiling on vertical surfaces, proposing theoretical model with interfacial wave disturbances taken into account for heat transfer calculation

04 p0686 A71-15527

Gravitational and forced convection effects in saturated liquids laminar boundary layer film boiling, presenting analytical solutions for common fluids

04 p0686 A71-15528

Leidenfrost film boiling for various liquids over velocity, plate temperature and surface roughness range, noting velocity effect on vaporization rate

04 p0687 A71-15529

Subcooled nitrogen tube flow film boiling, investigating heat transfer and hydraulic resistance

04 p0687 A71-15530

Vapor bubble growth on heated surface with random temperature distribution and liquid microfilm for water and boiling potassium

17 p2836 A71-34306

Boiling heat transfer to cryogenic fluids, considering pool convective, nucleate, film and forced convective subcooled boiling

19 p3162 A71-37463

Corresponding states fluids film boiling with cylindrical heaters, studying pressure and diameter effects

20 p3312 A71-39283

Pressure, subcooling and diameter effects on heat transfer and circumferential flow transition of thin wire film boiling of liquid nitrogen in pool

20 p3313 A71-39284

Swirl flow augmented heat transfer to liquid nitrogen in dispersed film boiling, using twisted tape inserts

20 p3313 A71-39285

Buoyancy effects on heat transfer coefficients in liquid nitrogen film boiling in vertical flow

20 p3313 A71-39286

Liquid nitrogen drops anomalous behavior in Leidenfrost film boiling, investigating vapor instabilities effect on total vaporization time

20 p3313 A71-39287

Liquid-liquid or solid-liquid interface Leidenfrost film boiling, deriving heat transfer coefficient for liquid drop floating on cryogenic fluid

20 p3313 A71-39288

Floating times of liquid/solid sphere on evaporative fluid /liquid nitrogen/ in metastable Leidenfrost film boiling

21 p3476 A71-40892

Film boiling liquid hydrogen vertical flowing system, determining buoyancy effects on hydrodynamic and heat transfer characteristics

21 p3476 A71-40895

Forced flow laminar film boiling heat transfer coefficients from vertical surface in terms of interfacial shear at liquid-vapor interface

21 p3476 A71-40896

Heat transfer from incandescent platinum wires in saturated liquid nitrogen, examining film boiling from atmospheric to critical pressure

21 p3476 A71-40899

Mass diffusivity effects in film boiling of water droplets vaporizing in air, Ar, N₂ He and steam

23 p3782 A71-43907

Heat transfer characteristics of two phase nitrogen film boiling in tubes with tape-generated swirl flow

23 p3783 A71-44195

FILM CONDENSATION

Moving condensate film effect on velocity profile and mass transfer rate from gas-vapor mixture by Crank-Nicholson method

06 p1006 A71-18070

Laminar film condensation thickness and Nusselt number on arbitrary axisymmetric bodies in nonuniform gravity

07 p1225 A71-20655

Water aerosol flux interaction and drop capture with particles of solid reagent, considering agaroid films and precipitation on thin wires

19 p3094 A71-38699

Film condensation heat transfer coefficients measurements on vertical heat pipes for cryogenic nitrogen, hydrogen and deuterium

20 p3313 A71-39290

FILM COOLING

Blowing air conditions and flow parameters effects on film cooling efficiency for rotating cylinder

01 p0178 A71-10416

Film cooling effectiveness in hypersonic turbulent flow from downstream surface equilibrium temperature measurement

01 p0180 A71-10961

Nozzle wall protection against high enthalpy gas flow effects by film cooling through parietal liquid injection

01 p0143 A71-11017

Critical heat release in water film on vertical pipe with inside cooling

01 p0181 A71-11244

Film cooling in gaseous medium, assuming turbulent boundary layer at blowing point

02 p0333 A71-12645

Film cooling effectiveness with He and refrigerant 12 injection into two dimensional turbulent boundary layer of supersonic airflow

03 p0517 A71-13453

Gas to gas film cooling, describing physical processes and performance prediction method based on heat and mass transfer analogy

04 p0676 A71-14978

Film cooling of flat plates by angled cold air injection for turbine blade applications

04 p0639 A71-15472

Thermal boundary layer thickness and momentum in turbulent flow over film cooled surface

04 p0680 A71-15473

Pressure gradients and slot Reynolds number effects on impervious wall film cooling effectiveness in constant density flow

04 p0680 A71-15474

Two dimensional and axisymmetric flow film cooling effectiveness in supersonic turbulent boundary layer, using Eckert reference enthalpy method

04 p0571 A71-15496

Various free stream turbulence levels at nonconverging and converging walls, investigating foreign gas film cooling

04 p0683 A71-15501

Injection film cooling effect on surface heat transfer downstream of flush nontangential injection holes and slots in turbine applications [AIAA PAPER 69-523]

06 p0945 A71-17695

Gaseous film cooling effectiveness under varying conditions of free stream turbulence intensity, hot gas acceleration, Mach number and film coolant flow rate

07 p1219 A71-18760

Mass transfer net rate /evaporation plus entrainment/ from thin liquid film, using methanol, water, butanol and RP-1 as coolants

07 p1222 A71-18997

Tangential body forces and pressure perturbation interactions in thin liquid film, considering destabilizing effect impairing film cooling efficiency

11 p1751 A71-25491

Two layer thermal and velocity model of gaseous film cooling with constant turbulent step slot flow [ASME PAPER 71-GT-3]

11 p1855 A71-25949

Three dimensional slot lip geometry effects on tangential and splash film cooling of gas turbines [ASME PAPER 71-GT-11]

11 p1855 A71-25957

Supersonic turbine design, presenting performance data for film cooled blunt leading edge rotor blades measured in two dimensional cascade experiments [ASME PAPER 71-GT-76]

11 p1704 A71-25990

Prediction analysis of downstream effectiveness in high speed laminar boundary layer for reentry vehicular surfaces film cooling, using reference enthalpy method

11 p1752 A71-26216

Two dimensional prediction of adiabatic wall temperature and heat transfer coefficient downstream of film cooling slots, using Prandtl mixing length forms

13 p2160 A71-28598

Annular vaporizing combustion chamber with film cooling, determining flame temperature under supersonic flight conditions

13 p2117 A71-28749

Data correlation and effectiveness prediction from film cooling injection geometries, considering finitely thick slot lip and boundary layers

13 p2161 A71-28751

Approximate method for calculating film cooling effectiveness of flat plate in presence of turbulent boundary layer with injection ratios less than unity

13 p2166 A71-29368

Approximate method for calculating film cooling effectiveness of flat plate at injection ratios exceeding 3.0

13 p2166 A71-29369

Film cooling as solid surfaces protection in high temperature environments, considering two and three dimensional secondary compressible and incompressible flow geometries

14 p2337 A71-30244

Cooling effectiveness of liquid film barrier injected into rocket thrust chamber with vortex motion, considering heat transfer and performance [AIAA PAPER 71-676]

14 p2291 A71-30740

Flat plate surface film cooling by two dimensional tangent slot injection in hypersonic turbulent flow, measuring equilibrium temperatures and skin friction [AIAA PAPER 71-599]

15 p2343 A71-31541

Gas turbine blades effusion cooling effectiveness, using boundary layer theory to calculate blade profile local heat transfer

15 p2472 A71-32716

Film cooling studies in subsonic and supersonic flows, using shock tunnel for gas turbine conditions simulation

16 p2551 A71-32882

Thermal protection of two dimensional supersonic nozzle fed with hot air by tangentially injected cold gaseous films for convergent and constant section ducts

20 p3314 A71-39415

Liquid film cooling for slender body type hyper-sonic reentry vehicles, comparing active mass injection cooling systems to ablation type passive systems 22 p3621 A71-42006

Operating characteristics of arc plasma generator with film and water cooling protected anode 22 p3484 A71-42784

Gas concentration measurement at wall with argon and helium injection at pipe entrance, investigating protecting film cooling efficiency 24 p3819 A71-44929

FILM THICKNESS

Vacuum deposited Bi thin films on glass substrates at liquid He temperature, investigating characteristics of critical thickness 03 p0466 A71-13291

Condensate film thickness and Nusselt number on axisymmetric vertical plates and cylinders, correcting for variable gravity and body form [ASME PAPER 70-HT-P] 03 p0519 A71-13699

Calorimetric measurements determining total hemispheric emittance of thin gold films as function of temperature, demonstrating film thickness effect [AIAA PAPER 70-63] 03 p0522 A71-14456

Light scattering from ultrathin free liquid films, calculating irradiance optical functions variation with geometry and film thickness 05 p0763 A71-16906

Supercritical Permalloy thin films thickness effect on magnetic domain structure 06 p0941 A71-17401

Two layer antireflection coatings on glass for He-Ne lasers, calculating optimal film thicknesses for various substrates and wavelengths 06 p0907 A71-18038

Film thickness effect on solid powdered graphite, molybdenum disulphide and calcium fluoride lubricants friction coefficients 07 p1116 A71-18998

Minimum squeeze film thickness in journal bearing under reversed periodic loading of double loop form [ASME PAPER 70-LUB-12] 07 p1117 A71-19505

Velocity distribution and Reynolds number relation to thickness in liquid films using turbulent viscosity 07 p1094 A71-20545

Evaporated Rh films preparation at various substrate temperatures in vacuum UV, determining reflectance and optical constants 08 p1343 A71-21183

Metal friction surface oxide thin films and secondary structures thickness determination using electron microscope method 09 p1454 A71-22311

Film thickness effects on stress magnitude in surface layers of bodies under external friction 09 p1455 A71-23078

Pulse echo ultrasonic measurement of thin film layer between thick media, using real time computation 09 p1458 A71-23439

Structural film adhesives peel-thickness correlation and cure rate study by torsion pendulum 10 p1614 A71-24074

Monograph on bulk flow theory for turbulent lubricant films, discussing flow rates, pressure gradients and shear stresses 11 p1772 A71-26462

EHD lubricant film thickness and friction forces effects on ball and roller bearings selection and design [ASME PAPER 71-DE-3] 12 p1911 A71-27322

Photographic emulsion thickness variation effect on wave front recording and reconstruction on holographic plate 14 p2241 A71-30132

Epitaxial film thickness and resistivity effect on transistor cut-off frequency, discussing collector junction space charge region boundary location 14 p2213 A71-30626

Photoelastic analysis of oil film effects on rolling/sliding contact stresses of plastic and glass cylinders on steel ring, showing discrepancy with Hertzian distribution 15 p2414 A71-31946

Electric field effect of epitaxial thin silver films on mica in vacuum as function of temperature, thickness and surface specularly 15 p2461 A71-32377

Gas-solid interaction by shock tube method, determining thickness and thermal accommodation effects on thin metal film resistance thermometer response 16 p2576 A71-32922

Optical properties of metallized fluorinated ethylene propylene Teflon films with various thicknesses, discussing suitability as spacecraft thermal control surface [ASME PAPER 71-AV-35] 18 p2869 A71-36402

Thickness monitoring technique for thin films, using silicon solar cell mounted adjacent to substrate with iron deposition 18 p2922 A71-36591

Magnetic thin film domain wall velocity dependence on magnetic field intensity as function of film thickness, discussing nonlinearity causes 18 p2955 A71-36938

IC applications to microwave frequencies, relating circuit performance to substrate roughness and thickness of thin film metal adhesion layers 18 p2895 A71-36981

Electron elastic scattering in thin films by impurities, noting conductivity dependence on film thickness 21 p3428 A71-41126

Tunnel MOS diode oxide thickness and thermal equilibrium considerations, emphasizing reverse bias case AC conductance, capacitance and DC I-V characteristics 23 p3652 A71-43937

Rheological factors and error sources in X ray measurements of lubricant film thickness in rolling contact 24 p3830 A71-44947

InTe thin films formation, growth kinetics and physical properties, determining vapor deposited film thickness dependence on glass substrate temperature 24 p3861 A71-45249

Non-Newtonian film thickness, load capacity and maximum viscoelastic stress effect in point contact with second order fluid lubricant for slide/roll ratio [ASLE PREPRINT 71LC-16] 24 p3832 A71-45293

FILMS

Film lubrication for angular contact ball bearings, taking rolling and spinning into account 04 p0604 A71-15768

Substrates, films and laser mirrors production, discussing material combinations and evaporation processes 13 p2080 A71-29087

Oxide films effect on metal particles ignition 15 p2511 A71-31378

FILTRING

U FILTRATION

FILTERS

Complex programmed control systems invariance for discrete times, synthesizing compensating filter with specific transfer function 01 p0063 A71-10725

Dissipative mechanical filter for rocket self excited vibrations to eliminate oscillatory instability, describing transfer function and modal characteristics 01 p0164 A71-11021

Sounding rocket dispersion reduction using optimum wind filter for impact prediction based wind statistics and measurement [AIAA PAPER 70-1394] 03 p0499 A71-13675

Meter and decimeter wavelength periodic filters with bent row arranged posts, deriving dispersion equations 09 p1415 A71-22460

Optimality in classification of stochastic processes in recognition system, using predicting filter rms error as discriminating function 19 p3038 A71-37779

German monograph on filters based on coupled lines covering computerized design, numerical approximation, rounding errors and matrix correction method 20 p3208 A71-39263

Pulse compression dispersive filters for signal processing 20 p3206 A71-39912

FILTRATION

NT SPATIAL FILTERING

French book on numerical filtering, data smoothing, parameter prediction and process identification, considering expansion, transform, least squares and Kalman methods 02 p0236 A71-11726

Stratified statistical filtering algorithm for numerical simulation of nonlinear systems behavior 07 p1081 A71-18836

Riemann surfaces use in plane boundary value problems and singular integral equations, considering plane elasticity and filtration theories 07 p1148 A71-20079

Porous glass hyperfiltration membranes stabilization by aluminum chloride solution, noting retreatment need 13 p2026 A71-29377

Optimal extrapolation and filtration for class of random processes, considering functionals of solutions of stochastic differential equations 17 p2765 A71-34863

Filtering methods for reducing systematic errors of measuring system with structural redundancy 17 p2740 A71-34964

FIN STABILIZERS

U FIN

U STABILIZERS [FLUID DYNAMICS]

FINANCIAL MANAGEMENT

Aerospace contractor management program projected through 1975 in terms of system engineering, configuration and financial management, with Minuteman Missile as example 04 p0691 A71-15291

Research and development project funds allocation, developing mathematical dynamic modeling method for cost management 10 p1699 A71-24539

Incentive contract with contractor profit based on achievement in cost, schedule and technical performance 23 p3786 A71-43467

FINE STRUCTURE

Radio sources fine structure at 81.5 MHz, examining angular structure by interplanetary scintillation 01 p0158 A71-10769

Cr-alloyed Fe powders fine crystalline structure from X ray analysis 01 p1002 A71-10789

Solar magnetic fine structure production by gas motion in supergranular convection 02 p0316 A71-12753

Solar radio astronomy decimeter wave multichannel spectrograph for solar bursts fine structure spectrum analysis 03 p0488 A71-13530

Atmospheric density curves by satellite observation, obtaining schematic models for fine structure of semiannual variation 03 p0414 A71-14023

Ultrafine-grain metals - Conference, Raquette Lake, New York, August 1969 03 p0445 A71-14486

Ultrafine grain metals strength properties at cryogenic temperatures and near melting point, discussing grain boundaries 03 p0446 A71-14487

Ultrafine grain metallic structures by solidification, describing various techniques 03 p0446 A71-14488

Grain size refinement by alloy solute additions inhibition effect on growth and recrystallization, reducing boundary migration 03 p0446 A71-14489

Powder metallurgy for fine grain metals and alloys, discussing grain size-mechanical properties relationship 03 p0446 A71-14490

Fine coherent precipitate morphologies by spinodal mechanism, reviewing clustering in binary solid solutions 03 p0446 A71-14491

Ultrafine grain alloys ductility from tensile tests, discussing grain size, temperature and strain rate effects 03 p0446 A71-14493

Parametric laser with single mode pumping, investigating emission spectra fine structure 04 p0608 A71-15120

IR radiation absorption by water vapor in atmospheric transmittance windows, discussing fine structure of absorption spectrum 05 p0778 A71-16841

Cloud fine structure using backscattered laser radiation, incorporating multiple scattering effects into data processing system 06 p0921 A71-17381

Jupiter surface features motions and changes, discussing planetary fine structure 06 p0971 A71-18247

Fine structure of geomagnetic Pc 1 micropulsations by cyclotron instability due to anisotropic energetic proton velocity 06 p0895 A71-18283

HF radio signal ionospheric propagation around world by sweep frequency CW sounding technique, observing fine structure in ionograms 07 p1062 A71-19682

Planetary nebulae NGC 6572, NGC 7009, NGC 7027 IR line emission, examining fine structure for Ne II, Cl IV, S IV and Ar III 07 p1199 A71-19836

Harmonic analysis of metals and alloys fine structure X ray photographs via digital computers 08 p1293 A71-21765

Fine structure and heat resistance of thin Ni-Cr alloys specimens after prolonged exposure to high temperatures under tensile loads 09 p1480 A71-23703

Quasar radio emission fine structure measurements by very long baseline interferometry, using Goldstone Mars antenna and Haystack radio telescope 10 p1671 A71-24325

Quiescent metallic and ordinary prominences continuous spectra measurements, showing hydrogen ionization dependence on fine structure 12 p1955 A71-26588

Ti alloys aging, noting hardness increase and fine structure alpha phase coherent with beta solid solution matrix 12 p1917 A71-27296

Fine structure of reddening interstellar extinction curves of stellar radiation, using photographic spectrophotometry 13 p2132 A71-27967

Solid bodies crack development theory, emphasizing crack tip fine and hyperfine structures concepts and time dependent effects 13 p2149 A71-28121

Sunspot penumbra displacements, emphasizing fine structure elements velocity and directional motion 14 p2308 A71-29972

- Strong level crossing signals in stepwise fluorescence, investigating fine and hyperfine structure of atomic Li 14 p2277 A71-30508
- Niobium fine structure, examining annealing in vacuum effects on strength 15 p2425 A71-31400
- Pc micropulsations spectra fine structure and diurnal variations, analyzing rubidium magnetometer recordings by power spectral density method 15 p2394 A71-31425
- Stoichiometric hydrogen-oxygen mixture spinning detonation fine structure determination by trace technique and high speed space-time photography 15 p2465 A71-32083
- Radio signals fine structure examination by instantaneous pulsed voltage measurements, describing fast response digital voltmeter circuit with memory element 15 p2409 A71-32188
- Transverse shock waves fine structure and saturation of ion-acoustic turbulence in collisionless plasma, using magnetic field probe and MHD equations 16 p2619 A71-33649
- Coronal line measurements on slit spectrogram during solar eclipse of 7 March 1970, showing fine structure in inner corona 16 p2642 A71-33784
- Deformation conditions and annealing temperature effects on fine structure of Mo single crystals, noting polygonization 16 p2595 A71-33884
- Cyclic heat treatment effect on fine structure and properties of Mo single crystals in He atmosphere 16 p2595 A71-33885
- Quasar internal kinematics and fine structure rapid time variations from radio interferometry 17 p2799 A71-34502
- Solar corona studies at Kiev University during 1952, 1954, 1961, 1965 and 1968 solar eclipses, showing coronal fine structure relation to chromosphere 17 p2802 A71-34827
- Chromium stainless steels fine structure, noting quenching and tempering temperatures effects 19 p3076 A71-37118
- Ni-Co alloy fine structure under plastic deformations, determining stacking fault energy effects with X ray diffraction lines 19 p3076 A71-37119
- Linear polarization of pulsar PSR 22 18 plus 47 radio emission pulses, attributing periodic fine structure of spectrum to rotation of polarization plane in interstellar medium 20 p3291 A71-39316
- Earth gravitational field fine structure via circular orbit satellite perturbations 20 p3220 A71-39660
- Lower thermosphere neutral composition fine structure data from rocket-borne time of flight mass spectrometer, emphasizing atomic nitrogen vertical distribution 20 p3222 A71-39697
- Zero field hyperfine splitting in carbon trifluorobromide photodissociation laser emission 21 p3391 A71-40215
- Morphological relationships in solar chromospheric H alpha fine structure involving bushes, fibrils, threads and filaments 22 p3597 A71-41457
- Strong current z discharge collisionless plasma, investigating ions distribution functions fine structure 23 p3708 A71-42890
- Fine structure dislocation and phase composition of Cr-Mo steel at elevated temperature in steam pipe applications, noting recrystallization stability 23 p3690 A71-43277
- Fine structure of energy distribution function for electron beam interacting with plasma 23 p3711 A71-43411
- Solar K-line profile absolute intensity calibration from elements of fine structure on surface, determining brightness temperature 23 p3767 A71-43836
- Fine structure at crack tip expanding in ideally elastoplastic material in plane deformation state and plane stressed state 23 p3778 A71-44061
- Grain boundary orientation effect on intergranular cracking, discussing crack introduction in purified iron by cathodic charging with hydrogen 23 p3695 A71-44285
- Microalloying effects on phase composition, surface phenomena, fine crystalline structure and microstructure of E1417L steel 24 p3836 A71-44374
- FINES**
- Amino acid contents of Apollo 11 and 12 fines, discussing laboratory syntheses 07 p1196 A71-19500
- Thermoluminescence glow curve and decay characteristics of Apollo 12 fines and soil samples, suggesting lower mean daytime surface temperature at site 10 p1672 A71-24395
- Thermal conductivity of Apollo 11 lunar fines as function of temperature, pressure and bulk density [AIAA PAPER 71-477] 11 p1833 A71-26255
- Apollo 11 lunar material characteristics and age, emphasizing fine lunar dust 13 p2138 A71-28765
- Carbon compounds in Apollo 12 lunar fines and core samples, using pyrolysis, mass spectrometry, ion exchange chromatography and optical and electron microscopy 17 p2801 A71-34649
- Spectral emittance ranges of Apollo 12 lunar fines dependent on density for 2.5-14 micron wavelengths [ASME PAPER 71-HT-21] 19 p3142 A71-37992
- Apollo 12 lunar rocks and fines mineralogy and petrology, using optical and electron microscopy, electron and X ray diffraction and electron probe microanalysis 23 p3741 A71-43630
- Mineralogical and petrographic investigation of olivines, feldspars and pyroxenes in Apollo 12 fines and igneous rocks, using optical and X ray diffraction 23 p3741 A71-43631
- Mineralogical composition, modal distribution and bulk chemical analysis on Apollo 12 lunar fines 23 p3744 A71-43652
- Lunar fines samples 10084,148 and 12070,98, investigating grain size, mineral and chemical composition and optical properties 23 p3744 A71-43655
- Gas-liquid chromatography and mass spectrometry of lunar fines and glass constitution by preparing trimethylsilyl derivatives of discrete silicate ions 23 p3746 A71-43668
- Primordial radionuclides K, Th and U concentrations in Apollo 12 lunar rocks, breccias and fines, using gamma ray spectrometry 23 p3748 A71-43679
- Apollo 12 lunar rocks and fines under high energy neutron activation analysis, determining O, Si, Al, Mg and Fe abundances 23 p3748 A71-43685
- Apollo 11 and 12 lunar fines 10084 and 12070 trace element determination, using multielement neutron activation analysis 23 p3749 A71-43690
- Re and Os abundance and meteoritic contamination levels in Apollo 11 and 12 rocks, fines and breccia 23 p3750 A71-43696
- Apollo 12 samples total C and N abundances suggesting indigenous lunar material with solar wind component 23 p3750 A71-43698
- Carbon and sulfur isotope content in Apollo 12 lunar fines 23 p3751 A71-43702
- Apollo 11 and 12 fines cosmogenic He, Ne and Ar radionuclides composition determination, using electron microprobe analysis 23 p3754 A71-43727
- Tritium activity measurement in Apollo 11 fines, breccia and crystalline rock, comparing with meteoritic values 23 p3755 A71-43735
- Organogenic elements and compounds abundances and distribution in Apollo 12 fines 23 p3756 A71-43744
- Long chain alkanes search in Apollo 12 lunar fines, using benzene-methanol extracts 23 p3756 A71-43745
- Apollo 12 fines sample 12057,72 particle size distribution determination procedures, discussing characteristic shapes, glassy agglomerates, smooth opaque particles and volume 23 p3757 A71-43752
- Gas interaction with lunar fines, investigating carbon monoxide, nitrogen, oxygen, argon and water vapor adsorption 23 p3758 A71-43754
- Particle size and shape distributions of Apollo 12 lunar fines by computer evaluation of scanning electron microscope images 23 p3758 A71-43755
- Regular particle morphology and petrostatistics in Apollo 11 and 12 lunar fines and conglomerates, using phase contrast and scanning microscopes 23 p3758 A71-43757
- Phase analysis of Apollo 12 fines, core tube samples and rocks by Mossbauer studies, noting nearly uniform distribution of major Fe containing phases 23 p3759 A71-43765
- Apollo 11 and 12 rocks dielectric constants, discussing far IR absorption spectrum of fines 23 p3760 A71-43772
- Physical characterization of Apollo 11 and 12 lunar fines and glasses by diffuse reflectance, Raman and X ray spectroscopy and thermally stimulated currents 23 p3760 A71-43773
- Lunar fines luminescence emission spectra in visible and near IR region under proton and electron excitations, discussing cause and plagioclase distribution 23 p3760 A71-43777
- Apollo 12 lunar fines 12001,19 thermal conductivity vacuum measurements, using line heat source method 23 p3761 A71-43781
- Apollo 12 fines and Apollo 11 microbreccias and rocks magnetic properties, discussing remanent magnetization 23 p3763 A71-43793
- Lunar fines transportation process in mare surface evolution, suggesting electrostatics role from photographic and seismic evidence 23 p3765 A71-43810
- FINGERS**
- Air temperature and wind speed role in finger-freezing time 02 p0197 A71-11669
- Human fingers coordination during teletype operation, examining temporal characteristics 02 p0205 A71-12055
- Human muscle power fluctuations under steady state physical activity, analyzing finger flexors strength 17 p2683 A71-35172
- Finger freezing time correlation with cooling rate, discussing effects of indeterminate skin supercooling 18 p2860 A71-36883
- FINISHES**
- NT ENAMELS**
- FINITE DIFFERENCE THEORY**
- Partial differential equations finite difference approximation, applying convergence theorems with probabilistic method 01 p0111 A71-10318
- Numerical integration finite difference methods stabilization for perturbed Keplerian motion differential equations 01 p0154 A71-10378
- Polynomial finite difference description of first order nonlinear dynamic control plants with incomplete information 01 p0058 A71-10405
- Thin elastic orthotropic plate in finite difference formulation, determining natural vibration mode and instability by summary representation method 01 p0168 A71-10410
- Nonlinear heat conduction problems, applying finite difference equation stability 01 p0179 A71-10616
- Quasi-plastic impact in shock interaction between free body and moving plane, using nonlinear finite difference equation 01 p0127 A71-10636
- Linear stability of finite difference approximations to no-slip boundary conditions in nonsteady fluid flow 01 p0071 A71-11161
- Downstream boundary condition on stream function, discussing sufficiency conditions in finite difference methods 01 p0071 A71-11162
- Marguerre equations for deflection and buckling of partially and fully loaded spherical caps, noting inaccuracy of finite difference approximation 03 p0503 A71-13428
- Time dependent finite difference solutions of steady state nonequilibrium quasi-one dimensional nozzle flows 03 p0400 A71-13458
- Postbuckling behavior of open cylindrical shells under uniform axial compression loads, solving finite difference equations by Newton-Raphson method 03 p0505 A71-13539
- Laminar boundary layer on spinning bodies of revolution in oncoming stream, using implicit finite difference technique [AIAA PAPER 70-1377] 03 p0341 A71-13660
- Radiation absorbing detonation waves calculation by finite difference techniques based on pseudoviscosities 03 p0439 A71-14064
- Soviet monograph on universal program for finite difference solution of Dirichlet problem of Poisson equation with enhanced accuracy formulas 04 p0619 A71-15450
- Nonlinear two dimensional free boundary problem of axisymmetric fluid flow in tubes with surface solidification, obtaining numerical solution based on finite difference equations 04 p0677 A71-15454
- Conical body laminar boundary layer heat transfer problem in supersonic flow, using quasi-linearization and implicit finite difference method 04 p0527 A71-15487
- Local heat transfer to transverse circular cylinder at low Reynolds numbers, using iterative finite difference approach 04 p0683 A71-15493
- Navier-Stokes equation solution in cylindrical coordinates, using finite difference scheme with brute force matrix methods 04 p0572 A71-15551
- Finite difference and initial value solutions of nonlinear boundary problems for ordinary differential equations, generating algorithms by quasi-linearization method 05 p0775 A71-16646
- Gravitational n-body calculation in discrete phase space using game model and finite difference scheme 06 p0927 A71-17555

Finite difference methods for time dependent Fokker-Planck equation conserving total system mass, energy and momentum

06 p0936 A71-17556

Viscous incompressible flow problems, using finite difference methods for solving Navier-Stokes equations

06 p0917 A71-17564

Parabolic equation for plate unsteady thermal conductivity during nonuniform heating, analyzing finite difference solution accuracy

06 p1006 A71-18007

Finite difference theory and other approximation methods convergence determination in nonlinear variational problems

06 p0919 A71-18202

Nonlinear finite difference computer program applied to elliptic cylinder collapse under uniform external pressure, comparing with theoretical bifurcation buckling

[AIAA PAPER 71-146]

06 p1003 A71-18589

Finite difference calculation for two dimensional compressible turbulent boundary layer flow with heat transfer, using mixing length concept

[AIAA PAPER 71-165]

06 p0885 A71-18607

Turbulent boundary layer laminarization prediction in moderate accelerations, using Pathankar-Spalding finite difference formulation and experimental results for shear stress model selection

07 p1085 A71-18767

Spalding-Patankar finite difference method application to combined free and forced convection turbulent boundary layer with variable fluid properties and chemical reaction

07 p1054 A71-18769

Soviet book on gas flow past blunt bodies, Part 1, Flow analysis and calculation methods covering finite difference theory, algorithms, etc

07 p1013 A71-19049

Numerical solution of nonself adjoint boundary value problems of electrodynamics using finite difference scheme and iterative processes

07 p1159 A71-19179

Landau viscous incompressible boundary layer separation formula comparison with Chudov finite difference method

07 p1090 A71-19751

Poiseuille pipe flow stability from finite difference equations approximation to nonlinear axisymmetric Navier-Stokes equations under stream function perturbation

07 p1094 A71-20611

Two nonlinear coupled second order differential equations finite difference solution, using nonsquare and nonuniform grids for minimum error

07 p1149 A71-20612

Planarly-rectangular shallow shells with double curvature geometry, analyzing natural oscillations by finite difference procedure

07 p1219 A71-20649

Simply supported double layered rectangular mesh grids, solving finite difference equations under arbitrary loading

08 p1370 A71-21409

Finite difference description for dynamic control plants with unknown disturbances based on integral transformation and extrapolation, applying to automatic control systems synthesis

08 p1270 A71-21975

Numerical solution of quasi-one dimensional viscous heat conducting compressible Laval nozzle flows by time dependent finite difference scheme

09 p1545 A71-22454

Asymmetric buckling of spherical caps with asymmetrical imperfections, using nonlinear relaxation technique for treatment of finite difference representation of differential equations

09 p1541 A71-23090

Duct thermal entrance region with axial conduction, evaluating laminar heat transfer rate with finite difference technique

10 p1696 A71-24409

Inviscid model for flow field within plumes of two-dimensional underexpanded jets calculated by time dependent finite difference method

11 p1853 A71-25160

Finite difference computer algorithm to solve vertical velocity equation of steady air flow about mesoscale obstacle in stably stratified atmosphere

11 p1793 A71-25169

Elastic collapse analysis of shell structures with variable rectangular grid spacing based on modified finite difference computer program

[AIAA PAPER 71-359]

11 p1844 A71-25338

Neutron transport equation in five dimensional tensor form, applying finite differencing by integration method via use of divergence theorem

11 p1791 A71-25741

Josephson junction I-V characteristics self resonant current peaks calculation by finite difference scheme simulation, comparing results with perturbation technique and experiment

11 p1742 A71-25800

Elliptical equation boundary value problems solution, using finite difference representation

11 p1792 A71-26156

Longitudinal waves propagation in viscoelastic semiinfinite rod under constant velocity impact, solving by characteristics and finite difference methods

11 p1850 A71-26178

Difference equations derivation for flat plates plane stress extension as localized Ritz process, providing common classification of finite difference and finite element methods

13 p2147 A71-27784

Computational efficiency comparison between finite element and finite difference methods for temperature distribution calculations

[ASME PAPER 69-WA/HT-38]

13 p2155 A71-28977

Steady laminar natural convective flow in concentric cylindrical annuli, using finite difference method for Navier-Stokes and energy equations solution

[ASME PAPER 70-WA/HT-9]

13 p2164 A71-28982

Direct Laval nozzle design problem solution using finite difference method

13 p1991 A71-29170

Convergence and accuracy of modified Gauss-Seidel finite difference scheme, calculating one dimensional Navier-Stokes shock structure

13 p2051 A71-29429

Finite difference scheme for calculating three dimensional incompressible turbulent boundary layer development on infinite yawed cylinder

[ASME PAPER 71-FE-19]

13 p2052 A71-29457

Three dimensional elastic plastic solid, calculating stress and deformation with finite difference procedure

14 p2322 A71-29737

Elastic displacement stress computation in cylindrical systems of isotropic homogeneous material by finite difference method

14 p2323 A71-29744

Transient and steady state creep of circular cylindrical shells loaded by internal pressure, using strain hardening hypotheses and finite difference method

14 p2328 A71-30379

Bending equations solution for arbitrarily shaped quadrilateral plates with simply supported edges, using finite difference method

14 p2329 A71-30485

Transonic flow past bodies of revolution, using finite difference scheme

14 p2171 A71-30876

Local short term mesoscale weather forecasting by finite difference solution of hydrothermodynamic equations

15 p2443 A71-31222

Finite difference and finite element methods for approximating elliptic boundary value problems solutions

15 p2440 A71-31346

Asymptotic error expansions of differential equations approximate solutions by finite difference schemes for use as technical devices in theoretical numerical analysis

15 p2440 A71-31347

Dirichlet problem for second order linear elliptic differential equations, considering convergence theory results for finite difference approximations

15 p2440 A71-31349

Time dependent partial differential equations solutions, considering hopscotch class algorithms, Galerkin type methods and finite difference schemes

15 p2441 A71-31352

Fluid flow equations problems, describing stability and convergence theory for finite difference approximations

15 p2441 A71-31353

Nonlinear hyperbolic equations integration, considering characteristic, mesh finite difference and particle in cell techniques

15 p2441 A71-31355

Harmonic mixed boundary value problem exact solution for rectangle with slit, outlining finite difference techniques convergence

15 p2441 A71-31356

Finite difference methods application to numerical weather prediction problems, describing frontal depression growth and boundary conditions for short gravity wave suppression

15 p2443 A71-31357

Plates analysis under static and dynamic loads based on finite difference, lattice analogs, mathematically consistent lumped parameters and finite element models

15 p2503 A71-31438

Input signal preservation in nonlinear dynamic system described by finite difference equation in presence of noise, deriving algorithms for discrete time computers

15 p2381 A71-31982

Arbitrarily shaped thin shell elastic-plastic deformation transient response prediction, using improved finite difference method

15 p2505 A71-32008

Unstable two dimensional incompressible flow and wake development, using finite difference calculations for Navier-Stokes equations

16 p2558 A71-32996

Vlasov theory application to nonshallow shells, suggesting discretization procedure with quadrilateral finite elements for calculation by finite differences

17 p2816 A71-34325

Laminar flow in incompressible fluid between rotating disk and fixed wall at small distances with radial mass stream, using finite difference method for Navier-Stokes equations

17 p2726 A71-34581

Boundary value problems solution for second order finite difference equations, applying second order orthonormal polynomials and related functions

17 p2764 A71-34843

Three dimensional boundary layers on axisymmetric bodies with large positive and negative crossflows, using finite difference method

17 p2727 A71-34875

On-off automatic control systems, using nonlinear finite difference equations for switching times and coordinate values determination

17 p2721 A71-35133

Natural vibration parameters of cantilevered isotropic plates, using finite difference method with matrix form solution

17 p2829 A71-35308

Finite difference method application to three dimensional boundary layer calculation on sphere-segment surfaces in supersonic flow

17 p2672 A71-35632

Convergence and error estimates for finite difference methods for approximately positive solutions of mildly nonlinear eigenvalue problems

17 p2768 A71-35683

Unsteady laminar boundary layers flow around three dimensional bodies, using finite difference techniques and power series expansion of time square root

[ONERA-TP-941]

18 p2901 A71-36019

Supersonic flow field computation for wing-body combinations by shock-capturing finite difference techniques, discussing improvement based on Runge-Kutta method

18 p2844 A71-36303

Difference methods for hyperbolic flow equations, using third order accuracy space and time split difference operators

18 p2844 A71-36305

Laminar boundary layer flow analysis from nonlinear difference equations solution by Newton method, using block-tridiagonal factorization

18 p2905 A71-36313

Prandtl three dimensional boundary layer equations in orthogonal curvilinear coordinates, applying implicit finite difference scheme to solution

18 p2906 A71-36318

Small disturbance transonic flows potential equations numerical solutions, using mixed finite difference theory

18 p2844 A71-36325

Finite difference technique for convective flow equations involving shock wave propagation, discussing heuristic analysis for truncation error

18 p2907 A71-36338

Implicit continuous fluid Eulerian time dependent multidimensional fluid flows calculation at arbitrary Mach number based on finite difference approximation

18 p2908 A71-36345

Finite difference approximation application to linear two-point boundary value problem differential equation for testing finite point suitability for infinity before computation

18 p2941 A71-36354

Finite difference approximation for discrete eigenvalues of clamped plate, using operator and perturbation technique

18 p2980 A71-36701

One dimensional nonsteady combustion processes accompanying self sustained detonation waves initiated by merger of two weak shock waves, using Lax finite difference method

19 p3170 A71-38127

Difference equations derivation for meteorological turbulent flow prediction, considering errors due to finite difference approximations

19 p3087 A71-38306

Convergence rate of finite difference schemes applied to initial value problems for hyperbolic equations

19 p3088 A71-38312

French monograph on similar solutions of laminar boundary layer problem in supersonic flow covering finite difference methods and convective heat flux

19 p2994 A71-38648

Iterative finite difference solution of Laplace operator interior eigenvalues and eigenfunctions, noting convergence in application to Helmholtz equation

20 p3201 A71-38755

Vortex flow through axial, axially radial and other three dimensional axisymmetric channels, using finite difference model for flow equations solution

20 p3211 A71-39465

- Numerical analysis of steady state creep of simply supported circular cylindrical shells by combined Newton and finite difference methods
21 p3463 A71-40752
- Critical evaluation of Schur-Cohn condition test for stability of multilevel finite difference schemes
21 p3408 A71-40851
- Hypersonic strong interaction boundary layer problem solution by implicit finite difference method
21 p3369 A71-40955
- Moderately thick plate transient response stability analysis, using finite difference equation
21 p3467 A71-40957
- Potential flow with free surface, comparing finite element and finite difference methods for liquid sloshing problem
21 p3369 A71-40974
- Two dimensional cylindrical stress propagation over viscoelastic body arbitrary cylindrical surface under instantaneous compression load, using finite difference method
22 p3613 A71-41564
- Galerkin approximation for boundary value problem finite difference scheme optimization by interpolation in Hilbert subspace
22 p3566 A71-42292
- Stability of finite difference approximation to mixed initial boundary value problems for linear parabolic system of equations
22 p3567 A71-42295
- Finite difference methods application to Euler non-linear elliptic differential equations, using symmetric and positive Jacobian
22 p3567 A71-42375
- Atmospheric circulation finite difference weather prediction model, investigating horizontal grid resolution effects
22 p3535 A71-42412
- Global numerical weather prediction model, using finite difference grid and operators with smoothing techniques
22 p3568 A71-42413
- Flow field calculation in intermediate altitude rocket exhaust plumes by modified Lagrangian finite difference technique
22 p3590 A71-42774
- Blade cascade design for meridional flow, using finite difference method for universal computer program
23 p3626 A71-43550
- Soviet book on computerized finite difference solutions for physically nonlinear plates and shells covering material anisotropy, creep, thermal, radiative and cyclic load effects
23 p3779 A71-44184
- Stress state of arbitrary contour body of revolution under torsion using finite difference method
23 p3779 A71-44218
- Finite difference scheme for elasticity theory boundary value problem in curvilinear region, estimating solution convergence rates
24 p3881 A71-44771
- Stability under uniform external pressure of closed spherical shell with axisymmetric initial imperfection in equatorial region, using finite difference technique
24 p3883 A71-44853
- Open cylindrical thermosiphon for laminar flow, predicting heat transfer performance by finite difference solution for comparison with Lighthill analysis
24 p3889 A71-44973
- FINITE ELEMENT METHOD**
- Nonconservative generalized nodal forces on finitely deformed finite elements
01 p0174 A71-10960
- Kirchoff triangular shell element design via linear shell theory
01 p0174 A71-10967
- Comparative shallow shell finite element analyses using different stiffness matrices
01 p0175 A71-11012
- Arbitrary shape and variable thickness cylindrical shell bending numerical solution by replacement of circular cylindrical strip elements
01 p0177 A71-11324
- Cylindrical shells finite element analysis by rectangular circular cylindrical elements replacement of actual structure
01 p0177 A71-11325
- Composite materials interaction stresses by ideal model with linearly elastic isotropic homogeneous inclusions and matrix, solving by finite element method
03 p0505 A71-13536
- Finite element method for composite materials anisotropic behavior, considering flat sheets plane stress and thin shells membrane and bending deformations
03 p0508 A71-13775
- Finite element program for structural design and stress analysis, introducing creep and plasticity into strain equations
[ASME PAPER 70-WA/DE-4] 03 p0511 A71-14140
- Finite element method approximations outside variational principle in elasticity problems, examining convergence to exact solution
[ASME PAPER 70-WA/APM-34] 03 p0512 A71-14160
- Plastic zone near crack end under forces causing plane deformation, calculating stress-strain state by finite element method
03 p0515 A71-14363
- Elastic solids mechanical characterization using finite element formulation of minimum potential energy theorem
04 p0671 A71-15751
- Consistent finite element model for two dimensional continuum problems on basis of virtual work principle
04 p0672 A71-15770
- Transient heat flow mean and first moments prediction by discontinuous linear or quadratic trial functions and variations
05 p0831 A71-16491
- Piecewise linear analysis of two connecting structures including connections with clearance, applying to engine crankshafts and pin-and-eye problems
05 p0829 A71-17116
- Stability analysis of structural systems subject to nonconservative forces, using finite element method
05 p0829 A71-17118
- Redundant structure dynamic analysis for forced and free vibrations, using finite element rank force method
05 p0829 A71-17120
- Rectangular panel acoustic response by variational finite element method, including radiated sound field effects on structural vibration
06 p0984 A71-17622
- Matrix displacement /finite element/ method for elastic structures analysis
06 p1001 A71-18050
- Plane or axisymmetric revolution geometry elasticity problems using finite element method and Fourier series
06 p1002 A71-18421
- Flat triangular elements for shell analysis, describing membrane and bending displacements by identical quadratic polynomials
06 p1003 A71-18564
- Unsteady supersonic aerodynamic coefficients evaluation to desired kinematic consistency level using finite element method
06 p0845 A71-18616
- Elasticity theory axisymmetrical problem, applying finite element method
07 p1210 A71-19161
- Rigid body motion implicit representation in curved finite elements
07 p1214 A71-19910
- Finite element solution of plane Poiseuille rarefied gas flow between parallel infinite plates
07 p1093 A71-20284
- Dielectric loaded waveguide electromagnetic field and coupling matrix derivation by finite element computer program, presenting dispersion curves and field plots
08 p1262 A71-20765
- Box type structure free vibrations investigation by rectangular finite elements, comparing with natural frequencies and normal modes solution
08 p1369 A71-20807
- Stiffened flat panel dynamic analysis, using finite element method
08 p1374 A71-22027
- Structural element for discrete element idealization of missile and liquid propellant as one composite structure
09 p1430 A71-22087
- [AIAA PAPER 70-23] Nonhomogeneous orthotropic beam Saint Venant bending, using finite element method
09 p1534 A71-22104
- Shallow shell triangular finite element method application to cylindrical shell theory
09 p1534 A71-22106
- Variational difference schemes construction by approximation method of finite elements
09 p1485 A71-22369
- Book on matrix structural analysis covering transformation, structure idealization, displacement method, finite element theory, nonlinear aspects, etc
09 p1539 A71-22873
- Comparative study of consistent and simplified finite element analyses of eigenvalue problems
09 p1541 A71-23203
- Automatic generator for finite rectangular/isoparametric element stiffness and mass matrices, discussing memory requirements and computation time optimization
09 p1542 A71-23280
- Computerized finite element techniques for stress and structural analysis for space communication and radar applications
10 p1684 A71-23756
- Nonconforming displacement triangular finite element derivation for plate bending problems, considering constant bending moment element
10 p1685 A71-23939
- Cruciform biaxial fatigue under alternate tensile and compressive forces, using finite element analysis and photoelastic-coating techniques
10 p1685 A71-23941
- Multilayer sandwich plates with transverse shear resistant inner layers and bending and twisting moment
10 p1686 A71-24020
- Arbitrary plates and axisymmetric bodies creep analysis by finite element method
10 p1691 A71-24820
- Variational principle for continua dynamic analysis by hybrid finite element method, considering consistent inertia properties of elements obtainable from assumed stress functions
10 p1692 A71-25047
- Duality in doubly curved shells analysis by finite element method, applying Kirchhoff-Love shells boundary conditions and energy variational principle
10 p1693 A71-25049
- Strain energy calculation of V notched crack in elastic continuum from finite element computer programs applied to fractures in solid propellant rocket motor cartridges or grains
10 p1693 A71-25056
- Collocation method predicting oscillatory subsonic pressure distributions on interfering parallel lifting surfaces, considering approach more economical than finite element method
11 p1701 A71-25309
- [AIAA PAPER 71-329] Finite element method for stiffness matrix free vibration analysis of thin rectangular plates under central planar loadings
11 p1842 A71-25313
- [AIAA PAPER 71-334] Initially curved thin elastic plates, predicting large deflection and postbuckling behavior with finite element procedure
11 p1844 A71-25336
- [AIAA PAPER 71-357] High precision finite element for static analysis of loaded thin elastic shells of revolution including shear deformations
11 p1844 A71-25339
- [AIAA PAPER 71-360] Coupled vibration modes for nonrotating blade-disk system in axial flow turbines and fans calculated by finite element method
11 p1845 A71-25348
- [AIAA PAPER 71-375] Incremental plastic analysis under large displacement and physical instabilizing effects, using finite element models and quadratic programming
11 p1849 A71-25679
- Conjugate approximations for piecewise functions of stress analysis using finite element method
11 p1792 A71-26103
- Nodal points stresses determination from finite element solved elastic problems, discussing thin disk stresses as function of mesh pattern regularity
11 p1851 A71-26312
- Finite element for torsion of thin walled open tubes, applying to matrix force analysis
12 p1974 A71-26871
- Plate and acoustic finite elements simulation of window-room system coupled transient response to sonic booms, discussing equations of motion and cavity depth effect
12 p1981 A71-27481
- Laminated plates transverse shear effects on deformation and stress distribution, using finite element analysis
12 p1982 A71-27571
- Difference equations derivation for flat plates plane stress extension as localized Ritz process, providing common classification of finite difference and finite element methods
13 p2147 A71-27784
- Consistent discrete models of continuous bodies electrothermoelastic behavior, using finite element formulations for general energy balance equations derivation
13 p2099 A71-27785
- Rectangular plate bending elements displacement functions representation by trigonometric expressions, using finite element method
13 p2147 A71-27790
- Computational efficiency comparison between finite element and finite difference methods for temperature distribution calculations
[ASME PAPER 69-WA/HT-38] 13 p2155 A71-28977
- Dielectric loaded waveguides electromagnetic fields solution by finite element method for cutoff modes determination
14 p2212 A71-30509
- Continuous system nonconservative stability examined by finite element Ritz method with extended Hamilton principle
14 p2330 A71-30687
- Convergent finite element equations for dynamic stability of plates dependent on vibration and buckling modes
14 p2331 A71-30696
- Finite difference and finite element methods for approximating elliptic boundary value problems solutions
15 p2440 A71-31346
- Variational principles and finite element method in partial differential equations, emphasizing basis functions fundamental to Galerkin procedure
15 p2441 A71-31351

Finite element midincrement stiffness matrices in postbuckling analysis of imperfect strut and rectangular plate 15 p2503 A71-31420

Finite element method application to transonic viscous flow through cascades and channels [AIAA PAPER 71-602] 15 p2388 A71-31542

Rectangular cylindrical shell finite element, deriving stiffness matrix with stress distribution 15 p2510 A71-32516

Elastic-plastic finite element analysis of near crack tip stress and strain field structure 16 p2590 A71-32940

Finite element method theory, discussing variational principle use, continuity requirements on interelement boundaries and incremental formulations of nonlinear problem in solid mechanics 16 p2651 A71-33077

Variational principles in solid continua mechanics, describing finite element models 16 p2651 A71-33078

Finite element analytical technique for calculating stress distribution in elastic body, using minimum potential energy principle 16 p2652 A71-33079

Mixed finite element formulation for shallow shells, discussing element matrix generation phase and governing variational principle 16 p2652 A71-33080

Matrix force analysis, discussing methods for expressing elastic behavior of semimonocoque polygon membrane and isotropic polygon bending elements 16 p2652 A71-33082

Stiffness matrices determination for flat plate elements under tangential and normal loadings by collocation, using exact polynomial solutions 16 p2652 A71-33083

Finite element analysis with material nonlinearities, obtaining linear incremental elastoplastic stress-strain relation 16 p2652 A71-33084

Finite element method application to stress distribution analysis at crack tip of rectangular plate under tension, obtaining elastoplastic response to cyclic loading 16 p2653 A71-33086

Geometrically nonlinear large deflection and structural stability problems, using finite element method 16 p2653 A71-33087

Combined finite element method and Rayleigh-Ritz procedure for geometrically nonlinear problems solution of elastic plates with arbitrary shape, boundary and load distribution 16 p2653 A71-33088

Unified finite element theory of geometrically nonlinear elasticity problems, noting restrictions applicable to different displacement formulations 16 p2653 A71-33089

Structural vibration and dynamic response analysis, applying finite element motion equations 16 p2653 A71-33090

Continuous media nonlinear thermomechanical behavior, presenting finite element formulation of deformation and irreversible thermodynamics problems 16 p2654 A71-33095

Hydrodynamic and plate structural analysis by finite element method, discussing diffusion, oil films and element couplings 16 p2654 A71-33096

Fluid mechanics problem of nonuniform meshes and complex boundary conditions, using finite element method 16 p2559 A71-33097

Arterioles and corneo-scleral shell structural response under various loading conditions, using finite element method for mechanical and hydrostatic stress distribution 16 p2528 A71-33099

Manipulation errors in structural systems finite element analyses, examining sources, magnitudes and characteristics 16 p2654 A71-33100

Thin elastic shells Koiter-Sanders mathematical model finite element analysis using Ritz method [ASME PAPER 71-APM-32] 16 p2655 A71-33197

Finite element method application to potential flow field problems governed by Laplace equation in fluid mechanics, developing computer program [ASME PAPER 71-APM-22] 16 p2520 A71-33207

Structural reliability predictions using finite element stress program and partial derivative method involving finite approximations 16 p2583 A71-33294

Vlasov theory application to nonshallow shells, suggesting discretization procedure with quadrilateral finite elements for calculation by finite differences 17 p2816 A71-34325

Circumferential notch effect on distribution of compressive self stresses produced by shallow skin layer expansion in round steel bars, using finite element method [SESA PAPER 1831] 17 p2819 A71-34529

Finite element method stress analysis for evaluating localized stress distributions in thick walled circular tube with step change in thermal expansion [SESA PAPER 1841A] 17 p2819 A71-34534

Three dimensional equilibrium finite element analysis, obtaining approximate stress solutions for symmetric laminates under inplane loading 17 p2824 A71-34812

Finite element procedure for plate large deflection by considering effects of element membrane forces due to initial deflection and bending on stiffness matrices 17 p2825 A71-34872

Stress hybrid finite element model for boundary conditions in solid continua with nodal values as final set of matrix equations 17 p2825 A71-34893

Finite element analysis codes for complex two layered linear elastic shells of revolution under static and dynamic loads 17 p2831 A71-35351

Continuous stress distributions across interelement boundaries, using finite element approximations based on displacement assumptions 17 p2831 A71-35352

Hybrid techniques combining continuum and finite element methods, noting application to stress concentration singularities 17 p2831 A71-35354

Elasticity theory axisymmetrical problem, applying finite element method 17 p2834 A71-35657

Convergence rate for finite element method, considering Neumann problem for second-order elliptic differential equations with constant coefficients in m dimensional Euclidean space 17 p2769 A71-35688

Kernel function for nonplanar oscillating surfaces in supersonic flow, using finite element method for interfering configurations 19 p2991 A71-37295

Simple structures large elastic-plastic transient deformations, using finite element method 19 p3157 A71-37874

Finite element method for elliptic differential equations solution, avoiding incidental technical difficulties 19 p3087 A71-38303

Computer programs for nonlinear finite element analysis with applications to large displacement and small strain problems 19 p3088 A71-38309

Viscoelastically damped structures finite element modeling and analyzing methods [ASME PAPER 71-VIBR-36] 21 p3458 A71-40288

Distributed mass and elastic damping finite element model for turborotor system on fluid film bearings [ASME PAPER 71-VIBR-56] 21 p3385 A71-40301

Transfer matrix and finite element combination technique for plates and shells vibration analysis [ASME PAPER 71-VIBR-85] 21 p3461 A71-40321

Free radial vibrations of curved beams by finite element method, using model to investigate variation with subtended angle of six lowest natural frequencies 21 p3462 A71-40529

Static characteristics and free vibration of doubly curved honeycomb sandwich plates, using finite element method 21 p3462 A71-40534

Creep stress and strain analysis in double edged V-shaped notched plates and circumferential V-shaped notched round bars by finite element method 21 p3400 A71-40840

Elastoplastic thermal stress analysis in axisymmetric bodies by finite element method, calculating residual stresses 21 p3466 A71-40841

High order finite element solution roundoff error reduction, using discretization of elliptic equations 21 p3409 A71-40962

Potential flow with free surface, comparing finite element and finite difference methods for liquid sloshing problem 21 p3369 A71-40974

High precision displacement functions for finite element models of rotational shell and plate bending problems 21 p3470 A71-41019

Curved finite elements application to circular arches, examining convergence properties of various shape functions used in stress resultant calculations 21 p3474 A71-41425

Elastoplastic indentation of half space by infinitely long rigid circular cylinder, using finite element method 21 p3474 A71-41426

Stress intensity factors determination for notched structures, using finite element technique 22 p3613 A71-41431

Elastic shells of revolution displacement analysis, using incremental variational theory with finite element method 22 p3613 A71-41434

Koiter theory for structural snap-through buckling behavior, using discretized matrix procedure based on finite element idealization 22 p3613 A71-41436

Finite element method for stress intensity factors calculation in cracked plates under bending 22 p3614 A71-41639

GWU-FAP computer program for rigid frame elastic-inelastic analysis based on finite element method and plastic initial strain concept 22 p3516 A71-41867

Finite element method application to convective heat transfer between parallel planes for arbitrary surface temperatures and Nusselt number 22 p3619 A71-41874

Discrete approximations for continuous fields in solid body nonlinear theory with differential and nonlinear equations replaced by algebraic and linear equations respectively 22 p3616 A71-42218

Functional methods in numerical solution of heat transfer problems, including finite element and local variation methods 22 p3621 A71-42290

Eigenvalues and eigenvectors error estimation in vibration and stability finite element analysis as function of mesh size, using Birkhoff perturbation method 22 p3617 A71-42541

Nonlinear finite element analysis of sandwich arches elastic buckling, using straight beam-column type model 22 p3618 A71-42586

Stress concentration factors of bonded single lap joints by finite element method as functions of dimensionless, geometric and material parameters 22 p3619 A71-42835

Stiffness and consistent mass matrices for beam bending finite element containing integration parameters 23 p3776 A71-43374

Dynamic response of thin walled structures natural frequency analyzed for formulating potential and kinetic energy for stiffness and mass matrices by minimization principle 24 p3878 A71-44555

Compressible viscous flow calculation, deriving finite element analog of Navier-Stokes and energy equations 24 p3818 A71-44617

Convergence and strain accuracy of finite element solutions for nodal displacements in plane elastic mesh 24 p3842 A71-44633

Curved finite element for elastic-plastic analysis of thin toroidal shells of revolution with discontinuous meridional slope under axisymmetric loadings 24 p3879 A71-44634

Discrete element finite deflection analysis of shallow arches using numerical method of potential energy minimization 24 p3879 A71-44636

Stiffness matrix algorithm for triangular plate bending elements using hierarchy of interpolation polynomials 24 p3879 A71-44637

Global-local finite element combined Ritz methods for beam and plate vibration analysis 24 p3880 A71-44638

Hermite polynomials application to stiffness matrix determination in plate finite element method for disk under plane stress, presenting digital computer program flow diagram 24 p3880 A71-44641

FINITE-STATE MACHINES

U TURING MACHINES

FINLAND

Morphology and geology of Lappajarvi structure /Finland/, suggesting meteorite impact evidence 19 p3049 A71-37652

FINNED BODIES

Radiative and convective heat transfer from conducting fins on plane surface, describing interactions among heat conduction and radiant exchange [ASME PAPER 70-HT-F] 03 p0519 A71-13701

Nonguided finned rocket initial stability problem, evaluating axis and tangent trajectory 05 p0817 A71-16638

Finned missiles aerodynamics at high angle of attack, examining body vortex wake region interaction with fins 06 p0980 A71-18511

Dynamic instability of finned missiles occurring as angle of attack undamping and caused by differential lift from windward and leeward fins [AIAA PAPER 70-206] 09 p1530 A71-22075

Finned configurations with nonlinear aerodynamic properties, obtaining solutions for angular motion at and near resonance 09 p1532 A71-22099

Stability and stress analysis of elastic finned circular cylindrical shells reinforced by stringers 14 p2332 A71-30852

Finned solid cylinders surface layers, determining residual axial stresses distribution and amount with induction sensor 15 p2503 A71-31480

FINS

Perfectly effective boiling fin design in horizontal right circular cylinder shape, deriving formulas at peak heat flux operation

15 p2514 A71-32264

FINS

NT COOLING FINS

Nike-Apache sounding rocket vehicle with canted fins, examining pitch-roll coupling characteristics by equilibrium and dynamic simulation methods

[AIAA PAPER 70-1376] 03 p0497 A71-13659

Launch vehicle under influence of random fin misalignments, predicting roll rate by statistical analysis

[AIAA PAPER 70-1382] 03 p0498 A71-13665

Transient heat transfer in fins undergoing phase transformation, obtaining approximate solution to temperature distribution and interface motion by perturbation technique

04 p0678 A71-15457

Free flight measurement of aerodynamic coefficients on fixed cruciform fin stabilized bombs, determining aerodynamic forces and moments dependence on angular velocity components

07 p1015 A71-19872

FIRE CONTROL

Navigator role in TACAN of reconnaissance and fighter aircraft, noting Weapon System Officer functions

01 p0123 A71-10503

Crotale low altitude ground to air missile, discussing target acquisition and fire control units, maintenance and operation

06 p0979 A71-17567

Cheyenne attack helicopter weapons system, discussing night vision capability, armament, fire control and navigation equipment integration

[AHS PREPRINT 530] 14 p2178 A71-31091

Weapons delivery computer for attack helicopters, using planar distributed function generator for general closed form instantaneous solution capability

[AHS PREPRINT 531] 14 p2209 A71-31092

Avionics systems for weapons control in F-14 fighter aircraft, discussing track multiple targets, sighting aids, radar, computer navigation, communications and built-in self testing

16 p2527 A71-34155

Sight line autopilot/SLAP/ for side-firing aircraft pointing accuracy improvement, using optimal regulator theory to generate control gains

[AIAA PAPER 71-960] 19 p3099 A71-37201

One man Jaguar aircraft navigation, weapon aiming system and pilot operational tasks, noting inertial platform alignment, displays and target attack modes

20 p3261 A71-39825

FIRE FIGHTING

Soviet book on aircraft power plant systems and devices covering layout, engine attachment, propellers, control, fuel and oil systems, fire fighting, monitoring, etc

02 p0299 A71-12722

Commercial sodium bicarbonate powder for methane air diffusion flames extinction, noting particle surface areas

07 p1182 A71-19248

Fire fighter protective clothing, considering efficiency as function of garment weight and heat stress loading

17 p2690 A71-34785

Aerial land rover for special needs of developing countries as passenger and freight aircraft, crop spraying and dusting, aerial survey and fire fighting

21 p3325 A71-40701

IR radiation sensors application to fire protection and rescue operations

22 p3545 A71-42157

Airport crash fire fighting equipment requirements and rescue operations

23 p3629 A71-43389

FIRE POINT

Flash points, fire points and impact sensitivity of materials under gaseous oxygen pneumatic and mechanical impact

14 p2222 A71-30550

FIRE PREVENTION

Aircraft fire hazard reduction, discussing early detection, extinguishing equipment and emergency landing survival

01 p0004 A71-10399

Fire retardant glass reinforced polyester resins optimum formulation, examining burning properties, volatility, extinction time and flame propagation

02 p0274 A71-12483

Book on chemistry and uses of fire retardants covering P, Sb, B, Cl, Br, cellulose, coatings and synthetic polymers

02 p0275 A71-12775

Counterflow diffusion flame applied in studies of gaseous and powdered agents in chemically inhibiting fires

07 p1182 A71-19244

Cargo aircraft crew safety and survival, describing restraint, escape, flight deck interior doors, fire and smoke hazards and personnel environmental protection

[SAE-ARP-1139] 07 p1019 A71-19643

Concorde power plant fire protection system, describing prototype engine bay overheat detection system and additional UV optical fire detection system

14 p2288 A71-30300

Space shuttle operation phases hazards, emphasizing propellant loading, fire suppression systems, survival equipment and self contained life support devices

17 p2813 A71-34784

Simulator for operating decision rules for control of airborne IR forest fire detection system

19 p3066 A71-38409

NASA program fire safety goals, discussing development of nonflammable materials covering fibrous asbestos, glass, polyimides, Teflon, metallics and halogenated materials

[AIAA PAPER 71-1011] 24 p3841 A71-44595

FIREBALLS

Prairie Network bright meteors, discussing constraints on meteoroid structure, photometric and dynamic masses and classical single body theory variations

03 p0490 A71-13934

Three dimensional Monte Carlo simulation of extensive air shower development, comparing fireball and mathematical models for mean total hadronic energy spectra

12 p1951 A71-27388

Fireball model at various energies, describing multiple meson production at very high energy

13 p2058 A71-28049

Fireballs existence, discussing maxima in angular distribution due to secondary particles transversal momenta limitation

13 p2058 A71-28062

Fireball transverse momentum effect on angular distribution of secondary particles, considering high energy nuclear interactions

13 p2058 A71-28063

Lost City/Oklahoma/ meteorite photometric and trajectory data, comparing flight characteristics with other fireballs

15 p2489 A71-32360

Ural fireball observations, noting accompanying meteorite falls

17 p2810 A71-35727

Fireball model of meson production in high energy nucleons collisions

18 p2949 A71-36210

Fireball identification method in accelerator and cosmic ray produced jets, considering model improvement for Lorentz factor determination

21 p3439 A71-41396

Light spark plasma in gas cloud, considering directed ejection to vacuum chamber and fireball acceleration

22 p3581 A71-41816

FIREPROOFING

Cylindrical transparent plastic antismoke hood with metallized dome, noting respiratory volume and air supply

01 p0028 A71-11599

Counterflow diffusion flame applied in studies of gaseous and powdered agents in chemically inhibiting fires

07 p1182 A71-19244

Flame retardant silicone elastomers for use as aircraft construction materials, describing fabrication techniques, mechanical, aging and weathering properties

12 p1921 A71-27412

NASA program fire safety goals, discussing development of nonflammable materials covering fibrous asbestos, glass, polyimides, Teflon, metallics and halogenated materials

[AIAA PAPER 71-1011] 24 p3841 A71-44595

FIRES

Apollo 13 in flight emergencies and countermeasures, discussing fire in Service Module oxygen tank causes and effects on spacecraft systems and solutions

07 p1206 A71-19087

Impact reaction intensity test, determining fire or explosion hazards of materials exposed to liquid oxygen

14 p2222 A71-30549

FIREWORKS

U PYROTECHNICS

FIRING (IGNITING)

NT RETROFIRING

NT ROCKET FIRING

NT TEST FIRING

Optimal firing temperature schedule during gas turbine loading for minimal thermal fatigue of hot gas path components, considering hollow stationary airfoils

[ASME PAPER 70-WA/GT-2] 03 p0470 A71-14116

Shock induced combustion by firing spheres or cone cylinders into air- or oxygen-hydrogen mixtures, taking shadow photographs of resulting disturbances

11 p1860 A71-26268

FIRING TIME

U BURNING TIME

FIRST AID

Medical planning and first aid in disasters at airports

11 p1725 A71-26128

FISH

U FISHES

FISHES

NT SHARKS

Salmonid fishes from Great Britain and southern Germany, analyzing visual pigments and liver retinols

01 p0008 A71-10229

Rudd vision mechanism, considering daylength effect on spectral sensitivity and visual pigment retinal extract proportions

01 p0009 A71-10271

African lungfish retina electron microscopy for Landolt club location, mitochondria, glycogen and microtubule content, considering relation to receptors and possible functions

01 p0009 A71-10272

Elasmobranch fish labyrinth electrophysiology, analyzing semicircular canals linear acceleration response

04 p0536 A71-14755

Semicircular canal and otolithic organ function in free swimming fish angular orientation behavior

21 p3328 A71-39996

Blind goldfish gravity reference response under linear accelerations on motor car and parallel swing from movie camera recording

22 p3487 A71-42228

FISHTAILING

U YAW

FISSION

Lunar origin by earth-moon fission, deriving parent planet characteristics from geochemical considerations

02 p0306 A71-11991

FISSION ELECTRIC CELLS

NT SNAP 8

FISSION PRODUCTS

Dynamic simulation of fission product heating in reactor using multigroup Way-Wigner method

07 p1158 A71-20350

Radioisotopes as energy source for power conversion systems, discussing future availability of fission products and transuranium elements from commercial nuclear power reactors

20 p3265 A71-38948

High altitude thermonuclear explosion fission fragments locating method, considering magnetogravitational trap as potential well for heavy charged fragments

20 p3279 A71-39143

Carbonaceous chondrite fission producing super-heavy element decay half life

22 p3605 A71-42398

Fission track analyses of uranium enriched phases in Apollo 11 and 12 basaltic rocks

23 p3739 A71-43615

FITNESS

NT FLIGHT FITNESS

NT PHYSICAL FITNESS

FITZGERALD-LORENTZ CONTRACTION

U LORENTZ CONTRACTION

FIX

U FIXING

FIXED POINTS [MATHEMATICS]

Two fixed centers problem generalization for case of material point attracted to coordinates origin by force proportional to radius

01 p0155 A71-10445

Lagrange equations of motion of gyroscope having fixed point in presence of constant gyrostatic moment, obtaining particular solution

03 p0457 A71-13582

Equations of motion of gyroscope body having fixed point, determining conditions for existence of quadratic invariant correlation

03 p0457 A71-13583

Heavy gyrostat equations of motion having fixed point and zero momentum integral constant, obtaining polynomial solutions

03 p0457 A71-13585

Integrodifferential equations of motion of body with fixed point, obtaining solution and geometrical interpretation

03 p0457 A71-13587

Hess solution for motion of heavy solid body with fixed point, surveying various methods

03 p0458 A71-13590

Dynamically symmetrical gyrostat steady state motion stability in force field of two fixed centers, using Raus-Liapunov theorem

10 p1683 A71-24579

Nonautonomous nonlinear functional differential equations periodic solutions, reducing problem to existence proof of fixed point for operator in suitable space of periodic functions

22 p3567 A71-42691

Suboptimal fixed point data smoothing algorithm for parameter and initial state estimation of nonlinear dynamic systems

23 p3659 A71-44113

FIXED WINGS

- Medical transportation by ambulance, helicopter and fixed wing aircraft, considering vibration damping and acceleration 05 p0715 A71-16932
- Book on fixed and rotary winged aircraft air cooled piston engine design, performance and maintenance in business and military operators manual terminology 05 p0796 A71-17125
- Canadian R and D on fixed wing civil STOL aircraft, discussing augmentor wing concept using jet powered lift augmentor system 16 p2523 A71-33470

- Augmentor wing high-lift aerodynamics, discussing results of wind tunnel tests and simulation studies [CASI PAPER 72/20] 19 p2993 A71-37606

FIXED-WING AIRCRAFT

- U AIRCRAFT CONFIGURATIONS
- U FIXED WINGS

FIXING

- Photopolymer recording materials fixing by flashing holograms with Xe light or deactivating catalyst with thermal methods 17 p2745 A71-35591

FIXTURES

- Airport lighting facilities in Japan, considering fixtures, marker and obstruction lights and apron floodlight 07 p1084 A71-20355

FLAME FRONTS

- U FLAME PROPAGATION

FLAME HOLDERS

- Combustion chamber flame tube cooling by swirling air flow, determining radial and longitudinal temperature distributions for various swirler hub ratios and jet angles 11 p1813 A71-26052
- Turbulence and flow pattern in wake of bluff body flame stabilizers, using hot-wire anemometer measurements and Prandtl-Kolmogorov model 19 p3168 A71-38102

FLAME INTERACTION

- U CHEMICAL REACTIONS
- U FLAME PROPAGATION

FLAME IONIZATION

- Enclosed diffusively turbulent flames, determining area of maximum ion concentration 01 p0178 A71-10338
- Maximum ion concentration zone in diffusively turbulent flames in fuel gas free jets, using mass exchange processes analysis 01 p0178 A71-10341
- Ionization rates in low pressure hydrocarbon flames produced by colliding burning gas jets 01 p0180 A71-11113
- Excited radical and ion formation in unperturbed acetylene-air and superimposed HF discharge flames, determining activation energy 09 p1402 A71-22379
- Combustion flame plasma reactions, considering collisional and chemical ionization, ion decay, electron temperatures and additives 16 p2540 A71-32969
- Chem-ionization induced by cyanogen in stoichiometric atmospheric pressure carbon monoxide-oxygen-nitrogen flames 19 p3013 A71-38089
- Carbon and methyl radical formation, studying emission intensities and chemi-ionization rates in hydrogen-oxygen flames with hydrocarbons 19 p3013 A71-38090
- Negative ion and compound formation in premixed fuel-rich laminar atmospheric pressure hydrogen-oxygen-nitrogen flames with molybdenum and potassium atoms 19 p3167 A71-38092
- Area measurement on steady, fluctuating, turbulent and expanding premixed flames, using saturation current method 19 p3168 A71-38103

FLAME PROBES

- Turbulent flame structures from ionization current measurements 08 p1376 A71-21911
- High sensitivity flame sensor for high temperature ambients, using Geiger-Muller tube triggered by photoelectron released by UV photon from flame 12 p1906 A71-27048
- UV radiation sensitive flame sensor for high temperature ambients, consisting of Geiger-Muller tube triggered by photoelectron released from photocathode 14 p2248 A71-30707
- Acoustic wave detection in K-seeded methane-oxygen flame plasma, using I-V characteristic modulation of fixed electrostatic probe 22 p3580 A71-41622

FLAME PROPAGATION

- Flame propagation and inhibition in polymers and unsaturated polyester resins, considering component and composition effect on flammability 02 p0275 A71-12492

- Cool flames theoretical model, formulating flame propagation equations based on mass, momentum and energy conservation and Fick mass diffusion law 02 p0210 A71-12859

- Flame propagation along interface between fuel slab/polymers, aluminum and tungsten powders/ and oxidizer slab/inorganic salts and oxides/ 03 p0521 A71-14278

- Detonation front at Chapman-Jouguet velocity demonstration by numerical transient flow calculations 05 p0834 A71-16510

- Gaseous mixtures turbulent combustion, considering turbulent flame propagation velocity 05 p0836 A71-16536

- Subsurface flow generation by surface tension variation due to flame spreading over liquid fuel at large Reynolds number, using hydrodynamical analysis [AIAA PAPER 71-207] 06 p1009 A71-18643

- Accelerating flame front generation and propagation controlling mechanism in porous propellant [AIAA PAPER 71-210] 06 p0948 A71-18646

- Flame propagation process, investigating transfer in turbulent flow, combustion times and burning in channel 07 p1220 A71-18778

- Lowered ignition temperature and fire propagation of polyester containing bromides 07 p1182 A71-19243

- Commercial sodium bicarbonate powder for methane air diffusion flames extinction, noting particle surface areas 07 p1182 A71-19248

- Turbulent flame propagation at high Reynolds numbers, discussing nonthermal hydrodynamic mechanism, laminar front and fine structure 07 p1223 A71-19249

- Methane and ethane binary mixtures with chlorine, determining main combustion products under flame propagation 07 p1054 A71-19280

- Axisymmetric wake diffusion flame response to HF periodic velocity oscillations at combustor boundaries 08 p1375 A71-20863

- Flame propagation dynamics of layered methane-air mixtures in vertical tubes, using interferometric techniques 08 p1346 A71-20864

- Stagnation point flow flame sheet model, showing density-viscosity product variation for injection rate effect on velocity profile 08 p1375 A71-20865

- Flame structure and propagation studied by modified Mach-Zehnder interferometers with He-Ne laser source, describing optical arrangements 10 p1623 A71-25125

- One dimensional premixed turbulent flame energy equation as function of heat release rate curve, temperature, velocity, composition and density 12 p1985 A71-26741

- Flame propagation speed, combustion zone extent and distance from front to maximum brightness surface in turbulent gasoline-air flames 13 p2162 A71-28956

- Combustion, reaction and flame propagation during gas mixtures burning, allowing for disruption of Maxwell-Boltzmann molecular velocity distribution 13 p2162 A71-28957

- Normal rates of flame propagation in two stage burning of gasoline-air mixtures 13 p2162 A71-28958

- Flame propagation rate in gasoline-air flow with tubular and grid-induced turbulence during two-stage burning process 13 p2162 A71-28959

- Combustion acceleration of molar oxygen-methane mixtures in cylindrical chamber during flame-shock wave interaction, using motion picture techniques 15 p2511 A71-31381

- Burning velocity measurement of laminar conical hydrogen-air flames on 10.3 mm diam water cooled nozzle burner, using schlieren and particle tracking techniques 15 p2465 A71-32085

- Turbulent swirling flames nonisotropic exchange coefficients determination from time mean velocity, pressure, temperature and concentration distributions 15 p2514 A71-32087

- Flame quenching device for distances determination by burning premixed laminar propane-air at atmospheric pressures between nonparallel walls 15 p2385 A71-32089

- Laminar flame speeds in chlorine-fluorine mixtures, predicting low temperature isothermal rates and spontaneous ignition limits 15 p2465 A71-32090

- Flame, laser and shock wave plasma generation, considering afterglows, ionized gas flows and high temperature effects 16 p2617 A71-32958

- Turbulent combustion stability in rocket engine with allowance for walls reflecting acoustic waves excited by flame 16 p2663 A71-33605

- Electric field effects on town gas and hydrocarbon flame reaction rate, burning velocity and propagation speed due to free electrons in flame front 17 p2840 A71-35704

- Oblique shock-combustion wave polar investigation of stationary two dimensional flow of fuel mixture in compressed gas 18 p2985 A71-36133

- Laser illuminated Mach-Zehnder interferometer system including high speed cameras for studying flame propagation among polythene particles suspended in air 19 p3064 A71-38063

- Vibratory flame propagation and pressure measurements in short closed tubes and vessels, using high speed schlieren cinematography and quartz piezoelectric transducer 19 p3167 A71-38097

- Hydrogen bromide effect on argon diluted propane-oxygen flame structure 19 p3167 A71-38100

- Area measurement on steady, fluctuating, turbulent and expanding premixed flames, using saturation current method 19 p3168 A71-38103

- Chlorine-fluorine flame, determining adiabatic propagation speed, refractive index field, temperature profile, composition distribution and atom concentrations 19 p3168 A71-38105

- Inhibitory effects of halogen compounds on hydrogen-air and hydrogen-nitrous oxide flames, measuring burning velocities and temperature/ composition profiles 19 p3013 A71-38106

- Monosized oil droplet streams combustion in stationary free flames, examining burning times and constants 19 p3169 A71-38112

- Low pressure trimethylaluminum vapor and oxygen flat diffusion flame structure, observing separation, formation and growth 19 p3121 A71-38299

- Steady propagation of plane laminar flame through uniform mixture of hydrogen and bromine gases, obtaining temperature and concentration profiles 21 p3474 A71-40524

- Steady laminar flame propagation speed prediction computation, applying to hydrazine decomposition 22 p3621 A71-42098

- Spherical hydrocarbon fuel droplet combustion in air, considering mass burning rates and flame zone locations as function of drop size [AIAA PAPER 71-989] 24 p3887 A71-44584

- Thermal energy requirement for homogeneous solid propellant ignition, measuring flame formation time and temperature 24 p3863 A71-44762

- Solid propellant combustion simplified laminar flame theory, calculating pressure effect on burning rate, surface energy loss and temperature effects 24 p3888 A71-44938

- FLAME QUENCHING
- U EXTINGUISHING
- U QUENCHING [COOLING]

- FLAME SPRAYING
- Cohesive strength of flame sprayed metallic coatings of various thicknesses 08 p1297 A71-21064

- Flame or plasma sprayed ceramic coating porosity estimation, using statistical distribution of breakdown voltage in coating 15 p2438 A71-31285

- Thermal conductivity and coating emittance measurements by stationary substrate heater method suitable for materials applied by flame vaporization 15 p2512 A71-31501

- FLAME STABILITY
- Cooled porous plug burner for flame recombination of oxygen and hydrogen, noting boiling water reactor off-gas application 03 p0517 A71-13367

- Turbulence intensity in combustion zone of stabilized air-kerosene flame from annular burner, using He diffusion measurements 03 p0520 A71-13994

- Diffusion flame stability, investigating critical dependencies for ignition point coordinates for fuel gas burning 07 p1220 A71-18779

- Flame stabilization by plasma jets increasing electrical input power 07 p1168 A71-19579

- Depressurization extinguishment of composite solid propellants for thrust termination, considering flame structure, surface characteristics and restart capability [DFVLR-SONDDR-129] 13 p2113 A71-28615

- Grid-induced turbulence effect on flameout characteristics for kerosene-air flames stabilized by bluff bodies of different sizes 13 p2163 A71-28961

- Stabilizer structure effect on flame stability of atomized liquid fuel, studying excess air ratio relation to air flow velocity 13 p2163 A71-28963

- Jet induced flame stabilization in combustible kerosene-air mixture flow of variable composition, discussing stable burning range and excess air content
13 p2163 A71-28965
- Gas dynamic antechambers flame stabilization at various flow rates and temperatures, calculating mixing factor vs flow and jet parameters
13 p2163 A71-28966
- Combustion chamber design with flame stabilizers, deriving gas flow, energy conservation equations and propellant combustion rates
13 p2163 A71-28967
- Aerodynamic flame stabilization by secondary air jets obliquely directed toward combustion chamber main flow, comparing with mechanical devices characteristics [DFVLR-SONDDR-120]
15 p2472 A71-32719
- Artificially induced unsteady flows effects on flame stabilization by model opposed jet stabilizer employing premixed propane-air combustible flow and opposed air jet
17 p2840 A71-35706
- Vibratory flame propagation and pressure measurements in short closed tubes and vessels, using high speed schlieren cinematography and quartz piezoelectric transducer
19 p3167 A71-38097
- Fuel rich premixed hydrogen-oxygen flame stabilization on cooled porous plate burners at 10 mm Hg
19 p3168 A71-38107
- Jet flame stability characteristics of propane-air mixture ejected into counter air stream by temperature and concentration measurements and visual observation
21 p3475 A71-40758
- FLAME TEMPERATURE**
- Cool flames theoretical model, formulating flame propagation equations based on mass, momentum and energy conservation and Fick mass diffusion law
02 p0210 A71-12859
- Flame temperature and combustion characteristics of model fuel-oxidizer-metal powder systems, using spectral and photometric techniques
03 p0376 A71-13988
- Metal oxide particle temperature determination in flames
03 p0376 A71-14283
- German monograph on open turbulent methane-oxygen flame temperature and concentration distribution determination from jet density measurements, using radiometric method
05 p0831 A71-16123
- Electron temperature in hydrocarbon air flame, discussing extra equilibrium excitation, energy relaxation rate and chemiluminescent emission
07 p1182 A71-19250
- Post reaction zone properties of premixed fuel rich propane-oxygen flames on torch, measuring temperature, composition and hydroxyl radicals
08 p1345 A71-20858
- Plasma flame temperature and flow characteristics in plasma jet transfer-type metal cutters from spectroscopic measurement and high speed streak camera photography
09 p1454 A71-23032
- Flame plasma temperature determination by microwave attenuation measurements, discussing measured values comparison with predictions by thermal ionization equation
11 p1804 A71-25193
- Composite propellant flame temperature and emission spectra during depressurization by rarefaction waves, using rapid scanning spectrometer [AIAA PAPER 70-663]
12 p1945 A71-27564
- Annular vaporizing combustion chamber with film cooling, determining flame temperature under supersonic flight conditions
13 p2117 A71-28749
- Combustion process in mixing zone of kerosene-air mixture and hot combustion products, deriving flameout time relation to characteristic temperature in mixing region
13 p2163 A71-28964
- UV radiation sensitive flame sensor for high temperature ambients, consisting of Geiger-Muller tube triggered by photoelectron released from photocathode
14 p2248 A71-30707
- Low flame temperature propellants, investigating temperature and humidity aging effects on physical and ballistic properties [AIAA PAPER 71-664]
14 p2286 A71-30732
- Magnesium vapor-oxygen low pressure diffusion flames temperature profile measurement, using subminiature thermocouple [WSS/CI PAPER 71-22]
15 p2464 A71-31631
- Monograph on flame form and temperature field at burners with nozzle for oxygen addition, using water model
17 p2837 A71-34795
- Flame temperature measurement by radiation and gas dynamic methods
17 p2745 A71-35440

- Radial temperature profiles in low pressure oxygen-calcium wire diffusion flames from optical measurements based on radiative transfer equation
19 p3170 A71-38115
- Thermal energy requirement for homogeneous solid propellant ignition, measuring flame formation time and temperature
24 p3863 A71-44762

FLAMES

- NT DIFFUSION FLAMES**
- NT PREMIXED FLAMES**
- AP composite solid propellant combustion model based on multiple flame structure surrounding individual oxidizer crystals
03 p0469 A71-13440
- Air-acetylene and air-propane-butane flames absorption spectra, determining distribution of free Ca and Na atoms and OH hydroxyl radicals
03 p0518 A71-13501
- LiOH dissociation energy in acetylene-air flames
03 p0376 A71-14281
- Flame structure in laminar condensed systems, noting burning rate dependence on pressure and specimen layer thickness, composition and mechanical condition
08 p1376 A71-21906
- Turbulent flame structures from ionization current measurements
08 p1376 A71-21911
- Nonresonant noise from turbulent nonpremixed flames, discussing burner diameter, impingement angle and equivalence ratio effects on acoustic power radiated [AIAA PAPER 71-732]
14 p2295 A71-30779
- Unmixed gases burning at finite reaction rate, analyzing steady laminar flames developing in mixing zone of fuel seminfinitesimal flow past static oxidizer
15 p2511 A71-31379
- Turbulent gas flame length in motionless air of various ambient temperatures, comparing calculation with measurement
15 p2511 A71-31380
- Hydrocarbon flame radicals excitation nature observation by photoelectric measurements, noting irrelevance to electron-ion recombination
15 p2463 A71-31389
- CH free radicals detection in oxyacetylene flame magnetic resonance absorption spectrum by IR water vapor laser
15 p2420 A71-32380
- Metal additives catalytic effect on free radicals recombination rates in hydrogen-oxygen-nitrogen flames
15 p2515 A71-32552
- Open singing flame from propane-butane and oxygen jet mixture, constructing oscillogram model of sound emission
17 p2839 A71-35696

FLAMMABILITY

- Flame propagation and inhibition in polymers and unsaturated polyester resins, considering component and composition effect on flammability
02 p0275 A71-12492
- Flame retardant effects on smoke density and oxygen index of polystyrene, acrylonitrile-butadiene-styrene (ABS) and polyester systems
07 p1144 A71-19572
- Flammability and heat transfer characteristics of flame retardant cotton, Nomex and polybenzimidazole (PBI) protective fabrics
07 p1145 A71-19573
- Flame resistant properties of phosphorus containing organic and inorganic high polymers
07 p1145 A71-19841
- Inflammable cylindrical channel ignition in semiclosed space, examining steady pressure development
08 p1376 A71-21907
- High pressure gaseous oxygen impact testing method incorporating drop plummet system for specimens flammability screening
14 p2222 A71-30547
- Flammability limits measurement of hydrogen-oxygen mixtures containing fluorocarbon diluents
15 p2465 A71-32086
- Glass fiber reinforced flame retardant thermoplastic resins, tabulating flammability resistance and mechanical properties
22 p3565 A71-42076
- FLAMMABLE GASES**
- Ionization rates in low pressure hydrocarbon flames produced by colliding burning gas jets
01 p0180 A71-11113
- Sulfur trioxide catalytic formation in gases from fuel-rich propane-air flames containing sulfur
03 p0376 A71-14279
- Shock induced ignition in explosive homogeneous hydrogen-oxygen gaseous mixtures
19 p3171 A71-38130
- Coherence theory of strong shock induced explosive gas ignition limit
22 p3621 A71-42099

FLANGES

- Flange joint moments magnitude due to bolts nonuniform tightening during assembly based on probability theory
07 p1116 A71-19359
- Minimum weight design of statically determinate wide flange beams, using Lagrange multipliers
13 p2151 A71-28210
- Stress distribution over elements of boss or collar tightened flange joints of circular thin walled shells during bending
17 p2829 A71-35306

FLAP CONTROL

- U AIRCRAFT CONTROL**
- U FLAPS [CONTROL SURFACES]**

FLAPPING

- Comparative vertical turbulence and loss restrictive stochastic models for threshold crossing rotor blade flapping vibrations at low lift high advance ratio [AIAA PAPER 71-389]
11 p1846 A71-25351

FLAPPING HINGES

- Rigid rotor hub flapping stiffness tailoring for controllability, considering length and fatigue/structural strength
15 p2348 A71-31601

FLAPS [CONTROL SURFACES]

- NT JET FLAPS**
- NT LEADING EDGE SLATS**
- NT TRAILING-EDGE FLAPS**
- NT WING FLAPS**
- Cambered and symmetric wing profiles and flap configurations, discussing wind tunnel tests at moderate Reynolds numbers
02 p0185 A71-11950
- Airfoil profiles with flaps at medium Reynolds numbers, determining performance characteristics in wind tunnel tests
04 p0526 A71-15025
- Performance characteristics of horizontal and vertical stabilizers at medium Reynolds number from wind tunnel measurements, considering air foil and flap effects
06 p0842 A71-18249
- Variable camber flap automatic control equipment for glider, considering combinations of mechanical, electrical and electronic approaches
06 p0847 A71-18250
- Multicomponent plane flap mechanism with transmission angles diverging minimally from ninety degrees, discussing synthesis by least squares method
07 p1117 A71-19361
- Multielement flap mechanism design, considering drive angles which deflect least from 90 degrees
09 p1386 A71-22652
- Flap induced flow deflection effects in hypersonic shock tunnel, obtaining turbulent heating, skin friction and pressure data [AIAA PAPER 71-598]
15 p2343 A71-31540
- Externally blown flap powered transport high lift wind tunnel model visual flow field investigation with multiple filament smoke streamlines [AIAA PAPER 71-577]
15 p2345 A71-31567
- Pressure distribution over deflected flap as function of boundary layer separation, flap geometry, Reynolds number and Mach number
18 p2972 A71-36435
- Aerodynamic heating tests of cone flap reentry vehicle using temperature sensitive paint
20 p3311 A71-39197
- Flap span length effects on boundary layer separation, giving streamwise pressure distributions
21 p3323 A71-40967
- Sailplane circling cross-country speed increase by variable geometry in high lift flap form for better compromise between cruise and climb performance
23 p3630 A71-44342

FLARED BODIES

- Flare induced laminar boundary layer/shock wave interactions on axisymmetric bodies at zero incidence in supersonic flow under adiabatic conditions
24 p3789 A71-44604

FLARES

- Quasars PKS 2345-16 and NRAO 512 optical flares photometric observation
02 p0317 A71-12864
- Flare stars in solar neighborhood, obtaining time averaged energy radiation upper bounds
06 p0976 A71-18474
- Photographic observations of meteors with flares, noting particle, solar and earth atmosphere role
07 p1193 A71-19315
- Flare characteristics of UV Ceti type stars from statistical analysis of photoelectric light curves
07 p1204 A71-20627
- Photoelectric and radio observations of flares of UV Ceti and YZ CMi stars
07 p1204 A71-20628
- Photoelectric observations of EV Lac flares in spectral U, H beta, G and V regions
07 p1204 A71-20629
- Meteoric masses evaporation during flare, showing discrepancies for luminosity factors
09 p1520 A71-22830

- BY Dra stellar flare characteristics by photoelectric observations, noting duration 12 p1971 A71-27750
- Reversal bleaching process for low flare light and high diffraction efficiencies and SNR in holograms 14 p2241 A71-30134
- Photographic observations of meteors with flares, noting particle, solar and earth atmosphere role 15 p2486 A71-31895
- UV Cet and YZ CMi star flare activity data, noting Poisson distribution of time sequence 19 p3134 A71-37510
- X ray flare regions structure, temperature and density, showing directed electron beams presence 19 p3126 A71-37622
- Flare stars X ray emission by fast electrons nonthermal bremsstrahlung 19 p3128 A71-38157
- Cygnus X-1 X ray data with temporal resolution, examining pulsations and flare activity 20 p3278 A71-39110
- Visual performance in simulated target acquisition tasks as function of flare-ignition altitude 22 p3503 A71-42196
- Red dwarf flare stars sporadic outbursts, considering light and radio emission curves, outburst energy and galactic emission 22 p3607 A71-42881
- FLASH**
- CdS single crystals with Cu and Cl additives, observing optical flash and thermoluminescence in IR band 03 p0468 A71-14385
- Computer simulation of thermal diffusivity measurements by flash method, considering errors due to boundary conditions 04 p0607 A71-14964
- Heat conduction equation for thermal diffusivity measurements by flash method in two layer composites 04 p0595 A71-14965
- Crab Nebula pulsar NP 0532 light flash arrival times, suggesting oscillations due to growing amplitude instabilities 05 p0806 A71-16201
- Brief light flash duration discrimination, discussing luminance and time between flashes 10 p1570 A71-24607
- Spatial and temporal patterned light flashes effects on dark adapted subjects, discussing cortical response changes in contrast depth 10 p1565 A71-24680
- Human rods dark adaptation, investigating rhodopsin resynthesis and bright light flash effects 11 p1718 A71-25635
- Apollo astronauts light flashes observation during lunar flight, discussing interpretation as scintillations in eye lens by multiply charged cosmic rays focusing on retina 19 p3001 A71-37299
- Flash photolysis initiated gaseous explosions detonation effects, observing ionization and radical emission spectra, absorption intensities and induction periods 19 p3169 A71-38110
- Flashing lights perception and application - Conference, London, April 1971 22 p3497 A71-41476
- Visual processes involved in flash perception, considering attention attraction at suprathreshold levels, unreliability at threshold levels and latency effects 22 p3497 A71-41477
- Subjective brightness of flashing light stimulus within fovea as function of stimulus size, noting edge effects contribution at suprathreshold levels 22 p3497 A71-41478
- Flash threshold perception in relation to flicker, showing flicker/flash sensitivity ratio constancy over large intensity level range 22 p3497 A71-41479
- Absolute foveal thresholds as function of flashes pulse length and null period 22 p3497 A71-41480
- Flash light angular size, adaptation luminance, pulse shape and color effects on Blondel-Rey constant tested on observers with good binocular vision 22 p3498 A71-41483
- Flashing lights effective intensity at threshold and suprathreshold levels, discussing Broca-Sulzer effect observance conditions 22 p3498 A71-41484
- Probability approach to visual effectiveness of signal flashing lights, showing graphically Broca-Sulzer effect 22 p3498 A71-41485
- Flashing lights attention attraction classification based on experimental results conversion into psychometric scale 22 p3498 A71-41486
- Successively presented flashing lights detection, discrimination and brightness measurements with four channel binocular Maxwellian viewing system 22 p3498 A71-41488
- Flashing civil aviation lights history, progress and photometric characteristics, discussing navigation and landing aids 22 p3499 A71-41489
- Color defective vision and aviation color signal light flashes recognition, indicating Farnsworth Lantern performance prediction test superiority 22 p3499 A71-41490
- Canadian Forces experiments on aircraft flashing lights covering warning signals, navigation and anticollision displays and autokinetic phenomenon 22 p3499 A71-41491
- Flashing lights radiation characteristics photometric measurement, discussing measuring apparatus sensitivity and errors analysis 22 p3499 A71-41496
- Flashing lights vision threshold systematic variations, using quadrant adaptometer for continuous tracking of sensitivity fluctuations 22 p3500 A71-41498
- Aircraft anticollision flashing lights, discussing current practices within national and international air traffic regulations regarding flash frequency, color and light sources 22 p3483 A71-41499
- FLASH BLINDNESS**
- Parafoveal sensitivity disruption /flash blindness/ due to retinal location and high intensity short duration adapting flash 06 p0851 A71-17605
- Flash blindness recovery with/without protection in simulated flight conditions, using aircraft instrument reading criteria 08 p1246 A71-20815
- Electroretinogram b-wave slope reduction by cooling of dark adapted frogs during serial flash stimulation 10 p1564 A71-24442
- Postexcitatory inhibition of monochromatic flickering potentials on electroretinogram in man under intensive dazzling stimuli 10 p1564 A71-24443
- Flash field size effect on flash blindness of aircraft crews, measuring recovery time 16 p2535 A71-33113
- FLASH LAMPS**
- Flash light excited dye solutions in liquid lasers, investigating wavelength and energy dependence of forced emission 02 p0261 A71-12322
- Nd-YAG pulsed laser, comparing Kr and Xe flash lamps for pumping performance 03 p0437 A71-13880
- Thermal conductivity determination for materials by pulsed laser or flash lamp energy absorption 04 p0595 A71-14961
- Organic dye lasers flash lamp pumped system for tunable coherent light production in visible and near IR spectrum 07 p1125 A71-19796
- Xe flash tube discharge saturable absorption effects, using YAG-Nd laser radiation for plasma attenuation measurements 09 p1465 A71-23484
- Two flash threshold measurement of comparison stimulus duration of Bloch law for anticollision strobe lights 11 p1725 A71-26116
- Flashtube pumped rhodamine 6G dye laser with four prism tuner, giving reflection losses equations and performance characteristics 14 p2254 A71-30135
- Xe plasma flash tubes with very low discharge current magnetic field for spectroscopic and laser applications in presence of Zeeman effect 14 p2243 A71-30272
- Automatic analyzer for rapid counting and sizing of raindrops, using collimated flashtube source for illumination 18 p2918 A71-36076
- Dye lasers developments and applications, including flash lamp pumps, frequency narrowing and tuning and picosecond pulse mode locking 18 p2931 A71-36602
- Repetitively pulsed flashtube pumped dye laser, noting high average outputs in red end of spectrum with rhodamine B 20 p3246 A71-39760
- Flashing light stimuli application to clinical instrument design for detection and quantitative assessment of early pathological visual loss based on minimum discernible luminance difference 22 p3498 A71-41482
- Apparent motion effects associated with stationary flashing lights configurations, noting frequency response characteristics analogous to real motion effects in human visual system model 22 p3498 A71-41487
- Effective flashes by scintillating Xe arc flash tube, considering perception by human eye 22 p3499 A71-41492
- Aircraft flash light designs, discussing tandem oscillating lights, fixed lamp rotating reflectors and lamps, xenon flashtube, quartz-iodine lamp and flash frequencies 22 p3483 A71-41494
- Visual masking effects in cat striate cortex single cell activity, using moving slit and diffuse flashing light stimuli 24 p3799 A71-45140
- FLASH POINT**
- Anomalous ignition and flash point measurements of halogenated hydrocarbon-flammable liquid mixtures [WSS/CI PAPER 70-20] 06 p0943 A71-17662
- Diffusion flame stability, investigating critical dependencies for ignition point coordinates for fuel gas burning 07 p1220 A71-18779
- Liquid fuel pool ignition at superflash and subflash temperatures involving adjacent heat source, cross wind and fluid motion 07 p1182 A71-19245
- High flash point polyalkylene glycol base synthetic quenchants for high strength alloy heat treatment, noting application to aluminum, titanium and steel parts 13 p2073 A71-28144
- Flash points, fire points and impact sensitivity of materials under gaseous oxygen pneumatic and mechanical impact 14 p2222 A71-30550
- FLASH TUBES**
- U FLASH LAMPS**
- FLASH WELDING**
- Mo alloy welding by continuous flashing method, discussing welded joints microstructure, plastic properties and strength 15 p2413 A71-31220
- FLASHING [VAPORIZING]**
- Photopolymer recording materials fixing by flashing holograms with Xe light or deactivating catalyst with thermal methods 17 p2745 A71-35591
- FLAT LAYERS**
- Heat transfer by radiation, convection and molecular thermal conductivity in gray absorbing medium flat layer bounded by parallel diffusively radiating planes 07 p1219 A71-18757
- Impulsive energy deposition generated stress waves in composite media formed by two plane layers with interfacial molecular bond joining 12 p1983 A71-27575
- Isotropic light scattering in unsteady plane layer of finite optical thickness, obtaining reflection and transmission coefficients for radiative transfer 22 p3607 A71-42869
- FLAT PLATES**
- Flutter analysis of plates with inplane boundary support flexibility exposed to transverse pressure loading or buckled by uniform thermal expansion 01 p0173 A71-10940
- Heat and gas curtain efficiency in turbulent boundary layer on flat plate, including heat transfer data 02 p0331 A71-11886
- Sound pressure radiation from infinite plate with rigid or pressure release baffles perpendicular to surface, using steepest descent method 02 p0325 A71-11997
- Boundary layer separation at free streamline attachment to sharp trailing edge of flat plate, deducing terminal velocity profile for two dimensional flow 02 p0185 A71-12376
- Natural convective heat transfer from fin-flat in vertical rectangular arrays, comparing duct and open channel coefficients 02 p0333 A71-12605
- Flat plate film boiling heat transfer under forced boundary layer convection, examining nonstationary wall temperature effects 02 p0333 A71-12646
- Nitrogen plasma flow over flat plate, comparing probe and probeless methods for boundary layer concentration profile measurement 02 p0254 A71-12648
- Nonlinear problem of fully and partially cavitating flow past oblique flat plates, solving via conformal mapping theory and Riemann-Hilbert method 03 p0398 A71-13106
- Three dimensional incompressible wake behind blunt obstacle at leading edge of flat plate compared with mathematical model by Oseen linearization [AIAA PAPER 69-747] 03 p0341 A71-13434
- Laminar boundary layer downstream heat transfer to sharp and blunt nosed isothermal flat plates under upstream mass injection, discussing insulating effect [ASME PAPER 70-HT-L] 03 p0519 A71-13700
- Stress distribution around elliptical hole in thin flat rectangular elastic plate under axial in-plane edge loads [ASME PAPER 70-DE-M] 03 p0506 A71-13705
- Finite element method for composite materials anisotropic behavior, considering flat sheets plane stress and thin shells membrane and bending deformations 03 p0508 A71-13775

Compressible turbulent boundary layer skin friction measurements on adiabatic flat plate, discussing drag balance calibration
[ASME PAPER 70-WA/FE-26] 03 p0403 A71-14134

Flat sheet under uniform radial tension, varying thickness reinforcement around hole for high stress concentration avoidance 03 p0513 A71-14238

Discrete vortex formation above perforated flat plate in wind tunnel, examining unsteady boundary layer 03 p0345 A71-14568

Book on flat plate stability covering initial buckling stresses, compressive and shear loads, holes, various reinforcements and shapes, sandwiching, etc 04 p0667 A71-15074

Wave formation behavior on melting surface of flat plate in heated air stream 04 p0678 A71-15455

Heat transfer in laminar MHD boundary layers on moving flat plate in magnetic field 04 p0635 A71-15468

Film cooling of flat plates by angled cold air injection for turbine blade applications 04 p0639 A71-15472

Prandtl number measurement in turbulent thermal boundary layer along flat plate with stepwise wall temperature variation 04 p0680 A71-15477

Temperature profiles in high velocity compressible turbulent boundary layer over flat plate without pressure gradients 04 p0681 A71-15480

Uniformly blown turbulent boundary layer on flat plate, investigating unheated solid starting length effect on heat transfer 04 p0572 A71-15500

Heat transfer in flat plate, considering acoustic resonance vibration effect 04 p0684 A71-15505

Viscous incompressible MHD fluid steady laminar flow past semiinfinite flat plate, noting heat transfer characteristics 04 p0635 A71-15508

Thermal radiation absorbing and emitting medium in flow between parallel plates, examining heat transfer for simultaneous radiation and convection 04 p0685 A71-15517

Mach-Zehnder interferometer measurements of average temperature and heat transfer rate in free convection on heated vertical flat plate 04 p0599 A71-15522

Semiempirical differential equation derived for turbulence scale behavior and turbulent boundary layer on flat plate 04 p0575 A71-15606

Nongray thermal radiation effect on laminar forced convection over heated horizontal flat plate, determining temperature profiles for optically thin and thick boundary layers 04 p0688 A71-15741

Uniform thin orthotropic skew flat plates free undamped vibration based on classical plate theory, using Rayleigh-Ritz method 05 p0820 A71-15987

Dissociated diatomic gas nonequilibrium boundary layer flow over catalytic flat plate, examining velocity profiles, temperature and concentration 05 p0735 A71-16389

Monte Carlo simulation for studying rarefied hypersonic gas flow about slender cones and flat plates [AIAA PAPER 69-651] 05 p0694 A71-16562

Incompressible turbulent boundary layer flow over steadily rotating flat plate blade, discussing centrifugal pumping and shear stress 05 p0694 A71-16581

Critical loads in flat plates under elastic strains 05 p0825 A71-16649

Heat transfer from finite flat plate in channel flow for vanishing Prandtl number, using Fourier transform and Wiener-Hopf technique [DFVLR-SONDR-98] 05 p0837 A71-16710

Supersonic flow field around flat plate at various angles of attack, comparing Brieden and Lighthill approximations 05 p0694 A71-16713

Longitudinal turbulent air flow past plate, applying heat transfer and drag calculations 05 p0838 A71-16784

Flat plate wake displacement sources in potential flow, considering high Reynolds numbers outside boundary layer 05 p0695 A71-16960

Steady two dimensional flow past flat plate in rectangular channel for low Reynolds number 05 p0738 A71-17249

Supersonic turbulent boundary layer separation on flat plate by forward facing step, measuring mean flow field characteristics [AIAA PAPER 71-127] 06 p0844 A71-18571

Turbulent skin friction and boundary layer velocity measurements on nonadiabatic flat plates at hypersonic Mach numbers [AIAA PAPER 71-167] 06 p0885 A71-18609

Hydromagnetic boundary layer free convection past vertical flat plate, discussing flow rates, temperature profiles and skin friction for high and low Prandtl numbers 07 p1165 A71-18744

High velocity liquid flow past rough plate surface, investigating boundary layer cavitation effects on convective heat and mass transfer 07 p1086 A71-18774

Seaplane step/flat plate/ricochet off ideal incompressible fluid surface, determining free surface shape by accounting for trailing vortices effects 07 p1088 A71-19355

Viscosity effects on three dimensional supersonic flow around circular half cones on flat plate, examining turbulent boundary layer separation 07 p1014 A71-19743

Unsteady viscous incompressible electrically conducting fluid flow past accelerated conductor or insulator flat plate in uniform transverse magnetic field 07 p1169 A71-20022

Elastico-viscous liquid laminar free convection flow along nonuniformly heated vertical flat plate, using momentum integral method for boundary layer velocity and temperature distributions 07 p1091 A71-20031

Cavitation flow of fluid with free surface past flat plate between parallel walls 07 p1092 A71-20081

Heavy fluid flow past partially cavitating flat plate with cavity closed by fictitious plate, considering lifting force under gravity 07 p1092 A71-20087

Jet reattachment to adjacent flat plate, investigating back pressure effects 07 p1094 A71-20606

Flat rectangular plate under plane stress, solving boundary condition problems with displacements and stresses from two neighboring edges 08 p1369 A71-20846

Elastic and elastic-plastic surface strain fields around skewed circular holes in flat plate under uniaxial tension 08 p1372 A71-21654

Stiffened flat panel dynamic analysis, using finite element method 08 p1374 A71-22027

Stress profiles measurement in opaque tempered glass and ion exchanged glass-ceramic flat plates from length change during etching 09 p1480 A71-22115

Supersonic collisionless plasma flow around flat plate and expansion into vacuum, using Poisson equation 09 p1500 A71-22233

EM induction in flat plates with two dimensional conductivity distribution, describing approximation method 09 p1492 A71-22425

Twin vortex development in unsteady separated flow past thin flat plate, using flow visualization 09 p1432 A71-22582

Edge loading effects on shallow hyperbolic parabolic shell elastic damping, discussing flat plate theory analog solution 10 p1686 A71-23995

Supersonic turbulent boundary layer density profile over flat plate at single Reynolds number, using Mach-Zehnder interferometer 10 p1593 A71-24270

Point matching technique applied to two dimensional solidification of viscous flow over semiinfinite flat plate, transforming moving free boundary problem to stationary domain [ASME PAPER 70-APM-R] 10 p1596 A71-24733

C-5A cargo box side wall deformations, examining square plates center deflections with elastic beams 10 p1557 A71-24871

Low Prandtl number laminar compressible boundary layer flow over flat plate, obtaining recovery temperature profile and heat transfer by matched asymptotic expansions method 10 p1597 A71-25066

Mean and fluctuating forces on flat plates normal to turbulent flow, giving power spectral density measurements of drag fluctuating component 10 p1598 A71-25085

Velocity, temperature and concentration profiles correlation for compressible turbulent boundary layer along porous flat plate, with carbon dioxide injection, discussing cooling applications 10 p1598 A71-25095

Uniform surface blowing effects on hypersonic boundary layer with viscous interaction, calculating heat transfer on flat plate and slender wedge 10 p1598 A71-25096

Boundary layer equation for free convective diffusion on flat vertical plate in translation motion in viscous incompressible fluid 11 p1854 A71-25240

Weight minimization of semiinfinite flat sandwich panel at constant dynamic pressure in supersonic flow subject to flutter constraint, using finite element model [AIAA PAPER 71-330] 11 p1842 A71-25310

Flat plate trailing edge problem solution consistent with second order boundary layer theory, establishing laminar wake evolution nature and upstream influence 11 p1701 A71-25469

Pressure orifices inclination in low density flow from experiments with cooled flat plate model in hypersonic low density wind tunnel 11 p1751 A71-25490

Radiatively interacting adjacent plates in presence of collimated solar flux, considering surface roughness effects on equilibrium temperature distribution [AIAA PAPER 70-817] 11 p1854 A71-25511

Time dependent shear stress, temperature and boundary layer pressure in laminar flow over stepwise accelerated flat plate at hypersonic speed 11 p1856 A71-26193

Metastable state gas flow experiment, investigating laminar boundary layer change in presence of flat plate surface catalytic reaction 11 p1705 A71-26276

Dynamic stress and strain concentration in flat plate at sharp change of section, assuming diffuse bending wave field 12 p1973 A71-26703

Steady Oseen flow past semiinfinite flat plate with force singularity, deriving integral equation solution 12 p1896 A71-26938

Horizontal flat plate moving transversely in rotating stratified fluid, calculating boundary layer blocking conditions for entire Rossby and Russell numbers range 12 p1897 A71-27222

Hypersonic wakes of two dimensional slender wedges and flat plate, testing stability in transition region in wind tunnel 12 p1866 A71-27561

Supersonic flutter of two dimensional flat plate in presence of chordwise tensile in-plane stresses 12 p1983 A71-27585

Difference equations derivation for flat plates plane stress extension as localized Ritz process, providing common classification of finite difference and finite element methods 13 p2147 A71-27784

Conjugate steady convective aerodynamic heating of plate in longitudinal compressible gas flow, taking into account boundary layer enthalpy distribution 13 p1989 A71-27890

Edge restraint effects on postbuckling behavior of thin flat plates under uniformly distributed compressive loads, noting buckling load and stiffness increase 13 p2153 A71-28466

Potential flow of incompressible inviscid liquid film along inclined semiinfinite flat plate for large Froude number values, using matched asymptotic expansions method 13 p2047 A71-28485

Compressible laminar boundary layer flow over semiinfinite isothermal porous flat plate in nearly quasi-steady motion, considering skin friction and heat transfer 13 p2048 A71-28600

Air stream injection from circular hole in flat plate into supersonic flow, measuring heat transfer 13 p1992 A71-29184

Asymptotic limiting viscous flow pattern and drag on flat plate with stationary separation zones at large Reynolds numbers 13 p2050 A71-29204

Approximate method for calculating film cooling effectiveness of flat plate in presence of turbulent boundary layer with injection ratios less than unity 13 p2166 A71-29368

Approximate method for calculating film cooling effectiveness of flat plate at injection ratios exceeding 3.0 13 p2166 A71-29369

Two dimensional vortex filament development artificially shed in laminar boundary layer on flat plate without pressure gradient, using hydrogen bubble visualization technique 13 p2051 A71-29428

Skin friction drag and velocity profile measurements on flat plate in two phase circular pipe flow in subsonic wind tunnel for gas-solid media, using photographic technique [ASME PAPER 71-FE-32] 13 p2053 A71-29467

Nonlinear stability of saddle-like deformed circular and square flat plates and shallow shells under transverse loadings 14 p2322 A71-29692

Turbulent skin friction and heat transfer prediction on flat plates and wind tunnel walls at supersonic and hypersonic Mach numbers, using Van Driest theory 14 p2334 A71-29868

Thermal boundary layer instability near heated vertical flat plate in poorly conducting liquid under horizontal DC electric field 14 p2337 A71-30407

High velocity boundary layer on flat plate, deriving equations analytical solution by flow variables expansion in powers of inversely squared Mach numbers 14 p2226 A71-30441

Monograph on crack problems in mathematical theory of thermoelasticity covering crack effects on

stress distribution in circular cylinders, thick plates and infinite solid bodies

14 p2329 A71-30501

Laminated plate flexural mode free vibration analysis by asymptotic method, obtaining phase velocity for comparison with experiment

14 p2330 A71-30684

Unsteady incompressible laminar viscous flow past infinite flat plate with arbitrary time dependent velocity, using Laplace transformation

15 p2387 A71-31184

Flat plate surface film cooling by two dimensional tangent slot injection in hypersonic turbulent flow, measuring equilibrium temperatures and skin friction [AIAA PAPER 71-599]

15 p2343 A71-31541

Flat plate span effects on ramp induced adiabatic laminar boundary layer separation at supersonic and hypersonic speeds, measuring surface pressure distribution

[AIAA PAPER 71-559] 15 p2344 A71-31557

Low density hypersonic flow on flat plate, discussing surface pressure measuring techniques

[AIAA PAPER 71-606] 15 p2346 A71-31580

Incompressible laminar boundary layer on flat plate, calculating flow oscillation effect on time-mean heat transfer

15 p2513 A71-31929

Laminar boundary layer growth along moving flat plate wall, obtaining series solution relating shear stress to velocity ratio

15 p2390 A71-32018

Attaching jet flow on inclined flat plate with small offset, obtaining centerline shape and velocity profile

15 p2391 A71-32056

Two dimensional MHD flow past flat plate with magnetic field aligned with flow field, using method of matched asymptotic expansions

16 p2615 A71-32860

Turbulent boundary layer growth over flat plate and compression corner model in hypersonic gun tunnels, measuring pressure and heat transfer rate distributions

16 p2554 A71-32880

Approximation analysis for laminar two dimensional boundary layer behind plane shock wave moving over infinite flat plate

16 p2556 A71-32914

Aeroelastic stability of flat plates and shells, considering panel flutter

16 p2648 A71-32987

Coupled elastic buckling in continuous systems, determining postbuckling paths for strut, spherical shell and flat plate

16 p2650 A71-33017

Heat transfer and drag calculations in longitudinal turbulent air flow around plate with constant or variable physical properties

16 p2662 A71-33036

Stiffness matrices determination for flat plate elements under tangential and normal loadings by collocation, using exact polynomial solutions

16 p2652 A71-33083

Wall shear stress, momentum and displacement thickness of shock induced boundary layer interaction in tube and over flat plate, using integral method

[ASME PAPER 71-APM-21] 16 p2559 A71-33208

Solid disk supported above flat plate by thin layer of gas flowing from central orifice, studying vertical motion equilibrium and dynamic data

[ASME PAPER 71-APM-3] 16 p2559 A71-33220

Stress-strain dependence on surface deflection and nonlinearity during bending of elliptic flat plate under plastic deformation

16 p2659 A71-33994

Constant velocity flow past semiinfinite flat plate trailing edge, emphasizing wake region structure

16 p2560 A71-34140

Uniform shear flow past semiinfinite flat plate, studying diffuse and heat transfer near leading edge

16 p2561 A71-34162

Detachment prediction in turbulent incompressible plane flows on thick bodies applied to wall with disconnections and flat plate normal to wind

17 p2669 A71-34189

Cold combustible gas mixture ignition temperature at flat plate forward stagnation point, investigating inert gas concentration, activation energy and first Damkohler number effects

17 p2837 A71-34436

Flow visualization and hot-wire measurements, showing vortex shedding association with turbulent air jet issuing from flat plate into cross wind

17 p2670 A71-34659

Circular symmetry stressed state for flat disk with flat circular crack, detailing potential and elasticity theories

17 p2824 A71-34844

Plate temperature fluctuations effect on convective flow and heat transfer from horizontal plate, presenting solutions for LF and HF

17 p2838 A71-35419

Singular perturbation theory for finite rate chemical kinetics effect on regression rate of semiinfinite flat fuel plate in gas oxidizer stream

17 p2792 A71-35796

Transient laminar two dimensional boundary layer induced pressures due to suddenly accelerated hyper-sonic semiinfinite flat plate

18 p2901 A71-35856

Liquid flow about oscillating flat plates, determining drag coefficient relationships to low Reynolds number and period parameter from graphical representation

18 p2902 A71-36033

Two dimensional laminar incompressible fluid flow past flat plate at various angles of attack, studying vortex shedding characteristics

18 p2844 A71-36311

Shock wave interaction with laminar boundary layer on flat plate using modified Lax-Wendroff difference technique

18 p2906 A71-36320

Longitudinal vortex rolls onset for laminar forced convection between two horizontal flat plates subjected to uniform axial wall temperature gradient

[ASME PAPER 71-HT-1] 19 p3163 A71-37979

Velocity and temperature profiles at near-critical point of nitrogen turbulent boundary layer flow over heated flat plate by thermocouple/pitot-static probe

[ASME PAPER 71-HT-23] 19 p3165 A71-37994

Checking method for reflection-type holographic system behavior, emphasizing critical stability of glass plate

20 p3236 A71-39194

Variable suction effects on two dimensional fluctuating slip flow of incompressible rarefied gas past infinite flat plate

20 p3211 A71-39466

Natural convection boundary layer stability on vertical flat plate with uniform heat flux, using numerical computer solutions for large Grashof number range

20 p3314 A71-39501

Sloping flat plate impulsively started constant velocity motion through slightly diffusive viscous density-stratified fluid, investigating transient and oscillatory viscous boundary layer flow

20 p3212 A71-39503

Conjugate steady convective aerodynamic heating of plate in longitudinal compressible gas flow, taking into account boundary layer enthalpy distribution

21 p3317 A71-40080

Laminar-turbulent inverse transition in divergent radial flow between two parallel flat disks

21 p3366 A71-40101

Dynamic influence of isotropic flat plates on spatial vibratory structures containing rigid bodies, considering compatibility and modal coupling

[ASME PAPER 71-VIBR-3] 21 p3456 A71-40267

Mean velocity profile and wall friction coefficients of perturbed turbulent boundary layer on flat plate

21 p3366 A71-40511

Unsteady boundary layer of viscous incompressible rotating fluid flow due to infinite flat plate accelerated motion, calculating velocity and skin friction

21 p3367 A71-40657

Boundary layer disturbances influence on three dimensional hypersonic flow about infinite triangular flat plate, investigating pressure effects on heat transfer and friction coefficients

21 p3322 A71-40681

Laminar viscous flow past semiinfinite flat plate to second Oseen type approximation, obtaining shear stress on plate

21 p3368 A71-40707

Crack shapes and stress intensity factors for deep edge crack in plate under tension or bending

21 p3467 A71-40907

Moderately thick plate transient response stability analysis, using finite difference equation

21 p3467 A71-40957

Hypersonic flat plate under impulsive loads, calculating time dependent transient wall shear stress and boundary layer induced pressure

21 p3369 A71-40964

Surface roughness and mass transfer influence on boundary layer and friction coefficient for turbulent flow over flat plate

21 p3371 A71-40997

Nominal stress prediction for plastic tensile instability occurrence in flat orthotropic sheet loaded by biaxial stress system, considering localized and diffuse necking

21 p3469 A71-41005

Liapunov-type analysis of linear systems dynamic stability under stochastic parametric excitation, noting application to rectangular flat plates

21 p3469 A71-41008

Supersonic collisionless plasma flow around flat plate and expansion into vacuum, using Poisson equation

21 p3424 A71-41113

Flat supported plate in plane supersonic oscillating flow, calculating forced vibration with potential flow theory

21 p3473 A71-41367

Oscillatory free convection laminar boundary flow from semiinfinite vertical flat plate, investigating surface temperature variations as distance function from leading edge

22 p3619 A71-41602

Infinite sandwich plate under concentrated torque load on one side, determining stress distribution with double infinite Fourier transform

22 p3614 A71-41604

Approximate motion equations of gas flow behind detonation front in flat explosive plate covered by inert coating

23 p3781 A71-43358

Heat exchange between two fluid streams in concurrent, countercurrent, laminar or turbulent boundary layer flow separated by flat plate, determining temperature distribution

23 p3783 A71-44193

Acoustic resonance excitation by vortex shedding from flat plate trailing edge in low speed wind tunnel

24 p3848 A71-44557

Vortex shedding from blunt trailing edge of flat plate spanning wind tunnel under oscillating flap and acoustic resonance excitations

24 p3848 A71-44558

Free convection heat transfer from vertical flat plate with sinusoidal wall temperature distribution

[AIAA PAPER 71-988] 24 p3887 A71-44583

Divergence behavior of flat rectangular panel at subsonic speeds, discussing boundary conditions, natural vibration modes and temperature effects

24 p3878 A71-44611

Previous plastic loading deformation effect on contact area, print number, size distribution and thermal conductivity for flat surfaces

24 p3830 A71-44943

Laminar boundary layer calculation for simultaneous heat and mass transfer in evaporating liquid layer on flat plate in parallel gas flow, considering variable material parameters

24 p3888 A71-44965

FLAT SURFACES

Radially loaded bearings rolling on flat track, determining slip-stick areas and creep conditions

01 p0086 A71-10298

Arsenic doped Si single crystal impurity segregation striae and central fractured area observations by scanned laser IR microscope

04 p0608 A71-15039

Turbulent flow structure and properties near flat wall, confirming turbulent friction damping by statistical analysis

04 p0576 A71-15611

Natural convection heat transfer coefficients from isothermal flat surfaces, using Boelter-Schmidt type heat flux meters

07 p1222 A71-18996

Electromagnetic pulse propagation over flat impedance surface, determining similarity parameters

07 p1060 A71-19187

Cross and single polarized light techniques revealing coarse grained fractures cleavage facets

07 p1111 A71-19582

Kinetic theory of transient condensation and evaporation at plane surface, using Maxwell moment formulation

09 p1545 A71-22852

FLATTENING

Thick strips widening by rolling, deriving formula for maximum widening from plastic deformation process description by displacement-rate fields

04 p0602 A71-14608

FLAW DETECTION

U NONDESTRUCTIVE TESTS

FLAWS

U DEFECTS

FLEXIBILITY

Glass reinforced polyester laminates under static and repeated loading, investigating resin flexibility effects on fatigue strength

02 p0274 A71-12479

Semiempirical bending, axial and torsional flexibility coefficients for structural joint assemblies, noting dependence on assembly diameter

07 p1209 A71-18903

Brittle alumina ceramic tensile and flexural strengths comparison based on statistical surface flaw distribution theory of fracture

09 p1484 A71-23699

Structural system analysis by partial decomposition of flexibility and stiffness matrices, obtaining coordinate deformations for computer and hand applications

10 p1691 A71-24693

Spar box structure under pure bending noting flexural rigidity and stress and stability analysis with Karman nonlinear equations

12 p1981 A71-27498

Reinforced plates flexural and torsional rigidity characteristics for stiffeners design, considering oblique angular coordinates system

12 p1982 A71-27509

Dual spin spacecraft bearing assembly flexibility effects on attitude stability, discussing time constant

[AIAA PAPER 70-1043] 12 p1973 A71-27569

Stainless steel wire fibers in refractory castables, noting flexural and compressive strength improvements

13 p2093 A71-28663

Longitudinal and transverse rib reinforced plates with parallel cracks extending to edge, obtaining flexural rigidity and stress-strain state

13 p2156 A71-29070

Helicopter rotor stall characteristics, investigating blade flexibility, unsteady aerodynamics and variable inflow effects

[AHS PREPRINT 520]

14 p2171 A71-31086

Strain rate effects on composite material tensile and flexural properties measured by load sensors and streak photography

17 p2737 A71-34345

Dynamic flexibility method based on Green resolvent, presenting applications to linear damped/un-damped forced/free harmonic/periodic vibration

18 p2947 A71-36177

Rotor elements eccentricity effect on rotor dynamic deflection, discussing rotor unbalance determination

24 p3884 A71-45010

FLEXIBLE BODIES

Flexible Storable Tubular Extendible Member /STEM/ in-plane bending vibrations under solar heating

01 p0173 A71-10941

Curvature matching method for two dimensional flexible plate nozzle contour of trisonic wind tunnel, obtaining overdetermined simultaneous equations

01 p0068 A71-10970

Cable-connected spinning and orbiting satellite spring-mass system, deriving in-plane motion equations by Hamilton principle for numerical analysis

01 p0165 A71-11587

LAMS flight control systems for gust load alleviation and structural mode stabilization on large flexible aircraft, using aerodynamic surfaces

02 p0188 A71-11659

Dynamical investigation of deformable gyrostats stability in circular orbit subject to gravitational torques, noting equilibrium states and damping effects

04 p0662 A71-15142

Flexible bar as spatial filter for measuring wave number-frequency spectra of distributed random processes

05 p0822 A71-16405

Equilibrium equations for flexible plates and shells with nonlinear terms in one dimensional case

06 p0989 A71-17782

Flexible plates and shallow shells supercritical deformation in high temperature field, taking into account modulus of elasticity and thermal expansion coefficient temperature dependence

06 p0990 A71-17796

Flexible aircraft to atmospheric turbulence transfer functions, discussing in-flight measurements

06 p0847 A71-18021

Semiempirical bending, axial and torsional flexibility coefficients for structural joint assemblies, noting dependence on assembly diameter

07 p1209 A71-18903

Flexible elastoplastic shallow shell theory, using mixed variational principle for flexure velocity and stress function

09 p1535 A71-22179

Hybrid coordinate formulation for flexible space vehicle attitude control system design

[AIAA PAPER 70-20]

09 p1532 A71-22907

Thin flexible panel acoustic power radiation due to turbulent boundary layer wall pressure fluctuations excitation

10 p1596 A71-24814

Validity range of response prediction methods for large flexible aircraft to continuous atmospheric turbulence, discussing power spectral densities and fatigue life

[AIAA PAPER 71-342]

11 p1707 A71-25321

Computer program for aerodynamic forces on flexible plate undergoing transient motion in shear flow, applying to panel flutter

12 p1866 A71-27559

Flexible spacecraft attitude control and classification systems based on mathematical models

12 p1973 A71-27604

Approximate critical stresses during longitudinal compression of nonmetallic rods of medium flexibility, using stability loss curve tangent to Euler hyperbola

13 p2091 A71-28295

Approximate method for nonlinear ordinary differential equations with variable coefficients applied to cylinder oscillation and flexible ring deformation

14 p2324 A71-29881

Time independent three dimensional streaming secondary motion due to vibrating flexible plate

14 p2325 A71-30061

Flexible spherical domes elastic-plastic deformation, using variational equation and iterative algorithm

14 p2331 A71-30840

High precision safety couplings performance, discussing flexible clutches enhancing effects

15 p2413 A71-31481

Rectangular flexible plate displacement theory, solving boundary value problems with fractional step method

17 p2824 A71-34848

Redundancy method for correct performance of flexible structure with faulty elements prepared from microelectronic information media

17 p2720 A71-34955

Aerodynamic control surfaces optimal location for flexible aircraft disturbed by random wind gusts, using matrix minimum principle and calculus of variations

19 p2998 A71-38713

Lumped parameter simulation model for flexible turbine rotor dynamics in nonspinning coordinate system, discussing bearing constraints modeling methods and eigenanalysis applicability

[ASME PAPER 71-VIBR-71]

21 p3385 A71-40309

Flexible rotating shafts high speed, rigid body and modal balancing machines

[ASME PAPER 71-VIBR-73]

21 p3460 A71-40311

Flexible rotor multiplane field balancing analysis, investigating test validity and accuracy and sensing instruments effects

[ASME PAPER 71-VIBR-74]

21 p3460 A71-40312

Flexible rotor balancing by exact point speed influence coefficient method

[ASME PAPER 71-VIBR-91]

21 p3386 A71-40324

Transient and steady state flexible rotor dynamics analysis

[ASME PAPER 71-VIBR-92]

21 p3461 A71-40325

Vibration characteristics of cantilever beam about nonlinear equilibrium state, showing flexibility and prestressed state effect

21 p3468 A71-40968

Motion stability analysis for force-free spinning satellites with flexible appendages by Liapunov direct method

[AAS PAPER 71-345]

23 p3772 A71-43018

Attitude stability of dual spin spacecraft with energy dissipation in flexible momentum wheel having two degrees of freedom

[AAS PAPER 71-347]

23 p3772 A71-43020

Analysis and stability of multiloop attitude control systems for flexible spacecraft

23 p3773 A71-44091

Geometrically nonlinear elastoplastic bending of rectangular flexible plates with various side ratios, using finite difference and strain theory

24 p3883 A71-44849

FLEXIBLE WINGS

NT PARAWINGS

Aerodynamic decelerator technology, emphasizing ribbon parachutes and flexible wings

06 p0846 A71-17692

Flexible ram air inflated keel and leading edge parawing design optimization for increased stability and reliability, introducing semirigid member concept

[AIAA PAPER 71-986]

24 p3791 A71-44582

FLEXING

Variational equation of motion for thin walled open section bars coupled flexure and torsion, considering thermal effects

[ASME PAPER 70-WA/APM-51]

03 p0513 A71-14169

Pure bending and flexure in plane stress with moment stress effects taken into account, considering Saint Venant principle

04 p0672 A71-15769

Torsional-flexural stability of stiffened Ti panels for application to supersonic transport, using small deflection energy methods

[AIAA PAPER 71-338]

11 p1843 A71-25317

Laminated plate flexural mode free vibration analysis by asymptotic method, obtaining phase velocity for comparison with experiment

14 p2330 A71-30684

Shear modulus, flexure and buckling of web stiffened sandwich structures, using core layer model based on continuum theory

[ASME PAPER 71-APM-8]

16 p2656 A71-33217

Wrinkled flat membranes analogy to very thin plates in flexure

18 p2982 A71-36836

Partial thickness cracks of preselected depths and shapes by axial and flexural fatigue methods, yielding preferred propagation path

20 p3248 A71-38780

Dynamic flexures in beam during massive extended load motion with allowance for inertial forces, using Bubnov-Galerkin method

23 p3778 A71-44046

Wanshaff vertical circle flexure determination at Goloseyev, using collimator tube, plane mirror and autocollimation ocular

23 p3680 A71-44262

FLEXORS

Cerebrospinal knee and flexor reflex suppression observations in rabbits and cats during blood circulation disorders

09 p1391 A71-22480

Human muscle power fluctuations under steady state physical activity, analyzing finger flexors strength

17 p2683 A71-35172

FLEXOWRITERS [TRADEMARK]

U AUTOMATIC TYPEWRITERS

FLEXURE

U FLEXING

FLICKER

Postexcitatory inhibition of monochromatic flickering potentials on electroretinogram in man under intensive dazzling stimuli

10 p1564 A71-24443

Retinal sine wave flicker transient response obtained with circular uniform field and counterphase grating targets

11 p1799 A71-26141

Cat type I and II optic nerve fibers response to flicker stimulation, noting receptive field organization, conduction velocity and temporal and spatial information processing

13 p2008 A71-28459

Flash threshold perception in relation to flicker, showing flicker/flash sensitivity ratio constancy over large intensity level range

22 p3497 A71-41479

Test field size, brightness and retinal location effect on observer assessment of stimulus at subvisual frequencies flicker suggesting inherent clock mechanism within human brains

22 p3499 A71-41497

Flicker adaptation effect on visual sensitivity to temporal fluctuations of light intensity

23 p635 A71-43974

Human eyes macular pigment optical density curves through spectral sensitivity measurements, noting differences due to race, environment, age, skin, eye and hair color

24 p3794 A71-44466

FLICKER FUSION FREQUENCY

U CRITICAL FLICKER FUSION

FLIGHT

Flying motivation loss, considering psychogenesis and physiological causes

05 p0715 A71-16933

FLIGHT ALTITUDE

Man machine considerations in all-weather low level navigation system design, noting off-course error reduction by command information display to pilot

01 p0125 A71-10515

Sounding rocket design parameters optimization, investigating apogee-payload relations, thrust as function of time, total weight, maximum altitude and acceleration

09 p1531 A71-22127

Jet transport aircraft design for safety under air turbulence conditions, considering cruise altitude limitations and pitch and g excursion reduction by special autopilot mode

14 p2173 A71-29777

Frequency modulated radio altimeters, discussing problems of altitude measurement independent of airplane motions in pitch and roll and immunity to fog effects

15 p2408 A71-31918

Altitude, bank angle and thrust program for minimizing time required by supersonic aircraft to turn through specified heading angle and reach required energy

[AIAA PAPER 71-796]

16 p2525 A71-34021

FLIGHT CHARACTERISTICS

Aircraft flying qualities research program, discussing navy test pilot evaluations and longitudinal handling characteristics for simulated carrier landing task

[AIAA PAPER 69-897]

02 p0189 A71-12678

Acrostar acrobatic aircraft design and performance

03 p0346 A71-13016

Clear air turbulence effects on flight and structural response of aircraft, using gust loads model

[ONERA-TP-867]

03 p0346 A71-13136

Sandhawk research sounding rocket performance, aerodynamic and flight characteristics for heavy payload transport to high altitude

[AIAA PAPER 70-1398]

03 p0499 A71-13679

Sounding rocket vehicle static stability reduction due to aeroelastic bending, using flight characteristics and wind tunnel test data for computerized analysis

[AIAA PAPER 70-1400]

03 p0499 A71-13681

Airfoil profiles with flaps at medium Reynolds numbers, determining performance characteristics in wind tunnel tests

04 p0526 A71-15025

Tilt-rotor VTOL aircraft design, discussing ground proximity effects on blade bending moments and flying qualities

04 p0531 A71-15404

Rotorcraft ideal height-velocity boundary and critical decision point height prediction, discussing pilots optimal control under emergency conditions

04 p0527 A71-15414

Air transportation systems ride vibration environments in relation to human comfort

04 p0532 A71-15421

Hovering and low speed flight capabilities of tilt wing VTOL aircraft in terminal area under near-zero visibility instrument landing conditions

[AIAA PAPER 71-7]

06 p0847 A71-18481

Design objectives for subsonic, transonic and supersonic civil transport flying characteristics based on MIL-F-8785, considering aircraft control

[SAE-ARP-842B]

07 p1019 A71-19645

Turbulent/total flight mile ratio in high altitude clear air turbulence /HICAT/ program 07 p1022 A71-20314

Flight testing of Diamant 18 glider, discussing aircraft behavior at low and high flight speed, stall, spin, stability and control characteristics, design and construction 08 p1230 A71-20686

Noise reduction at source, flight methods adjustments and airport compatible land use for jet noise abatement 08 p1378 A71-21815

Land use strategies and noise reduction by source control and flight procedures for noise exposed areas minimization 08 p1378 A71-21818

Flight time, path and fuel consumption in climb at constant radius turn, variable or constant velocity and constant engine power, deriving approximate simple formulas 08 p1232 A71-22050

Lifting body vehicle handling qualities, considering X-24A, M2-F3 and HL-10 reentry vehicles flight characteristics and simulation requirements [AIAA PAPER 71-310] 09 p1532 A71-22622

Effect of asymmetrical inviscid flow from Trail-blazer flight measurements, discussing windward leeward attenuation variation in transmitted VHF signal 09 p1406 A71-22916

Concorde airworthiness requirements and Air Registration Board participation in flight test program, considering supersonic flight characteristics 09 p1385 A71-23579

Soviet book on aircraft flight with incomplete and asymmetrical thrust covering probabilistic characteristics, stability, landing and takeoff with partial engine failures, etc 10 p1554 A71-24013

FAA flying and handling qualities program, discussing development of optimum and minimum acceptable flight characteristics criteria for new civilian and military aircraft designs [SAE PAPER 710372] 10 p1554 A71-24241

Light general aviation airplanes flying qualities in-flight simulation, considering longitudinal short period frequency and damping, pitch control sensitivity and lift curve slope [SAE PAPER 710373] 10 p1554 A71-24242

Light aircraft longitudinal stability control systems, discussing downspring and bobweight effects on flight characteristics [SAE PAPER 710388] 10 p1555 A71-24252

Wind gradient effect on flight characteristics during aircraft landing approach, particularly path deviation 11 p1706 A71-25194

Aircraft handling rating scales efficiency, noting difficulty in understanding and interpreting pilot opinion 12 p1875 A71-27253

Cruising flight range as function of supersonic/subsonic transport fuselage geometrical parameters 12 p1868 A71-27494

Aircraft flight characteristics dependence on angle of attack, roll and pitch 13 p1997 A71-29043

Flight characteristics of ion engine powered automatic laboratories in upper ionosphere 13 p2146 A71-29210

Flight characteristics under atmospheric turbulence conditions, analyzing analog trace records of airspeed, normal acceleration, altitude, air temperature, control surface and flight attitude parameters 14 p2173 A71-29771

German monograph on linear theory of optimization problems for low thrust rockets covering orbital calculations, flight characteristics and Coast Arc problem 14 p2319 A71-30233

Forward flight performance of coaxial rigid rotor in NASA wind tunnel, comparing to aerodynamic stability with conventional rotors [AHS PREPRINT 524] 14 p2178 A71-31090

STOL aircraft flight characteristics in proximity to ground, comparing analytical results with wind tunnel test data [AIAA PAPER 71-579] 15 p2349 A71-32281

Concorde flight characteristics, discussing performance flight test data relationship to design 15 p2350 A71-32690

Flying qualities military specification, discussing longitudinal static stability, transonic flight relaxation, control forces in maneuvering flight, lateral-directional oscillations, etc 16 p2523 A71-34004

Civil V/STOL aircraft projects, discussing design, lift fan engines, weights, flight performance, noise levels, safety and comfort standards 16 p2525 A71-34101

High speed aircraft maneuvers stability determination by constant angular pitching/rotation velocity, angle of attack and flight speed, using Liapunov method 18 p2849 A71-36176

Thermal design, analysis, testing and flight performance of ITOS-1 spacecraft, noting fail-safe temperature regulation [ASME PAPER 71-AV-23] 18 p2868 A71-36390

Three day mission biosatellite environmental thermal control system design and flight performance [ASME PAPER 71-AV-33] 18 p2869 A71-36400

Subsonic flight characteristics of LB 21 reentry vehicle, discussing lateral directional stability and lifting fuselage 18 p2972 A71-36436

Flight dynamics for aircraft noise reduction, gust effects decrease and dynamic stability of parachute load systems 18 p2850 A71-36752

Flight investigation of turbulence effects on aircraft longitudinal flying qualities, evaluating pilot ratings for ILS approach task [AIAA PAPER 71-905] 19 p2995 A71-37156

Discrete time digital flight control systems design resulting in closed loop aircraft response characteristics approximation to prescribed flying quality specifications [AIAA PAPER 71-955] 19 p3024 A71-37196

Soviet book on practical aerodynamics of aircraft with turboprop engines covering piloting, forces and moments, stability, controllability, takeoff, landing, etc 19 p2994 A71-38534

Tilt-fold-proprotor VTOL aircraft stability and control, emphasizing pylon tilt and rotor stop-fold effects on flying qualities 19 p2998 A71-38652

Reflex mechanisms and programmed command in insect flight stabilization, discussing gravity proprioceptors, wind sensing and optomotor control 21 p3326 A71-39987

Vortex wakes transport and decay for various aircraft types, flight modes and meteorological conditions 21 p3320 A71-40499

Atmospheric wind, temperature, turbulence, hydrometeors, ozone, cosmic radiation and radio activity effects on commercial SST Concorde flight 21 p3325 A71-40829

Variable stability aircraft lateral directional flying qualities, investigating turbulence effects 22 p3483 A71-42833

FLIGHT CLOTHING

Flight helmet sound attenuation test, using Manikin method 01 p0026 A71-11189

Flight personnel green protection system from nuclear weapons high intensity thermal effects 06 p0858 A71-17609

Properly fitting flight helmets for U.S. Army aviation personnel in Vietnam 06 p0859 A71-17616

Skylab and space station crew garments, discussing personal preference and style integration with function and overall system impact [AIAA PAPER 71-875] 18 p2870 A71-36630

FLIGHT CONDITIONS

Soviet book on meteorological conditions and supersonic aircraft flight covering atmospheric composition and structure, temperature distribution, wind effects, etc 02 p0278 A71-12840

Flash blindness recovery with/without protection in simulated flight conditions, using aircraft instrument reading criteria 08 p1246 A71-20815

Reevaluation of emergency pressurization requirements for brief flights over 50,000 feet, considering pressure suit requirement 08 p1247 A71-20822

Flight characteristics under atmospheric turbulence conditions, analyzing analog trace records of airspeed, normal acceleration, altitude, air temperature, control surface and flight attitude parameters 14 p2173 A71-29771

Dog uropespin excretion dynamics under extremal flight conditions, detailing hypoxia, high temperature radical accelerations and impact G forces effects 15 p2358 A71-31322

Mathematical models of distance perception under flight conditions according to visible brightness of luminous surface 17 p2691 A71-35166

Automatic flight control accommodation to dynamic characteristics variations of airframe, providing uniform response for all flight conditions 19 p2996 A71-37296

Gravity effect and lift perception in flying insects and animals, discussing flapping flight and aerial locomotion in aerodynamic balance weightless state 21 p3327 A71-39988

Emotional stress of pilots in difficult flight conditions, noting pulse rate increase and biopotentials amplitude changes 24 p3800 A71-44473

FLIGHT CONTROL

NT AUTOMATIC FLIGHT CONTROL

NT AUTOMATIC LANDING CONTROL

NT FLY BY WIRE CONTROL

NT POINTING CONTROL SYSTEMS

NT THRUST VECTOR CONTROL

LAMS flight control systems for gust load alleviation and structural mode stabilization on large flexible aircraft, using aerodynamic surfaces 02 p0188 A71-11659

LAMS flight control systems for turbulence induced fatigue damage reduction in B-52 and C-5A aircraft, using mathematical models 02 p0188 A71-11660

Model performance index /Pi/ providing criterion for approximating one dynamic flight control system by another based on geometrical representation of linear autonomous systems [AIAA PAPER 69-885] 02 p0189 A71-12682

Flight control systems influence on military aircraft design and performance, discussing static stability, ride quality, flutter margin and maneuver load controls [AIAA PAPER 69-767] 02 p0190 A71-12683

Army avionics technology transfer to civil aviation, discussing communication systems, flight control and landing aids 04 p0557 A71-15017

Space launchers flight control and guidance systems technology, emphasizing use of onboard digital computers 05 p0817 A71-16678

Time vector method extension to equations of motion with real roots, noting applications to aircraft flight control problems 06 p0925 A71-18049

Interceptor missiles minimum flight time control, describing modified steepest descent algorithm for optimal trajectories [AIAA PAPER 71-19] 06 p0979 A71-18486

ATC automated systems, discussing National Airspace System En Route Stage A and Advanced Radar Terminal System [AIAA PAPER 71-244] 07 p1156 A71-19719

Late model F-4 air superiority aircraft and electronic flight control systems protection against lightning discharges damage to electric and electronic systems 07 p1021 A71-19940

VOR/DME ground station oriented aircraft area navigation horizontal guidance capability, discussing digital input/output flight control 08 p1331 A71-21166

Control and instrumentation fluidics, describing equipment, circuits and applications to jet engine controls, missile guidance, flight control, ordnance and machine tool control 09 p1386 A71-22775

Fluidic inertial instruments, describing sensor or transducer components, flight control systems, rate damper systems and attitude control systems 09 p1387 A71-22785

Experimental flight mechanics in terms of data processing quality, discussing subsystems control 10 p1581 A71-23928

Terminal area control, discussing geographically grouped visual information displays, controllers coordination, plan position indicators and telecommunication 10 p1639 A71-23945

Adaptive flight control systems, emphasizing bionics approach to self organizing systems 10 p1682 A71-24227

Constant attitude light aircraft flight control system, describing design studies for minimum pilot command requirements [SAE PAPER 710393] 10 p1555 A71-24257

Six degree of freedom hybrid digital computer program for complex flight control and associated mode logic design and training 11 p1736 A71-25852

Military aircraft flight test establishments, discussing airframe, engine, flight control and weapons delivery systems tests work flow integration requirements 11 p1708 A71-26315

Area navigation facility, discussing control and display and navigation standards 12 p1927 A71-26879

Hydraulically powered duplex input servos for flight control system of VFW-Fokker V/STOL fighter aircraft 12 p1867 A71-26884

L-1011 aircraft flying stabilizer, discussing choice of longitudinal flight control systems [SAE PAPER 710426] 13 p1996 A71-28312

Optimality conditions for initial functions of time lag control systems onboard flight vehicles with transient response dependent on preceding trajectory coordinates 13 p2043 A71-28733

VTOL aircraft minimum climb-to-cruise time transition optimal open loop and suboptimal closed loop control synthesis 14 p2220 A71-30799

Heavy lift helicopter flight control system design, emphasizing fly by wire electrical analog [AHS PREPRINT 503] 14 p2178 A71-31079

Concorde flight simulator at Toulouse, discussing flight control system, air navigation and certification 15 p2384 A71-31881

FLIGHT CREWS

- Spacecraft reentry trajectory angle of attack control by mechanically varying center of mass for axial loads
16 p2645 A71-33443
- Control configured vehicle design longitudinal requirements due to application of relaxed static stability and maneuver load control
[AIAA PAPER 71-786] 16 p2525 A71-34016
- Discrete time digital flight control systems design resulting in closed loop aircraft response characteristics approximation to prescribed flying quality specifications
[AIAA PAPER 71-955] 19 p3024 A71-37196
- Power by wire actuators and fly by wire flight controls, discussing systems configuration, reliability, economy and durability
20 p3183 A71-39150
- Aircraft wake turbulence relation to CAT, discussing flight control loss, jumbo jets trailing vortex wakes breakup and detection and safe aircraft spacing
21 p3325 A71-40704
- Minimal time climb velocity optimization for stratospheric and tropospheric jet aircraft flights
22 p3482 A71-41972
- Commercial ATC, considering VFR, flight control and inertial navigation
22 p3570 A71-42078
- Microwave scanning beam guidance receiver design for aircraft landing aid, discussing time sharing and flight control
22 p3572 A71-42091
- Minimum order state vector reconstruction linear filters for constant plants optimal control, applying to aircraft flight multiple control-point problem
23 p3657 A71-44077
- Stability augmentation system for aircraft elastic modes control, discussing active flutter suppression technology
23 p3629 A71-44107
- Technology developments in rotor, drive, flight controls and cargo handling systems of heavy lift helicopter system, noting military and commercial applications
[AIAA PAPER 71-994] 24 p3792 A71-45296
- STOI, aircraft flight control problems, discussing Mach trim, artificial feel, stability, feedback system responses and lateral/directional laws
[AIAA PAPER 71-993] 24 p3792 A71-45297
- FLIGHT CREWS**
- Aircraft compartment glare minimization for flight crew visibility conditions and visual performance improvement
01 p0004 A71-10028
- Flight crew training process oriented systems approach through multimedia instruction
01 p0023 A71-10524
- Statistical analysis of airline flight crew psychological unfitness
01 p0028 A71-11598
- Aircrew radiological examination of spinal anatomical state, emphasizing traumatism due to vibration, acceleration, ejection and crashes
05 p0715 A71-16936
- Flight personnel green protection system from nuclear weapons high intensity thermal effects
06 p0858 A71-17609
- Hypoxia tolerance of aircrew with previous impaired flight consciousness in high altitude high performance aircraft
06 p0859 A71-17617
- Aircrews coronary insufficiency diagnosis via electrocardiographic modifications after exertion, observing ischemia
06 p0860 A71-18192
- Chlorates use in breathable oxygen production for aircrews
06 p0860 A71-18193
- Female aircrews under moderate hypoxia, noting uterine rheography modification
06 p0860 A71-18194
- Flight crews medicophysiological preparation for international glider competition
06 p0860 A71-18195
- Cargo aircraft crew safety and survival, describing restraint, escape, flight deck interior doors, fire and smoke hazards and personnel environmental protection
[SAE-ARP-1139] 07 p1019 A71-19643
- Recreational preferences among potential space crews from questionnaire analysis
08 p1248 A71-21231
- Soyuz 9 spacecraft crew medical support and post-flight examination, discussing earth environment readaptation
09 p1397 A71-22197
- Auditory analyzer functional changes in flight crews as result of long flights and emotional stress, noting cumulative effects of various harmful factors
10 p1569 A71-24340
- Operational preparation and commissioning of IL-62 long distance jet aircraft, considering flight crew and maintenance personnel training at U.S.S.R. plant
11 p1743 A71-25256

- Flight and operation of IL-62 long distance jet aircraft, considering flight crew composition and training, passenger and cargo handling and refueling
11 p1706 A71-25260
- Aircraft crew without pressure suits, noting abrupt ambient pressure drop tolerance in trained and untrained subjects
12 p1876 A71-27659
- Flight crew training, describing systematic tools, learning elements, managing systems and course organization
[SAE PAPER 710474] 13 p2016 A71-28303
- Flight crew training ground school programs, featuring automated instruction in cockpit classroom with audio visual machines
[SAE PAPER 710478] 13 p2017 A71-28343
- Personnel training in airline operations technology at Friedrich List Transportation Institute for aircraft pilots, flight safety engineers and systems engineers
13 p2021 A71-29143
- Aircraft personnel radiation hazards from radioactive luminous paint on instrument dials, signs and operational elements
13 p2021 A71-29145
- Soviet book on aviation medicine covering human anatomy and physiology, atmospheric physics, flight effects, respiratory systems, crew diets, etc
14 p2188 A71-29943
- DC 10 flight crew individualized ground training program, emphasizing hands-on equipment and instruction hardware
[SAE PAPER 710472] 14 p2176 A71-30538
- Flash field size effect on flash blindness of aircraft crews, measuring recovery time
16 p2535 A71-33113
- Long term spaceflight crew personal hygiene, discussing human waste processing and/or utilization, microbiological control and medical infirmary-dispensary-laboratory requirements
[AIAA PAPER 71-878] 18 p2870 A71-36631
- Ergonomic evaluation of flight crew working conditions from viewpoint of static and dynamic adaptation of aircraft system design to human psychophysical capabilities
19 p3007 A71-38016
- Aircraft noise effect on hearing impairment of cockpit crews in civil aviation, using audiometric evaluation
19 p3008 A71-38222
- Transport aircrew sleep patterns effects on fatigue and sleep disturbances, discussing physiologic debt and stresses
21 p3342 A71-40341
- In-flight study of work/rest cycle effects on double crew performance and fatigue in flying transport missions
22 p3501 A71-41829
- Cumulative /chronic/ and acute skill fatigue and physical fitness in aircrews, considering relationship to pilot error accidents
23 p3639 A71-43390
- FLIGHT FATIGUE**
- Electroencephalographic evaluation of brain functions disturbances in response to stress in flying personnel, relating fatigue and rest periods allocation
19 p3008 A71-38223
- Transport aircrew sleep patterns effects on fatigue and sleep disturbances, discussing physiologic debt and stresses
21 p3342 A71-40341
- Sleep related fatigue in pilot performance and flight safety, considering sleep lack and disruption and irregular duty patterns
21 p3343 A71-40590
- Cumulative /chronic/ and acute skill fatigue and physical fitness in aircrews, considering relationship to pilot error accidents
23 p3639 A71-43390
- FLIGHT FITNESS**
- Physical exercises to increase cosmonaut space environment tolerance, discussing effects of acceleration, altitude and hypoxia
01 p0027 A71-11556
- Statistical analysis of airline flight crew psychological unfitness
01 p0028 A71-11598
- Flight crews medicophysiological preparation for international glider competition
06 p0860 A71-18195
- Flight surgeons guidance criteria for flying personnel, detailing individual areas examination, documentation and clinical findings
08 p1245 A71-20719
- Preventive and clinical medicine effect on aircrew health maintenance
08 p1245 A71-20725
- Civil aviation medicine practice, discussing airman certification for flight fitness, government legislation, accidents and carrier operations
08 p1245 A71-20728
- Cosmonauts selection with regard to psychological and physical fitness, discussing clinical examination, hospital tests and training
09 p1397 A71-22192

- EKG examination of healthy aircrew for high performance aircraft flying fitness evaluation, stressing hyperventilation factor importance
12 p1876 A71-27631
- Aircrew static reach reduction caused by upper and lower limb orthopedic disabilities
12 p1876 A71-27632
- Tolerance tests including EEG, glucose test, thermal stress and G stress for aircrew fitness assessment after cranio-cerebral incidents
12 p1871 A71-27633
- Functions of medical services charged with ensuring flying personnel fitness, stressing aging process
13 p2018 A71-28487
- Airline flight personnel fitness downgrading, presenting statistical breakdown by age and physiological or psychological causes
13 p2019 A71-28509
- Physical fitness relation to flight requirements, pilot performance and age, considering muscular strength, cardio-respiratory capacity, body weight and mental aspects
16 p2528 A71-33114
- FLIGHT HAZARDS**
- NT METEOROID HAZARDS**
- Radiological risks of cosmic radiation during high altitude supersonic flights, considering galactic, solar and incident particles in aircraft atmosphere
03 p0473 A71-13099
- Lightning hazards for helicopters, discussing components vulnerability and protective design requirements
04 p0531 A71-15412
- Aeromedical requirements, control limitations and hazards of aircraft pressure cabins and rapid decompression
08 p1244 A71-20715
- Aerial transportation of patients, potential hazards due to motion sickness, decreased atmospheric pressure and oxygen tension, fatigue, inactivity and dehydration
08 p1245 A71-20726
- Materials and structural design development by high velocity impact testing due to transport and subsonic military aircraft susceptibility to bird collision damage
14 p2221 A71-29642
- Thunderstorm gust fronts from Oklahoma surface mesonet network and weather radar data, considering hazard to aircraft
14 p2267 A71-29757
- Pioneer Jupiter probe missions as precursor to subsequent outer planets exploration, discussing primary objective of asteroid belt and Jupiter radiation belt hazards evaluation
19 p3152 A71-37911
- Epidemiology statistics of USAF spatial disorientation aircraft accidents, noting pilot training, flight environment and indoctrination remedy programs
21 p3342 A71-40359
- Physiological factors in fatal aircraft accidents, discussing pilot incapacitation and transient functional disturbances
22 p3502 A71-41834
- Cervical vertebral distortion during acrobatic flight, discussing clinical and medico-legal aspects and preventive measures
23 p3632 A71-43219
- Water vapor-droplet transitional state and halo observation around light sources in radiative fog formation, applying to flight weather forecasts
24 p3844 A71-44866
- FLIGHT INSTRUMENTS**
- NT APPROACH INDICATORS**
- NT ATTITUDE INDICATORS**
- NT AUTOMATIC PILOTS**
- NT FLIGHT TEST INSTRUMENTS**
- NT GYRO HORIZONS**
- NT HORIZON SCANNERS**
- NT RADIO ALTIMETERS**
- Man machine considerations in all-weather low level navigation system design, noting off-course error reduction by command information display to pilot
01 p0125 A71-10515
- Three axis flight director for precise helicopter control, deflected slipstream STOL or VTOL attitude and power under low ceiling and visibility landing
04 p0624 A71-15428
- Pilot visual perception time of instrument readings after viewing external features and landmarks
07 p1053 A71-20540
- Navy pilots performance improvement through symbolic flight displays
09 p1453 A71-23675
- Turn rate gyro installation angle and airspeed effects on instrument reliability, presenting in-flight investigation results relative to turn rate information usefulness under various flight conditions
[SAE PAPER 710380] 10 p1610 A71-24245
- Flight helmets speech intelligibility evaluation using in-flight manikin recording
10 p1572 A71-25069
- Onboard area navigation systems in ATC environment, discussing route structure and flight instruments
[SAE PAPER 710455] 13 p2098 A71-28332

- Frequency modulated radio altimeters, discussing problems of altitude measurement independent of air-plane motions in pitch and roll and immunity to fog effects 15 p2408 A71-31918
- Pressure altimeter, airspeed and vertical velocity instruments, discussing selection, installation, pilot verification, error identification, repair and use 23 p3675 A71-43385

FLIGHT LOAD RECORDERS

- Boeing 747 flight loads measurements, describing aircraft instrumentation with strain gages and pressure pickups 03 p0348 A71-13766
- Bonded and weldable strain gages for aircraft flight loads measurements at high temperatures, discussing installation, calibration and performance tests 03 p0426 A71-13781
- Aircraft structural fatigue life in-flight monitoring, describing sensor installation on aircraft fin structure and measurement results 10 p1685 A71-23938
- Aircraft flight load measurements in high temperature environment, determining optimal strain gage installation and calibration 14 p2248 A71-30681

FLIGHT MECHANICS

- Soviet book on rocket flight dynamics covering center of mass motion characteristics, guided missiles, external ballistics, multistage design and flight optimization 02 p0320 A71-12724
- German report on activities of DFVLR covering flow and flight mechanics, navigation, aerospace structures, propulsion systems, space simulation and flight medicine 03 p0394 A71-12975
- Soviet book on space flight mechanics covering vehicle motion, engine systems, gravitational fields and trajectories 08 p1361 A71-21050
- Glider flight mechanics for turning flight, discussing relationships between turning radius, flight speed, sink rate and aerodynamic characteristics 08 p1232 A71-21770
- Experimental flight mechanics in terms of data processing quality, discussing subsystems control 10 p1581 A71-23928
- Aircraft integrated command and control system, discussing vertical, aerodynamic and horizontal situations, flight mechanics, power setting, telecommunications, etc 15 p2349 A71-31878
- Flight mechanics of point with limited power propulsion system and energy storage unit, investigating variational maximum payload problem with singular control optimization 20 p3288 A71-39125
- Correlation system of equations for mathematical expectations and phase coordinate correlation moments for accuracy analysis in flight vehicle dynamics problems 24 p3792 A71-44692
- Flight dynamics of noise optimal flight profiles for V/STOL aircraft, minimization of gust effects on aircraft and nonlinear dynamic stability of parachute-load systems 24 p3792 A71-44761

FLIGHT OPTIMIZATION

- Reentry lifting body hypersonic and subsonic flight enhancement by configuration modifications with compound curvatures minimization, giving wind tunnel model data 02 p0319 A71-11974
- Optimum flight paths for V/STOL aircraft operating in short haul transportation near city centers 04 p0624 A71-15443
- Flight simulator efficiency for optimal vehicle characteristics, considering in-flight, digital and manned techniques involving horizon indication and maneuver applications [DGLR-70-072] 05 p0732 A71-15960
- Flight range and optimum angle of attack under wind conditions of constant velocity and direction, considering fuel consumption for given distance 06 p0847 A71-18325
- Large flexible booster launch vehicle autopilots automated design and optimization by computerized technique in frequency and time domain 08 p1332 A71-21337
- Supersonic airplane minimum time turns at constant altitude, determining thrust, bank angle and angle of attack programs with optimal control theory 08 p1232 A71-22032
- Minimum propellant optimal rendezvous maneuver of two cosmic vehicles on circular orbits, considering tracking vehicle motion equations 10 p1672 A71-24335
- Optimal stochastic control and gust alleviation for jet aircraft response for flight through turbulent upwash field 10 p1557 A71-24870

- High altitude probe design and optimization, discussing hybrid propellant propulsion system peak altitude payloads and combustion temperatures 11 p1811 A71-25575
- Two stage rocket flight optimization for minimum propellant consumption, using calculus of variations 13 p2145 A71-28734
- Approximate multi-impulse large amplitude optimal rendezvous between neighboring elliptical orbits 17 p2807 A71-35472
- Aircraft performance and optimal energy flight path control in combat environment 19 p2997 A71-37724
- Automatic multi-satellite ephemeris maintenance by mathematical procedures, describing computer automated scheduling system program [AAS PAPER 71-355] 23 p3728 A71-43026
- Design parameter optimization for two-stage space shuttle atmospheric flight from spherical nonrotating earth by sequential straight line approximation 23 p3774 A71-44115

FLIGHT PATHS

- NT GLIDE PATHS
- Missiles and aircraft trajectories computation time reduced via time sharing and hybridization 02 p0227 A71-11794
- Aircraft propulsive thrust moment effect on phugoid motion, examining angle of attack and flight path variations with resulting instability 03 p0347 A71-13340
- Rocket probe with constant tangential acceleration in planetary gravitational field, investigating flight direction 03 p0495 A71-14388
- Unmanned scientific missions to outer planets in late 1970s, discussing instruments requirements, flight paths, spacecraft designs and payloads 04 p0649 A71-15347
- Frequency and amplitude during longitudinal control surface pumping by pilots in precise flight path handling for aircraft design [AIAA PAPER 70-567] 06 p0847 A71-17699
- Mars lander deorbit trajectory sensitivity analysis for fixed flight path and communications angles at atmospheric entry, comparing with Monte Carlo simulation [AIAA PAPER 71-190] 06 p0978 A71-18628
- Aircraft navigation system requiring computer and display for approach guidance to circular orbit over fixed ground area [AIAA PAPER 69-986] 07 p1156 A71-20305
- Supersonic airplane minimum time turns at constant altitude, determining thrust, bank angle and angle of attack programs with optimal control theory 08 p1232 A71-22032
- Cut-off Mach number of sonic bang propagation on ground for flight track in relation to atmospheric parameters 09 p1383 A71-23577
- Sounding rocket flight accurate trajectory data, determining cost effective radar tracking system 10 p1610 A71-24149
- Engine inlet noise prediction from static test and flyover data as function of time at various observer locations, examining suppression effects on total spectra [SAE PAPER 710386] 10 p1659 A71-24250
- Flight path optimization with multiple time scales, discussing decoupling of high order three dimensional aircraft flight problem into several low order problems 10 p1556 A71-24858
- Supersonic flight path curvature effects on local shock wave production, considering no boom zone and ground rules 11 p1708 A71-26310
- V/STOL aircraft flight path and attitude controls in turbulence, discussing design based on state variable methods of control theory 14 p2173 A71-29776
- Satellite flight trajectories construction, proposing algorithms for computer and automatic curve plotter 16 p2605 A71-33444
- STOL aircraft guidance capability with onboard digital computer, maintaining time of arrival envelope at way points along complex flight paths [AIAA PAPER 71-770] 17 p2775 A71-35528
- Passive mapping of terrain with sidelooking radiometry by storing received signals from various elements over extended flight path 17 p2746 A71-35763
- Omega navigation application to general aviation aircraft, presenting diurnal course shift to overcome deficiencies 17 p2776 A71-35767
- Dynamic positioning stationkeeping and stability criteria for formation flight systems extended to helicopter and V/STOL transports 18 p2849 A71-35923
- Cost effective high speed projectile trajectory plotting system for gunnery range instrumentation, applying to aircraft path recording during automatic landing control 18 p2924 A71-36613

- Jet aircraft flyover noise measurement, determining average intrusion level in residential communities under approach and departure corridors 19 p2996 A71-37497
- Sonic boomless transonic transports design, performance, economics and airline routes at Mach 1.2 and 0.98 [CASI PAPER 72/8] 19 p2996 A71-37598
- Two body orbits problem concerning satellite flightpath transfer possibility to orbit touching cyclic or elliptical trajectories 20 p3287 A71-38849
- Aircraft lateral dynamics effect on positioning accuracy along straight flight path, using Loran C data 20 p3261 A71-38864
- Analytical model for air navigation and ATC system design, demonstrating system parameters effects on lateral separation standards for parallel flight lanes 22 p3571 A71-42083
- Computer graphic interactive flight path design program for planetary flyby missions [AAS PAPER 71-380] 23 p3702 A71-43050
- Prop rotor and lift fan VTOL aircraft ground noise level reduction, using flight trajectory management [AIAA PAPER 71-991] 24 p3792 A71-45295

FLIGHT PERFORMANCE

U FLIGHT CHARACTERISTICS

- Commercial V/STOL aircraft area navigation system requirements, discussing airborne computer, flight plan data storage and control subsystems and horizontal orientation display 10 p1639 A71-24150
- Tu-154 responsibilities of three-man crews, considering flight plan, refueling, cargo loading and unloading 11 p1744 A71-25258
- French ATC, discussing automatic coordinator systems, computer utilization and flight plan data processing 14 p2272 A71-30382

FLIGHT RECORDERS

- Civil aircraft accident and maintenance recording regulations and systems, discussing airborne equipment 03 p0348 A71-13735

FLIGHT RULES

NT INSTRUMENT FLIGHT RULES

- Sonic boom implications and decision on acceptability with alternative policies of complete barring, controlled corridors and overflight limitations [CASI PAPER 72/4] 19 p2996 A71-37595

FLIGHT SAFETY

- Avionics system maximizing pilot chances of surviving mission and destroying selected target by removing mental limitations 01 p0124 A71-10506
- ATC system improvement by procedural changes, applying probability concepts to flight safety 02 p0278 A71-11699
- General aviation safety and effectiveness enhancement through electronic technology applications, discussing airspace control system based on beacon transponder, LF-VLF area navigation and vertical radar 05 p0780 A71-17228
- Apollo 13 in flight emergencies and countermeasures, discussing fire in Service Module oxygen tank causes and effects on spacecraft systems and solutions 07 p1206 A71-19087
- Aerospace Recommended Practice criteria for flight deck crew escape systems applicable to all commercial aircraft propulsion systems, design speeds and payloads [SAE-ARP-808A] 07 p1019 A71-19646
- Preventive and clinical medicine effect on aircrew health maintenance 08 p1245 A71-20725
- Space shuttle safety, discussing rocket engine durability, turbine life, flaw detection, radiation hazards, etc [AIAA PAPER 71-302] 09 p1511 A71-22616
- Space shuttle design, emphasizing reliability and safety [AIAA PAPER 71-303] 09 p1531 A71-22617
- Jet aircraft airworthiness standards, discussing airline fleet maintenance resources, inspection systems and future requirements 11 p1772 A71-26308
- Soviet book on space biology and medicine covering cosmonaut selection and training, flight safety, normal life support factors, interplanetary space sojourn, etc 17 p2689 A71-34475
- Psychosociological and medical evaluation of private pilots to promote flight safety 17 p2690 A71-34824
- ATC system safety problems from user standpoint, considering requirements by pupil, test and airline pilots and light, private, business, taxi and military aircraft 17 p2774 A71-35372

Sleep related fatigue in pilot performance and flight safety, considering sleep lack and disruption and irregular duty patterns

21 p3343 A71-40590

Space flight safety, discussing escape, rescue and survival design approaches for astronauts

22 p3611 A71-42037

Aircraft ditching and flying personnel survival, stressing passenger briefing and crew jacket equipment with VHF transceiver for rescue operations coordination

23 p3628 A71-43229

FLIGHT SIMULATION

Motion simulation in flight training devices, discussing basic phenomena, minimum requirements and methods of mechanization with regard to equipment design features and maintainability

01 p0066 A71-10017

Flight simulation in various degrees of environmental realism by visual and other physiological cues, discussing available devices and techniques relative to specific training tasks

01 p0066 A71-10020

Real time six degree of freedom aircraft flight digital simulation using SL-I continuous system simulation language

02 p0226 A71-11786

Six degree of freedom flight vehicle kinematics digital simulation using CSSL-II language

02 p0227 A71-11789

Hybrid real time computer simulation of external visual display cues for Apollo Command and Service Modules

02 p0237 A71-11791

Apollo Command and Service Module simulation of flight phases in lunar landing missions

02 p0237 A71-11792

N-body real time trajectory simulation of Apollo Command and Service module G and C systems and mission

02 p0237 A71-11793

Flight simulation requirements and design, considering analog computers, moiyon platforms and visual systems

04 p0566 A71-14996

Ground and airborne aircraft flight simulation methods, discussing simulator layouts and application to Concorde project

04 p0566 A71-15206

Rotary wing and VTOL aircraft controllability requirements definition through in-flight simulation of visual and kinetic impressions and environmental conditions by BO-105 helicopter

05 p0696 A71-16135

Piloted lunar escape to orbit systems simulation using simplified manual guidance and attitude control

06 p0977 A71-18519

Ground based flight simulation as engineering aid in aircraft design for evaluation of aircraft dynamics, handling qualities and control system characteristics over entire flight envelope

07 p1084 A71-20309

High turbulent flow simulation in hypervelocity wind tunnel for reentry vehicles operational testing, discussing nozzle gas dynamic and mechanical design

08 p1273 A71-21982

Stored arc heated air true temperature, flight and altitude simulation facility in Mach number 8 to 10 region for air breathing propulsion research

08 p1273 A71-21983

Lifting body vehicle handling qualities, considering X-24A, M2-F3 and HL-10 reentry vehicles flight characteristics and simulation requirements

09 p1532 A71-22622

Light general aviation airplanes flying qualities in flight simulation, considering longitudinal short period frequency and damping, pitch control sensitivity and lift curve slope

10 p1554 A71-24242

Human response to and perception of angular acceleration, discussing implications for motion capability in flight simulator

10 p1571 A71-24860

Positive/latero-lateral accelerations and acute hypoxic hypoxia effects on central visual fields behavior in simulated flight

10 p1571 A71-24978

Hybrid computer operating system for piloted aircraft simulation and optimization studies

11 p1736 A71-25853

Reentry heating simulation, noting UV radiation effects as shock layer thickness decreases

11 p1859 A71-26248

Total normal emittance under simulated reentry conditions, using emissometer with aluminum oxide reference cavity integral within sample

11 p1764 A71-26249

Hypersonic reentry flow over blunt nosed bodies, using water oxygen mixture to achieve simulation at lower stagnation temperatures

11 p1705 A71-26270

Roll rate variation and lift effect on reentry vehicle impact, comparing analytic treatment with six degree of freedom trajectory simulation

13 p2144 A71-27977

Relaxation distance for sharp cone behavior from chemical nonequilibrium laminar boundary layer effects on simulated space shuttle configuration during reentry

13 p2146 A71-29504

V/STOL aircraft gust effects prediction with mathematical models based on nonlinear hybrid simulation at takeoff and landing altitudes

14 p2173 A71-29775

Computerized simulation techniques for investigating aircraft accidents due to atmospheric turbulence

14 p2221 A71-29779

Motion platform systems evolution for flight research and training simulation

15 p2384 A71-31887

Flight simulation, discussing low training cost, maintenance, reliability and instructors certification standards

15 p2385 A71-32465

Solid propellant missiles underground silo self eject mode launching simulation, obtaining heat transfer, pressure and acoustic measurements

[AIAA PAPER 71-707] 15 p2385 A71-32576

Simulation tests of multiagency reconnaissance sensor operations, including multisensor data base, imagery processing laboratory, flight testing and ground truth activities

17 p2775 A71-35764

Space flight aerodynamic problems and wind tunnel simulation, considering satellites, maneuverability for landing and synergetic orbit rotation, hypersonic problems of reentry, etc

18 p2846 A71-36408

Long duration orbital simulator for technical planning activities, discussing capabilities, options, accuracy and central processing unit usage

18 p2885 A71-36460

Secondary visual tracking tasks utility in assessing lag effect in simulated combat aircraft dynamics

18 p2873 A71-36973

Augmentor wing high-lift aerodynamics, discussing results of wind tunnel tests and simulation studies

[CASI PAPER 72/20] 19 p2993 A71-37606

VTOL and fan lift STOL aircraft, discussing simulation and head-up displays for roll demand, vertical speed and ILS beam

21 p3413 A71-40134

Instrumentation in aerospace simulation facilities - Conference, Rhode-Saint-Genese, Belgium, June 1971

21 p3362 A71-40380

Nonlinear flight dynamic simulation using wind tunnel and aircraft model as analog function generator and computer for motion equation processing and command orientation

21 p3363 A71-40392

Heat transfer and pressure distribution of cone shaped model at different angles of attack in hypersonic flow simulating reentry flight in wind tunnel

22 p3480 A71-41965

FLIGHT SIMULATORS

NT COCKPIT SIMULATORS

Airline flight simulators and associated pilot training equipment, discussing improvements in flying control systems, computers, visual systems and power supplies

01 p0066 A71-10013

Flight simulators use in UK military flight training, discussing Full Mission Simulators concept and Royal Navy viewpoints

01 p0066 A71-10014

Flight simulators procurement and commissioning, discussing difficulties due to different aircraft configurations, advantages of equipment and procedures standardization, etc

01 p0066 A71-10015

Flight simulator visual systems, discussing improvement objectives in terms of current technology, image quality, system reliability and maintainability

01 p0066 A71-10016

Flight simulator ancillary features using computer data storing and processing capabilities for flight instructor decision making process improvement

01 p0066 A71-10018

Flight training by simulator, discussing justification and effectiveness criteria, transfer of learning to real flight situations, information flow models, full mission simulation, etc

01 p0066 A71-10019

Flight simulators pilot performance monitoring and recording, discussing multichannel data acquisition and use in specific training tasks performance evaluations

01 p0066 A71-10021

Spaceflight astronaut training, discussing guidance and navigation methodology of Apollo Mission Simulators

01 p0067 A71-10516

Aircraft navigator training, examining flight and ground trainer balance from cost effectiveness standpoint

01 p0022 A71-10521

Airborne trainer and ground simulator for undergraduate navigator training system

01 p0023 A71-10522

Moving cockpit flight simulator design with force and rotational acceleration vectors at pilot head location

[DFVLR-SONDDR-82] 03 p0396 A71-13343

Flight simulator efficiency for optimal vehicle characteristics, considering in-flight, digital and manned techniques involving horizon indication and maneuver applications

[DGLR-70-072] 05 p0732 A71-15960

Airborne flight simulator /helicopter/ as aircraft development aid

[DGLR-70-075] 05 p0733 A71-15965

Pilot training flight simulators without visual or motion cues, discussing validity for aircraft handling qualities assessment and pilot role in simulation process

[DGLR-70-070] 05 p0733 A71-15968

Flight simulators simulation width and parameter sensitivity analysis by state vector feedback method, using multiparameter control root-locus technique

05 p0733 A71-15970

Airborne variable stability helicopter flight simulator for V/STOL aircraft design

05 p0697 A71-16954

Shadow projector creating visual illusion of space surrounding flying aircraft for aviation training, relating perceived distortions to system parameters

06 p0864 A71-18716

Pilot physiological responses as indicators of pitch motion cues effect on flight simulator fidelity

07 p1047 A71-19465

Interactive Saturn flight program simulator for real time graphics operations of navigation, guidance, engine control, event sequencing and communications

08 p1272 A71-21237

Concorde economic flight testing methods, discussing Blagnac flight simulator mobile cabin visualization and color TV terrain model

12 p1868 A71-27608

Visual flight simulation devices, considering high resolution photographic films and digital memories

13 p2046 A71-29483

Low altitude turbulence simulation in piloted flight simulators, discussing turbulence induced aircraft disturbances and effects on pilot

14 p2188 A71-29781

Concorde flight simulator at Toulouse, discussing flight control system, air navigation and certification

15 p2384 A71-31881

Pilot training efficiency increase through advanced simulation technology utilization, discussing computerized flight simulators, CRT display systems and automated briefings

15 p2384 A71-31886

Reusable nuclear shuttle navigation systems evaluation by mission simulation, discussing reduced NERVA cooldown thrust pulses uncertainty effects

17 p2774 A71-35075

Total in-flight simulator (TIFS) in variable stability C-131 aircraft, describing potential as design tool

[AIAA PAPER 71-794] 17 p2675 A71-35529

Link 747 simulator with six degrees of motion system for engineers and pilot training

18 p2900 A71-36970

Boeing 747 digital computer type flight simulator with four degrees of movement for engineer and pilot training

18 p2901 A71-36971

Adaptive technique feasibility for flight simulator training of pilots

18 p2873 A71-36974

Operating principles of spaceflight simulators, considering star coordinates errors in collimator simulator of stellar sky

19 p3062 A71-37150

USAF total in-flight simulator model-following feedback control system, discussing conceptual design and flight test results

[AIAA PAPER 71-961] 19 p2995 A71-37202

Full mission engineering simulator/flight controls integration laboratory utilization in Apollo program, describing equipment for control systems testing, monitoring and troubleshooting

[AIAA PAPER 71-970] 19 p3040 A71-37211

FLIGHT STABILITY TESTS

Rapid hybrid frequency response method for aircraft flight flutter testing based on hybrid computing system

01 p0049 A71-10228

F-8D aircraft transonic flight and wing tunnel tests for buffet onset prediction, considering effects of g level and fluctuation amplitude and frequency

[AIAA PAPER 70-341] 10 p1557 A71-24863

Transient dynamic characteristics of aircraft under unsteady flight, using Laplace-Carson integral transforms

24 p3792 A71-45016

FLIGHT STRESS

Soviet book on aviation medicine covering human anatomy and physiology, atmospheric physics, flight effects, respiratory systems, crew diets, etc

14 p2188 A71-29943

- Transport aircrew sleep patterns effects on fatigue and sleep disturbances, discussing physiologic debt and stresses 21 p3342 A71-40341
- FLIGHT STRESS [BIOLOGY]**
 NT SPACE FLIGHT STRESS
 In-flight telemetric ECG recordings of aircraft pilots during normal, abnormal and aerobatic flight, analyzing heart rate variations as function of stresses 03 p0370 A71-13064
 Physiopathological and otolaryngological repercussions of supersonic flight on SST passengers 03 p0371 A71-13098
 Jet pilots flight stresses assessment via biotelemetric transmission of pulse rate, respiratory rate, electrocardiographic data, flight altitude and velocity 10 p1567 A71-23880
 Vestibular system functions physical analog model, predicting responses to motion inputs and possible problems for flight situations 10 p1569 A71-24237
 Auditory analyzer functional changes in flight crews as result of long flights and emotional stress, noting cumulative effects of various harmful factors 10 p1569 A71-24340
 Cardiovascular functional reactions in pilot trainees during training flights, presenting case histories 10 p1570 A71-24341
 Flight concomitant pathogenetic effects on urinary tract conditions, noting kidney descent, inflammatory episodes and calculus 10 p1566 A71-24977
 Flight stress effects on blood pressure and eye accommodation from frequent takeoffs and landing of AN-24 aircraft 11 p1723 A71-25261
 Nervous/cardiovascular systems and blood composition changes in moderate duration military transport flights 12 p1874 A71-27163
 Functional diagnostics in aerospace medicine for evaluating pilot ability and flight stresses 13 p2018 A71-28488
 EEG and derivative spectral characteristics evaluation in determining pilot mental activity during flight 15 p2362 A71-31250
 Pilot psychic states in flight, including preliminary demobilization, drowsiness, stunning, euphoria and phobias 16 p2536 A71-33576
 Literature survey of nervous-emotional stress effects on pilot during flight, discussing premature fatigue, cardiovascular disorders, psychic disturbances and circadian rhythms 19 p3002 A71-37763
 Electroencephalographic evaluation of brain functions disturbances in response to stress in flying personnel, relating fatigue and rest periods allocation 19 p3008 A71-38223
 Unfavorable high intensity noise effects on auditory and motor analysts during space flight 22 p3495 A71-42793
- FLIGHT SURGEONS**
 Physical and physiopathological effects of high altitude supersonic flight in TF-104G aircraft told by flight surgeon 10 p1572 A71-24980
- FLIGHT TEST INSTRUMENTS**
 LAMS flight demonstration, discussing instrumentation, flutter boundary and dynamic response, aerodynamic testing and structural response to turbulence 02 p0188 A71-11662
 Space shuttle flight test instrumentation for launcher, spacecraft and airplane triple operational and maintenance system requirements, discussing digital data bus monitoring concept [AIAA PAPER 71-313] 10 p1609 A71-23974
 Flight test program, facilities and instrumentation for F-14 aircraft structural, powerplant, avionics, performance and carrier suitability evaluation 16 p2526 A71-34153
 Instrumentation in aerospace simulation facilities - Conference, Rhode-Saint-Genese, Belgium, June 1971 21 p3362 A71-40380
- FLIGHT TEST VEHICLES**
 B-52 LAMS test vehicle structural modification and instrumentation in flight phase 02 p0188 A71-11661
 LAMS flight demonstration, discussing instrumentation, flutter boundary and dynamic response, aerodynamic testing and structural response to turbulence 02 p0188 A71-11662
 Post Apollo program European participation in space tug design and orbiter model flight tests, considering mini shuttle support applications 11 p1839 A71-26331
- FLIGHT TESTS**
 NT FLIGHT STABILITY TESTS
 Inertial navigation system augmented by digital distance measuring equipment in FAA flight inspection aircraft for performance evaluation 01 p0124 A71-10507

- Aircraft turbine engine development, considering mismatch reduction between engine and airframe in flight tests 01 p0143 A71-11180
 B-52 LAMS test vehicle structural modification and instrumentation in flight phase 02 p0188 A71-11661
 Collision avoidance system flight test and evaluation program for airline industry CAS specification 02 p0280 A71-12896
 Standard-Cirrus glider flight test performance, noting cockpit design and instrumentation 03 p0346 A71-13019
 Flight test evaluation of onboard automatic computer controlled jet engine monitoring system with reduced fault detection time 03 p0395 A71-13080
 Time vector method for aircraft flight test data evaluation, discussing control deflections effects on phugoid motion, lateral stability derivatives and error estimation 03 p0347 A71-13341
 DC-10 aircraft test program effectiveness, discussing performance, operational envelope, airworthiness, noise measurements, etc [SAE PAPER 700830] 03 p0348 A71-13726
 Lifting body flight test program applications in manned space shuttle 04 p0661 A71-14819
 Skylab, space station and shuttle programs covering economics, international participation and ground and flight tests 04 p0661 A71-14928
 UH-1B helicopter flight test noise measurements data reduction and analysis, presenting sound pressure vs frequency and time plots 04 p0531 A71-15405
 Helicopter in-flight noise radiation pattern and spectra measurements for various operating parameters 04 p0531 A71-15406
 V/STOL aircraft visual aids flight evaluation concerning minimum landing area operations 04 p0534 A71-15445
 Flight testing of automatic orbital operations system for satellites and space probes [DGLR-70-080] 05 p0779 A71-15958
 Europa I third stage flight testing for onboard control system performance parameters [DGLR-70-061] 05 p0815 A71-15963
 Elfe S-3 glider flight test, pointing out imperfections in cockpit and wing design 05 p0696 A71-16128
 Concorde progress toward certification, discussing SST airworthiness requirements, flight test program, takeoff and landing operational experience and stability problems at high incidence 05 p0696 A71-16487
 Meteor meteorological rocket flight testing, describing performance, instrumentation and technical and organizational problems 05 p0817 A71-16639
 FAA full scale aircraft vortex wake turbulence flight test programs [AIAA PAPER 71-97] 06 p0848 A71-18552
 Hypersonic flight test base pressure results at high Reynolds numbers for slender cone in turbulent flow, noting implications for ground test simulation [AIAA PAPER 71-134] 06 p0883 A71-18578
 Phase locked automatic direction finder (ADF)/flight test results, indicating signal to noise threshold reduction by coherent detection 07 p1057 A71-18815
 ESRO 1 small scientific satellite attitude measurement system, discussing design and flight test results 07 p1154 A71-18840
 Flight tests - Conference, Beverly Hills, September 1970 07 p1017 A71-19076
 Naval aircraft testing, discussing weapons systems, funding commitments, outfitting schedules, time frames, contracts and management problems 07 p1018 A71-19077
 ARAVA STOL aircraft, describing payloads, configuration, design flight testing, stability and landing characteristics 07 p1018 A71-19082
 DC-10 flight test program, discussing handling, takeoff and landing, and flutter, stall and stability characteristics 07 p1018 A71-19085
 Height velocity (H-V) flight testing, giving results from OH-58A Kiowa and AH-1G Huey Cobra helicopters 07 p1018 A71-19093
 USAF F-4E Stall/Near Stall Investigation, discussing testing requirements, fighter aircraft improvement, spin avoidance and high angle of attack limitations 07 p1019 A71-19095
 ESRO 2 satellite program reliability prediction and procedures in design and manufacture, defects during development and tests and performance in orbit 07 p1207 A71-19552
 Electrostatic charging noise measurement, reduction and flight test verification 07 p1021 A71-19937
 Flight testing of Diamant 18 glider, discussing aircraft behavior at low and high flight speed, stall, spin, stability and control characteristics, design and construction 08 p1230 A71-20686
 Hawker Siddeley Trident 3B flight test program, booster engine, structural features, power plants, systems and landing gear 09 p1385 A71-22890
 SERT 2 spacecraft ion thruster ground tests and flight operation, tabulating performance data [AIAA PAPER 70-1125] 09 p1511 A71-22899
 Space shuttle development test program, discussing low cost dynamic structural and flight testing [AIAA PAPER 71-308] 09 p1532 A71-23017
 Concorde airworthiness requirements and Air Registration Board participation in flight test program, considering supersonic flight characteristics 09 p1385 A71-23579
 Light aircraft standard fuel flight evaluation, discussing compatibility with grades 80/87 and 100/130 certified engines and comparative operational fuel consumption [SAE PAPER 710369] 10 p1657 A71-24239
 Light aircraft qualification for icing conditions from flight test data, considering increase in instrument rated pilots and IFR flying activity [SAE PAPER 710394] 10 p1555 A71-24258
 Parachutes for low density atmospheres, describing low and high altitude test results [AIAA PAPER 70-1164] 11 p1707 A71-25525
 Flight test completed on onboard real time engine performance monitoring system, discussing thermodynamic analysis technique [ASME PAPER 71-GT-77] 11 p1813 A71-25991
 Military aircraft flight test establishments, discussing airframe, engine, flight control and weapons delivery systems tests work flow integration requirements 11 p1708 A71-26315
 European airbus, considering flight trials of first A.300B high capacity transport aircraft 12 p1867 A71-26921
 Flight tests of inertial navigation system in aerial geodetic mapping, achieving automatic side-lap, verticality and line position control 12 p1927 A71-27256
 Sounding rockets aerodynamic characteristics, comparing wind tunnel and flight test data 12 p1864 A71-27474
 Concorde economic flight testing methods, discussing Blagnac flight simulator mobile cabin visualization and color TV terrain model 12 p1868 A71-27608
 Yak 40 aircraft flight test program, discussing airworthiness requirements, static structural, vibration and wind tunnel tests 14 p2174 A71-29911
 Concorde SST flight test equipment installation with PCM recording and visual instruments 14 p2174 A71-30055
 In-flight deployment balloon launching system with load lowering friction brake, discussing flight test results 14 p2175 A71-30071
 Integrated flight test data system combining digital airborne data acquisition/recording system with telemetry/microwave link to computerized ground station 14 p2243 A71-30318
 Airborne integrated data system capabilities based on flight tests with commercial aircraft 14 p2208 A71-30319
 High temperature capacitance strain gage development for aircraft testing, discussing instrument configuration and data reliability 14 p2248 A71-30682
 High performance UH-1 compound helicopter high speed flight research, considering rotor loads, stability, control and flying qualities [AHS PREPRINT 570] 14 p2180 A71-31111
 SYDAC ILS systems flight tests 15 p2446 A71-31911
 Concorde flight characteristics, discussing performance flight test data relationship to design 15 p2350 A71-32690
 DC-10 design dispatch and component reliability through flight test and follow-up fault isolation programs 16 p2522 A71-33297
 F-4E stall/spin development and flight tests, relating mass distribution and angle of attack aerodynamic design [AIAA PAPER 71-772] 16 p2524 A71-34008
 Harrier aircraft development from flight test viewpoint, discussing conventional flight envelope problems caused by V/STOL concept imposed constraints [AIAA PAPER 71-773] 16 p2524 A71-34009

FLIGHT TIME

- F-15 aircraft integrated data system for flight test program information, discussing development and major elements
[AIAA PAPER 71-774] 16 p2524 A71-34010
- DC 10 flight test program improvement using data acquisition/processing with real time monitoring, instrument landing and laser tracking
[AIAA PAPER 71-788] 16 p2553 A71-34018
- Flight test program, facilities and instrumentation for F-14 aircraft structural, powerplant, avionics, performance and carrier suitability evaluation
16 p2526 A71-34153
- French flight test center role in development and certification of Concorde aircraft, considering cooperation with industry
[AIAA PAPER 71-784] 17 p2675 A71-35526
- Total in-flight simulator (TIFS) in variable stability C-131 aircraft, describing potential as design tool
[AIAA PAPER 71-794] 17 p2675 A71-35529
- L-1011 flight test program, describing aircraft design and performance
[AIAA PAPER 71-789] 17 p2675 A71-35531
- Performance evaluation of variable geometry external fuel tank prototypes by static structural tests, wind tunnel tests and flight tests on F-11 aircraft
[AIAA PAPER 71-763] 17 p2675 A71-35533
- Experimental and theoretical aeroelastic analysis of Fokker F-28 T tail, using flutter model and flight flutter tests
17 p2676 A71-35649
- Flight test of hybrid strapdown inertial navigator with Doppler radar and occasional position fixes through Kalman filter mechanized in small computer
17 p2776 A71-35765
- ALOFT computer language for checkout and operation of complex space oriented equipment such as space shuttle
18 p2885 A71-36446
- TOTAL checkout computer language for future space vehicles, considering objectives, characteristics and merits
18 p2885 A71-36447
- Space shuttle tests and flight operation, discussing launching, maintenance, booster/orbiter mating, payload installation and orbital mechanics
18 p2974 A71-36490
- BAC 111 autopilot development, discussing computer compatible system for digital representation of airborne flight test data and direct transmission to ground-based computers
18 p2946 A71-36672
- Flight test results for CACTUS accelerometer launched by rocket probe at Guiana Space Center, considering atmospheric density profile in 120-150 km altitude zone
18 p2924 A71-36755
- Pilot workload reduction in steep approach landing of light aircraft from flight test data analysis
[AIAA PAPER 71-904] 19 p3095 A71-37155
- Flight investigation of turbulence effects on aircraft longitudinal flying qualities, evaluating pilot ratings for ILS approach task
[AIAA PAPER 71-905] 19 p2995 A71-37156
- USAF total in-flight simulator model-following feedback control system, discussing conceptual design and flight test results
[AIAA PAPER 71-961] 19 p2995 A71-37202
- Flight test measurements of shock cell noise loading of aircraft tail planes, noting alleviation by nozzle and mirror structural modifications
19 p2998 A71-38467
- Reliable and low cost electrical solar array/silver zinc battery power system for Agena satellite, discussing design features and flight tests results
20 p3182 A71-38943
- Blunt planetary entry probe full scale flight test base pressure measurements, noting insensitivity to angle of attack variations up to 10 degrees
20 p3176 A71-39353
- Low noise levels of DC-10 aircraft with CF6-6D turbofan engines, discussing design, flyover tests and FAA requirements
[CASI PAPER 72/5] 20 p3178 A71-39424
- Macaca nemestrina monkey bone density change during Biosatellite 3 mission
21 p3330 A71-40343
- Gun tunnel free flight testing system and components, discussing model dropping, magnetic suspension and light beam and RF tracing
[DFVLR-SONDDR-136] 21 p3362 A71-40382
- Trailing vortices behind wing tip with vortex dissipator, using wind tunnel flow visualization and flight tests
21 p3319 A71-40496
- Boeing 747, Lockheed C-5A and other aircraft vortex wake characteristics by tower flyby technique
21 p3320 A71-40498
- Flight tests for hazard evaluation to other aircraft from wake turbulence generated by large jet transport airplanes
21 p3321 A71-40506
- Flight test experiment to evaluate mechanized automatic control system to minimize wake turbulence effects on aircraft
21 p3321 A71-40509

- German VAK 191B combat VTOL aircraft development program, describing prototype ground tests, autopilot preoptimization and hover flight tests
22 p3482 A71-41517
- Flight test measurements for improved estimates of aircraft states and aerodynamic parameters, using relinearized Kalman filter
23 p3629 A71-44089
- Active flutter mode control system synthesis for flight test, showing mass balancing as possible artificial symmetrical wing destabilization
23 p3629 A71-44106
- Folding sidewall aircraft tires design, construction and flight tests, noting advantages and disadvantages
24 p3792 A71-44975

FLIGHT TIME

- Circadian rhythms synchronization changes in human biological and physiological functions during transmeridian flights
01 p0020 A71-11568
- High energy fast Grand Tour multiplanet flyby missions to outer planets omitting Jupiter, noting identical arrival date at Neptune
[AIAA PAPER 71-188] 12 p1958 A71-26697
- Orbital flight time in terms of isochronism kinematic theory, discussing Lambert and Hamilton hodographic representations
13 p2135 A71-28351
- Modeling of differences between actual and estimated flight times over radio beacon, obtaining cumulative frequency distributions
13 p2167 A71-28490
- Minimum time profiles for F-104 aircraft by Balakrishnan epsilon technique, comparing solutions with energy method
13 p1996 A71-28831
- STOL vehicle and systems air transportation expansion by reducing trip time, congestion, noise exposures and pollution for DOT, DOD and NASA roles
[SAE PAPER 710464] 14 p2176 A71-30535
- Apollo 15-17 CSM design modifications, discussing increased mission duration capability, lunar orbital science instruments operation and weight increase
[AIAA PAPER 71-821] 17 p2812 A71-34723
- Book on astrodynamics covering n body equations of motion, orbital elements, differential corrections, time of flight, ballistic missiles and interplanetary transport
18 p2963 A71-36248
- Central terminal rapid processing and high speed VTOL aircraft effects on airport design, flight time, cost and ATC
20 p3210 A71-39394

FLIGHT TRAINING

- NT SPACE FLIGHT TRAINING
Flight training simulators - Conference, London, October 1970
01 p0065 A71-10012
- Flight simulators use in UK military flight training, discussing Full Mission Simulators concept and Royal Navy viewpoints
01 p0066 A71-10014
- Motion simulation in flight training devices, discussing basic phenomena, minimum requirements and methods of mechanization with regard to equipment design features and maintainability
01 p0066 A71-10017
- Flight simulator ancillary features using computer data storing and processing capabilities for flight instructor decision making process improvement
01 p0066 A71-10018
- Flight training by simulator, discussing justification and effectiveness criteria, transfer of learning to real flight situations, information flow models, full mission simulation, etc
01 p0066 A71-10019
- Flight simulation in various degrees of environmental realism by visual and other physiological cues, discussing available devices and techniques relative to specific training tasks
01 p0066 A71-10020
- Simulated low visibility landing training, discussing airborne and ground based simulators
01 p0067 A71-10022
- Flight training simulator use in airline operations, discussing economics of various simulator types with projection toward ultimate simulator
01 p0183 A71-10023
- Aircraft navigator training, examining flight and ground trainer balance from cost effectiveness standpoint
01 p0022 A71-10521
- Airborne trainer and ground simulator for undergraduate navigator training system
01 p0023 A71-10522
- Complex navigation systems training philosophy emphasizing functional approach to system and components
01 p0023 A71-10523
- Flight crew training process oriented systems approach through multimedia instruction
01 p0023 A71-10524
- Air navigational training simulators, discussing navigation aids, civilian navigator use, visual simulation and land-mass radar
01 p0125 A71-10526

- Link 747 simulator design and operation, describing cockpit layout, motion picture system and malfunction insertion and display unit
06 p0881 A71-18663
- Light source displacement distortions in shadow visualization for flight trainers involving terrain scale and landing simulation
08 p1271 A71-20796
- Operational preparation and commissioning of IL-62 long distance jet aircraft, considering flight crew and maintenance personnel training at U.S.S.R. plant
11 p1743 A71-25256
- Ground based flight equipment evaluation in routine primary pilot training
12 p1875 A71-27249
- Flight crew training, describing systematic tools, learning elements, managing systems and course organization
[SAE PAPER 710474] 13 p2016 A71-28303
- Boeing 747 crew members training program, describing ground training, classrooms, inertial navigation system and cockpit trainers
[SAE PAPER 710473] 13 p1996 A71-28339
- Commercial airlines flight training program, using simulation and improved techniques for safety and economy
[SAE PAPER 710475] 13 p2044 A71-28340
- Training simulators as substitutes for airborne training, considering limitations and future developments
[SAE PAPER 710476] 13 p2044 A71-28341
- Flight crew training ground school programs, featuring automated instruction in cockpit classroom with audio visual machines
[SAE PAPER 710478] 13 p2017 A71-28343
- Airline pilot training specific behavioral objective concept, noting introduction with Boeing 744
[SAE PAPER 710479] 13 p2017 A71-28344
- Flight training program for twin-engine transition, using commercially available training device
[SAE PAPER 710480] 13 p2017 A71-28345
- Personnel training in airline operations technology at Friedrich List Transportation Institute for aircraft pilots, flight safety engineers and systems engineers
13 p2021 A71-29143
- Case histories of pilot failure during training or operational flight due to cerebral cortical dysfunction
13 p2023 A71-29365
- DC 10 flight crew individualized ground training program, emphasizing hands-on equipment and instruction hardware
[SAE PAPER 710472] 14 p2176 A71-30538
- Motion platform systems evolution for flight research and training simulation
15 p2384 A71-31887
- Flight simulation, discussing low training cost, maintenance, reliability and instructors certification standards
15 p2385 A71-32465
- Aircraft accidents due to engine-out simulation, discussing human factors, minimum control speed certification requirements and pilot flight training procedures
[AIAA PAPER 71-793] 16 p2525 A71-34025
- Serotonin metabolism of helicopter pilots, showing effects of emotional factors due to flight inexperience
23 p3632 A71-43220
- Psychological screening of pilot trainees, showing neurosis noncorrelation with learning ability to fly
23 p3639 A71-43221
- Corporate aircraft pilot ground and flight phase training, errors and accidents
23 p3629 A71-43388
- Continued flight training correlation with general aviation aircraft accident rates reduction
23 p3641 A71-44252

FLIGHT VEHICLES

- Elastic flight vehicles feedback control systems synthesis by invariance theory
01 p0163 A71-10714
- Soviet book on antenna radomes of flight vehicles covering electromagnetic wave transmission through dielectric media, fabrication, construction materials, etc
01 p0057 A71-11322
- Book on foam polyurethanes synthesis and use in flight vehicles
09 p1455 A71-23162
- Flight vehicle adaptive control systems with on-board digital computers, considering control algorithm complexity, processing rates, weight and geometry restrictions, accuracy and adaptability requirements, etc
12 p1883 A71-26715
- Nonlinear self adjusting and variable structure automatic control systems for piloted and pilotless flight vehicles, considering oscillations due to electric servosystems nonlinear characteristics
12 p1926 A71-26716
- Flight vehicles nonsearching self adjusting control systems synthesis, using gradient method with simplified sensitivity models
12 p1926 A71-26729
- Longitudinal proper motions of flight vehicle based on equivalent dynamic systems for trajectory coincident with nonsingular transformation in phase space
13 p2145 A71-28731

Flight characteristics of ion engine powered automatic laboratories in upper ionosphere
13 p2146 A71-29210

Flight vehicle equations of motion for computer simulation, calculating optimal servosystem parameters and optimal range control by hybrid computer scheme
14 p2319 A71-30001

Unmanned flight vehicles recovery system, describing built-in rotor design for navigation and high precision landing
[DGLR-71-020] 15 p2351 A71-32787

Hyperballistic free flight test facilities using light gas guns, considering wake of flight vehicle at hypersonic velocity and aerothermal phenomena
18 p2898 A71-36411

Correlation system of equations for mathematical expectations and phase coordinate correlation moments for accuracy analysis in flight vehicle dynamics problems
24 p3792 A71-44692

FLIP-FLOPS

High performance LSI main frame MOS flip-flops memory module for digital computers
01 p0047 A71-10210

Multiphase multivibrator with nanosecond pulse duration and parallel transistorized inductive correction, analyzing flip-flop circuit
02 p0230 A71-11831

Flow and dynamic pressure recovery in wall-attachment fluid amplifiers, considering large scale flip-flop
[ASME PAPER 70-WA/FLCS-9] 03 p0354 A71-14085

Jet switching dynamic behavior in bistable fluidic devices, examining flow field, response and switching time
[ASME PAPER 70-WA/FLCS-20] 03 p0355 A71-14093

Unstable high speed optronic /photoelectric/ flip-flop memory elements with positive optical feedback
07 p1075 A71-19303

Supersonic fluidic bistable switch, developing improved pressure recovery
07 p1029 A71-20590

Supersonic pitot fluidistor in bistable mode, investigating improved pressure and flow recovery at large expansion ratios
07 p1029 A71-20591

Delay compensation in flip-flop element of optimal relay system with self oscillations, using optimal control algorithm constructed by phase space method
11 p1742 A71-26095

Malfunction probabilities in presence of wideband noise for tunnel diode binary logic element /flip-flop/ pulse triggered into either of two output states
11 p1740 A71-26543

Flowmeter based on oscillating bistable fluid amplifier, discussing Mach number, Reynolds number and Strouhal number effects on measuring characteristics
15 p2352 A71-32066

Glass switching elements with storage properties for electronically controlled flip-flop circuitry, noting composition and fabrication
21 p3355 A71-40742

Flip-flop circuits nonlinear distributed network mathematical model, investigating oscillations nonexistence
22 p3527 A71-42626

FLOATING

Supporting fluid effects in floated inertial instruments, examining cause, frequency, extent and solution
02 p0253 A71-12462

Floating times of liquid/solid sphere on evaporative fluid /liquid nitrogen/ in metastable Leidenfrost film boiling
21 p3476 A71-40892

FLOATING POINT ARITHMETIC

Real polynomial quadratic divisors determination with maximum accuracy in floating point arithmetic, using Bairstow method algorithm
03 p0450 A71-13118

Floating point arithmetic units design for large high speed digital computer
12 p1884 A71-27151

Hybrid binary floating point digital differential analyzer technology, noting speed, cost and utility
14 p2207 A71-30021

Polynomial equation roots determination, analyzing floating point arithmetic errors
23 p3698 A71-43097

FLOATS

Floating airport structural design, using hollow concrete blocks filled with polystyrene foam as runway basic unit
09 p1428 A71-22949

FLOCCULATING

Floccule theory three dimensional planetary formation model of collapsing cloud leading to nonplanar system with protoplanets in retrograde orbits
23 p3769 A71-43991

FLOORS

Bent structure failure under pulse floor acceleration shocks, concerning aircraft seat damage during crash landing
08 p1367 A71-20747

FLORA

U PLANTS [BOTANY]

FLOTATION SYSTEMS

U FLOATS

FLOW

Flow patterns modification through space charges, demonstrating laminarization of turbulent flow and boundary layer separation prevention
04 p0569 A71-14985

FLOW CHAMBERS

Magnetic field effect on boundary temperature in axisymmetric MHD flow in vortex chamber, using dissipationless approximation
02 p0293 A71-12633

Optimum two fluid mixing chamber length for energy efficiency of conical diffusers in straight pipe jet pump systems
03 p0399 A71-13369

Aircraft fuel and air conditioning systems vortex valves and diodes, examining flow patterns into and out of chambers
07 p1025 A71-20556

Variable gap and chamber width effect on load bearing capacity of radial hydrostatic bearing with capillary throttling
16 p2584 A71-33616

Double-diaphragm shock tube optimal parameters with allowance for boundary layer effect behind shock wave propagating in central chamber
17 p2730 A71-35634

Optimum conical mixing chambers configuration in supersonic ejectors, showing cylindrical exhaust channel requirement
18 p2903 A71-36121

FLOW CHARACTERISTICS

NT BOUNDARY LAYER STABILITY

NT FLAME STABILITY

NT FLOW DISTRIBUTION

NT FLOW STABILITY

NT FLOW VELOCITY

NT MAGNETOHYDRODYNAMIC STABILITY

Blowing air conditions and flow parameters effects on film cooling efficiency for rotating cylinder
01 p0178 A71-10416

Steady three dimensional ideal dissociative gas flow along stream lines, examining velocity components, pressure gradients, density and mass fraction variable
02 p0239 A71-12124

Channel flow boundary layers, discussing parabolic differential equations, pressure gradients, friction coefficients, Stanton numbers, velocity and temperature profiles, etc
02 p0241 A71-12644

Flow characteristics in turbomachine blade cascades with transonic regime, emphasizing shock-boundary layer interaction phenomena
03 p0340 A71-13140

Unsteady flow induced by circular cylinder impulsive motions, examining vortices formation and interaction
03 p0399 A71-13197

Vortex sheet behavior in inviscid subsonic flow of lifting wing with nonzero trailing edge angle
03 p0342 A71-13738

Axial compressor flow characteristics by computerized calculation methods, considering annular duct swirling flow model
03 p0342 A71-13828

Input-output flow characteristics of direct and transverse fluidic impact modulators, using static model
[ASME PAPER 70-WA/FLCS-2] 03 p0354 A71-14077

Nonvented vortex fluid amplifier receiver tubes flow and performance characteristics
[ASME PAPER 70-WA/FLCS-18] 03 p0354 A71-14091

Air jet mixing with low velocity stream in constant diameter pipe, measuring flow characteristics for non-separating conditions
[ASME PAPER 70-WA/FE-2] 03 p0402 A71-14124

Vortex angular rate sensor flow characteristics, solving Navier-Stokes equations by numerical technique
[ASME PAPER 70-WA/FE-5] 03 p0402 A71-14127

Two dimensional wall jet and wall wake flow turbulence characteristics, considering mean and fluctuating flow properties
[ASME PAPER 70-WA/APM-35] 03 p0403 A71-14161

Axially symmetrical two phase turbulent air jet, examining small liquid droplets effect on flow structure
[ASME PAPER 70-WA/APM-45] 03 p0404 A71-14166

Energetic proton bursts in magnetotail, examining flow direction and intensity, spectral energies and origin
03 p0482 A71-14517

Hypersonic perfect gas flow past thin three dimensional body with strong viscous interaction, obtaining aerodynamic characteristics and drag and heat coefficients
03 p0345 A71-14563

Plane ideal incompressible fluid jet impact on curvilinear surface, considering flow characteristics near stagnation point
04 p0567 A71-14592

Flow characteristics behind reflected shock wave flow and heat transfer at tube wall, noting unsteady and nonlinear effects
04 p0567 A71-14665

High performance shock tube driving techniques, determining effectiveness and flow properties predictability
04 p0564 A71-14669

Flow and radiative properties of air in high explosive shock tube
04 p0586 A71-14700

Reflected shock wave interaction with boundary layer and contact surface in shock tube, examining flow uniformity
04 p0568 A71-14703

Scale effect in cavitation flow, discussing flow parameters and model size effects on similar flows
04 p0570 A71-15063

Variable properties effects on MHD flow in ducts with finite aspect ratio and electrically insulating walls, noting current distribution
04 p0634 A71-15179

Thermal boundary layer thickness and momentum in turbulent flow over film cooled surface
04 p0680 A71-15473

Binary gas mixture rarefied hypersonic flow structure near blunt body, investigating diffusive effects on recovery temperature dependence
04 p0528 A71-15488

Error estimates for turbulent flow characteristics determination by visualization and solid particle photography
04 p0573 A71-15562

Closed system of differential equations derived for kinematic characteristics of turbulent flow in pressurized smooth pipe
04 p0575 A71-15608

Aqueous acid solution turbulent boundary layer characteristics during alkali solution injection through porous surface in presence of positive pressure gradient
04 p0576 A71-15614

Convective mass transfer, velocity and concentration fields during nonNewtonian fluid motion in circular pipe with diffusion flow at wall
04 p0579 A71-15798

Finite electrical conductivity effects on solar flare-induced interplanetary shock waves, discussing solar wind time dependent bulk flow characteristics
05 p0810 A71-16634

Steady diabatic inviscid gas flow properties, emphasizing vortex lines geometry
05 p0839 A71-17047

Two dimensional supersonic turbulent burning mixing layer, measuring physical properties and growth rate
[WSS/CI PAPER 70-16] 06 p0943 A71-17657

Supersonic wind tunnel design, discussing flexible nozzle flow aspects
06 p0880 A71-17700

Gas turbine air cooling systems hydraulic characteristics by graph-analytical method
06 p0945 A71-18001

Convective heat transfer in coolant with constant velocity in ring channel with heat sources, deriving expressions for flow and wall temperature
06 p1006 A71-18004

Irreversibility control in two gas flows mixture, discussing jet engines thrust increase by air-exhaust gases admixture
06 p0945 A71-18051

Supersonic jet noise suppressor with tubes and shrouds, examining flow and acoustic characteristics
[AIAA PAPER 71-153] 06 p0884 A71-18595

Saturn launch vehicle gust penetration loads, presenting separated flow and associated time lag effects
[AIAA PAPER 71-178] 06 p1004 A71-18617

Secondary losses in plane compressor grid with low aspect vanes, discussing flow characteristics dependence on fins, protruding elements and smoothed junctions
06 p0846 A71-18705

Turbulent flow main characteristics calculation based on maximum stability hypothesis with respect to most dangerous perturbation, presenting numerical solutions by digital computer
07 p1085 A71-18755

Two dimensional flow MHD in plasmas with anisotropic pressure, considering weak shock waves parameter changes in linear approximation
07 p1168 A71-19726

Transonic gas flows in axisymmetric small throat curvature radius Laval nozzle with appreciable flow parameters variation in transverse direction
07 p1014 A71-19732

Magnetic annular arc accelerator for high pressure high enthalpy flow test facility

07 p1083 A71-19880

Jet pipe valve characteristics, discussing pressure and flow recovery for various loads, nozzle diameter ratios and spacings

07 p1025 A71-20559

Two dimensional supersonic fluid amplifier flow field density and characteristics determined by differential interferometry

07 p1028 A71-20588

Compressible two dimensional laminar and turbulent free jet characteristics, presenting unitary method with similarity transformation

07 p1029 A71-20593

Plasma flame temperature and flow characteristics in plasma jet transfer-type metal cutters from spectroscopic measurement and high speed streak camera photography

09 p1454 A71-23032

CERCHAR low speed wind tunnel design details, operational characteristics and utilization of facility for coal mine safety

10 p1589 A71-24287

Incident thermal flux parameters and wall temperature effects on flow characteristics in prepreparation zone of laminar boundary layer and separation point location

10 p1551 A71-24368

Collisionless ion exosphere kinetic and hydrodynamic models comparison for polar wind supersonic flow characteristics

10 p1605 A71-24796

Plenum chamber with nozzle wind tunnel model, noting jet flow phenomena at various angles of attack

10 p1590 A71-24865

Supersonic conical inlet additive drag formula, using flow data in freestream

10 p1553 A71-24866

Traveling shock waves interaction with orifice inside ducts, noting anomalous phenomena probably due to unsteady boundary layer growth or time lag

10 p1596 A71-24923

Flush mounted electrostatic probes behavior under different flow regimes, studying bias, area, geometry and position effects on collected current density

11 p1743 A71-25148

Flow patterns within centrifugal and mixed flow impeller channel, examining velocity distributions, blade surface pressure and flow behavior

[ASME PAPER 71-GT-41]

11 p1704 A71-25974

Equilibrium air boundary layer flows at three dimensional stagnation points, discussing flow characteristics and real gas heat transfer parameters

[AIAA PAPER 70-809]

12 p1866 A71-27582

Laminar flow breakdown in circular tubes, noting disturbance level effect on intermittent flow parameters and turbulent zone length distribution

13 p2046 A71-27827

Flow momentum losses during gas mixture chemically nonequilibrium expansion in nozzle

13 p2158 A71-27880

Truncated conical diffusers with various geometrical configurations and incompressible inlet flow conditions, noting reduced pressure recovery

13 p2047 A71-28468

Monograph on free and confined vortex gas burner flow characteristics covering pressure distribution, velocity, power law, mass flow in boundary layers, etc

13 p2047 A71-28496

Plane one dimensional steady compressible ideally charged gas flow characteristics in electric field

13 p2107 A71-28567

Vessels mechanical behavior and blood flow dynamics in aorta bifurcation zone, using Navier-Stokes and continuity equations

13 p2019 A71-28657

Longitudinal space-time correlation function of turbulent near wall pressure pulsations with hydrodynamic wavelength exceeding boundary layer thickness at streamlined model

13 p2049 A71-28846

Supersonic gas ejector characteristics of mixing gases with different adiabatic exponents, heat capacities and stagnation temperatures

13 p1994 A71-29233

Air flow past small aspect ratio thick-section wing at small angles of attack, investigating vortex system effect on flow characteristics in absence of lift

13 p1994 A71-29234

Bounded flow incident on cylindrical body in transverse magnetic field, determining constraints effects on dynamic and structural characteristics

14 p2278 A71-29609

Incompressible planar fluid flow magnitude, direction and turbulent shear stress measurement by hot-wire anemometer

14 p2239 A71-29928

Nonlinear dynamical evolution of two dimensional unstable shear flows, using numerical integration of time dependent incompressible Navier-Stokes equations

14 p2226 A71-30409

Reattachment of single two dimensional turbulent air jet, investigating gas flow characteristics in combustion chambers

14 p2170 A71-30419

Gas injectors characteristics investigation by cold flow simulation, using flow field visualization techniques and velocity and mass concentration profiles measurements

[AIAA PAPER 71-675]

14 p2291 A71-30739

Helicopter rotor stall characteristics, investigating blade flexibility, unsteady aerodynamics and variable inflow effects

[AHS PREPRINT 520]

14 p2171 A71-31086

Book on pressure losses in ducted flows covering subsonic flow in straight or curved ducts, constrictions flow characteristics, etc

15 p2386 A71-31149

Low area ratio ejectors internal flow phenomena synthesis, increasing thrust augmentation by mixing and diffusion

[AIAA PAPER 71-576]

15 p2468 A71-31566

Slow switching in wall attachment fluidic devices, determining flow characteristics

15 p2391 A71-32057

Similarity solutions describing flow characteristics behind plane hydromagnetic shock propagating into uniform ideal gas at rest in presence of transverse magnetic field

15 p2391 A71-32074

Swirling flow in gas turbine engine combustion chamber forward part, considering air flow characteristics behind blade swirler

16 p2624 A71-33606

Laminar boundary layer on wing profiles and bodies of revolution, calculating flow characteristics based on integral momentum relation

17 p2670 A71-34424

Solid particle impurity effects on hypersonic wind tunnel flow characteristics

17 p2671 A71-35116

Mesh method for supercritical transonic flow calculation with normal or oblique shock wave at trailing edge

17 p2674 A71-35799

Bursting phenomenon measurement in turbulent boundary layer by hot wire, noting spottiness, HF intermittency and energy balance dynamics

18 p2985 A71-36036

Base flow characteristics in four-nozzle rocket exhaust as functions of nozzle axis interspaces, nozzle exit section-base surface distance and Mach number

18 p2903 A71-36117

Laser beam operation, light scattering in gases, holography applications and flow analyses

18 p2931 A71-36420

Flow simulation with digital computer by Monte Carlo computation methods based on interacting molecular gas kinetics, noting application to gas flow

18 p2941 A71-36427

Inclined wedges in rarefied hypersonic flow conditions, investigating base and wake pattern geometrical and aerodynamic characteristics

18 p2849 A71-36756

Rarefied gas flow characteristics through pipe orifice in intermediate range of rarefaction between free molecular flow and continuum flow

18 p2849 A71-37023

Two and three dimensional pistons motion in stationary gas, calculating potential flow characteristics near weak discontinuities as function of piston geometry and acceleration

19 p3043 A71-37099

Axisymmetric plane transonic flow past convex corner point, obtaining characteristics by mapping into hodograph plane

19 p2991 A71-37103

Hydrogen near-critical point flow in heated cylindrical tube, measuring flow parameters radial profiles by combination pitot tube/thermopile/hot-wire sensor probe

[ASME PAPER 71-HT-25]

19 p3165 A71-37995

Three ideal incompressible fluid jets collision induced flow, reducing discontinuity region analytic functions to nonlinear system with two numerical parameters and singular integrals

21 p3367 A71-40684

Small mesoscale waves development in steady stratified plane parallel flow, assuming mean flow characteristics dependence on vertical coordinate

21 p3412 A71-41391

Second order viscous liquid pulsating flow superposed on steady laminar flow through circular pipe, examining non-Newtonian effects on flow characteristics

22 p3530 A71-41562

Centrally-fed circular inherently-compensated aerostatic gas thrust bearing flow behavior in inlet region, obtaining graphs for design optimization

22 p3551 A71-41663

Centrifugal compressor bladeless diffuser parameters, flow kinematics and energy losses, noting effects of friction coefficient and expansion angle

23 p3626 A71-43551

Transient pressure measurement in plasma exhaust flow of 500 microsec duration, discussing discharge temporal behavior and cold gas pressure front existence

23 p3711 A71-43598

Calculation method for flow about bodies with injection, presenting parameters approximation formulas derived from Cauchy problem solution for Helmholtz equation

24 p3789 A71-44478

Navier-Stokes equations solutions expressing flow conditions through blade cascade

24 p3817 A71-44523

Two dimensional incompressible turbulent wall jet in moving stream, describing viscous flow characteristics and various boundary layer parameters

24 p3818 A71-44605

Dimensionless parameters effect on divided blood flow characteristics in large arterial bifurcation

24 p3801 A71-44622

Turbulent stress distribution relationship to averaged characteristics of incompressible fluid boundary layer flow with positive pressure gradient

24 p3818 A71-44748

Natural trihedrons associated with stationary or nonstationary flows in hydrodynamics and MHD, using moving reference theory

24 p3856 A71-44795

Flow and strain analysis and engineering design of porous cylindrical gas film foil bearing at low pressures

24 p3830 A71-44944

Pressure and flow direction defects behind Mach reflected shock near three shock intersection, considering steady flow theoretical model

24 p3820 A71-44953

Thermal dissociation reactions and radiation effects on flow variables in front of and behind strong normal shock, using gray gas approximation

24 p3822 A71-45368

Compressors and turbines centripetal stages operational characteristics, investigating airflow rate and pressure ratio effects on power

24 p3790 A71-45380

FLOW CHARTS

Digital structures simulation system as computer systems design aid, discussing basic building blocks, flow charts, task assignments, cost and performance constraints, etc

01 p0048 A71-10222

Fluid logic circuit network analysis, utilizing classical synthesis technique with primitive flow table and maps

15 p2351 A71-31686

Programming languages expansion by users, considering language elements important in flow control or formulation of translation processes

19 p3025 A71-37423

FLOW COEFFICIENTS

NT DISCHARGE COEFFICIENT

Contraction coefficient of orifice for subsonic and supersonic flows, including velocity-of-approach and compressibility effects upstream and downstream

[ASME PAPER 70-WA/FM-1]

03 p0402 A71-14103

Flow coefficient equations of square edged orifices, comparing graphically computed and test values

[ASME PAPER 70-WA/FM-2]

03 p0402 A71-14104

Low speed two dimensional axial flow compressor cascade data, considering lift drag ratio and minimum loss coefficient

[ASME PAPER 70-WA/GT-10]

03 p0343 A71-14118

Unsteady coefficient measurements to corroborate theory for coefficient distribution about little elongated two dimensional wings with control surfaces

05 p0694 A71-16737

Small curvature radius/throat radius ratio supersonic nozzles mass flow rate coefficients at high Reynolds numbers, appraising isentropic flow prediction methods

07 p1015 A71-19877

Computer programmable flow coefficient formulas for standard constrictions, orifice gages and Venturi nozzles

10 p1595 A71-24640

Flow parameters behind shock waves propagating in carbon dioxide-nitrogen mixtures at Mach numbers from 5 to 10

19 p3044 A71-37583

Heat transfer in turbulent boundary layer separation zones ahead of step, using local flow parameters at wall boundary layer limit

24 p3887 A71-44746

FLOW DEFLECTION

Plane supersonic overexpanded jet interaction with obstacle, using hodographs for flow pattern construction

01 p0001 A71-10425

Supersonic laminar boundary layer structure near convex corners for large turning angles

01 p0069 A71-10461

Two dimensional potential flow theory for incompressible unsteady flow about multiple lifting bodies in small amplitude motion

01 p0071 A71-10929

Impulsively started time dependent transonic flow of ideal compressible gas past circular cylinder, using finite difference method

01 p0003 A71-11160

Supersonic underexpanded jet-plane obstacle flow interaction patterns, discussing pressure and distance effects

02 p0186 A71-12643

Soviet book on nonlinear conical gas flow theory covering flows with different characteristics past bodies of various geometries and positions

02 p0187 A71-12719

Boundary layer solution for unsteady compressible incompressible flow past body, discussing momentum conservation equation solution by series expansion

02 p0241 A71-12848

Steady incompressible flow past oblate and prolate spheroids for Reynolds numbers up to 100, using spherical coordinates and finite difference method

03 p0400 A71-13729

V/STOL aircraft wing-propeller interaction, using mean flow deflection angle in lift and drag characteristics prediction

04 p0526 A71-14988

Supersonic reactive gas flow free expansion over sharp corner into region of constant pressure, using linearized theory and numerical method of characteristics

05 p0836 A71-16535

Initial structure of wing-body interaction in steady inviscid supersonic flow, obtaining asymptotic expansion from canonical problem solution

05 p0696 A71-17219

Channel flow and flow past bodies turbulent/laminar reverse transition for friction drag and heat transfer reduction

06 p0881 A71-17584

Wing-canard configurations nonlinear vortex interactions, using Sacks method of vortex sheet simulation with discrete vortices distribution

06 p0844 A71-18550

Two dimensional supersonic surface jet-hypersonic flow interaction with axial symmetry

06 p0845 A71-18575

Far wake asymptotic structure in rarefied plasma flow past charged bodies

07 p1165 A71-18878

Hypersonic radiating gas inviscid flow past blunt bodies, using spherical harmonics approximation

07 p1013 A71-19183

Viscous incompressible axisymmetrical flow, examining vortices near stagnation point of infinite flat obstacle

07 p1089 A71-19737

Flow pattern around arbitrary star-shaped contour, deriving expression for complex potential as velocity function

07 p1014 A71-19745

Jet engine contribution to lift at supersonic flight velocities via air mass heating, studying three dimensional flow with heat supply and stream deflection

07 p1014 A71-19746

Cavitation flow of fluid with free surface past flat plate between parallel walls

07 p1092 A71-20081

Cavitation flow of fluid with free surface past underwater wing with jet flap, solving equations of motion for thin foil with jet emergent from trailing edge

07 p1092 A71-20086

Heavy fluid flow past partially cavitating flat plate with cavity closed by fictitious plate, considering lift force under gravity

07 p1092 A71-20087

Beam deflection type fluidic amplifiers with single and symmetric control jets, considering free streamline flow theory

07 p1025 A71-20557

Jet flow deflection by cross flowing stream applied to low velocity anemometers

07 p1030 A71-20596

Continuous flow past plate located perpendicular to wall with inviscid incompressible fluid having linear variation of velocity with height

08 p1227 A71-20828

Unsteady analogy for hypersonic flows past blunt bodies with shock deformation

08 p1227 A71-21863

Inviscid incompressible vortex-free axisymmetric pipe flow near arbitrary shape body symmetrically located near axis

09 p1431 A71-22180

Multielement flap mechanism design, considering drive angles which deflect least from 90 degrees

09 p1386 A71-22652

Steady nonrotational flow around rectilinear profile in finite width uniform current in linear theory, calculating fluid exerted forces

10 p1549 A71-23822

Soviet book on MHD flow of incompressible electrically conducting fluid past bodies covering inviscid flows and viscous flows of Stokes and Oseen type

10 p1596 A71-24669

Annular free jets application as air curtains, formulating relations for plane and conical jets to calculate deflection of particles

[DFVLR-SONDDER-106] 10 p1596 A71-24938

Inviscid incompressible two phase concave type corner flows embedded with small spherical particles, examining streamlines, critical collision conditions and approximate viscous effects

10 p1598 A71-25081

Inviscid incompressible two dimensional jet deflection by various dimension segments, investigating potential flow with Schwarz-Christoffel transformation and free streamline theory

11 p1753 A71-26444

Numerical analysis of steady symmetric incompressible flow past elliptical cylinders for Reynolds numbers up to 90

12 p1895 A71-26739

Uniform transonic ideal gas flow past finite bodies approximated by Karman equation

13 p1989 A71-27902

Stratified fluid flow over barrier, obtaining stationary solution for initial value problem

13 p2047 A71-28481

Weakly rarefied gas flow past bodies of various geometry, deriving equations of motion with approximate macroscopic integrodifferential equations

13 p1991 A71-29148

Boundary conditions formulation for energy and mass transfer in weakly rarefied gas flows past bodies

13 p1991 A71-29149

Steady hypersonic nearly free molecular rarefied gas flow about convex body, applying kinetic operator

13 p1991 A71-29152

Gas particle radial reflection model application to hypersonic nearly-free molecular flow about convex bodies, solving steady state problem

13 p1991 A71-29153

Transonic gas flow around profile, proving uniqueness of Frankl solution

13 p1993 A71-29221

Two dimensional jet flap cascades, presenting stream deflection angles as function of jet to mainstream momentum flux

[ASME PAPER 71-FE-14] 13 p1995 A71-29453

Small spherical solid or liquid particles deceleration, melting and shattering due to spherical and conical bodies in compressible hypersonic shock layer flow field

[AIAA PAPER 69-712] 14 p2334 A71-29873

Three dimensional spatial unsteady hypersonic gas flow about bodies behind strong shock wave front

14 p2169 A71-30182

Hypersonic shockless gas flow past circular cone and cylindrical surfaces, reducing Vallander equations to nonlinear integral

14 p2169 A71-30183

Transonic flow past bodies of revolution, using finite difference scheme

14 p2171 A71-30876

Asymptotic behavior of boundary layer equations solution for viscous incompressible flow past curvilinear obstacle

14 p2227 A71-30878

Flap induced flow deflection effects in hypersonic shock tunnel, obtaining turbulent heating, skin friction and pressure data

[AIAA PAPER 71-598] 15 p2343 A71-31540

Small disturbance equations for steady transonic flows past thin lifting airfoils and slender bodies

[AIAA PAPER 71-566] 15 p2344 A71-31560

Proportional fluid amplifier, measuring deflection angle, jet turbulence and noise level

15 p2390 A71-32052

Unsteady viscous flow around oscillating cylinders, calculating fluctuating lift, drag and moment effects with Navier-Stokes equations

16 p2520 A71-33098

Constant velocity flow past semiinfinite flat plate trailing edge, emphasizing wake region structure

16 p2560 A71-34140

Supersonic flow past V-shaped wings with leading edges, applying method of establishment to space variable for pressure distribution

17 p2673 A71-35647

Asymptotic solution of viscous incompressible flow past uniformly heated paraboloid of revolution with constant surface temperature

17 p2730 A71-35800

Two dimensional laminar incompressible fluid flow past flat plate at various angles of attack, studying vortex shedding characteristics

18 p2844 A71-36311

Subcritical nonlinear potential flows over two dimensional subsonic airfoils by multistrip method of integral relations

18 p2845 A71-36330

Initial flow past circular cylinder in viscous incompressible fluid calculation by numerical integration using boundary layer coordinates

18 p2908 A71-36341

Viscous compressible flow around slender body in hypersonic slip flow regime, using finite difference method

18 p2908 A71-36344

Flow processes around body of hypersonic velocity, studying plasma diagnostics in ionized wake

18 p2952 A71-36421

Frictionless hypersonic flow around body by time dependent numerical processes and method of characteristics

18 p2846 A71-36423

Supersonic flow past steady and oscillating blunt bodies of revolution, using singularity transformation and series truncation methods

19 p2993 A71-37878

Heated jet interaction with deflecting flow in subsonic wind tunnel, presenting flow visualization and temperature and velocity profiles

[ASME PAPER 71-HT-2] 19 p3163 A71-37980

Unsteady analogy for hypersonic flows past blunt bodies with shock deformation

20 p3176 A71-39362

Water tunnel walls effect on supercavitating flows past slender bodies

20 p3213 A71-39786

Supercavitating bounded flow of weightless fluid past slender bodies, deriving singular integral equations in terms of pressure gradient and cavern thickness derivative

20 p3213 A71-39787

Laminar viscous flow past semiinfinite flat plate to second Oseen type approximation, obtaining shear stress on plate

21 p3368 A71-40707

Two dimensional supersonic moist air expansion around sharp corner, investigating water vapor condensation by homogeneous nucleation

21 p3369 A71-40952

Steady slow free molecule flow past sphere, obtaining distribution function and surface boundary conditions

21 p3370 A71-40987

Boundary layer solution for initial flow around impulsively started sphere in viscous fluid at high Reynolds numbers

23 p3664 A71-44144

Chemically reacting gas mixture supersonic flow characteristics around blunt body, using differential equations

23 p3784 A71-44336

Dynamic behavior of dissociating gas supersonic flow past blunt bodies at angle of attack

24 p3790 A71-44775

FLOW DIRECTION INDICATORS
Nonsteady air flow direction generation and measurement, comparing three-tube probe with hot-wire anemometer data

14 p2244 A71-30326

FLOW DISTORTION
Centrifugal compressor impeller exit flow velocity distribution distortion based on equations of motion involving entropy gradient terms

03 p0343 A71-13831

Fluid transmission lines terminated by orifice with nonlinear pressure flow characteristics, calculating harmonic distortion frequency response by perturbation method

[ASME PAPER 70-WA/FE-6] 03 p0402 A71-14128

Subsonic fan noise, using helicopter rotor noise theory for analysis of phase related and randomly time varying flow distortions

05 p0796 A71-17161

Small scale spatially periodic auroral arc distortion observations, using low light level TV reception

06 p0893 A71-17981

Gas-particle mixtures weak disturbances, applying linearized hydrodynamic and phase transformation kinetic equations

07 p1088 A71-19191

Hanging shock wave in small supersonic flow past profile with broken generatrix in plane ideal gas

08 p1228 A71-21872

Incompressible flow stability to axisymmetric disturbances in circular pipe

09 p1434 A71-23165

Normal shock wave interaction with deformable solid walls, determining explosion or sonic booms effects on elastic structures and protection devices

10 p1556 A71-24483

Supersonic boundary layer flow profile distortion due to oblique shock during separation

10 p1552 A71-24592

Velocity and static pressure redistribution in distorted flow field upstream of axial flow compressors

[AIAA PAPER 69-485] 10 p1553 A71-24856

Ideal incompressible fluid flow around fixed obstacle near rectilinear wall, investigating plane motion with profile couple method

11 p1705 A71-26258

Spatial MHD flow in diffuser bounded by two diverging and two parallel walls, showing solutions with axial symmetry in cylindrical and spherical coordinate systems

14 p2278 A71-29605

MHD flow abrupt widening and narrowing, considering M shaped velocity profiles

14 p2278 A71-29606

Ideally conducting compressible liquid flow near arbitrary geometrical thin profile form in transverse magnetic field

14 p2278 A71-29608

Bounded flow incident on cylindrical body in transverse magnetic field, determining constraints effects on dynamic and structural characteristics

14 p2278 A71-29609

HF rake probes with high temperature integrated sensor for inflight aircraft engine intake air flow distortion measurements

14 p2243 A71-30321

Miniature integrated sensor pressure transducers for inlet air flow distortion and buffet studies of wind tunnel models

14 p2245 A71-30336

Time variant distortions in supersonic inlet on J-85-GE-13 turbojet engine from wind tunnel test, considering instantaneous distortion amplitudes and contours

14 p2290 A71-30733

Plane Couette flow with finite disturbances, investigating stability in nonlinear terms

16 p2558 A71-32986

Aerodynamic perturbation due to single hot-wire probes, comparing with evaluations derived from potential flow scheme

18 p2904 A71-36262

Karman vortex street breakdown under deceleration, noting vortices distortion and annihilation followed by vortex street formation of different frequency

19 p3046 A71-38202

Hanging compression shock wave in plane supersonic ideal gas flow past body with broken generatrix

20 p3176 A71-39371

Nonstationary ideal gas flow in variable section axisymmetric channel, noting flow disturbances during sudden changes in conditions at outlet section

21 p3368 A71-40696

Oscillatory free convection laminar boundary flow from semiinfinite vertical flat plate, investigating surface temperature variations as distance function from leading edge

22 p3619 A71-41602

Flat face cylinders in rarefied supersonic gas flow, investigating perturbed region evolution

24 p3790 A71-45096

FLOW DISTRIBUTION

Plane supersonic overexpanded jet interaction with obstacle, using hodographs for flow pattern construction

01 p0001 A71-10425

Wind flow patterns in severe thunderstorms structures, using Doppler radar

01 p0117 A71-10573

In- and outflow fields in hurricane Debbie, using airborne radar echoes and ATS 3 satellite pictures

01 p0118 A71-10589

Flow field of two dimensional nozzle exhausting to vacuum, describing computer program based on BGK equation and plotting exhaust region density, temperature and velocity

01 p0002 A71-10932

Whitham supersonic flow theory application to mid-or near-field sonic boom of slender bodies in wind tunnel research

01 p0005 A71-10956

Inviscid fluid flow in cylindrical channel excited by internal hydrodynamic energy source, calculating velocity and density distribution

01 p0071 A71-11045

Global atmospheric circulation theory relation to flow pattern of free thermal convection in rotating fluid subjected to horizontal temperature gradient

01 p0122 A71-11359

Approximate calculation for far field flow distribution of nozzle exhausting into vacuum

01 p0072 A71-11595

Frictionless rotationally symmetrical free supersonic gas jets with thermodynamic relaxation, applying approximate method for shape and flow parameters at boundary

02 p0241 A71-12407

Sweptback turboblades in parallel wall channel, investigating thickness, camber and leading edge curvature effects on flow and pressure distributions and vortex movement

02 p0186 A71-12606

Supersonic underexpanded jet-plane obstacle flow interaction patterns, discussing pressure and distance effects

02 p0186 A71-12643

Numerical analysis of flow field around thin airfoil in two dimensional nonuniform stream, using finite difference method

02 p0187 A71-12680

Diverging flow structure in conical diffuser using two Townsend turbulent parameters

03 p0399 A71-13456

Modified Coles compressibility transformation for wake mapping with Howarth-Dorodnitsyn scaling suppression

03 p0400 A71-13460

Two dimensional cascade flow, discussing methods of flow field idealization, nonviscous incompressible flow theoretical methods, compressibility and viscosity effects

03 p0342 A71-13826

Fast multiple point measurement of fluid temperature and flow speed fields using bead thermistors and digital system

03 p0427 A71-13921

Jet switching dynamic behavior in bistable fluidic devices, examining flow field, response and switching time

[ASME PAPER 70-WA/FLCS-20]

03 p0355 A71-14093

Supersonic inviscid flow fields associated with conical premixed flame sheet

03 p0521 A71-14242

Boundary layer flow field exposed to oscillating stream, determining third term of Fourier series expansion

03 p0405 A71-14295

Pressure wave propagation through annular and mist flow patterns, noting virtual mass effects in interphase momentum transport of rarefaction and compression waves

03 p0405 A71-14418

Boundary layer growth effects on two dimensional flow field in low pressure test gas of circular and rectangular shock tubes

04 p0568 A71-14667

Angiotensin I infusion effect on intrarenal blood flow distribution, using krypton 85 method and autoradiography

04 p0538 A71-15088

Blunt body stagnation point heat transfer in hypersonic flow, describing gas dynamic equations flow field viscosity and conductivity

04 p0528 A71-15490

Hot laminar round inert gaseous jet entraining fuel-air mixture, obtaining velocity, temperature and concentration profiles

04 p0683 A71-15495

Multitube condensers of various geometries, investigating tube flow stability, distribution and gravitational effects

04 p0688 A71-15538

Ring flow expansion of incompressible viscous fluid in cylindrical channel

04 p0573 A71-15561

Two dimensional hypersonic flow field density gradient distribution measurement by space-time resolved laser schlieren system

04 p0600 A71-15592

Nonself-similar wave type gas dynamic equations solutions, considering flow fields due to Riemann waves interaction in polytropic gas

05 p0693 A71-16376

Nongray absorption and radiation cooling on smooth symmetric blunt bodies included in modified Maslen flow field method for radiation and large blowing

[AIAA PAPER 69-637]

05 p0694 A71-16566

Global stability of closed plasma configurations relation to dynamical principle of least constraint and space-time and gage symmetries of flow fields

05 p0789 A71-16651

Supersonic flow field around flat plate at various angles of attack, comparing Brieden and Lighthill approximations

05 p0694 A71-16713

Supersonic flow field downstream of turbofan aircraft engine fan nozzle over bodies of revolution, using boundary layer theory and method of characteristics

05 p0796 A71-17150

Submerged moving body in nonviscous incompressible fluid, evaluating finite potential flow field momentum with rigid and free far distant outer boundary

06 p0841 A71-17419

Forced convection over infinite periodically overheated plane on basis of mesometeorological vertical wind velocity

06 p0923 A71-17515

Premixed laminar flames in flow fields, amplifying fluid mechanical disturbances including vibratory motion and overall feedback loop

06 p1007 A71-18221

Heat transfer from rotating disk to parallel nonrotating disk, investigating turbulence effect from air flow pattern observation

06 p1007 A71-18315

Centerline velocity and concentration decay predictions of free and confined jet models with/without secondary flows, considering turbulent mixing

[AIAA PAPER 71-3]

06 p0883 A71-18478

Nonuniform plug nozzle flow field calculated for closed wake, using flow model divided into near wake and adjacent regions

[AIAA PAPER 71-41]

06 p0946 A71-18502

Supersonic axisymmetric wake-like and two dimensional shear nonuniform free stream flows effects on inviscid flow fields and aerodynamic coefficients of sharp and spherically blunted cones

[AIAA PAPER 71-51]

06 p0843 A71-18512

Three dimensional transonic shear flow structure in turbomachine cascade, using time dependent numerical solution

[AIAA PAPER 71-83]

06 p0843 A71-18540

Three dimensional inviscid supersonic flow fields with primary and embedded shock and expansion waves determined over and behind wings and wing-body configurations

[AIAA PAPER 71-99]

06 p0844 A71-18554

Human mitral valve fluid mechanics, confirming existence of vortex forms during diastasis by vitro flow patterns

[AIAA PAPER 71-102]

06 p0863 A71-18556

Supersonic turbulent boundary layer separation on flat plate by forward facing step, measuring mean flow field characteristics

[AIAA PAPER 71-127]

06 p0844 A71-18571

Separation patterns over inclined body of revolution from symmetry-plane boundary layer solutions, discussing bubble type

[AIAA PAPER 71-130]

06 p0845 A71-18574

Subsurface flow generation by surface tension variation due to flame spreading over liquid fuel at large Reynolds number, using hydrodynamical analysis

[AIAA PAPER 71-207]

06 p1009 A71-18643

Hypersonic flow over cones with attached and detached shock waves, using Lax differencing technique and time dependent formulation for reentry flow fields

[AIAA PAPER 71-55]

06 p0846 A71-18655

Flow field behind two dimensional roughness element in rectangular channel, discussing wall effects, reattachment point position, velocity distribution and turbulence intensity

07 p1086 A71-18775

Free convection turbulent flow under supercritical conditions, investigating convection heat transfer and flow patterns

07 p1220 A71-18780

Supersonic air flow pattern over rectangular indentations on plane and axisymmetric surfaces, examining static pressure and adiabatic temperature distributions

07 p1014 A71-19744

Flow pattern around arbitrary star-shaped contour, deriving expression for complex potential as velocity function

07 p1014 A71-19745

Transient and turbulent flow structure in wake behind thin plates in wind tunnel, noting velocity fields, temperature and initial boundary layers

07 p1089 A71-19750

Pulsed laser holography physical principles and applications in stress and vibration analysis, flow pattern visualization, biophysical and medical research

07 p1113 A71-19783

Liquid rocket propellant engine exhaust plume flow field, discussing mathematical models for combustion chamber, throat region and nozzle

[AIAA PAPER 70-844]

07 p1183 A71-19861

Two dimensional flow field in secondary sonic transverse jet injection port vicinity, studying free stream Mach number, total pressure and specific heats ratio

07 p1090 A71-19896

Aircraft fuel and air conditioning systems vortex valves and diodes, examining flow patterns into and out of chambers

07 p1025 A71-20556

Two dimensional supersonic fluidic amplifier flow field density and characteristics determined by differential interferometry

07 p1028 A71-20588

Flowfield isentropes in conical gas flow with singular current surfaces

08 p1227 A71-21864

Hot wire total temperature probe at hypersonic speeds for flow field measurements

[AIAA PAPER 71-273]

08 p1377 A71-21999

External store surface pressure distributions during captive flight aboard F-4B aircraft, considering carrying aircraft effects on flow field about airborne ordnance

[AIAA PAPER 71-295]

08 p1232 A71-22015

Cross flow profiles for compressible turbulent boundary layers with and without flow reversal via hodograph models family

08 p1229 A71-22033

Mach disk in underexpanded exhaust plume predicted by dividing flow field into subregions

[AIAA PAPER 70-231]

09 p1382 A71-22097

Proportional fluidic element static characteristics, calculating main jet interaction with control jet

09 p1386 A71-22655

Circular gas jet path lines in nonuniform velocity side field drift flow, using auxiliary curve values and correction coefficients

09 p1432 A71-22730

Linear mountain lee wave model with nonlinear lower boundary condition for arbitrary basic flow and two dimensional topography, computing flow field

09 p1487 A71-23024

- Incompressible viscous fluid nonsteady three dimensional flow, obtaining velocity field and pressure distribution in boundary layer
09 p1433 A71-23092
- Linear coastal hydrostatic boundary layers of lake with no horizontal motion, discussing flow conditions under wind stress and interior velocity
10 p1600 A71-23961
- Regional pulmonary vasomotor activity in sitting man, determining pulmonary flow distribution with Xe 133 technique
10 p1561 A71-24126
- Aerodynamic characteristics and flow pattern in wake behind star-shaped body at supersonic speed, determining drag and shock waves location
10 p1551 A71-24371
- Incompressible nonviscous rotating fluid in toroidal shell, obtaining flow patterns steady state solutions for turbomachinery design
10 p1552 A71-24520
- Inviscid flow distribution of high temperature jet of optically thick radiating gas exhausting from two-dimensional nozzle into low temperature quiescent medium
10 p1552 A71-24588
- Flow field properties of impinging free jets from circular convergent nozzle, measuring velocity, surface pressure and momentum flux
10 p1552 A71-24616
- Velocity and static pressure redistribution in distorted flow field upstream of axial flow compressors
[AIAA PAPER 69-485] 10 p1553 A71-24856
- Temperature distribution inside solid sphere rotating in viscous incompressible liquid with constant strength heat source at center, discussing flow field around sphere
11 p1853 A71-25146
- Anisotropic homogeneous two-point double-velocity correlation tensor model for turbulent flow field, deriving relation between micro and macro scale
11 p1748 A71-25153
- Inviscid model for flow field within plumes of two-dimensional underexpanded jets calculated by time dependent finite difference method
11 p1853 A71-25160
- Time asymptotic solutions for hypervelocity blunt body flow field with coupled nongray radiation, treating shock as discrete surface
[AIAA PAPER 70-865] 11 p1701 A71-25453
- Underexpanded transverse sonic jet-hypersonic stream three dimensional flowfield based on inviscid rotational flow model
11 p1701 A71-25472
- Two dimensional analysis of isentropic perfect gas flow fields in axisymmetric nozzles for transonic two phase flow initial values, calculating particle trajectories
[AIAA PAPER 69-572] 11 p1751 A71-25508
- Multiphase two dimensional mixing and combustion of flow fields suspended in gaseous medium for propulsion systems problems, obtaining governing equations
[AIAA PAPER 70-145] 11 p1854 A71-25509
- Flow patterns within centrifugal and mixed flow impeller channel, examining velocity distributions, blade surface pressure and flow behavior
[ASME PAPER 71-GT-41] 11 p1704 A71-25974
- Ideal incompressible fluid flow around fixed obstacle near rectilinear wall, investigating plane motion with profile couple method
11 p1705 A71-26258
- Two dimensional incompressible turbulent boundary layer, determining velocity distribution with Cole law of wake
11 p1752 A71-26259
- Nonself-similar wave type gas dynamic equations solutions, considering flow fields due to Riemann waves interaction in polytropic gas
12 p1898 A71-27453
- Lifting force of wing with rotating flap, deriving lift increase due to circulation redistribution at surface
12 p1865 A71-27491
- Flow field model for steady asymmetric vortex system shed from slender body of revolution in coning motion
[AIAA PAPER 70-52] 12 p1865 A71-27552
- Flowfields behind reflected shock waves, predicting end-wall pressure, radiative heat transfer and radiative gas dynamic coupling effects
[AIAA PAPER 70-774] 12 p1986 A71-27562
- Integral kinetic equation for flow distribution past body and surface heat flow, noting representation in form for computer solution
13 p1991 A71-29156
- Flow and heat transfer measurements in dihedrons simulating patterns about supersonic conical edge and shock wave interaction line, using thermodynamic-coating technique
13 p1992 A71-29174
- Asymptotic limiting viscous flow pattern and drag on flat plate with stationary separation zones at large Reynolds numbers
13 p2050 A71-29204
- Interaction between viscous mixing shear layer induced by tangential injection and external supersonic flow field, obtaining spark schlieren photographs and wall pressure distributions
[ASME PAPER 71-FE-24] 13 p2053 A71-29461
- MHD flow in rectangular channel with two conducting walls, investigating velocity structure
14 p2278 A71-29607
- Stratospheric air flow patterns and CAT measurements onboard aircraft over and downwind of Western U.S. mountain terrain
14 p2267 A71-29755
- Flowfields calculation in inlet design, using flow variable gradients from equations of motion
14 p2170 A71-30608
- Nonreacting gases supersonic turbulent mixing flowfields, calculating turbulent kinetic energy as function of injection angle and jet velocity
[AIAA PAPER 71-725] 14 p2295 A71-30774
- Flowfield production by fluid injection into supersonic crossflow, occurring with liquid/gas jet control of vehicle with combustion ramjets
[AIAA PAPER 71-728] 14 p2295 A71-30775
- Hypersonic flow pattern past windward side of delta wing with supersonic leading edges, joining potential and vortex regions behind shock wave
14 p2171 A71-30874
- Nonlinear mathematical model for dynamical behavior of extensible towing cable subjected to aerodynamic forces generated by uniform flow field, discussing system stability
14 p2171 A71-31026
- Flow field velocity distribution at rotating wing devices tip vortices
[AHS PREPRINT 522] 14 p2172 A71-31088
- Space shuttle vehicle models, calculating surface flow patterns and pressure and aerodynamic heating distributions for comparison with test data
[AIAA PAPER 71-594] 15 p2343 A71-31539
- Viscous flow fields around pointed cones at angle of attack in nonuniform supersonic flow, using axisymmetric analog for three dimensional boundary layer
[AIAA PAPER 71-624] 15 p2344 A71-31552
- Flow field measurement about sharp and slightly blunted slender cone at hypersonic speed and zero angle of attack
15 p2344 A71-31553
- Near field flow pattern of inclined slender body of revolution, using Whitham far field theory of supersonic flow
[AIAA PAPER 71-626] 15 p2344 A71-31554
- Externally blown flap powered transport high lift wind tunnel model visual flow field investigation with multiple filament smoke streamlines
[AIAA PAPER 71-577] 15 p2345 A71-31567
- Multicomponent nonequilibrium air flow past axisymmetric blunt body, calculating flow distribution at various attack angles with time dependent technique
[AIAA PAPER 71-595] 15 p2512 A71-31575
- Inviscid supersonic flow field structure over blunt delta wing, determining attack angle effects on shock layer surface pressure distributions and streamline patterns
[AIAA PAPER 71-596] 15 p2512 A71-31576
- Submerged free air jet with laminar parabolic profile, investigating pressure recovery characteristics for various tube diameters, spacing and Reynolds number
15 p2389 A71-31683
- Inviscid compressible transonic flow field equations for perfect gas in conical rocket nozzles, measuring wall and center line pressures
15 p2390 A71-32040
- Two dimensional viscous incompressible fluid flow field calculation in fluidic element, giving Navier-Stokes equations solution in finite difference form
15 p2390 A71-32054
- DC equivalent circuit, describing pressure and flow distribution at input ports of fluidic line branchings
15 p2352 A71-32067
- Stokes second problem solution, obtaining transient and steady state fluid flow pattern near cylinder executing harmonic rotational oscillations around axis
15 p2393 A71-32263
- Turbulent compressible underexpanded two dimensional jet interaction with crossflowing free stream, analyzing flow field by numerical solution of Navier-Stokes equations
[AIAA PAPER 71-611] 15 p2514 A71-32277
- Two dimensional jet interaction flow field, investigating gas dynamic and transport phenomena
[AIAA PAPER 71-561] 15 p2514 A71-32279
- Slender cone at Mach 10 with underexpanded exhaust plume, determining flow field interactions separation pattern and aerodynamic coefficients
[AIAA PAPER 71-562] 15 p2347 A71-32280
- German monograph on incompressible potential flow field calculation about thick rectangular wings with control surfaces and ground effects
15 p2347 A71-32307
- Finite element method application to potential flow field problems governed by Laplace equation in fluid mechanics, developing computer program
[ASME PAPER 71-APM-22] 16 p2520 A71-33207
- Steady inhomogeneous axisymmetric nozzle flow, determining pattern by simultaneous solution of radial equilibrium and continuity equations
16 p2521 A71-33614
- Skin friction, trailing edge boundary profiles and tuft flow patterns on model F-4D aircraft in transonic flow
[AIAA PAPER 71-762] 16 p2521 A71-34001
- Transonic flow fields in slender symmetric profiles, incorporating shock relations at trailing edge
16 p2522 A71-34163
- Flow field induced by aircraft trailing vortices near ground during takeoff and landing, noting experimental departure from theory
17 p2671 A71-34900
- Hypersonic viscid-inviscid internal flow field interaction with laminar boundary layer in circular ducts, using method of characteristics and implicit finite difference scheme
17 p2671 A71-35281
- Flow distribution behind laminar boundary layer separation point in supersonic flow, calculating plateau region pressure
17 p2672 A71-35629
- Droplet pairs collision efficiencies and coalescence parameters, computing flow fields from nonlinear time dependent Navier-Stokes equations
17 p2770 A71-35805
- Circular cylinder resistance in oscillating stream of second order fluid, calculating flow distribution
18 p2843 A71-36042
- Weakly interacted laminar MHD flow growth in entrance region of plane channel with wall conductances investigated by momentum integral method
[ASME PAPER 71-APM-A] 18 p2951 A71-36251
- Mach number effects on flow field in gas bearings at high subsonic and supersonic tangential speeds based on perturbation theory
[ASME PAPER 71-APM-U] 18 p2926 A71-36263
- Supersonic flow field computation for wing-body combinations by shock-capturing finite difference techniques, discussing improvement based on Runge-Kutta method
18 p2844 A71-36303
- Planar supersonic near wake flow field problem with variable viscosity and base injection, investigating boundary errors spatial decay rate
18 p2906 A71-36321
- Dynamic parameters of supersonic flow incident on conical bodies at large angles of attack, considering flow field and entropy distribution
18 p2845 A71-36328
- Continuous hypersonic wind tunnels with low gas density simulating flow states during reentry phase of space vehicles
18 p2898 A71-36412
- Aerodynamic probes for determining flow state of high enthalpy hypersonic flow fields, considering pitot pressure, total enthalpy and current density
18 p2921 A71-36414
- Flow field and model wall on slender bodies in low density hypersonic flows ranging from free molecular flow to continuum flow
18 p2846 A71-36418
- Iterated double integrals for subsonic flow patterns bounded by segments of straight lines and free boundaries, using FORMAC
18 p2909 A71-36703
- Near wake streamline configuration in symmetry plane of slender cone in hypersonic flow at free stream Mach number 7
18 p2848 A71-36754
- Polooidal Hall current calculation in hydrodynamic approximation for stationary weakly interacting and conducting cylindrical plasma flow with uniform transverse flow parameter distribution
19 p3109 A71-37138
- Interference loading linear prediction on aircraft stores at supersonic speeds, considering flow field due to jet fighter bomber
19 p2996 A71-37290
- Wakes of freely falling water drops, discussing flow patterns, kinetic energy, vorticity decay and velocity profiles
19 p3089 A71-37733
- Tollmien-Schlichting waves in flow field of mixed coaxial laminar air diffusion flames, using flow visualization and hot-wire anemometry
19 p3167 A71-38094
- Turbulence and flow pattern in wake of bluff body flame stabilizers, using hot-wire anemometer measurements and Prandtl-Kolmogorov model
19 p3168 A71-38102
- Gaseous hydrogen and methane injection into supersonic air stream heated by plasma burner, studying combustion effects on flow field
19 p3168 A71-38104
- Predicted flow nonuniformities due to laminar and turbulent boundary layer buildup in shock tubes, studying effects on dissociation rates of bromine in argon mixture
19 p3046 A71-38225

FLOW EQUATIONS

Flow patterns on Poincare sphere as aid to qualitative study of polarization and intensity of quasi-stationary laser mode in anisotropic resonator

20 p3243 A71-39095

Electron guns with band shaped flow, improving klystron performance and increasing pervance by anodic aperture action

20 p3204 A71-39155

Flow field isentropes in conical ideal gas flow with singular stream surfaces

20 p3176 A71-39363

Longitudinal diffusivity of turbulent flows in open channels and circular pipes, discussing experiments

20 p3212 A71-39504

Generalized hodograph transformation with velocity potential as function of continuous second derivatives

21 p3406 A71-40154

Aircraft trailing vortex pair linear stability, obtaining flow field near curved vortex filament with swirl and axial velocities

21 p3320 A71-40500

Cutaneous and intestinal blood flow differentiation during hypothalamic heating and cooling in anesthetized dogs

21 p3335 A71-40632

Conical diffusers outlet flow profile and performance, investigating swirling inlet flow effects on pressure recovery

21 p3323 A71-40950

Free shear layer similarity flow profiles correlation for turbulent isobaric jet mixing by spread rate parameters, using viscosity models

21 p3371 A71-41032

Streamline pattern deduction for sun large scale flow from Doppler line of sight velocities

22 p3596 A71-41454

Two dimensional supersonic flow pattern, velocity and loss in shock waves in front of blade cascade

22 p3479 A71-41842

Monograph on hypersonic low temperature ablation covering cross hatched surface patterns, flow field, turbulent boundary layer, angle of attack, etc [VKI-TN-64]

22 p3621 A71-42031

Symmetrical and unilateral sticking flow modes of nozzle air jets expelled into plane-parallel and parabolic ducts

22 p3480 A71-42681

Flow field calculation in intermediate altitude rocket exhaust plumes by modified Lagrangian finite difference technique

22 p3590 A71-42774

Dynamic coupling response between convectively controlled burning process and nonsteady flow field with pressure, density and gas velocity periodic variations

23 p3782 A71-43593

Flow field generation by coaxial turbulent jets, determining velocity distribution, turbulence intensities and shear stresses by hot-wire anemometers

23 p3627 A71-44198

FLOW EQUATIONS

NT HELMHOLTZ VORTICITY EQUATION

NT VON KARMAN EQUATION

NT VORTICITY EQUATIONS

NonNewtonian /second order/ fluids motion equation derivation based on statistical nonequilibrium distribution

01 p0068 A71-10026

Unsteady cavitation flow, presenting physical mechanism of cavity formation in liquid flow and formulation of governing equations

01 p0069 A71-10110

Gas dynamic equations of arbitrary materials detonation, without allowance for transport phenomena, deriving stability criteria from boundary value problem steady solution

01 p0070 A71-10490

Flow field of two dimensional nozzle exhausting to vacuum, describing computer program based on BGK equation and plotting exhaust region density, temperature and velocity

[AIAA PAPER 69-658]

01 p0002 A71-10932

Adiabatic compressible turbulent boundary layer equations for two dimensional and axisymmetric flow, discussing methods of solution based on eddy viscosity formulation

[AIAA PAPER 69-687]

01 p0071 A71-10933

Cylindrical shock waves generation from instantaneous energy release along line in quiescent atmosphere studied by numerical integration of flow equations

01 p0072 A71-11471

Atmospheric general circulation model for numerical climate digital simulation and weather forecasting, using fluid flow equations

02 p9277 A71-11808

Self similar solutions of nonlinear partial differential equations, applying group invariance under infinitesimal transformation

03 p0449 A71-13075

Transonic flow equations for chemically inert gases binary mixture, considering diffusion effect on dissipative process

03 p0401 A71-13906

Boundary layer equations existence and convergence theorems, using von Mises transformation for conversion into parabolic differential equation boundary value problem

04 p0568 A71-14810

Stokes multipliers first approximations for outer expansions of Orr-Sommerfeld flow equation solutions

04 p0570 A71-15096

Linearized equation for stability and heat transfer of two dimensional incompressible laminar boundary layer in water flow

04 p0679 A71-15469

Subsonic compressible flow equations solution in terms of velocity potential, obtaining reliable convergence

05 p0737 A71-17115

Laminar flow heat transfer in circular pipes, solving for Graetz equation eigenvalues and eigenfunctions

06 p1007 A71-18304

Friction, heat transfer and mass transfer theory of flow represented by two dimensional parabolic boundary layer equations

07 p1085 A71-18766

Numerical integration of equations of three dimensional laminar boundary layer on spreading lines

07 p1087 A71-19182

Compressible turbulent flows free mixing based on two dimensional viscous flow equations

[AIAA PAPER 71-4]

Multicomponent gas laminar boundary layer equations, deriving asymptotic formulas for friction coefficient, concentration, temperature and diffusion flows

07 p1089 A71-19735

Equations systems for free turbulent boundary layer in incompressible fluid, deriving semiempirical formulas for turbulent viscosity coefficient

07 p1091 A71-20027

Self preserving solutions of Stewart-Townsend and Ogura-Meakoda equations for isotropic turbulence decay, discussing asymptotic nature for small and large wavenumbers

07 p1091 A71-20027

Equations of motion for Poiseuille flow in circular tubes, solving Gromeko problem with integral Laplace transforms and Bubnov-Galerkin method

08 p1277 A71-21935

Nondegenerate and degenerate semiconductor current flow equilibrium at low temperatures based on Boltzmann transport equation

09 p1414 A71-22251

French book on hypersonic aerodynamics covering thermochemistry, flow equations, heat transfer, etc

09 p1382 A71-22278

Two dimensional incompressible laminar boundary layer with longitudinal surface curvature, examining equations with particular attention to pressure boundary conditions and pressure gradient formulation

09 p1433 A71-23098

Emitting, absorbing and scattering gray gas flow through plane stationary normal shock wave, presenting governing equations linearized analysis

09 p1546 A71-23164

Flow equations of vertical shear modes in inertial waves on rotating earth, comparing chemical release ionospheric wind profiles

09 p1489 A71-23449

Axisymmetric steady diabatic flow equations exact solutions

09 p1434 A71-23545

Orr-Sommerfeld hydrostatic stability equation derivation for nonparallel flow in wake from Goldstein velocity distribution, noting lateral direction velocity component magnitude

10 p1592 A71-24025

Incompressible fluid plane laminar unsteady boundary layers equations solution through reduction to nonlinear partial differential equation and series expansion

10 p1592 A71-24025

Incompressible fluid plane laminar unsteady boundary layer, obtaining Falkner-Skan equation as special case for similar solutions in steady flow case

10 p1592 A71-24026

Unsteady incompressible laminar boundary layer universal equation form for solution through reduction to ordinary differential equations and series coefficients determination

10 p1593 A71-24027

Conducting fluid in transverse magnetic field at low Reynolds numbers, deriving laminar boundary layer universal equations in Crocco or Mises variables

10 p1648 A71-24028

Upper atmosphere semidiurnal pressure variation calculation from hydrodynamic equations similar to atmospheric tides theory

10 p1600 A71-24038

Nozzle area rated two component flow properties, combining integrated solution equations into single transcendental equation for equilibrium condensation

10 p1550 A71-24336

Quasi-one dimensional approximation equations derivation for electrohydrodynamic channel flows with small interaction parameter, obtaining I-V characteristics

10 p1649 A71-24365

Boundary layer equations for radiating and absorbing gas flow at large Reynolds numbers

10 p1593 A71-24367

Compressor surge effect on mixed compression inlet flow from numerical solution of one dimensional unsteady inviscid flow equations in variable area duct

[AIAA PAPER 69-484]

10 p1553 A71-24855

Universal equations of two dimensional incompressible unsteady laminar boundary layer

10 p1597 A71-25017

Detonation wave of gas in circular cylinder with nonsimultaneous axisymmetric initiation at plane boundary, obtaining solution for small perturbation flow behind detonation front

11 p1853 A71-25152

Finite difference computer algorithm to solve vertical velocity equation of steady air flow about mesoscale obstacle in stably stratified atmosphere

11 p1793 A71-25169

Boundary layer equation for free convective diffusion on flat vertical plate in translation motion in viscous incompressible fluid

11 p1854 A71-25240

Plane unsteady polytropic MHD flow equations reduced to time independent system, using complex variable techniques

11 p1804 A71-25439

Compressible laminar boundary layer flow including second order longitudinal surface curvature effects, deriving flow equations from Navier-Stokes equations

11 p1750 A71-25473

Compressible similar laminar boundary layer equations for zero wall shear and mass addition, describing heat transfer reduction and boundary layer growth by asymptotic analysis

11 p1750 A71-25479

Laminar boundary layer equations integration for jet propagating along porous surface, determining transverse velocity component effect

12 p1896 A71-27114

Laminar boundary layer equations for rotating plate with surface of arbitrary curvilinear shape, determining external flow pressure gradient leading to separation

12 p1865 A71-27502

Unsteady one dimensional time-dependent diabatic gas flow equations reduced to single partial differential equation, deriving solutions for entropy distribution

13 p2158 A71-27829

Supersonic flow around porous-wall conical body with uniform gas injection through wall, deriving equations for pressure at contact surface

13 p1990 A71-28182

Group properties of laminar boundary layer equations for incompressible binary fluid under various magnetic field distributions and reaction rates

13 p2048 A71-28735

Critical and near critical two phase flow in venturi tube, applying one dimensional flow equations

[ASME PAPER 71-4]

13 p2051 A71-29447

Boundary layer equations based on eddy viscosity model for turbulent free shear flow, solving numerically in Crocco coordinate plane

[ASME PAPER 71-FE-17]

13 p2052 A71-29456

Pipe gas flow with heated solid particles injection, presenting flow equations numerical solution by digital computer

[ASME PAPER 71-FE-22]

13 p2166 A71-29460

Numerical solution of coupled boundary layer equations describing strongly cooled turbulent flow of gas between parallel plates with property variation

[ASME PAPER 71-FE-38]

13 p2166 A71-29477

Existence theorem for nonlinear boundary value problems involving two dimensional incompressible boundary layer equations

14 p2264 A71-29523

Group-invariant properties of boundary layer flow differential equation for electrically conducting fluid in magnetic field

14 p2279 A71-29629

Stokes flow equations solutions existence and completeness, considering vector and scalar potentials

14 p2224 A71-30094

Similarity solution of boundary layer equations for nonuniform external flow

14 p2225 A71-30217

Axisymmetrical three component flow equations for incompressible viscous fluid in cylinder with rotating disk

14 p2227 A71-30855

Turbulent flow asymmetrical mechanics equations derivation from conservation laws, discussing Navier-Stokes equation, angular momentum and transport theory

14 p2227 A71-30877

Asymptotic behavior of boundary layer equations solution for viscous incompressible flow past curvilinear obstacle

14 p2227 A71-30878

Gas dynamic and irrotational flow equations system transformation into Cauchy-Riemann equations via Beltrami coordinate transformation for simple representation of transonic flows

[DFVLR-SONDDR-124]

14 p2228 A71-31127

Two dimensional hypersonic boundary layer equations solution upper and lower bounds determination as initial value problem 15 p2386 A71-31161

Supersonic potential flow at large distance from slender body of revolution at angle of attack, deriving nonlinear partial differential equations system 15 p2343 A71-31170

Fluid flow equations problems, describing stability and convergence theory for finite difference approximations 15 p2441 A71-31353

Compressible transonic flow about two dimensional airfoils, developing inviscid nonlinear potential equations by relaxation procedures [AIAA PAPER 71-569] 15 p2345 A71-31562

Constant density and viscosity fluid steady plane two dimensional flow under no external forces, deriving partial differential equations for vorticity, energy and pressure 15 p2389 A71-31728

Fluid mechanics problem of nonuniform meshes and complex boundary conditions, using finite element method 16 p2559 A71-33097

Difference schemes for approximating system of one dimensional gas dynamics equations in Eulerian coordinates, taking into account mass conservation law and viscosity 17 p2729 A71-35370

Self similar numerical and asymptotic solutions of laminar multicomponent isothermal boundary layer equations for large blowing rates 17 p2673 A71-35633

Asymptotic solution of viscous incompressible flow past uniformly heated paraboloid of revolution with constant surface temperature 17 p2730 A71-35800

Unsteady laminar boundary layers flow around three dimensional bodies, using finite difference techniques and power series expansion of time square root [ONERA-TP-941] 18 p2901 A71-36019

Hyperbolic and parabolic system three dimensional boundary layer equations, discussing characteristics and subcharacteristics roles in influence and dependence zones determination 18 p2902 A71-36039

Difference methods for hyperbolic flow equations, using third order accuracy space and time split difference operators 18 p2844 A71-36305

Numerical analysis of plasma expansion confined by magnetic field, emphasizing boundary oscillation and temperature rise, based on hyperbolic and parabolic system equations 18 p2952 A71-36308

Numerical solution of time dependent incompressible flow differential transport equations including turbulence effects 18 p2905 A71-36312

Stefan problem reduction to order n differential flow equation solution using Runge-Kutta method 18 p2905 A71-36314

Finite difference technique for convective flow equations involving shock wave propagation, discussing heuristic analysis for truncation error 18 p2907 A71-36338

Two dimensional flow equations for incompressible viscous fluid in square cavity 18 p2907 A71-36340

Compressible boundary layer equations similarity solutions uniqueness proof, using asymptotic behavior 18 p2909 A71-36814

MHD equations of motion solved for conducting fluid interaction with electromagnetic field in porous media in range of Darcy law 18 p2953 A71-36948

Dissipative fluid motion, discussing approaches to analysis of real fluids time dependent complex flow equations 19 p3089 A71-37499

Inviscid swirling nozzle flow equations from Crocco relation 19 p2993 A71-37890

Laminar boundary layer flows on bodies with suction or injection, solving equations using Goertler series solution for impermeable wall 20 p3210 A71-39027

Short shock wave equations solutions for two dimensional steady flow of ideal gas 20 p3211 A71-39370

Compressor blade hodography and profile equations for subsonic two dimensional flow calculated on graphic visualization console 20 p3176 A71-39420

Second order viscoelastic fluid two dimensional stagnation point flow, solving boundary layer equations 20 p3213 A71-39564

Three dimensional nonlinear subsonic flow over finite wings of arbitrary planform, solving transonic small disturbance equation by integral method 20 p3177 A71-39568

Gas-solid particles flow pseudofluid equations, discussing difference of species and partial density and various flow phases 21 p3365 A71-40018

Radially symmetric shocked flows computation method, using momentum equation in conservation form in original Cartesian coordinates 21 p3368 A71-40848

Unsteady state boundary layer equations solution in laminar flow systems with free surface and transfer of heat or mass 21 p3370 A71-40990

Plane diabatic Prim gas flow, reducing hodograph equations in elliptic regions to Cauchy-Riemann equations via Baeklund transformations 23 p3662 A71-43121

Navier-Stokes equations solutions for incompressible laminar viscous fluid flow produced by vortex filament placed on cone axis 23 p3664 A71-44004

Flow models for turbomachinery, averaging equations for flow through blade cascades across pitch 23 p3627 A71-44348

Compressible viscous flow calculation, deriving finite element analog of Navier-Stokes and energy equations 24 p3818 A71-44617

Self similar solution to Cauchy problem of gas dynamics equations in nonisentropic media 24 p3819 A71-44774

Interaction between two incompressible fluid flows in plane duct, deriving parametric equations for free stream line and flow interface 24 p3820 A71-45005

Unsteady state MGD equations and Alfven velocity behavior, examining triple orthogonal curves system formed by magnetic, principal normal and binormal lines 24 p3857 A71-45186

FLOW FIELDS

U FLOW DISTRIBUTION

FLOW GEOMETRY

High gain proportional fluid amplifier, examining defined region geometry with flow visualization and quantitative data [ASME PAPER 70-WA/FLCS-12] 03 p0354 A71-14087

Projectile entry into water vertically from air, predicting cavity shape as function of time based on hydraulic flow model [ASME PAPER 70-WA/FE-8] 03 p0402 A71-14129

Unsteady one dimensional isentropic gas flows, discussing nonlinear pressure waves geometry 03 p0405 A71-14345

Shock wave interaction with wedge moving at supersonic speed, calculating geometry of regions formed intersecting wavefronts 07 p1014 A71-19741

Numerical solution of nonuniform enthalpy mixed axisymmetric gas flow in curvilinear regions with upper boundary and discontinuity using build-up method 10 p1551 A71-24376

Curvature effects on laminar and turbulent free jet boundary between irrotational flow and stagnant fluid, discussing pressure effects 11 p1702 A71-25482

Three dimensional slot lip geometry effects on tangential and splash film cooling of gas turbines [ASME PAPER 71-GT-11] 11 p1855 A71-25957

Asymptotic expansions for viscous flow along right angle corner, satisfying layer equations and boundary conditions 11 p1752 A71-26104

Reattachment angle of supersonic laminar mixed boundary layer, using revolution model with Reynolds number allowance 11 p1704 A71-26194

Rarefied gas Poiseuille flow in parallel plates, cylindrical tube and annulus geometries, deriving subsonic flow velocity profiles by third order constitutive relations 14 p2227 A71-30574

Flow stability in differentially heated inclined rectangular box of small depth/length ratio, examining thermal convection and transition to turbulent flow as function of inclination angle 15 p2513 A71-31930

Tube or duct confined submerged turbulent jet exit cone angle calculation for various expansion area ratios 15 p2390 A71-32016

Reaction kinetic studies using hydrodynamic flow structure due to spherical shock wave from laser induced spark 16 p2616 A71-32903

Aperture angle effect on flow separation in inlet section of diffuser with cylindrical to conical channel transition 16 p2521 A71-33611

Streamwise wall curvature and transition effects in turbulent boundary layers, using modified eddy viscosity and mixing length concepts 19 p3045 A71-37891

Karman vortex street geometry calculation for single circular cylinder, using pressure drag coefficient, Strouhal number and Kronauer criterion [ASME PAPER 71-VIBR-11] 21 p3457 A71-40273

Circle, half plane and cylinder theorems for slow viscous flows involving hydrodynamic singularities under rigid boundary 23 p3625 A71-43237

Cavities geometry in steady or periodic supercavitating flow from light beam transmission in flow tunnel 23 p3664 A71-44005

Flow angularity prediction near supersonic fuselage forebody with arbitrary cross section and zero sideslip, using small perturbation theory [AIAA PAPER 71-996] 24 p3789 A71-44588

Extendible, variable profile nozzle for various flow regimes operation, developing numerical design algorithm 24 p3821 A71-45339

FLOW GRAPHS

Algorithm for higher order loops determination in flow graph from subgraphs of linear graph model, considering circuits with ladder/nonladder structures 03 p0382 A71-14310

Dynamic response with feedback characterization of human musculoskeletal frameworks by linegraph-flow graph procedure 05 p0713 A71-16485

Boolean algebra and flow diagram nomenclature for sequential logic design 13 p2035 A71-28912

FLOW MEASUREMENT

Hydrogen exchange between pial arteries for measuring local cerebral blood flow quantitatively in anesthetized cats 01 p0008 A71-10075

Real vortices velocity, density and temperature distribution determination, discussing flow measurements by hot-wire anemometer, multiple spark camera interferography and smoke visualization techniques 01 p0069 A71-10107

Arterial branches pulsating flow and wave propagation in large blood vessels, considering flow measurements from simulated model experiments 01 p0008 A71-10111

Ultrasonic flowmeters for unsteady flow, discussing beam deflection method, phase difference systems, etc 01 p0079 A71-10302

Laser schlieren crossed beam measurements in shear layer of shock free Mach 2.46 jet 01 p0094 A71-10953

Viscosity model application to turbulent plane Couette flow velocity profile and shear stress values, obtaining skin friction relation 01 p0071 A71-10954

Dog blood flow telemetric measurement with TV system using ultrasonic signals Doppler effect 01 p0024 A71-11059

Liquid flow velocity fluctuations measuring methods based on liquid-electrode contact potential dependence on flow velocity-electrolyte conductivity temperature relationship 01 p0072 A71-11225

Swirling flow through multiple nozzles of simulated solid propellant rocket motors, determining thrust and mass flow effects on passage 01 p0072 A71-11592

Relaxation method for direct measurement of molecular oxygen quenching rate constants in discharge flow system 02 p0287 A71-12493

Small gas discharge coefficient of venturi tubes 02 p0253 A71-12557

Turbulent fluid flow through pipe, measuring circumferential velocity component close to wall by electrochemical techniques 03 p0400 A71-13733

Fast multiple point measurement of fluid temperature and flow speed fields using bead thermistors and digital system 03 p0427 A71-13921

Air jet mixing with low velocity stream in constant diameter pipe, measuring flow characteristics for non-separating conditions [ASME PAPER 70-WA/FE-2] 03 p0402 A71-14124

Mean velocity profile measurements in turbulent wake behind single or parallel arbitrarily spaced and sized cylinders with adverse pressure gradient [ASME PAPER 70-WA/FE-10] 03 p0403 A71-14131

Turbulent mixing of two parallel similar and dissimilar fluid streams, comparing velocity and density profiles measurements with similarity solution [ASME PAPER 70-WA/AFM-38] 03 p0404 A71-14163

Liquid flow rate measurement based on tank-filling method, discussing factors affecting accuracy 03 p0356 A71-14328

Shock tube diagnostics, instrumentation and rapid photography in nonequilibrium gas dynamics 04 p0565 A71-14699

Hydrodynamic and thermal measurements in turbulent boundary layer of liquid drop flow past plate for mineral oil-water mixtures 04 p0576 A71-15617

Turbulent boundary layer development and heat transfer in parallel wall passage entrance region, comparing measurement results with computer solution 04 p0689 A71-15920

Variable viscosity fluid laminar flow, measuring tube resistance at critical Reynolds numbers as function of energy dissipation 05 p0737 A71-17037

Transonic jets pressure and density fluctuations dependence on air humidity, discussing flow field measurements by differential and Mach-Zehnder interferometry and wall pressure distributions 05 p0737 A71-17153

Vortex breakdown in swirling conical flows, determining swirl angle distribution, flow rates and Reynolds number effects 06 p0843 A71-18513

Optical crossed-beam measurements of turbulence intensities in cold subsonic air jet shear layer [ALAA PAPER 71-137] 06 p0902 A71-18580

Supersonic turbulent boundary layer measurements in moderate adverse pressure gradient region along two dimensional ramp model 06 p0884 A71-18604

Turbulent skin friction and boundary layer velocity measurements on nonadiabatic flat plates at hypersonic Mach numbers 06 p0885 A71-18609

Parallel plate plasma accelerator energy deposition, considering kinetic and thermal modes based on flow velocity, temperature and Mach number measurements 06 p0939 A71-18635

Disturbances within hypersonic transitional boundary layer in Mach 7 gun tunnel observed with hot-wire anemometer, comparing results with surface heat transfer measurement 06 p0886 A71-18637

Turbulent He jet measurements using hot-wire anemometry and digital recording techniques, assessing accuracy 06 p0886 A71-18639

Turbulent boundary layers near-wall measurements for single phase incompressible flows 07 p1105 A71-18781

Turbulent cylindrical boundary layer velocity distribution, determining power law functional relationship by wind and water tunnel experimental measurements 07 p1088 A71-19420

Supersonic molecular beams with cycling-pressure sources, investigating mass flow rate effects on skimmer interference 07 p1164 A71-19900

Wind tunnel experiments on vortex shedding from circular cylinders in oscillating free stream 07 p1090 A71-19908

Computerized capillary model for fluidic restrictors in multipoint concurrent air flow measurements 07 p1025 A71-20563

Hydrogen slush storage and transfer density and flow measuring instrumentation, emphasizing capacitance measurement 08 p1292 A71-21695

Mean flow measurement of cone laminar supersonic wake 09 p1381 A71-22091

Effect of asymmetrical inviscid flow from Traill-blazer flight measurements, discussing windward leeward attenuation variation in transmitted VHF signal 09 p1406 A71-22916

Coronary blood flow measurements during strenuous upright exercise, using nitrous oxide method 09 p1400 A71-23362

One component two phase flow in tubes with increasing pressure gradient, investigating flow choking and correlating measurements with analytical results 09 p1434 A71-23464

Turbulent supersonic flow measured by laser anemometry, stressing advantages over optical heterodyning 09 p1453 A71-23693

Laser fluid flow velocimeter pulse output resolution approximation, using spectrum analyzer or discriminator measurements 09 p1453 A71-23726

Fast miniature shielded pitot pressure transducer for spatial resolution of flow details 09 p1453 A71-23728

Sonic nozzle design for precise mass flow measurement, determining nozzle profile for axial velocity distribution in conformity with laminar boundary layer equations solution 10 p1597 A71-24944

Two dimensional flow in radial turbomachine bladed impeller, comparing numerical solution based on potential theory with experimental results [ASME PAPER 71-GT-20] 11 p1703 A71-25964

Shock tube facility with two-phase system of solid particles and gases as primary driven fluid, applying to hypervelocity impact phenomena observation 11 p1745 A71-26266

Parallel light beam triangular path interferometer with linear compressive shear effect for flow measurement applications, describing prism system and interference patterns 12 p1905 A71-26816

Thermosensitive quartz anemometer operating in vibrational mode, discussing design and applications in low airflow velocity measurement 12 p1906 A71-26826

Errors due to air flow pulsation in orifice meters, discussing various diameter ratios 12 p1906 A71-26872

Nonbleeding blood flow measurement by magnetorheography, using electromagnetic flowmeter principle 12 p1874 A71-27137

Vortex shedding characteristics of circular cylinders at low Reynolds numbers from experiment on tapered models wake structure 12 p1897 A71-27220

Unsteady flow measurement around wing sections during rapid angle of attack variations, emphasizing helicopter rotor blades 12 p1864 A71-27468

Nozzle wall hypersonic turbulent boundary layers at free stream Mach number, using pitot, hot wire, wall pressure fluctuation and static pressure measurements [ALAA PAPER 70-746] 12 p1898 A71-27558

Hot-wire flowmeters calibration for low density flow measurements, describing method for hot wire end loss determination 12 p1908 A71-27595

Rarefied hypersonic flow in blunt body bow region, measuring density and rotational temperature fields by electron beam method 13 p1989 A71-27841

Fluid velocity measurements by electroacoustic transducers using phase difference relation 13 p2069 A71-28901

Gas dynamic test assemblies experiments for demonstrating theoretical basis of supersonic nozzle design with radial flow section 13 p1992 A71-29173

Flow and heat transfer measurements in dihedrons simulating patterns about supersonic conical edge and shock wave interaction line, using thermoincandescence coating technique 13 p1992 A71-29174

Transient flow measurement with sharp-edged orifices, considering pump trip accidents simulation in water cooled nuclear reactors 13 p2053 A71-29465

Monograph on hypersonic shock tunnel supersonic combustion research techniques covering test facilities, optical and electromagnetic flow measurement methods, etc 14 p2334 A71-29578

Electromagnetic flowmeters readings for boundary effects of current equalization 14 p2279 A71-29616

Supersonic mass flux probe description, discussing inlet geometry, angle of attack and Reynolds and Mach numbers effects on performance 14 p2239 A71-29925

Nonsteady air flow direction generation and measurement, comparing three-tube probe with hot-wire anemometer data 14 p2244 A71-30326

Gas injectors characteristics investigation by cold flow simulation, using flow field visualization techniques and velocity and mass concentration profiles measurements 14 p2291 A71-30739

Holographic interferometry for observing transparent media in supersonic gas flow, comparing results with Mach-Zehnder interferometry 15 p2404 A71-31275

Flow field measurement about sharp and slightly blunted slender cone at hypersonic speed and zero angle of attack 15 p2344 A71-31553

Low density hypersonic flow on flat plate, discussing surface pressure measuring techniques [ALAA PAPER 71-606] 15 p2346 A71-31580

Noise and spectral analysis for measuring fluid flow with random temperature fluctuations by transit times 15 p2406 A71-31596

Direct measurement of spatial velocity correlation functions in turbulent flow by conditional probability of scattered light 15 p2449 A71-31866

Vortex type pneumatic angular rate sensor with vanes and hydrodynamic viscous coupling, determining differential pressure outputs 15 p2352 A71-32063

Flow measurements in axisymmetric turbulent wake of sphere in low speed wind tunnel 15 p2346 A71-32123

Cryogenic fluids flow measurement, discussing various fluids, pressures, temperatures and flow rates 15 p2412 A71-32701

Heat transfer, density and pressure measurements of hypersonic two dimensional centered nonequilibrium corner expansion oxygen flow with frozen boundary in shock tunnel 16 p2555 A71-32906

Nonequilibrium nozzle flow determination for vibrationally relaxing gas, describing sudden freeze approximation method validity 16 p2556 A71-32907

Unsteady compressible flow measurement, determining local lift coefficient from pressure distribution along airfoil 16 p2520 A71-33342

Hot-wire anemometer design for measuring forced expiratory flow and volume, testing dynamic nonlinearity on hybrid computer 17 p2738 A71-34441

Flow visualization and hot-wire measurements, showing vortex shedding association with turbulent air jet issuing from flat plate into cross wind 17 p2670 A71-34659

Vortex laser Doppler velocimeter system for aircraft wake turbulence velocity profile mapping, describing optical arrangements, back and forward scattering modes and prototype design 17 p2754 A71-35756

Bursting phenomenon measurement in turbulent boundary layer by hot wire, noting spottiness, HF intermittency and energy balance dynamics 18 p2985 A71-36036

Turbulent multispecie gas mixing measurements using dark field laser schlieren system 18 p2930 A71-36059

Unsteady multispecie gas mixture concentration flow measurement, using Raman scattering of pulsed nitrogen laser light 18 p2930 A71-36060

Gas flow through hypersonic conical nozzle in shock-gun tunnel, measuring pressure ratio and Mach number distributions at test section 18 p2849 A71-37024

Backscattering laser Doppler velocimeter for water flow and moving opaque object measurements, discussing velocity resolution and optical geometry 19 p3072 A71-37552

Turbulent boundary layer and heat transfer measurements along cooled conical convergent-divergent nozzle [ASME PAPER 71-HT-4] 19 p2993 A71-37982

Hydrogen near-critical point flow in heated cylindrical tube, measuring flow parameters radial profiles by combination pitot tube/thermopile/hot-wire sensor probe [ASME PAPER 71-HT-25] 19 p3165 A71-37995

Capacitance measurement technique for density and mass flow measurements for hydrogen slush storage and transfer 20 p3237 A71-39276

Turbulence measurement in subsonic wind tunnel gas jet flows containing dust particles, using Doppler difference laser velocimeter 21 p3392 A71-40397

Turbulent jet flow concentration, velocity and direction measurements, describing cold and hot wire techniques and data reduction system 21 p3378 A71-40401

Hot split-film anemometer sensors for three dimensional air velocity vector measurement 21 p3378 A71-40487

Book on turbulence covering measurement techniques, equations of motion, Newtonian viscous fluids, Reynolds stresses, flow visualization, random processes, turbulent energy, boundary layers, etc 21 p3371 A71-41248

Unbounded turbulent jet transducer element fluidic sensors, measuring ambient velocity and density from pressure data 22 p3531 A71-42768

Sonic line position measurement in supersonic flow behind detached shock wave preceding axisymmetric or plane blunt bodies 23 p3625 A71-43092

Flow field generation by coaxial turbulent jets, determining velocity distribution, turbulence intensities and shear stresses by hot-wire anemometers 23 p3627 A71-44198

Diffusion from continuous line source in turbulent boundary layer, comparing calculation based on Lagrangian similarity with measurements 23 p3664 A71-44200

Helicopter, tilt wing and jet lift hovering aircraft outflow measurements to determine suitability as rescue vehicles [ALAA PAPER 71-992] 24 p3791 A71-44586

Shielded hot-wire probe for mean and rms flow velocities in highly turbulent and rapidly reversing flows 24 p3828 A71-45075

Flow NETS
Flow lines construction in two dimensional supersonic flow region with rarefaction waves interaction from several disturbance sources 08 p1230 A71-22052

FLOW PATTERNS
U FLOW DISTRIBUTION

- FLOW RATE**
U FLOW VELOCITY
- FLOW REGULATORS**
NT FUEL FLOW REGULATORS
Continuous flow oxygen regulators construction, performance and testing SAE standard, covering automatic, adjustable and preset types [SAE-AS-1197] 07 p1049 A71-19648
Gas chromatography techniques, discussing carrier tank, flow control, injector, reactor, column, detector, recorder, flowmeter, etc 11 p1729 A71-26291
Fluid interface Rayleigh-Taylor type instability, considering control as optimal regulator problem 11 p1742 A71-26413
Hydrostatic bearings for large optical and radio telescopes, explaining lubricant flow control systems 23 p3661 A71-43862
Passive gas flow control with compensation for ambient temperature and supply pressure variations, using choked orifice with area variation linearly proportional to diaphragm deflection [ASME PAPER 70-WA/AUT-14] 24 p3828 A71-45137
- FLOW RESISTANCE**
NT AERODYNAMIC DRAG
NT FRICTION DRAG
NT VISCOUS DRAG
Low resistance nozzles for complete power compensation in rate of climb indicators 01 p0079 A71-10350
Circular pipe gas laminar flow at constant wall temperature, determining heat exchange and drag by motion and energy equations integration in boundary layer approximations 02 p0240 A71-12192
Gas and fluid flow through flat and cylindrical porous cermet walls, determining permeation energy loss and radial flow hydraulic resistance 02 p0240 A71-12277
Shear flow turbulent friction in boundary layer, deriving Navier-Stokes equation integrodifferential formulation 02 p0241 A71-12411
Blood pressure and velocity waveform recording for patients during cardiac catheterization, interpreting relationships to vascular impedance 02 p0201 A71-12915
Plastic impact principle of hydraulic losses in turbulent viscous flow, using Navier-Stokes equation with friction term 03 p0397 A71-13006
Heat transfer and fluid friction of hydrogen and helium gas flows undergoing turbulent to laminar flow transition in heated pipe [ASME PAPER 69-HT-54] 03 p0405 A71-14291
Variable viscosity fluid laminar flow, measuring tube resistance at critical Reynolds numbers as function of energy dissipation 05 p0737 A71-17037
Plane grid condenser movement through magnetized plasma, calculating resistance by quasi-hydrodynamic approximation for plasma dielectric tensor 06 p0936 A71-17731
Transients estimation for measuring lines of LF pressure sensors, taking into account hydraulic resistance in inlet channel 08 p1286 A71-20834
Plastic anisotropy in bcc metal crystals, measuring flow strength for various plane strain compression states 08 p1308 A71-21513
Turbulent air flow in cooled tubes, studying local heat transfer and hydraulic resistance 08 p1377 A71-21924
Mathematical model for brain arteries hemodynamic resistance, using blood pressure data 09 p1390 A71-22261
Cardiac output in relation to peripheral resistance in borderline hypertension 09 p1392 A71-22591
Volume, compliance and flow resistance of pulmonary vascular compartments of dogs 10 p1560 A71-24122
Heart rate and diastolic inflow coronary resistance extravascular component, discussing heart artificial stimulation and pharmacological maximal dilation effects 10 p1565 A71-24679
Turbulent photosphere and chromosphere, investigating finite resistivity effects on solar flare phenomena 11 p1832 A71-26173
Resistance and heat transfer coefficients in hydrodynamically and thermally developed MHD pipe flow 12 p1941 A71-27740
Gas flow heat loss through porous metals, deriving hydraulic resistance and heat release coefficients 13 p2165 A71-29218
Turbulent gas flow through duct with alternating pressure gradient, considering heat transfer and frictional resistance 13 p2166 A71-29370
- Incompressible liquid laminar boundary layer flow velocity profile and normal friction stress calculation by successive approximation method 14 p2169 A71-29630
Nondimensional entrance loss equation for radial turbulent flows without swirl between parallel disks 14 p2226 A71-30415
Friction in compressible turbulent boundary layers at isothermal adiabatic wall 15 p2510 A71-31163
Circular pipe gas laminar flow at constant wall temperature, determining heat exchange and drag by motion and energy equations integration in boundary layer approximations 15 p2388 A71-31498
Low Reynolds number turbulent flow in large aspect ratio rectangular ducts, investigating Blasius and Prandtl circular tube friction factor relations 15 p2392 A71-32261
Heat transfer and hydraulic resistance in cross flow heat exchanger with slitlike channels 17 p2836 A71-34212
Turbulent air flow in cooled tubes, studying local heat transfer and hydraulic resistance 17 p2838 A71-35268
Fluidic viscometer using laminar impedance element for output signal amplification 17 p2677 A71-35289
Turbulent boundary layer interaction with supersonic outer flow behind step, calculating pressure distribution, momentum thickness and friction 17 p2672 A71-35631
Circular cylinder resistance in oscillating stream of second order fluid, calculating flow distribution 18 p2843 A71-36042
Ideally conducting magnetostatic equilibria and associated time dependent resistive flows from two dimensional solution for MHD equations 19 p3115 A71-38211
Potassium concentrations and osmolality levels changes effects on vascular resistance in subcutaneous adipose tissue blood flow 20 p3189 A71-39379
Velocity and resistance profiles for unsteady turbulent flow in rough pressure channels, using Prandtl hypothesis 20 p3214 A71-39797
Electrically conducting fluid flow resistance in plane insulated channel in presence of transverse magnetic field, determining pressure, velocity and electric potential distributions 21 p3422 A71-40677
Room temperature evaporating water drop shape history on cooper, lucite, stainless steel and Teflon, observing wetting dynamics effects 21 p3476 A71-40903
Unsteady laminar flow in polygonal ducts, calculating velocity profiles, friction factors and energy dissipation 21 p3371 A71-40994
Fluid flow friction and combined free and forced convective heat transfer characteristics in rotating curved circular tube, using finite difference scheme and iterative solution 23 p3783 A71-44192
Hydraulic resistance and heat transfer in annular channel with rotating flow, comparing to axial flow 24 p3888 A71-44747
Polytropic process description for gas flow by introducing resistance and heat transfer coefficients 24 p3820 A71-45020
Unsteady gas pulsations in compliant tube, predicting pressure amplitude extremum as function of mean flow by linear theory with frictional effect 24 p3820 A71-45073
Hydraulic resistance of laminar isothermal flow of fluid with structural viscosity in circular cylindrical rigid channel 24 p3821 A71-45227
- FLOW SEPARATION**
U BOUNDARY LAYER SEPARATION
U SEPARATED FLOW
- FLOW STABILITY**
NT BOUNDARY LAYER STABILITY
NT FLAME STABILITY
NT MAGNETOHYDRODYNAMIC STABILITY
Gas dynamic equations of arbitrary materials detonation without allowance for transport phenomena, deriving stability criteria from boundary value problem steady solution 01 p0070 A71-10490
Optically thin medium convective instability, examining radiant pressure and magnetic field effects 01 p0158 A71-10804
Continuous zonal flow nonlinear baroclinic instability, noting amplitude vacillations and flow-wave interactions 01 p0120 A71-10855
Shear wave propagation into heat conducting viscoelastic fluids, considering steady one dimensional flow stability 01 p0181 A71-11188
Plane laminar flow stability along flexible boundary, obtaining numerical and asymptotic solutions 03 p0399 A71-13198
- Stability theory for pair of trailing vortices, investigating induced field convection, modes, amplification, cut-off distance, etc 03 p0341 A71-13436
Cavity fluid oscillation near convecting field, calculating onset velocity as hydrodynamic stability problem 03 p0399 A71-13438
Uniform flow stability near two dimensional stagnation region formed by blunt body immersion in cross flow 03 p0400 A71-13728
Couette flow stability between coaxial rotating cylinders, calculating eigenvector in first approximation small perturbation equations 03 p0404 A71-14231
Finite amplitude instability of compressible laminar wake with strongly amplified disturbances, discussing nonlinear theory in terms of von Karman equation 04 p0569 A71-15028
Thermal conductive liquid hydrodynamic stabilized Hartmann flow in rectangular canal with transverse field, examining magnetic effect on heat transfer 04 p0635 A71-15509
Multitube condensers of various geometries, investigating tube flow stability, distribution and gravitational effects 04 p0688 A71-15538
Laminar flow stability and transition to turbulent flow, giving nonlinear theory for perturbations development 04 p0574 A71-15602
Viscoelastic fluids flow stability between arbitrary spaced concentric cylinders, noting critical Taylor number dependence on gap size 05 p0735 A71-16715
Nonadiabatic gas acoustic oscillation instability, examining heat release fluctuations 05 p0838 A71-16777
Plane Poiseuille viscoelastic liquids flow stability, using method of inner and outer expansions based on Chun and Schwarz asymptotic solution of Orr-Sommerfeld equation 05 p0737 A71-17102
Transonic jets pressure and density fluctuations dependence on air humidity, discussing flow field measurements by differential and Mach-Zehnder interferometry and wall pressure distributions 05 p0737 A71-17153
Plane Poiseuille flow stability to finite amplitude periodic disturbances, using Orr-Sommerfeld eigenfunctions 06 p0881 A71-17429
Uniform magnetic field parallel alignment effects on incompressible electrically conducting free two dimensional jet flow stability at large Reynolds number 07 p1084 A71-18745
Turbulent flow main characteristics calculation based on maximum stability hypothesis with respect to most dangerous perturbation, presenting numerical solutions by digital computer 07 p1085 A71-18755
Monograph on transonic shock free potential flow around quasi-elliptical airfoil sections, investigating flow stability under unsteady disturbances 07 p1015 A71-19773
Nongeostrophic and nonhydrostatic stability of baroclinic fluid for small Richardson numbers 07 p1153 A71-20220
Cylindrical viscous jet surrounded by flowing gas, investigating flow stability by linear perturbation theory 07 p1093 A71-20281
Stability of two concentrically flowing fluids in straight circular tube, investigating axisymmetric and asymmetric disturbances by small perturbation method 07 p1093 A71-20282
Laminar-turbulent bounded jet stability, examining transition zone shift with smoke visualization 07 p1029 A71-20594
Poiseuille pipe flow stability from finite difference equations approximation to nonlinear axisymmetric Navier-Stokes equations under stream function perturbation 07 p1094 A71-20611
Hydrodynamically stabilized turbulent viscous incompressible fluid flow in circular tube, examining nonstationary convective heat transfer by numerical methods 08 p1276 A71-21923
Velocity profile in viscous sublayer at wall based on maximum stability principle applied to Karman constant for turbulent channel flow 08 p1277 A71-21950
Plane Poiseuille flow bounded by solid walls, applying Fourier expansion method to stability problem 09 p1432 A71-22583
Laminar mixing region stratified free shear layer stability between two uniform streams from numerical solution of linear sixth order equation for disturbance amplitude function 09 p1432 A71-22851

Incompressible flow stability to axisymmetric disturbances in circular pipe 09 p1434 A71-23165

Incompressible inviscid fluid flow in presence of two homogeneous porous layers, examining hydrodynamic instability 10 p1591 A71-23754

Nonlinear stability of incompressible laminar flows involving perturbation in Banach space 10 p1591 A71-23914

Orr-Sommerfeld hydrostatic stability equation derivation for nonparallel flow in wake from Goldstein velocity distribution, noting lateral direction velocity component magnitude 10 p1592 A71-24024

Fluid rotational stability between coaxial cylinders rotating at same angular velocity in presence of radial temperature gradient 10 p1696 A71-24374

Laminar incompressible boundary layer flow stability, emphasizing wall curvature and flexibility effects 10 p1594 A71-24548

Flow instability and secondary circulation in pressure-driven rotating rectangular channel 10 p1595 A71-24617

Asymptotic stability of rapidly rotating horizontally bounded fluid heated from below, considering conductive state and Ekman layers 10 p1595 A71-24618

Nonlinear stability analysis of inviscid and viscous liquid film adjacent to compressible gas flow, using gravity and pressure perturbation models 10 p1595 A71-24620

Stratified shear flow stability, investigating diffuse interface between two miscible fluids 10 p1595 A71-24623

Local instability of curved flow, considering stability of fluid flow between rotating cylinders for instability onset criterion establishment 10 p1597 A71-24941

Intrinsic helical and quasi-rigid hydrodynamic motions of incompressible, ideal and viscous fluids, using mobile frame method 11 p1804 A71-25175

Massive stars evolutionary models, exploring convective instability effects 11 p1818 A71-25205

Stabilization effect of rotation on Rayleigh-Taylor instability of stratified compressible inviscid fluid of variable density for noncritical wave numbers 11 p1749 A71-25434

Variational formulation for hydrodynamic stability based on local potential motion, determining transition from laminar to turbulent flow 11 p1749 A71-25441

Magnetically suspended laminar supersonic cone wake stability from hot wire fluctuation and spectral components amplitude/phase measurements 11 p1702 A71-25475

Stellar free neutrino and antineutrino emission thermodynamics under hot matter neutronization and hydrodynamic stability during late evolutionary stages 12 p1954 A71-26576

Nonviscous fluid isotropic turbulent motion concept, and structural stability role in steady state flow statistical properties 12 p1895 A71-26827

Boussinesq stratified fluid zonal flow with vertical and horizontal shear, studying stability to hydrostatic neutral wave perturbations 12 p1925 A71-27194

Inviscid compressible fluid jet flow, calculating instability boundaries characteristics by linear perturbation analysis and numerical solution 12 p1897 A71-27219

Directional acoustic radiation from supersonic jet, discussing generation mechanism theory based on shear layer instability close to nozzle 12 p1945 A71-27221

Plane parallel Couette flow stability with respect to small perturbations, considering positive wave numbers and Reynolds numbers 12 p1897 A71-27307

Hydrodynamic instabilities of MHD plasma with current, using two fluid model in crossed magnetic-electric fields 13 p2105 A71-28789

Neutral fluctuations of zonal winds in stratosphere and mesosphere from flow equations, noting flow instability role in generation mechanism 13 p2057 A71-28020

Nonzonal atmospheric motion effects on meteorological elements 26-month oscillations stability in equatorial zone from linear hydrothermodynamic equations 13 p2057 A71-28022

Surface evaporation and condensation effects on stability of thin liquid film flowing down heated inclined plane at critical Reynolds number 13 p2160 A71-28596

Correlation model of stability and onset of turbulent motions for incompressible fluid, noting inconsistency of Keller-Friedman equations 13 p2050 A71-29206

Stability theory for thermal stratified viscous parallel flows at Prandtl number of unity, considering atmospheric boundary layer and jet stream mechanisms 13 p2165 A71-29246

Quasi-one dimensional nonlinear model of electrohydrodynamic stability and control of current carrying seminsulating jets at supercritical and subcritical regimes 13 p2118 A71-29249

Synoptic scale processes effect on high level clear air turbulence production, considering Kelvin-Helmholtz instability role in flow transition 14 p2268 A71-29762

Short conical diffusers with radial splitters for flow stabilization with high pressure recovery performance 14 p2225 A71-30304

Convection stability in arbitrarily shaped fluid containers heated from below with temperature gradient above critical value 14 p2337 A71-30408

Nonlinear dynamical evolution of two dimensional unstable shear flows, using numerical integration of time dependent incompressible Navier-Stokes equations 14 p2226 A71-30409

Exothermic hypersonic blunt body flow periodic instability mechanism, using ballistic range with schlieren photographic equipment 14 p2337 A71-30455

Plane horizontal fluid film convective stability with free boundaries in vertical circular cylinder for periodic modulation of vertical temperature gradient or gravitational field 14 p2338 A71-30873

Flow stability in differentially heated inclined rectangular box of small depth/length ratio, examining thermal convection and transition to turbulent flow as function of inclination angle 15 p2513 A71-31930

Nonlinear stability theory, considering velocity and vorticity perturbations in circular Couette plane Poiseuille and shear layer flows 15 p2393 A71-32568

Stationary nonparallel plane flow stability with horizontal shear to three dimensional nondivergent disturbances in Boussinesq fluid, using Arnold method 15 p2393 A71-32637

Hydrodynamic instability generation by stable layer tilting at high altitude, considering clear air turbulence 15 p2445 A71-32712

Hydrodynamic stability, determining velocity field bounds in laminar boundary layer by Nagumo-Westphal theory of parabolic differential operators [DFVLR-SONDDR-131] 16 p2557 A71-32982

Cellular convective fluid flow stability regions between concentric cylinders, considering nonuniqueness features with asymptotic stationary solution 16 p2557 A71-32983

Gravity waves over flow with nonuniform velocity distribution, investigating neutral stability problem of generation and momentum transport 16 p2557 A71-32984

Viscous incompressible flow stability between concentric rotating cylinders, developing nonlinear model of two disturbance interaction 16 p2558 A71-32985

Plane Couette flow with finite disturbances, investigating stability in nonlinear terms 16 p2558 A71-32986

Closed circuit electrical, mass and heat flow stability analysis, showing capacities or inductances trace effects 16 p2607 A71-32991

Global hydrodynamic stability theory, discussing energy methods and nonlinear Boussinesq equations for disturbed motion 16 p2558 A71-32995

Unstable two dimensional incompressible flow and wake development, using finite difference calculations for Navier-Stokes equations 16 p2558 A71-32996

Nonlinear hydrodynamic stability of incompressible Newtonian fluid, comparing linear and energy theories 16 p2558 A71-33005

Pipe Poiseuille flow instability with respect to finite amplitude disturbances, calculating Reynolds stress by linear wall mode 16 p2558 A71-33021

Damping disturbances structure in unbounded laminar flow stability at large Reynolds numbers, demonstrating damping modes eigensolutions in form of concentrated wave packets 16 p2559 A71-33022

Hydrodynamically stabilized turbulent viscous incompressible fluid flow in circular tube, examining unsteady convective heat transfer by numerical methods 17 p2729 A71-35267

Plane Poiseuille flow stability evaluation for finite amplitude periodic disturbances, using harmonic analysis 17 p2729 A71-35389

Ideally incompressible fluid with free surface, analyzing interfacial tension forces effects on rotational-translational motion stability 17 p2730 A71-35648

Turbulent plane flow velocity profile stability characteristics covering parabolic Poiseuille flow under infinitesimal disturbances 18 p2901 A71-35855

Large amplitude whistler as collisionless laminar shock model, showing instability for oblique perturbation propagation 18 p2950 A71-35865

Impulsively started time-dependent rotational Couette flow stability analysis by initial value problem and quasi-steady approaches 18 p2902 A71-36038

Joseph type theorems derivation for parallel fluid flow with wave perturbation stability governed by Orr-Sommerfeld equation 18 p2902 A71-36041

Smallest Taylor number corresponding to Couette flow stability between two rotating cylinders subjected to rotationally symmetrical perturbation 18 p2902 A71-36093

Plane laminar flow linear stability problem, using Orr-Sommerfeld equation with Volterra integral equation 18 p2904 A71-36136

Second order accuracy and stability analysis of method of characteristics application to three dimensional steady supersonic flow 18 p2907 A71-36329

Plane MHD Couette flow stability with asymmetric velocity profile shaped by transverse magnetic field, considering Hartmann flow 19 p3108 A71-37077

Variable density effect on inviscid free shear layer instability at small Mach numbers, deriving difference equation for inviscid disturbance [DFVLR-SONDDR-114] 19 p3043 A71-37300

Plane Couette-Poiseuille flow stability between porous walls with fluid injection and suction causing uniform crossflow 19 p3044 A71-37728

Laminar compressible wakes instability behind planar and axisymmetric slender bodies, solving integral conservation equations for fluctuation amplitude variations 19 p2993 A71-37879

Plane parallel Couette flow stability with respect to small perturbations, considering positive wave numbers and Reynolds numbers 19 p3046 A71-38263

Acoustical oscillations effect on free jet flow stability and structure, using inviscid Orr-Sommerfeld equation for flow disturbances frequency, wavelength and velocity 20 p3175 A71-38806

Turbulent flow stability with respect to small disturbances, applying maximum stability principle to stable averaged flow 20 p3210 A71-38895

Wing tip vortex control device, discussing design, operation and effectiveness 20 p3175 A71-39084

Unstable thermal stratification and critical Reynolds number effects on dynamic instability of Ekman boundary layer vortex rolls 20 p3257 A71-39438

Flow instability in stagnation point region of circular cylinder in turbulent channel flow, using hydrogen bubble method for flow visualization 20 p3211 A71-39454

Oscillatory modes of perturbation in onset of flow instability for Newtonian liquid between concentric rotating cylinders with transverse pressure gradient 20 p3212 A71-39484

Stability problem in hydrodynamics of perturbed heterogeneous shear flow, solving initial value problem for Couette flow 20 p3213 A71-39783

Compressible circular free jet instability allowing for turbulent boundary layer thickness, considering influence of axisymmetry on spatial growth rate and disturbance phase velocity 21 p3365 A71-40013

Aircraft trailing vortex pair linear stability, obtaining flow field near curved vortex filament with swirl and axial velocities 21 p3320 A71-40500

Self induction function and stability for vortex with finite core at aircraft wing, confirming Crow theory 21 p3320 A71-40502

Flow visualization of aircraft trailing vortex wakes in towing tank with electrochemically activated dye, noting flow instability 21 p3321 A71-40505

Thermal convection induced perturbations in unstably stratified horizontal shear Couette flow of Boussinesq fluid in rectangular channel heated from below 21 p3475 A71-40641

Vertical magnetic field effects on stability of variable density compressible inviscid fluid, solving by variational principle 21 p3415 A71-40666

Buoyancy and surface-tension induced fluid instabilities in open and closed vertical circular cylindrical

containers from series solution by Jeffreys-Goldstein method

21 p3367 A71-40667

MHD flow stability under arbitrary three dimensional disturbances, considering energy estimate for interaction between magnetic field and velocity field at critical Reynolds number

21 p3422 A71-40676

Hydrodynamic stability of incompressible conducting fluid flow between two moving linearly and rotating coaxial cylinders in longitudinal magnetic field

21 p3367 A71-40688

Spectral density functions of velocity pulsations and frequency dependent stability in turbulent plane and axisymmetric channel air flows at different Reynolds numbers

21 p3368 A71-40697

Two axisymmetric annular flows linear hydrodynamic stability analysis, using Navier-Stokes system

21 p3370 A71-40991

Mesoscale perturbations in wind velocity field in jet streams, interpreting data in terms of hydrodynamic stability theory

21 p3412 A71-41392

Inhomogeneous plasma shear flow instability with ion-ion collision, using BGK model

22 p3579 A71-41581

Lower boundary condition effects on quasi-geostrophic baroclinic instability, showing vertical wind shear as function of pressure and wavelength

22 p3569 A71-42544

Viscous incompressible flow between concentric rotating spheres, investigating hydrodynamic stability

23 p3663 A71-43443

Electrification induced instabilities, breakup and drop size of charged cylindrical liquid jets, using small perturbation method

23 p3663 A71-43445

Variational formulation for stability of parallel flows with imposed temperature gradient

23 p3783 A71-44180

Reflected shock wave interaction with tangential discontinuity curve for supersonic incalculable jets, examining flow instability

23 p3665 A71-44337

Taylor vortex flow stability between rotating concentric cylinders, using fifth order amplitude expansions in matrix form

24 p3817 A71-44420

Stability of dissipative shear flow of inviscid incompressible electrically conductive fluid in presence of magnetic field, deriving instability modes phase velocity limiting conditions from MHD equations

24 p3855 A71-44645

Flow instability due to viscosity variation in high pressure two dimensional laminar flow of Newtonian fluid between rigid parallel plates

24 p3819 A71-44945

Hartmann number for velocity pulsation free transition from turbulent MHD flow to laminar, noting difference relative to linear stability theory

24 p3856 A71-45059

Small perturbation development of plane potential motion of ideal incompressible fluid in elliptical region, confirming instability

24 p3821 A71-45219

FLOW THEORY

NT MIXING LENGTH FLOW THEORY

Unsteady cavitation flow, presenting physical mechanism of cavity formation in liquid flow and formulation of governing equations

01 p0069 A71-10110

Unsteady flow theory, describing milestone experiments in aerodynamics

01 p0001 A71-10266

Nonsimilarity boundary layer solutions applicable locally and independently of information from other streamwise positions

01 p0070 A71-10928

Two dimensional potential flow theory for incompressible unsteady flow about multiple lifting bodies in small amplitude motion

01 p0071 A71-10929

Whitham supersonic flow theory application to mid-or near-field sonic boom of slender bodies in wind tunnel research

01 p0005 A71-10956

Elastoplastic constitutive laws with nonassociated flow laws and work hardening, nonhardening and softening behavior

01 p0174 A71-10999

Fredholm method for reversible transonic flow in computing aircraft wing and turbomachine or helicopter blade airfoils for compressibility law

01 p0003 A71-11022

Incompressible fluid flow calculations, describing simplified marker-and-cell technique

01 p0071 A71-11163

Turbulent transport equations derivation for incompressible fluid unsteady flow in arbitrary geometry, considering application to flow between parallel plates

01 p0072 A71-11469

Thermoplasticity plane problems with complex edge loading, deriving algorithm based on theory of flow with translational hardening

02 p0323 A71-11746

Channel flow boundary layers, discussing parabolic differential equations, pressure gradients, friction coefficients, Stanton numbers, velocity and temperature profiles, etc

02 p0241 A71-12644

Soviet book on nonlinear conical gas flow theory covering flows with different characteristics past bodies of various geometries and positions

02 p0187 A71-12719

Nonlinear problem of fully and partially cavitating flow past oblique flat plates, solving via conformal mapping theory and Riemann-Hilbert method

03 p0398 A71-13106

Flow research on blading - Conference, Baden, Switzerland, March 1969

03 p0339 A71-13139

Navier-Stokes equations numerical integration in Eulerian coordinates, applying results to compressible and incompressible fluids steady flow

[AIAA PAPER 70-2] 03 p0399 A71-13426

Modified Coles compressibility transformation for wake mapping with Howarth-Dorodnitsyn scaling suppression

03 p0400 A71-13460

Two dimensional cascade flow, discussing methods of flow field idealization, nonviscous incompressible flow theoretical methods, compressibility and viscosity effects

03 p0342 A71-13826

Thin plane wings with mixed leading edges, applying linearized supersonic flow theory

03 p0344 A71-14241

Heuristic flow acoustics, discussing noise frequency spectrum in reference to moving singularities

04 p0569 A71-14980

Flows on 3-manifolds near isolated invariant sets

04 p0620 A71-15727

Wall jet and wake flow prediction, using Prandtl-Kolmogoroff turbulence model

04 p0578 A71-15766

Perturbations effect on tube flow and density variations due to noninstantaneous shock wave formation

05 p0836 A71-16529

Supersonic reactive gas flow free expansion over sharp corner into region of constant pressure, using linearized theory and numerical method of characteristics

05 p0836 A71-16535

Unsteady coefficient measurements to corroborate theory for coefficient distribution about little elongated two dimensional wings with control surfaces

05 p0694 A71-16737

Streaming birefringence theory, discussing incompressible fluids, shear and Couette flows, fading memory, deformations

05 p0784 A71-17244

Inviscid mixed subsonic-supersonic gas flows with shocks, developing time dependent numerical method

[AIAA PAPER 71-45] 06 p0883 A71-18506

Turbulent boundary layer theories and classification according to prediction ability relative to heat transfer rates, shear stress distribution and fields of concentration

07 p1085 A71-18752

Vortex flow theory, developing computer program for various separation flows

07 p1086 A71-18776

Soviet book on gas flow past blunt bodies, Part 1, Flow analysis and calculation methods covering finite difference theory, algorithms, etc

07 p1013 A71-19049

Stationary Navier-Stokes equations solution vorticity asymptotic behavior in three and two dimensional neighborhoods of infinity

07 p1147 A71-19640

Exact numerical solution for laminar compressible boundary layers with nonuniform wall temperatures compared with Luxton-Young approximate method results, noting skin friction effects

09 p1545 A71-22940

Linear theory of weakly perturbed supersonic plane axisymmetric flows of gas-particles mixture, deriving partial differential equation for perturbation potential

10 p1551 A71-24373

Numerical simulation of developing and decaying two dimensional isotropic turbulence consistent with Batchelor predictions

10 p1595 A71-24619

Circular turbulent liquid jet in external stream, considering Reichardt theory, jet expansion law, asymptotic similarity and constant eddy viscosity hypotheses

10 p1597 A71-24940

Flow theorem as circulation extension for closed curves in autobarotropic fluids in meteorology and hydrography

10 p1639 A71-25113

Constant property fluid laminar flow between rotating and stationary infinite disks for limiting Reynolds numbers based on gap width

11 p1748 A71-25154

Ideal compressible fluid slow motion in permanent and nonpermanent regime, discussing velocity field geometrical interpretation

11 p1748 A71-25173

Turbulence research retrospective and new developments, reviewing contributions by Reynolds, Rayleigh, Prandtl, Taylor and Tollmien

11 p1751 A71-25578

Temperature dependence of flow stress of cold worked heavily deformed doped W

11 p1781 A71-26296

Approximation of flow around jet flapped airfoil, discussing ground effect on lift coefficient increments

11 p1705 A71-26314

Three dimensional turbulent boundary layer calculations, using two dimensional method based on turbulent energy equation empirical conversion into shear stress transport equation

11 p1753 A71-26443

Monograph on bulk flow theory for turbulent lubricant films, discussing flow rates, pressure gradients and shear stresses

11 p1772 A71-26462

Nonviscous fluid isotropic turbulent motion concept, and structural stability role in steady state flow statistical properties

12 p1895 A71-26827

Bifurcation solutions of Navier-Stokes equations for time periodic motions of viscous incompressible fluid at critical Reynolds number

12 p1922 A71-26867

Laminar incompressible entry flow in plane channel based on modern boundary layer theory

12 p1897 A71-27223

Soviet book on MHD flows in channels covering one dimensional theory, viscous fluids, boundary layers, electric fields, laminar flow, etc

12 p1940 A71-27294

Emmons spot theory extension for boundary layer flow on blunt bodies, deducing spot formation rate dependence on transition Reynolds and Mach numbers

12 p1865 A71-27557

Monograph on potential flow interaction between blade rows in axial flow compressors covering mathematical model, numerical analysis and experiment

13 p1990 A71-28883

Flow theory of steady separation zone near body at high Reynolds numbers, determining vortex parameters counterflow inviscid region

13 p2049 A71-29171

Unsteady curvilinear motion of lifting surface, calculating induced gas flow velocities in terms of vortex densities

13 p1992 A71-29188

Propeller vortex theory, calculating vortex streets pitch distributions and wake configuration

14 p2170 A71-30443

Incompressible fluid turbulence theory based on space-time Hopf characteristic functional integral representation for velocity field statistical ensemble

15 p2388 A71-31477

Two dimensional steady gas flows with heat addition, using reduction to partial differential equations

16 p2662 A71-33168

Finite element method application to potential flow field problems governed by Laplace equation in fluid mechanics, developing computer program

[ASME PAPER 71-APM-22] 16 p2520 A71-33207

Approximate elastoplastic problems solutions by method analogous to antiplane deformation of circular incompressible region in flow theory

16 p2657 A71-33594

Laminar boundary layer on wing profiles and bodies of revolution, calculating flow characteristics based on integral momentum relation

17 p2670 A71-34424

Hypothetical gases transonic flow higher approximation, expressing flow solutions by Airy functions

17 p2726 A71-34508

Systems concept formalization, including structural relations on basis of set theory, topological considerations and flow theory

17 p2777 A71-34599

Supersonic jet interaction with turbulent wake, calculating plane and axisymmetric flow behind body butt face

17 p2672 A71-35630

Shock wave formation in stationary flow adjacent to supersonic flow region, using Friedrich simple wave theory

17 p2673 A71-35645

Laminar and turbulent incompressible entry flows in channel with jets along walls, determining filling length

18 p2904 A71-36135

Laminar boundary layer flow theory for arbitrary curved surfaces, predicting shear stress, thickness and velocity and pressure distributions

18 p2844 A71-36319

Flow mechanics with emphasis on reentry problems - Conference, Goettingen, West Germany, March 1971, Volume 1

18 p2845 A71-36407

FLOW VELOCITY

Unsteady approach to nonisothermal flow theory for Couette flow, making general assumptions concerning rheological law and temperature dependence of fluidity
19 p3043 A71-37386

German papers on gas dynamics covering Oswatitch expansion method of characteristics, subsonic flow, transonic flow, hypersonic flow, unsteady compressible flow and detonation processes
19 p2992 A71-37451

Hypersonic flow theory evolution, considering friction and high temperature effects and flows about slender, blunt and bluff bodies
19 p2992 A71-37455

Dissipative fluid motion, discussing approaches to analysis of real fluids time dependent complex flow equations
19 p3089 A71-37499

Linear theory of weakly perturbed supersonic plane axisymmetric flows of gas-particles mixture, deriving partial differential equation for perturbation potential
20 p3175 A71-38898

Concentrated vorticity regions motion in turbulent flow, calculating mean displacement velocity relationship to turbulent velocity fluctuation
20 p3212 A71-39473

Unsteady viscous compressible flow through straight channel with flat porous walls under time varying pressure
21 p3367 A71-40591

Viscous fluid layer surface waves nonlinear theory, analyzing surface friction and gravity force angle effects on wave characteristics
21 p3367 A71-40682

Incompressible flow hydrodynamic time dependent problems for moving walls and free surfaces, using Marker-Cell computing method
21 p3368 A71-40849

Continuum dislocation theory, discussing initial stress couple problem, slip motion and dislocation rate tensor
21 p3468 A71-41000

Design and technological calculations in machine building, analyzing flow, creep and elastoplastic deformation theories
21 p3472 A71-41144

Orthotropic shells of revolution limit analysis, considering yield conditions and flow rules
22 p3614 A71-41605

Obstruction effects in rarefied gas flow through cylindrical ducts by numerical analysis, considering specular reflection, adsorption, absorption and finite molecular mean free path
22 p3531 A71-42343

Approximate nonlinear theory of steady incompressible fluid flow about cylindrical bodies from vortex method for thin lifting surfaces
22 p3481 A71-42867

Nonlinear theory of wave resistance in supersonic ideal gas flow past finite flat axisymmetric bodies, establishing drag relation to flow rate deficit
24 p3790 A71-44773

FLOW VELOCITY

Two dimensional wake laminar-turbulent transition by single and double frequency sounds imposition and wind tunnel natural disturbance, inducing velocity fluctuations
01 p0001 A71-10132

Plane linear cascades of thin curved profiles, obtaining potential flow velocities and lifting force on leading edge
01 p0001 A71-10339

Liquid flow velocity fluctuations measuring methods based on liquid-electrode contact potential dependence on flow velocity-electrolyte conductivity temperature relationship
01 p0072 A71-11225

Circular cone with cross shaped wings in supersonic flow, determining flow characteristics, velocities and pressure
02 p0185 A71-11958

Blood pressure and velocity waveform recording for patients during cardiac catheterization, interpreting relationships to vascular impedance
02 p0201 A71-12915

Cavity fluid oscillation near convecting field, calculating onset velocity as hydrodynamic stability problem
03 p0399 A71-13438

Turbulent flow mean velocity beyond rotating disk edge, using momentum integral method
[ASME PAPER 70-FE-C] 03 p0400 A71-13702

Laminar shock induced boundary layers, examining velocity, pressure gradients and enthalpy
03 p0400 A71-13739

Steady incompressible laminar pipe flow within porous wall cylinder, determining velocity, pressure distribution and shear stress
[ASME PAPER 70-WA/FLCS-3] 03 p0401 A71-14079

Unsteady flow about solid cylinder falling through viscous fluid in vertical tube, obtaining velocity profiles via solution of Navier-Stokes equation
[ASME PAPER 70-WA/FE-9] 03 p0403 A71-14130

Single stage axial flow turbocompressor with trips, examining viscosity effects on flow velocity profiles
[ASME PAPER 70-WA/FE-24] 03 p0343 A71-14133

Nonuniform flow in straight channel inlet section initiated by Fourier expandable nonuniform profile, linearizing Navier-Stokes equations about mean velocity
[ASME PAPER 70-WA/FE-27] 03 p0403 A71-14135

Superfluid flow through parallel channel, obtaining critical velocity measurements by phase coupling
03 p0404 A71-14199

Liquid flow rate measurement based on tank-filling method, discussing factors affecting accuracy
03 p0356 A71-14328

Plastic flow rates in materials under complex loads producing constant stress intensity, considering plastic deformation
03 p0515 A71-14364

Hot-wire anemometer velocity measurement in slow air flow
03 p0430 A71-14374

Heavy ion diffusion in solar corona, emphasizing flow velocity and density
03 p0495 A71-14503

Microwave systems for cryogenic liquid and slush density and flow velocity measurements
04 p0586 A71-14659

Laminar and turbulent boundary layer effects on flow velocity and Mach number behind shock front
04 p0567 A71-14664

Temperature profiles in high velocity compressible turbulent boundary layer over flat plate without pressure gradients
04 p0681 A71-15480

Hot laminar round inert gaseous jet entraining fuel-air mixture, obtaining velocity, temperature and concentration profiles
04 p0683 A71-15495

Leidenfrost film boiling for various liquids over velocity, plate temperature and surface roughness range, noting velocity effect on vaporization rate
04 p0687 A71-15529

Pulsed velocity longitudinal component in water flow turbulent boundary layer, investigating intensity, spectral characteristics and drag reduction
04 p0576 A71-15616

Velocity distribution equation for steady incompressible two dimensional turbulent flow, taking pressure gradients and surface roughness effects into account
04 p0578 A71-15764

Two component hydromagnetic system Kelvin instability due to tangential velocities discontinuity, using normal mode analysis
05 p0788 A71-16626

Gas and liquid flows local velocity measurements, using Doppler frequency shifts due to wave scattering at solid microparticles suspended in flow
05 p0753 A71-16786

Two dimensional wake laminar-turbulent transition, emphasizing velocity fluctuation nonlinear interaction
05 p0695 A71-16964

Inviscid incompressible flow velocity distribution in conical configurations with water as working fluid, using method of integral relations
05 p0737 A71-17103

Laser Doppler heterodyning system for bidirectional pulsatile fluid flow velocity magnitude and direction measurement
05 p0756 A71-17233

Centerline velocity and concentration decay predictions of free and confined jet models with/without secondary flows, considering turbulent mixing
[AIAA PAPER 71-3] 06 p0883 A71-18478

Separated turbulent eddy viscosity models incompressible similar reverse flow velocity profiles from Falkner-Skan equations
[AIAA PAPER 71-203] 06 p0886 A71-18641

Flow between parallel planes of dissimilar surface texture, obtaining mixing length models velocity profiles, skin friction coefficients and zero shear stress position
07 p1086 A71-18773

Vertical air motions velocity in rainfall from Doppler spectrum total radar reflectivity and median velocity
07 p1150 A71-18798

Turbulent velocity field in noncircular cross section rectilinear duct, determining relation between viscosity ratio and dimensionless velocity by integral transformation
07 p1087 A71-18992

Nonstationary isentropic low density flows with axial or central symmetry, suggesting characteristics with flow rate and sound speed variation as in stationary source flow
07 p1014 A71-19729

Unsteady MHD channel flow between two semi-infinite harmonically oscillating and perfectly conducting solids, determining liquid velocity profile curves
07 p1169 A71-20032

Viscous incompressible slow unsteady flow through circular tube with small axial roughness, obtaining velocity components by integral transform technique
07 p1092 A71-20093

Beam laser operational efficiency relation to molecule /atom/ interaction in focusing system, explaining lasing power drop at large flow rates
07 p1126 A71-20186

Moving part pneumatic logic element static and dynamic characteristics, determining air flow rate and output pressure
07 p1027 A71-20574

Microwave methods for nitrogen or hydrogen densities and flow rate measurement in single phase liquid and slush state
[NAS PAPER M-1] 08 p1292 A71-21696

Laser Doppler velocimeter, determining basic operational parameters including required particle density, number, type, size, output signal to noise ratio, etc
[AIAA PAPER 71-288] 08 p1304 A71-22011

Flow in channel with abrupt asymmetric widening, calculating expanding flow velocity profile by Prandtl semiempirical turbulence theory
08 p1277 A71-22041

Detonation products expansion in vacuum, measuring gas flow speeds and pressure profiles far from charge
09 p1545 A71-22690

Rarefied gas flow density and velocity by total head and flow rate adapters, noting isentropic flow core region
09 p1382 A71-22728

Turbulent air flow velocity and temperature fluctuations, determining mean fields, Prandtl number distributions and correlation moments and coefficients
09 p1432 A71-22729

Circular gas jet path lines in nonuniform velocity side field drift flow, using auxiliary curve values and correction coefficients
09 p1432 A71-22730

Asymptotic far field velocity component in Prandtl boundary layer equations for steady laminar two dimensional flow past rigid body
09 p1486 A71-23578

Wall jets over concave surfaces, obtaining average velocity profiles
10 p1591 A71-23842

Pulsed subsonic wind tunnel, calculating instantaneous flow velocity with allowance for boundary layer thickness at walls
10 p1549 A71-23855

Numerical calculation of Oseen hydrodynamic fields around sphere in unbounded fluid for various Reynolds numbers, obtaining flow velocity and drag
10 p1592 A71-23935

Linear coastal hydrostatic boundary layers of lake with no horizontal motion, discussing flow conditions under wind stress and interior velocity
10 p1600 A71-23961

Unsteady inward and outward velocities of subsonic radial air flow between two disks, using hot-wire anemometer and cylindrical wave equation
10 p1550 A71-24000

Orr-Sommerfeld hydrostatic stability equation derivation for nonparallel flow in wake from Goldstein velocity distribution, noting lateral direction velocity component magnitude
10 p1592 A71-24024

Ideal incompressible holomorphic fluid plane irrotational motion velocity due to deformable constant area airfoil displacement
10 p1594 A71-24453

Flow with time harmonic function velocity in wind tunnel, controlling rate by sonic striction of varying cross section
10 p1552 A71-24454

Velocity profiles for flows with laminar heat transfer in circular tube and rectangular duct inlet region with wall suction and injection
10 p1597 A71-25064

Water drops deformation and fragmentation due to shock wave impact in high velocity air stream
[AIAA PAPER 71-392] 11 p1749 A71-25354

Laser-blowoff metal plasma interaction with strong transverse magnetic field, observing velocity reduction due to inhibited ambipolar electron-ion energy transfer
11 p1805 A71-25794

Reynolds number effects on centrifugal compressor performance characteristics, discussing power losses in compressor, impeller and diffuser stages and compressor adiabatic efficiency
[ASME PAPER 71-GT-25] 11 p1703 A71-25967

Three dimensional boundary layer flow and velocity profiles in mixed diffuser with equal angle walls
[ASME PAPER 71-GT-40] 11 p1704 A71-25973

Vapor flow passage wall shear stress effect on sonic velocity limit in Na heat pipes
[AIAA PAPER 71-407] 11 p1856 A71-26202

Two dimensional incompressible turbulent boundary layer, determining velocity distribution with Cole law of wake
11 p1752 A71-26259

Radiating laminar convective flow in vertical heated channel, noting radiation effects on temperature and velocity
11 p1860 A71-26446

Hot wire dual probes directional sensitivity for measuring mean flow velocity angles ranges
12 p1903 A71-26574

Large amplitude wave propagation in arteries, deriving aorta mathematical model consistent with heart pressure and flow pulses and wavefront velocity
12 p1870 A71-26937

Condenser microphones aerodynamically induced noise, investigating acoustic pressure lower limit dependence on air flow velocity and turbulence
12 p1888 A71-27063

Laminar boundary layer equations integration for jet propagating along porous surface, determining transverse velocity component effect
12 p1896 A71-27114

Conservation theorem of velocity circulation along moving contours in continuous steady ideal gas flows
12 p1863 A71-27305

Laminar boundary layers with large wall heating and flow acceleration, considering heat transfer parameter increase
12 p1987 A71-27589

Aerofoil cascades with axial velocity change in incompressible flow, determining turbine blade force dependence on circulation
13 p1990 A71-28467

Boundary layers velocity distribution measurements, using scattered laser radiation Doppler shift
13 p2078 A71-28574

Fluid velocity measurements by electroacoustic transducers using phase difference relation
13 p2069 A71-28901

Stabilizer structure effect on flame stability of atomized liquid fuel, studying excess air ratio relation to air flow velocity
13 p2163 A71-28963

Gas dynamic antechambers flame stabilization at various flow rates and temperatures, calculating mixing factor vs flow and jet parameters
13 p2163 A71-28966

Unsteady curvilinear motion of lifting surface, calculating induced gas flow velocities in terms of vortex densities
13 p1992 A71-29188

Two coaxial axisymmetric subsonic gas jets of different density mixed during expulsion from convergent nozzles with high compression, using flow rate ratio
13 p2050 A71-29215

Isothermal flow under capillary forces in heat pipe with zero gravity, deriving relation between flow rate and duct parameters
13 p2050 A71-29219

Plane stationary constant-vorticity incompressible flow region surrounded by potential flow, determining two dimensional velocity distribution by numerical calculation
13 p2050 A71-29220

Laminar boundary layer separation by free stream with large amplitude oscillating velocity, using multiple hot-wire anemometer arrays
13 p2050 A71-29247

Wind noise reduction by windshields, considering effect of mean flow velocity, turbulence, flow direction, windscreen shape and size, covering material and microphone location
13 p2040 A71-29283

Hodograph models family for cross flow velocity component of three dimensional turbulent boundary layers, applying integral method to curved rectangular channels data
[ASME PAPER 71-FE-1] 13 p2051 A71-29445

Skin friction drag and velocity profile measurements on flat plate in two phase circular pipe flow in subsonic wind tunnel for gas-solid media, using photographic technique
[ASME PAPER 71-FE-32] 13 p2053 A71-29467

Soviet book on liquid metals nonstationary flow in ducts of MHD devices covering laminar flow at constant and variable flow rates
14 p2277 A71-29526

MHD flow abrupt widening and narrowing, considering M shaped velocity profiles
14 p2278 A71-29606

Ion probe measurements of very low fluid velocities, improving accuracy by marking technique
14 p2223 A71-29745

Thermal diffusion effect on gas flow velocity measurements with anemometers with heat convection signals
14 p2239 A71-29815

Stationary Gaussian Markovian form randomly fluctuating pressure gradient effects on steady incompressible channel flow velocity
14 p2223 A71-29924

Steady state wind driven currents velocity in Lake Erie, using shallow lake level model in numerical calculation
14 p2231 A71-29935

Circular air jet velocity, turbulence intensity and energy spectra distributions, investigating longitudinal acoustic field influence
14 p2225 A71-30226

German monograph on particle motion in symmetric rotation flow velocity covering potential vorticity, track curves, resistance laws, transition region, drag and pressure effects
14 p2170 A71-30234

Rarefied gas Poiseuille flow in parallel plates, cylindrical tube and annulus geometries, deriving subsonic flow velocity profiles by third order constitutive relations
14 p2227 A71-30574

Flow field velocity distribution at rotating wing devices tip vortices
[AHS PREPRINT 522] 14 p2172 A71-31088

Density and velocity profiles of transonic flow past wavy wall at various channel heights, using Mach-Zehnder interferometer
15 p2386 A71-31165

Velocity profile of steady two dimensional incompressible laminar boundary layer flow with suction or injection, noting wall shear function
15 p2388 A71-31441

Rotational temperature and density measurements in high speed gas flow by electron beam fluorescence technique
[AIAA PAPER 71-605] 15 p2406 A71-31544

Velocity profiles of oscillating flow in wake of blunt based body, using finite difference solutions of vorticity transport and Poisson equations
[AIAA PAPER 71-603] 15 p2345 A71-31579

Shearing flows in steady vortex around airfoil in perturbed velocity, considering aerodynamic forces torque
15 p2346 A71-31903

Flow velocity field in main plastic deformation zone during orthogonal cutting from continuity equation
15 p2415 A71-31986

Attaching jet flow on inclined flat plate with small offset, obtaining centerline shape and velocity profile
15 p2391 A71-32056

Hydromechanical analysis of jet spreading in low pressure planar fluid amplifiers for low Reynolds numbers and finite aspect ratios, deriving velocity distribution equations
15 p2391 A71-32058

Thrust and flow rate control in choked convergent nozzles by potential vortex generation, verifying swirling nozzle flow analytical model
15 p2391 A71-32061

Flutter of thin walled cylindrical shells conveying fluid above critical flow velocity
15 p2508 A71-32135

Turbulent flow field mean velocity components measurements near thin rotating disk
15 p2392 A71-32253

Laser Doppler turbulent and laminar flow velocity measurement model, using optical mixing spectroscopy theory
15 p2423 A71-32589

Temporal and spatial flow velocity profiles produced by shock tube generated pressure wave propagation in open-end pipe
16 p2556 A71-32921

Gravity waves over flow with nonuniform velocity distribution, investigating neutral stability problem of generation and momentum transport
16 p2557 A71-32984

Gas and liquid flows local velocity measurements, using Doppler frequency shifts due to wave scattering at solid microparticles suspended in flow
16 p2576 A71-33038

High temperature high Mach number expansion tube flows, determining impurities by time integrated spectroscopic measurements
16 p2551 A71-33155

Viscous fluid flow velocities instantaneous potential based on continuous medium, energy conservation and classic kinetic matter theories
16 p2560 A71-34055

Molecular jet velocity measurement, using periodic spatial variation modulation of radio frequency field
16 p2614 A71-34063

Constant velocity flow past semiinfinite flat plate trailing edge, emphasizing wake region structure
16 p2560 A71-34140

Stream function and velocity of shear flow vortex in infinitely thin profile from linearized Euler equations for boundary value problem
16 p2561 A71-34161

Viscous incompressible fluid flow between two rotating nonconcentric cylinders, presenting transverse velocity profiles
17 p2725 A71-34177

Wall roughness effects on laminar boundary layer velocity profile and Reynolds number, using Hankel functions and integrals
17 p2725 A71-34180

Undulating laminar and turbulent liquid film flows down vertical surface, determining velocity fields and local heat transfer coefficients
17 p2725 A71-34210

Cold plasma flow rate determination from emission inhomogeneities, using time of flight method and high speed streak photography for instantaneous velocity measurements
17 p2787 A71-34286

Steady plasma flow velocity measurements, describing two channel high resolution spectrometer
17 p2787 A71-34390

Boundary effects on gaseous detonation velocity deficit and limit using approximation into boundary layer equations, comparing to experimental data
17 p2837 A71-34437

Statistical evaluation of Doppler ultrasonic blood flowmeter, determining correlation between Doppler signal zero crossing density and fluid flow velocity
17 p2689 A71-34448

Exit stream velocity increase in propulsion units by adding latent heat of vaporization by condensation in supersonic nozzle
17 p2728 A71-34882

Magnetic annular arc continuous operation at atmospheric pressure, determining arc velocity and rotational frequency as functions of magnetic flux density and arc current
17 p2788 A71-34901

Simple gas thermal creep/velocity slip and temperature jump coefficients by applying variational technique to linearized Boltzmann equation with boundary conditions
17 p2785 A71-35446

Reynolds differential equations for three dimensional gas lubrication flows, noting linear velocity at rotating cylinder surface
17 p2749 A71-35639

Flow velocity measurement by laser differential Doppler heterodyning, obtaining SNR from frequency difference between shifted beams
18 p2914 A71-35848

Space-time correlation measurements in grid-generated isotropic turbulence, determining full- and narrow-band velocity signals Eulerian time correlation
18 p2902 A71-36035

Plane Poiseuille flow at constant rate, developing numerical simulation of transition and turbulence
18 p2845 A71-36337

Low density hypersonic flow around blunt bodies, considering total pressure and flow velocity on stagnation point line
18 p2846 A71-36417

Rarefied hypersonic flow density, velocity and temperature determination by electron beam technology, including ion production, calibration curves, collisions and spectroscopic analysis
18 p2949 A71-36419

Gas flow velocity measurements in channel, using electromagnetic technique
19 p3061 A71-37090

Viscous incompressible conducting fluid at constant flow rate under magnetic field variation, investigating laminar unsteady MHD Couette flow problem with approximate solution
19 p3108 A71-37092

Comet Tago-Sato-Kosaka isophotometry, obtaining surface brightness distribution and solar wind velocity estimate
19 p3130 A71-37228

Air flow in pipe with double screw thread, calculating tangential forces and turbulent viscosity coefficient along isotachs
19 p3043 A71-37266

Air injection into trailing vortex core, noting jet flow effect on circumferential velocity
19 p2991 A71-37291

Solar wind plasma density and flow speed semiannual variations from Vela 3 and 4 satellite observations, noting dependence on heliographic latitude
19 p3124 A71-37351

Homogeneous turbulence decay calculation from multipoint velocity correlations or spectral equivalents at initial time
19 p3044 A71-37370

Small scale turbulence structure in atmospheric boundary layers over open ocean, noting velocity derivatives probability density function lognormality
19 p3044 A71-37371

Thermal creep slip velocity expression in power series for arbitrary fraction of molecules diffusely reflected from surface by Bhatnagar-Gross-Krook model solution
19 p3163 A71-37374

Conservation theorem of velocity circulation along moving contours in continuous steady ideal gas flows
19 p3046 A71-38258

Automatic regulation of volumetric blood flow rate during artificial blood circulation, using electromechanical system for controlling arterial pump of cardiopulmonary machine
19 p3010 A71-38641

Swedish monograph on low air flow velocity measurement with hot-wire anemometer under free and forced convection, using schlieren method
19 p3172 A71-38645

Two phase flow speed transit time measurements by correlation methods with randomly fluctuating signals, noting use in small bore tubes and strip steel production
19 p3067 A71-38658

Radar measurements of vertical structure and motion trajectories of cumulus-rain clouds, studying vertical flows velocities and radar echo characteristics
19 p3094 A71-38701

Small signal gain and saturation intensity measurement of carbon dioxide laser as function of gas flow velocity 20 p3244 A71-39099

Monograph on blood flow rates instantaneous measurement from ultrasound signals of Doppler flowmeter, discussing steady laminar flow test results 20 p3193 A71-39262

Microwave instrumentation for measuring cryogenic fluids density and flow rate, noting slush 20 p3237 A71-39277

Flow velocity measurement in electromagnetically driven unsteady shock tube from charged particles extraction, using ionization gages 20 p3239 A71-39432

Concentrated vorticity regions motion in turbulent flow, calculating mean displacement velocity relationship to turbulent velocity fluctuation 20 p3212 A71-39473

Viscous fluid stirring due to small amplitude rigid circular cylinder rotation, calculating steady flow velocity relationship to Reynolds number 20 p3177 A71-39481

Laser dye cell optical quality dependence on light pumping and liquid dye flow velocity, using schlieren method 20 p3246 A71-39489

Velocity profiles of plane turbulent flow of incompressible fluid on porous surface in presence of suction 20 p3213 A71-39790

Boundary layer approximation for isothermal turbulent plane semibounded jet expanding over porous surface, deriving friction stresses and flow velocity in skin and stream regions 20 p3214 A71-39795

Highly uniform inlet velocity profile influence on conical diffuser characteristics 20 p3177 A71-39798

Turbulent jet flow concentration, velocity and direction measurements, describing cold and hot wire techniques and data reduction system 21 p3378 A71-40401

Viscous vortex rings of small cross section, considering velocity in ideal fluid with arbitrary vorticity in core and arbitrary circumferential velocity 21 p3366 A71-40484

Perturbation velocity of laminar wake downstream of two dimensional body in boundary layer, considering transition behind trip wire 21 p3322 A71-40640

Unsteady boundary layer of viscous incompressible rotating fluid flow due to infinite flat plate accelerated motion, calculating velocity and skin friction 21 p3367 A71-40657

Unsteady laminar flow in polygonal ducts, calculating velocity profiles, friction factors and energy dissipation 21 p3371 A71-40994

Numerically simulated turbulent velocity flow field, covering Navier-Stokes and energy conservation equations 21 p3371 A71-40996

Ni and Ni-base alloys gaseous calorization by circulation method, investigating gas flow velocity effect on metal diffusive saturation 21 p3389 A71-41165

Fluid velocity gradient measurement by laser-Doppler techniques based on signal spectrum bandwidth or frequency shift corresponding to position shift near wall 22 p3541 A71-41792

Centrifugal pump pressure characteristics calculation by pressure quality coefficient dependence on relative flow rate, assuming arbitrary number of blades 22 p3554 A71-41848

Flow rate and heating analysis of centrifugal pumps with variable cross section impeller blade ring inlet 22 p3554 A71-41850

Model prediction for magnetospheric electric field dependence on solar wind velocity, comparing results with plasmaspheric measurements for different Kps 23 p3721 A71-43177

Laminar incompressible flow velocities and heat transfer by radiation and convection in inlet section of parallel plate duct 23 p3781 A71-43313

Class of steady viscous incompressible axisymmetric nonrotating flows with axial velocity component dependent on distance along axis from reference point 23 p3663 A71-43489

Liquid flow rate measurement by determining fall time of emf generated in sensor coil by fluid nuclei precessing freely in magnetic field 23 p3678 A71-43536

Flow acceleration coefficient effect at inlet on centrifugal compressor wheel characteristics during axial-radial rotation 23 p3626 A71-43553

Centrifugal wheel flow swirl effect on pressure/flow rate characteristic in input zone 23 p3626 A71-43555

Jet mixing in cross flow at different velocity ratios and incidence angles, calculating momentum and mass flow 23 p3664 A71-43831

Optical anemometers for local nondestructive flow velocity measurements, discussing signal analysis possibilities 23 p3679 A71-43952

Free axisymmetric turbulent annular nozzle jet propagation, detailing velocity distribution variation due to momentum loss in stall region 23 p3664 A71-44335

Minute blood and stroke volumes dynamics during prolonged hypokinesia by acetylene method 24 p3796 A71-44536

Ideal gas and liquid droplets two phase flow continuity and motion one dimensional equations, describing relations between velocity, density, pressure and bulk component concentrations 24 p3818 A71-44709

Photogrammetric flow rate determination in centrifugal pump impeller, using rotating camera 24 p3825 A71-44754

Shielded hot-wire probe for mean and rms flow velocities in highly turbulent and rapidly reversing flows 24 p3828 A71-45075

Incompressible fluid impulsive laminar flow, developing velocity law and tangential stresses by approximate method 24 p3821 A71-45183

Gaseous media parameters in wave energy exchanger, examining compression cycles, temperature ratios and flow velocities for maximum conversion efficiency 24 p3891 A71-45199

Liquid transition through critical value, considering self oscillation mode frequency 24 p3821 A71-45340

FLOW VISUALIZATION

Multiple spark camera for unsteady compressible flow investigations, considering geometrical optical design, parallax, spark producing electric circuitry, etc 01 p0078 A71-10106

Transonic flow through planar cylinder lattices, discussing flow pattern visualization and recording techniques by high speed camera 01 p0001 A71-10108

Shock wave propagation in bent and branched ducts, discussing schlieren method flow visualization, diffraction measurement with differential interferometer and interaction between shock and vortex 03 p0400 A71-13696

High gain proportional fluid amplifier, examining defined region geometry with flow visualization and quantitative data [ASME PAPER 70-WA/FLCS-12] 03 p0354 A71-14087

Photographic study of early vortex formation in flow started by shock diffracting over edge 04 p0586 A71-14702

Error estimates for turbulent flow characteristics determination by visualization and solid particle photography 04 p0573 A71-15562

Turbulent pressurized and open channel flows analysis by flow visualization, using solid particles and dynamic ball rate sensors 04 p0578 A71-15627

Schlieren device for visualization of thermal gradients in boundary layer of any orientation, replacing natural astigmatism with arbitrarily adjustable one 05 p0749 A71-16266

Turbulent wall flow, observing flux and heat transfer conditions with stroboscopic visualization 07 p1105 A71-18782

Multiple source schlieren system for flow visualization in Canadian trisonic wind tunnel, using integrated logic circuitry for control 07 p1083 A71-19924

Caret wing serial tests in Mach 8 to 15 hypersonic flow, including three component force, spanwise direction pressure distribution and shock wave angular measurements by flow visualization 07 p1016 A71-20015

Laminar-turbulent bounded jet stability, examining transition zone shift with smoke visualization 07 p1029 A71-20594

Two phase Hg tunnel for shock wave visualization by RF discharge between test model body and external ring, comparing measurements with supersonic flow theory 08 p1272 A71-21751

Schlieren system conversion to holographic visualization in operational wind tunnels and test facilities 09 p1449 A71-22788

Instantaneous aerodynamic force measurements and flow visualization on flapping wing, showing increase of thrust force mean value over maximum steady state value 10 p1550 A71-24362

Flow visualization and velocity measurements in repeatedly branching tube systems representative of

human lung, estimating viscous dissipation and pressure drop 10 p1571 A71-24625

Wind tunnel hypersonic flow visualization by schlieren and phase contrast methods at low volumetric mass 11 p1764 A71-26273

Hele-Shaw flow viscous tails from airfoil, observing high Reynolds number trailing edge flow for separation and initiation of Kutta condition 11 p1705 A71-26447

Schlieren visualization for supersonic annular fixed cascade and freon compressor wind tunnels, using vane holding cylinder devices [ONERA-TP-948] 12 p1867 A71-27717

Hydraulic analogy for visualization of flow through moving plane cascade for rotor section of compressor stage 12 p1898 A71-27720

Flow visualization of free convection laminar-to-turbulent transition along vertical heated plate in water induced by two dimensional forced disturbances [DFVLR-SONDDR-116] 12 p1987 A71-27739

Diagnostic flow visualization, using chemiluminescent radiation in mixing region between aqueous luminol and potassium ferricyanide solutions 13 p2044 A71-27853

Turbulence level effects on mixing of three plane parallel slipstreams with equal velocities and temperature from smoke visualization 13 p2163 A71-28962

Helicopter rotor vortex system and induced velocity field for various angles of attack, flight conditions and unit loads, using smoke visualization technique 13 p1994 A71-29235

Two dimensional vortex filament development artificially shed in laminar boundary layer on flat plate without pressure gradient, using hydrogen bubble visualization technique 13 p2051 A71-29428

Flow visualization by cathodic hydrogen bubble technique, using electric pulsing for regular pattern formation for flow distortion tracing [ASME PAPER 71-FE-36] 13 p2053 A71-29471

AEDC test facilities laser instrumentation for flow field diagnostics by Doppler velocimeter, holographic flow visualization and particle studies 14 p2245 A71-30332

Holographic recording of optical inhomogeneities in gas flow in hypersonic wind tunnels, using Mach-Zehnder interferometer and schlieren apparatus 15 p2404 A71-31274

Holographic interferometry for flow visualization within aerodynamic wind tunnels with retrodiffuser apparatus 15 p2405 A71-31276

Lee side air flow from cone-cylinder model, determining vortex core regions from subsonic wind tunnel smoke visualization techniques 15 p2346 A71-32117

Rotating arc plasma jet exhaust flow pattern visualization, using bifocal lens system and photographic flash technique in particle track photography 16 p2579 A71-33339

Flow visualization and hot-wire measurements, showing vortex shedding association with turbulent air jet issuing from flat plate into cross wind 17 p2670 A71-34659

Supersonic cylindrical freon compressor with low blade height for elementary compression and flow visualization aerodynamic and thermodynamic tests 17 p2793 A71-35467

Interference holography, discussing precision displacement measurement, fringe localization, multiple beam techniques, contour generation and flow visualization 18 p2920 A71-36148

Space shuttle aerothermodynamics, discussing heat transfer measurements, phase change patterns, electron beam flow visualization and boundary layer transition 18 p2847 A71-36430

High speed neutral buoyancy bubble generators for aerodynamic flow visualization, investigating tip vortex from wing or helicopter rotor blade 19 p3064 A71-37725

Heated jet interaction with deflecting flow in subsonic wind tunnel, presenting flow visualization and temperature and velocity profiles [ASME PAPER 71-HT-2] 19 p1663 A71-37980

Laser Doppler holographic technique for fluid velocity field visualization and quantitative two dimensional vector velocity measurement 20 p3235 A71-39183

Complex three dimensional shock waves about space shuttle configuration, visualizing hypersonic nitrogen flow with electron beams 20 p3211 A71-39356

Flow instability in stagnation point region of circular cylinder in turbulent channel flow, using hydrogen bubble method for flow visualization 20 p3211 A71-39454

- Gortler-Taylor vortices visualization in liquids between rotating concentric cylinders using pulverized aluminum
20 p3213 A71-39781
- Vortex flow over helicopter rotor square tips, using visualization technique with ammonia vapor boundary layer flow over diazonium salt solution
21 p3318 A71-40169
- Gas density measurement and flow visualization in hypersonic wind tunnel by electron beam probe, noting isobaric boundary layer application
21 p3364 A71-40395
- Trailing vortices behind wing tip with vortex dissipator, using wind tunnel flow visualization and flight tests
21 p3319 A71-40496
- Vortex wake development and aircraft dynamics, using computer graphics and flow visualization techniques
21 p3319 A71-40497
- Flow visualization of aircraft trailing vortex wakes in towing tank with electrochemically activated dye, noting flow instability
21 p3321 A71-40505
- Delta wing shock envelope visualization at hypersonic speed, obtaining flow field photographs by vapor screen technique
21 p3324 A71-40973
- Photogrammetric recording of helicopter rotor induced aerodynamic effects using wind tunnel test smoke visualization technique
23 p3678 A71-43588
- Heat transfer visualization, discussing shadowgraph, schlieren and interference methods
24 p3890 A71-45147
- FLOWMETERS**
- NT GAS METERS**
- NT HOT-WIRE FLOWMETERS**
- NT RHEOMETERS**
- Ultrasonic flowmeters for unsteady flow, discussing beam deflection method, phase difference systems, etc
01 p0079 A71-10302
- Turbine flowmeters for liquids with different viscosity and wide range of flow rates, calculating static characteristics
03 p0428 A71-13958
- Compressible subsonic and supercritical flows, developing flowmeter orifice expansion factors [ASME PAPER 70-WA/FM-3]
03 p0402 A71-14105
- Simultaneous comparison and calibration of ultrasonic Doppler telemetry and electromagnetic flowmeters implanted on peripheral arteries of dogs
04 p0545 A71-15164
- Digital fluidic metering system for composition control of liquid batch mixing from circuit design to final product
07 p1028 A71-20581
- Apparatus for vapor-liquid flow studies, discussing measurement system and energy dissipation
08 p1273 A71-19311
- Spectral analysis of laser Doppler flowmeter signals, considering time independent systems
09 p1463 A71-22691
- Book on fluid meter theory and applications covering quantity and rate measurements and differential pressure meters
10 p1610 A71-24148
- Hydrodynamic study of systematic errors of mass flowmeters, considering effects of working fluid, sensitive elements and secondary motions
10 p1610 A71-24168
- Optimum calibration of turbine flow sensors AC voltage signals with volume proportional frequency by weighted least squares techniques
11 p1762 A71-25934
- Gas chromatography techniques, discussing carrier tank, flow control, injector, reactor, column, detector, recorder, flowmeter, etc
11 p1729 A71-26291
- Directional laser Doppler velocimeter measurements in perturbed circular flow, noting use in cardiovascular research
11 p1766 A71-26303
- Calibration test rig for high accuracy liquid hydrogen flowmeter, discussing design and operation
12 p1906 A71-26836
- Nonbleeding blood flow measurement by magnetorheography, using electromagnetic flowmeter principle
12 p1874 A71-27137
- Blood pressure measurement with Doppler ultrasonic flowmeter, providing sensitive and accurate noninvasive approach for continuous measurement of systemic arterial pressure
12 p1874 A71-27139
- Electromagnetic flowmeters readings for boundary effects of current equalization
14 p2279 A71-29616
- Electrode voltage of rectangular cross section MHD channel in conductive flowmeter, investigating magnetic field inhomogeneity and velocity profile effects
14 p2279 A71-29617
- Small turbine type flowmeters for liquid hydrogen, discussing design, inspection, calibration and reliability
14 p2239 A71-29926
- Flowmeter based on oscillating bistable fluid amplifier, discussing Mach number, Reynolds number and Strouhal number effects on measuring characteristics
15 p2352 A71-32066
- Statistical evaluation of Doppler ultrasonic blood flowmeter, determining correlation between Doppler signal zero crossing density and fluid flow velocity
17 p2689 A71-34448
- French monograph on thermal microflowmeters covering anemometers, fluid mechanics, Nusselt number, thermocouple flowmeters
17 p2744 A71-35228
- Batch unit for investigation of injectors in vapor-liquid flows, discussing measurement system and energy dissipation
17 p2724 A71-35275
- Miniature battery operated electromagnetic blood flowmeter for data acquisition from unrestrained animals
24 p3801 A71-44783
- FLUCTUATION THEORY**
- Fluctuation-dissipation thermodynamics with variables changing sign during time reversal
04 p0676 A71-15118
- Fluctuating circulation, lift and flow induced structural vibrations of two dimensional bodies, including vortex shedding on sluice gates
07 p1014 A71-19592
- Signal fluctuation noise reduction with input screen inertia by lagging component introduction to introsopic system
08 p1294 A71-21903
- Type one fluctuations sustained by large air showers at sea level, describing simulation method for influence of first nuclear interaction altitude on shower morphology
10 p1660 A71-23853
- Fluctuations in numerical computations of discontinuous solutions of differential equations
14 p2265 A71-29556
- Asymptotic intensity fluctuations of plane light wave propagating in turbulent medium, using parabolic equation and Markov model
15 p2387 A71-31190
- Laminar compressible wakes instability behind planar and axisymmetric slender bodies, solving integral conservation equations for fluctuation amplitude variations
19 p2993 A71-37879
- Fluctuations in parametrically excited subharmonic oscillator, deriving steady state probability distribution for amplitude and phase transitions analogous to Brownian motion of particle in potential well
20 p3203 A71-39094
- Phase-space theory of macroscopic fluctuations in nonlinear systems far from thermodynamic equilibrium, using chemical kinetics model
21 p3416 A71-40856
- Hydrodynamic equations for dense system fluctuations with stochastic terms in pressure tensor and heat flux vector evaluated for dilute gas
22 p3530 A71-41893
- Fluctuation in synchronized reflex klystron oscillators due to shot noise in electron beams
22 p3521 A71-42264
- FLUERIC**
- Fluoric oscillators as sensors for carbon dioxide concentration detection in exhaled breathing gases, noting frequency dependence on gas properties [ASME PAPER 70-WA/FLCS-10]
03 p0372 A71-14086
- Fluidic ammeter for measuring electric current in uninsulated wire, using fluoric oscillator sensor
16 p2576 A71-32974
- FLUID AMPLIFICATION**
- U FLUID AMPLIFIERS**
- FLUID AMPLIFIERS**
- NT JET AMPLIFIERS**
- Fluidic systems as digital devices, considering stream interaction, vortex and turbulence measurements
01 p0006 A71-10801
- Fluidics component operation and characteristics, including turbulent reattachment, jet deflection and vortex amplifiers
03 p0353 A71-13132
- Input-output flow characteristics of direct and transverse fluidic impact modulators, using static model [ASME PAPER 70-WA/FLCS-2]
03 p0354 A71-14077
- Flow and dynamic pressure recovery in wall-attachment fluid amplifiers, considering large scale flip-flop [ASME PAPER 70-WA/FLCS-9]
03 p0354 A71-14085
- High gain proportional fluid amplifier, examining defined region geometry with flow visualization and quantitative data [ASME PAPER 70-WA/FLCS-12]
03 p0354 A71-14087
- Nonvented vortex fluid amplifier receiver tubes flow and performance characteristics [ASME PAPER 70-WA/FLCS-18]
03 p0354 A71-14091
- Static and dynamic testing of fluidic elements as function of geometrical and operating parameters
03 p0355 A71-14296
- Fluidics, discussing wave operated sensors, control systems, future developments and applications
07 p1024 A71-20208
- Digital turbulence amplifiers, investigating dynamic switching response
07 p1024 A71-20552
- Turbulence amplifier optimal dimensioning for maximum fan-out factor and minimal signal transport time
07 p1024 A71-20554
- Internally ported vortex amplifier, presenting dynamic equivalent circuit with transfer functions
07 p1025 A71-20555
- Beam deflection type fluidic amplifiers with single and symmetric control jets, considering free streamline flow theory
07 p1025 A71-20557
- Large model fluid proportional amplifier, investigating optimum static and dynamic pressure gain by methodological and transmission line approach
07 p1025 A71-20558
- Computerized capillary model for fluidic restrictors in multipoint concurrent air flow measurements
07 p1025 A71-20563
- Beam deflection fluidic circuit design by linear static matching method, considering servoamplifier feedback control system
07 p1026 A71-20569
- Hybrid fluidic binary counter, using commercially available fluidic bistable amplifier in conjunction with free disk steering gate
07 p1026 A71-20572
- Fluidic proportional amplifier circuit with two bistable element stages, using pulse width modulation techniques
07 p1027 A71-20579
- Missile fluidic attitude control system, discussing integrator, transducer amplifiers and circuits
07 p1028 A71-20583
- Missile roll axis attitude control system based on fluid amplifiers, describing fluidic integrator and chain
07 p1028 A71-20584
- Two dimensional supersonic fluidic amplifier flow field density and characteristics determined by differential interferometry
07 p1028 A71-20588
- Two axisymmetric jets impingement in fluid amplifiers, discussing velocity profiles of radial jet
07 p1029 A71-20592
- Fluidic coincidence position sensors, using wall attachment amplifiers and nozzle displacement
07 p1030 A71-20601
- Proportional fluid amplifier, measuring deflection angle, jet turbulence and noise level
15 p2390 A71-32052
- Facility for signal noise measurement in proportional fluidic amplifiers, discussing stored sweep spectra interpretation
15 p2351 A71-32053
- Hydromechanical analysis of jet spreading in low pressure planar fluid amplifiers for low Reynolds numbers and finite aspect ratios, deriving velocity distribution equations
15 p2391 A71-32058
- Laminar square jet from turbulence amplifier, analyzing centerline velocity distribution and supply pressure recovery
15 p2391 A71-32060
- Operating characteristics of high performance vortex amplifiers, discussing turnaround ratios, noise reduction, linearity and stability
15 p2352 A71-32062
- Flowmeter based on oscillating bistable fluid amplifier, discussing Mach number, Reynolds number and Strouhal number effects on measuring characteristics
15 p2352 A71-32066
- Fluid amplifiers in logic circuits and control and monitoring systems, discussing operating principles and performance features
18 p2850 A71-36137
- Directional hydraulic control switching fluid amplifier at various Reynolds numbers, including cavitation effects
18 p2851 A71-36205
- Fluid amplifier digital elements dynamic switching, noting back pressure effects
18 p2851 A71-36207
- Active digital and proportional fluidic devices design and manufacture including turbulence, wall-attachment, focused jet, beam deflection and vortex amplifiers
22 p3483 A71-42783
- Fluid amplifiers theory and use as temperature and pressure sensors, discussing applications in chemical and ammunition industries and jet aircraft control [IEEE PAPER 70-TP-120-IGA]
23 p3630 A71-42921

FLUID BOUNDARIES

- Operational amplifier design with fluidic Schmitt trigger and linear resistor feedback network
23 p3631 A71-44098
- FLUID BOUNDARIES**
 NT GAS-SOLID INTERFACES
 NT JET BOUNDARIES
 NT LIQUID-LIQUID INTERFACES
 NT LIQUID-SOLID INTERFACES
 NT LIQUID-VAPOR INTERFACES
 Capillary ball game phenomenon under weightlessness, showing photographs of mercury droplet reflection from fluid boundary
02 p0239 A71-11925
 Ground effect vehicles limiting volumetric dissipations from air cushion and propulsion systems with fluid boundary by Coanda effect
07 p1019 A71-19923
 Viscous fluid horizontal motion due to moving heat source and boundary
07 p1091 A71-20030
 Propulsion, guidance and stability of ground effect vehicle with perimetric Coanda fluid boundary
13 p1997 A71-29308
 Steady nonlinear regime of Benard convection in uniformly rotating fluid, using two-dimensional primitive equation numerical model with rigid boundaries
15 p2393 A71-32638
 Boundary effects on gaseous detonation velocity deficit and limit using approximation into boundary layer equations, comparing to experimental data
17 p2837 A71-34437
 Control strategies for space shuttle transition at 45,000-150,000 ft, emphasizing terminal conditions and stability and control boundaries
19 p3147 A71-37170
 Dissolution rate of vertical nickel cylinder in liquid aluminum under free convection, showing fluid boundary layer mass transfer role
19 p3079 A71-37709
- FLUID DYNAMICS**
 NT AERODYNAMICS
 NT AEROTHERMODYNAMICS
 NT ELASTOHYDRODYNAMICS
 NT ELECTROHYDRODYNAMICS
 NT GAS DYNAMICS
 NT HYDRODYNAMICS
 NT HYPERSONICS
 NT MAGNETOHYDRODYNAMICS
 NT RAREFIED GAS DYNAMICS
 NT ROTOR AERODYNAMICS
 Lagrangian invariants of inviscid compressible fluid applied to hydrodynamic equations
02 p0239 A71-11923
 Jet fluid dynamics under various boundary conditions and velocity distributions
03 p0341 A71-13579
 Heated glass free jet characteristics at low Reynolds numbers, evaluating temperature distribution and two dimensional fluid dynamic effects
03 p0521 A71-14125
 Lorentz invariants in relativistic fluid dynamics and thermodynamics in nonvacuo, suggesting determination through earth-moon space flight experiments
04 p0661 A71-14872
 Round cylinder in viscous fluid asymmetrically disturbed flow, calculating dynamic and temperature conditions with difference method
04 p0571 A71-15492
 Relativistic electromagnetic field analysis, using fluid dynamic approach
04 p0628 A71-15917
 Friction, heat transfer and mass transfer theory of flow represented by two dimensional parabolic boundary layer equations
07 p1085 A71-18766
 Centrifugal compressor fluid dynamics, discussing unresolved problems governing design and performance prediction
10 p1550 A71-24216
 Dynamics of planetary atmospheres large scale motions, using similarity theory and dimensional analysis methods for atmospheric circulation characteristics calculation
11 p1826 A71-25720
 German monograph on accelerating grids in wind tunnel and axial flow turbine, covering plane/secondary flows past cascades and stator/rotor blading
15 p2347 A71-32303
 Fluid dynamics numerical methods - Conference, University of California at Berkeley, September 1970
18 p2904 A71-36301
 Numerical fluid dynamics problems in Hele-Shaw cell secondary flow, blast wave and plane jet electrostatic pinching, presenting algorithms and error estimates
18 p2905 A71-36310
 Weightless environment effects on fluid behavior and heat transfer in life support systems, obtaining analytical models
18 p2909 A71-36652
 Fuel slosh energy dissipation and dynamic stability of Intelsat 4, discussing spacecraft and tank selection
19 p3148 A71-37195

Fronts and frontal clouds evolution theory as nonstationary two dimensional problem with allowance for dynamics and thermodynamics
19 p3091 A71-38682

Gravitational radiation interaction with uniform incompressible inviscid fluid in simple motion, considering response in linearized approximation to general relativity
21 p3446 A71-40421

Fluid dynamics in elastic complex geometry tanks, obtaining liquid mass and stiffness matrices for gravitational effects
21 p3467 A71-40948

Dynamical formation and structure of plasma focus, using two dimensional numerical fluid model
22 p3581 A71-41892

FLUID FILMS

Liquid film formation at base of bubbles and effects on heat transfer during nucleate boiling
01 p0181 A71-11404

Fluid mechanics of shallow liquid fuel layer near burning wick, deriving continuity, momentum and convective diffusion equations to obtain extinction condition
02 p0334 A71-12855

Heat transfer measurements in thin water films on brass tube, using electrically heated elements
04 p0680 A71-15475

Liquid metals vapor drag and electromagnetic fields effects on laminar film condensation, using finite difference method
04 p0688 A71-15539

Light scattering from ultrathin free liquid films, calculating irradiance optical functions variation with geometry and film thickness
05 p0763 A71-16906

Turbulent boundary layers transpiration cooling prediction with coolant fluid serving as heat sink within structure wall and as protective film
07 p1220 A71-18768

Mass transfer net rate /evaporation plus entrainment/ from thin liquid film, using methanol, water, butanol and RP-1 as coolants
07 p1222 A71-18997

Steady boundary layer flow in viscous liquid thin down variable incline for large Reynolds and Froude numbers
09 p1432 A71-22451

Potential flow of incompressible inviscid liquid film along inclined semiinfinite flat plate for large Froude number values, using matched asymptotic expansions method
13 p2047 A71-28485

Surface evaporation and condensation effects on stability of thin liquid film flowing down heated inclined plane at critical Reynolds number
13 p2160 A71-28596

Plane horizontal fluid film convective stability with free boundaries in vertical circular cylinder for periodic modulation of vertical temperature gradient or gravitational field
14 p2338 A71-30873

Crosshatched wave patterns in liquid films, discussing supersonic wind tunnel experiments aimed at elimination of sublimation or vaporization as pattern generating mechanisms
15 p2389 A71-31551

Compliant surface fluid film thrust and journal bearing analysis, using coupled flow-elasticity model and load tests
17 p2747 A71-34192

Undulating laminar and turbulent liquid film flows down vertical surface, determining velocity fields and local heat transfer coefficients
17 p2725 A71-34210

Meniscus induced thinning of tear films due to fluid film fracture and straining
17 p2687 A71-35803

Turbulent flow of air film between rotating circular and stationary plane surfaces, determining pressure distributions, inertial forces effects and velocity profiles
18 p2926 A71-36185

Corresponding states fluids film boiling with cylindrical heaters, studying pressure and diameter effects
20 p3312 A71-39283

Distributed mass and elastic damping finite element model for turborotor system on fluid film bearings
21 p3385 A71-40301

Computerized analysis of fluid film behavior, load capacity and center locus of journal bearing under dynamic load
21 p3386 A71-40322

Externally pressurized double thrust bearings with variable gas film laminar restrictor increasing stiffness at low eccentricity ratios
22 p3553 A71-41680

Thin liquid films under simultaneous shear and gravity forces, noting data incorporation into transport equations for heat and mass transfer
22 p3620 A71-41884

Flow and strain analysis and engineering design of porous cylindrical gas film foil bearing at low pressures
24 p3830 A71-44944

Liquid properties and ambient pressure effects on cavitation erosion in thin film
24 p3819 A71-44946

Fixed and free sinusoidally driven hydraulic squeeze film bearing design for improved load gyroscope performance
24 p3832 A71-45291

FLUID FILTERS

NT AIR FILTERS

Light aircraft engine lubricating oil filter types and model specification, noting dirt holding ratings
10 p1617 A71-24248

Theoretical and experimental performance studies of quadrupole mass analyzers with round and hyperbolic field forming surfaces, noting resolving power superiority of hyperbolic rods
11 p1760 A71-25219

Three micron absolute main oil filter for aircraft gas turbine lubrication system, discussing indicator system and bench and engine tests
17 p2793 A71-35488

Fluid contamination and protective filter in hydraulic power components for design service life
18 p2851 A71-36204

Hydraulic servo equipment filtration systems design, discussing contamination effects and servo components physical characteristics effects on tolerance level
19 p2999 A71-38320

Hydraulic components and equipment contamination control and effects on system efficiency, discussing filter ratings and location
19 p2999 A71-38321

Hydraulic equipment fluid contamination control, discussing sample bottle cleaning, fluid sampling, component tolerance profiles and filtration performance specifications
19 p2999 A71-38322

Hydraulic fluids contribution to system contamination, discussing precipitate formation due to reaction with water, filtration inability and contaminant elimination
19 p2999 A71-38323

Hydraulic fluid filtering and maintenance techniques, discussing component life optimization and adverse environment handling problems
19 p3000 A71-38325

FLUID FLOW

- NT ADIABATIC FLOW
 NT AIR CURRENTS
 NT AIR FLOW
 NT AIR JETS
 NT ANNULAR FLOW
 NT AXIAL FLOW
 NT AXISYMMETRIC FLOW
 NT BAROTROPIC FLOW
 NT BASE FLOW
 NT BELTRAMI FLOW
 NT BLOOD FLOW
 NT BOUNDARY LAYER FLOW
 NT BOUNDARY LAYER SEPARATION
 NT CAPILLARY FLOW
 NT CASCADE FLOW
 NT CAVITATION FLOW
 NT CHANNEL FLOW
 NT COAXIAL FLOW
 NT COMBUSTIBLE FLOW
 NT COMPRESSIBLE FLOW
 NT CONTINUUM FLOW
 NT CONVECTIVE FLOW
 NT CORE FLOW
 NT COUETTE FLOW
 NT COUNTERFLOW
 NT CRITICAL FLOW
 NT DUCTED FLOW
 NT EQUILIBRIUM FLOW
 NT FREE FLOW
 NT FREE MOLECULAR FLOW
 NT FUEL FLOW
 NT GAS FLOW
 NT HARTMANN FLOW
 NT HEAD FLOW
 NT HELICAL FLOW
 NT HYPERVELOCITY FLOW
 NT INCOMPRESSIBLE FLOW
 NT INLET FLOW
 NT INVISCID FLOW
 NT ISOTHERMAL FLOW
 NT JET FLOW
 NT JET MIXING FLOW
 NT JET STREAMS [METEOROLOGY]
 NT KNUDSEN FLOW
 NT LAMINAR FLOW
 NT LIQUID FLOW
 NT MAGNETOHYDRODYNAMIC FLOW
 NT MASS FLOW
 NT MERIDIONAL FLOW
 NT MOLECULAR FLOW
 NT MULTIPHASE FLOW
 NT NONEQUILIBRIUM FLOW
 NT NONNEWTONIAN FLOW
 NT NONUNIFORM FLOW
 NT NOZZLE FLOW
 NT ONE DIMENSIONAL FLOW
 NT OPEN CHANNEL FLOW
 NT ORIFICE FLOW

NT OSCILLATING FLOW
 NT PERIPHERAL JET FLOW
 NT PIPE FLOW
 NT PLASTIC FLOW
 NT POTENTIAL FLOW
 NT PROPELLANT TRANSFER
 NT RADIAL FLOW
 NT REATTACHED FLOW
 NT RECIRCULATIVE FLUID FLOW
 NT REVERSED FLOW
 NT SECONDARY FLOW
 NT SEPARATED FLOW
 NT SHEAR FLOW
 NT SINGLE-PHASE FLOW
 NT SLIP FLOW
 NT STAGNATION FLOW
 NT STEADY FLOW
 NT STOKES FLOW
 NT STRATIFIED FLOW
 NT SUBCRITICAL FLOW
 NT SUPERCAVITATING FLOW
 NT SUPERCRITICAL FLOW
 NT SUPERSONIC JET FLOW
 NT THREE DIMENSIONAL FLOW
 NT TRANSITION FLOW
 NT TRESKA FLOW
 NT TURBULENT FLOW
 NT TWO DIMENSIONAL FLOW
 NT TWO PHASE FLOW
 NT UNIFORM FLOW
 NT UNSTEADY FLOW
 NT VERTICAL AIR CURRENTS
 NT VISCOUS FLOW
 NT WALL FLOW
 NT WATER FLOW
 NT WEDGE FLOW
 Liquid flow velocity fluctuations measuring methods based on liquid-electrode contact potential dependence on flow velocity-electrolyte conductivity temperature relationship
 01 p0072 A71-11225
 Hydromagnetic waves interaction with time dependent inhomogeneous background fluid, using Hamilton principle
 01 p0136 A71-11475
 Gas and fluid flow through flat and cylindrical porous cermet walls, determining permeation energy loss and radial flow hydraulic resistance
 02 p0240 A71-12277
 Laminar and turbulent mixing of two parallel streams of dissimilar fluids, using similarity transformation
 [ASME PAPER 70-WA/APM-37]
 03 p0403 A71-14162
 Turbulent mixing of two parallel similar and dissimilar fluid streams, comparing velocity and density profiles measurements with similarity solution
 [ASME PAPER 70-WA/APM-38]
 03 p0404 A71-14163
 Slender deformable airfoil in bounded fluid flow, determining lift coefficient by one dimensional integrodifferential equation for elastic large aspect ratio wing
 04 p0567 A71-14590
 Radiative/convective heat transfer in moving media, reducing boundary problem to integral equations
 04 p0685 A71-15514
 Laser Doppler heterodyning system for bidirectional pulsatile fluid flow velocity magnitude and direction measurement
 05 p0756 A71-17233
 Fluid inertia effect on porous thrust plate, using mathematical model for prediction
 [ASME PAPER 70-LUB-18]
 07 p1088 A71-19625
 Fluid flow around two parallel circular cylinders moving in ideal liquid, deriving exact solution for flow velocity and kinetic energy
 07 p1089 A71-19736
 Viscous fluid horizontal motion due to moving heat source and boundary
 07 p1091 A71-20030
 Viscous incompressible fluid partly filling rotating cylindrical cavity, considering motion under centrifugal forces in adjoining unperturbed free surface region
 07 p1093 A71-20467
 Multiple wave propagation in acoustic duct with winds, using perturbation Lagrangian for ideal fluid flow
 08 p1276 A71-21651
 Laser fluid flow velocimeter pulse output resolution approximation, using spectrum analyzer or discriminator measurements
 09 p1453 A71-23726
 Concentration profile in incompressible viscous fluid flow across plane plate in oscillating motion, considering gravity diffusion
 09 p1434 A71-23729
 Rapidly rotating fluid flows, calculating inertia waves by geometrical optics method
 10 p1591 A71-23854
 Book on fluid meter theory and applications covering quantity and rate measurements and differential pressure meters
 10 p1610 A71-24148

Incompressible nonviscous rotating fluid in toroidal shell, obtaining flow patterns steady state solutions for turbomachinery design
 10 p1552 A71-24520
 Critical velocity of fluid flow in cantilever tube, applying Galerkin method to modal type analysis
 11 p1748 A71-25163
 Relativistic fluid thermodynamics for compressible fluid reversible adiabatic flow, using variational principle to derive stress-energy tensor
 11 p1798 A71-25739
 Rotationally symmetric flow above infinite rotating disk by nonexistence proof and uniqueness theorem
 12 p1896 A71-26924
 Sharp circular edged orifice dynamic characteristics under high amplitude periodic fluid flow conditions, discussing hydraulic resistance coefficients
 12 p1898 A71-27506
 Lift and particle displacement around lifting body with stream function as fluid motion equation integral
 12 p1866 A71-27577
 Transformed boundary layer equation solution for power law fluid flows of Falkner-Skan type by gamma functions series
 13 p2053 A71-29470
 [ASME PAPER 71-FE-35]
 Heterogeneous fluid flow-chemical processes interaction in low density plasma flow two phase boundary layer seeding, using physicochemical model
 14 p2279 A71-29878
 German monograph on particle motion in symmetric rotation flow velocity covering potential vorticity, track curves, resistance laws, transition region, drag and pressure effects
 14 p2170 A71-30234
 Steady state flow of viscous incompressible fluid, proposing difference scheme for numerical solution of Navier-Stokes equations
 14 p2226 A71-30437
 Fluid flow equations problems, describing stability and convergence theory for finite difference approximations
 15 p2441 A71-31353
 Noise and spectral analysis for measuring fluid flow with random temperature fluctuations by transit times
 15 p2406 A71-31596
 Stokes second problem solution, obtaining transient and steady state fluid flow pattern near cylinder executing harmonic rotational oscillations around axis
 15 p2393 A71-32263
 Cryogenic fluids flow measurement, discussing various fluids, pressures, temperatures and flow rates
 15 p2412 A71-32701
 Viscous fluid flow velocities instantaneous potential based on continuous medium, energy conservation and classic kinetic matter theories
 16 p2560 A71-34055
 Dirichlet problem in hodograph plane of compressible fluid flow from aircraft, helicopter blades or turbine blade airfoils
 17 p2672 A71-35470
 Joseph type theorems derivation for parallel fluid flow with wave perturbation stability governed by Orr-Sommerfeld equation
 18 p2902 A71-36041
 Circular cylinder resistance in oscillating stream of second order fluid, calculating flow distribution
 18 p2843 A71-36042
 Boundary conditions discretization on fluid flow moving discontinuities for analytical or numerical integration
 18 p2906 A71-36315
 Implicit continuous fluid Eulerian time dependent multidimensional fluid flows calculation at arbitrary Mach number based on finite difference approximation
 18 p2908 A71-36345
 Dissipative fluid motion, discussing approaches to analysis of real fluids time dependent complex flow equations
 19 p3089 A71-37499
 Flow around obstacle in plasma with ions cold relative to electrons and with directed subsonic, considering relative density measurement
 19 p3115 A71-38207
 Dimensional analysis of wear by solid particle impact in fluid flows in pumps and ducts
 19 p3046 A71-38273
 Slide valve slot fluid flow oscillation frequency range estimate for quasi-stationarity
 20 p3183 A71-39168
 Papers on cryogenics covering materials behavior, heat transfer, fluid flow, superconductive magnets, cryosorption pumping, rocket propulsion and low temperature measurement
 20 p3269 A71-39239
 Heat transfer, fluid flow and pressure loss, noting application to cryogenic heat exchangers and process plants
 20 p3312 A71-39245
 Microwave instrumentation for measuring cryogenic fluids density and flow rate, noting slush
 20 p3237 A71-39277
 Buoyancy effects on heat transfer coefficients in liquid nitrogen film boiling in vertical flow
 20 p3313 A71-39286

Flow induced vibrations of metal bellows with internal cryogenic fluid flow, noting effects of heat transfer, liquid state properties, external damping and condensation
 [ASME PAPER 71-VIBR-14]
 21 p3457 A71-40276
 Buoyancy and surface-tension induced fluid instabilities in open and closed vertical circular cylindrical containers from series solution by Jeffreys-Goldstein method
 21 p3367 A71-40667
 Quasi-steady three dimensional ideal compressible fluid flow between convex and concave sides of neighboring blade profiles in axial flow turbine
 21 p3322 A71-40687
 Time-space description of steady and homogeneous turbulence in incompressible fluid flow
 21 p3367 A71-40690
 Convective heat transfer between laminar fluid flow and circular flat tubes, considering wall thermophysical properties effect
 22 p3619 A71-41873
 Heat transfer measurements in differentially heated fluid annulus for nonrotating and rotating flow
 23 p3781 A71-43335
 Discrete slot pressurized fluid journal bearing design for low L/D ratios and small size configuration
 24 p3830 A71-44942
FLUID INJECTION
 NT GAS INJECTION
 NT LIQUID INJECTION
 NT WATER INJECTION
 Fluid flow turbulent boundary layer development in channel inlet under injection, obtaining friction coefficient and dynamic characteristics at subsonic velocities
 01 p0070 A71-10794
 Incompressible fluid laminar flow between stationary and rotating porous disks with equal suction and injection
 02 p0240 A71-12337
 Compressible turbulent boundary layers with fluid injection, considering transpiration cooling, skin friction coefficient, etc
 03 p0398 A71-13128
 Film cooling effectiveness with He and refrigerant 12 injection into two dimensional turbulent boundary layer of supersonic airflow
 03 p0517 A71-13453
 Gas flow parameter changes under partially vaporized fluid injection, considering effects on pressure, temperature and rate of resultant mixture
 03 p0521 A71-14252
 Liquid/gas repeated injection into ideal gas plane supersonic flow, determining resultant shock wave radius relation to Mach number and temperature
 03 p0404 A71-14254
 Axisymmetrical, optically thick nonNewtonian, power law boundary layer with injection and suction, obtaining similarity transformations for simultaneous convection and radiation
 04 p0685 A71-15516
 Blunt body nose protection from radiation-convective heat transfer, using porous injection of radiation absorbing substance
 04 p0685 A71-15518
 Injection film cooling effect on surface heat transfer downstream of fluid nontangential injection holes and slots in turbine applications
 [AIAA PAPER 69-523]
 06 p0945 A71-17695
 Heat transfer in turbulent boundary layer for arbitrary surface temperature with fluid injection and pressure gradient
 07 p1220 A71-18765
 Heat transfer in Couette flow with/without injection, taking into account wall conduction effects
 11 p1856 A71-26049
 Laminar source flow between rotating parallel porous disks with equal suction/injection rates solved for infinite radius series, discussing radial velocity and shear stress distributions
 12 p1896 A71-27052
 Turbulent boundary layers calculation downstream of compressible relaxing slot injection flows, using finite difference method based on eddy viscosity model
 13 p2046 A71-27986
 Heat exchange at large Prandtl numbers near porous flat wall with liquid injection, calculating Stanton number
 13 p2046 A71-28181
 Mass injection effect on heat transfer reduction to three dimensional stagnation points as function of shape, enthalpy and gas properties
 14 p2335 A71-29891
 Flowfield production by fluid injection into supersonic crossflow, occurring with liquid/gas jet control of vehicle with combustion ramjets
 [AIAA PAPER 71-728]
 14 p2295 A71-30775
 Velocity profile of steady two dimensional incompressible laminar boundary layer flow with suction or injection, noting wall shear function
 15 p2388 A71-31441
 Laminar boundary layer flow at stagnation point with intensive injection of different absorbing medi-

- um, calculating temperature profiles and thermal fluxes
17 p2725 A71-34215
- Supersonic jet expansion in variable geometry channels, obtaining pressure dependence on injection rate and similarity parameters
17 p2669 A71-34216
- Liquid jet injection into transverse two-phase vapor-liquid flow, calculating penetration path and depth from semiempirical theory
20 p3210 A71-38896
- Modular slot fed fluid bearing using jacking gas effects for pumping power conservation under high speed steady state, discussing design and application
22 p3552 A71-41669
- Perturbation and projection operator algorithms for Navier-Stokes equations for incompressible flow in rectangular cavities and injection into cylindrical ducts
23 p3662 A71-43238
- Calculation method for flow about bodies with injection, presenting parameters approximation formulas derived from Cauchy problem solution for Helmholtz equation
24 p3789 A71-44478

FLUID JET AMPLIFIERS
U FLUID AMPLIFIERS
U JET AMPLIFIERS

- FLUID JETS**
NT AIR JETS
NT FREE JETS
NT GAS JETS
NT HYDRAULIC JETS
- Bending-torsional flutter stability of cantilevered bar subjected to transverse follower force of fluid jet, using Frobenius method
01 p0166 A71-10125
- Fluid jets disintegration into uniform droplets with and without satellite formation, using stroboscopic photography
03 p0399 A71-13292
- Dynamic characteristics of submerged twisted jet flow of incompressible viscous fluid
04 p0573 A71-15560
- Ideal fluid jets theory, discussing cavitation flows calculation, jet flow and plane steady potential incompressible fluid flow
07 p1091 A71-20080
- Fluidic rotational speed sensor, using boundary layers attached to rotating disk surfaces to deflect fluid jets
07 p1031 A71-20604
- Fluid jets disintegration into uniform droplets with and without satellite formation, using stroboscopic photography
09 p1434 A71-23267
- Circular turbulent liquid jet in external stream, considering Reichardt theory, jet expansion law, asymptotic similarity and constant eddy viscosity hypotheses
10 p1597 A71-24940
- Breakup mechanism of liquid sheets and jets in supersonic gas stream, using spark photomicrographs and high speed movies
11 p1750 A71-25471
- Fluid jets along curved or straight walls with non-zero external potential flow, analyzing Coanda effect
15 p2390 A71-32055
- Jet edge tone sensor and internal feedback fluidic oscillator for temperature measurement, using dependence of sound speed in gas
15 p2352 A71-32065

- Fluidic devices with combined pneumatic and hydraulic components, describing jet-siphon liquid flow frequency transducer with pneumatic pulse counting device
15 p2353 A71-32071
- Fluid jet control by acting on thin guiding filament, noting electromagnetic deflections by ferromagnetic wire
15 p2353 A71-32073
- Fluid jets and droplets deformation in transverse supersonic two phase gas flow
17 p2673 A71-35638

- Three ideal incompressible fluid jets collision induced flow, reducing discontinuity region analytic functions to nonlinear system with two numerical parameters and singular integrals
21 p3367 A71-40684

FLUID LOGIC

- Papers on fluid power and logic devices covering pumps, motors, gages, etc
01 p0007 A71-11430
- Fluid logic automatic control systems troubleshooting, discussing circuit and components design for quick malfunction analysis and repair
07 p1023 A71-19995
- Fluidic control systems, discussing basic concepts, static and dynamic, input, transfer and output characteristics of fluidic devices
07 p1023 A71-20002
- Static fluid logic elements, discussing short circuit during switchover, snap action, pressure loss and circuit examples
07 p1027 A71-20573

- Digital fluidic metering system for composition control of liquid batch mixing from circuit design to final product
07 p1028 A71-20581

- Book on fluidics components and circuits covering fluid logic devices, fluid mechanics, analog devices, moving and nonmoving part digital devices, switching elements, etc
09 p1386 A71-22070

- FLE-251 fluidic NOR gate impact modulator developing equivalent circuit model for pressure gain recovery and cut-off, output capacitance and step response
15 p2351 A71-31684

- Fluid logic random input, irregularly activated or stochastic control network analysis, using digital control network synthesis technique /DICONESYN III/
15 p2351 A71-31685

- Fluid logic circuit network analysis, utilizing classical synthesis technique with primitive flow table and maps
15 p2351 A71-31686

- Fluid amplifiers in logic circuits and control and monitoring systems, discussing operating principles and performance features
18 p2850 A71-36137

- Sequential control with fluid logic programmers, considering decimal and binary counters, shift registers, gray code generator and integrated devices
24 p3793 A71-45087

FLUID MECHANICS

- NT AERODYNAMICS
NT AEROTHERMODYNAMICS
NT ELASTOHYDRODYNAMICS
NT ELECTROHYDRODYNAMICS
NT FLUID DYNAMICS
NT GAS DYNAMICS
NT HYDRODYNAMICS
NT HYDROMECHANICS
NT HYDROSTATICS
NT HYPERSONICS
NT MAGNETOHYDRODYNAMICS
NT MAGNETOHYDROSTATICS
NT PNEUMATICS
NT RAREFIED GAS DYNAMICS
NT ROTOR AERODYNAMICS
- Fluid mechanics of shallow liquid fuel layer near burning wick, deriving continuity, momentum and convective diffusion equations to obtain extinction condition
02 p0334 A71-12855

- Fluid mechanical and gas dynamic experimentation by Slingshot aerodynamic test facility
04 p0564 A71-14675

- French book on fluid mechanics, Volume 3, covering nonsteady phenomena, boundary layer and viscous flow
06 p0882 A71-18019

- Premixed laminar flames in flow fields, amplifying fluid mechanical disturbances including vibratory motion and overall feedback loop
06 p1007 A71-18221

- Human mitral valve fluid mechanics, confirming existence of vortex forms during diastasis by vitro flow patterns
06 p0863 A71-18556

- Boundary value problems and applications in fluid and gas mechanics - Conference, Kazan, U.S.S.R., May 1969
07 p1091 A71-20076

- Book on plasma physics, Volume 1, covering electromagnetic fields, fluid mechanics and theory, mathematical analysis and thermodynamics
08 p1341 A71-21892

- Modified brute force technique application boundary layer stability
13 p2050 A71-29203

- Stochastic modification of binary fluid mixtures hydrodynamic dissipative equations, considering nonequilibrium entropy
13 p2051 A71-29354

- Clear air turbulence mechanics, considering thermal convection, shear layers, Coriolis and centrifugal instability, billons and rotors
14 p2267 A71-29758

- Book on fluid mechanics covering rotating fluids, flow between concentric cylinders, emulsions, standing waves on water, etc
14 p2226 A71-30554

- Excess energy in fluid mechanics, breaking up equation into different orders by small perturbation approach and Rankine-Hugoniot shock relation
14 p2227 A71-30818

- Turbulent flow asymmetrical mechanics equations derivation from conservation laws, discussing Navier-Stokes equation, angular momentum and transport theory
14 p2227 A71-30877

- Papers on fluid mechanics, Volume 3, covering magnetohydrodynamics, plasma shocks, gas radiation, nonlinear viscoelastic fluids, laminar combustion, measurement techniques, etc
15 p2393 A71-32558

- Stability of governing parameters critical values /Taylor, Rayleigh or Reynolds numbers/ and periodic solutions in fluid mechanics
16 p2558 A71-33002

- Fluid mechanics problem of nonuniform meshes and complex boundary conditions, using finite element method
16 p2559 A71-33097

- Fluid mechanics of human whistling as function of resonant cavity and orifice jet velocities, comparing Rayleigh bird call and Pfeiftonone
18 p2910 A71-36935

- Dense fluids linearized general transport equations solution, obtaining explicit expressions for shear viscosity
18 p2950 A71-37061

- Eigenfunctions of curl operator, rotationally invariant Helmholtz theorem and applications to electromagnetic theory and fluid mechanics
20 p3255 A71-39575

- Book on statistical mechanics of turbulent fluid flows covering gas oscillations, correlation function, Reynolds equation, laminar flow, particle dispersion, etc
20 p3213 A71-39774

- Quasi-fluid mechanical formulation generation for ionized gases dispersive transport coefficients by linear dynamic response function technique
21 p3423 A71-40800

- Chemical kinetics and fluid mechanics interaction effects in stagnation point boundary layer
21 p3475 A71-40860

- Fluid and solid mechanics - Conference, University of Notre Dame, South Bend, Indiana, August 1971
21 p3468 A71-40982

FLUID POWER

- Papers on fluid power and logic devices covering pumps, motors, gages, etc
01 p0007 A71-11430

- Book on fluid power circuits and systems covering switching theory, closed loop systems, pneumatic circuits, servo systems and pressure control
02 p0190 A71-11871

- Steady one dimensional MHD flow under transverse magnetic induction, determining maximum power of incompressible fluid generator
16 p2620 A71-34144

- Fluid power transmissions and control systems - Conference, Hanover, West Germany, April 1971
18 p2850 A71-36201

- Fluid contamination and protective filter in hydraulic power components for design service life
18 p2851 A71-36204

- Aerospace fluid power - Conference, Detroit, Michigan, October 1970
20 p3183 A71-39147

FLUID ROTOR GYROSCOPES

- Two stage integrating float gyroscopes with reactive moment meters and sensors, examining feedback design for stabilization systems
06 p0899 A71-17930

- Motion stability of symmetric rotor of gyroscope with inviscid incompressible liquid filled cylindrical annular cavity around coaxial rigid rod
13 p2065 A71-29778

- Low cost high performance rate gas bearing gyroscope development, emphasizing large scale production and overall instrument design optimization
22 p3551 A71-41664

- Two-axis pneumatic rate gyroscope with externally pressurized gas bearing for airborne vehicle fluidic autostabilizer sensor
22 p3551 A71-41666

FLUID SWITCHING ELEMENTS

- Two dimensional jets forced and induced switching by vortex flow
[ASME PAPER 70-WA/FLCS-13]
03 p0354 A71-14088

- Jet switching dynamic behavior in bistable fluidic devices, examining flow field, response and switching time
[ASME PAPER 70-WA/FLCS-20]
03 p0355 A71-14093

- Plane discrete fluidic switching element external static characteristics tests in relay and trigger modes
07 p1023 A71-19362

- Digital turbulence amplifiers, investigating dynamic switching response
07 p1024 A71-20552

- Fluidic diverting valve independent of turbulent reattachment, examining large scale model and digital element characteristics in closed loop system
07 p1024 A71-20553

- Fluidic element fabrication techniques, discussing concrete and epoxy molds and stainless steel chemical milling
07 p1121 A71-20562

- Digital active fluid amplifiers static and dynamic behavior, defining complex parameters for system engineering
07 p1026 A71-20564

- Fluidic proportional amplifier circuit with two bistable element stages, using pulse width modulation techniques
07 p1027 A71-20579

Boundary layer pressure distributions for supersonic fluidics bistable devices 07 p1029 A71-20589

Supersonic fluidic bistable switch, developing improved pressure recovery 07 p1029 A71-20590

Fluidic OR-NOR element multiple regression analysis, investigating wall attachment, hysteresis switch pressure and percentage recovery 07 p1031 A71-20607

Fluidic passive and, exclusive-or logic gate, investigating switching, input and output characteristics 07 p1031 A71-20610

Book on fluidics components and circuits covering fluid logic devices, fluid mechanics, analog devices, moving and nonmoving part digital devices, switching elements, etc 09 p1386 A71-22070

Discrete fluidic element dynamic tests, using magnified models with similarity criteria 09 p1386 A71-22653

Two dimensional discrete fluidic element with Coanda effect, calculating switching discharge, jet gap and circulation zone length 09 p1386 A71-22654

Proportional fluidic element static characteristics, calculating main jet interaction with control jet 09 p1386 A71-22655

Slow switching in wall attachment fluidic devices, determining flow characteristics 15 p2391 A71-32057

Hydraulic resistance control and actuation switching system designs and classifications, using bridge half components and loop combinations 18 p2850 A71-36203

Directional hydraulic control switching fluid amplifier at various Reynolds numbers, including cavitation effects 18 p2851 A71-36205

Fluid amplifier digital elements dynamic switching, noting back pressure effects 18 p2851 A71-36207

FLUID TRANSMISSION LINES

Fluid lines transient response to frequency modulated signal inputs, considering Newtonian fluids or perfect gases [ASME PAPER 70-WA/FLCS-1] 03 p0354 A71-14078

Fluid transmission lines terminated by orifice with nonlinear pressure flow characteristics, calculating harmonic distortion frequency response by perturbation method [ASME PAPER 70-WA/FE-6] 03 p0402 A71-14128

Fluid lines transient response obtained in infinite series form [ASME PAPER 70-WA/FE-22] 03 p0403 A71-14132

Blocked and series connected pneumatic fluidic transmission lines, determining amplitude frequency response 07 p1026 A71-20566

External feedback fluidic oscillators design and analysis using branched pneumatic transmission line arrangements 07 p1027 A71-20578

RC analog fluidic circuits design for arbitrary transfer functions generation 15 p2351 A71-31682

DC equivalent circuit, describing pressure and flow distribution at input ports of fluidic line branchings 15 p2352 A71-32067

Fuel cell system steam/hydrogen mixture mass ratio detector using fluidic delay line oscillator 17 p2745 A71-35294

Hydrostatic power transmission systems classifications, considering transformation, transport and accumulation of energies /mass, heat, optical, chemical, pneumatic, hydraulic, etc/ 18 p2850 A71-36202

Transportation lag simulation by fluidic transmission lines and bubble tubes 24 p3793 A71-45086

FLUID TRANSPIRATION

U TRANSPIRATION

FLUIDIC CIRCUITS

NT FLIP-FLOPS

FLUIDICS

NT FLUERICS

Fluidic systems as digital devices, considering stream interaction, vortex and turbulence amplifiers 01 p0006 A71-10801

Reliability test for fluidic digital comparison device 01 p0006 A71-10925

Papers on fluid power and logic devices covering pumps, motors, gages, etc 01 p0007 A71-11430

Fluidic sensors for automatic control systems parameter measurement 02 p0196 A71-12625

Fluidics component operation and characteristics, including turbulent reattachment, jet deflection and vortex amplifiers 03 p0353 A71-13132

Proportional fluidic elements jet nozzle discharge coefficients as function of control pressure and geometrical parameters 03 p0354 A71-13959

Fluidic instrument pressure regulator, noting pressure sensing circuit, confined jet amplifier and control valve [ASME PAPER 70-WA/FLCS-4] 03 p0428 A71-14080

Fluidic acoustic signal detector for output determination of HF fluid oscillators, discussing performance, constant loading effect and signal amplitude [ASME PAPER 70-WA/FLCS-7] 03 p0428 A71-14083

Fluidic ID transmission line characteristic impedance measurement as function of signal frequency, noting correlation with Nichols theory [ASME PAPER 70-WA/FLCS-14] 03 p0354 A71-14089

Computer aided design for fluidic-pneumatic sequential control circuits synthesis, discussing algorithms and computer programs [ASME PAPER 70-WA/FLCS-17] 03 p0354 A71-14090

Liquid cooled space suit fluidic temperature control, using pressure differential variations across garment for cooling level modulation [ASME PAPER 70-WA/FLCS-19] 03 p0355 A71-14092

Jet switching dynamic behavior in bistable fluidic devices, examining flow field, response and switching time [ASME PAPER 70-WA/FLCS-20] 03 p0355 A71-14093

Static and dynamic testing of fluidic elements as function of geometrical and operating parameters 03 p0355 A71-14296

Fluidic inertial instruments for space sensing, guidance and control including gyroscopes, accelerometers and rate sensors 04 p0535 A71-15322

German monograph on hot-wire anemometry in fluidics, taking into account partial differential equation solution for temporal and spatial temperature distribution along wire 05 p0753 A71-16899

Solid propellant rocket motor combustion control by fluidic vortex valve, considering thrust variation [AIAA PAPER 70-643] 07 p1183 A71-18904

Various configuration fluid jet amplifiers, investigating cavitation conditions in water tunnels and open duct 07 p1023 A71-19198

Fluidic control systems, discussing basic concepts, static and dynamic, input, transfer and output characteristics of fluidic devices 07 p1023 A71-20002

Fluidics applications noting liquid level regulation, press control, alarm, windshield wiper, hydrofoil stabilization, pneumatic conveyor belt, respirator, stepping motor and tape centering control 07 p1023 A71-20003

Fluidics, discussing wave operated sensors, control systems, future developments and applications 07 p1024 A71-20208

Subsonic tactical missile hydraulic and fluidic autopilot systems for directional control, considering costs, reliability, vulnerability, maintainability, weight and mobility [SME PAPER MS-70-524] 07 p1024 A71-20547

Fluidics - Conference, Coventry, March 1970, Volumes 1, 2, 3 07 p1024 A71-20551

Fluidic diverting valve independent of turbulent reattachment, examining large scale model and digital element characteristics in closed loop system 07 p1024 A71-20553

Beam deflection type fluidic amplifiers with single and symmetric control jets, considering free streamline flow theory 07 p1025 A71-20557

Fluidic 8 track punched tape reader, discussing design simplicity, flexibility, accuracy, wear and long life operation 07 p1025 A71-20560

Fluidics application to weapon systems safety and arming devices, investigating reliability and immunity to environmental conditions 07 p1025 A71-20561

Fluidic element fabrication techniques, discussing concrete and epoxy molds and stainless steel chemical milling 07 p1121 A71-20562

Optimal design and manufacture of wall attachment fluidic devices, noting thermoplastics injection molding followed by ultrasonic bonding 07 p1121 A71-20565

Blocked and series connected pneumatic fluidic transmission lines, determining amplitude frequency response 07 p1026 A71-20566

Fluidic pneumatic control system compensator for digital signal processing 07 p1026 A71-20567

Fluidic Helmholtz resonator for FM signal analysis, showing instantaneous phase difference between input and output pressures 07 p1026 A71-20568

Beam deflection fluidic circuit design by linear static matching method, considering servoamplifier feedback control system 07 p1026 A71-20569

Transfer function synthesis by RC fluidic circuits, presenting transfer function element circuits analysis and experimental verification 07 p1026 A71-20570

Piezoelectric and capacitive transducer pressure measurements in low pressure fluidic elements 07 p1026 A71-20571

Hybrid fluidic binary counter, using commercially available fluidic bistable amplifier in conjunction with free disk steering gate 07 p1026 A71-20572

Fluidic relaxation oscillator experimental and theoretical analysis, investigating pressure and temperature effects on frequency stability 07 p1027 A71-20576

Monostable fluidic feedback oscillator analysis, using mathematical models describing function, feedback control theory and analog computer simulation to determine oscillation frequency 07 p1027 A71-20577

External feedback fluidic oscillators design and analysis using branched pneumatic transmission line arrangements 07 p1027 A71-20578

Pressure regulator design and construction, using high pressure fluidic proportional chain 07 p1027 A71-20580

Digital fluidic metering system for composition control of liquid batch mixing from circuit design to final product 07 p1028 A71-20581

Missile fluidic attitude control system, discussing integrator, transducer amplifiers and circuits 07 p1028 A71-20583

Pneumatic and hydraulic fluidic power control systems, discussing moving part position servos and cold gas reaction systems 07 p1028 A71-20585

High performance fighter aircraft engine pressure ratio and turbine inlet temperature measurement, using fluidic sensors 07 p1028 A71-20586

Fluidic pressure ratio control for vertical takeoff aircraft lift engine fuel system, describing breadboard circuit, test bed and flight standard 07 p1028 A71-20587

Two dimensional supersonic fluidic amplifier flow field density and characteristics determined by differential interferometry 07 p1028 A71-20588

Supersonic fluidic bistable switch, developing improved pressure recovery 07 p1029 A71-20590

Supersonic pitot fluidistor in bistable mode, investigating improved pressure and flow recovery at large expansion ratios 07 p1029 A71-20591

Fluidic ambient velocity and pressure measurement sensors, using unbounded turbulent jets 07 p1029 A71-20595

Low pressure air jet sensing power pneumatic and fluidic circuits and interface valves for low pressure signal stepup to main line pressure, considering circuit design 07 p1030 A71-20597

Pneumatic resistance transducer for fluidic measurement of mechanical quantities 07 p1030 A71-20598

Fluidic noncontact position sensor, investigating flap insertion effect on laminar jet flow 07 p1030 A71-20599

Fluidic coincidence position sensors, using wall attachment amplifiers and nozzle displacement 07 p1030 A71-20601

Volume variations detection by Hartmann air jet fluidic oscillator 07 p1030 A71-20602

Fluidic/electronic pressure ratio computer prototype, using two free jets interaction for instrument error reduction 07 p1031 A71-20603

Fluidic rotational speed sensor, using boundary layers attached to rotating disk surfaces to deflect fluid jets 07 p1031 A71-20604

Gas-liquid fluidic timing control device, discussing media combination, oscillator complete clock, bubble counter and pressure gages 07 p1031 A71-20605

Fluidic OR-NOR element multiple regression analysis, investigating wall attachment, hysteresis switch pressure and percentage recovery 07 p1031 A71-20607

Fluidic passive and, exclusive-or logic gate, investigating switching, input and output characteristics 07 p1031 A71-20610

Book on fluidics components and circuits covering fluid logic devices, fluid mechanics, analog devices, moving and nonmoving part digital devices, switching elements, etc 09 p1386 A71-22070

Discrete fluidic element dynamic tests, using magnified models with similarity criteria
09 p1386 A71-22653

Two dimensional discrete fluidic element with Coanda effect, calculating switching discharge, jet gap and circulation zone length
09 p1386 A71-22654

Proportional fluidic element static characteristics, calculating main jet interaction with control jet
09 p1386 A71-22655

Control and instrumentation fluidics, describing equipment, circuits and applications to jet engine controls, missile guidance, flight control, ordnance and machine tool control
09 p1386 A71-22775

Fluidic inertial instruments, describing sensor or transducer components, flight control systems, rate damper systems and attitude control systems
09 p1387 A71-22785

Temperature measurement techniques annual progress survey including contact and radiation thermometers, IR thermography, microwave radiometry, fluidic sensors, and liquid crystals
10 p1612 A71-24685

Reentry vehicles fluidically controlled hydrazine rocket engine modules for roll rate control
[AIAA PAPER 70-650] 11 p1810 A71-25503

Control jets interaction with airstream surrounding typical tactical missile configuration, considering rear mounted bistable fluidic thrusters and circular sonic jets
11 p1837 A71-25506

Fluidic fuel control valve for uniform fuel distribution to gas turbine annular combustor, providing sufficient pressure drop at low fuel flow rates
[ASME PAPER 71-GT-44] 11 p1812 A71-25977

Fluidic diodes designs with and without fluid discharge
13 p1998 A71-28010

Fluidic cabin pressure automatic control systems for military and civil aircraft, discussing design, operation and performance
14 p2182 A71-30308

RC analog fluidic circuits design for arbitrary transfer functions generation
15 p2351 A71-31682

Fluidics - Conference, Prague, June-July 1971
15 p2351 A71-32051

Two dimensional viscous incompressible fluid flow field calculation in fluidic element, giving Navier-Stokes equations solution in finite difference form
15 p2390 A71-32054

Surface roughness causes and effects in planar fluidic elements, using large scale models
15 p2351 A71-32059

Jet edge tone sensor and internal feedback fluidic oscillator for temperature measurement, using dependence of sound speed in gas
15 p2352 A71-32065

DC equivalent circuit, describing pressure and flow distribution at input ports of fluidic line branchings
15 p2352 A71-32067

Design algorithms for fluidic combinational and sequential circuits
15 p2352 A71-32068

Fluidic servo amplifier operation by PWM mode with PD computation and ripple removal circuit
15 p2352 A71-32069

Heading reference system feedback linear control circuits containing fluidic vortex rate sensor applied to turbine drive
15 p2353 A71-32070

Fluidic devices with combined pneumatic and hydraulic components, describing jet-siphon liquid flow frequency transducer with pneumatic pulse counting device
15 p2353 A71-32071

Electro-pneumatic transducer for conversion of electrical into fluidic signals, using temperature dependence of laminar gas jet deflection angle in flow along heated curved wall
15 p2353 A71-32072

Fluid jet control by acting on thin guiding filament, noting electromagnetic deflections by ferromagnetic wire
15 p2353 A71-32073

Fluidic ammeter for measuring electric current in insulated wire, using fluoric oscillator sensor
16 p2576 A71-32974

Hot-wire anemometers design and operation in fluidics, discussing temperature gradient due to heat transfer effects
16 p2579 A71-33435

Book on fluidic systems design covering analog and digital control, application to aircraft, spacecraft, computers, tracking devices and equivalent circuits
16 p2526 A71-33475

Series and bypass fluidic pressure regulators, discussing component selection, performance details, sensing circuits, feedback amplifier and flow controller
16 p2579 A71-33526

Fluidic viscometer using laminar impedance element for output signal amplification
17 p2677 A71-35289

Fuel cell system steam/hydrogen mixture mass ratio detector using fluidic delay line oscillator
17 p2745 A71-35294

Fluid amplifiers in logic circuits and control and monitoring systems, discussing operating principles and performance features
18 p2850 A71-36137

Fluidics analog to digital signal techniques, discussing data transmission, acquisition and processing
18 p2851 A71-36206

Aerospace pneumatic and fluidic developments, discussing high speed and response air motors, control functions, thrust reverser actuator and various drive systems
18 p2851 A71-36208

Fluidic gyroscope technology, reviewing current development and problems associated with severe environmental conditions affecting inertial guidance and spacecraft control
18 p2922 A71-36482

Fluidic inertial platform feasibility model for line of sight guidance of air to surface missile
18 p2945 A71-36483

Aerodynamic compensation for ambient medium temperature effect on fluidic standard components and timing devices
19 p2998 A71-37570

Fluidic diodes designs with and without fluid discharge into atmosphere
21 p3326 A71-41140

Two-axis pneumatic rate gyroscope with externally pressurized gas bearing for airborne vehicle fluidic autostabilizer sensor
22 p3551 A71-41666

Unbounded turbulent jet transducer element fluidic sensors, measuring ambient velocity and density from pressure data
22 p3531 A71-42768

Fluidic element input impedance measurement, noting aperiodic nature of transient response in input channel
23 p3631 A71-44019

Pneumatic passive lead networks for fluidic systems, presenting transfer functions, equivalent circuits and design information
23 p3631 A71-44096

Pure fluidic gas detectors for monitoring gas density changes
23 p3680 A71-44097

FLUIDIZED BED PROCESSORS

Lunabase regions origin, suggesting volcanic dust masses fluidized by volcanic gases
09 p1528 A71-23550

Fiber reinforced thermoplastics fabrication by fluidized bed techniques, fusing powder matrix to fiber surface for continuous coating
11 p1768 A71-25415

FLUIDS

Density and temperature dependences of viscosity and thermal conductivity of dense fluids
05 p0831 A71-16408

Nonlinear interaction between three weakly coupled waves with well defined phases in dissipative media /fluids, plasmas or crystals/
13 p2106 A71-28453

Continuity equation properties for incoherent fluid, obtaining linear partial differential equation
19 p3105 A71-38584

FLUORESCENCE

NT X RAY FLUORESCENCE
Photodissociation produced O/P3 atoms detection and reaction rate measurements by resonance fluorescence scattering
01 p0130 A71-10369

Cross sections for fluorescence production in carbon dioxide photoionization by 58.4 nm radiation, deriving emission spectra
06 p0963 A71-17255

Tissue typing instrumentation with fluorochromatic cytotoxicity assay for quantitative data analysis, eliminating visual counting
07 p1050 A71-20050

Chlorine dioxide induced fluorescence spectra, using argon ion laser
08 p1300 A71-20667

Comet 1969g spectrum at 3800-8500 A, noting upper H alpha surface brightness limit consistency with chromospheric resonance fluorescence model
09 p1517 A71-22335

Book on glass lasers covering absorption and fluorescence of glasses, glass structure, energy transfer, nonradiative transitions, quenching, etc
11 p1772 A71-25450

Human lens fluorescent pigment O-beta-D-glucoside of L-3-hydroxykynurenine, discussing preparation, electrophoresis and paper chromatograms
11 p1718 A71-25634

Jupiter upper atmosphere extreme UV dayglow, involving resonant scattering and fluorescence of incident solar flux
12 p1961 A71-26888

Upper atmosphere radiative energy transport equation derivation with allowance for deviations from

Kirchhoff law, examining fluorescence mechanism and effect on radiative heating
13 p2057 A71-28025

Strong level crossing signals in stepwise fluorescence, investigating fine and hyperfine structure of atomic Li
14 p2277 A71-30508

Rotational temperature and density measurements in high speed gas flow by electron beam fluorescence technique
15 p2406 A71-31544

[AIAA PAPER 71-605]
Hexamethylindotricarbocyanine iodide ethanol dye solution stimulated fluorescence during excitation by ruby laser radiation in spike generation quasi-continuous monopulse modes
15 p2421 A71-32406

Optical fluorescence spectra of rock forming minerals for quantitative analysis of lunar surface
15 p2411 A71-32471

Optical fluorescence of lunar transients in UV to IR range for rock forming silicates, using electron microprobe with cathode luminescence capability
15 p2492 A71-32472

Ruby laser pumped tunable organic dye laser to excite atomic flame fluorescence of 5535.5 A barium resonance line, obtaining intensity vs concentration
15 p2422 A71-32582

Upper atmosphere temperatures from barium oxide fluorescence emissions in ion cloud rocket experiments, studying thermal response to geomagnetic disturbances
16 p2562 A71-32808

Ultrafast laser pulses, revealing fluorescence decay, stimulated Raman scattering and plasma formation transient details
16 p2588 A71-33873

Flame atomic fluorescence-atomic emission DC spectrometer for trace wear metals analysis in jet engine oils, covering spectral wavelengths below and above 3500 A
17 p2695 A71-35150

Coherent electromagnetic excitation of optical transition levels by fluorescence measurement, obtaining dipole moment and relaxation times
18 p2929 A71-35903

Fluorescence spectra of anthracene ethyl alcohol solution and powdery crystalline anthracene by single and two photon ruby laser excitation
19 p3071 A71-37263

Temperature dependent differential quenching rates of vibrationally excited CO fluorescence by ortho and para hydrogen, using Born-Bethe approximation
19 p3107 A71-38052

H II region formation from type II supernovae explosion, detecting with fluorescence model
20 p3287 A71-39052

Airglow optical emission processes covering resonance scattering, fluorescence, chemical association, ionic reactions and excitation transfer
20 p3226 A71-39827

Bicolor cathode ray display tubes with triple-layer bombarding electron beam energy-dependent red-green fluorescent screen
21 p3347 A71-40109

Fluorescence phenomena in celestial bodies, considering atomic lines and molecular bands in stellar and nebulae emissions
22 p3597 A71-41515

Fluorescence of iodine molecule excited at 5017 and 5145 A by ionized Ar laser, observing magnetic depolarization/Hanle effect/
22 p3555 A71-41623

UV absorber dyes in fluorescent tracers, discussing theory of dimensional sensitivity and use in liquid film developers to quench background fluorescence
23 p3681 A71-43194

Nd positive ion cross section for stimulated emission with glass composition determined by laser and fluorescence measurements
23 p3685 A71-43938

FLUORESCENT EMISSION

U FLUORESCENCE

FLUORIDES

NT BARIUM FLUORIDES
NT CALCIUM FLUORIDES
NT CESIUM FLUORIDES
NT CHLORINE FLUORIDES
NT CRYOLITE
NT DIFLUORIDES
NT HYDROFLUORIC ACID
NT LITHIUM FLUORIDES
NT MAGNESIUM FLUORIDES
NT OXYGEN FLUORIDES
NT SODIUM FLUORIDES
NT SULFUR FLUORIDES
NT TUNGSTEN FLUORIDES

Undoped and Nd doped synthetic fluorapatite single crystals heat capacity, thermal expansion and thermal conductivity measurements, yielding Debye temperature
07 p1180 A71-20164

Fluoride overcoated Al reflectance measurements and polarization effects at various angles of incidence, noting utilization in vacuum UV instrumentation
08 p1335 A71-21381

- Variable spacing thermionic converter consisting of fluoride vapor deposited W emitter and Nb collector, considering cesiated work function of electrode pair
11 p1714 A71-25905
- Line shifts in first overtone band of DF perturbed by HF, studying pressure induced transitions and partial pressures
11 p1729 A71-26139
- Solid and fluid states oxyal fluoride vibrational spectra and structure
14 p2191 A71-30575
- Carbon difluoride in ablating air-teslon laminar boundary layers by spectrally and spatially resolved UV thermal radiation measurements
19 p3163 A71-37881
- FLUORINATION**
Rh alloys thermodynamic reactions with fluorinating agents including fluorine, bromine, pentafluoride and chlorine trifluoride
06 p0904 A71-17949
- Fluorinated ethylene propylene covers for silicon solar cells, describing processing parameters effects on optical and electrical characteristics
20 p3182 A71-38944
- FLUORINE**
Fluorine ions excited levels mean lives from beam-foil line spectrum analysis
01 p0129 A71-10138
- Lunar Module AG coated stranded Cu wire, analyzing fluorine contamination with proton microprobe
02 p0209 A71-12592
- Compressed liquid and gaseous fluorine constant volume specific heat measurements, tabulating results
04 p0674 A71-14729
- Fluorine liquid-vapor coexistence boundary and critical point parameters, considering thermodynamic and transport properties
05 p0831 A71-16409
- Liquid fluorine feed system valves, seals and seats, discussing design criteria for flight weight components [AIAA PAPER 70-705]
11 p1709 A71-25519
- Fluorine chemical shift tensor measurements in magnesium fluoride, using multiple pulse NMR technique
13 p2025 A71-28031
- Laminar flame speeds in chlorine-fluorine mixtures, predicting low temperature isothermal rates and spontaneous ignition limits
15 p2465 A71-32090
- Launch facility requirements for liquid fluorine upper stage, considering propellant storage and transfer, vapor disposal, leak detection, spills, aborts and range safety
18 p2898 A71-36457
- Vibrational energy distribution and emission lines of fluorine atoms plus chloroform reactions in chemical laser, using equal gain measurements
19 p3071 A71-37331
- Jupiter orbiter spacecraft propulsion system design, noting advantages of fluorine/hydrizine propellant combination [AAS PAPER 71-154]
19 p3122 A71-37925
- Chlorine-fluorine flame, determining adiabatic propagation speed, refractive index field, temperature profile, composition distribution and atom concentrations
19 p3168 A71-38105
- Pulsed laser oscillation from F atoms in mixed helium-fluorine gases using electric discharge excitation
20 p3244 A71-39107
- Fluorine and other trace elements in lunar plagioclase concentrates from Apollo 11 fines, and anorthosite inclusion from Apollo 12 breccia
20 p3292 A71-39383
- F, Na and Al origin in galactic cosmic radiation, investigating production as spallation fragments and generation in source
23 p3719 A71-42943
- Time dependent progress of vibrational rotational transitions in chemical laser using hydrogen-fluorine mixture investigated by oscillography with IKM-1 monochromator
23 p3684 A71-43405
- FLUORINE COMPOUNDS**
NT BARIUM FLUORIDES
NT CALCIUM FLUORIDES
NT CARBON TETRAFLUORIDE
NT CESIUM FLUORIDES
NT CHLORINE FLUORIDES
NT CRYOLITE
NT DIFLUORIDES
NT FLUORIDES
NT FLUORINE ORGANIC COMPOUNDS
NT FLUORO COMPOUNDS
NT FLUOROAMINES
NT FLUOROCARBONS
NT FLUOROHYDROCARBONS
NT FLUOROSILICATES
NT HYDROFLUORIC ACID
NT LITHIUM FLUORIDES
NT MAGNESIUM FLUORIDES
NT OXYGEN FLUORIDES
NT POLYTETRAFLUOROETHYLENE
NT SODIUM FLUORIDES
NT SULFUR FLUORIDES
NT TUNGSTEN FLUORIDES
- Transverse gas flow effects on deuterium fluoride-carbon dioxide chemical laser output, discussing amplifier medium homogeneity factor
10 p1619 A71-23834
- Silicon difluoride reactions and properties, describing production from commercial silicon tetrafluoride and versatility of reactions with organic and inorganic compounds
19 p3011 A71-37647
- Permittivity increase in fluor-substituted barium titanate solid solutions for ceramic capacitor microminiaturization
24 p3859 A71-44387
- Carbonyl fluorine thermal decomposition in excess Ar behind incident and reflected shock waves, analyzing reaction rate variation with temperature and total pressure
24 p3802 A71-44941
- FLUORINE ORGANIC COMPOUNDS**
NT CARBON TETRAFLUORIDE
NT FLUOROAMINES
NT FLUOROCARBONS
NT FLUOROHYDROCARBONS
Time dependent Q switched energy storage of trifluoromonoiodomethane photodissociation laser
06 p0910 A71-18661
- Fluid sealing capabilities of silicone, fluorosilicone and fluorocarbon elastomers above 250 F [ASLE PREPRINT 71AM 3B-1]
13 p2093 A71-29488
- FLURO COMPOUNDS**
NT CARBON TETRAFLUORIDE
NT CRYOLITE
NT FLUORINE ORGANIC COMPOUNDS
NT FLUOROAMINES
NT FLUOROCARBONS
NT FLUOROHYDROCARBONS
NT POLYTETRAFLUOROETHYLENE
Beta-Li hexafluoroaluminate heat capacity and thermodynamic properties from 15 to 380 K
04 p0674 A71-14727
- Fluorapatite single crystals absorption spectra and luminescent characteristics under activation by rare earth ions, noting line widening dependence on crystal composition
09 p1507 A71-22390
- Electroencephalogram alterations in dogs and monkeys during bromotrifluoromethane exposure, correlating brain wave patterns with CNS depression [AMRL-TR-69-14]
09 p1398 A71-22475
- Low compression set and volume swell of vulcanizates of fluoroelastomer at elevated temperatures for sealing applications
10 p1632 A71-24099
- Performance testing of fluorosilicone hydraulic fluid in high temperature supersonic aircraft piston pumps
12 p1921 A71-27040
- Fluorochlorosilane preparation and identification by Raman laser spectroscopy, establishing line to vibration mode relation
14 p2189 A71-29746
- High purity lithium hexafluoroarsenate preparation methods and hexafluoroarsenic acid properties
23 p3642 A71-43540
- FLUROAMINES**
Hydrogen fluoride elimination chemical laser from difluoromethylamine using temperatures below 268 K and flash photolysis
07 p1123 A71-19372
- FLUROCARBONS**
Accelerated testing of jet fuel containment sealant, using reduced pressure and hybrid fluorocarbon silicone
10 p1632 A71-24083
- Nonflammable self extinguishing nontoxic fluorocarbon elastomers as adhesives and coatings for Apollo program
10 p1632 A71-24097
- Fluid sealing capabilities of silicone, fluorosilicone and fluorocarbon elastomers above 250 F [ASLE PREPRINT 71AM 3B-1]
13 p2093 A71-29488
- Flammability limits measurement of hydrogen-oxygen mixtures containing fluorocarbon diluents
15 p2465 A71-32086
- Zero field hyperfine splitting in carbon trifluorobromide photodissociation laser emission
21 p3391 A71-40215
- FLUROHYDROCARBONS**
NT CARBON TETRAFLUORIDE
Fluoro-alkyl s-triazines as high temperature lubricants and energy transfer fluids for aerospace systems [ASLE PREPRINT 70LC-5]
08 p1322 A71-21155
- IR and Raman vibrational spectra and structure of tetrafluorocyclobutane
17 p2695 A71-35520
- FLUROMICA**
U FLUROSILICATES
U MICA
- FLUROSCOPY**
Fluorometric microvolumetric test for unconjugated 11-hydroxycorticosteroids distribution in plasma, noting concentrations in capillary and venous blood
11 p1718 A71-25627
- Aircraft parts testing by NDT methods, considering ultrasonic system for valve defects and fluorescent particle system for crack detection
18 p2929 A71-37056
- FLUROSILICATES**
Fluorosilicone sealants for aircraft fuel containment, discussing resistance to heat, jet fuel, moisture and heat aging
10 p1631 A71-24080
- FLUTTER**
NT PANEL FLUTTER
NT SUPERSONIC FLUTTER
NT TRANSONIC FLUTTER
DC-10 flight test program, discussing handling, takeoff and landing, and flutter, stall and stability characteristics
07 p1018 A71-19085
- FLUTTER ANALYSIS**
Bending-torsional flutter stability of cantilevered bar subjected to transverse follower force of fluid jet, using Frobenius method
01 p0166 A71-10125
- Rapid hybrid frequency response method for aircraft flight flutter testing based on hybrid computing system
01 p0049 A71-10228
- Critical flutter of wing with rigid aileron studied by analog computer modeling
01 p0169 A71-10606
- Flutter analysis of plates with inplane boundary support flexibility exposed to transverse pressure loading or buckled by uniform thermal expansion
01 p0173 A71-10940
- LAMS flight demonstration, discussing instrumentation, flutter boundary and dynamic response, aerodynamic testing and structural response to turbulence
02 p0188 A71-11662
- Tip vortex effects on rotor blade flutter in hovering flight, discussing compressibility and oscillation frequency
05 p0694 A71-16564
- Defense of damping theory applications in flutter analysis, discussing energy dissipation
06 p0984 A71-17623
- Flutter analysis of stressed flat simply supported skew panels in supersonic flow, using small deflection thin plate theory
08 p1370 A71-21302
- Flutter analysis of rotating thin cylindrical shell with outer surface exposed to inviscid helical air flow field
09 p1533 A71-22078
- Nonlinear panel flutter analysis and response under random excitation or nonlinear aerodynamic loading, using Rayleigh-Ritz approximation to Hamilton variational principle
09 p1534 A71-22080
- Spring supported circular cylinder stability in wake flow of similar cylinder at various spacings using quasi-static aerodynamic derivatives and flutter theory
09 p1539 A71-22942
- T tail flutter analysis, considering dihedral, angle of attack and aerodynamic force effects
11 p1706 A71-25188
- Sweepback thin cantilever wing transonic flutter density and velocity coefficients, investigating engine pod shaped concentrated mass location effects
11 p1706 A71-25189
- Wing-fuselage-tail interacting low speed flutter, considering mechanical tuning and aerodynamic interference couplings [AIAA PAPER 71-326]
11 p1842 A71-25306
- Nonstationary random analysis of flight vehicle response to atmospheric turbulence, using Priestley evolutionary spectral method [AIAA PAPER 71-341]
11 p1836 A71-25320
- Flutter analysis of long thin cylindrical shells rotating in circular helical air flow field [AIAA PAPER 71-373]
11 p1845 A71-25346
- Flutter analysis of clamped thin skew panels with midplane forces in supersonic flow, using Galerkin method
12 p1974 A71-26766
- Flutter of buckled plate exposed to static pressure differential and streamwise applied in-plane load, comparing experimental results with stability boundary calculations
12 p1983 A71-27584
- Supersonic flutter of two dimensional flat plate in presence of chordwise tensile in-plane stresses
12 p1983 A71-27585
- Thermal flutter of satellite storable tubular extendible members, determining static flexural and torsional vibrations due to solar radiation
12 p1984 A71-27736
- Cascading turbomachine blade row coupled flutter, correlating camber angle, cascade condition and elasticity
13 p2157 A71-29128
- Supersonic flutter analysis of clamped skew panels with in-plane forces by Galerkin method, using two dimensional static approximation for aerodynamic loading
14 p2177 A71-30607

- Vertically cantilevered column weight and follower force effects on flutter and buckling instabilities respectively
14 p2330 A71-30685
- Mechanical support system role in determination of aeroelastic stability of leeward cylinder immersed in wake using undamped flutter theory
14 p2334 A71-31021
- Cylindrical membrane aeroelastic stability and flutter analysis at high supersonic or low hypersonic Mach numbers
15 p2506 A71-32019
- Flutter of thin walled cylindrical shells conveying fluid above critical flow velocity
15 p2508 A71-32135
- Aircraft structural parameters optimization satisfying flutter velocity constraint and minimum mass, applying to box beam design
17 p2825 A71-34874
- Experimental and theoretical aeroelastic analysis of Fokker F-28 T tail, using flutter model and flight flutter tests
17 p2676 A71-35649
- Turbine alternating fan failure due to flutter by coupling of vibration modes and effect of mass distribution in blade
18 p2980 A71-36696
- Structural analysis trends, considering strain and force methods, flutter, dynamic response, atmospheric turbulence and random phenomena problems
20 p3308 A71-39400
- Flow induced flutter and buckling instability of elastic tube with displacement spring support [ASME PAPER 71-VIBR-39]
21 p3459 A71-40289
- Nonlinear flutter of hinged closed cylindrical shells in supersonic gas flow, comparing with wind tunnel tests on panels
21 p3473 A71-41155
- Vibration amplitudes and phases/excitation modes/during flutter for weakly inhomogeneous annular cascade flow with blade interaction and random inhomogeneity
22 p3615 A71-41846
- Variable structure digital control servomechanism flutter mode analysis, using nonlinear differential equation
22 p3528 A71-42878
- Active flutter mode control system synthesis for flight test, showing mass balancing as possible artificial symmetrical wing destabilization
23 p3629 A71-44106
- Stability augmentation system for aircraft elastic modes control, discussing active flutter suppression technology
23 p3629 A71-44107
- Control surfaces and direct jet force flutter suppression system shown to increase flutter speed of wing
23 p3630 A71-44108
- Active feedback wing/store flutter control for fighter aircraft, using computer programs based on frequency and time domains for linear analysis
23 p3630 A71-44109
- FLUX**
Single fluxon drift through superconductors, describing observation technique
07 p1179 A71-20158
- FLUX [RATE PER UNIT AREA]**
U FLUX DENSITY
- FLUX [RATE]**
NT HEAT FLUX
NT MAGNETIC FLUX
NT SOLAR FLUX
Low energy cosmic ray deuteron flux, examining energy spectral shapes of sources
02 p0303 A71-12871
- Convection schemes finite difference formulation for nonlinear instability prevention by absolute spatial conservation rather than flux form
06 p0917 A71-17552
- High energy muon flux diurnal variations related to lunar time
06 p0960 A71-18169
- Polar auroras, lower magnetosphere and geomagnetic perturbations, as effect of corpuscular fluxes penetration into lower ionosphere
07 p1104 A71-20046
- Quasi-captured and escaped electron flux angular dependence and latitudinal variations observations at low altitudes by Cosmos 228 satellite
09 p1512 A71-22362
- Antimatter body size determination, using primary high energy cosmic ray flux
09 p1515 A71-23535
- Ion production rates during electron flux-atmosphere interactions based on atmospheric models with different energy and angular distributions
13 p2061 A71-28541
- Sound propagation in sheared fluid in duct, determining energy flux from linearized gas dynamic equations
21 p3366 A71-40536
- FLUX DENSITY**
NT CURRENT DENSITY
NT ELECTRON FLUX DENSITY
NT ILLUMINANCE
NT IRRADIANCE

- NT LUMENS
NT LUMINANCE
NT LUMINOUS INTENSITY
NT NEUTRON FLUX DENSITY
NT PARTICLE FLUX DENSITY
NT PHOTON DENSITY
NT PROTON FLUX DENSITY
NT RADIANCE
NT RADIANT FLUX DENSITY
NT SOLAR CONSTANT
NT SOLAR FLUX DENSITY
NT SOUND INTENSITY
Cosmic radiation origin, discussing inner and extragalactic energy density and elements distribution
02 p0300 A71-12372
- Chromospheric flare north-south asymmetry aspects, calculating radio flux density correlation indices
03 p0417 A71-14193
- Admittance first derivative interpretation in flux sounding by electromagnetic field stabilization
04 p0581 A71-15068
- High pressure rare gas UV emission spectra, examining wavelength cut-offs and flux ratios
04 p0549 A71-15691
- Planetary nebulae radio spectra observations by Jodrell Bank interferometer and total power instruments, using variable radius spherical shell model for flux density
04 p0658 A71-15836
- Sagittarius A region observations with 80 MHz radioheliograph, noting radio sources flux density
05 p0805 A71-16116
- Radio emission from small galactic nebulosities, describing position, flux densities, identification and exciting stars
05 p0811 A71-16683
- Radio galaxies flux density measurements at 800 MHz
08 p1357 A71-20869
- Small diameter radio sources, determining positions, flux densities and diameters
08 p1357 A71-20870
- Multicharge nuclei fluxes from satellite observation, plotting energy and rigidity spectra from latitudinal dependences
08 p1350 A71-20955
- Scorpius XR-1 simultaneous radio and optical measurements, discussing correlation of fluxes
08 p1360 A71-20985
- Nonisothermal plasma ion acoustic oscillations spectral energy density in electromagnetic wave field, calculating HF conductivity and absorption coefficient
09 p1500 A71-22243
- Gunn diodes temperature, calculating power density dissipation by simple domain mode models and accumulation mode operation
09 p1414 A71-22249
- Power density spectrum of longitudinal velocity fluctuations in pretransition pulsed boundary layer
10 p1591 A71-23836
- Ultrasonic energy density measurement over various frequencies in liquids, using instrument unperturbed by standing acoustic waves
10 p1612 A71-24682
- Pulsar CP 0328 data at 1420 MHz, examining mean intensity and long term fluctuation due to interstellar scintillations
10 p1680 A71-25008
- Seyfert galaxies NGC 1275 and NGC 4151 X ray flux detection, determining position and emission intensity
11 p1814 A71-25214
- Energy flux of tropospheric mesoscale waves and heat influx into upper mesosphere caused by energy absorption, discussing wavelength and latitude effects
12 p1924 A71-26735
- Extensive air showers nuclear active component energy flux lateral distribution and spectrum based on Monte Carlo simulation of elementary interactions
13 p2123 A71-28077
- Interplanetary medium characteristics during geomagnetic storms, discussing changes in pressures, energy flux densities, acoustic velocities and static/magnetic pressure ratio
13 p2058 A71-28236
- Extended galactic radio sources in anticenter quadrant, obtaining 408 MHz integrated flux densities and spectral indices
13 p2135 A71-28298
- Flux flow noise spectra measurement in pairs of magnetically coupled superconducting films, noting frequency response
13 p2111 A71-28502
- Strong planetary nebulae measurement at short centimeter wave lengths, observing flux densities and thermal spectra
13 p2138 A71-28760
- Distant geomagnetic tail longitudinal magnetic field gradient model based on pressure balance between internal field and solar wind, discussing tail flux content
13 p2064 A71-29162
- Absolute calibration of radio sources with variable flux density in microwave region
14 p2316 A71-30976

- Scattering effects on decimeter wavelength quiet sun emissions flux densities, frequencies and brightness temperatures
15 p2485 A71-31737
- Compact pulsed carbon dioxide laser with uniform volume excitation, obtaining output energy as function of discharge voltage, gas composition and pressure
15 p2424 A71-32659
- Analytical model for molecular flow of reactive gaseous species through cylindrical reactors with apertures at either end, evaluating surviving flux magnitude
17 p2695 A71-35133
- Stellar convective shell plane gas layer, noting time dependence of energy flux
19 p3134 A71-37555
- Rechargeable cylindrical hydrogen-oxygen fuel cell for synchronous satellites, determining energy density as function of current, pressure and electrolytes with computer model
20 p3182 A71-38944
- Incident meteor flux density seasonal variations from radio reflections from trains and light scattering from micrometeoroids
20 p3298 A71-39644
- Crab Nebula integrated electromagnetic emission spectra, noting flux density spectral index at various frequencies
20 p3301 A71-39911
- Galactic nucleus map and flux at 10 microns scanned with 5.5 arcsec beam on Catalina observatory telescope
20 p3305 A71-39955
- Nonisothermal turbulent plasma ion acoustic oscillations spectral energy density in electromagnetic wave field, calculating HF conductivity and absorption coefficient
21 p3424 A71-41132
- Laser emission absorption in surface layer of optical glass, determining surface temperature dependence on emission energy density
21 p3394 A71-41297
- Angular distribution of outgoing short wave radiation field intensity as function of sun height on basis of actinometric data from Cosmos 184 satellite
21 p3374 A71-41299
- FLUX MAPPING**
U FLUX DENSITY
U MAPPING
- FLUX QUANTIZATION**
Ozone flux measurement in atmospheric surface layer by profile method as function of destruction coefficient, friction velocity and concentration
09 p1438 A71-23023
- Quark flux measurement by simulating fractional charge particle pulses, testing calibration procedures by comparing simulated and genuine quarklike events
10 p1613 A71-24957
- Radar echoes maximal intensity measurements from meteorological formations, describing pulse by pulse recording system
24 p3826 A71-44883
- FLUXMETERS**
U MAGNETIC MEASUREMENT
U MEASURING INSTRUMENTS
- FLY BY WIRE CONTROL**
Aircraft flaps and ailerons actuators electronic fly by wire control as alternative to mechanical linkages for maneuverability and reliability in flight
01 p0006 A71-10823
- Heavy lift helicopter flight control system design, emphasizing fly by wire electrical analog
14 p2178 A71-31079
- Computerized automatic redundancy management for space shuttle guidance, navigation and control, using fly by wire control technique for in-flight failure detection and correction
19 p3098 A71-37187
- Aircraft electronic or fly by wire control systems, discussing aircraft design fuel-structure weight reduction cycle and control system redundancy requirements
19 p3099 A71-37200
- Power by wire actuators and fly by wire flight controls, discussing systems configuration, reliability, economy and durability
20 p3183 A71-39150
- FLYBY MISSIONS**
NT GRAND TOURS
NT MARINER VENUS-MERCURY 1973
NT MARINER-MERCURY 1973
Space station and interplanetary flight research programs, discussing design, grand tour and Jupiter flyby
05 p0817 A71-16644
- Time series approximation of acceleration functions for analytical solution of low thrust interplanetary transfers, treating flyby and rendezvous mission modes
06 p0977 A71-18566
- Grand Tour mission design, discussing navigation trajectory parameters, launch vehicles and satellite flybys
06 p0978 A71-18620
- Multiple interplanetary flyby trajectories precision targeting, using sequence of alternate heliocentric and

planetocentric trajectory segments with position and time matching constraints
[AIAA PAPER 71-191] 06 p0978 A71-18629

Space vehicle motion on planetary flyby trajectories, using Chebyshev polynomial series and Picard successive approximations method to solve two point boundary value problem
[AIAA PAPER 71-192] 06 p0978 A71-18630

Space shuttle application to periodic interplanetary orbit making flyby without stopping, discussing trajectory requirements and relative orientation of earth, Venus and Mars
10 p1676 A71-24515

Venus-Mercury flyby vehicle solar cells, cover glasses, adhesives and Kapton film, investigating space radiation effects on solar absorptance and transmittance
[AIAA PAPER 71-452] 11 p1859 A71-26236

High energy fast Grand Tour multiplanet flyby missions to outer planets omitting Jupiter, noting identical arrival date at Neptune
[AIAA PAPER 71-188] 12 p1958 A71-26697

German book on models and constructions for interplanetary space flights covering Helios project, grand tour, Mars landing, planetary exploration, etc
16 p2645 A71-33523

Mariner 1969 flyby Mars UV spectrum observations, interpreting data in terms of atmospheric, topographic and polar cap adsorptive characteristics
17 p2799 A71-34501

Requirements and opportunities for comet and asteroid missions including flyby, rendezvous, docking and sample return
[AAS PAPER 71-104] 19 p3139 A71-37906

Shuttle/Centauro injection stage, considering application to comet rendezvous mission via Jovian powered swingby
[AAS PAPER 71-113] 19 p3139 A71-37912

Terminal guidance sensing from spinning spacecraft in swingby mission to outer planets
[AAS PAPER 71-121] 19 p3101 A71-37916

Pioneer F and G spacecraft Jupiter flyby postencounter mission options ranging from solar system escape to high-inclination low-perihelion trajectories
[AAS PAPER 71-136] 19 p3139 A71-37921

Mission analysis for multi-planet flyby and major satellites close encounter to determine solar system planetary evolution data, presenting Grand Tour trajectory parameters
[AAS PAPER 71-137] 19 p3139 A71-37922

Jupiter orbiter missions, considering satellite emphasis and planetary environment and planetology missions
[AAS PAPER 71-140] 19 p3140 A71-37923

Outer planet exploration spacecraft subsystems reliability and ten year flight requirements for planet orbiting and flyby missions
[AAS PAPER 71-112] 19 p3140 A71-37934

Outer planets combined orbiter/flyby missions, investigating single launch feasibility with INT-20/Centauro launch vehicle
[AAS PAPER 71-114] 19 p3140 A71-37935

Launch opportunities for Grand Tour outer planets missions using Saturn-Jupiter instead of Jupiter-Saturn flyby sequence
[AAS PAPER 71-139] 19 p3140 A71-37943

Atmospheric entry probe from flyby mission to Jupiter, considering descent trajectory feasibility and instrument package
[AAS PAPER 71-142] 19 p3153 A71-37945

Jupiter entry probe integration on TOPS and Pioneer outer planet spacecraft for flyby missions, discussing design feasibility and spacecraft modification requirements
[AAS PAPER 71-153] 19 p3153 A71-37955

Ground based studies of Jupiter at optical frequencies, determining atmospheric chemical composition, temperature and stratification, aerosol layers structure and flyby/penetration experiments results
20 p3297 A71-39631

Trajectory aiming plane in optimum satellite orbit selection for planetary flyby and orbiter missions
[AAS PAPER 71-305] 23 p3724 A71-42981

Jupiter atmospheric probe using relay-link communications geometry between probe and flyby spacecraft for 3.5 hr intervals
[AAS PAPER 71-321] 23 p3726 A71-42995

Bi-injection earth departure mode analysis for combined flyby/orbiter Jupiter-Saturn-Pluto and Jupiter-Uranus-Neptune Grand Tour missions
[AAS PAPER 71-322] 23 p3726 A71-42996

Multiple outer planets flyby opportunities during 1976-1980 Grand Tour missions launch period, presenting computer generated specific encounter dates and flyby distances
23 p3729 A71-43029

Asteroids flyby approaches during Jupiter missions and Grand Tours, obtaining gravitational deflection of spacecraft trajectories and mass cost estimates
[AAS PAPER 71-360] 23 p3729 A71-43030

Earth-Jupiter-Saturn-earth trajectories, determining mission planning parameters
[AAS PAPER 71-361] 23 p3729 A71-43031

Computer graphic interactive flight path design program for planetary flyby missions
[AAS PAPER 71-380] 23 p3702 A71-43050

Solar system escape trajectory analysis for Jupiter-Saturn-Pluto and Jupiter-Uranus-Neptune Grand Tour missions, presenting flyby characteristics and heliocentric postencounter directions
[AAS PAPER 71-383] 23 p3731 A71-43053

FLYING
U FLIGHT
FLYING BEDSTEAD AIRCRAFT
U FLYING PLATFORMS
FLYING PERSONNEL
NT AIRCRAFT PILOTS
NT ASTRONAUTS
NT COSMONAUTS
NT FLIGHT CREWS
NT ORBITAL WORKERS
NT PILOTS [PERSONNEL]
NT SPACECREWS
NT TEST PILOTS

Sensorimotor performance of flight and nonflight personnel, investigating motions speed and accuracy
01 p0024 A71-11110

Hemorrhagic reticulosis in flying personnel in terms of etiologic, evolutive and therapeutic aspects
01 p0028 A71-11596

Flying personnel urinary lithiasis relationship with aeronautical activity, discussing etiopathological factors and augmented fluid intake
01 p0028 A71-11600

Flight surgeons guidance criteria for flying personnel, detailing individual areas examination, documentation and clinical findings
08 p1245 A71-20719

Clinical aspects of aerospace neurology, considering central nervous system diseases among flying personnel
08 p1238 A71-20723

Functions of medical services charged with ensuring flying personnel fitness, stressing aging process
13 p2018 A71-28487

Near and intermediate vision in civil aircraft crews, presenting statistical evaluation of age factor effect on visual acuity in professional and nonprofessional personnel
13 p2019 A71-28507

Airline flight personnel fitness downgrading, presenting statistical breakdown by age and physiological or psychological causes
13 p2019 A71-28509

Electroencephalographic evaluation of brain functions disturbances in response to stress in flying personnel, relating fatigue and rest periods allocation
19 p3008 A71-38223

Psychological training for personality development of aircraft stewards for conscious passenger relation establishment
19 p3008 A71-38224

Potential epilepsy determination in flight personnel, suggesting systematic EEG with hyperventilation and photic stimulation tests and personal history data of head trauma and unconsciousness
21 p3331 A71-40357

Hyperventilation syndrome in flying personnel, discussing symptoms of paresthesia and extremities contraction, psychoemotional causes and control mechanism
22 p3500 A71-41569

Flying personnel equilibrium tests with pendulum armchair, investigating labyrinth reflex by induced nystagmus
22 p3500 A71-41570

Psychopathological causes for French Air Force flying personnel inaptitude, considering motivational problems and age factor
22 p3500 A71-41575

EEG characteristics of cadets and flying personnel, noting spike wave paroxysmal screening and epilepsy detection
22 p3502 A71-41836

ST segment elevation spectrum in ECG of healthy male USAF flying personnel
22 p3504 A71-42417

FLYING PLATFORM STABILITY
U AERODYNAMIC STABILITY
U FLYING PLATFORMS
FLYING PLATFORMS
Geomagnetic components measurement from moving platforms, discussing coordinate system stabilization methods for errorless time averaging of measurements
05 p0756 A71-17194

Geomagnetic components measurement from moving platforms, discussing coordinate system stabilization methods for errorless time averaging of measurements
13 p2067 A71-28249

Radio controlled small aircraft as measurement platform for meteorological sensors, discussing development and performance from field tests
17 p2675 A71-35334

FLYING QUALITIES
U FLIGHT CHARACTERISTICS

FLYING SPOT SCANNERS

Computer controlled encoding device with laser flying spot scanning for automatic photographic image measurement
17 p2741 A71-34998

Flying spot digitizer angle encoding system, describing multispeed transducer output conversion to digital format
18 p2925 A71-36914

Three dimensional display with multicolor capability, continuously variable intensity and random accessed flying spot, exhibiting fixed or moving objects
20 p3234 A71-39063

Pattern recognition problems, using on-line picture language program with flying spot scanner
22 p3519 A71-42767

FLYWHEELS
Hodograph of asymmetrical gyrost with self excitation, determining angular velocity dependence on flywheel momentum
01 p0163 A71-10656

Motion components about center of mass of body using flywheel attitude control by small parameter method
02 p0279 A71-11906

Motion components about center of mass of body using flywheel attitude control by small parameter method
13 p2098 A71-28193

Gyro platform orientation control system, using inertial flywheels
13 p2068 A71-28634

Hodograph of asymmetrical gyrost with self excitation, determining angular velocity dependence on flywheel momentum
14 p2275 A71-30990

Three axis and dual-spin attitude control subsystems for communications satellites, considering flywheel stabilization advantage
21 p3454 A71-40478

FOAMING
Foamy properties at various temperatures of nonaqueous hydroliquids based on petroleum fractions and organic silicon and phosphorus oligomers
01 p0088 A71-11107

FOAMS
Sandwich structure cores of foamglass granulate filled unsaturated polyester paste, discussing development of highly thixotropic paste mixtures
01 p0172 A71-10699

Rapid mass transport to Pt electrodes in foamed electrolytes, examining current density-anode overpotential relationship
02 p0210 A71-12957

Mechanical properties and performance characteristics comparison of syntactic foams fabricated by conventional mixing or vacuum impregnation, including filler packing factors
11 p1784 A71-25394

Ablation residue, including silicone elastomer foam heat shield material ablative degradation
11 p1855 A71-26040

Cryogenic propellant tank thermal insulation system based on polypropylene oxide, polyurethane polyvinylchloride and polymethacrylimide foams, discussing design, technology and model tests
12 p1985 A71-26834

High energy hydrogen-oxygen launch vehicle thermal insulation system, discussing closed cell rigid polyvinyl chloride foam mechanical characteristics, use and tests
12 p1985 A71-26835

Modified low density polyisocyanurate foams for low heating rate thermal protection, considering high char yield with reduced surface recession
13 p2091 A71-28178

Pyrrone foams molding, considering chemically blown and syntactic foams mechanical properties
14 p2262 A71-29650

Jet noise reduction by foam injection, developing mathematical model for foam behavior in sound field
[AIAA PAPER 71-734] 15 p2388 A71-31327

Polyvinyl chloride foam insulation system for liquid hydrogen-liquid oxygen space vehicles tested under groundhold and simulated flight conditions
20 p3253 A71-39269

Spray foam insulation for Saturn S-2 stage, consisting of phenolic honeycomb core composite purged with helium
20 p3312 A71-39270

FOCI
Wide angle paraboloid reflector electromagnetic field intensity distribution measurements in focal region
19 p3035 A71-38601

FOCUSING
NT DEFOCUSING
NT SELF FOCUSING
Nondissipative focusing and ionospheric reflecting effects on MF radio wave absorption measurements for magnetically quiet and disturbed periods
03 p0409 A71-13391

FOG

- Interelectrode focusing voltage effect on electron beam and tube efficiency in TW and backward wave tubes with electrostatic focusing systems
03 p0385 A71-13793
- Carbon dioxide laser induced thermal lensing /focusing/ reduction in liquid carbon disulfide with DC electric field
03 p0436 A71-13877
- Camera focal distance, optical center position and distortion determination of Zeiss Astrogaphic objective by moving star pairs method
03 p0428 A71-13941
- Minimum image size in parallel plate electrostatic spectrograph under focusing with small angular aberrations
04 p0600 A71-15593
- Laser beam focusing and defocusing by thermal gas lens, deriving wave optics equations for electromagnetic fields with allowance for temperature distribution
04 p0628 A71-15808
- Carbon dioxide laser beam thermal focusing effects on deflection in absorbing gas
05 p0763 A71-16902
- Sonic boom near field behavior, discussing N wave focusing
[AIAA PAPER 71-185]
06 p0886 A71-18624
- Plasma produced by focused Q switched ruby laser beam, considering use for minimum ignition energy measurement
07 p1123 A71-19577
- Focused ruby laser beam degradation of various gaseous aliphatic and alicyclic hydrocarbons
07 p1124 A71-19789
- Beam laser operational efficiency relation to molecule /atom/ interaction in focusing system, explaining lasing power drop at large flow rates
07 p1126 A71-20186
- Focused aperture antenna arrays near field radiation patterns, determining minimum focusing distance
08 p1266 A71-21464
- Highly directive radio telescope antenna parameters in near zone, using focusing at minimum distance
09 p1414 A71-22218
- Constant period discrete holograms features, investigating laser visualization, recording, reconstruction and image focusing
10 p1608 A71-23810
- Holographic generation of high efficiency, extended range spatial filters, applying to defocused images restoration
10 p1612 A71-24585
- Lateral separation focus sensors for high angular resolution optical systems, reviewing autocollimating optics and operational patterns
10 p1644 A71-25090
- Single thin lens for Gaussian laser mode matching, discussing position and focal length determination
12 p1905 A71-26809
- Fresnel hologram focusing method, considering Leith and Upatniekss wave front reconstruction with diffused illumination
12 p1907 A71-27212
- Traveling wave tube magnetic field focusing and accelerating voltage effects on power output
12 p1889 A71-27627
- Focused laser coherent light beam expansion in turbulent atmosphere
13 p2080 A71-29016
- Power and focusing requirements in recording and reading with Gaussian laser beam in TEM mode
14 p2254 A71-30136
- Radar duct surface interference phenomena and focusing effects on radar beam energy propagation
14 p2201 A71-30936
- Electron cluster formation in klystron buncher, calculating focusing longitudinal magnetic field variation for maximum electron radial stability
15 p2376 A71-31742
- Periodic electrostatic focusing of high perveance electron beams for high power klystrons
19 p3028 A71-37696
- Fresnel hologram focusing method, considering Leith and Upatniekss wave front reconstruction with diffused illumination
19 p3067 A71-38624
- Long object photography with lens array in non-coherent light and subsequent integrated image focus holography in laser beam for reconstruction in white light
19 p3068 A71-38708
- High energy neutralized ion beam generation by focusing ultrashort laser pulses on thin foils, applying to nuclear reaction for superheavy nuclei production
22 p3555 A71-41595
- Laser beam focusing at various distances from caustic surfaces by spherical resonator formed by mirrors or lenses
22 p3557 A71-42063
- Asymptotic expansion of axisymmetric electromagnetic beams with azimuthal dependence near internal caustic /focal line/
23 p3647 A71-44330

FOG

- Millimeter waves attenuation in fog, showing strong temperature dependence and correlation with visibility
01 p0117 A71-10580
- CW He-Ne laser beam scattering observation for artificial fog droplet size distribution during evolution stages
01 p0094 A71-10831
- Fog phenomena systematics, describing physical classification according to substrate and function
02 p0277 A71-12371
- Airport runway mechanical fog dispersal, using trailer mounted rotating wire mesh sieves
04 p0566 A71-14983
- Soviet monograph on atmospheric boundary layer covering compressible turbulent air flow, diurnal fluctuations, fog, air pollution and lower atmosphere electric field
04 p0621 A71-15399
- Turbulent diffusion of impurity from infinite linear source in clouds and fog, allowing for particle entrainment
05 p0776 A71-16422
- Space charge effects on fog precipitation, taking droplet size into account
05 p0779 A71-17141
- Atmospheric absorption by clouds, fog and rain on earth-space path at 90 GHz, using sun tracker
07 p1060 A71-19215
- Soviet book on fog, cloud and humidity measuring instruments, discussing artificial fog formation and natural fog dispersion problems
07 p1114 A71-20298
- Fog removal by high power carbon dioxide lasers, evaluating possibility of clearing airport runways
[AIAA PAPER 69-670]
07 p1153 A71-20308
- IR laser propagation through fog with droplet vaporization, assuming incident electromagnetic radiation as plane harmonic wave
08 p1302 A71-21392
- Meteorological observations for terminal weather modification in aviation, noting airport fog dispersal
08 p1329 A71-21732
- Warm fog modification by condensation nucleus seeding, discussing droplet concentrations, cloud height and aerosol content effects on salt seeding material optimal size and dosage
09 p1488 A71-23253
- Submillimeter wave extinction in clouds and fogs, using spectrometric results of water optical properties
09 p1408 A71-23375
- Sound attenuation by warm air fog, using droplet measurements in Wilson cloud chamber
09 p1490 A71-23556
- Fog droplet and rain effects on propagation of echo location signals from bats
10 p1638 A71-24423
- Fog clearance from airport runways, discussing available techniques, economic aspects and importance for military operations
12 p1925 A71-27247
- Fog evolution and droplet radii spectrum determination by scattered laser beam angular distribution measurement
13 p2082 A71-29484
- Fog drop size distribution measurement with laser hologram camera
16 p2604 A71-33535
- Supercooled fog dissipation by liquid propane, determining effectiveness in providing operational support to aircraft landing and takeoff
16 p2604 A71-33536
- Radiation attenuation volume coefficients for water clouds and fogs thermal sources and laser outputs
16 p2543 A71-33708
- Rain and fog modification concerning natural and artificial nuclei role, warm fog clearing and supercooled cloud experimentation
17 p2769 A71-34545
- Lidar observations of artificial warm fog seeding operations, analyzing spatial and temporal variations
17 p2770 A71-35741
- Fog dissipation programs by commercial and military agencies
18 p2944 A71-36450
- Decane and hexadecane fog detonation propagation in gaseous oxygen
19 p3170 A71-38128
- Artificial fog thermodynamic conditions and evolution data, using scattered laser beam angular distribution measurements
19 p3091 A71-38586
- Fog droplet size spectral distribution from artificial fog induced He-Ne laser beam scatter, using five photometers for angular distribution measurements
19 p3091 A71-38657
- Helicopter experimental fog clearing by downwash mixing at Greenbrier Valley Airport, Lewisburg, West Virginia
20 p3256 A71-39206
- Fog formation and dispersal by velocity field induced by helicopter trailing vortices, presenting dynamic model with droplet depletion, evaporation and condensation
21 p3321 A71-40510

Wind velocities and directions, air temperature and visibility range in atmospheric boundary layer under fog conditions
22 p3569 A71-42064

Persistent and semipersistent thick and dense fog visibility definitions and tabulated data for London/Heathrow Airport and Kingsway/Holborn during 1950-1969
23 p3701 A71-43899

Water vapor-droplet transitional state and halo observation around light sources in radiative fog formation, applying to light weather forecasts
24 p3844 A71-44806

Laser IR radiation attenuation in natural and artificial fogs, noting dependence on particle size distribution
24 p3835 A71-45172

FOIL BEARINGS

Externally pressurized gas-lubricated foil bearing rotation speed effects on gap topography and clearance variation
22 p3552 A71-41653

Flow and strain analysis and engineering design of porous cylindrical gas film foil bearing at low pressures
24 p3830 A71-44940

FOILS [MATERIALS]
NT METAL FOILS

Neutron spectra measurement in epithermal energy range by activation of threshold and resonance foils using expansion in orthonormal polynomials
04 p0594 A71-14911

High speed gas lubricated foil supported nonmetallic rotor for nuclear magnetic resonance research
22 p3553 A71-41676

Polycrystalline beta silicon nitride foils containing glide dislocations from room temperature fracture determining Burgers vectors and slip planes
24 p3842 A71-45191

FOKKER AIRCRAFT

F-28 TRANSPORT AIRCRAFT
Hydraulically powered duplex input servos for flight control system of VFW-Fokker V/STOL fighter aircraft
12 p1867 A71-26808

FOKKER BOND TESTERS

U ADHESION TESTS

FOKKER F 28 AIRCRAFT

U F-28 TRANSPORT AIRCRAFT

FOKKER-PLANCK EQUATION

Distribution function for two circularly polarized modes in laser with axial magnetic field derived by master equation transformation to Fokker-Planck equation
01 p0094 A71-1074

Electron velocity distribution in fully ionized plasma under crossed electric and magnetic fields, assuming Fokker-Planck expression for Lorentz gas
02 p0293 A71-1274

Laser light statistical properties including Fokker-Planck equation, photoelectron counting distribution and quantum mechanical equation from Weidlich and Haake theory
05 p0762 A71-1648

Absolute value type early-late gate bit synchronization steady state phase noise performance evaluation by Fokker-Planck method
05 p0730 A71-1706

Pitch angle distribution of protons and helium ions in magnetosphere from numerical solution of Fokker-Planck equation
06 p0964 A71-1728

Finite difference methods for time dependent Fokker-Planck equation conserving total system mass energy and momentum
06 p0936 A71-1755

Fokker-Planck equation for convection dominated transport of solar cosmic rays solved for exponential decay phase of solar particle events
07 p1185 A71-1965

Nonlinear Fokker-Planck equation solution by Mott-Smith bimodal distribution function method, investigating fully ionized nonequilibrium plasma relaxation time
07 p1171 A71-2029

Fokker-Planck boundary value solutions to transient phase error response of nonlinear phase locked tracking systems
07 p1082 A71-2042

Eigenfunction expansions of reduced nonGaussian phase error transition probability density function for first order tracking loop, analyzing spectral properties of Fokker-Planck equation
08 p1324 A71-2134

Sequence solution to multidimensional time varying Fokker-Planck equation for phase locked nonlinear systems
08 p1324 A71-2134

Information-theoretical approach to lasers theory avoiding Fokker-Planck equation method
10 p1619 A71-2391

Multimode laser with multilevel atoms, deriving Fokker-Planck equation for laser light statistics
10 p1622 A71-2492

Auroral electrons interaction with atmosphere from Fokker-Planck equation, considering angular diffusion, energy loss and geomagnetic field convergence effects

14 p2235 A71-30345

Coulomb collisions in high density plasma beams from numerical integration of Fokker-Planck equation for three initial distribution functions, studying relaxation time

14 p2283 A71-30674

Fokker-Planck equation for Compton scattering in hot plasma, considering energy exchange rates for scattering in relativistic Maxwellian plasma

14 p2283 A71-30859

Nonlinear Fokker-Planck equation numerical tests for collision effects on self consistent field first order component and plasma electron distribution function perturbation

15 p2453 A71-31146

Dust grain orientation in interstellar space from Fokker-Planck equation, taking into account collisions with gas atoms and magnetic interactions

15 p2485 A71-31715

Ray statistics of electromagnetic wave scattering in homogeneous isotropic turbulent medium with ellipsoidal inhomogeneities of refractive index, using Fokker-Planck equation

19 p3020 A71-38364

Superradiant laser stationary characteristics description by Fokker-Planck equation for classical distribution function, taking into account phase destroying effects

21 p3421 A71-41398

Fokker-Planck-Kolmogoroff equation for radar tracking meter with nonlinear discriminator and second-order smoothing loops, obtaining steady solution by separated variables method

24 p3815 A71-44702

FOLDING STRUCTURES

NT SAIL WINGS

Unfurlable spacecraft antenna design and electrical characteristics, using Gregorian geometry with conical main and parabolic subreflector

02 p0232 A71-12324

Folding sidewall aircraft tires design, construction and flight tests, noting advantages and disadvantages

24 p3792 A71-44975

FOLIAGE

Gravity effects on auxin transport, growth and foliage spread of green plants for efficient radiation capture, using horizontal climostat experiments

21 p3341 A71-40005

FOOD

Gamma irradiation effects on physicochemical and organoleptic properties of food products

06 p0861 A71-18367

Potential foods synthesis for long duration space missions by physicochemical methods, discussing regeneration of carbohydrates from metabolic waste carbon dioxide and electrolytic byproduct hydrogen

07 p1056 A71-20375

Soyuz 9 spacecraft crew food diet description including products and packaging

09 p1397 A71-22205

Food utility calculation for various formose sugar treatments as valid qualitative measure of relative effects of dietary materials

19 p3007 A71-37575

Microelement extraction from mineralized biological samples in food rations and human excretions

24 p3800 A71-44540

FOOD INTAKE

Dog blood leucocyte composition relation to alimentary satiation and adrenocorticotrophic and reticuloendothelial systems, considering effect of ACTH and india ink injections

01 p0008 A71-10092

Combined glucose-sodium chloride solution consumption by rats during normal and food deprivation conditions

02 p0201 A71-12874

Telemetric techniques for pharmacological effects of body temperature, motor activity and food and fluid intake on rat brain, describing recording and monitoring equipment

05 p0716 A71-17112

Internal osmotic balance and stress induced body fluid osmolality changes due to food or water deprivation, reporting on experimental results with rats

08 p1240 A71-21750

Body fluid osmolality control of food intake initiation in rehydrated rats injected with hypertonic sodium chloride solution

11 p1719 A71-26073

Food choice, consumption control and metabolism, discussing homeostatic alimentary theories, nerve signals and appetite regulation

13 p2010 A71-28719

Food and water intake changes associated with interruption of hypothalamus anterior or posterior fiber connections

13 p2011 A71-28802

Solid and liquid diets during thiamine deficiency, noting hunger dependence on novelty

13 p2011 A71-28808

Oxygen exposure effect on food consumption/ utilization efficiency, growth and biochemical parameters

13 p2015 A71-29360

Polysomal RNA disaggregation and attendant reduction in hepatic protein synthesis in rats as result of decreased feed ingestion during hypoxia

16 p2529 A71-33190

Human body water metabolism during acute high altitude exposure with heavy physical activity and high food intakes

16 p2530 A71-33240

Human energy requirements in weightless environments, correlating metabolic data from Gemini and Apollo missions with food consumption and energy balance measurements

16 p2532 A71-33778

Skylab habitability considerations in Orbital Workshop design, discussing waste management, food management and sleeping compartments

[AIAA PAPER 71-872]

18 p2870 A71-36628

Human adaptation to high altitude, considering effects of physical preconditioning, exercise, high carbohydrate diets and normal food intake maintenance

18 p2859 A71-36867

Chronic centrifugation effects on water intake and urine output in mice, considering food intake and growth rate

20 p3186 A71-38984

Chronic acceleration effects on animals, considering growth rate, food intake, oxygen metabolism and life expectancy

21 p3328 A71-40003

Diurnal water and food intake and body weight changes pattern in rats with hypothalamic lesions

22 p3486 A71-41936

FORBIDDEN BANDS

Total free electron energy disparity with energy radiated in forbidden O I lines in supernova spectra explained by nova luminescence formation

01 p0151 A71-10067

Electron states in highly doped semiconductors, describing energies in conduction and forbidden bands

02 p0297 A71-12616

Plasma satellites near He I forbidden lines during turbulent heating

06 p0936 A71-17592

Solar X-ray resonance, intercombination and forbidden lines variations of O VII emission

06 p0968 A71-17910

G5-K5 stars 3600-4000 A region, determining forbidden Fe/H lines for G8-K3 giants

07 p1201 A71-20436

Total free electron energy disparity with energy radiated in forbidden O I lines in supernova spectra explained by nova luminescence formation

09 p1525 A71-23260

Two group model of stationary plasma flow in magnetosphere with space charges due to inertia drift and forbidden regions

09 p1529 A71-23710

Sunspots forbidden Fe I lines, calculating magnetic dipole and electric quadrupole transition probabilities

11 p1830 A71-26112

Solar inner corona forbidden emission lines and continuum enhancement during 30 May 1965 eclipse as function of heliocentric position angle

12 p1969 A71-27650

Altitude variation of forbidden line of 5577 A and 3914 A auroral emissions intensities ratio from rocket sounding

16 p2566 A71-33748

Sunspot forbidden Fe I line spectra, showing high solar iron abundance

18 p2961 A71-35944

Dumb-bell Nebula forbidden O III line profiles observation with two-etalon scanning Fabry-Perot

19 p3144 A71-38171

Heat treated thallium bismuth sulfide, selenide and telluride amorphous and polycrystalline thin films electrical conductivity, differential thermal emf and forbidden bandwidth

20 p3276 A71-39076

Electroabsorption spectra of cadmium telluride at photon energies smaller than forbidden band width, observing energy levels

21 p3429 A71-41212

Semiconductor radiation-induced electrical conductivity changes correlation to forbidden band from theoretical model, considering radiation defects as conductivity compensators

21 p3431 A71-41230

Quasi-binary InAs-GaP single crystals absorption and diffuse reflection spectra, determining forbidden bandwidth as function of compound composition

21 p3434 A71-41332

Helium-like ion forbidden line emission and transition probabilities, deriving solar densities in active regions

19 p3136 A71-37621

Electron temperature and density vs ionization potential in bright planetary gaseous nebulae, using forbidden emission line intensity ratios and level populations

21 p3440 A71-40059

Deactivation and radiative lifetime of CO Cameron forbidden transition spectral bands produced by photon absorption

21 p3418 A71-40232

FORBUSH DECREASES

Forbush decreases vertical cutoff rigidity dependence, comparing cosmic ray intensities from Pioneer 8 detector and ground based neutron monitors

03 p0481 A71-14501

Forbush midlatitude microdecreases effects on diurnal cosmic ray intensity, using neutron monitor

05 p0799 A71-16624

Cosmic ray neutron component intensity increases dependence on corpuscular stream velocity before Forbush effects

06 p0954 A71-18124

Forbush decrease rigidity dependence relation to cosmic ray solar modulation, using neutron monitors counting rate variations at different vertical cut-off rigidities

06 p0956 A71-18136

Forbush decreases and long term cosmic ray particle intensity changes, investigating spectral variations

06 p0956 A71-18137

Cosmic ray solar modulation anisotropy during 23 March 1966, 25 May 1967 and 26 January 1968 events in preForbush phase, evaluating multidirectional meson observations

06 p0956 A71-18138

Cosmic rays transient north-south polar asymmetry, confirming time lag between Forbush decrease onsets

06 p0956 A71-18140

Atmospheric fast neutron flux, discussing solar proton events and Forbush decreases effects

06 p0963 A71-18183

Cosmic ray intensity Forbush decrease on 23 September 1966 coincidence with magnetic storm sudden commencement from satellite and ground based monitors data

07 p1184 A71-18750

Chromosphere-flare and galactic cosmic ray hypotheses of Forbush decrease and strong shock waves in interplanetary medium

08 p1352 A71-20967

Cosmic ray modulation spectrum function properties during Forbush decrease by spectrographic analysis

08 p1352 A71-20968

Forbush decreases effects on radio wave absorption, cosmic ray variations and ionization in lower ionosphere cosmic layer

08 p1353 A71-20981

Mean neutron monitor multiplicity time variations for solar cosmic ray events and Forbush decreases with modulation spectrum allowance

11 p1816 A71-25753

Rigidity dependence of Forbush decreases and 11 year variation in cosmic ray intensity at Calgary and Sulphur Mountain and other neutron monitor stations

12 p1949 A71-27374

Anisotropy during cosmic radiation Forbush decreases modulation mechanism onset

12 p1950 A71-27376

Cosmic ray mean intensity drop observation after Forbush decrease, noting rigidity dependence and daily variation from exponential recovery curve

15 p2474 A71-31777

Cosmic ray flux diurnal variation from radial number density gradient, showing Forbush decrease profiles strong dependence on shock radial approach velocity

15 p2480 A71-32755

Forbush decreases comparison with 11 year cosmic ray intensity variation, examining rigidity dependence and modulation functions

20 p3277 A71-38742

Jupiter decametric radio emission relation to solar wind, geomagnetic activity and shock waves causing Forbush decreases

20 p3291 A71-39312

Electron flux time dependence, observing flare increases, Forbush decreases, counting rate changes and intensity variations

20 p3281 A71-39733

FORBUSH EFFECT

U FORBUSH DECREASES

FORCE

Liquid propellant rockets with rotating reactive force vectors, improving equations of motion

12 p1972 A71-27492

FORCE DISTRIBUTION

Mechanical systems free motion, comparing effects of external and delayed action internal forces

01 p0155 A71-10446

Nonconservative generalized nodal forces on finitely deformed finite elements

01 p0174 A71-10960

Cylindrical shell deflection under concentrated radial force expressed in terms of algebraic polynomials

02 p0326 A71-12295

Impeller radial forces in volute casing centrifugal pumps, using potential theory 03 p0431 A71-13145

Einstein universe fictitious forces in noninertial frames, deriving equations from classical formulas by general covariance 03 p0490 A71-13942

Lifting and side force distributions acting on body in transonic flow 03 p0344 A71-14232

Thin spherical shell with circular cutout under HF axisymmetric excitation by concentrated radial force 04 p0667 A71-15181

Liquid droplet elliptical deformation in gas flow upon external flow force application, presenting solution as ellipsoid semiaxes plot of dimensionless time functions at various Weber numbers 05 p0736 A71-16749

Gyrostatic in circular orbit in Newtonian force field, solving for optimal rotational motion stabilization 05 p0817 A71-16997

Elastic spherical shell three dimensional stress-strain state asymptotic behavior near concentrated force as function of parameter characterizing relative thickness and curvature 06 p0995 A71-17830

Force field model for galactic cosmic rays modulation by solar cycles, noting agreement with Fokker-Planck equation analytic and numerical solutions 06 p0952 A71-18110

Stress-strain state of large inhomogeneous bodies of revolution, considering deformation due to arbitrary surface and mass forces in temperature field 07 p1210 A71-19158

Stress relaxation characteristics obtained by compensation principle, force measuring techniques and sample unloading for stress-strain state determination 07 p1210 A71-19160

Elastic, inertial and aerodynamic forces aeroelastic triangle, examining lift changes due to aircraft structure deformation, dynamic flight stability and space shuttle development problems 07 p1215 A71-20063

Aircraft systems assembly methods, discussing rigidity effects on error redistribution in external and internal force field application 08 p1295 A71-20792

Force moment method estimation of atmospheric circulation effect on earth polar movement 08 p1284 A71-21674

Electrodynamic forces distribution in conducting bodies in two traveling magnetic fields with different frequencies and pole spacings 09 p1499 A71-22137

Steady nonrotational flow around rectilinear profile in finite width uniform current in linear theory, calculating fluid exerted forces 10 p1549 A71-23822

Spherical and paraboloid shells of revolution internal and external forces correlation, considering boundary value problem differential solution 10 p1686 A71-23996

Mean and fluctuating forces on flat plates normal to turbulent flow, giving power spectral density measurements of drag fluctuating component 10 p1598 A71-25085

Room temperature rated coercive force measurements of Ni sheet specimens in torsional bending cycles for saturation value, using ballistic method 11 p1778 A71-25563

Lunar geometrical and dynamical properties, deriving force function from density distribution and surface equation 11 p1822 A71-25687

Steady Oseen flow past semiinfinite flat plate with force singularity, deriving integral equation solution 12 p1896 A71-26938

High lift wing characteristics with/without additional devices, emphasizing lift control and load distribution 12 p1864 A71-27476

Circular viscoelastic plate under in-plane forces, determining increase in curvature as function of time 12 p1983 A71-27574

Distributed inertial forces due to cyclic loading in minimum volume beams cross sectional stress calculations 13 p2154 A71-28643

Shimmying wheel with elastic tire, investigating motion equations for wobble and forces exerted by ground 13 p1997 A71-29230

Nonconservative dynamic instability of columns under distributed tangential force, using analog computer 13 p2158 A71-29430

Wind tunnel test models and force measuring balances design, fabrication, inspection and calibration 15 p2413 A71-31440

Unsteady force and pressure measurements by molecular and parametric transducers including strain gage, drag, moment and piezoelectric balance instruments 15 p2411 A71-32563

Hamilton-Jacobi equation application to forces selection for mechanical systems asymptotic stabilization, minimizing functional by Euler-Lagrange equations 16 p2602 A71-32814

Elastic stability theory for perfectly elastic materials with couple stresses, deriving exact functional for overall conservative systems of forces and couples 16 p2648 A71-32989

Optimal bar design for tangential load transmission into sheet, determining stress distribution 17 p2821 A71-34591

Stress relaxation characteristics obtained by compensation principle, force measuring techniques and sample unloading for stress-strain state determination 17 p2834 A71-35656

Elastoviscoplastic system with components undergoing effects of external, resistance and attraction forces, determining motion 18 p2977 A71-36194

Force and heat transfer measurement in hypersonic flows of low gas density, using electromagnetic balances for horizontal and vertical forces and pendulum method for measuring resistance 18 p2921 A71-36416

Elastic beam dynamic buckling stability under transverse follower force, considering force direction dependence on cross sectional twist angle 18 p2980 A71-36679

Gyrostatic in circular orbit in Newtonian force field, solving for optimal rotational motion stabilization 18 p2976 A71-36797

Air flow in pipe with double screw thread, calculating tangential forces and turbulent viscosity coefficient along isostachs 19 p3043 A71-37266

Infinite elastic plate forcing by time varying radial pressure in circular hole at center 20 p3309 A71-39563

Generalized continuum of interleaved microstructures coupled by forces, investigating equations of motion, tensor indices and asymmetrical effects 20 p3309 A71-39566

Total mass density in neighborhood of sun and Galactic force law from stellar motions perpendicular to Galactic plane, using King pseudomoments method 21 p3440 A71-40061

Fluctuating aerodynamic force measurement on stationary circular cylinder spanning wind tunnel, using direct method without support interference 21 p3363 A71-40393

Spanwise lift distribution over wings and wake formation in thin airfoils of finite aspect ratio in linear subsonic potential flow 21 p3319 A71-40495

Stress intensity factors determination for notched structures, using finite element technique 22 p3613 A71-41431

Satellites explosion debris distribution and orbital characteristics as data base for earth force field and geopotential resonance phenomena analysis [AAS PAPER 71-351] 23 p3728 A71-43023

Control surfaces and direct jet force flutter suppression system shown to increase flutter speed of wing 23 p3630 A71-44108

Fibers-matrix force interaction effects in metal composites, analyzing stress-strain state of reinforced plate 23 p3697 A71-44202

FORCE FIELDS

U FIELD THEORY (PHYSICS)

FORCE-FREE MAGNETIC FIELDS

Plane plasma layer stabilization by force-free magnetic field 17 p2789 A71-35342

FORCED CONVECTION

Pipe bends effects on heat transfer coefficient of turbulent forced convection 02 p0330 A71-11650

Flat plate film boiling heat transfer under forced boundary layer convection, examining nonstationary wall temperature effects 02 p0333 A71-12646

Variable viscosity effect on laminar forced convective heat transfer in rectangular duct, using ethylene glycol and aqueous solutions 03 p0518 A71-13616

Binary liquid metal forced convection boiling heat transfer, determining axial and radial temperature distribution in two phase flow 04 p0676 A71-15173

Viscous heating effects on laminar combined free and forced convection through vertical circular tubes 04 p0676 A71-15177

Heat transfer - Conference, Versailles, August-September 1970, Volume 2, Forced convection 04 p0679 A71-15466

Heat transfer - Conference, Versailles, August-September 1970, Volume 3, Forced convection and radiation 04 p0681 A71-15484

Gravitational and forced convection effects in saturated liquids laminar boundary layer film boiling, presenting analytical solutions for common fluids 04 p0686 A71-15528

Nongray thermal radiation effect on laminar forced convection over heated horizontal flat plate, determining temperature profiles for optically thin and thick boundary layers 04 p0688 A71-15741

Forced convection over infinite periodically over-heated plane on basis of mesometeorological vertical wind velocity 06 p0923 A71-17515

Forced convective heat transfer in laminar flow fluid of vanishing viscosity in constant wall temperature pipe, discussing velocity distribution effects 06 p0882 A71-18073

Spalding-Patankar finite difference method application to combined free and forced convection turbulent boundary layer with variable fluid properties and chemical reaction 07 p1054 A71-18769

Thermally induced modifications of high power CW laser beam, considering heat losses by forced and free convection 07 p1122 A71-19207

Forced convection in atmosphere boundary layer, considering nonlinear unsteady vertical airflow velocity increments over temperature spot on earth surface 11 p1793 A71-25170

Forced convection effects on characteristics of steady state cross flow arc in presence of applied transverse magnetic field 12 p1938 A71-27265

Viscous dissipation effects on Nusselt number in combined free and forced convection through vertical concentric annuli 13 p1260 A71-28601

Flow direction effect on combined forced and free convective heat transfer from cylinders to air 13 p1264 A71-28985

Forced and free convective equations combination to represent combined heat transfer coefficients for horizontal cylinder 13 p1264 A71-28986

Local forced convection heat transfer data and empirical correlations for boiling Hg in single wetted Ta tube with composite helical inserts [GESP-450] 15 p2447 A71-32216

Boiling at solid heated surfaces, discussing nucleation, bubble formation, pool boiling factors, heat transfer correlation and forced convection 15 p2515 A71-32565

Boiling heat transfer to cryogenic fluids, considering pool convective, nucleate, film and forced convective subcooled boiling 19 p3162 A71-37463

Longitudinal vortex rolls onset for laminar forced convection between two horizontal flat plates subjected to uniform axial wall temperature gradient [ASME PAPER 71-HT-1] 19 p3163 A71-37979

Heat transfer due to combined free and forced convection in horizontal isothermal tube flow [ASME PAPER 71-HT-3] 19 p3163 A71-37981

Gravity effect on developing laminar flow with forced convection in vertical isothermal tube, investigating velocity and temperature profiles and heat transfer rate [ASME PAPER 71-HT-6] 19 p3164 A71-37983

Free stream turbulence effects on local heat transfer from sphere situated in forced convection air flow [ASME PAPER 71-HT-8] 19 p3164 A71-37985

Turbulent forced-convection heat transfer coefficient for supercritical fluid, extending Prandtl mixing length concept [ASME PAPER 71-HT-26] 19 p3165 A71-37996

Swedish monograph on low air flow velocity measurement with hot-wire anemometer under free and forced convection, using schlieren method 19 p3172 A71-38645

French monograph on free and forced convection and external radiation from hot gas oscillating in resonance tube, considering heat balance and mass exchange 19 p3172 A71-38649

Forced convection to hydrodynamically and thermally fully developed laminar flow in eccentric annuli, determining energy equation approximate solutions 22 p3620 A71-41880

Laminar convective heat transfer from rotating isothermal disk in uniform forced stream, using pressure distribution measurements 23 p3781 A71-43314

Fluid flow friction and combined free and forced convective heat transfer characteristics in rotating curved circular tube, using finite difference scheme and iterative solution 23 p3783 A71-44192

Forced convection steady heat transfer across laminar incompressible constant-property boundary layers over wedges with step discontinuity in surface temperature 23 p3784 A71-44196

Combustion and chemical reactions near wall, in forced convection, boundary layer transition, radiation and ablation of missile reentry 24 p3890 A71-45148

FORCED OSCILLATION U FORCED VIBRATION

FORCED VIBRATION

Nonlinear viscoelastic beam with hereditary properties, analyzing forced harmonic vibration propagation 01 p0169 A71-10638

Forced random oscillations of nonholonomic systems about equilibrium positions, deriving stability conditions in white noise disturbances 01 p0176 A71-11042

Nonautonomous vibrations of self excited cantilever beam with tangential force 01 p0177 A71-11295

Flexural-torsional vibration stability of thin walled elastic bars under longitudinal periodic force, using parametric resonance theory 02 p0321 A71-11687

Oscillator frequency synchronization by injection locking, considering nonlinear oscillation model 02 p0230 A71-11818

Nonlinear closed loop-shape characteristics of vibrational mechanical systems, using forced vibration analysis 02 p0284 A71-12284

Circular plates forced vibrations, considering internal damping and free and supported boundaries in thin plate wave equation solutions 03 p0502 A71-13300

Small forced flexural elastoplastic vibrations of structural beam, deriving approximate partial differential equation based on stress-strain relation 03 p0503 A71-13403

Console rod free and forced transverse vibrations amplitude dependent damping, considering longitudinal tensile force effect and hysteresis 03 p0502 A71-13405

Machine assemblies forced vibrations equations of motion determination, considering elastic dissipative qualities, structural hysteresis and damping 03 p0503 A71-13410

Optimal relaxation time existence for Maxwell solid cylinder bonded to thin casing during forced vibration of rocket assembly, discussing Voigt solid 03 p0497 A71-13469

Thin circular cylindrical plate reinforced by longitudinal rigid stringers, deriving computer algorithm for calculating forced vibration 03 p0515 A71-14367

Forced resonant vibration in nonlinear gyroscope in gimbal suspension 05 p0751 A71-16587

Complex modulus of elasticity relation to viscoelastic cantilever beams stress or strain under forced vibration, considering fiber reinforced plastics 05 p0826 A71-16738

Forced vibrations of three layer plates and shells made from physically nonlinear materials, deriving nonlinear equations with allowance for rigid filler tangential displacement 06 p0991 A71-17797

Two-body satellite of axisymmetric rigid bodies interconnected by lossy universal joint, calculating transient oscillation damping of forced precession under external torque 07 p1205 A71-18895

Forced thickness-stretch vibrations of plated elastic plate, involving time derivatives in boundary conditions 07 p1212 A71-19589

Incompressible viscous liquid forced oscillations stability, developing linearization procedure for nonlinear operator equation of perturbations 08 p1275 A71-21051

Free flexural vibrations of orthotropic rectangular plates subjected to large amplitude free or forced oscillations, using von Karman nonlinear equations 08 p1370 A71-21307

Free and forced vibrations of three layer freely suspended plate with allowance for energy dissipation 08 p1372 A71-21707

Subharmonic forced vibrations of one degree of freedom nonlinear mechanical systems, deriving formulas for oscillation amplitude, phase shift and shape factor 09 p1536 A71-22410

Nonlinear forced vibrations of aeroelastic plate in two dimensional supersonic flow under harmonic pressure near critical Mach number 10 p1690 A71-24643

Forced rotational oscillations of plane-convex glass lens pressed against brass plate, determining contact frictional and elastic characteristics from resonance and hysteresis 11 p1849 A71-25621

Acoustically induced cylindrical shell vibrations, solving differential equation derived for expression of system axisymmetric forced vibrations 13 p2150 A71-28136

Forced vibrations of circular cylindrical shell under random normal load and internal pressure, noting stability of transversely pressurized flexible vs rigid structures 13 p2150 A71-28140

Forced axisymmetric vibrations of composite cylindrical shell with spherical bottom, obtaining influence coefficients and inhomogeneous boundary conditions 13 p2150 A71-28141

Viscoelastic and elastic shells boundary value problems relation, studying natural and forced oscillations of isotropic viscoelastic shells 13 p2155 A71-28656

Damping characteristics /absorption coefficient/ of dissipative systems, defining authentic value of energy dissipation characteristic determination from forced and free vibrations 14 p2321 A71-29618

Thin hyperelastic tube forced large amplitude radial oscillations, deriving exact solution for general forcing function 14 p2322 A71-29690

Nonlinear damped vibratory system with two degrees of freedom excited by two external harmonic forces of different frequencies, investigating summation tones stability 14 p2322 A71-29693

Nonlinear /mixed/ damping forces on forced vibration system response, developing recursion procedure for equation of motion coefficients 14 p2327 A71-30203

Deterministic and random nonlinear forced vibrations of one degree of freedom system with broken line elastic response 14 p2328 A71-30378

Pulsating follower loads implementation by pulsating gas or liquid jets, using Mettler differential equations for forced vibrations of elastic bodies 15 p2502 A71-31172

Forced vibration damping of satellites in elliptical orbits by variable cantilevers and rotor 15 p2499 A71-31177

Isotropic elastic thin oval rings nonlinear free and forced flexural vibrations calculation by Galerkin method 15 p2503 A71-31436

Long thin spacecraft antennas and gravity gradient booms, explaining solar induced oscillations with lumped parameter and Lagrangian equation models 15 p2504 A71-31598

Complex molecules forced vibrations as material points system with quasi-elastic valence bonds 15 p2452 A71-32624

Forced oscillations of system governed by one dimensional nonlinear wave equations, using perturbation procedure for solutions near linear resonant frequencies 16 p2606 A71-32857

Forced transverse vibration damping of end loaded elastic cantilever beam, determining hysteresis loop contour from resonance curves 16 p2658 A71-33977

Stationary small elastoplastic longitudinal forced vibrations of rods with internal resonance, obtaining asymptotic solution of nonlinear partial differential equations 16 p2659 A71-33980

Cylindrical shells partially filled with liquid, calculating forced vibration under random loads and deterministic internal pressure 17 p2817 A71-34333

Free and forced nonlinear oscillations differential equations approximate solution by orthogonal polynomial linearization, applying method to systems analysis near singular points 17 p2780 A71-34917

Free and forced nonlinear oscillatory systems with harmonic perturbations, noting amplitude dependence on force frequency and friction coefficients 17 p2782 A71-34935

Small forced flexural elastoplastic vibration of structural beam, deriving approximate partial differential equation based on stress-strain relation 17 p2825 A71-35013

Cantilever bar free and forced transverse vibrations amplitude dependent damping, considering longitudinal tensile force effect and hysteresis 17 p2825 A71-35015

Clamped-clamped sandwich beam with thin face sheets and soft viscoelastic core, investigating forced, damped, nonlinear and LF flexural vibrations 17 p2826 A71-35032

French book on linear vibrations covering systems with one or more degrees of freedom in free and forced vibration, propagation in discontinuous and continuous media, etc 17 p2784 A71-35737

Dynamic flexibility method based on Green resolvent, presenting applications to linear damped/undamped forced/free harmonic/periodic vibration 18 p2947 A71-36177

Nonstationary resonance analysis of forced flexural elastoplastic vibrations of beam of hardening/softening material under cyclic strain 18 p2981 A71-36709

Force equations for static and dynamic friction under external forced vibration, determining mean values from mechanical model 19 p3068 A71-37346

Forced axisymmetric motion of circular viscoelastic plate, including effects of rotatory inertia, transverse shear and time dependent boundary conditions 19 p3157 A71-37848

Free and forced nonlinear vibrations of rigidly clamped thin circular plate, deriving ordinary differential equations 20 p3307 A71-38795

Forced and free vibrations of shallow cylindrical shell in rectangular duct filled with ideal fluid 20 p3310 A71-39785

Nonlinear free and forced vibration response and stability of simply supported restrained buckled beams, using analog computer simulation [ASME PAPER 71-VIBR-17] 21 p3458 A71-40277

Wake formation behind circular cylinders undergoing self excited and forced transverse oscillations [ASME PAPER 71-VIBR-25] 21 p3458 A71-40282

Deflection equations and bending stress for forced vibration of beam with time dependent boundary condition [ASME PAPER 71-VIBR-32] 21 p3458 A71-40286

Steady state performance of two degrees of freedom system consisting of main linear spring mass system under periodic forcing [ASME PAPER 71-VIBR-49] 21 p3459 A71-40298

Viscous incompressible flow past semiinfinite slender body with upper and lower surface forced vibrations, solving ideal fluid and boundary layer equations by Shkadov method 21 p3367 A71-40683

Free and forced finite amplitude nonlinear oscillations of thin elastic annular plate with free inner and clamped immovable boundaries 21 p3471 A71-41026

Nonlinear Volterra integral equation system solution using almost periodic forced oscillations 21 p3409 A71-41081

Flat supported plate in plane supersonic oscillating flow, calculating forced vibration with potential flow theory 21 p3473 A71-41367

Forced vibration of internally damped circular and annular plates with clamped boundaries, obtaining driving point and transfer impedances and force transmissibility 23 p3775 A71-43204

Laser vibration noise produced by piezoelectric transducer induced forced vibrations of resonator mirror, determining translational and rotational amplitude limits for laser output fluctuation 23 p3686 A71-43999

Boundary value problems of forced vibration of nonconservatively loaded dynamic elastic system, using William method 24 p3878 A71-44554

Finite cylinder forced longitudinal axisymmetric vibrations with prescribed surface stresses, reducing problem to quasi-regular infinite system of linear algebraic equations 24 p3880 A71-44723

Natural and forced joint vibrations of liquid and shallow spherical shells 24 p3881 A71-44829

FORCED VIBRATORY MOTION EQUATIONS
U FORCED VIBRATION

FOREARM
Human muscular control patterns during forearm precision cyclic bending on ergograph 02 p0204 A71-12053

FOREBODIES
NT ABLATIVE NOSE CONES
NT NOSE CONES
NT NOSES [FOREBODIES]
NT ROCKET NOSE CONES
Flow angularity prediction near supersonic fuselage forebody with arbitrary cross section and zero sideslip, using small perturbation theory [AIAA PAPER 71-996] 24 p3789 A71-44588
Stowed shaped tip on plastic sphere front portion, detailing hydrodynamic drag reduction at various Reynolds numbers 24 p3818 A71-44711

FORECASTING
NT LONG RANGE WEATHER FORECASTING
NT NUMERICAL WEATHER FORECASTING
NT PERFORMANCE PREDICTION
NT PREDICTION ANALYSIS TECHNIQUES
NT STATISTICAL WEATHER FORECASTING
NT TECHNOLOGICAL FORECASTING
NT WEATHER FORECASTING
Long range prediction of minimum and maximum of sunspot cycle, including Wolf number 02 p3033 A71-11715
Science and technology trend forecasting for planning, organization and program selection 02 p3335 A71-11852
Technological forecasting by evaluating patent significance, applying to earth moving equipment development 02 p3335 A71-11858
Quantitative and qualitative philosophical aspects of measure and forecasting applied to patent handling 02 p3336 A71-11861
Verification, control and forecasting information characteristics for random process mixed with additive noise 13 p2041 A71-27942

FORECASTS

FORECASTS

U FORECASTING

FOREIGN BODIES

Ultrasonic/radiographic method for intraocular foreign body localization 13 p2013 A71-29031

FOREIGN POLICY

NT INTERNATIONAL COOPERATION

NT INTERNATIONAL RELATIONS

Space station program characteristics, discussing technology, sciences, exploration, public services, foreign relations and national defense 04 p0689 A71-14930

FORENSIC SCIENCES

U LAW [JURISPRUDENCE]

FOREST FIRE DETECTION

Simulator for operating decision rules for control of airborne IR forest fire detection system 19 p3066 A71-38409

Latent forest fire detection, describing airborne IR surveillance system 19 p3066 A71-38410

FORESTS

Airborne remote sensing application to agriculture and forestry for crop forecasting, soil mapping, insect infestation detection and range surveys 06 p0896 A71-18406

Forested area landscape characteristics from remote sensed imagery, establishing base line information for vegetation mapping 09 p1438 A71-23209

Space photos for land use and forestry, considering IR color photographs from Apollo 9 flight 13 p2064 A71-29398

Aerial color photography in forestry for species identification, reforestation areas development, watershed studies and land planning 17 p2737 A71-34272

ERTS remote sensing techniques, discussing objectives for southeastern U.S. in terms of agriculture, forestry, strip mine land reclamation and thermal pollution 22 p3534 A71-41967

FORGING

Ti alloys isothermal forging, using precision-cast superalloy dies [SME PAPER MF-70-122] 01 p0089 A71-11255

High velocity metal working, discussing airfoil forging, ausforming of bearing race blanks, tooling, etc [SME PAPER MF-70-228] 01 p0090 A71-11267

Large Al forgings machining cost reduction via stress relief involving mechanical working following quench 01 p0091 A71-11547

High strength stress-corrosion resistant Al alloy forgings fabrication processes, noting chemical composition and physical properties 03 p0441 A71-13255

Titanium alloys for drop and press forged airframe, engine, rocket and spacecraft components, presenting physical and mechanical properties for various alloys and applications 05 p0757 A71-16136

Closed die forgings for aircraft industry, discussing technology, tolerances, materials and costs 07 p1119 A71-20075

Titanium-steel bimetal part fabrication using explosive and drop forging 08 p1295 A71-20840

Aircraft engines and stationary gas turbines high precision components, discussing die forging and machining combined with joining processes 09 p1456 A71-23299

Forging conditions effects on Ti alloys mechanical properties, considering ingot conversion to semifinished product 09 p1475 A71-23304

Steels, Ni alloys and Ti alloys deformation resistance and deformability, discussing temperature effects on forging rate 09 p1475 A71-23305

Forge phase rigid and plastic region model of friction welding, deriving interfacial dispersion parameter of weld quality optimization 09 p1459 A71-23456

Precision forging and pressing of Al alloy and Ti alloy parts of aircraft structures at cost effective prices 09 p1459 A71-23691

Three dimensional isostatic pressing process, discussing equipment, tooling and forging preforms and finished parts production 10 p1618 A71-24764

Cast cobalt base superalloys extrusion and forging, noting hot deformation effects on tensile properties, stress rupture strength and ductility 11 p1778 A71-25854

High strength Al alloy forgings processing for stress corrosion cracking prevention, including plane relocation and compressive relief techniques 13 p2073 A71-28146

Forgeability and tensile properties of spark sintered unstrained Ti-Al-V preforms from prealloyed powders in uncontrolled atmosphere 13 p2084 A71-28147

Ti-Al-V alloy forgings fatigue strength improvements, discussing surface finish, heat treatments and alpha and beta grain size [AHS PREPRINT 553] 14 p2261 A71-31105

Unsteady press forging process in dies with material extrusion through plane strained slot, describing deformation stages, slip line patterns and hodographs 16 p2581 A71-32818

Closed die forgings of vacuum remelted carbon and low alloy steels to improve transverse ductility and microcleanness for aircraft industry 17 p2749 A71-35336

Ti alloys diffusion bonding and forging, discussing joints testing and material utilization improvement through die forging process [SME PAPER AD-71-244] 18 p2927 A71-36656

Carburizing steels cold forging, investigating pressure requirement relationship to compressive stress from comparison of backward extrusion and laboratory compression tests 18 p2935 A71-36669

Statistical analysis of endurance limits for castings and forgings of die forged and cast steel, using rotating beam fatigue tests 21 p3388 A71-40754

FORM

U SHAPES

FORM FACTORS

Proton form factors and radius determination from experimental data analysis of cross sections of electron scattering by protons over wide transferred-momentum range 12 p1901 A71-27180

Computer algorithms for gamma algebra of electromagnetic form factors in terms of Chebyshev polynomials with photon 4-momentum 21 p3415 A71-40842

Proton form factors and radius determination from experimental data analysis of cross sections of electron scattering by protons over wide momentum transfer range 22 p3578 A71-42454

FORM PERCEPTION

U SPACE PERCEPTION

FORMALDEHYDE

Amino acids synthesis by formaldehyde-ammonia heating and hydrolysis, simulating reactants in weakly reducing atmosphere at volcanic temperatures 03 p0357 A71-13014

Adsorbed formaldehyde levels from vaporized paraformaldehyde on various surfaces as function of relative humidity and chemical concentration 07 p1055 A71-19593

Formaldehyde line emission observed from trapezium H II region of Orion nebula, attributing to 140 GHz rotational transition 08 p1360 A71-20983

Ablative polymers synthesis from formaldehyde, phenols and ethers reaction products, discussing char yield, thermally stable fillers incorporation and thermogravimetric analysis 11 p1855 A71-26034

Formaldehyde vapor photodecomposition modes by end product analysis, utilizing mixed isotope, radical scavenger, inert gas pressurization and lamp intensity attenuation 12 p1877 A71-27758

Catalytic effect of lanthanide hydroxides on formaldehyde conversion to pentoses and hexoses at 110°C in life support systems 13 p2018 A71-28408

Reaction rate controlling mechanisms in shock wave initiated oxidation of formaldehyde 13 p2113 A71-28617

Radical and formaldehyde daytime concentrations predictions from steady state model of unpolluted surface atmosphere 16 p2575 A71-34048

Possible prebiotic synthesis of thymine by heating uracil, paraformaldehyde and hydrazine in ammoniacal solution for three days at 70°C 18 p2855 A71-36231

Radio emission detection of para-formaldehyde and 2 mm formaldehyde distribution in Orion IR nebula 20 p3287 A71-39112

Formaldehyde absorption and emission lines in Orion IR nebula, indicating pumping suppression by neutral particle collisions 20 p3288 A71-39113

Formaldehyde transitions in ground and excited states at 6 cm, attaining line widths and hyperfine structure at 1-3 kHz 23 p3723 A71-42953

Monosaccharides effect on catalytic synthesis of carbohydrates from formaldehyde 24 p3800 A71-44527

FORMAT

Prisoner dilemma game matrix, noting response patterns to various formats 18 p2863 A71-37017

FORMATION HEAT

U HEAT OF FORMATION

FORMATIONS

Dynamic positioning stationkeeping and stability criteria for formation flight systems extended to helicopter and V/STOL transports 18 p2849 A71-35923

FORMING TECHNIQUES

NT AUSFORMING

NT BLANKING [CUTTING]

NT CASTING

NT COINING

NT COLD ROLLING

NT COLD WORKING

NT ELECTROFORMING

NT EXPLOSIVE FORMING

NT EXTRUDING

NT FORGING

NT HOT WORKING

NT INVESTMENT CASTING

NT MAGNETIC FORMING

NT METAL DRAWING

NT METAL SPINNING

NT PRESSING [FORMING]

NT ROLL FORMING

NT STAMPING

Peen forming of large complex parts from sheet and plate, illustrating dihedral break in airplane wing skin 01 p0091 A71-11550

Stiffened integrally formed panel stability evaluation based on compression structural efficiency and manufacturing costs [AIAA PAPER 69-760] 02 p0329 A71-12686

Energy balance during ring blanks widening by electromagnetic pulses, establishing theoretical limit of mechanical efficiency 06 p0906 A71-18712

Magnetic pulse technique connecting Al pipe with steel pipe, determining mechanical and physical parameters 06 p0906 A71-18713

Ball forming technique application to Al alloys structural part contouring, discussing L-1011 wing panel forming and prestress tooling 08 p1299 A71-21681

Refractory metals forming, coating, machining and joining operations, discussing parts manufacture 08 p1299 A71-21683

Beta Ti alloy sheet and foil mechanical property tests, honeycomb core fabrication, forming and welding evaluations [ASM PAPER W71-23.1] 09 p1455 A71-23095

Refractory metals and alloys products fabrication for aerospace applications, discussing hydrostatic bulge forming and aluminide coating in Nb alloy nozzle extension production 10 p1618 A71-24766

Failure and forming limit diagrams in biaxial tension for sheet metal with preexisting inhomogeneities based on Marciniak concept 15 p2505 A71-31945

Aluminum-boron composite forming and cutting processes covering milling, grinding, abrasive cutoff, drilling, piercing, electrodischarge machining, blanking, punching and shearing 18 p2928 A71-36666

Metal deformation processing in solid mechanics, discussing plastic idealization for viscous behavior theorems, Ekstein paradox, free surface problems and incremental forging 21 p3389 A71-40983

Superplasticity and materials forming methods for metal alloys, considering reformation speed increase by finer grained and stable alloys development 22 p3563 A71-42323

FORMULAS [MATHEMATICS]

Algorithm and computer program generating formats and logic equations for addressable remote multiplexed time division telemetry systems 01 p0050 A71-10880

Two-point iteration formulas with one calculation step requiring successive solution of two linear equations 06 p0921 A71-18347

Approximate analytical formulas for free oscillations of nonstationary linear control systems using canonical transformations 10 p1643 A71-24896

Light wave attenuation in fog, mist, rainfall and snowfall during propagation through atmosphere deriving semiempirical formulas for attenuation rate relationship to visibility 22 p3569 A71-42522

Magnetic shell parameter L approximation simplifying McIlwain expression 23 p3669 A71-43175

FORMULATIONS

Chronometrically invariant formulation of relativistic thermodynamics second law distinguishing between three dimensional space and time 01 p0156 A71-10556

FORTRAN

LEAF /LISP Extended Algebraic Facility/ as FORTRAN dialect in list structure, extending LISP arithmetic functions to algebraic language level 01 p0045 A71-10192

- FORTRAN-based list processor subroutines for computing Poisson series used in celestial mechanics 04 p0660 A71-15890
- MESY systems programming with PL/I, comparing with ALGOL and FORTRAN 19 p3025 A71-37422
- NTWO as FORTRAN 4 family of subroutines developed on 7094-7044 system for determining thermodynamic and transport properties of nitrogen 20 p3253 A71-39268
- Fortran source listing for computer program approximating system reliability 21 p3351 A71-40371
- FORWARD SCATTERING**
- Mars surface features contrast reduction, discussing forward scattering haze as possible cause 15 p2491 A71-32418
- Pulsed signal secondary forward scattering in optical fiber transmission lines 23 p3646 A71-43968
- FOSSIL METEORITE CRATERS**
- U FOSSILS
- U METEORITE CRATERS
- FOSSILS**
- Rotaformidae of upper cretaceous Nassellarina /radiolaria/ from Great Valley Sequence, California Coast Ranges 07 p1104 A71-20013
- Gas rich Kapoeta howardite composition, evolution, high particle fossil track densities and normal track rich crystals spatial relations 10 p1672 A71-24392
- Superheavy transuranic elements in meteorites and lunar dust by fossil track microscopy 10 p1673 A71-24424
- Preterinary invertebrate fossil remnants and microcoprolites found in Lower Himalayan Basin 11 p1721 A71-26318
- Microfossil structures from morphological alterations of proteinoid microspheres due to inclusion of organic or synthetic polyamino acids 14 p2190 A71-30178
- Lunar magnetic fields measured by magnetometers placed by Apollo 12 and 14 astronauts, considering permanent fields due to fossil magnetic material and transient fields 17 p2811 A71-35734
- FOUNDATIONS**
- Variable thickness anisotropic annular plates bending on generalized elastic foundation, using numerical method 05 p0823 A71-16423
- Von Karman equations analogs solution for nonlinear large amplitude vibrations of circular plate on uniform elastic foundation [ASME PAPER 71-VIBR-9] 21 p3457 A71-40271
- Stochastically imperfect columns on nonlinear elastic foundations, obtaining approximate asymptotic expression for buckling stresses and lateral displacement autocorrelation 24 p3884 A71-44962
- FOUR BODY PROBLEM**
- Equations of motion of restricted four body problem numerically integrated for positions of three primaries 04 p0653 A71-15711
- Earth-moon libration point space station optimal control, considering restricted four body problem 08 p1363 A71-21323
- Restricted four body problem, obtaining graphs for Hill surface of zero relative velocity 13 p2137 A71-28478
- FOURIER ANALYSIS**
- NT FOURIER SERIES
- Pulsar PSR 1237 plus 25, noting correlated subpulse structure with Fourier analysis method 02 p0318 A71-12951
- Left ventricular performance Fourier analysis, obtaining ventricular and ascending aortic pressure and flow from closed and open chest dog measurements 07 p1041 A71-19636
- Elliptical motion series representation, presenting methods for estimating values of Bessel functions, Fourier and Hansen coefficients 09 p1486 A71-23336
- Geomagnetic disturbance field asymmetry Fourier analysis for amplitude G and local time phase of first diurnal harmonic for IGY 10 p1600 A71-24295
- Multiple Fourier method for plate bending compared with least squares and boundary collocation solutions 14 p2325 A71-29888
- Image spatial frequency content of speckle patterns on illuminated diffuse screen and photographic film by optical Fourier analysis 14 p2242 A71-30152
- Clamped anisotropic symmetrically laminated plate bending, buckling and free vibration exact solution, using Fourier analysis 15 p2506 A71-32013
- Searchlight problem with isotropic scattering for semiinfinite and finite geometries, computing transmission functions for Fourier intensity components by kernel approximation method 17 p2839 A71-35571
- Two dimensional optical Fourier approach diagnosing interpretation-limiting pictorial noise patterns in ERTS image output 18 p2919 A71-36082
- Van der Pol equation periodic solutions using approximation scheme for all Fourier amplitudes 20 p3254 A71-38800
- Visible optical pulsars search with Fourier and correlation techniques in X ray sources, supernova remnants, white dwarfs, IR stars, planetary nebulae, etc 20 p3304 A71-39939
- Acoustical harmonic point source in motion relative to surrounding fluid, using Fourier integrals for mathematical representation 24 p3847 A71-44418
- FOURIER LAW**
- Transient heat conduction of solids obeying Fourier law, deriving numerical solution for boundary value problem by Laplace transformation 01 p0180 A71-10937
- FOURIER SERIES**
- German monograph on Fourier coefficients of modulus forms, presenting theorem reducing infinite number of equations to limited number of equations 01 p0110 A71-10126
- Fourier series in almost periodic Bohr functions, examining uniform convergence definitiveness 03 p0450 A71-13294
- Polyvibrating equation boundary value problem solution in Fourier series form, obtaining Green function 06 p0928 A71-18226
- Plane or axisymmetric revolution geometry elasticity problems using finite element method and Fourier series 06 p1002 A71-18421
- Plane Poiseuille flow bounded by solid walls, applying Fourier expansion method to stability problem 09 p1432 A71-22583
- Axisymmetric stressed-state problem of finite length hollow circular cylinder in Fourier and Fourier-Dini series form 12 p1984 A71-27692
- Book on antenna admittance problem covering iterative solution of integral equations, Fourier series solution, Wiener Hopf methods, transmission line theory, etc 14 p2193 A71-29932
- Root-mean-square and uniform approximations of signals by Fourier and Haar series 16 p2550 A71-33720
- German monograph on Fourier-Chebyshev approximation of primary functions, giving quadrature method 17 p2764 A71-34484
- Fourier coefficients and integral operators S numbers of summable functions 17 p2765 A71-34864
- Functional analytical iteration methods for calculating nonlinear vibrations of several degrees of freedom and error estimation improvement, considering uniformly converging Fourier series expansion 17 p2782 A71-34939
- Circular loop antenna array of N elements with arbitrary circumference, analyzing by Fourier series expansion 19 p3023 A71-38588
- Fundamental frequency of star shaped membrane with boundaries described by polar coordinates in Fourier series form 20 p3308 A71-39039
- Nonlinear second order differential equations periodic solutions in terms of Fourier series, applying method to calculation of charged particle orbit in radial electric field 20 p3255 A71-39081
- Periodic functions complete orthogonal sequences class as linear combinations of Fourier expansions, obtaining convergence theorem 21 p3410 A71-41083
- Fourier series approach to gravity anomaly data representation [AAS PAPER 71-342] 23 p3666 A71-43015
- Continuous signal representations in time and frequency domains by Fourier series 23 p3644 A71-43284
- FOURIER TRANSFORMATION**
- Gravitating particle system phase density, finding differential and integral equations for Fourier transform 01 p0150 A71-10064
- Fourier transform chart showing interrelationships between data block length, frequency resolution sampling rate, fast Fourier transform (FFT) stages and other related variables 02 p0215 A71-12045
- Fourier transform formalism of sampling theorem in frequency domain used in coherent optical processor, obtaining multiple reproduction of space limited functions 04 p0627 A71-15686
- Picture transmission by Fourier transform based data reduction system, considering law of module probability and spatial distribution, statistical analysis and degradation 05 p0722 A71-16746
- Multiple acoustic evoked responses coherence time course using mathematical correlation and Fourier transforms 05 p0714 A71-16922
- Millimeter wave lensless Fourier transformation /LFT/ holographic imaging, discussing equipment and performance 05 p0754 A71-17081
- Digital computer operated from remote terminal for signal analysis including Fourier transform, complex multiplication and conjugation 05 p0727 A71-17144
- Multispectral and multitemporal digital imagery spatial registration using fast Fourier transform techniques, applying to earth resources satellite imagery preprocessing 05 p0756 A71-17147
- Unstable electrostatic waves propagating in uniform infinite plasma with weak beam, Fourier transforming space dependent variables 07 p1166 A71-18881
- Discrete Fourier transform associated with discrete function theory 07 p1147 A71-19324
- Cylindrical shell with elastic core under annular sliding load, solving for critical velocity via Fourier transformation 07 p1212 A71-19533
- Bessel transform and corresponding inversion formula, showing relationship to Fourier, Watson and Kontorovich-Lebedev transforms for boundary value problems solution 08 p1324 A71-21355
- Coherent optical target recognition through phase distorting medium, using holography, Fourier transform and autocorrelation functions 08 p1335 A71-21377
- Fabry-Perot interferograms analysis by Fourier transforms, considering mirror defects, light incident angle spread and spectral lines Lorentzian and Gaussian shapes 08 p1289 A71-21378
- Fourier transform hologram recording by quasi-monochromatic incoherent source, resolving bias problem at expense of resolution 08 p1290 A71-21386
- Optical information processing systems, considering spherical lens derivation of two dimensional Fourier transform 09 p1493 A71-22776
- Holography principles, discussing formation and reconstruction for in-line, off-axis and Fourier transform type holographic systems 09 p1449 A71-22787
- Mathematical model for fields and currents calculation for asynchronous linear motors and MHD converters by Fourier transformation 09 p1387 A71-23650
- Photomaterial nonlinear effects on contour distortion in holographic recording of Fourier image slit for graphic memory use 10 p1612 A71-24716
- Digital control systems for electrodynamic vibration exciters, discussing computer ranged instrumentation amplifier, digitally controlled sine wave oscillator and FFT processor 11 p1746 A71-26503
- Frequency analysis and Fourier transform evaluation of mechanical shocks and single impulses, outlining theory for filter response to pulses 11 p1853 A71-26521
- High resolution holographic Fourier transform spectroscopy, discussing interferometer localized interference fringes direct recording method and heterodyning technique 12 p1905 A71-26805
- Optical Fourier transformers zero order removal for low spatial frequency signal components detectability improvement 12 p1906 A71-26818
- Submillimeter wave region solar radiation atmospheric absorption by Fourier spectrometry and double output Michelson interferometer with Goley cell detectors 14 p2307 A71-29740
- Phase modulation theory for two-beam far IR Michelson interferometers, discussing application to Fourier transform spectrometry 14 p2238 A71-29741
- Phase modulation in far IR interferometers applied to Fourier spectrometry and metrology, obtaining modulus, phase, absorption and refraction spectra 14 p2238 A71-29742
- Arbitrary dynamic load problem for elastic infinite bodies, solving with Lamé equations and Fourier and Laplace transforms in distribution space 14 p2323 A71-29817
- Polarization Fourier spectrometry for circular dichroism spectroscopy, stressing IR application 14 p2242 A71-30156

FOVEA

Fourier transform holography with partially coherent light from incoherent quasi-monochromatic source, considering bias problem

15 p2402 A71-31256

Diffraction technique for three dimensional frequency spectra of photographic images using computer program based on Fourier transformation of optical density distribution

15 p2406 A71-31645

Discrete group symmetric linear control systems reduction to elementary cell, generalizing Fourier transform to groups without operational constraints

15 p2381 A71-31978

Soviet book on multilayered media elasticity theory three dimensional problems covering Fourier and Hankel integral transformations, compression, bending, normal and tangential loads, etc

15 p2506 A71-32020

Structural panel under acoustic loading by supersonic convected turbulence, deriving responses with finite Fourier transforms

15 p2507 A71-32131

German monograph on spatial elasticity problems solution by multidimensional Fourier transformation covering stress concentration on hollow and solid cones for given load distribution

15 p2509 A71-32300

Holographic lens magnification aberrations in various Fourier transform optical data storage geometries

15 p2412 A71-32592

Two dimensional pictorial information Fourier transform generation by coherent optics method, applying to imageries in earth sciences

17 p2737 A71-34271

Book on optical holography covering basic concepts, Fourier transform, propagation and diffraction, pulsed lasers, interferometry, geometric analysis of point source hologram, etc

17 p2738 A71-34450

Wide angle microwave antenna radiation beam steering with fixed parabolic reflectors, using adaptive primary feed for intercepted field spatial Fourier transformation

17 p2708 A71-35493

Human visual system biological model for pattern recognition based on spatial filtering covering Fourier transform modification for application to discrete case

17 p2694 A71-35793

Astronomical data correction for smearing effects applying Fast Fourier Transform algorithm

18 p2960 A71-35933

Computerized digital techniques for image motion compensation as function of additive noise level, using Fourier transform image filtering and half-tone display

18 p2919 A71-36083

Density fluctuation dispersal in uniform magnetoplasma, obtaining expressions for Fourier-Laplace transforms of perturbed density, potential field and flux distribution

19 p3113 A71-37745

Fourier transform holograms as complex matched filter for pattern recognition and signal detection in coherent optical systems

19 p3066 A71-38239

Random vibration testing digital computer control system and experiment design, considering discrete Fourier transform techniques application

[ASME PAPER 71-VIBR-30] 21 p3360 A71-40285

Quasi-static thermoelasticity and dynamic thermal stress equations solution in matrix form by Fourier transform and Hilbert-Levy method

22 p3614 A71-41567

Infinite sandwich plate under concentrated torque load on one side, determining stress distribution with double infinite Fourier transform

22 p3614 A71-41604

Optical transfer function measurement by holographic techniques, describing Fourier transform method useful for lens production testing

22 p3539 A71-41738

Fourier transform spectrometers in IR astronomy, including rapid scan interferometer

22 p3545 A71-42146

Fast Fourier transform calculating discrete Fourier transform, considering optimized algorithm for digital computers

22 p3566 A71-42249

Book on interference of electromagnetic waves covering Michelson-Fizeau and Fabry-Perot interferometers, Fourier transform spectroscopy, etc

22 p3576 A71-42429

Finite Fourier transforms from finite dimensional algebraic viewpoint, deriving fast Fourier transform algorithm via tensor products induced matrix factorization

23 p3698 A71-42920

Physical and technological aspects of holographic recording including optical data processing, Fourier hologram reconstruction and random structure information determination

23 p3679 A71-43896

FOVEA

Summation coefficient determination inside and outside fovea by critical fusion frequency measurement, showing inverse relation to test surface size

01 p0010 A71-10275

Foveal vision absolute thresholds for various duration light pulses and flash pairs at different separations

10 p1560 A71-23992

Human central fovea theoretical model for target stimuli threshold detection performance prediction

17 p2693 A71-33325

Foveal perceptive fields for human vision, using measurements of contrast illusions in grids and bars

18 p2857 A71-36687

Increment thresholds for foveally viewed square and circular visual stimuli, suggesting availability of more than one spatial integration pattern

19 p3003 A71-38277

Detectability measurement of foveal stimulus, suggesting nonuniformity of retinal illuminance in visual task

19 p3003 A71-38278

Surround luminance effect on relative perceptual latency of response, using test stimuli confined to rod free area of fovea

20 p3184 A71-38774

Subjective brightness of flashing light stimulus within fovea as function of stimulus size, noting edge effects contribution at suprathreshold levels

22 p3497 A71-41478

Absolute foveal thresholds as function of flashes pulse length and null period

22 p3497 A71-41480

FR-1 SATELLITE

Electrical stability of double sphere dipole antennas for FR-1 satellite ionospheric plasma electric fields measurements

02 p0229 A71-11714

FRACTIONATION

Cysteamine AET, serotonin and hexamine antiradiation drugs, investigating protective effect against fractionated lethal gamma irradiation

07 p1037 A71-18969

Gas-liquid chromatographic milligram preparative separation of steranes and triterpanes from hydrocarbon fraction of Green River oil shale

11 p1729 A71-26067

Chemical fractionations in meteorites, considering trace elements abundance in L chondrites and implications for cosmochemistry

13 p2141 A71-29097

Chondrite classification, primordial matter composition and early solar system chemical processes, discussing cosmic gas condensation and refractory element fractionation

18 p2967 A71-37027

Oxygen isotope fractionation in Apollo 12 rocks and soils, noting plagioclase ilmenite isotopic temperature

23 p3751 A71-43704

Crystal Al powder electrolytic production in inert atmosphere, discussing fractional composition, current efficiency, gravimetric density and particle morphology

24 p3837 A71-44734

Aviation fuels lubricating characteristics, discussing refining methods, viscosity, service performance and load testing

24 p3864 A71-45383

FRACTIONS

Cerebral lipid fractions, examining relation between physiological functions and metabolism

09 p1391 A71-22481

FRACTOGRAPHY

Physical-metallurgical nature of brittle fracture of steels from phenomenological and atomic/dislocation approach

03 p0516 A71-14576

Macro- and microfractographic methods in failure analysis

06 p0911 A71-17347

Fractography of thermoset resins toughened with Hycar carboxyl terminated butadiene acrylonitrile, using electron microscope

11 p1785 A71-25406

Fractographic analysis of failure kinetics and crack formation in Al alloys, showing microfatigue intrusions and extrusions for various initial stress levels

12 p1919 A71-27682

Fractographic investigation of fatigue crack propagation in pure monocrystalline and polycrystalline Al

16 p2599 A71-34095

Remote sensing for geologic problems, using side-looking radar for fracture and fault detection and IR images for limestone, dolomite and granite discrimination

18 p2911 A71-35890

High strength metastable austenitic steels fractography, showing alloy composition, strain rate and temperature effects

19 p3080 A71-37717

Thick Al alloy sheet with central slot under cyclic loads, examining striation spacings and fatigue crack propagation rates with electron fractography

22 p3561 A71-41708

FRACTURE MECHANICS

Metal fatigue relationship to cyclic plastic deformation resistance, considering fracture behavior, stress-strain curve, hardening and ductility

01 p0098 A71-10162

Cleavage fracture equations of motion solved for constant moment, force and deflection, discussing plate crack propagation

01 p0167 A71-10291

Mathematical model for laser-induced supersonic crack propagation in crystals with weak cleavage planes

01 p0092 A71-10293

Al-Zn-Mg-Cu type high strength Al alloys mechanical properties evaluation by fracture mechanics methods

01 p0104 A71-11540

Triple point crack nucleation and growth at zero time by grain boundary sliding, estimating time to fracture

02 p0329 A71-12715

Zr and zircaloy 2 fracture mode, examining grain boundaries and strain rates effects

02 p0268 A71-12887

Anisotropic materials ductile fracture involving crack initiation and propagation, using Dugdale mathematical model

[SESA PAPER 1729] 03 p0507 A71-13760

Composite viscoelastic materials fracture energy determination using equations for line crack in linear materials from spherical flaw theory and Griffith concept

[SESA PAPER 1647] 03 p0508 A71-13764

Soviet book on fracture physics /crack growth in solid bodies/ covering glass, polymers, single crystals and polycrystalline metals, etc

03 p0515 A71-14398

Fracture of bumper protected fuel tanks subjected to hypervelocity meteoroid impact, applying method of characteristics to stress wave propagation in tank walls

[AIAA PAPER 69-369] 03 p0500 A71-14431

Crack growth relation to grain boundaries, considering transgranular cleavage in plain carbon steels and ductile intergranular fracture in Al-Zn alloy

03 p0447 A71-14497

Fractures - Conference, Marienbad, Czechoslovakia, October 1970, Part 2

03 p0516 A71-14577

Brittle fracture mechanics, discussing shape, stress and dynamic toughness factors, crack-defect interaction and crack barriers

03 p0516 A71-14578

Crack initiation and propagation in fracture of plastic materials

03 p0516 A71-14580

Laser radiation metal fracture, using pulsed X ray metallography and high speed photography for cavity depth and material ejection time dependences

04 p0608 A71-15116

Fatigue and fracture in elastic cylindrical shells with circumferential crack under axial tension, noting precracked specimens

04 p0670 A71-15386

Crack opening displacement concept in fracture mechanics, considering crack tip radius as measure of extension potential

04 p0670 A71-15392

AlZnMgCu alloys fracture behavior, examining aging conditions, rolling, forging, cracking, tensile strength and chemical composition

04 p0613 A71-15745

Damage and fracture mechanisms in high temperature low cycle fatigue of cast nickel-based superalloys, noting grain boundaries oxidation role in crack nucleation and propagation

04 p0615 A71-15789

Three dimensional elastic body fracture analysis, considering lateral constraint factor contour plots

05 p0822 A71-16412

Inverse variational principles of brittle body fracture derived by extending inverse variational principles of mechanics and thermodynamics

05 p0825 A71-16609

Be impact strength temperature dependence and fracture structure, noting grain boundaries cohesion role

05 p0768 A71-16773

Brittle fracture propagation velocity and branching, using high speed photography, electrical and ultrasonic methods

06 p0981 A71-17296

Stress distribution at cracks in solid bodies, discussing crack models, plasticity and elasticity theories and continuum mechanical basis of fracture theory

06 p0911 A71-17413

Li concentration effect on CdS single crystals brittle fracture anisotropy by metallographic techniques

06 p0941 A71-18083

Linear elastic fracture mechanics based on elasticity theory, discussing Griffith theory for crack behavior

06 p1001 A71-18091

Ti alloy embrittlement by prolonged high temperature exposure, using substandard fracture mechanics test for time-temperature dependence

06 p0915 A71-18686
Forged superhigh density sinters steel strength and fracture mechanism

08 p1304 A71-20995
Fracture kinetics, emphasizing plastic deformation, dislocation and diffusion micromechanics, point defects effects and microcrack formation

08 p1371 A71-21606
Fracture location in brittle solids, using stress wave propagation in slender rod

09 p1538 A71-22699
Fracture models of stress field produced by accelerating crack under shear loading, using pulse diffraction method

10 p1684 A71-23932
Fracture mechanics application to structural adhesives test methods, considering joints crack extension resistance and plane strain fracture toughness

10 p1615 A71-24088
Brittle fracture mechanism models and connection with rheological properties of material, deriving relations for Griffith energy criterion

10 p1688 A71-24388
Linear elastic fracture mechanics in presence of notch stress concentration, considering crack formation and propagation under cyclic stresses

10 p1628 A71-24686
Crack dislocations nature and significance, density equations, instability conditions, fracture mechanics, including cohesive forces and plastic zone equilibrium

10 p1628 A71-25026
Stable cracks initiation by piled up dislocations groups or by impeded strong shear bands

10 p1629 A71-25031
Stress intensity factor of flat toroidal crack under internal pressure, using approximate solution of axisymmetric problems in fracture mechanics

10 p1693 A71-25057
Failure analysis of notched unidirectional composites under tensile load parallel to fiber, considering Griffith-Irwin-Orowan fracture theory applicability [AIAA PAPER 71-369]

11 p1784 A71-25343
Elastic-plastic fracture behavior engineering model based on surface flaw severity by crack length dimensions measurements [AIAA PAPER 71-371]

11 p1845 A71-25345
Seminfinite crack perpendicular to elastic half plane surface under pressure distribution on faces or remote loading, obtaining fracture mechanics solution with Wiener-Hopf method

11 p1847 A71-25444
Spacecraft structures weight optimization based on fracture mechanics and reliability cost constraints applied to pressure vessel design

11 p1847 A71-25464
Fracture-safe design, discussing strength transition, ratio analysis diagram, R-curve resistance, weldability and computer techniques

11 p1778 A71-25747
Gas turbine wheel design fracture mechanics, discussing buried and surface flaws analysis for rotor failure prediction applications [ASME PAPER 71-GT-10]

11 p1811 A71-25956
Fracture mechanics and time dependent strength of elastic or viscoelastic solids adhesively jointed by soft polymeric bonding layer

11 p1851 A71-26383
Boron and carbon fracture and debonding in epoxy matrix, using acoustic emission analysis

11 p1772 A71-26392
Fracture mechanics of metal matrix composite with ductile stainless steel reinforcing fibers

12 p1985 A71-27775
Diffused fracture model as basis for plotting delayed fracture curves in space of principal stresses

13 p2149 A71-28119
Crack kinematics for bodies with time dependent deformation and strength characteristics in brittle fracture, discussing tip region, crack models and energy equation

13 p2149 A71-28123
Papers on fracture mechanics covering engineering fundamentals, environment effects, crack growth, photoelastic analysis, nondestructive testing, etc

13 p2151 A71-28212
Crack growth and fracture mechanics, discussing linear stress field and plasticity analyses for three dimensional and dynamic problems

13 p2151 A71-28213
Solids continuum mechanics and fracture criteria, emphasizing intermixed elastic, plastic or viscoelastic types materials behavior idealization

13 p2151 A71-28214
Notch analysis of fracture, discussing elasticity theory of stress concentration and applications to brittle inhomogeneous materials and fatigue crack propagation

13 p2151 A71-28215
Two and three dimensional static and dynamic photoelasticity and birefringent coating techniques applications in linear fracture mechanics

13 p2152 A71-28217

High strength alloys, discussing fracture mechanics concepts applicability to environmental cracking under static load and combined effects of cyclic stress and aggressive environment

13 p2152 A71-28222
Temperature variations of effective fracture surface energy of metals and alloys and relation to crack growth in high temperature creep

13 p2085 A71-28505
Ni-Ni Nb eutectic composite, investigating monotonic mechanical response, deformation and fracture mechanisms

13 p2088 A71-29401
Stage 1 fatigue fracture mechanism in Ni-based superalloy single crystals, observing air and vacuum effects

13 p2088 A71-29405
Hot ductility correlation with microstructure from nickel softening and fracture mechanisms interaction

13 p2089 A71-29410
Polycrystalline Hf under tension at various temperatures, determining H effects on fracture, operative deformation modes and hydride habit planes

13 p2090 A71-29417
Thin shallow initially curved sheets fracture theory, extending Griffith analysis

14 p2322 A71-29738
Brittle structures and materials fracture strength, using linear fracture mechanics as analytical basis for testing

14 p2258 A71-29895
Crack tip strain problem in elastic body, relating fracture energy criterion with mathematical models

14 p2334 A71-31002
Deformation work for strained copper during tensile testing until fracture as function of slenderness in neck

15 p2427 A71-31700
Monograph on ductile fracture covering electron microscopy of fracture surfaces and microstructures of Al alloys

15 p2434 A71-32301
Fracture mechanics macroscopic aspects in terms of continua mechanics to provide practical criteria for fracture toughness estimates

15 p2510 A71-32557
Alternative approach to fracture mechanics, discussing thickness dependence of residual strength, crack initiation and crack propagation stability

15 p2510 A71-32725
Time dependent fracture and failure criteria for aluminum under stress pulse loading in uniaxial strain, using exploding foil spallation tests in air and vacuum

16 p2590 A71-32943
Atomic bond rupture and molecular mechanisms of polymer fracture, using EPR spectroscopy

16 p2600 A71-32944
Wells COD /crack opening displacement/ criterion for notch root deformation and fracture measurements

16 p2591 A71-32949
Numerical stress analysis of elastic three-dimensional fracture specimen with edge crack, using singular integral equations analogous to Green boundary formula in potential theory

16 p2655 A71-33181
Iron single crystals plastic deformation under tension, studying ductile/brittle fractures mechanisms and transition temperature

16 p2591 A71-33369
Crack interaction effect along straight line on critical equilibrium and fracture of plate relative to crack-piece length

16 p2658 A71-33685
Recrystallized and unrecrystallized deformed semiminished Al base alloy under cyclic and static loads, investigating macrofracture kinetics

16 p2594 A71-33713
Fracture mechanics, considering toughness /energy absorption/ factor, applied stress, crack size, operating temperature and state of stress

17 p2828 A71-35299
Microcracks analysis by micropolar continua theory, presenting solution for circular hole in infinite plate

17 p2832 A71-35421
Brittle fracture under stress concentrations, calculating scale factor based on technical cohesive strength statistical theory

17 p2833 A71-35619
Fracture kinetics, emphasizing plastic deformation, dislocation and diffusion micromechanics, point defects effects, microcrack formation and interstitial mechanisms

17 p2834 A71-35667
Polymer type, temperature, crystallinity and orientation effects on fracture mode, discussing macroload carrying capacity, nylon fiber tie chains and molecular behavior

18 p2939 A71-35889
Viking Mars spacecraft pressure vessel design, incorporating linear elastic fracture mechanics for long life

18 p2979 A71-36487
Microradiographic and acoustic evaluation of fracture in boron filament aluminum matrix composite under tensile stress

19 p3081 A71-37903

Fracture mechanics for design procedures, producing approximate expressions for stress intensity factors

19 p3158 A71-38019
Linear-elastic fracture mechanics limits concerning toughness based on elastic-plastic rupture model for yielding materials

19 p3161 A71-38726
Dynamic tear fracture toughness test and fracture mechanics parameter correlation for high strength Al alloys

20 p3248 A71-38771
Semiempirical modification of Irwin fracture analysis for semielliptical surface crack in metal plate

20 p3248 A71-38781
Linear elastic fracture mechanics for design against high cycle fatigue failure, considering stress intensification, crack initiation and propagation

20 p3307 A71-38813
Fracture mechanics application to proof testing for components life determination, exemplifying concept by flawed pressure vessel

20 p3308 A71-39459
Fracture mechanics analysis of metal fatigue crack growth as function of stress intensity factor

22 p3560 A71-41641
Hertzian fracture test for strong solid surface properties measurement based on crack growth in nonuniform stress field due to contact loading

23 p3777 A71-43934

FRACTURE RESISTANCE **U FRACTURE STRENGTH** **FRACTURE STRENGTH**

Turbine disks and shafts for low temperature operation, examining brittle fracture tendency by acceleration testing

01 p0098 A71-10078
Steel cylinders with circumferential cracks under repeated impact tensile loads, investigating plain strain fracture toughness index temperature dependence

01 p0166 A71-10079
Materials and welded joints brittle fracture resistance estimation from impact bending tests

01 p0085 A71-10084
High strength steels fracture toughness, investigating loading rate and temperature effects

03 p0442 A71-13625
Notched tensile plate steel specimens, investigating temperature and stress state effects on nil ductility transition and fracture strength [SESA PAPER 1735]

03 p0443 A71-13752
Brittle fracture resistance of mild steel after low cycle fatigue damage

03 p0516 A71-14579
Fracture toughness tests and brittle failure of high strength structural steels under thermomechanical treatment

03 p0447 A71-14581
Static and dynamic fracture toughness of tempered low alloy high strength steels in low temperature range

03 p0448 A71-14582
Steel brittle fracture tests using explosive charge stress wave absorption measurements

03 p0517 A71-14583
Low temperature steel welded joints resistance to brittle fracture, discussing Niblink dynamic loading, deep notch static loading and Charpy V tests

03 p0433 A71-14585
Whisker composites tensile and fatigue properties, fracture toughness and mechanical properties at high temperatures

04 p0611 A71-14951
Martensite formation and fracture toughness in TRIP steels, examining effects of plastic zone ahead of crack tip and triaxiality ahead of notch

04 p0615 A71-15792
Unidirectional glass-epoxy filament wound composite material fracture strength based on three dimensional stress components of fiber-containing plane

05 p0826 A71-16740
Fracture strength of helical wound glass-epoxy composite cylinder under axial tension, determining tensile strength

05 p0826 A71-16741
Managing steel weldability, examining crack origin and fracture toughness

05 p0770 A71-17246
Mechanical property data for silicon nitride-silicon carbide fiber ceramic composites having high fracture values

06 p0916 A71-18035
High temperature ductility of low alloy ferritic steels, correlating tensile elongation values to crack nucleation resistance

07 p1134 A71-19517
Microstructural variables effects on fracture stress in alpha beta Ti alloy having Widmanstatten structure

07 p1139 A71-19992
Additive elements and heat treatment effects on Al-Zn-Mg alloy fracture characteristics, using tensile and stress corrosion tests

07 p1143 A71-20488
Fracture toughness of aluminum oxide composite containing ductile Mo fibers

08 p1304 A71-20700

High speed ball impact tests and fracture energy of carbon fiber reinforced plastics
[PLASTICS INST. PAPER 25]

08 p1322 A71-20922

Heat resistant materials strength characteristics with long service periods, formulating equation for time dependence of rupture resistance

08 p1306 A71-21111

Long time strength and creep recilinear diagrams constructed for heat resistant alloys to obtain extrapolation values

08 p1306 A71-21113

Test results extrapolation for heat resistant alloys long time strength using exponential relation between time to rupture and value for initial stress decrease

08 p1306 A71-21114

Aluminum alloy deformations and rupture strength under complex stress at low temperatures, observing anisotropy decrease with temperature

08 p1306 A71-21117

Thermomechanical treatment effects on microstructure and fracture toughness of extruded Beta III titanium alloy

08 p1313 A71-21558

Co base superalloys fracture toughness microstructural aspects, considering effects of interdentritic carbides and carbide precipitation on aging at elevated temperatures

08 p1314 A71-21572

Fracture toughness relationship to microstructure in alpha-beta Ti alloy heat treated to constant yield strength, considering crack propagation

09 p1472 A71-23126

Ti alloys in aircraft industry, considering jet engines applications and structural stability improvements related to fracture toughness, fatigue and stress corrosion

09 p1474 A71-23292

Welded steel structures fracture safe design, considering continuity conditions responsible for catastrophes resulting from crack initiation

09 p1458 A71-23453

Fracture mechanics application to structural adhesives test methods, considering joints crack extension resistance and plane strain fracture toughness

10 p1615 A71-24088

Processing variables effects on epoxy adhesive joints fracture toughness and crack extension resistance

10 p1632 A71-24089

Kinetic crack propagation theory of fatigue fracture toughness for notched and unnotched asformed high strength and heat treated ball bearing steels

10 p1687 A71-24307

High strength steel fracture toughness, investigating stress wave emission during crack growth

10 p1627 A71-24534

Carboxyl terminated butadiene-acrylonitrile/epoxy carbon fiber composites fracture energy, noting fracture strength, short beam shear strength and tensile strength at cryogenic temperatures

11 p1785 A71-25403

Interfacial bonding effect on fracture toughness of glass sphere filled epoxy and polyester resins, using tapered cleavage specimen

11 p1846 A71-25413

Orientation dependent impact toughness and crack resistance of brittle fiber-ductile matrix composite of solidified carbide reinforced Co-Cr eutectic

11 p1782 A71-26386

Fracture toughness and critical strain rate measurements in unidirectional glass reinforced plastics as function of resin, hardener, fiber and degree of cure

11 p1790 A71-26387

Fiber composites monofilament and strand tests, considering fracture, fatigue, stress, corrosion and microstructure

12 p1921 A71-27635

Ductility and susceptibility to brittle fracture of alloys under stress at low temperatures

12 p1919 A71-27685

Multiaxial stress state effects on materials fracture strength, ductility and structural design

13 p2151 A71-28216

Tensile strength and fracture toughness of carbon fiber polyester composites, using mechanical testing and scanning electron microscopy

13 p2092 A71-28625

Notch effect on ductile fracture, considering plastic stress and strain concentration in stainless steel, brass, copper and mild steel

13 p2088 A71-29343

Brittle structures and materials fracture strength, using linear fracture mechanics as analytical basis for testing

14 p2258 A71-29895

Steel structural elements resistance reserve to brittle fracture, considering critical temperatures and breaking stresses

15 p2504 A71-31852

Steels resistance to brittle fracture at various temperatures, determining failure stress and transition temperatures for nonuniform stress distribution

15 p2428 A71-31855

Heat treatment effects on high strength maraging steel tensile, fracture toughness and stress corrosion properties, discussing reversion to austenite

15 p2433 A71-32175

Fracture mechanics macroscopic aspects in terms of continua mechanics to provide practical criteria for fracture toughness estimates

15 p2510 A71-32557

Notch effect on stainless steel and alpha brass rods and plates ductility and fracture strength

16 p2591 A71-32947

Crack propagation resistance-cyclic fracture strength relation for austenitic and Mn-Cr-V steels, considering thermomechanical working effects

16 p2592 A71-33408

Scale factor effect on brittle fracture strength for Ti and Al alloys and high strength steels

16 p2657 A71-33409

Turbine wheels and shafts for low temperature operation, examining brittle fracture by acceleration testing

16 p2593 A71-33634

Steel cylinders with circumferential cracks under repeated impact tensile loads, investigating plane strain fracture toughness index temperature dependence

16 p2658 A71-33635

Materials and welded joints low temperature operation reliability prediction by estimating brittle fracture resistance from impact bending tests

16 p2584 A71-33640

Tensile properties, plane strain fracture toughness and stress corrosion threshold of high strength precipitation hardening stainless steels

17 p2755 A71-34438

Heat treatment effect on fracture behavior of aged Al alloy sheet, investigating toughness dependence on microstructure

17 p2756 A71-34486

Image distortion technique for viewing surface deformation zones at precracked specimens under monotonic loading during fracture test [SESA PAPER 1799]

17 p2738 A71-34547

Toughness testing for low ductility fracture due to crack development in elastic stress field

17 p2757 A71-34557

Anisotropic bolt bearing specimens failure mode and strength prediction, evaluating relative merits of maximum stress, maximum strain and distortional energy as failure criteria

17 p2824 A71-34820

Thickness effect on fracture toughness and crack propagation of Al alloy sheets used for aircraft skins

17 p2758 A71-35153

Center cracked tension panels residual strength evaluation and prediction, deriving analysis technique based on stress intensity factor

17 p2827 A71-35155

Damage tolerant aircraft structures material toughness and residual strength, presenting fracture test results on precracked panels reinforced with crack stoppers

17 p2827 A71-35157

Fatigue crack initiation and growth and residual strength of F-100 wing, comparing service failure data with full scale fatigue test results

17 p2827 A71-35159

DC-10 fuselage pressure shell fail-safe design, presenting analysis methods for residual strength prediction of damaged stiffened panels

17 p2827 A71-35160

Helicopter rotor blades fail-safe design, presenting criteria for fatigue loaded structures residual strength and life based on crack propagation rate methods

17 p2828 A71-35163

Industrial Ni alloys and steels rupture strength by short time data extrapolation

17 p2760 A71-35651

Elastic adhesive interlayer effect on bond fracture strength, considering propellant-liner-steel combination in solid rocket motors

18 p2977 A71-36245

High strength Al alloys in structural design, taking into account fracture toughness

18 p2937 A71-36849

Aluminum alloy gas tungsten arc welds, determining defect size and distribution effects on fracture strength

18 p2929 A71-36857

Ti alloys heat resistant properties evaluation for long service under various heat treatment conditions, considering tensile properties, fracture toughness and microstructure

19 p3082 A71-38420

Transition temperature behavior in plane strain fracture toughness tests on A517-F steel, comparing with Charpy tests

20 p3248 A71-38770

Dynamic tear fracture toughness test and fracture mechanics parameter correlation for high strength Al alloys

20 p3248 A71-38771

Evaporated pure Ni coatings effects on carbon fiber fracture strength and microstructure at room temperature

20 p3248 A71-38815

Tensile properties and notch toughness of Al alloys at low temperature, considering fracture toughness and weld strength

20 p3251 A71-39266

Charpy impact test measurement of maraging steel thermal embrittlement, observing fracture mode and toughness changes with heat treatment

21 p3398 A71-40467

Fracture testing, discussing fracture toughness, proof testing assemblies, crack identification, growth, catastrophic failure probability, etc

21 p3463 A71-40673

Cryogenic fracture toughness testing - ASTM-ASME Conference, Toronto, June 1970

21 p3401 A71-40914

Cryogenic steels, Al and Ti alloys plane strain fracture toughness at room and subzero temperatures, discussing tensile and notch bend results

21 p3401 A71-40915

High strength Al alloys at cryogenic temperatures, presenting plane strain fracture toughness tests results

21 p3401 A71-40916

Specimen design effects on Al and Ti alloy plane strain fracture toughness at room and cryogenic temperatures, discussing crack propagation and rolling directions orientations

21 p3401 A71-40917

Ti-Al-Sn and Al alloys thin sectioned specimens cryogenic fracture strength, discussing surface crack fracture behavior

21 p3401 A71-40918

Al alloys tensile deformation and fracture characteristics relation to stress-strain diagrams, discussing strain hardening indices

22 p3560 A71-41642

Kossel line technique application to intergranular fragility study, discussing lattice constant measurement to determine difference in impurity distribution

22 p3563 A71-42324

Fatigue, necked-out and intermediate fracture types observation in load-controlled low-cycle fatigue tests of rolled steel

22 p3617 A71-42496

Epoxy-alumina trihydrate composite system fracture energy data, noting interdependence of surface topography, phase dispersion volume fraction, particle size and spacing

23 p3696 A71-43102

Hertzian fracture test for strong solid surface properties measurement based on crack growth in nonuniform stress field due to contact loading

23 p3777 A71-43934

Cast heterophase Mo and alloys fracture strength and plastic characteristics, investigating crystal growth texture, orientation and substructure

23 p3693 A71-44215

FRACTURE TOUGHNESS U FRACTURE STRENGTH FRACTURES [MATERIALS]

Cracked metals brittle fracture statistical analysis, discussing plastic deformation under load

01 p0166 A71-10080

Ductile Ni deformation and fracture, examining simultaneous cyclic and monotonic strain effects

01 p0098 A71-10164

Weibull density functions applied to fracture location distribution in brittle solids

01 p0167 A71-10294

Glass fiber reinforced plastics stress and fracture analysis, using approximate and iterative methods for strength estimates and nonlinear stress-strain relationships

01 p0172 A71-10697

Continuous filament composite materials fabrication and tests for dynamic deformation, fracture and wave propagation properties, considering axially reinforced cylindrical body compression

03 p0508 A71-13768

Metal and glass composites with similar residual stress states under axial loading, examining yielding and fracture behavior

03 p0443 A71-14186

Fractures - Conference, Marienbad, Czechoslovakia, October 1970, Part 3

03 p0433 A71-14584

Thin Al and plexiglass sheets biaxial stress field effect on fatigue and fracture [ASME PAPER 70-PVP-17]

04 p0665 A71-14768

Heat treated low carbon steel fatigue tests at low cycle tension compression loads, determining durability relationships to load and total work to fracture

04 p0666 A71-14878

Carbon steel and heat treated duraluminum fatigue fracture microstructure observation using electron microscope, determining crack propagation relationships to loading sequence

04 p0610 A71-14880

Fiber reinforced plastics testing and mechanical parameters measurement, considering materials strength and fracture probability

04 p0618 A71-14887

Bond rupture and fracture in semicrystalline polymers, noting agreement with random length molecular tie chain scission model

04 p0670 A71-15388

Stress analysis of multilayered composite structures with flaws, emphasizing application to fracture studies 04 p0671 A71-15753

Cross and single polarized light techniques revealing coarse grained fractures cleavage facets 07 p1111 A71-19582

Probability theory for viable microorganism exposure in fractured contaminated solid, using quantal response model 07 p1048 A71-19600

Rhenium effect on tungsten sensitivity to brittle fracture, measuring amplitude dependence of internal friction at temperatures from 77 to 1273 K 07 p1141 A71-20247

Low temperature impact toughness test as criteria for metal susceptibility to brittle fracture 09 p1468 A71-22509

Applied transducer signals from surface and internal fractures of various lengths, depths and positions 09 p1450 A71-22896

Adhesive fracture blister tests, using energy balance for treating stress singularities in brittle elastic materials 10 p1631 A71-24077

Al alloy and carbon steel low cycle fatigue and fracture surface topography transition from static dimple to striation type by electron fractography 11 p1777 A71-25266

Fracture under hot creep rupture, discussing grain boundary structure, high temperature region, creep deformation and recovery, void formation and intercrystalline failure 13 p2152 A71-28220

Metals dynamic fracture model, discussing critical incubation time and temperature dependence 15 p2503 A71-31446

Fabrication, texture, alloying, substructure and fracture effects on bend ductility and toughness of beryllium sheet 15 p2436 A71-32509

Metal matrix composites fractured and cut surfaces analysis using scanning electron microscopy [ASM PAPER W71-3.4] 16 p2579 A71-33541

Cracked metals brittle fracture statistical analysis, discussing plastic deformation under loading 16 p2658 A71-33636

Flexural-torsional fatigue fracture of duraluminum, noting dependence on cyclic stress, frequency and medium 16 p2593 A71-33689

Mechanical properties, fracture and limited high temperature oxidation resistance of carbon fiber reinforced Ni composites 16 p2599 A71-34086

Boron-aluminum composites fracture behavior, using conventional metallography and scanning electron microscope 16 p2599 A71-34087

Stochastic character of metal fatigue fracture and fatigue life dependence on stress cycle amplitude, using equiprobability curves 18 p2936 A71-36694

Plastic deformation and fracture of beta Ti alloy under tensile tests at room and low temperatures 19 p3077 A71-37464

Recovery creep properties and intercrystalline fracture in precipitation hardened alloys heat treated on relative stable conditions 20 p3250 A71-39024

Iron response to dynamic loads, discussing pressure induced phase changes, constitutive equation relationship to dislocation processes and dynamic fracture criteria 21 p3399 A71-40789

Pulse attenuation in composite materials, discussing stress waves geometric dispersion and compressive fracturing effects 21 p3465 A71-40791

Tensile strain response for spallation fracture in metals by impact and electron beam heating of Al, Cu and Ti alloys 21 p3466 A71-40798

Tensile fracture in grip section of fiber reinforced reduced cross section plastic composite specimens 22 p3564 A71-41591

Fracture mode transition under varied mean stress levels in metal fatigue at constant crack growth rate 22 p3561 A71-41711

Hold time effects on plastic deformation and fracture in high temperature low cycle metal fatigue 22 p3561 A71-41942

Carbon effects on fracture phenomena in martensitic transformation of steels under heat and thermomechanical treatments 22 p3563 A71-42322

Fatigue, necked-out and intermediate fracture types observation in load-controlled low-cycle fatigue tests of rolled steel 22 p3617 A71-42496

Aerospace materials and structures shock sensitivity from derivation of dynamic fracture propagation relationship to stress wave 24 p3886 A71-45370

FRACTURING

Pressure-bonded trilayer insulator stress analysis, using computer model for explaining alumina component fracturing during fabrication 02 p0256 A71-12249

Steels brittle fracture susceptibility by notch impact bending test, considering plastic deformation zone and crack propagation 04 p0610 A71-14889

Macroscopically ductile and brittle fracture via electron microscope photographs, considering brittle fracture and embrittlement temperature under uniaxial and multiaxial stress 10 p1627 A71-24595

High strength steel delayed fracture, applying Yokobori stochastic-kinetic theory of fatigue crack propagation for time to fracture calculation 13 p2155 A71-28790

Fatigue process analysis through crack initiation and propagation and final fracture, considering ductility, tensile strength and fracture toughness roles 14 p2258 A71-29896

FRAGMENTATION

Laser heated surface layer fragmentation taking into account particles dispersion due to vaporization, reactive force and mechanical recoil moment 01 p0070 A71-10796

Mass spectroscopic determination of geometric isomers of alpha, beta-unsaturated carboxylic acids, noting various modes of fragmentation 01 p0028 A71-11304

Synthesized amino esters and ketones with varying distance between functionalities, examining mass spectral fragmentation 02 p0209 A71-12574

Reduced pressure effects on thermal expansion and fragmentation of rocks 03 p0418 A71-14460

Runaway pulsar formation and ejection in supernova collapse, fragmentation, condensation, radiation and disruption 04 p0643 A71-15046

Normal shock wave acceleration of water droplets by external pressure, observing distortion and breakup through shadowgraph techniques [AIAA PAPER 71-325] 11 p1749 A71-25305

Water drops deformation and fragmentation due to shock wave impact in high velocity air stream [AIAA PAPER 71-392] 11 p1749 A71-25354

Small meteor bodies fragmentation, using radar diffractional pictures 16 p2639 A71-33697

Liquid hydrocarbon fuel drop interaction with incident shock wave in oxidizing and inert atmospheres, investigating aerodynamic shattering and combustion 17 p2836 A71-34435

Galaxy active nucleus and quasar fragmentation based on model of rotating supermassive star releasing thermal radiation 21 p3449 A71-40610

Criticism of paper on spallation cross section for Be 10 production from oxygen high energy fragmentation in meteorites 22 p3508 A71-42350

FRAME PHOTOGRAPHY

High speed photographic assembly with turbine drive for continuous recording and frame photography 10 p1613 A71-24872

Serial edge absolute coded and parallel alphanumeric timing on engineering sequential films, discussing frame selection, marking, offset, pull down and exposure correction 18 p2919 A71-36085

FRAMES

NT AIRFRAMES

NT UNDERCARRIAGES

Frame structures linear-mode failure probability estimation by reliability analysis 02 p0327 A71-12347

Minimum weight design for beams and frames with compliance constraints from constitutive relation 04 p0671 A71-15754

Dynamic stress measurement of cantilever beams, frame structures and rings under impulsive loads 07 p1210 A71-19046

Book on computer methods of structural analysis concentrating on frame systems, stiffness matrix techniques and Fortran IV 07 p1210 A71-19099

Arbitrary solid cross section frames and arches shakedown analysis including axial forces effects on stress through reduction to linear programming 11 p1849 A71-25678

Stress analysis of thin walled framed cylindrical beams under deformation beyond proportionality limit by iteration method 14 p2321 A71-29540

Work hardening material planar frame inelastic load deformation and buckling, using finite difference method and variational principle 14 p2330 A71-30693

Rigid plastic framed structures minimum weight design and analysis formulation by network-topological approach based on yielding concept 17 p2831 A71-35356

Micropolar continuum, potential energy, stresses and constitutive relations for buckling of large rectangular grid frameworks under axial load 21 p3469 A71-41009

Displacement fields for two dimensional minimum weight frames for load dispositions analogous to perfectly plastic plane flow in metal working 21 p3391 A71-41428

GWU-FAP computer program for rigid frame elastic-inelastic analysis based on finite element method and plastic initial strain concept 22 p3516 A71-41867

Static, kinematic and uniqueness theorems of incremental collapse of frames extended to variable repeated loading 22 p3619 A71-42593

Nonlinear structural frame analysis by dynamic relaxation for use with computers 24 p3879 A71-44632

FRAMING CAMERAS

Portable self contained Imacon image converter high speed camera system capable of framing and streak operation 18 p2924 A71-36614

Ultrafast camera with picosecond framing times for photographic measurement of light pulses 20 p3235 A71-39189

FRANCK-CONDON PRINCIPLE

Franck-Condon factors, r-centroids and absolute band transition probabilities of NH, SiH, molecular sulfur and SO 10 p1645 A71-24544

Isotope effects in Lyman and Werner systems of molecular hydrogen, HD and molecular deuterium, calculating band strengths, oscillator strengths and Franck-Condon factors 11 p1803 A71-26072

Solar photosphere vibrational temperature determination, using Franck-Condon factor with equivalent line widths for five CN vibrational bands 12 p1963 A71-27081

Franck-Condon factors, densities and r-centroids for diatomic molecules, computing vibrational wave functions by FORTRAN V 14 p2276 A71-30297

Solar photosphere vibrational temperature determination, using Franck-Condon factor with equivalent line widths for five CN vibrational bands 19 p3133 A71-37431

FRAUNHOFER LINES

Solar magnetic field regions, bright line structures and faculae from Fraunhofer lines analysis, discussing magnetic downward velocities 01 p0152 A71-10328

Linearly polarized light measurements of solar spectral lines Zeeman effects, describing calibration method based on Fraunhofer lines broadening due to magnetic fields 04 p0642 A71-14903

Fraunhofer line resonance polarization from solar spectral bands statistical analysis, noting collisional depolarization 06 p0969 A71-17973

Solar Na I Fraunhofer lines empirical constants and abundance, discussing van der Waal attraction, stark broadening and radiative damping 06 p0969 A71-17974

Solar photosphere macroturbulence effects on Fraunhofer lines and central intensities of various absorption lines 06 p0975 A71-18443

Weak and average intensity Fraunhofer lines contours variation over solar disk 07 p1200 A71-20038

Fraunhofer line profiles, determining optical depth at various points in photosphere 09 p1524 A71-23191

Solar center-limb Fraunhofer line profile variations observed with double diffraction monochromator 09 p1524 A71-23192

Fraunhofer lines at solar disk center and near limb, investigating profiles for asymmetry 09 p1524 A71-23194

Solar photosphere macroturbulence effects on Fraunhofer lines and central intensities of various absorption lines 12 p1955 A71-26593

Sunspot umbra, calculating vertical magnetic field strength distribution from Fraunhofer lines 14 p2308 A71-29979

Interferometric observation of photon fluctuation during Fraunhofer diffraction by small round hole, considering light granular structure at low intensities 15 p2421 A71-32405

Excess red shift of Fraunhofer lines at extreme limb explained by mechanism of radial currents in solar atmosphere 16 p2629 A71-32807

Solar atmosphere mean radial velocity relation to low excitation potential based on Fraunhofer lines blue shifts observations 17 p2808 A71-35576

Solar Fraunhofer line wavelengths shifts at disk center and at limb, evaluating Stark broadening contribution 18 p2962 A71-36106

Telescopic phase retardation effect on polarization in Zeeman split Fraunhofer line, discussing consequence for solar magnetic field determination 18 p2965 A71-36732

True central intensities of Fraunhofer lines, describing solar telescope and Czerny-Turner spectrometer 19 p3146 A71-38661

Fraunhofer diffraction apparatus design based on He-Ne laser, testing performance in distorted point lattices photography 23 p3686 A71-43956

FRAUNHOFER REGION
U FAR FIELDS
FREDHOLM EQUATIONS
 Initial value method for Fredholm integral equations with displacement kernels on infinite interval, using invariant imbedding 03 p0450 A71-13622

Thin shallow shell theory boundary value problem, discussing reduction to Fredholm integral equations system 05 p0828 A71-16893

Axisymmetrical potential theory for two spherical circular disks system, using X-analytic functions for reducing to Fredholm equation 06 p0928 A71-18345

Two dimensional Laplace equation solution by Fredholm integral equation method for Dirichlet problem 07 p1148 A71-20096

Fredholm integral equation stabilization methods for atmospheric IR transfer in vertical temperature profile determination 08 p1286 A71-21877

Fredholm integral equations solutions in atmospheric optics, proposing algorithm for optimal parameter regularization values 09 p1487 A71-22378

Steady electromagnetic oscillation amplitude calculation from solution kernel to Maxwell equations boundary value problems through orthogonal coordinate transformation to Fredholm integral equations 09 p1495 A71-23431

Linear one dimensional system with infinite degrees of freedom, discussing optimal control by Fredholm integral equation 09 p1424 A71-23457

Fredholm equation solution for radiative transfer between parallel plate configuration at midpoint 13 p2159 A71-27981

Conditions for obtaining analytical expressions for eigenvalues and eigenfunctions of homogeneous Fredholm equation 13 p2096 A71-28015

Hypersonic flow around delta wing at small angles of attack, using pressure sources method and Fredholm integral equation 13 p1992 A71-29189

Baffled piston source sound radiation impedance from numerical solution of Fredholm integral equation for vibrating disk in finite rigid concentric baffle 19 p3104 A71-37849

Fredholm integral equation stabilization methods for atmospheric IR transfer in vertical temperature profile determination 19 p3060 A71-38470

Atmospheric thermal sounding radiation data interpretation, determining integral Fredholm equation solution, absorption characteristics and temperature profiles 20 p3258 A71-39670

First kind Fredholm integral equation approximation by numerical quadrature formulas plus collocation, using singular value decomposition for solution 22 p3567 A71-42296

Convolution integral equation unique solution in second kind Fredholm equation form, applying to plane polarized electromagnetic wave diffraction on infinitely thin band 24 p3804 A71-44769

FREDHOLM OPERATORS
U FREDHOLM EQUATIONS
U OPERATORS [MATHEMATICS]
FREE ATMOSPHERE
 Energy transport over turbulence spectrum of free atmosphere, using aircraft experiments 04 p0622 A71-15634

Temperature stratification effects on free atmosphere turbulence structure under Archimedean forces, noting energy dissipation buoyancy forces and adiabatic gradients 07 p1150 A71-18796

Radiosonde with radiation sensor, minimizing temperature measurement errors in free atmosphere 08 p1293 A71-21745

Nongeostrophic wind behavior in free atmosphere during cyclogenesis, noting maximum development during cyclone lifetime middle stage 15 p2400 A71-31969

Turbulence energy balance and temperature pulsations in free atmosphere in presence of water phase transformation in clouds of given microstructure 21 p3412 A71-41394

Long term vertical and horizontal variations of long wave radiation field in free atmosphere over U.S.S.R., using actinometric sounding data 22 p3570 A71-42848

FREE BOUNDARIES
 Nonlinear free surface effects in low gravity tank draining, finding domains of validity for linearized and nonlinear analysis [AIAA PAPER 69-680] 03 p0399 A71-13439

Nonlinear two dimensional free boundary problem of axisymmetric fluid flow in tubes with surface solidification, obtaining numerical solution based on finite difference equations 04 p0677 A71-15454

Viscous incompressible fluid flow with free boundary at large Reynolds numbers, deriving asymptotic expansion solution for wave motion 05 p0737 A71-16989

Three-part mixed boundary problem concerning equilibrium of semiinfinite two dimensional elastic medium containing Griffith cracks parallel to free boundary 07 p1214 A71-20021

Free boundary problems for heat equation involving interface coinciding initially with fixed face, proving existence, uniqueness and continuous dependence theorems 08 p1324 A71-20879

Plasma-free point magnetic dipole in field-free stationary plasma, determining magnetopause or free boundary by moment technique 09 p1503 A71-22865

Singular perturbation problems for linear second order elliptic equation, obtaining asymptotic approximations for simple unbounded regions with free boundary layer terms 10 p1636 A71-23934

Point matching technique applied to two dimensional solidification of viscous flow over semiinfinite flat plate, transforming moving free boundary problem to stationary domain [ASME PAPER 70-APM-R] 10 p1596 A71-24733

Stationary points of functional corresponding to boundary value problem with free boundary 12 p1930 A71-27167

Neutral stability of laminar free boundary layer in mixing incompressible MHD half jets at low Reynolds number 13 p2103 A71-27842

Air inlet for simulation of shock wave separated flow in supersonic diffusers, deriving pressure variation profile along free boundary 13 p1992 A71-29175

Geomagnetic tail natural oscillations, applying model of plasma cylinder with free boundary immersed in interplanetary medium 16 p2564 A71-33673

General Stefan problem for heat conduction with melting and free boundary problems occurring in control and statistical decision theories 17 p2841 A71-35794

Numerical solution algorithm for parabolic free boundary problem in statistical decision theory, comparing convergence with asymptotic expansions 18 p2941 A71-36352

Iterated double integrals for subsonic flow patterns bounded by segments of straight lines and free boundaries, using FORMAC 18 p2909 A71-36703

Asymptotic expansions for solution of wave motions of viscous incompressible fluid flow with free boundary at large Reynolds number 18 p2909 A71-36789

Potential flow with free surface, comparing finite element and finite difference methods for liquid sloshing problem 21 p3369 A71-40974

One dimensional two phase parabolic free interface /Stefan/ problem numerical solution, using method of lines to approximate partial differential equations at discrete time levels 22 p3575 A71-42294

Thermally driven motion of water with free surface in rotating annulus, investigating steady wave flow by three dimensional nonlinear Navier-Stokes equations numerical integration 24 p3844 A71-44417

FREE CONVECTION
 Laminar boundary layer free convection at vertical plate with exponentially decreasing surface temperature, determining thermal flux and shear stress 01 p0179 A71-10610

Free convection in turbulent Ekman layer, discussing kinetic energy budget above surface layer 01 p0119 A71-10742

Natural convection turbulent boundary layer temperature profile measurements along isothermal vertical plate, indicating temperature distribution independence of altitude in fully developed turbulent region 01 p0180 A71-10994

Global atmospheric circulation theory relation to flow pattern of free thermal convection in rotating fluid subjected to horizontal temperature gradient 01 p0122 A71-11359

Free nonlinear air convective motion in two dimensional cloud banks along vertical wind shift 02 p0277 A71-11690

Lunar solid state thermal convection throughout interior, noting pressure release production of basaltic magmas consistent with Apollo 11 rocks composition 02 p0305 A71-11988

Free convection in compressible viscous heat conducting liquid near critical point, discussing temperature gradients, layer heights, density distribution and inhomogeneity effect 02 p0331 A71-12190

Laminar natural convective heat transfer from baseplates of vertical rectangular fin arrays, taking temperature and fin geometry effects into account 02 p0333 A71-12601

Natural convective heat transfer from fin edges in vertical rectangular arrays, noting temperature and fin thickness effects 02 p0333 A71-12604

Natural convective heat transfer from fin-flat in vertical rectangular arrays, comparing duct and open channel coefficients 02 p0333 A71-12605

Mathematical models for heat transfer by laminar free convection to rotating central plate passing through synchronously rotating surroundings, considering Coriolis effect 03 p0518 A71-13617

Natural convection inside horizontal circular cylinder, selecting fluid, geometry and thermal boundary condition for high Prandtl and Grashof numbers 03 p0519 A71-13732

Free convection in compressible viscous heat conducting fluid, determining parameters leading to onset 03 p0521 A71-14292

Buoyancy effects on transient free convection heat transfer in revolving tube for zero to 100 g centrifugal acceleration [ASME PAPER 70-HT-10] 03 p0521 A71-14292

Vibration effects on free convection heat transfer from fluid filled horizontal cylinder 04 p0675 A71-14784

Viscous heating effects on laminar combined free and forced convection through vertical circular tubes 04 p0676 A71-15177

Heat transfer - Conference, Versailles, August-September 1970, Volume 4, Natural convection and rheology 04 p0685 A71-15521

Mach-Zehnder interferometer measurements of average temperature and heat transfer rate in free convection on heated vertical flat plate 04 p0599 A71-15522

Free convection temperature field about isothermal spheres in air, using interferometer for axisymmetric field 04 p0686 A71-15523

Differential phenomenological theory for turbulent free convection along heated vertical plate 04 p0686 A71-15524

Free convective flow in plane channel by boundary layer approximation, deriving continuity equations for viscous stress tensor 04 p0689 A71-15814

Incompressible fluid steady laminar flow free convection and various gas species mass diffusion from hot horizontal plate surface 06 p1007 A71-18074

Hydromagnetic boundary layer free convection past vertical flat plate, discussing flow rates, temperature profiles and skin friction for high and low Prandtl numbers 07 p1165 A71-18744

Spalding-Patankar finite difference method application to combined free and forced convection turbulent boundary layer with variable fluid properties and chemical reaction 07 p1054 A71-18769

Free convection turbulent flow under supercritical conditions, investigating convection heat transfer and flow patterns 07 p1220 A71-18780

Vapor bubbles radius at heating surface separation moment at boiling under free convection and forced motion through channel 07 p1221 A71-18923

Natural convection heat transfer between two isothermal concentric spheres, using water and silicone oils as convective fluids 07 p1222 A71-18995

Natural convection heat transfer coefficients from isothermal flat surfaces, using Boelter-Schmidt type heat flux meters 07 p1222 A71-18996

Closed axisymmetric vessel filled with viscous incompressible fluid, calculating integral heat release coefficients in free convection 07 p1222 A71-19196

Thermally induced modifications of high power CW laser beam, considering heat losses by forced and free convection 07 p1122 A71-19207

Elastico-viscous liquid laminar free convection flow along nonuniformly heated vertical flat plate, using momentum integral method for boundary layer velocity and temperature distributions
07 p1091 A71-20031

Boundary layer equation for free convective diffusion on flat vertical plate in translation motion in viscous incompressible fluid
11 p1854 A71-25240

Flow visualization of free convection laminar-to-turbulent transition along vertical heated plate in water induced by two dimensional forced disturbances [DFVLR-SONDDR-116]
12 p1987 A71-27739

Viscous dissipation effects on Nusselt number in combined free and forced convection through vertical concentric annuli
13 p2160 A71-28601

Laminar free convection heat transfer in vertical rectangular corner, considering velocity and temperature distribution
13 p2161 A71-28621

Critical Rayleigh numbers for natural convection of water confined in square cells, noting heat transfer modes
[ASME PAPER 70-WA/HT-7] 13 p2164 A71-28981

Vibration effect on heat transfer by natural convection from oscillating horizontal wire in air
13 p2164 A71-28984

Flow direction effect on combined forced and free convective heat transfer from cylinders to air
13 p2164 A71-28985

Forced and free convective equations combination to represent combined heat transfer coefficients for horizontal cylinder
13 p2164 A71-28986

Monograph on boundary layer theory covering unsteady heat transfer from rotating disk, thermal free convection in corners, etc
14 p2223 A71-29934

Free convection in horizontally positioned, water filled circular cylindrical cavity
14 p2336 A71-30228

Free convection in compressible viscous heat conducting liquid near critical point, discussing temperature gradients, layer heights, density distribution and inhomogeneity effect
15 p2512 A71-31497

Boundary velocity and temperature field of unsteady natural periodic convection over three dimensional obstacle for arbitrary Prandtl numbers
18 p2984 A71-35950

Heat transfer coefficients calculation for human body in cold water from heat balance equations, comparing with free convection coefficients in cross-flowing water
18 p2862 A71-36900

Dissolution rate of vertical nickel cylinder in liquid aluminum under free convection, showing fluid boundary layer mass transfer role
19 p3079 A71-37709

Heat transfer due to combined free and forced convection in horizontal isothermal tube flow
[ASME PAPER 71-HT-3] 19 p3163 A71-37981

Swedish monograph on low air flow velocity measurement with hot-wire anemometer under free and forced convection, using schlieren method
19 p3172 A71-38645

French monograph on free and forced convection and external radiation from hot gas oscillating in resonance tube, considering heat balance and mass exchange
19 p3172 A71-38649

German monograph on free convective heat transfer from heated tubes in air in presence of bounding walls parallel to tube axis
20 p3311 A71-39043

Free convective heat transfer in cryogenic liquid filled enclosure, studying effects of vibration near resonant frequency
20 p3314 A71-39292

Gravity induced free convection effects in melting phenomena for thermal control, predicting temperature distributions and solid-liquid interface profiles by two dimensional model
20 p3314 A71-39354

Laminar free convection from line heat source for Prandtl number 2 based on differential equation solution
20 p3314 A71-39491

Natural convection boundary layer stability on vertical flat plate with uniform heat flux, using numerical computer solutions for large Grashof number range
20 p3314 A71-39501

Thermal convection induced perturbations in unstably stratified horizontal shear Couette flow of Boussinesq fluid in rectangular channel heated from below
21 p3475 A71-40641

Oscillatory free convection laminar boundary flow from semiinfinite vertical flat plate, investigating surface temperature variations as distance function from leading edge
22 p3619 A71-41602

Boundary layer asymptotic solutions for free convection in laminar three dimensional systems, determining rapid mass transfer and centrifugal forces effects
22 p3619 A71-41870

Centrifugally driven thermal convection in rotating cylinder of fluid heated from above, calculating heat flux through wall and effect on Nusselt number
22 p3620 A71-41879

Laminar free convective heat transfer on vertical cylinder with concentration gradients, considering mass transfer effects prediction
22 p3620 A71-41882

Generalized solutions existence proof for viscous incompressible fluids free convection, investigating smoothness properties dependence on initial values and forces
22 p3622 A71-42863

Convective heat transfer by laminar and turbulent free convection in air on large horizontal and vertical planes
23 p3781 A71-43324

Fluid flow friction and combined free and forced convective heat transfer characteristics in rotating curved circular tube, using finite difference scheme and iterative solution
23 p3783 A71-44192

Vertical laminar natural convection boundary layer stability during thermal expansion at large Prandtl number
24 p3886 A71-44422

Free convection heat transfer from vertical flat plate with sinusoidal wall temperature distribution [AIAA PAPER 71-988]
24 p3887 A71-44583

Heat and mass transfer in binary laminar boundary layer with free convection on vertical porous surface, integrating momentum and energy equations for upper limits
24 p3887 A71-44744

Natural convection contribution to strong gravitational fields affecting astrophysical objects evolution and mass ejection
24 p3868 A71-44749

FREE ELECTRONS

Short wave broadcasting and ionospheric reflection during solar eclipse of 7 March 1970, relating to nighttime free electron distributions
01 p0151 A71-10119

Low temperature weakly ionized molecular plasma kinetic equation in electric field, considering free electron distribution function for molecule-electron inelastic collisions
04 p0634 A71-15114

Production rates for beat and sum frequencies mixing from interaction of two parallel laser beams with free electrons, using nonrelativistic radiation theory
09 p1465 A71-23546

Graphite lubricants superconducting properties under high pressures and low temperatures, suggesting new superconductors developments and metal free electron model modification
10 p1656 A71-24299

Magnetic corrections to Boltzmann distribution function by power expansion, determining current density in system of free electrons accelerated by crossed electric and magnetic fields
13 p2109 A71-29288

Nonlinear optical effects associated with free holes and electrons in semiconductors, including higher harmonics generation and frequency mixing
16 p2621 A71-33375

Electromagnetic absorption cross sections from wave function of free carriers in semiconductors with point defects
16 p2623 A71-34031

Hall coefficient and electrical resistivity increase during aging of Al-Zn alloys, suggesting free electron energy reduction due to solute atoms clustering
17 p2759 A71-35227

Electric field effects on town gas and hydrocarbon flame reaction rate, burning velocity and propagation speed due to free electrons in flame front
17 p2840 A71-35704

VLF emissions and low energy electrons relation to other auroral phenomena from satellite-borne data associating midnight maximum with particles from plasma sheet
20 p3229 A71-39855

Optical mixing and higher harmonics generation by free carriers in semiconductors, using carbon dioxide laser
21 p3393 A71-40663

Free electron distribution function, atomic level population and ionization rate in low voltage arc near electrodes
23 p3709 A71-43266

Carbon ion and free electrons three body recombination rate coefficient measurement in carbon monoxide flows
24 p3802 A71-44607

Predawn effect on hot and cold electrons at magnetoconjugate point in F2 layer, discussing electron shock wave speed and thermal collisionless wave energy dissipation
24 p3824 A71-45321

FREE ENERGY

NT GIBBS FREE ENERGY

Perovskite crystals phase transition with unit cells atom displacement, considering permittivity anomalies, structure and free energy expansion coefficients
01 p0138 A71-10430

Quasi-means definition and auxiliary system introduction for models including negative four-fermion interaction, solving limiting expressions problem for free energy
05 p0775 A71-16865

Kinetic coefficients calculation for gas with internal degrees of freedom during free energy exchange between translational and internal motion
08 p1338 A71-21918

Hafnium and zirconium sulfides, determining partial molar free energy of sulfur at metal saturation with electromotive force cell
09 p1387 A71-23129

Thermochemistry data changes influence in form of heat of formation, partition functions, specie free energy or specific heat on high temperature gas mixtures composition
15 p2514 A71-32097

Temperature dependent electron structure model of free energy decomposition of beta phase in Ti alloys
16 p2599 A71-34085

Kinetic coefficients calculation for gas with free energy exchange between translational and internal degrees of freedom
17 p2785 A71-35263

Carbon activity, free energy entropy and enthalpy in fcc solid solution of Fe-Ni-C alloy
19 p3080 A71-37714

FREE FALL

Free fall speed characteristics of simulated hailstones measured by tracking radar, discussing roughness effects on speed and drag
01 p0115 A71-10556

Free-fall periodic orbits /interplanetary trajectories/ connecting earth and Mars, using patched conic analysis
[AIAA PAPER 71-92] 06 p0977 A71-18547

Free fall of sphere in viscous fluid, expressing fluctuations frequency as function of interfacial tension, sphere density and diameter
08 p1276 A71-21878

Spark ignition of polystyrene suspensions during free fall in air, investigating ignition mechanism by high speed photography
12 p1986 A71-26967

Radiative heat transfer effects on small fires in zero gravity spacecraft and free falling chamber environments from diffusion flame models
15 p2514 A71-32084

Analog mass center estimator for spinning drag-free orbiting satellite, using free-falling proof mass shielded from external forces inside satellite cavity as reference
[AIAA PAPER 71-947] 19 p3148 A71-37188

Free falling spheres rocking/lateral motions, deriving nonlinear damped pendulum equation with motion coupling expressed as Reynolds number dependent phase shift effect
21 p3416 A71-40953

Fluctuating lift and drag forces on accelerating free falling sphere, discussing relation to asymmetrical wake vortex shedding
21 p3324 A71-40970

FREE FLIGHT

Critique of Chapman-Kirk iterative method for differential equations yielding aerodynamic coefficients from free flight data
01 p0002 A71-10971

Nonlinear aerodynamic moments for arbitrary motions of bodies of revolution in free flight
[AIAA PAPER 70-205] 03 p0341 A71-13435

Free flight space vehicle nonlinear bending vibrations due to harmonic and pulse excitation
05 p0825 A71-16679

Space station experiments fine pointing and stability, discussing attached or coorbiting free flying mode with zero G conditions
[AIAA PAPER 71-62] 06 p0980 A71-18521

Free flight measurement of aerodynamic coefficients on fixed cruciform fin stabilized bombs, determining aerodynamic forces and moments dependence on angular velocity components
07 p1015 A71-19872

Angle of attack vertical variations of free flight trajectory missile, estimating missile, trajectory and atmospheric parameters effects on fluctuations relative to center of mass
08 p1367 A71-22051

Aerodynamic effects of bluntness on slender cones in free flight tests at Mach 17
[AIAA PAPER 70-554] 09 p1381 A71-22090

Rigid towed and free flight glider, considering loads and turbulent atmosphere effects
09 p1385 A71-23669

Ballistic wind tunnel for drag measurement on models during free flight at supersonic speeds
13 p2045 A71-29201

Free flight static and dynamic stability tests on lightweight cone shaped models in longshot tunnel at hypersonic speeds, using spark recording

16 p2519 A71-32879

Free flight hypersonic wind tunnel model testing in Ludwig tube, discussing launching device and recording setup

21 p3362 A71-40381

Analytic solution to range deviations along descending branch of free flight trajectory of ballistic vehicle in planetary atmosphere

24 p3872 A71-45015

FREE FLIGHT TEST APPARATUS

Comparative sting supported and free flight tests in hypersonic wind tunnel on modified Apollo launch configuration

[AIAA PAPER 71-265]

08 p1274 A71-21991

Launch and data reduction in supersonic wind tunnel free flight testing of high fineness ratio bodies

[AIAA PAPER 71-278]

08 p1228 A71-22003

Free flight ranges application to high temperature gas dynamics, using mathematical model to relate sub and full scale observations

11 p1705 A71-26269

Hypersonic free flight test facilities using light gas guns, considering wake of flight vehicle at hypersonic velocity and aerothermal phenomena

18 p2898 A71-36411

Gun tunnel free flight testing system and components, discussing model dropping, magnetic suspension and light beam and RF tracing

[DFVLR-SONDDR-136]

21 p3362 A71-40382

Free flight model accelerations, forces and trajectory measurements in short duration facilities, using optical methods and digital recording

21 p3362 A71-40383

Sequential electric spark technique for hypervelocity projectiles turbulent wake velocity measurements at ballistic ranges in free flight regime

21 p3362 A71-40385

Cooled film anemometer techniques for hypersonic wake temperature and velocity distribution measurements for projectiles in free flight range

21 p3363 A71-40386

Hypersonic turbulent wake density measurements in free flight hypersonic ranges by electron beam fluorescence probe technique

21 p3363 A71-40389

FREE FLOW

Frictionless rotationally symmetrical free supersonic gas jets with thermodynamic relaxation, applying approximate method for shape and flow parameters at boundary

02 p0241 A71-12407

Two free homogeneous turbulent coaxial air jet mixing, showing mass transfer between boundary layers and interface presence

02 p0185 A71-12409

German monograph on radiative transport in freely expanding gas clouds covering analytical and numerical calculations and experiments

03 p0418 A71-14369

Free stream turbulence enhanced stagnation line heat and mass transfer on two dimensional blunt body

04 p0681 A71-15481

Various free stream turbulence levels at nonconverging and converging walls, investigating foreign gas film cooling

04 p0683 A71-15501

Shock induced exothermic reactions on boundary layer transition in shock tube, investigating free stream thermal energy release effects

04 p0572 A71-15503

Supersonic axisymmetric wake-like and two dimensional shear nonuniform free stream flows effects on inviscid flow fields and aerodynamic coefficients of sharp and spherically blunted cones

[AIAA PAPER 71-51]

06 p0843 A71-18512

Wind tunnel experiments on vortex shedding from circular cylinders in oscillating free stream

07 p1090 A71-19908

Beam deflection type fluidic amplifiers with single and symmetric control jets, considering free stream-line flow theory

07 p1025 A71-20557

Laminar mixing region stratified free shear layer stability between two uniform streams from numerical solution of linear sixth order equation for disturbance amplitude function

09 p1432 A71-22851

Thin airfoils theory in nonequilibrium magnetogasdynamics with nonuniform nonequilibrium free stream, using Green function technique

09 p1383 A71-23200

Supersonic conical inlet additive drag formula, using flow data in freestream

10 p1553 A71-24866

Compressible flow in two dimensional boundary layers in arbitrary pressure gradient, using turbulent energy equation for skin frictions and free stream Mach numbers

10 p1598 A71-25082

Centrifugal particle separation limit in free vortex, stressing particle interference with vortex flow and viscous effects

11 p1750 A71-25467

Loads induced on infinite aspect ratio wing by straight infinite free vortex in subsonic compressible freestream, using planar lifting surface theory

11 p1702 A71-25474

Boundary layer separation at free streamline attached to body sharp trailing edge, comparing asymptotic solution with numerical analysis of flow on flat plate

12 p1896 A71-27218

Nozzle wall hypersonic turbulent boundary layers at free stream Mach number, using pitot, hot wire, wall pressure fluctuation and static pressure measurements

[AIAA PAPER 70-746]

12 p1898 A71-27558

Monograph on free and confined vortex gas burner flow characteristics covering pressure distribution, velocity, power law, mass flow in boundary layers, etc

13 p2047 A71-28496

Laminar boundary layer separation by free stream with large amplitude oscillating velocity, using multiple hot-wire anemometer arrays

13 p2050 A71-29247

Freestream density field in nonequilibrium dissociating nitrogen flow over circular cylinder, using free piston shock tunnel and optical interferometry measurements

14 p2169 A71-29884

Equation for motion of buoyant free vortices in inviscid fluid subjected to gravity

[AIAA PAPER 71-604]

15 p2388 A71-31543

Turbulent compressible underexpanded two dimensional jet interaction with crossflowing free stream, analyzing flow field by numerical solution of Navier-Stokes equations

[AIAA PAPER 71-611]

15 p2514 A71-32277

Low speed testing of VTOL models in wind tunnels, describing method for estimating free air approach velocity and angle of attack

15 p2386 A71-32724

Aerodynamic free vortex loading on two dimensional wing at zero incidence at low speeds in incompressible flow

16 p2521 A71-33420

Continuous flush electrostatic probe for weakly ionized flowing gas surface density gradient and charged particle free stream density determination, obtaining I-V characteristics

18 p2950 A71-35858

Noise generation due to inlet free stream turbulence incident on isolated stators and rotors, using flat plate cascade blade row model

18 p2956 A71-36498

Near wake streamline configuration in symmetry plane of slender cone in hypersonic flow at free stream Mach number 7

18 p2848 A71-36754

Free stream turbulence effects on local heat transfer from sphere situated in forced convection air flow

[ASME PAPER 71-HT-8]

19 p3164 A71-37985

Supercritical carbon dioxide free convective heat transfer, investigating heater surface material and flow effects

[ASME PAPER 71-HT-27]

19 p3165 A71-37997

Modified asymptotic perturbation expansion method application to free flow rotation effect on boundary layer for hypersonic flow about blunt body

20 p3177 A71-39483

Free vortices from slender wings, controlling strength, position, core stability and thickness on basis of one dimensional flow model

21 p3319 A71-40492

Shock wave diffraction at symmetric lenticular wing profile with free stream critical Mach number of 0.87, using Godunov difference scheme

21 p3322 A71-40679

Blunt and hemispherical base axisymmetric bodies in Mach 4 free stream, investigating turbulent near wakes generation

21 p3324 A71-40999

Free shear layer similarity flow profiles correlation for turbulent isobaric jet mixing by spread rate parameters, using viscosity models

21 p3371 A71-41032

FREE JETS

Maximum ion concentration zone in diffusively turbulent flames in fuel gas free jets, using mass exchange processes analysis

01 p0178 A71-10341

One dimensional motion of unsteady incompressible conducting free jet in transverse magnetic field, noting computer solution by characteristics method

01 p0133 A71-10792

Two dimensional free gas jet expansion into quiescent medium, predicting terminal shock position

03 p0400 A71-13466

Free and impinging axisymmetric turbulent jet characterization model providing continuous transition from nozzle exit through fully developed region

[ASME PAPER 70-WA/FLCS-6]

03 p0401 A71-14082

Heated glass free jet characteristics at low Reynolds numbers, evaluating temperature distribution and two dimensional fluid dynamic effects

[ASME PAPER 70-WA/FE-3]

03 p0521 A71-14125

Turbulent pulsation mixing of free gas jets in mechanical vortex generator with turbulization level control

04 p0577 A71-15621

Critical nozzle pressure ratio and geometry effects on free exhaust gas jets of jet engine models

[DGLR-70-055]

05 p0831 A71-15966

Aerodynamic sound generation by turbulent circular free jets, presenting solution to inhomogeneous acoustic wave equation by Lighthill

[DFVLR-SONDDR-87]

06 p0881 A71-17421

Centerline velocity and concentration decay predictions of free and confined jet models with/without secondary flows, considering turbulent mixing

[AIAA PAPER 71-3]

06 p0883 A71-18478

Uniform magnetic field parallel alignment effects on incompressible electrically conducting free two dimensional jet flow stability at large Reynolds number

07 p1084 A71-18745

Free nitrogen jets ejected from small orifices, measuring acoustic emission level and spectral pattern dependence on pressure

07 p1161 A71-20058

Compressible two dimensional laminar and turbulent free jet characteristics, presenting unitary method with similarity transformation

07 p1029 A71-20593

Fluidic/electronic pressure ratio computer prototype, using two free jets interaction for instrument error reduction

07 p1031 A71-20603

Aeroacoustic phenomena in free turbulent gas jets, discussing structure, noise-turbulence correlations and acoustic field generation at subsonic/critical velocities

09 p1384 A71-23607

Turbulent characteristics of circular subsonic free jet impinging normal to flat plate, measuring heat transfer rates

10 p1694 A71-23951

Circular subsonic free jet impinging on wall, investigating high intensity frequency noise and turbulence spectrum

10 p1594 A71-24594

Flow field properties of impinging free jets from circular convergent nozzle, measuring velocity, surface pressure and momentum flux

10 p1552 A71-24616

Entrainment induced potential flow near free jets, using equivalent sink distribution derived from known boundary layer solutions

10 p1596 A71-24937

Annular free jets application as air curtains, formulating relations for plane and conical jets to calculate deflection of particles

[DFVLR-SONDDR-106]

10 p1596 A71-24938

Turbulent free jets expansion, presenting method for velocity distribution calculation via suitable correlations between average velocity and turbulent fluctuations

10 p1596 A71-24939

Curvature effects on laminar and turbulent free jet boundary between irrotational flow and stagnant fluid, discussing pressure effects

11 p1702 A71-25482

Diffusive separation of binary gas mixture in free jet expelled into vacuum, comparing theory and experimental results

13 p2050 A71-29216

Approximate calculation for axisymmetric interaction between freely expanding jet and obstacle by reduction to problem of uniform gas flow past sphere

13 p1994 A71-29232

Carbon dioxide free jet plumes issuing from supersonic nozzle into high vacuum, measuring densities and temperature

13 p2026 A71-29355

Liquid phase evaporation rates in free turbulent air-liquid droplet jet, giving droplet dynamic characteristics determination criterion

14 p2227 A71-30613

Submerged free air jet with laminar parabolic profile, investigating pressure recovery characteristics for various tube diameters, spacing and Reynolds number

15 p2389 A71-31683

Free jet expansion of liquid-gas bubble mixture suspended in glycerine

17 p2728 A71-34891

Main parameters of free supersonic jets of ideal compressible fluid, comparing with numerical calculations and experimental data

19 p2991 A71-37081

Translational freezing in free expanding jets of Ar, nitrogen and carbon dioxide from molecular beam intensity measurements, deriving perpendicular temperature

19 p3045 A71-37882

Acoustical oscillations effect on free jet flow stability and structure, using inviscid Orr-Sommerfeld equation for flow disturbances frequency, wavelength and velocity
20 p3175 A71-38806

Compressible circular free jet instability allowing for turbulent boundary layer thickness, considering influence of axisymmetry on spatial growth rate and disturbance phase velocity
21 p3365 A71-40013

Direct local density gradient measurement in rarefied free jet flow using electron beam deflection signal processed with lock-in amplifier
21 p3364 A71-40394

Diagnostics of Ar free jet expansion from high pressure inductive arc source into low density wind tunnel, observing background gas effects
22 p3583 A71-42048

Temperature and electron density measurements for free jet of ionized nitrogen at atmospheric pressure by plasma spectroscopy, estimating Prandtl numbers
23 p3664 A71-44197

Free axisymmetric turbulent annular nozzle jet propagation, detailing velocity distribution variation due to momentum loss in stall region
23 p3664 A71-44335

Two dimensional potential flow model of Pitot static probe and subsonic free jet interaction, using conformal mapping and hodograph method
[AIAA PAPER 71-998]
24 p3817 A71-44589

FREE MOLECULAR FLOW

Spheres drag coefficient at hypersonic Mach numbers for near free molecular flow
01 p0002 A71-10969

Electron density measurement behind shock waves in air/argon mixture by free molecular Langmuir probes
04 p0629 A71-14705

Monte Carlo method for ultrahigh vacuum free molecule flow transmission probability for straight tubes
05 p0785 A71-16395

Approximate bridging relations for heat transfer, surface shear and drag in transitional regime between free molecule and continuous flows
07 p1087 A71-18894

Velocity distribution measurement of Cs gas flow from orifice in near-free molecule regime, using apparatus based on time of flight method
09 p1432 A71-22682

Free molecular flow on cryosurface in cylindrical space simulation chamber with spherical test object
09 p1433 A71-23005

Steady hypersonic nearly free molecular rarefied gas flow about convex body, applying kinetic operator
13 p1991 A71-29152

Gas particle radial reflection model application to hypersonic nearly-free molecular flow about convex bodies, solving steady state problem
13 p1991 A71-29153

Photoelectric, bolometric and photographic recording assembly for measurement of light pressure and aerodynamic forces on complex shape body in free molecular flow
13 p2071 A71-29155

Aerodynamic characteristics similarity and variation in hypersonic flow transition region from free molecular flow to solid medium
13 p1991 A71-29172

Density distribution of neutral matter in cometary atmosphere in transition region between hydrodynamic and free molecular flow
15 p2484 A71-31662

Conical converging nozzle flow of perfect monatomic gas in rarefied near continuum, transition and near free molecular regimes, using finite difference methods
15 p2390 A71-32045

Spherical free-molecular electrostatic probe surrounded by finite sheath, calculating I-V characteristic saturation current regimes
15 p2409 A71-32100

Sphere drag in hypersonic jet transition flow near free molecule limit, using magnetic suspension method
15 p2347 A71-32124

Flow field and model wall on slender bodies in low density hypersonic flows ranging from free molecular flow to continuum flow
18 p2846 A71-36418

Rarefied gas flow characteristics through pipe orifice in intermediate range of rarefaction between free molecular flow and continuum flow
18 p2849 A71-37023

Shock tunnel drag measurements on sharp slender cones in near free molecule hypersonic flow in air and He
19 p2993 A71-37897

Steady slow free molecule flow past sphere, obtaining distribution function and surface boundary conditions
21 p3370 A71-40987

FREE OSCILLATIONS
U FREE VIBRATION

FREE RADICALS

Free radical activity in white mice tissues under hyperbaric oxygenation, examining antioxidants effects
01 p0012 A71-11075

Free radicals role in photodynamic inactivation of Rhodotorula glutinis subjected to high intensity light irradiation
01 p0019 A71-11560

Air-acetylene and air-propane-butane flames absorption spectra, determining distribution of free Ca and Na atoms and OH hydroxyl radicals
03 p0518 A71-13501

Free radical effect on exchange reaction between ammonia and deuterium in high diluted argon shock tube
04 p0548 A71-14698

Reactivity measurements of protective agent selenourea toward primary water radiolysis radicals
07 p1033 A71-18934

Organic free radical radioprotective and radiosensitizing effect, reporting Chinese hamster cell line survival characteristics after treatment
07 p1035 A71-18949

Organic free radical photographic films for biomedical microimaging
07 p1110 A71-19475

Methyl radicals reactions produced by azomethane or ethane pyrolysis in reflected shock waves, describing chain reaction mechanism
08 p1250 A71-20668

Halogen molecules electron affinities by measuring negative ion average translational energy and appearance potentials, noting free radicals heat of formation
09 p1498 A71-23376

French book on macromolecular chemistry covering solid state polymers, polymerization reactions involving free radicals, linear viscoelasticity, vitreous transition of macromolecular polymers, electrical conductivity, etc
11 p1729 A71-26152

Reacting gases analysis by mass spectroscopy, discussing stable products microprobe and molecular beams effective samplings for free radicals and active atoms
11 p1765 A71-26278

Temperature and radical concentration measurements for high temperature flowing gas streams in rig simulating conditions in ramjet combustion chamber and nozzle
13 p2162 A71-28758

Hydrocarbon flame radicals excitation nature observation by photoelectric measurements, noting irrelevance to electron-ion recombination
15 p2463 A71-31389

CH free radicals detection in oxacetylene flame magnetic resonance absorption spectrum by IR water vapor laser
15 p2420 A71-32380

Metal additives catalytic effect on free radicals recombination rates in hydrogen-oxygen-nitrogen flames
15 p2515 A71-32552

CN radical red system molecular constants, considering degenerate perturbation effects in shifts between electronic states
19 p3106 A71-37405

Metal additives catalytic effects on premixed hydrogen-oxygen-nitrogen flames free radical recombination rates, discussing heterogeneous and homogeneous schemes
19 p3012 A71-38082

Activation energy and temperature dependence of radiation induced free radical destruction in N-acetyl-DL-valine, using Arrhenius plots
21 p3345 A71-40203

Visible coherent radiation generation mechanism in ionized oxygen and nitrogen, considering free radical stabilized on discharge tube wall and metastable atom creation
23 p3706 A71-42889

CH radical 10 cm line frequency determination by photographic Fabry-Perot interferometry
23 p3733 A71-43082

FREE STREAM EFFECTS
U FREE FLOW
FREE STREAMS
U FREE FLOW
FREE VIBRATION

Thin elastic orthotropic plate in finite difference formulation, determining natural vibration mode and instability by summary representation method
01 p0168 A71-10410

Uniformly turbulized incompressible heavy fluid sloshing and free oscillations in rigid rotating vessel, using linear surface wave theory
01 p0069 A71-10411

Spheroidal solutions near center for free oscillations of self gravitating rheological spherical mass
01 p0127 A71-10462

Thermal prestress effect on natural vibrations of hinge supported isotropic cylindrical shell, integrating equations of motion by Bubnov-Galerkin method
02 p0322 A71-11738

Free lateral vibration of viscoelastic metallic beam under axial creep, considering elastic deformation
02 p0324 A71-11996

Axisymmetric and unsymmetric free vibrations of orthotropic sandwich cylindrical or conical shells under various boundary conditions
02 p0325 A71-11999

Equations of motion for free vibrations of three layer plate, considering energy dissipation in soft low modulus of elasticity middle layer
03 p0502 A71-13404

Console rod free and forced transverse vibrations amplitude dependent damping, considering longitudinal tensile force effect and hysteresis
03 p0502 A71-13405

Astatic gyroscope with viscous friction at suspension system axes, noting free nonlinear vibrations and motion
03 p0423 A71-13411

Rotor and rotor-disk system response to constant and pulsating torque, experimentally examining critical whirling speed and lateral vibration
[ASME PAPER 70-WA/DE-14]
03 p0511 A71-14146

Buckled beam nonlinear vibration under harmonic excitation, solving governing partial differential equation by Galerkin and harmonic balance methods
[ASME PAPER 70-WA/APM-48]
03 p0512 A71-14167

Nonlinear partial differential equation solution for natural free-free vibrations of beam structures
[ASME PAPER 70-WA/APM-55]
03 p0513 A71-14172

Single axis gyroscopic stabilizer with floating type integrating gyro, describing natural oscillations by differential equations of motion
03 p0429 A71-14237

Gas flow past straight airfoil, analyzing damped natural oscillations
03 p0345 A71-14561

Axisymmetric free transverse vibration frequencies of centrally clamped spinning membrane disks
04 p0668 A71-15186

Free transverse oscillations of closed prismatic shell of flexible rectangular panels filled with compressible inviscid liquid
04 p0573 A71-15564

Multilayered anisotropic cylindrical shells free vibration modes
05 p0819 A71-15982

Uniform thin orthotropic skew flat plates free undamped vibration based on classical plate theory, using Rayleigh-Ritz method
05 p0820 A71-15987

Isotropic circular plate natural vibrations for inhomogeneous boundary conditions, using net point method to derive finite difference equations
05 p0821 A71-16353

Orthotropic shells of revolution free vibration theory, including transverse shear and rotary inertia effects
05 p0823 A71-16495

Singly curved rectangular plate free vibration characteristics obtained by partial differential equations of motion
05 p0825 A71-16605

Thin walled shell free linear vibrations frequency density calculation using asymptotic method
05 p0829 A71-16994

Natural transverse vibrations of beam with variable cross section and parameters exhibiting small random deviations
06 p0983 A71-17368

Circular cylindrical sandwich shell natural vibrations reduced to shell and filler contact problem, using two and three dimensional models
06 p0990 A71-17792

Natural vibrations of partially liquid filled closed spherical shell for arbitrary boundary conditions, using approximate method
06 p0991 A71-17798

Thin elastic shell of revolution with negative Gaussian curvature, discussing free nonaxisymmetric oscillations
06 p0992 A71-17811

Thin elastic partially liquid filled shells of revolution, applying asymptotic integration method to free vibrations case
06 p0995 A71-17834

Thin paraboloidal shells of revolution under external hydrostatic pressure loading, analyzing free vibrations by finite element method
[AIAA PAPER 71-214]
06 p1004 A71-18650

Free vibration of spherical sandwich shell under axisymmetric static and dynamic loading
07 p1212 A71-19590

Spherical sandwich shells free vibration motion equations, taking into account transverse shear deformation and rotatory inertia effects
07 p1215 A71-20095

Thin cylindrical shell of revolution delamination detection model, using free vibration natural frequency parameter under clamped-clamped conditions
07 p1216 A71-20135

Planarly-rectangular shallow shells with double curvature geometry, analyzing natural oscillations by finite difference procedure

07 p1219 A71-20649

Box type structure free vibrations investigation by rectangular finite elements, comparing with natural frequencies and normal modes solution

08 p1369 A71-20807

Energy dissipation in free oscillations of multilayer shells consisting of alternating rigid elastic layers and soft fillers, deriving equations of motion

08 p1369 A71-21123

Book of tables and graphs for circular cylindrical shells free vibrations

08 p1370 A71-21234

Free flexural vibrations of orthotropic rectangular plates subjected to large amplitude free or forced oscillations, using von Karman nonlinear equations

08 p1370 A71-21307

Clamped-free and clamped-ring-stiffened cylindrical shells free vibrations analysis for digital computer programming, using Rayleigh-Ritz technique for approximate solution

08 p1371 A71-21427

Free and forced vibrations of three layer freely suspended plate with allowance for energy dissipation

08 p1372 A71-21707

Free vibrations of closed spherical shell immersed in ideal incompressible fluid at arbitrary depth

09 p1535 A71-22182

Small natural vibrations effect of solar sail-propelled system on heliocentric orbit motion

09 p1531 A71-22559

Thin simply supported polygonal and rhombic plates critical hydrostatic buckling loads and free vibration frequency calculation by conformal mapping and power series expansion

10 p1686 A71-24018

Orthotropic shells of revolution with concentrated masses and oscillator inclusions and reinforced by stringers and ribs, calculating free vibration by Ritz method

10 p1690 A71-24570

Hinged sandwich beams loaded by concentrated masses, calculating natural vibration frequencies with and without allowance for rotatory mass inertia

10 p1690 A71-24571

Approximate analytical formulas for free oscillations of nonstationary linear control systems using canonical transformations

10 p1643 A71-24898

Nonstationary linear systems analysis over finite time interval and graphical method for differential equation, comparing exact and approximate solutions for free oscillations

10 p1643 A71-24908

Heterogeneous orthotropic cylindrical shells, calculating free natural vibration frequency spectra from refined equations of motion in Love and Donnell type theories

11 p1841 A71-25184

Finite element method for stiffness matrix free vibration analysis of thin rectangular plates under central planar loadings

11 p1842 A71-25313

Nonlinear elastic shells free vibrations, obtaining phase trajectories with finite bending within Hooke's law

12 p1975 A71-27106

Free vibrations of three dimensional system of rods subjected to transverse vibrations in two planes of symmetry

12 p1930 A71-27172

Oscillation theorem for natural vibrations of thin shells of revolution, considering boundary value problem eigenvalues

12 p1977 A71-27304

Initial thermal stresses effect on natural vibrations of orthotropic cylindrical shells

12 p1979 A71-27360

Kane-Mindlin differential equations solved by perturbation techniques for free extensional vibrations in elastic plates

12 p1981 A71-27483

Free vibrations of isotropic nonhomogeneous circular plates, deriving closed form expressions for nodal frequencies

12 p1983 A71-27587

Adaptive automatic control systems, determining damping coefficient and natural oscillation frequencies with second order differential equations

13 p2041 A71-28639

Viscoelastic and elastic shells boundary value problems relation, studying natural and forced oscillations of isotropic viscoelastic shells

13 p2155 A71-28656

Cylindrical shells of revolution with various boundary conditions, calculating free vibrations with differential equations

13 p2156 A71-29067

Damping characteristics (absorption coefficient) of dissipative systems, defining authentic value of energy dissipation characteristic determination from forced and free vibrations

14 p2321 A71-29618

Nonlinear differential equations system for one degree of freedom isochronous and anisochronous conservative oscillators resonance behavior during natural perturbation solved by coordinate transformations

14 p2265 A71-29687

Transverse free vibrations of beam with one end fixed and other supported on bilinear spring and carrying concentrated mass

14 p2323 A71-29847

Radial free vibration frequency of pressurized orthotropic shells with bending terms

14 p2325 A71-29886

Nonlinear free oscillations, discussing linearization for nonlinear functions by weighted mean square method

14 p2325 A71-30060

Curvature effects on shallow shell free vibration frequencies, solving linear eigenvalue problem

14 p2325 A71-30062

Imperfect circular disks large amplitude free transverse vibration calculation by Galerkin procedure

14 p2326 A71-30064

Laminated plate flexural mode free vibration analysis by asymptotic method, obtaining phase velocity for comparison with experiment

14 p2330 A71-30684

Free vibrations of beam-like structures, deducing equations of motion

15 p2502 A71-31419

Isotropic elastic thin oval rings nonlinear free and forced flexural vibrations calculation by Galerkin method

15 p2503 A71-31436

Integrally stiffened five bay panel, calculating free vibration and random response to jet noise excitation [AIAA PAPER 71-585]

15 p2504 A71-31532

Clamped anisotropic symmetrically laminated plate bending, buckling and free vibration exact solution, using Fourier analysis

15 p2506 A71-32013

Rectangular plates under direct and shear in-plane forces, considering free lateral vibrations

15 p2509 A71-32512

Imperfect circular cylindrical shell under external hydrostatic pressure loads, determining free and resonant vibration modes

16 p2651 A71-33062

Free vibrations of linear structure with arbitrary support by Rayleigh-Ritz method using unconstrained normal modes

16 p2656 A71-33218

Missiles free flexural vibrations on moving or stationary launching pad calculated by matrix method

16 p2656 A71-33340

Isoperimetric problem upper bounds for fundamental frequencies in free oscillations of incompressible fluid in container

16 p2559 A71-33483

Lunar forced motions and free oscillations, considering inertia moments effects on rotational and translational movements

16 p2636 A71-33502

Elastic spherical shell coupled to rigid body, calculating asymmetric free vibration natural frequencies and mode shapes from boundary conditions

17 p2817 A71-34339

Concave thin shell of revolution lowest natural vibration spectra frequency corresponding to simple inflection point

17 p2817 A71-34341

Hydraulic system self acting valves natural vibration dynamic characteristics, showing energy transfer by phase shift of variable hydrostatic compression component

17 p2677 A71-34349

Finite length thin circular cylindrical shells with clamped or simply supported edges, calculating flexural free vibration natural frequencies

17 p2822 A71-34643

Freely vibrating supported elastic isotropic oval cylindrical shells natural frequencies and mode shapes

17 p2825 A71-34873

Free and forced nonlinear oscillations differential equations approximate solution by orthogonal polynomial linearization, applying method to systems analysis near singular points

17 p2780 A71-34917

Free and forced nonlinear oscillatory systems with harmonic perturbations, noting amplitude dependence on force frequency and friction coefficients

17 p2782 A71-34935

Equations of motion for free vibrations of three layer plate, considering energy dissipation in soft low modulus of elasticity middle layer

17 p2825 A71-35014

Cantilever bar free and forced transverse vibrations amplitude dependent damping, considering longitudinal tensile force effect and hysteresis

17 p2825 A71-35015

Nonlinear free oscillations of astatic gyroscope with viscous friction at suspension system axes

17 p2743 A71-35019

Finite length heterogeneous thin layered cylindrical shell axisymmetric free vibration frequency spectrum analysis

17 p2826 A71-35083

Natural vibration parameters of cantilevered isotropic plates, using finite difference method with matrix form solution

17 p2829 A71-35300

Partially liquid filled cylindrical shells with elastically supported end rims, deriving algorithm for nonaxisymmetric natural vibration frequency calculations

17 p2833 A71-35614

French book on linear vibrations covering systems with one or more degrees of freedom in free and forced vibration, propagation in discontinuous and continuous media, etc

17 p2784 A71-35753

Dynamic flexibility method based on Green resolvent, presenting applications to linear damped/un-damped forced/free harmonic/periodic vibration

18 p2947 A71-36177

Spinning centrally clamped thin shallow spherical shell free vibration numerical analysis by considering perturbation about equilibrium configuration [ASME PAPER 71-APM-G]

18 p2977 A71-36254

Beam column with probabilistic material and geometric properties, axial loads and boundary conditions, obtaining free vibration and natural frequency stochastic equations

18 p2979 A71-36358

Thin walled shell free linear vibrations frequency density calculation using asymptotic method

18 p2982 A71-36794

Free vibrations frequencies and mode shapes of anisotropic elastic thin plates, using Galerkin method

18 p2983 A71-36931

Natural axisymmetric vibration of thin elastic shell of revolution, deriving eigenvalues convergence to spectrum lower bound by asymptotic method

19 p1354 A71-37097

Natural vibrations of two coaxial rotors with unbalanced disk and different angular velocities, solving equations of motion by energy balance method

19 p1356 A71-37536

Rectangular cantilever plate free vibration under in-plane acceleration loads, calculating frequencies and mode shapes by Ritz method and computer technique

19 p1357 A71-37850

Minimum mass design of two dimensional plate-like structure with free vibration fundamental frequency or aeroelastic constraints, using optimal theory for extremum

19 p1358 A71-37877

Oscillation theorem for natural vibrations of thin shells of revolution, considering boundary value problem eigenvalues

19 p1359 A71-38264

Natural oscillations existence in cross section of cylindrical waveguide with resonant cavity based on Hilbert space operators, solving boundary value problem

19 p3019 A71-38336

Free and forced nonlinear vibrations of rigidly clamped thin circular plate, deriving ordinary differential equations

20 p3307 A71-38795

Vibrational behavior of nonlinear systems subjected to finite duration pulse excitation, transforming original differential equation into Lighthill method solvable form

20 p3267 A71-38798

Plasma layer effect on natural oscillations of magnetosphere tail, using infinite plasma cylinder model immersed in interplanetary plasma

20 p3216 A71-39137

Numerical analysis of natural frequency spectrum of elastic plate free vibrations in compressible inviscid fluid

20 p3310 A71-39784

Forced and free vibrations of shallow cylindrical shell in rectangular duct filled with ideal fluid

20 p3310 A71-39785

Lumped parameter models for description of continuous one dimensional and Bernoulli-Euler beam vibration, compared on basis of maximum system strain energy

21 p3456 A71-40268

Nonlinear free and forced vibration response and stability of simply supported restrained buckled beams, using analog computer simulation

21 p3458 A71-40277

Wake formation behind circular cylinders undergoing self excited and forced transverse oscillations

21 p3458 A71-40282

Lightweight free oscillating cone shaped model design for intermittent wind tunnel facilities, discussing dynamic stability derivatives measuring techniques

21 p3363 A71-40390

Hot-wire anemometer measurement of free oscillation damping of viscous and sluggish fluid in U tube, determining velocity distribution

21 p3366 A71-40512

Thin truncated conical shells axisymmetric free vibrations, considering shear deformation and rotary inertia effects
21 p3462 A71-40528

Free radial vibrations of curved beams by finite element method, using model to investigate variation with subtended angle of six lowest natural frequencies
21 p3462 A71-40529

Curved sandwich beams free flexural vibration by finite element method, noting parameters effects on natural frequencies
21 p3462 A71-40533

Static characteristics and free vibration of doubly curved honeycomb sandwich plates, using finite element method
21 p3462 A71-40534

Clamped circular elastic plate nonlinear free vibrations, obtaining mode shapes and amplitude-frequency relationships
21 p3471 A71-41025

Free and forced finite amplitude nonlinear oscillations of thin elastic annular plate with free inner and clamped immovable boundaries
21 p3471 A71-41026

Natural vibrations of closed reinforced cylindrical shell clamped at end faces
21 p3473 A71-41153

Velocity profiles of heavy viscous fluid free oscillatory motion in U-tube by hot-wire anemometry
22 p3531 A71-42242

Free axisymmetric torsional vibrations of thick hollowed conical frustums cantilevered at small end, considering conicity and cone thickness effects
22 p3618 A71-42590

Oval cross sectioned cylindrical shells, deriving free oscillation solution
23 p3775 A71-43310

Resonance equation for rotating shaft natural vibration, using Timoshenko beam theory and gyroscopic moments
23 p3776 A71-43377

Thin elastic shell of revolution with waves along parallel, considering small free nonaxisymmetric vibrations
24 p3877 A71-44406

Natural vibrations of complex shape plates with clamped edge on resilient base, deriving approximate solution via R functions
24 p3877 A71-44481

Free elastic vibrations and waves in laminated orthotropic circular cylinders
24 p3878 A71-44561

Natural and forced joint vibrations of liquid and shallow spherical shells
24 p3881 A71-44829

Structural materials ability for irreversible conversion of mechanical to thermal energy from free longitudinal vibrations attenuation measurements in rod
24 p3817 A71-45200

Shell of revolution natural vibration spectrum, investigating moment and momentless type systems of differential equations
24 p3886 A71-45342

Elastic momentless shell completely filled with ideal incompressible liquid, detailing small steady natural vibrations
24 p3821 A71-45344

FREEZING
NT VIBRATIONAL FREEZING
Air temperature and wind speed role in finger-freezing time
02 p0197 A71-11669

Halophilic bacteria growth in freeze-thaw environment, investigating cooling and warming rates and solute concentrations
09 p1388 A71-22131

One dimensional heat conduction with freezing or melting in bodies with variable cross sectional areas, using phase boundary rate of propagation equations
10 p1698 A71-25099

Finger freezing time correlation with cooling rate, discussing effects of indeterminate skin supercooling
18 p2860 A71-36883

Frozen bipropellants as self supporting structural member for booster weight reduction, considering mechanical and thermal properties and melting rate requirement
20 p3276 A71-39609

Hydrazine-hydrazine azide blending for propellant performance improvement and freezing point reduction, presenting engine test data
22 p3588 A71-42778

Combined and individual effects of UV light, X ray irradiation and freezing-thawing cycles on ribonuclease
22 p3496 A71-42830

FREEZING POINTS
U MELTING POINTS
FREIGHT COSTS
Air freight economics and growth forecast, discussing rates, cost and technological aspects
22 p3623 A71-41840

FRENCH SATELLITE
NT FR-1 SATELLITE

FRENCH SPACE PROGRAMS

Satellites applications in French space programs, discussing telecommunication, meteorology, air navigation aids, space geodesy and earth resources
02 p0337 A71-12918

Diamant B French satellite booster development program, discussing general aims, specific objectives, program implementation, organization and industrial facilities
04 p0664 A71-15820

Low, medium and high specific impulse microthrusters development in France, using cold gases, subliming solids, hydrazine, ammonia and cesium ions
07 p1184 A71-19865

[AIAA PAPER 70-617] French space telecommunication policy report, noting European, autonomous and educational options
11 p1861 A71-26522

Eole project for atmospheric phenomena studies, describing meteorological satellite/balloons arrangements, equipment and operational methods
15 p2500 A71-31824

French space programs review with emphasis on compatibility with European and international programs
15 p2495 A71-32689

French aerospace research for aircraft, missiles, spacecraft and related power plant developments, discussing optimization methods, materials, reentry phenomena, etc
15 p2500 A71-32691

Report to COSPAR on French space program covering ionosphere and magnetosphere physics, meteorology, cosmic rays and earth resources
16 p2666 A71-33861

Ion propulsion R and D at ONERA, discussing ionizer test control procedures, attitude control simulation and neutral fraction measurements
17 p2793 A71-35536

[DGLR-71-027] Mixed satellite TV broadcasting system for France, estimating cost
18 p2988 A71-36505

Ground acquisition of digital rate synchronization during experiments in French Dioscours project
18 p2946 A71-36512

Data transmission system of Franco-German Symphonie communication satellite
18 p2889 A71-36523

Franco-German Symphonie communication satellite reliability measures, describing component selection methods
18 p2889 A71-36524

French space programs, discussing European and international activities, telecommunication, meteorology, data collecting, natural resources and air and sea traffic control
18 p2975 A71-36753

Meteosat satellite for taking earth photographs and relaying between weather stations
19 p3154 A71-38474

Project management methods oversophistication, discussing French space activity and managerial apprenticeship
23 p3785 A71-43454

CNES hypotheses and methods determining current delivered by solar generator of FR 1 satellite, discussing electrical performance due to electron and proton irradiation
24 p3793 A71-44760

French-American Eole project for meteorological prediction systems development, discussing balloon sounding and satellite data transmission
24 p3876 A71-45274

FRENKEL DEFECTS
Dynamic carrier density instabilities for semiconductor-metal electronic phase transition by Frenkel-Poole effect in seminsulator with donors
23 p3716 A71-43478

FREON
Supersonic cylindrical freon compressor with low blade height for elementary compression and flow visualization aerodynamic and thermodynamic tests
17 p2793 A71-35467

Mass flow rate measurements and calibration in heterogeneous medium with hot wires tested on Freon mixtures
19 p3163 A71-37894

N-heptane, carbon dioxide and Freon 13 droplet vaporization measurements at supercritical pressure, comparing with film theory calculation
24 p3890 A71-45072

FREQUENCIES
NT AUDIO FREQUENCIES
NT BEAT FREQUENCIES
NT BROADBAND
NT C BAND
NT CARRIER FREQUENCIES
NT CRITICAL FREQUENCIES
NT CYCLOTRON FREQUENCY
NT EXTREMELY HIGH FREQUENCIES
NT EXTREMELY LOW RADIO FREQUENCIES
NT HIGH FREQUENCIES
NT INFRASONIC FREQUENCIES
NT INTERMEDIATE FREQUENCIES
NT IONIZATION FREQUENCIES

NT LOW FREQUENCIES
NT MAXIMUM USABLE FREQUENCY
NT MICROWAVE FREQUENCIES
NT NYQUIST FREQUENCIES
NT P BAND
NT PLASMA FREQUENCIES
NT RADIO FREQUENCIES
NT RESONANT FREQUENCIES
NT SUPERHIGH FREQUENCIES
NT SWEEP FREQUENCY
NT ULTRAHIGH FREQUENCIES
NT VERY HIGH FREQUENCIES
NT VERY LOW FREQUENCIES
Frequency correlation between amplitude and phase fluctuations of different-frequency spherical waves propagating in turbulent medium
01 p0073 A71-10545

Automatic frequency spectrum recorder to monitor radio emissions in space service allocated bands
10 p1578 A71-24583

FREQUENCY AMPLIFIERS
U AMPLIFIERS
FREQUENCY ANALYZERS
Solid state circuit digital frequency discriminator with low pass filter in ESRO stations telemetry receivers AFC and antisideband system
05 p0720 A71-16326

Frequency analysis of open loop transfer function, determining combustion instability for catalytic monopropellant thrusters
14 p2286 A71-30759

FREQUENCY ASSIGNMENT
Frequency allocations for radio astronomy
01 p0153 A71-10362

Communication satellite earth station technology, considering steerable antenna subsystems, high power amplifiers, terminal equipment and frequency bands allocation
02 p0222 A71-12787

NASA program concerning determination of RF spectrum sharing criteria and automatic data processing in aerospace systems
03 p0381 A71-14588

Electromagnetic compatibility in space age, discussing effects of spectrum crowding, wider bandwidths, coding forms and growing use of microelectronics and solid state devices
04 p0555 A71-15342

Randomly used shared communication channels capacity, calculating probability function dependence on frequency assignment policy
05 p0721 A71-16467

UHF sharing between space and terrestrial services, discussing relationships between frequency choice, satellite relay performance, RF power requirements and system costs
07 p1065 A71-20419

International radio regulations adopted by Geneva space conference with reference to frequency band allocations in 1-10 GHz range with equal rights to space and terrestrial services
17 p2697 A71-34246

Maritime operational and frequency requirements for satellite system having worldwide coverage
17 p2697 A71-34251

Short wave frequency-diversity radio communication systems operating at extremal frequencies of group, estimating noise reduction effectiveness
17 p2698 A71-34395

European regional satellite communication system, discussing TV coverage, spot beam antennas, frequency reuse, speech interpolation and circuits allocation
17 p2700 A71-34679

Satellite voice communications system for small terminals in remote areas, discussing feasibility, design, cost and frequency allocation
17 p2706 A71-35123

Unilateralism in U.S. satellite communications policy, suggesting international cooperation for frequency spectrum management
18 p2986 A71-36165

Satellite telecommunications problems, discussing frequency assignment and power efficiency
18 p2877 A71-36515

European regional satellite communication system, discussing TV coverage, spot beam antennas, frequency reuse, speech interpolation and circuits allocation
18 p2877 A71-36516

European 12 GHz regional satellite telecommunications systems, discussing band assignment limitation and frequency reuse
18 p2877 A71-36517

Adaptive frequency selection for reduction of effects of noise differing irregularly from useful pulse signals, estimating error probabilities
18 p2882 A71-36622

Performance characteristics and reuse intervals of high capacity mobile radio systems with dynamic channel assignment, using computer simulations
19 p3014 A71-37216

Wideband spectrum utilization above 10 GHz for high rate digital communications and ecology monitoring of sea state, earth surface contour and atmospheric pollutants
19 p3020 A71-38407

Electromagnetic compatibility in radio astronomy, discussing frequency spectrum pollution and national radio quiet zone 19 p3032 A71-38454

Tabular listing of frequency allocations for space services and radio astronomy made at Extraordinary Administrative Radio Conference 21 p3348 A71-40476

Radio regulation planning and frequency assignments for operational earth exploration satellite service 22 p3623 A71-41974

FREQUENCY BANDS U FREQUENCIES

FREQUENCY COMPRESSION DEMODULATORS
Communication satellite ground station receiver-demodulator equipment using frequency double transposition and compression 17 p2717 A71-35514

FREQUENCY CONTROL

NT AUTOMATIC FREQUENCY CONTROL
Radiation frequency control in cyclotron resonance maser via TEM wavelength oscillations in Fabry-Perot resonator produced by screw electron beam 01 p0095 A71-11212

High power argon laser single frequency emission, discussing dividing mirror reflection coefficient and degree of gain saturation 03 p0435 A71-13504

Air traffic control radar separation by pulse repetition frequency discrimination for double and triple stagger configurations 05 p0720 A71-16347

Automatic phase control system with separating capacitance containing low and high frequency electric filters 06 p0866 A71-17375

IR difference frequency generation using tunable dye laser 06 p0910 A71-18663

Single frequency carbon dioxide laser cavity length computer aided selection for reduced line competition, considering heterodyne communications systems 07 p1121 A71-18811

Emission frequency tunable organic dye laser development and construction 07 p1123 A71-19239

Tunable organic dye laser with dispersion prism for increased radiation spectral density and luminescence band smooth frequency control 12 p1912 A71-26757

Hybrid M-type microwave oscillators including backward and traveling wave tubes with crossed fields in large amplitude mode, considering power efficiency and frequency control 12 p1888 A71-27620

Axial mode locking and equidistant frequency generation in solid state lasers due to active medium saturation, using self consistent equations with broadened amplification line 15 p2418 A71-31189

Synchronization time of nine solid state lasers as function of frequency alignment 15 p2375 A71-31226

Condensed media investigated by variable frequency laser via induced radiative processes, discussing laser design, induced radiation divergence control and induced emission spectroscopy 15 p2419 A71-31383

Ne 20 isotope for selective frequency absorption to obtain monofrequency radiation in He-Ne laser with naturally isotope-doped Ne as active medium 15 p2419 A71-31398

Resonant energy exchanges between gaseous media and externally applied radiation fields from wavelength-tunable lasers 16 p2586 A71-33164

Coupled oscillator circuits simultaneous tuning by plane relationship between circuit currents/voltages/ 16 p2548 A71-34034

Intelsat 3 and 4 RF demodulator design with tracking filters, using varactor for frequency control and discriminator for frequency drift compensation 18 p2890 A71-36558

Asynchronous generators classification based on primary distinction by independent or self operated excitation and stabilized or controlled frequency 19 p3000 A71-38639

Parasitic speed controller for alternator rotational speed and frequency regulation in dynamic space power systems, investigating phase controlled loading improvement 20 p3262 A71-38916

FREQUENCY CONVERSION

U FREQUENCY CONVERTERS

FREQUENCY CONVERTERS

NT DOWN-CONVERTERS

NT FREQUENCY DIVIDERS

NT FREQUENCY MULTIPLIERS

NT FREQUENCY SYNTHESIZERS

NT PARAMETRIC FREQUENCY CONVERTERS

Thyristor circuitry for AC controllers and single phase frequency converter 01 p0051 A71-10262

Earth station mixers design as wideband millimeter wave up- and down-converters for satellite communication systems 02 p0234 A71-12818

High speed homopolar alternators as static frequency converter supplies, optimizing design parameters by computer geometric programming 03 p0352 A71-13052

Aircraft DC to AC converters frequency stabilization systems, describing circuit diagrams and operation principles 03 p0355 A71-14247

Continuous optical conversion to IR and directional stellar radiation flow conversion to diffused radiation fields in circumstellar dust envelopes 07 p1187 A71-19821

Frequency generators using RC (RL) designs with odd selective quadrupole element numbers as converters 07 p1078 A71-20062

Short term frequency stability of precision oscillators and frequency generators, discussing conversion from frequency to time domain and among time domain measures 11 p1739 A71-26422

Receiving system for phase measurement on coherent signals from satellites, discussing frequency conversion through phase locked filter 13 p0303 A71-29275

Planar and nonplanar transistors noise factor dependence on signal source impedance and emitter current, considering amplification and frequency conversion application 14 p2213 A71-30628

Communication satellite ground station transmitting equipment, discussing carrier waves, FM, frequency converters and microwave amplifiers characteristics 17 p2717 A71-35515

Noise temperature in microwave frequency mixers using nonlinear resistors, giving rectifier and diode loss formulas for rectangular and sinusoidal waves 19 p0207 A71-37494

K band satellite transmit/receive frequency converters, describing design features and performance tests under simulated environmental conditions 19 p0328 A71-37697

Solid state RC network for single sideband frequency converter using phase difference carrier suppression 19 p0322 A71-38497

Conversion losses as function of signal power and circuit impedance in narrow band triode frequency converter 19 p0322 A71-38499

Intermodulation distortion in abrupt junction current pumped varactor frequency converter 20 p3202 A71-38848

Satellite-borne minimum bulk and weight K-band transmitter and receiver frequency converters design features and performance 22 p3524 A71-42522

Frequency conversion/division, multiplication and shifting/ application to multistable phase- frequency elements design 22 p3524 A71-42573

Design and performance of semiconductor devices with heterojunctions, covering injection laser without cooling, emission frequency converter and negative resistance triode 24 p3808 A71-44383

FREQUENCY DISTRIBUTION

Microwave scattering from plasma fluctuations produced by forcing gas in turbulent flow through discharge tube, investigating frequency spectrum broadening 01 p0136 A71-11480

Frequency spectra and cosinor for circadian rhythms in rodents and in man during Gemini and Vostok flights, considering future biosatellites 01 p0020 A71-11569

Uniform frequency distribution pseudorandom digital sequences, using shift register generator 04 p0560 A71-14745

Time interval maximum transmittable energy under spectral limitation, deriving time limited pulse functions for minimum energy loss 05 p0720 A71-16393

Thin walled shell free linear vibrations frequency density calculation using asymptotic method 05 p0829 A71-16994

Pc 1 pulsations occurrence frequency diurnal annual and 11 year variations at midlatitudes, relating distribution with carrier frequencies of perturbation 06 p0894 A71-18266

Vapor bubbles during nucleate boiling, deriving formation frequency relationship with departure diameter 07 p1222 A71-19197

Relative spectral sensitivity/ amplitude frequency characteristics/ applicability to describing nonlinear systems 07 p1043 A71-20111

Planar-epitaxial IC resistors p-n junction parasitic effects on cut-off frequency, obtaining design formulas for capacitance and geometry 08 p1264 A71-21074

Laser modulator with multilayer dielectric mirror coating on piezoelectric substrate, investigating vibration distribution and maximum frequency deviation 08 p1303 A71-21806

Image restoration from random fluctuations/ developing analog procedure from time dependent functions of spatial frequencies and approximation 09 p1407 A71-23040

Cumulative frequency curves of terrain slopes/ radar shadow frequency method 09 p1439 A71-23212

Soft X ray radiation correlations to radio emission flux at various frequencies in 20th solar activity cycle 09 p1515 A71-23520

Monocular vision field structural color in violet and yellow region under increasing light frequency and periodic electric stimulation 10 p1560 A71-23999

Frequency equation for harmonic waves with circumferential nodes traveling in composite traction free circular cylindrical shells, using IBM 7094 computer 11 p1847 A71-25464

Distribution curves of F 2 critical frequency variations, considering probability density functions interpretation via asymmetric model 11 p1757 A71-25777

Dye emission frequency variation during quasi-stationary emission process 11 p1774 A71-26000

Universe global structure and quasar frequency distribution based on red shifts and cosmological interpretations 12 p1968 A71-27644

Frequency vs time spectral shapes of magnetospheric VLF discrete emissions for field line and electron stream parameters 13 p0207 A71-27910

Air shower radio pulse amplitude variations with zenith and azimuth angle, distance from shower axis and primary energy, examining frequency spectrum characteristics 13 p2127 A71-28105

Modeling of differences between actual and estimated flight times over radio beacon, obtaining cumulative frequency distributions 13 p2167 A71-28490

Sporadic E layer occurrence frequency distribution during 1958-1960, investigating characteristics over equatorial, temperate and auroral zones 13 p2061 A71-28540

Frequency and temperature variations of active diode region in pulsed GaAs laser, using Fabry-Perot interferometer 13 p2079 A71-28923

Sensible heat meridional transport frequency spectra wavenumber in Southern Hemisphere midtroposphere 13 p2063 A71-29100

Angular momentum meridional transport flux wavenumber-frequency spectral characteristics in midtroposphere of Southern Hemisphere 13 p2063 A71-29100

Surface impedance of sphere based on received electromagnetic field amplitude-frequency characteristics 14 p2191 A71-29511

Aircraft design and fatigue life monitoring, investigating effects of gust velocity frequency distribution in patches of atmospheric turbulence 14 p2174 A71-29785

Radial free vibration frequency of pressurized orthotropic shells with bending terms 14 p2325 A71-29886

Noctilucent cloud incidences relation to solar activity variations, determining frequency spectrum and four year occurrence cycles 14 p2233 A71-29967

Man made radio noise sources frequency-distance dependence and location, noting vehicular ignition power transmission and electrical pulsing 14 p2203 A71-30962

Diffraction technique for three dimensional frequency spectra of photographic images using computer program based on Fourier transformation of optical density distribution 15 p2406 A71-31644

Frequency composition in glass laser with Fabry-Perot resonator producing polarized radiation components, discussing transverse modes selection 15 p2420 A71-32000

Arbitrary shape pulsed AM systems prediction technique improvement, using time-domain signal 15 p2373 A71-32327

Solar microwave burst frequency occurrence statistical analysis 15 p2495 A71-32688

Combination frequency spectrum asymmetry in interaction between high and low frequency plasma oscillations, noting Doppler effect role 16 p2618 A71-33044

Frequency spectrum of lightning discharges/ developing mathematical model to account for at

atmospherics difference between cloud-ground and cloud-cloud discharges 16 p2604 A71-33070

Uniform convergence of frequencies of events in independent tests sequence to probabilities of occurrence 17 p2764 A71-34573

Steady oscillation frequencies in systems described by nonlinear differential equations, including external perturbations 17 p2782 A71-34931

Bistatic radar frequency spectra and cross sections dependence on surface scattering laws, studying echo bandwidth 17 p2702 A71-35026

Finite length heterogeneous thin layered cylindrical shell axisymmetric free vibration frequency spectrum analysis 17 p2826 A71-35035

Radiometric measurements of frequency distribution of solar emission attenuation due to troposphere, noting sun-earth communication paths 17 p2707 A71-35124

Dynamic properties of turbine wheels under bending vibrations, classifying resonant frequencies on basis of vibration modes 18 p2981 A71-36722

Thin walled shell free linear vibrations frequency density calculation using asymptotic method 18 p2982 A71-36794

Wave propagation in three layered plates, giving frequency spectrum 19 p3158 A71-37884

Jet turbulence orderly structure enhancement, control and relation to noise, studying response to periodic surging of frequency and amplitude 19 p3056 A71-38204

Discrete frequency sound radiation from rotating periodic sources covering rotor blade noise in near field and from disk loading asymmetries 19 p2997 A71-38466

Frequency distribution of heart sounds in precordium, studying slope of attenuation and relative peak-
ing 20 p3185 A71-38803

Frequency dependent conductor coating matrices for lossy cylindrical conductors with circular section, using diffusion equation 20 p3197 A71-39450

Numerical analysis of natural frequency spectrum of elastic plate free vibrations in compressible inviscid fluid 20 p3310 A71-39784

Structure and polarization differences of strong pulses from pulsar NP 0532, showing discontinuous frequency spectrum 20 p3302 A71-39926

RR Lyrae variables period-frequency distribution in Oosterhoff types I and II globular clusters, interpreting in terms of pulsation theory 21 p3445 A71-40413

Free radial vibrations of curved beams by finite element method, using model to investigate variation with subtended angle of six lowest natural frequencies 21 p3462 A71-40529

Frequency and temperature variation with time in active region of pulsed GaAs laser diode, using Fabry-Perot interferometer 21 p3394 A71-41318

Distribution curves of F 2 critical frequency variations, considering probability density functions interpretation via asymmetric model 22 p3532 A71-41539

Open clusters membership probabilities and frequency distribution function parameters calculation by fitting relative proper motions to model with maximum likelihood procedure 22 p3601 A71-42165

Geomagnetic index Kp frequency distribution tables [1932-1970] 23 p3670 A71-43192

FREQUENCY DIVIDERS

Frequency multipliers and dividers with step-recovery diodes, calculating steady state behavior as function of circuit parameters and input frequency 01 p0052 A71-10322

Diffraction frequency splitting of opposed waves produced by diaphragm in He-Ne laser resonator 02 p0260 A71-11938

Prismatic absorption type wavemeter consisting of frequency divider and Fabry-Perot interferometer, considering tests in millimeter and submillimeter range 03 p0386 A71-13801

Electronic frequency divider with discrete correction of negative quartz clock rate 04 p0592 A71-14859

Dynamic systems oscillation period doubling in presence of C bifurcations 05 p0782 A71-16985

Harmonic oscillations frequency dividers with small asynchronous component of nonlinear element conductance, showing self excitation and wide synchronization bandwidth 09 p1413 A71-22152

Frequency multiplier or divider output signal spectral line form and width conversion from monochromatic input signal 16 p2542 A71-33490

Phase control circuits used in frequency division and multiplication, noting applications as filters and demodulators 20 p3208 A71-39433

Tunnel diode harmonic relaxation frequency divider, obtaining large division factors and wide synchronization bands with sinusoidal output signal 20 p3206 A71-39818

Frequency conversion /division, multiplication and shifting/ application to multistable phase- frequency elements design 22 p3524 A71-42573

Subharmonic frequency division for neon discharge plasma oscillations under resonance due to nonuniform electric field 24 p3858 A71-45263

FREQUENCY DIVISION MULTIPLEXING

Frequency division multiplexing of antenna feeder ducts without resonators using bridge circuits 01 p0054 A71-11084

Frequency division multiplexing methods for wide-band optical communications systems, calculating approximate information capacity 02 p0214 A71-12022

Satellite communication system earth station transmitter with FDM-FM and SPADE carriers, noting intermodulation effect on channel capacity 02 p0223 A71-12810

Data transmission via FDM/FM troposcatter channels, predicting system performance in error rate terms 05 p0723 A71-17052

Sequence spectrum of phase modulated discrete signal for frequency division multiplex filters 07 p1064 A71-20264

Electronically tunable compact X band triplexer, consisting of four port nonreciprocal directional YIG filters in cascade 09 p1418 A71-23416

German-French Symphony synchronous communication satellites, discussing frequency and time division multiple access subsystems characteristics 14 p2193 A71-29824

Digital FM techniques for combined time and frequency division multiplexing, improving telemetry sampling channel bandwidth utilization 14 p2193 A71-30020

Nonlinear gain and AM/PM conversion in FDMA communication through satellite repeater, using traveling wave tubes plus postzonal filter 17 p2703 A71-35082

FDMA single channel per carrier satellite communication system voice processing and modulation techniques, discussing analog frequency modulation and phase shift keying 17 p2704 A71-35086

PSK signals time division multiplexing and frequency multiplexed subcarrier systems equivalence and efficiency for digital communications 17 p2706 A71-35107

FREQUENCY MEASUREMENT

Summation coefficient determination inside and outside fovea by critical fusion frequency measurement, showing inverse relation to test surface size 01 p0010 A71-10275

High input impedance wideband frequency measurement probe with bipolar and unipolar transistor circuits 01 p0051 A71-10284

Sinusoidal pressure generator for determining frequency response of small pressure transducers, pressure probes and characteristics of small diameter infinite lines 01 p0067 A71-10478

Wall shift measurement of unperturbed hydrogen hyperfine transition frequency against cesium reference 04 p0585 A71-14652

Portable photoelectric recorder for solar limb vibration frequency spectrum and amplitude measurements 04 p0590 A71-14844

Instantaneous radar pulse frequency measurement for microwave bands, discussing multiplexed filters, wideband discriminators, dissipative frequency sensitive attenuators and band division receivers 04 p0555 A71-15360

Cantilever beam resonant frequencies measurement using electrodynamic vibration exciter 04 p0672 A71-15823

Flexible bar as spatial filter for measuring wave number-frequency spectra of distributed random processes 05 p0822 A71-16405

Alouette 2 ionograms frequency interpolation correction allowing measurement accuracy comparable to sounder system resolution 05 p0725 A71-17083

Receiving equipment for direct differential Doppler frequency measurement via beacon satellites observation 07 p1059 A71-19012

Microwave frequency measuring techniques extension into IR, developing Si point contact diode with nonlinear I-V characteristics 07 p1125 A71-19797

Photodetector frequency response measurement, using beat light signals from mixed single mode He-Ne laser 09 p1460 A71-22227

Efficiency evaluation of large parabolic antenna reflector by frequency scaling 09 p1409 A71-23496

Frequency counted measurements and phase locking to noisy oscillators, showing counted frequency method sample variance slow convergence to actual variance 10 p1574 A71-23763

High temperature fatigue test assembly for symmetric tension compression cycles at 10 kHz 10 p1589 A71-24201

Stationary and dynamic characteristics of integrators with dosage capacitor for analog frequency measurements, analyzing dynamic response at large modulation depth via analog computer simulation 10 p1589 A71-24502

Frequency equation of flexural vibration of fluid filled circular cylindrical shells, using linear elasticity 12 p1974 A71-26928

Vacuum tube frequency meters to measure oscillator stability, calculating beat period modulation characteristics 12 p1883 A71-27619

Quasi-optimum frequency measurement with linearly dispersive delay line, introducing variance factor for real-ideal systems comparison 14 p2192 A71-29806

Automatic amplitude control dynamic performance of system with oscillating frequency determination by ring gain bandpass behavior 14 p2210 A71-29809

Threshold SNR for signal frequency meter based on zero number count method, determining reliability 14 p2194 A71-30088

Frequency measurements of square wave signal with unknown amplitude by two mismatched channels, comparing rms error with effective estimate variance 14 p2195 A71-30106

Absorbed energy spectra and absorption frequencies from elastic constants of vibrating metals with cubic lattice structure, using cold neutron scattering 14 p2190 A71-30149

VLF and LF time and frequency international comparison, noting diurnal shifts and SID constant magnitude ratio 14 p2204 A71-30972

Absolute measurement of laser frequencies in IR range, using extended harmonic heterodyne technique 14 p2255 A71-30979

Radio frequency measurements below 30 GHz, considering power, impedance, phase shift, voltage and current data 14 p2205 A71-30981

Finite skin-stringer structures natural frequencies determination, using free flexural wave groups 15 p2510 A71-32518

Solar microwave bursts spectrum, calculating maximum radiation fluxes and frequencies from statistical data 15 p2480 A71-32749

Millimeter wave klystron single-loop phase locking using final 4th-harmonic mixer in reference chain for submillimeter laser frequency measurement 16 p2589 A71-34126

Nonnoise whistlers noise frequency and minimum group delay measurements 17 p2732 A71-34323

Edge clamped spherical shell natural vibration frequency determination using Vlasov shell theory equations 19 p3155 A71-37532

Loran-C pulse hyperbolic navigation system application to time and frequency measurements, evaluating errors 22 p3570 A71-41524

HCN and water vapor submillimeter and far IR laser frequency measurement against fundamental frequency standard by harmonic generation and beat frequency detection 22 p3557 A71-42152

Velocity and frequency drifting measurement apparatus developed for rotating machinery study 22 p3523 A71-42474

FREQUENCY MODULATION

NT FEEDBACK FREQUENCY MODULATION

NT FREQUENCY SHIFT KEYING

NT PULSE FREQUENCY MODULATION

NT PULSE FREQUENCY MODULATION TELEMETRY

Modified integrate and dump detector using FM click mechanism for improving bit decision and reducing error rates in FSK system 01 p0032 A71-10879

Magnetic tape recording system FM distortion derivation from head-to-tape spacing transfer function 01 p0033 A71-10892

Constant bandwidth FM subcarrier oscillators signal preemphasis for FM and PM transmitters
01 p0033 A71-10897

Harmonic and independent subcarrier DSB/FM telemetry systems implementation and utilization
01 p0033 A71-10898

Digital FM discriminator for demodulating FM signals with high deviation percentage
01 p0033 A71-10899

Projectile P band FM/FM telemetry system for in-barrel data acquisition
01 p0034 A71-10912

Reception and transmission of reduced sidelobe pseudorandom FM signals using quaternary S-sequence synthesis
01 p0037 A71-11082

Single sideband phase modulation compared with conventional PM or FM effect on spectrum conservation
01 p0037 A71-11164

Noise stability in single-channel FM transmission system via maximum SNR obtained with optimal predistortion
02 p0212 A71-11836

Semiconductor lasers direct amplitude, pulse and frequency modulation methods, comparing advantages and limitations
02 p0260 A71-12004

Gain/temperature measurement for earth station antenna and receiving subsystem by FM method, determining Y-factor [noise power proportional increase]
02 p0222 A71-12798

Linear low noise wideband frequency modulator for Intelsat 4 satellite telephony communication, considering channel capacity
02 p0234 A71-12819

Narrow band FM modems with high carrier frequency stability for satellite communication terminals with small dish antennas
02 p0234 A71-12820

Dynamic FM demodulator with tracking filter for threshold extension
02 p0235 A71-12821

Noiselike signals frequency modulation via pseudorandom sequence, deriving relationships for spectra and combined frequency-lag/ correlation functions
03 p0378 A71-13393

Nd-YAG laser with intracavity lithium niobate phase modulator, investigating frequency sweeping/modulation/ mode operation
03 p0437 A71-13878

Homogeneously broadened pulsed laser mode locking with internal frequency or amplitude modulation
03 p0437 A71-13882

Nd-YAG pulsed laser mode locking with internal FM modulation
03 p0437 A71-13883

Fluid lines transient response to frequency modulated signal inputs, considering Newtonian fluids or perfect gases
[ASME PAPER 70-WA/FLCS-1]
03 p0354 A71-14078

FM radio link fluctuating intermodulation distortions reduction by additive superpositioning of several compensating echoes with adaptive equalizer
03 p0380 A71-14334

FM data recording system with transducers for converting varying parameters into frequency and tape recorder capable of playback for computer analysis
03 p0383 A71-14344

Nonlinear electron beam bunching in zero temperature plasma during modulation by two frequencies, using klystron model
04 p0631 A71-14625

Frequency modulation and compression of ultrashort light pulses by optical Kerr effect
04 p0552 A71-15035

FM converter for tape recording of LF biological data
04 p0545 A71-15163

Gas laser axial modes mutual synchronization for frequency modulation, considering stability condition and even/odd harmonics
05 p0760 A71-16005

FM radio relay system modulation-demodulation equipment for multichannel FDM or TV signal transmission
05 p0728 A71-16146

Homogeneous pulsed laser with intracavity FM modulator, predicting modulation frequency detuning effect on mode locking behavior
05 p0762 A71-16340

Signals measurement distortions in FM recording-reproducing channel due to recorder magnetic tape speed fluctuations, discussing compensation methods
05 p0752 A71-16724

FM optical signals detection using Fabry-Perot interferometer with air gap between mirrors
05 p0753 A71-16875

Optimal quasi-regular signal detection on amplitude and frequency modulated noise background
05 p0723 A71-17020

Data transmission via FDM/FM troposcatter channels, predicting system performance in error rate terms
05 p0723 A71-17052

Quantized multiple access voice communications, comparing QPPM-AM and FM performances concerning transmitter power, RF bandwidth, circuit complexity, etc
[IEEE PAPER 69-TP-448-COM]
05 p0724 A71-17056

Time shared FSK FM modulator using second order digital filter with one variable multiplier
05 p0725 A71-17066

FM discriminator with nonideal limiting, calculating signal to noise ratio under white Gaussian noise input
05 p0730 A71-17071

PAM/FM radio telemetry coder including electronic commutator for sampling and sequential time control, discussing design, operation, performance and reliability
06 p0870 A71-18399

Waveguide cavity CW Gunn microwave oscillator bias voltage controlled amplitude and frequency modulation
07 p1073 A71-19110

Phase locked avalanche transit time oscillators FM noise spectra
07 p1074 A71-19124

Frequency modulation technique based on injection phase locking theory applied to microwave oscillator Q measurement
07 p1074 A71-19127

Real noise stability of coherent FM receiver for case of spectrum limited signals due to passage through channel and selective networks
07 p1061 A71-19508

FM discriminator detection, calculating false click probability and effect on output signal to noise ratio
07 p1061 A71-19535

Quasi-single sideband frequency modulation system response to noise above threshold for Gaussian signal
[IEEE PAPER 70-TP-70-COM]
07 p1062 A71-19537

Noise thermometry by Josephson effect, demonstrating self excitation random frequency modulation with thermal noise and thermometer having microkelvin noise temperature measurement capability
07 p1114 A71-20157

Statistical dynamic response of FM receiver with frequency feedback
07 p1064 A71-20261

Baseband recorder flutter, pilot and AGC noise effects on quadrature double sideband IQDSB/ FM systems
07 p1066 A71-20430

Fluidic Helmholtz resonator for FM signal analysis, showing instantaneous phase difference between input and output pressures
07 p1026 A71-20568

FM demodulator system with parametric tracking filters for threshold improvement, discussing reception performance
08 p1265 A71-21279

FM type system for measurement of wear narrow band noise power based on phase components processing
08 p1253 A71-21289

Multipath effects on FM communication systems performance, using analog computer simulation
08 p1255 A71-21597

Analog information systems frequency modulators, describing network design consisting of phase shifting RC network, amplifier and inerteless resistor
09 p1415 A71-22296

Mode synchronization in laser with uniform broadening by asymmetrical internal frequency modulation
09 p1462 A71-22397

Ionospheric dispersion of FM electromagnetic pulse, examining distortion of amplitude, pulse length and modulation in terms of integrated electron density along transmission path
09 p1410 A71-23523

CW X band frequency-locked Gunn oscillators as frequency demodulator with millivolt range detection sensitivity
09 p1421 A71-23720

Threshold-extension phase-lock demodulator design for optimizing satellite communication ground station systems, using FM carriers
10 p1580 A71-25106

Diversified frequency radio data transmission and reception by linear modulation, considering error rate in white noise and selective/flat fading
10 p1580 A71-25109

Low power density modulated RF energy illumination effects on mammalian biological functions, noting possible hazards to personnel
11 p1716 A71-25282

Dual laser ranging for distance measurements superimposing beams modulated at different frequencies
11 p1774 A71-25936

TWT amplifiers in radar and communication systems, investigating AM and FM noise theory and reduction
11 p1734 A71-26435

Millimeter backward wave oscillators, discussing cooling, operating characteristics, frequency pulling and pushing, life and reliability
11 p1739 A71-26436

Cavity controlled Gunn effect oscillators FM-current noise ratio, studying device current and domain capacitance as functions of carrier concentration and GaAs layer internal field
11 p1739 A71-26437

Heterodyne oscillator instability free frequency drift measurement of mixed FM signals in circuits with supplementary conversion
12 p1885 A71-26842

Broadband FM systems behavior, calculating transmission deviations via transfer functions obtained from measurements and linear network analysis
12 p1878 A71-26993

Electron beam high frequency modulation effects on hot ions production in cold plasma
12 p1938 A71-27207

Interference threshold probabilities of pseudorandom frequency hopped signals in conventional spread spectrum communications relative to Gaussian receiver bandwidth
12 p1881 A71-27428

Vacuum tube frequency meters to measure oscillator stability, calculating beat period modulation characteristics
12 p1883 A71-27619

Mathematical model for harmonic emission spectrum in FM and PM communication transmitters modulated by random signal
13 p2032 A71-28875

Meteorological tower high resolution CW-FM radar measurements for studies of temperature inversions, waves, thermal plumes and convection in atmospheric boundary layer
14 p2192 A71-29707

Digital FM techniques for combined time and frequency division multiplexing, improving telemetry sampling channel bandwidth utilization
14 p2193 A71-30020

Optico-acoustic autocorrelator for linear FM signals spatial compression, discussing design and performance
14 p2194 A71-30085

Low power vertical-incidence solid state pulse compression FM ionosonde
14 p2246 A71-30480

Linear passive network steady state FM distortion numerical calculation, applying to Chebyshev-response bandpass filter
14 p2197 A71-30806

FM threshold extension bounds during click elimination, considering pulse-averaging type discriminator
14 p2198 A71-30906

Microwave responders in FM or AM modes with cavity resonator, considering use in medium distance telemetering or telemonitoring
14 p2215 A71-30911

Low frequency noise spectra measurement in varicaps by frequency modulation of harmonic oscillator, noting application to diode and p-n transistors
15 p2369 A71-31232

Frequency modulated radio altimeters, discussing problems of altitude measurement independent of airplane motions in pitch and roll and immunity to fog effects
15 p2408 A71-31918

Laser beam CW self-induced frequency modulation and switching observation in liquids with low surface tension
15 p2420 A71-32381

Quasi-stationary method applicability for determining distortion of FM signal passing through linear circuit
15 p2373 A71-32631

FM radio receiver SNR and noise spectra for arbitrary transmission band characteristics
17 p2701 A71-34778

Transmission performance of thin route satellite communication system for northern Canada, comparing FM, PCM and delta modulation techniques
17 p2703 A71-35081

Digital phase locked loop for FM signals demodulation, considering system nonlinear difference equation
17 p2704 A71-35084

Intelsat 4 transponder for broadband multicarrier operation with frequency and pulse modulation, considering TWT, tunnel diode amplifiers, filters, equalizers, mixers, multiplexers and antennas
17 p2705 A71-35099

FM-PM conversion by frequency locking of free running Gunn oscillator
17 p2717 A71-35339

Communication satellite ground station transmitting equipment, discussing carrier waves, FM, frequency converters and microwave amplifiers characteristics
17 p2717 A71-35515

Temperature and bias circuit frequency modulation in CW X band Gunn oscillators 18 p2888 A71-36132

X-band Gunn oscillator equivalent circuit parameters determination for baseband and RF noise contribution to AM and FM noise 18 p2888 A71-36270

Spectrum limitation of FM carrier in case of accidental overloading of modulating signal arising in Intelsat 4 communication system 18 p2891 A71-36559

Double electron-nuclear resonance spectrometer using HF modulation of magnetic field for observation of electron paramagnetic resonance signal 18 p2924 A71-36626

Remote double resonance coupling of radar energy to ionospheric irregularities by sweeping radar modulation frequency through whole range 18 p2914 A71-36929

X band output power and FM noise of parallel multicontact Gunn oscillators 19 p3029 A71-38074

FM noise in output spectrum of low level operating IMPATT diode microwave oscillators 19 p3029 A71-38217

Phase locked loop models with off-tuned binary PSK interfering signal and angle modulated signal and noise at input, noting performance degradation 19 p3020 A71-38429

Electron beam HF modulation effects on hot ions production in cold plasma 19 p3117 A71-38619

Cortical responses of awake cat to narrow-band FM noise stimuli, proposing neuronal model 20 p3190 A71-39767

Electron beam modulation at optical frequencies, calculating excited radiation characteristics with quantum theory 21 p3420 A71-41254

Finite amplitude monochromatic wave self modulation in nonlinear medium, showing excitation process dependence on initial conditions 21 p3417 A71-41261

Solid state modulation for spacecraft horizon sensing via IR carbon dioxide atmospheric radiation, proposing Fabry-Perot structure with controlled plate separation 22 p3537 A71-41475

Nonlinear electron beam bunching in zero temperature plasma during modulation by two frequencies, using klystron model 22 p3583 A71-42265

Probability density and distribution functions of click amplitudes for rectangular IF, determining frequency modulation effect 22 p3513 A71-42386

Combined injection locking with indirect synchronization for FM signals in noisy environment with allowance for bias oscillator LF time constant effect 22 p3514 A71-42393

Gas laser axial modes mutual locking for frequency modulation, considering stability condition and even/odd harmonics 22 p3559 A71-42754

CW avalanche microwave oscillator frequency modulation/pulling/ by injected RF signal, discussing theory and experiment 23 p3646 A71-43903

Transmission and reaction cavity stabilized Gunn microwave oscillators AM and FM noise spectra, extending calculations based on Kurokawa theory to high modulation frequencies 23 p3653 A71-43967

Magnetic energy pumping into plasma by slowly modulating plasmon frequency-dependent external magnetic field 24 p3851 A71-44485

Demodulator interference noise in FM modulation radio relay system as function of ratio between interfered and interfering carrier powers and AM sensitivity 24 p3804 A71-44988

FREQUENCY MULTIPLIERS

Frequency multipliers and dividers with step-recovery diodes, calculating steady state behavior as function of circuit parameters and input frequency 01 p0052 A71-10322

Multioctave microwave frequency synthesizer by subharmonic synthesis and frequency multiplication under digital programmed commands 01 p0054 A71-10972

Klystron and frequency multiplier submillimeter harmonic emission determination, using lamellar grating Fourier spectrometer 02 p0250 A71-12143

Tunnel diode frequency multiplier circuit, analyzing harmonic I-V characteristics by equivalent network method 03 p0384 A71-13396

Carbon dioxide laser frequency doubling by Te crystal reflector output element, discussing shortcomings for conversion efficiency enhancement by power density increase 05 p0761 A71-16273

Semiconductor devices for frequency multiplication including variable capacitance, charge storage effect and composite varactor diodes 06 p0873 A71-17541

Superhigh multiplicity wideband tunable parametric diode frequency multipliers for decimeter range 06 p0873 A71-17542

Diffusion varactor and Schottky barrier semiconductor diodes for frequency multiplication at millimeter wave frequency range 06 p0873 A71-17545

Current spectral noise density in nonlinear element transmitter stage, examining vacuum tube frequency multiplier phase and amplitude fluctuations 09 p1405 A71-22469

X- to K-band harmonic generator using nonlinear capacitance of varactor diode, deriving maximum efficiency, optimum load and generator impedances 09 p1417 A71-23036

Energy spectrum minimization of intrinsic phase fluctuations in multistage vacuum tube frequency multiplier, using graphic analysis 11 p1738 A71-25940

Single diode microwave circuit for simultaneous function as frequency doubler and parametric up-converter 12 p1887 A71-26999

Nd-YAG laser operation with simultaneous intracavity frequency doubling and mode locking, observing mode-locked pulse lengthening and circulating power decrease 13 p2081 A71-29335

In-line harmonic tripler with GaAs varactor diode, detailing waveguide mount fabrication, power extraction filter and reverse bias voltage effects 14 p2211 A71-29857

Ninety degree phase shifter and frequency multiplier for square waves 15 p2376 A71-32025

Frequency doubling of 2.06 micron holmium doped oxyapatite laser output by proustite single crystal 15 p2348 A71-32610

Frequency multiplier or divider output signal spectral line form and width conversion from monochromatic input signal 16 p2542 A71-33490

Nonlinear optics of combination scattering of IR laser radiation in crystals and statistical frequency mixing-multiplication of polarons and longitudinal phonons 16 p2588 A71-33997

HF anodic oscillation tube tripler circuit optimization under constraints due to heat losses in grid electrode 17 p2714 A71-34572

Dynamic piecewise-continuous linear systems oscillation period doubling in presence of C bifurcations 18 p2948 A71-36785

Carbon dioxide laser radiation frequency doubling, using Te for second harmonic generation 18 p2933 A71-37010

Te coefficient for frequency doubling with pulsed carbon dioxide lasers, considering peak second harmonic generation conversion efficiency due to absorption of fundamental 18 p2933 A71-37011

Design and fabrication of frequency multipliers from 10 to 30 GHz on silica substrates by scaling and integrated circuit processing 19 p3026 A71-37219

Energy spectrum minimization of intrinsic phase fluctuations in multistage vacuum tube frequency multiplier, using graphic analysis 20 p3205 A71-39260

Phase control circuits used in frequency division and multiplication, noting applications as filters and demodulators 20 p3208 A71-39433

Short-pulse high-rate space digital laser communication components technology, discussing mode locked and frequency doubled Nd-YAG laser source 21 p3348 A71-40806

Magnetron crossed field amplifier multistage frequency multiplier HF field properties, obtaining numerical solutions for nonlinear governing equations 22 p3522 A71-42315

Design and performance optimization of series mode step recovery diode frequency multipliers, using computer aided analysis 22 p3523 A71-42358

Frequency conversion/division, multiplication and shifting/ application to multistable phase-frequency elements design 22 p3524 A71-42573

Second harmonic mode locked frequency doubled pulsed neodymium-yttrium-aluminum oxide garnet laser using single intracavity barium sodium niobate 23 p3683 A71-42957

FREQUENCY RANGES

NT OCTAVES

NT RADIO RANGE

Bonn 100 meter radio telescope, describing frequency range, antenna array, steering accuracy, construction and design 02 p0239 A71-12913

Monopole antenna with continuous resistive loading, studying broadband characteristics over frequency range by thin film evaporation techniques 06 p0867 A71-17710

Autoparametric oscillator with tunnel diode and variable capacitors, considering effective frequency range extension 09 p1414 A71-22258

Frequency domain spectral energy equations for large scale atmospheric motions, discussing earth rotation effects on kinetic energy spectrum 10 p1638 A71-23963

Riser whistlers observed at low latitude ground station, noting time delay increase with frequency 10 p1579 A71-25009

Weissenberg rheogoniometer modifications, providing upper cone motion elimination, unsteady/steady state measurements in constant stress field and amplitude/frequency variations 11 p1763 A71-26058

Fast shock waves electromagnetic production in light gases, discussing interferometric measurements at optical and microwave frequencies in H 11 p1764 A71-26272

Frequency analysis and Fourier transform evaluation of mechanical shocks and single impulses, outlining theory for filter response to pulses 11 p1853 A71-26521

Pulsars CP 0950 and CP 1133, examining pulse spectra characteristics in 83-111 MHz frequency range 12 p1963 A71-27076

Active antennas for frequency range 100 kHz to 250 MHz, discussing transistor circuitry optimization with respect to noise and linearity 14 p2210 A71-29822

Electromagnetic wave propagation on Yagi-Uda structure, obtaining current distribution, free space vs guided wavenumbers diagram and cutoff frequencies 14 p2196 A71-30514

Error reduction in automatic systems using computers and measuring network parameters over broad frequency ranges 14 p2205 A71-30983

Nonlinear control systems stochastic stability frequency conditions based on one and multidimensional cases 15 p2379 A71-31293

Restrictions on signals effective bandwidth, determining uniform upper bounds for use in design of systems with minimum distortion 16 p2542 A71-33458

Space radio astronomy, discussing frequency range in terrestrial atmosphere, RAE-1 satellite, cosmic and solar emissions and magnetopause generation, propagation and absorption processes 17 p2797 A71-34243

Uniform inhomogeneous waveguides with linear time invariant passive medium, determining functional behavior in frequency domain of electromagnetic waves propagation constant 17 p2708 A71-35492

Airborne communications with AN/ARC-154 transceiver in single radio, discussing extended frequency coverage, multimode operation, navigation and input/output provisions 17 p2775 A71-35758

Bispectral analysis of EEG frequency bands interrelations 18 p2863 A71-35896

Parametric amplifiers for ground station low-noise receivers in communication satellite systems, considering frequency range extension effect on noise temperature and passband requirements 18 p2890 A71-36557

Remote double resonance coupling of radar energy to ionospheric irregularities by sweeping radar modulation frequency through whole range 18 p2914 A71-36929

Transferred electron/Gunn/amplifiers and oscillators for microwave applications, considering electronic and mechanical tuning over large frequency ranges 18 p2894 A71-36977

Semiconductor device with stable negative conductance over wide range of microwave frequencies and power levels, using transferred electron effect in epitaxial GaAs 18 p2895 A71-36985

Pulsars CP 0950 and CP 1133, examining pulse spectra characteristics in 83-111 MHz frequency range 19 p1333 A71-37426

Large amplitude monochromatic electron cyclotron wave broadening in plasma, producing shifted phases in finite frequency range 19 p3114 A71-37855

Physical nature and measurement of broadband noise, considering rms value directly proportional to square root of frequency bandwidth 19 p3020 A71-38428

Slide valve slot fluid flow oscillation frequency range estimate for quasi-stationarity 20 p3183 A71-39168

Flat thin films in stripline cavity resonator with TEM mode, expressing bandwidth and resonance as frequency difference 20 p3239 A71-39426

Magnetospheric VLF waves growth rate variations, calculating frequency spectrum and intensity with self consistent solution 21 p3346 A71-40046

Logarithmic rate meter computer aided design, taking into account components tolerances for desired accuracy over selected frequency range 21 p3379 A71-40650

Solar radio bursts and noise storms frequency band spectra, investigating warm plasma wave propagation and mode coupling theories 22 p3579 A71-41462

High resolution full spatial frequency range optical image by incoherent superposition of low resolution partial frequency range component photographs, using optical aperture synthesis 22 p3538 A71-41735

Pyroelectric IR detectors performance, investigating strontium barium nitrate, lithium sulphate and triglycine sulfate materials effects on frequency range and sensitivity 22 p3542 A71-42122

Monochromatic radio wave propagation in interplanetary plasma, deriving frequency spectrum and phase and amplitude fluctuations 22 p3511 A71-42302

Multilayer epitaxial InP transferred electron microwave oscillator I-V characteristics and frequency dependence on layer thickness 23 p3649 A71-42912

IR spectra of oxamide and dithioxamide, studying Raman spectrum in LF range 23 p3642 A71-43825

FREQUENCY REGULATION U FREQUENCY CONTROL FREQUENCY RESPONSE

Rapid hybrid frequency response method for aircraft flight flutter testing based on hybrid computing system 01 p0049 A71-10228

Low pass active filters with various characteristics, comparing amplitude-frequency responses 01 p0051 A71-10259

Active filters of triple layer rectangular-shaped distributed RC elements, calculating components geometric variation effect on frequency response 01 p0058 A71-10312

Frequency multipliers and dividers with step-recovery diodes, calculating steady state behavior as function of circuit parameters and input frequency 01 p0052 A71-10322

Sinusoidal pressure generator for determining frequency response of small pressure transducers, pressure probes and characteristics of small diameter infinite lines 01 p0067 A71-10478

Computer methods for calculating sensitivity of amplitude and phase frequency response functions in automatic control systems to system parameter changes 01 p0059 A71-10529

Atmospheric extinction coefficients dependence on wavelength, comparing theoretical prediction to observational data 01 p0119 A71-10832

Rotating accelerometer with magnetic amplifier for angular acceleration detection, investigating static, dynamic and frequency response characteristics 02 p0252 A71-12421

LF EM wave absorption in disordered semiconductors, calculating frequency dependence of conductivity due to electron transitions between discrete local levels 02 p0297 A71-12618

Modal coupling in thermally stressed plates, obtaining solution for frequencies and stiffness 02 p0329 A71-12685

Frequency response characteristics of nonlinear oscillatory circuits with inductive and complex capacitance couplings 03 p0379 A71-13812

Group delay measurements accuracy, using Nyquist method as function of FM and response characteristics of measured two-terminal pair network 03 p0386 A71-13814

Normal mode helix antenna with rectangular and tapered Al strip conductors, measuring impedance variation with frequency at VHF range 03 p0387 A71-13820

Fluid transmission lines terminated by orifice with nonlinear pressure flow characteristics, calculating harmonic distortion frequency response by perturbation method [ASME PAPER 70-WA/FE-6] 03 p0402 A71-14128

Aircraft fuselage internal noise, and structural frequency response due to random excitation, using transfer matrix analysis [ASME PAPER 70-WA/DE-9] 03 p0348 A71-14143

First and second order lag system frequency response to pulse width modulated input signals [ASME PAPER 70-WA/AUT-8] 03 p0380 A71-14149

Soviet book on frequency method of calculating nonlinear systems covering continuous and pulsed automatic control 03 p0393 A71-14425

Regenerative feedback amplifier with maximally flat amplitude-frequency response 04 p0556 A71-14621

Gunn oscillator frequency characteristics vs displacement voltage in low Q factor resonance circuits 04 p0557 A71-14634

Modified constant temperature hot-wire anemometer for extended bandwidth operation, discussing improved frequency response test 04 p0596 A71-14971

Thin spherical shell with circular cutout under HF axisymmetric excitation by concentrated radial force 04 p0667 A71-15181

Clamped circular plates axisymmetric nonlinear resonant frequency response under uniform static pressure 04 p0668 A71-15187

Laguerre networks design optimization with threshold frequency and time limit based on pulse/frequency responses energy distribution, representing low pass filters 04 p0561 A71-15700

Auditory meatus sound pressure levels measurements in subjects with fabricated human ear molds with canal modifications, considering frequency responses and resonance 05 p0712 A71-16279

Human vision in communication system analysis, discussing psychophysical investigation, brightness functions, spatial frequency response and modulation transfer function 05 p0713 A71-16484

Thermoanemometer frequency characteristic determination, simulating turbulent oscillations by plane acoustic waves 05 p0753 A71-16845

Multiplexed PAM signal transmission over random time multichannel and diversity systems, discussing optimization for receiver frequency response by numerical solution [IEEE PAPER 70-TP-47-COM] 05 p0723 A71-17053

Bandpass limiter output envelope fluctuations dependence on input form and bandwidth 05 p0730 A71-17061

D region electron density profile relation to radio wave absorption frequency dependence 05 p0746 A71-17204

Inhomogeneous crystals frequency properties calculation by admittance averaging method, deriving expressions for metal semiconductor contact impedance 07 p1175 A71-19222

Nighttime ionospheric absorption frequency dependence during solar activity cycle 07 p1100 A71-19400

Ring laser beat frequency response near parametric resonance 07 p1125 A71-19810

Blocked and series connected pneumatic fluidic transmission lines, determining amplitude frequency response 07 p1026 A71-20566

Interdigital capacitors frequency response and application to lumped element microwave integrated circuits 08 p1261 A71-20753

Telephone channel phase-frequency distortions effects on discrete signal transmission quality from phase-delay-time frequency characteristics criterion 08 p1253 A71-20774

Bipolar silicon microwave transistors process technology improvements related to extensions of frequency, power handling or low noise performance 08 p1263 A71-20991

Periodically supported and damped closed circular beam structure, determining frequency response matrix 08 p1374 A71-22026

Frequency characteristics calculation of regenerative two cavity microwave bandpass amplifiers, applying to parametric and quantum amplifiers and underexcited microwave relaxation oscillators 09 p1413 A71-22157

Beat and synchronization modes of opposed waves in rotating gas ring laser, examining frequency response asymptotic behavior 09 p1460 A71-22222

Frequency characteristics determination of fixed piezoaccelerometers, using three mass equivalent system 09 p1450 A71-22797

Amplitude-frequency characteristics of physically similar piezoelectric accelerometric converters 09 p1450 A71-22798

Waveguide and stripline bandstop filters for pass-band loss minimization, using Chebyshev response curves 09 p1418 A71-23158

Optimum frequency for detection of acoustic sources in upper atmosphere as function of altitude and turbulence 10 p1642 A71-24818

Symmetrical amplitude-frequency characteristics of microwave reflection amplifiers with active resonators connected in series by nonhalf wave transmission lines 10 p1584 A71-24819

Internal asynchronous modulation of He-Ne laser with Doppler broadened line of working transition in multifrequency mode 10 p1621 A71-24818

Dynamic frequency characteristics of built-up structures by transient rapid sweep testing 11 p1841 A71-25111

Structural system frequency response measurements under environmental noise conditions, discussing autocorrelation function for transient excitation damping 11 p1797 A71-25111

Transient ion sheath effects on spherical metallic plasma probe complex admittance at different frequencies, comparing numerical results with experiment 11 p1805 A71-25804

Frequency response of velocity and acceleration transducers for oscillatory environments instrumentation 11 p1762 A71-25933

Ni-based superalloy stress cycle frequency effects on elevated temperature fatigue life 11 p1779 A71-26011

Nonlinear systems response to arbitrary multiple frequency inputs, deriving series expansion for nonlinear modulation products 11 p1793 A71-26422

Camera shutter spatial frequency spectrum and components light scattering effects on negatives quality based on composite image representation system theory 11 p1767 A71-26469

Dielectric layer surface electric charge movement determination by measuring metal-insulator-semiconductor (MIS) capacity response at very low frequencies 12 p1942 A71-26829

Computer synthesis of nondegenerate parametric amplifiers with single mesh filter for maximum flat Chebyshev frequency response applicable to quantum devices 12 p1886 A71-26844

Photocurrent frequency dependence in thin-base silicon photodiodes for carrier optical generation between p-n junction and depleted region 12 p1886 A71-26845

Rayleigh wave propagation along edge of thin plate, calculating velocity dependence on frequency 12 p1929 A71-26929

Wideband transistor amplifier frequency response at low frequencies, discussing gain increase, thermal pull-in effect, barrier layer geometry and switching control functions 12 p1887 A71-27042

Jet fighter-bomber aircraft noise survey, discussing sound pressure levels and frequency analysis during ground running, speech interference levels and ear protectors requirements 12 p1875 A71-27629

Monomode laser frequency fluctuations, considering line width separation 12 p1915 A71-27644

Variable structure automatic control system dynamic properties, using frequency response method 13 p2041 A71-27943

Physical pendulum normalized error variance as irregularity function in excitation with narrow band frequency spectrum 13 p2065 A71-27947

Revolving cylindrical surface reflected energy from scanning fixed laser beam, noting signal frequency 13 p2077 A71-27948

Lower ionosphere magnetic fields generated by three dimensional Alfvén waves, examining amplitude and phase spatial distribution and frequency dependence 13 p2059 A71-28254

D region electron density profile relation to radio wave absorption frequency dependence 13 p2059 A71-28255

Flux flow noise spectra measurement in pairs of magnetically coupled superconducting films, noting frequency response 13 p2111 A71-28502

Electron density profile determination in D region based on frequency dependence of radio waves absorption, discussing lower ionosphere anomalous ionization 13 p2061 A71-28539

Light combination scattering in organic liquids, measuring frequency dependence with dye laser technique 13 p2080 A71-29021

Frequency-length relationship for bulk InGaAsP microwave oscillators in 10-100 micron thickness 13 p2080 A71-29022

range, obtaining threshold field and average transit velocity
14 p2210 A71-29791

Optical synthetic aperture analogs of Covington-Drane and thin annular radio interferometers, discussing aperture resolution and spatial frequency response
14 p2238 A71-29802

Structural steady state vibration frequency response and resonance testing, investigating nonlinearity effects of large deflections
14 p2326 A71-30065

HF response of point excited cylindrical shell, converting normal-mode series to integral representation with Watson transformation
14 p2327 A71-30201

Frequency response of five component strain gage oscillating balance for dynamic wind tunnel stability testing
14 p2221 A71-30333

Equivalent circuit parameters of microwave planar power transistors at high injection levels, indicating parameters frequency dependence determination
14 p2213 A71-30627

Decameter solar radio bursts time splitting data, presenting high time and frequency resolution on double bursts
15 p2473 A71-31720

Decomposing method for linear transfer functions identification from frequency or time response, using Caue form continued fraction expansion
15 p2379 A71-31821

Structural panel under acoustic loading by supersonic convected turbulence, deriving responses with finite Fourier transforms
15 p2507 A71-32131

Plate excitation by supersonic turbulent and shock boundary layers, measuring wall pressure fluctuation and panel displacement
15 p2507 A71-32132

Active all-pass networks with shaped group-frequency delay characteristics, discussing design based on automatic synthesis
15 p2372 A71-32323

Frequency response of rainfall attenuation for various dropsize distributions, plotting measured values at 890 and 110 GHz
15 p2374 A71-32696

Rat irradiated spinal cord, detailing orthodontic ventral root and monosynaptic reaction to rhythmic and increasing frequency stimulation
15 p2362 A71-32735

Continuous systems stability analysis under parametric excitation, using time dependent Liapunov functional for frequency response
16 p2607 A71-32992

Volume hologram formation in photopolymer materials with bright low noise images, considering sensitivity, spatial frequency response, particle scattering noise and nonlinearities
16 p2577 A71-33144

Digital filters, describing transfer function, frequency response, stability and design
16 p2546 A71-33478

Electro-optical Fabry-Perot modulator with KDP and ADP crystals as optical resonators, determining modulation and frequency response characteristics
16 p2587 A71-33493

Thermostable and heat resistant steels and alloys vibration loading frequency effects on fatigue at high temperatures
16 p2598 A71-33992

Frequency and level dependent discrepancy between free field and pressure thresholds at low frequencies due to physiological noise produced under earcap
17 p2681 A71-34699

Sinusoidal image distributions generation by changing frequency response of optical system by exit pupil function /incoherent spatial filtering/ modification
18 p2918 A71-36073

Silicon IMPATT microwave oscillators, calculating CW power as function of frequency by scaling approximation
18 p2888 A71-36129

Continuously variable microwave stripline phase shifter with linear shift vs frequency by dielectric constant variation
18 p2889 A71-36272

Silicon microwave transistors frequency response theory, considering application as small-signal and power amplifiers
18 p2894 A71-36978

Gain and stability of MOS transistor small signal amplifier as function of frequency, using lumped element equivalent circuit
19 p3028 A71-37563

Nighttime ionospheric absorption frequency dependence during solar activity cycle
19 p3053 A71-37824

Filter design for optimal transient performance, comparing with steady state frequency response
19 p3038 A71-38487

Spectral analysis of solar microwave bursts, examining flux and energy variation with frequency
19 p3146 A71-38577

Frequency domain stability criteria for dynamical systems with random parameters, considering open loop stability, stochastic gain element rms value and linear element effective bandwidth
19 p3039 A71-38710

Lithium niobate hypersound attenuation and reflection coefficients frequency dependence determination by scattering laser light at hypersonic oscillations
20 p3244 A71-39162

Light ponderability in gravitation theory, discussing hypothetical Freudlich effect of light velocity dependence on radiation field intensity, based on Maxwell electrodynamics nonlinear generalization
20 p3270 A71-39457

Drifting whistler frequency cutoff phenomena /striations/ observation in low latitude by POGO satellites, discussing interpretation based on propagation effect
20 p3198 A71-39746

Multilayer microwave semiconducting film piezoelectric acoustic transducer loss and frequency response derivation from electromechanical power conversion theory
20 p3240 A71-39764

Frequency response of nonlinear feedback control systems, using modified polar plot of open loop transfer function
20 p3208 A71-39914

Frequency response optimization of one dimensional damped linear continuous systems, requiring initial value numerical integration of state and adjoint differential equations
21 p3456 A71-40265

[ASME PAPER 71-VIBR-1] Damped isolation and undamped vibration absorber model for dynamic control, discussing frequency response and tuning and damping performance
21 p3459 A71-40294

[ASME PAPER 71-VIBR-45] Real operational amplifier analysis application to state variable filter design emphasizing high-Q HF phenomena, noting undesirable behavior by heuristic argument
21 p3360 A71-40808

Semiconductor surface state effects on p-n junction photodiode frequency characteristics under short and open circuit conditions, noting nonequilibrium capacitance during illumination
21 p3358 A71-41215

X band Gunn diode oscillator pulsed operation starting delay time relationship to CW operation frequency/temperature characteristics, suggesting contact resistance role
21 p3359 A71-41411

Apparent motion effects associated with stationary flashing lights configurations, noting frequency response characteristics analogous to real motion effects in human visual system model
22 p3498 A71-41487

Variable sweep rate frequency response and vibration testing for test time reduction, using closed loop controller for sweep rate modulation
22 p3537 A71-41635

Spiral grooved thrust and spherical gas bearings, predicting stability and frequency response by Newton-Raphson and orthonormalization methods
22 p3551 A71-41668

Rigid rotor whirl dynamics in externally pressurized gas journal bearings, calculating frequencies in terms of stiffness and other parameters
22 p3552 A71-41670

Regenerative feedback amplifier with maximally flat amplitude-frequency response
22 p3521 A71-42261

Gunn oscillator frequency characteristics vs displacement voltage in low Q factor resonance circuits
22 p3521 A71-42274

Design technique based on frequency response loci associated with characteristic transfer functions for linear time-invariant multivariable feedback control system
22 p3526 A71-42284

Dynamic frequency and phase response of digital communications system of synchronized oscillators from time-incremental computer simulation
22 p3523 A71-42376

Vergence eye movements control, discussing transient and frequency responses
22 p3489 A71-42446

Temperature and frequency dependence of electron phonon interaction maxima in rhenium, explaining transverse and longitudinal waves ultrasonic attenuation by two band theory
22 p3578 A71-42597

Frequency dependence of Rayleigh wave propagation velocity along rough surfaces, based on smooth surface mass loading
23 p3703 A71-43203

Continuous signal representations in time and frequency domains by Fourier series
23 p3644 A71-43284

Impedance and capacitance frequency dependence of p-i-n junction diodes at microwave frequencies with high injection levels
23 p3650 A71-43308

Temperature effects on long wavelength photon frequency and linewidth in diamond, using Raman scattering techniques
23 p3715 A71-43471

Frequency and power limits of field effect triodes, noting application to gridistor for millimeter waves
23 p3653 A71-43950

Reflection and scattering properties of two dimensional periodic arrays of loaded dipoles with bandpass filter characteristics as function of frequency
23 p3654 A71-44159

Electrohydraulic stand for vibration strength testing, discussing system design, specifications, frequency-amplitude characteristics and applications
23 p3662 A71-44235

HF and LF transistors suitability for integrated high Q LC circuits, studying inductivity, Q and component frequency dependence
24 p3807 A71-44377

Temperature and frequency effects on permittivity and dielectric loss angle tangent in glasses and pyroceramics
24 p3859 A71-44379

Plasma LF oscillations in Sirius stellator, showing fundamental frequency dependence on density temperature and magnetic field strength
24 p3853 A71-44504

Isothermal gas rotation in circular cylinder, calculating symmetric normal frequency modes
24 p3818 A71-44590

Movable metal iris with nearly frequency independent susceptance, relating characteristics to centered capacitive obstacle in waveguide
24 p3809 A71-45095

Sound field measurement in circular and rectangular air duct with sound-absorbing walls /mufflers/, deriving empirical formula for attenuation frequency characteristics
24 p3849 A71-45271

FREQUENCY SCANNING

Radiation spectral and kinetic characteristics in neodymium glass laser in frequency scanning mode
01 p0095 A71-11029

Swept electron beam scanning in microwave beam-wave interaction devices via periodic magnetic fields
03 p0385 A71-13794

Data reading function synchronized digital mass spectrometer with incremental scan by magnetic field sweeping, describing method for polynomial fitting of data
11 p1762 A71-25663

Linear frequency beam scanning array antenna excited by individual phase shifter, studying rectangular waveguide in magnetic field plane
11 p1741 A71-26552

High speed electronic phase and frequency scanned linear, static fed and monopulse arrays element and angular error analysis
14 p2205 A71-31049

Doppler scanning landing microwave system for air-derived azimuth and elevation angle aircraft guidance by frequency coding and reference carrier transmission
22 p3572 A71-42089

Antenna impedance measurements using frequency sweep generator and oscillograph
24 p3810 A71-45127

FREQUENCY SHIFT

Abel-Tauber theorems predicting asymptotic behavior of source functions for resonance lines formed by frequency redistribution in semiinfinite atmosphere
01 p0131 A71-11350

Sunspot spectrograms analysis, observing wavelength shift in Zeeman triplet circular components and magnetic splitting inequality under different circular polarizations
03 p0484 A71-13210

Homogeneous pulsed laser with intracavity FM modulator, predicting modulation frequency detuning effect on mode locking behavior
05 p0762 A71-16340

Gas and liquid flows local velocity measurements, using Doppler frequency shifts due to wave scattering at solid microparticles suspended in flow
05 p0753 A71-16786

Western frequency drift effects on spectrum time evolution azimuthal asymmetry in diminishing period geomagnetic pulsation intervals
05 p0747 A71-17214

Frequency variation with temperature in coaxial cavity avalanche transit time microwave oscillators explained by diode junction capacitance and cavity length changes with temperature
07 p1074 A71-19120

Pressure dependent shift of He-Ne laser radiation, observing beat frequencies
07 p1123 A71-19486

FREQUENCY SHIFT KEYING

Coupling loss factor estimation, using wave transmission or natural frequency shift methods in statistical energy analysis

07 p1161 A71-19962

Frequency agile waveforms effects on detection and tracking radars performance, decorrelating distributed clutter echoes

08 p1253 A71-20798

Electronic equipment for measuring resonant frequency drift during slow wave structure impedance measurements, considering mean square errors

08 p1264 A71-21073

Oscillation frequency shift and gas discharge tube design relation in He-Ne DC lasers

09 p1462 A71-22402

Single-mode He-Ne laser, investigating longitudinal magnetic field effect on output amplitude, frequency and polarization characteristics

10 p1620 A71-24343

Internal combustion engine gas temperature measurement, using ultrasonic wave frequency shift method

11 p1810 A71-25269

Line shifts in first overtone band of DF perturbed by HF, studying pressure induced transitions and partial pressures

11 p1729 A71-26139

Western frequency drift effects on spectrum time evolution azimuthal asymmetry in decreasing period geomagnetic pulsation intervals

13 p2060 A71-28269

Rotating mirror wavelength shifter of laser light source for use in electronic spectroscopy, noting measurements with high speed Doppler wheel in vacuum

13 p2067 A71-28445

Ion wave frequency shift and instability suppression by RF electric field, examining wave-field coupling

13 p2110 A71-29334

Preferential pairing detection in CDS at 4.2 K through electron radiation damage of donor-acceptor pair green edge emission, discussing resulting wavelength shift

14 p2284 A71-29818

Dispersionless delay line design producing signal frequency shifts for calibration tests of wideband Doppler shift measuring equipment

15 p2373 A71-32632

Gas and liquid flows local velocity measurements, using Doppler frequency shifts due to wave scattering at solid microparticles suspended in flow

16 p2576 A71-33038

Reflected short wave signal frequency shift due to reflecting ionospheric layer movement and electron concentration changes, considering oblique incidence on isotropic and anisotropic layers

16 p2542 A71-33484

Radiative width of laser transition in Ne 20 atom and line frequency shift vs pressure in dual He-Ne laser assembly effectuating atom collisions

17 p2752 A71-34403

Nonlinear frequency shift in GaAs electroacoustic domains, using Bommel-Dransfeld analysis technique

17 p2791 A71-34447

Holography with single transverse longitudinal mode pulsed ruby laser, emphasizing carrier frequency shift as limiting factor on depth of field

17 p2745 A71-35587

Solar Fraunhofer line wavelengths shifts at disk center and at limb, evaluating Stark broadening contribution

18 p2962 A71-36106

Tuning range extension of doubly resonant lithium iodate parametric oscillator by upconversion, using simultaneous pumping by single ruby laser beam

19 p3071 A71-37477

Rotating waveplate optical frequency shifting in lithium niobate, producing light beam with moderate requirements on modulator adjustment

20 p3204 A71-39097

Differential line shifts in spectrum of superelemental beta Ori attributed to radial spreading of stellar atmosphere

20 p3290 A71-39302

Doppler carrier frequency shift measurement accuracy

20 p3198 A71-39808

Laser system for atmospheric wind velocity and turbulence, using Doppler frequency shift undergone by radiation beam scattered by particles suspended in flows

21 p3319 A71-40490

Wavelength shifts of intensity minima in type I supernova spectra

21 p3449 A71-40606

Fluid velocity gradient measurement by laser-Doppler techniques based on signal spectrum bandwidth or frequency shift corresponding to position shift near wall

22 p3541 A71-41792

Characteristic energies of exponential band tails in GaAs junction lasers from wavelength shift with cavity Q and spontaneous emission line width

22 p3558 A71-42360

Frequency conversion/division, multiplication and shifting/application to multistable phase-frequency elements design

22 p3524 A71-42573

Solar chromosphere spectrum analysis, measuring H alpha line relative shifts variation with altitude

22 p3607 A71-42872

Electromagnetic wave reflection from ferrite plate in external alternating magnetic field, showing frequency change due to moving domain wall

23 p3645 A71-43568

Neon red lines Stark widths and shifts in function of electron and neutral Ne densities in shock tube

23 p3707 A71-43585

Frequency shift in air-coupled surface waves during Saturn 5 launches, computing apparent phase velocity experienced by ground

23 p3672 A71-43883

SHF resonator small resonant frequency shift and Q factor changes measurement based on FM signal envelope shape analysis

24 p3858 A71-45237

FREQUENCY SHIFT KEYING

Modified integrate and dump detector using FM clock mechanism for improving bit decision and reducing error rates in FSK system

01 p0032 A71-10879

Wideband FSK system involving direct and reflected path transmission, predicting diversity performance from mathematical model

05 p0724 A71-17057

All-digital multichannel narrow band FSK data receiver with time-shared arithmetic processor, discussing prototype design and performance [IEEE PAPER 70-TP-49-COM]

05 p0724 A71-17064

Time shared FSK FM modulator using second order digital filter with one variable multiplier

05 p0725 A71-17066

Low data rate m-ray frequency shift keyed (MFSK)/modulation system design

07 p1061 A71-19534

Spectrum economy by passing signal through symmetrical bandpass filter using FSK keyer

10 p1574 A71-23769

Noise stability during noncoherent reception of frequency shift keyed signal by receiver with finite Q predetector integrators in presence of fading

11 p1733 A71-25938

Error detection coding limitations at high error rates, discussing forward error correcting codes and multiple frequency shift keying techniques

12 p1880 A71-27146

Binary, uncoded and M-ary FSK with convolutional codes for low powered planetary entry probes communicating to earth

14 p2200 A71-30921

Cochannel interference reduction in FSK system by applying Hilbert transform techniques

17 p2703 A71-35079

Bandlimiting effects on coherent detection of PSK, ASK and FSK signals in presence of white Gaussian noise, using SNR as performance criterion

17 p2704 A71-35085

FSK L-level or duobinary system performance evaluation under intersymbol interference, using limiter-discriminator without postdetection filter as detector

17 p2707 A71-35479

Noise stability and rejection probability of code sequence in real multifrequency communications systems with multipositional frequency shift keying

19 p3022 A71-38495

Noise stability during noncoherent reception of frequency shift keyed signal by receiver with finite Q predetector integrators in presence of fading

20 p3196 A71-39258

Power spectral density of N-ary orthogonal continuous phase FSK waveforms for ELF/VLF communications

22 p3513 A71-42385

Electronic broad banding of VLF/LF antennas for FSK radio communication through switched magnetically coupled reactor, determining antenna transient response

22 p3513 A71-42388

FREQUENCY STABILITY

Opposed wave synchronization mode stability in gas laser undergoing torsional vibrations

01 p0093 A71-10604

Frequency stability of molecular beam laser with stimulated coherent emission

01 p0093 A71-10681

Quartz crystal HF resonator unit for high g environments, discussing tradeoff between stiff support and stress-induced frequency instability

01 p0054 A71-10913

Optically pumped rubidium maser short term frequency instability caused by thermal noise and resonator temperature and pumping power fluctuation

01 p0095 A71-11211

Frequency stability of three-loop oscillator with time lag on coupling coefficient plane used for optimal circuit configuration

02 p0230 A71-11835

Noise stability in single-channel FM transmission system with maximum SNR obtained with optimal predistortion

02 p0212 A71-11836

Miniaturized Rb atomic frequency source having 1 in 10 to 8th power stability in year and 5 minute warm-up time

02 p0252 A71-12422

Narrow band FM modems with high carrier frequency stability for satellite communication terminals with small dish antennas

02 p0234 A71-12820

Magnetron oscillators frequency and oscillation stability, examining phase mismatch angle, filament current and cathode thermal balance

03 p0386 A71-13805

Aircraft DC to AC converters frequency stabilization systems, describing circuit diagrams and operation principles

03 p0355 A71-14247

Frequency stabilization and measurement of single frequency He-Ne laser at 0.6328 microns, using Michelson interferometer as mode selector and reference cavity

05 p0760 A71-16006

Oscillator signal frequency instability relationship with spectral purity based on thermal noise effects [ONERA-TP-912]

05 p0722 A71-16706

Gunn diode generated signal frequency jumps as function of voltage variations, basing explanation on high field domain formation and decay

05 p0729 A71-16999

Frequency stability of automatic control system with hydraulic actuating mechanism external load, taking into account fluid compressibility

05 p0705 A71-17033

Sampled phase lock loop filter for tracking short pulses, deriving frequency stability criterion and margins

05 p0725 A71-17080

Thermal noise perturbed oscillator RF spectrum determination from frequency instability in time domain [ONERA-TP-927]

07 p1075 A71-19265

Frequency shift in hydrogen maser due to atomic collisions with storage bulb surface/wall shift, investigating temperature dependence

07 p1124 A71-19686

Transistorized ultrasonic oscillator active conductances and other circuit parameters effects on self oscillation frequency stability

07 p1078 A71-20060

Frequency stability of molecular beam laser with stimulated coherent emission

07 p1125 A71-20142

Magnetoplasma modulated waves nonlinear instability, taking into account relativistic effects

07 p1171 A71-20296

Fluidic relaxation oscillator experimental and theoretical analysis, investigating pressure and temperature effects on frequency stability

07 p1027 A71-20576

Multivibrator frequency stability as function of circuit parameters, using stability/parametric errors sensitivity coefficients for general algorithm

08 p1264 A71-21072

Two oscillation mode He-Ne gas laser, discussing frequency stabilization by strong competition effect at gain curve center

09 p1461 A71-22387

Doppler jitter stabilization of carbon dioxide laser without internal modulation to inverted Lamb dip in extracavity absorption cell

09 p1463 A71-22759

HF stability audio multichannel oscillators design and operation, comparing frequency synthesizer systems for optimal circuitry characteristics

09 p1417 A71-23029

Avalanche diode microwave oscillator stabilized by two external resonant circuits, investigating self oscillation characteristics

10 p1582 A71-23808

Phase and frequency instabilities in electromagnetic wave propagation - NATO/AGARD Conference, Ankara, Turkey, October 1967

10 p1576 A71-24185

Frequency stabilized lasers as absolute wavelength standards, discussing perturbation causes for optical resonant cavities and atomic transitions

10 p1621 A71-24581

Digital synthesizers design and operation for radio communications, discussing reception and transmission noise performance, frequency stability and acquisition time

10 p1579 A71-24757

He-Ne laser with stable thermally tunable single frequency referenced to Kr 86 primary wavelength, describing construction details, calibration and performance characteristics

11 p1776 A71-26302

X band reflex klystron oscillator with frequency stability comparable to high quality quartz clock by coupling to superconducting cavity

11 p1739 A71-26368

Short term frequency stability of precision oscillators and frequency generators, discussing conversion from frequency to time domain and among time domain measures

11 p1739 A71-26422

Ne absorption tube in alternating magnetic field for He-Ne laser frequency stabilization reference, discussing laser output SNR effects

12 p1913 A71-26926

High stability frequency standard distribution system involving use of geostationary satellites and two-way microwave transmission, discussing errors

12 p1882 A71-27439

Vacuum tube frequency meters to measure oscillator stability, calculating beat period modulation characteristics

12 p1883 A71-27619

Single loop quartz vacuum tube oscillators, calculating oscillation spectral line width due to thermal and shot noise and circuit parameters fluctuations

12 p1889 A71-27622

Temperature compensation for frequency changes stabilization of avalanche transit time diode microwave oscillator, using loop circuits and high dielectric constant ceramics

13 p2036 A71-27938

Subpicosecond structure and frequency sweep observation results of single pulse of Nd-glass laser, considering explanation by mode locking theory

13 p2079 A71-28712

Quartz-tube LF measuring generator with low linear instability, using frequency divider and narrow band RC filter

13 p2040 A71-28936

Geomagnetic Pc-1 type micropulsations appearance and development due to proton belt cyclotron instability

14 p2301 A71-30350

Random multiple access technique for satellite data collection, taking advantage of frequency instability associated with oscillator circuits

14 p2199 A71-30908

Doubly resonant optical parametric oscillator frequency instabilities and threshold, studying non-resonant mode feedback effects

15 p2423 A71-32605

Long term single frequency stabilization of composite cavity argon laser by mirror separation, using reference He-Ne laser

15 p2423 A71-32611

He-Ne laser frequency stabilization through Ne resonance absorption, using optical amplification for comparison resonance enhancement

16 p2589 A71-34134

Optically pumped rubidium maser short term frequency instability caused by thermal noise and resonator temperature and pumping power fluctuations

17 p2750 A71-34262

Frequency criteria for absolute stability of equilibrium states and processes in nonlinear automatic control systems

17 p2783 A71-35130

Soviet book on self adjusting systems dynamics with frequency stabilization characteristics, covering linearized motion equations, narrow band processes, etc

17 p2722 A71-35175

Random noise effects on oscillator short term frequency stability and velocity measurement by Doppler effect

18 p2879 A71-36531

Intelsat 3 and 4 RF demodulator design with tracking filters, using varactor for frequency control and discriminator for frequency drift compensation

18 p2890 A71-36558

HF radio communication receiver performance requirements and realization, considering gain, noise, interference, filtering, reciprocal mixing, intermodulation and frequency stability

18 p2895 A71-36998

Short term timing stability of Crab pulsar clock from telescope observations at 256 and 405 MHz

19 p3144 A71-38173

Asynchronous generators classification based on primary distinction by independent or self operated excitation and stabilized or controlled frequency

19 p3000 A71-38639

Dual input null networks application in RC feedback oscillators, examining frequency stability

20 p3206 A71-39915

Frequency stability definition for signal generator, proposing spectral density measure

21 p3414 A71-40222

HCN CW laser design, considering factors affecting short and long term power and frequency stabilities

22 p3557 A71-42134

N-type In-Sb continuous coherent microwave oscillation under transverse magnetic field, discussing helical frequency instability on threshold and growing wave conditions

22 p3586 A71-42347

Frequency stabilization and instability measurement of single frequency He-Ne laser at 0.6328 microns,

using Michelson interferometer as mode selector and reference cavity

22 p3559 A71-42755

German monograph on Gunn oscillators frequency stabilization by synchronization with external oscillator emitting HF signals

23 p3649 A71-43045

Weakly ionized cesium plasmas produced in sealed diodes, examining LF instabilities with fluid equations

23 p3708 A71-43083

Single frequency He-Ne laser stabilization by Lorentz absorption contour in external gas cell, obtaining error signal based on absorption line scanning

23 p3683 A71-43396

Gunn oscillator frequency stabilization at minus 10 to 60 C by high Q single tuned oscillator circuit, considering requirements for 20 GHz radio relay system

23 p3651 A71-43438

Gas lasers application to length measurement technology, discussing temperature, air pressure and vibration effects on laser frequency stabilization

24 p3833 A71-44449

Single phase stable frequency AC current power supplies, using stable master oscillator and asynchronous generator

24 p3793 A71-44717

FREQUENCY STANDARDS

Hydrogen maser time and frequency standards at Agassiz observatory for long baseline interferometry via radio telescope, discussing Loran C

02 p0261 A71-12334

Miniaturized Rb atomic frequency source having 1 in 10 to 8th power stability in year and 5 minute warm-up time

02 p0252 A71-12422

Comparative national time standards by overflight synchronization method

04 p0585 A71-14653

Quartz clock nonsystematic and frequency fluctuation statistical properties compared with GBR radio station

04 p0600 A71-15664

Frequency stabilized lasers as absolute wavelength standards, discussing perturbation causes for optical resonant cavities and atomic transitions

10 p1621 A71-24581

High stability frequency standard distribution system involving use of geostationary satellites and two-way microwave transmission, discussing errors

12 p1882 A71-27439

Frequency stabilized He-Ne laser wave secondary length standard for automatic measurements, discussing electronic control, accuracy, line width, pressure, current and magnetism effects

16 p2588 A71-34119

Satellite time and frequency dissemination, discussing deficiencies of HF broadcasts for navigation and communication systems

18 p2878 A71-36530

Standard frequency and UTC time signal transmission coherent with SI /atomic/ second

22 p3509 A71-42087

Australian National Radio Astronomy Observatory integrated time and frequency system with cesium beam frequency standard and digital computer for real time operation

22 p3547 A71-42498

Radio astronomic intercontinental base interferometry, discussing independent local oscillators requirements and atomic clock frequency standards

23 p3674 A71-43087

FREQUENCY SYNCHRONIZATION

Oscillator frequency synchronization by injection locking, considering nonlinear oscillation model

02 p0230 A71-11818

Loran C transmissions for long baseline time and frequency synchronization

02 p0216 A71-12328

ATA Collision Avoidance System based on time and frequency synchronization via ground stations or other aircraft

02 p0280 A71-12895

Optically coupled GaAs injection lasers emission spectra, determining maximum frequency difference in gain bandwidths for mode synchronization

03 p0435 A71-13506

Gas laser axial modes mutual synchronization for frequency modulation, considering stability condition and even/odd harmonics

05 p0760 A71-16005

IMPATT and Gunn microwave oscillators injection phase locking, discussing stationary state synchronization theory and phase vs frequency deviation measurements

08 p1263 A71-20990

Solid state laser with slow relaxation bleachable filter, calculating modes self synchronization probability statistics relationship to relaxation time

14 p2253 A71-30109

German monograph on Gunn oscillators frequency stabilization by synchronization with external oscillator emitting HF signals

23 p3649 A71-43045

Radio pulse synchronous detection with wideband preamplifier, evaluating frequency mismatch effects on signal distortion by transient response analysis

23 p3644 A71-43287

FREQUENCY SYNTHESIZERS

Multioctave microwave frequency synthesizer by subharmonic synthesis and frequency multiplication under digital programmed commands

01 p0054 A71-10972

Electronic time scale converters for frequency synthesizers

04 p0592 A71-14861

Coded control circuit for digital frequency synthesizer

06 p0870 A71-17494

HF stability audio multichannel oscillators design and operation, comparing frequency synthesizer systems for optimal circuitry characteristics

09 p1417 A71-23029

FREQUENCY TRANSLATION

U FREQUENCY CONVERTERS

FRESNEL DIFFRACTION

Fresnel annular zone objective lens for multichannel Fabry-Perot interferometer

03 p0425 A71-13651

Holographic multiplexing by Fresnel diffraction based on aperture field division, discussing reconstructed image quality

03 p0429 A71-14179

Kirchhoff integral evaluation for Gaussian incident field in Fresnel diffraction from plane wave beams truncated by circular apertures

04 p0627 A71-15688

Laser irradiance pattern from aperture with truncated Gaussian field distribution, evaluating diffraction integral subject to Fresnel approximation

05 p0763 A71-16904

Stable single mode cavity resonators of high Fresnel number with increased fundamental transverse mode for carbon dioxide laser oscillators

09 p1466 A71-23727

Fresnel hologram focusing method, considering Leith and Upatnieks wave front reconstruction with diffused illumination

12 p1907 A71-27212

Book on laser physics covering radiation theory, atomic system interactions, Fresnel diffraction, Gaussian beam, Lamb theory and cavity engineering

13 p2078 A71-28429

Fresnel diffraction on opaque absorbing screen half planes with small rough surfaces, deriving field attenuation factor and structure/correlation functions

14 p2194 A71-30099

Fresnel hologram focusing method, considering Leith and Upatnieks wave front reconstruction with diffused illumination

19 p3067 A71-38624

Fresnel diffraction model appropriateness for stellar occultation by moon

24 p3871 A71-44912

FRESNEL REGION

Hologram Fresnel zone with monochromatic signal and background noise, determining precision of object image coordinates

04 p0584 A71-14633

Design and spark erosion production for circular Fresnel zone plates under He-Ne laser illumination, considering plates as optical reference elements

08 p1289 A71-21374

Hologram Fresnel zone with monochromatic signal and background noise, determining precision of object image coordinates

22 p3546 A71-42273

Optical modeling of antenna radiation patterns from radio hologram of Fresnel region field

22 p3522 A71-42310

FRETTING

Logarithmic damping of flexural oscillations produced by residual fretting stresses in circular plates

03 p0503 A71-13415

Pinned steel lug joints fretting fatigue, examining cumulative damage under constant amplitude and narrow band random loading

03 p0513 A71-14244

Slip front mechanisms in clamped or bolted double lap joints from photoelastic analysis of stress environments, discussing fretting fatigue

11 p1845 A71-25344

Logarithmic damping of bending oscillations produced by residual fretting stresses in circular plates

17 p2826 A71-35022

FRETTING CORROSION

Metal fretting corrosion energy analysis in terms of thermodynamics of irreversible process

06 p0904 A71-17942

Metal surface layers structural changes during fretting corrosion, analyzing strain effects

09 p1455 A71-23081

Thermal emf measurement of Ti alloy, steel, bronze and duraluminum subjected to fretting corrosion tests

13 p2082 A71-27820

Fretting corrosion relationship to mechanical vibrations damping capacity for Fe and Cu alloys, noting energy dissipation

13 p2082 A71-27822

Three greases in oscillatory bearings under various conditions of speed, load and angle of oscillation, determining effects on fretting corrosion prevention [ASLE PREPRINT 71AM 1B-1]

13 p2076 A71-29490
Fretting fatigue test apparatus with load monitoring as function of cycles for relating quantitatively damage to life

14 p2248 A71-30883
Unlubricated instrument ball bearing axial vibration frequency and amplitude effect on fretting corrosion at constant temperature and humidity [ASLE PREPRINT 71LC-7]

FRICITION

NT AERODYNAMIC DRAG
NT DRY FRICTION
NT FLOW RESISTANCE
NT FRICTION DRAG
NT INTERNAL FRICTION
NT KINETIC FRICTION
NT SKIN FRICTION
NT SLIDING FRICTION
NT STATIC FRICTION
NT VISCOUS DRAG

Soviet book on friction welding of metals covering theory, equipment and quality control

02 p0255 A71-11849
Elasticity theory two dimensional contact problems, examining cohesion or friction in contact area

03 p0513 A71-14229
Soviet book on friction and heat transfer covering interaction of bodies with internal/external liquid/gas laminar/turbulent boundary layer flows

04 p0571 A71-15264
Friction, mass and heat transfer in turbulent boundary layers of fluid flows past obstacles

04 p0577 A71-15619
Turbulent boundary layer approximate analytical method based on momentum and energy integral correlations and limiting laws of friction and heat transfer

07 p1085 A71-18756
Friction role in impact dampers for elastic systems out of static equilibrium

08 p1372 A71-21619
Metal friction surface oxide thin films and secondary structures thickness determination using electron microscope method

09 p1454 A71-22311
Forge phase rigid and plastic region model of friction welding, deriving interfacial dispersion parameter of weld quality optimization

09 p1459 A71-23456
Gyroscopic drift in gimbal suspension on moving base in presence of friction force proportional to dynamic reactions

10 p1612 A71-24578
Forced rotational oscillations of plane-convex glass lens pressed against brass plate, determining contact frictional and elastic characteristics from resonance and hysteresis

FRICITION COEFFICIENT U COEFFICIENT OF FRICTION

FRICITION DRAG
NT AERODYNAMIC DRAG
NT VISCOUS DRAG

Heat transfer and friction drag calculation for turbulent boundary layer of gas with temperature dependent physical properties

02 p0185 A71-11884
Media resistance effects on three body problem three dimensional periodic orbits, discussing implications to solar system formation from surrounding nebula

09 p1527 A71-23534
Skin friction drag and velocity profile measurements on flat plate in two phase circular pipe flow in subsonic wind tunnel for gas-solid media, using photographic technique

[ASME PAPER 71-FE-32] 13 p2053 A71-29467
Flow transition to laminar drag law for thin cylinder freely suspended in Hg in rotating vertical cylindrical MHD channel

14 p2279 A71-29615
Stationary longitudinal turbulent flow of air with equilibrium ionization and dissociation around plate, calculating heat exchange and frictional drag

17 p2671 A71-35266
Turbulent skin friction drag for tapered wings as function of root chord Reynolds number

22 p3481 A71-42839

FRICITION FACTOR

Unwanted gimbal rotation friction torques in gyro wheel bearings due to lubrication viscous friction, ball wedging and contamination

02 p0253 A71-12459
Test time and contact stresses effect on jet fuels antiwear properties under rolling friction

02 p0298 A71-12570
Soviet book on mechanical oscillator threshold sensitivity to small moment of forces, covering light friction and radiometric oscillatory instability effects and estimates

02 p0285 A71-12839

Plastic impact principle of hydraulic losses in turbulent viscous flow, using Navier-Stokes equation with friction term

03 p0397 A71-13006
Downstream heat transfer and wall friction predictions for quasi-developed strongly heated turbulent pipe flow, using mixing length model

[ASME PAPER 70-HT-8] 03 p0405 A71-14294
Coolants Prandtl number effect on pressure drop, heat transfer and friction of rough surfaces

04 p0675 A71-14779
Pure metal structure effect on friction and lubrication under steady slip in ultrahigh vacuum at low temperatures

05 p0757 A71-16185
Counterface nature effect on friction and wear processes of carbon fiber reinforced polymers, discussing formation of transfer film of wear debris

05 p0773 A71-17245
Multimass system oscillations due to viscous friction factor and kinematic random disturbances, considering dynamic behavior of wheeled vehicle on rough roadbed

07 p1162 A71-20469
Comparative review of friction welding mechanisms, including inertia and metallurgical aspects [SME PAPER AD-70-574]

07 p1121 A71-20548
Local turbulent friction factors and heat transfer coefficients for fluid flows through ducts of arbitrary cross section with prescribed wall heat flux distribution

07 p1224 A71-20654
Complex hydrodynamic systems nonlinear differential motion equations integration, taking friction forces into account

08 p1299 A71-21620
Film thickness effects on stress magnitude in surface layers of bodies under external friction

09 p1455 A71-23078
Polarographic measurements of secondary Couette flow between coaxial cylinders for diffusion coefficient effects on mean friction factor, using wall flush microelectrodes

10 p1592 A71-23978
Machine tool friction slides dynamics simulation for phase diagrams analysis, using Szoke model

10 p1614 A71-23994
Smooth annuli correlation equation for friction factor, discussing Prandtl turbulence based Spalding inner velocity profile modification

12 p1896 A71-27053
EHD lubricant film thickness and friction forces effects on ball and roller bearings selection and design [ASME PAPER 71-DE-3]

12 p1911 A71-27322
Piecewise-linear approximation of nonlinear friction effect on interferometric servosystem stability, deriving formulas for harmonic linearization coefficient of linearity

13 p2041 A71-28375
Reynolds analogy of heat transfer applied to disk rotating near stator, including frictional dissipation and radial outflow in compressible or incompressible flow

13 p2048 A71-28599
Friction forces between expansion die sectors and blank, describing effect on closed contour shell stress-strain state and shaping process

13 p2074 A71-28939
Friction factor for low Reynolds number turbulent flow in large aspect ratio rectangular ducts, comparing Blasius and Prandtl relations [ASME PAPER 71-FE-A]

13 p2051 A71-29378
Complex media and plasticity theory deformation models based on central friction mechanism, discussing elastic spring analog

14 p2332 A71-30879
Numerical heat transfer and wall friction results, demonstrating gas transport property variation effects on three laminar flow situations

14 p2338 A71-30931
Low Reynolds number turbulent flow in large aspect ratio rectangular ducts, investigating Blasius and Prandtl circular tube friction factor relations

15 p2392 A71-32261
Friction role in impact shock absorbers for elastic systems out of static equilibrium and resonance excitation in vibrations, noting harmful effects

17 p2834 A71-35679
Friction forces in complex hydrodynamic systems nonlinear differential motion equations integration

17 p2749 A71-35680
Temperature limit determination of rotating neutron stars based on heat dissipation due to slowing by frictional forces, noting Crab and Vela pulsars

19 p3131 A71-37337
Force equations for static and dynamic friction under external forced vibration, determining mean values from mechanical model

19 p3068 A71-37346
Undisturbed ionospheric ion and electron temperature warming, investigating frictional heating effect by neutral winds

19 p3048 A71-37399

Brazing roughness effects on rectangular plate fin heat exchanger surfaces heat transfer and flow friction characteristics, noting fin surface geometry influence [ASME PAPER 71-HT-29]

19 p3166 A71-37995
Surface cover materials thermal radiation characteristics and radiation resistance of plastics and solar cells, discussing friction in vacuum and spacecraft surface contamination by outgassing

20 p3210 A71-39455
Lubricated friction of steel ball on commercial tempered aluminum plate as function of time

21 p3396 A71-40100
Friction, wear and adhesion of filler and matrix polymer composite bearing materials including glass, carbon, lamellar solids, metal powders, carbons, nylons, PTFE, polyimides, etc

21 p3405 A71-40600
Natural frequencies and vibration mode shapes of missile with idealized air friction force tangent to instantaneous neutral axis

21 p3455 A71-41012
Aircraft parts damage by corrosive friction forces, hot gases and intercrystalline attack, noting worm universal joint and blade grain boundary damage

24 p3836 A71-44574
Humidity effects on molybdenum disulfide bonded solid film lubricant friction properties at low load and slow speed, noting mechanical escapement timers accuracy [ASLE PREPRINT 71LC-2]

24 p3831 A71-45285
FRICTION LOSS COEFFICIENT
U FRICTION FACTOR

FRICTION MEASUREMENT
Compressible turbulent boundary layer skin friction measurements on adiabatic flat plate, discussing drag balance calibration

[ASME PAPER 70-WA/FE-26] 03 p0403 A71-14134
Gyroscopic bearings friction moments constant and variable components experimental determination by method of compensation, using test equipment based on electric spring principle

05 p0758 A71-16355
Metals and alloys internal friction meter based on intense ultrasonic vibration, discussing error compensation

09 p1426 A71-22320
Friction and wear tests on materials of various speeds, loads and temperatures at high relative humidity

09 p1426 A71-22325
Spectral density of friction pulsations in turbulent channel wall flow for various length to height ratios and Reynolds numbers, using electrochemical method

12 p1897 A71-27306
Turbulent boundary layer friction and heat transfer under longitudinal pressure gradient

13 p2048 A71-28590
Instrument for skin friction measurements in adiabatic turbulent compressible boundary layers [ASME PAPER 71-FE-27]

13 p2072 A71-29463
Friction in compressible turbulent boundary layers at isothermal adiabatic wall

15 p2510 A71-31163
Preston skin friction measuring tube calibration, presenting Patel analytic method simplification

17 p2729 A71-35284
Spectral density of friction pulsations in turbulent channel wall flow for various length to height ratios and Reynolds numbers, using electrochemical method

19 p3046 A71-38262
Device for dry friction determination at low temperatures

23 p3678 A71-43537

FRICTION PRESSURE DROP U SKIN FRICTION FRICTION REDUCTION

Elastic body-vibrating surface interaction, examining friction coefficient under various modes

01 p0088 A71-10626
Antifriction effects of heteroorganic compounds in medium-distillation hydrocarbon fuels for rocket engines

01 p0141 A71-11108
Frictional resistance reduction in hydrodynamics, considering critical shear stress in duct flow

04 p0571 A71-15209
Polybenzothiazole as solid film formulations binder for friction wear improvements, noting thermal and oxidative stability, toughness, adhesive properties and handling ease

05 p0772 A71-16375
Arbitrary direction harmonic vibration effects on kinetic friction coefficient between sliding bodies

11 p1767 A71-25267
Mechanical design of frictionless bimetal actuated louver system for spacecraft thermal control [ASME PAPER 71-AV-39]

18 p2870 A71-36406
Plasma metal coating facility, noting antifriction and mechanical properties

24 p3816 A71-44864

FRICTIONLESS ENVIRONMENTS

Frictionless hypersonic flows by transforming partial differential equations into ordinary, noting detonation wave analogy

18 p2846 A71-36424

FRINGE PATTERNS
U DIFFRACTION PATTERNS
FROGS
Frog eye response to UV light stimulation, investigating sensitivity from electroretinogram 03 p0363 A71-13484
Histochemical investigation of enzymes activity during various cardiac cycle phases in frogs, noting effects of ion concentration 16 p2533 A71-33913
Refraction and image forming qualities of frog eye using measurement of intensity profile /point spread function/, confirming hyperopia 18 p2857 A71-36690

FRONTAL AREAS [METEOROLOGY]
U FRONTS [METEOROLOGY]
FRONTS [METEOROLOGY]
Land breeze fronts observed by X and S band radars at Wallops Island 01 p0116 A71-10563
Anticyclonic eddy formation and emergence within severe thunderstorm observed by radar and surface data, noting wave development along pseudocold front 01 p0118 A71-10588
Diagnostic numerical model of frontal vertical circulation in atmospheric boundary layer using local parameters 08 p1326 A71-21448
Numerical integration of motion equations for two layer atmospheric fronts model with baroclinicity along frontal surface separating two incompressible fluids in stable stratification 10 p1638 A71-23965
Microbarometric oscillations enhancement due to atmospheric pressure waves generation and cold fronts passage, considering relationship to sporadic E critical frequency 10 p1606 A71-24918
Soviet papers on aviation and synoptic meteorology problems covering vertical motions near cold fronts, cloud development, latitude effect, temperature conditions above mountains, etc 11 p1795 A71-26557
Cold front zone meteorological elements, calculating temperature gradients, dew point deficit, and wind vector vertical distribution 11 p1795 A71-26558
Atmospheric jet stream reinforcement by cold pseudofronts and convective energy from local source 12 p1924 A71-26824
Atmospheric frontogenesis models with air velocity fields acting on initially large scale temperature distributions 13 p2097 A71-28722
Temperature effects on cosmic rays muon component variations during cold fronts passage 13 p2131 A71-29485
Thunderstorm gust fronts from Oklahoma surface mesonetwork and weather radar data, considering hazard to aircraft 14 p2267 A71-29757
Finite difference methods application to numerical weather prediction problems, describing frontal depression growth and boundary conditions for short gravity wave suppression 15 p2443 A71-31357
Fronts and frontal clouds evolution theory as nonstationary two dimensional problem with allowance for dynamics and thermodynamics 19 p3091 A71-38682
Precipitation formation and regulation from supercooled and frontal clouds, noting crystalline cloud seeding effects 19 p3092 A71-38689

FROST
Carbon dioxide frosts spectral absolute reflectance measurements at 0.5-12 microns, applying results to problems associated with cryogenically cooled surfaces 15 p2514 A71-32098
Subsurface moisture and frost detection by capacitive measurement of ground permittivity from landed planetary probes and surface vehicles 15 p2411 A71-32473
Jupiter Galilean satellites surface optical polarization measurement, noting bright transparent material cover possibly frost 18 p2964 A71-36290

FROUDE NUMBER
Steady boundary layer flow in viscous liquid thin down variable incline for large Reynolds and Froude numbers 09 p1432 A71-22451
Potential flow of incompressible inviscid liquid film along inclined semiinfinite flat plate for large Froude number values, using matched asymptotic expansions method 13 p2047 A71-28485
Vertical acceleration effect on gas-hydraulic analogy for turbulent flows with and without jumps with error dependence on Froude number and length to depth ratio 16 p2560 A71-33598

FRUSTUMS
Double frustum phenomenon in mushrooming of cylindrical Al projectiles upon high speed impact with hardened steel anvil 21 p3474 A71-41424
Free axisymmetric torsional vibrations of thick hollowed conical frustums cantilevered at small end, considering conicity and cone thickness effects 22 p3618 A71-42590

FUEL CELL CATALYSTS
U ELECTROCATALYSTS
FUEL CELLS
NT HYDROGEN OXYGEN FUEL CELLS
NT REGENERATIVE FUEL CELLS
Book on fuel cells covering types, applications, thermodynamics, chemical reactions, direct electrical generation, etc 01 p0006 A71-11192
Book on direct energy conversion principles and methods covering fusion, fuel cells, MHD, thermoelectric, thermionic, photovoltaic, electrohydrodynamic, piezoelectric and ferroelectric power generation 01 p0006 A71-11193
Hydrazine-hydrogen peroxide fuel cells coulombic efficiency measurement 02 p0197 A71-12960
Oxide bronzes as oxygen reduction catalysts in batteries and fuel cells, considering effects of varying compositions and crystal faces 03 p0374 A71-13054
Phosphoric acid corrosion resistant alloys for electrolyte fuel cells, discussing materials selection and optimization 03 p0440 A71-13055
Fuel cell electrodes preparation by sputtering thin Ta and Pt layers on porous Vycor 03 p0353 A71-13056
Ni-Ti system electrocatalysts for fuel cell and accumulator electrodes 03 p0355 A71-14318
Hydrazine-oxygen fuel cells energy costs minimization by optimizing diaphragm thickness, hydrazine concentration and load 03 p0355 A71-14321
Earth-moon mission fuel cells, discussing development of direct, indirect and redox cells 04 p0535 A71-15082
Fuel cell technology in astronautics, reviewing design and operational characteristics, functional and economic merits as spacecraft power supply sources 05 p0705 A71-16140
Electrochemical properties of Na-W bronzes for use as electrocatalysts in acid electrolyte fuel cells 09 p1387 A71-23648
Aircraft self sealing fuel tank and fuel cell systems damage control, considering chemical, precompressed foam and swellable elastomer seal concepts 10 p1534 A71-24079
Hydrazine feed control in hydrazine-oxygen fuel cells, discussing continuous measurement of limiting diffusion current for determining fuel concentration in electrolyte 11 p1708 A71-25241
High temperature fuel cell in hot gas mixtures analysis, presenting porous silver and palladium electrodes cathodic polarizations 15 p2367 A71-31648
Fuel cell system steam/hydrogen mixture mass ratio detector using fluidic delay line oscillator 17 p2745 A71-35294
Hydrogen depolarized fuel cell for space station prototype carbon dioxide concentrator, describing modular design concept and operation [ASME PAPER 71-AV-37] 18 p2870 A71-36404

FUEL COMBUSTION
Detonation propagation velocity through tubes with walls coated with thin fuel film, using turbulent boundary layer theory 01 p0181 A71-11305
Combustion velocity of burning liquid fuel droplets as function of number and distance 01 p0182 A71-11445
Vaporization and combustion kinetics of condensed single drop kerosene and gasoline thickened by polyisobutylene 01 p0142 A71-11446
Solid fuels and propellants heterogeneous ignition mechanism, using local similarity and related methods 02 p0333 A71-12853
Fluid mechanics of shallow liquid fuel layer near burning wick, deriving continuity, momentum and convective diffusion equations to obtain extinction condition 02 p0334 A71-12855
Flame temperature and combustion characteristics of model fuel-oxidizer-metal powder systems, using spectral and photometric techniques 03 p0376 A71-13988
Shape effect of compressed solid fuel on thermal ignition delay time in heated gas flow for pyroxyline 03 p0520 A71-13993
Diffusion controlled combustion of liquid fuel droplet in oxygen-steam oxidizer mixture 03 p0468 A71-13996

Jet engine liquid fuel wall layer combustion stimulation by repeated oxidizer injection into supersonic section of nozzle 03 p0472 A71-14256
Sulfur trioxide catalytic formation in gases from fuel-rich propane-air flames containing sulfur 03 p0376 A71-14279
Dispersion model of turbulent mixing of isothermal and nonisothermal slipstreams of air-gasoline combustion products in nozzles 04 p0577 A71-15622
Particulate B fuels combustion and ignition working models in air at ambient pressures, using levitation cell and pulsed Nd doped laser [WSS/CI PAPER 70-13] 06 p0943 A71-17659
Luminometer numbers of hydrocarbons and reactive fuels as function of molecular weight and structure 06 p0913 A71-18471
Incident shock wave interaction with liquid hydrocarbon fuel drops in oxidizing and inert atmospheres, considering combustion characteristics and ignition mechanism [AIAA PAPER 71-206] 06 p0886 A71-18642
Subsurface flow generation by surface tension variation due to flame spreading over liquid fuel at large Reynolds number, using hydrodynamical analysis [AIAA PAPER 71-207] 06 p1009 A71-18643
Liquid fuel droplets in heterogeneous detonation of dilute sprays, noting deformation and fragmentation in reaction zone 07 p1222 A71-19189
Liquid fuel pool ignition at superflash and subflash temperatures involving adjacent heat source, cross wind and fluid motion 07 p1182 A71-19245
Post reaction zone properties of premixed fuel rich propane-oxygen flames on torch, measuring temperature, composition and hydroxyl radicals 08 p1345 A71-20858
Oxygen-kerosene fuel combustion products, calculating thermal and physical constants 08 p1346 A71-21263
Gaseous fuel mixtures containing nitrogen oxides, discussing combustion mechanism 09 p1403 A71-22531
Ignition delay times behind reflected shock wave of alkanes methane through pentane in stoichiometric argon simulated air mixture 10 p1657 A71-24047
Fuel evaporation in combustion chambers L-shaped and annular vaporizers, determining operational parameters effect on evaporation ratio 10 p1658 A71-25123
Heterogeneous detonation propagation in mixture of liquid fuel droplets suspended in gaseous oxidizer, discussing droplets disintegration time and shock wave parameters 10 p1698 A71-25124
Shock wave ignition of liquid fuel drop in oxidizing atmosphere, discussing combustion process [AIAA PAPER 70-9] 12 p1986 A71-27566
Laser light scattering by fuel droplets in flame combustion zone, measuring intensity distribution with contactless optical probe 13 p2065 A71-27886
Piezoelectric transducer/oscillograph technique for simultaneously rating fuels knock properties and detonation intensity 13 p2113 A71-28228
Transient nature of fuel droplet combustion, discussing burning rates and flame to drop diameter ratio 13 p2161 A71-28614
Kerosene type fuels for aircraft gas turbine engines, discussing combustion problems, smoke emission reduction and bacterial or fungal contamination 13 p2113 A71-28754
Liquid fuel atomizers for gas turbine combustion system model experiments, considering droplet sheet photography and molten wax spray technique 13 p2117 A71-28755
Turbulent flame boundaries and maximum brightness surface position in gasoline-air mixtures, using photography and gas analysis measurements of carbon dioxide concentrations 13 p2162 A71-28955
Flame propagation speed, combustion zone extent and distance from front to maximum brightness surface in turbulent gasoline-air flames 13 p2162 A71-28956
Combustion, reaction and flame propagation during gas mixtures burning, allowing for disruption of Maxwell-Boltzmann molecular velocity distribution 13 p2162 A71-28957
Normal rates of flame propagation in two stage burning of gasoline-air mixtures 13 p2162 A71-28958
Flame propagation rate in gasoline-air flow with tubular and grid-induced turbulence during two-stage burning process 13 p2162 A71-28959

Gasoline-air combustion zone extent as function of inlet temperature for plane turbulent flame in square-section channel 13 p2163 A71-28960

Stabilizer structure effect on flame stability of atomized liquid fuel, studying excess air ratio relation to air flow velocity 13 p2163 A71-28963

Combustion process in mixing zone of kerosene-air mixture and hot combustion products, deriving flame-out time relation to characteristic temperature in mixing region 13 p2163 A71-28964

Jet induced flame stabilization in combustible kerosene-air mixture flow of variable composition, discussing stable burning range and excess air content 13 p2163 A71-28965

Combustion rates of ammonium perchlorate mixtures with organic acids, alcohols, cyclic hydrocarbons, amines, nitroso compounds and nitrimines, studying relationship to fuel chemical composition 15 p2366 A71-31370

Unmixed gases burning at finite reaction rate, analyzing steady laminar flames developing in mixing zone of fuel semiinfinite flow past static oxidizer 15 p2511 A71-31379

Styrene-methyl methacrylate and -acrylonitrile copolymers linear and mass regression rates in hybrid rocket fuels combustion 15 p2464 A71-31640

Individual liquid fuel droplets ignition factors, introducing heating-up and evaporation delay 15 p2516 A71-32709

Liquid hydrocarbon fuel drop interaction with incident shock wave in oxidizing and inert atmospheres, investigating aerodynamic shattering and combustion 17 p2836 A71-34435

Soviet papers on fuel vibrational combustion in model devices covering applications to gases, powder and coal particles 17 p2839 A71-35694

Exhaust pipe or diffusion kinetic flame type relaxation autooscillatory fuel combustion system, calculating vibration frequency, amplitude and mode 17 p2839 A71-35695

Solid fuel vibrational combustion devices and operational analysis, considering various chamber configurations 17 p2840 A71-35702

Oblique shock-combustion wave polar investigation of stationary two dimensional flow of fuel mixture in compressed gas 18 p2985 A71-36133

Unsteady burning rate response of condensed phase fuel plate adjacent to reacting gaseous boundary layer with oscillating external flow 19 p3123 A71-38095

Free fuel droplet spherical combustion in freely falling chamber under zero gravity condition 19 p3169 A71-38111

Ethyl alcohol combustion effect on laminar boundary layer structure near flat plate, assuming thermal cracking of fuel 19 p3169 A71-38113

Detonation propagation through tubes with thin fuel film coated walls, obtaining heat transfer coefficients, friction, evaporation rate, reaction zone length and propagation velocity 19 p3171 A71-38129

Electric fields for solid and liquid fuels dispersion and trajectory manipulation of charged particles to control mixing with air, vaporization and burning 19 p3171 A71-38193

Soviet book on fuel burning process physicochemical fundamentals covering combustion gases thermophysical and thermochemical characteristics, methane, formaldehyde and carbon monoxide combustion reaction kinetics, etc 20 p3194 A71-39089

German monograph on flow and combustion changes during hydrogen and methane transverse injection into hot supersonic air jet 21 p3475 A71-40750

Homogeneous fuel combustors with multistage reaction rate controlled system, determining linear relationships and heat release 21 p3437 A71-41049

Emissivity calculation for radiant heat flux from isothermal gas mixture of hydrocarbon fuel combustion products 23 p3718 A71-43918

Lithium deuteride nuclear fuel autocatalytic burning via proton and beryllium isotope resonance in fusion chain reactions 24 p3847 A71-44497

Spherical hydrocarbon fuel droplet combustion in air, considering mass burning rates and flame zone locations as function of drop size [AIAA PAPER 71-989] 24 p3887 A71-44584

Fuel droplet burning rate variation with ambient temperature and oxygen concentration in combustion gas environment 24 p3887 A71-44606

Combustion of homogeneous reacting gas mixture with solid or liquid fuel particles, describing motion by multiveLOCITY and multitemperature model 24 p3891 A71-45216

Solid fuel combustion in presence of unsteady heat propagation in heated layer, solving fuel heat conduction equation for sudden combustion rate change 24 p3891 A71-45218

FUEL CONSUMPTION

Axisymmetric spacecraft fuel optimal reorientation control by reaction jets determined using Pontryagin maximum principle 01 p0165 A71-11586

Orbiting vehicle state variables at ballistic transfer termination for known injection errors, calculating fuel consumption for final adjustments 03 p0485 A71-13249

Second order variational endpoint condition numerical application used for low thrust minimum fuel orbital transfer problems 03 p0450 A71-13445

Spin stabilized spacecraft fuel optimal direction cosine attitude control, considering relation to inertial system 03 p0500 A71-14448

Aircraft propulsion, discussing piston, turbojet, turboprop and turbofan engines in terms of thrust to weight ratio, specific fuel consumption and propulsive efficiency 04 p0638 A71-14977

Two-phase detonations, discussing importance of stripping mechanism and droplets deformation in reaction zone fuel consumption 05 p0834 A71-16515

Minimum propellant deterministic guidance law for bounded-thrust constant jet exhaust velocity spacecraft, using neighboring extremal theory [AIAA PAPER 71-118] 06 p0978 A71-18568

Rocket engine thermodynamic characteristics and parameters determination, using extrapolation formulas with initial fuel composition 08 p1346 A71-21264

High pressure ratio centrifugal compressors for small gas turbine engines, investigating power and specific fuel consumption variation with pressure and temperature 10 p1658 A71-24218

Light aircraft standard fuel flight evaluation, discussing compatibility with grades 80/87 and 100/130 certified engines and comparative operational fuel consumption [SAE PAPER 710369] 10 p1657 A71-24239

Soft lunar landing powered descent optimal control for cost functional minimization, considering linear analytic approach with fuel consumption reduction 10 p1682 A71-24330

Low thrust minimum fuel space vehicle transfer from initial circular orbit to coplanar elliptic orbit of given energy and angular momentum 10 p1671 A71-24334

Minimum propellant optimal rendezvous maneuver of two cosmic vehicles on circular orbits, considering tracking vehicle motion equations 10 p1672 A71-24335

Nonlinear satellite system attitude control for minimum fuel consumption, deriving linear programming algorithm based on optimal control theory 10 p1683 A71-24522

Soviet book on liquid propellant rocket engines non-stationary operation covering dynamic processes, transient conditions, component elements, fuel delivery, etc 10 p1659 A71-24649

Two stage rocket flight optimization for minimum propellant consumption, using calculus of variations 13 p2145 A71-28734

Fuel optimal noncoplanar orbital transfers of thrust limited rocket 13 p2139 A71-28828

Jet-supported VTOL aircraft fuel-time-optimal landing control, using mathematical model, Pontryagin maximum principle and analog computer solution 13 p1997 A71-29281

Subsonic and supersonic turbojet aircraft engines development, discussing design, operation, reliability, weight, fuel consumption and cost 14 p2287 A71-29811

Symphonie geostationary satellite fuel-optimal injection problem, employing Tschauner-Hempel differential equations and Monte Carlo simulation 15 p2498 A71-31157

Constant-thrust trajectory problem with gravitational acceleration as linear function of radius vector, obtaining minimum fuel solution in integrals 15 p2488 A71-32043

Two-spool turbojet engine nozzle diameter adjustment system for increasing thrust, fuel economy and reliability, describing automatic clamshell shutter control mechanism 15 p2471 A71-32527

French SNECMA M56 turbofan engine design for medium capacity airliners, featuring low specific fuel consumption and low noise level 15 p2471 A71-32692

Turbojet engines thrust and fuel economy improvement by gas-air jet mixing, discussing efficiency increase and noise reduction 15 p2472 A71-32715

Air transport propulsion systems economics, considering first cost, specific weight, fuel consumption and maintenance effect on direct operating cost 16 p2523 A71-33460

Heated tank under axial compression and internal pressure, noting fuel expenditure effects on stream strain state 16 p2658 A71-33625

Three dimensional minimum fuel turns for supersonic aircraft by energy state approximation [AIAA PAPER 71-913] 19 p3096 A71-37116

Onboard approach guidance instrument for Grand Tour to outer planets missions reducing fuel for corrective maneuvers by estimating trajectories [AAS PAPER 71-119] 19 p3101 A71-37914

Suboptimal design of closed loop least upper bound fuel control for dynamic systems, minimizing fuel consumption on basis of fixed ultimate error 20 p3206 A71-38971

Spacecraft interplanetary guidance trajectory correction, deriving algorithm for optimal accuracy and minimum fuel expenditure 20 p3288 A71-39124

Minimum propellant guidance laws comparison for impulsive and bounded thrust spacecraft, considering jump and controllability conditions for one burn trajectories 22 p3611 A71-42025

Fuel optimal analytic multiburn transfer trajectories and shuttle rendezvous, assuming gravity vector linear dependence on position vector for burn arcs [AAS PAPER 71-306] 23 p3724 A71-42982

Fuel optimal transfer from circular orbit space station to rendezvous with vehicles in different circular orbits [AAS PAPER 71-365] 23 p3729 A71-43035

Optimal singular control conditions for intermediate rocket thrust arc nonoptimality in Newtonian gravitational field for minimum fuel fixed time trajectory 23 p3718 A71-43378

FUEL CONTAMINATION

Aircraft fuel tank nitrogen inerting, fire and explosion suppression for foreign particle contamination, sludge and lacquering reduction [ASME PAPER 71-GT-45] 11 p1810 A71-25978

Polyurethane foam effects on fuel contamination during installation for fuel system fire and explosion protection [ASME PAPER 71-GT-54] 11 p1708 A71-25981

Microbiological contamination of jet aircraft fuel tanks in tropical regions, considering maintenance [SAE PAPER 710438] 13 p1996 A71-28320

Kerosene type fuels for aircraft gas turbine engines, discussing combustion problems, smoke emission reduction and bacterial or fungal contamination 13 p2113 A71-28754

FUEL CONTROL

Out-of-pile experiment for measuring uranium dioxide fuel redistribution rates, determining vent hole plugging time and thermal cycling 02 p0296 A71-12247

Inertial and semiinertial propulsion systems output power and efficiency, taking into account continuous kinetic and potential energy buildup and fuel release 06 p0979 A71-17583

Liquid fuel atomization spectrum in nozzles, examining proportion control of droplet size 08 p1348 A71-21262

Hydrazine feed control in hydrazine-oxygen fuel cells, discussing continuous measurement of limiting diffusion current for determining fuel concentration in electrolyte 11 p1708 A71-25241

Fluidic fuel control valve for uniform fuel distribution to gas turbine annular combustor, providing sufficient pressure drop at low flow rates [ASME PAPER 71-GT-44] 11 p1812 A71-25977

Annular vaporizing combustion chambers, considering aerodynamic control of fuel distribution and mechanical simplifications 13 p2116 A71-28744

Energy state approximation and supersonic aircraft minimum fuel fixed range trajectory optimization, noting not convex velocity set 14 p2177 A71-30609

Turbine engine fuel control stability on CH-47C helicopter, using flight tests and lag damper simulation [AHS PREPRINT 560] 14 p2297 A71-31107

Suboptimal design of closed loop least upper bound fuel control for dynamic systems, minimizing fuel consumption on basis of fixed ultimate error 20 p3206 A71-38971

Cryogenic propellant control system, discussing hot wire sensors, fuel state in fueling and tank pressurizing and feed stage 22 p3588 A71-41504

Spinning and dual spin spacecraft angular momentum and axis control, investigating optimal fuel and small angle reorientation techniques 22 p3611 A71-42045

FUEL CORROSION

Jet fuel soluble corrosion inhibitors evaluation by potentiostatic polarization methods 03 p0377 A71-14323

Jet fuels thermal stability and corrosive properties during prolonged storage 07 p1182 A71-19492

Antiwear properties of jet fuels as function of dissolved oxygen, resin and heteroorganic compound content and temperature, considering antioxidant additives 16 p2623 A71-33579

Book on external corrosion and deposits on boiler tubes and gas turbine blades covering mineral matter in fuels, oxidation, additives, etc 18 p2935 A71-36247

Soviet monograph on carbon deposits in jet engines covering distribution, formation, fuel properties, reduction and removal and harmful effects in gas turbines 21 p3437 A71-40871

FUEL ECONOMY

U FUEL CONSUMPTION

FUEL ELEMENTS [NUCLEAR REACTORS]

U NUCLEAR FUEL ELEMENTS

FUEL FLOW

NT PROPELLANT TRANSFER

Fuel rod bundle boundary layer in longitudinal fluid flow, investigating turbulent temperature and pressure pulsations 04 p0684 A71-15504

Rocket fuel lines disruptive cavitation oscillations, considering rocket body mechanical vibrations and fuel line oscillation frequency characteristics 08 p1366 A71-21753

Optimal gas temperature in bypass and turbojet engines afterburners ensuring minimum fuel flow rate dependence on thrust augmentation 16 p2624 A71-33607

Singular perturbation theory for finite rate chemical kinetics effect on regression rate of semiinfinite flat fuel plate in gas oxidizer stream 17 p2792 A71-35796

Volume fraction analysis of coaxial flow gas core nuclear rocket for mass flow ratios, fuel radius and density, using free jet computer code and eddy viscosity equations 22 p3573 A71-41638

Rocket fuel lines disruptive cavitation oscillations, considering rocket body mechanical vibrations and fuel line oscillation frequency characteristics 24 p3876 A71-44926

FUEL FLOW REGULATORS

D-30 bypass engine hydraulic control system for Tu-134 aircraft, discussing fuel flow regulator assembly and operation 09 p1511 A71-22947

Propulsion system and fuel regulator design effect on thrust change during air ejection for VTOL aircraft stabilization in hovering flight 10 p1659 A71-24753

Fluidic fuel control valve for uniform fuel distribution to gas turbine annular combustor, providing sufficient pressure drop at low fuel flow rates [ASME PAPER 71-GT-44] 11 p1812 A71-25977

FUEL GAGES

Electrical and physical nature of microbial membranes implicated in aircraft fuel quantity probe malfunction [SAE PAPER 710439] 13 p2113 A71-28321

Zero-g propellant tank quantity gaging methods, suggesting large cryogenic propellant tanks for space shuttle orbiter stage 18 p2922 A71-36455

FUEL INJECTION

Internal mixing scheme for continuous fuel injection in Wankel engine via swirl nozzle during intake-compression cycle 02 p0298 A71-12559

Hydrogen fuel injection into hot oncoming air flow, investigating boundary layer chemical behavior at stagnation point of diffusion flame 02 p0334 A71-12857

Supersonic combustion ramjet engine with liquid fuel injection, considering atomization process and ignition criteria 05 p0836 A71-16531

Mg slurry fuel mixing, ignition and combustion characteristics for injection into high speed air flow [AIAA PAPER 71-6] 06 p1007 A71-18480

Oxygen difluoride/diborane propellant thrust chamber and injector technology, discussing engine duty cycles and performance [AIAA PAPER 70-717] 07 p1183 A71-18890

Stagnation point flow flame sheet model, showing density-viscosity product variation for injection rate effect on velocity profile 08 p1375 A71-20865

Rocket engine propellant injectors with noncircular orifice geometry, presenting experimental spray patterns and predicted performance for noncircular and circular orifice configurations 11 p1810 A71-25520

Low pressure drop fuel liquid injectors for jet engine combustors, using gas turbine vaporizer design [ASME PAPER 71-GT-38] 11 p1812 A71-25972

Annual vaporizing combustion chambers, considering aerodynamic control of fuel distribution and mechanical simplifications 13 p2116 A71-28744

Combustion efficiencies of staged rocket motor consisting of gas generator, secondary combustor and converging-diverging nozzle [AIAA PAPER 71-739] 14 p2296 A71-30782

Supersonic combustion flowfield transverse hydrogen jet injection into Mach 2.5 airstream, discussing recirculation region upstream [WSS/CI PAPER 71-15] 15 p2463 A71-31624

FUEL PUMPS

Concorde aircraft fuel system and fuel pumps, considering center of gravity and center of pressure relationship to maintain trim 09 p1512 A71-23581

High speed vane type main engine fuel pump for small gas turbine engines [ASME PAPER 71-GT-24] 11 p1812 A71-25966

FUEL SYSTEMS

NT AIRCRAFT FUEL SYSTEMS

Bellows for aerospace feed line ducting, discussing liquid propellant rocket engines, cryogenic valves, etc 01 p0007 A71-11433

Saturn 5 S-2 stage propellant feedlines and V-2 engines simulating structural longitudinal oscillation by analog computer [AIAA PAPER 70-626] 03 p0472 A71-14430

Fluidic pressure ratio control for vertical takeoff aircraft lift engine fuel system, describing breadboard circuit, test bed and flight standard 07 p1028 A71-20587

Double ended full length external fuel thermionic converter, describing component fabrication, assembly sequence, joining methods, vacuum test procedures and converter load control 11 p1715 A71-25910

Soviet book on aircraft and rocket engines control automation, discussing nuclear power plant/fuel systems design and control simulation methods 11 p1814 A71-26403

Soviet book on liquid rocket engines covering combustion chambers, fuel supply systems, static and dynamic characteristics, control and reliability 15 p2466 A71-31296

Material, design and operating principles of rotary seals used in gas ducts, bearing elements and fuel systems of aircraft gas turbine engines 19 p3069 A71-38015

FUEL TANK PRESSURIZATION

Optimal model of pressurization system for liquid propellant on Surveyor lunar landing spacecraft 03 p0472 A71-14447

Liquid hydrogen fueled space vehicle fluorine-hydrogen main tank injection pressurization system performance prediction by computerized analysis [AIAA PAPER 71-645] 14 p2290 A71-30722

Liquid rocket propellants pressurization by injected cryogenic liquids evaporation, using water and liquefied air for experimental investigation [DFVLR-SONDDR-117] 15 p2466 A71-32721

Fuel tank gas cushion minimum volume during refueling, using method of successive approximations 16 p2623 A71-33610

Valves and regulators development and testing for liquid hydrogen propellant tank pressurization system 22 p3588 A71-41503

Cryogenic propellant control system, discussing hot wire sensors, fuel state in fueling and tank pressurizing and feed stage 22 p3588 A71-41504

FUEL TANKS

NT WING TANKS

Fracture of bumper protected fuel tanks subjected to hypervelocity meteoroid impact, applying method of characteristics to stress wave propagation in tank walls [AIAA PAPER 69-369] 03 p0500 A71-14431

Outgassing of multilayer insulation materials for use in cryogenic fuel tanks 03 p0522 A71-14441

Carbon fiber reinforced composite cryogenic fuel tanks development for post-Apollo programs, discussing fiber and resin physical properties 05 p0819 A71-15946

Optimal viscous damping effect of cylindrical filled fuel tanks on satellite nutations 06 p0979 A71-17417

Supersonic transport fuel tank environments and sealant requirements, describing Boeing laboratory environment approach 09 p1385 A71-23424

Elastomers for aerospace vehicles extreme environments, discussing fuel tank integral high temperature sealants 10 p1631 A71-24078

Aircraft self sealing fuel tank and fuel cell systems damage control, considering chemical, precompressed foam and swellable elastomer seal concepts 10 p1554 A71-24079

Fluorosilicone sealants for aircraft fuel containment, discussing resistance to heat, jet fuel, moisture and heat aging 10 p1631 A71-24080

Long term exposure effects on high temperature resistant supersonic aircraft fuel tank sealants 10 p1631 A71-24081

Accelerated testing of jet fuel containment sealant, using reduced pressure and hybrid fluorocarbon silicone 10 p1632 A71-24083

Automated fueling for Kennedy jet airport, using computer controlled underground bulk storage-satellite tank pipeline system 10 p1589 A71-24300

Variable geometry external fuel tanks for high performance aircraft with drag reduction upon fuel transfer [AIAA PAPER 71-395] 11 p1707 A71-25271

Pressure vessel flaw detection at high stress and cryogenic temperatures, noting Lunar Module fuel tanks experience [AIAA PAPER 71-336] 11 p1777 A71-25315

Aircraft fuel tank nitrogen inerting, fire and explosion suppression for foreign particle contamination, sludge and lacquer reduction [ASME PAPER 71-GT-45] 11 p1810 A71-25978

Microbiological contamination of jet aircraft fuel tanks in tropical regions, considering maintenance [SAE PAPER 710438] 13 p1996 A71-28320

Quasi-stationary one dimensional thermoplastic stress strain state in cylindrical fuel tank during emptying process, allowing for Bauschinger effect 13 p2157 A71-29196

Heated tank under axial compression and internal pressure, noting fuel expenditure effects on stress-strain state 16 p2658 A71-33620

Performance evaluation of variable geometry external fuel tank prototypes by static structural tests, wind tunnel tests and flight tests on F-111 aircraft [AIAA PAPER 71-763] 17 p2675 A71-35533

FUEL TESTS

Antifiction effects of heteroorganic compounds in medium-distillation hydrocarbon fuels for rocket engines 01 p0141 A71-11108

Test time and contact stresses effect on jet fuels antiwear properties under rolling friction 02 p0298 A71-12570

Liquid fuel drop evaporation under pressure on hot surface, measuring lifetime and transient interface temperature at subcritical and supercritical conditions 04 p0689 A71-15919

Soviet book on automotive and jet aircraft engine fuel chemical stabilizers under storage, transit and operational conditions, examining additives in relation to stability ratings 06 p0942 A71-17433

FUEL VALVES

Fluidic fuel control valve for uniform fuel distribution to gas turbine annular combustor, providing sufficient pressure drop at low fuel flow rates [ASME PAPER 71-GT-44] 11 p1812 A71-25977

Soviet book on liquid rocket engines fuel valves design and development covering hydraulic characteristics, control cavities, shut-off devices, operational stability, etc 15 p2466 A71-31295

Valves and regulators development and testing for liquid hydrogen propellant tank pressurization system 22 p3588 A71-41503

FUEL-AIR RATIO

Turbulence intensity in combustion zone of stabilized air-kerosene flame from annular burner, using He diffusion measurements 03 p0520 A71-13994

Hot laminar round inert gaseous jet entraining fuel-air mixture, obtaining velocity, temperature and concentration profiles 04 p0683 A71-15495

Flame propagation dynamics of layered methane-air mixtures in vertical tubes, using interferometric techniques 08 p1346 A71-20864

Burning velocity measurement of laminar conical hydrogen-air flames on 10.3 mm diam water cooled nozzle burner, using schlieren and particle tracking techniques 15 p2465 A71-32085

Artificially induced unsteady flows effects on flame stabilization by model opposed jet stabilizer employing premixed propane-air combustible flow and opposed air jet 17 p2840 A71-35706

Test bed engine studies of overall excess air ratio permissible deviation, obtaining diagram for constraints calculation 24 p3864 A71-45022

FUELING

U REFUELING

FUELS

NT AIRCRAFT FUELS

NT CRYOGENIC ROCKET PROPELLANTS

NT GASOLINE

FULL SCALE FATIGUE TESTS

- NT HYDROCARBON FUELS
 NT HYDROGEN FUELS
 NT HYPERGOLIC ROCKET PROPELLANTS
 NT JET ENGINE FUELS
 NT LIQUID ROCKET PROPELLANTS
 NT METAL FUELS
 NT METAL PROPELLANTS
 NT MONOPROPELLANTS
 NT NUCLEAR FUELS
 NT SLURRY PROPELLANTS
 NT SOLID ROCKET PROPELLANTS
 Liquid fuel droplet transient evaporation in high temperature environment, examining vaporization process with coupled heat and mass transfer [AIAA PAPER 71-126] 06 p1008 A71-18570
- FULL SCALE FATIGUE TESTS
 U FATIGUE TESTS
 U FULL SCALE TESTS
 FULL SCALE TESTS
 Sounding rockets nonlinear aerodynamic characteristics from full scale and supersonic wind tunnel free flight data, using wobble analysis [AIAA PAPER 70-1383] 03 p0498 A71-13666
 FAA full scale aircraft vortex wake turbulence flight test programs [AIAA PAPER 71-97] 06 p0848 A71-18552
 Airfoil profile drag measurements, correlating full scale flight tests and scale model tests in transonic and high Reynolds number wind tunnels [AIAA PAPER 71-289] 08 p1229 A71-22012
 Free flight ranges application to high temperature gas dynamics, using mathematical model to relate sub and full scale observations 11 p1705 A71-26269
 Design, analysis and testing of F-111 complex fuselage full scale section of composite materials, noting weight savings [SAWE PAPER 889] 17 p2835 A71-35825
 Blunt planetary entry probe full scale flight test base pressure measurements, noting insensitivity to angle of attack variations up to 10 degrees 20 p3176 A71-39353
- FUNCTION GENERATORS
 Chain reversible functional transducer design, obtaining reversibility by additional resistances without changing operating voltage level 13 p2041 A71-27950
 Nonlinear analog function generators using semiconductor junctions and combined diode-resistor network 13 p2039 A71-28914
 RC analog fluidic circuits design for arbitrary transfer functions generation 15 p2351 A71-31682
 Lame function generation within ellipsoidal coordinates by computerized formula manipulation techniques 22 p3565 A71-41501
 Multiple Walsh function generator design for improved time response relative to digital components, comparing with Rademacher device 23 p3646 A71-43962
 Recurrence techniques for generation of Bessel functions of complex order and argument 23 p3648 A71-43966
- FUNCTION SPACE
 NT BANACH SPACE
 NT HILBERT SPACE
 Orthogonal transforms and feature selection using pattern, Harr, Walsh, Fourier and Karhunen-Loeve spaces for providing efficient classification algorithms in pattern recognition 08 p1258 A71-21354
 Partial ordering of normed space, using positive element cone construction method 09 p1485 A71-22368
 Expansive mappings as generalizations of expansive homeomorphisms, proving nonexistence of expansive functions on open unit interval 09 p1485 A71-22587
 General Markov processes, considering topological space E and semigroup t equal to or greater than zero 12 p1922 A71-26819
 Bubnov-Galerkin method convergence prediction, discussing J spaces and orthonormal bases 15 p2439 A71-31154
 Normal mode vibrations of system with trajectories of unit mass in Euclidean space, determining modal subspaces by potential function 17 p2776 A71-34295
 Geometric theory of linear multivariable systems extension by controllable output subspace introduction 17 p2723 A71-35295
 Boundary value problems solution in optimal control theory, discussing gradient descent method in state space 19 p3037 A71-37534
 Function classes of n -dimensional nonlinear mappings generalizing matrices, including convergence for Jacobi and Gauss-Seidel process 19 p3088 A71-38311
 Stationary signal space topology concept in special relativity, considering points neighborhoods as independent of signal sending time 21 p3346 A71-40091

- Cauchy problem theory covering analytic and nonanalytic functions, Gevrey function spaces, hyperbolic operators and differentiable functions spaces 22 p3566 A71-41513
 Conditions definition for nonexistence of continuous right inverse for surjective linear partial differential operators on Frechet spaces 22 p3568 A71-42693
 Local dynamical system behavior in perturbed Tikhonov space, showing fundamental cycle periods continuous variations 22 p3568 A71-42695
 Degenerate critical points Morse index type characteristics, considering maximum points of functional on surface of another 24 p3843 A71-44707
 Orthogonality and positive operators on space of almost periodic and quasi-periodic functions, using frequency-power formulas 24 p3843 A71-44961
- FUNCTION TESTS
 U TESTS
 FUNCTIONAL ANALYSIS
 NT BANACH SPACE
 NT CONVOLUTION INTEGRALS
 NT FOURIER TRANSFORMATION
 NT FREDHOLM EQUATIONS
 NT HARMONIC ANALYSIS
 NT HILBERT SPACE
 NT HILBERT TRANSFORMATION
 NT INTEGRAL EQUATIONS
 NT INTEGRAL TRANSFORMATIONS
 NT LAPLACE TRANSFORMATION
 NT SINGULAR INTEGRAL EQUATIONS
 NT TESSERAR HARMONICS
 NT VOLTERRA EQUATIONS
 NT WIENER HOPE EQUATIONS
 NT ZONAL HARMONICS
 Variational and boundary value problems for functionals depending on functions with deviating argument 01 p0111 A71-10488
 Equations of state for materials with memory, discussing derivation methods based on nonlinear functional analysis and applications 01 p0175 A71-11037
 Book on approximate methods in optimization problems covering nonlinear extremum, functional analysis, algorithms, optimal control theory and finite dimensional spaces 01 p0113 A71-11323
 Weakly differentiable functional systems related to analytic functions with parametric representation via Stieltjes integral, discussing range theorems 02 p0276 A71-11724
 Multiple integrals-numerical evaluation techniques survey, discussing Monte Carlo, number-theoretical and functional analysis methods 02 p0276 A71-11801
 Convex functions theory of rigid perfectly plastic structures, formulating strain rate and stress fields relation in subgradients 02 p0326 A71-12339
 Minimization of unconstrained function of several variables by gradient dependent techniques, discussing applications to boundary value problems in optimal control [AIAA PAPER 69-951] 03 p0450 A71-13444
 Measurability and nonmeasurability of composition function, considering Borel sets 03 p0451 A71-13784
 Convex Taylor series truncations minimization by iterative method based on approximating initial functional 03 p0452 A71-14058
 Iterative functional minimization methods using Lagrange multipliers, examining convergence 03 p0452 A71-14059
 Equilibrium points and periodic orbits, using qualitative theory of autonomous functional differential equations 06 p0927 A71-17639
 Functional method application to ultrarelativistic particles in external fields quantum electrodynamics, discussing electromagnetic field superposition 07 p1162 A71-20549
 Komkov class of boundary value problems and associated variational principles, discussing necessary conditions for basic functional or potential extremal behavior 08 p1323 A71-20878
 Multistage rockets terminal control synthesis based on linear functionals 09 p1532 A71-22660
 Stationary points of functional corresponding to boundary value problem with free boundary 12 p1930 A71-27167
 Specialized version of Jones direct stiffness structural analysis method, deriving functional substitutions in variational formulation for displacement discontinuities 12 p1983 A71-27597
 Stability of feedback systems with backlash, deriving stability criterion in form of existence theorem for multiplier function 13 p2042 A71-28703

- Calculus of variations sudden expansion and decentralization, minimizing convex functional on closed group in reflexive Banach space 13 p2095 A71-28824
 Quality functional analysis for self adaptive filtration of random signal sequences 13 p2040 A71-28919
 Approximate methods for optimal control problems solution in terms of functionals differentiable only with respect to direction 14 p2265 A71-29554
 Signal detection in stationary, Markov and other noise background, discussing functional method of statistical and probabilistic representation 15 p2370 A71-31589
 Elastic structure dynamic stability problem, determining optimum inequality relating energy functional to displacement, and considering beam column with various boundary conditions 15 p2506 A71-32015
 High order optimality conditions of singular controls, considering Pontryagin maximum principle, Bellman dynamic programming and functional analysis 16 p2550 A71-33701
 Optimal extrapolation and filtration for class of random processes, considering functionals of solutions of stochastic differential equations 17 p2765 A71-34863
 Functional analytic methods for periodic and quasi-periodic solution of differential equations in nonlinear oscillation theory 17 p2780 A71-34921
 Periodic solutions existence for autonomous system of ordinary differential equations, modifying parameter functionalization of vector fields in phase spaces 17 p2766 A71-34934
 Functional analysis of nonlinear nonautonomous and autonomous periodic oscillations by treating equations and periodicity conditions for initial displacements and velocities as generalized operator equation 17 p2782 A71-34936
 Smooth solutions of functional and differential-difference equations in neighborhood of singular points with deviation of argument tending to zero 17 p2767 A71-34938
 Functional analytical iteration methods for calculating nonlinear vibrations of several degrees of freedom and error estimation improvement, considering uniformly converging Fourier series expansion 17 p2782 A71-34939
 Nonlinear feedback control system with two nonlinear memoryless energyless elements separated by linear device, discussing grapho-analytical method for self sustained oscillation determination 17 p2722 A71-35183
 Uniform inhomogeneous waveguides with linear time invariant passive medium, determining functional behavior in frequency domain of electromagnetic waves propagation constant 17 p2708 A71-35492
 Linear functional equations bounded solutions stability by reflexive Banach space mapping, applying to elliptical and parabolic differential equations ill-posed problems 18 p2941 A71-36351
 Computer programs for functional analysis, planning and control of space stations and shuttles operation 18 p2885 A71-36459
 Time optimal control of systems with magnitude and impulse limited constraints on control forces 18 p2896 A71-36788
 Nonlinear functional analysis - Conference, University of Wisconsin, Madison, October 1970 18 p2943 A71-36951
 Functional analysis application to nonlinear integral equations, stressing Schauder fixpoint theorem 18 p2943 A71-36952
 Nonlinear operators properties, considering differential role in nonlinear functional analysis 18 p2943 A71-36954
 Numerical solutions of boundary value problems for linear elliptic partial differential equations by function theoretic methods 19 p3087 A71-38308
 Extremal problems approximation conditions in functional optimal value and elements set senses, applying to study of convergence in presence of constraints 19 p3088 A71-38413
 Optimal control with minimax cost for systems of n first-order state equations with performance measured by Chebyshev type functional over state trajectory 19 p3039 A71-38716
 Neutral functional equation including scalar differential-difference equation, determining sufficient conditions for zero solution 20 p3254 A71-38899
 Solutions near equilibrium point of finitely retarded autonomous functional differential equation, noting bifurcation 21 p3407 A71-40208

- Ascoli theorem generalization and application to functional differential equations, proving existence theorem
21 p3410 A71-41188
- Functional methods in numerical solution of heat transfer problems, including finite element and local variation methods
22 p3621 A71-42290
- Deterministic system optimal control with single control and several cost functionals by Pontryagin maximum principle
23 p3656 A71-43858
- Vector functionals optimization, programming optimal trajectories
23 p3657 A71-44017
- Smoothed randomized functionals and algorithms in adaptation and learning theory, accounting for constraints by generalized penalty function method
23 p3657 A71-44018
- Suboptimal control laws calculation, using functional form of variables for algorithm
24 p3813 A71-44615

FUNCTIONAL INTEGRATION

- Differential equations systems construction from given integral manifold, deriving steady state functionals and stability conditions
01 p0111 A71-10487
- Unique solution of certain classes of linear and nonlinear functional-integral equations reducible to Volterra integral equations
11 p1793 A71-26562
- Incompressible fluid turbulence theory based on space-time Hopf characteristic functional integral representation for velocity field statistical ensemble
15 p2388 A71-31477
- Transition probabilities for Ar I, using Coulomb approximation values of radial wave function integral
20 p3271 A71-38776
- Functional converters for logic circuits synthesis, determining mutual value order of input functions
23 p3631 A71-43830

FUNCTIONS [MATHEMATICS]

- NT ABEL FUNCTION
- NT AIRY FUNCTION
- NT ANALYTIC FUNCTIONS
- NT APERIODIC FUNCTIONS
- NT ASYMPTOTES
- NT BOOLEAN FUNCTIONS
- NT CONFORMAL MAPPING
- NT COORDINATE TRANSFORMATIONS
- NT DELTA FUNCTION
- NT DISCRETE FUNCTIONS
- NT DISTRIBUTION FUNCTIONS
- NT DISTURBING FUNCTIONS
- NT ELLIPTIC FUNCTIONS
- NT ENTIRE FUNCTIONS
- NT ERROR FUNCTIONS
- NT EXPONENTIAL FUNCTIONS
- NT FOURIER TRANSFORMATION
- NT GAMMA FUNCTION
- NT GREEN FUNCTION
- NT HAMILTONIAN FUNCTIONS
- NT HANKEL FUNCTIONS
- NT HARMONIC FUNCTIONS
- NT HYPERBOLIC FUNCTIONS
- NT HYPERGEOMETRIC FUNCTIONS
- NT KERNEL FUNCTIONS
- NT LAGUERRE FUNCTIONS
- NT LAME FUNCTIONS
- NT LAPLACE TRANSFORMATION
- NT LEGENDRE FUNCTIONS
- NT LIAPUNOV FUNCTIONS
- NT LINEAR TRANSFORMATIONS
- NT LOGARITHMS
- NT LORENTZ TRANSFORMATIONS
- NT MATHIEU FUNCTION
- NT MAXWELL-BOLTZMANN FUNCTION DENSITY
- NT MEROMORPHIC FUNCTIONS
- NT MONOTONE FUNCTIONS
- NT NORMAL DENSITY FUNCTIONS
- NT ORTHOGONAL FUNCTIONS
- NT ORTHONORMAL FUNCTIONS
- NT PEARSON DISTRIBUTIONS
- NT PERIODIC FUNCTIONS
- NT POISSON DENSITY FUNCTIONS
- NT PROBABILITY DENSITY FUNCTIONS
- NT PROBABILITY DISTRIBUTION FUNCTIONS
- NT RATIONAL FUNCTIONS
- NT RAYLEIGH DISTRIBUTION
- NT RECURSIVE FUNCTIONS
- NT SCHWARZ-CHRISTOFFEL TRANSFORMATION
- NT SINE SERIES
- NT SPACE-TIME FUNCTIONS
- NT SPHERICAL HARMONICS
- NT SPLINE FUNCTIONS
- NT STEP FUNCTIONS
- NT STRESS FUNCTIONS
- NT TIME FUNCTIONS
- NT TRANSCENDENTAL FUNCTIONS
- NT TRIGONOMETRIC FUNCTIONS
- NT WALSH FUNCTION
- NT WEIBULL DENSITY FUNCTIONS

NT WEIGHTING FUNCTIONS

NT WHITTAKER FUNCTIONS

- Quadratically convergent algorithms for function minimization tested by numerical examples
01 p0112 A71-10847
- Ionospheric nondeviative absorption diurnal variation describing function suitable for computer methods
03 p0378 A71-13315
- Automatic determination of linear pattern recognition and evaluation functions, computing coefficients for half space problem
03 p0450 A71-13621
- Axisymmetric load problems in Cosserat medium, expressing displacement states by mathematical functions
03 p0509 A71-13899
- Three dimensional opacity function for phase objects measurements using interferometry, holography or schlieren methods
04 p0596 A71-14969
- Fourier transform formalism of sampling theorem in frequency domain used in coherent optical processor, obtaining multiple reproduction of space limited functions
04 p0627 A71-15686
- Markov process optimal stoppage, using strongly supermedian functions
05 p0773 A71-16157
- Hunt process equilibrium potentials /special supermartingales processes/, obtaining additive functionals
05 p0773 A71-16158
- Complex configuration solid bodies boundary value problems numerical solution algorithm using R functions
05 p0775 A71-17013
- Constrained function extremization, taking into account modified quasi-linearization algorithm
05 p0776 A71-17088
- Optimal control problems for functional extremization, developing modified quasi-linearization algorithm
05 p0776 A71-17089
- Neutron monitors multiplicity yield function calculation, using Monte Carlo method for nucleonic cascade in atmosphere
06 p0960 A71-18165
- Power series uniformization by transformations of perturbation functions irregular part, considering compatibility problem
06 p0919 A71-18197
- Square root function approximation in interval, using Heron iteration and Chebyshev method
06 p0919 A71-18206
- Numerical approximation of continuous real function in interval by polynomials using appropriate nets, estimating error
06 p0920 A71-18209
- Gas mixture transmission function, determining multiplication method accuracy
07 p1151 A71-18910
- Soviet papers on special problems of differential equations and functions theory covering approximation, complex variables, integral operators, etc
07 p1146 A71-19038
- Existence theorem and optimal approximation of functions of many variables by superimposing sums of smaller number of variables in complex region
07 p1146 A71-19039
- Optimal algorithm for searching minimum of single variable convex function
07 p1146 A71-19177
- Solid mechanics boundary value problems solution by cylindrical functions addition theorem in polar and curvilinear orthogonal coordinates
07 p1162 A71-20648
- Perturbation theory for reduced density matrices representable as functions of independent parameters
08 p1332 A71-20660
- Heuristic search algorithm for highest and lowest values of functions, considering Algol program
09 p1485 A71-22313
- Earth international compartmentalization into equal area elements on reference sphere for spherical functions utilization
10 p1601 A71-24460
- Lagrange implicit functions generalization to n dimensions, developing inversion as power series
10 p1637 A71-24933
- Body of revolution potential expanded in spherical function series, showing analytical density limited by surface
10 p1679 A71-24934
- Minimization of convex functions without derivative calculation, proving superlinear convergence
13 p2094 A71-27895
- Physical pendulum normalized error variance as irregularity function in excitation with narrow band frequency spectrum
13 p2065 A71-27947
- Search for saddle points of function, presenting subgradient and penalty methods for solving differential, finite and infinite games
13 p2095 A71-28813

Dual methods for calculating minimum of convex function on intersection of convexes, considering reflexive Banach space and normalized vector space
13 p2095 A71-28822

Minimization of functions with unconstrained variables, using memory gradient method
13 p2095 A71-28826

Criterion on types of extrema of singular solutions of conditional equations in calculus of variations from Euler function behavior with respect to integration path
13 p2096 A71-29322

Minimization of convex maxmin functions, obtaining formula for derivative with respect to direction
14 p2265 A71-29553

Differentiation of maxmin function with respect to direction, analyzing theorems on differentiability
14 p2265 A71-29563

Angular function computation in Mie theory of light scattering, considering sequential computer programming economics
14 p2207 A71-30150

Conjugate functions theory variational application to solid mechanics, generalizing concept of potential for nonlinear behavior laws in viscosity and plasticity
14 p2329 A71-30447

One variable unimodal function minimization, describing adaptive algorithm with iterative four point interpolation process
15 p2440 A71-31156

Sensitivity functions of phase canonical form for single input linear time invariant controllable systems, using frequency domain techniques
15 p2382 A71-32442

Hamilton-Jacobi equation application to forces selection for mechanical systems asymptotic stabilization, minimizing functional by Euler-Lagrange equations
16 p2602 A71-32814

Geometric object concept in third principle of relativity, obeying identity functional equations for infinitesimal general coordinate transformations
16 p2611 A71-33273

Scalar function expansion in relativistic invariant functions in pseudoeuclidian space, deriving direct and inverse formulas for spherical, hyperbolic and Lobachevskii coordinates
16 p2612 A71-33459

Sum rule functions for expressions of atomic or molecular quantum mechanical properties
16 p2603 A71-33527

Asymptotic expansion of spectral functions expressed by Cauchy integral over smooth open segment
17 p2763 A71-34419

German monograph on Fourier-Chebyshev approximation of primary functions, giving quadrature method
17 p2764 A71-34484

Convergence characteristics of sequential and combined conjugate gradient restoration algorithms for mathematical programming, studying constrained function minimization
17 p2764 A71-34520

Definite interval values calculations of integral of smooth functions, using quadrature formulas with high algebraic degree of accuracy
17 p2765 A71-34845

Differential equations optimization method based on auxiliary functional and minimization at simple structure manifold
17 p2765 A71-34849

Fourier coefficients and integral operators S numbers of summable functions
17 p2765 A71-34864

Classes of n dimensional functions nonlinear matrix mapping, emphasizing block-Jacobi and block-Gauss-Seidel process convergence for continuous surjective M functions
17 p2767 A71-35524

Unique linear product approximations of continuous functions of several variables extended to general convex sets
17 p2768 A71-35682

Generalized computing machines deductive systems, introducing sequence of partial functions
18 p2886 A71-36823

Sobolev function Q in radiative transfer, using invariant imbedding approach for integral equation transform
19 p3133 A71-37506

Balance function concept extension to optimal control problem for finding numerical iterative solutions, considering low thrust orbit transfer problem
19 p3037 A71-37557

Disconjugacy criterion for self adjoint linear differential equations containing nonnegative continuous function in interval under study
21 p3410 A71-41187

Spectra and correlation functions for ion sound turbulence, calculating anomalous resistivity for plasma in external electric field
22 p3579 A71-41582

FUNGI

- Temporal frequency spectra for spherical wave propagating through atmospheric turbulence, using covariance functions and Taylor hypothesis 22 p3575 A71-41788
- One and two dimensional function values calculation for curve systems by continued fraction interpolation from point grids, using computer program 22 p3518 A71-42394
- Equations of motion averaging method, constructing series representation of function [AAS PAPER 71-334] 23 p3727 A71-43007
- Function construction procedure for ring-shaped structure conformal mapping onto doubly connected regions with simple contours, applying to prismatic rod torsion problem 23 p3776 A71-43419
- Functional converters for logic circuits synthesis, determining mutual value order of input functions 23 p3631 A71-43830
- N-step conjugate gradient minimization algorithm for nonquadratic functions, giving numerical example of application to double precision arithmetic 24 p3842 A71-44623
- Optimal strategies in search of function global maximum 24 p3843 A71-44770
- FUNGI**
- NT NEUROSPORA
- NT SPORES
- NT STREPTOMYCETES
- NT YEAST
- Bacteria and yeast strains, fungus specimens and seaweed species high vacuum resistance, noting microorganisms interplanetary transport in outer space 13 p2009 A71-28689
- FURAN RESINS**
- NT POLYAMIDE RESINS
- FURNACES**
- NT IMAGE FURNACES
- NT VACUUM FURNACES
- FUSELAGE MOUNTING**
- U AIRCRAFT PRODUCTION
- FUSELAGES**
- Lift of slender aircraft with rectangular cross section fuselage and high wing 03 p0342 A71-13377
- Aircraft fuselage internal noise and structural frequency response due to random excitation, using transfer matrix analysis [ASME PAPER 70-WA/DE-9] 03 p0348 A71-14143
- Aircraft fuselage vibration response to turbulent boundary layers, measuring structural wavelengths and phase velocities as functions of frequency [ASME PAPER 70-WA/DE-10] 03 p0348 A71-14144
- Helicopter fuselage design for crashworthiness under specific conditions 04 p0532 A71-15416
- Biological oscillating propulsion systems, investigating plate propeller, boundary layer control, low drag fuselage shapes and VTOL engine installations 10 p1569 A71-24235
- Representative Thorneil fiber aircraft fuselage component nondestructive testing and repair, and Thorneil fiber, polysulfone and polyamide-imide composites fabrication and evaluation 11 p1787 A71-25427
- Prototype graphite fiber/plastic fuselage component design, test and performance prediction, using structural analysis methods 11 p1787 A71-25428
- Cruising flight range as function of supersonic/subsonic transport fuselage geometrical parameters 12 p1868 A71-27494
- Fuselage influence on total aircraft drag in subsonic passenger aircraft, considering high aspect ratio cylindrical fuselages 14 p2177 A71-30821
- Automated ultrasonic inspection system for L-1011 adhesive bonded fuselage panels using through transmission technique [SME PAPER IQ-71-746] 15 p2417 A71-32437
- DC-10 fuselage pressure shell fail-safe design, presenting analysis methods for residual strength prediction of damaged stiffened panels 17 p2827 A71-35160
- Design, analysis and testing of F-111 complex fuselage full scale section of composite materials, noting weight savings [SAWE PAPER 889] 17 p2835 A71-35825
- Near field noise measurement on quarter-scale model to estimate fuselage pressure in VTOL aircraft for conventional, short and vertical takeoff configurations 19 p2997 A71-37844
- In-flight noise radiation by wing-mounted jet engines on aircraft fuselage based on correlation with turbulent boundary layer pressure fluctuations 19 p2997 A71-37846
- Aircraft fuselage design with marine type bulkhead construction, discussing advantages in cabin decompression and fire hazards reduction 20 p3178 A71-38752

- Real weight formula for shell fuselages based on theoretical similarity considerations 20 p3178 A71-39411
- Agusta helicopter design and testing criteria, discussing four-blade rotor, fuselage and radio navigation equipment 22 p3482 A71-42224
- Flow angularity prediction near supersonic fuselage forebody with arbitrary cross section and zero sideslip, using small perturbation theory [AIAA PAPER 71-996] 24 p3789 A71-44588
- Aircraft fuselage antisymmetric loading strain effects on small aspect delta wing performance 24 p3885 A71-45018
- Ideal weight of axisymmetric fuselage shells, taking into account load distribution and cabin pressurization 24 p3885 A71-45180
- FUSES**
- High acceleration resistant electronic trigger fuse for in-flight gun launched projectile payloads ignition and ejection [AIAA PAPER 70-1389] 03 p0468 A71-13671
- FUSES [ORDNANCE]**
- Electronic time delay fuses with high-g components for gun launched projectiles for placing payloads at high altitudes 18 p2851 A71-36281
- FUSIBILITY**
- Fusibility and thermal emf of ternary intermetallic TiFe-TiCo-TiNi system 01 p0103 A71-11090
- FUSIFORM SHAPES**
- U CONES
- FUSION**
- Seizing of flat and flat/spherical steel samples pairs in vacuum as function of temperature, pressure and time of contact, using compression-tension machine 24 p3838 A71-44857
- FUSION [MELTING]**
- Cr-chromium nitride fusion phase diagram analysis, establishing nonvariant eutectic and dissociative transformations 02 p0266 A71-12673
- Atmospheric heating effects on thermoluminescence output variations with depth below Ucera meteorite fusion crust, noting nonuniform cosmic rays shielding 10 p1675 A71-24470
- Net fusion energy from laser heated deuterium-tritium particles dependent on plasma temperature, electrical energy and electron-ion thermalization through collisions 11 p1805 A71-25799
- Thermally activated crystal microcrack initiation by fusion of leading and following dislocations 13 p2149 A71-28118
- Residual stresses for fused contacts between metals and Si or gallium arsenide from polarization measurements in principal crystallographic planes 15 p2461 A71-31510
- Heating, fusion and atomization of meteoric bodies in earth atmosphere 17 p2810 A71-35724
- FUSION WELDING**
- NT ARC WELDING
- NT BRAZING
- NT ELECTRON BEAM WELDING
- NT ELECTROSLAG WELDING
- NT GAS TUNGSTEN ARC WELDING
- NT GAS WELDING
- NT PLASMA ARC WELDING
- NT ULTRASONIC SOLDERING
- Ductility of simulated weld fusion zones in Inconel 718 04 p0617 A71-15911
- Forge phase rigid and plastic region model of friction welding, deriving interfacial dispersion parameter of weld quality optimization 09 p1459 A71-23456
- Modulated power control for fusion welding, considering modification to conventional magnetic amplifier controlled power sources 13 p2076 A71-29093
- Book on fusion welding covering workshop problems, production processes, miniature casting and resistance welding techniques 13 p2076 A71-29444
- F4H AIRCRAFT**
- U F-4 AIRCRAFT
- F8U AIRCRAFT**
- U F-8 AIRCRAFT

G

- Apollo 12 lunar rock 12013 petrologic and mineralogic characteristics, discussing data on isotopic Xe and Gd composition 03 p0494 A71-14222
- Gadolinium isotopic composition and neutron capture effects in meteorites 08 p1365 A71-21652
- Emission spectra, wavelengths and photoelectric intensities of triply-ionized gadolinium, using hollow cathode source with Czerny-Turner vacuum spectrograph 11 p1801 A71-25132
- Gadolinium molybdate-neodymium ions stimulated emission, noting luminescence, absorption and spectroscopic properties 13 p2111 A71-28412
- Gadolinium molybdate-neodymium ions stimulated emission, noting luminescence, absorption and spectroscopic properties 21 p3427 A71-40082
- GAGES**
- U MEASURING INSTRUMENTS
- GAIN [AMPLIFICATION]**
- U AMPLIFICATION
- GALACTIC EVOLUTION**
- Galactic nuclei composition of dense core with small subunits generating relativistic particles 01 p0162 A71-114212
- Galaxies dynamic parameters formation associated with cosmological turbulence in expanding hot universe 02 p0307 A71-120832
- Computerized simulation of disk galaxies evolution using doubly periodic model for stellar motions 02 p0318 A71-129292
- Intense X radiation source in Cetus region observation by Black Brant rocket 04 p0640 A71-150452
- Transient annular structures in galaxies with nuclear explosion and fragmentation, examining radiogalaxy dynamics 04 p0655 A71-157242
- Momentum conservation in metagalactic astronomy, considering magnetoid ejection from active galactic nuclei 04 p0657 A71-158272
- Galaxies and universe evolution, discussing expansion, isotropic black body radiation, present matter distribution, radio source population density and galactic nuclei instability 04 p0661 A71-158952
- Expanding universe adiabatic density fluctuation evolution, describing photon distribution function collision equation for plasma recombination 05 p0801 A71-159292
- Quasars primordial He abundance, discussing relation to galactic evolution 05 p0808 A71-164022
- Galaxy gaseous disk as low mode dynamo, calculating turbulent diffusion coefficient for passive magnetic fields 05 p0811 A71-166882
- Galaxy cluster expansion theory, noting dispersion in radial velocities of members 05 p0812 A71-166942
- Elliptical and spiral galactic angular momentum and velocity dispersion relations, considering cosmological turbulence during formation 06 p0971 A71-182442
- Interstellar gas dynamic characteristics, discussing galactic large scale features 06 p0971 A71-183282
- Galactic magnetic fields and cosmic ray gas, investigating origin and dynamical effects 06 p0972 A71-183322
- Interstellar gas and star mass interchange, discussing balance and galactic and stellar evolution models 06 p0972 A71-183342
- Interstellar grain formation relation with stellar evolution in terms of density wave theory of spiral structure origin 06 p0973 A71-183392
- Color changes and absorption line variations in M31, M32 and NGC 4472, attempting synthesis of M31 disk population 07 p1197 A71-198142
- Galaxies dynamic parameters formation associated with cosmological turbulence in expanding hot universe 08 p1362 A71-211352
- Galactic spiral structure production mechanism observation by method based on photometry of individual stars 09 p1517 A71-223312
- Galaxy chemical evolution, discussing stellar mass loss, supernova explosions, white dwarf formations nucleosynthesis, cosmochronology, etc 09 p1521 A71-228692
- Explosive nucleosynthesis in Galaxy, discussing carbon detonation, uniform density models, supernova rates and massive stars 09 p1521 A71-229292

- Cosmological evolution in radio galaxies, discussing stellar populations, optical luminosity, model choice, red shift uncertainties, etc 09 p1522 A71-22974
- Nonhomogeneous cosmological model with equations describing universe relative density variation, demonstrating thermal instability role in galaxies formation 10 p1667 A71-23856
- German book on variable stars covering supernovae, novae, pulsating variable stars, symbiotic objects, galactic nebulae, stellar and galactic evolution, astronomical photometry, etc 10 p1675 A71-24479
- Gravitational instability picture for galactic rotation, examining numerical model for protogalaxy separation in expanding universe 11 p1820 A71-25535
- Galaxy M33 density wave velocity and detection, discussing star distribution, H II regions red and blue supergiant and hot stars 11 p1821 A71-25540
- Spiral arms formation on galactic scale in terms of density waves produced by gravitational perturbations 11 p1832 A71-26184
- Galaxy structure and evolution - NATO Conference, Athens, September 1969 12 p1958 A71-26771
- Galactic and plasma dynamics similarities, considering collisionless and collisional relaxation of stellar systems, stability problems, etc 12 p1960 A71-26782
- Stellar evolution, discussing mass loss to interstellar medium, galactic distances determination and supernova explosions 12 p1960 A71-26784
- Galaxies chemical evolution and aging mechanisms, considering He nucleosynthesis, galactic nuclei and clusters dense core origin 12 p1960 A71-26787
- Statistical space density and velocity perturbations of galaxies relative to origin of rotation in range of Friedman cosmological model 12 p1966 A71-27235
- Spiral galaxy structure formation and stability explanation in terms of wave theory of stellar subsystems interaction 12 p1967 A71-27309
- Source count statistics of radio galaxy lifetimes and intergalactic heating, assuming multiple explosions 12 p1968 A71-27540
- Stellar explosive nucleosynthesis and element abundances in Galactic chemical evolution 13 p2133 A71-27970
- Necessary and sufficient global stability criteria for axisymmetric perturbations of stellar dynamic disk models of galaxies 13 p2138 A71-28775
- Strong gravitational wave bursts in galaxy, suggesting collapsed relativistic body cluster burning gravitational potential energy 13 p2142 A71-29137
- Matter density in universe, comparing delayed galactic growth with observed radio sources and quasars 14 p2305 A71-29675
- Quasars as nuclei of nascent galaxies, proposing protogalaxy model from spectroscopic or color observations 15 p2482 A71-31328
- Extragalactic nebulae, considering galactic formation stages and energy supply problems 15 p2486 A71-31925
- Turbulent gaseous nonmagnetic protogalaxies under external torques, calculating angular velocity distribution 15 p2490 A71-32400
- Spiral density wave structure in computer simulations of evolution of galaxies, showing azimuthal dependence on gravitational and radial forces 15 p2497 A71-32769
- Galaxy formation in expanding universe, discussing primordial plasma and photon gas turbulent medium for magnetic field amplification by dynamo mechanism 16 p2625 A71-33052
- Galaxy formation by weak and strong primeval turbulence in relation to velocity and density perturbation 16 p2631 A71-33232
- Scientific cosmology principles, considering distant galaxies red shift and galactic evolution 16 p2611 A71-33279
- Exploding universe phenomena, considering supernovae, exploding galaxies, Crab Nebula, pulsars, quasars and radio galaxies 16 p2643 A71-34036
- Galactic clusters evolution in universe with zero rest mass particles, showing size dependence on cosmic dust energy density 18 p2969 A71-37040
- Fast hydrogen clouds in galactic halo related to galaxies formation model 20 p3293 A71-39448
- Energy in universe from stellar and galactic evolution, discussing flow mechanisms, entropy, arresting factors and catastrophic phenomena 20 p3301 A71-39916
- Computer model for dynamical evolution of isolated disks of stars with initial velocity dispersions corresponding to Toomre criterion, noting instability relative to large scale modes 21 p3445 A71-40410
- Galaxy active nucleus and quasar fragmentation based on model of rotating supermassive star releasing thermal radiation 21 p3449 A71-40610
- Stellar population data, discussing star distribution and galactic evolution 22 p3599 A71-41931
- Small circle geometry of Galactic continuum loops, noting consistency with neutral hydrogen and supernova remnant hypothesis 22 p3601 A71-42168
- Quasars as nuclei of nascent galaxies, proposing test of protogalaxy model from spectroscopic or color observations 22 p3606 A71-42603
- Radio galaxies cosmological evolution, discussing rate and spectrophotometric data 23 p3766 A71-43823
- Thermal history of universe traced from assumption of photon and plasma turbulence for galactic formations, discussing thermal instability and heating effects 23 p3770 A71-44181
- Soviet papers on astrophysics covering variable stars and galactic structure, stellar atmospheres, cometary physics and evolution, stellar and solar spectroscopic observations, etc 23 p3771 A71-44302
- GALACTIC MAGNETIC FIELDS**
U INTERSTELLAR MAGNETIC FIELDS
GALACTIC RADIATION
NT GALACTIC RADIO WAVES
 Galactic EM energy radiation, discussing flux upper limits in Low model 01 p0153 A71-10364
- Galactic soft X rays role in interstellar dust grains alignment producing starlight polarization 01 p0145 A71-11344
- Diffuse galactic X ray background intensity as function of galactic scattering and discrete sources 01 p0145 A71-11345
- Galactic radio emission sources high resolution observation by telescope, obtaining contour maps with positions and flux densities 02 p0303 A71-11820
- Structural characteristics of light absorbing matter near sun from optical observations 02 p0308 A71-12096
- Spiral galaxies mass-luminosity relationship from optical and radio astronomy data 02 p0308 A71-12102
- Very long baseline interferometry of galactic hydroxyl radical microwave emission sources 02 p0310 A71-12327
- Mean cosmic density determinations, obtaining field galaxy luminosity function moments with red shift catalogs 02 p0313 A71-12499
- Galactic and extragalactic sources of far IR radiation, discussing spectral distribution and luminosities 02 p0315 A71-12656
- Radio emission upper limits from galaxies in Markarian catalog 02 p0317 A71-12866
- X ray sources location and grouping into supernova remnants and loose cluster categories, accounting for galactic background 03 p0483 A71-13187
- Fossil nuclear charged particle tracks in lunar rock 12013 Ca-feldspar, K-feldspar and pyroxene attributed to galactic cosmic rays 03 p0494 A71-14216
- Galactic sources 18 cm OH emission and/or absorption observation 04 p0657 A71-15759
- OH absorption line measurements for longitude range near galactic center, suggesting existence of radial velocity gradient 04 p0657 A71-15760
- Quasars as images of Seyfert galaxies nuclei resulting from gravitational lens mechanism 04 p0658 A71-15829
- Galactic Lyman alpha observation by Vela 7, discussing error possibility of data interpretation based on interstellar hydrogen shock wave 04 p0658 A71-15831
- Mn 53 age measurement of galactic cosmic rays 05 p0797 A71-15930
- Radio emission from small galactic nebulosities, describing position, flux densities, identification and exciting stars 05 p0811 A71-16683
- Semidiurnal variation of galactic cosmic ray intensity, using neutron and meson monitor data 05 p0800 A71-17008
- Galactic cosmic ray solar modulation in interplanetary medium, discussing spherically symmetric model 06 p0949 A71-17275
- Atlas of 21 cm H I emission line profiles of outer part of Galaxy in Galactic anticenter region, plotting brightness temperature vs radial velocity 06 p0964 A71-17348
- Galactic cosmic rays nonlinear interactions with solar wind, taking into account autofocusing effect 06 p0951 A71-18103
- Models for solar wind modulation of galactic cosmic rays by anisotropic diffusion approximation 06 p0951 A71-18104
- Force field model for galactic cosmic rays modulation by solar cycles, noting agreement with Fokker-Planck equation analytic and numerical solutions 06 p0952 A71-18110
- Galactic cosmic ray proton and He spectrum measurements in 1968 compared to electron spectra, explaining solar modulation features by models incorporating energy loss effects 06 p0952 A71-18112
- Diurnal intensity variations of high energy galactic cosmic rays, taking into account particle trajectories in sectorial interplanetary magnetic field 06 p0952 A71-18115
- Isotropic galactic cosmic ray diffusion in interplanetary space from solar wind velocity and diffusion coefficient dependence on heliolatitude and heliointitude 06 p0953 A71-18118
- Galactic cosmic ray solar modulation with 20 year periodicity, suggesting nearby galactic magnetic field direction 06 p0955 A71-18130
- Sunspot heliographic latitude role in 11 year galactic cosmic ray modulation 06 p0955 A71-18133
- Galactic cosmic ray modulation region dimensions calculated during various solar activity cycles 06 p0955 A71-18134
- Solar and galactic cosmic rays interactions with interplanetary magnetic field 28 January-25 February 1967 based on Explorer 33 and 28 satellite observations 06 p0957 A71-18145
- Low energy solar and galactic cosmic ray propagation in interplanetary medium from Zond 3 and Venus 2-4 space probes measurements 06 p0958 A71-18152
- Galactic cosmic rays solar modulation effects on fast neutron flux in atmosphere 06 p0962 A71-18182
- Markarian galaxies spectra, analyzing emission line characteristics 07 p1191 A71-19283
- Galactic and solar cosmic rays diffusion as function of solar activity and interstellar medium properties, considering particle velocity and proton scattering transport 07 p1185 A71-19379
- Soviet book on active protection of space vehicles covering measures against penetrating radiation from Van Allen belts, solar flares and galactic cosmic rays 07 p1207 A71-19474
- Ammonia inversion radiation at 1.25 cm in direction of three galactic center sources, setting upper limits on densities in other areas 07 p1188 A71-19834
- X ray observations of NP0532 and other radio pulsars and galactic X ray sources 07 p1200 A71-20052
- Soft galactic X rays role in interstellar grains alignment 07 p1188 A71-20056
- Galactic primary cosmic rays nuclei tracks in meteorite olivine, studying intensity of VH and VVH groups 08 p1351 A71-20961
- Chromosphere-flare and galactic cosmic ray hypotheses of Forbush decrease and strong shock waves in interplanetary medium 08 p1352 A71-20967
- Eleven year galactic cosmic ray amplitude variation, determining modulation by sunspot groups and latitude 08 p1352 A71-20972
- Galactic cosmic ray density space-time variations in interplanetary space with solar wind, using spherically symmetrical model with diffusion approximation 08 p1352 A71-20974
- Galactic cosmic ray density modulation by solar wind, assuming heliointitudinal asymmetry 08 p1353 A71-20975
- Solar activity heliointitudinal distribution effect on interplanetary space electromagnetic conditions governing galactic cosmic ray intensity 08 p1353 A71-20977
- Galactic cosmic rays interaction with interplanetary magnetic field from Venera 4 measurements June-October 1967 08 p1354 A71-21015
- Structural characteristics of light absorbing matter near sun from optical observations 08 p1362 A71-21146

Quiet time galactic component of geomagnetic field variations excluding solar-terrestrial disturbances 08 p1363 A71-21199

Galactic cosmic ray proton and He nuclei spectra measurements aboard Pioneer 8 spacecraft over large energy range, considering solar modulation parameters 08 p1355 A71-21626

Balmer emission lines in hydrogen cloud in bright galactic nucleus 09 p1518 A71-22351

Interplanetary magnetic field inhomogeneities structure from galactic cosmic rays intensity fluctuations observation 09 p1513 A71-22424

Giant elliptical galaxy Maffei I continuous radiation emission data at 1415 MHz, examining radio luminosity magnitude 09 p1523 A71-22982

OSO 3 satellite observations of diffuse X ray emission from galactic plane, eliminating straight line interpolation of spectrum between 3-10 keV X ray range and 100 MeV energy range 10 p1665 A71-23750

NGC 2655 galaxy nucleus emissive gas/absorption line widths and stellar population, using network spectrographs 10 p1667 A71-23827

Flux and shape variability of X ray emission from M87 using proportional counters onboard Aerobee-Hi rocket 10 p1661 A71-24421

Galactic wind as steady radial perfect gas flow from stars and central gravitating source 11 p1818 A71-25207

Galactic plane X ray scan by NASA small astronomy satellite Uhuru, discussing satellite instrumentation, detector and sensor sensitivity and preliminary measurements 11 p1814 A71-25212

Real and observable radius of roughly dispersed liquid aerosols correlated by electrophotographic method, assessing galactic cosmic rays energy 11 p1815 A71-25582

Neutral pion decay and galactic gamma radiation from demodulated cosmic ray spectrum, discussing neutral pion meson production 11 p1815 A71-25593

Contour map of galactic radio emission in Cassiopeia and Cepheus region, noting discrete sources 11 p1831 A71-26132

Galactic radio source Sagittarius optically thick component evidence based on flux density measurement 12 p1956 A71-26612

NGC 3351 galaxy core spectrophotometry of optical spectrum covering emission and absorption lines 12 p1960 A71-26831

X ray flux variability of massive elliptical galaxy M87 from rocket flight measurement, considering synchrotron, inverse Compton and thermal bremsstrahlung 12 p1962 A71-26931

Cosmic ray diffusion from discrete sources in random galactic location, studying chemical constituents anisotropy and age with scattering model 12 p1948 A71-27367

Cosmic soft X rays diffuse component dependence on galactic latitude related to interstellar absorption 12 p1949 A71-27370

Galactic and albedo X rays measurement by balloon-borne instruments and sounding rockets 12 p1949 A71-27371

Satellite-borne anisotropy and energy spectra measurement instruments for cosmic ray electrons and protons and solar and galactic X-rays 12 p1954 A71-27711

Differential energy spectrum of cosmic ray deuterium flux of galactic origin from IMP 5 satellite measurements 13 p2120 A71-27974

Line emission in X ray background in galactic plane and at galactic pole based on rocket flight data 13 p2120 A71-28005

Extended galactic radio sources in anticenter quadrant, obtaining 408 MHz integrated flux densities and spectral indices 13 p2135 A71-28298

Cosmic rays galactic component intensity observed on earth correlated with solar phenomena 13 p2130 A71-29061

Galactic IR background emission mechanisms, considering electrons, protons and cosmic rays role 13 p2131 A71-29272

Galactic cosmic ray intensity solar diurnal and semidiurnal variations outside magnetosphere 13 p2131 A71-29437

Galactic LF nonthermal radio emission origin, considering mechanisms of synchrotron radiation from cosmic ray electrons and enhanced bremsstrahlung 14 p2304 A71-29593

Galactic H II regions 35 cm wave source emission line profile observation, noting frequency and intensity variations 14 p2304 A71-29594

Interstellar 21 cm and Na D lines comparison in directions of 30 stars at intermediate and high galactic latitudes 14 p2304 A71-29595

Galactic Lyman alpha emission, describing radiative transfer in radiation diffusion 14 p2306 A71-29683

Soft X ray background source, discussing north polar galactic spur as supernova outburst remnant 14 p2298 A71-29732

Galactic cosmic ray transport equation numerical solution for interplanetary region, considering modulation, diffusion, convection and energy loss effects 14 p2301 A71-30387

Extragalactic X ray sources from Explorer 42 flight, confirming explosive nature of Seyfert galaxies revealed by optical telescopes 14 p2313 A71-30401

Elliptical and spiral galaxies in coma cluster central zone, presenting observed radius vs magnitude diagrams 14 p2313 A71-30429

Galactic discrete X ray sources identification with black nebulae, H II regions, close binary stars, Wolf-Rayet stars and planetary nebulae 15 p2482 A71-31330

Galactic cosmic rays electron density, discussing incompatibility of local data estimates with galactic radio background 15 p2473 A71-31721

High energy cosmic gamma ray point sources identification near galactic plane from balloon flights data 15 p2478 A71-31826

Galactic brightness, color distribution and ellipticity data from photometry and colorimetry observations 15 p2486 A71-32028

Line emission in diffuse X ray background at high galactic latitudes, interpreting rocket observations 15 p2480 A71-32760

Galactic nucleus thermal emission due to dirty ice or silicate grains, explaining far IR radiation power output and spectral dependence 15 p2498 A71-32773

IR stars and galaxies measurements, determining 3.5 mm continuum radiation intensity 15 p2498 A71-32775

Galactic H II regions radio sources observations by high resolution radio telescopes, comparing with optical appearance 16 p2632 A71-33326

Aperture synthesis observations of neutral hydrogen radio emission in spiral galaxy M 101, using twin-element interferometer 16 p2632 A71-33329

IR line radiation from galactic center thermal radio sources, determining element abundances 16 p2633 A71-33336

Solar wind modulation effects on galactic protons and cosmic rays, using radial magnetic field mathematical model and Monte Carlo method 17 p2795 A71-34373

Galactic center isolated radio pulse search at 151.5 MHz, correlating with Weber gravitational events 17 p2805 A71-35378

Galactic weak X ray sources observation in Southern Hemisphere for flux and energy spectrum 17 p2796 A71-35408

H beta fluxes of planetary nebulae along southern Milky Way from photoelectric telescope 17 p2809 A71-35593

Neutron star cooling behavior models based on neutrino emission theory, explaining galactic steady state cosmic rays and pulsar radiation 18 p2959 A71-35931

Cosmic ray injection by clusters of dense magnetic neutron stars, giving particle number for Galaxy 18 p2957 A71-35962

Magellanic clouds X rays observation, interpreting spectrum analysis data as due to few strong sources 18 p2959 A71-37051

GX 17 X ray observation, noting exponential spectrum characteristic of thermal bremsstrahlung and resemblance with Sco X-1 radiation 18 p2959 A71-37054

H alpha emission photometry for galactic H II region, obtaining contour diagrams 19 p3130 A71-37227

Soft galactic X rays role in interstellar grains alignment, taking into account interstellar absorption 19 p3124 A71-37336

Galactic and solar cosmic rays diffusion coefficient as function of solar activity and interstellar medium properties, considering particle velocity and proton scattering transport 19 p3127 A71-37804

Galactic high energy electron differential spectrum, estimating spatial distribution and random magnetic field intensity 19 p3129 A71-38358

Outer space and earth surface galactic cosmic ray intensity data correlation analysis for studying interplanetary magnetic field structure 20 p3278 A71-39129

X ray background model based on photons bremsstrahlung emission by subcosmic metagalactic electrons or protons 20 p3279 A71-39292

Galactic cosmic rays interaction with interplanetary magnetic field from Venera 4 measurements of June-October 1967 20 p3280 A71-39555

Galactic cosmic ray propagation earth-surface distance determination by observing charge spectrum 20 p3280 A71-39555

Galactic cosmic ray effects on interplanetary dust particles erosion and spurious counts in micrometeroid sensors, microphones and capacitor detectors 20 p3280 A71-39555

Galactic cosmic rays and interplanetary magnetic field flux measurements onboard Venera 4 spacecraft, noting lack of correspondence with Forbush decrease 20 p3282 A71-39774

Planetary, stellar, galactic, sky and extragalactic UV radiation from OAO-2 spectrophotometric observations, noting interstellar extinction curves 20 p3300 A71-39744

Cosmic soft X ray detection by proportional counters with thin polypropylene windows onboard sounding rocket, estimating galactic emission possibility 20 p3283 A71-39752

Galactic nucleus map and flux at 10 microns scanned with 5.5 arcsec beam on Catalina observatory telescope 20 p3305 A71-39955

Book on cosmic gamma rays covering secondary particle decay, electron-positron annihilation, proton-antiproton interactions, galactic radiation and cosmology 21 p3438 A71-40450

Spectrum and galactic isotropy of diffuse cosmic X rays by balloon-borne detector 21 p3438 A71-40602

Seyfert galaxy micron photometry measurements determining IR radiation flux changes with time 21 p3449 A71-40611

Stellar UVB photometric investigation, determining brightness, coordinates, B-V and U-B color indexes of faint blue objects near galactic North Pole 21 p3451 A71-40721

Galactic cosmic rays solar modulation and particle intensity gradient in interplanetary space from satellite observation data 22 p3591 A71-41534

Small circle geometry of Galactic continuum loops, noting consistency with neutral hydrogen and supernova remnant hypothesis 22 p3601 A71-42168

Galactic diffuse radiation in far UV, discussing consistency of findings on optical properties of interstellar grains 22 p3593 A71-42337

Cosmic rays origin, discussing nuclear, electron and electromagnetic components, supernovae, pulsars, white dwarfs and gas motions in Galactic Center 22 p3594 A71-42550

Galactic discrete X ray sources identification with black nebulae, H II regions, close binary stars, Wolf-Rayet stars and planetary nebulae 22 p3606 A71-42605

Spiral galaxy M33 observations at 21 cm, deriving hydrogen atoms distribution and kinematic properties 23 p3722 A71-42938

F, Na and Al origin in galactic cosmic radiation, investigating production as spallation fragments and generation in source 23 p3719 A71-42943

Maffei 2 spiral galaxy hydrogen line and adjacent continuum observation by radio interferometry 23 p3733 A71-43080

Apollo 11 and 12 lunar samples history of irradiation exposure to galactic cosmic rays and solar wind, using rare gas and Gd isotope measurements 23 p3754 A71-43724

Solar and galactic iron group cosmic ray track distributions in Apollo 12 lunar rocks, investigating surface residence times 23 p3764 A71-43800

Diffuse cosmic X rays small scale structure, comparing Wolfe-Burbridge theoretical autocorrelation functions for galaxies clusters and superclusters with experimental value 23 p3722 A71-44013

Galactic and solar cosmic ray effects on Apollo 11 lunar soil and rock samples, analyzing Xe isotopic anomalies 23 p3722 A71-44016

Galactic radio spur association with soft X ray emission 24 p3865 A71-44444

Photographic monitoring of radio sources with flat or peaked spectra, identifying as quasars or unstable galactic nuclei by optical variations 24 p3872 A71-44920

Seyfert galaxies optical polarization, investigating time and wavelength dependences by multicolor polarimetric and photometric observations 24 p3873 A71-45078

GALACTIC RADIO WAVES

Physical processes in galactic and extragalactic sources of nonthermal radio emission, assuming pulsars as principal magnetic field and cosmic rays sources

03 p0483 A71-13201

Galactic radio corona existence, measuring northern galactic hemisphere sky brightness and cosmic ray distribution

03 p0483 A71-13204

Gravitational radiation events-galactic microwave emission pulses relation, comparing with Weber gravitational wave experiment

11 p1820 A71-25298

Anomalous OH emission in direction of planetary nebula NGC 2438 and optically radio-weak galactic nebulae S 247, S 269, IC 2162 and NGC 2264

14 p2313 A71-30431

M87 nucleus radio flux density variations observation at 5 GHz

14 p2301 A71-30451

Radio astronomy signals reception and interpretation, detailing solar, galactic and extragalactic spectrum sources

17 p2797 A71-34242

Galactic neutral hydrogen absorption line spectra at 21 cm wavelength by radio sources interferometric observations, discussing cool gas temperature, ionization rate and Cetus Arc distance

24 p3873 A71-45084

GALACTOSE

Gangliosides inhibitory effects on active Ca ion transport in rat brain mitochondria, using succinate as respiratory substrate

21 p3338 A71-41075

GALAXIES

NT ANDROMEDA GALAXIES

NT MILKY WAY GALAXY

NT RADIO GALAXIES

NT SPIRAL GALAXIES

Energy spectra of expanding relativistic particle clouds producing quasar and Seyfert galaxy nuclei outbursts

02 p0307 A71-12082

Galactic models from neutral H line profiles at 21 cm wavelength

02 p0307 A71-12084

Mass estimation for quasars and galactic nuclei with absorption line shift into long wave region

02 p0307 A71-12090

Gas heating near quasars, Seyfert galaxies nuclei and pulsars by induced Compton effect

02 p0317 A71-12872

Galaxies pairs motions, considering disintegrating, rotational and oscillatory types for comparison with observational data

03 p0484 A71-13207

Stellar magnitude equation from corrected catalog data to determine absolute proper motions relative to galaxies

03 p0484 A71-13218

Galaxy clusters stabilization by cosmological constant, considering clusters mass discrepancy

03 p0489 A71-13561

BL Lacertae photometric data, noting object brightness and optical similarity to N galaxy 3C371

04 p0643 A71-15045

Spectral classification parameters, discussing spectral-type indicators, luminosity indicators, spectra of clusters and galaxies, abundance, population and low metal objects

04 p0646 A71-15231

X ray background angular structure comparison with optical galaxies spatial distribution, ruling out universe models with sources following cosmological mass distribution

04 p0657 A71-15826

Quasars as images of Seyfert galaxies nuclei resulting from gravitational lens mechanism

04 p0658 A71-15829

Small elliptical galaxy associated with radio source 3C 386, noting luminosity, internal velocity dispersion and low metal abundance

05 p0805 A71-16109

Strong and weak emission red shifts of N galaxy 3C 390.3 in Balmer lines, indicating nonisothermal source and gas ejection

05 p0807 A71-16210

IR object Maffei 1 observational data indicating highly reddened giant elliptical galaxy of Local Group

05 p0807 A71-16211

North Galactic Pole soft X ray flux measurements, using Teflon windowed proportional counter

05 p0799 A71-16699

Coma Berenices galaxy clusters, discussing radio sources detection

05 p0813 A71-17090

Double galaxies mass distribution from pair components motion dependence on radial velocity

06 p0966 A71-17750

Cosmic accretion gas dynamics, discussing star, galaxies and galactic cluster effects

06 p0972 A71-18333

Preferable orientation of physical galactic pairs, obtaining equatorial plane inclinations and great axes positional angles distribution

06 p0974 A71-18432

Markarian galaxies spectra, analyzing emission line characteristics

07 p1191 A71-19283

Supernovae in late morphological type galaxies, discussing photometric and colorimetric observations

07 p1192 A71-19284

Supernovae as indicators of distances to galaxy clusters based on Karpowicz and Rudnicki catalog and angular measurement

07 p1192 A71-19288

Stellar intrinsic motions with respect to galaxies, including solar apex coordinates, secular parallax and Oort constants

07 p1194 A71-19331

Large Magellanic Cloud stellar associations system physical properties from object characteristics and spatial distribution

07 p1197 A71-19723

Nuclei reddening of Seyfert galaxies NGC 1068 and 1275 from photoelectric spectrophotometric observations

07 p1197 A71-19813

Ionized gas galactic cluster stabilization model construction, considering ionizing radiation enhanced cosmic flux and quasar PKS 1116 plus 12 absorption spectrum

07 p1198 A71-19830

External galaxies radial velocity relationship to extragalactic nebulae spectral lines red shift

07 p1200 A71-20054

Multicolor photographic photometry of NGC 4254 galaxy using electro-optical converter, observing H alpha emission and H II regions at galactic center

07 p1205 A71-20634

Galactic optical radial velocity measurements compared to 21 cm red shifts derived velocity

08 p1357 A71-20873

Cosmic objects and phenomena research, considering matter and galaxy compacting and dispersing processes, red shift, quasars, etc

08 p1358 A71-20890

Energy spectra of expanding relativistic particle clouds producing quasar and Seyfert galaxy nuclei outbursts

08 p1362 A71-21132

Galactic models from neutral H line profiles at 21 cm wavelength

08 p1362 A71-21134

Mass estimation for quasars and galactic nuclei with absorption line shift into long wave region

08 p1362 A71-21140

Modulation of long scale time variations of quasi-stellar radio sources and Seyfert galaxies due to intergalactic scintillations

08 p1364 A71-21414

Expanding source model verification for radio outbursts in quasars and Seyfert galaxy nuclei

08 p1365 A71-21424

Mean luminous cosmic matter density calculations, using galaxy counts and mass data eliminating luminosity functions

09 p1516 A71-22060

Local mean cosmic density from double galaxy data

09 p1516 A71-22061

Mean cosmic density based on galactic clusters masses

09 p1516 A71-22062

Field galaxy cosmological reddening from red shift data at faint magnitudes

09 p1516 A71-22063

Giant elliptical galaxy Maffei I continuous radiation emission data at 1415 MHz, examining radio luminosity magnitude

09 p1523 A71-22982

Soviet book on stars, galaxies and metagalaxy covering stellar luminosities, spectra, novae and supernovae

10 p1668 A71-24015

Book on relativity and discretization in astronomy covering cosmic structures, galactic isopleths equilibrium theory, red shift discretizations, etc

10 p1670 A71-24210

Seyfert galaxies NGC 1275 and NGC 4151 X ray flux detection, determining position and emission intensity

11 p1814 A71-25214

Seyfert galaxy 3C120 photometric behavior, investigating light variations

11 p1831 A71-26168

Galactic clusters statistical analysis for relative sky areas at various distances, discussing inverse apparent diameters and interstellar obscuration effects

11 p1833 A71-26329

Preferential orientation of physical galactic pairs, obtaining equatorial plane inclinations and major axes positional angles distribution

12 p1955 A71-26582

Radio quiet compact galaxy I Zw 1 /0051 plus 12/ photometric data, noting variability and brightness levels

12 p1957 A71-26622

Galaxy structure and evolution - NATO Conference, Athens, September 1969

12 p1958 A71-26771

Galactic structure historical approach, discussing stellar astronomy foundations, Milky Way, cluster and spiral position, etc

12 p1958 A71-26772

Spherically symmetric galactic and star clusters at Hubble expansion, deriving spatial density

12 p1962 A71-26909

Coma galactic cluster, investigating nuclei oblateness, diagrams and tables of variables

12 p1962 A71-26910

Hercules galaxies cluster rotation, determining radial velocities, axis position angle and center position

12 p1962 A71-26911

Astronomical methods for determination of distances to planets, stars and galaxies, considering human distance perception

12 p1962 A71-26955

Statistical analysis of gravitational instability for isotropic cosmological models, examining density perturbations as random functions of coordinates and comparing with galactic mass statistics

12 p1965 A71-27178

Galaxy nuclei and quasars model, considering supernova explosions, neutron stars matter accretion and energy radiation

12 p1968 A71-27541

Radio source and associated elliptical galaxy major axes position angles correlation

13 p2135 A71-28299

Expanding metagalaxy closed model with changing gravitational constant, noting matter motion in moving and central reference systems

13 p2136 A71-28423

Radio mapping of Maffei 1 and 2 galaxies, confirming previously detected small diameter source

13 p2136 A71-28428

Large scale clustering of galaxies and galactic clusters, comparing observed and Poisson distributions

13 p2138 A71-28759

Mass distribution of compact galaxies, obtaining average mass/luminosity ratio

13 p2138 A71-28762

X ray evidence of limit amount of hot intracuster gas for gravitational binding of Coma cluster of galaxies

13 p2130 A71-29094

Compton effect in variable radio sources, considering models of Seyfert galaxies 3C 84 and 3C 120 from baseline interferometry

13 p2141 A71-29100

Galactic structure and spectra, examining universe expansion, Hubble law and quasar distances

13 p2142 A71-29129

Seyfert galaxy NGC 1068 IR observations, noting angular extent and size

14 p2303 A71-29585

Flat galaxies dynamics via linearized Vlasov equation integration and Poisson equation exact solution

14 p2303 A71-29590

Coma galaxy clusters missing mass observations by gravitational lens effect

14 p2305 A71-29676

Galaxy Maffei 2 observations in 21 cm neutral hydrogen line and in continuum at 1415 MHz with Nancy radio telescope

14 p2305 A71-29681

Quasar-like N-type and Seyfert galaxies optical characteristics, discussing optical variability and radio spectrum characteristics

14 p2307 A71-29866

Star and galaxy clusters total kinetic energy content, using line of sight velocity data and astronomical models

14 p2312 A71-30390

Extragalactic X ray sources from Explorer 42 flight, confirming explosive nature of Seyfert galaxies revealed by optical telescopes

14 p2313 A71-30401

Elliptical and spiral galaxies in coma cluster central zone, presenting observed radius vs magnitude diagrams

14 p2313 A71-30429

External galaxies neutral hydrogen distribution from interferometric observations, discussing interpretation consistent with optically derived rotation curves

14 p2314 A71-30638

Galactic nebula YM 29 radiometric observations showing thermal source, mass and Balmer line fluxes comparable to planetary nebula

14 p2314 A71-30643

Large and small red shift quasars relative probability correlation with cataloged galaxies clusters direction

14 p2315 A71-30656

Globular star clusters and spherical galaxies stability, proposing rotating gravitating masses spherically symmetrical system model

15 p2482 A71-31331

Galactic brightness, color distribution and ellipticity data from photometry and colorimetry observations

15 p2486 A71-32028

Aperture synthesis of neutral hydrogen in M 101 galaxy, suggesting close connection between surface density of light and H I

16 p2632 A71-33330

Extragalactic cosmic X ray sources at high galactic latitude from sounding rocket experiments, correlating with galactic clusters

16 p2626 A71-33357

Extragalactic gravitational radiation focusing by galactic core acting as lens

17 p2798 A71-34399

Galactic clusters characteristics tabulation and statistical analysis, calculating dimensions, luminosity and radial velocities dispersion

17 p2804 A71-34841

Distribution functions of observed and true spherities (axis ratios) of Sculptor-type dwarf galaxies

17 p2804 A71-34842

Radio source PKS 1514-25 identification as E galaxy, investigating rapid optical variability and light curves

17 p2805 A71-35379

Coma cluster X ray source data from Uhuru satellite, observing size, luminosity, spectra, thermal bremsstrahlung mass and stability

17 p2796 A71-35413

Double galaxies relative number determination, taking into account differences of components absolute magnitudes

17 p2808 A71-35578

Quasars as proto-blackholes in galactic nuclei blackhole model, discussing lifetimes, dust and IR radiation using models

17 p2811 A71-35745

Galaxy type correlated with rotational velocity using Hubble sequence

18 p2960 A71-35941

Newcomb precession determination from Bradley stars proper motions, evaluating neglect of galactic rotation

18 p2961 A71-35942

Synchrotron radiation reabsorption in inhomogeneous sources, considering IR spectra of quasars and galactic nuclei

18 p2963 A71-36158

Local group stellar systems including Galaxy, Magellanic Cloud, Andromeda galaxy, triangulum and spherical dwarf galaxies

18 p2966 A71-36759

Dwarf elliptical and irregular galaxies of small intrinsic size, small absolute luminosity and low surface brightness

18 p2967 A71-37028

Galactic clusters evolution in universe with zero rest mass particles, showing size dependence on cosmic dust energy density

18 p2969 A71-37040

Supermassive double galaxy spectrographic and photometric data for cluster Abell 1775, showing radial velocity difference, visual magnitude and mass estimates

18 p2969 A71-37041

Magellanic clouds X rays observation, interpreting spectrum analysis data as due to few strong sources

18 p2959 A71-37051

Extragalactic Faraday rotation models, examining galactic plane and Galaxy supercluster

19 p3142 A71-38005

Emission lines of star S22 in Large Magellanic Cloud, identifying H, Fe II and forbidden Fe II and Ni II lines

19 p3144 A71-38167

Planetary capture in restricted three body problem and bridge formation between galaxies

20 p3286 A71-38761

Entropy generation and survival of protogalaxies in expanding universe, deriving bulk/shear viscosity, heat transport and sound waves damping rate in relativistic fluid

20 p3287 A71-39051

Extragalactic background soft X ray diffuse flux consistent with absorption by Small Magellanic Cloud

20 p3278 A71-39108

Gas heating by LF radiation due to Compton scattering near quasars, Seyfert galaxies nuclei and pulsars

20 p3289 A71-39293

Stability of plane rotating galaxies in magnetic field parallel to axis of rotation, showing linearized MHD equations self conjugate for radial disturbance case

20 p3289 A71-39298

Statistical investigation of 1500 galaxies in MCG catalog with weak surface brightness, noting sculpture type spheroidal galaxies in Virgo cluster

20 p3289 A71-39299

Papers on astronomy covering eclipsing binaries, eclipse functions computations, silicon in sun, Magellanic clouds and stellar kinematics

20 p3300 A71-39819

Stellar composition analysis of Small and Large Magellanic clouds using Hertzprung-Russell, color magnitude and two color diagrams

20 p3301 A71-39823

Expanding metagalaxy closed model with changing gravitational constant, noting matter motion in moving and central reference systems

21 p3441 A71-40078

Spectral analysis of Markarian galaxies, observing emission and absorption lines and hydrogen reversal

21 p3441 A71-40105

H beta and UVB photoelectric photometry of southern galactic cluster, deriving absolute magnitude calibrations and intrinsic color relations

21 p3443 A71-40194

Total to selective extinction ratio determination, obtaining distance to galactic center

21 p3445 A71-40245

Radio observation for radial velocities in center region of Perseus cluster of galaxies

21 p3445 A71-40408

Galaxies clusters mass determination with aid of virial theorem based on velocity dispersion, emphasizing black holes existence

21 p3450 A71-40713

Coma cluster X ray observations implying limits on gas density in intergalactic space and Friedmann models

22 p3599 A71-41926

Mean ratio of mass to three-halves power of luminosity for elliptical and lenticular galaxies based on catalog mass data emphasizing uncertainties

22 p3599 A71-41935

Statistical analysis of gravitational instability for isotropic cosmological models, examining density perturbations as random functions of coordinates and comparing with galactic mass statistics

22 p3605 A71-42452

Globular star clusters and spherical galaxies stability, modeling as rotating gravitating masses in spherically symmetrical system

22 p3606 A71-42606

Absolute spectral energy distribution and K-corrections for giant elliptical galaxies in Virgo cluster

23 p3722 A71-42935

Absolute spectral energy distribution and K-corrections for giant elliptical galaxies from scanner observations

23 p3722 A71-42936

H II regions kinematic properties in Large Magellanic Cloud, presenting emission line profiles and radial velocities

23 p3723 A71-42939

Photometric study of light variation and variable stars in luminous supergiants in Large Magellanic Cloud

23 p3723 A71-42940

Stellar density function outside symmetry plane of galactic phase-space model

24 p3868 A71-44461

Seyfert galaxy NGC 5548 H alpha profile spectroscopic observations, discussing broad emission lines

24 p3870 A71-44901

GALAXY AIRCRAFT

U C-5 AIRCRAFT

GALERKIN METHOD

Pontryagin space and convergence of Bubnov-Galerkin method for equations with involution operators

01 p0112 A71-11092

Linear and nonlinear parabolic equations approximate solutions by Galerkin methods, leading to linear algebraic equations

06 p0917 A71-17558

Elastic rectangular and thin plates design under dynamic loading, using Bubnov-Galerkin method for computer solutions

06 p0992 A71-17808

Ritz-Galerkin method for solving nonlinear operator equations in Hilbert space, discussing convergence and error estimate

06 p0919 A71-18204

Partial differential equation solution for aircraft hydraulic lines flexural vibration by Bubnov-Galerkin method, reducing to Duffing equation analysis

08 p1286 A71-20783

Shallow spherical shell thermal stability, investigating factors affecting Galerkin method validity

10 p1690 A71-24574

Dynamic analysis of vibrating beams on viscoelastic supports, using Galerkin approximate method

10 p1694 A71-25088

Stable limit cycles and triggering limits of first radial mode in nonlinearly unstable liquid propellant rocket motors, using wave equation and Galerkin method

11 p1836 A71-25162

Critical velocity of fluid flow in cantilever tube, applying Galerkin method to modal type analysis

11 p1748 A71-25163

Soviet book on variational methods in mathematical physics covering energy method, Ritz process, Bubnov-Galerkin method and least squares method

12 p1931 A71-27292

Imperfect circular disks large amplitude free transverse vibration calculation by Galerkin procedure

14 p2326 A71-30064

Time dependent problems involving parabolic and hyperbolic differential equations, discussing formulation for approximate solution by Galerkin methods

14 p2265 A71-30294

Ridged waveguide complete eigenvalue solution by integral equation formulation and Ritz-Galerkin method

14 p2212 A71-30516

Bubnov-Galerkin method convergence prediction discussing J spaces and orthonormal bases

15 p2439 A71-31154

Variational principles and finite element method in partial differential equations, emphasizing basis functions fundamental to Galerkin procedure

15 p2441 A71-31351

Time dependent partial differential equations solutions, considering hopscotch class algorithms, Galerkin type methods and finite difference schemes

15 p2441 A71-31352

Existence and uniqueness of weak solution of wave equation with nonlinear boundary condition, using Galerkin method

18 p2940 A71-36094

Alternating-direction Galerkin methods application to parabolic and hyperbolic differential equations for obtaining efficient iterative solution of heat equation on rectangle

19 p3087 A71-38305

Galerkin/spectral/ method accuracy for numerical simulation of incompressible boundary flows, testing scalar-convection and Taylor-Green vortex decay problems

21 p3367 A71-40638

Galerkin approximation for boundary value problem finite difference scheme optimization by interpolation in Hilbert subspace

22 p3566 A71-42292

GALLIUM

Thin gallium films metastable gamma and delta phase ring diagrams using electron diffraction techniques

12 p1942 A71-26821

Ga spreading over Ag and Au thin films surfaces from electronographic and optical experiments, noting volume heterodiffusion

20 p3276 A71-39155

Nucleate boiling of liquid helium I on gallium single crystal surfaces

20 p3312 A71-39282

GALLIUM ALLOYS

Zr-Ga phase diagram eutectoid region metallographic analysis, discussing solubility, reactions and compound formation

04 p0614 A71-15779

Gallium oxide particles effects on Ag-Ga matrix single crystals critical resolved shear stress

08 p1311 A71-21543

Yttrium effect on phase composition of V-Ga alloys from microstructural, X ray structural and microdilatometric analysis

16 p2622 A71-33909

GALLIUM ANTIMONIDES

Degenerate n-type GaSb, calculating electron mobility dependence on impurities concentration for comparison with experiment

09 p1507 A71-22361

Gallium antimonide synthesis without antimony evaporation stoichiometry disturbances, describing zone refining procedures and quality control

16 p2621 A71-33473

Gallium antimonide-germanium system solid solution lattice constant determination, using X ray and microstructural analysis and microhardness measurements

17 p2791 A71-34566

Optical pumping and detection of spin polarized electrons created in p-type GaSb conduction band by excitation with light

17 p2791 A71-35583

Te-doped n-type GaSb semiconductor negative magnetoresistance and magnetothermoelectric power dependence on longitudinal magnetic field

21 p3436 A71-41349

GALLIUM ARSENIDE LASERS

GaAs injection lasers phenomenological theory and internal parameters physical meanings, giving maximum optical gain dependence on current density

03 p0434 A71-13349

GaAs heterojunction diode injection lasers, predicting high order transverse cavity modes and far field patterns from theoretical model

03 p0434 A71-13482

Optically coupled GaAs injection lasers emission spectra, determining maximum frequency difference in gain bandwidths for mode synchronization

03 p0435 A71-13506

- Injection breakdown in Fe and Cr-doped high resistance GaAs laser due to increased electron-hole plasma during electron heating 03 p0467 A71-13979
- Near-bandgap narrow spectrum low loss volume-excited GaAs laser with time-uniform output 03 p0440 A71-14462
- Large optical cavity low loss n-type GaAs injection laser with reduced degradation 05 p0763 A71-16499
- Daytime pulsed optical communication within line-of-sight using GaAs IR laser 06 p0907 A71-17570
- Low threshold large optical cavity /LOC/ GaAs injection lasers with high quantum efficiencies at room temperature 06 p0909 A71-18660
- GaAs lasers self-induced pulses signal structure, measuring pulse width, repetition rate and amplitude fluctuations 06 p0910 A71-18671
- GaAs-GaAsP heterostructure injection lasers performance tests [ECS PAPER 71] 07 p1123 A71-19570
- Light pulses from tandem bisected GaAs lasers nonuniform excitation, determining width by intensity correlation in lithium iodate crystal 07 p1126 A71-20167
- CW GaAs semiconductor laser fabrication by liquid epitaxy, noting Ag plating role in output power 07 p1126 A71-20196
- Stimulated emission wavelength tuning from GaAs and CdSe electron beam pumping laser crystals as function of time and current 07 p1128 A71-20393
- Partial mode locking in picosecond self pulsing GaAs injection lasers 07 p1128 A71-20394
- GaAs lasers p-n junction active region thickness from minority carrier mobility and spontaneous emission measurements in threshold current determination 09 p1460 A71-22305
- GaAs junction laser continuous operation, investigating reflectivity dependence of temperature rise, stimulated light output and power efficiency 09 p1464 A71-22988
- Multilayer liquid phase epitaxy heterostructures growth with crystalline solid solutions of aluminum gallium arsenide for injection lasers 09 p1464 A71-23122
- Uncooled GaAs injection laser with high pulse repetition rate, discussing structural features and current-power characteristics 10 p1619 A71-23811
- Mode hopping due to GaAs lasers longitudinal mode inhomogeneous sequential excitations perpendicular to junction at injection levels above threshold 10 p1619 A71-24039
- Pulse rate and pumping power effects on emission spectra and I-V characteristics of multielement GaAs injection lasers 10 p1622 A71-24884
- Spatial-temporal emission of n-GaAs laser pumped by electron beam at liquid nitrogen temperatures 10 p1622 A71-24889
- Logical GaAs integrated laser circuits, discussing integrated laser modules with electron-hole junctions fabricated by diffusion techniques 11 p1773 A71-25917
- GaAs multiple beam injection laser amplifier avoiding light flux saturation by periodic signal release 12 p1913 A71-26852
- Population inversion in Cs133 ground state hyperfine levels, using CW GaAs laser at 77 K for optical pumping 12 p1913 A71-26977
- Frequency and temperature variations of active diode region in pulsed GaAs laser, using Fabry-Perot interferometer 13 p2079 A71-28923
- Time dependence of peak emission energy shift due to junction temperature rise in GaAs junction lasers operated with flat topped current pulse 15 p2420 A71-32027
- Laser action internal differential quantum yield estimation using GaAs injection lasers near field emission patterns 15 p2422 A71-32461
- SiO antireflection coatings for GaAs injection lasers, discussing single layer quarter-wave coatings for loss minimization and bandwidth maximization 16 p2585 A71-33136
- GaAs laser arrays for beam addressable memories, discussing efficiency, junction width, beam spread and polarization 18 p2929 A71-35957
- High power GaAs injection laser diodes characteristics and array module design for pulsed operation, using confinement junction formation and reflective end coating 18 p2931 A71-36604
- GaAs laser diode junction temperature measurement methods for verification of stimulated emission quenching due to heating 19 p3074 A71-38231
- Peak optical flux density for catastrophic damage in close confined and double heterojunction injection Al-GaAs-GaAs lasers 19 p3075 A71-38507
- Neutron irradiation effects on radiative, nonradiative and threshold currents in epitaxial GaAs laser diodes at room temperature 20 p3275 A71-38785
- Spontaneous emission decreases at CdS and GaAs lasing onset observed visually in internal reflection cavity under electron beam pumping 20 p3243 A71-39007
- Logical GaAs integrated laser circuits, discussing integrated laser modules with diffused p-n junctions 21 p3394 A71-41228
- Waveguide structure effect on electron beam pumped GaAs laser characteristics, considering diffraction losses and laser threshold reduction 21 p3394 A71-41233
- GaAs injection laser radar for measuring cloud height, determining required laser output power as function of state of atmosphere and receiver sensitivity 21 p3394 A71-41238
- Spatial-temporal emission of n-GaAs laser pumped by electron beam at liquid nitrogen temperatures 21 p3394 A71-41258
- Frequency and temperature variation with time in active region of pulsed GaAs laser diode, using Fabry-Perot interferometer 21 p3394 A71-41318
- Temperature dependent threshold current density and doping gradient at p-n junction in epitaxial GaAs injection laser diodes 22 p3555 A71-41686
- Electromagnetic field distributions and far field radiation patterns of three layer waveguide GaAs heterostructure injection lasers, using Maxwell equations 22 p3555 A71-41688
- GaAs lasers filamentary coupling, investigating various mode perturbations in temporal output 22 p3558 A71-42346
- Characteristic energies of exponential band tails in GaAs junction lasers from wavelength shift with cavity Q and spontaneous emission line width 22 p3558 A71-42360
- Bulk quantum efficiency in electron beam pumped n-type GaAs lasers at 300 K as function of impurity concentration 22 p3558 A71-42362
- Numerical analysis of large signal output characteristics for directly modulated GaAs junction injection lasers, investigating resonance phenomenon 23 p3683 A71-43351
- Room temperature GaAlAs close confinement /single heterojunction/ laser diode performance and applications 23 p3684 A71-43503
- Staircase array and diode stacking moderate power GaAlAs injection laser light sources at room temperature 23 p3685 A71-43504
- High order transverse cavity mode selection and propagation in homojunction and heterojunction GaAs injection lasers, using five layer dielectric model 24 p3832 A71-44432
- Double heterostructure GaAs injection laser mode reflectivity and waveguide properties, discussing threshold current density and wavelength dependence on mirror reflectivity 24 p3832 A71-44433
- GALLIUM ARSENIDES**
- High efficiency epitaxial growth of GaAs by system using substrates oriented along /111/ Ga face 01 p0137 A71-10314
- Hall constant and resistivity of impurity centers in semiconducting n-type GaAs during illumination and heating 01 p0138 A71-10776
- Thermodynamic distribution of amphoteric Ge impurities in sublatitudes of GaAs semiconductor for compensation by acceptor vacancies 01 p0139 A71-10778
- Visible and IR reflection spectra of p- and n-type GaAs under fast neutron irradiation 01 p0139 A71-10783
- Electroacoustic properties of GaAs diffusion layer transducers as function of resistivity and charge carrier concentration in single crystals 01 p0140 A71-11122
- GaAs strongly doped p-n junctions, examining I-V characteristics changes under electron bombardment and mixed reactor field irradiation 01 p0140 A71-11458
- GaAs S diodes with negative differential resistance, examining selectivity and oscillation characteristics 01 p0057 A71-11460
- Electron mobility in gallium arsenide phosphide solid solutions, discussing temperature effects 01 p0141 A71-11465
- GaAs high resistivity n-type Cr doped samples, examining field domains shape and motion by visual observation 01 p0141 A71-11467
- Gallium arsenide devices in microwave communications, discussing Gunn oscillators, FET, varactors and radar applications 02 p0231 A71-12049
- Solid state traveling wave amplifier using thin n-type epitaxial GaAs layer 03 p0384 A71-13316
- Hall effect, conductivity, thermal emf and Nerst-Ettingshausen transfer in n-type highly doped compensated GaAs 03 p0466 A71-13398
- Noise-induced current fluctuations on S-shaped I-V curve in Cr-doped GaAs diodes 03 p0387 A71-13982
- Polarization of spontaneous emission in Zn-doped GaAs p-n junctions as function of electric field strength 03 p0467 A71-13985
- High resistance single crystal light sensitive n-type GaAs wafer for obtaining long wave photographic images via electric photosensitivity control 03 p0428 A71-13986
- Photomitter technology based on GaAs/Cs photocathodes 03 p0468 A71-14466
- Silicon and gallium arsenide photovoltaic solar cells, examining performance at high illumination intensities 04 p0535 A71-15006
- P-type aluminum gallium arsenide phosphide growth on gallium arsenide phosphide from solution, noting lattice match preservation and heterostructure junction devices 04 p0608 A71-15041
- Anomalous Cu concentration profile due to migrating Cu ions-GaAs crystal defects interaction 05 p0794 A71-16877
- GaAs FET design and performance, discussing fabrication techniques and scattering and noise parameter measurements 05 p0729 A71-16916
- CW microwave reflection-type amplification from circuit stabilized epitaxial GaAs transferred electron devices, observing gain and hysteresis 05 p0729 A71-16918
- CaAs Schottky tunnel junctions properties and bias independent structure evaluation by excess noise generation 06 p0940 A71-17312
- Coplanar n-type GaAs Gunn effect microwave oscillators failure mechanism, suggesting role of current filament formation in thermal breakdown 06 p0874 A71-17665
- Microwave Gunn diodes made from GaAs single crystals, describing fabrication by diffusion process 06 p0876 A71-18082
- Large signal oscillation mode model for GaAs devices operational prediction, including space charge and intervalley transfer time effects 07 p1070 A71-18867
- GaAs transmutational doping by slow neutrons irradiation, using Cd and In screens for impurities distribution control 07 p1175 A71-19219
- Electrophysical properties of Ga-In-As single crystals in varying mixture ratios at 78-380 K, determining electrical conductivity, Hall coefficient and electron mobility 07 p1176 A71-19224
- Optical absorption spectra in Cu-doped p-type GaAs samples 07 p1177 A71-19498
- Germanium distribution coefficient in GaAs epitaxial crystals by radiotracer, mass spectroscopy and electron probe analysis noting total impurity concentration from Hall mobility 07 p1180 A71-20176
- K band double-tuned nondegenerative parametric amplifier using single-packaged GaAs varactor diode, discussing design and performance 08 p1262 A71-20763
- GaAs-InAs type single crystals, polycrystals and epitaxial films solid solutions, studying optical, electrical and luminescent properties 08 p1344 A71-21443
- High density DC effects on displacement of solid GaAs-liquid metal interface, considering Peltier effect and dislocation density 08 p1344 A71-21444
- Limited space charge accumulation layer diodes operating characteristics, using GaAs devices with uniform doping for microwave peak power 08 p1266 A71-21624
- GaAs epitaxial layers growth in open system, noting spontaneous crystallization on reactor walls at high temperatures 09 p1506 A71-22161
- GaAs epitaxial layers inhomogeneous doping in continuous chloride system, discussing electron concentration with respect to gas flow direction 09 p1506 A71-22167
- Wideband UHF amplification in bulk n-type GaAs during domain generation, comparing cut-off and Gunn frequency 09 p1507 A71-22223

GALLIUM COMPOUNDS

Hysteresis effects during retuning of n-type GaAs Gunn oscillator with bias source and RLC circuit, showing range of domain damping by low field 09 p1414 A71-22228

FET transistors on epitaxial GaAs as input and output transducers for acoustic surface waves 09 p1417 A71-22755

Spectral mode and CW operation of stripe geometry double heterostructure GaAs junction lasers above room temperature 09 p1463 A71-22763

Gamma radiation effect on electrical properties of n-type GaAs single crystals with doping impurities, calculating defect introduction rate and forbidden zone energy levels 10 p1656 A71-24141

Gamma radiation influence on photomechanical effect in GaP and GaAs single crystals, using microhardness tester 10 p1656 A71-24143

GaAs single crystals conductivity and surface capacitance under transverse electric field at low temperatures 10 p1657 A71-24322

Cu doped GaAs electron radiative capture mechanisms based on photoconductivity and photoluminescence dependence on temperature and excitation intensity 10 p1657 A71-24324

High purity GaAs transverse magnetophonon amplitudes, investigating magnetic field dependence and Landau level collision broadening 10 p1621 A71-24537

Unilateral GaAs traveling wave microwave amplifier based on space charge growth in domain-stabilized transferred electron semiconductor, considering power, noise, gain and efficiency 11 p1736 A71-25234

Hall effect measurements and electron microscope examination of Te-doped gallium arsenide crystals annealed at various temperatures 13 p2111 A71-28503

Power gain of Q-band GaAs FET with Schottky-barrier gate, giving amplifier and oscillator designs 14 p2210 A71-29800

In-line harmonic tripler with GaAs varactor diode, detailing waveguide mount fabrication, power extraction filter and reverse bias voltage effects 14 p2211 A71-29857

Measuring instrument for solar radio emission at 8 mm, using GaAs Schottky barrier diode mixer for system noise temperature reduction 14 p2239 A71-29916

GaAs solar cells photoelectric energy characteristics as function of light flux, comparing with Si cells 14 p2181 A71-29952

Pulsed GaAs point contact diodes quick response performance, obtaining contact electrical characteristics and Schottky-type rectifying barriers by half period currents 14 p2211 A71-30093

GaAs single crystals real surface electrical characteristics, using pulsed field effect techniques 14 p2284 A71-30403

Characteristics of field effect and surface barrier GaAs transistor (MESFET) operating at 4.2 K, noting very low temperature hyperfrequency amplifier application 14 p2212 A71-30439

Residual stresses for fused contacts between metals and Si or gallium arsenide from polarization measurements in principal crystallographic planes 15 p2461 A71-31510

Physical model of Zn diffused GaAs electroluminescent diodes gradual degradation, establishing formation of new recombination centers through injected carrier lifetime measurement 15 p2377 A71-32607

Radiation defects isochronal annealing effects on absorption spectral distribution of gallium arsenide irradiated with fast neutron flux 16 p2620 A71-33184

GaAs single crystals defects formation during low temperature gamma photons and electron irradiation, considering electrical properties 16 p2620 A71-33185

GaAs epitaxial layer growth process parameters relationship to electrical properties 16 p2621 A71-33563

Electroconductivity and Hall effect in doped GaAs at low temperatures, studying temperature dependence of electron concentration, mobility and localization 16 p2623 A71-34030

Spectral dependence of GaAs-CdSe alloys optical reflection coefficient 17 p2790 A71-34203

Low noise operation of CW devices with GaAs vapor grown p-n junctions, observing optimum AM SNR of minus 140 dB 17 p2713 A71-34445

Nonlinear frequency shift in GaAs electroacoustic domains, using Bommel-Dransfeld analysis technique 17 p2791 A71-35447

Impure GaAs and InP semiconductors compensation by introducing diffusible temperature dependent impurities 18 p2953 A71-35871

Al distribution in gallium aluminum arsenide films obtained by epitaxial growth from liquid phase, showing temperature variation dependence during deposition 18 p2954 A71-36161

Fabrication and noise performance of high power Schottky barrier GaAs IMPATT diodes with double epitaxial layer structure on low-etch-pit density substrates 18 p2895 A71-36982

Semiconductor device with stable negative conductance over wide range of microwave frequencies and power levels, using transferred electron effect in epitaxial GaAs 18 p2895 A71-36985

Peroxide-alkaline polishing solution for GaAs, evaluating optical quality, surface damage, polishing rate and metallic contact resistance 18 p2955 A71-37004

Photolithographic fabrication and electrical characteristics of GaAs Schottky barrier diodes for pulse operation 19 p3027 A71-37259

Photovoltaic and electron-voltaic properties of diffused and Schottky barrier GaAs diodes, considering irradiance in 0.001-10,000 microwatt/sq cm range 19 p3027 A71-37484

Temperature dependence of ionization rates in aluminum gallium arsenides for samples with varying Al contents 19 p3117 A71-37486

Semiconductor lasers, noting AlGaAs-GaAs p-n heterojunction structure contribution to room temperature efficiency of diode lasers 19 p3074 A71-38230

Spurious emissions from CW and pulsed GaAs solid state oscillators as function of material active layer thickness and contacting procedure 19 p3032 A71-38460

Hall coefficient and resistivity in undoped heteroepitaxial GaAs on aluminum oxide films grown by trimethylgallium arsine process 20 p3276 A71-38881

GaAs solar batteries for spacecraft power supplies, comparing effectiveness with Si cells for optimum utilization 20 p3183 A71-39133

Low voltage IR image converter display system using scanned line array of GaAsP light-emitting junction diodes 21 p3352 A71-40117

Thin single crystalline film deposition by molecular beam epitaxy of GaAs, describing surface structure observation with high energy electron diffraction 21 p3427 A71-40217

GaAs and silicon IMPATT diodes applications and performance, discussing power levels, amplifier applications, injection locked oscillators and microwave signal source 21 p3357 A71-40818

Energy levels and vacancy association of defects in annealed GaAs at 600-1100 C under controlled vapor pressures, using cathodoluminescence measurements 21 p3428 A71-41044

Light intensity distribution inhomogeneity in transmission by GaAs single crystals, using schlieren method 21 p3428 A71-41201

Electron concentration and degeneracy effect on threshold photon energy for optical transitions onset from splitoff valence band to conduction band in n-type GaAs 21 p3429 A71-41211

Temperature dependence of impurity photoluminescence of Cr-doped GaAs single crystals, measuring activation energy 21 p3430 A71-41214

Deep level impurity compensation of high resistivity epitaxial films of GaAs by chromium, complex lattice defects and copper acceptors, using cathodoluminescence spectra 21 p3430 A71-41220

Current-voltage characteristics of n-GaAs epitaxial structures at various temperatures, indicating use in memory devices and high power switches 21 p3430 A71-41223

High resistance undoped GaAs samples at different temperatures, investigating energy spectra, Hall effect and electron conductivity 21 p3431 A71-41227

High resistivity Fe-doped GaAs, investigating carrier lifetime dependence on Fe atoms concentration 21 p3431 A71-41234

Au-n-GaAs surface barrier diode space charge layer strong electric field effects on photoconductivity quantum efficiency 21 p3432 A71-41302

GaAs luminescent p-n junction diode spontaneous emission measurement in magnetic field, noting redistribution in Lorentz force direction 21 p3432 A71-41303

Sn-N-GaAs semiconductor surface barrier structure electrical properties measurement over wide electron density range, determining energy band diagram - current flow mechanism 21 p3433 A71-41304

Cr-doped n-type seminsulating GaAs single crystal photoconductivity measurement, noting spectral peaks dependence on temperature 21 p3434 A71-41305

GaAs-InAs solid solutions single crystal ingots, investigating optical absorption and reflection spectral energy gap width and carrier mobility temperature dependence 21 p3435 A71-41306

GaAs contacts fabrication by successive metals alloy evaporation, examining surface distribution by ray microprobe 22 p3585 A71-41702

Double-heterostructure injection laser radiation transverse polarization from reflectivity analysis in GaAs-air interface vs TE and ME mode incidence angle 22 p3558 A71-42222

Supercritical transfer electron amplifier using GaAs CW Gunn diode with cathode doping notch as a profiles sloping upward for stabilization 22 p3521 A71-42223

X band GaAs diffused IMPATT diodes for high C efficiencies 22 p3523 A71-42424

IMPATT diodes noise performance lower limit deriving optimization theorem for GaAs diodes under assumption of equal ionization coefficients for electrons and holes 22 p3524 A71-42616

GaAs LSA mode V band oscillator CW and pulsed operations power and efficiency limitations 23 p3649 A71-42919

Acoustoelectrical current oscillations in GaAs film at low temperature under ultrasonic Rayleigh wave amplification 23 p3716 A71-43474

Neutron irradiation effects on dissociative high temperature zinc diffusion in indium and gallium arsenide 23 p3716 A71-43484

Wideband phase-matched carbon dioxide laser second harmonic generation in GaAs thin film waveguide through dielectric dispersion 23 p3687 A71-44133

Gallium arsenide phosphide electroluminescent junction diode pumped Nd-YAG laser room temperature CW and pulsed outputs 23 p3687 A71-44133

Cryogenic n-type GaAs residual photoconductivity produced repeatedly after heating to room temperature and renewed cooling 24 p3859 A71-44466

Kinetic parameters and conditions for optimum epitaxial growth of GaAs from liquid phase, observing solution cooling rate effect on p-n junction quality 24 p3808 A71-44722

Noise voltage power spectrum of GaAs bulk diodes at LF as function of bias field approaching negative resistance region 24 p3804 A71-44959

Structural and electrical properties of sublimation deposited GaAs films on sapphire and seminsulating substrate in vacuum 24 p3863 A71-45353

GALLIUM COMPOUNDS

NT GALLIUM ANTIMONIDES

NT GALLIUM ARSENIDES

NT GALLIUM PHOSPHIDES

NT GALLIUM SELENIDES

Quadrupole interaction in crystals of diamond-like semiconductors gallium telluride and indium telluride 07 p1177 A71-19277

Electroluminescent semiconductor diodes based on GaP and GaAlAs, discussing design, properties, uses and production 11 p1737 A71-25566

P-type Al-GaAs-p-type GaAs-n-type GaAs single heterostructure preparation and properties, discussing effect on injection laser diode characteristics 12 p1914 A71-27024

NiGa intermetallic compound electrical transport and resistance, Hall coefficient and optical absorption, discussing defect structure and electron scattering 14 p2260 A71-30474

GALLIUM PHOSPHIDES

Electron mobility in gallium arsenide phosphide solid solutions, discussing temperature effects 01 p0141 A71-11461

Single crystal indium gallium phosphide solid solution synthesis, discussing crystallographical and electrophysical properties 03 p0467 A71-13474

P-type aluminum gallium arsenide phosphide grown on gallium arsenide phosphide from solution, noting lattice match preservation and heterostructure junction devices 04 p0608 A71-15044

Gallium phosphide current carriers radiative recombination, discussing electro- and photoluminescence phenomena 06 p0940 A71-17350

GaAs-GaAsP heterostructure injection lasers performance tests [ECS PAPER 71] 07 p123 A71-19570

Single crystal indium gallium phosphide p-n junction preparation by epitaxial vapor phase growth technique, determining energy gap dependence on alloy composition 09 p1510 A71-23121

Gamma radiation influence on photochemical effect in GaP and GaAs single crystals, using microhardness tester 10 p1656 A71-24143

Oxygen contamination effect on GaP solar cell electroluminescence and photoluminescence characteristics from electrical and mass spectroscopic analysis data 19 p2998 A71-38143

Red and green light emitting GaP junction diodes and monolithic arrays for display devices, discussing fabrication and properties 21 p3352 A71-40110

Electrical, photoelectric and electroluminescent properties of reverse biased GaP p-n structures at room temperature, considering isolated microplasmas 21 p3430 A71-41217

Electrical properties and electroluminescence measurements for p-n junctions in Au- and Ag-doped GaP, noting negative resistance in I-V characteristics 21 p3433 A71-41312

Quasi-binary InAs-GaP single crystals absorption and diffuse reflection spectra, determining forbidden bandwidth as function of compound composition 21 p3434 A71-41332

Metal film ohmic contacts to n-type GaP devices operating at high ambient temperatures 22 p3520 A71-41687

GaP diodes with metal-semiconductor potential barriers manufactured by chemical deposition of metal on n-GaP surface 23 p3653 A71-43960

Indium gallium phosphide p-n junction laser operation at 4.2 and 77 K, considering threshold currents magnitude 23 p3687 A71-44138

Gallium arsenide phosphide electroluminescent junction diode pumped Nd-YAG laser room temperature CW and pulsed outputs 23 p3687 A71-44139

GALLIUM SELENIDES

P-type gallium selenide crystals impurity photoconductivity measurements by Q switched ruby laser 13 p2077 A71-27959

Copper gallium diselenide point contact diodes I-V characteristics temperature and illumination dependence, considering high temperature and photoelectric devices applications 21 p3434 A71-41327

Gallium selenide excitation by ruby laser radiation, investigating impurity photoconductivity dependence on radiation intensity 21 p3395 A71-41352

GALVANIC CELLS

U ELECTROLYTIC CELLS

GALVANIC SKIN RESPONSE

Extraordinary effects of sound on senses, concerning visual functions, nystagmus, galvanic skin response and audioanalgesic use 03 p0359 A71-13158

Orienting response and apparent motion toward and away from observer, using galvanic skin response and finger pulse volume studies 07 p1048 A71-19515

Human nervous system stimulus trace retention in various age groups, using skin galvanic reaction 08 p1240 A71-21788

Fear measurement and mastery, investigating relationship between experience and electrodermal arousal in responses to stimulus words of varying relevance 18 p2862 A71-36944

GALVANOMAGNETIC EFFECTS

NT NERNST-ETTINGSHAUSEN EFFECT

Semiconductor developments, discussing field effect transistors, MOS, microwave components, piezoelectric effects, optoelectronics and galvanomagnetism 03 p0384 A71-13534

Metal galvanomagnetic properties for specific Fermi surface and conduction electron scattering model, solving linearized Boltzmann equation 05 p0792 A71-16317

Thermal and electrical transport in tungsten crystal for strong magnetic fields and liquid helium temperatures 08 p1344 A71-21365

Galvanomagnetic properties of solid refractory zirconium and titanium compounds in two-band representation, measuring Hall effect and reluctance vs external magnetic field 15 p2426 A71-31512

GALVANOMAGNETISM

U GALVANOMAGNETIC EFFECTS

GALVANOMETERS

Quartz astatic galvanometer resistant to geomagnetic field variations, vibrations or microseismic noise 06 p0901 A71-18286

Geomagnetic PP type oscillations recordings, using fluxmetric rings and galvanometer 07 p1104 A71-20049

Tungsten crystal Fermi surface galvanomagnetic coefficients in scattering process by semiempirical scheme 08 p1344 A71-21366

Pen actuators prototype models for fast response graphic recording instruments, using DC servomotors or galvanometers 09 p1452 A71-23386

GAME THEORY

NT MINIMAX TECHNIQUE

NT SADDLE POINTS [GAME THEORY]

Extremal strategies of differential pursuit game for nonlinear controlled plants 01 p0128 A71-10654

Generalized control theory, discussing criterion function, pareto-optimal set determination, information structure, etc 01 p0112 A71-10846

Pursuit game strategy based on Hamilton-Jacobi formalism, considering internal and external potential fields, optimum trajectories and gravitational and electromagnetic fields 03 p0483 A71-13116

Controller characteristic adaptive control by disturbance of plant operation under random non-manipulated action, considering cognitive system as Markovian automation-nature game 03 p0389 A71-13516

Two controlled motions rendezvous problems treated as game between partners using quality criterion as payoff, deriving optimal strategies 03 p0392 A71-14405

N person nonzero sum differential games with linear dynamics, proving existence of equilibrium strategies 04 p0620 A71-15864

Sufficient conditions for differential game encounter 05 p0782 A71-16976

Continuous deflection strategies in game problems with motion encounters, discussing absorption sets 05 p0782 A71-16978

Controlled objects convergence game, constructing optimal minimax pursuer strategy 05 p0782 A71-16979

Differential games with information lag, considering pursuit problems and capture conditions 05 p0782 A71-16980

Differential game of convergence, constructing extremal strategy for ensuring motion encounter with given set 05 p0783 A71-17011

Efficient evasion strategies for vehicle pursuit-evasion games with imperfect information, using computer solution 06 p0846 A71-17331

Soviet monograph on differential games of encounter of motions covering optimal control, rendezvous, pursuit, evasion, extremal guidance, etc 06 p0926 A71-17438

Two countable systems of differential inequalities, applying to stability of feedback controls synthesizing equilibrium solutions to linear quadratic differential games 06 p0919 A71-18198

Recursively defined infinite system convergence solutions for initial and boundary value inequalities, applying to differential game stability problems 06 p0920 A71-18237

Pursuit and evasion games, proving existence and approximation theorems 06 p0921 A71-18238

Mixed player convergence game of conflicting controlled motion under phase constraint 08 p1336 A71-21860

Multistage two player zero-sum games with state determined by difference equations, deriving optimal strategy pair satisfying saddle point condition 10 p1637 A71-24842

Game theory application to spacecraft reentry problem, obtaining optimal control algorithms 12 p1972 A71-27017

Differential guidance game with aftereffects, investigating extremal strategies 12 p1931 A71-27522

Linear control of systems governed by second order equations, discussing games in operational partial differential equations 13 p2095 A71-28823

German monograph on game theory and planning techniques for aircraft evaluation 13 p1996 A71-28880

Algorithm for minimax and maximin problems in theory of differential games 14 p2265 A71-29555

Extremal strategies of differential pursuit game for nonlinear controlled plants 14 p2266 A71-30988

Radio engineering of signal detection, filtration, information processing and recognition, discussing game theory methods for problems solution 17 p2698 A71-34393

Equilibrium strategies for linear games with quadratic costs in Hilbert space, deriving nonlinear equation in allowed operator feedback spaces 17 p2723 A71-35297

Measurement uncertainty effects in linear multistage games, considering state variables construction from player measurement sequences 17 p2767 A71-35298

Sufficient conditions for differential game encounter, considering conflict controlled motion guidance onto given set 18 p2947 A71-36776

Continuous deflection strategies in game problems with motion encounters, discussing absorption sets 18 p2948 A71-36778

Controlled objects convergence game, constructing optimal minimax pursuer strategy 18 p2948 A71-36779

Differential games with information lag, considering pursuit problems and capture conditions 18 p2948 A71-36780

Prisoner dilemma game matrix, noting response patterns to various formats 18 p2863 A71-37017

Differential games with deviation from encounter, considering strategies for continuous, programmed and discontinuous control classes to bring motion to given set 19 p3103 A71-37093

Conflict rendezvous, pursuit and deviation game problems, obtaining optimal control strategies approximation by continuous functions 19 p3103 A71-37104

Game theory application to spacecraft reentry problem, obtaining optimal control algorithms 19 p3152 A71-37687

Unmanned spacecraft pursuit of evading manned vehicle by game theory, assuming full information availability to both players 19 p3038 A71-38014

Mixed strategy convergence game of conflicting controlled motion under phase constraint 20 p3270 A71-39359

Direct search penalty function algorithm for treating general mathematical programming form of optimal design problem 21 p3350 A71-40340

Zero sum differential game solution for aerial combat problem, applying direct gradient methods 23 p3699 A71-44103

Second order differential guidance game, formulating strategy for optimal feedback control 24 p3849 A71-45338

GAMMA FUNCTION

Service life testing and reliability estimation, using ordinary and empirical Bayes approach in failure model with gamma probability distribution 12 p1910 A71-26685

Transformed boundary layer equation solution for power law fluid flows of Falkner-Skan type by gamma functions series [ASME PAPER 71-FE-35] 13 p2053 A71-29470

Error evaluation for incomplete gamma function calculated by truncated asymptotic series 21 p3408 A71-40852

GAMMA GLOBULIN

Human gamma globulin polymorphism, discussing characteristics, statistical distribution and potential utilization for gene frequency studies in paternity serology 05 p0710 A71-16943

GAMMA RADIATION

U GAMMA RAYS

GAMMA RAYS

Li quantitative determination in soaps and lubricants by gamma spectroscopy of nuclear reactions with alpha particles from radioactive source 01 p0106 A71-10093

Bone marrow physiological regeneration after chronic gamma irradiation, noting effect on fission processes and chromosome apparatus of cells 01 p0014 A71-11146

Gas-Cerenkov balloon-borne detector for low energy gamma rays, calculating efficiency and angular response by Monte Carlo program 01 p0083 A71-11222

Nd 147 decay gamma-gamma directional correlations, using coaxial Ge/Li and NaI/Tl detectors in conjunction with multichannel coincidence configuration 02 p0285 A71-11646

Reactor gammas effects on thermionic diode output simulated in electron accelerator 02 p0238 A71-12228

Soviet book on material analysis by nuclear radiation covering heavy elements concentration in ores,

radioisotope devices and gamma ray capture spectroscopy

02 p0283 A71-12721

Diffuse cosmic gamma ray background origin, using simple photon production model

02 p0303 A71-12837

Omnidirectional intensity of atmospheric gamma rays at balloon altitudes at various energy thresholds, noting integral spectrum flattening at lower energies

03 p0473 A71-13306

Electromagnetic mechanism of direct muon and gamma quanta production by collision of strongly interacting particles

03 p0462 A71-13864

Compton scattering in quasars, discussing gamma rays effects on core chemical abundances

03 p0481 A71-14266

Ionization chamber for high intensity isotopic gamma radiation dose measurement, discussing saturation current and Compton interaction process

04 p0594 A71-14917

Ultrasonic viscosimeter for gamma irradiation effects on materials structure, determining fluid viscosity changes from rate of damping of plate vibrations

04 p0594 A71-14918

Cosmic objects relativistic plasma X ray and gamma ray background radiation increase, considering bremsstrahlung effect on radiation spectrum

04 p0657 A71-15747

Supernovae high energy gamma rays detection by extensive air shower arrays

04 p0641 A71-15830

Gamma radiation flux distribution and spectral composition by satellite observation, analyzing background effects

05 p0798 A71-16047

Near space annihilation gamma radiation intensity and spectral energy composition by satellite observation, considering possible antimatter nature of comets and meteor streams

05 p0798 A71-16048

X ray source Sco X-1 gamma radiation due to Compton synchrotron process, comparing flux observation for synchrotron origin validity

05 p0799 A71-16476

Primary immune response chemical radioprotection in white mice during gamma irradiation, using serotonin as chemical protective and sheep red blood cells as immunizing agents

05 p0710 A71-16816

Spacecraft sterilization by microbial inactivation, comparing thermoradiation and dry heat methods

06 p0853 A71-17959

Balloon-borne telescopes to detect pulsed gamma rays from Crab Nebula, graphing data and diagramming telescope

06 p0950 A71-18034

Neutron and gamma ray production by nuclear interactions in solar flares

06 p0961 A71-18175

Extraterrestrial gamma ray and neutron flux and energy spectrum at balloon altitudes over equatorial latitudes, using pulse shape discriminator during solar flares

06 p0962 A71-18177

Atmospheric gamma rays energy spectrum and implication on high energy interactions characteristics

06 p0962 A71-18181

Gamma irradiation effects on physicochemical and organoleptic properties of food products

06 p0861 A71-18367

Radioreistant yeast strain *Saccharomyces cerevisiae*, discussing cycloheximide and gamma irradiation treatment influence on growth

07 p1034 A71-18943

Mouse Ehrlich ascites tumor cells, examining Co-60 gamma ray influence in presence of radiosensitizing 5,8-dihydroxypsoralen

07 p1035 A71-18953

Cysteamine AET, serotonin and mexamine antiradiation drugs, investigating protective effect against fractionated lethal gamma ray irradiation

07 p1037 A71-18969

O-benzoylacetic and methyl-o-benzoylacetic acids effects on mice radiosensitivity to fast neutrons and gamma rays

07 p1038 A71-18976

Failure criteria percentages for bipolar transistors, determining adequacy of Weibull distribution for low gamma ray dose survival probability

07 p1071 A71-19064

Isotropic diffuse cosmic X rays and gamma radiation background origin

07 p1184 A71-19321

Isotropic component of diffuse gamma ray background, discussing possible dense intergalactic medium coexistence with universal cosmic ray flux

07 p1185 A71-19549

Atmospheric high energy gamma rays, pion production and electron energy spectra over Hyderabad, using stack nuclear emulsions

07 p1189 A71-20497

Primary gamma radiation flux measurement, using spark chamber on satellite

08 p1350 A71-20954

Cystamine effects on lymphocytes chromosomal aberrations in human peripheral blood during local fractionated gamma irradiation

08 p1240 A71-21797

Magnetic Compton spectrometer for high intensity pulsed gamma ray environments and nuclear device spectral measurement

08 p1294 A71-21840

Gamma ray spectrometers made from high purity p-type Ge crystal, observing performance

08 p1345 A71-21843

Acceptable gamma radiation dosages for extended manned space flights based on prolonged irradiation of dogs

09 p1388 A71-22193

Large gamma radiation doses effect on neodymium activated glass laser emission properties

09 p1460 A71-22256

Radiative transfer theory extended to cosmological red shift and expansion effects on uniform isotropic X rays and gamma rays in homogeneous intergalactic medium

09 p1512 A71-22333

SNAP 15A heat source gamma ray intensity measurements and identification of gamma ray producing isotopes, describing measurement apparatus

09 p1491 A71-22456

Primary cosmic gamma-quanta fluxes measured using telescope consisting of Cerenkov counters

09 p1513 A71-22556

Corneal transparency in metabolic activity absence, using acid mucopolysaccharide depletion and prolonged gamma irradiation

09 p1393 A71-22985

Carrier concentration, radiation dose and temperature effects on radiation defect formation in Si and Ge during gamma irradiation

10 p1655 A71-24138

Gamma radiation effect on electrical properties of n-type GaAs single crystals with doping impurities, calculating defect introduction rate and forbidden zone energy levels

10 p1656 A71-24141

Formation kinetics of radiation defects produced by gamma rays in Sb doped n-type Ge single crystals at 77 K

10 p1656 A71-24142

Gamma radiation influence on photomechanical effect in GaP and GaAs single crystals, using microhardness tester

10 p1656 A71-24143

Dry heat and Co 60 gamma radiation combined effects on spacecraft sterilization, discussing kinetic analysis of spore inactivation

10 p1565 A71-24613

High energy gamma rays in steady state universe assuming primary cosmic ray spectrum in extragalactic space by simple power law

10 p1664 A71-25045

Neutral pion decay and galactic gamma radiation from demodulated cosmic ray spectrum, discussing neutral pion meson production

11 p1815 A71-25593

Compton electrons produced ring current effects on geomagnetic fields for gamma quantum source and air molecular interactions, considering exact analytical model

11 p1817 A71-25777

FORTTRAN 4 computer program for gamma ray energy spectra, determining peak locations, peak areas and elemental abundances

11 p1729 A71-26069

Calorimetric determination of reactor gamma source heating as function of specimens thickness and atomic number, discussing slab and cylindrical geometrical effects

11 p1797 A71-26078

Gamma irradiation effect on conductivity of varistors made of p-type black SiC

12 p1886 A71-26897

X ray and gamma ray astronomy, considering intensity monotonic decline in cosmic electromagnetic spectrum

12 p1949 A71-27369

Radio source 3C120 gamma quanta with energy above 100 MeV from Cosmos satellites scintillation and Cerenkov counter measurements

12 p1953 A71-27417

Cerenkov light distribution calculation from gamma ray initiated air shower model obtained from Monte Carlo computer program

13 p1225 A71-28093

Average energy electron capture coefficient dependence on air density, temperature and altitude under gamma radiation

13 p2061 A71-28543

Flux estimates of gamma quanta with energies of 5 TeV from celestial objects due to bremsstrahlung and inverse Compton scattering of relativistic electrons

14 p2299 A71-29985

Cosmic gamma ray background flux for photon energies greater than 100 MeV, considering Compton collisions

14 p2301 A71-30435

Mossbauer gamma spectrometer for operation at constant and adjustable velocities, incorporating springless vibrator and automatic zero stabilization

14 p2247 A71-30577

Cosmic ray shower evolution model based on passive baryon existence and direct energy transfer to gamma quanta hypotheses

14 p2302 A71-30593

Transparency of extragalactic space to very high energy photons, considering background gamma ray effects

15 p2472 A71-31190

Erythrocytes life span and bone marrow production in dogs subjected to gamma irradiation in doses simulating prolonged space flight conditions

15 p2356 A71-31301

Peripheral blood and bone marrow morphological composition in dogs subjected to chronic and repeated gamma irradiation

15 p2357 A71-31308

Amytetravite and ATP effect on hemopoiesis of dogs subjected to chronic and repeated gamma irradiation

15 p2357 A71-31312

Chronic and acute gamma irradiation facilities used in animal experiments simulating steady cosmic radiation and powerful solar flare radiation expected in prolonged space flight

15 p2357 A71-31313

Pulsed gamma radiation from rotating neutron star, discussing synchrotron emission mechanism based on electron pulses incident on high intensity sharply localized magnetic field

15 p2474 A71-31724

Gamma ray emission from individual interactions of hadrons in carbon at 10 TeV, using ionization spectrometer-emulsion chamber combination

15 p2407 A71-31808

High energy cosmic gamma ray point sources identification near galactic plane from balloon flights data

15 p2478 A71-31826

Isotropic cosmic gamma ray flux, discussing extragalactic point sources detection by high resolution spectrometers

15 p2478 A71-31837

High energy pulsed gamma rays detection from pulsars emission based on time averaged phase histograms

15 p2479 A71-31838

Low energy gamma ray measurements by balloon flights, detecting peak energy due to electron-positron annihilation

15 p2479 A71-32077

Cosmic ray produced radionuclides in Lost City meteorite, determining concentrations by nondestructive two-parameter gamma ray analysis

15 p2479 A71-32363

Hydrogen atoms trapped in gamma irradiated calcium phosphates, studying radiation yields, electron paramagnetic resonance line widths, dose saturation and relaxation

16 p2538 A71-32873

GaAs single crystals defects formation during low temperature gamma photons and electron irradiation, considering electrical properties

16 p2620 A71-33185

Neutron and gamma radiation effects on electrophysical properties of high resistivity Si single crystals grown in hydrogen atmosphere

16 p2621 A71-33186

Pulsating gamma ray flux from pulsar NP 0532 in energy range from 250 keV to 2.3 MeV

16 p2626 A71-33338

Gamma radiation flux distribution and spectral composition from Cosmos satellite observation, analyzing background effects

16 p2626 A71-33451

Near space annihilation gamma radiation intensity and spectral energy composition by Cosmos satellite observation, considering possible antimatter nature of comets and meteor streams

16 p2626 A71-33452

Gamma radiation induced changes in parameters of black silicon carbide nonlinear semiconductor resistors/varistors

16 p2546 A71-33464

Background phonon X ray and gamma quanta intensities dependence on solar activity from Geiger counter recordings in outer space

16 p2626 A71-33675

ESRO report to COSPAR on sounding rockets and geostationary satellites development, orbits and decay during extraterrestrial gamma radiation

16 p2667 A71-33867

Carrier diffusion length change in damaged gamma irradiated silicon solar cells by numerical analysis, using experimentally obtained voltage or current

17 p2677 A71-35050

Gamma rays in Crab Nebula pulsar, considering synchrotron radiation and inverse Compton scattering as production mechanisms

17 p2796 A71-35335

Thermoluminescent dosimeter for skin basal layer dose measurement in mixed beta and gamma radiation fields 17 p2693 A71-35450

Extragalactic objects luminosity upper limits in hard gamma ray band, using Cosmos 208 scintillation Cerenkov telescope 17 p2796 A71-35736

Compton synchrotron spectra of gamma rays produced in Crab Nebula by photons scattered by relativistic electrons, assuming magnetic field due to pulsar 18 p2963 A71-36154

Pulsed gamma radiation detection from Crab Nebula by balloon-borne telescope 19 p3124 A71-37333

Diurnal variations in equatorial and precipitating low energy solar proton-produced gamma rays in magnetosphere 19 p3125 A71-37359

Solar flare X and gamma rays, radio and far UV emission, discussing model for chromospheric cool plasma heating by flow through magnetic instability 19 p3126 A71-37620

Proposed model with with neutrons as energy source for solar corona, discussing validity based on capture gamma ray flux expectation 19 p3127 A71-38009

Radioisotopic power applications of beta and gamma emitting Co 60, noting powder ceramic fabrication of dense wafers for irradiation to convert natural Cn 59 20 p3265 A71-38938

Crab pulsar NP 0532 low energy gamma radiation emission data, observing flux ratios and pulsations 20 p3278 A71-39109

Comparative abdomen and head shield effect during gamma irradiation of dogs on protein fractions in blood serum, noting increased globulins and glutamate aspartate transferases 20 p3188 A71-39222

Combined action of vibration and gamma irradiation on sporulation dynamics, survival rate and mutability of *Chlorella* 20 p3193 A71-39237

Gamma ray production by pulsar-emitted particles interaction with surrounding nebula matter, investigating radiation intensity time variation 20 p3279 A71-39325

Gamma radiation due to cosmic rays interaction with Mars surface/atmosphere and natural radioactive rocks elements decay, calculating intensity and spectral composition 20 p3280 A71-39630

Diffuse background 0.1-1 MeV gamma ray component observed by balloon-borne counter system, finding no positive evidence for cosmic component existence 20 p3283 A71-39752

Primary cosmic rays high energy gamma ray intensity spectrometric measurements onboard Cosmos 208 satellite, allowing for charged particles effects 20 p3283 A71-39753

Crab Nebula pulsar NP 0532 pulsed gamma emission from balloon flight measurements with spark chamber equipped gamma ray telescope 20 p3283 A71-39754

Crab Nebula and pulsar gamma ray emission from synchrotron or inverse Compton mechanism 20 p3301 A71-39919

Biosatellite 2 onboard experiments studying weightlessness effects on biological processes and interaction with radiation from Sr 85 gamma ray source 21 p3341 A71-40007

Book on cosmic gamma rays covering secondary particle decay, electron-positron annihilation, proton-antiproton interactions, galactic radiation and cosmology 21 p3438 A71-40450

Cosmic X and gamma radiation, discussing galactic and extragalactic sources, generation processes and spectrometric characteristics 21 p3438 A71-40522

Kinematic theory of resonant gamma rays diffraction by single crystals, calculating differential cross sections of Bragg scattering for total degeneracy and Zeeman splitting 21 p3420 A71-41123

Solar flares gamma ray flux, describing production by downward moving high energy particles 22 p3590 A71-41468

Compton electrons produced ring current effects on geomagnetic fields for gamma quantum source and air molecular interactions, considering exact analytical model 22 p3532 A71-41545

Balloon obtained Crab pulsar gamma ray emission data searched for pulsation above 50 MeV 22 p3592 A71-42220

Ultrahigh energy electrons and gamma quanta in ground produced by primary cosmic rays, plotting mean free path vs energy 22 p3595 A71-42669

Death rates, median life span and weight in mice exposed to gamma radiation after intra-abdominal injections of cysteamine 22 p3505 A71-42712

Chemical agents protective properties on albino mice under gamma-neutron radiation, noting dose and composition effects 22 p3492 A71-42713

Gamma emission effect on cystamine toxicity elimination in rats organism 22 p3492 A71-42715

Partial body shielding effects on rats radiation sickness survival rates under gamma-neutron radiation, comparing head and belly shielding effectiveness at different intensities 22 p3492 A71-42716

Reactivity changes to pharmacochimical preparations under total proton and gamma ray irradiation of abdomen and head shielded rats 22 p3492 A71-42717

Head and abdomen shielding effects on radiation sickness evolution in dogs under lethal gamma irradiation 22 p3493 A71-42718

Abdomen shielding effects on chromosome aberrations in bone marrow cells of guinea pigs and rats under gamma irradiation 22 p3493 A71-42719

Glutamicosapartic and glutamicoalanine aminotransferases activity in blood serum of dogs under gamma irradiation with shielded abdomen or head, observing hyperfermentemia 22 p3493 A71-42720

Rat organs pathomorphological changes under gamma neutron irradiation with head and abdomen shielding, noting intestines early damage 22 p3493 A71-42722

Acceleration tolerance of gamma irradiated mice with and without radioprotectors 22 p3493 A71-42724

Mice under combined gamma radiation and vibration and acceleration dynamic factors, studying radioresistance recovery rate 22 p3494 A71-42725

Mice acceleration before and after gamma irradiation, determining protective effect of cystamine in adrenaline and amphetamine mixture 22 p3494 A71-42726

Dogs peripheral blood reaction to complex action of transverse accelerations and gamma irradiation 22 p3494 A71-42727

Vibration influence on peripheral blood reaction to gamma radiation in dogs, using clinico- hematological indices 22 p3494 A71-42728

Aminothiols class radiation protector influence on tissue damage of white rats under single and two-fold gamma irradiation at various test conditions 22 p3494 A71-42729

Radioprotective effectiveness of cystamine and S beta-aminoethylisothiuronium in mice under combined gamma irradiation and transverse acceleration loads 22 p3494 A71-42730

Relative biological effectiveness of fast neutrons, allowing for gamma component contribution 22 p3494 A71-42735

Inelastic scattering alpha-gamma angular correlations from C 12, Mg 24, Ni 58 and Sn 120 decay measurements 23 p3706 A71-43198

Balloon flight detected gamma ray source Lib gamma-1, discussing possible identification with PKS 1514-24 radio galaxy 24 p3865 A71-44444

Low energy primary cosmic gamma ray measurements for spectrum latitude dependence and time variations near earth by Cosmos satellite scintillation spectrometer 24 p3865 A71-44564

Quasar and pulsar gamma ray absorption by critical energy collisions with low energy photons 24 p3866 A71-44917

High energy gamma quanta flux measurements in primary cosmic rays, using Cosmos 208 satellite data 24 p3866 A71-45026

GANGLIA

NT NERVES 01 p0009 A71-10234

NT NEURONS

Cat retina ganglion cell /YCC-1/ threshold intensity, obeying reversed Weber law 01 p0009 A71-10234

Transganglionic degeneration in vestibular nerve resulting from transection of peripheral sensory nerve branch of bipolar neurone 04 p0537 A71-14766

Sensitivity, size and receptive fields position in cat retina ganglion cells 05 p0706 A71-16341

Vagal sensitive neurons unitary activity, applying microelectrode technique to nodose ganglion ventral part 05 p0707 A71-16342

Adrenergic neurons in intramural cardiac ganglia in rabbits, using histochemical luminescent microscopy 09 p1391 A71-22533

Cerebral speech mechanisms division into cortical centers and basal ganglia centers 10 p1563 A71-24229

Cochlear/vestibular apparatus, ganglion cells, spinal roots and nerve trunk damage from ionizing radiation based on neural elements transirradiation in neoplasms 10 p1566 A71-25039

Cardiovascular responses to hypothalamic, spinal cord and stellate ganglion stimulation as function of intensity, pulse duration and frequency in cats 16 p2531 A71-33367

Gangliosides inhibitory effects on active Ca ion transport in rat brain mitochondria, using succinate as respiratory substrate 21 p3338 A71-41075

GAPS

NT SPARK GAPS

Bioelectric potential in gap between abutting cardiac muscle cells, using differential equation for active to inactive cell transmission 01 p0025 A71-11177

GARNETS

NT YTTRIUM-ALUMINUM GARNET

NT YTTRIUM-IRON GARNET

Ferrimagnetic vanadate garnet IR Faraday rotation as function of wavelengths and temperature, considering ions multivalence and multilattice site modifications 06 p0941 A71-18040

Epitaxial garnet films magnetic anisotropic models, describing mobile cylindrical domains 12 p1943 A71-26854

Longitudinal and transverse magneticstriction of polycrystalline iron garnets containing Gd, Tb, Dy and Ho in high magnetic fields 21 p3428 A71-41116

Compact optical Faraday rotation isolator using terbium-aluminum garnet and high field permanent magnets of rare earth alloys 22 p3559 A71-42566

Second harmonic mode locked frequency doubled pulsed neodymium-yttrium-aluminum oxide garnet laser using single intracavity barium sodium niobate 23 p3683 A71-42957

GAS ANALYSIS

NT OZONOMETRY

Human blood gases continuous measurement in vivo by mass spectrography, considering arterial nitrogen washout and cerebral blood flow determination 01 p0021 A71-10237

Venera-borne gas analyzers for parachute descent probing of Venus atmosphere, describing design and operation 02 p0248 A71-11916

Shadow and interference methods sensitivity for low density gas flows improved via monochromatic light source 02 p0248 A71-11937

Capillary plasma heating source processes, using textolite and fiberglass-reinforced textolite dielectric discharge chambers 02 p0292 A71-12556

Computerized outgassing analyzer for nuclear rocket graphite fuel elements at various temperatures in vacuum 05 p0780 A71-16243

Gas concentration determination for mixture by UV energy absorption measured in terms of photomultiplier tube output current, describing oxygen sensor 08 p1287 A71-20987

Electrochemical detection of hydrogen, carbon monoxide and hydrocarbons in inert or oxygen atmospheres, using electrical biasing technique 08 p1250 A71-21473

Computer program for selected gases outgassing rates calculation, tabulating and plotting for NERVA fuel elements gas evaluation 09 p1492 A71-23348

Ultrahigh vacuum gas analysis by mass spectrometry, discussing quadrupole and omegatron mass spectrometers performance with special reference to reversible adsorption characteristics 11 p1763 A71-26187

Reacting gases analysis by mass spectroscopy, discussing stable products microprobe and molecular beams effective samplings for free radicals and active atoms 11 p1765 A71-26278

Propulsion system atom and radical concentrations measurements, using low pressure gas discharge flow system for combustion environment control 11 p1729 A71-26285

Computer program for interpretation of residual gas analyzer mass spectra, considering vacuum environmental testing of spacecraft 11 p1730 A71-26505

Venera-borne gas analyzers for parachute descent probing of Venus atmospheric composition, describing design and operation 13 p2067 A71-28203

GAS BAGS

Turbulent flame boundaries and maximum brightness surface position in gasoline-air mixtures, using photography and gas analysis measurements of carbon dioxide concentrations 13 p2162 A71-28955

Chronic hypoxia effects on blood oxygen and carbon dioxide tensions and pH changes in unanesthetized chickens at high altitude compared to sea level control 14 p2186 A71-30565

High temperature fuel cell in hot gas mixtures analysis, presenting porous silver and palladium electrodes cathodic polarizations 15 p2367 A71-31648

Cosmic radiation and gas retention ages of Chassigny achondrite by measuring Al, K and noble gases contents and production rates in meteorites 17 p2800 A71-34514

UV Raman remote gas sensors incorporating laser scattered radiation with high resolution monochromator 17 p2753 A71-35292

High temperature creep of niobium alloy, obtaining creep limit, microhardness and gas analysis data 18 p2936 A71-36715

Simultaneous calibration of gas analyzers and meters for continuous process gas stream composition monitoring 19 p3010 A71-38566

Venus atmosphere chemical composition from gas analyzers onboard Venera automatic stations, determining element abundance, water vapor density and cloud layer structure 20 p3296 A71-39625

Graphite properties in high and ultrahigh vacuum, suggesting use as electrode material in vacuum gages and residual gas analyzers 21 p3405 A71-40221

Mass spectrometer application to gas analysis of samples from turbulent wake of hypervelocity projectiles 21 p3362 A71-40384

Photoionization mass spectrometry, considering application to appearance potentials determination, ion-neutral reactions and gas analysis 22 p3537 A71-41649

Sequential dual wavelength IR gas analyzers for anesthetics research and chemical plant process streams analysis 22 p3545 A71-42156

Oxygen, hydrogen and nitrogen determination in high melting point metals 22 p3563 A71-42364

Apollo 12 lunar soil samples trapped rare gas analysis, observing solar wind He local variation from breccia 23 p3754 A71-43723

GAS BAGS

Cargo airship standard atmosphere operation modes, discussing long range gas capacity and short range applications for large compact loads 11 p1708 A71-26309

Two dimensional steady potential incompressible flow past elastic expandable gas filled envelope fastened to edge of plate normal to flow 17 p2730 A71-35640

GAS BEARINGS

Externally pressurized gas thrust bearings, examining performance and pressure distribution in film 02 p0256 A71-12412

Glow discharge cleaning for surface contaminants removal from hydrodynamic gas bearing components, discussing equipment application to thin film lubricant vapor deposition 02 p0256 A71-12461

Gyros and accelerometers with hydrostatic gas bearings, discussing design and adjustments, drift measurement methods and environmental tests [AGARDOGRAPH-128] 05 p0751 A71-16314

Air lubricated bearing elements lifting force, restoring moment and translational rigidity, considering dependence on minimum clearance, sliding rate, pressing force and geometric parameters 05 p0758 A71-16351

Gaseous squeeze-film bearings analysis for large squeeze numbers 05 p0759 A71-16975

Load carrying capacity of finite length self acting gas lubricated journal bearings [ASME PAPER 70-LUB-23] 07 p1117 A71-19502

Spherical hydrostatic gas bearings for two axis gyros, using Al die castings [ASME PAPER 70-LUB-6] 07 p1117 A71-19504

Air bearings design for laser scanner high speed rotating mirror in vacuum, describing static and dynamic tests for rotor inversion point [ASME PAPER 70-LUB-15] 07 p1117 A71-19506

Tilting pad hydrodynamic and porous hydrostatic gas lubricated journal bearings for miniature cryogenic turbomachinery [ASLE PREPRINT 70LC-10] 08 p1298 A71-21158

Three degree of freedom gas bearing for wind tunnel dynamic measurements, allowing models simultaneous spin, pitch and yaw motions [AIAA PAPER 71-279] 08 p1275 A71-22004

Surface geometry effect of polycentric gas bearing on rotor stability in dynamic equilibrium without radial load 09 p1454 A71-22799

Time dependent clearance changes effects on aerodynamic characteristics of sectorially grooved gas bearings, describing lift and drag coefficients calculation 14 p2252 A71-30227

Hot performance tests of three identical Brayton rotating units on gas bearings 15 p2355 A71-32226

Gas dynamic elastically mounted bearing, describing stability analysis of unloaded rotor central equilibrium position 15 p2417 A71-32457

Herringbone grooved gas lubricated journal bearing load capacity, attitude angle and power loss measurements 17 p2749 A71-35487

Mach number effects on flow field in gas bearings at high subsonic and supersonic tangential speeds based on perturbation theory [ASME PAPER 71-APM-U] 18 p2926 A71-36263

Miniature high speed expansion turbines for helium liquefiers and refrigerators, discussing turbine flow passages and gas lubricated bearings 20 p3184 A71-39246

Quasi-static pressure characteristics of gas lubricated thrust bearing with shrouded Rayleigh step pads, solving nonlinear equation of motion [ASME PAPER 71-VIBR-75] 21 p3385 A71-40313

Gas bearing - Conference, University of Southampton, England, March 1971, Volumes 1 and 2 22 p3550 A71-41658

Air pressurized bearing mounted rotor with vertical shaft, discussing elastically suspended foundation mass and damping effect on self excited vibration 22 p3550 A71-41659

Automatic control theory application to pneumatic self vibration /hammer/ occurrence criteria derivation for externally-pressurized gas-lubricated thrust collar bearings 22 p3551 A71-41660

Gas bearing ground clearance effects on pivoted pad resonance, pitching vibration mode, static journal displacement and friction 22 p3551 A71-41661

Externally pressurized gas journal bearing whirl instability stabilization system, predicting whirl onset threshold speed 22 p3551 A71-41662

Centrally-fed circular inherently-compensated aerostatic gas thrust bearing flow behavior in inlet region, obtaining graphs for design optimization 22 p3551 A71-41663

Low cost high performance rate gas bearing gyroscope development, emphasizing large scale production and overall instrument design optimization 22 p3551 A71-41664

Ion machining techniques for cutting accurate and repeatable pumping grooves in gas bearing component materials typified by boron carbide 22 p3551 A71-41665

Two-axis pneumatic rate gyroscope with externally pressurized gas bearing for airborne vehicle fluidic autostabilizer sensor 22 p3551 A71-41666

Hemispherical and spherical pressurized gas bearing design with narrow circumferential feed slot as laminar flow restrictors, predicting static load performance 22 p3551 A71-41667

Spiral grooved thrust and spherical gas bearings, predicting stability and frequency response by Newton-Raphson and orthonormalization methods 22 p3551 A71-41668

Modular slot fed fluid bearing using jacking gas effects for pumping power conservation under high speed steady state, discussing design and application 22 p3552 A71-41669

Rigid rotor whirl dynamics in externally pressurized gas journal bearings, calculating frequencies in terms of stiffness and other parameters 22 p3552 A71-41670

Externally pressurized gas-lubricated foil bearing rotation speed effects on gap topography and clearance variation 22 p3552 A71-41671

Computerized step-jump and time-transient dynamic analysis application to gimbal mounted Rayleigh-step gas-lubricated thrust bearing design 22 p3552 A71-41672

Stiffness and load capacity control by self compensating flow restrictor for externally pressurized gas lubricated thrust bearing design 22 p3552 A71-41673

Gyro wheels cleaning by ion bombardment applied to ceramic gas bearings, comparing with chemical cleaning 22 p3552 A71-41674

Externally pressurized air lubricated bearing boring spindle performance tests, considering circular accuracy, maintenance, tool life and cost effectiveness 22 p3552 A71-41675

Computerized design procedures for externally pressurized flexibly mounted gas lubricated journal bearings, predicting steady state performance, vibration capacity and translational stability 22 p3553 A71-41676

Opposed hemispherical self acting gas bearings fabrication for gyro wheels, using machine lapping and sputter etching 22 p3553 A71-41677

High speed gas lubricated foil supported nonmetallic rotor for nuclear magnetic resonance research 22 p3553 A71-41678

Plain externally pressurized thrust air bearings with porous inserts and high supply pressures, comparing with discrete orifice feed 22 p3553 A71-41679

Externally pressurized double thrust bearings with variable gas film laminar restrictor increasing stiffness at low eccentricity ratios 22 p3553 A71-41680

Inclined radial jet drive systems for noiseless gas bearings, comparing with turbine driven device 22 p3553 A71-41681

Pneumatic hammer /self oscillation/ occurrence in gas lubricated externally pressurized annular thrust bearing, comparing experimental and theoretical stability data 24 p3830 A71-44948

GAS CHROMATOGRAPHY

Human gas metabolism under rarefied atmosphere via gas chromatography, discussing pulmonary ventilation determination and exhaled samples collection equipment 01 p0025 A71-11142

Life detection for space missions based on detecting optical asymmetry in biogenic molecules by gas chromatography involving diastereomeric esters synthesis 01 p0025 A71-11162

Carbon fiber surface reactivity relationship to various organic compounds using gas-solid chromatography, evaluating molecular absorption enthalpies 02 p0209 A71-12537

Ion source for double focusing magnetic mass spectrometer for use with gas chromatograph on Mars mission, requiring electron beam stabilization in space 07 p1113 A71-19851

Phenylalkylcarbinol steric purity determination from asymmetric secondary alcohol derivatives separation by gas chromatographic resolution 09 p1403 A71-22478

Carbonaceous chondrite and Precambrian chert amino acids detection, using simultaneous optical configuration determination and gas chromatography 09 p393 A71-22984

Pyrolysis-gas chromatography locating degradation front in phenolic ablative plastics, giving percent phenolic resin vs distance normal to surface 11 p1728 A71-26044

Gas-liquid chromatographic milligram preparative separation of steranes and triterpanes from hydrocarbon fraction of Green River oil shale 11 p1729 A71-26067

Gas chromatography techniques, discussing carrier tank, flow control, injector, reactor, column, detector, recorder, flowmeter, etc 11 p1729 A71-26291

Quantitative determination of phenylalanine in serum by gas-liquid chromatographic analysis method 13 p0206 A71-29477

Sterols isolation and identification from Pleistocene sediment by gas-liquid chromatography and combined gas chromatography-mass spectrometry 15 p2366 A71-31367

Polynuclear aromatic hydrocarbons in Murchison meteorite, determining distribution by gas chromatography and mass spectrometry 17 p2799 A71-34503

Bound sugar content in marine sediments by capillary gas chromatographic-mass spectrometric analysis of trimethylsilyl derivatives 19 p3055 A71-38146

Evaporative injector system for capillary column gas chromatography for solutes in dilute solution 20 p3194 A71-39257

Iron meteorites total N abundances determination by inert carrier gas fusion extraction gas chromatography 23 p3734 A71-43243

Gas-liquid chromatography and mass spectrometry of lunar fines and glass constitution by preparing trimethylsilyl derivatives of discrete silicate ions 23 p3746 A71-43668

Apollo 12 lunar surface samples analysis for organic compounds by mass spectroscopy and pyrolysis-gas chromatography 23 p3756 A71-43741

GAS COMPOSITION

NT CARBON DIOXIDE CONCENTRATION Gas phase composition effect on CdS deposits crystalline perfection by Knudsen effusion apparatus and mass spectrometry 06 p0942 A71-18084

Flow-through carbon dioxide lasers population inversion relation to individual gas components and electron velocity distribution functions 07 p1126 A71-20187

Pressure and gas composition effects on sodium acetate-C 14 incorporation into liver lipids, indicating metabolic relationships to decomposition sickness
08 p1238 A71-20814

Molybdenite oxidation kinetics by thin layer technique with close temperature and gas composition control, measuring temperature, gas composition and particle size effects
09 p1472 A71-23128

Multiphase gas flow, measuring gas concentration by laser Raman spectroscopy
[AIAA PAPER 71-286] 09 p1464 A71-23308

Alveolar air samples of human subjects at various altitudes, determining gas composition and partial pressure
12 p1876 A71-27658

Exhaled air microimpurities composition of humans exposed to stress effects including bed rest, starvation, lyophilized diet feeding, high temperature and humidity
13 p2007 A71-28412

Ion source of mass spectrometer for high temperature composition studies of gas phase
14 p2247 A71-30588

Gaseous oxygen/hydrogen injector element modeling based on composition profile measurements for cold flows
[AIAA PAPER 71-674] 14 p2291 A71-30738

Analytical model for performance and pollutant emissions of gas turbine combustors, predicting gas composition and temperature
[AIAA PAPER 71-711] 14 p2294 A71-30765

Human blood pH and gas composition regulation mechanism under response to carbon dioxide partial pressure changes in inhaled air
15 p2357 A71-31316

Thermochemistry data changes influence in form of heat of formation, partition functions, specie free energy or specific heat on high temperature gas mixtures composition
15 p2514 A71-32097

Compact pulsed carbon dioxide laser with uniform volume excitation, obtaining output energy as function of discharge voltage, gas composition and pressure
15 p2424 A71-32698

Radiation heat transfer volume interchange factors approximation for gases with nonuniform temperature, composition or pressure, comparing with exact numerical computations
[ASME PAPER 71-HT-19] 19 p3164 A71-37990

Pulsed atmospheric pressure carbon dioxide laser, studying pulse power and shape as functions of energy storage capacitor value, charging voltage and gas composition
22 p3557 A71-42159

Gaseous medium composition and multiple freezing temperature effects on catalase activity
22 p3497 A71-42831

Composition effects on binary gas mixtures thermal conductivity coefficient, considering Hirschfelder-Eucken formula
24 p3886 A71-44369

Equilibrium equations solutions for ideal gas composition, pressure, volume and temperature based on Newton-Raphson method, outlining programming method
24 p3887 A71-44635

Nitriding process on Nb alloy, presenting gas phase temperature, time and composition effects
24 p3838 A71-44894

Gas accumulation mechanisms in porous lunar surface layer, discussing ground samples from Sea of Tranquility
24 p3875 A71-45189

GAS COOLED REACTORS

NT HIGH TEMPERATURE NUCLEAR REACTORS

Nuclear light bulb reactor and coaxial flow reactor for gas core nuclear rocket engines
[AIAA PAPER 70-708] 03 p0456 A71-14427

GAS COOLING

Relaxation method for direct measurement of molecular oxygen quenching rate constants in discharge flow system
02 p0287 A71-12493

Various free stream turbulence levels at nonconverging and converging walls, investigating foreign gas film cooling
04 p0683 A71-15501

Gaseous film cooling effectiveness under varying conditions of free stream turbulence intensity, hot gas acceleration, Mach number and film coolant flow rate
07 p2129 A71-18760

Turbulent air flow in cooled tubes, studying local heat transfer and hydraulic resistance
08 p1377 A71-21924

Sulfide formation process from solar composition cooling gas, examining constrained equilibrium theory
10 p1676 A71-24505

Metal temperatures in rotating cooled gas turbine blades, discussing coolant flow aerodynamics
13 p2117 A71-28748

Gas cooled porous plate unsteady temperature field during high temperature action, considering ther-

moradiative, convective and mixed radiative-convective heat transfer
16 p2662 A71-32833

Turbulent air flow in cooled tubes, studying local heat transfer and hydraulic resistance
17 p2838 A71-35268

Gas controlled variable conductance heat pipe for OAO-C onboard processor temperature stabilization, describing thermal performance tests under simulated flight conditions
[AIAA PAPER 71-411] 18 p2975 A71-36775

Large cobalt 60 gas cooled radioisotope heat source, including test loop, operations, control and safety
20 p3265 A71-38937

Film ablative cooled gas pressure feed liquid rocket engine unstationary process analysis with digital computer, detailing engine dynamics, heat transfer and temperature profile
22 p3589 A71-42054

GAS DENSITY

Modified Ashby-Jephcott laser interferometer schlieren system for HF gas density measurements
03 p0427 A71-13922

Plane shock wave propagation in polytropic gas of variable density, using successive approximation technique
03 p0345 A71-14558

Hemispherical imploding shock wave reflection, noting cold wall presence and gas density effects
04 p0568 A71-14682

Parallel incompressible gas jets mixing of variable densities based on dimensional analysis
04 p0577 A71-15623

Density and compressibility of oxygen in critical region, using capacitance measurements
05 p0781 A71-16703

Polar region atmospheric ozone density profile measurements, using rocket sounding
05 p0743 A71-17007

Polytropic gas spheres gravitational instability under external pressure, obtaining critical masses and densities
05 p0813 A71-17091

Onsager relations for Sorot-Dufour and diffusion coefficients in moderately dense gas mixtures based on kinetic theory, considering symmetry relations for transport properties
06 p0929 A71-18036

Thin gas optical limit isothermal curves, discussing Planck mean emission coefficients
07 p1222 A71-18993

Self similar shock wave propagation in exponentially varying density at constant pressure, solving by method of successive approximation
07 p1089 A71-19731

Annihilation quanta detector and positron source for gas density measurement, noting sensitivity, counting interval and Be covering thickness
07 p1164 A71-20178

Rotating nonvibrating diatomic low density gas molecules rotational relaxation time and viscosity, based on quantum mechanics
08 p1336 A71-20659

Molecular and atomic oxygen properties in nonequilibrium flows, determining vibrational temperature and number density by electron beam fluorescence technique
[AIAA PAPER 71-271] 08 p1338 A71-21997

Rarefied gas flow density and velocity by total head and flow rate adapters, noting isentropic flow core region
09 p1382 A71-22728

Multiphase gas flow, measuring gas concentration by laser Raman spectroscopy
[AIAA PAPER 71-286] 09 p1464 A71-23308

Plane shock wave formation in dense Ar, using molecular dynamics numerical technique
10 p1694 A71-23953

Gas phase ignition of solid propellants involving gas phase variable density for constant density based equations by Howarth transformation
10 p1695 A71-24332

Thermospheric gas density determined from solar UV absorption measurement at grazing ray and near vertical incidence
10 p1676 A71-24551

Monograph on dense gases state parameters measurement at high temperatures, applying to nitrogen
10 p1697 A71-24676

Viscous flow in supersonic de Laval nozzle, measuring gas density and rotational temperatures by electron beam techniques
[AIAA PAPER 70-810] 12 p1865 A71-27555

Carbon dioxide free jet plumes issuing from supersonic nozzle into high vacuum, measuring densities and temperature
13 p2026 A71-29355

Interstellar gas absorption correlation with dust extinction, obtaining gas to dust density ratio
16 p2632 A71-33323

Relativistic and/or degenerate electron gas equation of state formulæ for density, temperature, entropy and internal energy
18 p2960 A71-35937

Continuous hypersonic wind tunnels with low gas density simulating flow states during reentry phase of space vehicles
18 p2898 A71-36412

Rarefied hypersonic flow density, velocity and temperature determination by electron beam technology, including ion production, calibration curves, collisions and spectroscopic analysis
18 p2949 A71-36419

Cs and Hg vapors compressibility factor in supercritical range as function of density, considering charged particles and atoms polarization interactions in ionized metal vapors
19 p3111 A71-37590

Expanding metal vapor density-radius measurements in wire explosions, using twin tube flash X ray unit
20 p3311 A71-38827

Gas density measurement and flow visualization in hypersonic wind tunnel by electron beam probe, noting isobaric boundary layer application
21 p3364 A71-40395

Interstellar carbonyl sulfide transition at 109.5 GHz, noting column density
21 p3447 A71-40447

Hydrodynamic equations for dense system fluctuations with stochastic terms in pressure tensor and heat flux vector evaluated for dilute gas
22 p3530 A71-41893

Coma cluster X ray observations implying limits on gas density in intergalactic space and Friedmann models
22 p3599 A71-41926

Solar cycle variation effects on interstellar hydrogen within solar system, discussing thermal motion, density, far UV ionization and charge transfer reactions
22 p3601 A71-42169

Nitrogen, argon and helium viscosity measurements, obtaining density expansion by statistical analysis
22 p3621 A71-42369

Interplanetary magnetic shock front location and geometry determination, using interstellar hydrogen density measurements
23 p3720 A71-43133

Isentropic ideal compressible vortical gas flow in axisymmetric channel, determining stream function and gas density
23 p3625 A71-43549

Cosmic ray exposure ages and rare gas concentration profiles in Apollo 12 lunar rocks, discussing spallation products and neutron capture effects
23 p3753 A71-43719

Pure fluidic gas detectors for monitoring gas density changes
23 p3680 A71-44097

Gas concentration measurement at wall with argon and helium injection at pipe entrance, investigating protecting film cooling efficiency
24 p3819 A71-44929

Gas density distributions in argon and carbon dioxide supersonic jets with low angular divergence in vacuum, using Laval supersonic nozzle
24 p3858 A71-45241

GAS DETECTORS

Gas-Cerenkov balloon-borne detector for low energy gamma rays, calculating efficiency and angular response by Monte Carlo program
01 p0083 A71-11222

Thermoconductometric portable hydrogen analyzer for air around industrial centers, using bridge tungsten sensor network
04 p0601 A71-15675

Gas proportional counting system gas stabilization, using feedback loop radioactive X ray emitter and correction signal
06 p0901 A71-18225

High vacuum mass spectrometric hazardous gas detection system used during cryogenic loading of Saturn vehicles, discussing application to environmental pollution detection
22 p3542 A71-41988

Pure fluidic gas detectors for monitoring gas density changes
23 p3680 A71-44097

GAS DISCHARGE COUNTERS

U COUNTERS

U GAS DISCHARGE TUBES

GAS DISCHARGE TUBES

Microwave scattering from plasma fluctuations produced by forcing gas in turbulent flow through discharge tube, investigating frequency spectrum broadening
01 p0136 A71-11480

Heat transfer to walls of quartz discharge tube in Ne, Ar and Xe, measuring integral energy flux
02 p0290 A71-12191

Relaxation method for direct measurement of molecular oxygen quenching rate constants in discharge flow system
02 p0287 A71-12493

- He-Ne laser with hemispherical nontunable internal cavity resonator formed by mirrors bonded to discharge tubes 03 p0439 A71-13999
- Argon ion laser plasma tube anodic coherent oscillations and noise suppression, using secondary discharge between anode and auxiliary cathode 06 p0906 A71-17306
- Carbon dioxide laser with Ge Brewster windows equipped sealed gas discharge tube, comparing with NaCl and KBr windows 06 p0908 A71-18080
- Stable ellipsoidal plasma configurations in alternating electrode annular system, considering longitudinal magnetic field strength, electrode voltage and gas discharge chamber pressure 07 p1171 A71-20185
- High energy narrow pulsewidth HF chemical laser emission from transverse multiple electrode nitrogen fluoride and nitric tetrafluoride discharge 07 p1128 A71-20397
- Oscillation frequency shift and gas discharge tube design relation in He-Ne DC lasers 09 p1462 A71-22402
- Xe flash tube discharge saturable absorption effects, using YAG-Nd laser radiation for plasma attenuation measurements 09 p1465 A71-23484
- Plasma display panel with rectangular gas discharge cells array separated by thin dielectric sheets, discussing operation principles 14 p2249 A71-31030
- He-Ne lasers stimulated emission, studying optical resonant cavities and discharge tubes construction 15 p2422 A71-32572
- Electron density gradient and radial compression waves in pulsed IR laser gas discharge tube 16 p2585 A71-32795
- Power gain distribution in He-Ne laser cuvettes at 0.63 and 3.39 microns wavelength, noting current density dependent laser power gain shifts 17 p2752 A71-34405
- Helium-cadmium laser discharge, discussing possible He trapping mechanisms and improved tube design to eliminate He cleanup 18 p2933 A71-37013
- Carbon dioxide laser, measuring focal length of gas defocusing lens in active medium as function of gas pressure and discharge tube diameter 19 p3073 A71-37771
- He-Ne laser discharge tube using water cooled mercury cathode with supplementary molybdenum anode 19 p3073 A71-37789
- He-Ne laser emission modulation through active element excitation source, using tube for discharge gap characteristics changes 22 p3558 A71-42266
- ### GAS DISCHARGES
- #### NT RING DISCHARGE
- #### NT TOROIDAL DISCHARGE
- Similar gas discharges for carbon dioxide lasers, including thermal effects and particle distributions over energy levels 01 p0093 A71-10682
- Spark discharge ignition in air by Q switched ruby laser 01 p0093 A71-10684
- Saha equilibrium deviations in wall stabilized rare gas arc plasmas under normal pressure, describing numerical method for temperature and density distributions evaluation 01 p0133 A71-10746
- Gain measurement on pulsed radiation from high voltage discharges in mixtures of carbon dioxide, nitrogen and helium 01 p0096 A71-11423
- Nonequilibrium plasma from pulsed discharge in crossed electric and magnetic fields 02 p0288 A71-11882
- Multiatomic molecules emission spectra excitation by superhigh frequency short duration pulsed gas discharges 02 p0286 A71-11889
- Cylindrical Xe filled thermionic diodes breakdown and low voltage arcs at various pressures and interelectrode distances 02 p0190 A71-11942
- Low pressure Cs vapor discharge in positive column, determining electron energy distribution function 02 p0289 A71-11956
- Nitrogen inductive low pressure discharge, determining vibrational and rotational temperatures, ionization degree, electron temperature and energy balance by spectroscopic technique 02 p0286 A71-12178
- Small gas discharge coefficient of venturi tubes 02 p0253 A71-12557
- Multimode ionization wave growth and saturation in finite length positive plasma column of gas discharge, investigating feedback and external driving signal effects 06 p0933 A71-17469

- Large volume high pressure gas uniform electrical discharges, applying to laser amplifier [AIAA PAPER 71-65] 06 p0909 A71-18524
- He-Cd laser output description by rate equations, investigating saturation effects, discharge processes and optimization 06 p0910 A71-18666
- Similar gas discharges for carbon dioxide lasers, including thermal effects and particle distributions over energy levels 07 p1125 A71-20143
- Spark discharge ignition in air by Q switched ruby laser 07 p1125 A71-20146
- Sparks induced in gases by transversely excited atmospheric pressure carbon dioxide IR pulsed lasers, observing plasma filament forward propagation 07 p1129 A71-20619
- High microwave power for studying interactions in high concentration linear Ar discharge plasma waveguide in magnetic field 08 p1339 A71-21479
- Transistorized gas laser discharge current stabilizer using double feedback circuit, discussing schematic diagram and operation principles 08 p1303 A71-21807
- High pressure electrodeless HF gas discharge plasmas, investigating effects of external magnetic field, gas and pressure on discharge rotation frequency 08 p1342 A71-21915
- Cd atoms excited state populations in nonequilibrium gas discharge plasma 09 p1500 A71-22267
- Carbon dioxide lasers gas discharges positive column, studying electron energy distribution by probe method 09 p1461 A71-22381
- Uniform continuous electric discharge in large volume high pressure near-sonic carbon dioxide-nitrogen-helium flowstream, describing closed cycle continuous laser amplifier channel design 09 p1505 A71-23485
- Atmospheric pressure carbon dioxide laser electrode design for uniform pulse excitation discharge 10 p1621 A71-24508
- Ionization wave varieties in nitrogen glow discharge at various pressures and current densities from phase and group velocity measurements 10 p1654 A71-24973
- Propulsion system atom and radical concentrations measurements, using low pressure gas discharge flow system for combustion environment control 11 p1729 A71-26285
- Electron energy distribution for spectroscopic determination in hollow cathode discharge helium-mercury plasma based on Druyvesteyn function 12 p1937 A71-27050
- Semiconductor or gas-discharge two-component plasmas, calculating permittivity variation due to carrier heating and diffusion during strong plane monochromatic, electromagnetic wave propagation 12 p1937 A71-27184
- Similarity laws for gas discharges in carbon dioxide lasers verified by longitudinal electric field measurements 12 p1914 A71-27209
- Microwave propagation in cylindrical waveguide containing inhomogeneous gas discharge plasma 13 p2029 A71-28363
- Nonlinear skin effects in gas discharge plasma during electromagnetic wave propagation with dissipation, obtaining wave amplitude and carrier temperature dependence on reflection parameters 13 p2108 A71-29042
- Electron avalanche processes in gas discharges, deriving electron energy distribution function and similarity laws 13 p2103 A71-29079
- Average energy of electron avalanches in gases for linear inelastic collision cross sections, including ionization coefficient and Stoletov constant for atomic hydrogen 13 p2103 A71-29080
- Stoletov constant for gas mixture, discussing average avalanche energy at reduced electric field with maximum ionization coefficient and Penning effect for Ne-Ar 13 p2103 A71-29081
- Voltage breakdown in scientific spacecraft systems during test and flight, discussing factors affecting gas discharges 14 p2181 A71-29863
- Magnetic field generation from coaxial plasma gun, discussing mechanism in terms of azimuthal plasma mass motion imparted during initial gas discharge 14 p2281 A71-30543
- Nitrogen inductive low pressure discharge, determining vibrational and rotational temperatures, ionization degree, electron temperature and energy balance by spectroscopic technique 15 p2451 A71-31487

- Carbon dioxide laser flow-through discharge, measuring electron density and collision rates with heavy particles as function of tube parameters 15 p2419 A71-31764
- Soviet papers on gas discharge plasmas and strong magnetic fields covering plasmatrons, MHD generators, electric arc combustion, etc 15 p2457 A71-32266
- German monograph on electron production effect on channel breakdown in nitrogen, showing positive space charge accumulation near anode in gas discharges 17 p2788 A71-34775
- German monograph on spark discharge behavior in nitrogen, carbon dioxide and argon at excess pressures covering Toepler, Weizel-Rompe and Braginskii laws applicability 17 p2779 A71-34781
- High pressure electrodeless HF gas discharges plasmas, investigating effects of external magnetic field, gas and pressure on discharge rotation frequency 17 p2789 A71-35260
- High intensity continuous gas discharge line sources for extreme UV with low electromagnetic interference 18 p2914 A71-35845
- Externally excited moving striations measurements in low pressure Ar discharge, comparing with ion acoustic wave propagation derivation from model 18 p2948 A71-35859
- Supersonic spherical viscous heat conducting gas discharge into vacuum, solving Navier-Stokes equations by buildup method 19 p3042 A71-37087
- Temperature and pressure of optically dense plasma from vaporizing wall gas discharge 19 p3110 A71-37577
- Radial temperature profiles of long induction discharge in argon at atmospheric pressure 19 p3111 A71-37579
- Gas discharge-current modulation noise of He-Ne laser, using sinusoidal signal at various frequencies 19 p3072 A71-37698
- Gas concentration, field frequency and applied power level for control over electron temperature and emission spectra in microwave gas discharge plasma 19 p3113 A71-37764
- Similarity laws for gas discharges in carbon dioxide lasers verified by longitudinal electric field measurements 19 p3075 A71-38621
- Transient RF pulse dispersion along plasma loaded coaxial gas discharge, noting group delay 20 p3272 A71-38783
- Striated discharge column behavior in nitrogen with moving and stationary striations 20 p3273 A71-39046
- Stability conditions for square wave sustaining voltage, including complex rectangular waveforms with pulsed discharges in plasma display 20 p3233 A71-39060
- High resolution gas discharge plasma display panel, discussing design, capabilities and performance 20 p3233 A71-39061
- AC plasma panel /gas discharge matrix/ display, discussing operation principles, static and switching characteristics and driving circuitry 21 p3352 A71-40120
- Oscillations in He, Ne and Ar glow discharges, obtaining I-V characteristics 21 p3426 A71-41290
- Semiconductor or gas-discharge two-component plasmas, calculating permittivity variation due to carrier heating and diffusion during strong plane monochromatic electromagnetic wave propagation 22 p3584 A71-42461
- Spectroscopic analysis of pulsed gas discharge in crossed electric and magnetic fields of gas magnetron diode in 3100-4660 Å wavelength range 23 p3712 A71-43933
- Self magnetic impulses in gas discharge configuration as function of current and anode-cathode radius ratio 24 p3851 A71-44431
- Visible and near UV spectra of vacuum Ar, Kr and Xe microwave discharge lamps with magnesium fluoride windows 24 p3849 A71-45211
- Stepwise ionization effects on ionic wave propagation and oscillation stability in inert gas DC discharges 24 p3857 A71-45230
- He-Ne laser discharge gap oscillation modes observation, noting applied magnetic field, gas parameters and cathode type effects on stimulated emission 24 p3835 A71-45235
- Microwave radiation intensity and spectral frequencies of Knudsen discharge in cesium plasma 24 p3858 A71-45244
- Subharmonic frequency division for neon discharge plasma oscillations under resonance due to nonuniform electric field 24 p3858 A71-45263

GAS DISSOCIATION

Thermodynamic equations of state for dissociating and ionizing high temperature air applied to vertical and oblique compression shocks

02 p0331 A71-12067

Steady three dimensional ideal dissociative gas flow along stream lines, examining velocity components, pressure gradients, density and mass fraction variable

02 p0239 A71-12124

Carbon dioxide molecules dissociative excitation processes by low energy electrons, examining light emission mechanism in VUV

02 p0261 A71-12318

IR radiation effect on gas molecular dissociation, showing dissociation temperature decrease due to IR photon absorption

02 p0288 A71-12850

Ozone atmospheric concentration, dissociation in SST air conditioning systems and biochemical poisoning

03 p0358 A71-13096

Reactive molecule and atom attack of refractory materials in dissociated gases at filament temperatures up to sublimation threshold

03 p0374 A71-13124

Atmospheric air breakdown by mode-locked Q switched laser pulse train, investigating threshold electric field dependence on characteristic diffusion length

03 p0440 A71-14178

Mars atmosphere carbon dioxide photodissociation via pressure independent one step process

03 p0497 A71-14548

Helium effects on dissociation and population inversion dynamics in pulsed carbon dioxide lasers

04 p0605 A71-14628

Hypersonic flow with nonequilibrium oxygen dissociation around blunt and conical bodies, considering temperature, pressure, density and compressibility factor behind normal shock

04 p0525 A71-14982

Dissociated diatomic gas nonequilibrium boundary layer flow over catalytic flat plate, examining velocity profiles, temperature and concentration

05 p0735 A71-16389

Shock wave propagation through converging nozzle, predicting real gas dissociation and vibrational excitation effects for comparison with shock tube measurement

05 p0735 A71-16528

Carbon dioxide dissociation plasma composition as function of gas mixture, flow rate, pressure and discharge current in sealed and flow-through laser systems

07 p1122 A71-19134

Molecular hydrogen cations collisions with hydrogen and helium, determining dissociation cross section dependence on kinetic energy from threshold to 100 eV

07 p1163 A71-19233

Dissociating airflow over two dimensional blunt body, determining laminar boundary layer chemical reaction suppression effects on heat exchange

07 p1015 A71-19748

Organic impurities effects on carbon dioxide dissociation activation energy, considering magnitude dependence on experimental conditions and data reduction techniques

08 p1251 A71-21783

Stationary longitudinal turbulent flow of air with equilibrium ionization and dissociation around plate, calculating heat exchange and frictional drag

08 p1228 A71-21922

Body temperature effects on intracellular carbon dioxide dissociation, pH and buffer capacity in hypothermic and hyperthermic dogs

10 p1559 A71-23897

Molecular gases dissociation due to pulsed carbon dioxide laser radiation, observing luminescence temporal, spatial and spectral characteristics prior to breakdown

10 p1620 A71-24040

Lighthill model applications to dissociating gas, considering function related to Riemann variables and nondissociating gas presence

10 p1593 A71-24269

Atomic nitrogen far UV emission excitation in auroral ionosphere due to electron impact dissociations

10 p1605 A71-24792

Positive diatomic nitrogen ions dissociation during collisions with inert gas atoms, measuring mass and energy distributions from focusing parabolic spectrograph

11 p1801 A71-25227

Dissociation and particle velocity in shock heated molecular beams of oxygen or hydrogen and argon mixtures, using mass spectroscopic measurements

11 p1765 A71-26282

Molecular hydrogen cations collisions with hydrogen and helium, determining dissociation cross section dependence on kinetic energy from threshold to 100 eV

12 p1932 A71-26751

Deuterium gas breakdown by ruby laser, using quantum kinetic equation for electron interactions with molecules and photon field

12 p1915 A71-27284

Dissociative recombination source of atomic oxygen green line excitation in day airflow, considering differential photoelectron flux

13 p2055 A71-27919

Chemical nonequilibrium flows in supersonic nozzle for mixture of dissociated gases and inert diluent [ASME PAPER 71-FE-8]

13 p2166 A71-29449

Bromine dissociation rates in presence of He, Ne, Ar, Kr and Xe, determining rate constant expressions from light absorption measurements behind incident shock waves

13 p2027 A71-29508

Freestream density field in nonequilibrium dissociating nitrogen flow over circular cylinder, using free piston shock tunnel and optical interferometry measurements

14 p2169 A71-29884

Equilibrium constant and heat of dissociation from dynamic viscosity of dissociating gas, noting dependence on composition and temperature

15 p2366 A71-31484

Viscosity of dissociating oxygen, carbon-air and argon plasmas at high temperature range, including error estimates and expansion up to 12,000 K

15 p2512 A71-31502

Thermal dissociation rate of undiluted nitrogen in shock tube over 5700 to 12,000 K range, using pressure measurements

[ALAA PAPER 71-620]

15 p2451 A71-31549

Random walk theory applied to electron motion in early stage of He breakdown in electric field, based on integral and differential cross section data

15 p2452 A71-31921

Nonequilibrium dissociating gas flow past blunt body using time dependent shock layer analysis

15 p2346 A71-32049

Oxygen dissociation and recombination rate constants at high temperatures from gas density interferometric measurement in relaxation zone of normal shock waves

15 p2367 A71-32570

Rare gas ions molecular and dissociative charge transfer reactions with nitrogen, using statistical phase-space theory of chemical reactions

16 p2538 A71-32813

High temperature singly and doubly ionized monatomic gas and partially dissociated and singly ionized diatomic gas, showing adiabatic and isentropic exponents relationship

16 p2662 A71-32837

Pure carbon monoxide dissociation rate behind incident shock wave in high temperature environment, using two wavelength IR emission data

16 p2539 A71-32909

Time of flight energy spectra of high lying and Rydberg metastable atoms by electron impact dissociation of molecular oxygen, noting atmospheric applications

16 p2614 A71-34043

Cometary dissociative recharging and recombination dissociation of water and hydrogen peroxide molecules in comets, giving empirical relation for effective cross sections

17 p2803 A71-34830

Stationary longitudinal turbulent flow of air with equilibrium ionization and dissociation around plate, calculating heat exchange and frictional drag

17 p2671 A71-35266

Temperature and pressure effects on viscosity and thermal conductivity of dissociating air at high temperatures

17 p2785 A71-35277

Normal and oblique shock thermodynamic equilibrium state variables calculation, taking into account air dissociation and ionization

18 p2909 A71-36678

Gas dissociation in carbon dioxide laser by IR absorption method, investigating role in population inversion

18 p2932 A71-37008

Diatomic gas molecules three body recombination and dissociation rate coefficients from modified phase-space theory of reaction rates

19 p3107 A71-38078

Relaxation equations for dilute diatomic gas dissociation-recombination reactions, transforming kinetic equations to normal modes

19 p3107 A71-38079

Dissociation reaction in presence of halogen atoms produced in shock wave by thermal decomposition of hydrogen fluoride

19 p3012 A71-38085

Predicted flow nonuniformities due to laminar and turbulent boundary layer buildup in shock tubes, studying effects on dissociation rates of bromine in argon mixture

19 p3046 A71-38225

Vacuum UV emission features dissociative excitation by electron impact on molecular hydrogen and oxygen, measuring excitation cross sections from threshold to 350 eV

19 p3107 A71-38344

Helium effects on dissociation and population inversion dynamics in pulsed carbon dioxide lasers

22 p3558 A71-42268

Hydrogen three-body recombination and dissociation rates in presence of molecular hydrogen, helium, argon and xenon collision partners

23 p3706 A71-42902

Molecular oxygen dissociative excitation in vacuum UV by electron impact, discussing resonance triplet atomic emission cross section

23 p3706 A71-42903

Carbon dioxide photolysis at 1849 A and various pressures, suggesting gas dissociation at wavelengths with appreciable absorption

23 p3641 A71-43328

Carbon dioxide UV absorption and dissociation processes and reaction kinetics of dissociation products

23 p3642 A71-43329

Mars atmospheric carbon dioxide dissociation, solving and comparing diffusion equations to Mariner oxygen and carbon dioxide observations

23 p3735 A71-43332

Nitrous oxide dissociation as natural source of stratospheric nitric oxide, noting estimates use as yardstick for artificial source

23 p3642 A71-43347

Molecular gas dissociation in constricted DC glow discharge plasma sac/sheath boundary, discussing characteristics and potential uses

23 p3712 A71-43931

Self focusing in gas breakdown produced by nanosecond laser pulses, using schlieren photography and laser light forward transmission measurements

24 p3832 A71-44358

Molecular gas dissociation equilibrium and carbon monoxide overtone line widths dependences on magnetic field strength in sunspots

24 p3868 A71-44459

Dynamic behavior of dissociating gas supersonic flow past blunt bodies at angle of attack

24 p3790 A71-44775

Oxygen dissociation in He, Ar, Kr and Xe gas mixtures behind incident shock waves, calculating density gradients and vibrational relaxation time

24 p3802 A71-44924

Molecular oxygen dissociation rate constant determination during interaction with He atoms in cylindrical shock tube

24 p3850 A71-45056

GAS DYNAMICS

NT AERODYNAMICS

NT AEROTHERMODYNAMICS

NT HYPERSONICS

NT RAREFIED GAS DYNAMICS

NT ROTOR AERODYNAMICS

Gas dynamics of fuel boundary layer combustion and surface pyrolysis in hybrid rocket motors

01 p0178 A71-10131

Atomic and molecular collisions in gases, considering E and F regions processes, auroras and applications

01 p0129 A71-10133

Gas temperature measurement behind strong shocks in diaphragmless electric shock tube by spectral line inversion method, noting application to gas dynamics

01 p0078 A71-10156

Gas dynamic equations of arbitrary materials detonation without allowance for transport phenomena, deriving stability criteria from boundary value problem steady solution

01 p0070 A71-10490

Radiative transfer equations averaging over quantum angles and energies, discussing use for nonsteady gas dynamic problems

01 p0179 A71-10666

Interstellar gas cloud spherically symmetrical collapse, considering computer program for density, temperature, flow velocity, cooling rate and gravity force

01 p0157 A71-10758

Boltzmann equation solution for isotropic heat velocity distribution in molecular gas kinetics

03 p0401 A71-13907

Plane nonsteady gas dynamic flows, reducing to system of time dependent equations system, presenting Chaplygin equation generalization

03 p0401 A71-13908

Plane straight shock wave stability in inviscid compressible medium, discussing gas dynamic equation discontinuous solution

03 p0401 A71-13967

Fluid mechanical and gas dynamic experimentation by Slingshot aerodynamic test facility

04 p0564 A71-14675

Shock tube diagnostics, instrumentation and rapid photography in nonequilibrium gas dynamics

04 p0565 A71-14699

German monograph on loss estimation for nonsteady gasdynamic duct-drum pressure exchangers, discussing design and optimization problems

04 p0568 A71-14925

Supersonic combustion thermogasdynamic analysis, presenting combustion processes via pressure-velocity diagram

04 p0676 A71-14986

- Pressure boundary layer profile numerical solution for transient and steady hydrodynamic gas film under high speed and small trailing edge thickness 04 p0570 A71-15178
- Blunt body stagnation point heat transfer in hypersonic flow, describing gas dynamic equations flow field viscosity and conductivity 04 p0528 A71-15490
- Steady two dimensional ideal gas flow past blunt body at incident infinite Mach number, obtaining gas dynamic variable asymptotic expansions as kappa approaches infinity 04 p0528 A71-15553
- Linearized shock waves and periodic disturbances propagation by discrete ordinates method in planar radiative gas dynamics 04 p0689 A71-15742
- Laser torch plasma dispersion gas dynamics from motion and kinetics of ionization processes 05 p0760 A71-16181
- Nonself-similar wave type gas dynamic equations solutions, considering flow fields due to Riemann waves interaction in polytropic gas 05 p0693 A71-16376
- Gas dynamics of explosions - Conference, Novosibirsk, U.S.S.R., August 1969 05 p0832 A71-16501
- Gas dynamic conditions resulting in reacting gases detonation waves at high initial temperatures, simulating internal combustion engine knock 05 p0833 A71-16506
- Gas dynamic processes effects on hydrogen-oxygen explosion chemical kinetics, calculating ignition delays under steady conditions behind plane reflected shock waves 05 p0716 A71-16514
- Radiatively driven acoustic waves, studying radiative transfer-gas motion interaction under local molecular equilibrium for vibrational rate processes 05 p0836 A71-16532
- Holographic interferometry application to gas dynamics, analyzing interferential patterns in monochromatic and achromatic light 05 p0695 A71-17166
- H I gas kinematics in Galactic anticenter region from Gaussian components of emission line profiles at 21 cm observations 06 p0964 A71-17349
- Low energy magnetoacoustic wave with finite conductivity, determining gas parameters near singular points 06 p0936 A71-17652
- Interstellar gas dynamics - Conference, Yalta, September 1969 06 p0971 A71-18326
- Cosmic gas dynamics, discussing galactic mass balance, dark matter and interstellar gas kinetic energy, temperature and density 06 p0971 A71-18327
- Interstellar gas dynamic characteristics, discussing galactic large scale features 06 p0971 A71-18328
- Galactic magnetic fields and cosmic ray gas, investigating origin and dynamical effects 06 p0972 A71-18332
- Cosmic accretion gas dynamics, discussing star, galaxies and galactic cluster effects 06 p0972 A71-18333
- Nitrogen-carbon dioxide thermally pumped gas dynamic lasers, using high speed flow for waste energy removal [AIAA PAPER 71-23] 06 p0908 A71-18490
- Laminar boundary layer effect on gasdynamic laser gain, considering vibrational relaxation time and population inversion [AIAA PAPER 71-24] 06 p0908 A71-18491
- Carbon dioxide-nitrogen-water vapor gas dynamic laser, discussing generation, power and gain [AIAA PAPER 71-25] 06 p0908 A71-18492
- Soviet book of gas dynamic function tables for two and three dimensional flows past blunt bodies 07 p1013 A71-19050
- Comparison of experimental and gas dynamic fluid parameter jumps across earth bow shock, suggesting reappraisal of gas dynamic analog from satellite observation 07 p1103 A71-19678
- Boundary value problems and applications in fluid and gas mechanics - Conference, Kazan, U.S.S.R., May 1969 07 p1091 A71-20076
- Laser beam evaporation of dense substances, examining luminous flux densities with gas dynamic equations 07 p1127 A71-20253
- Powerful laser beam and material interaction, investigating gas dynamics of plasma heating and dispersion 07 p1127 A71-20254
- Pneumatic and hydraulic fluidic power control systems, discussing moving part position servos and cold gas reaction systems 07 p1028 A71-20585
- Gas dynamic lasers design and operation, discussing pumping techniques, waste energy removal and mode control 08 p1301 A71-20693
- Aircraft turbine engines strength and gas dynamic characteristics improved by vibration decrease using elastic elements 08 p1349 A71-21710
- High turbulent flow simulation in hypervelocity wind tunnel for reentry vehicles operational testing, discussing nozzle gas dynamic and mechanical design [AIAA PAPER 71-253] 08 p1273 A71-21982
- Transparent radiating gas thermal instability criteria derivation from gasdynamic equations 09 p1519 A71-22528
- Gas dynamic test stand analyzing elastoplastic strains in aircraft gas turbine disks and liquid propellant rocket engines turbopumps under alternating nonisothermal loads 09 p1427 A71-22603
- Burger model equations for MHD turbulence with analog in gas dynamics for nondissipative case 09 p1432 A71-22703
- French book on thermodynamics and gas dynamics covering theoretical and applied thermodynamics, air compressors, combustion, internal combustion engines, water vapor, compressible fluid cooling, etc 09 p1545 A71-22965
- Dissipation and nonlinearity effects on linear three dimensional wave front, obtaining Burger equation for gas dynamics 09 p1433 A71-23053
- Gas dynamic solutions of plane shock wave propagation in moving medium, considering conservation laws 09 p1525 A71-23198
- Supernovae light curves theory based on numerical integration of gas dynamics and radiative heat conductivity equations 09 p1528 A71-23591
- CW carbon dioxide gasdynamic laser gain for mixture of carbon dioxide, nitrogen and helium 10 p1620 A71-24043
- Small amplitude resonant thermal acoustic oscillations of inviscid polytropic gas contained in finite length tube 11 p1798 A71-25446
- Gas dynamic effects of reaction center in explosive gas mixture, using model and numerical computation [AIAA PAPER 70-147] 11 p1854 A71-25452
- Kinetic and ionization phenomena in Q switched laser produced plasmas, considering gas dynamic plasma parameters /velocity, density distribution, pressure and temperature/ 11 p1806 A71-26086
- Gas dynamics models for plasma production by irradiating solids with laser beams, taking into account spatial inhomogeneity of absorption process 11 p1775 A71-26090
- Free flight ranges application to high temperature gas dynamics, using mathematical model to relate sub and full scale observations 11 p1705 A71-26269
- Nonself-similar wave type gas dynamic equations solutions, considering flow fields due to Riemann waves interaction in polytropic gas 12 p1898 A71-27453
- Holographic interferometry application to gas dynamics, analyzing interferential patterns in monochromatic and achromatic light 12 p1864 A71-27458
- Gas flow in nozzle, stages and gas dynamic systems, discussing motion in cross sectional plane 13 p1990 A71-28588
- Gas dynamic antechambers flame stabilization at various flow rates and temperatures, calculating mixing factor vs flow and jet parameters 13 p1263 A71-28966
- Amorphous particle rarefied gas in bounded volume, analyzing kinetic equation existence and uniqueness 13 p2103 A71-29146
- Gas dynamic effects associated with unboundedness of solution of quasi-linear hyperbolic systems 14 p2223 A71-29560
- Temperature and thermal flux measurement with calorimetric heat receivers during gas dynamic processes, determining physical properties and geometry effects on errors 14 p2335 A71-30184
- Planetary mass distribution, considering accretional theory of gas condensation into particles and particle accretion by growing embryo 14 p2312 A71-30389
- Radiative transfer equations averaging over quantum angles and energies, discussing use for nonsteady gas dynamic problems 14 p2339 A71-30999
- Gas dynamic and irrotational flow equations system transformation into Cauchy-Riemann equations via Beltrami coordinate transformation for simple representation of transonic flows [DFVLR-SONDDR-124] 14 p2228 A71-31127
- Kinetic equation for gases with rotational degrees of freedom under equality of probabilities of direct and inverse transitions and stereoisomerism of molecules 15 p2387 A71-31192
- Boltzmann kinetic equation for imperfect gases in a pair collision approximation, including terms proportional to time and coordinate derivatives and van der Waal constants 15 p2387 A71-31193
- Pulsed gas dynamic laser for radiation generation at high power levels, using shock tube [AIAA PAPER 71-572] 15 p2419 A71-31564
- Acoustic and gas dynamic characteristics of jet noise muffler, using adapters at outlet section of exhaust nozzle 15 p2469 A71-31710
- Large gas bubble migration in rotating liquid without gravity, noting velocity dependence on stagnation point distance and radius of curvature 15 p2392 A71-32119
- Two dimensional jet interaction flow field, investigating gas dynamic and transport phenomena [AIAA PAPER 71-561] 15 p2514 A71-32279
- Gas dynamic elastically mounted bearing, describing stability analysis of unloaded rotor central equilibrium position 15 p2417 A71-32457
- Coupled radiative transfer-gas dynamic interactions in unsteady wave propagation, two dimensional steady flows and atmospheric motions 15 p2515 A71-32562
- Gas dynamics of explosions, considering electromagnetic fields and chemical reactions effects on blast wave propagation in unbounded media 15 p2515 A71-32567
- Slow MHD shock wave profile discontinuity corresponding to conventional gas dynamics isothermal jump 16 p2615 A71-32793
- Milky Way galaxy interstellar neutral hydrogen rolling motion phenomenon confirmed by 21 cm line survey data 16 p2630 A71-33053
- Optical methods in gas dynamic research - Conference, Syracuse University, New York, May 1970 16 p2586 A71-33151
- Gases refractive behavior, discussing constitutive properties, wave propagation, Lorentz electron theory of dispersion, spectral interferometry and hook method 16 p2608 A71-33156
- Resonant energy exchanges between gaseous media and externally applied radiation fields from wavelength-tunable lasers 16 p2586 A71-33164
- Kinetic theory of gases in general relativity, including model of matter particle structure 16 p2610 A71-33267
- Vertical acceleration effect on gas-hydraulic analogy for turbulent flows with and without jumps with error dependence on Froude number and length to depth ratio 16 p2560 A71-33598
- Gas bubble in liquid under surface tension, weightlessness and rotation, determining angular velocity for fluid system disintegration 16 p2560 A71-34142
- Difference schemes for approximating system of one dimensional gas dynamics equations in Eulerian coordinates, taking into account mass conservation law and viscosity 17 p2729 A71-35370
- Flame temperature measurement by radiation and gas dynamic methods 17 p2745 A71-35440
- Simple gas thermal creep/velocity slip and temperature jump coefficients by applying variational technique to linearized Boltzmann equation with boundary conditions 17 p2785 A71-35446
- Transparent radiating gas thermal instability criteria derivation from gasdynamic equations 17 p2807 A71-35504
- Soviet papers on gas dynamics and heat transfer covering turbulent boundary layers, supersonic ideal-gas jets, rocket exhaust base pressure, base flow characteristics, etc 18 p2902 A71-36111
- Complex wave structure development upon underexpanded jet impact on plane obstruction at small incidence angles, determining gas dynamics parameters of supersonic jet 18 p2903 A71-36120
- Shock wave profile nonlinear one dimensional problems in gas dynamics, using monotonic difference scheme 18 p2907 A71-36333
- High temperature gas dynamics, including hypersonic wind tunnel nozzles, air-breathing/chemical rocket propulsion systems, thermodynamic models and relaxation boundary layers 18 p2846 A71-36425
- Solar corona model for structure and dynamic properties, investigating gas-magnetic field interactions 18 p2966 A71-36737

Molecular dynamics data from neutron scattering techniques for gas mixing 18 p2949 A71-36958

Close binary systems evolutionary processes, considering mass transfer and gas dynamics 18 p2968 A71-37033

Aerodynamic testing for space transport vehicle design, discussing experimental gas dynamics role in high stagnation enthalpy systems 19 p3161 A71-37315

German papers on gas dynamics covering Oswatich expansion method of characteristics, subsonic flow, transonic flow, hypersonic flow, unsteady compressible flow and detonation processes 19 p2992 A71-37451

Radiation gas dynamics covering monatomic and molecular gases, chemical dissociation and vibrational relaxation 19 p3043 A71-37459

Galactic central region gas motions, discussing hypothetical explosive expulsion of matter from galactic nucleus 19 p3143 A71-38165

Nighttime polar atmospheric structure and temperature variations due to gas kinetic and electron energy changes 19 p3056 A71-38361

Initial viscous heat conducting gas dynamic state one dimensional decay problem solution, using kinetic theory with Boltzmann equation 19 p3046 A71-38541

Atmospheric gases effective electron collision frequency calculations, using momentum transfer cross sections 20 p3271 A71-38743

Time-of-flight measurements for relationship between velocity, mass and temperature in molecular gas motion and electron-atom collision kinematics 20 p3271 A71-38789

Hydrodynamic effects on laser beam propagation through gases by finite difference solution, applying to trapping, acoustic and light amplifications and banana self focusing 20 p3242 A71-38838

Linearized unsteady gas dynamic differential equation, obtaining parameter characteristics from boundary values 20 p3211 A71-39032

Soviet book on unsteady motions of continuous media covering gas dynamics, thermodynamics, shock and plane detonation waves, three dimensional gas motions, etc 20 p3211 A71-39144

Gas dynamic model for coupled vibrational and radiative nonequilibrium in carbon dioxide, obtaining macroscopic collisional and radiative transfer equations 21 p3418 A71-40233

Sound propagation in sheared fluid in duct, determining energy flux from linearized gas dynamic equations 21 p3366 A71-40536

Dynamic problems for molecular gases with rotational degrees of freedom, deriving hydrodynamic equations from kinetic equations integration 21 p3420 A71-41121

Jump conditions across three dimensional curved shock in radiation gas dynamics, considering radiation pressure number effect 22 p3530 A71-41695

Fundamental derivative γ and other thermodynamic variables in gas dynamics, considering transonic passage variation, Prandtl-Meyer wave, adiabatic flow and nonlinear wave propagation 22 p3530 A71-41887

Semilinear hyperbolic systems analogous to differential-integral Boltzmann equations of gas dynamics, developing solutions existence for nonnegative initial data 22 p3531 A71-42690

Gas dynamics nonstationary linearized equation solutions based on nonstationary source- and vortex-like singularities 23 p3663 A71-43491

Medium compressibility effect on gas dynamic characteristics and aerodynamic forces and moments in centrifugal compressor end stage bladed diffuser 23 p3626 A71-43552

Self similar solution to Cauchy problem of gas dynamics equations in nonisotropic media 24 p3819 A71-44774

Dynamic behavior of dissociating gas supersonic flow past blunt bodies at angle of attack 24 p3790 A71-44775

**GAS EVACUATING
U EVACUATING [VACUUM]
GAS EVOLUTION**

Hydrogen outgassing from proton irradiated aluminum samples, determining gas evolution and blister formation during annealing 07 p1139 A71-20173

Comets Alcock 1963 III and Everhart 1964 IX brightness bursts, obtaining time curves for gas evolution 12 p1965 A71-27228

Comets Alcock 1963 III and Everhart 1964 IX brightness bursts, obtaining time curves for gas evolution 19 p3132 A71-37380

Preservative phenol derivative effects on toxic gas evolution from stored urine in sealed vessels 22 p3506 A71-42808

Inert gases release from breccia 10065 by lunar rock vacuum crushing at room temperature, suggesting breccia formation from gas-rich parent materials 23 p3754 A71-43725

GAS EXCHANGE

Hydrogen exchange between pial arteries for measuring local cerebral blood flow quantitatively in anesthetized cats 01 p0008 A71-10075

External respiration, gas exchange and energy expenditures during orthostatic tests involving immersion experiment 01 p0014 A71-11136

Pulmonary gas exchange relation to cyclical pattern of ventilatory flow, considering alveolar dead space and metabolic and respiratory rate effects 03 p0361 A71-13183

Conditioned reflex gas exchange shifts in persons under repeated local thermal stimuli 04 p0540 A71-15572

Oxygen diffusion in monoclinic zirconia as function of equivalent pressure, using oxygen 18 gas-solid exchange techniques 05 p0769 A71-17096

Air blast effects on pulmonary ventilation, gas exchange, venous-arterial shunt and blood gas parameters 06 p0851 A71-17601

Gas exchange and muscular thermoregulation activity in rats under environmental oxygen deficiency 08 p1242 A71-21963

German book on clinical pathophysiology of respiration covering respiratory physiology, pulmonary gas exchange, respiratory control, hypoxia, hyperoxia, pressure breathing, etc 09 p1394 A71-23069

Book on gravity and acceleration effects on lungs covering breathing mechanics, ventilation distribution, blood flow, gas exchange, arterial oxygen saturation and pulmonary shunting 09 p1402 A71-23620

Pressure effects on human ventilation and gas exchange, determining stratified inhomogeneity during deep diving 12 p1873 A71-27126

Pulmonary gas exchange studied in computer models with series inequality of ventilation 12 p1870 A71-27131

Alveolar gas exchanges and cardiovascular functions during breath holding with air, determining resting oxygen consumption 12 p1870 A71-27135

Pulmonary oxygen toxicity development rate and effects on lung volume and alveolar-arterial gas exchange during oxygen breathing 13 p2024 A71-29501

Gas exchange, thermoregulatory muscle tone and electrical activity in rat muscles in hyperoxic atmosphere 15 p2360 A71-32533

Gas exchange metabolic fluctuations of nitrogen fixation, hydrogen evolution and photoreduction in Rhodospirillum rubrum as function of culture conditions and age 16 p2528 A71-33059

Nitrogen and oxygen exit rate from subcutaneous gas pockets in rats during tissue blood flow elevation due to cobalt chloride injection 17 p2678 A71-34174

Gas exchange between air or gas mixture flows and terrestrial soil in extraterrestrial microorganisms detection, using continuous sampling and gas chromatography 21 p3346 A71-40575

Hypokinesia effects on gas exchange and oxygen consumption in rats, noting weight losses 24 p3795 A71-44526

External respiration, gas exchange and blood circulation during passive orthostatic tests 24 p3796 A71-44537

GAS EXPANSION

Digital simulation for translational and rotational equilibrium breakdown in gaseous molecules expansions by Monte Carlo method 01 p0130 A71-10936

Two dimensional free gas jet expansion into quiescent medium, predicting terminal shock position 03 p0400 A71-13466

Compressible subsonic and supercritical flows, developing flowmeter orifice expansion factors [ASME PAPER 70-WA/FM-3] 03 p0402 A71-14105

German monograph on radiative transport in freely expanding gas clouds covering analytical and numerical calculations and experiments 03 p0418 A71-14369

Laser power from carbon monoxide supersonic expansion in nitrogen and argon mixtures, comparing to carbon dioxide gas dynamic lasers 04 p0608 A71-15042

German monograph on centered two dimensional nonequilibrium hypersonic expansion flow, considering real gas flow with chemical reactions 05 p0693 A71-16124

Gas dynamic coupling effect on vibrational deexcitation of carbon monoxide at 1400 to 2200 K range in shock tube 05 p0835 A71-16523

Supersonic reactive gas flow free expansion over sharp corner into region of constant pressure, using linearized theory and numerical method of characteristics 05 p0836 A71-16535

Nozzle throat conditions at sound velocity discontinuity due to transition from one to two condensed phases during expansion 05 p0735 A71-16576

Ellipsoidal level surface gas cloud expansion into vacuum 05 p0783 A71-16991

Thermal separator type refrigerating machines design, discussing gas expansion under unsteady conditions 06 p0882 A71-18310

Supernovae expansion, investigating hydrodynamic model with interstellar magnetic fields and relativistic particles effects 06 p0973 A71-18335

Inviscid air nonequilibrium shock layer properties correlation based on plenum entropy, predicting composition of downstream converging-diverging nozzle expanding air flow [AIAA PAPER 70-866] 07 p1090 A71-19905

Ruby laser driven luminous waves during breakdown and heating within freely expanding gas jet observed with streak photography 07 p1126 A71-20168

Near equilibrium solutions of steady spherical expansion of monatomic gas into vacuum, using Lighthill technique for higher order analysis 09 p1430 A71-22086

Supersonic collisionless plasma flow around flat plate and expansion into vacuum, using Poisson equation 09 p1500 A71-22233

One dimensional plane adiabatic MHD free expansion of relativistic plasma 10 p1676 A71-24495

Nonreacting and reacting ideal gases expansion between interconnected chambers, considering nitrogen and carbon dioxide simultaneous pressure measurements 12 p1877 A71-27550

Computer simulated semiinfinite uniform plasma expansion in vacuum, showing inapplicability of thermal velocity burst ion model 13 p2104 A71-27846

Flow momentum losses during gas mixture chemically nonequilibrated expansion in nozzle 13 p2158 A71-27880

Chemical reactions occurrence during gas supersonic expansion into vacuum, calculating gas temperature, pressure and density 13 p2025 A71-28774

Transonic gas flow measurement during sudden expansion from circular nozzle into coaxial cylindrical channel, emphasizing flow attachment 13 p1993 A71-29192

Approximate calculation for axisymmetric interaction between freely expanding jet and obstacle by reduction to problem of uniform gas flow past sphere 13 p1994 A71-29232

Ejection explosion energy transfer to ambient media, examining effect of orifice distance from explosive charge center 15 p2511 A71-31386

Arc-heated nonequilibrium air expansion flow mass spectroscopic analysis, noting reservoir entropy effect [AIAA PAPER 71-621] 15 p2366 A71-31550

Steady state partially ionized monatomic gas expansion from sonic orifice, investigating electron-ion recombination effects on flow properties 15 p2457 A71-32101

Nonequilibrium corner expansion flow of ionized argon induced by normal shock waves in hypervelocity shock tube 16 p2555 A71-32905

High temperature high Mach number expansion tube flows, determining impurities by time integrated spectroscopic measurements 16 p2551 A71-33155

Supersonic jet expansion in variable geometry channels, obtaining pressure dependence on injection rate and similarity parameters 17 p2669 A71-34216

Supernovae underexpanded submerged gas jet at various Mach and Knudsen numbers and pressure ratios, observing trailing shock wave geometry 17 p2669 A71-34218

- Free jet expansion of liquid-gas bubble mixture suspended in glycerine 17 p2728 A71-34891
- Shock tubes and shock tunnels, considering equilibrium expansion, relaxation phenomena and real gas effects 18 p2897 A71-36410
- Ellipsoidal level surface gas cloud expansion into vacuum 18 p2948 A71-36791
- Pulsed combustion heated carbon dioxide gas dynamic laser with expansion separation, showing composition and stagnation pressure dependent gain and energy variations 19 p3071 A71-37144
- Translational freezing in free expanding jets of Ar, nitrogen and carbon dioxide from molecular beam intensity measurements, deriving perpendicular temperature 19 p3045 A71-37882
- Fully ionized plasma expansion from spherical source into vacuum, deriving equations of motion and collision integrals 19 p3115 A71-38212
- Partially ionized plasma expansion from spherical source into vacuum, obtaining equations of motion, collision integrals and recombination rate coefficient 19 p3115 A71-38213
- Expanding metal vapor density-radius measurements in wire explosions, using twin tube flash X ray unit 20 p3311 A71-38827
- Electromagnetic absorption in adiabatically expanding fully ionized cosmic plasma, using Einstein-De Sitter cosmology 21 p3442 A71-40161
- Supersonic collisionless plasma flow around flat plate and expansion into vacuum, using Poisson equation 21 p3424 A71-41113
- Microwave plasma generation in magnetic field, detecting expansion related to electron cyclotron frequency harmonics 21 p3426 A71-41287
- Carbon dioxide, nitrogen and water vapor hot mixture expansion through Laval nozzle, showing population inversion on carbon dioxide laser transition 22 p3556 A71-41726
- High beta laser produced spherical plasma expansion in background magnetic field and ambient plasma, treating electrons as inertial fluid 22 p3581 A71-41891
- Diagnostics of Ar free jet expansion from high pressure inductive arc source into low density wind tunnel, observing background gas effects 22 p3583 A71-42048
- Ion cloud expansion perpendicular to initially homogeneous magnetic field, estimating maximum radius with energy balance and expansion process 23 p3667 A71-43132
- ### GAS EXPLOSIONS
- Detonation waves in gases and two phase systems with nonideal wave front, calculating acetylene explosion parameters for different initial pressures 03 p0520 A71-13991
- Gases, condensed phases and blast simulation for high explosive driven shock tubes 04 p0565 A71-14677
- Ionizing shock waves and high speed gas flow generation in tubes using high explosives 04 p0674 A71-14683
- Gaseous explosives free detonation waves for hydrogen-oxygen, noting propagation velocity deficit and detonability limit 05 p0834 A71-16512
- Hydrogen-oxygen reaction kinetics behind steady state shock waves under isothermal branched chain explosion limits 05 p0834 A71-16513
- Gas dynamic processes effects on hydrogen-oxygen explosion chemical kinetics, calculating ignition delays under steady conditions behind plane reflected shock waves 05 p0716 A71-16514
- Spark ignited hydrogen-oxygen detonations in supersonic wind tunnel, using schlieren photographs 05 p0835 A71-16520
- Diamagnetic moment of strong shock waves from high temperature light spark explosion in gases 06 p0930 A71-17399
- Far field sonic boom pressure profiles simulation by methane-oxygen mixture detonation in balloons [AIAA PAPER 71-186] 06 p0886 A71-18625
- Spherical magnetogasdynamic shock production in conducting gas by explosion into homogeneous self gravitating system, assuming density dependence on inverse power of distance 09 p1505 A71-23585
- Gas dynamic effects of reaction center in explosive gas mixture, using model and numerical computation [AIAA PAPER 70-147] 11 p1854 A71-25452
- German monograph on gaseous detonations stability covering carbon dioxide thermal decomposition, initial temperature/pressure, reflected shock waves and water adsorption 13 p2049 A71-28878
- Boundary effects on gaseous detonation velocity deficit and limit using approximation into boundary layer equations, comparing to experimental data 17 p2837 A71-34437
- Flash photolysis initiated gaseous explosions detonation effects, observing ionization and radical emission spectra, absorption intensities and induction periods 19 p3169 A71-38110
- Explosion-pumped gas dynamic carbon dioxide laser, obtaining high pulse energy by common hydrocarbon fuels 23 p3687 A71-44135
- ### GAS FLOW
- NT AIR CURRENTS
- NT AIR FLOW
- NT CONTINUUM FLOW
- NT EQUILIBRIUM FLOW
- NT FREE MOLECULAR FLOW
- NT JET STREAMS (METEOROLOGICAL)
- NT KNUDSEN FLOW
- NT MERIDIONAL FLOW
- NT MOLECULAR FLOW
- NT NONEQUILIBRIUM FLOW
- NT SLIP FLOW
- NT TRANSITION FLOW
- NT VERTICAL AIR CURRENTS
- Tangential momentum transfer accommodation coefficient for gas flow based on monocrystalline molecular model of gas-solid interface 01 p0071 A71-10949
- Rotational temperature and density measurements in rarefied flow over sharp leading edge flat plate, obtaining shock layer static pressure 01 p0082 A71-10955
- Laser effect radiation power in gas mixture flow of carbon dioxide, nitrogen and traces of water vapor, presenting calculations based on kinetic theory 01 p0094 A71-10992
- Steady isothermal plane gas flow between infinite parallel plates at arbitrary Knudsen numbers, obtaining linear differential equations of mass transfer 01 p0071 A71-11114
- Impulsively started time dependent transonic flow of ideal compressible gas past circular cylinder, using finite difference method 01 p0003 A71-11160
- Ablative heat shield char layer, examining reacting nonequilibrium pyrolysis gas flow [AICHE PREPRINT 15B] 01 p0181 A71-1297
- Heat transfer in nongray radiating gas turbulent flow in circular tube 01 p0181 A71-11403
- Arc discharge plasma response to turbulent gas flow covering wide range of Reynolds numbers measured with Langmuir probes 01 p0136 A71-11479
- Light beam deflection due to temperature gradient in laminar gas flow in shielding pipe for laser communication, considering beam waveguide design 02 p0284 A71-11869
- Heat transfer and friction drag calculation for turbulent boundary layer of gas with temperature dependent physical properties 02 p0185 A71-11884
- Heat and gas curtain efficiency in turbulent boundary layer on flat plate, including heat transfer data 02 p0331 A71-11886
- Supersonic electrically conducting gas flow in flat channel with dielectric walls in inhomogeneous magnetic field 02 p0289 A71-11926
- Steady three dimensional ideal dissociative gas flow along stream lines, examining velocity components, pressure gradients, density and mass fraction variable 02 p0239 A71-12124
- Circular pipe gas laminar flow at constant wall temperature, determining heat exchange and drag by motion and energy equations integration in boundary layer approximations 02 p0240 A71-12192
- Gas permeable dispersion layer between impermeable solid wall and high temperature gas flow, calculating dimensionless heat flux equations 02 p0332 A71-12200
- Gas and fluid flow through flat and cylindrical porous cermets walls, determining permeation energy loss and radial flow hydraulic resistance 02 p0240 A71-12277
- German monograph on plane ideal gas flows calculation with allowance for unsteady gaseous walls and compression shocks using difference methods 02 p0240 A71-12400
- Frictionless rotationally symmetrical free supersonic gas jets with thermodynamic relaxation, applying approximate method for shape and flow parameters at boundary 02 p0241 A71-12407
- Soviet book on nonlinear conical gas flow theory covering flows with different characteristics past bodies of various geometries and positions 02 p0187 A71-12719
- Solar magnetic fine structure production by gas motion in supergranular convection 02 p0316 A71-12753
- Anharmonic oscillator diatomic molecule system, examining vibrational relaxation in expanding gas flow 03 p0460 A71-13499
- Correlation measurements by laser in turbulent gas flow, determining phase structure velocity distributions and coherence lengths 03 p0435 A71-13529
- Two dimensional annular flow of viscous heat conducting gas between coaxial cylinders, using Navier-Stokes equations 03 p0401 A71-14066
- Gas flow parameter changes under partially vaporized fluid injection, considering effects on pressure, temperature and rate of resultant mixture 03 p0521 A71-14252
- Vaporization rate of liquid injected into high temperature supersonic gas flow, considering relation to static pressure and distillation process 03 p0521 A71-14253
- Lateral drift of solid particles suspended in plane supersonic gas flow along wall with recess step, using successive approximation for equations 03 p0404 A71-14255
- Shock wave dynamic behavior in shock tube under variable diaphragm opening time for high pressure gas flow into lower pressure section 03 p0472 A71-14261
- Heat transfer and fluid friction of hydrogen and helium gas flows undergoing turbulent to laminar flow transition in heated pipe [ASME PAPER 69-HT-54] 03 p0405 A71-14291
- Unsteady one dimensional isentropic gas flows, discussing nonlinear pressure waves geometry 03 p0405 A71-14345
- Gas flow past straight airfoil, analyzing damped natural oscillations 03 p0345 A71-14561
- Hypersonic perfect gas flow past thin three dimensional body with strong viscous interaction, obtaining aerodynamic characteristics and drag and heat coefficients 03 p0345 A71-14563
- Symmetric airfoil profiles with sharp and rounded leading edges in inviscid gas unbounded uniform adiabatic transonic flow, solving by nonlinear approximation 04 p0525 A71-14591
- Wankel engine chamber gas leakage determination based on exit slot sample gas analysis, considering air to working fluid ratio 04 p0638 A71-14598
- Hypersonic rarefied nitrogen flow over wedge, investigating density field 04 p0570 A71-15033
- Steady two dimensional ideal gas flow past blunt body at infinite Mach number, obtaining gas dynamic variable asymptotic expansions as kappa approaches infinity 04 p0528 A71-15553
- Inviscid nonheat conducting gas flow parameters behind shock wave reflection from solid wall at obtuse angle using linear approximation from variable separation method 04 p0572 A71-15554
- Carbon dioxide laser gyro flowing gas system, considering stability, locking frequencies and ease of construction 05 p0761 A71-16271
- Magnetoacoustic instabilities in weakly ionized gas flow, using adiabatic approximation 05 p0788 A71-16600
- One dimensional gas flow with radiative transfer, using time dependent difference scheme 05 p0735 A71-16714
- Liquid droplet elliptical deformation in gas flow upon external flow force application, presenting solution as ellipsoid semiaxes plot of dimensionless time functions at various Weber numbers 05 p0736 A71-16749
- Test facility for fatigue and thermal fatigue of turbine blades in high temperature gas flow 05 p0734 A71-16762
- Gas and liquid flows local velocity measurements, using Doppler frequency shifts due to wave scattering at solid microparticles suspended in flow 05 p0753 A71-16786
- Steady diabatic inviscid gas flow properties, emphasizing vortex lines geometry 05 p0839 A71-17047
- Soviet book on supersonic turbulent boundary layer covering gas flow molecular theory, heat and mass transfer at porous surfaces, etc 06 p0841 A71-17439
- Irreversibility control in two gas flows mixture, discussing jet engines thrust increase by air-exhaust gases admixture 06 p0945 A71-18051
- Inviscid mixed subsonic-supersonic gas flows with shocks, developing time dependent numerical method [AIAA PAPER 71-45] 06 p0883 A71-18506

- Pressure distribution over blade in cascade nozzle for incompressible and compressible particulate gas flow
[AIAA PAPER 71-82] 06 p0883 A71-18539
- High temperature gaseous flow, discussing approximate methods of calculation of turbulent boundary layer
[AIAA PAPER 71-163] 06 p0885 A71-18605
- Soviet book on gas flow past blunt bodies, Part 1, Flow analysis and calculation methods covering finite difference theory, algorithms, etc
07 p1013 A71-19049
- Hypersonic radiating gas inviscid flow past blunt bodies, using spherical harmonics approximation
07 p1013 A71-19183
- Runge-Kutta type difference methods for calculating unsteady gas flow with shock waves
07 p1087 A71-19184
- Sunspot observations on 3 July and 14 September 1967, examining transverse magnetic field distribution and radial gas velocities and motion with magnetograph
07 p1195 A71-19338
- Transonic gas flows in axisymmetric small throat curvature radius Laval nozzle with appreciable flow parameters variation in transverse direction
07 p1014 A71-19732
- Viscous gas flow interaction on delta wing and oblique airfoil at Mach number of infinity
07 p1014 A71-19739
- Rarefied monatomic gas flow in axisymmetric jet exhaustion into vacuum, noting expansion to low densities at thermodynamic unequilibrium
07 p1090 A71-19894
- Gas discharge from curvilinear walled vessel of finite width and from symmetrical vessel with rectilinear parallel walls
07 p1092 A71-20082
- Approximation of Chaplygin equation for subsonic ideal gas plane adiabatic flow, applying to discharge from flat channel with contraction
07 p1016 A71-20083
- Surface construction of body of revolution in supersonic gas flow from distribution of velocity vector modulus along generatrix of body, using Frankl method of characteristics
07 p1016 A71-20089
- Mathematical model of nonstationary intake and exhaust gas motion in two cycle internal combustion engine cylinders
08 p1347 A71-20780
- One dimensional isentropic gas motion in acoustic wave reflection from cylindrical tube nonplane closed end under flow
08 p1276 A71-21478
- Flowfield isentropes in conical gas flow with singular current surfaces
08 p1227 A71-21864
- One dimensional nonstationary motion of compressible electrically conducting gas with allowance for heat conductivity and viscosity, solving MHD equations
09 p1499 A71-22129
- GaAs epitaxial layers inhomogeneous doping in continuous chloride system, discussing electron concentration with respect to gas flow direction
09 p1506 A71-22167
- Electric arc column in laminar gas flow, using integral method for stabilization conditions
09 p1544 A71-22266
- Carbon dioxide flow vacuum condensation on cryogenic pump surface, noting flow temperature and directionality effects on condensation rate
09 p1544 A71-22268
- Turbulent hot gas motion in round pipes from semiempirical turbulence theory, accounting for energy dissipation and thermodynamic parameter variability
09 p1431 A71-22370
- Laminar steady flow and heat transfer of viscous heat conducting gas moving between coaxial cylinders, using Runge-Kutta method
09 p1431 A71-22408
- Reinforced shells of revolution carrying capacity upper limit subjected to internal adiabatic ideal gas flow
09 p1538 A71-22632
- Velocity distribution measurement of Cs gas flow from orifice in near-free molecule regime, using apparatus based on time of flight method
09 p1432 A71-22682
- Detonation products expansion in vacuum, measuring gas flow speeds and pressure profiles far from charge
09 p1545 A71-22690
- Rarefied gas flow density and velocity by total head and flow rate adapters, noting isentropic flow core region
09 p1382 A71-22728
- Reactive equilibrium hypersonic gas flow over slender pointed body, neglecting rate chemistry
09 p1383 A71-23054
- Emitting, absorbing and scattering gray gas flow through plane stationary normal shock wave, presenting governing equations linearized analysis
09 p1546 A71-23164
- Rarefied gas flow along boundary wall with temperature gradient, determining thermal creep and temperature slip effects
09 p1547 A71-23167
- Multiphase gas flow, measuring gas concentration by laser Raman spectroscopy
[AIAA PAPER 71-286] 09 p1464 A71-23308
- Uniform continuous electric discharge in large volume high pressure near-sonic carbon dioxide-nitrogen-helium flowstream, describing closed cycle continuous laser amplifier channel design
09 p1505 A71-23485
- Axisymmetric steady diabatic flow equations exact solutions
09 p1434 A71-23545
- Plane sandwich plates in supersonic gas flow, investigating aeroelastic stability, transverse shear flexibility and axial loads
09 p1543 A71-23609
- Transverse gas flow effects on deuterium fluoride-carbon dioxide chemical laser output, discussing amplifier medium homogeneity factor
10 p1619 A71-23834
- Body profile low frequency oscillations in transonic gas flow, investigating nonlinear differential equation boundary value problem by approximation method
10 p1550 A71-24363
- Boundary layer equations for radiating and absorbing gas flow at large Reynolds numbers
10 p1593 A71-24367
- Numerical solution of axisymmetric minimum drag bodies in hypersonic viscous gas flow, obtaining coefficient of friction by local variations method
10 p1551 A71-24370
- Vortex layer near circular cone surface in supersonic axisymmetric steady flow of homogeneous inviscid gas
10 p1551 A71-24372
- Cylindrical shock wave in solid body rotating gas for angular variation effects on shock velocity, using similarity method
10 p1593 A71-24405
- Galactic wind as steady radial perfect gas flow from stars and central gravitating source
11 p1818 A71-25207
- Initially spherical liquid droplet transient response under surface tension accelerated by external gas flow
[AIAA PAPER 71-393] 11 p1749 A71-25355
- Metastable state gas flow experiment, investigating laminar boundary layer change in presence of flat plate surface catalytic reaction
11 p1705 A71-26276
- Destabilizing buoyancy forces effect on weak homogeneous shear flow turbulence in gases, discussing turbulence decay with time and turbulence energy growth
12 p1896 A71-26940
- Conservation theorem of velocity circulation along moving contours in continuous steady ideal gas flows
12 p1863 A71-27305
- Diaphragm opening time influence on gas flow in shock tubes
12 p1897 A71-27451
- Unsteady one dimensional time-dependent diabatic gas flow equations reduced to single partial differential equation, deriving solutions for entropy distribution
13 p2158 A71-27829
- Conjugate steady convective aerodynamic heating of plate in longitudinal compressible gas flow, taking into account boundary layer enthalpy distribution
13 p1989 A71-27890
- Unsteady large particle numerical solutions to vortical equations of plane and axisymmetric inviscid gas flow past blunt body for subsonic and hypersonic velocities
13 p1989 A71-27901
- Heat transfer on cylindrical antenna in supersonic high temperature gas flow, noting electromagnetic wave damping due to ablation
13 p1990 A71-28296
- Compressible viscous gas supersonic flow, observing near wake region behind perpendicular trailing face of plate with motion, state, energy and continuity equations
13 p2047 A71-28421
- Plane one dimensional steady compressible ideally charged gas flow characteristics in electric field
13 p2107 A71-28567
- Gas flow in nozzle, stages and gas dynamic systems, discussing motion in cross sectional plane
13 p1990 A71-28588
- Heat shield ablation under high enthalpy chemically active turbulent gas flow in hydrojet engine manifolds
13 p2160 A71-28589
- Monograph on shock wave structure in nonequilibrium partially ionized gas flow covering plasma diagnostics, electron temperature, ion density, induced potential gradient, etc
13 p2048 A71-28738
- Combustion chamber design with flame stabilizers, deriving gas flow, energy conservation equations and propellant combustion rates
13 p2163 A71-28967
- Gas turbine engine combustion chamber outlet, noting gas flow temperature field peripheral nonuniformity
13 p2118 A71-28972
- Weakly rarefied gas flow past bodies of various geometry, deriving equations of motion with approximate macroscopic integrodifferential equations
13 p1991 A71-29148
- Boundary conditions formulation for energy and mass transfer in weakly rarefied gas flows past bodies
13 p1991 A71-29149
- Three dimensional steady separated liquid and gas flows past low aspect ratio bodies, deriving similarity laws for reduction to two dimensional problem
13 p2049 A71-29169
- Heat transfer on spheres and sharp cones in rarefied hypersonic gas flow at zero angles of attack in wind tunnel vacuum
13 p1992 A71-29176
- Unsteady curvilinear motion of lifting surface, calculating induced gas flow velocities in terms of vortex densities
13 p1992 A71-29188
- Transonic gas flow measurement during sudden expansion from circular nozzle into coaxial cylindrical channel, emphasizing flow attachment
13 p1993 A71-29192
- Blowing and wall curvature effects on gas flow separation and critical pressure gradient in Couette flow examples
13 p1993 A71-29193
- Unsteady hypersonic self similar gas flow and drag on circular cone accelerated according to power law, using small perturbation theory
13 p1993 A71-29205
- Gas flow heat loss through porous metals, deriving hydraulic resistance and heat release coefficients
13 p2165 A71-29218
- Transonic gas flow around profile, proving uniqueness of Frankl solution
13 p1993 A71-29221
- Approximate calculation for axisymmetric interaction between freely expanding jet and obstacle by reduction to problem of uniform gas flow past sphere
13 p1994 A71-29232
- Compressible rarefied gas Couette flow over plane wall, calculating mean free path with Boltzmann equation relaxation model
13 p2051 A71-29357
- Turbulent gas flow through duct with alternating pressure gradient, considering heat transfer and frictional resistance
13 p2166 A71-29370
- Pipe gas flow with heated solid particles injection, presenting flow equations numerical solution by digital computer
[ASME PAPER 71-FE-22] 13 p2166 A71-29460
- Numerical solution of coupled boundary layer equations describing strongly cooled turbulent flow of gas between parallel plates with property variations
[ASME PAPER 71-FE-38] 13 p2166 A71-29473
- Soviet book on experimental aerodynamics covering wind tunnels, shock tubes, liquid and gas physical properties, flow parameter measurement equipment, etc
14 p2221 A71-29524
- Thermal diffusion effect on gas flow velocity measurements with anemometers with heat convection signals
14 p2239 A71-29815
- Nonequilibrium modeling of pyrolysis gas products flow through char layer of ablative heat shield
14 p2334 A71-29876
- Methane and natural gas flow through critical flow nozzles, calculating real gas effects on mass flow rate
14 p2224 A71-29937
- Viscous gas flow past semiinfinite porous plate with gas injection or suction and identical composition in outer flow
14 p2224 A71-30002
- Light propagation through moving gas, computing beam bending into wind and self defocusing due to gas heating
14 p2274 A71-30129
- Three dimensional spatial unsteady hypersonic gas flow about bodies behind strong shock wave front
14 p2169 A71-30182
- Hypersonic shockless gas flow past circular cone and cylindrical surfaces, reducing Vallander equations to nonlinear integral
14 p2169 A71-30183
- Couette flow two point boundary value problem solution using Navier-Stokes and Barnett viscous gas equations
14 p2224 A71-30185
- Method of characteristics application to steady rarefied gas flow from spherical source or sink
14 p2225 A71-30214
- Viscous gas unsteady flow between harmonically oscillating and nonoscillating walls
14 p2225 A71-30220

Melting body disintegration in hypersonic gas flow under radiation influence from shock layer, assuming optically thin boundary layer and intense vaporization 14 p2336 A71-30222

Heat transfer in rarefied gases, considering gas at rest between flat plates, concentric spheres and cylinders and flowing through tubes, nozzles and between parallel plates 14 p2336 A71-30242

Burning rate of Al particles suspended in polymer propellant gas flow with inorganic oxidizers 14 p2285 A71-30620

Acoustic waves reflection from nonplanar closed end of cylindrical tube with one dimensional isentropic gas flow from Riccati differential equation solution 14 p2227 A71-30665

Inert gases, hydrogen, deuterium and carbon dioxide flow in plane parallel glass slots over various Knudsen numbers, calculating slippage constants and volumetric discharge 14 p2227 A71-30673

Equations for radiative contribution to energy and mass transfer in monatomic and ionized gas flow in local thermodynamic nonequilibrium 14 p2338 A71-30819

Slender body interaction with interface forming after bursting of membrane separating low and high pressure gas supersonic flow in shock wave tube 15 p2386 A71-31162

Holographic recording of optical inhomogeneities in gas flow in hypersonic wind tunnels, using Mach-Zehnder interferometer and schlieren apparatus 15 p2404 A71-31274

Holographic interferometry for observing transparent media in supersonic gas flow, comparing results with Mach-Zehnder interferometry 15 p2404 A71-31275

Unmixed gases burning at finite reaction rate, analyzing steady laminar flames developing in mixing zone of fuel semiinfinite flow past static oxidizer 15 p2511 A71-31379

Circular pipe gas laminar flow at constant wall temperature, determining heat exchange and drag by motion and energy equations integration in boundary layer approximations 15 p2388 A71-31498

Gas permeable dispersion layer between impermeable solid wall and high temperature gas flow, solving dimensionless heat flux equations 15 p2512 A71-31505

Rotational temperature and density measurements in high speed gas flow by electron beam fluorescence technique [AIAA PAPER 71-605] 15 p2406 A71-31544

Nonreacting and equilibrium chemically reacting gas turbulent boundary layer flows through hypervelocity nozzles, comparing calculation with experiment [AIAA PAPER 71-597] 15 p2512 A71-31577

End wall sampling of high pressure shock tube, using abrupt pressure rise to drive test gas flow through duct to sample bottle [WSS/CI PAPER 71-18] 15 p2383 A71-31627

Pade fractions use in calculation of axisymmetric flow of perfect gas past blunt body of revolution, obtaining stream function Taylor expansion terms 15 p2346 A71-31222

Steady and unsteady modes of electric arc combustion in Ar and Ar-Cs flows produced by plasma accelerator in closed glass contour 15 p2457 A71-32269

Turbulent gaseous nonmagnetic protogalaxies under external torques, calculating angular velocity distribution 15 p2490 A71-32400

Colliding supersonic rarefied argon-helium jet flows diffusive separation in low density wind tunnel with electron beam diagnostics apparatus 16 p2554 A71-32800

Nonequilibrium nozzle flow determination for vibrationally relaxing gas, describing sudden freeze approximation method validity 16 p2556 A71-32907

Plane oblique shock wave diffraction on wedge moving in homogeneous gas flow at supersonic speed, reducing boundary value problem to Hilbert problem 16 p2519 A71-32930

Gas and liquid flows local velocity measurements, using Doppler frequency shifts due to wave scattering at solid microparticles suspended in flow 16 p2576 A71-33038

Optical diagnosis and measurements for radiation from gases in nonequilibrium flow 16 p2578 A71-33153

Two dimensional steady gas flows with heat addition, using reduction to partial differential equations 16 p2662 A71-33168

Solid disk supported above flat plate by thin layer of gas flowing from central orifice, studying vertical motion equilibrium and dynamic data [ASME PAPER 71-APM-3] 16 p2559 A71-33220

Droplet size and concentration in gas stream, discussing measurement error analysis and recording medium calibration procedure 16 p2663 A71-33363

Geometrical parameters effect on operation of high pressure two-stage nozzle ejector with conical mixing chamber, measuring gas flow rates, total pressures and stagnation temperatures 16 p2521 A71-33612

Gas flow behind cylindrical nozzles at roots and along periphery for narrow blades, using radial equilibrium equation 16 p2521 A71-33617

Fluid droplet collapse in two phase system gas flows, noting time dependence 16 p2663 A71-33893

Cascading turbomachine blades vibrations measurement in subsonic and sonic high temperature gas flows, describing test facility 16 p2553 A71-33993

Gas and liquid drop laminar, transition and turbulent flows heat transfer intensification in circular tubes, applying to hydraulic resistance design 17 p2835 A71-34205

Hypothetical gases transonic flow higher approximation, expressing flow solutions by Airy functions 17 p2726 A71-34508

Radiation field inhomogeneity effect on radiation gas jet flow, taking into account radiative energy transfer by differential approximation 17 p2728 A71-35117

Test apparatus for mechanical/thermal fatigue and vibration strength of turbine blades in high temperature gas flow 17 p2724 A71-35461

Tubular models sealed at one end with cavity facing oncoming steady gas flow, measuring increased stagnation temperature associated with shock wave formation 17 p2672 A71-35628

Method of characteristics application to supersonic jet and nozzle gas flow with allowance for equilibrium and nonequilibrium condensation 17 p2673 A71-35636

Viscous relaxing gas hypersonic flow around sphere in presence of nonequilibrium chemical reactions in shock layer 17 p2673 A71-35637

Fluid jets and droplets deformation in transverse supersonic two phase gas flow 17 p2673 A71-35638

Reynolds differential equations for three dimensional gas lubrication flows, noting linear velocity at rotating cylinder surface 17 p2749 A71-35639

Compressible electrically conducting gas boundary layer on MHD channel electrode, deriving equations for ambipolar region with finite ionization and recombination rates 17 p2790 A71-35644

Turbulent multispecies gas mixing measurements using dark field laser schlieren system 18 p2930 A71-36059

Unsteady multispecies gas mixture concentration flow measurement, using Raman scattering of pulsed nitrogen laser light 18 p2930 A71-36060

Secondary floating shock generation in supersonic ideal gas flow about blunt bodies, investigating body configuration and flight regime effects 18 p2845 A71-36331

Gas flow energy transport, discussing thermal radiation, radiant flux density, planetary atmosphere entry, thermodynamic equilibrium and differential approximations 18 p2847 A71-36426

Flow simulation with digital computer by Monte Carlo computation methods based on interacting molecular gas kinetics, noting application to gas flow 18 p2941 A71-36427

Gas flow through hypersonic conical nozzle in shock-gun tunnel, measuring pressure ratio and Mach number distributions at test section 18 p2849 A71-37024

Plane unsteady gas flow under action of dihedral angle shaped piston traveling at constant velocity 19 p3042 A71-37080

Gas flow velocity measurements in channel, using electromagnetic technique 19 p3061 A71-37090

Two and three dimensional pistons motion in stationary gas, calculating potential flow characteristics near weak discontinuities as function of piston geometry and acceleration 19 p3043 A71-37099

Plane transonic gas flows through Laval nozzle and symmetrical wedge-shaped profile, solving boundary value problem by reduction to singular integral equation 19 p2991 A71-37101

Gas flows with thermodynamic relaxation, considering expanding flows in hypersonic wind tunnel nozzles 19 p3162 A71-37458

Three dimensional rotational gas flows, using Berker compatibility equations 19 p3045 A71-37795

Conservation theorem of velocity circulation along moving contours in continuous steady ideal gas flow 19 p3046 A71-38222

Laminar-turbulent transition zone in boundary layer about bodies moving in gas at high Reynolds number using statistical physics methods 19 p3046 A71-38244

Gas resonant oscillations in closed end tube describing time-periodic motion by perturbation method with Mach number as flow parameter 20 p3211 A71-39073

Small signal gain and saturation intensity measurement of carbon dioxide laser as function of gas flow velocity 20 p3244 A71-39051

Flow field isentropes in conical ideal gas flow with singular stream surfaces 20 p3176 A71-39361

Short shock wave equations solutions for two dimensional steady flow of ideal gas 20 p3211 A71-39378

Flow velocity measurement in electromagnetically driven unsteady shock tube from charged particles extraction, using ionization gases 20 p3239 A71-39434

Wave reconstruction from gaseous flow holographic analysis with differential interferometry in polarized light and schlieren techniques with phase filter defocusing 20 p3239 A71-39466

Normal shock wave propagation in nonuniform gases with arbitrary property gradients based on modified method of infinitesimal contact discontinuities 20 p3212 A71-39482

Conjugate steady convective aerodynamic heating of plate in longitudinal compressible gas flow, taking into account boundary layer enthalpy distribution 21 p3317 A71-40088

Compressible viscous gas supersonic flow, observing near wake region behind perpendicular trailing face of rectangular plate with motion, state, energy and continuity equations 21 p3318 A71-40088

Electrode configuration and power output for transverse flow carbon dioxide laser consisting of two parallel water cooled copper tubes perpendicular to gas flow 21 p3391 A71-40181

Aerodynamic approximations for unsteady supersonic flow of perfect inviscid gas through flexible duct of revolution [ASME PAPER 71-VIBR-23] 21 p3458 A71-40288

Supersonic and hypersonic viscous gas flows with boundary layer induced pressure gradients, investigating disturbance upstream propagation by asymptotic theory 21 p3322 A71-40688

Plane acoustic wave transmission problem through finite chord plate array in subsonic gas flow, using factorization method in diffraction theory 21 p3322 A71-40688

Inviscid gas flow from supersonic nozzle into submerged region, considering specific heat ratio effect on dimensionless parameters, jet boundaries and suspended shock profiles 21 p3322 A71-40691

Pitot tube interaction with subsonic rarefied gas flow, considering impact pressure 21 p3323 A71-40691

Nonstationary ideal gas flow in variable section axisymmetric channel, noting flow disturbances during sudden changes in conditions at outlet section 21 p3368 A71-40691

German monograph on three dimensional steady hypersonic flow of perfect gas past pyramid shaped bodies of rhombic planform 21 p3323 A71-40777

Molecular beam extraction from equilibrium gas flows, describing shock beam formation model with associated escape probability 21 p3419 A71-40955

Nonlinear flutter of hinged closed cylindrical shell in supersonic gas flow, comparing with wind tunnel tests on panels 21 p3473 A71-41155

Ni and Ni-base alloys gaseous calorization by circulation method, investigating gas flow velocity effect on metal diffusive saturation 21 p3389 A71-41166

Kinetic and kinematic properties of steady diabatic complex lamellar gas flows 22 p3530 A71-41699

Streamline calculation of gas flow in bypass compressor with flow area divided by longitudinal partition 22 p3479 A71-41844

Hg condensation characteristics on Cs substrate in high velocity nitrogen carrier gas, formulating on dimensional flow model based on two phase three component gas dynamics 22 p3620 A71-41877

- Backflow region and shock interaction in rotating and swirling gas streams and jets in supersonic nozzle with separation and thrust effects 22 p3480 A71-42682
- Plane diabatic Prm gas flow, reducing hodograph equations in elliptic regions to Cauchy-Riemann equations via Baeklund transformations 23 p3662 A71-43121
- Plane steady rotational flow of inviscid gas with arbitrary state equation for straight or circular streamlines 23 p3662 A71-43236
- Approximate motion equations of gas flow behind detonation front in flat explosive plate covered by inert coating 23 p3781 A71-43358
- Liquid drop deformation and mass loss in high speed gas flow at high Weber numbers due to capillary surface waves 23 p3662 A71-43371
- Isentropic ideal compressible vortical gas flow in axisymmetric channel, determining stream function and gas density 23 p3625 A71-43549
- Self similar solutions for ideal gas flow driven by piston ahead of shock propagating in medium at rest with power law density distribution 23 p3719 A71-44143
- Chemically reacting gas mixture supersonic flow characteristics around blunt body, using differential equations 23 p3784 A71-44336
- Isothermal gas rotation in circular cylinder, calculating symmetric normal frequency modes [AIAA PAPER 71-999] 24 p3818 A71-44590
- Carbon ion and free electrons three body recombination rate coefficient measurement in carbon monoxide flows 24 p3802 A71-44607
- Nonlinear theory of wave resistance in supersonic ideal gas flow past finite flat axisymmetric bodies, establishing drag relation to flow rate deficit 24 p3790 A71-44773
- Shock initiation problem collisionless solution for transport properties of gas flow, considering departure from Navier-Stokes solution 24 p3819 A71-44791
- Laminar boundary layer calculation for simultaneous heat and mass transfer in evaporating liquid layer on flat plate in parallel gas flow, considering variable material parameters 24 p3888 A71-44965
- Compressible gas flow in two dimensional porous wall, calculating heat transfer and mass flow by conformal mapping for Laplace equation solution 24 p3889 A71-44972
- Polytropic process description for gas flow by introducing resistance and heat transfer coefficients 24 p3820 A71-45020
- Critical streamline length in axisymmetric and plane ideal gas flows past conical bodies as function of Mach number and form parameter 24 p3790 A71-45058
- Unsteady gas pulsations in compliant tube, predicting pressure amplitude extremum as function of mean flow by linear theory with frictional effect 24 p3820 A71-45073
- Flat face cylinders in rarefied supersonic gas flow, investigating perturbed region evolution 24 p3790 A71-45096
- Passive gas flow control with compensation for ambient temperature and supply pressure variations, using choked orifice with area variation linearly proportional to diaphragm deflection [ASME PAPER 70-WA/AUT-14] 24 p3828 A71-45137
- Monatomic gas flow in radiation field, noting effects on mass transfer 24 p3821 A71-45182
- Axisymmetric hypersonic flow of nonequilibrium ionized monatomic radiating inviscid gas past blunt body, using Clarke-Ferrari kinetic model 24 p3790 A71-45224
- GAS GENERATOR ENGINES**
U GAS GENERATORS
GAS GENERATORS
- Sinusoidal pressure generator for determining frequency response of small pressure transducers, pressure probes and characteristics of small diameter infinite lines 01 p0067 A71-10478
- Large gas turbine generator sets silencing, including silencer shells and doublewall acoustical/concrete enclosures [ASME PAPER 71-GT-26] 11 p1812 A71-25968
- Jet fuel starter, describing small gas turbine for starter, providing sufficient pressurized gas flow to rotate main engine [ASME PAPER 71-GT-43] 11 p1812 A71-25976
- Afterburning turbofan engine thrust calculation by gas generator method, using F-111A for comparison tests 14 p2292 A71-30744
- Combustion efficiencies of staged rocket motor consisting of gas generator, secondary combustor and converging-diverging nozzle [AIAA PAPER 71-739] 14 p2296 A71-30782
- Gas generator with high thrust-weight ratio, discussing thermodynamic cycles, mass flow rates and combustion chamber 15 p2471 A71-32571
- GAS GUNS**
NT LIGHT GAS GUNS
GAS HEATING
- Gas heating near quasars, Seyfert galaxies nuclei and pulsars by induced Compton effect 02 p0317 A71-12872
- Electrical shock tube performance with RF induction heating of downstream gas 04 p0564 A71-14672
- Stellar origin and evolution, discussing interstellar gas heating and condensation, star cluster formation and supersonic body decay 04 p0642 A71-14774
- Hypersonic shock wave production into air at one atmosphere in tube with electrical discharge gas heating 04 p0566 A71-14970
- Strong shock wave generation by detonation with simultaneous working gas heating and compression 05 p0735 A71-16381
- Intergalactic gas ionization and heating by UV radiation 06 p0974 A71-18429
- Interstellar gas acceleration and heating by cosmic rays streaming along uniform magnetic field faster than Alfvén speed 07 p1190 A71-18854
- Recombination emission by atoms or radicals used with population for inversion thermal gas laser production 07 p1128 A71-20529
- Twins tube gas heating resonator using bistable air wall attaching supersonic power jet 07 p1028 A71-20582
- Cellular convection in horizontal gas layer between solid walls and heated from below 08 p1376 A71-21789
- Transparent radiating gas thermal instability criteria derivation from gasdynamic equations 09 p1519 A71-22528
- Intergalactic gas ionization and heating by UV radiation 12 p1955 A71-26579
- Strong shock wave generation by detonation with simultaneous working gas heating and compression 12 p1898 A71-27460
- Two dimensional inviscid heated flows in terms of pressure, density, speed, direction and heating rate applied to supersonic duct combustion chambers 12 p1987 A71-27735
- Low pressure gas heating in shock tube, considering stagnation temperature increase 13 p2049 A71-29198
- Light propagation through moving gas, computing beam bending into wind and self defocusing due to gas heating 14 p2274 A71-30129
- Interstellar gas heating by soft X rays and cosmic rays for electron production, calculating heating rate with Boltzmann equation and Monte Carlo method 14 p2302 A71-30642
- Monatomic mercury gas excitation and ionization mechanisms ahead of and behind shock front, establishing electron gas heating kinetics in relaxation zone 16 p2616 A71-32902
- High temperature dense plasma formation by laser heating of gas target, noting fusion reaction in deuterium-tritium mixture 16 p2619 A71-33647
- Interelectrode gap position control of discharge in coaxial gas heater with arc rotated by magnetic field 17 p2676 A71-34309
- Radiation source consisting of porous wall heated internally by hot gas, noting application as high altitude or space flare 17 p2728 A71-34888
- Transparent radiating gas thermal instability criteria derivation from gasdynamic equations 17 p2807 A71-35504
- Radiative heat transfer in atomic lines through shock heated nonhomogeneous gases by analytical frequency integration, using separability approximation 19 p3162 A71-37407
- Gas heating and energy balance of HF ring discharge in rare gases within cylindrical vessel, discussing electron energy distribution functions 20 p3273 A71-39044
- Gas heating by LF radiation due to Compton scattering near quasars, Seyfert galaxies nuclei and pulsars 20 p3289 A71-39293
- Gum Nebula ionization and heating by energetic particles from Vela X supernova 22 p3598 A71-41917
- Optical line spectrum and ionization equilibria of hard UV radiation and energetic proton heated hydrogen, helium, nitrogen, oxygen and neon 22 p3601 A71-42160
- Laminar heat transfer losses effects on piston gas heater performance, computing heat transfer rate and thermal boundary layer thickness 24 p3887 A71-44603
- GAS INJECTION**
- Solar wind injection into magnetosphere, noting effects of magnetopause outward velocity and electric field strength 01 p0146 A71-11452
- Molecular mass gage with chambers interconnected by porous membranes for injected small gas samples 02 p0250 A71-12137
- Secondary gas injection at right angles into supersonic rocket nozzle, investigating side force characteristics 03 p0470 A71-13736
- Heat exchange in dissociating partly ionized gas flow over critical point on permeable surface with injection into laminar boundary layer 03 p0342 A71-13748
- Film cooling of flat plates by angled cold air injection for turbine blade applications 04 p0639 A71-15472
- Supersonic compressible turbulent boundary layer on porous cylinder with air injected through wall, investigating heat transfer 04 p0571 A71-15498
- Air, helium and carbon dioxide injection effect on turbulent boundary layer thermodynamic behavior by wind tunnel experiments 04 p0576 A71-15615
- Air injection into turbulent boundary layer flow through porous plate, examining heat transfer and shielding efficiency 05 p0838 A71-16783
- Noise reduction in turbulent jet by repeated air injection at boundary of jet core 06 p0848 A71-18704
- Two dimensional flow field in secondary sonic transverse jet injection port vicinity, studying free stream Mach number, total pressure and specific heats ratio 07 p1090 A71-19896
- Injected air cooled turbine blade trailing edges temperature, calculating thermal distribution with differential equations 08 p1348 A71-21265
- Boundary layer flow with large mass injection rate, presenting numerical method with rapid convergence for increasing blowing parameter 09 p1430 A71-22108
- Hypersonic flow interaction with transverse jet, discussing experimental investigation of Reynolds number, jet pressure ratio and mass flux effects 09 p1382 A71-22944
- Air and carbon dioxide intensive injection effect on turbulent boundary layer of subsonic channel air flow 10 p1551 A71-23478
- Velocity, temperature and concentration profiles correlation for compressible turbulent boundary layer along porous flat plate, with carbon dioxide injection, discussing cooling applications 10 p1598 A71-25095
- Heat and mass transfer in supersonic laminar boundary layers with light gas injection, deriving approximate solution for binary mixture flow with variable fluid properties 10 p1598 A71-25097
- Two layer thermal and velocity model of gaseous film cooling with constant turbulent step slot flow [ASME PAPER 71-GT-3] 11 p1855 A71-25949
- Cooling air injection effect on turbine efficiency, presenting experimental results for single stage air driven turbine with cylindrical stator and rotor blades 12 p1946 A71-27503
- Supersonic flow around porous-wall conical body with uniform gas injection through wall, deriving equations for pressure at contact surface 13 p1990 A71-28182
- Blowing angle effect on heat protection effectiveness of flat wall in slit injected low speed air flow with turbulent boundary layer in wind tunnel 13 p2159 A71-28420
- Gas turbine engine combustion chamber start-up and burning performance, considering air injection and propellant atomization 13 p2117 A71-28968
- Gas turbine engine startup igniter with modified propellant atomizer enhanced by air injection 13 p2118 A71-28969
- Viscous gas flow past semiinfinite porous plate with gas injection or suction and identical composition in outer flow 14 p2224 A71-30002
- Inert and reactive gas injection in near wake behind afterbodies in supersonic flow, considering influence on base pressure and temperature 14 p2336 A71-30213
- Thermionic converter output improvement by Ar injection at low Cs pressures 14 p2182 A71-30679

GAS IONIZATION

Cold flow tests of mixing and atomization characteristics of gas/liquid circular coaxial injector elements in pressurized facilities [AIAA PAPER 71-672] 14 p2291 A71-30736

Gas injectors characteristics investigation by cold flow simulation, using flow field visualization techniques and velocity and mass concentration profiles measurements [AIAA PAPER 71-675] 14 p2291 A71-30739

Two dimensional sonic nonreacting gaseous secondary injection into supersonic primary stream with turbulent boundary layer for application to thrust vector control [AIAA PAPER 71-750] 14 p2227 A71-30786

High pressure gaseous hydrogen oxygen auxiliary propulsion systems /APS/ thruster design and cold flow and hot fire testing for space shuttle requirements [AIAA PAPER 71-737] 15 p2470 A71-32291

Air injection into turbulent boundary layer flow through porous plate, examining heat transfer and shielding efficiency 16 p2662 A71-33035

Air injection into trailing vortex core, noting jet flow effect on circumferential velocity 19 p2991 A71-37291

Injection conditions effect on ignition temperature of methane and hydrogen in hot Mach 2 air stream 19 p3163 A71-37889

Gaseous hydrogen and methane injection into supersonic air stream heated by plasma burner, studying combustion effects on flow field 19 p3168 A71-38104

Thermal protection of two dimensional supersonic nozzle fed with hot air by tangentially injected cold gaseous films for convergent and constant section ducts 20 p3314 A71-39415

Pulmonary dissipation of gas emboli produced by oxygen, nitrogen and carbon dioxide intravenous injection in unanesthetized sheep with chronically implanted ultrasonic Doppler flow probes 21 p3330 A71-40342

German monograph on flow and combustion changes during hydrogen and methane transverse injection into hot supersonic air jet 21 p3475 A71-40750

Windward injection into supersonic stream at angle of attack, minimizing vortex disruption 22 p3481 A71-42787

Incompressible turbulent boundary layer with suction and surface injection computation by implicit finite difference method and turbulent kinetic energy equation for mixing length flow 24 p3820 A71-44954

Computer program for recirculating fluid flows applied to concentration curves obtained by gas injection on pipe center line with fully developed turbulent flow 24 p3820 A71-44956

GAS IONIZATION

NT ATMOSPHERIC IONIZATION

NT AURORAL IONIZATION

NT FLAME IONIZATION

Monograph on particle diffusion losses in contact ionization plasmas under Q machine conditions covering collisionless theory, thermalization, alkali metals, ion recombination, etc 01 p0131 A71-10102

Similar solution of strong shock wave propagation with nonequal heat coefficients, approximating energy of dissociation ionization and free molecular oscillation 01 p0070 A71-10663

Explosion shock wave induced short wave radio emission, deriving time related gas ionization state of wave front 02 p0284 A71-11927

Thermodynamic equations of state for dissociating and ionizing high temperature air applied to vertical and oblique compression shocks 02 p0331 A71-12067

Gas ionization in supersonic wake at throat, transition and breakthrough points in hyperballistic firing tunnel for atmospheric reentry study 03 p0462 A71-13131

Ionizing shock wave interaction with transverse magnetic field, examining magnetic field distribution behind shock front, interface discontinuity and wave reflection 03 p0462 A71-13234

Stellar variability emphasizing pulsations, noting role of He II critical ionization zone in maintaining self oscillations 03 p0485 A71-13259

Knocked out atomic electron energy during impact ionization, comparing Thomson and Drawin formulas 03 p0465 A71-13954

MHD shock waves structure capable of ionizing gases, using law of conductivity variation with temperature 03 p0465 A71-14063

High density atmospheric pressure plasma ionization measurement by negatively pulsed Langmuir probe, showing agreement with space charge controlled sheath expansion model 04 p0586 A71-14660

Ionizing shock wave propagation through MHD channel flow, determining induction emf current and electron density and concentration 04 p0632 A71-14691

Flat plate ion density probe with convection and ion production in electric sheath, comparing to shock waves in air 04 p0632 A71-14706

Angular distribution of atomic oxygen ions produced by electron bombardment of oxygen, showing electron energy dependence 04 p0631 A71-15657

Intergalactic gas photoionization by quasars UV radiation, using Friedman cosmological model 05 p0805 A71-16111

Laser torch plasma dispersion gas dynamics from motion and kinetics of ionization processes 05 p0760 A71-16181

Rare gases interaction with focused multimode Q switched laser beam, measuring orders of nonlinearity and multiphoton ionization probabilities 05 p0761 A71-16335

Planetary atmospheres ionosphere formation by cosmic rays, examining ionization of various gases 05 p0799 A71-16817

Cross sections for fluorescence production in carbon dioxide photoionization by 58.4 nm radiation, deriving emission spectra 06 p0963 A71-17255

Inelastic ionization cross sections for protonic and atomic hydrogen collisions with atomic and molecular gases in 0.5 keV to 5 MeV energy range 06 p0928 A71-17266

Intergalactic gas ionization and heating by UV radiation 06 p0974 A71-18429

Quiescent metallic and ordinary prominences continuum spectra measurements, showing hydrogen ionization dependence on microstructure 06 p0975 A71-18438

Static solar H II region ionization balance, energy, UV radiation transfer, gravitational equilibrium and interstellar gas temperature 06 p0975 A71-18442

Gas ionization relaxation phenomena behind strong shock waves, discussing ionization kinetics, radiation transfer effects, relaxation time and radiative heating 07 p1087 A71-19172

Shock waves with high equilibrium temperature, calculating structure during multiple ionization of atoms 07 p1087 A71-19186

Field ionization yield with single graphite whisker lateral surface as ionizer, using helium, ammonia, carbon monoxide and carbon dioxide 07 p1164 A71-19855

Collision free ionizing wave propagation into cold low density un-ionized gas, showing wave oscillations damping due to ion velocities phase mixing 07 p1171 A71-20289

Hydrogen and helium photoionization, calculating total cross section and transitions for soft X ray region 08 p1350 A71-20948

Book on gaseous ionization and plasma electronics covering atomic structure, electron emission, charged particle behavior, self sustaining discharge and breakdown mechanisms 08 p1341 A71-21700

Stationary longitudinal turbulent flow of air with equilibrium ionization and dissociation around plate, calculating heat exchange and frictional drag 08 p1228 A71-21922

Interaction between perfect gas ionizing shock wave and transverse magnetic field in coaxial channel, indicating incident wave attenuation and reflected shock wave formation 09 p1498 A71-22128

Phase transitions possibility in nonideal multiply ionized plasma, analyzing equation of state and ionization equilibrium equation for various ionization multiplicities 09 p1500 A71-22244

Gas ionization by fission fragments emitted by spherical or cylindrical sources, deriving analytical expressions for ion distribution via diffusion model 09 p1496 A71-22358

Atomic hydrogen equilibrium abundance in dense dark hydrogen clouds as function of low energy cosmic ray ionization rate 10 p1662 A71-24491

Kinetic and ionization phenomena in Q switched laser produced plasmas, considering gas dynamic plasma parameters /velocity, density distribution, pressure and temperature/ 11 p1806 A71-26086

Electrostatic probe measurements of charged particles and thermal ionization relaxation in shock heated low density supersonic monatomic gas flows 11 p1766 A71-26286

Intergalactic gas ionization and heating by UV radiation 12 p1955 A71-26579

Quiescent metallic and ordinary prominences continuous spectra measurements, showing hydrogen ionization dependence on fine structure 12 p1955 A71-26580

Static solar H II region ionization balance and energy, UV radiation transfer, gravitational equilibrium and interstellar gas temperature 12 p1955 A71-26592

Low temperature plasma collisional-radiative ionization and recombination coefficients, discussing nonequilibrium factors affecting electron density change rate 12 p1939 A71-27270

Thermal ion-atom charge transfer effects on ionization equilibrium of interstellar oxygen in H I regions using Bahcall-Wolf orbiting approximation 13 p2132 A71-27960

Monograph on shock and detonation waves ionization and structure covering diagnostic techniques, heat transfer, particle flow, pressure measurements, etc 14 p2335 A71-29933

Similar solution of strong shock wave propagation with nonequal heat coefficients, approximating dissociation, ionization and excitation energy of molecules vibrational degrees of freedom 14 p2228 A71-30996

Communication blackout during missile and spacecraft high altitude flight, considering convective effects on gas breakdown by microwaves 14 p2206 A71-31071

Nitrogen inductive low pressure discharge, determining vibrational and rotational temperatures, ionization degree, electron temperature and energy balance by spectroscopic technique 15 p2451 A71-31487

Ionization measurement in detonation and shock waves in reactive gas mixtures by microwave cavity techniques 15 p2411 A71-32556

Continuous light absorption, emission and ionization relaxation behind shock front in xenon 16 p2613 A71-32890

Fast argon plasma flow interaction with strong magnetic fields, describing ionization relaxation phenomena behind magnetically reflected shock fronts 16 p2615 A71-32898

Monatomic mercury gas excitation and ionization mechanisms ahead of and behind shock front, establishing electron gas heating kinetics in relaxation zone 16 p2616 A71-32902

Ionizing shocks in argon produced by pressure driven shock tube, measuring velocity and ionization within and behind nozzle 16 p2616 A71-32904

Argon gas ionization behind reflected shock wave front investigation by double probe method with HF multistep pulse voltage 16 p2576 A71-32911

Ionization profiles of shock heated argon with impurities, using microwave and pulsed Langmuir probe measurements 16 p2616 A71-32912

Shock wave generated plasmas elementary reactions, discussing shock tubes and noble and diatomic gases chemionization 16 p2540 A71-32970

Low temperature high conductivity nonequilibrium plasma creation in MHD generators by microwave ionization 17 p2676 A71-34193

Stationary longitudinal turbulent flow of air with equilibrium ionization and dissociation around plate, calculating heat exchange and frictional drag 17 p2671 A71-35266

MOS sandwich grid diode for gas ionization and field electrons generation at solid-gas phase boundaries 17 p2717 A71-35448

Flow processes around body of hypersonic velocity, studying plasma diagnostics in ionized wake 18 p2952 A71-36421

Normal and oblique shock thermodynamic equilibrium state variables calculation, taking into account air dissociation and ionization 18 p2909 A71-36678

Electron temperatures for lithium-like ions O VI, Ne VIII and Mg X formation in solar chromosphere and corona, using rocket spectrometric measurements 19 p3136 A71-37618

Numerical integration of Schroedinger equation for spontaneous ionization of hydrogen atom in electric field 19 p3107 A71-38056

Hydrogen ionization and excitation equilibrium, using slab model atmospheres irradiated from both sides by photospheric, chromospheric and coronal radiation 19 p3146 A71-38664

Electromagnetically driven shock tube with precursor effect due to ionization of impurities by UV radiation from discharge, using gages to tag gas flow 20 p3239 A71-39431

Gum Nebula conceived as hydrogen gas mass ionized by UV radiation from supernova explosion related to Vela X remnant, discussing fossil Stroemgren sphere model
20 p3294 A71-39572

Ionization relaxation phenomena behind strong shock waves, discussing ionization kinetics, radiation transfer effects, relaxation time and radiative heating
21 p3365 A71-40087

Acoustic pulse excited ionization waves and wakes measurement in glow discharge plasma, giving phenomenological explanation
21 p3421 A71-40089

Interstellar medium time dependent model, investigating supernovae and hot stars UV ionization effects on ion production and heating and cloud formation
21 p3445 A71-40248

Simultaneous CW microwave radiometer and laser probing of hypersonic wake ionization and turbulence, relating radiation temperature, radar echo and mechanical flow field structure
21 p3392 A71-40387

Reversible charge exchange reactions effects on ionization equilibrium of nitrogen in interstellar space
21 p3445 A71-40412

Shock free transonic deceleration of solar wind due to ionizing interactions, discussing plasma flow
21 p3438 A71-40604

Neutral gas acceleration to high velocity at low ionization level by electromagnetic plasma gun formed ionized shock wave
21 p3423 A71-40766

Phase transitions possibility in nonideal multiply ionized plasma, analyzing equations of state and ionization equilibrium equation for various ionization multiplicities
21 p3424 A71-41133

Gum Nebula ionization and heating by energetic particles from Vela X supernova
22 p3598 A71-41917

Spacecraft communication cut-off during atmospheric reentry due to thermal ionization of gas boundary layer, discussing sulfur hexafluoride injection alleviation and electrostatic probe
22 p3583 A71-41998

Optical line spectrum and ionization equilibria of hard UV radiation and energetic proton heated hydrogen, helium, nitrogen, oxygen and neon
22 p3601 A71-42160

Ne ionization relaxation time behind reflected shock waves from temperature and pressure measurements of combustion driven shock tube end wall
23 p3706 A71-42909

Interstellar He photoionization effect on solar wind abundance
23 p3721 A71-43182

Plane supersonic ionizing shock wave in magnetic field under small wave plane perturbation from equilibrium position, calculating stability from linearized equations
23 p3663 A71-43575

Stratified nonequilibrium plasma ionization instability in crossed fields investigated by physical model without diffusion processes and boundary effects, considering space-time behavior of perturbation
23 p3713 A71-44152

Electromagnetic wave propagation in gas with interdependent electron density and electric field strength, calculating transmitted power limit value
24 p3851 A71-44428

Dense discharge plasma temperature and ionization distributions in He, H and Ar, investigating pulsed arc emission dependence on current and pressure
24 p3855 A71-44520

He ionization and excitation in optically thick solar prominences, considering recombination excitation for observed triplet-level populations at 5000-10,000 K electron temperature
24 p3869 A71-44805

Atomic and molecular gases electron impact ionization, measuring secondary particle energy distribution and angular dependence
24 p3850 A71-44925

Low temperature kinetics of metastable He atom pair collisions, investigating temperature dependence of plasma ionization
24 p3856 A71-45054

Stepwise ionization effects on ionic wave propagation and oscillation stability in inert gas DC discharges
24 p3857 A71-45230

Langmuir electron oscillation excitation by ion beam at velocity exceeding average electron thermal velocity in plasma formed by residual gas ionization
24 p3858 A71-45234

GAS JETS

Maximum ion concentration zone in diffusively turbulent flames in fuel gas free jets, using mass exchange processes analysis
01 p0178 A71-10341

Compressible gas jet flow from vessel with parallel walls pointing in opposite directions, solving Chaplygin equations for stream functions
01 p0069 A71-10420

Ionization rates in low pressure hydrocarbon flames produced by colliding burning gas jets
01 p0180 A71-11113

Turbulent diffusion gas jet length in transverse flow and in stationary air medium
01 p0181 A71-11147

Two dimensional free gas jet expansion into quiescent medium, predicting terminal shock position
03 p0400 A71-13466

Parallel nonuniform supersonic flow of two coaxial gas jets past sphere
03 p0345 A71-14562

Axisymmetric supersonic overexpanded ideal gas jet calculation, using finite difference method based on buildup principle
03 p0346 A71-14573

Variable density turbulent jets, discussing compressible, high temperature gas, cryogenic and supersonic jets, Reynolds equations, etc
04 p0577 A71-15620

Turbulent pulsation mixing of free gas jets in mechanical vortex generator with turbulence level control
04 p0577 A71-15621

Parallel incompressible gas jets mixing of variable densities based on dimensional analysis
04 p0577 A71-15623

Ejector pump with gas-air jet, deriving momentum conservation equation
06 p0882 A71-18010

Free turbulent mixing of heated high speed central hydrogen jet and cold low speed annular air stream coupled with finite rate chemical reactions
06 p0866 A71-18479

Gas temperature in combustion chamber and jet nozzle exit, and gas jet velocity resulting from various pressures, temperatures and air excess factors combinations
06 p0948 A71-18702

Two link approximation of Chaplygin function by coupling to integral equations, applying to ideal gas jet separation flow past symmetrical arc
07 p1016 A71-20084

Ideal gas jet sonic flow past wedge according to Kirchhoff scheme, testing sine series solution for convergence
07 p1016 A71-20085

Ruby laser driven luminous waves during breakdown and heating within freely expanding gas jet observed with streak photography
07 p1126 A71-20168

Oscillations generating mechanism in resonance tube fed by subsonic gas jet, determining oscillations amplitude and frequency at resonance
09 p1382 A71-22406

Circular gas jet path lines in nonuniform velocity side field drift flow, using auxiliary curve values and correction coefficients
09 p1432 A71-22730

Aeroacoustic phenomena in free turbulent gas jets, discussing structure, noise-turbulence correlations and acoustic field generation at subsonic/critical velocities
09 p1384 A71-23607

High velocity airstream interaction with multiple gas jets from single row multihole wall injectors, discussing jet penetration and mixing in cross flow
11 p1750 A71-25478

Arc melter using Pyrex pipe cross for controlled atmosphere chamber, incorporating Ar jet into electrode holder for dynamic flushing and rapid quenching
13 p2044 A71-28154

Critical overexpanded jet conditions of gas ejector at large pressure gradients based on supersonic compressed layer theory
13 p1993 A71-29213

Two coaxial axisymmetric subsonic gas jets of different density mixed during expulsion from convergent nozzles with high compression, using flow rate ratio
13 p2050 A71-29215

Viscous gas jets in uniform oncoming flow, deriving similarity laws by dimensional analysis theory
13 p1994 A71-29223

Pulsating follower loads implementation by pulsating gas or liquid jets, using Mettler differential equations for forced vibrations of elastic bodies
15 p2502 A71-31172

Supersonic underexpanded submerged gas jet at various Mach and Knudsen numbers and pressure ratios, observing trailing shock wave geometry
17 p2669 A71-34218

Shock standoff distance and Mach disk diameter measurements in underexpanded sonic jets, using nitrogen dioxide-tetroxide working fluid
17 p2670 A71-34895

Approximate method for hydrodynamic parameters of supersonic ideal-gas jet, considering isentropic region and theoretical boundary of underexpanded jet
18 p2902 A71-36114

Base pressure of cluster rocket exhaust with several jets simultaneously ejecting from nozzles
18 p2903 A71-36116

Turbulence measurement in subsonic wind tunnel gas jet flows containing dust particles, using Doppler difference laser velocimeter
21 p3392 A71-40397

Solid particle or droplet admixture effect on turbulent gas jet structure
22 p3530 A71-41872

Supersonic Ar, He and molecular nitrogen jets, determining electron temperature and concentration and atomic state population in shock waves region by spectroscopic measurement
23 p3712 A71-43916

Laser pulse produced plasma in freely expanding high density nitrogen gas jets, measuring electron temperature and light-plasma interaction time
23 p3687 A71-44140

Knudsen effusion problem in thermal molecular gas jet mixing, using moment method based on velocity distribution function
24 p3817 A71-44354

GAS LASERS

NT CARBON DIOXIDE LASERS
NT HELIUM-NEON LASERS
He-Cd laser stable long life CW excitation by DC cathaphoresis to maintain spatially uniform and optimum Cd vapor concentration
01 p0091 A71-10007

He-Ne laser LF radiation parameters calculations verified experimentally
01 p0092 A71-10334

Pulsed hydrogen fluoride gas laser output line spectral distribution, describing experimental setup and measurements
01 p0092 A71-10371

Gas laser output allowing for energy exchange between levels using population balance method
01 p0093 A71-10603

Start-stop pulse generator for gas laser in quasi-steady monoimpulse mode with given emission duration
01 p0093 A71-10621

Laser effect radiation power in gas mixture flow of carbon dioxide, nitrogen and traces of water vapor, presenting calculations based on kinetic theory
01 p0094 A71-10992

Multifrequency gas laser spectrum structural changes caused by small external light signals
01 p0095 A71-11115

He-Ne IR laser resonator as quadratic receiver for modulated filtered laser emission, noting strong LF noise
01 p0096 A71-11218

Gain measurement on pulsed radiation from high voltage discharges in mixtures of carbon dioxide, nitrogen and helium
01 p0096 A71-11423

Output increase through waste energy dissipation improvement by forced convection via high speed flow for thermally pumped gas dynamic laser
01 p0096 A71-11626

He-Ne discharge regular oscillations effect on laser output power
02 p0259 A71-11930

Diffraction frequency splitting of opposed waves produced by diaphragm in He-Ne laser resonator
02 p0260 A71-11938

CW nitrous oxide laser action at 81.5 and 263.4 micrometers in optically pumped ammonia gas, measuring rotational and inversion frequencies
03 p0434 A71-13476

Limited scanning function of optical system consisting of He-Ne laser and Fabry-Perot interferometers with small effective apertures
03 p0435 A71-13514

Single mode polarization in simple gas laser for long path difference Michelson interferometry
03 p0436 A71-13653

IR gas pulsed lasers continuous self mode locking, observing optical spectra with scanning Fabry-Perot interferometer
03 p0438 A71-13889

CW laser output in carbon dioxide and nitrous oxide induced by vibrational energy transfer from excited carbon monoxide
03 p0438 A71-13893

Laser action on six lines of ionized Xe spectrum, discussing discharge tube, optical resonator and spectrograph characteristics
03 p0438 A71-13895

He-Ne laser with hemispherical nontunable internal cavity resonator formed by mirrors bonded to discharge tubes
03 p0439 A71-13999

IR Q switched gas laser with Michelson interferometer for plasma diagnostics, describing equipment operation
03 p0439 A71-14056

He-Ne laser light beam double slit experiments, investigating multimode operation effect on spatial coherence
03 p0440 A71-14177

He-Ne laser self-locked or mode-locked with Ne absorption cell, investigating phase relationships between modes
03 p0440 A71-14183

He-Ne laser emission modulation through active element excitation source 04 p0604 A71-14626

Gas laser technology developments, discussing UV CW noble gas ion lasers, high output IR carbon dioxide lasers, metal vapor and pure helium lasers 04 p0605 A71-14711

Laser Q-branch emission near 8 microns from flowing hydrogen-acetylene-helium mixture under pulsed electrical excitation 04 p0607 A71-15038

Laser power from carbon monoxide supersonic expansion in nitrogen and argon mixtures, comparing to carbon dioxide gas dynamic lasers 04 p0608 A71-15042

Optical signal amplifiers operational principles, discussing parametric, semiconductor laser, and solid state lasers and amplifiers using gas in Fabry-Perot resonator 04 p0608 A71-15079

Doppler effect in laser beam probe of scattering objects, using interferometer for scattered light intensity angular distribution relation to hologram sizes 04 p0608 A71-15117

Gas laser axial modes mutual synchronization for frequency modulation, considering stability condition and even/odd harmonics 05 p0760 A71-16005

Frequency stabilization and measurement of single frequency He-Ne laser at 0.6328 microns, using Michelson interferometer as mode selector and reference cavity 05 p0760 A71-16006

Laser torch plasma dispersion gas dynamics from motion and kinetics of ionization processes 05 p0760 A71-16181

He-Ne laser beam parameters and diffraction field measurement by holography 05 p0760 A71-16260

Two mode He-Ne gas laser irradiance autocorrelation function measurement, comparing time-to-amplitude converter techniques with frequency domain measurements 05 p0760 A71-16268

CO laser emission lines and nitrogen oxides absorption lines spectral coincidences observations 05 p0762 A71-16339

Operational characteristics, spectroscopy and inversion mechanisms of noble gas ion lasers in light of plasma theories and atomic data [AIAA PAPER 70-82] 05 p0763 A71-16551

He-Ne laser light intensity fast and slow modulation by thin acoustoelectric photoconducting CdS platelet oscillators 06 p0906 A71-17308

Gas laser radiation depolarization coefficient as function of radiation energy, cavity anisotropy and operating transition type 06 p0907 A71-17595

He-Ne laser atomic scattering theory 06 p0907 A71-17997

Two layer antireflection coatings on glass for He-Ne lasers, calculating optimal film thicknesses for various substrates and wavelengths 06 p0907 A71-18038

Lasers operating on rotation vibration of chemically formed carbon monoxide, discussing excitation methods 06 p0908 A71-18312

Nitrogen-carbon dioxide thermally pumped gas dynamic lasers, using high speed flow for waste energy removal [AIAA PAPER 71-23] 06 p0908 A71-18490

Laminar boundary layer effect on gasdynamic laser gain, considering vibrational relaxation time and population inversion [AIAA PAPER 71-24] 06 p0908 A71-18491

Carbon dioxide-nitrogen-vapor gas dynamic laser, discussing generation, power and gain [AIAA PAPER 71-25] 06 p0908 A71-18492

High power continuous and pulsed coherent radiation generation by gas lasers, discussing transmission by proton generators and transforming engines [AIAA PAPER 71-106] 06 p0946 A71-18557

Gas lasers pumping by nuclear energy, discussing heavy particle interactions, threshold densities, population inversion, etc. [AIAA PAPER 71-110] 06 p0909 A71-18560

Gas laser using nonequilibrium MHD generator with He, carbon dioxide and Cs mixture [AIAA PAPER 71-68] 06 p0940 A71-18656

Noise spectra of CW hollow cathode zinc ion laser comparison with conventional discharges, noting gain per unit length on transitions 06 p0910 A71-18662

He-Cd laser output description by rate equations, investigating saturation effects, discharge processes and optimization 06 p0910 A71-18666

He-Zn vapor lasers excitation mechanism, presenting Penning and charge transfer cross sections 06 p0910 A71-18670

Annular gas laser beat frequency as function of Doppler shift emission, examining mirrors feedback, cavity Q and pumping variational effects 07 p1122 A71-19137

Gas laser gain and loss coefficients measurement, using resonator staged calibrator plate for optimal and nonoptimal conditions 07 p1122 A71-19139

Hydrogen fluoride elimination chemical laser from difluoromethylamine using temperatures below 268 K and flash photolysis 07 p1123 A71-19372

Pressure dependent shift of He-Ne laser radiation, observing beat frequencies 07 p1123 A71-19486

Gas laser optical pumping based on photodissociation, calculating spatial temporal distributions of pump radiation absorption probability and main level population 07 p1125 A71-19806

He-Ne laser spontaneous emission intensity in N synchronized longitudinal modes as function of intermode beat frequency and longitudinal magnetic field strength 07 p1127 A71-20376

He-Ne laser coherence measurement by Young interference method, noting dependence on resonator mirror alignment 07 p1127 A71-20378

Scattered light depolarization measurement near carbon dioxide critical temperature, using He-Ne laser 07 p1127 A71-20379

Circularly polarized He-Ne ring laser operation, noting no traveling waves coupling via amplifying medium and locking due to cavity imperfections 07 p1127 A71-20388

CW helium-air-carbon monoxide laser with low flow rate and liquid nitrogen cooling, observing emission below 5 microns 07 p1128 A71-20398

Recombination emission by atoms or radicals used with population for inversion thermal gas laser production 07 p1128 A71-20529

Gas dynamic lasers design and operation, discussing pumping techniques, waste energy removal and mode control 08 p1301 A71-20693

IR laser action at 2-3 microns by low pressure discharge and gas mixtures containing molecular oxygen and sulfur dioxide 08 p1301 A71-21190

Design and spark erosion production for circular Fresnel zone plates under He-Ne laser illumination, considering plates as optical reference elements 08 p1289 A71-21374

Spurious inverse Lamb dip mode lock in saturated absorption stabilized He-Ne laser 08 p1302 A71-21406

Transistorized gas laser discharge current stabilizer using double feedback circuit, discussing schematic diagram and operation principles 08 p1303 A71-21807

Beat and synchronization modes of opposed waves in rotating gas ring laser, examining frequency response asymptotic behavior 09 p1460 A71-22222

Photodetector frequency response measurement, using beat light signals from mixed single mode He-Ne lasers 09 p1460 A71-22227

He-Ne ring laser in locking range, studying opposing waves amplitude and phase differences dependence on cavity rotation and oscillation frequency tuning 09 p1461 A71-22382

Two oscillation mode He-Ne gas laser, discussing frequency stabilization by strong competition effect at gain curve center 09 p1461 A71-22387

Helium role in populating upper levels of cadmium gas laser in discharge tube 09 p1462 A71-22401

Oscillation frequency shift and gas discharge tube design relation in He-Ne DC lasers 09 p1462 A71-22402

He-Ne laser as detectors in mine boring, quality/compensational control, data collection/reduction and positioning accuracies 09 p1458 A71-23409

Continuous wave HCl chemical laser, achieving large specific gain through high speed flow, rapid mixing and transverse geometry 09 p1465 A71-23480

Computer controlled electromechanical system for luminous projection on world map of satellite orbits, using Ne-He laser beam 09 p1430 A71-23627

Iterative technique using continuous gas laser for alignment of Mach-Zehnder interferometer for monochromatic and white light fringes 09 p1453 A71-23692

Transverse gas flow effects on deuterium fluoride-carbon dioxide chemical laser output, discussing amplifier medium homogeneity factor 10 p1619 A71-23834

High efficiency gas chamber for obtaining Raman spectra of corrosive gases at atmospheric pressure by He-Ne laser excitation 10 p1619 A71-23857

Mode locked He-Ne laser pulse compression and expansion by electro-optic internal modulator 10 p1619 A71-23858

He-Ne laser 0.63 micron line collisional broadening dependence on gas temperature 10 p1620 A71-24240

Single-mode He-Ne laser, investigating longitudinal magnetic field effect on output amplitude, frequency and polarization characteristics 10 p1620 A71-24330

High resolution laser homodyne interferometer for determining small time resolved optical path length variations, using Michelson interferometer with He-Ne laser 10 p1611 A71-24400

Superregenerative linear mode amplification in switched He-Xe laser as function of resonator phase length and signal angle 10 p1621 A71-24710

Amplitude characteristics of Q switched He-Ne laser at 3.5 microns, using rotating reflection prism and velocity equations 10 p1621 A71-24711

Internal asynchronous modulation of He-Ne laser with Doppler broadened line of working transition in multifrequency mode 10 p1621 A71-24888

Nonresonance vibrational exchange in molecular binary harmonic and one component anharmonic oscillators with beam laser applications 10 p1622 A71-24888

Heated mirrors and hot plasma column effects on diffraction losses and power output of gas lasers 10 p1623 A71-25099

Flame structure and propagation studied by modified Mach-Zehnder interferometers with He-Ne laser source, describing optical arrangements 10 p1623 A71-25121

Iodine photodissociation laser kinetic model for pumping, radiative and collisional processes, predicting reactant pressure and flashlamp parameters 11 p1773 A71-25799

Variable output coupling for IR gas lasers, using Michelson interferometer with polyethylene or polypropylene beam splitter 11 p1773 A71-25800

He-Zn ion laser, considering charge exchange and Penning collisions as primary excitation sources of Zn II levels 11 p1773 A71-25920

Longitudinal magnetic field effect on output power polarization and lasing frequency of He-Ne laser operating at 0.63 micron wavelength 11 p1774 A71-26000

Semiconductor wafers examination with He-Ne II laser scan microscope, producing oscilloscope shadowgraph displays of IR transmission variations in wafers 11 p1763 A71-26188

He-Ne laser with stable thermally tunable single frequency referenced to Kr 86 primary wavelength, describing construction details, calibration and performance characteristics 11 p1776 A71-26300

He-Ne laser cavity amplifier performance analysis indicating usefulness as scanning interferometer for high resolution analysis of other laser outputs 11 p1776 A71-26443

Carbon dioxide-nitrogen-helium laser optical heterodyne experiment, obtaining various laser transitions by controlling voltage applied to PZT ceramic transducer 12 p1912 A71-26600

Sidelight emission spectrum of He-Ne laser with/without oscillations, determining line intensity change and laser power dependence on discharge current 12 p1913 A71-26889

Ne absorption tube in alternating magnetic field for He-Ne laser frequency stabilization reference, discussing laser output SNR effects 12 p1913 A71-26920

Kr ion laser forced and self mode locking, using graphite bore plasma tube and acousto-optic modulator 12 p1914 A71-26988

Spectroscopy and collisional transfer in methyl chloride by microwave laser double resonance, measuring population changes in various rotation vibration levels 12 p1877 A71-27000

Laser designs with thermal pumping, obtaining electron states phototransition probability, cooling rate for population inversion and laser action threshold for diatomic gas molecules 12 p1914 A71-27020

High temperature aerodynamics with electromagnetic radiation, considering thermally radiating shock layers, electric arc driven wind tunnels and gas dynamic lasers 12 p1940 A71-27270

Vacuum UV laser emission from molecular hydrogen, discussing theory and experimental verification 12 p1914 A71-27280

Plasma refractive index and electron density measurements by He-Ne vernier interferometric laser 12 p1940 A71-27282

Pulsed Xe ion laser properties, considering emission divergence, coherence and cross section 13 p2080 A71-29028

Absorption gas dynamic laser operation based on polyatomic molecules vibrational relaxation process 13 p2081 A71-29347

Gas laser birefringence observation in active elements under pumping action, using light beam components polarization intensity measurements 14 p2255 A71-30586

Gas laser construction and processing techniques, considering operating temperature, cathode processing, bore design and Brewster window material 14 p2255 A71-30706

CW 28 micron signal resonant regenerative amplification in pulsed vapor laser, showing pulse to pulse frequency coherence 14 p2255 A71-30832

Cold cathode pulsed gas laser construction with glass plasma tube allowing operation with oxygen and variety gases 14 p2255 A71-30882

Pulsed gas dynamic laser for radiation generation at high power levels, using shock tube [AIAA PAPER 71-572] 15 p2419 A71-31564

Mode locking with internal phase modulation observed in He-Se ion laser emitting on many transitions in visible region 15 p2419 A71-31750

Ne 20 isotope for selective frequency absorption to obtain monofrequency radiation in He-Ne laser with naturally isotope-doped Ne as active medium 15 p2419 A71-31998

Carbon monoxide-helium-oxygen laser emission continuous self mode locking and temporal structure for various optical cavity lengths 15 p2420 A71-32379

Far IR coupled cavity HCN laser interferometer for measuring low density transient plasma 15 p2410 A71-32384

IR and submillimeter wave HCN laser radiation visual observation, using thermal image converter 15 p2420 A71-32385

Power output of stable sealed off CO lasers with semiconfocal cavities and totally reflecting spherical and dielectrically coated flat mirrors 15 p2420 A71-32387

Carbon monoxide gas dynamic laser oscillation generation, observing maximum power and vibrational exchange among single diatomic species states 15 p2422 A71-32583

Far IR sulfur dioxide laser line prediction from transitions involving irregular Fermi interactions between molecular energy levels 15 p2422 A71-32587

CW gain measurements on rotation-vibration P branch transitions of CO molecular laser, calculating gas temperature, Einstein coefficient and population densities 15 p2423 A71-32609

Pulsed output, delay time and rotational-vibrational transitions of high pressure transverse discharge CO laser 15 p2424 A71-32613

He-Ne laser mode self locking conditions and modulation characteristics 16 p2589 A71-34125

Dynamic amplification ranges of monochromatic signal by semiconductor, solid state and gas lasers in steady operation mode 17 p2750 A71-34270

HCN laser amplifier gain measurement at IR wavelengths in gas mixtures by recording with pyroelectric receiver 17 p2750 A71-34290

CO lasing processes using small signal single pass gain measurements on flowing CO-air-He laser 17 p2751 A71-34378

Longitudinal modes in standing wave gas laser with Brewster windows in presence of active level emission capture 17 p2753 A71-34412

Gasdynamic lasers optically active medium two-fluid model, deriving solutions for CW generators and quantum amplifiers 17 p2754 A71-35397

Vibrational population distribution in high power liquid nitrogen cooled CO laser by emission spectroscopy 17 p2754 A71-35751

Operating characteristics of Q switched CO-He laser, discussing energy transfer processes leading to population inversion 18 p2929 A71-35835

Helium-cadmium laser discharge, discussing possible He trapping mechanisms and improved tube design to eliminate He cleanup 18 p2933 A71-37013

Gas laser operating on mixture of He and Cd 114 for excitation of scattered light spectra 19 p3073 A71-37792

Gas lasers, discussing engineering developments for size and cost reduction, reliability, long life and high power 19 p3074 A71-38227

Integral equation for determination of nonuniform gain profile effect on resonant modes of ion laser cavity, considering ring modes at high current densities 19 p3074 A71-38228

Plasma optical refractivity, considering gas laser interferometry and holographic phase measurements 19 p3116 A71-38244

Retinal damage thresholds of rhesus monkeys to ocular radiation from yellow line 568.2 nm emitted by krypton CW gas laser 19 p3008 A71-38284

High repetition line selectable compact electrically pulsed hydrogen fluoride lasers operating on sulfur fluoride and hydrogen mixture 20 p3242 A71-38825

Kinetic modeling of vibrational state populations in high power direct discharge excited CO laser, using iterative technique 20 p3243 A71-39005

Collision effects on line shapes using quantum mechanical description of atomic center of mass motion, considering pressure effects in gas lasers 20 p3271 A71-39069

Polarization flip with hysteresis effect at zero magnetic field in CW far IR HCN laser 20 p3244 A71-39098

Low vibrational level CO transitions of flowing electrochemically excited liquid nitrogen cooled helium-air-methane-carbon monoxide laser in Q switched operation 20 p3244 A71-39100

High pressure transversely excited pulsed nitrous oxide laser active mode locking at subatmospheric pressures 20 p3244 A71-39101

Gas laser triggered switching causing propagating streamer to close by laser pulse introduction into gap 20 p3244 A71-39102

Pulsed laser oscillation from F atoms in mixed helium-fluorine gases using electric discharge excitation 20 p3244 A71-39107

Dual beam pulsed gas laser magnetic resonance spectrometer for magneto-optic studies of solids in far IR frequencies 20 p3244 A71-39177

Water cooled hollow cathode design for continuous emission HCN lasers 20 p3246 A71-39494

Crossbeam electric discharge convection laser, reviewing uniform and stable discharges in rectangular channel and laser optical properties 20 p3246 A71-39758

Gas laser asynchronous coupling modulation, examining dependence on lasing threshold, optical spectrum and transition line shape 20 p3199 A71-39811

He-Cd CW laser transitions, describing charge exchange and Penning ionization-excitation processes 21 p3393 A71-41038

Hollow dielectric waveguide gas laser with He-Ne mixtures at 6328 A 21 p3393 A71-41040

Gain and spectral characteristics of transverse flow CW chemical laser with hydrogen and deuterium fluorides active medium 21 p3393 A71-41041

Carbon monoxide laser emission from helium-air-cyanogen mixture 21 p3393 A71-41043

Unidirectional gas laser amplifier using monochromatic optical pumping of coupled Doppler broadened transition 21 p3394 A71-41048

Nonresonant vibrational exchange in molecular binary harmonic and one component anharmonic oscillators with beam laser applications 21 p3394 A71-41255

Photosensitive epoxy resin coating light path propagation variation measurements, using continuous radiation gas laser and Fabry-Perot interferometers 21 p3555 A71-41615

Gas dynamic laser, obtaining initial high temperature gas mixture by detonating solid 22 p3556 A71-41813

HCN CW laser design, considering factors affecting short and long term power and frequency stabilities 22 p3557 A71-42134

HCN and water vapor submillimeter and far IR laser frequency measurement against fundamental frequency standard by harmonic generation and beat frequency detection 22 p3557 A71-42152

Quantum fluctuations in gas laser radiation, obtaining photon diffusion coefficients for traveling and standing waves 22 p3558 A71-42456

Gas laser axial modes mutual locking for frequency modulation, considering stability condition and even/odd harmonics 22 p3559 A71-42754

Electrical CO laser performance prediction from pumping mechanism based on vibrational energy exchange under thermal nonequilibrium conditions 23 p3683 A71-42954

Electrically excited gas dynamic CO laser using glow discharge in supersonic nozzle plenum 23 p3683 A71-42958

Gas ring laser lock-in zone, showing dependence on resonator mirror curvature radius and mode competition between oppositely directed waves 23 p3683 A71-43393

Spatiotemporally coherent pulsed Ne and Ti vapor lasers superaddition, showing coherence time dependence on pulse length and gas pressure 23 p3683 A71-43395

Population inversion development and breakdown in active medium produced by plasma generation during pulsed discharge in molecular nitrogen laser 23 p3684 A71-43406

Gas laser power gain time dependence on molecular rotational relaxation under tight pulse excitation 23 p3684 A71-43415

Vacuum UV traveling wave excitation by high voltage pulse and hydrogen laser technology 23 p3684 A71-43502

Quantum phase fluctuations in IR gas lasers, noting nearly Lorentzian power spectrum with bandwidth inversely proportional to output power 23 p3688 A71-44269

Pulsed neon laser high gain oscillation at 486.1 and 434.0 nm identified as Balmer beta and gamma lines of atomic hydrogen 23 p3688 A71-44296

R-branch multiline performance of transversely excited pulsed HF chemical laser 23 p3688 A71-44297

Turbulent defocusing and displacement fluctuations of focused He-Ne laser beam in atmosphere over paths near ground 23 p3688 A71-44329

Gas lasers application to length measurement technology, discussing temperature, air pressure and vibration effects on laser frequency stabilization 24 p3833 A71-44449

Low loss mode selection and wavelength regulation of gas lasers with electro-optical intracavitator 24 p3834 A71-45163

GAS LIQUEFACTION U CONDENSING GAS LUBRICANTS

Pressure boundary layer profile numerical solution for transient and steady hydrodynamic gas film under high speed and small trailing edge thickness 04 p0570 A71-15178

Gold sliding electric contacts friction behavior, studying adsorbed gas lubrication in ultrahigh purity environments 12 p1912 A71-27637

Reynolds differential equations for three dimensional gas lubrication flows, noting linear velocity at rotating cylinder surface 17 p2749 A71-35639

GAS LUBRICATED BEARINGS U GAS BEARINGS GAS MASERS

Multiple region hydrogen maser using Teflon coated cylindrical vessel to reduce atom-wall collision frequency shift 01 p0096 A71-11223

Hydrogen maser time and frequency standards at Agassiz observatory for long baseline interferometry via radio telescope, discussing Loran C 02 p0261 A71-12334

Frequency shift in hydrogen maser due to atomic collisions with storage bulb surface /wall shift/, investigating temperature dependence 07 p1124 A71-19686

Hydrogen maser relaxation time measurement, using oscillator amplitude response 10 p1623 A71-25023

Oscillations in second cavity of ammonia maser containing two resonators successively traversed by molecular beam, studying polarization and radioelectric emission 14 p2254 A71-30440

Hydrogen maser research, discussing H atom hyperfine structure, frequency characteristics and potential use as atomic clock 14 p2255 A71-30987

Atomic hydrogen maser wall shift elimination by operating at temperature to obtain zero average phase shift per atomic collision 21 p3391 A71-40201

Atomic time standards, discussing Cs 133, hydrogen maser, ammonia maser and rubidium gas cell equipment 24 p3827 A71-44994

GAS METERS

Simultaneous calibration of gas analyzers and meters for continuous process gas stream composition monitoring 19 p3010 A71-38566

GAS MIXTURES NT DETONABLE GAS MIXTURES

Steam-air mixture viscosity, deriving empirical formula from experimental data 01 p0118 A71-10620

Kinetic theory of gas mixtures and thermodynamic laws of irreversible processes, deriving hydrodynamic equations and Onsager relations 01 p0130 A71-10793

Laser effect radiation power in gas mixture flow of carbon dioxide, nitrogen and traces of water vapor, presenting calculations based on kinetic theory 01 p0094 A71-10992

Gain measurement on pulsed radiation from high voltage discharges in mixtures of carbon dioxide, nitrogen and helium 01 p0096 A71-11423

EM pulse distortion in resonant and nonresonant gases, discussing applications to homogeneous tropospheric propagation 01 p0040 A71-11608

Russian book on perception of respiratory medium and gas preference in man and animals covering hypoxic or hypercapnic media, inhalation times, gas mixtures, etc 02 p0198 A71-11823

Multicomponent gaseous mixtures and plasmas transport analysis improved formalism consisting of N moment Boltzmann equation and N parameter distribution function representation 02 p0290 A71-12229

Multicomponent ionized gases mixture transport coefficients for field-free and strong magnetic field cases 03 p0463 A71-13471

CW chemical laser operation with HF and DF in subsonic electric discharge mixing device, obtaining 5.5 W output 03 p0434 A71-13479

High power carbon dioxide electric discharge mixing laser with vibrationally excited nitrogen providing population inversion 03 p0434 A71-13480

Thermal conductivity of binary gas mixtures with/without hydrogen to 1100 K, using molecular kinetic theory and structure model 03 p0520 A71-13749

Transonic flow equations for chemically inert gases binary mixture, considering diffusion effect on dissipative process 03 p0401 A71-13906

Hydrogen-oxygen induction period kinetics behind shock waves, monitoring OH concentration by UV line absorption method 03 p0376 A71-14276

Hydrogen-sensitized decomposition of hydrogen peroxide, taking oxygen inhibiting effect into account 03 p0376 A71-14277

Burning velocities in 50 percent hydrogen-air mixtures 03 p0376 A71-14282

Inviscid binary gas mixture steady supersonic two dimensional flow past convex corner, taking into account spontaneous condensation 03 p0345 A71-14559

Shock wave attenuation delay in arc heated shock tube by use of He-Ar mixture as driver gas 04 p0673 A71-14670

Shock tube measurements of vibrational energy transfer in molecular carbon dioxide-nitrogen-water system 04 p0629 A71-14693

Laser Q-branch emission near 8 microns from flowing hydrogen-acetylene-helium mixture under pulsed electrical excitation 04 p0607 A71-15038

Binary gas mixture rarefied hypersonic flow structure near blunt body, investigating diffusive effects on recovery temperature dependence 04 p0528 A71-15488

Hot laminar round inert gaseous jet entraining fuel-air mixture, obtaining velocity, temperature and concentration profiles 04 p0683 A71-15495

Models for partially mixed stars at He flash time, determining mixture degree effects, carbon production and total mass 05 p0801 A71-15932

One dimensional unsteady flows of combustible gas mixtures with detonation waves generation, noting electromagnetic effects 05 p0833 A71-16502

Shock waves and chemical reactions due to plane, cylindrical and spherical point explosions in combustible gaseous mixtures 05 p0833 A71-16503

Shock waves in nitrogen, carbon dioxide and mixtures, measuring Mach number for deviation evaluation from vibrational and dissociation equilibria 05 p0835 A71-16522

Gaseous mixtures turbulent combustion, considering turbulent flame propagation velocity 05 p0836 A71-16536

Electron-ion recombination in dense molecular gas, presenting semiquantitative method for hydrogen, nitrogen, carbon dioxide and damp gas mixtures 05 p0785 A71-16726

Laminar or turbulent chemically reacting gas mixture flow in circular tube, examining heat transfer with enthalpy equation 05 p0838 A71-16791

German monograph on ignition and combustion processes in rapidly flowing gas mixtures covering supersonic flow, ramjet parameters, flow heating, etc 05 p0838 A71-16900

Laser emission from helium-air-methane mixture identification by comparing with vibrational rotational transition 06 p0906 A71-17307

Isotopic helium atmospheric composition determination, using mixtures of He 3 and He 4 for comparison 06 p0921 A71-17390

Ejector pump with gas-air jet, deriving momentum conservation equation 06 p0882 A71-18010

Onsager relations for Sorot-Dufour and diffusion coefficients in moderately dense gas mixtures based on kinetic theory, considering symmetry relations for transport properties 06 p0929 A71-18036

Irreversibility control in two gas flows mixture, discussing jet engines thrust increase by air-exhaust gases admixture 06 p0945 A71-18051

Low density monatomic gases mixtures multicomponent thermal diffusion coefficients, demonstrating for heat conductivity and dissociated air equations 06 p0929 A71-18072

Gas laser using nonequilibrium MHD generator with He, carbon dioxide and Cs mixture [AIAA PAPER 71-68] 06 p0940 A71-18656

Gas mixture transmission function, determining multiplication method accuracy 07 p1151 A71-18910

Gas-particle mixtures weak disturbances, applying linearized hydromechanic and phase transformation kinetic equations 07 p1088 A71-19191

Zirconium droplet combustion in oxygen-rare gas mixtures, observing transient burning phenomena, oxidation conditions and luminosity-time records 07 p1223 A71-19623

Spacecraft attitude control microthrusters utilizing catalytically reactive gas mixtures during pulse mode and steady state operation 07 p1183 A71-19859

Laser induced Raman scattering as diagnostic technique for measuring specie concentrations in gas mixtures [AIAA PAPER 70-224] 07 p1125 A71-19897

Binary gas mixtures shock tube flow kinetic theory, indicating shock wave formation, contact layer diffusion and expansion wave dispersion 07 p1093 A71-20287

Gaseous nitromethane-oxygen mixtures detonation characteristics, determining reaction time by schlieren technique 08 p1346 A71-20862

Combustion kinetics of premixed laminar graphite dust-oxygen-nitrogen flames with/without hydrocarbon 08 p1346 A71-20866

Gas concentration determination for mixture by UV energy absorption measured in terms of photomultiplier tube output current, describing oxygen sensor 08 p1287 A71-20987

Soviet book on thermal conductivity of monatomic and polyatomic gases and hot and cold mixtures, comparing molecular kinetic theory collision integral formulas with experimental data 08 p1375 A71-21656

Boltzmann kinetic equations for gas mixtures reacting according to detail balance principle 09 p1496 A71-22376

Gaseous fuel mixtures containing nitrogen oxides, discussing combustion mechanism 09 p1403 A71-22531

Solar radiation energy distribution simulated by vacuum monochromator, discussing Ar-Kr-Xe-methane mixture 09 p1513 A71-22557

Italian book on mixed plasmas equilibrium compositions and thermodynamic properties, covering numerical values tabulation for nitrogen mixtures with He, Ar and Xe 09 p1505 A71-23353

Quenching rates for oxygen during 1470 A pulse photolysis in carbon dioxide, nitrogen and helium mixtures 09 p1404 A71-23382

Thermal conductivity of Ar binary mixtures with He, N and Ne, using secondary concentric cylinders cell 09 p1547 A71-23463

High pressure laser action in gas mixtures with pulsed transverse excitation, observing molecular and atomic transitions 10 p1620 A71-24045

Spherical shell potential extension to shells of differing diameters for intermolecular forces in globular molecules, considering binary gaseous mixtures 11 p1801 A71-25369

Hydrogen-helium gas mixtures high pressure phase behavior, considering solidified gas core under Jupiter and Jovian planets atmospheres 11 p1827 A71-25728

Gasoline-air mixtures normal combustion velocity by photographic observations of flame propagation in transparent tubes 12 p1986 A71-27499

Low alloy alpha Ti alloy ignition during breaking in oxygen containing gases, considering partial oxygen pressure and tensile loads 13 p2082 A71-27815

Flow momentum losses during gas mixture chemically nonequilibrated expansion in nozzle 13 p2158 A71-27880

Temperature, concentration and heat conductivity profiles of chemically reacting gas mixtures with thermal gradient, using classical transfer equations 13 p2025 A71-27884

Heat and mass transfer in monatomic molecular gases and gas mixtures, discussing energy exchange during collision and thermal diffusion effect on thermal conductivity 13 p2159 A71-28186

Multicomponent ionized gas mixtures chemically equilibrated flows over nonporous and ablating surfaces, using Navier-Stokes and Prandtl equations for asymptotically thin boundary layer 13 p2048 A71-28570

Partially ionized binary gas mixture temperature development during nonequilibrium ion formation, solving heat and ionization balance equations 13 p2062 A71-28573

Transversely excited atmospheric pressure carbon dioxide laser operation at 9.6 microns, describing proper gas mixture for power adjustment 13 p2079 A71-28674

Collision induced hydrogen spectra for overtone absorptions by gas mixtures under temperature and density conditions matching planetary atmospheres 13 p2138 A71-28773

Combustion, reaction and flame propagation during gas mixtures burning, allowing for disruption of Maxwell-Boltzmann molecular velocity distribution 13 p2162 A71-28957

Flame propagation rate in gasoline-air flow with tubular and grid-induced turbulence during two-stage burning process 13 p2162 A71-28959

Gasoline-air combustion zone extent as function of inlet temperature for plane turbulent flame in square-section channel 13 p2162 A71-28960

Grid-induced turbulence effect on flameout characteristics for kerosene-air flames stabilized by bluff bodies of different sizes 13 p2163 A71-28961

Velocity measurements in gas mixtures by hot-wire and hot-film anemometers, inferring transport properties from direct calibrations 13 p2069 A71-29008

Supersonic gas ejector characteristics of mixing gases with different adiabatic exponents, heat capacities and stagnation temperatures 13 p1994 A71-29233

In-flight UV spectrometric measurements of simulated Jupiter atmosphere, using sunlight gas mixture released from Mariner spacecraft in interplanetary space 14 p2308 A71-29914

Radiative and convective heat transfer for stagnation point flow of emitting carbon dioxide and nitrogen gas mixture, assuming thermodynamic equilibrium in shock layer 14 p2335 A71-30212

Multicomponent gas nonequilibrium viscous flow near blunt body stagnation point, presenting shock layer parameter variations effects on heat exchange 14 p2336 A71-30224

Nitrogen-carbon dioxide system molecular resonant energy exchange vibration-vibration probability measurement by shock tube and IR emission monitoring, noting temperature effects 14 p2276 A71-30399

Nonreacting gases supersonic turbulent mixing flowfields, calculating turbulent kinetic energy as function of injection angle and jet velocity [AIAA PAPER 71-725] 14 p2295 A71-30774

Liquefied gas solutions of methane in carbon tetrafluoride and propylene, calculating pressure and temperature dependence of density 15 p2462 A71-31246

Convectively cooled carbon dioxide-nitrogen-helium electric discharge laser theory based on excitation and relaxation processes, comparing with experiment [AIAA PAPER 71-588] 15 p2419 A71-31574

Ethane-oxygen-argon mixtures ignition behind reflected shock wave, deriving composition temperature dependences correlation [WSS/CI PAPER 71-16] 15 p2463 A71-31625

High temperature fuel cell in hot gas mixtures analysis, presenting porous silver and palladium electrodes cathodic polarizations 15 p2367 A71-31648

Stoichiometric hydrogen-oxygen mixture spinning detonation fine structure determination by trace technique and high speed space-time photography

15 p2465 A71-32083

Flammability limits measurement of hydrogen-oxygen mixtures containing fluorocarbon diluents

15 p2465 A71-32086

Stoichiometric hydrogen-carbon monoxide-oxygen mixtures detonation wave propagation at critical Mach number, noting explosion limit chemical kinetics role

15 p2465 A71-32088

Thermal conductivity, diffusion and viscosity of gases and multicomponent gaseous mixtures at high temperatures

15 p2515 A71-32450

Ionization measurement in detonation and shock waves in reactive gas mixtures by microwave cavity techniques

15 p2411 A71-32556

Shock tube measurements of vibration-vibration energy exchange probability in nitrogen-carbon monoxide-argon mixtures

16 p2613 A71-32896

Laminar or turbulent chemically reacting gas mixture flow in circular tube, examining heat transfer with enthalpy equation

16 p2662 A71-33041

Minima and maxima in composition dependence of thermal diffusion factor and conductivity of gas mixtures

16 p2614 A71-33104

Vibrational population inversions due to molecular energy exchanges from rapid heating behind normal shock wave in carbon dioxide-nitrogen-helium mixtures

17 p2728 A71-34883

Transversely excited carbon dioxide lasers gain measurements for linear and helical electrodes at various gas mixtures and pressures as function of time

17 p2754 A71-35404

Open singing flame from propane-butane and oxygen jet mixture, constructing oscillogram model of sound emission

17 p2839 A71-35696

Combustion systems ionic wind velocities, investigating gauze parameters, magnetic fields and mixture inhomogeneity effects

17 p2785 A71-35703

Methane-oxygen-argon mixture ignition behind reflected shock waves in single pulse shock tube

17 p2792 A71-35707

Pulsed chain reaction chemical lasers using flash photolysis of hydrogen-fluorine-helium mixtures

17 p2754 A71-35750

Anharmonic effects in time dependent vibrational relaxation of diatomic molecules in rapidly expanding flows, considering N-CO-Ar mixtures

18 p2948 A71-35837

Unsteady multispecie gas mixture concentration flow measurement, using Raman scattering of pulsed nitrogen laser light

18 p2930 A71-36060

Pressure change accompanying mixing of two ideal gases, assuming constant specific heats

18 p2904 A71-36280

Molecular dynamics data from neutron scattering techniques for gas mixing

18 p2949 A71-36958

Carbon dioxide-helium mixture IR laser action and power gain increase by nitrogen addition

18 p2932 A71-37006

Detonation processes in gases, considering Zel'dovich-Doering-Neumann model and reaction kinetics

19 p3162 A71-37437

Flow parameters behind shock waves propagating in carbon dioxide-helium mixtures at Mach numbers from 5 to 10

19 p3044 A71-37583

Spectroscopic study of imploding shock waves in hemispherical chamber filled with oxygen-hydrogen-helium mixture at high pressure

19 p3163 A71-37735

Mass flow rate measurements and calibration in heterogeneous medium with hot wires tested on Freon mixtures

19 p3163 A71-37894

Air and jet fuel-air mixtures, calculating temperature dependent laminar and turbulent heat transfer parameters and transport properties

[ASME PAPER 71-HT-41] 19 p3166 A71-38002

NO, CO and Ar mixtures IR spectral emission radiant intensities behind shock tube generated reflected shock waves

19 p3012 A71-38087

Ion formation in photochemically initiated combustion of acetylene-oxygen-nitric oxide mixtures, measuring carbon, CH and OH emission spectra and ion current time change

19 p3013 A71-38091

Combustion driven acoustic oscillations in gas fired burner of premixed methane, nitrogen and oxygen, noting mixture ratio and flow rate effects

19 p3123 A71-38098

Buoyant centrifugal force effect on combustion of homogeneous propane-air mixtures at stoichiometric proportions, using steel pipe as centrifuge

19 p3167 A71-38101

Inhibitory effects of halogen compounds on hydrogen-air and hydrogen-nitrous oxide flames, measuring burning velocities and temperature/ composition profiles

19 p3013 A71-38106

Ignition delays of propane-oxygen-argon mixtures in shock tubes from pressure and heat flux measurements in reflected region

19 p3169 A71-38109

Cystine synthesis in simulated primitive conditions by UV irradiation of methane, ethane, ammonia, water vapor and hydrogen sulfide in spherical vessel

19 p3014 A71-38678

Brayton cycle power conversion system using He-Xe gas mixture, discussing compressor net engine and turbine static efficiencies

20 p3180 A71-38908

Human expiratory oxygen and carbon dioxide partial pressure and dissociation curves for intrapulmonary gas mixing, using mass spectrometry

21 p3328 A71-40098

Hyperbaric normoxic breathing helium, nitrogen and neon gas mixture effects on EEG and reaction time in man

21 p3342 A71-40347

Steady propagation of plane laminar flame through uniform mixture of hydrogen and bromine gases, obtaining temperature and concentration profiles

21 p3474 A71-40524

Diffusing gas mixtures slipping rate along wall at arbitrary accommodation coefficients, deriving expression based on molecule distribution functions from linearized Boltzmann equations solution

21 p3418 A71-40678

Jet flame stability characteristics of propane-air mixture ejected into counter air stream by temperature and concentration measurements and visual observation

21 p3475 A71-40758

Critical atomic carbon to oxygen ratio measurement for incipient soot formation in shock heated acetylene, ethylene and ethane/oxygen/argon mixtures

21 p3436 A71-40859

High performance electric arc driven shock tube for shock velocities to 45 km/sec and test times over 4 microseconds, using 80/20 helium-hydrogen mixture

21 p3365 A71-40975

Molecular gas mixtures inelastic collision integral spectra, describing internal degrees of freedom with correlation functions

21 p3420 A71-41271

Carbon dioxide, nitrogen and water vapor hot mixture expansion through Laval nozzle, showing population inversion on carbon dioxide laser transition

22 p3556 A71-41726

Chemical laser action at atmospheric pressure from vibrational rotational transitions of HF produced by multiple transverse spark discharges in propane-helium-sulfur fluoride mixtures

22 p3556 A71-41727

Heat transfer from platinum wires in He and He-Ar mixtures, plotting Nusselt number variations with Reynolds number for various He concentrations

22 p3620 A71-41875

Organic synthesis in simulated Jovian atmosphere by passing semicorona discharge through methane-ammonia mixture

22 p3602 A71-42180

Moment analysis of atomic spectral lines of Cs-Ar and Cs-He systems, using adiabatic approximation

22 p3578 A71-42462

Time dependent progress of vibrational rotational transitions in chemical laser using hydrogen-fluorine mixture investigated by oscillography with IKM-1 monochromator

23 p3684 A71-43405

Emissivity calculation for radiant heat flux from isothermal gas mixture of hydrocarbon fuel combustion products

23 p3718 A71-43918

N-hexane-air mixture ignition by giant pulse laser beam, analyzing probability and development time to formation of measurable nucleus

23 p3686 A71-43998

Ignitability limits of hydrogen/air and hydrocarbon/oxygen mixtures at high temperatures near self ignition range

23 p3782 A71-44007

Chemically reacting gas mixture supersonic flow characteristics around blunt body, using differential equations

23 p3784 A71-44336

Composition effects on binary gas mixtures thermal conductivity coefficient, considering Hirschfelder-Eucken formula

24 p3886 A71-44369

Combustion of homogeneous reacting gas mixture with solid or liquid fuel particles, describing motion by multiveLOCITY and multitemperature model

24 p3891 A71-45216

Ideal gases and binary monatomic gas mixtures heats of transport derivation from kinetic theory expressions for thermal transpiration

24 p3891 A71-45384

GAS PHASES

U VAPOR PHASES

GAS PIPES

Material, design and operating principles of rotary seals used in gas ducts, bearing elements and fuel systems of aircraft gas turbine engines

19 p3069 A71-38015

GAS POCKETS

Nitrogen and oxygen exit rate from subcutaneous gas pockets in rats during tissue blood flow elevation due to cobalt chloride injection

17 p2678 A71-34174

GAS PRESSURE

Tubular powder channel gas velocity distribution and pressure buildup during burning

04 p0638 A71-15680

Gas pressure conversion for spacecraft outgassing products investigation by mass spectrometer analysis, noting plastic decomposition products calibration

07 p1023 A71-20067

Pulsed coaxial plasma accelerator, measuring longitudinal gas pressure distribution, particle emission and magnetic fields characteristics under various operating conditions

08 p1341 A71-21498

Hollow cathode arc discharge parameters at active zone level, examining gas pressure and electron density

10 p1646 A71-23843

Light scattering from gas thermal fluctuations, deriving density-density correlation function over various pressures

10 p1642 A71-24836

Reflecting oven for very high temperatures under gas pressure, describing apparatus, heat source and possible contamination

10 p1613 A71-25040

HF electromagnetic waves absorption as function of discharge current intensity in ionized H₂ using gas pressure or uniform magnetic field as parameters

11 p1805 A71-25598

Air cooled turbine blades activated diffusion brazing and gas pressure welding, using composite finned configuration model

11 p1770 A71-25969

Artificial respiration in elevated gas pressure chamber to revive organism after clinical death by rapid decompression

12 p1876 A71-27745

Formaldehyde vapor photodecomposition modes by end product analysis, utilizing mixed isotope, radical scavenger, inert gas pressurization and lamp intensity attenuation

12 p1877 A71-27758

Functional-biochemical shifts in rats central nervous system during initial stage of increased oxygen pressure exposure

13 p2002 A71-27810

Ar, N and Ne partial pressure tolerance in dogs, plotting saturation curves

13 p2005 A71-28038

Gas pressure gradient and transmittance of sunspots, obtaining contours of D2 Na I and 5173 Å Mg I lines

14 p2309 A71-29983

Fluidic cabin pressure automatic control systems for military and civil aircraft, discussing design, operation and performance

14 p2182 A71-30308

Hertzian radiometry experimental aspects covering background and medium temperature measurements, sky radiometry and absorbing gas total pressure measurements

14 p2204 A71-30969

Pulsed coaxial plasma accelerator, measuring longitudinal gas pressure distribution, particle emission and magnetic fields characteristics under various operating conditions

16 p2618 A71-33046

German monograph on spark discharges behavior in nitrogen, carbon dioxide and argon at excess pressure covering Toepler, Weizel-Rompe and Braginskii laws applicability

17 p2779 A71-34799

Polyatomic gases thermal conductivity and rotational relaxation number from thermomolecular pressure differences across capillary tubes

17 p2785 A71-34946

Pressure change accompanying mixing of two ideal gases, assuming constant specific heats

18 p2904 A71-36280

Low density hypersonic flow around blunt bodies, considering total pressure and flow velocity on stagnation point line

18 p2846 A71-36417

Temperature and pressure of optically dense plasma from vaporizing wall gas discharge

19 p3110 A71-37577

GAS REACTORS

Thermodynamic measurement of cryogenic temperatures based on gases at low pressures or platinum electrical resistance

20 p3270 A71-39243

Quasi-static pressure characteristics of gas lubricated thrust bearing with shrouded Rayleigh step pads, solving nonlinear equation of motion

[ASME PAPER 71-VIBR-75] 21 p3385 A71-40313

Film ablative cooled gas pressure feed liquid rocket engine unstationary process analysis with digital computer, detailing engine dynamics, heat transfer and temperature profile

22 p3589 A71-42054

Equilibrium equations solutions for ideal gas composition, pressure, volume and temperature based on Newton-Raphson method, outlining programming method

24 p3887 A71-44635

Passive gas flow control with compensation for ambient temperature and supply pressure variations, using choked orifice with area variation linearly proportional to diaphragm deflection

[ASME PAPER 70-WA/AUT-14] 24 p3828 A71-45137

GAS REACTORS

Reacting gases atom concentration quantitative measurements with electron spin resonance, discussing microwave power, saturation and modulation amplitude effects

11 p1765 A71-26284

GAS SPECTROSCOPY

Portable direct reading spectrometer for monitoring oxygen-hydrogen containing contaminants in gas tungsten arc welding process

02 p0247 A71-11712

Flow and radiative properties of air in high explosive shock tube

04 p0586 A71-14700

Gas phase atomic hydrogen, nitrogen and oxygen detection by photoelectron spectroscopy of ground state, suggesting application to gas phase kinetics

04 p0548 A71-14799

Gas phase acidities of aliphatic alcohols by ion cyclotron resonance spectroscopy

07 p1055 A71-19597

Pulsed plasma accelerator energy balance determination by spectroscopic measurement

09 p1498 A71-22100

High efficiency gas chamber for obtaining Raman spectra of corrosive gases at atmospheric pressure by He-Ne laser excitation

10 p1619 A71-23857

IR radiative heat transfer in nongray nonequilibrium gases, giving solutions for radiative equilibrium and combined conduction and radiation

10 p1698 A71-25094

High resolution far IR interferometer in Michelson configuration for measuring gas optical properties in symmetric or asymmetric operation mode, testing performance

12 p1904 A71-26799

Absorption spectra enhancement by organic dye laser quenching, considering applications for absorbing species spectroscopic detection

13 p2082 A71-29439

Carbon dioxide photodissociation in vacuum UV, using time-of-flight spectroscopy and metastable photofragment detection by electron emission from metal surfaces

14 p2190 A71-30571

Gases high resolution Raman spectroscopy, using mirror system for exciting laser beam multiplication

15 p2423 A71-32600

Interferometric gas diagnostics by hook method, using Mach-Zehnder interferometer and stigmatic spectrograph

16 p2578 A71-33157

Circumstellar dust clouds and Bok globules examined for gaseous emission lines, emphasizing forced diffusion process

16 p2643 A71-34077

K-L Auger spectra of nitrogen, oxygen, carbon monoxide, nitrogen oxide, water and carbon dioxide, using double focusing electrostatic electron spectrometer

21 p3345 A71-40235

Arc driven hypersonic wind tunnels total enthalpy measurement from blunt body gas cap emission, using rapid scan spectrometer for gray gas continua

21 p3364 A71-40403

Effective cross section and excitation functions measurements for molecular nitrogen ion first negative system spectral bands by fast electrons

21 p3419 A71-41108

Oxygen Schumann-Runge bands system from photographic and photoelectric spectra recording for arc jet heated air and oxygen-noble gas mixtures

[ASME PAPER 71-RR-354] 24 p3850 A71-45088

GAS STREAMS

Breakup mechanism of liquid sheets and jets in supersonic gas stream, using spark photomicrographs and high speed movies

11 p1750 A71-25471

Temperature and radical concentration measurements for high temperature flowing gas streams in rig simulating conditions in ramjet combustion chamber and nozzle

13 p2162 A71-28758

Gas stream-wall interaction for Maxwell model by scattering element-detector system with specular reflection and diffusion separation

15 p2389 A71-31702

Close binary star systems U Gem, VV Pup and UX UMa, calculating gas streams trajectory movement

19 p3134 A71-37509

GAS TEMPERATURE

Partially ionized binary gas mixture temperature development during nonequilibrium ion formation, solving heat and ionization balance equations

13 p2062 A71-28573

Gas temperature measurement in aircraft combustion chambers, using calorimetric probe

13 p2117 A71-28757

Carbon dioxide free jet plumes issuing from supersonic nozzle into high vacuum, measuring densities and temperature

13 p2026 A71-29355

German monograph on time dependent gas temperature in decaying plasmas, using frequencies of standing acoustic wave stimulated by pulsed discharges in rarefied gases

13 p2110 A71-29423

Analytical model for performance and pollutant emissions of gas turbine combustors, predicting gas composition and temperature

14 p2294 A71-30765

Combustion characteristics of single boron carbide particles, studying minimum gas temperatures for self-ignition and burning times

15 p2464 A71-31630

Jet edge tone sensor and internal feedback fluidic oscillator for temperature measurement, using dependence of sound speed in gas

15 p2352 A71-32065

Temperature measurements in shock heated carbon monoxide by IR emission-absorption technique

15 p2411 A71-32554

Optimal gas temperature in bypass and turbojet engines afterburners ensuring minimum fuel flow rate dependence on thrust augmentation

16 p2624 A71-33607

Gas turbine engine combustion chamber outlet gas temperature field peripheral nonuniformity, detailing jets disruptive capacity effects in mixing zone

16 p2625 A71-33609

Simple gas thermal creep/velocity slip and temperature jump coefficients by applying variational technique to linearized Boltzmann equation with boundary conditions

17 p2785 A71-35446

Relativistic and/or degenerate electron gas equation of state formulae for density, temperature, entropy and internal energy

18 p2960 A71-35937

Rarefied hypersonic flow density, velocity and temperature determination by electron beam technology, including ion production, calibration curves, collisions and spectroscopic analysis

18 p2949 A71-36419

Gas and surface temperature distributions for laminar flow in circular tube, considering conduction, convection and radiation effects

[ASME PAPER 71-HT-17] 19 p3164 A71-37988

Room temperature and heated driver gas low attenuation electric shock tube, investigating diaphragm opening process and effect on shock wave motion

20 p3209 A71-38837

Electric discharge carbon dioxide laser gas temperature, electron and current densities radial distribution from mathematical model

20 p3242 A71-38844

Lower thermospheric density and molecular nitrogen partial density rocket measurements, obtaining neutral gas temperature vertical distribution and ion density profile

20 p3222 A71-39699

Microwave water emission in Comet Bennett, deriving column density for various temperatures of cometary gas

21 p3443 A71-40190

Interferometric measurement of gas temperature in positive column of discharges used for carbon dioxide lasers

22 p3374 A71-41725

Equilibrium equations solutions for ideal gas composition, pressure, volume and temperature based on Newton-Raphson method, outlining programming method

24 p3887 A71-44635

Nitriding process on Nb alloy, presenting gas phase temperature, time and composition effects

24 p3838 A71-44894

Chemical lasers diatomic and multiatomic molecules dissociation in nonequilibrium conditions, discussing vibrational energy exceeding gas temperature

24 p3834 A71-45112

GAS TRANSPORT

Transport analysis of collision dominated relaxation plasma in ignited mode thermionic converter

02 p0291 A71-12237

Oxygen transport and consumption, ventilation and cardiac index in natives and sojourners at high altitudes

06 p0853 A71-18060

PH conditional ammonia assimilation deficient mutants isolation and growth properties, studying nitrogen transport in *Hydrogenomonas eutropha*

06 p0857 A71-18672

Cardiac output variations in regulation of arterial oxygen transport during hypoxia

08 p1241 A71-21939

Molecular flux distributions and capture by cryopanel in space simulation chamber using homogeneously emitting spherical gas source

09 p1428 A71-23006

Decompression sickness physical and physiological aspects, discussing gas transport quantification, inert gas elimination and metabolic gas exchange in recompression therapy, work performance, etc

09 p1394 A71-23236

Dutch monograph on nonstationary hot-wire method determining thermal conductivity coefficient of gases, using recorded temperature vs time relation

10 p1697 A71-24677

Thermionic converter performance from theoretical model, considering transport, ionization-recombination, and electrostatic sheath phenomena

11 p1711 A71-25880

Mass injection effect on heat transfer reduction to three dimensional stagnation points as function of shape, enthalpy and gas properties

14 p2335 A71-29891

Mycardial ischemia and necrosis without major coronary arteries obstruction, investigating possible deranged hemoglobin-oxygen transport

14 p2185 A71-30286

Numerical heat transfer and wall friction results, demonstrating gas transport property variation effects on three laminar flow situations

14 p2338 A71-30931

Galactic central region gas motions, discussing hypothetical explosive expulsion of matter from galactic nucleus

19 p3143 A71-38165

GAS TUBES

Quarter wave tube in off- and near-resonance regimes, dissipating energy by jet formation during flow emergence from cavity into duct

[AIAA PAPER 71-87] 06 p0881 A71-18543

X band gas tube attenuator for ruby maser saturation protection in pulsed high power radar

07 p1070 A71-18866

GAS TUNGSTEN ARC WELDING

Gas tungsten arc, manual, machine and resistance welding in assembly of gas turbine parts

[SME PAPER AD-70-147] 01 p0089 A71-11258

Portable direct reading spectrometer for monitoring oxygen-hydrogen containing contaminants in gas tungsten arc welding process

02 p0247 A71-11712

Stainless steel-Al joining techniques, describing gas tungsten arc process

04 p0603 A71-14920

Ni maraging steels weld heat-affected zone, showing liquid grain boundary film formation due to titanium sulfide inclusions constitutional liquation

04 p0603 A71-14921

Cathode tip shape influence on temperature and velocity fields in gas tungsten arc welding, noting effect on weldment area and penetration

04 p0603 A71-14922

Residual stress measurement in Hastelloy N gas tungsten arc welds by Sachs boring-out method, permitting stress distribution determination over short distance increments

06 p0912 A71-18043

Porosity in gas tungsten arc aluminum weldments and elimination by hydrogen reduction

07 p1119 A71-19969

Strength, toughness and hardness of gas tungsten arc multipass welds in titanium alloy plates

07 p1119 A71-19970

Metal droplet motion in mercury weld pool in tungsten arc, noting cause by Lorentz force and surface arc plasma jet

11 p1769 A71-25748

DC straight polarity gas tungsten aluminum alloys

13 p2076 A71-29090

Nickel alloys susceptibility to pores formation in tungsten inert gas welding in argon-nitrogen mixture, considering influence of Cr, Mo and W

14 p2260 A71-30487

Stress rupture ductility of electron beam, gas tungsten arc and gas metal arc welds, considering creep crack initiation

15 p2437 A71-32617

Ti alloys argon TIG welding to Nb alloys, detailing joint impact strength, fusion zone ductility and bending tests

15 p2418 A71-32668

- Corrosion resistance of Ar TIG welded joints in Ti alloys, discussing chemical and mechanical slag film removal effects 17 p2757 A71-34804
- Aluminum alloy gas tungsten arc welds, determining defect size and distribution effects on fracture strength 18 p2929 A71-36857
- Manual pulsed and continuous arc TIG welding in controlled atmosphere chamber, examining joint quality 19 p3070 A71-38422
- Electron beam hearth refined ferritic stainless steel, presenting weldability with gas tungsten arc process 21 p3388 A71-40623
- Tungsten and tungsten alloys weldability by gas tungsten arc, electron beam and chemical vapor deposition techniques 21 p3388 A71-40624
- AS TURBINE ENGINES**
- NT BRISTOL-SIDDELEY OLYMPUS 593 ENGINE 01 p0099 A71-10166
- NT DUCTED FAN ENGINES 01 p0142 A71-10479
- NT J-57 ENGINE 01 p0142 A71-10820
- NT J-85 ENGINE 02 p0299 A71-12852
- NT JET ENGINES 02 p0271 A71-12939
- NT RAMJET ENGINES 03 p0469 A71-13370
- NT SUPERSONIC COMBUSTION RAMJET ENGINES 03 p0469 A71-13370
- NT TURBOFAN ENGINES 03 p0469 A71-13370
- NT TURBOJET ENGINES 03 p0469 A71-13370
- NT TURBOPROP ENGINES 03 p0469 A71-13370
- NT TURBORAMJET ENGINES 03 p0469 A71-13370
- Ni base superalloys fatigue strength improvement for gas turbine engine components, discussing homogeneous deformation distribution, grain size control, etc 01 p0099 A71-10166
- Computerized analysis of seal temperature, elastic displacements and seal force balance in iterative design method for gas turbine mainshaft seals 01 p0142 A71-10479
- Gas turbines air pollution control, discussing exhaust composition, combustion chamber design, engine efficiency, etc 01 p0142 A71-10820
- Tubular gas turbine engine combustor design by combining turbulent flame speed, microvolume burning and stirred reactor models 02 p0299 A71-12852
- Niobium alloys for gas turbine blades, examining working temperatures, protective coatings and ductility 02 p0271 A71-12939
- Automatic antisurge control of axial compressor using partial gas recycling bypass method 03 p0469 A71-13370
- High temperature tests of gas turbine engine with transpiration air cooled blades, discussing blade design, fabrication, ductility and oxidation resistance [ASME PAPER 70-WA/GT-1] 03 p0470 A71-14115
- Nozzle system elements size relation to passage cross section in full size two cascade and miniaturized gas turbine engine power plant 03 p0472 A71-14258
- Gas turbine engines nozzles flow passage cross sections area measurement, using gas flowmeter, pipes system and vacuum pump 03 p0472 A71-14258
- Sand and dust erosion on small VTOL gas turbine engines, discussing effects on inlets, compressor housing and blades 04 p0639 A71-15436
- Soviet book on aircraft gas turbine engine assembly covering organization, specified accuracy, automatic systems, mechanization problems, quality control, etc 04 p0639 A71-15449
- Aircraft turbine engines with elevated gas inlet temperatures 04 p0639 A71-15670
- Gas turbine engines materials and components equivalent service life estimation 05 p0796 A71-16753
- Gas turbine engine Ni alloys heat resistance, examining fatigue life and creep properties at various temperatures and test durations 05 p0767 A71-16754
- Gas turbine engine nozzle guide vanes under pulsed thermal operation, discussing service life evaluation and increase 05 p0827 A71-16756
- Aircraft gas turbine engine components equivalent testing by shortening testing time required to increase service life 05 p0796 A71-16761
- Helicopter gas turbine engine health indication using instrument panel for correcting gas temperature and producer speed 06 p0945 A71-17690
- Injection film cooling effect on surface heat transfer downstream of flush nontangential injection holes and slots in turbine applications [AIAA PAPER 69-523] 06 p0945 A71-17695
- Gas turbine aircraft engine compressor blades foreign object ingestion control by inlet vortex flow suppression jets, indicating wind tunnel air intake applications 06 p0945 A71-17696
- Small gas turbines for helicopters and fixed wing aircraft, discussing designs, materials, lubrication, etc 06 p0945 A71-18052
- Aircraft gas turbine engines nitric oxide emission model, describing flow behavior and chemical processes [AIAA PAPER 71-123] 06 p0948 A71-18659
- Aerospace Recommended Practice for gas turbine engine steady state performance presentation for digital computer programs, describing engine type, operating and control characteristics [SAE-ARP-681B] 07 p1183 A71-19647
- Soviet book on aircraft gas turbine and internal combustion engines covering structural design schemes, inlet devices, combustion chambers, materials, compressors, etc 08 p1347 A71-20674
- Gas dynamic test stand for cyclic thermal load testing of gas turbine engine materials and components at variable heating and cooling rates and mechanical loads 08 p1271 A71-20839
- Combustor design for minimum exhaust smoke emission from aircraft gas turbine jet engines, considering air pollution 08 p1347 A71-20867
- Book on aircraft gas turbine engine technology covering combustion chambers, exhaust systems, lubricating oils, thrust augmentation, inlet ducts and overhaul procedures 08 p1348 A71-21625
- Aircraft turbine engines strength and gas dynamic characteristics improved by vibration decrease using elastic elements 08 p1349 A71-21710
- Gas turbine engines emission characteristics, discussing methods for pollutants reduction 08 p1349 A71-21820
- Probabilistic estimate of aerodynamic imbalance of aircraft gas turbine rotors due to production errors in compressor blade angle 08 p1349 A71-22045
- Cost reduction concepts in gas turbine engine design and fabrication for general aviation aircraft 09 p1511 A71-22811
- High temperature corrosion in aircraft engine components and gas turbines by sulfur in fuels, vanadium pentoxide and NaCl 09 p1474 A71-23288
- High temperature steel and alloys metallurgical processes for stationary and aircraft gas turbine engine components, discussing production-quality control-research interrelationship 09 p1456 A71-23301
- Concorde environmental testing, considering endurance tests, thermal shock rigs and plant for simulating air supply from compressor stages of aircraft gas turbine engines 09 p1430 A71-23583
- High pressure ratio centrifugal compressors for small gas turbine engines, investigating power and specific fuel consumption variation with pressure and temperature 10 p1658 A71-24218
- High speed vane type main engine fuel pump for small gas turbine engines [ASME PAPER 71-GT-24] 11 p1812 A71-25966
- Jet fuel starter, describing small gas turbine for starter, providing sufficient pressurized gas flow to rotate main engine [ASME PAPER 71-GT-43] 11 p1812 A71-25976
- Metal matrix composite fabrication procedures for gas turbine engine fan blades, stressing diffusion bonding process susceptibility to blades volume producibility [ASME PAPER 71-GT-46] 11 p1770 A71-25979
- Resin matrix composite airfoils in gas turbine engines, considering performance, fabrication and cost [ASME PAPER 71-GT-47] 11 p1770 A71-25980
- Lightweight high performance regenerative gas turbine designs for aircraft propulsion, comparing various compressor, turbine, combustor and recuperator arrangements [ASME PAPER 71-GT-67] 11 p1812 A71-25983
- Gas turbine engine combustor stability dynamic model, representing premixing and combustion chambers as Helmholtz resonators for stability criteria derivation [ASME PAPER 71-GT-73] 11 p1813 A71-25987
- Aircraft gas turbine condition analysis instrumentation used for status diagnosis of naval turbine engines, discussing sensor and electronic data interpretation progress [ASME PAPER 71-GT-86] 11 p1813 A71-25994
- Gas field nonuniformity as function of turbine engine combustion chamber design parameters, discussing hot tube circumferential holes total area effect 12 p1945 A71-27501
- VTOL propulsion, discussing gas turbine pressure ratio inlet temperature and lifting and high bypass fans 13 p2114 A71-27838
- Commercial aircraft powerplant development, discussing engine and components test programs and techniques [SAE PAPER 710449] 13 p2114 A71-28327
- Silicide coated Nb alloys for gas turbine engine components operating at temperatures above 2000 F [SAE PAPER 710460] 13 p2115 A71-28334
- High temperature aircraft gas turbine engine design, discussing developments in manufacturing processes, materials, cooling techniques, aerodynamic and mechanical design improvements [SAE PAPER 710462] 13 p2115 A71-28335
- Air bypass behind compressor into variable area exhaust nozzle, obtaining energy losses from gas turbine jet engine indices 13 p2115 A71-28586
- Diffusion and thermal mechanism ignition theories, applying to altitude relighting of gas turbine engine combustors 13 p2116 A71-28745
- Kerosene type fuels for aircraft gas turbine engines, discussing combustion problems, smoke emission reduction and bacterial or fungal contamination 13 p2113 A71-28754
- Soviet papers on combustion processes in turbulent and laminar flows of kerosene and gasoline mixtures, stressing gas turbine engines problems 13 p2162 A71-28954
- Gas turbine engine combustion chamber start-up and burning performance, considering air injection and propellant atomization 13 p2117 A71-28968
- Gas turbine engine startup igniter with modified propellant atomizer enhanced by air injection 13 p2118 A71-28969
- Carbon deposition rates in gas turbine engine combustion chambers with airstream-mechanical propellant atomization 13 p2118 A71-28970
- Optimal penetration effect on peripheral gas flow temperature field at outlet of turbine combustion chamber with circular flame tubes 13 p2118 A71-28971
- Gas turbine engine combustion chamber outlet, noting gas flow temperature field peripheral nonuniformity 13 p2118 A71-28972
- Gas turbine auxiliary power unit accessories, discussing high energy igniters, cables and connectors, thermocouples and speed and temperature monitoring equipment 13 p2071 A71-29262
- Metal coated superalloys evaluation for gas turbine engine components, including corrosion, impact and fatigue tests 14 p2256 A71-29635
- Chemical kinetic calculation of nitric oxide formation in spark ignition automobile engines and gas turbine combustors 14 p2190 A71-30454
- Aircraft JT9D engine development for airline operation, discussing construction, condition monitoring, maintenance, noise and smoke reduction [SAE PAPER 710434] 14 p2289 A71-30528
- Gas turbine engine condition analysis by digital computer and fault isolation techniques [SAE PAPER 710448] 14 p2289 A71-30532
- Turbopropulsion systems thrust augmentor combustion instability, discussing physical causes due to various pressure oscillation modes [AIAA PAPER 71-697] 14 p2293 A71-30756
- Jet engines nitric oxide air pollutant emission formation, developing gas turbine combustor models [AIAA PAPER 71-712] 15 p2470 A71-32289
- Flight mission severity in cumulative damage/low cycle fatigue and creep stress rupture/ not detected by usual nondestructive testing in aircraft gas turbine industry 16 p2624 A71-33298
- Statistical analysis of durability data of heat resistant alloys for gas turbine engines, using long term mass creep strength tests on industrial melts 16 p2592 A71-33413
- Gas turbine design advances for helicopter powerplants, illustrating by Turbomeca engines 16 p2624 A71-33416
- Swirling flow in gas turbine engine combustion chamber forward part, considering air flow characteristics behind blade swirler 16 p2624 A71-33606
- Gas turbine engine combustion chamber outlet gas temperature field peripheral nonuniformity, detailing jets disruptive capacity effects in mixing zone 16 p2625 A71-33609
- Soviet book on subsonic gas turbine passenger planes power supply systems covering Boeing 747, short haul aircraft, DC-10, L-1011, etc 17 p2677 A71-34472
- Gas turbine with high velocity combustor, pure impulse compressor and turbine and isothermal burner 17 p2793 A71-34590

Gas turbine engines materials and components equivalent service life estimation 17 p2793 A71-35452

Gas turbine engine steels and Ni alloys heat resistance, examining fatigue life and creep properties at various temperatures and test durations 17 p2759 A71-35453

Gas turbine engine nozzle guide vanes under pulsed thermal operation, discussing service life evaluation and increase 17 p2832 A71-35455

Aircraft gas turbine engine components equivalent testing by shortening testing time required to increase service life 17 p2793 A71-35460

Three micron absolute main oil filter for aircraft gas turbine lubrication system, discussing indicator system and bench and engine tests 17 p2793 A71-35488

Propulsion systems trends for 1980s, discussing environmental noise levels, stoichiometric gas turbine engines for military aircraft, high bypass ratio engines for V/STOL aircraft, etc 17 p2795 A71-35625

Book on external corrosion and deposits on boiler tubes and gas turbine blades covering mineral matter in fuels, oxidation, additives, etc 18 p2935 A71-36247

Computerized solutions of gas turbine engines motion equations, considering Euler, fourth order and fifth order Runge-Kutta, Adams, Bashforth and implicit methods 18 p2957 A71-36809

Material, design and operating principles of rotary seals used in gas ducts, bearing elements and fuel systems of aircraft gas turbine engines 19 p3069 A71-38015

Vacuum brazing for nozzle guide vanes repair in aircraft gas turbine engines, noting economic advantages 19 p3069 A71-38313

Multivariable frequency response methods for feedback control design for aircraft gas turbines, involving digital test bed trials 20 p3277 A71-38989

Gas turbine engine adjustable nozzle ring flat arrays aerodynamic characteristics determination from profile loss factor dependence on setting angle 20 p3175 A71-39172

Higher pressure ratios trend in aircraft gas turbines leading to higher exit temperatures from compressor, noting real gas effects 21 p3437 A71-40170

Sum and difference frequencies in vibration incident on gas turbine engine, considering synchronous and asynchronous excitation [ASME PAPER 71-VIBR-103] 21 p3462 A71-40329

Brazing filler metals as cost effective replacement for Au-Ni in aircraft gas turbine engine component 21 p3387 A71-40621

Soviet monograph on carbon deposits in jet engines covering distribution, formation, fuel properties, reduction and removal and harmful effects in gas turbines 21 p3437 A71-40871

Gas turbine engine turbine blades service life increase by Cr and Al vacuum diffusion metallization, presenting full scale endurance test results 21 p3390 A71-41173

Book on aircraft propulsion covering design, dynamics, control, installation, gas turbine, ramjet, rocket and piston engines, compressors, combustion and energy cycles, etc 22 p3589 A71-42427

High temperature gas turbine engines rotor blades cooling, deriving generalized dimensionless relations for heat transfer data extension from static tests to operational conditions 23 p3718 A71-44066

Gas turbine blades of cast Zr56K heat resistant alloy, investigating structural strength from fatigue test data 23 p3779 A71-44208

Gas turbine blade models of heat resistant Zr56K alloy under operational temperature variations, observing fatigue strength 23 p3779 A71-44209

Failure and crack formation in gas turbine engine compressor disks under variable stresses from fatigue tests, considering safety factors 23 p3779 A71-44210

Operational characteristics of starting igniters for gas turbine engine combustion chambers 24 p3864 A71-45003

Volume-weight characteristics of cross flow heat exchangers for heat regenerating gas turbine engines 24 p3889 A71-45007

Gas/turbine casing heat transfer coefficient distribution 24 p3889 A71-45008

Temperature field profiling along radius in front of gas turbine stage, applying to regeneratively cooled turbine engine 24 p3864 A71-45011

GAS TURBINES

Small gas turbines for aircraft auxiliary power unit, considering compressor and combustor design, noise, fuel consumption and specific weight problems 01 p0006 A71-10751

Rotor loss coefficients for prediction of radial gas turbine performance using one dimensional analysis 01 p0143 A71-11016

Closed hermetic air cooling system for high temperature gas turbines 01 p0143 A71-11246

Gas tungsten arc, manual, machine and resistance welding in assembly of gas turbine parts [SME PAPER AD-70-147] 01 p0089 A71-11258

Solidified Ni-Mo-Al gas turbine guide vane alloy with improved melting point, creep rupture strength and structural stability 03 p0431 A71-13256

Optimal firing temperature schedule during gas turbine loading for minimal thermal fatigue of hot gas path components, considering hollow stationary airfoils [ASME PAPER 70-WA/GT-2] 03 p0470 A71-14116

Thin gas turbine disk strength under axisymmetric flexural vibrations, noting agreement of calculated and experimental rotor rpm danger zone 04 p0671 A71-15639

Soviet book on air driven microturbines covering design, operation, energy losses, efficiency, economy and applications 06 p0848 A71-17446

Gas turbine air cooling systems hydraulic characteristics by graph-analytical method 06 p0945 A71-18001

Gas turbine cascade radial gap inverse heat transfer, calculating release coefficients 06 p1006 A71-18002

Swirling effects on turbulent flow recirculation zone behavior in gas turbine main burners [AIAA PAPER 71-2] 06 p0946 A71-18477

Multistage gas turbine design optimization, using parameter and component analysis with computer calculations 08 p1348 A71-21267

Gas turbine rotor axial load determination, using static pressure distribution 08 p1348 A71-21268

Columnar grain and single crystal high temperature gas turbine elements development through directional solidification 08 p1314 A71-21565

Gas turbine blades design and exploitation processes, discussing long time fatigue strength, static durability and heating effects at elevated temperatures 08 p1299 A71-21708

Gas dynamic test stand analyzing elastoplastic strains in aircraft gas turbine disks and liquid propellant rocket engines turbopumps under alternating nonisothermal loads 09 p1427 A71-22603

Welding rods chemical composition and welding procedures for heat resistant austenitic and martensitic steels for gas turbines, considering maraging steels heat treatment influence 09 p1456 A71-23291

Gas turbine components precision casting, discussing high temperature alloys and casting techniques in manufacture of components subject to high thermal and mechanical stresses 09 p1456 A71-23293

High temperature Fe, Co and Ni alloys for gas turbine components, considering tensile and creep rupture strength increase by thermal mechanical processing 09 p1475 A71-23298

Aircraft engines and stationary gas turbines high precision components, discussing die forging and machining combined with joining processes 09 p1456 A71-23299

High temperature Ni and Co alloys for stationary gas turbines and jet engine parts, considering microstructure and mechanical behavior under stress and temperature 09 p1475 A71-23302

Gas turbine blades local heat transfer, correlating experimental surface temperature, heat transfer coefficient and internal coolant temperature with theoretical estimates 09 p1547 A71-23658

Supersonic gas turbine nozzles with condensed particles, determining optimal contour geometries by direct variational procedures 10 p1551 A71-24379

Gas turbine exhaust silencer performance prediction by transmission line theory, considering LF requirements effect on size and cost [ASME PAPER 71-GT-8] 11 p1811 A71-25954

Heat transfer coefficients of various jet systems impinging on gas turbine blade inner surfaces, discussing cooling flow rates and solid particles injection into air flow [ASME PAPER 71-GT-9] 11 p1811 A71-25955

Gas turbine wheel design fracture mechanics, discussing buried and surface flaws analysis for rotor failure prediction applications [ASME PAPER 71-GT-10] 11 p1811 A71-25956

Three dimensional slot lip geometry effects on tangential and splash film cooling of gas turbines [ASME PAPER 71-GT-11] 11 p1855 A71-25957

Low alloy steels and superalloys inertia welding in gas turbine field, discussing microstructure tensile strength and stress rupture [ASME PAPER 71-GT-21] 11 p1770 A71-25958

Large gas turbine generator sets silencing, including silencer shells and doublewall acoustical/concrete enclosures [ASME PAPER 71-GT-26] 11 p1812 A71-25959

High subsonic flow two dimensional turbine cascade design by approximate hodograph method noting pressure distribution measurements [ASME PAPER 71-GT-34] 11 p1704 A71-25960

Low pressure drop fuel liquid injectors for jet engine combustors, using gas turbine vaporizer design [ASME PAPER 71-GT-38] 11 p1812 A71-25961

Low cost short life gas turbine design based on parametric performance and component selection outlining turbojet production [ASME PAPER 71-GT-69] 11 p1813 A71-25962

Coolant combustion effects in transpiration cooling of gas turbine components, using hydrogen, ammonia and nitrogen coolants [ASME PAPER 71-GT-72] 11 p1855 A71-25963

Standard equipment and procedures for aircraft gas turbine engine exhaust smoke measurement [ASME PAPER 71-GT-88] 11 p1813 A71-25964

Steady transonic flow through two dimensional gas turbine cascades predicted with time dependent formulation of flow equations, giving airfoil surface pressure distributions [ASME PAPER 71-GT-89] 11 p1704 A71-25965

Nozzle vane air cooling system for deflector type gas turbines, estimating profile perimeter average temperature for given coolant air flow rates 11 p1856 A71-26055

Gas turbine blades cast heat treated superalloys high temperature mechanical properties during aging 12 p1919 A71-27778

Gas turbine blades fatigue crack development and failure analysis under thermal cycling tests, considering chemical processes and thermal and mechanical stresses 13 p2149 A71-28117

Continuous combustion gas turbine with stepwise heat release, investigating ideal thermal efficiency cycle of gas overexpansion, cooling and compression 13 p2115 A71-28581

Combustion and heat transfer in gas turbine systems - Conference, Cranfield, England, April 1969 13 p2116 A71-28739

Air mass flow rate in can type gas turbine combustion chambers 13 p2117 A71-28747

Metal temperatures in rotating cooled gas turbine blades, discussing coolant flow aerodynamics 13 p2117 A71-28748

High temperature gas turbine alloys corrosion tests describing laboratory facilities for preliminary screening 13 p2086 A71-28755

Liquid fuel atomizers for gas turbine combustion system model experiments, considering droplet size photography and molten wax spray technique 13 p2117 A71-28755

Soviet monograph on turbines and jet nozzles for two phase flows covering gas-particle velocity and temperature differences, turbine design, etc 13 p2117 A71-28899

Analytical model for performance and pollutant emissions of gas turbine combustors, predicting gas composition and temperature [AIAA PAPER 71-711] 14 p2294 A71-30766

Nitric oxide formation analytical model for gas turbine combustion chamber, considering influence of primary zone equivalence ratio, combustor residence time and initial fuel droplet size [AIAA PAPER 71-715] 14 p2191 A71-30766

Pressure gain resonant combustion chambers in gas turbines, discussing thermal efficiency and power output 15 p2467 A71-31444

Axial flow steam and gas turbines performance estimations over ranges of loading, velocity/blade ratio Reynolds number and aspect ratio 15 p2469 A71-31733

Single phase and evaporative systems for liquid cooling high temperature gas turbine rotor blades reviewing heat transfer performance evaluation 15 p2469 A71-31733

Three stage potassium vapor turbine for space systems electric power generation, discussing erosion and endurance tests 15 p2415 A71-32211

Thermal fatigue cracking of gas turbine blades in fuel combustion product flow, investigating surface composition, microhardness and structure under simulated loads 15 p2469 A71-32222

- Gas turbine blades effusion cooling effectiveness, using boundary layer theory to calculate blade profile local heat transfer 15 p2472 A71-32716
- Film cooling studies in subsonic and supersonic flows, using shock tunnel for gas turbine conditions simulation 16 p2551 A71-32882
- Thermal stresses in gas turbine rotor blade with two dimensional temperature field, using closed /Saint Venant/ plate solutions 16 p2657 A71-33543
- Transverse flow in cavity ensurance by air exhaust cooling of trailing edges of gas turbine blades with deflector 16 p2624 A71-33544
- Axial flow gas turbines blade cascades forming arrays with convergent channels, discussing contours design 16 p2521 A71-33615
- Gas turbine blades dynamic characteristics determination, investigating vibrational stresses, thermal cycles, alloy physicomechanical properties and coatings effects 16 p2659 A71-33987
- Pressure ratios and surface effects on regenerative heat exchanger in Brayton gas turbine cycles with intercooling or reheating 16 p2663 A71-34037
- Stream lines construction in meridional plane of blade nozzle annular cascades of steam and gas turbines in subsonic and supersonic flow 17 p2670 A71-34446
- Two dimensional stress and temperature fields in cooled gas turbine blades with allowance for elasticity, plasticity and creep 18 p2980 A71-36704
- On-design performance characteristics of radial gas turbines, investigating blade geometry, rotor losses and pressure ratio effects 19 p3123 A71-38269
- Miniature high speed expansion turbines for helium liquefiers and refrigerators, discussing turbine flow passages and gas lubricated bearings 20 p3184 A71-39246
- Tensile, impact and fatigue properties of welded Ti alloys, determining joint quality and friction welding sensitivity in highly stressed gas turbine components 21 p3387 A71-40619
- Gas turbine blades cast heat treated superalloys high temperature mechanical properties during aging 21 p3403 A71-41103
- High temperature creep characteristics and strain curves of heat resistant Fe and Ni alloys in turbine components 21 p3403 A71-41158
- Heavy load transportation Mi 12 helicopter design and performance, noting gas turbine rigid shaft connection 23 p3627 A71-42926
- Multiple rig rolling fatigue life test, evaluating aviation gas turbine lubricants [ASLE PREPRINT 71LC-15] 24 p3832 A71-45292
- GAS VISCOSITY**
- Steam-air mixture viscosity, deriving empirical formula from experimental data 01 p0118 A71-10620
- German monograph on differential solar rotation resulting from anisotropic turbulent viscosity in hydrogen convection zone 02 p0317 A71-12846
- Normal shock wave stability in perfect gas with viscosity and heat conduction under arbitrary small one dimensional disturbances, formulating eigenvalue problem 07 p1224 A71-20288
- Rotating nonvibrating diatomic low density gas molecules rotational relaxation time and viscosity, based on quantum mechanics 08 p1336 A71-20659
- One dimensional nonstationary motion of compressible electrically conducting gas with allowance for heat conductivity and viscosity, solving MHD equations 09 p1499 A71-22129
- Nitrogen-oxygen and nitrogen-argon mixtures viscosity, using oscillating disk viscometer to test corresponding states principle validity 09 p1546 A71-23010
- Viscosity effect on initial highly underexpanded jets in Mach 1 to 5.7 nozzles for laminar, turbulent and rarefied air flows 13 p1989 A71-27889
- Shock tube high temperature air viscosity from laminar boundary layer heat exchange data 14 p2224 A71-30047
- Viscous gas unsteady flow between harmonically oscillating and nonoscillating walls 14 p2225 A71-30220
- Equilibrium constant and heat of dissociation from dynamic viscosity of dissociating gas, noting dependence on composition and temperature 15 p2366 A71-31484
- Viscosity of dissociating oxygen, carbon-air and argon plasmas at high temperature range, including error estimates and expansion up to 12,000 K 15 p2512 A71-31502
- Heating effects on wing tip vorticity diffusion rate in gas vortex, causing outward radial convection and increased kinematic viscosity [AIAA PAPER 71-616] 15 p2512 A71-31556
- Thermal conductivity, diffusion and viscosity of gases and multicomponent gaseous mixtures at high temperatures 15 p2515 A71-32450
- Temperature and pressure effects on viscosity and thermal conductivity of dissociating air at high temperatures 17 p2785 A71-35277
- Supersonic spherical viscous heat conducting gas discharge into vacuum, solving Navier-Stokes equations by buildup method 19 p3042 A71-37087
- Viscosity effect on initial part of highly underexpanded jets in Mach 1 to 5.7 nozzles for laminar, turbulent and rarefied air flows 21 p3317 A71-40079
- Nitrogen, argon and helium viscosity measurements, obtaining density expansion by statistical analysis 22 p3621 A71-42369
- Oxygen viscosity variation under strong magnetic field, comparing angular dependence of Senfleben effect 24 p3802 A71-45116
- GAS WELDING**
- NT BRAZING**
- NT ULTRASONIC SOLDERING**
- Pressurized inert gas metal arc welding of Al, determining voltage, filler metal speed and chamber pressure effects by multiple regression analysis 02 p0255 A71-11709
- High strength steel weldability with shielded and gas metal arc processes, discussing hardness, tensile, bend, impact and fatigue tests 04 p0603 A71-14922
- Inert gas welding of Al with He as oxidation inhibitor, discussing penetration, welding rate and cost compared to Ar use 04 p0604 A71-15815
- Heat affected zone crack filling and weld metal-base metal interactions of high strength alloys in dissimilar gas arc welding 11 p1769 A71-25749
- Air cooled turbine blades activated diffusion brazing and gas pressure welding, using composite finned configuration model [ASME PAPER 71-GT-32] 11 p1770 A71-25969
- Ti alloys semiautomatic pulsed arc MIG welding, showing increased productivity and reduced distortion 19 p3070 A71-38423
- GAS-GAS INTERACTIONS**
- Chemically interacting gases transfer properties at varying temperatures, determining collision parameters by viscosity, diffusion coefficients, molecular beam scattering and vibrational relaxation time 02 p0286 A71-12186
- Nitric oxide vibrational relaxation times in Ar from IR emission measurements at high temperature 02 p0287 A71-12495
- Carbon dioxide vibrational relaxation in Ar at high temperature, using shock tube method 02 p0287 A71-12496
- Film cooling in gaseous medium, assuming turbulent boundary layer at blowing point 02 p0333 A71-12645
- Atomic oxygen-nitrogen shock tube endothermic reaction under high translational and low vibrational energy, noting ozone loss 03 p0375 A71-13493
- Initial vibrational energy level distribution of hydrogen fluoride formed in reaction between atomic fluorine and molecular hydrogen, using IR chemiluminescence 03 p0375 A71-13495
- Oxygen-nitrogen synergistic interactions in rats in hyperbaric environment, determining lung damage by total water measurement 04 p0538 A71-15054
- Interaction flowfield of two dimensional supersonic airstream with transversely injected jets of various gases, presenting wall static pressure, gas concentration and temperature measurements 09 p1382 A71-22111
- Energy dependence of integral scattering cross sections of noble gas atoms in carbon dioxide 13 p2102 A71-27809
- Chemically interacting gases transfer properties at various temperatures, determining collision parameters and interaction cross sections and energies 15 p2451 A71-31494
- Two dimensional jet interaction flow field, investigating gas dynamic and transport phenomena [AIAA PAPER 71-561] 15 p2514 A71-32279
- Velocity dependent HD beam scattering by inert gases, measuring total effective cross section in thermal energy range 23 p3707 A71-43879
- He, HD and deuterium scattering by various gas molecules, measuring total effective cross sections for comparison with calculation 23 p3707 A71-43880
- GAS-ION INTERACTIONS**
- Comparative numerical capture and experimental reaction cross sections for ion-molecule ammonia 01 p0028 A71-10476
- Light emission during ion-molecule collisions, using low energy nitrogen and argon ion beams 04 p0630 A71-15655
- Isotope effects on collision dynamics of molecular hydrogen-argon ion reactions, using chemical accelerator 05 p0784 A71-15974
- Fully ionized hydrogen cosmic plasma interaction with surrounding neutral gas, noting minimum temperature and power input 05 p0810 A71-16637
- Molecular N ion production, studying cross sections, collisions kinetic energies and isotopic substitution 06 p0929 A71-17407
- Oxygen ion-molecule reactions at thermal energies, using drift tube mass spectrometer 07 p1164 A71-19689
- Kinetic energy dependent charge transfer rates for ion-molecule reactions in ammonia, using cyclotron ejection and impulse methods 08 p1249 A71-20657
- Electron loss and capture by hydrogen atoms, protons and negative ions during collisions between atoms and molecules in gases, interpreting cross section data 08 p1338 A71-21491
- Gas phase ion-molecule phosphine reactions in pure and binary mixtures by ion cyclotron resonance spectroscopy, considering acidity and basicity 08 p1251 A71-21699
- Crossed beam model of nitrogen ion-molecular oxygen reactions in upper atmosphere as function of collision energy 08 p1251 A71-21784
- Slow negative atomic oxygen ion production in collisions between fast protons or hydrogen atoms and gas molecules 09 p1496 A71-22230
- Shock and turbulent ray interactions of plasma streams with neutral gas cloud, noting comet tail similarity 10 p1652 A71-24653
- Tropospheric ionization mechanism for gas to particle condensation embryos existence, using positive and negative ions ground level and altitude profiles 10 p1604 A71-24704
- Cross sections of metastable H formation by charge transfer of hydrogen ion beam on helium, argon, nitrogen and oxygen targets 11 p1803 A71-26371
- Three body ion-neutral association reactions of NO ions with oxygen, nitrogen and carbon dioxide, noting temperature effect on rate constant 13 p2026 A71-29507
- Electron production by proton impact on nitrogen, oxygen, neon and argon, measuring cross sections angular and energy distribution by electrostatic analysis and electron counting 14 p2277 A71-30660
- Molecular rotational excitation during CO ion-Argon interactions by ion beam collision spectroscopy, observing energy loss spectra 15 p2452 A71-32551
- Positive NO ion formation with excess internal energy in positive atomic oxygen ion-nitrogen collisions 16 p2538 A71-32810
- Rare gas ions molecular and dissociative charge transfer reactions with nitrogen, using statistical phase-space theory of chemical reactions 16 p2538 A71-32813
- Electron loss and capture by hydrogen atoms, protons and negative ions during collisions between atoms and molecules in gases, interpreting cross section data 16 p2614 A71-33042
- Slow negative atomic oxygen ion production in collisions of fast protons and hydrogen atoms with oxygen molecules, measuring scattering cross sections 21 p3419 A71-41109
- Mean charge measurement for heavy ions moving through He and air with aid of gas-filled mass separator, noting anomalies in nuclear charge dependence 21 p3419 A71-41112
- Statistical phase space cross sections for helium ion-nitrogen molecule reactions, including dispersion and short range forces in intramolecular potential energy function 23 p3706 A71-43119
- Electron transfer cross sections for low energy negative oxygen ion collisions with oxygen molecules measured by single-collision beam technique 23 p3707 A71-43930
- GAS-LIQUID INTERACTIONS**
- Gas bubble growth and dissolution due to pressure fluctuations in turbulent diffusion liquid flow 07 p1094 A71-20475

Gas-liquid fluidic timing control device, discussing media combination, oscillator complete clock, bubble counter and pressure gages

07 p1031 A71-20605

Tangential body forces and pressure perturbation interactions in thin liquid film, considering destabilizing effect impairing film cooling efficiency

11 p1751 A71-25491

Liquid-vapor interactions in constant area steam-water condensing ejector mixing section, measuring axial static and stagnation pressure profiles

13 p2052 A71-29459

Gas-filled spherical cavity in infinite compressible liquid, deriving radial oscillations by numerical solution

14 p2225 A71-30229

Hydrogen sorption capacity by sulfur dioxide frost from cryodeposit formation on stainless steel sphere in vacuum chamber and equilibrium isotherms measurement

17 p2695 A71-35142

Two phase gas-liquid ejectors with cylindrical mixing chamber, discussing ejection equations, jet flow parameters, operation modes and diffusor substitution

22 p3479 A71-41851

GAS-METAL INTERACTIONS

Oxygen diffusion coefficient during metal/Ti oxidation in unsteady high temperature region, allowing for interfacial phase boundary shift

01 p0101 A71-10673

Imaging gas-metal surface interaction in evaporation field by ion microscopy, discussing molecular ion identification and dipole attraction due to electronic rearrangement

02 p0209 A71-12735

Ti-Al-V hydrogen induced fatigue crack growth at room temperature under sustained load

02 p0268 A71-12891

Chemisorption layer kinetics of oxygen on thin Ta films at room temperature and low pressures

03 p0441 A71-13359

Chemisorption and sticking probability of nitrogen on Ta films, considering relationship to temperature and pressure

03 p0441 A71-13360

Chemisorption rate and physical adsorption of nitrogen on Ta films as function of temperature

03 p0441 A71-13361

High melting point metal systems with nitrogen or oxygen, discussing engassing and degassing reactions kinetics and thermodynamic equilibrium

03 p0442 A71-13362

Limiting temperature and size conditions for aluminum particle ignition in mixtures of oxygen with argon and nitrogen

03 p0468 A71-13990

Ultrahigh vacuum deposited Ni, Fe, W and Mo films, determining molecular oxygen adsorption efficiencies

04 p0636 A71-15015

Refractory metal surface-gas reactions at high temperatures in vacuum, determining activation energies

05 p0766 A71-16241

Hydrogen and carbon monoxide coadsorption on platinum single crystal surface, examining interactions and species formation by thermal flash and electron impact techniques in ultrahigh vacuum

07 p1055 A71-19844

Hydrogen and nitrogen chemisorbed species interactions on $100/\text{tungsten}$ crystals, using flash desorption methods

07 p1056 A71-19846

Mo, W and Zr effects on niobium reaction with residual gases during heating in vacuum

09 p1469 A71-22846

Hydrogen-nickel reaction in presence of CO adsorbed gas, increasing total desorption cross section and eliminating monotonic relation between uptake and H ion current

10 p1573 A71-24540

Thermal relaxation effects on thermal adjustment between gas and wall, comparing with thermograms from shock tube experiments

13 p2161 A71-28619

Adsorption states of Mo and Re surfaces during oxidation at low oxygen pressures and temperatures up to 2300 K, using noble gas molecular beams

14 p2190 A71-30402

Vibration fatigue of metallic materials in vacuum and different gas atmospheres, considering fcc metals, Al alloys and steels

[DFVLR-SONDDR-62]

14 p2259 A71-30466

Two phase oxygen adsorption on molybdenum surface from secondary ion-ion emission

14 p2260 A71-30678

Oxidation kinetics of pure Al in dry oxygen as function of pressure and temperature, using manometric method

15 p2426 A71-31408

Binding states, adsorbate densities and desorption kinetics of hydrogen on crystal planes of tungsten

15 p2367 A71-31676

Metallic Ni trace effects on oxygen chemisorption forms on nickel oxide in various temperature regions

15 p2367 A71-31901

Oxygen adsorption kinetics at Nb single crystal surface at high temperatures and low pressures

15 p2436 A71-32547

Gas-solid interaction by shock tube method, determining thickness and thermal accommodation effects on thin metal film resistance thermometer response

16 p2576 A71-32922

Oxygen sorption rate by Ti at low pressure from measurement in stainless steel ultrahigh vacuum chamber

17 p2695 A71-35139

In situ metal-gas secondary standard assembly for ultrahigh vacuum gage calibration, using repeatable pressure generation from binary erbium-hydrogen system

17 p2744 A71-35140

Rotating disk flow system for Fe vaporizing into cold Ar atmosphere, investigating effect of condensation in boundary layer on mass transfer

19 p3162 A71-37727

Inert gases energy accommodation coefficients dependence on clean metal surface temperature based on lattice theory

21 p3415 A71-40538

Nitrogen adsorption on single crystal W planes by flash desorption experiment, noting work function change dependence on planes

21 p3345 A71-40539

Oxygen diffusion coefficient during metal/titanium/oxidation in unsteady high temperature region, allowing for interfacial phase boundary shift

21 p3401 A71-41054

Ni and Ni-base alloys gaseous carburization by circulation method, investigating gas flow velocity effect on metal diffusive saturation

21 p3389 A71-41165

Quasi-equilibrium prediction of rate of volatilization/erosion/ of solid tungsten by reaction with gaseous oxygen at high temperature and low pressure

21 p3404 A71-41419

Nitrogen ions surface interactions with Al surfaces at and above earth satellite speeds, measuring normal and tangential momentum accommodation coefficients

22 p3577 A71-41980

Gas molecular interactions, energy and momentum transfer and scattering from clean metal surfaces

22 p3577 A71-41996

Metal embrittlement by gaseous hydrogen, discussing countermeasures against hydrogen metal interaction and cracking

22 p3562 A71-41999

Gas-metal reactions in refractory metals purification, discussing reaction kinetics, thermodynamic equilibria and dissolved gases induced mechanical properties changes

22 p3564 A71-42423

Oxygen interaction with polycrystalline W, calculating sticking probabilities and desorption spectra at various temperatures

23 p3641 A71-42906

Corrosive oxide layer formation kinetics during interaction of oxygen with polycrystalline W at 500-1000 K, using desorption mass spectrometry

23 p3641 A71-42907

GAS-SOLID INTERFACES

Tangential momentum transfer accommodation coefficient for gas flow based on monocrystalline molecular model of gas-solid interface

01 p0071 A71-10949

Shape effect of compressed solid fuel on thermal ignition delay time in heated gas flow for pyroxyline

03 p0520 A71-13993

Gas phase reactions near solid-gas interface of deflagrating double base propellant causing abrupt changes in burning rate-pressure curve

[AIAA PAPER 70-124]

05 p0837 A71-16571

Solid particle impurity effects on hypersonic shock tube flow, determining error in blunt body measurements

07 p1013 A71-18916

Solid/vapor surface energies of metals at melting point related to heat of sublimation

07 p1134 A71-19518

Cadmium telluride epitaxial films on potassium bromide, investigating external gases effects on photovoltaic properties

07 p1179 A71-19919

Elementary particle recombination probabilities on solid body surface, using reactive gas model in form of quantum mechanics three body problem

12 p1934 A71-27546

Gas atoms collisions with linear harmonic oscillator and solid surface simulated by semiinfinite elastically coupled atomic lattice, using combined asymptotic expansions method

13 p2103 A71-29227

Classical and quantum mechanical theories of gas atom-solid surface scattering with applications to different physical regimes

14 p2276 A71-30405

Two dimensional unsteady heat conduction in solid with subliming surface, replacing original boundary value problem by ordinary integrodifferential equation

14 p2338 A71-30933

Slender body interaction with interface formation after bursting of membrane separating low and high pressure gas supersonic flow in shock wave tube

15 p2386 A71-31141

Monatomic gas interaction with solid phase surface deriving three dimensional theoretical model including hard spheres collision and surface energy

15 p2451 A71-31625

Gas stream-wall interaction for Maxwell model by scattering element-detector system with specular reflection and diffusion separation

15 p2389 A71-31707

Sulfur effervescing molten slag/gas systems causing planetary vulcanism, examining patterns on earth, moon and Mars

15 p2496 A71-32725

Heat and mass transfer during deposition on heated surfaces in nonisothermal gas flow with suspended solid particles, using motion of continuous Newtonian medium

17 p2836 A71-34300

Solid particle impurity effects on hypersonic wind tunnel flow characteristics

17 p2671 A71-35116

MOS sandwich grid diode for gas ionization and field electrons generation at solid-gas phase boundaries

17 p2717 A71-35448

Kinetic models for gas-surface interactions, considering distribution functions of molecules at solid wall

18 p2874 A71-35900

Monatomic gas beams scattering from gas surfaces interface with randomly distributed energy states, confirming reciprocity or detailed balance principle

19 p3104 A71-38057

Gas-solid particles flow pseudoflow equations, discussing difference of species and partial density and various flow phases

21 p3365 A71-40018

Nonablating inelastic deformable material surface interaction with external supersonic turbulent boundary layer, observing crosshatch patterns

21 p3323 A71-40941

Macroscopic values of energy exchange between polyatomic gas and solid wall, considering heat transfer rate and wall temperature change

23 p3781 A71-43105

Gas interaction with lunar fines, investigating carbon monoxide, nitrogen, oxygen, argon and water vapor adsorption

23 p3758 A71-43754

Sintered construction material with high SiC content, investigating thermal stability in nitrogen, air, carbon dioxide and water vapor above 2000 K

23 p3696 A71-44020

Hydrogen solubility in alpha phase Ti-Al alloys, using resistometric technique and electron microscopy

23 p3694 A71-44282

GASEOUS CAVITATION

U CAVITATION FLOW

U GAS FLOW

GASEOUS DIFFUSION

Pt electrode oxygen diffusion and consumption systematic errors effect on oxygen partial pressure measurement in perfused tissues

01 p0021 A71-10073

Oxygen diffusion coefficient during metal/Ti oxidation in unsteady high temperature region, allowing for interfacial phase boundary shift

01 p0101 A71-10673

Gas permeable dispersion layer between impermeable solid wall and high temperature gas flow, calculating dimensionless heat flux equations

02 p0332 A71-12200

Spherical hydrogen-oxygen diffusion flame structure, discussing combustion processes chemical kinetics

02 p0210 A71-12856

Gaseous impurities diffusion into silicon via open tube microelectronic method

02 p0297 A71-12922

Oxygen uptake by hemoglobin solution, considering diffusion rate and chemical reaction by mathematical model numerical solution

03 p0360 A71-13180

Atmospheric air breakdown by mode-locked Q-switched laser pulse train, investigating threshold electric field dependence on characteristic diffusion length

03 p0440 A71-14178

Nitrogen diffusion and solubility in W, deriving expression for permeation constant

04 p0614 A71-15784

High strength steel reversible hydrogen embrittlement mechanisms, noting role of hydrogen diffusion

04 p0615 A71-15790

Oxygen diffusion in monoclinic zirconia as function of equivalent pressure, using oxygen 18 gas-solid exchange techniques

05 p0769 A71-17090

Niobium oxide defect structure, correlating electrical conductivity and oxygen diffusional properties with nonstoichiometry degree

05 p0770 A71-17097

Incompressible fluid steady laminar flow free convection and various gas species mass diffusion from horizontal plate surface

06 p1007 A71-18074

Metals electronic structure effects on hydrogen diffusion mobility

09 p1471 A71-23082

Titanium-containing steels nitriding in ammonia, discussing hydrogen diffusion layers brittleness, cracking, peeling and thickness

12 p1919 A71-27776

Diffusive separation of binary gas mixture in free jet expelled into vacuum, comparing theory and experimental results

13 p2050 A71-29216

Position, exercise and lung volume effects on healthy males pulmonary diffusing capacity for CO at rest and during exercise

13 p2015 A71-29493

Alveolar-arterial oxygen pressure gradient derivation as sum of shunt, ventilation/perfusion inequalities and membrane and airway diffusions

15 p2363 A71-31444

Gas permeable dispersion layer between impermeable solid wall and high temperature gas flow, solving dimensionless heat flux equations

15 p2512 A71-31505

Heating effects on wing tip vorticity diffusion rate on gas vortex, causing outward radial convection and increased kinematic viscosity

15 p2512 A71-31556

Plasma decay due to charged particles recombination, linearizing nonlinear equations describing diffusion of singly ionized two-component gas undergoing recombination

15 p2456 A71-31999

Thermal conductivity, diffusion and viscosity of gases and multicomponent gaseous mixtures at high temperatures

15 p2515 A71-32450

Gas permeability of polymeric foils reduction by vapor metallization in vacuum, noting dependence on surface state, diffusion layer and macroporosity

16 p2601 A71-33684

Circumstellar dust clouds and Bok globules examined for gaseous emission lines, emphasizing forced diffusion process

16 p2643 A71-34077

Oxygen pulmonary diffusion capacity estimation by rebreathing procedure based on gas-blood partial-oxygen-pressure equilibration

17 p2678 A71-34173

Cesium vapor diffusion condensations from laminar argon flows in tubes and turbulent movement on banks, considering boundary layer mist formation effect

17 p2785 A71-34206

Space station life support prototype vapor diffusion water reclamation system for pure and sterile water distillation from urine process stream

18 p2869 A71-36398

Diffusing gas mixtures slipping rate along wall at arbitrary accommodation coefficients, deriving expression based on molecule distribution functions from linearized Boltzmann equations solution

21 p3418 A71-40678

Oxygen diffusion coefficient during metal/titanium oxidation in unsteady high temperature region, allowing for interfacial phase boundary shift

21 p3401 A71-41054

Titanium-containing steels nitriding in ammonia, discussing hydrogen diffusion layers brittleness, cracking, peeling and thickness

21 p3424 A71-41097

Nb nitriding kinetics and external effects observations, noting nitrogen diffusion through crystal lattices

21 p3404 A71-41163

Alloy steels supercooled austenite nitriding in ammonia flow, examining diffusion layers by X ray analysis and hardness tests

21 p3404 A71-41164

Austenitic stainless steels diffusion layer formation and structure by gaseous calorization with FeAl-ammonium chloride powder mixture, describing elements redistribution

21 p3390 A71-41166

Delta-zirconium hydride hydrogen engassing experiment, investigating hydrogen absorption rate and diffusion constant temperature dependence

23 p3688 A71-42929

Pulmonary carbon monoxide diffusing capacity of sea level and high altitude dwellers at various altitudes, noting early postnatal lung growth effects

24 p3797 A71-44778

Pulmonary blood flow and carbon monoxide diffusing capacity uneven distribution measurements, determining body position effects

24 p3798 A71-44782

NUCLEAR FISSION REACTORS

Analytical model for molecular flow of reactive gaseous species through cylindrical reactors with apertures at either end, evaluating surviving flux magnitude

17 p2695 A71-35137

Critical mass calculation for open cycle gas core rocket reactors, considering cavity size, fuel radius, reflector thickness and hydrogen bypass flow

22 p3573 A71-41637

Volume fraction analysis of coaxial flow gas core nuclear rocket for mass flow ratios, fuel radius and density, using free jet computer code and eddy viscosity equations

22 p3573 A71-41638

GASEOUS ROCKET PROPELLANTS

Stored gas retrorocket total impulse expression, deriving from flow continuity equation in closed duct

08 p1366 A71-21308

Long term life test and vacuum tests of high temperature resistojets, using ammonia and hydrogen propellants

[ALAA PAPER 70-1136]

11 p1811 A71-25523

Nuclear light bulb engine based on thermal radiation energy transfer from gaseous uranium fuel through internally cooled transparent wall to seeded hydrogen

[ALAA PAPER 71-642]

14 p2274 A71-30719

Gaseous oxygen/gaseous hydrogen auxiliary propulsion engines, considering cold flow experiments with nonreactive simulant gases

[ALAA PAPER 71-673]

14 p2291 A71-30737

Gaseous oxygen/hydrogen injector element modeling based on composition profile measurements for cold flows

[ALAA PAPER 71-674]

14 p2291 A71-30738

Low pressure gaseous hydrogen/gaseous oxygen APS rocket engines operating with propellant stored as liquids and fed to thruster without pressure augmentation

[ALAA PAPER 71-738]

15 p2467 A71-31326

GASES

NT ARGON

NT ARGON ISOTOPES

NT CARBON DIOXIDE

NT CARBON MONOXIDE

NT COLD GAS

NT COMPRESSED GAS

NT COSMIC GASES

NT DETONABLE GAS MIXTURES

NT DEUTERIUM

NT DEUTERIUM PLASMA

NT DIATOMIC GASES

NT EXHAUST GASES

NT FLAMMABLE GASES

NT GAS MIXTURES

NT GAS STREAMS

NT GRAY GAS

NT HELIUM

NT HELIUM ATOMS

NT HELIUM ISOTOPES

NT HIGH TEMPERATURE AIR

NT HIGH TEMPERATURE GASES

NT HYDROGEN

NT HYDROGEN ATOMS

NT HYDROGEN IONS

NT HYDROGEN ISOTOPES

NT HYDROGEN PLASMA

NT IDEAL GAS

NT INTERPLANETARY GAS

NT INTERSTELLAR GAS

NT IONIZED GASES

NT LIQUEFIED GASES

NT LIQUID HELIUM

NT LIQUID HYDROGEN

NT LIQUID NITROGEN

NT LIQUID OXYGEN

NT LORENTZ GAS

NT MOLECULAR GASES

NT MONATOMIC GASES

NT NEON

NT NEON ISOTOPES

NT NITROGEN

NT NONCONDENSIBLE GASES

NT NONGRAY GAS

NT ORTHO HYDROGEN

NT OXYGEN

NT PARA HYDROGEN

NT POLAR GASES

NT POLYATOMIC GASES

NT RADON

NT RADON ISOTOPES

NT RARE GASES

NT RAREFIED GASES

NT REAL GASES

NT RESIDUAL GAS

NT SOLIDIFIED GASES

NT TRITIUM

NT XENON

NT XENON ISOTOPES

NT XENON 133

Interatomic forces and gas theories from Newton to Lennard-Jones, discussing hypothetical deductive atomic models relation to gas properties

01 p0129 A71-11401

Simple gases and liquids thermodynamic properties, calculating isotopic effects by corresponding states law with quantum corrections

02 p0331 A71-12187

Microwave scattering from gaseous plasmas, discussing EM waves, fluctuation and diagnostics problems

07 p1172 A71-20503

Gaseous plasma diagnostics by light scattering for localized minimal perturbing measurement of temperature and density parameters

07 p1172 A71-20504

Kinetic coefficients calculation for gas with internal degrees of freedom during free energy exchange between translational and internal motion

08 p1338 A71-21918

Monograph on dense gases state parameters measurement at high temperatures, applying to nitrogen

10 p1697 A71-24676

Kinetic coefficients calculation for gas with free energy exchange between translational and internal degrees of freedom

17 p2785 A71-35263

Quantum counter action in various media including trivalent and divalent rare earth ions, Fe group transition metal ions, semiconductors and gases

18 p2930 A71-36145

Gaseous media parameters in wave energy exchanger, examining compression cycles, temperature ratios and flow velocities for maximum conversion efficiency

24 p3891 A71-45199

GASOLINE

Book on aviation fuels covering gasoline and turbine fuel properties, handling problems and future fuels

03 p0469 A71-14298

Gasoline-air mixtures normal combustion velocity by photographic observations of flame propagation in transparent tubes

12 p1986 A71-27499

Turbulent flame boundaries and maximum brightness surface position in gasoline-air mixtures, using photography and gas analysis measurements of carbon dioxide concentrations

13 p2162 A71-28955

Flame propagation speed, combustion zone extent and distance from front to maximum brightness surface in turbulent gasoline-air flames

13 p2162 A71-28956

Normal rates of flame propagation in two stage burning of gasoline-air mixtures

13 p2162 A71-28958

Flame propagation rate in gasoline-air flow with tubular and grid-induced turbulence during two-stage burning process

13 p2162 A71-28959

GASTROINTESTINAL SYSTEM

NT INTESTINES

NT RECTUM

NT STOMACH

Electronic instrumentation for monitoring intragastric pH, temperature, motility and electrical activity

01 p0023 A71-10887

Human gastrointestinal tract functional disturbances after prolonged work in UHF field

08 p1249 A71-21955

Antiradiation drugs effects on healthy and irradiated rats gastrointestinal tract evacuatory motor function

22 p3492 A71-42707

Gastrointestinal tract reactions to atropine sulfate, acetylcholine and carbacholine in rats after acceleration exposures, using roentgenograms

22 p3495 A71-42796

GATES [CIRCUITS]

NT THRESHOLD GATES

FET insulating layer electrical properties requirements, considering threshold voltage, dielectric constant, breakdown voltage and insulated gate FET instabilities

02 p0229 A71-11813

Absolute value type early-late gate bit synchronizer steady state phase noise performance evaluation by Fokker-Planck method

05 p0730 A71-17060

N and p junction field effect transistor (JFET) gate current measurement leading to understanding of impact ionization mechanism and field distribution

07 p1081 A71-20542

Fluidic passive and, exclusive-or logic gate, investigating switching, input and output characteristics

07 p1031 A71-20610

Gate voltage drift in enhanced p-channel MIS transistors having either pure silicon dioxide insulation or silicon dioxide with silicon nitride

09 p1413 A71-22156

Memory behavior in floating gate avalanche injection MOS structure, considering long term charge storage in insulated gate field effect device

13 p2036 A71-28045

Gated phase locked loop system characteristics based on sampled data model, comparing with continuous loop operation

14 p2214 A71-30795

FLE-251 fluidic NOR gate impact modulator developing equivalent circuit model for pressure gain recovery and cut-off, output capacitance and step response

15 p2351 A71-31684

Analog computer application for determination of charge centers in multilayer gate structure of variable threshold FET, deriving equations yielding position of internally stored charge

15 p2462 A71-32639

Three color photoelectric photometer improvements by introducing synchronous signal detection and electronic gates by field effect transistors

16 p2579 A71-33434

Silicon gate process effect on MOS circuits application, noting bipolar compatibility, circuit layout compactness and reliability

21 p3354 A71-40729

Switched power limitation due to thermal processes in p-n-p-n devices turned off by gate current pulse

21 p3430 A71-41219

Microwave Si MESFET for 15 GHz oscillation with reduced gate metallization resistance and pad parasitics, improving gain and noise figure

22 p3520 A71-41683

Distributed gate multielectrode MOS transistor, presenting negative resistance operation mode

22 p3520 A71-41685

Probabilistic analysis of random pulse signal gating on time selective zero lag converter with rectangular pulse input

23 p3647 A71-44322

Ion implantation technique utilization for reducing MOSFET devices threshold voltage and gate drain capacitance

24 p3808 A71-44725

Input admittance, drain noise and induced gate noise measurements in search for excess gate noise in large geometry MOSFET

24 p3863 A71-45355

GAUGE INVARIANCE

Electrodynamics Lagrangian with gauge invariant electron operator, obtaining free field nonequal time commutators and photon propagator for perturbation theory

16 p2610 A71-33269

Gauge equations in general relativity theory for tetrad gravitational potential formulation, based on algebraic invariants method

17 p2778 A71-34636

GAUSS EQUATION

Laminar boundary layer convective heat transfer with constant wall temperature, using Gaussian quadrature formulas

02 p0332 A71-12394

Growth minimization of nonzero elements in sparse matrix during reduction to Hessenberg triangular form by Gaussian similarity transformations

10 p1635 A71-23775

GAUSS FUNCTION

U GAUSS EQUATION

GAUSS-MARKOV THEOREM

Scalar Gaussian channel information optimal input capacity as function of random variable, assuming finite number of values for amplitude and variance constraints

11 p1730 A71-25374

GAUSSIAN DISTRIBUTIONS

U NORMAL DENSITY FUNCTIONS

GAUSSIAN NOISE

U RANDOM NOISE

GAUSSMETERS

U MAGNETOMETERS

GAUZE

Combustion systems ionic wind velocities, investigating gauze parameters, magnetic fields and mixture inhomogeneity effects

17 p2785 A71-35703

GC-130 AIRCRAFT

U C-130 AIRCRAFT

GCR [REACTORS]

U GAS COOLED REACTORS

GEAR TEETH

Geometrical conditions for contact without interference in internal gear stages with small tooth number differences

03 p0431 A71-13024

Transition curve equation for end cross section of slant-toothed wheel cut by rack type instrument with protuberance and rounded edge

07 p1117 A71-19360

GEARS

Gear drives operating in vacuum conditions, calculating friction coefficient with dimensional analysis

02 p0258 A71-12598

Geometrical conditions for contact without interference in internal gear stages with small tooth number differences

03 p0431 A71-13024

External-internal gear stages contact ratio on basis of gear wheels working drawing geometrical quantities

03 p0431 A71-13025

High stress cycles and impact fatigue behavior of common case hardened carburized gear steels under loading

03 p0441 A71-13253

Power train systems gear induced noise analysis, using in-flight vibration and noise measurements for comparison with calculated noise spectra

[ASME PAPER 70-WA/DGP-1] 03 p0471 A71-14137

Lubrication considerations concerning mechanical and service variables for obtaining optimum gear performance under severe operating conditions

06 p0904 A71-17576

Oleopneumatic accumulators in gearboxes for rationalizing installed power

07 p1023 A71-20004

Aircraft gear pumps bearing elements design for increasing service life

08 p1295 A71-20793

VTOL aircraft gear systems, discussing bearings, shaft connection, Ti alloy components, etc

09 p1454 A71-22963

Reduction gearbox reliability problems from development and service experience with PT6A turboprop engine

[SAE PAPER 710433] 13 p2073 A71-28318

GEGENSCHEIN

Gegenschein photographic and photoelectric scan observations, considering origin in light reflection from interplanetary dust outside earth orbit

04 p0659 A71-15853

Bibliography on Gegenschein covering observations, theories, models, review papers, etc

11 p1835 A71-26461

Gegenschein observational history and characteristic features, discussing theories regarding origin

14 p2308 A71-29904

OSO-6 measurements of gegenschein, comparing relative sky brightness data with ground based observations

18 p2966 A71-36766

Gegenschein as zodiacal light illuminated lunar dust ejected from meteorite impacts

20 p3286 A71-38730

GEIGER COUNTERS

High sensitivity flame sensor for high temperature ambients, using Geiger-Muller tube triggered by photoelectron released by UV photon from flame

12 p1906 A71-27048

UV radiation sensitive flame sensor for high temperature ambients, consisting of Geiger-Muller tube triggered by photoelectron released from photocathode

14 p2248 A71-30707

GEIGER-MUELLER TUBES

U GEIGER COUNTERS

GELATINS

Stress distribution in gelatin disk and rectangular plate compressed between horizontal slabs, using tangential difference method

02 p0328 A71-12512

Photographic gelatin microimpurities quantitative analysis and removal techniques

04 p0585 A71-14645

Hologram formation in gelatin, photopolymeric and photochromic materials for high diffraction efficiency, in-place real-time processing and erasability

04 p0596 A71-15167

Light effect on dielectric constant of thin hardened dichromated gelatin films for holographic recordings

07 p1110 A71-19482

Phototechnology for phase holograms recording and information storage in hardened gelatin

07 p1116 A71-20620

GELS

Gel permeation chromatography for polymer molecules size / hydrodynamic volume / separation

04 p0548 A71-15265

Amino silica gels absorption properties with respect to carbon dioxide, hydrogen sulfide and water vapor, comparing affinity

20 p3193 A71-39233

GEMINI FLIGHTS

NT GEMINI 4 FLIGHT

NT GEMINI 10 FLIGHT

GEMINI PROJECT

Electron microprobe analysis of cavity surface and lip of cosmic dust impact craters in stainless steel plates exposed at 400 km altitude in Gemini S-010 experiment

20 p3299 A71-39652

GEMINI 4 FLIGHT

Trapped protons east-west asymmetry observations during Gemini 4 flight, using on-board high sensitivity plastic-scintillation spectrometer

03 p0479 A71-14041

GEMINI 10 FLIGHT

Ionospheric wake spacecraft potential, electron current and temperature observations, using Agena/Gemini manned two body system sensors

09 p1517 A71-22175

GEMINID METEOROIDS

Geminid meteoroids characteristics observation by radio, noting distributions of major semiaxes, plane inclination, elliptic eccentricities and day-by-day number variations

12 p1963 A71-26965

Geminid meteoroid dust particles detection, determining velocity and orbital elements from OGO 3 flux measurements

16 p2640 A71-33741

Geminid meteoroids characteristics observation by radio, noting distributions of semiaxes, plane inclina-

tion elliptic eccentricities and day-by-day number variations

19 p3144 A71-38888

Meteor bodies mass distribution function / Geminid stream, determining parameter S from radar echoes

19 p3145 A71-38889

GENERAL AVIATION AIRCRAFT

NT YAK 40 AIRCRAFT

Civil aircraft accident and maintenance record regulations and systems, discussing airborne equipment

03 p0348 A71-13773

General aviation safety and effectiveness enhancement through electronic technology applications, discussing airspace control system based on beacon transponder, LF-VLF area navigation and weather radar

05 p0780 A71-17575

Metro commuter aircraft specifications, performance and CAB certification problems

06 p0846 A71-17576

Book on general aviation future and economic impact covering fleet size and distribution, aircraft types, passenger and cargo profiles, etc

06 p1010 A71-17676

Avionics for gliders and touring aircraft, considering safety and VHF radio equipment

08 p1261 A71-20690

Avionics for gliders and touring aircraft, surveying available electronic equipment for 1971

08 p1294 A71-21777

Cessna Citation twin turbofan business aircraft design, performance characteristics, communications, navigation and automatic flight control equipment and flight evaluation

09 p1385 A71-22181

Cost reduction concepts in gas turbine engine design and fabrication for general aviation aircraft

09 p1511 A71-22888

FAA flying and handling qualities programs, discussing development of optimum and minimum acceptable flight characteristics criteria for new civil and military aircraft designs

10 p1554 A71-24242

Light general aviation airplanes flying qualities / flight simulation, considering longitudinal short period frequency and damping, pitch control sensitivity and lift curve slope

10 p1554 A71-24242

Executive jet landing approach lateral-directional handling under IFR ILS simulated conditions, investigating Dutch roll control power effect on cross wind component

10 p1554 A71-24242

NASA aerodynamic research applicable to business aircraft concerning wind tunnel and flight tests, STO performance and high speed cruise technology

10 p1554 A71-24242

Business jet aircraft noise certification, discussing test programs and cost reduction

10 p1555 A71-24242

Crashworthy personnel restraint systems for general aviation including upper torso restraint

10 p1569 A71-24262

General aviation aircraft accidents involving seat belt and shoulder harness restrained occupants, discussing vertical force effects on survivability and injuries in severe crashes

10 p1555 A71-24262

Wing structure fatigue substantiation procedure under fail-safe concept for general aviation aircraft

10 p1555 A71-24262

Lateral-directional handling qualities and roll control power requirements for executive jet and military class II airplanes in landing approach flight phase

16 p2524 A71-34006

Omega navigation application to general aviation aircraft, presenting diurnal course shift to overcome deficiencies

17 p2776 A71-35766

Aerial land rover for special needs of developing countries as passenger and freight aircraft, crop spraying and dusting, aerial survey and fire fighting

21 p3325 A71-40706

Corporate aircraft 1970 accident statistics analysis stressing pilot selection, training and supervision

23 p3628 A71-43224

Corporate aircraft safety - Conference, San Antonio, May 1970

23 p3628 A71-43377

General aviation aircraft altimeter errors, tolerance and static system tests

23 p3629 A71-43388

Corporate aircraft pilot ground and flight phase training, errors and accidents

23 p3629 A71-43388

Continued flight training correlation with general aviation aircraft accident rates reduction

23 p3641 A71-44222

GENERAL DYNAMICS AIRCRAFT

NT C-131 AIRCRAFT

NT F-111 AIRCRAFT

GENERATION

Automatic generator for finite rectangular/oparametric element stiffness and mass matrices, discussing memory requirements and computation me optimization 09 p1542 A71-23280
Element stiffness matrix generator in terms of material and geometric properties by computer algorithm, using displacement functions, transformation matrices and strain energy expression 09 p1542 A71-23281

GENERATORS

Noise temperature measurement of mismatched cryogenic generator, using compensation method 01 p0056 A71-11198
Short term frequency stability of precision oscillators and frequency generators, discussing conversion from frequency to time domain and among time domain measures 11 p1739 A71-26422

GENETICS

GENETIC MUTATIONS

Genetics and temporal autogenic seizures in mice, noting age and exposure effects on susceptibility 03 p0360 A71-13161
Space travel genetic effects, discussing radiation, weightlessness, vibration and acceleration 09 p1394 A71-23149
Electrophoretic mobility of tear lysozyme in human subjects, noting applicability to genetics 13 p2013 A71-29033

GENITOURINARY SYSTEM

BLADDER

UTERUS

ASTROPHYSICS

ASTROPHYSICS

ASTROPHYSICS

ASTROPHYSICS

ASTROPHYSICS

ASTROPHYSICS

ASTROPHYSICS

ASTROPHYSICS

ASTROPHYSICS

ASTROPHYSICS

ASTROPHYSICS

ASTROPHYSICS

ASTROPHYSICS

ASTROPHYSICS

ASTROPHYSICS

ASTROPHYSICS

ASTROPHYSICS

ASTROPHYSICS

ASTROPHYSICS

ASTROPHYSICS

ASTROPHYSICS

ASTROPHYSICS

ASTROPHYSICS

ASTROPHYSICS

ASTROPHYSICS

ASTROPHYSICS

ASTROPHYSICS

ASTROPHYSICS

ASTROPHYSICS

ASTROPHYSICS

ASTROPHYSICS

ASTROPHYSICS

ASTROPHYSICS

ASTROPHYSICS

ASTROPHYSICS

ASTROPHYSICS

ASTROPHYSICS

ASTROPHYSICS

ASTROPHYSICS

ASTROPHYSICS

ASTROPHYSICS

ASTROPHYSICS

ASTROPHYSICS

ASTROPHYSICS

ASTROPHYSICS

ASTROPHYSICS

ASTROPHYSICS

ASTROPHYSICS

ASTROPHYSICS

ASTROPHYSICS

ASTROPHYSICS

ASTROPHYSICS

ASTROPHYSICS

ASTROPHYSICS

ASTROPHYSICS

ASTROPHYSICS

ASTROPHYSICS

ASTROPHYSICS

ASTROPHYSICS

ASTROPHYSICS

ASTROPHYSICS

ASTROPHYSICS

ASTROPHYSICS

ASTROPHYSICS

ASTROPHYSICS

ASTROPHYSICS

ASTROPHYSICS

ASTROPHYSICS

ASTROPHYSICS

ASTROPHYSICS

ASTROPHYSICS

ASTROPHYSICS

ASTROPHYSICS

GEOCHEMISTRY

Lunar origin by earth-moon fission, deriving parent planet characteristics from geochemical considerations 02 p0306 A71-11991
Porphyrins and amino acids chemical bonding under geochemically plausible conditions, considering diagenesis of biogenic compounds and life processes prebiotic chemical evolution 02 p0198 A71-12047
Mineralogy and chemistry of earth upper mantle, using partial fusion-partial crystallization model 04 p0583 A71-12566

Book on geochemical exploration of moon and planets covering orbital, compositional and surface studies, Apollo missions, Lunar Receiving Laboratories and data processing 05 p0813 A71-16950

Archaeon volcanics geochemistry and modern basalts chemical and geographic characteristics, considering trace element model 06 p0892 A71-17895

Terrestrial and stony meteorite carbon, investigating similarity in isotopic composition 07 p1201 A71-20399

Lighter-than-iron elements in earth iron core, assuming formation timed chemical equilibrium with mantle 10 p1607 A71-24986

Venus ferrous chloride hydrate cloud production, examining geochemical problems 11 p1824 A71-25704

Gas-liquid chromatographic milligram preparative separation of steranes and triterpanes from hydrocarbon fraction of Green River oil shale 11 p1729 A71-26067

Lunar samples mineralogy, petrology and geochemistry, considering lunar surface processes, cosmic ray flux and solar wind 12 p1967 A71-27414

Igneous rocks origin associated with shock metamorphism, considering geochemical investigations of Canadian craters 19 p3051 A71-37668

GEOCHRONOLOGY

Fission track and K-Ar ages of coexisting minerals in drill core from heat-flow boreholes in western central Sierra Nevada batholith 21 p3374 A71-40649

GEOCORONAL EMISSIONS

Lyman alpha radiation scattering observation by satellites, obtaining geocoronal atomic hydrogen distribution in thermosphere and exosphere 03 p0415 A71-14028

Earth hydrogen geocorona models comparison with solar Lyman alpha spectrographic data from Aerobee rocket flight measurements 03 p0496 A71-14509

Solar Lyman alpha emission line absorption by geocoronal atomic hydrogen, comparing observational data with prediction from models 03 p0496 A71-14510

Brightness ratio near solar horizon from Ly alpha predawn and postdawn rocket observations consistent with radiation multiple scattering geocoronal model 10 p1605 A71-24794

Wind transport effect on redistribution of ionization produced by geocoronal and interplanetary UV emissions in nighttime ionosphere, using electron density sounding rocket data 14 p2230 A71-29709

Ionospheric geocoronal L sub alpha emission intensity related to solar activity level from Cosmos 215 satellite data 16 p2564 A71-33667

GEODESY

Higher geodesy problems, determining earth dimensions and figure, gravitational field and absolute and relative point positions with artificial earth satellites 01 p0159 A71-10809

Soviet book on gyroscopes in geodesy and aerial photography based on structural analysis for automatic control systems, covering gyro error, theodolites, etc 01 p0083 A71-11321

Long baseline radio interferometry, discussing phase difference measurement principles in terms of signal characteristics and wave forms, astronomy and geodesy applications 03 p0484 A71-13244

Geometric satellite geodesy, discussing simultaneous ranging from tracking station network 03 p0418 A71-14207

Earth ellipsoid physical constants using satellite measurements of geocentric gravitational constant, earth-moon mass ratio and geopotential harmonic coefficients 04 p0581 A71-15066

International Polar Motion Service stations residual latitudes variation by other than polar motion, considering dependence on earth figure deformation 06 p0890 A71-17880

Selenodesy and planetary geodesy of moon, inner and outer planets, including sun-planet mass ratios 08 p1366 A71-21798

Earth gravity field in physical geodesy, considering satellite geodesy, gravitation-inertia interrelation, etc 08 p1285 A71-21799

Satellite geodesy, discussing reference orbits calculation, gravity field spherical harmonics, station positions, etc 08 p1285 A71-21800

Satellite geodesy for determining tracking station coordinates and gravity field 08 p1285 A71-21801

Satellite laser tracking for geodetic data acquisition 08 p1285 A71-21802

Stokes earth shape formula derivation without removing continental masses for regularization requirement 09 p1438 A71-23181

Optimal synchronous plane accuracy for space triangulation as function of geometrical position of artificial satellite relative to earth sphericity 11 p1758 A71-25812

Satellite geodesy progress over 12 years since artificial earth satellites, considering gravitational field and station position measurement accuracies 11 p1759 A71-25820

Second order difference approximations with large viscosity coefficient for primitive barotropic model over spherical geodesic grid, comparing with first order approximations 13 p2097 A71-28231

Long baseline radio interferometers, considering quasars, interstellar masers, geodesy and geology applications 15 p2412 A71-32705

Satellite geodesy in Netherlands, discussing measurement and instrumentation techniques and ground station equipment and operation 16 p2563 A71-33368

Netherlands space research including solar, stellar and cosmic radiation observations, photometry and satellite geodesy 16 p2666 A71-33858

German book on satellite geodesy covering two body problem, perturbation theory, earth gravitational field, gravitational effects of sun and moon, radiation pressure, etc 17 p2799 A71-34470

Gravimetric geodesy theory offering anomalous gravity potential solution for smoothed topography 17 p2733 A71-35028

Base triangle determination by geometric geodesy, using laser telemetry and satellite optical observations with cataphotic reflecting prisms 20 p3220 A71-39661

Earth rotational and deformational motion equations in extended Kalman-Schmidt filter for geodetic data processing [AAS PAPER 71-339] 23 p3666 A71-43012

Quadrature errors in satellite geodesy via geopotential simple layer model, investigating different size surface elements and methods of subdivision [AAS PAPER 71-340] 23 p3666 A71-43013

GEODETIC COORDINATES

Astronomical-geodetic observations of direction of instantaneous earth rotation vector at South Pole 03 p0406 A71-13007

Astronomical-geodetic networks processing in three dimensional rectangular coordinates, considering advantages and accuracy 06 p0889 A71-17674

High target geodetic coordinates determination by measuring vertical angles without using azimuth 06 p0889 A71-17675

Geodetic geographic coordinate transformations and ellipsoid heights, azimuth and length determination from synchronous photographic observations and distance measurements of artificial satellites 11 p1759 A71-25813

Geodetic azimuth between two remote points on earth surface based on synchronous satellites positions and photographs 11 p1759 A71-25817

Translation of geodetic geographical coordinates and ellipsoidal altitudes by synchronous photographic satellite observations and satellite-distance measurements from two ground stations 12 p1903 A71-27753

Earth gravity field and satellite tracking stations positions geodetic parameters in geocentric reference frame 17 p2733 A71-35027

Space-time model of torsion tensor effect on geodetic lines under Schwarzschild metric, evaluating orbital perihelion motion of planets and light ray bending 18 p2967 A71-36826

Astronomical geodetic networks equalization, using Laplace azimuths 19 p3056 A71-38174

Atmosphere meteorological sounding, measuring geodetic quadrangle sides and diagonals by aircraft radio direction finder 19 p3065 A71-38175

Geodetic parameters describing earth gravity field and satellite tracking stations positions in geocentric reference frame, using satellite observation and deep space probes 20 p3220 A71-39659

Differential correction for redetermination of satellite observation stations geodetic coordinates as related to earth center of gravity and terrestrial potential coefficients 22 p3534 A71-42023

Geodetic grid points coordinates accuracy estimate based on normal equations system cracovian matrix, determining arbitrary elements by numerical process without error equations linearization 24 p3822 A71-44768

GEODETIC SATELLITES

GEODETIC SATELLITES

- NT GEOS 1 SATELLITE
- NT GEOS 2 SATELLITE
- NT GEOS-C SATELLITE
- NT PAGEOS SATELLITE
- Geocentric coordinates from dynamic satellite geodesy, using gravimetric Stokes and Venning-Meinesz functions
 - 03 p0406 A71-13010
- Geometric satellite geodesy, discussing simultaneous ranging from tracking station network
 - 03 p0418 A71-14207
- French Geole spatial system utilization in polar zones, combining satellite with ground beacons, telemetry ground receiving station and computer
 - 10 p1599 A71-23860
- Satellite geodetic global networks employing triangulation, trilateration and height measurements, deriving dominant point observation stations /Hazay-Tarczy method/
 - 11 p1759 A71-25816
- Automatic camera for international synchronous observations of geodetic satellites
 - 14 p2250 A71-31117
- Geodetic and oceanographic surface mapping by satellite radar altimeter system, discussing measurement technique, orbital parameters and data processing equipment
 - [AIAA PAPER 71-845] 17 p2733 A71-34708
- Geodetic satellite data utilization for test range specific point positioning, control densification, earth gravitational model determination and tracking station locations
 - 18 p2913 A71-36492
- Geodetic system with satellites and automatic radio beacons, establishing network on earth surface to track isolated points
 - 18 p2913 A71-36529
- Satellite applications to cartographic and geodetic surveys, discussing photographic difficulties
 - 19 p3047 A71-37302
- Satellite data techniques and instrumentation in earth geometry and kinetics, reviewing geopotential models, pole positions, tides, ocean physics and international cooperation
 - 20 p3219 A71-39656
- GEOS-C geodetic satellite purpose and equipment, discussing earth gravitational field study, radar altimeter possibility and tracking systems usefulness
 - 20 p3306 A71-39657
- Geodetic satellite observational data condensation by substitution for all measurements of pass above station with pseudomeasurement expressed by vector with almost six components
 - 20 p3220 A71-39663
- Space triangulation and orbital methods of geodetic surveying of earth with satellites, using simultaneous observations from two and three stations
 - 21 p3374 A71-40584
- Quadrature errors in satellite geodesy via geopotential simple layer model, investigating different size surface elements and methods of subdivision
 - [AAS PAPER 71-340] 23 p3666 A71-43013
- GEODETIC SURVEYS
 - Very long baseline interferometry /VLBI/ one-bit instrumentation using videotape recorders in geodetic and geophysical measurements
 - 02 p0251 A71-12332
 - European ground stations geodetic surveys by laser range measurements and photographic observations of satellites with reflectors
 - 03 p0413 A71-14008
 - Geodetic survey adjustment and accuracy improvement using satellite radar range and ballistic camera data
 - 04 p0583 A71-15302
 - Geodetic position rapid determination accuracy by Doppler satellite observation
 - 04 p0583 A71-15304
 - Statistical method in geodetic surveying including equilibration calculations, error theory, estimation, verification, distributionless tests, etc
 - 04 p0584 A71-15900
 - Integrated data processing of stereotriangulation system providing automatic map plotting
 - 08 p1281 A71-21249
 - Geodetic marker preservation program establishing horizontal and vertical control networks in U.S.
 - 08 p1281 A71-21251
 - French Geole spatial system utilization in polar zones, combining satellite with ground beacons, telemetry ground receiving station and computer
 - 10 p1599 A71-23860
 - Doppler geodetic measurements, discussing ionospheric wave diffraction errors, refractive index and electromagnetic wave propagation
 - 11 p1732 A71-25831
 - Relativistic effects and optimization in Doppler geodetic measurements, using model computations for satellite azimuth-elevation relation
 - 11 p1732 A71-25832
 - Flight tests of inertial navigation system in aerial geodetic mapping, achieving automatic side-lap, verticality and line position control
 - 12 p1927 A71-27256

- Airport geodetic control stations, discussing obstruction charting program
 - 12 p1895 A71-27537
- Soviet geodetic network construction and compensation, noting triangulation of first and second class in each polygon
 - 15 p2395 A71-31464
- Geodetic boundary value problem reformulation, using measured gravity values on known earth surface and potential theory
 - 16 p2563 A71-33476
- Space triangulation and orbital methods of geodetic surveying of earth with satellites, using simultaneous observations from two and three stations
 - 21 p3374 A71-40584
- Geodetic locations of Doppler satellite observing stations consistent with CIO pole and astronomical determinations
 - [AAS PAPER 71-341] 23 p3666 A71-43014
- GEODIMETERS
 - Model 6A geodimeter /photometric range finders/ laboratory and field tests
 - 15 p2405 A71-31466
- GEOELECTRICITY
 - Geoelectric effects on plants geotropic reaction chain, discussing hormone auxin asymmetric distribution due to gravity
 - 21 p3340 A71-39984
 - External indole-3-acetic acid effect on elongation and geotropic bending of Avena coleoptiles related to auxin induced electrical responses
 - 21 p3340 A71-39986
- GEOGRAPHY
 - NT OROGRAPHY
 - Martian features nomenclature based on Schiaparelli application of ancient geographical and mythological names
 - 21 p3448 A71-40520
- GEIDS
 - Satellite geodetic data interpretation of geoid undulations and gravity anomalies
 - 08 p1285 A71-21803
 - Earth ellipsoid gravitational potential selection influence on geoid height determination, using near-geoid model
 - 23 p3674 A71-44051
- GEOLOGICAL FAULTS
 - Remote sensing for geologic problems, using side-looking radar for fracture and fault detection and IR images for limestone, dolomite and granite discrimination
 - 18 p2911 A71-35890
- GEOLOGY
 - NT GEOCHRONOLOGY
 - NT GEOMORPHOLOGY
 - NT HYDROGEOLOGY
 - NT LUNAR GEOLOGY
 - NT OROGRAPHY
 - NT PETROGRAPHY
 - NT PETROLOGY
 - NT PHOTOGEOLOGY
 - NT TECTONICS
 - NT VOLCANOLOGY
 - Nimbus AVCS imagery applied to studies of bedrock geology, geomorphology and climate
 - 04 p0597 A71-15309
 - Side-looking radar, thermal IR scanner and passive microwave radiometers for remote sensors for geologic mapping
 - 09 p1452 A71-23215
 - Integral coefficient of correlation between gravitational and magnetic fields with geological element
 - 14 p2235 A71-30189
 - Papers on geological problems in lunar and planetary research covering sensing techniques, phenomenology, exploration methods, etc
 - 15 p2492 A71-32469
 - Planetological terminology for geological processes and features of earth, moon and planets
 - 15 p2516 A71-32499
 - Long baseline radio interferometers, considering quasars, interstellar masers, geodesy and geology applications
 - 15 p2412 A71-32705
 - Sikhote-Alin expedition geological survey, examining crater and pit structural characteristics
 - 17 p2810 A71-35717
 - Tektites atmospheric and geological history, noting fragmentation and surface sculpturing processes
 - 17 p2811 A71-35728
 - Manua Islands /Samoa/ lavas chemical composition, geology and probable history
 - 18 p2911 A71-35887
 - Lunar Orbiter photographs utilization in earth science courses, illustrating geologic features, stratigraphy and historical geology
 - 18 p2915 A71-35888
 - Side-looking airborne radars and image recording scanners design for geoscience applications, discussing gray scale improvement, multispectral sensing, target discrimination, etc
 - 18 p2875 A71-36366
 - Aircraft and satellite remote sensing techniques in geology, soil science, geography and hydrology
 - 18 p2913 A71-36539

- Morphology and geology of Lappajarvi structure /Finland/, suggesting meteorite impact evidence
 - 19 p3049 A71-37303
- Pulsed Nd laser source mass spectroscopy application to geological material analysis, tabulating assessed limits of detection for various elements
 - 20 p3245 A71-39658
- Earth orbital photography for geologic applications, discussing advantages over aerial photography
 - 22 p3534 A71-41111
- GEOMAGNETIC ANOMALIES
 - U MAGNETIC ANOMALIES
- GEOMAGNETIC CROTCHETS
 - U SUDDEN IONOSPHERIC DISTURBANCES
- GEOMAGNETIC EFFECTS
 - U MAGNETIC EFFECTS
- GEOMAGNETIC EQUATOR
 - U MAGNETIC EQUATOR
- GEOMAGNETIC FIELD
 - U GEOMAGNETISM
- GEOMAGNETIC HOLLOW
 - Solar wind torque on geomagnetic cavity by rotational unipolar induction currents, including Joule heating of ionospheric plasma and directional magnetic fields
 - 15 p2474 A71-31710
- GEOMAGNETIC LATITUDE
 - Directional cosmic ray cut-off and loop-cone folding distribution at geomagnetic midlatitude sites
 - 01 p0146 A71-11414
 - Ion reflection and whistler trace shapes as function of magnetic latitude from satellite observations
 - 03 p0408 A71-13331
 - Solar cosmic ray diurnal variations latitude effect explained by two way anisotropy model
 - 06 p0952 A71-18111
 - Equatorial zone daytime F 2 maximum height diurnal variation latitude change with decreasing solar activity from vertical sounding
 - 07 p1100 A71-19444
 - Electron and proton whistlers polarization reversal and mode coupling, explaining magnetic latitude dependence
 - 07 p1062 A71-19644
 - Low geomagnetic latitude night airglow characteristics, using Cosmos 215 measurements in 1225 1350 A range
 - 08 p1277 A71-21064
 - Low latitude geomagnetic substorm development model due to increased resistance in magnetospheric tail current sheath
 - 08 p1278 A71-21065
 - Geomagnetic latitude-longitude coordinates, examining field lines intersections at height of 100 km
 - 08 p1285 A71-21717
 - Geomagnetic distributions of VLF hiss intensity and drifting frequency bursts near inner boundary of plasmapause on middle latitudes
 - 09 p1411 A71-23666
 - Latitudinal profiles of geomagnetic H and Z components due to return current of auroral zone electrojet during polar substorms
 - 11 p1756 A71-25777
 - Primary component corrections for global cosmic ray variations from latitudinal expeditions, discussing method adaptation to computer
 - 13 p2128 A71-28555
 - Suprathermal electron temperature and ion composition as function of geomagnetic latitude in polar ionosphere, using Explorer 31 mass spectrometer measurements
 - 14 p2234 A71-30044
 - F 2 layer peak electron density diurnal and seasonal variations, noting geomagnetic latitude and solar activity effects
 - 15 p2394 A71-31414
 - Plasmapause position during stormtime increase trapped energetic electrons, measuring near prime geomagnetic meridian by whistler techniques
 - 16 p2629 A71-33999
 - Earth gravitational and magnetic field correlation considering nondipole geomagnetic potential latitudinal rotation effects
 - 17 p2735 A71-35735
 - Equatorial zone daytime F 2 maximum height diurnal variation latitude change with decreasing solar activity from vertical sounding
 - 19 p3053 A71-37888
 - Latitudinal distribution of electron temperature in 2 layer during summer daytime period of low solar activity from electron density profile geometric parameters
 - 19 p3057 A71-38333
 - Geomagnetic activity daily variability index statistical dependence on geomagnetic latitude, noting maximum below equatorial electrojet
 - 20 p3217 A71-39555
 - Ionospheric electric field strength at equatorial medium geomagnetic latitudes during twilight from barium-ion cloud drift measurements
 - 20 p3218 A71-39556
 - Low geomagnetic latitude night airglow characteristics, using Cosmos 215 measurements at 1225 1350 A in oxygen spectrum
 - 20 p3219 A71-39557

Low latitude geomagnetic substorm development model due to increased resistance in magnetosphere tail current sheath

20 p3219 A71-39597

Trapped protons flux vs L profile measurement on-board sounding rocket near equator, comparing results with calculation from neutron albedo source and atmospheric losses

20 p3284 A71-39881

Comparative north and south polar F layer electron density dependence on universal time and latitude, using ionosonde data

23 p3669 A71-43172

GEOMAGNETIC MICROPULSATIONS

Geomagnetic microfluctuations noting magnetospheric dimensions, solar wind velocity, magnetic activity indicators and latitude effects on rapid variations

04 p0584 A71-15369

Pi2 geomagnetic pulsation polarization characteristic observations, using photoelectric fluxmeters

05 p0747 A71-17213

Pc 1 micropulsation source region relation to plasmopause, using amplitude and polarization measurements

06 p0964 A71-17263

Fine structure of geomagnetic Pc 1 micropulsations by cyclotron instability due to anisotropic energetic proton velocity

06 p0895 A71-18283

Magnetospheric boundary Pc2-4 pulsations period relationship based on Explorer 12 daytime magnetosphere data

07 p1101 A71-19416

Pc 3-4 period range geomagnetic micropulsations simultaneous recordings at Canadian stations spanning auroral and polar regions

07 p1102 A71-19665

Alfven irregularities near plasmopause, discussing significance in relation to geomagnetic micropulsations based on OGO-3 and ground station observations correlation

07 p1104 A71-20008

Polarization of short period oscillations Pc2-Pc4 dependence on time of day, oscillation type and geoelectromagnetic field activity

09 p1436 A71-22449

Geomagnetic micropulsations distribution in magnetosphere, using OGO 3 and 5 data

09 p1440 A71-23635

Pc and Pi micropulsations, correlating magnetospheric cavity eigenmodes with sunspot activity

09 p1440 A71-23637

Pc1 propagation in magnetosphere model accounting for ionization gradients aligned along geomagnetic field

10 p1599 A71-23849

Magnetic field components of local ionospheric current for LF oscillation range including micropulsation frequencies, discussing spatial and frequency distribution

11 p1758 A71-25790

Earth plasmasphere annual and sunspot cycle variations, considering observations with respect to whistler paths and Pc4 pulsations mean period variations

12 p1902 A71-27669

Band limited micropulsations observed in space during magnetospheric substorm by fluxgate magnetometer on OGO 5

13 p2119 A71-27913

Auroral sporadic E layer events relationship to Pi 1 type irregular magnetic pulsations generation in Arkhangelsk region

13 p2059 A71-28244

Pi2 geomagnetic micropulsation polarization characteristics, using photoelectric fluxmeters

13 p2060 A71-28268

Decreasing period micropulsations during elementary magnetospheric substorms, discussing relation to ring current asymmetry development

13 p2061 A71-28546

Geomagnetic Pc-1 type micropulsations appearance and development due to proton belt cyclotron instability

14 p2301 A71-30350

Pc micropulsations spectra fine structure and diurnal variations, analyzing rubidium magnetometer recordings by power spectral density method

15 p2394 A71-31425

Pc-type micropulsation amplitude variation correlation at separate places up to 10,000 km distances, suggesting pi-type as cause

15 p2395 A71-31435

Hydromagnetic waves, micropulsations and temporal variations in vector geomagnetic field at 6.25 earth radii

15 p2397 A71-31759

Long period quasi-monochromatic geomagnetic micropulsations amplitude spectra and polarization as function of geomagnetic latitude

15 p2397 A71-31760

Pc 2-4 pulsations relationship to interplanetary magnetic field strength and orientation, using IMP 3 and 4 satellite data

15 p2401 A71-32732

Temporal and spatial relations between impulsive Pi bursts near midnight at polar substorms onset and IPDP micropulsation events in afternoon-evening hours

16 p2573 A71-33952

Geomagnetic micropulsation data, emphasizing behavior during 11 year solar cycle

17 p2732 A71-34671

Coherent periodic compressional micropulsations of geomagnetic field intensity and energetic electron fluxes at synchronous altitude during quiet day

19 p3016 A71-37361

Pc 3 and 4 micropulsations period structure data, observing multiple frequencies during magnetically active times

19 p3048 A71-37397

Magnetospheric boundary Pc2-4 pulsations period relationship based on Explorer 12 daytime magnetosphere data

19 p3054 A71-37840

Geomagnetic micropulsation periods variation with latitude and plasmopause presence, calculating uncoupled toroidal and poloidal modes eigenperiods of hydromagnetic waves

20 p3215 A71-38735

Magnetic field components of local ionospheric current for LF oscillation range including micropulsation frequencies, discussing spatial and frequency distribution

22 p3532 A71-41558

GEOMAGNETIC PULSATIONS

NT GEOMAGNETIC MICROPULSATIONS

Geomagnetic field perturbation as function of 11-year solar activity cycle, using magnetic observatory

01 p0073 A71-10921

Rapid geomagnetic field variations relationship with auroral luminosity fluctuations at 4278 A

01 p0076 A71-11501

SD geomagnetic variations and electron jet spread over polar cap stream during solar cycle

02 p0243 A71-11763

Simultaneous sudden magnetospheric compressions and geomagnetic bay onsets correlation, using IGY data

02 p0245 A71-11967

Sudden impulses in geomagnetic field, discussing synchronous equatorial orbit-satellite magnetometer observations

03 p0421 A71-14537

Ionospheric transmission model vs current model for examination of low latitude geomagnetic pulsation origin

05 p0743 A71-17002

Auroral sporadic E layer events relationship to pi 1 type irregular magnetic pulsations generation in Arkhangelsk region

05 p0744 A71-17187

Western frequency drift effects on spectrum time evolution azimuthal asymmetry in diminishing period geomagnetic pulsation intervals

05 p0747 A71-17214

Pc 1 pulsations occurrence frequency diurnal annual and 11 year variations at midlatitudes, relating distribution with carrier frequencies of perturbation

06 p0894 A71-18266

Magnetospheric plasma concentration from geomagnetic pulsations periods

06 p0894 A71-18270

Diurnal variations in polarization axis direction of Pc 1 pulsations

06 p0895 A71-18282

Interplanetary space solar wind flux variations-earth electromagnetic field pulsations comparison by spacecraft and geophysical station observations

07 p1187 A71-19677

Geomagnetic secular variation as main field drift superposition and strength changes, reflecting drift and convection in earth fluid core

07 p1103 A71-19763

Geomagnetic field quiet solar diurnal variations, examining dynamo theory in lower ionosphere at middle latitudes

07 p1104 A71-20045

Polar auroras, lower magnetosphere and geomagnetic perturbations, as effect of corpuscular fluxes penetration into lower ionosphere

07 p1104 A71-20046

Geomagnetic solar quiet field and terrestrial currents diurnal variations, discussing interrelations and vector polarization

07 p1104 A71-20047

Geomagnetic PP type oscillations recordings, using fluxmetric rings and galvanometer

07 p1104 A71-20049

Solar wind flux correlation with earth EM field pulsations, noting flare-generated shock front effects on magnetosphere

09 p1513 A71-22422

Pi 2 type geomagnetic pulsations relationship to auroral zone morphological features

09 p1435 A71-22448

Low latitude atmospheric vertical density variations, comparing solar and geomagnetic activities effects

09 p1436 A71-22578

Geomagnetic field measurements by ATS 1 in synchronous equatorial orbit, determining pulsations types during magnetically quiet and geomagnetic storm periods

09 p1440 A71-23636

Magnetospheric electric field diagnosis, using geomagnetic disturbances in equatorial plane and pulsations in middle and high latitudes

09 p1441 A71-23639

Geomagnetic Pc1 pulsations propagation in F region, deriving hydromagnetic waves equations by ray tracing method and waves refractivity index in extraordinary mode

10 p1607 A71-25118

DP 2 fluctuations and polar substorm activity morphological distinctions, using worldwide magnetograms

11 p1753 A71-25545

Long period, pearls and irregular geomagnetic pulsations for plasma diagnostics in magnetosphere

11 p1756 A71-25647

Comparative proton flux and Pc-1 pulsations from Explorer 26 satellite and ground observations

11 p1756 A71-25648

Outer radiation belt energetic electron flux intensity correlation with auroral activity and Kp index

11 p1816 A71-25760

Geomagnetic crochet associated solar optical flares and microwave bursts during four year period, showing north-south asymmetry over disk

12 p1947 A71-26768

Western frequency drift effects on spectrum time evolution azimuthal asymmetry in decreasing period geomagnetic pulsation intervals

13 p2060 A71-28269

Plasma electron and proton motion in equatorial plane of magnetosphere under geomagnetic disturbance generated electric field

13 p2060 A71-28530

Geomagnetic field horizontal component daily variation due to ionospheric E region dynamo, magnetopause surface and magnetospheric tail/partial ring currents

13 p2064 A71-29161

Magnetospheric model calculation for self oscillation period and amplitude dependence on longitude and plasma density estimation from observed geomagnetic pulsation period

14 p2228 A71-29531

Quasi-biennial oscillation in low latitude geomagnetic Sq field, showing larger amplitude under equatorial electrojet by harmonic analysis

14 p2231 A71-29719

Geomagnetic pulsation effect on charged particles motion, based on Mead magnetosphere analytic model, using Parker perturbation method

14 p2235 A71-30346

ULF geomagnetic pulsations interpretation based on Kelvin-Helmholtz magnetospheric instability mechanism and bounce resonance wave excitation, considering energy exchange with energetic protons

14 p2202 A71-30954

Solar eclipse on 7 March 1970, determining midlatitude geomagnetic pulsations with dynamic power spectral analysis

15 p2397 A71-31761

Model interpretation of Pc pulsations during geomagnetic storms, analyzing plane HM-wave resonance in horizontally stratified middle-low geomagnetic latitude lower magnetosphere

17 p2734 A71-35190

Steady LF geomagnetic pulsations, deriving dispersion equation relating plasma electron frequency, hot ion velocity and particle radii and drift frequencies

17 p2735 A71-35243

French monograph on ULF geomagnetic field variations covering plasmopause, geomagnetic pulsations, WKB limit and magnetospheric density

17 p2735 A71-35248

Sunspot cycle effect on solar and lunar daily geomagnetic variations

18 p2966 A71-36745

Solar effects contradictory relationships with earth atmosphere, discussing geomagnetic disturbance, annual variations, stratospheric transport and high energy particles

19 p3128 A71-38354

Arctic polar region geomagnetic perturbations during IQSY, noting diurnal variations

19 p3059 A71-38399

Geomagnetic Pi 2 pulsations association with magnetic storm onset in quiet conditions, discussing plasma sheet and pause theories

22 p3535 A71-42051

Geophysical data analysis for high latitude negative geomagnetic disturbances revealing geomagnetic pulsations during auroral arcs passage

24 p3823 A71-45037

GEOMAGNETIC STORMS

U MAGNETIC STORMS

GEOMAGNETIC TAIL

Solar flare particles entrance into geomagnetic tail, modifying diffusion model

01 p0147 A71-11494

Geomagnetic tail configuration during substorms from Imp 4 magnetic field and auroral index measurements

03 p0419 A71-14516

Energetic proton bursts in magnetotail, examining flow direction and intensity, spectral energies and origin

03 p0482 A71-14517

Auroral oval electrojet poleward expansion correlation to energetic electron enhancement in magnetotail during substorm from satellite observation

03 p0419 A71-14518

Magnetotail energetic electron event simultaneous observations by Vela 3A and Imp 3 satellites, evaluating plasma sheet boundary motion hypotheses

03 p0421 A71-14545

Lower limit of neutral line in geomagnetic tail merging, noting inconclusiveness of direct spacecraft observations

03 p0421 A71-14551

Geomagnetic tail tearing instability nonlinear evolution, discussing quasi-linear theory

05 p0742 A71-16630

High energy particle interaction with magnetospheric tail neutral layer, determining limiting shape of pitch angle particle distribution

05 p0800 A71-17176

Resonant proton drift in axisymmetric rotating magnetosphere, discussing flow from boundary or tail to auroral region

05 p0800 A71-17178

Magnetotail plasma sheet electron and proton energy spectra and angular distribution over auroral zone, comparing Vela satellite and rocket measurements

06 p0887 A71-17260

Geomagnetic tail structure near null sheet, indicating decrease and/or dissipation of plasma sheet particle energy density at lunar distances

06 p0893 A71-17994

Energetic electrons distribution in magnetotail plasma sheet from Explorer 35 satellite observation data

07 p1186 A71-19657

Energetic electrons in magnetospheric tail plasma sheet, investigating flux time profiles and correlation with local magnetic fields from Imp 3 satellite observation data

07 p1186 A71-19658

Low latitude geomagnetic substorm development model due to increased resistance in magnetosphere tail current sheath

08 p1278 A71-21017

Electric currents in undisturbed magnetospheric tail, discussing interplanetary magnetic field polarity effect and neutral sheet characteristics

08 p1280 A71-21214

Substorm related magnetic field variations in near geomagnetic tail from OGO 5 inbound pass

08 p1283 A71-21643

Pressure conditions across distant magnetopause from interplanetary magnetic field measurements, comparing Pioneer 7 plasma data with Explorer 33 distant geomagnetic tail field magnitudes

08 p1285 A71-21692

Polar H ion plasma escape from ionosphere into magnetospheric tail effect on plasmopause formation, using hydrodynamic approximation

11 p1756 A71-25756

Geomagnetic horizontal field decrease from magnetospheric tail field annihilation, considering polar ionospheric current generation mechanism

11 p1758 A71-25792

Hydromagnetic wave coupled solar wind-plasma sheet effects on resonant oscillations of geomagnetic tail, using two dimensional model

13 p2119 A71-27910

Temporal history of 25-26 August 1967 magnetospheric substorm, discussing magnetotail plasma sheet thinning, partial ring current buildup and magnetic bays development

13 p2132 A71-27912

High energy particle interaction with magnetospheric tail neutral layer, determining particle pitch angle distribution limiting shape

13 p2128 A71-28233

Resonant proton drift in asymmetric rotating magnetosphere, discussing flow from boundary or tail to auroral zone

13 p2128 A71-28235

Auroral absorption and DR currents development during magnetic storms, discussing corpuscular fluxes arrival from magnetospheric tail into lower ionosphere

13 p2062 A71-28563

Geomagnetic field horizontal component daily variation due to ionospheric E region dynamo, magnetopause surface and magnetospheric tail/partial ring currents

13 p2064 A71-29161

Distant geomagnetic tail longitudinal magnetic field gradient model based on pressure balance between internal field and solar wind, discussing tail flux content

13 p2064 A71-29162

Magnetospheric tail models for Uranus type planet with viscous and magnetic coupling compared to geomagnetic configuration

14 p2305 A71-29664

Magnetosphere structure, considering geomagnetic field lines configuration in magnetotail

14 p2229 A71-29669

Solar wind compressed magnetic field in sunward magnetosphere and extended geomagnetic tail observation by Pioneer 7 spacecraft

14 p2234 A71-30028

Low energy electron and proton fluxes in geomagnetic tail of equatorial magnetosphere forming plasma sheet related to auroral oval

14 p2299 A71-30029

Geomagnetic tail influence on polar ionosphere proton and electron precipitation, considering ionospheric ionization and polar cap absorption

14 p2300 A71-30034

Magnetospheric tail regions, investigating McIntosh effect in AE and Dst indices daily variations

14 p2236 A71-30354

Radiation from electrostatic waves in thin current sheet in geomagnetic tail into cold magnetized plasma, noting wave damping for wide frequency range

16 p2562 A71-32805

Geomagnetic tail natural oscillations, applying model of plasma cylinder with free boundary immersed in interplanetary medium

16 p2564 A71-33673

Magnetotail changes relationship to solar wind magnetic field and magnetospheric substorms from ground and satellite data

16 p2629 A71-33944

Time variations of magnetotail plasma sheet from electron energy spectral measurements on Vela satellites

16 p2629 A71-33945

Magnetospheric observations by Imp 3 satellite of energetic electron and magnetotail field variations near neutral sheet as function of substorm time

16 p2574 A71-33971

Bibliography and review of interplanetary magnetic fields and plasmas, considering solar wind properties, magnetosheath, bow shock and magnetospheric tail

17 p2799 A71-34460

Bibliography on magnetosphere covering structure, magnetopause, geomagnetic tail, plasma sheet, convection plasmopause, storm and substorms, ring current and energetic particles

17 p2732 A71-34468

Solar proton trajectories calculations in Williams-Mead geomagnetic field model, showing longitude difference in tail region

20 p3216 A71-38747

Charged particles interaction with geomagnetic field, discussing plasma equations of motion, ionospheric current induction, transition layer and magnetotail rotation

20 p3216 A71-39118

Plasma layer effect on natural oscillations of magnetosphere tail, using infinite plasma cylinder model immersed in interplanetary plasma

20 p3216 A71-39137

Low latitude geomagnetic substorm development model due to increased resistance in magnetosphere tail current sheath

20 p3219 A71-39597

Cosmic rays cutoff daily variations at ATS geostationary satellite altitude, noting role of magnetospheric tail in lowering cutoff below calculated value

20 p3282 A71-39739

Magnetotail plasma sheet variations association with auroral display features during substorms from all sky photography

20 p3230 A71-39880

Magnetosphere aerodynamic parameters, discussing lift and drag coefficient, shape, magnetic field gradients and tail

21 p3374 A71-41353

Geomagnetic horizontal field decrease from magnetospheric tail field annihilation during magnetic storm, considering polar ionospheric current generation mechanism

22 p3533 A71-41560

Magnetospheric substorms observations by satellite and balloon-borne X ray detectors, considering auroral arc brightening and energetic electron flux enhancement in magnetotail

23 p3668 A71-43163

Earth corotating plasma tail evidence in plasmopause variations from high resolution proton distribution data obtained by Ogo 4 satellite during magnetic storm

23 p3668 A71-43166

Magnetotail magnetic fluctuation observation during polar magnetic substorms, noting localized character

23 p3669 A71-43178

Vela 4A and 4B satellite observation of impulsive energetic electron fluxes in distant magnetotail associated with magnetospheric polar substorms

23 p3670 A71-43184

Plasma current driven sheet at neutral point of cusps and quadrupole magnetic field for space physics simulation of solar flare and geomagnetic tail

23 p3714 A71-44282

GEOMAGNETICALLY TRAPPED PARTICLES U RADIATION BELTS GEOMAGNETISM

Conjugate mirror point locations for world geomagnetic contour maps, noting use for particle tracing

01 p0077 A71-11511

Oscillating satellite orientation from geomagnetic field strength vector, using least squares method

02 p0319 A71-11911

Plasma motion in magnetosphere under undisturbed geomagnetic conditions, taking solar wind into account

02 p0244 A71-11919

Earth and Jupiter magnetic fields relationship to core motional induction

02 p0310 A71-12160

Boundary position and thickness between geomagnetic field and solar wind plasma, simulating interaction with magnetosphere

03 p0473 A71-13100

ESRO 1 satellite hydrogen and ionized nitrogen auroral emissions photometric measurements, discussing electron/proton phenomena relation to geomagnetic activity

03 p0406 A71-13248

E layer atmospheric densities from decaying satellites observation, discussing solar activity and geomagnetic correlations

03 p0414 A71-14022

Polar orbiting satellite observed transient plasma density enhancements relation to geomagnetic activity

03 p0417 A71-14042

Solar radio centers and interplanetary sector structures in connection with recurrent geomagnetic storms

03 p0496 A71-14512

Quiet day variations in earth surface magnetic field, examining magnetopause, neutral sheet and ring current nonionospheric current models

03 p0421 A71-14535

Ancient geomagnetic intensity in Japan by comparing natural remanent magnetization with known thermomagnetic magnetization induction, using stepwise heating method on antique pottery

04 p0582 A71-15127

Auroral ionosphere, examining low energy proton fluxes parallel to geomagnetic field lines of force

05 p0738 A71-16160

Geomagnetic field effects on cosmic radiation, determining muon component momentum distribution and charge ratio

05 p0798 A71-16219

Lunar semimonthly oscillations in solar daily F range related to midday F2 critical frequency at equatorial stations, analyzing lunar tides in ionosphere

05 p0740 A71-16432

Geomagnetic field secular variation subdivision based on time effect, noting harmonic processes with 20 year period

05 p0745 A71-17191

Geomagnetic field intensity during past 2000 years from global data, noting cyclic variations

05 p0745 A71-17193

Geomagnetic components measurement from moving platforms, discussing coordinate system stabilization methods for errorless time averaging of measurements

05 p0756 A71-17194

Geomagnetic activity diurnal variation dependence on latitude and longitude during IGY

05 p0746 A71-17210

Geomagnetic field anomalous variations due to solar eclipse of 22 September 1968

05 p0746 A71-17211

Earth variable electromagnetic field spatial harmonics asymptotic properties

05 p0746 A71-17212

Geomagnetic field secular variations in Drake passage (Antarctic Ocean), applying absolute magnetic surveys

05 p0747 A71-17215

Quartz magnetometer design and operation for simultaneous geomagnetic field declination and horizontal component measurements

05 p0756 A71-17216

Geomagnetic T and Z components variation measurements, discussing design and operation principles of magnetic survey device

05 p0756 A71-17217

Ionospheric irregularity structure boundary variations shown by scintillation from satellite and radio star observations during quiet and disturbed magnetic conditions

06 p0887 A71-17269

Ionospheric geomagnetic field inclination measurement by incoherent scatter method

06 p0887 A71-17270

International geomagnetic reference field 1965 geomagnetic potential rate of change and transformation to dipole coordinates

06 p0888 A71-17282

- Spherical superconducting geomagnetic field generating layer under ultrahigh pressure in earth center 06 p0889 A71-17734
- Indirectly stabilized magnetometers on moving carrier, examining techniques for geomagnetic field vector component measurements 06 p0899 A71-17932
- Geomagnetic field daily variation, discussing ambient field weakening on night side 06 p0893 A71-17992
- Geomagnetic storm on 24 March 1969, obtaining upper atmosphere emission data in middle latitude zone 06 p0894 A71-17996
- Twenty-seven day variations in cosmic ray intensity and geomagnetic activity index, using filter and power spectrum methods 06 p0953 A71-18122
- Solar proton entry into geomagnetic field during 9 June 1968 event 06 p0958 A71-18153
- Geomagnetic activity relation to large scale variations in interplanetary magnetic field and solar wind deformation velocity, using satellite and space probe observations 06 p0963 A71-18254
- Spherical harmonic analysis of geomagnetic field strength for global magnetic anomaly charts 06 p0894 A71-18267
- Nondipole geomagnetic field effect on magnetospheric boundary, presenting graphs for distance dependence on polar angle 06 p0895 A71-18271
- Geomagnetic field variations recording by two variometers, correcting for variation components effects by instruments orientation 06 p0901 A71-18284
- Twilight helium emission diurnal and seasonal variations relationship to geomagnetic activity and solar depression, using Abastumani observations 07 p1099 A71-19389
- Three dimensional electromagnetic induction problem of magnetovariational and magnetotelluric sounding at flat earth 07 p1099 A71-19394
- Cyclic variations in geomagnetic field from 1550 through 1960 using spherical harmonic analysis of magnetic declination 07 p1099 A71-19395
- Geomagnetic field modeling facility based on nine-dipole model parameters 07 p1100 A71-19406
- Geomagnetic activity effects on atomic oxygen emissions in green and red light, noting radiant intensity, strong dispersion, local and planetary Kp indices 07 p1101 A71-19413
- Energetic electrons in magnetospheric tail plasma sheet, investigating flux time profiles and correlation with local magnetic fields from Imp 3 satellite observation data 07 p1186 A71-19658
- Quiet day geomagnetic field measurements at synchronous orbit ATS 1, calculating equatorial component of interaction force between solar wind and earth 07 p1102 A71-19664
- Artificial solar wind experiments, describing interaction between hydrogen plasma shock wave and simulated geomagnetic field 08 p1354 A71-21010
- Geomagnetic activity indices-overall diurnal interplanetary magnetic field strength correlation by satellite magnetometer data 08 p1360 A71-21016
- Solar flare EUV radiation and ionospheric currents dynamo region ground based detection by geomagnetic crochets time structure analysis 08 p1355 A71-21198
- Quiet time galactic component of geomagnetic field variations excluding solar-terrestrial disturbances 08 p1363 A71-21199
- Magnetic field of currents in earth induced by external field with known distribution, representing earth conductivity by thin conducting spherical shell 08 p1278 A71-21200
- Geomagnetic cavity heuristic model with solar wind driven unipolar induction current in ionosphere 08 p1280 A71-21218
- Geomagnetic activity winter-summer difference in Northern and Southern Hemisphere middle latitudes 08 p1283 A71-21645
- Earth and sun magnetic field production models as function of dynamo states, discussing solar field effects on terrestrial space environment 09 p1517 A71-22334
- Laminar geoelectromagnetic field excited by coaxial ring current, determining impedance and magnetic field ratios of spherical harmonics 09 p1435 A71-22434
- Lower ionosphere electromagnetism induction effect on geomagnetic field guided MHD wave propagation, considering Hall effect 09 p1435 A71-22436
- Ionospheric current flow past circular inhomogeneous spot with Pederson and Hall conductivities, calculating earth surface magnetic field by Lipshitz-Hankel integral 09 p1436 A71-22549
- Hydrogen ion flux detected along earth magnetic force lines in Northern Hemisphere midlatitudes, determining flux magnitude 09 p1436 A71-22561
- Adiabatic drawing of quasi-captured charged particles by geomagnetic trap field during phase recovery period of magnetic storm 09 p1513 A71-22572
- Plasmasphere ion concentration measurements on-board Elektron 2 and 4 satellites, observing dependence on geomagnetic activity 09 p1513 A71-22574
- Interplanetary magnetic field intensity and geomagnetic activity level correlation with 27-day solar activity cycle based on Venera 4 and Mariner 5 data comparison 09 p1519 A71-22577
- High energy electrons in near space excess radiation from high altitude balloon and satellite data 09 p1513 A71-22667
- Critique of paper on earth gravitational field correlations to dipole part of magnetic field 09 p1437 A71-22930
- Earth gravitational field correlations to dipole part of magnetic field, rejecting modifications to statistical procedures 09 p1437 A71-22931
- Geomagnetically trapped particles radial diffusion across L shells, considering influence on steady state structure and dynamics of radiation belts 09 p1514 A71-23460
- Geomagnetic field measurements by ATS 1 in synchronous equatorial orbit, determining pulsations types during magnetically quiet and geomagnetic storm periods 09 p1440 A71-23636
- Geomagnetic solar quiet day horizontal current and electrostatic potential field model in ionosphere, using dynamo equations 09 p1442 A71-23708
- Pc1 propagation in magnetosphere model accounting for ionization gradients aligned along geomagnetic field 10 p1599 A71-23849
- Ionospheric propagation forecasting as function of solar and magnetic activity conditions for maximum usable communications frequencies, using F2 layer peak electron density 10 p1575 A71-23865
- Geomagnetic disturbance field asymmetry Fourier analysis for amplitude G and local time phase of first diurnal harmonic for IGY 10 p1600 A71-24295
- Geomagnetic reversals in volcanic flows, computing paleomagnetic pole positions similar to Tertiary rocks 10 p1601 A71-24397
- Solar geomagnetic seasonal ionization control of upper ionosphere longitudinal composition variations from polar satellite observations 10 p1602 A71-24555
- Geomagnetic quadrupole field secular oscillation causing earth rotation change, discussing earth core induced velocity field and field attenuation 10 p1603 A71-24599
- Atmospheric electrical structure control by lower ionosphere force, considering interaction between neutral atmosphere tidal circulations and ionospheric plasma in presence of geomagnetic field 10 p1604 A71-24702
- Magnetic field and trapped electron/proton correlated pulsations due to magnetospheric field line resonance, using model based on Maxwell equation two dimensional solution 10 p1664 A71-24786
- Geomagnetic field inclination determination by incoherently scattered signal Faraday rotation calibration and simultaneous ionosonde measurements of ionospheric electron density 10 p1605 A71-24798
- Attenuation and phase velocity of ELF and VLF radio waves propagating under anisotropic ionosphere, discussing geomagnetic field effect 11 p1731 A71-25602
- Extraterrestrial ring current under very quiet magnetic conditions from mean long term diurnal horizontal intensities 11 p1755 A71-25616
- Earth radiation belts high energy electron flux intensity monotonic decrease during magnetically quiet periods from satellite data analysis 11 p1816 A71-25759
- Quasi-linear theory of inhomogeneities generation in equatorial jet, considering space charge waves excitation by electric current perpendicular to geomagnetic field 11 p1757 A71-25772
- Geomagnetic and interplanetary magnetic fields, considering inverse direction of electric currents in Northern and Southern Hemispheres 11 p1757 A71-25776
- Compton electrons produced ring current effects on geomagnetic fields for gamma quantum source and air molecular interactions, considering exact analytical model 11 p1817 A71-25777
- Geomagnetic field calculation for intermediate ionosphere altitudes, applying Dirichlet sphere problem to rectangular magnetic field components 11 p1757 A71-25778
- Geomagnetic field intensity maps of vertical, horizontal, northern and eastern components of geomagnetic field and of magnetic inclination for 1965 11 p1757 A71-25779
- Geomagnetic horizontal field decrease from magnetospheric tail field annihilation, considering polar ionospheric current generation mechanism 11 p1758 A71-25792
- Solar wind effects on space around earth, discussing dipole image of magnetic field, radiation belt feeding and atmospheric phenomena based on artificial satellite observations 11 p1817 A71-26337
- Terrestrial, solar and galactic magnetic fields, discussing generation by combined nonuniform rotation and cyclonic turbulence based on dynamo equation 12 p1961 A71-26859
- Antarctic auroral ovals, determining time-longitude coordinates, statistical mean position and polewards and equatorwards boundaries for various Kp 12 p1900 A71-27056
- Hamiltonian optics based model of ionospheric radio propagation, discussing earth magnetic field effects on radio wave angle-of-arrival changes 12 p1879 A71-27058
- Geomagnetic effects on radio signals mechanism in extensive air showers, discussing scintillators array for east-west to north-south ratio polarization measurements 12 p1967 A71-27390
- Multiple midlatitude auroral arcs during geomagnetic storm recovery phase 8/9 March 1970, noting correlation with recorded geomagnetic field intensity variations 12 p1902 A71-27670
- Geomagnetic field effects on directional propagation of LF and VLF radio waves in ionosphere, taking into account ion types effects 13 p2029 A71-28026
- Oscillating artificial earth satellite orientation determination from geomagnetic field strength vector, using least squares method 13 p2145 A71-28205
- Plasma motion in magnetosphere under undisturbed geomagnetic conditions, taking into account solar wind 13 p2058 A71-28206
- Interplanetary medium characteristics during geomagnetic storms, discussing changes in pressures, energy flux densities, acoustic velocities and static/magnetic pressure ratio 13 p2058 A71-28236
- Geomagnetic field secular variation subdivision based on time effect, noting harmonic processes with 20 year period 13 p2059 A71-28247
- Geomagnetic secular variations from various surveys, noting negative value for Gulf of Aden anomaly chart 13 p2059 A71-28248
- Geomagnetic components measurement from moving platforms, discussing coordinate system stabilization methods for errorless time averaging of measurements 13 p2067 A71-28249
- Geomagnetic activity diurnal variation dependence on latitude and longitude during IGY 13 p2060 A71-28265
- Geomagnetic field anomalous variations due to solar eclipse of 22 September 1968 13 p2060 A71-28266
- Earth variable electromagnetic field spatial harmonics asymptotic properties 13 p2060 A71-28267
- Quartz magnetometer design and operation for simultaneous geomagnetic field declination and horizontal component measurements 13 p2067 A71-28270
- Geomagnetic T and Z components variation measurements, discussing design and operation of magnetic survey device 13 p2067 A71-28271
- Hall effect and magnetic field characteristics in lower ionosphere by vertical magnetospheric currents, using gyrotronic model 13 p2061 A71-28534
- Earth magnetosphere boundary position, head shock wave, transition region width and current magnetic field changes during magnetopause in geomagnetic storm periods 13 p2061 A71-28549
- Daily Ap activity response of magnetosphere to sunspots, using 38 year geomagnetic storminess levels 13 p2062 A71-28785

Spherical harmonic expansion for volumes of tubes of unit flux in geomagnetic field for use in magnetospheric dynamics

14 p2229 A71-29668

Magnetosphere structure, considering geomagnetic field lines configuration in magnetotail

14 p2229 A71-29669

Geomagnetic disturbance vector distribution, computing three dimensional ring and ionospheric currents system models

14 p2229 A71-29672

Upper atmosphere aeronomy historical review, considering meteor trails, radio waves, auroral photography, terrestrial magnetic field and spectroscopy

14 p2229 A71-29704

Auroral precipitation electron energetic and angular distributions as function of geomagnetic activity from Cosmos 261 measurements

14 p2230 A71-29713

Ionospheric currents due to electric polarization field transfer from magnetosphere under quiet and disturbed conditions, using Ba ion cloud and geomagnetic measurements

14 p2230 A71-29715

Geomagnetic field models validity from satellite data

14 p2231 A71-29903

Trapped charged particle cyclotron, bounce and drift motion in distorted geomagnetic field

14 p2300 A71-30033

Auroral electrons interaction with atmosphere from Fokker-Planck equation, considering angular diffusion, energy loss and geomagnetic field convergence effects

14 p2235 A71-30345

Planetary magnetic activity measure based on K indices of antipodal observations

14 p2235 A71-30353

Optically pumped magnetometers for earth and interplanetary magnetic fields measurement, using Zeeman effect

15 p2405 A71-31409

Magnetospheric plasma clouds equatorial observation by ATS 5 satellite, revealing plasma injection during substorms and dispersion by earth magnetic and electric fields

15 p2397 A71-31755

Proton measurements in ring current by OGO-3 satellite compared with geomagnetic field data at low and high latitudes

16 p2626 A71-33663

Northern high latitude electron trapping boundary position diurnal, seasonal and geomagnetic Kp variations based on ESRO 1/Aurora polar satellite observations

16 p2627 A71-33753

Geomagnetic field daily variation amplitude increase under equatorial electrojet during 7 July 1966 solar proton flare

16 p2567 A71-33768

Electron temperature profiles in ionosphere from rocket probes, noting correlation with geomagnetic activity indexes

16 p2569 A71-33798

Atmospheric density variation response time measurement to geomagnetic activity by satellites - borne low-G accelerometer calibration system, considering atmospheric heating mechanism

16 p2571 A71-33839

Thermosphere structure and motion from neutral atmospheric density data, noting correlation with enhanced geomagnetic activity

16 p2571 A71-33840

German Democratic Republic space research, reviewing meteorological, ionospheric, geomagnetic and solar physics studies

16 p2666 A71-33864

Earth upper mantle electrical conductivity as function of depth based on geomagnetic variation field spatial distribution data

16 p2572 A71-33907

Shock normal calculation by applying least squares technique to combined geomagnetic field and plasma data from single satellite, assuming Rankine-Hugoniot conservation relations

16 p2560 A71-33941

Earth bow shock internal structure based on correlated observations of magnetic field, ELF magnetic fluctuations and suprathermal electrons by OGO 5 satellite

16 p2628 A71-33943

Sq day to day variability relation to interplanetary plasma parameters including magnetic field and solar wind velocity and kinetic energy

17 p2801 A71-34625

German monograph on self consistent ring current models of geomagnetic field interaction with charged particles

17 p2733 A71-34789

Solar corona formation relation to geomagnetic storm generation

17 p2734 A71-35191

French monograph on ULF geomagnetic field variations covering plasmopause, geomagnetic pulsations, WKB limit and magnetospheric density

17 p2735 A71-35248

Earth gravitational and magnetic field correlations, considering nondipole geomagnetic potential latitudinal rotation effects

17 p2735 A71-35383

Geomagnetic diurnal variations near Sq current vortex focus, indicating existence of ionospheric diverging or converging currents

18 p2912 A71-36298

German monograph on geomagnetic reference field for rocket measurements covering mathematical model for northern Scandinavia

18 p2913 A71-36682

Magnetopause current layer equilibrium based on numerical solution of uniform magnetic field confinement by warm plasma with net parallel velocity

19 p3132 A71-37355

Magnetospheric electric field dynamics, examining resonant protons role in magnetic storms

19 p3127 A71-37760

Twilight helium emission diurnal and seasonal variations relationship to geomagnetic activity and solar depression, using A bastumani observations

19 p3053 A71-37814

Three dimensional electromagnetic induction problem of magnetovariational and magnetotelluric sounding at flat earth

19 p3053 A71-37818

Cyclic variations in geomagnetic field from 1550 through 1960, using spherical harmonic analysis of magnetic declinations

19 p3053 A71-37819

Electromagnetic and thermal energy fluxes during magnetic storms, using interplanetary spacecraft and D variation data

19 p3053 A71-37821

Geomagnetic field modeling facility based on nine-dipole model parameters

19 p3053 A71-37830

Geomagnetic activity effects on atomic oxygen emissions in green and red light, noting radiant intensity, strong dispersion, local and planetary Kp indices

19 p3054 A71-37837

Five component electromagnetic field station to record geomagnetic field magnetic and electric components variations

19 p3042 A71-38374

Noncircular ionospheric current conversion into longitudinal currents in magnetosphere along lines of force of geomagnetic field

19 p3057 A71-38380

Electrical conduction in orthogonal coordinates from nondipole nature of geomagnetic field on conductivity tensor of ionospheric dynamo region

19 p3057 A71-38381

Ionospheric currents fields, determining Hall conductivity and geomagnetic lines of force slope effects

19 p3058 A71-38387

Magnetospheric current effects on geomagnetic field structure, noting electron and proton precipitation into auroral zone

19 p3059 A71-38396

ESRO-1A /Aurora/ observations of variations in low energy electron spectrum, noting relationship to magnetic activity

19 p3060 A71-38576

German monograph on electron flux properties in polar atmosphere, discussing pitch angle distribution, energy spectrum and relation to geomagnetic field disturbances

19 p3130 A71-38646

Stable earth core geomagnetic dynamo model consisting of disk oscillating about symmetry axis with coil connected to brushes on axle and at disk edge

19 p3061 A71-38676

Solar proton trajectories calculations in Williams-Mead geomagnetic field model, showing longitude difference in tail region

20 p3216 A71-38747

Charged particles interaction with geomagnetic field, discussing plasma equations of motion, ionospheric current induction, transition layer and magnetotail rotation

20 p3216 A71-39118

Interplanetary and magnetospheric magnetic force lines reconnection and effects on geomagnetic activity

20 p3289 A71-39126

Jupiter decametric radio emission relation to solar wind, geomagnetic activity and shock waves causing Forbush decreases

20 p3291 A71-39312

Solar regular daily geomagnetic variations - Conference, Potsdam, East Germany, April 1970

20 p3216 A71-39508

Magnetospheric interactions with ionosphere for solar regular daily geomagnetic variations, discussing dynamo region electric fields effects

20 p3217 A71-39509

Midlatitude solar quiet geomagnetic field dynamics morphology, emphasizing regular diurnal and annual changes and irregular fluctuations

20 p3217 A71-39510

Daily geomagnetic variations ionospheric current systems calculation from total magnetic field data obtained at ground stations during IGY

20 p3217 A71-39511

Geomagnetic activity daily variability index statistical dependence on geomagnetic latitude, noting maximum below equatorial electrojet

20 p3217 A71-39512

Lunar and solar daily geomagnetic variability morphology correlation based on atmospheric dynamo model

20 p3217 A71-39513

Diurnal variations of Sq currents in terms of electroconductivity model of ionosphere and geomagnetic field, using two dimensional dynamo theory

20 p3217 A71-39514

Atmospheric dynamo equations derivation based on Maxwell equations and Ohm law with anisotropic asymmetric electric conductivity tensor for quasi-geomagnetic variations explanation

20 p3217 A71-39515

Equatorial electrojet region ionospheric current during magnetically quiet day and nighttime from rocket measurements

20 p3218 A71-39516

Equivalent current systems at 115 km parallel to earth surface profile based on ground observations of geomagnetic field, comparing with auroral electrojet

20 p3218 A71-39517

Artificial solar wind experiments, describing interaction between hydrogen plasma shock wave and simulated geomagnetic field

20 p3279 A71-39518

Geomagnetic activity indices-overall diurnal interplanetary magnetic field strength correlation by satellite magnetometer data

20 p3294 A71-39519

Ionospheric model for magnetic perturbation field global distribution during polar magnetic substorms considering ground level geomagnetic effects from Birkeland and Pedersen currents

20 p3229 A71-39848

Magnetic field aligned striations of Ba ion clouds artificially injected into ionosphere, investigating physical processes based on model

20 p3230 A71-39849

Night and daytime auroral zone ionospheric electric field measurement by rocket-borne Langmuir probe noting components parallel and perpendicular to magnetic field

20 p3231 A71-39848

Time dependent plasmopause motion after increases and decrease in magnetic activity based on analytical model of plasma flow

20 p3232 A71-39849

Magnetospheric plasma observation by Sirio 1 satellite, measuring protons, electrons and magnetic field with sensors

20 p3307 A71-39955

Geomagnetic field horizontal component H daily variation nature, using graphs to show increases above or decreases below given level

21 p3373 A71-40055

Radiation belt particles nonadiabatic changes, calculating rigidity as function of magnetic field lines

21 p3439 A71-41355

Earth radiation belts high energy electron flux intensity monotonic decrease during magnetically quiet periods from satellite data analysis

22 p3591 A71-41522

Outer radiation belt energetic electron flux intensity correlation with auroral activity and Kp index

22 p3591 A71-41522

Quasi-linear theory of inhomogeneities generation in equatorial jet, considering space charge waves excitation by electric current perpendicular to geomagnetic field

22 p3532 A71-41544

Geomagnetic and interplanetary magnetic fields considering inverse direction of electric currents in Northern and Southern Hemispheres

22 p3532 A71-41544

Compton electrons produced ring current effects on geomagnetic fields for gamma quantum source and molecular interactions, considering exact analytical model

22 p3532 A71-41544

Geomagnetic field calculation for intermediate ionosphere altitudes, applying Dirichlet sphere problem to rectangular magnetic field components

22 p3532 A71-41544

Global geomagnetic field intensity maps of vertical, horizontal, northern and eastern components of geomagnetic field and of magnetic inclination for 1960

22 p3532 A71-41544

Geomagnetic horizontal field decrease from magnetospheric tail field annihilation during magnetospheric storm, considering polar ionospheric current generation mechanism

22 p3533 A71-41545

Magnetospheric VLF transverse wave propagation along geomagnetic field, examining dispersion relation

22 p3533 A71-41545

Interplanetary magnetic sector polarity effects on polar geomagnetic field diurnal variation

22 p3604 A71-42222

- Steady state transition layer between cold solar plasma flow and geomagnetic field in one dimensional model
22 p3536 A71-42622
- Localized abnormal geomagnetic disturbance near polar cap and simultaneous ionospheric variation during auroral zone weak magnetic activity periods
22 p3536 A71-42625
- Quiet and stormy day diurnal variations of geomagnetic field, investigating ionospheric contribution
23 p3665 A71-42968
- Lunar daily geomagnetic variations separation into oceanic and ionospheric origin in Indian region
23 p3667 A71-43149
- Magnetic shell parameter L approximation simplifying McIlwain expression
23 p3669 A71-43179
- Premidnight asymmetry in directional 40 keV ionospheric electron flux profiles in magnetic local time observed on Azur satellite
23 p3721 A71-43185
- Midlatitude sporadic E layer changes during increased geomagnetic activity, considering skin effect and current shear
23 p3670 A71-43189
- Geomagnetic index Kp frequency distribution tables (1932-1970)
23 p3670 A71-43192
- Auroral conjugacy observations over Alaska and south of New Zealand, noting correlation with geomagnetic field lines
23 p3671 A71-43325
- High energy particle environment model at synchronous altitudes during quiet geomagnetic periods from satellite observation, establishing outer radiation belt distribution function
23 p3722 A71-43978
- Least geomagnetic diurnal variation effects period determination by statistical method
23 p3673 A71-43984
- Large geomagnetic diurnal variations effects period determination by statistical method, considering partial ring currents in night magnetosphere
23 p3673 A71-43985
- Longitudinal dependence of solar quiet geomagnetic field horizontal component at equator, discussing discrepancy between theory and observation
23 p3673 A71-43986
- Extensive air shower radio pulse emission by geomagnetic charge separation mechanism, using antenna and scintillation counters arrays
23 p3646 A71-44012
- Comet brightness variations correlation with geomagnetic field and solar corpuscular flux variations in interplanetary space
24 p3870 A71-44814
- Solar unipolar magnetic regions relation to geomagnetic disturbances variability, discussing 11 year cycle
24 p3823 A71-45036
- Digital computer numerical procedure to solve dynamo theory MHD equations for earth nucleus, using combination of Fourier and finite difference methods for integration
24 p3823 A71-45038
- Solar activity effects on biosphere, examining solar-geomagnetic and medico-biological indexes relationships and clinico-statistical evidence of human organism effects
24 p3799 A71-45197
- Magnetospheric midday boundary width dependence on geomagnetic dipole axis orientation, discussing different positions for magnetosphere boundary
24 p3824 A71-45319
- Nonadiabatic and atmosphere induced energy losses as causes of proton capture in geomagnetic field
24 p3867 A71-45320
- GEOMETRICAL HYDROMAGNETICS**
U MAGNETOHYDRODYNAMICS
GEOMETRICAL OPTICS
U OPTICS
GEOMETRODYNAMICS
U RELATIVITY
GEOMETRY
NT ANALYTIC GEOMETRY
NT ANGLES [GEOMETRY]
NT BRAGG ANGLE
NT BREWSTER ANGLE
NT CARTESIAN COORDINATES
NT CHORDS [GEOMETRY]
NT CIRCLES [GEOMETRY]
NT COLLINEARITY
NT COPLANARITY
NT CURL [VECTORS]
NT CURVATURE
NT CURVES [GEOMETRY]
NT DIFFERENTIAL GEOMETRY
NT EUCLIDEAN GEOMETRY
NT FIXED POINTS [MATHEMATICS]
NT FLOW GEOMETRY
NT GREAT CIRCLES
NT HEXAGONS
NT HYPERBOLAS
NT IMBEDDINGS [MATHEMATICS]
NT INVARIANT IMBEDDINGS
NT LIE GROUPS
- NT LINES [GEOMETRY]
NT LOCI
NT MERCATOR PROJECTION
NT METRIC SPACE
NT NOZZLE GEOMETRY
NT OBLATE SPHEROIDS
NT PARALLELEPIPEDS
NT POINTS [MATHEMATICS]
NT POLYGONS
NT POLYHEDRONS
NT PROJECTIVE GEOMETRY
NT PROLATE SPHEROIDS
NT RADII
NT RECTANGLES
NT RHOMBOHEDRONS
NT RIEMANN MANIFOLD
NT S CURVES
NT SPHEROIDS
NT SPINOR GROUPS
NT TANK GEOMETRY
NT TENSOR ANALYSIS
NT TETRAHEDRONS
NT TOPOLOGY
NT TORUSES
NT TRAPEZOIDS
NT TRIANGLES
NT VECTOR ANALYSIS
NT VORTICITY
- Book on optimization methods covering matrix algebra, n dimensional geometry, search techniques, linear and nonlinear programming, etc
05 p0774 A71-16475
- Cosmic ray telescopes geometric factor determination, taking into account particle incidence angle
06 p0898 A71-17705
- Relation uniaxial stressed state relationship to internal geometry of flexible shell
06 p0993 A71-17814
- Channel form determination from circles family envelopes, discussing turbine duct geometries
06 p0841 A71-18009
- Partial ordering of normed space, using positive element cone construction method
09 p1485 A71-22368
- Lie group differential equation application to gravitation theory, rejecting Riemann geometry in favor of Klein geometry
09 p1495 A71-23073
- British Aircraft Corporation Numerical Master Geometry system using parameter surface mathematics and digital computer
10 p1580 A71-23759
- Theory of form based on geometric probabilities, leading to two dimensional retinal type computer programmed to exhibit elementary form perception aspects
10 p1567 A71-23997
- Soviet papers on geometrical and group methods in gravitational and elementary particles theory, covering relativity and electromagnetic and quantum fields
19 p3104 A71-38578
- Electromagnetic and gravitational fields geometry, using compensating fields concept
19 p3105 A71-38581
- Apollo core tube geometry effect on quantity and quality of lunar sample recovery
23 p3757 A71-43750
- GEOMORPHOLOGY**
Lunar hot spots surface distribution-geomorphic index relationship, discussing maria, terrae and regolith evolutionary stage
05 p0809 A71-16462
- Morphology and dynamics of low intensity monochromatic midlatitude auroral arcs of 6300 A /O I/, comparing results with observation during IGY
07 p1103 A71-19766
- Pi 2 type geomagnetic pulsations relationship to auroral zone morphological features
09 p1435 A71-22448
- Recording and interpretation of aerial photographs applied to geomorphology
10 p1599 A71-23872
- Apollo lunar sea geomorphic data agreement with Luna 16 data
15 p2488 A71-32325
- Small lunar maria craters morphological maturity as function of age and dimensions
16 p2638 A71-33670
- Monograph on satellite-borne orbital photographic imaging techniques application to natural resources survey, discussing remote areas geomorphological and geological reconnaissance maps preparation
18 p2915 A71-35905
- Morphology and geology of Lappajarvi structure /Finland/, suggesting meteorite impact evidence
19 p3049 A71-37652
- Charlevoix structure impactite description, discussing meteoritic impact origin from petrographic and chemical data
19 p3049 A71-37656
- Tuff rings from Fort Rock-Christmas Lake Valley basin, investigating morphologic and volcanic features for surface water role in genesis
19 p3051 A71-37671
- Midlatitude solar quiet geomagnetic field dynamics morphology, emphasizing regular diurnal and annual changes and irregular fluctuations
20 p3217 A71-39510
- Auroral morphology, covering static and dynamic ovals, polar cap and dayside auroras, auroral zones, substorms and electron precipitation
20 p3227 A71-39838
- Near side lunar mare surfaces ages interpretation in terms of geomorphic indices based on crater number density
21 p3444 A71-40205
- GEON [TRADEMARK]**
U POLYVINYL CHLORIDE
GEOGRAPHICAL OBSERVATORIES
NT OGO
NT OGO-B
NT OGO-C
NT OGO-D
NT OGO-E
NT OGO-F
NT OGO-G
- Worldwide geophysical observatories network for observing solar optical, radio, particle X rays and geomagnetic and ionospheric effects
[AIAA PAPER 70-1354] 02 p0239 A71-12692
- GEOGRAPHICAL SATELLITES**
NT EXPLORER 12 SATELLITE
NT OGO
NT OGO-B
NT OGO-C
NT OGO-D
NT OGO-E
NT OGO-F
NT OGO-G
- Intercosmos 3 satellite for radiophysical and geophysical observations of radiation belts and ionosphere, discussing design, configuration and instrumentation
03 p0423 A71-13419
- GEOPHYSICS**
Geothermometer based on plagioclase-magmatic liquid equilibrium
05 p0751 A71-16411
- Geoscience electronics - IEEE Conference, Washington, D.C., April 1970
05 p0754 A71-17126
- Global radiation temperature distribution inhomogeneities in underlying surfaces, atmosphere and radiation absorbing areas
06 p0924 A71-17518
- Earth rotation pole coordinates from International Latitude Service stations and International Polar Motion Service data
06 p0890 A71-17878
- International Time Bureau /Paris/ astronomical and geophysical research based on universal time and latitude observations of earth rotation
06 p0890 A71-17879
- Geophysical and astronomical consequences of core-mantle interactions, considering earth rotation changes
06 p0891 A71-17887
- Long base line radio interferometry principles and geophysical applications
06 p0892 A71-17893
- Earth studies by astronomy and geophysics methods - Conference, Poltava, U.S.S.R., October 1967
08 p1283 A71-21670
- Unitary potential method for numerical separation of subterranean three dimensional gravitational and magnetic fields
09 p1436 A71-22608
- Polar cap as distinct geophysical entity, considering open magnetic field lines for connectedness to interplanetary plasma and particle input to lower latitudes
10 p1600 A71-24308
- Solar and lunar modulation of geophysical parameters, atmospheric electricity and thunderstorms in complex space-meteorology scope
10 p1604 A71-24706
- Theoretical equations of state in geophysics, considering systematics approach to laboratory data, seismic velocity profiles, finite strain and atomistic approach
12 p1931 A71-27415
- Errors in spectral estimates by single-mode filters using analog computer for geoscientific data processing
14 p2246 A71-30482
- Geophysical map preparation by automatic procedure using polynomial representation of fields in iteration process
16 p2563 A71-33460
- Atmospheric optics and geophysics problems modeling arrangement reproducing radiation field within light scattering medium
16 p2605 A71-34106
- Ries structure in southern Germany, considering complicated crater geometry revealed by surface topography and geophysical investigations
19 p3049 A71-37654

GEOPOTENTIAL

Satellite data techniques and instrumentation in earth geometry and kinetics, reviewing geopotential models, pole positions, tides, ocean physics and international cooperation

20 p3219 A71-39656

Geophysical cartesian coordinate system transformation, using vector-matrix formalism

21 p3375 A71-41355

Geothermic processes determination and registration in volcanic activity range by satellite IR measurements

22 p3534 A71-42004

GEOPOTENTIAL

NT GEOPOTENTIAL HEIGHT

Earth spherical and ellipsoidal gravity potential coefficients association using Lamé orthogonal function properties

01 p0155 A71-10388

Geopotential coefficient recovery, using resonant satellite orbits long arc elements

02 p0245 A71-11995

Earth surface density distribution, using earth gravity field representation as potential of simple layer determined from combined satellite and gravity anomalies observations

02 p0246 A71-12463

Earth gravitational environment critical parameters at synchronous altitudes by satellite drift observation, discussing geopotential field determination

04 p0583 A71-15306

Automatic computer verification of diurnal temperature and geopotential observations on principal isobaric surfaces by statistical data analysis, describing computer algorithm

06 p0922 A71-17504

Upper troposphere and lower stratosphere geopotential field short range forecast quasi-geostrophic model

06 p0889 A71-17516

Satellite orbital elements perturbation due to tesseral and sectorial harmonics of earth gravitational potential

06 p0976 A71-18451

External geopotential expansion coefficients and zonal harmonics estimation

06 p0976 A71-18453

Satellite orbital elements, examining resonance due to earth potential

08 p1366 A71-21778

Weather satellite data for numerical analysis and forecasts, reconstructing geopotential field

09 p1486 A71-22300

Satellite orbital elements perturbation due to tesseral and sectorial harmonics of earth gravitational potential

12 p1955 A71-26601

External geopotential zonal harmonics expansion coefficients estimate

12 p1898 A71-26603

Artificial satellites eccentric orbits commensurable with earth rotation, noting resonance effects of geopotential

13 p2135 A71-28354

Satellite orbital elements perturbations, examining resonance due to earth geopotential

15 p2495 A71-32683

Lumped fifteenth order spherical harmonics in geopotential from Ariel 3 satellite orbital inclination corrected for lunar-solar oscillatory perturbations

16 p2563 A71-33387

Geopotential temporal variations from earth Baker-Nunn satellite observations

20 p3219 A71-39658

Conservative Hamiltonian systems with infinitely deep potential wells, obtaining periodic solutions with variational technique

[AAS PAPER 71-332] 23 p3698 A71-43005

Gravity coefficients of geopotential expansion in ellipsoidal harmonics via Lamé functions, noting application to earth, Jupiter and Saturn

[AAS PAPER 71-338] 23 p3666 A71-43011

Quadrature errors in satellite geodesy via geopotential simple layer model, investigating different size surface elements and methods of subdivision

[AAS PAPER 71-340] 23 p3666 A71-43013

Satellites explosion debris distribution and orbital characteristics as data base for earth force field and geopotential resonance phenomena analysis

[AAS PAPER 71-351] 23 p3728 A71-43023

Orbital equations of motion and associated variational equations numerical integration, calculating geopotential in terms of spherical harmonics

[AAS PAPER 71-390] 23 p3666 A71-43058

Helmholtz vorticity equation application for indirect determination of inaccessible area geopotential field from satellite data

23 p3700 A71-43305

GEOPOTENTIAL HEIGHT

Complex monitoring of aerological information on geopotential and temperature of principal isobaric surfaces by static method and optimal interpolation on semiautomatic basis

17 p2769 A71-34299

Areal precipitation correlation with 850 mb geopotential height over Northern Hemisphere

22 p3535 A71-42414

GEOS 1 SATELLITE

Orbital solutions based on critical optical tracking and Doppler observations, comparing with GEOS 1 and 2 satellite orbits

04 p0553 A71-15305

Space triangulation corrections of equatorial topocentric coordinates and radius vector of Jupiter in Baker-Nunn net, using Geos A satellite optical and laser observations

11 p1732 A71-25819

GEOS 2 SATELLITE

Orbital solutions based on critical optical tracking and Doppler observations, comparing with GEOS 1 and 2 satellite orbits

04 p0553 A71-15305

GEOS-C SATELLITE

GEOS-C geodetic satellite purpose and equipment, discussing earth gravitational field study, radar altimeter possibility and tracking systems usefulness

20 p3306 A71-39657

GEOSTROPHIC WIND

Nongeostrophic and nonhydrostatic stability of baroclinic fluid for small Richardson numbers

07 p1153 A71-20220

Planetary boundary layer stationary air flow over plane homogeneous surface under geostrophic wind conditions, solving for thermal turbulence field stabilization by iterative method

08 p1330 A71-21874

Conditional instability of second kind /CISK/ in three dimensional quasi-geostrophic low latitude flow, examining Yamasaki model

09 p1490 A71-23561

Balance equation solution in spherical coordinate form, applying vector alterations to geostrophic wind field from pressure-height observations grid point analysis

10 p1638 A71-23964

Global monsoon atmospheric response model in geostrophic terms for heating input function parameterization, including Himalayas mountains effects

10 p1638 A71-23966

Planetary boundary layer stationary air flow over plane homogeneous surface under geostrophic wind conditions, solving for thermal turbulence field stabilization by iterative method

19 p3091 A71-38468

Geostrophic wind measurements by radiosondes at various altitudes over British Isles, relating deviations from geostrophic equilibrium to vertical motions near tropospheric trough

20 p3258 A71-39551

Lower boundary condition effects on quasi-geostrophic baroclinic instability, showing vertical wind shear as function of pressure and wavelength

22 p3569 A71-42544

Ageostrophic deviations and advection corrections to geostrophic wind velocity and shear stresses above water surface

22 p3570 A71-42849

Horizontal velocity and temperature spectra at high wavenumbers in three dimensional quasi-geostrophic turbulent flow

23 p3701 A71-43346

GEOTROPISM

Geotropic stimulus in plants, describing method to test correlations between microscopically visible cell particles and geotropic bending direction

21 p3339 A71-39974

Gravity receptors in Phycomyces sporangioophores, considering transient and long term geotropic responses

21 p3339 A71-39976

Gravity susception by higher plants, analyzing geotonic data for georeception theories

21 p3340 A71-39978

Auxin transport and geotropic response of roots and shoots, discussing plant growth mechanisms under stimulation-inhibition conditions

21 p3340 A71-39980

Hormone movement in geotropism, discussing supraoptimal auxin content and indoleacetic acid in wheat roots

21 p3340 A71-39981

Geotropic mechanisms of lateral auxin movement and polar transport of growth substances /ethylene/ without differential cell enlargement

21 p3340 A71-39982

Linkage mechanism between gravity perceptrors and auxin redistribution causing differential growth and geotropic curvatures in plants

21 p3340 A71-39983

Geoelectric effects on plants geotropic reaction chain, discussing hormone auxin asymmetric distribution due to gravity

21 p3340 A71-39984

External indole-3-acetic acid effect on elongation and geotropic bending of Avena coleoptiles related to auxin induced electrical responses

21 p3340 A71-39986

Gravity influence on plant growth, lateral development, apical dominance, bud initiation, orientation and flower morphology

21 p3340 A71-39999

Geopinnastic bending of *Fritillaria Meleagris* axes as prototype of geinduced plagiotropic growth

21 p3341 A71-40000

Plants behavioral reactions to continuous gravitational field directional reorientation by clinostat, discussing gravity compensation effects on tropism and forces required for geotropic response

21 p3341 A71-40004

Gravity effects on auxin transport, growth and foliage spread of green plants for efficient radiation capture, using horizontal clinostat experiments

21 p3341 A71-40005

Gravity responses and geotropic behavior at ontogenetic stages of higher green plants, noting tendril movement under mechanical stimulation

21 p3341 A71-40008

Lettuce seedlings growth reduction and geotropic and phototropic behavior modification by 3-*primo* chlorophenyl 3-methoxy phthalide, noting gravity response elimination through action on statoliths

23 p3639 A71-43143

GEP TELESCOPES

U PARTICLE TELESCOPES

GERDIEN ARC HEATERS

U ARC HEATING

U HEATING EQUIPMENT

GERMANIDES

Chemical properties of titanium, zirconium and hafnium germanides exposed to acids, oxidizers, complex salts, alkaline solutions and water

19 p3075 A71-37106

GERMANIUM

NT SILICON

NT TELLURIUM

Thermodynamic distribution of amphoteric Ge impurities in sublatitudes of GaAs semiconductor for compensation by acceptor vacancies

01 p0139 A71-10778

Magnetic field effects on electron heating by strong electric field in n-Ge single crystals

01 p0140 A71-11459

Free hole drag in p-type Ge by photons in optical transitions between valence band subbands, examining magnetic field effects

02 p0296 A71-12613

Transport mechanism for holes in polycrystalline Ge films based on Matthiessen rule, considering surface scattering and dislocation

03 p0468 A71-14464

Gold plated Ge surfaces, investigating LEED patterns and electronic properties

04 p0636 A71-15016

Transducer with single crystal Ge for high heat flux measurement, noting calibration by direct conduction

04 p0599 A71-15589

Superconducting niobium aluminide and niobium aluminide-Ge films formation on Nb substrate

05 p0792 A71-16238

N-type Ge semiconductor low temperature breakdown potential dependence on neutral impurity concentration

05 p0793 A71-16420

Carbon dioxide laser with Ge Brewster windows equipped sealed gas discharge tube, comparing with NaCl and KBr windows

06 p0908 A71-18080

Germanium distribution coefficient in GaAs epitaxial crystals by radiotracer, mass spectrography and electron probe analysis noting total impurity concentration from Hall mobility

07 p1180 A71-20176

Multiple valued Sasaki effect concerning electron transitions in multivalley Ge semiconductors

07 p1181 A71-20537

Carbon dioxide laser Ge windows thermal runaway characteristics

08 p1302 A71-21391

High purity Ge crystals growth, studying Hall effect and resistivity for semiconductor detector fabrication

08 p1345 A71-21841

Gamma ray spectrometers made from high purity p-type Ge crystal, observing performance

08 p1345 A71-21843

Satellite-borne Ge radiation detectors, investigating design criteria and performance at elevated temperatures

08 p1267 A71-21847

Carrier concentration, radiation dose and temperature effects on radiation defect formation in Si and Ge during gamma irradiation

10 p1655 A71-24138

Formation kinetics of radiation defects produced by gamma rays in Sb doped n-type Ge single crystals at 77 K

10 p1656 A71-24142

N-type germanium Seitz coefficients relationship based on anisotropic electron scattering theory

13 p2110 A71-27958

Gallium antimonide-germanium system solid solution lattice constant determination, using X ray and

microstructural analysis and microhardness measurements 17 p2791 A71-34566

Heavily Ge doped p-InSb photoelectric and electric properties, showing impurity concentration effects 19 p3120 A71-38526

Thin dielectric films on germanium substrates, using oxygen diffusion through silicon dioxide 20 p3205 A71-39435

Stress-strain curves of dual slip orientation in Ge single crystals deformed in compression, using interference, optical and electron microscopy 21 p3397 A71-40457

Surface acoustic waves in layered substructure of piezoelectric epitaxial film of cadmium sulfide on germanium substrate 21 p3429 A71-41208

Crystal dislocations and impurity atmospheres role in kinetics of accumulation of radiation defects in Ge under fast electron bombardment 21 p3429 A71-41209

Ge and Si point contact semiconductor diodes anisotropic deformation, investigating pressure effects on current and negative resistance in forward branch of I-V characteristics 21 p3430 A71-41222

Pure and doped Ge dumbbell p and n type samples at liquid helium temperatures, investigating electric breakdown 21 p3430 A71-41224

Monte Carlo method computer simulation for displacement cascades energy and space structure in Ge, Si and PbS, interpreting semiconductor electrical properties under hard radiation 21 p3432 A71-41304

Photocurrent for two stage transition in space charge layer in p-n junctions of germanium with radiation defects 21 p3435 A71-41333

Solid and liquid Ge thermal conductivity measurement at high temperatures by coaxial cylinder and flat layer methods 21 p3435 A71-41334

Photoelectric properties of gold doped germanium semiconductor structures, investigating long wavelength background illumination effect on nonequilibrium conductivity 21 p3435 A71-41336

Cubic nonlinearity in p-type germanium semiconductor in constant magnetic field 21 p3435 A71-41337

Germanium single crystal surface conductivity, observing carbon monoxide adsorption effects at various pressures 21 p3435 A71-41341

N-type germanium Seitz coefficients relationship based on anisotropic electron scattering theory 21 p3436 A71-41347

Electron transitions between excited states of donors in Ge, investigating photoconductivity in 500-1300 micron band 22 p3585 A71-41817

Microwave biased germanium IR photoconductive detector for optical communication systems, describing operation principles, signal demodulation and performance 22 p3543 A71-42123

Spherical avalanche diodes in silicon and silicon-germanium mixed crystals, describing IR detection properties 22 p3543 A71-42125

P-type germanium photon drag detectors with carbon dioxide lasers, discussing response speed and sensitivity 22 p3543 A71-42129

Experimental observation of 10.6 micron guided waves in Ge thin films, noting application to carbon dioxide laser communication 22 p3587 A71-42568

Neutron bombardment effect on dislocation mobility in Ge single crystals investigated by bending and etching techniques 23 p3715 A71-43309

Germanium extrinsic photoconductive IR detectors with Au, Hg and Cu doping, discussing preparation and electrical and optical characteristics 24 p3860 A71-45070

GERMANIUM ALLOYS

PbTe-GeTe-PbSe solid solution alloyed by lead chloride, investigating structure, composition and distribution of basic elements 15 p2460 A71-31283

Performance tests of high temperature silicon-germanium alloy thermoelectric generator for outer planet mission spacecraft 20 p3264 A71-38928

Protective xenon atmospheres in sealed silicon-germanium alloy thermoelectric generators, discussing leakage and pressure levels 20 p3265 A71-38934

Mn-Ge solid solutions coercive force and magnetization, investigating temperature dependence and heat treatment effects 21 p3432 A71-41264

GERMANIUM COMPOUNDS

NT GERMANIDES

Switching effects in diode structure formed by two tungsten point contacts on glassy cadmium germanium arsenide surface 21 p3358 A71-41207

GeTe alloyed with Zn, Cd or Hg, measuring electrical conductivity and thermoelectric power temperature dependence 21 p3435 A71-41345

N-type cadmium germanium arsenide single crystal semiconductor electron and hole effective mass determination from thermoelectric power measurement 21 p3436 A71-41350

GERMANIUM DIODES

High Q microwave diodes on n-type germanium using carrier counterdiffusion in reducing atmosphere 06 p0873 A71-17539

Ge diodes double injection experiments, measuring I-V characteristics, AC small signal admittance and noise 06 p0876 A71-18037

Annealing and white light illumination effect on I-V characteristics of long Ge diodes irradiated by 5 MeV electrons at 77 K 10 p1583 A71-24144

Schottky barrier, point contact and Ge back diodes for microwave mixers and detectors, noting burnout characteristics 18 p2894 A71-36979

Noise, admittance and I-V characteristics of hot holes in space charge limited Ge diodes at high voltage and frequencies to 22 MHz 19 p3029 A71-38141

Li-drifted Ge p-n diode for low noise IR detectors, describing spectral sensitivity and NEP value 22 p3543 A71-42127

Low frequency phase method application to fast electron processes and characteristic relaxation times in quick response Ge and Si junction diodes 23 p3650 A71-43307

GERMANIUM RECTIFIERS

U GERMANIUM DIODES

GERMANY

German space radio monitoring service, describing facilities for receiving and evaluating 20 MHz to 1 GHz transmissions 09 p1407 A71-23046

West German parachute research, discussing stretching/filling shock, fabric material properties and static stability 15 p2350 A71-32373

GERMICIDES

U BACTERICIDES

GERMINATION

Neurospora germination and growth in medium of low water activity due to NaCl or nonelectrolyte addition 11 p1721 A71-26146

Stearothermophilus spore germination stimulation, investigating effects of preheating and amino acid and carbohydrate concentration 13 p2010 A71-28695

Hawaiian silversword seed germination and inhibition showing extraordinary heat sensitivity 16 p2527 A71-33049

GESTALT THEORY

Gestalt psychology perceptual organization, analyzing contextual background and residual stimuli, interaction concepts, configurational principles and organismic factors 07 p1042 A71-19696

GHOSTS

Ghost images due to reflection between interference filters and Fabry-Perot etalons during measurement of radial velocities 04 p0593 A71-14911

GIACOBINI-ZINNER COMET

Periodic comets Giacobini-Zinner and Borrelly motions, determining orbits with nonNewtonian motion equations and three orthogonal nongravitational terms 08 p1358 A71-20877

GIANT STARS

Quark regions in massive stars internal structure, discussing plasma superconductivity and spectral line emission 01 p0160 A71-11112

Mira Ceti type long period variable giant stars emission spectra, emphasizing UVB photometry and IR electrophotometry 03 p0486 A71-13267

MHD parameters in photospheric plasmas of giant and dwarf stars, noting electric conductivity, Joule dissipation, Reynold and Lundquist numbers 03 p0490 A71-13938

Red giant star s-process and subsequent delayed electron capture, accounting for large Li abundances 07 p1198 A71-19822

G5-K5 stars 3600-4000 A region, determining forbidden Fe/H lines for G8-K3 giants 07 p1201 A71-20436

Population II red giant stars evolution models, investigating relativistic degeneracy, neutrino losses core critical mass and helium flash 08 p1359 A71-20940

Massive stars evolutionary models, exploring convective instability effects 11 p1818 A71-25205

K giants, subgiants, M67 and NGC 188 abundances, noting high metallicities 13 p2136 A71-28431

Super metal rich K giant stars atmospheric model, obtaining abundances and turbulent velocity parameter 14 p2305 A71-29674

Hydrogen burning supermassive stars hydrostatic equilibrium models from numerical integration of stellar structure equations 15 p2485 A71-31718

Stellar evolution, discussing semiconvective regions, mass loss, red giants and supergiants, He flash structures and globular clusters 18 p2967 A71-36999

Differential line shifts in spectrum of supergiant beta Ori attributed to radial spreading of stellar atmosphere 20 p3290 A71-39302

Spectrophotometric observations of asymptotic giant and red giant branch stars in metal weak globular clusters 21 p3440 A71-40063

G and K giant stars iron abundances from narrow band indices, using spectrophotometer, red-IR colors and independent luminosity estimates 21 p3444 A71-40240

Massive main sequence stars in rapid differential rotation, investigating structure, energy transport, luminosity and circulation time scale 21 p3444 A71-40241

Galaxy active nucleus and quasar fragmentation based on model of rotating supermassive star releasing thermal radiation 21 p3449 A71-40610

Massive main sequence stars pulsation kinetics, examining amplitude growth, time scale ratios and evolutionary stabilization 22 p3596 A71-41447

Structure and stability of rapidly uniformly rotating supermassive star, using post-Newtonian hydrodynamic equations and standard model 22 p3604 A71-42328

GIBBS FREE ENERGY

Thermodynamical properties computation for binary mixture in equilibrium at constant pressure and temperature based on Gibbs free energy 11 p1851 A71-26380

Thermodynamic properties of dilute solutions of oxygen in liquid Fe-Co and Fe-Ni binary mixtures, obtaining Gibbs energy variation with temperature 15 p2432 A71-32174

Viscoelastic materials property inequalities as consequence of Gibbs free energy minimum, disproving interpretation as indication of second order phase transition 20 p3310 A71-39867

GIMBALLESS INERTIAL NAVIGATION

Gimballess inertial navigation system, discussing initial alignment by strap-down system at standstill 11 p1796 A71-26416

Strapdown or gimbaled inertial measurement units for space shuttle program, considering reliability, redundancy and cost of ownership 17 p2772 A71-35059

GIMBALS

Astatic gyroscope with gimbal system on rocking base, discussing effects of Cardan joint adjustment to insensitivity zone on instrument drift 01 p0080 A71-10631

Gimbaled reaction boom attitude control systems for gravity gradient stabilization of earth-pointing satellites, investigating performance by dynamic model simulation 01 p0165 A71-11585

Unwanted gimbal rotation friction torques in gyro wheel bearings due to lubrication viscous friction, ball wedging and contamination 02 p0253 A71-12459

Three axis long life satellite attitude control, describing double gimbaled reaction wheel system 04 p0663 A71-15299

Forced resonant vibration in nonlinear gyroscope in gimbal suspension 05 p0751 A71-16587

Gyroscope in gimbal system with elastic rotor bearings, determining dynamic stability in Newtonian central force field 06 p0899 A71-17929

Heavy gyroscope motion in gimbal suspension for arbitrary housing gravity center, showing steady solutions with respect to nutation angle 08 p1294 A71-21870

Forced rotation influence of gimbal suspension on astatic gyroscope motion with respect to inertial coordinates, demonstrating pseudoregular precession 09 p1451 A71-23172

Gyroscopic drift in gimbal suspension on moving base in presence of friction force proportional to dynamic reactions 10 p1612 A71-24578

Three degrees of freedom gyrocompass with common drive and gimbal bearing, exhibiting westerly deviation from drive axis

11 p1763 A71-26188

Gimbal suspended gyrocompass in elastically damped frame with dynamically unbalanced rotor, noting oscillations and drifts

13 p2065 A71-27945

Disk rotating in gimbal system, describing gyroscopic moments and precession

13 p2068 A71-28632

Liapunov stability of gyroscopic stabilizers as electromechanical systems, assuming nonrigidity of rotor, gimbal and platform suspension

13 p2069 A71-28726

Weak damping of free gyro motion in static coordinate system under dry friction in gimbal joint, deriving equations of motion by Lagrange method

13 p2069 A71-28932

Stabilization of solid body orientation with twin gyros under slave engine drive, producing control moments to gimbal axis

13 p2145 A71-28935

Systematic drift of astatic gyroscope in gimbal suspension during rundown

13 p2070 A71-29076

Algorithm providing three-gimbal inertial system all-attitude capability by protecting against gimbal lock

14 p2272 A71-30802

High speed spin effect on amplified or damped nutations in low friction rotary gyroscopes mounted on gimbals

15 p2401 A71-31178

Space shuttle guidance, evaluating performance of strapdown and gimbaled systems by nominal and abort trajectories

17 p2773 A71-35061

Asymptotic solution to nonlinear motion of heavy gyro in gimbal suspension, noting convergence within finite time interval

17 p2746 A71-35066

Lightweight precision gimbal design for spaceborne star tracker with arc-second accuracy for stellar updated inertial system independent of spacecraft stabilization

19 p3062 A71-37204

Heavy gyrocompass motion in gimbal suspension for arbitrary housing gravity center, showing steady solutions with respect to nutation angle

20 p3238 A71-39369

Computerized step-jump and time-transient dynamic analysis application to gimbal mounted Rayleigh-step gas-lubricated thrust bearing design

22 p3552 A71-41672

Gyrocompass in gyropendulum stabilized Cardan suspension, deriving system undamped oscillations equations

24 p3847 A71-44415

Precession rate of balanced gyrocompass in Cardan suspension with elastic gimbal couplings

24 p3826 A71-44833

Kinematic method for deriving formula for gimbal error of directional gyroscope with allowance for main axis inclination to horizontal plane

24 p3828 A71-45157

GIRDERS

Symmetric three-layer girder with contact deformations and transverse compression of filler, calculating vibration under elastic impact by numerical analysis

09 p1538 A71-22522

Girder system transverse bending under axial and lateral loads, deriving stability conditions by direct Liapunov method

13 p2153 A71-28519

GLANDS [ANATOMY]

NT ADRENAL GLAND
NT ENDOCRINE GLANDS
NT PANCREAS
NT PINEAL GLAND
NT PITUITARY GLAND
NT THYROID GLAND

Prenatal exposure to hypoxia, showing prolonged suppression of labeled amino acid incorporation into developing submandibular gland and pancreas in neonatal period

07 p1042 A71-19698

Human sweat gland duct filling and skin epidermal hydration behavior by analysis of time delays between sweat emergence and steady state, using electrical stimulation

18 p2858 A71-36865

GLANDS [SEALS]

Material, design and operating principles of rotary seals used in gas ducts, bearing elements and fuel systems of aircraft gas turbine engines

19 p3069 A71-38015

GLARE

Aircraft compartment glare minimization for flight crew visibility conditions and visual performance improvement

01 p0004 A71-10028

Monochromatic light glare effect on human eye as function of wavelength, using visual threshold variation as criterion

01 p0016 A71-11389

Lunar transients in Aristarchus region with respect to tidal, sunrise, illumination, magnetic tail, bow shock and solar activity hypotheses

15 p2492 A71-32479

GLASS

NT BOROSILICATE GLASS
NT GLASS FIBERS
NT S GLASS
NT SILICA GLASS

Sandwich structure cores of foamglass granulate filled unsaturated polyester paste, discussing development of highly thixotropic paste mixtures

01 p0172 A71-10699

Glass properties and applications, discussing strengthening, surface etching and structure modification

01 p0109 A71-11432

Surface destruction of glass dielectric by pulsed laser beam, considering plasma clouds, shock waves, ablation and crack formation

02 p0258 A71-11640

Glass substrates for thin film circuits compared to other materials for properties and suitability, emphasizing surface properties

02 p0230 A71-11816

Nd glass laser radiation time and spectral structure

03 p0437 A71-13885

Heated glass free jet characteristics at low Reynolds numbers, evaluating temperature distribution and two dimensional fluid dynamic effects

[ASME PAPER 70-WA/FE-3] 03 p0521 A71-14125

Metal and glass composites with similar residual stress states under axial loading, examining yielding and fracture behavior

03 p0443 A71-14186

Glass ceramics manufacture, chemical composition and properties, and applications

03 p0448 A71-14352

Thermal expansion of dilute binary composites concerning ceramic-glass, glass-metal, metal-metal and organic-metal systems

03 p0449 A71-14458

Glass laser types, properties and applications, noting welding and cutting, plasma generation, controlled thermonuclear reactions, neutron generation, intense short duration X ray fields, etc

04 p0605 A71-14709

Glass and glass ceramics for large astronomical telescopes, examining fabrication, absorption coefficient and applications

04 p0617 A71-14865

Lunar glasses of impact origin, considering occurrence, abundance, optical properties and chemical composition for determination of regolith bulk, age and origin

04 p0644 A71-15130

Hydrogen impregnated glass covers of solar cells preventing irradiation caused darkening and loss of power output under space environment conditions

05 p0700 A71-16066

Si solar cell cover glass assembly and packaging improvements using Teflon

05 p0702 A71-16079

Glass lasers characteristics and applications, discussing material compositions, ion imbeddings and manufacturing techniques

05 p0761 A71-16327

Molten glass inclusion and stress concentrator/empty hole/ effects on Arco iron electrode potential

05 p0766 A71-16384

Neodymium glass lasers, investigating pump-induced birefringence effect on polarization and radiation distribution

06 p0907 A71-17398

Neodymium glass solid state laser transverse mode locking and capture due to active medium nonlinear properties

06 p0907 A71-17400

Nd glass traveling wave laser single frequency emission luminescence stability as function of pumping power, using dispersive ring resonator

07 p1122 A71-19136

Giant pulse amplification in Nd ion doped glass analysis using model, taking into account sublevels and multiplicity

07 p1127 A71-20387

Mode locked Nd-glass laser, describing dispersion and Kerr effects on pulse frequency modulation

08 p1301 A71-21125

Stress profiles measurement in opaque tempered glass and ion exchanged glass-ceramic flat plates from length change during etching

09 p1480 A71-22115

Interfacial bonding effect on fracture toughness of glass sphere filled epoxy and polyester resins, using tapered cleavage specimen

11 p1846 A71-25413

Book on glass lasers covering absorption and fluorescence of glasses, glass structure, energy transfer, nonradiative transitions, quenching, etc

11 p1772 A71-25450

Ovonic systems involving electrothermal switching effects on semiconductor glasses, discussing threshold voltage characteristics as function of temperature distribution and glass thickness

12 p1944 A71-27638

Glazed lunar rocks, explaining origin as result of nearby meteoritic impact

13 p2137 A71-28519

Steatites replicas electron microscopy for microstructure variations with composition and firing conditions differences, discussing protoenstatite crystallization and glass phase formation

13 p2093 A71-28666

Laser emission absorption in surface layer of optical glass, determining surface temperature dependence on emission energy density

13 p2079 A71-28859

Porous glass hyperfiltration membranes stabilization by aluminum chloride solution, noting retreatment need

13 p2026 A71-29377

Frequency composition in glass laser with Fabry-Perot resonator producing polarized radiation components, discussing transverse modes selection

15 p2420 A71-32000

Quartz, organic glass and plexiglass luminescence under giant pulse ruby laser radiation

15 p2422 A71-32462

Microhardness dependent saturation of glass powders by iron, nickel and titanium during sintering of cermet metal matrix materials in vacuum

16 p2601 A71-33573

Microcrater morphology in lunar soil glass, oligoclase and olivine, determining projectile velocity, impact angle and shape effects

18 p2961 A71-35947

Emission characteristics of neodymium glass laser with polymethylene dye passive shutters of finite relaxation time, investigating ultrashort pulse separation

18 p2929 A71-35983

Extruding complex structural shapes of Ti alloys, considering use of glass as lubricant

18 p2927 A71-36662

Large deformation stress and mechanical resistance of thin glass circular plates by bending test involving concentric rings

18 p2940 A71-36697

Diaplectic glass formation by experimental shock loading of orthoclase in porous mixtures

19 p3084 A71-37662

Scanning electron microscope and petrographic observations of glass particles from Apollo 12 lunar soil sample, revealing surface features and origin

19 p3137 A71-37674

Photochromic glass activation process for recording three dimensional holograms, using radiation with maximum spectral brightness coincidence with absorption band edge

19 p3064 A71-37772

Inorganic polymers and glasses at high temperatures, detecting LF internal friction

19 p3084 A71-38050

Checking method for reflection-type holographic system behavior, emphasizing critical stability of glass plate

20 p3236 A71-39194

Capacitive thermometry characteristics of dielectric crystallized titanate-containing glass ceramic at cryogenic temperatures

20 p3253 A71-39279

Viscoelastic materials with varying glass transitions, free and constrained layer damping and damping of LF vibrations in massive structure

21 p3405 A71-40296

Glass switching elements with storage properties for electronically controlled flip-flop circuitry, noting composition and fabrication

21 p3355 A71-40742

Mechanical and frictional properties of sintered copper matrix glass compacts, considering lubricating or seizure preventing effects of glass presence

21 p3406 A71-40759

Laser emission absorption in surface layer of optical glass, determining surface temperature dependence on emission energy density

21 p3394 A71-41297

Glass spheres formation on moon, suggesting mineral melt atomization in high speed gas stream

21 p3454 A71-41421

Mode locked Nd-glass laser transient effects, examining pulse width limitations by side band generation

22 p3556 A71-41801

Flatband voltage stabilization of metal-glass-oxide-silicon composites for phosphosilicate glass

22 p3587 A71-42532

Glass particles crystallization in sintered metal matrix glass materials, examining microcracks and temperature and cyclic heating effects

23 p3696 A71-43251

Neodymium glass laser emission kinetics controlled with positive and negative feedback by introducing nonlinear media into plane-parallel resonator with two positive lenses

23 p3684 A71-43418

Apollo 12 Mare Procellarum soil glasses analyzed by ion and electron microprobe, discussing rock ages

23 p3744 A71-43653

Lunar glassy objects and mineral grains surface microstructure by optical and scanning electron

microscopy, comparing with tektites and terrestrial volcanic analogs

23 p3745 A71-43664

Morphological, physical and chemical characteristics of basaltic and anorthositic glassy spheroids in Apollo 12 lunar fines

23 p3746 A71-43666

Gas-liquid chromatography and mass spectrometry of lunar fines and glass constitution by preparing trimethylsilyl derivatives of discrete silicate ions

23 p3746 A71-43668

Glass spherical particles formation mechanisms for lunar surface, discussing size limitation factors

23 p3757 A71-43753

Apollo 12 lunar glass spherules chemical composition, homogeneity, densities and thermal histories, using electron probe analysis

23 p3758 A71-43758

Pressure histories from densification and relaxation measurements on lunar glass and synthetic samples, investigating refractive index changes after annealing

23 p3758 A71-43760

Visible and near IR spectral reflectivity measurements of basalt separates, glass and anorthositic fragments from Apollo 12 mare samples

23 p3760 A71-43770

Physical characterization of Apollo 11 and 12 lunar fines and glasses by diffuse reflectance, Raman and X ray spectroscopy and thermally stimulated currents

23 p3760 A71-43773

Lunar glass spheres cratering origin hypothesis from target temperature effects on crater morphology in targets impacted by high velocity Al projectiles

23 p3765 A71-43808

Apollo 12 returned Surveyor 3 surface sampler examination for micrometeorite pits and soil, glassy spheres and other granular materials adhesion to paint

23 p3766 A71-43817

Strength and deformation characteristics of glass plastic under torsional and compressive shear loads, investigating temperature effects on elastic modulus

23 p3697 A71-44204

Temperature and frequency effects on permittivity and dielectric loss angle tangent in glasses and pyroceramics

24 p3859 A71-44379

Crack propagation kinetics in organic glass subjected to monotonically increasing tension perpendicular to crack plane, examining crack contour prior to spontaneous rupture

24 p3883 A71-44858

Glass rods loading tests after exposure to hydrogen, nitrogen and argon under high pressure, noting strength improvement by Ar impregnation

24 p3841 A71-44868

Surface electronic conductivity in oxide glasses for microchannel electron multipliers, noting heat treatment and chemical composition effects

24 p3862 A71-45327

Glass multichannel perforated plate manufacture technology, discussing drawing and hollow fiber techniques

24 p3832 A71-45335

GLASS COATINGS

Mechanical stability of self healing viscous glass layer in porous oxidation protection coating on Ni under high acceleration

02 p0272 A71-12945

Facility backscattered material effect on performance of glass-coated accelerator grids for Kaufman electron bombardment thrusters

06 p0947 A71-18598

Reflecting Au films deposition on glass substrates by evaporation in vacuo, discussing optical devices, reproduction and bonding improvements

11 p1809 A71-26431

IR filters and coatings, describing vacuum deposited layer properties of II/VI, heavy halide and V/VI glass compounds

22 p3544 A71-42135

GLASS ELECTRODES

Oxygen partial pressure measurements in myocardium of beating heart by miniature glass needle and surface electrodes

05 p0714 A71-16598

GLASS FIBERS

Glass fiber-epoxy resin composites shear strength, considering fiber length and interfacial bond effects

01 p0106 A71-10277

Fiberglass-reinforced plastics loading conditions effects on tensile strength, determining creep rupture strength from test data

01 p0107 A71-10413

Fiberglass reinforced plastics heavy duty structural parts quality control, discussing strength parameters, safety coefficients, testing methods, etc

01 p0088 A71-10689

Epoxy resin reinforcement by various fiberglass types, discussing effects of bond-enhancing agents, fatigue strength properties, etc

01 p0108 A71-10691

Glass fiber reinforced thermoplastics application possibilities and limitations, considering physical and mechanical properties

01 p0108 A71-10695

Glass fiber reinforced plastics strain properties under multiaxial loads, considering long and short time loading, temperature and environmental conditions

01 p0109 A71-10696

Glass fiber reinforced plastics stress and fracture analysis, using approximate and iterative methods for strength estimates and nonlinear stress-strain relationships

01 p0172 A71-10697

Glass fiber reinforced durometer and hard foam sandwich structures deformation characteristics under static loads, presenting theoretical and experimental results

01 p0172 A71-10700

Deformation and strength of pipes manufactured from oriented glass fiber reinforced plastics under axial tension

01 p0177 A71-11237

Fiberglass reinforced plastic materials in steady temperature fields, determining creep and load carrying capacity

02 p0272 A71-11753

Fiberglass reinforced plastic cylindrical shells, investigating rheological effects during heating and concentrated radial loads

02 p0324 A71-11754

Corrosion resistant fiberglass reinforced plastic fluid storage vessels, noting structural characteristics, fabrication techniques, etc

02 p0256 A71-12348

Glass reinforced polyester laminates under static and repeated loading, investigating resin flexibility effects on fatigue strength

02 p0274 A71-12479

Fire retardant glass reinforced polyester resins optimum formulation, examining burning properties, volatility, extinction time and flame propagation

02 p0274 A71-12483

Glass fiber reinforced plastics tensile strength under various continuous loading rates and elevated temperatures

02 p0275 A71-12667

Thin glass fibers relaxation characteristics, discussing shear modulus, internal friction and temperature effects

03 p0448 A71-13298

Thermal cycle stresses at interface of composite glass tape-epoxy casting resin cylinder, using strain gages

03 p0508 A71-13763

Glass textile materials strength during cooling under tensile, high rate tension and impact loads

05 p0771 A71-16362

Elastic and compression strength characteristics of fiberglass-reinforced plastics prepared by cold solidification

05 p0771 A71-16364

Orthotropic cylindrical shell stability under variable compression loads, considering glass fiber reinforced plastic tube

05 p0822 A71-16368

Low shear rigidity effect on stability of glass fiber reinforced plastic cylindrical shells under loads and elevated temperature

05 p0822 A71-16369

Elasticity and strength anisotropy changes of unidirectional fiberglass reinforced plastics during winding

05 p0759 A71-16372

Glass fiber reinforced plastic plates static tensile and low cycle fatigue tests under pulsating tension

05 p0772 A71-16739

Unidirectional glass-epoxy filament wound composite material fracture strength based on three dimensional stress components of fiber-containing plane

05 p0826 A71-16740

Fracture strength of helical wound glass-epoxy composite cylinder under axial tension, determining tensile strength

05 p0826 A71-16741

Tensile test equipment for fiberglass reinforced plastics strength measurement under shear

05 p0772 A71-16888

Injection molded thermoplastics with fiberglass reinforcement, examining mechanical properties and thermal and stress cracking resistance

05 p0773 A71-17123

Fiberglass-reinforced plastics with and without water content, studying ablation performance

06 p0915 A71-17681

Anisotropic fiberglass reinforced plastic shell stability under short term and prolonged loading, using geometrically nonlinear formulation and Galerkin method

06 p0994 A71-17825

ND and Yb ions stimulated emission from spirally wound glass fibers, comparing activator pumping energy peaks

07 p1122 A71-19135

Light attenuation and depolarization measurements on glass fibers in index matching oil

07 p1159 A71-19212

Glass fiber reinforced thermoplastics with increased room temperature mechanical properties, noting effect of heat, aging and chemical environment exposure

07 p1145 A71-19692

Fiberglass reinforced plastic strength and deformability under tension as function of loading rate and test temperature

07 p1145 A71-20466

Filament winding manufacturing methods using unidirectional glass reinforcements for design and fabrication of aircraft wing structure

07 p1120 A71-20546

Organofunctional silane interfacial coupling for high strength glass reinforced thermoplastics

08 p1318 A71-20695

Failure analysis of unidirectionally reinforced fiberglass composites due to winding, using critical stress distribution function

08 p1323 A71-21701

Specimen width effect on ultimate fiberglass tensile strength for specimens cut from tubes and oriented at certain angle to symmetry axes

09 p1482 A71-22504

Interlayer shear modulus relation to thermal conductivity coefficient in oriented glass fiber reinforced plastics

09 p1482 A71-22814

Filament winding geodesic characteristics of shells of revolution made of glass fiber reinforced plastics

09 p1482 A71-22815

Numerical analysis of winding and heat treatment effects on residual stress distribution in cylindrical glass fiber reinforced plastic products

09 p1482 A71-22816

Steady multifiber winding process conditions in compact glass fiber packing for glass fiber reinforced plastic tubes

09 p1482 A71-22817

Stress concentration near hole in transversely isotropic cylindrical and spherical shells made of oriented glass fiber reinforced plastics

09 p1539 A71-22820

Stability characteristics of glass fiber reinforced plastic orthotropic cylindrical shell with elastic filler under torsion

09 p1539 A71-22821

Residual stresses in ring shaped specimens of wound glass fiber plastic products, using radial cutting technique

09 p1482 A71-22822

Optimal design parameters in minimization of reinforcement elements weight in cylindrical glass fiber reinforced orthotropic plastic shells under axial compression

09 p1539 A71-22826

Thin glass fibers relaxation characteristics, discussing shear modulus, internal friction and temperature effects

09 p1483 A71-23271

Unidirectional fibrous composites brittle and ductile failures prediction under tension and torsion, comparing results with tests on glass-epoxy composites

10 p1686 A71-24017

High temperature honeycomb woven fiberglass reinforced polyimide resin, asbestos reinforced composites and high modulus graphite materials, discussing specific strength and stiffness

10 p1618 A71-24771

Short carbon and glass fiber reinforced composites, calculating modulus of elasticity from mathematical model

10 p1635 A71-24806

Hardened and glass reinforced epoxy resin mechanical properties after 180 day hold in water, acid and alkaline solutions

10 p1635 A71-24827

Fiber length, diameter, bundle size, glass content and sizing effects on fiberglass reinforced plastic systems flexural, tensile and impact strength

11 p1784 A71-25395

SVAM glass reinforced plastics production and properties, discussing drawing, coating and forming oriented laminate on drum

11 p1784 A71-25396

Longitudinal tensile strength of unidirectional fibrous glass/polymeric matrix composites under high loading rates

11 p1785 A71-25405

Carbon fiber reinforcement in carbon fiber/glass fiber mat sandwich beams increasing tensile and compressive strength

11 p1846 A71-25412

Fiberglass reinforced plastic rocket launcher tubes with internal helical rails to impart spin to missiles, discussing design, fabrication and testing

11 p1786 A71-25419

Papers on glass fiber reinforced plastics covering end products and design criteria

11 p1788 A71-25651

Glass fiber reinforced plastics aerospace applications covering radomes, dielectric panels, aircraft ducting, secondary structures, furnishings, mouldings and tooling

11 p1788 A71-25652

Glass fiber reinforced plastics reinforcement techniques, emphasizing E glass filament manufacture, properties, advantages and products

11 p1788 A71-25653

Plastics reinforcement by combining high plastic deformation and fracture resistances with stiffness, discussing ceramics, whiskers, carbon and glass fibers 11 p1788 A71-25654

Glass fiber reinforced plastics mechanical properties, strain-stress characteristics and anisotropy, deriving orthotropic laminates tensile stiffness under deformation 11 p1849 A71-25656

Glass fiber reinforced plastics, discussing adhesion, wetting and adsorption effects on chemical reactions in glass-resin interfaces 11 p1788 A71-25657

Glass fiber reinforced plastics fatigue tests, discussing closed loop hydraulic servomechanism equipment, testing methods and materials and mean stress effects 11 p1789 A71-25658

Thermal stability of cylindrical laminated fiberglass reinforced plastic shells, solving by linear shell stability theory 11 p1790 A71-26175

Elastic properties of bonded orthotropic layer plates, finding good agreement with fiberglass reinforced plastic laminates 11 p1851 A71-26199

Glass fiber rotor blades design with longitudinal pressure tapings for cascade wind tunnel and turbomachinery flow research applications 11 p1772 A71-26316

Load-deformation characteristics in tension, compression and bending of two thin cement laminates reinforced with short random glass fibers, discussing stiffness and residual strain 11 p1790 A71-26384

Unidirectional glass fiber epoxy composite material nonlinear viscoelastic behavior, using isothermal uniaxial creep and recovery tests with thermodynamic constitutive equations 11 p1851 A71-26385

Fracture toughness and critical strain rate measurements in unidirectional glass reinforced plastics as function of resin, hardener, fiber and degree of cure 11 p1790 A71-26387

Filament winding techniques for glass fiber reinforced plastics, discussing processes, configurations and materials for achieving optimum strength 12 p1920 A71-27011

Stiffness factor in reinforced thermoplastics mechanical properties as function of glass fiber content, working temperature and duration of loading 12 p1920 A71-27012

Fiberglass reinforced plastic structural elements heat induced deformation and carrying capacity due to material macroinhomogeneity and rigidities asymmetry 12 p1921 A71-27346

Perpendicularly woven fiberglass reinforced plastics stability, elasticity and viscoelasticity as function of temperature 12 p1921 A71-27347

Hand/machine sanded surfaces moderate environment exposure time effects on adhesive bonding of glass fiber reinforced plastic joints 12 p1921 A71-27411

Fiber reinforcements for structural composites, considering glass, polycrystals, vapor deposition, whiskers and metals 12 p1922 A71-27636

Fiberglass reinforced plastics under constant strain rate, deriving failure models as random process for microscopic crack propagation 13 p2148 A71-28115

Probability characteristics of glass/epoxy plastics mechanical properties, considering tangential and axial tensile and bending strength, modulus of elasticity, buckling and compression strength 13 p2092 A71-28653

Stability loss, critical load and wave numbers for smooth conical and cylindrical shells of fiberglass reinforced plastics under uniform axial compression 13 p2157 A71-29181

Aboveground liquid storage tanks design with fiberglass-reinforced composites based on pressure vessels requirements [DFVLR-SONDDR-93] 13 p2157 A71-29307

Stress-time superposition creep data for unfilled and coupled glass reinforced polypropylene at 23-80 C 14 p2264 A71-29835

Mechanical properties of fiberglass-epoxy cross-ply laminates, considering tensile strength, crack propagation and ultimate stress and strain 14 p2264 A71-29837

Soviet book on glass-reinforced plastic plates and shells covering engineering methods for anisotropic plates and shells stability and stress analysis 14 p2327 A71-30245

Geometrical parameters and load carrying capacity of fiberglass reinforced plastic composites with elastoplastic adhesive bonding, deriving relations for stress distribution 14 p2264 A71-30270

Fatigue strength of polyester laminates reinforced with glass cloth and mats 14 p2264 A71-30484

Fiberglass shift moduli based on twist tests, using ratio of deformations on adjacent faces 15 p2438 A71-31654

Sealing materials adhesion to fiberglass and metals based on rupturing force in loading tests 15 p2414 A71-31655

Epoxy and unsaturated polyester resin compounds for embedding glass fibers in fiberglass-reinforced plastics 15 p2439 A71-32737

Prestressing of two layer fiberglass-reinforced plastic cylindrical shell under internal pressure 16 p2657 A71-33410

Stress-strain diagrams for oriented fiberglass-reinforced plastic under tension, taking into account temperature and anisotropy effects 16 p2601 A71-33411

Polymer binder setting degree effect on maximum strength of fiberglass cross reinforced plastic, analyzing compressive, bending, hardness, impact, thermal and porosity properties 16 p2601 A71-33682

Glass fibers and rods from thallium-sodium ion exchanging, investigating flexibility, focusing and light conduction without distortion 16 p2588 A71-34120

Fatigue strength anisotropy in glass fiber materials with epoxy-phenol binders under symmetric and pulsed compression-tension cyclic loads 17 p2762 A71-34783

Filament wound glass-reinforced plastic struts for cryogenic tank supports in long term planetary missions, testing thermal and mechanical properties 17 p2762 A71-35205

Low thermal flux lightweight glass fiber composite tubing for cryogenic propulsion plumbing systems 17 p2762 A71-35206

Oriented glass fiber-plastics plates and shells design, noting zero moment stress shells and filament overwrapped metallic pressure vessels 17 p2830 A71-35315

Thin multilayer pressurized glass fiber-plastic cylindrical shells, calculating stress redistribution due to crack initiation and prestressing effects 17 p2830 A71-35319

Boron, carbon, sapphire and glass fiber composite materials, considering brittleness, anisotropic properties, filament winding and plastic and metallic matrices 18 p2939 A71-35915

Mechanical properties in glass fiber optics, measuring tensile strength and modulus, Poisson ratio and fatigue 18 p2939 A71-36074

Uniaxially aligned glass and carbon fiber reinforced nylon composites prepared from caprolactam by anionic polymerization 19 p3083 A71-37339

Polyamides reinforced with finely chopped glass fiber, noting mechanical strength, Martens yield temperature and heat stability 19 p3085 A71-38476

Glass-fiber/glass-bead/resin beam stiffness and strength improvement with sandwicheing between layers of unidirectional carbon fiber composite 21 p3405 A71-40597

Nondestructive test for fiberglass reinforced plastic tank, using percussion method 21 p3466 A71-40838

Fatigue properties of satin woven fiberglass reinforced plastic cloth under various stress directions 21 p3406 A71-40839

Glass fiber reinforced flame retardant thermoplastic resins, tabulating flammability resistance and mechanical properties 22 p3565 A71-42076

Weakly guiding glass fiber parameters design formulas and functions for optical communication, considering propagation constant, mode delay, cladding field depth and power distribution 22 p3576 A71-42557

Anisotropic glass fiber plastic material stress, strain and crack formation threshold measurements under long term static and cyclic axial loads 23 p3696 A71-43424

Glass fibers durability in air and vacuum conditions, showing stress concentration coefficients at various tensile stresses 23 p3697 A71-44031

GLAUBER THEORY

Glauber and Vainshtein approximations for cross sections of 1s-2p excitation during inelastic electron-atomic hydrogen scattering 20 p3272 A71-39470

Glauber approximations for elastic and inelastic scattering of protons by ground state hydrogen atoms, comparing with measurements 20 p3272 A71-39578

Glauber scattering amplitudes for atomic hydrogen excitation by electrons or protons, presenting closed form expressions requiring no numerical integration 21 p3420 A71-41195

GLAUCOMA

Spatial field of vision in healthy subjects and glaucoma patients, noting age effect 06 p0853 A71-17950

Intraocular pressure self regulating nervous system components, discussing fluctuation sensors, corneal centers to eye impulse conveyors and glaucoma diagnostic applications 11 p1716 A71-25655

GLAUERT COEFFICIENT

U AERODYNAMIC FORCES

U MACH NUMBER

GLIDE ANGLES

U GLIDE PATHS

GLIDE LANDINGS

NT HORIZONTAL SPACECRAFT LANDING

GLIDE PATHS

Maximum stagnation temperature on swept wing leading edge for equilibrium glide entry of space shuttle 07 p1013 A71-18181

Light aircraft spoilers to minimize landing run discussing spoiler/dive brake area effects on glide path angular control 10 p1555 A71-24222

[SAE PAPER 710387]

Aircraft approach and landing under low altitude wind shear conditions, discussing flying hazards and glide path correction procedures 11 p1708 A71-26334

Psychophysical evaluation of glide slope detection accuracy by diamond vs square shape in runway centerline stripping as aircraft landing aid 12 p1875 A71-27222

Quasi-stationary gliding trajectories of aircraft planetary atmosphere during constant control of attack and bank angles 13 p2143 A71-29181

GLIDE SLOPES

U GLIDE PATHS

GLIDERS

NT BOOSTGLIDE VEHICLES

NT FLEXIBLE WINGS

NT HYPERSONIC GLIDERS

NT PARAGLIDERS

NT PARAWINGS

Sailplane fatigue testing determining load spectra fail safe structures and damage calculation 02 p0324 A71-11949

Standard-Cirrus glider flight test performance, noting cockpit design and instrumentation 03 p0346 A71-13011

Trailing edge flap automatic control for glider performance improvement 03 p0346 A71-13021

Elfe S-3 glider flight test, pointing out imperfections in cockpit and wing design 05 p0696 A71-16121

Flight crews medicophysiological preparation for international glider competition 06 p0860 A71-18191

Human factors in glider accidents, discussing drug fatigue, oxygen lack, nervous tension, etc 06 p0860 A71-18191

Balloon and glider vertical speed indicators, considering barometric devices and electric variometer 06 p0901 A71-18244

Variable camber flap automatic control equipment for glider, considering combinations of mechanical and electronic approaches 06 p0847 A71-18251

Avionics for gliders and touring aircraft, considering safety and VHF radio equipment 08 p1261 A71-20681

Glider flight in thermal air currents, discussing aircraft behavior, pilot sensory perceptions and reaction and use of variometers for ascent rate determination 08 p1230 A71-20681

Flight testing of Diamant 18 glider, discussing aircraft behavior at low and high flight speed, stall, spin stability and control characteristics, design and construction 08 p1230 A71-20681

Avionics for gliders and touring aircraft, surveying available electronic equipment for 1971 08 p1294 A71-21761

Motorized glider equipped with Wankel engine for self powered takeoff, describing prototype design and flight test data 08 p1232 A71-21761

Glider flight mechanics for turning flight, discussing relationships between turning radius, flight speed, sink rate and aerodynamic characteristics 08 p1232 A71-21771

In-flight profile drag measurement of gliders with total and static pressure sensors in boundary layer wake, using moments method 09 p1384 A71-23661

Rigid towed and free flight glider, considering load and turbulent atmosphere effects 09 p1385 A71-23661

Sailplanes tail load static derivation for instantaneous unchecked longitudinal maneuver, considering aperiodic response 11 p1708 A71-26441

Sailplanes control, deriving incremental aerodynamic load on horizontal tail produced by instantaneous elevator deflection 11 p1708 A71-26441

Sailplane elevator induced maneuvering and horizontal tail surface loads, discussing airworthiness requirements 13 p1997 A71-29256

Wind tunnel tests of geometrically compatible airfoils for variable chord sailplane 13 p1994 A71-29257

Two dimensional wind tunnel tests on airfoil fastened between tunnel walls, investigating variable chord concept applicability in sailplane design 15 p2350 A71-32294

Book on fatal civil aircraft accidents medical and pathological investigation covering transport, light and glider aircraft case histories and statistics 23 p3638 A71-42910

High lift device application to high performance competition gliders, considering merit of design for conflicting climb/cruise requirements 23 p3627 A71-43089

Sailplane circling cross-country speed increase by variable geometry in high lift flap form for better compromise between cruise and climb performance 23 p3630 A71-44342

GLIDING

Gliding guided ribbon parachute for transonic speed deployment, investigating turn capability, opening reliability, structural integrity and effective drag 10 p1557 A71-24868

World championship gliding team medicophysiological problems during competition at Marfa, Texas, discussing climatic adaptation, nutrition, hypoxia and pilots general physical and psychomotor conditions 22 p3500 A71-41576

GLINT

Atmospheric high pressure axis determination from satellite photographed sea surface sunglint reflection patterns, using model calculations 05 p0778 A71-17045

Radar target direction variation /glint/ sensed by amplitude monopulse tracking antenna receiving nonuniform waves 14 p2214 A71-30807

Radar glint reduction by diversity techniques, indicating tracking improvement by error signal choice 19 p3022 A71-38587

GLOBAL TRACKING NETWORK

Satellite geodetic global networks employing triangulation, trilateration and height measurements, deriving dominant point observation stations /Hazay-Tarczy method/ 11 p1759 A71-25816

GLOBULES

Cometary nebulae and globules, discussing ionized and neutral gas densities, temperatures and morphological classifications 06 p0974 A71-18433

Cometary nebulae and globules, discussing ionized and neutral gas densities, temperatures and morphological classifications 12 p1955 A71-26583

GLOBULINS

NT GAMMA GLOBULIN

Comparative abdomen and head shield effect during gamma irradiation of dogs on protein fractions in blood serum, noting increased globulins and glutamate aspartate transferases 20 p3188 A71-39222

GLOMERULUS

Renal hemodynamic factors in whole kidney glomerulotubular balance in anesthetized dogs by manipulating filtration rate through constriction of aorta, thoracic vena cava, etc 16 p2529 A71-33194

Oxygen tension distribution in cats glomus caroticum under influence of varying arterial oxygen partial pressure, using platinum microelectrodes 24 p3796 A71-44562

GLOSSARIES

U DICTIONARIES

GLOTRAC [TRACKING NETWORK]

U GLOBAL TRACKING NETWORK

GLOW

U LUMINESCENCE

GLOW DISCHARGES

Glow discharge microphone for acoustic pressure detection and measurement at ultrasonic frequencies 02 p0232 A71-12140

Glow discharge cleaning for surface contaminants removal from hydrodynamic gas bearing components, discussing equipment application to thin film lubricant vapor deposition 02 p0256 A71-12461

Ionization wave varieties in nitrogen glow discharge at various pressures and current densities from phase and group velocity measurements 10 p1654 A71-24973

Steady state RF glow, abnormal glow and DC arc discharges in air at atmospheric pressure 12 p1881 A71-27274

Glow discharge, ion and excited state properties of laser plasmas, including CW conditions for argon 14 p2253 A71-29542

Thermal electrodeless plasma generation below RF range through magnetic induction heating, applying to argon glow and arc discharges 17 p2788 A71-34869

Inertialless glow discharge ignition in triotron controllable crossed field cold cathode tube, comparing with magnetic coil initiation 19 p3028 A71-37785

Acoustic pulse excited ionization waves and wakes measurement in glow discharge plasma, giving phenomenological explanation 21 p3421 A71-40089

Computerized tabular data display with cross-bar addressed glow discharge panel, discussing system details 21 p3350 A71-40115

Oscillations in He, Ne and Ar glow discharges, obtaining I-V characteristics 21 p3426 A71-41290

Plasma anodization of Si in positive column of DC oxygen glow discharge, considering silicon dioxide growth rate in negative glow, Faraday dark space and anode fall 22 p3581 A71-41809

Electrically excited gas dynamic CO laser using glow discharge in supersonic nozzle plenum 23 p3683 A71-42958

Plasma acceleration of low pressure toroidal gas discharge, measuring plasma velocity as function of radial magnetic field for different pressures 23 p3711 A71-43874

Molecular gas dissociation in constricted DC glow discharge plasma sac /sheath boundary/, discussing characteristics and potential uses 23 p3712 A71-43931

Hollow cathode lasers based on negative glow discharge excitation including charge exchange ion-atom collisions and Penning excitation 23 p3686 A71-43955

GLUCOSE

Glucose reduction in human musculus vastus lateralis during bicycle exercise below pulse endurance limit, noting glucose infusion effect 01 p0016 A71-11400

Lower fasting blood glucose levels in high altitude acclimatization 02 p0197 A71-11664

Glucose intestinal absorption, blood glucose and hematocrit in hamsters, relating physiologic modifications to pregnancy 02 p0201 A71-12608

Combined glucose-sodium chloride solution consumption by rats during normal and food deprivation conditions 02 p0201 A71-12874

Arterial glucose and lactate levels and heart rate in human males during intermittent running, discussing anaerobic capacity and anoxidative glycolytic processes 05 p0708 A71-16619

Absorption and incorporation rates of C 14 glucose in rats under acute hypoxia 08 p1242 A71-21964

Heterotrophic growth in dim light of blue green alga Agmenellum quadruplicatum and Lyngbya lagerheimii with glucose as carbon source 09 p1402 A71-23472

Glucose and fructose extraction from formose sugar mixtures by enzymatic methods using hexokinase reaction 19 p3011 A71-37574

Heart rate variation during and after muscular exercise, discussing correlated measurements of rectal and mean skin temperatures, blood lactate, pyruvate and glucose 20 p3185 A71-38891

GLUCOSIDES

Human lens fluorescent pigment O-beta-D- glucoside of L-3-hydroxykynurenine, discussing preparation, electrophoresis and paper chromatograms 11 p1718 A71-25634

Ouabain insensitive effects of metabolism on ion and water content of red blood cells 17 p2681 A71-34943

GLUES

Vinoflex glue for Constantan strain gauges in low temperature tensometry, showing satisfactory recording at single and multiple loadings 07 p1116 A71-20481

GLUTAMATES

Glycine conversion into serine, aspartate and glutamate in cerebrum under normal and hypoxia conditions 09 p1391 A71-22482

Comparative abdomen and head shield effect during gamma irradiation of dogs on protein fractions in blood serum, noting increased globulins and glutamate aspartate transferases 20 p3188 A71-39222

GLUTAMIC ACID

Physical training effects on human plasma glutamic-oxalacetic transaminase, creatine phosphokinase and lactic dehydrogenase enzyme levels 17 p2683 A71-35143

GLUTAMINE

Glutaminase isoenzyme activators in mitochondrial brain fractions of rabbits 03 p0361 A71-13235

Cytocidal effect of L-glutaminase distribution in leukemic lymphocytes by slide chamber method 18 p2864 A71-35994

Amino acid levels in fasted and fed rats plasma, liver, muscle and kidney during and after exercise, noting glutamine decrease in liver tissue 20 p3186 A71-38982

GLYCERIDES

Erythrocytes diposphoglycerate increase mechanisms during hypoxia and anemia, studying hemoglobin oxygenation state effects 17 p2685 A71-35368

Prolonged strenuous physical exercise effect on triglycerides, phospholipids and glycogen concentration in human femoral muscle 18 p2856 A71-36238

Glycerides metabolism in rats brain under normal conditions and during hypoxia, showing diglycerides role in triglycerides and phospholipids biosynthesis 21 p3337 A71-41056

GLYCERINS

U GLYCEROLS

GLYCEROLS

Free jet expansion of liquid-gas bubble mixture suspended in glycerine 17 p2728 A71-34891

NaI-glycerol solution resistivity values, determining measurement frequency, temperature, outgas procedures, purity and doping level effects 24 p3802 A71-44614

GLYCINE

Glycine conversion into serine, aspartate and glutamate in cerebrum under normal and hypoxia conditions 09 p1391 A71-22482

Peptides formation from glycine in presence of trimetaphosphate, investigating mechanism 21 p3345 A71-40175

GLYCOGENS

African lungfish retina electron microscopy for Landolt club location, mitochondria, glycogen and microtubule content, considering relation to receptors and possible functions 01 p0009 A71-10272

C 14 incorporation from labeled glucose into cerebral glycogen of normal and X ray irradiated rats 01 p0011 A71-10850

Glycogen reduction in human musculus vastus lateralis during bicycle exercise below pulse endurance limit, noting glucose infusion effect 01 p0016 A71-11400

Myocardial glycogen stores increase protective role in rat cardiac anoxia studied in isolated perfused heart 03 p0363 A71-13489

Glucocorticoid metabolite excretion with urine in healthy people as function of age and sex 06 p0858 A71-18727

Muscle adenosine triphosphate, creatine phosphate, adenosine diphosphate, glycogen, and lactate concentrations during intermittent exercise 15 p2358 A71-31726

Normal muscle lactate concentration after prolonged exercise resulting in decrease in glycogen content 15 p2359 A71-31727

Prolonged strenuous physical exercise effect on triglycerides, phospholipids and glycogen concentration in human femoral muscle 18 p2856 A71-36238

High muscle glycogen content effect on human performance in prolonged heavy physical exercise 19 p3009 A71-38554

GLYCOLS

Para-aminopropiophenone and propylene glycol radiation protective effect on hematopoietic stem cells of mice 07 p1036 A71-18959

GLYCOLYSIS

Radioprotective drugs relationship to modification of glycolysis in Ehrlich ascites tumor cells 07 p1035 A71-18954

Rats hypoxia tolerance, noting smoke effects on survival, respiratory rate, body temperature and glycolytic parameters 09 p1396 A71-23364

Cerebrospinal fluid changes due to isocarbic hypoxia, discussing electrochemical potential, lactate concentration and anaerobic glycolysis 11 p1722 A71-26360

Human erythrocyte 2, 3-diphosphoglycerate concentration elevation effects on glycolytic metabolism and intracellular pH 16 p2533 A71-34090

GLYCOSIDES

U GLUCOSIDES

GNEISS

Rochechouart meteorite impact structure located in granites and gneisses of Hercynian age in south-central France 19 p3049 A71-37655

GOALS

GOALS

Experimental plan group characteristics, describing main goals, construction methods, mathematical models and data analysis procedures

12 p1988 A71-26706

Low speed aerodynamics, detailing relevance tree technological forecasting method of Canadian science council national goals list

22 p3481 A71-42766

GODDARD EXPERIMENT PACKAGE TELESCOPE U PARTICLE TELESCOPES GOLAY DETECTOR CELLS

Submillimeter wave region solar radiation atmospheric absorption by Fourier spectrometry and double output Michelson interferometer with Golay cell detectors

14 p2307 A71-29740

GOLD

Calorimetric measurements determining total hemispheric emittance of thin gold films as function of temperature, demonstrating film thickness effect [AIAA PAPER 70-63]

03 p0522 A71-14456

Gold and Aquadag contacts with single crystal nickel oxide surfaces, determining I-V characteristics

04 p0637 A71-15588

Epitaxial deposition of Au on ultrahigh vacuum cleaved mica during early nucleation and growth

14 p2284 A71-30072

Platinum, palladium and gold detection in silver assay buttons by atomic absorption spectrophotometry

15 p2367 A71-31649

Thin gold films strain distribution determination from X ray diffraction peaks, noting elasticity theory

20 p3276 A71-39012

Spatially periodic inhibition of gold vapor condensation by intense optical standing wave using Q switched laser radiation

20 p3245 A71-39403

Laser beam ionization of gold investigated by proportional electron counter

21 p3392 A71-40516

Au-n-GaAs surface barrier diode space charge layer strong electric field effects on photoconductivity quantum efficiency

21 p3432 A71-41302

Electrical properties and electroluminescence measurements for p-n junctions in Au- and Ag-doped GaP, noting negative resistance in I-V characteristics

21 p3433 A71-41312

Au diffusion parameters in CdS determined under Cd and sulfur vapor atmospheres at 540-1000 C, explaining profile difference by dissociative mechanism

21 p3433 A71-41315

Photoelectric properties of gold doped germanium semiconductor structures, investigating long wavelength background illumination effect on nonequilibrium conductivity

21 p3435 A71-41336

Gold doping effect on minority carrier lifetime and other electrical properties of epitaxial Si transistors

22 p3520 A71-41702

GOLD ALLOYS

Au-Ba intermetallic compound electron work function temperature dependence

07 p1179 A71-19922

Thin film compound Au-Al intermetallic structure of CsCl type with lattice period of 3.140 plus or minus 0.003 A from electronographic measurement

12 p1917 A71-27308

Slip line deformation of ordered and disordered Cu-Au intermetallic single crystals from microstrain and electron micrographic studies

20 p3249 A71-38967

Brazing filler metals as cost effective replacement for Au-Ni in aircraft gas turbine engine component

21 p3387 A71-40621

GOLD COATINGS

Au plated contacts deterioration by pore corrosion, noting resistance relation to basis or underplated metals porosity

01 p0102 A71-10800

Plastic low emittance Au coating for spacecraft, controlling thickness via electron bombardment method

01 p0109 A71-11271

Gold plated Ge surfaces, investigating LEED patterns and electronic properties

04 p0636 A71-15016

Reflectance measurements of dielectric coating on metallic substrate, comparing with analytical model [AIAA PAPER 71-448]

11 p1799 A71-26233

Reflecting Au films deposition on glass substrates by evaporation in vacuo, discussing optical devices, reproduction and bonding improvements

11 p1809 A71-26431

Gold sliding electric contacts friction behavior, studying adsorbed gas lubrication in ultrahigh purity environments

12 p1912 A71-27637

Dry reed sealer transfer contact design, operation and embodiment, noting Au diffused and Rh contacts with hydrogen gas

13 p2038 A71-28838

Ga spreading over Ag and Au thin films surfaces from electronographic and optical experiments, noting volume heterodiffusion

20 p3276 A71-39153

Electron microscopic investigation of Au thin film deposits on Si single crystals in ultrahigh vacuum, noting semiconductor-like resistance/temperature behavior at liquid He temperatures

24 p3862 A71-45347

GOLD PLATE

U GOLD COATINGS

GONIOMETERS

NT PHOTOGONIOMETERS

Laser gyro goniometry for fluctuations and angular measurements at low rotational velocities, noting countup/countdown detection systems

02 p0262 A71-12924

Weissenberg rheogoniometer modifications, providing upper cone motion elimination, unsteady/steady state measurements in constant stress field and amplitude/frequency variations

11 p1763 A71-26058

GOSS [SUPPORT SYSTEM]

U GROUND OPERATIONAL SUPPORT SYSTEM

GOVERNMENT PROCUREMENT

Maintenance aids evaluation for government contracting and decision making, including cost model based on life cycle economics

16 p2552 A71-33311

GOVERNMENT/INDUSTRY RELATIONS

Noise pollution control and airport noise levels abatement regulation by state government, taking into account economic and technical feasibility

08 p1379 A71-21825

Federal legislation and regulatory activities for control and abatement of aircraft noise

08 p1379 A71-21827

State, local government and airport proprietor legal role in regulating aircraft noise at airports

08 p1379 A71-21828

Commercial spinoff from government sponsored R and D, considering productivity and industry benefits

14 p2342 A71-31133

Airport environmental protection, discussing area-wide agency, FAA planning grant program and legal aspects

15 p2385 A71-32247

French flight test center role in development and certification of Concorde aircraft, considering cooperation with industry

[AIAA PAPER 71-784]

17 p2675 A71-35526

V/STOL airworthiness certification, considering standards developed by FAA in cooperation with industry

[CASI PAPER 72/21]

19 p2997 A71-37607

Multinational consortiums of industrial firms from member states for ESRO satellite programs

23 p3786 A71-43463

GOVERNMENTS

NASC future active role, discussing advisory capacity to Executive Branch, problems handled and space programs

04 p0689 A71-14926

GRADIENTS

NT ELECTRON DENSITY PROFILES

NT POTENTIAL GRADIENTS

NT PRESSURE GRADIENTS

NT TEMPERATURE GRADIENTS

M-dimensional gradient extremal system under non-random and random noises of inertial control plant, using difference equation

01 p0064 A71-10922

Convex functions theory of rigid perfectly plastic structures, formulating strain rate and stress fields relation in subgradients

02 p0326 A71-12339

Wind gradient effect on flight characteristics during aircraft landing approach, particularly path deviation

11 p1706 A71-25194

Steepest gradient method for optimum structural design, using search for unconstrained maximum or minimum of function with many independent variables

13 p2147 A71-27789

Cosmic ray annual intensity variations indicating gradient perpendicular to solar equatorial plane

16 p2625 A71-32801

Gradient shape influence on connectivity in two phase graded structures, considering polyphase structure of filament reinforced composites

17 p2763 A71-35226

Gradient search procedures application for non-linear system unknown parameters identification from system dynamic response observations

[ASME PAPER 71-VIBR-50]

21 p3460 A71-40299

Zero sum differential game solution for aerial combat problem, applying direct gradient methods

23 p3699 A71-44103

GRADIOMETERS

U MAGNETOMETERS

GRADUATION

U CALIBRATING

GRAIN BOUNDARIES

Polycrystalline semiconductors Hall effect by grain structure model for low and high resistivity boundaries, giving vapor deposited cadmium selenide film data

01 p0137 A71-10228

Cu addition effects in solid solution on grain boundary sliding in Al at constant shear stress, considering accompanying crystal dislocations

01 p0102 A71-10739

Soviet book on crystallite boundaries in cast metals and alloys covering solute distribution, lattice imperfections, fracture mechanisms, etc

02 p0263 A71-11845

Triple point crack nucleation and growth at zero time by grain boundary sliding, estimating time to fracture

02 p0329 A71-12713

Creep failure model, using wedge crack nucleation in polycrystalline materials due to grain boundary sliding

02 p0329 A71-12716

W and thoriated W grain boundaries topography by trace analysis and field evaporation, observing curved surface with ledges, protrusions and serrations

02 p0266 A71-12737

Zr and zircaloy 2 fracture mode, examining grain boundaries and strain rate effects

02 p0268 A71-12887

Grain boundary sliding on Mg-Al alloy polycrystalline specimens measured at successive strains during creep under 2800 psi stress

03 p0443 A71-14184

High purity Mg deformation by remelting and rolling, investigating grain growth based on size measurement

03 p0445 A71-14341

Ultrafine grain metals strength properties at cryogenic temperatures and near melting point, discussing grain boundaries

03 p0446 A71-14487

Grain size refinement by alloy solute additions inhibition effect on growth and recrystallization, reducing boundary migration

03 p0446 A71-14489

Powder metallurgy for fine grain metals and alloys, discussing grain size-mechanical properties relationship

03 p0446 A71-14490

Steels prior austenite and martensite grain size control by thermal cycling

03 p0446 A71-14492

Ultrafine grain alloys ductility from tensile tests, discussing grain size, temperature and strain rate effects

03 p0446 A71-14493

Work hardening model for grain size effects on metals flow stress, discussing dislocation density as stress-strain function

03 p0447 A71-14494

Grain size effects on metal fatigue, considering work hardening and crack initiation and propagation

03 p0447 A71-14495

Intergranular failure modes in polycrystalline metals and alloys, discussing boundary sliding, cracking and structure

03 p0447 A71-14496

Crack growth relation to grain boundaries, considering transgranular cleavage in plain carbon steels and ductile intergranular fracture in Al-Zn alloy

03 p0447 A71-14497

Superplastic alloys fabrication and applications, discussing grain size and surface area roles

03 p0516 A71-14498

Ni maraging steels weld heat-affected zone, showing liquid grain boundary film formation due to titanium sulfide inclusions constitutional liquidation

04 p0603 A71-14921

Al alloys grain boundary precipitation pattern relationship to stress corrosion sensitivity

04 p0613 A71-15746

CdS thin film grain boundaries and stacking faults effects on electrical resistivity

05 p0791 A71-16055

Subgrain volume and orientation effects at tip of fatigue crack on propagation rate

05 p0821 A71-16348

Be impact strength temperature dependence and fracture structure, noting grain boundaries cohesion role

05 p0768 A71-16773

Polycrystalline semiconductors grain boundaries effect on conductivity, Hall mobility and current carriers concentration

06 p0942 A71-18187

Grain growth inhibition in niobium diboride by TiN addition

07 p1144 A71-19390

Austenitic stainless steel intergranular corrosion model for thermodynamic analysis leading to grain boundary diffusion and Cr concentration profiles determination

07 p1134 A71-19566

- Lattice defect and grain boundary influence on metal dissolution in electrolyte and stress corrosion cracking
07 p1134 A71-19604
- Microporosity morphology relationship to grain size and boundaries in alloys solidification and pores removal kinetics from castings by sintering
07 p1119 A71-19977
- Ternary Al-B-Ti system, investigating Al corner and B effect on grain refinement
07 p1138 A71-19981
- Maraging steels thermal embrittlement, discussing austenite grain boundaries inclusions, carbide networks precipitation and carbon concentration
08 p1305 A71-21027
- Grain boundary hardening in relation to electrical resistivity, magnetic permeability and yield stress in iron and Fe dilute alloys
08 p1309 A71-21529
- Bcc metals single and multilayer stacking faults, twin boundaries and screw dislocations observations, using central force atomic model
08 p1310 A71-21537
- Bubble raft model for atomic configurations in ordered grain boundary and grain boundary dislocation at high temperatures, discussing Al-Mg alloys
08 p1345 A71-21575
- Grain boundary sliding and shear deformation in bicrystal Al and Al-Co solid solutions
08 p1345 A71-21576
- Tilt boundary intersections during creep in Mo single crystals
08 p1315 A71-21577
- Ultrasonic effects on dislocations and grain boundaries in vacuum annealed polycrystalline Al specimens
09 p1467 A71-22288
- Granulometric composition effects on stainless steel powders bulk weight, friability and compactability, taking into account particle shape
09 p1470 A71-23062
- Phosphorus segregation to prior austenite grain boundaries in ferrite, considering effect on Ni-Cr-C-P steel temper embrittlement
09 p1471 A71-23123
- Strain hardening and grain size effects on early fatigue damage of polycrystalline metal under fluctuating stress, using micromechanics theory
10 p1685 A71-23933
- Coarse grained recrystallized Mo ductile brittle transition temperature due to dislocation substructure and grain boundary state, noting low temperature annealing and critical straining
10 p1629 A71-25029
- Crystal imperfections effect on MC carbide precipitation on coherent twin boundaries and regions close to grain boundaries in austenitic steels, using electron microscopy
11 p1780 A71-26027
- Metal carbide grain boundary precipitates effect on austenitic stainless steels high temperature fatigue fracture behavior
11 p1782 A71-26439
- Long duration high temperatures rated stress effects on Ti beta alloy IVT-1, correlating creep with beta granular boundaries migration
11 p1782 A71-26471
- Titanium nitride sintering in vacuum, noting strain by grain sliding to pore center under surface tension force effects
12 p1918 A71-27527
- Fracture under hot creep rupture, discussing grain boundary structure, high temperature region, creep deformation and recovery, void formation and intercrystalline failure
13 p2152 A71-28220
- Two stage creep cavity growth by grain boundary sliding as shear crack and Griffith-Orowan fracture, using energy balance argument
13 p2085 A71-28504
- Grain boundary precipitation in austenitic steels during creep deformation and ordinary aging treatment
13 p2086 A71-28623
- Tempered martensite and lower bainite in high purity carbon steels, discussing impact toughness due to internal twinning, grain boundary precipitation and carbide morphology
15 p2432 A71-32173
- Tensile stress and compressive effects on grain boundary precipitate morphology in Ni-base superalloy during creep
15 p2433 A71-32179
- Grain size effect on fatigue life during tension and compression tests of alpha brass, copper and aluminum, considering slip character
15 p2437 A71-32578
- Crystal structure defects of W samples containing small and large angle grain boundaries, using field ion emission microscopes
16 p2580 A71-33927
- Refining and hardening reactive additions effect on slow cooling grain boundary embrittlement response of maraging steel
17 p2756 A71-34490
- Elastic seismic waves attenuation in polycrystalline ceramics and rocks by grain boundary relaxation, noting strong frequency dependence of earth mantle internal friction
17 p2735 A71-35390
- Fe-Ni base alloy heat treatment for optimum high temperature stress-rupture properties, noting Ni-Nb/Ni-Ti intermetallics precipitation at grain boundaries
19 p3080 A71-37712
- Grain boundary dislocations generation and motion in deformed Nb steel in relation to sliding, using electron microscope analysis
21 p3395 A71-40021
- Field induced changes in W specimens during field ion microscope operation, considering behavior of dislocations and grain boundaries
21 p3395 A71-40024
- Inconel-600 under heat treatment and tension tests, examining grain boundaries slip interaction
21 p3397 A71-40458
- Lattice and grain boundary diffusion of Ce and Nd in Ni using radioactive tracer sectioning technique
21 p3398 A71-40468
- Grain scattering in unstable spin wave region of parametrically excited magnons in polycrystalline YIG
21 p3428 A71-41047
- Kossel line technique application to intergranular fragility study, discussing lattice constant measurement to determine difference in impurity distribution
22 p3563 A71-42324
- Computer programs based on least squares numerical analysis for complex internal friction spectra due to Snoek and grain boundary relaxation
23 p3648 A71-43927
- Grain boundary orientation effect on intergranular cracking, discussing crack introduction in purified iron by cathodic charging with hydrogen
23 p3695 A71-44285
- Aircraft parts damage by corrosive friction forces, hot gases and intercrystalline attack, noting worn universal joint and blade grain boundary damage
24 p3836 A71-44574
- Recrystallized metalceramic W plastic deformation effects on brittleness temperature threshold, revealing relationship to impurity segregations at grain boundaries
24 p3837 A71-44674
- GRAINS**
Square cross section rectangular rotating grains dynamic behavior in magnetic fields, obtaining orientation data with Monte Carlo method
15 p2498 A71-32772
- GRAINS [FOOD]**
Autotrophic cultivation of cereals with high photosynthetic activity under intensive illumination as biological components in life support systems
13 p2017 A71-28405
- Wheat seedling responses to chronic acceleration, considering total height, coleoptile diameter, root length, sensitivity to growth retardation and histological changes
21 p3341 A71-40001
- GRAMMARS**
Time-bounded grammars and languages capable of simulation by Turing acceptors in automata theory
20 p3202 A71-39050
- GRAND TOURS**
Space station and interplanetary flight research programs, discussing design, grand tour and Jupiter flyby
05 p0817 A71-16642
- Grand Tour mission design, discussing navigation, trajectory parameters, launch vehicles and satellite flybys
06 p0978 A71-18626
- PCM TV photographic data communication for grand tour of outer planets, emphasizing adaptive information-preserving data compression system for optimal performance
08 p1254 A71-21346
- Spacecraft computer centered data systems with standby redundancy, automated flexibility and LSI devices for grand tour mission
08 p1260 A71-21846
- Jupiter gravitational potential mapping for Grand Tours spacecraft, discussing Jovian satellites effect on orbit and trajectory perturbations
09 p1525 A71-23222
- High energy fast Grand Tour multiplanet flyby missions to outer planets omitting Jupiter, noting identical arrival date at Neptune
12 p1958 A71-26697
- Jupiter, Saturn, Uranus and Neptune space missions, discussing acceleration constraints, time, radio communication, navigation and control of grand tour spacecraft
13 p2141 A71-29085
- German book on models and constructions for interplanetary space flights covering Helios project, grand tour, Mars landing, planetary exploration, etc.
16 p2645 A71-33523
- Jupiter grand tour mission, discussing objectives and technical aspects of unmanned Pioneer F and G vehicle
18 p2965 A71-36684
- Outer planets Grand Tour spacecraft onboard optical guidance instruments, discussing vidicon and image dissector systems designs
19 p3098 A71-37186
- Grand Tour meteoroid environment analysis, considering different asteroid and cometary particle models
19 p3139 A71-37910
- Onboard approach guidance instrument for Grand Tour to outer planets missions reducing fuel for corrective maneuvers by estimating trajectories
19 p3101 A71-37914
- Magnetic field measurements on Outer Planets Grand Tour to yield solar system origin and evolution and interstellar medium data
19 p3139 A71-37918
- IR experiments planning for Outer Planets Grand Tour including investigations of planetary radiation balance and atmospheric composition and satellites composition and physical properties
19 p3011 A71-37920
- Mission analysis for multi-planet flyby and major satellites close encounter to determine solar system planetary evolution data, presenting Grand Tour trajectory parameters
19 p3139 A71-37922
- Grand Tour spacecraft configuration design involving system requirements, communications, power, guidance, etc.
19 p3152 A71-37924
- Multiplanet gravity assist grand tours in outer solar system, discussing launch opportunities and mission effects on spacecraft design
19 p3140 A71-37932
- Navigation, orbit and trajectory analysis of 1979 Jupiter-Uranus-Neptune Grand Tour mission, assuming deep space network tracking
19 p3101 A71-37936
- Outer planets Grand Tour X ray investigation of planetary magnetospheres to obtain flux and energy spectrum of electrons precipitated from Jovian magnetosphere
19 p3127 A71-37941
- Launch opportunities for Grand Tour outer planets missions using Saturn-Jupiter instead of Jupiter-Saturn flyby sequence
19 p3140 A71-37943
- Grand Tour missions centralized data handling, describing computer aided telemetry system and self testing and repairing control computer
19 p3025 A71-37954
- Planetary LF radio emission experiments on Grand Tours, discussing models and spectrum, polarization, position and time variation measurements
19 p3141 A71-37965
- Grand tour missions radioisotope thermoelectric generator power source, presenting optimization technique for hot thermocouple junction operation
20 p2644 A71-38932
- Outer planet explorers design for Grand Tour mission, discussing launch parameters, flight paths, environmental hazards, communications, ground control, navigation and power generation
22 p3601 A71-42028
- Radiation effects on components of science instruments used on outer planets Grand Tour mission
22 p3574 A71-42299
- Grand Tour interplanetary trajectories regularization, removing singularities in equations of motion of space vehicles
23 p3725 A71-42990
- Planetary quarantine constraint on 1977 Jupiter-Saturn-Pluto mission, determining fuel loading penalties, optimum biasing strategies and outer planet navigational characteristics
23 p3726 A71-42993
- Bi-injection earth departure mode analysis for combined flyby/orbiter Jupiter-Saturn-Pluto and Jupiter-Uranus-Neptune Grand Tour missions
23 p3726 A71-42996
- Grand Tour missions set optimization for 1976 to 1982, defining flight opportunity launch/arrival date space for various mission types
23 p3728 A71-43028
- Multiple outer planets flyby opportunities during 1976-1980 Grand Tour missions launch period, presenting computer generated specific encounter dates and flyby distances
23 p3729 A71-43029
- Asteroids flyby approaches during Jupiter missions and Grand Tours, obtaining gravitational deflection of spacecraft trajectories and mass cost estimates
23 p3729 A71-43030
- Monte Carlo simulation of navigation and guidance for Grand Tour Jupiter-Saturn-Uranus 1977 mission, using graphics computer program/STEP VI
23 p3701 A71-43044
- Grand Tour mission satellite planetary imaging analyses and science scan platform pointing requirements, utilizing computer graphic techniques
23 p3731 A71-43049
- Solar system escape trajectory analysis for Jupiter-Saturn-Pluto and Jupiter-Uranus-Neptune Grand Tour missions, presenting flyby characteristics and heliocentric postencounter directions
23 p3731 A71-43053

GRANITE

Midcourse and planetary approach guidance by on-board optical measurements, noting application to earth-Mars trajectories and Grand Tour missions [AAS PAPER 71-393] 23 p3702 A71-43061

Onboard optical tracking effectiveness for Grand Tour deep space navigation, considering star-planet angles, plane diameter angles and natural satellite observations [AAS PAPER 71-394] 23 p3732 A71-43062

GRANITE

Rochechouart meteorite impact structure located in granites and gneisses of Hercynian age in south-central France 19 p3049 A71-37655

GRANULAR MATERIALS

Sandwich structure cores of foamglass granulate filled unsaturated polyester paste, discussing development of highly thixotropic paste mixtures 01 p0172 A71-10699

Soft galactic X rays role in interstellar grains alignment 07 p1188 A71-20056

WC-Co system binder phase composition and properties, studying W content as function of initial carbide grain size, Co content, sintering and quenching time 09 p1466 A71-22170

Meteoritic graphite, silicon carbide and silicates to explain observed interstellar grains properties 10 p1675 A71-24471

Grain size effect on corrosion resistance and mechanical properties of Al alloy sheets between final annealing and quenching 15 p2434 A71-32329

Electrolytic production of metal powder in continuously operating facility, using vibrating cathodes with chambers filled with granulated anode metal 19 p3068 A71-37105

Exposing light and resulting density distribution and granularity in lower photographic emulsion layer, investigating modulation transfer function and power spectrum 22 p3538 A71-41733

Granular lithium hydroxide as carbon dioxide absorbent for closed cycle life support systems, considering porosity, carrier gas and water vapor pressure and bed temperature 22 p3508 A71-41773

Grainy composite material structural analysis, presenting statistical mathematical model 23 p3698 A71-44224

Heat generating granular layer tube, obtaining temperature distribution across cross section and boundary conditions 23 p3719 A71-44338

GRAPHIC ARTS

Man-machine graphics, discussing research in mass data reduction, production scheduling, speech synthesis, etc 03 p0372 A71-13500

Map preparation techniques and cartographic design for cost reduction and production speeding 08 p1280 A71-21247

GRAPHITE

NT PYROLYTIC GRAPHITE

High modulus graphite fiber composites, considering production, properties, utilization, availability and price/performance [SME PAPER EM-70-114] 01 p0109 A71-11251

Boron vs graphite fiber reinforced composites, noting design application role 01 p0104 A71-11280

Liquid Cs graphite integral reservoir effect on thermionic converter performance 02 p0196 A71-12271

Titanium carbide ingots production for laminar and flake precipitation of graphite, using electric arc furnace with consumable electrode 02 p0238 A71-12281

Thermal expansion of unidirectional, angle-ply and complex laminated graphite-epoxy composites, considering fiber orientation, hysteresis and interlayer stress relaxation 03 p0449 A71-14459

Thermal lattice expansion measurements on carbon powders up to graphitization temperatures, using X ray diffraction 04 p0618 A71-14960

Graphite/epoxy composite structural spacecraft panels, discussing design analysis and fabrication procedure 04 p0618 A71-15344

Computerized outgassing analyzer for nuclear rocket graphite fuel elements at various temperatures in vacuum 05 p0780 A71-16243

Single layer graphite oxidation kinetics evaluated by electron microscopy, discussing removal rate 06 p0915 A71-17302

Graphite fiber reinforced Al-Si alloy composite tensile strength and microstructure, observing tension failure modes 06 p0914 A71-18678

Field ionization yield with single graphite whisker lateral surface as ionizer, using helium, ammonia, carbon monoxide and carbon dioxide 07 p1164 A71-19855

Lightning protective coatings for boron and graphite fiber reinforced plastics 07 p1021 A71-19944

High intensity electric current damage in boron and graphite filament reinforced epoxy resin composites 07 p1145 A71-19945

Combustion kinetics of premixed laminar graphite dust-oxygen-nitrogen flames with/without hydrocarbon 08 p1346 A71-20866

Graphite fiber reinforced plastics adhesion and orientation effects on mechanical properties [PLASTICS INST. PAPER 27] 08 p1320 A71-20906

High performance graphitized carbon/carbon composites, discussing mechanical properties improvement by fiber content optimization and heat treatment [PLASTICS INST. PAPER 37] 08 p1321 A71-20910

High modulus graphite fiber reinforced composites tensile and compressive test methods and results [PLASTICS INST. PAPER 23] 08 p1321 A71-20913

Crack opening mechanism for high temperature creep of polycrystalline graphite 08 p1323 A71-21584

Elastic characteristics of graphite plastics and graphite materials impregnated with synthetic resins, considering aging effect on elastic modulus 09 p1483 A71-22824

Graphite fiber reinforced ablative composites fabricated into rocket propulsion test units for oxidative liquid high temperature and pressure environments 09 p1459 A71-23685

Graphite lubricants superconducting properties under high pressures and low temperatures, suggesting new superconductors developments and metal free electron model modification 10 p1656 A71-24299

Mass entrainment products effect on radiative and convective heat transfer during decomposition of graphite blunt body in steady hypersonic flow of radiating air 10 p1696 A71-24364

High temperature honeycomb woven fiberglass reinforced polyimide resin, asbestos reinforced composites and high modulus graphite materials, discussing specific strength and stiffness 10 p1618 A71-24771

Thornel graphite fibers modulus of elasticity, mechanical properties, applications and price 10 p1635 A71-24773

Transverse impact resistive graphite fiber reinforced plastic /GFRP/ lightweight sandwich panels and beam structures, using thin inner core facings 11 p1846 A71-25417

Prototype graphite fiber/plastic fuselage component design, test and performance prediction, using structural analysis methods 11 p1787 A71-25428

Composite materials fiber-matrix interfacial behavior, determining polymer concentration on graphite fibers surface by Raman spectroscopy and composite shear strength increase 11 p1787 A71-25430

Thermally stable polyimide graphite fiber reinforced composites from solutions of monomeric reactions, comparing amide acid prepolymers 11 p1788 A71-25560

Graphite fiber surfaces atomic composition data, using Auger electron spectroscopy in ultrahigh vacuum low energy electron diffraction system 11 p1788 A71-25633

Graphite heat shield ablation during low velocity low altitude portion of satellite reentry trajectories [AIAA PAPER 71-415] 11 p1857 A71-26208

Graphite ablation under high temperatures for large outer planets entry probes, correlating mass loss rates with surface temperatures and specimen nose cone radii [AIAA PAPER 71-418] 11 p1857 A71-26209

Graphite materials for nosetip/reentry applications, discussing isotactically pressed short fiber-pitch composites and binderless graphites, ablation data and NDT procedures [AIAA PAPER 71-417] 11 p1790 A71-26341

Graphite arc radiation temperature measurements with submillisecond resolution, using high speed photoelectric and photographic pyrometers 12 p1905 A71-26812

Air Force development programs with graphite reinforced composites, discussing matrix materials and cost and weight savings [ASME PAPER 71-DE-13] 12 p1921 A71-27323

Graphite-epoxy composite skins for commercial aircraft flight spoiler, discussing multiangle ply design and fabrication 12 p1921 A71-27413

Ti, B and graphite fiber composites application in aircraft design, discussing mechanical properties and market competition 12 p1918 A71-27600

Industrial polycrystalline graphites monochromator emissivity in visible and IR spectral regions at high temperatures 13 p2090 A71-27800

Interferometric studies of focused Nd laser radiation interaction with thin graphite absorbing surface layer, discussing time behavior of plasma expansion and density distribution 13 p2078 A71-28400

Turbulent submerged wall air jet on ablating graphite surface, examining friction and heat and mass exchange in boundary layer 13 p2160 A71-28500

Graphite epoxy composites fiber microstructure as surface condition, noting tensile fracture, crack propagation and brittleness 13 p2092 A71-28550

Al alloy matrix-graphite fiber reinforcement composites, discussing strength, temperature properties and processing techniques 13 p2092 A71-28600

Hybrid boron-graphite filaments in epoxy matrix composite, describing increased tensile strength and modulus of elasticity 14 p2261 A71-29630

Solid additives, graphite and molybdenum disulfide concentration effects on liquid lubricants and greases antiwear performance 14 p2251 A71-29820

Graphite fiber composite structures nondestructive testing, discussing liquid penetrants, X ray radiography sonic methods, acoustic emission and IR tests 15 p2414 A71-31810

Polyacrylonitrile and rayon precursor graphite fibers diameter relation to Young modulus and tensile strength 15 p2438 A71-31810

Carbide coating formation on graphite from vapor gas phase, calculating thermodynamics and kinetics by digital computer for comparison with experiment 15 p2438 A71-32140

Optimum temperature for Zr and Mo soldering of graphite materials with formation of carbide interlayer for ensuring maximum heat resistance 15 p2439 A71-32140

Boron and graphite fiber reinforced plastics machining, discussing tools, operating parameters and process limitations [SME PAPER MR-71-820] 15 p2416 A71-32420

Polycrystalline graphite total creep time dependent effects based on mathematical model of nonlinear hereditary theory 16 p2600 A71-32790

Specific heat measurement in magnetic field for graphite under neutron irradiation at low temperatures noting Schottky anomaly 16 p2600 A71-33370

Anisotropic carbon-graphite materials and metal temperature dependence of thermal expansion coefficients, noting approximation by Debye heat capacity function 16 p2601 A71-33710

High porosity carbon-graphite materials thermal and electrical conductivities at high temperatures by potentiometric method 17 p2761 A71-34200

High modulus graphite composites application for structural weight reduction and stiffness requirements without strength loss 17 p2762 A71-35200

High modulus graphite-boron composites design and application to lightweight structures, illustrating sandwich construction for race boat main boom stiffness and compressive strength 17 p2762 A71-35200

Graphite solubility in Co and Ni, discussing solution energies and entropies 19 p3081 A71-37720

Microfriction anisotropy of graphite at small load for sliding on basal and edge planes, using scanning electron microscope 20 p3253 A71-39410

Graphite properties in high and ultrahigh vacuum suggesting use as electrode material in vacuum gauges and residual gas analyzers 21 p3405 A71-40220

Carbon fibers grown on graphite by thermal decomposition of hydrocarbons, investigating external morphology and structure 21 p3406 A71-40830

Fibrous carbon structure determination by high resolution electron microscopy, establishing relationship between graphite planes and catalyst particle orientation 23 p3696 A71-43140

Zirconium carbide eutectic and supraeutectic alloy preparation with graphite addition, determining heat resistance under thermal cycling tests 23 p3697 A71-44020

Thermal and mechanical stresses concentration near peripheral notches on ring-shaped graphite, noting notch sensitivity relationship to tip curvature and graphite grain size

23 p3698 A71-44230

Niobium carbide film formation in pseudoliquidified layer on graphite at 3000 C in argon metal vapor mixtures with/without hydrogen

23 p3696 A71-44317

Limiting chemical reaction rate of graphite and carbon containing material combustion at high temperatures

24 p3890 A71-45108

GRAPHITIZATION

Tensile, shear, bulk density and electrical properties of pitch based strain graphitized glassy carbon fibers [PLASTICS INST. PAPER 13]

08 p1319 A71-20897

Microstructural defects responsible for tensile strength reduction in carbon fibers subjected to high temperature graphitization, using transmission electron microscopy

09 p1483 A71-23653

Graphitizing and nongraphitizing substances carbonization, observing cokes chemical structure changes and thermal decomposition

15 p2368 A71-32733

GRAPHS [CHARTS]

NT MOLLIER DIAGRAM

Solution search strategy optimization by analytic graphic techniques for problem with several approaches involving Bernoulli type trials

01 p0110 A71-10088

Iterative graphical method for broadband N way TEM mode power divider design, using Smith chart

01 p0055 A71-11194

Fourier transform chart showing interrelationships between data block length, frequency resolution sampling rate, fast Fourier transform (FFT) stages and other related variables

02 p0215 A71-12045

Rigid plane skeletal structures combinational properties, considering analytic geometry criteria and graphs from algorithm

02 p0327 A71-12395

Strain energy curves in generalized coordinates, discussing deformable body state, stress-strain relation, etc

05 p0827 A71-16760

Random graphs probabilistic characteristics, deriving algorithms for graph connectivity probability estimation

05 p0731 A71-16795

Illumination charts for operational satellite, discussing orbit geometry and times, evolution trajectories and launch parameters

06 p0966 A71-17702

Electromagnetic transducer DC rotor magnetic state diagram, describing simulation procedure for moment pickup

06 p0899 A71-17933

Design curve for estimating conduction heat transfer liquid He cryostats with vapor-cooled vent tubes

07 p1115 A71-20359

Two finite undirected linear graphs, determining isomorphism

07 p1148 A71-20370

Book of tables and graphs for circular cylindrical shells free vibrations

08 p1370 A71-21234

Logical functions for constructing graph with fundamental cutset matrix equal to given fundamental cutset matrix

08 p1268 A71-21282

Rational scale selection for theoretical and experimental graphs, investigating slopes and angles between line segments for various parameters

09 p1439 A71-23347

Geomagnetic field intensity maps of vertical, horizontal, northern and eastern components of geomagnetic field and of magnetic inclination for 1965

11 p1757 A71-25779

Energy spectrum minimization of intrinsic phase fluctuations in multistage vacuum tube frequency multiplier, using graphic analysis

11 p1738 A71-25940

Multicomponent exponential curves analysis by Post-Widder equation, providing continuous distribution function of time constants in inhomogeneous systems

12 p1870 A71-27129

Restricted four body problem, obtaining graphs for Hill surface of zero relative velocity

13 p2137 A71-28478

Design charts relating time response characteristics to parameters of closed loop transfer functions possessing conjugate pair of poles

13 p2042 A71-28706

Graphical method for predicting intermodulation components and spurious responses

13 p2038 A71-28867

Stochastic dynamic meteorological prediction depicted in graphical formats

14 p2269 A71-29947

Anisotropic composite materials failure surface criteria in three dimensional space, using graphical representation

17 p2824 A71-34817

Nonlinear feedback control system with two nonlinear memoryless energyless elements separated by linear device, discussing grapho-analytical method for self sustained oscillation determination

17 p2722 A71-35183

Computer algorithm for simulating dynamic systems by functional graphs, noting extension to complex systems

18 p2884 A71-35917

Two dimensional structures of 76 extragalactic radio sources at 1425 MHz in tabular and graphical forms

18 p2970 A71-37064

Light curve and apsidal motion of AR Cas from photoelectric photometry

18 p2971 A71-37069

Sensitivity formula and graphical interpretation for IR scanner, assuming object and ambient medium as Lambertian radiators

19 p3068 A71-38707

Creep strength extrapolation for high temperature steels, suggesting combined numerical and graphic methods

20 p3249 A71-39017

Energy spectrum minimization of intrinsic phase fluctuations in multistage vacuum tube frequency multiplier, using graphic analysis

20 p3205 A71-39260

Low, medium and high carbon steels hardenability determination from composition, using charted data

20 p3251 A71-39336

Multiplying factors charts for hardenability prediction of Cr, Ni, Si, Mo and Mn steels containing carbon

20 p3251 A71-39337

Geomagnetic field horizontal component H daily variation nature, using graphs to show increases above or decreases below given level

21 p3373 A71-40050

Graph-analytical method of determining optimal adjustment of real differentiating units and components introduced into single loop automatic control system with time lag

22 p3525 A71-41440

Global geomagnetic field intensity maps of vertical, horizontal, northern and eastern components of geomagnetic field and of magnetic inclination for 1965

22 p3532 A71-41547

GRASHOF NUMBER

Natural convection boundary layer stability on vertical flat plate with uniform heat flux, using numerical computer solutions for large Grashof number range

20 p3314 A71-39501

GRASSES

Turbulent energy budget and velocity dissipation spectrum near grass surface as function of atmospheric stability

22 p3569 A71-42546

GRASSMANN ALGEBRA

U VECTOR SPACES

GRATINGS

Ideal reflector simulation of periodically supported infinite plane metallic wire gratings with rectangular mesh showing small sag

09 p1409 A71-23503

GRATINGS [SPECTRA]

NT ECHELETTE GRATINGS

Far IR spectrophotometry improvement with lamellar grating, describing construction, alignment and performance

01 p0082 A71-10836

Plane acoustic wave diffraction by dense periodic grating, using crimped surface scattering with Neumann and mixed boundary conditions

01 p0128 A71-11120

Diffraction properties of three dimensional asymmetric gratings for reflected and transmitted E-polarized waves

01 p0038 A71-11215

Klystron and frequency multiplier submillimeter harmonic emission determination, using lamellar grating Fourier spectrometer

02 p0250 A71-12143

Commercially produced metallic wire gratings reflection spectra measurement, determining use as high performance filters and light polarizers in far IR region

03 p0457 A71-13507

Photoresist for hologram recording and diffraction gratings formation, using Ar laser output

03 p0425 A71-13640

Coherent optical data processing systems resolution testing, using multifrequency linear diffraction gratings

03 p0425 A71-13644

Constant dispersion rotating grating Q switch for carbon dioxide laser with simultaneous band selection and cavity adjustment

03 p0436 A71-13652

Plane electromagnetic wave inhomogeneous diffraction field from multilayer metal band gratings

05 p0722 A71-16829

Fourier resonance associated with electromagnetic wave diffraction from multilayer gratings

06 p0870 A71-18349

Error allowance of photoelectric sighting grating with incline slits in stellar observations at Pulkovo

07 p1108 A71-19330

Stereoscopic vision dependent on vertical grating of different spatial frequency of retinal images

09 p1394 A71-23013

Retinal sine wave flicker transient response obtained with circular uniform field and counterphase grating targets

11 p1799 A71-26141

Two wavelength holographic interferometry for transparent media with high or low sensitivity, using diffraction grating

12 p1904 A71-26796

Savart plates use in grating interferometers, deriving expressions for phase retardations for arbitrary angles between optical axis and plate normal

12 p1904 A71-26798

Auroral spectroscopy, considering grating spectrometers, Fabry-Perot and Michelson spectrometers, filter photometers, etc

13 p2058 A71-28039

Electromagnetic wave diffraction at multilayer wire grating, discussing computer program for diffraction field calculation

14 p2194 A71-30086

Cartesian shear and rigid rotation moire patterns by spatial filtering of superposed diffraction gratings

14 p2329 A71-30464

Holographic diffraction shearing interferometer scheme, considering gratings arrangement and calculation method

15 p2403 A71-31261

Matched/mismatched crossed beam interference field combination with sinusoidal holographic diffraction grating, studying metric properties and moire-obtured bands

15 p2410 A71-32404

Compact monochromatic rhodamine doped polymethyl methacrylate dye laser with internal diffraction grating resonator, describing frequency selection from emission spectrum

15 p2422 A71-32585

Shearing interferometer based on moire method using Fourier image of grating, considering applications to phase gradient and lens aberration measurements

16 p2577 A71-33133

Light diffraction by holographic gratings in pink ruby due to absorption coefficient spatial variations

16 p2578 A71-33149

Optical grating measuring systems high resolution interpolation using phase analog and digital counter techniques

17 p2745 A71-35293

Holographic diffraction gratings on plane or concave spherical surface photographic plate, investigating interference fringes and aberration properties

17 p2745 A71-35588

Holographic fiber optics image-guiding structures preparation in sensitized polymethyl methacrylate cast sheet by refractive index gratings pair recording

18 p2946 A71-35852

Monochromatic plane electromagnetic wave reflection by electrically perfectly conducting diffraction grating

21 p3415 A71-40665

Transmission coefficient calculations for infinite grating of conducting circular cylinders, considering parallel and perpendicular polarizations

23 p3655 A71-44170

GRAVIMETERS

Gravitational acceleration measurement, using gravimetric recordings on moving base at sea

08 p1294 A71-21787

Terrestrial spectroscopy by cryogenic gravity meter with hollow superconducting niobium sphere in cylindrically symmetric magnetic field, detecting earth spheroidal oscillations

10 p1598 A71-23737

Gravimeters calibration by inclination method with astronomical theodolite, tabulating relative errors and temperature corrections

24 p3826 A71-44767

GRAVIMETRY

Soviet book on random functions theory in gravimetric observations over water covering ship dynamics, meter design, instrument damping, optimal linear filtering, etc

02 p0254 A71-12841

Geocentric coordinates from dynamic satellite geodesy, using gravimetric Stokes and Vening-Meinesz functions

03 p0406 A71-13010

Gravimetric geodesy theory offering anomalous gravity potential solution for smoothed topography

17 p2733 A71-35028

Satellite and gravimetric data combination procedure for determining geocentric station coordinates and earth gravitational field

17 p2734 A71-35031

Crystal Al powder electrolytic production in inert atmosphere, discussing fractional composition, current efficiency, gravimetric density and particle morphology

24 p3837 A71-44734

GRAVIRECEPTORS

NT OTOLITH ORGANS

Plants and animals reactions to environment gravitational component, showing organisms perception of accelerating force

21 p3326 A71-39970

Gravitational and other forces involved in equilibrium of growing plants, showing gravity sensing ability lower limit existence

21 p3339 A71-39971

Physical determinants of gravity receptor mechanisms, discussing hydrostatic stress effects on membranes and gravity influence on enzymatic transport

21 p3339 A71-39972

Geotropic stimulus in plants, describing method to test correlations between microscopically visible cell particles and geotropic bending direction

21 p3339 A71-39974

Gravity receptors in lower plants including *Phycomyces* sporangiophores and *Chara* rhizoids

21 p3339 A71-39975

Gravity receptors in *Phycomyces* sporangiophores, considering transient and long term geotropic responses

21 p3339 A71-39976

Gravity susception by higher plants, proving starch statolith hypothesis

21 p3339 A71-39977

Gravity susception by higher plants, analyzing geotonic data for georeception theories

21 p3340 A71-39978

Arguments against statolith theory of gravitational perception in plants

21 p3340 A71-39979

Linkage mechanism between gravity receptors and auxin redistribution causing differential growth and geotropic curvatures in plants

21 p3340 A71-39983

Reflex mechanisms and programmed command in insect flight stabilization, discussing gravity proprioceptors, wind sensing and optomotor control

21 p3326 A71-39987

Gravity effect and lift perception in flying insects and animals, discussing flapping flight and aerial locomotion in aerodynamic balance weightless state

21 p3327 A71-39988

Proprioceptive gravity perception in Hymenoptera, noting joint located hair plates and constant angle space orientation in dark

21 p3327 A71-39989

Gravity orientation in insects, discussing different mechanoreceptor role

21 p3327 A71-39990

Gravity receptor evolution in invertebrates, considering cilia role in reception and transduction into responses

21 p3327 A71-39991

Gravity receptors and locomotion orientation in Crustacea, discussing statocyst, stimulation, input and compensatory eye movements with respect to gravitational field

21 p3327 A71-39992

Integrative action of central nervous system in converting gravity sensation into crustacean equilibrium reactions

21 p3327 A71-39993

Functional anatomy of vertebrate gravity receptor system in spatial orientation, discussing otolith organs, sensory cells and hair cell topography in elasmobranch labyrinth

21 p3327 A71-39994

Gravity sensing mechanism of inner ear, discussing statoceptors existence in vestibule

21 p3327 A71-39995

Gravity sensors and intracellular conduction mechanisms in animals, noting contradictory hypotheses on function of hair cell in labyrinth

21 p3328 A71-40009

GRAVITATION

NT ARTIFICIAL GRAVITY

NT GRAVITY ANOMALIES

NT LUNAR GRAVITATION

NT PLANETARY GRAVITATION

NT REDUCED GRAVITY

NT SOLAR GRAVITATION

Action at distance gravitation as alternative to general relativity, discussing gravitational frequency shift and light bending

07 p1189 A71-18747

GRAVITATION THEORY

Gravitational theory with variable constant, examining local energy momentum tensor conservation law and celestial mechanics effects

01 p0155 A71-10440

Relativistic correction for planet perihelion rotation within Einstein gravitation theory, using proper magnitudes in terms of chronometric invariants

01 p0159 A71-10920

Static solutions to equations of gravity, showing nonequilibrium universe with negatively determinate time-similar Ricci curvature

01 p0160 A71-11117

Motion equations of spherical gyroscope in gravitational field of larger mass derived from Gupta quantum theory of gravitation

01 p0161 A71-11274

Gravitation theory equations with higher order derivatives based on two point geometry, using differential equations systems

02 p0285 A71-12664

Gravitational stresses derived for Friedmann-Lobachevskii and Schwarzschild spaces

03 p0456 A71-13297

Extraterrestrial vestibular research, discussing geocentric and heliocentric otolith regulation and gravitation theory

04 p0542 A71-14759

Inconsistency in covariant gravitation theory with scalar field, considering limitation to forces of inertia and contradiction of macroscopic physics deterministic principle

04 p0625 A71-15098

Newtonian gravitational system of n mass particles, noting solutions by deterministic approach analysis and Poincare theory

04 p0652 A71-15707

Arbitrary surface gravitational potential function normal derivative determination, using Tikhonov regularization method for obtaining integrodifferential equation

05 p0739 A71-16421

Perturbation growth in free particle expanding Universe with critical density, considering Newton gravitation theory

06 p0974 A71-18427

Equivalence principle in Einstein general relativity, discussing gravitation and inertial forces, cosmological postulate and metagalactic evolution

07 p1189 A71-18739

Theoretical frameworks for testing relativistic gravity, using presence of metric and gravitational response equation from Dicke approach as postulates of parameterized postNewtonian formalism

07 p1190 A71-18859

Parameterized postNewtonian formalism for perfect fluids applied to Nordtvedt effect in relativistic gravity

07 p1190 A71-18860

Relativistic gravitation theory and experimentation, surveying literature on gravity waves, EM propagation, gyroscopic precession, etc

07 p1158 A71-19096

Time variable physical singularity in general relativistic cosmological solution of gravitation equations, constructing simplified models

07 p1191 A71-19173

Einstein equations of gravitational field for universe filled with radiation, obtaining spherical symmetrical inhomogeneous solutions

07 p1203 A71-20530

Newton inverse square law of gravitation in solar system, considering closed orbit trajectories

08 p1363 A71-21320

Conformally flat universe class with short ranged scalar gravity, satisfying Einstein field equations

08 p1334 A71-21360

Interstellar dust density, constructing cosmological model with gravitational equations

08 p1366 A71-21785

Coordinate conditions necessary for Einstein gravitation equations system completion

08 p1336 A71-21796

Near field approximation for strong gravitational fields, noting close similarities to electromagnetic fields

09 p1493 A71-22803

Lie group differential equation application to gravitation theory, rejecting Riemann geometry in favor of Klein geometry

09 p1495 A71-23073

Gravitational field equations in classical Newtonian mechanics within framework of macroscopic gravitation theory

09 p1523 A71-23074

Gravitational stresses derived for Friedmann-Lobachevskii and Schwarzschild spaces

09 p1495 A71-23270

Planetary rotational and translational motion interrelation in Einstein gravitation theory, describing orbital elements secular disturbances in two body problem

09 p1526 A71-23339

Thirring effect experimental measurements in gravitation theory, magnetic suspension system or torsion balance with two rotating disks generating angular momentum

10 p1642 A71-24467

Relativity - Conference, Cincinnati, June 1969

11 p1798 A71-25279

Perturbation growth in free particle expanding universe with critical density, considering Newton gravitation theory

12 p1954 A71-26577

Gravitational field quantum fluctuations role in general theory of relativity and cosmological model

12 p1965 A71-27171

Zerilli equation solutions for even-parity gravitational perturbations on Schwarzschild geometry, considering gravitational collapse and black hole effects

13 p2133 A71-27990

Gravitational theory for black holes, presenting relativistic collapse in three dimensions identical to general relativity

14 p2303 A71-29500

Newton gravitation theory, showing extension to relativistic mass and vector gravitation potential addition

14 p2305 A71-29600

Relativistic gravitation theory quantitative study of space vehicle experiments, discussing earth orbit and deep space investigations

14 p2319 A71-29990

Gravitation theory with universe reference frame concept consistent with general relativity theory based on equivalence principle

14 p2315 A71-30846

Field theoretic approach of Jordan-Brans-Dicke theory within Lorentz invariant gravitation theory framework, solving linear motion equations inconsistency

15 p2451 A71-32646

Relativity and gravitation - Conference, Technion City, Israel, July 1969

16 p2609 A71-33220

Landau-Lifshitz pseudotensor analogs of telemechanical conservation laws in Einstein theory of gravitation

16 p2611 A71-33278

Gravitational fields invariant evolution, noting Einstein equations constraints effects on initial values of variables

16 p2611 A71-33288

Gravitation phenomena based on uniformly expanding universe cosmological model for acceleration field

16 p2612 A71-33288

Geodetic boundary value problem reformulation using measured gravity values on known earth surface and potential theory

16 p2563 A71-33470

Nonlinear correction in Lagrangian density of gravitational field, deriving dusty cosmological model with no singularity

16 p2638 A71-33544

Coordinate conditions necessary for Einstein gravitation equations system

16 p2612 A71-33544

Action-at-a-distance theory of gravitation generalized to tensor interactions of all orders, considering special relativity demands and perihelion advance of Mercury

17 p2797 A71-34360

Brans-Dicke gravitation theory, applying unitary transformation to field equations

17 p2777 A71-34390

Linearized gravitation theory in macroscopic media deriving refraction of gravitational waves based on classical electromagnetism

17 p2777 A71-34580

Soviet papers on gravitation and elementary particle theory covering unified and quantum field theories geometrical models, mass spectrum, internal space etc

17 p2777 A71-34620

Simultaneous solution of Einstein and elementary particle motion equations for space-time curvature within particle resulting from self gravitation

17 p2778 A71-34620

Scalar-tensor field self consistent interaction theory eliminating Einstein gravitational model paradox

17 p2801 A71-34620

Gravitational equations in Maxwellianized form, investigating Bianchi qualities

17 p2778 A71-34630

Fourth order differential gravitational field equations for non-Einsteinian cosmological model, considering linearly expanding universe

17 p2801 A71-34630

Bounded system gravitational fields Debye potentials, using linearized gravitation theory field equations in form similar to Maxwell equations

17 p2784 A71-35340

Homogeneous isotropic universe, analyzing cosmological solutions with linear theory of gravitation

19 p3104 A71-38119

Soviet papers on geometrical and group methods in gravitational and elementary particles theory, covering relativity and electromagnetic and quantum fields

19 p3104 A71-38570

Tensors in relativistic asymmetrical field theory generalizing Einstein gravitation and Maxwell electromagnetic equations for electrogravitational fields

19 p3105 A71-38580

Mass of virtual particle responsible for gravitation of vacuum and expansion of universe, considering correspondence to red shift in quasar spectra

19 p3146 A71-38640

German monograph on static fields in general relativity theory covering covariant equilibrium conditions, two body problems, vacuum fields and Newtonian gravity principles 20 p3269 A71-39077

Light ponderability in gravitation theory, discussing hypothetical Freundlich effect of light velocity dependence on radiation field intensity, based on Maxwell electrodynamics nonlinear generalization 20 p3270 A71-39457

Galaxies spiral structure interpretation in terms of gravitation theory of pressure and density waves 20 p3293 A71-39528

Time variable physical singularity in general relativistic cosmological solution of gravitation equations, constructing simplified models 21 p3441 A71-40088

Gravitation theory within Lorentz covariant and second quantized formalism framework from gravity interaction with binding energy, discussing graviton behavior 21 p3416 A71-41035

Lorentz invariant theory for relativistic gravity testing, deriving conservation laws and parameter constraints from parametrized post-Newtonian equations of motion 22 p3575 A71-41919

Relativistic gravity in solar system, predicting Newtonian gravitational constant anisotropy measurements by Cavendish experiments 22 p3575 A71-41920

Relativistic gravitation theory, using Lorentz invariant scalar potential and gravitational metric 22 p3575 A71-42355

Gravitational field quantum fluctuations role in general theory of relativity and cosmological models 22 p3605 A71-42453

Initial singularity removal in model big bang universe compatible with 3K black body radiation in terms of renormalized gravitational theory 23 p3770 A71-44182

Natural convection contribution to strong gravitational fields affecting astrophysical objects evolution and mass ejection 24 p3868 A71-44749

GRAVITATIONAL COLLAPSE

Interstellar gas cloud spherically symmetrical collapse, considering computer program for density, temperature, flow velocity, cooling rate and gravity force 01 p0157 A71-10758

Electromagnetic wave fields in outer space during gravitational collapse of aspherical mass 01 p0160 A71-11064

General relativity and gravitational collapse, discussing experimental tests, waves, use of Riemann geometry and Einstein field equations 03 p0482 A71-12972

Nonspherical stellar gravitational collapse to black hole state, discussing event horizon concept 03 p0486 A71-13324

Light propagation in spherically symmetric cosmic dust distribution, obtaining conditions for escape from region of gravitational collapse to one of expansion 04 p0642 A71-14813

Black hole model for gravitational collapse of universe according to Einstein theory 05 p0813 A71-16956

Polytropic gas spheres gravitational instability under external pressure, obtaining critical masses and densities 05 p0813 A71-17091

Black hole model accounting for epsilon Aur eclipsing binary secondary component observations 06 p0970 A71-18031

Cosmic objects and phenomena research, considering matter and galaxy compacting and dispersing processes, red shift, quasars, etc 08 p1358 A71-20890

Nonspherical finite amplitude pulsations of uniform gas cloud in smooth gravitational contraction 08 p1364 A71-21413

Star formation angular momentum and magnetic flux problem, investigating collapsing dust cloud theory 11 p1830 A71-26108

Gravitational theory for black holes, presenting relativistic collapse in three dimensions identical to general relativity 14 p2303 A71-29583

Very low mass gravitationally collapsed objects, formed as fluctuation effects in early universe 14 p2307 A71-29865

Neutrino emission from collapsing stars, discussing possibility of detection by large mass organic scintillator 15 p2478 A71-31802

Thermal X ray sources associated with rotating collapsed stars with surrounding plasma shells, discussing plasma density profile and electron distribution in stellar magnetosphere 15 p2497 A71-32762

Kerr-Newman black hole as generic final state of gravitational collapse developed from Schwarzschild

geometry and mass, angular momentum and charge parameters 16 p2631 A71-33177

Collapsing white dwarf stars, investigating detonation wave formation for thermonuclear explosion 16 p2631 A71-33228

Star formation at interstellar gas cloud stage, discussing gravitational collapse, Bok dust globules, spectroscopic and IR peculiarities and models 17 p2801 A71-34696

Black holes in binary star systems from orbital eccentricity observations 19 p3142 A71-38006

Halos around black holes, showing luminosities caused by synchrotron radiation of magnetized plasma 20 p3289 A71-39295

Multiple pulsar ejection in supernova core collapse and neutron star formation energy loss 20 p3305 A71-39947

Collapsing dust cloud with small differential rotation described in normal Gaussian coordinate system 22 p3605 A71-42499

Neutron star limiting mass based on soft hadron matter resistance to gravitational collapse in stellar structural stability consideration 23 p3732 A71-43073

Floccule theory three dimensional planetary formation model of collapsing cloud leading to nonplanar system with protoplanets in retrograde orbits 23 p3769 A71-43991

GRAVITATIONAL CONSTANT

Gravitational theory with variable constant, examining local energy momentum tensor conservation law and celestial mechanics effects 01 p0155 A71-10440

Electron charge dependence on universe age, considering possible gravitational constant dependence on time 02 p0313 A71-12547

Earth ellipsoid physical constants using satellite measurements of geocentric gravitational constant, earth-moon mass ratio and geopotential harmonic coefficients 04 p0581 A71-15066

Eddington theory validity based on formulas connecting light velocity, Planck and gravitational constants and electron, proton and neutron masses 04 p0626 A71-15136

Gravitational constant time variation based on planetary radar echo time delay in comparison with atomic time, discussing accuracy limits 05 p0807 A71-16227

Gravitational constant determination, using rotating mounted W sphere and gas tight chamber with cylinder suspended from quartz fiber 12 p1931 A71-27245

Expanding metagalaxy closed model with changing gravitational constant, noting matter motion in moving and central reference systems 13 p2136 A71-28423

Electron charge dependence on universe age, considering possible gravitational constant dependence on time 15 p2494 A71-32503

Gravitational constant measurement by resonance method, describing experimental device 16 p2575 A71-34060

Jordan theory of gravitational constant variation, showing nonreducibility to Einstein model 17 p2778 A71-34633

Weyl and Schwarzschild field metric equivalence, showing nonreducibility from one to other by coordinate transformation 17 p2778 A71-34637

Cosmological upper limit on gravitational constant time variation, extending Dicke theoretical bound to pressure filled cosmologies in flat space 17 p2801 A71-34651

Mass and discrepant red shifts theory, discussing time dependent gravitational constant, Friedmann cosmological model and Dirac equation 20 p3305 A71-39956

Expanding metagalaxy closed model with changing gravitational constant, noting matter motion in moving and central reference systems 21 p3441 A71-40078

Geogravitational acceleration constant determination using two falling interferometer reflectors illuminated by laser light 22 p3574 A71-41650

Relativistic gravity in solar system, predicting Newtonian gravitational constant anisotropy measurements by Cavendish experiments 22 p3575 A71-41920

Experimental determination of gravitational constant in orbiting space laboratory by gravitational centrifugal balance of test objects [AAS PAPER 71-350] 23 p3728 A71-43022

GRAVITATIONAL EFFECTS

Uniform matter fragmentation under gravitational influence, examining approximate solution for density perturbations 01 p0150 A71-10062

Gravitating particle system phase density, finding differential and integral equations for Fourier transform 01 p0150 A71-10064

Gravitating point motion under attraction by two fixed centers, investigating hyperbolic case 01 p0156 A71-10449

Thick walled slowly rotating viscoelastic cylinder deformation under varying gravitational loads, using theory of elasticity 01 p0169 A71-10500

Three body gravitational capture of interstellar dust in solar system, examining zodiacal cloud 01 p0158 A71-10771

Self gravitating fluid spheroid oscillations in hydrostatic equilibrium with magnetic fields using variational principle 01 p0129 A71-11336

Helicopter pilot and passengers emergency survival, considering gravitation force, human tolerances, design factors, etc 01 p0026 A71-11376

Gravitational fields and atmospheric pressure effects on soils subjected to static and dynamic loading, using aircraft parabolic gravity simulation [AIAA PAPER 69-1009] 01 p0068 A71-11581

Gravitational acceleration effects on hemodynamics, describing mechanocardiographic equipment 02 p0198 A71-11900

Boiling under weightlessness, examining gravitational effects on bubbles formation frequency and diameters 02 p0331 A71-11922

Uniaxial satellite rotational motion, examining magnetic and gravitational torque effects on gyro dynamic properties 02 p0320 A71-11975

Lunar tides and precession effects on model earth fluid core dynamics 02 p0245 A71-11994

Optimal control of exhaust velocity for plane motion of variable mass point along trajectory under gravitational and resisting forces 02 p0284 A71-12292

Gravitational stresses derived for Friedmann-Lobachevskii and Schwarzschild spaces 03 p0456 A71-13297

Anisotropic plasma stability, taking into account self gravitation, finite ion Larmor radius, Hall current and rotation 03 p0465 A71-14263

Gravity effects on human caloric and rabbits rotational nystagmus, noting semicircular canals role 04 p0542 A71-14757

Gravity effects on experimental nystagmus in rabbits under electrical, rotatory and caloric vestibular stimulation, taking into account semicircular canals and otolith organs 04 p0536 A71-14758

Hydrodynamic equations for isothermal atmosphere stratified by uniform gravitational field, obtaining traveling wave solutions 04 p0570 A71-15030

Dynamical investigation of deformable gyrostats stability in circular orbit subject to gravitational torques, noting equilibrium states and damping effects 04 p0662 A71-15142

Stellar structure theory, examining particle aggregates gravitational and pressure forces, energy flow, generation and opacity and equations of state 04 p0648 A71-15246

Exposed rock bodies thickness determination using normalized peak gravity effect diagrams 04 p0583 A71-15271

Gravitational and forced convection effects in saturated liquids laminar boundary layer film boiling, presenting analytical solutions for common fluids 04 p0686 A71-15528

Two phase heat transfer in thermosyphon counterflow under simulated gravities of 0.1 to 100 earth gravity, measuring critical heat flow rates and convection coefficients 04 p0687 A71-15531

Multitube condensers of various geometries, investigating tube flow stability, distribution and gravitational effects 04 p0688 A71-15538

Three body stellar problem libration calculation using nonlinear mechanics methods, and application to lunar satellite perturbation by earth and lunar gravitational effects 04 p0655 A71-15728

Gravitational and tidal torque effects on Mercury spin rate as model of passage through resonance 04 p0657 A71-15738

Quasars as images of Seyfert galaxies nuclei resulting from gravitational lens mechanism 04 p0658 A71-15829

Interstellar gas cloud equilibrium and gravitational stability, examining evaporation, condensation, thermal balance and pressure 04 p0658 A71-15837

Lense-Thirring effect in test masses approaching in same orbit around rotating body, noting correction de-

GRAVITATIONAL EFFECTS

pendence on central body geometry and angular velocity

05 p0806 A71-16183

Gravitationally induced electric field shielding using whisker model with conducting metal surface for reducing strain dependence on altitude

05 p0792 A71-16315

Lunar satellite motion semianalytic solution, considering perturbative effects due to gravitational fields, solar radiation pressure and libration

05 p0809 A71-16541

Pointed body of revolution in gravitationally stratified atmosphere, discussing supersonic boom and minimum drag

[DFVLR-SONDDR-97] 05 p0694 A71-16712

Fermi particles /fluid/ oscillations in external gravitational field, discussing hydrodynamic equations, acoustic modes and sonic waves due to turbulent effects

05 p0813 A71-16833

Gravitational n-body calculation in discrete phase space using game model and finite difference scheme

06 p0927 A71-17555

Monocular and binocular vision comparison under moderate whole body Gz sinusoidal vibration stress environments

06 p0858 A71-17606

Heavy liquid shells of revolution, determining equilibrium form in gravitational and surface tension forces from condition of minimal functional of total free energy

06 p0994 A71-17827

General relativity theory tests, discussing Einstein effects existence and light velocity in gravitational field

06 p0971 A71-18246

Gravity stratified compressible fluid spin-up in sphere, analyzing by increase in container angular velocity and linearization about uniform rotation

06 p0883 A71-18320

Satellite orbital elements perturbation due to tesseral and sectorial harmonics of earth gravitational potential

06 p0976 A71-18451

Gravity gradient torque and near earth environment effects on rotationally damped dual spin satellite attitude motion

[AIAA PAPER 71-90] 06 p0980 A71-18546

White dwarfs, neutron stars and black holes origin and characteristics, discussing density, mass radius, gravitation and structure

07 p1199 A71-19999

Planetary diurnal rotation, discussing motion of small particle in solar and planet gravitational fields

07 p1201 A71-20437

Saturn rings radial structure model featuring purely gravitational forces association with primary and perturbations, using planar restricted three body problem formalism

07 p1202 A71-20518

Gravitational stability analysis based on Boltzmann-Vlasov collisionless kinetic equation solution by trajectory integration method in plasma physics

07 p1173 A71-20531

Laminar film condensation thickness and Nusselt number on arbitrary axisymmetric bodies in nonuniform gravity

07 p1225 A71-20655

Global cluster star velocities distribution, examining dynamic evolution models and gravitational effects

08 p1362 A71-21153

Gravitational acceleration measurement, using gravimetric recordings on moving base at sea

08 p1294 A71-21787

Human biomechanical and vegetative reactions to hypotonic suggestion of gravitational effects

08 p1243 A71-21971

Random gravitational encounter effects of passing stars on dynamical evolution of spherically symmetric stellar system, using modified Monte Carlo method

09 p1517 A71-22330

Gravitational field effect on phase difference of moving waves and polarization in rotating ring laser

09 p1462 A71-22398

Intermediate orbit calculation, allowing for spacecraft large gravitational perturbation during motion near planetary sphere of influence

09 p1519 A71-22663

Nomograms for meteor geocentric velocity and trajectory with correction for zenith attraction and radiant

09 p1520 A71-22831

Gravitational field effect on relativistic charge emission, noting gravitational waves detection

09 p1494 A71-22887

Artificial earth satellite orbit perigee motion, calculating perturbation effect due to gravitational and magnetic fields on orientation and rotation

09 p1523 A71-23150

Mitral valve systolic prolapse aggravation due to G acceleration and aeromedical significance

09 p1395 A71-23246

Gravitational stresses derived for Friedmann-Lobachevskii and Schwarzschild spaces

09 p1495 A71-23270

Satellite orbital period variation under earth gravitational potential tesseral and sectorial harmonics

09 p1526 A71-23341

Liquid shell about solid spherical core, analyzing vibrations and sphere gravitational effects on material particle motion

09 p1495 A71-23342

Stability of regular motions of dynamically symmetrical body with equatorial symmetry plane in Newtonian force field of spherical planet by Liapunov second method

09 p1526 A71-23346

Algol secondary component gravity darkening observations, examining IR light curve

09 p1527 A71-23530

Rotating self gravitating axisymmetric fluid mass structure steady state equations, examining Clairaut theory asymptotic nature

09 p1527 A71-23532

Radiative flux effect on magnetogasdynamical shock in self-gravitating gaseous stars

09 p1506 A71-23589

Book on gravity and acceleration effects on lungs covering breathing mechanics, ventilation distribution, blood flow, gas exchange, arterial oxygen saturation and pulmonary shunting

09 p1402 A71-23620

Gravitational instability of nonhomogeneous cosmological model, establishing density perturbation growth as function of time for model containing matter and radiation

10 p1667 A71-23851

Astrophysics - Conference, University of Nice, France, April 1969

10 p1670 A71-24186

Inhomogeneous rotating self-gravitating system kinetic theory, linearizing collisionless Boltzmann equation to two dimensional linear integral equation for obtaining small oscillation modes

10 p1641 A71-24278

Nonlinear stability analysis of inviscid and viscous liquid film adjacent to compressible gas flow, using gravity and pressure perturbation models

10 p1595 A71-24620

Galactic wind as steady radial perfect gas flow from stars and central gravitating source

11 p1818 A71-25207

Newtonian gravitational system n body problem infinite time approach, obtaining spatial distribution of star clusters

11 p1819 A71-25208

Earth-moon distance perturbations from anisotropic gravitational mass effect

11 p1819 A71-25209

Gravitational radiation events-galactic microwave emission pulses relation, comparing with Weber gravitational wave experiment

11 p1820 A71-25298

Gravitational instability picture for galactic rotation, examining numerical model for protogalaxy separation in expanding universe

11 p1820 A71-25535

Gravitational red shift in standard and isotropic forms of Schwarzschild metric

11 p1822 A71-25592

Spherical harmonics of secular perturbations in artificial satellites motion due to atmospheric gravitation

11 p1829 A71-25808

Spiral arms formation on galactic scale in terms of density waves produced by gravitational perturbations

11 p1832 A71-26184

Satellite orbital elements perturbation due to tesseral and sectorial harmonics of earth gravitational potential

12 p1955 A71-26601

Temperature gradients effect on density distribution in material near critical point, using classical and scaling-law theories and Ising model

12 p1929 A71-27031

Earth outward winding by cosmic particle gravitational accretion, examining individual meteor counts crossing celestial meridian in WE and EW directions

12 p1966 A71-27232

Boiling under weightlessness, examining gravitational effects on bubbles formation frequency and diameters

13 p2159 A71-28209

Tumbling triaxial satellite in elliptical orbit about spherical planet, determining resonant and nonresonant gravity gradient perturbations

13 p2145 A71-28356

Abdominal pressure decrease resulting in transpulmonary pressure cranio-caudal gradient increase under gravitational effect simulation

13 p2008 A71-28437

Suspended hollow cylinder under force of gravity, calculating stresses and displacements by linear elastic theory differential equations

13 p2153 A71-28518

EM field and wave propagation in static and spherical gravitation, obtaining modified Debye potentials and amplitude and eikonal equations

13 p2139 A71-28999

X ray evidence of limit amount of hot intracluster gas for gravitational binding of Coma cluster of galaxies

13 p2130 A71-29095

Equations of motion of infinitesimal particles attracted by Newtonian gravitation of two mutually revolving masses in circular orbits

13 p2101 A71-29114

Gravitohydrodynamic instability of static and constricting composite systems composed of infinitely conducting fluids, using normal modes analysis

13 p2108 A71-29164

Isothermal flow under capillary forces in heat pipes with zero gravity, deriving relation between flow rate and duct parameters

13 p2050 A71-29211

Cosmological models for creation of hierarchy of clusters within clusters, involving gravitational interactions

14 p2303 A71-29588

Coma galaxy clusters missing mass observations by gravitational lens effect

14 p2305 A71-29676

Gravitational instability of heat conducting compressible fluid relative to class of axisymmetric perturbations, considering viscosity, magnetic field and uniform rotation

14 p2226 A71-30397

Electromagnetic and gravitational waves scattering by static gravitational field, comparing classical general relativistic and quantum field theoretic results

14 p2275 A71-30861

White dwarf star gravity mode stability, considering hydrogen-helium transition sorting zone

14 p2318 A71-31018

Plane photogravitational restricted circular three body problem symmetrical periodic orbits closing on rotating plane after revolutions

15 p2483 A71-31340

Equation for motion of buoyant free vortices in inviscid fluid subjected to gravity

15 p2388 A71-31543

Heat pipes design and applications, examining pressure losses in steam and liquid phases and capillarity and gravity effects

15 p2513 A71-31637

Falling body problem solution, considering curvilinear motion effects of earth rotation axis

15 p2450 A71-32039

Constant-thrust trajectory problem with gravitational acceleration as linear function of radius vector obtaining minimum fuel solution in integrals

15 p2488 A71-32043

Automatic leveling instrument gravity intensity and compensator support tilt angle variations effects on measurement error

15 p2410 A71-32353

Arbitrary gravitational field effects on natural frequencies of rotating ring laser with traveling electromagnetic wave

15 p2421 A71-32408

Gravitating continuous medium instability in presence of delta shaped point density perturbations, discussing cloud structure development in interstellar gas

15 p2495 A71-32642

Magnetogravitational instability model with allowance for finite Larmor radius effect, considering plasma rotation parallel to magnetic field

15 p2459 A71-32654

Photoelastic determination of stress distribution in thin square plates subjected to gravitational force multiplied by immersion in Hg

16 p2647 A71-32824

Manufacturing processes in orbital workshop, considering metal and optical lenses casting crystal growth and gravity lack effects

16 p2606 A71-32856

Self gravitating time independent disk-like stellar system model, investigating mass and velocity distributions

16 p2630 A71-33054

Gravity decrease effects on planetary orbits, considering two bodies in circular and elliptical orbits and many bodies solar system with interaction between planets

16 p2631 A71-33167

Particle motion in combined gravitational field of monopole and prolate quadrupole, deriving exact solution in Newtonian mechanics and general relativity

16 p2609 A71-33256

Chemical equilibria susceptibility to gravitational field effects, suggesting coincidence with conditions derived from relativistic thermodynamics

16 p2540 A71-33257

Elektron 2 and 4 satellites rotary motion with orbital variance of precession parameters and kinetic angular momentum vector, considering gravitational and magnetic effects

16 p2645 A71-33438

Graviplane flight theory, spacecraft center of mass motion in central gravitational field with continuous mass geometry variation

16 p2646 A71-33661

General relativistic time delay of electromagnetic radiation propagation due to solar gravitational field measured from Mariner 6 and 7 range and Doppler data

16 p2640 A71-33737

Simultaneous solution of Einstein and elementary particle motion equations for space-time curvature within particle resulting from self gravitation

17 p2778 A71-34628

Stresses and deformation in solid propellants charges under gravitational load, assuming homogeneous isotropic and linearly viscoelastic charge material

17 p2829 A71-35307

Galactic center isolated radio pulse search at 151.5 MHz, correlating with Weber gravitational events

17 p2805 A71-35378

Periodic orbits around Lagrange libration points of restricted three body problem disturbed by gravitational and radiative influences

17 p2809 A71-35599

Nonstatic model of universe based on Newtonian cosmology, considering central body effects on interstellar dust motion

17 p2809 A71-35600

Lens test facility calibrating Mipir radar boresight fences by measuring deviations due to gravitational effects

18 p2897 A71-36072

Gravitational stimuli due to variations in angular velocity and radius, noting effects on behavioral control

[AIAA PAPER 71-884]

18 p2871 A71-36635

Structural development in rat bone under earth gravity, hypergravity and simulated weightlessness, discussing physical dimensions, density, rigidity, microhardness and ash content

[AIAA PAPER 71-895]

18 p2856 A71-36640

Weightless environment effects on fluid behavior and heat transfer in life support systems, obtaining analytical models

[AIAA PAPER 71-864]

18 p2909 A71-36652

Elastic stability and buckling modes of cylindrical shell under critical gravity load, using double Fourier series and linear theory

18 p2983 A71-36847

Earth outward winding by cosmic particle gravitational accretion, examining individual meteor counts crossing celestial meridian in WE and EW directions

19 p3132 A71-37384

Relativistic hydrodynamic solution for gravitational interaction of vortex and potential motion of homogeneous medium

19 p3134 A71-37515

Arbitrary amplitude magnetoacoustic waves under gravitational field effects, obtaining exact Riemann wave solutions to MHD equations for compressible medium

19 p3112 A71-37741

Gravity effect on developing laminar flow with forced convection in vertical isothermal tube, investigating velocity and temperature profiles and heat transfer rate

[ASME PAPER 71-HT-6]

19 p3164 A71-37983

Solar semi-diurnal atmospheric tide theory based on gravitational action only, taking into account atmospheric stratification

19 p3055 A71-38044

Mimas-Tethys resonance motions under short period gravitational perturbations and tidal dissipation functions

20 p3286 A71-38760

Motor and vestibular analyzers and frontal hypothalamus role in gravitational loads compensation during orthostasis, noting respiration, arterial pressure and brain bioelectric activity changes

20 p3188 A71-39223

Gravity induced free convection effects in melting phenomena for thermal control, predicting temperature distributions and solid-liquid interface profiles by two dimensional model

20 p3314 A71-39354

Nonhomogeneous flow stratification in fluid region under thermal and gravitational forces, considering steady state and time dependent density fields

20 p3212 A71-39502

Papers on gravitation effects on properties and behavior of living matter

21 p3326 A71-39969

Gravitational and other forces involved in equilibrium of growing plants, showing gravity sensing ability lower limit existence

21 p3339 A71-39971

Physical determinants of gravity receptor mechanisms, discussing hydrostatic stress effects on membranes and gravity influence on enzymatic transport

21 p3339 A71-39972

Circumnutations in plants under gravitational stimulation

21 p3339 A71-39973

Gravity receptors in lower plants including *Phycomyces sporangiophores* and *Chara rhizoids*

21 p3339 A71-39975

Gravity susception by higher plants, proving starch statolith hypothesis

21 p3339 A71-39977

Geoelectric effects on plants geotropic reaction chain, discussing hormone auxin asymmetric distribution due to gravity

21 p3340 A71-39984

Gravity effect and lift perception in flying insects and animals, discussing flapping flight and aerial locomotion in aerodynamic balance weightless state

21 p3327 A71-39988

Integrative action of central nervous system in converting gravity sensation into crustacean equilibrium reactions

21 p3327 A71-39993

Central nervous tissue sensitivity, considering direct sensing of gravitational stimuli of vibratory character

21 p3328 A71-39997

Gravity influence on plant growth, lateral development, apical dominance, bud initiation, orientation and flower morphology

21 p3340 A71-39999

Geocipinastic bending of *Fritillaria Meleagris* axes as prototype of geoinduced plagiotropic growth

21 p3341 A71-40000

Animals physiological responses to gravity chronic acceleration

21 p3328 A71-40002

Plants behavioral reactions to continuous gravitational field directional reorientation by clinostat, discussing gravity compensation effects on tropism and forces required for geotropic response

21 p3341 A71-40004

Pinto beans circadian leaf movements in simulated weightless environment, relating rotational treatment time to rhythm phase

21 p3341 A71-40006

Gravity responses and geotropic behavior at ontogenetic stages of higher green plants, noting tendril movement under mechanical stimulation

21 p3341 A71-40008

Binary fluid mixtures density gradients near critical point due to gravity effect, deriving expression as linear function of height with thermodynamic equilibrium as starting point

21 p3345 A71-40236

Viscous fluid layer surface waves nonlinear theory, analyzing surface friction and gravity force angle effects on wave characteristics

21 p3367 A71-40682

Cosmological models of universe based on expansion-gravitational interaction, including red shift, radio sources, quasars and background radiation measurements

21 p3451 A71-40776

Fluid dynamics in elastic complex geometry tanks, obtaining liquid mass and stiffness matrices for gravitational effects

21 p3467 A71-40948

Gravitation theory within Lorentz covariant and second quantized formalism framework from gravity interaction with binding energy, discussing graviton behavior

21 p3416 A71-41035

Electromagnetic radiation active gravitational mass relationship to particle mass from decay of particle into two radiation pulses

21 p3417 A71-41402

Thin liquid films under simultaneous shear and gravity forces, noting data incorporation into transport equations for heat and mass transfer

22 p3620 A71-41884

Alouette and Isis satellites flight data comparison with attitude and spin dynamics theory, considering solar radiation pressure and gravitation and magnetic field effects

22 p3609 A71-41997

Time optimal semiactive attitude control for circular orbiting satellite pitch motion, using gravitational and aerodynamic torques

22 p3570 A71-42001

Blind goldfish gravity reference response under linear accelerations on motor car and parallel swing from movie camera recording

22 p3487 A71-42228

Nonlinear photometric effects of limb darkening and gravity darkening dominance in eclipsing variables from light minima observations

22 p3604 A71-42332

Schwarzschild constants evaluation from coupled gyroscopes spin axes observation, noting axes high angular velocities due to gravomagnetic effect in gravitational interaction

22 p3605 A71-42338

Plane photogravitational restricted circular three body problem symmetrical periodic orbits closing on rotating plane after revolutions

22 p3606 A71-42615

Earth gravitational field effect on dual spin satellite motion in circular orbit, using Vigneron averaging method for linearized equations of motion

22 p3612 A71-42782

Healthy males immersion in water containing NaCl, determining modified gravitational field effect on motor functions

22 p3505 A71-42792

Gravitational and aerodynamic perturbation moment effects on nonsymmetric solid body rotary motion near mass center, using precession model

22 p3612 A71-42870

Pulsar speedup due to neutron starquakes, deriving self gravitating elastic incompressible sphere model for time prediction

23 p3722 A71-42894

Long term orbit calculation by superposition of gravity and drag perturbations, taking into account solar and geomagnetic induced density variations

23 p3730 A71-43046

Lunar orbit space station lifetime, using averaged variational equations numerical integration for terrestrial, solar and lunar gravitational field effects

23 p3730 A71-43047

Earth mantle material chemical differentiation from structural model, considering gravitational instability relationship to low density layer formation at core boundary

23 p3671 A71-43579

Cone penetration resistance tests on granular lunar soil simulants for in-place shear strength and packing characteristics under various gravity conditions

23 p3757 A71-43751

Interplanetary time delay and light deflection measurements anomalies, investigating gravitational and electromagnetic fields interaction

23 p3766 A71-43824

Solar gravitational deflection of radio waves measured by Cambridge one-mile telescope, observing radio source 3C 279 before/after 8 October 1970 occultation

23 p3769 A71-43990

Cometary nucleus outbursts and splitting moments spatial distribution, indicating solar radiation and tidal action effects

24 p3868 A71-44457

Natural convection contribution to strong gravitational fields affecting astrophysical objects evolution and mass ejection

24 p3868 A71-44749

Gravitational system dynamics, discussing massive-light star mixtures with collisions and systems with equal mass objects

24 p3869 A71-44803

Saturn ring motion stability factors for atomized material resistance to gravitational field, discussing ring thickness, density and other parameters

24 p3869 A71-44810

Sirius B white dwarf star effective temperature, radius and gravitational red shift determination from H-alpha and H-gamma line profile analysis

24 p3871 A71-44908

Artificial lunar satellite motion in gravitational fields of nonspherical moon, earth and sun, deriving orbit perturbations

24 p3874 A71-45174

GRAVITATIONAL FIELDS

Elliptic integrals for gravitational potential in symmetry plane of Milky Way galaxy

01 p0148 A71-10033

Lunar gravitational field parameters from Lunar Orbiters trajectory measurement, discussing theoretical basis

01 p0149 A71-10048

Autocorrelation function for gravity anomaly stochastic field outside earth spherical surface

01 p0127 A71-10358

Earth spherical and ellipsoidal gravity potential coefficients association using Lamé orthogonal function properties

01 p0155 A71-10388

Spheroidal solutions near center for free oscillations of self gravitating rheological spherical mass

01 p0127 A71-10462

Earth gravity anomalies calculation, discussing normal field structure

01 p0074 A71-11060

Motion equations of spherical gyroscope in gravitational field of larger mass derived from Gupta quantum theory of gravitation

01 p0161 A71-11274

Celestial body gravitational field from satellite photogrammetry

01 p0083 A71-11326

Gravitational fields and atmospheric pressure effects on soils subjected to static and dynamic loading, using aircraft parabolic gravity simulation

01 p0068 A71-11581

Earth surface density distribution, using earth gravity field representation as potential of simple layer determined from combined satellite and gravity anomalies observations

02 p0246 A71-12463

Electromagnetic repulsion of conducting and dielectric bodies within liquid metal and electrolyte in crossed field under gravitational acceleration

02 p0293 A71-12630

Motion stability of double-gyro inertial frame in Newtonian central force field, applying Liapunov and Chetaev methods

02 p0253 A71-12638

Gyroscopic and physical pendulum stability with gimbal suspension centers moving in Newtonian central force field, using Raus method
02 p0254 A71-12639

Earth gravitational and magnetic field correlation, determining undulations on core-mantle interface
02 p0247 A71-12953

Pursuit game strategy based on Hamilton-Jacobi formalism, considering internal and external potential fields, optimum trajectories and gravitational and electromagnetic fields
03 p0483 A71-13116

Body motion with liquid filled cavities in central Newtonian force field, using hodography
03 p0458 A71-13595

Gravitational field due to point mass, proving Newton space existence
03 p0458 A71-13606

Satellite dynamics applications in determination of atmospheric drag, earth and moon gravitational fields and Mars and Venus mass from trajectory construction
03 p0491 A71-14003

Rocket probe with constant tangential acceleration in planetary gravitational field, investigating flight direction
03 p0495 A71-14388

Static axially symmetric gravitational field equations, presenting Weyl solutions for standard coordinates
04 p0625 A71-14730

Gravitational anomaly distributions of rectangular prismatic bodies, using tables
04 p0581 A71-15069

Earth gravitational environment critical parameters at synchronous altitudes by satellite drift observation, discussing geopotential field determination
04 p0583 A71-15306

Classical and relativistic forces of inertia based on exact solution of Einstein nonlinear gravitational field equations, using general covariance principle
04 p0628 A71-15903

Chronometrically invariant formulation of Petrov gravitational fields algebraic classification at spacetime fixed point in general relativity
05 p0781 A71-16182

Arbitrary surface gravitational potential function normal derivative determination, using Tikhonov regularization method for obtaining integrodifferential equation
05 p0739 A71-16421

Static thin shells and disks gravitational fields in general relativity
05 p0781 A71-16447

Gyroscope in gimbal system with elastic rotor bearings, determining dynamic stability in Newtonian central force field
06 p0899 A71-17929

Autocorrelation functions of anomalous gravitational and magnetic fields for ocean lines, relating Mohorovičić boundary and Curie isotherm
06 p0894 A71-18268

Inhomogeneous plasma flute instability in presence of gravitational field and supported by magnetic fields
06 p0938 A71-18425

Particle motion in gravitational field for disk-like configurations, solving kinetic equation for quadratic potential
07 p1192 A71-19286

Space environment and operations from medical viewpoint, discussing gravitation, magnetic fields, particle rays, planetary atmospheres, etc.
08 p1357 A71-20703

Lunar gravitational field parameters from Lunar Orbiters trajectory measurement, discussing theoretical basis
08 p1361 A71-21042

Static cylindrically symmetric universes consisting of Einstein-Maxwell gravitational and electromagnetic fields, discussing central axial mass and charge or current density
08 p1334 A71-21361

Earth gravity field in physical geodesy, considering satellite geodesy, gravitation-inertia interrelation, etc.
08 p1285 A71-21799

Satellite geodesy, discussing reference orbits calculation, gravity field spherical harmonics, station positions, etc.
08 p1285 A71-21800

Satellite geodesy for determining tracking station coordinates and gravity field
08 p1285 A71-21801

Coplanar transfer orbits optimal trajectories in central Newtonian gravitational field, using Krotov sufficient criteria
09 p1519 A71-22566

Unitary potential method for numerical separation of subterranean three dimensional gravitational and magnetic fields
09 p1436 A71-22608

Near field approximation for strong gravitational fields, noting close similarities to electromagnetic fields
09 p1493 A71-22803

Weak gravitational field negative energy possibility from energy momentum leakages consideration for asymptotically flat solutions of Einstein equations
09 p1494 A71-22807

Near earth motion equations for electrically charged dust particles in gravitating dipole magnetic fields, using zero-relative-velocity surfaces and energy integral
09 p1437 A71-22832

Critique of paper on earth gravitational field correlations to dipole part of magnetic field
09 p1437 A71-22930

Earth gravitational field correlations to dipole part of magnetic field, rejecting modifications to statistical procedures
09 p1437 A71-22931

Jupiter gravitational potential mapping for Grand Tours spacecraft, discussing Jovian satellites effect on orbit and trajectory perturbations
09 p1525 A71-23222

Nonlinear electrostatic theory Lagrangian analogous to gravitational Lagrangian from correspondence between Maxwell electromagnetism and Einstein gravitation
10 p1667 A71-23815

Scalar theory for nonstatic gravitational fields, using tensor and linearized equations
10 p1641 A71-23975

General relativity theory applicability limits for strong gravitational fields and near singularities in cosmology
10 p1668 A71-24002

Computer simulation model for stars motion in plane of disk-like stellar systems, investigating dynamics of Jeans and gravitational two-stream instability
10 p1670 A71-24181

Debye-Huckel gravitational potential in Lemaitre universe
10 p1680 A71-25019

Infinite universe compatibility with gravity potential satisfying Poisson equation, avoiding cosmological difficulties by universal gravitational field sources and sinks introduction
10 p1681 A71-25074

Gravitational radiation damping of slowly moving systems, discussing treatment as singular perturbation problem with approximation solution by method of matched asymptotic expansions
11 p1797 A71-25139

Carnot cycles generalization for thermodynamic systems with stationary gravitational fields, deriving temperature, thermodynamic equilibrium and entropy definitions for general relativistic systems
11 p1798 A71-25738

Rotating plane layer viscous incompressible conducting fluid flow between two parallel walls with temperature gradient subject to perpendicular gravitational and magnetic fields
11 p1757 A71-25767

Satellite geodesy progress over 12 years since artificial earth satellites, considering gravitational field and station position measurement accuracies
11 p1759 A71-25820

Stellar mass relativistic integral theorems and upper and lower bounds for gravitational potential theory
11 p1830 A71-26106

Optimal control of material point motion in thin spherical layer of central gravitational field, solving by approximation
12 p1957 A71-26631

Homogeneous isotropic zero-pressure cosmological problem of gravitational field solved in Jordan-Dicke equations framework
12 p1963 A71-27030

Statistical analysis of gravitational instability for isotropic cosmological models, examining density perturbations as random functions of coordinates and comparing with galactic mass statistics
12 p1965 A71-27178

Gravitational field quantum fluctuations role in general theory of relativity and cosmological model
12 p1965 A71-27179

General relativity gravitational field equations, giving composite sphere internal structure for core and shell
12 p1932 A71-27643

Zerilli equation solutions for even-parity gravitational perturbations on Schwarzschild geometry, considering gravitational collapse and black hole effects
13 p2133 A71-27972

Kinetic equations for particle motion in gravitational fields, discussing stellar configurations evolution
13 p2100 A71-27973

Closed universes quantization and gravitational field in general relativity, emphasizing superspace concept and finite-dimensional model quantum theories construction
13 p2100 A71-28395

Routh-Liapunov stability of lasting rotation of dynamically symmetrical gyrost at in force field of two stationary centers
13 p2145 A71-28729

Stationary motions of holonomous five degree of freedom mechanical system of rod suspended homogeneous symmetrical body in central gravitational field
13 p2100 A71-28729

Minimum time low thrust rocket transfer between elliptic orbits in strong gravity field, using averaging method
13 p2139 A71-28816

Massive body gravitational to inertial mass ratio from equilibrium assembly model of particle interactions
13 p2139 A71-28999

Gravitational radiation theory, discussing mechanisms, wave properties and analogies with EM fields
13 p2130 A71-29141

Point motion in axisymmetrical planet equatorial plane gravitational field, taking into account orbital elliptical elements osculation
14 p2310 A71-30188

Integral coefficient of correlation between gravitational and magnetic fields with geological element
14 p2235 A71-30188

Gravity field determination from satellite orbit analysis, using surface gravity and astrometric data
14 p2313 A71-30488

Plane horizontal fluid film convective stability with free boundaries in vertical circular cylinder for periodic modulation of vertical temperature gradients or gravitational field
14 p2338 A71-30871

Subluminous star spectroscopic data, determining temperature and surface gravity
14 p2317 A71-31011

Equilibrium position stability of nonlinear two body satellite system in circular orbits in gravitational central force field, using linearized equations of motion
15 p2499 A71-31174

Gravitational potential tensor and equations of motion of relativistic mechanics for isolated system of masses
15 p2481 A71-31187

Numerical analysis of accretion growing grain segregation in gravitational field with resisting gas, discussing motion equation, evaporation rate and planetary evolution
15 p2489 A71-32397

Normal gravity field parameters from harmonic coefficients and satellite observation data
15 p2492 A71-32463

Spherically symmetric initial solutions for coupled gravitation and massless field system generated by physical particle source
16 p2610 A71-33264

Classical gravitational field equations modification for virtual quantized matter, taking into account additional mass due to attractive forces
16 p2610 A71-33271

Classification of curvature tensor of relativistic Riemann space-time gravitational metric field
16 p2611 A71-33276

Gravitational fields invariant evolution, noting Einstein equations constraints effects on initial values of variables
16 p2611 A71-33288

Normal terrestrial gravitational field potential, taking into account second order variables and distances from earth ellipsoid
16 p2563 A71-33466

Geodetic boundary value problem reformulation using measured gravity values on known earth surface and potential theory
16 p2563 A71-33476

Nonlinear correction in Lagrangian density of gravitational field, deriving dusty cosmological model with no singularity
16 p2638 A71-33554

Spherical and ellipsoidal functions relationship for terrestrial gravitational field anomalies
16 p2564 A71-33577

Lunar gravity measurements by Apollo 14 Doppler radio tracking during low altitude orbits, correlating variations with surface features
16 p2641 A71-33777

Lunar gravity field global model from moon orbital secular and long period trends, noting large anomalies on far side
16 p2642 A71-33811

Oceanic masses vertical gravity gradient, noting slight decrease with depth
16 p2575 A71-34066

German book on satellite geodesy covering two body problem, perturbation theory, earth gravitational field, gravitational effects of sun and moon, radiation pressure, etc.
17 p2799 A71-34477

Gravitational field equations derivation from least action principle, interpreting additional vector field generalization as vector potential of electromagnetic field
17 p2778 A71-34633

- Fourth order differential gravitational field equations for non-Einsteinian cosmological model, considering linearly expanding universe 17 p2801 A71-34634
- Gauge equations in general relativity theory for tetrad gravitational potential formulation, based on algebraic invariants method 17 p2778 A71-34636
- Moller gravitational field energy-momentum pseudotensor comparison with Einstein canonical and Landau-Lifshitz pseudotensors and Minkewitsch quasitensor, noting chronometric invariance 17 p2778 A71-34638
- Earth gravity field and satellite tracking stations positions geodetic parameters in geocentric reference frame 17 p2733 A71-35027
- Gravimetric geodesy theory offering anomalous gravity potential solution for smoothed topography 17 p2733 A71-35028
- Satellite and gravimetric data combination procedure for determining geocentric station coordinates and earth gravitational field 17 p2734 A71-35031
- Bounded system gravitational fields Debye potentials, using linearized gravitation theory field equations in form similar to Maxwell equations 17 p2784 A71-35341
- Earth gravitational and magnetic field correlations, considering nondipole geomagnetic potential latitudinal rotation effects 17 p2735 A71-35383
- Uniformly rotating thin relativistic disks structure, stability and gravitational fields within general relativity framework 17 p2806 A71-35405
- Optimal transfer in central field between coplanar circular orbits, allowing for errors in velocity changes and phase variables 18 p2962 A71-36107
- Geodetic satellite data utilization for test range specific point positioning, control densification, earth gravitational model determination and tracking station locations 18 p2913 A71-36492
- Cepheid beta Doradus color photometry data, detailing temperature, mean radius, absolute magnitude and surface gravity variations 18 p2971 A71-37070
- Position determination on planetary surface from gravity and star line-of-sight direction measurements, presenting numerical results for Apollo lunar landing missions [AAS PAPER 71-900] 19 p3095 A71-37151
- Electromagnetic and gravitational fields geometry, using compensating fields concept 19 p3105 A71-38581
- Invariant characteristics of Einstein spaces according to Petrov classification, determining gravitational fields described by covariant equation involving space curvature tensor and arbitrary scalar 19 p3105 A71-38585
- Critique of cosmological theories based on spontaneous matter creation in strong gravitational fields, deriving particles discrete number constancy in general relativity 20 p3268 A71-38834
- Critique of Woodward-Younger hypothesis of frequency dependence of light velocity in gravitational fields based on variable stars observations, considering photon rest mass 20 p3286 A71-38836
- Time optimal transfer trajectory in central Newtonian force field between two arbitrary points under jet acceleration 20 p3289 A71-39135
- Gravitational fields of giant planets in hydrostatic equilibrium, solving equations for linear and quadratic density distributions 20 p3290 A71-39310
- Lense-Thirring spin-spin gravitational forces measurement between disks and cylinders, using weak field low velocity relativity approximation 20 p3292 A71-39409
- Theorem proved for monotonic behavior of pressure within relativistic rotating star, assuming stationary axisymmetric gravitational field of Euclidean topology 20 p3293 A71-39447
- Gyroscope apparent precession due to reference star light deflection by solar gravitational field 20 p3270 A71-39559
- GEOS-C geodetic satellite purpose and equipment, discussing earth gravitational field study, radar altimeter possibility and tracking systems usefulness 20 p3306 A71-39657
- Geodetic parameters describing earth gravity field and satellite tracking stations positions in geocentric reference frame, using satellite observation and deep space probes 20 p3220 A71-39659
- Earth gravitational field fine structure via circular orbit satellite perturbations 20 p3220 A71-39660
- BCD Cepheids observations, examining data with quasi-static interpretation approximation for gravity and stellar masses 21 p3441 A71-40065
- Global lunar gravity field from weighted least squares analysis of Lunar Orbiters elements, deriving zonal and sectorial harmonics from libration data 21 p3443 A71-40183
- Statistical space velocity distributions, gravitation field strength and vertex deviation for nearby young stars, using density wave theory of galactic spirals 21 p3444 A71-40196
- Artificial gravity field produced by rotating spacecraft in earth orbit, examining astronaut physical responses and centrifugal force effects on work tasks 21 p3342 A71-40255
- Rotating plane layer viscous incompressible conducting fluid flow between two parallel walls with temperature gradient subject to perpendicular gravitational and magnetic fields 22 p3532 A71-41535
- Characteristic initial data for gravitational vacuum fields invariant of two initial null hypersurfaces and space-like section sigma 22 p3576 A71-42404
- Statistical analysis of gravitational instability for isotropic cosmological models, examining density perturbations as random functions of coordinates and comparing with galactic mass statistics 22 p3605 A71-42452
- Gravitational field quantum fluctuations role in general theory of relativity and cosmological models 22 p3605 A71-42453
- Planetary gravitational fields variations determination by onboard gravity gradiometer instrumentation [AAS PAPER 71-364] 23 p3729 A71-43034
- High velocity H alpha ejections in association with important solar flare on 12 March 1969, suggesting mass motions control by gravitational field 23 p3721 A71-43848
- Earth ellipsoid gravitational potential selection influence on geoid height determination, using near-geoid model 23 p3674 A71-44051
- Translational and rotational vibrational motion correlation of solid body mass center in Newtonian force field 24 p3872 A71-45047
- GRAVITATIONAL POTENTIAL**
U GRAVITATIONAL FIELDS
GRAVITATIONAL RADIATION
U GRAVITATIONAL FIELDS
GRAVITATIONAL WAVES
Pulsars as rotating neutron stars with frozen-in magnetic field, accounting for energy and angular momentum losses due to gravitational radiation 02 p0300 A71-12473
- General relativity and gravitational collapse, discussing experimental tests, waves, use of Riemann geometry and Einstein field equations 03 p0482 A71-12972
- Gravitational waves properties and detection, discussing relationship between electromagnetism and special relativity theory 03 p0459 A71-13950
- Angular momentum flux from confined gravitational radiator, using linear approximation with Landau-Lifshitz energy-momentum pseudotensor 04 p0625 A71-14731
- Gravitational waves collision analysis using coordinate system for general relativity 04 p0658 A71-15832
- Lunar mascons interpretation as meteorites impact, discussing use as gravitational waves detectors 04 p0661 A71-15904
- Gravitational radiation experimentation, discussing detector, directivity, equations of motion, etc 08 p1333 A71-21175
- Gravitational field effect on relativistic charge emission, noting gravitational waves detection 09 p1494 A71-22887
- Viscous compressible fluid response to incident gravitational wave, deriving governing equations in linearized approximation to general relativity 10 p1676 A71-24496
- Cosmological enhancement of density perturbations and amplitude variation of acoustic and gravitational waves in anisotropic homogeneous universe 10 p1678 A71-24886
- Long period gravitational radiation detection, using relative velocity discrepancies of earth and Mariner 6 and 7 10 p1664 A71-25007
- Gravitational radiation events-galactic microwave emission pulses relation, comparing with Weber gravitational wave experiment 11 p1820 A71-25298
- Gravitational shock waves from tachyons, considering capability for Weber gravitational radiation detection apparatus excitation across astronomical distances 11 p1798 A71-25591
- Gravitational wave bursts emanating from direction of center of Milky Way Galaxy, considering pulsating neutron star as source 12 p1958 A71-26694
- Maxwell equations analog for gravitational fields, considering Malybaeva equation as condition for gravitational waves existence in Riemann manifold 12 p1931 A71-27243
- Gravitational waves from rotating relativistic neutron stars/pulsars in far field region, assuming small velocity and spherical deformation 13 p2133 A71-27971
- Constant space curvature perturbations, considering density, rotational and propagation of gravitational waves with Lifshitz method 13 p2137 A71-28479
- Rotating Jacobi ellipsoid evolution by gravitational waves emission, discussing triaxial nonaxisymmetrical configurations for rapidly rotating pulsars 13 p2140 A71-29000
- Gravitational radiation theory, discussing mechanisms, wave properties and analogies with EM fields 13 p2130 A71-29117
- Strong gravitational wave bursts in galaxy, suggesting collapsed relativistic body cluster burning gravitational potential energy 13 p2142 A71-29137
- LF gravitational waves search based on light intensity fluctuations after traveling over transmission paths 14 p2274 A71-29856
- Electromagnetic and gravitational waves scattering by static gravitational field, comparing classical general relativistic and quantum field theoretic results 14 p2275 A71-30861
- Gravitational radiation existence from Riemann curvature tensor Fourier transform measurements, giving antenna directivity theory 16 p2612 A71-33283
- Stability analysis of nonradial oscillations of cold nonrotating relativistic neutron stars by linearized Einstein equations with coupled gravitational waves 16 p2635 A71-33482
- Extragalactic gravitational radiation focusing by galactic core acting as lens 17 p2798 A71-34399
- Energy momentum stress tensors for harmonic oscillator model, calculating energetic interaction with plane gravitational wave of same frequency 18 p2946 A71-35982
- Gravitational radiation antenna consisting of disk cylinder in radial mode of circular symmetry 19 p3104 A71-38190
- Gravitational radiation interaction with uniform incompressible inviscid fluid in simple motion, considering response in linearized approximation to general relativity 21 p3446 A71-40421
- HF gravitational radiation due to quantum transitions, studying absorption, emission and sources 21 p3439 A71-40612
- Cosmological enhancement of density perturbations and amplitude variation of acoustic and gravitational waves in anisotropic homogeneous universe 21 p3453 A71-41251
- Gravitational wave impingement upon static magnetic field, noting EM waves excitation 21 p3417 A71-41397
- Heat balance effects of acousto-gravitational waves in upper atmosphere, concerning infrasonics from earthquakes, polar auroral arcs and magnetic storms 22 p3533 A71-41656
- Gravitational wave astronomy, discussing phenomenon relationship to Einstein relativity theory and detector configurations 23 p3733 A71-43120
- Bondi condition gravitational waves, investigating radiation and energy transfer in given coordinate system 23 p3704 A71-43300
- Gravitational shock waves study by tensor distribution technique including Einstein equations solution 23 p3770 A71-44006
- Photon noise limited interferometer transducer for gravitational radiation antenna, using piezoelectric driver to generate subangstrom vibrations 24 p3835 A71-45209
- GRAVITONS**
Gravitation theory within Lorentz covariant and second quantized formalism framework from gravity interaction with binding energy, discussing graviton behavior 21 p3416 A71-41035
- GRAVITY**
U GRAVITATION
GRAVITY ANOMALIES
Autocorrelation function for gravity anomaly stochastic field outside earth spherical surface 01 p0127 A71-10358
- Earth gravity anomalies calculation, discussing normal field structure 01 p0074 A71-11060

Lunar surface mascon structure and origin from mass estimates, noting contributions to lunar gravity field variations

02 p0306 A71-11990

Earth surface density distribution, using earth gravity field representation as potential of simple layer determined from combined satellite and gravity anomalies observations

02 p0246 A71-12463

Gravitational anomaly distributions of rectangular prismatic bodies, using tables

04 p0581 A71-15069

Satellite geodetic data interpretation of geoid undulations and gravity anomalies

08 p1285 A71-21803

Gravitational anomaly of mascons formation on lunar surface from geological data analysis

09 p1519 A71-22532

Earth gravitational field anomalies relation to atmospheric circulation and tropical perturbations

15 p2443 A71-31223

Normal terrestrial gravitational field potential, taking into account second order variables and distances from earth ellipsoid

16 p2563 A71-33466

Gravity anomaly and lunar radius measurement at Apollo 12 landing site, using data telemetered to earth from surface module

16 p2636 A71-33507

Spherical and ellipsoidal functions relationship for terrestrial gravitational field anomalies

16 p2564 A71-33571

Lunar gravity field global model from moon orbiters secular and long period trends, noting large anomaly on far side

16 p2642 A71-33815

Oceanic masses vertical gravity gradient, noting slight decrease with depth

16 p2575 A71-34065

Gravimetric geodesy theory offering anomalous gravity potential solution for smoothed topography

17 p2733 A71-35028

Earth masses substitution by nearly minimum number of point sources of gravity anomalies

17 p2734 A71-35188

Least squares prediction of gravity anomalies, tabulating interpolation coefficients and mean square errors

17 p2734 A71-35189

Fourier series approach to gravity anomaly data representation

23 p3666 A71-43015

GRAVITY GRADIENT SATELLITES

NT APPLICATIONS TECHNOLOGY SATELLITES

NT ATS 1

NT ATS 5

NT ATS 6

NT ATS 7

Gravity gradient satellite librational dynamics under solar radiation pressure, using analytical and numerical integration methods

01 p0163 A71-10755

Gimballed reaction boom attitude control systems for gravity gradient stabilization of earth-pointing satellites, investigating performance by dynamic model simulation

01 p0165 A71-11585

Damping in gravity gradient satellite passive stabilization systems under eddy currents and dry friction induced by magnet motion

02 p0319 A71-11908

Satellite time optimal attitude control, using gravity gradient technique with active libration damping

03 p0500 A71-14434

Gravity oriented satellites librational dynamics in elliptic orbits, emphasizing atmosphere adverse effects

06 p0980 A71-18545

Rigid body stability studies with Hamiltonian as Liapunov function, noting application to flexible compact gravity gradient satellite planar motion

06 p0981 A71-18648

Stochastic Liapunov stability of satellite motion influenced by aerodynamic and gravity gradient torques, considering atmospheric density uncertainty

07 p1208 A71-19883

Equilibrium orientations of gravity gradient stabilized gyrostabilized satellites with rotor axis in principal plane, using Hamiltonian as Liapunov testing function

10 p1684 A71-24929

Inertia effects on coupled librations and stability bounds of axisymmetric gravity oriented satellites in circular orbits, using integral manifold

11 p1838 A71-26195

Damping in gravity gradient satellite passive stabilization systems under eddy currents and dry friction induced by magnet motion

13 p2144 A71-28195

Damped gravity orientated satellite linearized analysis for vibrational response to large amplitude motion

14 p2320 A71-30307

Gravity stabilized satellite in elliptic orbit, examining rotational motion equations stability

15 p2499 A71-31159

Stroboscopic and analytical studies of oscillations and stability regions of gravity gradient satellite in eccentric orbit

18 p2963 A71-36282

Worldwide data acquisition and tracking of meteorological balloon stations by flyby gravity stabilized satellite

18 p2878 A71-36528

Attitude control of gravity orientated satellite in arbitrary orbit by solar pressure, showing libration damping characteristics of radiation force

20 p3306 A71-39396

Artificial gravity field produced by rotating spacecraft in earth orbit, examining astronaut physical responses and centrifugal force effects on work tasks

21 p3342 A71-40255

Rotating space station simulator for translational and rotational motion determination under gravity gradient torque action and control under input state conditions

22 p3529 A71-41970

Planar librational motion prediction for gravity gradient satellite with extendible booms during deployment

22 p3610 A71-42014

Coupled librational dynamics of gravity oriented cylindrical satellite, calculating solar radiation pressure effects on attitude control behavior

22 p3611 A71-42042

Altitude dynamics and motion stability analysis of gravity oriented synchronous satellite under perturbation effects of environmental forces due to sun, earth, albedo and cosmic rays

22 p3612 A71-42050

Earth pointing satellites gravity gradient stabilization by thin inextensible fibers with end tip masses

22 p3590 A71-42779

GRAVITY GRADIOMETERS

Planetary gravitational fields variations determination by onboard gravity gradiometer instrumentation

23 p3729 A71-43034

GRAVITY WAVES

NT BAROCLINIC WAVES

Midlatitude atmospheric gravity waves generation by auroral heating during magnetic substorms

02 p0245 A71-11965

Lower F region ionospheric response to internal gravity waves as function of azimuth of wave propagation, noting anisotropy

03 p0420 A71-14534

Plane potential incompressible fluid flow in channel with rough bottom and variable surface pressure, allowing for gravitational and surface tension forces

03 p0406 A71-14567

Clear air turbulence due to large amplitude Kelvin-Helmholtz billows, noting simultaneous measurements by instrumented aircraft and radar

04 p0621 A71-15043

Internal gravity waves in atmospheres with realistic dissipation and temperature, considering thermal tides excited below mesopause

05 p0739 A71-16425

Shearing gravity waves /Kelvin-Helmholtz/ instability in isothermal layer model discontinuous interface application to CAT

05 p0777 A71-16667

Internal gravity wave propagation in neutral wind stratified atmospheric model

06 p0888 A71-17274

Ionization disturbances caused by gravity waves in neutral air propagating through ionosphere in electrostatic field and background wind

06 p0888 A71-17278

Quasi-stagnation levels in ion motion induced by internal atmospheric gravity waves at ionospheric height

06 p0888 A71-17280

Ionospheric response to internal gravity waves isotropic spectrum, presenting computer produced tonal value plots

06 p0893 A71-17986

Ionospheric electron content observation by ATS-3 radio signals, noting gravity waves effect

07 p1098 A71-19034

Sporadic E layer and critical frequency relationship to traveling ionospheric disturbances, suggesting role of atmospheric internal gravity waves

07 p1100 A71-19402

Book on aeronomy covering earth upper atmosphere structure, tidal oscillations, gravity waves, airglow, aurora, ionospheric disturbances, electric currents and turbulence

09 p1437 A71-22778

Motion effects on atmospheric density altitude distribution, discussing vertical waves, gravity, temperature and winds

09 p1441 A71-23645

Horizontal and vertical trace velocities of traveling ionospheric disturbances, interpreting in terms of atmospheric gravity waves

10 p1602 A71-24462

Soviet book on nonstationary waves covering gravity waves development, moving periodic pressure systems, seismic disturbances and nonhomogeneous ideal liquids

10 p1595 A71-24650

Earth eigen vibrations excitation by gravity waves tabulating energy content of even and odd harmonics overtones

10 p1607 A71-25000

Phase velocities and vertical amplitude profile nonsingular mesoscale gravity waves produced stratified jet flows by floating and deflecting earth rotation forces

11 p1793 A71-25177

Mesoscale gravity waves and jet stream stability temperature-stratified atmosphere with small wave perturbations, estimating wave phase velocities and amplitude functions

12 p1924 A71-26177

Hydrodynamic wave modes calculation for solar atmospheric model with ionization effects, noting trapped resonant gravity waves calculation agreement with observed oscillations

12 p1969 A71-27660

Similarities between ion waves in plasmas and gravity waves in incompressible fluid/steady water flow with allowance for surface tension

13 p2046 A71-27840

Rotating solar wind nonradial oscillations and energy transport, showing internal solar gravity waves effects

13 p2130 A71-29111

F 2 ion velocity and electron density perturbations in terms of gravity waves, comparing incoherent scatter techniques

14 p2230 A71-29711

Internal gravity waves numerical model allowing momentum transport interaction with mean flow

14 p2269 A71-29950

Ionospheric electron density variation at neutral acoustic gravity wave passage from continuity equation, noting ionization in wake

14 p2236 A71-30355

Atmospheric synoptic and mesoscale motions dynamic theory, including baroclinic instabilities gravity/planetary waves, tides and sea breezes

14 p2236 A71-30493

Atmospheric turbulence structure, cloud convection, gravity waves, clear air flow and surface/planetary boundary layers

14 p2270 A71-30499

Galactic spirals density wave theory based on three models rotation curve patterns observation

14 p2314 A71-30635

Finite difference methods application to numerical weather prediction problems, describing frontal depression growth and boundary conditions for short gravity wave suppression

15 p2443 A71-31357

Bondi condition gravity waves, investigating radiation and energy transfer in given coordinate system

15 p2451 A71-32726

Internal gravity waves vertical propagation in lower ionosphere from temperature and wind profiles measurements

16 p2561 A71-32800

Gravity waves over flow with nonuniform velocity distribution, investigating neutral stability problem of generation and momentum transport

16 p2557 A71-32984

Low degree gravity harmonics sources, discussing upper mantle hypothesis of mass anomalies location

16 p2563 A71-33150

Bounded sources gravitational waves generation and propagation, noting refraction phenomenon in matter presence

16 p2612 A71-33282

Orbiting satellites VHF radio signal transmission enhancement, considering focusing effect of electron density contours resulting from gravity or acoustic wave in ionosphere

16 p2543 A71-33811

Neutral atmosphere density profile data from satellite-borne accelerometer experiment, observing gravity waves propagating in north-south direction at high latitudes

16 p2570 A71-33822

Neutral winds in F region from traveling ionospheric disturbance data, investigating gravity wave hypothesis

16 p2570 A71-33822

Sporadic E layer enhancement by horizontal transport within layer, considering gravity waves interaction effect on ion density horizontal redistribution

16 p2573 A71-33960

Traveling ionospheric disturbances due to gravity wave interactions during solar eclipse of 7 March 1970, confirming electron content variations from ATS 3 polarization data

16 p2575 A71-33977

Linearized gravitation theory in macroscopic media deriving refraction of gravitational waves based on classical electromagnetism

17 p2777 A71-34588

Tropospheric stratification structure from high resolution FM/CW radar sounder, comparing with internal gravity wave atmospheric models

17 p2771 A71-35800

Weber antenna sensitivity for short pulses of gravitational radiation, giving limit for connection coefficient of piezotransducer with detector 18 p2946 A71-35979

Aircraft observed stratospheric gravity waves spectral analysis, noting differentiation between atmospheric turbulence and waves 19 p3089 A71-37500

Sporadic E layer and critical frequency relationship to traveling ionospheric disturbances, suggesting role of atmospheric internal gravity waves 19 p3053 A71-37826

Polar mesosphere internal gravity waves generation and propagation, using temperature and wind profiles from rocket grenade method 20 p3221 A71-39693

Gravity waves effects on ionospheric columnar electron content data, using Faraday rotation and differential Doppler measurements of geostationary satellite radio signals 20 p3224 A71-39717

Internal gravity wave parameters calculation from total electron content short term variations, comparing ionospheric disturbance models 21 p3373 A71-40049

Traveling ionospheric disturbances excitation in F 2 layer by passing acoustic gravity waves 23 p3665 A71-42966

Solar eclipse induced atmospheric gravity waves interference, considering resulting bow wave discrepancy with wavelike ionospheric disturbance 23 p3670 A71-43190

Sporadic E layer ionization relation to thundersquall surface pressure disturbance, considering gravity wave propagation 23 p3670 A71-43322

GRAY GAS

Steady state node simplification technique for thermal radiation in gray enclosures, including computer program 03 p0522 A71-14446

Temperature distributions and heat flux for gray gas in radiative equilibrium bounded by walls with different temperatures, using differential approximation [AIAA PAPER 70-834] 09 p1516 A71-22094

Emitting, absorbing and scattering gray gas flow through plane stationary normal shock wave, presenting governing equations linearized analysis 09 p1546 A71-23164

Periodic disturbances propagation in radiating gray gas, using singular eigenfunction expansions 13 p2165 A71-29356

Gray air flow in turbulent optically thin boundary layer, determining radiant energy transport by Patankar-Spalding finite difference procedure 14 p2338 A71-30932

Gray radiative transfer equations, bridging Planck and Rosseland mean absorption coefficients 17 p2839 A71-35557

Greenhouse effect in gray planetary atmosphere, showing thermal radiation generation and scattering with principles of invariance 18 p2970 A71-37049

Arc driven hypersonic wind tunnels total enthalpy measurement from blunt body gas cap emission, using rapid scan spectrometer for gray gas continua 21 p3364 A71-40403

Thermal dissociation reactions and radiation effects on flow variables in front of and behind strong normal shock, using gray gas approximation 24 p3822 A71-45368

GREASES

High speed low power loss spiral groove bearings self sealing grease lubricants with high shear stability and good boundary lubrication [ASLE PREPRINT 70LC-6] 08 p1322 A71-21157

Military aviation greases for subsonic commercial airplane lubricants, discussing economic and technical benefits based on service experience and testing [SAE PAPER 710411] 13 p2091 A71-28304

Yield pressure, starting torque, consistency and rheology of lubricating greases at low temperature in ball bearings [ASLE PREPRINT 71AM 1B-2] 13 p2076 A71-29489

Three greases in oscillatory bearings under various conditions of speed, load and angle of oscillation, determining effects on fretting corrosion prevention [ASLE PREPRINT 71AM 1B-1] 13 p2076 A71-29490

Solid additives, graphite and molybdenum disulfide concentration effects on liquid lubricants and greases antiwear performance 14 p2251 A71-29827

Glass transition temperature and specific heat of Apiezon N and T greases used as thermal bonding agent at cryogenic temperatures 20 p3253 A71-39267

GREAT BRITAIN

Air pollution emissions at Heathrow Airport, London, from aircraft operations, heating installations and road traffic 08 p1378 A71-21823

GREAT CIRCLES

Object constant speed motion in terrestrial orthodromy, examining Shuler vertical small oscillations stability 01 p0125 A71-10628

GREAT POLAR CAPS

U POLAR CAPS

GREEN FUNCTION

Neutron linear transport theory boundary value problems, using Green function approach 01 p0111 A71-10333

Electron gas problem in metal physics by self consistent Green function formalism, presenting momentum-space Feynman rules and integral equations derivation 04 p0631 A71-15795

Elliptical boundary value problems with conditions not in direction normal to boundary, deriving theorems on homomorphisms and Green formula 05 p0774 A71-16418

Polyvibrating equation boundary value problem solution in Fourier series form, obtaining Green function 06 p0928 A71-18226

Nonlinear approximation for coherent Green function behavior in randomly fluctuating, unbounded and statistically homogeneous medium, emphasizing large scale fluctuations 08 p1325 A71-21883

Boundary value problems in noncylindrical domains investigated by Green matrix 09 p1484 A71-22176

Thin airfoils theory in nonequilibrium magnetogasdynamics with nonuniform nonequilibrium free stream, using Green function technique 09 p1383 A71-23200

Helmholtz reciprocity theorem extension to clear turbulent atmosphere, defining Green functions to characterize optical propagation in opposite directions between parallel planar apertures 10 p1641 A71-23949

Rectangular plate and circular cylindrical shell segment under rotating moment and dynamic loads evaluated by Green function 10 p1691 A71-24812

Coupled and uncoupled versions of Hartree-Fock theory, calculating atomic system linear response to external time dependent perturbation and Green function 11 p1802 A71-26057

Adjoint Green operator use in parabolic problems with normal boundary conditions 13 p2094 A71-27804

Green tensor for large initial deformations of isotropic elastic body 13 p2152 A71-28277

Numerical solution of nonclassical problem of calculus of variations, reducing nonlinear integral equation with Green function 13 p2095 A71-28819

Two dimensional contact problem for isotropic body in triangle form on half plane, calculating elastic constants with difference Green function 13 p2156 A71-29071

Green function or Huygens principle for radiation and diffraction of electromagnetic or acoustic waves in anisotropic media 15 p2449 A71-31869

Linear two-point boundary value problem solution through integral transformation into Cauchy system with Green function as auxiliary dependent variable 15 p2443 A71-32441

Orthotropic semiinfinite elastic solid under plane strain, calculating thermal stresses in terms of Green functions [ASME PAPER 71-APM-18] 16 p2655 A71-33211

Laminar boundary layer past continuous moving surface with constant wall velocity, deriving perturbation solution in terms of Green function 16 p2560 A71-34074

Perturbation theory of invariant manifolds of dynamic systems based on Green function, deriving new existence theorems 17 p2781 A71-34930

Green functions difference interpretation for finite and semiinfinite heat receiving rods, using dimensionless unsteady heat transfer parameter 18 p2985 A71-36124

Dynamic flexibility method based on Green resolvent, presenting applications to linear damped/undamped forced/free harmonic/periodic vibration 18 p2947 A71-36177

Green tensor function for waveguides, resonators and radiating devices with boundaries coinciding with orthogonal cylindrical coordinate systems surfaces 19 p3104 A71-38339

Zero-charge and scale-invariance problems in solvable field theory model, considering Green function and vertex parts behavior under perturbation theory invariance 21 p3420 A71-41128

Singularities of Green matrix in steady state wave propagation in homogeneous anisotropic media 21 p3416 A71-41245

GRINDING [MATERIAL REMOVAL]

Stochastic, random and ordinary Green function relations for two point correlation functions in mathematical physics 23 p3698 A71-43114

Approximate periodic Green matrix solution to equilibrium equations in displacements for shell of revolution under linear loads 24 p3881 A71-44826

GREEN THEOREM

U GREEN FUNCTION

GREENHOUSE EFFECT

Space vehicle observation effect on Mars and Venus conceptions, considering origins of life, runaway greenhouse effect on earth and atmospheric circulation 14 p2308 A71-29909

Refutation of greenhouse model of Venus atmosphere from Venus 4 and Mariner 5 data, proposing volcanic activity burst hypothesis 17 p2803 A71-34835

Greenhouse effect in gray planetary atmosphere, showing thermal radiation generation and scattering with principles of invariance 18 p2970 A71-37049

GRIDS

Moire contour map enhancement by removal of unwanted noncontour obscuring patterns, considering preferability of continuously moving grid to discrete translation 05 p0749 A71-16267

Secondary losses in plane compressor grid with low aspect vanes, discussing flow characteristics dependence on fins, protruding elements and smoothed junctions 06 p0846 A71-18705

Reduction or disappearance of visual aftereffect of movement without patterned surrounding consisting of dots, concentric circles, grid pattern or vertical bars 10 p1558 A71-23744

Long term atmospheric circulation prediction model, considering horizontal grid resolution effect on truncation error 14 p2269 A71-29946

GRIFFITH CRACK

Partially closed Griffith crack shape and stress intensity factor in infinite elastic solid 01 p0172 A71-10842

Displacement and stress distribution in infinite elastic medium weakened by Griffith crack 03 p0509 A71-13909

Linear elastic fracture mechanics based on elasticity theory, discussing Griffith theory for crack behavior 06 p1001 A71-18091

Three-part mixed boundary problem concerning equilibrium of semiinfinite two dimensional elastic medium containing Griffith cracks parallel to free boundary 07 p1214 A71-20021

Brittle fracture mechanism models and connection with rheological properties of material, deriving relations for Griffith energy criterion 10 p1688 A71-24388

Two stage creep cavity growth by grain boundary sliding as shear crack and Griffith-Orowan fracture, using energy balance argument 13 p2085 A71-28504

Thin shallow initially curved sheets fracture theory, extending Griffith analysis 14 p2322 A71-29738

Stress field in elastic strip of finite width under pressure applied to faces of symmetrically situated Griffith crack 16 p2654 A71-33170

Thermoelastic axisymmetric equilibrium of elastic semiinfinite two dimensional medium with Griffith crack under prescribed heat flux 19 p3159 A71-38189

GRINDING [COMMUNITION]

Pulverized volcanogenic products and chemicals polarizing properties determination, applying to lunar surface layer 07 p1107 A71-19201

Normal albedo and polarization maximum degree wavelength dependence from terrestrial volcanic pulverized samples 14 p2305 A71-29677

GRINDING [MATERIAL REMOVAL]

NT METAL GRINDING

Grinding characteristics charts of aerospace alloys wheel-workpiece pairs for comparison with single point turning and electrochemical machining [SME PAPER EM-70-100] 01 p0090 A71-11262

Turbine and compressor blade profiles grinding, formulating mathematical rules for shaping links adaptable to programmed control 02 p0258 A71-12569

Coated abrasive grinding of Ti alloys using water, various soluble cutting oils and inorganic phosphate solutions as coolants and lubricants 11 p1771 A71-26142

Milling, band grinding, final manual polishing and tumbler polishing effect on fatigue life and surface finish of steel compressor blades 12 p1912 A71-27680

GRINDING MACHINES

Heat resistant alloys face polishing with ultrasonically cleaned grinding wheel abrasive rim surface
13 p2075 A71-28942

Carbon-graphite bound electrochemical grinding wheel, describing composition formulation, fabrication techniques, mechanical and electrical properties and performance criteria
14 p2263 A71-29654

Centerless grinding control high precision automatic invariant systems synthesis, outlining machine tool working elements inductive setters
15 p2415 A71-32185

Jet engine high pressure turbine high temperature alloy blades and vanes grinding operation, discussing testing, operating conditions and coolant application [SME PAPER MR-71-802]
15 p2416 A71-32432

Plastic deformation in hot compressed Ti, Zr and Nb carbides during diamond grinding, studying fine structure on diffractometer
16 p2584 A71-33896

GRINDING MACHINES

Submicron sectioning apparatus for studying slow carbon self diffusion in dense polycrystalline tungsten carbide
03 p0429 A71-14187

Helicopter component surface finish smoothness and residual stress requirements, using abrasive grinding belt machines with gear link mechanisms
13 p2075 A71-28943

GROOVES

NT V GROOVES
Groove depth/residual deformation/ in vibrational rolling of Ti cylindrical samples, considering impression force, cylinder and steel spheres diameters
02 p0258 A71-12641

Tall thin strip rolling in ribbed grooves, determining critical area reductions causing plastic stability loss
08 p1295 A71-20841

Self acting herringbone journal bearings optimization program for maximum radial load capacity and wide operating range via groove configurations
11 p1769 A71-25836

Ion machining techniques for cutting accurate and repeatable pumping grooves in gas bearing component materials typified by boron carbide
22 p3551 A71-41665

GROUND BASED CONTROL

NT AIR TRAFFIC CONTROL
NT RADAR APPROACH CONTROL

Steep approach to landing for jet transport aircraft noise abatement, using ground based equipment and onboard TV display
01 p0126 A71-11311

Ground based biomedical supervision of crew members during extended space missions, discussing data acquisition and transmission, astronaut medical competence, etc
01 p0027 A71-11451

Ground station central control and monitoring of satellite communications systems
02 p0224 A71-12822

Large earth station control for satellite communications system, including traffic capacity, TV transmission path breaks and logic equipment
02 p0224 A71-12824

Ground based data derivation and transmission system for multicontrol satellite communication system
02 p0225 A71-12834

Optimum VTOL aircraft landing maneuverability, using short range three dimensional surveillance system and ground computer
03 p0454 A71-13574

OAO for observations of stars, galaxies, planets and nebulae, discussing ground system and men and data systems integration
05 p0734 A71-17130

OAO simulation system including prototype spacecraft and digital computer for verifying ground system performance
05 p0734 A71-17131

Intelsat 3 Ground Control System functions, design and operation of tracking, telemetry and command stations subsystems
06 p0870 A71-18394

NASA ground based digital data processing facility for Earth Resources Technology Satellite system
07 p1067 A71-18804

Computer controlled ground based command and data acquisition software system for OAO-A2 spacecraft remote control stations, discussing interface with monitor and interrupt capabilities
08 p1259 A71-21658

Apollo real time control center large software systems development management covering implementation, integration, testing, operation and maintenance
17 p2710 A71-34620

Satellite observations for earth resources management, discussing operational ground-based remote sensor system and information extraction techniques
22 p3534 A71-41973

Extended launch windows for ground based rescue missions, using bi-elliptic rendezvous technique [AAS PAPER 71-304]
23 p3638 A71-42980

GROUND CREWS

Operational preparation and commissioning of IL-62 long distance jet aircraft, considering flight crew and maintenance personnel training at U.S.S.R. plant
11 p1743 A71-25256

Aircraft personnel radiation hazards from radioactive luminous paint on instrument dials, signs and operational elements
13 p2021 A71-29145

GROUND EFFECT

Tilt-rotor VTOL aircraft design, discussing ground proximity effects on blade bending moments and flying qualities
04 p0531 A71-15404

VHF/UHF satellite transmission, predicting multiple ground reflection effects on signal fading and effective antenna gain by computerized method
06 p0868 A71-17732

Ground effects on pressure distribution on slender wing bodies with low aspect ratio and thick cross sections
06 p0842 A71-18047

Ground boundary layer effects of fixed ground plane for powered STOL wind tunnel model, discussing flow breakdown criteria, contraction lag, strut fading interference, etc [AIAA PAPER 71-266]
08 p1232 A71-21992

Approximation of flow around jet flapped airfoil, discussing ground effect on lift coefficient increments
11 p1705 A71-26314

Longitudinal stability of ground effect airplane, discussing influence on aerodynamic characteristics of height, ground surface roughness and wing aspect ratio
13 p1997 A71-29228

Point and large sources acoustic free field measurement, predicting reflecting ground surface effects on accuracy
14 p2274 A71-30066

STOL aircraft flight characteristics in proximity to ground, comparing analytical results with wind tunnel test data [AIAA PAPER 71-579]
15 p2349 A71-32281

German monograph on incompressible potential flow field calculation about thick rectangular wings with control surfaces and ground effects
15 p2347 A71-32307

Aerodynamic characteristics of arbitrary planform wing moving near screen, ground or water surface, using vortex model
16 p2521 A71-33596

Flow field induced by aircraft trailing vortices near ground during takeoff and landing, noting experimental departure from theory
17 p2671 A71-34900

Trailing wake hazards of large transports in takeoff and landing, examining configuration stability of vortex pair in ground effect
17 p2674 A71-35757

Conical monopole antenna imaging above hemispherical ground of variable radius, plotting finite screen effectiveness from analytical and numerical solutions
23 p3655 A71-44168

GROUND EFFECT MACHINES

Forward horizontal speed influence on aerodynamic characteristics of air cushion vehicle with circular nozzles and cylindrically or conically shaped curtains
02 p0186 A71-12551

Edge jet Hovercraft dynamic stability in heaving motion, deriving two dimensional mathematical model [ASME PAPER 70-APM-QQ]
03 p0348 A71-13712

Ground effect vehicles limiting volumetric dissipations from air cushion and propulsion systems with fluid boundary by Coanda effect
07 p1019 A71-19923

Air cushion vehicle technology, considering economics, propulsion, structures, controllability, flexible skirt systems and R and D [SAE PAPER 710183]
08 p1231 A71-21713

Nuclear surface effect vehicle and subsonic aircraft for transoceanic cargo shipping, discussing mobile reactor safety tests under high speed impact conditions
09 p1492 A71-22779

High speed tracked air cushion vehicles dynamic interactions with guideways, considering model of lumped double-sprung vehicle masses traveling in tandem along simply supported beams [AIAA PAPER 71-386]
11 p1846 A71-25350

Lunar ground effect machine, discussing operation principles, design, construction, terrain advantage and scale model testing
11 p1747 A71-26528

Propulsion, guidance and stability of ground effect vehicle with perimetric Coanda fluid boundary
13 p1997 A71-29308

Air breathing nuclear propulsion, considering reactor safety in air cushion vehicles and aircraft
14 p2273 A71-29930

SK-5 air cushion vehicles evaluation including search/rescue, aids to navigation, law enforcement, safety logistics and oil pollution [AHS PREPRINT 572]
14 p2180 A71-31113

Life cycle cost optimization of STOL aircraft air tracked air cushion vehicles for operating transportation system
16 p2522 A71-33308

Digital simulation for predicting static directional aerodynamic forces and moments characteristics of air cushion vehicle configuration through 180 degrees of sideslip [AIAA PAPER 71-907]
19 p2995 A71-37111

Critical forward speed effects on two dimensional peripheral jet ground effect support systems, comparing theoretical analysis with wind tunnel model data [AIAA PAPER 71-908]
19 p2995 A71-37111

GROUND HANDLING

Boeing 747 aircraft passenger handling measurements, Frankfurt airport, discussing loading, unloading, baggage claim and customs control
09 p1430 A71-23610

Frankfurt terminal baggage conveyor system describing passenger capacity and luggage handling equipment
13 p2045 A71-29313

Lockheed L-1011 passenger jumbo jet layout ground handling and servicing
18 p2849 A71-35995

Narita site Tokyo international airport, discussing transportation, runways, ground handling, navigational aids, lighting, etc
18 p2897 A71-35995

GROUND OPERATIONAL SUPPORT SYSTEMS

Satellite communications system earth station operation and reliability, discussing staffing, main and supporting communication equipment maintenance, utilities and redundancy
02 p0224 A71-12823

Ground operations computer system for German Aeros, Symphonie and Helios satellite projects discussing communication and data processing systems integration [DGLR-70-079]
05 p0733 A71-15961

Bare base shelter/bangar expandable structures for rapid worldwide Tactical Fighter Organization deployment, noting foam and honeycomb fabrication [AIAA PAPER 71-398]
11 p1744 A71-25270

Skylab checkout and launch facilities and operations, describing modifications required for Apollo lunar missions facilities utilization at Cape Kennedy
18 p2899 A71-36474

Lunar impact targeting technique improvement for Apollo 14 mission preflight analyses and flight support operations [AAS PAPER 71-392]
23 p3732 A71-43066

GROUND RESONANCE

U GROUND EFFECT
U RESONANCE
GROUND RUN-UP
U ENGINE TESTS
U GROUND TESTS
GROUND STATE

Perturbation theory of Hookes law model for H atom, obtaining ground state energy through third order
02 p0287 A71-12499

Gas phase atomic hydrogen, nitrogen and oxygen detection by photoelectron spectroscopy of ground state, suggesting application to gas phase kinetics
04 p0548 A71-14799

Average energies of ground and excited configurations in highly ionized atoms, using orthogonalized screened hydrogenic radial functions
04 p0630 A71-14999

Atomic system ground state energy upper bound considering internuclear distances and removal of restriction for negative definite potential energy operator
04 p0630 A71-15266

Ground state energy approximate eigenvalues calculation for electron in stationary finite electric dipole field by variational approach
07 p1163 A71-19688

Rayleigh-Schrodinger perturbation energies for ground state of two electron atomic Hookes law model through tenth order
11 p1803 A71-26151

Population inversion in Cs133 ground state hyperfine levels, using CW GaAs laser at 77 K for optical pumping
12 p1913 A71-26977

Nitrogen dioxide ground and excited state self consistent fields energy calculations, discussing electronic transitions probable assignments in spectrum
12 p1934 A71-27775

Interstellar SH search for ground state main line transitions at 111 MHz
14 p2313 A71-30433

Ionization and excitation kinetics of Hg in relaxation flow zone behind shock wave front, considering electron impact role in ground state atoms ionization
18 p2951 A71-35998

Nonempirical LCAO-SCF-MO method for potential energy surface for ground state of linear helium hydrogen ion system
19 p3117 A71-37333

Filippov-Ovcharenko wave functions in form of interaction constant inverse power series for calculating two and three nucleon ground state binding energies
22 p3578 A71-42056

Formaldehyde transitions in ground and excited states at 6 cm, attaining line widths and hyperfine structure at 1-3 kHz
23 p3723 A71-42953

Zero temperature relativistic plasma ground state energy calculation using Fermi momentum and Green function
24 p3857 A71-45115

GROUND STATIONS
NT DEEP SPACE INSTRUMENTATION FACILITY
NT SPACE DETECTION AND TRACKING SYSTEM
NT STADAN [SATELLITE TRACKING NETWORK]

Automatic aerological ground station with processing and transmission facilities for radio probe and radar data

Unified S band communication system for manned space flight network ground stations

Skyнет telemetry and command stations configuration and equipment functions, discussing antenna subsystem parabolic reflector and positioning, PCM demodulation and computer systems

Skyнет ground stations design, equipment and operations, discussing antennas movement control, Cassegrain reflectors, receiving system amplifier noise temperature and tracking demodulator

Skyнет ground stations operations and equipment, discussing receiving systems parametric amplifiers, local oscillators, demodulators, noise temperature, frequency flexibility and reliability

Skyнет and SCAT ground stations system noise temperature, considering receiver, antenna and sky sources, measurement techniques and error analysis

Skyнет type 3 and 4 transportable ground stations, describing antenna, radio cabin with IF and control equipment and channeling cabin with baseband equipment

Skyнет types 3 and 4 ground stations performance, discussing antenna gain, FM carrier to noise ratio, channel capacity, error rates and system reliability

Skyнет project earth station effective radiated power and gain by dual satellite access measurements

Microwave radiometry for earth terminal and communication satellite performance measurements, including gain, tracking, noise temperature, radome attenuation, power and transfer characteristics

Earth station technology - IEE Conference, London, October 1970

INTELSAT IV earth stations communications standards, discussing receiver gain-noise temperature ratio, feed polarization, radiation power and control, transmission modes, etc

Satellite operating conditions effects on INTELSAT IV earth station design, emphasizing communications aspects

Satellite and earth station parameters effects on SPADE communication systems link budget, considering carrier power statistics, amplitude and phase nonlinearities

INTELSAT earth station operations via SPADE demand-assignment system, discussing interference requirements, frequency stability, gain flatness, etc

Skyнет types III and IV ground stations design, discussing signal flow, antenna system, SNR, tracking and transmitter channels and test facilities

Earth station modifications for INTELSAT IV operation, discussing transmission parameters, distortion control, amplifier design, etc

Communication satellite earth station technology, considering steerable antenna subsystems, high power amplifiers, terminal equipment and frequency bands allocation

Electric power supplies for communication satellite earth stations, considering methods for power availability and stability

Communication satellite autotracking by step track technique for exclusion of tracking feeds and multiple receiver channels in earth stations

Communication satellite earth station steerable antennas drive train resonance and traction drive wheel slippage control by differential velocity feedback, discussing analog simulation

Communication satellite ground station steerable antenna autotracking, evaluating on-line optimal search techniques by digital simulation

High efficiency spherical reflector antennas with scanning and multiple feed properties for communication satellite portable earth stations

Gain/temperature measurement test set for earth station receiving system by radio sources program tracking unit, noting antenna power ratios determination by attenuator

Gain/temperature measurement for earth station antenna and receiving subsystem by FM method, determining Y-factor/noise power proportional increase/

Atmosphere effects on antenna noise temperature variations in G/T value for earth station performance in satellite communication system

Waveguide feeder system design for antenna receive path of Intelsat 3 satellite ground station, considering system noise temperature

Antenna primary feed design and sample and store technique tracking system with conical scan control for Intelsat 3 satellite ground station

Earth station antennas structural parameters and performance prediction, considering autotrack loop stability optimization by multiple lag compensation using single axis model

Skyнет satellites earth stations design, structure, transportation and erection ease, considering operational and stowed position survivability in high velocity winds

Frequency selective conical scanning for direction finding earth station antennas for communication satellite automatic tracking, using waveguide mode conversion

Satellite communication system earth station transmitter with FDM-FM and SPADE carriers, noting intermodulation effect on channel capacity

Uncooled low noise microwave parametric amplifier for small receiving earth stations, describing three stage design, gain and bandwidth

Satellite ground station autotracking receivers, discussing antenna position control systems

Ground station integrated receiver cabinet formed by down-converter, demodulator and baseband equipment packaging

Earth station mixers design as wideband millimeter wave up- and down-converters for satellite communication systems

Ground station central control and monitoring of satellite communications systems

Ground station power control in multiple access satellite communication system

Communication satellite systems ground stations operating personnel training, outlining basic and specialized study and on-job training program

Military earth communication station maintenance, noting mobility, environment, logistics and reliability

Large earth station operation and maintenance for international communications, noting control consoles, static tracking, aerial flexibility, transmitter reliability, etc

Earth station equipment for Intelsat 4, discussing thermal noise, transmitters, wideband receivers and demodulators

Earth station communication system planning for Intelsat 4, discussing telephony and TV transmission

Microstrip double down-converter receiver for satellite earth stations, describing thin film integrated circuits and carrier selection

European ground stations geodetic surveys by laser range measurements and photographic observations of satellites with reflectors

Three dimensional traverse in geocentric Cartesian coordinates for connection of two adjacent satellite observation stations

Intelsat system earth station on-site planning considerations for integration with existing wideband communication system and traffic ground demand

Range and range rate measurement errors between ground station and artificial satellite, investigating atmospheric refraction effects

Orbiting satellite targets assignment and scheduling to ground stations, presenting mathematical formulation and numerical example

OAD for observations of stars, galaxies, planets and nebulae, discussing ground system and men and data systems integration

OAD simulation system including prototype spacecraft and digital computer for verifying ground system performance

Intelsat global network demand assignment multiple access system, discussing traffic density and earth station functional requirements

Intelsat 3 Ground Control System functions, design and operation of tracking, telemetry and command stations subsystems

Buitrago /Spain/ earth station for Intelsat operation, discussing tracking antenna design and performance

Indonesian Intelsat 3 earth station equipment, operation and performance

Intelsat 4 satellite optimum channel capacity as function of earth station performance

Central station of German ground system for satellite data acquisition, tracking and telecommand

Propagation modes involved in HF or VHF reception at ground station of beyond-horizon satellite transmission

Statistical model for interference to terrestrial radio relay systems from geostationary satellites

Ground space facilities protection from lightning and electromagnetic interference

Communication satellite station at Fucino /Italy/, testing receiving and transmitting equipment transmission quality

Group delay and amplitude equalized bandpass elliptic function filters for ground stations of communications satellite system

VOR/DME ground station oriented aircraft area navigation horizontal guidance capability, discussing digital input/output flight control

Guiana Space Center facilities and equipment, describing computerized and automated real time telemetering and data processing systems for spacecraft tracking

Satellite communications earth station antennas, describing antenna elements and subsystems analysis, design and performance

French Geole spatial system utilization in polar zones, combining satellite with ground beacons, telemetry ground receiving station and computer

Riser whistlers observed at low latitude ground station, noting time delay increase with frequency

Ground stations for communication satellites, discussing radio transmitter and receiver systems using low noise parametric amplifiers at low temperatures and extended demodulator threshold

Communication satellite ground station radio receiver and transmitter systems including parametric amplifier and phase lock demodulators applications

Measurement system for communication satellite ground station equipment including parametric amplifier, wideband receiver, power oscillators, and radio transmitters and receivers

Intelsat system ground station equipment testing including antenna radiometric gain, noise temperature, energy dissipation, telephone and TV performance measurements

Parametric amplifier design and construction for communication satellite ground station, discussing noise temperature, distortions, bandwidth and antenna gain

Threshold-extension phase-lock demodulator design for optimizing satellite communication ground station systems, using FM carriers

International coordinated measurements of solar activity geophysical effects in upper atmosphere, discussing synchronized observations of Cosmos 261 satellite and ground based ionospheric station network 11 p1816 A71-25762

Satellite geodetic global networks employing triangulation, trilateration and height measurements, deriving dominant point observation stations /Hazy-Tarczy method/ 11 p1759 A71-25816

Intelsat 4 transmission subsystems design, discussing alternative high power amplifier configurations, redundancy and emergency routing of transmitted RF carriers 12 p1894 A71-26992

Satellite communication earth stations time division multiple access systems, discussing operational principles and configurations 12 p1895 A71-27000

Satellite communication earth stations tracking receiver, describing operational principles with special attention to down-converter and demodulator circuits 12 p1887 A71-27001

Insufficient auroral electron spectra and pitch angle distributions from ground based altitude luminosity profiles 13 p2054 A71-27802

Microwave receiving antenna with solid state power rectifier for converting energy from space solar cell array into DC power on earth 13 p2000 A71-28671

Raisting ground radio station second antenna system, discussing design for all weather performance 14 p2214 A71-30812

Satellite telemetry systems for data transmission to developing nations ground stations decoding equipment 14 p2199 A71-30910

ATC satellites providing communications channels between aircraft and ground control stations and aircraft localization 16 p2605 A71-32849

Millimeter broadband high power traveling wave transmitter tubes with stub voltage tuning for ground stations of satellite communication systems 16 p2545 A71-32975

Satellite systems for educational TV program distribution, discussing orbit utilization, ground stations and ATS program 16 p2645 A71-33588

UK space research programs, discussing ground based, satellite and rocket-borne experiments 16 p2666 A71-33859

Daytime occurrence of maximum wave reflection frequency and blanketing frequency for period of two solar cycles at Rarotonga and Christchurch stations 16 p2574 A71-33970

Space radio communications, considering radio links reliability between multistage launcher rocket and ground stations 17 p2696 A71-34228

Intelsat system, describing organization, satellites, space segment support elements and ground stations 17 p2811 A71-34230

Satellite telecommunication systems, considering standard and small transportable ground stations and Intelsat system 17 p2696 A71-34233

Satellite communications use of geostationary orbit, considering ground station antennas radiation patterns, signal processing, stationkeeping, etc 17 p2696 A71-34234

Low noise FET amplifiers for earth station radio receivers 17 p2715 A71-34687

Communications capability of Canadian domestic satellite system, outlining performance parameters of satellite and earth stations 17 p2703 A71-35080

Reduced cost ground stations for satellite communications system and applicability to small nations, using single channel per carrier FM and companders 17 p2704 A71-35087

Earth stations operating in Intelsat System, discussing mandatory performance requirements and design approaches 17 p2705 A71-35100

NASA ERTS program, discussing system concept automatic data processing capability, compatibility with tracking ground stations and international cooperation 17 p2805 A71-35329

Intelsat satellite-earth station communications technology, considering microwave line of sight techniques 17 p2707 A71-35333

Satellite communication ground station center in conjunction with Intelsat 3 satellites system for transcontinental telephone links 17 p2708 A71-35508

Second Pleumeur-Bodou /France/ ground station for Telstar satellite communication, discussing equipment specifications, Cassegrain antenna and parabolic reflector 17 p2708 A71-35509

Pleumeur-Bodou /France/ ground station steerable parabolic reflector Cassegrain antenna for communication satellites, discussing specifications and radioelectric and mechanical characteristics 17 p2717 A71-35510

Electronic and hydraulic devices for communication satellite ground station steerable antenna servocontrol, driving and pointing, discussing tracking error signals 17 p2724 A71-35511

Intelsat 3 satellite communication ground station radio receiving and transmitting equipment design 17 p2724 A71-35512

Low noise parametric amplifiers for communication satellite ground station radio receivers, considering components characteristics 17 p2709 A71-35513

Communication satellite ground station receiver-demodulator equipment using frequency double transposition and compression 17 p2717 A71-35514

Communication satellite ground station transmitting equipment, discussing carrier waves, FM, frequency converters and microwave amplifiers characteristics 17 p2717 A71-35515

Communication satellite ground station terminal equipment, discussing carrier current telephone, video and sound TV apparatus 17 p2717 A71-35516

Communication satellite ground station electric power generation and distribution equipment characteristics, emphasizing reliability 17 p2724 A71-35517

Remote control and surveillance equipment for communication satellite ground station, discussing console and engineering service circuit designs 17 p2709 A71-35518

Communication satellite ground station equipment modifications for second station compatible with Intelsat 3 17 p2709 A71-35519

Meteorological objectives, radiometry and ground stations for Meteosat weather prediction system using geostationary satellite 18 p2878 A71-36527

Antenna system design for communication satellite ground station operating in 10.7-35 GHz range 18 p2881 A71-36556

Low noise parametric amplifier design and construction for Intelsat 4 satellite communications earth stations 19 p3027 A71-37496

Cloud cover charts for North Atlantic-European-North African region, comparing satellite and ground station visual observations 20 p3258 A71-39552

Ground based optical observation of raylike artificial auroras produced by rocket-borne accelerator generated electron beams, using image orthicon TV system 20 p3231 A71-39886

Satellite tracking ground antenna servocontrol, discussing system requirements and automatic and programmed operating modes 22 p3483 A71-41520

International coordinated measurements of solar activity geophysical effects in upper atmosphere, discussing synchronized observations of Cosmos 261 satellite and ground based ionospheric station network 22 p3591 A71-41530

Differential correction for redetermination of satellite observation stations geodetic coordinates as related to earth center of gravity and terrestrial potential coefficients 22 p3534 A71-42023

Geodetic locations of Doppler satellite observing stations consistent with CIO pole and astronomical determinations 23 p3666 A71-43014

GROUND SUPPORT EQUIPMENT
NT GROUND OPERATIONAL SUPPORT SYSTEM

Space systems aerospace ground support equipment environmental testing criteria under varying conditions for optimal operation and deterioration reduction in use and storage 01 p0067 A71-10104

Ground space facilities protection from lightning and electromagnetic interference 07 p1084 A71-19947

Components field failure rates assessment methods for ground support equipment 09 p1454 A71-22618

Space shuttle onboard vs ground checkout systems, considering vehicle autonomy and cost reduction 09 p1427 A71-22623

Ground deicing system for transport aircraft, discussing antifreeze liquid spray application after mechanical snow removal 09 p1428 A71-22948

Soviet book on aircraft ground support and onboard radio equipment operation and reliability increase by redundancy and rational methods, discussing preventive maintenance 10 p1583 A71-24670

Equatorial CECLES/ELDO base management a study of launch operations, discussing installation facilities, equipment and personnel 12 p1894 A71-26992

Tacsat 1 telecommunications relay system, discussing UHF-SHF antenna radiation pattern, ground terminal equipment, nutation dampers and attitude and orbital correction procedures 12 p1882 A71-27616

Mobile LF air navigation AN/MRN-13 equipment operation and maintenance 23 p3702 A71-43811

GROUND SUPPORT SYSTEMS
NASA Office of Tracking and Data Acquisition mission support and ground and spacecraft communication networks 04 p0551 A71-14914

Space shuttle ground operations analysis emphasizing cost effectiveness, discussing breakdown in ground support activities, facilities and equipment 09 p1427 A71-22616

Lunar Mapping Camera ground support operations, describing pre and post mission assistance, stellar field calibration and data reduction 09 p1429 A71-23222

Space shuttle program sustaining engineering and hardware logistics support 12 p1894 A71-26656

NASA earth resources technology satellites system, discussing ERTS A and B development, payloads and ground support systems and international aspects 16 p2630 A71-32859

German space operations center for performing ground operations for Azur research satellite 16 p2553 A71-33740

Airline operations approach to Cape Kennedy launch processing system for reduced hardware and operational costs of shuttle support 18 p2899 A71-36470

Skylab program data management systems, discussing onboard data collection, transmission and ground facilities 22 p3610 A71-42008

Operations and equipment of NASA ground data handling system for earth resources technology satellites 22 p3509 A71-42011

Climatological studies and weather forecast support for Apollo 14 mission prelaunch, launch, emergency landing and terminal areas 24 p3845 A71-44981

GROUND TESTS
NT COLD FLOW TESTS
NT PRELAUNCH TESTS

Skylab, space station and shuttle programs covering economics, international participation and ground and flight tests 04 p0661 A71-14923

Automatic excitation forces generation for aircraft structure ground vibration tests using digital computers [ONERA-TP-870] 04 p0669 A71-15351

Ground test reactor design based on colloid fuel reactor concept 07 p1158 A71-19861

Space shuttles thermal-structural cost effective ground testing 09 p1531 A71-22620

SERT 2 spacecraft ion thruster ground tests and flight operation, tabulating performance data 09 p1511 A71-22889

Continuous flow arc air heater for reentry vehicle components ground testing, achieving combined high pressure and enthalpy 09 p1429 A71-23061

Aircraft continuous elastomechanical system parameters determination by ground vibration tests using integral equation, phase resonance and separation technique 10 p1692 A71-24946

Driver terrestrial in-core thermionic reactor dynamic behavior, discussing computerized simulation with respect to coolant loop 11 p1711 A71-25881

Ground based flight equipment evaluation in routine primary pilot training 12 p1875 A71-27241

Jet fighter-bomber aircraft noise survey, discussing sound pressure levels and frequency analysis during ground running, speech interference levels and ear protectors requirements 12 p1875 A71-27621

Thermal ground testing of Concorde and Veras considering static and fatigue testing in heat environment 18 p2899 A71-36461

German VAK 191B combat VTOL aircraft development program, describing prototype ground tests, at topilot preoptimization and hover flight tests 22 p3482 A71-41511

Dynamic stability analysis, ground testing and corrective accumulator devices for POGO oscillations in space booster structure 22 p3609 A71-41999

Apollo/Saturn 5 propulsion system design, development, testing and integration 22 p3589 A71-42021

Apparatus for dynamically equivalent ground tests of satellite instrumentation and attitude control system
24 p3817 A71-45273

GROUND TRUTH
Ground relief representation by contour lines and by profiles, noting error possibilities
01 p0074 A71-11328
Ground truth role in remote sensing surveys from space, considering field measurement techniques in calibrating sensor imagery and unknown terrestrial environment
11 p1760 A71-26532
Simulation tests of multiagency reconnaissance sensor operations, including multisensor data base, imagery processing laboratory, flight testing and ground truth activities
17 p2775 A71-35764

GROUND WAVE PROPAGATION
Tropospheric diffraction fields computation in atmospheres with modified refractive index increasing monotonically with height, discussing IF and LF ground wave propagation
04 p0552 A71-15020
Spatial statistical coherence of X band propagation over path near ground
04 p0552 A71-15211
Ground wave propagation over nonuniform overburden with arbitrarily varying complex dielectric coefficient and depth, discussing application to water table mapping
09 p1436 A71-22644
Pseudoacoustic energy flux influence on accessibility of ground emitted wave to plasma resonance in F region, using adiabatic approximation with scalar pressure
10 p1602 A71-24465
Interference pattern of ground and sky waves at 16 kHz during summer near solar maximum
12 p1880 A71-27155
C band SYDAC system compatible with conventional ILS, considering transmission sensitivity to ground reflection and lateral obstacles
15 p2445 A71-31910
Geometrical-optical approximation for residue series of obstacle/terminal/gain in radio wave propagation over inhomogeneous earth
22 p3511 A71-42281
Amplitude prediction for terrestrial radar echoes from ground using topographical data
22 p3514 A71-42469

GROUND WIND
Synoptic and microscale variance spectrum of horizontal wind velocity at 50 m above ground, comparing with perturbations models
20 p3257 A71-39439

GROUND-AIR-GROUND COMMUNICATIONS
ATC station ground to air communication via VHF tropospheric scatter, discussing high power radio transmitters and low noise over the horizon receivers combination
10 p1576 A71-24175
Low carrier power aircraft antenna module for airborne UHF communications system, considering range/field strength measurements
14 p2216 A71-31046
Airborne videodisc visual communication system for transmitting single frame TV information in digital form from air to ground over narrow and wideband circuits
17 p2709 A71-35760
Omnidirectional one slot aerial energized by dielectric waveguide for hypersonic vehicle-ground communication through ionized shock layer
[ONERA-TP-949] 18 p2887 A71-36022
Ground-aircraft link via synchronous communication satellite, discussing transmission frequency selection, ionospheric effect on propagation and satellite antenna
19 p3016 A71-37314
Space communications period forecasting algorithm for limited power ground based transmitters and spacecraft in earth orbit
19 p3022 A71-38502
Swept frequency or chirp signals for data transmission and pulse compression, considering long range air ground communication in HF band
22 p3510 A71-42277

GROUND-TO-AIR MISSILES
U SURFACE TO AIR MISSILES

GROUP BEHAVIOR
U GROUP DYNAMICS

GROUP DYNAMICS
Psychoreactive action caused by flying accident in group, discussing repercussions in civil and military aviation fields
10 p1572 A71-24982
Fighting between male mice isolated at early age or reared in small groups, considering ontogenetic and experiential determinants
13 p2011 A71-28805

GROUP THEORY
NT AUTOMORPHISMS
NT HOMOMORPHISMS
NT SUBGROUPS

Shear-invariant mean value of positive-definite operator on bicompart group in form function of integral sequence, considering ergodic theorem
01 p0110 A71-10097
Commutative nilpotent semigroups, discussing necessary and sufficient conditions for freedom within manifolds
02 p0276 A71-11725
Orthotropic plate dynamics, examining plane vibrations with group theory approximate equations
06 p0993 A71-17818
Lorentz group infinite dimensional representation, establishing forms for all irreducible unitary representations
08 p1324 A71-21359
Self similar invariant group solutions to Belman nonlinear partial differential equation for optimal correction problems of control systems motion with random disturbances
16 p2549 A71-32935
Elementary particle geometrical-group model assuming negative curvature de Sitter space inside and flat space outside
17 p2778 A71-34627
Basis functions for arbitrary time variable network symmetries for large scale integration, using group theory
19 p3038 A71-38488
Soviet papers on geometrical and group methods in gravitational and elementary particles theory, covering relativity and electromagnetic and quantum fields
19 p3104 A71-38578
Wave and elementary particles equations invariance properties relationship with respect to Lie group and conservation laws
19 p3105 A71-38579
Viscometric motions of continuous bodies, studying kinematics and dynamics of d'Alembert, homogeneous and circulation preserving groups
20 p3309 A71-39567
Exact solutions of elasticity theory nonlinear differential equations by Lie group theory methods
24 p3877 A71-44480
Finite sigma groups complemented with quasi-permutable operators
24 p3843 A71-44796
Frobenius group theorem, discussing invariant and additional Frobenius multipliers, Schmidt criteria and theorem applications
24 p3843 A71-44823
Type CS finite groups characterized by nonexpandability into Silov subgroups, defining group order divided into two different prime numbers
24 p3843 A71-44824
Minimax groups relation to group classes with maximality and minimality conditions
24 p3843 A71-44825
Microwave structures symmetry analysis based on group theoretic concepts application to vector electromagnetic fields, investigating single wire helix
24 p3809 A71-45090

GROUP VELOCITY
Magnetospheric whistlers, deriving group refractive index and velocity, propagation time and various L values
05 p0721 A71-16443
Group delay times criterion of multibeam propagation of ionospheric radio echoes for communications systems
06 p0869 A71-18281
Radio signal receiving system design for group delay experiments with geostationary ATS-F for ionospheric and magnetospheric electron content
07 p1206 A71-19033
Group delay and amplitude equalized bandpass elliptic function filters for ground stations of communications satellite system
07 p1082 A71-20412
Group delay time differences in locating sources of atmospheric dependent on arrival azimuth, time of day and season
14 p2237 A71-30959
Ultrashort pulse formation in short pulse stimulated Raman oscillator, achieving partial group velocity matching
19 p3071 A71-37475
Radio signal group trajectory in ionosphere expressed as series expansion in terms of increasing power of beam reflection height
19 p3020 A71-38371
Microwave radio signals refraction angles and group delay times for biexponential model of ionospheric electron density profile
24 p3805 A71-45253

GROUP 1A COMPOUNDS
U ALKALI METAL COMPOUNDS

GROUP 2A COMPOUNDS
U ALKALINE EARTH COMPOUNDS

GROUP 3A COMPOUNDS
Group 3A suboxides IR absorption spectra at liquid helium temperatures, measuring bending frequencies and modes
16 p2538 A71-32875

GROUP 4B COMPOUNDS
Group 4 and 5 transition metal carbides thermal expansion determined on quartz dilatometer at various temperatures
05 p0768 A71-16789

GROUP 5B COMPOUNDS
Group 4 and 5 transition metal carbides thermal expansion determined on quartz dilatometer at various temperatures
05 p0768 A71-16789
Internal friction solid solution weakening of bcc group V-B alloys
08 p1309 A71-21524

GROUP 6A COMPOUNDS
Low temperature and composition effects on alloy softening in group 6A metals alloyed with Re
11 p1781 A71-26293

GROUP 7A COMPOUNDS
U HALOGEN COMPOUNDS

GROWTH
NT CROP GROWTH
NT CRYSTAL GROWTH
NT CZOCHRALSKI METHOD
NT EPITAXY
NT HYDROTHERMAL CRYSTAL GROWTH
Algae survival and growth under adverse conditions, considering high and low temperatures, desiccation and halophilism
07 p1048 A71-19522
Mitotic activity of kidney undergoing compensatory hypertrophy in high mountain nonadapted rats
08 p1242 A71-21965
Neurospora germination and growth in medium of low water activity due to NaCl or nonelectrolyte addition
11 p1721 A71-26146
Chronic centrifugation effects on water intake and urine output in mice, considering food intake and growth rate
20 p3186 A71-38984
Auxin transport and geotropic response of roots and shoots, discussing plant growth mechanisms under stimulation-inhibition conditions
21 p3340 A71-39980
Geotropic mechanisms of lateral auxin movement and polar transport of growth substances/ethylene/without differential cell enlargement
21 p3340 A71-39982
Linkage mechanism between gravity receptors and auxin redistribution causing differential growth and geotropic curvatures in plants
21 p3340 A71-39983
External indole-3-acetic acid effect on elongation and geotropic bending of Avena coleoptiles related to auxin induced electrical responses
21 p3340 A71-39986
Gravity influence on plant growth, lateral development, apical dominance, bud initiation, orientation and flower morphology
21 p3340 A71-39999
Chronic acceleration effects on animals, considering life expectancy
21 p3328 A71-40003
Gravity effects on auxin transport, growth and foliage spread of green plants for efficient radiation capture, using horizontal clinostat experiments
21 p3341 A71-40005
Soviet book on experimental research on human higher nervous activity from growth aspect covering normal and pathological states, cerebral cortex interaction with central nervous system
21 p3339 A71-41374
Lettuce seedlings growth reduction and geotropic and phototropic behavior modification by 3-4prime chlorophenyl 3-methoxy phthalide, noting gravity response elimination through action on statoliths
23 p3639 A71-43143

GRUMMAN AIRCRAFT
NT F-14 AIRCRAFT
NT F-111 AIRCRAFT

GRUNEISEN CONSTANT
Temperature effects on tungsten lattice and Gruneisen parameters and thermal expansion coefficients at low temperatures by X ray method
22 p3561 A71-41724

GUIDANCE [MOTION]
NT AIRCRAFT GUIDANCE
NT COMMAND GUIDANCE
NT INERTIAL GUIDANCE
NT INJECTION GUIDANCE
NT MAP MATCHING GUIDANCE
NT MIDCOURSE GUIDANCE
NT REENTRY GUIDANCE
NT RENDEZVOUS GUIDANCE
NT SATELLITE GUIDANCE
NT SPACECRAFT GUIDANCE
NT STRAPDOWN INERTIAL GUIDANCE
NT TERMINAL GUIDANCE
Indirect, linear and nonlinear optimal guidance schemes from precomputed reference trajectory, using iterative techniques for boundary equations
03 p0454 A71-13449

GUIDANCE SENSORS

- Automatic solar and lunar reference guidance system with balanced photoelectric measuring equipment 04 p0591 A71-14846
- Soviet monograph on differential games of encounter of motions covering optimal control, rendezvous, pursuit, evasion, extremal guidance, etc 06 p0926 A71-17438
- Unmanned lunar roving vehicle remote guidance, discussing onboard vs on-earth steering and velocity control, imaging system, obstacle detection and avoidance 08 p1331 A71-21325
- High speed tracked air cushion vehicles dynamic interactions with guideways, considering model of lumped double-sprung vehicle masses traveling in tandem along simply supported beams [AIAA PAPER 71-386] 11 p1846 A71-25350
- Quasi-optimal proportional navigation, deriving feedback guidance laws for interceptor aerodynamically controlled missiles 11 p1796 A71-26409
- Differential guidance game with aftereffects, investigating extremal strategies 12 p1931 A71-27522
- Automatic telescope guidance system for faint light source tracking, using cumulative photocurrent mismatch signal storage 14 p2271 A71-29994
- Control, navigation and guidance review, considering application of earth reference coordinates for aircraft, missiles and spacecraft 14 p2272 A71-30710
- ## GUIDANCE SENSORS
- Stellar photoelectric servo guide with photon counting in mismatch sensor for telescope positioning 04 p0590 A71-14845
- Optimum orientation and accuracy of redundant sensor arrays in space navigation, guidance and attitude reference systems [AIAA PAPER 71-59] 06 p0925 A71-18518
- Space vehicles solar orientation sensors, discussing construction, configuration and direction finding characteristics 12 p1972 A71-27485
- Sensing and communications technologies for short wayside headways, considering applicable equipment for personal rapid transit systems, modulation, coding and data transmission techniques 14 p2195 A71-30337
- Pulsed relay control system for stabilizing spacecraft orientation in flight, allowing for changes in characteristics of guidance sensor systems and slave mechanisms 16 p2646 A71-33660
- Space shuttle scanning beam landing guidance system, discussing accuracy in penetration, alignment, flare out and touchdown maneuvers and trajectories 17 p2773 A71-35068
- Star sensor telescope, employing digitally coded silicon photocell detector for precise optical image location 18 p2925 A71-36910
- Space transport rendezvous and docking techniques, emphasizing guidance, propulsion system configuration and sensors 19 p3149 A71-37306
- Onboard silicon detector TV guidance sensor for establishing outer planet mission spacecraft orientation with precise targeting, based on patched conic trajectory simulation [AAS PAPER 71-120] 19 p3101 A71-37915
- Terminal guidance sensing from spinning spacecraft in swingby mission to outer planets [AAS PAPER 71-121] 19 p3101 A71-37916
- Solid state modulation for spacecraft horizon sensing via IR carbon dioxide atmospheric radiation, proposing Fabry-Perot structure with controlled plate separation 22 p3537 A71-41475
- Vehicle attitude determination and guidance sensor orientation by vector space matrix method, minimizing errors by weighted least squares affine transformation technique [AAS PAPER 71-396] 23 p3773 A71-43064
- ## GUIDANCE STABILITY
- ### U CONTROL STABILITY
- ### U GUIDANCE [MOTION]
- ## GUIDE VANES
- ### NT JET VANES
- Guide vanes small aspect ratio effect on high pressure stages of axial flow compressors 02 p0186 A71-12558
- Solidified Ni-Mo-Al gas turbine guide vane alloy with improved melting point, creep rupture strength and structural stability 03 p0431 A71-13256
- Superalloy turbine engine guide vane thermal fatigue cracks repair by plasma arc fusion method 03 p0432 A71-13257
- Gas turbine engine nozzle guide vanes under pulsed thermal operation, discussing service life evaluation and increase 05 p0827 A71-16756

- Nozzle vane air cooling system for deflector type gas turbines, estimating profile perimeter average temperature for given coolant air flow rates 11 p1856 A71-26053
- Gas turbine engine nozzle guide vanes under pulsed thermal operation, discussing service life evaluation and increase 17 p2832 A71-35455
- Cascade displacements and stresses in nozzle ring guide vanes with sectional diaphragm under axial and circumferential flow 18 p2980 A71-36706
- Vacuum brazing for nozzle guide vanes repair in aircraft gas turbine engines, noting economic advantages 19 p3069 A71-38313
- Transonic and supersonic turbine guide vanes, noting air as flow medium in experiment and steam in actual turbine 20 p3176 A71-39455
- Normal shock existence in blade spacings of rotor and guide vanes of axial flow supersonic compressor as function of pressure nonuniformity 22 p3479 A71-41843
- Circumferentially nonuniform flow in front of axial compressor stage with stepwise two zone pressure and velocity distribution resulting in increased guide vane losses 22 p3479 A71-41845
- Axial flow compressors stable operation, using rotating guide vanes regulation 23 p3626 A71-43554
- Plane cascades efficiency and exit blade angles dependence on cooling air admitted to air-gas flow area from exhaust nozzle guide vanes 24 p3864 A71-45009
- ## GUIDED MISSILES
- ### U MISSILES
- ## GUINEA PIGS
- Guinea pigs vestibular adaptation to repeated angular acceleration dependent on acceleration direction 01 p0012 A71-11056
- Methionine S 35 uptake rate changes in auditory analyzer receptors and neurons due to sonic stimulation in guinea pigs 06 p0850 A71-17393
- Young guinea pigs thermal adaptation tests at different temperatures and environmental conditions, observing threshold temperature shifting for shivering and heat polypnea 18 p2858 A71-36863
- ## GULF STREAM
- Atlantic Ocean surface temperature distribution data for Gulf Stream meanders and eddies, usingITOS 1 satellite direct readout IR images 17 p2734 A71-35216
- ## GUM VULCANIZATES
- ### U VULCANIZED ELASTOMERS
- ## GUMBEL THEORY
- ### U RANGE [EXTREMES]
- ## GUN PROPELLANTS
- Thermodynamic calculation of chemical equilibrium of rocket propellants and gun powders using computer program in Fortran IV 01 p0141 A71-10343
- Rocket propellants and gun powders performance calculation, using FORTRAN IV program 04 p0637 A71-15678
- Surface temperature discrepancy during flameless vacuum burning of trinitroglycerin gunpowder due to vaporization of volatile components 15 p2462 A71-31373
- Gunpowder mean burning rate at constant pressure with periodic variation of heat influx into flame zone 15 p2462 A71-31374
- Gunpowder unsteady burning as closed dynamic system, studying frequency characteristics and transient processes 15 p2462 A71-31375
- Burning gunpowder temperature measurement in gaseous phase, describing thermocouple method 15 p2463 A71-31388
- ## GUNN EFFECT
- Shift register based on coplanar Gunn diodes for pulse processing, considering diodes application to logic circuits of digital instrumentation and communication systems 01 p0052 A71-10323
- Varactor-tuned Gunn diode oscillators, discussing computerized design, circuit analysis and device characteristics 01 p0054 A71-10974
- Microwave Gunn diodes I-V characteristics as function of carrier concentration 01 p0057 A71-11213
- Gunn diodes I-V characteristics width as function of carrier concentration/mobility and diode length, noting role of impact ionization in strong electric field 02 p0231 A71-11877
- Gallium arsenide devices in microwave communications, discussing Gunn oscillators, FET, varactors and radar applications 02 p0231 A71-12049

- Stable tunable microwave source for spectroscopy using Gunn diode, giving microwave cavity spectrometer block diagram 03 p0428 A71-13929
- Gunn oscillator frequency characteristics vs displacement voltage in low Q factor resonance circuits 04 p0557 A71-14634
- Gunn diode generated signal frequency jumps as function of voltage variations, basing explanation on high field domain formation and decay 05 p0729 A71-16999
- Coplanar n-type GaAs Gunn effect microwave oscillators failure mechanism, suggesting role of current filament formation in thermal breakdown 06 p0874 A71-17661
- Microwave Gunn diodes made from GaAs single crystals, describing fabrication by diffusion process 06 p0876 A71-18083
- Neutron irradiation induced degradation in epitaxial Gunn diode performance 07 p1071 A71-19069
- Gunn diodes impedance measurement at bias voltage above threshold, using broadband equivalent circuit model for mount and package 07 p1072 A71-19103
- Parasitic reactances in Gunn effect device packages from microwave equivalent circuit parameters 07 p1072 A71-19104
- Frequency saturation effects in transferred electron/Gunn/microwave oscillators mechanical tuning characteristics in conventional waveguide cavities 07 p1072 A71-19105
- Postcoupled waveguide cavity Gunn effect microwave oscillator equivalent circuit analysis, using lumped constant elements 07 p1072 A71-19106
- Waveguide cavity CW Gunn microwave oscillator bias voltage controlled amplitude and frequency modulation 07 p1073 A71-19110
- Broadband pulling cavity stabilized X band Gunn oscillator, using measured circuit and diode admittance 07 p1073 A71-19112
- Self pumped parametric amplification and oscillation of Gunn effect diodes 07 p1075 A71-19262
- IMPATT and Gunn microwave oscillators injection phase locking, discussing stationary state synchronization theory and phase vs frequency deviation measurements 08 p1263 A71-20990
- Microwave oscillators with Gunn effect device resonant circuit and YIG tuning, discussing design and performance 08 p1263 A71-20991
- Wideband UHF amplification in bulk n-type GaAs during domain generation, comparing cut-off and Gunn frequency 09 p1507 A71-22223
- Hysteresis effects during retuning of n-type GaAs Gunn oscillator with bias source and RLC circuit, showing range of domain damping by low field 09 p1414 A71-22228
- Gunn diodes temperature, calculating power density dissipation by simple domain mode models and accumulation mode operation 09 p1414 A71-22249
- Second harmonic voltage effects on quenched domain mode Gunn effect oscillator for DC to RF conversion efficiency, discussing negative device conductance at multiharmonic frequencies 09 p1417 A71-22696
- CW X band frequency-locked Gunn oscillators as frequency demodulator with millivolt range detection sensitivity 09 p1421 A71-23720
- Varactor tuned X band Gunn oscillator with lumped thin film microwave circuits, discussing GaAs materials, output powers and bandwidths 09 p1421 A71-23722
- Gunn diode with capacitive probe on side surface for signaling strong field domain passage, calculating maximum permissible microwave coupling 10 p1584 A71-24721
- Gunn diodes and heterojunction laser applications in optical pulse communication systems synthesis 11 p1772 A71-25235
- Tunable Gunn oscillator obtained by semiconductor surface loading, discussing oscillation frequency as function of anode to edge distance 11 p1738 A71-26365
- Cavity controlled Gunn effect oscillators FM-current noise ratio, studying device current and domain capacitance as functions of carrier concentration and GaAs layer internal field 11 p1739 A71-26433
- Gunn diode operation at below threshold bias voltage, investigating microwave oscillations amplification 13 p2036 A71-27955
- Microwave integrated stripline Gunn oscillator with fixed/variable frequency tuning in X band 13 p2039 A71-28911

Gunn effect diode in portable Doppler radar, describing electron transfer, negative resistance and domains formation and propagation 13 p2040 A71-29238

Integrated S band microstrip parametric amplifier modules with self contained Gunn effect pump oscillator for space flight applications 14 p2210 A71-29570

Dispersion and boundary equation concerning space-charge wave propagation under diffusion effect in Gunn semiconductors with anisotropic conductivity and finite thickness 14 p2283 A71-29793

Double cavity tuning of Gunn oscillators at mm wavelengths achieving output power improvements 14 p2215 A71-30831

High speed pulse response and power-delay product of planar Gunn diodes, noting delay time and power delay product 14 p2215 A71-30834

Book on hot electron microwave generators covering semiconductor physics, collision theory, Gunn effect, domain dynamics, avalanche breakdown, etc 15 p2375 A71-31509

Varactor tuned FM pulsed Gunn oscillator for testing X band delay lines for pulse compression radar 16 p2546 A71-33415

Phased array pulsed X band microstrip Gunn diode transmitters with temperature stabilization at 9.4 GHz 16 p2547 A71-33555

Ku band monopulse receiver with electronically tunable Gunn oscillator, discussing negative resistance diodes dynamic impedance properties 16 p2547 A71-33557

Microwave Gunn diodes I-V characteristics as function of carrier concentration and power efficiency 17 p2713 A71-34264

High power efficiency solid state UHF sources, comparing Gunn and avalanche diodes performance 17 p2715 A71-34685

Sensitive mm wave receivers, using local oscillator and mixer functions in single Gunn diode for large dynamic signal input range and wide IF bandwidth capability 17 p2717 A71-35111

FM-PM conversion by frequency locking of free running Gunn oscillator 17 p2717 A71-35339

Broadband varactor tuned X band Gunn oscillator, investigating output power and temperature stability 17 p2717 A71-35340

Temperature and bias circuit frequency modulation in CW X band Gunn oscillators 18 p2888 A71-36132

X-band Gunn oscillator equivalent circuit parameters determination for baseband and RF noise contribution to AM and FM noise 18 p2888 A71-36270

Waveguide mounted X band CW Gunn effect oscillators load impedance characteristics, proposing lumped equivalent circuit 18 p2894 A71-36830

Transferred electron /Gunn/ amplifiers and oscillators for microwave applications, considering electronic and mechanical tuning over large frequency ranges 18 p2894 A71-36977

Overcritically doped Gunn diode I-V characteristics stability under constant voltage, discussing use as subnanosecond switching element 18 p2895 A71-36989

Equivalent circuit parameters determination for baseband and microwave noise from Gunn oscillator, using AM-FM correlation coefficient 19 p3028 A71-37699

Gunn diodes stable high field domains parameters and behavior, considering hole effects in various carriers 19 p3028 A71-37861

Contact materials effects on X band FM noise and current fluctuations of Gunn elements 19 p3029 A71-38073

X band output power and FM noise of parallel multicontact Gunn oscillators 19 p3029 A71-38074

High-power high-efficiency CW X band Gunn oscillators on diamond heat sinks, noting operation in waveguide cavities 19 p3029 A71-38219

High electric field Gunn effect in n-type InAs under hydrostatic pressure due to transferred carrier mechanism 20 p3275 A71-38786

Gunn effect devices properties and applications, discussing microwave energy sources tunable and local oscillators, parametric amplifier pumps and radar transmitters 21 p3357 A71-40819

Gunn diode operation at below threshold bias voltage, investigating microwave oscillations amplification 21 p3358 A71-41339

X band Gunn diode oscillator pulsed operation starting delay time relationship to CW operation frequency/temperature characteristics, suggesting contact resistance role 21 p3359 A71-41411

Supercritical transfer electron amplifier using GaAs CW Gunn diode with cathode doping notch and profiles sloping upward for stabilization 22 p3521 A71-42204

Gunn oscillator frequency characteristics vs displacement voltage in low Q factor resonance circuits 22 p3521 A71-42274

Microwave planar Gunn oscillators performance in X band, giving pulsed and CW I-V characteristics 23 p3649 A71-42913

German monograph on Gunn oscillators frequency stabilization by synchronization with external oscillator emitting HF signals 23 p3649 A71-43045

Reactive impedance matching of Gunn or IMPATT diodes for microwave oscillators by dielectric tuning 23 p3650 A71-43071

Gunn oscillator frequency stabilization at minus 10 to 60 C by high Q single tuned oscillator circuit, considering requirements for 20 GHz radio relay system 23 p3651 A71-43438

Transmission and reaction cavity stabilized Gunn microwave oscillators AM and FM noise spectra, extending calculations based on Kurokawa theory to high modulation frequencies 23 p3653 A71-43967

X band microwave oscillator design for matched cavity reactance and maximized power by coupling Gunn and IMPATT diodes to coaxial transmission line 24 p3807 A71-44362

GUNPOWDER
U GUN PROPELLANTS
GUNS [ORDNANCE]
Cheyenne attack helicopter weapons system, discussing night vision capability, armament, fire control and navigation equipment integration [AHS PREPRINT 530] 14 p2178 A71-31091

Electronic time delay fuses with high-g components for gun launched projectiles for placing payloads at high altitudes 18 p2851 A71-36281

GUST ALLEVIATIONS
LAMS flight control systems for gust load alleviation and structural mode stabilization on large flexible aircraft, using aerodynamic surfaces 02 p0188 A71-11659

Sensitivity analysis and optimal control theory used to design optimal gust alleviation systems, discussing gain and gear ratios [AIAA PAPER 71-9] 06 p0848 A71-18483

Aircraft elastic mode control for turbulence /gust/ alleviation, noting riding quality, structural fatigue life and peak loads 07 p1022 A71-20301

Optimal stochastic control and gust alleviation for jet aircraft response for flight through turbulent upwash field 10 p1557 A71-24870

Automatic gust alleviation system employing inertial sensors and feedback devices with wing flaps and elevators, considering linkage control, noninteracting control and split control 11 p1706 A71-25195

Aircraft gust alleviation, considering movement correction based real time atmospheric turbulence measurement 14 p2174 A71-29785

GUST LOADS
Aircraft response to atmospheric gust, discussing spectral analysis procedures and calculation results on T-tail aircraft design 01 p0005 A71-10752

Clear air turbulence effects on flight and structural response of aircraft, using gust loads model [ONERA-TP-867] 03 p0346 A71-13136

Inertial aircraft lateral guidance system limitations in stochastic gust environment, comparing configurations using aileron or differential spoilers [AIAA PAPER 71-22] 06 p0925 A71-18489

Saturn launch vehicle gust penetration loads, presenting separated flow and associated time lag effects [AIAA PAPER 71-178] 06 p1004 A71-18617

Two dimensional rigid wings, investigating response characteristics to gust loads 09 p1383 A71-23440

Optimal control stabilization under continuous small disturbances applied to aircraft stability in horizontal flight under vertical gust loads 10 p1586 A71-24726

Plane rigid airfoil with fixed center of gravity, discussing motion in turbulent air and gust loads 10 p1557 A71-24947

Separated flow and time lag effects on sinusoidal gust penetration loads and elastic launch vehicle response of Apollo-Saturn class [AIAA PAPER 71-344] 11 p1836 A71-25323

Wind gust effect on autotracking antenna servosystem tracking error, evaluating torque disturbance admittance 12 p1868 A71-27002

Atmospheric turbulence effect on turbine powered transport aircraft, discussing gust accelerations, avoidance, detection, forecasting and pilot control 14 p2172 A71-29750

Aircraft structural design requirements based on statistical analysis of air turbulence intensity and gust loads records from large number of research flights 14 p2173 A71-29784

Gust transfer functions relating lift and moments to upwash in single sinusoidal wave for large aspect ratio rectangular wings in turbulent incompressible flow 14 p2176 A71-30604

Gust loading on two dimensional thin airfoil in compressible flow, deriving closed-form lift expression 17 p2671 A71-35285

Flight dynamics for aircraft noise reduction, gust effects decrease and dynamic stability of parachute load systems 18 p2850 A71-36752

Aerodynamic control surfaces optimal location for flexible aircraft disturbed by random wind gusts, using matrix minimum principle and calculus of variations 19 p2998 A71-38713

Flight dynamics of noise optimal flight profiles for V/STOL aircraft, minimization of gust effects on aircraft and nonlinear dynamic stability of parachute-load systems 24 p3792 A71-44761

GUSTATORY PERCEPTION
U TASTE
GUSTS
Stochastic analysis of wind gusts applied to prediction of long term maximum velocities 04 p0621 A71-15168

Numerical variational analysis with weak constraint for surface analysis of severe storm gust 05 p0776 A71-16155

Pulsed air gust generator for sinusoidal streamwise perturbation of wind tunnel test stream, describing upstream blowing air jet array, flow calibration and mathematical model [AIAA PAPER 71-281] 08 p1275 A71-22005

Extreme turbulence measurement during low level flights of Mirage A3-76 fighter aircraft, determining true gust velocities and power spectral energy distributions 14 p2267 A71-29756

Thunderstorm gust fronts from Oklahoma surface mesonet and weather radar data, considering hazard to aircraft 14 p2267 A71-29757

V/STOL aircraft gust effects prediction with mathematical models based on nonlinear hybrid simulation at takeoff and landing altitudes 14 p2173 A71-29775

Aircraft with T tail configuration, examining dynamic response to lateral gusts 14 p2174 A71-29786

Aircraft design and fatigue life monitoring, investigating effects of gust velocity frequency distribution in patches of atmospheric turbulence 14 p2174 A71-29789

Discrete gust and power spectrum models of atmospheric turbulence, considering energy distribution effect on aircraft dynamic response 14 p2174 A71-29790

High rotor advance ratio from multiblade general coordinates method in linear analysis of lifting rotor dynamic stability and gust ratio [AHS PREPRINT 512] 14 p2178 A71-31083

Nonadiabatic convection parameters calculation allowing for vertical wind shear, determining effect on thunderstorm maximum possible duration, gusts and precipitation quantity 15 p2444 A71-31361

German monograph on lower atmospheric turbulence and gustiness coefficients in connection with large scale parameters, deriving climatological flow characteristics from wind measurements 17 p2770 A71-35233

Performance limitation of simplified rigid-inertial lateral control guidance system subject to stochastic gusts for automatic landing [AIAA PAPER 71-957] 19 p3099 A71-37198

Gust factor variation as function of height and atmospheric stability, deriving simple power law expression from meteorological tower wind measurements 19 p3091 A71-38289

Atmospheric and wake turbulence effects on aircraft from discrete gust and spectral interpretations, discussing load production and uncontrollable rolling moments 21 p3321 A71-40507

GUY WIRES
Optimum positioning and structure of light hogged antenna masts for radio communications and broadcasting networks 01 p0068 A71-11085

GYMNASTICS
U EXERCISE [PHYSIOLOGY]
GYRATION
NT AUTOROTATION
NT EARTH ROTATION
NT LARMOR PRECESSION
NT MOLECULAR ROTATION

GYRATORS

NT PRECESSION
 NT PROTON PRECESSION
 NT ROTATION
 NT SATELLITE ROTATION
 NT SOLAR ROTATION
 NT STELLAR ROTATION
 Normally incident electromagnetic wave propagation in inhomogeneous gyration medium, obtaining reflection and transmission coefficients and discussing resonance 13 p2108 A71-29088
 Particle gyration in homogeneous magnetic field and perpendicularly propagating electrostatic wave, calculating wave-particle energy transfer and wave-amplitude limiting effects 18 p2950 A71-35862

GYRATORS
 NT MICROWAVE FILTERS
 Gyrotron circuit design with two antiparallel transistor amplifier stages for minimal DC current reception 18 p2888 A71-36223

GYRO HORIZONS
 Laser gyro goniometry for fluctuations and angular measurements at low rotational velocities, noting countup/countdown detection systems 02 p0262 A71-12924
 Inertial navigation system consisting of gyro horizon compass, directional gyro and computer, considering errors due to compass vibrations 12 p1927 A71-27169
 Geckeler-Anschutz gyrohorizon compass element motion with uncoupled gyrocompasses, obtaining equations of motion with quadratures solution 24 p3827 A71-45049

GYROCOMPASSES
 Gyropendulum and two-rotor gyrocompass equations equivalence conditions, formulating and proving theorem 01 p0080 A71-10627
 Two-rotor gyrocompass accelerated reduction to meridian 01 p0080 A71-10630
 Tied aether existence hypothesis determination, comparing gyrocompass precessional couple at earth surface and at 3300 m depth for negative results 03 p0456 A71-13358
 Single rotor gyrocompass with electromagnetic correction during random interactions involving intercardinal deviation, constructing correcting device to obtain optimal dynamic characteristics 03 p0430 A71-14353
 Two-rotor gyrocompass equations of motion under perturbation, demonstrating reducibility to canonical form 03 p0430 A71-14354
 Liapunov stability of unperturbed motion of single rotor correctable gyrocompasses with liquid-torsion suspension 05 p0751 A71-16586
 Decaying oscillations of sensitive element in ground based gyrocompasses with suspension system permitting Euler angle and translational displacement 07 p1108 A71-19304
 Single rotor gyrocompass dynamics under LF three component linear vibration of base, using precessional equations 07 p1108 A71-19305
 Orbiting spacecraft local attitude determination, analyzing second order gyrocompass filter, third order steady state filter and fourth order time varying gyrocompass filter 07 p1207 A71-19531
 Gyrocompass strapdown three coil synchro sensor magnetometer in conjunction with vertical gyro, eliminating azimuth detector inertial platforms 07 p1156 A71-20340
 Three stage astatic gyrocompass design with pendulum correction, considering equations of motion 09 p1449 A71-22795
 Small parameter method in gyrocompass theory, deriving differential equations for motion of sensitive element of two rotor gyrocompass 10 p1608 A71-23804
 Three degrees of freedom gyrocompass with common drive and gimbal bearing, exhibiting westerly deviation from drive axis 11 p1763 A71-26188
 Inertial navigation system consisting of gyro horizon compass, directional gyro and computer, considering errors due to compass vibrations 12 p1927 A71-27169
 Gyrocompass stability during circulations and arbitrary periodic maneuvers, taking into account translational motion vertical inertia component 17 p2746 A71-35604
 Reduced state estimator for satellite orbital heading reference, describing decoupled single-skewed-gyro gyrocompass design for attitude control 19 p3148 A71-37206
 Gyrocompass with optimal error correction under rapid acceleration change 23 p3675 A71-43297

Gyrocompass in gyropendulum stabilized Cardan suspension, deriving system undamped oscillations equations 24 p3847 A71-44415
 Two rotor gyrocompass with random parameter excitation, calculating angular velocity random variation effects on drift 24 p3825 A71-44700
 Geckeler-Anschutz gyrohorizon compass element motion with uncoupled gyrocompasses, obtaining equations of motion with quadratures solution 24 p3827 A71-45049

GYROFREQUENCY
 Radio wave propagation at frequencies near proton gyrofrequency in horizontally stratified ionosphere, taking into account intermediate coupling 07 p1102 A71-19666
 Wave propagation with frequency inferior to gyrofrequency of ions in collisionless hydrogen plasma, showing Alfvén wave reflection on discontinuity surface parallel to magnetic field 10 p1599 A71-23846
 Coupled longitudinal-transverse wave modifications of electrostatic dispersion relation with ion gyrofrequency instabilities in magnetized plasma 18 p2950 A71-35866
 Electric field fluctuations in magnetospheric plasma at multiples of local electron gyrofrequency due to plasma instability 19 p3048 A71-37368
 Particle collisions and relativistic effects on electromagnetic wave propagation within plasma in direction normal to external magnetic field near gyrofrequencies 23 p3645 A71-43559
 Wide wavelength parametric plasma instability in constant magnetic and weak HF electric fields above ion gyroscopic frequency 23 p3714 A71-44327

GYROINTERACTION
 U MAGNETIC RIGIDITY
GYROMAGNETISM
 NT GYROFREQUENCY
GYROPLANES
 U HELICOPTERS
GYROS
 U GYROSCOPES
GYROSCOPES
 NT ATTITUDE GYROS
 NT CONTROL MOMENT GYROSCOPES
 NT CRYOGENIC GYROSCOPES
 NT FLUID ROTOR GYROSCOPES
 NT GYRO HORIZONS
 NT GYROCOMPASSES
 NT GYROSCOPIC PENDULUMS
 NT GYROSTABILIZERS
 NT OPTICAL GYROSCOPES
 NT ROTARY GYROSCOPES
 Lunar surface vehicle navigation system, describing dead reckoning and sun aspect compass for initial gyro alignment 01 p0124 A71-10514
 Free three degrees of freedom gyroscope motion with exponential attenuation of rotor kinetic moment 01 p0079 A71-10532
 Cardan suspension axes nonperpendicularity and misalignment effects on precision of gyroscope motion in presence of system angular vibrations 01 p0083 A71-11043
 Motion equations of spherical gyroscope in gravitational field of larger mass derived from Gupta quantum theory of gravitation 01 p0161 A71-11274
 Soviet book on gyroscopes in geodesy and aerial photography based on structural analysis for automatic control systems, covering gyro error, theodolites, etc 01 p0083 A71-11321
 Dissipative gyroscopic system with servo link, obtaining steady motion stability 02 p0252 A71-12402
 Soviet book on gyroscopic devices statistical synthesis covering dynamic characteristics, automatic systems, etc 03 p0423 A71-13371
 Astatic gyroscope with viscous friction at suspension system axes, noting free nonlinear vibrations and motion 03 p0423 A71-13411
 Equations of motion of heavy gyrostat with fixed point in uniform force field 03 p0457 A71-13580
 Lagrange equations of motion of gyroscope having fixed point in presence of constant gyrostatic moment, obtaining particular solution 03 p0457 A71-13582
 Equations of motion of gyroscope body having fixed point, determining conditions for existence of quadratic invariant correlation 03 p0457 A71-13583
 Heavy gyroscope equations of motion solution, assuming center of mass on major axis 03 p0457 A71-13584

Heavy gyrostat equations of motion having fixed point and zero momentum integral constant, obtaining polynomial solutions 03 p0457 A71-13580
 Traveling angular velocity hodograph equations solution to gyrostat motion problem 03 p0457 A71-13581
 Heavy gyrostat motion problem, using Mozairevskaya particular solution characterized by algebraic invariant relation 03 p0458 A71-13582
 Liquid filled gyroscope motion stability, examining experimental data, design and testing procedures 03 p0426 A71-13717
 Satellite optimal guidance, discussing gyroscope application for stabilization and orientation control 03 p0500 A71-14271
 Gyrostatic system with center of mass in uniform circular motion, deriving rotary motion equations in a variant 03 p0460 A71-14386
 Fluidic inertial instruments for space sensing guidance and control including gyroscopes, accelerometers and rate sensors 04 p0535 A71-153222
 Precision gyro and accelerometer testing evolution, noting instrument performance and electrical and mechanical equipment 05 p0749 A71-163030
 Gyroscopic reliable performance life testing economic justification, noting cost lowering by efficient gyro rejection 05 p0749 A71-163040
 Gyroscopes motor couple scale factor measurement 05 p0750 A71-16311
 Gyroscopic bearings friction moments constant and variable components experimental determination by method of compensation, using test equipment based on electric spring principle 05 p0758 A71-16355
 Equations of motion solution of heavy solid body about stationary point applied to Hess gyroscope 05 p0754 A71-16998
 Inertial grade floated rate integrating gyroscope surface temperature control by closed loop feedback controller 06 p0983 A71-17362
 Free Lagrangian gyroscope, discussing numerical relations between precessions and nutations 06 p0899 A71-17930
 Numerical and graphic drive shaft motion trajectories in dynamic gyroscopic system with four degrees of freedom 06 p0928 A71-18232
 Static friction influence on readings of gyrotachometer with pulse width modulated torque sensor current 07 p1108 A71-19306
 Spherical hydrostatic gas bearings for two axis gyros, using Al die castings 07 p1117 A71-19504
 Soviet book on supports and suspensions of aircraft gyroscopic devices covering accuracy, reliability and lifetime factors related to quality and operational conditions 07 p1115 A71-20299
 Gyrostat with center of gravity on ellipsoid axis, determining motion by two invariant algebraic equations 07 p1209 A71-20645
 Inertial sensors, considering electromechanical devices, single and two degrees of freedom floated gyros and electromagnetic rebalance pendulous accelerometers 09 p1443 A71-22594
 Precessional equation of gyroscopic systems with rigid structural elements connected by single degree of freedom axial hinges 10 p1611 A71-24577
 Gyroscopic drift in gimbal suspension on moving base in presence of friction force proportional to dynamic reactions 10 p1612 A71-24578
 Gimbal suspended gyroscope in elastically damped frame with dynamically unbalanced rotor, noting oscillations and drifts 13 p2065 A71-27945
 Disk rotating in gimbal system, describing gyroscopic moments and precession 13 p2068 A71-28632
 Gyro platform orientation control system, using inertial flywheels 13 p2068 A71-28634
 Systematic drift of astatic gyroscope in gimbal suspension during rundown 13 p2070 A71-29076
 French book on optimal inertial navigation and statistical filtering covering Wiener and Kalman filters, gyroscopes, accelerometers, inertial platforms, data processing, computer programming, etc 14 p2271 A71-29940
 Low-power long-life high-accuracy digital inertial reference assembly, using dual voltage spinmotor

operated pulse rebalanced temperature compensated gas bearing gyroscopes

14 p2272 A71-30803

Motion characteristics of elastically supported gyroscope, presenting linearized equation of motion for eight degrees of freedom system

15 p2401 A71-31180

Gyroscopic system nonstationary operation mode analysis, utilizing asymptotic method with linear matrix equation

15 p2410 A71-32454

Elastically suspended gyroscope dynamics, using Euler equations of motion allowing for casting rotation

15 p2410 A71-32455

Ideal laser gyro sensitivity against background of natural emission fluctuations

17 p2737 A71-34411

Structural design of gyroscope ball bearings, considering additional sliding friction force moment

17 p2739 A71-34561

Nonlinear free oscillations of astatic gyroscope with viscous friction at suspension system axes

17 p2743 A71-35019

Asymptotic solution to nonlinear motion of heavy gyro in gimbal suspension, noting convergence within finite time interval

17 p2746 A71-35066

Fluidic gyroscope technology, reviewing current development and problems associated with severe environmental conditions affecting inertial guidance and spacecraft control

18 p2922 A71-36482

Equations of motion solution of heavy solid body about stationary point applied to Hess gyroscope

18 p2925 A71-36798

Gyroscope rotor axial moment of inertia of measurement by connection to small vibrator device

19 p3062 A71-37148

Fail operational control moment gyro configuration of four single gimbal gyros, eliminating cross coupling by simple analog steering law

19 p3097 A71-37181

Gyro and star tracker precision attitude determination system, assessing computational and other error effects on system performance

19 p2996 A71-37205

Gyro drift rate acceptance test design to reflect system performance, using Bayes philosophy for derivation of test cost, product yield and quality

19 p3068 A71-37209

Low temperature viscous lubricants from mixed pentaerythritol esters for precision inertial guidance gyroscope bearings and instrument applications

20 p3254 A71-39800

Gyro wheels cleaning by ion bombardment applied to ceramic gas bearings, comparing with chemical cleaning

22 p3552 A71-41674

Opposed hemispherical self acting gas bearings fabrication for gyro wheels, using machine lapping and sputter etching

22 p3553 A71-41677

Optimal gyroscopic servosystems feasibility analysis, using approximation technique for finite memory optimal filter transfer function

23 p3675 A71-43296

Statistical optimization of spherical gyroscope regarded as servocontrol system under random perturbation, using measured values of relative angles between sphere and inner gimbal

24 p3825 A71-44691

Kinematic method for deriving formula for gimbal error of directional gyroscope with allowance for main axis inclination to horizontal plane

24 p3828 A71-45157

Astatic gyroscope mounted on aircraft moving arbitrarily near earth surface, obtaining integrals of kinematic equations

24 p3828 A71-45160

Motion integrals conservation under Hamiltonian function variations, examining gyroscope equations of motion with parameter disturbances

24 p3849 A71-45343

GYROSCOPIC COUPLING

Helicopter stability, using Lockheed rotor system with gyro coupled to cantilevered blades

15 p2348 A71-31599

Reaction wheel satellite attitude control, describing nondimensional parameter for interaxis gyroscopic coupling effects in preliminary design estimates

17 p2722 A71-35185

Motion equations of statically unbalanced two degree of freedom gyroscope excited by base linear vibrations, determining instrument errors as function of casing/body coupling

24 p3828 A71-45159

GYROSCOPIC DRIFT

U GYROSCOPES

U GYROSCOPIC STABILITY

GYROSCOPIC PENDULUMS

Gyropendulum and two-rotor gyrocompass equations equivalence conditions, formulating and proving theorem

01 p0080 A71-10627

Random vibrations nonlinear effects on gas bearing pendulous-integrating gyroscopic accelerometer response, using digital simulation

02 p0252 A71-12454

Gyroscopic and physical pendulum stability with gimbal suspension centers moving in Newtonian central force field, using Raus method

02 p0254 A71-12639

Three stage astatic gyrocompass design with pendulum correction, considering equations of motion

09 p1449 A71-22795

Gyroscopic integrating accelerometer dynamics on high frequency angular vibrating base, determining self oscillations and drift motions

13 p2065 A71-27946

Gyrocompass in gyropendulum stabilized Cardan suspension, deriving system undamped oscillations equations

24 p3847 A71-44415

Rotating solid body nutations damping by pendulums system oscillating in plane normal to rotation axis, deriving optimal conditions

24 p3848 A71-44855

Stability of gyropendulum damped by astatic gyroscope

24 p3828 A71-45158

GYROSCOPIC STABILITY

Orbiting gyrostats stability elementary cases analysis, examining existing methods and developing new method involving less computational labor

01 p0163 A71-10123

Free three degrees of freedom gyroscope motion with exponential attenuation of rotor kinetic moment

01 p0079 A71-10532

Drift causes in floated-rotor integrating gyros used as accelerometers, discussing gyromotor magnetic field effects

01 p0080 A71-10535

Astatic gyroscope with gimbal system on rocking base, discussing effects of Cardan joint adjustment to insensitivity zone on instrument drift

01 p0080 A71-10631

Gyrosystems motion equations, obtaining nutation, precession and drift components as asymptotic expansions by small parameter technique

01 p0080 A71-10632

Cardan suspension axes nonperpendicularity and misalignment effects on precision of gyroscope motion in presence of system angular vibrations

01 p0083 A71-11043

Soviet book on rotary and oscillatory vibrational gyroscopes covering equations of motion, stability, error correction, applications, etc

02 p0247 A71-11824

Superfluid gyroscope for general relativity tests, using resonant phonon force field for drift reduction

02 p0248 A71-11943

Gyroscopic precession effects in earth polar orbital satellite experiments for Einstein general relativity tests

02 p0312 A71-12369

Gyro dynamic errors in strapdown inertial guidance system due to body rate

02 p0279 A71-12457

Law of motion for two degrees of freedom integrating gyro mounted on oscillating base, using averaging method

02 p0253 A71-12637

Motion stability of double-gyro inertial frame in Newtonian central force field, applying Liapunov and Chetaev methods

02 p0253 A71-12638

Gyroscopic and physical pendulum stability with gimbal suspension centers moving in Newtonian central force field, using Raus method

02 p0254 A71-12639

Single degree of freedom strapdown gyroscope performance and drift model, considering steady and vibrational inputs

[DFVLR-SONDDR-80]

03 p0422 A71-13342

Single axis gyroscopic stabilizer with floating type integrating gyro, describing natural oscillations by differential equations of motion

03 p0429 A71-14237

Dynamical investigation of deformable gyrostats stability in circular orbit subject to gravitational torques, noting equilibrium states and damping effects

04 p0662 A71-15142

Stability problems of free rotor and driven rotor gyrostats, considering spin stabilized spacecraft

04 p0662 A71-15192

Test instrumentation for inertial gyros performance evaluation, describing turntables, holding fixtures, electronic equipment, automation, environment simulation, etc

[AGARDOGRAPH-128]

05 p0750 A71-16305

Inertial gyro testing, measuring coefficients for performance model equation

[AGARDOGRAPH-128]

05 p0750 A71-16306

Gyro testing in UK, discussing equipment, methods, errors, etc

[AGARDOGRAPH-128]

Gyroscopes diagnostic tests for design shortcomings, discussing spin-axis ball and gas bearings,

spin-motor reaction torque, flotation fluid and ligament creep

[AGARDOGRAPH-128]

05 p0750 A71-16310

Gyroscopic drift tests, using sinusoidal linear VLF acceleration

[AGARDOGRAPH-128]

05 p0750 A71-16312

Gyros and accelerometers with hydrostatic gas bearings, discussing design and adjustments, drift measurement methods and environmental tests

[AGARDOGRAPH-128]

05 p0751 A71-16314

Precession equations of gyroscope onboard near earth satellite, comparing Schiff and Brans-Dicke theories

05 p0781 A71-16488

Stability of steady motions of satellite gyroscope in Newtonian central force field, allowing for rotor bearing elasticity

05 p0751 A71-16585

Liapunov stability of unperturbed motion of single rotor correctable gyrocompasses with liquid-torsion suspension

05 p0751 A71-16586

Forced resonant vibration in nonlinear gyroscope in gimbal suspension

05 p0751 A71-16587

Gyrostat in circular orbit in Newtonian force field, solving for optimal rotational motion stabilization

05 p0817 A71-16997

Gyroscope in gimbal system with elastic rotor bearings, determining dynamic stability in Newtonian central force field

06 p0899 A71-17929

Two stage integrating float gyroscopes with reactive moment meters and sensors, examining feedback design for stabilization systems

06 p0899 A71-17930

Single rotor gyrocompass dynamics under LF three component linear vibration of base, using precessional equations

07 p1108 A71-19305

Orbiting gyroscope de Sitter precession in different versions of Brans-Dicke theory, discussing term arising from anomalous scalar force in equations of motion

07 p1160 A71-19550

Heavy gyroscope motion in gimbal suspension for arbitrary housing gravity center, showing steady solutions with respect to nutation angle

08 p1294 A71-21870

Damping effects in three frame rotary gyroscope due to force originated by static joint housing design

09 p1449 A71-22794

Dynamic characteristics of two degree of freedom gyroscopes with positional and integral negative feedback for simultaneous angular velocity and displacement measurement

09 p1451 A71-23171

Forced rotation influence of gimbal suspension on astatic gyroscope motion with respect to inertial coordinates, demonstrating pseudoregular precession

09 p1451 A71-23172

Gyroscopic drift in gimbal suspension on moving base in presence of friction force proportional to dynamic reactions

10 p1612 A71-24578

Dynamically symmetrical gyrostat steady state motion stability in force field of two fixed centers, using Raus-Liapunov theorem

10 p1683 A71-24579

Equilibrium orientations of gravity gradient stabilized gyrostat satellites with rotor axis in principal plane, using Hamiltonian as Liapunov testing function

10 p1684 A71-24929

Methods for reducing integrating gyroscope errors caused by angular oscillations of base, considering use of two identical gyros with opposite kinetic moment vectors

13 p2065 A71-27951

Gyroscopic systems equations of motion solution by Bogoliubov averaging method, considering free gyroscope on rotating base

13 p2065 A71-27952

Motion stability of symmetric rotor of gyroscope with inviscid incompressible liquid filled cylindrical annular cavity around coaxial rigid rod

13 p2065 A71-27978

Liapunov stability of gyroscopic stabilizers as electromechanical systems, assuming nonrigidity of rotor, gimbal and platform suspension

13 p2069 A71-28726

Routh-Liapunov stability of lasting rotation of dynamically symmetrical gyrostat in force field of two stationary centers

13 p2145 A71-28729

Positional motion rigidity of gyroscopic systems with cyclic coordinates and low spin, using Liapunov second method

13 p2069 A71-28732

Weak damping of free gyro motion in static coordinate system under dry friction in gimbal joint, deriving equations of motion by Lagrange method

13 p2069 A71-28932

Gravity center effect on drift of gyro linear acceleration integrator on vibrating base, showing errors at frequencies near nutations

13 p2069 A71-28933

Stabilization of solid body orientation with twin gyros under slave engine drive, producing control moments to gimbal axis

13 p2145 A71-28935

Elastically mounted gyroscope stability under parameter excited vertical vibrations, using vector differential equation and multichannel oscillograph

15 p2502 A71-31173

High speed spin effect on amplified or damped nutations in low friction rotary gyroscope mounted on gimbals

15 p2401 A71-31178

Motion characteristics of elastically supported gyroscope, presenting linearized equation of motion for eight degrees of freedom system

15 p2401 A71-31180

Holographic interferometry fringe patterns in interpretation for small displacements measurement, considering precision gyro stability

17 p2744 A71-35286

Dynamic stabilization of undamped gyrosystems with elastically pliable structural elements by inertial damper mounted on gimbal suspension

17 p2746 A71-35602

Gyrocompass stability during circulations and arbitrary periodic maneuvers, taking into account translational motion vertical inertia component

17 p2746 A71-35604

Gyrostat in circular orbit in Newtonian force field, solving for optimal rotational motion stabilization

18 p2976 A71-36797

Optimal Kalman filter gyro drift rate mathematical models for limiting inertial navigation errors [AIAA PAPER 71-971]

19 p3100 A71-37212

Pioneer Jupiter spacecraft, noting low weight, radioisotope thermoelectric generators and gyroscopic stabilization by spinning with antenna pointed at earth [AAS PAPER 71-167]

19 p3141 A71-37964

Energy and variational principles, studying local stability of equilibrium of elastic body subjected to conservative and gyroscopic forces

20 p3232 A71-38797

Heavy gyroscope motion in gimbal suspension for arbitrary housing gravity center, showing steady solutions with respect to nutation angle

20 p3238 A71-39369

Gyroscope apparent precession due to reference star light deflection by solar gravitational field

20 p3270 A71-39559

Gyroscopic systems dynamic drift reduction by inertial damping, using astatic and static stabilizers

23 p3675 A71-43295

Gyrocompass in gyropendulum stabilized Cardan suspension, deriving system undamped oscillations equations

24 p3847 A71-44415

Two rotor gyrocompass with random parameter excitation, calculating angular velocity random variation effects on drift

24 p3825 A71-44700

Precession rate of balanced gyroscope in Cardan suspension with elastic gimbal couplings

24 p3826 A71-44833

Stability of gyropendulum damped by astatic gyroscope

24 p3828 A71-45158

Motion equations of statically unbalanced two degree of freedom gyroscope excited by base linear vibrations, determining instrument errors as function of casing/body coupling

24 p3828 A71-45159

Fixed and free sinusoidally driven hydraulic squeeze film bearing design for improved load gyroscope performance [ASLE PREPRINT 71LC-14]

24 p3832 A71-45291

GYROSTABILIZERS

Power gyro stabilizer optimal controlling section with random base frame oscillations, solving filtration problem as function of platform structure by Wiener method

01 p0079 A71-10427

Nonlinear control law for increased powered stabilization system accuracy in single-axis gyro stabilizer

01 p0079 A71-10533

Sounding rocket attitude monitoring and control, using digital output roll stabilized gyro platform

03 p0455 A71-13686

Optimal synthesis of rational composite system for gyro stabilizer stabilization

05 p0751 A71-16588

Gyrostat in circular orbit in Newtonian force field, solving for optimal rotational motion stabilization

05 p0817 A71-16997

Maximum deviations of corrected uniaxial gyro stabilizer under disturbances on stabilization and precession axes with modulus constraints

09 p1450 A71-22796

Gyrostat satellite steady motion and relative position optimal stabilization by additional forces application

14 p2275 A71-30871

Digital systems synthesis for stabilization of triaxial gyro stabilizer consisting of three uniaxial gyro stabilizers with cross couplings

17 p2738 A71-34559

Uniaxial gyroscopic stabilizer errors in presence of base random vibration, taking into account dry friction forces in bearings

17 p2738 A71-34560

Symphonie telecommunication satellite attitude control system, describing operational principle based on gyroscopic inertial reference and redundant IR sensors

18 p2974 A71-36525

Gyrostat in circular orbit in Newtonian force field, solving for optimal rotational motion stabilization

18 p2976 A71-36797

GYROSTATS U GYROSCOPES

GYROTROPISM

Design algorithm for gyrotropic waveguide consisting of symmetrical rectangular coaxial with magnetized ferrite rods

19 p3019 A71-38333

Solar magnetic field generation by gyrotropic turbulence, noting inadequacy of Steenbeck explanation for quantitative estimates of solar cycle parameters

20 p3291 A71-39317

H

H ALPHA LINE

Solar chromospheric flares observations tabulation /1969/ and H alpha line width curves graph

01 p0144 A71-10870

H alpha line emission in ionization zones encircling neutron stars, suggesting accretion-induced UV luminosity

02 p0308 A71-12091

Orion Nebula /NGC 1976/ physical characteristics from H alpha line radio telescopic observation, discussing energy level population, electron density, collision mechanisms, etc

02 p0308 A71-12094

Solar magnetic field polarity mapping from H-alpha filtergrams, using magnetic configurations in flare location and time forecasting

02 p0316 A71-12696

Real time solar flare locations and region activity levels prediction based on hydrogen alpha inferred magnetic configuration [AIAA PAPER 70-1373]

02 p0301 A71-12700

Spicule horizontal component motion from H alpha spectra movies with slit tangential to solar limb

02 p0316 A71-12756

Solar H alpha prominences on 29, 30, 31 July and 1 August 1967, using filtergrams and spectroheliograms

04 p0641 A71-15661

Sunspot region birth and growth, noting arch filament systems with H alpha time lapse movies

05 p0801 A71-15935

Sco X-1 optical spectroscopic and photometric observations, noting H alpha and H ion emission lines pattern-continuum brightness relationship

05 p0812 A71-16698

Stark induced quantum beats in H Ly alpha emission, using beam foil excited hydrogen

05 p0785 A71-16701

Morning and evening H alpha hydrogen line in twilight glow, establishing connection with solar activity level

07 p1105 A71-20439

Multicolor photographic photometry of NGC 4254 galaxy using electro-optical converter, observing H alpha emission and H II regions at galactic center

07 p1205 A71-20634

H alpha line emission in ionization zones encircling neutron stars, suggesting accretion-induced UV luminosity

08 p1362 A71-21141

Orion Nebula /NGC 1976/ physical characteristics from H alpha line radio telescopic observation, discussing energy level population, electron density, collision mechanisms, etc

08 p1362 A71-21144

H Lyman alpha auroras during May 18-27, 1967 magnetic disturbance from satellite observation

08 p1283 A71-21637

Diffuse interstellar features in spectrum of reddened star in Cygnus OB2 stellar association, tabulating equivalent widths of H alpha and stellar He I line

10 p1665 A71-23749

Sunspot group magnetic field distribution and radial velocities, investigated at H alpha and 6302.499 A atmospheric levels

10 p1666 A71-23788

Solar flares explosive phase in photometric terms for flash onset correlations with 10.7 cm radio and hard X ray bursts, using H alpha film records

10 p1660 A71-23793

Soft X ray bursts involving solar flares from satellite observations, discussing thermal nature and total activity related H-alpha emission rates

10 p1660 A71-23794

Extraterrestrial hydrogen Lyman alpha emission source, investigating interstellar wind with OGO satellite

10 p1601 A71-24438

Type 3 solar radio bursts in absence of H alpha flares, noting soft X-ray emission

12 p1946 A71-26612

Solar chromospheric flares in 1969, constructing tables of observation data commencement and end times and H alpha line maximum width

13 p2128 A71-28408

Atmospheric and cosmic origin of noctilucent clouds, discussing solar wind effects on H₂O and water vapor molecules in mesosphere and thermosphere

14 p2232 A71-29955

Motions in chromospheric limb and disk flares based on H alpha photography

14 p2298 A71-29970

H85 alpha recombination line in planetary nebulae NGC 7027, considering IR physical parameters consistent with radio observations

14 p2313 A71-30432

Upper atmosphere atomic hydrogen H sub alpha emission, correlating intensity and hydroxyl vibrational temperature

16 p2564 A71-33665

Stark widening in hydrogen Lyman alpha line, considering atomic state operator of evolution thermal mean effects

16 p2614 A71-34061

Real time system for solar spectrophotometry, noting application for scanning H alpha and other Balmer series lines profiles in solar flare regions

17 p2741 A71-34994

Videometer instrument for solar flares quantitative measurement, eliminating red sensitive vidicon for real time operation in H alpha region

17 p2742 A71-35003

NGC 2024 direction H I region H 137 alpha recombination line emission detection, determining ionized hydrogen fraction

17 p2807 A71-35415

H alpha emission photometry for galactic H II region, obtaining contour diagrams

19 p3130 A71-37227

Solar flare observations /14-19 November 1969/, obtaining H alpha line profile

19 p3124 A71-37229

Interstellar absorption at H alpha line wavelength in Orion nebula, obtaining contour map for comparison with radio intensity

19 p3131 A71-37230

Solar limb H alpha spicules spectrograms, noting oscillations and time intervals

19 p3147 A71-38665

Be star theta Corona Borealis UBVY H alpha filter observations, noting spectroscopic changes of light variation due to particles in stellar atmosphere

21 p3443 A71-40193

Electron density and temperature in diffuse interstellar medium from H alpha and beta radio recombination lines near galactic plane

21 p3445 A71-40411

Solar limb high resolution photography at different H-alpha wavelengths, using tunable I-8A and IA Halle filters in tandem for parasitic light elimination

22 p3596 A71-41455

Oscillations of visible chromosphere boundary and regularity in position of spicule groups along limb, studying H alpha filtergrams

22 p3597 A71-41456

Morphological relationships in solar chromospheric H alpha fine structure involving bushes, fibrils, threads and filaments

22 p3597 A71-41457

Spiral topology of chromospheric fibrils and filaments in H alpha near sunspots, noting similarity with axisymmetric force free magnetic field configuration

22 p3597 A71-41458

Solar chromosphere spectrum analysis, measuring H alpha line relative shifts variation with altitude

22 p3607 A71-42872

Pole-on Be star envelope models, comparing H alpha line profiles with line of sight perpendicular to rotation axis

23 p3723 A71-42945

Atmospheric atomic hydrogen H alpha emission correlation with hydroxyl vibrational temperature

23 p3665 A71-42961

Solar rotation evidence from H alpha and K line spectra of quiescent prominences for westward wind

23 p3767 A71-43841

High velocity H alpha ejections in association with important solar flare on 12 March 1969, suggesting mass motions control by gravitational field

23 p3721 A71-43848

Seyfert galaxy NGC 5548 H alpha profile spectroscopic observations, discussing broad emission lines

24 p3870 A71-44901

H BETA LINE

Ionized gas flow temperature distribution effects on half width of H beta line

04 p0633 A71-15064

H I and H beta emission, Sco-Cen association stellar members near Sco X-1, discussing X ray heating and ionization
07 p1187 A71-19818

Night sky H beta photometry, showing solar type spectrum at high galactic latitudes and net emission at low latitudes
08 p1350 A71-20946

H beta, H gamma and H delta Stark broadened profiles, investigating perturbing electron-radiating atom inelastic collisions, Gaunt factors and half widths
09 p1496 A71-22413

Young cluster NGC 2264 main sequence A and F stars four color and H beta observation, suggesting evidence of circumstellar gas shells
12 p1956 A71-26615

Temperature dependence of H-beta emission from hot hydrogen-helium plasmas, calculating production rate at 10,000-100,000,000 K
15 p2455 A71-31722

H beta fluxes of planetary nebulae along southern Milky Way from photoelectric telescope
17 p2809 A71-35593

Four-color and H beta photometric data tabulation for bright B type stars in Southern Hemisphere
21 p3443 A71-40192

H beta and UVB photoelectric photometry of southern galactic cluster, deriving absolute magnitude calibrations and intrinsic color relations
21 p3443 A71-40194

Electron density and temperature in diffuse interstellar medium from H alpha and beta radio recombination lines near galactic plane
21 p3445 A71-40411

Pulsed neon laser high gain oscillation at 486.1 and 434.0 nm identified as Balmer beta and gamma lines of atomic hydrogen
23 p3688 A71-44296

H GAMMA LINE
H beta, H gamma and H delta Stark broadened profiles, investigating perturbing electron-radiating atom inelastic collisions, Gaunt factors and half widths
09 p1496 A71-22413

Pulsed neon laser high gain oscillation at 486.1 and 434.0 nm identified as Balmer beta and gamma lines of atomic hydrogen
23 p3688 A71-44296

H LINES
NT H ALPHA LINE
NT H BETA LINE
NT H GAMMA LINE
NT K LINES
NT LYMAN SPECTRA
NT RYDBERG SERIES
NT TELLURIC LINES
Electrostatic vibrations from turbulent plasma heating on basis of Stark broadening of hydrogen spectral lines, obtaining electric field strength
01 p0131 A71-10069

Visual, photographic and photoelectric observations of polar auroras and hydrogen emission at conjugate points
02 p0242 A71-11757

Galactic models from neutral H line profiles at 21 cm wavelength
02 p0307 A71-12084

Spectrophotometry of star EW Lac, showing variability by H line profiles
02 p0311 A71-12356

Hydrogen lines of spectrally variable star alpha squared CVn from spectrograms, determining atom concentration, electron density and acceleration of gravity on surface
02 p0311 A71-12357

Atlas of 21 cm H I emission line profiles of outer part of Galaxy in Galactic anticenter region, plotting brightness temperature vs radial velocity
06 p0964 A71-17348

Stark broadening of hydrogen lines in plasma, noting role of amplitude modulation and nonadiabaticity
06 p0930 A71-17406

Powerful solar flare H lines spectrophotometric observation, noting H lines atom upper energy levels overexcitation
07 p1188 A71-20033

Galactic models from neutral H line profiles at 21 cm wavelength
08 p1362 A71-21134

Auroral protons and substorm resonance concept, eliminating discrepancy between hydrogen emission spectroscopic and direct measurements
09 p1513 A71-22674

Electrostatic vibrations from turbulent plasma heating on basis of Stark broadening of hydrogen spectral lines, obtaining electric field strength
09 p1504 A71-23264

Solar simplified geometrical model, observing emission peak center to limb variation of Mg II, H and K lines and optical thickness
10 p1666 A71-23782

Taurus dust cloud magnetic field line of sight component observations and M17 and Cyg A absorption spectra data noting Zeeman splitting at 21 cm H lines
12 p1957 A71-26623

Calcium H and K line anomaly in faint meteor spectra, discussing brightness correlation with aerodynamic flow and resonant charge exchange with ionized nitrogen
12 p1957 A71-26626

Spectral line broadening theory applications to qualitative interpretation and quantitative determination of spectrograms from hydrogen line profiles of stellar atmospheric parameters
12 p1969 A71-27667

Solar spicules H alpha and beta, D3 and K line profiles, considering radial and turbulent velocities, optical thickness, atomic density and He emission
13 p2140 A71-29049

Interstellar H II regions high quantum number recombination line measurements, indicating Stark broadening
13 p2143 A71-29268

Galaxy Maffei 2 observations in 21 cm neutral hydrogen line and in continuum at 1415 MHz with Nançay radio telescope
14 p2305 A71-29681

Integral equations for source functions of Ca II H, K and IR triplet lines for transfer through homogeneous stellar atmosphere
14 p2276 A71-30298

Solar atmosphere structure inhomogeneities, describing Ca II H and K line spectra profiles
15 p2497 A71-32743

Stark contours of hydrogen spectral lines in turbulent plasma with high noise level due to HF Langmuir oscillations
19 p3110 A71-37388

Solar Mg II H and K line profiles from rocket-borne echelle interferometer spectrograph and densitometer data
19 p3135 A71-37612

Stellar chromosphere detection through H, K and metastable He lines observation, noting importance for solar physics
19 p3136 A71-37627

Stable auroral red and hydrogen arcs simultaneous spectrographic triangulation, noting correlation
20 p3232 A71-39895

Small circle geometry of Galactic continuum loops, noting consistency with neutral hydrogen and supernova remnant hypothesis
22 p3601 A71-42168

Maffei 2 spiral galaxy hydrogen line and adjacent continuum observation by radio interferometry
23 p3733 A71-43080

H WAVES
H wave propagation in waveguide consisting of two parallel plates with longitudinal rectangular grooves, determining electric and magnetic fields by reduction method
19 p3019 A71-38331

Anisotropic plasma half space moving normal to interface, investigating incident H waves reflection and transmission coefficients
19 p3024 A71-38610

H-53 HELICOPTER
Night rescue terminal navigation, considering design, development and tests of Limited Night Recovery System for HH-53 helicopter
[AHS PREPRINT 534] 14 p2273 A71-31095

H-56 HELICOPTER
AH-56A Cheyenne compound helicopter icing spray rig tests, discussing ice protection systems design and operating performance
04 p0534 A71-15438

Cheyenne attack helicopter weapons system, discussing night vision capability, armament, fire control and navigation equipment integration
[AHS PREPRINT 530] 14 p2178 A71-31091

AH-56A compound helicopter rigid rotor stability and handling qualities, using flight, whirl tower and wind tunnel tests
[AHS PREPRINT 574] 14 p2180 A71-31115

HABITABILITY
Space station crew operations, discussing vehicle and research duties, habitability, etc
02 p0203 A71-11976

Venus surface alteration for human habitation
04 p0539 A71-15346

Skylab habitability facilities for astronaut work effectiveness and physical well being
15 p2363 A71-31456

Orbital maintenance in pressurized environment, incorporating limited habitability, electronic/pneumatic bench access, critical spares storage racks, extravehicular activity manipulators and repair area
18 p2899 A71-36468

Skylab habitability considerations in Orbital Workshop design, discussing waste management, food management and sleeping compartments
[AIAA PAPER 71-872] 18 p2870 A71-36628

Shower habitability requirements for adequate cleansing of body and hair to satisfy physiological,

psychological and social needs of crew members on long space missions
[AIAA PAPER 71-873] 18 p2870 A71-36629

Architectural and environmental design tools for space system habitability, discussing work and living areas, hygienic facilities, etc
[AIAA PAPER 71-879] 18 p2871 A71-36632

Earth-like ecology for habitation in space, considering hollow sunlit rotating space chamber for life cycles in controlled weather environment
21 p3343 A71-40360

Skylab life support, habitability and thermal comfort system, discussing ventilation, humidity, carbon dioxide and odor control and water, food and waste management
22 p3609 A71-41976

HABITS
Human behavior during machine control learning, modeling habit development as automatic control system
03 p0368 A71-12997

Human operator psychophysiological analysis by memory-activity interdependence simulation, noting buffer memory, reflex system and habit acquisition
07 p1050 A71-20107

HABITUATION [LEARNING]
Vestibular habituation retention, showing nystagmic response reduction to repetitive rotatory and caloric tests
04 p0537 A71-14764

Critical period and habituation in control precision performance response to startle due to pistol shots
11 p1723 A71-25181

Habituation and dishabituation of human vertex response, using auditory or somatosensory stimuli
13 p2012 A71-28890

Visual attention automatization due to repeated stimulus experience, noting fixation rate habituation concomitance with fixations spatial distribution uncertainty reduction
20 p3193 A71-39545

HADRONS
TeV hadrons lateral energy distributions in air shower cores from Ne hodoscope measurements for fluctuations between primary energy and shower size, discussing French alpine scintillators array
12 p1951 A71-27386

Three dimensional Monte Carlo simulation of extensive air shower development, comparing fireball and mathematical models for mean total hadronic energy spectra
12 p1951 A71-27388

Proton-proton interactions at 70-600 GeV in Echo Lake cosmic ray experiment, discussing multiplicity, prongs, hadron flux and ionization calorimeter
12 p1933 A71-27391

Unaccompanied hadron vs primary proton spectra in atmosphere and proton-air inelastic cross sections above 500 GeV from cosmic ray measurements
12 p1951 A71-27394

Cosmic hadron flux measurements and energy spectra at various altitudes in atmosphere, using calorimeters
13 p2122 A71-28066

Sidereal distribution of arrival directions of extensive air showers containing high energy hadrons
13 p2123 A71-28074

TeV hadronic component in air shower cores, comparing energy spectra and lateral distributions to Monte Carlo simulations
13 p2123 A71-28078

High energy hadrons energy flow fluctuations and chemical composition of cosmic rays in air shower cores, comparing to Monte Carlo calculations
13 p2123 A71-28079

Extensive air showers hadronic component observation by nuclear emulsion chambers combined with scintillation detectors
13 p2124 A71-28080

Hadron matter thermodynamical properties at high temperatures, developing dual resonance dynamic model of high energy particle interactions
14 p2304 A71-29597

Gamma ray emission from individual interactions of hadrons in carbon at 10 TeV, using ionization spectrometer-emulsion chamber combination
15 p2407 A71-31808

Neutron star limiting mass based on soft hadron matter resistance to gravitational collapse in stellar structural stability consideration
23 p3732 A71-43073

Statistical system formation in fast hadrons collision process and multiple hadron production
24 p3851 A71-45170

HAFNIUM
Hafnium droplets burning in ultrapure oxygen at various pressures, considering combustion induced natural mode periodic oscillations
[WSS/C/PAPER 70-14] 06 p0942 A71-17654

Anomalous thermal diffusivity measurements of Hf, Nb and Zircalloys, using modulated electron beam technique
10 p1624 A71-23909

HAFNIUM ALLOYS

- Polycrystalline Hf under tension at various temperatures, determining H effects on fracture, operative deformation modes and hydride habit planes
13 p2090 A71-29417
- Columnar grained Ni superalloy lifetimes and transverse creep ductilities enhancement and microstructural alterations due to Hf additions
17 p2759 A71-35394

HAFNIUM ALLOYS

- Precipitation reactions in concentrated Ta-Hf and Nb-Hf alloys at 600-1400 C from X ray diffraction and transmission microscopy, discussing phase relations
06 p0914 A71-18679
- Mo-Re-Hf ternary alloys physical and mechanical properties, considering workability, electrical resistivity and expansion coefficient
07 p1140 A71-20237
- Mo-Hf alloy dispersion hardening by internal nitriding, examining structure and high temperature mechanical behavior
08 p1311 A71-21546
- Nb-Hf alloys alpha precipitation strengthening via aging at various temperatures, examining mechanical properties
08 p1312 A71-21549
- Ternary Mo-Hf-C alloys thermomechanical and mechanical property relationship, obtaining yield strength at various temperatures
08 p1313 A71-21557
- Hf alloys containing transition metals, discussing phase transformations and solid solutions
09 p1473 A71-23225
- High temperature tensile strength of Ta-W-Hf alloy sheet with protective Si-Ti coating in vacuum and air
18 p2933 A71-35951
- Ti-W-B, Hf-Ta-B and Ta-W-B alloys isothermal phase diagrams at 1400 C, using X ray analysis and metallographic techniques
19 p3076 A71-37112
- Monocrystalline and polycrystalline Ta-Hf oxidation at 750-1050 C, noting orientation
22 p3563 A71-42363

HAFNIUM CARBIDES

- Temperature dependence of Vickers pyramid hardness for Ti, Zr and Hf carbides at wide temperature range in vacuum
07 p1142 A71-20483
- Molybdenum and tungsten alloys, detailing strengthening with hafnium carbide
15 p2428 A71-31840
- High temperature vaporization of titanium, zirconium, hafnium and thorium carbides by Knudsen effusion mass spectrometry, measuring ion intensities, formation enthalpies and dissociation energies
16 p2540 A71-33251
- Zirconium uranium carbide and zirconium hafnium carbide thermodynamic properties, using time-of-flight mass spectrometer
[ECS PAPER 120]
20 p3252 A71-39555

HAFNIUM COMPOUNDS
NT HAFNIUM CARBIDES
NT HAFNIUM OXIDES

- High purity hafnium titanate, discussing preparation and DTA, electron microscopy wet chemical and X ray analyses
02 p0275 A71-12595
- Electrical conductivity of strontium zirconate and hafnate at 1400-2600 K measured by two-probe method with alternating and direct currents, calculating activation energy
08 p1323 A71-21934
- Hafnium and zirconium sulfides, determining partial molar free energy of sulfur at metal saturation with electromotive force cell
09 p1387 A71-23129
- Chemical properties of titanium, zirconium and hafnium germanides exposed to acids, oxidizers, complex salts, alkaline solutions and water
19 p3075 A71-37106

HAFNIUM OXIDES

- Alkoxy derived yttria stabilized hafnia composition, using DTA, X ray diffraction, electron microscopy and emission spectrographic analysis
02 p0275 A71-12596
- Air sintered oxides stabilized hafnia body compositions and phases from X ray diffraction and electron microprobe correlation, noting monoclinic and cubic grains
10 p1630 A71-23976
- Electrolytic behavior of yttria-hafnia solid solutions from X ray analysis and electroconductivity measurements
18 p2874 A71-37001

HAIR

- Hair detection by dual wavelength radar overcoming prior limitations, discussing equipment design and technique limitations
01 p0115 A71-10552
- Hair cells aloft interactions and radar detectability inferred from surface data, giving statistically random model
01 p0115 A71-10553

Reflectivity and attenuation observations of hail and radar bright band during storms, discussing rain effects
01 p0115 A71-10554

Microwave attenuation cross section of wet ice spheres, tabulating as function of wavelength, sphere diameter and water thickness
01 p0030 A71-10555

Free fall speed characteristics of simulated hailstones measured by tracking radar, discussing roughness effects on speed and drag
01 p0115 A71-10556

Radar reflectivities in South Dakota hailstorms from hailstone momentum data, applying microwave scattering theory
01 p0115 A71-10557

Radar and air flow structure of Alberta hailstorms from radiosonde data, aircraft measured cloud base updrafts and weak echo region concept
01 p0115 A71-10558

Surface and aircraft radar observations of updrafts within weak echo region of Alberta hailstorm, discussing adiabatic flow breakdown into turbulent flow
01 p0115 A71-10559

Updraft vault dynamic in hailstorms using one dimensional cumulonimbus entraining jet model, observing initial conditions steady state
01 p0119 A71-10744

Freezing nucleus concentrations in hail and rain from different storms, showing dependence on precipitation type and intensity
08 p1326 A71-21451

Dry radar reflectivity and attenuation due to wet ice spheres exponential distributions, noting hail detection procedures
11 p1794 A71-25379

Hail precipitation process from cumulonimbus clouds based on aircraft and ground observations
19 p3093 A71-38692

Ice forming effectiveness and dispersion of reagent particle aerosols through explosion of Elbrus 2 antihail iodide artillery shells in free and clear atmosphere
19 p3094 A71-38697

Cumulonimbus cloud hail danger, precipitation and water content measurements with scattering and attenuation of centimeter radar waves, including automated echo subtraction device
19 p3094 A71-38700

Atmospheric physics of cloud formation, rain, hail and snow precipitation, discussing intracloud temperature variations electric fields and air impurities on water condensation
21 p3410 A71-40146

Atmospheric conditions for hailstone evolution process, using convection theory and kinetic particle model
23 p3701 A71-43909

HAIRSTONES

U HAIR

HAIR

Mammalian hair effectiveness as insulation, using biotelemetry for deep body temperature measurement
01 p0023 A71-10886

Vestibular physiology, discussing endolymph chemical composition, cupola structure and function and hair cells
04 p0536 A71-14752

HALF LIFE

Long life radioisotope thermoelectric generator, discussing mathematical model to simulate expected performance profiles
20 p3266 A71-38958

Carbonaceous chondrite fission producing super-heavy element decay half life
22 p3605 A71-42398

HALF PLANES

Isotropic half plane weakened by circular holes normal to boundary, calculating stress-strain state created by concentrated force
03 p0506 A71-13604

Stress state elastic equilibrium of ponderable anisotropic half plane with free and ring reinforced elliptic hole near rectilinear boundary
10 p1690 A71-24567

Stress and displacement fields in elastic half plane containing edge crack normal to free surface, using integral equations
11 p1847 A71-25440

Semiinfinite crack perpendicular to elastic half plane surface under pressure distribution on faces or remote loading, obtaining fracture mechanics solution with Wiener-Hopf method
11 p1847 A71-25444

Contact stress between half plane and elastic cover plate, reducing problem to Prandtl type integrodifferential equation with Hilbert kernel
12 p1982 A71-27526

Two dimensional contact problem for isotropic body in triangle form on half plane, calculating elastic constants with difference Green function
13 p2156 A71-29071

Fresnel diffraction on opaque absorbing screen half planes with small rough surfaces, deriving field at attenuation factor and structure/correlation functions
14 p2194 A71-30098

Stress-strain state of finite length elastic rod free end bending moments and coupled to semiinfinite plate
14 p2332 A71-30809

Maximum stress concentration in two dimensional elasticity theory for half plane and circle as function of contour distribution, using Cauchy-Buniakovskii inequality in Banach space
16 p2648 A71-32925

Periodically laminated elastic half plane response to rapid internal heating, obtaining far field composite stress waves variation due to dispersion
[ASME PAPER 71-APM-28]
16 p2663 A71-33202

Acoustical field from streamlined body of revolution moving in homogeneous gaseous medium past semiinfinite rigid screen, using Wiener-Hopf method for diffraction radiation
20 p3175 A71-38809

Book on complex variable methods in elasticity, covering boundary value problems for half planes and circular regions
21 p3456 A71-40264

Stress intensity factors of periodically spaced elastic cover plates bonded to elastic half plane, solving contact problem by Fredholm integral equation
21 p3470 A71-41020

Elastic field generation in two bonded isotropic half planes with circular or rectangular inclusion
23 p3774 A71-43146

HALF SPACES

Axisymmetric mixed boundary value problem of thermoelasticity for hot stamp penetration into transversely isotropic half space, deriving contact stresses
01 p0175 A71-11036

Elastic half space transient response to normal impulsive surface line load
02 p0321 A71-11677

Covering plate steady state response to acoustic vibrations in viscoelastic half space, calculating interface displacement frequency spectra under zero shear stress assumption
03 p0459 A71-13719

Couple stress effects on thermoelastic problem for half space with heat doublet on bounding plane, discussing singularity behavior and order
03 p0510 A71-13910

Nonlinear unsteady heat conduction problems, investigating thermophysical property dependence on temperature and body coordinates by half space and approximate methods
06 p1006 A71-17749

Main mixed axisymmetric stress for elastic half space with single line separation between boundary conditions, using p-analytic functions
06 p1001 A71-18341

Pulse propagation from time-step point force at surface of transversely isotropic elastic half space, obtaining solutions by integral transforms
08 p1371 A71-21428

Elastic half space two dimensional unsteady temperature and stress fields under induction heating and convective heat transfer
09 p1537 A71-22519

Admittance of aperture antenna radiating into lossy warm overdense plasma half space, considering electron energy
09 p1505 A71-23521

Input resistance of electric dipole above metallic disk lying on homogeneous conducting half space at HF, using compensation theorem
09 p1495 A71-23573

Elastic half space with plane boundary subjected to transient temperature field, calculating temperature distribution and thermoelastic strain through Laplace transform
10 p1688 A71-24351

Penny shaped crack in elastic layer bonded to two dissimilar half spaces, investigating stress intensity factors and fracture propagation direction
11 p1841 A71-25301

Dissimilar bonded anisotropic half spaces with flat crack under arbitrary loads, determining stress distribution
11 p1842 A71-25303

Two dimensional effects of cylinders rolling on elastic half space, investigating inflated tire shear stress and slip region
11 p1850 A71-26101

Boundary value problems of steady state thermoelasticity and axisymmetric Boussinesq stress concentration for half space in linear Cosserat elasticity
12 p1974 A71-26942

Elastic plane shear wave diffraction on elliptical cylinders in half space, using elliptical wave function series and linear algebraic equations
12 p1978 A71-27332

Parabolic systems solutions asymptotic behavior with dissipation in half space greater than zero, considering Cauchy problem
13 p2094 A71-27805

One dimensional wave propagation at low temperatures in thermoelastic half space under step strain at free surface
13 p2148 A71-27828

Plane longitudinal stress waves propagation in plane-parallel viscoelastic partition of finite thickness dividing two linear half spaces with different elastic properties
13 p2155 A71-28655

Dynamic damping of plane one dimensional unsteady stress wave passing through viscoelastic layer separating linearly elastic half spaces
13 p2155 A71-28848

Coupled thermoelastic disturbances in half space due to thermal shock incident on surface at finite heat expansion rates
14 p2335 A71-30191

Dissimilar elastic half spaces joined over circular region, calculating interfacial traction stresses induced by arbitrary loading from coupled integral equations
14 p2328 A71-30293

Displacements produced by impulsive torsional body force situated within elastic half space bonded to half space of different material properties
16 p2647 A71-32859

Plane thermal waves in heat conducting and radiating/ emitting and absorbing/ medium occupying half space x greater than zero
[DFVLR-SONDDR-133] 16 p2664 A71-34141

Stress distribution in isotropic and anisotropic half spaces with crack in interface bonding, reducing boundary value problem to Hilbert problem
17 p2819 A71-34509

Nonlinear unsteady heat conduction problems, investigating thermophysical property dependence on temperature and body coordinates by half space and approximate methods
17 p2838 A71-35115

Mathematical model of hemispherical inclusion in elastic half space for estimating plastic deformation
18 p2937 A71-36772

Circular planform punch pressure on elastic half space, solving system of two dimensional dual integral equations
19 p3160 A71-38478

Electromagnetic fields of finite linear antennas in dissipative half space, obtaining antenna patterns from computer results
19 p3023 A71-38589

Anisotropic plasma half space moving normal to interface, investigating incident H waves reflection and transmission coefficients
19 p3024 A71-38610

Principal boundary value problems solution for Helmholtz equation in half space with spherical cavities, reducing problems to infinite systems of algebraic equations
20 p3268 A71-38808

Harmonic excitation response of masses on elastic half space, considering Poisson ratio effect, vibration amplitudes and resonant frequencies
[ASME PAPER 71-VIBR-59] 21 p3460 A71-40304

Elastoplastic indentation of half space by infinitely long rigid circular cylinder, using finite element method
21 p3474 A71-41426

Half space with periodic continuous distributed dislocations and plastic distortions, calculating stress fields and free surface orientation with cartesian coordinate system
22 p3613 A71-41432

Coupled thermoelastic problem of homogeneous isotropic elastic half space with embedded spherical cavity
22 p3613 A71-41566

Axially symmetric flow in half space above rotating disk, proving boundary value problem solution existence by fixed point technique
22 p3531 A71-42402

Nonaxisymmetric boundary value problem solution for transversely isotropic half space with circular separation line between boundary conditions, determining tangential stresses
22 p3617 A71-42576

Micropolar elasticity plane problems equilibrium equations system solution, considering elastic half space deformation and steady thermoelasticity
23 p3775 A71-43316

Stresses and displacements in elastic half space with variable modulus of elasticity under axisymmetrical shifting load distributed along ring
23 p3778 A71-44045

Stress and displacement analysis in linear elastic half space consisting of one or two layers bonded to another homogeneous half space
23 p3779 A71-44178

Deformations and stresses in elastoplastic half space indented by rigid sphere, using finite element method
24 p3879 A71-44631

Axisymmetric contact problem of elastic half space stress-strain state, seeking displacements in Hankel integral expansion form
24 p3885 A71-45222

HALIDES

NT ALKALI HALIDES
NT ALUMINUM CHLORIDES
NT AMMONIUM CHLORIDES
NT BARIUM FLUORIDES
NT BORON CHLORIDES
NT BROMIDES
NT CALCIUM CHLORIDES
NT CALCIUM FLUORIDES
NT CARBON TETRACHLORIDE
NT CESIUM FLUORIDES
NT CESIUM IODIDES
NT CHLORIDES
NT CHLORINE FLUORIDES
NT CHROMIUM BROMIDES
NT COPPER CHLORIDES
NT DICHLORIDES
NT DIFLUORIDES
NT FLUORIDES
NT HYDROCHLORIC ACID
NT HYDROCHLORIDES
NT HYDROFLUORIC ACID
NT IRON CHLORIDES
NT LEAD CHLORIDES
NT LITHIUM FLUORIDES
NT MAGNESIUM CHLORIDES
NT MAGNESIUM FLUORIDES
NT OXYGEN FLUORIDES
NT POTASSIUM BROMIDES
NT POTASSIUM CHLORIDES
NT SILICON TETRACHLORIDE
NT SILVER HALIDES
NT SILVER IODIDES
NT SODIUM CHLORIDES
NT SODIUM FLUORIDES
NT SODIUM IODIDES
NT SULFUR FLUORIDES
NT TETRACHLORIDES
NT TUNGSTEN FLUORIDES
NT ZIRCONIUM IODIDES

Ti alloy hot salt stress corrosion under simulated engine environmental conditions, presenting threshold data based on residual tensile ductility
02 p0268 A71-12885

Cuprous halides nonlinear properties in near and medium IR regions
08 p1302 A71-21435

Dissociation reaction in presence of halogen atoms produced in shock wave by thermal decomposition of hydrogen fluoride
19 p3012 A71-38085

IR filters and coatings, describing vacuum deposited layer properties of II/VI, heavy halide and V/VI glass compounds
22 p3544 A71-42135

HALL ACCELERATORS
Aerodynamic probe measurements for plasma jets produced by electrothermal and Hall current accelerators
11 p1764 A71-26275

HALL COEFFICIENT
U HALL EFFECT
HALL CURRENTS
U ELECTRIC CURRENT
U HALL EFFECT
HALL EFFECT
Polycrystalline semiconductors Hall effect by grain structure model for low and high resistivity boundaries, giving vapor deposited cadmium selenide film data
01 p0137 A71-10283

Hall constant and resistivity of impurity centers in seminsulating n-type GaAs during illumination and heating
01 p0138 A71-10776

Hall electron mobility in cadmium arsenide as function of concentration and temperature
01 p0141 A71-11466

Transverse current leakage effect on energy conversion and Hall characteristics of MHD generator
02 p0290 A71-12195

Hall ion thruster using electron neutralized positive space charge in acceleration zone
02 p0283 A71-12312

Plane and cylindrical MHD wave propagation in conducting compressible fluid under Hall effect, examining flow perturbation
02 p0291 A71-12533

Hall effect, conductivity, thermal emf and Nernst-Ettingshausen transfer in n-type highly doped compensated GaAs
03 p0466 A71-13398

Conducting fluids Rayleigh-Taylor instability in vertical magnetic field, taking into account Hall currents
03 p0463 A71-13473

Varying electrical resistivity incompressible fluid flow with Hall effect in presence of thin airfoil
03 p0343 A71-13903

Anisotropic plasma stability, taking into account self gravitation, finite ion Larmor radius, Hall current and rotation
03 p0465 A71-14263

HALL EFFECT

Radioelectric /Hall/ effect due to electromagnetic wave propagation in semiconductors, noting longitudinal electric field generation by thermoelectric forces
05 p0794 A71-16882

Nonstoichiometric VC, studying thermal and electrical conductivities, thermoelectric properties and Hall coefficient
06 p0912 A71-18085

Polycrystalline semiconductors grain boundaries effect on conductivity, Hall mobility and current carriers concentration
06 p0942 A71-18187

Nonhomogeneous arbitrarily formed semiconductor layers, using Van der Pauw method for measuring conductivity and Hall mobility
07 p1175 A71-19221

Electrophysical properties of Ga-In-As single crystals in varying mixture ratios at 78-380 K, determining electrical conductivity, Hall coefficient and electron mobility
07 p1176 A71-19224

HF Hall current instability, discussing short wavelength backscatter for equatorial and auroral electrojets in disturbed ionosphere
08 p1279 A71-21205

High purity Ge crystals growth, studying Hall effect and resistivity for semiconductor detector fabrication
08 p1345 A71-21841

Plasma blowing and suction through channel wall electrodes in two dimensional stationary flow, taking into account Hall effect
09 p1502 A71-22537

Ionospheric current flow past circular inhomogeneous spot with Pederson and Hall conductivities, calculating earth surface magnetic field by Lipshitz-Hankel integral
09 p1436 A71-22549

Plasma flow interaction with nozzle-shaped magnetic field generated by current loop with strong Hall effect
09 p1504 A71-23309

Hall current effects on plasma screw pinch stability, obtaining dispersion relation from perturbations characteristic equations
10 p1647 A71-23889

Hall effect mechanical vibration transducer with indium arsenide semiconductors and elastically suspended magnets
10 p1612 A71-24639

Magnetohydrodynamic Kelvin-Helmholtz problem in Hall plasma, discussing case of hot unmagnetized fluid juxtaposed to cold magnetized plasma
10 p1653 A71-24664

Electrical conductivity, thermal emf, expansion and Hall coefficient of hot compressed powdered diborides of group IV and V transition metals
13 p2084 A71-28036

Hall effect measurements and electron microscope examination of Te-doped gallium arsenide crystals annealed at various temperatures
13 p2111 A71-28503

Hall effect and magnetic field characteristics in lower ionosphere by vertical magnetospheric currents, using gyrotropic model
13 p2061 A71-28534

Electrode nonlinear current distribution in plasma with anisotropic conductivity, noting Hall parameter effect on electric field structure
13 p2107 A71-28566

Potentiometric measurement of temperature effects on electrical resistance and Hall effect in Ni-Co alloys
14 p2259 A71-30188

NiGa intermetallic compound electrical transport and resistance, Hall coefficient and optical adsorption, discussing defect structure and electron scattering
14 p2260 A71-30478

Molybdenum doped zirconium monocarbide, investigating Hall coefficient, thermal emf and resistivity measurements
15 p2460 A71-31284

Galvanomagnetic properties of solid refractory zirconium and titanium compounds in two-band representation, measuring Hall effect and reluctance vs external magnetic field
15 p2426 A71-31512

Hall effect and reluctance of TiN and ZrN specimens obtained by hot compression
15 p2427 A71-31515

Electric field in flow of medium with tensor conductivity due to Hall effect, studying eddy currents structure in magnetic field variation region
16 p2616 A71-32929

Electroconductivity and Hall effect in doped GaAs at low temperatures, studying temperature dependence of electron concentration, mobility and localization
16 p2623 A71-34030

Hall coefficient and electrical resistivity increase during aging of Al-Zn alloys, suggesting free electron energy reduction due to solute atoms clustering
17 p2759 A71-35227

HALL GENERATORS

Reynolds magnetic number effect on MHD channel conducting gas flow current distribution, taking into account Hall effect

17 p2790 A71-35642

Hall fields effect on interaction of MHD waves in inhomogeneous plasma, considering MHD wave dispersion

19 p3109 A71-37134

Poloidal Hall current calculation in hydrodynamic approximation for stationary weakly interacting and conducting cylindrical plasma flow with uniform transverse flow parameter distribution

19 p3109 A71-37138

Stationary plasma flow interaction with axisymmetric spatially periodic magnetic field in presence of Hall effect, determining electric currents structure

19 p3109 A71-37139

Hall effect measurements utilization for simultaneous determination of donors and acceptors concentration in semiconductors, applying to n-type silicon

19 p3118 A71-37487

Free carrier surface density and mobility in large MOS transistors from conductivity and Hall measurements

19 p3028 A71-37564

Ionospheric currents fields, determining Hall conductivity and geomagnetic lines of force slope effects

19 p3058 A71-38387

Hall coefficient and resistivity in undoped heteroepitaxial GaAs on aluminum oxide films grown by trimethylgallium arsine process

20 p3276 A71-38881

Polar cap magnetic variation mechanism based on electric field aligned continuity of Hall current auroral electrojets, noting ionospheric electron density gradients effects

20 p3230 A71-39862

Temperature, magnetic field and pressure dependence of electrical conductivity, thermal emf, Hall effect and transverse Nernst-Ettingshausen effect in indium-doped lead telluride

21 p3429 A71-41210

Impurity photoconductivity, generation-recombination noise and temperature dependences of Hall coefficient and equilibrium carrier mobility in p-type cobalt-doped germanium

21 p3429 A71-41213

High resistance undoped GaAs samples at different temperatures, investigating energy spectra, Hall effect and electron conductivity

21 p3431 A71-41227

Optical investigation of metal-semiconductor interface blocking layer and photo-Hall effect in high resistivity crystals

21 p3433 A71-41316

Electrodynamics of turbulently moving electrically conducting medium, allowing for Hall effect

21 p3453 A71-41356

Four electrodes Hall effect isolator equivalent circuit, describing impedance matrix elements frequency dependence

22 p3520 A71-41705

Subequatorial ionospheric upward moving irregularities during high sunspot activity, explaining phenomenon at F2 region level by Hall drift from daytime west-east electric field

23 p3665 A71-42971

Zirconium monocarbide electrical conductivity, Hall coefficient, thermal emf and magnetic susceptibility measurements for temperature dependence at 500-1000 C in homogeneity region

23 p3692 A71-44021

Nd-Bi phase diagrams from thermal differential, metallographic and X ray analyses, discussing carrier concentration and mobilities, Hall coefficients, conductivity and thermal emf

23 p3692 A71-44022

Current carrier mobility and concentration measurements in inversion metal dielectric semiconductor channels by Hall method

24 p3808 A71-44384

HALL GENERATORS

One dimensional steady supersonic motion of partially ionized two temperature argon-cesium plasma in disk type Hall MHD generator channel

07 p1023 A71-19728

Hall MHD generator duct optimization, using digital calculation for Carter integral minimum for size under required power output

09 p1512 A71-23441

HALO PARACHUTING

U PARACHUTE DESCENT

HALOGEN COMPOUNDS

NT ALKALI HALIDES
NT ALUMINUM CHLORIDES
NT AMMONIUM CHLORIDES
NT AMMONIUM PERCHLORATES
NT BARIUM FLUORIDES
NT BORON CHLORIDES
NT BROMIDES
NT BROMINE COMPOUNDS
NT CALCIUM CHLORIDES
NT CALCIUM FLUORIDES
NT CARBON TETRACHLORIDE
NT CARBON TETRAFLUORIDE

NT CESIUM FLUORIDES
NT CESIUM IODIDES
NT CHLORATES
NT CHLORIDES
NT CHLORINE COMPOUNDS
NT CHLORINE FLUORIDES
NT CHLORINE OXIDES
NT CHLOROSILANES
NT CHROMIUM BROMIDES
NT COPPER CHLORIDES
NT CRYOLITE
NT DICHLORIDES
NT DIFLUORIDES
NT FLUORINE ORGANIC COMPOUNDS
NT FLUORO COMPOUNDS
NT FLUOROAMINES
NT FLUOROCARBONS
NT FLUOROHYDROCARBONS
NT HALIDES
NT HYDROCHLORIC ACID
NT HYDROCHLORIDES
NT HYDROFLUORIC ACID
NT HYDROXYLAMMONIUM PERCHLORATES
NT IODATES
NT IODIDES
NT IODINE COMPOUNDS
NT IODOACETIC ACID
NT IRON CHLORIDES
NT LEAD CHLORIDES
NT LITHIUM FLUORIDES
NT MAGNESIUM CHLORIDES
NT MAGNESIUM FLUORIDES
NT NITRONIUM PERCHLORATE
NT OXYGEN FLUORIDES
NT PERCHLORATES
NT POLYTETRAFLUOROETHYLENE
NT POTASSIUM BROMIDES
NT POTASSIUM CHLORIDES
NT POTASSIUM PERCHLORATES
NT SILICON TETRACHLORIDE
NT SILVER HALIDES
NT SILVER IODIDES
NT SODIUM CHLORIDES
NT SODIUM FLUORIDES
NT SODIUM IODIDES
NT SULFUR FLUORIDES
NT TETRACHLORIDES
NT TUNGSTEN FLUORIDES
NT ZIRCONIUM IODIDES

Inhibitory effects of halogen compounds on hydrogen-air and hydrogen-nitrous oxide flames, measuring burning velocities and temperature/ composition profiles

19 p3013 A71-38106

Stainless steels nitriding in presence of halogen compounds with heat treatment, observing thermodynamic potential shift

21 p3389 A71-41099

HALOGENATION

NT CHLORINATION

NT FLUORINATION

HALOGENS

NT BROMINE
NT CHLORINE
NT FLUORINE

Halogens atomic transition probabilities spectroscopic measurements in visible and near IR spectra, using gas driven shock tube

09 p1163 A71-19685

Halogen molecules electron affinities by measuring negative ion average translational energy and appearance potentials, noting free radicals heat of formation

09 p1498 A71-23376

Ground state dissociation energies and long range internuclear potentials of diatomic molecules of halogens from spectroscopic vibrational spacings

11 p1728 A71-26065

Dissociation reaction in presence of halogen atoms produced in shock wave by thermal decomposition of hydrogen fluoride

19 p3012 A71-38085

Apollo 12 lunar samples halogen and trace element composition, investigating chemical and physical processes affecting surface halides, platinum group metals and Hg

23 p3749 A71-43689

HALOPHILES

Halophilic bacteria growth in freeze-thaw environment, investigating cooling and warming rates and solute concentrations

09 p1388 A71-22131

Halophilic bacteria electron transport chain, studying protein, phospholipids, flavoproteins and cytochromes sedimentation properties by electron microscopy and light scattering technique

21 p3334 A71-40593

Electron transport chain of extremely halophilic bacteria, investigating cytochrome oxidase activity dependence on pH

23 p3633 A71-43525

HALOS

Venus halo as photometric evidence for hexagonal ice in cloudtops

04 p0660 A71-15862

Milky Way galaxy radio halo, investigating background brightness distribution and local spiral arm magnetic field structure

12 p1963 A71-27800

Optical effects observation by air traveler during takeoff, including haze or cloud droplet scattering halos, shock wave shadows, shallow watercolors and twilight wedge

13 p2022 A71-29105

Brightness dependence on heliocentric distance of cometary hydroxyl and hydrogen halos, using the step production mechanism

14 p2318 A71-31120

Milky Way galaxy radio halo, investigating background brightness distribution and local spiral arm magnetic field structure

19 p3133 A71-37400

Halos around black holes, showing luminosities caused by synchrotron radiation of magnetized plasmas

20 p3289 A71-39252

RR Lyrae stars instability strip for halo population variables, presenting linear nonadiabatic approximation calculations with emphasis on blue edges location in H-R diagram

22 p3602 A71-42170

Apollo 11 and 12 rock samples examination, failing to observe radioactive halos

23 p3739 A71-43615

Water vapor-droplet transitional state and halo observation around light sources in radiative fog formation, applying to flight weather forecasts

24 p3844 A71-44860

HAMILTON-JACOBI EQUATION

Generalized Hamilton-Jacobi theorem extension to dynamic equations of motion for holonomic mechanical systems of variable mass with impulse connections

01 p0128 A71-11115

Pursuit game strategy based on Hamilton-Jacobi formalism, considering internal and external potential fields, optimum trajectories and gravitational and electromagnetic fields

03 p0483 A71-13111

Nonlinear systems optimal control, presenting Hamilton-Jacobi equations analytical solutions for quadratic cost function minimization

11 p1742 A71-26420

Quasi-classical ionization model under assumption of straight-line electron trajectories, presenting Hamilton-Jacobi equations solution

12 p1932 A71-27240

Hamilton-Jacobi type theorem on equations of motion with factors of constraints, giving proof for stationary mechanical systems

12 p1923 A71-27525

Hamilton-Jacobi equation application to forced selection for mechanical systems asymptotic stabilization, minimizing functional by Euler-Lagrange equations

16 p2602 A71-32810

Canonical quantization, discussing Schroedinger equation, Hamilton-Jacobi theory, Feynman integrals and sandwich conjecture

16 p2609 A71-33258

Nonlinear optimal closed loop system control problems equivalence relations as one-to-one correspondences between Hamilton-Jacobi equations solutions

17 p2719 A71-34740

Equations of multiple periodic motions, considering quantification of parameters with Hamilton-Jacobi equation

18 p2948 A71-36940

HAMILTONIAN FUNCTIONS

Hamiltonian systems properties in relation to Poisson care function and canonical variables in bilinear form discussing periodic orbits

01 p0128 A71-10660

Optimal piecewise constant control of continuous time systems with time varying delay, deriving restrictive condition on Hamiltonian integrated between switching instants

03 p0389 A71-14070

Deep resonance problem of conservative periodic Hamiltonian reduction to ideal form in celestial mechanics

04 p0657 A71-15730

Hamiltonian of two center libration, including resonant circular orbits and Garfinkel formalism

04 p0620 A71-15730

Von Zeipel procedure convergence for proving theorem pertaining to conditionally periodic motion equations with small change in Hamiltonian

04 p0661 A71-15890

Recursive triangular algorithm for Lie transformation from introduction of small parameter into generating function and Hamiltonian

05 p0774 A71-16540

Canonical linear Hamiltonian systems normalization algorithm, applying to restricted three body problem

05 p0810 A71-16540

Rigid body stability studies with Hamiltonian as Liapunov function, noting application to flexible compact gravity gradient satellite planar motion

06 p0981 A71-18640

Equilibrium position stability of Hamiltonian systems with one and two degrees of freedom in resonance

08 p1336 A71-21859

Two-degree of freedom Hamiltonian system stability and motion about equilibrium point for two-to-one commensurability

10 p1679 A71-24936

Optimization of nonclassical equations of state systems, considering concepts of adjoint and Hamiltonian states

13 p2043 A71-28830

Hamiltonian systems properties in relation to Poincaré function and canonical variables in bilinear form, discussing periodic orbits

14 p2276 A71-31001

Polynomial Hamiltonian for type VIII and IX vacuum cosmologies, suggesting quantized versions involving fluctuations of 3-space signature and topology

18 p2946 A71-35983

Hamiltonian systems equilibrium position stability conditions in presence of resonances, assuming neutrality in linear approximation

19 p3103 A71-37096

Linear and nonlinear two-stream instability under relative motion between cold plasma components from Hamiltonian derivation for plasmons

19 p3112 A71-37744

Equilibrium position stability of Hamiltonian systems with one and two degrees of freedom in resonance

20 p3270 A71-39358

Periodic solutions to Hamiltonian systems with convex potential, considering application to n-body problem

22 p3568 A71-42694

Conservative Hamiltonian systems with infinitely deep potential wells, obtaining periodic solutions with variational technique

[AAS PAPER 71-332] 23 p3698 A71-43005

First order variational equations of Hamiltonian systems with two degrees of freedom for symmetric periodic orbit

23 p3699 A71-43240

Kruskal transformation canonization of perturbed periodic systems with Hamiltonian

24 p3843 A71-44789

Motion integrals conservation under Hamiltonian function variations, examining gyroscope equations of motion with parameter disturbances

24 p3849 A71-45343

HAMSTERS

Microcathodes measurement of oxygen tension on arterioles external surface in hamster cheek pouch and hamster/rat cremaster muscle for blood flow regulation mechanism

03 p0363 A71-13487

HAND [ANATOMY]

Differential equations for control and adaptation of hand motion in cubital joint under weightlessness and accelerations

03 p0357 A71-12990

Human hand anthropometric and biomechanical characteristics, discussing data utilization for human factors engineering

12 p1875 A71-27250

Speed and accuracy relation of hand movement aimed at target, showing error as function of length of uncontrolled terminal phase

16 p2536 A71-33372

Coordination structure of human hand arbitrary movements during stimulation of horizontal semicircular canals in vestibular apparatus by negative angular acceleration

24 p3796 A71-44545

HANDEDNESS

Handedness formula for elliptical polarization after specular metallic reflection of linearly polarized light

07 p1111 A71-19485

HANDLING

U MATERIALS HANDLING

HANDLING EQUIPMENT

NT CRANES

Melbourne/Tullamarine airport, describing facilities, capacity, road system, cargo and passenger handling areas and runway layout

13 p2045 A71-29310

Frankfurt terminal baggage conveyor system, describing passenger capacity and luggage handling equipment

13 p2045 A71-29312

System engineering techniques application to end-to-end space shuttle cargo handling system

18 p2899 A71-36466

HANDLING QUALITIES

U CONTROLLABILITY

HANDWRITING

Handwritten graphical data computer input device with pen position coordinate measurement from acoustic signal propagation delay time in piezoelectric solid plate

21 p3376 A71-40122

Orthonormal series expansion for features generation with predetermined properties, applying to handwritten numerals recognition

22 p3515 A71-41512

HANGARS

Bare base shelter/hangar expandable structures for rapid worldwide Tactical Fighter Organization deployment, noting foam and honeycomb fabrication

[AIAA PAPER 71-398] 11 p1744 A71-25274

International airport planning, considering runways, hangars, second level loading, cargo handling and safety

20 p3209 A71-39388

HANKEL FUNCTIONS

Locally illuminated diffracting edge near field calculation in terms of Hankel function asymptotic solution

09 p1409 A71-23514

Soviet book on multilayered media elasticity theory three dimensional problems covering Fourier and Hankel integral transformations, compression, bending, normal and tangential loads, etc

15 p2506 A71-32020

Degree reduction of scattering matrix by factorization, deriving necessary and sufficient conditions by methods based on Hankel matrices and on Smith-MacMillan form

18 p2941 A71-36237

Generalized finite Hankel transform method for engineering problems with complicated boundary conditions

20 p3255 A71-39034

Axisymmetric contact problem of elastic half space stress-strain state, seeking displacements in Hankel integral expansion form

24 p3885 A71-45222

HANSEN LUNAR THEORY

Hansen method for partial anomalies applied to orbit perturbation equations

01 p0155 A71-10439

Celestial mechanics, discussing fourth order linear differential equation for Hansen coefficients

09 p1486 A71-23340

Computer implementation for Hansen theory of general perturbations, constructing program based on automatic Poisson series processor

21 p3445 A71-40257

HARDENING

Material properties, impregnation, shaping, hardening and structural design in mass production of reinforced laminates for aircraft construction

12 p1920 A71-26954

HARDENING [MATERIALS]

NT CARBURIZING

NT COLD HARDENING

NT HOT PRESSING

NT MARAGING

NT NITRIDING

NT PRECIPITATION HARDENING

NT PULSE HEATING

NT SILICONIZING

NT STRAIN HARDENING

NT WORK HARDENING

Annealed steels strengthening and structural changes under explosive shock wave

01 p0085 A71-10037

Hardening effects of various Ta proportions in Fe-Ni-Ta alloys, noting austenitic nature after homogenization and quenching at high temperature

01 p0105 A71-11619

Cu-Ni-Mn alloys hardening by heat treatment, describing various critical temperature measurement methods and micrographic analysis

01 p0105 A71-11622

Metal hardening under cyclic thermal loads, determining deformation, breakdown, creep and stress-strain relation

02 p0324 A71-11752

Titanium dichloride phase modifications under hardening at various temperatures, using thermal and X ray analysis

02 p0266 A71-12674

Nb alloys hardening due to interstitial atoms interactions with dislocations, obtaining stress-strain relationship for various impurities, precipitates, strain rates and temperature

02 p0270 A71-12929

Austenitized oil hardened annealed chromium steels with electrolytically isolated carbides, determining structure by X ray analysis

04 p0610 A71-14886

High strength multiphase Co-Ni-Cr-Mo alloy hardening, noting deformation and aging induced strengthening

06 p0913 A71-18098

Segmented slip theory of hardening application to bcc metals, discussing dislocation locking and virtual athermal dislocation model

08 p1308 A71-21516

Solid solution hardening theories, discussing point obstacles random distribution effect on strength and superposition of multiple hardening mechanisms

08 p1309 A71-21522

Solid solution hardening of Ta base alloys as function of elastic interaction between dislocations and solute atoms

08 p1309 A71-21523

Grain boundary hardening in relation to electrical resistivity, magnetic permeability and yield stress in iron and Fe dilute alloys

08 p1309 A71-21529

Radiation-anneal hardening and radiation effects on yield stress temperature dependence in bcc metals

08 p1312 A71-21550

Co-Ni-Cr-Mo alloys hardening mechanisms, noting martensitic transformation role

08 p1312 A71-21551

Aligned fibers reinforced material hardening rate, taking into account elastic energy and external potential due to internal stress interaction with applied stress

09 p1467 A71-22286

Electron microscope investigation of packing defect energy effect on structure of crystal dislocations in hardened metals during annealing and deformation

09 p1473 A71-23226

Hardened and glass reinforced epoxy resin mechanical properties after 180 day hold in water, acid and alkaline solutions

10 p1635 A71-24827

Refining process of Fe-NiCu-Mn alloys, discussing aging kinetics, hardening mechanism and strength properties

11 p1781 A71-26159

Bleached hologram lifetime extension, decreasing light induced decay rate by gelatin hardening

12 p1905 A71-26815

Solid solution hardening in Nb alloys single crystals, explaining in terms of elastic interaction of dislocations with substitutional atoms

12 p1916 A71-26927

Ti alloys aging, noting hardness increase and fine structure alpha phase coherent with beta solid solution matrix

12 p1917 A71-27296

Physically nonlinear bent rod, deriving strain method equations for plasticity with hardening according to broken line law

12 p1978 A71-27336

Solution hardening and softening of single crystals, considering deformation in Nb-Mo and Nb-Re alloys

13 p2088 A71-29344

Vacuum melted Ni base superalloys, determining Mo and hardener effects on gamma prime solvus temperature and solutioning rate

13 p2090 A71-29418

Hardened low alloy steel ultrasonic attenuation under magnetic field due to thermally introduced residual stresses

15 p2414 A71-31641

Creep tests on heat resistant steels, studying elongation/rupture strength and temper hardening

20 p3251 A71-39026

Low, medium and high carbon steels hardenability determination from composition, using charted data

20 p3251 A71-39336

Plasticity with noncoincident yield and loading surfaces, noting isothermal isotropic hardening

20 p3309 A71-39565

Solid solution hardening in Ta alloy single crystals, investigating temperature effects on interstitial impurities scavenging and lattice mechanism

21 p3395 A71-40027

High purity Ni wire hardening by lucunae agglomeration during tempering, using comparative tension curves

22 p3562 A71-42245

Hardened cast Al alloys with Cu additions, investigating correlation between mechanical properties and structure at room temperature

24 p3840 A71-45377

HARDNESS

NT MICROHARDNESS

High compressive residual stress and high hardness for long life fatigue strength in nonrotating bending of notched machine parts

01 p0167 A71-10171

Al-Zn-Mg alloys hardness and conductivity behavior as function of aging time and temperature

04 p0610 A71-14884

Nitriding effects on short time tensile strength, plastic properties and hardness of niobium

04 p0612 A71-15549

Nitriding effect on hardness and wear resistance of Mo alloys

06 p0912 A71-17936

MOS large scale IC phosphosilicate glass substrate vapor deposits effects, including hardness, pinhole density and electromigration

07 p1070 A71-18868

Aging effect on tensile mechanical properties and hardness of high purity binary Ni-Cr alloys at 290-530 C

07 p1138 A71-19986

Temperature dependence of Vickers pyramid hardness for Ti, Zr and Hf carbides at wide temperature range in vacuum

07 p1142 A71-20483

HARDNESS TESTS

Optimum tip vertex angles measurement for determining steels tensile strength and yield point from hardness

09 p1467 A71-22314

Fe-Cr-Zr ternary alloys, investigating Zr effect on high temperature hardness and heat resistance

09 p1473 A71-23228

Friction and wear of steels, Ti, Al, Cu and copper beryllium in sliding over hardness range of steel plates in vacuum and air

11 p1771 A71-26143

Tungsten carbide advantages in hard metals structure, including high pressure strength, high elasticity modulus and plastic properties

14 p2255 A71-29517

Ta nitriding temperature and duration effects on tensile strength, elongation and surface hardness

15 p2424 A71-31240

Titanium carbide based cermet materials with alloy steel binder, investigating production conditions, hardness, machining and quenching properties

15 p2429 A71-32139

High temperature tests of short time strength, hardness, moduli of elasticity of W-Mo alloys subject to plastic deformation and annealing

18 p2936 A71-36712

Low, medium and high carbon steels hardenability determination from composition, using charted data

20 p3251 A71-39336

Multiplying factors charts for hardenability prediction of Cr, Ni, Si, Mo and Mn steels containing carbon

20 p3251 A71-39337

Hardness, internal friction, microstress, martensite lattice and density changes during aging of precipitation hardening Fe-Cr-Ni steel, using dilatometric and X ray analysis

21 p3402 A71-41086

HARDNESS TESTS

Superficial residual stresses measurement in plastic region by Hertzian hardness method, considering indentation by ball and proportionality to load variations

02 p0328 A71-12535

Al alloys nucleation and precipitation hardening, examining quenching rate effects with hardness measurements and electron microscopy

04 p0613 A71-15744

TSh-2 hardness test gage, investigating deformation of steel under increasing loads

07 p1106 A71-19141

Gamma radiation influence on photomechanical effect in GaP and GaAs single crystals, using microhardness tester

10 p1656 A71-24143

Graphite epoxy composites fatigue testing, including loaded and unloaded shear, hardness and tensile strength in wet and dry environments

11 p1785 A71-25402

Oxygen and nitrogen thermotransport in transition metals by microindentation hardness testing for concentration determination

11 p1778 A71-25533

Stress distribution during plastic deformation of steel turbine disk from hardness measurements

15 p2505 A71-31863

Cast ZrC hot hardness measurement by static tests at high temperatures, comparing with hot-pressed samples

15 p2431 A71-32161

Hot pressed transition metal carbide samples microhardness measurement, interpreting results in terms of atomic electron configurations

15 p2431 A71-32162

Surfacing materials based on transition metal borides with boron carbide additions, testing brittleness, hardness and abrasive wear resistance

15 p2431 A71-32163

Hot pressed boron carbide and titanium diboride for use as indenter materials for tungsten carbide hardness measurements at high temperatures

15 p2409 A71-32165

German monograph on correlation of Vickers and Rockwell C hardness testing methods covering indentation form measurements, deformation work, etc

17 p2739 A71-34797

Recrystallization behavior of thorium dispersion hardened W-Re alloy compared to pure W by X ray diffraction, hardness tests, metallographic and electron microscopy methods

20 p3247 A71-38763

Heat treatment for weldability and formability improvement of Udimet 700, evaluating by bend, hardness and tensile tests

21 p3388 A71-40622

Brittle transition temperature of steels by Vickers hardness testing, comparing with tensile properties and impact fracture process in Charpy impact test

21 p3388 A71-40751

Transition metal / particularly Ti / carbide hardness temperature dependence explained from dislocation theory viewpoint, relating hardness to electronic structure

22 p3565 A71-41657

HARDWARE

Computer memory reduction through Fortran higher level language, discussing tradeoff between costs saved and additional logic hardware

03 p0382 A71-13450

Space shuttle integrated information management system, emphasizing software element requirements and data processor hardware

[AIAA PAPER 71-222]

Service support for hardware engineering models from breadboard to preproduction stages, determining spare parts location, quantity and cost requirements

09 p1430 A71-23477

Attitude control loop and inertial guidance hardware, studying system dynamic performance hybrid simulation

11 p1796 A71-25846

Microprogrammable hardware interpreter design in LSI multiprocessing system, emulating instruction set with software functions

17 p2712 A71-35776

Higher order computer language architecture for aerospace software production problems, discussing real time constraints, hardware tradeoffs, memory, computer design and logic circuitry

17 p2712 A71-35777

Hardware executive control with associative memory for avionic digital computer system, comparing computation speed, cost and reliability with software method

17 p2712 A71-35778

Reliability in key project decision making, including failure mode/effect analyses, design tradeoff, baseline meetings, hardware storage and data bases

18 p2926 A71-36491

Apollo lunar explorations, reviewing landing, trajectories, hardware, mission problems and scientific studies

20 p3295 A71-39613

HARMONIC ANALYSIS

NT TESSERAL HARMONICS
NT ZONAL HARMONICS

Complex control nonlinear systems invariance and stability conditions, discussing harmonic balance analysis method

01 p0063 A71-10729

Earth poles motion harmonic analysis, using observational data

03 p0406 A71-13245

Tunnel diode frequency multiplier circuit, analyzing harmonic I-V characteristics by equivalent network method

03 p0384 A71-13396

Approximate optimal control law formulation by harmonic linearization for nonlinear time invariant state regulator problem with high performance index

03 p0390 A71-14299

Soviet book on self adjusting control systems with reference models covering harmonic linearization method, phase plane technique, deterministic signals, etc

04 p0560 A71-14641

Asynchronous spatial harmonics effect on O-type interaction in comb-type slow wave structure, obtaining transcendental dispersion equation

05 p0728 A71-16011

Earth variable electromagnetic field spatial harmonics asymptotic properties

05 p0746 A71-17212

Spherical harmonic analysis of worldwide cosmic ray variations during geomagnetic storms, using ground station and satellite data

06 p0949 A71-17253

Periodically supported beams response to random loading, using space-harmonic analysis

08 p1371 A71-21429

Harmonic analysis of metals and alloys fine structure X ray photographs via digital computers

08 p1293 A71-21765

Frequency analysis and Fourier transform evaluation of mechanical shocks and single impulses, outlining theory for filter response to pulses

11 p1853 A71-26521

Earth variable electromagnetic field spatial harmonics asymptotic properties

13 p2060 A71-28267

Quasi-biennial oscillation in low latitude geomagnetic Sq field, showing larger amplitude under equatorial electrojet by harmonic analysis

14 p2231 A71-29719

Lunar center figure position determination by harmonic analysis, comparing with Mills III catalog

15 p2483 A71-31344

Synchronous data transmission system digital signal harmonic analysis based on stochastic process theory, applying to amplitude and phase modulation

15 p2372 A71-32321

Fine structure variations of Al alloy after aging, using harmonic analysis for calculating matrix microdeformation for correlation with mechanical properties

15 p2435 A71-32332

Harmonic analysis of F 2 region critical frequency in antarctic region, emphasizing solar activity effects

17 p2731 A71-34317

Plane Poiseuille flow stability evaluation for finite amplitude periodic disturbances, using harmonic analysis

17 p2729 A71-35388

Harmonic residuum of solar gravity, considering mean deviation and correlation coefficients

20 p3217 A71-39548

Harmonic analysis of signal processing radar antennas spatial filtering process, noting application of physical optics theory

20 p3200 A71-39905

Polarimeter for simultaneous determination of Stokes parameters, analyzing electric signal frequency and phase

22 p3537 A71-41444

Lunar center figure position determination by harmonic analysis, comparing with Mills III catalog

22 p3607 A71-42615

Asynchronous spatial harmonics effect on O-type interaction in comb-type slow wave structure, obtaining transcendental dispersion equation

22 p3524 A71-42757

Covariance analysis of Mars gravity harmonics, ephemeris and radiation pressure from Mariner 1979 range and Doppler radio tracking data

23 p3727 A71-43011

Harmonic analysis applicability to amplitude-modulated frequency characteristics of plasma current fluctuations, governing spectral characteristics determination accuracy by passband filter delineation precision

24 p3851 A71-44394

Statistical and combined harmonic and statistical linearization methods for piecewise-linear nonlinear system characteristics analysis

24 p3814 A71-44699

Current harmonics in passively nonlinear resistance subject to simultaneous DC and AC fields

24 p3860 A71-44877

HARMONIC EXCITATION

Stimulated emission from stilbenyloxazole solution: under pumping by second harmonic of ruby laser; determining emission thresholds

03 p0434 A71-13502

Buckled beam nonlinear vibration under harmonic excitation, solving governing partial differential equation by Galerkin and harmonic balance methods [ASME PAPER 70-WA/APM-48]

03 p0512 A71-14167

Free flight space vehicle nonlinear bending vibrations due to harmonic and pulse excitation

05 p0825 A71-16675

Combinational optic third harmonic generation enhancement by simultaneous coupled nonlinear absorption in liquid dye medium with anomalous dispersion

07 p1128 A71-20392

Nonlinear damped vibratory system with two degrees of freedom excited by two external harmonic forces of different frequencies, investigating summation tones stability

14 p3222 A71-29697

Subharmonic oscillations excited by horizontal vibrations of mathematical pendulum suspension

16 p2607 A71-32934

Harmonic excitation response of masses on elastic half space, considering Poisson ratio effect, vibration amplitudes and resonant frequencies

21 p3460 A71-40304

Second harmonic aperture in ultrashort pulse length measurement by mixing two AM light beams in nonlinear crystals

23 p3683 A71-43397

HARMONIC FUNCTIONS

Analog device for harmonic functions modeling and electron plasma dispersion function computation

01 p0135 A71-11078

Flow with time harmonic function velocity in wind tunnel, controlling rate by sonic striction of varying cross section

10 p1552 A71-24454

German monograph on iterative procedure for sectional parameters of shells of revolution with meridional form under peripheral loads described by harmonic functions

15 p2509 A71-32374

Harmonic stress function and stress intensity factor for elliptical crack embedded in elastic solid and subjected to arbitrary internal pressure

20 p3307 A71-38787

Random analogs of boundary value problems class for biharmonic functions, demonstrating unique solution existence

21 p3410 A71-41187

Gravity coefficients of geopotential expansion in ellipsoidal harmonics via Lamé functions, noting application to earth, Jupiter and Saturn

23 p3666 A71-43011

HARMONIC GENERATIONS

Laser emission nonchromaticity effect on second harmonic generation in ADP, KDP, RDP and lithium niobate crystals

02 p0259 A71-1193

Klystron and frequency multiplier submillimeter harmonic emission determination, using lamellar grating Fourier spectrometer

02 p0250 A71-1214

Fluid transmission lines terminated by orifice with nonlinear pressure flow characteristics, calculating harmonic distortion frequency response by perturbation method
[ASME PAPER 70-WA/FE-6] 03 p0402 A71-14128

Nonlinear materials and optics, second harmonic generation, optical parametric oscillators and IR converters
04 p0635 A71-14721

Second harmonic generation with focused pump beams of optimum phase mismatch and confocal parameters values for obtaining high conversion efficiency
05 p0762 A71-16337

Nonsteady third harmonic generation due to plasma interaction with microwave
06 p0937 A71-18041

Cold bounded nonuniform magnetoplasma harmonic generations model for small collision frequencies
07 p1166 A71-18889

Second spherical harmonic generation mechanisms in axisymmetric diurnal and semidiurnal cosmic ray spectrum variations
08 p1352 A71-20969

One dimensional plasma wave nonlinear dispersion relation, stability and harmonic generation from statistical properties of trapped particle orbits in random potential
09 p1503 A71-22862

Electromagnetic second harmonic wave generation in inhomogeneous magnetoactive plasma, using HF probe and horn antenna for detection
10 p1654 A71-24974

Quantitative analysis of secondary harmonic generation in DC polarized isotropic laser beam, emphasizing molecular mechanisms and symmetrical effects
11 p1773 A71-25566

Second harmonic generation in magnetized ferrite, considering nonlinear interaction between electromagnetic field and medium
12 p1879 A71-26996

Si p-n-n junction avalanche diode, investigating experimental evidence of microwave generation at subharmonics of transit time excitation and trapped-plasma mode
12 p1887 A71-27047

Second harmonic generation experiments, considering limited focused laser beam diameter and crystal sample shape
12 p1915 A71-27641

Third harmonic component generation in reflected and transmitted waves from magnetoplasma slab, using Boltzmann transport equation and Maxwell equation
13 p2109 A71-29243

Laser radiation second harmonic generation susceptibility in molecular crystals due to charge transfer accompanied lowest energy electronic transitions
15 p2421 A71-32402

Nonlinear optical effects associated with free holes and electrons in semiconductors, including higher harmonics generation and frequency mixing
16 p2621 A71-33375

Neodymium-yttrium-aluminate laser for high average power operation and second harmonic and parametric generation
17 p2753 A71-34802

Harmonic generation due to strong microwaves nonlinear mixing in He plasma, noting resonances at fundamental frequencies
18 p2951 A71-35932

Harmonic generation in trapped-plasma-mode IMPATT diode microwave oscillators with waveguide-coaxial cavity
18 p2894 A71-36828

Carbon dioxide laser radiation frequency doubling, using Te for second harmonic generation
18 p2933 A71-37010

Te coefficient for frequency doubling with pulsed carbon dioxide lasers, considering peak second harmonic generation conversion efficiency due to absorption of fundamental
18 p2933 A71-37011

Self induced thermal distribution due to laser beam, discussing effects on refractive index inhomogeneities and second harmonic generation
20 p3196 A71-39105

Laser beam frequency mixing, discussing optical harmonics generation, light reflection/transmission and picosecond pulse measurements
21 p3392 A71-40661

Optical mixing and higher harmonics generation by free carriers in semiconductors, using carbon dioxide laser
21 p3393 A71-40663

High power tunable second harmonic and UV sum frequency generation from rhodamine 6G dye laser and ADP crystal
22 p3556 A71-41803

Pulse shape of mode locked frequency doubled Nd-YAG laser, using single crystal for second harmonic generation and phase modulation
22 p3558 A71-42348

Optical second harmonic generation in excised tissues by Q switched ruby laser irradiation, observing narrow band emission line in collagenous tissues
22 p3559 A71-42567

Second harmonic mode locked frequency doubled pulsed neodymium-yttrium-aluminum oxide garnet laser using single intracavity barium sodium niobate
23 p3683 A71-42957

Nonlinear optical properties of phase matchable crystal cadmium germanium arsenide for carbon dioxide laser second harmonic generation and parametric interactions
23 p3714 A71-42960

Nonlinear sum and difference frequency and second harmonic generations of current density in homogeneous magnetoplasma by nonuniform microwave electric fields
23 p3712 A71-44002

Wideband phase-matched carbon dioxide laser second harmonic generation in GaAs thin film waveguide through dielectric dispersion
23 p3687 A71-44136

Plasma microwave harmonic generation conversion efficiency, applying field gradient theory to case of positive column placed through rectangular waveguide
24 p3803 A71-44648

HARMONIC GENERATORS

Combinational optic third harmonic generation enhancement by simultaneous coupled nonlinear absorption in liquid dye medium with anomalous dispersion
07 p1128 A71-20392

X- to K-band harmonic generator using nonlinear capacitance of varactor diode, deriving maximum efficiency, optimum load and generator impedances
09 p1417 A71-23036

Harmonic pressure generator design based on plane sound waves principle
13 p2071 A71-29293

In-line harmonic tripler with GaAs varactor diode, detailing waveguide mount fabrication, power extraction filter and reverse bias voltage effects
14 p2211 A71-29857

Harmonic extraction from high power efficiency avalanche diodes, discussing circuit in terms of multiple reflection triggering process
18 p2895 A71-36983

Dielectrics breakdown under ultrashort neodymium laser pulses at fundamental and second harmonic frequencies
24 p3834 A71-45120

HARMONIC MOTION

Exponentially decaying intensity averaging time and introscope inertia effect on image unsharpness during object uniform or harmonic motion
08 p1294 A71-21902

HARMONIC OSCILLATION

Krylov-Bogolubov integration theory for first-order perturbation analysis of multidimensional harmonic oscillator applied to body motion in earth gravity
01 p0151 A71-10113

Nonlinear viscoelastic beam with hereditary properties, analyzing forced harmonic vibration propagation
01 p0169 A71-10638

Three dimensional wings harmonic oscillation with arbitrary frequency in subsonic flow, presenting approximation method for singular integral equation
01 p0173 A71-10844

Elastic harmonic waves propagation in composite circular elastic cylinder
07 p1214 A71-19956

Unsteady MHD channel flow between two semi-infinite harmonically oscillating and perfectly conducting solids, determining liquid velocity profile curves
07 p1169 A71-20032

Laser dynamic theory with uniformly broadened and Doppler spectral lines based on nonlinear interactions between harmonic oscillations
07 p1127 A71-20255

Horizontal pendulum angular velocity and motion due to harmonic vibrations at base
07 p1162 A71-20651

Harmonic oscillations frequency dividers with small asynchronous component of nonlinear element conductance, showing self excitation and wide synchronization bandwidth
09 p1413 A71-22152

Optical parametric oscillator, observing simultaneous oscillation and second harmonic and difference frequency generation
09 p1493 A71-22760

Aerodynamic forces on harmonically oscillating wing in subsonic flow of ideal gas
09 p1384 A71-23615

Angular dependence of specularly parameter/probability of specular scattering of electron incident upon surface/ via magnetic field dependence of magnetomorphic harmonic oscillations
10 p1655 A71-23771

Earth eigen vibrations excitation by gravity waves, tabulating energy content of even and odd harmonics overtones
10 p1607 A71-25005

Cavitation microstreaming near spherical drop or bubble performing translational harmonic oscillations in liquid at rest
11 p1749 A71-25183

Arbitrary direction harmonic vibration effects on kinetic friction coefficient between sliding bodies
11 p1767 A71-25267

Harmonic vibrations of rib reinforced rectangular elastic plates with two freely supported parallel edges, deriving method for natural frequencies and forced vibration
11 p1848 A71-25580

Forced rotational oscillations of plane-convex glass lens pressed against brass plate, determining contact frictional and elastic characteristics from resonance and hysteresis
11 p1849 A71-25621

P-n avalanche diode trapped plasma avalanche triggered transit /TRAPATT/ oscillations characteristics and voltage waveform under square wave driving current, using computer program
12 p1887 A71-27046

Airfoils unsteady stall by testing two dimensional model in harmonic pitching oscillation for helicopter rotor blades characteristics
12 p1866 A71-27609

Geomagnetic field secular variation subdivision based on time effect, noting harmonic processes with 20 year period
13 p2059 A71-28247

Harmonic vibration analysis methods, discussing mathematical model, ground tests, structure suspension exciter and pickup location eigenvalue measurement and mode research
14 p2175 A71-30058

Viscous gas unsteady flow between harmonically oscillating and nonoscillating walls
14 p2225 A71-30220

Energy dissipation in harmonically oscillating spherical annulus filled with viscous fluid
15 p2391 A71-32104

Subharmonic oscillations excited by horizontal vibrations of mathematical pendulum suspension
16 p2607 A71-32936

Free and forced nonlinear oscillatory systems with harmonic perturbations, noting amplitude dependence on force frequency and friction coefficients
17 p2782 A71-34935

Dynamic piecewise-continuous linear systems oscillation period doubling in presence of C bifurcations
18 p2948 A71-36785

Interference of transferred electron device operation involving harmonic tuning, considering EMC aspects
19 p3032 A71-38461

Perturbations generated by two dimensional super-sonic channel flows with walls oscillating with harmonic time dependence and small pressure amplitude computed, using linearized method of characteristics
24 p3819 A71-44951

HARMONIC OSCILLATORS

Projected Hartree-Fock energy spectra using basis wave functions with harmonic oscillator and Wood-Saxon radial dependence
06 p0929 A71-17577

Second harmonic voltage effects on quenched domain mode Gunn effect oscillator for DC to RF conversion efficiency, discussing negative device conductance at multiharmonic frequencies
09 p1417 A71-22696

Analog to digital converters employing subharmonic oscillator phase as recording medium, discussing parametron application as phase comparator
11 p1743 A71-26541

Vibration mode patterns of acoustoelectric oscillators, describing detecting apparatus
13 p2036 A71-28469

Gas atom collisions with linear harmonic oscillator and solid surface simulated by semiinfinite elastically coupled atomic lattice, using combined asymptotic expansions method
13 p2103 A71-29227

Low frequency noise spectra measurement in varicaps by frequency modulation of harmonic oscillator, noting application to diode and p-n transistors
15 p2369 A71-31232

Energy momentum stress tensors for harmonic oscillator model, calculating energetic interaction with plane gravitational wave of same frequency
18 p2946 A71-35982

Tunnel diode harmonic relaxation frequency divider, obtaining large division factors and wide synchronization bands with sinusoidal output signal
20 p3206 A71-39818

Nonresonant vibrational exchange in molecular binary harmonic and one component anharmonic oscillators with beam laser applications
21 p3394 A71-41255

HARMONIC RADIATION

Two dimensional distribution moments of harmonic signal and normal narrow band noise mixture envelope, deriving expressions by power series expansion
09 p1404 A71-22293

HARMONICS

High order harmonic mixing of klystron microwave and far IR laser radiation using Josephson junction
09 p1464 A71-22766

Frequency equation for harmonic waves with circumferential nodes traveling in composite traction free circular cylindrical shells, using IBM 7094 computer
11 p1847 A71-25461

Mathematical model for harmonic emission spectrum in FM and PM communication transmitters modulated by random signal
13 p2032 A71-28875

Electron beam interaction with external harmonic microwave field in planar diode gap, calculating electric field current and voltage distribution functions
14 p2211 A71-30084

Frequency equations for trains of axisymmetric harmonic waves traveling in infinitely long three layered elastic circular cylindrical shells and rods
14 p2327 A71-30202

Ionospheric VLF and ELF wave observations, noting ion cyclotron resonance and harmonics effects on propagation
14 p2202 A71-30946

Radioheliographic 80 MHz observations of harmonic type 2 solar burst near limb flare
15 p2472 A71-31688

Culgoora 80 MHz radioheliographic observations of 13 October 1969 harmonic solar type 2 burst attributed to explosive flare behind west limb
15 p2472 A71-31689

Solar type 3 bursts with fundamental and second harmonic structure for corona reflected and direct rays at 80 MHz observed with Culgoora radioheliograph
15 p2473 A71-31690

Propagation angle effect on time harmonic wave dispersion in periodically laminated medium, using two dimensional equations of elasticity
[ASME PAPER 70-WA/APM-47]
15 p2506 A71-32010

Laser radiation second harmonic generation susceptibility in molecular crystals due to charge transfer accompanied lowest energy electronic transitions
15 p2421 A71-32402

Ion cyclotron harmonic waves development in simulated low density and temperature space plasma, determining propagation upper and lower bounds
15 p2491 A71-32448

Harmonic electromagnetic field outside closed surface perfectly conducting antenna, using Kirchhoff formula
16 p2544 A71-34171

Vector synchronism for interaction between ordinary and extraordinary wave during second harmonic emission and frequency mixing in He-Ne laser
17 p2752 A71-34408

Deuterium fluoride overtone vibration-rotation chemical laser emission, studying frequency doubling and rate constant ratios
17 p2753 A71-34801

Time harmonic waves oblique propagation in periodically laminated composite, using coupled thermoelasticity theory for plane strain
22 p3613 A71-41433

Acoustical harmonic point source in motion relative to surrounding fluid, using Fourier integrals for mathematical representation
24 p3847 A71-44418

HARMONICS

NT HARMONIC EXCITATION
NT SPHERICAL HARMONICS
NT SUPERHARMONICS
NT TESSERAL HARMONICS
NT ZONAL HARMONICS

Satellite orbital elements perturbation due to tesseral and sectorial harmonics of earth gravitational potential
06 p0976 A71-18451

Accurate single-sideband radio receiver tuning, observing reconstitution of harmonic tones in human speech strong vowel sounds
08 p1254 A71-21318

Whistlers with harmonic bands caused by multiple stroke lightning, using Injun 5 VLF data
08 p1283 A71-21649

First and second frequency harmonics and form shapes of liquid filled cylindrical shell axisymmetric vibrations, analyzing effect of pressure and shell dry portion on vibration frequencies
08 p1374 A71-22055

Short wave HF instabilities in strongly inhomogeneous plasma with hot electrons, considering ion acoustic oscillations and electron cyclotron harmonics
10 p1650 A71-24525

Satellite orbital elements perturbation due to tesseral and sectorial harmonics of earth gravitational potential
12 p1955 A71-26601

Absolute measurement of laser frequencies in IR range, using extended harmonic heterodyne technique
14 p2255 A71-30979

Systematic phase variation in second harmonic of daily variation of cosmic ray intensity in one year, recorded by neutron monitor at Deep River
15 p2441 A71-31410

Low degree gravity harmonics source, discussing upper mantle hypothesis of mass anomalies location
16 p2563 A71-33150

Mars surface harmonics and continental drift from radar and spectroscopic topographic height determination
16 p2638 A71-33519

Short wave HF instabilities in strongly inhomogeneous plasma with hot electrons, considering ion acoustic oscillations and electron cyclotron harmonics
19 p3116 A71-38251

Decarbonization monitoring of ball bearing steel bars, describing defectoscope based on eddy current higher harmonics method
22 p3553 A71-41768

Unified electrical machine theory with allowance for space harmonics effects, transforming time-dependent linear differential equations into linear time-invariant equations
24 p3793 A71-44657

HARNESSES

Primate restraint harness of nylon jacket and cotton cot on aluminum frame padded seat for bone resorption and calcium metabolism studies
09 p1398 A71-22476

Automated electrical wire harness manufacturing for Boeing 747 aircraft, discussing development of numerical control program
21 p3386 A71-40441

HARRIER AIRCRAFT

Supersonic staggered gutter colander combustion system for plenum chamber burning on high bypass Pegasus turbofan engine of Harrier VTOL aircraft, noting performance improvement
13 p2116 A71-28743

Harrier aircraft development from flight test viewpoint, discussing conventional flight envelope problems caused by VSTOL concept imposed constraints
16 p2524 A71-34009

HARTMANN FLOW

Thermal conductive liquid hydrodynamic stabilized Hartmann flow in rectangular canal with transverse field, examining magnetic effect on heat transfer
04 p0635 A71-15509

Plane MHD Couette flow stability with asymmetric velocity profile shaped by transverse magnetic field, considering Hartmann flow
19 p3108 A71-37077

HARTMANN NUMBER

MHD Rayleigh-Taylor instability in galvanic approximation, demonstrating Hartmann number stabilizing effect
07 p1167 A71-19188

Wall conductivity effects in MHD rectangular duct flow at high Hartmann numbers with uniform magnetic field applied parallel to one pair of duct sides
10 p1649 A71-24419

MHD rectilinear two dimensional flows at high Hartmann number, including extension to three dimensional problems
15 p2459 A71-32560

Hartmann number for velocity pulsation free transition from turbulent MHD flow to laminar, noting difference relative to linear stability theory
24 p3856 A71-45059

HARTREE APPROXIMATION

Projected Hartree-Fock energy spectra using basis wave functions with harmonic oscillator and Woods-Saxon radial dependence
06 p0929 A71-17577

Nucleus energy spectra projection from Hartree-Fock intrinsic wave functions model space, using coupled orbital matrix elements
06 p0929 A71-17578

Term splitting of Li I, B I, Na I and other sequences with one electron spectra, using screening parameters obtained from Hartree-Fock calculations
08 p1337 A71-21182

Coupled and uncoupled versions of Hartree-Fock theory, calculating atomic system linear response to external time dependent perturbation and Green function
11 p1802 A71-26057

Hartree-Fock energy levels, transition probabilities and wave functions for highly ionized atoms in B I isoelectronic sequences, including spin-orbit interactions
15 p2452 A71-32597

HARTREE-APPLETON APPROXIMATION

U HARTREE APPROXIMATION

HARTREE-FOCK APPROXIMATION

U HARTREE APPROXIMATION

HASTELLOY (TRADEMARK)

Residual stress measurement in Hastelloy N gas tungsten arc welds by Sachs boring-out method, permitting stress distribution determination over short distance increments
06 p0912 A71-18043

Air- and vacuum-melted Hastelloy-N/Ni-based alloy/creep-rupture properties dependence on irradiation temperature
11 p1781 A71-26066

HAWKER SIDDELEY AIRCRAFT

NT BUCCANEER AIRCRAFT
NT COMET 4 AIRCRAFT
NT DH 121 AIRCRAFT
NT HARRIER AIRCRAFT

VSTOL lift fan airliner project HS 141 for intercontinental transport, describing features, weight and performance data, noise characteristics and reliability criteria
15 p2348 A71-31414

VSTOL developments at Hawker Siddeley Aviation, noting circulation controlled rotor concept for HS-141 aircraft
19 p2997 A71-37600

HAZARDS

NT AIRCRAFT HAZARDS
NT FLIGHT HAZARDS
NT METEOROID HAZARDS
NT OPERATIONAL HAZARDS
NT RADIATION HAZARDS
NT TOXIC HAZARDS

Plug-in relay hazards and minimization for aircraft flight safety applications
13 p2001 A71-28848

Hazard rate functions of systems with identically distributed subsystem failure times in sequential continuous simultaneous operation
22 p3566 A71-42111

HAZE

Similarity comparisons of isotropic and anisotropic scattering patterns in cloudy atmospheres for haze effects on Mars image contrast, using asymptotic method
11 p1825 A71-25717

Optical effects observation by air traveler during takeoff, including haze or cloud droplet scattering, halos, shock wave shadows, shallow watercolors and twilight wedge
13 p2022 A71-29350

Mars surface features contrast reduction, discussing forward scattering haze as possible cause
15 p2491 A71-32441

Standard visibility and scattering coefficient changes due to humidity variation from maritime aerosol particles equilibrium radii calculations
16 p2605 A71-34088

Haze scattering effect on solar radiative heating rate due to water vapor absorption in near IR
17 p2736 A71-35556

Martian blue haze clearings and flash phenomena meteorological mechanism, considering atmospheric clearing due to water precipitation
18 p2966 A71-36767

HC-1 HELICOPTER

U CH-47 HELICOPTER

HEAD [ANATOMY]

NT CRANIUM
NT OCCIPITAL LOBES
NT SKULL

Moulting of Calpodus ethlius larvae head and thorax isolated with prothoracic glands dependent on molting hormone injection
01 p0016 A71-11344

Water cooled head cap for heat stress amelioration in subjects working in warm environments
06 p0859 A71-17611

Hind limb antagonistic muscles bioelectric activity dependence on animal rotation direction and head fixation
09 p1388 A71-22199

Dogs intrapleural and intraesophageal pressures dependence on head positions
19 p3010 A71-38566

Visual sensations produced by cosmic ray muons passing in different directions through human eyes and hand
19 p3005 A71-38677

Physiological responses to head and neck vs trunk and leg cooling under hyperthermic stress
21 p3331 A71-40350

Afferent oculomotor pathways to extraocular muscle nuclei, considering discrete unilateral lesion role in head posture disturbance production
22 p3488 A71-42433

Head and abdomen shielding effects on radiation sickness evolution in dogs under lethal gamma irradiation
22 p3493 A71-42711

HEAD [FLUID MECHANICS]

Fluctuating pressure measurement in mixing zone of axisymmetric jet, using total head and static probe coupled to 1/8 inch microphone
13 p2053 A71-29466

HEAD FLOW

Head end secondary flows in solid propellant rocket motor combustion chamber due to transverse acoustic waves in quiescent fluid
14 p2335 A71-29877

HEAD MOVEMENT

Guinea pigs head and eye movements produced by vestibular apparatus stimulation via static pressure changes

01 p0010 A71-10347

Head spatial position effects on vestibular compensation rates in rabbits

01 p0012 A71-11074

Heat rotation induced eye movements in cats by neuron level determination, considering vestibular apparatus of signal transmission loop for mathematical model

03 p0356 A71-12983

Coriolis effects on endolymph shift direction in semicircular canals of man under rotation with head movements in sagittal plane, involving nystagmus and illusory sensations

09 p1392 A71-22640

Coronary hemodynamic responses to postural changes in hemorrhaged dogs involving head-up and head-down tilts

11 p1720 A71-26114

Instantaneous postural reaction of cattle to brain concussion indicating mechanoreceptor HF discharge impulse pathophysiological mechanism

11 p1720 A71-26122

Mathematical model for short term adaptation to vestibular stimuli, deriving transfer function relating angular velocities of nystagmus and head rotation

14 p2182 A71-30250

Rotational ocular nystagmus phases induced by head rotation, developing vestibulo-ocular system mathematical model

17 p2691 A71-35045

Eye-point-of-regard system including eye and head movements devices and analog computer for pilot scanning and display research

18 p2864 A71-36091

Eye-head coordination in monkeys by recordings from neck and eye muscles, noting central neural command role

18 p2856 A71-36232

Vestibulo-colic reflex control of head movement in seated man under sinusoidal and stepwise rotational velocity stimulation, comparing with ocular stabilization

22 p3501 A71-41822

HEAD-UP DISPLAYS

Head- or helmet-mounted display/control system in V/STOL aircraft for pilot workload and training reduction

14 p2189 A71-31093

[AHS PREPRINT 532] Aircraft head-up display systems for providing pilot information focused at infinity within pilot normal field of view

21 p3413 A71-40131

VTOL and fan lift STOL aircraft, discussing simulation and head-up displays for roll demand, vertical speed and ILS beam

21 p3413 A71-40134

HEALING

NT WOUND HEALING

HEALTH

Flight surgeons guidance criteria for flying personnel, detailing individual areas examination, documentation and clinical findings

08 p1245 A71-20719

Preventive and clinical medicine effect on aircrew health maintenance

08 p1245 A71-20725

Aircraft noise as public health problem, discussing effects on physical, mental and social well-being

08 p1249 A71-21816

Epidemiological aspects of airport medicine in relation to global public health and international cooperation

11 p1725 A71-26129

HEARING

NT ACOUSTIC FATIGUE

NT BINAURAL HEARING

Inner ear basilar membrane motions estimation for lower hearing threshold, using nonlinear model

02 p0201 A71-12474

Plethysmographical study of noise effects on hearing and peripheral vasoconstriction in man and animals

03 p0359 A71-13155

Argyrophil sphincter formations in intraorganic vascular channels of hearing organ

08 p1243 A71-21967

Cortical potentials evoked by weak acoustic signals below hearing threshold in man

10 p1564 A71-24440

Interaural phase angle control, using equal masker/signal narrow noise bands and phase shifting network between channels

12 p1871 A71-27534

Quick-check audiometry reliability for testing hearing ability according to fitness regulations, comparing to complete tone and speech audiometry

14 p2188 A71-29821

Spatial and temporal discrimination functions in vision, audition and touch, establishing and controlling stimuli by vibrators

14 p2188 A71-30252

Community aircraft noise intensity indexes from annoyance and physiological reaction standpoint, discussing sleep interruption, hearing loss, communication interference, etc

15 p2364 A71-32242

Book on noise effects on man covering audiometry, aural reflex, hearing damage risk, physiological responses, motor performance and speech communication

20 p3193 A71-39874

Aircraft noise effects on hearing acuity and perceptual and intellectual judgment tasks

21 p3342 A71-40351

HEARING LOSS

U AUDITORY DEFECTS

HEART

NT CARDIAC VENTRICLES

NT MYOCARDIUM

Cardiac cells electrical interaction mathematical simulation, calculating gap region resistance and current

01 p0025 A71-11176

Electro-optic monitoring method for single isolated heart cell activity

02 p0202 A71-11672

Heart electric generator system simulation by dipolar or multipolar generators

10 p1569 A71-24238

Human heart, kidneys, liver and spleen tissues antigen composition analysis by isolation of pure antibodies

12 p1872 A71-27723

HEART DISEASES

Mortality of myocardial infarction patients on diet low in saturated fats and cholesterol

01 p0015 A71-11299

Abnormal left ventricular contour with late systolic murmur at apex preceded by click and with abnormal T waves in electrocardiogram

02 p0197 A71-11694

Mitral valve muscular fibers, investigating pathological changes of myocardium of left heart ventricle

02 p0198 A71-11695

Complete heart block associated with acute myocardial infarction, discussing high mortality rate and transvenous pacemaker applications

02 p0198 A71-11696

Coronary artery heart disease detection in aircraft pilots to age 45 during physical examinations

02 p0208 A71-12392

Thrombosis and coronary heart disease - Conference, Porvoo, Finland, September 1969

02 p0199 A71-12413

Coronary sclerosis morphology, discussing myocardium microcirculation disturbances

02 p0200 A71-12414

Antithrombotic agent search, finding anticoagulants useful for Venous system

02 p0200 A71-12418

ECG changes and coronary risk of acquired bundle branch block in healthy population

03 p0363 A71-13490

Submaximal exercise ECG test in screening high risk populations for occult ischemic heart disease

03 p0372 A71-13491

Clinical and hemodynamic profile of cardiogenic shock after acute myocardial infarction

04 p0541 A71-15914

Autopsies compared to ECG for diagnosis accuracy for acute recurrent myocardial infarction

05 p0711 A71-16951

Acoustic phenomena accompanying pericardial disease, considering heart valves and chordae tendinae

05 p0711 A71-16953

Myocardial infarction acute stage, noting carbohydrate metabolism disturbances

06 p0849 A71-17291

Myocardial infarction, investigating alpha-dehydroxybutyric acid dehydrogenase enzymatic activity

06 p0849 A71-17292

Myocardial infarction noting serum prealbumins changes

06 p0849 A71-17293

Human valvular heart disease, examining work load effects on oxygen demand

06 p0849 A71-17294

Cinearteriographically demonstrated coronary artery disease severity correlation with myocardial blood flow response to treadmill exercise or isoproterenol infusion

06 p0852 A71-17874

Aircrews coronary insufficiency diagnosis via electrocardiographic modifications after exertion, observing ischemia

06 p0860 A71-18192

Arm to tongue blood circulation time for heart disease and failure diagnosis in aged people

07 p1043 A71-20215

Myocardial lysosomal enzymes activity in adaptation to high altitude hypoxia and during cardiac diseases, using albino rats

08 p1239 A71-21058

Hemodynamic correlation of Austin Flint murmur and a-wave of apexcardiogram in aortic regurgitation

09 p1392 A71-22589

Carotid pulse wave slope variations in normal subjects, aortic valvular diseases and hypertrophic sub-aortic stenosis

09 p1392 A71-22590

Mitral valve systolic prolapse aggravation due to G acceleration and aeromedical significance

09 p1395 A71-23246

Cardiac arrhythmias simulated by concealed bundle of His extrasystoles in open chest intact dog hearts

09 p1395 A71-23256

Cardiac hypertrophy in animals, discussing increased cardiac work load compensation and muscle cell alterations

10 p1565 A71-24674

Myocardial oxygen reduction by stimulating carotid sinus nerves and angina pectoris treatment application

11 p1718 A71-25437

Hypertensive heart and pulmonary vascular disease, examining chronic alveolar hypoxia effects

11 p1719 A71-25931

Heart size estimated from chest X rays related to corrected orthogonal ECG findings in patients with congestive heart failure symptoms

12 p1875 A71-27288

Extrinsic factors in pathogenesis of congenital heart diseases, considering morphogenetic processes in heart and great vessels development

13 p2002 A71-27811

Ultrasonic echocardiograms of anterior cusp of mitral valve in aortic valve disease

13 p2002 A71-27814

Pulmonary circulation regulating factors, examining heart disease effects on lung capillary blood flow

13 p2003 A71-27861

Ventricular septal defect, discussing incidence, human physiological responses, morbidity and mortality in various age groups

13 p2004 A71-27862

Myocardial hypertrophy, discussing various forms and mechanisms in myocardial fiber growth and eventual failure

13 p2004 A71-27863

Cardiac hyperfunction, hypertrophy and insufficiency, discussing physiological mechanism and cause and effect relationships

13 p2004 A71-27864

Mild hypertension risks, presenting results of case studies over ten year period of mortality rate associated with cardiovascular diseases

13 p2004 A71-27865

Hypertension and heart or arterial disease relationships, discussing cause and effect mechanisms in coronary diseases

13 p2004 A71-27866

Myocardial infarction and coronary heart disease, considering incidence, mortality and preventive measures

13 p2004 A71-27867

Analog simulation of cardiac malfunctions associated with A-V conduction block and Wenckebach phenomenon, using P and R wave and internal function generators

13 p2020 A71-29001

Sudden death and syncope mechanism in aortic valve stenosis, noting presence of baroreceptors in left ventricular wall

13 p2014 A71-29301

Myocardial ischemia and necrosis without major coronary arteries obstruction, investigating possible deranged hemoglobin-oxygen transport

14 p2185 A71-30286

Myocardial ischemia observations, utilizing morphologic and pathophysiologic correlations with cinecoronary arteriography, left ventriculography and hemodynamic examination

14 p2185 A71-30287

T wave abnormalities in electrocardiograms of athletes without organic heart diseases

14 p2187 A71-30708

Human radioisotopic angiocardiology, emphasizing identification and physiological diagnosis of congenital and acquired cardiovascular defects

15 p2361 A71-32537

Atrioventricular and intra-ventricular conduction disturbances in acute myocardial infarction, discussing heart block

15 p2361 A71-32540

Right ventricular end-diastolic volume as index of myocardial fiber length and correlation with ventricular work at rest and exercise with and without right ventricular failure

15 p2361 A71-32541

LVET/EICT ratio usefulness compared to EICT for left ventricular contractility in patients with mitral valve disease

15 p2361 A71-32659

Efferent vagal activity increase prior to intermittent cardiac block due to rise in blood pressure

16 p2529 A71-33192

Physiologic and pathologic cardiomegaly, noting myocardial blood flow oxygen uptake and lengthening and widening of coronary vessels

16 p2531 A71-33423

Nonlinear analysis of arterial flow pulses and shock waves, simulating aortic insufficiency under pathological conditions by mathematical model
16 p2538 A71-34145

Hemodynamic evaluation of glucagon in symptomatic heart disease, comparing to isoproterenol
17 p2682 A71-35040

Human ventricular activation correlation with canine model in chronic myocardial infarction
17 p2682 A71-35041

Primary cardiomyopathy, discussing obstructive and nonobstructive cases, myocardial inflammation, chronic alcoholism and age relationships
17 p2682 A71-35120

Myocardial inotropism index, using left ventricle time varying pressure/volume ratio in systole
17 p2683 A71-35121

Electrocardiographic evidence of false complete bilateral bundle branch block with impaired atrioventricular conduction in patient with hypertensive heart disease
18 p2853 A71-35912

Correlative ECG survey of surgically proven constrictive pericarditis involving left ventricle with T wave inversion
18 p2853 A71-35913

Acute fatal nontraumatic collapse during physical work and sports due to pathological processes
18 p2855 A71-36214

Acute fatal nontraumatic collapse during physical exertion due to circulatory diseases
18 p2855 A71-36215

Unconsciousness, confusion, amnesia, syncope and sudden death of pilots in flight due to silent ischemic heart diseases
18 p2855 A71-36216

Frequency phonocardiography technique for heart sounds and murmurs registration, producing analog voltage proportional to frequency by zero crossing detector
19 p3006 A71-37234

Diastolic heart sounds and filling waves in coronary artery disease, relating graphic abnormalities and clinical, arteriographic and hemodynamic findings
19 p3002 A71-37550

Myocardial blood flow and oxidative metabolism in cyanotic congenital heart disease patients, using lactate/pyruvate ratios and coronary sinus catheterization
22 p3484 A71-41521

Antecedent clinical statistics of myocardial infarction and sudden death in actively employed middle aged men, noting cardiac rate, rhythm and conduction abnormalities
22 p3485 A71-41798

Photoplethysmographic analysis of pulse wave velocity in healthy subjects and in patients with hypertension, heart disease, diabetes and anemia
22 p3490 A71-42518

Ultrasonic evaluation of heart anatomical abnormalities in congenital and acquired heart diseases including myocardium hypertrophy and tissue degeneration
23 p3639 A71-43118

Midsystolic clicks and papillary muscle dysfunction evidence in arteriosclerotic heart disease from ECG, carotid pulse tracing and phonocardiography
23 p3635 A71-44126

Ejection fraction relation to left ventricular dimensional changes in patients with heart disease, using angiograms
23 p3635 A71-44128

Preclinical coronary heart disease detection by near maximal treadmill exercise ECG
23 p3636 A71-44129

Diagnostic import of QRS notching in HF ECG of living subjects with heart disease, noting notch count correlation with ventricular enlargement
23 p3636 A71-44130

Cardiac arrest or arrhythmia due to coronary arteriosclerosis in young aviator, examining causes, prevention and predictive measures
23 p3637 A71-44250

Cardiovascular system functional disorders relationship to nervous activity disturbances
24 p3795 A71-44472

HEART FUNCTION

NT HEART MINUTE VOLUME

Catheter inserted wire basket device for creation of reversible aortic insufficiency in animal
01 p0022 A71-10248

Right heart ventricle activity in patients with hypertension recorded by electrokymograph
01 p0014 A71-11138

Computer differential analysis of cardiac rhythm irregularities involving comparison of EKG RR intervals
01 p0025 A71-11154

Physical exercise effect on mitochondrial energy production in heart muscle and liver in rats
01 p0017 A71-11542

Coronary perfusion pressure, heart performance and homeometric autoregulation in intact dogs
03 p0361 A71-13224

Anatomy and function of normal pericardium including removal effect in mammals, fish and amphibians
03 p0362 A71-13328

Fiberoptic indicator-dilution assessment of myocardial function
03 p0362 A71-13329

Gap in atrioventricular conduction in humans by catheter technique for recording electrical activity of His bundle
03 p0363 A71-13488

Left ventricular volume and cardiac work evaluation by thermomodulation technique, employing thermocatheter for temperature measurement [ASME PAPER 70-WA/TEMP-2]
03 p0372 A71-14102

Human left ventricle mathematical models, determining physiological response oriented mechanical parameters with diagnostic significance [ASME PAPER 70-WA/BHF-14]
03 p0373 A71-14112

Concentric layer model for estimating energy expenditure of left ventricle
05 p0713 A71-16486

Atrial and ventricular dimensional analysis in animals and man, discussing angiocardiographic, biplane, X ray, indicator dilution, radioisotopic and noninvasive methods
05 p0715 A71-16925

Epinephrine infusion in man, examining systolic time intervals and sympathetic stimulation in cardiovascular dynamics
06 p0850 A71-17440

High environmental carbon dioxide effects on cardiac depression and respiratory rate in rhesus monkeys and chimpanzees
06 p0851 A71-17612

Oxygen transport and consumption, ventilation and cardiac index in natives and sojourners at high altitudes
06 p0853 A71-18060

Dog cardiac output measurement by using ethyl ether dissolved in saline solution as indicator, comparing to Fick method results
06 p0856 A71-18389

Myocardial ventricle contraction in high altitude hypoxia adaptation, using barochamber trained rats
06 p0857 A71-18467

Human mitral valve fluid mechanics, confirming existence of vortex forms during diastasis by vitro flow patterns [AIAA PAPER 71-102]
06 p0863 A71-18556

Cardiac impulse conduction measurements noting delay, block and one way block in excised canine Purkinje fibers with depressed responsiveness
07 p1041 A71-19637

Left ventricular function analysis by atrial pacing in subjects with normal and elevated left ventricular filling pressure, relating stroke volume to end diastolic pressure
07 p1044 A71-20352

Premature pulmonary valve closure due to severe mitral insufficiency by left atrial V wave retrograde transmission
08 p1240 A71-21888

Cardiac output variations in regulation of arterial oxygen transport during hypoxia
08 p1241 A71-21939

Heart, lungs and erythropoiesis optimum functional parameters mathematical model based on oxygen transport minimum losses
09 p1388 A71-22126

Book on clinical physiology techniques and anesthesiology measurements covering electronics, ECG analysis, blood pressure measurement, cardiac function, respiratory mechanics, etc
09 p1398 A71-22459

Cardiac output in relation to peripheral resistance in borderline hypertension
09 p1392 A71-22591

Excitation-contraction coupling of papillary muscles from hypertrophied right ventricles of cats with pulmonary artery artificial stenosis
09 p1395 A71-23257

Human steady and unsteady state treadmill exercise, comparing cardiac output, heart rate and oxygen uptake interrelationships
09 p1401 A71-23367

Aging effects on blood pressure-flow relations and cardiac output/ventricular end diastolic pressure, discussing pulmonary vascular bed capacity dependence on increasing flow during supine exercise
10 p1561 A71-24128

Age effect on pulmonary circulation in normal subjects, measuring oxygen consumption, cardiac output and pulmonary arterial pressure by floated catheter technique
10 p1561 A71-24129

Cardiac hypertrophy in animals, discussing increased cardiac work load compensation and muscle cell alterations
10 p1565 A71-24674

Thermomodulation and indocyanine green dye technique comparison for cardiac output measurement in man
11 p1724 A71-25458

Rat heart muscle series elasticity compliance, showing hypoxia effects
11 p1719 A71-25858

Chemical release from traumatized tissue in dogs under cross circulation with lethal cardiac depression response
11 p1720 A71-26118

Cardiovascular system response to swimming exercise by dogs, measuring left ventricular internal diameter and pressure, cardiac output and heart rate
12 p1873 A71-27111

Cardiac output and arterial pressure control presence or absence of functional nervous system discussing dog experiments
13 p2003 A71-27838

Normal myocardium structure and function discussing cardiac performance and output control
13 p2003 A71-27851

Cardiac hyperfunction, hypertrophy and insufficiency, discussing physiological mechanism and cause and effect relationships
13 p2004 A71-27864

Trained college and recreational swimmers cardiac output and maximum oxygen consumption during tethered swimming and treadmill running
13 p2024 A71-29490

Hypoxia, high altitude and heart - Conference: Aspen, Colorado, January 1970
14 p2183 A71-30272

Left ventricular power as product of pressure and volume change rate, relating peak values to end diastolic mass
14 p2187 A71-30709

Cardiac activity changes during prolonged hypodynamia, discussing clinical and experimental investigations results with humans and animals
15 p2358 A71-31320

Energy output of left ventricle and congestive heart failure mechanism, approximating blood velocity in aortic system by mathematical model
15 p2363 A71-31443

Upright tilt stress effects on cardiac cycle phases in healthy subjects, using noninvasive techniques
15 p2358 A71-31455

Lowered cardiac output and arterial pressure response to exercise after autonomic heart blockade in man, noting retained work capability
15 p2358 A71-31454

Vagus nerve effects on cardiac output adaptation to exercise in sympathectomized dogs
15 p2360 A71-32001

Left ventricular posterior wall motion measurements in myocardial infarction, using ultrasonic echogram time-motion data
15 p2365 A71-32536

Maximal treadmill stress test correlation with postexercise phonocardiogram, ECG and double master test in normal subjects, discussing third and fourth heart sound incidence
15 p2361 A71-32538

Concealed and supernormal atrioventricular conduction data, using His bundle electrogram recordings
15 p2366 A71-32539

Atrioventricular and intraventricular conduction disturbances in acute myocardial infarction, discussing heart block
15 p2361 A71-32540

LVET/EICT ratio usefulness compared to EICT for left ventricular contractility in patients with mitral valve disease
15 p2361 A71-32659

Lower cardiac nerve unmyelinated afferent fibers detection and functional property characteristics
15 p2362 A71-32736

Cardiac output and regional blood flow in hypoxic woodchucks, noting no change in heart rate, diaphragm, kidney, liver, stomach and intestines
16 p2529 A71-33189

Myocardium ultrastructural and metabolic alterations in altitude acclimated rats, considering heart muscle mitochondria
16 p2529 A71-33193

Validity and reproducibility of cardiac output determination by thermomodulation, using dual thermistor catheter introduced in pulmonary artery
16 p2531 A71-33366

Heart myocardium contractility assessment based on pressure rise rate relation to intraventricular pressure during isovolumic systole
17 p2681 A71-35039

Functioning aortic valve orifice size relation to configuration and flow
17 p2682 A71-35042

Electrical medical apparatus with electrodes and intracardiac catheters, considering electric current danger threshold, electrocution hazards and safety precautions
17 p2693 A71-35484

Monophasic action potential recording of intact human heart, using bipolar electrode catheter for explanation of ECG abnormalities

18 p2853 A71-35910

Sagittal path of moving electrical center of human heart from measurements of surface ECG potentials

18 p2853 A71-35911

First heart sound changes, discussing sound vibration and transmission and cardiac function

19 p3000 A71-37232

Second heart sound changes due to position and magnitude variations of aortic or pulmonary component

19 p3001 A71-37233

Frequency phonocardiography technique for heart sounds and murmurs registration, producing analog voltage proportional to frequency by zero crossing detector

19 p3006 A71-37234

Noradrenaline concentration in myocardium of rats subjected to high altitude hypoxia, considering heart regulation in presence of hyperfunction and hyper trophy

19 p3001 A71-37393

Analog computer analysis of radiocardiograms, determining cardiac function and pulmonary blood volume

20 p3191 A71-38802

Frequency distribution of heart sounds in precordium, studying slope of attenuation and relative peaking

20 p3185 A71-38803

Heart maximal aerobic and anaerobic power and stroke volume, discussing cardiac output and blood oxygen capacity measurements in subalpine population subjects

20 p3185 A71-38887

Isoproterenol, atrial pacing, ouabain and methoxamine effects on dogs during experimental cardiac tamponade, observing arterial pressure, cardiac output and heart rate changes

20 p3186 A71-38968

Polycythemia and altitude hypoxia effects on rats heart and sea level exercise tolerance

20 p3186 A71-38980

Bed rest effects on human hemodynamic and gaseous metabolism, observing increased cardiac output and decreased oxygen consumption and carbon dioxide production

20 p3188 A71-39231

Jet and turbulence mechanism of vascular murmurs associated with stenosis for minimum flow Reynolds numbers, using aorta orifice plates in dogs

21 p3336 A71-40864

Heart excitation and membrane permeability effects on two component action potentials in human atrial muscle strips, using microelectrodes

21 p3336 A71-40865

Anoxia effect on laboratory animals cardiac action, discussing ECG injury current relation to myocardium phosphorylcreatine content

22 p3484 A71-41568

Magnetic recording of heart electrical activity by cryogenic magnetometer with two Josephson junction quantum interference reduction device

22 p3504 A71-42341

Vectorcardiographic analysis of patients with ECG diagnosed inferior atrial rhythm

22 p3490 A71-42519

Aminothiol group radioprotective drugs effect on guinea pigs cardiac function during lateral acceleration

22 p3491 A71-42702

Long term effects of hypoxic stimulus suppression upon heart rate, cardiac output and pulmonary artery pressure of highlanders, observing bradycardia

23 p3631 A71-43117

Ejection fraction relation to left ventricular dimensional changes in patients with heart disease, using angiocardiograms

23 p3635 A71-44128

Cholinesterase activity and acetylcholine level dependence on adrenaline dose injected in heart during rats experimental myocardiodystrophy

24 p3800 A71-44500

HEART MINUTE VOLUME

Left ventricular volume determination by high speed cineangiography, using optical scanning and automatic data processing

02 p0203 A71-11705

Canine heart rate Frank-Starling mechanism effects on ventricular volumes during natural and artificial cardiac pacing

10 p1565 A71-24681

Short term high altitude exposure, determining coronary blood flow reduction relationship to cardiac output and stroke volume

14 p2184 A71-30284

Right ventricular end-diastolic volume as index of myocardial fiber length and correlation with ventricular work at rest and exercise with and without right ventricular failure

15 p2361 A71-32541

Thermomodulation method instrument using cold indicator depot with heat exchanger for standardization of heart-time-volume measurements

18 p2872 A71-36692

Right and left heart and pulmonary blood volume determination, using radiocardiograms and analog computer analysis

20 p3191 A71-38801

Heart maximal aerobic and anaerobic power and stroke volume, discussing cardiac output and blood oxygen capacity measurements in subalpine population subjects

20 p3185 A71-38887

Atrial shortening during volume loading by infusion in animal, using Frank-Starling approach

22 p3485 A71-41718

HEART RATE

NT ARRHYTHMIA

NT BRADYCARDIA

NT SYSTOLE

NT TACHYCARDIA

Arterial blood pressure changes due to bilateral carotid occlusion or electrical heart pacing, considering effects on kidney blood flow and circumference in dogs

01 p0008 A71-10074

Linear beat by beat cardiograph, describing amplifier design and operation

01 p0021 A71-10242

Heart rhythm coordinate curves for continuous EKG analysis using digital computer

01 p0025 A71-11153

Military parachutists physiological and force field responses to aerospace recovery environment, using multichannel FM/FM telemetry for heart rates

02 p0207 A71-12389

Long term day and night ECG recordings of healthy human subjects, analyzing heart rate and amplitude variations during normal wakefulness and sleep periods

03 p0370 A71-13061

In-flight telemetric ECG recordings of aircraft pilots during normal, abnormal and aerobatic flight, analyzing heart rate variations as function of stresses

03 p0370 A71-13064

Telemetric ECG recordings of workers under high and strongly varying temperature conditions, discussing heart rate variations under heat stress

03 p0370 A71-13065

High intensity sonic boom effects on heart rate of dogs, noting conditioning benefit

03 p0358 A71-13097

Pulsus alternans study by noninvasive techniques for assessing cardiovascular function in hemodynamics and muscular physiology

03 p0372 A71-13492

Instantaneous cardiac acceleration in man induced by voluntary muscle contraction

04 p0544 A71-15152

Human heart rates long term measurement by cumulative counters activation by electrical signals from precordial electrodes

04 p0544 A71-15153

Previous heavy work effect on central hemodynamics and autonomic nervous system, discussing ensuing heart rate changes

04 p0545 A71-15156

Oxygen partial pressure measurements in myocardium of beating heart by miniature glass needle and surface electrodes

05 p0714 A71-16598

Physical fitness in prolonged muscular work tolerance evaluation by oxygen consumption for 170 beat/min heart rate, considering age, sex and occupation

05 p0708 A71-16614

Oxygen intake, ventilation and heart rate during various intensity and duration tests

05 p0708 A71-16615

Arterial glucose and lactate levels and heart rate in human males during intermittent running, discussing anaerobic capacity and anoxidative glycolytic processes

05 p0708 A71-16619

Human work capacity in hot environment irrelevance to normal conditions, considering physiological reactions to exercise in heat by heart rate criterion

05 p0709 A71-16621

Right and left ventricular systolic time intervals from high fidelity pulmonary arterial pulse wave measurements

06 p0852 A71-17875

Cardiac output during submaximal bicycle exercise in children and teen-agers, discussing oxygen transport function of blood

06 p0857 A71-18722

Human work capacity measurements by graded step test and bicycle ergometer, considering heart rate and oxygen uptake

07 p1046 A71-19457

Multiple sensor heart rate telemetry using automatic data acquisition and management in squirrel ecology

07 p1049 A71-19626

Respiratory rate and cardiac responses to exercise in man

07 p1052 A71-20326

Myocardial depressant factor purified preparation effect on isolated perfused cat heart, studying coronary vascular, dromotropic and inotropic actions

08 p1239 A71-21176

In-flight monkey cardiovascular observations, discussing central venous pressure, urine volume, electrolyte imbalances and heart rate

09 p1395 A71-23244

Human steady and unsteady state treadmill exercise, comparing cardiac output, heart rate and oxygen uptake interrelationships

09 p1401 A71-23367

High altitude submaximal and maximal work by humans, noting time required for steady state oxygen consumption, ventilation and heart rate

09 p1401 A71-23368

Stroke-pulmonary blood volume relation and vascular recruitment and distensibility in dogs, allowing independent control of flow, heart rate and left atrial pressure

10 p1561 A71-24123

Heart rate and diastolic inflow coronary resistance extravascular component, discussing heart artificial stimulation and pharmacological maximal dilation effects

10 p1565 A71-24679

Canine heart rate Frank-Starling mechanism effects on ventricular volumes during natural and artificial cardiac pacing

10 p1565 A71-24681

Negative heart rate response during low level microwave irradiation of dorsal head in rabbits

11 p1717 A71-25284

Human heart beat phase frequency changes after acoustic stimulation during natural sleep from EEG, EKG, EMG of musculus hypoglossus and eye motions

11 p1721 A71-26292

Transient dynamics of ventilation and heart rate following positive and negative sustained step changes in work load initiated from different load levels

11 p1722 A71-26357

Ventilation and heart rate responses to muscular exercise by work load ramp function changes studies

11 p1722 A71-26359

Cardiovascular system response to swimming exercise by dogs, measuring left ventricular internal diameter and pressure, cardiac output and heart rate

12 p1873 A71-27130

Human heart rate, minute ventilation and oxygen uptake measurement during treadmill and track running at three speeds

12 p1874 A71-27134

Ectopic right atrial rhythms in ECG vectorial analysis

12 p1870 A71-27289

Dipole, quadrupole and octapole measurements in isolated beating hearts

13 p2016 A71-28150

Preavoidance blood pressure elevations accompanied by heart rate decreases in dogs

13 p2008 A71-28516

Set and uncertainty as factors influencing anticipatory cardiovascular response in humans, monitoring heart rate and vasomotor activity

13 p2011 A71-28809

Baroreflex regulation of pulse interval during bicycling exercise, using systolic pressure-pulse relation to express reflex sensitivity

13 p2012 A71-28951

Sitting and supine position effect on exercise tolerance, heart rate, systolic pressure and respiration rate in male subjects with coronary insufficiency, noting onset of angina pectoris

13 p2014 A71-29303

Heart rate variability in REM sleep, stage 4 sleep and wakeful state from ECG of normal males, calculating coefficient of temporal variability for each state

13 p2014 A71-29319

Short term high altitude exposure, determining coronary blood flow reduction relationship to cardiac output and stroke volume

14 p2184 A71-30284

Computer analysis of ECG compared to cardiologist conclusions, noting discordance in rhythm analysis

15 p2366 A71-32543

Operator mental performance reliability prediction from heart beat rate and electromyogram

16 p2534 A71-32826

Hypoxia effects on cardiovascular reflexes during hypoxia, measuring response of heart rate to lower body negative pressure

16 p2529 A71-33191

Muscular fatigue of healthy Bengali males with increasing work loads under varying environmental conditions, considering ventilation, heart rate and oxygen consumption

17 p2688 A71-34360

Physiological tests for psychic stress effects on aircraft pilot tracking performance, respiration and heart rate

17 p2693 A71-35199

- Heart sounds duration, intervals and Q-I lengths, studying displacement, velocity, acceleration tracings and filtration 18 p2854 A71-36140
- Human physiological responses to rotating environment, evaluating heart rates, blood pressure, pulmonary functions, visual observations and vital capacities [AIAA PAPER 71-890] 18 p2856 A71-36639
- Afferent nerve impulse traffic from atrial A-type receptor fibers in cats in relation to heart rate control 18 p2857 A71-36688
- Brain temperature change effects on cardiovascular responses, examining heart rate and systemic arterial blood pressure 18 p2860 A71-36880
- Physiological strains due to industrial heat stress, investigating heart rate and body temperature 18 p2860 A71-36882
- Maximum oxygen uptake measurement by two techniques, calculating heart rate 19 p3008 A71-38553
- World champion marathon runner metabolic responses during submaximal and maximal treadmill running, recording oxygen consumption, heart rate and lactic acid 20 p3185 A71-38890
- Heart rate variation during and after muscular exercise, discussing correlated measurements of rectal and mean skin temperatures, blood lactate, pyruvate and glucose 20 p3185 A71-38891
- Isopterol, atrial pacing, ouabain and methoxamine effects on dogs during experimental cardiac tamponade, observing arterial pressure, cardiac output and heart rate changes 20 p3186 A71-38968
- Psychophysiological reactions to understimulation and overstimulation, noting catecholamine output, heart rate and performance efficiency in humans 21 p3329 A71-40177
- Cardiac automatic rhythms, discussing diastolic depolarization in Purkinje fibers and factor controlling automaticity 21 p3330 A71-40250
- Altitude and cold acclimatization effects on human basal heart rate, blood pressure, respiration and breath-holding 21 p3330 A71-40349
- Electrical heart activity and ECG mathematical model with nonlinear oscillator system construction for normal and abnormal rhythms 21 p3336 A71-40986
- Heart rate and systolic pressure variability control through visual feedback of physiological information, obtaining respiratory measurements and ECG 21 p3344 A71-41037
- Transient heart rate response to square wave breathing in man under zero G parabolic flight 22 p3501 A71-41828
- Mercaptoalkylamine group radiation protection preparations on resistance of rats and mice to lateral acceleration rate 22 p3491 A71-42700
- Hemodynamic evaluation of heart rate augmentation produced by atrial pacing and isoproterenol in early postoperative phase of cardiac valve surgery 23 p3640 A71-44131
- Posture and lower body negative pressure effects on human heart rate and blood pressure 23 p3636 A71-44241
- Moderate heat exposure effects on human circadian variations in body temperature, heart and metabolic rates and water loss 24 p3797 A71-44779
- Respiratory sinus arrhythmia by spectral analysis and digital filtering, using linear model to approximate lung volume relationship to heart rate during normal breathing 24 p3802 A71-45067
- HEAT**
NT DRY HEAT
NT HEAT OF DISSOCIATION
HEAT ACCLIMATIZATION
U ACCLIMATIZATION
U HEAT TOLERANCE
HEAT BALANCE
Algorithm for nonstationary thermal regime of electronic equipment using heat balance method for variation in thermal coefficients and source power 01 p0052 A71-10536
- Martian exospheric temperatures diurnal variations during Mariner 4, 6 and 7 observations by solving time dependent heat balance equations 02 p0305 A71-11972
- Heat balance measurements at collector of heat pipe thermionic converter 02 p0196 A71-12268
- Diurnal variations due to actual heat output, oxygen consumption and carbon dioxide production in rats undergoing eating habit changes 04 p0539 A71-15157
- Atmospheric radiating gas components contribution to thermal balance at various altitudes, geographic latitudes and seasons 06 p0923 A71-17509
- Iterative solution for radiation-dominated heat balance about heat shield or superinsulation nodes, testing performance in thermal analyzer program 07 p1221 A71-18905
- Heat balance of human body submerged in water, determining body temperature reduction as function of ambient temperature 13 p2019 A71-28508
- Solar prominences formation, discussing coronal thermal instability, chromospheric heat balance, magnetic field and gas heating 15 p2482 A71-31334
- Heat balance and 8.22 mm radio emission of Mars, evaluating surface thermal and electrical parameters including brightness temperature 15 p2490 A71-32411
- Azur satellite flight data evaluation, discussing heat balance and temperature monitoring 15 p2501 A71-32780
- Simultaneous plasma internal energy, temperature and volume determination based on energy balance analysis during pulsed heating 17 p2789 A71-35272
- Electric power and efficiency of thermoelements with temperature dependent thermoelectric properties by heat balance technique 18 p2852 A71-36965
- Solar cycle variation of planetary exospheric temperature from heat balance equation solution 19 p3131 A71-37334
- French monograph on free and forced convection and external radiation from hot gas oscillating in resonance tube, considering heat balance and mass exchange 19 p3172 A71-38649
- Annual heat balance in Martian northern polar cap, considering atmospheric, ground and solar heat flux absorbed by snow 20 p3290 A71-39309
- Heat balance effects of acousto-gravitational waves in upper atmosphere, concerning infrasonics from earthquakes, polar auroral arcs and magnetic storms 22 p3533 A71-41656
- Martian polar caps heat balance, noting albedo differences due to irregularities in solid carbon dioxide cover 22 p3603 A71-42190
- Solar prominences formation, discussing coronal thermal instability, chromospheric heat balance, magnetic field and gas heating 22 p3606 A71-42609
- Solar coronal plasma radiative capacity and temperature structure from cooling function in thermal balance equation 24 p3869 A71-44806
- HEAT BUDGET**
NT ATMOSPHERIC HEAT BUDGET
HEAT CAPACITY
U SPECIFIC HEAT
HEAT CONDUCTION
U CONDUCTIVE HEAT TRANSFER
HEAT CONTENT
U ENTHALPY
HEAT DISSIPATION
U COOLING
HEAT DISSIPATION CHILLING
U COOLING
HEAT EFFECTS
U TEMPERATURE EFFECTS
HEAT EQUATIONS
U THERMODYNAMICS
HEAT EXCHANGERS
NT TUBE HEAT EXCHANGERS
Heat transfer - Conference, Versailles, August-September 1970, Volume 1, Conduction and heat exchangers 04 p0677 A71-15451
- Boiling cryogenic gas-liquid cross-current heat exchanger unit surface power transmission optimization 04 p0626 A71-15463
- Spiral plate heat exchanger temperature-length profile calculation by Runge-Kutta technique 04 p0678 A71-15464
- Heat transfer in exchangers with forced laminar or turbulent flows with linear pressure drop and exponential thermal flux distribution 04 p0688 A71-15740
- Al 27 for heating working body in heat exchangers of jet engines 06 p0926 A71-18706
- Nozzle parameters effects on conical vortex heat exchanger characteristics, considering optimal area in critical cross section for maximum energy and temperature efficiency 08 p1233 A71-20835
- Concorde thermal fatigue test installation, controlling temperature by transfer temperature variation in single heat exchanger block 09 p1430 A71-23580
- Heat pipe applications for space vehicle thermal control, discussing spacecraft radiators, thermal exchangers and structure isothermalization [AIAA PAPER 71-410] 11 p1856 A71-26205
- Airlock thermal capacitor for radiator performance augmentation by absorbing heat on orbit hot side and rejecting on cold, providing coolant temperature level damping 11 p1858 A71-26210
- Vibratory stresses in heat exchangers due to pressure pulsation induced acoustic resonances, calculating flow pulsations from Karman vortex streets [HEAT EXCH. CONF. PAPER 13] 15 p2513 A71-31638
- Heat exchanger miniaturization for avionics applications, discussing design and fabrication [HEAT EXCH. CONF. PAPER 15] 15 p2376 A71-31638
- Performance tests of two identical Brayton cycle heat exchanger units consisting of recuperator, heat sink exchanger and ducting in combination with turbine 15 p2355 A71-322131
- Pressure ratios and surface effects on regenerative heat exchanger in Brayton gas turbine cycles with intercooling or reheating 16 p2663 A71-34379
- Cooling fin shape optimization for minimum volume, considering convective and radiative heat exchange for assumed temperature distribution 17 p2837 A71-34442
- Thermomodulation method instrument using cold indicator depot with heat exchanger for standardization of heart-time-volume measurements 18 p2872 A71-36692
- Brazing roughness effects on rectangular plate fin heat exchanger surfaces heat transfer and flow friction characteristics, noting fin surface geometry influence [ASME PAPER 71-HT-29] 19 p3166 A71-37999
- Brayton cycle electric space power supply systems, describing shielded reactor and heat exchanger design 20 p3263 A71-38924
- Heat transfer, fluid flow and pressure loss, noting application to cryogenic heat exchangers and process plants 20 p3312 A71-39245
- Variable thickness ice film water-to-cryogen heat exchanger design, presenting mathematical model for performance calculation by modified integration digital analog simulator computer program 20 p3314 A71-39291
- Li-filled vacuum-deposited W heat pipes for efficient heat extraction from nuclear reactors, discussing design, fabrication and testing 23 p3682 A71-43599
- Volume-weight characteristics of cross flow heat exchangers for heat regenerating gas turbine engines 24 p3889 A71-45007
- HEAT FLOW**
U HEAT TRANSMISSION
HEAT FLUX
Laminar boundary layer free convection at vertical plate with exponentially decreasing surface temperature, determining thermal flux and shear stress 01 p0179 A71-10610
- Gas permeable dispersion layer between impermeable solid wall and high temperature gas flow, calculating dimensionless heat flux equations 02 p0332 A71-12200
- Yaw sphere and thermometer combination, examining proportional vertical heat flux 03 p0422 A71-13231
- Horizontal cylindrical heaters heat transfer to pool boiling Hg at heat fluxes up to burnout [ASME PAPER 70-HT-R] 03 p0519 A71-13698
- Heat exchange in dissociating partly ionized gas flow over critical point on permeable surface with injection into laminar boundary layer 03 p0342 A71-13748
- Ablative materials performance in high radiative heat flux environments produced by CW carbon dioxide laser [AIAA PAPER 70-864] 03 p0449 A71-14437
- Critique of thermoelastic problem solution for thermal stress in semiinfinite body under step heat input 04 p0669 A71-15193
- Mach-Zehnder interferometer measurements of average temperature and heat transfer rate in free convection on heated vertical flat plate 04 p0599 A71-15522
- Transducer with single crystal Ge for high heat flux measurement, noting calibration by direct conduction 04 p0599 A71-15589
- Heat transfer boundary conditions determination in studying heat protective coatings effectiveness, discussing measurement methods for stagnation temperatures and heat fluxes from exhaust gases 04 p0600 A71-15643
- Heat transfer in exchangers with forced laminar or turbulent flows with linear pressure drop and exponential thermal flux distribution 04 p0688 A71-15740
- Heat pipe operating principle, design and applications, discussing liquids for different temperature ranges, heat flux density and temperature control 04 p0689 A71-15816

- Rigid heat conductors, using controllable states for heat flux-temperature gradient materials response function measurements 05 p0837 A71-16721
- Plasma confinement in Tokamak, calculating particle and heat fluxes due to conductivity current and electric field 06 p0930 A71-17405
- Monolith thermal flux sensors inertia characteristics on various surfaces 06 p0899 A71-18005
- Natural convection heat transfer coefficients from isothermal flat surfaces, using Boelter-Schmidt type heat flux meters 07 p1222 A71-18996
- Temperature distributions and heat flux for gray gas in radiative equilibrium bounded by walls with different temperatures, using differential approximation [AIAA PAPER 70-834] 09 p1516 A71-22094
- Heating rate effect on parameters of resistance wire strain gages subjected to temperature gradients 09 p1443 A71-22634
- Heat flux measuring device using Wollaston prism schlieren interferometer 09 p1444 A71-22713
- Heat fluxes from premixed methane-oxygen and propane-oxygen flames measurement by transient calorimetric method, comparing forward stagnation point results with calculated values 10 p1695 A71-24049
- Incident thermal flux parameters and wall temperature effects on flow characteristics in preseparation zone of laminar boundary layer and separation point location 10 p1551 A71-24368
- Jupiter cloud structure observations near 8.5 microns from thermal flux measurement along polar and equatorial scans 11 p1827 A71-25727
- High heating rate thermogravimetric analyzer for ablative plastics, predicting response with semiempirical analytical model 11 p1744 A71-26042
- RF transparent ablator of silica filled elastomeric silicone, describing thermal, mechanical and electrical properties at various heating rates 11 p1790 A71-26046
- Reentry spherical vehicles with variable wall thickness, determining heat flux absorption without surface ablation and wake contamination [AIAA PAPER 71-424] 11 p1858 A71-26215
- Centerline loss, transient sink temperature and thermal conductivity design constant considerations for thin foil copper-Gardon heat flux sensors [AIAA PAPER 71-470] 11 p1764 A71-26251
- Energy flux of tropospheric mesoscale waves and heat influx into upper mesosphere caused by energy absorption, discussing wavelength and latitude effects 12 p1924 A71-26735
- Turbulent boundary layer thermal flux fluctuation spectral distribution determination by applying fluctuation diagram method to filtered signals 12 p1985 A71-26828
- Hot plasma oscillations analysis for instabilities as function of magnetic viscosity and heat fluxes, using inertial waves dispersion equations 12 p1937 A71-27202
- Surface evaporation and condensation effects on stability of thin liquid film flowing down heated inclined plane at critical Reynolds number 13 p2160 A71-28596
- Vertical variations of Reynolds stress and heat flux in atmospheric surface layer attributed to sub-mesoscale circulations, using sonic, thermometer and drag measurements 13 p2097 A71-28724
- Nonuniform sidewall heat flux effect on thermal stratification 13 p2165 A71-29010
- Heat flux between parallel plates in rarefied gas at various temperature ratios and Knudsen numbers, using Monte Carlo method 13 p2165 A71-29226
- Iterative solution for quasi-linear heat equation, examining convergence for equation describing self similar heat wave from instantaneous plane source 14 p2334 A71-29564
- Laminar incompressible fully developed pulsating flow between parallel flat plates effects on local time-average heat flux 14 p2334 A71-29603
- Time variable effect on synthetic wind speed and air temperature profiles based on sensible heat flux density and stress at surface layer 14 p2266 A71-29705
- Temperature and thermal flux measurement with calorimetric heat receivers during gas dynamic processes, determining physical properties and geometry effects on errors 14 p2335 A71-30184
- Shear stress distribution and local heat flux at surface of axisymmetric bodies for laminar and turbulent boundary layer flow 14 p2170 A71-30219
- Plasma accelerator central electrode erosion and heat flux, describing measurement techniques and results 14 p2280 A71-30266
- Reactive solids ignition by constant energy flux from asymptotic analysis of activation energy limit 14 p2337 A71-30458
- Two dimensional unsteady heat conduction in solid with subliming surface, replacing original boundary value problem by ordinary integrodifferential equation 14 p2338 A71-30933
- Gunpowder mean burning rate at constant pressure with periodic variation of heat influx into flame zone 15 p2462 A71-31374
- Gas permeable dispersion layer between impermeable solid wall and high temperature gas flow, solving dimensionless heat flux equations 15 p2512 A71-31505
- Third approximation to Boltzmann equation for heat flux vector of gas of rigid spheres, using Brooker-Green technique 15 p2513 A71-31687
- Perfectly effective boiling fin design in horizontal right circular cylinder shape, deriving formulas at peak heat flux operation 15 p2514 A71-32264
- Laminar boundary layer flow at stagnation point with intensive injection of different absorbing medium, calculating temperature profiles and thermal fluxes 17 p2725 A71-34215
- Thermal flux model of lithium plasma source at various temperatures and pressures, using arc channel model with conducting cross section 17 p2787 A71-34303
- Composite rocket engine casing thermal flux approximation from multilayer plate heat conductivity 17 p2837 A71-34568
- Transverse magnetic field influence on heat transfer of conductive fluid /mercury/ in electrically insulated pipe subjected to uniform heat flux 17 p2788 A71-34660
- Low thermal flux lightweight glass fiber composite tubing for cryogenic propulsion plumbing systems 17 p2762 A71-35206
- Pressure and heat flux measurements at wall of nose cone in hypersonic wind tunnel flow with high generatrix enthalpy 18 p2844 A71-36182
- Atmospheric radiant heat influx spectral distribution, evaluating vertical profiles of short wave radiation and aerosol effects 19 p3047 A71-37281
- Friction velocity in stably stratified constant flux layer with known heat flux, using log-linear velocity profile with fixed Monin-Obukhov parameter value 19 p3089 A71-37502
- Heat transfer and drag during air laminar flow in circular pipe with constant heat flux density at wall 19 p3044 A71-37585
- Radiation energy density and radiation heat flux in small rectangular cavity, assuming modes excitation spectrum according to Planck distribution function [ASME PAPER 71-HT-16] 19 p3164 A71-37987
- Plasma radiation effects in gas tube electric arc heating, obtaining temperature and heat flux profiles and I-V characteristics from energy transport mathematical model [ASME PAPER 71-HT-18] 19 p3164 A71-37989
- Surface heat flux for incipient boiling in liquid metal heat pipes, determining nucleation site radius upper limit in Na heat pipes 19 p3171 A71-38349
- Hot plasma oscillations analysis for instabilities as function of magnetic viscosity and heat fluxes, using inertial waves dispersion equations 19 p3116 A71-38614
- Cloud physics, comparing observational and theoretical values of wave parameter determining heat influx properties 19 p3094 A71-38703
- Natural convection boundary layer stability on vertical flat plate with uniform heat flux, using numerical computer solutions for large Grashof number range 20 p3314 A71-39501
- Parametric differentiation solution accuracy and stability for temperature profile and heat flux behind one dimensional hypersonic shock, including thermal radiation 21 p3409 A71-41016
- Homogeneous fuel combustors with multistage reaction rate controlled system, determining linear relationships and heat release 21 p3437 A71-41049
- Radiative and turbulent heat transfer in atmospheric surface layer, measuring radiative heat flux divergence and temperature fluctuations at different heights 22 p3534 A71-41860
- Centrifugally driven thermal convection in rotating cylinder of fluid heated from above, calculating heat flux through wall and effect on Nusselt number 22 p3620 A71-41879
- Hydrodynamic equations for dense system fluctuations with stochastic terms in pressure tensor and heat flux vector evaluated for dilute gas 22 p3530 A71-41893
- Emissivity calculation for radiant heat flux from isothermal gas mixture of hydrocarbon fuel combustion products 23 p3718 A71-43918
- Radiant heat flux measurement during pulsed processes from surface in high temperature emitting gas, using thin film sensor with small time constant 23 p3782 A71-43922
- ### HEAT GAIN
- #### U HEATING
- #### HEAT GENERATION
- Thermal environment loads in lunar ambulation, discussing Apollo EVA suit system and internally produced heat 02 p0207 A71-12386
- Steady heat conduction with generation, discussing boundary value problem transformation by change of variables 04 p0677 A71-15453
- Living human tissue thermal behavior analytical modeling including internal heat generation and blood flow effects 04 p0539 A71-15460
- Laminar turbulent tube flow heat transfer, investigating internal radiation exchange and wall heat conduction and generation effects 04 p0685 A71-15519
- Zn-Ag oxide cell discharge, determining heat generation rate and voltage production model 08 p1235 A71-21099
- Heat generation in hinged orthotropic viscoelastic cylindrical shells under transverse vibrations and cyclic surface load 12 p1978 A71-27343
- Adenosine triphosphate addition effects on heat production in intact muscular fibers by calorimetry 17 p2683 A71-35247
- Heat release from elemental decay in radioactive layer from radio astronomical observations and lunar rock chemical analysis 20 p3295 A71-39620
- Expanding D-T plasma laser heating equations derivation, allowing for heat produced by associated thermonuclear fusion 23 p3710 A71-43320
- Heat generating granular layer tube, obtaining temperature distribution across cross section and boundary conditions 23 p3719 A71-44338
- Volume-weight characteristics of cross flow heat exchangers for heat regenerating gas turbine engines 24 p3889 A71-45007
- ### HEAT MEASUREMENT
- High temperature calorimetry of solids for heat capacity and thermal processes thermodynamic and thermokinetic characteristics, considering calorimeter design engineering 01 p0083 A71-11226
- Compressed liquid and gaseous fluorine constant volume specific heat measurements, tabulating results 04 p0674 A71-14729
- Heat transfer - Conference, Versailles, August-September 1970, Volume 7, Combined heat transfer and measuring techniques 04 p0688 A71-15540
- Measuring instrument for lunar surface layer heat flow, temperature and thermal conductivity 04 p0599 A71-15543
- W-Mo alloy enthalpy and specific heat measurement at high temperatures by drop calorimetry 04 p0613 A71-15580
- Liquid hypergolic propellants heat and gas release determination by calorimetric and PVT measurements, using impinging free jets for propellant mixing [WSS/CI PAPER 70-26] 06 p0943 A71-17658
- Reaction heat for flameless combustion of double-base propellant using differential scanning calorimetry and thermogravimetric analysis, noting pressure effects [AIAA PAPER 70-125] 07 p1183 A71-19898
- Chlorine trifluoride standard heat of formation by fluorine flame calorimetry, deriving from measured enthalpies of reactions 07 p1056 A71-20656
- Heat quantity to atmospheric circulation ratio over period of decades, using positive temperature sums for long range forecasting method 08 p1326 A71-21445
- Heat flux measuring device using Wollaston prism schlieren interferometer 09 p1444 A71-22713
- High gas temperatures calorimetric measurement, providing probes with industrial temperature range capability 09 p1449 A71-22791
- Temperature and pressure effects on phase transformations, structural changes and related processes in metals, comparing thermographic and calorimetric methods 09 p1547 A71-23227

HEAT OF COMBUSTION

- Tungsten high temperature thermal diffusivity at 1000-2500 K by flash technique
10 p1624 A71-23911
- Composite solid propellant binders thermal decomposition investigation by differential scanning calorimetry method, discussing kinetic data relevance to solid propellant combustion
10 p1657 A71-24046
- Heat resistance, thermal stability, thermal conductivity coefficient and specific heat measured in cylindrical hollow specimens of corundum materials
10 p1634 A71-24200
- Jupiter cloud structure observations near 8.5 microns from thermal flux measurement along polar and equatorial scans
11 p1827 A71-25727
- Heat flux measurement in high pressure arc heated wind tunnel flow by swept null point calorimetry, describing calorimeter configurations and test results [AIAA PAPER 71-428]
11 p1763 A71-26217
- Air stream injection from circular hole in flat plate into supersonic flow, measuring heat transfer
13 p1992 A71-29184
- Calorimetrically measured energy feedback heat of reaction dependence from laminar diffusion flames above water cooler
15 p2463 A71-31621
- Magnesium vapor-oxygen low pressure diffusion flames temperature profile measurement, using subminiature thermocouple
15 p2464 A71-31631
- Heat content measurement of tantalum carbide in homogeneity range at high temperatures by mixing method using bulk calorimeter
15 p2431 A71-32155
- Truncated-cone hot-pressed silicon carbide samples, measuring enthalpy and heat capacity as temperature function at high temperatures
15 p2431 A71-32160
- Specific heat measurement in magnetic field for graphite under neutron irradiation at low temperatures, noting Schottky anomaly
16 p2600 A71-33379
- Enthalpy probe heat response dependence on surface thermal load amplitude
16 p2581 A71-34033
- Ammonium chloride specific heat measurement near order-disorder transition, comparing results to Ising model behavior
17 p2791 A71-35743
- Convective heat exchange coefficient determination for human body immersed in turbulent water flow, using fractional calorimetry
18 p2858 A71-36862
- Turbulent boundary layer and heat transfer measurements along cooled conical convergent-divergent nozzle
19 p2993 A71-37982
- Ignition delays of propane-oxygen-argon mixtures in shock tubes from pressure and heat flux measurements in reflected region
19 p3169 A71-38109
- Particle model measurements of collision and heating times in two dimensional thermal computer plasma
21 p3423 A71-40843
- Radiant heat flux measurement during pulsed processes from surface in high temperature emitting gas, using thin film sensor with small time constant
23 p3782 A71-43922
- HEAT OF COMBUSTION**
- Reaction heat for flameless combustion of double-base propellant using differential scanning calorimetry and thermogravimetric analysis, noting pressure effects [AIAA PAPER 70-125]
07 p1183 A71-19898
- Experimental method for determining condensed phase heat of reaction of deflagrating double-base propellant, defining minimum surface temperature at solid surface without heat feedback
11 p1809 A71-25493
- Pulsed combustion heated carbon dioxide gas dynamic laser with expansion separation, showing composition and stagnation pressure dependent gain and energy variations
19 p3071 A71-37144
- HEAT OF DISSOCIATION**
- Mass spectrometric determination of vapor phase dissociation energies of scandium dicarbide and scandium tetracarbide
08 p1250 A71-20673
- Equilibrium constant and heat of dissociation from dynamic viscosity of dissociating gas, noting dependence on composition and temperature
15 p2366 A71-31484
- HEAT OF FORMATION**
- LiOH dissociation energy in acetylene-air flames
03 p0376 A71-14281
- Chlorine trifluoride standard heat of formation by fluorine flame calorimetry, deriving from measured enthalpies of reactions
07 p1056 A71-20656
- Halogen molecules electron affinities by measuring negative ion average translational energy and appearance potentials, noting free radicals heat of formation
09 p1498 A71-23376
- Thermochemistry data changes influence in form of heat of formation, partition functions, specie free energy or specific heat on high temperature gas mixtures composition
15 p2514 A71-32097
- HEAT OF SOLUTION**
- Crystal lattice energies of solvation of alkali metal perchlorate in water
22 p3508 A71-42530
- HEAT OF VAPORIZATION**
- Vaporization heat transfer mechanism from capillary wick covered heated surface, considering applicability to heat pipes
03 p0353 A71-13615
- Solid/vapor surface energies of metals at melting point related to heat of sublimation
07 p1134 A71-19518
- Exit stream velocity increase in propulsion units by adding latent heat of vaporization by condensation in supersonic nozzle
17 p2728 A71-34882
- Large volume liquid oxygen pool boiling, investigating heat exchange coefficient dependence on flux density and pressure
23 p3705 A71-44339
- HEAT PIPES**
- Reinforced tube bundles thermal efficiency and convective heat transfer, discussing inter-rib cavity depth effects
01 p0181 A71-11229
- Nuclear electric space power plant rejecting waste heat by heat pipes
01 p0126 A71-11576
- Heat pipes structural material and heat carrier for various temperature ranges in satellite technology
02 p0331 A71-12069
- Isothermal irradiators of neon filled stainless steel heat pipes with Na as working fluid, discussing laboratory and reactor feasibility tests
02 p0280 A71-12250
- Heat balance measurements at collector of heat pipe thermionic converter
02 p0196 A71-12268
- Heat pipe improvement of capacitor energy storage and I-V, analyzing in terms of heat loss vs conducted heat
03 p0352 A71-13045
- Vaporization heat transfer mechanism from capillary wick covered heated surface, considering applicability to heat pipes
03 p0353 A71-13615
- Cryogenic heat pipes with parallel capillary channel wicks [ASME PAPER 70-WA/ENER-1]
03 p0520 A71-14106
- Viscous heating effects on laminar combined free and forced convection through vertical circular tubes
04 p0676 A71-15177
- Heat pipe operating principle, design and applications, discussing liquids for different temperature ranges, heat flux density and temperature control
04 p0689 A71-15816
- Out-of-core thermionic converter system using heat pipes as electrical resistive elements, discussing design and performance
11 p1710 A71-25875
- Design optimization of out-of-core cylindrical thermionic converter module with heat pipes and integral finned radiator
11 p1711 A71-25876
- Radioisotope thermionic power supply for unmanned electric propulsion missions to outer planets, using 69 modules consisting of thermionic converter and emitter heat pipe
11 p1811 A71-25897
- Out-of-core heat pipe heated and cooled thermionic converter module mechanical design, fabrication and subcomponent performance evaluation
11 p1715 A71-25912
- Reassessment of Cotter model startup in Li heat pipe, modifying model by moving sonic point to end of hot zone and including wall friction and condensation
11 p1715 A71-25914
- Vapor flow passage wall shear stress effect on sonic velocity limit in Na heat pipes [AIAA PAPER 71-407]
11 p1856 A71-26202
- Life tests and properties of organic working fluids heat pipes for electronic component cooling [AIAA PAPER 71-408]
11 p1856 A71-26203
- Grooved Al heat pipes experimental performance in moderate temperature for space vehicle applications [AIAA PAPER 71-409]
11 p1856 A71-26204
- Heat pipe applications for space vehicle thermal control, discussing spacecraft radiators, thermal exchangers and structure isothermalization [AIAA PAPER 71-410]
11 p1856 A71-26205
- Elemental maximum energy transport formula for wick heat pipe evaporators under artificial gravity and external acceleration, testing by laboratory centrifuge [AIAA PAPER 71-419]
11 p1857 A71-26210

- Noncondensable gas temperature controlled heat pipe systems design, considering working fluid, reservoir wicks and ambient thermal environment [AIAA PAPER 71-420]
11 p1857 A71-26212
- Variable conductance heat pipes feedback mechanisms for spacecraft electrical temperature control system design, using steady state analysis based performance model [AIAA PAPER 71-421]
11 p1857 A71-26213
- Variable conductance inert gas type heat pipe for spacecraft electronic equipment fine temperature control, noting design to eliminate start-up problems [AIAA PAPER 71-422]
11 p1857 A71-26214
- Capillary and electro-osmotic flow pumping in heat pipes, discussing capacity increase [AIAA PAPER 71-423]
11 p1857 A71-26215
- Corrosion mechanism in Ta-Li high temperature heat pipes by ion analysis, demonstrating oxygen and yttrium diffusion into heating zone
12 p1916 A71-26974
- High temperature heat pipes material corrosion problems, considering mass transfer from cooling zone into heating zone
12 p1917 A71-26975
- Multiple circumferential heat pipes construction and tests for spacecraft thermal control, using simulated space environment [AIAA PAPER 71-412]
12 p1972 A71-27408
- Heat pipes steady state and dynamic behavior, noting pressure balance, vapor flow, transport capability and applications
12 p1987 A71-27741
- High power linear beam tube devices for space power generation station, considering use of klystron with heat pipes for low weight and high efficiency
13 p2000 A71-28669
- Isothermal flow under capillary forces in heat pipe with zero gravity, deriving relation between flow rate and duct parameters
13 p2050 A71-29219
- Heat transfer processes in heat pipes, examining heat and mass transport mechanisms between heat source and sink
14 p2336 A71-30243
- Heat pipe application to OAO as structural isothermalizer, considering overall spacecraft thermal network analysis
15 p2512 A71-31594
- Heat pipes design and applications, examining pressure losses in steam and liquid phases and capillarity and gravity effects [HEAT EXCH. CONF. PAPER 23]
15 p2513 A71-31637
- Out-of-core nuclear thermionic converter system design feature concerning heat pipes, vapor-cooled radiators, modularity and reliability
15 p2448 A71-32224
- Temperature stabilization with self controlled water and radiation cooled heat pipes using argon in addition to K heat transfer medium
16 p2663 A71-34039
- Design and performance testing of arterial wick circular heat pipes for OAO-C spacecraft [ASME PAPER 71-AV-26]
18 p2868 A71-36393
- Steady state and transient response of heat source with temperature regulated by electrical feedback controlled variable conductance heat pipe [ASME PAPER 71-AV-27]
18 p2868 A71-36394
- ATS F and G thermal control, discussing heat pipe, lower and model tests [ASME PAPER 71-AV-28]
18 p2868 A71-36395
- Thermal control using nitrogen, circuit board, switching, flexible, transformer and segmented evaporator heat pipes [ASME PAPER 71-AV-29]
18 p2868 A71-36396
- Space station thermal control systems design, discussing pumped loop, air cooled semipassive and heat pipe systems [ASME PAPER 71-AV-36]
18 p2869 A71-36403
- Gas controlled variable conductance heat pipe for OAO-C onboard processor temperature stabilization, describing thermal performance tests under simulated flight conditions [AIAA PAPER 71-411]
18 p2975 A71-36775
- Surface heat flux for incipient boiling in liquid metal heat pipes, determining nucleation site radius upper limit in Na heat pipes
19 p3171 A71-38345
- Cascaded thermoelectric generator using Si-Ge and Pb-Te elements with heat pipe interstage coupling
20 p3264 A71-38925
- Film condensation heat transfer coefficients measurements on vertical heat pipes for cryogenic nitrogen, hydrogen and deuterium
20 p3313 A71-39298
- Dynamic analysis of ATS 5 heat pipe fluid energy dissipation, confirming estimated stability of planned rescue approach configuration
22 p3611 A71-42033
- Li-filled vacuum-deposited W heat pipes for efficient heat extraction from nuclear reactors, discussing design, fabrication and testing
23 p3682 A71-43559

- HEAT PUMPS**
 Cascade thermoelectric cooler /heat pump/ transient response for various geometries, materials and environmental conditions 03 p0355 A71-14320
- HEAT RADIATORS**
ANT SPACECRAFT RADIATORS
 In-core thermionic power system for manned space station application, discussing driver fuel elements, nuclear radiation shield, heat rejection and coolant outlet temperature 11 p1710 A71-25869
 Design optimization of out-of-core cylindrical thermionic converter module with heat pipes and integral finned radiator 11 p1711 A71-25876
 Spacecraft radiator thermal scale model, using forced convection, conduction and radiation heat transfer 11 p1860 A71-26517
 Thin shallow annular radiating fins for heat removal from sphere or polyhedron with isothermal surfaces, determining optimal weight and geometrical parameters 12 p1986 A71-27331
 Optimal shape of single radiative cooling elements without self irradiation relative to cross sections and linear generatrices of radiator 13 p2165 A71-29179
 Out-of-core nuclear thermionic converter system design feature concerning heat pipes, vapor-cooled radiators, modularity and reliability 15 p2448 A71-32224
 Optimal radiative capacity of star shaped radiator with mirror reflecting surfaces for vacuum cooling of elongated finned bodies 17 p2836 A71-34311
- HEAT REGULATION**
U TEMPERATURE CONTROL
HEAT REJECTION DEVICES
U HEAT RADIATORS
HEAT RESISTANCE
U THERMAL RESISTANCE
HEAT RESISTANT ALLOYS
NT MOLYBDENUM ALLOYS
NT NIOBIUM ALLOYS
NT OSMIUM ALLOYS
NT REFRACTORY METAL ALLOYS
NT RHENIUM ALLOYS
NT TANTALUM ALLOYS
NT TUNGSTEN ALLOYS
NT UDIMET ALLOYS
 Ni base superalloys fatigue strength improvement for gas turbine engine components, discussing homogeneous deformation distribution, grain size control, etc 01 p0099 A71-10166
 Materials for spacecraft design requirements, considering composite and refractory metals, Ti and heat resistant alloys 01 p0102 A71-10816
 Microstructure and mechanical properties of weldable heat resistant Ni alloy containing carbon and boron 01 p0103 A71-11068
 Ti alloys isothermal forging, using precision-cast superalloy dies [SME PAPER MF-70-122] 01 p0089 A71-11255
 Combined vacuum furnace brazing with diffusion welding for joining high strength Ni base superalloys 02 p0255 A71-11708
 Soviet papers on plastic deformation of high melting metals and alloys covering tungsten, molybdenum, titanium and stainless steels 02 p0264 A71-12511
 Oxidation potential criterion for metal sticking to rolls during rolling in vacuum, considering Ta, Zr, Mo, W, Ni, Cu, Nb and V 02 p0256 A71-12515
 Ni base superalloy single crystal fatigue crack propagation 02 p0268 A71-12886
 Heat resistant materials long term strength characteristics, determining optimum parameters from creep data statistical analysis by least squares method 03 p0440 A71-13194
 Superalloy turbine engine guide vane thermal fatigue cracks repair by plasma arc fusion method 03 p0432 A71-13257
 Damage and fracture mechanisms in high temperature low cycle fatigue of cast nickel-based superalloys, noting grain boundaries oxidation role in crack nucleation and propagation 04 p0615 A71-15789
 German monograph on Co-free heat resistant austenitic steel alloys precipitation hardening and creep strength properties as function of chemical composition 05 p0764 A71-15973
 Aircraft construction materials for 1990s, discussing need for high temperature resistant materials for supersonic and hypersonic airframe and engine structural components 05 p0839 A71-16141
- Ti and Ni base high temperature alloys welded joints efficiency, discussing fatigue, storage, long time heat and corrosion tests 05 p0765 A71-16172
 Monograph on cobalt base superalloys covering mechanical properties relation to microstructure, carbides, heat treatment, aging, intermetallic precipitation and dislocation 05 p0765 A71-16198
 Stress rupture properties at elevated temperature of nickel base superalloys with varying Ti and Al additions, investigating microstructural and age hardening effects 06 p0913 A71-18676
 Uniaxial stress effect on morphology changes of coherent gamma prime precipitates in nickel base superalloy crystals 06 p0914 A71-18682
 Ni base superalloys mechanical properties relationship to microstructure, considering precipitate dispersion and phase state effects on flow stress and creep strength 07 p1133 A71-19445
 Ni base superalloys fatigue behavior, emphasizing role of ordered gamma prime precipitate in two phase materials 07 p1133 A71-19447
 Optimal heat resistance, mechanical properties and microstructure of steam pipe Cr-Mo-V steel 07 p1135 A71-19618
 Oxide films effect on heat resistant steels hydrogen permeability, using mass spectrometer 07 p1136 A71-19920
 Stress annealed Ni-base superalloy crystals, investigating orientation and applied uniaxial stress sense effect on coherent gamma prime precipitates morphology 07 p1138 A71-19987
 W-Mo-Re high temperature alloys, discussing high strength, elastic properties, creep, thermal resistivity and expansion coefficient 07 p1141 A71-20243
 Mechanical, heat resistant and thermoelectric properties of W-Re alloys for thermocouples 07 p1144 A71-20250
 Energy dissipation in heat resistant Ni steels under cyclic tension and compression at room temperature 07 p1142 A71-20479
 Cyclic creep and relaxation of heat resistant alloys at high temperatures, showing inapplicability of static load conditions 07 p1142 A71-20480
 Microstructure and mechanical properties of weldable heat resistant Ni alloy containing carbon and boron 08 p1305 A71-21035
 Heat resistant materials strength characteristics with long service periods, formulating equation for time dependence of rupture resistance 08 p1306 A71-21111
 Long time static strength, durability and thermal stability relations determined for heat resistant alloys at operational temperatures 08 p1306 A71-21112
 Long time strength and creep rectilinear diagrams constructed for heat resistant alloys to obtain extrapolation values 08 p1306 A71-21113
 Test results extrapolation for heat resistant alloys long time strength using exponential relation between time to rupture and value for initial stress decrease 08 p1306 A71-21114
 High strength corrosion resistant superalloy structure and mechanical properties 08 p1314 A71-21566
 Ni superalloys plane front cast structure through controlled unidirectional solidification, discussing improved mechanical properties 08 p1314 A71-21567
 Ni superalloys strengthening by body centered tetragonal gamma double prime phase precipitation, investigating various alloying components and ratios 08 p1314 A71-21568
 Precipitation hardened Ni base superalloys fatigue deformation, investigating correlation between metallurgical structure characteristics and high-cycle fatigue behavior 08 p1314 A71-21570
 Co base superalloys fracture toughness microstructural aspects, considering effects of intermetallic carbides and carbide precipitation on aging at elevated temperatures 08 p1314 A71-21572
 High temperature alloys oxidation resistance and strength characteristics, considering influence of various alloying compositions via use of oxide mapping method 08 p1314 A71-21573
 Stacking fault formation and mechanical twinning in Ni base superalloy during tensile deformation at high temperature 08 p1315 A71-21581
 Solidification process for unidirectionally cast airfoil shaped turbine components from Ni superalloys, discussing mold withdrawal 08 p1299 A71-21682
- Cyclic heating and thermal stresses effect on fatigue strength and durability of turbine blade alloys and structural elements 08 p1372 A71-21702
 Microstructure and mechanical properties of heat resistant alloy under homogenization and subsequent isothermal heat treatment 08 p1317 A71-21764
 Heat resistant Ni alloys intermetallic gamma prime phase analysis by electrolytic separation 09 p1467 A71-22322
 Yield point temperature dependence in heat resistant austenitic alloys, showing tendency to brittle failure under short term overloads 09 p1468 A71-22598
 Heat resistant alloys low cycle fatigue tests at 20-800 C, establishing residual strain change patterns as function of stress and temperature 09 p1468 A71-22600
 Kovpak method for estimating and extrapolating heat resistance characteristics, considering alloy long term strength 09 p1538 A71-22627
 Thermal fatigue tests of high temperature Ni and Co base alloys by fluidized bed technique 09 p1469 A71-22812
 High temperature precipitation hardening of Ni-Cr alloys, discussing effect on creep rupture strength 09 p1470 A71-23044
 Directionally solidified Ni base superalloys, determining stress and temperature effect on primary creep strain 09 p1472 A71-23130
 Martensitic transformation in NiAl oxidation-resistant coatings on Ni superalloys heated for 300 hr at 1093 C 09 p1472 A71-23132
 Chemical precipitation techniques for dispersion hardened high temperature alloys, considering Co, Ni, Cr, Mo and W multicomponent alloys 09 p1455 A71-23285
 High temperature Ni alloys structural stability, computing gamma prime phase coagulation and average electron vacancy number 09 p1474 A71-23289
 Welding rods chemical composition and welding procedures for heat resistant austenitic and martensitic steels for gas turbines, considering maraging steels heat treatment influence 09 p1456 A71-23291
 Gas turbine components precision casting, discussing high temperature alloys and casting techniques in manufacture of components subject to high thermal and mechanical stresses 09 p1456 A71-23293
 High temperature austenitic steels, Ni and Co alloys machining, considering deformation resistance and strain hardening 09 p1456 A71-23297
 High temperature Fe, Co and Ni alloys for gas turbine components, considering tensile and creep rupture strength increase by thermal mechanical processing 09 p1475 A71-23298
 High temperature Ni and Co alloys powder metallurgy, discussing production, preparation, pressing and sintering 09 p1456 A71-23300
 High temperature Ni and Co alloys for stationary gas turbines and jet engine parts, considering microstructure and mechanical behavior under stress and temperature 09 p1475 A71-23302
 Cold prestraining effect on steady state creep strength and rate of precipitation hardened heat resistant steel 09 p1477 A71-23331
 Prediction of metals heat resistance increase by thermomechanical treatment, considering Ni-Al alloy 09 p1477 A71-23332
 Heat resistant dispersion strengthened and fiber reinforced metal matrix superalloys for high temperature applications, considering superstrength alloys development 09 p1478 A71-23397
 Hot deformation of superrefractory austenitic Ni alloy, considering elastic and plastic limits 09 p1479 A71-23625
 Intracrystalline liquefaction in Ni alloys containing Nb studied with microanalyses 09 p1480 A71-23702
 Ternary compositions for high temperature alloys Ni-Cr-Al and Co-Cr-Al, using superimposed oxidation data on phase diagrams /oxide mapping/ 10 p1625 A71-23972
 Thermal resistance estimation for machine parts of heat resistant alloys under real working conditions 10 p1686 A71-24190
 Oxidation resistant high temperature Ni-Al system preparation using powder metallurgy and thermomechanical treatments without sintering 10 p1626 A71-24401
 Powder metallurgy superalloy parts, discussing production methods and mechanical properties comparison with conventional process products 10 p1618 A71-24763

Superalloy dispersion strengthened and fused slurry silicic coatings for aircraft gas turbine engines and space shuttle heat shields

11 p1778 A71-25555

Cast cobalt base superalloys extrusion and forging, noting hot deformation effects on tensile properties, stress rupture strength and ductility

11 p1778 A71-25854

Chemical vapor deposition process for preparing W-Re alloys having uniform Re content and dense coherent grain structure

11 p1797 A71-25862

Low alloy steels and superalloys inertia welding in gas turbine field, discussing microstructure tensile strength and stress rupture

[ASME PAPER 71-GT-21] 11 p1770 A71-25965

Ni-based superalloy stress cycle frequency effect on elevated temperature fatigue life

11 p1779 A71-26012

TD NiC nickel based alloy high temperature oxidation control, discussing thorium dispersion effect on Ni-Cr oxidation properties

11 p1779 A71-26015

High chromium hot corrosion resistant superalloys in sheet form, noting precipitation hardening and creep resistance equivalent to Nimonic alloys

12 p1916 A71-26922

Long term aged heat resistant Ni base alloys, investigating gamma prime phase chemical composition

12 p1917 A71-27298

Ni-Cr and Ni-W alloys high temperature strength properties, considering stacking fault energy, diffusion velocity, Young modulus and dislocation locking

12 p1919 A71-27762

Gas turbine blades cast heat treated superalloys high temperature mechanical properties during aging

12 p1919 A71-27778

Heat resistant alloys strengthened elements, studying high temperatures prolonged exposure effects on surface layers strengthening and residual stresses relaxation

12 p1919 A71-27780

Composite heat resistant Ni alloy production using refractory oxide phase dispersion hardening

13 p2083 A71-27893

Chemical composition effects on microstructure and high temperature properties of cast Cr-Ni-Al steels containing Ti, B, Ce and Zr

13 p2084 A71-28035

Heat resisting Ni base alloy stress rupture strength and fatigue life, observing corrosive high temperature environment effect

13 p2084 A71-28111

High temperature gas turbine alloys corrosion tests, describing laboratory facilities for preliminary screening

13 p2086 A71-28752

Heat resistant alloys face polishing with ultrasonically cleaned grinding wheel abrasive rim surface

13 p2075 A71-28942

Stage I fatigue fracture mechanism in Ni-based superalloy single crystals, observing air and vacuum effects

13 p2088 A71-29405

Gamma phase composition estimation in Ni base superalloys by phase rule principles and analytic geometry

13 p2089 A71-29407

Vacuum melted Ni base superalloys, determining Mo and hardener effects on gamma prime solvus temperature and solutioning rate

13 p2090 A71-29418

High strength Ni base superalloy workability, investigating microstructure relation to mechanical properties

13 p2090 A71-29419

Metal coated superalloys evaluation for gas turbine engine components, including corrosion, impact and fatigue tests

14 p2256 A71-29635

Impact strength of Cu, Cu-Ni alloy and superalloy matrices reinforced with W fibers, studying temperature, heat treatment and fiber content and toughness effects

14 p2258 A71-29919

Ti-Al-V alloys heat resistance relationship to phase structure from bending test at high temperature

15 p2426 A71-31404

Intermetallic compounds application in structural materials, emphasizing role in superalloys development for gas turbine engine parts and high temperature environments

15 p2427 A71-31531

Tensile stress and compressive effects on grain boundary precipitate morphology in Ni-base superalloy during creep

15 p2433 A71-32179

Jet engine high pressure turbine high temperature alloy blades and vanes grinding operation, discussing testing, operating conditions and coolant application [SME PAPER MR-71-802]

15 p2416 A71-32432

Age hardenable Inconel X-750 superalloy mechanical response to tensile loads for identifying microstructural changes due to deformation

15 p2437 A71-32616

Single crystal Ni-base superalloy anisotropic hollow cylinder creep under biaxial loading, studying rate dependence on crystallographic axis orientation and stresses ratio

[ASME PAPER 71-APM-1] 16 p2591 A71-33222

Program parameters effects on fatigue life of turbine blade heat resistant alloys at high temperatures under cyclic loading

16 p2592 A71-33407

Statistical analysis of durability data of heat resistant alloys for gas turbine engines, using long term mass creep strength tests on industrial melts

16 p2592 A71-33413

Structural shapes extrusion technique with superalloy powders, noting fine grain, chemical homogeneity and elevated temperature mechanical properties

[ASM PAPER W71-5.4] 16 p2592 A71-33540

Heat resistant weldable dispersion hardened Ni base alloy, discussing intermetallic phase hardening

16 p2594 A71-33715

Stress-strain diagrams of heat resistant alloys at high temperatures, describing test facility

16 p2598 A71-33988

Thermostable and heat resistant steels and alloys vibration loading frequency effects on fatigue at high temperatures

16 p2598 A71-33992

Room temperature ultrasonic frequency fatigue behavior of Ni-base superalloy single crystals

17 p2756 A71-34493

High temperature Ti alloys welding, discussing strength, ductility, beta stabilizing elements and chemical compositions

17 p2758 A71-34806

Columnar grained Ni superalloy lifetimes and transverse creep ductilities enhancement and microstructural alterations due to Hf additions

17 p2759 A71-35394

Titanium and superalloy radiative heat shield design for space shuttle booster, recommending postsupported honeycomb configuration

18 p2973 A71-36462

Superalloy investment casting, discussing production processes, shell molding technique, applications, cost control, solidification, ductility improvement and cooling rate

[SME PAPER CM-71-160] 18 p2927 A71-36659

Diffusion bonding in production of shuttle type vehicles, considering fluxless brazing of refractory superalloys for heat shielding

[SME PAPER AD-71-246] 18 p2927 A71-36660

Semifinished product production technology influence on heat resistant alloys mechanical properties, considering forging, rolling, casting, melting, diffusion welding and powder metallurgy

18 p2937 A71-36725

Refractory, superalloy and composite materials brazing process for space shuttle orbiter heat shield

18 p2928 A71-36854

Precipitation strengthened Fe-Ni-base superalloy microstructure, investigating phase relationships

19 p3079 A71-37711

Ni-base heat resistant alloys loading frequency effect on fatigue resistance, noting linear relationship between creep strain and cycles to failure in logarithmic coordinates

19 p3082 A71-38348

Heat resistant material properties under power and chemical plant conditions - Conference, Mala Fatra, Czechoslovakia, September 1971

20 p3249 A71-39013

High temperature properties of weld metals formed by electrodes for welding of low alloy heat resistant Cr-Mo and Cr-Mo-V steels

20 p3249 A71-39014

Structural stability and creep properties of heat resistant steel weld joints, considering substitutional and precipitation hardening and dislocation effects

20 p3249 A71-39015

Creep strength extrapolation for high temperature steels, suggesting combined numerical and graphic methods

20 p3249 A71-39017

Creep tests on heat resistant steels, studying elongation/rupture strength and temper hardening

20 p3251 A71-39026

Mo and high temperature Mo alloys thermally activated deformation mechanisms from flow stress thermal component and effective stress temperature dependence observation

21 p3396 A71-40030

Composite heat resistant Ni alloy production using refractory oxide phase dispersion hardening

21 p3396 A71-40084

German monograph on creep buckling tests of finned and unfinned thin walled pipes of heat resistant breeder reactor cladding materials

21 p3464 A71-40781

High heat resistance of austenitic Cr-Ni-V-B steel by polygonization and recrystallization, using thermomechanical treatment

21 p3403 A71-41102

Gas turbine blades cast heat treated superalloys high temperature mechanical properties during aging

21 p3403 A71-41103

High temperatures prolonged exposure effects on surface layers hardening and residual stresses relaxation in heat resistant alloys

21 p3403 A71-41105

High temperature creep characteristics and stress curves of heat resistant Fe and Ni alloys in turbine components

21 p3403 A71-41150

Heat resistant and refractory materials contact eutectic melting for surface coating production

21 p3390 A71-41175

Oxidation resistance and scale fracture healing by Al additions to Co-Cr alloys at high temperatures, using electron probe and scanning electron microscope analyses

21 p3405 A71-41414

Heat resistant Ni alloys hot strength level and temperature dependence as function of gamma-prime phase particle size, discussing aging effect on creep rate

22 p3561 A71-41841

High temperature Ti-Ni alloy stacking variation stability, studying size, shear and valence electron concentration effects

22 p3586 A71-42367

Inconel superalloy microscopic observation of local melting and hot ductility behavior during weld thermal cycles to clarify cracking cause in heat affected zone

22 p3564 A71-42494

Boron addition effects on scaling resistance of Ni-Cr steel at high temperatures

23 p3690 A71-43278

Phase transformations and mechanical properties of heat resistant martensitic stainless steel during precipitation aging at prolonged high temperature exposures

23 p3690 A71-43280

Sintering of Ni based heat resistant alloy, determining phase composition, lattice constant and microhardness of compressed specimens

23 p3691 A71-43521

Zirconium carbide eutectic and supraeutectic alloys preparation with graphite addition, determining heat resistance under thermal cycling tests

23 p3697 A71-44025

Mo and Co alloying effects on high temperature chromium ball bearing steels contact strength

23 p3692 A71-44037

Gas turbine blades of cast ZhS6K heat resistant alloy, investigating structural strength from fatigue test data

23 p3779 A71-44208

Gas turbine blade models of heat resistant ZhS6K alloy under operational temperature variations, observing fatigue strength

23 p3779 A71-44209

Heat resistant steels long time strength determination by graph-analytical time-temperature extrapolation

23 p3693 A71-44213

Heat resistant Ni-base composite stiffened with W wires, investigating interaction between alloy and fibers from metallographic and X ray diffraction microscopy data

23 p3693 A71-44214

Heat resistant ZhS6K alloy precision and ground cast specimens, determining short and long term strength and fatigue

23 p3780 A71-44236

Sodium role in accelerated oxidation behavior/sulfidation/ of Ni-base superalloys and binary alloys coated with sodium sulfate or carbonate

23 p3695 A71-44288

High temperature aging, structural stability and tensile properties of hot rolled Co-W heat resistant alloy for space applications

24 p3836 A71-44443

Mechanical properties of fiber reinforced heat resistant alloys

24 p3837 A71-44726

Tungsten filaments as reinforcing agent of heat resistant composite chromium alloy, investigating long term high temperature effects

24 p3837 A71-44728

Heat resistant Nichrome composite alloy with tungsten filament reinforcement, discussing manufacturing and mechanical properties at 1100 C

24 p3837 A71-44730

Aluminized layer phase and chemical composition of heat resistant iron and nickel alloys

24 p3837 A71-44733

Ni-base superalloys metallography, investigating catastrophic cracking in weld heat affected zones by electron microscopy

24 p3839 A71-45133

HEAT SHIELDING

NT REENTRY SHIELDING

Ablative heat shield char layer, examining reaction nonequilibrium pyrolysis gas flow

[AICHE PREPRINT 15B] 01 p0181 A71-11299

Air injection into turbulent boundary layer flow through porous plate, examining heat transfer and shielding efficiency

05 p0838 A71-1678

Iterative solution for radiation-dominated heat balance about heat shield or superinsulation nodes, testing performance in thermal analyzer program
07 p1221 A71-18905

Transient stresses in heat shield generated by short duration pressure pulses, using method of characteristics for interface stresses
[AIAA PAPER 71-351] 11 p1844 A71-25330

In-core thermionic reactor flight system for space base applications, providing electric power and thermal shielding
11 p1710 A71-25870

Test streams and chemical composition effects on ablative composites for hypervelocity heat protection of manned atmospheric entry vehicles
11 p1855 A71-26031

Epoxy resin heat shield performance prediction based on chemical structure relation to ablative properties, discussing thermal degradation mechanism and char forming reactions
11 p1855 A71-26038

Ablation residue, including silicone elastomer foam heat shield material ablative degradation
11 p1855 A71-26040

Graphite heat shield ablation during low velocity low altitude portion of satellite reentry trajectories
[AIAA PAPER 71-415] 11 p1857 A71-26208

Viking rocket heat shield material mechanical properties, examining time-temperature superposition with continuous stress relaxation data measured in vacuum
11 p1791 A71-26518

Blowing angle effect on heat protection effectiveness of flat wall in slit injected low speed air flow with turbulent boundary layer in wind tunnel
13 p2159 A71-28420

Heat shield ablation under high enthalpy chemically active turbulent gas flow in hydrojet engine manifolds
13 p2160 A71-28589

Hypersonic reentry heat shielding problem, considering axisymmetric laminar boundary layer flow with local coolant mass injections at multiple stations
13 p1990 A71-29127

Nonequilibrium modeling of pyrolysis gas products flow through char layer of ablative heat shield
14 p2334 A71-29876

Air injection into turbulent boundary layer flow through porous plate, examining heat transfer and shielding efficiency
16 p2662 A71-33035

Heat shields for space applications, reviewing heat sinks, double wall cooling techniques and radiative, transpiration and ablation cooling systems
18 p2848 A71-36433

Titanium and superalloy radiative heat shield design for space shuttle booster, recommending postsupported honeycomb configuration
18 p2973 A71-36462

Diffusion bonding in production of shuttle type vehicles, considering fluxless brazing of refractory superalloys for heat shielding
[SME PAPER AD-71-246] 18 p2927 A71-36660

Filament wound carbon/carbon composite heat shields, describing fabrication process involving winding, carbonization, pyrolytic carbon infiltration and graphitization
[SME PAPER EM-71-204] 18 p2939 A71-36664

Refractory, superalloy and composite materials brazing process for space shuttle orbiter heat shield
18 p2928 A71-36854

Shock layer parameters of supersonic viscous gas flow past blunt bodies of heat insulated and cooled surfaces, using Navier-Stokes equations
19 p2991 A71-37089

Space shuttle structural heat problems, discussing shield design configurations and cooling systems
19 p3150 A71-37311

Graphitic ablative heat shield fractions and forebody configurations for probe entry into atmospheres of Saturn, Uranus and Neptune
[AAS PAPER 71-145] 19 p3141 A71-37948

Jupiter atmosphere entry probes graphite ablative heat shields performance, indicating convective and radiative blockage and graphite sublimation processes in surface heat balance
[AAS PAPER 71-146] 19 p3084 A71-37949

Reflecting and ablating Teflon heat shields for radiative environment of outer planets atmosphere
[AAS PAPER 71-147] 19 p3084 A71-37950

Reinforced plastics for aerospace applications, giving special attention to heat shield and inflatable structures materials
19 p3085 A71-38069

Meteorological rocket nose thermal shield, discussing design and effectiveness
19 p3172 A71-38636

Pressure sensors thermal protection by porous Zr disk as heat shield, considering acoustic transparency, linearity, transient response and air flow resistance
[ONERA-TP-957] 22 p3547 A71-42501

HEAT SINKS

Tropospheric and stratospheric turbulence, discussing energy sources and sinks and energy spectra pattern at different atmospheric conditions
05 p0741 A71-16625

Turbulent boundary layers transpiration cooling prediction with coolant fluid serving as heat sink within structure wall and as protective film
07 p1220 A71-18768

Organo-ceramic composites for thermal protection of aerospace vehicles, discussing heat sink property
09 p1483 A71-23206

Hydrocarbon fuel for hypersonic vehicle cooling, discussing use of endothermic reactions to achieve maximum heat sinks
[AIAA PAPER 68-997] 10 p1658 A71-24852

Annular solid state microwave diodes temperature distribution at diode/heat sink interface, presenting closed form solution for calculation of absolute temperature rise
12 p1889 A71-27699

Seasonal-climatic vertical distributions of radiative heat sources and sinks calculation for Northern Hemisphere stratosphere and lower mesosphere
13 p2057 A71-28023

Heat sink requirements in transistor devices, examining temperature dependence of thermal resistivity and electrical capacitance
14 p2284 A71-30631

Performance tests of two identical Brayton cycle heat exchanger units consisting of recuperator, heat sink exchanger and ducting in combination with turbine
15 p2355 A71-32213

Temperature control in presence of varying heat sources or sinks through thermal conductance
16 p2576 A71-32973

Heat shields for space applications, reviewing heat sinks, double wall cooling techniques and radiative, transpiration and ablation cooling systems
18 p2848 A71-36433

Temperature distribution from line sources and sinks in infinite medium during finite time
18 p2986 A71-36594

Experimental comparison between double drift and single drift region mm wave IMPATT diodes on room temperature metal heat sinks
18 p2895 A71-36984

Temperature variations effect on TRAPATT microwave oscillator parameters, considering upper temperature limit dependence on heat dissipated in diode and heat sink thermal resistance
18 p2895 A71-36988

High-power high-efficiency CW X band Gunn oscillators on diamond heat sinks, noting operation in waveguide cavities
19 p3029 A71-38219

HEAT SOURCES

Space nuclear power developments, reviewing radioisotope heat sources, reactors and power conversion systems
04 p0624 A71-15284

Al 27 for heating working body in heat exchangers of jet engines
06 p0926 A71-18706

Steady state thermal stresses and deformations in infinite hollow circular cylinder by sinusoidal internal heat source and Newtonian radiation boundary condition outer surface cooling
07 p1214 A71-20026

Viscous fluid horizontal motion due to moving heat source and boundary
07 p1091 A71-20030

Evaporation rate of droplet with internal heat source from Maxwell-Langmuir theory extension
08 p1377 A71-21926

Incompressible laminar boundary layer flow with mass and heat sources, calculating thermal and friction stress distribution
08 p1277 A71-22037

SNAP 15A heat source gamma ray intensity measurements and identification of gamma ray producing isotopes, describing measurement apparatus
09 p1491 A71-22456

Hybrid integral microcircuits with thin film resistor heat sources, determining temperature fields on substrate and boundaries
09 p1416 A71-22495

Reflecting oven for very high temperatures under gas pressure, describing apparatus, heat source and possible contamination
10 p1613 A71-25040

Temperature distribution inside solid sphere rotating in viscous incompressible fluid with constant strength heat source at center, discussing flow field around sphere
11 p1853 A71-25146

Liquid water natural occurrence on Martian surface, considering possibility of ice melting by sunlight or other heat sources
11 p1826 A71-25718

Temperature distribution in metal sheets due to point and circular surface heat sources for laser welding applications, using power supply approximation model
12 p1985 A71-26571

Seasonal-climatic vertical distributions of radiative heat sources and sinks calculation for Northern Hemisphere stratosphere and lower mesosphere
13 p2057 A71-28023

Thermal stresses in infinite viscoelastic plate due to external heat source
13 p2152 A71-28278

Radioisotope heat sources protection from reentry ablation and thermal stress with outer anisotropic pyrolytic graphite shield
13 p2099 A71-29259

Thermoelastic stress analysis of circular perforated plate under point heat source
14 p2326 A71-30195

Equatorial electrojet as supplementary heat source for tropical region upper atmosphere based on thermal energy release calculation
15 p2399 A71-31964

Temperature control in presence of varying heat sources or sinks through thermal conductance
16 p2576 A71-32973

Acoustic vibrations generation and transmission in nonadiabatic gas containing heat sources, taking into account conductive and radiative heat transfer and momentum loss
16 p2662 A71-33029

Nuclear reactor design as heat source for electric power generation in space
16 p2606 A71-33249

Radiation attenuation volume coefficients for water clouds and fogs thermal sources and laser outputs
16 p2543 A71-33708

Lunar interior thermal history models for setting radioactive heat sources upper limits consistent with proposed temperature distribution
16 p2642 A71-33797

Evaporation rate of droplet with internal heat source from Maxwell-Langmuir theory extension
17 p2838 A71-35270

Transient thermal stresses in infinite cylinder of rectangular cross section with heat sources, using integral transforms
18 p2976 A71-36127

Steady state and transient response of heat source with temperature regulated by electrical feedback controlled variable conductance heat pipe
[ASME PAPER 71-AV-27] 18 p2868 A71-36394

Temperature distribution from line sources and sinks in infinite medium during finite time
18 p2986 A71-36594

Convective clouds development stimulation by artificial ascending jets forming above stationary heat and momentum source, discussing propagation in atmosphere
19 p3093 A71-38694

Multihundred watt radioisotope thermoelectric generator heat source survivability in multiple skip reentry
20 p3264 A71-38931

Large cobalt 60 gas cooled radioisotope heat source, including test loop, operations, control and safety
20 p3265 A71-38937

Laminar free convection from line heat source for Prandtl number 2 based on differential equation solution
20 p3314 A71-39491

Axisymmetric small Rossby number flow driven by axially distributed heat sources, examining core multiboundary layer structure
20 p3212 A71-39507

Time periodic convection development in incompressible viscous fluid with distributed heat sources
21 p3475 A71-40689

Thermal stresses in infinite elastic plate with circular hole and single heat source, considering steady state heat conduction
21 p3464 A71-40753

Closed form solution for quasi-static thermal stress field due to moving point heat source in circular disk, noting application to welding problems
21 p3467 A71-40966

Aerodynamic nonstationary conjugate heat transfer of thin plate with heat sources in incompressible fluid flow
22 p3622 A71-42684

Planetary atmospheric motions, discussing solar radiation, internal heat sources, planetary rotation and magnetic field effects
23 p3672 A71-43891

Diffusion from continuous line source in turbulent boundary layer, comparing calculation based on Lagrangian similarity with measurements
23 p3664 A71-44200

Bulk boiling studies with motion picture camera and quartz envelope of KIO 220/2500-2 tube for heat releasing surface
24 p3890 A71-45025

Heat transfer in transpiration cooled porous heat sources, deriving dimensionless temperature profiles
24 p3891 A71-45185

HEAT TESTS

U HIGH TEMPERATURE TESTS

HEAT TOLERANCE

Thermal state symptoms characterizing limit of human tolerance to heat loads at rest and during physical exercise
01 p0014 A71-11135

- Human tolerances to thermal environment extremes in aerospace activities 02 p0207 A71-12388
- Carbon fiber composites, examining epoxy resin matrix effects on mechanical performance and heat tolerance 02 p0274 A71-12486
- Heat tolerance for resting subjects in event of air conditioning system failure in SST passenger cabin 03 p0371 A71-13095
- Positive effect of physical training on heat endurance of man 03 p0361 A71-13193
- Tolerance time for hot humid conditions, considering acclimatized and unacclimatized men at rest and at work with moderate rate of energy expenditure 05 p0705 A71-16153
- Voluntary body water and salt deficits decreasing human heat tolerance 05 p0708 A71-16597
- Human work capacity in hot environment irrelevance to normal conditions, considering physiological reactions to exercise in heat by heart rate criterion 05 p0709 A71-16621
- Physiological effects of cooling measured by men wearing air and water cooling garment under external heat loads or large metabolic heat 08 p1248 A71-21232
- Oxygen deficiency and body temperature effects on work capacity of human subjects in hot humid environment 09 p1399 A71-22922
- Hawaiian silversword seed germination and inhibition showing extraordinary heat sensitivity 16 p2527 A71-33049
- Acute renal failure due to heat stress and physical exercise, noting discrepancy between physiological alterations and histopathological abnormalities 18 p2855 A71-36218
- Sweat and time constant response of human thermostat to linear gradient heat load, using analog computer experiment 18 p2859 A71-36874
- Heat acclimatization by evaporative cooling prevention in men wearing vapor barrier suits, considering body temperature and heart and sweat rates 21 p3331 A71-40355
- Training cycle in altitude chamber for human adaptation to hypoxia, high temperatures and transverse myogenic loads 22 p3505 A71-42805
- Moderate heat exposure effects on human circadian variations in body temperature, heart and metabolic rates and water loss 24 p3797 A71-44779
- HEAT TRANSFER**
- NT AERODYNAMIC HEAT TRANSFER
- NT CONDUCTIVE HEAT TRANSFER
- NT CONVECTIVE HEAT TRANSFER
- NT HYPERSONIC HEAT TRANSFER
- NT LAMINAR HEAT TRANSFER
- NT RADIATIVE HEAT TRANSFER
- NT SUPERSONIC HEAT TRANSFER
- NT TURBULENT HEAT TRANSFER
- Temperature effects on heat transfer in turbulent boundary layer on cooled plate at various Reynolds numbers 01 p0179 A71-10609
- Heat transfer between rarefied monatomic gas and porous wall, examining temperature jump with model kinetic equation for Knudsen layer 01 p0179 A71-10612
- Porous metal fiber laminar vacuum insulation, calculating steady state heat and mass transfer 01 p0179 A71-10615
- Resonance tube heat losses, discussing thermal exchange mechanism and wall temperature limits 01 p0180 A71-10993
- Human heat exchange and body overheating mechanism at high ambient temperatures at sea level and lowered pressures 01 p0013 A71-11134
- Critical heat release in water film on vertical pipe with inside cooling 01 p0181 A71-11244
- Heat transfer literature (1969) covering conduction, boundary layer, channel and separated flows, convection, mass transfer, radiation, etc 01 p0181 A71-11402
- Liquid film formation at base of bubbles and effects on heat transfer during nucleate boiling 01 p0181 A71-11404
- Nonlinear heat transfer in rarefied gas between concentric cylinders, using modified discrete ordinate method based on BGK model equation 01 p0182 A71-11405
- Inverse problems for parameters and optimal heat transfer model in thermophysical processes 02 p0331 A71-11731
- Heat transfer to walls of quartz discharge tube in Ne, Ar and Xe, measuring integral energy flux 02 p0290 A71-12191

- Circular pipe gas laminar flow at constant wall temperature, determining heat exchange and drag by motion and energy equations integration in boundary layer approximations 02 p0240 A71-12192
- Thermionic diode with integral guard ring, measuring emitter and collector work functions and heat transfer 02 p0195 A71-12236
- Body heat loss in water immersion, using heat transfer model 02 p0207 A71-12387
- Uniform magnetic field effects on electroconducting fluids turbulent flow and heat transfer characteristics 02 p0293 A71-12649
- Heat transfer analysis literature survey, including bibliography of perturbation, asymptotic and integral equations methods 02 p0333 A71-12650
- German monograph on heat transfer in Prandtl-Bjerring fluid flows through flat channels with allowance for dissipation and asymmetrical thermal boundary 02 p0241 A71-12675
- Geometry and oncoming boundary layer characteristics effects on heat transfer rate in reattached wall of cavity exposed to hypersonic flow 03 p0517 A71-13464
- Heat transfer - ASME/AICHE Conference, Minneapolis, August 1969 03 p0518 A71-13614
- Vaporization heat transfer mechanism from capillary wick covered heated surface, considering applicability to heat pipes 03 p0353 A71-13615
- Horizontal cylindrical heaters heat transfer to pool boiling Hg at heat fluxes up to burnout [ASME PAPER 70-HT-8] 03 p0519 A71-13698
- Laminar boundary layer downstream heat transfer to sharp and blunt nosed isothermal flat plates under upstream mass injection, discussing insulating effect [ASME PAPER 70-HT-1] 03 p0519 A71-13700
- Boltzmann equation solution for isotropic heat velocity distribution in molecular gas kinetics 03 p0401 A71-13907
- Tissue cooling with liquid nitrogen, determining film boiling transition temperature and heat transfer rates [ASME PAPER 70-WA/HT-16] 03 p0372 A71-14096
- Heat transfer and fluid friction of hydrogen and helium gas flows undergoing turbulent to laminar flow transition in heated pipe [ASME PAPER 69-HT-54] 03 p0405 A71-14291
- Downstream heat transfer and wall friction predictions for quasi-developed strongly heated turbulent pipe flow, using mixing length model [ASME PAPER 70-HT-8] 03 p0405 A71-14294
- Nuclear rocket nozzle cooling passages, discussing heat transfer and friction correlations for single-phase hydrogen turbulent flow [AIAA PAPER 70-661] 03 p0456 A71-14444
- One dimensional steady heat transfer in rarefied gas between infinite parallel laws, using Boltzmann kinetic equation 03 p0462 A71-14570
- Flow characteristics behind reflected shock wave flow and heat transfer at tube wall, noting unsteady and nonlinear effects 04 p0567 A71-14665
- Heat transfer correlations for turbulent flow in ducts with rough surfaces 04 p0674 A71-14778
- Coolants Prandtl number effect on pressure drop, heat transfer and friction of rough surfaces 04 p0675 A71-14779
- Surface roughness effects on gas to wall heat transfer in conical converging diverging nozzles, using heated air 04 p0675 A71-14780
- Heat transfer and pressure drop in air flowing in square tube with two dimensional discrete turbulence promoters applied to opposite walls 04 p0675 A71-14781
- Heat transfer intensification under forced one and two phase flow in channels 04 p0675 A71-14782
- Gas to gas film cooling, describing physical processes and performance prediction method based on heat and mass transfer analogy 04 p0676 A71-14978
- Heat transfer to concentric annular turbulent mercury flow, determining wetting effect, velocity profiles, eddy diffusivity of momentum transfer and friction factors 04 p0570 A71-15172
- Soviet book on friction and heat transfer covering interaction of bodies with internal/external liquid/gas laminar/turbulent boundary layer flows 04 p0571 A71-15264
- Wave formation behavior on melting surface of flat plate in heated air stream 04 p0678 A71-15455
- Bulk solids melting on inclined plane heated surface, investigating heat transfer and mass flow rates, fluid driving force and pressure gradient 04 p0678 A71-15456

- Transient heat transfer in fins undergoing phase transformation, obtaining approximate solution to temperature distribution and interface motion by perturbation technique 04 p0678 A71-15457
- Living human tissue thermal behavior analytical modeling including internal heat generation and blood flow effects 04 p0539 A71-15460
- Heat transfer differential equations numerical solution, using latin square experimental design plans for reducing repetitions 04 p0678 A71-15461
- Heat transfer through phase change in metallic heat carrier exposed to strong centrifugation encountered turbine blades 04 p0639 A71-15462
- Heat transfer in laminar MHD boundary layers on moving flat plate in magnetic field 04 p0635 A71-15468
- Linearized equation for stability and heat transfer of two dimensional incompressible laminar boundary layer in water flow 04 p0679 A71-15469
- Temperature distribution and heat transfer across transitional separated shear layer under subsonic air flow, using interferometric measurements 04 p0679 A71-15470
- Heat transfer measurements in thin water films on brass tube, using electrically heated elements 04 p0680 A71-15475
- Turbulent boundary layer equations for heat and mass transfer in incompressible and compressible flows, using eddy viscosity formulation 04 p0680 A71-15479
- Free stream turbulence enhanced stagnation line heat and mass transfer on two dimensional blunt body 04 p0681 A71-15481
- Turbulent compressible two dimensional boundary layer flows with heat transfer, pressure gradients and wall blowing or suction 04 p0681 A71-15482
- Air flow turbulence effect on heat transfer and boundary layer growth around flat plate, aerodynamic profile and cylinder 04 p0681 A71-15483
- Started supersonic axisymmetric parallel diffuser, examining wall static pressure and heat transfer 04 p0528 A71-15489
- Supersonic compressible turbulent boundary layer on porous cylinder with air injected through wall, investigating heat transfer 04 p0571 A71-15498
- Uniformly blown turbulent boundary layer on flat plate, investigating unheated solid starting length effect on heat transfer 04 p0572 A71-15500
- Nonuniform blowing and surface temperature turbulent boundary layer, investigating heat transfer 04 p0684 A71-15502
- Heat transfer in flat plate, considering acoustic resonance vibration effect 04 p0684 A71-15505
- Laminar boundary layer on porous plane plate situated in plasma jet, examining transfer phenomena with chemical reaction 04 p0572 A71-15507
- Viscous incompressible MHD fluid steady laminar flow past semiinfinite flat plate, noting heat transfer characteristics 04 p0635 A71-15508
- Thermal conductive liquid hydrodynamic stabilized Hartmann flow in rectangular canal with transverse field, examining magnetic effect on heat transfer 04 p0635 A71-15509
- Heat transfer - Conference, Versailles, August-September 1970, Volume 4, Natural convection and rheology 04 p0685 A71-15521
- Heat transfer - Conference, Versailles, August-September 1970, Volume 5, Boiling 04 p0686 A71-15522
- Turbulent film boiling on vertical surfaces, proposing theoretical model with interfacial wave disturbances taken into account for heat transfer calculation 04 p0686 A71-15523
- Subcooled nitrogen tube flow film boiling, investigating heat transfer and hydraulic resistance 04 p0687 A71-15533
- Heat transfer - Conference, Versailles, August-September 1970, Volume 6, Boiling and condensation 04 p0687 A71-15533
- Translatory vapor bubbles motion in binary liquid mixtures under heat and mass transfers 04 p0687 A71-15533
- Liquid-vapor system in closed container, investigating transient pressure rise under heat and mass transfer interactions including incipient and nucleate boiling 04 p0687 A71-15533
- Cryogenic liquids boiling peculiarities concerning heated surface material thermophysical properties effects on cavity stability, density and heat transfer rate 04 p0688 A71-15533

- Heat transfer - Conference, Versailles, August-September 1970, Volume 7, Combined heat transfer and measuring techniques
04 p0688 A71-15540
- Nonlinear integrodifferential equations of heat and mass transfer problems, discussing asymptotic solution method
04 p0688 A71-15542
- Friction, mass and heat transfer in turbulent boundary layers of fluid flows past obstacles
04 p0577 A71-15619
- Heat transfer boundary conditions determination in studying heat protective coatings effectiveness, discussing measurement methods for stagnation temperatures and heat fluxes from exhaust gases
04 p0600 A71-15643
- Soviet book on fundamentals of heat transfer theory covering thermodynamic equations, steady, unsteady, turbulent, incompressible and MHD flows, etc
05 p0831 A71-16196
- Heat transfer from finite flat plate in channel flow for vanishing Prandtl number, using Fourier transform and Wiener-Hopf technique
05 p0837 A71-16710
- Rarefied gas Couette flow between concentric cylinders and heat transfer from wire to external cylinder, applying momentum method
05 p0736 A71-16723
- Air injection into turbulent boundary layer flow through porous plate, examining heat transfer and shielding efficiency
05 p0838 A71-16783
- Longitudinal turbulent air flow past plate, applying heat transfer and drag calculations
05 p0838 A71-16784
- Laminar or turbulent chemically reacting gas mixture flow in circular tube, examining heat transfer with enthalpy equation
05 p0838 A71-16791
- Steady diabatic inviscid gas flow properties, emphasizing vortex lines geometry
05 p0839 A71-17047
- Soviet book on supersonic turbulent boundary layer covering gas flow molecular theory, heat and mass transfer at porous surfaces, etc
06 p0841 A71-17439
- Laminar pulsating ducted flow heat transfer, taking into account velocity distribution time dependence
06 p1005 A71-17682
- Injection film cooling effect on surface heat transfer downstream of flush non tangential injection holes and slots in turbine applications
06 p0945 A71-17695
- Gas-particle mixture cascade flow over turbine blades, considering momentum/heat transfer and particle trajectories
06 p0841 A71-17701
- Plane incompressible MHD boundary layer on porous plate, considering heat and mass transfer in blowing or suction velocity distribution
06 p0936 A71-17736
- Anomalous viscous fluid in channel with nonconducting walls, considering magnetic field effect on heat transfer
06 p0937 A71-17738
- Infinite elastic plate with rectilinear crack, determining heat exchange effect on thermoelastic stresses
06 p1000 A71-17939
- Mesosphere and lower thermosphere heat input rates and circulation, calculating worldwide average eddy diffusion coefficient
06 p0892 A71-17978
- Gas turbine cascade radial gap inverse heat transfer, calculating release coefficients
06 p1006 A71-18002
- Unsteady heat transfer in nonlinear systems, solving hyperbolic equation by net-point method
06 p1006 A71-18006
- Cellulose, explosives and propellants thermal surface ignition, using heat transport and chemical kinetic equations
06 p0944 A71-18298
- Heat transfer from rotating disk to parallel nonrotating disk, investigating turbulence effect from air flow pattern observation
06 p1007 A71-18315
- Thermal resistance to heat transfer at interface between hard smooth flat surface and softer turned surface
06 p1008 A71-18537
- Plasma torch stagnation point heat transfer measurements, using heat pipe calorimetry
06 p0902 A71-18538
- Finite difference calculation for two dimensional compressible turbulent boundary layer flow with heat transfer, using mixing length concept
06 p0885 A71-18607
- Nonadiabatic compressible turbulent boundary layer heat transfer to rough surfaces under arbitrary pressure gradient
06 p0885 A71-18608
- Heat and mass transfer in turbulent boundary layers
Conference, Herceg Novi, Yugoslavia, September 1968, Volume 1
07 p1219 A71-18751
- Turbulent boundary layer theories and classification according to prediction ability relative to heat transfer rates, shear stress distribution and fields of concentration
07 p1085 A71-18752
- Turbulent boundary layer approximate analytical method based on momentum and energy integral correlations and limiting laws of friction and heat transfer
07 p1085 A71-18756
- Transpiration cooling heat transfer in incompressible turbulent boundary layer, using Couette flow model, boundary layer model and combinations of both
07 p1219 A71-18758
- Heat transfer and thermal entrance length in annular channel with rounded and sharp inlet edges
07 p1220 A71-18763
- Heat transfer in turbulent boundary layer for arbitrary surface temperature with fluid injection and pressure gradient
07 p1220 A71-18765
- Wall flow boundary layer, observing external turbulent field effect on velocity and temperature distribution and heat exchange
07 p1086 A71-18771
- Turbulent wall flow, observing flux and heat transfer conditions with stroboscopic visualization
07 p1105 A71-18782
- Heat transfer from circular cylindrical hot wire and film anemometer probes, examining calibration steadiness
07 p1106 A71-18783
- Heat and mass transfer investigation in nucleate boiling boundary layer by salt depositions
07 p1221 A71-18787
- Post burnout heat transfer to mist flow for nuclear reactor design, using two step model
07 p1221 A71-18789
- Boiling in two-phase layer on heated wall in relation to thermal exchange mechanisms
07 p1221 A71-18790
- Binary fluids boiling heat and mass transfer in boundary layer, discussing bubble growth rate, surface roughness effects and burnout heat flux
07 p1221 A71-18791
- Flux divergence in optically thin outer layers of model moving stellar atmospheres using weighting functions in energy balance equation
07 p1190 A71-18863
- Approximate bridging relations for heat transfer, surface shear and drag in transitional regime between free molecule and continuous flows
07 p1087 A71-18894
- Inhomogeneous heat transfer lines analysis by matrix method in form of power converging series by Laplace operator
07 p1221 A71-18925
- Dissociating airflow over two dimensional blunt body, determining laminar boundary layer chemical reaction suppression effects on heat exchange
07 p1015 A71-19748
- Rarefied gas flow and heat transfer in plane Couette flow using Bhatnagar-Gross-Krook model with ellipsoidal distribution
07 p1224 A71-20024
- Viscous incompressible fluid flow between two cofocal elliptic cylinders, discussing temperature distribution and heat transfer in annulus
07 p1224 A71-20029
- MHD Couette flow at stationary plate under transverse magnetic field, discussing effect on heat transfer between electrically conducting walls
07 p1170 A71-20099
- Turbulent transfer model in wall region, estimating mean surface renewal frequency for mass momentum and heat transfer rates and velocity, temperature and concentration profiles
07 p1092 A71-20224
- Density distribution, heat transfer and drag measurements in rarefied Ar cylindrical Couette flow, comparing results with Navier-Stokes and Burnett equations solutions
07 p1093 A71-20286
- Gas-particle mixture cascade flow over turbine blades, considering momentum/heat transfer and particle trajectories
07 p1017 A71-20311
- Turbulent pipe flow, developing analogy between momentum and heat transfer
07 p1224 A71-20371
- Stationary longitudinal turbulent flow of air with equilibrium ionization and dissociation around plate, calculating heat exchange and frictional drag
08 p1228 A71-21922
- Turbulent air flow in cooled tubes, studying local heat transfer and hydraulic resistance
08 p1377 A71-21924
- Thermodynamic system with concentrated loads due to heat and mass transfer or chemical reactions, analyzing wave processes and system stability
09 p1544 A71-22269
- French book on hypersonic aerodynamics covering aerothermochemistry, flow equations, heat transfer, etc
09 p1382 A71-22278
- Book on dynamic characteristics of aerosol particles in terms of classical mechanics covering continuum approximation, single particles heat and mass transfer, diffusion, dispersion, etc
09 p1431 A71-22284
- Heat transfer in rarefied gases, discussing applicability of molecular-kinetic gas theory
09 p1544 A71-22287
- Laminar steady flow and heat transfer of viscous heat conducting gas moving between coaxial cylinders, using Runge-Kutta method
09 p1431 A71-22408
- Rarefied gases heat transfer and density distribution between parallel plates at different temperatures
09 p1432 A71-22854
- Diffusion-ion capture and heat transfer by phonons in solid and liquid metals
09 p1494 A71-22882
- Heat transfer to slender bodies in hypersonic flow, comparing wind tunnel measurements with modified reference enthalpy method predictions for laminar and turbulent flow
09 p1545 A71-22941
- Axisymmetric steady diabatic flow equations exact solutions
09 p1434 A71-23545
- Gas turbine blades local heat transfer, correlating experimental surface temperature, heat transfer coefficient and internal coolant temperature with theoretical estimates
09 p1547 A71-23658
- Book on homogeneous flows aerothermochemistry covering chemical reactions, heat and mass transfer, entropy production, species continuity, momentum and energy equation
09 p1547 A71-23674
- Classic fourth and lower order Runge-Kutta formulas with stepsize control, applying to heat transfer problems
10 p1636 A71-23924
- Turbulent characteristics of circular subsonic free jet impinging normal to flat plate, measuring heat transfer rates
10 p1694 A71-23951
- Thermal ignition theory review, discussing mathematical problem statement, ignition characteristics approximate calculation methods, heat transfer mechanisms, geometrical and critical conditions, experimental tests, etc
10 p1695 A71-24050
- Book on heat transfer measurement techniques, discussing cryogenic temperature measurements, optical, spectroscopic and probe methods
10 p1695 A71-24187
- Intelsat 4 satellite transponder, examining receivers, transmitters, mechanical stability and heat transfer
10 p1578 A71-24509
- Heat transfer in cylindrical cavity with circulating flow as function of time and Peclet number
10 p1696 A71-24615
- Heat transfer at high Peclet number from sphere freely rotating in shear flow field at low Reynolds numbers
10 p1697 A71-24621
- Soviet book on physics of interaction between atmosphere and ocean covering heat transfer, wave formation, vertical mixing in upper sea layer, etc
10 p1639 A71-24671
- Low Prandtl number laminar compressible boundary layer flow over flat plate, obtaining recovery temperature profile and heat transfer by matched asymptotic expansions method
10 p1597 A71-25066
- Uniform surface blowing effects on hypersonic boundary layer with viscous interaction, calculating heat transfer on flat plate and slender wedge
10 p1598 A71-25096
- Heat and mass transfer in supersonic laminar boundary layers with light gas injection, deriving approximate solution for binary mixture flow with variable fluid properties
10 p1598 A71-25097
- Axisymmetric incompressible boundary layer flow, temperature distribution and heat exchange near critical point of rotating body with varying surface temperature
11 p1854 A71-25239
- Papers on heat transfer and spacecraft thermal control covering solid-vacuum interfaces thermal and visible radiation properties, multilayer insulation, thermal control devices, etc
11 p1854 A71-25360
- Compressible similar laminar boundary layer equations for zero wall shear and mass addition, describing heat transfer reduction and boundary layer growth by asymptotic analysis
11 p1750 A71-25479
- Lateral heat transfer along parallel conducting and radiating plates spaced by absorbing and isotropically scattering dielectric
11 p1788 A71-25524
- In-pile tests of multielement thermionic converter with Mo- and W-based alloy cathodes, noting output electric power dependence on internal heat release
11 p1711 A71-25877

Cross flowing air stream effects on heat transfer characteristics of single lines of air jets impinging on plane surfaces

11 p1854 A71-25947

Heat transfer in Couette flow with/without injection, taking into account wall conduction effects

11 p1856 A71-26049

One dimensional premixed turbulent flame energy equation as function of heat release rate curve, temperature, velocity, composition and density

12 p1985 A71-26741

Heat transfer in laminar free-convection boundary layers adjacent to plane and axisymmetric walls at constant temperature, deriving skin friction and mass flow rate

12 p1985 A71-26941

Rocket propulsion systems local heat transfer investigation, comparing experimental data to Bartz formula estimates over wide combustion chamber pressure range

12 p1945 A71-26983

Equilibrium air boundary layer flows at three dimensional stagnation points, discussing flow characteristics and real gas heat transfer parameters

12 p1866 A71-27582

Laminar boundary layers with large wall heating and flow acceleration, considering heat transfer parameter increase

12 p1987 A71-27589

Longitudinal solid surface curvature effects on heat transfer, calculating velocity and temperature fields by similarity analysis via boundary layer equations

12 p1987 A71-27737

Unsteady one dimensional time-dependent diabatic gas flow equations reduced to single partial differential equation, deriving solutions for entropy distribution

13 p2158 A71-27829

Heat exchange at large Prandtl numbers near porous flat wall with liquid injection, calculating Stanton number

13 p2046 A71-28181

Heat and mass transfer in monatomic molecular gases and gas mixtures, discussing energy exchange during collision and thermal diffusion effect on thermal conductivity

13 p2159 A71-28186

Local and mean heat transfer at initial thermal segment for stabilized turbulent air flow in circular tubes and rectangular channels

13 p2159 A71-28419

Collisionless plasma thermal shock wave, showing heat in electron component transportable along magnetic field at lower rates than thermal velocity

13 p2106 A71-28425

Two dimensional turbulent boundary layer before rectangular step, investigating heat exchange in separation regions

13 p2048 A71-28572

Local heat transfer in tubes under nonstationary conditions, calculating coefficients from wall temperature gradient at surface

13 p2160 A71-28587

Reynolds analogy of heat transfer applied to disk rotating near stator, including frictional dissipation and radial outflow in compressible or incompressible flow

13 p2048 A71-28599

Laminar free convection heat transfer in vertical rectangular corner, considering velocity and temperature distribution

13 p2161 A71-28621

Optimal control synthesis of one dimensional stochastic heat and mass transfer processes with distributed parameters

13 p2161 A71-28727

Combustion and heat transfer in gas turbine systems - Conference, Cranfield, England, April 1969

13 p2116 A71-28739

Monograph on heat transfer from rotating heated surface with induced turbulent boundary layers covering disk, cone and sphere geometries

13 p2162 A71-28882

Two phase critical flow of one component mixtures in nozzles, orifices and short tubes, considering interphase heat, mass and momentum transfer rates

13 p2049 A71-28980

Heat and mass transfer in triple interline region of stationary evaporating meniscus on flat plate immersed in liquid pool

13 p2164 A71-29006

Exact method for low Peclet number thermal entry region heat transfer in channel flow, considering transverse nonuniformity of fluid velocity and axial conduction

13 p2164 A71-29009

Sensible heat meridional transport frequency spectra wavenumber in Southern Hemisphere midtroposphere

13 p2063 A71-29108

Flow and heat transfer measurements in dihedrons simulating patterns about supersonic conical edge and shock wave interaction line, using thermodynamic-coating technique

13 p1992 A71-29174

Heat transfer on spheres and sharp cones in rarefied hypersonic gas flow at zero angles of attack in wind tunnel vacuum

13 p1992 A71-29176

Air stream injection from circular hole in flat plate into supersonic flow, measuring heat transfer

13 p1992 A71-29184

Structural model of mature hurricane, determining heat and moisture transfer, boundary layer dynamics and thermodynamic balance

13 p2097 A71-29250

Turbulent gas flow through duct with alternating pressure gradient, considering heat transfer and frictional resistance

13 p2166 A71-29370

Heat transfer within resonant cavities at subsonic and supersonic flow, discussing wind tunnels, test procedures and data reduction

[ASME PAPER 71-FE-9]

13 p2166 A71-29450

Heat transfer through human peripheral tissue based on one dimensional steady state continuum model combining effects of conduction, convection, vascular heat exchange and metabolism

13 p2025 A71-29502

IR radiation role in limiting central heater maximum temperature and heat transfer to high density oxygen in cryogenic storage systems

13 p2166 A71-29505

Spacecraft propane boiler system, obtaining heat transfer behavior under simulated aerospace conditions

14 p2319 A71-29726

Mass injection effect on heat transfer reduction to three dimensional stagnation points as function of shape, enthalpy and gas properties

14 p2335 A71-29891

Shock tube high temperature air viscosity from laminar boundary layer heat exchange data

14 p2224 A71-30047

Heat exchange and temperature distribution between two liquids divided by plate, discussing possible errors

14 p2335 A71-30048

Heat and mass transfer optimization in hydrogen-oxygen fuel cells with ion exchange membrane

14 p2181 A71-30050

Papers on heat transfer covering theoretical and experimental heat transfer in liquids, gases and liquid-solid interfaces, transport phenomena, heat pipes, electrochemical method, etc

14 p2336 A71-30240

Heat transfer near critical point, examining continuity, momentum and energy equations for variable thermodynamic and transport properties effects

14 p2336 A71-30241

Heat transfer in rarefied gases, considering gas at rest between flat plates, concentric spheres and cylinders and flowing through tubes, nozzles and between parallel plates

14 p2336 A71-30242

Heat transfer processes in heat pipes, examining heat and mass transport mechanisms between heat source and sink

14 p2336 A71-30243

Thermal boundary layer instability near heated vertical flat plate in poorly conducting liquid under horizontal DC electric field

14 p2337 A71-30407

Extended flat body thermal conductivity determination by local heating at constant heater helix temperature

14 p2338 A71-30622

Cooling effectiveness of liquid film barrier injected into rocket thrust chamber with vortex motion, considering heat transfer and performance

[AIAA PAPER 71-676]

14 p2291 A71-30740

Numerical heat transfer and wall friction results, demonstrating gas transport property variation effects on three laminar flow situations

14 p2338 A71-30931

Surface renewal and penetration model in heat and momentum transfer analogy for incompressible turbulent boundary layer flow

14 p2227 A71-30935

Heterogeneous detonations literature review, indicating need for research on heat transfer processes in subsonic and supersonic flows

15 p2511 A71-31387

Circular pipe gas laminar flow at constant wall temperature, determining heat exchange and drag by momentum and energy equations integration in boundary layer approximations

15 p2388 A71-31498

Heat transfer and pressure drop characteristics of He in two phase and supercritical flow, calculating He heat exchangers for superconductive devices

[HEAT EXCH. CONF. PAPER 24]

15 p2513 A71-31638

Heat transfer surfaces performance measurements, considering tube bundles with fluid flow perpendicular to tube generatrices

[HEAT EXCH. CONF. PAPER 25]

15 p2383 A71-31639

Single phase and evaporative systems for liquid cooling high temperature gas turbine rotor blades - reviewing heat transfer performance evaluation

15 p2469 A71-31711

Surface roughness effects on heat transfer to ablating cones, using calculation method adaptable to computer routines for smooth wall

15 p2514 A71-32060

German monograph on viscous fluids heat transfer in pipes covering Prandtl number dependence, turbulent boundary layer flow and transition areas

15 p2514 A71-32060

Boiling at solid heated surfaces, discussing nucleation, bubble formation, pool boiling factors, heat transfer correlation and forced convection

15 p2515 A71-32061

Heat transfer through stationary monatomic rarefied gas in annular space between coaxial cylinders using two-flow Maxwellian function for approximate molecular velocity distribution

16 p2661 A71-32872

Gas cooled porous plate unsteady temperature field during high temperature action, considering thermal radiative, convective and mixed radiative-convective heat transfer

16 p2662 A71-32872

Heat transfer, density and pressure measurements of hypersonic two dimensional centered nonequilibrium corner expansion oxygen flow with frozen boundary in shock tunnel

16 p2555 A71-32900

Temperature fields and mass and heat transfer in surface of solid spherical particle in laminar viscous fluid flow

16 p2557 A71-32931

Plasma heat transport associated with matter, momentum, energy and electrical charge transfer

16 p2617 A71-32951

Air injection into turbulent boundary layer flow through porous plate, examining heat transfer and shielding efficiency

16 p2662 A71-33070

Heat transfer and drag calculations in longitudinal turbulent air flow around plate with constant or variable physical properties

16 p2662 A71-33070

Laminar or turbulent chemically reacting gas mixture flow in circular tube, examining heat transfer with enthalpy equation

16 p2662 A71-33070

Two dimensional steady gas flows with heat addition, using reduction to partial differential equations

16 p2662 A71-33166

Hot-wire anemometers design and operation in fluidics, discussing temperature gradient due to heat transfer effects

16 p2579 A71-33434

Thermoelastic critical equilibrium of plate with rectilinear crack under heat transfer from edge surface and tensile stress

16 p2658 A71-33688

Linear heat transfer boundary value problem series solution in Cartesian and cylindrical coordinates systems

16 p2663 A71-33900

Dynamic bubble growth and diameter at detachment during liquid boiling at heating surfaces, using force equilibrium, laser Mach-Zehnder interferometer and temperature measurements

16 p2663 A71-34030

Heat transfer in interstitial solid solutions, interpreting thermal diffusion measurements in transition metals mixed crystals

16 p2599 A71-34099

Nonlinear heat transfer in plane rarefied isothermal Couette gas flow, using BGK model

16 p2561 A71-34141

Uniform shear flow past semiinfinite flat plate, studying diffuse and heat transfer near leading edge

16 p2561 A71-34166

Transient matrix heat transfer test data reduction discussing direct curve matching methods implementation by distance function minimization

17 p2835 A71-34177

Gas and liquid drop laminar, transition and turbulent flows heat transfer intensification in circular tubes applying to hydraulic resistance design

17 p2835 A71-34200

Heat transfer and hydraulic resistance in cross flow heat exchanger with slitlike channels

17 p2836 A71-34211

Heat and mass transfer during deposition on heated surfaces in nonisothermal gas flow with suspended solid particles, using motion of continuous Newtonian medium

17 p2836 A71-34300

Lateral surface heat transfer effect on thermophysical characteristics in thin layer coatings, discussing temperature gradients in corundum and zirconium oxide on copper

17 p2836 A71-34300

Transverse magnetic field influence on heat transfer of conductive fluid/mercury in electrically insulated pipe subjected to uniform heat flux

17 p2788 A71-34600

German monograph on heat transfer from vertical heating surfaces to liquids at rest in nucleate boiling, showing microstructure interaction with interfacial tension 17 p2838 A71-34852

Laminar constant pressure boundary layer hypersonic limits, estimating skin friction and heat transfer 17 p2728 A71-34885

Heat exchange between atmosphere and earth surface, calculating nonadiabatic term size and spatial distribution 17 p2734 A71-35193

Stationary longitudinal turbulent flow of air with equilibrium ionization and dissociation around plate, calculating heat exchange and frictional drag 17 p2671 A71-35266

Turbulent air flow in cooled tubes, studying local heat transfer and hydraulic resistance 17 p2838 A71-35268

Supersonic aircraft propulsion by external heat addition, discussing numerical method for suitable caret wing design 17 p2793 A71-35398

Clear air turbulence in midstratosphere, analyzing heat and momentum transports and temperature fluctuations spectra 18 p2943 A71-36008

Soviet papers on gas dynamics and heat transfer covering turbulent boundary layers, supersonic ideal-gas jets, rocket exhaust base pressure, base flow characteristics, etc 18 p2902 A71-36111

Green functions difference interpretation for finite and semiinfinite heat receiving rods, using dimensionless unsteady heat transfer parameter 18 p2985 A71-36124

R and C parameters determination for electric circuit simulating heat transfer in rod by amplitude-frequency characteristics 18 p2985 A71-36125

Force and heat transfer measurement in hypersonic flows of low gas density, using electromagnetic balances for horizontal and vertical forces and pendulum method for measuring resistance 18 p2921 A71-36416

Laminar hypersonic boundary layer equations, calculating heat transfer and shear stress in stagnation point 18 p2847 A71-36428

Space shuttle aerothermodynamics, discussing heat transfer measurements, phase change patterns, electron beam flow visualization and boundary layer transition 18 p2847 A71-36430

Weightless environment effects on fluid behavior and heat transfer in life support systems, obtaining analytical models [AIAA PAPER 71-864] 18 p2909 A71-36652

Asymptotic solution of nonlinear Volterra integral equation, examining nonlinear heat conduction and boundary layer heat transfer 18 p2942 A71-36747

Turbulent rotating tube flows kinematic similarities, deriving heat and mass transfer, swirl damping and axial and rotational velocity profile 19 p3043 A71-37127

Boiling heat transfer to cryogenic fluids, considering pool convective, nucleate, film and forced convective subcooled boiling 19 p3162 A71-37463

Heat transfer and drag during air laminar flow in circular pipe with constant heat flux density at wall 19 p3044 A71-37585

Heat transfer due to combined free and forced convection in horizontal isothermal tube flow [ASME PAPER 71-HT-3] 19 p3163 A71-37981

Gravity effect on developing laminar flow with forced convection in vertical isothermal tube, investigating velocity and temperature profiles and heat transfer rate [ASME PAPER 71-HT-6] 19 p3164 A71-37983

Curvature effect on heat and mass transfer from isothermal sphere in potential flow [ASME PAPER 71-HT-7] 19 p3164 A71-37984

Free stream turbulence effects on local heat transfer from sphere situated in forced convection air flow [ASME PAPER 71-HT-8] 19 p3164 A71-37985

Heat and mass transfer through porous plate into turbulent two dimensional incompressible boundary layer, using van Driest damped mixing length [ASME PAPER 71-HT-10] 19 p3045 A71-37986

Brazing roughness effects on rectangular plate fin heat exchanger surfaces heat transfer and flow friction characteristics, noting fin surface geometry influence [ASME PAPER 71-HT-29] 19 p3166 A71-37999

Vaporization heat transfer in saturated liquid capillary flow through wick structure, describing test facility and procedure [ASME PAPER 71-HT-35] 19 p3166 A71-38000

Heat transfer to transpired turbulent boundary layer, reviewing theoretical models and experimental results for friction coefficient and Stanton number [ASME PAPER 71-HT-44] 19 p3166 A71-38003

Thermal behavior simulation of cooling biological system, describing heat generation and transfer at nor-

mothermic to hibernating body temperatures with mathematical model 19 p3003 A71-38199

Cold climate clothed human windchill tables, considering various heat transfer modes and skin temperature 20 p3192 A71-39205

Heat transfer, fluid flow and pressure loss, noting application to cryogenic heat exchangers and process plants 20 p3312 A71-39245

Lateral heat transfer measurements in cryogenic multilayer insulation, considering effective thermal conductivity 20 p3312 A71-39272

Temperature decay method for determining superinsulation thermal conductivity, equating insulation heat transfer rate to calorimeter plate heat loss 20 p3312 A71-39273

Pressure, subcooling and diameter effects on heat transfer and circumferential flow transition of thin wire film boiling of liquid nitrogen in pool 20 p3313 A71-39284

Heat and mass transfer calculation in turbulent boundary layer on rough surface 20 p3315 A71-39793

Collisionless plasma thermal shock wave, showing heat in electron component transportable along magnetic field at lower rates than thermal velocity 21 p3421 A71-40083

Gas nature effect on wall temperature and heat transfer in Hartmann-Sprenger tube 21 p3366 A71-40102

Heat transfer of short hot wire normal to ambient incompressible air flow, using small perturbation energy equation 21 p3379 A71-40664

Long wavelength ion acoustic instability of two temperature collisional fully ionized plasma with heat transfer, noting additional destabilizing currents 21 p3422 A71-40708

Laminar and rotationally symmetrical flow of viscous incompressible fluid in circular pipe of constant temperature, considering inlet swirl effects and heat transfer to wall 21 p3368 A71-40756

Film boiling liquid hydrogen vertical flowing system, determining buoyancy effects on hydrodynamic and heat transfer characteristics 21 p3476 A71-40895

Heat transfer from incandescent platinum wires in saturated liquid nitrogen, examining film boiling from atmospheric to critical pressure 21 p3476 A71-40899

Unsteady state boundary layer equations solution in laminar flow systems with free surface and transfer of heat or mass 21 p3370 A71-40990

Two phase flow in asymmetrically roughened ducts, investigating secondary flow effects on heat transfer characteristics 21 p3477 A71-40995

Resonant oscillations effect on heat transfer across mixing length in cavities spanned by low speed turbulent shear layers 21 p3371 A71-41033

Flow rate and heating analysis of centrifugal pumps with variable cross section impeller blade ring inlet 22 p3554 A71-41850

Heat transfer and temperature field calculation in turbulent flows through channels of noncircular cross sections, allowing for secondary flow 22 p3619 A71-41871

Heat transfer from platinum wires in He and He-air mixtures, plotting Nusselt number variation with Reynolds number for various He concentrations 22 p3620 A71-41875

Spalding-Patankar numerical integration for heat transfer from air cooled disk rotating near stator, considering frictional heating, disk temperature distribution and nonunity Prandtl numbers 22 p3620 A71-41878

Centrifugally driven thermal convection in rotating cylinder of fluid heated from above, calculating heat flux through wall and effect on Nusselt number 22 p3620 A71-41879

Thin liquid films under simultaneous shear and gravity forces, noting data incorporation into transport equations for heat and mass transfer 22 p3620 A71-41884

Heat transfer and pressure distribution on biconic and hemispherical geometries with sharp and blunt noses in Mach 15-20 flow 22 p3480 A71-41964

Functional methods in numerical solution of heat transfer problems, including finite element and local variation methods 22 p3621 A71-42290

Approximate solutions to Stefan nonlinear heat and mass transfer problem under various boundary conditions and phase transformation temperature 22 p3622 A71-42687

Hypersonic nozzle convergent section heat transfer optimization by Euler method, using Lagrange undetermined multiplier and pipe flow approximation 22 p3622 A71-42781

Conical nozzle roughness on heat transfer in supersonic region 22 p3622 A71-42785

Macroscopic values of energy exchange between polyatomic gas and solid wall, considering heat transfer rate and wall temperature change 23 p3781 A71-43105

Plane diabatic Prim gas flow, reducing hodograph equations in elliptic regions to Cauchy-Riemann equations via Baeklund transformations 23 p3662 A71-43121

Heat transfer measurements in differentially heated fluid annulus for nonrotating and rotating flow 23 p3783 A71-43335

Viscous heating and non-Newtonian behavior of incompressible steady pipe flow with variable transport properties, using perturbation method 23 p3662 A71-43370

High temperature gas turbine engines rotor blades cooling, deriving generalized dimensionless relations for heat transfer data extension from static tests to operational conditions 23 p3718 A71-44066

Heat transfer characteristics of two phase nitrogen film boiling in tubes with tape-generated swirl flow 23 p3783 A71-44195

Slip, surface permeability and temperature gradient effects on surface friction and heat transfer in boundary layer near cylinder critical point 24 p3887 A71-44743

Heat and mass transfer in binary laminar boundary layer with free convection on vertical porous surface, integrating momentum and energy equations for upper limits 24 p3887 A71-44744

Laminar-turbulent boundary layer transition at Mach number 2-10, observing stabilizing effect of transition Reynolds number at increasing heat transfer intensity 24 p3818 A71-44745

Heat transfer in turbulent boundary layer separation zones ahead of step, using local flow parameters at wall boundary layer limit 24 p3887 A71-44746

Hydraulic resistance and heat transfer in annular channel with rotating flow, comparing to axial flow 24 p3888 A71-44747

Liquid flow and heat transfer in thermosiphons in centrifugal and Coriolis force fields 24 p3888 A71-44931

Heat transfer with dissipation from longitudinal surface curvature, numerically integrating all equations for parameters 24 p3889 A71-44968

Surface of revolution annular elements thermal radiation and heat exchange for propellant schematization, attachment to missile wall and opening into ambient medium 24 p3889 A71-44970

Compressible gas flow in two dimensional porous wall, calculating heat transfer and mass flow by conformal mapping for Laplace equation solution 24 p3889 A71-44972

Heat transfer - Conference, Versailles, August-September 1970, Volume 9 24 p3890 A71-45146

Heat transfer visualization, discussing shadowgraph, schlieren and interference methods 24 p3890 A71-45147

Federal German Republic heat transfer research programs at universities, institutes, chemical industries and in nuclear process engineering 24 p3890 A71-45149

Heat transfer in transpiration cooled porous heat sources, deriving dimensionless temperature profiles 24 p3891 A71-45185

HEAT TRANSFER COEFFICIENTS

Mean heat transfer coefficients determination at surface front of built-in alpha calorimeter from wall temperature data 01 p0179 A71-10611

Similar solution of strong shock wave propagation with nonequal heat coefficients, approximating energy of dissociation ionization and free molecular oscillation 01 p0070 A71-10663

Pipe bends effects on heat transfer coefficient of turbulent forced convection 02 p0330 A71-11650

Cylindrical wall with variable heat conductivity coefficient, solving temperature distribution by asymptotic method 02 p0333 A71-12540

Direct measurement of convective heat transfer coefficient by realizing proportionality to sublimation rate of naphthalene ball near body surface 04 p0545 A71-15158

Lifting body leeward surface maximum heat transfer coefficient in hypersonic flow, considering Reynolds number, incidence and shape effects 04 p0527 A71-15486

Single disk rotating in still air, calculating temperature profiles and local heat transfer coefficients
04 p0683 A71-15494

Liquid oxygen nucleate boiling in simulated reduced gravity fields, obtaining heat transfer coefficients, departure frequency and bubble growth rate
04 p0687 A71-15536

Dilatometric thermal expansion method for determining cylindrical solid body thermal conductivity coefficient
05 p0838 A71-16790

Polyatomic gases thermal conductivity coefficient, examining magnetic field effect
06 p1005 A71-17316

Thermal shock physiological effects, determining skin-air convective heat exchange coefficient
06 p0860 A71-18190

Unsteady temperature fields in thin anisotropic plates with variable coefficient of heat exchange from side surfaces
06 p1009 A71-18730

Heat and mass exchange coefficients and critical separation for turbulent boundary layer during nonuniform blowing under nonisothermal conditions
07 p1087 A71-18918

Natural convection heat transfer coefficients from isothermal flat surfaces, using Boelter-Schmidt type heat flux meters
07 p1222 A71-18996

Closed axisymmetric vessel filled with viscous incompressible fluid, calculating integral heat release coefficients in free convection
07 p1222 A71-19196

Local turbulent friction factors and heat transfer coefficients for fluid flows through ducts of arbitrary cross section with prescribed wall heat flux distribution
07 p1224 A71-20654

Convective heat transfer coefficient for supersonic flow past sphere, considering kinetic heating by flow
08 p1378 A71-22047

Interlayer shear modulus relation to thermal conductivity coefficient in oriented glass fiber reinforced plastics
09 p1482 A71-22814

Temperature stress distribution in infinite plate with time varying heat transfer coefficient
10 p1687 A71-24197

Thin isotropic plates with time and temperature dependent surface heat exchange coefficients, presenting heat conduction equations
10 p1695 A71-24361

Duct thermal entrance region with axial conduction, evaluating laminar heat transfer rate with finite difference technique
10 p1696 A71-24409

Dutch monograph on nonstationary hot-wire method determining thermal conductivity coefficient of gases, using recorded temperature vs time relation
10 p1697 A71-24677

Temperature distribution in composite media sections involving solid interfacial sources, using Vodka orthogonality equations
10 p1697 A71-24694

Hot-wire anemometry for measuring velocity-temperature coefficients in turbulent flow with heat transfer
10 p1597 A71-25016

Mathematical model for heat transfer coefficients between two identical metal surfaces in contact
11 p1853 A71-25157

Oxygen and nitrogen thermotransport in transition metals by microindentation hardness testing for concentration determination
11 p1778 A71-25533

Heat transfer coefficients of various jet systems impinging on gas turbine blade inner surfaces, discussing cooling flow rates and solid particles injection into air flow
11 p1811 A71-25955

Uniformly and nonuniformly spaced circular cylinders contacting two planes, calculating conductive heat transfer coefficient under vacuum conditions
11 p1858 A71-26224

Pressure and wall temperature gradients effects on equilibrium enthalpy profiles and heat transfer coefficients of incompressible turbulent boundary layers, using eddy conductivity model
12 p1986 A71-27553

Resistance and heat transfer coefficients in hydrodynamically and thermally developed MHD pipe flow
12 p1941 A71-27740

Pyrolytic graphite heat conductivity coefficients in direction perpendicular to deposition surface at high temperatures
13 p2090 A71-27883

Two dimensional prediction of adiabatic wall temperature and heat transfer coefficient downstream of film cooling slots, using Prandtl mixing length forms
13 p2160 A71-28598

Transport coefficients interrelations, using irreversible process thermodynamics
13 p2161 A71-28620

Forced and free convective equations combination to represent combined heat transfer coefficients for horizontal cylinder
13 p2164 A71-28986

Gas flow heat loss through porous metals, deriving hydraulic resistance and heat release coefficients
13 p2165 A71-29218

Similar solution of strong shock wave propagation with nonequal heat coefficients, approximating dissociation, ionization and excitation energy of molecules vibrational degrees of freedom
14 p2228 A71-30996

Heated or cooled wall surface layers temperature anomaly, noting fluid-wall heat exchange coefficients
15 p2513 A71-31905

Low density collisionally ionized plasma at equilibrium, calculating permitted, forbidden and semiforbidden radiative cooling coefficients
15 p2460 A71-32776

Turbulent boundary layer growth over flat plate and compression corner model in hypersonic gun tunnels, measuring pressure and heat transfer rate distributions
16 p2554 A71-32880

Coolant thermophysical properties effect on heat transfer intensity in porous metals, analyzing differential equations
17 p2835 A71-34204

Undulating laminar and turbulent liquid film flows down vertical surface, determining velocity fields and local heat transfer coefficients
17 p2725 A71-34210

Convective heat exchange coefficient determination for human body immersed in turbulent water flow, using fractional calorimetry
18 p2858 A71-36862

Thyroidectomy and cold adaptation effects on hibernating hamsters thermoregulation and heat transfer coefficient
18 p2860 A71-36881

Heat transfer coefficients calculation for human body in cold water from heat balance equations, comparing with free convection coefficients in cross-flowing water
18 p2862 A71-36900

Moment and heat transfer coefficients for disks rotating in rarefied environment, noting transport characteristics decrease with increasing rarefaction
19 p3161 A71-37292

Air and jet fuel-air mixtures, calculating temperature dependent laminar and turbulent heat transfer parameters and transport properties
19 p3166 A71-38002

Detonation propagation through tubes with thin fuel film coated walls, obtaining heat transfer coefficients, friction, evaporation rate, reaction zone length and propagation velocity
19 p3171 A71-38129

Heat and mass exchange coefficients and critical separation for turbulent boundary layer with secondary fluid injection under nonisothermal conditions
20 p3210 A71-38897

Buoyancy effects on heat transfer coefficients in liquid nitrogen film boiling in vertical flow
20 p3313 A71-39286

Liquid-liquid or solid-liquid interface Leidenfrost film boiling, deriving heat transfer coefficient for liquid drop floating on cryogenic fluid
20 p3313 A71-39288

Film condensation heat transfer coefficients measurements on vertical heat pipes for cryogenic nitrogen, hydrogen and deuterium
20 p3313 A71-39290

Heat transfer rate correlation with local surface pressure for blunt cones at angle of attack
20 p3176 A71-39355

Blunt body heat transfer predictions for atmospheric reentry, discussing coupled effects of real gas behavior and slip/jump boundary conditions
21 p3474 A71-40256

Forced flow laminar film boiling heat transfer coefficients from vertical surface in terms of interfacial shear at liquid-vapor interface
21 p3476 A71-40896

Roughness role in liquid He-solid boundary thermal resistance, calculating heat transfer coefficient
21 p3416 A71-41122

Vertical heat transfer coefficient of flat and cylindrical walls in fluidized bed from wall vertical temperature distribution
23 p3783 A71-44069

Large volume liquid oxygen pool boiling, investigating heat exchange coefficient dependence on flux density and pressure
23 p3705 A71-44339

Composition effects on binary gas mixtures thermal conductivity coefficient, considering Hirschfelder-Eucken formula
24 p3886 A71-44369

Laminar heat transfer losses effects on piston gas heater performance, computing heat transfer rate and thermal boundary layer thickness
24 p3887 A71-44603

Gas/turbine casing heat transfer coefficient distribution
24 p3889 A71-45008

Polytropic process description for gas flow by introducing resistance and heat transfer coefficients
24 p3820 A71-45020

Ideal gases and binary monatomic gas mixtures heats of transport derivation from kinetic theory expressions for thermal transpiration
24 p3891 A71-45368

HEAT TRANSMISSION

NT AERODYNAMIC HEAT TRANSFER
NT CONDUCTIVE HEAT TRANSFER
NT CONVECTIVE HEAT TRANSFER
NT HEAT TRANSFER
NT HYPERSONIC HEAT TRANSFER
NT LAMINAR HEAT TRANSFER
NT RADIATIVE HEAT TRANSFER
NT SUPERSONIC HEAT TRANSFER
NT TURBULENT HEAT TRANSFER

Heat propagation rate effect on dynamic thermal stress distribution in thin plate, using Hankel and Laplace transforms
01 p0168 A71-10414

Thermal conductance of contacts between dissimilar solids with interstitial fluids, calculating heat flow direction effect by double constriction model
04 p0678 A71-15459

Heat flow in unidirectional solidification of vacuum cast alloy turbine blades, using analog thermal model
05 p0758 A71-16244

Transient heat flow mean and first moments prediction by discontinuous linear or quadratic trial functions and variations
05 p0831 A71-16491

Rectangular thin elastic plate with circular holes under heat flow, solving thermoelastic problem by point matching
05 p0823 A71-16492

Oceanic rise crest heat flow model, examining vertical velocity distribution of mass transport
06 p0889 A71-17635

Microwave energy dissipation as heat in eye, using agar for eye model construction
10 p1572 A71-25078

Collisionless heat propagation along plasma magnetic field, showing relation to ion sound velocity
13 p2107 A71-28568

Integral kinetic equation for flow distribution past body and surface heat flow, noting representation in form for computer solution
13 p1991 A71-29156

Closed circuit electrical, mass and heat flow stability analysis, showing capacities or inductances trace effects
16 p2607 A71-32991

Thermal distortion effect on heat flow between two contacting semiinfinite solids of different materials
17 p2837 A71-34691

Two dimensional dynamic thermal stresses in Al plate, allowing for Newtonian surface heat exchange
18 p2981 A71-36720

Chill level index for skin temperature effects on rate of evaporative heat loss and thermal information to central controller during heavy work
18 p2860 A71-36876

Thermal stresses and couples in micropolar elastic solid cavity and rigid inclusion during uniform heat flow
20 p3309 A71-39566

Ionospheric heating Q calculation of electron gas evaluating heat inflow at various altitudes
20 p3281 A71-39725

One dimensional propagation and multiple reflection of plane thermoelastic wave in Lamé elastic isotropic plate with finite heat transmission
22 p3615 A71-41911

Thermoviscoelastic problem for semiinfinite plate determining temperature field and stresses permitting heat propagation
23 p3780 A71-44223

Thermal stresses produced by steady heat flow in two layer plate simply supported at contour
24 p3886 A71-45363

HEAT TREATMENT

NT ANNEALING
NT MARAGING
NT NITRIDING
NT PULSE HEATING
NT STRESS RELIEVING
NT TEMPERING

Al alloys improved fatigue resistance via thermomechanical processing, considering microstructure and deformation characteristics
01 p0099 A71-10166

Discrete coatings, surface diffusion and thermomechanical surface treatments for metal fatigue strengthening
01 p0099 A71-10166

P-n junction formation in zinc mercury telluride samples, using heat treatment to control carrier concentration
01 p0140 A71-11466

Homogenization and dehomogenization phenomena at high temperature of Cr-Ni austenitic steels, discussing electron microscope microstructural examinations after heat treatment
01 p0105 A71-11611

- Cu-Ni-Mn alloys hardening by heat treatment, describing various critical temperature measurement methods and micrographic analysis 01 p0105 A71-11622
- Mechanical properties of Ti alloys subjected to rolling and heat treatment 02 p0265 A71-12522
- Reduction-elongation relation in plastic deformation of tensile test samples of Ti alloys subject to thermomechanical treatment 02 p0265 A71-12523
- Ni maraging steel cantilever beams intergranular stress corrosion cracking in aqueous solutions, noting heat treatment effects 02 p0267 A71-12881
- Refractory Nb alloys with high creep strength, good ductility and moderate density, heat treatment and workability 02 p0271 A71-12937
- Ta spectral emissivity in red and green and relationship to surface structure change induced by heat treatment 03 p0460 A71-14465
- Steels prior austenite and martensite grain size control by thermal cycling 03 p0446 A71-14492
- Heat, solution and cooling treatment of Ti-Al-V-Sn alloy for high strength and plastic properties 05 p0765 A71-16199
- Magnesium and manganese ferrite ion states under heat treatment using X ray and Mossbauer methods 05 p0793 A71-16832
- Hard metals and WC-Co alloy stress and heat treatment effect on coercive force, crack formation energy and abrasive resistance 06 p0911 A71-17342
- Forced convection over infinite periodically over-heated plane on basis of mesometeorological vertical wind velocity 06 p0923 A71-17515
- Alloy melting technique and heat treatment effects on elastic limit and modulus of elasticity 06 p0912 A71-17947
- Sintered Al-Ni-Co alloys, investigating magnetic properties and density after heat treatment 06 p0913 A71-18099
- Explosive metal welding bond interface, investigating heat treatment effect on microstructure 06 p0914 A71-18680
- Kinetics of transformation to long range ordering in Ni-V as function of heat treatment 07 p1131 A71-19433
- Volume spectra during heat treatment in metallic systems, using automatic dilatometry 07 p1112 A71-19613
- Alloying elements, mechanical working and heat treatment effects on vibration damping of Mg-Zr alloys, using Fastov device 07 p1136 A71-19634
- Glass fiber reinforced thermoplastics with increased room temperature mechanical properties, noting effect of heat, aging and chemical environment exposure 07 p1145 A71-19692
- Heat treatment and deformation effects on blended metal powder compacts homogenization, using mathematical model 07 p1137 A71-19976
- Mo-Re alloy wire structure and properties, observing heat treatment effect with metallographic techniques and X ray analysis 07 p1141 A71-20242
- High performance graphitized carbon/carbon composites, discussing mechanical properties improvement by fiber content optimization and heat treatment [PLASTICS INST. PAPER 37] 08 p1321 A71-20910
- Heat sterilizable separator material for development of heat sterilizable Ag-Zn batteries meeting contamination requirements in interplanetary exploration 08 p1235 A71-21095
- Thermomechanical treatment effects on microstructure and fracture toughness of extruded Beta III titanium alloy 08 p1313 A71-21558
- Composition, microstructure, heat treatment and properties of Ni alloy with high rupture strength and hot corrosion resistance for turbine blade applications 08 p1299 A71-21687
- Soviet papers on physics of metals and metallography covering residual stresses, energy dissipation after plastic deformation, heat treatment, etc 08 p1317 A71-21759
- Microstructure and mechanical properties of heat resistant alloy under homogenization and subsequent isothermal heat treatment 08 p1317 A71-21764
- Molybdenum Permalloy powder cores heat treatment effects on permeability, magnetic loss and brittleness control, using metallographic techniques 09 p1466 A71-22171
- Numerical analysis of winding and heat treatment effects on residual stress distribution in cylindrical glass fiber reinforced plastic products 09 p1482 A71-22816
- Cr steel cyclic strength and elastic properties after combined high temperature thermomechanical treatment and cold working 09 p1471 A71-23079
- Shallow conical shells local heat treatment, determining optimal temperature fields 09 p1546 A71-23084
- Fracture toughness relationship to microstructure in alpha-beta Ti alloy heat treated to constant yield strength, considering crack propagation 09 p1472 A71-23126
- Soviet book on metal alloys plasticity gaps covering crystallization, thermomechanical treatment, heat induced brittleness zones formation, etc 09 p1472 A71-23161
- Prediction of metals heat resistance increase by thermomechanical treatment, considering Ni-Al alloy 09 p1477 A71-23332
- Hot deformation of superrefractory austenitic Ni alloy, considering elastic and plastic limits 09 p1479 A71-23625
- Alloy and heat treatment effect on Ti bondability for adhesive bonded aircraft structure, using annealed and aged Ti-6Al-4V and Ti-6Al-6V-2Sn alloys for testing 10 p1615 A71-24093
- Macroheterogeneous carbon materials elastic characteristics during heat treatment process 10 p1634 A71-24203
- Oxidation resistant high temperature Ni-Al system preparation using powder metallurgy and thermomechanical treatments without sintering 10 p1626 A71-24401
- Carburized steel surface stresses and fatigue behavior, correlating stress distribution measurements and notched bar bending fatigue tests after several heat treatment steps 11 p1777 A71-25388
- Maraging steel structural analysis under heat treatment, noting age hardening time and temperature 11 p1778 A71-25855
- Fast heated titanium-vanadium martensite beta-phase transformations comparison with slow heated structures 11 p1782 A71-26472
- Gas turbine blades cast heat treated superalloys high temperature mechanical properties during aging 12 p1919 A71-27778
- Mechanical properties and heat treatment of Ti-V and Ti-V-Al alloys in quenched and quenched-aged states 13 p2083 A71-27872
- Beta stabilizers effect on mechanical properties of alpha structure Ti-Al-V alloys subjected to different heat treatments 13 p2083 A71-27874
- High flash point polyalkylene glycol base synthetic quenchants for high strength alloy heat treatment, noting application to aluminum, titanium and steel parts 13 p2073 A71-28144
- Vacuum heat treatment of brazed and diffusion bonded jet engine components near melting temperature 13 p2073 A71-28145
- Superconductive Nb-Al alloy critical temperature as function of chemical composition and heat treatment 13 p2085 A71-28576
- Postweld heat treatment cracking of high Ni alloys using mechanical testing and metallography 13 p2087 A71-29092
- Soviet book on aircraft materials science and treatment covering steel/cast iron processing, metallography, heat/thermochemical conditioning, surface protection and corrosion prevention 14 p2256 A71-29529
- Heat treatment effect on electrochemical behavior of Ni-Co-Mo maraging steel in sulfuric acid aqueous solution, studying anodic polarization 14 p2257 A71-29840
- Beta stabilizing Mo and Cr effects on mechanical properties of welded and heat treated Ti alloys 14 p2260 A71-30490
- Cast Nb-W-Mo-Zr-C alloys heat treatment effect on microstructure and phase composition, noting ductility improvement 15 p2426 A71-31406
- Fe-Ni alloys with Cr, investigating heat treatment effect on thermoelectric coefficient 15 p2426 A71-31482
- Aging of cast iron components by thermal shocks, considering heat treatment for machine elements dimensional stabilization 15 p2414 A71-31527
- Unidirectionally solidified Ti-base eutectic composites and alloys strength and microstructural stability under heat treatment 15 p2432 A71-32170
- Heat treatment effects on high strength maraging steel tensile, fracture toughness and stress corrosion properties, discussing reversion to austenite 15 p2433 A71-32175
- Al alloys high temperature thermomechanical treatment, discussing mechanical properties, enhanced plasticity and roughness 15 p2434 A71-32327
- Thermomechanical treatment effect on mechanical properties of high strength Al-Mg-Zn-Cu alloys, considering subsequent aging and state before deformation 15 p2434 A71-32328
- Heat treatment effectiveness in reducing residual stress from stress relaxation data analysis 15 p2436 A71-32506
- Complex alloyed steel under electroslog welding, investigating heat treatment effect on heat affected zone phase composition 15 p2437 A71-32661
- Optimum heat treatment for welds, investigating residual stress relief with higher harmonics method 15 p2417 A71-32664
- Alloying elements, mechanical working and heat treatment effects on vibration damping of Mg-Zr alloys 16 p2593 A71-33630
- Cyclic heat treatment effect on fine structure and properties of Mo single crystals in He atmosphere 16 p2595 A71-33885
- Austenitic high nitrogen chromium-nickel steels plastic deformation and heat treatment in plasma arc furnaces 16 p2596 A71-33910
- Thermal strain hardening influence on structural changes in coarse grain Ni under creep tests during heat treatment 16 p2598 A71-33990
- Composition transformations at interface levels in iron-nickel alloys as function of thermal treatment, using potentiokinetic method 16 p2598 A71-34050
- Recrystallization of heat treated Fe-Ni alloys microstructures after hammer hardening 16 p2598 A71-34051
- Electrodeposited Ni-Mo coatings corrosion resistance improvement by heat treatment, showing crystal structure degree of perfection role 16 p2599 A71-34052
- Reinforcing fiber weaknesses, considering stress concentrators, cracks and steps due to handling damage and interaction with contaminants during heat treatment 17 p2817 A71-34343
- Heat treatment effect on fracture behavior of aged Al alloy sheet, investigating toughness dependence on microstructure 17 p2756 A71-34486
- German book on welding conditions and material composition effects on structural changes and heat-affected zone mechanical properties of high strength structural steels 17 p2748 A71-34851
- Fiber volume content, fiber-matrix bonding, heat treatment and age hardening effects on transverse modulus and tensile strength of unidirectional Al matrix fibrous composites 18 p2935 A71-36597
- Salt bath application to steels and Al alloys heat treatment, discussing carburizing, neutral hardening, austempering, martempering, annealing and brazing 18 p2927 A71-36665
- Nb and Nb-Zr alloy tubular and sheet samples cyclic loading tests, determining heat treatment effects on notch sensitivity and fatigue strength 18 p2937 A71-36724
- Phase transformations in superconductive Nb-Ti alloys with Zr during heating or isothermal annealing 19 p3078 A71-37469
- Fe-Ni base alloy heat treatment for optimum high temperature stress-rupture properties, noting Ni-Nb/Ni-Ti intermetallics precipitation at grain boundaries 19 p3080 A71-37712
- Ti alloys heat resistant properties evaluation for long service under various heat treatment conditions, considering tensile properties, fracture toughness and microstructure 19 p3082 A71-38420
- Creep fracture of Cr-Mo-V steel after operational heat treatment and power plant operation, noting intercrystalline and transcrystalline fracture 20 p3249 A71-39016
- Austenitic stainless steels susceptibility to intergranular corrosion under unwelded, welded and heat treated conditions in process environments 20 p3241 A71-39341
- Ni-Cu-Nb age hardenable steel mechanical properties, examining hot rolling and heat treatment effects 21 p3387 A71-40455
- Inconel-600 under heat treatment and tension tests, examining grain boundaries slip interaction 21 p3397 A71-40458
- Charpy impact test measurement of maraging steel thermal embrittlement, observing fracture mode and toughness changes with heat treatment 21 p3398 A71-40467
- Heat treatment for weldability and formability improvement of Udimet 700, evaluating by bend, hardness and tensile tests 21 p3388 A71-40622

HEATERS

- Shatter crack incubated nucleation in relation to heat treatment effects on hydrogen elimination in steels, comparing with thermal explosion mechanism 21 p3402 A71-41090
- Stainless steels nitriding in presence of halogen compounds with heat treatment, observing thermodynamic potential shift 21 p3389 A71-41099
- Austenitic stainless steels diffusion layer formation and structure by gaseous carburization with Fe-Al-manganese chloride powder mixture, describing elements redistribution 21 p3390 A71-41166
- Prior stressing and thermal treatments effect on shock induced substructures in polycrystalline Mo, using transmission electron microscopy 21 p3404 A71-41416
- Ni-Cr-Mo-Co steel microstructures after austenitizing, quenching and tempering, correlating with mechanical properties 22 p3560 A71-41594
- Intense ionizing radiation and thermal treatment effects on electrical parameters of Si semiconductor devices 22 p3584 A71-41619
- Intergranular corrosion of chromium carbide sensitized Ni base alloys, noting surface effect during solution heat treatment 22 p3560 A71-41626
- Carbon effects on fracture phenomena in martensitic transformation of steels under heat and thermomechanical treatments 22 p3563 A71-42322
- Oxygen concentration and heat treatment effects on structure and mechanical properties of Nb-Zr alloys 22 p3563 A71-42366
- Accelerated intergranular corrosion tests under high humidity on Zn-Al alloy with lamellar eutectoid microstructure due to postforming heat treatment 22 p3564 A71-42534
- Increased microplastic deformation resistance, relaxation stability and aging of beryllium by cyclic heat treatment 23 p3690 A71-43281
- Ni-based alloy strength characteristics dependence on heat treatment during melting and casting in vacuum and in air 23 p3691 A71-43425
- Heat treatment specifications selection for Ni alloy by mathematical method based on cylindrical specimens elongation under tensile loads 23 p3691 A71-43523
- Heat treatment effect on tensile and bending fatigue strength of Al alloy thin sheet 23 p3693 A71-44217
- High cycle fatigue resistance improvement of age hardened Al-Zn-Mg-Cu alloys through thermomechanical treatments 23 p3695 A71-44290
- Age hardenable Mg-Y alloys, investigating impurity phase in solution heat treatment 23 p3696 A71-44292
- Cr-Ni alloy heat treated cast specimens microstructure, metallographic, X ray and spectral investigation, noting chemical inhomogeneity 24 p3836 A71-44484
- ## HEATERS
- Compressive creep behavior of yttria rare earth stabilized zirconia storage heater refractories, determining stress time to failure 09 p1484 A71-23686
- IR radiation role in limiting central heater maximum temperature and heat transfer to high density oxygen in cryogenic storage systems 13 p2166 A71-29505
- Heater and nozzle design of ONERA/S4MA hypersonic wind tunnel for supersonic combustion ramjet tests [ONERA-TP-924] 18 p2956 A71-36017
- ## HEATING
- NT AERODYNAMIC HEATING
- NT ARC HEATING
- NT ATMOSPHERIC HEATING
- NT BAKING
- NT BASE HEATING
- NT GAS HEATING
- NT INDUCTION HEATING
- NT IONOSPHERIC HEATING
- NT KINETIC HEATING
- NT LASER HEATING
- NT PLASMA HEATING
- NT PULSE HEATING
- NT RADIANT HEATING
- NT RADIO FREQUENCY HEATING
- NT RESISTANCE HEATING
- NT SHOCK HEATING
- NT SOLAR HEATING
- NT SUPERHEATING
- NT TRANSIENT HEATING
- Turbine disks failure under nonuniform heating, deriving expression for critical rpm 05 p0826 A71-16755
- Turbulent boundary layer on porous plate with suction and heating, measuring mean velocity and tem-

- perature profiles at various locations along wall as function of suction rate 07 p1219 A71-18759
- Rapid heating effects on hot pressed TiC cylinders stability, calculating temperature fields and stress distribution 07 p1130 A71-19168
- Closed spherical shell, calculating optimal internal temperature fields for keeping thermal stresses at low level under local axisymmetric heating 09 p1537 A71-22520
- Molybdenum alloy under annealing and heating by AC electric current, investigating structure change effects on strength properties 09 p1475 A71-23312
- Time optimal control for massive solids heating or cooling from initial into prescribed finite state with constraints 10 p1695 A71-24159
- Al coating of Nb and Nb alloys by pack cementation, discussing coating structural states, heating cycle temperatures and growth kinetics 11 p1781 A71-26295
- ## HEATING EQUIPMENT
- NT BOILERS
- NT EVAPORATORS
- NT IMAGE FURNACES
- NT OVENS
- NT VACUUM FURNACES
- NT VAPORIZERS
- Gas flame heater for heat resistant samples under fatigue tests, simulating gas turbine engine operating conditions 01 p0657 A71-10041
- High speed wind tunnels air heating system optimization, considering pebble bed air heater for intermittent operations 20 p3209 A71-39086
- ## HEAVING
- Edge jet Hovercraft dynamic stability in heaving motion, deriving two dimensional mathematical model [ASME PAPER 70-APM-QQ] 03 p0348 A71-13712
- ## HEAVY COSMIC RAY PRIMARIES
- U HEAVY NUCLEI
- U PRIMARY COSMIC RAYS
- ## HEAVY ELEMENTS
- NT CALIFORNIUM ISOTOPES
- NT PLUTONIUM
- NT PLUTONIUM 238
- NT TRANSURANIUM ELEMENTS
- Soviet book on material analysis by nuclear radiation covering heavy elements concentration in ores, radioisotope devices and gamma ray capture spectroscopy 02 p0283 A71-12721
- Solar corona and wind composition, accounting for He flux and heavy elements from diffusion equations solution 02 p0303 A71-12770
- URCA neutrino emission processes explaining anomalous isotopic heavy element abundance in solar system 04 p0651 A71-15660
- Superheavy elements formation due to fast neutron capture during supernova outbursts, discussing meteorites fission produced noble gases 08 p1337 A71-20959
- Rare earth and heavy elements determination in olivine hypersthene and enstatite chondrites by spark source mass spectroscopy, noting Fe meteorite silicate inclusions composition 11 p1819 A71-25225
- Carbonaceous chondrite fission producing superheavy element decay half life 22 p3605 A71-42398
- Neutron activation analysis of Apollo 11 lunar fines, determining Pb 204, U, Bi and Ti contents 23 p3753 A71-43715
- Superheavy elements search in lunar fine grains from Apollo 12 mission by measuring kinetic energy spectrum of nuclear fission fragments 23 p3753 A71-43718
- Rapid neutron capture products evidence on peculiar A star surfaces from observation of promethium and heaviest elements abundance 24 p3865 A71-44567
- ## HEAVY IONS
- Cosmic ray heavy ion component biological effect, describing histological and radioautographic high altitude balloon experiment with black mice and rabbits 01 p0019 A71-11555
- Heavy ion diffusion in solar corona, emphasizing flow velocity and density 03 p0495 A71-14503
- Primary cosmic rays heavy ion tracks from balloon-borne emulsion 04 p0641 A71-15368
- Plastic track detectors calibration for heavy charged particles in cosmic ray experiments, considering track etching rates as function of particle charge and velocity 07 p1113 A71-20042

- Heavy ion track registration in nonconducting minerals, discussing radiation damage and atomic species along trajectory 07 p1158 A71-20270
- Spark discharge enhancement of heavy ion track etching in Lexan polycarbonate 07 p1114 A71-20270
- Heavy ion tracks in silicate minerals, using thermoluminescence annealing to identify origins 07 p1158 A71-20270
- Lunar rock analysis, discussing heavy ion impact traces and amorphous skin relation to solar wind 10 p1677 A71-24690
- Solar wind heavy ion data, using Heos-1 satellite observations of 31 March 1970 interplanetary shock 13 p2130 A71-29001
- Mean charge measurement for heavy ions moving through He and air with aid of gas-filled mass separator, noting anomalies in nuclear charge dependence 21 p3419 A71-41111
- ## HEAVY NUCLEI
- C, N and O nuclei abundances in radiation belt near geomagnetic equator, using data obtained byOGO-7 satellite in 1968 03 p0473 A71-13477
- Primary cosmic rays heavy ion tracks from balloon-borne emulsion 04 p0641 A71-15368
- Heavy cosmic ray nuclei intensity and energy spectra, investigating solar modulation effects 06 p0954 A71-18129
- Large Z primary cosmic rays charge spectra, using semiautomatic photometer 08 p1350 A71-20955
- Superheavy transactinide isotopes in outer space: discussing single standard composition of cosmic material bulk 08 p1351 A71-20958
- Heavy cosmic rays slowing in balloon-borne stack: discussing high resolution measurement and synthesis in rapid neutron capture 08 p1354 A71-21038
- Heavy cosmic rays identification by charge spectrum analysis of balloon-borne combined plastic detectors and nuclear emulsions, noting astrophysical implications 09 p1514 A71-22804
- Energy spectrum of iron group solar cosmic ray particles determined from glass removed from Surveyor 3 spacecraft, considering lunar erosion implications 09 p1515 A71-23656
- Type I fluctuations experienced by extensive air showers generated by protons or heavy nuclei: discussing effect on primary cosmic ray energy determination 10 p1661 A71-23854
- Heavy cosmic ray nuclei track counts in plastics: examining Apollo mission 8 and 12 helmets 10 p1665 A71-25121
- Iron nuclei emission during 1967-1969 solar flares from spacecraft window and lunar camera lens etched tracks, discussing Fe/He ratio and lunar soil densities 11 p1815 A71-25299
- Mass spectrum of stopping heavy cosmic ray particles at sea level observed, interpreting flux as deuteron production by high energy protons and neutrons 13 p2122 A71-28067
- Air shower properties from Monte Carlo simulations, determining electron and muon numbers at sea level for primary protons and copper nuclei 13 p2124 A71-28085
- Cosmic radiation heavy nuclei intensity and composition measurement, treating nuclear emulsions in calcium bromide solutions 22 p3596 A71-42733
- Large area parallel-plate pulse ionization chamber for high altitude balloon measurements of relativistic cosmic ray heavy nuclei 22 p3550 A71-42887
- Ultraheavy cosmic ray nuclei existence inferred from Apollo 12 lunar rock pigeonite crystal track length distribution 23 p3765 A71-43805
- ## HEAVY WATER
- Harmful induced stimulated emission losses in rhodamine unpumped ethyl alcohol and heavy water solutions of various excitation energies 09 p1461 A71-22383
- ## HEIGHT
- NT SCALE HEIGHT
- Nighttime F layer true height profiles reduction from routine ionograms, discussing error corrections 03 p0408 A71-13387
- Atmospheric model phase ionograms for true height reduction technique tests, using ionosonde data 10 p1602 A71-24461
- ## HEISENBERG THEORY
- Heisenberg ferromagnet with applied external magnetic field, investigating thermodynamic properties near Curie point 11 p1807 A71-25555
- Anisotropic Heisenberg antiferromagnet sublattice magnetization, obtaining temperature dependence 13 p2100 A71-28677

Quantum electrodynamics on null planes in Minkowski space, discussing applications to lasers, wave packet construction, Heisenberg and Furry pictures and Compton scattering

13 p2080 A71-28998

Extension of Heisenberg model for spectral transfer to second order fluids in turbulent shear flow, noting accompanying weakening of anisotropic influences

17 p2725 A71-34181

Diffraction phenomena numerical modeling by Monte Carlo statistical analysis, using Heisenberg uncertainty principle

22 p3576 A71-42556

HELICAL ANTENNAS

Normal mode helix antenna with rectangular and tapered AI strip conductors, measuring impedance variation with frequency at VHF range

03 p0387 A71-13820

Resonant circularly polarized quadrifilar helix antenna with antiphase feed, noting cardioid shaped radiation patterns

04 p0559 A71-15877

Input impedance of cylindrical and helical antennas in cold lossy magnetoplasma, discussing sensitivity to current distribution

07 p1065 A71-20323

Tape helix radiators for spacecraft phased antenna arrays, analyzing performance for proposed L band system

14 p2217 A71-31057

Short helical antenna performance and characteristics, discussing radiation patterns, efficiency, bandwidth and space vehicle use [ONERA-TP-950]

18 p2888 A71-36023

Quadrifilar helix antenna pitch angle and ground plane size optimization based on beam pattern data

19 p3036 A71-38603

Broadband helical antenna feeds for millimeter wave parabolic reflectors and lenses, determining bandwidths and polarizations as functions of helix parameters and frequency

21 p3359 A71-41408

Microwave structures symmetry analysis based on group theoretic concepts application to vector electromagnetic fields, investigating single wire helix

24 p3809 A71-45090

HELICAL FLOW

Electromagnetic waves phase velocity in helical waveguides in magnetodielectric medium with cylindrical void interspace

05 p0722 A71-16827

Finite amplitude helical instability effect on microwave beam phase propagated through plasma column

07 p1166 A71-18888

Helical circulations in unstable planetary boundary layer measurements, using constant volume balloons and air parcel tracking

07 p1103 A71-19761

Flutter analysis of rotating thin cylindrical shell with outer surface exposed to inviscid helical air flowfield

09 p1533 A71-22078

Primary/secondary flow density ratio effect on rotary jet flow induction, describing experimental results with 1/7-1/1 density ratios

10 p1553 A71-24853

Intrinsic helical and quasi-rigid hydrodynamic motions of incompressible, ideal and viscous fluids, using mobile frame method

11 p1804 A71-25175

Helical motions with vorticity-velocity and conduction current-free force magnetic vectors parallelisms

11 p1804 A71-25177

Flutter analysis of long thin cylindrical shells rotating in circular helical air flow field [AIAA PAPER 71-373]

11 p1845 A71-25346

Helical wave deceleration with inhomogeneous plasma approximated by anisotropically conducting plane

14 p2279 A71-30115

Incompressible frictionless helical flows hydromagnetic stability in cylindrical circular space

15 p2387 A71-31166

HELICAL INDUCERS

Helical induction boiler feed electromagnetic pump design, fabrication and testing for potassium Rankine cycle space power system [GESP-455]

15 p2415 A71-32202

HELICAL WINDINGS

Helical channel multipliers encapsulation for space flight applications

04 p0600 A71-15597

Fracture strength of helical wound glass-epoxy composite cylinder under axial tension, determining tensile strength

05 p0826 A71-16741

High resolution X ray diffraction patterns of yeast phenylalanyl transfer RNA crystals, discussing double helical regional distribution characteristics

11 p1727 A71-25834

HELICOPTER ATTITUDE INDICATORS

U ATTITUDE INDICATORS

U HELICOPTERS

HELICOPTER CONTROL

Airborne radar as helicopter approach aid

04 p0624 A71-15425

Three axis flight director for precise helicopter control, deflected slipstream STOL or VTOL attitude and power under low ceiling and visibility landing

04 p0624 A71-15428

Sand and dust effects on military helicopter flight controls and equipment service life, discussing relief program

04 p0533 A71-15430

Airborne variable stability helicopter flight simulator for V/STOL aircraft design

05 p0697 A71-16954

Single rotor helicopter directional stability in rectilinear flight with constant angle of side slip

06 p0847 A71-18307

Helicopter longitudinal stability in forward flight and hover modes under attitude, height and speed constraints, noting need for cyclic pitch control due to instabilities

07 p1019 A71-19421

Helicopter handling under ASW flight conditions, discussing sea state effect on low altitude hover stability

13 p1998 A71-29384

Rotor blade stall induced helicopter control loads, combining unsteady aerodynamics with aeroelastic rotor analysis

[AHS PREPRINT 513] 14 p2178 A71-31084

AN/ASN-86 inertial navigation system consisting of inertial platform, digital computer and control indicator

[AHS PREPRINT 533] 14 p2273 A71-31094

Electromechanical control system synthesis for compound hingeless rotor helicopter, using root locus method with transfer functions from airframe motion linear model

[AHS PREPRINT 536] 14 p2179 A71-31096

Heavy lift helicopters IFR hover capability with slung load, discussing sensors controls and displays

[AHS PREPRINT 540] 14 p2250 A71-31097

Hingeless rotor helicopter stability and control characteristics, considering induced flow field, flapwise bending modes and blade-fuselage dynamic coupling

[AHS PREPRINT 541] 14 p2179 A71-31098

Handling qualities and control sensitivity of high performance helicopters, considering pitch and collective control

[AHS PREPRINT 542] 14 p2179 A71-31099

Fail-safe helicopter rotor control design, discussing damage tolerant components, redundant system, failure warning and maintenance

[AHS PREPRINT 550] 14 p2179 A71-31102

High performance UH-1 compound helicopter high speed flight research, considering rotor loads, stability, control and flying qualities

[AHS PREPRINT 570] 14 p2180 A71-31111

AH-56A compound helicopter rigid rotor stability and handling qualities, using flight, whirl tower and wind tunnel tests

[AHS PREPRINT 574] 14 p2180 A71-31115

Helicopter automatic flight control equipment, discussing autopilot stabilizer, localization system, ground approach guidance coupler and flight director

15 p2446 A71-31916

Large crane heavy lift helicopter stability and controllability, considering effects of slung loads, performance improvement, automatic flight control and physical size

19 p2998 A71-38651

Tilt-fold-prop rotor VTOL aircraft stability and control, emphasizing pylon tilt and rotor stop-fold effects on flying qualities

19 p2998 A71-38652

Model following technique for optimal control applied to hovering motion of CH-3 helicopter

20 p3178 A71-39000

U.S. Army ATC cost-effective system developments for high density low altitude helicopter tactical operations to avoid enemy radar under near-all weather conditions

22 p3571 A71-42084

Helicopter optimal autorotation landing parameters for touchdown at zero speed, including rotor rpm drop due to flow separation on blades

23 p3627 A71-43090

HELICOPTER DESIGN

Helicopter pilot and passengers emergency survival, considering gravitation force, human tolerances, design factors, etc

01 p0026 A71-11376

NACA/NASA rotating wing aircraft research history during 1955-1970 period, discussing wind tunnel research

01 p0005 A71-11377

Carbon fiber reinforced epoxy composites, evaluating application as helicopter tail rotor blade material

02 p0273 A71-12477

NACA/NASA rotary wing aircraft research, considering rotor loads and configurations, ground resonance, blade flutter and flapping, motion equations and VTOL

04 p0529 A71-15171

WG.13 Lynx battlefield helicopter design and performance

04 p0529 A71-15394

Helicopter downwash velocities, noise and airloads, examining rotor tip modification effects

04 p0527 A71-15410

Lightning hazards for helicopters, discussing components vulnerability and protective design requirements

04 p0531 A71-15412

Helicopter fuselage design for crashworthiness under specific conditions

04 p0532 A71-15416

Helicopters safe antitorque control, describing Fenestron ducted fan design

04 p0532 A71-15417

Helicopter design for cabin noise level reduction

04 p0532 A71-15423

Helicopter structural damage due to icing, discussing secondary effects on tail rotor, horizontal tail and engine from ice shed by main rotor

04 p0533 A71-15432

Environmental development and testing of OH-58A light observation helicopter for close ground support, noting particle separator and injection seals

04 p0534 A71-15439

Military helicopter design and weaknesses correction, considering man/machine combat survivability and operational accidents reduction

04 p0534 A71-15447

Do 132 turbine powered helicopter, discussing icing problems solution

06 p0847 A71-17745

Aerodynamic synthesis of helicopter rotor under hover and vertical ascent conditions, using nonlinear vortex approach

07 p1014 A71-19740

Materials and construction techniques in lightning protection for aircraft and helicopters

07 p1020 A71-19930

Lightning and static electricity effects on helicopter design, considering rotor protection, cargo hook operation and passive dischargers for radio interference reduction

07 p1021 A71-19938

Helicopter vibrational behavior prediction in flight with known aerodynamic loads, using branch modes method

09 p1385 A71-23606

Stability analysis and design optimization with dynamics and aeroelastic constraints for helicopter rotor blade minimum weight with bending torsion flutter and favorable frequency placements

11 p1846 A71-25352

Helicopter auxiliary power unit (APU) life cycle cost computation

12 p1988 A71-26679

Costs-reliability relationships in helicopter development testing and demonstration, emphasizing decision making in program management

13 p2167 A71-28330

Helicopter design for use as crane and for carrying external loads

13 p1996 A71-28489

Helicopter component surface finish smoothness and residual stress requirements, using abrasive grinding belt machines with gear link mechanisms

13 p2075 A71-28943

Soviet book on helicopter design covering aerodynamic properties, power plants, control systems, fatigue minimization and strength analysis

14 p2174 A71-29944

Westland WG 13 Lynx helicopter, discussing design features, performance characteristics and civil and military applications

14 p2175 A71-30301

Soviet Mil V-12 heavy lift helicopter for civil and military missions, noting turbine engines, rotor configuration, cargo hold and navigation system

14 p2175 A71-30420

Advancing Blade Concept helicopter lifting rotor development, discussing full scale analysis, design, fabrication and wind tunnel tests

14 p2178 A71-31080

High rotor advance ratio from multiblade general coordinates method in linear analysis of lifting rotor dynamic stability and gust ratio

14 p2178 A71-31083

Optimal turboprop engine and reaction drive rotor combinations for helicopter design

14 p2297 A71-31108

Strain gage torque meter as primary power indicating instrument in helicopter transmission systems, providing advantages for helicopter designer and operator

14 p2250 A71-31110

French helicopters design and performance, considering Alouette 2 and 3 and military versions

15 p2350 A71-32694

Lynx military helicopter design high reliability and low maintenance demands

16 p2523 A71-33457

Helicopter rotor blades fail-safe design, presenting criteria for fatigue loaded structures residual strength and life based on crack propagation rate methods

17 p2828 A71-35163

HELICOPTER ENGINES

- Analytical weight determination of articulated shaft driven helicopter main rotor blades, presenting computer program 17 p2835 A71-35826 [SAWE PAPER 893]
- Tilt-fold-propotor VTOL aircraft stability and control, emphasizing pylot tilt and rotor stop-fold effects on flying qualities 19 p2998 A71-38652
- Mil Mi-12 Soviet giant rigid rotor helicopter with 30,000 kg load or 250 passenger capacity 20 p3178 A71-39375
- Agusta helicopter design and testing criteria, discussing four-blade rotor, fuselage and radio navigation equipment 22 p3482 A71-42224
- Heavy load transportation Mi 12 helicopter design and performance, noting gas turbine rigid shaft connection 23 p3627 A71-42926
- Technology developments in rotor, drive, flight controls and cargo handling systems of heavy lift helicopter system, noting military and commercial applications [AIAA PAPER 71-994] 24 p3792 A71-45296
- HELICOPTER ENGINES**
- Helicopter turbine engine protection device design guidelines 04 p0533 A71-15434
- Book on fixed and rotary winged aircraft air cooled piston engine design, performance and maintenance in business and military operators manual terminology 05 p0796 A71-17125
- Helicopter gas turbine engine health indication using instrument panel for correcting gas temperature and producer speed 06 p0945 A71-17690
- Helicopter jet propulsion systems, considering turbocompressors, gas generators, turbine air jet systems, pulsed jet engines, ramjet engines and rocket engines 11 p1706 A71-25259
- Helicopter power transmission failure modes, presenting field experiences correlation with conventional design stress analysis and bench test data [SAE PAPER 710454] 13 p2074 A71-28331
- Soviet book on helicopter design covering aerodynamic properties, power plants, control systems, fatigue minimization and strength analysis 14 p2174 A71-29944
- Gas turbine design advances for helicopter powerplants, illustrating by Turbomeca engines 16 p2624 A71-33416
- HELICOPTER PERFORMANCE**
- Helicopter noise minimization by various piloting maneuvers, discussing takeoff and landing, transition to forward flight, route selection, etc 04 p0531 A71-15408
- Helicopter pilot and passenger comfort/vibration tolerance criteria 04 p0532 A71-15420
- Airborne flight simulator /helicopter/ as aircraft development aid [DGLR-70-075] 05 p0733 A71-15965
- Height velocity /H-V/ flight testing, giving results from OH-58A Kiowa and AH-1G Huey Cobra helicopters 07 p1018 A71-19093
- Helicopter noise minimization by various piloting maneuvers, discussing takeoff and landing, transition to forward flight, route selection, etc 08 p1230 A71-21049
- Westland WG 13 Lynx helicopter, discussing design features, performance characteristics and civil and military applications 14 p2175 A71-30301
- Soviet Mil V-12 heavy lift helicopter for civil and military missions, noting turbine engines, rotor configuration, cargo hold and navigation system 14 p2175 A71-30301
- Noise production during aerodynamic tests on helicopter rotor in wind tunnel 14 p2176 A71-30519
- Army rotorcraft performance data, discussing hovering and forward flight performance out of ground and level flight power requirements and drag and compressibility effects [AHS PREPRINT 500] 14 p2177 A71-31076
- Helicopter fuselage vertical and in-plane main rotor head vibratory forces isolation with hydropneumatic servocentered system at transmission/airframe interface [AHS PREPRINT 514] 14 p2253 A71-31085
- Helicopter rotor stall characteristics, investigating blade flexibility, unsteady aerodynamics and variable inflow effects [AHS PREPRINT 520] 14 p2171 A71-31086
- High performance UH-1 compound helicopter high speed flight research, considering rotor loads, stability, control and flying qualities [AHS PREPRINT 570] 14 p2180 A71-31111
- Helicopter stability, using Lockheed rotor system with gyro coupled to cantilevered blades 15 p2348 A71-31599

- French helicopters design and performance, considering Alouette 2 and 3 and military versions 15 p2350 A71-32694
- Helicopter rotor noise due to blade-vortex interaction, using linear gust model 18 p2849 A71-36934
- Large crane heavy lift helicopter stability and controllability, considering effects of slung loads, performance improvement, automatic flight control and physical size 19 p2998 A71-38651
- Helicopter wake and boundary layer effects on rotor aerodynamic performance in hovering, low and high speed forward flight [AIAA PAPER 71-581] 22 p3479 A71-41500
- Heavy load transportation Mi 12 helicopter design and performance, noting gas turbine rigid shaft connection 23 p3627 A71-42926

HELICOPTER PROPELLER DRIVE

- Helicopter rotor system vibratory and mechanical stability characteristics, investigating anisotropically mounted flexible swash plate and blade out of track effects [AHS PREPRINT 511] 14 p2178 A71-31082
- Optimal turbofan engine and reaction drive rotor combinations for helicopter design [AHS PREPRINT 561] 14 p2297 A71-31108
- HELICOPTER ROTORS**
- U ROTARY WINGS**
- HELICOPTER WAKES**
- Helicopter wake impulsive noise calculation based on rotor tip vortex interaction 04 p0531 A71-15407

- Helicopter and V/STOL aircraft external noise and downwash measurements during simulated jungle rescue mission 04 p0531 A71-15409

- Wake model and computer program to compute geometries, flows and velocity influence coefficients for helicopter blade load calculations [AHS PREPRINT 523] 14 p2172 A71-31089
- Helicopter experimental fog clearing by downwash mixing at Greenbrier Valley Airport, Lewisburg, West Virginia 20 p3256 A71-39206

- Fog formation and dispersal by velocity field induced by helicopter trailing vortices, presenting dynamic model with droplet depletion, evaporation and condensation 21 p3321 A71-40510

- Helicopter wake and boundary layer effects on rotor aerodynamic performance in hovering, low and high speed forward flight [AIAA PAPER 71-581] 22 p3479 A71-41500

HELICOPTERS

- NT ALOUETTE HELICOPTERS
- NT BO-105 HELICOPTER
- NT CH-3 HELICOPTER
- NT CH-46 HELICOPTER
- NT CH-47 HELICOPTER
- NT CH-54 HELICOPTER
- NT COMPOUND HELICOPTERS
- NT H-53 HELICOPTER
- NT H-56 HELICOPTER
- NT MILITARY HELICOPTERS
- NT OH-6 HELICOPTER
- NT RIGID ROTOR HELICOPTERS
- NT UH-1 HELICOPTER
- Do-132 light five seat tip drive turbine helicopter, discussing applications, flight testing, design and major components 01 p0004 A71-10465
- Helicopter operations integration into civil air traffic system, noting special requirements for mixed fixed and rotary wing terminal environments 02 p0279 A71-12892
- VTOL systems for commercial short haul air transportation, discussing large helicopters and compound aircraft applications for system capacity profitability and efficiency increases 03 p0347 A71-13575
- Helicopter in-flight noise radiation pattern and spectra measurements for various operating parameters 04 p0531 A71-15406
- Helicopters, heliports and helistops, discussing need for public facilities 04 p0692 A71-15440
- Public-use ground level and rooftop helicopter and STOL aircraft landing facilities for city and suburban traffic 04 p0567 A71-15442
- Medical transportation by ambulance, helicopter and fixed wing aircraft, considering vibration damping and acceleration 05 p0715 A71-16932
- Helicopter automatic and manual low visibility landing systems evaluation by hybrid computer simulation 06 p0880 A71-18423
- Helicopter charging mechanisms, considering engine and rain precipitation charging 07 p1020 A71-19933
- Boundary layer discontinuity on helicopter rotor blade in hovering using flow visualization [AIAA PAPER 69-197] 07 p1017 A71-20307

- Helicopter rotor inertial system kinetic energy, examining takeoff advantages 09 p1385 A71-2389

- Mutual aerodynamic effects of SM-1 helicopter during simultaneous takeoff and landing, determining minimum distances between helicopters 12 p1867 A71-2658

- Helicopter operation as cranes and for external air transportation, discussing operational and economic aspects 12 p1867 A71-2730

- Aircraft accident rescue system with helicopter, discussing cooperation between helicopter service and ground personnel 13 p2020 A71-2817

- Helicopters as cranes and external load carriers, considering operational costs and investment returns 13 p1997 A71-2919

- Soviet book on airplane and helicopter electric power supply systems covering storage batteries, D generators, alternators, voltage regulators, current and frequency control, etc 14 p2180 A71-2959

- Helicopter systems operations in, around and between major metropolitan areas, considering performance of New York Airways [AIAA PAPER 71-507] 14 p2339 A71-2950

- Helicopter aerial design problems, considering antenna multiplicity use of nonmetallic structures and complexity of airborne radio systems 14 p2217 A71-31010

- Heavy lift helicopter flight control system design, emphasizing fly by wire electrical analog [AHS PREPRINT 503] 14 p2178 A71-31010

- Helicopter rotor blade airload by applying lift/surface solution [AHS PREPRINT 510] 14 p2171 A71-31010

- Tethered, ground supplied, rotor-borne, self stabilized surveillance platform /Kiebitz/ systems, discussing reconnaissance tasks, fire and communication control and data acquisition transmission and evaluation 15 p2347 A71-3122

- Helicopter radar equipment for obstacle avoidance in all-weather low altitude flight, describing components installation, cockpit display and controls 15 p2446 A71-31938

- Ice formation and prevention on helicopters, taking into account presence of big drops of undercooled rain 20 p3178 A71-3933

- Spine radiological examination for helicopter pilot fitness determination, discussing spinal weakness symptoms, special exercises, medical examinations and vibration reducing seat construction 22 p3500 A71-41578

- Longitudinal stability of plate-like load towed beneath helicopter in horizontal forward flight 23 p3630 A71-4434

- Helicopter, tilt wing and jet lift hovering aircraft, outflow measurements to determine suitability as rescue vehicles [AIAA PAPER 71-992] 24 p3791 A71-4458

HELICENTRIC ORBITS**U SOLAR ORBITS****HELIOGRAPHS****U SPECTROHELIOGRAPHS****HELIOGRAPHY****U SPECTROHELIOGRAPHS****HELIOMAGNETISM****U SOLAR MAGNETIC FIELD****HELIOMETERS****NT PYROHELIOMETERS**

- Radioheliographic 80 MHz observations of harmonic type 2 solar burst near limb flare 15 p2472 A71-3168

- Culgoora 80 MHz radioheliographic observations of 13 October 1969 harmonic solar type 2 burst attributed to explosive flare behind west limb 15 p2472 A71-3168

- Harmonic type 3 solar bursts radioheliographic observations, discussing polarization characteristics 15 p2473 A71-3169

- Moving type 4 solar radio burst observation on 1 October 1969 with radioheliograph, noting circular polarization, movement direction, speed and structure 15 p2473 A71-3169

- Active cavity radiometric and international pyrheliometric scales comparison and solar constant from simultaneous solar irradiance measurements 16 p2581 A71-3393

- Compensation pyrheliometers and thermoelectric actinometers response lag and irregular operation after instantaneous shadowing, discussing techniques for determining instrument inertial characteristics 20 p3237 A71-3933

- Culgoora radioheliograph electronic imaging system for diffraction pattern generation 24 p3828 A71-4520

HELIOIMETRY**U HELIOIMETERS****U PYROHELIOIMETERS****HELIOPORTS**

- Helicopters, heliports and helistops, discussing need for public facilities 04 p0692 A71-15440

- Aircraft noise propagation in city streets due to intertown VISTOL and helicopter ports, using small scale models 20 p3178 A71-39264
- HELIUM**
- NT HELIUM ATOMS
- NT HELIUM ISOTOPES
- NT LIQUID HELIUM
- High electron temperature H and He I and II, calculating partition functions 01 p0158 A71-10806
- Solar wind elemental and isotopic He and Ne compositions from mass spectrometry of ions collected in metal foils deployed during Apollo 11 and 12 landings 01 p0146 A71-11486
- Solar corona and wind composition, accounting for He flux and heavy elements from diffusion equations solution 02 p0303 A71-12770
- Film cooling effectiveness with He and refrigerant 12 injection into two dimensional turbulent boundary layer of supersonic airflow 03 p0517 A71-13453
- Turbulent boundary layer recovery factor for wedge model in hypersonic helium flow at high Reynolds and Mach numbers 03 p0517 A71-13461
- He excitation by He, Ne, Ar and Kr collisions, calculating first Born wave cross section 03 p0460 A71-13498
- Helium effects on dissociation and population inversion dynamics in pulsed carbon dioxide lasers 04 p0605 A71-14628
- Inert gas welding of Al with He as oxidation inhibitor, discussing penetration, welding rate and cost compared to Ar use 04 p0604 A71-15815
- Modified buried collector gauge performance over He pressure range, determining sensitivity dependence on filament geometry 05 p0748 A71-16231
- Quasars primordial He abundance, discussing relation to galactic evolution 05 p0808 A71-16406
- He I 584 A dayglow radiation measurement by retarding potential photoelectron analyzer on Javelin sounding rocket 06 p0887 A71-17267
- Superconductors applications, noting low cost reliable closed cycle He refrigerators 06 p0941 A71-18017
- Galactic cosmic ray proton and He spectrum measurements in 1968 compared to electron spectra, explaining solar modulation features by models incorporating energy loss effects 06 p0952 A71-18112
- Turbulent He jet measurements using hot-wire anemometry and digital recording techniques, assessing accuracy [AIAA PAPER 71-201] 06 p0886 A71-18639
- Twilight helium emission diurnal and seasonal variations relationship to geomagnetic activity and solar depression, using Abastumani observations 07 p1099 A71-19389
- Pressure dependent shift of He-Ne laser radiation, observing beat frequencies 07 p1123 A71-19486
- He shell burning termination in solar mass stars evolution to white dwarf stage 07 p1198 A71-19823
- Hydrogen and helium photoionization, calculating total cross section and transitions for soft X ray region 08 p1350 A71-20948
- Lower limit helium abundance envelope models of hydrogen deficient stars, using mixing length theory 08 p1364 A71-21418
- Twilight helium 10,830 A emission observations and calculations, using grille spectrometer 08 p1283 A71-21638
- Horizontal He distribution in upper atmosphere fromOGO 6 mass spectrometric data normalization for altitude by Jacchia model atmosphere 08 p1283 A71-21647
- Helium role in populating upper levels of cadmium gas laser in discharge tube 09 p1462 A71-22401
- Normal shock wave in He, comparing measured and predicted molecular velocity distribution functions 09 p1433 A71-22857
- Helium and nitrogen breathing effects upon intraocular pressure during and after near vacuum exposure in anesthetized and unanesthetized dogs 09 p1400 A71-23359
- Trapped solar wind He and Ne in Surveyor 3 unpaired Al tube, comparing with Apollo 11 and 12 solar wind composition 10 p1672 A71-24390
- He I absorption line profiles in normal main sequence B star spectra, discussing He abundance and LTE 11 p1821 A71-25536
- Jupiter occultation of beta Scorpii on 13 May 1971, determining hydrogen/helium ratio 12 p1961 A71-26876
- Ar, N and Ne partial pressure tolerance in dogs, plotting saturation curves 13 p2005 A71-28038
- Helium for nitrogen substitution effects on body temperature of rats exposed to high carbon dioxide concentrations at different ambient temperatures 13 p2006 A71-28402
- Stellar core evolution of initial mass 1.5 solar mass, starting from He-burning phase 13 p2140 A71-29013
- Spatial variations in cosmic He abundance attributed to primordial temperature fluctuations at early epochs in Friedmann universe 14 p2303 A71-29587
- Electron and ion concentrations, electron temperature and electrical conductivity of ionized air before shock wave, using shock tube with He driver gas 14 p2225 A71-30225
- Arc welding apparatus for chemically active high-melting metals in controlled superpure He atmosphere 14 p2253 A71-30486
- Solid helium and molecular/metallic hydrogen thermodynamic properties and phase diagrams as functions of pressures corresponding to Jupiter and Saturn 15 p2511 A71-31338
- Heat transfer and pressure drop characteristics of He in two phase and supercritical flow, calculating He heat exchangers for superconductive devices [HEAT EXCH. CONF. PAPER 24] 15 p2513 A71-31638
- Holographic investigation of laser sparks in hydrogen and helium, determining electron concentration spatial distribution and plasma dispersion dynamics 15 p2419 A71-31738
- Random walk theory applied to electron motion in early stage of He breakdown in electric field, based on integral and differential cross section data 15 p2452 A71-31921
- Stars with central He burning and loop occurrence in H-R diagram, suggesting secular instabilities with high stellar mass 16 p2633 A71-33332
- Interplanetary hydrogen and helium from cosmic dust deionizing effect on solar wind, calculating gas density and flux 16 p2628 A71-33940
- Turbulent He jet time resolved velocity and He mass fraction measurements, using hot-wire anemometry and digital recording techniques 17 p2670 A71-34878
- Proton flares in McMath Region 8461 /August-September 1966/, describing solar wind plasma ejection and helium enriched interplanetary medium 18 p2958 A71-36743
- Carbon dioxide-helium mixture IR laser action and power gain increase by nitrogen addition 18 p2932 A71-37006
- Helium-cadmium laser discharge, discussing possible He trapping mechanisms and improved tube design to eliminate He cleanup 18 p2933 A71-37013
- Nonempirical LCAO-SCF-MO method for potential energy surface for ground state of linear helium-hydrogen ion system 19 p3117 A71-37332
- Gas laser operating on mixture of He and Cd 114 for excitation of scattered light spectra 19 p3073 A71-37792
- Twilight helium emission diurnal and seasonal variations relationship to geomagnetic activity and solar depression, using Abastumani observations 19 p3053 A71-37814
- Stellar rotation effects on radiation spectral characteristics, calculating He line profiles by LTE method 19 p3143 A71-38158
- Solar limb D3 He line intensity distribution measurements during eclipse of 22 September 1968 19 p3147 A71-38666
- Brayton cycle power conversion system using He-Xe gas mixture, discussing compressor net engine and turbine static efficiencies 20 p3180 A71-38908
- Transition period for variable stars, considering helium sensitive relationship to luminosity obtained with nonlinear theory 20 p3287 A71-39054
- High Arctic latitude thermospheric helium and hydrogen rocket-borne mass spectrometric measurements, showing concentrations and winter bulge 20 p3222 A71-39698
- Stellar models with He envelopes and carbon-oxygen cores, discussing interior structures and evolution of helium and R CrB stars 21 p3440 A71-40055
- Hollow dielectric waveguide gas laser with He-Ne mixtures at 6328 A 21 p3393 A71-41040
- Carbon monoxide laser emission from helium-air-cyanogen mixture 21 p3393 A71-41043
- Mean charge measurement for heavy ions moving through He and air with aid of gas-filled mass separator, noting anomalies in nuclear charge dependence 21 p3419 A71-41112
- Heat transfer from platinum wires in He and He-air mixtures, plotting Nusselt number variation with Reynolds number for various He concentrations 22 p3620 A71-41875
- Helium effects on dissociation and population inversion dynamics in pulsed carbon dioxide lasers 22 p3558 A71-42268
- Positive column He-Cd/plus/ laser discharge, determining electron temperature and density 22 p3558 A71-42345
- Solar corona O VII and Ne IX helium line triplets observations, examining electron density limits 22 p3605 A71-42352
- Nitrogen, argon and helium viscosity measurements, obtaining density expansion by statistical analysis 22 p3621 A71-42369
- Solid helium and molecular metallic hydrogen thermodynamic properties and phase diagrams as functions of pressures corresponding to Jupiter and Saturn interiors 22 p3606 A71-42613
- Gas metabolism and electrical activity of skeletal muscles of rats in He/O medium at room temperature, noting rectal temperature drop 22 p3496 A71-42803
- Beta cephei stars atmospheric He and metal abundances, comparing line spectra data with other early B stars sample 23 p3723 A71-42947
- Reduced nebular helium abundances, using capture-cascade and collisional excitation calculations 23 p3733 A71-43081
- Coalescence /collapse/ of overlapping spectral lines due to nonadiabatic broadening for Stark structure of hydrogen and helium lines in discharge plasma 23 p3707 A71-43407
- Apollo 12 lunar soil samples trapped rare gas analysis, observing solar wind He local variation from breccia 23 p3754 A71-43723
- Solar chromospheric data for 1952, 1958, 1962 and 1966 eclipses, showing helium abundance in prominences 23 p3767 A71-43842
- Neutral helium short wave solar radiation in quiescent and loop prominences 23 p3768 A71-43844
- He, HD and deuterium scattering by various gas molecules, measuring total effective cross sections for comparison with calculation 23 p3707 A71-43880
- He excitation and ionization in chromospheric flares, performing calculations for 10,000-50,000 K electron temperatures and 0.5-9.0 times 10 to 13th power per cc electron densities 23 p3722 A71-44310
- Model computations for Population I star in evolutionary phase from He exhaustion in stellar center up to carbon ignition 24 p3872 A71-45076
- HELIUM AFTERGLOW**
- Microwave noise emission in He negative glow plasma frequency range, discussing high energy electron densities near cathode 09 p1502 A71-22694
- Helium plasma afterglow at low temperatures, describing triatomic ion recombination and dissociation 15 p2460 A71-32730
- Nonthermal electron population of energy levels in cool dense helium afterglow for small principal quantum number, using Saha equation and optical spectroscopy techniques 16 p2620 A71-34044
- Helium plasma afterglow at low temperatures, describing triatomic ion recombination and dissociation 23 p3710 A71-43301
- HELIUM ATOMS**
- Perturbation theory of Hookes law model for He atom, obtaining ground state energy through third order 02 p0287 A71-12494
- Cross sections for simultaneous ionization and charge transfer in fast proton-helium atom collisions, using Born approximation 09 p1497 A71-22416
- Bright quiescent solar prominences metastable He excitation, studying electron temperatures and densities in interfilament areas 09 p1525 A71-23197
- Diffuse interstellar features in spectrum of reddened star in Cygnus OB2 stellar association, tabulating equivalent widths of H alpha and stellar He I line 10 p1665 A71-23749
- Electron impact excitation rates of bound electronic states of hydrogen, helium and alkali atoms 10 p1645 A71-24543
- H and He concentrations upper limit for Titan atmosphere from molecular diffusion time constant 11 p1828 A71-25732
- He I lines in OB spectra, examining main sequence stars 11 p1830 A71-26111

HELIUM IONS

- S wave scattering from H and He positron systems at low energies, applying Kohn and Harris variational methods 11 p1803 A71-26373
- Non-LTE physics of He atoms in hot stellar atmospheres, presenting numerical results for He I and II line spectra variations explanation 17 p2808 A71-35558
- Atmospheric neutral and singly ionized He extreme UV emission altitude distribution measurement by sounding rocket-borne thin film photon counters 20 p3231 A71-39891
- Molecular nitrogen ions collisions with He and Ne gas atoms, discussing processes based on atomic N ion fragment velocity distribution measurements at varying electron energies 21 p3421 A71-41405
- Low temperature kinetics of metastable He atom pair collisions, investigating temperature dependence of plasma ionization 24 p3856 A71-45054
- Molecular oxygen dissociation rate constant determination during interaction with He atoms in cylindrical shock tube 24 p3850 A71-45056

HELIUM IONS

- Solar He II Lyman alpha line, measuring long term absolute intensity variations 03 p0496 A71-14507
- Anomalous low magnetospheric He alpha/proton flux ratio in terms of electrostatic radial diffusion taking into account charge exchange and pitch angle loss processes 06 p0964 A71-17284
- Pitch angle distribution of protons and helium ions in magnetosphere from numerical solution of Fokker-Planck equation 06 p0964 A71-17285
- Earth immersion in glowing He ions, studying magnetosphere structural dynamics by observations from cavity 07 p1095 A71-18742
- He ion vertical concentration profiles from space probe mass spectrometer measurements 08 p1278 A71-21020
- Electron emission from He ion by proton bombardment, calculating double differential cross sections relative to ejection energy and angle 09 p1497 A71-22415
- Solar wind origin of auroral ions from low energy hydrogen and helium ion spectral measurements 10 p1664 A71-24791
- Positive H, He and O ions in exosphere from mass spectrometers mounted on Elektron 4 satellite 12 p1899 A71-26644
- Helium-like ion forbidden line emission and transition probabilities, deriving solar densities in active regions 19 p3136 A71-37621
- Light production by 2.5-490 eV helium ion collisions with nitrogen, considering 1200 and 3200 Å emission 19 p3107 A71-38055
- He II alpha lines scanned by electromagnetically driven T tube, comparing with Stark broadening theory 20 p3272 A71-39576

- He ion vertical concentration profiles from space probe mass spectrometer measurements 20 p3219 A71-39600
- H, He and O ion fluxes along exospheric magnetic field lines, determining flux energy and direction from RF mass spectrometer measurements onboard Elektron 4 satellite 20 p3226 A71-39742
- Plasmaspheric ambient hydrogen and helium atomic cations density measurement byOGO 5 ion mass spectrometer during magnetic storm, noting relationship to auroral red arcs 20 p3227 A71-39833
- Low energy hydrogen and helium ions composition of primary aurora precipitation from rocket-borne spectrometer experiment, suggesting direct solar wind origin of primaries 20 p3301 A71-39850
- Atmospheric neutral and singly ionized He extreme UV emission altitude distribution measurement by sounding rocket-borne thin film photon counters 20 p3231 A71-39891
- Cosmic ray and soft X ray steady state models of interstellar gas, determining He/H ions concentration ratio 22 p3601 A71-42167
- Interstellar He photoionization effect on solar wind abundance 23 p3721 A71-43182
- He ionization and excitation in optically thick solar prominences, considering recombination excitation for observed triplet-level populations at 5000-10,000 K electron temperature 24 p3869 A71-44805

HELIUM ISOTOPES

- Mechanical transducers for generating and detecting second sound in He isotopes at millidegree temperatures, discussing construction and performance 02 p0250 A71-12135

- Strain free insulated mounting technique for semiconductor onto cold finger at liquid He 3 temperatures 02 p0294 A71-12142
- Solar flare relative abundance and energy spectra of He 3 and He 4, using charged particle telescope on IMP 4 05 p0797 A71-15943
- Interplanetary space He 3 differential energy spectrum in 10-30 MeV range from IMP 4 satellite observations, noting solar contributions 05 p0802 A71-15944
- Isotopic helium atmospheric composition determination, using mixtures of He 3 and He 4 for comparison 06 p0921 A71-17390
- Tritium and He-3 nuclei measurements in Al targets from Soyuz spacecraft observation 08 p1354 A71-21021
- Low energy cosmic ray H 2 and He 3 nuclei intensities /1967-1968/ from Pioneer 8 and IMP 4 measurements 09 p1512 A71-22336
- Cosmic rays produced He, Ne and Ar isotope concentrations in iron meteorite separated phases, using Rudstam spallation model 10 p1676 A71-24506
- Surface wave velocity at interface between liquid He 4 and saturated vapor 13 p2101 A71-28769
- Absolute production rates of He 3 and Ne 21 in average chondrites, determining radiation ages of stony meteorites aged less than two million years 15 p2486 A71-31991
- He 4 burning nucleosynthesis, noting Ne 20 buildup in massive stars 16 p2633 A71-33335
- He, Ne and Ar isotopic distribution and origin in Apollo 12 lunar samples, considering solar wind implantation 17 p2695 A71-35030
- Adsorption cryopumped He 3 cooled IR detector without encumbrance of external diffusion or mechanical pump 18 p2922 A71-36588
- Soyuz observation of tritium and He-3 nuclei in Al targets exposed to space radiation 20 p3280 A71-39601
- Limiting He 3 abundances in four H II regions 21 p3448 A71-40449

HELIUM PLASMA

- Thermal insulation and confinement of resistance heated He plasma in Uranus stellarator with large shear 01 p0132 A71-10678
- Electron temperature determination in low density helium plasma 01 p0134 A71-11005
- Decaying helium gas plasma particles diffusion across magnetic fields by combined microwave and Langmuir electron density probes, considering instabilities 03 p0463 A71-13470
- Spectroscopic studies of helium-hydrogen plasmas in first reflected shock region in electromagnetic T-tube 04 p0631 A71-14684
- H-He partially ionized plasma bremsstrahlung, radiative and dielectronic recombination, discrete levels excitation and collisional ionization 05 p0787 A71-16489
- Dynamic stabilization of magnetoplasma drift dissipative instability by HF oscillating magnetic field, discussing helium and hydrogen afterglow plasmas 06 p0934 A71-17481
- Plasma satellites near He I forbidden lines during turbulent heating 06 p0936 A71-17592
- Ion collection by spherical and cylindrical probes in collisional He plasma, comparing saturation current measurements with transitional regime probe theories 07 p1169 A71-19909
- Pulsed discharge path in He at 100 atm and air atmosphere pressures, determining electrical conductivity dependence on discharge time by high speed photography 08 p1341 A71-21497
- Homogeneous equilibrium low temperature dense helium plasma ionization composition and radiative energy losses, calculating ionization potential 09 p1501 A71-22380
- Microwave noise emission in He negative glow plasma frequency range, discussing high energy electron densities near cathode 09 p1502 A71-22694
- Metastable atom destruction, collision-radiative recombination and electron heating in low temperature decaying helium plasmas, using spectroscopic resonance line measurements 10 p1654 A71-24896
- Electron energy distribution for spectroscopic determination in hollow cathode discharge helium-mercury plasma based on Druyvesteyn function 12 p1937 A71-27050

- Mixed plasmas transport properties at one atmosphere and 5000-35,000 K, considering helium, nitrogen, argon-nitrogen and xenon-nitrogen plasmas 12 p1986 A71-27159
- V groove cathode discharge produced He plasma parameters studied for reentry electron density and temperature simulation, correlating energy flux and microwave noise emission 12 p1895 A71-27772
- Collisional radiative volume recombination atom ionization coefficients for quasi-stationary helium considering singlet and triplet systems as two coupled individual systems 13 p2106 A71-28483
- Temperature dependence of H-beta emission from hot hydrogen-helium plasmas, calculating production rate at 10,000-100,000,000 K 15 p2455 A71-31728
- Cesium spectral lines luminescence and population during helium-cesium discharge plasma decay 15 p2458 A71-32401
- Helium plasma afterglow at low temperatures, describing triatomic ion recombination and dissociation 15 p2460 A71-32734
- Electron-ion recombination and ambipolar diffusion, disruption of electron density in cryogenic helium plasma, using cavity resonator measurements 16 p2619 A71-33644
- Harmonic generation due to strong microwave nonlinear mixing in He plasma, noting resonances at fundamental frequencies 18 p2951 A71-35933
- Multipass laser interferometry sensitivity improvement for He plasma electron density determination by increasing effective path length of laser beam in medium 18 p2931 A71-36584
- Helium plasma interaction with inhomogeneous transverse magnetic field, noting plasma electron temperature and density increase 19 p3112 A71-37744
- Metastable atom destruction, collision-radiative recombination and electron heating in low temperature decaying helium plasmas, using spectroscopic resonance line measurements 21 p3425 A71-41270
- LF waves and instabilities on positive column in magnetic field, comparing three theories for helicon modes for He at low pressures 22 p3582 A71-41899
- Helium plasma afterglow at low temperatures, describing triatomic ion recombination and dissociation 23 p3710 A71-43300
- Ar-K and He-R plasma conductivity measurements at atmospheric pressure from equilibrium to nonequilibrium conditions, using electrostatic probes 23 p3714 A71-44277
- Energy losses of collisional He plasma with ohmic heating in Uranus stellarator with large shear, comparing plasma lifetime to Bohm confinement time 24 p3855 A71-44664

HELIUM 2

U HELIUM ISOTOPES

HELIUM 3

U HELIUM ISOTOPES

HELIUM 4

U HELIUM ISOTOPES

HELIUM-NEON LASERS

- Output power stabilization of He-Ne laser, using vacuum photodiodes or semiconductor diodes for discharge current regulation 12 p1915 A71-27733
- Industrial helium-neon laser emission noise characteristics, defining amplitude fluctuations by variable proportional to photoelectric multiplier current random modulation factor 13 p2077 A71-27933
- Atmospheric turbulence effects on focused coaxial carbon dioxide and He-Ne laser beam propagation 13 p2078 A71-28523
- Cylindrical lithium niobate single crystal acoustic propagation, determining speed, damping and sound reflection with He-Ne laser light scattering at hypersonic oscillations 13 p2080 A71-29024
- Optical and microwave multifrequency autooscillatory drift and reflex klystrons, TWT and electronic oscillators, comparing to He-Ne lasers 14 p2211 A71-30099
- He-Ne lasers stimulated emission, studying optical resonant cavities and discharge tubes construction 15 p2422 A71-32572
- High sensitivity helium neon laser interferometer for transient phase objects designed for shock tubes and tunnel experiments 16 p2576 A71-32913
- Three dimensional hologram recording, showing He-Ne laser reconstruction of Q switched ruby laser hologram image of mosquito flight 16 p2579 A71-33528
- Frequency stabilized He-Ne laser wave secondary length standard for automatic measurements

discussing electronic control, accuracy, line width, pressure, current and magnetism effects
16 p2588 A71-34119

He-Ne laser frequency stabilization through Ne resonance absorption, using optical amplification for comparison resonance enhancement
16 p2589 A71-34134

Temporal distribution of photons radiated by He-Ne laser operating in five modes
17 p2750 A71-34202

He-Ne IR laser resonator as quadratic detector for modulated filtered laser radiation, noting strong LF noise
17 p2750 A71-34269

He-Ne laser emission spectra with AM by reflected Doppler shifted signal and matched/mismatched three-mirror resonator/mobile outer mirror/
17 p2750 A71-34289

Controllable phase locked frequency splitting in two-frequency lasers by anisotropic or nonreciprocal resonator elements
17 p2751 A71-34380

Photoelectric system for recording Raman spectra with He-Ne laser excitation source suitable for liquid, solution, crystal and powder and depolarization measurements
17 p2751 A71-34383

Pulsed emission and modulation of output power of He-Ne laser at 0.63 and 1.15 micron wavelengths as function of external longitudinal magnetic field
17 p2751 A71-34385

He-Ne laser emission and discharge plasma parameters, detailing variable magnetic field effects on modulation
17 p2752 A71-34389

Ne 20 transition line width behavior vs pressure in He-Ne laser at 3.19 microns wavelength
17 p2752 A71-34402

Radiative width of laser transition in Ne 20 atom and line frequency shift vs pressure in dual He-Ne laser assembly effectuating atom collisions
17 p2752 A71-34403

Power gain distribution in He-Ne laser cuvettes at 0.63 and 3.39 microns wavelength, noting current density dependent laser power gain shifts
17 p2752 A71-34405

Saturation effects and mode selection for monofrequency He-Ne lasers with nonlinear absorption
17 p2752 A71-34406

Frequency selection in He-Ne laser with Ne cell inside resonator effecting nonlinear frequency absorption
17 p2752 A71-34407

Vector synchronism for interaction between ordinary and extraordinary wave during second harmonic emission and frequency mixing in He-Ne laser
17 p2752 A71-34408

Cd ion laser with He-Ne, suggesting Cd ion excitation by Penning process
18 p2929 A71-35981

Gas discharge-current modulation noise of He-Ne laser, using sinusoidal signal at various frequencies
19 p3072 A71-37698

He-Ne lasers, investigating possible saturation effect usage in strong field to obtain single-mode operation
19 p3072 A71-37769

Diagnostic He-Ne laser interferometer for measuring electron concentration in cross section of argon plasma jet
19 p3073 A71-37786

He-Ne laser discharge tube using water cooled mercury cathode with supplementary molybdenum anode
19 p3073 A71-37789

Machining integrated circuit metal film masks with continuously operating carbon dioxide laser and high pressure pulsed He-Ne laser
19 p3069 A71-38234

Electro-optic He-Ne laser microscope for high-speed high-precision edge detection for IC masks
19 p3075 A71-38236

Fog droplet size spectral distribution from artificial fog induced He-Ne laser beam scatter, using five photometers for angular distribution measurements
19 p3091 A71-38657

He-Ne laser output noise due to mode competition, predicting behavior by Lamb three mode laser equation numerical solution
20 p3242 A71-38883

He-Ne lasers noise modulation at DC excitation, confirming existence of critical frequency related to metastable atom lifetime
21 p3392 A71-40373

Optical phase variations, temperature structure and wind velocity measurements in atmosphere using He-Ne laser beam on 70 m propagation path
22 p3509 A71-41787

He-Ne laser emission modulation through active element excitation source, using tube for discharge gap characteristics changes
22 p3558 A71-42266

He-Ne-Zn laser oscillations in red, yellow or blue spectral regions with total output power of nearly 10 mW
22 p3558 A71-42344

Frequency stabilization and instability measurement of single frequency He-Ne laser at 0.6328 microns, using Michelson interferometer as mode selector and reference cavity
22 p3559 A71-42755

Single frequency He-Ne laser stabilization by Lorentz absorption contour in external gas cell, obtaining error signal based on absorption line scanning
23 p3683 A71-43396

He-Ne laser insertion loss effect on power variation of two operation modes during cavity frequency tuning
23 p3684 A71-43401

Transistorized amplifier circuit for measuring power of CW emission from He-Ne laser
23 p3685 A71-43532

Fraunhofer diffraction apparatus design based on He-Ne laser, testing performance in distorted point lattices photography
23 p3686 A71-43956

He-Ne laser coherent radiation photodetection by variable diaphragm photomultiplier, analyzing photocurrent spectra as function of diaphragms aperture size and shape
23 p3687 A71-44175

Dispersion characteristics of He-Ne laser at 3.39 microns
24 p3834 A71-45046

Single mode output power multiplication in standard commercial He-Ne laser with cavity extension and etalon
24 p3835 A71-45214

He-Ne laser discharge gap oscillation modes observation, noting applied magnetic field, gas parameters and cathode type effects on stimulated emission
24 p3835 A71-45239

He-Ne laser radiation modulator at 1.5 GHz using X and Z cut lithium niobate crystals in toroidal microwave cavity
24 p3835 A71-45265

HELIX TUBES
U TRAVELING WAVE TUBES
HELIXES
U CURVES [GEOMETRY]
HELMETS
Flight helmet sound attenuation test, using Manikin method
01 p0026 A71-11189

Heavy cosmic particle dosage measurement by chemical etching of particle tracks on Apollo astronauts plastic helmets
04 p0543 A71-14822

Properly fitting flight helmets for U.S. Army aviation personnel in Vietnam
06 p0859 A71-17616

Astronaut electrode-amplifier helmet harness for cable and radiotelemetry acquisition of EEG, EGO, EMG and blood pressure data on noninterference basis
10 p1570 A71-24475

Flight helmets speech intelligibility evaluation using in-flight manikin recording
10 p1572 A71-25069

Heavy cosmic ray nuclei track counts in plastics, examining Apollo mission 8 and 12 helmets
10 p1665 A71-25121

HELMHOLTZ EQUATIONS
Boundary value problems solution of Helmholtz and Poisson equations for parallelepiped, applying to elasticity theory
02 p0328 A71-12542

Neumann boundary value problem for region D Helmholtz equation, considering parameter dependence
04 p0619 A71-14649

Neumann problem for Helmholtz equation in complex configuration region, developing variational solution method
05 p0782 A71-16884

Integral equation solution for air flow over mountain system, considering boundary value problems of Helmholtz equation
07 p1149 A71-18794

Arbitrarily shaped waveguide analysis computer program EHPOL for polynomial approximation to eigenfunctions of Helmholtz equation, considering homogeneous Neumann and Dirichlet boundary conditions
08 p1261 A71-20752

Neumann boundary value problem for Helmholtz equation in region complementary to highly jagged set in fixed surface neighborhood
08 p1325 A71-21698

Helmholtz and relativistic electrodynamics, discussing kinetic interaction potential using Lorentz invariance
10 p1644 A71-25110

Rellich uniqueness theorem for Helmholtz equation for steady state wave propagation in inhomogeneous anisotropic media subject to Sommerfeld radiation
12 p1929 A71-26865

HEMISPHERE CYLINDER BODIES

Integral equation methods application to exterior boundary value problems solution for Laplace and Helmholtz equations
15 p2441 A71-31350

Modified method of cross sections applied to scalar Helmholtz equation solution in infinite symmetrical waveguides
15 p2449 A71-31711

Nonhomogeneous Helmholtz vibration equation for sectorial-annular membranes and plates under arbitrary load, using Fourier method
15 p2508 A71-32231

Approximate solutions to quasi-linear n dimensional Helmholtz equation by asymptotic methods
19 p3088 A71-38477

Principal boundary value problems solution for Helmholtz equation in half space with spherical cavities, reducing problems to infinite systems of algebraic equations
20 p3268 A71-38808

Calculation method for flow about bodies with injection, presenting parameters approximation formulas derived from Cauchy problem solution for Helmholtz equation
24 p3789 A71-44478

HELMHOLTZ VORTICITY EQUATION
Helmholtz vorticity equation application for indirect determination of inaccessible area geopotential field from satellite data
23 p3700 A71-43305

HEMATOCRIT
Glucose intestinal absorption, blood glucose and hematocrit in hamsters, relating physiologic modifications to pregnancy
02 p0201 A71-12608

HEMATOCRIT RATIO
Age effects on whole blood viscosity with Wells-Brookfield microviscometer, investigating role of hematocrit and plasma protein
11 p1722 A71-26362

Long term immersion effects on human water-salt metabolism, noting increased erythrocyte water contents and hematocrit index
13 p2006 A71-28403

HEMATOLOGY
Acute inhalation toxicity of monomethylhydrazine vapor on rats, mice, beagles, squirrels and rhesus monkeys, considering hematology and blood chemistry tests
07 p1046 A71-19000

Carbon dioxide absorption of dog blood and plasma under anoxia at simulated high altitudes, deriving equations for protein concentration rated buffer values
07 p1043 A71-20327

Dehydration effects on blood parameters in Somali donkeys and zebu steers, observing increases in plasma osmolality, sodium chloride, hemoglobin, packed cell volume, etc
17 p2681 A71-34940

Hematological characteristics of emotional stresses during parachute jump, studying leucocyte, erythrocyte and eosinophil populations changes
24 p3800 A71-44413

HEMATOPOIESIS
Mumie preparation effect on DNA and RNA contents in hemopoietic organs during acute radiation sickness due to low power radiation
01 p0013 A71-11118

Mitomycin C radiosensitizing effect on hematopoietic colony forming cells, using technique based on bone marrow cells spleen colonies forming ability
07 p1036 A71-18958

Amytetravite and ATP effect on hemopoiesis of dogs subjected to chronic and repeated gamma irradiation
15 p2357 A71-31312

Hematopoietic injury and recovery from radiation exposure for dogs and monkeys, showing dose protraction effects
16 p2532 A71-33774

Hemopoiesis and anoxybiotic processes comparative characteristics in brain and muscular tissues of heterothermal and homoiothermal rodents during prolonged hypoxia
17 p2679 A71-34221

HEMATOPOIETIC SYSTEM
Para-aminopropiophenone and propylene glycol radiation protective effect on hematopoietic stem cells of mice
07 p1036 A71-18959

Hematoporphyrin chlorhydrate radioprotective effects on mice, removing, weighing and fixing spleens for hematopoietic colonies count
07 p1036 A71-18960

Irradiation protection in mice, dogs and sheep by bacterial endotoxin injection, discussing hematopoietic system stimulation and leukocyte counts
07 p1038 A71-18974

HEMISPHERE CYLINDER BODIES
Hypersonic flow past freely vibrating hemisphere-cylinder-cone, noting Reynolds and Mach numbers dependence and conical stabilizer aperture angle
03 p0345 A71-14571

HEMISPHERES

Laminar convective heat transfer rates on hemisphere cylinder in rarefied hypersonic flow, comparing experimental results with Cheng, Davis and Lees theories

17 p2671 A71-34902

Opposed hemispherical self acting gas bearings fabrication for gyro wheels, using machine lapping and sputter etching

22 p3553 A71-41677

HEMISPHERES

Blunt and hemispherical base axisymmetric bodies in Mach 4 free stream, investigating turbulent near wakes generation

21 p3324 A71-40999

Conical monopole antenna imaging above hemispherical ground of variable radius, plotting finite screen effectiveness from analytical and numerical solutions

23 p3655 A71-44168

Thermal radiation hemi-ellipsoidal and hemispherical collectors efficiency characteristics from Monte Carlo simulation for focusing photon bundle trajectories

23 p3783 A71-44191

HEMISPHERICAL SHELLS

Pulsating liquid filled hemispherical shell dynamic characteristics, determining hydrodynamic pressure and shell displacements

06 p0882 A71-17837

Metallic diaphragms design, fabrication and testing for cryogenic fluid and positive expulsion systems [AIAA PAPER 70-683]

11 p1768 A71-25518

Spherical head projectiles collision with hemispherical shells and square plates with and without protective covering, calculating stress distribution

12 p1976 A71-27160

HEMODYNAMIC RESPONSES

Eating and digestion effects on conscious dog coronary and visceral vasoactivity

01 p0015 A71-11183

Previous heavy work effect on central hemodynamics and autonomic nervous system, discussing ensuing heart rate changes

04 p0545 A71-15156

Middle cerebral artery occlusion effect on cortical blood flow, tissue oxygen pressure and acid base equilibrium in animals under extended ligations

05 p0708 A71-16617

Hypokinesia and acceleration effects on plasma proteins displacement and bioelectric activity of striated muscles of rats

06 p0853 A71-17960

Fluorescein permeability of hemato-ophthalmic barrier of rabbits after acceleration exposure

06 p0854 A71-18364

Multifactor correlation analysis of systemic circulation effects on brain blood filling level, using linear regression equations

06 p0855 A71-18373

Rheoencephalography of cerebral hemodynamics during mental work, showing left hemisphere hyperemia

08 p1242 A71-21960

Pancreas pathomorphology under acute hyperthermia in animals, showing hemodynamic changes of vessel dilatation and intravascular leukocytosis

08 p1243 A71-21968

Hemodynamic correlation of Austin Flint murmur and a-wave of apexcardiogram in aortic regurgitation

09 p1392 A71-22589

Central nervous system role in body metabolism effects on cardiac output, measuring 2,4-dinitrophenol (DNP) dosage effect on arterial pressure and oxygen consumption in dogs

09 p1396 A71-23541

Hypodynamia effects on human hemodynamics under various microclimatic conditions, noting hormonal activity changes in sympathoadrenal system

10 p1563 A71-24339

Coronary hemodynamic responses to postural changes in hemorrhaged dogs involving head-up and head-down tilts

11 p1720 A71-26114

Diastolic and mean blood pressure responses to exercise after beta-adrenergic blockade in normal and labile hypertensive subjects, using Trascior

13 p2014 A71-29320

Myocardial ischemia observations, utilizing morphologic and pathophysiologic correlations with cinecoronary arteriography, left ventriculography and hemodynamic examination

14 p2185 A71-30287

Hemodynamic changes in healthy pilots with excess weight investigated by mechanocardiograph, showing decreased cardiac output, left ventricle strength and volume rate

15 p2357 A71-31319

Systolic and diastolic blood pressures and urinary catecholamines under stress in normotensive and hypertensive subjects

15 p2358 A71-31451

Upright tilt stress effects on cardiac cycle phases in healthy subjects, using noninvasive techniques

15 p2358 A71-31453

Lowered cardiac output and arterial pressure response to exercise after autonomic heart blockade in man, noting retained work capability

15 p2358 A71-31454

Renal hemodynamic factors in whole kidney glomerulotubular balance in anesthetized dogs by manipulating filtration rate through constriction of aorta, thoracic vena cava, etc

16 p2529 A71-33194

M-cholinergic and adrenergic subcortical structures blockage effects on blood flow rate in dog pulmonary circulation system

16 p2534 A71-34113

Bed rest effects on human hemodynamic and gaseous metabolism, observing increased cardiac output and decreased oxygen consumption and carbon dioxide production

20 p3188 A71-39231

Vasomotor effects of vagus nerve on canine lung blood content in response to electrical stimulation of vagosympatheticus

22 p3490 A71-42581

HEMODYNAMICS

Soviet book on blood hydrodynamics covering circulatory system structure, rheology and mathematical models, pulsating flows, concentration effects and mass transfer

02 p0203 A71-11846

Gravitational acceleration effects on hemodynamics, describing mechanocardiographic equipment

02 p0198 A71-11900

Pulsus alternans study by noninvasive techniques for assessing cardiovascular function in hemodynamics and muscular physiology

03 p0372 A71-13492

Mathematical model for brain arteries hemodynamic resistance, using blood pressure data

09 p1390 A71-22261

Coronary blood flow regulation, discussing local and remote control mechanisms and disturbance effects due to obstructive arteriosclerosis

13 p2003 A71-27860

Automation in cardiology, discussing analog and digital computer techniques for on-line hemodynamic analysis and collection and manipulation of cardiovascular data

13 p2016 A71-27868

High altitude blood coagulation, determining hypercoagulability relationship to altered pulmonary hemodynamics

14 p2183 A71-30278

Cortical neurodynamics during vestibular afferent activity and associated cardiovascular and respiratory reactions, noting EEG correlation to hemodynamics

16 p2527 A71-32828

Arterial or venous blood oxygen tension continuous measurement, describing electrode cuvette design with response time of less than 3 sec

16 p2535 A71-33248

Hemodynamic evaluation of glucagon in symptomatic heart disease, comparing to isoproterenol

17 p2682 A71-35040

Cardiac sympathetic nervous control of right ventricular pressure-flow dynamics in outflow tract in anesthetized dogs

22 p3484 A71-41522

Hemodynamic evaluation of heart rate augmentation produced by atrial pacing and isoproterenol in early postoperative phase of cardiac valve surgery

23 p3640 A71-44131

Coriolis acceleration effect on human organism from optic functions and retinal hemodynamics study

24 p3795 A71-44534

HEMOGLOBIN

NT CARBOXYHEMOGLOBIN

NT OXYHEMOGLOBIN

Electron density maps of human deoxyhemoglobin revealing C-terminal residues configurations of beta chain by three dimensional Fourier synthesis

01 p0015 A71-11343

Oxygen uptake by hemoglobin solution, considering diffusion rate and chemical reaction by mathematical model numerical solution

03 p0360 A71-13180

Hemoglobin-sodium nitrite reaction in absence of oxygen, discussing methemoglobin formation by autocatalysis

03 p0363 A71-13486

Carbon dioxide reduction and hemoglobin saturation rates of blood flow in curved channel membrane exchanger

13 p2013 A71-29004

Oxygen dissociation curve shift, hemoglobin affinity and diphosphoglycerate concentration in blood of acidotic and normal subjects at altitude

13 p2016 A71-29494

Erythrocytes diphosphoglycerate increase mechanisms during hypoxia and anemia, studying hemoglobin oxygenation state effects

17 p2685 A71-35368

Oxygen uptake kinetics by hemoglobin layers, using Hill advancing front equation

19 p3010 A71-38567

HEMOLYSIS

Streptococcal flora in pharynx of men during prolonged enclosure noting concomitant hemolytic microbes

06 p0854 A71-18322

Composition and colicinogenic and hemolytic activities changes of *Escherichia* isolated from man during long term confinement

21 p3333 A71-40594

HEMORRHAGES

Hemorrhagic reticulolysis in flying personnel in terms of etiological, evolutive and therapeutic aspects

01 p0028 A71-11573

Coronary hemodynamic responses to postural changes in hemorrhaged dogs involving head-up and head-down tilts

11 p1720 A71-26114

HEOS A SATELLITE

Highly eccentric satellite orbit, determining analytical solution for HEOS 1 launch window

01 p0154 A71-10360

Solar wind heavy ion data, using Heos-1 satellite observations of 31 March 1970 interplanetary shock

13 p2130 A71-29040

HEOS A-1 satellite telecommunication system describing command, telemetry and ranging subsystems

18 p2875 A71-35919

HEOS-A2 eccentric orbit satellite for interplanetary space and high latitude magnetosphere data, discussing onboard experiments, major subsystems and design philosophy

22 p3607 A71-41540

HEOS SATELLITES

NT HEOS A SATELLITE

International HEOS project organizations discussing communication, task delegation, decision making and structure

23 p3785 A71-43430

HEPARINS

Heparin efficacy in burns, considering healing time and pain relief, etc

02 p0207 A71-12345

HEPTANES

Polymethyl methacrylate lifetime tested in water and heptane, showing increase with orientation degree

16 p2601 A71-33686

N-heptane, carbon dioxide and Freon 13 droplet vaporization measurements at supercritical pressures comparing with film theory calculation

24 p3890 A71-45070

HERCULES AIRCRAFT

C-130 AIRCRAFT

HEREDITY

Chromosome radiation injury preservation of generations of X ray irradiated cells of human diploid strains

08 p1242 A71-21960

Eye movements and visual images evoked by verbal stimuli, considering hereditary factors contribution to image formation

24 p3796 A71-44540

HERMETIC SEALS

Waist seal design providing discrete anatomical placement, subject comfort, ingress/egress ease and size accommodation for lower body negative pressure devices

11 p1725 A71-26114

Dynamic seal development for space base rotational hubs, describing simulated environmental tests for elastomer inflatable seals and lubricants evaluation [AIAA PAPER 71-863]

18 p2927 A71-36690

HERMITIAN POLYNOMIAL

Partial differential equations approximate solutions using Hermitian functions and collocation for improved numerical accuracy

05 p0776 A71-17222

Nonlinear boundary value problems numerical solutions using spline and Hermitian functions in Ritz-Galerkin setting

06 p0917 A71-17566

Kato upper and lower bounds formula application to Hermitian operator eigenvalues

07 p1146 A71-18740

Tchebycheffian spline functions, solving Hermite Birkhoff interpolation as stochastic prediction and filtering

07 p1147 A71-19322

Hermite polynomials application to stiffness matrix determination in plate finite element method for displacement plane stress, presenting digital computer program flow diagram

24 p3880 A71-44640

HERTZSPRUNG-RUSSELL DIAGRAM

Hertzsprung-Russell diagram calibration in terms of age and mass for main sequence B and A stars

04 p0646 A71-15233

Variable emission star BD plus 28.637 deg three color photographic observation data evaluation, giving light curves and H-R position

07 p1201 A71-20433

Horizontal and post-horizontal branch hydrodynamic rich stellar atmospheric models, presenting emergent fluxes and H and He line profiles

14 p2314 A71-30640

- Trigonometric white dwarf star parallax measurements, using astrometric reflector to derive H-R diagram
14 p2316 A71-31007
- Population II stars evolution models from main sequence to supergiant stage, constructing time constant loci in H-R diagram
16 p2635 A71-33432
- Stellar composition analysis of Small and Large Magellanic clouds using Hertzprung-Russell, color magnitude and two color diagrams
20 p3301 A71-39823
- Short period variables, considering Scuti stars evolution, pulsations, magnitude and positions in H-R diagram
21 p3440 A71-40054
- HERZBERG BANDS**
Night airglow oxygen Herzberg I bands covariation with O I 5577 Å line, evaluating NASA 1968 airborne auroral measurements
23 p3670 A71-43186
- HERETOCYCLIC COMPOUNDS**
NT ACETAZOLAMIDE
NT ADENINES
NT ADENOSINE DIPHOSPHATE [ADP]
NT ADENOSINE TRIPHOSPHATE [ATP]
NT ADENOSINES
NT ASCORBIC ACID
NT ATROPINE
NT AZINES
NT BIOTIN
NT CYANURATES
NT INDOLES
NT NICOTINE
NT OXAZOLE
NT PHTHALOCYANIN
NT PHYLLQUINONE
NT PILOCARPINE
NT PYRIDOXINE
NT RETINENE
NT THIAMINE
NT THYMIDINE
NT THYMINE
NT TRYPTOPHAN
NT URACIL
Amidoximes dehydration with and without rearrangement, suggesting carbodiimide formation from O-benzenesulfonyl ester
06 p0865 A71-17550
Gaseous 3-oxetanone ring compound, investigating IR and vibrational spectra and molecular structure
09 p1403 A71-22473
Murchison meteorite heterocyclic compounds contents, using gas chromatography-mass spectrometry
17 p2801 A71-34650
- HETERODYNING**
NT OPTICAL HETERODYNING
IR photodiode heterodyne detection, deriving noise equivalent power, conversion gain, frequency response, local oscillator power and IF amplifier noise factor
02 p0249 A71-12035
Carbon dioxide laser heterodyne plasma density length product measuring with microsecond response in Astron controlled fusion experimental area
07 p1126 A71-20166
Heterodyne oscillator instability free frequency drift measurement of mixed FM signals in circuits with supplementary conversion
12 p1885 A71-26842
Absolute measurement of laser frequencies in IR range, using extended harmonic heterodyne technique
14 p2255 A71-30979
- HETEROGENEITY**
Nondissipative heterogeneous shear flow stability in presence of uniform magnetic field in streaming direction
07 p1169 A71-20023
Heterogeneity effects on thin composite cylindrical shells axisymmetric vibration characteristic, considering material and geometric symmetry deviations influence on frequency spectra
08 p1368 A71-20805
Heterogeneous orthotropic cylindrical shells, calculating free natural vibration frequency spectra from refined equations of motion in Love and Donnell type theories
11 p1841 A71-25184
Inclusions diffusive motion effects on heterogeneous systems creep properties, determining creep rate as function of stress and temperature
13 p2148 A71-27960
Transhorizon radio propagation by atmospheric heterogeneities, discussing effect on attenuation, antenna gain reduction and transmission bandwidth
13 p2033 A71-29239
Creep test results scatter, considering non-homogeneity of specimen properties and deviation from test conditions
20 p3250 A71-39021
- HETEROSPHERE**
Atmospheric modeling for earth and Venus heterosphere structure using multicomponent radiative hydrodynamic equations, determining atmospheric temperature and constituents height variation
11 p1828 A71-25764
- Semiannual density variation in heterosphere as function of height based on satellite drag and atmospheric models
16 p2564 A71-33723
Heterosphere semiannual density variation with amplitude as function of height, noting dependence on temperature distribution and sunspot cycle
16 p2574 A71-33963
Atmospheric modeling for earth and Venus heterosphere structure using multicomponent radiative hydrodynamic equations for atmospheric temperature and constituents height variation determination
22 p3598 A71-41532
- HETEROTROPHUS**
Heterotrophic growth in dim light of blue green alga Agmenellum quadruplicatum and Lyngbya lagerheimii with glucose as carbon source
09 p1402 A71-23472
- HEURISTIC METHODS**
Search procedures selection from heuristic methods of solving design development problems by computer
01 p0087 A71-10408
Decision making heuristic program reflecting human brain function in problems with listed requirements and unspecified goal
03 p0369 A71-13002
Biological heuristic programming in cybernetics, discussing solid state logic elements limiting factors in modeling
03 p0383 A71-14394
Heuristic flow acoustics, discussing noise frequency spectrum in reference to moving singularities
04 p0569 A71-14980
Heuristic method for phase velocities and growth rates of ion and electron plasma oscillations generalized to multicomponent plasmas
07 p1166 A71-18887
Geomagnetic cavity heuristic model with solar wind driven unipolar induction current in ionosphere
08 p1280 A71-21218
Heuristic search algorithm for highest and lowest values of functions, considering Algol program
09 p1485 A71-22313
Control systems optimization via heuristic approach based on Pontryagin maximum principle and pseudotrajectory concept
09 p1423 A71-22968
Nervous system modeling, considering cybernetic brain functions, neuroheuristic programming and modes of distributed information processing pertinent to neuropsychological experiments
10 p1568 A71-24222
Heuristic algorithm for computation of failures detection tests in asynchronous sequential logic circuits
14 p2218 A71-29520
Heuristic signal design for digital communication over fast-fading Gaussian channels, stressing nonorthogonal signaling schemes
14 p2193 A71-30010
Compressible three dimensional nonsimilar laminar boundary layers numerical analysis using two layer heuristic model
18 p2845 A71-36336
Finite difference technique for convective flow equations involving shock wave propagation, discussing heuristic analysis for truncation error
18 p2907 A71-36338
Heuristic approaches for generating perturbations to automatically evaluate partial derivatives for interplanetary space missions
19 p3135 A71-37561
Nonlinear wave packet and modulated beam propagation description in approximate heuristic theories, considering chimeras as neoclassical approximation for equations solution
23 p3705 A71-44122
- HEXAGONAL CELLS**
Silicidization on Nb-Ta alloys, considering formation of niobium disilicide phase with hexagonal lattice
15 p2425 A71-31401
- HEXAGONS**
Eighteen layer hexagonal ferrite magnetic properties in various fields and temperatures, noting magnetization and crystal structure
12 p1943 A71-26862
- HEXOKINASE**
Glucose and fructose extraction from formose sugar mixtures by enzymatic methods using hexokinase reaction
19 p3011 A71-37574
- HEXOSSES**
Hexosamines biosynthesis control mechanism, considering UDP-N-acetylglucosamine function
05 p0706 A71-16217
- HEXYL COMPOUNDS**
Mass spectral properties of alkoxy cyclohexanol trimethylsilyl ethers and alkoxy cyclohexyl trimethylsilanes, using deuterium labeling
02 p0209 A71-12575
- HMX HELICOPTER**
U H-53 HELICOPTER
- HIBERNATION**
Ultrastructure changes of membrane and sarcoplasmic reticulum of myocardial cells in squirrels during hibernation
06 p0850 A71-17412
- Hyperresponsiveness in hibernating mammals, discussing responsiveness increase with body temperature decrease as compensating mechanism for sensitivity loss
07 p1041 A71-19524
Animals tissue activity during winter hibernation under Alaskan environmental conditions, discussing sense of time, anticipation of seasonal changes, etc
07 p1041 A71-19525
Circannual biological clock operation without environmental signals based on squirrel hibernation and bird migration studies
10 p1563 A71-24298
Marmot ketone bodies concentration during activity, deep hibernation and early arousal, discussing increased oxidative metabolism effects
13 p2014 A71-29125
Adrenocortical function in garden dormouse during autumnal preparation for hibernation, considering environmental temperature factors
13 p2014 A71-29315
Venous and arterial blood gases in hibernating and normothermic ground squirrels, showing venous oxygen and carbon dioxide partial pressures reduction in hibernation
17 p2681 A71-34941
Thyroidectomy and cold adaptation effects on hibernating hamsters thermoregulation and heat transfer coefficient
18 p2860 A71-36881
Thermal behavior simulation of cooling biological system, describing heat generation and transfer at normothermic to hibernating body temperatures with mathematical model
19 p3003 A71-38199
Autoclave chronic catheter system and restraining box for blood sampling and pressure measurement for hibernating marmots
19 p3010 A71-38568
Low temperature effects on succinate oxidase activity of mitochondrial membranes in hibernating squirrels
21 p3336 A71-40854
Hibernation effects on hedgehog electrolyte distributions and renal function, determining Na, K, Mg and Cl concentrations in muscles, liver, kidney, plasma red blood cells and bladder urine
22 p3488 A71-42416
Ambient temperature effects on spontaneous rewarming of ground squirrels during awakening after hibernation
22 p3491 A71-42582
Preoptic and environmental temperature effects on hibernator thermoregulatory responses, noting changes in metabolic rates
23 p3637 A71-44301
- HIERARCHIES**
NT BBGKY HIERARCHY
NT DICHOTOMIES
Hierarchical systems effectiveness estimation algorithm, taking into account reliability
05 p0731 A71-16796
NonMarkoffian kinetic theory for hierarchical structure of clusters in expanding universe
06 p0964 A71-17314
Time optimal hierarchical failure-search systems by varying structure for four different search algorithms
10 p1585 A71-24161
Motivation principles in industry based on Maslov theory of hierarchy of needs, discussing selection of supervisory personnel
13 p2167 A71-28798
Hierarchical systems compromise controls selection by decomposition method
15 p2379 A71-31843
Algorithm for dual compromise control problems arising from each subsystem of inner level in multilevel static hierarchical system
24 p3812 A71-44393
- HIGH ACCELERATION**
Mechanical stability of self healing viscous glass layer in porous oxidation protection coating on Ni under high acceleration
02 p0272 A71-12945
Interchangeable head vibration exciter for 200g large object testing and measurement of structural modes, impedances, transfer functions and calibration
11 p1746 A71-26495
Optical tracking system for high angular acceleration missile flights, using movable mirrors with motion picture camera interfaced with computer
18 p2900 A71-36906
- HIGH ALTITUDE**
Turbulent/total flight mile ratio in high altitude clear air turbulence/HICAT/program
07 p1022 A71-20314
Reevaluation of emergency pressurization requirements for brief flights over 50,000 feet, considering pressure suit requirement
08 p1247 A71-20822
Physical and physiopathological effects of high altitude supersonic flight in TF-104G aircraft told by flight surgeon
10 p1572 A71-24980

HIGH ALTITUDE BALLOONS

HIGH ALTITUDE BALLOONS

High energy electrons in near space excess radiation from high altitude balloon and satellite data
09 p1513 A71-22667

Vertical and horizontal atmospheric electric fields measurements at balloon altitudes, considering magnetospheric processes effect and potential differences
10 p1603 A71-24699

High altitude balloon gore meridional stresses effects on film response by analyzing cylindrical elastic membrane under uniform hydrostatic pressure and axial loads
12 p1976 A71-27121

High altitude balloons pressure-altitude transducer assembly, discussing electronic circuitry, calibration and temperature and vibration effects
14 p2240 A71-30070

Belgian report to COSPAR, reviewing experiments with gas release at high altitudes and stratospheric balloons
16 p2667 A71-33870

High altitude balloon cosmic dust collection, considering individual particle chemical composition and ablation
20 p3299 A71-39653

Alcyon project PTA 1, considering balloon stabilization efficiency during night-day transition and system reliability
22 p3483 A71-42400

HIGH ALTITUDE BREATHING

Oxygen transport and consumption, ventilation and cardiac index in natives and sojourners at high altitudes
06 p0853 A71-18060

Aircraft crew without pressure suits, noting abrupt ambient pressure drop tolerance in trained and untrained subjects
12 p1876 A71-27659

High altitude aerobic working capacity limitations, examining oxygen transport system and circulator factors
14 p2183 A71-30276

High altitude pulmonary edema in unacclimatized humans, discussing symptoms, etiology incidence and prevention
14 p2183 A71-30277

High altitude pulmonary edema syndrome, investigating increased alveolar-arterial oxygen gradients of humans during treadmill exercise
14 p2184 A71-30279

Systemic arterial blood pressure response to chronic high altitude and hypoxia effects
14 p2184 A71-30280

High altitude acclimatized humans, noting decreased coronary blood flow and increased oxygen extraction
14 p2184 A71-30283

Short term high altitude exposure, determining coronary blood flow reduction relationship to cardiac output and stroke volume
14 p2184 A71-30284

High altitude residents cardiovascular evaluations, showing right ventricular enlargement and reactive pulmonary hypertension
14 p2184 A71-30285

Human hypoxic ventilatory drive data for high altitude breathing, noting motivation reduction inversely related to time and altitude
14 p2185 A71-30288

Physical exercise oxygen uptake and debt in dogs at ground level and high altitude, investigating beta adrenergic blocking agent effects
16 p2530 A71-33242

Trained young runners maximum oxygen consumption rate at sea level and high altitude
16 p2530 A71-33244

Noradrenaline concentration in myocardium of rats subjected to high altitude hypoxia, considering heart regulation in presence of hyperfunction and hypertrophy
19 p3001 A71-37393

Ventilatory response to progressively increasing inspired carbon dioxide tensions at ground level and acetazolamide pretreatment before high altitude exposure
23 p3636 A71-44242

Pulmonary carbon monoxide diffusing capacity of sea level and high altitude dwellers at various altitudes, noting early postnatal lung growth effects
24 p3797 A71-44778

Hypoxic respiratory reactions of highland natives and recently arrived residents to oxygen concentration change in inhaled mixtures
24 p3798 A71-45065

HIGH ALTITUDE ENVIRONMENTS

Temperature controlled zinc-silver oxide reserve battery, describing design for high power/energy density, broad operating temperature range and high altitude environmental capability
03 p0352 A71-13044

Radiological risks of cosmic radiation during high altitude supersonic flights, considering galactic, solar and incident particles in aircraft atmosphere
03 p0473 A71-13099

Muons spatial distribution function in mountain level extensive air showers
03 p0476 A71-13855

Aerial stowaway clinical case covering unconsciousness, deafness, hypoxia, hypothermia, acidosis and other effects due to 9 hr flight in unpressurized landing gear cell
04 p0544 A71-15058

Chronic hypoxia effects on capillary development during high altitude exposure in decompression chamber and maintenance at sea level
08 p1237 A71-20679

Supersonic transport air traffic meteorology, considering high altitude and flight velocities, applications technology satellites for lower stratosphere thunderstorms, clear air turbulence, etc
09 p1488 A71-23070

IR astronomy high altitude sites, discussing optimal geographic locations, observation conditions criteria, transportation and survival measures
11 p1743 A71-25242

Parachutes for low density atmospheres, describing low and high altitude test results
[AIAA PAPER 70-1164] 11 p1707 A71-25525

Atomic Ba excitation, ionization and oxidation during release in sunlight at high altitudes
13 p2026 A71-29038

Hydrodynamic instability generation by stable layer tilting at high altitude, considering clear air turbulence
15 p2445 A71-32712

High-mountain altitudes inhibition of inflammation and wound healing in rabbits
16 p2531 A71-33522

Environmental radiation exposure in air travel, comparing integral radiation dosages for conventional jet transport aircraft and SST
20 p3192 A71-38976

Muons lateral distribution function in mountain level extensive air showers
22 p3595 A71-42656

HIGH ALTITUDE FLIGHT

U FLIGHT

U HIGH ALTITUDE

HIGH ALTITUDE NUCLEAR DETECTION

Nuclear interactions of neutral cosmic particles with carbon target at mountain altitudes
03 p0476 A71-13848

High altitude thermonuclear explosion fission fragments locating method, considering magnetogravitational trap as potential well for heavy charged fragments
20 p3279 A71-39143

Nuclear interactions of neutral cosmic particles with carbon target at mountain altitudes
22 p3595 A71-42649

HIGH ALTITUDE PRESSURE

Rat left ventricle isolated papillary muscles contractile force in pressure chamber under high altitude adaptation
09 p1388 A71-22125

Escaping photoelectrons effect on polar wind exospheric model, suggesting kinetic pressure predominance at very high altitudes
16 p2569 A71-33814

HIGH ALTITUDE TESTS

Carbon dioxide absorption of dog blood and plasma under anoxia at simulated high altitudes, deriving equations for protein concentration rated buffer values
07 p1043 A71-20327

High altitude radiosonde thermometer and pressure sensor construction, discussing radiation error and wire lag
08 p1293 A71-21740

High altitude submaximal and maximal work by humans, noting time required for steady state oxygen consumption, ventilation and heart rate
09 p1401 A71-23368

Oxygen red-green line emission intensity in quiet auroral arc, using rocket-borne photometers
11 p1754 A71-25551

Hypoxia, high altitude and heart - Conference, Aspen, Colorado, January 1970
14 p2183 A71-30275

High altitude blood coagulation, determining hypercoagulability relationship to altered pulmonary hemodynamics
14 p2183 A71-30278

Chronic hypoxia effects on blood oxygen and carbon dioxide tensions and pH changes in unanesthetized chickens at high altitude compared to sea level control
14 p2186 A71-30565

Cellular respiration and high altitude adaptation effect on cytochrome content and on oxidation and oxidative phosphorylation parameters of brain homogenates in rats
15 p2357 A71-31310

Human body water metabolism during acute high altitude exposure with heavy physical activity and high food intakes
16 p2530 A71-33240

Electronic time delay fuses with high-g components for gun launched projectiles for placing payloads at high altitudes
18 p2851 A71-30282

Temperature pulsation measurements by high altitude aircraft in presence of lower troposphere convection elements
21 p3412 A71-41939

Ventilatory response to progressively increasing inspired carbon dioxide tensions at ground level and acetazolamide pretreatment before high altitude exposure
23 p3636 A71-44242

Age effects on plasma aldosterone levels, red cell plasma and total blood volume at sea level and high altitude
24 p3797 A71-44740

HIGH ASPECT RATIO

Turbine blades with high aspect ratios, calculating behavior at small Reynolds number
[ASME PAPER 70-WA/GT-11] 03 p0343 A71-14141

Large aspect ratio rectangular duct with nonuniform surface texture, investigating turbulent flow, maximum velocity positions and zero shear stress
07 p1086 A71-18793

High aspect ratio jet flap lifting-line theory, using matched asymptotic expansions method
09 p1381 A71-22022

Three dimensional jet flapped wing matched asymptotic expansion solution for high aspect ratios based on thin airfoil theory assuming inviscid and incompressible flow
12 p1863 A71-27272

Friction factor for low Reynolds number turbulent flow in large aspect ratio rectangular ducts, comparing Blasius and Prandtl relations
[ASME PAPER 71-FE-A] 13 p2051 A71-29339

Gust transfer functions relating lift and moments to upwash in single sinusoidal wave for large aspect ratio rectangular wings in turbulent incompressible flow
14 p2176 A71-30600

Fuselage influence on total aircraft drag in subsonic passenger aircraft, considering high aspect ratio cylindrical fuselages
14 p2177 A71-30608

Low Reynolds number turbulent flow in large aspect ratio rectangular ducts, investigating Blasius and Prandtl circular tube friction factor relations
15 p2392 A71-32222

Flat modulation transfer functions obtained by spatial filtering of high aspect ratio annular aperture images in coherent optical processor
22 p3549 A71-42552

HIGH ASPECT RATIO WINGS

U SLENDER WINGS

HIGH CURRENT

High power regulated energy transfer by inductor transformers with single and multiple stages using trapezoidal current waveshapes
03 p0352 A71-13080

Integrated circuit conductors short pulse high current rating, identifying three failure regimes
04 p0559 A71-15888

High intensity electric current damage in boron and graphite filament reinforced epoxy resin composites
07 p1145 A71-19999

Niobium nitride thin films very high critical currents and field characteristics, noting deposition by sputtering
07 p1179 A71-20101

Time delay in pulsed optical carbon dioxide laser pumping mechanism in high current gaseous discharge
11 p1773 A71-25777

Thermal load capacity and nozzle shape for guiding and constricting high current plasmas from electric arc data, using Ar as discharge gas
14 p2279 A71-29848

Substrate emitter monolithic inverted transistor structure for low-power high-current gain applications
15 p2375 A71-31444

HIGH EFFICIENCY

U EFFICIENCY

HIGH ENERGY

U ENERGY

HIGH ENERGY ELECTRONS

Energetic electron magnetospheric motion and acceleration during substorms, examining fault line existence at near local midnight
03 p0419 A71-14515

Midlatitude nighttime D region ionization source considering precipitating energetic electrons
03 p0420 A71-14516

Suprathermal electron flux and temperature in 5-2 eV range at high latitude with Explorer 31 potential analyzer
03 p0420 A71-14517

Radiation intensity produced by inverse Compton effect between solar flux and Van Allen belt trapped high energy electrons
04 p0640 A71-14888

Pulsars relationship to very high energy cosmic ray electron propagation, examining far IR background and radiation sources
05 p0797 A71-15999

- White light flares due to photosphere heating by flux of energetic ions and electrons impinging from above
05 p0797 A71-16028
- High energy electron penetration and scattering in solids, obtaining beam density profiles by polymethyl methacrylate resist exposure
06 p0940 A71-17305
- Solar flare electrons at 10-200 MeV region, discussing energy spectra and time history
06 p0961 A71-18170
- Solar flare delayed relativistic electron appearance, comparing radio, optical and X ray data for particle intensities
06 p0961 A71-18171
- Solar flare high energy electrons, examining rise time and decay
06 p0961 A71-18173
- Energetic solar electron emission and cone propagation by IMP satellites, noting relation to proton and relativistic energy events
06 p0961 A71-18174
- Energetic electrons distribution in magnetotail plasma sheet from Explorer 35 satellite observation data
07 p1186 A71-19657
- Energetic electrons in magnetospheric tail plasma sheet, investigating flux time profiles and correlation with local magnetic fields from Imp 3 satellite observation data
07 p1186 A71-19658
- High energy electron injection into magnetosphere inner region during magnetic storms
08 p1350 A71-20956
- High energy electron background flux in F 2 layer, discussing grouped particle acceleration
08 p1354 A71-21012
- Quantum mechanical theory of nonrelativistic fast electron backscattering from continuous media, considering scattering cross sections
09 p1496 A71-22236
- High energy electrons in near space excess radiation from high altitude balloon and satellite data
09 p1513 A71-22667
- Microwave noise emission in He negative glow plasma frequency range, discussing high energy electron densities near cathode
09 p1502 A71-22694
- Satellite instruments to measure intensity and energy spectrum of high energy electrons and protons
10 p1683 A71-24464
- Intense solar microwave burst indication of high energy electron production, discussing synchrotron radiation, interplanetary medium particle propagation and cosmic ray modulation
12 p1950 A71-27381
- Ion sources designs involving high energy electron beam injections, discussing input power continuous and pulsed modes optimal efficiencies
12 p1940 A71-27507
- Relativistic electrons associated with solar particle events, measuring occurrence frequency, electron propagation and diffusion anisotropy
13 p2129 A71-29057
- Electromagnetic showers triggered in lead by 6 GeV primary cosmic ray electrons, calculating spatial distribution with Monte Carlo method
14 p2302 A71-30594
- Primary cosmic ray electron energy and intensity measuring equipment, using Cerenkov and scintillation counters, spark chamber, lead absorber and photorecorder
14 p2247 A71-30598
- Electromagnetic showers in lead, using 20 GeV primary cosmic ray electrons to calculate spatial evolution
14 p2302 A71-30603
- Interstellar gas heating by soft X rays and cosmic rays for electron production, calculating heating rate with Boltzmann equation and Monte Carlo method
14 p2302 A71-30642
- Moving type 4 solar radio burst, describing bipolar magnetic structure and origin in synchrotron radiation from relativistic electrons
15 p2473 A71-31692
- Fast charged particles measurement in inner radiation belt by Cerenkov counter mounted on Cosmos 137 satellite indicating presence of high energy electrons
16 p2626 A71-33664
- Relativistic electron precipitation during magnetic storms, showing cyclotron resonances with electromagnetic ion cyclotron waves
16 p2629 A71-33948
- Plasmopause position during stormtime increase in trapped energetic electrons, measuring near prime geomagnetic meridian by whistler techniques
16 p2629 A71-33969
- Magnetospheric observations by Imp 3 satellite of energetic electron and magnetotail field variations near neutral sheet as function of substorm time
16 p2574 A71-33971
- Energetic electrons pitch angle scattering during magnetic storms due to resonant interaction with proton generated Doppler shifted ion cyclotron waves
16 p2574 A71-33972
- Velocity determination in hypersonic low density wind tunnel based on high energy electron beam produced nitrogen ions time of flight
17 p2670 A71-34887
- Relativistic and/or degenerate electron gas equation of state formulae for density, temperature, entropy and internal energy
18 p2960 A71-35937
- Hydrazine formation from ammonia in constricted plasma discharge using electron source in selected high energy range
18 p2955 A71-35968
- Energetic electrons, protons and alpha particle measurements by Azur satellite over polar cap and in radiation belt during March 1970 solar particle event
19 p3126 A71-37419
- Flare stars X ray emission by fast electrons nonthermal bremsstrahlung
19 p3128 A71-38157
- Galactic high energy electron differential spectrum, estimating spatial distribution and random magnetic field intensity
19 p3129 A71-38358
- Dynamic energy spectra of nonthermal electrons in solar flares from balloon-borne high resolution hard X ray observations
19 p3130 A71-38673
- Intense relativistic electron beam propagation in drift tube with neutral gas and plasma background, determining front velocity and energy transport
20 p3272 A71-38784
- Foiled diode for production of high power relativistic electron beams, using multicathode system
20 p3202 A71-38831
- High energy electron background flux in F 2 layer, discussing grouped particle acceleration
20 p3280 A71-39592
- Quantum mechanical theory of nonrelativistic fast electron backscattering from continuous media, considering scattering cross sections
21 p3419 A71-41118
- Relativistic neutralized cylindrical electron beam paraxial motion through uniform longitudinal magnetic field
21 p3426 A71-41289
- Earth radiation belts high energy electron flux intensity monotonic decrease during magnetically quiet periods from satellite data analysis
22 p3591 A71-41527
- Outer radiation belt energetic electron flux intensity correlation with auroral activity and Kp index
22 p3591 A71-41528
- Ultrahigh energy electrons and gamma quanta in ground produced by primary cosmic rays, plotting mean free path vs energy
22 p3595 A71-42669
- Magnetospheric substorms observations by satellite and balloon-borne X ray detectors, considering auroral arc brightening and energetic electron flux enhancement in magnetotail
23 p3668 A71-43163
- Vela 4A and 4B satellite observation of impulsive energetic electron fluxes in distant magnetotail associated with magnetospheric polar substorms
23 p3670 A71-43184
- Electromagnetic waves excitation in coaxial resonator by relativistic electron beam, assuming presence of steady longitudinal magnetic field
24 p3833 A71-44663
- Relativistic electron beam propagation in decelerating medium in crossed electric and magnetic fields, noting nonrelativistic instability condition
24 p3856 A71-44669
- Microchannel plates detection efficiency for 2-150 keV electrons from C 14 pellet and electron gun
24 p3829 A71-45336
- ### HIGH ENERGY INTERACTIONS
- Soviet papers on cosmic rays and high energy nuclear interactions
01 p0145 A71-11362
- High energy multiple birth inelastic interactions between cosmic ray particles and atomic nucleus targets, using Wilson chamber and ionization calorimeter
01 p0083 A71-11363
- High energy inelastic interactions in cosmic ray showers, using Wilson chamber
01 p0145 A71-11365
- Extensive atmospheric showers and energy transfer from interacting nucleons to electron photon cascades at high energy levels
01 p0146 A71-11366
- Radiation measuring instruments assembly for extensive air showers and cosmic ray particle nuclear interactions at high energies
01 p0084 A71-11367
- Quasi-nucleon nuclear interactions of high energy protons in photoemulsion irradiated in pulsed magnetic field
01 p0131 A71-11368
- High energy interaction multiperipheral theories, examining inelastic events
03 p0461 A71-13834
- Strong cosmic ray interactions, considering meson production in accelerators
03 p0475 A71-13835
- High energy cosmic particle interactions with LiH target, discussing relation between longitudinal and transverse momenta of generated pions
03 p0476 A71-13844
- High energy pN interactions, using emulsion technique in strong magnetic field
03 p0461 A71-13846
- Negative pi-N NN interactions in emulsion at high energies, plotting angular distributions of secondary particles in cosmic ray showers
03 p0476 A71-13847
- High energy nucleon passage through lower atmosphere during chemical composition changes of primary cosmic rays, using Proton satellite observations
03 p0476 A71-13851
- Pion interactions with nucleons and nuclei in emulsions irradiated by high energy pion beams
03 p0461 A71-13852
- Momenta measurements of particles produced by high energy quasi-nucleon interactions of pions on photoemulsion layers, using primary particle tracks scanning
03 p0461 A71-13854
- Soviet book on cosmic ray physics covering high energy particles interactions, origin, acceleration mechanism, etc
03 p0481 A71-14424
- High energy particle interaction with magnetospheric tail neutral layer, determining limiting shape of pitch angle particle distribution
05 p0800 A71-17176
- High energy albedo neutron production by cosmic ray collisions, investigating balloon altitude flux variations near atmospheric top
06 p0962 A71-18179
- Atmospheric gamma rays energy spectrum and implication on high energy interactions characteristics
06 p0962 A71-18181
- Soviet papers on elementary particle and cosmic ray physics covering elastic and nonelastic collisions at high and superhigh energies
10 p1662 A71-24665
- Nuclear interactions superhigh energy measurements in cosmic particles on high mountain large sandwich assembly
10 p1662 A71-24666
- Cerenkov detectors and He filled spark chambers with large interelectrode spaces in high energy nuclear interaction studies, noting cosmic ray applications
10 p1612 A71-24667
- Very high energy cosmic ray muons, discussing recent experiments with mu-meson anomalous couplings, triplets and intermediate vector bosons
11 p1815 A71-25356
- Laser pulse produced energetic ion and plasma measurements fore and aft side of targets including Al and Au foils
11 p1775 A71-26084
- Proton-proton interactions at 70-600 GeV in Echo Lake cosmic ray experiment, discussing multiplicity, prongs, hadron flux and ionization calorimeter
12 p1933 A71-27391
- Surviving high energy primary protons of cosmic ray nuclear bursts in atmosphere without air shower at Chacaltaya
12 p1933 A71-27393
- High energy interactions at 10 to 12 power eV, discussing muon-pion showers, incoherent muons and horizontal air showers
12 p1933 A71-27395
- Two temperature model of cosmic ray high energy jets, predicting one particle accelerator momentum spectra
12 p1951 A71-27397
- Cosmic rays - Conference, Budapest, August-September 1969, Volume 3, High energy interactions and extensive air showers
13 p2120 A71-28048
- High energy nuclear bursts without accompanying air showers, considering surviving primary protons without inelastic collision in atmosphere
13 p2121 A71-28054
- Regular multiplicities of particle production in high energy collisions and antineutron-nucleon annihilation, comparing cosmic ray jet data and pion-nucleon difference
13 p2102 A71-28061
- Fireball transverse momentum effect on angular distribution of secondary particles, considering high energy nuclear interactions
13 p2058 A71-28063
- Local high energy events in extensive air showers core region, using scintillators and multiplate cloud chambers
13 p2124 A71-28081
- Air shower properties from Monte Carlo simulations, determining electron and muon numbers at sea level for primary protons and copper nuclei
13 p2124 A71-28085
- Monte Carlo simulation of high energy atmospheric extensive air shower nuclear cascade based on Aleph model of nuclear interactions
13 p2125 A71-28089

Extensive air showers muons angular distribution, considering high energy nuclear reactions 13 p1216 A71-28097

High energy particle interaction with magnetospheric tail neutral layer, determining particle pitch angle distribution limiting shape 13 p1218 A71-28233

Hadron matter thermodynamical properties at high temperatures, developing dual resonance dynamic model of high energy particle interactions 14 p2304 A71-29597

Nucleon-nucleon and nucleon-nucleus interaction energy measuring system at mountain elevation, discussing components and design 14 p2247 A71-30600

Nuclear soft core potential reproduction by isoscalar vector meson in nonlocal field theory of fireball in high energy cosmic ray collisions 15 p2472 A71-31151

High energy muons production by cosmic rays, discussing advantages of moon based experiments over earth surface measurements 15 p2475 A71-31780

High energy penetrating component of cosmic radiation at mountain level recorded in underground ionization calorimeter, showing muon production in vertical and horizontal direction 15 p2476 A71-31787

Energy spectrum of cosmic ray showers from high energy muon interactions with nuclear emulsion chamber 15 p2476 A71-31789

Anomalous cosmic ray muon interactions at very high energies, using zenith angle distribution data at sea level and deep underground 15 p2476 A71-31791

Ultrahigh energy muons intensity distribution as function of zenith angle at fixed slant depth of rock 15 p2476 A71-31793

High energy primary cosmic ray program of Goddard Space Flight Center involving charge composition and energy spectra studies in balloon and satellite experiments 15 p2478 A71-31804

Gamma ray emission from individual interactions of hadrons in carbon at 10 TeV, using ionization spectrometer-emulsion chamber combination 15 p2407 A71-31808

Cosmic ray high energy pion and nucleon nuclear interaction observations, determining statistical fluctuations in secondary particles angular distribution 15 p2479 A71-32076

Fireball model of meson production in high energy nucleons collisions 18 p2949 A71-36210

Cosmic ray nuclear interactions in 10-300 GeV energy range, using balloon-borne emulsion target, spark chambers and ionization spectrometer 19 p1214 A71-37286

Near sea level cosmic ray high energy interactions from data recorded by interleaved stack of cloud and ionization chambers and carbon and iron plates 19 p1214 A71-37287

Magnetospheric high energy protons relaxation due to interaction with Alfvén waves, presenting Einstein-Kolmogoroff equation numerical solution for particle momentum distribution function 20 p3278 A71-39074

High energy cosmic ray spectrometer onboard Proton 4, discussing ionization calorimeter, nuclear targets, particle charge and radiation detectors and primary measurements 20 p3283 A71-39755

Monte Carlo generation method for phase-space integrals of multiperipheral models for high energies and particle multiplicities 21 p3408 A71-40850

Electromagnetic interactions of high energy cosmic ray muons from combined calorimeter-spectrograph investigation 22 p3594 A71-42409

High energy interaction multiperipheral theories, examining inelastic events 22 p3578 A71-42635

Strong cosmic ray interactions and meson production in accelerators 22 p3594 A71-42636

Inelastic particle collisions with energies exceeding 10 to 13th eV, considering cosmic rays, nucleons and hadrons 22 p3594 A71-42638

High energy cosmic particle interactions with LiH target, discussing relation between longitudinal and transverse momenta of generated pions 22 p3594 A71-42645

PN interactions, using emulsion technique in strong magnetic field 22 p3579 A71-42647

Negative pi minus N and NN interactions in emulsion at high energies, plotting angular distributions of secondary particles in cosmic ray showers 22 p3594 A71-42648

High energy nucleon passage through lower atmosphere during chemical composition changes of primary cosmic rays, using Proton satellite observations 22 p3595 A71-42652

Pion interactions with nucleons and nuclei in emulsions irradiated by high energy pion beams 22 p3579 A71-42653

Momenta measurements of particles produced by high energy quasi-nucleon interactions of pions on photoemulsion layers, using primary particle tracks scanning 22 p3579 A71-42655

High energy proton spallation cross sections for several radionuclides from Ti targets, discussing application to lunar materials and meteoritic analysis 23 p3706 A71-43199

High energy proton spallation cross sections for several radionuclides from Fe targets, discussing application to beam monitoring and meteoritic studies 23 p3706 A71-43200

HIGH ENERGY PROPELLANTS

High energy three stage booster system for geostationary orbiter, discussing interstage propellant transfer, apogee impulse system and mission rated payload modular configurations 11 p1838 A71-25574

High energy solid propellants use in Europa 2 launch vehicle perigee-apogee motor, considering synchronous satellite payload increase 16 p2645 A71-33365

HIGH EXPLOSIVES

U EXPLOSIVES

HIGH FIELD MAGNETS

Hysteresis loop measurements and functional measurements correlation on periodic permanent magnet stacks of TWT ring magnets of Sm-Co alloy 14 p2285 A71-30705

Cu clad Nb-Ti wire wound superconducting solenoids with large fields at 1.6-5.2 K 24 p3809 A71-45105

HIGH FREQUENCIES

Rodents bimodal cochlear microphonic response to high frequencies recorded from round window membrane 01 p0016 A71-11346

F region ionospheric modification by heating from high power HF ground based transmission, discussing ionosonde observations 01 p0078 A71-11535

Auroral absorption of HF radar waves over high latitude ionospheric paths 01 p0041 A71-11610

Corrugated theta pinch stabilization, considering variable axial HF current and quadrupole magnetic field 03 p0464 A71-13930

Automated precision polarimeter for HF-VHF range 04 p0586 A71-14654

Flat HF radio spectra from optically thin sources with low electron energy distribution indexes 05 p0808 A71-16399

Oscillatory systems slow monotonic motion due to carrying elements performing HF low amplitude relative oscillations 06 p0897 A71-17364

Nonequilibrium plasma HF conductivity, introducing dressed ion expression in terms of dielectric permittivity 07 p1165 A71-18743

HF radio signal ionospheric propagation around world by sweep frequency CW sounding technique, observing fine structure in ionograms 07 p1062 A71-19682

Combined HF compensation of single stage transistor amplifier with RC feedback in emitter circuit 07 p1079 A71-20262

HF plasma instabilities driving mechanisms and distribution types, considering beam plasma computer simulation example 07 p1173 A71-20508

HF Hall current instability, discussing short wavelength backscatter for equatorial and auroral electrojets in disturbed ionosphere 08 p1279 A71-21205

HF backscattering by plane electromagnetic wave at oblique incidence from perfectly conducting right circular cone, applying geometrical theory of diffraction 08 p1257 A71-21884

Waves arrival directional fluctuations effect on power gain of horizontal rhombic antennas for high frequencies and various antenna and wave parameters 09 p1420 A71-23676

Haag synchronization theory application to HF vacuum tube oscillators, considering LF perturbation 10 p1609 A71-23852

Pulsed HF chemical laser output as function of fluorine source, flow rate and output coupling 10 p1620 A71-24153

Short wave HF instabilities in strongly inhomogeneous plasma with hot electrons, considering ion acoustic oscillations and electron cyclotron harmonics 10 p1650 A71-24525

Microwave/high frequencies safe exposure limits, discussing radiating aerial near field, radio hazards and human body absorption 10 p1573 A71-25081

Signal stability in distributed active lines of MCM semiconductor devices with negative leakage resistance 12 p1878 A71-26946

Man-made HF noise interference with satellite broadcasting, giving special consideration to automotive ignition systems 12 p1878 A71-26949

Receiver triangle size effect on ionospheric drift near 2 MHz, using partial and total reflections from lower ionosphere 14 p2230 A71-29717

Fluctuation power spectra of CW phase path HF sounders in ionosphere compared with Vaisala frequency curve for upper atmosphere monitoring 14 p2230 A71-29717

HF response of point excited cylindrical shell, converting normal-mode series to integral representation with Watson transformation 14 p2327 A71-30202

Transmission loss measurements at HF over 960 km temperate latitude path for wave polarization calculations and ionospheric absorption estimation 14 p2196 A71-30464

Performance and cost design tradeoff between HF and synchronous meteorological satellite data collection systems, considering platform transmitting power and SNR 14 p2198 A71-30909

Tropospheric refraction effects and field strength dependence on height at frequencies below 10 MHz 19 p3017 A71-37864

Short wave HF instabilities in strongly inhomogeneous plasma with hot electrons, considering ion acoustic oscillations and electron cyclotron harmonics 19 p3116 A71-38251

Physical interpretation of electromagnetic waves attenuation function HF singularity during diffraction over spherical surface, applying to short wave diffraction in tropospheric model 20 p3198 A71-39809

HF electric signal detection, using acoustoelectric surface wave field in piezo semiconducting crystal 21 p3436 A71-41369

Statistical HF electron heating at oscillating plasma boundary with acceleration of double Langmuir layer 23 p3709 A71-43269

Diagnostic import of QRS notching in HF ECG of living subjects with heart disease, noting notch correlation with ventricular enlargement 23 p3636 A71-44139

HF dispersion, power and energy storage in periodic slow wave waveguides of resonator chains coupled through openings 24 p3805 A71-45291

HIGH IMPULSE

NERVA XE-Prime test series, discussing computer simulation full power and high specific impulse operation and startup under varying initial conditions [AIAA PAPER 70-709] 03 p0456 A71-14422

HIGH LATITUDES

U POLAR REGIONS

HIGH LIFT DEVICES

U LIFT DEVICES

HIGH MELTING COMPOUNDS

U REFRACTORY MATERIALS

HIGH PASS FILTERS

Low- and high-pass active filters theory and design describing positive and negative feedback circuits 02 p0231 A71-11861

Third order correlations in grid turbulence, investigating high pass filtering effect at small cut-off frequencies 04 p0569 A71-15027

HIGH POLYMERS

Polarization-optical method of stress analysis problems, explaining high polymers physicochemical properties with Boltzmann-Volterra integral equations 04 p0671 A71-15557

Flame resistant properties of phosphorus containing organic and inorganic high polymers 07 p1145 A71-19843

HIGH PRESSURE

Dwell or dark pause measurements of shock tube driver high pressure arc discharge for various gases 05 p0788 A71-16578

Spherical superconducting geomagnetic field generating layer under ultrahigh pressure in earth center 06 p0889 A71-17734

Large volume high pressure gas uniform electrical discharges, applying to laser amplifier [AIAA PAPER 71-65] 06 p0909 A71-18524

Pressure regulator design and construction, using high pressure fluidic proportional chain 07 p1027 A71-20588

Continuous flow arc air heater for reentry vehicle components ground testing, achieving combined high pressure and enthalpy [AIAA PAPER 71-259] 09 p1429 A71-23061

High pressure laser action in gas mixtures with pulsed transverse excitation, observing molecular and atomic transitions

10 p1620 A71-24045

Graphite lubricants superconducting properties under high pressures and low temperatures, suggesting new superconductors developments and metal free electron model modification

10 p1656 A71-24299

Atomic scale elastic structure equations of state for Thomas-Fermi model extension to high pressures, considering earth core iron-silicates composition

11 p1802 A71-25572

Shock tunnel extremely high enthalpy and pressure for scramjet engine combustion research

11 p1860 A71-26267

Jet stream axis position from cumulusiform cloud structural differentiation observed over Central Europe on 22 May 1970, noting coincidence with high pressure near ground

12 p1924 A71-26575

Artificial respiration in elevated gas pressure chamber to revive organism after clinical death by rapid decompression

12 p1876 A71-27745

Superpressurization mechanism in hollow cathode active zone, calculating upstream pressure variation as function of discharge current

13 p2106 A71-28399

Biological effects of inert gases in elevated pressure respiratory mixtures on human central nervous system

16 p2536 A71-33577

Elevated atmospheric pressure effects on human psychophysiological qualities including attention, memory and time-estimating capabilities and nervous processes equilibrium

16 p2536 A71-33578

Thin layers shear strength and friction under high pressure, describing rotating-anvil shear press with high sensitivity strain gage equipped load and torque rolls

20 p3241 A71-38878

Soviet book on high pressure centrifugal pumps design and calculation covering industrial applications, systems engineering, components, etc

21 p3391 A71-41371

Plain externally pressurized thrust air bearings with porous inserts and high supply pressures, comparing with discrete orifice feed

22 p3553 A71-41679

HIGH PRESSURE OXYGEN

Nonflammable elastomeric materials and coatings for oxygen enriched atmospheres

10 p1632 A71-24098

German monograph on high pressure oxygen toxicity and hyperbaric treatment of gas gangrene

11 p1716 A71-25200

High pressure gaseous oxygen impact testing method incorporating drop plummet system for specimens flammability screening

14 p2222 A71-30547

Impact sensitivity tester for engineering materials in liquid and gaseous oxygen at high pressures

14 p2222 A71-30548

Adrenalectomy influence on electrical activity of cortex and subcortical areas in rats under hyperbaric oxygen, using implanted electrode electroencephalographic recordings

16 p2528 A71-33118

HIGH Q

U Q FACTORS

HIGH RESISTANCE

High resistance semiconductors minority carriers mean diffusion length based on induced charge dependence on applied voltage during illumination by absorbable light

02 p0294 A71-11898

HIGH RESOLUTION

Three electrode image translator with electrostatic electron beam focusing, rendering high uniform resolution over entire viewfield

06 p0897 A71-17531

Spatial resolution improvement by utilizing temporal degree of freedom of transmitted signal, discussing hologram plate recording during exposition intervals

08 p1287 A71-21191

High resolution measurement of carbon dioxide broadened half widths for water vapor lines in fundamental band

10 p1645 A71-24965

Real time high resolution mass spectroscopy using digital computer techniques for data acquisition, processing and presentation

11 p1761 A71-25220

Lunar landing site suitability, using stereoscopic medium and high resolution photography

11 p1836 A71-26533

High resolution far IR interferometer in Michelson configuration for measuring gas optical properties in symmetric or asymmetric operation mode, testing performance

12 p1904 A71-26799

Wide field high resolution birefringent filter based on Fabry-Perot etalon and Lyot-Ohman filter, discussing limitations and applications

12 p1904 A71-26802

High resolution holographic Fourier transform spectroscopy, discussing interferometer localized interference fringes direct recording method and heterodyning technique

12 p1905 A71-26805

Interferential spectrometer with selection by amplitude modulation with double passage mirrors arrangement for obtaining double resolution

12 p1905 A71-26811

Reversal processing technique for producing high diffraction efficiency, low noise and good light stability phase holograms on silver halide emulsions

13 p2068 A71-28713

Visual flight simulation devices, considering high resolution photographic films and digital memories

13 p2046 A71-29483

Pulsed semiconductor laser as high resolution optical range spectroscopy, noting application to Cs hyperfine absorption

15 p2421 A71-32403

Modified Young interferometer for measuring separation between centers of two nearly coincident slits with high resolution

16 p2577 A71-33132

Martian surface relief details observation from earth distance, showing telescope resolution requirements above dense atmospheric layers

16 p2639 A71-33698

High resolution microdensitometry image interpretation and manipulation by digital computer, discussing radiation coherence problems

17 p2742 A71-35002

Optical grating measuring systems high resolution interpolation using phase analog and digital counter techniques

17 p2745 A71-35293

Red blood cell image hologram reconstruction and superresolution based on coherent physical optics, using computer program

17 p2693 A71-35586

High resolution 16mm pulse mode cine reconnaissance camera design features, discussing dynamic balance and reaction forces cancellation

17 p2746 A71-35761

High resolution gas discharge plasma display panel, discussing design, capabilities and performance

20 p3233 A71-39061

High resolution charged particle detector with wire cathode for synchrotron applications, discussing design and advantages

20 p3238 A71-39423

High resolution astronomical radiointerferometry, discussing radio telescope system design

21 p3452 A71-41052

Solar limb high resolution photography at different H-alpha wavelengths, using tunable 1-8A and 1A Halle filters in tandem for parasitic light elimination

22 p3596 A71-41455

High resolution full spatial frequency range optical image by incoherent superposition of low resolution partial frequency range component photographs, using optical aperture synthesis

22 p3538 A71-41735

Display system for scanning medical thermometer covering temperature range 28.0-37.4 C with 0.2 C accuracy, using liquid nitrogen cooled indium antimonide photoresistive detector

22 p3545 A71-42149

Optical system superresolution by reduction of temporal degrees of freedom using holography

24 p3824 A71-44453

HIGH SENSITIVITY

U SENSITIVITY

HIGH SPEED

High velocity metal working, discussing airfoil forging, ausforming of bearing race blanks, tooling, etc [SME PAPER MF-70-228]

01 p0090 A71-11267

High speed tracked air cushion vehicles dynamic interactions with guideways, considering model of lumped double-sprung vehicle masses traveling in tandem along simply supported beams [AIAA PAPER 71-386]

11 p1846 A71-25350

Direct impulse response method application to function optimization, using high speed hybrid computer

11 p1735 A71-25841

High speed roller bearing design with long fatigue life and weight reduction for high temperature operation in inert environment [ASME PAPER 71-DE-50]

12 p1912 A71-27328

HIGH SPEED CAMERAS

NT FRAMING CAMERAS

Multiple spark camera for unsteady compressible flow investigations, considering geometrical optical design, parallax, spark producing electric circuitry, etc

01 p0078 A71-10106

Submerged arc welding process, observing arc motion and metal transfer with X ray high speed photography

06 p0905 A71-18090

HIGH STRENGTH ALLOYS

Pure hydrocarbon droplets heating, expansion, vapor phase fuel storage and gasification in oxidizing gas at elevated pressures, using high speed cinematography

06 p1007 A71-18300

High speed photographic assembly with turbine drive for continuous recording and frame photography

10 p1613 A71-24872

Q switched ruby laser time dependent spectrum analysis by high speed camera with Fabry-Perot interferometer, noting holographic interferometry application

10 p1622 A71-24962

Slave sweep plane-parallel mirror systems design for maximum picture taking rates in high speed cameras

11 p1767 A71-26467

Portable self contained Imacon image converter high speed camera system capable of framing and streak operation

18 p2924 A71-36614

Laser illuminated Mach-Zehnder interferometer system including high speed cameras for studying flame propagation among polythene particles suspended in air

19 p3064 A71-38063

Ultrafast camera with picosecond framing times for photographic measurement of light pulses

20 p3235 A71-39189

Optically sensitive epoxy resin based high polymers under pulsed loads, observing deformation and mechanical displacement with high speed photography

22 p3614 A71-41610

Duralumin rods deformation and stress propagation study under dynamic pulse loads, using photosensitive epoxy coatings and high speed photography

22 p3537 A71-41612

Holography capabilities of hypervelocity projectiles with front surface resolution, discussing fringes intensity and position from projectile spin

22 p3549 A71-42569

Objects in motion measurement by photogrammetry in Japan noting stir, rocket tracking, snow, roof deformation, avalanches, car collisions, water and air turbulence applications

24 p3826 A71-44758

HIGH SPEED FLIGHT

U FLIGHT

U HIGH SPEED

HIGH SPEED TRANSPORTATION

U RAPID TRANSIT SYSTEMS

HIGH STRENGTH

High strength ceramics for high temperature applications, reviewing oxides, nitrides and carbides

01 p0109 A71-11601

High strength polyimide resin composites, discussing commercial and aerospace applications, chemistry, void content, volatiles and moisture absorption

02 p0274 A71-12487

High strength and modulus continuous carbon fibers, discussing preparation and quality control [PLASTICS INST. PAPER 5]

08 p1297 A71-20925

Stress redistribution and static inerteolastic instability of rotating beams and disks of low modulus high yield strength materials

11 p1848 A71-25495

HIGH STRENGTH ALLOYS

NT HIGH STRENGTH STEELS

NT MARAGING STEELS

Al-Zn-Mg-Cu type high strength Al alloys mechanical properties evaluation by fracture mechanics methods

01 p0104 A71-11540

Combined vacuum furnace brazing with diffusion welding for joining high strength Ni base superalloys

02 p0255 A71-11708

High strength stress-corrosion resistant Al alloy forgings fabrication processes, noting chemical composition and physical properties

03 p0441 A71-13255

Heat, solution and cooling treatment of Ti-Al-V-Sn alloy for high strength and plastic properties

05 p0765 A71-16199

High strength Al alloys stress corrosion resistance testing in various heat treatment conditions, using precracked cantilever beam specimens

06 p0912 A71-18012

High strength multiphase Co-Ni-Cr-Mo alloy hardening, noting deformation and aging induced strengthening

06 p0913 A71-18098

Wrought high strength Al alloy nonequilibrium second phase particles formation effect on mechanical behavior during solidification

07 p1137 A71-19978

Hard alloys electrolyte selection for electrochemical dimensional machining

07 p1120 A71-20206

Equilibrium diagrams of Re with W, Mo, Co, Ni, discussing high strength system elastic components with torsional support applications

07 p1140 A71-20232

HIGH STRENGTH STEELS

- W-Mo-Re high temperature alloys, discussing high strength, elastic properties, creep, thermal resistivity and expansion coefficient 07 p1141 A71-20243
- High strength martensite beta Ti alloy microstructure, discussing ductility and age hardening 08 p1312 A71-21552
- High strength corrosion resistant superalloy structure and mechanical properties 08 p1314 A71-21566
- Heat resistant dispersion strengthened and fiber reinforced metal matrix superalloys for high temperature applications, considering superstrength alloys development 09 p1478 A71-23397
- Point defects and fine precipitates effects on fatigue strength of high strength alloys, exhibiting higher fatigue strength in isothermally aged samples 10 p1625 A71-24009
- Heat affected zone crack filling and weld metal-base metal interactions of high strength alloys in dissimilar gas arc welding 11 p1769 A71-25749
- Ni-Cr and Ni-W alloys high temperature strength properties, considering stacking fault energy, diffusion velocity, Young modulus and dislocation locking 12 p1919 A71-27762
- High flash point polyalkylene glycol base synthetic quenchants for high strength alloy heat treatment, noting application to aluminum, titanium and steel parts 13 p2073 A71-28144
- High strength Al alloy forgings processing for stress corrosion cracking prevention, including plane relaxation and compressive relief techniques 13 p2073 A71-28146
- High strength corrosion resistant multiphase Co-Ni-Cr-Mo alloys with fcc structure hardened to hcp by mechanical deformation 13 p2084 A71-28148
- High strength alloys fatigue in terms of irreversible microplastic deformations accumulations, discussing fatigue crack mechanisms and cyclic straining effects on bulk properties 13 p2152 A71-28219
- High strength alloys, discussing fracture mechanics concepts applicability to environmental cracking under static load and combined effects of cyclic stress and aggressive environment 13 p2152 A71-28222
- High-strength low-cost moderate-conductivity cobalt modified aluminum brass for electrical contacts, terminals and relay springs 13 p2086 A71-28836
- High strength Ni base superalloy workability, investigating microstructure relation to mechanical properties 13 p2090 A71-29419
- Thermomechanical treatment effect on mechanical properties of high strength Al-Mg-Zn-Cu alloys, considering subsequent aging and state before deformation 15 p2434 A71-32328
- Magnetic field perturbation and electric current injection techniques for characterizing high strength alloys fatigue microcracks 16 p2581 A71-32865
- High strength Al alloys in structural design, taking into account fracture toughness 18 p2937 A71-36849
- Small holes effect on Ni base superalloy wrought thin sheets fatigue strength under pulsating tension load, analyzing crack initiation, propagation and critical length 18 p2938 A71-36850
- Plastic zones and stable crack growth at notches in thin high strength sheet alloys, using replication technique 18 p2938 A71-36853
- Dynamic tear fracture toughness test and fracture mechanics parameter correlation for high strength Al alloys 20 p3248 A71-38771
- High strength Al alloys at cryogenic temperatures, presenting plane strain fracture toughness tests results 21 p3401 A71-40916
- Structure, hardness, density and electrical resistance of binary alloys V-Ti, V-Cr, V-Al and V-Sn 23 p3691 A71-43283
- HIGH STRENGTH STEELS**
- NT MARAGING STEELS**
- High strength steel weld metal, determining gaseous impurities effects on mechanical properties degradation 02 p0262 A71-11710
- High strength steels fracture toughness, investigating loading rate and temperature effects 03 p0442 A71-13625
- Fracture toughness tests and brittle failure of high strength structural steels under thermomechanical treatment 03 p0447 A71-14581
- Static and dynamic fracture toughness of tempered low alloy high strength steels in low temperature range 03 p0448 A71-14582

- High strength steel butt welds surface geometry effect on fatigue durability under cyclic loads, using photoelastic analysis 04 p0602 A71-14881
- High strength steel weldability with shielded and gas metal arc processes, discussing hardness, tensile, bend, impact and fatigue tests 04 p0603 A71-14922
- High strength steel reversible hydrogen embrittlement mechanisms, noting role of hydrogen diffusion 04 p0615 A71-15790
- Lambda rocket motor case weight reduction through use of MB 130 instead of HT 100 steel, presenting structural strength test results 05 p0821 A71-16297
- High yield strength steel stress corrosion crack tip electrochemical and pH potential conditions, using AgCl reference electrode 07 p1137 A71-19973
- Martensitic high strength steels composition effect on environmentally induced delayed failure 07 p1139 A71-19990
- Ductile metals fatigue crack propagation model applications to brittle metals, discussing crack initiation effects on high strength steels failure modes 09 p1467 A71-22285
- Metallic coating effects on aircraft high strength steel fatigue, considering chromium plating, shot peening and plasma spraying [NACE PAPER 23] 09 p1469 A71-22889
- Ultrahigh tensile steels for landing gear and other aircraft design applications, discussing composition, mechanical properties, quality requirements, manufacture and testing 09 p1454 A71-22996
- Hot strain cycle recording in single and multipass welds for C-Mn steel using welding simulation, surface pressed plug and microscopic techniques 09 p1459 A71-23455
- Kinetic crack propagation theory of fatigue fracture toughness for notched and unnotched asurfmed high strength and heat treated ball bearing steels 10 p1687 A71-24307
- High strength steel fracture toughness, investigating stress wave emission during crack growth 10 p1627 A71-24534
- High strength stainless steel dislocation structure and mechanical properties, discussing tempering, tensile strength, precipitation hardening and temperature effects 11 p1776 A71-25167
- Carburized steel surface stresses and fatigue behavior, correlating stress distribution measurements and notched bar bending fatigue tests after several heat treatment steps 11 p1777 A71-25388
- Optical holographic interferometry for radial microcracks detection from bolt holes in high strength aircraft steel [ASME PAPER 71-MET-C] 12 p1911 A71-27312
- Vanadium containing high strength low alloy steel thermomechanical processing by last hot mill pass temperature control [ASME PAPER 71-MET-I] 12 p1918 A71-27320
- Mechanical properties, hardness and dislocation structure of Ti bearing maraging steels, considering Mo role in strength and plastic properties improvement 13 p2086 A71-28581
- High strength steel delayed fracture, applying Yokobori stochastic-kinetic theory of fatigue crack propagation for time to fracture calculation 13 p2155 A71-28790
- German monograph on hot machining of high temperature steels by flame heating with propane-oxygen and plasma arc burners 14 p2252 A71-30232
- High tensile strength maraging steels aging, discussing dispersed precipitates formation by homogeneous nucleation 15 p2427 A71-31525
- Microcracks detection in high strength steel by optical holographic interferometry, comparing results with magnaflex, eddy current and X ray inspection methods 15 p2409 A71-32258
- High strength steels and Ti alloys machining, discussing hardness levels, cutting speeds, tool chip contact area, and reasonable production rates [SME PAPER MR-71-819] 15 p2416 A71-32426
- Low alloy high strength steels undetected fabrication originated anomalies, causing brittle behavior and crack propagation susceptibility [SME PAPER EM-71-706] 15 p2435 A71-32435
- Scale factor effect on brittle fracture strength for Ti and Al alloys and high strength steels 16 p2657 A71-33409
- High strength structural stainless steels with good toughness and little crack sensitivity, noting brittleness due to oxidation, precipitation and carbide network 16 p2597 A71-33916

- Tensile properties, plane strain fracture toughness and stress corrosion threshold of high strength precipitation hardening stainless steels 17 p2755 A71-34444
- Stress corrosion cracking in high strength steels showing occurrence along zero isoclinic surfaces 17 p2755 A71-34444
- Strength and toughness optimization in high strength stainless steels by austenitizing and removal of delta ferrite by isothermal transformation 17 p2756 A71-34444
- German book on welding conditions and material composition effects on structural changes and heat affected zone mechanical properties of high strength structural steels 17 p2748 A71-34444
- Mo effect on high temperature strength, heat resistance, plasticity and toughness of austenitic Cr-Ni-Al steel 19 p3077 A71-37444
- High strength Cr-Mo-Co stainless steels with improved toughness and ductility by austenitizing temperature selection 19 p3079 A71-37444
- High strength metastable austenitic steels fracture toughness, showing alloy composition, strain rate and temperature effects 19 p3080 A71-37444
- Ni-Mo-V, Ni-Cr-Mo-V and Cr-Mo-V high strength rotor forging steels fatigue crack growth characteristics tests at room temperature 20 p3247 A71-38744
- Fatigue crack propagation in high yield strength steels at room temperature in air environments, considering primary influence of applied stress intensity range 20 p3248 A71-38744
- Transition temperature behavior in plane strain fracture toughness tests on A517-F steel, comparing with Charpy tests 20 p3248 A71-38744
- Acoustic emission technique for nondestructive cracking rate determination in hydrogen embrittled steel, using crack-tip stress intensity factor as critical parameter 20 p3241 A71-38744
- Stress corrosion crack branching in high strength steels, considering constant crack velocity and critical stress intensity 20 p3248 A71-38744
- High strength stainless steel dislocation structure and mechanical properties, discussing tempering, site strength, precipitation hardening and temperature effects 21 p3402 A71-41044
- High strength steel structural transformations under arc melting, cooling and electroslag remelting, noting delta ferrite precipitation with hot stage microscope 21 p3402 A71-41044
- Bimetallic plated high strength steel, noting transition zone effects on mechanical properties 23 p3692 A71-44044
- Strength and plasticity characteristics of hardened multilayer structural steels, investigating layer thickness effect 24 p3837 A71-44744
- HIGH TEMPERATURE**
- High temperature calorimetry of solids for heat capacity and thermal processes thermodynamic and thermokinetic characteristics, considering calorimetric design engineering 01 p0083 A71-11274
- Thermophysical properties of solids at high temperatures - Conference, Salford, England, July-August 1970, Part I 04 p0594 A71-14944
- High temperature specific heat of refractory molybdenum and uranium dioxide 04 p0612 A71-14944
- Single pulse shock tube in high temperature chemical reaction kinetics, considering shock reflection theory 05 p0836 A71-16544
- Protective oxide formation on single phased Cu-Al-Si alloys during high temperature oxidation 05 p0770 A71-17044
- Metal gluing with synthetic polymer based adhesives, discussing history, technology and high temperature resistance 06 p0905 A71-18044
- Carbon fiber and carbon fiber polytetrafluoroethylene composites high temperature mechanical properties [PLASTICS INST. PAPER 35] 08 p1319 A71-20844
- High temperature ultraminiature pressure transducers, reviewing p-n junctions thermal limitations and thermal properties of dielectric oxides used with so state epitaxially grown sensors 09 p1448 A71-22744
- Prototype two stage maser extended passband broadening and stability increase at high cooling temperature 13 p2078 A71-28344

HIGH TEMPERATURE AIR

Thermodynamic equations of state for dissociating and ionizing high temperature air applied to vertical and oblique compression shocks

02 p0331 A71-12067

Nonequilibrium recombination of dissociated combustion products of hydrogen in oxygen enriched heated air in supersonic nozzle

10 p1696 A71-24381

High temperature aerodynamics with electromagnetic radiation, considering thermally radiating shock layers, electric arc driven wind tunnels and gas dynamic lasers

12 p1940 A71-27277

Chemically nonequilibrium laminar boundary layer profiles in axisymmetric hypersonic conical nozzle at high air stagnation temperature, calculating wall friction, displacement and momentum loss thickness

13 p1989 A71-27904

Shock tube high temperature air viscosity from laminar boundary layer heat exchange data

14 p2224 A71-30047

Injection conditions effect on ignition temperature of methane and hydrogen in hot Mach 2 air stream

19 p3163 A71-37889

Thermal protection of two dimensional supersonic nozzle fed with hot air by tangentially injected cold gaseous films for convergent and constant section ducts

20 p3314 A71-39415

German monograph on flow and combustion changes during hydrogen and methane transverse injection into hot supersonic air jet

21 p3475 A71-40750

HIGH TEMPERATURE ALLOYS

U HEAT RESISTANT ALLOYS

HIGH TEMPERATURE ENVIRONMENTS

Human heat exchange and body overheating mechanism at high ambient temperatures at sea level and lowered pressures

01 p0013 A71-11134

Heat resistant roller bearings for vacuum applications at high temperature, discussing cage design and self lubricating materials

02 p0258 A71-12599

Engine vibration high temperature transducer, discussing piezoelectric materials properties and design considerations relative to temperature, pressure, acoustic noise, humidity environment

02 p0255 A71-12911

Helios solar probe satellite solar array techniques for high temperature and illumination intensity

05 p0702 A71-16080

Doped tungsten high temperature behavior, discussing hypotheses regarding doping agents microstructural effects

05 p0767 A71-16599

German monograph on high energy propellant-oxidizer systems changes of state under high temperature conditions with chemical relaxation taken into account

05 p0795 A71-17106

Ti alloy deformation through surface oxidation at elevated temperature, considering lattice parameter and alpha concentration effects

06 p0913 A71-18677

Extensometer for evaluating remote reading strain gage performance at high and rapidly changing temperatures

09 p1445 A71-22720

Ni-Mo alloys electron transfer and ion diffusion at high temperatures

09 p1471 A71-23077

High temperature corrosion in aircraft engine components and gas turbines by sulfur in fuels, vanadium pentoxide and NaCl

09 p1474 A71-23288

High temperature oxidation protective coatings behavior, emphasizing jet engine applications

09 p1483 A71-23296

Ti alloys structural high temperature applications in fighter aircraft, considering fabrication and assembly methods

09 p1458 A71-23427

Impact composite materials with reactive resins as binders for polyester fabric, determining peel resistance, tensile shear strength and high temperature aging effect

11 p1786 A71-25416

Venus life forms, describing algae grown in pure carbon dioxide under pressure in acidic nutrient media at high temperatures

11 p1724 A71-25701

Reradiative and high temperature insulative space shuttle thermal protection systems with actively cooled, passively cooled and uncooled substructures [AIAA PAPER 71-443]

11 p1838 A71-26228

Dissociative recombination rates in partially ionized gases at elevated gas temperatures, using shock tube for limited ionization introduction

11 p1765 A71-26283

High sensitivity flame sensor for high temperature ambients, using Geiger-Muller tube triggered by photoelectron released by UV photon from flame

12 p1906 A71-27048

Resilient metal seals for extreme temperatures or minimum leakage and weight

12 p1911 A71-27060

High speed roller bearing design with long fatigue life and weight reduction for high temperature operation in inert environment

[ASME PAPER 71-DE-50] 12 p1912 A71-27328

Heat resisting Ni base alloy stress rupture strength and fatigue life, observing corrosive high temperature environment effect

13 p2084 A71-28111

Polyimide plastics, considering mechanical properties high temperature applications and cost effectiveness

13 p2091 A71-28165

Long-life self-contained solid lubricated ball bearing systems operating under combined high-temperature, high-speed, high-load conditions

14 p2252 A71-30192

Film cooling as solid surfaces protection in high temperature environments, considering two and three dimensional secondary compressible and incompressible flow geometries

14 p2337 A71-30244

Aircraft flight load measurements in high temperature environment, determining optimal strain gage installation and calibration

14 p2248 A71-30681

High temperature capacitance strain gage development for aircraft testing, discussing instrument configuration and data reliability

14 p2248 A71-30682

UV radiation sensitive flame sensor for high temperature ambients, consisting of Geiger-Muller tube triggered by photoelectron released from photocathode

14 p2248 A71-30707

High temperature permeameter for measuring magnetizing force or magnetic induction in vacuum or inert atmosphere

15 p2401 A71-31194

Thermal dissociation rate of undiluted nitrogen in shock tube over 5700 to 12,000 K range, using pressure measurements

[AIAA PAPER 71-620] 15 p2451 A71-31549

Al alloys high temperature thermomechanical treatment, discussing mechanical properties, enhanced plasticity and roughness

15 p2434 A71-32327

Gas cooled porous plate unsteady temperature field during high temperature action, considering thermoradiative, convective and mixed radiative-convective heat transfer

16 p2662 A71-32833

Shock tube investigation of cyanogen and CN molecule dissociation at high temperatures, considering kinetics of CN decomposition

16 p2538 A71-32891

Pure carbon monoxide dissociation rate behind incident shock wave in high temperature environment, using two wavelength IR emission data

16 p2539 A71-32909

Fatigue measurements in hot working conditions on subjects wearing self contained breathing apparatus in heat chamber

17 p2688 A71-34361

Ceramic fibrous materials for high temperature insulation, discussing practical approach to obtain lower thermal conductivity

18 p2939 A71-36668

Male and female physiological responses to heat stress, discussing sweating, skin and body temperature, heart rate and metabolism

18 p2859 A71-36871

Physiological strains due to industrial heat stress, investigating heart rate and body temperature

18 p2860 A71-36882

Ionic conduction in perovskite-type oxide solid solution, discussing application to high temperature hydrogen oxygen fuel cells

18 p2852 A71-36966

Ni-Cr alloys sulfidation at 700 C from inert and radioactive marker techniques

18 p2938 A71-37003

Carbon-fiber-reinforced carbon composites for high temperature applications, describing filament orientation, matrix composition and heat treatment effects on ablation performance

19 p3085 A71-38350

Integrated absorption coefficient of pressure induced pure rotational and vibrational transitions in binary collisions of homonuclear diatomic molecules at high temperatures

19 p3108 A71-38719

Transition metals addition effect on W sintering behavior in 1000-2000 C range, explaining by electron exchange between alloy components

21 p3396 A71-40031

Polymer materials for aerospace construction, considering behavior in cryogenic and high temperature environments

22 p3564 A71-41510

Mean body temperature computation in neutral and hot environments from rectal and skin temperatures

22 p3485 A71-41723

Water-salt metabolism in human blood and urine under high temperature conditions after residence in different climatic zone

24 p3794 A71-44414

HIGH TEMPERATURE FLUIDS

NT HIGH TEMPERATURE AIR

NT HIGH TEMPERATURE GASES

Viscosity measurement apparatus for molten materials, presenting block diagram of logic circuit for recording pendulum behavior

05 p0754 A71-16968

HIGH TEMPERATURE GASES

NT HIGH TEMPERATURE AIR

Nongray equilibrium radiative heat transfer in viscous radiating shock layer around blunt body entering high temperature nonisothermal carbon dioxide-nitrogen atmosphere

[AIAA PAPER 69-636] 01 p0180 A71-10938

Nozzle wall protection against high enthalpy gas flow effects by film cooling through parietal liquid injection

01 p0143 A71-11017

Gas permeable dispersion layer between impermeable solid wall and high temperature gas flow, calculating dimensionless heat flux equations

02 p0332 A71-12200

High temperature gases radiative heat exchange, evaluating approximation methods

03 p0519 A71-13744

Vaporization rate of liquid injected into high temperature supersonic gas flow, considering relation to static pressure and distillation process

03 p0521 A71-14253

Soviet book on optical properties of hot air covering spectral lines, radiative transfer, cross sections, pressure effects and absorptivity

03 p0460 A71-14397

High temperature bypass piston shock tube for helium and nitrogen

04 p0564 A71-14673

Radiation effects on compression shock in hot gases, considering hypersonic flow around blunt body during planetary atmosphere entry

[DFVLR-SONDDR-60] 04 p0526 A71-15101

Aircraft turbine engines with elevated gas inlet temperatures

04 p0639 A71-15670

Gas dynamic conditions resulting in reacting gases detonation waves at high initial temperatures, simulating internal combustion engine knock

05 p0833 A71-16506

Test facility for fatigue and thermal fatigue of turbine blades in high temperature gas flow

05 p0734 A71-16762

Shock tube research instrumentation with fast response time for data on thermodynamic and transport properties, relaxation times and kinetics of high temperature gases

06 p0897 A71-17430

High temperature gaseous flow, discussing approximate methods of calculation of turbulent boundary layer

[AIAA PAPER 71-163] 06 p0885 A71-18605

Gaseous film cooling effectiveness under varying conditions of free stream turbulence intensity, hot gas acceleration, Mach number and film coolant flow rate

07 p1219 A71-18760

Columnar grain and single crystal high temperature gas turbine elements development through directional solidification

08 p1314 A71-21565

Turbulent hot gas motion in round pipes from semiempirical turbulence theory, accounting for energy dissipation and thermodynamic parameter variability

09 p1431 A71-22370

High gas temperatures calorimetric measurement, providing probes with industrial temperature range capability

09 p1449 A71-22791

Inviscid flow distribution of high temperature jet of optically thick radiating gas exhausting from two-dimensional nozzle into low temperature quiescent medium

10 p1552 A71-24588

Free flight ranges application to high temperature gas dynamics, using mathematical model to relate sub and full scale observations

11 p1705 A71-26269

Hot water vapor curve of growth, using statistical band model with exponential line intensity distribution yielding spectral absorption coefficients

12 p1904 A71-26793

Temperature measurement methods using thermocouples and hot-wire anemometers for rapidly changing hot gases

12 p1906 A71-26990

Atmospheric pressure electrical and thermal conductivities on nitrogen and hydrogen up to 26,000 K from argon arc measurements

12 p1939 A71-27271

Heat transfer on cylindrical antenna in supersonic high temperature gas flow, noting electromagnetic wave damping due to ablation

13 p1990 A71-28296

Gas temperature measurement in aircraft combustion chambers, using calorimetric probe
13 p2117 A71-28757

Temperature and radical concentration measurements for high temperature flowing gas streams in rig simulating conditions in ramjet combustion chamber and nozzle
13 p2162 A71-28758

Ion source of mass spectrometer for high temperature composition studies of gas phase
14 p2247 A71-30588

Gas permeable dispersion layer between impermeable solid wall and high temperature gas flow, solving dimensionless heat flux equations
15 p2512 A71-31505

High temperature fuel cell in hot gas mixtures analysis, presenting porous silver and palladium electrodes cathodic polarizations
15 p2367 A71-31648

Thermochemistry data changes influence in form of heat of formation, partition functions, specie free energy or specific heat on high temperature gas mixtures composition
15 p2514 A71-32097

Electronic excitation contribution to thermodynamic properties of high temperature gases according to partition function cutoff criteria
15 p2515 A71-32647

High temperature singly and doubly ionized monatomic gas and partially dissociated and singly ionized diatomic gas, showing adiabatic and isentropic exponents relationship
16 p2662 A71-32837

Radiative heat transfer effects behind reflected and incident shock waves in high temperature air and xenon respectively
16 p2662 A71-32888

Shock tube production of vibrationally excited molecules for mass spectra studies in hot gases
16 p2613 A71-32894

High temperature high Mach number expansion tube flows, determining impurities by time integrated spectroscopic measurements
16 p2551 A71-33155

Cascading turbomachine blades vibrations measurement in subsonic and sonic high temperature gas flows, describing test facility
16 p2553 A71-33993

Radiation source consisting of porous wall heated internally by hot gas, noting application as high altitude or space flare
17 p2728 A71-34888

Test apparatus for mechanical/thermal fatigue and vibration strength of turbine blades in high temperature gas flow
17 p2724 A71-35461

High temperature gas dynamics, including hypersonic wind tunnel nozzles, air-breathing/chemical rocket propulsion systems, thermodynamic models and relaxation boundary layers
18 p2846 A71-36425

Chromium sesquioxide instability towards oxygen at high temperature, using spring thermobalance
18 p2937 A71-36763

High temperature gas dispersed Al particle flow, investigating electrical conductivity and radiation properties
19 p3161 A71-37265

Shock tube investigation of solid polymeric hydrocarbon fuel ignition in hot oxidizing gas stream
19 p3121 A71-38124

French monograph on free and forced convection and external radiation from hot gas oscillating in resonance tube, considering heat balance and mass exchange
19 p3172 A71-38649

Transient pressure, temperature and density measurement of dense hot gas
21 p3364 A71-40402

Quasi-equilibrium prediction of rate of volatilization /erosion/ of solid tungsten by reaction with gaseous oxygen at high temperature and low pressure
21 p3404 A71-41419

Carbon dioxide, nitrogen and water vapor hot mixture expansion through Laval nozzle, showing population inversion on carbon dioxide laser transition
22 p3556 A71-41726

Gas dynamic laser, obtaining initial high temperature gas mixture by detonating solid
22 p3556 A71-41813

Radiant heat flux measurement during pulsed processes from surface in high temperature emitting gas, using thin film sensor with small time constant
23 p3782 A71-43922

Aircraft parts damage by corrosive friction forces, hot gases and intercrystalline attack, noting worn universal joint and blade grain boundary damage
24 p3836 A71-44574

Thermodynamic properties and nozzle flow calculations for high temperature and pressure hydrogen, presenting results in Mollier diagram
24 p3887 A71-44629

Liquid droplet vaporization under exposure to hot gas, obtaining time dependent temperature and concentration profiles in vicinity from coupled diffusion equations
24 p3888 A71-44963

HIGH TEMPERATURE LUBRICANTS

Fluoro-alkyl s-triazines as high temperature lubricants and energy transfer fluids for aerospace systems [ASLE PREPRINT 70LC-5]
08 p3322 A71-21155

High temperature plastic lubricants thermal stability, discussing thickening agent-dispersed medium interaction effects
12 p1922 A71-27663

NaK lubricated segmented hydrodynamic fluid film tilting pad type journal bearings and Kingsbury type self aligning thrust bearings
15 p2447 A71-32210

HIGH TEMPERATURE MATERIALS

U REFRACTORY MATERIALS

Turbo-MHD cycle technology of nuclear electric power systems with high temperature reactor for space and terrestrial applications
14 p2273 A71-30716

Future space flight energy requirements for onboard power supplies and propulsion, considering high temperature reactors with nuclear fuel in plasma state
19 p3122 A71-37319

HIGH TEMPERATURE PLASMA

Steady high power plasma flows using three phase AC generator
04 p0632 A71-14794

Dense hot plasma generation by laser beam focusing on gas or solid targets, discussing experimental setups, diagnostic methods and ionization theories
10 p1647 A71-23920

Homogeneous spherical hot hydrogen plasma cloud at various temperatures and optical depths, presenting electron scattering effects on optical and X ray spectral emission
18 p2951 A71-36012

HIGH TEMPERATURE PLASMAS

High temperature plasma electron density and ion signal intensity measuring apparatus for reaction rate evaluation
04 p0600 A71-15591

High temperature laboratory plasmas diagnostics, noting time resolution for growth and decay mechanisms
06 p0896 A71-17297

Solar corona emissions, discussing very high temperatures origin, eclipses and electromagnetic radiation spectrum
06 p0970 A71-18058

Plasma physics, obtaining very high temperatures and electron/ion densities by power laser heating
06 p0908 A71-18066

Extraordinary waves propagating perpendicularly to uniform magnetic field in hot electron plasma, discussing wave interaction
07 p1166 A71-18884

Obliquely incident p-polarized plane electromagnetic wave interaction with hot plasma half space, using linearized relativistic Vlasov equation and Laplace transform technique
07 p1171 A71-20292

Hot plasma production by strong shock wave heating, using EM shock tubes under laboratory controlled conditions
07 p1172 A71-20506

High temperature nitrogen plasma, calculating thermodynamic and electrical parameters dependence on pressure and temperature
08 p1342 A71-21917

Hot Cs plasma parametric resonance in variable electric field related to plasma heating
09 p1499 A71-22229

Dispersion equations of plane parallel waveguide filled with hot magnetized plasma, using linear approximation
09 p1503 A71-22883

Spatially uniform external periodic magnetic field effect on wave propagation perpendicular to hot electron plasma, obtaining dispersion relation from hydrodynamic equations
10 p1578 A71-24655

Shock wave propagation in electronically excited hot plasma in electromagnetic field, assuming negligible electron-ion collisions
10 p1653 A71-24828

Book on high temperature plasma diagnostics methods covering measurement errors, holographic interferometers and light scattering
11 p1804 A71-25280

Spectroscopic measurement of high temperatures for ionized gases /plasmas/ in local thermodynamic equilibrium
11 p1761 A71-25571

Nonuniform density cosmic plasma heating allowing energy losses by radiation and heat conduction, using filament-structured high temperature plasma region model
11 p1828 A71-25765

Mixed plasmas transport properties at one atmosphere and 5000-35,000 K, considering helium-nitrogen, argon-nitrogen and xenon-nitrogen plasmas
12 p1986 A71-27188

Hot plasma oscillations analysis for instabilities as function of magnetic viscosity and heat fluxes, using inertial waves dispersion equations
12 p1937 A71-27202

Rate constant measurements of hot plasma electron attachment from ion current collection plots for communication during atmospheric entry
12 p1939 A71-27202

High temperature plasmas optical properties measurement by plasma spectroscopy, using gas driven shock tube as light source
12 p1940 A71-27202

Helicon and magnetoacoustic waves instability during passage through hot collisionless plasma with current transverse to weak external magnetic field
13 p2107 A71-28888

Soviet monograph on wave propagation in cold and hot magnetoplasmas covering particle collision, plasma control and instability and plasma-particle interactions
14 p2280 A71-30242

Longitudinal waves correlation damping in high temperature plasma under magnetic field, calculating dielectric constant by quantum statistical method
14 p2280 A71-30450

RF power absorption of uniform hot ion-electron plasma column, considering collision effects and EM radiation
14 p2281 A71-30559

Fokker-Planck equation for Compton scattering in hot plasma, considering energy exchange rates for scattering in relativistic Maxwellian plasma
14 p2283 A71-30858

Nitrogen plasma electrical and thermal conductivities and radiative source strength at atmospheric pressure and 9,000-12,500 K, using Hall probe and optical methods
15 p2454 A71-31536

Economical fusion reactor requirements, considering ultrahigh temperature plasma containment for nuclei reaction and energy extraction
15 p2455 A71-31682

Temperature dependence of H-beta emission from hot hydrogen-helium plasmas, calculating production rate at 10,000-100,000,000 K
15 p2455 A71-31720

Porous refractory materials for thermochemical protection against high temperature plasma flows, discussing effectiveness in erosive wear reduction
15 p2432 A71-32164

High temperature nitrogen plasma emission spectrum in 2500-5000 A range, estimating negative ion photoionization cross sections
16 p2613 A71-32904

Plasma chemistry, discussing low and high temperature plasmas, nuclear fusion reactions and chemical molecular and nuclear synthesis
16 p2539 A71-32960

Nuclear reactions in high temperature laboratory and stellar plasmas, discussing pinches, thermonuclear burning and star evolution
16 p2613 A71-32977

Quasi-neutral inhomogeneity /particle cloud/ in collisionless hot or cold plasmas without magnetic field
16 p2619 A71-33522

High temperature dense plasma formation by laser heating of gas target, noting fusion reaction in deuterium-tritium mixture
16 p2619 A71-33644

Axisymmetric blunt body heating by high temperature plasma flow as function of geometry, pressure and stagnation enthalpy
17 p2669 A71-34204

High temperature nitrogen plasma, calculating thermodynamic and electrical parameters dependence on pressure and temperature
17 p2789 A71-35264

Magnetic field aligned electric field production by hot magnetospheric plasma interaction with cold ionosphere
19 p3048 A71-37401

Plasma guns hot and cold plasma separation, describing diverter operation principles
19 p3112 A71-37639

Hot plasma oscillations analysis for instabilities as function of magnetic viscosity and heat fluxes, using inertial waves dispersion equations
19 p3116 A71-38614

Solar coronal X ray spectrum calculation of high temperature low-density plasma, considering line emission from electron collisional excitation and radiation
20 p3278 A71-39054

Crab Nebula pulsar and extra emission from collapsed star magnetosphere, accounting for physical characteristics with nonthermal plasma mechanism
20 p3285 A71-39954

Highly ionized hot Cs plasma parametric resonance in alternating electric field related to plasma heating
21 p3424 A71-41107

Nonelectrostatic helicon and magnetoacoustic waves instability during passage through hot collisionless plasma with current transverse to weak external magnetic field
21 p3425 A71-41280

Hot plasma fast ions energy distributions in toroidal accelerators with quasi-stationary discharge
21 p3426 A71-41286

Nonuniform density cosmic plasma heating allowing for energy losses by radiation and heat conduction, using filament-structured high temperature plasma region model
22 p3598 A71-41533

Laminar collisionless shock propagation perpendicular to magnetic field into hot plasma, calculating temperature effects on leading edge growth rate
22 p3579 A71-41580

Transverse current conduction through MHD generator seeded hot plasma flow, showing Joule heating dominance in cathode boundary layer due to thermal instability
22 p3584 A71-42596

German monograph on experimental determination of noble gas plasma conductivity under normal pressure in high temperature range, covering measurements under electric arc conditions
23 p3711 A71-43475

Monochromatic absorption coefficients determination for Ar heated in wall-stabilized arc at high temperatures and pressures
23 p3712 A71-43915

Multispecies high temperature Tokamak plasma heating by energetic particle injection, using Balescu-Lenard kinetic equation
24 p3852 A71-44490

RF power absorption by magnetized uniform hot electron-ion plasma column submitted to TE and TM waves
24 p3852 A71-44498

Injected ion beam interaction with hot plasma in cylindrical magnetic mirror, noting acoustic frequency oscillation heating effect
24 p3854 A71-44514

HIGH TEMPERATURE RESEARCH

Refractory metal surface-gas reactions at high temperatures in vacuum, determining activation energies
05 p0766 A71-16241

Bursting diaphragm shock tube as research tool for high temperature phenomena in energy transfer processes, reaction kinetics, hypersonic flow and astrophysics
05 p0734 A71-17240

GaAs epitaxial layers growth in open system, noting spontaneous crystallization on reactor walls at high temperatures
09 p1506 A71-22161

Mass spectrometer ion source modifications for temperature range extension in high temperature research
09 p1450 A71-23068

Thermodynamic calculation of silicon chloride gas for high temperature two stage molybdenum silicification in glowing discharge under vacuum conditions
11 p1770 A71-25944

High temperature tensile strength, creep rupture behavior and high temperature exposure effects on subsequent room temperature properties of maraging steel plates and welds
12 p1918 A71-27314

[ASME PAPER 71-MET-E]

Hadron matter thermodynamical properties at high temperatures, developing dual resonance dynamic model of high energy particle interactions
14 p2304 A71-29597

Plasma as fourth state of matter, including high temperature behavior, radiation emission, applied electric/magnetic fields effects and laboratory generation
16 p2617 A71-32953

High porosity carbon-graphite materials thermal and electrical conductivities at high temperatures by potentiometric method
17 p2761 A71-34208

Thermobalance for studying high temperature silicon-carbon reaction kinetics, incorporating HF current, coaxial shielding of electrical connections and electromagnetic balance
17 p2838 A71-35475

High temperature oxidation of ammonia, carbon monoxide and methane by nitrous oxide in shock tubes, using optical interferometry and UV/IR emissions
19 p3012 A71-38086

HIGH TEMPERATURE TESTS

Cu compatibility with refractory Ta-W alloy interface at high temperature, noting eutectic formation
01 p0100 A71-10374

Viscoelastic behavior of boron fiber-epoxy resin composites at high temperature from torsion pendulum study, proposing linear model for damping peak effect
01 p0107 A71-10460

Ta thermal properties at high temperature in cast cylinder, powder and wire specimens
01 p0100 A71-10547

Austenitic Cr-Ni-Ne stabilized steel, evaluating high temperature oxidation and creep process interaction
01 p0104 A71-11603

High temperature thermophysical properties of vanadium, establishing heat conductivity coefficient,

electric resistivity, Lorentz number, monochromatic and total hemispherical emission coefficients
02 p0263 A71-12189

High temperature neutron irradiation properties of uranium oxides, carbides and nitrides coated with tungsten-rhenium
02 p0296 A71-12246

Cobalt 60 oxides as thermionic fuels, discussing high temperature properties, fabrication and irradiation techniques
02 p0280 A71-12256

Soviet optomechanical instruments for metallurgy and high temperature metallography
02 p0254 A71-12711

Structure and durability of self healing silicide based coatings for niobium oxidation protection at high temperatures
03 p0272 A71-12947

Vaporization chemistry in C, Si, Cr, Mo and Nb high temperature oxidation, using thermochemical diagrams
03 p0374 A71-13123

Reactive molecule and atom attack of refractory materials in dissociated gases at filament temperatures up to sublimation threshold
03 p0374 A71-13124

Elevated temperature strain gages using capacitance changes as indication, discussing design and response tests
03 p0426 A71-13770

Bonded and weldable strain gages for aircraft flight loads measurements at high temperatures, discussing installation, calibration and performance tests
03 p0426 A71-13781

High temperature tests of gas turbine engine with transpiration air cooled blades, discussing blade design, fabrication, ductility and oxidation resistance [ASME PAPER 70-WA/GT-1]
03 p0470 A71-14115

Ni-Cr foil resistance strain gages for high temperature operation, discussing performance test data
03 p0430 A71-14327

High temperature permeameters for measuring magnetizing force and magnetic induction, presenting normal induction curves as function of temperature
03 p0430 A71-14413

Spectral emittance of Ti at high temperatures in visible region under vacuum
04 p0611 A71-14956

High speed measurements of thermophysical properties at high temperatures, including photoelectric and photographic methods
04 p0595 A71-14957

Apparatus for thermal diffusivity measurements under gas atmosphere at high temperature, using flash method
04 p0595 A71-14962

Thermal diffusivity and total emissivity measurements of solids between 1500 K and melting point, using arc image furnace
04 p0595 A71-14966

Multiproperty apparatus for high temperature determination of tungsten thermal properties, using direct electrical heating methods
04 p0595 A71-14967

Thermophysical properties of solids at high temperatures concerning zirconium carbide, corundum, metals and Ba-Cs system
04 p0612 A71-15578

Thermal conductivity and emittance of arc cast and powdered W at 1800-2800 K
04 p0612 A71-15579

W-Mo alloy enthalpy and specific heat measurement at high temperatures by drop calorimetry
04 p0613 A71-15580

Tungsten, molybdenum and rhenium single crystals hemispherical emissivity at high temperatures by electron beam heating, considering grain boundary contribution
04 p0613 A71-15581

Creep strength of Nb alloys with Mo at high temperatures in vacuum, noting Zr-C complex alloying effect
04 p0613 A71-15642

Damage and fracture mechanisms in high temperature low cycle fatigue of cast nickel-based superalloys, noting grain boundaries oxidation role in crack nucleation and propagation
04 p0615 A71-15789

Soviet monograph on refractory materials elasticity at high temperatures covering elastic and shear moduli, Poisson coefficient and resonance methods
05 p0766 A71-16400

Pure W monochromatic emissivity measurements at 0.4 to 4 microns and at high temperatures
05 p0767 A71-16600

Solid metal plates breakdown mechanism at high temperatures and supersonic plasma jet action
05 p0768 A71-16778

W, Nb, Mo and Ta spectral radiative power at wavelengths from 0.66 to 5.12 mu at various high temperatures
05 p0768 A71-16780

High temperature creep comparison of single phase Fe and Ni alloys subjected to constant load tensile tests, measuring strain as function of time
06 p0911 A71-17345

Ti alloy embrittlement by prolonged high temperature exposure, using substandard fracture mechanics test for time-temperature dependence
06 p0915 A71-18686

High temperature creep behavior of nickel base alloys with L12 and B2 type lattices, discussing single crystals of beta-NiAl
07 p1133 A71-19446

High temperature ductility of low alloy ferritic steels, correlating tensile elongation values to crack nucleation resistance
07 p1134 A71-19517

Metal film resistors rapid evaluation method including thermal, load and shock tests devised by British electronic component manufacturers
07 p1076 A71-19553

Refractory metals and alloys fabrication and mechanical and physical properties at high temperatures
07 p1134 A71-19581

X ray Debye chambers and diffractometer cameras for high temperature investigations of metal systems phase equilibrium
07 p1112 A71-19620

Stainless steel fatigue crack growth characteristics at liquid metal fast breeder type nuclear reactors elevated temperatures
07 p1138 A71-19983

Asymmetric three layer cylindrical shells with orthotropic layers under deflection due to high temperature, deriving differential bending equations
07 p1217 A71-20456

Cyclic creep and relaxation of heat resistant alloys at high temperatures, showing inapplicability of static load conditions
07 p1142 A71-20480

High temperature blank heating and cutting during magnetic alloy machining for optimal cutter stability
08 p1296 A71-20844

Recrystallized and nitrided Mo alloy microstructure under plastic deformation by tension at high temperatures
08 p1305 A71-21029

Mo microstructure changes at high temperatures noting polygonization, grain migration and crack propagation during failure
08 p1305 A71-21032

Multisample test equipment for steels and alloys oxidation resistance at high temperatures in corrosive gaseous atmospheres
08 p1292 A71-21440

V-Ti alloys high temperature behavior dependence on Ti content, examining interstitial impurities effects on mechanical properties
08 p1310 A71-21532

Ni-Cr thoria dispersion strengthened alloys, determining texture effects on high temperature mechanical properties
08 p1311 A71-21545

Aged Al alloys dislocation substructure effect on mechanical properties at elevated temperatures
08 p1313 A71-21559

Stacking fault formation and mechanical twinning in Ni base superalloy during tensile deformation at high temperature
08 p1315 A71-21581

Crack opening mechanism for high temperature creep of polycrystalline graphite
08 p1323 A71-21584

Ternary systems Hf-W-B, Hf-Re-B and Nb-Re-B isothermal sections phase diagrams at high temperature, using X ray analysis
08 p1317 A71-21858

Hg vapor thermal conductivity measurement at 300-900 C and atmospheric pressure, using hot wire method
08 p1376 A71-21919

Single crystal W thermal conductivity measurement at 1200-2500 K, discussing apparatus and error sources
08 p1318 A71-21920

Pyrolytic graphite hemispherical emissivity measurement on surface parallel and perpendicular to deposition surface at 1200-2300 K
08 p1323 A71-21921

Electrical conductivity of strontium zirconate and hafnate at 1400-2600 K measured by two-probe method with alternating and direct currents, calculating activation energy
08 p1323 A71-21934

High temperature apparatus for enthalpy and specific heat measurements of refractory metals
08 p1273 A71-21936

Tensile-compressive testing apparatus for low cycle load at high temperatures
09 p1426 A71-22499

Nb alloy high temperature creep and long term strength, determining exponential relations between stress, strain rate and durability
09 p1468 A71-22628

HIGH TEMPERATURE TESTS

Measuring apparatus for cyclic plastic strains at high temperatures, discussing data processing techniques

09 p1443 A71-22636

Piezoelectric accelerometers for high temperature vibration measurements, examining materials critical characteristics, design minimal weights and vibration system test methods

09 p1443 A71-22707

High temperature measurement by photographic technique using radiation-sensitive color film for unpredictable exposure conditions

09 p1444 A71-22712

High temperature dynamic strain gage test equipment for evaluating precision, life and environmental limitations

09 p1445 A71-22719

High temperature thermal null strain gage with sensing unit and electronic control unit to measure mechanical strain in terms of induced thermal strain

09 p1445 A71-22721

Miniature pressure transducer with extended temperature capability, discussing design and operation

09 p1445 A71-22723

High temperature tensile strength testers for metallic and carbon filaments

09 p1446 A71-22735

Stacking faults and fcc precipitation of Ti beta alloys after high temperature heating

09 p1469 A71-22850

Metals and welded joints corrosion resistance at high temperatures and pressures, describing tests in autoclave with pneumatic loading

09 p1429 A71-23050

Aerodynamic heating effects on fatigue and creep properties of supersonic aircraft alloys at high temperatures, considering deformation mechanisms interaction

09 p1472 A71-23204

Fe-Cr-Zr ternary alloys, investigating Zr effect on high temperature hardness and heat resistance

09 p1473 A71-23228

Cr specimens containing Y, investigating microscopic breakdown at high temperatures as function of deformation during vacuum rolling

09 p1474 A71-23235

Aluminum high temperature resistant diffusion type coatings structure and chemical composition, outlining turbine blades testing for thermal shock, oxidation and sulfur and sea salt corrosion

09 p1474 A71-23287

Ni-Al alloy strain hardening, observing high intensity ultrasonic irradiation effect on high temperature creep

09 p1475 A71-23315

Thermophysical properties of solids at high temperatures - Conference, University of Salford, England, April 1970

10 p1624 A71-23906

Edge losses effects on thermal conductivity of thermal insulations at high temperature measured by guarded hot plate method

10 p1694 A71-23907

Ti thermal conductivity, electrical resistivity and total emittance at high temperatures in ultrahigh vacuum, discussing phase transformation effect

10 p1624 A71-23910

Tungsten high temperature thermal diffusivity at 1000-2500 K by flash technique

10 p1624 A71-23911

Mo high temperature melting point and electrical resistivity measurement by pulse heating method

10 p1624 A71-23912

Potting compounds service life estimation based on accelerated hydrolytic reversion data at high temperatures and humidities

10 p1633 A71-24117

High temperature fatigue test assembly for symmetric tension compression cycles at 10 kHz

10 p1589 A71-24201

High temperature testing assembly for reinforced plastics and binders in oxidizing and inert media under tension, compression, bending and cleavage loads

10 p1589 A71-24202

Monograph on dense gases state parameters measurement at high temperatures, applying to nitrogen

10 p1697 A71-24676

Al alloys one step fatigue tests under combined high temperature and structural vibration conditions

10 p1628 A71-24821

Reflecting oven for very high temperatures under gas pressure, describing apparatus, heat source and possible contamination

10 p1613 A71-25040

Graphite ablation under high temperatures for large outer planets entry probes, correlating mass loss rates with surface temperatures and specimen nose cone radii

[AIAA PAPER 71-418]

Polycrystalline NbC and TaC Young, shear and bulk moduli determination at high temperature, noting porosity and temperature effects

11 p1857 A71-26209

Hot pressed boron carbide and titanium diboride for use as indenter materials for tungsten carbide hardness measurements at high temperatures

11 p1781 A71-26294

General dislocation model for high temperature creep of pure metals, discussing strain rate effects

11 p1782 A71-26476

Nb and Mo doped Ni-Al alloy with Ni-Nb additions, obtaining diagrams of composition versus heat resistance in high temperature bending tests

12 p1916 A71-26968

Corrosion mechanism in Ta-Li high temperature heat pipes by ion analysis, demonstrating oxygen and yttrium diffusion into heating zone

12 p1916 A71-26974

High temperature heat pipes material corrosion problems, considering mass transfer from cooling zone into heating zone

12 p1917 A71-26975

Performance testing of fluorosilicone hydraulic fluid in high temperature supersonic aircraft piston pumps

12 p1921 A71-27040

Strain gages of annealed tantalum wire resting on quartz paper base for prolonged tests at high temperatures

12 p1908 A71-27363

Fibrous composite materials experimental failure studies at high temperatures and cyclic loading

12 p1922 A71-27683

Heat resistant alloys strengthened elements, studying high temperatures prolonged exposure effects on surface layers strengthening and residual stresses relaxation

12 p1919 A71-27780

Mechanical properties and strain rates determination at high temperature, using automatic loading system with strain gage dynamometer and oscillograph

13 p2045 A71-29375

High temperature creep in alpha-Fe, Fe-Mo and Fe-Co alloys, investigating stress dependence and alloying effects in ferromagnetic and paramagnetic temperature ranges

13 p2089 A71-29409

Cyclic strain effects on creep for steel at elevated temperatures, discussing overload frequency effects on plastic strain buildup

14 p2256 A71-29626

Nickel under diffusion controlled reactions at high temperatures, reviewing parabolic oxidation rate law

14 p2256 A71-29634

Creep-fatigue analysis by strain range partitioning, considering metals inelastic deformation at high temperature due to plastic flow

14 p2325 A71-29923

Radiative capacity of materials with low thermal conductivity at high temperatures determination from reflectivity measurements for oblique light incidence

14 p2240 A71-30051

Nb single and polycrystalline thermal conductivity/diffusivity, specific heat, electrical resistivity and monochromatic/integrated degree of blackness at high temperatures

14 p2258 A71-30052

Shape instabilities for eutectic alloys composite microstructure at elevated temperatures

14 p2259 A71-30413

Methane high temperature oxidation in steady flow system, predicting change rate of species concentrations and gas properties during reaction

14 p2285 A71-30457

Nitrogen solubility in W at high temperature, using metal high vacuum apparatus and mass filter partial pressure measuring instrument

14 p2260 A71-30475

Hf-W-B, Hf-Re-B and Nb-Re-B ternary systems isothermal phase diagrams at high temperature, using X ray analysis

14 p2261 A71-30837

High temperature thermophysical properties of vanadium, establishing heat conductivity coefficient, electric resistivity, Lorentz number, monochromatic and total hemispherical emission coefficients

15 p2426 A71-31496

High temperature creep in Al-Zn solid solution, using isothermal tests

15 p2429 A71-31997

Heat content measurement of tantalum carbide in homogeneity range at high temperatures by mixing method using bulk calorimeter

15 p2431 A71-32155

Thermodynamic properties of titanium carbide of variable composition at high temperature, considering enthalpy, specific heat and entropy change due to thermal vacancies

15 p2431 A71-32159

Truncated-cone hot-pressed silicon carbide samples, measuring enthalpy and heat capacity as temperature function at high temperatures

15 p2431 A71-32160

Cast ZrC hot hardness measurement by static tests at high temperatures, comparing with hot-pressed samples

15 p2431 A71-32161

Hot pressed boron carbide and titanium diboride for use as indenter materials for tungsten carbide hardness measurements at high temperatures

15 p2409 A71-32165

Hot performance tests of three identical Brayton rotating units on gas bearings

15 p2355 A71-32292

Creep rupture behavior and high temperature exposure effects on room temperature properties of Ni-Cr-Mo maraging steel plates and welds

15 p2434 A71-32293

Tensile strength of boron, silicon carbide coated boron, silicon carbide, stainless steel and tungsten fibers after exposure to air, argon and aluminum at high temperatures

15 p2435 A71-32294

Thermal conductivity, diffusion and viscosity of gases and multicomponent gaseous mixtures at high temperatures

15 p2515 A71-32401

Oxygen dissociation and recombination rate constants at high temperatures from gas density interferometric measurement in relaxation zone of normal shock waves

15 p2367 A71-32512

Point defects relation to thermoelectric emission at high temperatures in yttrium oxide

15 p2462 A71-32717

Solid metal plates erosion mechanism at high temperatures under supersonic plasma jet action, noting dependence on specific heat and latent heat of fusion

16 p2591 A71-33010

W, Nb, Mo and Ta spectral emissive power wavelengths from 0.66 to 5.12 μ m at various high temperatures

16 p2591 A71-33020

Continuous nitrogen and oxygen ion spectra due to photoionization and free ion transfers at high temperatures, calculating absorption coefficient

16 p2662 A71-33040

High temperature vaporization of titanium, zirconium, hafnium and thorium carbides by Knudsen effusion mass spectrometry, measuring ion intensities, formation enthalpies and dissociation energies

16 p2540 A71-33242

Program parameters effects on fatigue life of turbine blade heat resistant alloys at high temperatures under cyclic loading

16 p2592 A71-33440

Structural changes and phases nucleation during growth in metal alloys during prolonged loading at high temperatures, examining steel strengthening precipitates coagulation kinetics

16 p2597 A71-33900

Stress-strain diagrams of heat resistant alloys at high temperatures, describing test facility

16 p2598 A71-33908

Electrical conductivities of Apollo 11 and 12 lunar rocks and chondritic meteorites at 300-1100 K

17 p2796 A71-34180

Electrical conductivity of pyrographite at high temperatures along and across deposition plane, using optical pyrometer measurements

17 p2761 A71-34300

Materials stability testing in high temperature propane-butane combustion product flow, selecting compact silicon carbide for structural use in redox medium

17 p2761 A71-34310

High temperature stress measurements with electrical resistance strain gages, describing test apparatus and gages evaluation

17 p2738 A71-34550

Co-Cr-W alloy sulfidation at high temperatures, performing weight gain, metallographic X ray and electron probe analysis

17 p2758 A71-35140

Single crystal W thermal conductivity measurements at 1200-2500 K, discussing apparatus and error sources

17 p2759 A71-35260

Pyrolytic graphite hemispherical emissivity measurement on surface parallel and perpendicular to deposition surface at 1200-2300 K

17 p2763 A71-35260

Temperature and pressure effects on viscosity and thermal conductivity of dissociating air at high temperatures

17 p2785 A71-35277

High temperature apparatus for enthalpy and specific heat measurements of refractory metals

17 p2724 A71-35278

Annealed Mo creep and stress rupture at high temperatures for typical deformation

17 p2760 A71-35660

High temperature tensile strength of Ta-W-Hf alloy sheet with protective Si-Ti coating in vacuum and air

18 p2933 A71-35950

High temperature oxidation protection of niobium by molybdenum disilicide coatings applied by hot pressing powder metallurgy method

18 p2934 A71-35950

German monograph on high temperature measurement of thermal and electrical conductivity of W and Mo single crystals

18 p2915 A71-35960

Surface temperatures and ablation mechanism of combustion protective plastics reinforced by silicon under intense heating measured by IR micropyrometry [ONERA-TP-962]

18 p2984 A71-36020

- Damping characteristics of Ni base refractory alloys at high temperatures, showing increase with cyclic strain amplitude 18 p2936 A71-36708
- High temperature tests of short time strength, hardness, moduli of elasticity of W-Mo alloys subject to plastic deformation and annealing 18 p2936 A71-36712
- Carbon effects on strength, ductility, brittle transition and plastic strains of tungsten at high temperatures 18 p2936 A71-36713
- High temperature creep of niobium alloy, obtaining creep limit, microhardness and gas analysis data 18 p2936 A71-36715
- Electron concentration and mobility of heavily doped n-type InSb single crystals at high temperatures, investigating temperature dependence of Hall coefficient 18 p2954 A71-36803
- High speed system for thermophysical properties measurement of electrical conductors above 2000 K in subsecond experiments 19 p3062 A71-37246
- High temperature strengthening of vacuum melted W-Ti alloys with Mo and Zr additions 19 p3076 A71-37267
- Age hardening of Mo alloys with titanium and zirconium carbides at high temperatures after quenching 19 p3077 A71-37268
- Mo effect on high temperature strength, heat resistance, plasticity and toughness of austenitic Cr-Mn-Ni-Al steel 19 p3077 A71-37465
- High temperature four point bending vacuum furnace machine testing thin refractory sheets, noting strain rate, velocity jump and relaxation on tantalum carbide 19 p3063 A71-37554
- Electroconductivity, thermal conductivity and diffusivity, specific heat and emissivities of Ti at 1000-1700 K 19 p3078 A71-37582
- Test facility for thermal diffusivity measurements in solids by method of plane temperature waves using periodic optical heating at 1500 K 19 p3063 A71-37589
- Stress effect on hydrogen distribution at high temperatures in titanium and Ti-Al-Mo-V alloy 19 p3080 A71-37720
- Inorganic polymers and glasses at high temperatures, detecting LF internal friction 19 p3084 A71-38050
- Elevated temperature testing problem areas - ASME-ASTM Conference, Toronto, June 1970 19 p3065 A71-38131
- High temperature creep testing facilities and techniques, evaluating statistically interlaboratory variability and significance of testing and material variables affecting creep results 19 p3081 A71-38132
- Interlaboratory program to evaluate thermocouple pyrometric practices in metals high temperature testing 19 p3065 A71-38136
- Thermocouple drift effect on creep and tension rupture life at high temperature 19 p3065 A71-38137
- Characteristic smooth test bar ductility correlation and prediction in high temperature creep rupture tests, noting application to material quality control 19 p3082 A71-38138
- Gripping method for short length tubing during high temperature tensile tests 19 p3069 A71-38139
- Al, Cu and Ni high temperature creep noting diffusivity, shear and dislocation deformation mechanisms 19 p3083 A71-38525
- Sealed and vented fusing devices, testing vacuum effects on performance at high and low temperatures 19 p3035 A71-38536
- Thermophysical properties of Ta, W and Ta-W alloy at high temperatures, using automatic high vacuum facility 20 p3247 A71-38764
- SNAP 19 TAGS thermoelectric generator life tests at high temperature in Ar, predicting long term performance including thermoelectric material and isotope fuel decay effects 20 p3266 A71-38963
- High temperature properties of weld metals formed by electrodes for welding of low alloy heat resistant Cr-Mo and Cr-Mo-V steels 20 p3249 A71-39014
- Al alloy tensile tests at high temperature and constant elongation and loading rates, noting creep strain 20 p3251 A71-39167
- Chemical vapor deposited tungsten or other refractory metal alloys mechanical properties evaluation at high temperature, describing hoop stress measurement apparatus for induction heated specimens [ECS PAPER 384-RPN] 20 p3252 A71-39553
- Retained lattice strain and substructure domain size effects on tensile strength at room and elevated temperature in dispersion strengthened Ni alloys 21 p3397 A71-40453
- High temperatures prolonged exposure effects on surface layers hardening and residual stresses relaxation in heat resistant alloys 21 p3403 A71-41105
- High temperature creep characteristics and strain curves of heat resistant Fe and Ni alloys in turbine components 21 p3403 A71-41158
- Solid body contact interaction devices at high temperatures in vacuum, gas and air for evaluation of surface coatings, adhesion, diffusion, mechanical properties, etc 21 p3382 A71-41174
- Thermal conductivity determination of Ar at extremely high temperatures, using temporal development of thermal boundary layer at shock tube wall 22 p3619 A71-41523
- Superhigh vacuum apparatus for creep and long term strength tests on metals at high temperatures, giving results for niobium alloys 22 p3538 A71-41699
- Hold time effects on plastic deformation and fracture in high temperature low cycle metal fatigue 22 p3561 A71-41942
- Monocrystalline and polycrystalline Ta-Hf oxidation at 750-1050 C, noting orientation 22 p3563 A71-42363
- Lithium additions effect on hydrogen content and mechanical properties of molten aluminum specimens 23 p3691 A71-43522
- High temperature phase transition and composition of Apollo 12 pigeonite/augite clinopyroxene crystal rock 12021 from X ray diffraction 23 p3738 A71-43607
- Tektite organic constituents evidence from high temperature mass spectrometry, investigating relation to formation process and terrestrial contamination 23 p3769 A71-43926
- Ignitability limits of hydrogen/air and hydrocarbon/oxygen mixtures at high temperatures near self ignition range 23 p3782 A71-44007
- Sintered construction material with high SiC content, investigating thermal stability in nitrogen, air, carbon dioxide and water vapor above 2000 K 23 p3696 A71-44020
- Tungsten filaments as reinforcing agent of heat resistant composite chromium alloy, investigating long term high temperature effects 24 p3837 A71-44728
- Heat resistant Nichrome composite alloy with tungsten filament reinforcement, discussing manufacture and mechanical properties at 1100 C 24 p3837 A71-44730
- Composite materials thermal diffusivity at high temperatures by quasi-stationary and monotonic methods, determining validity domain of differential heat conduction equation without heat sources 24 p3889 A71-44967
- Free radical induced high temperature oxidation degradation curtailment of polyphenyl ethers by oxides, hydroxides and carbonates of alkali metals and Ba [ASLE PREPRINT 71LC-11] 24 p3842 A71-45290
- ### HIGH THRUST
- FOILAC solid propellant rocket motors for high thrust short action time propulsion, reviewing development status and performance [AIAA PAPER 70-1385] 03 p0470 A71-13668
- High thrust density colloid emitting source development as basic microthruster for electrostatic propulsion systems [AIAA PAPER 71-694] 14 p2293 A71-30753
- Civil aircraft future propulsion requirements, considering larger engine sizes, higher takeoff thrusts and lower noise levels [CASI PAPER 72/10] 19 p3122 A71-37600
- High and low propulsion for optimal transfers between coplanar coaxial elliptic orbits, determining impulse number and timing [AAS PAPER 71-368] 23 p3729 A71-43038
- ### HIGH VACUUM
- High vacuum low temperature fatigue tests, describing design and operation of equipment for microstructural observation 09 p1427 A71-22511
- Bacteria and yeast strains, fungus specimens and seaweed species high vacuum resistance, noting microorganisms interplanetary transport in outer space 13 p2009 A71-28689
- German book on metallurgy, production and application of rare metals, discussing high vacuum technology 21 p3399 A71-40783
- Electrical breakdown initiation in high vacuum by electron beam, investigating discharge delay time dependence on beam parameters 21 p3420 A71-41292
- ### HIGH VOLTAGES
- Transistor collector pulse response characteristics measurement at high voltages in avalanche multiplication region, considering dissipated power curve 01 p0051 A71-10282
- High voltage thermionic module eliminating power conditioning and multiple units series connection, discussing design and coating technologies 02 p0195 A71-12244
- High voltage power supply for NASA orbital gravity substitute electrostatic workbench, including abnormal load and oxygen environment tests 03 p0394 A71-13050
- High voltage DC power supplies for aerospace detectors operation, considering different resonant configurations for performance 03 p0352 A71-13051
- Field aligned currents and high potential drop space charge regions above aurora associated with electron acceleration 03 p0419 A71-14525
- Integrated high voltage CdS solar batteries with interconnected cells in series without grid 05 p0699 A71-16058
- Modified Ebers-Moll equivalent circuit model for saturation characteristics of high voltage transistors 07 p1174 A71-19058
- Model of curved channel multipliers saturation gain at high applied voltages 09 p1446 A71-22736
- Laser triggered switching, discussing ability to trigger high voltage spark gaps with nsec delay and subnsec jitter 11 p1775 A71-26083
- Radioactive decay energy conversion of beta particle emitting cerium 144 into high voltage electricity in coaxial cylinder cell 15 p2447 A71-32211
- High voltage power supply for optically pumped solid state lasers, including water cooling of ruby and discharge tube jacket 16 p2585 A71-33074
- Multiple scattering of VHF and UHF radio waves from bundle conductor high voltage power transmission lines 19 p3021 A71-38446
- High voltage source model for fast neutral particles, showing energy and yield as function of potential, pressure and magnetic field 21 p3421 A71-41295
- ### HILBERT SPACE
- #### U AIR RACRY
- #### HILBERT SPACE
- #### NT BANACH SPACE
- Boundary value problems solution by partial absorption method for elastic oscillations in inhomogeneous media, discussing Hilbert space methods 04 p0665 A71-14809
- Ritz-Galerkin method for solving nonlinear operator equations in Hilbert space, discussing convergence and error estimate 06 p0919 A71-18204
- Admissible translations of probability measures on sigma algebra of Borel sets of Hilbert space 07 p1147 A71-19200
- Bifurcation points in equation $Au = \lambda u$ with A as monotonic nonlinear operator and T as completely continuous nonlinear operator in real separable Hilbert space 13 p2094 A71-28274
- Hilbert space valued systems and elliptic boundary value problems stability, employing circle criterion 16 p2549 A71-32978
- Feedback stabilization of linear distributive systems in form of second-order evolutionary equation in Hilbert space, applying to plasma stabilization 16 p2618 A71-33006
- German monograph on upper and lower bounds in elastomechanics covering elastostatic, natural vibration and stability problems, elastic states Hilbert space, numerical methods, etc 17 p2818 A71-34480
- Distributed parameter systems described by parabolic differential equations in Hilbert space, discussing existence of optimal control based on quadratic cost criteria 17 p2719 A71-34738
- Unbounded linear operator in Hilbert space, constructing characteristic function for transformation 17 p2765 A71-34865
- Equilibrium strategies for linear games with quadratic costs in Hilbert space, deriving nonlinear equation in allowed operator feedback spaces 17 p2723 A71-35297
- Multiply connected domain with Hilbert reduced problem, applying to MHD problems 18 p2953 A71-36950
- Diffraction by perfectly conducting plane screens solved by Hilbert space formulation of EM diffraction 19 p3018 A71-38192
- Galerkin approximation for boundary value problem finite difference scheme optimization by interpolation in Hilbert subspace 22 p3566 A71-42292
- Linear dynamic systems suboptimal control determination from lower dimension models, characterizing system and model outputs as Hilbert space elements 23 p3660 A71-44121

HILBERT TRANSFORMATION

Electromagnetic wave diffraction properties by ribbon metallic lattice in optically active media using Riemann-Hilbert method 24 p3804 A71-44716

HILBERT TRANSFORMATION

Cochannel interference reduction in FSK system by applying Hilbert transform techniques 17 p2703 A71-35079

Phase object visualization by Hilbert transformation, noting image properties evolution as function of various experimental parameters 18 p2947 A71-36043

HILL CURVES

U HILL METHOD

HILL METHOD

Planetary satellites intermediate orbits calculation in three dimensional Hill problem, allowing for solar disturbances 01 p0156 A71-10447

Periodicity solutions of Whittaker-Hill equation in trigonometric series form by three term recurrence relations 03 p0450 A71-13372

Hill lunar solution of a planet problem in rectangular heliocentric coordinates 04 p0656 A71-15733

Restricted four body problem, obtaining graphs for Hill surface of zero relative velocity 13 p2137 A71-28478

Two spheroid rigid bodies rotational and translational motion, using linear and Hill type differential equations for angular variables and coordinates 14 p2312 A71-30384

HIMALAYAS

Global monsoon atmospheric response model in geostrophic terms for heating input function parameterization, including Himalayas mountains effects 10 p1638 A71-23966

Pretertiary invertebrate fossil remnants and microcoprolites found in Lower Himalayan Basin 11 p1721 A71-26318

HINDRANCE

U CONSTRAINTS

HINGE MOMENTS

U TORQUE

HINGED ROTOR BLADES

U HINGES

U ROTARY WINGS

HINGELESS ROTORS

U RIGID ROTORS

HINGES

NT FLAPPING HINGES

Precessional element of gyroscopic systems with rigid structural elements connected by single degree of freedom axial hinges 10 p1611 A71-24577

HIPPOCAMPUS

Orientation reflexes neuronal activity due to various stimuli, noting hippocampus reaction to sound and light 17 p2685 A71-35361

Hypothalamus anterior and hippocampus limbic system relation and oxytocin effect in rabbits, using EEG analysis 22 p3490 A71-42577

HISS

Polar chorus background hiss generation, investigating VLF wave characteristics responsible for harder electron precipitation from magnetosphere 05 p0743 A71-17004

VLF hiss directions from Injun 5 Poynting flux observations, proposing propagation across plasmapause boundary 08 p1282 A71-21633

Geomagnetic distributions of VLF hiss intensity and drifting frequency bursts near inner boundary of plasmapause on middle latitudes 09 p1411 A71-23634

Midlatitude VLF hiss distinction from discrete emissions /chorus/ based on event tape recording and spectrum analysis 12 p1878 A71-26892

Electron lifetime in earth radiation belt due to resonant scattering with hiss VLF radiation 16 p2626 A71-33674

Auroral ELF and VLF emission at high latitudes, discussing chorus and hiss generation regions and noise mechanism 20 p3229 A71-39854

HISTAMINES

Histamine importance in nervous system activity, discussing synaptic mediation, reception processes and pharmacological action 12 p1869 A71-26652

HISTIDINE

Chemoautotrophic Thiobacillus neapolitanus growth inhibition by histidine, methionine, phenylalanine and threonine under imbalance conditions 04 p0537 A71-14776

HISTOGRAMS

High energy pulsed gamma rays detection from pulsar emission based on time averaged phase histograms 15 p2479 A71-31838

Neuron response to stimuli compared with background activity on histograms 16 p2532 A71-33898

HISTOLOGY

Morphological and histological changes in liver and kidneys of rats exposed to long term hypothermy 01 p0013 A71-11131

Human coronary arteries fibrinolytic activity, considering histochemical and quantitative methods for arteriosclerosis and occlusion investigations 02 p0200 A71-12416

Oxidative and hydrolytic enzymes localization in rhesus monkey brain, investigating glutaraldehyde fixation effect with histochemistry 07 p1042 A71-20017

Myocardial ischemic lesions age, discussing validity of histopathological criteria and margin of error 15 p2361 A71-32542

Histochemical investigation of enzymes activity during various cardiac cycle phases in frogs, noting effects of ion concentration 16 p2533 A71-33913

Acute renal failure due to heat stress and physical exercise, noting discrepancy between physiological alterations and histopathological abnormalities 18 p2855 A71-36218

Postflight histological analysis of turtles aboard Zond 7, noting decrease in cell nuclei size due to space flight conditions adaptation 21 p3334 A71-40568

Brachial plexus bundle structural and histological characteristics in man and monkey, noting lack of intraneural network in monkey 23 p3634 A71-43911

HISTORIES

NT CASE HISTORIES

NACA/NASA rotating wing aircraft research history during 1955-1970 period, discussing wind tunnel research 01 p0005 A71-11377

Satellite design developments by U.S. Navy 02 p0336 A71-11980

Astronautics and rocket technology history - Conference, Belgrade, September 1967, covering rocket engines, fuels and materials, ramjet engines, control systems, etc 05 p0816 A71-16500

HMX

Combustion model of solid composite propellants containing monopropellant oxidizers ammonium perchlorate, cyclotetramethylene-tetranitramine and potassium perchlorate 19 p3121 A71-38122

HO-6 HELICOPTER

U OH-6 HELICOPTER

HODOGRAPHS

Plane supersonic overexpanded jet interaction with obstacle, using hodographs for flow pattern construction 01 p0001 A71-10425

Hodograph of asymmetrical gyrostator with self excitation, determining angular velocity dependence on flywheel momentum 01 p0163 A71-10656

Reversible transonic fluid flow through cylindrical blades cascade by hodographic singularities solution of potential and stream function 01 p0003 A71-11023

Traveling angular velocity hodograph equations in solution to gyrostat motion problem 03 p0457 A71-13588

Kinematic interpretation of body motion about fixed point for case of traveling angular velocity hodograph integrable in closed form 03 p0457 A71-13589

Heavy solid body rotation about fixed point, using fixed and traveling hodograph 03 p0458 A71-13592

Body motion with liquid filled cavities in central Newtonian force field, using hodography 03 p0458 A71-13595

Transonic wing profiles analog determination by hodograph method 05 p0694 A71-16735

Normalized hodographic mapping for constrained trajectory families, discussing mapping concepts, information content and applications [AIAA PAPER 69-924] 07 p1199 A71-19884

Terrestrial electrical current distribution diagram based on solar quiet variation hodographs 07 p1104 A71-20048

Cross flow profiles for compressible turbulent boundary layers with and without flow reversal via hodograph models family 08 p1229 A71-22033

Differential equations of root loci motions for stationary linear automatic control design by hodograph and Evan method 10 p1637 A71-24906

High subsonic flow two dimensional turbine cascade design by approximate hodograph method, noting pressure distribution measurements [ASME PAPER 71-GT-34] 11 p1704 A71-25971

Orbital flight time in terms of isochronism kinematic theory, discussing Lambert and Hamilton hodograph representations 13 p2135 A71-2902

Hodograph models family for cross flow velocity component of three dimensional turbulent boundary layers, applying integral method to curved rectangular channels data 13 p2051 A71-2902

Hodograph of asymmetrical gyrostator with self excitation, determining angular velocity dependence on flywheel momentum 14 p2275 A71-3004

Book on hodograph equations covering both transonic flow, Tricomi boundary value problems, weak shocks and pressure density relations 15 p2394 A71-3274

Axisymmetric plane transonic flow past corner point, obtaining characteristics by mapping in hodograph plane 19 p2991 A71-3747

Subsonic flow direct and indirect methods including Oswatich integral equation, thickness parameter expansion, Janzen-Rayleigh method and stream a potential functions in hodograph plane 19 p2992 A71-3747

Transonic flow theory and experiment, considering hodograph method, integral equation method, parabolic method and method of characteristics 19 p2992 A71-3747

Compressor blade hodography and profile equation for subsonic two dimensional flow calculated by graphic visualization console 20 p3176 A71-3948

Generalized hodograph transformation with velocity potential as function of continuous second derivatives 21 p3406 A71-4010

Plane diatomic Prim gas flow, reducing hodograph equations in elliptic regions to Cauchy-Riemann equations via Baeklund transformations 23 p3662 A71-4318

HODOSCOPES

Extensive air showers multiple core and transverse momenta observations with Kiel neutron hodoscope 13 p2123 A71-2800

Underground interactions of primary cosmic ray produced atmospheric muon neutrinos, using large area liquid scintillation detector hodoscope 19 p3105 A71-3729

HOHMANN TRAJECTORIES

U ELLIPTICAL ORBITS

U TRANSFER ORBITS

HOHMANN TRANSFER ORBITS

U ELLIPTICAL ORBITS

U TRANSFER ORBITS

HOLDERS

NT FLAME HOLDERS

Elastomer O ring vacuum device for positive holding of Schumann film for precise microdensitometry during rocket flight in 7 March 1970 solar eclipse 14 p2249 A71-3080

HOLE DISTRIBUTION (ELECTRONICS)

Thermodynamic distribution of amphoteric Ge impurities in sublatitudes of GaAs semiconductor for compensation by acceptor vacancies 01 p0139 A71-1077

Hole effect on residual resistivity of crystalline binary ordered substitution alloy with bcc lattice 03 p0467 A71-1392

Highly ordered pressure-annealed pyrolytic graphite majority carrier electrons and holes locations in Brillouin zone from measurements in magnetic fields 08 p1344 A71-2131

Gunn diodes stable high field domains parameterization and behavior, considering hole effects in various carriers 19 p3028 A71-3784

HOLE DISTRIBUTION (MECHANICS)

Isotropic nonlinearly elastic plate weakened by doubly periodic reinforced curvilinear holes, calculating stress-strain state by Cauchy integrals 01 p0168 A71-10414

Transversely isotropic spherical shell of small shear modulus material, deriving stress concentration at circular holes 01 p0175 A71-11031

Three-layer spherical shell, determining filler effects on stress-strain state at circular hole 01 p0176 A71-11041

Stress concentration at free and reinforced curvilinear holes with random surface roughness applied to plane under hydrostatic tension 02 p0326 A71-1229

Thin circular cylindrical perforated shell, analyzing stress distribution around circular hole by coordinate transformation and partial differential equations 02 p0326 A71-1234

Aircraft assembly accuracy parameters, using hole as reference points 02 p0257 A71-1256

Isotropic half plane weakened by circular holes normal to boundary, calculating stress-strain state created by concentrated force 03 p0506 A71-1360

- Stress distribution around elliptical hole in thin flat rectangular elastic plate under axial in-plane edge loads
[ASME PAPER 70-DE-M] 03 p0506 A71-13705
- Hollow annular inserts for stress concentration and alternating stress range reduction around holes in thin flat plates, taking friction coefficient into account
[ASME PAPER 70-DE-L] 03 p0506 A71-13706
- Ring reinforced circular holes in cylindrical shells examining stress concentrations due to internal pressure
03 p0507 A71-13740
- Shallow shell theory boundary value problems, calculating stress concentration for domes and shells with holes
03 p0513 A71-14230
- Interaction between supersonic flow and transverse sonic or supersonic jet blown perpendicular to main stream through circular hole in wall
03 p0345 A71-14572
- Assembling accuracy of three dimensional joints using assembly holes in aircraft construction
04 p0602 A71-14609
- Shallow spherical shells with periodically spaced holes, discussing stress analysis by least squares method for curved perforated plates
[ASME PAPER 70-PVP-11] 04 p0665 A71-14771
- German monograph on stress distribution around cutouts in disks, plates and cylindrical shells
05 p0820 A71-16121
- Stress-strain state of isotropic three-layer plates and shells with rigid and light weight fillers, noting weakening by curvilinear holes
06 p0987 A71-17769
- Stress concentration at holes in plates and shells with multiply connected regions
06 p0999 A71-17863
- Circular and elliptical holes and inclusions effects on stress concentration in elastic beams under uniform compression
06 p1002 A71-18414
- Circular membranes and plates with arbitrary hole distribution, deriving natural vibrations frequency characteristic equations by infinite determinants
07 p1218 A71-20464
- Stress concentration in planar rectangular shallow shells and plates with polygonal holes
07 p1218 A71-20470
- Hardened plasticity zone around circular hole in creep deformed plate under normal forces, determining stress-strain relation and time dependent variations
07 p1219 A71-20647
- Stressed state in region of strain raisers /round holes/ in plate subjected to two axial tension associated with plastic yield
08 p1372 A71-21703
- Two dimensional stress-strain fields under elastic and elastic-plastic strains and steady state creep, calculating stress distribution around hole in cylindrical shell
09 p1538 A71-22631
- Stress concentration near hole in transversely isotropic cylindrical and spherical shells made of oriented glass fiber reinforced plastics
09 p1539 A71-22820
- Approximate trigonometric solution to thermoelastic boundary value problem of plane with doubly periodic system of holes, deriving unsteady temperature and thermstress fields
10 p1687 A71-24195
- Metal strip with circular hole under tension, calculating plastic strain and stress concentration coefficients
10 p1687 A71-24199
- Stress state elastic equilibrium of ponderable anisotropic half plane with free and ring reinforced elliptic hole near rectilinear boundary
10 p1690 A71-24567
- Infinite thin plate containing circular holes with elastic inclusions under biaxial tension, calculating maximum stresses on common boundaries based on Airy function
11 p1841 A71-25265
- Spherical shell stressed state weakened by holes, investigating shear deformation effect
12 p1975 A71-27107
- Spherical shallow shell with hole, noting natural vibration frequency
12 p1975 A71-27108
- Anisotropic plate with curvilinear holes, noting stress concentrations
12 p1975 A71-27110
- Nonlinear physical and geometrical thermoelasticity for plane strain and stressed state at circular hole in infinite space, using approximation in Lagrangian coordinates
12 p1978 A71-27349
- Two dimensional periodic and doubly periodic boundary value problems solution in theory for stable oscillations of elastic and viscoelastic bodies perforated by circular holes
12 p1980 A71-27447
- Stress concentrations over smooth perimeters of curvilinear holes in infinite isotropic plates subjected to loads
12 p1984 A71-27694
- Reflection, diffraction and transmission of plane microwave incident on conducting screen perforated periodically with circular holes, using transmission line analysis and dipole moments method
14 p2192 A71-29568
- Stress distribution in cylindrical shell with two unequal diametrically opposite reinforced circular holes under internal pressure
16 p2661 A71-34159
- Propagating crack arrest capability of circular hole in plate, studying dynamic stress intensity and concentration factors changes
[SESA PAPER 1827A] 17 p2820 A71-34546
- Small holes effect on Ni base superalloy wrought thin sheets fatigue strength under pulsating tension load, analyzing crack initiation, propagation and critical length
18 p2938 A71-36850
- Excited states drift and diffusion effects on spatial hole burning and laser oscillation, solving rate equation for population inversion
20 p3242 A71-38842
- Stress concentration in layers of sandwich beams with holes under bending and tension
21 p3473 A71-41156
- Algorithm for pure torsion of doubly connected square profile prismatic bars with hole, using R functions and variational technique
24 p3881 A71-44834
- Critical bending moments for elastic beam weakened by elliptical crack in tensile stress region
24 p3882 A71-44847
- HOLE MOBILITY**
- Transport mechanism for holes in polycrystalline Ge films based on Matthiessen rule, considering surface scattering and dislocation
03 p0468 A71-14464
- Noise, admittance and I-V characteristics of hot holes in space charge limited Ge diodes at high voltage and frequencies to 22 MHz
19 p3029 A71-38141
- HOLES**
- Elastoplastic stress analysis for samples with notches and holes under tension, discussing boundary condition calculation by finite element method
03 p0510 A71-13949
- Successive approximation algorithm for stress concentrations at holes in nonlinear shallow shells, applying to cylindrical and spherical shells with circular and elliptical holes
04 p0664 A71-14602
- Transient axisymmetrical rotary shear wave propagation in nonhomogeneous viscoelastic media with cylindrical hole
04 p0671 A71-15752
- Elliptical cylindrical shell under internal pressure, investigating stress concentration near surface hole
06 p0994 A71-17821
- Plasticity zone changes near circular hole, examining material structure inhomogeneity effects in presence of creep
09 p1535 A71-22183
- Kerr-Newman black hole as generic final state of gravitational collapse developed from Schwarzschild geometry and mass, angular momentum and charge parameters
16 p2631 A71-33177
- Stress concentration formulas for elliptical hole in spherical shell with or without cap
19 p3156 A71-37540
- Laser-drilled transparent material hole geometry dependence on beam focus and intensity, computing laser power, mode and work positioning
20 p3246 A71-39492
- HOLES [ELECTRON DEFICIENCIES]**
- Free hole drag in p-type Ge by photons in optical transitions between valence band subbands, examining magnetic field effects
02 p0296 A71-12613
- Electron-hole plasma in current carrying wire azimuthal magnetic field, noting electric field intensity by hydrodynamic approximation
05 p0790 A71-16880
- Electron-hole plasmas feedback stabilization, considering instability coefficients measurement
06 p0933 A71-17470
- Dynamic stabilization of helical and sausage instabilities of p-indium antimonide electron-hole plasmas, using Ioffe type RF energized magnetic quadrupoles
06 p0935 A71-17489
- High temperature Ni alloys structural stability, computing gamma prime phase coagulation and average electron vacancy number
09 p1474 A71-23289
- MgO single crystals dominant coloration in solar spectral region by electron hole pair diffusion, trapping and recombination
11 p1808 A71-26234
- Electron hole n-p plasma conductivity in cylindrical germanium specimens as function of current produced azimuthal magnetic field
12 p1936 A71-27036
- Electron-hole scattering effect on carrier heating and I-V characteristics in semiconductors, using relaxation time and self consistent analysis
13 p2111 A71-28921
- Soviet monograph on EM waves in solid state plasma covering propagation, amplification, generation and generation
13 p2112 A71-29078
- Electron hole plasma in plate shaped semiconductor under rapidly increasing external magnetic field, examining density
15 p2453 A71-31247
- Nonlinear optical effects associated with free holes and electrons in semiconductors, including higher harmonics generation and frequency mixing
16 p2621 A71-33375
- Electron-hole scattering effect on carrier heating and I-V characteristics in semiconductors, using relaxation time and self consistent analysis
21 p3433 A71-41308
- Cyclotron resonance measurement for holes in uniaxially compressed Si, determining pressure and temperature effects on relative half width of hole line by relaxation time
21 p3433 A71-41309
- HOLLOW CATHODES**
- Superpressurization mechanism in hollow cathode active zone, calculating upstream pressure variation as function of discharge current
13 p2106 A71-28399
- Ion engine development at Farnborough /England/, considering 10 mN mercury electron bombardment thruster system with hollow cathode
22 p3588 A71-41508
- Electric parameters of cold hollow cathode discharge and effect, controlling electron free paths by electric or magnetic field
23 p3710 A71-43276
- Hollow cathode lasers based on negative glow discharge excitation including charge exchange ion-atom collisions and Penning excitation
23 p3686 A71-43955
- HOLMIUM**
- Energy transmission mechanism in calcium fluoride-europium ion plus holmium ion system, investigating luminescence and absorption spectra
09 p1461 A71-22388
- High efficiency room temperature lasing operation assisted by energy transfer in holmium doped yttrium lithium fluoride
20 p3247 A71-39761
- HOLOGRAPHY**
- Holography theory, analyzing coherent, incoherent and modulated incoherent forms in SNR terms
01 p0078 A71-10142
- Spatial filtering equipment for unwanted images and diffraction in holography, interferometry, etc
01 p0092 A71-10336
- Parallel matched spatial filtering by optically superposed Fourier holograms, detecting simultaneously different image details
01 p0081 A71-10686
- Thin aligned holograms superposition for image intensification of diffusely scattered object, noting degradation in resolution and contrast
01 p0082 A71-10838
- Holographic filters for optical automatic pattern recognition systems, discussing reconnaissance target and fingerprint
02 p0247 A71-11702
- Microwave holography with artificial reference wave and receiver multiplier, improving linear resolution in image
02 p0248 A71-11876
- Holographic amplitude modulation procedure for pulse compression in synthetic aperture radar
02 p0215 A71-12037
- Spatial and temporal coherence effects in holography, giving general formula for reconstructed virtual image
02 p0251 A71-12148
- Holographic display applications in portraiture, data storage and retrieval, motion pictures, TV, etc
02 p0253 A71-12597
- Multiple exposure holographic interferometer for static and dynamic photomechanics
03 p0422 A71-13171
- Optimum beam ratio producing maximum contrast photographic reconstructions from double exposure holographic interferograms
03 p0424 A71-13639
- Photoreist for hologram recording and diffraction gratings formation, using Ar laser output
03 p0425 A71-13640
- Holographic interferometry with both beams traversing transparent object, providing variable sensitivity and directional phase detection
03 p0425 A71-13654
- Limited parallax holograms of silhouetted objects for bandwidth reduction properties, considering suitability for viewing with extended incoherent sources
03 p0425 A71-13655
- Holographic twin image elimination by nonlinear method based on statistical differences in objects and diffraction fields
03 p0425 A71-13656
- Holographic interferometry application to photoelasticity, discussing absolute retardation in

terms of plane or circularly polarized light fringe pattern interpretation
[SESA PAPER 1719] 03 p0426 A71-13767

Three dimensional hologram reconstruction and recording, using extended source
03 p0428 A71-14057

Hologram and optical elements insertion in Q switched laser for generation switching, using YAG /Nd/ basic laser
03 p0439 A71-14176

Holographic multiplexing by Fresnel diffraction based on aperture field division, discussing reconstructed image quality
03 p0429 A71-14179

Two point resolution in Fourier holography with partially coherent recording and illuminating light
03 p0429 A71-14180

Translational vs deformation displacement motion in sensitivity of double exposure holographic interferometry
03 p0429 A71-14181

Small phase differences amplification in holographic interferometry, using nonlinear development of recordings
03 p0429 A71-14182

Synthetic endfire hologram radar for small target and clear air turbulence detection
03 p0381 A71-14476

Synthetic aperture holographic techniques in continuous wave bistatic radars for moving targets
03 p0381 A71-14477

Hologram Fresnel zone with monochromatic signal and background noise, determining precision of object image coordinates
04 p0584 A71-14633

Photographic material information capacity in holography
04 p0585 A71-14643

Holography developments concerning interferometry, microscopy, display systems, data storage and ultrasonic tests
04 p0587 A71-14724

Holographic measurement of moving cloud droplets size distribution from aircraft using Q switched ruby laser
04 p0596 A71-14968

Three dimensional opacity function for phase objects measurements using interferometry, holography or schlieren methods
04 p0596 A71-14969

Doppler effect in laser beam probe of scattering objects, using interferometer for scattered light intensity angular distribution relation to hologram sizes
04 p0608 A71-15117

Electron microscope micrographs enhancement by holographic image deblurring
04 p0596 A71-15135

Hologram formation in gelatin, photopolymeric and photochromic materials for high diffraction efficiency, in-place real-time processing and erasability
04 p0596 A71-15167

Supported rectangular plates HF transverse vibrations by holographic interferometry
04 p0668 A71-15188

Pulsed laser holography, discussing illumination source and holocameras for high contrast recording with Q switched ruby lasers
04 p0597 A71-15363

Image contrast limits in thin phase hologram reconstruction of diffuse objects with large reference-object irradiance ratios
04 p0601 A71-15687

Image polarity in holography and carrier frequency photography
04 p0601 A71-15696

Classical and hologram interferometry, considering fringe localization and visibility
05 p0747 A71-16190

Holographic interferometry of diffusely reflecting surfaces, analyzing homologous rays concept
05 p0747 A71-16192

Holography applications, recording and reconstructing three dimensional objects by split laser beams interference technique
05 p0747 A71-16194

He-Ne laser beam parameters and diffraction field measurement by holography
05 p0760 A71-16260

Single and multiple exposure storage holograms with comparable diffraction efficiency
05 p0748 A71-16261

Optical fields holographic subtraction for SNR enhancement
05 p0748 A71-16262

Radiation energy deposition profiles in transparent liquids, using holographic interferometer
05 p0748 A71-16263

Two wavelength nondiffuse holography for interferometry of transparent media
05 p0748 A71-16264

Double pulse laser holographic interferometry for large noisy vibrating subjects, including demonstration on Al plate
05 p0751 A71-16580

Photoelastic model stress analysis by holographic interferometry and automatic measurement of light shapes, discussing slicing technique
05 p0752 A71-16733

Phase objects holography using pulsed ruby laser with plane-parallel and hemispherical cavity
05 p0752 A71-16748

Nomographs for point source holographic imaging, discussing recording and reconstruction geometry
05 p0753 A71-16913

Millimeter wave lensless Fourier transformation /LFT/ holographic imaging, discussing equipment and performance
05 p0754 A71-17081

Book on optical data processing covering light characteristics, Fourier transforms, spectrum analysis, photographic film, filtering, holography, etc
05 p0754 A71-17124

Holographic interferometry application to gas dynamics, analyzing interferential patterns in monochromatic and achromatic light
05 p0695 A71-17166

Microwave holography application to monopole antenna radiation field mechanism, using liquid crystals for optical reconstruction
05 p0756 A71-17231

Electron thermal diffusion effects during light interference patterns exposure, generating strong electric fields and holographic storage in electro-optic materials
06 p0940 A71-17309

Holography development, discussing three dimensional images, fine grain recording emulsions and beam switching during reconstruction
06 p0897 A71-17369

Antenna synthesis by microwave holography, using interference pattern approximations for series of holograms construction
06 p0898 A71-17723

Holographic optical memory and computer output applications for rapid bulk data storage, considering various laser visualization systems
06 p0908 A71-18067

Holography and shapes recognition, considering optical memory, information density advantages and optical correlators
06 p0900 A71-18068

Holographic interferometric recording of vibration patterns of plexiglass core construction mirrors [AIAA PAPER 71-180]
06 p0903 A71-18619

Matched spatial filters for holographic image recognition in biological studies
06 p0903 A71-18695

Strain field measurement near crack tip in polymethyl methacrylate by holographic interferometry
07 p1209 A71-19043

Photoelastic fringe patterns in double exposure holography interferometric technique for stress wave analysis
07 p1209 A71-19044

Holographic lens used with pulsed ruby laser for machining single and multiple spots on Ti thin film on glass
07 p1122 A71-19205

Interferometric holography application to elastic stress and surface corrosion of two dimensional objects and metals, discussing stretching
07 p1107 A71-19209

Axisymmetric phase object holographic interferometry, showing light beam refraction effect on interference pattern
07 p1108 A71-19237

Photographic materials in holography, examining resolving power dependence on size and on angle between reference and signal light beams
07 p1108 A71-19238

Hologram modulation for spatial channel selection by putting together signal hologram and carrier hologram
07 p1108 A71-19259

TV holography systems, discussing camera and reproducer resolution and operation methods at real time scan rates
07 p1109 A71-19452

Holographic multiple beam interferometry, considering phase retardation role in hologram diffracted waves for fringes irradiance distribution definition
07 p1110 A71-19479

Light effect on dielectric constant of thin hardened dichromated gelatin films for holographic recordings
07 p1110 A71-19482

Hologram recording material characterization concerning maximum diffraction, linearity and sensitivity
07 p1110 A71-19483

Nonredundant two dimensional square and hexagonal point arrays with optimal autocorrelative properties, considering high resolution imaging systems in holography
07 p1111 A71-19490

Faraday and polar Kerr reconstruction effects in stored magnetic holography [IEEE PAPER 8.1]
07 p1112 A71-19609

Magnetic hologram reconstruction processes discussing diffracted field, polarization properties and efficiency
07 p1112 A71-19610

Coherent optical data processing technique discussing diffraction phenomena, spectral analysis and holography
07 p1067 A71-19652

Pulsed laser holography physical principles and applications in stress and vibration analysis, flow pattern visualization, biophysical and medical research
07 p1113 A71-19783

Holography and interferometry industrial applications, considering three dimensional imaging, precision distance measurement, nondestructive testing and structural strains and failures detection
07 p1113 A71-19784

Holographic microscopy technique fundamentals and electrically activated integrated circuit changes in inspection
07 p1113 A71-19786

Hologram interferometer methods classification according to diffuse elements in objects and illumination sources, considering effect on interference fringe interpretation
07 p1114 A71-20144

Light scatterers use behind phase object in double exposure holography, determining laser radiation wave front dynamics effect on image quality
07 p1114 A71-20189

Phototechnology for phase holograms recording and information storage in hardened gelatin
07 p1116 A71-20620

Optical data storage photodetector output signal to noise and signal to background ratios, using Fourier transform amplitude and phase holograms
08 p1287 A71-21186

Holographic recording intermodulation noise suppression by image wave field distortion and retrieval, considering signal to noise ratio
08 p1287 A71-21187

Photographic emulsion model for signal to average noise irradiance ratio analysis in hologram reconstruction
08 p1287 A71-21188

Spatial resolution improvement by utilizing temporal degree of freedom of transmitted signal, discussing hologram plate recording during exposition intervals
08 p1287 A71-21191

Coherent optical target recognition through phase distorting medium, using holography, Fourier transform and autocorrelation functions
08 p1335 A71-21377

Photographic materials holographic exposure index improvement due to increased sensitometric speed and macroscopic transfer characteristics
08 p1290 A71-21385

Fourier transform hologram recording by quasi-monochromatic incoherent source, resolving bias problem at expense of resolution
08 p1290 A71-21386

Hologram imagery and aberrations computer based analysis, considering hologram geometries and nonchromatic aberrations
08 p1290 A71-21387

Optical elements aspheric testing, using computer generated synthetic holograms
08 p1290 A71-21388

Holographic recording media low signal energy densities comparison, determining peak values of diffraction efficiency and normal contrast ratio divided by signal beam exposure
08 p1290 A71-21389

Gaussian shaped laser pulse holographic brightness analysis, presenting theoretical and experimental holographic coherence length curves for Q switched laser oscillator and amplifier system
08 p1290 A71-21390

Information search and retrieval by superimposed holograms, describing coding detection and image reconstruction methods
08 p1291 A71-21397

Hologram fifth order aberrations, deriving equation and coefficients as functions of hologram construction and reconstruction geometry
08 p1291 A71-21398

Efficiency improvement of holograms with very high reference beam to object beam intensity ratio by constructing copy from first hologram
08 p1291 A71-21399

Holography with fiber optics, allowing three dimensional photography of inaccessible objects in biomedical research and other applications
08 p1291 A71-21400

Optical data processing by incoherent matched filtering with Fourier holograms
08 p1291 A71-21401

Holographic images of moving objects, extending theory to objects moving with constant acceleration
08 p1291 A71-21402

Phase quantization in holograms, presenting experimental verification of Goodman and Silvestri theory
08 p1291 A71-21404

- Holographic interferometry at two wavelengths for phase objects dispersion characteristics
08 p1292 A71-21487
- Image reconstruction from three dimensional holograms
08 p1292 A71-21488
- Stress analysis of elastic bending plates by holographic interferometry, comparing results to theory
08 p1373 A71-21752
- Holographic spectrum analyzer for plasma diagnostics in microwave band, deriving formulas for emission spectrum based on interference patterns intensities in waveguide
09 p1499 A71-22150
- Holography of focused images, using arbitrarily shaped off-axis reference wave and white light for image restoration
09 p1442 A71-22393
- Radiant flux diffraction effectiveness of amplitude holograms with allowance for nonlinearity of photo-material
09 p1442 A71-22400
- Ground based coherent radar synthetic aperture procedure against uniform velocity targets, discussing airborne holographic synthetic gain applications to stationary antennas
09 p1405 A71-22697
- Real time and double exposure holographic interferometry measurements of strain on aluminum cylinder under internal pressure, noting discrepancy with strain gage values
09 p1444 A71-22711
- Thermal deflection tests of fused silica mirror blanks by holographic interferometry
09 p1447 A71-22745
- Holography principles, discussing formation and reconstruction for in-line, off-axis and Fourier transform type holographic systems
09 p1449 A71-22787
- Schlieren system conversion to holographic visualization in operational wind tunnels and test facilities
09 p1449 A71-22788
- Fringe interpretation in stress-holo- interferometry, emphasizing isopachic-isochromatic interaction effects in photoelastic analysis
09 p1542 A71-23538
- [SESA PAPER 1642]
- Lens-prism model for holographic image processing in space-frequency domains with chirp signal interferometric compression
09 p1452 A71-23565
- Constant period discrete holograms features, investigating laser visualization, recording, reconstruction and image focusing
10 p1608 A71-23810
- Ultrarapid holographic recording in IR light at 1.06 micron
10 p1608 A71-23838
- Classical vs holographic interferometry comparing same fringe profiles
10 p1608 A71-23844
- Holography utilization to data processing, discussing factors affecting recording and matched filters creation for pattern recognition
10 p1581 A71-23917
- Three-beam holographic interferometry featuring sensitivity increase and aberrations compensation
10 p1611 A71-24345
- Holography as quantitative tool for photoelastic measurements, using moire theory of interference phenomena
10 p1611 A71-24473
- Frequency-contrast characteristics of holographic systems, studying image contrast and angular spread as function of hologram aperture
10 p1611 A71-24529
- Holographic generation of high efficiency, extended range spatial filters, applying to defocused images restoration
10 p1612 A71-24585
- Photomaterial nonlinear effects on contour distortion in holographic recording of Fourier image slit for graphic memory use
10 p1612 A71-24716
- Holographic image recording and reconstruction in two and three dimensions, including light wavelike nature, Huygens principle, wavefront reproduction and spectral composition
10 p1613 A71-24849
- German monograph on holographic method to increase effective aperture in optical imaging covering optical systems resolving power increase holography, etc
10 p1613 A71-24875
- Nematic liquid crystals in optical holography, obtaining speckle free projection screens and data input in holographic memories
10 p1622 A71-24961
- Metrological holographic interferometry, discussing speckle pattern application for wavefront phase samples
10 p1613 A71-25092
- Thin holographic recording and retrieval from semipermanent optical memories
11 p1762 A71-25624
- Asymmetric three dimensional aerodynamic density fields from holographic interferograms, applying to supersonic flow from free jet
11 p1762 A71-25802
- Pulsed laser holographic applications to aerospace components nondestructive testing, inspecting electron beam welds and internal structural flaws
[ASME PAPER 71-GT-74] 11 p1770 A71-25988
- Surface strain measurements in turbine blades by time average holographic interferometry, reviewing resonant modes and holographic fringe patterns
[ASME PAPER 71-GT-84] 11 p1762 A71-25992
- Plasma diagnostics covering magnetic, electron beam, electrostatic, laser, holography, interferometry, Thomson scattering, microwave and electroacoustic techniques
11 p1766 A71-26287
- Lens phase aberration correction in optical system, using holograms
11 p1766 A71-26305
- Holography principles development, history, wave field recording, processing and reconstructing techniques for image quality improvement, laser applications, etc
11 p1767 A71-26352
- Plane and three dimensional dynamic holograms recording in bleachable dyes, using ruby laser with gallium chloride phthalocyanin in chlorobenzene as Q switch
11 p1767 A71-26565
- Axisymmetric phase object holographic interferometry, showing light beam refraction effect on interference pattern
12 p1903 A71-26755
- Photographic materials in holography, examining resolving power dependence on size and angle between reference and signal light beams
12 p1903 A71-26756
- Aberration reduction and optimal in-line and off-axis recording geometry in acoustical holography
12 p1904 A71-26794
- Optical beam propagation, determining turbulent medium effects with holographic wave front reconstruction technique
12 p1904 A71-26795
- Two wavelength holographic interferometry for transparent media with high or low sensitivity, using diffraction grating
12 p1904 A71-26796
- High resolution holographic Fourier transform spectroscopy, discussing interferometer localized interference fringes direct recording method and heterodyning technique
12 p1905 A71-26805
- Bleached hologram lifetime extension, decreasing light induced decay rate by gelatin hardening
12 p1905 A71-26815
- Holographic interferometry method application to plasma electron concentration measurements
12 p1906 A71-27211
- Fresnel hologram focusing method, considering Leith and Upatniekss wave front reconstruction with diffused illumination
12 p1907 A71-27212
- Hologram mensuration, discussing photogrammetric stereo model differences, close range objects, pointing, geometric fidelity, computerized plate analysis and reconstruction shift
12 p1907 A71-27262
- Optical holographic interferometry for radial microcracks detection from bolt holes in high strength aircraft steel
[ASME PAPER 71-MET-C] 12 p1911 A71-27312
- Holographic interferometry application to gas dynamics, analyzing interferential patterns in monochromatic and achromatic light
12 p1864 A71-27458
- Holographic narrow beam VHF antenna design and testing, using X band scale model
13 p2036 A71-27999
- Continuous relative phase control between reference and object beams in holographic interferometry
13 p2066 A71-28161
- Vibration analysis by holography, discussing recording media, maximum light utilization, stroboscopic and time-averaged techniques and alterations in sensitivity
13 p2067 A71-28396
- Holographic method for coding and decoding three dimensional information
13 p2067 A71-28443
- Signal to noise ratio measurement in hologram reconstructions by vibration interferograms
13 p2068 A71-28447
- Real time holography using moving groundglass or fluorescent layer suitable for coherent matched filtering and seeing through fog
13 p2068 A71-28709
- Information reduction for three dimensional image projection holography, using horizontally direction selective stereoscreen
13 p2068 A71-28710
- Plane wave holographic recording and reconstruction, investigating effects of photosensitive medium as three dimensional diffractive pupil
13 p2068 A71-28711
- Reversal processing technique for producing high diffraction efficiency, low noise and good light stability phase holograms on silver halide emulsions
13 p2068 A71-28713
- Phase hologram nonlinearities effects, determining signal to noise power ratio in terms of Chebyshev series coefficients
13 p2069 A71-28714
- Image quality improvement by successive hologram acquisition process
13 p2070 A71-29026
- High quality hologram copies, using photosensitive emulsion layer technique
13 p2070 A71-29027
- Computer phase hologram synthesis simplified modification, using EM field vector transformation for points
13 p2070 A71-29029
- Acoustic holography for simultaneous three-dimensional image and internal structure insight, discussing applications to submarine exploration and medical diagnostics
13 p2071 A71-29299
- Holography background, classification and application to microscopy, particle size analysis, interferometry, optical elements and data storage
13 p2071 A71-29349
- Diffraction-limited electromagnetic theory of image formation for point reference arbitrary shape hologram
13 p2072 A71-29440
- Holographic interferometer for photoelastic stress analysis, eliminating isochromatic pattern interference from isopachic interferogram by double pass object beam and optical rotator
14 p2239 A71-29845
- Aberration-free wave front reconstruction from holograms illuminated at wavelengths differing from forming wavelength
14 p2240 A71-30130
- Hologram size and film type limitations effects on resolution of reconstructed image in edgeline holography
14 p2241 A71-30131
- Photographic emulsion thickness variation effect on wave front recording and reconstruction on holographic plate
14 p2241 A71-30132
- Reference/object wave temporal modulation effect on fringe formation in holographic interferometry
14 p2241 A71-30133
- Reversal bleaching process for low flare light and high diffraction efficiencies and SNR in holograms
14 p2241 A71-30134
- Recorded wave front aperture sharing technique for space division multiplexing of small holograms
14 p2242 A71-30151
- In situ double exposure differential interferometry, using photoconductive thermoplastic sandwich in place of film, allowing second hologram inscription
14 p2242 A71-30153
- Single and multibeam holography application to size, trajectory, distribution, population density and velocity measurements of water and electric arc welding sprays droplets
14 p2243 A71-30299
- Holographic techniques, optical data processing and laser properties for aerospace instrumentation
14 p2244 A71-30329
- Optical surfaces contamination analysis by holographic interferometry, using fringe patterns for contaminant film thickness and uniformity
14 p2244 A71-30330
- AEDC test facilities laser instrumentation for flow field diagnostics by Doppler velocimeter, holographic flow visualization and particle studies
14 p2245 A71-30332
- Holographic stroboscope using ruby laser with passive shutter for HF vibration measurement
14 p2254 A71-30584
- Two-wavelength holographic interferometry for phase objects dispersion characteristics, noting plasma diagnostics application
14 p2248 A71-30675
- Plane wave and virtual image reconstruction from three dimensional holograms
14 p2248 A71-30676
- Holography in nondestructive materials testing, describing laser interferometry and reproduction techniques for deformation and torsional, bending, thermal and vibrational behavior
15 p2402 A71-31217
- Holography applications - Conference, Besancon, France, July 1970
15 p2402 A71-31252
- Three dimensional hologram relationship to object optical properties and structure, considering hologram imaging properties
15 p2402 A71-31253

Laser radiation source time and spatial coherence effect on brightness distribution of image produced by hologram

15 p2402 A71-31254

Pulsed lasers coherence measurements by holographic techniques, considering high fraction of near field pattern with appreciable coherence

15 p2419 A71-31255

Fourier transform holography with partially coherent light from incoherent quasi-monochromatic source, considering bias problem

15 p2402 A71-31256

Two beam holographic interferometer based on spherical mirrors with laser beam splitting by semitransparent plate and image reconstruction in monochromatic and nonmonochromatic light

15 p2402 A71-31257

High sensitivity three beam holographic interferometry using Zernike method, applying to small deformation measurement

15 p2402 A71-31258

Holographic multiple pass two-beam optical interferometer with greater sensitivity than single pass instrument/Mach-Zehnder

15 p2402 A71-31259

Lateral shearing interferometry sensitivity improvement by amplifying phase difference with nonlinear holograms

15 p2403 A71-31260

Holographic diffraction shearing interferometer scheme, considering gratings arrangement and calculation method

15 p2403 A71-31261

Holographic interferometry, discussing deformation second derivatives mapping and fringes formation and visibility

15 p2403 A71-31262

Diffusely reflecting object element three dimensional displacement measurement from single hologram nonlocalized patterns

15 p2403 A71-31263

Three dimensional deformation surface displacement measurement by holographic interferometry, using equal inclination fringes

15 p2403 A71-31264

Diffusely reflecting in-plane surface displacement measurement by holographic interferometry, comparing static and dynamic methods for accuracy

15 p2403 A71-31265

Fringe order determination in holographic interferometry, discussing zero motion object region identification

15 p2403 A71-31266

In-plane strain measurement by three beam holography using two incident wave fronts

15 p2404 A71-31267

Stress analysis by holographic interferometry and automatic light forms analysis

15 p2502 A71-31268

Optical methods for measuring mechanical strain by observing shift and deformation of elemental surface areas, using holographic techniques

15 p2404 A71-31269

Normal time average holography amplitude range extension by integration over vibration cycle fraction

15 p2404 A71-31270

Real time stroboscopic vibration analysis technique involving holographic interferometry

15 p2404 A71-31271

Holographic vibration analysis by generalized stroboscopy, combining high reconstruction brightness with time average holograms interpretation

15 p2404 A71-31272

Vibration analysis for static and rotating objects by stroboscopic holography, considering axial flow compressor blades and two-mass system with torsional vibration

15 p2404 A71-31273

Holographic recording of optical inhomogeneities in gas flow in hypersonic wind tunnels, using Mach-Zehnder interferometer and schlieren apparatus

15 p2404 A71-31274

Holographic interferometry for observing transparent media in supersonic gas flow, comparing results with Mach-Zehnder interferometry

15 p2404 A71-31275

Holographic interferometry for flow visualization within aerodynamic wind tunnels with retrodiffuser apparatus

15 p2405 A71-31276

Two interferograms holographic laser recording on same emulsion by double exposure with ruby and harmonic wavelengths

15 p2454 A71-31277

Holographic interferograms for determining spatial configuration and absolute electron density of fully ionized transient plasmas

15 p2405 A71-31278

Moiré patterns generation by two frequency image plane holographic contouring, discussing multiple source and variable refractive index techniques

15 p2405 A71-31279

Binary optical detour phase holograms formation in measurements with centimeter electromagnetic waves, describing dielectric diffusers for microwaves

15 p2405 A71-31280

Optical wave reconstruction from microwave holograms and application to interferometry, considering resolving power and visible images of microwave transparencies

15 p2405 A71-31281

Interferometric holograms of vibrating body via numerical analysis of oscillations amplitude and phases

15 p2406 A71-31706

Holographic investigation of laser sparks in hydrogen and helium, determining electron concentration spatial distribution and plasma dispersion dynamics

15 p2419 A71-31738

Optical techniques for holographic NDT inspection speeds increase in laminate structures flaw detectability

15 p2408 A71-31815

Microcracks detection in high strength steel by optical holographic interferometry, comparing results with magnaflox, eddy current and X ray inspection methods

15 p2409 A71-32258

Applied optics, reviewing homogeneous and inhomogeneous optical conversion elements, fiber and Fresnel optics, lens properties, programmed optical reliefs, holography, etc

15 p2410 A71-32299

Matched/mismatched crossed beam interference field combination with sinusoidal holographic diffraction grating, studying metric properties and moiré/obturated bands

15 p2410 A71-32404

Holography applications in aeronautics and astronautics, discussing advantages of three dimensional information in aircraft navigation, space missions and astronomical experiments

15 p2411 A71-32528

Phase holographic data storage in doped barium sodium niobate crystal, detailing decay times, energy density and diffraction efficiency

15 p2412 A71-32586

Binary intensity holographic information storage system, investigating nonlinearity effects

15 p2412 A71-32591

Holographic lens magnification aberrations in various Fourier transform optical data storage geometries

15 p2412 A71-32592

Time average holographic interferometric fringes of circular plate vibrating in two rationally related modes

15 p2412 A71-32593

Holograms of physical objects, calculating irradiance statistical distribution from reference-object beam powers ratio

15 p2412 A71-32594

Continuous holographic recording of wave front temporal variations for nonstationary processes

15 p2413 A71-32788

Pulsed laser double exposure holographic interferometry for measuring transverse wave propagation in beams

15 p2413 A71-32790

Holographic interferometry measurements of mean and localized fluctuating wake density field of cones fired at Mach 6 at ballistic range, using pulsed laser

[AIAA PAPER 71-564]

Insufficient spatial and temporal coherence effects on holographic image reconstruction by injection laser, noting application to optical data processing

16 p2577 A71-33142

Diffraction limited circular holographic determination of Airy radius by photoelectric scanning of image irradiance

16 p2577 A71-33143

Volume hologram formation in photopolymer materials with bright low noise images, considering sensitivity, spatial frequency response, particle scattering noise and nonlinearities

16 p2577 A71-33144

Light diffraction by holographic gratings in pink ruby due to absorption coefficient spatial variations

16 p2578 A71-33149

Optical interferometry and schlieren photography involving high power pulsed lasers, discussing applications to plasma diagnostics and holography

16 p2586 A71-33159

Pulse laser holographic interferometry for refractivity measurement, considering wave front reconstruction principles

16 p2578 A71-33160

Three dimensional hologram recording, showing He-Ne laser reconstruction of Q switched ruby laser hologram image of mosquito flight

16 p2579 A71-33528

Fog drop size distribution measurement with laser hologram camera

16 p2604 A71-33535

Three dimensional hologram recording and reconstruction, discussing image geometry, reference beam intensity, size finiteness, transition limits and photosensitive materials

16 p2580 A71-33623

Holographic analysis of periodic microobjects and ray wavelengths, obtaining high contrast

17 p2737 A71-34240

Book on optical holography covering basic concepts, Fourier transform, propagation and diffracted pulsed lasers, interferometry, geometric analysis of point source hologram, etc

17 p2738 A71-34400

Holographic interferometer for photoelastic stress analysis by simultaneous acquisition of isochromatic and isopachic fringe patterns without mutual interference, providing increased sensitivity

[SESA PAPER 1792]

Holography applications to complete stress analysis of three dimensional photoelastic models, using double exposure in conjunction with immersion tank

[SESA PAPER 1852]

Holographic interferometry fringe patterns interpretation for small displacements measurements considering precision gyro stability

17 p2744 A71-35253

Plane and three dimensional dynamic holograms recording in bleachable dyes, using ruby laser with gallium chloride phthalocyanin in chlorobenzene as switch

17 p2745 A71-35566

Red blood cell image hologram reconstruction and superresolution based on coherent physical optical using computer program

17 p2693 A71-35580

Holography with single transverse longitudinal mode pulsed ruby laser, emphasizing carrier frequency shift as limiting factor on depth of field

17 p2745 A71-35588

Holographic diffraction gratings on plane or concave spherical surface photographic plate, investigating interference fringes and aberration properties

17 p2745 A71-35589

Phase-only complex valued spatial filter for holographic wave front construction involving amplitudes and phase modulations, investigating performance

17 p2745 A71-35590

Photopolymer recording materials fixing by flashing holograms with Xe light or deactivating catalyst with thermal methods

17 p2745 A71-35592

Minimum aberrations in image wave front due to wavelength shift between recording and reconstruction beams in holography, using computer program

18 p2914 A71-35840

Holographic fiber optics image-guiding structures preparation in sensitized polymethyl methacrylate cast sheet by refractive index gratings pair recording

18 p2946 A71-35850

Total diffraction efficiency of transmittance storage holograms, using space dependent contrast function

18 p2915 A71-35900

Sequence of double exposure holograms corresponding to repetition laser to study objects undergoing perturbation

18 p2916 A71-36040

Pattern recognition multiplex arrangement with optical relay tube and point hologram for image distribution onto spatially separated channels to obtain SNR improvement

18 p2917 A71-36050

Holographic interferometry for speckle pattern interpretation in metrology, using video techniques

18 p2917 A71-36050

Ruby laser sources of short duration and high energy emission in holography, considering oscillator amplifier illuminator, contour spacings, transmission holocameras, etc

18 p2930 A71-36060

Holographic display for blind landing system with variable image perspective over wide field of view using collimated or cylindrical laser beam

18 p2945 A71-36060

High resolution holographic image deblurring methods involving coherent optical analog processing and Fourier transform division filter

18 p2918 A71-36070

Q switched ruby laser holography, using controlled multimode emission for contour recordings of reflected light scenes

18 p2920 A71-36100

Papers on quantum electronics, Volume 1, covering carbon dioxide and YAG lasers, quantum counter action and interference holography

18 p2930 A71-36140

Interference holography, discussing precision displacement measurement, fringe localization, multiple beam techniques, contour generation and flow visualization

18 p2920 A71-36140

Double exposure pulsed laser holographic interferometry application to transverse wave propagation in Al plate

18 p2977 A71-36230

Laser beam operation, light scattering in gases, holography applications and flow analyses

18 p2931 A71-36420

Electronic processing of coherent optical data for measurement and display using holography, speckle

- patterns, interferograms, image intensifiers and TV systems 18 p2923 A71-36608
- Wavefront reconstruction interferometry with acoustical holography using ultrasound camera, surface deformation and mechanically scanned detector methods 18 p2923 A71-36609
- Stroboscopic coherent light source for vibrational analysis by holographic interferometry using Pockels cell laser modulator 18 p2923 A71-36610
- Holography as nondestructive testing tool, considering application in vibration analysis, stress/strain measurement, bond inspection, internal flaw detection and displacement measurement [SME PAPER IQ-71-121] 18 p2927 A71-36657
- Adhesively bonded structures inspected by laser holography, producing diffraction pattern recording of amplitude and phase shift 18 p2925 A71-37057
- Laser Curie point writing characteristics and diffraction efficiencies of MnBi thin films for holographic recording 19 p3062 A71-37143
- Laser holographic inspection of silicon bond in pressure sensors for process control systems 19 p3068 A71-37245
- High efficiency inline multiple imaging by means of multiple phase holograms, giving diffraction patterns 19 p3063 A71-37482
- Photochromic glass activation process for recording three dimensional holograms, using radiation with maximum spectral brightness coincidence with absorption band edge 19 p3064 A71-37772
- Recording device with Fourier hologram memory based on optical spatial filtration principle for identifying chemical compounds by IR absorption spectra 19 p3064 A71-37773
- Real time holographic interferograms, achieving required beam intensities relationship by ordinary neutral light filters near collimator focus 19 p3065 A71-38196
- High density redundant information storage in magnetic holography with Curie point writing on thin films and magneto-optic readout 19 p3065 A71-38237
- Holographic matched filter correlator using liquid gate precision plate holder to eliminate necessity for hologram movement 19 p3065 A71-38238
- Fourier transform holograms as complex matched filter for pattern recognition and signal detection in coherent optical systems 19 p3066 A71-38239
- Frequency power and resolution effects on ultrasonic holography for medical diagnosis involving information processing on computer 19 p3066 A71-38240
- Plasma optical refractivity, considering gas laser interferometry and holographic phase measurements 19 p3116 A71-38244
- Frequency-contrast characteristics of holographic systems, studying image contrast and angular spread as function of hologram aperture 19 p3066 A71-38257
- Acoustic or microwave hologram reconstruction into visible three dimensional image in real time 19 p3066 A71-38412
- Holographic interferometry application to vibration mode pattern analysis of steam turbine and centrifugal compressor blades and disks 19 p3067 A71-38419
- Holographic method of correlation and spectral analysis of radio signals applied to stable RF generator, random fields and stereophonic radio transmission measurements 19 p3067 A71-38492
- Holographic interferometry method application to plasma electron concentration measurements 19 p3067 A71-38623
- Fresnel hologram focusing method, considering Leith and Upatnieks wave front reconstruction with diffused illumination 19 p3067 A71-38624
- Long object photography with lens array in non-coherent light and subsequent integrated image focus holography in laser beam for reconstruction in white light 19 p3068 A71-38708
- Holography applications in science and technology, considering plasma diagnostics, particle motion pictures, stress and vibration measurements, flow visualization, data processing and aeronautical navigation 19 p3068 A71-38725
- Holographic investigation of acoustical fields, describing shadowgraph recording apparatus for sound pressure amplitude distribution 20 p3232 A71-38811
- Aspheric lenses and mirrors testing by single and double exposure two-wavelength visible light holography for obtaining interferogram 20 p3235 A71-39182
- Laser Doppler holographic technique for fluid velocity field visualization and quantitative two dimensional vector velocity measurement 20 p3235 A71-39183
- Real time lensless holographic recognition of spatially incoherent and self luminous patterns on diffusing backgrounds using optical matched multiple filters 20 p3235 A71-39184
- Three dimensional surface displacement measurement by hologram interferometry, applying to cantilever 20 p3235 A71-39187
- Moire equivalence device for simulating fringe patterns in hologram interferometry, using loci of constant pathlength 20 p3235 A71-39188
- Multicolor images with volume dielectric holograms in photopolymer materials, reconstructing complex three dimensional images with high resolution in white light 20 p3236 A71-39192
- Pre- or postexposure effect in holographic recording and reconstruction in reference to object beam intensity ratio 20 p3236 A71-39193
- Checking method for reflection-type holographic system behavior, emphasizing critical stability of glass plate 20 p3236 A71-39194
- Photographic phase holograms including printout effect, bleaching, conversion with iodine compound and light stability 20 p3236 A71-39195
- Laser holography and interferometry in materials science, evaluating displacement and deformation within nondestructive testing 20 p3245 A71-39342
- Sound to light image conversion, emphasizing liquid surface acoustical holography 20 p3238 A71-39343
- Holographic interferometry equipment design for NDT and vibrational and deformation analysis, discussing apparatus construction, optical quality and industrial applications 20 p3238 A71-39344
- Holographic interferometry application to photoelasticity, interpreting fringe patterns for two dimensional stress analysis 20 p3238 A71-39345
- Holographic interferometry for structure and material deformation measurement, presenting static loading and resonant vibration surveys 20 p3238 A71-39346
- Pulsed ruby laser holographic instrumentation for materials tests, detailing reflected wave front complex amplitude characterization 20 p3245 A71-39347
- Laser beams amplitude-phase correction by holographic method, obtaining beams with plane fronts and Gaussian amplitude distribution 20 p3245 A71-39413
- Wave reconstruction from gaseous flow hologram analysis with differential interferometry in polarized light and schlieren techniques with phase filter defocusing 20 p3239 A71-39461
- Holographic applications in mechanics - ASME Conference, University of Southern California at Los Angeles, August 1971 21 p3377 A71-40226
- Holographic interferometry application to two step static displacement measurement of diffusely reflecting surface of rigid body in motion 21 p3377 A71-40227
- Holographic interferometry application to photoelasticity, discussing relationship between isochromatic and isopachic fringes and fringe families separation method 21 p3456 A71-40228
- Real time mechanical strain measurement by optical correlation techniques, using coded matched-filter hologram and incoherent illumination 21 p3377 A71-40229
- Vibration analysis of simulated axial flow turbine disks by holography, illustrating advantages of full field modal and deflection information [ASME PAPER 71-VIBR-105] 21 p3377 A71-40330
- Ultrarapid color holography using continuous synchronized coherent light sources of different wavelengths 21 p3378 A71-40514
- Multibeam holographic interference Gabor theory construction, using variational principle and potential theory 21 p3379 A71-40626
- IR holography with cholesteric liquid crystals as recording medium and carbon dioxide laser as light source, discussing demagnification and image reconstruction 21 p3379 A71-40703
- Holographic methods for etching masks of IC and other semiconductor components 21 p3354 A71-40731
- French book on optical holography covering interference phenomena, image reconstruction from interferograms, geometrical and mathematical aspects, image quality and color holography 21 p3379 A71-40778
- Laser development and applications in telephone communications, manufacturing and holographic memory 21 p3393 A71-40877
- Holographic developments - Conference, Boston, April 1971 21 p3380 A71-40919
- Hologram recording materials within and outside visible spectrum, considering sensitivity, reconstruction efficiency, resolution limitations, nonlinear and noise effects 21 p3380 A71-40920
- Binary computer holograms construction, discussing two and three dimensional objects, wave propagation, plotter instrumentation, photographic reduction and diffusers 21 p3380 A71-40921
- Holographic optical memory broadband development system based on CW Ar ion laser, discussing component operating, power requirement and cost problems 21 p3380 A71-40922
- Bioholographic animal information processing model, considering nervous system as diffractive medium and neural network as Fourier analyzer 21 p3380 A71-40923
- Holographic process theoretical and experimental optimization, considering object/reference beam ratio and photographic emulsion thickness effects 21 p3380 A71-40924
- Pulsed ruby laser holography improvement by coherence length increase with temperature controlled multilayers and beam uniformity through ruby crystals improvement 21 p3393 A71-40925
- High resolution portable hologram recording camera with pulsed ruby laser light source and rechargeable storage batteries as self contained power supply 21 p3380 A71-40926
- Photopolymer holography systems and holograms fixing techniques, discussing polymer films image storing and fixing processes 21 p3381 A71-40927
- Holography review covering photon, grain and speckle noises limitations, large 3D picture production and various applications 21 p3381 A71-40930
- Acoustical holography principles properties and applications, discussing liquid surface levitation, Bragg diffraction and undersea and seismic utilization 21 p3381 A71-40931
- Deformation and translation measurements with holographic interferometry, considering flat surface moved with precision differential screw micrometer 21 p3381 A71-40933
- Real time holographic interferometry of steady state mechanical vibrations of engineering structural components applicable to arbitrary small amplitude and large mode numbers 21 p3381 A71-40934
- Self referencing holographic system for image compensation in fluctuating random medium, describing homodyning procedure 21 p3382 A71-40935
- Three frame pulsed holographic interferometry of plasma radial density profiles and helical displacement for use with theta pinch device 21 p3423 A71-40937
- Holographic detection of transient phase objects in Nd oxide doped laser glass 21 p3382 A71-40938
- Holographic interferometry application to laser NDT of objects with nonoptical surfaces, describing techniques and industrial uses 21 p3382 A71-40939
- Optical field contouring techniques using holographic interferometry for obtaining objects shapes on contour maps 21 p3382 A71-40940
- Axisymmetric imperfect conical shells vibration analysis using time average holographic interferometry technique 21 p3382 A71-41028
- Pre- and post-exposure recording in holographic measurement of high object velocities for enhanced image reconstruction 22 p3537 A71-41597
- Stress analysis of photosensitive coatings and transparent birefringent materials, applying holography to optical polarization method 22 p3537 A71-41614
- Holography applications - Conference, Washington, D.C., October 1969 22 p3538 A71-41731
- Holographic electron microscopy, discussing speckle-free illuminated plane object reconstruction from holograms 22 p3538 A71-41732
- Three dimensional imaginary object reconstruction by holographic stereogram method 22 p3538 A71-41734

HOLOMORPHISM

- Imaging with low redundancy arrays, noting holography role in image processing 22 p3538 A71-41736
- Holographic correction of lens aberration in optical system, considering turbulence effect correction 22 p3538 A71-41737
- Optical transfer function measurement by holographic techniques, describing Fourier transform method useful for lens production testing 22 p3539 A71-41738
- Hologram interference fringes formation and location using grating model of diffusely reflecting surface 22 p3539 A71-41739
- Holographic image reconstruction analysis based on two beam interferometry by spatially incoherent light source, obtaining optical transfer function 22 p3539 A71-41740
- Holographic interferometry application to plate Poisson ratio determination and bending vibration analysis 22 p3539 A71-41741
- Q-switched ruby laser holographic interferometry for hypersonic flame combustion recording 22 p3539 A71-41742
- Pulsed ruby laser transmission and reflection holography in single transverse and axial electromagnetic mode, stressing safety aspects 22 p3556 A71-41743
- Nonlinear hologram application to interferometry, discussing phase difference amplification 22 p3539 A71-41744
- Digital picture processing and holography, considering spatial filtering computer simulation and image synthesis 22 p3539 A71-41745
- Computer synthesis of holograms and spatial filters for coherent optical data processing systems, noting large computational volume required for three dimensional objects 22 p3539 A71-41746
- Optical information processing holographic techniques, describing random masks correlation method for pattern classification 22 p3539 A71-41747
- Fingerprint identification by holographic correlator pattern recognition techniques, discussing reconstructed image visual observation and photoelectric measurement 22 p3539 A71-41748
- Coherent microwave holographic radar systems, discussing mono and bistatic versions, far field performance, pulse compression techniques and signal processing 22 p3540 A71-41751
- Acoustical holographic opaque structures visualization techniques and applications, discussing ultrasound qualities, image converters, detector arrays and medical diagnostic utilization 22 p3540 A71-41752
- Holography applications in ophthalmology to determine optical constants of living eye, including retinal receptors 22 p3540 A71-41753
- High capacity holographic storage system including frequency doubled Nd-YAG laser, Si integrated photodetector array and digital light deflector 22 p3540 A71-41754
- Acoustical holography - Conference, Newport Beach, California, July 1970, Volume 3 22 p3540 A71-41776
- Ultrasonic holography in nondestructive testing, using single transducer or separate focussed transducers for transmission and reception 22 p3541 A71-41780
- Nondestructive testing evaluation of graphite epoxy composites and adhesive bonded Al composite structures using acoustical holography 22 p3554 A71-41781
- Holographic ultrasonic imaging method for flaw detection in aerospace materials and structures 22 p3554 A71-41782
- Optical holographic detection and measurement of ultrasonic waves, providing practical method of investigating LF sound waves 22 p3541 A71-41785
- Multibeam holographic interferometry, using variational principle and potential theory 22 p3574 A71-41786
- Holographic spectral analysis to determine modes oscillating in multilongitudinal and multitransverse mode laser 22 p3541 A71-41791
- Hologram storage in evaporated thin films of arsenic trisulfides, considering simple diffraction gratings and complex data masks 22 p3542 A71-41811
- Hologram Fresnel zone with monochromatic signal and background noise, determining precision of object image coordinates 22 p3546 A71-42273
- Optical modeling of antenna radiation patterns from radio hologram of Fresnel region field 22 p3522 A71-42310

Minimum elements number on discrete two dimensional hologram with constant distance between emitters, considering reduction of matrix elements 22 p3546 A71-42311

Computer technique for synthesizing binary holograms used in wave beams analysis in quasi-optical communication channels 22 p3546 A71-42320

Rotated pattern detection by optical spatial filtering with superposed holograms, obtaining optimal rotation angle for triangle with digital computer 22 p3546 A71-42475

Holography, covering thin, thick, transmission, reflection, amplitude and phase type holograms principles and applications in interferometry, microscopy, imaging, optical data processing, etc 22 p3546 A71-42476

Microwave quasi-holographic techniques, discussing synthetic aperture, chirp radar, rotating target imaging system and beam forming method 22 p3546 A71-42477

Acoustic holography imaging technology, discussing sound field visualization and applications in nondestructive testing, medical diagnostics, ultrasonic microscopy, seismology and underwater viewing 22 p3546 A71-42478

Digital computer holography, discussing generation, reconstruction, applications in optical spatial filtering and surface testing and sampling and quantization effects 22 p3546 A71-42479

Millimeter wave holographic imaging for concealed weapon detection by phase-only hologram, discussing recording and reconstruction systems configurations 22 p3546 A71-42485

Two dimensional holography application to fault-tolerant high density mass data storage design for digital information retrieval system 22 p3548 A71-42517

Diffuse object scanned illumination hologram recording, discussing intermodulation flare light elimination for speed and reconstruction efficiency 22 p3549 A71-42561

Holography capabilities of hypervelocity projectiles with front surface resolution, discussing fringes intensity and position from projectile spin 22 p3549 A71-42569

Holographic inspection of bond between inert solid propellant grain and polymer liner, using double exposure to record surface deformation of fiberglass case 22 p3549 A71-42570

Noise-free linear wave front reconstruction from nonlinearly recorded holograms, noting importance of amplitude transfer function 22 p3550 A71-42571

Photoactivated electric field effects in nematic liquid crystals for recording real time transparent phase holograms 22 p3674 A71-42955

Reproduction accuracy of holographic model, discussing coordinates origin and X-Y-Z errors 22 p3675 A71-43303

Formulas derived for object conjugate points coordinates and holographic image 22 p3675 A71-43304

Hologram recording by optical wave field scanning with arbitrary aperture and point source at center of entrance pupil and photoreceiver 22 p3675 A71-43398

Holographic interferometry flaw detection sensitivity on cylinders under hoop stress, comparing with strain gages 22 p3676 A71-43508

Holographic evaluation of low power ruby laser emitted wave spatial coherence factor via fringe visibility measurements 22 p3679 A71-43894

Physical and technological aspects of holographic recording including optical data processing, Fourier hologram reconstruction and random structure information determination 22 p3679 A71-43896

Holographic nondestructive testing of materials, using laser for object illumination and interferometry 22 p3682 A71-43951

Radio-optics prospects in signal and information processing, image reconstruction, data transmission, computer storage, display and holographic movies and TV 22 p3681 A71-44344

Three dimensional imaging of objects from white light or X ray shadowgraphs by holographic phase implantation 22 p3824 A71-44356

Optical system superresolution by reduction of temporal degrees of freedom using holography 22 p3824 A71-44453

Ultrarapid motion photogrammetry using three dimensional holography with pulsed laser recording 22 p3825 A71-44757

Interference patterns from hologram interferometer related to aberration theory 22 p3826 A71-44980

Holographic method for investigating piston type oscillations with phase modulated reference light beam 24 p3829 A71-45272

Laser holographic inspection for disbonded metal/phenolic rocket nozzles of two divergent geometries, corroborating by ultrasonics and dye penetrants 24 p3829 A71-45272

HOLOMORPHISM
U ANALYTIC FUNCTIONS
HOMEOSTASIS

Psychobiological stress of prolonged weightlessness/bed rest/ in man in terms of adaptive homeostatic state and decreased sensory-motor-muscular input 11 p1725 A71-26111

Food choice, consumption control and metabolism: discussing homeostatic alimentary theories, nerve signals and appetite regulation 13 p2010 A71-28710

Hypothalamus and cerebral cortex electric stimulation effects on temperature homeostasis under hyperoxia 17 p2680 A71-34646

HOMING DEVICES

Nonlinear proportional navigation guided homing missile and minimum time to turn, developing quadratic equation with close larger positive root approximation 07 p1156 A71-19873

HOMODYNE RECEPTION

Optical homodyne detection of light signal wavefront scattered by moving surface with normally distributed roughness, calculating conditions for optimum SNR 18 p2930 A71-36051

Self referencing holographic system for image compensation in fluctuating random medium, describing homodyning procedure 21 p3382 A71-40931

HOMOGENEITY

Homogenization and dehomogenization phenomena at high temperature of Cr-Ni austenitic steels: discussing electron microscope microstructural examinations after heat treatment 01 p0105 A71-11611

Homogeneous and composite polycrystalline materials macroscopic thermoelastic characteristics: determination based on structural model 02 p0324 A71-11755

Titanium and niobium monocarbides electron work function relation to homogeneity region composition: considering electron structure and thermal emission 02 p0263 A71-12199

Transition metals carbides and nitrides homogeneity regions relation to nonlocalized valence electrons in lattice and configuration stabilizing ability 02 p0264 A71-12280

Boundary value problems transformation into initial value problems, obviating homogeneity in boundary conditions 03 p0451 A71-13711

Homogeneous isotropic elastic body stresses after imposing small deformation on strain configuration: obtained from initial small deformation of original configuration 10 p1689 A71-24503

Existence theorems in micropolar elastostatics three dimensional boundary value problems relating to isotropic and homogeneous bodies equilibrium 11 p1847 A71-25442

Homogeneous anisotropic body elasticity theory: calculating boundary value problem for arbitrary conditions 13 p2153 A71-28422

Light transmission homogeneity measurements of optical materials, using Murty interferometer 14 p2242 A71-30154

Laboratory method assessing homogeneity and interchangeability of thermocouple wires, considering thermoelectric properties of widely separated wires from same spool 18 p2852 A71-36990

Homogeneous isotropic universe, analyzing cosmological solutions with linear theory of gravitation 19 p3104 A71-38191

Homogeneous anisotropic body elasticity theory: calculating boundary value problem for arbitrary conditions 21 p3455 A71-40086

Micropolar, homogeneous, isotropic and centrosymmetric medium under external mechanical factors and embedded in magnetic field, investigating magnetoelasticity problems 21 p3417 A71-41361

HOMOGENEOUS TURBULENCE

Homogeneous turbulence decay formulation using multipoint velocity correlations, initial time derivatives and time evolution 03 p0405 A71-14411

Phythan perturbation theory for stationary homogeneous turbulence of incompressible fluid 10 p1594 A71-24511

Homogeneous wave turbulence-MHD tangential discontinuity structures interaction, resulting in shear stress across discontinuity surface

10 p1652 A71-24663

Second order correlation functions of velocity and magnetic field for homogeneous unsteady isotropic hydromagnetic turbulence in incompressible conducting fluid

11 p1805 A71-25599

Monograph on statistical theory for weak homogeneous turbulence covering mathematical model, wave correlation functions, Bogoliubov expansion method, kinetic equation, nonlinear interactions, etc

17 p2727 A71-34771

Homogeneous turbulence decay calculation from multipoint velocity correlations or spectral equivalents at initial time

19 p3044 A71-37730

Ray statistics of electromagnetic wave scattering in homogeneous isotropic turbulent medium with ellipsoidal inhomogeneities of refractive index, using Fokker-Planck equation

19 p3020 A71-38364

HOMOGENIZATION U HOMOGENIZING HOMOGENIZING

Heat treatment and deformation effects on blended metal powder compacts homogenization, using mathematical model

07 p1137 A71-19976

Microstructure and mechanical properties of heat resistant alloy under homogenization and subsequent isothermal heat treatment

08 p1317 A71-21764

HOMOLOGY

Principal homogeneous spaces above elliptical curves over discretely normalized local field

06 p0918 A71-17572

HOMOMORPHISMS NT AUTOMORPHISMS NT SUBGROUPS

Elliptical boundary value problems with conditions not in direction normal to boundary, deriving theorems on homomorphisms and Green formula

05 p0774 A71-16418

HONEYCOMB CORES

Honeycomb sandwich core elastic modulus measurement under transverse compression

09 p1470 A71-22994

Beta Ti alloy sheet and foil mechanical property tests, honeycomb core fabrication, forming and welding evaluations

09 p1455 A71-23095

Metal-metal bonded structures corrosion resistance improvement by use of primers or Al alloy honeycomb core

10 p1626 A71-24110

Spray foam insulation for Saturn S-2 stage, consisting of phenolic honeycomb core composite purged with helium

20 p3312 A71-39270

Static characteristics and free vibration of doubly curved honeycomb sandwich plates, using finite element method

21 p3462 A71-40534

HONEYCOMB STRUCTURES NT HONEYCOMB CORES

Metallurgical and structural production of diffusion bonded titanium honeycomb sandwich panels for aerospace hardware weight saving

01 p0090 A71-11270

Composite materials testing, standards and design, considering flat laminates, honeycombs and construction weight savings

03 p0448 A71-13535

Solar cell array fabrication for operation at 173- 383 K, discussing honeycomb sandwich substrate using epoxy-novolac-fiberglass facings and Al core

05 p0756 A71-16097

Sandwich panels with conical shell or elongated honeycomb fillers, calculating stability and elastic properties

06 p0986 A71-17757

Static computations of thin walled shells and honeycombs, examining variational, matrix, finite element, initial function, small parameter and plate bending methods

06 p0999 A71-17867

Complex Al brazing alloy for honeycomb core joining to Ti alloy face sheets, discussing fillet formation and strength optimization

08 p1299 A71-21686

Metallic and nonmetallic objects phase separation and honeycomb structures adhesion lack, analyzing defects by surface temperatures distribution determination

09 p1450 A71-22893

High peel strength epoxy and urethane adhesives for aircraft bonding, discussing high temperature curing and honeycomb panel repair

10 p1630 A71-24064

Single ply sandwich composite prepregs for use with honeycomb reinforcement, noting one step curing for light weight structural panels

10 p1630 A71-24065

Climbing drum peel adhesion test anomaly in spacecraft adhesive bonded honeycomb structure under lap shear and flatwise tension

10 p1614 A71-24075

Variable weight composite materials for aircraft optimal adhesive bonding structural designs, discussing C-5A tow weight saving Ti honeycomb applications

10 p1686 A71-24084

High temperature honeycomb woven fiberglass reinforced polyimide resin, asbestos reinforced composites and high modulus graphite materials, discussing specific strength and stiffness

10 p1618 A71-24771

Boron-epoxy structural skins design for F-14 honeycomb horizontal stabilizer, using computer program

11 p1786 A71-25420

Elastic characteristics of multilayer structures with honeycomb fillers, discussing deflection, tensile and compression tests

12 p1980 A71-27362

Honeycomb cell multilayer and reinforced structures, examining temperature field radiative heat transport and thermal conductivity and emissivity

13 p2165 A71-29180

Titanium and superalloy radiative heat shield design for space shuttle booster, recommending postsupported honeycomb configuration

18 p2973 A71-36462

HOOKES LAW

Perturbation theory of Hookes law model for He atom, obtaining ground state energy through third order

02 p0287 A71-12494

Rayleigh-Schrodinger perturbation energies for ground state of two electron atomic Hookes law model through tenth order

11 p1803 A71-26151

Nonlinear elastic shells free vibrations, obtaining phase trajectories with finite bending within Hookes law

12 p1975 A71-27106

Buckling under compressive loads of incompressible neo-Hookean plates for homogeneous initial deformation, using variational principle

14 p2333 A71-30993

Closed profile thin walled curvilinear rods, deriving static and strain integrals with Hookes law

24 p3877 A71-44410

HOOPS

Holographic interferometry flaw detection sensitivity on cylinders under hoop stress, comparing with strain gages

23 p3676 A71-43508

HORIZON

NT RADIO HORIZONS

Earth surface nighttime, twilight and daytime horizons visual observations by Soyuz 9 spacecraft

13 p2060 A71-28426

Brightness profiles of earth daytime horizon from Soyuz spacecraft photographic photometry, deriving atmospheric scattering coefficient relation to optical thickness vertical distribution

19 p3054 A71-37967

HORIZON SCANNERS

Flight simulator efficiency for optimal vehicle characteristics, considering in-flight, digital and manned techniques involving horizon indication and maneuver applications

05 p0732 A71-15960

Satellite onboard local vertical detection, emphasizing IR horizon sensors role

06 p0892 A71-17964

IR horizon sensors design, taking into account earth radiation properties

06 p0892 A71-17965

Two-horizon-sensors system for low orbit satellite with three-axis attitude stabilization

06 p0899 A71-17966

Distribution functions of errors in earth and moon horizon sighting due to planetary surface unevenness

09 p1523 A71-23147

Solid state modulation for spacecraft horizon sensing via IR carbon dioxide atmospheric radiation, proposing Fabry-Perot structure with controlled plate separation

22 p3537 A71-41475

HORIZON SENSING

U HORIZON SCANNERS

HORIZONTAL FINS

U FINS

HORIZONTAL FLIGHT

Forward horizontal speed influence on aerodynamic characteristics of air cushion vehicle with circular nozzles and cylindrically or conically shaped curtains

02 p0186 A71-12551

Optimum automatic flight control techniques in horizontal guidance of aircraft at terminal

07 p1156 A71-20306

Optimal control stabilization under continuous small disturbances applied to aircraft stability in horizontal flight under vertical gust loads

10 p1586 A71-24726

Point target horizontal speed determination with circular beam radar for measuring signal intensity and range, noting application to insects in atmospheric waves

17 p2706 A71-35122

Longitudinal stability of plate-like load towed beneath helicopter in horizontal forward flight

23 p3630 A71-44346

HORIZONTAL SPACECRAFT LANDING

Space shuttle scanning beam landing guidance system, discussing accuracy in penetration, alignment, flare out and touchdown maneuvers and trajectories

17 p2773 A71-35068

Propulsive lift augmentation for horizontal landing of low and medium L/D reentry vehicles, determining optimum thrust program

22 p3612 A71-42046

HORIZONTAL STABILIZERS

U STABILIZERS [FLUID DYNAMICS]

HORIZONTAL TAIL SURFACES

Aft vs canard horizontal tail locations for fighter/attack configuration at sub and supersonic speeds, observing lift coefficient, L/D and longitudinal stability [AIAA PAPER 71-8]

06 p0848 A71-18482

Supersonic flow separation around cross shaped horizontal tail plane with subsonic leading edge, obtaining pressure distribution and aerodynamic characteristics

09 p1384 A71-23608

Sailplane elevator induced maneuvering and horizontal tail surface loads, discussing airworthiness requirements

13 p1997 A71-29256

HORIZONTAL TAILS

U HORIZONTAL TAIL SURFACES

U TAIL ASSEMBLIES

HORMONE METABOLISMS

Pineal gland endocrine functions, discussing melatonin synthesis and secretion in response to environmental illumination

05 p0712 A71-17108

Glucocorticoid metabolite excretion with urine in healthy people as function of age and sex

06 p0858 A71-18727

Hypodynamia effects on human hemodynamics under various microclimatic conditions, noting hormonal activity changes in sympathoadrenal system

10 p1563 A71-24339

Urinary metabolites relationship to fatigue, considering excretion of proteins, electrolytes, simple organic compounds and hormones

17 p2679 A71-34357

Hormonal activity during hypodynamia

24 p3796 A71-44538

HORMONES

NT ALDOSTERONE

NT CORTICOSTEROIDS

Moulting of Calpodex ethiulus larvae head and thorax isolated with prothoracic glands dependent on molting hormone injection

01 p0016 A71-11347

Biological radioprotectants in space flights including amino acids, bacterial polysaccharides, hormones and vitamins

06 p0861 A71-18358

Physiological and biochemical characterization of natriuretic hormone in human urine and blood plasma

13 p2013 A71-28952

Adrenal medulla biochemistry and morphology, discussing epinephrine synthesis control by glucocorticoid hormones

14 p2187 A71-30809

Ascorbic acid reduction in organs due to thyroid hormones saturation under hypothermia

17 p2680 A71-34646

Auxin transport and geotropic response of roots and shoots, discussing plant growth mechanisms under stimulation-inhibition conditions

21 p3340 A71-39980

Hormone movement in geotropism, discussing supraoptimal auxin content and indoleacetic acid in wheat roots

21 p3340 A71-39981

Geotropic mechanisms of lateral auxin movement and polar transport of growth substances /ethylene/ without differential cell enlargement

21 p3340 A71-39982

Linkage mechanism between gravity perceptrors and auxin redistribution causing differential growth and geotropic curvatures in plants

21 p3340 A71-39983

Geoelectric effects on plants geotropic reaction chain, discussing hormone auxin asymmetric distribution due to gravity

21 p3340 A71-39984

External indole-3-acetic acid effect on elongation and geotropic bending of Avena coleoptiles related to auxin induced electrical responses

21 p3340 A71-39986

- Gravity effects on auxin transport, growth and foliage spread of green plants for efficient radiation capture, using horizontal clinostat experiments
21 p3341 A71-40005
- Rat thyroid gland changes during acclimatization to simulated high altitude environments, observing high hormone stimulation
23 p3637 A71-44300

HORN ANTENNAS

- Pyramidal or conical horn antenna E plane aperture distribution and radiation pattern control by flare angle changes
01 p0054 A71-10973
- Plane infinite horn antenna with small aperture angle coupled to waveguide, considering wave excitation
01 p0038 A71-11207
- Hybrid mode flare feed horns for parabolic antennas, discussing horn parameters and angular aperture effects on gain factor or aperture transmission efficiency
02 p0234 A71-12807
- Irregular waveguide and horn construction using asymptotic two beam sum theory
05 p0719 A71-15998
- Out of phase conical horn radiating element amplitude and phase diagrams at short distances
06 p0872 A71-17374
- Horn antennas phase centers calculation by vector method from far field expressions
06 p0867 A71-17708
- Rudimentary broadband linearly polarized horn antenna design, impedance and radiation characteristics
09 p1419 A71-23509
- Asymptotic solution for conical horn modes, comparing with exact solution for eigenfunctions and eigenvalues
09 p1420 A71-23677
- Polarization distortion of partially polarized wave emission and reception by two channel horn antennas, noting radio astronomy, radar and optics applications
10 p1584 A71-24876
- Microwave biological exposure systems implementation in limited space, describing focused prolate spheroid, absorber-lined horn and compact range illumination system
11 p1723 A71-25288
- High speed airborne scanning navigational radar antenna with matched patterns, using offset horn feed reflector and polarization modes for improved visual display
14 p2216 A71-31036
- Plane infinite horn antenna with small aperture angle coupled to waveguide, discussing wave excitation and field strength
17 p2697 A71-34259
- Horn array electrically respun antenna design, testing and radiation characteristics, noting excitation by feed system consisting of phase shifters and circular switches
17 p2713 A71-34433
- Wideband Cassegrain microwave antenna for space communication, discussing reflecting horn for maximum radiation gain
17 p2715 A71-34686
- Long conical multimode horn with corrugated surface throat to suppress sidelobes and equalize E and H plane beamwidths
17 p2716 A71-35095
- Near field radiation characteristics of corrugated feed by spherical mode expansion method
19 p3018 A71-38218
- Double refracting dielectric microwave lenses design for horn antennas in SHF applications
19 p3036 A71-38643
- Radiation patterns due to four pyramidal horns used in sum and difference comparison monopulse radar from single horn pattern for design optimization
20 p3203 A71-39092
- Irregular waveguide and horn construction using asymptotic two beam sum theory
22 p3515 A71-42747
- Aperture field and radiation pattern of conical horns with large flare angles, using vector diffraction formula
23 p3654 A71-44166
- Polarization transforming feed horns for rapid scan X-band radar antenna, allowing transmission in various polarization modes and parallel and orthogonal-polarized return reception
23 p3655 A71-44167
- HOSES**
Dynamic response of hydraulic hoses, considering tests with closed loop electrohydraulic position servo
03 p0356 A71-14443
- HOT AIR**
U HIGH TEMPERATURE AIR
- HOT CATHODES**
Re based W alloys for electronic tube hot cathodes, discussing reduction and annealing effects on mechanical and plastic properties
07 p1140 A71-20238
- Ion sources with oscillating electrons, discussing operating principles and characteristics of sources

with cold and incandescent cathodes and Penning ionization chamber
08 p1343 A71-22043

V groove cathode discharge produced He plasma parameters studied for reentry electron density and temperature simulation, correlating energy flux and microwave noise emission
12 p1895 A71-27273

Knudsen arc firing potential in plane gas filled diode with hot cathode as function of electrode gap and atom concentration
15 p2455 A71-31739

Pulsed high permeance electron gun with hot lanthanum boride cathode
20 p3204 A71-39156

HOT CYCLE PROPULSION SYSTEM

U TIP DRIVEN ROTORS

HOT ELECTRONS

Hot electron gas on metal surface under strong heat flux as function of crystal lattice temperature at Fermi level
02 p0332 A71-12196

Density thresholds for anisotropy and loss-cone instabilities onset in hot electron plasmas as function of frequency, wavelength and propagation direction of oscillations
05 p0790 A71-16937

Hot electron plasma, observing flute instabilities with feedback
06 p0933 A71-17471

Hot electron plasma confinement in cusped magnetic field, considering production in electron cyclotron resonance region by pulsed microwaves
06 p0935 A71-17491

Short wave HF instabilities in strongly inhomogeneous plasma with hot electrons, considering ion acoustic oscillations and electron cyclotron harmonics
10 p1650 A71-24525

Magnetic mirror confined plasma diagnostics, considering hot electron density, X ray pulse height and synchrotron radiation measurement techniques
10 p1651 A71-24651

LF hot-electron noise during quasi-elastic scattering in semiconductor with simple band structure, evaluating convective fluctuations contribution to noise temperature
13 p2112 A71-29082

Wave propagation near upper hybrid frequency in mirror-confined hot electron unstable plasma
13 p2109 A71-29242

Ion beam collisionless relaxation in hot electron plasma, observing oscillation spectra and velocity distributions
15 p2453 A71-31245

Book on hot electron microwave generators covering semiconductor physics, collision theory, Gunn effect, domain dynamics, avalanche breakdown, etc
15 p2375 A71-31509

Free-free bremsstrahlung emission in anisotropic hot electron plasma in magnetic mirror, measuring polarization by Compton scattering
17 p2788 A71-34853

Short wave HF instabilities in strongly inhomogeneous plasma with hot electrons, considering ion acoustic oscillations and electron cyclotron harmonics
19 p3116 A71-38251

Schottky barrier diodes as photodetectors in hot electron mode, deriving ballistic transport model for scattering mechanisms effects
20 p3236 A71-39191

Cyclotron absorption and resonance spectra of hot electrons in p-type InSb samples cut from single crystals containing different amounts of impurities
21 p3430 A71-41226

Electron distributions in afterglow of hot electron mirror contained plasma as function of time, using bremsstrahlung spectra measurement
22 p3582 A71-41903

Rollin InSb hot electron bolometer performance and calibration
22 p3543 A71-42124

Hot electrons in semiconductors within crossed and parallel electric and quantizing magnetic fields, examining collision frequencies and energy relaxation
24 p3861 A71-45165

HOT EXTRUDING

U EXTRUDING

HOT FORMING

U HOT WORKING

HOT GAS SYSTEMS

U HIGH TEMPERATURE GASES

HOT GASES

U HIGH TEMPERATURE GASES

HOT JET EXHAUST

U HIGH TEMPERATURE GASES

U JET EXHAUST

HOT JETS

U JET FLOW

HOT MACHINING

Material thermal removal by electrical discharge, electron beam and laser machining, discussing effects on surface integrity
09 p1458 A71-23411

German monograph on hot machining of high temperature steels by flame heating with propane-oxygen and plasma arc burners
14 p2252 A71-30274

HOT PLASMAS

U HIGH TEMPERATURE PLASMAS

HOT PRESSING

Transition metals powders and carbides sintering by high temperature hot pressing in homogeneity regions, determining optimum conditions and activation energy
02 p0256 A71-12270

Hydraulic hot pressing equipment for producing large parts from high melting point metal powders and compounds by induction heating of dies
02 p0238 A71-12280

Continuous filament metal matrix composites fabrication from hot pressed composites by diffusion reaction process
06 p0915 A71-18683

Niobium carbides sintering by hot pressing at various temperatures, discussing kinetics, relative compactness and activation energy
09 p1466 A71-22160

Thermal conductivity, electrical resistivity and specific heat of hot pressed beryllium
10 p1624 A71-23900

Hot pressed transition metal carbide samples: microhardness measurement, interpreting results in terms of atomic electron configurations
15 p2431 A71-32162

Hot pressed boron carbide and titanium diboride for use as indenter materials for tungsten carbide hardness measurements at high temperatures
15 p2409 A71-32165

Hot compaction of tungsten and pseudobinary powders in terms of volumetric-viscous flow dependences on isothermal exposure time, using Kovalchenko-Samsonov equation
16 p2592 A71-33572

Plastic deformation in hot compressed Ti, Zr and Nb carbides during diamond grinding, studying fine structure on diffractometer
16 p2584 A71-33890

Hot pressed W-Cu pseudobinary strength and ductility under tension and compression
17 p2760 A71-35670

Nichrome powder microstructure characteristics effect on hot compaction kinetics, considering temperature, pressure and preliminary heat treatment effects
19 p3075 A71-37100

Transparent scandium oxide powder development by hot pressing, plotting IR transmission vs wavelength
20 p3253 A71-38819

HOT STARS

NT A STARS

NT B STARS

NT O STARS

NT WHITE DWARF STARS

Radiation transfer equation in extended hot stellar atmospheres, discussing scattering effects due to free electrons
01 p0158 A71-10802

Wolf-Rayet star atmospheres, discussing matter density distribution, light pressure effects on particle motion and H and He ionization levels
01 p0158 A71-10802

Hot stellar atmospheres, calculating mean radiation absorption coefficients as function of temperature and electron pressure
01 p0158 A71-10805

Wolf-Rayet WN6 stars emission line spectral profiles observation by spectrograms and photoelectric scanning
02 p0314 A71-12584

RV Tau type stars general and spectral classification, covering color indices, line-of-sight velocities, kinematics and spatial distribution
03 p0485 A71-13262

High galactic latitude faint blue stars from Tonantzintla and Asiago catalogs, finding quasars and subdwarfs by spectroscopy and UVB photoelectric photometry
04 p0651 A71-15659

Hot stars, supergiants and quasars extended and expanding atmospheres, examining resonance line profile formation by coherent scattering
05 p0806 A71-16203

Dust history and physical environment near hot stars associated with nebulosity, discussing optical depths and IR energy
07 p1198 A71-19819

Book on stellar spectroscopy for peculiar stars covering hot star spectra emission lines, novae, magnetic, metallic line and related stars
10 p1675 A71-24477

B and O hot dwarf stars ionic UV line spectra, observing electron and ion damping constants with impact and semiclassical approximations
16 p2633 A71-33338

Wolf-Rayet stars evolution due to stellar matter mixing and escape from nuclei
17 p2800 A71-34571

Symmetrically distributed nebulae around Wolf-Rayet stars, detailing Nge 7635 and associated star BD plus 60 deg 2522

17 p2806 A71-35410

Non-LTE physics of He atoms in hot stellar atmospheres, presenting numerical results for He I and II line spectra variations explanation

17 p2808 A71-35558

UV radiation in space and Venus atmosphere, studying L-alpha lines luminescence hot stars intensity, Milky Way brightness and hydrogen envelope existence

20 p3282 A71-39748

Interstellar medium time dependent model, investigating supernovae and hot stars UV ionization effects on ion production and heating and cloud formation

21 p3445 A71-40248

Young dust-filled planetary nebulae models with hot central stellar black body radiation, evaluating IR radiation absorption and reradiation in H I region

21 p3446 A71-40417

Interstellar Lyman alpha absorption equivalent widths in hot stars spectra, examining rocket and satellite observations

22 p3598 A71-41913

Orion constellation hot stars UV spectra observation by photography from stratospheric balloon gondola using geomagnetic field for stabilization

23 p3735 A71-43249

Evolutionary meaning of nitrogen and carbon sequences in Wolf-Rayet stars

23 p3770 A71-44064

NOT SURFACES

Incompressible fluid steady laminar flow free convection and various gas species mass diffusion from hot horizontal plate surface

06 p1007 A71-18074

Hot wire and tubes nondestructive eddy current testing as cybernetic process, noting high speeds with high on-line data flow

17 p2749 A71-35494

NOT WORKING

NT AUSFORMING

Hot forming/die quenching of aluminum and titanium alloy integrally stiffened panels [SME PAPER EM-70-178]

01 p0089 A71-11259

Oxidation potential criterion for metal sticking to rolls during rolling in vacuum, considering Ta, Zr, Mo, W, Ni, Cu, Nb and V

02 p0256 A71-12515

Fracture toughness tests and brittle failure of high strength structural steels under thermomechanical treatment

03 p0447 A71-14581

Abnormal microstructure in hot rolled plates and sheets of alpha plus beta Ti alloys

05 p0766 A71-16349

Mechanical and plastic properties of Ni-Mo alloys subjected to hot working, determining tensile strength as function of test temperature

07 p1136 A71-19635

Hot working cast nickel based alloy for thin gage sheet, noting electroslog remelting increased temperature range

07 p1136 A71-19964

Re hot rollability under low vacuum conditions as function of temperature, comparing with cold rolling

07 p1120 A71-20240

Cold and hot working effects on Al alloys elastic properties, discussing crystallographic systems reference points

10 p1628 A71-24822

Hot rolled powder metallurgy Mo, noting texture during annealing and cold rolling

15 p2425 A71-31396

Al alloys high temperature thermomechanical treatment, discussing mechanical properties, enhanced plasticity and roughness

15 p2434 A71-32327

Thermomechanical treatment effect on mechanical properties of high strength Al-Mg-Zn-Cu alloys, considering subsequent aging and state before deformation

15 p2434 A71-32328

Mechanical and plastic properties of Ni-Mo alloys subjected to hot working, determining tensile strength as function of test temperature

16 p2593 A71-33631

AMg6M alloy hot rolling butt joints, showing ductility and strength of welds

19 p3070 A71-38424

Hot extrusion properties of free machining Al alloys with low melting point Pb as chip breakers

21 p3384 A71-40026

Ni-Cu-Nb age hardenable steel mechanical properties, examining hot rolling and heat treatment effects

21 p3387 A71-40455

Microstructural characteristics of Fe-Ni alloy plastic deformation at 20-500 C during cold and hot rolling, noting intergranular shear processes

21 p3402 A71-41095

HOT-FILM ANEMOMETERS

Ascending aorta blood flow sequential velocity measurement using conical hot-film probe with linearized constant temperature anemometer circuit [ASME PAPER 70-WA/BHF-13]

03 p0373 A71-14111

Pressure effects on calibration characteristics of hot-film anemometers, discussing heat loss from sensing element

04 p0601 A71-15765

Heat transfer from circular cylindrical hot wire and film anemometer probes, examining calibration steadiness

07 p1106 A71-18783

Velocity measurements in gas mixtures by hot-wire and hot-film anemometers, inferring transport properties from direct calibrations

13 p2069 A71-29008

Hot split-film anemometer sensors for three dimensional air velocity vector measurement

21 p3378 A71-40487

HOT-WIRE ANEMOMETERS

Hot-wire anemometer velocity measurement in slow air flow

03 p0430 A71-14374

Modified constant temperature hot-wire anemometer for extended bandwidth operation, discussing improved frequency response test

04 p0596 A71-14971

German monograph on hot-wire anemometry in fluidics, taking into account partial differential equation solution for temporal and spatial temperature distribution along wire

05 p0753 A71-16899

Disturbances within hypersonic transitional boundary layer in Mach 7 gun tunnel observed with hot-wire anemometer, comparing results with surface heat transfer measurement

06 p0886 A71-18637

Turbulent He jet measurements using hot-wire anemometry and digital recording techniques, assessing accuracy

06 p0886 A71-18639

Heat transfer from circular cylindrical hot wire and film anemometer probes, examining calibration steadiness

07 p1106 A71-18783

Hot-wire anemometer calibration, measuring shear stress and turbulence distributions in circular channel

07 p1106 A71-18785

Airborne hot wire measurements of small scale structure of atmospheric turbulence

07 p1153 A71-20276

Hot-wire anemometry for measuring velocity-temperature coefficients in turbulent flow with heat transfer

10 p1597 A71-25016

Velocity distributions in axisymmetric air jets submerged in coaxial oscillating stream measured by hot-wire anemometer

11 p1748 A71-25156

Temperature measurement methods using thermocouples and hot-wire anemometers for rapidly changing hot gases

12 p1906 A71-26990

Velocity measurements in gas mixtures by hot-wire and hot-film anemometers, inferring transport properties from direct calibrations

13 p2069 A71-29008

Incompressible planar fluid flow magnitude, direction and turbulent shear stress measurement by hot-wire anemometer

14 p2239 A71-29928

Nonsteady air flow direction generation and measurement, comparing three-tube probe with hot-wire anemometer data

14 p2244 A71-30326

Bridge-feedback amplifier constant-temperature hot-wire anemometer static and dynamic response determination

15 p2408 A71-31931

Hot-wire anemometers design and operation in fluidics, discussing temperature gradient due to heat transfer effects

16 p2579 A71-33435

Dynamic small perturbation calibration of constant temperature hot-wire anemometers for turbulence measurements in Karman vortex streets, comparing static method

16 p2581 A71-34166

Hot-wire anemometer design for measuring forced expiratory flow and volume, testing dynamic non-linearity on hybrid computer

17 p2738 A71-34449

Aerodynamic perturbation due to single hot-wire probes, comparing with evaluations derived from potential flow scheme [ASME PAPER 71-APM-T]

18 p2904 A71-36262

Swedish monograph on low air flow velocity measurement with hot-wire anemometer under free and forced convection, using schlieren method

19 p3172 A71-38645

Hot-wire anemometer measurement of free oscillation damping of viscous and sluggish fluid in U tube, determining velocity distribution

21 p3366 A71-40512

Hot-wire anemometer remote operation, discussing coaxial cable length, terminal connection and bridge current

22 p3541 A71-41794

Velocity profiles of heavy viscous fluid free oscillatory motion in U-tube by hot-wire anemometry

22 p3531 A71-42242

Shielded hot-wire probe for mean and rms flow velocities in highly turbulent and rapidly reversing flows

24 p3828 A71-45075

HOT-WIRE FLOWMETERS

Hot wire total temperature probe at hypersonic speeds for flow field measurements

08 p1377 A71-21999

Hot wire signal interpretation using universal calibration law, studying yaw and incidence angles effects

09 p1453 A71-23694

Dutch monograph on nonstationary hot-wire method determining thermal conductivity coefficient of gases, using recorded temperature vs time relation

10 p1697 A71-24677

Hot wire dual probes directional sensitivity for measuring mean flow velocity angles ranges

12 p1903 A71-26574

Hot-wire flowmeters calibration for low density flow measurements, describing method for hot wire end loss determination

12 p1908 A71-27595

X-type hot-wire probe thermal turbulent wake interference, discussing wind tunnel investigation of wire distance effect on pitch angle sensitivity

14 p2339 A71-31022

Random turbulent signals from hot wires across pipe flow, studying form, skewness and flatness factors

15 p2391 A71-32108

Mass flow rate measurements and calibration in heterogeneous medium with hot wires tested on Freon mixtures

19 p3163 A71-37894

Turbulent jet flow concentration, velocity and direction measurements, describing cold and hot wire techniques and data reduction system

21 p3378 A71-40401

Heat transfer of short hot wire normal to ambient incompressible air flow, using small perturbation energy equation

21 p3379 A71-40664

Cryogenic propellant control system, discussing hot wire sensors, fuel state in fueling and tank pressurizing and feed stage

22 p3588 A71-41504

HOT-WIRE TURBULENCE METERS

U HOT-WIRE FLOWMETERS

U TURBULENCE METERS

HOUSINGS

NT RADOMES

Heat resistant roller bearings for vacuum applications at high temperature, discussing gage design and self lubricating materials

02 p0258 A71-12599

Meteorological rocket nose portion thermal regime, determining housing, insulation coating and compartments temperature

19 p3172 A71-38632

HOVERCRAFT

U GROUND EFFECT MACHINES

HOVERING

Army rotorcraft hot day standard design hover criterion, developing analytical models for hovering aircraft, cost, climatology and environmental features

04 p0533 A71-15431

Hovering and low speed flight capabilities of tilt wing VTOL aircraft in terminal area under near-zero visibility instrument landing conditions

[AIAA PAPER 71-7]

06 p0847 A71-18481

Boundary layer discontinuity on helicopter rotor blade in hovering using flow visualization

[AIAA PAPER 69-197]

07 p1017 A71-20307

Army rotorcraft performance data, discussing hovering and forward flight performance out of ground and level flight power requirements and drag and compressibility effects

[AHS PREPRINT 500]

14 p2177 A71-31076

Heavy lift helicopters IFR hover capability with slung load, discussing sensors controls and displays

[AHS PREPRINT 540]

14 p2250 A71-31097

German VAK 191B combat VTOL aircraft development program, describing prototype ground tests, autopilot preoptimization and hover flight tests

22 p3482 A71-41517

Helicopter, tilt wing and jet lift hovering aircraft outflow measurements to determine suitability as rescue vehicles

[AIAA PAPER 71-992]

24 p3791 A71-44586

HOVERING STABILITY

HOVERING STABILITY

Aircraft ultrasonic altitude and vertical velocity sensor for low flight, discussing VTOL aircraft automatic hovering control and time lag

01 p0084 A71-11624

Attitude and velocity control for VTOL aircraft takeoff and landing operations in hovering flight, discussing simulation devices and testing operations [DGLR-70-073]

05 p0779 A71-15948

Tip vortex effects on rotor blade flutter in hovering flight, discussing compressibility and oscillation frequency

05 p0694 A71-16564

Helicopter longitudinal stability in forward flight and hover modes under attitude, height and speed constraints, noting need for cyclic pitch control due to instabilities

07 p1019 A71-19421

Propulsion system and fuel regulator design effect on thrust change during air ejection for VTOL aircraft stabilization in hovering flight

10 p1659 A71-24753

Helicopter handling under ASW flight conditions, discussing sea state effect on low altitude hover stability

13 p1998 A71-29384

Model following technique for optimal control applied to hovering motion of CH-3 helicopter

20 p3178 A71-39000

HRB-1 HELICOPTER

U CH-46 HELICOPTER

HU-1 HELICOPTER

U UH-1 HELICOPTER

HUBS

Rigid rotor hub flapping stiffness tailoring for controllability, considering length and fatigue/structural strength

15 p2348 A71-31601

Dynamic seal development for space base rotating hubs, describing simulated environmental tests for elastomer inflatable seals and lubricants evaluation [AIAA PAPER 71-863]

18 p2927 A71-36651

Axisymmetric stress and strain states calculation for linear elastic field in cylindrical tight fits between hub and shaft

21 p3463 A71-40656

HUECKEL THEORY

Chemisorption energies of organics on Pb surface by extended Hueckel molecular orbital technique

07 p1055 A71-19845

HUGHES AIRCRAFT

NT OH-6 HELICOPTER

HUGONIOT ADIABAT

U HUGONIOT EQUATION OF STATE

HUGONIOT EQUATION OF STATE

Composites and mechanical systems dynamic behavior prediction, calculating Hugoniot with effective modulus

21 p3465 A71-40792

Porous Cu and W shock loading properties, discussing principal Hugoniot data for P alpha dynamic response model

21 p3466 A71-40796

HUMAN BEHAVIOR

Confidential information management, discussing designer and data system user role as foundation for basic privacy control system

01 p0044 A71-10189

Task difficulty involving simple and choice reaction time under stress of shock, threat of shock and noise

01 p0026 A71-11414

Conference report on impact of man on global environment, assessing actions covering climatic and ecological effects, pollution monitoring, etc

02 p0246 A71-12350

Operator behavior in man/machine system, using multidimensional manual control system model with random sampling time and information theory method

03 p0368 A71-12996

Human operator thinking and decision making model for man-machine interaction

03 p0368 A71-12999

Long term human biomedical and behavioral characteristics research, examining enhanced physiological fitness in space

04 p0543 A71-14933

Three element model for choice behavior binary prediction consisting of logical, experiential and error components

07 p1048 A71-19595

Psychopathology identification by manifest phenotypic behavior, discussing syndrome identification, misperceptions and distorted impressions

07 p1042 A71-19697

Human operator psychophysiological characteristics as cybernetic man machine system components, emphasizing human memory activity

07 p1050 A71-20117

Sonic boom effects on human physiology and behavior and structures, based on theoretical studies and simulators

08 p1232 A71-21812

Influence sources affecting self organization of man machine systems, discussing human pilot model

10 p1571 A71-24760

Prolonged perceptual deprivation effects on behavioral, physiological and chemical reactions, discussing EEG mean frequency changes

11 p1724 A71-25362

Rabbits and humans behavioral reactions and EEG changes relation to hypoxia in pressure chamber

12 p1871 A71-27488

Multicategory bibliographic classification of human behavior computer simulation models

14 p2189 A71-30461

Aircraft noise reduction criteria, examining noise measurements relation to human behavior and physical measures connection to subjective judgments

15 p2349 A71-31879

Factor analysis in construction of human fatigue rating scale from individual appearance and comportment

17 p2687 A71-34355

Human thermoregulator set point under physical exercise, using behavioral indicator

17 p2686 A71-35388

Time sense modifications among human groups isolated in underground environment and deprived of timekeeping means, evaluating average individual behavior

22 p3500 A71-41577

Human adaptive behavior under psychological stress of astronauts tasks posture-motor characteristics, discussing stabilographic platform test results

22 p3503 A71-42041

HUMAN BEINGS

Humans and animals acute hypoxia effects on EEG pattern and behavioral reactions

09 p1390 A71-22210

HUMAN BODY

Data processing analog for human vertical position regulation via afferent nervous system control of skeletal muscles

02 p0206 A71-12064

Human left ventricle mathematical models, determining physiological response oriented mechanical parameters with diagnostic significance [ASME PAPER 70-WA/BHF-14]

03 p0373 A71-14112

Computer simulation of human body kinematics under rapid decelerations

04 p0542 A71-14786

Human legs thermal response during cooling for refrigeration anesthesia, deriving analytical model for temperature level prediction as function of time

04 p0545 A71-15160

Computerized human body anatomical geometrical model with life size skeleton and organs scaling for radiation dosage analyses in space missions

04 p0546 A71-15282

Human alveolar-arterial oxygen pressure differences, investigating inert gas effects

04 p0540 A71-15576

Human gamma globulin polymorphism, discussing characteristics, statistical distribution and potential utilization for gene frequency studies in paternity serology

05 p0710 A71-16943

Human erythrocytes phosphate metabolism in hyperthermia

05 p0711 A71-16944

Human organ thermal properties prediction by measuring water content of equal fat/protein tissues

06 p0851 A71-17603

Human mitral valve fluid mechanics, confirming existence of vortex forms during diastasis by vitro flow patterns

06 p0863 A71-18556

Human temperature control computer simulation, considering sudomotor, vasomotor and metabolic as error signals from hypothalamic and cutaneous thermoreceptors

07 p1048 A71-19585

Resistance and mathematical modeling of human body control concerning brain, cardiovascular, arteriolar muscle contraction and protein metabolism systems

10 p1571 A71-24955

Human body thermal behavior modeling, obtaining steady state analytical solution for various boundary conditions and parameters

12 p1875 A71-27563

Human inner organic system simulation by digital computer, using overall quantitative heuristic model

12 p1876 A71-27742

Heat transfer through human peripheral tissue based on one dimensional steady state continuum model combining effects of conduction, convection, vascular heat exchange and metabolism

13 p2025 A71-29502

Human body attitude control in space, using ten body complex geometry system, noting astronaut training jig

14 p2188 A71-29832

Soviet book on aviation medicine covering human anatomy and physiology, atmospheric physics, flight effects, respiratory systems, crew diets, etc

14 p2188 A71-29943

Convective heat exchange coefficient determination for human body immersed in turbulent water flow using fractional calorimetry

18 p2858 A71-3684

Human thermoregulation, discussing experimental determination of equation for mean body temperature calculation in neutral and warm environments

18 p2858 A71-3684

Mathematical model for human thermal system checking accuracy

18 p2873 A71-3684

Heat transfer coefficients calculation for human body in cold water from heat balance equations, comparing with free convection coefficients in cross-flowing water

18 p2862 A71-3684

Experimental analysis of information content of aural electric field of human body, considering electrotonic and triboelectric components

21 p3338 A71-41601

Dynamic sampling calorimeter for continuous measurement of human radiative, convective and evaporative heat loss, enabling closed loop control system analysis

22 p3503 A71-42102

HUMAN CENTRIFUGES

Rotation perception in dark and oculogyral illusion, using power law to describe subjective vestibular sensation relation to angular acceleration stimulus pulse

13 p2022 A71-29384

HUMAN ENGINEERING

U HUMAN FACTORS ENGINEERING

HUMAN FACTORS ENGINEERING

Role of man in navigation - Conference, Colorado Springs, July 1970

01 p0122 A71-10534

Man role in future navigation from SAC viewpoint, considering relationships to mission and machine

01 p0123 A71-10534

Navigator role in Military Airlift Command (MA) as navigator, weather analyst, fuel manager and flight planner

01 p0123 A71-10534

Flight crew training process oriented systems approach through multimedia instruction

01 p0023 A71-10534

Electronic control indicator for human pilot capability enhancement using color coded cathode ray display, presenting information from seven different instruments

01 p0081 A71-10734

Psychophysiological, strict engineering-psychological and systems engineering analyses, solving engineering-psychological problems in large control systems for human operators

03 p0369 A71-13046

German monograph on digital simulation system for ergonomic investigation of radar observational problems covering flight plan data with density variation

04 p0551 A71-14946

Human factors engineering in man machine systems, evaluating biotechnology and aeronautics medicine relationship

05 p0715 A71-16943

Fiber optic faceplates for contrast enhancement under high ambient light conditions for commercial and military cockpits, eliminating ghost, halo and direct sunlight problems

07 p1107 A71-19171

General information system model, producing human performance simulator for various equipment personnel and procedure mixes

07 p1046 A71-19457

Aerospace Recommended Practice criteria for flight deck crew escape systems applicable to all commercial aircraft propulsion systems, design speeds and payloads [SAE-ARP-808A]

07 p1019 A71-19644

Representative data of actual forces and moments applicable to large spacecraft attitude control system for typical crew activities obtained through simulation programs [AIAA PAPER 69-1006]

07 p1208 A71-19864

Human skin vibratory sensibility consideration as analyzer receptor for stimuli conversion into nervous processes

07 p1043 A71-20117

Human eye information processing algorithm mathematical model technological materialization

07 p1051 A71-20117

Aerospace emergency escape systems and procedures, discussing physical, biophysical and physiological aspects related to increased flight speeds and altitudes

08 p1245 A71-20717

Human factors engineering cost effectiveness, citing inspector and assembler performance improvement and warning system audibility verification

08 p1378 A71-21222

Book on human factors application in teleoperator design and operation covering aerospace environments, transportation, remote control, sensors and actuator subsystems

09 p1399 A71-22644

Large aperture telescope on-orbit maintainability packaging, examining optical systems replacement tolerances and astronauts EVA mode accessibility 09 p1446 A71-22742

German book on space medicine covering stresses on human organism during ascent into space, weightlessness and radiation effects, spacecraft environment, nutritional problems, etc 10 p1558 A71-23753

Psychometric measurements approaches for pilot training questionnaires, considering personality traits standard model 10 p1559 A71-23929

Aerospace research bionics and bioengineering, considering adaptation of man to environment and matching of man and machine 10 p1568 A71-24221

Displaced and delayed retinal feedback adaptation theory for human factors problems in man machine systems 10 p1571 A71-24825

Anthropometry for aircraft cockpit and pressure suit design compatible with mission requirements 11 p1724 A71-26115

Statistical survey of aeromedical and human aspects of airports, discussing population, facilities, accident treatment, design guide and requirements 11 p1725 A71-26127

Waist seal design providing discrete anatomical placement, subject comfort, ingress/egress ease and size accommodation for lower body negative pressure devices 11 p1725 A71-26130

Automated facility for electronic equipment production reliability environmental testing, discussing human engineering and test and failure mode designs 11 p1746 A71-26512

Human hand anthropometric and biomechanical characteristics, discussing data utilization for human factors engineering 12 p1875 A71-27250

Human nervous reactions to monochromatic red, yellow green and blue light for optimal color climate in spacecraft cabins 13 p2018 A71-28411

Community aircraft noise intensity indexes from annoyance and physiological reaction standpoint, discussing sleep interruption, hearing loss, communication interference, etc 15 p2364 A71-32242

ONR human engineering research program concerning information input, display and processing concepts, decision making and motor output and control 16 p2536 A71-33529

Aircraft accidents due to engine-out simulation, discussing human factors, minimum control speed certification requirements and pilot flight training procedures [AIAA PAPER 71-793] 16 p2525 A71-34025

Electronic equipment maintenance simplification by proceduralized troubleshooting method for malfunction isolation and tests and checks selection and sequencing, noting technician training cost reduction 17 p2689 A71-34702

Visual search performance as function of color coding for information location tested on aeronautical charts 17 p2689 A71-34703

Aircraft pilots anthropometric survey for human factors engineering, discussing measurement techniques and arrangements for training 17 p2692 A71-35198

Velocity transposition theory based on velocity perception constancy effects, noting importance for human engineering guidance in sea, land, air and space traffic fields [DFVLR-SONDDR-107] 18 p2863 A71-35829

Human factors engineering, discussing industrial, engineering and experimental psychology, human relations, research on attention, perceptual motor skills and control systems laboratory 18 p2864 A71-36296

Ergonomic evaluation of flight crew working conditions from viewpoint of static and dynamic adaptation of aircraft system design to human psychophysical capabilities 19 p3007 A71-38016

Physicotechnical and biomedical aspects of human efficiency under weightlessness, discussing physical exercise role in adaptation 20 p3192 A71-39217

Air safety standards and objectives, discussing human factors as accident causes, piloting aids and management 20 p3178 A71-39395

Artificial ecological regenerative life support system design for space environments, discussing biotechnological properties 21 p3343 A71-40563

Flashing lights vision threshold systematic variations, using quadrant adaptometer for continuous tracking of sensitivity fluctuations 22 p3500 A71-41498

Manned 90 day test of closed chamber regenerative life support system simulator, describing subsystems,

crew nutrition, hygiene, maintenance and leisure activities 22 p3503 A71-42043

Visual information discernibility measurement for suprathreshold transfer in display to observer system, noting use for color contrast scaling and disturbance evaluation 22 p3547 A71-42504

HUMAN PATHOLOGY

Chronic posttraumatic changes in central nervous system in pugilists from brain damage due to head injuries 01 p0010 A71-10393

Statistical analysis of airline flight crew psychological unfitness 01 p0028 A71-11598

Metabolic processes in bone tissues as basis for fighting bone disease, emphasizing enzymes role 05 p0710 A71-16858

Patients transportation pathology, discussing accelerations and vibrations in ambulances, helicopters and fixed wing aircraft 06 p0860 A71-18191

Psychopathology identification by manifest phenotypic behavior, discussing syndrome identification, misperceptions and distorted impressions 07 p1042 A71-19697

Computer aided statistical model of visual evoked potential in man as normality criterion for pathological indicator 09 p1397 A71-22253

Alloisoleucine configuration in blood serum of maple syrup urine disease patients, using gas liquid chromatography 09 p1403 A71-22477

Endolymph and perilymph fluid systems pathophysiology from induced and spontaneous disorders changes observed in inner ear 14 p2183 A71-30254

Nonlinear analysis of arterial flow pulses and shock waves, simulating aortic insufficiency under pathological conditions by mathematical model 16 p2538 A71-34145

Acute renal failure due to heat stress and physical exercise, noting discrepancy between physiological alterations and histopathological abnormalities 18 p2855 A71-36218

Sick and injured transportation aboard regular airliners, considering pathological and psychological contraindications 22 p3500 A71-41572

Antecedent clinical statistics of myocardial infarction and sudden death in actively employed middle aged men, noting cardiac rate, rhythm and conduction abnormalities 22 p3485 A71-41798

Ultrasonics use in physiological and pathophysiological experiments on human organism, considering ultrasonic vibration physical properties 22 p3502 A71-41941

Book on fatal civil aircraft accidents medical and pathological investigation covering transport, light and glider aircraft case histories and statistics 23 p3638 A71-42910

HUMAN PERFORMANCE

NT ASTRONAUT PERFORMANCE

NT OPERATOR PERFORMANCE

NT PILOT PERFORMANCE

Aircraft compartment glare minimization for flight crew visibility conditions and visual performance improvement 01 p0004 A71-10028

Background nonequivalence during long term photopic dark adaptation 01 p0008 A71-10143

Commercial and military aircraft navigator future role, considering increasing task requirement stringency and growing navigational aids availability 01 p0124 A71-10505

Human survivability and work capacity in aerospace environments, discussing sudden unprotected exposure to vacuum 01 p0022 A71-10512

Human foot-balancing reflex as basis for hands-free EVA control system [RE-352J] 01 p0068 A71-11306

Target detection facilitation by adjacent border control involving distance between inducing visual fields and duration of presentation 01 p0026 A71-11416

Visual task vigilance deterioration under hypoxia, considering work-rest schedule effect and IQ scores 01 p0017 A71-11418

Visual images induced in aircraft crew members, during pressure chamber experiments, discussing latent period and persistence of sequences 02 p0198 A71-11899

Soviet papers on movement control covering rate regulation, human rhythms, finger coordination, etc 02 p0203 A71-12051

Human temporal performance of homogeneous discrete motor acts sequence, suggesting central nervous mechanism for movement rate generation 02 p0204 A71-12052

Human muscular control patterns during forearm precision cyclic bending on ergograph 02 p0204 A71-12053

Human discrete and continuous rhythmical movements rate control 02 p0204 A71-12054

Human fingers coordination during teletype operation, examining temporal characteristics 02 p0205 A71-12055

Time interval tracking in humans during steady and transient performance of homogeneous discrete motor acts sequence 02 p0205 A71-12056

Human tracking of external targets and body point projections, examining visual feedback role 02 p0205 A71-12057

External acoustic signals for human cyclic movements temporal structure control 02 p0205 A71-12058

Aural and visual limitations effects on athletes rowing rhythms, examining afferent systems interactions 02 p0205 A71-12059

Isolated synthesized vowel fundamental tone duration, intensity and frequency imitation by human voice 02 p0205 A71-12060

Human voice imitation of tonal signals pitch interval 02 p0206 A71-12061

Synthesized glottal consonant imitation by human voice, analyzing stimulus and response intensity levels relationship 02 p0206 A71-12062

Human muscle hardness as isometric stress force indicator 02 p0198 A71-12065

Human operator adaptive response characteristics to step changes in compensatory tracking system dynamics 02 p0207 A71-12349

Human motor skills acquisition during manual control problem solving, modeling operator as single channel data processing system 03 p0368 A71-12998

Neural activities during simultaneous contrast and information processing in visual system 03 p0364 A71-14188

Neurophysiological aspects of human optical and acoustical perception, discussing pattern recognition and cognizance role in optical image evaluation 03 p0373 A71-14331

Human vigilance performance in brightness discrimination task under hypoxia, considering reaction time in signal detection 04 p0541 A71-14740

Performance decrement during bimodal vigilance task, discussing arousal and selective attention constructs 04 p0541 A71-14741

Human rotation perception, discussing man-carrying rotation device, angular acceleration threshold, etc 04 p0541 A71-14756

Respiratory features for conscious or unconscious warning of impending exhaustion, noting work load-performance decrement relation 04 p0545 A71-15159

Stereophotogrammetric system for human motion measurement, describing design and operation 04 p0547 A71-15844

Practice effects on visual vigilance task performance with and without search 04 p0540 A71-15845

Human strength decrement and recovery for repetitive maximal muscular exertions with various intertrial intervals 04 p0540 A71-15846

Human sleep deprivation research, discussing task performance, man machine interaction and work-rest cycles 04 p0540 A71-15848

Visual alignment task performance for marks with vertical separation under various illuminations 04 p0547 A71-15849

Alcohol effects on complex task performance including monitoring, compensatory tracking and mental arithmetic 04 p0547 A71-15850

Human eye optical performance, noting retina anatomy and physiology, visual acuity, resolving power and reflectometry 05 p0713 A71-16482

Pursuit tracking skill acquisition in humans, considering sex, initial ability, age, aptitude and proficiency levels and psychomotor performances 05 p0713 A71-16549

Knowledge of results and rest pauses effect on sensorimotor skills at different training conditions 05 p0714 A71-16618

Human work capacity in hot environment irrelevance to normal conditions, considering physiological reactions to exercise in heat by heart rate criterion 05 p0709 A71-16621

Blood lactate levels in human males after bicycle rides, considering altitude effects on oxygen consumption and glycolytic and aerobic activity 05 p0709 A71-16623

Human physical exercise with stepwise increasing load noting working capacity, cardiovascular and respiratory system performance and blood composition interrelations

05 p0709 A71-16805

Multiple acoustic evoked responses coherence time course using mathematical correlation and Fourier transforms

05 p0714 A71-16922

Human factors in glider accidents, discussing drugs, fatigue, oxygen lack, nervous tension, etc

06 p0860 A71-18196

General information system model, producing human performance simulator for various equipment, personnel and procedure mixes

07 p1046 A71-19456

Human work capacity measurements by graded step test and bicycle ergometer, considering heart rate and oxygen uptake

07 p1046 A71-19457

Subjective and electromyographic estimation of fatigue and muscle activity physiological levels, considering isometric muscle contraction task endurance

07 p1047 A71-19458

Complex psychomotor task time duration relation to subtask performance and psychological measures

07 p1047 A71-19459

Human performance in pursuit tracking task with realistic structured and blank backgrounds

07 p1047 A71-19460

Human performance in continuous pursuit tracking with temporary target obscurations, noting positional and velocity control systems

07 p1047 A71-19461

Motor learning error performance with discrimination reaction timer, discussing commitment to wrong response, group observations and specific error repetition

07 p1047 A71-19462

Human work load assessments by time study of officers and physiologists, noting disagreeing values

07 p1047 A71-19466

Irrelevant information with no activity purpose, discussing detrimental effect on human memory

07 p1050 A71-20104

Complex human memory processes large scale simulation/cybernetic modeling/ based on information handling probability and retrieval

07 p1050 A71-20105

Human operator psychophysiological analysis by memory-activity interdependence simulation, noting buffer memory, reflex system and habit acquisition

07 p1050 A71-20107

Mathematical simulation of human recognition by black box approach as information conversion process

07 p1050 A71-20109

Redundancy effects on human memorization working capacity, noting application to memory systems design

07 p1043 A71-20113

Space vehicle apparent distance magnitude estimation judgments, investigating stimulus range effects on response range and Stevens type power function exponent

07 p1051 A71-20217

Manned aircraft crew long range navigation, discussing sensor, information processing and display systems for future commercial and military missions

07 p1157 A71-20343

Somatic concentration and brief sensory deprivation effects on rod and frame and embedded figures test performance

07 p1045 A71-20382

Visual-tactile dominance relationship as function of tactual judgment accuracy

07 p1045 A71-20385

Average minimum time for incorrect movement amendment, based on performer ability to process visual feedback

07 p1045 A71-20386

Target detection performance in simulated real time airborne reconnaissance mission, taking into account search time and image type, contrast and rate of motion

08 p1248 A71-21227

Human operators performance under control problem programs, determining training and fatigue effects

09 p1398 A71-22483

Atmospheric ions effects on human visual performance, taking into account ozone concentration and humidity

09 p1493 A71-22741

Crew performance as information input factor based on USAF two man space cabin research

09 p1400 A71-23245

Night vision visual systems with image intensifiers, noting effect on human eye performance at low light levels

10 p1641 A71-24057

Intermittent noise effects on performance of visual search tasks of varying complexity, measuring test subjects target detection time under various noise/time ratio conditions

10 p1562 A71-24206

Human time estimation tests, describing methods of reproduction, verbal estimation and production in randomized blocks of trials

10 p1562 A71-24207

Pretask instructions effect on vigilance task performance, measuring time related signal detection correct and incorrect response percentages

10 p1571 A71-24808

Critical period and habituation in control precision performance response to startle due to pistol shots

11 p1723 A71-25181

Information support system for physiological studies of human performance, including indexing approach for references categorization, microfiche file and data bank

11 p1860 A71-25253

Diurnal variations in catecholamine excretion, alertness and performance of subjects with different working habits

11 p1722 A71-26356

Carbon monoxide methods for studying diffusing capacity of human lungs

12 p1869 A71-26654

Diurnal rhythms of human physiological functions and performance during frequently alternating sleep-work cycles

13 p2006 A71-28410

Engineering management, discussing technical men work effort, time/intellectual changes, performance measurements, motivational factors and relationship to company

13 p2167 A71-28799

Human performance after awakening at different times of night, considering reaction time and muscular coordination

15 p2362 A71-31201

Human performance in various locomotive tasks under simulated lunar reduced gravity conditions, classifying test stands and equipment

15 p2362 A71-31304

Human vigilance performance and personality traits characterization by EEG alpha frequencies, correlating rest and task period recordings

15 p2359 A71-31954

German monograph on human mental performance under simultaneous mental and above normal muscular stress involving signal response in double choice reaction problems

15 p2360 A71-32306

Man machine system dynamic properties and biomechanical model concepts, determining random vibration effects on sitting and working human body

15 p2366 A71-32728

Psychological tests for aerial photograph interpreter selection and performance prediction

16 p2534 A71-32829

Human auditory signal detection related to averaged evoked potential in scalp by electrophysiological measurements

16 p2534 A71-32951

Human inferences based on partially reliable reports, studying likelihood ratio estimates and probabilistic relations in nature

16 p2534 A71-33103

Optical tracking task performance and nystagmus during angular acceleration in yaw and pitch, comparing differences due to vertical and horizontal canal response

16 p2535 A71-33107

Maximal human anaerobic power, discussing unsplit phosphagen concentration in muscles during steady state exercise

16 p2530 A71-33247

Human performance reliability data system using taxonomic structure for classifying behavioral studies and predicting man-machine performance

16 p2536 A71-33318

Redundancy information effect on human performance in forced pace cognitive tasks under overload stimulus presentation rates

16 p2536 A71-33679

Partial reinforcement effect in visual vigilance task, varying knowledge of results as incentive

16 p2537 A71-33680

Sounds effects on natural nocturnal sleep of healthy humans with normal hearing

17 p2679 A71-34479

Frequency tolerance of vibration stress effects on human performance, considering body resonance, visual acuity, manual tracking and neural capacities

17 p2689 A71-34701

Visual search performance as function of color coding for information location tested on aeronautical charts

17 p2689 A71-34703

Magnification level for optimum performance at microminiature inspection with binocular microscope, minimizing time

17 p2689 A71-34704

Two dimensional adaptive model of human operator control in visual-manual compensatory tracking task using pattern recognition

17 p2691 A71-35046

Methodological features of programmed control of human upper extremities movements, using six-channel bioelectric system

17 p2692 A71-35158

Mathematical model of human visual system linear adaptive signal transformation

17 p2692 A71-35159

Variables affecting processing mode of serial or parallel of complex stimuli information

17 p2684 A71-35255

Human central fovea theoretical model for target stimuli threshold detection performance prediction

17 p2693 A71-35358

Human power output during short duration exercise, relating to body size and composition

17 p2686 A71-35451

Human violent exercise burst effect on cognitive task, noting mild hypoxia irrelevance to skills decrements

17 p2686 A71-35452

Psychological correlates of pattern identification tasks and invariance of pattern recognition under rotation, using Kabrisky model of human visual system

17 p2694 A71-35744

Human performance in rotating environments, discussing Stromberg Dexterity, pursuit rotor, mental arithmetic, verbal learning and NAMI Ataxia tests

18 p2871 A71-36644

Human physiological responses to rotating environment, evaluating heart rates, blood pressure, pulmonary functions, visual observations and vital capacities

18 p2856 A71-36644

Manned earth-orbital missions performance assessment experiments, studying effects of artificial zero gravity spacecraft environments on humans

18 p2857 A71-36644

Weightlessness simulation for orbital man machine experimentation, discussing telerboard and cargo transfer examples

18 p2871 A71-36644

Human performance in optical high inertia tracking system interface, considering proprioceptive feedback, display magnification, control dynamics visual field and anticipatory processes effects

18 p2873 A71-36916

Mental reactive exertion increase phenomenon, investigating achievement under various degrees of carefulness and fatigue

18 p2862 A71-36948

Fatigue effects on standing broad jump and other body movements patterns

18 p2873 A71-36948

Human psychomotor performance measurements in rotating environments, using Langley complex coordinator and decision response time devices

19 p3006 A71-37273

Positive and negative deflections in human electroretinogram off response to stimuli

19 p3007 A71-38050

High muscle glycogen content effect on human performance in prolonged heavy physical exercise

19 p3009 A71-38555

Alkalosis effect on human maximal performance and lactic acid formation in blood under supramaximal exercise conditions

20 p3185 A71-38888

Noise exposure effects on human physiological and psychological functions and performance

20 p3192 A71-38959

Physicotechnical and biomedical aspects of human efficiency under weightlessness, discussing physical exercise role in adaptation

20 p3192 A71-39211

Color and music distraction for operator in isolated environment and counteract psychophysiological activity impairment

20 p3193 A71-39222

Psychophysiological reactions to understimulation and overstimulation, noting catecholamine output, heart rate and performance efficiency in humans

21 p3329 A71-40177

Human perceptual motor skill development in tracking performance, using feedback control system gain and effective time delay as measures

21 p3343 A71-40908

Functional lability of human tactual analyzer by measuring minimum interval between two discrete controlled stimuli

21 p3344 A71-41066

Human performance as function of task and environmental factors, using psychological and physiological references

22 p3503 A71-42199

Visual performance in simulated target acquisition tasks as function of flare-ignition altitude

22 p3503 A71-42199

Human observer performance in imaging systems: detailing contrast, ambient illumination, resolution exposure time, display size, field of view and image blur and enhancement

22 p3547 A71-42505

Comparative residual and reversed microinterval masking signals and human auditory perception capacity measurements using sound level estimates

22 p3490 A71-42571

Human olfactory perception of inspired air composition, noting sensory differentiation improvement with subsequent exposures in space flight training 22 p3505 A71-42800

Alpha activity parameters during human performance of motor tasks with open and closed eyes 23 p3631 A71-43108

Presentation modality as encoding variable in short term memory, obtaining mean recall score as function of trials 23 p3639 A71-43113

Man machine system dynamic properties and biomechanical model concepts, determining random vibration effects on sitting and working human body 23 p3639 A71-43299

Human motor system control mechanism for stretch reflex loop gain with simplified central nervous system computation 23 p3639 A71-43354

Apparent movement due to closely spaced sequentially flashed dots in human peripheral field of vision, considering eye movement role 23 p3634 A71-43970

Scanpaths in saccadic eye movements during pattern vision and recognition 23 p3635 A71-43973

Low grade hypoxia effects on human physiological responses and performance in vigilance/display monitoring tasks 23 p3636 A71-44238

Affect adjective checklist assessment of mood changes as function of stress in air traffic controllers 23 p3640 A71-44240

Combined heat, noise and vibration stress effects on human performance and physiological functions including heart rate, body temperature and mental arithmetic 23 p3637 A71-44247

Human adaptation to Coriolis and linear accelerations, investigating habituation effect 24 p3795 A71-44533

Coriolis acceleration effect on human organism from optic functions and retinal hemodynamics study 24 p3795 A71-44534

HUMAN REACTIONS

Human subjective responses to approaching and receding aircraft sounds during flight over stationary observer 01 p0127 A71-10345

Monochromatic light glare effect on human eye as function of wavelength, using visual threshold variation as criterion 01 p0016 A71-11389

Human eye cyclofusional movement response measurement in terms of disparity threshold for diplopia 01 p0016 A71-11391

Cardiovascular and ventilatory responses to room air and pure oxygen breathing under various exercise work load conditions 01 p0016 A71-11407

Human work level adjustment to specific energy expenditures during hard work on servocontrolled treadmill 02 p0202 A71-11665

Fatigue factor of lactate, ATP and creatine phosphate/CP accumulation in working muscles during short exhaustive exercise in man 02 p0202 A71-11666

Human thermoregulatory response to ambient temperature variations, considering deep body and skin temperature interrelations 02 p0202 A71-11667

Water intake effects on human thermal sweat rate and composition in environmental chamber at specific temperature and humidity 02 p0202 A71-11670

Reaction time diurnal variations to optical and acoustic stimuli, investigating disturbed natural sleep-waking rhythm effects 02 p0197 A71-11684

Russian book on perception of respiratory medium and gas preference in man and animals covering hypoxic or hypercapnic media, inhalation times, gas mixtures, etc 02 p0198 A71-11823

Military parachutists physiological and force field responses to aerospace recovery environment, using multichannel FM/FM telemetry for heart rates 02 p0207 A71-12389

Skin temperature and metabolism changes magnitude, duration and variability in unacclimatized male subjects during cold stress 02 p0208 A71-12836

Healthy subjects physical training effects on blood flow and enzymatic activity in skeletal muscle 02 p0201 A71-12916

Human neuromuscular activity description by model for muscle spindles functions, considering systems parameters oscillations relation to mean muscle stress 03 p0366 A71-12978

Human motor reactions sequential systems control characteristics, considering effects of external stimulus and repetition time interval 03 p0357 A71-12988

Human cardiovascular control system model by analog computer program for various work loads up to submaximal, estimating correspondence to real life 03 p0368 A71-12995

Long term day and night ECG recordings of healthy human subjects, analyzing heart rate and amplitude variations during normal wakefulness and sleep periods 03 p0370 A71-13061

Acoustic stimulation effect on electroretinogram of man 03 p0361 A71-13191

Gap in atrioventricular conduction in humans by catheter technique for recording electrical activity of His bundle 03 p0363 A71-13488

Light-dark cycle strength as Zeitgeber for circadian rhythms in isolated man 03 p0364 A71-14249

Soyuz 9 prolonged space flight biomedical effects on human organism, emphasizing weightlessness 03 p0365 A71-14392

Human orthostatic tolerance measurement via leg and lower body negative pressure, discussing heart rate and stroke volume variations 04 p0543 A71-15052

Time zone change effects on worldwide schedule flight crews sleep patterns, considering biological functions Circadian rhythm changes 04 p0544 A71-15057

Conditioned reflex gas exchange shifts in persons under repeated local thermal stimuli 04 p0540 A71-15572

Changing rotational velocity recording device for vestibular apparatus tests, examining stimulus reaction speed 05 p0714 A71-16810

Magnetic field effects on biological systems, discussing ergometer measurements of human subjects muscular contractions 05 p0714 A71-16896

Topography of acoustically evoked potentials triggered by alpha activity in man 05 p0710 A71-16942

Visual analyzer functional state during latent motion sickness on rocking devices simulating moving aircraft 05 p0711 A71-17026

Electrophysiological audiometry noting average brain response in man 06 p0858 A71-17295

Human circadian rhythms in continuous darkness, noting social cues entrainment sufficiency 06 p0849 A71-17303

Mean period spontaneous EEG as psychophysiological characteristics of higher nervous activity in human individuals 06 p0858 A71-17600

Four-electrode impedance plethysmograph system for evaluating conduction variations of upper and lower body segments relative to blood volume displacement 06 p0853 A71-17958

LF vibration effects on human beings, discussing circulatory reactions 06 p0859 A71-18188

Immunological reactivity of human body during 120 day feeding on dehydrated diet 06 p0861 A71-18368

Clinical, physiological and metabolic changes in human body during 120 day bed rest 06 p0855 A71-18371

Time constant for collateral ventilation in human, dog and pig lungs under various physiological conditions 06 p0856 A71-18385

Cardiovascular, respiratory and thermoregulatory mechanisms in aqualung diver drillers 06 p0864 A71-18721

Free and systematic horizontal visual search target detection times, testing human subjects with mixed stimulus schedules on high and low contrast targets 07 p1047 A71-19463

Toxic substances absorption, metabolism and excretion by man, discussing role of solubility, transfer through membrane tissue, liver and kidney as metabolizing and excreting organs 07 p1042 A71-19700

Respiratory rate and cardiac responses to exercise in man 07 p1052 A71-20326

Chemosensitivity in normal, hypoxia and hypocapnia cases, using rebreathing techniques to construct isoxic carbon dioxide response curves and isocapnic oxygen response curves 07 p1052 A71-20329

Chlorophenoxisobutyric acid action on human cholesterol metabolism, suggesting cholesterol synthesis inhibition 07 p1044 A71-20353

Hyperemic skeletal muscle capillaries restricted diffusion, obtaining permeability data for chromium 51 labeled EDTA and inulin in exercising human forearm 08 p1237 A71-20677

Human biodynamics during deceleration, impact and blast, discussing body positions and protective restraints for crash safety, aircraft ejection, etc 08 p1244 A71-20707

Neuroendocrine and metabolic responses to rotating workshift schedules, using urinalysis to assess physiological disturbances and adaptive changes 08 p1239 A71-20817

Soyuz 9 flight manned biomedical mission, evaluating 18 day exposure effect on human physiology and work capacity 08 p1246 A71-20820

Mechanical, physiological and psychological responses of man to sinusoidal whole body vibration 08 p1248 A71-21230

Physiological effects of cooling measured by men wearing air and water cooling garment under external heat loads or large metabolic heat 08 p1248 A71-21232

Human nervous system stimulus trace retention in various age groups, using skin galvanic reaction 08 p1240 A71-21788

Community reactions to aircraft noise, discussing short term interim alleviation measures in airport operations and runway usage scheduling 08 p1378 A71-21819

Visceral system regulation processes investigation in human organism during manual labor and environmental adaptation, using multichannel biotelemetry and computer processing 08 p1241 A71-21941

Temperature analyzer function under ambient temperatures in children 08 p1242 A71-21961

Vascular effector structure in orientation reaction of peripheral vessels to sound, using plethysmogram and rheoencephalogram indications 08 p1242 A71-21962

Human conditioned reflexes to time and EEG responses under acute hypoxia 08 p1243 A71-21970

Human biomechanical and vegetative reactions to hypnotic suggestion of gravitational effects 08 p1243 A71-21971

Human spinal reflex effects during static work, suggesting cord segmental chiasmatic connections interaction with spinobulbar-spinal tract 08 p1249 A71-21973

Human panel comparison of aircraft engine noise tape recordings with synthetic broadband noise approximating pure jet 09 p1398 A71-22255

Hyperthermia effects on conduction velocity of nerve fibers and peripheral motor neuron-muscular activity in man 09 p1399 A71-22924

Regional pulmonary vasomotor activity in sitting man, determining pulmonary flow distribution with Xe 133 technique 10 p1561 A71-24126

Ambient temperature effects on flicker fusion threshold, using constant stimuli and forced choice methods for determination of test subjects sensory sensitivity to heat and cold exposure 10 p1568 A71-24184

Hypodynamia effects on human hemodynamics under various microclimatic conditions, noting hormonal activity changes in sympathoadrenal system 10 p1563 A71-24339

Human response to and perception of angular acceleration, discussing implications for motion capability in flight simulator [AIAA PAPER 70-350] 10 p1571 A71-24860

Human visual system response to moving spatially periodic stimuli, developing mathematical model for motion perception 10 p1572 A71-24999

Isotonic training effects on circulation for limb muscular strength characteristics, using peak blood flow and venous compliance measurements 11 p1719 A71-26071

Thermal environment effect on human skin temperature and final temperature and tolerance time prediction from early exposure 11 p1725 A71-26117

Human heart beat phase frequency changes after acoustic stimulation during natural sleep from EEG, EKG, EMG of musculus hypoglossus and eye motions 11 p1721 A71-26292

Subsonic jet aircraft noise and simulated sonic booms awakening effects on human sleep 11 p1726 A71-26510

Astronaut selection and training, considering acceleration, hypoxia, weightlessness and temperature variation tolerance 12 p1873 A71-26951

Response strategies in two-choice reaction task with continuous cost for time, confirming fast-guess model prediction 12 p1873 A71-27008

Pressure effects on human ventilation and gas exchange, determining stratified inhomogeneity during deep diving 12 p1873 A71-27126

HUMAN TOLERANCES

- Human heart rate, minute ventilation and oxygen uptake measurement during treadmill and track running at three speeds 12 p1874 A71-27134
- Space flight factors effects on human physiology and psychology, discussing spacecraft gaseous medium control, food supply, closed ecological systems and weightlessness effects 13 p2016 A71-27876
- Human brain subcortical formations slow electrical processes during memory tests 13 p2005 A71-28377
- Long term immersion effects on human water-salt metabolism, noting increased erythrocyte water contents and hematocrit index 13 p2006 A71-28403
- Human nervous reactions to monochromatic red, yellow green and blue light for optimal color climate in spacecraft cabins 13 p2018 A71-28411
- Exhaled air microimpurities composition of humans exposed to stress effects including bed rest, starvation, lyophilized diet feeding, high temperature and humidity 13 p2007 A71-28412
- Human afterimage and pupillary activity in darkness after strong light exposure, noting dependence on stimulus intensity and duration 13 p2018 A71-28463
- Human visual geometrical illusions and figural aftereffects, determining mechanism locations for spatial patterns physical and phenomenal properties 13 p2018 A71-28464
- Heat balance of human body submerged in water, determining body temperature reduction as function of ambient temperature 13 p2019 A71-28508
- Soviet book on vestibular reactions covering functional relationship between stimulus parameters and labyrinth nonauditory part, adaptation to Coriolis forces and response to ionizing radiation 13 p2008 A71-28672
- Set and uncertainty as factors influencing anticipatory cardiovascular response in humans, monitoring heart rate and vasomotor activity 13 p2011 A71-28809
- Visual evoked cortical response in man related to rate, spatial frequency and wavelength of alternating barred pattern with background illumination 13 p2012 A71-28888
- Noise exposure index from mean sound intensity measurement, considering harmful effects on humans 13 p2021 A71-29284
- Heart rate variability in REM sleep, stage 4 sleep and wakeful state from ECG of normal males, calculating coefficient of temporal variability for each state 13 p2014 A71-29319
- Diastolic and mean blood pressure responses to exercise after beta-adrenergic blockade in normal and labile hypertensive subjects, using Trascior 13 p2014 A71-29320
- Multiple starlike flashes and short streaks reported by subjects exposed to neutrons under 25 mev, discussing interaction with retinal rods by proton recoils 13 p2022 A71-29353
- Human physiological responses comparison between work with concentric and eccentric muscle contractions, observing oxygen debt in short term exercise 13 p2024 A71-29495
- Pilot subjective evaluation of XB-70 aircraft response to atmospheric turbulence in comparison with measured accelerations 14 p2173 A71-29774
- Atmospheric turbulence induced aircraft vibrations effects on aircrew performance, discussing physiological and psychological responses 14 p2187 A71-29778
- Human electroretinographic dark adaptation recovery curves rod-cone break time dependence on bleach intensity 14 p2185 A71-30503
- Cardiac activity changes during prolonged hypodynamia, discussing clinical and experimental investigations results with humans and animals 15 p2358 A71-31320
- Computer quantitation of ST segment response to graded exercise in untrained and trained subjects, continuously recording amplitude of selected points on ECG waveform 15 p2358 A71-31452
- Human muscle blood flow measurement by Xe 133 clearance method during rhythmic exercise, noting work load effects 15 p2358 A71-31455
- Human subjects REM sleep characteristics under 5-hydroxytryptophan influence, analyzing continuous polygraphic recordings of parietal EEG, horizontal eye movement and submental electromyographic activity 15 p2359 A71-31952
- Cortical neurodynamics during vestibular afferent activity and associated cardiovascular and respiratory reactions, noting EEG correlation to hemodynamics 16 p2527 A71-32828
- Young pilot performance in emergency situations including communication system failure and other equipment breakdowns, noting emotional reactions 16 p2534 A71-32831
- Elevated atmospheric pressure effects on human psychophysiological qualities including attention, memory and time-estimating capabilities and nervous processes equilibrium 16 p2536 A71-33578
- Cardiovascular and respiratory systems, motor and muscular activity, metabolism and body energetics functional changes due to prolonged weightlessness 16 p2531 A71-33676
- Human erythrocyte 2, 3-diphosphoglycerate concentration elevation effects on glycolytic metabolism and intracellular pH 16 p2533 A71-34090
- Human fatigue with emphasis on chronic conditions unrelieved by rest or sleep, recommending elimination of conditions resulting in excessive stress, anxiety or boredom 17 p2687 A71-34353
- Subjective fatigue feeling correlation to symptoms based on bank clerks and broadcasting workers work load assessment ratings 17 p2688 A71-34367
- Human motor control behavior sampling hypothesis of open loop system at voluntary effort initiation, discussing validity based on ankle rotation physiological test 17 p2690 A71-34741
- Antixposure suits physiological evaluation for subjective comfortableness, oral and skin temperatures and pulse rate, determining optimum environmental temperature 17 p2692 A71-35195
- Human sweat gland duct filling and skin epidermal hydration behavior by analysis of time delays between sweat emergence and steady state, using electrical stimulation 18 p2858 A71-36865
- Male and female physiological responses to heat stress, discussing sweating, skin and body temperature, heart rate and metabolism 18 p2859 A71-36871
- Sweat and time constant response of human thermostat to linear gradient heat load, using analog computer experiment 18 p2859 A71-36874
- Water temperature effect on body thermoregulation in swimming, comparing swimmers responses to track man on treadmill at same metabolic rate 18 p2861 A71-36893
- Fear measurement and mastery, investigating relationship between experience and electrodermal arousal in responses to stimulus words of varying relevance 18 p2862 A71-36944
- Prisoner dilemma game matrix, noting response patterns to various formats 18 p2863 A71-37017
- Human response to auditory stimuli start and cessation, noting time lag and perception duration 19 p3001 A71-37283
- Conditioned motor reactions characterizing higher nervous activity, using logokinetic method 19 p3006 A71-37447
- Human heat stress evaluation indices, discussing acclimatization, dehydration, clothing, age, physical fitness, health and sex effects 19 p3006 A71-37483
- Human response to space environment, discussing prolonged weightlessness, extravehicular work and lunar surface activity 19 p3002 A71-37492
- Visually evoked cerebral cortex responses to on- and off-set of patterned light and contour density and sharpness in humans 19 p3004 A71-38282
- Bed rest effects on human hemodynamic and gaseous metabolism, observing increased cardiac output and decreased oxygen consumption and carbon dioxide production 20 p3188 A71-39231
- Book on noise effects on man covering audiometry, aural reflex, hearing damage risk, physiological responses, motor performance and speech communication 20 p3193 A71-39874
- Vibration effects on human body, discussing neurophysiological data, safe exposure limits, therapeutic applications, motion sickness, muscular responses and biomechanical effects 21 p3342 A71-40147
- Normal females electrophysiological changes during sensory isolation of water tank variety from EEG, EMG, EOG, EKG and electrodermal measurements, considering cortical activities reduction 21 p3330 A71-40346
- Young adult males split-period sleep regimes dependence on intervening wakefulness time intervals periods length and onset sidereal time 21 p3330 A71-40346
- Human microbial flora and immunologic responses long term space missions, describing environmental parameters and factors and work-rest schedules effects 21 p3332 A71-40347
- Human body immune status normalization in prolonged space flight, investigating ribonucleic acid stimulated antibody formation 21 p3332 A71-40348
- Spacecraft cabin artificial atmospheric composition and variation effects on human immunocompetence examining lymphoid cell immunity reactions after lymphocytes blast transformations 21 p3332 A71-40350
- Human microflora variation in long term confinement, examining anaerobic and aerobic microorganisms responses 21 p3333 A71-40351
- Excitability, reactivity, adequacy, creativity and guidance at molecular, cellular, systemic and psychologic levels in human biophysical neurodynamics, plotting stimulus magnitude vs response duration 21 p3344 A71-41046
- Transient heart rate response to square wave breathing in man under zero G parabolic flight 22 p3501 A71-41876
- Human cerebral EEG phenomena and evoked potential relationships to eye and retinal image movements 22 p3488 A71-42436
- Radiation damage diagnosis in humans, investigating free amino acid excretion with urine by paper chromatography method 22 p3495 A71-42717
- Healthy males immersion in water containing NaCl determining modified gravitational field effect on motor functions 22 p3505 A71-42718
- Unfavorable high intensity noise effects on auditory and motor analyzers during space flight 22 p3495 A71-42719
- Water immersion or bed rest effects on basal metabolism and external respiration under simulated weightlessness 22 p3495 A71-42720
- Humans under constant diet feeding in closed ecological system, demonstrating instability elimination process of various elements 22 p3506 A71-42818
- Manned spacecraft life support system dehydrated food ration effects on human organisms health metabolism and immunoreactivity during long space flight 22 p3507 A71-42819
- Auditory stimulus conditioning of human skin resistance responses on escape-avoidance schedule 22 p3497 A71-42866
- Human visual system color and edge-sensitive channels confirmation by psychological tests of tuning for orientation 23 p3640 A71-43546
- Human reaction to externally induced body vibration, discussing vibration exposure limits 23 p3640 A71-43906
- Metric characteristics of horizontal saccadic eye movements in normal humans from electrooculographic recordings, discussing dysconjugacy mechanisms 23 p3635 A71-43977
- Ventilatory response to progressively increasing inspired carbon dioxide tensions at ground level and acetazolamide pretreatment before high altitude exposure 23 p3636 A71-44244
- Human auditory adaptation to medium intensity noise complex action under relative isolation and hypokinesia conditions from monaural hearing threshold measurement 24 p3799 A71-44400
- High blood pressure and age effect on human baroreflex arc controlling pulse interval sensitivity showing systolic pressure response to phenylephrine intravenous injection 24 p3794 A71-44433
- Emotional stress of pilots in difficult flight conditions, noting pulse rate increase and biopotentials amplitude changes 24 p3800 A71-44477
- Chronic hypoxia exposure effects on human ventilatory response to carbon dioxide and oxygen deficiency 24 p3797 A71-44778
- Hypoxic respiratory reactions of highland natives and recently arrived residents to oxygen concentration change in inhaled mixtures 24 p3798 A71-45066
- HUMAN TOLERANCES**
- Human survivability and work capacity in aerospace environments, discussing sudden unprotected exposure to vacuum 01 p0022 A71-10511

- Thermal state symptoms characterizing limit of human tolerance to heat loads at rest and during physical exercise
01 p0014 A71-11135
- External respiration, gas exchange and energy expenditures during orthostatic tests involving immersion experiment
01 p0014 A71-11136
- Aspartic aminotransferase activity relation to clinical and biochemical indices of human tolerance to impact accelerations
01 p0014 A71-11140
- Helicopter pilot and passengers emergency survival, considering gravitation force, human tolerances, design factors, etc
01 p0026 A71-11376
- Human tolerances to thermal environment extremes in aerospace activities
02 p0207 A71-12388
- Heat tolerance for resting subjects in event of air conditioning system failure in SST passenger cabin
03 p0371 A71-13095
- Simulated sonic booms effects on sleeping humans, considering intensity levels, age factors, sleep stage, adaptability and housing
03 p0371 A71-13165
- Physiological and psychological human responses to sonic booms in France, UK and U.S. considered as acceptability criteria
03 p0371 A71-13167
- Positive effect of physical training on heat endurance of man
03 p0361 A71-13193
- Helicopter pilot and passenger comfort/vibration tolerance criteria
04 p0532 A71-15420
- Air transportation systems ride vibration environments in relation to human comfort
04 p0532 A71-15421
- Tolerance time for hot humid conditions, considering acclimatized and unacclimatized men at rest and at work with moderate rate of energy expenditure
05 p0705 A71-16153
- Impulse-noise human ear damage-risk criterion correction factor for single impulse, studying temporary threshold shift
05 p0712 A71-16284
- Voluntary body water and salt deficits decreasing human heat tolerance
05 p0708 A71-16597
- Physical fitness in prolonged muscular work tolerance evaluation by oxygen consumption for 170 beat/min heart rate, considering age, sex and occupation
05 p0708 A71-16614
- Vibration and buffeting effects on man, discussing aerospace environments, biomechanics, human tolerances and performance, etc
08 p1244 A71-20709
- Cardiopulmonary and circulatory mechanisms, adaptation limits and response to aerospace flight stress
08 p1238 A71-20720
- Human gastrointestinal tract functional disturbances after prolonged work in UHF field
08 p1249 A71-21955
- Dark adaptation in humans under Arctic conditions, noting role of physiological disorders
08 p1242 A71-21958
- Acceptable gamma radiation dosages for extended manned space flights based on prolonged irradiation of dogs
09 p1388 A71-22193
- Acceleration tolerance improvement in human subjects by gymnastics, games, athletics and aviation pilot training
09 p1399 A71-22920
- Oxygen deficiency and body temperature effects on work capacity of human subjects in hot humid environment
09 p1399 A71-22922
- Thermal environment effect on human skin temperature and final temperature and tolerance time prediction from early exposure
11 p1725 A71-26117
- CO exposure effects on human psychomotor performance for blood carboxyhemoglobin saturation levels, using sleep monitored EEG methods
11 p1726 A71-26509
- Book on electromagnetic fields and life environment covering biological effects of radio waves, protection, radiation sources, permissible intensities, working conditions
12 p1873 A71-26868
- Somatic and autonomic responses in vestibular tolerance of human subjects, using Coriolis acceleration test
13 p2007 A71-28414
- High altitude pulmonary edema in unacclimatized humans, discussing symptoms, etiology and prevention
14 p2183 A71-30277
- Beta inflection in darkness adaptation curve, postulating stimulus thresholds in mono and binocular examinations for perception time and sensitivity
16 p2527 A71-32866
- Frequency tolerance of vibration stress effects on human performance, considering body resonance, visual acuity, manual tracking and neural capacities
17 p2689 A71-34701
- Medical physiological requirements of angular velocity and g level for artificial gravity creation by rotating space vehicle, considering human tolerances and vehicle design
18 p2870 A71-36627
- Human adaptation to high altitude, considering effects of physical preconditioning, exercise, high carbohydrate diets and normal food intake maintenance
18 p2859 A71-36867
- Sweat and time constant response of human thermostat to linear gradient heat load, using analog computer experiment
18 p2859 A71-36874
- Human temperature tolerance during exposure to hot and cold environments, using skin temperature as indicator
18 p2859 A71-36875
- Heat acclimatization by evaporative cooling prevention in men wearing vapor barrier suits, considering body temperature and heart and sweat rates
21 p3331 A71-40355
- Microbial contamination of human skin and upper respiratory tract during long term isolation in sealed environment
21 p3333 A71-40559
- Human orthostatic and vestibular stability responses to weightlessness during extended space flights noting acceleration tolerance, physical efficiency, infection resistance and medication sensitivity
22 p3495 A71-42790
- Training cycle in altitude chamber for human adaptation to hypoxia, high temperatures and transverse myogenic loads
22 p3505 A71-42805
- ### HUMAN WASTES
- #### NT URINE
- Carbon dioxide elimination across human skin, investigating perspiration effects
14 p2186 A71-30567
- Artificial mineralization of water regenerated from human waste products in space flight
15 p2362 A71-31309
- Long term spaceflight crew personal hygiene, discussing human waste processing and/or utilization, microbiological control and medical infirmity-dispensary-laboratory requirements
18 p2870 A71-36631
- Circadian rhythms of human renal excretions in polar, temperate and equatorial regions
20 p3190 A71-39477
- Biologically mineralized human waste products utilization in nutrient solutions for higher and lower autotrophs cultivation
22 p3507 A71-42819
- Human waste product utilization possibility through mineralization by wet combustion method
22 p3507 A71-42820
- Group analysis of impurities in water regenerated from liquid human wastes
24 p3800 A71-44529
- Microelement extraction from mineralized biological samples in food rations and human excretions
24 p3800 A71-44540
- Adrenaline, noradrenaline and catecholamine excretion in railroad men during daytime and nighttime work
24 p3799 A71-45085
- ### HUMIDITY
- Solid molybdenum disulfide lubricants antifriction properties and performance under atmospheric and high vacuum conditions, noting humidity effects and composition of friction-evolved gases
01 p0106 A71-10036
- Al-Si alloys corrosion resistance in humid atmosphere and acid medium, investigating effects of refining process and hydrogen content
01 p0097 A71-10040
- Meteorological observations during solar eclipse of 7 March 1970 concerning temperature, wind, humidity, pressure, air circulation and optical phenomena
01 p0151 A71-10118
- Atmospheric refractometry anomaly at high relative humidities observed in controlled environment for causes
01 p0113 A71-10252
- Aerosol-induced solar radiation attenuation correlation to humidity in atmospheric boundary layer
04 p0641 A71-15119
- Pilot performance under helicopter cabin high temperature and humidity
04 p0547 A71-15422
- Ti-Ag and Ti-Pd-Ag solar cell contacts structure and degradation dependence on high temperature and humidity environmental exposure
05 p0699 A71-16060
- Solderless Ag-Ti solar cell contacts humidity degradation mechanism
05 p0699 A71-16061
- Tolerance time for hot humid conditions, considering acclimatized and unacclimatized men at rest and at work with moderate rate of energy expenditure
05 p0705 A71-16153
- Relative humidity augmentation for triggering convection in two dimensional numerical cumulus cloud model
06 p0924 A71-18412
- Adsorbed formaldehyde levels from vaporized paraformaldehyde on various surfaces as function of relative humidity and chemical concentration
07 p1055 A71-19593
- Potting compounds service life estimation based on accelerated hydrolytic reversion data at high temperatures and humidities
10 p1633 A71-24117
- Humidity effects on sound velocity in air at constant temperature and normal atmospheric pressure in lower audio frequency range
10 p1642 A71-24815
- Corrosive contaminants, oxygen, humidity and temperature environment simulation
11 p1746 A71-26496
- Time and frequency statistics of turbulent fluctuations of wind, temperature and humidity in atmospheric surface layer
14 p2266 A71-29706
- Low flame temperature propellants, investigating temperature and humidity aging effects on physical and ballistic properties
14 p2286 A71-30732
- Surface cracking resistance of polymethyl methacrylate glass in vacuum, air and nitrogen, noting humidity effect
16 p2601 A71-33690
- Standard visibility and scattering coefficient changes due to humidity variation from maritime aerosol particles equilibrium radii calculations
16 p2605 A71-34084
- Water vapor electrolysis for oxygen generation and humidity control in long term manned space flight
18 p2868 A71-36391
- Vertical atmospheric humidity profile variations relationship to clouds water vapor content from thermal radio emission measurements onboard Cosmos 243 satellite
23 p3673 A71-44048
- Atmospheric vertical humidity profile from ground measurements of radio wave absorption at 1.35 cm water vapor line
24 p3822 A71-44820
- Humidity effects on molybdenum disulfide bonded solid film lubricant friction properties at low load and slow speed, noting mechanical escapement timers accuracy
24 p3831 A71-45285
- ### HUMIDITY MEASUREMENT
- Atmospheric total moisture content from Cosmos 243 satellite, describing onboard equipment calibration
01 p0074 A71-11101
- Nimbus 3 and 4 satellites IR grating spectrometers for remote sensing of vertical temperature and humidity profiles of stratosphere and troposphere near Philippines
05 p0818 A71-17137
- Atmospheric total moisture content from Cosmos 243 satellite, describing onboard equipment calibration
07 p1102 A71-19650
- Soviet book on fog, cloud and humidity measuring instruments, discussing artificial fog formation and natural fog dispersion problems
07 p1114 A71-20298
- Dew point hygrometer with constant resistance humidity transducer, using salt solution phase transition principle
08 p1292 A71-21456
- Book on atmospheric boundary layer dynamics considering theoretical models of vertical distribution of wind velocity, temperature and humidity
09 p1488 A71-23175
- Low hygrometer calibration for water vapor measurements smaller than 3 mm
11 p1761 A71-25244
- Ceramic semiconductor atmospheric humidity detector with hydrophilic properties, using complex capillary porous body composed of crystals and amorphous substance
21 p3383 A71-41237
- Dew point/frost point/ reference hygrometer for humidity gage testing in thermohygrostat hygrochamber
21 p3384 A71-41379
- Atmospheric vertical humidity profile determination by measuring microwave radiation from satellite
24 p3822 A71-44350
- ### HURRICANES
- In- and outflow fields in hurricane Debbie, using airborne radar echoes and ATS 3 satellite pictures
01 p0118 A71-10589

HUYGENS PRINCIPLE

Hurricane Gladys structure and dynamics observations by Apollo 7 spacecraft, satellites and radar, noting large cloud feature

05 p0777 A71-16662

Airborne severe storm surveillance, including radar detection hurricane model

07 p1058 A71-18826

Tropical hurricane central pressure drop to maximal wind velocity ratio, discussing thermal to mechanical energy transfer as function of ocean surface temperature

08 p1330 A71-21873

Structural model of mature hurricane, determining heat and moisture transfer, boundary layer dynamics and thermodynamic balance

13 p2097 A71-29250

Equatorial upper troposphere and lower stratosphere hurricane and wavelike motions numerical predictions, analyzing heating, friction, cloud physics and ozone dynamics

14 p2270 A71-30500

HUYGENS PRINCIPLE

Shadow photography applied to Mach reflections in argon, carbon dioxide and Freon 12 in shock tube, using Huygens principle for transfer mechanism

02 p0239 A71-11635

Green function or Huygens principle for radiation and diffraction of electromagnetic or acoustic waves in anisotropic media

15 p2449 A71-31869

HYBRID COMBUSTION

U HYBRID PROPELLANT ROCKET ENGINES

HYBRID COMPUTERS

MOBSSL-UAF block structured simulation language for digital and hybrid computers

01 p0046 A71-10200

Hybrid computer programming for continuous systems simulation

01 p0046 A71-10201

Hybrid executive programs for simulation, discussing I/O processing, potentiometer evaluation, data conversions, etc

01 p0046 A71-10202

Partial differential equations hybrid computer solution by extended space technique for overcoming slow convergence of Galerkin method

01 p0048 A71-10223

Hybrid computers solution of linear differential equations, analyzing Taylor series /derivatives/ use for compensation

01 p0048 A71-10224

Hybrid computer simulation program for analyzing large circuits intractable by conventional methods using PACTOLUS language

01 p0048 A71-10225

Time shared input/output I/O processor with hybrid I/O separation from hybrid computation

01 p0048 A71-10226

Digital hybrid systems simulator /DHYSYS/ program, examining subsystems sampling and execution time and applications

02 p0226 A71-11780

Missiles and aircraft trajectories computation time reduced via time sharing and hybridization

02 p0227 A71-11794

Large hybrid simulation and analog section replacement by digital model, considering digital simulation techniques for economical solution of special problems class

02 p0227 A71-11797

Missile six degree of freedom simulation by hybrid computer, discussing roll and pitch dynamics

02 p0227 A71-11798

Soviet analog computer modifications for iterative and hybrid computations, describing memory system alterations

02 p0228 A71-12489

High speed automated network design method for optimum value determination of system parameters, using sensitivity analysis and hybrid computer optimization techniques

03 p0390 A71-14305

Analog/hybrid programming of stimulus sequence for cardiac excitation study

04 p0546 A71-15166

Hybrid computer systems, describing interface, analog output and program design

06 p0871 A71-17744

Direction finding problems involving several waves of same frequency, discussing nonlinear computation methods with hybrid computers

06 p0927 A71-18205

Hybrid computer simulation for cardio-circulatory assist device, discussing atrium to aorta and ventricle to aorta optimal output, time tension index and flow control

07 p1048 A71-19584

Iterative computation of variational optimization problems by analog computers with digital logic control /hybrid computers/

09 p1413 A71-23665

Quasi-analog and hybrid computers, describing ARKUS hybrid integrator effectiveness in solving

boundary value problems and ordinary differential equations

10 p1581 A71-24382

Hybrid computation - Conference, Brussels, August-September 1970

11 p1734 A71-25839

Parameter optimization in linear control systems subject to random disturbances, using hybrid computer

11 p1735 A71-25840

Direct impulse response method application to function optimization, using high speed hybrid computer

11 p1735 A71-25841

Dynamic optimization with constrained state and control vectors, solving problems by hybrid method with partial derivatives

11 p1735 A71-25842

Hybrid computer Monte Carlo technique for simulation and optimization of system with random parameters

11 p1735 A71-25843

Apollo command module guidance computer and environment hybrid simulation for flight software and crew procedures verification

11 p1744 A71-25845

Attitude control loop and inertial guidance hardware, studying system dynamic performance hybrid simulation

11 p1796 A71-25846

Complex real time hybrid computer simulator for captive two blade rotor platform dynamic problem solving

11 p1744 A71-25847

Hybrid simulation to increase hit possibility of rocket fired from military tanks at moving targets

11 p1735 A71-25848

Viscous fluid flows determination by network calculator consisting of hybrid resistor with electronically switching active nodes

11 p1744 A71-25849

Apollo hybrid simulator for man-machine interface in low orbit lunar landmark tracking

11 p1796 A71-25850

Six degree of freedom hybrid digital computer program for complex flight control and associated mode logic design and training

11 p1736 A71-25852

Hybrid computer operating system for piloted aircraft simulation and optimization studies

11 p1736 A71-25853

Hybrid computer program for data reduction or on-line analysis of nystagmus during closed loop experiment involving visual and/or vestibular function

13 p2022 A71-29359

Flight vehicle equations of motion for computer simulation, calculating optimal servosystem parameters and optimal range control by hybrid computer scheme

14 p2319 A71-30001

Hybrid computer solutions for optimal control of time varying systems with parameter uncertainties, exemplifying minimax load relief for large launch vehicles

14 p2319 A71-30019

Hybrid binary floating point digital differential analyzer technology, noting speed, cost and utility

14 p2207 A71-30021

German monograph on PHENO hybrid computing elements for nonlinear operations covering ADC and DAC, level and time quantization effects on computational accuracy, etc

14 p2207 A71-30238

Hybrid computer use for dynamic system probabilistic modeling, determining hydraulic actuator output statistics

16 p2549 A71-33295

Hybrid computer continuous space methods for time dependent partial differential equations involving solution of sequence of two point boundary value problems

19 p3025 A71-38292

On-line identification for nonlinear system from noisy measurements, applying stochastic algorithm to hybrid simulation of chemical process models

20 p3207 A71-38974

Hybrid computer control of engine start-up using adaptive logic, adaptive programming and self organizing storage

20 p3208 A71-38998

Hybrid computer simulation of nonlinear ion-acoustic shocks in diaphragms

22 p3577 A71-41896

Analog data computation with hybrid and logic operational elements, applying to periodic function arithmetic mean determination and transistor characteristics representation

22 p3518 A71-42430

HYBRID NAVIGATION SYSTEMS

Flight test of hybrid strapdown inertial navigator with Doppler radar and occasional position fixes through Kalman filter mechanized in small computer

17 p2776 A71-35765

HYBRID PROPELLANT ROCKET ENGINES

Gas dynamics of fuel boundary layer combustion and surface pyrolysis in hybrid rocket motors

01 p0178 A71-10100

Hybrid rocket propulsion engine combustion efficiency, burnout patterns and operating conditions using nitric acid oxidizer

02 p0298 A71-12028

Ammonium nitrate, ammonium perchlorate and nitronium perchlorate as liquid oxidizers for hybrid propellant rocket engines, discussing oxidizer/kerosene mixing ratio

10 p1657 A71-24214

High altitude probe design and optimization, discussing hybrid propellant propulsion system peak altitude payloads and combustion temperatures

11 p1811 A71-25555

Time constant dependence of hybrid rocket combustion chamber on engine parameters and structure

16 p2625 A71-33640

Polymer thermal degradation theory of pressure sensitive hybrid combustion, calculating linear regression rates

19 p3170 A71-38121

HYBRID PROPELLANTS

Gas dynamic analysis of hybrid boundary layer combustion with nonequilibrium surface pyrolysis using Rayleigh analogy

05 p0837 A71-16535

Styrene-methyl methacrylate and -acrylonitrile copolymers linear and mass regression rates in hybrid rocket fuels combustion

15 p2464 A71-31646

HYBRID ROCKET ENGINES

Small hybrid rocket engine using aromatic amines mixture as fuel and nitric acid as oxidizer, discussing regression rate relations and internal ballistics design

22 p3589 A71-42011

Hybrid rocket /Barbarella I/ design, tests, engine feed system oxidizer tank, fairings fins, propellant and launch facilities

22 p3589 A71-42048

HYDRATES

Carbon dioxide clathrate in Martian ice cap suggested from hydrate stability relative to solid phases and water ice as function of temperature

01 p0148 A71-10000

Hydrated hydronium ions in D region, discussing sources and production mechanisms

03 p0421 A71-14548

Venus cloud composition, noting partially hydrated iron chloride as principal constituent

11 p1824 A71-25700

Venus ferrous chloride hydrate cloud production, examining geochemical problems

11 p1824 A71-25700

Aminazine and chloral hydrate effects on metabolism intensity of rats brain gangliosides components including N-acetylneuramine acid and N-acetylglucosamine

21 p3337 A71-41055

HYDRATION

Equilibration rate of uncatalyzed carbon dioxide hydration reaction in open system at constant carbon dioxide partial pressure, examining buffering capacity effect

10 p1559 A71-23898

Human body temperature regulation under various hydration regimes during exercise, noting changes related to sweating

16 p2530 A71-33243

Hydrated electrons photoexcitation by giant pulses Q-switched ruby laser, investigating absorbency over wide range of light intensities

17 p2753 A71-34950

Human sweat gland duct filling and skin epidermal hydration behavior by analysis of time delays between seat emergence and steady state, using electrical stimulation

18 p2858 A71-36865

HYDRAULIC ACTUATORS

U ACTUATORS

U HYDRAULIC EQUIPMENT

HYDRAULIC ANALOGIES

Hydraulic analogy for visualization of flow through moving plane cascade for rotor section of compressor stage

12 p1898 A71-27720

Reynolds analogy of heat transfer applied to disk rotating near stator, including frictional dissipation and radial outflow in compressible or incompressible flow

13 p2048 A71-28595

Surface renewal and penetration model in heat and momentum transfer analogy for incompressible turbulent boundary layer flow

14 p2227 A71-30935

Approximate elastoplastic problems solutions by method analogous to antiplane deformation of circular incompressible region in flow theory

16 p2657 A71-33594

Vertical acceleration effect on gas-hydraulic analogy for turbulent flows with and without jumps with

error dependence on Froude number and length to depth ratio

16 p2560 A71-33598

Metal joint explosive bonding, investigating wavy interface formation mechanism by aerohydrodynamic analogy

17 p2748 A71-34494

Transverse curvature effect on singularity at separation for laminar boundary layer from analogy with flat-plate compressible boundary layer

19 p3044 A71-37726

HYDRAULIC CONTROL

Electrohydraulic thrust control system for super-sonic transport aircraft engines, considering reliability, performance and weight

[SAE PAPER 700819] 01 p0143 A71-11546

Solar telescope coelostat and auxiliary mirror hydropneumatic unloading mechanism

04 p0566 A71-14870

Electro-hydraulic servomechanisms dynamic performance variation probabilistic model, presenting sixth order system variable parameters for Monte Carlo simulation

06 p0848 A71-17318

Aircraft electronic control systems, considering hydraulic servocontrol, force simulation and reliability models

07 p1156 A71-20064

Pneumatic and hydraulic fluidic power control systems, discussing moving part position servos and cold gas reaction systems

07 p1028 A71-20585

Hydraulic resistance control and actuation switch system designs and classifications, using bridge half components and loop combinations

18 p2850 A71-36203

Directional hydraulic control switching fluid amplifier at various Reynolds numbers, including cavitation effects

18 p2851 A71-36205

Electrohydraulic stand for vibration strength testing, discussing system design, specifications, frequency-amplitude characteristics and applications

23 p3662 A71-44235

HYDRAULIC EQUIPMENT

NT AIRCRAFT HYDRAULIC SYSTEMS

Hydraulic vane pumps, including variable displacement, double and compound pumps

01 p0006 A71-10815

Hydraulic system axial- and radial-piston pumps design and operation principles, considering cost reduction

01 p0006 A71-10817

Rotary hydraulic motors dynamic behavior during pressure and fluid flow control

01 p0006 A71-10823

Hydraulic servomechanism with piston-type control valve, examining oil compressibility and sustained oscillations effects on system stability

01 p0007 A71-11378

Hydraulic hot pressing equipment for producing large parts from high melting point metal powders and compounds by induction heating of dies

02 p0238 A71-12282

Dynamic response of hydraulic hoses, considering tests with closed loop electrohydraulic position servo

03 p0356 A71-14443

Frequency stability of automatic control system with hydraulic actuating mechanism external load, taking into account fluid compressibility

05 p0705 A71-17033

Subsonic tactical missile hydraulic and fluidic autopilot systems for directional control, considering costs, reliability, vulnerability, maintainability, weight and mobility

[SME PAPER MS-70-524] 07 p1024 A71-20547

Vertical hydraulic press for metal extrusion at temperatures from 4 to 77 K, discussing design

08 p1299 A71-21809

Hydrodynamic forces on pistons in sharp-edged spool valves with double throttling gaps at Reynolds numbers from 60 to 240

09 p1434 A71-23664

Vapor pressure measurements of mineral oils for hydraulic power systems, using transpiration method

09 p1484 A71-23666

Listening method for hydraulic drive systems, using vibration signature analysis with rolling, sliding, impact and flow

13 p2000 A71-28720

Optimal quick response control synthesis for hydraulic drive with throttle, using two step phase space method

13 p2002 A71-28937

Third Chance flight control system, discussing aircraft control capability with backup hydraulic system after loss of dual main hydraulic systems due to combat damage

13 p1998 A71-29382

Dynamic characteristics of hydraulic fatigue testing machines, using hydraulic activation efficiency factor

14 p2221 A71-29625

Thrust measurement of aircraft propulsion systems, considering hydraulic piston device, edge clearance, oil quantity and calibration

14 p2251 A71-29860

Fluidic devices with combined pneumatic and hydraulic components, describing jet-siphon liquid flow frequency transducer with pneumatic pulse counting device

15 p2353 A71-32071

Hybrid computer use for dynamic system probabilistic modeling, determining hydraulic actuator output statistics

16 p2549 A71-33295

Hydraulic system self acting valves natural vibration dynamic characteristics, showing energy transfer by phase shift of variable hydrostatic compression component

17 p2677 A71-34349

Runner and cavitation characteristics of hydraulic machine with finite blade number and ideal frictionless incompressible working fluid determination by potential theory

17 p2727 A71-34668

Electronic and hydraulic devices for communication satellite ground station steerable antenna servocontrol, driving and pointing, discussing tracking error signals

17 p2724 A71-35511

Fluid contamination and protective filter in hydraulic power components for design service life

18 p2851 A71-36204

Hydraulic system cleanliness - ASTM Conference, Toronto, June 1970

19 p2999 A71-38318

Hydraulic system and fluid cleanliness maintenance, discussing contamination sources and prevention techniques including filtration, dehydration and degasification

19 p2999 A71-38319

Hydraulic servo equipment filtration systems design, discussing contamination effects and servo components physical characteristics effects on tolerance level

19 p2999 A71-38320

Hydraulic components and equipment contamination control and effects on system efficiency, discussing filter ratings and location

19 p2999 A71-38321

Hydraulic equipment fluid contamination control, discussing sample bottle cleaning, fluid sampling, component tolerance profiles and filtration performance specifications

19 p2999 A71-38322

Hydraulic fluids contribution to system contamination, discussing precipitate formation due to reaction with water, filtration inability and contaminant elimination

19 p2999 A71-38323

HYDRAULIC FLUIDS

Liquid volume deformation effect on hydraulic drive under continuous or jumpwise pressure

01 p0007 A71-11243

Soviet book on aviation fuels, lubrication materials and special fluids covering compositions, physicochemical properties, filtration, etc

01 p0142 A71-11320

Oleo-pneumatic accumulators in gearboxes for rationalizing installed power

07 p1023 A71-20004

Ultrasonic waves propagation in hydraulic and lubricating oils, testing shear resistance

09 p1484 A71-23673

Performance testing of fluorosilicone hydraulic fluid in high temperature supersonic aircraft piston pumps

12 p1921 A71-27040

Hydraulic system and fluid cleanliness maintenance, discussing contamination sources and prevention techniques including filtration, dehydration and degasification

19 p2999 A71-38319

Hydraulic equipment fluid contamination control, discussing sample bottle cleaning, fluid sampling, component tolerance profiles and filtration performance specifications

19 p2999 A71-38322

Hydraulic fluids contribution to system contamination, discussing precipitate formation due to reaction with water, filtration inability and contaminant elimination

19 p2999 A71-38323

Hydraulic fluid filtering and maintenance techniques, discussing component life optimization and adverse environment handling problems

19 p3000 A71-38325

Fixed and free sinusoidally driven hydraulic squeeze film bearing design for improved load gyroscope performance

24 p3832 A71-45291

HYDRAULIC HEATING SOURCES

U HEAT SOURCES

U HYDRAULIC EQUIPMENT

HYDRAULIC JETS

Hollow cone water spray from pressure jet swirl atomizer into uniform air stream, observing drop velocities and trajectories by high speed photography

13 p2049 A71-28753

Pulsating follower loads implementation by pulsating gas or liquid jets, using Mettler differential equations for forced vibrations of elastic bodies

15 p2502 A71-31172

Surface patterns of ablating bodies from water jet flow experiment simulation, discussing vortices detection

21 p3317 A71-40019

HYDRAULIC PUMPS

U HYDRAULIC EQUIPMENT

U PUMPS

HYDRAULIC SYSTEMS

U HYDRAULIC EQUIPMENT

HYDRAULIC TEST TUNNELS

Trajectories prediction for subsonic spin stabilized projectiles via water tunnel tests, considering blunt nose and tail and rounded nose right circular cylinders

08 p1275 A71-22016

Helicopter rotor model testing in water tunnel, discussing advantages over wind tunnel testing due to Reynolds number scaling and avoidance of wall interference effects

16 p2526 A71-34151

Water tunnel walls effect on supercavitating flows past slender bodies

20 p3213 A71-39786

Water tunnel study of turbulent boundary layers structure in incompressible fluid with longitudinal pressure gradient at inlet section of converging and diverging nozzles

20 p3213 A71-39789

Wall effects and correction rules for cavitation flow past wedge in closed water tunnel, deriving drag coefficient from various theoretical models

23 p3663 A71-43442

HYDRAULIC VALVES

U HYDRAULIC EQUIPMENT

U VALVES

HYDRAZIDES

Book on hydrazino-hydrazide groups covering experimental details and applications of various analysis methods

05 p0718 A71-17009

HYDRAZINE ENGINES

Monopropellant hydrazine propulsion catalysts evaluation, considering catalyst durability improvement and breakup

07 p1183 A71-19858

Reentry vehicles fluidically controlled hydrazine rocket engine modules for roll rate control

11 p1810 A71-25503

Liquid hydrazine catalytic reactor startup characteristics as function of catalyst adsorbed gas condition and temperature by high speed motion picture observation

14 p2294 A71-30760

High thrust throttleable monopropellant hydrazine catalytic reactors for planetary landing vehicles, considering engine designs, dynamic characteristics and response to commanded duty cycles

14 p2294 A71-30762

Catalytic hydrazine thruster design, fabrication and testing for TOPS spacecraft single-axis attitude control simulation program

14 p2294 A71-30763

HYDRAZINE NITRATE

Engine pressure spiking restart preignition products, determining hydrazine nitrate and dinitrate presence by spectrum analysis

06 p0945 A71-18296

Water diluent effect on molten hydrazine mononitrate critical diameter and condensed explosive detonation stability

15 p2463 A71-31383

HYDRAZINE NITROFORM

Solid propellant oxidizers hydroxylammonium perchlorate and hydrazine nitroform self deflagration, determining combustion temperatures and burning rate pressure relationships

06 p0944 A71-18299

HYDRAZINES

NT DIMETHYLHYDRAZINES

NT METHYLHYDRAZINE

Hydrazine-hydrogen peroxide fuel cells coulombic efficiency measurement

02 p0197 A71-12960

Hydrazine-oxygen fuel cells energy costs minimization by optimizing diaphragm thickness, hydrazine concentration and load

03 p0355 A71-14321

Stillman rubber elastomers tests by cyclic exposure to hydrazine and air, water vapor or carbon dioxide, considering suitability as valve seat

05 p0772 A71-16466

Book on hydrazino-hydrazide groups covering experimental details and applications of various analysis methods

05 p0718 A71-17009

HYDRAZONES

Rocket engines with nitrogen tetroxide/hydrazine injectors destructive instability due to pressure disturbances, establishing origin, propagation velocity and pops extent by streak photography [WSS/CI PAPER 70-25] 06 p0942 A71-17653

Nitrogen tetroxide/hydrazine pulse mode rocket engines structural failure due to chemically reactive gaseous hot spots causing high pressure spiking and detonation initiation 06 p0944 A71-17663

Hydrazine concentration measurement in potassium hydroxide, describing instrument design and operation 06 p0900 A71-18014

Acute hydrazine hydrate poisoning morphological effects on internal organs and blood in guinea pigs, noting pronounced changes in liver and kidneys 09 p1393 A71-22921

Hydrazine feed control in hydrazine-oxygen fuel cells, discussing continuous measurement of limiting diffusion current for determining fuel concentration in electrolyte 11 p1708 A71-25241

Mass spectrometric technique for investigation of hydrazine catalytic decomposition on heated platinum at low pressure, considering advantages of quadrupole spectrometer 11 p1765 A71-26280

Iridium-based long life hydrazine catalyst with multiple cold start capability, describing development program for substrate evaluation and physical properties and process optimization [AIAA PAPER 71-704] 14 p2286 A71-30761

Inflammability, burning rates and exothermal decomposition of compact hydroxylamine and hydrazine sulfate and chloride with/without copper chloride additions, plotting pressure variations curves 15 p2463 A71-31377

Hydrazine formation from ammonia in constricted plasma discharge using electron source in selected high energy range 18 p2955 A71-35968

Possible prebiotic synthesis of thymine by heating uracil, paraformaldehyde and hydrazine in ammoniacal solution for three days at 70 C 18 p2855 A71-36231

Jupiter orbiter spacecraft propulsion system design, noting advantages of fluorine/hydrazine propellant combination [AAS PAPER 71-154] 19 p3122 A71-37925

Steady laminar flame propagation speed prediction computation, applying to hydrazine decomposition 22 p3621 A71-42098

Hydrazine-hydrazine azide blending for propellant performance improvement and freezing point reduction, presenting engine test data 22 p3588 A71-42778

HYDRAZONES

Valeraldehyde o-nitrophenylhydrazones mass spectrum with low intensity peak due to combined hydroxyl and water loss from molecular ion 02 p0209 A71-12573

HYDRIDES

NT ALUMINUM HYDRIDES

NT BERYLLIUM HYDRIDES

NT BORANES

NT BORON HYDRIDES

NT CHLOROSILANES

NT DIBORANE

NT LITHIUM HYDRIDES

NT METAL HYDRIDES

NT NITROGEN HYDRIDES

NT PHOSPHINES

NT SILANES

NT SODIUM HYDRIDES

NT ZIRCONIUM HYDRIDES

Hydride thermionic reactor system transient behavior dynamic mathematical model and digital simulation 02 p0281 A71-12262

Nb strips siliconization by silicon hydride decomposition and silicide or silicon oxidation, noting Si surface enrichment and bulk diffusion processes 02 p0272 A71-12943

Temperature dependent absorption line width and secondary moments of nuclear magnetic resonance spectra of Ti-Zr-H system 14 p2258 A71-30009

Titanium, vanadium and niobium carbohydrides, investigating electronic structure effects on atomic behavior 15 p2429 A71-32140

SiH molecular ion identification in solar atmosphere by solar absorption spectra 20 p3294 A71-39547

Titanium dihydride room temperature polymorphic transition from fcc to body centered tetragonal, noting different transition temperatures 22 p3563 A71-42368

HYDROACOUSTICS

U UNDERWATER ACOUSTICS

HYDROAEROMECHANICS

U AERODYNAMICS

HYDROCARBON COMBUSTION

Ionization rates in low pressure hydrocarbon flames produced by colliding burning gas jets 01 p0180 A71-11113

Hydrocarbon fuels high temperature oxidation behind shock waves, investigating reaction process by combustion products IR emissions and density gradient 02 p0298 A71-12860

Acetylene pyrolysis kinetics, considering isothermal vs adiabatic conditions and surface catalyzed vs homogeneous reactions [WSS/CI PAPER 70-18] 06 p0943 A71-17660

Anomalous ignition and flash point measurements of halogenated hydrocarbon-flammable liquid mixtures [WSS/CI PAPER 70-20] 06 p0943 A71-17662

Pure hydrocarbon droplets heating, expansion, vapor phase fuel storage and gasification in oxidizing gas at elevated pressures, using high speed cinematography 06 p1007 A71-18300

Back mixing effects on hydrocarbons combustion, comparing well-stirred reactor with flat flame soot yields 07 p1181 A71-19240

Electron temperature in hydrocarbon air flame, discussing extra equilibrium excitation, energy relaxation rate and chemiluminescent emission 07 p1182 A71-19250

Water vapor condensation effects on methane-air combustion gases for aerodynamic test medium [AIAA PAPER 71-258] 08 p1377 A71-21986

Optimal inlet parameters of MHD generator channel employing kerosene-gaseous oxygen combustion products 09 p1386 A71-22136

Ignition delay times behind reflected shock wave of alkanes methane through pentane in stoichiometric argon simulated air mixture 10 p1657 A71-24047

Heat fluxes from premixed methane-oxygen and propane-oxygen flames measurement by transient calorimetric method, comparing forward stagnation point results with calculated values 10 p1695 A71-24049

Soviet papers on combustion processes in turbulent and laminar flows of kerosene and gasoline mixtures, stressing gas turbine engines problems 13 p2162 A71-28954

Combustion acceleration of molar oxygen-methane mixtures in cylindrical chamber during flame-shock wave interaction, using motion picture techniques 15 p2511 A71-31381

Hydrocarbon flame radicals excitation nature observation by photoelectric measurements, noting irrelevance to electron-ion recombination 15 p2463 A71-31389

Elementary reactions in hydrocarbon combustion, using shock tube as chemical reactor to determine rate of reaction in 1600 to 2100 K range 16 p2539 A71-32892

Materials stability testing in high temperature propane-butane combustion product flow, selecting compact silicon carbide for structural use in redox medium 17 p2761 A71-34310

Open singing flame from propane-butane and oxygen jet mixture, constructing oscillogram model of sound emission 17 p2839 A71-35696

Electric field effects on town gas and hydrocarbon flame reaction rate, burning velocity and propagation speed due to free electrons in flame front 17 p2840 A71-35704

Combustion products and temperature distributions along axis of hexane/air diffusion flame 18 p2984 A71-35867

Air-methane supersonic diffusion flame in duct, comparing pressure measurement and gas sampling data with two dimensional combustion analysis [ONERA-TP-961] 18 p2984 A71-36027

Ion formation in photochemically initiated combustion of acetylene-oxygen-nitric oxide mixtures, measuring carbon, CH and OH emission spectra and ion current time change 19 p3013 A71-38091

Buoyant centrifugal force effect on combustion of homogeneous propane-air mixtures at stoichiometric proportions, using steel pipe as centrifuge 19 p3167 A71-38101

Gaseous hydrogen and methane injection into supersonic air stream heated by plasma burner, studying combustion effects on flow field 19 p3168 A71-38104

Monosized oil droplet streams combustion in stationary free flames, examining burning times and constants 19 p3169 A71-38112

Decane and hexadecane fog detonation propagation in gaseous oxygen 19 p3170 A71-38128

Jet flame stability characteristics of propane-air mixture ejected into counter air stream by temperature 19 p3170 A71-38128

and concentration measurements and visual observation 21 p3475 A71-40757

Soot emission suppression from propane diffusion flame by metallic additives 22 p3588 A71-42127

Emissivity calculation for radiant heat flux from isothermal gas mixture of hydrocarbon fuel combustion products 23 p3718 A71-43915

N-hexane-air mixture ignition by giant pulse laser beam, analyzing probability and development time to formation of measurable nucleus 23 p3686 A71-43995

Ignitability limits of hydrogen/air and hydrocarbon/oxygen mixtures at high temperatures near self ignition range 23 p3782 A71-44003

Spherical hydrocarbon fuel droplet combustion in air, considering mass burning rates and flame zone locations as function of drop size [AIAA PAPER 71-989] 24 p3887 A71-44585

HYDROCARBON FUELS

NT GASOLINE

NT JET ENGINE FUELS

Turbojet engine design for methane element or liquefied natural gas as aircraft fuel, discussing supersonic transport applications 01 p0141 A71-10484

Antifriture effects of heteroorganic compounds in medium-distillation hydrocarbon fuels for rocket engines 01 p0141 A71-11104

Vaporization and combustion kinetics of condensed single drop kerosene and gasoline thickened by polyisobutylene 01 p0142 A71-11444

Oxygen and homologous hydrocarbon mixture detonation limits, discussing propagation, fuel molecule structure, critical temperature, initial cracking mechanism and carbonaceous solids condensation 02 p0331 A71-11959

Hydrocarbon fuel ignitability, investigating molecular structural characteristics and homogeneous additives effect [WSS/CI PAPER 70-19] 06 p0943 A71-17660

Luminometer numbers of hydrocarbons and reactive fuels as function of molecular weight and structure 06 p0913 A71-18477

Incident shock wave interaction with liquid hydrocarbon fuel drops in oxidizing and inert atmospheres, considering combustion characteristics and ignition mechanism [AIAA PAPER 71-206] 06 p0886 A71-18642

Post reaction zone properties of premixed fuel rich propane-oxygen flames on torch, measuring temperature, composition and hydroxyl radicals 08 p1345 A71-20852

HCN, acetylene and ethylene formation by propane in mixed jet staged flames 08 p1346 A71-20861

Flame propagation dynamics of layered methane-air mixtures in vertical tubes, using interferometric techniques 08 p1346 A71-20861

Hydrocarbon fuel for hypersonic vehicle cooling, discussing use of endothermic reactions to achieve maximum heat sinks [AIAA PAPER 68-997] 10 p1658 A71-24852

Liquid hydrocarbon fuel drop interaction with incident shock wave in oxidizing and inert atmospheres, investigating aerodynamic shattering and combustion 17 p2836 A71-34432

Shock tube investigation of solid polymeric hydrocarbon fuel ignition in hot oxidizing gas stream 19 p3121 A71-38124

Thermal stability of naphthenes up to 1000 F, considering hypersonic aircraft fuel applications 22 p3588 A71-42837

Explosion-pumped gas dynamic carbon dioxide laser, obtaining high pulse energy by common hydrocarbon fuels 23 p3687 A71-44135

Liquid hydrogen as future replacement for hydrocarbon fuels in surface and air transportation, noting advantages in energy per unit weight and pollution-free combustion 24 p3863 A71-44365

HYDROCARBONS

NT ACETYLENE

NT ALKANES

NT ALKENES

NT ANTHRACENE

NT BENZENE

NT BUTADIENE

NT BUTENES

NT CAROTENE

NT CYCLIC HYDROCARBONS

NT CYCLOBUTANE

NT CYCLOPROPANE

NT ETHANE

NT ETHYLENE

NT HEPTANES

NT METHANE
 NT METHYLENE
 NT NAPHTHALENE
 NT NAPHTHENE
 NT OXYACETYLENE
 NT PARAFFINS
 NT PROPANE
 NT PROPYLENE
 NT TOLUENE

Extraterrestrial abiotic amino acids and hydrocarbons in type II carbonaceous chondrite at Murchison, Australia
 03 p0493 A71-14209

Complex hydrocarbon molecular formation by physical adsorption on interstellar grains in dense clouds
 04 p0650 A71-15396

Synthesized hydrocarbon oil antiwear and extreme pressure additives effects on bearing spinning torque and endurance
 06 p0904 A71-17580

Focused ruby laser beam degradation of various gaseous aliphatic and alicyclic hydrocarbons
 07 p1124 A71-19789

Phase change solidification phenomena in n-hexadecane for spacecraft thermal control systems, considering two or three dimensional models
 07 p1223 A71-19876

Electrochemical detection of hydrogen, carbon monoxide and hydrocarbons in inert or oxygen atmospheres, using electrical biasing technique
 08 p1250 A71-21473

Type III carbonaceous chondrite Murchison meteorite, obtaining amino acids, aliphatic and aromatic hydrocarbons from specimen
 09 p1393 A71-22983

Hydrocarbons pyrolysis in Knudsen cells at low pressures, using mass spectrometry to study reactions and products
 11 p1727 A71-25229

Gas-liquid chromatographic milligram preparative separation of steranes and tripterpanes from hydrocarbon fraction of Green River oil shale
 11 p1729 A71-26067

Hydrocarbons as foundation for life development universe, discussing chemical composition of galaxy, antimatter existence, interstellar medium and cosmic age factors
 13 p2009 A71-28678

Hydrocarbons, amino acids and large molecule organic compounds formation in chondrite meteorites by abiogenic reactions
 13 p2010 A71-28692

Polynuclear aromatic hydrocarbons in Murchison meteorite, determining distribution by gas chromatography and mass spectrometry
 17 p2799 A71-34503

HYDROCHLORIC ACID
 Aqueous HCl refractive indices determined for room temperature to Venus cloud temperature and various concentrations
 09 p1522 A71-22937

Continuous wave HCl chemical laser, achieving large specific gain through high speed flow, rapid mixing and transverse geometry
 09 p1465 A71-23480

Aqueous HCl solutions refractive index calculation from concentration dependence for Venus clouds composition
 10 p1680 A71-25012

Photolysis of HCl photosensitized evolution from dichlorobutane in solution by aliphatic ketones
 11 p1728 A71-25937

Exponential approximation of rotational relaxation of polar HCl and DCl at 300 and 500 K by molecular dynamics, comparing with perturbation calculations
 15 p2451 A71-31673

Peak contour positions of rotation lines of hydrogen chloride as function of spectral slitwidth for wavenumber calibration of far IR spectrometers
 16 p2577 A71-33134

IR chemiluminescence from HCl formed in atomic hydrogen reaction with sulfur dichloride, noting energy distribution among reaction products
 18 p2874 A71-35832

Collisional broadening of IR absorption lines in vibration-rotation bands of carbon monoxide and hydrochloric acid
 19 p3106 A71-37374

Venusian photochemistry, discussing hydrogen source from HCl, loss of water in relation to HCl, carbon dioxide stability and COS and hydrogen sulfide in visible clouds
 23 p3736 A71-43341

HYDROCHLORIDES
 Water distribution in space, natural satellites and terrestrial planets, discussing Clarke abundance values and hydrochlorosphere concept
 15 p2494 A71-32493

HYDROCYANIC ACID
 U HYDROGEN CYANIDES
 HYDRODYNAMIC EQUATIONS
 NT HELMHOLTZ VORTICITY EQUATION

Lubrication hydrodynamics differential equation of solving analytic solutions for essential practical cases by use of suitable gap profile expressions
 01 p0085 A71-10121

Kinetic theory of gas mixtures and thermodynamic laws of irreversible processes, deriving hydrodynamic equations and Onsager relations
 01 p0130 A71-10793

Lagrangian invariants of inviscid compressible fluid applied to hydrodynamic equations
 02 p0239 A71-11923

Acoustic turbulence spectrum in compressible fluid with potential motion, using complex traveling wave amplitudes in hydrodynamic equations
 02 p0239 A71-11924

Moving plasma hydrodynamic equations of motion, continuity and energy in axially symmetric coordinate system
 03 p0464 A71-13904

Nonlinear large vibrations of ideal incompressible homogeneous fluid in cylindrical sector tanks, determining hydrodynamic equations coefficients and relation to tank geometry
 03 p0405 A71-14565

Hydrodynamic equations for isothermal atmosphere stratified by uniform gravitational field, obtaining traveling wave solutions
 04 p0570 A71-15030

Hydrodynamic equations for discontinuity problems of origin and disruption of vortices, transonic gas flow and shock wave formation, using Lagrange equations
 04 p0579 A71-15813

Fermi particles /fluid/ oscillations in external gravitational field, discussing hydrodynamic equations, acoustic modes and sonic waves due to turbulent effects
 05 p0813 A71-16833

Macroscale atmospheric vorticity model, using nonlinear system hydrodynamic and addends free motion equations
 06 p0923 A71-17513

Wind field from macroscale atmospheric whirlpools /typhoons/ pressure fields by nonlinear hydrodynamic equations
 06 p0923 A71-17514

Earth macroclimate mean zonally averaged state equilibrium solution, using thermohydrodynamic equations
 08 p1325 A71-20882

Complex hydrodynamic systems nonlinear differential motion equations integration, taking friction forces into account
 08 p1299 A71-21620

Hydrodynamic equations for behavior of thermally conducting viscous compressible fluid in first post-Newtonian approximation to general relativity, obtaining conservation laws
 09 p1518 A71-22338

Burger model equations for MHD turbulence with analog in gas dynamics for nondissipative case
 09 p1432 A71-22703

Thermohydrodynamic equations for viscous incompressible lubricant flow in hydrostatic thrust bearings, considering inertia and temperature effects
 10 p1617 A71-24482

Spatially uniform external periodic magnetic field effect on wave propagation perpendicular to hot electron plasma, obtaining dispersion relation from hydrodynamic equations
 10 p1578 A71-24655

Weber differential hydrodynamic equations with earth rotation allowance related to Bjerknes circulation theorem and Ertel variational principle of atmospheric dynamics
 10 p1607 A71-25111

Linear vector differential Fridman equations for cosmic and telluric effects on earth atmosphere facilitating dynamic climate forecasts
 10 p1639 A71-25115

Intrinsic helical and quasi-rigid hydrodynamic motions of incompressible, ideal and viscous fluids, using mobile frame method
 11 p1804 A71-25175

Atmospheric modeling for earth and Venus heterosphere structure using multicomponent radiative hydrodynamic equations, determining atmospheric temperature and constituents height variation
 11 p1828 A71-25764

Expanding laser generated plasma self similarity model from hydrodynamic equations, describing thermokinetic properties
 11 p1806 A71-26092

Magnetoactive spatially homogeneous plasma parallel and perpendicular waves derivation from hydrodynamic equations in quasi-linear approximation, noting resonances and nonlinear effects
 12 p1937 A71-27181

Sound dispersion in monatomic gases from viewpoint of linearized hydrodynamic, Boltzmann and model equations
 12 p1930 A71-27190

Hydrodynamic model of coalescing meteors substantiating cosmogonic Laplace-Schmidt hypotheses of solar system planetary formation from cosmic dust
 13 p2131 A71-27892

Upper atmosphere neutral components temperature differences estimates from gas hydrodynamic equations solution by disturbances method
 13 p2057 A71-28019

Rarefied collisionless plasma, obtaining hydrodynamic equations for magnetic viscosity and thermal conductivity
 13 p2106 A71-28564

Stochastic modification of binary fluid mixtures hydrodynamic dissipative equations, considering nonequilibrium entropy
 13 p2051 A71-29354

Collisionless plasmas stationary flow hydrodynamic equations applied to plasma waves analysis
 14 p2280 A71-30211

Local short term mesoscale weather forecasting by finite difference solution of hydrothermodynamic equations
 15 p2443 A71-31222

Hydrometeorological fields derivatives transformation in hydrothermodynamic equations numerical integration
 15 p2443 A71-31224

Solar wind outflow from active regions by numerical integration of hydrodynamics equations, using corona temperature distribution
 15 p2480 A71-32753

Numerical integration of quasi-static system of hydrodynamic equations, considering economical production of short range high resolution meteorological forecasts
 16 p2604 A71-33532

Friction forces in complex hydrodynamic systems nonlinear differential motion equations integration
 17 p2749 A71-35680

Equilibrium diffusion of rotating plasma in toroidal systems, deriving two fluid hydrodynamic equations with allowance for ion temperature perturbation
 19 p3109 A71-37140

Relativistic hydrodynamic solution for gravitational interaction of vortex and potential motion of homogeneous medium
 19 p3134 A71-37515

Hydrodynamic equations for anisotropic plasma in magnetic fields, considering collisionless and collisional transport effects
 19 p3111 A71-37634

Splitting-up method with variational optimization for time independent nonstationary hydrodynamic transfer equations for use in meteorology, oceanology, etc
 19 p3088 A71-38310

Nonlinear hydrodynamic field equations transformations into complex wave equations for application to ideal compressible fluids
 20 p3211 A71-39031

Beta processes effect on detonation and postdetonation evolution of degenerate carbon-oxygen core supernovae, using numerical hydrodynamic calculations
 20 p3287 A71-39053

Hydrodynamic model of adhering meteors substantiating cosmogonic Laplace-Schmidt hypotheses of solar system planetary formation from cosmic dust
 21 p3441 A71-40076

Dynamic problems for molecular gases with rotational degrees of freedom, deriving hydrodynamic equations from kinetic equations integration
 21 p3420 A71-41121

Atmospheric modeling for earth and Venus heterosphere structure using multicomponent radiative hydrodynamic equations for atmospheric temperature and constituents height variation determination
 22 p3598 A71-41532

Hydrodynamic equations for dense system fluctuations with stochastic terms in pressure tensor and heat flux vector evaluated for dilute gas
 22 p3530 A71-41893

Magnetoactive spatially homogeneous plasma parallel and perpendicular waves derivation from hydrodynamic equations in quasi-linear approximation, noting resonances and nonlinear effects
 22 p3583 A71-42458

Viscous hydrodynamic equations functional type boundary value problem, investigating uniqueness theorem for elliptic equations
 22 p3531 A71-42629

Circle, half plane and cylinder theorems for slow viscous flows involving hydrodynamic singularities under rigid boundary
 23 p3625 A71-43237

Hydrodynamic equations for ions and electrons of ionized collision plasma in strong nonuniform magnetic field from Boltzmann kinetic equations
 24 p3855 A71-44521

Boundary conditions determined for hydrodynamic equations from solution of Boltzmann kinetic equation in Knudsen layer, obtaining distribution function in Enskog function superposition form
 24 p3821 A71-45226

HYDRODYNAMIC TUNNELS

HYDRODYNAMIC TUNNELS

U PLASMA JET WIND TUNNELS

HYDRODYNAMICS

NT ELASTOHYDRODYNAMICS

NT ELECTROHYDRODYNAMICS

NT MAGNETOHYDRODYNAMICS

Locally isotropic hydrodynamic turbulent fields statistical properties for kinetic energy and temperature dissipation fluctuations

01 p0120 A71-11106

Supporting fluid effects in floated inertial instruments, examining cause, frequency, extent and solution

02 p0253 A71-12462

Steam turbine blade metal removal rates by repetitive water drop impact, using hydrodynamic model

03 p0405 A71-14290

German monograph on mass transfer between close binaries from hydrodynamic standpoint

04 p0644 A71-15099

Frictional resistance reduction in hydrodynamics, considering critical shear stress in ducted flow

04 p0571 A71-15209

Turbulent hydrodynamics and heat transfer in rotating flows of incompressible fluid

04 p0578 A71-15631

One dimensional detonation hydrodynamics of condensed high explosives and small inert particles mixtures on basis of mathematical flow model

05 p0834 A71-16518

Spiral structure of galaxies identified with growing wave propagation in finite thickness axisymmetric disk hydrodynamic theory

05 p0813 A71-17036

Supernovae expansion, investigating hydrodynamic model with interstellar magnetic fields and relativistic particles effects

06 p0973 A71-18335

Boundary layer nonlinear stability theory, considering hydrodynamic problems associated with laminar flow transition into turbulent flow

07 p1086 A71-18777

Locally isotropic hydrodynamic turbulent fields statistical properties for kinetic energy and temperature dissipation fluctuations

08 p1325 A71-20850

Centrifugal compressor vaneless diffuser, estimating energy losses with hydrodynamic model

08 p1348 A71-21266

Hydrodynamically stabilized turbulent viscous incompressible fluid flow in circular tube, examining nonstationary convective heat transfer by numerical methods

08 p1276 A71-21923

Light ion flow from polar caps in hydrodynamic and evaporative forms, noting pressure gradient force, exospheric electric field and realistic boundary conditions

09 p1440 A71-23459

Numerical calculation of Oseen hydrodynamic fields around sphere in unbounded fluid for various Reynolds numbers, obtaining flow velocity and drag

10 p1592 A71-23935

Hydrodynamic study of systematic errors of mass flowmeters, considering effects of working fluid, sensitive elements and secondary motions

10 p1610 A71-24168

Hydrodynamic Stokes flow around body of revolution, using least squares method for fluid sticking on wall

10 p1594 A71-24455

Laminar incompressible boundary layer flow stability, emphasizing wall curvature and flexibility effects

10 p1594 A71-24548

Self consistent hydrodynamic heating of solid substance by laser pulse for nonequilibrium ionization

10 p1653 A71-24887

Hydrodynamic lubrication temporary breakdown during initiation of extrusion process

10 p1618 A71-24924

Hydrodynamics of matter-antimatter in contact, discussing coalescence, particles annihilation pressure and energy balance

11 p1821 A71-25539

Earth atmospheric zonal circulation model, using hydrothermodynamic equations with Newton law for radiative heat sources

11 p1795 A71-25919

Reaction kinetic studies using hydrodynamic flow structure due to spherical shock wave from laser induced spark

16 p2616 A71-32903

Global hydrodynamic stability theory, discussing energy methods and nonlinear Boussinesq equations for disturbed motion

16 p2558 A71-32995

Hydrodynamic and plate structural analysis by finite element method, discussing diffusion, oil films and element couplings

16 p2654 A71-33096

Difference analog of nonlinear hydrodynamic boundary value problem from Navier-Stokes steady state theory

17 p2728 A71-35241

Earth atmospheric zonal circulation model, using hydrothermodynamic equations with Newton law for radiative heat sources

20 p3256 A71-39210

Stability problem in hydrodynamics of perturbed heterogeneous shear flow, solving initial value problem for Couette flow

20 p3213 A71-39783

Incompressible flow hydrodynamic time dependent problems for moving walls and free surfaces, using Marker-Cell computing method

21 p3368 A71-40849

Soviet book on hydrodynamics of nonstationary motions of viscoplastic media covering mechanical properties of clay, mortar, cement, lubricating oil, petroleum and disperse media, etc

21 p3369 A71-40872

Film boiling liquid hydrogen vertical flowing system, determining buoyancy effects on hydrodynamic and heat transfer characteristics

21 p3476 A71-40895

Self consistent hydrodynamic heating of solid substance by laser pulse for nonequilibrium ionization

21 p3424 A71-41253

Hydrodynamic model of momentum, heat and mass transport for turbulent flow in straight circular pipes, tabulating velocity profiles and eddy diffusivity

23 p3780 A71-43091

Sword shaped tip on plastic sphere front portion, detailing hydrodynamic drag reduction at various Reynolds numbers

24 p3818 A71-44711

Natural trihedrons associated with stationary or nonstationary flows in hydrodynamics and MHD, using moving reference theory

24 p3856 A71-44795

Atmosphere hydrodynamic simulation model for cascade energy transfer in turbulent flow, using Euler gyro equations

24 p3844 A71-44818

HYDROELASTICITY

Lubrication hydrodynamics differential equation offering analytic solutions for essential practical cases by use of suitable gap profile expressions

01 p0085 A71-10121

HYDROFLUORIC ACID

Pulsed hydrogen fluoride gas laser output line spectral distribution, describing experimental setup and measurements

01 p0092 A71-10371

CW chemical laser operation with HF and DF in subsonic electric discharge mixing device, obtaining 5.5 w output

03 p0434 A71-13479

Initial vibrational energy level distribution of hydrogen fluoride formed in reaction between atomic fluorine and molecular hydrogen, using IR chemiluminescence

03 p0375 A71-13495

Laser action in visible and near IR on atomic fluorine transitions based on collisional dissociation of hydrogen fluoride

04 p0608 A71-15040

Hydrogen fluoride elimination chemical laser from difluoromethylamine using temperatures below 268 K and flash photolysis

07 p1123 A71-19372

High energy narrow pulsedwidth HF chemical laser emission from transverse multiple electrode nitrogen fluoride and nitric tetrafluoride discharge

07 p1128 A71-20397

Intense superradiant emission in HF and DF molecules high gain IR transitions, examining spectral distributions with pneumatically tuned Fabry-Perot interferometer

09 p1498 A71-23478

Hydrogen fluoride vibrational excitation behind incident shock waves at 1400-4100 K, describing experimental procedure and results

15 p2463 A71-31626

Electronic to vibrational energy transfer in mercury vapor reaction with hydrogen fluoride, studying IR emission and scattering cross section

18 p2874 A71-35834

Dissociation reaction in presence of halogen atoms produced in shock wave by thermal decomposition of hydrogen fluoride

19 p3012 A71-38085

High repetition line selectable compact electrically pulsed hydrogen fluoride lasers operating on sulfur fluoride and hydrogen mixture

20 p3242 A71-38825

Gain and spectral characteristics of transverse flow CW chemical laser with hydrogen and deuterium fluorides active medium

21 p3393 A71-41041

R-branch multiline performance of transversely excited pulsed HF chemical laser

23 p3688 A71-44297

Hydrogen fluoride vibrational relaxation times behind incident shock waves at various temperatures

24 p3802 A71-44922

HYDROFOILS

Cavitation flow of fluid with free surface past underwater wing with jet flap, solving equations of motion for thin foil with jet emergent from trailing edge

07 p1092 A71-20069

HYDROGEN

NT DEUTERIUM

NT DEUTERIUM PLASMA

NT HYDROGEN ATOMS

NT HYDROGEN IONS

NT HYDROGEN ISOTOPES

NT HYDROGEN PLASMA

NT LIQUID HYDROGEN

NT ORTHO HYDROGEN

NT PARA HYDROGEN

NT TRITIUM

Hydrogen exchange between pial arteries for measuring local cerebral blood flow quantitatively in anesthetized cats

01 p0008 A71-10071

High electron temperature H and He I and II, calculating partition functions

01 p0158 A71-10800

Multiple region hydrogen maser using Teflon coated cylindrical vessel to reduce atom-wall collision frequency shift

01 p0096 A71-11222

Photochemistry, diffusion and escape of atomic and molecular hydrogen on Mars, noting water vapor spectroscopy consistent with temperature profiles

01 p0162 A71-11488

Molecular hydrogen thermodynamic properties in ideal state from spectroscopic data, using WKE method

02 p0286 A71-12189

Interstellar molecular hydrogen formation by physical adsorption on grains, determining H atoms adsorptive potentials on silicates, graphite, solid hydrocarbons and ice

02 p0287 A71-12582

Ti-Al alloy hot salt stress corrosion cracking due to hydrogen production and absorption

02 p0267 A71-12880

Ti-Al-V hydrogen induced fatigue crack growth at room temperature under sustained load

02 p0268 A71-12899

Nb binary alloys room temperature brittleness in hydrogen atmosphere

02 p0270 A71-12932

Vacuum UV laser emission from molecular hydrogen in Lyman band using short risetime traveling wave discharge

03 p0434 A71-13479

Thermal conductivity of binary gas mixtures with/without hydrogen to 1100 K, using molecular kinetic theory and structure model

03 p0520 A71-13749

Stress intensity factors of hollow notched bars and hydrogen embrittled solid specimens [SESA PAPER 1671]

03 p0443 A71-13751

Hydrogen-oxygen induction period kinetics behind shock waves, monitoring OH concentration by UV line absorption method

03 p0376 A71-14276

Burning velocities in 50 percent hydrogen-air mixtures

03 p0376 A71-14282

Nuclear rocket nozzle cooling passages, discussing heat transfer and friction correlations for single-phase hydrogen turbulent flow

03 p0456 A71-14444

Supersonic solar wind flow termination, examining interstellar neutral hydrogen effect

03 p0481 A71-14502

Wall shift measurement of unperturbed hydrogen hyperfine transition frequency against cesium reference

04 p0585 A71-14652

Plasma accelerator self ionizing current free stable radiative shock wave structure in hydrogen, using time resolved spectroscopic measurements

04 p0548 A71-14696

Reversible hydrogen brittleness of steels in terms of dislocation theory

04 p0612 A71-15550

Thermoconductometric portable hydrogen analyzer for air around industrial centers, using bridge tungsten sensor network

04 p0601 A71-15675

High strength steel reversible hydrogen embrittlement mechanisms, noting role of hydrogen diffusion

04 p0615 A71-15790

Galactic Lyman alpha observation by Vela 7, discussing error possibility of data interpretation based on interstellar hydrogen shock wave

04 p0658 A71-15831

Isotope effects on collision dynamics of molecular hydrogen-argon ion reactions, using chemical accelerator

05 p0784 A71-15974

Small scale vacuum stream degassing of molten aluminum for hydrogen removal

05 p0758 A71-16247

- Hydrogen-slow electron collision cross sections, calculating Jovian upper atmosphere Lyman alpha and Balmer H alpha emission 06 p0929 A71-17679
- Cr-Ni stainless steel tensile and compressive stresses effect on hydrogen permeability at elevated temperatures 06 p0912 A71-17946
- Galactic structure derived from neutral hydrogen observations, using kinematic models based on density wave theory 06 p0969 A71-17972
- Hydrogen and nitrogen binding states and desorption kinetics on /100/ plane of Mo, using flash mass spectrometry 06 p0865 A71-18302
- Interstellar medium characteristics, examining H I and II regions thermal properties and shock waves 06 p0972 A71-18329
- Free turbulent mixing of heated high speed central hydrogen jet and cold low speed annular air stream coupled with finite rate chemical reactions [AIAA PAPER 71-5] 06 p0866 A71-18479
- Dissolved hydrogen effects on mechanical properties, modulus of elasticity, lattice constants and X ray lines of Ti alloys, showing cold brittleness at high strain rates 07 p1130 A71-19298
- Theoretical and observed Balmer alpha distributions over solar cycle by Lyman beta scattering on hydrogen in upper atmosphere 07 p1187 A71-19671
- Frequency shift in hydrogen maser due to atomic collisions with storage bulb surface (wall shift), investigating temperature dependence 07 p1124 A71-19686
- Hydrogen adsorption behavior on polycrystalline nickel surfaces, using electron impact desorption flash filament with gas phase and ion spectrometer and vapor deposition 07 p1055 A71-19843
- Hydrogen and carbon monoxide coadsorption on platinum single crystal surface, examining interactions and species formation by thermal flash and electron impact techniques in ultrahigh vacuum 07 p1055 A71-19844
- Hydrogen and nitrogen chemisorbed species interactions on /100/ tungsten crystals, using flash desorption methods 07 p1056 A71-19846
- Oxide films effect on heat resistant steels hydrogen permeability, using mass spectrometer 07 p1136 A71-19920
- Porosity in gas tungsten arc aluminum weldments and elimination by hydrogen reduction 07 p1119 A71-19969
- Hydrogen solubility in alpha Ti, using electrical resistivity measurement at liquid nitrogen temperature 07 p1139 A71-19991
- TiH metallographic and lattice parameters variation with hydrogen content 07 p1139 A71-19993
- Hydrogen and deuterium oscillator strengths and transition probabilities for Lyman and Werner system individual bands by electronic dipole moment functions 07 p1164 A71-20019
- Hydrogen outgassing from proton irradiated aluminum samples, determining gas evolution and blister formation during annealing 07 p1139 A71-20173
- Hydrogen embrittlement in hot salt stress corrosion of Ti alloy 07 p1142 A71-20372
- Rayleigh-Brillouin light scattering in compressed hydrogen, hydrogen deuteride and deuterium, noting discrepancy between observed and theoretical spectra 08 p1301 A71-20743
- Hydrogen and helium photoionization, calculating total cross section and transitions for soft X ray region 08 p1350 A71-20948
- Electrochemical detection of hydrogen, carbon monoxide and hydrocarbons in inert or oxygen atmospheres, using electrical biasing technique 08 p1250 A71-21473
- Steels in stressed state, determining hydrogen saturation and occlusion 09 p1467 A71-22309
- Neutral hydrogen subsystem rotation in inner Galaxy from equal angular velocity surfaces 09 p1518 A71-22375
- Hydrogen condensation and evaporation on liquid helium cooled surfaces in cryopump with reduced thermal radiation loading 09 p1546 A71-23008
- Metals electronic structure effects on hydrogen diffusion mobility 09 p1471 A71-23082
- Fe-Ni alloys, determining hydrogen permeability, diffusion coefficient and solubility as function of composition by electrochemical method 09 p1472 A71-23127
- Comets gaseous atmospheres related to 1970 OAO discovery of vast hydrogen atmosphere, indicating molecular hydrogen abundance and gas production rate 10 p1665 A71-23745
- Electron exchange and nuclear symmetry for 2s and 2p collisional excitations of hydrogen by H atom based on symmetrized atomic orbitals set 10 p1644 A71-23925
- Hydrogen-nickel reaction in presence of CO adsorbed gas, increasing total desorption cross section and eliminating monotonic relation between uptake and H ion current 10 p1573 A71-24540
- Equilibrium adsorption isotherms correlation for low temperature cryodeposits, using Dybinin-Raduschkevich equilibrium equation to estimate hydrogen capacity of cryosorption pumping system 10 p1643 A71-25011
- Pair correlation function for gaseous hydrogen at low density and temperature from quantum mechanical calculation, using Lennard-Jones potential 11 p1801 A71-25367
- Uranus atmospheric molecular hydrogen abundance from pressure induced overtone spectra, using quadrupole moment and polarizability matrix elements theoretical values 11 p1827 A71-25731
- Hydrogen effects on low temperature solution strengthening and ductility of Nb-H single crystals, noting effects of normal and strain induced hydride precipitation 11 p1780 A71-26020
- Isotope effects in Lyman and Werner systems of molecular hydrogen, HD and molecular deuterium, calculating band strengths, oscillator strengths and Franck-Condon factors 11 p1803 A71-26072
- Succinic dehydrogenase activity inhibition and pentobarbital sodium protection of lung tissue in mouse breathing oxygen at atmospheric pressure 11 p1721 A71-26125
- Resistance increases in thin film Evanhm resistors due to hydrogen gas absorption and desorption 11 p1738 A71-26162
- Shock induced combustion by firing spheres or cone cylinders into air- or oxygen-hydrogen mixtures, taking shadow photographs of resulting disturbances 11 p1860 A71-26268
- Jupiter occultation of beta Scorpii on 13 May 1971, determining hydrogen/helium ratio 12 p1961 A71-26876
- Jovian atmosphere radio observations, discussing helium- and ammonium-hydrogen molecules ratio, brightness temperature spectra and RF wavelength absorbing agents 12 p1964 A71-27087
- Vacuum UV laser emission from molecular hydrogen, discussing theory and experimental verification 12 p1914 A71-27281
- Collision induced hydrogen spectra for overtone absorptions by gas mixtures under temperature and density conditions matching planetary atmospheres 13 p2138 A71-28773
- Polycrystalline Hf under tension at various temperatures, determining H effects on fracture, operative deformation modes and hydride habit planes 13 p2090 A71-29417
- Spiral galaxy NGC 2403 neutral hydrogen distribution model fitting of observed velocity profiles 14 p2303 A71-29589
- Solar atmosphere line broadening by neutral hydrogen, noting discrepancy in van der Waals interaction 14 p2306 A71-29686
- Interstellar SH search for ground state main line transitions at 111 MHz 14 p2313 A71-30433
- External galaxies neutral hydrogen distribution from interferometric observations, discussing interpretation consistent with optically derived rotation curves 14 p2314 A71-30638
- Horizontal and post-horizontal branch hydrogen rich stellar atmospheric models, presenting emergent fluxes and H and He line profiles 14 p2314 A71-30645
- Pressure-induced absorption in planetary atmospheres from hydrogen-methane collisions, stressing resulting thermal opacity 14 p2315 A71-30659
- Inert gases, hydrogen, deuterium and carbon dioxide flow in plane parallel glass slots over various Knudsen numbers, calculating slippage constants and volumetric discharge 14 p2227 A71-30673
- Gaseous oxygen/hydrogen injector element modeling based on composition profile measurements for cold flows 14 p2291 A71-30738
- [AIAA PAPER 71-674] 14 p2291 A71-30738
- Hydrogen maser research, discussing H atom hyperfine structure, frequency characteristics and potential use as atomic clock 14 p2255 A71-30987
- Brightness dependence on heliocentric distance of cometary hydroxyl and hydrogen halos, using three step production mechanism 14 p2318 A71-31124
- Industrial Ti and beta-Ti alloy hydrogen thermodynamic and effects on brittleness 15 p2424 A71-31238
- Low pressure gaseous hydrogen/gaseous oxygen APS rocket engines operating with propellant stored as liquids and fed to thruster without pressure augmentation [AIAA PAPER 71-738] 15 p2467 A71-31326
- Solid helium and molecular/metallic hydrogen thermodynamic properties and phase diagrams as functions of pressures corresponding to Jupiter and Saturn 15 p2511 A71-31338
- Molecular hydrogen thermodynamic properties in ideal state from spectroscopic data, using WKB method 15 p2451 A71-31493
- Holographic investigation of laser sparks in hydrogen and helium, determining electron concentration spatial distribution and plasma dispersion dynamics 15 p2419 A71-31738
- Flammability limits measurement of hydrogen-oxygen mixtures containing fluorocarbon diluents 15 p2465 A71-32086
- Stoichiometric hydrogen-carbon monoxide-oxygen mixtures detonation wave propagation at critical Mach number, noting explosion limit chemical kinetics role 15 p2465 A71-32088
- Hydrogen absorption by molten aluminum and Al alloys, considering equilibrium delay in metal-gas system 15 p2435 A71-32334
- Hydrogen and nitrogen pores formation in welds, considering gas concentration redistribution between liquid and solid metal 15 p2417 A71-32663
- Low temperature shock waves in molecular hydrogen, discussing Rankine-Hugoniot equation behavior 16 p2555 A71-32895
- Milky Way galaxy interstellar neutral hydrogen rolling motion phenomenon confirmed by 21 cm line survey data 16 p2630 A71-33053
- Aperture synthesis observations of neutral hydrogen radio emission in spiral galaxy M 101, using twin-element interferometer 16 p2632 A71-33329
- Hydrogen condensation in interstellar gas clouds onto solid dust grains from vapor pressure measurements of solid hydrogen at low temperatures 16 p2634 A71-33392
- Ion-membrane hydrogen oxygen fuel cell, using microbially or biochemically produced hydrogen by enzymatic reactions 16 p2527 A71-33550
- Thermospheric hydrogen density and temporal variations from Explorer 32 measurements, discussing dependence on exospheric temperature 16 p2565 A71-33731
- Neutral hydrogen interstellar wind parameters from Lyman alpha sky background measurements outside geocorona by photometers on OGO 5 16 p2643 A71-33834
- Interplanetary hydrogen and helium from cosmic dust deionizing effect on solar wind, calculating gas density and flux 16 p2628 A71-33940
- Bibliography on upper atmosphere hydrogen covering Lyman alpha and beta and Balmer alpha measurements, non-Maxwellian distribution, diurnal variations and oxygen evolution 17 p2732 A71-34463
- Molecular hydrogen sorption pumping by cold carbon dioxide cryodeposits, showing absorbed molecules surface diffusion into disordered frost structure 17 p2695 A71-35138
- Hydrogen sorption capacity by sulfur dioxide frost from cryodeposit formation on stainless steel sphere in vacuum chamber and equilibrium isotherms measurement 17 p2695 A71-35142
- Perchloric acid reactivity with respect to hydrogen, methane, ethane and ethylene by flow method, using twin concentric jet reactor of Pyrex glass 17 p2792 A71-35709
- Interstellar molecular hydrogen gas near IR emission detection in dark clouds 18 p2969 A71-37042
- Vacuum deposited thin Cr films on glass substrate, describing hydrogen adsorption effects 19 p3076 A71-37116
- S-wave elastic positron-hydrogen scattering in ionization region, estimating error in extrapolated t matrix from complex energy 19 p3106 A71-37375
- Jovian atmosphere radio observations, discussing helium- and ammonium-hydrogen molecules ratio,

HYDROGEN ATOMS

brightness temperature spectra and RF wavelength absorbing agents

19 p3133 A71-37437

Bulk and surface hydrogen concentration comparison in NBS hydrogen-in-titanium standards

19 p3080 A71-37718

Stress effect on hydrogen distribution at high temperatures in titanium and Ti-Al-Mo-V alloy

19 p3080 A71-37720

Injection conditions effect on ignition temperature of methane and hydrogen in hot Mach 2 air stream

19 p3163 A71-37889

Hydrogen near-critical point flow in heated cylindrical tube, measuring flow parameters radial profiles by combination pitot tube/thermopile/hot-wire sensor probe

[ASME PAPER 71-HT-25] 19 p3165 A71-37995

Hydrogen-oxygen reaction sensitized by ammonia, comparing with nitrogen dioxide and nitrosyl chloride activators

19 p3012 A71-38081

Gaseous hydrogen and methane injection into supersonic air stream heated by plasma burner, studying combustion effects on flow field

19 p3168 A71-38104

Inhibitory effects of halogen compounds on hydrogen-air and hydrogen-nitrous oxide flames, measuring burning velocities and temperature/ composition profiles

19 p3013 A71-38106

Pressure induced hydrogen collisions vibrational spectra absorption coefficients at high temperatures and local thermodynamic equilibrium

19 p3108 A71-38720

Hydrogen content effect on annealed and work hardened palladium wire tensile properties, determining yield/tensile stress and elongation

20 p3247 A71-38765

Close coupling calculation for low energy hydrogen atom-molecule collision, discussing cross section, transition probabilities and elastic scattering

20 p3272 A71-39579

High Arctic latitude thermospheric helium and hydrogen rocket-borne mass spectrometric measurements, showing concentrations and winter bulge

20 p3222 A71-39698

Hydrogen molecule Lyman band continuous emission spectrum with fluctuations due to wave functions maxima, corresponding to transitions from vibrational levels

20 p3305 A71-39968

Solid Ni-Co and Ni-Cu alloys, investigating hydrogen solubility

21 p3398 A71-40466

Spiral wave dispersion, wave number and amplitude relationship in Galaxy near inner Lindblad resonance, noting correlation with ionized hydrogen density

21 p3451 A71-40855

HD rotational relaxation collision number temperature dependence calculation from excitation probability, comparing with experiment

21 p3419 A71-40911

Shatter crack incubated nucleation in relation to heat treatment effects on hydrogen elimination in steels, comparing with thermal explosion mechanism

21 p3402 A71-41090

Metal embrittlement by gaseous hydrogen, discussing countermeasures against hydrogen metal interaction and cracking

22 p3562 A71-41999

Shock wave initiation of hydrogen-oxygen at 1200-1800 K, using UV absorption spectroscopy in shock tube studies

22 p3587 A71-42097

Solar cycle variation effects on interstellar hydrogen within solar system, discussing thermal motion, density, far UV ionization and charge transfer reactions

22 p3601 A71-42169

Oxygen, hydrogen and nitrogen determination in high melting point metals

22 p3563 A71-42364

Hydrogen autoionization rates for molecular vibrational transitions near threshold, using internal conversion model

22 p3578 A71-42464

Solid helium and molecular metallic hydrogen thermodynamic properties and phase diagrams as functions of pressures corresponding to Jupiter and Saturn interiors

22 p3606 A71-42613

Phenylpropargylene and phenylethynylacetylene intermediacy, abstracting hydrogen to produce benzylacetylene, phenylallene and 1-methyl-2-phenylacetylene

22 p3508 A71-42886

High power hydrogen thyratron grid-anode structure without gradient grids, discussing design and performance tests

23 p3649 A71-42916

Delta-zirconium hydride hydrogen engassing experiment, investigating hydrogen absorption rate and diffusion constant temperature dependence

23 p3688 A71-42929

Interplanetary magnetic shock front location and geometry determination, using interstellar hydrogen density measurements

23 p3720 A71-43133

Hydrogen evacuation with He condensation pump in ultrahigh vacuum region

23 p3661 A71-43272

Time dependent progress of vibrational rotational transitions in chemical laser using hydrogen-fluorine mixture investigated by oscillography with IKM-1 monochromator

23 p3684 A71-43405

Coalescence /collapse/ of overlapping spectral lines due to nonadiabatic broadening for Stark structure of hydrogen and helium lines in discharge plasma

23 p3707 A71-43407

Lithium additions effect on hydrogen content and mechanical properties of molten aluminum specimens

23 p3691 A71-43522

Apollo 11 and 12 lunar samples O 18/O 16, Si 30/Si 28, D/H and C 13/C 12 ratio determination, examining whole rocks, breccias, soils, plagioclases and fines

23 p3751 A71-43705

Velocity dependent HD beam scattering by inert gases, measuring total effective cross section in thermal energy range

23 p3707 A71-43879

He, HD and deuterium scattering by various gas molecules, measuring total effective cross sections for comparison with calculation

23 p3707 A71-43880

Radiation quenching and depopulation of excited Hg atoms by collisions with ground state hydrogen molecules, using steady state flowing afterglow method

23 p3712 A71-43996

Hydrogen solubility in alpha phase Ti-Al alloys, using resistometric technique and electron microscopy

23 p3694 A71-44282

Molecular hydrogen primary ionization coefficient measurement in non-self sustained Townsend discharge, using light detection method based on radiant flux vs electron density proportionality

24 p3850 A71-44370

Thermodynamic properties and nozzle flow calculations for high temperature and pressure hydrogen, presenting results in Mollier diagram

24 p3887 A71-44629

Hydrogen dissolution in fused silica, investigating temperature effects during impregnation on reactive defect sites number

24 p3841 A71-44869

Werner band system and Lyman alpha radiation emission from molecular hydrogen excitation by electron impact

24 p3850 A71-44923

Galactic neutral hydrogen absorption line spectra at 21 cm wavelength by radio sources interferometric observations, discussing cool gas temperature, ionization rate and Cetus Arc distance

24 p3873 A71-45084

Hydrogen solubility in liquid Cr, Ni and Co alloys containing Si for various concentrations and temperatures

24 p3840 A71-45371

HYDROGEN ATOMS

Large fluxes of energetic neutral atomic hydrogen at 800 km preceding geomagnetic disturbance, using sounding rocket electrostatic analyzer

01 p0148 A71-11526

Hydrogen molecule-atom short range interaction energy, calculating multicenter integrals for screening constants

02 p0286 A71-11954

Interatomic electric dipole moment coefficient derivation by approximation involving accessible atomic properties, noting application to H atoms

02 p0287 A71-12708

Atomic H excitation by electron impact, deriving cross sections for anomalous recombination lines in H II regions radio frequency spectrum

02 p0317 A71-12873

Slow positive ion and electron production in collisions of protons and hydrogen atoms with gases of planetary atmospheres

03 p0460 A71-13494

Lyman alpha radiation scattering observation by satellites, obtaining geocoronal atomic hydrogen distribution in thermosphere and exosphere

03 p0415 A71-14028

Solar Lyman alpha emission line absorption by geocoronal atomic hydrogen, comparing observational data with prediction from models

03 p0496 A71-14510

Rate constant measurement for atomic hydrogen reaction with carbon dioxide yielding OH and CO, considering near IR emission spectroscopy applicability

04 p0548 A71-14697

Gas phase atomic hydrogen, nitrogen and oxygen detection by photoelectron spectroscopy of ground state, suggesting application to gas phase kinetics

04 p0548 A71-14799

Interstellar H I region Lyman alpha production by suprathermal protons, determining temperature and ionization equilibrium

04 p0640 A71-14878

Lunar atomic hydrogen atmosphere from solar wind proton bombardment, considering detection by scattered Lyman alpha radiation measurements

04 p0659 A71-15898

Inelastic ionization cross sections for protonic and atomic hydrogen collisions with atomic and molecular gases in 0.5 keV to 5 MeV energy range

06 p0928 A71-17262

H I gas kinematics in Galactic anticenter region from Gaussian components of emission line profiles in 21 cm observations

06 p0964 A71-17373

UV absorption line spectra from HI regions evaluating X ray and photoionization heating models

07 p1190 A71-18858

Upper atmosphere H atoms concentration maxima and minima from topside to bottomside ionospheric electron contents ratio, using coupled continuity and thermal equations

07 p1098 A71-19037

Contour maps of antenna temperature in W31 region, discussing H I absorption features

07 p1198 A71-19814

H I and H beta emission, Sco-Cen association stellar members near Sco X-1, discussing X ray heating and ionization

07 p1187 A71-19814

Powerful solar flare H lines spectrophotometric observation, noting hydrogen atom upper energy level overexcitation

07 p1188 A71-20035

Hydrogen atoms upper energy levels overexcitations in solar flare, suggesting role of stimulated photoionizations

07 p1188 A71-20035

Nonadiabatic H-H collisions cross sections in two state time dependent impact parameter approximation, including electron exchange

08 p1337 A71-21197

Atomic and molecular hydrogen yields of propyne photolysis at 1470 Å Xe resonance line

09 p1403 A71-23377

Vibrational relaxation of CO and hydrogen atom effects in nonequilibrium nozzle flow using shock tunnel IR detection system

09 p1404 A71-23377

Atomic hydrogen equilibrium abundance in dense dark hydrogen clouds as function of low energy cosmic ray ionization rate

10 p1662 A71-24499

Electron impact excitation rates of bound electronic states of hydrogen, helium and alkali atoms

10 p1645 A71-24543

H and He concentrations upper limit for Titan atmosphere from molecular diffusion time constant

11 p1828 A71-25732

Quenched and tempered steel, investigating embrittlement as function of temperature in partially dissociated atomic hydrogen environment

11 p1779 A71-26013

Cross sections of metastable H formation by charge transfer of hydrogen ion beam on helium, argon, nitrogen and oxygen targets

11 p1803 A71-26373

Positron-hydrogen scattering below positronium pickup threshold by Hylleraas bound technique, discussing phase shifts and linear parameters

11 p1803 A71-26373

S wave scattering from H and He positron systems at low energies, applying Kohn and Harris variational methods

11 p1803 A71-26373

Neutral H concentration in upper atmosphere during solar minimum, using ion thermal energies from rocket and satellite mass spectrometric, radio and proton whistler measurements

12 p1898 A71-26637

Galactic radio emission, considering continuum radiations, radio polarization, H I regions structure and physics, recombination and absorption lines

12 p1959 A71-26778

German monograph on bimolecular reactions of H and O atoms in shock waves with hydrogen peroxide and dioxide and nitrous oxide

13 p2102 A71-28881

Average energy of electron avalanches in gases for linear inelastic collision cross sections, including ionization coefficient and Stoleto constant for atomic hydrogen

13 p2103 A71-29080

Lyman alpha emission cross sections for collisions of hydrogen ion and atom beams with thin target nitrogen and oxygen relevant to proton auroral analysis

15 p2397 A71-31763

Energy dependence of collisional time delay functions computed for H/IS atoms interacting via hydrogen potential, determining scattering cross sections

16 p2613 A71-32811

- Hydrogen atoms trapped in gamma irradiated calcium phosphates, studying radiation yields, electron paramagnetic resonance line widths, dose saturation and relaxation 16 p2538 A71-32873
- Na D lines broadening by atomic H, discussing interatomic forces between Na and H atoms in terms of NaH molecular potentials 16 p2614 A71-33101
- Aperture synthesis of neutral hydrogen in M 101 galaxy, suggesting close connection between surface density of light and H I 16 p2632 A71-33330
- Upper atmosphere atomic hydrogen H sub alpha emission, correlating intensity and hydroxyl vibration temperature 16 p2564 A71-33665
- Lyman alpha resonant radiation in regions distant from cometary tails due to additional atomic hydrogen production from dust particles 17 p2809 A71-35595
- Vibrationally excited hydroxyl formation by atomic hydrogen reaction with ozone, using Fourier transform spectroscopy 18 p2874 A71-35833
- Numerical integration of Schroedinger equation for spontaneous ionization of hydrogen atom in electric field 19 p3107 A71-38056
- Added inert gases effect on gas phase H atoms recombination rate at room temperature, using electron spin resonance spectroscopy 19 p3011 A71-38080
- Reactions of H and O with hydrogen peroxide and water in discharge flow systems, measuring rate coefficients 19 p3012 A71-38083
- Glauber and Vainshtein approximations for cross sections of 1s-2p excitation during inelastic electron-atomic hydrogen scattering 20 p3272 A71-39470
- H atoms generation by photodissociation of molecules evaporated from cometary core, basing analysis on hydrogen atmosphere line spectra 20 p3293 A71-39538
- Glauber approximations for elastic and inelastic scattering of protons by ground state hydrogen atoms, comparing with measurements 20 p3272 A71-39578
- Interplanetary H scattered solar Lyman alpha background observations by Vela 7 andOGO 3 satellites, showing 27 day correlation with intensity curve 20 p3300 A71-39736
- Thermospheric atomic hydrogen concentration temporal variations in situ measurement by Explorer 32 satellite 20 p3232 A71-39898
- Atomic hydrogen maser wall shift elimination by operating at temperature to obtain zero average phase shift per atomic collision 21 p3391 A71-40201
- Fast hydrogen atoms penetration into fusion reactor plasma, calculating collision cross section rates coefficients 21 p3422 A71-40765
- Glauber scattering amplitudes for atomic hydrogen excitation by electrons or protons, presenting closed form expressions requiring no numerical integration 21 p3420 A71-41195
- Spiral galaxy M33 observations at 21 cm, deriving hydrogen atoms distribution and kinematic properties 23 p3722 A71-42938
- Atmospheric atomic hydrogen H alpha emission correlation with hydroxyl vibrational temperature 23 p3665 A71-42961
- Atomic hydrogen dayglow Lyman alpha structure of Mars exosphere from Mariner 6 and 7 UV spectrometric observations 23 p3734 A71-43156
- H transition excitation during atomic hydrogen collision with alkali elements and inert gases, discussing inner electron excitement 23 p3707 A71-43268
- Atomic oxygen and hydrogen identification in Mars upper atmosphere emission spectra by Mariner UV spectrometer, inferring carbon monoxide presence by self absorption 23 p3735 A71-43330
- Hydroxyl emission of upper atmosphere, considering atomic hydrogen and ozone near thermosphere base 23 p3673 A71-43982
- Trapped hydrogen atoms detection in proton irradiated KCl and NaCl single crystals at 77 K, using electron paramagnetic resonance spectroscopy 24 p3802 A71-44425
- Atomic hydrogen cloud densities determined by interstellar absorption lines of early stars 24 p3874 A71-45145
- Binding states, adsorbate densities and desorption kinetics of hydrogen on crystal planes of tungsten 15 p2367 A71-31676
- HYDROGEN CHLORIDE**
U HYDROCHLORIC ACID
- HYDROGEN CLOUDS**
Balmer emission lines in hydrogen cloud in bright galactic nucleus 09 p1518 A71-22351
- Atomic hydrogen equilibrium abundance in dense dark hydrogen clouds as function of low energy cosmic ray ionization rate 10 p1662 A71-24491
- Fast hydrogen clouds in galactic halo related to galaxies formation model 20 p3293 A71-39448
- HYDROGEN COMPOUNDS**
NT ALUMINUM HYDRIDES
NT BERYLLIUM HYDRIDES
NT BORANES
NT BORON HYDRIDES
NT CHLOROSILANES
NT DEUTERIDES
NT DEUTERIUM COMPOUNDS
NT DIBORANE
NT HEAVY WATER
NT HYDRIDES
NT HYDROGEN CYANIDES
NT HYDROGEN PEROXIDE
NT HYDROGEN SULFIDE
NT LITHIUM HYDRIDES
NT METAL HYDRIDES
NT NITROGEN HYDRIDES
NT PHOSPHINES
NT SILANES
NT SODIUM HYDRIDES
NT ZIRCONIUM HYDRIDES
- Line shifts in first overtone band of DF perturbed by HF, studying pressure induced transitions and partial pressures 11 p1729 A71-26139
- HBr positive ion formation by Ar ion beam collision with HBr, using predissociation to establish dissociation limit 13 p2026 A71-29039
- Hydrogen bromide effect on argon diluted propane-oxygen flame structure 19 p3167 A71-38100
- HYDROGEN CYANIDES**
Plasma refractive index effects in pulsed HCN lasers, calculating stable cavity mirror curvatures constriction as function of electron density by ray matrix approach 07 p1124 A71-19795
- HCN, acetylene and ethylene formation by propane in mixed jet staged flames 08 p1346 A71-20861
- Far IR coupled cavity HCN laser interferometer for measuring low density transient plasma 15 p2410 A71-32384
- IR and submillimeter wave HCN laser radiation visual observation, using thermal image converter 15 p2420 A71-32385
- HCN laser amplifier gain measurement at IR wavelengths in gas mixtures by recording with pyroelectric receiver 17 p2750 A71-34290
- Polarization flip with hysteresis effect at zero magnetic field in CW far IR HCN laser 20 p3244 A71-39098
- Water cooled hollow cathode design for continuous emission HCN lasers 20 p3246 A71-39494
- HCN CW laser design, considering factors affecting short and long term power and frequency stabilities 22 p3557 A71-42134
- HCN and water vapor submillimeter and far IR laser frequency measurement against fundamental frequency standard by harmonic generation and beat frequency detection 22 p3557 A71-42152
- HYDROGEN DEUTERIUM OXIDE**
U HEAVY WATER
- HYDROGEN FLUORIDES**
U HYDROFLUORIC ACID
- HYDROGEN FUELS**
Hydrogen fuel injection into hot oncoming air flow, investigating boundary layer chemical behavior at stagnation point of diffusion flame 02 p0334 A71-12857
- Hydrogen-oxygen catalytic ignition system steady state model for predicting temperature and concentration profiles 05 p0795 A71-16350
- Hypersonic ramjet reaction mechanisms for H combustion, discussing computational models, operation principles and atomic, radical and molecular collisions 06 p0865 A71-17410
- Hydrogen slush storage and transfer density and flow measuring instrumentation, emphasizing capacitance measurement [NAS PAPER M-2] 08 p1292 A71-21695
- Nonequilibrium recombination of dissociated combustion products of hydrogen in oxygen enriched heated air in supersonic nozzle 10 p1696 A71-24381
- Open cycle gas core nuclear rocket engine, considering reactor critical experiments and cold and hot flow tests [AIAA PAPER 71-641] 14 p2273 A71-30718
- Nuclear light bulb engine based on thermal radiation energy transfer from gaseous uranium fuel through internally cooled transparent wall to seeded hydrogen [AIAA PAPER 71-642] 14 p2274 A71-30719
- Supersonic hydrogen combustion in vitiated air stream with stepped wall injection, considering temperature, pressure and composition measurements [AIAA PAPER 71-721] 14 p2286 A71-30772
- Supersonic combustion flowfield transverse hydrogen jet injection into Mach 2.5 airstream, discussing recirculation region upstream [WSS/CI PAPER 71-15] 15 p2463 A71-31624
- Burning velocity measurement of laminar conical hydrogen-air flames on 10.3 mm diam water cooled nozzle burner, using schlieren and particle tracking techniques 15 p2465 A71-32085
- Supersonic hydrogen diffusion flames ignition aids at near-thermal self ignition point, discussing catalytically induced prereactions [DFVLR-SONDDR-118] 15 p2466 A71-32718
- Energy requirements for anthydrogen production in interstellar photonic drives, discussing feasibility 18 p2956 A71-36683
- Fuel rich premixed hydrogen-oxygen flame stabilization on cooled porous plate burners at 10 mm Hg 19 p3168 A71-38107
- Capacitance measurement technique for density and mass flow measurements for hydrogen slush storage and transfer 20 p3237 A71-39276
- Liquid hydrogen as future replacement for hydrocarbon fuels in surface and air transportation, noting advantages in energy per unit weight and pollution-free combustion 24 p3863 A71-44365
- HYDROGEN IONS**
Transform for hydrogen ion exchange perturbation problem, involving first order partial differential equations and method of characteristics 01 p0130 A71-10368
- Effective cross sections for molecular hydrogen positive ion formation in collision between He, Ne and Ar ions or atoms 02 p0287 A71-12503
- Planetary nebula NGC 7027 mapping at 11.1 cm, examining structure, ionized H mass and electron density 02 p0317 A71-12869
- Interstellar hydrogen ion production and destruction by electron recombination or photodissociation 02 p0317 A71-12870
- H II region high velocity observations by two etalon, propane scanned photoelectric Fabry-Perot spectrometer with reflecting telescope 04 p0581 A71-15044
- H II regions compact radiation sources flux densities observation at centimeter wavelengths 05 p0812 A71-16690
- Sco X-1 optical spectroscopic and photometric observations, noting H alpha and H ion emission lines pattern-continuum brightness relationship 05 p0812 A71-16698
- Neutral condensations and protostars in H II regions noting original density distributions 06 p0973 A71-18340
- Quiescent metallic and ordinary prominences continuum spectra measurements, showing hydrogen ionization dependence on microstructure 06 p0975 A71-18438
- Static solar H II region ionization balance, energy, UV radiation transfer, gravitational equilibrium and interstellar gas temperature 06 p0975 A71-18442
- Molecular hydrogen cations collisions with hydrogen and helium, determining dissociation cross section dependence on kinetic energy from threshold to 100 eV 07 p1163 A71-19233
- Multicolor photographic photometry of NGC 4254 galaxy using electro-optical converter, observing H alpha emission and H II regions at galactic center 07 p1205 A71-20634
- Formaldehyde line emission observed from trapezium H II region of Orion nebula, attributing to 140 GHz rotational transition 08 p1360 A71-20983
- Zeta Aurigae chromospheric lines observed radial velocities mean variations, taking into account H ion gas acceleration, K star mass ejection and rotation 08 p1364 A71-21417
- Hydrogen ion flux detected along earth magnetic force lines in Northern Hemisphere midlatitudes, determining flux magnitude 09 p1436 A71-22561

HYDROGEN ISOTOPES

Far IR fluxes from H II regions with solar luminosities at .02-2 times 10 to 7th

10 p1675 A71-24488

Hydrogen ion concentration measurements by OGO 5 in plasmasphere during intense magnetic storms accompanied by stable auroral red arcs

10 p1605 A71-24787

Solar wind origin of auroral ions from low energy hydrogen and helium ion spectral measurements

10 p1664 A71-24791

Galaxy M33 density wave velocity and detection, discussing star distribution, H II regions red and blue supergiant and hot stars

11 p1821 A71-25540

HF electromagnetic waves absorption as function of discharge current intensity in ionized H, using gas pressure or uniform magnetic field as parameters

11 p1805 A71-25598

Polar H ion plasma escape from ionosphere into magnetospheric tail effect on plasmopause formation, using hydrodynamic approximation

11 p1756 A71-25756

Quiescent metallic and ordinary prominences continuous spectra measurements, showing hydrogen ionization dependence on fine structure

12 p1955 A71-26588

Static solar H II region ionization balance and energy, UV radiation transfer, gravitational equilibrium and interstellar gas temperature

12 p1955 A71-26592

Positive H, He and O ions in exosphere from mass spectrometers mounted on Elektron 4 satellite

12 p1899 A71-26644

Molecular hydrogen cations collisions with hydrogen and helium, determining dissociation cross section dependence on kinetic energy from threshold to 100 eV

12 p1932 A71-26751

Galactic H II regions 35 cm water source emission line profile observation, noting frequency and intensity variations

14 p2304 A71-29594

Triatomic hydrogen positive ion surface crossing effects in chemical reactions based on potential energy surfaces calculation using diatomics-in- molecules approach

14 p2191 A71-30573

Lyman alpha emission cross sections for collisions of hydrogen ion and atom beams with thin target nitrogen and oxygen relevant to proton auroral analysis

15 p2397 A71-31763

Galactic H II regions radio sources observations by high resolution radio telescopes, comparing with optical appearance

16 p2632 A71-33326

Ab initio calculations on trajectories and nonadiabatic transitions in reactions of hydrogen atomic ions with hydrogen molecules

18 p2949 A71-35897

Contour maps of radio source CTB 1 at UHF, suggesting supernova remnant superimposed on broad faint H II region

18 p2962 A71-36153

H alpha emission photometry for galactic H II region, obtaining contour diagrams

19 p3130 A71-37227

Nonempirical LCAO-SCF-MO method for potential energy surface for ground state of linear helium-hydrogen ion system

19 p3117 A71-37332

H II region formation from type II supernovae explosion, detecting with fluorescence model

20 p3287 A71-39052

H II regions near O and R stars effect on interstellar electron density in solar vicinity

20 p3294 A71-39542

Gum Nebula conceived as hydrogen gas mass ionized by UV radiation from supernova explosion related to Vela X remnant, discussing fossil Stromgren sphere model

20 p3294 A71-39572

Associative ionization and dissociative recombination cross sections of hydrogen molecular ions as function of vibrational coupling restricted to Rydberg states

20 p3272 A71-39577

H, He and O ion fluxes along exospheric magnetic field lines, determining flux energy and direction from RF mass spectrometer measurements onboard Elektron 4 satellite

20 p3226 A71-39742

Plasmaspheric ambient hydrogen and helium atomic cations density measurement by OGO 5 ion mass spectrometer during magnetic storm, noting relationship to auroral red arcs

20 p3227 A71-39833

Proton auroras ionization and excitation cross sections of atmospheric constituents by energetic hydrogen ions and atoms, presenting recent measurements and H emission laboratory results

20 p3228 A71-39845

Low energy hydrogen and helium ions composition of primary aurora precipitation from rocket-borne

spectrometer experiment, suggesting direct solar wind origin of primaries

20 p3301 A71-39850

Spiral galaxies N/O abundance gradients across disks from H II regions spectra

21 p3445 A71-40409

Cosmic ray and soft X ray steady state models of interstellar gas, determining He/H ions concentration ratio

22 p3601 A71-42167

H II regions kinematic properties in Large Magellanic Cloud, presenting emission line profiles and radial velocities

23 p3723 A71-42939

HYDROGEN ISOTOPES

NT DEUTERIUM

NT TRITIUM

Low energy cosmic ray H 2 and He 3 nuclei intensities /1967-1968/ from Pioneer 8 and IMP 4 measurements

09 p1512 A71-22336

Hydrogen isotopes around terrestrial planets, discussing H and deuterium dynamic behavior in Venus and Mars coronas

10 p1668 A71-24001

Apollo 12 lunar dust and rocks carbon and hydrogen amount and isotopic composition determination, using in vacuo outgassing and combustion in oxygen

23 p3751 A71-43703

HYDROGEN OXYGEN ENGINES

NT J-2 ENGINE

Space based reusable manned/unmanned tug, discussing potential missions, system requirements and auxiliary hydrogen oxygen propulsion system

09 p1511 A71-22902

Nuclear, hydrogen/oxygen and solid propellant satellite interceptors effectiveness measurement, considering warhead kill radius, propellant weight and specific impulse

13 p2144 A71-27982

High pressure gaseous hydrogen oxygen auxiliary propulsion systems /APS/ thruster design and cold flow and hot fire testing for space shuttle requirements

15 p2470 A71-32291

Rocket engine burning oxygen and hydrogen propellants at 3000 psia combustion chamber pressure for space shuttle booster and orbiter stages

16 p2624 A71-33106

Cryogenic liquids thermal behavior under operational conditions, discussing Europa 3 second stage liquid hydrogen and oxygen engine

22 p3588 A71-41502

HYDROGEN OXYGEN FUEL CELLS

Biosatellite hydrogen oxygen fuel cell/silver zinc battery combination power system for long aerospace missions, discussing optimal design tradeoff

04 p0535 A71-15286

High energy hydrogen-oxygen launch vehicle thermal insulation system, discussing closed cell rigid polyvinyl chloride foam mechanical characteristics, use and tests

12 p1985 A71-26835

Heat and mass transfer optimization in hydrogen-oxygen fuel cells with ion exchange membrane

14 p2181 A71-30050

Stoichiometric hydrogen-oxygen mixture spinning detonation fine structure determination by trace technique and high speed space-time photography

15 p2465 A71-32083

Carbon dioxide traces effects on composition, volume and electrochemical characteristics of trapped electrolyte hydrogen oxygen alkaline fuel cells

15 p2354 A71-32205

Ion-membrane hydrogen oxygen fuel cell, using microbially or biochemically produced hydrogen by enzymatic reactions

16 p2527 A71-33550

Advanced communications satellites system engineering, including configuration based on active body stabilization, rechargeable hydrogen oxygen fuel cells and ion engines

17 p2812 A71-34710

Ionic conduction in perovskite-type oxide solid solution, discussing application to high temperature hydrogen oxygen fuel cells

18 p2852 A71-36966

Transistor circuit driven hydrogen-oxygen fuel cell, testing internal impedance effect on power supply noise for comparison with lumped parameter model

19 p3000 A71-38463

Rechargeable cylindrical hydrogen-oxygen fuel cell for synchronous satellites, determining energy density as function of current, pressure and electrolytes with computer model

20 p3182 A71-38947

Dead ended compartments concentration and current distributions calculation in space hydrogen-oxygen fuel cells, using mathematical model with convective diffusion equation

21 p3326 A71-41249

Continuous impurities purging from hydrogen oxygen fuel cells gas compartments, describing operation mode and design techniques

21 p3326 A71-41250

HYDROGEN PEROXIDE

Hydrazine-hydrogen peroxide fuel cells coulombic efficiency measurement

02 p0197 A71-12989

Hydrogen-sensitized decomposition of hydrogen peroxide, taking oxygen inhibiting effect into account

03 p0376 A71-14272

Hydrogen peroxide decomposition acceleration in carbon monoxide, discussing reaction mechanisms and rate coefficients

03 p0376 A71-14282

Hydrogen peroxide immersion effects on dimethylsilicone seal rubber tensile properties and tear strength

10 p1631 A71-24090

Cometary dissociative recharging and recombination dissociation of water and hydrogen peroxide molecules in comets, giving empirical relation for effective cross sections

17 p2803 A71-34828

Reactions of H and O with hydrogen peroxide in water in discharge flow systems, measuring rate coefficients

19 p3012 A71-38080

Titanium carbide powder corrosion resistance to sulphuric acid-hydrogen peroxide system at various temperatures

24 p3838 A71-44730

HYDROGEN PLASMA

NT DEUTERIUM PLASMA

Kinetic equations derivation for computer calculation of nonuniform hydrogen plasma decay, considering hydrogen recombination, electron temperature and ambipolar diffusion

03 p0463 A71-13508

Spectroscopic studies of helium-hydrogen plasmas in first reflected shock region in electromagnetic tube

04 p0631 A71-14680

Hydrogen plasma turbulent heating, simulating ion-acoustic instability

05 p0786 A71-16222

H-He partially ionized plasma bremsstrahlung, radiative and dielectronic recombination, discrete levels excitation and collisional ionization

05 p0787 A71-16480

Fully ionized hydrogen cosmic plasma interaction with surrounding neutral gas, noting minimum temperature and power input

05 p0810 A71-16634

Dynamic stabilization of magnetoplasma drift dissipative instability by HF oscillating magnetic field, discussing helium and hydrogen afterglow plasmas

06 p0934 A71-17488

H lines Stark broadening in turbulent plasma, considering Langmuir vibrations monadiabatic action and energy density

07 p1168 A71-19277

Spatial potential measurements in magnetized non-Maxwellian hydrogen plasma, using Zaitsev-Mnezhnev method

07 p1171 A71-20199

Artificial solar wind experiments, describing interaction between hydrogen plasma shock wave and simulated geomagnetic field

08 p1354 A71-21014

Microwave electromagnetic emission in the pinch hydrogen plasma by sensitive superheterodyne receivers, noting discharge azimuthal current

08 p1339 A71-21477

Plasma fluxes transport in vacuum chamber by quadrupole magnetic field, studying H plasmas motion

08 p1340 A71-21481

Computer simulation of strongly ionized potassium and hydrogen plasmas relaxation during rapid electrode cooling by He atoms, noting population inversions

08 p1342 A71-21913

Conductivity measurement of hot ion hydrogen plasma for runaway electric field, comparing Spitzer and Buneman formulas

09 p1502 A71-22860

Wave propagation with frequency inferior to gyrofrequency of ions in collisionless hydrogen plasma, showing Alfvén wave reflection on discontinuity surface parallel to magnetic field

10 p1599 A71-23848

Electron collisional-radiative ionization and recombination rate coefficients, using hydrogenic plasma model with resonance radiation trapping

10 p1653 A71-24672

Pulsed magnetic piston produced shock waves propagation along field in collisionless hydrogen plasma

10 p1654 A71-24894

Hydrogen plasma simulation of solar wind-planetary body interaction, showing electric fields behind moon and Venus

11 p1816 A71-25755

Hydrogen plasma internal magnetic field determination, using spectral characteristic measurements due to level intersection

13 p2108 A71-29030

- Electron scattering effects on spectral emission at optical and X ray wavelengths for homogeneous spherical ionized hydrogen plasma cloud, discussing radiation transfer
14 p2297 A71-29592
- H lines Stark broadening in turbulent plasma, considering Langmuir vibrations nonadiabatic action and energy density
14 p2280 A71-30171
- Azimuthal current growth and microwave radiation in theta pinch hydrogen plasma discharge from sensitive superheterodyne receivers
14 p2282 A71-30663
- Hydrogen plasma HF heating boundaries by magnetic traps, noting diamagnetic effects due to ion and electron heating
14 p2282 A71-30667
- Hydrogen plasma transport in linear magnetic quadrupole field, studying polarization potential and density distribution
14 p2282 A71-30669
- Temperature dependence of H-beta emission from hot hydrogen-helium plasmas, calculating production rate at 10,000-100,000,000 K
15 p2455 A71-31722
- Three-phase plasmatrons with hot W electrodes for obtaining plasma of inert gases, nitrogen and hydrogen
15 p2457 A71-32267
- Computer simulation of strongly ionized potassium and hydrogen plasmas relaxation during rapid electrode cooling by He atoms, noting population inversions
17 p2788 A71-35257
- Homogeneous spherical hot hydrogen plasma cloud at various temperatures and optical depths, presenting electron scattering effects on optical and X ray spectral emission
18 p2951 A71-36012
- Sweep Langmuir probe with sweep speeds greater than 150 V/microsec, considering electron cyclotron resonance heated hydrogen plasma confined in toroidal quadrupole
18 p2952 A71-36582
- Nonlinear radiative heat transfer in hydrogen plasma gas, obtaining temperature distributions
19 p3161 A71-37404
- Positive ion composition of collision dominated weakly ionized HF hydrogen plasma discharge, measuring abundance ratio as function of extraction voltage and gas density
20 p3275 A71-39429
- Artificial solar wind experiments, describing interaction between hydrogen plasma shock wave and simulated geomagnetic field
20 p3279 A71-39590
- Temperature control bracket energy equation as measure of temperature distribution in pure hydrogen stellar atmosphere, considering electron energy and radiation field
21 p3446 A71-40419
- Enhanced scattering signal observation at electrostatic plasma wave frequency by focusing Q switched laser beam on hydrogen plasma
22 p3580 A71-41596
- Hydrogen plasma Balmer spectrum measurement for emission coefficients, comparing results with theories
22 p3583 A71-42373
- Magnetosonic wave excitation and electron heating in magnetically confined hydrogen plasma hybrid resonance region
24 p3853 A71-44502
- High current pulsed arc in hydrogen plasma at 400 atm, showing instability with rising pressure and arc length
24 p3854 A71-44519
- Electron temperature and density of HF inductive discharge in hydrogen plasma
24 p3855 A71-44524
- Artificial magnetosphere interaction with 8 keV electrons in hydrogen plasma beam simulating solar wind, noting penetration caused by boundary instability
24 p3823 A71-45043
- Hydrogen plasma generation by microwave field in magnetic-mirror device due to electron cyclotron resonance, measuring transverse diffusion coefficient dependence on magnetic field
24 p3858 A71-45235
- HYDROGEN RECOMBINATIONS**
Atomic H excitation by electron impact, deriving cross sections for anomalous recombination lines in H II regions radio frequency spectrum
02 p0317 A71-12873
- Cooled porous plug burner for flame recombination of oxygen and hydrogen, noting boiling water reactor off-gas application
03 p0517 A71-13367
- Kinetic equations derivation for computer calculation of nonuniform hydrogen plasma decay, considering hydrogen recombination, electron temperature and ambipolar diffusion
03 p0463 A71-13508
- Molecular hydrogen formation on dust grain surfaces, discussing recombination efficiency as function of surface temperature
05 p0784 A71-16205
- Sealed secondary Ag cells, controlling H and O recombination by auxiliary electrode
08 p1236 A71-21106
- Hydrogen recombination and molecule formation by nonactivated chemisorption on iron grains surfaces
10 p1573 A71-25006
- Diffuse interstellar medium hydrogen radio recombination lines radiation transfer, investigating thermodynamic equilibrium effects
15 p2498 A71-32770
- Dense interstellar cloud radio recombination lines in H I regions, calculating quadrupole effects on line splitting
15 p2498 A71-32771
- Hydrogen oxygen recombination rate constants from hydroxyl radical decay measurements in shock tube steady expansion
16 p2539 A71-32908
- NGC 2024 direction H I region H 137 alpha recombination line emission detection, determining ionized hydrogen fraction
17 p2807 A71-35415
- Associative ionization and dissociative recombination cross sections of hydrogen molecular ions as function of vibrational coupling restricted to Rydberg states
20 p3272 A71-39577
- Hydrogen three-body recombination and dissociation rates in presence of molecular hydrogen, helium, argon and xenon collision partners
23 p3706 A71-42902
- HYDROGEN SULFIDE**
Ultrasonic absorption in hydrogen sulfide, measuring vibrational and rotational relaxation times as function of temperature
03 p0459 A71-13718
- Long wavelength UV photoproduction of amino acids on primitive earth, using hydrogen sulfide as photon acceptor
18 p2855 A71-36229
- Amino silica gels absorption properties with respect to carbon dioxide, hydrogen sulfide and water vapor, comparing affinity
20 p3193 A71-39233
- HYDROGEN 2**
U DEUTERIUM
HYDROGEN 3
U TRITIUM
HYDROGENATION
Benzoylformic and alpha-acetamidooacrylic acid hydrogenation, using modified ion exchange resin-palladium catalysts
03 p0375 A71-13199
- Binary Ti alloys hydrogenation-dehydrogenation treatment effect on alloying element activity
04 p0615 A71-15801
- Internal friction from hydrogen dissolved in Ti-Mn alloys, considering solute interstitial atoms caused asymmetrical distortion decrease with increased Mn concentration
10 p1625 A71-24008
- Crystallites in hydrogenated hydroxy terminated polybutadiene from polarized light examination, viscosity-temperature curve discontinuity and elastomer modulus-temperature curve
10 p1573 A71-25126
- [JPL-TR-32-1512]
Reversible hydrogen embrittlement mechanism in hydrogenated steels
17 p2757 A71-34496
- HYDROGENOLYSIS**
Asymmetric synthesis of alanine by hydrogenolytic asymmetric transamination, noting temperature effect
13 p2026 A71-29376
- HYDROGENOMONAS**
PH conditional ammonia assimilation deficient mutants isolation and growth properties, studying nitrogen transport in *Hydrogenomonas eutropha*
06 p0857 A71-18672
- Hydrogenomonas eutropha* mutants deficient amination due to ammonia-nitrogen permeation defect
06 p0857 A71-18673
- Mineral composition optimization of nutrient medium for *Hydrogenomonas*, using steepest ascent method for mathematical planning of experiments
20 p3193 A71-39236
- Bicarbonate requirement for elimination of lag period of chemoautotrophically grown *Hydrogenomonas eutropha*
21 p3329 A71-40213
- HYDROGEOLOGY**
Lunar and Martian subsurface liquid water under porous rock layers and permafrost, using terrestrial hydrogeology analogs
15 p2494 A71-32491
- Remote sensors for hydrogeologic prospecting in arid terrains, recommending vertical and horizontal polarized microwave radiometers
18 p2913 A71-36362
- Operational calibration of airborne IR spectrometer over hydrogeologically significant terrains, obtaining radiance spectra
18 p2920 A71-36363
- HYDROGRAPHY**
Flow theorem as circulation extension for closed curves in autobarotropic fluids in meteorology and hydrography
10 p1639 A71-25113
- HYDROKINETICS**
U HYDROMECHANICS
HYDROLOGY
NT HYDROGEOLOGY
Ecological interpretation of daytime data from Nimbus 3 high resolution IR radiometer for hydrologic and plant distribution mapping
08 p1277 A71-20884
- Aircraft and satellite remote sensing techniques in geology, soil science, geography and hydrology
18 p2913 A71-36359
- HYDROLYSIS**
Oxidative and hydrolytic enzymes localization in rhesus monkey brain, investigating glutaraldehyde fixation effect with histochemistry
07 p1042 A71-20017
- Plastics as potting compounds in military aircraft electrical systems, investigating resistance to reversion and hydrolytic stability
10 p1633 A71-24115
- Potting compounds service life estimation based on accelerated hydrolytic reversion data at high temperatures and humidities
10 p1633 A71-24117
- Proteins hydrolysis, investigating temperature effect on reaction, determining optimum conditions for maximum amino acids yields
11 p1728 A71-26066
- Titanium and silicon tetrachlorides oxygen-containing impurities determination without hydrolysis, describing measuring device design
15 p2383 A71-31659
- Compounds hydrolyzable to amino acids in aqueous extracts of Apollo 11 and 12 lunar fines, noting presence of glycine and alanine
18 p2855 A71-36230
- Urea hydrolysis reaction rates by urease at low water activity, noting use for Mars surface bioassay
22 p3487 A71-42226
- Polymerized and hydrolyzed polypeptides from condensed amino acid adenylates for prebiological synthesis model
22 p3508 A71-42232
- HYDROMAGNETIC FLOW**
U MAGNETOHYDRODYNAMIC FLOW
HYDROMAGNETIC STABILITY
U MAGNETOHYDRODYNAMIC STABILITY
HYDROMAGNETIC WAVES
U MAGNETOHYDRODYNAMIC WAVES
HYDROMAGNETICS
U MAGNETOHYDRODYNAMICS
HYDROMAGNETISM
U MAGNETOHYDRODYNAMICS
HYDROMECHANICS
NT ELASTOHYDRODYNAMICS
NT ELECTROHYDRODYNAMICS
NT HYDRODYNAMICS
NT HYDROSTATICS
NT MAGNETOHYDRODYNAMICS
NT MAGNETOHYDROSTATICS
Gas-particle mixtures weak disturbances, applying linearized hydromechanic and phase transformation kinetic equations
07 p1088 A71-19191
- Boundary value problems of analytic functions and singular integral equations, considering hydromechanics and elasticity theory applications
07 p1148 A71-20077
- Small scale flow and surface effects in multiphase media hydromechanics, obtaining entropy production in mixture for interphase transformations characterization
19 p3042 A71-37098
- HYDROMETEOROLOGY**
Hydrometeorological fields derivatives transformation in hydrothermodynamic equations numerical integration
15 p2443 A71-31224
- Airborne Doppler velocity sensors, considering hydrometeors effects on HF signal attenuation and reflection
17 p2747 A71-35768
- HYDRONIUM IONS**
Energetic electron precipitation effects on upper D region water cluster ion population at various vapor mixing ratios
02 p0245 A71-11961
- Hydrated hydronium ions in D region, discussing sources and production mechanisms
03 p0421 A71-14546
- HYDROPLANING**
Aircraft aquaplaning skidding prevention by runway resurfacing and water depth sensor warning indicators
10 p1609 A71-23946

HYDROPONICS

HYDROPONICS

Hydroponic plant cultivation with keramzit substrate, investigating replacement time effect and regenerative power of nutrient solution 22 p3506 A71-42816

HYDROSPHERE [EARTH] U EARTH HYDROSPHERE

HYDROSTATIC PRESSURE

Circular shallow cylindrical panel stability and creep buckling under hydrostatic pressure 01 p0171 A71-10649

Nonlinearly elastic rings and arches under hydrostatic pressure, examining equilibrium with sixth order differential equations 02 p0325 A71-12125

Internal friction measurement under hydrostatic pressure, describing apparatus to determine phase angle between stress and strain 02 p0255 A71-12132

Stress concentration at free and reinforced curvilinear holes with random surface roughness applied to plane under hydrostatic tension 02 p0326 A71-12291

Universal endurance test machine for tubular samples torsion testing under hydrostatic pressure 04 p0673 A71-15899

Cylindrical shell reinforced by transverse ribs under hydrostatic pressure, determining elastoplastic deformation 06 p0988 A71-17774

Cylindrical shells buckling under subcritical loads, considering internal and external hydrostatic pressure and axial compression 06 p0988 A71-17779

Thin paraboloidal shells of revolution under external hydrostatic pressure loading, analyzing free vibrations by finite element method [AIAA PAPER 71-214] 06 p1004 A71-18650

Hydrostatic pressure effects on Al polycrystals stress-strain behavior at room temperature, using magnetostrictive load cell 07 p1143 A71-20490

Pulmonary arterial blood flow regulation by hydrostatic pressure in low resistance circulatory system 10 p1561 A71-24127

High altitude balloon gore meridional stresses effects on film response by analyzing cylindrical elastic membrane under uniform hydrostatic pressure and axial loads 12 p1976 A71-27121

Stress concentration in variable-modulus perforated plate of isotropic elastic material under hydrostatic pressure 13 p2151 A71-28142

Cylindrical shell laminar plastic structure effect on stability under hydrostatic pressure, applying Kirchhoff-Love hypothesis 13 p2155 A71-28654

Hydrostatic extrusion, emphasizing prismatic products fabrication from industrial metals and alloys 14 p2252 A71-30469

Plastically deformed Ni powder specimens residual microstresses as function of applied hydrostatic pressure, using X ray diffraction measurements 15 p2429 A71-31996

Thin infinite isotropic elastic plate on nonlinear elastic foundation under uniform two dimensional hydrostatic pressure, detailing imperfection effects on initial postbuckling behavior 16 p2648 A71-32979

Imperfect circular cylindrical shell under external hydrostatic pressure loads, determining free and resonant vibration modes 16 p2651 A71-33062

Yield point thermal component in bcc metals at low temperatures as function of hydrostatic compression, noting interionic reaction potential nonspericity 16 p2596 A71-33889

Hydraulic system self acting valves natural vibration dynamic characteristics, showing energy transfer by phase shift of variable hydrostatic compression component 17 p2677 A71-34349

Cavitation erosion of aluminum at high hydrostatic pressure, using chamber focusing acoustic system 18 p2910 A71-36932

Hydrostatically loaded noncircular pressurized cylindrical shells with nonuniform rings, using asymptotic expansion procedure 19 p3157 A71-37875

High electric field Gunn effect in n-type InAs under hydrostatic pressure due to transferred carrier mechanism 20 p3275 A71-38786

Physical determinants of gravity receptor mechanisms, discussing hydrostatic stress effects on membranes and gravity influence on enzymatic transport 21 p3339 A71-39972

Flexural vibration of rectangular orthotropic plates under in-plane hydrostatic forces 21 p3464 A71-40768

Rh and Ag-Pd alloys magnetic susceptibility, investigating hydrostatic pressure effects 21 p3432 A71-41269

Computer program for nonuniform thickness ring structure stress distribution under uniform radial line load based on reinforced circular cylindrical shell interaction under hydrostatic pressure 22 p3516 A71-41866

Apollo 12 basalts porosity and volume compressibility under hydrostatic pressure 23 p3759 A71-43768

Hydrostatic bearings for large optical and radio telescopes, explaining lubricant flow control systems 23 p3661 A71-43862

Noncircular cylindrical shells stress and displacement under hydrostatic loads, applying Donnell equations 24 p3879 A71-44618

HYDROSTATICS

NT MAGNETOHYDROSTATICS

Self gravitating fluid spheroid oscillations in hydrostatic equilibrium with magnetic fields using variational principle 01 p0129 A71-11336

Finite wall conductance effect on performance /pressure and load capacity/ of MHD hydrostatic thrust bearings 07 p1117 A71-19503

Spherical hydrostatic gas bearings for two axis gyros, using Al die castings 07 p1117 A71-19504

Proportional fluidic element static characteristics, calculating main jet interaction with control jet 09 p1386 A71-22655

Linear coastal hydrostatic boundary layers of lake with no horizontal motion, discussing flow conditions under wind stress and interior velocity 10 p1600 A71-23961

Orr-Sommerfeld hydrostatic stability equation derivation for nonparallel flow in wake from Goldstein velocity distribution, noting lateral direction velocity component magnitude 10 p1592 A71-24024

Variable gap and chamber width effect on load bearing capacity of radial hydrostatic bearing with capillary throttling 16 p2584 A71-33616

Hydrostatic power transmission systems classifications, considering transformation, transport and accumulation of energies /mass, heat, optical, chemical, pneumatic, hydraulic, etc/ 18 p2850 A71-36202

HYDROTHERMAL CRYSTAL GROWTH

High quality quartz single crystal synthesis by hydrothermal recrystallization in autoclave 02 p0229 A71-11718

HYDROGEN ENGINES

U HYDROGEN OXYGEN ENGINES

HYDROXIDES

NT LITHIUM HYDROXIDES

NT POTASSIUM HYDROXIDES

Lime refractory fabrication and properties for high temperature applications, describing production of calcium oxide grain by sintering process from commercial calcium hydroxide 21 p3405 A71-40246

Free radical induced high temperature oxidation degradation curtailment of polyphenyl ethers by oxides, hydroxides and carbonates of alkali metals and Ba [ASLE PREPRINT 71LC-11] 24 p3842 A71-45290

HYDROXYCORTICOSTEROID

Fluorometric microvolumetric test for unconjugated 11-hydroxycorticosteroids distribution in plasma, noting concentrations in capillary and venous blood 11 p1718 A71-25627

HYDROXYL COMPOUNDS

NT ALCOHOLS

NT BISPHENOLS

NT ETHYL ALCOHOL

NT GLYCOLS

NT METHYL ALCOHOLS

NT PHENOLS

Valeraldehyde o-nitrophenylhydrazone mass spectrum with low intensity peak due to combined hydroxyl and water loss from molecular ion 02 p0209 A71-12573

Air-acetylene and air-propane-butane flames absorption spectra, determining distribution of free Ca and Na atoms and OH hydroxyl radicals 03 p0518 A71-13501

Intermediates structure and IR spectrum in OH reaction with CO by vacuum UV photolysis, studying refractive product absorptions and valence force potentials 08 p1336 A71-20661

Zinc-hydroxy system spectrum analysis, using laser source Raman spectrometer and modified IR reflectance accessory 08 p1233 A71-21079

Crystallites in hydrogenated polybutadiene from polarized light examination, viscosity-temperature curve discontinuity and elastomer modulus-temperature curve [JPL-TR-32-1512] 10 p1573 A71-25126

Polyester formation by Escherichia coli ribosome catalyzed alpha-hydroxy acid incorporation into polymer chain 17 p2686 A71-35574

HYDROXYL EMISSION

Very long baseline interferometry of galactic hydroxyl radical microwave emission sources 02 p0310 A71-12250

Hydroxyl and water vapor emission properties in interstellar medium attributed to maser action 02 p0313 A71-12450

Nocturnal intensity and excitation temperature variation of hydroxyl vibrational rotational band in air glow 04 p0581 A71-15020

Galactic sources 18 cm OH emission and/or absorption observation 04 p0657 A71-15700

OH absorption line measurements for long distance range near galactic center, suggesting existence of radial velocity gradient 04 p0657 A71-15700

Vibrationally excited ground state hydroxyl in fast flow system, considering mean radiative lifetime and reaction rate with ozone 08 p1250 A71-20660

Upper atmosphere hydroxyl emission mechanisms discussing absorption band, energy balance, atomic hydrogen and ozone in lower thermosphere and nitrogen oxides 08 p1277 A71-21000

Astrophysics - Conference, University of Nice, France, April 1969 01 p1670 A71-24180

Organic compounds astrochemistry, discussing hydroxyl absorption lines and molecular abundances in interstellar space 10 p1678 A71-24818

Vibrational and rotational temperatures diurnal variations of upper atmospheric OH emissions from IR spectroscopic measurements, discussing earth shadow effects on mean intensity 11 p1753 A71-25546

Double resonator ruby maser for observing transitions of interstellar hydroxyl, noting incorporation in modulation radiometer of astronomical telescope 13 p2077 A71-28377

Twilight OH emission intensity and rotational temperature in mesosphere as function of solar position below horizon 14 p2232 A71-29958

Anomalous OH emission in direction of planetary nebula NGC 2438 and optically radio-weak galactic nebulae S 247, S 269, IC 2162 and NGC 2264 14 p2313 A71-30433

Brightness dependence on heliocentric distance of cometary hydroxyl and hydrogen halos, using three-step production mechanism 14 p2318 A71-31120

Hydrogen oxygen recombination rate constant from hydroxyl radical decay measurements in shock tube steady expansion 16 p2539 A71-32900

Upper atmosphere atomic hydrogen H sub alpha emission, correlating intensity and hydroxyl vibration temperature 16 p2564 A71-33661

OH emission column density upper limit from rocket-borne UV spectrometer measurement of resonantly scattered sunlight intensity in electronic transition vibrational band 16 p2574 A71-33961

Vibrationally excited hydroxyl formation by atomic hydrogen reaction with ozone, using Fourier transform spectroscopy 18 p2874 A71-35833

Reaction rate of vibrationally excited hydroxyl with ozone, obtaining hydroxyl emission spectra by Fourier transform spectroscopy 18 p2874 A71-35836

Upper atmosphere hydroxyl emission nocturnal average vibrational temperature correlation with molecular oxygen emission intensities 19 p3049 A71-37400

Hydroxyl emission at T Tauri stars positions in Taurus-Auriga region, discussing radial velocities of stars and dust clouds 19 p3144 A71-38172

Upper atmosphere hydroxyl emission mechanism discussing absorption band, energy balance, atomic hydrogen and ozone in lower thermosphere and nitrogen oxides 20 p3218 A71-39586

Dayglow emissions for OH, molecular oxygen, sodium, lithium, potassium, atomic oxygen and nitrogen considering height profiles and diurnal variations 20 p3226 A71-39828

D region night airglow OH emissions and IR at atmospheric diatomic oxygen bands excitation mechanism with aid of model involving solar photodissociation 20 p3226 A71-39831

Nighttime hydroxyl airglow emission intensity and excitation temperature measurements, noting seasonal and nocturnal variations 20 p3227 A71-39834

IR auroral/airglow study covering hydroxyl emission and dipole moment function determination and at 20 p3227 A71-39834

ospheric nitrogen vibrational temperature measurement
20 p3240 A71-39843
Atmospheric atomic hydrogen H alpha emission correlation with hydroxyl vibrational temperature
23 p3665 A71-42961
Hydroxyl emission of upper atmosphere, considering atomic hydrogen and ozone near thermosphere base
23 p3673 A71-43982
OH transitions excitation temperatures in absorbing cloud from observations of W12
24 p3871 A71-44906

HYDROXYLAMINE SULFATE

Inflammability, burning rates and exothermal decomposition of compact hydroxylamine and hydrazine sulfate and chloride with/without copper chloride additions, plotting pressure variations curves
15 p2463 A71-31377

HYDROXYLAMMONIUM PERCHLORATES

Solid propellant oxidizers hydroxylammonium perchlorate and hydrazine nitroform self deflagration, determining combustion temperatures and burning rate pressure relationships
06 p0944 A71-18299

HYGIENE

Preventive medicine for air travelers in flight and at route stops, considering disease dissemination and control, international quarantinable diseases, sanitation, etc
08 p1245 A71-20727

Jet aircraft and hygiene, considering communicable diseases spread control measures and sanitation methods by airlines
09 p1400 A71-23071

Zero gravity whole body shower system for space station, describing air drag and vacuum methods for water collection
[ASME PAPER 71-AV-2] 18 p2865 A71-36369

Shower habitability requirements for adequate cleansing of body and hair to satisfy physiological, psychological and social needs of crew members on long space missions
[AIAA PAPER 71-873] 18 p2870 A71-36629

Long term spaceflight crew personal hygiene, discussing human waste processing and/or utilization, microbiological control and medical infirmity-dispensary-laboratory requirements
[AIAA PAPER 71-878] 18 p2870 A71-36631

Engineering aspects of zero gravity personal hygiene and waste management systems, noting controlled air flows, surface tension and artificial gravity use
[AIAA PAPER 71-865] 18 p2872 A71-36653

Polymer odor threshold determination for hygienic considerations in sealed/pressurized chamber construction, comparing static and dynamic methods
24 p3800 A71-44539

HYGROMETERS

NT PSYCHROMETERS

Dew point hygrometer with constant resistance humidity transducer, using salt solution phase transition principle
08 p1292 A71-21456

Low hygrometer calibration for water vapor measurements smaller than 3 mm
11 p1761 A71-25244

Dew point /frost point/ reference hygrometer for humidity gage testing in thermohygrostat hygrochamber
21 p3384 A71-41379

HYGROSCOPICITY

Cloud control and modification through seeding with hygroscopic compounds
14 p2271 A71-30611

HYPERBARIC CHAMBERS

Free radical activity in white mice tissues under hyperbaric oxygenation, examining antioxidants effects
01 p0012 A71-11075

Oxygen-nitrogen synergistic interactions in rats in hyperbaric environment, determining lung damage by total water measurement
04 p0538 A71-15054

German monograph on high pressure oxygen toxicity and hyperbaric treatment of gas gangrene
11 p1716 A71-25200

Chronic inability of succinate for protection against paralysis of rats exposed to hyperbaric oxygen toxicity, correlating thermocontrol response
11 p1720 A71-26124

Respiratory aspects of hyperbaric thermal environments, considering heat exchange by convection
18 p2860 A71-36878

HYPERBOLAS

Halley method of tangential hyperbolas in Banach space, deriving local existence, uniqueness and convergence theorems
04 p0620 A71-15668

HYPERBOLIC FUNCTIONS

Weak periodic solutions of hyperbolic partial differential equation with quadratic dissipative term for biharmonic waves
02 p0276 A71-12000

Papers on hyperbolic equations and waves covering Cauchy problem, Feynman integrals, general relativistic hydrodynamics, flow stability, etc
04 p0626 A71-15575

MOSFET inverter pulse response analysis using hyperbolic functional description
05 p0726 A71-17086

Unsteady heat transfer in nonlinear systems, solving hyperbolic equation by net-point method
06 p1006 A71-18006

Optimal control for distributed parameter system described by linear hyperbolic partial differential equation, deriving existence theorem and cost function
07 p1147 A71-19471

Optimal solution existence theorem for control system described by linear hyperbolic partial differential equation
07 p1148 A71-19770

Second order hyperbolic partial differential equation in canonical form solution by iterative method
09 p1485 A71-22277

Tricomi problem for elliptic-hyperbolic Chaplygin equation extended to mixed Lavrentev-Bitsadze equation
10 p1635 A71-23802

Time dependent asymptotic solution for transonic flows in hyperbolic nozzle and turbine cascades with oblique shock
[ASME PAPER 71-GT-42] 11 p1704 A71-25975

Bogoliubov generalization principle applicability conditions for second order hyperbolic equations with functionally perturbed argument, using Wendroff-Bellman lemma
11 p1792 A71-26154

Gas dynamic effects associated with unboundedness of solution of quasi-linear hyperbolic systems
14 p2223 A71-29560

Time dependent problems involving parabolic and hyperbolic differential equations, discussing formulation for approximate solution by Galerkin methods
14 p2265 A71-30294

Nonlinear hyperbolic equations integration, considering characteristic, mesh finite difference and particle in cell techniques
15 p2441 A71-31355

Mixed problem for hyperbolic type linear non-homogeneous second order partial differential equation with delayed arguments, obtaining asymptotic solution for derived Cauchy problem
19 p3086 A71-38011

Alternating-direction Galerkin methods application to parabolic and hyperbolic differential equations for obtaining efficient iterative solution of heat equation on rectangle
19 p3087 A71-38305

Convergence rate of finite difference schemes applied to initial value problems for hyperbolic equations
19 p3088 A71-38312

Critical time calculation for singularity in solutions of homogeneous nonlinear hyperbolic differential equations with smooth initial data, discussing application examples
20 p3254 A71-38790

Theorems on parabolic and hyperbolic differential equations solutions continuous dependence on elliptic operator coefficients, deriving proof by hypothesis of existence and uniqueness
21 p3408 A71-40651

Optimal control of linear systems with distributed parameters, using hyperbolic type equation
22 p3526 A71-41909

Uniform progressing wave expansions solutions, using comparison equation method for hyperbolic and mixed type equations
22 p3567 A71-42630

Asymptotic expansion method for hyperbolic and parabolic differential equations fundamental solutions featuring validity near surface and in interior of characteristic conoid
23 p3698 A71-43096

Validity proof of asymptotic methods in one dimensional dynamic systems described by hyperbolic and parabolic differential equations
24 p3844 A71-45063

HYPERBOLIC NAVIGATION

NT LORAN

NT LORAN C

Long range hyperbolic navigation in U.S., discussing loran and Omega systems
14 p2272 A71-30711

HYPERBOLIC REENTRY

Spacecraft trajectories for reentry at hyperbolic velocity, examining aerodynamic control loads and characteristics in atmospheric skip
20 p3288 A71-39122

Landing control algorithm using onboard digital computer for spacecraft hyperbolic velocity reentry, discussing simulation test results
24 p3846 A71-45303

HYPERBOLIC SYSTEMS

Quasi-H-analytic function classes sufficient conditions for second order linear hyperbolic type H /Hadamard/ operator
06 p0918 A71-17575

Lightning flash-ground strokes VHF radio pictures by hyperbolic position fixing system, obtaining three dimensional sferics fixes as function of time
08 p1325 A71-20880

Higher dimensional wave equation boundary value control, investigating hyperbolic problems in several space dimensions with application of Holmgren and John uniqueness theorems
09 p1424 A71-23467

Boiling of relativistic heat conducting fluid in normal space-time manifold for nonstrict hyperbolic system, using Eckart scheme
10 p1694 A71-23831

Hyperbolic and parabolic system three dimensional boundary layer equations, discussing characteristics and subcharacteristics roles in influence and dependence zones determination
18 p2902 A71-36039

Difference methods for hyperbolic flow equations, using third order accuracy space and time split difference operators
18 p2844 A71-36305

Asymptotic expansion for hyperbolic Cauchy problem solution, proving correctness
21 p3409 A71-41079

Semilinear hyperbolic systems analogous to differential-integral Boltzmann equations of gas dynamics, developing solutions existence for nonnegative initial data
22 p3531 A71-42690

HYPERBOLIC TRAJECTORIES

Hyperbolic, elliptical and parabolic heliocentric motion, determining location of body in orbit with unitary method
03 p0493 A71-14194

Optimal acceleration from earth orbit to hyperbolic velocities of low thrust space vehicle, constructing asymptotic expansions near and far from central field
09 p1519 A71-22545

Energy optimal single impulse transfer from hyperbolic trajectory to circular orbit
20 p3288 A71-39119

Optimal impulsive transfer of minimum characteristic velocity between hyperbolic asymptotes associated with real planet
22 p3600 A71-41969

HYPERCAPNIA

Russian book on perception of respiratory medium and gas preference in man and animals covering hypoxic or hypercapnic media, inhalation times, gas mixtures, etc
02 p0198 A71-11823

Chronic hypercapnia oxygen dissociation curves and red cell cation exchange in rats, considering compensated/uncompensated phases of respiratory acidosis
03 p0360 A71-13181

Hypoxia-hypercapnia interplay as respiratory chemoreceptors stimulants and depressants by investigating arterial oxygen and carbon dioxide tensions effects on phrenic nerve activity
06 p0854 A71-18061

Hypoxic and hypercapnic ventilatory control and oxygen uptake in athletes, noting chemoreceptor function
06 p0862 A71-18384

Carbon dioxide tolerance after hypercapnia adaptation of rhesus monkeys in upright position
09 p1395 A71-23250

Prolonged hypoxia, hypercapnia and combination effects on rats circulating red cell volume
10 p1559 A71-23970

Gradual unilateral hypoxia effects on pulmonary blood flow partition, noting interaction with hypercapnia
10 p1561 A71-24125

Hypercapnia in rat, measuring carbon dioxide concentration effect on tidal and minute volumes, respiratory rate, pH depression, blood gases, hematocrit and percent oxyhemoglobin saturation
13 p2015 A71-29364

Factors affecting respiratory waves formation, modulating arterial blood pressure recordings and photoplethysmograms
14 p2185 A71-30411

Hypoxic hypoxia and hypercapnia effect on calcium, inorganic phosphorus and total protein in rats blood during hypodynamic syndrome
15 p2356 A71-31306

Chronic hypercapnia effects on oxygen affinity and 2,3-diphosphoglycerate in red cell from tests on guinea pigs
20 p3189 A71-39440

Hypoxia and hypercapnia induced asphyctic differentiation of cutaneous and visceral sympathetic activity in anesthetized paralyzed rabbits
21 p3334 A71-40629

Coronary blood flow at increased arterial carbonic acid partial pressure, noting induced hypercapnia
21 p3335 A71-40633

HYPERFINE STRUCTURE

HYPERFINE STRUCTURE

Wall shift measurement of unperturbed hydrogen hyperfine transition frequency against cesium reference

04 p0585 A71-14652

Optical hyperfine splitting of Rb resonance lines of atomic beam light source, using Fabry-Perot interferometer

07 p1111 A71-19488

Population inversion in Cs133 ground state hyperfine levels, using CW GaAs laser at 77 K for optical pumping

12 p1913 A71-26977

Solid bodies crack development theory, emphasizing crack tip fine and hyperfine structures concepts and time dependent effects

13 p2149 A71-28121

Strong level crossing signals in stepwise fluorescence, investigating fine and hyperfine structure of atomic Li

14 p2277 A71-30508

Mossbauer effect applications to magnetic thin films, discussing electric and magnetic hyperfine interactions and experimental difficulties

18 p2955 A71-36939

Ion pairing study in unresolved metal hyperfine splitting spectral region, using electron spin resonance line shape analysis

21 p3345 A71-40372

Atomic level interference and hyperfine splitting effects on angular and polarization distributions of resonantly scattered light in magnetic field

21 p3420 A71-41120

Formaldehyde transitions in ground and excited states at 6 cm, attaining line widths and hyperfine structure at 1-3 kHz

23 p3723 A71-42953

HYPERGEOMETRIC FUNCTIONS

Spherical harmonics differential approximation generalized from one dimensional radiation specific intensity angular dependence Jacobi polynomial expansion

10 p1696 A71-24536

Singularity free refractive index profiles, using hypergeometric function

10 p1642 A71-24590

Jacobi polynomial series analytic continuity properties based on relation with corresponding Taylor series

17 p2764 A71-34421

French monograph on variable-structure automatic control systems covering algorithms, stability, nonlinear hypersurface slip, minimum time, switching elements, analog simulation, etc

17 p2767 A71-35249

Extreme eigenvalues of Toeplitz matrices associated with Laguerre and Jacobi polynomials, using finite difference operators

21 p3410 A71-41084

Earth-moon and other trajectories calculation in planar elliptic restricted three body problem by slowly varying Jacobi function

23 p3731 A71-43051

HYPERGEOMETRY

U HYPERSPACES

HYPERGLYCEMIA

Total body adipose tissue mass and composition variations, examining hyperglycemic, obese, exercised and centrifuged animals

23 p3637 A71-44299

HYPERGOLIC ROCKET PROPELLANTS

Adsorption role in empirical ignition laws of various solid nitric acid based hypergolic propellant systems, discussing ignition delay relation to acid concentration

04 p0548 A71-14825

Liquid bipropellant rocket engine ignition and start transient calculation for hypergolic and externally ignited starts at sea level and high altitude pressures

06 p0943 A71-17655

Liquid hypergolic propellants heat and gas release determination by calorimetric and PVT measurements, using impinging free jets for propellant mixing

06 p0943 A71-17658

Hypergolic rocket propellant system gas phase ignition, measuring ambient pressure, flow parameters and propellant temperature effects on delay characteristics

19 p3123 A71-38297

Q-switched ruby laser holographic interferometry for hypergolic flame combustion recording

22 p3539 A71-41742

HYPERON

Neutron star matter equations of state involving hyperon formation effects for maximal stable mass models, tabulating moments of inertia

10 p1671 A71-24302

Hyperon stars thermodynamics, deriving hot neutron stars equation of state with particular reference to center singularities

11 p1828 A71-25737

HYPEROPIA

Refraction and image forming qualities of frog eye using measurement of intensity profile /point spread function/, confirming hyperopia

18 p2857 A71-36690

HYPEROXIA

Short term pure oxygen exposure effects on rats proximal convoluted tubular cell structure

01 p0011 A71-10768

Hypobaric pressure and hypoxic or hyperoxic atmospheres effect on mice resistance to pneumococcal pneumonia

02 p0199 A71-12382

Metal ions effect on oxygen toxicity in rats, noting convulsions and lung edema alleviation through mixed Mg-Mn ion treatment

04 p0537 A71-15053

Lipid peroxidation in pulmonary hyperoxia, noting effects of hyperbaric oxygen, ascorbic acid and ferrous iron

06 p0851 A71-17604

Generalized hyperoxia and local effects of oxygen on lungs in etiology of pulmonary damage due to oxygen, noting nitrogen and carbon monoxide effects

08 p1237 A71-20681

Central nervous system functions under high oxygen concentrations at normal and elevated pressures

08 p1241 A71-21938

Pyridine nucleotide concentration in cerebral hemispheres of rats under hyperoxia

09 p1391 A71-22534

Pathological effects of pure oxygen on animal organism at atmospheric pressure, noting perivascular edema, diapedesis hemorrhages, respiratory and metabolic disorders

09 p1392 A71-22641

Oxygen tension effect on pulmonary diffusion capacity and postnatal lung growth in rats under hypoxic, normoxic and hyperoxic atmospheres

10 p1559 A71-23899

Prolonged hyperoxia effects on lipid synthesis in rat liver and adipose tissue slices

10 p1559 A71-23969

German monograph on high pressure oxygen toxicity and hyperbaric treatment of gas gangrene

11 p1716 A71-25200

Chronic inability of succinate for protection against paralysis of rats exposed to hyperbaric oxygen toxicity, correlating thermocontrol response

11 p1720 A71-26124

Acetylsalicylic and ascorbic acids effects on mice susceptibility to oxygen toxicity, discussing in vitro sensitivity of red cells to hydrogen peroxide

11 p1721 A71-26126

Pulmonary oxygen toxicity development rate and effects on lung volume and alveolar-arterial gas exchange during oxygen breathing

13 p2024 A71-29501

Gas exchange, thermoregulatory muscle tone and electrical activity in rat muscles in hyperoxic atmosphere

15 p2360 A71-32533

Dietary antioxidant vitamin level effects on fine structure of proximal convoluted tubules in rats, studying changes due to oxygen toxicity

16 p2528 A71-33116

Hypothalamus and cerebral cortex electric stimulation effects on temperature homeostasis under hyperoxia

17 p2680 A71-34645

Cerebral gamma-aminobutyric acid metabolism and hyperbaric oxygen induced seizures in chicks during brain development, noting increased membrane permeability

20 p3186 A71-38970

EEG study of hyperoxemic convulsions in Macacus nemestrinus and Papio primates, considering preventive effect of Diazepam and derivatives

21 p3339 A71-41418

Stimulatory effects of hypobaric hyperoxia on lipid synthesis in rat liver and adipose tissues under free feeding

22 p3486 A71-41825

Hyperoxic medium effects on experimental animal cells, tissues and organs morphology, infrastructure and histochemistry

22 p3495 A71-42801

Hyperoxia pathological effects on albino rats subcutaneous connective tissue, noting oxidizing enzyme activity depression and cellular metabolism suppression

22 p3496 A71-42802

Hyperoxia effects on thermoregulation and neurochemical functions, showing temperature increases in cerebrum and decreases in cortical and subcortical formations

23 p3633 A71-43582

Hypoxic respiratory reactions of highland natives and recently arrived residents to oxygen concentration change in inhaled mixtures

24 p3798 A71-45065

HYPERPLANES

N-dimensional phase spaces of nonlinear nth order automatic control systems at parameter space sections /hyperplanes/, considering nonlinearities effects in servomechanisms

17 p2783 A71-35129

Necessary conditions of optimality for control problems with state variable inequality constraints using separating hyperplane theorem

21 p3359 A71-40267

HYPERPNEA

Neural stimuli contribution to increasing respiration and hyperpnea during exercise

06 p0862 A71-18366

HYPERSONIC AIRCRAFT

NT HYPERSONIC GLIDERS

Hyperonic conventional and rocket transport aircraft, discussing costs and air and noise pollution

01 p0184 A71-11302

Aircraft construction materials for 1990s, discussing need for high temperature resistant materials for supersonic and hyperonic airframe and engine structural components

05 p0839 A71-16141

Hyperonic ramjet reaction mechanisms for H combustion, discussing computational models, operation principles and atomic, radical and molecular collisions

06 p0865 A71-17410

Hyperonic cruise aircraft configuration reliability Reynolds numbers extrapolation from laminar boundary to turbulent layer

06 p0883 A71-18576

Optimal weight of aerodynamic heat protection layers of stressed skin and optimal efficiency of cooling system for hyperonic aircraft compartments

08 p1375 A71-20836

Hyperonic air transportation future prospects, discussing technical problems and feasibility in view of space shuttle development

10 p1699 A71-24285

Hyperonic aircraft design usable as transport or space shuttle, determining aerodynamic behavior in viscous flow

18 p2847 A71-36431

Feasibility assessment of hyperonic transports with actively cooled airframe structure, considering liquid hydrogen fuel use as coolant

19 p2995 A71-37123

Hyperonic air transportation based on superonic combustion ramjet development, discussing economic feasibility

19 p2995 A71-37124

Thermal stability of naphthenes up to 1000 F, considering hyperonic aircraft fuel applications

22 p3588 A71-42837

HYPERSONIC BOUNDARY LAYER

Three dimensional attached compressible laminar boundary layer on slender cones in hyperonic flight at high angles of attack derived by numerical integration

01 p0070 A71-10926

Geometry and oncoming boundary layer characteristics effects on heat transfer rate in reattached wall of cavity exposed to hyperonic flow

03 p0517 A71-13464

Hyperonic boundary layer of spinning circular cone at angle of attack, using finite difference method

06 p0843 A71-18516

Slender cone hyperonic laminar three dimensional boundary layer separation at angle of attack, proposing helical vortex model

06 p0845 A71-18573

Nozzle wall hyperonic boundary layers in helium tunnel, presenting skin friction measurements and heat transfer rates

06 p0884 A71-18603

Turbulent skin friction and boundary layer velocity measurements on nonadiabatic flat plates at hyperonic Mach numbers

06 p0885 A71-18609

Disturbances within hyperonic transitional boundary layer in Mach 7 gun tunnel observed with hot-wire anemometer, comparing results with surface heat transfer measurement

06 p0886 A71-18637

Pressure gradient and roughness effects on laminar, transition and turbulent boundary layer in hyperonic shock tunnel

08 p1377 A71-22031

Uniform surface blowing effects on hyperonic boundary layer with viscous interaction, calculating heat transfer on flat plate and slender wedge

10 p1598 A71-25096

Shear stress and eddy viscosity distribution in Mach 20 compressible turbulent boundary layer, using mixing length flow theory

11 p1751 A71-25499

Time dependent shear stress, temperature and boundary layer pressure in laminar flow over stepwise accelerated flat plate at hyperonic speed

11 p1856 A71-26193

Slender cone boundary layer transition under angle of attack at Mach 21 with promoted leeward and fixed windward ray

14 p2335 A71-29887

Two dimensional hyperonic boundary layer equations solution upper and lower bounds determination as initial value problem

15 p2386 A71-31161

Monograph on dynamic viscous pressure interaction in hyperonic flow covering boundary layer effect on

oscillating body unsteady pressure distribution in continuum hypersonic flow 17 p2671 A71-35217

Binary laminar boundary layer in hypersonic axisymmetric stagnation point flow with temperature dependent material properties, presenting exact and approximate calculation methods 17 p2671 A71-35422

Transient laminar two dimensional boundary layer induced pressures due to suddenly accelerated hypersonic semiinfinite flat plate 18 p2901 A71-35856

Laminar hypersonic boundary layer equations, calculating heat transfer and shear stress in stagnation point 18 p2847 A71-36428

Incompressible two dimensional turbulent hypersonic boundary layer flow velocity, pressure, temperature and density distributions 18 p2908 A71-36429

Modified asymptotic perturbation expansion method application to free flow rotation effect on boundary layer for hypersonic flow about blunt body 20 p3177 A71-39483

Hypersonic strong interaction boundary layer problem solution by implicit finite difference method 21 p3369 A71-40955

Monograph on hypersonic low temperature ablation covering cross hatched surface patterns, flow field, turbulent boundary layer, angle of attack, etc [VKI-TN-64] 22 p3621 A71-42031

HYPERSONIC FLIGHT

Statics and aerodynamics of lifting decelerators /parawings and sailings/ at supersonic and hypersonic speeds [AIAA PAPER 68-945] 01 p0002 A71-10927

Reentry lifting body hypersonic and subsonic flight enhancement by configuration modifications with compound curvatures minimization, giving wind tunnel model data 02 p0319 A71-11974

Hypersonic flight test base pressure results at high Reynolds numbers for slender cone in turbulent flow, noting implications for ground test simulation [AIAA PAPER 71-134] 06 p0883 A71-18578

Nonequilibrium multicomponent ionization calculations for stagnation merged shock layer of hypersonic blunt body by successive accelerated replacement [AIAA PAPER 69-655] 07 p1015 A71-19890

Hypersonic minimum drag slender wing leading edge shape for given airfoil section, using Newtonian theory 08 p1229 A71-22039

Shock interaction effects on flapped delta wing at hypersonic speed, presenting method for estimating reflected expansion wave impingement boundaries and resulting aerodynamic coefficients 12 p1868 A71-27598

Hypersonic flight load bearing refractory alloy control surface protective coatings, emphasizing oxidation screening tests 14 p2262 A71-29646

Hyperballistic free flight test facilities using light gas guns, considering wake of flight vehicle at hypersonic velocity and aerothermal phenomena 18 p2898 A71-36411

HYPERSONIC FLOW

Film cooling effectiveness in hypersonic turbulent flow from downstream surface equilibrium temperature measurement 01 p0180 A71-10961

Spheres drag coefficient at hypersonic Mach numbers for near free molecular flow 01 p0002 A71-10969

Leading edge bluntness and boundary layer displacement effects on attached and separated laminar boundary layers in high temperature hypersonic flow over compression corner [AIAA PAPER 68-68] 03 p0341 A71-13437

Turbulent boundary layer recovery factor for wedge model in hypersonic helium flow at high Reynolds and Mach numbers 03 p0517 A71-13461

Hypersonic viscous air flow past blunt bodies with radiation, obtaining solution for Navier-Stokes equations by finite difference scheme 03 p0343 A71-14062

Hypersonic conical flow with attached shock waves over delta wings 03 p0344 A71-14243

Hypersonic aerodynamic characteristics of flat delta and caret wing models at high incidence angles for space shuttles 03 p0344 A71-14445

Hypersonic perfect gas flow past thin three dimensional body with strong viscous interaction, obtaining aerodynamic characteristics and drag and heat coefficients 03 p0345 A71-14563

Hypersonic flow past freely vibrating hemisphere-cylinder-cone, noting Reynolds and Mach numbers dependence and conical stabilizer aperture angle 03 p0345 A71-14571

Nonreflected shock tunnels hypersonic air flow, determining beginning and end times for optimum testing periods 04 p0563 A71-14666

Hypersonic flow with nonequilibrium oxygen dissociation around blunt and conical bodies, considering temperature, pressure, density and compressibility factor behind normal shock 04 p0525 A71-14982

Hypersonic rarefied nitrogen flow over wedge, investigating density field 04 p0570 A71-15033

Lifting body leeward surface maximum heat transfer coefficient in hypersonic flow, considering Reynolds number, incidence and shape effects 04 p0527 A71-15486

Binary gas mixture rarefied hypersonic flow structure near blunt body, investigating diffusive effects on recovery temperature dependence 04 p0528 A71-15488

Steady two dimensional ideal gas flow past blunt body at incident infinite Mach number, obtaining gas dynamic variable asymptotic expansions as kappa approaches infinity 04 p0528 A71-15553

Two dimensional hypersonic flow field density gradient distribution measurement by space-time resolved laser schlieren system 04 p0600 A71-15592

German monograph on centered two dimensional nonequilibrium hypersonic expansion flow, considering real gas flow with chemical reactions 05 p0693 A71-16124

Leading edge bluntness and boundary layer displacement effects on attached and separated laminar boundary layers in high temperature hypersonic flow over compression corner [AIAA PAPER 68-68] 05 p0735 A71-16561

Monte Carlo simulation for studying rarefied hypersonic gas flow about slender cones and flat plates [AIAA PAPER 69-651] 05 p0694 A71-16562

Steady state mixed subsonic-supersonic flow near blunt leading edge in hypersonic internal flow, using asymptotic solution by time-dependent method [AIAA PAPER 71-85] 06 p0843 A71-18542

Two dimensional supersonic surface jet-hypersonic flow interaction with axial symmetry [AIAA PAPER 71-131] 06 p0845 A71-18575

High accuracy hypersonic low density cone drag measurements, using method with advantages of free jet and wind tunnel electromagnetic balance [AIAA PAPER 71-133] 06 p0845 A71-18577

Hypersonic flow over cones with attached and detached shock waves, using Lax differencing technique and time dependent formulation for reentry flow fields [AIAA PAPER 71-55] 06 p0846 A71-18655

Hypersonic radiating gas inviscid flow past blunt bodies, using spherical harmonics approximation 07 p1013 A71-19183

Interaction between radiation from shock wave region and oncoming cold air flow in hypersonic flow past blunt body 07 p1014 A71-19730

Incompressible hypersonic laminar boundary layer flow over sharp cone, based on asymptotic inner and outer flow field expansion 07 p1015 A71-19892

Caret wing serial tests in Mach 8 to 15 hypersonic flow, including three component force, spanwise direction pressure distribution and shock wave angular measurements by flow visualization 07 p1016 A71-20015

Unsteady analogy for hypersonic flows past blunt bodies with shock deformation 08 p1227 A71-21863

Viscous similitude reduction to Mach number independent Birkhoff binary scaling for hypersonic flow over slender bodies [AIAA PAPER 71-252] 08 p1377 A71-21981

Static pressure port errors in hypersonic turbulent flow, using approximate shear layer momentum balance for pressure increase derivation [AIAA PAPER 71-270] 08 p1228 A71-21996

Hypersonic strong interaction flow over inclined surface, using asymptotic expansion in powers of hypersonic interaction parameter for boundary layer equations reduction 09 p1382 A71-22109

French book on hypersonic aerodynamics covering aerothermochemistry, flow equations, heat transfer, etc 09 p1382 A71-22278

Heat transfer to slender bodies in hypersonic flow, comparing wind tunnel measurements with modified reference enthalpy method predictions for laminar and turbulent flow 09 p1545 A71-22941

Hypersonic flow interaction with transverse jet, discussing experimental investigation of Reynolds number, jet pressure ratio and mass flux effects 09 p1382 A71-22944

Reactive equilibrium hypersonic gas flow over slender pointed body, neglecting rate chemistry 09 p1383 A71-23054

Turbulent wakes from subsonic-hypersonic bodies for downstream mean flow predictions analysis, considering eddy viscosity function 10 p1550 A71-24338

Mass entrainment products effect on radiative and convective heat transfer during decomposition of graphite blunt body in steady hypersonic flow of radiating air 10 p1696 A71-24364

Numerical solution of axisymmetric minimum drag bodies in hypersonic viscous gas flow, obtaining coefficient of friction by local variations method 10 p1551 A71-24370

Unsteady hypersonic flow around melting axisymmetric blunt bodies of revolution with profile depending on wall temperature, calculating temperature distribution and wall pressure 10 p1698 A71-25087

Underexpanded transverse sonic jet-hypersonic stream three dimensional flowfield based on inviscid rotational flow model 11 p1701 A71-25472

Reentry vehicles configuration lift and drag coefficients in hypersonic flow from pressure distribution and balance measurements, comparing with isolated cone data 11 p1702 A71-25487

Mach reflection of strong shock waves by sharp compressive corner in real gas in hypersonic tube, using laser Mach-Zehnder interferometer 11 p1752 A71-26190

Small surface curvature effect on unsteady hypersonic flow over thin oscillating wedge, using perturbation theory 11 p1705 A71-26197

Hypersonic reentry flow over blunt nosed bodies, using water oxygen mixture to achieve simulation at lower stagnation temperatures 11 p1705 A71-26270

Wind tunnel hypersonic flow visualization by schlieren and phase contrast methods at low volumetric mass 11 p1764 A71-26273

Newtonian limit of hypersonic flow over elliptic cylinder, finding standoff distance by Freeman result 12 p1863 A71-27055

Thin delta wing in hypersonic inviscid flow at small angles of attack, calculating motion equations and boundary conditions at small perturbations 12 p1863 A71-27330

Nozzle wall hypersonic turbulent boundary layers at free stream Mach number, using pitot, hot wire, wall pressure fluctuation and static pressure measurements [AIAA PAPER 70-746] 12 p1898 A71-27558

Radiative emission effects on viscous flow in shock structure of low density hypersonic flow around blunt body 12 p1986 A71-27583

Rarefied hypersonic flow in blunt body bow region, measuring density and rotational temperature fields by electron beam method 13 p1989 A71-27841

Unsteady large particle numerical solutions to vortical equations of plane and axisymmetric inviscid gas flow past blunt body for subsonic and hypersonic velocities 13 p1989 A71-27901

Steady hypersonic nearly free molecular rarefied gas flow about convex body, applying kinetic operator 13 p1991 A71-29152

Gas particle radial reflection model application to hypersonic nearly-free molecular flow about convex bodies, solving steady state problem 13 p1991 A71-29153

Aerodynamic characteristics similarity and variation in hypersonic flow transition region from free molecular flow to solid medium 13 p1991 A71-29172

Heat transfer on spheres and sharp cones in rarefied hypersonic gas flow at zero angles of attack in wind tunnel vacuum 13 p1992 A71-29176

Hypersonic flow around delta wing at small angles of attack, using pressure sources method and Fredholm integral equation 13 p1992 A71-29189

Unsteady hypersonic self similar gas flow and drag on circular cone accelerated according to power law, using small perturbation theory 13 p1993 A71-29205

Wind tunnel simulation of viscous hypersonic flow-laminar boundary layer interactions, presenting similarity parameter effects on aerodynamic characteristics 13 p1994 A71-29224

High entropy layer in hypersonic flow with arbitrary large freestream Mach number behind shock 14 p2334 A71-29559

Monograph on hypersonic shock tunnel supersonic combustion research techniques covering test facilities, optical and electromagnetic flow measurement methods, etc 14 p2334 A71-29578

Turbulent skin friction and heat transfer prediction on flat plates and wind tunnel walls at supersonic and hypersonic Mach numbers, using Van Driest theory
14 p2334 A71-29868

Three dimensional spatial unsteady hypersonic gas flow about bodies behind strong shock wave front
14 p2169 A71-30182

Hypersonic shockless gas flow past circular cone and cylindrical surfaces, reducing Vallander equations to nonlinear integral
14 p2169 A71-30183

Melting body disintegration in hypersonic gas flow under radiation influence from shock layer, assuming optically thin boundary layer and intense vaporization
14 p2336 A71-30222

Exothermic hypersonic blunt body flow periodic instability mechanism, using ballistic range with schlieren photographic equipment
14 p2337 A71-30455

Hypersonic flow pattern past windward side of delta wing with supersonic leading edges, joining potential and vortex regions behind shock wave
14 p2171 A71-30874

Entropy layer in hypersonic flows, determining body configuration from shock wave shape described by coordinates power function
14 p2171 A71-30875

Pitching stability derivatives of sharp oscillating wedges at zero incidence in viscous hypersonic flow from perturbation method, including thickness and wave reflection effects
14 p2171 A71-31023

Hypersonic flow of dust containing gases at low density for distribution accuracy of cosmic dust collection by sounding rockets
15 p2387 A71-31171

Flat plate surface film cooling by two dimensional tangent slot injection in hypersonic turbulent flow, measuring equilibrium temperatures and skin friction [AIAA PAPER 71-599]
15 p2343 A71-31541

Low density hypersonic flow on flat plate, discussing surface pressure measuring techniques [AIAA PAPER 71-606]
15 p2346 A71-31580

Slipstream due to supersonic source in hypersonic stream, determining shape of limiting surface
15 p2346 A71-32116

Sphere drag in hypersonic jet transition flow near free molecule limit, using magnetic suspension method
15 p2347 A71-32124

Two dimensional viscous hypersonic flow past thin, needle shaped and highly blunted bodies with strong boundary layer interaction on outer stream
15 p2347 A71-32569

Turbulent boundary layer growth over flat plate and compression corner model in hypersonic gun tunnels, measuring pressure and heat transfer rate distributions
16 p2554 A71-32880

Heat transfer, density and pressure measurements of hypersonic two dimensional centered nonequilibrium corner expansion oxygen flow with frozen boundary in shock tunnel
16 p2555 A71-32906

Rarefaction and angle of attack effects on delta wing in hypersonic flow in wind tunnel
16 p2520 A71-33376

Hypersonic small perturbation flow past two dimensional or axisymmetric slender bodies supporting logarithmic shock waves
17 p2670 A71-34658

Laminar constant pressure boundary layer hypersonic limits, estimating skin friction and heat transfer
17 p2728 A71-34885

Laminar convective heat transfer rates on hemisphere cylinder in rarefied hypersonic flow, comparing experimental results with Cheng, Davis and Lees theories
17 p2671 A71-34902

Monograph on dynamic viscous pressure interaction in hypersonic flow covering boundary layer effect on oscillating body unsteady pressure distribution in continuum hypersonic flow
17 p2671 A71-35217

Hypersonic viscid-inviscid internal flow field interaction with laminar boundary layer in circular ducts, using method of characteristics and implicit finite difference scheme
17 p2671 A71-35281

Viscous relaxing gas hypersonic flow around sphere in presence of nonequilibrium chemical reactions in shock layer
17 p2673 A71-35637

Pressure and heat flux measurements at wall of nose cone in hypersonic wind tunnel flow with high generatrix enthalpy
18 p2844 A71-36182

V shaped conical wing in supersonic and hypersonic flow with shock attached to leading edge, investigating complex wave system with time dependent and analytical methods
18 p2845 A71-36339

Viscous compressible flow around slender body in hypersonic slip flow regime, using finite difference method
18 p2908 A71-36344

Aerodynamic probes for determining flow state of high enthalpy hypersonic flow fields, considering pitot pressure, total enthalpy and current density
18 p2921 A71-36414

Pitot and static pressure measurement in low density hypersonic flows, considering thermal transpiration, gas nonequilibrium near measurement cavity and nature of inlet geometry
18 p2921 A71-36415

Force and heat transfer measurement in hypersonic flows of low gas density, using electromagnetic balances for horizontal and vertical forces and pendulum method for measuring resistance
18 p2921 A71-36416

Low density hypersonic flow around blunt bodies, considering total pressure and flow velocity on stagnation point line
18 p2846 A71-36417

Flow field and model wall on slender bodies in low density hypersonic flows ranging from free molecular flow to continuum flow
18 p2846 A71-36418

Rarefied hypersonic flow density, velocity and temperature determination by electron beam technology, including ion production, calibration curves, collisions and spectroscopic analysis
18 p2949 A71-36419

Frictionless hypersonic flow around body by time dependent numerical processes and method of characteristics
18 p2846 A71-36423

Frictionless hypersonic flows by transforming partial differential equations into ordinary, noting detonation wave analogy
18 p2846 A71-36424

Near wake streamline configuration in symmetry plane of slender cone in hypersonic flow at free stream Mach number 7
18 p2848 A71-36754

Lift and drag coefficients for arbitrary body form in hypersonic flow calculated for cylindrical surface with reference to space shuttle reentry
19 p2992 A71-37320

Hypersonic flow theory evolution, considering friction and high temperature effects and flows about slender, blunt and bluff bodies
19 p2992 A71-37455

Vortex-induced heating alleviation to lee side of slender wings in hypersonic flow by contouring leading edge planform
19 p2993 A71-37892

Hypersonic lee surface vortex heating alleviation on delta wing by apex alignment with free stream
19 p2993 A71-37895

Complex three dimensional shock waves about space shuttle configuration, visualizing hypersonic nitrogen flow with electron beams
20 p3211 A71-39356

Unsteady analogy for hypersonic flows past blunt bodies with shock deformation
20 p3176 A71-39362

Supersonic and hypersonic viscous gas flows with boundary layer induced pressure gradients, investigating disturbance upstream propagation by asymptotic theory
21 p3322 A71-40680

Boundary layer disturbances influence on three dimensional hypersonic flow about infinite triangular flat plate, investigating pressure effects on heat transfer and friction coefficients
21 p3322 A71-40681

German monograph on three dimensional steady hypersonic flow of perfect gas past pyramid shaped bodies of rhombic planform
21 p3323 A71-40774

Hypersonic flow over rearward facing step by rotational characteristics method, describing inviscid and viscous dominated regions
21 p3324 A71-40969

Delta wing shock envelope visualization at hypersonic speed, obtaining flow field photographs by vapor screen technique
21 p3324 A71-40973

Heat transfer and pressure distribution on biconic and hemispherical geometries with sharp and blunt noses in Mach 15-20 flow
22 p3480 A71-41964

Apollo command module aerodynamic characteristics in hypersonic low density flow, measuring drag, three component force and heat transfer
22 p3480 A71-42027

Electron beam fluorescence probe with modulation technique for measuring density disturbance near sharp wedge in rarefied hypersonic flow
22 p3529 A71-42052

Slender two dimensional wedge wings aerodynamic characteristics in hypersonic strong interaction flow, determining wall shear stress and lift drag ratio effects
24 p3789 A71-44621

Laminar-turbulent boundary layer transition at Mach number 2-10, observing stabilizing effect of transition Reynolds number at increasing heat transfer intensity
24 p3818 A71-44745

Axisymmetric hypersonic flow of nonequilibrium ionized monatomic radiating inviscid gas past blunt body, using Clarke-Ferrari kinetic model
24 p3790 A71-4522-02

HYPERSONIC GLIDERS

Nb alloys in hypersonic glider fabrication, discussing mechanical properties, oxidation resistances and sandwich panel design
02 p0270 A71-129358

Thermal ground testing of Concorde and Verano, considering static and fatigue testing in heat environment
18 p2899 A71-36464-5

HYPERSONIC HEAT TRANSFER

Blunt body stagnation point heat transfer in hypersonic flow, describing gas dynamic equations flow field viscosity and conductivity
04 p0528 A71-15490-9

Hypersonic laminar cavity heat transfer, including upstream boundary layer thickness, unequal core and wall temperature effects
04 p0528 A71-15491-9

Turbulent heat transfer measurements on blunt cone in nitrogen flow at high Mach number under various angles of attack
06 p1008 A71-18499-9

Nozzle wall hypersonic boundary layers in helium tunnel, presenting skin friction measurements and heat transfer rates
06 p0884 A71-18603-9

Heat conduction role in leading edge heating of wing in hypersonic flight, using conducting plate theory
13 p2165 A71-29282-7

Heat transfer and pressure distribution of cone shaped model at different angles of attack in hypersonic flow simulating reentry flight in wind tunnel
22 p3480 A71-41965-5

HYPERSONIC INLETS

Supersonic and subsonic combustion ramjet engines inlet calibration, using gun tunnel to establish hypersonic throat flow
11 p1860 A71-26271-1

Axisymmetric inlet design for turbo ramjet powered hypersonic cruise vehicle, examining effects of spillage and cowl drags on air flow characteristics
16 p2521 A71-34145-5

HYPERSONIC NOZZLES

Viscosity effect on initial highly underexpanded jets in Mach 1 to 5.7 nozzles for laminar, turbulent and rarefied air flows
13 p1989 A71-27889-5

Chemically nonequilibrium laminar boundary layer profiles in axisymmetric hypersonic conical nozzle at high air stagnation temperature, calculating wall friction, displacement and momentum loss thickness
13 p1989 A71-27904-5

Nonreacting and equilibrium chemically reacting gas turbulent boundary layer flows through hypervelocity nozzles, comparing calculation with experiment
15 p2512 A71-31577-5

Vibrational nonequilibrium Prandtl-Meyer expansion flows, discussing vibration energy associated with change of state and hypersonic nozzle flow calculation
18 p2909 A71-36440-5

Gas flow through hypersonic conical nozzle in shock-gun tunnel, measuring pressure ratio and Mach number distributions at test section
18 p2849 A71-37024-5

Viscosity effect on initial part of highly underexpanded jets in Mach 1 to 5.7 nozzles for laminar turbulent and rarefied air flows
21 p3317 A71-40079-5

Hypersonic nozzle convergent section heat transfer optimization by Euler method, using Lagrange undetermined multiplier and pipe flow approximation
22 p3622 A71-42781-5

HYPERSONIC REENTRY
Spacecraft reentry aerodynamics regarding hypersonic high altitude lifting bodies, shock wave and flow field, heat, mass and energy transfer, etc [ICAS PAPER 70-01]
02 p0185 A71-11686

Radiation effects on compression shock in hot gases, considering hypersonic flow around blunt body during planetary atmosphere entry [DFVLR-SONDDR-60]
04 p0526 A71-15101-5

Hypersonic body optimum lift control during atmospheric entry, taking into account drag coefficients and density
06 p0842 A71-18488-5

Hypersonic lifting entry vehicle turbulent heat transfer and boundary layer transition at various angles of attack and Reynolds numbers [AIAA PAPER 71-100]
06 p0844 A71-18555-5

Thoria dispersed Ni-Cr alloy hypersonic entry ablation model, accounting for Cr oxidation [AIAA PAPER 71-34]
06 p1009 A71-18654-5

Transpiration cooling of reentry vehicle nose tips, noting two dimensional aspects of porous wall coolant flow and matrix-coolant energy exchange [AIAA PAPER 69-96]
07 p1223 A71-19689-5

Hypersonic reentry heat shielding problem, considering axisymmetric laminar boundary layer flow with local coolant mass injections at multiple stations 13 p1990 A71-29127

Heat transfer and pressure distribution of cone shaped model at different angles of attack in hypersonic flow simulating reentry flight in wind tunnel 22 p3480 A71-41965

Liquid film cooling for slender body type hypersonic reentry vehicles, comparing active mass injection cooling systems to ablation type passive systems 22 p3621 A71-42006

Optimal lift control of hypersonic lifting body during atmospheric entry by singular perturbation method [AAS PAPER 71-366] 23 p3773 A71-43036

HYPersonic SHOCK

Hypersonic shock wave production into air at one atmosphere in tube with electrical discharge gas heating 04 p0566 A71-14970

Hypersonic shock tube for aerodynamic measurements at high Reynolds numbers [DFVLR-SONDDR-95] 06 p0880 A71-18046

Chemical nonequilibrium effects on hypersonic, blunt body shock layers flow in reacting planetary carbon dioxide-nitrogen atmospheres 06 p0866 A71-18496

Solid particle impurity effects on hypersonic shock tube flow, determining error in blunt body measurements 07 p1013 A71-18916

Newtonian limit of hypersonic flow over elliptic cylinder, finding standoff distance by Freeman result 12 p1863 A71-27055

Small spherical solid or liquid particles deceleration, melting and shattering due to spherical and conical bodies in compressible hypersonic shock layer flow field [AIAA PAPER 69-712] 14 p2334 A71-29873

Flap induced flow deflection effects in hypersonic shock tunnel, obtaining turbulent heating, skin friction and pressure data [AIAA PAPER 71-598] 15 p2343 A71-31540

Parametric differentiation solution accuracy and stability for temperature profile and heat flux behind one dimensional hypersonic shock, including thermal radiation 21 p3409 A71-41016

Hypersonic shock wave front motion into air at one atmosphere, measuring reflectivity and curvature for comparison with theory 23 p3626 A71-43929

HYPersonic SPEED

Hot wire total temperature probe at hypersonic speeds for flow field measurements [AIAA PAPER 71-273] 08 p1377 A71-21999

Aerodynamic effects of bluntness on slender cones in free flight tests at Mach 17 [AIAA PAPER 70-554] 09 p1381 A71-22090

Unperturbed atmospheric parameters calculation from surface measurements of blunt body at hypersonic speeds under various aerodynamic conditions 09 p1437 A71-22678

Unsteady vibrations of rotating free solid body entering atmosphere at hypersonic velocity, taking into account nonlinearity of aerodynamic moments 12 p1972 A71-27171

Axisymmetric flow effects on surface mass injection at supersonic and hypersonic speeds, streamline inclinations and surface pressures generation by turbulent viscous dissipation 14 p2223 A71-29874

Flow field measurement about sharp and slightly blunted slender cone at hypersonic speed and zero angle of attack [AIAA PAPER 71-625] 15 p2344 A71-31553

Flat plate span effects on ramp induced adiabatic laminar boundary layer separation at supersonic and hypersonic speeds, measuring surface pressure distribution [AIAA PAPER 71-559] 15 p2344 A71-31557

Slender cone at Mach 10 with underexpanded exhaust plume, determining flow field interactions separation pattern and aerodynamic coefficients [AIAA PAPER 71-562] 15 p2347 A71-32280

Free flight static and dynamic stability tests on lightweight cone shaped models in longshot tunnel at hypersonic speeds, using spark recording 16 p2519 A71-32879

Free piston double diaphragm shock tube for hypersonic speeds without attenuation in argon, discussing time resolved channeled spectra measurements of electron density 16 p2551 A71-32916

Flow processes around body of hypersonic velocity, studying plasma diagnostics in ionized wake 18 p2952 A71-36421

Flow parameters behind shock waves propagating in carbon dioxide-nitrogen mixtures at Mach numbers from 5 to 10 19 p3044 A71-37583

Hypersonic flat plate under impulsive loads, calculating time dependent transient wall shear stress and boundary layer induced pressure 21 p3369 A71-40964

HYPersonic TEST APPARATUS

Stored arc heated air true temperature, flight and altitude simulation facility in Mach number 8 to 10 region for air breathing propulsion research [AIAA PAPER 71-254] 08 p1273 A71-21983

Hypersonic magnetic spectrometer-relaxometer, comparing direct and indirect recording methods for hypersonic in metals at helium temperatures 16 p2580 A71-33928

HYPersonic VEHICLES

NT HYPersonic AIRCRAFT

NT HYPersonic GLIDERS

Sandwich metal construction with welded Norsial corrugated core for light weight and strength, discussing fabrication and application to hypersonic research vehicles 04 p0603 A71-15207

Hypersonic vehicles low speed handling qualities, describing test flights approach and landing operations 05 p0697 A71-16680

Cone roll dynamics-ablation patterns coupling in hypersonic wind tunnels [AIAA PAPER 70-562] 07 p1208 A71-19868

Composite rocket cum hypersonic airbreathing propulsion reducing space exploration program cost 08 p1348 A71-21301

Hydrocarbon fuel for hypersonic vehicle cooling, discussing use of endothermic reactions to achieve maximum heat sinks [AIAA PAPER 68-997] 10 p1658 A71-24852

Hypersonic cruise vehicles viscous interactions areas, examining compression corners, shock interactions, laminar and turbulent flow, boundary layer separation, etc [AIAA PAPER 70-781] 12 p1865 A71-25551

Axisymmetric inlet design for turbofanjet powered hypersonic cruise vehicle, examining effects of spillage and cowl drags on air flow characteristics 16 p2521 A71-34149

Omnidirectional one slot aerial energized by dielectric waveguide for hypersonic vehicle-ground communication through ionized shock layer [ONERA-TP-949] 18 p2887 A71-36022

Matched asymptotic solutions for optimum lift controlled atmospheric entry of hypersonic lifting vehicles 24 p3876 A71-44609

HYPersonic WAKES

Spherical and cylindrical electrostatic probes for point ion density measurements in continuum flowing plasmas in hypersonic wake, discussing shock tube program for calibration 03 p0423 A71-13441

Two dimensional hypersonic laminar wakes incipient transition region calculation based on boundary layer approximation and von Karman integral formulation [AIAA PAPER 71-202] 06 p0846 A71-18640

Hypersonic wakes conductivity measurements behind models in argon and air, using electrodynamic technique 12 p1863 A71-27208

Hypersonic wakes of two dimensional slender wedges and flat plate, testing stability in transition region in wind tunnel 12 p1866 A71-27561

Hypersonic wakes behind wedges for various angles of attack, determining near and far wakes [AIAA PAPER 71-563] 15 p2344 A71-31558

Holographic interferometry measurements of mean and localized fluctuating wake density field of cones fired at Mach 6 at ballistic range, using pulsed laser [AIAA PAPER 71-564] 16 p2520 A71-33105

Hypersonic free flight test facilities using light gas guns, considering wake of flight vehicle at hypersonic velocity and aerothermal phenomena 18 p2898 A71-36411

Inclined wedges in rarefied hypersonic flow conditions, investigating base and wake pattern geometrical and aerodynamic characteristics 18 p2849 A71-36756

Hypersonic wakes conductivity measurements behind models in argon and air, using electrodynamic technique 19 p2994 A71-38620

Cooled film anemometer techniques for hypersonic wake temperature and velocity distribution measurements for projectiles in free flight range 21 p3363 A71-40386

Simultaneous CW microwave radiometer and laser probing of hypersonic wake ionization and turbulence, relating radiation temperature, radar echo and mechanical flow field structure 21 p3392 A71-40387

Charge density fluctuation measurements in ionized turbulent hypersonic sphere wakes, using Langmuir and continuum electrostatic probes and microwave interferometric and scattering equipment 21 p3363 A71-40388

Hypersonic turbulent wake density measurements in free flight hypersonic ranges by electron beam fluorescence probe technique 21 p3363 A71-40389

Turbulent hypersonic wake density and temperature measurement for slender cone model in shock tunnel, using dual electron beam excitation technique 21 p3364 A71-40396

Two dimensional and three dimensional wakes in supersonic and hypersonic rarefied gas wind tunnels, comparing cone and dihedral configurations 23 p3625 A71-43357

Hypersonic axisymmetric slender body near wake shear layer determination by shock expansion method for numerical computation accuracy and efficiency 23 p3626 A71-44194

HYPersonic WIND TUNNELS

U HYPersonic VELOCITY WIND TUNNELS

HYPersonic

Solid state phenomena investigation by hypersonic methods, discussing frequency and temperature dependence of hypersonic phonons damping in crystals, elastic wave interactions in semiconductors, etc 06 p0942 A71-18199

Nose bluntness, angle of attack and oscillation amplitude effect on hypersonic unsteady aerodynamics of slender cones [AIAA PAPER 70-216] 07 p1016 A71-19895

HYPERSPACES

Misconceptions and distortions in n dimensional covariance matrices interpretation regarding probability confidence levels to error ellipsoid and hyperellipsoid 11 p1791 A71-25485

Einstein equations solution as hypersurface of four dimensions in Euclidean space, investigating imbedded manifold deformations 16 p2610 A71-33272

Strassen algorithm as matrix products representation in seven dimensional space 18 p2942 A71-36700

Characteristic initial data for gravitational vacuum fields invariant of two initial null hypersurfaces and space-like section sigma 22 p3576 A71-42404

HYPERTENSION

Renin level in renal venous and peripheral blood in patients with renovascular hypertension 01 p0010 A71-10391

Right heart ventricle activity in patients with hypertension recorded by electrocardiograph 01 p0014 A71-11138

Behaviorally induced hypertension in squirrel monkey following conditioned key-pressing response schedules 01 p0015 A71-11330

Endocrine and metabolic effects of noise in normal, hypertensive and psychotic subjects, considering increased corticoadrenal and adrenergic activity 03 p0359 A71-13154

Cardiovascular and biochemical effects of chronic intermittent neurogenic stimulation, noting alaphamethyltyrosine antihypertension agent 03 p0359 A71-13157

Physiological characteristics in llamas pulmonary circulation at sea level and changes after 5 and 10 weeks at 3,420 m above sea level, noting arterial hypertension 08 p1237 A71-20678

Cardiac output in relation to peripheral resistance in borderline hypertension 09 p1392 A71-22591

Hypertensive effects and tissue metal levels due to Cd, Hg and Zn intraperitoneal injection in rats 09 p1397 A71-23543

Hypertensive heart and pulmonary vascular disease, examining chronic alveolar hypoxia effects 11 p1719 A71-25931

Mild hypertension risks, presenting results of case studies over ten year period of mortality rate associated with cardiovascular diseases 13 p2004 A71-27865

Hypertension and heart or arterial disease relationships, discussing cause and effect mechanisms in coronary diseases 13 p2004 A71-27866

Whole body blood flow autoregulation relationship to hypertension in reflex dogs 13 p2013 A71-28953

Diastolic and mean blood pressure responses to exercise after beta-adrenergic blockade in normal and labile hypertensive subjects, using Trasicor 13 p2014 A71-29320

Coronary vasculature development under hypoxia and pulmonary hypertension as possible cause of right ventricle phasic flow contour changes 14 p2184 A71-30282

High altitude residents cardiovascular evaluations, showing right ventricular enlargement and reactive pulmonary hypertension 14 p2184 A71-30285

Systolic and diastolic blood pressures and urinary catecholamines under stress in normotensive and hypertensive subjects 15 p2358 A71-31451

Plasma renin activity in hypertonic and normotonic persons exposed to exogenous stress, comparing with measurements at rest and in orthostasis 20 p3185 A71-38893

- Parasympathetic inhibition effects on hyperkinetic borderline hypertension, measuring cardiac output, resting heart rate and intraarterial blood pressure
21 p3332 A71-40407
- Photoplethysmographic analysis of pulse wave velocity in healthy subjects and in patients with hypertension, heart disease, diabetes and anemia
22 p3490 A71-42518

HYPERTHERMIA

- Human heat exchange and body overheating mechanism at high ambient temperatures at sea level and lowered pressures
01 p0013 A71-11134
- Cerebral oxygenation and metabolism during progressive hyperthermia
04 p0538 A71-15092
- Human erythrocytes phosphate metabolism in hyperthermia
05 p0711 A71-16944
- Pancreas pathomorphology under acute hyperthermia in animals, showing hemodynamic changes of vessel dilatation and intravascular leukocytosis
08 p1243 A71-21968
- Hyperthermia effects on conduction velocity of nerve fibers and peripheral motor neuron-muscular activity in man
09 p1399 A71-22924
- Physiological responses to head and neck vs trunk and leg cooling under hyperthermic stress
21 p3331 A71-40356

HYPERTONIA

U OSMOSIS

HYPERTROPHY

U GROWTH

HYPERVELOCITY ACCELERATORS

U HYPERVELOCITY GUNS

HYPERVELOCITY CRATERING

U HYPERVELOCITY PROJECTILES

U PROJECTILE CRATERING

HYPERVELOCITY FLOW

- Time asymptotic solutions for hypervelocity blunt body flow field with coupled nongray radiation, treating shock as discrete surface
[AIAA PAPER 70-865] 11 p1701 A71-25453
- Three dimensional hypervelocity reentry trajectories, using aerodynamic lift and vehicle bank angle as optimal control parameter
[AIAA PAPER 71-920] 19 p3096 A71-37169

HYPERVELOCITY GUNS

- Small caliber smoothbore powder sabot guns generating planar shock wave in solids, using streak camera monitoring of impact and recoil velocities
14 p2223 A71-30885
- Gun tunnel free flight testing system and components, discussing model dropping, magnetic suspension and light beam and RF tracing
[DFVLR-SONDDR-136] 21 p3362 A71-40382

HYPERVELOCITY IMPACT

- Spherical shells deformation subjected at elevated temperature to high velocity impact on planar rigid target
03 p0503 A71-13427
- Projectile impacts into laminated targets consisting of plastic layers backed by Al substrates using SHAPE code with hydrodynamic elastoplastic distortional model
[AIAA PAPER 69-356] 03 p0504 A71-13431
- Fracture of bumper protected fuel tanks subjected to hypervelocity meteoroid impact, applying method of characteristics to stress wave propagation in tank walls
[AIAA PAPER 69-369] 03 p0500 A71-14431
- Jetting collision effect on structural changes at interface between Ti and steel in explosive bonding, considering plastic deformation and residual stresses
10 p1629 A71-25030
- Construction and hypervelocity impact tests of penetration resistive dual bumper wall for spacecraft meteoroid protection
[AIAA PAPER 71-339] 11 p1843 A71-25318
- Hypervelocity impact produced metallic plasmas equilibrium composition and radiation, calculating radiative energy as function of wavelength and internal partition functions
11 p1804 A71-25510
- Micrometeoroid detector design for hypervelocity particle impacts, discussing solar radiation pressure effects on satellite measurements
11 p1761 A71-25544
- Hypervelocity projectile material impact on ultimate reflectance of bombarded polished metals from shock tube tests
11 p1799 A71-25835
- Shock tube facility with two-phase system of solid particles and gases as primary driven fluid, applying to hypervelocity impact phenomena observation
11 p1745 A71-26266
- Rigid spherical projectile hypervelocity impact with compressible strain-hardening target material, obtaining analytic solution based on dynamic cavity expansion and deep penetration theories
12 p1982 A71-27570
- Lunar, meteoroid and asteroid surface erosion, investigating hypervelocity impact, solar wind flux and ion sputtering effect
16 p2642 A71-33818

Hypervelocity impact melts, considering meteorite crater igneous rocks or glasses associated with shock deformation
19 p3051 A71-37666

Micrometeoroid flux determination from impact sites on Surveyor 3 TV camera optical filter surfaces, noting agreement with Pioneer, Cosmos and Pegasus spacecraft measurements
23 p3766 A71-43820

Spherical projectile hypervelocity impact on compressible fluid, showing viscous effects on velocity and stress distribution behind shock front
24 p3877 A71-44426

HYPERVELOCITY LAUNCHERS

Implosion driven hypervelocity launcher performance prediction, considering loss mechanisms, hydrodynamic calculations and shock phenomena
05 p0733 A71-16505

HYPERVELOCITY PROJECTILES

Velocity and density measurements in hypervelocity ballistic projectile turbulent wakes, using hot film anemometers
[AIAA PAPER 68-701] 07 p1015 A71-19891

Rigid spherical projectile hypervelocity impact with compressible strain-hardening target material, obtaining analytic solution based on dynamic cavity expansion and deep penetration theories
12 p1982 A71-27570

Pulsed ruby laser high speed photography for accuracy measurements of models contours in hypervelocity flight within aeroballistic range
18 p2923 A71-36612

Cost effective high speed projectile trajectory plotting system for gunnery range instrumentation, applying to aircraft path recording during automatic landing control
18 p2924 A71-36613

Mass spectrometer application to gas analysis of samples from turbulent wake of hypervelocity projectiles
21 p3362 A71-40384

Sequential electric spark technique for hypervelocity projectiles turbulent wake velocity measurements at ballistic ranges in free flight regime
21 p3362 A71-40385

Holography capabilities of hypervelocity projectiles with front surface resolution, discussing fringes intensity and position from projectile spin
22 p3549 A71-42569

Laser optical system for hyperballistic range hypervelocity models surface erosion measurement, describing instrumentation of front-lighted, silhouette and stereo stations
23 p3677 A71-43513

HYPERVELOCITY WIND TUNNELS

NT CASCADE WIND TUNNELS

NT PLASMA JET WIND TUNNELS

NT SHOCK TUNNELS

Axisymmetric hypersonic wind tunnel nozzle design by determining inviscid contour and correcting for turbulent boundary layer growth
[AIAA PAPER 69-337] 01 p0003 A71-11578

Gas ionization in supersonic wake at throat, transition and breakthrough points in hyperballistic firing tunnel for atmospheric reentry study
03 p0462 A71-13131

ONERA hypersonic wind tunnels used for ballistic and aerodynamic research kinetic heating problems and control surface efficiency
[ONERA-TP-877] 06 p0841 A71-18025

Hypersonic low pressure wind tunnel design and operation, describing instrumentation
[DFVLR-SONDDR-94] 06 p0880 A71-18045

Blunt cylinder with small thread in anomalous seeded flow in hypersonic wind tunnels, observing separated shock wave distortion
07 p1013 A71-18924

Wind tunnel history, evolution and use, covering low speed variable density, high speed transonic, supersonic, hypersonic and hypervelocity wind tunnels
08 p1272 A71-21666

High turbulent flow simulation in hypervelocity wind tunnel for reentry vehicles operational testing, discussing nozzle gas dynamic and mechanical design
[AIAA PAPER 71-253] 08 p1273 A71-21982

Comparative sting supported and free flight tests in hypersonic wind tunnel on modified Apollo launch configuration
[AIAA PAPER 71-265] 08 p1274 A71-21991

Aerodynamic support interference in wind tunnel testing of configurations involving bulbous base, mass addition, transition near base and hypersonic low density flows
[AIAA PAPER 71-277] 08 p1228 A71-22002

Pressure orifices inclination in low density flow from experiments with cooled flat plate model in hypersonic low density wind tunnel
11 p1751 A71-25490

Wind tunnel hypersonic flow visualization by schlieren and phase contrast methods at low volumetric mass
11 p1764 A71-26273

Wind tunnel simulation of viscous hypersonic flow-laminar boundary layer interactions, presenting

SUBJECT INDEX

- similarity parameter effects on aerodynamic characteristics
13 p1994 A71-29220
- Holographic recording of optical inhomogeneities in gas flow in hypersonic wind tunnels, using Mach-Zehnder interferometer and schlieren apparatus
15 p2404 A71-31274
- Rarefaction and angle of attack effects on delta wing in hypersonic flow in wind tunnel
16 p2520 A71-33378
- Velocity determination in hypersonic low density wind tunnel based on high energy electron beam produced nitrogen ions time of flight
17 p2670 A71-34889
- Solid particle impurity effects on hypersonic wind tunnel flow characteristics
17 p2671 A71-35116
- Heater and nozzle design of ONERA/S4MA hypersonic wind tunnel for supersonic combustion ramjet tests
[ONERA-TP-924] 18 p2956 A71-36017
- Intermittent hypersonic wind tunnels, considering pressure and vacuum storage, blowdown tunnels and pressure tubes
18 p2897 A71-36409
- Continuous hypersonic wind tunnels with low gas density simulating flow states during reentry phase of space vehicles
18 p2898 A71-36412
- High temperature gas dynamics, including hypersonic wind tunnel nozzles, air-breathing/chemical rocket propulsion systems, thermodynamic models and relaxation boundary layers
18 p2846 A71-36425
- Gas flows with thermodynamic relaxation, considering expanding flows in hypersonic wind tunnel nozzles
19 p3162 A71-37458
- Free flight hypersonic wind tunnel model testing in Ludwieg tube, discussing launching device and recording setup
21 p3362 A71-40381
- Gas density measurement and flow visualization in hypersonic wind tunnel by electron beam probe, noting isobaric boundary layer application
21 p3364 A71-40395
- Arc driven hypersonic wind tunnels total enthalpy measurement from blunt body gas cap emission, using rapid scan spectrometer for gray gas continua
21 p3364 A71-40403
- Hypersonic wind tunnel air condensation detection by light scattering instrumentation, discussing stagnation temperature condensation
21 p3364 A71-40405
- Conical ablation surface models in hypersonic wind tunnel tests, describing Mach number and nose tip bluntness effects on cross hatching
21 p3476 A71-40965
- Heat transfer and pressure distribution of cone-shaped model at different angles of attack in hypersonic flow simulating reentry flight in wind tunnel
22 p3480 A71-41965

HYPERVENTILATION

Blood plasma volume reduction by voluntary hyperventilation, associating with hypovolemia of status asthmaticus
04 p0545 A71-15155

Hyperventilation and isoproterenol infusion, investigating T wave abnormalities, arterial blood gases and plasma electrolyte concentration
07 p1042 A71-19837

EEG examination of healthy aircrew for high performance aircraft flying fitness evaluation, stressing hyperventilation factor importance
12 p1876 A71-27631

Respiratory responses and hyperventilation mechanism during static muscular work in maximal voluntary contraction, noting chemoreceptor and alarm-defense reaction
13 p2008 A71-28436

Ventilatory acclimatization to chronic hypoxia in high altitude natives by cerebrospinal fluid pH decrease
17 p2683 A71-35144

Alveolar-arterial oxygen pressure difference during controlled hyperventilation and posthyperventilatory phase
19 p3003 A71-38200

Potential epilepsy determination in flight personnel, suggesting systematic EEG with hyperventilation and photic stimulation tests and personal history data of head trauma and unconsciousness
21 p3331 A71-40357

Hyperventilation syndrome in flying personnel, discussing symptoms of paresthesia and extremities contraction, psychoemotional causes and control mechanism
22 p3500 A71-41569

HYPNOSIS

Human biomechanical and vegetative reactions to hypnotic suggestion of gravitational effects
08 p1243 A71-21971

HYPOBARIC ATMOSPHERES

Visual performance and retinal vascular changes under hypobaric elevation and hypoxia, noting stereopsis, binocular depth perception, critical flicker fusion, dark adaptation, etc

22 p3485 A71-41719

Stimulatory effects of hypobaric hyperoxia on lipid synthesis in rat liver and adipose tissues under free breathing

22 p3486 A71-41825

HYPOCAPNIA

Chemorensitivity in normal, hypoxia and hypocapnia cases, using rebreathing techniques to construct toxic carbon dioxide response curves and isocapnic oxygen response curves

07 p1052 A71-20329

HYPODYNAMIA

Hypodynamia effects on human hemodynamics under various microclimatic conditions, noting horizontal activity changes in sympathoadrenal system

10 p1563 A71-24339

Cardiac activity changes during prolonged hypodynamia, discussing clinical and experimental investigations results with humans and animals

15 p2358 A71-31320

Human nitrogen and water-salt metabolisms and respiratory activity during prolonged confinement in small volume chamber with cyclic varying hypoxic air

22 p3495 A71-42799

Hormonal activity during hypodynamies

24 p3796 A71-44538

HYPOELASTICITY

Longitudinal acceleration and distinct transverse waves propagation in Hadamard and Green hypoeplastic materials

01 p0165 A71-10025

Yield conditions and flow rules derivation from hypoeplasticity, regarding constitutive equation as linear transformation on six dimensional inner product space of symmetrical tensors

21 p3455 A71-40090

HYPOKINESIA

Hypokinetic effect on sarcoplasmic and myofibrillar protein composition of skeletal muscles in rats

01 p0013 A71-11130

Hypokinesia and acceleration effects on plasma proteins displacement and bioelectric activity of striated muscles of rats

06 p0853 A71-17960

Ischemic deafferentation of transversostriated muscle quadriceps femoris in cats contributing to hypokinesia and psychophysiological disturbances

06 p0854 A71-18362

Liver and skeletal musculature morphology during hypokinesia and protein deficiency in mice

06 p0855 A71-18377

Reduced diaphragmatic muscle tissue resistance in rats during prolonged hypokinesia, showing sorption of basic vital neutral red stain

13 p2007 A71-28417

Hypokinesia effect on formation and elimination of ketones, aldehydes, carbon monoxide and ammonia in rats

15 p2356 A71-31305

Prolonged hypokinesia effect on rats serotonin (5-HT) metabolism, noting pronounced blood content deviation from normal during first to third and thirteenth to fifteenth day

20 p3187 A71-39218

Nasal vascular system reactions during 120-day bed rest hypokinesia under drug affected metabolism

20 p3188 A71-39229

Shin muscle electrical activity during standing after 120 day bed rest hypokinesia from EMG measurement

20 p3188 A71-39230

Morphological and cytochemical changes in red and mixed skeletal muscles of animals exposed to hypokinesia

23 p3636 A71-44237

Hypokinesia effects on gas exchange and oxygen consumption in rats, noting weight losses

24 p3795 A71-44526

Minute blood and stroke volumes dynamics during prolonged hypokinesia by acetylene method

24 p3796 A71-44536

HYPOTENSION

Carotid sinus hypotension in dogs under fasting/digestion conditions, considering effect on splanchnic circulation and vasoconstrictor response

04 p0538 A71-15090

Antihistamine treatment of hypotension and early transient incapacitation in monkeys under supralethal mixed gamma-neutron radiation

11 p1720 A71-26118

HYPOTHALAMUS

Blood cholesterol and protein fraction concentrations in pathogenesis of hypothalamic atherosclerosis patients

02 p0201 A71-12531

Rabbit hypothalamic neuron stimulation by changes in ambient temperature

03 p0361 A71-13225

Phospholipid composition of lipid extracts of hypothalamo-neurohypophyseal system of cattle

03 p0362 A71-13237

Hypothalamus and adrenal glands catecholamines relationship for hypophysectomized rats

03 p0362 A71-13293

Ascending pathways from spinal thermosensitive region to hypothalamic temperature control center, considering spinothalamic tract impulse frequency temperature response and bilateral RF coagulations

04 p0539 A71-15094

Retinohypothalamic projection in rats by light microscope observations in unilateral retinal destruction

05 p0707 A71-16344

Retinohypothalamic projection in rats by electron microscope observations of degenerating nerve fibers and boutons in arcuate nucleus after bilateral retinal destruction

05 p0707 A71-16345

Polymorphic nucleus leukocytes pyrogenic protein fraction effects on rabbits hypothalamic thermal control structures

05 p0707 A71-16386

Prolonged water deprivation effects on hypothalamic self stimulation of rats with electrodes chronically implanted in posterior lateral hypothalamus

05 p0711 A71-17087

Oxygen respiration effect on self stimulation and emotional reactions in rabbits during hypothalamus electrical stimulation

06 p0855 A71-18376

Antagonistic descending characteristics of medial and lateral hypothalamic nuclei on excitation of spinal cord motoneurons

06 p0856 A71-18465

Hypothalamus supraoptic nucleus morphological changes in rats under prolonged transverse acceleration

09 p1388 A71-22195

Physiological and biochemical changes arising in allergic reactions and hypothalamic neurohumoral regulation disorders role, comparing with diencephalic syndromes

11 p1718 A71-25667

Food and water intake changes associated with interruption of hypothalamus anterior or posterior fiber connections

13 p2011 A71-28802

Cardiovascular responses to hypothalamic, spinal cord and stellate ganglion stimulation as function of intensity, pulse duration and frequency in cats

16 p2531 A71-33367

Hypothalamus and cerebral cortex electric stimulation effects on temperature homeostasis under hyperoxia

17 p2680 A71-34645

Skin surface burns effect on neurosecretory processes in hypothalamus supraoptic and paraventricular nuclei and neurosecretory admission into hypophysis

17 p2680 A71-34647

Differentiation of hypothalamic drive and reward centers, applying electric stimulation via chronically implanted electrodes

17 p2681 A71-34944

Human sweating regulation at rest, evaluating thermal inputs effects on thermoregulatory center and internal hypothalamic and skin temperatures

17 p2683 A71-35146

Hypothalamic unit activity relation to thermoregulation, investigating preoptic area response to local and peripheral temperature changes

18 p2859 A71-36869

Preoptic anterior hypothalamic area temperature sensitive neurons, showing integrative center for thermoregulation

18 p2859 A71-36870

Cats preoptic and skin temperature change effects on posterior hypothalamic neurons

18 p2861 A71-36888

Guinea pig thermoregulation of shivering and nonshivering thermogenesis, showing intrahypothalamic noradrenaline injection effects on threshold temperature elevation

18 p2862 A71-36901

Postexercise elevated tissue temperatures contributions to oxygen consumption in rats, suggesting hypothalamic adjustment

20 p3186 A71-38981

Motor and vestibular analyzers and frontal hypothalamus role in gravitational loads compensation during orthostasis, noting respiration, arterial pressure and brain bioelectric activity changes

20 p3188 A71-39223

Cutaneous and intestinal blood flow differentiation during hypothalamic heating and cooling in anesthetized dogs

21 p3335 A71-40632

Incentive goal and extensive stimulation experience effects on proportion increase of hypothalamic electrode sites yielding elicited eating and drinking behavior

21 p3336 A71-40706

Purine and pyrimidine derivatives of cattle hypothalamus determined by gel filtration and subsequent spectral analysis and chromatography

21 p3338 A71-41071

Coronary dilating substances of low molecular weight separated through dialysis from hypothalamus protein carriers

21 p3338 A71-41072

Diurnal water and food intake and body weight changes pattern in rats with hypothalamic lesions

22 p3486 A71-41936

Hypothalamus anterior and hippocampus limbic system relation and oxytocin effect in rabbits, using EEG analysis

22 p3490 A71-42577

HYPOTHERMIA

Enzyme activity reduction in thyroid gland tissue of albino rats under deep hypothermia

01 p0012 A71-11057

Morphological and histological changes in liver and kidneys of rats exposed to long term hypothermy

01 p0013 A71-11131

Oxygen consumption and carbonic acid output in hypothermic rats cooled under diethyl ether anesthetics, investigating physiological indices during hypothermia

06 p0852 A71-17667

Coagulative and delayed cumulative cataract production by microwaves investigated by hypothermic technique

10 p1572 A71-25077

Hypothermia effect on lipid synthesis of hamster tissue following intravenous injection of acetate-C 14

14 p2182 A71-29582

Hypothermia effects on cat and dog vascular tone vasomotor reflex regulation, suggesting role of inhibition due to changed afference from cooled tissues

16 p2533 A71-34111

Ascorbic acid reduction in organs due to thyroid hormones saturation under hypothermia

17 p2680 A71-34646

Alpha adrenergic inhibition of immunoreactive insulin release during deep hypothermia in puppies given glucose infusions

17 p2681 A71-34942

Rat plasma creatine phosphokinase activity, hypothermia and stress, considering cold restraint

22 p3486 A71-41938

Hypothermia effect on brain nutritive processes and regulator activity, considering changes in brain blood supply, respiration and carbohydrate metabolism

22 p3486 A71-41940

Caffeine, ephyllin, cordiamin, morphine, calcium chloride, adrenaline and mesaton effects on organism physiology during hypothermia

22 p3492 A71-42709

HYPOTHESES

NT EXPECTANCY HYPOTHESIS

NT LAGRANGE SIMILARITY HYPOTHESIS

NT VORTICITY TRANSPORT HYPOTHESIS

Superconducting Nb experimental tests for hypothesis concerning relations between anisotropic critical field and dislocation cell structure

07 p1138 A71-19988

Hypothetical geocentric /interplanetary/ dust cloud concentration detection possibility by earth shadow

10 p1601 A71-24449

Spiral galaxies orientation anisotropy explanation by hypothetical model of cosmological magnetic field

11 p1831 A71-26166

Respiratory air flow optimal regulation hypothesis, testing analytic prediction model results with experiment under stress and rest conditions

13 p2023 A71-29491

Bayesian estimate of signal parameters in random noise background under mutually exclusive hypotheses about statistical properties

15 p2370 A71-31584

Cartesian diver atmospheric model hypothesis for Jupiter Red Spot longitude, size and intensity variations

18 p2964 A71-36288

HYPOVOLEMIA

Blood plasma volume reduction by voluntary hyperventilation, associating with hypovolemia of status asthmaticus

04 p0545 A71-15155

Somatosensory cortical and cuneate evoked responses and EEG amplitude/frequency changes due to hypovolemic shock

13 p2003 A71-27836

HYPOXEMIA

Hypoxemia reflex neurogenic vasoconstrictor factors competition with local vasodilator mechanisms in skeletal muscle

08 p1237 A71-20680

HYPOXIA

Hypoxia effects on cerebral vascular autoregulation to arterial perfusion pressure in dogs

01 p0015 A71-11185

Visual task vigilance deterioration under hypoxia, considering work-rest schedule effect and IQ scores

01 p0017 A71-11418

Russian book on perception of respiratory medium and gas preference in man and animals covering hypoxic or hypercapnic media, inhalation times, gas mixtures, etc

02 p0198 A71-11823

Hypobaric pressure and hypoxic or hyperoxic atmospheres effect on mice resistance to pneumococcal pneumonia

02 p0199 A71-12382

Human vigilance performance in brightness discrimination task under hypoxia, considering reaction time in signal detection

04 p0541 A71-14740

Long term hypoxia effects on granuloma and various organs in rats, noting collagen and noncollagenous proteins formation stimulation and/or inhibition

05 p0706 A71-16293

Training effect on oxygen tension dynamics in rats brain cortex under progressive high altitude hypoxia conditions, noting adaptation influence on motor activity and survival rate

06 p0850 A71-17394

Acute mountain sickness due to oxygen deficiency, discussing control by acetazolamide, placebo or furosemide pretreatment

06 p0851 A71-17613

Hypoxia tolerance of aircrew with previous impaired flight consciousness in high altitude high performance aircraft

06 p0859 A71-17617

Hypoxia-hypercapnia interplay as respiratory chemoreceptors stimulants and depressants by investigating arterial oxygen and carbon dioxide tensions effects on phrenic nerve activity

06 p0854 A71-18061

Female aircrews under moderate hypoxia, noting uterine rheography modification

06 p0860 A71-18194

Hypoxic and hypercapnic ventilatory control and oxygen uptake in athletes, noting chemoreceptor function

06 p0862 A71-18384

Myocardial ventricular contraction in high altitude hypoxia adaptation, using barochamber trained rats

06 p0857 A71-18467

Cardiovascular responses of hypoxic hypoxia in mongrels with catecholamine induced coronary dilation

06 p0857 A71-18723

Hypoxia protection against ionizing irradiation by anaerobic glycolysis stimulation, lactic acid increase and blood glucose level elevation

07 p1037 A71-18966

Prenatal exposure to hypoxia, showing prolonged suppression of labeled amino acid incorporation into developing submandibular gland and pancreas in neonatal period

07 p1042 A71-19698

Chemosensitivity in normal, hypoxia and hypercapnia cases, using rebreathing techniques to construct isoxic carbon dioxide response curves and isocapnic oxygen response curves

07 p1052 A71-20329

Simulated high altitude chronic hypoxia and long term sideropenic anemia adapted animals, investigating acute anoxia tolerance of myocardium

07 p1044 A71-20331

Barometric pressure and exercise effects on erythropoietin titer in normal and hypoxic rat plasma, noting lactic acid concentration and acid base balance changes

08 p1237 A71-20676

Chronic hypoxia effects on capillary development during high altitude exposure in decompression chamber and maintenance at sea level

08 p1237 A71-20679

Hypoxia from aerospace medicine viewpoint, discussing respiration physiology, oxygen transport, altitude effects, psychomotor functions, etc

08 p1238 A71-20705

Altitude range for supplemental aircraft continuous flow, diluter and pressure demand oxygen systems, discussing regulations and pressure breathing

08 p1244 A71-20714

Myocardial lysosomal enzymes activity in adaptation to high altitude hypoxia and during cardiac diseases, using albino rats

08 p1239 A71-21058

Cardiac output variations in regulation of arterial oxygen transport during hypoxia

08 p1241 A71-21939

Pilots hypoxic hypoxia occurrence and treatment

08 p1249 A71-21959

Gas exchange and muscular thermoregulation activity in rats under environmental oxygen deficiency

08 p1242 A71-21963

Absorption and incorporation rates of C 14 glucose in rats under acute hypoxia

08 p1242 A71-21964

Human conditioned reflexes to time and EEG responses under acute hypoxia

08 p1243 A71-21970

Humans and animals acute hypoxia effects on EEG pattern and behavioral reactions

09 p1390 A71-22210

Myocardium ultrastructure and histochemistry in dogs under hypoxic hypoxia

09 p1390 A71-22262

Glycine conversion into serine, aspartate and glutamate in cerebrum under normal and hypoxia conditions

09 p1391 A71-22482

Oxygen deficiency and body temperature effects on work capacity of human subjects in hot humid environment

09 p1399 A71-22922

Dynamic respiratory and circulatory responses to hypoxia in anesthetized dogs, recording oxygen partial pressures, heart rate, blood pressure, blood flows, respiratory rate, etc

09 p1396 A71-23358

Rats hypoxia tolerance, noting smoke effects on survival, respiratory rate, body temperature and glycolytic parameters

09 p1396 A71-23364

Arterial hypoxia effects on regional blood circulation in anesthetized dogs, measuring aortic blood flow under controlled artificial ventilation and after sinoaortic denervation

09 p1396 A71-23542

Altitude acclimatization of albino rats and guinea pigs, measuring chronic and acute hypoxia effect on oxygen affinity and red cell 2,3 diphosphoglycerate concentration

10 p1558 A71-23894

Oxygen tension effect on pulmonary diffusion capacity and postnatal lung growth in rats under hypoxic, normoxic and hyperoxic atmospheres

10 p1559 A71-23899

Prolonged hypoxia, hypercapnia and combination effects on rats circulating red cell volume

10 p1559 A71-23970

Pulmonary vasoconstrictor response to temperature dependent acute hypoxia, using isolated rat lungs with heparinized homologous blood under constant volume pulsatile inflow

10 p1561 A71-24124

Gradual unilateral hypoxia effects on pulmonary blood flow partition, noting interaction with hypercapnia

10 p1561 A71-24125

Positive/latero-lateral accelerations and acute hypoxic hypoxia effects on central visual fields behavior in simulated flight

10 p1571 A71-24978

Tissue respiration and hemopoiesis in heterothermic and homothermic rodents under hypoxia

11 p1719 A71-25670

Pulmonary arterial system impedance and transmission properties, noting hypoxia and serotonin infusion vasoconstrictor effects

11 p1719 A71-25929

Rat heart muscle series elasticity compliance, showing hypoxia effects

11 p1719 A71-25930

Hypertensive heart and pulmonary vascular disease, examining chronic alveolar hypoxia effects

11 p1719 A71-25931

Cerebrospinal fluid changes due to isobaric hypoxia, discussing electrochemical potential, lactate concentration and anaerobic glycolysis

11 p1722 A71-26360

Dynamics of increasing organism resistance to hypoxia, considering reactions occurring in various tissues during adaptation

12 p1869 A71-26653

Rabbits and humans behavioral reactions and EEG changes relation to hypoxia in pressure chamber

12 p1871 A71-27488

Benzodiazepine series tranquilizers effect on mice resistance to hypoxia and lifetime, noting diazepam as most effective

12 p1872 A71-27722

Hypoxia effects on organism resistance and immunobiological reactivity, noting bacterial and protozoa infections aggravation

13 p2006 A71-28401

Spleen role as erythrocytic depot in reticulocytic reaction to acute hypoxia in splenectomized dogs inhaling air with reduced partial oxygen pressure

13 p2007 A71-28418

Lung diffusing capacity for oxygen during exercise and alveolar hypoxia measured without blood samples by ear oximeter

13 p2023 A71-29492

Hypoxia, high altitude and heart - Conference, Aspen, Colorado, January 1970

14 p2183 A71-30275

Systemic arterial blood pressure response to chronic high altitude and hypoxia effects

14 p2184 A71-30280

Coronary blood flow response to acute and chronic hypoxia, observing vascular smooth muscle relaxation relation to released adenosine

14 p2184 A71-30281

Coronary vasculature development under hypoxia and pulmonary hypertension as possible cause of right ventricle phasic flow contour changes

14 p2184 A71-30282

Human hypoxic ventilatory drive data for high altitude breathing, noting motivation reduction inversely related to time and altitude

14 p2185 A71-30288

Ventilatory control in acute hypoxia, detailing polycythemia effects on respiratory chemoreceptor sensitivity

14 p2185 A71-30289

Chronic hypoxia effects on blood oxygen and carbon dioxide tensions and pH changes in anaesthetized chickens at high altitude compared to sea level control

14 p2186 A71-30300

Conditioned reflexes developed by prolonged training in two genetic strains of mice during adaptation to altitude hypoxia

15 p2356 A71-31242

Immunobiological reactivity inhibition in mice under partial adaptation to high altitude hypoxia, observing decreased phagocytic activity, antibody production, hypoplasia and lymph cell number

15 p2356 A71-31242

Hypoxic hypoxia and hypercapnia effect on calcium, inorganic phosphorus and total protein in rat blood during hypodynamic syndrome

15 p2356 A71-31303

Cardiac output and regional blood flow in hypoxic woodchucks, noting no change in heart rate, diaphragm, kidney, liver, stomach and intestines

16 p2529 A71-33181

Polysomal RNA disaggregation and attendant reduction in hepatic protein synthesis in rats as result of decreased feed ingestion during hypoxia

16 p2529 A71-33191

Hypoxia effects on cardiovascular reflexes during hypoxia, measuring response of heart rate to lowered body negative pressure

16 p2529 A71-33191

Hypoxia effects on myocardial potassium balance in dogs during cardioaccelerator nerve and atrial stimulation

16 p2529 A71-33191

Physical exercise oxygen uptake and debt in dogs at ground level and high altitude, investigating beta adrenergic blocking agent effects

16 p2530 A71-33240

Functional systems changes in intact anaesthetized rats during increasing hypoxia in decompression chamber

16 p2532 A71-33911

Erythrocyte disintegration products role in blood regeneration, showing erythropoiesis link to erythroidesis for different forms of hypoxia

17 p2679 A71-34210

Factors affecting tissue oxygen supply in old people, showing capillary circulation disturbance role in hypoxia development during aging

17 p2679 A71-34228

Hemopoiesis and anoxobiotic processes comparative characteristics in brain and muscular tissues of heterothermic and homoiothermal rodents during prolonged hypoxia

17 p2679 A71-34222

Ventilatory acclimatization to chronic hypoxia in high altitude natives by cerebrospinal fluid pH decrease

17 p2683 A71-35144

Erythrocytes diphosphoglycerate increases mechanisms during hypoxia and anemia, studying hemoglobin oxygenation state effects

17 p2685 A71-35364

Human violent exercise burst effect on cognitive task, noting mild hypoxia irrelevance to skills decrements

17 p2686 A71-35430

Monograph on peripheral chemoreceptors and central chemosensitive area control of ventilation during chronic blood acid base changes and hypoxia in mammals

18 p2852 A71-35865

Noradrenaline concentration in myocardium of rats subjected to high altitude hypoxia, considering heart regulation in presence of hyperfunction and hypertrophy

19 p3001 A71-37393

Physiological responses of burro Equus asinus to oxygen lack in mountain altitudes, studying red blood cell and plasma volumes

19 p3005 A71-38566

Polycythemia and altitude hypoxia effects on rat heart and sea level exercise tolerance

20 p3186 A71-38988

Respiratory chemoreceptors and acid-base alterations effects on adrenocortical activation during hypoxia in dogs

20 p3187 A71-38988

Hypoxia and hypercapnia induced asphyctic differentiation of cutaneous and visceral sympathetic activity in anesthetized paralyzed rabbits

21 p3334 A71-40622

Glycerides metabolism in rats brain under normal conditions and during hypoxia, showing diglyceride role in triglycerides and phospholipids biosynthesis

21 p3337 A71-41053

Gangliosides and cerebroside content in rat brain under normal conditions, during hypoxia and under small X ray doses action

21 p3337 A71-41053

Hypoxia effects on response time to peripheral visual signals, noting direct relation to exposure severity and duration
22 p3499 A71-41495

World championship gliding team medicophysiological problems during competition at Marfa, Texas, discussing climatic adaptation, nutrition, hypoxia and pilots general physical and psychomotor conditions
22 p3500 A71-41576

Visual performance and retinal vascular changes under hypobaric elevation and hypoxia, noting stereopsis, binocular depth perception, critical flicker fusion, dark adaptation, etc
22 p3485 A71-41719

Power derived from aerobic, lacticid and alactacid energy sources during human muscular work under normoxic and hypoxic conditions, noting oxygen consumption
22 p3485 A71-41721

Cold pressor response tests under altitude acclimatization and simultaneous hypoxic acclimatization and cold in man
22 p3502 A71-41831

Peritoneal macrophagocytic ingestive capacity decrease in mice under hypobaric hypoxia, indicating infection susceptibility in altitude environments
22 p3486 A71-41832

Pathomorphological and histochemical changes in rat lungs, liver, heart, diaphragm and adrenal glands from acceleration and cysteamine caused tissue oxygen deficiency
22 p3491 A71-42703

Radiation protection drugs effects on albino rats hypoxia resistance, discussing hypoxic hypoxia response to intraperitoneally and perorally administered cysteamine and aminoethylisothionium
22 p3491 A71-42704

White rats resistance to acute anoxic, anemic and histotoxic hypoxia during various phases of X radiation sickness, studying adrenal cortex histophysiological state
22 p3494 A71-42731

Human nitrogen and water-salt metabolisms and respiratory activity during prolonged confinement in small volume chamber with cyclic varying hypoxic air
22 p3495 A71-42799

Toxic gaseous compounds effects on low pressure tolerance of rats under hypoxia in atmosphere containing polymer decomposition products
22 p3506 A71-42806

Animal tolerance to carbon monoxide, nitrogen oxide, triethylamine and freon-12 toxic effects after adaptation to hypoxia from tests on albino mice
22 p3496 A71-42810

Erythropoietic activity dosage in polycythemic mice after intermittent hypobaric hypoxia
23 p3632 A71-43216

Hypobaric hypoxia effect on polycythemic mice erythropoietic hyperactivity, evaluating iron content in peripheral erythrocytes
23 p3632 A71-43217

Extrarenal production of erythropoietin in binephrectomized rats after hypobaric hypoxia
23 p3632 A71-43218

Electron microscopic quantitative analysis of myocardium sections from male dogs exposed to general hypoxia, considering mitochondrion sizes, numbers and areas
23 p3634 A71-43912

Low grade hypoxia effects on human physiological responses and performance in vigilance/display monitoring tasks
23 p3636 A71-44238

Elevated basal metabolism in man under simultaneous altitude hypoxia and cold acclimatization
23 p3636 A71-44239

Rat thyroid gland changes during acclimatization to simulated high altitude environments, observing high hormone stimulation
23 p3637 A71-44300

Arthropoda /Daphnia, crawfish, wood lice, cockroaches, flies and ants/ hypoxia survival time and resistance to explosive decomposition
24 p3797 A71-44719

Chronic hypoxia exposure effects on human ventilatory response to carbon dioxide and oxygen deficiency
24 p3797 A71-44780

Hypoxic respiratory reactions of highland natives and recently arrived residents to oxygen concentration change in inhaled mixtures
24 p3798 A71-45065

HYPSOMETERS

Simple sensitive multichannel servo system thermobarometer for volume changes corrections, noting adaptation to five channel closed circuit respiratory apparatus
12 p1874 A71-27138

Selenodetic catalog centers mutual positions determination from lunar near side hypsometric charts
24 p3875 A71-45316

HYSTERESIS

Cryogenic fluids nucleate boiling dependence on solid surface characteristics, considering hysteresis, boiling site spreading and radiation effects
01 p0178 A71-10005

Satellite oscillations about center of mass, allowing for energy dissipation due to magnetic hysteresis
02 p0319 A71-11907

Hysteresis loop parameters for energy dissipation in material, considering relation to calculated values for oscillations of system
03 p0502 A71-13402

Cyclic deformations and internal energy dissipation effect on hysteresis loop shape equations derivation in terms of three components including nonlinear and inelastic materials properties
03 p0502 A71-13407

Residual modulation from 1954-1964 solar cycle, considering 19th cycle hysteresis loop from cosmic ray balloon data
06 p0955 A71-18131

Structural hysteresis in split root fir tree turbine blade attachment under centrifugal forces and cyclic bending moments
07 p1211 A71-19162

Thin uniaxial ferromagnetic metal films blocking curve verification using rotational hysteresis and transverse susceptibility measurements
07 p1180 A71-20171

Elastic systems vibrations calculated with allowance for amplitude and frequency dependent energy dissipation, using hysteresis loop contour expression
07 p1218 A71-20476

Martensitic stainless steels structure related to energy dissipation capability, obtaining damping mechanism as magnetomechanical hysteresis
07 p1142 A71-20477

Electronic recording of cyclic strain diagrams of metals in wide loading frequency range using dynamic hysteresis method
07 p1218 A71-20485

Fluidic OR-NOR element multiple regression analysis, investigating wall attachment, hysteresis switch pressure and percentage recovery
07 p1031 A71-20607

Cosmic rays amplitude hysteresis dependence on sunspot mean heliographic latitude and cluster number
08 p1353 A71-20979

Hysteresis effects during retuning of n-type GaAs Gunn oscillator with bias source and RLC circuit, showing range of domain damping by low field
09 p1414 A71-22228

Temperature field influence on hysteresis in Cs surface ionization on metal surfaces, observing adsorption phase fine structure and ion current density increase
10 p1657 A71-24542

Structural materials dynamic analysis, considering viscous, hysteresis and viscoelastic damping [ALAA PAPER 71-349]
11 p1843 A71-25328

Energy calculation for oscillatory systems with nonlinear, hysteretic and parametric elements
11 p1743 A71-26537

Nonlinear hysteretic element narrow band resonant system operating in steady state at fundamental resonance
11 p1743 A71-26538

Automatic control systems with nonlinear hysteresis characteristics, deriving frequency conditions for absolute system stability
12 p1892 A71-27025

Area analysis of pressure-volume hysteresis in mammalian lungs by slowly filling with air and saline
12 p1870 A71-27132

Satellite rotation about center of mass, allowing for energy dissipation due to magnetic hysteresis
13 p2144 A71-28194

Polycrystalline Nb cyclic yield point behavior under strain softening and hardening, noting stable hysteresis loop
13 p2087 A71-29123

Energy dissipation measurement in materials during cyclic fatigue testing by dynamic hysteresis loop method
14 p2238 A71-29619

Hysteresis loop measurements and functional measurements correlation on periodic permanent magnet stacks of TWT ring magnets of Sm-Co alloy
14 p2285 A71-30705

Dynamic hysteresis loop measurement of energy dissipation in materials, showing deformation effects on accuracy
15 p2508 A71-32233

Forced transverse vibration damping of end loaded elastic cantilever beam, determining hysteresis loop contour from resonance curves
16 p2658 A71-33977

Vibration simulation of elastohysteretic systems on analog computers using photocurrent-voltage relationship of polycrystalline photoresistors
16 p2658 A71-33978

Structural hysteresis in gas turbine blade herringbone scarf joints under centrifugal forces and cyclic bending moments
17 p2834 A71-35658

Thermally stabilized volcanic rock magnetic properties and coupling hysteresis effect changes due to reheating in weak magnetic field
18 p2912 A71-36197

Hysteresis loop analysis with allowance for material imperfect elasticity in mechanical vibration problems, using strain amplitude decrement relation
18 p2981 A71-36707

Automatic control systems with nonlinear hysteresis characteristics, deriving frequency conditions for absolute system stability
19 p3038 A71-37694

Parametric resonance of single degree of freedom system with double bilinear hysteresis
20 p3267 A71-38793

Polarization flip with hysteresis effect at zero magnetic field in CW far IR HCN laser
20 p3244 A71-39098

Hysteresis to strength relationship and particulate filler effect on reinforcement of rubbers and plastics
21 p3405 A71-40601

Current-voltage hysteresis and memory properties of silicon-silicon nitride capacitors as function of oxide layer and stacking fault traps
22 p3516 A71-41684

Ferrite and dielectric element waveguide phase shifters with rectangular hysteresis loop, deriving differential phase and attenuation constants for wave propagation
22 p3512 A71-42308

Ionospheric propagation hysteresis relationship to secular variation in F region response to sunspot number, noting differences in succeeding solar cycles
22 p3536 A71-42419

Hysteresis effect at solar cycle maximum for midlatitude E layer electron density response to solar activity
24 p3824 A71-45125

I

I BEAMS

I-beam plastic moment under shear force, using empirical curve for interaction between bending moment and shear force
01 p0174 A71-11000

Nonuniform cross section tapered, stepped rectangular and I section cantilever beams elastic lateral stability
14 p2330 A71-30689

Orthotropic thin walled bars with rigidly connected rectangular elements, applying displacement under torsion with allowance for shear to H beam
17 p2823 A71-34782

IAPETUS

Saturn satellite Iapetus periodic light variation curve explanation in terms of meteoroids impact erosion
04 p0660 A71-15861

Iapetus magnitude variations due to orientation changes in poles, comparing visual and photometric observations
13 p2136 A71-28389

Iapetus photometric observations, obtaining light curve by plotting rotational phase angle against magnitude
13 p2136 A71-28390

IBM COMPUTERS

NT IBM 360 COMPUTER
Distributed computer system at McDonald observatory, discussing experience with IBM 1800 process control computer time shared operation
17 p2711 A71-35011

IBM 9020 multiprocessing computer application to ATC, discussing control sectors for inflight control at air route traffic control centers in U.S.
23 p3702 A71-43888

IBM 360 COMPUTER

Mathematically oriented digital computer system implemented on IBM 360 with graphic remote consoles for engineering problems
17 p2710 A71-34622

ICARUS ASTEROID

Minor planet Icarus earth approach observations with reflector and TV camera, determining spherical coordinates by comparison with reference stars
14 p2309 A71-29993

Icarus photographic observations, determining general relativity effects on orbital motion
21 p3443 A71-40187

ICBM (MISSILES)

U INTERCONTINENTAL BALLISTIC MISSILES

ICE

Venus halo as photometric evidence for hexagonal ice in cloutdops
04 p0660 A71-15862

Evaporation of dirty ice particles surrounding early type stars, using dust grains model for explanation of anomalous reddening of Orion Nebulae
08 p1364 A71-21415

Ice, solid carbon dioxide and alcohols oxygen K spectra from long wave X ray spectroscopy
09 p1498 A71-23479

Temperature field measurements above porous surface during ice-water sublimation into vacuum, showing

ICE FORMATION

ing discontinuities due to external heat and mass transfer 23 p3784 A71-44340

ICE FORMATION NT CLOUD GLACIATION

Helicopter structural damage due to icing, discussing secondary effects on tail rotor, horizontal tail and engine from ice shed by main rotor 04 p0533 A71-15432

VTOL operation under snow and ice conditions, discussing adhesion, radiation absorption and electrical properties of ice 04 p0533 A71-15437

AH-56A Cheyenne compound helicopter icing spray rig tests, discussing ice protection systems design and operating performance 04 p0534 A71-15438

Do 132 turbine powered helicopter, discussing icing problems solution 06 p0847 A71-17745

Gasoline icing inhibitors effect on light aircraft piston engine carburetor icing [SAE PAPER 710371] 10 p1658 A71-24240

Light aircraft qualification for icing conditions from flight test data, considering increase in instrument rated pilots and IFR flying activity [SAE PAPER 710394] 10 p1555 A71-24258

Dry radar reflectivity and attenuation due to wet ice spheres exponential distributions, noting hail detection procedures 11 p1794 A71-25379

Liquid wastes venting into space environment, producing ice particle clouds interference with spacecraft optical instruments 11 p1753 A71-26506

Ice forming nuclei in atmosphere during severe convective storms from aged background aerosol and soil particles aerosolized by storm turbulence 12 p1925 A71-27197

Fincap communication antennas design and environmental tests for vibration, acceleration, waterproofing, salt corrosion, ice formation and compass safe distance 14 p2216 A71-31047

Cloud elements evolution, investigating electrical charges effects on ice crystal growth rate in water vapor by laboratory experiment 19 p3092 A71-38688

Ice forming effectiveness and dispersion of reagent particle aerosols through explosion of Elbrus 2 antihail iodide artillery shells in free and clear atmosphere 19 p3094 A71-38697

Ice formation and prevention on helicopters, taking into account presence of big drops of undercooled rain 20 p3178 A71-39374

Arctic ocean pack ice terrain profiling by airborne laser altimeter and coincident photography, analyzing data for ice development stages interpretation 24 p3833 A71-44986

ICE MAPPING

Side-looking airborne radar /SLAR/ for sea ice identification, mapping and ship routing in Northwest Passage 09 p1439 A71-23448

ICE NUCLEI

Freezing nucleus concentrations in hail and rain from different storms, showing dependence on precipitation type and intensity 08 p1326 A71-21451

Warm fog modification by condensation nucleus seeding, discussing droplet concentrations, cloud height and aerosol content effects on salt seeding material optimal size and dosage 09 p1488 A71-23253

Ice forming nuclei in atmosphere during severe convective storms from aged background aerosol and soil particles aerosolized by storm turbulence 12 p1925 A71-27197

Light pulses reflection from water and ice in clouds, using Monte Carlo technique for all orders of multiple scattering 13 p2031 A71-28795

Ice crystal and cloud drop nuclei origin and physical characteristics, discussing nucleation pollution products, weather modification and microphysical processes 14 p2270 A71-30496

Methane, ammonia and silicate effects on 3.07 micron ice absorption in interstellar grains, using cesium iodide window deposited sample measurements 15 p2498 A71-32774

Ice particles initial concentration effect on coagulation growth kinetics, considering distribution function variation with time 19 p3095 A71-38705

ICE OBSERVATION

U ICE REPORTING

ICE PREVENTION

Aircraft ice protection problems, considering one dimensional Stefan method for cyclic deicing system 17 p2838 A71-34850

Ice formation and prevention on helicopters, taking into account presence of big drops of undercooled rain 20 p3178 A71-39374

ICE REPORTING

Cirrus ice cloud detection from remote emission measurements in far IR by satellite radiometer 09 p1487 A71-23022

Side-looking airborne radar /SLAR/ for sea ice identification, mapping and ship routing in Northwest Passage 09 p1439 A71-23448

ICING

U ICE FORMATION

IDADO

Dribble spires in Snake River Plain, Idaho, discussing basalt lava features and remnants in lunar areas 22 p3533 A71-41839

IDEAL FLUIDS

Hess solution for heavy body rotating about fixed point, considering cavities filled with ideal incompressible fluid in turbulent and irrotational motion and linear invariant relation 03 p0458 A71-13591

Symmetry axis motion of solid body with ellipsoidal cavity filled with ideal incompressible uniformly turbulent fluid 03 p0458 A71-13596

Ideal incompressible fluid plane jets interaction with flow discontinuity at jet boundaries, deriving nonlinear system of integral equations 03 p0405 A71-14564

Nonlinear large vibrations of ideal incompressible homogeneous fluid in cylindrical sector tanks, determining hydrodynamic equations coefficients and relation to tank geometry 03 p0405 A71-14565

Variational principle for MHD of ideal fluid, determining canonical variables and Hamiltonian 06 p0529 A71-17378

Dynamic stability of cylindrical shell with freely supported edges partly filled with ideal compressible fluid and undergoing steady longitudinal vibrations 06 p0997 A71-17846

Parameterized postNewtonian formalism for perfect fluids applied to Nordtved effect in relativistic gravity 07 p1190 A71-18860

Fluid flow around two parallel circular cylinders moving in ideal liquid, deriving exact solution for flow velocity and kinetic energy 07 p1089 A71-19736

Thin shallow spherical shell vertical impact against ideal incompressible liquid surface, calculating axisymmetric deformation and hydrodynamic load distribution 07 p1089 A71-19738

Ideal fluid jets theory, discussing cavitation flows calculation, jet flow and plane steady potential incompressible fluid flow 07 p1091 A71-20080

Free vibrations of closed spherical shell immersed in ideal incompressible fluid at arbitrary depth 09 p1535 A71-22182

Villat problem of ideal incompressible two dimensional fluid flow around plate, determining stagnation point location 10 p1594 A71-24452

Ideal incompressible holomorphic fluid plane irrotational motion velocity due to deformable constant area airfoil displacement 10 p1594 A71-24453

Incompressible nonviscous rotating fluid in toroidal shell, obtaining flow patterns steady state solutions for turbomachinery design 10 p1552 A71-24520

Relativistic MHD waves based on ideal fluid compressibility and statistical mechanics for given spacetime 10 p1650 A71-24586

Soviet book on nonstationary waves covering gravity waves development, moving periodic pressure systems, seismic disturbances and nonhomogeneous ideal liquids 10 p1595 A71-24650

Airfoil profiles coupling method for determining complex potential of two dimensional ideal incompressible fluid flow due to arbitrary airfoil section movement near rectilinear wall 10 p1597 A71-25015

Ideal compressible fluid slow motion in permanent and nonpermanent regime, discussing velocity field geometrical interpretation 11 p1748 A71-25173

Small cross section viscous vortex ring velocity in ideal fluid with arbitrary vorticity distribution in core 11 p1749 A71-25357

Ideal incompressible fluid flow around fixed obstacle near rectilinear wall, investigating plane motion with profile couple method 11 p1705 A71-26258

Steady barotropic motion of ideal fluid, determining conditions for unit vector serviceability as velocity direction field 11 p1753 A71-26563

Variational principle for ideal fluid MHD, determining canonical variables and Hamiltonian 12 p1940 A71-27456

Three dimensional incompressible flow about slender foil in perfect fluid, stressing vortex field defect 12 p1865 A71-27222

Electrohydrodynamic ideal incompressible flow in flat and circular channels, determining electric potential and field distribution 12 p1941 A71-27744

Cavity cross sections deformation in heavy liquid, deriving nonlinear system of equations for dependence within framework of small perturbation theory 13 p2047 A71-28111

Ideally conducting compressible liquid flow near arbitrary geometrical thin profile form in transverse magnetic field 14 p2278 A71-29244

Gromeka-Beltrami ideal incompressible fluid flow in semiinfinite circular cylindrical tube 14 p2225 A71-30744

Small monochromatic disturbances propagation in stable ideal MHD fluid by geometric optics method solving point source radiation at short wavelengths 15 p2459 A71-32674

Einstein field equations solution for universe filled with perfect fluid of position-dependent density 16 p2611 A71-33222

Initial interaction phase between thin shallow conical shell vibrating axisymmetrically and ideal incompressible fluid, determining hydrodynamic pressure effects 16 p2560 A71-33522

Perfect incompressible fluid steady rotation linearized three dimensional flows, calculating complex waves system 16 p2560 A71-34044

Steady barotropic motion of ideal fluid, determining conditions for unit vector serviceability as velocity direction field 17 p2729 A71-35558

MHD detonation waves in relativistic perfect fluid of magnetic permeability μ immersed in electromagnetic field 18 p2951 A71-36158

Main parameters of free supersonic jets of ideal compressible fluid, comparing with numerical calculations and experimental data 19 p2991 A71-37044

Nonlinear hydrodynamic field equations transformations into complex wave equations for application to ideal compressible fluids 20 p3211 A71-39044

Forced and free vibrations of shallow cylindrical shell in rectangular duct filled with ideal fluid 20 p3310 A71-39774

Viscous vortex rings of small cross section, considering velocity in ideal fluid with arbitrary vorticity in core and arbitrary circumferential velocity 21 p3366 A71-40444

Plane steady irrotational flow of ideal compressible fluid around jet profile, obtaining Kutta-Joukowski theorem 21 p3322 A71-40514

Three ideal incompressible fluid jets collision induced flow, reducing discontinuity region analysis functions to nonlinear system with two numerical parameters and singular integrals 21 p3367 A71-40644

Quasi-steady three dimensional ideal compressible fluid flow between convex and concave sides of neighboring blade profiles in axial flow turbine 21 p3322 A71-40644

Ideal compressible fluid plane unsteady vortex flow self-similar flow, obtaining particular solutions familiar to Riemann waves and Prandtl-Meyer flows 22 p3532 A71-42804

Small perturbation development of plane potential motion of ideal incompressible fluid in elliptical region, confirming instability 24 p3821 A71-45218

IDEAL GAS

Impulsively started time dependent transonic flow of ideal compressible gas past circular cylinder, using finite difference method 01 p0003 A71-11118

Steady three dimensional ideal dissociative gas flow along stream lines, examining velocity components pressure gradients, density and mass fraction variables 02 p0239 A71-12122

Molecular hydrogen thermodynamic properties in ideal state from spectroscopic data, using WKB method 02 p0286 A71-12118

German monograph on plane ideal gas flows calculation with allowance for unsteady gaslight walls and compression shocks using difference methods 02 p0240 A71-12404

Ideal gas isentrope mean value exponent, calculating state variables 03 p0520 A71-13904

Liquid/gas repeated injection into ideal gas plane supersonic flow, determining resultant shock wave radius relation to Mach number and temperature 03 p0404 A71-14252

- Hypersonic perfect gas flow past thin three dimensional body with strong viscous interaction, obtaining aerodynamic characteristics and drag and heat coefficients
03 p0345 A71-14563
- Axisymmetric supersonic overexpanded ideal gas jet calculation, using finite difference method based on buildup principle
03 p0346 A71-14573
- German monograph on shock wave diffraction wedge angular changes in ideal gas region, comparing experimental with perturbation theoretical results
05 p0737 A71-17107
- Approximation of Chaplygin equation for subsonic ideal gas plane adiabatic flow, applying to discharge from flat channel with contraction
07 p1016 A71-20083
- Two link approximation of Chaplygin function by coupling to integral equations, applying to ideal gas jet separation flow past symmetrical arc
07 p1016 A71-20084
- Ideal gas jet sonic flow past wedge according to Kirchhoff scheme, testing sine series solution for convergence
07 p1016 A71-20085
- Normal shock wave stability in perfect gas with viscosity and heat conduction under arbitrary small one dimensional disturbances, formulating eigenvalue problem
07 p1224 A71-20288
- Short shock wave equations for two dimensional steady motions of ideal gas
08 p1276 A71-21871
- Interaction between perfect gas ionizing shock wave and transverse magnetic field in coaxial channel, indicating incident wave attenuation and reflected shock wave formation
09 p1498 A71-22128
- Shock wave shape attached to cone moving in ideal gas studied by Pade-Shanks approximation method, considering angle of attack
09 p1431 A71-22405
- Aerodynamic forces on harmonically oscillating wing in subsonic flow of ideal gas
09 p1384 A71-23615
- Galactic wind as steady radial perfect gas flow from stars and central gravitating source
11 p1818 A71-25207
- Steady supersonic isoelectric flow of thermally and calorically perfect gas past circular cones at zero angle of attack, using dimensional perturbation method
12 p1863 A71-26939
- Conservation theorem of velocity circulation along moving contours in continuous steady ideal gas flows
12 p1863 A71-27305
- Nonreacting and reacting ideal gases expansion between interconnected chambers, considering nitrogen and carbon dioxide simultaneous pressure measurements
12 p1877 A71-27550
- Uniform transonic ideal gas flow past finite bodies approximated by Karman equation
13 p1989 A71-27902
- Algorithm for numerical analysis of cylindrical shock wave propagation in stationary ideal gas
13 p2046 A71-27903
- Molecular hydrogen thermodynamic properties in ideal state from spectroscopic data, using WKB method
15 p2451 A71-31493
- Third approximation to Boltzmann equation for heat flux vector of gas of rigid spheres, using Brooker-Green technique
15 p2513 A71-31687
- Inviscid compressible transonic flow field equations for perfect gas in conical rocket nozzles, measuring wall and center line pressures
15 p2390 A71-32040
- Similarity solutions describing flow characteristics behind plane hydromagnetic shock propagating into uniform ideal gas at rest in presence of transverse magnetic field
15 p2391 A71-32074
- Approximate method for hydrodynamic parameters of supersonic ideal-gas jet, considering isentropic region and theoretical boundary of underexpanded jet
18 p2902 A71-36114
- Pressure change accompanying mixing of two ideal gases, assuming constant specific heats
18 p2904 A71-36280
- Secondary floating shock generation in supersonic ideal gas flow about blunt bodies, investigating body configuration and flight regime effects
18 p2845 A71-36331
- Conservation theorem of velocity circulation along moving contours in continuous steady ideal gas flows
19 p3046 A71-38258
- Flow field isentropes in conical ideal gas flow with singular stream surfaces
20 p3176 A71-39363
- Short shock wave equations solutions for two dimensional steady flow of ideal gas
20 p3211 A71-39370
- Hanging compression shock wave in plane supersonic ideal gas flow past body with broken generatrix
20 p3176 A71-39371
- Aerodynamic approximations for unsteady supersonic flow of perfect inviscid gas through flexible duct of revolution
[ASME PAPER 71-VIBR-23] 21 p3458 A71-40280
- Nonstationary ideal gas flow in variable section axisymmetric channel, noting flow disturbances during sudden changes in conditions at outlet section
21 p3368 A71-40696
- German monograph on three dimensional steady hypersonic flow of perfect gas past pyramid shaped bodies of rhombic planform
21 p3323 A71-40774
- Self similar solutions for ideal gas flow driven by piston ahead of shock propagating in medium at rest with power law density distribution
23 p3719 A71-44143
- Equilibrium equations solutions for ideal gas composition, pressure, volume and temperature based on Newton-Raphson method, outlining programming method
24 p3887 A71-44635
- Nonlinear theory of wave resistance in supersonic ideal gas flow past finite flat axisymmetric bodies, establishing drag relation to flow rate deficit
24 p3790 A71-44773
- Critical streamline length in axisymmetric and plane ideal gas flows past conical bodies as function of Mach number and form parameter
24 p3790 A71-45058
- Ideal gases and binary monatomic gas mixtures heats of transport derivation from kinetic theory expressions for thermal transpiration
24 p3891 A71-45384
- IDENTIFYING**
- NT TIMBER IDENTIFICATION
- Rapid identification of steels and other metals by chemical, instrumental and organoleptic methods
01 p0183 A71-10256
- Rapid internal standard identification method for metals by atomic absorption spectrophotometry, using diluted acid solution of specimen
01 p0028 A71-10257
- Nondestructive high reliability rapid comparison and identification of metals by electrical interpretation method for product variation control and laboratory unknowns determination
01 p0085 A71-10258
- Discrete linear plant identification, using generalized Kalman models
02 p0236 A71-12624
- Simultaneous identification and control by separation method of two separate problems solution, one being set of unknown parameters estimation
03 p0394 A71-14485
- Relevant cue placement effects in concept identification tasks employing enforced verbal encoding
07 p1048 A71-19514
- Moving magnetic field lines identification, applying to moving nonrigid conductor
08 p1283 A71-21648
- Dynamic control plants parametric identification theory for linear and nonlinear systems
09 p1423 A71-22874
- One dimensional linear stationary systems described by linear differential equations, discussing identification procedure with transformation into integral equations
10 p1585 A71-24157
- Continuous identification algorithm for system containing two delays for signal represented by stationary random process with autocorrelation function approximation
10 p1585 A71-24160
- Identification algorithm for linear discrete time systems difference equations with input-output measurements coefficients
10 p1586 A71-24737
- Second order system with structure perturbation affected parameter value, studying identification and autoadaptation by sign functions
10 p1586 A71-24740
- System identification problems, discussing approximation by polynomial integral operators, determinable classes in spectral decompositions, observation noise and stochastic systems stationary in observation time
10 p1587 A71-24742
- Nonlinear systems parameter identification schemes using first and second order extended Kalman-Bucy linear filters and sensitivity functions, comparing performance by two examples
10 p1587 A71-24745
- Model theory identification application to aeronautical systems, discussing transfer function representation, state variable and direct methods
10 p1587 A71-24748
- Algorithm for subclass identification in image recognition
13 p2034 A71-27835
- Image parameters identification and estimation problems /in learning without teacher/, deriving error
- variance lower bounds and spurious solution probabilities
19 p3024 A71-37225
- Specific banding patterns for identification and structural detection of human chromosomes, using differential staining method
21 p3336 A71-40853
- Fireball identification method in accelerator and cosmic ray produced jets, considering model improvement for Lorentz factor determination
21 p3439 A71-41396
- IDENTITIES**
- Identities required for classification of Newman-Penrose formalism equations, using tensor description
16 p2612 A71-34068
- IFR (RULES)**
- U INSTRUMENT FLIGHT RULES
- IGNEOUS ROCKS**
- NT ANDESITE
- NT ANORTHOSITE
- NT BASALT
- NT ENSTATITE
- NT GRANITE
- NT LAVA
- NT MAGMA
- NT OLIVINE
- NT PYROXENES
- NT QUARTZ
- NT SERPENTINE
- Apollo 11 crystalline igneous rocks mineralogy and petrology, suggesting origin from pyroxenite mantle melting
02 p0305 A71-11982
- Apollo 12 lunar rock 12013 preliminary examination and preparation for instrumental analysis, noting feldspar content and igneous nature
03 p0493 A71-14213
- Apollo 11 igneous rocks potassium content vs irradiation exposure age, comparing lunar geology models
06 p0966 A71-17897
- Apollo 11 igneous rock vug clinopyroxene composite crystal with tabular pigeonite nucleus and subcalcic augite precipitation
10 p1673 A71-24412
- Igneous and metamorphic rocks as simulated lunar rocks, determining elastic and attenuation symmetry by quasi-longitudinal pulse velocity and amplitude measurements on spherical specimens
11 p1834 A71-26454
- Canary Islands volcanic rocks, investigating lead isotope compositions for upper mantle multistage history
13 p2062 A71-28698
- Hypervelocity impact melts, considering meteorite crater igneous rocks or glasses associated with shock deformation
19 p3051 A71-37666
- Igneous rocks origin associated with shock metamorphism, considering geochemical investigations of Canadian craters
19 p3051 A71-37668
- Apollo 11 lunar crystalline igneous rock samples electrical conductivity temperature dependence, noting age of moon
20 p3295 A71-39619
- Rare earth, alkali and alkaline earth elements content of phenocrysts and acidic igneous magma
23 p3734 A71-43246
- Lunar plagioclases, tridymite and cristobalite feldspar crystal structure and chemical analyses from Apollo igneous rocks by X ray and electron diffraction
23 p3738 A71-43611
- Apollo 12 lunar igneous rocks and breccia opaque minerals examined by optical and electron microprobe techniques
23 p3739 A71-43621
- Luminescence petrography of Apollo 12 lunar igneous rocks, comparing to meteorites and terrestrial basalts
23 p3740 A71-43624
- Mineralogical, petrological and chemical features of four Apollo 12 lunar microgabbros
23 p3740 A71-43625
- Mineralogy and petrology of Apollo 12 igneous rocks 12004, 12008, 12009 and 12022, noting ilmenite, olivine and spinel content and metal grains composition
23 p3740 A71-43627
- Mineralogical and petrographic investigation of olivines, feldspars and pyroxenes in Apollo 12 fines and igneous rocks, using optical and X ray diffraction
23 p3741 A71-43631
- Lunar maria igneous rock compositions and magmatic liquid viscosity from samples 12021 and 12022, using microprobe analyses
23 p3741 A71-43633
- Pyroxenes morphological significance in Apollo 12 lunar igneous rock samples petrogenesis, analyzing crystallization process history
23 p3742 A71-43642
- Apollo 12 lunar soil, breccia and igneous rock samples, determining elemental abundances with spark

IGNIMBRITE

source mass spectrometry and neutron activation analysis

23 p3748 A71-43680

Apollo 12 lunar soils and igneous rocks from Ocean of Storms, determining major, minor and trace element composition with chemical, X ray fluorescence and spectrographic techniques

23 p3748 A71-43683

Bulk elemental composition of Apollo 12 samples of lunar igneous and breccia rocks and soils from instrumental and radiochemical neutron activation analysis

23 p3748 A71-43684

Rare earth elements and trace elements abundance in Apollo 12 igneous rocks, breccia and lunar soil

23 p3750 A71-43695

Apollo 12 lunar soil and igneous rocks magnetic properties

23 p3763 A71-43792

IGNIMBRITE

U LAVA

IGNITERS

NT INITIATORS [EXPLOSIVES]

Gas turbine engine startup igniter with modified propellant atomizer enhanced by air injection

13 p2118 A71-28969

Gas turbine auxiliary power unit accessories, discussing high energy igniters, cables and connectors, thermocouples and speed and temperature monitoring equipment

13 p2071 A71-29262

Energy requirement measurements for bridge wire igniters at low voltage, using capacitor discharge

22 p3587 A71-41448

Low thrust long burning solid rocket propellant motor for orbit insertion maneuvers, discussing design, static tests, nozzle composition, igniter and performance

22 p3589 A71-42016

Operational characteristics of starting igniters for gas turbine engine combustion chambers

24 p3864 A71-45003

IGNITION

NT ELECTRIC IGNITION

NT SOLID PROPELLANT IGNITION

NT SPARK IGNITION

Propellant low temperature preignition reactions during simulated engine shutdown conditions, discussing IR spectroscopic observation method

02 p0298 A71-12861

Black Brant 4 rocket second stage motor, investigating high altitude ignition problems by postflight analysis

03 p0470 A71-13667

Ignition and nondetonating decomposition of liquid nitromethane explosive at 10 bar pressure

05 p0795 A71-16517

Supersonic combustion ramjet engine with liquid fuel injection, considering atomization process and ignition criteria

05 p0836 A71-16531

German monograph on ignition and combustion processes in rapidly flowing gas mixtures covering supersonic flow, ramjet parameters, flow heating, etc

05 p0838 A71-16900

Explosion products population inversion by combining vibrational chemical excitation with thermal ignition

06 p0865 A71-17402

Liquid bipropellant rocket engine ignition and start transient calculation for hypergolic and externally ignited starts at sea level and high altitude pressures

[WSS/CI PAPER 70-23] 06 p0943 A71-17655

Hydrocarbon fuel ignitability, investigating molecular structural characteristics and homogeneous additives effect

[WSS/CI PAPER 70-19] 06 p0943 A71-17661

Cellulose, explosives and propellants thermal surface ignition, using heat transport and chemical kinetic equations

06 p0944 A71-18298

Incident shock wave interaction with liquid hydrocarbon fuel drops in oxidizing and inert atmospheres, considering combustion characteristics and ignition mechanism

[AIAA PAPER 71-206] 06 p0886 A71-18642

Diffusion flame stability, investigating critical dependencies for ignition point coordinates for fuel gas burning

07 p1220 A71-18779

Plasma produced by focused Q switched ruby laser beam, considering use for minimum ignition energy measurement

07 p1123 A71-19577

Metal powders hypergolic ignition in gaseous chlorine trifluoride, examining use in air augmented rockets primary combustors

07 p1183 A71-19875

Inflammable cylindrical channel ignition in semiclosed space, examining steady pressure development

08 p1376 A71-21907

Polyfraction Mg particles suspension in active gaseous medium, studying ignition and burnout

08 p1376 A71-21909

Ignition delay times behind reflected shock wave of alkanes methane through pentane in stoichiometric argon simulated air mixture

10 p1657 A71-24047

Thermal ignition theory review, discussing mathematical problem statement, ignition characteristics approximate calculation methods, heat transfer mechanisms, geometrical and critical conditions, experimental tests, etc

10 p1695 A71-24050

Shock wave ignition of liquid fuel drop in oxidizing atmosphere, discussing combustion process

[AIAA PAPER 70-9] 12 p1986 A71-27566

Low alloy alpha Ti alloy ignition during breaking in oxygen containing gases, considering partial oxygen pressure and tensile loads

13 p2082 A71-27815

Reactive solids ignition by constant energy flux from asymptotic analysis of activation energy limit

14 p2337 A71-30458

Ignition and combustion tests of storable boron/magnesium/hexane slurry injected directly in high speed air stream

[AIAA PAPER 71-723] 14 p2286 A71-30773

Oxide films effect on metal particles ignition

15 p2511 A71-31378

Ethane-oxygen-argon mixtures ignition behind reflected shock wave, deriving composition temperature dependencies correlation

[WSS/CI PAPER 71-16] 15 p2463 A71-31625

Boron particles ignition theory and shock tube experiments, measuring ignition delay as function of temperature, pressure, gas composition and particle size

[WSS/CI PAPER 71-20] 15 p2464 A71-31629

Red fuming nitric acid-sulfur dioxide as oxidizer for auxiliary ignition in liquid rocket motors

15 p2465 A71-32110

Individual liquid fuel droplets ignition factors, introducing heating-up and evaporation delay

15 p2516 A71-32709

Supersonic hydrogen diffusion flames ignition aids at near-thermal self ignition point, discussing catalytically induced preeractions

[DFVLR-SONDDR-118] 15 p2466 A71-32718

Methane-oxygen-argon mixture ignition behind reflected shock waves in single pulse shock tube

17 p2792 A71-33507

Inertialless glow discharge ignition in triatron controllable crossed field cold cathode tube, comparing with magnetic coil initiation

19 p3028 A71-37785

Ignition delays of propane-oxygen-argon mixtures in shock tubes from pressure and heat flux measurements in reflected region

19 p3169 A71-38109

Aluminum particles ignition by focused laser flux in controlled oxygen-Argon environment, observing by cinephotomicrography throughout entire burning time

19 p3169 A71-38114

Shock induced ignition in explosive homogeneous hydrogen-oxygen gaseous mixtures

19 p3171 A71-38130

Hypergolic rocket propellant system gas phase ignition, measuring ambient pressure, flow parameters and propellant temperature effects on delay characteristics

19 p3123 A71-38297

N-hexane-air mixture ignition by giant pulse laser beam, analyzing probability and development time to formation of measurable nucleus

23 p3686 A71-43998

IGNITION LIMITS

Oxygen and homologous hydrocarbon mixtures detonation limits, discussing propagation, fuel molecule structure, critical temperature, initial cracking mechanism and carbonaceous solids condensation

02 p0331 A71-11957

Anomalous ignition and flash point measurements of halogenated hydrocarbon-flammable liquid mixtures

[WSS/CI PAPER 70-20] 06 p0943 A71-17662

Liquid fuel pool ignition at superflash and subflash temperatures involving adjacent heat source, cross wind and fluid motion

07 p1182 A71-19245

Inhibiting mechanism of ethane in hydrogen-oxygen mixtures ignition, discussing lower limits, carbon monoxide effect and chain lengthening reactions

11 p1730 A71-26566

Coherence theory of strong shock induced explosive gas ignition limit

22 p3621 A71-42099

Ignitability limits of hydrogen/air and hydrocarbon/oxygen mixtures at high temperatures near self ignition range

23 p3782 A71-44007

IGNITION SYSTEMS

High acceleration resistant electronic trigger fuse for in-flight gun launched projectile payloads ignition and ejection

[AIAA PAPER 70-1389] 03 p0468 A71-13671

Hydrogen-oxygen catalytic ignition system steady state model for predicting temperature and concentration profiles

05 p0795 A71-16517

Particulate B fuels combustion and ignition models in air at ambient pressures, using levitation and pulsed Nd doped laser

[WSS/CI PAPER 70-13] 06 p0943 A71-17655

Dual magneto ignition system for business and military aircraft, describing development, design and test program

[SAE PAPER 710382] 10 p1659 A71-24047

Diffusion and thermal mechanism ignition theory applying to altitude relighting of gas turbine engines combustors

13 p2116 A71-28969

Critical parameters in two component thermal ignition system based on Bowes computer evaluation dimensionless temperature formula

14 p2337 A71-30458

Broadband radiated interference measurements on nonhyperbolic propellant rocket engine spark gap ignition for electromagnetic compatibility

15 p2471 A71-32718

IGNITION TEMPERATURE

NT FLASH POINT

Self ignition temperature of aerogels of Al-Mg alloys during heating of powders

01 p0182 A71-11111

Self ignition temperature of aerosols of Al-Si powders as function of dispersion and alloy composition

01 p0182 A71-11111

Limiting temperature and size conditions for minimum particle ignition in mixtures of oxygen with argon and nitrogen

03 p0468 A71-13667

Shock initiated detonation wave propagation in combustible hydrogen oxygen flow in constant area duct, considering wave initiation Mach number and ignition temperature

05 p0834 A71-16517

Lowered ignition temperature and fire propagation of polyester containing bromides

07 p1182 A71-19245

Metals bulk ignition temperature in oxygen atmospheres, emphasizing preignition surface oxidation effects

14 p2337 A71-30458

Particle size effect on self ignition temperatures of powdered Al-Mg alloys

14 p2285 A71-30458

Cold combustible gas mixture ignition temperature at flat plate forward stagnation point, investigating inert gas concentration, activation energy and Damkohler number effects

17 p2837 A71-34007

Injection conditions effect on ignition temperature of methane and hydrogen in hot Mach 2 air stream

19 p3163 A71-38114

IGY [GEOPHYSICAL YEAR]

U INTERNATIONAL GEOPHYSICAL YEAR 1957-1962 AIRCRAFT

Operational preparation and commissioning of 62 long distance jet aircraft, considering flight crew and maintenance personnel training at U.S.S.R. plant

11 p1743 A71-25111

Flight and operation of IL-62 long distance jet aircraft, considering flight crew composition and training, passenger and cargo handling and refueling

11 p1706 A71-25111

ILLIAC COMPUTERS

NT ILLIAC 4 COMPUTER

ILLIAC 4 COMPUTER

Illiac 4 and Spectra 70 computers comparison in terms of logic circuit noise immunity and system noise sources

03 p0388 A71-13667

ILLUMINANCE

Peak diameter differences of sensitization by annular surrounds in subjects, concerning scotopic increment threshold and retinal illuminance

03 p0365 A71-14007

Full photographic spectral range spaceborne cameras photometric calibration, involving determination of absolute magnitude and illuminance space variation in image plane

09 p1447 A71-22111

Luxmeters and photoelectric receptors for illumination measurement of light beams in limited solid angle in image systems, considering automatic photogrammetry

14 p2246 A71-30458

Visual latencies at photopic levels as function of binocular differences in retinal illuminance, using Limulus adaptation model and ERG correspondence

16 p2527 A71-32811

Detectability measurement of foveal stimulus, suggesting nonuniformity of retinal illuminance in visual task

19 p3003 A71-38297

ILLUMINATING

Electroluminescent aircraft instrument lighting effects on pilots dark adaptation taking into account color, panel legibility, scotopic sensitivity and acuity

08 p1248 A71-21211

- Artificial satellite illumination by sun, calculating height, time and position of earth shadow by nomogram 13 p2145 A71-28511
- Speed overestimation in intermittent illumination of moving bars and textures as function of frequency, using Piaget and brightness enhancement phenomena 15 p2366 A71-32713
- Crystal laser pyrotechnic illumination lamps with noncompacted explosive mixture, noting Nd ion doped calcium tungstate and YAG laser tests 19 p3073 A71-37788
- ILLUMINATION**
- Aircraft emergency evacuation illumination standards, considering independent power source, crash survivable installation, operation initiation and exit visibility 01 p0004 A71-10030
- Circular apertures with Besinc correlated illumination, examining far field diffraction properties and intensity distribution 05 p0781 A71-16193
- Illumination charts for operational satellite, discussing orbit geometry and times, evolution trajectories and launch parameters 06 p0966 A71-17702
- Illumination level effect on corneo-retinal potential and electro-oculography (EOG) recording 08 p1246 A71-20812
- Natural illumination and irradiance levels for photoelectric device design and specifications in nocturnal light conditions 10 p1641 A71-24056
- Comparative contrast and cues for illumination effects on perception of surface lightness, using target cast shadow experiments 12 p1872 A71-26613
- Fiber optics for spectroscopic illumination, discussing absolute and angular transmission measurements and optical angular transfer function calculation 12 p1905 A71-26806
- Quantitative measurement of speckle contrast for illumination with laser oscillating simultaneously in multilongitudinal modes on rough surface, determining coherence length 16 p2589 A71-34130
- Partially spatially coherent illumination influence on measurement of correlation function of two dimensional patterns, obtaining formula for optical filtering 18 p2929 A71-35973
- Automatic analyzer for rapid counting and sizing of raindrops, using collimated flashlamp source for illumination 18 p2918 A71-36076
- Coherence in image plane of incoherent optical system, considering illumination conditions and component impulse response 18 p2920 A71-36104
- Photosystem resolution of coherent laser illuminated objects, discussing experimental investigation of image quality dependence on relative aperture 19 p3073 A71-38194
- Image visual observation in coherent diffuse illumination, discussing human eye angular resolution deterioration and depth vision threshold dependence on light characteristics 19 p3074 A71-38195
- Spectral density modulation visibility at Michelson interferometer exit illuminated with white light parallel beam 21 p3375 A71-40072
- Depth perception variability under central and peripheral illumination conditions, using Duncan multiple range test for data analysis 22 p3498 A71-41481
- Artificial illumination for Venus surface pictures from landed space vehicle 22 p3608 A71-41953
- Illumination effects on drain current for p channel enhancement type MOS transistor, attributing photoresponse to electron excitation in conduction band 22 p3523 A71-42481
- Illumination wavelength effect and supply voltage dependence of photomultiplier area sensitivity map 23 p3676 A71-43505
- Photoelectric localization of features via optical signal modulation, noting sensitivity dependence on illumination type 23 p3679 A71-43895
- ILLUMINATORS**
- Ruby laser sources of short duration and high energy emission in holography, considering oscillator amplifier illuminator, contour spacings, transmission holocameras, etc 18 p2930 A71-36057
- Elliptical laser illuminator pumping efficiency dependence on light source focal displacement, using optical systems image forming theory 20 p3243 A71-39075
- ILLUSIONS**
- NT OCULOGRAPHIC ILLUSIONS**
- Auditory illusions, investigating phonemic restorations, verbal transformations and perceptual organization 07 p1051 A71-20212

- Pilots illusory attitude perception causes, suggesting psychological and medical remedies 16 p2534 A71-32830
- ILMENITE**
- Lunar and terrestrial ilmenite basalt, considering hornfels from Keweenaw Duluth complex in Minnesota and Apollo 11 samples 09 p1529 A71-23657
- Chromite and ilmenite analysis in pallasites, mesosiderites, achondrites and meteorites with electron microprobe 14 p2310 A71-30173
- Armalcolite and ilmenite basalt in Apollo 11 lunar samples, discussing formation process of titanium, potassium and silicon oxides 23 p3734 A71-43247
- Zirconium liquid-crystal distribution in phase ilmenite of Apollo 11 and 12 lunar rocks 23 p3739 A71-43618
- Opaque mineral compositions in Apollo 12 lunar rocks, noting ilmenite, spinels, native iron and troilite 23 p3739 A71-43620
- Single crystal structure of shocked terrestrial and lunar ilmenite from X ray precession and Laue analyses 23 p3740 A71-43623
- Surface morphology of free-growing ilmenites and chromites from lunar vuggy rocks by scanning electron microscopy and electron microprobe 23 p3745 A71-43665
- Oxygen isotope fractionation in Apollo 12 rocks and soils, noting plagioclase ilmenite isotopic temperature 23 p3751 A71-43704
- Critique of paper on Apollo 11 ilmenite basalts petrology and lunar bodies origin and form 23 p3769 A71-43886
- ILS (LANDING SYSTEMS)**
- U INSTRUMENT LANDING SYSTEMS**
- ILYUSHIN AIRCRAFT**
- NT IL-62 AIRCRAFT**
- Flexible runway surfaces classification by LCN method, calculating for Ilyushin aircraft 11 p1745 A71-26201
- ILYUSHIN IL-62 AIRCRAFT**
- U IL-62 AIRCRAFT**
- IMAGE CONTRAST**
- Thin aligned holograms superposition for image intensification of diffusely scattered object, noting degradation in resolution and contrast 01 p0082 A71-10838
- Microwave holography with artificial reference wave and receiver multiplier, improving linear resolution in image 02 p0248 A71-11876
- Filter effect on CRT display resolution and relation to photometric and color contrast 02 p0249 A71-12073
- Direction indicating color schlieren system displaying radial refractive index gradients, comparing with knife edge monochrome image resolution 03 p0423 A71-13459
- Optimum beam ratio producing maximum contrast photographic reconstructions from double exposure holographic interferograms 03 p0424 A71-13639
- Holographic multiplexing by Fresnel diffraction based on aperture field division, discussing reconstructed image quality 03 p0429 A71-14179
- Contour effects on brightness paradox, investigating contrast and perception of luminance gradients in space by constant sum estimation method 03 p0365 A71-14377
- Pulsed laser holography, discussing illumination source and holocameras for high contrast recording with Q switched ruby lasers 04 p0597 A71-15363
- Image contrast limits in thin phase hologram reconstruction of diffuse objects with large reference-object irradiance ratios 04 p0601 A71-15687
- Suprathreshold vision retinal image contrast loss measurement, suggesting role of balance between optical unsharpness and neural oversharpness 04 p0540 A71-15833
- Aircraft cockpit instrumentation display media research, discussing brightness and contrast ratio requirements for gray scale displays 07 p1046 A71-18736
- Fiber optic facelates for contrast enhancement under high ambient light conditions for commercial and military cockpits, eliminating ghost, halo and direct sunlight problems 07 p1107 A71-19175
- Linear mathematical model for human visual edge contrast by delineating and emphasizing image contours 07 p1043 A71-20101
- Mathematical model of visual information of edge contrast effects in human eye as functions of image brightness and viewing angle 07 p1051 A71-20123

- Optimum AM reticle-detector models, discussing image resolution, electrical bandwidth and detection problems 07 p1115 A71-20368
- Stellar image quality at Abastumani on Mount Kanobli, considering image diffraction picture at 755 magnification 07 p1201 A71-20440
- Image quality degradation studied with interference-polarization filter of Abastumani telescope, discussing photography of solar spectrum around H alpha line and artificial light source 07 p1115 A71-20443
- Image scale of photoelastic device model and negative in photographic camera 07 p1116 A71-20544
- Holographic recording media low signal energy densities comparison, determining peak values of diffraction efficiency and normal contrast ratio divided by signal beam exposure 08 p1290 A71-21389
- Astronomical IR telescopes image quality and observing efficiency gain 08 p1290 A71-21394
- Exponentially decaying intensity averaging time and intrascope inertia effect on image unsharpness during object uniform or harmonic motion 08 p1294 A71-21902
- Frequency-contrast characteristics of holographic systems, studying image contrast and angular spread as function of hologram aperture 10 p1611 A71-24529
- Spatial and temporal patterned light flashes effects on dark adapted subjects, discussing cortical response changes in contrast depth 10 p1565 A71-24680
- Photomaterial nonlinear effects on contour distortion in holographic recording of Fourier image slit for graphic memory use 10 p1612 A71-24716
- Model of retinal information in cats from physiological and anatomical evidence, considering processing of contrast and eye movement information 11 p1723 A71-25254
- Similarity comparisons of isotropic and anisotropic scattering patterns in cloudy atmospheres for haze effects on Mars image contrast, using asymptotic method 11 p1825 A71-25710
- Electro-optical and high contrast properties of structurally stabilized anil-type nematic liquid crystals in display devices 11 p1729 A71-26070
- Camera shutter spatial frequency spectrum and components light scattering effects on negatives quality based on composite image representation systems theory 11 p1767 A71-26469
- Comparative contrast and cues for illumination effects on perception of surface lightness, using target cast shadow experiments 12 p1872 A71-26613
- Visual contrast sensitivity and fundus oculi pattern changes due to accelerations in pelvis-head axis 12 p1870 A71-27165
- Spatio-temporal patterns in visual contrast sensitivity, noting exaggerated eye movements effects 13 p2018 A71-28462
- Visual perception theoretical models for liminal contrast prediction 13 p2023 A71-29442
- Noisy image visual discrimination and detection, investigating Bayes criterion ideal statistical method validity for pattern recognition 14 p2197 A71-30815
- Imagery of periodic objects through interposed turbulent medium, investigating diffraction images irradiance distribution and contrast 14 p2275 A71-30827
- Mars surface features contrast reduction, discussing forward scattering haze as possible cause 15 p2491 A71-32418
- Light adaptation and visual latency, discussing temporal resolving properties of eye as function of binocular differences and target background contrast 16 p2527 A71-32868
- Quantitative measurement of speckle contrast for illumination with laser oscillating simultaneously in multilongitudinal modes on rough surface, determining coherence length 16 p2589 A71-34130
- Holographic analysis of periodic microobjects at X ray wavelengths, obtaining high contrast 17 p2737 A71-34292
- GALAXY machine for measuring image position and brightness and converting Schmidt telescope photographic data into computer form, outlining design and development 17 p2741 A71-34996
- High performance solar prominence telescope, showing objective diameter effect on image contrast 18 p2915 A71-35977

IMAGE CONVERTERS

- High resolution holographic image deblurring methods involving coherent optical analog processing and Fourier transform division filter 18 p2918 A71-36079
- Foveal perceptive fields for human vision, using measurements of contrast illusions in grids and bars 18 p2857 A71-36687
- Scanning densitometer for spectral transmission density continuous recording at low image contrast, discussing design and performance tests 19 p3063 A71-37248
- Visual system image blur and lateral inhibition effects on visual performance, convolving luminance profiles of targets with point spread functions 19 p3007 A71-38059
- Frequency-contrast characteristics of holographic systems, studying image contrast and angular spread as function of hologram aperture 19 p3066 A71-38257
- Cathode ray tube, including electron beam peak power, resolution elements, luminescent materials, fabrication techniques, contrast preservation and reliability 20 p3234 A71-39062
- Gaussian and Poisson noise and SNR effects on subjective image quality rating, using transparency aerial scenes 20 p3235 A71-39190
- Pseudotransfer function for interference contrast of coherent illuminated phase edge object 20 p3245 A71-39427
- Contrast level reading tests of CRT and self luminous display devices with optical filters at high ambient light for cockpit applications 21 p3376 A71-40127
- Information producing capabilities of various combinations of SNR, bandwidth and contrast in simulated digital encoding TV systems 21 p3347 A71-40130
- Visual information discernibility measurement for suprathreshold transfer in display to observer system, noting use for color contrast scaling and disturbance evaluation 22 p3547 A71-42504
- Image detail reproduction quality and resolution, describing signal to noise and modulation transfer function effects 22 p3547 A71-42505
- Atmospheric contrast reduction of aerial images, predicting quality under various target and meteorological conditions 22 p3547 A71-42506
- Large path difference laser interferometry, discussing test tower instrumentation problems of interference fringe flicker and loss of contrast due to laser mode instability 23 p3683 A71-43356
- Incoherent light bandpass filter to amplify detail contrast of optical system 23 p3679 A71-44010
- IMAGE CONVERTERS**
- NT IMAGE TUBES**
- Stellar spectrograph with image converter, obtaining optimal ratio between telescope and collimator diameters 04 p0589 A71-14833
- Precision systems oscillations measurement by transistorized two channel photoelectric image converter, discussing circuit diagram 05 p0751 A71-16356
- Three electrode image translator with electrostatic electron beam focusing, rendering high uniform resolution over entire viewfield 06 p0897 A71-17531
- Shock wave free surface velocity measurement using moire method for photographic recording with image converter streak camera 09 p1444 A71-22715
- Folded all-reflecting Schmidt camera UV image converter system for space astronomy applications, discussing pressure sensitivity effects on UV direct recording emulsion 09 p1447 A71-22751
- Schlieren system conversion to holographic visualization in operational wind tunnels and test facilities 09 p1449 A71-22788
- Distant artificial cosmic objects coordinate determination by image converter/closed TV system screen photography and TV observations of space probes 14 p2309 A71-29992
- Retina photosensitive cells properties and functions compared with films photosensitive chemicals, emphasizing retinal image transformation 18 p2864 A71-36068
- Portable self contained Imacon image converter high speed camera system capable of framing and streak operation 18 p2924 A71-36614
- Sound to light image conversion, emphasizing liquid surface acoustical holography 20 p3238 A71-39343

- Low voltage IR image converter display system using scanned line array of GaAsP light-emitting junction diodes 21 p3352 A71-40117
- Dynamic active element model of electroluminescent image converter with positive optical feedback, using voltage-brightness approximation 24 p3808 A71-44389

IMAGE CORRELATORS

- Holography and shapes recognition, considering optical memory, information density advantages and optical correlators 06 p0900 A71-18068
- Coherent optical multichannel profiling correlator for increasing automatic stereocompilation speed by X parallax profiles simultaneous measure and display 07 p1114 A71-20209
- Instant profile image correlator for coherent optical parallel processing, describing laboratory and aerial stereophotographs results 13 p2071 A71-29351
- Signal processing operation of real time optical correlator, using ultrasonic light modulators 17 p2708 A71-35484
- Fingerprint identification by holographic correlator pattern recognition techniques, discussing reconstructed image visual observation and photoelectric measurement 22 p3539 A71-41748

IMAGE DISSECTOR TUBES

- Image dissector photomultiplier for acquisition, guiding, focusing and photometric monitoring in telescope control 17 p2741 A71-34992
- Image intensifier tube coupled to smoothing disector to improve SNR in electronic scanning spectrometer 18 p2914 A71-35850
- Image dissectors in optical tracking applications, discussing design, operation, SNR performance, tracking modes, relative merits and disadvantages 18 p2883 A71-36915

IMAGE ENHANCEMENT

- Solar corona radio emission enhancement, comparing thermal and nonthermal streamer models 01 p0152 A71-10332
- Thin aligned holograms superposition for image intensification of diffusely scattered object, noting degradation in resolution and contrast 01 p0082 A71-10838
- Optical design of image selector for Cassegrain telescope recording difference spectrum of targets in focal plane 03 p0425 A71-13646
- Holographic twin image elimination by nonlinear method based on statistical differences in objects and diffraction fields 03 p0425 A71-13656
- Electron microscope micrographs enhancement by holographic image deblurring 04 p0596 A71-15135
- Moire contour map enhancement by removal of unwanted noncontour obscuring patterns, considering preferability of continuously moving grid to discrete translation 05 p0749 A71-16267
- Mariner near encounter pictures with maximum discriminability, applying algorithms for contrast and resolution enhancement and noise removal 06 p0898 A71-17634
- Light scatterers use behind phase object in double exposure holography, determining laser radiation wave front dynamics effect on image quality 07 p1114 A71-20189
- Wide angle high gain image amplification by organic dye solution lasers using rhodamine or fluorescein disodium salt 09 p1463 A71-22752
- Side-looking airborne radar and IR line scan systems, discussing instrumental correction of image distortion 09 p1450 A71-22967
- Image restoration from random fluctuations, developing analog procedure from time dependent functions of spatial frequencies and approximation 09 p1407 A71-23048
- Stabilized image movement control by mounting object in electric synchronous motor and rotating eccentricity 10 p1567 A71-23989
- Lens phase aberration correction in optical system, using holograms 11 p1766 A71-26305
- Image quality improvement by successive hologram acquisition process 13 p2070 A71-29026
- Interferometric holograms of vibrating body via numerical analysis of oscillations amplitude and phases 15 p2406 A71-31706
- Solar image correction in high resolution radio interferometer by digital data processing technique maintaining required phase relations in antenna elements 15 p2373 A71-32446

- Volume hologram formation in photopolymer materials with bright low noise images, considering sensitivity, spatial frequency response, particle scattering noise and nonlinearities 16 p2577 A71-3328
- Electronic multimage processor for enhancement and interpretation of ERTS multiband remote sensing imagery data 17 p2737 A71-3488
- Image amplifier camera resolution as function of light level based on photon statistics and cathode quantum efficiency 17 p2746 A71-3489
- Time resolution enhancement in laser photogrammetry recording fast events with long pulse length laser without auxiliary shutters 18 p2914 A71-35850
- Pseudocolor image enhancement by two-separate photographic process, considering transformation curve alterations in CIE space by changes of photographic materials, filters and exposures 18 p2918 A71-36079
- Aerospace imagery enhancement for visual interpretation, considering ERTS applications 18 p2919 A71-36080
- Doppler velocity field recording method over two dimensional solar active region image, using narrow band filter with video photographic subtractive technique 18 p2924 A71-36081
- Photographic phase holograms including printout affect, bleaching, conversion with iodine compound and light stability 20 p3236 A71-39190
- Self referencing holographic system for image compensation in fluctuating random medium, describing homodyning procedure 21 p3382 A71-40949
- Photographically recorded image enhancement, discussing filtering, SNR and film grain noise 21 p3382 A71-40950
- Optical image deblurring methods, discussing coherent and incoherent optical analog, incoherent electronic analog and digital computer processing 22 p3539 A71-41748
- Isodensity mapping with digital computer system selection and cathode ray X-Y plotter, showing photographic image display and enhancement of density height information 24 p3826 A71-44748
- Mars surface mapping, discussing computer reconstruction process for Mariner 6 and 7 TV picture quality improvement 24 p3875 A71-45228
- IMAGE FILTERS**
- Spatial filtering equipment for unwanted images as diffraction in holography, interferometry, etc 01 p0092 A71-10330
- Straight and curved edges produced videodigital amplitude spectra discrimination in TV image scanning nuclear particle path photographs, using filter device 02 p0248 A71-11980
- Filter effect on CRT display resolution and relation to photometric and color contrast 02 p0249 A71-12020
- Spatial filtering for digitally deconvolving non degraded image by exploiting fundamental identity between vector convolution and polynomial multiplication 04 p0627 A71-15600
- Nonredundant array filtering and postdetected processing for aberration compensation in incoherent imaging 07 p1110 A71-19447
- Lens-prism model for holographic image processing in space-frequency domains with chirp signal interferometric compression 09 p1452 A71-23500
- Monopulse receiver design system and image base noise factors tradeoffs, discussing preselector and integrated front end trends 11 p1737 A71-25660
- Gaussian processes discrimination, considering correlation functions in integral control of nonlinear filter for image recognition 13 p2039 A71-28980
- High resolution holographic image deblurring methods involving coherent optical analog processing and Fourier transform division filter 18 p2918 A71-36079
- Computer best least square filtering and approximation by radial filter of noisy imagery using discrete array transmission from photographic film 18 p2884 A71-36080
- Computerized digital techniques for image motion compensation as function of additive noise level, using Fourier transform image filtering and half-tone display 18 p2919 A71-36081
- Solar chromosphere and corona manifold structure data, using high resolution filter photography 19 p3136 A71-37610
- Photographically recorded image enhancement, discussing filtering, SNR and film grain noise 21 p3382 A71-40949

- Nonlinear filtering for noise reduction of image data by mean-squared error minimization, discussing zero memory technique 22 p3547 A71-42507
- IMAGE FURNACES**
Thermal diffusivity and total emissivity measurements of solids between 1500 K and melting point, using arc image furnace 04 p0595 A71-14966
- Polymeric ablation materials testing in arc image furnace over various temperatures, pressures and thermal flux 11 p1790 A71-26045
- IMAGE INTENSIFIERS**
NT IMAGE ORTHICONS
Echelle grating and transmission optics spectrographs using image intensifier tubes for increased sensitivity 02 p0250 A71-12138
- Night vision visual systems with image intensifiers, noting effect on human eye performance at low light levels 10 p1641 A71-24057
- Four stage image intensifier testing for weak astronomical object photography in connection with 42 inch Cassegrain telescope 13 p2070 A71-29138
- Equatorward moving fast auroral waves recorded with image intensifier-TV system 14 p2229 A71-29660
- Image intensifier tube coupled to smoothing dissector to improve SNR in electronic scanning spectrometer 18 p2914 A71-35850
- Image intensifiers for color conversion, image deflection and scanning, shuttering and recording, defining information gain criterion for comparison with unaided photography 18 p2925 A71-36907
- Low light level TV system using Plumbicon tube and 3-stage image intensifiers 22 p3548 A71-42511
- Large display direct view low light level system with objective lens, image intensifiers and eyepiece 22 p3548 A71-42512
- IMAGE MOTION COMPENSATION**
Computer program for space and airborne optical imaging systems evaluation, emphasizing image motion compensation role 09 p1411 A71-22748
- Computerized digital techniques for image motion compensation as function of additive noise level, using Fourier transform image filtering and half-tone display 18 p2919 A71-36083
- Rectilinear correction of geometric errors of images transmitted from earth resources satellites, using digital computer 18 p2886 A71-36540
- Spaceborne astronomical telescope image stabilization system, utilizing field splitting technique 18 p2925 A71-36903
- Aerospace vehicles high resolution photography, introducing phase rate image tracking sensors for forward motion compensation 18 p2883 A71-36909
- Equatorial lunar radius determinations from image motion compensation sensor onboard Lunar Orbiter 1 spacecraft [AAS PAPER 71-337] 23 p3727 A71-43010
- Astronomical telescopes stellar image motion dependence on zenith distance, determining RMS value of jitter 23 p3771 A71-44259
- IMAGE ORTHICONS**
Transverse conductivity and temperature dependence of storage time during photographic scanning of astronomical objects with superorthicon camera 03 p0422 A71-13008
- Faint meteor spectra recording, using high sensitivity image orthicon 13 p2070 A71-29017
- Perseid meteors spectroscopic observations, using image orthicon technique for meteor spectral recording at luminosity thresholds below conventional spectroscopic capabilities 13 p2070 A71-29018
- Auroral conjugacy and time dependent geometry via all sky cameras and image orthicon TV onboard conjugate-flying aircraft 20 p3228 A71-39840
- Coherent optical processing system coupled to electronic readout system incorporating image orthicon TV camera, small digital computer and cell generator 21 p3381 A71-40929
- Computer controlled image orthicon tube for low light level spectroscopy of metastable excited ions transient absorption spectra 22 p3549 A71-42558
- IMAGE TRANSDUCERS**
Forty channel magnetography system including CRT display, digital controlled heliostat, real time computer and optical transducer 17 p2740 A71-34988
- Flying spot digitizer angle encoding system, describing multispeed transducer output conversion to digital format 18 p2925 A71-36914
- Solid state linear array piezoelectric hydroacoustic image transducer for underwater viewing in turbid oceanic environments 20 p3233 A71-38828
- Real time coherent optical data processing, describing spatial filtering and reactive processor and image converter designs 22 p3540 A71-41750
- IMAGE TUBES**
Closed system for air cooling of image converter tubes and superorthicons for wear light flux, using refrigerator or dry ice 01 p0080 A71-10622
- Space TV systems using SEC /secondary electron conduction/ camera tube 04 p0597 A71-15289
- Image tube for extrafocal photometry of faint galaxies, solving small scale sensitivity fluctuation problems 06 p0902 A71-18473
- Pattern recognition multiplex arrangement with optical relay tube and point hologram for image distribution onto spatially separated channels to obtain SNR improvement 18 p2917 A71-36054
- Semiconductor diode image tube system as digital multichannel photometer, noting cost, weight and size advantages over photomultiplier tube array with pulse counting electronics 22 p3541 A71-41793
- Electronic techniques in optronics /optoelectronics/, discussing CRT, image tubes, semiconductor and lasers 22 p3559 A71-42467
- Return beam vidicon characteristics and applications for reconnaissance, optical storage and scan conversion, data and signal processing 22 p3548 A71-42509
- High performance image isocan camera tube, noting resolution, contrast, service life, cost and TV applications 22 p3548 A71-42510
- Low light level TV system using Plumbicon tube and 3-stage image intensifiers 22 p3548 A71-42511
- Light pen optical writing and erasing with bistable phosphor storage tubes using screen photoconductivity 23 p3651 A71-43437
- Electronic optical astronomy, describing image detectors and computer controlled micrometers and telescope setting systems 23 p3678 A71-43542
- IMAGE VELOCITY SENSORS**
Aerospace vehicles high resolution photography, introducing phase rate image tracking sensors for forward motion compensation 18 p2883 A71-36909
- IMAGERY**
NT AERIAL PHOTOGRAPHY
NT ALL SKY PHOTOGRAPHY
NT ASTRONOMICAL PHOTOGRAPHY
NT CHRONOPHOTOGRAPHY
NT CINEMATOPHOTOGRAPHY
NT CLOUD PHOTOGRAPHY
NT COLOR PHOTOGRAPHY
NT ELECTRO-OPTICAL PHOTOGRAPHY
NT ELECTRON PHOTOGRAPHY
NT HOLOGRAPHY
NT INFRARED IMAGERY
NT INFRARED PHOTOGRAPHY
NT KINOFORM
NT LUNAR PHOTOGRAPHY
NT MICROWAVE IMAGERY
NT PHOTOMICROGRAPHY
NT PHOTORECONNAISSANCE
NT RADAR IMAGERY
NT RADAR PHOTOGRAPHY
NT RADIOGRAPHY
NT REPRODUCTION [COPYING]
NT ROCKET-BORNE PHOTOGRAPHY
NT SATELLITE-BORNE PHOTOGRAPHY
NT SCHLIEREN PHOTOGRAPHY
NT SHADOWGRAPH PHOTOGRAPHY
NT SPACEBORNE PHOTOGRAPHY
NT SPECTROHELIOGRAPHS
NT STEREOPHOTOGRAPHY
NT ULTRAVIOLET PHOTOMETRY
NT XEROGRAPHY
- Urban housing environment data acquisition from remote sensor imagery, stressing rapid surveys and data timeless attribute 09 p1439 A71-23213
- Ground truth role in remote sensing surveys from space, considering field measurement techniques in calibrating sensor imagery and unknown terrestrial environment 11 p1760 A71-26532
- Low loss surface oriented waveguide for millimeter IC, using high permittivity rectangular dielectric image line 17 p2714 A71-34603
- Earth resources technology satellites image processing system including electron beam recorder, image corrector, electro-optical systems and digital processors as design features [AIAA PAPER 71-977] 24 p3825 A71-44575
- IMAGES**
NT AFTERIMAGES
NT IMAGE VELOCITY SENSORS
NT RETINAL IMAGES
Visual images induced in aircraft crew members, during pressure chamber experiments, discussing latent period and persistence of sequences 02 p0198 A71-11899
- Eye movements and visual images evoked by verbal stimuli, considering hereditary factors contribution to image formation 24 p3796 A71-44548
- IMAGING TECHNIQUES**
NT IMAGE ENHANCEMENT
NT RADAR IMAGERY
Self reproduction of diffraction and reconstructed images of finite aperture in coherent radiation field by periodic transverse and longitudinal alternation 01 p0092 A71-10032
- Imaging with partially coherent light, generalizing optical transfer function in Fresnel approximation 01 p0078 A71-10144
- Parallel matched spatial filtering by optically superposed Fourier holograms, detecting simultaneously different image details 01 p0081 A71-10686
- Noncoherent optical analog image processing by constructive convolution integral techniques for removal of blur, defocus and noise 01 p0081 A71-10828
- Coherent optical data processing system imaging qualities photographic film requirements 01 p0050 A71-10900
- Underwater objects plotted in double projectors, reconstructing water surface optical refraction 01 p0083 A71-11327
- Long elevated horizontal line sources mutual impedance coupling, using image theory techniques 01 p0041 A71-11615
- Image transmission in isotropic photooptical channels, examining object-image brightness relationship 02 p0211 A71-11830
- Truncated periodic targets modulation in partially coherent light, deriving diffraction image formulas 02 p0260 A71-12146
- Spatial and temporal coherence effects in holography, giving general formula for reconstructed virtual image 02 p0251 A71-12148
- Laser image speckle interferometer design for observing vibrational modes on diffusely reflecting surfaces as alternative to holographic methods 02 p0254 A71-12718
- Solar radio bursts multifrequency observation using simple image forming system with multielement interferometer 02 p0302 A71-12765
- Holographic interferometry with both beams traversing transparent object, providing variable sensitivity and directional phase detection 03 p0425 A71-13654
- Holographic twin image elimination by nonlinear method based on statistical differences in objects and diffraction fields 03 p0425 A71-13656
- Microwave ultrasonic beam visualization techniques via Bragg diffraction of laser beam, investigating resolution capability 03 p0436 A71-13717
- High resistance single crystal light sensitive n-type GaAs wafer for obtaining long wave photographic images via electric photosensitivity control 03 p0428 A71-13986
- Three dimensional hologram reconstruction and recording, using extended source 03 p0428 A71-14057
- Hologram Fresnel zone with monochromatic signal and background noise, determining precision of object image coordinates 04 p0584 A71-14633
- Laser display technology, discussing recent systems, light beam deflectors and modulators 04 p0607 A71-14723
- TV techniques for solar optical image, describing equipment for recording and conversion 04 p0589 A71-14835
- Planned optical coincidence system for level bubble end image superimposition and transmittance to passage instrument ocular part 04 p0591 A71-14856
- Image polarity in holography and carrier frequency photography 04 p0601 A71-15696

IMAGING TECHNIQUES

Holography applications, recording and reconstructing three dimensional objects by split laser beam interference technique

05 p0747 A71-16194

Optical fields holographic subtraction for SNR enhancement

05 p0748 A71-16262

Phase objects holography using pulsed ruby laser with plane-parallel and hemispherical cavity

05 p0752 A71-16748

Nomographs for point source holographic imaging, discussing recording and reconstruction geometry

05 p0753 A71-16913

Millimeter wave lensless Fourier transformation /LFT/ holographic imaging, discussing equipment and performance

05 p0754 A71-17081

Multispectral and multitemporal digital imagery spatial registration using fast Fourier transform techniques, applying to earth resources satellite imagery preprocessing

05 p0756 A71-17147

USAF space missions information processing requirements relative to space transportation system, emphasizing real time image processing

05 p0727 A71-17229

Ultrasound propagation visualization in solids, describing sensitive schlieren apparatus

06 p0903 A71-17323

Holography development, discussing three dimensional images, fine grain recording emulsions and beam switching during reconstruction

06 p0897 A71-17369

Digital computer techniques for Mars surface imagery systematic video data distortions quantification and correction onboard Mariner 6 and 7

06 p0871 A71-17631

Photointerpretation automation, discussing computer pattern input system, image scanning and correlation, optical image transformations, trainable logic techniques, etc

06 p0900 A71-18095

Background effects on photographic stellar image photometry

06 p0902 A71-18445

Real time solar flare image production for Skylab astronaut training, using films of H alpha, XUV and X ray solar images [AIAA PAPER 71-73]

06 p0902 A71-18530

Matched spatial filters for holographic image recognition in biological studies

06 p0903 A71-18695

Memoscope for communications between operator and machine during biological image studies

06 p0864 A71-18696

Follow-up scanning systems and reading volume reduction in biological image descriptions facilitating computer aided microstructure analysis

06 p0871 A71-18697

Synchronous meteorological satellite mission goals and system design, describing imaging, data collection, facsimile, space environment, trilateration, ranging and transmission

07 p1067 A71-18807

Coherent noise elimination in coherent light imaging systems by time averaging noise concentrations through lens rotation about optical axis

07 p1107 A71-19208

TiNi antiphase boundaries direct observation using transmission electron dark field imaging technique

07 p1131 A71-19431

TV holography systems, discussing camera and reproducer resolution and operation methods at real time scan rates

07 p1109 A71-19452

Rotating modulation collimator as astronomical X ray camera, discussing data reduction techniques for image synthesis

07 p1109 A71-19455

Nonredundant two dimensional square and hexagonal point arrays with optimal autocorrelative properties, considering high resolution imaging systems in holography

07 p1111 A71-19490

Monograph on optical imaging of ultrasonic fields by acoustic Bragg diffraction covering heuristic plane wave and ray approach scattered fields

07 p1111 A71-19575

Pulsed laser holography physical principles and applications in stress and vibration analysis, flow pattern visualization, biophysical and medical research

07 p1113 A71-19783

Holography and interferometry industrial applications, considering three dimensional imaging, precision distance measurement, nondestructive testing and structural strains and failures detection

07 p1113 A71-19784

Kinescope light characteristics nonlinear effect of television system penetrating ability for image reproduction of faint stars

07 p1115 A71-20444

Lightning flash-ground strokes VHF radio pictures by hyperbolic position fixing system, obtaining three dimensional sferics fixes as function of time

08 p1325 A71-20880

Pulsed laser schlieren system for ultrasonic wave front imaging in nondestructive testing techniques

08 p1286 A71-20949

Statistical analysis of fiber optics imagery, considering resolution difference between static and dynamically scanned bundles

08 p1334 A71-21180

Photographic materials holographic exposure index improvement due to increased sensitometric speed and macroscopic transfer characteristics

08 p1290 A71-21385

Hologram imagery and aberrations computer based analysis, considering hologram geometries and nonchromatic aberrations

08 p1290 A71-21387

Information search and retrieval by superimposed holograms, describing coding detection and image reconstruction methods

08 p1291 A71-21397

Efficiency improvement of holograms with very high reference beam to object beam intensity ratio by constructing copy from first hologram

08 p1291 A71-21399

Image reconstruction from three dimensional holograms

08 p1292 A71-21488

Exponentially decaying intensity averaging time and intransparency effect on image unsharpness during object uniform or harmonic motion

08 p1294 A71-21902

Holography of focused images, using arbitrarily shaped off-axis reference wave and white light for image restoration

09 p1442 A71-22393

Full photographic spectral range spaceborne cameras photometric calibration, involving determination of absolute magnitude and illuminance spatial variation in image plane

09 p1447 A71-22744

Computer program for space and airborne optical imaging systems evaluation, emphasizing image motion compensation role

09 p1411 A71-22748

Photographic image acquisition from planet orbiters, examining systems performance and lens selection

09 p1447 A71-22749

Bands and gray levels number selection for Mars surface multispectral imaging

09 p1447 A71-22750

Portable xerographic unit construction and electric circuitry, discussing application for welded seams X ray imagery

09 p1450 A71-22895

ERTS-A imagery, Apollo 9 and high altitude aircraft photography applications to Land Management Bureau, Indian Affairs and Reclamation

09 p1451 A71-23208

Forested area landscape characteristics from remote sensed imagery, establishing base line information for vegetation mapping

09 p1438 A71-23209

Aerial photography vs orbital acquired imagery resolution for land use data

09 p1439 A71-23212

Image data coding by linear transformation and block quantization, considering Fourier, Hadamard and Karhunen-Loeve methods

10 p1580 A71-23766

Constant period discrete holograms features, investigating laser visualization, recording, reconstruction and image focusing

10 p1608 A71-23810

Papers on photoelectronic imaging devices covering radiometry, photometry, vision, electro-optical system evaluation, etc

10 p1609 A71-24055

Electro-optical systems in photoelectronic imaging devices, discussing electron gun, electrostatic focusing lens, spherical aberration, magnetic field computation and ray tracing

10 p1609 A71-24058

Electronic imaging devices specifications, emphasizing real time reconnaissance systems performance requirements

10 p1609 A71-24059

Photoelectric imaging devices resolution performance, considering modulation transfer function and measurement methods

10 p1610 A71-24060

Photoelectron noise limited low light level imaging sensors, investigating resolving power, signal degradation and camera tube performance

10 p1610 A71-24061

Electro-optical devices evaluation search model, considering imagery and image transmission

10 p1610 A71-24062

Holographic generation of high efficiency, extended range spatial filters, applying to defocused images restoration

10 p1612 A71-24585

Computer generated visual simulation of three dimensional objects, using geometric modeling technique for mathematical representation of photographic process

10 p1581 A71-24775

Holographic image recording and reconstruction two and three dimensions, including light wavelet structure, Huygens principle, wavefront reproduction spectral composition

10 p1613 A71-24261

German monograph on holographic method to increase effective aperture in optical imaging cover optical systems resolving power increase holography etc

10 p1613 A71-24262

Nematic liquid crystals in optical holography, attaining speckle free projection screens and data in holographic memories

10 p1622 A71-24263

Holography principles development, history, world recording, processing and reconstruction techniques for image quality improvement, laser applications, etc

11 p1767 A71-26261

Space photography for earth resource assessment discussing multi-band, -date and -stage techniques advantages, image analysis and conference systems

11 p1767 A71-26262

Plane and three dimensional dynamic hologram recording in bleachable dyes, using ruby laser with plium chloride phthalocyanin in chlorobenzene as a switch

11 p1767 A71-26263

Background effects in stellar photometry

12 p1903 A71-26264

Real time holography using moving groundglass fluorescent layer suitable for coherent matched filtering and seeing through fog

13 p2068 A71-28261

Information reduction for three dimensional projection holography, using horizontally directed selective stereoscreen

13 p2068 A71-28262

Computer phase hologram synthesis simplified modification, using EM field vector transformation for points

13 p2070 A71-29061

Diffraction-limited electromagnetic theory of image formation for point reference arbitrary shape hologram

13 p2072 A71-29062

Image distortion technique for viewing deformation zones at crack tips on highly polished surface

14 p2323 A71-29063

Hologram size and film type limitations effects on resolution of reconstructed image in edge-line holography

14 p2241 A71-30101

Spectrometric imager device providing information on spatial and spectral distribution of light from extended objects, discussing signal encoding and decoding devices and techniques

14 p2242 A71-30102

Inertial-inertial beam stabilization application for image surface mechanical coupling to instrument /photography/ and uncoupled surface /eye/

14 p2242 A71-30103

Optical aperture configurations effect on image performance, discussing large telescope systems design criteria

14 p2242 A71-30104

Image spatial frequency content of speckle pattern on illuminated diffuse screen and photographic film optical Fourier analysis

14 p2242 A71-30105

Luxmeters and photoelectric receptors for illumination measurement of light beams in limited solid angle in image systems, considering automatic photogoniometer

14 p2246 A71-30401

Plane wave and virtual image reconstruction from three dimensional holograms

14 p2248 A71-30601

Image classification by optical and electro-optical processing methods for spatial signal perception and treatment in natural form

14 p2248 A71-30801

Imagery of periodic objects through interposed turbulent medium, investigating diffraction images irradiance distribution and contrast

14 p2275 A71-30802

Three dimensional hologram relationship to object optical properties and structure, considering hologram imaging properties

15 p2402 A71-31201

Laser radiation source time and spatial coherence effect on brightness distribution of image produced hologram

15 p2402 A71-31202

Two interferograms holographic laser recording same emulsion by double exposure with ruby and harmonic wavelengths

15 p2454 A71-31203

Moire patterns generation by two frequency image plane holographic contouring, discussing multiple source and variable refractive index techniques

15 p2405 A71-31204

Optical wave reconstruction from microwave holograms and application to interferometry, considering

- resolving power and visible images of microwave transparencies 15 p2405 A71-31281
- Maastricht automatic data processing and display system concept for automatic management of reception and data transmission and information visualization 15 p2384 A71-31888
- Holography applications in aeronautics and astronautics, discussing advantages of three dimensional information in aircraft navigation, space missions and astronomic experiments 15 p2411 A71-32528
- Thermal imaging devices scanning systems for producing television-like images, noting alternate line scanning 15 p2412 A71-32759
- Random images transmission rates, comparing line-by-line and two dimensional encoding 16 p2541 A71-32819
- Scanning electron microscope in nondestructive testing, reviewing signal mode produced topographical data, image recording and inspection procedures 16 p2581 A71-32862
- Shearing interferometer based on moire method using Fourier image of grating, considering applications to phase gradient and lens aberration measurements 16 p2577 A71-33133
- Insufficient spatial and temporal coherence effects on holographic image reconstruction by injection laser, noting application to optical data processing 16 p2577 A71-33142
- Diffraction limited circular holographic determination of Airy radius by photoelectric scanning of image irradiance 16 p2577 A71-33143
- Electron-optical system with electro- and magneto-static lenses, ensuring large image reduction for producing printed microcircuits 16 p2579 A71-33500
- Three dimensional hologram recording, showing He-Ne laser reconstruction of Q switched ruby laser hologram image of mosquito flight 16 p2579 A71-33528
- Three dimensional hologram recording and reconstruction, discussing image geometry, reference beam intensity, size finiteness, transition limits and photosensitive materials 16 p2580 A71-33623
- Two dimensional pictorial information Fourier transform generation by coherent optics method, applying to imageries in earth sciences 17 p2737 A71-34271
- Holographic analysis of periodic microobjects at X ray wavelengths, obtaining high contrast 17 p2737 A71-34292
- Image distortion technique for viewing surface deformation zones at precracked specimens under monotonic loading during fracture test [SESA PAPER 1799] 17 p2738 A71-34547
- Synchronous meteorological satellite programs, noting earth imaging, data transmission, collection and relay and space environment monitoring 17 p2812 A71-34612
- High resolution microdensitometry image interpretation and manipulation by digital computer, discussing radiation coherence problems 17 p2742 A71-35002
- Automatic data reduction system for TV images of star fields acquired from OAO 17 p2743 A71-35009
- Statistical detection theory applied to images against background of laser produced speckle, using flying-spot type scanning machine 17 p2754 A71-35324
- Remote sensing imaging techniques for oil pollution survey, using airborne UV, IR, color and filtered panchromatic photography 17 p2735 A71-35386
- Plane and three dimensional dynamic holograms recording in bleachable dyes, using ruby laser with gallium chloride phthalocyanin in chlorobenzene as Q switch 17 p2745 A71-35507
- Simulation tests of multiagency reconnaissance sensor operations, including multisensor data base, imagery processing laboratory, flight testing and ground truth activities 17 p2775 A71-35764
- Real time reconnaissance cockpit display system for airborne sensor systems, providing night combat imagery 17 p2747 A71-35772
- Minimum aberrations in image wave front due to wavelength shift between recording and reconstruction beams in holography, using computer program 18 p2914 A71-35846
- Holographic fiber optics image-guiding structures preparation in sensitized polymethyl methacrylate cast sheet by refractive index gratings pair recording 18 p2946 A71-35852
- Monograph on satellite-borne orbital photographic imaging techniques application to natural resources survey, discussing remote areas geomorphological and geological reconnaissance maps preparation 18 p2915 A71-35905
- Remote subsurface oceanographic imagery from orbital altitudes in blue multispectral region, showing optimum filter passband 18 p2917 A71-36064
- High spectral resolution image recording instrument with postrecording bandpass selection, discussing signature data base and sensor modes 18 p2917 A71-36066
- Flat field condensing system for illuminating film projected on screen using Hg-Xe short arc lamp 18 p2918 A71-36071
- Sinusoidal image distributions generation by changing frequency response of optical system by exit pupil function/incoherent spatial filtering/modification 18 p2918 A71-36073
- Two dimensional optical Fourier approach diagnosing interpretation-limiting pictorial noise patterns in ERTS image output 18 p2919 A71-36082
- Side-looking airborne radars and image recording scanners design for geoscience applications, discussing gray scale improvement, multispectral sensing, target discrimination, etc 18 p2875 A71-36366
- ERTS-A and B pictorial data processing center, describing image processing system and available user services in terms of international participation 18 p2900 A71-36541
- Spaceborne astronomical telescope image stabilization system, utilizing field splitting technique 18 p2925 A71-36903
- Image intensifiers for color conversion, image deflection and scanning, shuttering and recording, defining information gain criterion for comparison with unaided photography 18 p2925 A71-36907
- Star sensor telescope, employing digitally coded silicon photocell detector for precise optical image location 18 p2925 A71-36910
- High quality continuous tone micromachining and image recording on metal thin films by low power pulsed gas laser heating 19 p3071 A71-37213
- High efficiency inline multiple imaging by means of multiple phase holograms, giving diffraction patterns 19 p3063 A71-37482
- Book on electron optics covering image formation principles, field plotting and ray tracing analog and computational methods, electrostatic and magnetic lenses, etc 19 p3103 A71-37522
- Two dimensional objects three dimensional image possibility based on self-reproduction effect for arbitrary periodic distribution function of transparency, using coherent light source 19 p3064 A71-37770
- Photochromic glass activation process for recording three dimensional holograms, using radiation with maximum spectral brightness coincidence with absorption band edge 19 p3064 A71-37772
- Outer planet satellite missions for optimal imaging conditions in terms of proximity and lighting [AAS PAPER 71-138] 19 p3140 A71-37942
- Image visual observation in coherent diffuse illumination, discussing human eye angular resolution deterioration and depth vision threshold dependence on light characteristics 19 p3074 A71-38195
- Computer aided digital transform natural image processing, using Fourier, Hadamard and Haar matrix algebra 19 p3026 A71-38404
- Astronomical telescopes image motion, distortion and scintillation, examining atmospheric refractive index and density/temperature variation effects 19 p3010 A71-38571
- Long object photography with lens array in non-coherent light and subsequent integrated image focus holography in laser beam for reconstruction in white light 19 p3068 A71-38708
- Multicolor images with volume dielectric holograms in photopolymer materials, reconstructing complex three dimensional images with high resolution in white light 20 p3236 A71-39192
- Photographic phase holograms including printout effect, bleaching, conversion with iodine compound and light stability 20 p3236 A71-39195
- Sound to light image conversion, emphasizing liquid surface acoustical holography 20 p3238 A71-39343
- Remote image-forming sensors on satellites and aircraft, considering resolving power, contrast rendition, dynamic range, SNR, sensitivity, and reliability as performance measures 20 p3240 A71-39608
- Walsh function imagery analysis by Hadamard-Walsh transform and eigenvector expansion technique 20 p3197 A71-39610
- Walsh functions in image processing, rotational feature selection and pattern recognition, defining set of orthogonal transformations 20 p3255 A71-39611
- Stereo viewing transmission/reflection display by producing stereopair image on CRT screen with polarizing polaroid sheets 21 p3376 A71-40126
- Large character set display terminal for public information service system, describing design, construction, components and operating characteristics for nonalpha languages 21 p3350 A71-40129
- Deformographic storage display tube system, describing construction, development, design, performance and operating principles 21 p3352 A71-40135
- French book on optical holography covering interference phenomena, image reconstruction from interferograms, geometrical and mathematical aspects, image quality and color holography 21 p3379 A71-40778
- Photopolymer holography systems and holograms fixing techniques, discussing polymer films image storing and fixing processes 21 p3381 A71-40927
- Holography review covering photon, grain and speckle noises limitations, large 3D picture production and various applications 21 p3381 A71-40930
- Optical field contouring techniques using holographic interferometry for obtaining objects shapes on contour maps 21 p3382 A71-40940
- High resolution full spatial frequency range optical image by incoherent superposition of low resolution partial frequency range component photographs, using optical aperture synthesis 22 p3538 A71-41735
- Imaging with low redundancy arrays, noting holography role in image processing 22 p3538 A71-41736
- Holographic image reconstruction analysis based on two beam interferometry by spatially incoherent light source, obtaining optical transfer function 22 p3539 A71-41740
- Acoustical holographic opaque structures visualization techniques and applications, discussing ultrasound qualities, image converters, detector arrays and medical diagnostic utilization 22 p3540 A71-41752
- Bragg imaging with optical heterodyne detection and bandpass filtering, considering resolution, SNR and dynamic range 22 p3540 A71-41777
- Phase aberrations in Bragg imaging for sound components projecting out of plane normal to light beam 22 p3540 A71-41778
- Brillouin scattering effect on noise of Bragg imaging in ultrasonic band at room temperature, using convergent illuminating light beam 22 p3541 A71-41779
- Holographic ultrasonic imaging method for flaw detection in aerospace materials and structures 22 p3554 A71-41782
- Active synthetic aperture coherent imaging technique to fill and double diameter of sparsely sampled aperture array 22 p3574 A71-41783
- Backward propagation method for ultrasonic image reconstruction, examining resolution in near field for high contrast objects 22 p3541 A71-41784
- Pyroelectric detector linear arrays for IR thermal imaging at room temperature 22 p3543 A71-42131
- Refractive imaging and scanning methods for thermal imaging systems, considering high performance IR lenses 22 p3544 A71-42137
- Scanning ultrasonic imaging technique for in vivo monitoring of microscopic bubble formation in decompression sickness, presenting image displays 22 p3504 A71-42250
- Hologram Fresnel zone with monochromatic signal and background noise, determining precision of object image coordinates 22 p3546 A71-42273
- Two dimensional probabilistic images generation and statistical characteristics determination, noting application to psychophysiological experiments 22 p3518 A71-42422
- Holography, covering thin, thick, transmission, reflection, amplitude and phase type holograms principles and applications in interferometry, microscopy, imaging, optical data processing, etc 22 p3546 A71-42476
- Microwave quasi-holographic techniques, discussing synthetic aperture, chirp radar, rotating target imaging system and beam forming method 22 p3546 A71-42477

IMBEDDINGS [MATHEMATICS]

Acoustic holography imaging technology, discussing sound field visualization and applications in nondestructive testing, medical diagnostics, ultrasonic microscopy, seismology and underwater viewing 22 p3546 A71-42478

Electronic imaging systems - Conference, Palo Alto, California, April 1970 22 p3547 A71-42502

Human observer performance in imaging systems, detailing contrast, ambient illumination, resolution, exposure time, display size, field of view and image blur and enhancement 22 p3547 A71-42503

Solid state charge controlled electroluminescent display panel with image memory capability, describing negative oxygen ions and photoconductive charge control methods 22 p3548 A71-42514

Laser beam image reproducer systems, emphasizing pattern generators, automatic calibration subsystems, raster line merging apparatus, scanners and continuous film transport mechanism 22 p3559 A71-42515

Electron beam image recorder applications, discussing superior resolution, dynamic range width and high precision controllability advantages over laser or CRT techniques 22 p3548 A71-42516

Defocused optical system imaging properties and optical transfer function improvement by shaded aperture, discussing necessary conditions and light absorption effect 22 p3548 A71-42551

Low loss images from smooth solid specimens in surface scanning electron microscope by collecting backscattered electrons 23 p3674 A71-42959

Grand Tour mission satellite planetary imaging analyses and science scan platform pointing requirements, utilizing computer graphic techniques [AAS PAPER 71-379] 23 p3731 A71-43049

Flash X ray technique for imaging of cavities formation during electron beam welding of Al alloy 23 p3681 A71-43195

Electro-optical techniques for particle size measurements from aircraft, noting imaging techniques superiority for nonaerosol and large particles 23 p3677 A71-43514

Latent photographic image formation mechanism, explaining neutral atoms drift towards negatively charged center with surrounding polarized silver atoms 23 p3678 A71-43580

Photoelectric localization of features via optical signal modulation, noting sensitivity dependence on illumination type 23 p3679 A71-43895

Incoherent light bandpass filter to amplify detail contrast of optical system 23 p3679 A71-44010

Radio-optics prospects in signal and information processing, image reconstruction, data transmission, computer storage, display and holographic movies and TV 23 p3681 A71-44344

Three dimensional imaging of objects from white light or X ray shadowgraphs by holographic phase implantation 24 p3824 A71-44356

Optical system superresolution by reduction of temporal degrees of freedom using holography 24 p3824 A71-44453

Cathode ray tube graphical display system as digital computer output terminal, using analog memory for flickerfree image 24 p3806 A71-44652

Telescope wave optical imaging performance, deriving point spread function, radial energy integral and modulation transfer functions for different wave front surface deviations 24 p3849 A71-45204

Culgoara radiotelescope electronic imaging system for diffraction pattern generation 24 p3828 A71-45205

Computer model of microchannel electron multiplier plates in imaging devices using Monte Carlo method 24 p3811 A71-45328

IMBEDDINGS [MATHEMATICS]

NT INVARIANT IMBEDDINGS

One dimensional optimum design lubrication treatment as imbeddings of nonlocal optimization problems 14 p2252 A71-30097

Einstein equations solution as hypersurface of four dimensions in Euclidean space, investigating imbedded manifold deformations 16 p2610 A71-33272

Quantum mechanics axiom system construction from physical theories, using imbedding operation 19 p3103 A71-37276

IMIDES

Imide-pyrone copolymers preparation by solution polymerization, considering base/acid degradation resistance and thermal stability in air and vacuum 04 p0549 A71-15749

Amidoximes dehydration with and without rearrangement, suggesting carbodiimide formation from O-benzenesulfonyl ester 06 p0865 A71-17550

Cytotoxic and radiosensitizing effect of thiol binding agents iodoacetamide /IAA/, N-ethylmaleimide /NEM/ and iodoacetic acid /IA/ on crypt cells of mice duodenum 07 p1038 A71-18975

Phenylated imide-quinoxaline copolymers, describing synthesis and thermal and solubility properties 11 p1787 A71-25425

IMMERSION

U SUBMERGING

IMMISCIBILITY

U SOLUBILITY

IMMITTANCE

U ELECTRICAL IMPEDANCE

IMMUNITY

Primary immune response chemical radioprotection in white mice during gamma irradiation, using serotonin as chemical protective and sheep red blood cells as immunizing agents 05 p0710 A71-16816

Active biological immunity development in long term space flights, discussing natural and nonspecific resistance to viruses and recurrent infections 21 p3332 A71-40552

Human body immune status normalization in prolonged space flight, investigating ribonucleic acid stimulated antibody formation 21 p3332 A71-40554

IMMUNOLOGY

In vitro lymphocyte antigen response measurements in cellular immunity evaluation under adverse logistical conditions, emphasizing RNA and DNA synthesis rates 02 p0199 A71-12390

Audiogenic stress effects on susceptibility to cytotoxic and oncogenic virus infections and host defense mechanisms 03 p0359 A71-13152

Antigenic properties of human vascular wall layers in atherosclerosis, using agar precipitation and immunoelectrophoretic measurements 04 p0540 A71-15574

Immunological reactivity of human body during 120 day feeding on dehydrated diet 06 p0861 A71-18368

Skin tissues automicroflora composition and natural immunity indices changes after 18 day orbital flight from microbiological and immunological examinations 09 p1389 A71-22204

Hypoxia effects on organism resistance and immunobiological reactivity, noting bacterial and protozoa infections aggravation 13 p2006 A71-28401

Immunochemical investigation of dogfish pepsinogens A, C and D, determining characteristics in terms of immunodiffusion, immuno-electrophoresis, complement fixation and enzymic activity inhibition 13 p2015 A71-29480

Immunobiological reactivity inhibition in mice under partial adaptation to high altitude hypoxia, observing decreased phagocytic activity, antibody production, hypoplasia and lymph cell number 15 p2356 A71-31289

Alpha adrenergic inhibition of immunoreactive insulin release during deep hypothermia in puppies given glucose infusions 17 p2681 A71-34942

Human microbial flora and immunologic response in long term space missions, describing environmental parameters and factors and work-rest schedules effects 21 p3332 A71-40553

Microflora simplification effects on immunocompetent organism systems, observing shifts in guinea pigs lymphoid tissue with limited flora 21 p3332 A71-40555

Spacecraft cabin artificial atmospheric composition and variation effects on human immunocompetence, examining lymphoid cell immunity reactions after lymphocytes blast transformations 21 p3332 A71-40556

Dispensing devices and error sources in radial immunodiffusion and electroimmunodiffusion techniques 22 p3508 A71-42888

IMP

MOSFET data systems evolution for IMP, discussing effects on system design and reliability approach 08 p1267 A71-21844

Interplanetary plasma and magnetic field observations by Vela 3 and Imp 3 satellites 23 p3708 A71-43154

IMP-C

U EXPLORER 28 SATELLITE

IMP-D

U EXPLORER 33 SATELLITE

IMP-E

U EXPLORER 35 SATELLITE

U IMP

IMPACT

NT ELECTRON IMPACT

NT HYPERVELOCITY IMPACT

NT ION IMPACT

NT POINT IMPACT

NT PROTON IMPACT

Elastoplastic impact, optimizing system with respect to mass kinetic energy with elastic and dry friction properties taken into account 05 p0821 A71-16398

Three mass vibrational impact system analysis by mathematical electronic analogs, examining system and excitation parameters influence on vibrational modes and dissipative properties 05 p0821 A71-16350

Single mass vibrational impact system optimization periodic motions, analyzing vibrorams productivity optimization via analog of sphere bouncing down stairs case 05 p0821 A71-16351

Impact craters crustal thickness and forms relationship to changing physical state of planetary surface during once-molten cooling 19 p3051 A71-37661

IMPACT ACCELERATION

Aspartic aminotransferase activity relation to clinical and biochemical indices of human tolerance to impact accelerations 01 p0014 A71-11144

Axially symmetric bodies impact landing on water surface, deriving acceleration for comparison with measurement 01 p0178 A71-11398

Bent structure failure under pulse floor acceleration shocks, concerning aircraft seat damage during crash landing 08 p1367 A71-20744

Small caliber smoothbore powder sabot gun generating planar shock wave in solids, using streak camera monitoring of impact and recoil velocities 14 p2223 A71-30888

IMPACT DAMAGE

NT METEORITIC DAMAGE

NT RAIN IMPACT DAMAGE

Spherical shells deformation subjected at elevated temperature to high velocity impact on planar rigid target 03 p0503 A71-13422

Impact induced closed brain injuries pathomorphology, considering dura mater, contusions, neuron and glial damage, brain stem lesions and hemorrhages 04 p0537 A71-14782

Helicopter structural damage due to icing, discussing secondary effects on tail rotor, horizontal tail and engine from ice shed by main rotor 04 p0533 A71-15432

Circular cylindrical orthotropic fiberglass reinforced shell buckling under longitudinal impact, assuming initial surface imperfections 06 p0985 A71-17684

Thin plate impact and plastic nonpenetrating deformation by blunt projectiles 07 p1209 A71-19043

Aircraft self sealing fuel tank and fuel cell system damage control, considering chemical, precompressed foam and swellable elastomer seal concepts 10 p1554 A71-24075

Bird impact hazard to general aircraft, discussing structural damage, flight safety and testing procedures 10 p1557 A71-24997

Instantaneous postural reaction of cattle to brain concussion indicating mechanoreceptor HF discharged impulse pathophysiological mechanism 11 p1720 A71-26122

Lunar impact cratering in geologic time, deriving meteoritic flux mass approximation and planetesimal origin 13 p2134 A71-28288

Materials and structural design development by high velocity impact testing due to transport and subsonic military aircraft susceptibility to bird collision damage 14 p2221 A71-29642

Viscoplastic cylindrical shell dynamic buckling during axial impact of rigid mass, discussing constitutive equations 14 p2331 A71-30841

Lunar craters formation impact vs volcanic theories, using lunar probes for recognizing moon surface shocked materials 15 p2493 A71-32481

Large meteoroids ablation and breakup mathematical model, estimating Mars atmosphere effectiveness as shield against surface impact craters production 16 p2643 A71-33968

Combat aircraft vulnerability to projectile impact, predicted by model giving target penetration, damage size and structural response [AIAA PAPER 71-777] 16 p2660 A71-34013

Two massive arbitrarily shaped hard bodies spatial collision, determining kinetic energy loss, motion and deformation of impact point 17 p2818 A71-34347

Wing structural elements ballistic damage tolerance and residual fracture strength characteristics, discussing projectile velocity, impact angle and target thickness effects

17 p2827 A71-35161

Impact craters and depressions on earth, examining meteoritic origin, characteristic features, energy release and cryptovolcanism

17 p2805 A71-35376

Microcrater morphology in lunar soil glass, oligoclase and olivine, determining projectile velocity, impact angle and shape effects

18 p2961 A71-35947

Meteorite impact and volcanism - Conference, Houston, October 1970

19 p3049 A71-37651

Australian Liverpool and Strang way craters as probable meteoritic impact origin from topographic and petrographic data

19 p3049 A71-37653

Rochechouart meteorite impact structure located in granites and gneisses of Hercynian age in south-central France

19 p3049 A71-37655

Charlevoix structure impactite description, discussing meteoritic impact origin from petrographic and chemical data

19 p3049 A71-37656

Igneous rocks origin associated with shock metamorphism, considering geochemical investigations of Canadian craters

19 p3051 A71-37668

Impact and explosive craters production in same target material under controlled laboratory conditions, determining depth of burst simulating impingement

19 p3156 A71-37682

Craters produced by oblique trajectory missile impact, suggesting crater dimension dependence on target material and missile kinetic energy

19 p3156 A71-37683

Pueblito de Allende meteorite craters, discussing crater formation and impact direction in comparison with experimental air-drop craters

19 p3052 A71-37684

Dimensional analysis of wear by solid particle impact in fluid flows in pumps and ducts

19 p3046 A71-38273

Electron microprobe analysis of cavity surface and lip of cosmic dust impact craters in stainless steel plates exposed at 400 km altitude in Gemini S-010 experiment

20 p3299 A71-39652

Physical chemistry of Aouellou impact crater glass, suggesting meteoritic origin of tektites

21 p3450 A71-40647

Double frustum phenomenon in mushrooming of cylindrical Al projectiles upon high speed impact with hardened steel anvil

21 p3474 A71-41424

Impact metamorphism effects in Apollo 12 microbreccias from Oceanus Procellarum

23 p3745 A71-43659

Cosmic dust particles impact craters searched for in lunar samples by binocular and electron scanning microscopes, relating to early solar system meteoroid flux

23 p3765 A71-43807

Lunar glass spheres cratering origin hypothesis from target temperature effects on crater morphology in targets impacted by high velocity Al projectiles

23 p3765 A71-43808

Micrometeoroid flux determination from impact sites on Surveyor 3 TV camera optical filter surfaces, noting agreement with Pioneer, Cosmos and Pegasus spacecraft measurements

23 p3766 A71-43820

Surveyor 3 unpainted Al tubing examination by replication electron microscopy for surface damage due to particle impact and ion bombardment in lunar environment

23 p3766 A71-43821

Craters produced by high speed hardened spherical particles, investigating depth and diameter relationship to impact speed

24 p3885 A71-45324

IMPACT DECELERATION

U DECELERATION

U IMPACT ACCELERATION

IMPACT LOADS

Steel cylinders with circumferential cracks under repeated impact tensile loads, investigating plain strain fracture toughness index temperature dependence

01 p0166 A71-10079

Quasi-plastic impact in shock interaction between free body and moving plane, using nonlinear finite difference equation

01 p0127 A71-10636

Critical static strength of Duralumin under cyclic impact loads, analyzing statistically load distribution function applicability

01 p0103 A71-11240

Nonlinear impact buckling of strut, using asymptotic small parameter method

01 p0177 A71-11296

High stress cycles and impact fatigue behavior of common case hardened carburized gear steels under loading

03 p0441 A71-13253

Mathematical stress wave model for sandwich plates under high velocity impact, considering structural multiple reflections and various material combinations

[SESA PAPER 1653] 03 p0508 A71-13774

Infinite elastic beam normal impact by semiinfinite elastic rod, using Timoshenko beam and one dimensional bar theory to describe elastic waves

[ASME PAPER 70-WA/APM-54] 03 p0513 A71-14171

Polish book on impact in discrete mechanical systems covering beams, curved rods, plates, nonlinear damping, numerical analysis, subjected to shock loading

03 p0513 A71-14297

Plastic wave propagation of combined stresses due to longitudinal impact of pretorqued tube

04 p0668 A71-15190

Structural behavior of rods and cylindrical shells under dynamic impact loads

06 p0989 A71-17783

Dynamic elastic-plastic buckling of rectangular plates in sustained flow involving mass impact

07 p1211 A71-19251

Symmetric three-layer girder with contact deformations and transverse compression of filler, calculating vibration under elastic impact by numerical analysis

09 p1538 A71-22522

Pendulum oscillations under impact force in low resistance medium

09 p1494 A71-22875

Dynamic response of beams to transverse impact, considering deflection curve

09 p1541 A71-23205

Dynamic plastic bending theory of thin circular annular plate with central hole under uniform impulse

10 p1689 A71-24519

Dynamic deformation of cylindrical shells by elastic body impact, using sequence boundary value solutions in plate theory

10 p1689 A71-24561

Asymmetrical three layer plate with filler under impact loading, examining material and layer thickness effects on deformation

12 p1975 A71-27111

Nonlinear equations of motion for cylindrical elastoplastic shell under axial impact

12 p1980 A71-27452

Dynamic snapthrough of shallow circular cylindrical shell undergoing plane motion in response to nearly symmetric impulsive pressure

13 p2146 A71-27781

Steel bar under longitudinal impact, deriving flexural half waves length formulas for critical force

13 p2158 A71-29435

Explosives in porous state under impact loads, obtaining adiabats, compressibility and temperatures

15 p2511 A71-31384

Thin conical shell under longitudinal impact, deriving theory for transverse and rotary inertias and transverse shear deformation effects

15 p2506 A71-32017

Room with windows and open doors under sonic boom, determining cavity resonance model for impulsive loading conditions

15 p2450 A71-32514

Near field dynamic response of semiinfinite elastic plate to lateral impact, comparing displacement field observations to numerical results

15 p2510 A71-32792

Maximum contact force dependence on rebound velocity, coefficient of restitution and impact duration during inelastic collision

16 p2647 A71-32816

Steel cylinders with circumferential cracks under repeated impact tensile loads, investigating plane strain fracture toughness index temperature dependence

16 p2658 A71-33635

Orthotropic laminated plates dynamic response to impulse loads, detailing flexural wave propagation

17 p2823 A71-34809

Dynamic loading of cantilever beams by magnetomotive and explosive loads and high bullet speed impact, noting elastic and plastic deformation modes

18 p2981 A71-36770

Penny shaped crack under time dependent impact wave loads, investigating transient response with integral transformations

21 p3468 A71-41002

Epoxy resin plate mechanical stress measurement under impact load, using laser light source three beam interferometric assembly with photographic recorder

22 p3555 A71-41613

Plane wave propagation following thin elastic rectangular plate impact against smooth rigid obstacle, using difference scheme

22 p3531 A71-41910

Circular conical shell initial deformation under impulsive load, using Timoshenko theory

24 p3883 A71-44852

IMPACT PREDICTION

Thrust vector control system of reduced impact dispersion of Skylark sounding rocket

[AIAA PAPER 70-1375] 03 p0497 A71-13658

Sounding rocket dispersion reduction using optimum wind filter for impact prediction based wind statistics and measurement

[AIAA PAPER 70-1394] 03 p0499 A71-13675

Thin shallow spherical shell vertical impact against ideal incompressible liquid surface, calculating axisymmetric deformation and hydrodynamic load distribution

07 p1089 A71-19738

Elastoplastic arresting device, predicting mass impact effect for optimal design in terms of deformation or contact time

08 p1367 A71-20688

Impact dispersion reduction of uncontrolled sounding rocket ZENIT with CUCKOO booster by canard control, noting flight path angle error by tracking radar

09 p1533 A71-23598

Campo del Cielo, Argentina meteorite crater structural analysis, discussing dimensions, energy of formation, mass, impact velocity, etc

15 p2488 A71-32352

Rigid body longitudinal impact against free end of variable cross sectioned viscoelastic cantilever beam, obtaining solution as rapidly converging Fourier series

19 p3160 A71-38485

IMPACT PRESSURES

U IMPACT LOADS

IMPACT RESISTANCE

Elastoplastic conical shells strain under longitudinal impact by large rigid body, analyzing plastic bending

06 p0996 A71-17842

Transverse impact resistive graphite fiber reinforced plastic (GFRP) lightweight sandwich panels and beam structures, using thin inner core facings

11 p1846 A71-25417

Impact resistant power packages for unmanned planetary probe landers, discussing radioisotope thermionic multiconverter array optimal configuration

11 p1713 A71-25898

Unidirectional fiber composites impact resistance, showing matrix modulus, fabrication process, fiber and void volume ratios and microresidual stress effects

14 p2264 A71-29920

Impact sensitivity tester for engineering materials in liquid and gaseous oxygen at high pressures

14 p2222 A71-30548

Impact reaction intensity test, determining fire or explosion hazards of materials exposed to liquid oxygen

14 p2222 A71-30549

Flash points, fire points and impact sensitivity of materials under gaseous oxygen pneumatic and mechanical impact

14 p2222 A71-30550

Quenching effects on glazed and unglazed alumina rods in various media, noting improved flexural and tensile strength, thermal shock resistance and impact resistance

22 p3565 A71-42342

IMPACT SENSITIVITY

U IMPACT RESISTANCE

IMPACT STRENGTH

Prealloyed hot formed Cr-Ni-Mo and Ni-Mo steels manufactured from powders, considering toughness, tensile properties, fatigue and impact strength

01 p0100 A71-10464

Projectile impacts into laminated targets consisting of plastic layers backed by Al substrates using SHAPE code with hydrodynamic elastoplastic distortional model

[AIAA PAPER 69-356] 03 p0504 A71-13431

Be impact strength temperature dependence and fracture structure, noting grain boundaries cohesion role

05 p0768 A71-16773

Charpy notched impact strength of carbon fiber reinforced epoxy resin composites over temperature range

[PLASTICS INST. PAPER 20] 08 p1318 A71-20891

Hot extruded W-Cu pseudosalloys under tension and compression, determining impact strength and plasticity

08 p1316 A71-21614

Low temperature impact toughness test as criteria for metal susceptibility to brittle fracture

09 p1468 A71-22509

Impact strength decrease of welded joints in Ti alloys due to air cooling rate after aging

09 p1478 A71-23421

Fiber length, diameter, bundle size, glass content and sizing effects on fiberglass reinforced plastic systems flexural, tensile and impact strength

11 p1784 A71-25395

Orientation dependent impact toughness and crack resistance of brittle fiber-ductile matrix composite of solidified carbide reinforced Co-Cr eutectic

11 p1782 A71-26386

Impact strength of Cu, Cu-Ni alloy and superalloy matrices reinforced with W fibers, studying temperature, heat treatment and fiber content and toughness effects
14 p2258 A71-29919

Tempered martensite and lower bainite in high purity carbon steels, discussing impact toughness due to internal twinning, grain boundary precipitation and carbide morphology
15 p2432 A71-32173

Ultralight magnesium based alloys classification by Li content, noting lattices, structural composition, specific weight, plastic properties and impact strength
15 p2435 A71-32336

Ti alloys argon TIG welding to Nb alloys, detailing joint impact strength, fusion zone ductility and bending tests
15 p2418 A71-32668

Al-Mg alloy with Ti, Zr, Mo and B additions under tensile and impact loads, investigating mechanical properties, strength and crack formation
16 p2594 A71-33712

Tensile, impact and fatigue properties of welded Ti alloys, determining joint quality and friction welding sensitivity in highly stressed gas turbine components
21 p3387 A71-40619

Alumina, boron carbide and silicon carbide notched and unnotched impact strength tests, using drop weight technique
22 p3565 A71-42542

IMPACT TESTING MACHINES

Launching intermediate velocity thin plastic sheets for short duration pressure pulse studies of dynamic materials properties
03 p0427 A71-13916

IMPACT TESTS

NT CHARPY IMPACT TEST

Materials and welded joints brittle fracture resistance estimation from impact bending tests
01 p0085 A71-10084

Bar impact against rigid obstacle, using method of characteristics for elastoplastic waves propagation and interaction
01 p0171 A71-10651

Axially symmetric bodies impact landing on water surface, deriving acceleration for comparison with measurement
01 p0178 A71-11398

Streak interferometry providing single impact test data for calculating dynamic stress-strain curve [SESA PAPER 1717]
03 p0509 A71-13777

Circular Al rings under radial impulsive loading by curved magnetically driven Al flyer plates, recording strain-time histories on oscilloscopes [SESA PAPER 1644]
03 p0509 A71-13778

Steam turbine blade metal removal rates by repetitive water drop impact, using hydrodynamic model
03 p0405 A71-14290

High speed ball impact tests and fracture energy of carbon fiber reinforced plastics [PLASTICS INST. PAPER 25]
08 p1322 A71-20922

High velocity microparticle simulation techniques for studying properties, dynamics and origin of micrometeoroids, considering accelerators and impact results
09 p1425 A71-22099

Nuclear surface effect vehicle and subsonic aircraft for transoceanic cargo shipping, discussing mobile reactor safety tests under high speed impact conditions [AIAA PAPER 70-1221]
09 p1492 A71-22779

Construction and hypervelocity impact tests of penetration resistive dual bumper wall for spacecraft meteoroid protection [AIAA PAPER 71-339]
11 p1843 A71-25318

Hypervelocity projectile material impact on ultimate reflectance of bombarded polished metals from shock tube tests
11 p1799 A71-25835

High strain rate effects on Al single crystals deformation, presenting overall and local strain and lattice rotation measurements in impact tested specimens
11 p1779 A71-26014

Izod impact testing of carbon fiber reinforced plastics, considering fiber volume loading, surface treatment and specimen and notch geometry
12 p1921 A71-27015

High pressure gaseous oxygen impact testing method incorporating drop plummet system for specimens flammability screening
14 p2222 A71-30547

Impact reaction intensity test, determining fire or explosion hazards of materials exposed to liquid oxygen
14 p2222 A71-30549

Dynamic response and perforation of thin plates subjected to projectile impact, measuring plastic deformation, dynamic strain and displacement with high speed camera
15 p2503 A71-31422

Bridge circuit for minimizing parasitic electrical disturbances in resistance strain gage measurements of dynamic stresses in impact tests
15 p2408 A71-31865

Reactor-shield-containment system models under impact tests, noting cracks, leaks and deformations
16 p2606 A71-33250

Materials and welded joints low temperature operation reliability prediction by estimating brittle fracture resistance from impact bending tests
16 p2584 A71-33640

Double frustum phenomenon in mushrooming of cylindrical Al projectiles upon high speed impact with hardened steel anvil
21 p3474 A71-41424

Mo alloy under impact tests, investigating notch sharpness effects on cold shortness threshold and strength
23 p3693 A71-44231

IMPEDANCE

NT ACOUSTIC IMPEDANCE

NT CONTACT RESISTANCE

NT ELECTRICAL IMPEDANCE

NT ELECTRICAL RESISTANCE

NT LC CIRCUITS

NT MECHANICAL IMPEDANCE

NT REACTANCE

NT RESPIRATORY IMPEDANCE

NT SKIN RESISTANCE

Total impedance plethysmography boundary value problems, developing computer program based on Jacobi iterative method
03 p0367 A71-12993

Surface impedance of thin metal plate excited by RF electromagnetic field as function of external DC magnetic field
04 p0636 A71-14972

Impedance antenna with slow wave structure of zig-zag shaped wires
07 p1079 A71-20260

IMPEDANCE MATCHING

Signal sources output impedance matching effect on phase difference measurement accuracy
02 p0212 A71-11842

Ni-Al-Ti alloys strength, investigating matrix precipitate lattice parameter mismatch effects
02 p0263 A71-11865

Single thermocouple temperature measurement, discussing millivoltmeters wiring method with resistance matching to ensure accuracy
03 p0430 A71-14329

Matched impedance microwave vacuum feedthrough
05 p0757 A71-16234

Radio communication system hypersonic delay lines, investigating coupled resonators matching efficiency in parallel and series connection
07 p1074 A71-19142

Traveling wave antenna arrays of mismatched elements, calculating element resistances and spacings
09 p1408 A71-23488

Radiation nulls suppression and broadband impedance matching of infinite rectangular waveguide phased arrays, giving numerical solutions
09 p1419 A71-23494

Arbitrary antenna arrays of not necessarily identical elements, deriving maximum realizable gain under impedance matching, and applying to spaced circular arrays
09 p1419 A71-23508

X band Schottky barrier diodes RF impedance mismatch and noise factor, calculating dependence on microwave oscillator voltage-standing wave ratio
09 p1421 A71-23723

Mutual impedance of interacting dipoles at wedge tip, determining errors for short spacing distances
13 p2036 A71-28370

Radio frequency power meters comparison, reducing mismatch and directivity errors with directional coupler
14 p2205 A71-30984

Thick unsymmetrically fed dipole antenna radiation pattern measurements and impedance matching
15 p2377 A71-32318

Microstrip microwave amplifier design using common emitter configuration and quarter wave impedance matching transformer
16 p2545 A71-33395

Book on microwave fields and circuits covering waveguides, transmission lines, impedance matching, sources, resonators, antennas, etc
17 p2716 A71-34772

Noise factor formula of multiple loop receiver input network with series connected stages for antenna matching and coupling parameters
19 p3022 A71-38498

Reactive impedance matching of Gunn or IMPATT diodes for microwave oscillators by dielectric tuning
23 p3650 A71-43071

Low noise IR range radiometer, including impedance matching and narrow band filtering
23 p3678 A71-43534

Electromagnetic wave amplification using coaxial line matching with plasma waveguide by charged particle beam
24 p3853 A71-44508

End line matching for high gain traveling wave amplifier constructed from heterogeneous transmission line with negative resistance
24 p3810 A71-45262

IMPEDANCE MEASUREMENTS

Planar diffused transistor characterization by equivalent circuit model using input impedance and amplification measurements
01 p0051 A71-10342

Complex permittivity and impedance of dielectric samples in coaxial lines and rectangular waveguides by moving probe and resonant Q factor measurements
02 p0229 A71-11710

Impedance measurement and standing wave ratio at microwave frequencies, using directional couplers
03 p0377 A71-13268

Normal mode helix antenna with rectangular wave tapered Al strip conductors, measuring impedance variation with frequency at VHF range
03 p0387 A71-13822

Fluidic ID transmission line characteristic impedance measurement as function of signal frequency, noting correlation with Nichols theory [ASME PAPER 70-WA/FLCS-14]
03 p0354 A71-14089

Short dipole antenna impedance in warm isotropic plasma using Vlasov theory
04 p0553 A71-15221

Gunn diodes impedance measurement at bias voltage above threshold, using broadband equivalent circuit model for mount and package
07 p1072 A71-19101

Series impedance elements in RF impedance measurements
07 p1112 A71-19777

Electronic equipment for measuring resonant frequency drift during slow wave structure impedance measurements, considering mean square errors
08 p1264 A71-21072

Reflex klystron electron beam admittance calculation, comparing results with measurement
08 p1264 A71-21277

Variational formula for input impedance of thin, asymmetrical cylindrical dipole antenna
09 p1408 A71-23490

Rough circular rod effective surface impedance and propagation constant, discussing guided electromagnetic wave attenuation on structure
10 p1578 A71-24399

Pulmonary arterial system impedance and transmission properties, noting hypoxia and serotonin infusion vasoconstrictor effects
11 p1719 A71-25922

Mechanical impedance measurement of artificial and human mastoids for bone vibrator calibration as function of frequency
11 p1725 A71-26185

Cross couplings in wideband antenna arrays, determining scattering coefficients, self/mutual impedances and admittances of two radiating elements
11 p1738 A71-26344

Dipole elements input impedance of wideband linear antenna arrays, using coupled circuits and induced emf
11 p1738 A71-26345

Microstrip microwave circuit design by complex admittance measurement and computer modeling
12 p1892 A71-27149

Antenna analysis method based on transmission line theory, yielding current distribution and input impedance of finite conical antenna
12 p1880 A71-27150

RF discharge quasi-homogeneous plasma device for measuring antenna impedance and sheath effects
13 p2105 A71-27996

Sharp peaking of wave impedance characterizing propagation in earth-ionosphere waveguide from atmospheric radio noise measurements near 2 kHz
13 p2029 A71-28471

Microwave oscillators Rieke diagram semiautomatic plotting by injection phase locking, using network analyzer for impedance measurement
14 p2211 A71-29823

Impedance testing techniques based on ratio of mechanical input force to velocity response for structures and systems behavior evaluation under dynamic loads
14 p2252 A71-30054

Small signal impedance of avalanche region in microwave IMPATT diode
14 p2215 A71-30833

Materials dynamic characteristics determination by acoustic input signal impedance measurement, presenting expressions as functions of reflection factor and signal propagation phase shift
15 p2409 A71-32186

Pure superconducting Al wire surface inductance measurement as function of temperature, noting penetration depth value
16 p2621 A71-33425

General media electrical properties from current and charge distributions and impedance characteristics of electrically thin cylindrical antennas
17 p2715 A71-34759

Current distribution and driving point admittances computation in certain antenna array with delta function generator driven electrically long elements
17 p2716 A71-35094

- R and C parameters determination for electric circuit simulating heat transfer in rod by amplitude-frequency characteristics 18 p2985 A71-36125
- Impedance determination for symmetrical spherical probes and spacecraft housing with flat screen separation, using partial capacitance formula 19 p3066 A71-38389
- Shielded enclosure resonance effects reduction on cavity impedance measurement by technique analogous to wave traps for notching out RF signal at selected frequencies 19 p3032 A71-38459
- Transistorized high power telemetry amplifier design, describing test equipment for input and collector load impedance 22 p3519 A71-41632
- Dummy S4 diode packages mounted in coaxial line, deriving model-independent equivalent circuit parameters from broadband admittance measurements 22 p3521 A71-42206
- Fluidic element input impedance measurement, noting aperiodic nature of transient response in input channel 23 p3631 A71-44019
- Azimuthal guiding surface wave attenuation with curvature applied to dielectric clad circular cylinder, including impedance tables 24 p3804 A71-44991
- Antenna impedance measurements using frequency sweep generator and oscillograph 24 p3810 A71-45127
- IMPEDANCE PROBES**
NT RADIO FREQUENCY IMPEDANCE PROBES
High impedance electric probes and floating double probes for plasma stream electric field, potential, density and temperature 01 p0134 A71-11002
Wideband four probe waveguide impedance meters design for standing wave structure measurement 15 p2378 A71-32634
- IMPELLER BLADES**
U ROTOR BLADES [TURBOMACHINERY]
IMPELLERS
NT PUMP IMPELLERS
Centrifugal compressor impeller exit flow velocity distribution distortion based on equations of motion involving entropy gradient terms 03 p0343 A71-13831
Flow variation effect on velocity and flow angle distribution at exit of shrouded radial flow impeller with backward swept blades, using streamline curvature method [ASME PAPER 71-GT-15] 11 p1703 A71-25961
Impeller blade loading vorticity on stream surface of revolution for mixed flow compressor, using annular cascade theory [ASME PAPER 71-GT-17] 11 p1703 A71-25962
Two dimensional flow in radial turbomachine bladed impeller, comparing numerical solution based on potential theory with experimental results [ASME PAPER 71-GT-20] 11 p1703 A71-25964
Inlet conditions for centrifugal compressor impeller covering pressure, temperature and velocity measurements on quasi-three dimensional model 22 p3480 A71-42035
- IMPERFECTIONS**
U DEFECTS
IMPERMEABILITY
U PERMEABILITY
IMPINGEMENT
NT JET IMPINGEMENT
Metals erosion by cavitation and liquid impingement, discussing test methods and resistance prediction 03 p0404 A71-14174
Gravitational wave impingement upon static magnetic field, noting EM waves excitation 21 p3417 A71-41397
- IMPLANTATION**
Brain electrodes rapid implantation method, using preassembled, stereotactically loaded, preconnected and pretested electrode and pedestal assemblies 04 p0538 A71-15059
Percutaneous access to implanted electrodes, discussing metal plaque-needle system and connection to instruments 11 p1724 A71-25436
Cardiovascular telemetry total implants, describing measurement problems, equipment design, low current operation, size and thermal and temporal stability 16 p2534 A71-33071
Charge neutrality in semiconductors with implanted dopant ions profiles, considering junction field penetration into Gaussian profile 19 p3118 A71-37489
- IMPLEMENTATION**
U PERFORMANCE
IMPLOSIONS
Hemispherical imploding shock wave reflection, noting cold wall presence and gas density effects 04 p0568 A71-14682
- Implosion driven hypervelocity launcher performance prediction, considering loss mechanisms, hydrodynamic calculations and shock phenomena 05 p0733 A71-16505
- Neutron star formation, calculating reimplosion mass fraction of thermonuclear supermova explosion 05 p0811 A71-16684
- Nonuniform self propagation of cylindrical imploding shock waves in electrically conducting gas 18 p2951 A71-36005
- Spectroscopic study of imploding shock waves in hemispherical chamber filled with oxygen-hydrogen-helium mixture at high pressure 19 p3163 A71-37735
- IMPREGNATING**
Hydrogen impregnated glass covers of solar cells preventing irradiation caused darkening and loss of power output under space environment conditions 05 p0700 A71-16066
Liquid-solid interface phenomena during sintering and porous materials impregnation by liquid metals, using spherical and nonspherical particle models 09 p1457 A71-23391
Material properties, impregnation, shaping, hardening and structural design in mass production of reinforced laminates for aircraft construction 12 p1920 A71-26954
Sealing porous metal castings and powdered parts, discussing impregnation by vacuum-pressure and internal circulatory methods and sealant types 18 p2928 A71-36838
Glass rods loading tests after exposure to hydrogen, nitrogen and argon under high pressure, noting strength improvement by Ar impregnation 24 p3841 A71-44868
Hydrogen dissolution in fused silica, investigating temperature effects during impregnation on reactive defect sites number 24 p3841 A71-44869
- IMPROVED TIROS OPERATIONAL SATELLITES**
NT ITOS I
IMPULSE GENERATORS
Electromagnetic interference measurements, considering direct reading with RI-FI receiver, impulse generators and spectrum analysis 14 p2193 A71-29915
- IMPULSE NOISE**
U ELECTROMAGNETIC NOISE
IMPULSE TRANSFER ORBITS
U TRANSFER ORBITS
IMPULSES
Optimal multipulse compensation for dynamic system external disturbances by minimax differential game approach, restricting impulse number and magnitude 01 p0059 A71-10429
Dynamic system impulse response model for goodness of fit and linearity hypothesis tests by computer simulation 17 p2722 A71-35181
Lagrangean equation of motion for crack wall driven by square tension impulse, obtaining deflection in terms of crack length and particle velocity 23 p3777 A71-43496
Self magnetic impulses in gas discharge configuration as function of current and anode-cathode radii ratio 24 p3851 A71-44431
- IMPURITIES**
Discontinuous yielding in annealed Al alloy resulting from negative slope in flow stress-strain rate relationship, discussing impurities diffusion role 01 p0105 A71-11606
High strength steel weld metal, determining gaseous impurities effects on mechanical properties degradation 02 p0262 A71-11710
Vapor deposited W impurities effect on crystal structure and preferred orientation, considering work function increase 02 p0296 A71-12241
Inelastic scattering by impurities and phonons in metals, determining energy level structure from nonlinear corrections to Ohm law 02 p0297 A71-12615
Gaseous impurities diffusion into silicon via open tube microelectronic method 02 p0297 A71-12922
Niobium with various interstitial and substitutional type impurities, examining plastic deformation and mechanical properties at various temperatures 02 p0269 A71-12927
Nb-impurity binary solid solutions, calculating interdiffusion and heterodiffusion coefficients 02 p0270 A71-12930
Space charge hypersurface layer conductance in semiconductors, allowing for three dimensional surface impurity fields 03 p0467 A71-13976
Photographic gelatin microimpurities quantitative analysis and removal techniques 04 p0585 A71-14645
- N-type Ge semiconductor low temperature breakdown potential dependence on neutral impurity concentration 05 p0793 A71-16420
- Turbulent diffusion of impurity from infinite linear source in clouds and fog, allowing for particle entrainment 05 p0776 A71-16422
- Semiconductors isoelectronic impurity states, using semiempirical delta-potential method to calculate bonding energy for GaP containing nitrogen as impurity 07 p1175 A71-19220
- Interstitial impurities effects on relation of activation energy to effective stress in iron, low carbon steel and other bcc metals 08 p1308 A71-21514
- Organic impurities effects on carbon dioxide dissociation activation energy, considering magnitude dependence on experimental conditions and data reduction techniques 08 p1251 A71-21783
- Nonequilibrium plasma molecular impurities effect on electron energy balance, considering importance in closed cycle MHD generators 08 p1342 A71-21916
- N-type single crystal silicon semiconductor resistors with high impurity concentrations and high accuracy 09 p1414 A71-22160
- Degenerate n-type GaSb, calculating electron mobility dependence on impurities concentration for comparison with experiment 09 p1507 A71-22361
- Turbulent diffusion in stationary thermally stratified atmospheric boundary layer, considering gravitational sedimentation and impurities lifetime 11 p1795 A71-25585
- Photoelectret effects in semiconductor materials containing deep lying impurity centers, discussing inhomogeneity regions and noise and reverse current levels 11 p1808 A71-25915
- Impurity lifetime broadening due to scattering at Fermi surfaces, calculating Dingle temperature in noble metals 11 p1808 A71-26145
- LiF single crystals temperature, strain rate and positive Mg ionic impurity effects on work hardening characteristics 11 p1809 A71-26478
- Multiple echo of impurity atom during collisions with solid body surface, contributing to vaporization from layer 12 p1932 A71-27034
- Base metal impurity effects on coercive force and contact properties of miniature multilayered diffused reed switches 13 p2038 A71-28837
- Carrier scattering related to orbiting and resonance states in screening impurity donor center of weakly doped homeopolar n-type semiconductor under injection 13 p2112 A71-28928
- Net impurity doping profile of double diffused transistors 14 p2210 A71-29792
- Test equipment for radiometric analysis of impurities concentration distribution in semiconductors, using thin plane-parallel layers continuous removal method 15 p2383 A71-31657
- Titanium and silicon tetrachlorides oxygen-containing impurities determination without hydrolysis, describing measuring device design 15 p2383 A71-31659
- High temperature high Mach number expansion tube flows, determining impurities by time integrated spectroscopic measurements 16 p2551 A71-33155
- Nonlinear dependence of resistance in metals on impurity concentration and temperature due to umklapp electron phonon interaction and anisotropy of phonon spectrum 16 p2593 A71-33654
- Nonequilibrium plasma molecular impurities effect on electron energy balance, noting importance in closed cycle MHD generators 17 p2789 A71-35261
- Impure GaAs and InP semiconductor compensation by introducing diffusible temperature dependent impurities 18 p2953 A71-35871
- High purity metals residual electrical resistivity, observing impurities, vacancies, dislocations, plastic strain and polyisotropy effects 19 p3076 A71-37115
- Beryllium impurities effects on ductile-brittle transition temperature, investigating fracture characteristics deformation mechanism 19 p3076 A71-37121
- Concentration broadening of impurity levels in compensated semiconductors, proposing averaging procedure 19 p3117 A71-37262

Ion and electron drift waves propagation and stability in nonhomogeneous plasma containing impurity ions

19 p3115 A71-38214

Electron elastic scattering in thin films by impurities, noting conductivity dependence on film thickness

21 p3428 A71-41126

Photoelectret effects in semiconductor materials containing deep lying impurity centers, discussing inhomogeneity regions and noise and reverse current levels

21 p3429 A71-41205

Crystal dislocations and impurity atmospheres role in kinetics of accumulation of radiation defects in Ge under fast electron bombardment

21 p3429 A71-41209

Temperature dependence of impurity photoluminescence of Cr-doped GaAs single crystals, measuring activation energy

21 p3430 A71-41214

Activator Mn impurity effect of carrier redistribution and partial photoionization of photoconductivity spectra of ZnS single crystals

21 p3430 A71-41218

Continuous impurities purging from hydrogen oxygen fuel cells gas compartments, describing operation mode and design techniques

21 p3326 A71-41250

Carrier scattering related to orbiting and resonance states in screened field of impurity donor center in weakly doped homeopolar n-type semiconductor under injection

21 p3434 A71-41331

Gallium selenide excitation by ruby laser radiation, investigating impurity photoconductivity dependence on radiation intensity

21 p3395 A71-41352

Electron scattering magnetic impurities effect in insulator layer of tunnel junction on superconductor current

22 p3585 A71-41818

Age hardenable Mg-Y alloys, investigating impurity phase in solution heat treatment

23 p3696 A71-44292

Group analysis of impurities in water regenerated from liquid human wastes

24 p3800 A71-44529

Impurity redistribution errors in C-V characteristics of MOS capacitors due to Si thermal oxidation

24 p3809 A71-44993

IMPURITY

U PURITY

IN-FLIGHT MONITORING

On-line software checkout facility for special purpose computers used in developing spaceborne programs

01 p0048 A71-10227

In-flight ECG telemetry for aircraft pilots diagnostics, discussing characteristic recordings and measuring probes development for simultaneous parameters transmission

03 p0370 A71-13062

Biotelemetry in aviation medicine, discussing telemetric methods and applications for continuous observation of physiological processes under environmental exercise and stress conditions

03 p0370 A71-13063

In-flight telemetric ECG recordings of aircraft pilots during normal, abnormal and aerobically flight, analyzing heart rate variations as function of stresses

03 p0370 A71-13064

Flight test evaluation of onboard automatic computer controlled jet engine monitoring system with reduced fault detection time

03 p0395 A71-13080

Helicopter gas turbine engine health indication using instrument panel for correcting gas temperature and producer speed

06 p0945 A71-17690

Strain level counter monitoring aircraft structural fatigue, describing system components consisting of sensors in critical structure areas and indicator unit with visual display

09 p1445 A71-22725

In-flight profile drag measurement of gliders with total and static pressure sensors in boundary layer wake, using moments method

09 p1384 A71-23667

Aircraft structural fatigue life in-flight monitoring, describing sensor installation on aircraft fin structure and measurement results

10 p1685 A71-23938

In-flight base heating and thermal environment measurements from Thor Delta launch vehicle using six straps-on solid propellant motors

14 p2320 A71-30721

Onboard computer for aircraft engine testing, monitoring and data reduction, emphasizing automatic in-flight recording for post-flight displays

14 p2290 A71-30727

Engine condition monitoring systems, discussing engineering design requirements with respect to accessibility, accuracy, economics, effectiveness, reliability and maintainability

14 p2290 A71-30728

Engine performance monitoring for jet engine troubleshooting, noting analyzable malfunctions

15 p2471 A71-32524

Aircraft engine in-flight thrust determination, discussing indirect and direct measurement methods

[DFVLR-SONDDR-119] 15 p2350 A71-32720

Flight test program, facilities and instrumentation for F-14 aircraft structural, powerplant, avionics, performance and carrier suitability evaluation

16 p2526 A71-34153

Total in-flight simulator (TIFS) in variable stability C-131 aircraft, describing potential as design tool

[AIAA PAPER 71-794] 17 p2675 A71-35529

Synoptic aerological conditions for occurrence of CAT, considering in-flight registrations and observations under jet stream conditions over North Atlantic

19 p3089 A71-37751

On-condition monitoring of aircraft hydraulic systems for component deterioration, applying to Boeing 747, L-1011 and DC 10 aircraft

22 p3483 A71-42075

Interplanetary navigation TV camera in-flight calibration, discussing instrument error sources elimination

22 p3573 A71-42771

In-flight monitoring of aircraft turbine engine reliability

23 p3718 A71-43233

Cosmic ray dosimetric monitoring in manned spacecraft, discussing ionization, thermoluminescent and nuclear photoemulsion methods of radiation measurement

24 p3826 A71-44888

IN-FLIGHT THRUST MEASUREMENT

U IN-FLIGHT MONITORING

U THRUST MEASUREMENT

INACTIVATION

U DEACTIVATION

INCENTIVES

Organizational climate inventories in R and D establishments, comparing obstacles and incentives to creativity in government and industrial laboratories

14 p2339 A71-29852

Partial reinforcement effect in visual vigilance task, varying knowledge of results as incentive

16 p2537 A71-33680

INCIDENCE

Obliquely incident radio wave absorptions measurements from January-October 1968 vertical ionospheric soundings, correlating diurnal variations with solar zenith angular changes

11 p1732 A71-25787

Ionospheric transverse inclinations from radio wave propagation characteristics obtained by circular oblique incidence sounding scans

11 p1758 A71-25788

Parallel plate electrostatic analyzer design, discussing second order focusing, angular aberrations and magnification

12 p1903 A71-26570

Weighted finite incidence systems construction using nonnegative integer functions and column vectors

16 p2603 A71-33591

INCIDENT RADIATION

Classification of electromagnetic wave scattering fluctuating objects from statistical scattering matrices, obtaining incident wave polarization

01 p0038 A71-11208

Electromagnetic scattering by oblique circular cylinder, deriving field equations

02 p0215 A71-12145

Antenna polar diagrams short range measurement, using far field approximation for incident plane waves source and radio star or satellite

02 p0223 A71-12801

Semitransparent spherical dielectric shell under diffuse incident radiation, determining absorptance and reflectance by Monte Carlo method

03 p0518 A71-13648

Electromagnetic wave glancing incidence on ideally conducting screen of infinitely thin strips by geometrical optics approximation

04 p0625 A71-14646

Kirchhoff integral evaluation for Gaussian incident field in Fresnel diffraction from plane wave beams truncated by circular apertures

04 p0627 A71-15688

Cosmic ray telescopes geometric factor determination, taking into account particle incidence angle

06 p0898 A71-17705

Complex incident fields analysis by ray diffraction method, using set of simple sources with same amplitude and phase characteristics as actual incident field

06 p0868 A71-17728

Thin polycrystalline CdTe film photovoltaic effect dependence on monochromatic light incidence angle

07 p1176 A71-19272

Fluoride overcoated Al reflectance measurements and polarization effects at various angles of incidence, noting utilization in vacuum UV instrumentation

08 p1335 A71-21381

Frequency and spectral composition effect of incident radiation on stimulated Raman scattering of organic compounds, using ruby laser harmonic emission

09 p1461 A71-27233

Optimum mounting angles for direct solar radiation flux on solar battery on circular orbit satellite

09 p1386 A71-27267

Electromagnetic HF potential effect on reflection waves obliquely incident on plasma with gas kinetic pressure nonlinearity

09 p1406 A71-27282

Kinetic theory of electromagnetic waves obliquely incident upon plasma slab considered as boundary value problem

09 p1409 A71-27282

Plane electromagnetic wave scattering, arbitrarily polarized and normally impinging on wedge shaped absorbing structure

09 p1409 A71-27282

Far field diffraction pattern of corner reflector for normally incident monochromatic light, considering polarization characteristics

10 p1640 A71-23982

Simply supported normal mode plate time response to traveling wave at oblique incidence, using numerical analysis

14 p2326 A71-30000

Incident sonic boom shock wave reflection factors off smooth surface, discussing pressure rise and flight near threshold Mach number

14 p2177 A71-30646

Ionosonde stations world distribution for vertical incidence soundings during IQSY and comparison with IGY

15 p2396 A71-31646

One dimensional acoustic tunnel effect for incident wave normal to barrier analogous to macroscopic spin waves and quantum mechanics

15 p2449 A71-31707

Radiative heat transfer effects behind reflected air incident shock waves in high temperature air and xenon respectively

16 p2662 A71-32844

Classification reliability of electromagnetic wave scattering fluctuating objects from statistical scattering matrices, obtaining incident wave polarization

17 p2698 A71-34202

Electromagnetic wave arbitrary incidence on conducting circular disk for polarization parallel and perpendicular to incidence plane, calculating backscattering cross section for comparison with measurement

20 p3194 A71-38844

Rayleigh scattering by obliquely oriented uniform thin cylindrical particles/needles, using dielectric needle approximation

20 p3196 A71-39404

Electromagnetic scattering of plane wave obliquely incident on infinitely long circular cylinder with radially varying permittivity and permeability

24 p3805 A71-45111

INCLINATION

Ionospheric geomagnetic field inclination measurement by incoherent scatter method

06 p0887 A71-17273

Preferable orientation of physical galactic pairs, obtaining equatorial plane inclinations and great axis positional angles distribution

06 p0974 A71-18434

Ionospheric transverse inclinations from radio wave propagation characteristics obtained by circular oblique incidence sounding scans

11 p1758 A71-25788

Apollo type asteroid with high orbital eccentricity and inclination and rough elongated shape, noting ephemerides

21 p3443 A71-40118

Ionospheric transverse inclinations from radio wave propagation characteristics obtained by circular oblique backscatter sounding scans

22 p3532 A71-41555

Odessa observatory meridian circle pivot irregularities effects determination on horizontal axis inclination and azimuth, using Challis method

23 p3680 A71-44266

INCLUSIONS

Micropolar elastic body with spherical inclusion, investigating thermal and couple stresses

01 p0181 A71-11288

Elastic elliptic inclusion stress state in plane elastic statics

02 p0321 A71-11688

Elastic field of cylindrical inclusion, using continuum dislocation theory

02 p0330 A71-12744

Composite materials interaction stresses by ideal model with linearly elastic isotropic homogeneous inclusions and matrix, solving by finite element method

03 p0505 A71-13533

Ni maraging steels weld heat-affected zone, showing liquid grain boundary film formation due to titanium sulfide inclusions constitutional liquation

04 p0603 A71-14922

Molten glass inclusion and stress concentration/empty hole/ effects on Armo iron electrode potential

05 p0766 A71-16388

Matrix and round inclusion two component composite equilibrium, considering crack effect on strength 06 p1000 A71-17938

Circular and elliptical holes and inclusions effects on stress concentration in elastic beams under uniform compression 06 p1002 A71-18414

W-Re alloy ingot nonmetallic inclusions complex phase structure, using electron probe, metallographic and electrolytic techniques 07 p1141 A71-20239

Dispersed alumina inclusions strengthening effect during nichrome alloy sintering 08 p1305 A71-21060

Orthotropic shells of revolution with concentrated masses and oscillator inclusions and reinforced by stringers and ribs, calculating free vibration by Ritz method 10 p1690 A71-24570

Infinite thin plate containing circular holes with elastic inclusions under biaxial tension, calculating maximum stresses on common boundaries based on Airy function 11 p1841 A71-25265

Bounds for effective dielectric constant of fiber reinforced materials, using Miller geometry of matrix and inclusion 11 p1782 A71-26388

Plastic deformation of elliptic inclusion in plane strain of infinite plate, using viscoelastic analogy 11 p1852 A71-26395

Steady thermoelastic equilibrium of infinite isotropic plate containing imbedded circular inclusion with cuts along circumference 12 p1984 A71-27693

Critical equilibrium of two component composite material with crack propagating along diameter of round inclusion 13 p2090 A71-27824

Inclusions diffusive motion effects on heterogeneous systems creep properties, determining creep rate as function of stress and temperature 13 p2148 A71-27960

Uniform torsion of elastic body weakened by spherical cut in form of rigid inclusion 13 p2150 A71-28139

Horse Creek, Mount Egerton and Norton County enstatitic meteorites metal phases and perthite inclusions from electron microprobe data 13 p2144 A71-29474

Mathematical model of hemispherical inclusion in elastic half space for estimating plastic deformation 18 p2937 A71-36772

Linearly deformable beams with distributed parameters and lumped inclusions, determining natural transverse vibration frequencies and mode shapes 19 p3155 A71-37535

Work hardening materials yield criterion derivation from mathematical model for inclusions embedded in elastoplastic matrix 19 p3078 A71-37644

Circular inclusion effects in infinite viscoelastic plate under monotonically increasing uniaxial tension, considering stress distribution 19 p3157 A71-37798

Rigid disk effect on thermal stress distribution in semiinfinite elastic solid under prescribed surface temperature and heat flux 19 p3159 A71-38188

Thermal stresses and couples in micropolar elastic solid cavity and rigid inclusion during uniform heat flow 20 p3309 A71-39560

Elastic field generation in two bonded isotropic half planes with circular or rectangular inclusion 23 p3774 A71-43146

Longitudinal shear induced stress field around rigid circular cylindrical inclusion and parallel crack, using Jacobi elliptic function in conformal mapping procedure 23 p3777 A71-43495

Petrology of Apollo 11 and 12 rock samples with silicate melt inclusions, discussing terrestrial equivalents 23 p3742 A71-43641

Stress field due to two rigid circular disk inclusions in isotropic homogeneous infinite plate 24 p3879 A71-44627

Elasticity theory for rectangular region with thin-walled inclusion under symmetrical external forces, reducing to three quasi-regular infinite systems of linear algebraic equations 24 p3880 A71-44722

INCOHERENCE

Mutual information between radiance of incoherently radiating object plane and field of observing system aperture, obtaining Shannon type formula 04 p0627 A71-15684

INCOHERENT SCATTERING

Noncoherent scattering, considering redistribution in continuous absorption and frequency dependent thermalization lengths 04 p0658 A71-15840

Ionospheric geomagnetic field inclination measurement by incoherent scatter method 06 p0887 A71-17270

Neutral ionospheric temperature profile diurnal variation at Arecibo from incoherent scatter measurements, considering relevance to 1400 hour density maximum 06 p0887 A71-17271

Turbulent plasma flame incoherent scatter calculation by modified first order Born approximation, considering attenuation due to absorption and scatter by energy conservation 07 p1171 A71-20294

Radar incoherent scatter technique for ionospheric propagation forecasting, using nocturnal and diurnal electron density profiles measurements 10 p1575 A71-23867

Geomagnetic field inclination determination by incoherently scattered signal Faraday rotation calibration and simultaneous ionosonde measurements of ionospheric electron density 10 p1605 A71-24798

Log normal random fluctuations of ionospheric electron concentration in F region from vertical sounding and incoherent scatter data 13 p2061 A71-28553

F region ionization drift and electric field observation by incoherent scatter techniques and data interpretation 14 p2236 A71-30942

Incoherent scatter measurements for ionospheric ion bulk velocity, thermospheric dynamics, F region gravity wave, photoelectron flux, ionic collision frequency and magnetic field direction 14 p2202 A71-30945

Simultaneous ionospheric electron density measurements from Isis satellite topside and incoherent scatter soundings 15 p2394 A71-31428

Thermal electron density fluctuations in weakly ionized gas from viewpoint of particle diffusion in single charged particle phase space, considering incoherent scattering 15 p2458 A71-32392

Diurnal variation of atmospheric parameters in thermosphere deduced from incoherent scatter and satellite drag, discussing atmospheric model correspondence to observed data 16 p2566 A71-33742

Geomagnetic equatorial ionospheric ion temperature, comparing incoherent scatter radar and OGO-D retarding potential analyzer values 16 p2573 A71-33956

Taurus X-1 X ray emission polarization from rocket-borne polarimeter measurements, utilizing incoherent scattering 20 p3302 A71-39921

Rocket measured exospheric temperatures correlation with global model values based on incoherent scatter measurements 23 p3670 A71-43187

Incoherent scatter observations of ion concentration and plasma line in F1 region 23 p3670 A71-43188

F region ion and electron temperature relationship to electron density, examining incoherent scatter data and physical processes 23 p3672 A71-43977

Simultaneous ionosphere measurements by incoherent ground radio wave scattering and coherent signals from Intercoms 2 and Cosmos 321 satellites 24 p3824 A71-45323

INCOMPRESSIBILITY

Infinitely small flexural oscillations of initially stretched incompressible elastic circular cylinder, showing stretch effect on wave propagation velocity 10 p1689 A71-24521

Large elastic deformations of incompressible materials shells with inclusion of transverse normal strain, considering thickness change at boundaries 12 p1976 A71-27159

Large deformation of incompressible elastic body reinforced by unidirectional system of elastic fibers 12 p1922 A71-27695

Approximate elastoplastic problems solutions by method analogous to antiplane deformation of circular incompressible region in flow theory 16 p2657 A71-33594

Finite elasticity theory for isotropic incompressible solids, formulating Ericksen problem for requirements of statically possible radially symmetric deformations in equilibrium 16 p2661 A71-34147

Incompressible materials weak compressibility effect in elastic theory, deriving displacement equation with average pressure function for any Poisson coefficient values 17 p2818 A71-34350

Temperature effects in incompressible elastic materials, adapting Adkins-Green isothermal successive approximation technique to thermoelasticity problems 19 p3157 A71-37800

Exact solutions for cord reinforced materials with thermomechanical constraints of incompressibility and inextensibility and thermal constraint on temperature gradient 20 p3310 A71-39869

INCOMPRESSIBLE FLOW

NT STOKES FLOW

Jet pump optimization for incompressible flow, considering friction losses, nonuniform densities and diffuser losses for overall energy conversion efficiency 01 p0085 A71-10105

Incompressible fluid flow calculations, describing simplified marker-and-cell technique 01 p0071 A71-11163

Boundary layer solution for unsteady compressible incompressible flow past body, discussing momentum conservation equation solution by series expansion 02 p0241 A71-12848

Three dimensional incompressible wake behind blunt obstacle at leading edge of flat plate compared with mathematical model by Oseen linearization [AIAA PAPER 69-747] 03 p0341 A71-13434

Steady incompressible flow past oblate and prolate spheroids for Reynolds numbers up to 100, using spherical coordinates and finite difference method 03 p0400 A71-13729

Varying electrical resistivity incompressible fluid flow with Hall effect in presence of thin airfoil 03 p0343 A71-13903

Three dimensional nonboundary layer laminar radially inward incompressible Newtonian fluid flow between corotating disks, using integral method [ASME PAPER 70-WA/FE-4] 03 p0402 A71-14126

Incompressible two dimensional inviscid stably stratified fluid flow over vertical step in channel bounded by rigid horizontal lid 03 p0453 A71-14201

Longitudinal surface curvature effect on steady two dimensional incompressible laminar thermal boundary layers 04 p0680 A71-15471

Turbulent boundary layer equations for heat and mass transfer in incompressible and compressible flows, using eddy viscosity formulation 04 p0680 A71-15479

Viscous incompressible MHD fluid steady laminar flow past semiinfinite flat plate, noting heat transfer characteristics 04 p0635 A71-15508

Dynamic characteristics of submerged twisted jet flow of incompressible viscous fluid 04 p0573 A71-15560

Ring flow expansion of incompressible viscous fluid in cylindrical channel 04 p0573 A71-15561

Soviet book on fundamentals of heat transfer theory covering thermodynamic equations, steady, unsteady, turbulent, incompressible and MHD flows, etc 05 p0831 A71-16196

Incompressible turbulent boundary layer flow over steadily rotating flat plate blade, discussing centrifugal pumping and shear stress 05 p0694 A71-16581

Velocity profiles of steady axial flow of homogeneous incompressible Newtonian liquid between infinitely long parallel eccentric circular cylinders 05 p0735 A71-16611

Incompressible boundary layers with specific velocity distribution, studying stability on straight and yawing wings 05 p0736 A71-16849

Plane incompressible boundary layer stability in presence of pressure gradient and suction 05 p0736 A71-16851

Asymptotic formulas for vortex and velocity field far from body in plane viscous incompressible fluid flow 05 p0737 A71-16990

Inviscid incompressible flow velocity distribution in conical configurations with water as working fluid, using method of integral relations 05 p0737 A71-17103

Viscous incompressible flow problems, using finite difference methods for solving Navier-Stokes equations 06 p0917 A71-17564

Plane incompressible MHD boundary layer on porous plate, considering heat and mass transfer in blowing or suction velocity distribution 06 p0936 A71-17736

Transpiration cooling heat transfer in incompressible turbulent boundary layer, using Couette flow model, boundary layer model and combinations of both 07 p1219 A71-18758

Viscous incompressible axisymmetrical flow, examining vortices near stagnation point of infinite flat obstacle 07 p1089 A71-19737

Viscous incompressible jet flow impinging on plane wall, considering negligibility of ambient medium viscosity within boundary layer equations framework 07 p1089 A71-19749

Landau viscous incompressible boundary layer separation formula comparison with Chudov finite difference method 07 p1090 A71-19751

INCOMPRESSIBLE FLOW

Skewed turbulent boundary layer and incompressible laminar flow on rotating disk, considering effective viscosity relations and applications domain

07 p1090 A71-19889

Incompressible hypersonic laminar boundary layer flow over sharp cone, based on asymptotic inner and outer flow field expansion

07 p1015 A71-19892

Viscous incompressible fluid flow between two cofocal elliptic cylinders, discussing temperature distribution and heat transfer in annulus

07 p1224 A71-20029

Ideal fluid jets theory, discussing cavitation flows calculation, jet flow and plane steady potential incompressible fluid flow

07 p1091 A71-20080

Solid foil small oscillations in unsteady incompressible flow, mapping physical plane and corresponding complex potential region onto curvilinear half strip

07 p1092 A71-20088

Computerized transonic airfoil design from predetermined supercritical velocity distribution, obtaining equivalent incompressible flow through streamline and potential line network transformation

07 p1017 A71-20304

Unsteady incompressible laminar boundary layer equations, obtaining similarity solutions from momentum integral equation

07 p1093 A71-20365

Low Reynolds number incompressible transient creep flow calculation by Marker-Cell numerical solution extension

07 p1094 A71-20613

Hydrodynamically stabilized turbulent viscous incompressible fluid flow in circular tube, examining nonstationary convective heat transfer by numerical methods

08 p1276 A71-21923

Incompressible laminar boundary layer flow with mass and heat sources, calculating thermal and friction stress distribution

08 p1277 A71-22037

Uniform two dimensional incompressible turbulent boundary layer with uniformly distributed surface mass injection, correlating results on basis of turbulent kinetic energy equation

09 p1430 A71-22105

Inviscid incompressible vortex-free axisymmetric pipe flow near arbitrary shape body symmetrically located near axis

09 p1431 A71-22180

Thin rectangular wing load distribution in nonstationary incompressible flow, using downwash integral equation Fourier transform

09 p1383 A71-22946

Incompressible viscous fluid nonsteady three dimensional flow, obtaining velocity field and pressure distribution in boundary layer

09 p1433 A71-23092

Two dimensional incompressible laminar boundary layer with longitudinal surface curvature, examining equations with particular attention to pressure boundary conditions and pressure gradient formulation

09 p1433 A71-23098

Incompressible flow stability to axisymmetric disturbances in circular pipe

09 p1434 A71-23165

Concentration profile in incompressible viscous fluid flow across plane plate in oscillating motion, considering gravity diffusion

09 p1434 A71-23729

Nonlinear stability of incompressible laminar flows involving perturbation in Banach space

10 p1591 A71-23914

Electrical resistive incompressible fluid motion past thin airfoils in oblique field, showing inverse dependence of lift on magnetic Reynolds number

10 p1648 A71-23956

Unsteady incompressible laminar boundary layer universal equation form for solution through reduction to ordinary differential equations and series coefficients determination

10 p1593 A71-24027

Integral equation for solving potential incompressible fluid flow past blade cascade on axisymmetric current surface in variable thickness layer

10 p1593 A71-24369

Plane unsteady convective motion of viscous incompressible liquid in infinite horizontal vessel of rectangular cross section due to wall temperature fluctuations

10 p1696 A71-24375

Thermohydrodynamic equations for viscous incompressible lubricant flow in hydrostatic thrust bearings, considering inertia and temperature effects

10 p1617 A71-24482

Turbulent incompressible air flow in-stream static pressure fluctuations measurement, describing bleed type pressure transducer theory, design and operational characteristics

10 p1611 A71-24516

Incompressible laminar boundary layer flow over parabolas and paraboloids, comparing results by local

truncation methods with results by finite difference method

10 p1594 A71-24524

Laminar incompressible boundary layer flow stability, emphasizing wall curvature and flexibility effects

10 p1594 A71-24548

Universal equations of two dimensional incompressible unsteady laminar boundary layer

10 p1597 A71-25017

Inviscid incompressible two phase concave type corner flows embedded with small spherical particles, examining streamlines, critical collision conditions and approximate viscous effects

10 p1598 A71-25081

Pulsating incompressible two dimensional laminar boundary layer flow past insulated plate at zero incidence, calculating skin friction and surface temperature

10 p1697 A71-25084

Viscous core of incompressible swirling flow through nozzle using momentum-integral equations [AIAA PAPER 70-51]

11 p1750 A71-25468

Prandtl first order boundary layer equations for two dimensional laminar incompressible flow past circulation controlled circular lifting rotor

11 p1702 A71-25494

Axisymmetrical incompressible and compressible fluid flow inverse problem formulation and solution with application to turbine blade design

11 p1752 A71-26051

Inviscid incompressible two dimensional jet deflection by various dimension segments, investigating potential flow with Schwarz-Christoffel transformation and free streamline theory

11 p1753 A71-26444

Numerical analysis of steady symmetric incompressible flow past elliptical cylinders for Reynolds numbers up to 90

12 p1895 A71-26739

Nonstationary three dimensional weakly ionized incompressible viscous gas plasma flow in homopolar device, noting effects on ionization-diffusion balance

12 p1935 A71-26753

Laminar incompressible entry flow in plane channel based on modern boundary layer theory

12 p1897 A71-27223

Three dimensional incompressible flow about slender foil in perfect fluid, stressing vortex field effect

12 p1865 A71-27477

Electrohydrodynamic ideal incompressible fluid flow in flat and circular channels, determining electric potential and field distribution

12 p1941 A71-27520

Pressure and wall temperature gradients effects on equilibrium enthalpy profiles and heat transfer coefficients of incompressible turbulent boundary layers, using eddy conductivity model [AIAA PAPER 69-689]

12 p1986 A71-27553

Quasi-axisymmetric and superposed fine fluctuating structure of ideal incompressible vortex flows in axial flow turbines, assuming infinite mutual blade proximity

12 p1866 A71-27714

Nonlinear limit rotation velocity and circulation induced by wheel in axial flow turbomachine for incompressible ideal fluid, using iterative numerical algorithm

12 p1866 A71-27715

Aerofoil cascades with axial velocity change in incompressible flow, determining turbine blade force dependence on circulation

13 p1990 A71-28467

Truncated conical diffusers with various geometrical configurations and incompressible inlet flow conditions, noting reduced pressure recovery

13 p2047 A71-28468

Plane stationary constant-vorticity incompressible flow region surrounded by potential flow, determining two dimensional velocity distribution by numerical calculation

13 p2050 A71-29220

Laminar incompressible fully developed pulsating flow between parallel flat plates effects on local time average heat flux

14 p2334 A71-29603

Incompressible liquid laminar boundary layer flow velocity profile and normal friction stress calculation by successive approximation method

14 p2169 A71-29630

Stationary Gaussian Markovian form randomly fluctuating pressure gradient effects on steady incompressible channel flow velocity

14 p2223 A71-29924

Incompressible planar fluid flow magnitude, direction and turbulent shear stress measurement by hot-wire anemometer

14 p2239 A71-29928

Incompressible fluid motion in laminar boundary layer on blade rotating uniformly about axis perpendicular to wing span

14 p2170 A71-30218

Gromeka-Beltrami ideal incompressible fluid flow in sem infinite circular cylindrical tube

14 p2225 A71-30221

Film cooling as solid surfaces protection in high temperature environments, considering two and three dimensional secondary compressible and incompressible flow geometries

14 p2337 A71-30222

Nonlinear dynamical evolution of two dimensional unstable shear flows, using numerical integration of time dependent incompressible Navier-Stokes equations

14 p2226 A71-30404

Steady state flow of viscous incompressible fluid, proposing difference scheme for numerical solution of Navier-Stokes equations

14 p2226 A71-30474

Asymptotic behavior of boundary layer equation solution for viscous incompressible flow past curvilinear obstacle

14 p2227 A71-30875

Incompressible laminar flow between rotating annular disks with small gap width and radial mass flow, using Navier-Stokes and continuity equations

15 p2387 A71-31161

Unsteady incompressible laminar viscous flow past infinite flat plate with arbitrary time dependent velocity, using Laplace transformation

15 p2387 A71-31181

Incompressible fluid turbulence theory based on space-time Hopf characteristic functional integral representation for velocity field statistical ensemble

15 p2388 A71-31471

Turbulent mixing between parallel incompressible air streams, using statistical investigation of pressure and velocity fields

15 p2389 A71-31581

Incompressible laminar boundary layer on flat plate, calculating flow oscillation effect on time-mean heat transfer

15 p2513 A71-31921

Two dimensional viscous incompressible fluid flow field calculation in fluidic element, giving Navier-Stokes equations solution in finite difference form

15 p2390 A71-32051

Incompressible laminar skin friction calculation over porous plate by Karman-Pohlhausen method, considering surface blowing

15 p2392 A71-32111

German monograph on incompressible potential flow field calculation about thick rectangular wing with control surfaces and ground effects

15 p2347 A71-32301

Incompressible viscous fluid flow between disk oscillating about state of rigid rotation, studying spin-up time effects

16 p2607 A71-32861

Viscous incompressible flow stability between concentric rotating cylinders, developing nonlinear model of two disturbance interaction

16 p2558 A71-32981

Unstable two dimensional incompressible flow and wake development, using finite difference calculations for Navier-Stokes equations

16 p2558 A71-32991

Incompressible laminar boundary layer on parabolic profile at angle of attack, noting singularity in advancing shear stress/separation points [ASME PAPER 71-APM-31]

16 p2520 A71-33191

Aerodynamic free vortex loading on two dimensional wing at zero incidence at low speeds in incompressible flow

16 p2521 A71-33421

Detachment prediction in turbulent incompressible plane flows on thick bodies applied to wall without disconnections and flat plate normal to wind

17 p2669 A71-34181

Viscous trailing vortices decay downstream of non-free axial flow fan, assuming steady axisymmetric incompressible laminar flow

17 p2725 A71-34191

Viscous stresses distribution in isothermal incompressible turbulent boundary layer with positive pressure gradient by diffusers in open jet wind tunnel

17 p2725 A71-34201

Viscous incompressible flow along right angled corner, using algebraic nature of asymptotic flow fields for numerical analysis boundary conditions

17 p2726 A71-34501

Viscous incompressible fluid flow downstream of paraboloid of revolution described by matching boundary layer approximations to potential flow solutions

17 p2727 A71-34673

Inviscid incompressible flow past thin circular arc airfoil at zero incidence, expanding for complex potential or velocity in powers of thickness ratio

17 p2670 A71-34674

Incompressible turbulent boundary layers at low Reynolds numbers, using eddy viscosity and mixing length concepts for computation

17 p2728 A71-34884

Steady incompressible flow with potential vortex over flat surface under suction

17 p2670 A71-34889

Hydrodynamically stabilized turbulent viscous incompressible fluid flow in circular tube, examining unsteady convective heat transfer by numerical methods

17 p2729 A71-35267

- Interior region of incompressible turbulent boundary layer with pressure gradient on permeable wall, discussing local similitude hypothesis 17 p2729 A71-35346
- Two dimensional steady potential incompressible flow past elastic expandable gas filled envelope fastened to edge of plate normal to flow 17 p2730 A71-35640
- Quasi-stationary viscous incompressible liquid flow in porous tube with deforming wall 17 p2694 A71-35641
- Asymptotic solution of viscous incompressible flow past uniformly heated paraboloid of revolution with constant surface temperature 17 p2730 A71-35800
- Incompressible turbulent shear boundary layer equations of motion, developing integrodifferential formulation of Navier-Stokes theory 18 p2904 A71-36184
- Plane laminar incompressible jet flow along parabola with no external stream, using second order boundary layer theory [ASME PAPER 71-APM-MM] 18 p2904 A71-36268
- Two dimensional laminar incompressible fluid flow past flat plate at various angles of attack, studying vortex shedding characteristics 18 p2844 A71-36311
- Numerical solution of time dependent incompressible flow differential transport equations including turbulence effects 18 p2905 A71-36312
- Laminar boundary layer structure under semi-infinite potential vortex maintained in incompressible steady flow by appropriate conditions at infinity 18 p2906 A71-36317
- Rotationally symmetric quasi-cylindrical viscous incompressible vortex flows at high swirl, discussing numerical integration with exponential functions 18 p2908 A71-36342
- Incompressible two dimensional turbulent hypersonic boundary layer flow velocity, pressure, temperature and density distributions 18 p2908 A71-36429
- Asymptotic formulas for vortex and velocity field far from body in plane viscous incompressible fluid flow 18 p2909 A71-36790
- Velocity field of viscous steady plane incompressible flow past body, linearizing by Oseen approximation 18 p2910 A71-36946
- Viscous incompressible conducting fluid at constant flow rate under magnetic field variation, investigating laminar unsteady MHD Couette flow problem with approximate solution 19 p3108 A71-37092
- Ergodic boundary in time evolution of two dimensional incompressible Navier-Stokes equations solution at large Reynolds numbers 19 p3045 A71-37841
- Heat and mass transfer through porous plate into turbulent two dimensional incompressible boundary layer, using van Driest damped mixing length [ASME PAPER 71-HT-10] 19 p3045 A71-37986
- Solid cylindrical particles interaction under entrainment in pipe by viscous incompressible fluid, obtaining numerical solution by reduction to flow past moving body 19 p3046 A71-38418
- Steady axisymmetric incompressible flow past sphere at low Reynolds numbers, reducing equations of motion to ordinary differential equations 20 p3212 A71-39506
- Regenerative kinematic-dynamo action under incompressible isotropic velocity turbulence, noting turbulent Lorentz force role 21 p3447 A71-40422
- Galerkin/spectral/ method accuracy for numerical simulation of incompressible boundary flows, testing scalar-convection and Taylor-Green vortex decay problems 21 p3367 A71-40638
- Heat transfer of short hot wire normal to ambient incompressible air flow, using small perturbation energy equation 21 p3379 A71-40664
- Viscous incompressible flow past semi-infinite slender body with upper and lower surface forced vibrations, solving ideal fluid and boundary layer equations by Shkadov method 21 p3367 A71-40683
- Incompressible potential cascade flow interaction, presenting approximate method based on blade profile flow expression by power series with distance between cascades as parameter 21 p3322 A71-40685
- Time-space description of steady and homogeneous turbulence in incompressible fluid flow 21 p3367 A71-40690
- Incompressible flow hydrodynamic time dependent problems for moving walls and free surfaces, using Marker-Cell computing method 21 p3368 A71-40849
- Laminar incompressible plane wall jet, calculating flow characteristics for potential core region with integral method 21 p3370 A71-40988
- Existence and uniqueness of boundary layer equations similarity solution for viscous incompressible fluid flow past paraboloid 22 p3531 A71-42197
- Aerodynamic nonstationary conjugate heat transfer of thin plate with heat sources in incompressible fluid flow 22 p3622 A71-42684
- Plane MHD boundary layer growth and separation in viscous incompressible flow past cylinder under abrupt motion and transverse magnetic field 22 p3584 A71-42685
- Approximate nonlinear theory of steady incompressible fluid flow about cylindrical bodies from vortex method for thin lifting surfaces 22 p3481 A71-42867
- Perturbation and projection operator algorithms for Navier-Stokes equations for incompressible flow in rectangular cavities and injection into cylindrical ducts 23 p3662 A71-43238
- Viscous incompressible flow between concentric rotating spheres, investigating hydrodynamic stability 23 p3663 A71-43443
- Lifting rectangular thin airfoil in symmetrical incompressible steady uniform orthogonal flow at small angle of attack, deriving Weissinger integral equation 23 p3625 A71-43487
- Class of steady viscous incompressible axisymmetric nonrotating flows with axial velocity component dependent on distance along axis from reference point 23 p3663 A71-43489
- Random fluctuating longitudinal pressure gradient effect on steady incompressible channel flow for arbitrary power spectrum and probability density 23 p3664 A71-43597
- Navier-Stokes equations solutions for incompressible laminar viscous fluid flow produced by vortex filament placed on cone axis 23 p3664 A71-44004
- Incompressible turbulent boundary layer with suction and surface injection computation by implicit finite difference method and turbulent kinetic energy equation for mixing length flow 24 p3820 A71-44954
- Interaction between two incompressible fluid flows in plane duct, deriving parametric equations for free stream line and flow interface 24 p3820 A71-45005
- ### INCOMPRESSIBLE FLUIDS
- Uniformly turbulent incompressible heavy fluid sloshing and free oscillations in rigid rotating vessel, using linear surface wave theory 01 p0069 A71-10411
- Turbulent transport equations derivation for incompressible fluid unsteady flow in arbitrary geometry, considering application to flow between parallel plates 01 p0072 A71-11469
- Incompressible fluid laminar flow between stationary and rotating porous disks with equal suction and injection 02 p0240 A71-12337
- Radially deforming sphere dynamic behavior during translational motion in infinite incompressible static medium 02 p0241 A71-12669
- Incompressible elastoviscous unsteady fluid flow past circular cylinder, confining calculations to non-zero vorticity region near cylinder 03 p0398 A71-13108
- Navier-Stokes equations numerical integration in Eulerian coordinates, applying results to compressible and incompressible fluids steady flow [AIAA PAPER 70-2] 03 p0399 A71-13426
- Hess solution for heavy body rotating about fixed point, considering cavities filled with ideal incompressible fluid in turbulent and irrotational motion and linear invariant relation 03 p0458 A71-13591
- Symmetry axis motion of solid body with ellipsoidal cavity filled with ideal incompressible uniformly turbulent fluid 03 p0458 A71-13596
- Unsteady MHD forced flow of viscous incompressible electrically conducting fluid against rotating disk 03 p0459 A71-13902
- Ideal incompressible fluid plane jets interaction with flow discontinuity at jet boundaries, deriving non-linear system of integral equations 03 p0405 A71-14564
- Plane potential incompressible fluid flow in channel with rough bottom and variable surface pressure, allowing for gravitational and surface tension forces 03 p0406 A71-14567
- Incompressible fluid turbulent boundary layer equations, examining approximate semiempirical calculations 04 p0573 A71-15555
- Statistical characteristics of pulsation pressure on surface in turbulent boundary layer of incompressible fluid, discussing effects near smooth flat wall 04 p0575 A71-15607
- Turbulent hydrodynamics and heat transfer in rotating flows of incompressible fluid 04 p0578 A71-15631
- Incompressible fluid boundary layer with negative pressure gradient near separation point, discussing stability characteristics and velocity profiles 05 p0736 A71-16847
- Viscous incompressible fluid flow with free boundary at large Reynolds numbers, deriving asymptotic expansion solution for wave motion 05 p0737 A71-16989
- Submerged moving body in nonviscous incompressible fluid, evaluating finite potential flow field momentum with rigid and free far distant outer boundary 06 p0841 A71-17419
- Incompressible fluid steady laminar flow free convection and various gas species mass diffusion from hot horizontal plate surface 06 p1007 A71-18074
- Incompressible unsteady viscous fluid flow through circular cross section curved pipe, noting centrifugal effects in interior 06 p0882 A71-18316
- Uniform magnetic field parallel alignment effects on incompressible electrically conducting free two dimensional jet flow stability at large Reynolds number 07 p1084 A71-18745
- Turbulent boundary layer in incompressible fluid with vanishing viscosity, analyzing degeneration of isothermal boundary layer, viscous sublayer and density pulsations 07 p1085 A71-18753
- Incompressible fluid nonuniform turbulence statistical approach, based on finite number of equations for high order single point correlations 07 p1087 A71-18920
- Incompressible turbulent circulatory fluid flow in plane curvilinear channel, deriving energy balance equations 07 p1088 A71-19199
- Seaplane step/flat plate/ricochet off ideal incompressible fluid surface, determining free surface shape by accounting for trailing vortices effects 07 p1088 A71-19355
- Unsteady viscous incompressible flow over impulsively started rotating disk by acceleration averaging method 07 p1088 A71-19356
- Equations systems for free turbulent boundary layer in incompressible fluid, deriving semiempirical formulas for turbulent viscosity coefficient 07 p1089 A71-19735
- Viscous incompressible slow unsteady flow through circular tube with small axial roughness, obtaining velocity components by integral transform technique 07 p1092 A71-20093
- Lifting surface nonstationary aperiodic motion in incompressible fluid solved by asymptotic method of function parameters, using algorithm for Cauchy problem 08 p1275 A71-20778
- Continuous flow past plate located perpendicular to wall with inviscid incompressible fluid having linear variation of velocity with height 08 p1227 A71-20828
- Incompressible viscous liquid forced oscillations stability, developing linearization procedure for nonlinear operator equation of perturbations 08 p1275 A71-21051
- Elastic solutions convergence in nonlinear problems of viscoelastic incompressible media, formulating and proving uniqueness theorem for certain conditions 08 p1369 A71-21053
- Inviscid incompressible electrically conducting fluid flow past slender profile investigated by asymptotic power expansion of reciprocal magnetic Reynolds number 09 p1382 A71-22135
- Free vibrations of closed spherical shell immersed in ideal incompressible fluid at arbitrary depth 09 p1535 A71-22182
- Incompressible inviscid fluid flow in presence of two homogeneous porous layers, examining hydrodynamic instability 10 p1591 A71-23754
- Incompressible fluid plane unsteady laminar boundary layers equations solution through reduction to nonlinear partial differential equation and series expansion 10 p1592 A71-24025
- Incompressible fluid plane laminar unsteady boundary layer, obtaining Falkner-Skan equation as special case for similar solutions in steady flow case 10 p1592 A71-24026
- Mixing layer of turbulent flows in homogeneous nonconducting and conducting incompressible fluids, extending approximate solution to flow in longitudinal magnetic field 10 p1593 A71-24366
- Villat problem of ideal incompressible two dimensional fluid flow around plate, determining stagnation point location 10 p1594 A71-24452

Ideal incompressible holomorphic fluid plane irrotational motion velocity due to deformable constant area airfoil displacement

10 p1594 A71-24453

Phythin perturbation theory for stationary homogeneous turbulence of incompressible fluid

10 p1594 A71-24511

Soviet book on MHD flow of incompressible electrically conducting fluid past bodies covering inviscid flows and viscous flows of Stokes and Oseen type

10 p1596 A71-24669

Airfoil profiles coupling method for determining complex potential of two dimensional ideal incompressible fluid flow due to arbitrary airfoil section movement near rectilinear wall

10 p1597 A71-25015

Temperature distribution inside solid sphere rotating in viscous incompressible liquid with constant strength heat source at center, discussing flow field around sphere

11 p1853 A71-25146

Series solution for unbounded mixing of two incompressible homogeneous coaxial flows with constant properties, using successive approximations method

11 p1748 A71-25159

Boundary layer equation for free convective diffusion on flat vertical plate in translation motion in viscous incompressible fluid

11 p1854 A71-25240

Second order correlation functions of velocity and magnetic field for homogeneous unsteady isotropic hydromagnetic turbulence in incompressible conducting fluid

11 p1805 A71-25599

Isotropic MHD turbulence in incompressible fluid by diagrammatic representation, obtaining approximation with transfer functions and scalar equations for correlation

11 p1805 A71-25600

Ideal incompressible fluid flow around fixed obstacle near rectilinear wall, investigating plane motion with profile couple method

11 p1705 A71-26258

Bifurcation solutions of Navier-Stokes equations for time periodic motions of viscous incompressible fluid at critical Reynolds number

12 p1922 A71-26867

Similarities between ion waves in plasmas and gravity waves in incompressible fluid/steady water flow with allowance for surface tension

13 p2046 A71-27844

Heat exchange during stabilized laminar flow of incompressible liquid in circular pipe with radiative cooling, deriving temperature profile and Nusselt number dependence

13 p2046 A71-28180

Characteristic equation of respiration vibrations of cylindrical ring in incompressible viscous fluid at rest, obtaining damping coefficient for large induced flow Reynolds numbers

13 p2047 A71-28397

Potential flow of incompressible inviscid liquid film along inclined semiinfinite flat plate for large Froude number values, using matched asymptotic expansions method

13 p2047 A71-28485

Group properties of laminar boundary layer equations for incompressible binary fluid under various magnetic field distributions and reaction rates

13 p2048 A71-28735

Correlation model of stability and onset of turbulent motions for incompressible fluid, noting inconsistency of Keller-Friedman equations

13 p2050 A71-29206

Acceleration covariance in turbulent flow of isotropic homogeneous incompressible viscous conducting fluid

13 p2109 A71-29295

Steady flow of electrically conducting incompressible viscous fluid in rotating parallel-plane channel under constant transverse magnetic field

13 p2110 A71-29296

Finite difference scheme for calculating three dimensional incompressible turbulent boundary layer development on infinite yawed cylinder [ASME PAPER 71-FE-19]

13 p2052 A71-29457

Conducting incompressible liquid in transverse magnetic field, considering plane steady motion of isothermal MHD boundary layer

14 p2278 A71-29604

Incompressible conducting fluid plane jet expansion in homogeneous slipstream, deriving partial differential equations for nonconduction approximation

14 p2278 A71-29610

Incompressible homogeneous isotropic fluid Couette flow between stationary inner and rotating concentric outer cylinders, examining Weissenberg effect

14 p2226 A71-30445

Axissymmetrical three component flow equations for incompressible viscous fluid in cylinder with rotating disk

14 p2227 A71-30855

Incompressible frictionless helical flows hydromagnetic stability in cylindrical circular space

15 p2387 A71-31166

Vertical magnetic field and Coriolis forces effect on equilibrium of heavy viscous incompressible infinitely conducting rotating fluid

15 p2453 A71-31183

Torsionally oscillating disk in steadily rotating incompressible second order fluid, calculating transverse and radial shear stress

15 p2387 A71-31185

Nonlinear hydrodynamic stability of incompressible Newtonian fluid, comparing linear and energy theories

16 p2558 A71-33005

Isoperimetric problem upper bounds for fundamental frequencies in free oscillations of incompressible fluid in container

16 p2559 A71-33483

Initial interaction phase between thin shallow conical shell vibrating axisymmetrically and ideal incompressible fluid, determining hydrodynamic pressure effects

16 p2560 A71-33901

Perfect incompressible fluid steady rotational linearized three dimensional flows, calculating complex waves system

16 p2560 A71-34056

Steady one dimensional MHD flow under transverse magnetic induction, determining maximum power of incompressible fluid generator

16 p2620 A71-34144

Viscous incompressible fluid flow between two rotating nonconcentric cylinders, presenting transverse velocity profiles

17 p2725 A71-34177

Scalar material transport in incompressible inhomogeneous turbulent fluid based on one point correlations equations

17 p2835 A71-34211

Laminar flow in incompressible fluid between rotating disk and fixed wall at small distances with radial mass stream, using finite difference method for Navier-Stokes equations

17 p2726 A71-34581

Plane laminar two phase jet flow consisting of small spherical particles suspended in incompressible carrier fluid in presence of adjacent parallel moving free stream

17 p2726 A71-34582

Ideally incompressible fluid with free surface, analyzing interfacial tension forces effects on rotational-translational motion stability

17 p2730 A71-35648

Two dimensional steady laminar boundary layer theory for incompressible medium, presenting error bounds for Prandtl equation solution

18 p2906 A71-36322

Two dimensional flow equations for incompressible viscous fluid in square cavity

18 p2907 A71-36340

Initial flow past circular cylinder in viscous incompressible fluid calculation by numerical integration using boundary layer coordinates

18 p2908 A71-36341

Asymptotic expansions for solution of wave motions of viscous incompressible fluid with free boundary at large Reynolds number

18 p2909 A71-36789

Unsteady flow of incompressible micropolar fluid due to sphere oscillations, calculating velocity, drag and stress components

19 p3045 A71-37799

One layer midlatitude beta plane channel model of incompressible fluid for study of systematic error propagation on nearly stationary synoptic scale wave

19 p3090 A71-38268

Laminar and turbulent incompressible viscous flow with spiral vortices between two parallel rotating disks

20 p3213 A71-39778

Water tunnel study of turbulent boundary layers structure in incompressible fluid with longitudinal pressure gradient at inlet section of converging and diverging nozzles

20 p3213 A71-39789

Velocity profiles of plane turbulent flow of incompressible fluid on porous surface in presence of suction

20 p3213 A71-39790

Stability characteristics and general transient motion of vertical finite width three lobe journal bearing, assuming incompressible fluid with cavitation [ASME PAPER 71-VIBR-76]

21 p3385 A71-40314

Gravitational radiation interaction with uniform incompressible inviscid fluid in simple motion, considering response in linearized approximation to general relativity

21 p3446 A71-40421

Turbulent fluids constitutive equations verification by Truesdell principle of material indifference in incompressible and compressible fluids

21 p3367 A71-40652

Three ideal incompressible fluid jets collision induced flow, reducing discontinuity region analytic

functions to nonlinear system with two numerical parameters and singular integrals

21 p3367 A71-40653

Time periodic convection development in incompressible viscous fluid with distributed heat sources

21 p3475 A71-40654

Turbulent viscosity, energy dissipation and diffusion parameters of steady plane boundary layer flow of incompressible fluids with transverse shift in closure system of differential equations

21 p3368 A71-40655

Laminar and rotationally symmetrical flow viscous incompressible fluid in circular pipe of constant temperature, considering inlet swirl effects and heat transfer to wall

21 p3368 A71-40711

Incompressible inviscid fluid free droplet surface layer tension determination as function of curvature from mechanical moment model

22 p3613 A71-41510

Turbulent flow of incompressible fluid in rough pipe, determining skin friction coefficient variation with Reynolds number

22 p3531 A71-42251

Approximate analytic solution for nonstationary heat transfer for viscous incompressible laminar fluid flow in annular cylindrical ducts

22 p3622 A71-42670

Generalized solutions existence proof for viscous incompressible fluids free convection, investigating smoothness properties dependence on initial values and forces

22 p3622 A71-42865

Plane vortex sheet in inviscid incompressible finitely conducting fluid under uniform magnetic field, considering hydromagnetic stability

23 p3663 A71-43450

Turbulent stress distribution relationship averaged characteristics of incompressible fluid boundary layer flow with positive pressure gradient

24 p3818 A71-44747

Heat exchange during stabilized laminar flow of incompressible liquid in circular pipe with radiative cooling, deriving temperature profile and Nusselt number dependence

24 p3888 A71-44937

Externally pressurized journal bearings fed with incompressible lubricant, determining feeding system and hydrodynamic effects on bearing stiffness

24 p3830 A71-44940

Two-dimensional asymptotic solutions to Navier-Stokes equations for weak vortex discontinuity flow with vanishing viscosity

24 p3820 A71-45064

General theory of relativity for symmetric field discussing De Donder incompressible fluid model and Tolman-Schwarzschild metrics

24 p3849 A71-45066

Incompressible fluid impulsive laminar flow developing velocity law and tangential stresses by asymptotic method

24 p3821 A71-45180

Small perturbation development of plane potential motion of ideal incompressible fluid in elliptical region, confirming instability

24 p3821 A71-45211

INCONEL [TRADEMARK]

Inconel 718 arc welding procedures and weldment mechanical properties, discussing impact strength and ductility improvement by heat treatment

02 p0255 A71-11711

Substructures and properties of Ni, Chromel A, Inconel 600 and TD-NiCr following explosive shock load deformation, using electron microscope

02 p0268 A71-12883

Titanium, Inconel and stainless steel alloys deep drawing press loads under various lubrication and temperature conditions, considering work hardening, friction and anisotropic coefficients [ASME PAPER 70-WA/PROD-26]

03 p0433 A71-14114

Ductility of simulated weld fusion zones in Inconel 718

04 p0617 A71-15911

Age hardenable Inconel X-750 superalloy mechanical response to tensile loads for identifying microstructural changes due to deformation

15 p2437 A71-32614

Rapid thermal fluctuations effect on Inconel 718 creep rate, noting strain rate decrease under cycling conditions

19 p3080 A71-37714

Inconel-600 under heat treatment and tension tests: examining grain boundaries slip interaction

21 p3397 A71-40458

Inconel superalloy microscopic observation of local melting and hot ductility behavior during weld thermal cycles to clarify cracking cause in heat affected zone

22 p3564 A71-42494

INDENTATION

Plastic deformation of aluminum oxide by indentation and abrasion at room temperature, using transmission electron microscopy

13 p2093 A71-28989

Critical stress and stability analysis of cylindrical shell with initial indentation of length comparable to radius under axial compression 14 p2321 A71-29536

Elastoplastic indentation of half space by infinitely long rigid circular cylinder, using finite element method 21 p3474 A71-41426

Deformations and stresses in elastoplastic half space indented by rigid sphere, using finite element method 24 p3879 A71-44631

DEPENDENT VARIABLES

NT LATTICE PARAMETERS

He-Ne laser LF radiation parameters calculations verified experimentally 01 p0092 A71-10334

Canonical theory of dynamics, examining independent variable transformations for perturbed two body problem 01 p0154 A71-10379

Inverse problems for parameters and optimal heat transfer model in thermophysical processes 02 p0331 A71-11731

Qualitative theory of unknown parameters selection electronic circuit synthesis, considering polynomial coefficients of transfer function 02 p0230 A71-11838

GaAs injection lasers phenomenological theory and internal parameters physical meanings, giving maximum optical gain dependence on current density 03 p0434 A71-13349

Diverging flow structure in conical diffuser using two Townsend turbulent parameters 03 p0399 A71-13456

Ideal gas isentropic mean value exponent, calculating state variables 03 p0520 A71-13900

Two shaft turbojet engine parameter plot techniques effectiveness, varying low pressure cascade rpm or nozzle system passage cross sections 03 p0472 A71-14259

Motor design parameters effects on solid propellant extinguishment predicted from mathematical combustion model [AIAA PAPER 70-664] 03 p0469 A71-14442

Action-angle variables for Euler-Poisson problem of solid body free rotation about stationary point 05 p0783 A71-16996

Plant parameter variations in linear optimal control systems along stability ray 06 p0878 A71-17334

Parameters influence on mercury hollow cathode neutralizers for Kaufman ion thruster [AIAA PAPER 70-1090] 07 p1184 A71-19863

Digital active fluid amplifiers static and dynamic behavior, defining complex parameters for system engineering 07 p1026 A71-20564

Perturbation theory for reduced density matrices representable as functions of independent parameters 08 p1332 A71-20660

Identification algorithm for estimating parameters in constant coefficient linear system independent of prior estimates [AIAA PAPER 70-34] 09 p1484 A71-22074

Distributed parameter systems under load disturbances regulatory control by feedforward feedback and state measures 09 p1422 A71-22282

Equation error approach to parameter identification in third order pitch plane dynamics for high performance aerodynamically controlled aerospace vehicle 11 p1742 A71-26418

Photographic materials characteristic curve description by sensitometric parameters including contrast, hardness and refinement 11 p1767 A71-26468

Chow parameters of switching functions in threshold logic, discussing basic properties and alternative definitions 13 p2035 A71-28975

Strong shock wave structure parameters variations calculation, considering various applications 13 p2049 A71-29200

Cauchy problem solution for elliptic equations of fourth order in two independent variables, improving Henri, Pucci and Colton results 14 p2266 A71-30811

Quality degradation and sensitivity standard of plant parameter definition accuracy in optimal open control system 15 p2379 A71-31520

Bayesian estimate of signal parameters in random noise background under mutually exclusive hypotheses about statistical properties 15 p2370 A71-31584

Optimal Bayesian system for simultaneous discrimination and parameter estimation of several signals in noise background 15 p2370 A71-31585

Normal gravity field parameters from harmonic coefficients and satellite observation data 15 p2492 A71-32468

Stability of governing parameters critical values [Taylor, Rayleigh or Reynolds numbers] and periodic solutions in fluid mechanics 16 p2558 A71-33002

Stability conditions approximation for assessment of single parameters effect and in making choices 16 p2607 A71-33003

Diurnal variation of atmospheric parameters in thermosphere deduced from incoherent scatter and satellite drag, discussing atmospheric model correspondence to observed data 16 p2566 A71-33742

Optimal parameters of Fabry-Perot etalon for error minimization in Doppler and dispersion portions determination of Voigt profile width 17 p2737 A71-34410

Parameter space sections method for nonlinear automatic control systems analysis, reducing initial system by linear transformation of variables to first and second order equations 17 p2783 A71-35127

Distributed parameter system measurement optimization devices location for error estimation cost minimization by disturbances statistical characteristics and boundary conditions 17 p2722 A71-35211

Optimal control of plant with varying parameters, obtaining suboptimal systems with feedback loops 17 p2722 A71-35214

Variables affecting processing mode /serial or parallel/ of complex stimuli information 17 p2684 A71-35255

Phase object visualization by Hilbert transformation, noting image properties evolution as function of various experimental parameters 18 p2947 A71-36043

Complex wave structure development upon underexpanded jet impact on plane obstruction at small incidence angles, determining gas dynamics parameters of supersonic jet 18 p2903 A71-36120

Action-angle variables for Euler-Poisson problem of solid body free rotation about stationary point 18 p2948 A71-36796

Approximation solution for elliptic boundary value problem with nondifferentiable parameters, considering second order linear partial differential equations in two independent variables 18 p2942 A71-36817

Regular boundary value problems singularities for linear second order analytic elliptic equations solutions in two independent variables 18 p2942 A71-36925

Baluns as electromagnetic compatibility control devices for signal and common mode currents, providing basic parameters and equivalent circuits 19 p3030 A71-38433

Collector/base current ratio degradation in bipolar transistors, describing mechanisms characteristics and protective techniques 19 p3034 A71-38522

Cloud physics, comparing observational and theoretical values of wave parameter determining heat influx properties 19 p3094 A71-38703

Book on fitting equations to data by computer analysis of multifactor data for scientists and engineers, covering independent variables selection and least squares method 21 p3406 A71-40166

Gradient search procedures application for non-linear system unknown parameters identification from system dynamic response observations [ASME PAPER 71-VIBR-50] 21 p3460 A71-40299

Algorithms for directional antenna boresight orientation estimation errors relative to spacecraft attitude sensor, based on measurement of received signal strength 22 p3525 A71-42775

Average number of real roots of polynomials consisting of independent random quantities with identical distribution 23 p3699 A71-43571

Parameters steady random variations effect on linear and nonlinear systems steady motion characteristics, using integral equation and averaging methods 24 p3815 A71-44696

INDEXES (DOCUMENTATION)

Information support system for physiological studies of human performance, including indexing approach for references categorization, microfiche file and data bank 11 p1860 A71-25253

NASA Scientific and Technical Information System, illustrating advantages of machine retrieval systems for legal profession 18 p2986 A71-35868

Aircraft industry license norms and standards, describing indexing procedures, storage techniques and data recovery operations with computer 18 p2886 A71-36810

INDEXES (RATIOS)

Airport sound prediction using Noise and Number Index deduced from noise logarithmic average and audible aircraft number 11 p1723 A71-25236

RR Lyrae type variable star statistical population indices evaluation based on space and radial velocities and position 11 p1820 A71-25247

Worldwide geomagnetic disturbance during magnetic storm using DR-indices to express magnetospheric ring current induced perturbation 22 p3536 A71-42624

Geomagnetic index Kp frequency distribution tables [1932-1970] 23 p3670 A71-43192

Psychophysiological loudness and annoyance indices application in sonic boom comfort level evaluation, pulsating noise estimation and sound insulation system effectiveness determination 24 p3799 A71-44399

INDIA

Total electron content over New Delhi by satellite beacons, discussing solar activity effects, electron production rates and seasonal variations 07 p1097 A71-19019

INDIAN OCEAN

Monsoonal response of Somali Current in Indian Ocean, using spacecraft IR observations of sea surface horizontal temperature gradients 16 p2562 A71-33068

Aerosol measurements over Atlantic and Indian Oceans, discussing aerosols optical thickness, effective radii, concentrations, sizes and optical properties variations with latitude and meteorological conditions 20 p3257 A71-39328

Latitudinal distribution of integral water drop content of clouds above Pacific, Atlantic and Indian oceans from Cosmos 243 measurements 22 p3568 A71-41653

INDICATING INSTRUMENTS

NT ANEMOMETERS
NT APPROACH INDICATORS
NT ATTITUDE INDICATORS
NT CLOUD HEIGHT INDICATORS
NT FLOW DIRECTION INDICATORS
NT GYRO HORIZONS
NT GYROCOMPASSES
NT HOT-FILM ANEMOMETERS
NT HOT-WIRE ANEMOMETERS
NT MICROWAVE SENSORS
NT PLAN POSITION INDICATORS
NT POSITION INDICATORS
NT RADIO DIRECTION FINDERS
NT SONIC ANEMOMETERS
NT SPACECRAFT POSITION INDICATORS
NT SPEED INDICATORS
NT STRAIN GAUGE BALANCES
NT THERMOBALANCES
NT WEIGHT INDICATORS

Severe thunderstorm warning by single pulse Doppler radar plan shear indicator 01 p0117 A71-10572

Aircraft visual warning indicating system, outlining design criteria, color and brightness recommendations [SAE-ARX-1088] 07 p1019 A71-19644

Electronic digital automatic defect indicator attachment to industrial echo defectoscope 08 p1300 A71-21897

Signaling sensitivity leveling by introduction of automatic defect indicator into defectoscope 08 p1273 A71-21904

Acoustic indicator for remote detection of microcracks in systems with high gas or vapor pressures 15 p2409 A71-32189

Mercury column electrochemical coulometer as amper-hour type of state-of-charge indicator for secondary batteries in space power applications 15 p2354 A71-32206

Thermomodulation method instrument using cold indicator depot with heat exchanger for standardization of heart-time-volume measurements 18 p2872 A71-36692

Broadcast sound loudness level monitor as measuring and indicating instrument, discussing technological and psychoacoustical evolution 20 p3271 A71-39763

INDICATORS

Servosystems errors of indicator-receiver for recording electromagnetic field pattern extremes in amplitude radio interferometers 04 p0557 A71-14635

INDIUM

Inelastic scattering of protons from In 115, using proton beam cyclotron 01 p0130 A71-10482

Atmospheric neutron production by cosmic rays, calculating cadmium-indium ratio 19 p3066 A71-38379

Spherical indium crystal manufacture in space, suspending and positioning weightless containerless melt in air and vacuum by adhesion and cohesion for crystal growth 20 p3247 A71-38767

INDIUM ALLOYS

High purity Sb, In and Ag by vacuum distillation, zone melting and electrolytic refining for semiconductor electronics

24 p3861 A71-45201

INDIUM ALLOYS

In-Bi alloys electrical conductivity measurement for compositions covering characteristic points of phase diagram at temperatures from liquidus line to 850 C

02 p0294 A71-11895

Magnesium indium alloys single crystal plastic deformation, investigating basal and prismatic slip at various temperatures

08 p1309 A71-21528

In-Bi whisker growth by squeeze technique, measuring crystal structure by X ray analysis and melting point method

23 p3689 A71-42956

INDIUM ANTIMONIDES

Te-doped In Sb single crystal growth in transverse magnetic fields, using Czochralski crystal puller

01 p0100 A71-10281

Microwave emission from InSb due to sound amplification by piezoelectric electron-phonon coupling at low magnetic fields

01 p0052 A71-10321

Diffusion and solubility of thermally induced acceptors in indium antimonide single crystals

04 p0636 A71-15085

Dynamic stabilization of helical and sausage instabilities of p-indium antimonide electron-hole plasmas, using Ioffe type RF energized magnetic quadrupoles

06 p0935 A71-17489

Magnetoreflexion of helicon wave from n-InSb semiconductor in microwave range

07 p1176 A71-19270

N-type InSb microwave noise radiation and attendant RF current oscillations under magnetic field

07 p1180 A71-20177

Type S bulk negative differential conductivity in n-InSb at 77 K and atmospheric pressure, showing associated large current due to strong impact ionization

09 p1508 A71-22756

High power single mode CW tunable spin-flip Raman laser in InSb using CO pump

10 p1620 A71-24041

Planetary disks brightness temperature measurement using 22 m radio telescope with indium antimonide detector at 1.4 mm

13 p2141 A71-29102

High intensity tunable InSb spin flip stimulated Raman scattering from pulsed high pressure carbon dioxide laser radiation pumping

13 p2081 A71-29336

Millimeter wave semiconductor isolator using circular waveguide with coaxial n-type InSb in longitudinal magnetic field

14 p2212 A71-30510

Multielement IR photoconductive detector arrays of InSb and mercury cadmium telluride operating at cryogenic temperatures

18 p2923 A71-36606

Electron concentration and mobility of heavily doped n-type InSb single crystals at high temperatures, investigating temperature dependence of Hall coefficient

18 p2954 A71-36803

Heavily Ge doped p-InSb photoelectric and electric properties, showing impurity concentration effects

19 p3120 A71-38526

Tellurium concentrations and photocurrent spectra in Te-doped InSb single crystal samples, determining Te diffusion after annealing

21 p3430 A71-41225

Cyclotron absorption and resonance spectra of hot electrons in p-type InSb samples cut from single crystals containing different amounts of impurities

21 p3430 A71-41226

Rollin InSb hot electron bolometer performance and calibration

22 p3543 A71-42124

Tunable spin-flip magneto-Raman IR laser, describing indium antimonide scattering, tuning range and applications

22 p3557 A71-42133

N-type In-Sb continuous coherent microwave oscillation under transverse magnetic field, discussing helical frequency instability on threshold and growing wave conditions

22 p3586 A71-42347

Microwave emission from plasmas in InSb with and without magnetic fields, deriving pseudolongitudinal wave interaction theory for explanation

23 p3714 A71-42914

INDIUM ARSENIDES

Te doped InAs single crystals structural characteristics investigation by X ray diffraction, noting laminar growth with alloying impurity varying concentrations

06 p0940 A71-17388

Electrophysical properties of Ga-In-As single crystals in varying mixture ratios at 78-380 K, determining electrical conductivity, Hall coefficient and electron mobility

07 p1176 A71-19224

GaAs-InAs type single crystals, polycrystals and epitaxial films solid solutions, studying optical, electrical and luminescent properties

08 p1344 A71-21443

InAs-AlAs pseudobinary system solidus boundary determination from pellet phase diagram

08 p1344 A71-21472

Capacitance voltage measurements on interface of pyrolytically deposited n-type silicon dioxide-InAs MOS diodes as function of admittance at room and 77 K temperatures

10 p1582 A71-23774

Hall effect mechanical vibration transducer with indium arsenide semiconductors and elastically suspended magnets

10 p1612 A71-24639

High electric field Gunn effect in n-type InAs under hydrostatic pressure due to transferred carrier mechanism

20 p3275 A71-38786

Auger recombination coefficient determination for nonequilibrium carriers in n-type InAs from photoconductivity and light absorption under laser excitation at high levels, noting electron mobility

21 p3433 A71-41310

Quasi-binary InAs-GaP single crystals absorption and diffuse reflection spectra, determining forbidden bandwidth as function of compound composition

21 p3434 A71-41332

GaAs-InAs solid solutions single crystal ingots, investigating optical absorption and reflection spectra, energy gap width and carrier mobility temperature dependence

21 p3435 A71-41335

Neutron irradiation effects on dissociative high temperature zinc diffusion in indium and gallium arsenides

23 p3716 A71-43480

INDIUM COMPOUNDS

NT INDIUM ANTIMONIDES

NT INDIUM ARSENIDES

NT INDIUM PHOSPHATES

NT INDIUM PHOSPHIDES

NT INDIUM SULFIDES

NT INDIUM TELLURIDES

Stimulated and spontaneous emission from InSe single crystal under focused fast electron beam bombardment

21 p3434 A71-41326

INDIUM PHOSPHATES

Epitaxial InP three level oscillators in K and Q bands /18-40 GHz/, suggesting optimum operating frequency determined by defined transit velocity

09 p1421 A71-23719

INDIUM PHOSPHIDES

Single crystal indium gallium phosphide solid solution synthesis, discussing crystallophysical and electrophysical properties

03 p0467 A71-13424

Single crystal indium gallium phosphide p-n junction preparation by epitaxial vapor phase growth technique, determining energy gap dependence on alloy composition

09 p1510 A71-23121

InP pulsed and CW millimeter wave oscillators at frequencies above 30 GHz

11 p1739 A71-26367

Frequency-length relationship for bulk InP microwave oscillators in 10-100 micron thickness range, obtaining threshold field and average transit velocity

14 p2210 A71-29791

Multilayer epitaxial InP transferred electron microwave oscillator I-V characteristics and frequency dependence on layer thickness

23 p3649 A71-42912

Indium gallium phosphide p-n junction laser operation at 4.2 and 77 K, considering threshold currents magnitude

23 p3687 A71-44138

INDIUM SULFIDES

Impure GaAs and InP semiconductors compensation by introducing diffusible temperature dependent impurities

18 p2953 A71-35871

INDIUM TELLURIDES

Irreversible processes during formation of contact between indium telluride thin film and metal in vacuum at high temperature

01 p0137 A71-10150

Electrical, photoelectrical and optical properties of crystalline cadmium telluride-indium telluride alloys, discussing temperature dependence, spectral characteristics and photoconductivity

05 p0793 A71-16824

Quadrupole interaction in crystals of diamond-like semiconductors gallium telluride and indium telluride

07 p1177 A71-19275

Copper-indium-tellurides homogeneity region components solubility in different cross sections of concentration triangle at room temperature

23 p3717 A71-44023

InTe thin films formation, growth kinetics and physical properties, determining vapor deposited film thickness dependence on glass substrate temperature

24 p3861 A71-45249

InTe thin films with 60-75 percent Te content, investigating phase composition and physical properties

24 p3862 A71-45250

INDOLES

NT TRYPTOPHAN

Biosynthesis control of melatonin and other methoxyindoles in mammalian pineal organ

14 p2182 A71-29600

Chlorella extracellular metabolites, identifying indole nature biologically active substances

19 p3004 A71-38800

External indole-3-acetic acid effect on elongation and geotropic bending of *Avena coleoptiles* related to auxin induced electrical responses

21 p3340 A71-39987

Indole vapor inhalation and direct injection in mice, rats and rabbits, examining toxic qualities

22 p3506 A71-42800

INDUCED FLUID FLOW

U FLUID FLOW

INDUCERS

U INTAKE SYSTEMS

INDUCTANCE

Tunnel diode trigger circuit, calculating effect of junction capacitance variation and small inductance on switching time

05 p0730 A71-17080

External circuit inductance effect on transverse discharge excited atmospheric pressure carbon dioxide-helium-nitrogen laser small signal gain

12 p1914 A71-26979

Inductive voltage divider bridge network for ferrite coils inductance and Q measurements

17 p2723 A71-35710

Plasma/magnetic field pressure ratio and inductance per unit length in Tokamak plasma pinch with arbitrary cross section

22 p3579 A71-41580

Design parameters optimization for flat spiral coils printed on dielectric substrates based on equivalent circuit analysis, emphasizing coil shape effects on inductance

22 p3520 A71-41710

HF and LF transistors suitability for integrated bipolar Q LC circuits, studying inductivity, Q and component frequency dependence

24 p3807 A71-44370

INDUCTION

Excitation schemes, fluid velocity and power of jet MHD induction generator

11 p1709 A71-25450

INDUCTION HEATING

Electrical shock tube performance with RF induction heating of downstream gas

04 p0564 A71-14670

Radiation effects on thermal decomposition induction period in ammonium perchlorate and other pseudostable inorganic solids

06 p0944 A71-18300

Al alloys thermal fatigue resistance measurements using testing apparatus involving HF induction heating

07 p1142 A71-20322

Elastic half space two dimensional unsteady temperature and stress fields under induction heating and convective heat transfer

09 p1537 A71-22510

Multilayered spherical model induced fields and static heating patterns, approximating primate cranial structure EM plane wave irradiation

11 p1717 A71-25280

Steam turbine blades induction brazing with programmed cycle, describing coil design

19 p3070 A71-38310

INDUCTION SYSTEMS

U INTAKE SYSTEMS

INDUCTORS

Optimal design of toroidal inductors with DC bias without repetitive trials

01 p0053 A71-10735

High power regulated energy transfer by inductor-transformers with single and multiple stages using trapezoidal current waveshapes

03 p0352 A71-13048

Nonlinear vector potential analysis of aerospace homopolar inductor alternators, considering fully armature currents

03 p0353 A71-13053

Laminar flow of viscous electrically conducting fluid in traveling magnetic field, examining channel flow in traveling wave field of one directional and two directional inductor

09 p1499 A71-22134

Electromagnetic effects in infinite conducting layers situated in field of inductors with mutually opposed traveling magnetic fields

09 p1499 A71-22138

Thick film flat spiral inductor filter design for television signals, using linear analysis computer program

13 p2039 A71-28913

Inductor winding dependent magnetic pulse deformation of cylindrical blanks allowing for mutual electromagnetic and mechanical coupling

15 p2417 A71-32523

INDUSTRIAL MANAGEMENT

NT ENGINEERING MANAGEMENT

NT PERSONNEL MANAGEMENT

Long term planning of technological and scientific development of machine design and construction on national industrial and enterprise levels
02 p0336 A71-11860

Aerospace industry engineering company management and marketing, discussing corporate strategy, production control, market analysis and professionally trained managers
05 p0840 A71-17148

Motivation principles in industry based on Maslov theory of hierarchy of needs, discussing selection of supervisory personnel
13 p2167 A71-28798

Industrial project management, defining functions and responsibilities of program director, contractor, subcontractor and manufacturer
23 p3785 A71-43460

Industrial project management executive work team for space programs, emphasizing responsibilities of prime contractor
23 p3786 A71-43461

INDUSTRIAL PLANTS
Man oriented program system for industrial facilities engineering design with modular structure, operating in time sharing mode
09 p1412 A71-23275

Physics and technology discoveries utilization in industrial control, considering semiconductors, thin films, lasers, holography, cryogenics, etc
24 p3827 A71-45071

INDUSTRIAL SAFETY
Explosive forming using compressed air as power source for safety and lower cost
01 p0091 A71-11549

Laser thermal/photochemical burns and electric shock prevention by preemployment/regular physical examinations and safety requirement education
09 p1402 A71-23412

Industry safe laser laboratory operating environments with reflection free walls, restrictive admittance and periodic personnel examinations
09 p1402 A71-23413

INDUSTRIES
NT AEROSPACE INDUSTRY
NT AIRCRAFT INDUSTRY
NT DEFENSE INDUSTRY
Book on high temperature materials covering vacuum or inert gas properties for industrial and aerospace applications
17 p2760 A71-35623

INELASTIC BODIES
U RIGID STRUCTURES

INELASTIC COLLISIONS
Quasi-plastic impact in shock interaction between free body and moving plane, using nonlinear finite difference equation
01 p0127 A71-10636

High energy multiple birth inelastic interactions between cosmic ray particles and atomic nucleus targets, using Wilson chamber and ionization calorimeter
01 p0083 A71-11363

High energy inelastic interactions in cosmic ray showers, using Wilson chamber
01 p0145 A71-11365

High energy interaction multiperipheral theories, examining inelastic events
03 p0461 A71-13834

Inelastic particle collisions with energies exceeding 10 to the 13th eV, considering cosmic rays, nucleons and hadrons
03 p0475 A71-13837

Inelastic ionization cross sections for protonic and atomic hydrogen collisions with atomic and molecular gases in 0.5 keV to 5 MeV energy range
06 p0928 A71-17266

Inelastic collision effects on vibrational excitation of diatomic molecules with conserved energy
08 p1338 A71-21781

H beta, H gamma and H delta Stark broadened profiles, investigating perturbing electron-radiating atom inelastic collisions, Gaunt factors and half widths
09 p1496 A71-22413

Al and Pb atoms nuclei inelastic interaction cross section with nuclear active particles, using ionization calorimeter and wide gap spark chambers
11 p1760 A71-25165

High energy nuclear bursts without accompanying air showers, considering surviving primary protons without inelastic collision in atmosphere
13 p2121 A71-28054

Pions-photographic emulsion nuclei inelastic collisions as function of energy, comparing multiplicity, produced particles angular distribution and evaporation prongs number
13 p2121 A71-28059

Electron energy distribution function in weakly ionized monatomic gas with inelastic collisions, using differential equation asymptotic resolution techniques
13 p2106 A71-28398

Average energy of electron avalanches in gases for linear inelastic collision cross sections, including ionization coefficient and Stoletoev constant for atomic hydrogen
13 p2103 A71-29080

Boltzmann equation approximate solution for molecular velocity distribution function perturbations by inelastic collisions
15 p2386 A71-31158

Maximum contact force dependence on rebound velocity, coefficient of restitution and impact duration during inelastic collision
16 p2647 A71-32816

Spatial relaxation of electron energy distribution with inelastic and Coulomb collisions, integrating Boltzmann equation
18 p2949 A71-36969

Low density plasma electron velocity distribution deviation due to Maxwellian photon radiation resulting from inelastic collisions with atoms
19 p3112 A71-37739

Fast charged particles inelastic collisions with atoms and molecules, investigating Bethe differential cross section theory
21 p3418 A71-40675

Molecular gas mixtures inelastic collision integral spectra, describing internal degrees of freedom with correlation functions
21 p3420 A71-41271

High energy interaction multiperipheral theories, examining inelastic events
22 p3578 A71-42635

Inelastic particle collisions with energies exceeding 10 to the 13th eV, considering cosmic rays, nucleons and hadrons
22 p3594 A71-42638

Electron production cross sections in inelastic atomic collisions, evaluating classical scaling law and quantum mechanical statistical methods against experimental results
24 p3850 A71-44587

[AIAA PAPER 71-995]
Rotationally inelastic molecular collisions in atom rigid rotor scattering, considering infinite order approximation of generalized phase shift treatment
24 p3850 A71-44921

INELASTIC SCATTERING
Inelastic scattering of protons from In 115, using proton beam cyclotron
01 p0130 A71-10482

Inelastic scattering by impurities and phonons in metals, determining energy level structure from nonlinear corrections to Ohm law
02 p0297 A71-12615

Inelastic alpha particle scattering experiment for studying energy spectrum and angular distribution of Sc-45 excited states
03 p0462 A71-14417

Born-Oppenheimer approximation for elastic and inelastic electron scattering by diatomic molecules
08 p1337 A71-20886

Symmetric excited state electron capture cross sections in ion-atom inelastic scattering, using two state approximation formulas
08 p1338 A71-21235

Inelastic scattering cross sections, using measured neutron leakage spectra from thick spherical shells of Ta, W, Mo and Be
11 p1802 A71-25556

Unaccompanied hadron vs primary proton spectra in atmosphere and proton-air inelastic cross sections above 500 GeV from cosmic ray measurements
12 p1951 A71-27394

Inelastic scattering transition densities in single particle operator reduced matrix elements between initial and final nuclear states for nucleon angular momentum calculations
14 p2276 A71-30013

Inelastic electron scattering cross sections and energy spectra from Al and Au targets, using magnetic analyzer with high resolution detector
16 p2614 A71-34042

Glauber and Vainshtein approximations for cross sections of 1s-2p excitation during inelastic electron-atomic hydrogen scattering
20 p3272 A71-39470

Glauber approximations for elastic and inelastic scattering of protons by ground state hydrogen atoms, comparing with measurements
20 p3272 A71-39578

Transport properties of low density gas of rotating diatomic molecules, deriving quantum mechanical expression for relaxation time via restricted distorted wave approximation method
23 p3706 A71-42908

Inelastic scattering alpha-gamma angular correlations from C 12, Mg 24, Ni 58 and Sn 120 decay measurements
23 p3706 A71-43198

Wave interference phenomena associated with elastic scattering of atoms, considering differential inelastic scattering cross sections anomalies
24 p3851 A71-45166

INELASTICITY
U ELASTIC PROPERTIES

INEQUALITIES
Coleman-Noll inequality, examining validity for all tensors G
05 p0826 A71-16720

Two countable systems of differential inequalities, applying to stability of feedback controls synthesizing equilibrium solutions to linear quadratic differential games
06 p0919 A71-18198

Complex zeros of complex polynomials, matrix inequalities and nonlinear programming, constructing areas intersection in complex plane defined by inequality bounds on eigenvalues of companion matrix
09 p1485 A71-22970

Laplace long period solar inequality effects on lunar ecliptic longitude, considering role in celestial mechanics
10 p1667 A71-23829

Elastic structure dynamic stability problem, determining optimum inequality relating energy functional to displacement, and considering beam column with various boundary conditions
15 p2506 A71-32015

Numerically stable algorithm for solving least squares problems with linear equalities and inequalities as additional constraints
17 p2769 A71-35693

Lower bound on distance between vertical asymptotes of second order differential equations solutions involving integral inequality
18 p2941 A71-36227

Pointwise bounds in Cauchy problem for fourth order quasi-linear equation using a priori inequality, applying Rayleigh-Ritz technique to elliptic partial differential equations
20 p3255 A71-39573

Viscoelastic materials property inequalities as consequence of Gibbs free energy minimum, disproving interpretation as indication of second order phase transition
20 p3310 A71-39867

Recurrent finitely converging algorithms for solving inequalities in automatic control systems involving adaptive filters
22 p3526 A71-41858

Nonlinear theory of nonlocal continuum mechanics, considering global energy balance, constitutive equations and Clausius-Duhem inequality
23 p3705 A71-43869

INERT ATMOSPHERE
Incident shock wave interaction with liquid hydrocarbon fuel drops in oxidizing and inert atmospheres, considering combustion characteristics and ignition mechanism
06 p0886 A71-18642

Helium from nitrogen substitution effects on body temperature of rats exposed to high carbon dioxide concentrations at different ambient temperatures
13 p2006 A71-28402

High temperature permeameter for measuring magnetizing force or magnetic induction in vacuum or inert atmosphere
15 p2401 A71-31194

Ti alloys inert gas shielded welding, determining relationship between welding current, electrode feed rate and electrode wire protruding length and diameter
15 p2413 A71-31219

Liquid hydrocarbon fuel drop interaction with incident shock wave in oxidizing and inert atmospheres, investigating aerodynamic shattering and combustion
17 p2836 A71-34435

INERT GASES
U RARE GASES

INERTIA
NT INERTIA PRINCIPLE
NT MACH INERTIA PRINCIPLE
Einstein universe fictitious forces in noninertial frames, deriving equations from classical formulas by general covariance
03 p0490 A71-13942

Inconsistency in covariant gravitation theory with scalar field, considering limitation to forces of inertia and contradiction of macroscopic physics deterministic principle
04 p0625 A71-15098

Shear deformation and rotary inertia in heterogeneous laminated plates of bonded anisotropic layers, discussing bending-extensional coupling
04 p0668 A71-15185

Classical and relativistic forces of inertia based on exact solution of Einstein nonlinear gravitational field equations, using general covariance principle
04 p0628 A71-15903

Inertial quantity sensors testing, discussing environmental control, calibration, inspection, etc
05 p0749 A71-16302

Slender beams transverse vibration, including nonlinear bending inertia in motion equation
05 p0825 A71-16716

Monolith thermal flux sensors inertia characteristics on various surfaces
06 p0899 A71-18005

Fluid inertia effect on porous thrust plate, using mathematical model for prediction
07 p1088 A71-19625

[ASME PAPER 70-LUB-18]
Ballistic reentry vehicle roll related to trim angles caused by inertia asymmetries
07 p1208 A71-19867

[AIAA PAPER 70-204]

INERTIA MOMENTS

- Inertia effect in failure mechanics for steadily developing equilibrium cracks in dynamic system with time dependent periodically variable load
08 p1372 A71-21705
- Helicopter rotor inertial system kinetic energy, examining takeoff advantages
09 p1385 A71-23670
- Rapidly rotating fluid flows, calculating inertia waves by geometrical optics method
10 p1591 A71-23854
- Inertia effects on coupled librations and stability bounds of axisymmetric gravity oriented satellites in circular orbits, using integral manifold
11 p1838 A71-26195
- Distributed inertial forces due to cyclic loading in minimum volume beams cross sectional stress calculations
13 p2154 A71-28643
- Massive body gravitational to inertial mass ratio from equilibrium assembly model of particle interactions
13 p2139 A71-28997
- Circular rings coupled twist bending vibrations, considering rotatory inertia and shearing deformation effects
15 p2510 A71-32517
- Inertial properties of segmented cadaver trunk for mathematical model of spinal response to impact in seat ejection acceleration injuries in high speed aircraft
16 p2528 A71-33117
- Compressible flow across shaft face seals and narrow slots, examining fluid inertia, viscous friction and entrance losses
23 p3663 A71-43592
- Dynamic flexures in beam during massive extended load motion with allowance for inertial forces, using Bubnov-Galerkin method
23 p3778 A71-44046
- INERTIA MOMENTS**
U MOMENTS OF INERTIA
INERTIA PRINCIPLE
NT MACH INERTIA PRINCIPLE
M-dimensional gradient extremal system under non-random and random noises of inertial control plant, using difference equation
01 p0064 A71-10922
- Jet engine components inertia welding, discussing process, equipment, low weight-cost advantage and mechanical properties reproducibility
11 p1770 A71-25970
- Inertial range transfer in two and three dimensional turbulence, using almost-Markovian Galilean-invariant model
15 p2445 A71-31928
- Inertial effects induced by rotating thin walled shell of finite thickness, considering general relativity equations of motion for test particle
18 p2970 A71-37059
- Spacecraft orientation angle measurement by inertial sensors, analyzing equipment kinematic efficiency and limitations
24 p3829 A71-45318
- INERTIA WHEELS**
U REACTION WHEELS
INERTIAL ACCELEROMETERS
U ACCELEROMETERS
INERTIAL COORDINATES
Forced rotation influence of gimbal suspension on astatic gyroscope motion with respect to inertial coordinates, demonstrating pseudoregular precession
09 p1451 A71-23172
- Tensor inertia conversion from principal to rotated coordinates system, obtaining negative products in aircraft
10 p1557 A71-24949
- Characteristic initial data for gravitational vacuum fields invariant of two initial null hypersurfaces and space-like section sigma
22 p3576 A71-42404
- INERTIAL FORCES**
U INERTIA
INERTIAL GUIDANCE
NT STRAPDOWN INERTIAL GUIDANCE
Inertially stabilized tactical missile control system performance analysis using hybrid computer simulation methods
02 p0226 A71-11785
- Inertial guidance problems - Conference, Cambridge, Mass., January 1970
02 p0252 A71-12451
- Analog inertial sensor digitizing methods, discussing pulse rebalancing and analog to digital conversion
02 p0279 A71-12453
- Inertial instruments temperature compensation vs control
02 p0253 A71-12460
- Supporting fluid effects in floated inertial instruments, examining cause, frequency, extent and solution
02 p0253 A71-12462
- Navigation, inertial guidance and position keeping terms definitions
02 p0280 A71-12897

- ELDO inertial guidance system digital computer, explaining guidance law subsystem formulation and programming
03 p0454 A71-13247
- Fluidic inertial instruments for space sensing, guidance and control including gyroscopes, accelerometers and rate sensors
04 p0535 A71-15322
- Cassiopee attitude control system for sounding rockets using stellar and inertial sensors for orientation and pointing
05 p0780 A71-16416
- Inertial aircraft lateral guidance system limitations in stochastic gust environment, comparing configurations using aileron or differential spoilers
06 p0925 A71-18489
- Prelaunch automatic azimuth alignment theodolites for Saturn 1B and Saturn 5 space vehicles inertial guidance system, discussing return images separation and error signal generation
08 p1289 A71-21375
- Attitude control loop and inertial guidance hardware, studying system dynamic performance hybrid simulation
11 p1796 A71-25846
- Special purpose computer mechanization of inertial attitude reference computation and transformation of body axis information into desired reference frame
14 p2271 A71-30317
- ST-224 redundant inertial measurement system, using conventional gimballed platforms, each with three skewed single-degree-of-freedom control gyro and one caged gyro
17 p2773 A71-35060
- Direct in-orbit alignment of integrated optical strapdown inertial guidance system for space application, considering self contained prelaunch alignment and calibration
17 p2774 A71-35071
- Fluidic gyroscope technology, reviewing current development and problems associated with severe environmental conditions affecting inertial guidance and spacecraft control
18 p2922 A71-36482
- Human performance in optical high inertia tracking system interface, considering proprioceptive feedback, display magnification, control dynamics view field and anticipatory processes effects
18 p2873 A71-36912
- Performance limitation of simplified radio-inertial lateral control guidance system subject to stochastic gusts for automatic landing
19 p3099 A71-37198
- Integrated test concept for terminal guidance subsystems and components evaluation, laboratory calibration and simulation tests
19 p3040 A71-37210
- Two dimensional seismic mathematical and scale techniques appropriate to inertial navigation devices test pads noise isolation examination
19 p3056 A71-38326
- Star comparator automatic azimuth system using long evacuated tunnel transfer to underground inertial guidance laboratory
19 p3102 A71-38328
- Low temperature viscous lubricants from mixed pentaerythritol esters for precision inertial guidance gyroscope bearings and instrument applications
20 p3254 A71-39800
- Aerospace guidance technology evolution at MIT with emphasis on inertial systems
22 p3570 A71-41993
- Pattern recognition technique for system error analysis, applying to inertial guidance system test
22 p3566 A71-42110
- INERTIAL MEASURING UNITS**
U INERTIAL PLATFORMS
INERTIAL NAVIGATION
NT GIMBALESS INERTIAL NAVIGATION
Inertial navigation system error reduction by gyroplatform rapid rotation
01 p0122 A71-10421
- Inertial navigation system augmented by digital distance measuring equipment in FAA flight inspection aircraft for performance evaluation
01 p0124 A71-10507
- Airborne inertial and area navigation systems performance requirements proposed for U.S. domestic airspace, including projection through 1995
01 p0124 A71-10508
- Airline experience with dual inertial systems as sole means of navigation, considering equipment reliability, cockpit design, training, etc
01 p0124 A71-10509
- Meridian direction autonomous inertial determination, using gyroplatform newtonometer data
01 p0125 A71-10629
- Kinematic error equations application to real inertial navigation systems analysis
02 p0253 A71-12636
- Heading of object moving on terrestrial sphere surface with inertial navigation aid, calculating asymptotic stability for position determination on computer
03 p0459 A71-14355

- Dry friction autocompensation in inertial navigation accelerometers by forced rotation of platform
05 p0751 A71-16589
- Soviet book on inertial navigation systems covering theory, design, construction, coordinate algorithms linear and angular accelerometers, etc
06 p0897 A71-17434
- Orientation vector differential equation formulations for strapdown inertial navigation, applying to rigid body rotation problem
07 p1154 A71-18859
- Gyrocompass strapdown three coil synchro sensor magnetometer in conjunction with vertical gyro eliminating azimuth detector inertial platforms
07 p1156 A71-20340
- U.S. domestic ATC airspace enroute and terminal area navigation system effects on pilot workload, projecting future FAA requirements
07 p1157 A71-20344
- Small factor errors of inertial navigation system for disturbed Keplerian motion of plant
07 p1158 A71-20464
- Strapdown inertial navigator alignment by digital filtering techniques, discussing application to aircraft and spacecraft
08 p1331 A71-21170
- Weather influence on long range radio navigation aids, considering supersonic aircraft operation and inertial navigation
10 p1640 A71-24965
- Aeronautical satellites, considering air-ground telecommunication, air traffic control and inertial navigation applications
12 p1971 A71-26822
- Inertial navigation system consisting of gyro horizon compass, directional gyro and computer, considering errors due to compass vibrations
12 p1927 A71-27165
- Flight tests of inertial navigation system in aerological mapping, achieving automatic side-lap, verticality and line position control
12 p1927 A71-27255
- Linear estimation with stochastic feedback control to cancel out disturbances or error signals effect, applying to integrated navigation systems involving inertial measurement
12 p1893 A71-27436
- Boeing 747 crew members training program describing ground training, classrooms, inertial navigation system and cockpit trainers
13 p1996 A71-28359
- French book on optimal inertial navigation and statistical filtering covering Wiener and Kalman filters, gyroscopes, accelerometers, inertial platforms and data processing, computer programming, etc
14 p2271 A71-29940
- German monograph on error analysis in strapdown inertial navigation system covering gimballed platforms, error propagation, Kalman filtering techniques and mathematical equations
14 p2271 A71-30236
- Inertial navigation systems improvements for commercial air transportation, noting digital computer program revision and increased functional capability
14 p2272 A71-30534
- Combined inertial and instrument landing aircraft navigation systems with reduced cross runway position and velocity errors, using optimal linear estimation
14 p2272 A71-30606
- Air navigation techniques history, considering radio, radar, loran Doppler and inertial navigation
14 p2272 A71-30712
- AN/ASN-86 inertial navigation system consisting of inertial platform, digital computer and control indicator
14 p2273 A71-31094
- Automatic landing systems using inertial navigation derived translational state information, discussing evaluation by simulation of transport aircraft operating with conventional instrument landing system
16 p2605 A71-34020
- Carousel IV inertial navigation system of Boeing 747 aircraft, discussing informational capabilities, accuracy and reliability
16 p2606 A71-34079
- ATC avionics equipment, discussing inertial area navigation, autopilots, airborne data acquisition, altitude reporting, collision avoidance, CAT, satellite communications, etc
17 p2771 A71-34615
- Optimum skew angle between redundant inertial systems, considering component weight, MTBF and duty cycle
17 p2773 A71-35062
- Skylab strapdown attitude navigation system using components designed for predecessor projects ATM and Saturn I Workshop
17 p2773 A71-35063
- Flight test of hybrid strapdown inertial navigator with Doppler radar and occasional position fixes through Kalman filter mechanized in small computer
17 p2776 A71-35763

Doppler satellite/airborne inertial navigation system integration with delayed state Kalman filter 17 p2776 A71-35766

Integrated airborne Omega/inertial navigation systems performance prediction using statistical models for position fix errors 17 p2776 A71-35769

Unified error analysis application to altimeter-aided terrestrial inertial navigation systems [AIAA PAPER 71-901] 19 p3095 A71-37152

Optimal Kalman filter gyro drift rate mathematical models for limiting inertial navigation errors [AIAA PAPER 71-971] 19 p3100 A71-37212

Radio and radar air navigation for civil aviation, discussing Doppler effect, inertia and satellite systems 19 p3100 A71-37344

Concorde aircraft navigation system comprising triple inertial systems, dual VOR/DME, dual ILS and dual ADF [CASI PAPER 72/9] 19 p3100 A71-37599

Motion measurements applications to facility design and inertial navigation hardware performance test problems concerning test platform response to ground motion, forces and disturbances [AIAA PAPER 71-923] 19 p3102 A71-38327

Errors equations for space stable inertial navigation systems, considering rotating platforms and velocity and altitude damping 20 p3261 A71-38854

Commercial ATC, considering VFR, flight control and inertial navigation 22 p3570 A71-42078

Inertial navigation impact on aircraft safety, discussing error sources and midair collision risks 22 p3571 A71-42079

Combined inertial navigation and VOR/DME systems contribution to area navigation accuracy and efficiency 22 p3571 A71-42080

Carrier aircraft inertial navigation system /CAINS/ design, noting thermal modeling, statistically filtered alignment modes and digital data links 22 p3571 A71-42081

INERTIAL PLATFORMS

Inertial navigation system error reduction by gyroplatform rapid rotation 01 p0122 A71-10421

Papers on inertial component testing including equipment, costs, etc [AGARDGRAPH-128] 05 p0749 A71-16301

Test instrumentation for inertial gyros performance evaluation, describing turntables, holding fixtures, electronic equipment, automation, environment simulation, etc [AGARDGRAPH-128] 05 p0750 A71-16305

Inertial gyro testing, measuring coefficients for performance model equation [AGARDGRAPH-128] 05 p0750 A71-16306

Inertial quality accelerometer tests, including mathematical models and error analysis [AGARDGRAPH-128] 05 p0750 A71-16307

Inertial instruments system-level tests under final use environment, discussing cost reduction [AGARDGRAPH-128] 05 p0750 A71-16308

Spring coupled inertially damped instrument servomechanisms design, applying phase margin maximization criterion 11 p1716 A71-26417

Gyro platform orientation control system, using inertial flywheels 13 p2068 A71-28634

French book on optimal inertial navigation and statistical filtering covering Wiener and Kalman filters, gyroscopes, accelerometers, inertial platforms, data processing, computer programming, etc 14 p2271 A71-29940

AN/ASN-86 inertial navigation system consisting of inertial platform, digital computer and control indicator [AHS PREPRINT 533] 14 p2273 A71-31094

Redundant strapdown Inertial Measurement Unit processor recovery requirements, investigating IMU information loss effects during recovery on spacecraft mission 17 p2772 A71-35058

ST-224 redundant inertial measurement system, using conventional gimbaled platforms, each with three skewed single-degree-of-freedom control gyro and one caged gyro 17 p2773 A71-35060

Autonomous location determination for rotating dynamic plant with inertial platform by constructing finite rotation vector 17 p2775 A71-35601

Fluidic inertial platform feasibility model for line of sight guidance of air to surface missile 18 p2945 A71-36483

Pneumatic isolation system for inertial instrument testing, using computer simulation model to evaluate physical parameter variation effect on pad suspension dynamic behavior [AIAA PAPER 71-910] 19 p3040 A71-37161

Inertial devices test pads geokinetic reference systems definition, using astronomical data [AIAA PAPER 71-911] 19 p3046 A71-37162

Motion measurements applications to facility design and inertial navigation hardware performance test problems concerning test platform response to ground motion, forces and disturbances [AIAA PAPER 71-923] 19 p3102 A71-38327

Errors equations for space stable inertial navigation systems, considering rotating platforms and velocity and altitude damping 20 p3261 A71-38854

Time optimal self alignment methods for inertial platforms, using mathematical model based on torque iteration and bang bang misalignment angles control 21 p3413 A71-40544

INERTIAL REFERENCE SYSTEMS

Service life and manufacturing yield of Apollo 25-IRIG /inertial reference integrating gyroscope/ ball bearing 02 p0252 A71-12458

Motion stability of double-gyro inertial frame in Newtonian central force field, applying Liapunov and Chetaev methods 02 p0253 A71-12638

Attitude control of spin stabilized satellite with autonomous maneuverability, discussing correction maneuver method with one quasi-constant inertial reference direction 12 p1971 A71-26985

Inertial-inertial beam stabilization application for image surface mechanical coupling to instrument /photography/ and uncoupled surface /eye/ 14 p2242 A71-30146

Special purpose computer mechanization of inertial attitude reference computation and transformation of body axis information into desired reference frame 14 p2271 A71-30317

Inertial instruments with outputs indicative of time integral and time double integral of vehicle acceleration for velocity and distance determination 14 p2245 A71-30343

Algorithm providing three-gimbaled inertial system all-attitude capability by protecting against gimbal lock 14 p2272 A71-30802

Low-power long-life high-accuracy digital inertial reference assembly, using dual voltage spinmotor operated pulse rebalanced temperature compensated gas bearing gyroscopes 14 p2272 A71-30803

Gravitation theory with universe reference frame concept consistent with general relativity theory based on equivalence principle 14 p2315 A71-30860

Very long baseline interferometry of radio emissions from geostationary satellites, determining orbital elements and inertial position 16 p2544 A71-33845

Electromagnetic wave propagation in uniform simple medium, demonstrating drag effects relative to inertial and accelerated frame 17 p2699 A71-34431

Quaternion representation of successive rotations in space vehicle control, locating final position of coordinate frame with respect to original position 17 p2773 A71-35066

Symphonic telecommunication satellite attitude control system, describing operational principle based on gyroscopic inertial reference and redundant IR sensors 18 p2974 A71-36525

Inertial devices test pads geokinetic reference systems definition, using astronomical data [AIAA PAPER 71-911] 19 p3046 A71-37162

Lightweight precision gimbal design for spaceborne star tracker with arc-second accuracy for stellar updated inertial system independent of spacecraft stabilization [AIAA PAPER 71-963] 19 p3062 A71-37204

Relativistic behavior of uniformly accelerated translational observer motion relative to inertial observer from space-time transformation 21 p3415 A71-40653

Spin stabilized spacecraft inversion by mass translation with momentum vector fixed in inertial space, calculating control mass dynamics 22 p3612 A71-42777

Misalignment estimation software system /MESS/ for in-flight celestial and inertial reference attitude sensor alignment and calibration on OAO [AAS PAPER 71-357] 23 p3648 A71-43027

Optical orientation determination and star pattern recognition for Skylab in solar inertial attitude by digital and hybrid simulations [AAS PAPER 71-397] 23 p3732 A71-43065

INFARCTION

Mortality of myocardial infarction patients on diet low in saturated fats and cholesterol 01 p0015 A71-11299

Complete heart block associated with acute myocardial infarction, discussing high mortality rate and transvenous pacemaker applications 02 p0198 A71-11696

Oxygen inhalation effects on intramyocardial oxygen tension in anesthetized dogs, investigating acute myocardial infarction therapy effectiveness 02 p0202 A71-12917

Clinical and hemodynamic profile of cardiogenic shock after acute myocardial infarction 04 p0541 A71-15914

Autopsies compared to ECG for diagnosis accuracy for acute recurrent myocardial infarction 05 p0711 A71-16951

Myocardial infarction acute stage, noting carbohydrate metabolism disturbances 06 p0849 A71-17291

Myocardial infarction, investigating alpha-dehydroxybutyric acid dehydrogenase enzymatic activity 06 p0849 A71-17292

Myocardial infarction noting serum prealbumins changes 06 p0849 A71-17293

Myocardial oxygen reduction by stimulating carotid sinus nerves and angina pectoris treatment application 11 p1718 A71-25437

Digital computer analysis of orthogonal ECG and VCG from patients with myocardial infarction 12 p1875 A71-27287

Myocardial infarction and coronary heart disease, considering incidence, mortality and preventive measures 13 p2004 A71-27867

Left ventricular posterior wall motion measurements in myocardial infarction, using ultrasonic echogram time-motion data 15 p2365 A71-32536

Atrioventricular and intraventricular conduction disturbances in acute myocardial infarction, discussing heart block 15 p2361 A71-32540

Human ventricular activation correlation with canine model in chronic myocardial infarction 17 p2682 A71-35041

Patients with selective cine coronary arteriography, statistically correlating vectorcardiographic diagnoses of myocardial infarcts with changes in arteries 18 p2854 A71-36139

Antecedent clinical statistics of myocardial infarction and sudden death in actively employed middle aged men, noting cardiac rate, rhythm and conduction abnormalities 22 p3485 A71-41798

INFECTIONS

U INFECTIOUS DISEASES

INFECTIOUS DISEASES

NT AIRBORNE INFECTION

NT TUBERCULOSIS

Hemorrhagic rectocolitis in flying personnel in terms of etiologic, evolutive and therapeutic aspects 01 p0028 A71-11596

Audioimmune stress effects on susceptibility to cytotoxic and oncogenic virus infections and host defense mechanisms 03 p0359 A71-13152

Botanical quarantine studies on Apollo 11 and 12 lunar soil samples effects on terrestrial plants, indicating absence of disease generating agents 04 p0539 A71-15393

Jet aircraft and hygiene, considering communicable diseases spread control measures and sanitation methods by airlines 09 p1400 A71-23071

Hypoxia effects on organism resistance and immunobiological reactivity, noting bacterial and protozoa infections aggravation 13 p2006 A71-28401

Cold environment exposure effect on mouse resistance to infection with Klebsiella pneumoniae 16 p2528 A71-33115

Active biological immunity development in long term space flights, discussing natural and nonspecific resistance to viruses and recurrent infections 21 p3332 A71-40552

Prolonged manned space flight infectious disease hazards, discussing confinement, zero gravity, high oxygen content, personal hygiene, waste disposal and preflight immune status 21 p3333 A71-40561

Microorganisms under closed environmental ecological conditions with reference to astronauts in infectious diseases, discussing bacteria growth in Biosatellite 2 and earth based closed chamber experiments 21 p3343 A71-40562

Peritoneal macrophagocytic ingestive capacity decrease in mice under hypobaric hypoxia, indicating infection susceptibility in altitude environments 22 p3486 A71-41832

INFILTRATION

Porous carbon and graphite substrates chemical vapor deposition carbon infiltration process, discussing isothermal and thermal and pressure gradients techniques 14 p2262 A71-29652

INFINITE SPAN WINGS

Potential flow past cylinder with sources and sinks singularities, deriving formulas for aerodynamic characteristics of infinite span wings with boundary layer control 08 p1227 A71-20777

INFINITY

INFINITY

Stationary Navier-Stokes equations solution vorticity asymptotic behavior in three and two dimensional neighborhoods of infinity 07 p1147 A71-19640

INFLATABLE DEVICES

U INFLATABLE STRUCTURES

INFLATABLE SPACECRAFT

NT BEACON SATELLITES

NT EXPLORER 22 SATELLITE

INFLATABLE STRUCTURES

NT BALLOONS

NT BALLUTES

NT BEACON SATELLITES

NT EXPLORER 22 SATELLITE

NT GAS BAGS

NT HIGH ALTITUDE BALLOONS

NT METEOROLOGICAL BALLOONS

Inflatable restraint collar for large balloons with heavy loads using winch driven cable launching 02 p0188 A71-11821

Multilobed inflated membranes stability under finite deformation, deriving system instability critical conditions 15 p2503 A71-31421

Contact problems of inflated cylindrical membranes with quadrature reduction under normal stress applied to loaded floating and submerged life raft [ASME PAPER 71-APM-11] 16 p2656 A71-33215

Reinforced plastics for aerospace applications, giving special attention to heat shield and inflatable structures materials 19 p3085 A71-38069

Stowable extendible structures for spacecraft and space experiments, discussing inflatable, rigidized cloth and mechanically deployable apparatus 22 p3609 A71-41981

Flexible ram air inflated keel and leading edge parawing design optimization for increased stability and reliability, introducing semirigid member concept [AIAA PAPER 71-986] 24 p3791 A71-44582

INFLATING

Inflation of initially spherical balloon of elastic rubber-like material, discussing tensile instability 11 p1707 A71-25445

Oxygen metabolic rate in isolated canine lungs at various static inflation levels and cyclic ventilation, examining mechanical deformation effects 17 p2683 A71-35145

Finite plane strain inflation of compressible hollow circular cylinder, using perturbation method for non-linear boundary value problem 24 p3884 A71-44955

INFLUENCE COEFFICIENT

NT STRUCTURAL INFLUENCE COEFFICIENTS

Branching model of scientific information propagation and influence networks, exemplifying problem of hypersonic flow around blunted bodies 02 p0335 A71-11854

Dipole antennas mutual influence near conducting intersecting circular cylinders, using geometrical diffraction theory 03 p0384 A71-13395

Influence coefficients for aircraft engine gas/air ducts parameter deviations, using statistical analysis 03 p0472 A71-14257

Influence coefficients closed forms for one and two sheet hyperboloids and ellipsoidal and paraboloidal shells under axisymmetrical edge loads 06 p1002 A71-18413

Forced axisymmetric vibrations of composite cylindrical shell with spherical bottom, obtaining influence coefficients and inhomogeneous boundary conditions 13 p2150 A71-28141

Wake model and computer program to compute geometries, flows and velocity influence coefficients for helicopter blade load calculations [AHS PREPRINT 523] 14 p2172 A71-31089

Influence coefficient matrix method for discretized Poisson equation solution 18 p2905 A71-36306

Externally pressurized thin walled elastic spherical shells influence coefficients singularity 19 p3158 A71-37886

Flexible rotor balancing by exact point speed influence coefficient method [ASME PAPER 71-VIBR-91] 21 p3386 A71-40324

INFORMATION

Irrelevant information with no activity purpose, discussing detrimental effect on human memory 07 p1050 A71-20104

INFORMATION DISSEMINATION

Confidential information management, discussing designer and data system user role as foundation for basic privacy control system 01 p0044 A71-10189

Information feedback distortion and countertraining effects on learning and performance in lever displacement-target test 01 p0026 A71-11415

Branching model of scientific information propagation and influence networks, exemplifying problem of hypersonic flow around blunted bodies 02 p0335 A71-11854

New information prediction in scientific research by data flow analysis 02 p0335 A71-11857

NASA Office of Technology Utilization, examining publications, information sources, data processing and dissemination facilities 04 p0690 A71-14938

Space station information management, examining data processing and distribution to space and ground users 04 p0661 A71-15001

User requirements for Earth Resources Satellite data, considering information dissemination and forest inventory application 07 p1106 A71-18802

International communications law development, discussing capital investment, information dissemination, 1967 space treaty and Intelsat program 18 p2986 A71-36163

Satellite communication role in disseminating information and promoting technology in underdeveloped countries 18 p2987 A71-36168

International satellite broadcasting practices and laws, discussing effect on free information dissemination 18 p2987 A71-36171

Satellite time and frequency dissemination, discussing deficiencies of HF broadcasts for navigation and communication systems 18 p2878 A71-36530

INFORMATION FLOW

Industrial bioscience research laboratory information flow, product ideas, procedural innovations and scientific/technical literature reading 08 p1378 A71-20775

Soviet book on science of science covering information concept, control, organization and economics of scientific labor and advances prognostication 10 p1699 A71-24730

INFORMATION MANAGEMENT

Tracking and data relay satellite system (TDRSS)/impact on spacecraft mission support information management [AIAA PAPER 71-224] 07 p1197 A71-19704

Information management system to schedule, control and status work on Apollo/Saturn Program at Kennedy Space Center [AIAA PAPER 71-239] 07 p1207 A71-19715

NASA 12-man 10-year space station program, discussing design, information management, environmental control and life support system 19 p3153 A71-38147

NASA technology utilization program, discussing technical information, spin-off benefits and various applications 19 p3173 A71-38408

Automated meteorological radar information operation methods for cloud fields, discussing data analysis and processing 19 p3094 A71-38702

Management information techniques, discussing project reports, meetings, decision process, work breakdown, planning schedules and computerization 23 p3785 A71-43457

INFORMATION RETRIEVAL

Computer microfilm data recorder for output speed increase and information retrieval, discussing cost reduction 01 p0048 A71-10219

Centralized inquiry-response systems for information retrieval, analyzing voice-data communications interaction 01 p0048 A71-10220

NASA Space Documentation Service on-line information retrieval system using direct access remote consoles 01 p0183 A71-10397

Information retrieval system at Extra-terrestrial Photographic Information Center (EPIC) for identification of extraterrestrial photographs from satellites and manned space explorations [NSSDC PAPER 69-09] 01 p0184 A71-11425

Communication technology development relation to NASA programs, discussing receivers, microwave tubes, solid state transmitters, lasers, information retrieval and frequency sharing 03 p0388 A71-14412

Data reduction for information retrieval, considering electron beams application for electronic circuit ultra-miniaturization 06 p0871 A71-17525

Complex human memory processes large scale simulation/cybernetic modeling/ based on information handling probability and retrieval 07 p1050 A71-20105

Information search and retrieval by superimposed holograms, describing coding detection and image reconstruction methods 08 p1291 A71-21397

Information specialists performance prediction, discussing multiple discriminate analysis of selected variables 09 p1548 A71-22479

Computerized registry of traumatic injuries IBM 360/44 system for use in mortality, paired probability and accidental risk factor analyses 16 p2535 A71-34444

NASA Scientific and Technical Information System, illustrating advantages of machine retrieval systems for legal profession 18 p2986 A71-36168

Large character set display terminal for public information service system, describing design, construction, components and operating characteristics nonalpha languages 21 p3350 A71-44444

Two dimensional holography application to tolerant high density mass data storage designs digital information retrieval system 22 p3548 A71-44444

INFORMATION SYSTEMS

NT MANAGEMENT INFORMATION SYSTEMS Information processing - Conference, Las Vegas, November 1969 01 p0041 A71-14444

NASA Space Documentation Service on-line information retrieval system using direct access remote consoles 01 p0183 A71-10397

Automatic control and information systems especially, generalizing Kotelnikov theorem on continuous signals reduction 01 p0060 A71-10444

Information retrieval system at Extra-terrestrial Photographic Information Center (EPIC) for identification of extraterrestrial photographs from satellites and manned space explorations [NSSDC PAPER 69-09] 01 p0184 A71-11425

Real time large scale display system with information image projection on reversible photochromic emulsion via IR laser 02 p0249 A71-12344

Holographic display applications in portraiture, storage and retrieval, motion pictures, TV, etc 02 p0253 A71-12344

Visual information industrial processing rates, correction tables with digits, letters, Landolt rings and geometrical figures 03 p0364 A71-13395

Data system environment simulator (DASYS), real time test bed capability for software development and testing 04 p0556 A71-18413

Nimbus 4 satellite telemetry information processing with data sampling and formatting flexibility 05 p0726 A71-15444

General information system model, producing human performance simulator for various equipment personnel and procedure mixes 07 p1046 A71-15444

Space shuttle integrated information management system, emphasizing software element requirements and data processor hardware 07 p1155 A71-19704

Extendable Computer System Simulator, discussing simulators as tools for integrated information system design [AIAA PAPER 71-228] 07 p1068 A71-19704

General purpose software inventory under simulated executive for application oriented information systems [AIAA PAPER 71-236] 07 p1225 A71-19704

Integrated project information and simulation system for management of aerospace vehicle development, discussing simulation models application [AIAA PAPER 71-238] 07 p1225 A71-19704

Information management system to schedule, control and status work on Apollo/Saturn Program at Kennedy Space Center [AIAA PAPER 71-239] 07 p1207 A71-19715

Three-phase time-ordered functional organization for ground based collision avoidance, discussing information flow, display capability and dynamic simulation model [AIAA PAPER 71-240] 07 p1155 A71-19704

Development program for multiple access real time tactical information distribution system, designing a constructing tactical air control system test facility [AIAA PAPER 71-243] 07 p1156 A71-19704

ESRO/ELDO space documentation service involving NASA file remote processing and data bank space component selection 07 p1225 A71-20044

Human eye optimum information reception assessment by Weber-Fechner law, threshold amount constancy and minimum continuous signal energy 07 p1043 A71-20105

Manned aircraft crew long range navigation/ discussing sensor, information processing and display systems for future commercial and military missions 07 p1157 A71-20105

Detectable information rate changes of photometer with finite observation time and background noise 08 p1289 A71-21397

Global meteorological systems, discussing variability information content, measurements frequency and 09 p1548 A71-22479

curacy, horizontal/vertical resolution, sensor bearing platform and cost

08 p1327 A71-21715

Observational data characteristics analysis as contributor to knowledge and utilization of all atmospheric physical occurrences

08 p1328 A71-21722

Crew performance as information input factor based on USAF two man space cabin research

09 p1400 A71-23245

Information support system for physiological studies of human performance, including indexing approach for references categorization, microfiche file and data bank

11 p1860 A71-25253

Computerized system evaluation and feedback data for assurance at hardware level, including reject and failure report documentation

12 p1890 A71-26673

Dynamic data processing systems with feedback and internal noise, evaluating carrying capacities, limiting parameters and optimal transfer function

12 p1893 A71-27455

ATC data automation, discussing flight plant processing system /FPPS/, radar data processing system /RDPS/ and signal automatic control system /SATCO/

15 p2446 A71-32523

Information model for simulating systems reliability estimates uncertainty, noting state transition matrix, methodology and sensitivity analysis of effectiveness

16 p2583 A71-33304

Optoelectronic elements for information system applications, discussing photomultipliers, photodiodes, photoresistors, avalanche and photoparametric diodes response and bandwidth characteristics

17 p2752 A71-34391

Soviet papers on information systems redundancy using redundant algorithms and structures and redundant coding theory

17 p2720 A71-34951

Redundancy approach to information systems synthesis

17 p2720 A71-34952

Statistical limits on reliability, informativeness, controllability and self organization of complex systems, determining minimum redundancy requirements for suppressing interfering factors

17 p2720 A71-34953

Redundancy method for correct performance of flexible structure with faulty elements prepared from microelectronic information media

17 p2720 A71-34955

Redundant information optimizer design, using nonlinear elements

17 p2720 A71-34957

Reliability analysis of redundant information systems, deriving formulas for risk of failure and faultless operation probability

17 p2721 A71-34966

Information effectiveness of redundant error detecting coding systems

17 p2702 A71-34968

Redundancy encoding with error correcting codes for controlling results of rational operations series in residual classes system

17 p2710 A71-34976

Information display device with electro-optical system for discrete deviation of monochromatic linearly polarized light beam, analyzing electronic control circuits energy characteristics

18 p2884 A71-35880

Automated information systems for electromagnetic compatibility analysis using computer

19 p3030 A71-38438

Computer automated systems development for electromagnetic compatibility analysis, noting interactive processing in near real time mode

19 p3030 A71-38439

French monograph on medium term planning process for large basic research laboratory based on information system of functional activities presentations

19 p3174 A71-38548

Information producing capabilities of various combinations of SNR, bandwidth and contrast in simulated digital encoding TV systems

21 p3347 A71-40130

Bioholographic animal information processing model, considering nervous system as diffractive medium and neural network as Fourier analyzer

21 p3380 A71-40923

Information organizer system of symbolic manipulation on model data structures, providing row and column creation, sorting and indexing

22 p3516 A71-41865

Planning organization for global remote sensing information system operated and financed through international cooperation

22 p3623 A71-41987

Computerized bacterial identification system to process Apollo spacecraft sample laboratory test results in NASA Planetary Quarantine Lunar Information System

22 p3504 A71-42233

Observer psychological response to air defense oriented visual information displays

23 p3640 A71-43904

INFORMATION THEORY

Cryptographic techniques applications to data processing systems, considering digital substitution and digital route transposition matrix

01 p0044 A71-10187

Information content and digital storage of aerial photography using assessing entropy of written English text

02 p0248 A71-11953

Muscle simulation by information theory for statistical analysis of behavior based on gas thermodynamics methods, showing stress relation to motor units excitation

03 p0366 A71-12979

Mutual information between radiance of incoherently radiating object plane and field of observing system aperture, obtaining Shannon type formula

04 p0627 A71-15684

Structural information propagation in optical wave fields arising in diffraction and scattering of quasinonchromatic light by fixed objects

05 p0753 A71-16903

Mathematical statistics methods application to incorrect problems in mathematical physics, using information theory

07 p1158 A71-19171

Mathematical simulation of human recognition by black box approach as information conversion process

07 p1050 A71-20109

Information-theoretical approach to lasers theory, avoiding Fokker-Planck equation method

10 p1619 A71-23919

Correlation estimates and optimal detector for incomplete a priori information signal reception on random and white noise background

10 p1579 A71-24878

Scalar Gaussian channel information optimal input capacity as function of random variable, assuming finite number of values for amplitude and variance constraints

11 p1730 A71-25374

Hybrid decoding technique for symmetrical binary input channels, using bootstrap algorithm across convolutionally encoded information streams

11 p1730 A71-25375

Multiplexer concentrators for data telecommunication systems with erratic information flow, concerning statistical assumptions, transient response, queueing tails and message clustering

12 p1880 A71-27072

Verification, control and forecasting information characteristics for random process mixed with additive noise

13 p2041 A71-27942

Signals detection of known form and unknown energy in Gaussian noise of unknown level, applying concept of invariance in hypothesis testing

16 p2541 A71-32820

Maximum likelihood estimates potential accuracy in presence of interfering parameters, presenting analysis method based on Fisher information matrix

16 p2542 A71-33489

Successive block decoding procedure for reduction of operations required for single information symbol decoding, noting substantial gains at equal error probabilities

17 p2702 A71-34970

Telecommunication developments covering coaxial cables, waveguides, error elimination, information theory, sound transmission and radars

19 p3016 A71-37340

Ear inherent channel capacity estimation by applying Shannon equations for binary signal transmission

20 p3191 A71-39769

Experimental analysis of information content of aural electric field of human body, considering electrotonic and triboelectric components

21 p3338 A71-41066

Data transmitting and receiving instruments and systems development problems covering signal shaping and converters and information channel and data reception theories

24 p3806 A71-44375

Accuracy analysis of statistically optimal dynamic system with modulus bounded control for discrete and continuous information input, using Fokker-Planck-Kolmogoroff equation

24 p3814 A71-44689

INFORMATION TRANSFER

U COMMUNICATING

INFORMATION TRANSMISSION

U DATA TRANSMISSION

INFRARED ASTRONOMY

IR astronomical telescope using six independent optical systems with path and phase controls for aperture synthesis

01 p0081 A71-10829

Galactic and extragalactic sources of far IR radiation, discussing spectral distribution and luminosities

02 p0315 A71-12656

Celestial sources far IR radiation detection using balloon-borne telescope

02 p0315 A71-12657

Mercury microwave and IR observations interpreted for thermophysical models for planetary subsurface, discussing rotation and heating

03 p0492 A71-14069

IR stars, discussing very young stars, circumstellar clouds and IR excesses

04 p0648 A71-15251

IR astronomy, considering basic principles, instrumentation energy production and radiation, spectroscopy, detectors and atmospheric absorption and emission

04 p0649 A71-15254

IR object Maffei 1 observational data indicating highly reddened giant elliptical galaxy of Local Group

05 p0807 A71-16211

IR object IRC plus 10216 carbon monoxide emission at 2.6 mm, noting spectral line width, thermal emission and mass

05 p0812 A71-16695

Compact nebulae IC 4997, VV 8 and FG Sge observed at 3.5 and 11.0 microns, noting IR wavelength energy

05 p0812 A71-16696

Dust history and physical environment near hot stars associated with nebulosity, discussing optical depths and IR energy

07 p1198 A71-19819

Four-color IR photometry of cool carbon, S and M stars

07 p1187 A71-19820

Galactic center region far IR map in 75-125 microns spectral interval with 6 minute resolution

07 p1199 A71-19835

Astronomical IR telescopes image quality and observing efficiency gain

08 p1290 A71-21394

Unlit lunar limb observations at IR wavelengths, presenting temperature charts and thermal abnormalities

09 p1530 A71-23716

Astronomy contributions to cosmology, considering universe nature, origin and evolution

10 p1668 A71-24004

IR astronomical background radiation measurements at very near IR and longer wavelengths for interplanetary, galactic and intergalactic sources

10 p1677 A71-24582

M stars mass loss, determining dust shells radii and densities with IR observations of circumstellar emission

11 p1818 A71-25204

IR astronomy high altitude sites, discussing optimal geographic locations, observation conditions criteria, transportation and survival measures

11 p1743 A71-25242

Daytime atmospheric water vapor measurements at IR astronomy mountain sites in southwestern U.S.

11 p1793 A71-25243

Martian surface pressure from 1967-1969 apparition observations, discussing micron bands carbon dioxide abundances

11 p1825 A71-25711

Ground based and airborne IR observation of comets over various wavelengths, determining flux distribution, luminous outbursts and color temperature

12 p1956 A71-26621

Saturn, Titan and ring IR photometric observations, examining brightness temperature albedos, optical thickness and individual particles

13 p2134 A71-28283

Photometric IR observations of Nova Serpentis 1970, showing visual flux decrease

14 p2303 A71-29576

Seyfert galaxy NGC 1068 IR observations, noting angular extent and size

14 p2303 A71-29585

H85 alpha recombination line in planetary nebula NGC 7027, considering IR physical parameters consistent with radio observations

14 p2313 A71-30432

IR study of thermal anomalies during lunar night, discussing ages and distribution on terrain

17 p2797 A71-34184

Star formation at interstellar gas cloud stage, discussing gravitational collapse, Bok dust globules, spectroscopic and IR peculiarities and models

17 p2801 A71-34696

Electronic circuit system for IR astronomy, describing noise figure, linearity and frequency response

17 p2744 A71-35229

Ganymede thermal inertia data from simultaneous visual photometry and IR radiometry observations during 17 March 1971 eclipse

17 p2807 A71-35418

IR astronomy review covering semiconductor detectors and astronomical radiation sources including thermal and nonthermal sources

18 p2959 A71-35909

IR radiation sources, discussing intermediate and early stars, galactic nucleus and extragalactic sources

18 p2958 A71-37029

Interstellar molecular hydrogen gas near IR emission detection in dark clouds

18 p2969 A71-37042

INFRARED DETECTORS

- N stars Y CVn, RY Dra and Psc IR synthetic cyanide radical spectrum analysis, determining C 12/C 13 ratio 18 p2969 A71-37044
- IR experiments planning for Outer Planets Grand Tour including investigations of planetary radiation balance and atmospheric composition and satellites composition and physical properties [AAS PAPER 71-131] 19 p3011 A71-37920
- StarLifter borne large aperture astronomical telescope for IR and submillimeter observations, discussing design and operation 20 p3234 A71-39173
- Photoelectric telescope observations of red stars in Cygnus at IR wavelength with threshold brightness detection 20 p3293 A71-39537
- Microwave molecular lines of CO, CN and CS emission from infrared object IRC plus 10216 22 p3599 A71-41929
- Fourier transform spectrometers in IR astronomy, including rapid scan interferometer 22 p3545 A71-42146
- Astronomical polarimetry at 5 and 10 microns for intensity measurements of IR sources 22 p3545 A71-42147
- Variations in 10 micron flux from NGC 1068, noting strong nucleus emission modulation 22 p3605 A71-42397
- Balloon-borne far IR survey of sky portions in Galactic plane 23 p3736 A71-43539

INFRARED DETECTORS

- Silicon avalanche photodiode detectors for near IR laser pulse receivers, discussing quantum efficiencies, internal gains and room temperature responsivities 01 p0092 A71-10011
- Solid state receiver for IR, using microwave biased Ge photoconductor 02 p0231 A71-12027
- IR photodiode heterodyne detection, deriving noise equivalent power, conversion gain, frequency response, local oscillator power and IF amplifier noise factor 02 p0249 A71-12035
- IR radiation measuring circuit with pneumatic detector usable on rockets and satellites [ONERA-TP-874] 06 p0900 A71-18023
- IR system with moving space filter, calculating detector output and noise due to background radiation 07 p1058 A71-18828
- Light transmitting vacuum deposited NaF polycrystal for IR measurements 08 p1343 A71-21288
- Miniature cryogenic systems for cooling IR detectors in upper atmosphere involving earth surface, air-glow and OH emission measurements 09 p1545 A71-23004
- Superfluid-helium-cooled rocket-borne far-IR radiometer for night sky radiation measurement, discussing cryogenic, optical detection and electronic systems design features and performance 12 p1903 A71-26791
- Airborne equipment for CAT detection ahead of aircraft, considering pulsed Doppler laser and IR detectors 14 p2268 A71-29765
- Snake IR receptor sense organs tested by IR stimulus from carbon dioxide laser, suggesting receptor operation on thermal principle 15 p2360 A71-32296
- IR transducer with detector for space applications, measuring capacitance on electronic bridge circuit based on temperature and pressure effects [ONERA-TP-963] 16 p2576 A71-32845
- Symphonic telecommunication satellite attitude control system, describing operational principle based on gyroscopic inertial reference and redundant IR sensors 18 p2974 A71-36525
- IR CdTe-HgTe detectors for laser space communications at 10.6 microns, using directivity of light waves in vacuo for wideband transmission 18 p2892 A71-36566
- Adsorption cryopumped He 3 cooled IR detector without encumbrance of external diffusion or mechanical pump 18 p2922 A71-36588
- Multielement IR photoconductive detector arrays of InSb and mercury cadmium telluride operating at cryogenic temperatures 18 p2923 A71-36606
- Thermal, pyroelectric and photoelectric detectors for middle IR wavelength range 19 p3064 A71-38064
- Simulator for operating decision rules for control of airborne IR forest fire detection system 19 p3066 A71-38409
- Low voltage IR image converter display system using scanned line array of GaAsP light-emitting junction diodes 21 p3352 A71-40117

- Remote sensing of chlorophyll and temperature in marine and fresh waters by spectroradiometer and differential and IR filter radiometers onboard airplane 22 p3534 A71-41986
- Pyroelectric IR detectors performance, investigating strontium barium nitrate, lithium sulphate and triglycine sulfate materials effects on frequency range and sensitivity 22 p3542 A71-42122
- Microwave biased germanium IR photoconductive detector for optical communication systems, describing operation principles, signal demodulation and performance 22 p3543 A71-42123
- Spherical avalanche diodes in silicon and silicon-germanium mixed crystals, describing IR detection properties 22 p3543 A71-42125
- Barium strontium lanthanum titanate thermistor bolometer for IR thermal detector, using positive temperature coefficient of resistance 22 p3543 A71-42126
- Li-drifted Ge p-n diode for low noise IR detectors, describing spectral sensitivity and NEP value 22 p3543 A71-42127
- Josephson junctions for far IR radiation detection, mixing and frequency measurement 22 p3543 A71-42128
- Pyroelectric detector linear arrays for IR thermal imaging at room temperature 22 p3543 A71-42131
- Cryogenic temperature cooling systems for IR detectors, describing Joule-Thomson liquefier and liquid transfer devices 22 p3544 A71-42139
- Pyroelectric, pneumatic and thermocouple detectors comparison, discussing IR detectors availability for use in spectrophotometers in 2-20 micron region 22 p3544 A71-42142
- IR radiation sensors application to fire protection and rescue operations 22 p3545 A71-42157
- Semiconductor package designs for high performance miniature IR sensors, including flat packs, TO, custom metal and glass dewar configurations 23 p3676 A71-43509
- IR radiometer experiment for Mariner 1971 Mars orbiter mission, describing objectives and instrumentation 23 p3676 A71-43510
- Precision calibration system with adjustable temperature extended radiance source for long wavelength IR radiometer, discussing performance tests 23 p3676 A71-43512
- Low noise IR range radiometer, including impedance matching and narrow band filtering 23 p3678 A71-43534
- Germanium extrinsic photoconductive IR detectors with Au, Hg and Cd doping, discussing preparation and electrical and optical characteristics 24 p3860 A71-45070
- INFRARED FILTERS**
- Commercially produced metallic wire gratings reflection spectra measurement, determining use as high performance filters and light polarizers in far IR region 03 p0457 A71-13507
- Solar IR spectra referencing procedure based on filter reference radiometer, discussing technique theoretical foundation 20 p3237 A71-39327
- IR filters and coatings, describing vacuum deposited layer properties of II/VI, heavy halide and V/VI glass compounds 22 p3544 A71-42135
- High performance bandpass and low pass interference filter for IR region above 40 microns, discussing metallic mesh and reflecting element properties 22 p3544 A71-42136
- Spacecraft-borne IR sequential filter radiometer design and performance for real time meteorological forecasting and atmospheric temperature measurements 22 p3544 A71-42143
- INFRARED HORIZON SCANNERS**
- U HORIZON SCANNERS**
- INFRARED SCANNERS**
- Thermal pattern visualizing and interpretation by imaging in far IR, noting equipment and uses of thermography in medicine, science and technology 01 p0078 A71-10135
- Real time large scale display system with information image projection on reversible photochromic emulsion via IR laser 02 p0249 A71-12072
- IR zoom lens design, discussing limitation of number of elements due to high scatter, absorption and surface reflection losses 07 p1109 A71-19451

- Ecological interpretation of daytime data from Nimbus 3 high resolution IR radiometer for hydrologic and plant distribution mapping 08 p1277 A71-20884
- Remote sensing for geologic problems, using side looking radar for fracture and fault detection and IR images for limestone, dolomite and granite discrimination 18 p2911 A71-35890
- Incoherent radiation distribution analysis by image multiplex coding with SNR gain applied to IR region [ONERA-TP-972] 18 p2916 A71-36031
- Latent forest fire detection, describing airborne IR surveillance system 19 p3066 A71-38410
- Optical characteristics of thermal IR scanners, using mirrors and prisms in parallel or converging ray pencils and rotating wedges 19 p3068 A71-38709
- Global, regional and local earth IR imagery for earth sciences from space TV, photography and spectrophotometry 20 p3220 A71-39665
- Earth surface effective temperature map from meteorological satellites IR imagery interpretation 20 p3260 A71-39866
- Meteorological satellite IR imagery for calculating spectral values of cloudiness radiation contrasts against underlying surface background 20 p3261 A71-39869
- Infrared techniques - Conference, University of Reading, Reading, Berkshire, England, September 1971 22 p3542 A71-42121
- Diffused slice Pb-Sn-Te photodiode arrays for IR detection and thermal imaging, evaporating Pb-Sn contacts onto n and p type surfaces 22 p3543 A71-42130
- Pyroelectric detector linear arrays for IR thermal imaging at room temperature 22 p3543 A71-42131
- Calibrated IR thermographic camera development and applications in medicine, X ray beam energy and reactor cooling rod measurements 22 p3545 A71-42148
- Gulf Stream and Middle Atlantic Bight complex synoptic sea surface temperature distribution from ITOS 1 satellite high resolution IR imagery 22 p3536 A71-42885
- INFRARED INSPECTION**
- Interference patterns obtained in transmitted light, determining surface parallelism of thin plates transparent in IR region using carbon dioxide laser 02 p0259 A71-11936
- Traversing Infrared Inspection System for C-5 aircraft fail-safe strap panels of bonded Ti-Al laminates, discussing design and application [ASME PAPER 71-DE-37] 12 p1911 A71-27327
- Infrared and thermal evaluation of tactical aircraft phased array radar antenna design with cooling air distribution for steady state operating temperature maintenance 21 p3352 A71-40434
- INFRARED INSTRUMENTS**
- IR flying spot telescope with CW laser beam scanning and target motion sensing capabilities 01 p0081 A71-10830
- Automatic testing of electro-optical systems including TV, IR and laser applications 03 p0395 A71-13082
- Nonlinear materials and optics, second harmonic generation, optical parametric oscillators and IR converters 04 p0635 A71-14721
- NASA satellites meteorological IR instruments, considering purpose, design, operation and performance 04 p0598 A71-15365
- Carbon dioxide lasers IR variable double prism attenuator with gap spacing determination by capacitance measurements 05 p0760 A71-16257
- Errors from multiple reflections between target environment viewed by IR thermometer or radiometer and background environment 05 p0752 A71-16672
- Infrared radiometer sea surface temperature measurements during oceanographic survey, examining inclination angle effect 09 p1440 A71-23590
- Temperature measurement techniques annual progress survey including contact and radiation thermometers, IR thermography, microwave radiometry, fluidic sensors, and liquid crystals 10 p1612 A71-24685
- Meteorological IR radiometer with thermosensitive element, chopper circuit and AC microvoltmeter, outlining calibration procedure 11 p1763 A71-26174
- High resolution far IR interferometer in Michelson configuration for measuring gas optical properties in symmetric or asymmetric operation mode, testing performance 12 p1904 A71-26799

Total emittance measurements by portable IR reflectometer, tabulating nongray error effects
13 p2159 A71-27979

Earth surface temperature measurement by airborne IR radiometers, discussing accuracy provided by narrow and wideband filters
14 p2240 A71-30126

Diffraction limited achromatic doublet lenses for IR instruments, discussing applications to compact optical systems
14 p2242 A71-30148

Optical, mechanical, thermal and electrical properties of IR sensor materials at low operating temperatures
14 p2284 A71-30545

Infrared Michelson interferometer system digital data processing by computer, developing spectral density plots
18 p2920 A71-36092

Infrared techniques - Conference, University of Reading, Reading, Berkshire, England, September 1971
22 p3542 A71-42121

Refractive imaging and scanning methods for thermal imaging systems, considering high performance IR lenses
22 p3544 A71-42137

IR modulator in space equipment, considering Fabry-Perot cavity with variable plate separation
22 p3544 A71-42138

Spacecraft-borne IR sequential filter radiometer design and performance for real time meteorological forecasting and atmospheric temperature measurements
22 p3544 A71-42143

Sequential dual wavelength IR gas analyzers for anesthetics research and chemical plant process streams analysis
22 p3545 A71-42156

Contactless determination of low temperatures by IR radiation thermometers, applying to measurement on transparent materials
22 p3546 A71-42158

INFRARED LASERS

Silicon avalanche photodiode detectors for near IR laser pulse receivers, discussing quantum efficiencies, internal gains and room temperature responsivities
01 p0092 A71-10011

Real time large scale display system with information image projection on reversible photochromic emulsion via IR laser
02 p0249 A71-12072

High rate electro-optical modulator for 10.6 micron IR laser beam consisting of GaAs crystal multitraversed by beam
02 p0262 A71-12923

IR gas pulsed lasers continuous self mode locking, observing optical spectra with scanning Fabry-Perot interferometer
03 p0438 A71-13889

IR Q switched gas laser with Michelson interferometer for plasma diagnostics, describing equipment operation
03 p0439 A71-14056

Gas laser technology developments, discussing UV CW noble gas ion lasers, high output IR carbon dioxide lasers, metal vapor and pure helium lasers
04 p0605 A71-14711

IR lasers, discussing carbon dioxide CW and Q-switched operation and semiconductor lasers
04 p0606 A71-14712

Arsenic doped Si single crystal impurity segregation striae and central faceted area observations by scanned laser IR microscope
04 p0608 A71-15039

Laser action in visible and near IR on atomic fluorine transitions based on collisional dissociation of hydrogen fluoride
04 p0608 A71-15040

IR laser beam atmospheric absorption, considering heating and cooling effects due to vibrational relaxation
04 p0609 A71-15681

Carbon dioxide lasers signature, considering 10.4 micron band P/20/ and P/16/ lines dominant modes for wide gain curve and operating conditions
05 p0760 A71-16255

Fusion reactor plasma feedback stabilization by nonlinear interaction of two carbon dioxide IR laser beams to produce difference frequency near hybrid resonance
06 p0931 A71-17457

Daytime pulsed optical communication within line-of-sight using GaAs IR laser
06 p0907 A71-17570

CW chemical operation in IR for hydrogen fluoride, deuterium fluoride, hydrogen fluoride-carbon dioxide and deuterium fluoride-carbon dioxide systems [AIAA PAPER 71-27]
06 p0909 A71-18493

IR laser action at 2-3 microns by low pressure discharge and gas mixtures containing molecular oxygen and sulfur dioxide
08 p1301 A71-21190

IR laser propagation through fog with droplet vaporization, assuming incident electromagnetic radiation as plane harmonic wave
08 p1302 A71-21392

Nonlinear effects of IR beam passage from continuous neodymium-yttrium garnet laser through defocusing media
09 p1460 A71-22231

Infrared laser output from giant pulse laser beam photoexcited alkali metal vapors, assuming buffer gas collisional mechanism
09 p1464 A71-23380

Strongly coherent Nd doped glass laser development by decreasing cavity Fresnel number, discussing maximized radiance and infrared output
09 p1465 A71-23564

Interstellar communication via IR laser beam, considering resolution and signal detection capabilities, reflectors structural size and accuracy, power requirements and cost
11 p1822 A71-25636

Variable output coupling far IR gas lasers, using Michelson interferometer with polyethylene or polypropylene beam splitter
11 p1773 A71-25805

Semiconductor wafers examination with He-Ne IR laser scan microscope, producing oscilloscope shadowgraph displays of IR transmission variations in wafers
11 p1763 A71-26186

Capacitor discharge excited atmospheric pressure carbon dioxide-nitrogen-helium pulsed IR laser, investigating laser output dependence on gas flow and electrical parameters
12 p1913 A71-26976

Absolute measurement of laser frequencies in IR range, using extended harmonic heterodyne technique
14 p2255 A71-30979

CH free radicals detection in oxyacetylene flame magnetic resonance absorption spectrum by IR water vapor laser
15 p2420 A71-32380

Frequency doubling of 2.06 micron holmium doped oxyapatite laser output by proustite single crystal
15 p2423 A71-32610

Electron density gradient and radial compression waves in pulsed IR laser gas discharge tube
16 p2585 A71-32795

Molecular spectral coincidences of carbon monoxide and carbon dioxide IR lasers for atmospheric pollutant detection by sensing of resonant absorption, thermal emission or fluorescence
16 p2585 A71-33129

IR carbon dioxide laser amplifier with fundamental mode output power in excess of 500 W, describing multistage mirror section design and test results
16 p2587 A71-33491

Nonlinear optics of combination scattering of IR laser radiation in crystals and statistical frequency mixing-multiplication of polarons and longitudinal phonons
16 p2588 A71-33997

HCN laser amplifier gain measurement at IR wavelengths in gas mixtures by recording with pyroelectric receiver
17 p2750 A71-34290

Optical radar aircraft tracking and position system, using IR Q switched flash pumped Nd-YAG laser transmitter and pulse receiver with magnetic tape recorder and real time computer
18 p2900 A71-36905

Carbon dioxide-helium mixture IR laser action and power gain increase by nitrogen addition
18 p2932 A71-37006

Polarization flip with hysteresis effect at zero magnetic field in CW far IR HCN laser
20 p3244 A71-39098

Nonlinear effects in high power Nd-YAG CW IR laser beam transmission through defocusing media
21 p3394 A71-41110

Millimeter wave klystrons phase locking to HCN far IR laser line via harmonic mixing in Si and metal-oxide-metal Josephson point contacts
22 p3555 A71-41599

Tunable spin-flip magneto-Raman IR laser, describing indium antimonide scattering, tuning range and applications
22 p3557 A71-42133

IR ring laser rotation sensor, describing design principles for alignment and eliminating locking phenomenon
22 p3557 A71-42153

Ni-Fe film exposure to continuous IR laser light for laser radiation structure
23 p3686 A71-44056

Quantum phase fluctuations in IR gas lasers, noting nearly Lorentzian power spectrum with bandwidth inversely proportional to output power
23 p3688 A71-44269

**INFRARED MASERS
U INFRARED LASERS**

INFRARED PHOTOGRAPHY

Environmental satellite data on-line processing and extraction procedures, including visible and IR imagery mapping and cloud pictures analysis
07 p1067 A71-18806

Coronal and prominence IR photography during 7 March 1970 solar eclipse
09 p1442 A71-22066

Ground water flow into Lehigh River, Pennsylvania identification by thermal IR imagery
09 p1439 A71-23217

Ultrarapid holographic recording in IR light at 1.06 micron
10 p1608 A71-23838

Photography date effects on intensive study sites airphoto interpretations, using color and color-IR films
12 p1907 A71-27258

Color and color IR films for soil identification, performing optical density measurements on film transparencies with densitometer
13 p2071 A71-29394

Dwelling unit estimation with color IR photos, applying aerial photointerpretation to urban analysis
13 p2064 A71-29396

Space photos for land use and forestry, considering IR color photographs from Apollo 9 flight
13 p2064 A71-29398

Diseased plants and crop loss per field from aerial IR-color photography
14 p2236 A71-30576

Satellite IR photography, discussing camera systems, photointerpretation, applications in glaciology, hydrology, oceanography, geology, volcanology and environmental protection
15 p2408 A71-31835

Urban environmental quality analysis using color IR aerial photography, considering film sensitivity and haze penetration
18 p2911 A71-36062

Cloud cover areal distribution estimation model using multichannel IR radiometer data from Nimbus 2 satellite
19 p3056 A71-38267

IR holography with cholesteric liquid crystals as recording medium and carbon dioxide laser as light source, discussing demagnification and image reconstruction
21 p3379 A71-40703

Geothermic processes determination and registration in volcanic activity range by satellite IR measurements
22 p3534 A71-42004

INFRARED RADIATION

NT FAR INFRARED RADIATION

NT NEAR INFRARED RADIATION

Pulsar distances tabulation, discussing possible IR emission
01 p0153 A71-10365

IR absorption edge measurement in cadmium antimonide crystals grown with various perfection degrees, considering forbidden band and phonon spectrum anisotropy
01 p0138 A71-10432

IR radiation effect on gas molecular dissociation, showing dissociation temperature decrease due to IR photon absorption
02 p0288 A71-12850

Be stars IR emission, noting thermal free-free radiation superposed upon stellar continuum
03 p0483 A71-13185

CW carbon dioxide laser beam IR absorption by sulfur hexafluoride, investigating saturation parameter relationship to pressure, temperature and relaxation time
03 p0437 A71-13879

Thermal emission from IR star shells calculated from circumstellar graphite dust model
03 p0495 A71-14267

IR radiation measurement of chain branching rates in hydrogen-oxygen mixtures ignited by reflected shock waves
04 p0548 A71-14695

Soviet monograph on visible and IR waves atmospheric propagation covering monochromatic radiation absorption and scattering, laser light beams under turbulence, etc
04 p0551 A71-14800

Visible and IR radiation attenuation in rain and snow, comparing calculation based on Mie diffraction formulas with measurement
05 p0718 A71-15992

Geography of upper atmospheric IR emission layers from Cosmos 65 observation
05 p0738 A71-16045

Simultaneous meteorological satellite IR radiation measurements and cloud photographs for superposition and mutual interpretation
05 p0752 A71-16676

IR radiation absorption by water vapor in atmospheric transmittance windows, discussing fine structure of absorption spectrum
05 p0778 A71-16841

INFRARED RADIATION

Optical properties of corundum for single and multiple layer antireflection achromatic coatings for IR below 5y6 microns

06 p0898 A71-17537

Ferrimagnetic vanadate garnet IR Faraday rotation as function of wavelengths and temperature, considering ions multivalence and multilattice site modifications

06 p0941 A71-18040

IR difference frequency generation using tunable dye laser

06 p0910 A71-18663

Calculation methods accuracy for spectral absorption of IR radiation by atmospheric gases, analyzing empirical, numerical integration and spectrum model methods

07 p1151 A71-19148

Microwave frequency measuring techniques extension into IR, developing Si point contact diode with nonlinear I-V characteristics

07 p1125 A71-19797

Carbon dioxide laser IR pulse transmission under moderate pressure conditions using four state model of molecular laser passive Q switching and double resonance

07 p1128 A71-20391

Carbon dioxide laser IR pulses self focusing in liquid carbon disulfide, calculating nonlinear refractive index

07 p1128 A71-20396

Cuprous halides nonlinear properties in near and medium IR regions

08 p1302 A71-21435

Fredholm integral equation stabilization methods for atmospheric IR transfer in vertical temperature profile determination

08 p1286 A71-21877

Upper atmosphere IR emission model with reference to thermal excitation, chemical reactions and electron excitation

09 p1437 A71-22670

Spectral distributions of absorption cross sections of IR radiation by quasi-local oscillations

09 p1494 A71-22885

Algol secondary component gravity darkening observations, examining IR light curve

09 p1527 A71-23530

Lunar equatorial region IR emission directional characteristics from brightness temperature measurements, developing cratered soil thermal model for negative surface relief studies

09 p1530 A71-23713

Nimbus 4 satellite selective chopper radiometer data on IR radiation emitted by carbon dioxide, considering stratospheric warming

10 p1598 A71-23743

Spectral transmittance of pressure induced and intrinsic absorption of IR energy by carbon dioxide and water due to Fermi bands and asymmetric molecules

10 p1644 A71-23950

IR polarization of Venus, providing Venus atmosphere effective particle size estimate

10 p1675 A71-24489

Carbon dioxide laser coherent radiation in IR region from Young double slit interference experiments, noting emergent beam spatial phase shift

10 p1622 A71-24959

Vibrational nonequilibrium influence on IR radiative energy transfer in nongray nonisothermal gases

10 p1643 A71-24967

Granular features of solar surface, describing television equipment used aboard balloon for image in 1.2-2 microns region

10 p1680 A71-25004

IR radiative heat transfer in nongray nonisothermal gases, giving solutions for radiative equilibrium and combined conduction and radiation

10 p1698 A71-25094

Model for relativistic electrons diffusion from IR sources, determining injected electron spectrum distortion due to inverse Compton losses and X ray spectrum

11 p1814 A71-25294

Interstellar communication via IR laser beam, considering resolution and signal detection capabilities, reflectors structural size and accuracy, power requirements and cost

11 p1822 A71-25636

Jupiter cloud structure observations near 8.5 microns from thermal flux measurement along polar and equatorial scans

11 p1827 A71-25727

Visible and IR radiative transfer in water and ice clouds, calculating radiance and polarization from Mie theory

11 p1800 A71-26299

Time dependent variation of IR polarization of eta Carinae and VY Canis Majoris with separation of interstellar scattering by associated nebula

12 p1956 A71-26611

Cosmic IR sources model based on assumption of cosmic ray particles emitting galactic sources surrounded by dust shells absorbing and reemitting energy

12 p1947 A71-26933

Water vapor dimer effects on atmospheric brightness temperature in cm and mm radiometric investigations from satellites above ocean areas

12 p1901 A71-27099

Earth radiation budget measurements, noting planetary albedo, IR radiant emittance and net balance

12 p1901 A71-27191

Low resolution measurements of IR absorption of sulfur dioxide at room temperature

[ASME PAPER 70-WA/HT-4] 13 p2025 A71-28979

Galactic IR background emission mechanisms, considering electrons, protons and cosmic rays role

13 p2131 A71-29272

Rotational line overlap effect on laser IR radiation absorption in high pressure carbon dioxide, comparing calculated absorption coefficient with measurements

13 p2081 A71-29337

IR radiation role in limiting central heater maximum temperature and heat transfer to high density oxygen in cryogenic storage systems

13 p2166 A71-29505

German book on radiation climate of earth covering EM, corpuscular IR radiation sources, spectral composition, biological effects, etc

14 p2298 A71-29941

BL Lac extragalactic source of radio, IR and visual radiation, estimating upper limit to distance based on spectrum model

14 p2313 A71-30452

IR and submillimeter wave HCN laser radiation visual observation, using thermal image converter

15 p2420 A71-32385

Meteorological satellite system for weather forecasting in Mediterranean area, including visible and IR ranges survey and automatic stations and buoys interrogation

16 p2604 A71-32846

Thermal decomposition kinetics of nitrous oxide in shock tube, measuring IR emission behind reflected wave

16 p2539 A71-32910

IR line radiation from galactic center thermal radio sources, determining element abundances

16 p2633 A71-33336

Spatial and angular distribution of upper atmospheric IR emission layers from Cosmos 65 observation

16 p2563 A71-33449

IR absorption of oxygenated dislocationless phosphorus doped fast neutron irradiated n-type silicon, investigating dominant defects for different radiation dosages

17 p2790 A71-34199

Radiative heat transfer in model water clouds by IR radiation, using method of discrete ordinates

17 p2735 A71-35560

Quasars as proto-blackholes in galactic nuclei blackhole model, discussing lifetimes, dust and IR radiation using models

17 p2811 A71-35745

IR chemiluminescence from HCl formed in atomic hydrogen reaction with sulfur dichloride, noting energy distribution among reaction products

18 p2874 A71-35832

Electronic to vibrational energy transfer in mercury vapor reaction with hydrogen fluoride, studying IR emission and scattering cross section

18 p2874 A71-35834

IR chemiluminescence of atomic nitrogen reaction with molecular oxygen, obtaining quantum efficiency

18 p2874 A71-35838

Atmospheric absorption of 10.6 micron laser beam radiation, noting effect on refractive index

18 p2910 A71-35843

Earth IR radiance at 5-20 microns from interferometric spectrometer /IRIS/ aboard NIMBUS 3 satellite

18 p2912 A71-36101

Collisional broadening of IR absorption lines in vibration-rotation bands of carbon monoxide and hydrochloric acid

19 p3106 A71-37374

IR pumped stimulated light emission in semiconductors, noting upconversion due to energy transfer between impurity ions

19 p3071 A71-37479

Combined lidar and radiometric techniques for high layer cumulus and cirrus clouds IR emissivity determination

19 p3089 A71-37501

Plasma diagnostics based on IR continuum intensity due to bremsstrahlung emission from plasma

19 p3113 A71-37765

Carbon dioxide IR radiation measurements of duration of constant reflected shock temperature in over-tailored shock tunnel

19 p3041 A71-37893

Azimuthal IR radiation distribution of atmospheric brightness cross sections at various zenith angles from balloon programmed-control radiometer data

19 p3054 A71-37969

Water vapor effect on vibrational relaxation of CO in shock tubes, measuring IR emissions

19 p3012 A71-38084

Fredholm integral equation stabilization methods for atmospheric IR transfer in vertical temperature profile determination

19 p3060 A71-38470

Carbon dioxide laser triggered pressurized spark gap producing high voltage fast risetime pulses for use in IR radiation control by electro-optic shutters

20 p3244 A71-39106

Formaldehyde absorption and emission lines from Orion IR nebula, indicating pumping suppression by neutral particle collisions

20 p3288 A71-39114

Closed cycle refrigeration system for cryogenic cooling of IR illuminator in helicopter mounted U.S. Army NVASS Night Vision System for night reconnaissance

20 p3184 A71-39273

Global atmospheric ozone distribution from inverted radiance measurements by IR interferometer spectrometer onboard Nimbus 3 satellite

20 p3220 A71-39668

Atmospheric temperature profile from satellite soundings of outgoing radiation in IR carbon dioxide band, using regularization and Chahine methods

20 p3258 A71-39669

Reflected radiation brightness field statistical structure in IR range from Cosmos 121 satellite measurements, calculating correlation functions and spectral densities

20 p3259 A71-39680

Solar and terrestrial IR reflected radiation from Cosmos satellites measurements, determining clouds upper boundary height

20 p3261 A71-39688

D region night airglow OH emissions and IR atmospheric diatomic oxygen bands excitation mechanism with aid of model involving solar photodissociation

20 p3226 A71-39831

IR auroral/airglow study covering hydroxyl emission and dipole moment function determination and atmospheric nitrogen vibrational temperature measurement

20 p3240 A71-39843

OH emission sources associated with long period variable IR stars emitting in 1665-1667 MHz lines

21 p3441 A71-40067

Young dust-filled planetary nebulae models with hot central stellar black body radiation, evaluating IR radiation absorption and reradiation in H I region

21 p3446 A71-40417

Methyl alcohol transitions in Orion at 1 cm noting emission source coincidence with IR nebula

21 p3447 A71-40445

Venus 3-4 micron region continuum absorption from high resolution spectra of Venus and sun

21 p3448 A71-40448

Compact radio sources in galactic nucleus, examining relation to IR emission

21 p3449 A71-40609

Seyfert galaxy micron photometry measurements, determining IR radiation flux changes with time

21 p3449 A71-40611

Global three dimensional atmospheric temperature mapping by selective chopper radiometer on Nimbus 4 satellite, measuring carbon dioxide IR emission

22 p3533 A71-41629

Partial quenching of radiation from ionized inert gases during bases irradiation by IR produced with carbon dioxide lasers

22 p3581 A71-41808

Balloon Sonde I experiment, discussing telemetry from flying body and temperature effects on earth IR radiation measurement

22 p3535 A71-42053

IR atmospheric temperature profiles sounding by selective chopper radiometer launched into polar orbit on Nimbus 4 satellite

22 p3544 A71-42144

UV and IR transmissivity and absorption coefficients of fused quartz between room temperature and 1500 C

22 p3565 A71-42559

Experimental observation of 10.6 micron guided waves in Ge thin films, noting application to carbon dioxide laser communication

22 p3587 A71-42568

Visible and IR radiation attenuation in rain and snow, comparing calculation based on Mie diffraction formulas with measurement

22 p3515 A71-42741

Martian height gradients from 1.6 micron carbon dioxide band intensity, using telescopes with prismatic quartz spectrometer

24 p3869 A71-44807

Dispersion characteristics of He-Ne laser at 3.39 microns

24 p3834 A71-45046

Lunar IR directional characteristics theory, noting agreement with observations at all observational and phase angles

24 p3874 A71-45188

- Laser IR radiation attenuation in natural and artificial fogs, noting dependence on particle size distribution 24 p3835 A71-45254
- Laser IR radiation attenuation in atmospheric precipitation, considering snow, rain and drizzle 24 p3835 A71-45255
- ## INFRARED REFLECTION
- Visible and IR reflection spectra of p- and n-type GaAs under fast neutron irradiation 01 p0139 A71-10783
- Cholesteric liquid crystal pitch from IR transmission measurements 02 p0209 A71-12572
- In vivo green soybean and corn leaves bidirectional IR reflection and transmission distribution functions 05 p0739 A71-16253
- Backscattered laser radar pulses and downward IR flux enhancements in clear air around small cumulus clouds, discussing hygroscopic aerosols for increased radiance 17 p2707 A71-35381
- Astigmatic image distortion in low temperature multiple reflection White cell with aluminum dewar assembly for Martian IR interpretation 18 p2914 A71-35844
- Semiconductors submillimeter and far IR reflection spectra and cyclotron resonance measurements 22 p3586 A71-42140
- ## INFRARED SCANNERS
- ### NT MULTISPECTRAL BAND SCANNERS
- Skyнет satellite attitude determination and adjustment by IR and solar sensors, electronics processing equipment, nutation damping and pulsed axial thrusters 02 p0320 A71-12430
- Sea surface temperature estimation by spatially scanning spaceborne systems operating in thermal IR atmospheric window spectral regions 06 p0898 A71-17560
- Satellite onboard local vertical detection, emphasizing IR horizon sensors role 06 p0892 A71-17964
- IR horizon sensors design, taking into account earth radiation properties 06 p0892 A71-17965
- Earth optical radiation environment observation from satellites, reviewing solar spectra, near IR cloud spectra and vacuum UV radiometer scans 09 p1437 A71-22739
- Side-looking airborne radar and IR line scan systems, discussing instrumental correction of image distortion 09 p1450 A71-22967
- Side-looking radar, thermal IR scanner and passive microwave radiometers for remote sensors for geologic mapping 09 p1452 A71-23215
- IR scanning vertical temperature profile radiometer forITOS meteorological satellites, describing electronic signal processing 14 p2200 A71-30916
- Noise equivalent irradiance equation for airborne IR scanner at peak response detector wavelength, involving target scene radiance and hot iodine emittance 18 p2917 A71-36053
- Thermal mapping performance of passive airborne IR scanners for remote environmental sensing, estimating SNR and noise equivalent irradiance 18 p2921 A71-36364
- Stray radiant flux effects on scanning IR radiometer for low temperature objects measurement 19 p3067 A71-38706
- Sensitivity formula and graphical interpretation for IR scanner, assuming object and ambient medium as Lambertian radiators 19 p3068 A71-38707
- Optical characteristics of thermal IR scanners, using mirrors and prisms in parallel or converging ray pencils and rotating wedges 19 p3068 A71-38709
- Noise equivalent irradiance evaluation of passive IR scanners for target thermal mapping systems operating in earth atmosphere, determining figure of merit 22 p3545 A71-42150
- Airborne IR linescan equipment for commercial aerial survey, discussing operational principle, temperature sensitivity, data processing and individual system components specifications 22 p3545 A71-42151
- IR linescan technique for airborne terrain mapping, discussing choice of waveband, system parameters and display techniques with emphasis on film recording 22 p3546 A71-42425
- ## INFRARED SPECTRA
- Far IR spectrophotometry improvement with lamellar grating, describing construction, alignment and performance 01 p0082 A71-10836
- Carbon dioxide IR absorption bands at elevated pressures, deriving transmission function 01 p0130 A71-11104
- Particulate silicates IR emission spectra under simulated lunar conditions, noting existence of nearly optimum conditions on moon surface 02 p0305 A71-11987
- Liquefied and solidified gas IR measurements describing versatile optical cell 02 p0250 A71-12133
- Hydrocarbon fuels high temperature oxidation behind shock waves, investigating reaction process by combustion products IR emissions and density gradient 02 p0298 A71-12860
- Computer controlled eclipse telescope for coronal thermal emission IR spectrum observation 03 p0424 A71-13633
- Characteristic energy absorption spectra of dielectric solids from direct IR measurements for single crystal and thin film specimens 03 p0385 A71-13645
- Lunar continent surface microstructure from UV and IR spectra, discussing photometric function determination by geometric shadows and diffraction effects 03 p0492 A71-14055
- Emission line spectra of halogens Cl I, Br I and I I in 4-micron region 05 p0717 A71-16911
- Photographic and IR multiband spectral discrimination for rock and soil mapping from orbiting ERTS satellites [AIAA PAPER 70-303] 06 p0898 A71-17562
- Electron temperature and concentration profiles behind shock front from IR emission and absorption simultaneous measurement, applying method to xenon ionization and recombination processes 06 p0936 A71-17594
- Atmospheric boundary layer IR transmittance spectra compared to spectrum calculated from transmittance functions 07 p1152 A71-19149
- IR lattice spectra of rare earth stannate and titanate pyrochlores 07 p1054 A71-19484
- Planetary nebulae NGC 6572, NGC 7009, NGC 7027 IR line emission, examining fine structure for Ne II, Cl IV, S IV and Ar III 07 p1199 A71-19836
- Intermediates structure and IR spectrum in OH reaction with CO by vacuum UV photolysis, studying refractive product absorptions and valence force potentials 08 p1336 A71-20661
- Carbon dioxide IR absorption bands at elevated pressures, deriving transmission function 08 p1337 A71-20848
- Comet Bennett 1969i IR narrow band filter photometry 09 p1442 A71-22067
- Gaseous 3-oxetanone ring compound, investigating IR and vibrational spectra and molecular structure 09 p1403 A71-22473
- Atmospheric attenuation in IR windows near sea level from transmittance spectral curves, discussing continuum absorbance 09 p1437 A71-22740
- Quenching rates for oxygen during 1470 A pulse photolysis in carbon dioxide, nitrogen and helium mixtures 09 p1404 A71-23382
- Intense superradiant emission in HF and DF molecules high gain IR transitions, examining spectral distributions with pneumatically tuned Fabry-Perot interferometer 09 p1498 A71-23478
- Venusian atmosphere subcloud layers intrinsic outgoing thermal radiation and IR spectrum transmissivity from satellite temperature, pressure, moisture content and chemical composition data 10 p1681 A71-25128
- IR and Raman spectra vibrational analysis of crystalline and fluidic oxalyl bromide, explaining observations by two geometrical isomers existence 11 p1727 A71-25363
- Spectral reflectance of water cryodeposits on liquid nitrogen cooled surfaces in vacuum IR integrating sphere 11 p1858 A71-26232
- [AIAA PAPER 71-447] Monoclinic, stabilized and metastable tetragonal and cubic zirconias, noting IR and Raman spectra 13 p2093 A71-28991
- Michelson interferometer onboard Nimbus 4 satellite for recording earth IR emission spectrum 14 p2241 A71-30140
- Integral equations for source functions of Ca II H, K and IR triplet lines for transfer through homogeneous stellar atmosphere 14 p2276 A71-30298
- Singly ionized magnesium CW laser oscillation in He-Mg discharge at micron wavelengths with possible extension to visible and UV spectrum 15 p2420 A71-32386
- Mars IR spectral geometric albedo of bright and dark regions for surface composition model 15 p2491 A71-32419
- IR stellar object HD 45677, discussing IR spectral energy distribution in terms of black body temperature range 15 p2497 A71-32765
- Methane, ammonia and silicate effects on 3.07 micron ice absorption in interstellar grains, using cesium iodide window deposited sample measurements 15 p2498 A71-32774
- Gaseous, liquid and polycrystalline biacetyl vibrational spectra and structure, noting mutual exclusion between IR and Raman radiation 16 p2538 A71-32874
- Group 3A suboxides IR absorption spectra at liquid helium temperatures, measuring bending frequencies and modes 16 p2538 A71-32875
- IR Fe XIII lines in solar corona during total eclipse of 12 November 1966 16 p2640 A71-33729
- Coronal IR emission lines during solar eclipse of 7 March 1970, using high altitude aircraft-borne Fourier transform spectrometer 16 p2640 A71-33751
- Raman and IR reflection spectra of zinc tungstate single crystals 17 p2790 A71-34201
- Deuterium fluoride overtone vibration-rotation chemical laser emission, studying frequency doubling and rate constant ratios 17 p2753 A71-34801
- IR and Raman vibrational spectra and structure of tetrafluorocyclobutane 17 p2695 A71-35520
- Synchrotron radiation reabsorption in inhomogeneous sources, considering IR spectra of quasars and galactic nuclei 18 p2963 A71-36158
- Gaseous and solid polycrystalline HNCS and DNCS IR and Raman spectra, studying LF of lattice vibrations 19 p3118 A71-37649
- Recording device with Fourier hologram memory based on optical spatial filtration principle for identifying chemical compounds by IR absorption spectra 19 p3064 A71-37773
- Atmospheric directional scattering coefficients from vertical measurements of IR spectral sky brightness near solar almucantar and direct radiation 19 p3090 A71-37976
- Water and ice clouds spectral brightness coefficients in IR region of spectra from aircraft measurements 19 p3090 A71-37977
- Flash photolysis produced gaseous carbon difluoride IR spectrum analysis by rapid scan IR spectroscopy 19 p3011 A71-38053
- NO, CO and Ar mixtures IR spectral emission radiant intensities behind shock tube generated reflected shock waves 19 p3012 A71-38087
- Comparative IR and Raman spectra of gaseous, liquid and polycrystalline symmetrical dimethylhydrazine and deuterium analogs 19 p3013 A71-38345
- Carbon dioxide lasers, covering molecular structure, IR spectra and laser transitions, population inversion mechanisms, gas discharge and longitudinal flow 20 p3243 A71-39067
- Interplanetary medium thermal emission detection, presenting diffuse background radiation upper limits in intermediate IR from sounding rocket data 20 p3288 A71-39114
- Polycrystalline barium titanates solid solutions with fluorine displacement of oxygen atoms, observing IR absorption spectra 20 p3276 A71-39151
- Solar IR spectra referencing procedure based on filter reference radiometer, discussing technique theoretical foundation 20 p3237 A71-39327
- Lunar surface microstructure inhomogeneities bimodal distribution from IR and UV spectral analysis 20 p3295 A71-39617
- IR spectrum of aurora, reviewing past and current experimental approaches 20 p3228 A71-39842
- G and K giant stars iron abundances from narrow band indices, using spectrophotometer, red-IR colors and independent luminosity estimates 21 p3444 A71-40240
- Mode locked transversely excited atmospheric carbon dioxide laser with Ge ultrasonic diffraction cell active loss modulator generating 10.6 micron wavelength pulses 22 p3557 A71-42132
- Atmospheric molecular absorption spectra in IR region, using 15 meter multiple pass absorption cell 22 p3544 A71-42141
- Mars IR spectra with Connex-type interferometer, noting atmospheric absorption and albedo drop due to surface water 22 p3602 A71-42176

Semiempirical model for molecular band mean transmission, applying to ammonia 10 and 16 micron lines 22 p3602 A71-42179

Venus water ice clouds existence possibility from high altitude IR spectra and ground based spectroscopic observations 22 p3603 A71-42189

Air pressure effects on absorption dependence at IR wavelengths, using water vapor transmittance windows 22 p3511 A71-42303

Far IR spectrum analysis using Michelson interferometer with beam splitter 23 p3676 A71-43400

IR vibrational spectroscopic analysis of Apollo 11 and 12 rocks and dust isolated silicate minerals, using LF absorption bands 23 p3759 A71-43766

Apollo 11 and 12 rocks dielectric constants, discussing far IR absorption spectrum of fines 23 p3760 A71-43772

IR spectra of oxamide and dithioxamide, studying Raman spectrum in LF range 23 p3642 A71-43825

Automated analysis of high resolution IR astronomical spectra by computer program, presenting procedures for spectral line width, depth and frequency determination 24 p3867 A71-44438

IR spectra temperature dependence of CsI crystals doped with sulfate and carbonate anions and Pb and Cd cations, observing intensive absorption bands 24 p3860 A71-44665

IR spectral geometric albedos of Jupiter Galilean satellites, noting resemblance to spectra of frosts 24 p3871 A71-44910

INFRARED SPECTROMETERS

Nimbus 3 and 4 satellites IR grating spectrometers for remote sensing of vertical temperature and humidity profiles of stratosphere and troposphere near Philippines 05 p0818 A71-17137

Twilight airglow measurements of hydroxyl and molecular oxygen bands by balloon-borne instruments including IR grating spectrometer and filter photometers 10 p1601 A71-24400

Phase modulation theory for two-beam far IR Michelson interferometers, discussing application to Fourier transform spectrometry 14 p2238 A71-29741

Phase modulation in far IR interferometers applied to Fourier spectrometry and metrology, obtaining modulus, phase, absorption and refraction spectra 14 p2238 A71-29742

Polarization Fourier spectrometer for circular dichroism spectroscopy, stressing IR application 14 p2242 A71-30156

Scanning system with hydropneumatic drive for Fabry-Perot spectrometers in IR region, describing He-Ne laser tests 14 p2247 A71-30587

IR spectrometer attachment for macromolecular investigation of polymer materials, describing constructional and operational features 15 p2383 A71-31658

Nimbus weather satellite with IR spectrometer, Michelson interferometer and selective chopping radiometer for atmospheric temperature remote sounding 15 p2445 A71-32295

Peak contour positions of rotation lines of hydrogen chloride as function of spectral slitwidth for wavenumber calibration of far IR spectrometers 16 p2577 A71-33134

Prism IR spectrometer calibration, using linear equation and dispersion formula for derivation of numerical calibration table 16 p2577 A71-33135

Earth radiance analysis by IR interferometric spectrometer of Nimbus 3 satellite, noting cloud cover as dominant variable 18 p2912 A71-36065

Operational calibration of airborne IR spectrometer over hydrogeologically significant terrains, obtaining radiance spectra 18 p2920 A71-36363

Dual beam pulsed gas laser magnetic resonance spectrometer for magneto-optic studies of solids in far IR frequencies 20 p3244 A71-39177

Atmospheric trace and pollutant molecules global survey, using airborne/spaceborne high resolution Fourier interference IR spectrometer 22 p3542 A71-41963

Fourier transform spectrometers in IR astronomy, including rapid scan interferometer 22 p3545 A71-42146

Nimbus 3 satellite IR spectrometer atmospheric pressure height profiles, comparing with nearby radiosonde data 22 p3535 A71-42410

Nimbus B-2 satellite-borne IR spectrometer lubrication using solid film technique, discussing real time and accelerated vacuum environmental tests [ASLE PREPRINT 71ILC-3] 24 p3831 A71-45286

INFRARED SPECTROPHOTOMETERS

Far IR spectrophotometry improvement with lamellar grating, describing construction, alignment and performance 01 p0082 A71-10836

BL Lacertae photometric data, noting object brightness and optical similarity to N galaxy 3C371 04 p0643 A71-15045

Pyroelectric, pneumatic and thermocouple detectors comparison, discussing IR detectors availability for use in spectrophotometers in 2-20 micron region 22 p3544 A71-42142

INFRARED SPECTROSCOPY

Satellite with onboard equipment for astronomical IR spectroscopy, considering stabilization accuracy and measurement duration effects on spectral resolution 01 p0163 A71-10395

Propellant low temperature preignition reactions during simulated engine shutdown conditions, discussing IR spectroscopic observation method 02 p0298 A71-12861

Active nitrogen afterglow complex spectrum analysis from vacuum UV to IR, proposing energy transfer mechanism 03 p0460 A71-13352

Zodiacal light IR spectroscopy by rocket-borne detector, providing information on interplanetary dust properties 03 p0491 A71-14013

Far IR materials optical constants analysis by channeled spectra, using Fourier spectroscopy single signature in interferogram to yield real and imaginary parts of refractive index 08 p1335 A71-21384

Vibrational and rotational temperatures diurnal variations of upper atmospheric OH emissions from IR spectroscopic measurements, discussing earth shadow effects on mean intensity 11 p1753 A71-25541

High density polyethylene composition oxidation rates and photodegradation resistance data, using IR spectroscopy 14 p2261 A71-29641

Planetary atmospheres composition from ground based IR spectroscopy, including multiple scattering, cloud layers, line formation and absorption 17 p2808 A71-35570

Atmospheric ozone data in tropical regions from Nimbus 3 IR interferometer spectrometer measurements, indicating easterly jet stream existence during summer monsoon period 17 p2771 A71-35810

Solid glyoxal Raman spectrum data, showing operativity of mutual exclusion principle by IR comparison to Raman bands 18 p2873 A71-35830

Venusian polar tropopause and cloud layer from IR spectral recording in carbon dioxide band near inferior conjunction for crescent regions 20 p3290 A71-39306

Spectral resolution of matrix Raman spectroscopy and depolarization measurements of isotope splitting, comparing with complementary IR data 20 p3194 A71-39404

Atmospheric temperature and water vapor profile calculation from Nimbus satellite IR spectrometer data, noting Southern Hemisphere tropospheric and stratospheric pressure analyses 20 p3258 A71-39667

IR spectroscopy of CO using tunable PbS₂ diode laser, measuring Doppler linewidth and room temperature absorption coefficient at line center 20 p3246 A71-39757

Electronic double differentiator for producing spectroscopic absorption curves second derivatives, considering application to polymers IR examination 22 p3545 A71-42154

INFRARED STARS

Interstellar dust, investigating starlight reddening by extinction, galactic light, IR star observations and polarization 12 p1959 A71-26775

High luminosity G supergiants at 0.4-18 micron wavelengths showing intense silicate emission shell 15 p2497 A71-32764

IR stars and galaxies measurements, determining 3.5 mm continuum radiation intensity 15 p2498 A71-32775

INFRASONIC FREQUENCIES

Infrasonic shock wave generation in troposphere by powerful earthquakes, causing upper atmosphere density rise due to heating 08 p1278 A71-21019

Aerodynamic infrasonic, considering atmospheric pressure variations in seconds to minutes period range 10 p1596 A71-24915

Infrasonic pulsations of optical auroral luminosity in 3914 A positive molecular nitrogen ion and 5577 A O I emission measurement by double photometer system 19 p3048 A71-37395

Infrasonic shock wave generation in troposphere by powerful earthquakes, causing upper atmosphere density rise due to heating 20 p3219 A71-39299

Seasonal stratospheric wind effects on infrasonic propagation to U.S. northeast coast from rocket launched at Cape Kennedy 20 p3306 A71-39793

Infrasonic waves correlation to supersonic aircraft motions and polar electrojet during substorm period 20 p3229 A71-39993

Heat balance effects of acousto-gravitational waves in upper atmosphere, concerning infrasonics from earthquakes, polar auroral arcs and magnetic storms 22 p3533 A71-41616

INGESTION (BIOLOGY)

NT DRINKING

Emotionally induced osmotic pressure and thirst increase of rats during stress, noting eating behavior 02 p0201 A71-12812

INGESTION (ENGINES)

Gas turbine aircraft engine compressor blade foreign object ingestion control by inlet vortex flow suppression jets, indicating wind tunnel air intake applications 06 p0945 A71-17694

F 101 30,000 lb thrust augmented turbofan engine for B-1 bomber, considering maintainability and bleed ingestion tolerance 19 p3122 A71-37494

INGOTS

Titanium carbide ingots production for laminar air flow precipitation of graphite, using electric arc furnace with consumable electrode 02 p0238 A71-12283

Al ingot level pouring casting, considering solidification effect on subsurface segregation and cyclic pattern of macrostructure 04 p0614 A71-15787

W-Re alloy ingot nonmetallic inclusions complex phase structure, using electron probe, metallography and electrolytic techniques 07 p1141 A71-20233

Forging conditions effects on Ti alloys mechanical properties, considering ingot conversion to semifinished product 09 p1475 A71-23301

Arc melted ingot high field superconductor, combining critical density and resistive critical field 10 p1655 A71-24044

Nb alloy ingots electron beam melting, investigating reverse zone liquation intensity and behavior dependence on melting parameters 15 p2424 A71-31204

Carbon impurity effects on molybdenum ingot formation, detailing crystal growth, size reduction and length 19 p3077 A71-37277

Commercial Ti alloys homogeneity as function of ingot diameter, noting mechanical properties of semifinished products 20 p3252 A71-39544

INHABITANTS

NT MOUNTAIN INHABITANTS

INHALATION

U RESPIRATION

INHIBITION

Cochlear nerve fibers two tone inhibition as signal suppressions inherent to bandpass nonlinearities, using modified analog model and mathematical analysis 05 p0712 A71-16284

Retinal neurons receptive field center, examining excitation and direct inhibition interaction 05 p0707 A71-16396

INHIBITION (PSYCHOLOGY)

Computerized simulation of lateral inhibitory networks for figural aftereffects, discussing light and dark adaptation mechanism 10 p1563 A71-24232

Visual suppression and intensity threshold changes during voluntary eye saccades with different luminance regions in visual field, discussing inhibition processes 11 p1718 A71-25583

Sense organs conditioned reflex and physiology, investigating mechanisms and functional localization of discrimination function and differentiating inhibition 15 p2360 A71-32529

Neural network hypothesis for mechanism of backward masking and disinhibition in visual perception 17 p2684 A71-35253

Soviet papers on higher nervous activity physiology, Part 1, Basic laws and mechanisms of conditioned reflex activity covering inhibition, and bioelectrical effects, with bibliography 17 p2684 A71-35357

Higher nervous activity physiology, discussing induction, protective and conditioned inhibition mechanisms in cerebrum and electrophysiological indices 17 p2684 A71-35359

Temperature effects on spinal excitation and inhibition in cats, investigating spinal motoneurons discharge frequency 18 p2861 A71-36890

Parasympathetic inhibition effects on hyperkinetic borderline hypertension, measuring cardiac output, resting heart rate and intraarterial blood pressure 21 p3332 A71-40407

Proactive reaction time inhibition as indicator of immediate memory retention intensity in subjects receiving interpolated acoustic stimuli 23 p3634 A71-43865

INHIBITORS

NT WEAR INHIBITORS

Jet fuel soluble corrosion inhibitors evaluation by potentiostatic polarization methods 03 p0377 A71-14323

Chemoautotroph *Thiobacillus neapolitanus* growth inhibition by histidine, methionine, phenylalanine and threonine under imbalance conditions 04 p0537 A71-14776

Respiratory inhibitor KCN for killing increase from single radiation doses and reduction of dose fractionation sparing effect 07 p1036 A71-18962

Fast brittle crack slowing by mechanical twins in transformer steel and by slip bands in LiF and NaCl crystals 09 p1468 A71-22625

Hawaiian silversword seed germination and inhibition showing extraordinary heat sensitivity 16 p2527 A71-33049

Inhibitory effects of halogen compounds on hydrogen-air and hydrogen-nitrous oxide flames, measuring burning velocities and temperature/ composition profiles 19 p3013 A71-38106

Phosphoenolpyruvate as enzyme inhibitor of phosphoribulokinase in *Pseudomonas facilis* with respect to ribulose-5-phosphate and ATP 20 p3185 A71-38820

INHOMOGENEITY

Statistical stability of structurally inhomogeneous material, analyzing weak spots effects on limiting state 01 p0166 A71-10081

Rayleigh wave propagation in stochastically inhomogeneous elastic medium 01 p0169 A71-10637

Two dimensional inhomogeneities effects on electrical resistance of plasma with nonuniform density in strong magnetic field 01 p0135 A71-11065

Inhomogeneous elasticity theory under spherical symmetry, using linear differential equations transformation into constant coefficient equations 03 p0507 A71-13714

Plane nonhomogeneous strain fields deformation tensor determination by moire equations for fringe pitch and angle measurement, considering rectangular block bending 03 p0508 A71-13772

Thermoelastic deformation of elastic media with stochastically inhomogeneous microstructure, characterizing physical properties as steady random variables 03 p0514 A71-14358

Boundary value problems solution by partial absorption method for elastic oscillations in inhomogeneous media, discussing Hilbert space methods 04 p0665 A71-14809

Inhomogeneous crystals frequency properties calculation by admittance averaging method, deriving expressions for metal semiconductor contact impedance 07 p1175 A71-19222

Ionospheric inhomogeneities effect on dipole current system produced magnetic field, deriving analytical expressions as function of distance from current carrying layer and inhomogeneity center 07 p1099 A71-19385

Small wavelength wave optics of media with inhomogeneous refractivity developed from geometric optics, representing probability amplitude of classical ray by wave function 07 p1110 A71-19476

First exchange energy inhomogeneity term numerical coefficient approximate derivation 07 p1164 A71-19690

Plasticity zone changes near circular hole, examining material structure inhomogeneity effects in presence of creep 09 p1535 A71-22183

Composition and composition inhomogeneity effects on plated wire memory elements strain sensitivity, considering tension and torsion sensitivities 09 p1509 A71-23115

Wave propagation through random inhomogeneous media, discussing mean wave profile modification due to scattering from density inhomogeneities 09 p1434 A71-23168

Inhomogeneous semiconductor model leading to anomalously high apparent mobility 09 p1510 A71-23486

Variational principles for initial boundary value problem of fully coupled linear thermoelasticity for inhomogeneous anisotropic materials with microstructure 10 p1689 A71-24512

Quasi-linear theory of inhomogeneities generation in equatorial jet, considering space charge waves excitation by electric current perpendicular to geomagnetic field 11 p1757 A71-25772

Lumped inhomogeneities reflections effect on characteristics of AM signal along transmission line 12 p1883 A71-27624

Notch analysis of fracture, discussing elasticity theory of stress concentration and applications to brittle inhomogeneous materials and fatigue crack propagation 13 p2151 A71-28215

Weak three dimensional plasma inhomogeneity effect on expression for mean force acting on plasma in HF field 13 p2108 A71-28853

Stationary saddle points phase method for wave diffraction problems in inhomogeneous medium, deriving asymptotic expansion for surface integrals 14 p2194 A71-30078

Electromagnetic wave scattering on inhomogeneities by Born approximation, estimating maximum error for small correlation radius 14 p2194 A71-30100

External field perturbations by local inhomogeneities in elastic medium, deriving expressions for interaction energy and forces between defects 14 p2332 A71-30869

Plane uniform waves reflected from layer with random permittivity inhomogeneities, determining distribution function and scattered wave propagation direction 16 p2543 A71-33568

Statistical analysis of structurally inhomogeneous material strength, analyzing weak spots effects on limiting state 16 p2658 A71-33637

Nonhomogeneous media electrodynamics, solving nonstationary equations by differential operators dependent on permittivity and permeability 17 p2776 A71-34277

Ionospheric inhomogeneities effect on dipole current system produced magnetic field, deriving analytical expressions as function of distance from current carrying layer and inhomogeneity center 19 p3052 A71-37810

Electromagnetic wave scattering on single ellipsoidal inhomogeneity in cylindrical waveguide, obtaining relationship for electric and magnetic waves reflection coefficient 19 p3019 A71-38330

Quasi-linear theory of inhomogeneities generation in equatorial jet, considering space charge waves excitation by electric current perpendicular to geomagnetic field 22 p3532 A71-41540

Bounded plasma ionization instability inhomogeneity scale evaluation, assuming negligible electron energy losses due to heat conduction as compared to elastic losses 23 p3712 A71-43923

Nonhomogeneous plate under pulsating and uniformly distributed loads, considering dynamic elasticity problem 24 p3880 A71-44712

Numerical analysis of electromagnetic wave diffraction on inhomogeneous transmitting bodies, reducing Maxwell equations boundary value problem to differential equations solution 24 p3804 A71-44772

Linearly polarized plane electromagnetic wave scattering by radially inhomogeneous spherical shell, presenting boundary value problems solutions and approximations 24 p3805 A71-45184

Micrononhomogeneous elastic media with moduli as coordinate random function, investigating stress and strain tensors 24 p3849 A71-45345

INITIAL VALUE PROBLEMS
U BOUNDARY VALUE PROBLEMS
INITIATION

Nitromethane detonation initiation by long duration low amplitude shock waves 07 p1182 A71-19242

INITIATORS (EXPLOSIVES)

Thermal conductance measurement in electroexplosive device by self balancing wire bridge, considering quality control or design applications 09 p1493 A71-22732

High voltage spark generating circuit design for studying electrostatic sensitivity of electroexplosive devices, considering pyrotechnic flash charges, bridgewire detonators and electric blasting caps 22 p3587 A71-41449

Nondestructive pulse technique for quality control of electroexplosive devices, noting cost reduction 24 p3864 A71-45279

INJECTION

NT CARRIER INJECTION

NT FLUID INJECTION

NT FUEL INJECTION

NT GAS INJECTION

NT ION INJECTION

NT LIQUID INJECTION

NT SECONDARY INJECTION

NT WATER INJECTION

Sandwich structures fabrication of foam core and solid polymer skin by automated injection molding 05 p0759 A71-16931

Approximate method for calculating film cooling effectiveness of flat plate at injection ratios exceeding 3.0 13 p2166 A71-29369

Pipe gas flow with heated solid particles injection, presenting flow equations numerical solution by digital computer [ASME PAPER 71-FE-22] 13 p2166 A71-29460

INJECTION CARBURETORS

U CARBURETORS

U FUEL INJECTION

INJECTION GUIDANCE

Orbiting vehicle state variables at ballistic transfer termination for known injection errors, calculating fuel consumption for final adjustments 03 p0485 A71-13249

INJECTION LASERS

Light pulse generator for amplitude-frequency analysis of photoreceivers, using wideband modulated semiconductor injection laser emission 01 p0093 A71-10624

Threshold currents of injection lasers with heterojunctions providing correction for optical thickness in terms of electromagnetic theory 01 p0094 A71-10779

Injection lasers as logic elements in optical communication systems with time division multiplexing, examining optimal switching and pulse duration reduction 02 p0259 A71-11875

GaAs injection lasers phenomenological theory and internal parameters physical meanings, giving maximum optical gain dependence on current density 03 p0434 A71-13349

GaAs heterojunction diode injection lasers, predicting high order transverse cavity modes and far field patterns from theoretical model 03 p0434 A71-13482

Optically coupled GaAs injection lasers emission spectra, determining maximum frequency difference in gain bandwidths for mode synchronization 03 p0435 A71-13506

Injection breakdown in Fe and Cr-doped high resistance GaAs laser due to increased electron-hole plasma during electron heating 03 p0467 A71-13979

Room temperature spatial distribution of emission from injection lasers with single and triple heterojunctions in AlAs-GaAs system 03 p0439 A71-13980

Large optical cavity low loss n-type GaAs injection laser with reduced degradation 05 p0763 A71-16499

Low threshold large optical cavity /LOC/ GaAs injection lasers with high quantum efficiencies at room temperature 06 p0909 A71-18660

GaAs-GaAsP heterostructure injection lasers performance tests [ECS PAPER 71] 07 p1123 A71-19570

Soviet papers on quantum radio physics covering injection lasers, high intensity beam and material interactions and laser dynamics 07 p1126 A71-20251

Semiconductor injection lasers, discussing energy characteristics of state density distribution, coherent emission, etc 07 p1126 A71-20252

Partial mode locking in picosecond self pulsing GaAs injection lasers 07 p1128 A71-20394

Multilayer liquid phase epitaxy heterostructures growth with crystalline solid solutions of aluminum gallium arsenide for injection lasers 09 p1464 A71-23122

Uncooled GaAs injection laser with high pulse repetition rate, discussing structural features and current-power characteristics 10 p1619 A71-23811

Mode hopping due to GaAs lasers longitudinal mode inhomogeneous sequential excitations perpendicular to junction at injection levels above threshold 10 p1619 A71-24039

Pulse rate and pumping power effects on emission spectra and I-V characteristics of multielement GaAs injection lasers 10 p1622 A71-24884

GaAs multiple beam injection laser amplifier avoiding light flux saturation by periodic signal release 12 p1913 A71-26852

P-type Al-Ga-As-p-type Ga-As-n-type Ga-As single heterostructure preparation and properties, discussing effect on injection laser diode characteristics 12 p1914 A71-27027

Transverse mode locking effect on radiation intensity of injection semiconductor laser as function of time and p-n junction refractivity 13 p2077 A71-28172

Semiconductor injection laser output transient response, analyzing stepshaped impressed current by differential rate equations 13 p2081 A71-29391

Laser action internal differential quantum yield estimation using GaAs injection lasers near field emission patterns 15 p2422 A71-32461

SiO antireflection coatings for GaAs injection lasers, discussing single layer quarter-wave coatings for loss minimization and bandwidth maximization 16 p2585 A71-33136

Insufficient spatial and temporal coherence effects on holographic image reconstruction by injection laser, noting application to optical data processing 16 p2577 A71-33142

Double heterojunction structure improvements in injection laser diodes and arrays 18 p2931 A71-36603

High power GaAs injection laser diodes characteristics and array module design for pulsed operation, using confinement junction formation and reflective end coating 18 p2931 A71-36604

Peak optical flux density for catastrophic damage in close confined and double heterojunction injection Al-GaAs-GaAs lasers 19 p3075 A71-38507

Electromagnetic field distributions and far field radiation patterns of three layer waveguide GaAs heterostructure injection lasers, using Maxwell equations 22 p3555 A71-41688

Double-heterostructure injection laser radiation transverse polarization from reflectivity analysis of GaAs-air interface vs TE and ME mode incidence angle 22 p3558 A71-42201

Injection laser range finder with avalanche photodiode for Mars rover obstacle sensing, discussing range data processing methods 22 p3529 A71-42772

Numerical analysis of large signal output characteristics for directly modulated GaAs injection laser, investigating resonance phenomenon 23 p3683 A71-43351

Staircase array and diode stacking moderate power GaAlAs injection laser light sources at room temperature 23 p3685 A71-43504

Design and performance of semiconductor devices with heterojunctions, covering injection laser without cooling, emission frequency converter and negative resistance triode 24 p3808 A71-44383

High order transverse cavity mode selection and propagation in homojunction and heterojunction GaAs injection lasers, using five layer dielectric model 24 p3832 A71-44432

Double heterostructure GaAs injection laser mode reflectivity and waveguide properties, discussing threshold current density and wavelength dependence on mirror reflectivity 24 p3832 A71-44433

Heterostructure /multisemiconductor junctions/injection laser with reduced current density requirement for continuous operation at room temperature 24 p3833 A71-44974

INJECTORS

NT VORTEX INJECTORS

Rocket engine propellant injectors with noncircular orifice geometry, presenting experimental spray patterns and predicted performance for noncircular and circular orifice configurations 11 p1810 A71-25520

Low pressure drop fuel liquid injectors for jet engine combustors, using gas turbine vaporizer design [ASME PAPER 71-GT-38] 11 p1812 A71-25972

Gaseous oxygen/hydrogen injector element modeling based on composition profile measurements for cold flows [AIAA PAPER 71-674] 14 p2291 A71-30738

Gas injectors characteristics investigation by cold flow simulation, using flow field visualization techniques and velocity and mass concentration profiles measurements [AIAA PAPER 71-675] 14 p2291 A71-30739

Throttleable bipropellant rocket engine, discussing cryogenic and space storable propellants and injection system optimization based on combustion mechanism photographic observation [AIAA PAPER 71-740] 14 p2296 A71-30783

Cold flow analysis of liquid propellant sprays from rocket engine injectors, relating propellant mixing and combustion performance 15 p2465 A71-32044

Vapor-liquid mixture steady flow from centrifugal injectors, determining kinetic energy loss relationship to phase separation 16 p2624 A71-33608

Batch unit for investigation of injectors in vapor-liquid flows, discussing measurement system and energy dissipation 17 p2724 A71-35275

INJUN SATELLITES

Color frequency-time spectrograms of VLF electric and magnetic field Poynting flux data from Injun 5 satellite 13 p2054 A71-27914

INJUN 5 SATELLITE

U EXPLORER 40 SATELLITE

INJURIES

NT BAROTRAUMA

NT BRAIN DAMAGE

NT BURNS [INJURIES]

NT CRASH INJURIES

NT EJECTION INJURIES

NT LESIONS

NT NOISE INJURIES

NT PARALYSIS

NT PULMONARY LESIONS

NT RADIATION INJURIES

Chemical radioprotective effectiveness modification by open skin wounds, discussing results with whole body X ray irradiated mice 07 p1037 A71-18964

U.S. General Aviation safety record, discussing National Transportation Safety Board and accident/injury prevention 10 p1557 A71-25132

Computerized registry of traumatic injuries with IBM 360/44 system for use in mortality, paired patient and accidental risk factor analyses 16 p2535 A71-33109

Lower extremity Army aviator amputee retention on flight status regarding service need, amputation and prosthetic fit, age, career, hours flown and time in military 16 p2535 A71-33120

INLET FLOW

Fluid flow turbulent boundary layer development in channel inlet under injection, obtaining friction coefficient and dynamic characteristics at subsonic velocities 01 p0070 A71-10794

Engine/compressor test inlet flow field simulation, considering ramp angle, screen location and diffuser length effects 02 p0299 A71-12909

Nonuniform flow in straight channel inlet section initiated by Fourier expandable nonuniform profile, linearizing Navier-Stokes equations about mean velocity [ASME PAPER 70-WA/FE-27] 03 p0403 A71-14135

Swirling flow in short cylindrical combustion chambers with diaphragm-free inlet section, examining momentum loss 03 p0405 A71-14382

Turbulent boundary layer development and heat transfer in parallel wall passage entrance region, comparing measurement results with computer solution 04 p0689 A71-15920

Cone shaped diffusers effectiveness, noting inlet conditions effect on pressure recovery coefficient 05 p0694 A71-16750

Plane steady laminar flow into channel between two semiinfinite parallel plates, constructing asymptotic solution for large Reynolds number 05 p0736 A71-16966

Inlet turbulence interaction with rotor potential flow as noise source in axial flow fans, developing expression for sound power radiated 05 p0738 A71-17163

Gas turbine aircraft engine compressor blades foreign object ingestion control by inlet vortex flow suppression jets, indicating wind tunnel air intake applications 06 p0945 A71-17696

Laminar incompressible flow heat transfer in inlet between parallel plates at constant temperature, considering pressure gradient effect on boundary layer velocity profile [AIAA PAPER 71-36] 06 p1008 A71-18497

Conical diffusers swirling inlet flow effects on pressure recovery and outlet flow profile [AIAA PAPER 71-84] 06 p0883 A71-18541

Heat transfer and thermal entrance length in annular channel with rounded and sharp inlet edges 07 p1220 A71-18763

Multistage axial flow turbine off-design performance prediction, exploring inlet temperature and pressure and exit pressure variation effects [ASME PAPER 70-PWR-2] 07 p1184 A71-20199

High performance fighter aircraft engine pressure ratio and turbine inlet temperature measurement, using fluidic sensors 07 p1028 A71-20586

Air temperature effects on internal combustion engines intake process, using similarity theory 08 p1347 A71-20782

Computerized simulation of inlet channel flow passage cross section effect on internal combustion engine filling 08 p1347 A71-20830

Optimal lining impedance for jet engine inlet duct yielding discrete frequency, flow velocity and geometry on basis of minimum radiated power 08 p1349 A71-21661

Optimal inlet parameters of MHD generator channels employing kerosene-gaseous oxygen combustion products 09 p1386 A71-22136

Turbulent flow in initial section of convergent axisymmetric nozzle based on logarithmic velocity law 09 p1431 A71-22409

Duct thermal entrance region with axial conduction, evaluating laminar heat transfer rate with finite difference technique 10 p1696 A71-24409

Coaxial jets development and mixing in axisymmetric twisted turbulent ring air flow injected through inlets 10 p1594 A71-24560

Compressor surge effect on mixed compression inlet flow from numerical solution of one dimensional unsteady inviscid flow equations in variable area duct [AIAA PAPER 69-484] 10 p1553 A71-24855

Velocity profiles for flows with laminar heat transfer in circular tube and rectangular duct inlet region with wall suction and injection 10 p1597 A71-25064

Three dimensional boundary layer flow and velocity profiles in mixed diffuser with equal angle walls [ASME PAPER 71-GT-40] 11 p1704 A71-25973

Truncated conical diffusers with various geometrical configurations and incompressible inlet flow conditions, noting reduced pressure recovery 13 p2047 A71-28468

Entrance region laminar flow development under suction or blowing at porous inner wall in concentric annular duct 13 p2160 A71-28602

Acoustic tone radiation from subsonic rotor near potential field by interaction with nonuniform inlet flow based on Lighthill aerodynamic sound equation 14 p2225 A71-30210

Nondimensional entrance loss equation for radial turbulent flows without swirl between parallel disks 14 p2226 A71-30415

Flowfields calculation in inlet design, using flow variable gradients from equations of motion 14 p2170 A71-30608

Slip flow development in parallel plate channel entrance, discussing center line velocity and excess pressure distributions 15 p2393 A71-32262

Aperture angle effect on flow separation in inlet section of diffuser with cylindrical to conical channel transition 16 p2521 A71-33611

Laminar and turbulent incompressible entry flows in channel with jets along walls, determining filling length 18 p2904 A71-36135

Noise generation due to inlet free stream turbulence incident on isolated stators and rotors, using flat plate cascade blade row model 18 p2956 A71-36498

Highly uniform inlet velocity profile influence on conical diffuser characteristics 20 p3177 A71-39798

Circular conical diffuser inlet velocity profile effect on efficiency, presenting experimental results for different cone angles and expansion ratios 20 p3177 A71-39799

Inlet circulation and swirl effect and optimum vane angle for maximum efficiency of subsonic straight conical diffusers 20 p3177 A71-39875

Uniform inlet flow inside centrifugal turbomachinery diffusers with flat parallel side walls, measuring pressure distribution and boundary layer velocity profiles 21 p3323 A71-40757

Conical diffusers outlet flow profile and performance, investigating swirling inlet flow effects on pressure recovery 21 p3323 A71-40950

Centrally-fed circular inherently-compensated aerostatic gas thrust bearing flow behavior in inlet region, obtaining graphs for design optimization 22 p3551 A71-41663

Inlet conditions for centrifugal compressor impeller covering pressure, temperature and velocity measurements on quasi-three dimensional model 22 p3480 A71-42035

Laminar incompressible flow velocities and heat transfer by radiation and convection in inlet section of parallel plate duct 23 p3781 A71-43313

Centrifugal wheel flow swirl effect on pressure/flow rate characteristic in input zone 23 p3626 A71-43555

LET NOZZLES
 Aircraft turbine engines with elevated gas inlet temperatures 04 p0639 A71-15670
 Supersonic and subsonic combustion ramjet engines inlet calibration, using gun tunnel to establish hypersonic throat flow 11 p1860 A71-26271
 Supersonic propulsion system inlet, engine and exhaust nozzle in wind tunnel and flight tests, discussing boundary layer effects on performance 23 p3718 A71-43599

LET PRESSURE
 Pitot type intake inlet additive drag in terms of capture area ratio, static and total pressure coefficients 02 p0187 A71-12688
 Engine surge pressure transients in mixed-compression supersonic inlet, describing scale wind tunnel model simulation and measurement techniques [AIAA PAPER 71-671] 14 p2291 A71-30735

LETS (DEVICES)

U INTAKE SYSTEMS

NER RADIATION BELT
 Inner belt electron flux variations following geomagnetic storms from satellite instrument data 03 p0418 A71-14212
 Inner radiation zone electrons loss and replenishment observation by Pegasus satellite during magnetically quiet and active periods 06 p0949 A71-17264
 Decay lifetimes of Starfish electrons in trapped radiation belt inner zone 08 p1356 A71-21646
 Geomagnetically trapped protons differential energy spectrum in Van Allen inner and outer radiation belts over various energies, using thin solid state detector 10 p1663 A71-24784
 Longitudinal variations of inner radiation belt particle flux density at low altitudes from Proton 2 satellite data 13 p2128 A71-28548
 Fast charged particles measurement in inner radiation belt by Cerenkov counter mounted on Cosmos 137 satellite indicating presence of high energy electrons 16 p2626 A71-33664
 Fast charged particle flux measurement in inner radiation belt by Cosmos 137 satellite in January-February 1967 20 p3278 A71-39140

OCULATION
 Subinoculations of bacterial strains under constant, varying and pulsed magnetic fields, producing sensitivity increase or decrease to antibiotics 08 p1247 A71-20856

ORGANIC COATINGS
 NT ANODIC COATINGS
 NT CERAMIC COATINGS
 Atmospheric and high vacuum performance tests of solid lubricant coatings based on molybdenum disulfide 05 p0757 A71-16174
 Metallographic examination of inorganic, metal plated and intermetallic coatings on martensitic stainless steels for pitting and surface corrosion prevention 19 p3081 A71-37902

ORGANIC COMPOUNDS
 NT AMMONIA
 Soviet book on chemistry of titanium covering intermetallic compounds, hydroxides, dioxide, titanates, halides, sulfates, titanium ores, deposit sites, etc 02 p0209 A71-11847
 Spontaneous polarization measurement of ferroelectric Rochelle salt near Curie point, using nuclear magnetic resonance for phase transitions 04 p0637 A71-15548
 Flame resistant properties of phosphorus containing organic and inorganic high polymers 07 p1145 A71-19841
 Coated abrasive grinding of Ti alloys using water, various soluble cutting oils and inorganic phosphate solutions as coolants and lubricants 11 p1771 A71-26142
 Physicochemical properties and applications of lubricant materials based on organic compounds, discussing developments in inorganic lubricants 16 p2600 A71-32839

ORGANIC MATERIALS
 Surface structure and environment effects on mechanical behavior of crystalline inorganic solids, giving stress-strain diagrams 11 p1808 A71-25999
 Refractory composite inorganic materials technology, covering gas phase, single crystal and hydrothermal synthesis, physicochemical analysis and fabrication methods 13 p2090 A71-28006
 Inorganic polymers and glasses at high temperatures, detecting LF internal friction 19 p3084 A71-38050
 Ion bombardment thinning apparatus for preparing electron microscope foils of inorganic nonmetallic samples including ceramics, minerals and rocks 20 p3233 A71-38826

Q switched inorganic Nd liquid laser oscillator, noting output capability 23 p3686 A71-43957

INORGANIC NITRATES
 NT AMMONIUM NITRATES
 NT HYDRAZINE NITRATE
INORGANIC PEROXIDES
 NT HYDROGEN PEROXIDE
 Respiratory gas reaction mechanism on potassium superoxide in closed circuit breathing apparatus 13 p2021 A71-29113
 Sodium superoxide isothermal decomposition, detailing metallic oxide effects with differential thermal analysis, thermogravimetry and differential thermogravimetry 17 p2694 A71-34672

INORGANIC SULFIDES
 NT CADMIUM SULFIDES
 NT COPPER SULFIDES
 NT HYDROGEN SULFIDE
 NT INDIUM SULFIDES
 NT LEAD SULFIDES
 NT MOLYBDENUM DISULFIDES
 NT MOLYBDENUM SULFIDES
 NT POLYSULFIDES
 NT ZINC SULFIDES
 NT ZINCBLLENDE

INPUT
 Optimal input stage interaction height in large scale operation of two-stage magnetron amplifier 03 p0385 A71-13791
 Discrete and analog electrical differentiators accuracy for input functions time derivatives determination, considering systematic errors and application suitability 04 p0599 A71-15567

INPUT/OUTPUT ROUTINES
 Programming language translator system, describing syntactic specifications for input-output relationships 01 p0045 A71-10190
 Time shared input/output I/O processor with hybrid I/O separation from hybrid computation 01 p0048 A71-10226
 Nonlinear time varying discrete feedback systems input-output properties, deriving stability criteria by generalized small gain and passivity theorems 03 p0389 A71-13327
 Minimal partial realizations of linear input/output map, discussing significance in regard to adaptive dynamics identification procedures 23 p3661 A71-44190

INSECTICIDES
 NT URETHANES

INSECTS
 NT BEETLES
 NT DROSOPHILA
 Space flight biological effects on parasitic wasp Habrobracon, investigating genetic, mutational, biochemical, behavioral and physiological parameters 01 p0019 A71-11553
 Photoperiodic effects on insect brain circadian clock control, investigating eclosion cycle initiation, stimulant hormone release and termination as functions of dark phase 09 p1392 A71-22648
 Reflex mechanisms and programmed command in insect flight stabilization, discussing gravity proprioceptors, wind sensing and optomotor control 21 p3326 A71-39987
 Gravity effect and lift perception in flying insects and animals, discussing flapping flight and aerial locomotion in aerodynamic balance weightless state 21 p3327 A71-39988
 Proprioceptive gravity perception in Hymenoptera, noting joint located hair plates and constant angle space orientation in dark 21 p3327 A71-39989
 Gravity orientation in insects, discussing different mechanoreceptors role 21 p3327 A71-39990

INSENSITIVITY
 U SENSITIVITY

INSERTION LOSS
 Low pass quiprille insertion loss functions roots for commensurate microwave filters with stubs and unit elements 13 p2038 A71-28610
 Insertion loss approach to doubly resistor terminated filters approximation-synthesis problem 14 p2209 A71-29544
 He-Ne laser insertion loss effect on power variation of two operation modes during cavity frequency tuning 23 p3684 A71-43401

INSERTS
 Hollow annular inserts for stress concentration and alternating stress range reduction around holes in thin flat plates, taking friction coefficient into account [ASME PAPER 70-DE-L] 03 p0506 A71-13706

INSOMNIA
 Rapid eye movements during nocturnal sleep of healthy human subjects, insomniacs and narcoleptics recorded on polygraphs 01 p0007 A71-10071

INSTRUCTION
 NT INFRARED INSPECTION

NT X RAY INSPECTION
 Two-unit redundant repairable system with standby, predicting periodic or random inspection effect on reliability through Laplace transforms 06 p0904 A71-18026
 MIL-STD-414 sampling procedures and tables for inspection by variables for percent defective 06 p0905 A71-18059
 Room temperature curing rubber for detection of cracks and other surface flaws in magnetic materials, revealing cracks in specimen by distinct dark lines 10 p1615 A71-24100
 Airport certification and safety inspection procedures and minimum safety standards [SAE PAPER 710413] 13 p2167 A71-28305
 Composites nature and assembly from inspection standpoint, discussing maturing process and comparison with ordinary metals 13 p2091 A71-28439
 Automatic control systems preventive inspection intervals examined from cost optimization viewpoint for various failure distribution rules 13 p2042 A71-28641
 Magnification level for optimum performance at microminiature inspection with binocular microscope, minimizing time 17 p2689 A71-34704
 Post test inspection of Brayton Rotating Unit for closed Brayton cycle electric power conversion system for long space missions 20 p3180 A71-38909
 Differential method of ultrasonic inspection and binary comparative search heads for implementation, combining mirror shadow and echo methods features 22 p3553 A71-41760

INSTABILITY
 U STABILITY

INSTALLATION
 U INSTALLING
 U INSTALLING
 Aircraft flight load measurements in high temperature environment, determining optimal strain gage installation and calibration 14 p2248 A71-30681

INSTRUCTION SETS (COMPUTERS)
 Instruction Set Design System /ISDS/ program for computer order code selection 01 p0047 A71-10217
 Computer program for compiling interpreter coded test instructions from high order pseudo-English language 03 p0381 A71-13078

INSTRUCTIONS
 U EDUCATION

INSTRUMENT APPROACH
 Cockpit simulator motion effects on ILS approach pilot guidance errors, using Erdmann model [DGLR-70-071] 05 p0779 A71-15956
 Aircraft ILS landing approaches, discussing approach area and surface and obstruction clearance surface and limit 21 p3325 A71-40891

INSTRUMENT COMPENSATION
 NT TEMPERATURE COMPENSATION
 Low resistance nozzles for complete power compensation in rate of climb indicators 01 p0079 A71-10350
 Digital control system for azimuthal optical telescope, using invariance techniques and photoelectric system to compensate for position and program errors 01 p0081 A71-10727
 Instrumentation magnetic tape recorder reproduce systems equalization using active circuits and signal processing to develop required transfer function 01 p0082 A71-10894
 Inertial instruments temperature compensation vs control 02 p0253 A71-12460
 Supporting fluid effects in floated inertial instruments, examining cause, frequency, extent and solution 02 p0253 A71-12462
 Stress dynamics of optimum high speed piezoelectric pressure probes utilizing backing rod material 03 p0427 A71-13913
 Iris photometer for star observations, discussing automatic compensation for plate background 04 p0590 A71-14840
 Photoelectric recording devices for star passages, describing automatic compensation for signal delay instability 04 p0592 A71-14864
 Signals measurement distortions in FM recording-reproducing channel due to recorder magnetic tape speed fluctuations, discussing compensation methods 05 p0752 A71-16724
 Electronic compensation of water vapor effects in respiratory mass spectrometry 07 p1052 A71-20335
 Paraboloidal, hyperboloidal and flattened spheroidal telescope mirrors testing with optical compensation lenses by Foucault shadow and Ronchi methods 07 p1116 A71-20641

INSTRUMENT DRIFT

Metals and alloys internal friction meter based on intense ultrasonic vibration, discussing error compensation

09 p1426 A71-22320

Electromagnetic propagation errors in radar tracking, photogrammetric cameras and laser range finders due to atmospheric refraction, discussing error compensation techniques

09 p1405 A71-22356

Side-looking airborne radar and IR line scan systems, discussing instrumental correction of image distortion

09 p1450 A71-22967

Three-beam holographic interferometry featuring sensitivity increase and aberrations compensation

10 p1611 A71-24345

Frequency response of velocity and acceleration transducers for oscillatory environments instrumentation

11 p1762 A71-25935

Delay compensation in flip-flop element of optimal relay system with self oscillations, using optimal control algorithm constructed by phase space method

11 p1742 A71-26095

Two-shaker single input sinusoidal and random vibration tests, considering Hunter-Helmuth solution with constant cross coupling compensation in frequency band

11 p1745 A71-26491

Tape recorder equalization techniques effects on attainable bit error probability in digital communication, considering asymptotic prediction recording PCM/FM case

14 p2249 A71-30918

Automatic coordinate compensation for systematic and random distortions of photographs on stereophotogrammetric devices

15 p2406 A71-31619

Laser interferometer techniques with automatic measurement and compensation for system inaccuracies, considering corrections for sine /Abbe/ errors for pitch and yaw, etc

[SME PAPER IQ-71-120]

18 p2924 A71-36655

Polarization compensator for Okayama Astrophysical Observatory solar Coude telescope, describing operational and design principles and performance characteristics

19 p3062 A71-37242

Broadband compensation of HF tunnel diode traveling wave amplifier using separate stages in transmission line

19 p3026 A71-37256

Compensation type reference pyrohelometer design and calibration, considering accuracy, constant characteristics and turbidity effects

21 p3384 A71-41383

Ferrite coercimeter with attached electromagnet and compensation winding, deriving analytical expressions for demagnetization and compensation currents

22 p3521 A71-41767

International zenith telescopes micrometer value, determining correction for ocular screw from latitude observations

23 p3680 A71-44261

INSTRUMENT DRIFT

U DRIFT [INSTRUMENTATION]

INSTRUMENT ERRORS

Probability method for gyroscope instrumental errors associated with inaccurate fabrication and components assembly, classifying external moments

01 p0080 A71-10534

Instrumentation tape recorder time base error effects on signal carrier amplitude and spectral purity

01 p0033 A71-10896

Cardan suspension axes nonperpendicularity and misalignment effects on precision of gyroscope motion in presence of system angular vibrations

01 p0083 A71-11043

Discrete servo position gage accuracy in presence of high uncorrelated noise level, using Markov chain

01 p0038 A71-11233

Riometers accuracy and stability, considering measurement error of ionospheric radio wave absorption

02 p0247 A71-11774

Phase meter channels correlation effect on mean phase difference measurements accuracy in heterodyne oscillators

02 p0212 A71-11837

Straight line approximation of random two dimensional discrete set containing large measurement errors, comparing to least squares results

02 p0304 A71-11902

Ionization gage detector signal interpretation as function of reflected molecule velocity distribution, noting shutter speed errors

02 p0286 A71-12128

Random vibrations nonlinear effects on gas bearing pendulous-integrating gyroscopic accelerometer response, using digital simulation

02 p0252 A71-12454

Electrical measuring device error caused by longitudinal instability of frame held in tensile suspension during casing transverse vibration

02 p0253 A71-12635

Soviet book on flight vehicle instruments and sensors static and dynamic characteristics, instrument errors and reliability

02 p0254 A71-12720

Stellar Tracking Rocket Attitude Positioning System /STRAP/ for sounding rocket payloads three-axis orientation control with accuracy

[AIAA PAPER 70-1402]

Noncircular cross section static pressure probes theoretically insensitive to pitch, yaw and Mach number, testing performance

03 p0341 A71-13730

ESCA /Electron Spectroscopy for Chemical Analysis/ spectrometer using small digital computer as process regulator

03 p0428 A71-13925

Spectrophotometric instrumentation in physics and chemistry, discussing developments in automation, accuracy and measurement time

03 p0429 A71-14326

Liquid flow rate measurement based on tank-filling method, discussing factors affecting accuracy

03 p0356 A71-14328

Servosystems errors of indicator-receiver for recording electromagnetic field pattern extremes in amplitude radio interferometers

04 p0557 A71-14635

Performance tests for guidance accuracy and tracking smoothness of Crimean Astrophysical Observatory radio telescope, discussing pointing and tracking errors

04 p0565 A71-14849

Atomic clock synchronization with high accuracy

04 p0596 A71-15208

Nondestructive test with high resolution instrumentation for observing long thin walled cylinder lateral displacements prior to buckling under axial compression

04 p0669 A71-15297

Intercept Ground Optical Recording telescope and Mobile Optical Tracking System for electro-optical photography, discussing measurement and system errors and CAMDAT computer program

04 p0554 A71-15320

Accelerometers linearity variations by centrifuge tests

[AGARDOGRAPH-128]

05 p0750 A71-16313

Wind speed measurement by cup and sonic anemometers, considering errors due to tower structure effect

05 p0752 A71-16663

Errors from multiple reflections between target environment viewed by IR thermometer or radiometer and background environment

05 p0752 A71-16672

Rocket-borne beta ray atmospheric densitometer errors due to cosmic rays

05 p0752 A71-16673

Turbulence measurement by electrothermoanemometry, discussing method errors

05 p0753 A71-16846

Mass spectrometer with electron impact ion source, evaluating instrument linearity and reproducibility

05 p0754 A71-16948

Alouette 2 ionograms frequency interpolation correction allowing measurement accuracy comparable to sounder system resolution

05 p0725 A71-17083

Universal testing machines dynamic load errors due to testing speed

05 p0734 A71-17247

High accuracy hypersonic low density cone drag measurements, using method with advantages of free jet and wind tunnel electromagnetic balance

[AIAA PAPER 71-133]

06 p0845 A71-18577

Turbulent He jet measurements using hot-wire anemometry and digital recording techniques, assessing accuracy

[AIAA PAPER 71-201]

06 p0886 A71-18639

Satellite radio interferometer multipath reflections effect on accuracy

07 p1106 A71-18839

Atmospheric propagation errors of satellite tracking system in VHF region

07 p1059 A71-19028

Third order aberrations in Cassegrain type telescopes and coma correction in servo-stabilized images

07 p1107 A71-19202

Static friction influence on readings of gyrotachometer with pulse width modulated torque sensor current

07 p1108 A71-19306

Null shift errors of compensated electromechanical pendulum accelerometers during random vibration of base

07 p1108 A71-19308

Static pressure measurements near oblique shock waves using short probe, evaluating readings accuracy

07 p1090 A71-19911

Photometric field error of Abastumani Schmidt camera determined from Hyad cluster photographs attributed to distance errors from vignetting of optics

07 p1115 A71-20442

Small factor errors of inertial navigation system in disturbed Keplerian motion of plant

07 p1158 A71-20442

Fluidic/electronic pressure ratio computer program type, using two free jets interaction for instrument error reduction

07 p1031 A71-20442

Soviet book on spacecraft motion parameters in measurements accuracy covering electronic systems and sources and reduction in design and data processing

08 p1251 A71-20442

Aircraft radio compass navigation errors due to local antenna inclinations during maneuvering

08 p1331 A71-20442

Temperature measurement inaccuracies in 30 to 1 km region by balloonsonde sensors, involving IR cooling of thermistor

08 p1277 A71-20442

Clock correction for Danjon prism astrolabe determination method description and verification

08 p1284 A71-21649

Meteorological instrument design, discussing response, errors, accuracy, range and standardization

08 p1293 A71-21747

Accuracy, calibration, maintenance and optimum design of scientific instruments for meteorological measurements

08 p1293 A71-21747

High altitude radiosonde thermometer and pressure sensor construction, discussing radiation error and wire lag

08 p1293 A71-21747

Fabry-Perot interferometer for dielectrics permittivity and loss measurements in millimeter and submillimeter ranges, discussing design, tests and accuracy

08 p1294 A71-21849

Single crystal W thermal conductivity measurements at 1200-2500 K, discussing apparatus and error sources

08 p1318 A71-21949

Static pressure port errors in hypersonic turbulent flow, using approximate shear layer momentum balance for pressure increase derivation

08 p1228 A71-21949

Electromagnetic propagation errors in radar tracking, photogrammetric cameras and laser range finders due to atmospheric refraction, discussing error compensation techniques

09 p1405 A71-22356

NBS traceable nonferrous conductivity standards for eddy current testing, discussing error analysis, long term drift, grain direction and stratification effects

09 p1469 A71-22747

High temperature dynamic strain gage test equipment for evaluating precision, life and environmental limitations

09 p1445 A71-22747

High accuracy temperature measurements using type K thermocouples

09 p1445 A71-22747

Error analysis of random and system degradation between calibrations for complex instrumentation digital computer models

09 p1449 A71-22747

Maximum deviations of corrected uniaxial gyrostat blazer under disturbances on stabilization and precision axes with modulus constraints

09 p1450 A71-22747

Ion orientation technique for attitude control based on counterflow sensing in earth upper atmosphere, discussing accuracy

09 p1523 A71-23117

Soviet book on navigation and control covering data processing, optimal stochastic self guidance, instrument errors, mean energy consumption and stabilization loop time lag

09 p1491 A71-23117

Screw run and period error stability of eyepiece micrometer of universal astronomical instrument showing dependence on attitudes in space

09 p1451 A71-23117

Electronic ergometer calibration equipment and errors at high work loads

09 p1401 A71-23370

Astrometric instruments optimal spatial sampling with parallel slits grill in focal plane, studying error minimization

10 p1608 A71-23822

Resistance thermometry measurements near wall in turbulent flow, considering error causes

10 p1591 A71-23844

AC power meters using electronic multiplier for overcoming limitations concerning frequency ranges, response times, power factor and distortion

10 p1609 A71-23911

Hydrodynamic study of systematic errors of mass flowmeters, considering effects of working fluid, sensitive elements and secondary motions

10 p1610 A71-24166

Turn rate gyro installation angle and airspeed effects on instrument reliability, presenting in-flight investigation results relative to turn rate information usefulness under various flight conditions

[SAE PAPER 710380]

10 p1610 A71-24244

Astronomical telescopes with Cassegrain two mirror optics, discussing optical aberrations and correction methods and modern testing procedures
10 p1612 A71-24690

Cloud base height estimation methods involving vertical radar, laser, stereotelemeter and ceilograph measurements with instrument error analyses
10 p1639 A71-25100

Ventilation rates and thermal factors of sensitive elements in radiosondes, using wind tunnel tests
11 p1761 A71-25382

Centerline loss, transient sink temperature and thermal conductivity design constant considerations for thin foil copper-Gardon heat flux sensors
[AIAA PAPER 71-470] 11 p1764 A71-26251

Quantum counting efficiency of commercial photomultiplier at 0328 A by direct measurements, including signal and background dependence
11 p1766 A71-26300

Pulsed optical range finders, predicting transmitter pulse waveshape effects on calibration, precision and efficiency by probability density function
12 p1903 A71-26792

Rapid scan astronomical spectrophotometer with 1024 channel for signal averaging on slow change in sky transparency for improving accuracy
12 p1904 A71-26803

Thermosensitive quartz anemometer operating in vibrational mode, discussing design and applications in low airflow velocity measurement
12 p1906 A71-26826

Calibration test rig for high accuracy liquid hydrogen flowmeter, discussing design and operation
12 p1906 A71-26836

Subsonic turbulent jet flow optical measurement by quantitative schlieren technique to overcome hot-body anemometry difficulties due to temperature and velocity fluctuations
12 p1896 A71-27215

Modulation cancellation altimeter error analysis and performance optimization
12 p1908 A71-27437

High stability frequency standard distribution system involving use of geostationary satellites and two-way microwave transmission, discussing errors
12 p1882 A71-27439

Insufficient auroral electron spectra and pitch angle distributions from ground based altitude luminosity profiles
13 p2054 A71-27802

Methods for reducing integrating gyroscope errors caused by angular oscillations of base, considering use of two identical gyros with opposite kinetic moment vectors
13 p2065 A71-27951

Straight line approximation of random two dimensional discrete set containing large measurement errors, comparing to least squares results
13 p2133 A71-28189

Gravity center effect on drift of gyro linear acceleration integrator on vibrating base, showing errors at frequencies near nutations
13 p2069 A71-28933

Improved accuracy electron temperature Langmuir probe by eliminating geomagnetic field, rocket velocity and random noise effects
14 p2238 A71-29532

Ion probe measurements of very low fluid velocities, improving accuracy by marking technique
14 p2223 A71-29745

Spectrophotometers photometric accuracy measurement technique, using Bouguer law and optical fields superposition
14 p2240 A71-30123

Monograph on oscillographic high accuracy technique for phase angle measurement covering applications for harmonic generator phase control
14 p2243 A71-30237

Aircraft barometric altimeter errors caused by atmospheric temperature deviations from International Standard Atmosphere
14 p2244 A71-30323

Double star measurements precision obtainable in space with stable and perfect instrument, comparing to ground observations
14 p2246 A71-30364

Orbit computation and measurement errors of visual binaries by wire micrometer distance method
14 p2312 A71-30372

Eye accommodation range limiting for increased adjustment accuracy of optico-mechanical instruments, considering spectacle lens, telescope, magnifying glass and microscope
14 p2189 A71-30416

Fan-produced sound pressure fluctuation in very low speed subsonic wind tunnel test stream, noting resulting anemometer calibration errors
14 p2275 A71-30526

Tape recorder equalization techniques effects on attainable bit error probability in digital communication, considering asymptotic prediction recording PCM/FM case
14 p2249 A71-30918

Radiometric errors in cosmic background radiation measurement
14 p2204 A71-30970

Coordinate measurement accuracy for star and satellite photographic observation using Zeiss Ascorecord
14 p2250 A71-31121

Diffusely reflecting in-plane surface displacement measurement by holographic interferometry, comparing static and dynamic methods for accuracy
15 p2403 A71-31265

Distance determination accuracy improvement by OTD double image range finder
15 p2405 A71-31467

Satellite skin potential and errors in electron density and temperature determinations by Langmuir probe measurements, using model ionosphere
15 p2398 A71-31768

Automatic leveling instrument gravity intensity and compensator support tilt angle variations effects on measurement error
15 p2410 A71-32353

Critique on photomultiplier tube for photon counting, considering pulse height distribution, SNR and electron collection efficiency errors
16 p2578 A71-33146

Schmidt telescope as astrometric instrument, comparing mean error with catalog positions
16 p2578 A71-33322

Dynamic small perturbation calibration of constant temperature hot-wire anemometers for turbulence measurements in Karman vortex streets, comparing static method
16 p2581 A71-34166

Quadrupole mass spectrometer ultimate characteristics concerning resolution, range, recording speed, working pressure and sensitivity
17 p2737 A71-34288

Instrument calibration, discussing statistical estimation of relationship and experimental design for precision improvement
17 p2738 A71-34526

Uniaxial gyroscopic stabilizer errors in presence of base random vibration, taking into account dry friction forces in bearings
17 p2738 A71-34560

Filtering methods for reducing systematic errors of measuring system with structural redundancy
17 p2740 A71-34964

Single crystal W thermal conductivity measurement at 1200-2500 K, discussing apparatus and error sources
17 p2759 A71-35264

Solar coronal line photometry eliminating inherent systematic measurement errors of previous methods
17 p2809 A71-35597

Gyroscope errors with gimbal suspension mounted on slowly moving base, discussing base steady rotation
17 p2746 A71-35605

Rotor asymmetry effect on errors of two degrees of freedom gyro mounted on dynamic platform
17 p2746 A71-35608

Mass and center of gravity determining system model, describing equipment, operation principle, calibration data and techniques accuracy and errors
[SAWE PAPER 879] 17 p2725 A71-35824

Spectral scanning method for determining temperature profile of jet- or rocket-engine exhaust stream by gas radiation and transmittance measurements, discussing radiometric errors effects
18 p2916 A71-36048

Telescopic phase retardation effect on polarization in Zeeman split Fraunhofer line, discussing consequence for solar magnetic field determination
18 p2965 A71-36732

Reentry vehicles trajectory reconstruction by computer program and Kalman filter estimation theory, analyzing instrument errors
[AIAA PAPER 71-933] 19 p3097 A71-37178

Testing apparatus contribution to bending in tension specimens, noting instrument errors role
19 p3065 A71-38133

Temperature gradients measurements in transit instrument pavilion and errors in time determination for two year period
20 p2337 A71-39314

Circumsolar scattered radiation effects on ozonometer reading accuracy, taking into account effect of sun angular altitude under cloudless conditions
20 p2337 A71-39329

Compensation pyrheliometers and thermoelectric actinometers response lag and irregular operation after instantaneous shadowing, discussing techniques for determining instrument inertial characteristics
20 p2337 A71-39332

Mirror meridian circle of zero expansion glass for reduction of flexure and refraction instrument errors in astrometry
20 p3240 A71-39539

Sensitivity requirements for attenuation measurement radio receivers, considering minimum input SNR for absolute measurement error not to exceed preestablished value
20 p3197 A71-39550

Galactic cosmic ray effects on interplanetary dust particles erosion and spurious counts in micrometeoroid sensors, microphones and capacitor detectors
20 p3280 A71-39635

Atmospheric transmittance measurement errors in determining temperature, water vapor and ozone distributions from satellite remote sensing
20 p3258 A71-39671

Instrument function for central spot distribution of Fabry-Perot etalon with finite aperture, comparing to Airy formula
21 p3379 A71-40636

Binary moving-window integrator radar target azimuth measurement error determination, presenting target detection probability curves obtained by digital simulation
21 p3348 A71-40725

Air temperature measurement errors, comparing thermometers with and without meteorological screening
21 p3383 A71-41240

Nonrandom measurement error analysis in vector form for mutually dependent and independent errors
21 p3383 A71-41241

Error factors of seasonal precipitation measurements by total precipitation gages
21 p3383 A71-41378

Circumsolar radiation and atmospheric turbidity effects on readings of compensation type pyroheliometers with allowance for receiver sensitivity
21 p3384 A71-41382

Loran-C pulse hyperbolic navigation system application to time and frequency measurements, evaluating errors
22 p3570 A71-41524

Spectral line intensity measurement errors due to electron-temperature fluctuations averaging in continuous plasma sources
22 p3581 A71-41790

Unaided, integrated and differential OMEGA radio navigation configurations, comparing accuracy and suitability for airways system operations
22 p3571 A71-42082

Tracking servosystems errors of indicator-receiver of amplitude radio interferometers for recording electromagnetic field pattern extremes
22 p3521 A71-42275

Interplanetary navigation TV camera in-flight calibration, discussing instrument error sources elimination
22 p3573 A71-42771

Pressure altimeter, airspeed and vertical velocity instruments, discussing selection, installation, pilot verification, error identification, repair and use
23 p3675 A71-43385

General aviation aircraft altimeter errors, tolerances and static system tests
23 p3629 A71-43386

Precision calibration system with adjustable temperature extended radiance source for long wavelength IR radiometer, discussing performance tests
23 p3676 A71-43512

Static and dynamic measurement errors in contact and contactless sensors of automatic dimensional control of finished product sorting
23 p3679 A71-43866

Soviet papers on astrometrical study methods, discussing instrument errors, stellar observation improvement, ambient medium conditions and automation
23 p3770 A71-44254

Odessa observatory meridian circle pivot irregularities effects determination on horizontal axis inclination and azimuth, using Challis method
23 p3680 A71-44263

Photographic recording for graduated circle readings during stellar observation, discussing method, errors and system
23 p3680 A71-44264

Solar spectrum photoelectric recording instrument signal ratio accuracy, discussing divider circuit analysis
23 p3681 A71-44312

Gravimetric calibration by inclination method with astronomical theodolite, tabulating relative errors and temperature corrections
24 p3826 A71-44767

Kinematic method for deriving formula for gimbal error of directional gyroscope with allowance for main axis inclination to horizontal plane
24 p3828 A71-45157

Motion equations of statically unbalanced two degree of freedom gyroscope excited by base linear vibrations, determining instrument errors as function of casing/body coupling
24 p3828 A71-45159

INSTRUMENT FLIGHT RULES

Maximum throughput-rate capacity for runway and final approach path airspace involving multiple IFR landings
02 p0279 A71-12893

IFR design requirements for STOL navigation equipment from flight tests
04 p0623 A71-15424

INSTRUMENT LANDING SYSTEMS

VTOL aircraft IFR airworthiness, noting necessity of higher safety levels for metropolitan air transit systems

04 p0533 A71-15426

VTOL handling qualities criteria for civil IFR qualifications, taking into account pilot abilities

04 p0533 A71-15427

ATC automation program for en route and terminal centers, discussing combined nationwide system features, IFR volume and video digitizer data links

08 p1332 A71-21659

Light aircraft qualification for icing conditions from flight test data, considering increase in instrument rated pilots and IFR flying activity

[SAE PAPER 710394]

10 p1555 A71-24258

Heavy lift helicopters IFR hover capability with slung load, discussing sensors controls and displays

[AHS PREPRINT 540]

14 p2250 A71-31097

INSTRUMENT LANDING SYSTEMS

NT AUTOMATIC LANDING CONTROL

STOL navigation equipment and microwave landing instruments test programs, noting data recording and flight operations

03 p0454 A71-13286

VC-10 aircraft ILS electronic equipment reliability tests

04 p0559 A71-15873

Cockpit simulator motion effects on ILS approach pilot guidance errors, using Erdmann model

[DGLR-70-071]

05 p0779 A71-15956

Blind landing by mobile beams and Doppler systems, superseding heavy infrastructure ILS

06 p0925 A71-17951

Hovering and low speed flight capabilities of tilt wing VTOL aircraft in terminal area under near-zero visibility instrument landing conditions

[AIAA PAPER 71-7]

06 p0847 A71-18481

Aircraft automatic landing improvement through use of space diversity ILS receiving system

07 p1153 A71-18830

Structures electromagnetic scattering and multipath transmission effects on aircraft instrument landing system localizer signals, using computer program

07 p1153 A71-18831

Aircraft final approach and landing aids, describing ILS, VHF omnidirectional radio range, distance measuring equipment and satellite systems for air navigation

07 p1154 A71-19014

Kalman filter application as observer of observable signals derivatives, using gain matrix to minimize variance estimate for instrument landing systems

08 p1269 A71-21343

Microwave and modular solid state ILS designs, discussing accelerated progress, international standard and present system life expectancy

10 p1639 A71-23943

Combined inertial and instrument landing aircraft navigation systems with reduced cross runway position and velocity errors, using optimal linear estimation

14 p2272 A71-30606

Handling qualities of V/STOL research vehicles during steep terminal area approaches, discussing powered lift fan VTOL aircraft limitations and instrument landing approach

[AHS PREPRINT 544]

14 p2179 A71-31101

Performance category III all-weather capability ILS landing equipment standards, discussing high directivity antennas and transmission and control system redundancy techniques for reliability

15 p2445 A71-31909

C band SYDAC system compatible with conventional ILS, considering transmission sensitivity to ground reflection and lateral obstacles

15 p2445 A71-31910

SYDAC ILS systems flight tests

15 p2446 A71-31911

Aircraft ILS signal reception system, obtaining category III reliability performance by circuit redundancy and automatic incoming information surveillance

15 p2446 A71-31912

DC 10 flight test program improvement using data acquisition/processing with real time monitoring, instrument landing and laser tracking

[AIAA PAPER 71-788]

16 p2553 A71-34018

Automatic landing systems using inertial navigation derived translational state information, discussing evaluation by simulation of transport aircraft operating with conventional instrument landing system

[AIAA PAPER 71-795]

16 p2605 A71-34020

Space shuttle scanning beam landing guidance system, discussing accuracy in penetration, alignment, flare out and touchdown maneuvers and trajectories

17 p2773 A71-35068

Air navigation and traffic control systems with application to Western Europe and Atlantic area, noting requirements for ILS successor

18 p2944 A71-35998

Holographic display for blind landing system with variable image perspective over wide field of view, using collimated or cylindrical laser beam

18 p2945 A71-36061

Concorde aircraft navigation system comprising triple inertial systems, dual VOR/DME, dual ILS and dual ADF

[CASI PAPER 72/9]

19 p3100 A71-37599

All-weather operations, including pilot role, instrument landing systems and guidance aids

[CASI PAPER 72/14]

19 p3100 A71-37601

Aircraft ILS landing approaches, discussing approach area and surface and obstruction clearance surface and limit

21 p3325 A71-40891

Doppler scanning landing microwave system for air-derived azimuth and elevation angle aircraft guidance by frequency coding and reference carrier transmission

22 p3572 A71-42089

Scanning microwave landing guidance system coordinates choice, discussing signal format, antennas planar or conical beams and V/STOL application

22 p3572 A71-42090

Aeronautical radio navigation aids photo-optical calibration, describing photogrammetric procedure and ground equipment for checking out airport ILS systems

23 p3702 A71-43587

INSTRUMENT ORIENTATION

Optimal axis alignment for strapdown inertial guidance system, suggesting alternate method of raised mounting pads and cylindrical alignment pins

02 p0279 A71-12456

Mayer formula time determinations from meridian passage instrument, using star program and equalization observations

03 p0422 A71-13009

Geomagnetic field variations recording by two variometers, correcting for variation components effects by instruments orientation

06 p0901 A71-18284

Quartz magnetic variometer allowing simultaneous recording of magnetic field variations and suspension axis inclination changes

06 p0901 A71-18285

Optimum orientation and accuracy of redundant sensor arrays in space navigation, guidance and attitude reference systems

[AIAA PAPER 71-59]

06 p0925 A71-18518

Optimum transmitted data volume, orientation accuracy and size of narrow beam parabolic spacecraft antennas, defining optimum parabola for approximate radiation pattern

07 p1078 A71-19871

Instrument tilt effect on atmospheric turbulence measurements, presenting transformation equations for turbulence characteristics

09 p1488 A71-23028

Ion orientation technique for attitude control based on counterflow sensing in earth upper atmosphere, discussing accuracy

09 p1523 A71-23151

Instrument orientation optimization for ballistic missile applications, emphasizing acceleration induced velocity and position errors

11 p1796 A71-26410

Gimballed inertial navigation system, discussing initial alignment by strap-down system at standstill

11 p1796 A71-26416

Satellite parallax mounted camera installation for adjusting axis parallel to earth rotation axis

13 p2070 A71-29120

Paraboloid-hyperboloid Cassegrain telescope mirror centering, describing stigmatic point position permanent control in focal plane by geometrical method

21 p3375 A71-40066

INSTRUMENT PACKAGES

NT APOLLO LUNAR SURFACE EXPERIMENTS PACKAGE

Atmospheric entry probe from flyby mission to Jupiter, considering descent trajectory feasibility and instrument package

[AAS PAPER 71-142]

19 p3153 A71-37945

Meteorological research rockets instrument composition and systematization, discussing functional schemes, arrangement and onboard location

19 p3067 A71-38637

INSTRUMENT TRANSFORMERS

Measuring transformer for AC input signal with pulse width modulated semiconductor multiplier feedback

08 p1261 A71-20737

INSTRUMENTAL ANALYSIS

U AUTOMATION

INSTRUMENTATION

U INSTRUMENTS

INSTRUMENTS

Aerospace systems instrumentation magnetic tape standardization and testing

04 p0597 A71-15298

Aerospace technology application to oceanic instrumentation and communication requirements

04 p0583 A71-15307

Inertial instruments system-level tests under final use environment, discussing cost reduction

[AGARDOGRAPH-128]

05 p0750 A71-16308

Instrumentation - Conference, Pittsburgh, October 1970, Part 2, Advances in Instrumentation

09 p1443 A71-232

Aerospace instrumentation - ISA Conference, Seattle, May 1970, Volume 3

09 p1448 A71-222

Aerospace instrumentation - Conference, Vegas, May 1969, Volume 2

09 p1449 A71-222

INSULATED STRUCTURES

Transient heat conduction in dual-layer insulating plate exposed to pulse heating, discussing temperature response

[AIAA PAPER 70-14]

03 p0522 A71-14

INSULATING MATERIALS

U INSULATION

INSULATION

NT ELECTRICAL INSULATION

NT MULTILAYER INSULATION

NT THERMAL INSULATION

Self generated turbulence in insulating liquids causing unipolar charge carrier injection, describing charge transport by Lagrangian diffusion process

19 p3044 A71-375

INSULATORS

FET insulating layer electrical properties requirements, considering threshold voltage, dielectric constant, breakdown voltage and insulated gate FET stabilities

02 p0229 A71-118

Wave functions of image potential induced surface states of insulators

04 p0630 A71-157

AIN insulating films electrical characteristics use in charge storage devices, presenting Al-AIN capacitor current-voltage-insulator thickness relationships

09 p1509 A71-231

Breakdown voltage and high power tests for pressure bonded collector sheath tubes with cracked alumina insulators and flowing liquid metal coolant

11 p1709 A71-259

INSULIN

Bovine pituitary proteinase I action on oxidized chain of insulin, noting preference for specific bonds

05 p0718 A71-17

Alpha adrenergic inhibition of immunoreactive insulin release during deep hypothermia in puppies given glucose infusions

17 p2681 A71-346

INTAKE SYSTEMS

NT AIR INTAKES

NT CONICAL INLETS

NT ENGINE INLETS

NT HELICAL INDUCERS

NT HYPERSONIC INLETS

NT INTERNAL COMPRESSION INLETS

NT SIDE INLETS

NT SUPERSONIC INLETS

Inlet particle separators for engine erosion prevention, discussing tests of various models for separator efficiency, clogging resistance, pressure loss and flow distortion

04 p0639 A71-154

S-IVB liquid rocket engine and propellant flow systems restart shutdown in orbital operations

[AIAA PAPER 70-672]

07 p1183 A71-198

INTEGERS

Weighted finite incidence systems constructed using nonnegative integer functions and column vectors

16 p2603 A71-335

INTEGRAL CALCULUS

Multiple integrals numerical evaluation technique survey, discussing Monte Carlo, number-theoretic and functional analysis methods

02 p0276 A71-118

Feinman integral definition and relation to Schrödinger equation for square summable potentials with lower bound

17 p2765 A71-348

INTEGRAL EQUATIONS

NT FREDHOLM EQUATIONS

NT SINGULAR INTEGRAL EQUATIONS

NT VOLTERRA EQUATIONS

NT WIENER HOPF EQUATIONS

Gravitating particle system phase density, finding differential and integral equations for Fourier transform

01 p0150 A71-100

Cauchy problem for nonlinear integrodifferential equations with time lag argument, estimating iterative solution existence and uniqueness

01 p0112 A71-104

Linear integral equations with difference and summation kernels in elasticity theory, developing approximate solution method

01 p0171 A71-106

Orthogonal polynomials method for integral equations solution in two dimensional mixed boundary value problems of elasticity theory

01 p0171 A71-106

Lifting surface in unsteady subsonic flow, describing integral equation calculation method including kernel logarithmic singularity 01 p0003 A71-11020

Mixed type nonlinear integral equations, using approximate method for numerical solutions 02 p0276 A71-12541

Heat transfer analysis literature survey, including bibliography of perturbation, asymptotic and integral equations methods 02 p0333 A71-12650

Satellite translational motion in circular problem of three bodies, discussing existence of equations integral 03 p0484 A71-13223

Integrodifferential equations of motion of body with fixed point, obtaining solution and geometrical interpretation 03 p0457 A71-13587

Linear integrodifferential time lag systems quick response problem approximate iterative solution, considering convergence and controllability conditions 03 p0452 A71-14060

First order nonlinear nonautonomous systems equivalence to second order linear autonomous systems through governing differential equations variables integral transformation 03 p0390 A71-14076

Polymer materials linear photo creep characteristics description in terms of differential and integral equations, discussing relationship between optical and mechanical properties 03 p0514 A71-14357

Radiative/convective heat transfer in moving media, reducing boundary problem to integral equations 04 p0685 A71-15514

Nonlinear integrodifferential equations of heat and mass transfer problems, discussing asymptotic solution method 04 p0688 A71-15542

Homogeneous integral equations of asymmetrical elasticity in steady state, using compound layer volume potentials 04 p0620 A71-15887

Arbitrary surface gravitational potential function normal derivative determination, using Tikhonov regularization method for obtaining integrodifferential equation 05 p0739 A71-16421

Integral equation eigenvalues extension from single to multiple interface Neumann problem 05 p0776 A71-17222

Mixed boundary value problem in elasticity theory for piecewise homogeneous isotropic plate with slits, reducing to integral equations 06 p0983 A71-17361

Advances in differential and integral equations - Conference, University of Wisconsin, August 1968 06 p0918 A71-17637

Zigzag antennas current distribution by integral equation analysis 06 p0874 A71-17709

Rib reinforced cylindrical shell stability under annular and axial stresses, determining eigenvalue of homogeneous integral equation 06 p0993 A71-17816

Approximation theory applications to differential and integral equations, considering nonlinear Chebyshev method in connection with hyperbolic and heat transfer equations 06 p0919 A71-18207

Triple integral equations solution based on analytic functions theory, applying to stress-strain state in plate with two equal collinear cracks 06 p1002 A71-18346

Transonic supercritical flow past arbitrary airfoils, using integral relations method [AIAA PAPER 71-98] 06 p0844 A71-18553

Unsteady motion of finite span wing in ideal incompressible liquid near solid surface by integral operator method in potential acceleration space 06 p0846 A71-18701

Integral equation solution for air flow over mountain system, considering boundary value problems of Helmholtz equation 07 p1149 A71-18794

Two link approximation of Chaplygin function by coupling to integral equations, applying to ideal gas jet separation flow past symmetrical arc 07 p1016 A71-20084

Unsteady incompressible laminar boundary layer equations, obtaining similarity solutions from momentum integral equation 07 p1093 A71-20365

Electromagnetic wave scattering by perfectly conducting sphere, using integral equation formulation 08 p1253 A71-21294

Random solution of stochastic integral equation of tagged point in continuous turbulent flow 08 p1276 A71-21357

Elastic plate with circular hole, solving contact problem in elasticity theory with integrodifferential equation 09 p1535 A71-22181

Compressible boundary layer separation near zero skin friction by Kaplun perturbation technique, studying nonlinear integral equation with Abel kernel 09 p1432 A71-22455

Book on applied diffraction theory covering scalar and vector wave theory, radio wave propagation, linear integral equations, microwave lens, Fabry-Perot interferometers, etc 09 p1494 A71-22959

One dimensional linear stationary systems described by linear differential equations, discussing identification procedure with transformation into integral equations 10 p1585 A71-24157

Inhomogeneous rotating self-gravitating system kinetic theory, linearizing collisionless Boltzmann equation to two dimensional linear integral equation for obtaining small oscillation modes 10 p1641 A71-24278

Linear elastokinetics tensorial field integral representation derivation from reciprocal dynamic theorem for equations of motion 10 p1687 A71-24350

Integral equation for solving potential incompressible fluid flow past blade cascade on axisymmetric current surface in variable thickness layer 10 p1593 A71-24369

System identification problems, discussing approximation by polynomial integral operators, determinable classes in spectral decompositions, observation noise and stochastic systems stationary in observation time 10 p1587 A71-24742

Closed-loop nonlinear systems synthesis, using mapping in Chebyshev series converging everywhere, multidimensional linearization and Volterra singular integral equations 10 p1587 A71-24744

Steady state photon transfer through homogeneous semiinfinite isothermal atmosphere with two level atoms, deriving linear integral equation for escape probability distribution 10 p1643 A71-24964

Integral equations inversion in geophysics, discussing ionospheric profile from electron content and Faraday rotation measurements 11 p1756 A71-25645

Normality-independence characterization of stochastic integrals in linear processes 11 p1792 A71-26102

Parallel and standby redundancy systems with priority or noninstantaneous switchover, applying renewal theory integral equation 11 p1772 A71-26163

Unique solution of certain classes of linear and nonlinear functional-integral equations reducible to Volterra integral equations 11 p1793 A71-26562

Steady Oseen flow past semiinfinite flat plate with force singularity, deriving integral equation solution 12 p1896 A71-26938

EM wave scattering in waveguide by active regular shape bodies, using integrodifferential equations 12 p1881 A71-27337

Convolution-type integral equations over arbitrary finite segment number with kernels, showing solvability in spaces, applications and correctness 12 p1982 A71-27519

Contact stress between half plane and elastic cover plate, reducing problem to Prandtl type integrodifferential equation with Hilbert kernel 12 p1982 A71-27526

Simultaneous dual integral equations coupled pairs with constant coefficients involving Bessel functions of orders zero and unity 13 p2094 A71-28484

Laser resonator with selector for Hermite-Gaussian TEM/22 mode, obtaining integral equation solutions for eigenmodes and eigenvalues on digital computer 13 p2078 A71-28608

Numerical solution of nonclassical problem of calculus of variations, reducing nonlinear integral equation with Green function 13 p2095 A71-28819

Existence theorems for eigenvalues of integral equations with continuous kernels 13 p2096 A71-28907

Integral kinetic equation for flow distribution past body and surface heat flow, noting representation in form for computer solution 13 p1991 A71-29156

Neutral particle gas integral kinetic equations numerical solution without integration on lag parameter 13 p1991 A71-29157

German monograph on spline functions interpolation for solving integral equations and stress calculation in curvilinear edged disks 13 p2157 A71-29420

Turbulent boundary layer parameters changes across normal shock wave, integrating energy integral equation [ASME PAPER 71-FE-16] 13 p2052 A71-29455

Book on antenna admittance problem covering iterative solution of integral equations, Fourier series

solution, Wiener Hopf methods, transmission line theory, etc 14 p2193 A71-29932

Dissimilar elastic half spaces joined over circular region, calculating interfacial traction stresses induced by arbitrary loading from coupled integral equations 14 p2328 A71-30293

Integral equations for source functions of Ca II H, K and IR triplet lines for transfer through homogeneous stellar atmosphere 14 p2276 A71-30298

Schwarz-Christoffel conformal transformation inversion for electrostatic field integral equation formulation, applying to stepped-guide junction 14 p2212 A71-30515

Ridged waveguide complete eigenvalue solution by integral equation formulation and Ritz-Galerkin method 14 p2212 A71-30516

Linear integral equations with difference and summation kernels in elasticity theory, developing approximate solution method 14 p2333 A71-30991

Orthogonal polynomials method for integral equations solution in two dimensional mixed boundary value problems of elasticity theory 14 p2333 A71-30994

Integral equation methods application to exterior boundary value problems solution for Laplace and Helmholtz equations 15 p2441 A71-31350

Dyson integral equation describing generalized field of normal waves in plane randomly inhomogeneous turbulent layer 15 p2388 A71-31513

Averaging of nonlinear integrodifferential equations, demonstrating uniform convergence of sequence by successive approximations 15 p2442 A71-31521

Degree of closeness estimates for initial and averaged systems of differential and integrodifferential equations with conditions on right members 15 p2442 A71-31523

Turbulent wall jet with initial boundary layer, calculating growth and separation in arbitrary pressure gradient by integral method 15 p2389 A71-31581

[AIAA PAPER 71-612] Integral analysis of incompressible turbulent boundary layer with mass transfer and pressure gradient, including Stevenson velocity profiles and skin friction law [ASME PAPER 71-APM-2] 16 p2559 A71-33221

Linear equations general form including difference, differential, deviating argument, aftereffect and integrodifferential equations 16 p2603 A71-33531

Numerical algorithm for Cauchy problem nonlinear partial differential integral equations solution by invariant imbedding 16 p2604 A71-34082

Rigorous solution for multiple arm conical log spiral antenna by numerical solution of integral equations, considering current distribution, half power beamwidth, etc 17 p2715 A71-34752

Fourier coefficients and integral operators S numbers of summable functions 17 p2765 A71-34864

Periodic or almost periodic small combination vibrations onset conditions by integral equations method and averaging principle 17 p2779 A71-34910

Laplace transform application to linear system of partial differential, integrodifferential and difference equations with periodic and quasi-periodic coefficients 17 p2780 A71-34911

Periodic solutions of singularly perturbed hereditary systems of ordinary nonlinear integrodifferential equations 17 p2780 A71-34920

Averaging methods of nonlinear differential and integrodifferential equations with fast and slow variables over finite and infinite segments 17 p2766 A71-34923

Non-LTE problems computation based on integral equation approach, using discrete operator for radiative transfer equation solution 17 p2808 A71-35552

Linear array antenna far field transient time response formulation, using concise vector field integral equations and generalization 17 p2717 A71-35584

Integral equation method for solving mixed boundary value problems 17 p2769 A71-35798

High subsonic potential flow calculation past circular cylinder by integral relations method 18 p2844 A71-36326

Iterated double integrals for subsonic flow patterns bounded by segments of straight lines and free boundaries, using FORMAC 18 p2909 A71-36703

Functional analysis application to nonlinear integral equations, stressing Schauder fixpoint theorem 18 p2943 A71-36952

Complementary variational principles, noting application to differential, integral and matrix equations 18 p2943 A71-36957

Subsonic flow direct and indirect methods including Oswatich integral equation, thickness parameter expansion, Janzen-Rayleigh method and stream and potential functions in hodograph plane 19 p2992 A71-37453

Transonic flow theory and experiment, considering hodograph method, integral equation method, parabolic method and method of characteristics 19 p2992 A71-37454

Transient simultaneous conductive and radiative heat transfer in plane gray layer bounded by black walls, yielding nonlinear integrodifferential equation [ASME PAPER 71-HT-22] 19 p3165 A71-37993

Integral equation for determination of nonuniform gain profile effect on resonant modes of ion laser cavity, considering ring modes at high current densities 19 p3074 A71-38228

Circular planform punch pressure on elastic half space, solving system of two dimensional dual integral equations 19 p3160 A71-38478

Nonlinear vibrating system characteristics relationship to transient process, deriving Abel integral equations for damping coefficient and restoring force 19 p3104 A71-38483

Accuracy modeling guidelines for analyzing thin wire scattering structures using electric field integral equation 19 p3035 A71-38598

Cloud particles coagulation kinetics, using integral equation for distribution function 19 p3095 A71-38704

Integrodifferential difference equation for isotropic portion of velocity distribution function resulting from electron excitation and Coulomb interaction 20 p3274 A71-39048

Error bounds and variational principles for nonlinear differential and integral equations, exemplifying by Liouville and Poisson-Boltzmann equations 20 p3255 A71-39496

Generalized Riccati equation reduction to integral equation, leading to asymptotic solution of second order linear differential equations 20 p3255 A71-39574

Steady and unsteady flow work and energy loss relationships expressed in integral form representing perturbation kinetic energy, internal energy and pressure work 21 p3317 A71-40011

Nearby high velocity stars energy and momentum data, determining orbital properties and integrals of motion 21 p3440 A71-40062

Shallow spherical cap and deep thin spherical shell buckling, solving integral equations by iterative procedure 21 p3463 A71-40542

Iterative solution of Hallen integral equation for current distribution on lossless cylindrical transmitting dipole antenna 21 p3348 A71-40578

Projective numerical solution of integral equations arising in boundary value problems of electric and magnetic field theory 21 p3416 A71-40846

Asymptotic behavior of nonlinear Volterra integrodifferential equation solution, noting application to nuclear reactor dynamics 21 p3409 A71-41077

Nonlinear Volterra integral equation system solution using almost periodic forced oscillations 21 p3409 A71-41081

Elastic cracks and screw dislocation pile-ups crossing bimaterial interface, deriving dual singular integral equations 22 p3615 A71-41710

Cosmic ray transport in random magnetic fields, deriving coupled integrodifferential equations for radiant intensity and flux 22 p3592 A71-41915

Lifting line theory extension to low aspect ratio wings, proposing formulation for Prandtl integral equation 22 p3480 A71-42288

Narrow strongly radiating slot voltage distribution, investigating cavity coupling with integral equation 22 p3522 A71-42305

Semilinear hyperbolic systems analogous to differential-integral Boltzmann equations of gas dynamics, developing solutions existence for nonnegative initial data 22 p3531 A71-42690

Distribution function integral representation application to steady motion of monocomponent rarefied gas containing amorphous particles, using successive approximation for kinetic equation solution 22 p3482 A71-42868

Dual integral equations solutions to electromagnetic wave diffraction at plane conducting slotted screen 23 p3644 A71-43258

Lifting rectangular thin airfoil in symmetrical incompressible steady uniform orthogonal flow at small angle of attack, deriving Weissinger integral equation 23 p3625 A71-43487

Integral quadratic control quality estimates in terms of system coefficients with allowance for system oscillation characteristics 24 p3812 A71-44483

Crack theory application to problems with circular boundaries, solving singular integral equations by Aleksandrov-Libatskii approximation method 24 p3880 A71-44721

Convolution integral equation unique solution in second kind Fredholm equation form, applying to plane polarized electromagnetic wave diffraction on infinitely thin band 24 p3804 A71-44769

Cylindrical space simulation chamber with spherical test subject, deriving molecular incidence rate from integral equations with probability matrix for finite partial surfaces 24 p3816 A71-45138

Motion integrals conservation under Hamiltonian function variations, examining gyroscope equations of motion with parameter disturbances 24 p3849 A71-45343

INTEGRAL FUNCTIONS

ENTIRE FUNCTIONS

INTEGRAL TRANSFORMATIONS

NT CONVOLUTION INTEGRALS

NT FOURIER TRANSFORMATION

NT HILBERT TRANSFORMATION

NT LAPLACE TRANSFORMATION

Mathematical physics multidimensional boundary value problems seminumerical solution, using differential-difference method and integral transformations 05 p0783 A71-17014

Turbulent velocity field in noncircular cross section rectilinear duct, determining relation between viscosity ratio and dimensionless velocity by integral transformation 07 p1087 A71-18992

Integral transform methods for analytic solutions to current and potential distribution on disk in infinite plane for four limiting cases 08 p1237 A71-21471

Finite difference description for dynamic control plants with unknown disturbances based on integral transformation and extrapolation, applying to automatic control systems synthesis 08 p1270 A71-21975

Integral transformations application to approximate elastic solutions for nonlinear hereditary media, considering elastoplastic deformations under active loads 13 p2154 A71-28649

Linear two-point boundary value problem solution through integral transformation into Cauchy system with Green function as auxiliary dependent variable 15 p2443 A71-32441

Three dimensional nonlinear heat conduction problem solving by perturbation theory and finite integral transformation method 17 p2838 A71-35271

Sobolev function Q in radiative transfer, using invariant imbedding approach for integral equation transform 19 p3133 A71-37506

Penny shaped crack under time dependent impact wave loads, investigating transient response with integral transformations 21 p3468 A71-41002

INTEGRATED CIRCUITS

NT LARGE SCALE INTEGRATION

Command system and associated algorithm for synthesis of integrated microcircuits composed of components with memories 01 p0051 A71-10090

Silicon-on-sapphire complementary MOS circuits for high speed associative memory arrays, discussing system, circuit and device processing concepts 01 p0047 A71-10209

Computer aided design system for integrated circuits including layouts and logic simulation 01 p0058 A71-10249

Thin film lumped element microwave integrated circuits from concept to final functional devices 01 p0053 A71-10735

Thin film methods applied to microwave integrated circuits for compactness, reliability and low cost 01 p0053 A71-10736

MOS multiphase LSI circuits design using computer program 02 p0228 A71-11651

MOS transistor inverters static and dynamic characteristics in IC assemblies 02 p0228 A71-11656

Inner FET and FET static and dynamic inverters in digital IC, discussing switching characteristics, gates, memory cells, etc 02 p0228 A71-11812

Basic digital circuits with integrated TTL and MOS structural elements, giving diagrams for dual counters, frequency dividers, adders and shift registers 02 p0231 A71-11863

Space shuttle integrated electronic onboard and ground reusable systems design, considering data flow, management, checkout, computer decentralization, electronic switching and redundancy 02 p0231 A71-11970

Integrated optical communication circuit technology adaptable to batch processing, considering encapsulated planar arrays of rectangular dielectric waveguides 02 p0231 A71-12000

Microstrip double down-converter receiver for satellite earth stations, describing thin film integrated circuits and carrier selection 02 p0235 A71-12835

Reciprocal thermal influence, temperature areas and conduction distance of electronic components in compact circuits 03 p0387 A71-14325

Radio sets integrated selection components, noting ceramic capacitors and filters and coil circuits 03 p0388 A71-14336

Computer controlled laser machining system for cutting integrated circuit masks in thin films deposited as fused silica substrates 03 p0433 A71-14342

Rationalized design of integrated circuits for control systems, noting cost reduction and quality improvement 03 p0388 A71-14575

Two-wire IC pressure transducer bridge circuit performance features based on circuit analysis 04 p0561 A71-15594

Integrated circuit conductors short pulse high current rating, identifying three failure regimes 04 p0559 A71-15874

Broadband hybrid UHF integrated power amplifiers providing high output, noting integration techniques, design, fabrication and characterization 04 p0559 A71-15876

Microwave integrated circuit technology, discussing substrates, conductors, dielectrics and resistors materials and design data and fabrication techniques 05 p0728 A71-16914

MOS large scale IC phosphosilicate glass substrate vapor deposits effects, including hardness, pinhole density and electromigration 07 p1070 A71-18868

Permanent IR electron radiation effects on hardened MOS integrated inverter circuits, using units with plasma grown and vapor deposited aluminum oxide 07 p1174 A71-19053

Ionizing radiation effects on monolithic metal oxide semiconductor inverters, including testing and hardening techniques 07 p1070 A71-19060

Dielectric thin optical film waveguides excitation for integrated optical circuitry by Gaussian laser beams 07 p1123 A71-19213

Power station electronic control equipment and integrated circuit computer reliability data analysis, emphasizing combined mathematical prediction and observation 07 p1077 A71-19565

Holographic microscopy technique fundamentals and electrically activated integrated circuit changes in section 07 p1113 A71-19786

Radiation tolerant monolithic amplifier design, considering IF amplifier 07 p1080 A71-20411

Interdigital capacitors frequency response and application to lumped element microwave integrated circuits 08 p1261 A71-20753

Superconductivity based cryogenic electronics, considering thin film IC, miniaturization, microwave circuits, memory elements, etc 08 p1263 A71-21067

Planar-epitaxial IC resistors p-n junction parasitic effects on cut-off frequency, obtaining design formulas for capacitance and geometry 08 p1264 A71-21074

Microwave multistage transistor amplifier with IC configuration, discussing design and performance 08 p1265 A71-21287

Phase locked loop as versatile building block for integrated circuit design, discussing basic principles and applications in analog and digital signal processing 09 p1415 A71-22354

Emitter coupled integrated transistorized logic elements, improving steady state noise stability by hysteresis in transfer characteristics 09 p1416 A71-22467

Semiconductor integrated circuit fabrication optimization, considering defect density, component number, crystal size and cost analysis 09 p1416 A71-22490

- Integrated circuit components equivalent circuits, considering transistor logic circuits and admissible noise 09 p1416 A71-22491
- MOS transistor cascade amplifiers, discussing monolithic integrated circuits 09 p1416 A71-22492
- Integrated circuits electrical parameters and design joint optimization, describing technological analysis, physical component characteristics, operating conditions and design factors 09 p1422 A71-22493
- Integrated dynamic digital computer elements, examining regenerative information storage, internal duration determination by clock pulse frequency and switching 09 p1411 A71-22494
- Integrated circuits semiconductor components, determining effects of heat energy production/withdrawal and strong field on electric current carriers mobility and concentration 09 p1416 A71-22496
- IC quality control by temperature fields contactless measurement, using microthermographs 09 p1450 A71-22894
- Integrated microwave circuits substrate materials, discussing fabrication techniques with attention to mechanical, thermal and electrical characteristics 09 p1418 A71-23059
- Substrate materials for microwave integrated circuits, comparing dielectric constants, surface finishes and thermal conductivity for alumina, sapphire, magnesium titanite, YIG and beryllium oxides 09 p1418 A71-23156
- Logical GaAs integrated laser circuits, discussing integrated laser modules with electron-hole junctions fabricated by diffusion techniques 11 p1773 A71-25917
- Computer aided reliability assurance system /CARAS/ for integrated circuits, correlating process and failure data 12 p1890 A71-26658
- Total reliability requirement procedure for design, development and production of medium- and large-scale integrated circuits 12 p1884 A71-26660
- Microwave integrated circuits lumped elements, including microstrip transmission lines configurations and electrical parameters 12 p1886 A71-26988
- Direct analysis of IC by laser beams, considering homogeneity test scanning of Ge semiconductor crystals through photovoltaic injector microscopy 12 p1914 A71-27041
- Book on integrated circuits and semiconductor devices covering MOSFET, optoelectronic devices, silicon controlled rectifiers and thyristors 13 p2036 A71-28042
- P channel enhanced MOS transistors, logic elements and digital integrated circuits in silicon films on sapphire substrates 13 p2038 A71-28716
- Compact head mounted six channel IC telemeter for artifact free EEG recording during laughter 13 p2020 A71-28889
- Semiconductor materials technologies, discussing optoelectronic and microwave components, photodiode arrays, HF diodes and transistors and IC Doppler radar units 13 p2111 A71-28908
- Thin film hybrid IC microwave component development, noting market and consumer applications 13 p2039 A71-28909
- Interface IC circuits for driving high voltage transistor switches from low level logic inputs, noting avionics application 13 p2039 A71-28910
- Microwave integrated stripline Gunn oscillators with fixed/variable frequency tuning in X band 13 p2039 A71-28911
- Integrated S band microstrip parametric amplifier modules with self contained Gunn effect pump oscillator for space flight applications 14 p2210 A71-29570
- Synthesis of linear antenna with integrated currents for specified ratio of antenna radiation to elementary radiator patterns 14 p2194 A71-30101
- Miniature integrated sensor pressure transducers for inlet air flow distortion and buffet studies of wind tunnel models 14 p2245 A71-30336
- Parallel pressure multiplexer and encoder for aerodynamic testing, employing zero pressure detectors coupled with IC digital electronics and reference pressure signal 14 p2222 A71-30342
- Substrate emitter monolithic inverted transistor structure for low-power high-current gain application 15 p2375 A71-31474
- Josephson and IC type superconducting tunneling junction neuristor devices performance tests, presenting bibliography 15 p2377 A71-32317
- Coupling effects between reliability components of integrated circuits by modeling failures in structures 15 p2377 A71-32345
- Ferrimagnetic components in microwave IC, considering junction circulators, planar phase shifters, etc 16 p2547 A71-33551
- Lumped elements in microwave IC, considering networks design, fabrication and performance in active and passive circuits 16 p2547 A71-33552
- Integrated wideband low-noise X-band sweeping superheterodyne receiver, demonstrating advantages of microwave IC techniques application 16 p2547 A71-33553
- S-band hybrid microwave IC module for phased arrays, presenting mechanical and electrical design details and performance test data 16 p2547 A71-33554
- L band microwave IC front end for identification friend or foe /IFF/ receiver, noting environmental and filtering requirements 16 p2547 A71-33556
- SHF low noise IC mixer, considering effects of series resistance and barrier capacitance in diode and internal resistance of local oscillator 16 p2548 A71-33558
- Microwave IC bandpass filters, utilizing dielectric resonators for high Q values 16 p2548 A71-33559
- Low loss surface oriented waveguide for millimeter IC, using high permittivity rectangular dielectric image line 17 p2714 A71-34603
- Integrated telescope computer system, including magnetic disk storage, digital encoding, drive control and automatic guiding 17 p2711 A71-34984
- Commercial production of high reliability components in plane transistors, bipolar integrated circuits and printed circuits technologies 18 p2889 A71-36355
- High reliability integrated complementary MOS circuit fabrication chain in Concerto satellite program, discussing technological process with account of physicochemical data 18 p2890 A71-36536
- Integrated complementary MOS circuit technology, discussing low power consumption, high speed, n and p regions realization on Si plates and design parameters relations 18 p2891 A71-36562
- Combinational possibilities of special application modules based on thin-film hybrid integrated circuits in standardized encapsulations 18 p2893 A71-36625
- Integrated digital emitter coupled logic /ECL/ circuits with transistors in nonsaturated mode 18 p2896 A71-36799
- Cellular array for multiplication and division of two binary numbers, discussing implementation with transistor-transistor logic integrated circuits 18 p2894 A71-36833
- IC applications to microwave frequencies, relating circuit performance to substrate roughness and thickness of thin film metal adhesion layers 18 p2895 A71-36981
- Design and fabrication of frequency multipliers from 10 to 30 GHz on silica substrates by scaling and integrated circuit processing 19 p3026 A71-37219
- Digital integrated circuits technology with MOS transistors packed on crystal wafer without isolation diffusions 19 p3028 A71-37566
- Panels and cassettes mechanical design for Camac modular construction of electronic analog and digital measuring instruments based on integrated circuits 19 p3029 A71-38065
- Machining integrated circuit metal film masks with continuously operating carbon dioxide laser and high pressure pulsed He-Ne laser 19 p3069 A71-38234
- Electro-optic He-Ne laser microscope for high-speed high-precision edge detection for IC masks 19 p3075 A71-38236
- Basis functions for arbitrary time variable network symmetries for large scale integration, using group theory 19 p3038 A71-38488
- Insulator surface ion migration effects on MOS and bipolar integrated circuits, describing inversion voltage and surface conductivity and recombination velocities 19 p3033 A71-38505
- Reliable plastic encapsulated semiconductor devices design, production and evaluation, noting application to IC 19 p3033 A71-38509
- Mass transport at high current densities in Al and Mo thin film conducting stripes, noting effect on IC life 19 p3119 A71-38511
- Ambient gas effects on Au-Al bonds life in integrated circuit package 19 p3119 A71-38514
- Integrated circuit life testing, comparing functional and pin-to-pin screening data 19 p3034 A71-38516
- Hybrid microelectronics IC S band double conversion phase locked receiver, discussing fabrication, process requirements and component selection criteria 19 p3035 A71-38538
- Cost effectiveness screening program for integrated circuits, considering four stages of life cycle 20 p3202 A71-38753
- Phase and amplitude error detection in photomasks for semiconductor integrated circuits with spatial frequency coherent optical filtering 20 p3246 A71-39449
- Book on electronic components covering radio, cathode ray and microwave tubes, telecommunication, ceramic materials, light conversion to electricity, integrated circuits, etc 20 p3205 A71-39775
- Monolithic alphanumeric array of planar light-emitting GaAsP diode matrix on common chip for programmed function keyboard use in display devices 21 p3349 A71-40108
- Red and green light emitting GaP junction diodes and monolithic arrays for display devices, discussing fabrication and properties 21 p3352 A71-40110
- Integrated circuits failures due to plastic or ceramic packaging methods, describing failure analysis technique 21 p3353 A71-40439
- Digital techniques for tactical radar signal processing functions, discussing low cost integrated circuitry, moving target indicators, and analog to digital converters 21 p3348 A71-40588
- Impurity diffusion self aligned MOS and lateral transistors used in IC 21 p3354 A71-40730
- Holographic methods for etching masks of IC and other semiconductor components 21 p3354 A71-40731
- C-MOS integrated circuit technology emphasizing reliability, design, failure mechanisms and performance parameters 21 p3355 A71-40737
- [DFVLR-SONDDR-100] Semiconductor components reliability assurance under assumption of failure rate decrease with time for IC quality and performance improvement 21 p3356 A71-40746
- Plastic encapsulated IC reliability tests, relating results to failure mechanism 21 p3356 A71-40747
- Subnanosecond digital computer with emitter-coupled fully integrated circuit packaging concept 21 p3351 A71-40748
- Beam-lead nitride-passivated IC seal junction chip reliability evaluation by life tests for optimum packaging into functional modules 21 p3357 A71-40813
- Beam-lead technology application to complementary MOS IC processing 21 p3357 A71-40814
- Hybrid integrated wideband linear microwave power amplifiers for S and C bands, discussing construction and performance 21 p3357 A71-40817
- Logical GaAs integrated laser circuits, discussing integrated laser modules with diffused p-n junctions 21 p3394 A71-41228
- Masking techniques in monolithic IC production in microelectronics, emphasizing contactless, lens, holographic and electron beam projection methods 22 p3525 A71-41713
- Wireless assembly methods for thin and thick film hybrid and monolithic IC, emphasizing flip-chip elements microelectronic devices fabrication and interconnection 22 p3525 A71-41714
- Book on thick film microelectronics covering microcircuit design, fabrication, packaging and applications 23 p3650 A71-43224
- Analog transistor model for IC simulation, discussing static characteristics and switching times 23 p3650 A71-43350
- Thin film silicide resistors in monolithic IC for high sheet resistance or radiation hardness using sputtering deposition without protective overlayer 23 p3655 A71-43428
- Interconnection Ta thin films and silicon encapsulation for solid state components in hybrid IC under high humidity 23 p3656 A71-43431
- Silicon thin film on sapphire for bipolar and MOSFET transistors for microwave IC and subnanosecond switching circuits 23 p3715 A71-43434
- HF and LF transistors suitability for integrated high Q LC circuits, studying inductivity, Q and component frequency dependence 24 p3807 A71-44377
- Thin film circuit microstructures and integrated microcircuits with distributed parameters, discussing analytical determination of microcell parameters 24 p3807 A71-44378

INTEGRATION [REAL VARIABLES] U MEASURE AND INTEGRATION INTEGRATORS

NT DIGITAL INTEGRATORS

Boxcar integrator attachment for oscilloscopes, improving S/N ratio of repetitive signal 03 p0427 A71-13918

Reversible point integrator circuits synthesis, using AB-102 universal ALGOL computer program 10 p1581 A71-24355

Quasi-analog and hybrid computers, describing ARKUS hybrid integrator effectiveness in solving boundary value problems and ordinary differential equations 10 p1581 A71-24382

Stationary and dynamic characteristics of integrators with dosage capacitor for analog frequency measurements, analyzing dynamic response at large modulation depth via analog computer simulation 10 p1589 A71-24502

Noise stability during noncoherent reception of frequency shift keyed signal by receiver with finite Q predetector integrators in presence of fading 11 p1733 A71-25938

Gravity center effect on drift of gyro linear acceleration integrator on vibrating base, showing errors at frequencies near nutations 13 p2069 A71-28933

Closed loop system analysis of triangular wave generator consisting of integrator, on-off element with hysteresis and multiplier 15 p2376 A71-32026

Noise stability during noncoherent reception of frequency shift keyed signal by receiver with finite Q predetector integrators in presence of fading 20 p3196 A71-39258

INTEGRITY

Metal microfinishing technique, evaluating surface integrity degrading effects and total time requirements 05 p0759 A71-16464

INTEGRAL DIFFERENTIAL EQUATIONS

U DIFFERENTIAL EQUATIONS

U INTEGRAL EQUATIONS

INTELLIGENCE

Three phase code transformation task reliability and correlation, representing general factor analytic intellectual abilities and personality characteristics 20 p3192 A71-39073

INTELLIGENCE

NT ARTIFICIAL INTELLIGENCE

NT INTELLIGENCE

INTELLIGIBILITY

NT SPEECH RECOGNITION

Flight helmets speech intelligibility evaluation using in-flight manikin recording 10 p1572 A71-25069

Computer simulation of automatic voice communication link intelligibility measurement, using speech recognition techniques 13 p2032 A71-28872

Speech intelligibility prediction in time varying aircraft noise based on test score relationship to articulation index for steady state noise 20 p3271 A71-39766

Time varying aircraft noise effect on speech intelligibility, discussing test for relation to articulation index 21 p3343 A71-40709

INTELSAT SATELLITES

INTELSAT IV earth stations communications standards, discussing receiver gain-noise temperature ratio, feed polarization, radiation power and control, transmission modes, etc 02 p0221 A71-12777

Satellite operating conditions effects on INTELSAT IV earth station design, emphasizing communications aspects 02 p0221 A71-12778

INTELSAT earth station operations via SPADE demand-assignment system, discussing interference requirements, frequency stability, gain flatness, etc 02 p0221 A71-12780

Earth station modifications for INTELSAT IV operation, discussing transmission parameters, distortion control, amplifier design, etc 02 p0221 A71-12786

Waveguide feeder system design for antenna receive path of Intelsat 3 satellite ground station, considering system noise temperature 02 p0223 A71-12800

Antenna primary feed design and sample and store technique tracking system with conical scan control for Intelsat 3 satellite ground station 02 p0223 A71-12802

Linear low noise wideband frequency modulator for Intelsat 4 satellite telephony communication, considering channel capacity 02 p0234 A71-12819

Earth station equipment for Intelsat 4, discussing thermal noise, transmitters, wideband receivers and demodulators 02 p0224 A71-12829

Earth station communication system planning for Intelsat 4, discussing telephony and TV transmission 02 p0225 A71-12830

Intelsat system earth station on-site planning considerations for integration with existing wideband communication system and traffic growth demand 03 p0380 A71-14343

Intelsat global network demand assignment multiple access system, discussing traffic density and earth station functional requirements 06 p0869 A71-18234

Intelsat 3 global satellite communication system design and performance 06 p0870 A71-18393

Intelsat 3 Ground Control System functions, design and operation of tracking, telemetry and command stations subsystems 06 p0870 A71-18394

Buitrago/Spain/earth station for Intelsat operation, discussing tracking antenna design and performance 06 p0880 A71-18396

Indonesian Intelsat 3 earth station equipment, operation and performance 06 p0880 A71-18397

Intelsat 3 satellite Communication, Telemetry, and Command system using transponders for multichannel voice and TV transmission 06 p0870 A71-18398

Microwave local oscillator and beacon generator for Intelsat 3, discussing design, operation and performance 06 p0877 A71-18400

Wideband mixer for Intelsat 3 satellite, describing design, operation and performance 06 p0877 A71-18401

Microwave transmitting and receiving duplexers for Intelsat 3 satellite, discussing design, operation and performance 06 p0877 A71-18402

Intelsat 3 satellite mechanical and electronic components fabrication, emphasizing quality and reliability assurance procedures and assembly techniques 06 p0905 A71-18403

Intelsat 3 satellite reliability program, discussing test procedures, redundancy, tradeoff against weight, etc 06 p0877 A71-18404

Intelsat 4 satellite optimum channel capacity as function of earth station performance 07 p1056 A71-18809

Digital multiple access communications for commercial transmission via Intelsat satellites 07 p1057 A71-18817

Satellite communication system parameters optimization based on economical and technical constraints, applying to Intelsat 3 07 p1063 A71-20040

Satellite communications systems international planning, discussing Intelsat system limitations 09 p1548 A71-23354

Intelsat 4 satellite transponder, examining receivers, transmitters, mechanical stability and heat transfer 10 p1578 A71-24509

Intelsat system ground station equipment testing including antenna radiometric gain, noise temperature, energy dissipation, telephone and TV performance measurements 10 p1580 A71-25104

Australian satellite domestic telecommunications network design, discussing population distribution, existing systems and Intelsat 3 F-4 11 p1730 A71-25264

Intelsat 4 transmission subsystems design, discussing alternative high power amplifier configurations, redundancy and emergency routing of transmitted RF carriers 12 p1894 A71-26992

Intelsat 4 satellite Spade communication system, using common reserve circuits and repeaters 15 p2373 A71-32640

International Telecommunications Satellite Consortium, reviewing legal order, organization structural framework, objectives and financial aspects 16 p2664 A71-33584

Intelsat system, describing organization, satellites, space segment support elements and ground stations 17 p2811 A71-34230

Satellite telecommunication systems, considering standard and small transportable ground stations and Intelsat system 17 p2696 A71-34233

Satellite communication technology in next decade covering Intelsat 4 characteristics, meteorological satellites, navigation aids, multichannel telephone and TV circuits and frequency assignment 17 p2699 A71-34677

PSK modem for multiple access communication system with time distribution, discussing performance tests on INTELSAT 3 17 p2700 A71-34688

Intelsat 4 transponder for broadband multicarrier operation with frequency and pulse modulation, considering TWT, tunnel diode amplifiers, filters, equalizers, mixers, multiplexers and antennas 17 p2705 A71-35099

Earth stations operating in Intelsat System, discussing mandatory performance requirements and design approaches 17 p2705 A71-35100

Intelsat communications satellite system network operation, describing reliability outages, maintenance and economy 17 p2705 A71-35101

Intelsat 4 communication system simulation a transponder engineering model to test performance objective concerning baseband distortion and modulation 17 p2705 A71-35102

Intelsat satellite-earth station communication technology, considering microwave line of sight techniques 17 p2707 A71-35103

Satellite communication ground station center conjunction with Intelsat 3 satellites system for transcontinental telephone links 17 p2708 A71-35104

Intelsat 3 satellite communication ground station radio receiving and transmitting equipment design 17 p2724 A71-35105

Communication satellite ground station equipment modifications for second station compatible with Intelsat 3 17 p2709 A71-35106

International communications law developments, discussing capital investment, information dissemination, 1967 space treaty and Intelsat program 18 p2986 A71-36160

East-West cooperation in space telecommunications, outlining Intelsat and Intersputnik organizational structure 18 p2987 A71-36161

Satellite broadcasting to West African countries, discussing communications policies, NASA tracking stations in Africa and U.S.-Nigeria agreement 18 p2987 A71-36162

PSK modem for PCM-TDMA system, discussing performance tests on INTELSAT 3 18 p2880 A71-36163

Intelsat 3 and 4 RF demodulator design with tracking filters, using varactor for frequency control and discriminator for frequency drift compensation 18 p2890 A71-36164

Spectrum limitation of FM carrier in case of accidental overloading of modulating signal arising in Intelsat 4 communication system 18 p2891 A71-36165

High power nickel cadmium battery for geostationary communications satellites for replacement in Intelsat 4 series 18 p2852 A71-36166

Fuel slosh energy dissipation and dynamic stability of Intelsat 4, discussing spacecraft and tank selection [AIAA PAPER 71-954] 19 p3148 A71-37100

Telecommunications satellites, discussing Intelsat series, multiple access, radio navigation, weather satellites and earth resources satellites 19 p3017 A71-37400

Low noise parametric amplifier design and construction for Intelsat 4 satellite communications earth stations 19 p3027 A71-37401

European research, development and production of solar cells, discussing Intelsat 4 program applications 20 p3179 A71-38840

Intelsat 1, 2, 3 and 4 satellite network developments for world telecommunication coverage, discussing expected future replacement and modulation and multiple access technologies 23 p3643 A71-43220

INTENSIFICATION

U AMPLIFICATION

INTENSIFIER TUBES

U IMAGE INTENSIFIERS

INTENSIFIERS

NT IMAGE INTENSIFIERS

NT IMAGE ORTHICONS

INTEPLANETARY SPACECRAFT

NT MARINER-MERCURY 1973

INTERACTIONS

Laser interaction and related plasma phenomena U.S. Army Conference, Hartford, June 1969 11 p1775 A71-26000

INTERATOMIC FORCES

Interatomic forces and gas theories from Newton to Lennard-Jones, discussing hypothetical deductive atomic models relation to gas properties 01 p0129 A71-11460

Hydrogen molecule-atom short range interaction energy, calculating multicenter integrals for screening constants 02 p0286 A71-11950

Interatomic electric dipole moment coefficients: derivation by approximation involving accessible atomic properties, noting application to H atoms 02 p0287 A71-12700

Adhesive joints bonding strength, discussing relative contribution of interatomic and intermolecular

forces and viscoelastic, viscous or plastic deformation effects
14 p2276 A71-29894

Na D lines broadening by atomic H, discussing interatomic forces between Na and H atoms in terms of NaH molecular potentials
16 p2614 A71-33101

Neutron diffraction analysis of atomic arrangements in maraging steel, discussing interatomic attractions
19 p3081 A71-37722

INTERCEPTION
Two impulse rendezvous between coplanar circular planetary orbits, considering mono-impulsive interception/flyby/ problem for optimality
05 p0812 A71-16731

INTERCEPTOR AIRCRAFT
U FIGHTER AIRCRAFT
INTERCEPTORS
Ballistic reentry warheads atmospheric interception, investigating defensive nuclear bursts effects
01 p0163 A71-10268

Modified steepest descent algorithm for optimum trajectory computation applied to interceptor missile control
14 p2207 A71-30018

INTERCONNECTION
U JOINING
INTERCONTINENTAL BALLISTIC MISSILES
NT MINUTEMAN ICBM
Instrumentation System Margin Analysis Program /ISMAP/ for ICBM telemetry data acquisition systems performance tests
01 p0032 A71-10882

Antenna and telemetry system for spherical shell ICBM reentry vehicles data link to ground
01 p0036 A71-10986

INTERFACE STABILITY
Glass fiber-epoxy resin composites shear strength, considering fiber length and interfacial bond effects
01 p0106 A71-10277

Carbon fiber surface treatment for reinforced plastic composites interlaminar strength increase, using wet oxidation process based on hypochlorous acid
02 p0274 A71-12485

Interfacial wetting, bonding and chemical and mechanical stabilities in whisker composites, discussing system stability
04 p0611 A71-14948

MOSFET transistors instabilities due to charge exchange near oxide-silicon interface states, determining energy levels distribution and time constants
05 p0791 A71-16165

Shearing gravity waves /Kelvin-Helmholtz/ instability in isothermal layer model discontinuous interface application to CAT
05 p0777 A71-16667

Tangential body forces and pressure perturbation interactions in thin liquid film, considering destabilizing effect impairing film cooling efficiency
11 p1751 A71-25491

Particle-metal matrix interface strength of dispersion strengthened Ni alloys, developing direct tensile stress measurement method
13 p2089 A71-29408

Fluid surface instability under perpendicular acceleration, presenting singular perturbation problem solution by successive approximations method
16 p2561 A71-34160

Turbulent wakes flow entrainment mechanism, investigating turbulence spreading near interface between laminar and turbulent regions
17 p2671 A71-34899

Upstream influence and interfacial waves in open channel two fluid small perturbation flow
23 p3663 A71-43446

INTERFACES
NT FLUID BOUNDARIES
NT GAS-SOLID INTERFACES
NT JET BOUNDARIES
NT LIQUID-LIQUID INTERFACES
NT LIQUID-SOLID INTERFACES
NT LIQUID-VAPOR INTERFACES
NT SOLID-SOLID INTERFACES
Boundary motion between media during transport phenomena under Stefan conditions, establishing shock front coordinates by Hadamard algorithm
03 p0520 A71-13951

Charging carriers of MOS structure interface states, considering effect on static transistor characteristics
08 p1265 A71-21291

Biharmonic problems solution in elasticity theory for piecewise homogeneous doubly connected media with interface in conformal mapping of ring onto doubly connected region
19 p3160 A71-38486

Stress concentrations and singularities at interface corners, presenting procedure for standardized mathematical formulation of conditions for different physical problems
23 p3777 A71-43494

INTERFACIAL ENERGY
Thin nickel aluminide sheets and small particles long range ordering, discussing antiphase boundary energy effects
07 p1133 A71-19441

INTERFACIAL STRAIN
U INTERFACIAL TENSION
INTERFACIAL TENSION
Plane potential incompressible fluid flow in channel with rough bottom and variable surface pressure, allowing for gravitational and surface tension forces
03 p0406 A71-14567

Surface tension effect on dispersion of Rayleigh waves in elastic body
04 p0673 A71-15882

Heavy liquid shells of revolution, determining equilibrium form in gravitational and surface tension forces from condition of minimal functional of total free energy
06 p0994 A71-17827

Subsurface flow generation by surface tension variation due to flame spreading over liquid fuel at large Reynolds number, using hydrodynamical analysis
06 p1009 A71-18643

[AIAA PAPER 71-207] Free fall of sphere in viscous fluid, expressing fluctuations frequency as function of interfacial tension, sphere density and diameter
08 p1276 A71-21878

Mercury intrusion porosimetry application to pore size and shape measurements for porous solids, discussing solid and air compressibilities, surface tension, contact angle, etc
09 p1453 A71-22168

Transient stresses in heat shield generated by short duration pressure pulses, using method of characteristics for interface stresses
11 p1844 A71-25330

Initially spherical liquid droplet transient response under surface tension accelerated by external gas flow
11 p1749 A71-25355

Strength transfer at glass-epoxy laminates interface in reference to critical surface tension of coupling agent on fabrics
11 p1786 A71-25414

S-shape lines of axial displacement field and interlaminar shear edge effect in laminated composites verified by moire technique
11 p1852 A71-26390

Interlaminar plane shear stress in fibrous composites under elastic deformation with edge effect, using membrane finite element analysis
11 p1852 A71-26394

Titanium nitride sintering in vacuum, noting strain by grain sliding to pore center under surface tension force effects
12 p1918 A71-27527

Interfiber stress model for elastic matrix-fiber reinforced composites under inplane shear and transverse normal loading
15 p2507 A71-32096

Unified raindrop breakup theory, examining spherical liquid drop transient response under surface tension accelerated by uniform external gas flow
16 p2557 A71-32924

Gas bubble in liquid under surface tension, weightlessness and rotation, determining angular velocity for fluid system disintegration
16 p2560 A71-34142

German monograph on heat transfer from vertical heating surfaces to liquids at rest in nucleate boiling, showing microstructure interaction with interfacial tension
17 p2838 A71-34852

Ideally incompressible fluid with free surface, analyzing interfacial tension forces effects on rotational-translational motion stability
17 p2730 A71-35648

Convergent approximations of impulsively loaded stable structures with account of geometry changes and discontinuity interfaces
18 p2978 A71-36267

[ASME PAPER 71-APM-KK] Engineering aspects of zero gravity personal hygiene and waste management systems, noting controlled air flows, surface tension and artificial gravity use
18 p2872 A71-36653

[AIAA PAPER 71-865] Mean curvature of deformed spherical surface in study of equilibrium configuration of water drops under surface tension, using differential geometry
19 p3045 A71-37899

Superconductivity, reviewing critical current/field concepts, Meissner effect, negative surface tension, zero resistance and applications
20 p3276 A71-39247

Buoyancy and surface-tension induced fluid instabilities in open and closed vertical circular cylindrical containers from series solution by Jeffreys-Goldstein method
21 p3367 A71-40667

Forced flow laminar film boiling heat transfer coefficients from vertical surface in terms of interfacial shear at liquid-vapor interface
21 p3476 A71-40896

Interlaminar shear stress and midsurface displacement of thin orthotropic laminated cylindrical shells, using linear deformation theory
21 p3470 A71-41018

Incompressible inviscid fluid free droplet surface layer tension determination as function of curvature from mechanical moment model
22 p3613 A71-41565

INTERFERENCE
Rocket/launcher aerodynamic interference effects investigation by wind tunnel simulation, determining interference coefficients for rockets ballistic dispersion calculations
08 p1274 A71-21995

[AIAA PAPER 71-269] Transonic wind tunnel wall interference effects experimental determination, investigating porous and slotted walls
08 p1229 A71-22013

[AIAA PAPER 71-292] Multiple-beam interference effects in Fabry-Perot interferometer with small wedge between mirrors, deriving expressions for light beams path
14 p2243 A71-30273

INTERFERENCE DRAG
Savart plates use in grating interferometers, deriving expressions for phase retardations for arbitrary angles between optical axis and plate normal
12 p1904 A71-26798

Interference analysis of wing with overlapping multipropellers in uniform velocity stream confined in elliptical cross section cylinder
15 p2346 A71-31583

[AIAA PAPER 71-614] Interference loading linear prediction on aircraft stores at supersonic speeds, considering flow field due to jet fighter bomber
19 p2996 A71-37290

INTERFERENCE GRATING
Strain analysis by moire-rosette method, using fringe patterns from pair of crossed gratings through optical spatial filtering
03 p0423 A71-13549

Plane wave diffraction by double grating of thin circular cylinders, determining field polarization in directions parallel and perpendicular to axis
05 p0718 A71-15995

Radial direction shearing interferometry, considering wave front radial phase derivative display by axicon or circular grating arrangements
07 p1110 A71-19477

Plane wave diffraction by double grating of thin circular cylinders, determining field polarization in directions parallel and perpendicular to axis
22 p3515 A71-42744

Plane electromagnetic wave diffraction by infinitely conductive grating at nonorthogonal incidence angles, using conformal mapping technique
24 p3847 A71-44357

INTERFERENCE LIFT
Upwash interference on two dimensional jet flap wing in slotted wall tunnel, using small disturbance theory
02 p0187 A71-12690

Jet interference effects on rectangular and swept wings, presenting wind tunnel test data for range of jet locations, inclinations and velocity ratios
05 p0693 A71-15951

[DGLR-70-052] Wind tunnel boundary interference on V/STOL model calculated in test section with solid vertical and slotted horizontal walls, using image method and Fourier transforms
08 p1229 A71-22029

[AIAA PAPER 70-575] Collocation method predicting oscillatory subsonic pressure distributions on interfering parallel lifting surfaces, considering approach more economical than finite element method
11 p1701 A71-25309

[AIAA PAPER 71-329] Wing-jet interference effects in cross wind on thrust and aerodynamic characteristics at large distance from and near ground
13 p1993 A71-29207

INTERFERENCE MONOCHROMATIZATION
U DIFFRACTION
U MONOCHROMATIZATION
INTERFEROGRAMS
U INTERFEROMETRY
INTERFEROMETERS
NT FABRY-PEROT INTERFEROMETERS
NT MACH-ZEHNDER INTERFEROMETERS
NT MICHELSON INTERFEROMETERS
NT MICROWAVE INTERFEROMETERS
NT PHASE SWITCHING INTERFEROMETERS
NT RADIO INTERFEROMETERS
Optical schemes of laser ring interferometer with selective characteristics, noting coupling via scattering at resonator optical elements
02 p0259 A71-11934

High resolution automatic measurement of ultrasonic velocity changes using interferometer and FM oscillator
02 p0250 A71-12134

Laser image speckle interferometer design for observing vibrational modes on diffusely reflecting surfaces as alternative to holographic methods
02 p0250 A71-12134

Multiple exposure holographic interferometer for static and dynamic photomechanics 03 p0422 A71-13171

Modified Ashby-Jephcott laser interferometer schlieren system for HF gas density measurements 03 p0427 A71-13922

Concave mirror interferometer for laser radiation spectra measurements, featuring piezoelectrically tuned optical system 03 p0439 A71-14000

Discrete radio sources precise declinations and optical identifications, using prototype space frequency interferometer 04 p0641 A71-14735

Unequal arm laser interferometer for high precision optics analysis of large astronomical devices 04 p0592 A71-14866

Aberration analysis for manual retouching of large objective lenses, using unequal arm laser interferometer 04 p0607 A71-14867

High precision large optical component surface visual monitoring with aid of small size etalons 04 p0593 A71-14869

Biaxial crystals utilization in polarized interferometers, noting Wollaston prisms useful beam aperture and Savart polariscopes streak linearity domain 07 p1109 A71-19453

Modified double point source differential shear interferometer for neutral reference light beam, using pinhole stop 07 p1110 A71-19478

Holograph interferometer methods classification according to diffuse elements in objects and illumination sources, considering effect on interference fringe interpretation 07 p1114 A71-20144

Heat flux measuring device using Wollaston prism schlieren interferometer 09 p1444 A71-22713

Variable shear interferometer for infinite fringe operation and velocity measurement, discussing refractive index distributions in stationary and moving media 10 p1613 A71-24994

Savart plates use in grating interferometers, deriving expressions for phase retardations for arbitrary angles between optical axis and plate normal 12 p1904 A71-26798

High resolution holographic Fourier transform spectroscopy, discussing interferometer localized interference fringes direct recording method and heterodyning technique 12 p1905 A71-26805

Parallel light beam triangular path interferometer with linear compressive shear effect for flow measurement applications, describing prism system and interference patterns 12 p1905 A71-26816

Phase modulation application to interferometers for submillimeter waves exceeding 10 microns 12 p1905 A71-26817

Phase modulation in far IR interferometers applied to Fourier spectrometry and metrology, obtaining modulus, phase, absorption and refraction spectra 14 p2238 A71-29742

Phase modulation in far IR interferometers applied to laser refraction measurements in solids and organic liquids 14 p2238 A71-29743

Optical interferometer with evacuated light paths, describing operating principles, cost efficiency and compactness 14 p2238 A71-29803

Holographic interferometer for photoelastic stress analysis, eliminating isochromatic pattern interference from isopachic interferogram by double pass object beam and optical rotator 14 p2239 A71-29845

Light transmission homogeneity measurements of optical materials, using Murty interferometer 14 p2242 A71-30154

Digital laser interferometer for vibration measurements, describing theory, transistorized circuitry and performance characteristics 15 p2401 A71-31138

Two beam holographic interferometer based on spherical mirrors with laser beam splitting by semitransparent plate and image reconstruction in monochromatic and nonmonochromatic light 15 p2402 A71-31257

Holographic multiple pass two-beam optical interferometer with greater sensitivity than single pass instrument /Mach-Zehnder/ 15 p2402 A71-31259

Holographic diffraction shearing interferometer scheme, considering gratings arrangement and calculation method 15 p2403 A71-31261

Far IR coupled cavity HCN laser interferometer for measuring low density transient plasma 15 p2410 A71-32384

Laser interferometer application in machine tool calibration, digital readout and feedback system, discussing advantages and limitations 15 p2421 A71-32433

[SME PAPER IQ-71-745] High sensitivity helium neon laser interferometer for transient phase objects designed for shock tube and tunnel experiments 16 p2576 A71-32913

Second-order degree of coherence measurement by compact wave front shearing interferometer 16 p2577 A71-33131

Modified Young interferometer for measuring separation between centers of two nearly coincident slits with high resolution 16 p2577 A71-33132

Shearing interferometer based on moire method using Fourier image of grating, considering applications to phase gradient and lens aberration measurements 16 p2577 A71-33133

Single plate interferometer tested by Na vapor anomalous dispersion near D lines, considering application to hook interferometry 16 p2578 A71-33158

Holographic interferometer for photoelastic stress analysis by simultaneous acquisition of isochromatic and isopachic fringe patterns without mutual interference, providing increased sensitivity [SESA PAPER 1792] 17 p2738 A71-34532

Airflow surveys using extended field large aperture interferometer-spectrometer with optical wedge compensators and digital recording 18 p2914 A71-35842

Light wave Rayleigh interferometer for concentration gradient measurements in liquid systems with mass transport 18 p2917 A71-36052

Automatic fringe counting pulsed ultrasonic interferometer for transit time measurement, using phase sensitive multiple echo detection 18 p2922 A71-36586

Laser interferometer techniques with automatic measurement and compensation for system inaccuracies, considering corrections for sine /Abbel/ errors for pitch and yaw, etc [SME PAPER IQ-71-120] 18 p2924 A71-36655

Diagnostic He-Ne laser interferometer for measuring electron concentration in cross section of argon plasma jet 19 p3073 A71-37786

Multiple channel fringe counting interferometer for remote monitoring of large diameter microwave antenna under test in simulated solar thermal and vacuum environment 20 p3235 A71-39186

Holographic interferometry equipment design for NDT and vibrational and deformation analysis, discussing apparatus construction, optical quality and industrial applications 20 p3238 A71-39344

Holographic interferometry application to photoelasticity, interpreting fringe patterns for two dimensional stress analysis 20 p3238 A71-39345

Geogravitational acceleration constant determination using two falling interferometer reflectors illuminated by laser light 22 p3574 A71-41650

Atmospheric trace and pollutant molecules global survey, using airborne/spaceborne high resolution Fourier interference IR spectrometer 22 p3542 A71-41963

Reflection coefficients measurement for scanning two-mirror interferometer with absorbing Ni film matched to external medium, discussing multilayered coatings 23 p3676 A71-43399

Photon noise limited interferometer transducer for gravitational radiation antenna, using piezoelectric driver to generate subangstrom vibrations 24 p3835 A71-45209

INTERFEROMETRY

NT DIFFERENTIAL INTERFEROMETRY

Spatial filtering equipment for unwanted images and diffraction in holography, interferometry, etc 01 p0092 A71-10336

Extended Spline Fit Technique for determining refractivity from interferograms of axisymmetric laminar diffusion flames 01 p0180 A71-10946

Electron concentration distribution over plasma discharge cross section, using interferometry 02 p0288 A71-11887

Interference patterns obtained in transmitted light, determining surface parallelism of thin plates transparent in IR region using carbon dioxide laser 02 p0259 A71-11936

Shadow and interference methods sensitivity for low density gas flows improved via monochromatic light source 02 p0248 A71-11937

Optimum frequency channels and delay estimates in very long baseline interferometry with large bandwidth for fringe and phase measurements 02 p0216 A71-12329

Hydrogen maser time and frequency standards at Agassiz observatory for long baseline interferometry via radio telescope, discussing Loran C 02 p0261 A71-12344

Optimum beam ratio producing maximum contrast photographic reconstructions from double exposure holographic interferograms 03 p0424 A71-13616

Holographic interferometry with both beams traversing transparent object, providing variable sensitivity and directional phase detection 03 p0425 A71-13654

Holographic interferometry application to photoelasticity, discussing absolute retardation in terms of plane or circularly polarized light fringe pattern interpretation [SESA PAPER 1719] 03 p0426 A71-13767

Streak interferometry providing single impact test data for calculating dynamic stress-strain curve [SESA PAPER 1717] 03 p0509 A71-13777

Radar interferometric mapping of Venus surface reflectivity in polarized mode at 70 cm wavelength 03 p0490 A71-13782

Translational vs deformation displacement motion in sensitivity of double exposure holographic interferometry 03 p0429 A71-141818

Small phase differences amplification in holographic interferometry, using nonlinear developments of recordings 03 p0429 A71-141828

Laser interferometry precision measurement and alignment techniques, describing application in optical lens manufacture and assembly 04 p0606 A71-147181

Holography developments concerning interferometry, microscopy, display systems, data storage and ultrasonic tests 04 p0587 A71-147249

Three dimensional opacity function for phase objects measurements using interferometry, holography or schlieren methods 04 p0596 A71-14969

Laser beam phase front distortion by atmospheric turbulence, discussing interferometric measurements 04 p0608 A71-151370

Supported rectangular plates HF transverse vibrations by holographic interferometry 04 p0668 A71-151824

Laser produced schlieren interferometry diffraction pattern determination, using Doppler frequency shift law 04 p0596 A71-15222

Thorium wavelength measurements by interferometry, noting weighted averages as secondary standards of length 04 p0627 A71-15692

Compressible flow density measurement using optical polarization interferometry with birefringent devices 04 p0601 A71-159181

Classical and hologram interferometry, considering fringe localization and visibility 05 p0747 A71-161909

Holographic interferometry of diffusely reflecting surfaces, analyzing homologous rays concept 05 p0747 A71-161922

Radiation energy deposition profiles in transparent liquids, using holographic interferometer 05 p0748 A71-16263

Two wavelength nondiffuse holography for interferometry of transparent media 05 p0748 A71-16264

Double pulse laser holographic interferometry for large noisy vibrating subjects, including demonstration on Al plate 05 p0751 A71-16580

Photoelectric photometer measurements of stellar interferometer fringes strength by light modulation 05 p0752 A71-16681

Photoelastic model stress analysis by holographic interferometry and automatic measurement of light shapes, discussing slicing technique 05 p0752 A71-16733

Holographic interferometry application to gas dynamics, analyzing interference patterns in monochromatic and achromatic light 05 p0695 A71-17166

Potassium niobate single crystals domain structures by interferometry, discussing surface deformations, dipole couplings and temperature dependent angles 06 p0941 A71-18039

Holographic interferometric recording of vibration patterns of plexiglass cored construction mirrors [AIAA PAPER 71-180] 06 p0903 A71-18619

Pulsed carbon dioxide laser amplifier, examining spatial and temporal refractive index variations with interferometric measurements 06 p0910 A71-18667

Strain field measurement near crack tip in polymethyl methacrylate by holographic interferometry 07 p1209 A71-19043

- Photoelastic fringe patterns in double exposure holography interferometric technique for stress wave analysis 07 p1209 A71-19044
- Interferometric holography application to elastic stress and surface corrosion of two dimensional objects and metals, discussing stretching 07 p1107 A71-19209
- System phase errors subtraction in interferometry, using modified laser unequal path interferometer and technique eliminating data reduction problem 07 p1107 A71-19210
- Axisymmetric phase object holographic interferometry, showing light beam refraction effect on interference pattern 07 p1108 A71-19237
- Fringe interferogram variable visibility control, eliminating vibration effects 07 p1109 A71-19467
- Holographic multiple beam interferometry, considering phase retardation role in hologram diffracted waves for fringes irradiance distribution definition 07 p1110 A71-19479
- Holography and interferometry industrial applications, considering three dimensional imaging, precision distance measurement, nondestructive testing and structural strains and failures detection 07 p1113 A71-19784
- Lens geometry history covering computerized design, prototype testing, optical shop aids and laser interferometry 08 p1333 A71-21177
- Multilayer interference optical minus filters low-ripple transmittance design, using equivalent layer concept 08 p1334 A71-21184
- Three mirror multiple beam interferometric rejection filter for laser Raman spectroscopy 08 p1289 A71-21379
- Far IR materials optical constants analysis by channeled spectra, using Fourier spectroscopy single signature in interferogram to yield real and imaginary parts of refractive index 08 p1335 A71-21384
- Freestanding wire grid manufacture of polarizing films for submillimeter interferometry 08 p1291 A71-21405
- Holographic interferometry at two wavelengths for phase objects dispersion characteristics 08 p1292 A71-21487
- Stress analysis of elastic bending plates by holographic interferometry, comparing results to theory 08 p1373 A71-21752
- Real time and double exposure holographic interferometry measurements of strain on aluminum cylinder under internal pressure, noting discrepancy with strain gage values 09 p1444 A71-22711
- Thermal deflection tests of fused silica mirror blanks by holographic interferometry 09 p1447 A71-22745
- Mirror reflection coefficients effect on fringe characteristics of multibeam series interferometer, showing improvement by Fabry-Perot etalon system 09 p1451 A71-23174
- Fringe interpretation in stress-holo- interferometry, emphasizing isopachic-isochromatic interaction effects in photoelastic analysis [SESA PAPER 1642] 09 p1542 A71-23538
- Two-wavelength interferometry of plasmas generated by Nd laser beam focalization, deriving electron and neutral particle densities 10 p1646 A71-23818
- Classical vs holographic interferometry comparing same fringe profiles 10 p1608 A71-23844
- Three-beam holographic interferometry featuring sensitivity increase and aberrations compensation 10 p1611 A71-24345
- Longitude precessional constant determined by long baseline interferometry through dynamical behavior observation of earth orbiting or interplanetary artificial spacecraft 10 p1674 A71-24437
- Holography as quantitative tool for photoelastic measurements, using moire theory of interference phenomena 10 p1611 A71-24473
- Metrological holographic interferometry, discussing speckle pattern application for wavefront phase samples 10 p1613 A71-25092
- Asymmetric three dimensional aerodynamic density fields from holographic interferograms, applying to supersonic flow from free jet 11 p1762 A71-25802
- Surface strain measurements in turbine blades by time average holographic interferometry, reviewing resonant modes and holographic fringe patterns [ASME PAPER 71-GT-84] 11 p1762 A71-25992
- Binary alpha Virginis interferometric data, noting distance, luminosity brightness ratio, angular size and diameter, orbits mass, temperature and gravity 11 p1830 A71-26107
- Quasar 3C 147 angular structure observations, using long baseline interferometer 11 p1830 A71-26113
- Fast shock waves electromagnetic production in light gases, discussing interferometric measurements at optical and microwave frequencies in H 11 p1764 A71-26272
- Plasma diagnostics covering magnetic, electron beam, electrostatic, laser, holography, interferometry, Thomson scattering, microwave and electroacoustic techniques 11 p1766 A71-26287
- Axisymmetric phase object holographic interferometry, showing light beam refraction effect on interference pattern 12 p1903 A71-26755
- Two wavelength holographic interferometry for transparent media with high or low sensitivity, using diffraction grating 12 p1904 A71-26796
- Two beam interferometry, measuring phase shift and dispersion at slit by channeled spectra 12 p1904 A71-26797
- Holographic interferometry method application to plasma electron concentration measurements 12 p1906 A71-27211
- Plasma refractive index and electron density measurements by He-Ne vernier interferometric laser 12 p1940 A71-27282
- Optical holographic interferometry for radial microcracks detection from bolt holes in high strength aircraft steel 12 p1911 A71-27312
- [ASME PAPER 71-MET-C] Holographic interferometry application to gas dynamics, analyzing interferential patterns in monochromatic and achromatic light 12 p1864 A71-27458
- Subnanosecond interferograms with high spatial resolution of plasma filaments in ruby laser produced spark 13 p2077 A71-28047
- Continuous relative phase control between reference and object beams in holographic interferometry 13 p2066 A71-28161
- Piecewise-linear approximation of nonlinear friction effect on interferometric servosystem stability, deriving formulas for harmonic linearization coefficient of linearity 13 p2041 A71-28375
- Gated light pulse technique for multiple-pass interferometry 13 p2067 A71-28444
- Interferometric studies of focused Nd laser radiation interaction with thin graphite absorbing surface layer, discussing time behavior of plasma expansion and density distribution 13 p2078 A71-28446
- Signal to noise ratio measurement in hologram reconstructions by vibration interferograms 13 p2068 A71-28447
- Holography background, classification and application to microscopy, particle size analysis, interferometry, optical elements and data storage 13 p2071 A71-29349
- Reference/object wave temporal modulation effect on fringe formation in holographic interferometry 14 p2241 A71-30133
- Penta prism angle reduplication by interferometric measurements 14 p2241 A71-30139
- Optical surfaces contamination analysis by holographic interferometry, using fringe patterns for contaminant film thickness and uniformity 14 p2244 A71-30330
- External galaxies neutral hydrogen distribution from interferometric observations, discussing interpretation consistent with optically derived rotation curves 14 p2314 A71-30638
- Two-wavelength holographic interferometry for phase objects dispersion characteristics, noting plasma diagnostics application 14 p2248 A71-30675
- Holography in nondestructive materials testing, describing laser interferometry and reproduction techniques for deformation and torsional, bending, thermal and vibrational behavior 15 p2402 A71-31217
- High sensitivity three beam holographic interferometry using Zernike method, applying to small deformation measurement 15 p2402 A71-31258
- Lateral shearing interferometry sensitivity improvement by amplifying phase difference with nonlinear holograms 15 p2403 A71-31260
- Holographic interferometry, discussing deformation second derivatives mapping and fringes formation and visibility 15 p2403 A71-31262
- Three dimensional deformation surface displacement measurement by holographic interferometry, using equal inclination fringes 15 p2403 A71-31264
- Diffusely reflecting in-plane surface displacement measurement by holographic interferometry, comparing static and dynamic methods for accuracy 15 p2403 A71-31265
- Fringe order determination in holographic interferometry, discussing zero motion object region identification 15 p2403 A71-31266
- Stress analysis by holographic interferometry and automatic light forms analysis 15 p2502 A71-31268
- Real time stroboscopic vibration analysis technique involving holographic interferometry 15 p2404 A71-31271
- Holographic interferometry for observing transparent media in supersonic gas flow, comparing results with Mach-Zehnder interferometry 15 p2404 A71-31275
- Holographic interferometry for flow visualization within aerodynamic wind tunnels with retrodiffuser apparatus 15 p2405 A71-31276
- Two interferograms holographic laser recording on same emulsion by double exposure with ruby and harmonic wavelengths 15 p2454 A71-31277
- Holographic interferograms for determining spatial configuration and absolute electron density of fully ionized transient plasmas 15 p2405 A71-31278
- Optical wave reconstruction from microwave holograms and application to interferometry, considering resolving power and visible images of microwave transparencies 15 p2405 A71-31281
- Interferometric holograms of vibrating body via numerical analysis of oscillations amplitude and phases 15 p2406 A71-31706
- Microcracks detection in high strength steel by optical holographic interferometry, comparing results with magnaflex, eddy current and X ray inspection methods 15 p2409 A71-32258
- Interferometric observation of photon fluctuation during Fraunhofer diffraction by small round hole, considering light granular structure at low intensities 15 p2421 A71-32405
- Time average holographic interferometric fringes of circular plate vibrating in two rationally related modes 15 p2412 A71-32593
- Pulsed laser double exposure holographic interferometry for measuring transverse wave propagation in beams 15 p2413 A71-32790
- Short length strain interferometric measurement from interference patterns of laser light diffracted from adjacent small reflecting surfaces 16 p2576 A71-32864
- Holographic interferometry measurements of mean and localized fluctuating wake density field of cones fired at Mach 6 at ballistic range, using pulsed laser [AIAA PAPER 71-564] 16 p2520 A71-33105
- Gases refractive behavior, discussing constitutive properties, wave propagation, Lorentz electron theory of dispersion, spectral interferometry and hook method 16 p2608 A71-33156
- Interferometric gas diagnostics by hook method, using Mach-Zehnder interferometer and stigmatic spectrograph 16 p2578 A71-33157
- Optical interferometry and schlieren photography involving high power pulsed lasers, discussing applications to plasma diagnostics and holography 16 p2586 A71-33159
- Pulse laser holographic interferometry for refractivity measurement, considering wave front reconstruction principles 16 p2578 A71-33160
- Very long baseline interferometry of radio emissions from geostationary satellites, determining orbital elements and inertial position 16 p2544 A71-33845
- Orthogonal bicolored moire fringes in mechanical interferometry, considering interpolation type determination of fractional fringe orders [SESA PAPER 1817A] 17 p2738 A71-34548
- Long baseline atomic clock interferometry with meter wavelength cross polarized antenna arrays for spacecraft propagation experiments 17 p2744 A71-35098
- Holographic interferometry fringe patterns interpretation for small displacements measurement, considering precision gyro stability 17 p2744 A71-35286
- Holographic interferometry for speckle pattern interpretation in metrology, using video techniques 18 p2917 A71-36056
- Interference holography, discussing precision displacement measurement, fringe localization, multiple beam techniques, contour generation and flow visualization 18 p2920 A71-36148

INTERGALACTIC MEDIA

Double exposure pulsed laser holographic interferometry application to transverse wave propagation in Al plate 18 p2977 A71-36233

Multipass laser interferometry sensitivity improvement for He plasma electron density determination by increasing effective path length of laser beam in medium 18 p2931 A71-36584

Wavefront reconstruction interferometry with acoustical holography using ultrasound camera, surface deformation and mechanically scanned detector methods 18 p2923 A71-36609

Stroboscopic coherent light source for vibrational analysis by holographic interferometry using Pockels cell laser modulator 18 p2923 A71-36610

Real time holographic interferograms, achieving required beam intensities relationship by ordinary neutral light filters near collimator focus 19 p3065 A71-38196

Plasma optical refractivity, considering gas laser interferometry and holographic phase measurements 19 p3116 A71-38244

Holographic interferometry application to vibration mode pattern analysis of steam turbine and centrifugal compressor blades and disks 19 p3067 A71-38419

Holographic interferometry method application to plasma electron concentration measurements 19 p3067 A71-38623

Transparent sample surfaces parallelism interferometric measurement using laser produced two beam nonlocalized fringes 20 p3245 A71-39181

Aspheric lenses and mirrors testing by single and double exposure two-wavelength visible light holography for obtaining interferogram 20 p3235 A71-39182

Three dimensional surface displacement measurement by hologram interferometry, applying to cantilever 20 p3235 A71-39187

Moiré equivalence device for simulating fringe patterns in hologram interferometry, using loci of constant pathlength 20 p3235 A71-39188

Laser holography and interferometry in materials science, evaluating displacement and deformation within nondestructive testing 20 p3245 A71-39342

Holographic interferometry for structure and material deformation measurement, presenting static loading and resonant vibration surveys 20 p3238 A71-39346

Condition equations for zonal harmonics using low inclination DIAL satellite interferometric measurements over perigee revolution 20 p3300 A71-39664

Stress state determination in birefringent elastic material for plane dynamic problems by photoelasticimetric and interferometric techniques 21 p3376 A71-40103

Holographic interferometry application to two step static displacement measurement of diffusely reflecting surface of rigid body in motion 21 p3377 A71-40227

Holographic interferometry application to photoelasticity, discussing relationship between isochromatic and isopachic fringes and fringe families separation method 21 p3456 A71-40228

Multibeam holographic interference Gabor theory construction, using variational principle and potential theory 21 p3379 A71-40626

Laser speckle interferometry for translational motions and vibrations detection, considering applications in radar and acoustics analysis 21 p3393 A71-40932

Deformation and translation measurements with holographic interferometry, considering flat surface moved with precision differential screw micrometer 21 p3381 A71-40933

Real time holographic interferometry of steady state mechanical vibrations of engineering structural components applicable to arbitrary small amplitude and large mode numbers 21 p3381 A71-40934

Three frame pulsed holographic interferometry of plasma radial density profiles and helical displacement for use with theta pinch device 21 p3423 A71-40937

Holographic interferometry application to laser NDT of objects with nonoptical surfaces, describing techniques and industrial uses 21 p3382 A71-40939

Optical field contouring techniques using holographic interferometry for obtaining objects shapes on contour maps 21 p3382 A71-40940

Axisymmetric imperfect conical shells vibration analysis using time average holographic interferometry technique 21 p3382 A71-41028

Interferometric measurement of gas temperature in positive column of discharges used for carbon dioxide lasers 22 p3574 A71-41725

Hologram interference fringes formation and location using grating model of diffusely reflecting surface 22 p3539 A71-41739

Holographic interferometry application to plate Poisson ratio determination and bending vibration analysis 22 p3539 A71-41741

Q-switched ruby laser holographic interferometry for hypergolic flame combustion recording 22 p3539 A71-41742

Nonlinear hologram application to interferometry, discussing phase difference amplification 22 p3539 A71-41744

Multibeam holographic interferometry, using variational principle and potential theory 22 p3574 A71-41786

Holography, covering thin, thick, transmission, reflection, amplitude and phase type holograms principles and applications in interferometry, microscopy, imaging, optical data processing, etc 22 p3546 A71-42476

Millimeter transverse electric wave diffraction by spherical plasma, interpreting interferometric measurements of electron density 23 p3708 A71-43085

Radio astronomical intercontinental base interferometry, discussing independent local oscillators requirements and atomic clock frequency standards 23 p3674 A71-43087

Large path difference laser interferometry, discussing test tower instrumentation problems of interference fringe flicker and loss of contrast due to laser mode instability 23 p3683 A71-43356

Holographic interferometry flaw detection sensitivity on cylinders under hoop stress, comparing with strain gages 23 p3676 A71-43508

Interferometric measurements of 142 solar absorption lines in light from solar disk center 23 p3767 A71-43835

Holographic nondestructive testing of materials, using laser for object illumination and interferometry 23 p3682 A71-43951

Interference patterns from hologram interferometer related to aberration theory 24 p3826 A71-44980

INTERGALACTIC MEDIA

Ionized intergalactic and pregalactic matter 3K microwave background, examining spectrum and degree of anisotropy 02 p0312 A71-12467

Intergalactic gas ionization and heating by UV radiation 06 p0974 A71-18429

Isotropic component of diffuse gamma ray background, discussing possible dense intergalactic medium coexistence with universal cosmic ray flux 07 p1185 A71-19549

Bubble of energetic charged particles embedded in interstellar or intergalactic magnetic field and in gas, discussing dynamic effects on radio astronomy observation 07 p1197 A71-19815

Cosmic objects and phenomena research, considering matter and galaxy compacting and dispersing processes, red shift, quasars, etc 08 p1358 A71-20890

Radiative transfer theory extended to cosmological red shift and expansion effects on uniform isotropic X rays and gamma rays in homogeneous intergalactic medium 09 p1512 A71-22333

High energy gamma rays in steady state universe assuming primary cosmic ray spectrum in extragalactic space by simple power law 10 p1664 A71-25045

Observational test of Planck constant variation on cosmic scale in terms of radiation absorption by interstellar and intergalactic gases 11 p1832 A71-26183

Intergalactic gas ionization and heating by UV radiation 12 p1955 A71-26579

Source count statistics of radio galaxy lifetimes and intergalactic heating, assuming multiple explosions 12 p1968 A71-27540

Transparency of extragalactic space to very high energy photons, considering background gamma rays effects 15 p2472 A71-31198

Time dependent multidimensional axisymmetric computations for extended extragalactic radio sources propagation into intergalactic media having different densities and temperatures 17 p2806 A71-35411

Extragalactic Faraday rotation models, examining galactic plane and Galaxy supercluster 19 p3142 A71-38005

Homogeneous large scale intergalactic magnetic field evidence in terms of Faraday rotation measurements of extragalactic radio sources 20 p3294 A71-39541

Intergalactic dust density limits using absorption magnitude and red shift of distant galaxies 22 p3599 A71-41924

Coma cluster X ray observations implying limits on gas density in intergalactic space and Friedmann models 22 p3599 A71-41924

Extragalactic radio sources polarized radiation intensity statistical analysis, calculating magnetic field scale 22 p3602 A71-42175

Book on cosmology covering stars, galaxies, radio galaxies, universe models, quasars, expansion, intergalactic matter and microwave radiation 22 p3607 A71-42773

INTERGRANULAR CORROSION

Al-Zn-Mg alloys intergranular failure due to aqueous stress corrosion cracking, fatigue and exfoliation, analyzing mud-crack pattern 03 p0441 A71-13319

Ni alloy corrosion tests, evaluating sensitization susceptibility and intergranular attack 06 p0911 A71-17414

Austenitic stainless steel intergranular corrosion model for thermodynamic analysis leading to grain boundary diffusion and Cr concentration profiles determination 07 p1134 A71-19566

Ti stress corrosion in organic liquids, considering intergranular and transgranular failure 11 p1781 A71-26262

C and Ni contents effects on water quenched tempered austenitic chromium nickel-stainless steels intercrystalline corrosion 12 p1919 A71-27777

High chromium low carbon steel, detailing oxygen content effects on high temperature reduction intercrystalline corrosion and grain growth 15 p2427 A71-31528

Steel joint weld decay mechanism, observing intergranular corrosion initiation and development in nitric acid solutions 15 p2417 A71-32665

Austenitic stainless steels susceptibility to intergranular corrosion under unwelded, welded and heat treated conditions in process environments 20 p3241 A71-39341

Dislocation arrays effects on heat treated austenitic stainless steel susceptibility to intercrystalline corrosion in sulfuric and nitric acids and cracking in magnesium chloride 21 p3402 A71-41087

C and Ni contents effects on water quenched tempered austenitic chromium nickel-stainless steels intercrystalline corrosion 21 p3403 A71-41100

Intergranular corrosion of chromium carbide sensitized Ni base alloys, noting surface effect during solution heat treatment 22 p3560 A71-41626

Accelerated intergranular corrosion tests under high humidity on Zn-Al alloy with lamellar eutectoid microstructure due to postforming heat treatment 22 p3564 A71-42534

INTERNAL BALLISTICS

Internal ballistics equations of powder solid fuel rocket motor treated as homogeneous chemical reactor 24 p3890 A71-45107

INTERLAYERS

NT MULTILAYER INSULATION

Interlayer rigidity effects on strength of fiber reinforced composite materials under plane loads 05 p0771 A71-16366

Grade 15 steel vacuum diffusion welding to AMTs alloy or AD1 aluminum, using nickel interlayer in joints 15 p2418 A71-32667

Elastic adhesive interlayer effect on bond fracture strength, considering propellant-liner-steel combination in solid rocket motors 18 p2977 A71-36245

INTERLOCKING

INTERMEDIATE FREQUENCIES

Varicap loop circuits for controllable IF phase corrector with independent delay suitable for automatic control 01 p0054 A71-11083

Optical heterodyne receiver design, using nonlinear recursive techniques to estimate atmospheric fluctuation effects on IF signal characteristics 02 p0249 A71-12026

Polarization of thunderstorm IF electromagnetic noise, taking into account earth electrical conductivity under detector 07 p1063 A71-19758

Computation of IF filter characteristics effect on angle modulation distortion 07 p1082 A71-20429

Intermediate band photometric system for three dimensional star classification based on published stellar spectral energy distribution data 10 p1681 A71-25129

Early stars Vilnius intermediate band and UVB systems comparison for color excess ratios and magnitudes, obtaining reddening line slopes by spectral energy distributions 10 p1682 A71-25131

Microwave discriminators with IF error signal ensuring high stabilization of master oscillator frequency without complex tuning operations 11 p1737 A71-25939

IF nonlinearities effect on Gaussian clutter rejection associated with noncoherent MTI radar receiver 17 p2708 A71-35483

Microwave discriminators with IF error signal ensuring high stabilization of master oscillator frequency without complex tuning operations 20 p3205 A71-39259

Probability density and distribution functions of click amplitudes for rectangular IF, determining frequency modulation effect 22 p3513 A71-42386

INTERMEDIATE FREQUENCY AMPLIFIERS

Low distortion gain-controlled 140 MHz IF main amplifiers for 2700-channel microwave repeaters, discussing design and performance 05 p0730 A71-17069

Radiation tolerant monolithic amplifier design, considering IF amplifier 07 p1080 A71-20411

Three-channel monopulse tracking receiver for automatic steering of satellite tracking antennas, noting gain controlled IF amplifier module 18 p2884 A71-36996

INTERMETALLICS

Intermetallic Ni-Al volume fraction dependent deformation of single crystals of binary Ni-Al system, using X ray and transmission electron microscopy 01 p0102 A71-10740

Fusibility and thermal emf of ternary intermetallic TiFe-TiCo-TiNi system 01 p0103 A71-11090

Soviet book on chemistry of titanium covering intermetallic compounds, hydroxides, dioxide, titanates, halides, sulfates, titanium ores, deposit sites, etc 02 p0209 A71-11847

Titanium dichromide phase modifications under hardening at various temperatures, using thermal and X ray analysis 02 p0266 A71-12674

Monograph on cobalt base superalloys covering mechanical properties relation to microstructure, carbides, heat treatment, aging, intermetallic precipitation and dislocation 05 p0765 A71-16198

Superconducting niobium aluminate and niobium aluminate-Ge films formation on Nb substrate 05 p0792 A71-16238

Europium hexaboride-high melting point metals reaction for intermetallic compounds production, noting evaporation kinetics 06 p0913 A71-18087

Intermetallic compounds structural component applications, considering crystal growth, alloy constitution and development, mechanical properties and processing technology 07 p1131 A71-19427

Ordered intermetallic CsCl compounds thermodynamic properties determination, noting linear relationship between intrinsic disorder and formation heat 07 p1131 A71-19428

Nickel molybdenide disorder to order early transition mechanism diffraction model, using transmission electron and field ion microscopy studies 07 p1132 A71-19436

Thin nickel aluminate sheets and small particles long range ordering, discussing antiphase boundary energy effects 07 p1133 A71-19441

Oxidation resistant Ni-Al intermetallic compounds as protective coating for high temperature nickel base superalloys 07 p1134 A71-19448

Intermetallic III-V compound semiconducting films and layers charge carrier transport phenomena and optical properties 07 p1178 A71-19850

Au-Ba intermetallic compound electron work function temperature dependence 07 p1179 A71-19922

Re intermetallic compounds structure and physical properties, examining chemical reactivity with transition metals as function of elements periodic table position 07 p1140 A71-20236

Heat resistant Ni alloys intermetallic gamma prime phase analysis by electrolytic separation 09 p1467 A71-22322

Ti-6Al-4V and solution treated and aged Ti-6Al-6V-2Sn alloys, investigating relationship between alpha grain size and crack initiation fatigue strength 09 p1472 A71-23131

Debye-Waller factors for Nb and Sn atoms in intermetallic niobium stannide by X ray intensity measurements on single crystal 10 p1655 A71-23770

Intermetallic compound precipitation processes in Ti-Cu alloys for high yield strengths, using electron microscopy 11 p1779 A71-26017

Al-Zn-Mg-Cu alloys, investigating minor elements Cr, Mn and Zr effects on quench sensitivity 11 p1780 A71-26018

All-beta Ti alloy Ti-V-Cr-Al, testing dynamic behavior of strain aging during stress relaxation period 11 p1780 A71-26026

Thin film compound Au-Al intermetallic structure of CsCl type with lattice period of 3.140 plus or minus 0.003 A from electronographic measurement 12 p1917 A71-27308

Electrical conductivity, thermal emf, expansion and Hall coefficient of hot compressed powdered diborides of group IV and V transition metals 13 p2084 A71-28036

NiGa intermetallic compound electrical transport and resistance, Hall coefficient and optical adsorption, discussing defect structure and electron scattering 14 p2260 A71-30478

Intermetallic compounds application in structural materials, emphasizing role in superalloys development for gas turbine engine parts and high temperature environments 15 p2427 A71-31531

Superconducting Nb-Sn intermetallic compound synthesis from elemental powders by converging shock waves 15 p2461 A71-32378

Heat resistant weldable dispersion hardened Ni base alloy, discussing intermetallic phase hardening 16 p2594 A71-33715

Metals and intermetallic chemical compounds, examining heat and oxidation resistance, magnetic and semiconductor properties, superconductivity and electron emissivity 16 p2597 A71-33924

Binary and ternary metal compounds superconductivity parameters comparison, considering crystal structure, valence electron concentration, component position and processing techniques 16 p2622 A71-33925

Al-Cu-Li-Mn and magnesium/rare-earth-element alloys heat resistance and microhardness, determining strengthening by intermetallics 16 p2597 A71-33926

Iron based Cr-Co-Mo alloys equilibrium diagrams and phase transformations at various temperatures, emphasizing intermetallic compounds effects on mechanical properties 17 p2758 A71-35148

Fe-Ni base alloy heat treatment for optimum high temperature stress-rupture properties, noting Ni-Nb/Ti-Ti intermetallics precipitation at grain boundaries 19 p3080 A71-37712

Intermetallic formation in Au-Al systems via diffusion couples, determining activation energy, silicon effect and tensile strength 19 p3119 A71-38513

Ambient gas effects on Au-Al bonds life in integrated circuit package 19 p3119 A71-38514

Ni-Cr thin film resistors reliability, describing deposits on silicon dioxide, intermetallic formation and electromigration 19 p3034 A71-38515

Slip line deformation of ordered and disordered Cu-Au intermetallic single crystals from microstrain and electron micrographic studies 20 p3249 A71-38967

Vacuum UV reflecting surfaces deterioration by intermetallic formation, recommending separation by dielectric barrier layer 20 p3236 A71-39196

Intermetallic compound Ti-Ni phase transformations, relating martensite crystal structure with premartensitic instability 21 p3397 A71-40433

Copper-indium-tellurides homogeneity region components solubility in different cross sections of concentration triangle at room temperature 23 p3717 A71-44023

Mechanical properties of Al-aluminum intermetallic eutectic alloys after rapid solidification in semicontinuous casting technique, noting flow stress and tensile strength increase 23 p3695 A71-44286

INTERMITTENCY

Digital systems intermittent failures effects and detection, using system simulation 01 p0046 A71-10204

Intermittency signals correlation, determining lateral motion of two dimensional jet boundaries 18 p2901 A71-35854

INTERMODULATION

Double balanced cross coupled transistor mixer, predicting conversion gain and inter and cross modulation distortion performances 02 p0233 A71-12345

TWT and klystron intermodulation reduction by amplitude and phase correction device 02 p0223 A71-12811

FM radio link fluctuating intermodulation distortions reduction by additive superpositioning of several compensating echoes with adaptive equalizer 03 p0380 A71-14334

Path intermodulation data distortion derivation from noise power ratio measurements over five tropospheric scatter paths during system acceptance tests 05 p0723 A71-17055

Holographic recording intermodulation noise suppression by image wave field distortion and retrieval, considering signal to noise ratio 08 p1287 A71-21187

Graphical method for predicting intermodulation components and spurious responses 13 p2038 A71-28867

Intelsat 4 communication system simulation by transponder engineering model to test performance objective concerning baseband distortion and intermodulation 17 p2705 A71-35102

HF radio communication receiver performance requirements and realization, considering gain, noise, interference, filtering, reciprocal mixing, intermodulation and frequency stability 18 p2895 A71-36998

Intermodulation distortion in abrupt junction current pumped varactor frequency converter 20 p3202 A71-38848

Diffuse object scanned illumination hologram recording, discussing intermodulation flare light elimination for speed and reconstruction efficiency 22 p3549 A71-42561

FET nonlinear and cross modulation characteristics, basing performance prediction on power series approximation to measured LF transfer characteristics 23 p3649 A71-43068

INTERMOLECULAR FORCES

Spherical shell potential extension to shells of differing diameters for intermolecular forces in globular molecules, considering binary gaseous mixtures 11 p1801 A71-25369

Adhesive joints bonding strength, discussing relative contribution of interatomic and intermolecular forces and viscoelastic, viscous or plastic deformation effects 14 p2276 A71-29894

High resolution differential cross section measurements for nonspherical potentials and molecular scattering of nitrogen and noble gases at thermal energies 18 p2949 A71-35898

Intermolecular forces and excited state from atomic line shape experiments, comparing numerical calculations with experimental data 22 p3578 A71-42463

Chaos propagation derivation from Boltzmann equation for dilute gas with intermolecular forces and collisions in pairs 23 p3705 A71-43873

INTERNAL COMBUSTION ENGINES

BRISTOL-SIDDELEY OLYMPUS 593 ENGINE

NT DIESEL ENGINES

NT DUCTED FAN ENGINES

NT GAS TURBINE ENGINES

NT J-57 ENGINE

NT J-85 ENGINE

NT JET ENGINES

NT RAMJET ENGINES

NT SUPERSONIC COMBUSTION RAMJET ENGINES

NT TURBOFAN ENGINES

NT TURBOJET ENGINES

NT TURBOPROP ENGINES

NT TURBORAMJET ENGINES

NT WANKEL ENGINES

Gas dynamic conditions resulting in reacting gases detonation waves at high initial temperatures, simulating internal combustion engine knock 05 p0833 A71-16506

Internal combustion engine exhaust system sound radiation, discussing pressure wave effects, energy flux and boundary conditions 05 p0796 A71-16604

Soviet book on aircraft gas turbine and internal combustion engines covering structural design schemes, inlet devices, combustion chambers, materials, compressors, etc 08 p1347 A71-20674

Mathematical model of nonstationary intake and exhaust gas motion in two cycle internal combustion engine cylinders 08 p1347 A71-20780

INTERNAL COMPRESSION INLETS

- Air temperature effects on internal combustion engines intake process, using similarity theory
08 p1347 A71-20782
- Computerized simulation of inlet channel flow passage cross section effect on internal combustion engine filling
08 p1347 A71-20830
- French book on thermodynamics and gas dynamics covering theoretical and applied thermodynamics, air compressors, combustion, internal combustion engines, water vapor, compressible fluid cooling, etc
09 p1545 A71-22965
- One dimensional flow models of internal combustion engine exhaust silencers in noisy systems
11 p1810 A71-25180
- Internal combustion engine gas temperature measurement, using ultrasonic wave frequency shift method
11 p1810 A71-25269
- Book on aircraft propulsion covering design, dynamics, control, installation, gas turbine, ramjet, rocket and piston engines, compressors, combustion and energy cycles, etc
22 p3589 A71-42427

INTERNAL COMPRESSION INLETS

- Analytical model of compressor sensitivity to transient and distorted transient flows, considering inlet duct, compressor stages and combustor up to turbine nozzles
[AIAA PAPER 71-670] 14 p2291 A71-30734

INTERNAL ENERGY

- Kinetic coefficients calculation for gas with internal degrees of freedom during free energy exchange between translational and internal motion
08 p1338 A71-21918
- Simultaneous plasma internal energy, temperature and volume determination based on energy balance analysis during pulsed heating
08 p1342 A71-21928
- Numerical integration procedure for calculating mixed phase transformation in continuum mechanics for given volume and internal energy increments
13 p2100 A71-28232
- Quantum-theoretical transport equation for dilute gases with internal degrees of freedom, generalizing for arbitrary spacing between internal energy levels
14 p2275 A71-30449
- Positive NO ion formation with excess internal energy in positive atomic oxygen ion-nitrogen collisions
16 p2538 A71-32810
- Kinetic coefficients calculation for gas with free energy exchange between translational and internal degrees of freedom
17 p2785 A71-35263
- Evaporation rate of droplet with internal heat source from Maxwell-Langmuir theory extension
17 p2838 A71-35270
- Simultaneous plasma internal energy, temperature and volume determination based on energy balance analysis during pulsed heating
17 p2789 A71-35272
- Steady and unsteady flow work and energy loss relationships expressed in integral form representing perturbation kinetic energy, internal energy and pressure work
21 p3317 A71-40011

INTERNAL FRICTION

- Internal friction measurement under hydrostatic pressure, describing apparatus to determine phase angle between stress and strain
02 p0255 A71-12132
- Thin glass fibers relaxation characteristics, discussing shear modulus, internal friction and temperature effects
03 p0448 A71-13298
- Rhenium effect on tungsten sensitivity to brittle fracture, measuring amplitude dependence of internal friction at temperatures from 77 to 1273 K
07 p1141 A71-20247
- Internal friction solid solution weakening of bcc group V-B alloys
08 p1309 A71-21524
- Dilute Al alloys single crystals amplitude dependent internal frictions measurement, obtaining binding energies between substitutional alloying atoms and dislocations
08 p1310 A71-21535
- Vibration decrement amplitude dependence study using internal friction method of freely attenuated transverse vibrations, considering energy dissipation
08 p1317 A71-21761
- Metals and alloys internal friction meter based on intense ultrasonic vibration, discussing error compensation
09 p1426 A71-22320
- Thin glass fibers relaxation characteristics, discussing shear modulus, internal friction and temperature effects
09 p1483 A71-23271
- Round cross section specimens flexural vibration damping decrement, determining amplitude dependent internal friction with allowance for stressed state
09 p1542 A71-23314

- Torsion pendulum for measuring internal friction and shear modulus of refractory metals and alloys
09 p1452 A71-23333
- Internal friction from hydrogen dissolved in Ti-Mn alloys, considering solute interstitial atoms caused asymmetrical distortion decrease with increased Mn concentration
10 p1625 A71-24008
- Nb-Ti alloys internal friction spectra due to oxygen content, applying graphical decomposition method
11 p1781 A71-26322
- Small elastoplastic cyclic strain effects on internal friction and energy dissipation in metals during vibrations
16 p2598 A71-33983
- Machine part surface layers properties effect on internal friction from transverse vibration decrement measurement
17 p2826 A71-35021
- Elastic seismic waves attenuation in polycrystalline ceramics and rocks by grain boundary relaxation, noting strong frequency dependence of earth mantle internal friction
17 p2735 A71-35390
- Vertical statically unbalanced rotating shaft with two degrees of freedom, investigating internal damping, flexural vibrations and equation of motion
19 p3154 A71-37348
- Friction velocity in stably stratified constant flux layer with known heat flux, using log-linear velocity profile with fixed Monin-Obukhov parameter value
19 p3089 A71-37502
- Inorganic polymers and glasses at high temperatures, detecting LF internal friction
19 p3084 A71-38050
- Cold work peak characteristics in undeformed aged niobium-nitrogen alloys from internal friction spectrum
20 p3252 A71-39464
- Hardness, internal friction, microstress, martensite lattice and density changes during aging of precipitation hardening Fe-Cr-Ni steel, using dilatometric and X ray analysis
21 p3402 A71-41086
- Boundary displacement conditions in linear elasticity with friction, using minimization of nondifferentiable convex functional and variational inequalities
23 p3775 A71-43239
- Computer programs based on least squares numerical analysis for complex internal friction spectra due to Snoek and grain boundary relaxation
23 p3648 A71-43927
- INTERNAL PRESSURE**
- Nonlinear viscoelastic material with stress dependent properties, solving for thick walled shells deformation under internal pressure
01 p0168 A71-10423
- Spherical shell plastic deformations under internal pressure, discussing stress instability condition
02 p0325 A71-12123
- Ring reinforced circular holes in cylindrical shells examining stress concentrations due to internal pressure
03 p0507 A71-13740
- Internal pressure load carrying capacity of intersecting spherical and cylindrical shells based on limit or plastic design concept
05 p0823 A71-16493
- Body weakening due to symmetrically expanding crack, discussing internal pressure, elastic equilibrium and stress-strain state
06 p0896 A71-17326
- Smooth cylindrical shell stability, considering internal pressure effect on critical axial stresses
06 p0993 A71-17819
- Elliptical cylindrical shell under internal pressure, investigating stress concentration near surface hole
06 p0994 A71-17821
- Solid propellant engine structural analysis, examining transient thermal loading and internal pressure effects
[AIAA PAPER 71-115] 06 p1003 A71-18565
- Stress distribution boundary value problem for long isotropic elastic cylinder with strip cracks due to internal pressure
07 p1215 A71-20100
- Low temperature plasticity of Al alloy thin walled tubular specimens under axial tension and internal pressure
10 p1626 A71-24193
- Stress intensity factor of flat toroidal crack under internal pressure, using approximate solution of axisymmetric problems in fracture mechanics
10 p1693 A71-25057
- Influence coefficients for thin walled finite length cylindrical shells subjected to uniform internal pressure and edge loads
12 p1983 A71-27586
- Forced vibrations of circular cylindrical shell under random normal load and internal pressure, noting stability of transversely pressurized flexible vs rigid structures
13 p2150 A71-28140

- Elastic sphere equilibrium with penny shaped crack under inner surface pressure, observing stress distribution
14 p2326 A71-30080
- Convolved nozzle extension in engine with low pressure exit seal released and blown off by venting internal pressure
[AIAA PAPER 71-677] 14 p2292 A71-30747
- Load carrying capacity of edge clamped spherical shells of revolution with Tresca yield condition under uniform internal pressure
14 p2332 A71-30846
- Circular stresses and concentration coefficient variations in star shaped elastic surface projected onto ring under internal pressure
14 p2287 A71-30850
- Thin walled tubes under external and internal pressures axial loads and torques, showing load capacity limit dependence
15 p2428 A71-31868
- Cylindrical shell under internal pressure, detailing axial thermal stresses relaxation
15 p2505 A71-31864
- Buckling and postbuckling loads of initially imperfect orthotropic cylindrical shells under axial compression and internal pressure, using potential energy principle
16 p2651 A71-33023
- Prestress of two layer fiberglass-reinforced plastic cylindrical shell under internal pressure
16 p2657 A71-33416
- Heated tank under axial compression and internal pressure, noting fuel expenditure effects on stress-strain state
16 p2658 A71-33620
- Closed circular cylindrical shell stability under dynamic axial compressive loading with static internal pressure
16 p2658 A71-33719
- Stress distribution in cylindrical shell with two unequal diametrically opposite reinforced circular holes under internal pressure
16 p2661 A71-34159
- Stress-strain state of homogeneous and inhomogeneous cylinders and disks with central axial curvilinear hole under internal pressure and thermal loads
17 p2816 A71-34333
- Equivalent reinforcement of contact area between spherical shell and radial outlet cylindrical pipe under internal pressure and axial force
17 p2817 A71-34333
- Cylindrical shells partially filled with liquid, calculating forced vibration under random loads and deterministic internal pressure
17 p2817 A71-34333
- Longitudinal edge stiffness and internal pressure effects on buckling and initial postbuckling behavior of axially compressed stringer reinforced cylindrical panels, discussing imperfection sensitivity
19 p3157 A71-37873
- Harmonic stress function and stress intensity factors for elliptical crack embedded in elastic solid and subjected to arbitrary internal pressure
20 p3307 A71-38782
- Internal pressure deformed star shaped crack, calculating stress intensity factor, crack energy and normal displacement
20 p3310 A71-39866
- INTERNAL STRESS**
- U RESIDUAL STRESS**
- INTERNATIONAL COOPERATION**
- Post-Apollo programs, discussing international participation aspects
01 p0183 A71-10266
- Compact radio sources of high angular resolution observed via joint U.S.-U.S.S.R. radio interferometry
02 p0307 A71-12086
- Airworthiness and Air Registration Board, discussing aims, objectives, technical changes and national and international control
03 p0524 A71-13734
- Skylab, space station and shuttle programs covering economics, international participation and ground and flight tests
04 p0661 A71-14928
- Ossa R and D program noting budget allocations, satellite programs and international projects
04 p0690 A71-14934
- Cooperative international space ventures, discussing mission programs, global needs, successes and deficiencies
04 p0690 A71-14935
- Economic trends of international air transport in 1970s
04 p0690 A71-14991
- Space applications international programs in 1970s, discussing political, legal, economic and management aspects of earth resources survey [ERS] satellite program
04 p0691 A71-15348
- U.S.-Europe cooperative space programs survey and experience from project management with ESRO-1 satellite
04 p0692 A71-15349

SUBJECT INDEX

Cooperative international scientific space programs, discussing NASA, ESRO and other foreign space activities 04 p0692 A71-15350

State definition international standardization for cold rolled Al sheets, examining yield curves and strain energy 05 p0764 A71-15923

Post-Apollo space programs European collaboration, discussing space shuttle and space tug projects [DGLR-70-067] 05 p0839 A71-15957

UK space program, discussing international cooperation, sounding rocket development and performance and military communication satellites 05 p0806 A71-16148

Magnetic disturbances effect on F2 critical frequencies in Australasian zone during IGY-IGC, correlating to equatorial electrojet 05 p0741 A71-16438

Aircraft nationality legal problems concerning regional cooperation and registration 06 p1009 A71-17423

NASA bilateral and multilateral international cooperation agreements in space research, discussing political objectives, program history, regulations and procedures 06 p1010 A71-17646

Cooperative international program of monochromatic coronal photography with interference filters for 1973-1976 06 p0968 A71-17911

Multinational corporate R and D laboratories, discussing problems with regard to language barriers, cultural differences and coordination 07 p1225 A71-19449

Information and technology transfer in multinational corporate R and D, discussing mechanisms of communication, use of common technical language and impediments due to attitude differences 07 p1225 A71-19450

Compact radio sources of high angular resolution observed via joint U.S.-U.S.S.R. radio interferometry 08 p1362 A71-21136

World Meteorological Organization global weather observing, discussing coordinate function, developing countries technical assistance, observing systems planning and UN relations 08 p1327 A71-21718

Satellite role in future observing systems for global atmospheric research program, describing satellite instrumentation 08 p1328 A71-21721

Aircraft noise abatement control on international basis by setting acoustic technological capability compulsory standards of quietness 08 p1379 A71-21826

Satellite communications systems international planning, discussing Intelsat system limitations 09 p1548 A71-23354

Legal principles and rules governing lunar and other extraterrestrial materials, considering establishment of international code 10 p1698 A71-23861

Microwave and modular solid state ILS designs, discussing accelerated progress, international standard and present system life expectancy 10 p1639 A71-23943

International coordinated measurements of solar activity geophysical effects in upper atmosphere, discussing synchronized observations of Cosmos 261 satellite and ground based ionospheric station network 11 p1816 A71-25762

International coordinated solar chromospheric flare effects on D region lower boundary and ionospheric propagation by Cosmos 261 satellite and ground based observatories 11 p1816 A71-25763

Epidemiological aspects of airport medicine in relation to global public health and international cooperation 11 p1725 A71-26129

Space shuttle phase B design, discussing British-American cooperation, fly-back orbital laboratory and Apollo 14 zero-gravity demonstration 11 p1839 A71-26320

International space transport systems, discussing shuttle system optimal sizing considerations 14 p2320 A71-30260

Manned space projects U.S./European cooperation, discussing economic and population factors involved in international space cooperation programs 14 p2341 A71-30261

Post-Apollo program European participation, discussing need for multilateral international agreements on space shuttle, space tug and space station projects 14 p2341 A71-30262

Air transport development trends, considering increased speed and capacity, STOL aircraft, urban service, and European cooperation for manufacturing 14 p2341 A71-30302

Global environmental monitoring system for at-mosphere, oceans, land and biology, considering international cooperation 14 p2198 A71-30897

Helios 6 interplanetary solar probe, investigating particle propagation, energy spectra, direction distributions and spatial gradients 15 p2499 A71-31211

French contribution to air transportation, discussing international cooperation on supersonic Concorde, medium range airbus and short range Mercure 15 p2350 A71-32688

French space programs review with emphasis on compatibility with European and international programs 15 p2495 A71-32689

NASA earth resources technology satellites system, discussing ERTS A and B development, payloads and ground support systems and international aspects 16 p2630 A71-32854

Organizing space activities for world needs - Conference, New York, October 1968 16 p2664 A71-33580

Symphonic communication satellite subsystem, discussing geostationary positions, launchers, frequency ranges and transmission zones 16 p2543 A71-33583

International Telecommunications Satellite Consortium, reviewing legal order, organization structural framework, objectives and financial aspects 16 p2664 A71-33584

International space telecommunication systems, emphasizing legal aspects of operation 16 p2665 A71-33585

International space exploration management and organization, emphasizing NASA cooperative programs 16 p2665 A71-33587

Space applications to world needs, emphasizing potential major agricultural production improvements 16 p2665 A71-33589

Swiss space research, surveying international cooperative scientific activity relative to upper atmosphere satellite geodesy, solar wind, lunar samples analysis, IR and UV astronomy and celestial mechanics 16 p2665 A71-33852

U.S. space program report to COSPAR covering organization, facilities, international activities, astronomy, lunar and planetary research, particles, fields, atmospheric, earth and life sciences 16 p2665 A71-33855

Italian report to COSPAR on 1970 space research, discussing 1971-72 programs for cosmic radiation, space plasma, meteorology, communications and international cooperation 16 p2666 A71-33862

Indian report to COSPAR on space activities, discussing organization, facilities, experiments, applications, international collaboration and future plans 16 p2666 A71-33863

Australian space research 1970 report to COSPAR covering rocket sounding, X ray and gamma ray astronomy, tracking stations and international cooperation 16 p2667 A71-33871

Satellite broadcasting defined by UN, discussing community and home direct reception modes and educational TV potentialities and problems 17 p2697 A71-34238

Satellite TV educational applications, outlining joint Indian Atomic Energy Department and NASA project 17 p2841 A71-34239

International radio regulations adopted by Geneva space conference with reference to frequency band allocations in 1-10 GHz range with equal rights to space and terrestrial services 17 p2697 A71-34246

Legal problems in space telecommunications, discussing UN and international nongovernmental organizations solutions for interference protection, pirate space stations and spacecraft distress or emergency 17 p2841 A71-34247

UN leadership in space communications international cooperation, emphasizing communication satellite systems application to educational TV 17 p2841 A71-34249

Global broadcasting from space, suggesting international cooperation and UN role 17 p2841 A71-34250

International cooperation in space radio science, considering real time telemetry application via Solrad, Tiros and Alouette satellites 17 p2697 A71-34252

NASA ERTS program, discussing system concept automatic data processing capability, compatibility with tracking ground stations and international cooperation 17 p2805 A71-35329

Unilateralism in U.S. satellite communications policy, suggesting international cooperation for frequency spectrum management 18 p2986 A71-36165

East-West cooperation in space telecommunications, outlining Intelsat and Intersputnik organizational structure 18 p2987 A71-36167

INTERNATIONAL COOPERATION

Satellite communication role in disseminating information and promoting technology in underdeveloped countries 18 p2987 A71-36168

Satellite broadcasting to West African countries, discussing communications policies, NASA tracking stations in Africa and U.S.-Nigeria agreement for Comsat and Intelsat programs 18 p2987 A71-36169

European space tug orbit to orbit autonomous shuttle system, discussing participation in post-Apollo programs 18 p2988 A71-36489

European space programs, presenting post-Apollo utilization views [AIAA PAPER 71-817] 18 p2988 A71-36500

Joint India-U.S. satellite instructional television experiment for national development using ATS-F spacecraft 18 p2988 A71-36502

Direct broadcast satellite TV communications, discussing international regulations and legal aspects 18 p2989 A71-36578

French space programs, discussing European and international activities, telecommunication, meteorology, data collecting, natural resources and air and sea traffic control 18 p2975 A71-36753

New IATA passenger and baggage international air transport conditions, discussing passenger/carrier legal relationships, with emphasis on differences between new and old regulations 18 p2989 A71-36918

Finnish air traffic law based on international civil aviation convention, discussing regulations relative to aircraft, personnel and airports 18 p2989 A71-36919

Warsaw air traffic convection agreements as amended at The Hague and Guatemala, presenting air transport regulations in present form 18 p2989 A71-36920

European contribution to space shuttle and tug reusable space transportation systems, discussing post-Apollo programs cost analysis and hardware 19 p3150 A71-37310

Space and orbital laboratories construction and operation legitimacy problem covering satellites, stations and space transport concepts and international management 19 p3151 A71-37323

Technical prospects of European aerospace industries participation in post-Apollo program, noting space shuttle development role 19 p3151 A71-37324

European contributions to post-Apollo space program, considering space station, space shuttle and space tug 19 p3151 A71-37325

European launcher programs and participation in post-Apollo shuttles and orbital stations development in partnership with U.S. 19 p3151 A71-37330

International Telecommunication Union report on telecommunication and peaceful uses of outer space, covering space programs, communication satellites, UN role, etc 19 p3172 A71-37517

Joint American-Soviet astronomical radio interferometry, discussing resolution and quasar and galaxies structural difference 19 p3145 A71-38569

Climatological European southern observatory in Chile, describing spectroscopic and photometric telescopes, grand prism objective and double astrophotograph 20 p3210 A71-39527

Broadband point-to-point communication satellite systems for 1970s, discussing R and D effort, economics and international and domestic applications 20 p3197 A71-39606

Unified international scaling for annual and seasonal precipitations measured by national gages, comparing U.S.S.R. and U.S. reduction coefficients 21 p3383 A71-41377

International coordinated measurements of solar activity geophysical effects in upper atmosphere, discussing synchronized observations of Cosmos 261 satellite and ground based ionospheric station network 22 p3591 A71-41530

International coordinated measurements of solar chromospheric flare effects on D region lower boundary and ionospheric propagation by Cosmos 261 satellite and ground based observatories 22 p3591 A71-41531

Planning organization for global remote sensing information system operated and financed through international cooperation 22 p3623 A71-41987

International cooperation in aerospace projects, discussing Concorde program organization 22 p3623 A71-42011

International cooperation in astronautics, reviewing European satellites launching and world distribution of lunar rock and soil samples 22 p3623 A71-42012

INTERNATIONAL GEOPHYSICAL YEAR

- International HEOS project organization, discussing communication, task delegation, decision making and structure 23 p3785 A71-43455
- Multinational consortiums of industrial firms from member states for ESRO satellite programs 23 p3786 A71-43463
- Balanced space programs for 1970s and beyond, discussing unmanned planetary missions, manned Apollo, Skylab and space shuttle projects, private, foreign and international programs [AIAA PAPER 71-1020] 24 p3892 A71-44598
- French-American Eole project for meteorological prediction systems development, discussing balloon sounding and satellite data transmission 24 p3876 A71-45274
- ## INTERNATIONAL GEOPHYSICAL YEAR
- Nighttime polar aurora zone during IGY and IQSY related to magnetic activity 02 p0242 A71-11759
- Magnetic disturbances effect on F 2 critical frequencies in Australasian zone during IGY-IGC, correlating to equatorial electrojet 05 p0741 A71-16438
- Geomagnetic activity diurnal variation dependence on latitude and longitude during IGY 05 p0746 A71-17210
- Ring current indices by IGY data, attributing differences during great magnetic storms main phase to asymmetry of magnetospheric ring current 10 p1603 A71-24598
- Geomagnetic activity diurnal variation dependence on latitude and longitude during IGY 13 p2060 A71-28265
- Ionospheric drifts during IQSY, discussing comparison with IGY, methods and D1 records analysis theory 15 p2396 A71-31612
- Daily geomagnetic variations ionospheric current systems calculation from total magnetic field data obtained at ground stations during IGY 20 p3217 A71-39511
- Automated diurnal variation analysis program applied to IGY observed solar quiet day geomagnetic variations 20 p3218 A71-39520
- Solar activity tabulation and review covering International Geophysical Year and International Quiet Sun Year 21 p3442 A71-40151
- Blanketing sporadic E layer diurnal and seasonal variations from equatorial stations ionosonde data obtained during IGY, discussing wind shear mechanism 23 p3667 A71-43134
- ## INTERNATIONAL LAW
- ### NT SPACE LAW
- Space rescue operations, discussing notification, emergency location, terminal guidance systems and techniques application, international codes, etc 01 p0164 A71-11438
- Aviation accidents liability limitation by treaty and statute for passengers personal injury or death, discussing Warsaw Convention revisions 03 p0523 A71-12966
- Air crash litigation liability limitations, noting international inequality 03 p0523 A71-12968
- Hijacking and acts of violence against civil aircraft, concerning draft convention by legal committee of International Civil Aviation Organization 04 p0691 A71-14997
- Air charter flights legal status, considering public, private and international laws and civil responsibility 06 p1009 A71-17422
- Revision of 1929 Warsaw Convention Articles 3 and 25 relative to air carrier liability, discussing possible U.S. secession 06 p1009 A71-17424
- International law for states jurisdiction in aerospace, emphasizing airspace lateral to national territories and high seas, vertical to earth surface and outer space 06 p1010 A71-17645
- Book on earth satellite telecommunications systems and international law covering historical, scientific, economic, legal and political background 06 p1010 A71-18020
- European view on liability and compensation limitation for death and injury in international commercial air transport 09 p1548 A71-22989
- U.S. view on legal liability and compensation for death and injury in international air transport 09 p1548 A71-22990
- Book on air law and civil air policy covering international regulation, air traffic market, passenger and cargo services, etc 14 p2340 A71-29938
- Copyright protection of communication satellite transmitted radio and TV programs, discussing involvement of UN agencies and other international organizations 17 p2841 A71-34248

- Papers on international communications law, covering technological environment, broadcasting control and satellite transmitted TV programs content 18 p2986 A71-36162
- International communications law development, discussing capital investment, information dissemination, 1967 space treaty and Intelsat program 18 p2986 A71-36163
- Technological environment for international communications law, examining system design, radio spectrum resource management and communication satellites 18 p2986 A71-36164
- Juridical and institutional aspects of problems raised by TV programs content transmitted by communication satellites, noting applicability of international law 18 p2986 A71-36166
- South American contributions to satellite communication juridical problems solution, suggesting adherence to international law 18 p2987 A71-36170
- International satellite broadcasting practices and laws, discussing effect on free information dissemination 18 p2987 A71-36171
- Air piracy/hijacking/bibliography, considering national and international law, extradition, punishment, prevention and safety assurance for passengers and crews 22 p3622 A71-41617
- ## INTERNATIONAL PRACTICAL TEMPERATURE
- ### U TEMPERATURE SCALES
- #### INTERNATIONAL QUIET SUN YEAR
- Nighttime polar aurora zone during IGY and IQSY related to magnetic activity 02 p0242 A71-11759
- Ionospheric absorption winter anomaly observation based on Loran-A pulse signals during IQSY, noting diurnal variation 06 p0889 A71-17685
- Latitude, mesons and radioactivity effects on planetary distribution of cosmic ray neutron component barometer coefficient during IQSY 06 p0960 A71-18166
- E and F region irregularities random movements over Waltair, India, during IQSY, obtaining diurnal and seasonal variations 13 p2056 A71-27931
- Spatial-temporal harmonics of noctilucent cloud occurrences during IQSY with maximum displays after summer solstice in both hemispheres 14 p2233 A71-29965
- Book on sources and availability of IQSY data, Volume 7, covering stations, sounding rockets, satellites, space probes and World Data Centers catalog 15 p2395 A71-31518
- Papers on IQSY observations and bibliography covering meteorology, geomagnetism, aurora, night airglow, solar activity, cosmic rays, absorption measurements and drift observations 15 p2395 A71-31606
- Magnetometer network operation during IQSY, establishing Sq variations in polar regions on quiet days and nature of geomagnetic disturbances 15 p2396 A71-31607
- Classification changes in IQSY Auroral Atlas, considering symbolism, synoptic map plotting and data reduction 15 p2396 A71-31608
- IQSY night airglow from multistation photometric observation network, discussing data processing, instruments, publications and catalogs 15 p2396 A71-31609
- Ionosonde stations world distribution for vertical incidence soundings during IQSY and comparison with IGY 15 p2396 A71-31610
- IQSY data analysis of pulse reflection measurements from midlatitude station, determining polar cap and auroral absorption 15 p2396 A71-31611
- Ionospheric drifts during IQSY, discussing comparison with IGY, methods and D1 records analysis theory 15 p2396 A71-31612
- IQSY solar magnetic field, radio emission and corona observations, including flare data reevaluation 15 p2483 A71-31613
- Rocket chemical release clouds into atmosphere during IQSY, discussing wind profiles, diffusion coefficients, turbulence, temperatures and atomic O distribution 15 p2396 A71-31615
- Solar UV radiation atmospheric absorption during IQSY by ion chamber measurements, considering upper atmosphere oxygen concentration 15 p2396 A71-31616
- Bibliographic references of articles on solar terrestrial research during IQSY, including geophysical phenomena, international projects and background material 15 p2397 A71-31617
- Upper atmosphere night sky luminescence observations during IQSY, discussing correlations between

- night airglow, solar activity, interstellar dust disturbances and meteor phenomena 15 p2400 A71-31987
- Arctic polar region geomagnetic perturbations during IQSY, noting diurnal variations 19 p3059 A71-38399
- Solar activity tabulation and review covering International Geophysical Year and International Quiet Sun Year 21 p3442 A71-40151
- E region irregularities drift and anisotropy at Waltair during IQSY, inferring trends of diurnal and seasonal variation 21 p3374 A71-40379
- ## INTERNATIONAL RELATIONS
- ### NT INTERNATIONAL COOPERATION
- International Time Bureau/Paris/ astronomical and geophysical research based on universal time and latitude observations of earth rotation 06 p0890 A71-17879
- ## INTERNATIONAL SATS FOR IONOSPHERIC STUDY
- ### U ISIS SATELLITES
- ## INTERNATIONAL TRADE
- Long haul international air transport, analyzing traffic growth rates 14 p2340 A71-30161
- ## INTERNUCLEAR PROPERTIES
- Molecular nitrogen ion potential energy curves based on valence bond method, calculating sextet and quartet states at intermediate internuclear separation distances 11 p1801 A71-25365
- Ground state dissociation energies and long range internuclear potentials of diatomic molecules of halogens from spectroscopic vibrational spacings 11 p1728 A71-26065
- Langer transformation effects on radial equation for internuclear potential curves calculation by Rydberg-Klein-Rees method 14 p2277 A71-30572
- ## INTERPLANETARY COMMUNICATION
- Wideband subcarrier frequencies demodulation technique for uncoded or coded PSK telemetry over large input SNR range for deep space interplanetary communication 08 p1254 A71-21316
- PCM TV photographic data communication for grand tour of outer planets, emphasizing adaptive information-preserving data compression system for optimal performance 08 p1254 A71-21346
- Earth-spacecraft radio communication requirements for future unmanned planetary missions, emphasizing imaging experiments and sensors 18 p2877 A71-36518
- ## INTERPLANETARY DUST
- ### NT METEOROID DUST CLOUDS
- ### NT ZODIACAL DUST
- Upper atmosphere micrometeorite research with sounding rockets, considering interplanetary particle flux 03 p0485 A71-13250
- Zodiacal light IR spectroscopy by rocket-borne detector, providing information on interplanetary dust properties 03 p0491 A71-14013
- Picogram dust particle flux measurements in selenocentric cislunar and interplanetary space by Mariner 4, OGO 3 and Explorer 35 03 p0491 A71-14014
- Gegenschein photographic and photoelectric scan observations, considering origin in light reflection from interplanetary dust outside earth orbit 04 p0659 A71-15853
- Hypothetical geocentric/interplanetary dust cloud concentration detection possibility by earth shadow 10 p1601 A71-24449
- Quasars as proto-blackholes in galactic nuclei blackhole model, discussing lifetimes, dust and IR radiation using models 17 p2811 A71-35745
- Dust environment estimation in asteroid belt during trans-Martian spacecraft missions, considering cosmological, dynamical and observational evidence 20 p3297 A71-39633
- Galactic cosmic ray effects on interplanetary dust particles erosion and spurious counts in micrometeoroid sensors, microphones and capacitor detectors 20 p3280 A71-39635
- Zodiacal light lines in interplanetary dust particle flux diagram, suggesting agreement with micrometeorite data 20 p3298 A71-39636
- Two-parametric models of interplanetary dust distribution predictions involving zodiacal light scattering measurements from space probes for in- and out-of-ecliptic missions 20 p3219 A71-39637
- ## INTERPLANETARY FLIGHT
- ### NT GRAND TOURS
- Solar system exploration, discussing planets characteristics, trajectory utilization, grand tours, etc 01 p0151 A71-10269

Optimal two impulse correction with minimum energy for planetary approach trajectory and subsequent satellite orbit transfer

02 p0304 A71-11901

Space station and interplanetary flight research programs, discussing design, grand tour and Jupiter flyby

05 p0817 A71-16642

Probable solar flare doses on interplanetary mission calculated by MCLFIRE computer program using Monte Carlo methods

09 p1399 A71-22809

High energy fast Grand Tour multiplanet flyby missions to outer planets omitting Jupiter, noting identical arrival date at Neptune

[AIAA PAPER 71-188] 12 p1958 A71-26697

Optimal two impulse correction with minimum energy for planetary approach trajectory and subsequent satellite orbit transfer

13 p2133 A71-28188

Space flight, discussing stellar trips, propulsion systems and planetary exploration

13 p2145 A71-29130

Spacecraft motion during flight toward planet, including trajectory correction energy loss, autonomous angular measurements and attractive forces

13 p2146 A71-29237

Manned mars exploration, discussing excursion module, surface rover and base construction

13 p2143 A71-29251

Manned planetary precursor missions size, cost and operational characteristics, discussing effects of transportation system for projection

14 p2319 A71-30247

Electrostatic ion propulsion systems for interplanetary missions, using experimental engine characteristics as basis for flight studies

[DFVLR-SONDDR-121] 15 p2496 A71-32722

German book on models and constructions for interplanetary space flights covering Helios project, grand tour, Mars landing, planetary exploration, etc

16 p2645 A71-33523

Lunar gravitational field application in interplanetary travel, investigating spacecraft orbits by data processing machine

17 p2797 A71-34186

Propulsion systems evaluation for Mars and Jupiter missions, using bundled ESKA 28 electrostatic ion thrusters and incore thermionic reactors

[DGLR-71-046] 17 p2794 A71-35545

Book on astrodynamics covering a body equations of motion, orbital elements, differential corrections, time of flight, ballistic missiles and interplanetary transport

18 p2963 A71-36248

Computer graphic interactive flight path design program for planetary flyby missions

[AAS PAPER 71-380] 23 p3702 A71-43050

Optimal timing for interplanetary midcourse guidance maneuvers for realistic cost function, indicating first and last maneuver sensitivity

23 p3702 A71-43939

INTERPLANETARY GAS

Interplanetary space He 3 differential energy spectrum in 10-30 MeV range from IMP 4 satellite observations, noting solar contributions

05 p0802 A71-15944

Extraterrestrial Lyman alpha radiation source attributed to solar Lyman alpha scattering on cold interplanetary hydrogen penetrating to inner solar system

09 p1526 A71-23462

Planetary system formation, examining particulate matter aggregation within dust cloud and gas around sun by computer simulation

11 p1835 A71-26459

Polish space research covering satellite tracking, solar physics interplanetary gas dynamics, meteorological rockets and aerospace medicine

16 p2666 A71-33856

Interplanetary hydrogen and helium from cosmic dust deionizing effect on solar wind, calculating gas density and flux

16 p2628 A71-33940

Interplanetary H scattered solar Lyman alpha background observations by Vela 7 and OGO 3 satellites, showing 27 day correlation with intensity curve

20 p3300 A71-39736

INTERPLANETARY MAGNETIC FIELDS

Interplanetary magnetic sector structure near sunspot maximum

01 p0163 A71-11521

Solar coronal structure and interplanetary magnetic fields prediction based on magnetic models, testing accuracy at solar eclipses

[AIAA PAPER 70-1363] 02 p0315 A71-12694

Solar radio centers and interplanetary sector structures in connection with recurrent geomagnetic storms

03 p0496 A71-14512

Magnetopause inward motion before substorm, showing association with interplanetary field vertical component reversal

03 p0496 A71-14515

Solar wind plasma power spectra noting frequency dependence, particle density and speed and interplanetary magnetic fields

05 p0802 A71-15942

Photospheric and interplanetary magnetic field polarity and magnitude comparison, using Explorer observations

05 p0802 A71-16012

Interplanetary magnetic field sectors correlated to solar coronal active centers and condensations in metric wavelengths from radio observations

05 p0802 A71-16015

Polarity pattern of interplanetary magnetic field near solar maximum, using poloidal model

05 p0810 A71-16017

Shock structure at Venus and Mars dependence on interplanetary magnetic field orientation from Mariner 4 and 5 data, indicating magnetosheaths existence

05 p0810 A71-16636

Meteorites as information sources on interplanetary space beyond Martian orbit and asteroid belt, discussing possible magnetic barrier and galactic field modulation

05 p0813 A71-16857

Lunar interior electrical conductivity and temperature from various conductivity models, considering interplanetary magnetic source field

06 p0964 A71-17281

Sun daily mean-interplanetary polarized magnetic fields correlation, using source surface model

06 p0968 A71-17920

Satellite cosmic ray monitors data, examining corotation with sun to obtain interplanetary magnetic field spatial structure

06 p0951 A71-18106

Diurnal intensity variations of high energy galactic cosmic rays, taking into account particle trajectories in sectorial interplanetary magnetic field

06 p0952 A71-18115

Heliocentric cosmic ray particle density gradient production of north-south streaming in interplanetary magnetic sector, using neutron monitor

06 p0953 A71-18116

Cosmic ray mu meson intensity power spectrum frequency dependence, comparing to interplanetary field spectra

06 p0954 A71-18125

Interplanetary magnetic field power spectra fluctuation measurements by Pioneer 6 satellite

06 p0956 A71-18141

Energetic solar wind particles, discussing interplanetary magnetic field curvature and gradient effects

06 p0956 A71-18142

Solar and galactic cosmic rays interactions with interplanetary magnetic field 28 January-25 February 1967 based on Explorer 33 and 28 satellite observations

06 p0957 A71-18145

Solar particles propagation to earth during solar proton event of 25 February 1969, discussing local interplanetary field

06 p0958 A71-18150

Geomagnetic activity relation to large scale variations in interplanetary magnetic field and solar wind deformation velocity, using satellite and space probe observations

06 p0963 A71-18254

Cosmic rays sidereal diurnal variations, considering interplanetary magnetic field shielding effect

07 p1185 A71-19378

Interplanetary magnetic field in plane perpendicular to ecliptic, investigating force lines configuration by solar proton events

07 p1189 A71-20640

Diurnal cosmic ray anisotropy, investigating solar wind velocity and interplanetary magnetic field effects

08 p1352 A71-20971

Irregularity levels changes in interplanetary magnetic field during solar activity cycle from cosmic ray neutron component measurement data obtained on azimuthal muon telescopes

08 p1353 A71-20976

Galactic cosmic rays interaction with interplanetary magnetic field from Venera 4 measurements June-October 1967

08 p1354 A71-21015

Geomagnetic activity indices-overall diurnal interplanetary magnetic field strength correlation by satellite magnetometer data

08 p1360 A71-21016

Electric currents in undisturbed magnetospheric tail, discussing interplanetary magnetic field polarity effect and neutral sheet characteristics

08 p1280 A71-21214

Dungey model generated by interplanetary magnetic field addition to closed magnetospheric model, discussing adiabatic theory breakdown for model current sheet

08 p1280 A71-21217

Magnetohydrodynamical effects of spirally twisted interplanetary field on solar wind velocity and density

08 p1355 A71-21420

Pressure conditions across distant magnetopause from interplanetary magnetic field measurements, comparing Pioneer 7 plasma data with Explorer 33 distant geomagnetic tail field magnitudes

08 p1285 A71-21692

Interplanetary magnetic field inhomogeneities structure from galactic cosmic rays intensity fluctuations observation

09 p1513 A71-22424

Interplanetary magnetic field intensity and geomagnetic activity level correlation with 27-day solar activity cycle based on Venera 4 and Mariner 5 data comparison

09 p1519 A71-22577

Cosmic rays propagation in solar wind, presenting statistical theory of interplanetary magnetic field effect on charged particles transport

09 p1515 A71-23461

Plasma intrusion into simulated magnetosphere compared with satellite observations, discussing spatial distribution and interplanetary magnetic field effects

09 p1529 A71-23707

Interplanetary magnetic field irregularities and solar proton diffusion mean free path during 25 February 1969 event

10 p1677 A71-24556

Solar wind-magnetosphere interaction modes from Explorer 33 and 35 interplanetary plasma and magnetic field data

10 p1663 A71-24780

Solar wind distribution with respect to interplanetary magnetic field structure, interaction with planets and effect on earth magnetosphere

11 p1814 A71-25262

Geomagnetic and interplanetary magnetic fields, considering inverse direction of electric currents in Northern and Southern Hemispheres

11 p1757 A71-25776

Interplanetary magnetic field parameters for various heliocentric distances from 1959-1967 satellite observations, discussing cavity position and solar activity phase correlations

11 p1829 A71-25782

Interplanetary magnetic field measurements from lunar surface and lunar orbit, discussing solar wind effects on bulk electrical conductivity of lunar crust

12 p1947 A71-26691

Interplanetary magnetic field north-south component from Mariner 2, 4 and 5 measurements

13 p2131 A71-27907

Interplanetary magnetic field angular gradient and sectorial effects on solar wind, discussing wind velocity

13 p2128 A71-28527

Polar magnetic disturbances, discussing correlation with interplanetary magnetic field and interaction effects between solar wind and magnetosphere

14 p2321 A71-29907

MHD processes of upper atmosphere in mesospheric cloud formation, discussing solar wind-magnetic field interactions and equilibrium for Pikelner bomb

14 p2332 A71-29960

Solar equatorial plane interplanetary plasma and magnetic field features from cosmic ray variation anomaly observation

14 p2299 A71-29988

Solar wind compressed magnetic field in sunward magnetosphere and extended geomagnetic tail observation by Pioneer 7 spacecraft

14 p2234 A71-30028

Optically pumped magnetometers for earth and interplanetary magnetic fields measurement, using Zeeman effect

15 p2405 A71-31409

Asymmetries in magnetospheric shock layer due to upstream interplanetary magnetic field, considering forward stagnation region of solar wind-magnetosphere interaction

[AIAA PAPER 71-610] 15 p2395 A71-31546

Simultaneous two magnetometer measurements of weak magnetic fields in interplanetary space, near moon and planets by satellites in presence of spacecraft field

15 p2406 A71-31753

Solar wind ion thermalization in earth bow shock by counterstreaming instability related to interplanetary magnetic field

15 p2399 A71-31774

Pc 2-4 pulsations relationship to interplanetary magnetic field strength and orientation, using IMP 3 and 4 satellite data

15 p2401 A71-32732

Coronal and interplanetary magnetic fields during 7 March 1970 solar eclipse, comparing calculated field line maps with coronal structure photographs

16 p2641 A71-33775

Solar modulation origin of sidereal diurnal variation in cosmic ray intensity anisotropies as function of interplanetary field direction, using underground muon telescopes

16 p2628 A71-33931

Solar wind rotational to tangential discontinuities ratio determination and hypothesis concerning origin in interplanetary magnetic field

16 p2628 A71-33942

Magnetotail changes relationship to solar wind magnetic field and magnetospheric substorms from ground and satellite data

16 p2629 A71-33944

INTERPLANETARY MEDIUM

- Bibliography and review of interplanetary magnetic fields and plasmas, considering solar wind properties, magnetosheath, bow shock and magnetospheric tail
17 p2799 A71-34460
- Sq day to day variability relation to interplanetary plasma parameters including magnetic field and solar wind velocity and kinetic energy
17 p2801 A71-34625
- Lunar electroconductivity, examining moon response to large discontinuity in interplanetary magnetic field
19 p3131 A71-37354
- Polar substorms relation to interplanetary magnetic field from IMP 3 satellite magnetic measurements
19 p3132 A71-37396
- Cosmic rays sidereal diurnal variations, considering interplanetary magnetic field shielding effect
19 p3127 A71-37803
- Magnetic field measurements on Outer Planets Grand Tour to yield solar system origin and evolution and interstellar medium data
[AAS PAPER 71-123] 19 p3139 A71-37918
- Interplanetary plasma and magnetic field interaction with earth magnetosphere using spacecraft measurements during storms
19 p3145 A71-38272
- Anomalous distribution in heliocentric longitude of solar injected cosmic radiation, suggesting interplanetary magnetic field lines of force stochastic wandering
19 p3130 A71-38674
- Interplanetary and magnetospheric magnetic force lines reconnection and effects on geomagnetic activity
20 p3289 A71-39126
- Outer space and earth surface galactic cosmic ray intensity data correlation analysis for studying interplanetary magnetic field structure
20 p3278 A71-39129
- Galactic cosmic rays interaction with interplanetary magnetic field from Venera 4 measurements of June-October 1967
20 p3280 A71-39595
- Geomagnetic activity indices-overall diurnal interplanetary magnetic field strength correlation by satellite magnetometer data
20 p3294 A71-39596
- Galactic cosmic rays and interplanetary magnetic field flux measurements onboard Venera 4 space probe, noting lack of correspondence with Forbush decrease
20 p3282 A71-39737
- Large scale spiral variations of interplanetary magnetic field related to structures in solar wind, including polar field and out of ecliptic models
21 p3453 A71-41181
- Metric frequency solar radio noise active regions relationship to interplanetary magnetic field polarity distribution
22 p3597 A71-41471
- Geomagnetic and interplanetary magnetic fields, considering inverse direction of electric currents in Northern and Southern Hemispheres
22 p3532 A71-41544
- Interplanetary magnetic field parameters for various heliocentric distances from 1959-1967 satellite observations, discussing cavity position and solar activity phase correlations
22 p3598 A71-41550
- Interplanetary magnetic sector polarity effects on polar geomagnetic field diurnal variation
22 p3604 A71-42221
- Interplanetary magnetic shock front location and geometry determination, using interstellar hydrogen density measurements
23 p3720 A71-43133
- Interplanetary plasma and magnetic field observations by Vela 3 and Imp 3 satellites
23 p3708 A71-43154
- Theta /north-south/ component in spherical polar coordinates of interplanetary magnetic field from Explorer 33 and 35 measurements
23 p3734 A71-43155
- Magnetospheric substorms relationship to interplanetary magnetic field and solar wind plasma parameters, noting dominant effect of interplanetary southward component
23 p3734 A71-43183
- Lunar atmosphere as source of lunar surface gaseous elements, calculating ions trajectory and impact energy as function of interplanetary magnetic field strength
23 p3754 A71-43728
- Outer radiation belt parameters dependence on interplanetary magnetic field sectorial structure and solar wind velocity
24 p3866 A71-45039

INTERPLANETARY MEDIUM

- NT INTERPLANETARY DUST
NT INTERPLANETARY GAS
NT METEOROID DUST CLOUDS
NT ZODIACAL DUST

Solar flare proton propagation, examining interplanetary shock wave effects on cosmic ray scattering
01 p0146 A71-11386

Proton fluxes at 300 keV associated with propagating interplanetary shock waves, noting alpha particle enhancement
01 p0146 A71-11487

Zodiacal light theoretical models, considering interplanetary particles optics, Mie theory and multicolor polarization
03 p0491 A71-14011

Solar wind microscopic structure, examining interplanetary wave-particle interactions
03 p0480 A71-14068

Low energy cosmic ray propagation anisotropies in interplanetary medium examined by unidirectional detectors on geostationary satellites
03 p0482 A71-14543

Interplanetary matter accumulations around Lagrangian libration points
05 p0808 A71-16455

Finite electrical conductivity role in interplanetary piston driven shock waves propagation in solar wind
05 p0810 A71-16635

Meteorites as information sources on interplanetary space beyond Martian orbit and asteroid belt, discussing possible magnetic barrier and galactic field modulation
05 p0813 A71-16857

Interplanetary medium during magnetic storm periods, noting pressure and density increases of various energy flows of media and static pressure/magnetic pressure ratio
05 p0744 A71-17179

Galactic cosmic ray solar modulation in interplanetary medium, discussing spherically symmetric model
06 p0949 A71-17275

Isotropic galactic cosmic ray diffusion in interplanetary space from solar wind velocity and diffusion coefficient dependence on heliolatitude and heliointensity
06 p0953 A71-18118

Low energy solar and galactic cosmic ray propagation in interplanetary medium from Zond 3 and Venus 2-4 space probes measurements
06 p0958 A71-18152

Radio wave propagation through extensive weakly scattering medium, presenting typical results for scintillation index, scintillation visibility and spatial autocorrelation function
07 p1196 A71-19576

VLF electric field data in interplanetary medium from Pioneer 8 space probe observation
07 p1196 A71-19655

Upstream discrete wave packets propagation interplanetary medium from Ogo 5 observation
07 p1197 A71-19656

Chromosphere-flare and galactic cosmic ray hypotheses of Forbush decrease and strong shock waves in interplanetary medium
08 p1352 A71-20967

Low energy cosmic ray intensity increase at propagating interplanetary shock wave front, discussing one dimensional model with particles undergoing convection and diffusion
08 p1356 A71-21630

Suprathermal electrons continuous stream release into interplanetary medium during hectometric solar noise storm activities
09 p1518 A71-22353

Interplanetary plasma disturbances in Venus proximity from Venera measurements
09 p1520 A71-22669

Interplanetary shock waves sounding and geomagnetic storm forecasting based on cosmic ray intensity increases from ground observations
09 p1515 A71-23633

Polar cap as distinct geophysical entity, considering open magnetic field lines for connectedness to interplanetary plasma and particle input to lower latitudes
10 p1600 A71-24308

Interplanetary medium small scale plasma irregularities by scintillation techniques, considering electron density deviations
10 p1674 A71-24434

Interplanetary magnetic field parameters for various heliocentric distances from 1959-1967 satellite observations, discussing cavity position and solar activity phase correlations
11 p1829 A71-25782

Interplanetary medium characteristics during geomagnetic storms, discussing changes in pressures, energy flux densities, acoustic velocities and static/magnetic pressure ratio
13 p2058 A71-28236

Solar wind heavy ion data, using Heos-1 satellite observations of 31 March 1970 interplanetary shock
13 p2130 A71-29059

Solar flare cosmic ray propagation, investigating bounded interplanetary diffusion medium effects
13 p2130 A71-29060

Dynamic nonshock properties of large amplitude microscale Alfvén waves in interplanetary medium, using plasma and magnetic field data from Mariner 5
15 p2456 A71-31752

Sun and interplanetary medium, considering pure atomic physics, radio emission, IR excess, solar wind, sunspots and solar radio astronomy
15 p2486 A71-31924

Radio sources 3C 48, 3C 144, 3C 161, 3C 273 and 3C 298 scintillations by interplanetary plasma at 60 MHz determining electron density fluctuations
15 p2487 A71-32020

Quasar 3C 48 observations at 408 MHz, noting scintillations due to interplanetary plasma inhomogeneities
15 p2487 A71-32020

Geomagnetic tail natural oscillations, applying model of plasma cylinder with free boundary immersed in interplanetary medium
16 p2564 A71-33620

Proton flares in McMath Region 8461/August-September 1966, describing solar wind plasma ejection and helium enriched interplanetary medium
18 p2958 A71-36701

Substorm signature in interplanetary medium relating southward component with solar wind energy transformation
19 p3132 A71-37359

Interplanetary plasma and magnetic field interaction with earth magnetosphere using spacecraft measurements during storms
19 p3145 A71-38272

Interplanetary medium thermal emission detection presenting diffuse background radiation upper limit in intermediate IR from sounding rocket data
20 p3288 A71-39111

Interplanetary magnetic field parameters for various heliocentric distances from 1959-1967 satellite observations, discussing cavity position and solar activity phase correlations
22 p3598 A71-41550

Monochromatic radio wave propagation in interplanetary plasma, deriving frequency spectrum and phase and amplitude fluctuations
22 p3511 A71-42303

Cosmic ray solar diurnal variation anomaly at 1959 minimum, discussing diffusion and scattering in interplanetary medium
23 p3720 A71-43133

Interplanetary plasma and magnetic field observations by Vela 3 and Imp 3 satellites
23 p3708 A71-43154

Interplanetary electron associations with type 1 solar bursts, using decametric OGO 3 and solar geophysical observations
23 p3721 A71-43170

Radio wave propagation characteristics in Venusian atmosphere and interplanetary plasma from Venera 4 probe data
24 p3805 A71-45312

INTERPLANETARY MONITORING PLATFORM
U IMP

INTERPLANETARY NAVIGATION

Jupiter atmospheric probe approach trajectory uncertainties and navigation requirements during 1979 mission
[AIAA PAPER 71-120] 06 p0926 A71-18566

Apollo simulator navigation and docking training techniques, discussing manned LM and CSM key role performance
07 p1156 A71-20342

Planetary quarantine constraint effect on multiple outer planet missions, considering navigation error sources and midcourse maneuvers
[AAS PAPER 71-122] 19 p3002 A71-37917

Navigation, orbit and trajectory analysis of 1979 Jupiter-Uranus-Neptune Grand Tour mission, assuming deep space network tracking
[AAS PAPER 71-117] 19 p3101 A71-37936

Navigation error sources and orbit determination accuracies for Jupiter planetary encounter, using earth-based radio tracking data
[AAS PAPER 71-118] 19 p3101 A71-37937

Interplanetary navigation TV camera in-flight calibration, discussing instrument error sources elimination
22 p3573 A71-42771

Planetary quarantine constraint on 1977 Jupiter-Saturn-Pluto mission, determining fuel loading penalties, optimum biasing strategies and outer planet navigational characteristics
[AAS PAPER 71-319] 23 p3726 A71-42993

Monte Carlo simulation of navigation and guidance for Grand Tour Jupiter-Saturn-Uranus 1977 mission, using graphics computer program [STEP VII]
[AAS PAPER 71-374] 23 p3701 A71-43044

INTERPLANETARY PROPULSION
U INTERPLANETARY SPACECRAFT
U ROCKET ENGINES

Slow mode shocks in interplanetary space detected by Mariner 5 spacecraft 3.5 and 27 million km from earth
01 p0148 A71-11527

Short duration proton energy increases observation by Explorer 34, considering interpretation as acceleration associated interplanetary shocks
06 p0949 A71-17254

Interplanetary cosmic ray gradients and anisotropies from Pioneer 8 probe
06 p0952 A71-18111

Low energy protons radial gradient in interplanetary space measured with intercalibrated solid state detectors
06 p0952 A71-18111

tors on Venus bound Mariner 5 and earth orbiting Explorer 33

Solar flares of 25-27 February 1969 effects on polar cap and interplanetary space flux rates, confirming magnetospheric modulation of proton density peaks

Plasma density irregularities in solar wind, showing wavelength dependence of interplanetary scintillation inconsistent with magnetic variations

Interplanetary space solar wind flux variations-earth electromagnetic field pulsations comparison by spacecraft and geophysical station observations

Interplanetary space cosmic ray currents global survey based on neutron component measurements, noting anisotropic diffusion, inhomogeneous solar wind and Forbush effect shell model

Interplanetary space cosmic ray density gradient from three dimensional anisotropic diffusion model

Galactic cosmic ray density space-time variations in interplanetary space with solar wind, using spherically symmetrical model with diffusion approximation

Solar activity heliolatitudinal distribution effect on interplanetary space electromagnetic conditions governing galactic cosmic ray intensity

Solar flare electron spectra in interplanetary space and within earth magnetosphere, investigating simultaneous observations by satellite-borne magnetic electron spectrometers

Interplanetary plasma electron density inhomogeneities formation explained by instability due to electron stream curvilinearity obtained from spacecraft data

Proton energy change effects on charged particles propagating in interplanetary space, using low energy solar flare proton fluxes observations

Polar cap cosmic radiation intensity measurement for deducing electromagnetic conditions near earth and in interplanetary space

Solar wind motion irregularities near sun from interplanetary scintillation observations, using receivers at Goldstone deep space tracking station

Interplanetary space low energy cosmic ray protons steady state anisotropy based on radial gradient model of outward convection at solar wind speeds

Photoelectron sheath and electric field around spacecraft in interplanetary space, considering typical sheath profiles and tenuous ambient plasma effects

Dust grain condensation and primordial elements transport into interplanetary space during early stage solar evolution

Galactic cosmic rays solar modulation and intensity gradient in interplanetary space from satellite observation data

Cosmic ray propagation in interplanetary space, deriving steady state transport equation with energy losses

Pioneer F spacecraft investigation of Jupiter regions and outer interplanetary space, discussing design, communication system and possible future missions

Pioneer 9 interplanetary observations, presenting deep space data for solar rotations and radial gradient in VLF electric field behavior

Extraterrestrial Lyman alpha radiation, showing interplanetary principal anisotropic effects

In-flight UV spectrometric measurements of simulated Jupiter atmosphere, using sunlight gas mixture released from Mariner spacecraft in interplanetary space

Galactic cosmic ray transport equation numerical solution for interplanetary region, considering modulation, diffusion, convection and energy loss effects

Electromagnetic waves in interplanetary space and effects on magnetosphere, considering solar wind characteristics due to wave interactions

Corotating solar plasma streams associated with variations of interplanetary scintillation from observed radio sources

Geolunar interorbital transportation based on shuttle trajectories, interorbital rendezvous, elliptic orbits and terminal transfer

Heuristic approaches for generating perturbations to automatically evaluate partial derivatives for interplanetary space missions

Direct measurements of cosmic dust particles in near earth environment and interplanetary space, noting reliability and calibration

Solar boundary conditions effect on interplanetary propagation of solar flare particles for anisotropic diffusion model

Interplanetary scintillation radio observations interpretation by theory for atmospheric scintillations optical observations

HEOS-A2 eccentric orbit satellite for interplanetary space and high latitude magnetosphere data, discussing onboard experiments, major subsystems and design philosophy

Galactic cosmic rays solar modulation and particle intensity gradient in interplanetary space from satellite observation data

Direct observation of cosmic ray kinetic energy losses in interplanetary region by measurements at separated spacecraft

Solar high energy particles directional and temporal properties, investigating single encounter model with propagating interplanetary shock waves

Interplanetary time delay and light deflection measurements anomalies, investigating gravitational and electromagnetic fields interaction

Comet brightness variations correlation with geomagnetic field and solar corpuscular flux variations in interplanetary space

INTERPLANETARY SPACECRAFT

NT JUPITER PROBES
NT MARINER SPACE PROBES
NT MARINER VENUS-MERCURY 1973
NT MARINER 5 SPACE PROBE
NT MARS PROBES
NT PIONEER SPACE PROBES
NT PIONEER 6 SPACE PROBE
NT PIONEER 7 SPACE PROBE
NT PIONEER 8 SPACE PROBE
NT PIONEER 9 SPACE PROBE
NT TOPS (SPACECRAFT)
NT VENERA SATELLITES
NT VENERA 3 SATELLITE
NT VENUS PROBES
NT VIKING LANDER SPACECRAFT
NT VIKING ORBITER SPACECRAFT
NT ZOND SPACE PROBES
NT ZOND 3 SPACE PROBE
NT ZOND 5 SPACE PROBE
NT ZOND 7 SPACE PROBE

Mathematical model for determining thrust interplanetary spacecraft orbit, considering time history of position, velocity and thrust acceleration

Manned artificial satellites, discussing problems of orbiting and interplanetary space stations with reference to U.S./U.S.S.R. future projects

Soviet book on interplanetary electric spacecraft covering chemical and nuclear jet engines and rockets, electrothermal engines, plasma thrusters, etc

Photoelectron sheath and electric field around spacecraft in interplanetary space, considering typical sheath profiles and tenuous ambient plasma effects

Optimal lunar springboard effect for maximum characteristics velocity savings on interplanetary missions utilizing gravitational field by departing spacecraft

Helios 6 interplanetary solar probe, investigating particle propagation, energy spectra, direction distributions and spatial gradients

Jovian turbopause probe mission, discussing atmospheric composition measurements and non-survivable system concept

Jupiter atmospheric entry probe mission, discussing descent depths, atmospheric pressure and temperature effects, data return techniques and Grand Tour Missions

Phobos and Deimos missions, examining lander and lander/orbiter configurations and Titan-Centaur and space shuttle-Centaur launch systems

Solar electric propulsion system design for interplanetary spacecraft, describing Hg bombardment ion engine

INTERPLANETARY TRANSFER ORBITS

Automatic interplanetary station adapter to obtain reflected signals amplitude-altitude-frequency characteristics during ionospheric probes

Orbit-to-orbit shuttles as earth capture systems for round trip planetary missions, using hyperbolic rendezvous technique with returning interplanetary spacecraft

Grand Tour interplanetary trajectories regularization, removing singularities in equations of motion of space vehicles

Low thrust interplanetary spacecraft tracking, using spectral factorization for Kalman filtering equations steady state solution

Balanced space programs for 1970s and beyond, discussing unmanned planetary missions, manned Apollo, Skylab and space shuttle projects, private, foreign and international programs

Motion equations numerical integration step as function of celestial object location and velocity in interplanetary probe orbit computation

INTERPLANETARY TRAJECTORIES

Recurrent Lagrange multipliers coordinate transformation for optimal low thrust Earth-Jupiter trajectories

Free-fall periodic orbits/interplanetary trajectories/ connecting earth and Mars, using patched conic analysis

Spacecraft midcourse guidance technique for lunar and interplanetary trajectories based on matched asymptotic expansions

Jupiter atmospheric probe approach trajectory uncertainties and navigation requirements during 1978 mission

Multiple interplanetary flyby trajectories precision targeting, using sequence of alternate heliocentric and planetocentric trajectory segments with position and time matching constraints

Space vehicle motion on planetary flyby trajectories, using Chebyshev polynomial series and Picard successive approximations method to solve two point boundary value problem

Spacecraft motion during flight toward planet, including trajectory correction energy loss, autonomous angular measurements and attractive forces

Onboard silicon detector TV guidance sensor for establishing outer planet mission spacecraft orientation with precise targeting, based on patched conic trajectory simulation

Mission analysis for multi-planet flyby and major satellites close encounter to determine solar system planetary evolution data, presenting Grand Tour trajectory parameters

Pioneer F/G spacecraft Jupiter missions, trajectories and objectives with relation to outer system

Interplanetary single impulse flight trajectories optimization and computation, determining geometrical and kinematic characteristics

Spacecraft interplanetary guidance trajectory correction, deriving algorithm for optimal accuracy and minimum fuel expenditure

Guidance system figure of merit determining relative effectiveness of launch vehicle in delivering spacecraft onto interplanetary trajectory

Grand Tour interplanetary trajectories regularization, removing singularities in equations of motion of space vehicles

N-body integrated reference trajectories and navigation requirements for extended Venus/Mercury 1973 mission midcourse correction

INTERPLANETARY TRANSFER ORBITS

Time series approximation of acceleration functions for analytical solution of low thrust interplanetary transfers, treating flyby and rendezvous mission modes

Space shuttle application to periodic interplanetary orbit making flyby without stopping, discussing trajectory requirements and relative orientation of earth, Venus and Mars

Geolunar interorbital transportation based on shuttle trajectories, interorbital rendezvous, elliptic orbits and terminal transfer

INTERPOLATION

INTERPOLATION

Coordinatograph control system transfer function and interpolation error calculation
05 p0732 A71-17040

Alouette 2 ionograms frequency interpolation correction allowing measurement accuracy comparable to sounder system resolution
05 p0725 A71-17083

Tchebycheffian spline functions, solving Hermite-Birkhoff interpolation as stochastic prediction and filtering
07 p1147 A71-19325

OSO 3 satellite observations of diffuse X ray emission from galactic plane, eliminating straight line interpolation of spectrum between 3-10 keV X ray range and 100 MeV energy range
10 p1665 A71-23750

Steady convergence analysis of generalized Chebyshev successive interpolation process, using functions of interpolative classes
10 p1635 A71-23801

Modified Landau-Lipschitz equation of thin ferromagnetic film for slowly reversing magnetic fields solved by interpolation, discussing magnetization curve subrelaxation segment
11 p1809 A71-26547

German monograph on spline functions interpolation for solving integral equations and stress calculation in curvilinear edged disks
13 p2157 A71-29420

Linear aperture antenna radiation pattern interpolation based on complex-valued function satisfying integral equations system
16 p2546 A71-33497

Orthogonal bicolored moire fringes in mechanical interferometry, considering interpolation type determination of fractional fringe orders
17 p2738 A71-34548

Limited spectrum random processes interpolation, considering unequivocal recovery from values in infinite sequence of equidistant moments of time
17 p2765 A71-34862

Optical grating measuring systems high resolution interpolation using phase analog and digital counter techniques
17 p2745 A71-35293

Errors resulting from linear interpolation use in opacity tables for stellar interior calculations
22 p3599 A71-41923

One and two dimensional function values calculation for curve systems by continued fraction interpolation from point grids, using computer program
22 p3518 A71-42394

INTERPOLATORS

U REPEATERS

INTERPLANAR COMMUNICATION

Interstellar communication via IR laser beam, considering resolution and signal detection capabilities, reflectors structural size and accuracy, power requirements and cost
11 p1822 A71-25636

Solar system interstellar communication with Galaxy, discussing information transmission, coding decoding, recording, display, pulse use and economics
15 p2371 A71-31747

Dynamic formulation for number of communicative civilizations in Milky Way galaxy suitable for digital simulation
18 p2965 A71-36295

Extraterrestrial civilizations, discussing cybernetic approach and development of languages for interstellar communications
19 p3134 A71-37521

INTERSTELLAR EXTINCTION

Rocket UV astronomy, discussing atmospheric and interstellar absorption, equipment design and OAO experiments
04 p0649 A71-15253

Interstellar extinction curve accounted for by graphite, iron and silicate grains, presenting refractive index values plotted as functions of wavelength
07 p1199 A71-20009

Interstellar silicate extinction related to 2200 A band from determination of enstatite optical constants
07 p1200 A71-20053

Silica minerals in interstellar dust as source of 2200 A interstellar absorption band from comparisons to 2250 A band in Fe or Al bearing quartz spectra
09 p1522 A71-22936

Diffuse interstellar bands polarization and extinction based on silicate and graphite grain composition and sizes
10 p1675 A71-24469

Diffuse interstellar absorption centered at 4430 A observed in reflection nebulae, using narrow band filters
11 p1831 A71-26135

Observational test of Planck constant variation on cosmic scale in terms of radiation absorption by interstellar and intergalactic gases
11 p1832 A71-26183

Galactic clusters statistical analysis for relative sky areas at various distances, discussing inverse apparent diameters and interstellar obscuration effects
11 p1833 A71-26329

Interstellar dust, investigating starlight reddening by extinction, galactic light, IR star observations and polarization
12 p1959 A71-26775

Cosmic soft X rays diffuse component dependence on galactic latitude related to interstellar absorption
12 p1949 A71-27370

Fine structure of reddening interstellar extinction curves of stellar radiation, using photographic spectrophotometry
13 p2132 A71-27967

Planetary nebulae observations in radio spectrum, determining interstellar extinction, electron temperature recombination theory and models
14 p2312 A71-30388

Methane, ammonia and silicate effects on 3.07 micron ice absorption in interstellar grains, using cesium iodide window deposited sample measurements
15 p2498 A71-32774

Interstellar gas absorption correlation with dust extinction, obtaining gas to dust density ratio
16 p2632 A71-33323

Interstellar absorption at H alpha line wavelength in Orion nebula, obtaining contour map for comparison with radio intensity
19 p3131 A71-37230

Soft galactic X rays role in interstellar grains alignment, taking into account interstellar absorption
19 p3124 A71-37336

Three color photometry of star field in Sagittarius cloud, determining interstellar absorption, density and luminosity for main sequence stars
19 p3144 A71-38169

Kinematic method for determining interstellar extinction/dilution ratio
20 p3293 A71-39533

Planetary, stellar, galactic, sky and extragalactic UV radiation from GAO-2 spectrophotometric observations, noting interstellar extinction curves
20 p3300 A71-39747

Identity relation of LF compact source to Crab pulsar NP 0532 with respect to interstellar scattering
20 p3302 A71-39924

Optical properties of graphite-iron-silicate grain mixtures from Mie theory for spherical particles, noting models consistency with interstellar extinction and backscattering observations
21 p3444 A71-40242

Total to selective extinction ratio determination, obtaining distance to galactic center
21 p3445 A71-40245

Interstellar Lyman alpha absorption equivalent widths in hot stars spectra, examining rocket and satellite observations
22 p3598 A71-41913

Intrinsic UV color variations of interstellar extinction laws due to stellar rotation, MK spectral type and photometric errors, using rocket observations
22 p3604 A71-42333

Interstellar spherical grains surface roughness model, noting far UV radiation extinction enhancement
22 p3605 A71-42340

OH transitions excitation temperatures in absorbing cloud from observations of W12
24 p3871 A71-44906

Atomic hydrogen cloud distances determined by interstellar absorption lines of early stars
24 p3874 A71-45145

INTERSTELLAR GAS

Mathematical model for interaction between solar wind and interstellar gas
01 p0144 A71-10066

Interstellar gas cloud spherically symmetrical collapse, considering computer program for density, temperature, flow velocity, cooling rate and gravity force
01 p0157 A71-10758

Interstellar hydrogen ion production and destruction by electron recombination or photodissociation
02 p0317 A71-12870

Supersonic solar wind flow termination, examining interstellar neutral hydrogen effect
03 p0481 A71-14502

Stellar origin and evolution, discussing interstellar gas heating and condensation, star cluster formation and superdense body decay
04 p0642 A71-14774

Interstellar H I region Lyman alpha production by suprathermal protons, determining temperature and ionization equilibrium
04 p0640 A71-14873

IR stars, discussing very young stars, circumstellar clouds and IR excesses
04 p0648 A71-15251

Galactic Lyman alpha observation by Vela 7, discussing error possibility of data interpretation based on interstellar hydrogen shock wave
04 p0658 A71-15831

Interstellar gas cloud equilibrium and gravitational stability, examining evaporation, condensation, thermal balance and pressure
04 p0658 A71-15837

Interstellar gas small scale irregularities in electron density, considering nonlinear processes in plasma causing turbulence in spectrum
05 p0805 A71-16286

Planetary nebulae and H II region dust density perturbation e-folding time, examining Lyman continuum radiation
05 p0812 A71-16666

H I gas kinematics in Galactic anticenter region from Gaussian components of emission line profiles
21 cm observations
06 p0964 A71-17306

Interstellar gas dynamics - Conference, Yalta, September 1969
06 p0971 A71-18338

Interstellar gas dynamic characteristics, discussing galactic large scale features
06 p0971 A71-18338

Interstellar gas and star mass interchange, discussing balance and galactic and stellar evolution models
06 p0972 A71-18338

Neutral condensations and protostars in H II regions noting original density distributions
06 p0973 A71-18341

Static solar H II region ionization balance, energy UV radiation transfer, gravitation equilibrium and interstellar gas temperature
06 p0975 A71-18444

UV absorption line spectra from H II regions evaluating X ray and photoionization heating models
07 p1190 A71-18858

Interstellar gas acceleration and heating by cosmic rays streaming along uniform magnetic field faster than Alfvén speed
07 p1190 A71-18858

Galactic and solar cosmic rays diffusion as function of solar activity and interstellar medium properties considering particle velocity and proton scattering transport
07 p1185 A71-19345

Neutral hydrogen subsystem rotation in inner Galaxy from equal angular velocity surfaces
09 p1518 A71-22375

Mathematical model for interaction between solar wind and interstellar gas
09 p1514 A71-23228

Cosmic rays observations, using particle interactions with interstellar gas and magnetic fields
09 p1515 A71-23535

Pulsar dispersion measures for spatial distributions above galactic plane, determining mean interstellar electron density of local spiral arm
10 p1671 A71-24308

Interstellar CO, constructing strip maps in declination and right ascension across W51, Sgr A and Sgr B4 for 115.2712 line radiation
11 p1818 A71-25204

Galaxy M33 density wave velocity and detection, discussing star distribution, H II regions red and blue supergiant and hot stars
11 p1821 A71-25544

Static solar H II region ionization balance and energy, UV radiation transfer, gravitational equilibrium and interstellar gas temperature
12 p1955 A71-26591

Young cluster NGC 2264 main sequence A and B stars four color and H beta observation, suggesting evidence of circumstellar gas shells
12 p1956 A71-26611

Galactic radio emission, considering continuum radiations, radio polarization, H I regions structure and physics, recombination and absorption lines
12 p1959 A71-26778

Interstellar matter, emphasizing H I and H II regions temperatures, dust, magnetic fields, intermediate and high velocity clouds
12 p1959 A71-26779

Measuring methods for internal velocities of stars and gas within spiral galaxy, considering emission lines and Fabry-Perot interferometer
12 p1960 A71-26786

One- and two-component gas models for explaining interstellar gas kinematics and 21 cm line emission brightness temperature dependence on galactic longitude
12 p1970 A71-27747

Thermal ion-atom charge transfer effects on ionization equilibrium of interstellar oxygen in H I regions using Bahcall-Wolf orbiting approximation
13 p2132 A71-27966

Double resonator ruby maser for observing transitions of interstellar hydroxyl, noting incorporation in modulation radiometer of astronomical telescope
13 p2077 A71-28375

Interstellar H II regions high quantum number recombination line measurements, indicating Stark broadening
13 p2143 A71-29266

Interstellar SH search for ground state main line transitions at 111 MHz
14 p2313 A71-30433

Interstellar gas heating by soft X rays and cosmic rays for electron production, calculating heating rate with Boltzmann equation and Monte Carlo method
14 p2302 A71-30642

Galactic discrete X ray sources identification with black nebulae, H II regions, close binary stars, Wolf-Rayet stars and planetary nebulae
15 p2482 A71-31330

Gravitating continuous medium instability in presence of delta shaped point density perturbations, discussing cloud structure development in interstellar gas
15 p2495 A71-32642

Diffuse interstellar medium hydrogen radio recombination lines radiation transfer, investigating thermodynamic equilibrium effects
15 p2498 A71-32770

Dense interstellar cloud radio recombination lines in H I regions, calculating quadrupole effects on line splitting
15 p2498 A71-32771

Milky Way galaxy interstellar neutral hydrogen rolling motion phenomenon confirmed by 21 cm line survey data
16 p2630 A71-33053

Interstellar gas absorption correlation with dust extinction, obtaining gas to dust density ratio
16 p2632 A71-33323

Magnetic stars as cosmic ray generators, considering interstellar gas particle acceleration by EM forces produced by rotating stellar magnetic field
16 p2625 A71-33324

Galactic H II regions radio sources observations by high resolution radio telescopes, comparing with optical appearance
16 p2632 A71-33326

Aperture synthesis observations of neutral hydrogen radio emission in spiral galaxy M 101, using twin-element interferometer
16 p2632 A71-33329

Hydrogen condensation in interstellar gas clouds onto solid dust grains from vapor pressure measurements of solid hydrogen at low temperatures
16 p2634 A71-33392

Spiral structure of Galaxy, using perturbation method for analysis of steady state interstellar gas with differential rotation due to coupling with stellar gas
16 p2643 A71-34069

Star formation at interstellar gas cloud stage, discussing gravitational collapse, Bok dust globules, spectroscopic and IR peculiarities and models
17 p2801 A71-34696

NGC 2024 direction H I region H 137 alpha recombination line emission detection, determining ionized hydrogen fraction
17 p2807 A71-35415

Interstellar silicon monoxide discovery from 130,246 MHz frequency line emission of galactic radio source Sag B2
17 p2807 A71-35416

Interstellar molecular hydrogen gas near IR emission detection in dark clouds
18 p2969 A71-37042

Galactic and solar cosmic rays diffusion coefficient as function of solar activity and interstellar medium properties, considering particle velocity and proton scattering transport
19 p3127 A71-37804

Galactic central region gas motions, discussing hypothetical explosive expulsion of matter from galactic nucleus
19 p3143 A71-38165

H II region formation from type II supernovae explosion, detecting with fluorescence model
20 p3287 A71-39052

Interstellar medium time dependent model, investigating supernovae and hot stars UV ionization effects on ion production and heating and cloud formation
21 p3445 A71-40248

Reversible charge exchange reactions effects on ionization equilibrium of nitrogen in interstellar space
21 p3445 A71-40412

Methyl alcohol transitions in Orion at 1 cm noting emission source coincidence with IR nebula
21 p3447 A71-40445

Millimeter emission lines from interstellar methyl cyanide transitions, noting kinetic temperature and hydrogen density
21 p3447 A71-40446

Interstellar carbonyl sulfide transition at 109.5 GHz, noting column density
21 p3447 A71-40447

Cosmic ray and soft X ray steady state models of interstellar gas, determining He/H ions concentration ratio
22 p3601 A71-42167

Solar cycle variation effects on interstellar hydrogen within solar system, discussing thermal motion, density, far UV ionization and charge transfer reactions
22 p3601 A71-42169

H II regions kinematic properties in Large Magellanic Cloud, presenting emission line profiles and radial velocities
23 p3723 A71-42939

Interstellar medium recombination line emission origin from discrete distribution of cold and dense clouds
23 p3723 A71-42942

Interplanetary magnetic shock front location and geometry determination, using interstellar hydrogen density measurements
23 p3720 A71-43133

Interstellar He photoionization effect on solar wind abundance
23 p3721 A71-43182

Cyclotron magnetoacoustic wave generation by planets and binary stars in circular orbits, deriving interstellar gas density variations
24 p3869 A71-44804

OH transitions excitation temperatures in absorbing cloud from observations of W12
24 p3871 A71-44906

Sgr B2 region interstellar gas microwave emission spectrum, observing inversion transitions in metastable rotational levels of ammonia
24 p3872 A71-44916

Galactic neutral hydrogen absorption line spectra at 21 cm wavelength by radio sources interferometric observations, discussing cool gas temperature, ionization rate and Cetus Arc distance
24 p3873 A71-45084

INTERSTELLAR MAGNETIC FIELDS

Linear MHD theory of inhomogeneities in axisymmetric models of universe with cosmological magnetic field
01 p0160 A71-11093

Physical processes in galactic and extragalactic sources of nonthermal radio emission, assuming pulsars as principal magnetic field and cosmic rays sources
03 p0483 A71-13201

Galactic magnetic field characteristics and cosmic rays origin, discussing gas clumping and star formation
04 p0641 A71-15758

Crab pulsar magnetic field structure measurements, using optical wavelengths linear polarization
05 p0808 A71-16454

Expanding universe magnetic field origin, examining Batchelor condition for spontaneous appearance in turbulent conducting fluid motion
05 p0809 A71-16470

Galactic magnetic field generation by dynamo process with nonuniform rotation and turbulence in gaseous disk
05 p0811 A71-16687

Galaxy gaseous disk as low mode dynamo, calculating turbulent diffusion coefficient for passive magnetic fields
05 p0811 A71-16688

North Galactic Pole soft X ray flux measurements, using Teflon windowed proportional counter
05 p0799 A71-16699

Meteorites as information sources on interplanetary space beyond Martian orbit and asteroid belt, discussing possible magnetic barrier and galactic field modulation
05 p0813 A71-16857

Galactic cosmic ray solar modulation with 20 year periodicity, suggesting nearby galactic magnetic field direction
06 p0955 A71-18130

Galactic magnetic field observation, investigating cluster polarization, Zeeman effect, pulsar rotation and signal dispersion, interstellar cloud elongation and models
06 p0972 A71-18331

Galactic magnetic fields and cosmic ray gas, investigating origin and dynamical effects
06 p0972 A71-18332

Supernovae expansion, investigating hydrodynamic model with interstellar magnetic fields and relativistic particles effects
06 p0973 A71-18335

Interstellar gas acceleration and heating by cosmic rays streaming along uniform magnetic field faster than Alfvén speed
07 p1190 A71-18854

Bubble of energetic charged particles embedded in interstellar or intergalactic magnetic field and in gas, discussing dynamic effects on radio astronomy observation
07 p1197 A71-19815

Linear MHD theory of inhomogeneities in axisymmetric models of universe with cosmological magnetic field
08 p1366 A71-21951

Cosmic rays observations, using particle interaction with interstellar gas and magnetic fields
09 p1515 A71-23536

Crab Nebula pulsar magnetic field structure, discussing linear polarization modifications and wisps
10 p1668 A71-23870

Taurus dust cloud magnetic field line of sight component observations and M17 and Cyg A absorption spectra data noting Zeeman splitting at 21 cm H lines
12 p1957 A71-26623

Interstellar matter, emphasizing H I and H II regions temperatures, dust, magnetic fields, intermediate and high velocity clouds
12 p1959 A71-26779

Terrestrial, solar and galactic magnetic fields, discussing generation by combined nonuniform rotation and cyclonic turbulence based on dynamo equation
12 p1961 A71-26859

Galactic dynamo generated magnetic field periodic modes based on mathematical model involving cyclonic turbulence and nonuniform rotation of gaseous disk
14 p2303 A71-29591

Cosmic rays compound diffusion, considering combined effects of one dimensional diffusion along interstellar magnetic field lines and field lines three dimensional random walk
14 p2301 A71-30434

Stellar and interstellar magnetic fields effects on plasma instabilities in Colgate cosmic ray model, using computer simulation
14 p2282 A71-30644

Magnetic field measurements on Outer Planets Grand Tour to yield solar system origin and evolution and interstellar medium data
19 p3139 A71-37918

Milky Way galaxy internal small scale magnetic field generation, relating strength to cyclonic turbulence properties and large scale shear
20 p3287 A71-39055

Milky Way galaxy poloidal magnetic field generation with hydromagnetic dynamos, showing galactic cosmic rays as major driving force
20 p3287 A71-39056

Polarization characteristics of pulsars, considering angular position changes due to interstellar magnetic field using Faraday rotation measurements
20 p3303 A71-39935

Pulsar high energy cosmic ray periodic flux detection with favorable interstellar magnetic field configuration along line of sight
24 p3865 A71-44569

Galactic stochastic magnetic field lines, deriving dynamic equation for probability density function
24 p3871 A71-44902

INTERSTELLAR MATTER

Interstellar dust grains temperature as intracloud position function under assumed radiative heating and cooling, discussing hydrogen formation
01 p0157 A71-10759

Three body gravitational capture of interstellar dust in solar system, examining zodiacal cloud
01 p0158 A71-10771

Galactic interstellar grains alignment by starlight, noting photon intrinsic angular momentum role
01 p0159 A71-10865

Interstellar medium polyatomic molecules formation, destruction and excitation processes by astronomical spectroscopy and interferometry
02 p0209 A71-11867

Structural characteristics of light absorbing matter near sun from optical observations
02 p0308 A71-12096

Luminescence of optically reflecting nebulas related to shape of light scattering indicatrix of interstellar dust particles
02 p0311 A71-12355

Interstellar dust, examining diffuse line and band origin, absorption spectra and silicate grains
02 p0312 A71-12466

Metal poor stars eccentric galactic orbits, considering interstellar medium accretion effect
02 p0312 A71-12468

Hydroxyl and water vapor emission properties in interstellar medium attributed to maser action
02 p0313 A71-12498

Interstellar molecular hydrogen formation by physical adsorption on grains, determining H atoms adsorptive potentials on silicates, graphite, solid hydrogen and ice
02 p0287 A71-12582

Complex hydrocarbon molecular formation by physical adsorption on interstellar grains in dense clouds
04 p0650 A71-15396

Interstellar medium characteristics, examining H I and II regions thermal properties and shock waves
06 p0972 A71-18329

Stellar mass loss, discussing consequences on interstellar medium and star evolution
06 p0973 A71-18337

Heliosphere boundary interactions with interstellar medium, considering galactic plasma shock front and boundary radius as function of solar activity level
06 p0977 A71-18495

Interstellar extinction curve accounted for by graphite, iron and silicate grains, presenting refractive index values plotted as functions of wavelength
07 p1199 A71-20009

Soft galactic X rays role in interstellar grains alignment 07 p1188 A71-20056

Long term fluctuations in pulsar radiation intensity due to interstellar scintillation 08 p1359 A71-20935

Structural characteristics of light absorbing matter near sun from optical observations 08 p1362 A71-21146

Media resistance effects on three body problem three dimensional periodic orbits, discussing implications to solar system formation from surrounding nebula 09 p1527 A71-23534

Interstellar medium molecular composition from ground based and spaceborne UV, visible light, IR, far IR and radio spectroscopy, discussing stellar formation 10 p1669 A71-24170

Diffuse interstellar bands polarization and extinction based on silicate and graphite grain composition and sizes 10 p1675 A71-24469

Meteoritic graphite, silicon carbide and silicates to explain observed interstellar grains properties 10 p1675 A71-24471

Scattered stellar clusters region stars and interstellar matter from photographic magnitudes diagrams and color indices, determining absorption fluctuations by color excess technique 10 p1681 A71-25127

Interstellar absorption and color excesses in Sco OB-1 from spectral observation and photometry for star cluster and association background 11 p1831 A71-26133

Interstellar dust, investigating starlight reddening by extinction, galactic light, IR star observations and polarization 12 p1959 A71-26775

Interstellar matter, emphasizing H I and H II regions temperatures, dust, magnetic fields, intermediate and high velocity clouds 12 p1959 A71-26779

Prestellar evolution, discussing interstellar medium, star development phases, cloud formation, gravitational/thermal instability and protostars 12 p1960 A71-26783

Stellar evolution, discussing mass loss to interstellar medium, galactic distances determination and supernova explosions 12 p1960 A71-26784

Interstellar formyl radical and carbon 13 formyl ion search in galactic radio sources 13 p2142 A71-29103

Interstellar grain temperatures, considering radiant energy distribution and optical properties effects 14 p2305 A71-29679

Interstellar grain temperatures, determining shape effects on emissivities 14 p2305 A71-29680

Dust grain orientation in interstellar space from Fokker-Planck equation, taking into account collisions with gas atoms and magnetic interactions 15 p2485 A71-31715

Laboratory approach to circumstellar mineral condensation, demonstrating fractional condensation 15 p2486 A71-31989

Methane, ammonia and silicate effects on 3.07 micron ice absorption in interstellar grains, using cesium iodide window deposited sample measurements 15 p2498 A71-32774

Interstellar medium dispersion and rotation measurements, calculating electron concentration fluctuation effects 16 p2608 A71-33227

Cosmic ray nuclei propagation through interstellar medium, solving transfer equation for simple model with allowance for boundary conditions 16 p2625 A71-33325

Neutral hydrogen interstellar wind parameters from Lyman alpha sky background measurements outside geocorona by photometers on OGO 5 16 p2643 A71-33834

Circumstellar dust clouds and Bok globules examined for gaseous emission lines, emphasizing forced diffusion process 16 p2643 A71-34077

Type I supernova broadband identification, examining interstellar medium spectra 17 p2806 A71-35384

Nonstatic model of universe based on Newtonian cosmology, considering central body effects on interstellar dust motion 17 p2809 A71-35600

Interstellar dust clouds physical and chemical constitution, discussing molecular gas chemical composition and abundances 18 p2968 A71-37037

Soft galactic X rays role in interstellar grains alignment, taking into account interstellar absorption 19 p3124 A71-37336

Astronomical models of solar wind interaction with interstellar medium, determining magnetic field effects on shock wave 20 p3278 A71-39139

Linear polarization of pulsar PSR 22 18 plus 47 radio emission pulses, attributing periodic fine structure of spectrum to rotation of polarization plane in interstellar medium 20 p3291 A71-39316

IAU Executive Committee, General Assembly and commissions reports on astronomy, including manuscripts preparation guidelines, handbook, etc 20 p3315 A71-39425

H II regions near O and R stars effect on interstellar electron density in solar vicinity 20 p3294 A71-39542

Vela pulsar interstellar scattering, studying pulse broadening, rotation measure and radiation origin near magnetic pole 20 p3303 A71-39937

Electron density and temperature in diffuse interstellar medium from H alpha and beta radio recombination lines near galactic plane 21 p3445 A71-40411

Interstellar clouds internal structure investigation by photographic photometry, determining maximum density 21 p3451 A71-40718

Internal structure investigation of interstellar clouds in Cassiopeia, discussing color equation, photographic plate characteristics and accuracy 21 p3451 A71-40719

Interstellar formamide detection in Sgr direction by microwave emission, showing hyperfine components and rest frequencies 22 p3599 A71-41930

Galactic diffuse radiation in far UV, discussing consistency of findings on optical properties of interstellar grains 22 p3593 A71-42337

Interstellar spherical grains surface roughness model, noting far UV radiation extinction enhancement 22 p3605 A71-42340

Interstellar silicate absorption search using VI Cyg No 12 spectrum observations 22 p3605 A71-42349

Pulsar 0833-45 LF radiation spectrum decrease explained by pulse broadening due to interstellar scattering 24 p3868 A71-44565

Pulsar CP 0950 radio emission intensity variation measurement, using dispersion removal technique for interstellar medium signal distortion 24 p3871 A71-44903

Pulsar JP 1933 distance lower limit from 21 cm absorption and galactic rotation model, noting scintillation parameters consistency with observations in thin screen model 24 p3873 A71-45141

INTERSTELLAR MICROWAVE SPECTRA

U INTERSTELLAR RADIATION

U MICROWAVE SPECTRA

INTERSTELLAR RADIATION

Pulsar radiation intensity time variations at radio frequencies, noting observations of CP 1133 04 p0649 A71-15273

Equivalent widths of CO lines in interstellar absorption spectrum of zeta Ophiuchi 08 p1360 A71-20982

Interstellar medium molecular composition from ground based and spaceborne UV, visible light, IR, far IR and radio spectroscopy, discussing stellar formation 10 p1669 A71-24170

Extraterrestrial hydrogen Lyman alpha emission source, investigating interstellar wind with OGO 5 satellite 10 p1601 A71-24438

Diffuse interstellar bands polarization and extinction based on silicate and graphite grain composition and sizes 10 p1675 A71-24469

Excess intensities of diffuse cosmic X rays related to characteristic line spectrum excitation and element abundances in interstellar region and nebulas 18 p2958 A71-36761

Radio pulse shapes from NP 0531 observed with swept frequency machine, showing broadening due to interstellar scattering 20 p3302 A71-39925

Interstellar medium recombination line emission origin from discrete distribution of cold and dense clouds 23 p3723 A71-42942

Microwave detection of anomalous interstellar electronic recombination line emission toward W49 A, using radio telescopes 24 p3871 A71-44904

INTERSTELLAR SPACE

Organic compounds astrochemistry, discussing hydroxyl absorption lines and molecular abundances in interstellar space 10 p1678 A71-24810

Pulsar CP 0328 data at 1420 MHz, examining mean intensity and long term fluctuation due to interstellar scintillations 10 p1680 A71-25008

Cosmic rays lifetime in Galaxy in presence of particle acceleration in interstellar space 16 p2626 A71-33431

Solar wind formation of heliosphere, discussing solar wind-interstellar medium interaction region probed by Pioneers F and G [AAS PAPER 71-165] 19 p3141 A71-37961

Microwave spectral line receivers for radio astronomy observation of molecular clouds in interstellar space 20 p3238 A71-39401

Reversible charge exchange reactions effects on ionization equilibrium of nitrogen in interstellar space 21 p3445 A71-40411

Electromagnetic wave dispersion in interstellar plasma, noting indistinguishable form from natural dispersion of photons with nonzero rest mass 22 p3574 A71-41596

INTERSTELLAR TRAVEL

Space flight, discussing stellar trips, propulsion systems and planetary exploration 13 p2145 A71-29133

Shortest transfer time interstellar propulsion systems, considering nuclear pulse and electric rockets, fusion and photon rockets, and ramjets 15 p2469 A71-31748

High relativistic speed interstellar starship navigation, considering darkness cones, barrel, starbow, and near light speed problems 15 p2445 A71-31749

Energy requirements for antihydrogen production in interstellar photonic drives, discussing feasibility 18 p2956 A71-36683

Ultraplanetary probes for exploration beyond solar system, discussing heliosphere, cometary, interstellar and stellar mission categories propulsion system selection 19 p3141 A71-37961

Scientific unmanned exploration of near stellar systems, discussing target star selection, extraterrestrial life, propulsion systems and kinematic and energy requirements [AAS PAPER 71-166] 19 p3141 A71-37961

Low gravity field phenomena, discussing vertical jump on moon, ball trajectories launched from asteroid and voyage to neutron star 22 p3600 A71-41982

Interstellar space flight kinematics near light speed, discussing theoretical requirements for relativistic rocket engines 22 p3600 A71-42000

INTERSTITIALS

Dislocation pinning by interstitial atoms during Cr and Cr-Ce strain aging, using amplitude dependent internal friction technique 02 p0263 A71-11897

Niobium with various interstitial and substitutional type impurities, examining plastic deformation and mechanical properties at various temperatures 02 p0269 A71-12927

Nb alloys hardening due to interstitial atoms interactions with dislocations, obtaining stress-strain relationship for various impurities, precipitates, strain rates and temperature 02 p0270 A71-12929

Deformed metals stage I recovery, considering plastic deformation microscopic description, defect creation, interstitials and experimental methods 03 p0441 A71-13348

Ta single crystals solution hardening, discussing interstitial impurities effects on bcc metals flow stress temperature dependence 05 p0765 A71-16162

Ta single crystals with interstitial carbon, nitrogen and oxygen, examining Peierls and interstitial hardening stresses additivity 08 p1307 A71-21503

Interstitial nitrogen effects on thermally activated flow in Nb single crystals, determining yield and flow stresses and strain-rate sensitivity dependences on temperature 08 p1307 A71-21504

Interstitial role in bcc metals slip anisotropy at low temperatures, examining stress differential effect in Nb-oxygen solid solutions 08 p1307 A71-21505

Interstitial impurities effects on relation of activation energy to effective stress in iron, low carbon steel and other bcc metals 08 p1308 A71-21514

V-Ti alloys high temperature behavior dependence on Ti content, examining interstitial impurities effects on mechanical properties 08 p1310 A71-21532

Guinier-Preston zone formation by mixed substitutional-interstitial solute-atom clustering in bcc metals, considering steel strengthening 08 p1311 A71-21541

Internal friction from hydrogen dissolved in Ti-Mn alloys, considering solute interstitial atoms caused asymmetrical distortion decrease with increased Mn concentration 10 p1625 A71-24008

Thermodynamic properties of interstitial solid solutions with fcc metals from atomically discrete model by computer simulation 11 p1778 A71-25531

Aged beta Ti alloy microstructure and mechanical properties, examining initial dislocation structure and interstitial concentration effects 12 p1917 A71-27297

Cr and Cr-Y alloy interstitial residual content and dynamic dislocation-interstitial interactions at various temperatures and strain rates 13 p2085 A71-28578

Plastic deformation and alloying effect of small additions of interstitial elements on decomposition of metastable beta phase 13 p2086 A71-28580

Binary interstitial solid solutions thermodynamic properties, examination with Kirkwood expansion, allowing crystal first order partition function measurement without degeneracy error 13 p2087 A71-29133

Heat transfer in interstitial solid solutions, interpreting thermal diffusion measurements in transition metals mixed crystals 16 p2599 A71-34093

Fracture kinetics, emphasizing plastic deformation, dislocation and diffusion micromechanics, point defects effects, microcrack formation and interstitial mechanisms 17 p2834 A71-35667

Interstitial solute thermomigration of C in Ti, V, Fe, Co, Ni and Pd, using radioactive tracer technique 19 p3079 A71-37710

Partial configurational thermodynamic functions of interstitial species in ternary solid solutions containing substitutional and interstitial solute atoms 20 p3194 A71-38804

Solid solution hardening in Ta alloy single crystals, investigating temperature effects on interstitial impurities scavenging and lattice mechanism 21 p3395 A71-40027

Interstitial solute carbon distribution in martensite, using generalized perfect lattice gas statistical mechanics 23 p3694 A71-44281

Bulk diffusion and glide and self climb mechanisms of vacancy and interstitial loop growth in Mo during neutron postirradiation annealing 24 p3839 A71-45193

INTERVALS

Threshold distribution of time intervals between atmospheric contradicting Poisson law 09 p1435 A71-22445

Failure prediction from interval data for reliability and inventory problems, considering irregular inspection and manufacture for aging in calendar time 12 p1911 A71-26687

Definite interval values calculations of integral of smooth functions, using quadrature formulas with high algebraic degree of accuracy 17 p2765 A71-34845

Time scale and time interval characteristics for scientific use, tabulating associated units 24 p3827 A71-44995

INTESTINES

NT RECTUM

Cellular mitosis role in daily mitotic activity in albino rats intestinal crypts and thyroid gland 01 p0012 A71-11058

Hemorrhagic rectocolitis in flying personnel in terms of etiological, evolutive and therapeutic aspects 01 p0028 A71-11596

Glucose intestinal absorption, blood glucose and hematocrit in hamsters, relating physiologic modifications to pregnancy 02 p0201 A71-12608

Intestinal muscle electrical behavior as series of loosely coupled oscillators, demonstrating slow wave frequency gradient and propagation velocity by computerized simulation 04 p0544 A71-15089

Cytotoxic and radiosensitizing effect of thiol binding agents iodoacetamide /IAA/, N-ethylmaleimide /NEM/ and iodoacetic acid /IA/ on crypt cells of mice duodenum 07 p1038 A71-18975

External oblique inguinal hernia due to acrobatic flying centrifugal accelerations, considering anatomical, clinical and medico-legal aspects 17 p2681 A71-34822

Cell contacts in canine duodenal smooth muscle layers, using perfusion with glutaraldehyde fixative 20 p3187 A71-38985

INTOXICATION

Alcohol effects on complex task performance including monitoring, compensatory tracking and mental arithmetic 04 p0547 A71-15850

INTRACRANIAL PRESSURE

Intracranial pressure measurement by miniature transducer with modifications for baseline reading and calibration checking throughout implantation period, giving circuit diagram 01 p0021 A71-10241

INTRAOCULAR PRESSURE

Helium and nitrogen breathing effects upon intraocular pressure during and after near vacuum exposure in anesthetized and unanesthetized dogs 09 p1400 A71-23359

Intraocular pressure self regulating nervous system components, discussing fluctuation sensors, cortical centers to eye impulse conveyors and glaucoma diagnostic applications 11 p1716 A71-25199

Arterial tonometry for atraumatic measurement of arterial blood pressure, considering transient effects of drugs or physiological interventions 12 p1874 A71-27140

Mechanical sterilization and cleansing of Goldmann applanation tonometer prisms contaminated with coliphage, comparing with germicidal immersion 13 p2020 A71-29036

Acoustical wave generation measurement during iris and retina photocoagulation and ruby laser burns, noting intraocular pressure surge simultaneous with ocular tissue explosion 15 p2365 A71-32346

Intraocular pressure distribution of healthy mental workers in 25-40 years age range, noting symmetry 20 p3189 A71-39234

Respiratory carbon dioxide and oxygen partial pressure effects on intraocular and blood pressure in rabbits under Somnifen narcosis 24 p3793 A71-44368

INTRAVASCULAR SYSTEM

Human cardiac intraventricular conduction measurements, using right and left bundle branch potentials during catheterization 07 p1044 A71-20351

INTRAVEHICULAR ACTIVITY

Medical flight information on astronauts response to space flight environment in confined and unconfined state and during intra- and extravehicular activities 08 p1246 A71-20731

Intravehicular manual cargo transfer, using water immersion technique for zero gravity simulation [AIAA PAPER 71-851] 18 p2871 A71-36642

INTRAVENOUS PROCEDURES

Pulmonary dissipation of gas emboli produced by oxygen, nitrogen and carbon dioxide intravenous injection in unanesthetized sheep with chronically implanted ultrasonic Doppler flow probes 21 p3330 A71-40342

INVARIANCE

NT GAUGE INVARIANCE

Shear-invariant mean value of positive-definite operator on bicompart group in form function of integral sequence, considering ergodic theorem 01 p0110 A71-10097

Local invariants under axial rotation, deriving recurrence relations for time series expansions and perturbation methods 01 p0154 A71-10387

Structural analysis of invariant automatic control systems characterized by coordinate pairs coupled through disturbed load operator 01 p0058 A71-10406

Light speed invariance in special theory of relativity concerning Galilean coordinates 01 p0127 A71-10601

Automatic control systems invariance theory - Conference, Kiev, May-June 1966, Volume I 01 p0059 A71-10701

Automatic control systems invariance theory, discussing Poncet principle, perturbation measurement, etc 01 p0060 A71-10702

Automatic control and information systems epsilon invariance, generalizing Kotelnikov theorem on continuous signals reduction 01 p0060 A71-10703

Multiloop discrete automatic control system invariant with respect to external perturbations 01 p0060 A71-10704

Controlled parameters invariance in automatic systems with bounded-coordinate components 01 p0060 A71-10706

Automatic control with twofold invariance properties, describing use as nonsearch self adaptive system 01 p0061 A71-10707

Finite automata systems invariance with respect to control actions 01 p0061 A71-10708

Nonminimal phase feedback control system synthesis by frequency methods, discussing invariance characteristics 01 p0061 A71-10709

Invariant automatic control structure for nonlinear plant, using inverse method 01 p0061 A71-10710

Automatic control systems analysis and synthesis, applying invariance conditions second form 01 p0061 A71-10711

Quasi-invariant automatic feedback control system, deriving basis for determination of perturbation compensating components parameters 01 p0061 A71-10713

Elastic flight vehicles feedback control systems synthesis by invariance theory 01 p0163 A71-10714

Linear continuous receiver and control systems resolution and statistical epsilon invariance 01 p0062 A71-10716

Invariant automatic control system performance improvement by signal predistortion for reproducibility increase 01 p0062 A71-10717

Automatic control systems without disturbance feedback, examining invariance under positive-zero-negative error transition 01 p0062 A71-10720

Invariance in nonminimum phase complex combined control systems synthesis, using root hodograph method 01 p0063 A71-10724

Complex programmed control systems invariance for discrete times, synthesizing compensating filter with specific transfer function 01 p0063 A71-10725

Pulsed analog and digital control systems invariance conditions at discrete times, using Laplace transform method 01 p0063 A71-10726

Nonlinear feedback control systems invariance, investigating coordinate and parametric disturbances compensation 01 p0063 A71-10728

Complex control nonlinear systems invariance and stability conditions, discussing harmonic balance analysis method 01 p0063 A71-10729

Invariance in automatic control systems nonlinear differential equations of motion 01 p0064 A71-10730

Lagrangian invariants of inviscid compressible fluid applied to hydrodynamic equations 02 p0239 A71-11923

Heavy gyrostator motion problem, using Mozalevskia particular solution characterized by algebraic invariant relation 03 p0458 A71-13593

Sun and planet system relative motion, using equations of invariant mechanics 03 p0492 A71-14190

Gyrostatic system with center of mass in uniform circular motion, deriving rotary motion equations invariant 03 p0460 A71-14386

Lorentz invariants in relativistic fluid dynamics and thermodynamics in nonvacuo, suggesting determination through earth-moon space flight experiments 04 p0661 A71-14872

Analytical techniques for invariant properties of families of moon-earth trajectories 04 p0660 A71-15891

Adiabatic invariant of nonlinear periodic wave described by partial differential equations in weakly inhomogeneous medium 05 p0780 A71-16177

Chronometrically invariant formulation of Petrov gravitational fields algebraic classification at spacetime fixed point in general relativity 05 p0781 A71-16182

Schwarz differential invariant in Kepler problem, describing point motion under Newtonian force effect 05 p0811 A71-16640

Automatic control systems with parametric invariance, describing method for quick response increase 05 p0731 A71-16797

Universe models topology, examining relation between CT and CP invariance 08 p1366 A71-21786

Control sets bound structure, discussing invariance theorems 09 p1422 A71-22377

Mode conversion in inhomogeneous plasma, discussing conservation laws relationships to differential equation invariants 09 p1501 A71-22535

Ordinary differential equations invariance properties, considering applications to stability problems 09 p1486 A71-23470

Nonperiodic orbit behavior in highly perturbed dynamic systems, examining invariant curve evolution 10 p1669 A71-24178

Monodispersed particle semifinite atmosphere, calculating invariance principles of diffused radiation based on Mie theory 12 p1960 A71-26823

Aircraft longitudinal coordinates invariance relative to atmospheric disturbances, giving simultaneous thrust variation, rudder deflection and flap deflection control rules 12 p1867 A71-27339

Stability and coarseness of one- and two-channel invariant control systems for various forms of parameter deviations 12 p1893 A71-27340

Soviet book on multiloop automatic control systems covering matrix notation, stability and accuracy, invariance principle, compensating cross couplings, etc 14 p2218 A71-29527

Group-invariant properties of boundary layer flow differential equation for electrically conducting liquid in magnetic field

14 p2279 A71-29629

Linearized shell theory, proposing improvement of Marguerre-Vlasov shallow shell equations in terms of invariant displacement and stress functions

16 p2649 A71-33000

Gravitational fields invariant evolution, noting Einstein equations constraints effects on initial values of variables

16 p2611 A71-33280

Morograph on algebraic theory for ordinary linear time invariant difference systems covering constant shift operators, matrix formalism, operational calculus, etc

16 p2602 A71-33397

Universe models topology, examining relation between CT and CP invariance

16 p2638 A71-33547

Continuum mechanics in differential forms, discussing material and spatial coordinates, compatibility conditions energy balance, entropy inequality and invariance principles

16 p2613 A71-34146

Perturbation theory of invariant manifolds of dynamic systems based on Green function, deriving new existence theorems

17 p2781 A71-34930

Modal control for linear multivariable time-invariant systems incorporating multiloop single input proportional controllers

18 p2896 A71-36235

Invariant characteristics of Einstein spaces according to Petrov classification, determining gravitational fields described by covariant equation involving space curvature tensor and arbitrary scalar

19 p3105 A71-38585

Zero-charge and scale-invariance problems in solvable field theory model, considering Green function and vertex parts behavior under perturbation theory invariance

21 p3420 A71-41128

Elastic shell strain energy calculation, using dimensional analysis and invariance properties for inversion of normal to middle surface

22 p3616 A71-42217

Noether invariance and conservation laws theorems extension to nonlocal calculus of variations, obtaining coordinate and point transformations effects on dependent functions domain space

23 p3700 A71-44177

Invariance theory for nonlocal variational principles, covering energy forms and identities, weak coordinate invariance, integral balance and conservation laws

23 p3700 A71-44179

Potential function, permissible transformations, geometrical, linguistic, optimal statistical and heuristic methods for pattern recognition, discussing unifying approach based on invariant decision functions

24 p3812 A71-44391

Frobenius group theorem, discussing invariant and additional Frobenius multipliers, Schmidt criteria and theorem applications

24 p3843 A71-44823

INVARIANT IMBEDDINGS

German monograph on invariant curves of annulus differentiable mappings covering existence theorem for closed curve within annulus transformed by mapping

01 p0110 A71-10127

Unstable linear initial value problem numerical solution, using Riccati equations of invariant imbedding

02 p0277 A71-12727

Initial value method for Fredholm integral equations with displacement kernels on infinite interval, using invariant imbedding

03 p0450 A71-13622

Flows on 3-manifolds near isolated invariant sets

04 p0620 A71-15727

Linear systems optimal control problems numerical solution methods comparison, noting accuracy advantage of invariant imbedding technique

07 p1081 A71-18834

Numerical algorithm for Cauchy problem nonlinear partial differential integral equations solution by invariant imbedding

16 p2604 A71-34082

Invariant imbedding for two point boundary value problems for difference equations, noting conversion to initial value problem

17 p2764 A71-34519

Sobolev function Q in radiative transfer, using invariant imbedding approach for integral equation transform

19 p3133 A71-37506

Radiative transfer in inhomogeneous anisotropically scattering spherical shell atmospheres with radial symmetry, using invariant imbedding technique

20 p3287 A71-39082

Equilibrium equations of elastic plates, reducing to Cauchy problem by use of invariant imbedding

22 p3618 A71-42584

INVENTIONS

Industrial innovations legal protection, discussing patents, registered designs, copyright and trademarks

01 p0183 A71-10756

INVENTORIES

NT TIMBER INVENTORY

Statistical methods for inventory boundary determination and data compression in automatic processing of multispectral scanner remote sensor earth observations from aircraft and spacecraft

[AIAA PAPER 71-234] 07 p1068 A71-19711

General purpose software inventory under single executive for application oriented information systems

[AIAA PAPER 71-236] 07 p1225 A71-19712

INVENTORY CONTROLS

Colorado Land Use and Environmental Resource Inventory Project /CLARI/ by computer methods, saving information retrieval time and cost

08 p1281 A71-21253

Failure prediction from interval data for reliability and inventory problems, considering irregular inspection and manufacture for aging in calendar time

12 p1911 A71-26687

INVENTORY MANAGEMENT

NT INVENTORY CONTROLS

INVERSIONS

NT CENTRIFUGING STRESS

NT POPULATION INVERSION

NT TEMPERATURE INVERSIONS

Error bounds for inverted nonsingular matrices using interval arithmetic in ALGOL-60

01 p0049 A71-10325

Ammonia inversion radiation at 1.25 cm in direction of three galactic center sources, setting upper limits on densities in other areas

07 p1188 A71-19834

Spacecraft motion parameters maximum probability estimates, using approximate weight-matrix inversion techniques

08 p1360 A71-21003

Lagrange implicit functions generalization to n dimensions, developing inversion as power series

10 p1637 A71-24933

Minimization algorithms unified derivation, using Hessian matrix inverse

12 p1923 A71-27727

INVERTEBRATES

NT ARTHROPODS

NT BEETLES

NT DROSOPHILA

NT INSECTS

NT PARAMECIA

NT PROTOZOA

NT SNAILS

NT SPORES

Preterian invertebrate fossil remnants and microprolites found in Lower Himalayan Basin

11 p1721 A71-26318

Gravity receptor evolution in invertebrates, considering cilia role in reception and transduction into responses

21 p3327 A71-39991

INVERTERS

NT STATIC INVERTERS

MOS transistor inverters static and dynamic characteristics in IC assemblies

02 p0228 A71-11656

Variable voltage and frequency thyristor inverter, describing series commutation power stage

03 p0352 A71-13047

MOSFET inverter pulse response analysis using hyperbolic functional description

05 p0726 A71-17086

Permanent IR electron radiation effects on hardened MOS integrated inverter circuits, using units with plasma grown and vapor deposited aluminum oxide

07 p1174 A71-19053

Ionizing radiation effects on monolithic metal oxide semiconductor inverters, including testing and hardening techniques

07 p1070 A71-19060

Pulse width modulated output voltage analysis in autonomous inverters, using Fourier series and digital computer

15 p2353 A71-32078

Optimum L shaped quadrupole filter for controlled valve voltage inverters

15 p2353 A71-32079

INVESTIGATION

NT AIRCRAFT ACCIDENT INVESTIGATION INVESTMENT

Air transport development, examining capital investment, traffic volume and facilities

03 p0524 A71-14246

INVESTMENT CASTING

Superalloy investment casting, discussing production processes, shell molding technique, applications, cost control, solidification, ductility improvement and cooling rate

[SME PAPER CM-71-160] 18 p2927 A71-36659

INVESTMENTS

Optimal investment model for R and D project evaluation and selection, using discrete cash flow and linear programming techniques

19 p3173 A71-37685

Costs/benefits strategy for investment in STC fleets reducing delay and airport congestion, using heuristic computer model

19 p3173 A71-38027

INVISCID FLOW

NT STAGNATION FLOW

Wing-body interference in supersonic inviscid flow extending Stewartson approach to arbitrary smooth convex cylinder

01 p0002 A71-10771

Slowly varying plane flows of highly conducting inviscid quasi-neutral gas plasma in channel with solid metallic walls as electrodes

01 p0133 A71-10799

Inviscid fluid flow in cylindrical channel excited by internal hydrodynamic energy source, calculating velocity and density distribution

01 p0071 A71-11040

Lagrangian invariants of inviscid compressible fluid applied to hydrodynamic equations

02 p0239 A71-11921

Inviscid ideally conducting fluid flow past thin foil in transverse magnetic field, using small parameter method

02 p0186 A71-12624

Steady supercritical planar inviscid transonic flow over lifting airfoils, generating unsteady flow by impulsively imposing airfoil boundary condition

[AIAA PAPER 70-47] 03 p0341 A71-13433

Incompressible two dimensional inviscid stably stratified fluid flow over vertical step in channel bounded by rigid horizontal lid

03 p0453 A71-14201

Aerodynamic characteristics of low aspect ratio wing in bounded inviscid fluid flow, considering planar form relation to lifting force derivative and angle of attack

04 p0525 A71-14589

Wall stability of parallel elastic plate duct in contact with inviscid compressible liquid flow

04 p0573 A71-15566

Inviscid incompressible flow velocity distribution in conical configurations with water as working fluid using method of integral relations

05 p0737 A71-17107

Supersonic axisymmetric wake-like and two dimensional shear nonuniform free stream flows effects on inviscid flow fields and aerodynamic coefficients of sharp and spherically blunted cones

[AIAA PAPER 71-51] 06 p0843 A71-18512

Three dimensional inviscid compressible flow past sharp shouldered blunt bodies at angle of attack presenting time dependent finite difference technique

[AIAA PAPER 71-56] 06 p0843 A71-18514

Three dimensional inviscid supersonic flow fields with primary and embedded shock and expansion waves determined over and behind wings and wing body configurations

[AIAA PAPER 71-99] 06 p0844 A71-18554

Hypersonic radiating gas inviscid flow past blunt bodies, using spherical harmonics approximation

07 p1013 A71-19182

Computer calculation of high Reynolds number viscous and inviscid flow over arbitrary shaped two dimensional bodies and airfoils

07 p1017 A71-20319

Continuous flow past plate located perpendicular to wall with inviscid incompressible fluid having linear variation of velocity with height

08 p1227 A71-20828

Inviscid incompressible electrically conducting fluid flow past slender profile investigated by asymptotic power expansion of reciprocal magnetic Reynolds number

09 p1382 A71-22135

Inviscid incompressible vortex-free axisymmetric pipe flow near arbitrary shape body symmetrically located near axis

09 p1431 A71-22180

MHD accelerator in pulsed mode with crossed fields, studying one dimensional steady inviscid flow

09 p1501 A71-22407

Effect of asymmetrical inviscid flow from Traill-blazer flight measurements, discussing windward leeward attenuation variation in transmitted VHF signal

09 p1406 A71-22916

Incompressible inviscid fluid flow in presence of two homogeneous porous layers, examining hydrodynamic instability

10 p1591 A71-23754

Vortex layer near circular cone surface in supersonic axisymmetric steady flow of homogeneous inviscid gas

10 p1551 A71-24372

Critical speeds for inviscid compressible potential flow past thin elastic cylindrical shells, using long wave approximation

10 p1689 A71-24565

Inviscid flow distribution of high temperature jet of optically thick radiating gas exhausting from two-dimensional nozzle into low temperature quiescent medium 10 p1552 A71-24588

Soviet book on MHD flow of incompressible electrically conducting fluid past bodies covering inviscid flows and viscous flows of Stokes and Oseen type 10 p1596 A71-24669

Inviscid incompressible two phase concave type corner flows embedded with small spherical particles, examining streamlines, critical collision conditions and approximate viscous effects 10 p1598 A71-25081

Small amplitude resonant thermal acoustic oscillations of inviscid polytropic gas contained in finite length tube 11 p1798 A71-25446

Steady three dimensional subsonic nonviscous flow through turbomachine with arbitrary hub and shroud shapes and finite blade number, using iterative blade to blade procedure [ASME PAPER 71-GT-2] 11 p1702 A71-25948

Inviscid incompressible two dimensional jet deflection by various dimension segments, investigating potential flow with Schwarz-Christoffel transformation and free streamline theory 11 p1753 A71-26444

Inviscid compressible fluid jet flow, calculating instability boundaries characteristics by linear perturbation analysis and numerical solution 12 p1897 A71-27219

Thin delta wing in hypersonic inviscid flow at small angles of attack, calculating motion equations and boundary conditions at small perturbations 12 p1863 A71-27330

Two dimensional inviscid heated flows in terms of pressure, density, speed, direction and heating rate applied to supersonic duct combustion chambers 12 p1987 A71-27735

Unsteady large particle numerical solutions to vortical equations of plane and axisymmetric inviscid gas flow past blunt body for subsonic and hypersonic velocities 13 p1989 A71-27901

Motion stability of symmetric rotor of gyroscope with inviscid incompressible liquid filled cylindrical annular cavity around coaxial rigid rod 13 p2065 A71-27978

Potential flow of incompressible inviscid liquid film along inclined semiinfinite flat plate for large Froude number values, using matched asymptotic expansions method 13 p2047 A71-28485

Entropy production in adiabatic flow in turbomachines, based on momentum equations for inviscid flow [ASME PAPER 71-FE-3] 13 p1994 A71-29446

Inviscid transonic rotational flow expansion around convex corner, applying to supersonic boundary layer over flat plate ending at sharp corner 14 p2226 A71-30444

Equation for motion of buoyant free vortices in inviscid fluid subjected to gravity [AIAA PAPER 71-604] 15 p2388 A71-31543

Separation controlled transonic drag-rise modification for V-shaped notches attributed to inviscid/viscid interaction controlling flow separation and reattachment [AIAA PAPER 71-568] 15 p2345 A71-31561

Compressible transonic flow about two dimensional airfoils, developing inviscid nonlinear potential equations by relaxation procedures 15 p2345 A71-31562

[AIAA PAPER 71-569] 15 p2345 A71-31562

Inviscid supersonic flow field structure over blunt delta wing, determining attack angle effects on shock layer surface pressure distributions and streamline patterns [AIAA PAPER 71-596] 15 p2512 A71-31576

Inviscid compressible transonic flow field equations for perfect gas in conical rocket nozzles, measuring wall and center line pressures 15 p2390 A71-32040

Inviscid incompressible flow past thin circular arc airfoil at zero incidence, expanding for complex potential or velocity in powers of thickness ratio 17 p2670 A71-34674

Hypersonic viscid-inviscid internal flow field interaction with laminar boundary layer in circular ducts, using method of characteristics and implicit finite difference scheme 17 p2671 A71-35281

Space time structure of acoustic waves propagating in cylindrical duct with weakly absorbing walls and axial inviscid time dependent fluid flow [ONERA-TP-965] 18 p2946 A71-36030

Streamlines geometry in hydromagnetic inviscid noneat conducting compressible flow in magnetic field, taking into account force vectors and energy/mass distributions 18 p2951 A71-36183

Steady inviscid fluid flows in plane channel and in axially symmetric nozzle, considering external magnetic field effects with electroconductive fluid 18 p2907 A71-36327

Variable density effect on inviscid free shear layer instability at small Mach numbers, deriving difference equation for inviscid disturbance [DFVLR-SONDDR-114] 19 p3043 A71-37300

Inviscid swirling nozzle flow equations from Crocco relation 19 p2993 A71-37890

Turbulent motions in fluids of small viscosity as inviscid flows with vortex sheets and rolled-up cores 21 p3317 A71-40010

Aerodynamic approximations for unsteady supersonic flow of perfect inviscid gas through flexible duct of revolution [ASME PAPER 71-VIBR-23] 21 p3458 A71-40280

Vertical magnetic field effects on stability of variable density compressible inviscid fluid, solving by variational principle 21 p3415 A71-40666

Inviscid gas flow from supersonic nozzle into submerged region, considering specific heat ratio effect on dimensionless parameters, jet boundaries and suspended shock profiles 21 p3322 A71-40693

Hypersonic flow over rearward facing step by rotational characteristics method, describing inviscid and viscous dominated regions 21 p3324 A71-40969

Plane steady rotational flow of inviscid gas with arbitrary state equation for straight or circular streamlines 23 p3662 A71-43236

Stability of dissipative shear flow of inviscid incompressible electrically conductive fluid in presence of magnetic field, deriving instability modes phase velocity limiting conditions from MHD equations 24 p3855 A71-44645

INVISIBILITY

U VISIBILITY

IODATES

Tuning range extension of doubly resonant lithium iodate parametric oscillator by upconversion, using simultaneous pumping by single ruby laser beam 19 p3071 A71-37477

Lithium iodate hexagonal and tetragonal form crystal growth conditions from aqueous solution and recorded refractivity 23 p3717 A71-43935

IODIDES

NT CESIUM IODIDES

NT SILVER IODIDES

NT SODIUM IODIDES

NT ZIRCONIUM IODIDES

Shock compressed tetranitromethane mixtures with various benzene ethyl iodide proportions, investigating lateral discharge wave effects on detonation process structure 15 p2511 A71-31382

Hexamethylindotricarbocyanine iodide ethanol dye solution stimulated fluorescence during excitation by ruby laser radiation in spike generation quasi-continuous monopulse modes 15 p2421 A71-32406

Ice forming effectiveness and dispersion of reagent particle aerosols through explosion of Elbrus 2 antihail iodide artillery shells in free and clear atmosphere 19 p3094 A71-38697

Beryllium preparation from liquid beryllium iodides, describing apparatus 24 p3840 A71-45373

IODINE

Emission line spectra of halogens Cl I, Br I and I I in 4-micron region 05 p0717 A71-16911

Iodine photodissociation laser kinetic model for pumping, radiative and collisional processes, predicting reactant pressure and flashlamp parameters 11 p1773 A71-25795

Iodine vapor bleaching under molecular electronic-vibrational transition due to ruby laser intense monochromatic radiation 15 p2421 A71-32409

Molecular iodine vapor absorption filter for stray laser light in Brillouin and Raman scattering 21 p3393 A71-41042

Fluorescence of iodine molecule excited at 5017 and 5145 A by ionized Ar laser, observing magnetic depolarization/Hanle effect/ 22 p3555 A71-41623

IODINE COMPOUNDS

NT CESIUM IODIDES

NT IODATES

NT IODIDES

NT IODOACETIC ACID

NT SILVER IODIDES

NT SODIUM IODIDES

NT ZIRCONIUM IODIDES

Radiosensitizing effect of iodine compounds in dilute solution on Ehrlich ascites tumor cells and SH enzymes 07 p1036 A71-18957

Cytotoxic and radiosensitizing effect of thiol binding agents iodoacetamide /IAA/, N-ethylmaleimide /NEM/ and iodoacetic acid /IA/ on crypt cells of mice duodenum 07 p1038 A71-18975

Lithium iodide and tetramethyl ammonium iodide additions effect on radical exchange between phenyl lithium and bromobenzene in diethyl ether 19 p3011 A71-37391

IDOACETIC ACID

Embryo chemical sensitization to low radiation doses damage by radiosensitizer iodoacetamide 07 p1037 A71-18963

ION ACCELERATORS

Cathode material ions acceleration during pulsed discharge in vacuum, discussing experimental investigation results 08 p1341 A71-21496

Fast plasma ions energy distributions in toroidal accelerators with quasi-stationary discharge 13 p2108 A71-28854

States stabilization in low density plasma layer in ion-accelerating constant external electric field 13 p2108 A71-28857

Ion accelerating system for minimum angular ion beam divergence with plasma ions ejection from source through slits in electrodes 19 p3109 A71-37133

Hot plasma fast ions energy distributions in toroidal accelerators with quasi-stationary discharge 21 p3426 A71-41286

Low density collisionless plasma stabilization in ion-accelerating external DC electric field 21 p3426 A71-41293

Stochastic ion acceleration by relativistic electron beam in plasma traveling waves with different phase velocities 22 p3578 A71-42065

ION ATOM INTERACTIONS

Thermal ion-atom charge transfer effects on ionization equilibrium of interstellar oxygen in H I regions, using Bahcall-Wolf orbiting approximation 13 p2132 A71-27966

Ion beam milling techniques for device fabrication involving atomic interactions on solid surfaces 21 p3384 A71-40219

ION BEAMS

Fluorine ions excited levels mean lives from beam-foil line spectrum analysis 01 p0129 A71-10138

Spectrograph design for simultaneous measurement of velocity spectra and charge-to-mass ratios of ions, using magnetic and electric fields deflection effects 02 p0249 A71-12126

Light emission during ion-molecule collisions, using low energy nitrogen and argon ion beams 04 p0630 A71-15655

Cs ion beam space charge and current neutralization by electron capture for partially ionized plasma formation, investigating longitudinal electrostatic wave excitation 07 p1171 A71-20193

Crossed beam model of nitrogen ion-molecular oxygen reactions in upper atmosphere as function of collision energy 08 p1251 A71-21784

Ion beam deceleration and effective energy transfer to plasma at nonisothermal acoustic velocities in presence of ion acoustic instability 10 p1653 A71-24892

Radiative mean lives and transition probabilities of electronic states in beam foil excited atomic and ionic carbon 11 p1803 A71-26061

Nonlinear explosive ion beam-plasma interaction, discussing coupling coefficients and Landau damping 12 p1935 A71-26912

Synthesized plasma of interpenetrating positive and negative ion beams, investigating oscillation amplification conditions 12 p1941 A71-27766

Ion beams heating by ion-ion two stream instability perpendicular to magnetic field with cold electron background 13 p2104 A71-27851

Spectrometer slit-width cancellation by Doppler shift of light emission by fast ion beams, resulting in spectral lines increased intensities 13 p2071 A71-29331

Monograph on instabilities in ion beam-plasma system covering surface wave propagation, magnetic effect and ion cyclotron radiation characteristics 14 p2281 A71-30507

Ion and electron beams technology application to microelectronics, discussing limitations imposed by electron/ion optical effects 14 p2277 A71-30701

Ion thruster ion beam current density profiles mathematical representation by two parameter equation [AIAA PAPER 71-693] 14 p2293 A71-30752

Coaxial magnetic beam polarization interaction in toroidal plasma field with diverter, showing axial stream trapping in hollow plasma cylinder 15 p2453 A71-31244

Ion beam collisionless relaxation in hot electron plasma, observing oscillation spectra and velocity distributions 15 p2453 A71-31245

ION CHAMBERS

Structural stability for two beam plasma model with proportional controller using distributed feedback
15 p2456 A71-31846

Molecular rotational excitation during CO ion-Ar interactions in ion beam collision spectroscopy, observing energy loss spectra
15 p2452 A71-32551

Energy necessary to produce beam ion in plasma discharge of Hg electron bombardment ion source
16 p2623 A71-32841

He ion beam space charge neutralization by thermal electrons injection
17 p2784 A71-34200

Moving plasma beam capture by transverse magnetic field due to polarization space charges electrostatic separation
17 p2786 A71-34280

French monograph on DC/DC transformers with controllable output voltage covering ion beam electrostatic deviation during attitude control, equivalent transformer circuits, etc
17 p2677 A71-35234

Lande g factors measurement of excited electronic states in Ne 20 II and III, using alignment of radiating particles in beam foil light source
18 p2949 A71-35978

Ion beam deposition of insulating carbon thin films on room temperature substrates, considering transparency, index of refraction, insulating capacity, glass scratching ability, etc
20 p3241 A71-39011

Electron removal from neutralizing emitter in cylindrical ion beam, determining I-V characteristics of plane diode with positive charge distribution
20 p3272 A71-39152

Ion beam milling techniques for device fabrication involving atomic interactions on solid surfaces
21 p3384 A71-40219

Ion beam deceleration and effective energy transfer to plasma at nonisothermal acoustic velocities in presence of ion acoustic instability
21 p3425 A71-41272

High energy neutralized ion beam generation by focusing ultrashort laser pulses on thin foils, applying to nuclear reaction for superheavy nuclei production
22 p3555 A71-41595

Gyro wheels cleaning by ion bombardment applied to ceramic gas bearings, comparing with chemical cleaning
22 p3552 A71-41674

Spatially separated plasma beams of different temperatures, determining amplified wave instability boundaries and growth increments by quasi-hydrodynamic approximation
23 p3711 A71-43557

Electron transfer cross sections for low energy negative oxygen ion collisions with oxygen molecules measured by single-collision beam technique
23 p3707 A71-43930

Injected ion beam interaction with hot plasma in cylindrical magnetic mirror, noting acoustic frequency oscillation heating effect
24 p3854 A71-44514

Transverse instability of charged particle beam in segmented linear accelerators due to beam encounter with wall
24 p3855 A71-44522

Langmuir electron oscillation excitation by ion beam at velocity exceeding average electron thermal velocity in plasma formed by residual gas ionization
24 p3858 A71-45234

ION CHAMBERS

U IONIZATION CHAMBERS

ION CHARGE

Spectrograph design for simultaneous measurement of velocity spectra and charge-to-mass ratios of ions, using magnetic and electric fields deflection effects
02 p0249 A71-12126

Structure and propagation of large amplitude modulated isolated compression waves in cold three component plasma with negatively charged ions
07 p1170 A71-20138

Spectral line emission from nitrogen ions, identifying charge by Doppler shift technique application to beam foil light source
16 p2615 A71-34129

Mass and charge dependent ion discrimination in linear pulsed time of flight mass spectrometer, using electric field for source storage and count enhancement
18 p2922 A71-36590

Ion charge composition in plasma-electron beam system in strong longitudinal magnetic field, noting multiply charged ions production under high temperature conditions
19 p3109 A71-37132

Charge neutrality in semiconductors with implanted dopant ions profiles, considering junction field penetration into Gaussian profile
19 p3118 A71-37489

Mean charge measurement for heavy ions moving through He and air with aid of gas-filled mass separator, noting anomalies in nuclear charge dependence
21 p3419 A71-41112

ION CONCENTRATION

Enclosed diffusively turbulent flames, determining area of maximum ion concentration
01 p0178 A71-10338

Maximum ion concentration zone in diffusively turbulent flames in fuel gas free jets, using mass exchange processes analysis
01 p0178 A71-10341

Sodium counterflow from serosal to mucosal surface of short-circuited acid-killed turtle bladder
01 p0015 A71-11182

Redox estimation from natural phase Eu ion concentrations in rocks
01 p0029 A71-11428

Diurnal variations and waves in ionospheric electron and ion temperatures and concentrations from Thomson scatter measurements
03 p0408 A71-13384

Carbonic acid effect on isolated skeletal muscle, discussing membrane potential and ion content measurements
05 p0710 A71-16941

Rarefied plasma disturbances produced by large slowly moving charged spherical body, deriving electric field, ion and electron concentrations in body vicinity
07 p1195 A71-19380

Ion collection by spherical and cylindrical probes in collisional He plasma, comparing saturation current measurements with transitional regime probe theories
07 p1169 A71-19909

He ion vertical concentration profiles from space probe mass spectrometer measurements
08 p1278 A71-21020

E region ion composition nighttime variations, examining nitrogen monoxide and oxygen ion nonequilibrium concentrations by ionic-molecular reactions
09 p1435 A71-22438

Hydrogen ion concentration measurements by OGO 5 in plasmasphere during intense magnetic storms accompanied by stable auroral red arcs
10 p1605 A71-24787

Electron and ion concentrations, electron temperature and electrical conductivity of ionized air before shock wave, using shock tube with He driver gas
14 p2225 A71-30225

Cluster ions concentration and nitric oxide in mesosphere D region, considering electron density profiles
15 p2394 A71-31430

Rarefied plasma disturbances produced by large slowly moving charged spherical body, deriving electric field, ion and electron concentrations in body vicinity
19 p3138 A71-37805

He ion vertical concentration profiles from space probe mass spectrometer measurements
20 p3219 A71-39600

Exospheric ion composition determination by vertical space probe mass spectrometer measurements, obtaining H, He, N, O and NO ion concentration vertical profiles
20 p3280 A71-39720

Photoelectric and photographic spectrophotometric observations of relatively bright moderate excitation planetary nebula NGC 6826, obtaining electron density and ion concentration
21 p3446 A71-40415

Cosmic ray and soft X ray steady state models of interstellar gas, determining He/H ions concentration ratio
22 p3601 A71-42167

Incoherent scatter observations of ion concentration and plasma line in F1 region
23 p3670 A71-43188

ION CURRENTS

NT ION BEAMS

Ionization gage with ion current linear dependence on pressure at room temperature
05 p0753 A71-16945

Turbulent flame structures from ionization current measurements
08 p1376 A71-21911

Satellite-borne spectrometer for low energy ion measurement
09 p1436 A71-22554

Ion currents to cylindrical electrodes in mobility dominated plasma flow from thin sheath theory involving convection currents
09 p1505 A71-23374

Magnetic field aligned currents during 18 March 1969 substorms, observing electric field by Ba plasma cloud motion for magnetic perturbation field
10 p1677 A71-24789

DC vacuum arc ion currents between copper electrodes, discussing wall geometry, plasma ionization, starvation phenomena and anode spot formation
12 p1939 A71-27269

Rate constant measurements of hot plasma electron attachment from ion current collection plots for communication during atmospheric entry
12 p1939 A71-27272

Ion and electron probe currents correlation for justification of electrostatic probes use for turbulent plasma diagnostics
14 p2280 A71-30170

Particle collision effects on electrostatic probe electron or ion current collection in transition regime as function of relative thermal energy
15 p2409 A71-32100

Electrical plasma probes, discussing ion-surface effects, geometry, cleaning procedures, collisionless regime and electron/ion current
16 p2617 A71-32969

Ionic conduction in perovskite-type oxide solid solution, discussing application to high temperature hydrogen oxygen fuel cells
18 p2852 A71-36969

Ion formation in photochemically initiated combustion of acetylene-oxygen-nitric oxide mixture: measuring carbon, CH and OH emission spectra and ion current time change
19 p3013 A71-38050

Thermodynamic ion current ratios of solid solution V-Ti alloys, using Knudsen effusion and time of flight mass spectrometric methods
21 p3398 A71-40469

High voltage source model for fast neutral particles showing energy and yield as function of potential, pressure and magnetic field
21 p3421 A71-41297

Electron beam interaction with plasma in ion sources with oscillating electrons, noting increased ion current
22 p3580 A71-41649

High vacuum ion source classification according to ionization technique, using permeance and current flow parameters
22 p3589 A71-42050

Field ion current angular distribution for large point emitter potentials as function of emitter geometry
22 p3578 A71-42050

Cesium ion sampling measurements in DC and RF plasma discharges, using mass spectrometry
24 p3851 A71-44479

Ion current sheath-convection effects with flux-mounted electrostatic probes in high pressure flowing plasmas
24 p3826 A71-44799

ION CYCLOTRON RADIATION

Nonpotential ion cyclotron waves propagation at very large angles to unperturbed magnetic field, obtaining dispersion relation numerical solutions
03 p0420 A71-14539

Subprotonospheric and ion cyclotron whistlers generated by same lightning discharge observed by OV1-10 satellite
06 p0869 A71-17998

Complex ray theory for ion cyclotron whistlers at proton and helium type in topside ionosphere
09 p1437 A71-22979

Negative ions photodetachment by continuous-tunable laser and ion cyclotron resonance spectrometer
11 p1772 A71-25379

Monograph on instabilities in ion beam-plasma system covering surface wave propagation, magnetic effect and ion cyclotron radiation characteristics
14 p2281 A71-30508

Ionospheric VLF and ELF wave observations, noting ion cyclotron resonance and harmonics effects on propagation
14 p2202 A71-30948

Stable auroral red arcs generation at plasmapause from ion cyclotron wave turbulent dissipation of ring current proton energy
16 p2572 A71-33941

Relativistic electron precipitation during magnetic storms, showing cyclotron resonances with electromagnetic ion cyclotron waves
16 p2629 A71-33941

Energetic electrons pitch angle scattering during magnetic storms due to resonant interaction with proton generated Doppler shifted ion cyclotron waves
16 p2574 A71-33971

Ion cyclotron resonance power absorption theory: application to reactive and nonreactive ions line shapes, using Wobbschall-Graham-Malone phenomenological equation of motion
17 p2695 A71-34949

Ion cyclotron resonance spectroscopy, discussing fundamentals, instrumentation and ion-molecule chemistry applications
17 p2695 A71-35521

Finite beta microinstabilities inherent in magnetized mirror confined plasmas, considering wave propagation across magnetic field at multiples of ion cyclotron frequency
18 p2950 A71-35869

Ion cyclotron resonance power absorption, deriving expression for average ion kinetic energy at saturation in steady state limit
21 p3418 A71-40231

Ring current location in magnetosphere, noting electromagnetic ion cyclotron instability region as stable proton trapping boundaries
22 p3532 A71-41444

Weakly damped Alfvén ion-cyclotron waves and fast magnetoacoustic waves in infinite plasma cylinder inserted into current bearing finite coil

24 p3858 A71-45245

ION DENSITY [CONCENTRATION]

NT IONOSPHERIC ION DENSITY

NT MAGNETOSPHERIC ION DENSITY

NT MAGNETOSPHERIC PROTON DENSITY

NT PROTON DENSITY [CONCENTRATION]

Magnetosphere thermal ion density and temperature in dawn and morning quadrants fromOGO 5 satellite measurements

01 p0147 A71-11498

Ionospheric artificial barium cloud growth and stability, considering ion density, internal electric field and velocity

01 p0077 A71-11508

Nighttime F region molecular ion concentrations of oxygen and nobelium and associated nightglow morphology, using numerical method for solving nonlinear equations

01 p0078 A71-11611

Spherical and cylindrical electrostatic probes for point ion density measurements in continuum flowing plasmas in hypersonic wake, discussing shock tube program for calibration

03 p0423 A71-13441

Atmospheric electrical properties derivation from continuity equation, considering ion concentration, conductivity, space charge density and electric field

03 p0409 A71-13610

Heavy ion diffusion in solar corona, emphasizing flow velocity and density

03 p0495 A71-14503

Mesosphere and lower thermosphere probing, noting electron and ion densities distributions, collision frequencies and ionospheric loss rates

05 p0740 A71-16427

Plasma physics, obtaining very high temperatures and electron/ion densities by power laser heating

06 p0908 A71-18066

Underlying and interlayer N/h ionization distribution in unobservable region, discussing single and multilayer approximation

07 p1101 A71-19410

Stratospheric small ion density measurements by level flight balloons

07 p1103 A71-19768

Cross field instability effect on weakly ionized plasmas with ionization density gradients under crossed electric and magnetic fields, using linear analysis

08 p1339 A71-21207

Hydrogen ion flux detected along earth magnetic force lines in Northern Hemisphere midlatitudes, determining flux magnitude

09 p1436 A71-22561

Plasmasphere ion concentration measurements on-board Elektron 2 and 4 satellites, observing dependence on geomagnetic activity

09 p1513 A71-22574

Weak ion concentration in stratosphere and mesosphere measured by accumulated capacity amplifier

09 p1443 A71-22676

Green line intensity and electron/ion density contours as function of height over solar limb for March 1970 coronal enhancement

12 p1969 A71-27651

Electric field potential near sphere moving through rarefied collisionless plasma in condensation zone, determining ion and electron concentrations

13 p1991 A71-29159

Vertical distribution of small ion density and of electric polar conductivity and ion temperature profiles in atmosphere at 1.5-19 km from balloon measurements

13 p2065 A71-29425

Nonequilibrium effects in Ar free jet plasma, using cooled Langmuir probe for electron temperature and ion density measurements through shock wave in front of blunt body

15 p2454 A71-31536

[AIAA PAPER 71-591] Langmuir probe measurement of ionization density of Ar plasma jet, suggesting electron-ion recombination in probe vicinity

17 p2789 A71-35338

Spatial distribution, ion density and space potential measurements in plasma boundary layer at conducting sphere

19 p3112 A71-37738

Underlying and interlayer N/h ionization distribution in unobservable region, discussing single and multilayer approximation

19 p3053 A71-37834

Stratospheric dust effect on electrical conductivity measurements, noting proportionality to ion concentration

20 p3216 A71-38792

Satellite data on solar wind velocity, ion composition, temperature and magnetic field characteristics near earth orbit

20 p3279 A71-39445

PCA due to solar proton event, measuring electron/ion densities and temperatures, proton/electron energy flux spectrum, Lyman alpha radiation and X rays

20 p3281 A71-39730

Charge density fluctuation measurements in ionized turbulent hypersonic sphere wakes, using Langmuir and continuum electrostatic probes and microwave interferometric and scattering equipment

21 p3363 A71-40388

Hybrid computer simulation of nonlinear ion-acoustic shocks in diaphragms

22 p3577 A71-41896

Nitrogen and neon cations number density time dependence during plasma decay in neon-nitrogen mixtures

23 p3711 A71-43881

Ram current effect in sounding rockets for plasma ion density measurement

24 p3822 A71-44793

ION DISTRIBUTION

Near earth solar wind Fe, Si and O ions, using electrostatic analyzer on Vela 5A satellite

01 p0148 A71-11520

Tropospheric positive and negative ions mobility distribution measurement from converging channel chamber data

02 p0247 A71-12849

Topside ionosphere O-H ions transition level altitude variation due to atmosphere winds

03 p0416 A71-14030

Magnesium and manganese ferrite ion states under heat treatment using X ray and Mossbauer methods

05 p0793 A71-16832

Plasma ions lifetime and energy spectra in quadrupole magnetic trap as function of energy and time

08 p1340 A71-21483

Temperature dependent ionic domain for yttrium oxide doped thoria as solid electrolytes at low oxygen activities

09 p1480 A71-22114

Sm double plus ion sites distribution in KCl by spectroscopy

09 p1506 A71-22147

Gas ionization by fission fragments emitted by spherical or cylindrical sources, deriving analytical expressions for ion distribution via diffusion model

09 p1496 A71-22358

Dynamo role in magnetospheric disturbances and ionospheric inhomogeneities, allowing for charged particle concentration height dependence

09 p1435 A71-22430

Metastable oxygen ion distribution and related optical emission rates in aurora, discussing line intensities, charge transfer efficiency and ionization peaks

09 p1441 A71-23642

E and F region positive ion composition, electron concentration and thermal balance vertical profile, discussing ionizing radiation spectrum, plasma cooling, primary chemical reaction rates and ionospheric formation

10 p1573 A71-24550

Papers on electronics and electron physics, Volume 29, covering plasma-RF field interactions, cluster ions formation and electron beams energy distribution

11 p1802 A71-25628

Anisotropic instability in velocity distribution of ions in plasmas under external RF electric field

12 p1934 A71-26572

Potential and ion charge distribution in proximity to conducting sphere moving in low density collisionless ion-electron plasma

12 p1958 A71-26647

Field aligned anisotropy for auroral ionospheric energetic ions, calculating pitchangle distributions

12 p1899 A71-26885

Plasma ions lifetime and energy spectra in quadrupole magnetic trap as function of energy and time

14 p2282 A71-30670

Midday ion composition altitude variations in midlatitude trough region and plasmasphere, observing light ion concentrations

15 p2398 A71-31767

Seasonal and annual longitudinal variations in ionospheric ion distribution, stressing solar geomagnetic control importance

16 p2567 A71-33762

Sporadic E layer enhancement by horizontal transport within layer, considering gravity waves interaction effect on ion density horizontal redistribution

16 p2573 A71-33960

Charge neutrality in semiconductors with implanted dopant ions profiles, considering junction field penetration into Gaussian profile

19 p3118 A71-37489

Digital simulation of pseudowaves and plasma sheath formation about grid by computer solution of ion Vlasov equation for ion distribution function time evolution

19 p3113 A71-37749

Plasma ion and electron distribution functions measurement on outer planet missions [AAS PAPER 71-124]

19 p3114 A71-37938

F1 region ion structure during ionospheric magnetic disturbances by numerical simulation of quiet and disturbed conditions based on electron concentration profiles

19 p3057 A71-38368

Linear antenna in anisotropic plasma, calculating reactance change with surrounding dielectric layer thickness with allowance for ion depletion

20 p3204 A71-39142

Positive ion composition of collision dominated weakly ionized HF hydrogen plasma discharge, measuring abundance ratio as function of extraction voltage and gas density

20 p3275 A71-39429

Turbulent low Mach number electrostatic ion shocks evolution, correlating turbulence spatial growth with reflected ions distribution

23 p3708 A71-42892

Oxidation state of iron and cation distribution over M1 and M2 sites in clinopyroxenes from Apollo 12 by Mossbauer absorption spectroscopy, noting cooling history

23 p3738 A71-43609

ION EMISSION

Field-ion, field emission microscopy - Conference, University of Florida, March 1970

02 p0287 A71-12732

Earth immersion in glowing He ions, studying magnetosphere structural dynamics by observations from cavity

07 p1095 A71-18742

Mass spectrometer application to study of secondary ion emission during metal surface bombardment by argon ion beam

07 p1112 A71-19621

Ion source emitter plasma column generated by electron beam injection through gas filled chamber, compensating ion space charge with fast discharge electrons

07 p1170 A71-20180

Secondary ion component on tungsten target surface during sputtering by alkali metal ions

09 p1494 A71-22878

Ionization mechanisms for deviation of experimental altitude vs velocity curves of meteor trails, considering various electron and ion emissions and dissociation effects

10 p1669 A71-24032

Linear and nonlinear laser induced ion emission from solid targets with and without magnetic field, considering electron space charge accelerator

11 p1775 A71-26085

Spectral line emission from nitrogen ions, identifying charge by Doppler shift technique application to beam foil light source

16 p2615 A71-34129

Photographic observations of plasma eruptions from metal and opaque dielectric targets subjected to neodymium laser pulses, discussing successive shock wave formation

19 p3070 A71-37085

Solar atmosphere electron densities from ion emission line intensities in Be isoelectronic sequence

23 p3721 A71-43839

ION ENGINES

NT CESTUM ENGINES

Submillipound mercury electron bombardment ion thruster efficiency, noting cathode pole piece, baffle position and geometry influence on ion chamber performance [AIAA PAPER 70-616]

01 p0143 A71-11577

Neutronic comparisons of design concepts for low power thermionic space power reactors based on uranium and uranium-based fuels

02 p0281 A71-12264

Thermionic reactor analytical model for systems analysis, considering complex interactions between reactor physics, thermionics and thermal/hydraulics

02 p0281 A71-12265

Thermionic performance influence on reactor design and operation, considering plant electrical ratings

02 p0281 A71-12266

Technology gap between thermionic converter physics and reactor engineering, emphasizing language problem

02 p0281 A71-12272

In-core thermionic reactor development for space applications

02 p0282 A71-12307

TV broadcast satellites with in-core thermionic reactor, discussing transmitting power, design and economy

02 p0283 A71-12308

Kaufman electrostatic ion thruster using electron bombardment ionized mercury vapor in cylindrical vessel and acceleration by electrostatic field

02 p0283 A71-12310

Hall ion thruster using electron neutralized positive space charge in acceleration zone

02 p0283 A71-12312

Radio frequency electrostatic ion thruster using mercury ion source electrodeless self sustaining discharge

02 p0283 A71-12313

Thermionic reactor development for space applications, discussing converter fuel elements, reliability and system weight [ASME PAPER 70-WA/ENER-13]

03 p0456 A71-14109

Facility backspattered material effect on performance of glass-coated accelerator grids for Kaufman electron bombardment thrusters [AIAA PAPER 71-156] 06 p0947 A71-18598

Electron bombardment ion thruster using hollow cathode and two-grid ion accelerating geometry, discussing performance tests [AIAA PAPER 71-158] 06 p0947 A71-18600

Oxide hollow cathode ion thruster power conditioner, evaluating electrical efficiency, weight, reliability integration and testing [AIAA PAPER 71-159] 06 p0947 A71-18601

Parameters influence on mercury hollow cathode neutralizers for Kaufman ion thruster [AIAA PAPER 70-1090] 07 p1184 A71-19863

Electron bombardment mercury ion thruster plasma properties and performance, computing ion beam current, discharge losses and propellant utilization efficiency [AIAA PAPER 69-256] 07 p1184 A71-19881

SERT 2 spacecraft ion thruster ground tests and flight operation, tabulating performance data [AIAA PAPER 70-1125] 09 p1511 A71-22899

Thermionic reactor electric propulsion for unmanned outer planets exploration, discussing spacecraft design, launch vehicle, weight factors, etc [AIAA PAPER 70-1122] 09 p1492 A71-22914

Optimal control of composite spacecraft propulsion system incorporating high thrust-weight ratio chemical engine and low thrust ion engine 09 p1512 A71-23138

Kaufman ion thruster providing electric propulsion for satellite spiraling from parking to synchronous orbit [AIAA PAPER 70-1101] 11 p1810 A71-25501

Low specific impulse hollow cathode mercury thruster for deep space electric propulsion, using SERT 2 configuration [AIAA PAPER 70-1099] 11 p1811 A71-25526

Thermionic reactor experiment design to evaluate U-235 fueled fast spectrum core dynamic and steady state characteristics, discussing system features 11 p1710 A71-25868

In-core thermionic reactor flight system for space base applications, providing electric power and thermal shielding 11 p1710 A71-25870

Thermionic reactor electric spacecraft propulsion system for unmanned outer planets missions, investigating voltage and radiator temperature effects on weight 11 p1811 A71-25872

Nuclear thermionic systems conceptual design with converters outside reactor to reduce weight 11 p1710 A71-25874

Driver terrestrial in-core thermionic reactor dynamic behavior, discussing computerized simulation with respect to coolant loop 11 p1711 A71-25883

Small fast spectrum thermionic reactor experiment open loop dynamics and control, discussing nonlinear transient simulation studies on closed loop plant 11 p1712 A71-25886

Automatic control, safety and dynamics of thermionic reactor experiment under simulated spacecraft load requirements 11 p1712 A71-25888

Space base 100 kw thermionic reactor power plant featuring interchange core replacement package 11 p1713 A71-25895

Electron energy distribution in plasma discharge of Hg electron bombardment ion engines, using Langmuir probe 13 p2114 A71-27985

Flight characteristics of ion engine powered automatic laboratories in upper ionosphere 13 p2146 A71-29210

Performance tests of electron bombardment ion thruster, using xenon, krypton, argon, neon, nitrogen, helium and carbon dioxide 14 p2287 A71-29922

NASA Lewis Research Center Hg electron bombardment ion thrusters research programs 14 p2288 A71-29931

Ion thruster technology and subsystem development program status, describing design and performance characteristics [AIAA PAPER 71-690] 14 p2293 A71-30750

Beam vector control from ion bombardment thrusters with dual grid electrostatic, movable screen electrode and discharge chamber extraction systems [AIAA PAPER 71-691] 14 p2293 A71-30751

Ion thruster ion beam current density profiles mathematical representation by two parameter equation [AIAA PAPER 71-693] 14 p2293 A71-30752

Magnetoelectrostatic containment ion thruster, considering adaptation for Hg operation based on discharge chamber loss comparison with Cs [AIAA PAPER 71-692] 15 p2470 A71-32288

Electrostatic ion propulsion systems for interplanetary missions, using experimental engine characteristics as basis for flight studies [DFVLR-SONDDR-121] 15 p2496 A71-32722

European geostationary telecommunication satellite stabilization using ion thrusters 16 p2623 A71-32851

Advanced communications satellites system engineering, including configuration based on active body stabilization, rechargeable hydrogen oxygen fuel cells and ion engines [AIAA PAPER 71-843] 17 p2812 A71-34710

Direct thrust measurement on electrostatic ion engine ESKA 18 P, comparing with values calculated from applied voltage and ionic current [DGLR-71-043] 17 p2793 A71-35538

Electron bombardment mercury ion rocket engine, considering mass flow rate and magnetic field strength effect on performance 17 p2794 A71-35540

Propulsion systems evaluation for Mars and Jupiter missions, using bundled ESKA 28 electrostatic ion thrusters and incore thermionic reactors [DGLR-71-046] 17 p2794 A71-35545

Solar electric propulsion system design for interplanetary spacecraft, describing Hg bombardment ion engine 17 p2794 A71-35546

RF ion thruster /RIT-10/ optimization, investigating energy balance and plasma diagnostics [DGLR-71-041] 17 p2794 A71-35547

Ion microthruster for satellite orbit and position corrections, describing optimum performance characteristics and test facility [DGLR-71-032] 17 p2795 A71-35548

Thermionic reactor technology, including insulator seal, nuclear fuel, emitter, tri-layer structure and interelectrode plasma 20 p3265 A71-38949

Ion engine development at Farnborough /England/, considering 10 mN mercury electron bombardment thruster system with hollow cathode 22 p3588 A71-41508

ION EXCHANGE MEMBRANE ELECTROLYTES

Closed cycle life support water electrolysis system using solid plastic sheet electrolyte /ion exchange membrane/ of sulfonated perfluoro polymer [ASME PAPER 71-AV-9] 18 p2866 A71-36376

ION EXCHANGE RESINS

Benzoylformic and alpha-acetamidooacrylic acid hydrogenation, using modified ion exchange resin-palladium catalysts 03 p0375 A71-13199

Heat and mass transfer optimization in hydrogen-oxygen fuel cells with ion exchange membrane 14 p2181 A71-30050

Ion exchange resin carbon dioxide removal and concentration system for space cabin environments, describing monitoring and control instrumentation 14 p2189 A71-30313

ION EXCHANGING

Transform for hydrogen ion exchange perturbation problem, involving first order partial differential equations and method of characteristics 01 p0130 A71-10368

Ion exchange kinetics during pulsating fluid flow, developing approximate mathematical model 01 p0070 A71-10619

Quantitative gas liquid chromatography analysis of amino acids in biological materials, discussing ion exchange techniques 11 p1729 A71-26068

Glass fibers and rods from thallium-sodium ion exchanging, investigating flexibility, focusing and light conduction without distortion 16 p2588 A71-34120

Oxidation state of iron and cation distribution over M1 and M2 sites in clinopyroxenes from Apollo 12 by Mossbauer absorption spectroscopy, noting cooling history 23 p3738 A71-43609

ION GAGES

U IONIZATION GAGES

ION IMPACT

White light flares due to photosphere heating by flux of energetic ions and electrons impinging from above 05 p0797 A71-16028

Singly tuned IMPATT diodes, examining noise and power saturation 05 p0729 A71-16919

Large signal microwave equivalent circuits analysis of IMPATT diodes, allowing carrier multiplication by impact ionization at every point in diode 07 p1072 A71-19108

X band IMPATT oscillator, discussing frequency stability, rms noise deviation, admittance characteristics, output power loss, temperature effects and power stability 07 p1073 A71-19111

Microwave oscillator circuit with cap structures for testing millimeter wave IMPATT diodes 07 p1073 A71-19119

Composite silicon IMPATT diode oscillator for 110 GHz operation with 140 mW output power 07 p1075 A71-19264

X band multiple IMPATT oscillator combining 12 packaged diodes in waveguide cavity for 10.5 watt CW output at 9.1 GHz, noting clean spectrum 07 p1075 A71-19266

IMPATT and Gunn microwave oscillators injection phase locking, discussing stationary state synchronization theory and phase vs frequency deviation measurements 08 p1263 A71-20949

Lunar rock analysis, discussing heavy ion impact traces and amorphous skin relation to solar wind 10 p1677 A71-24649

Silicon IMPATT microwave oscillators, calculating CW power as function of frequency by scaling approximation 18 p2888 A71-36124

Self consistent one dimensional large signal analysis of Read type IMPATT diode oscillator, taking into account device-circuit interaction 18 p2888 A71-36144

Microwave avalanche diodes, considering diode velocity and power efficiency limitations of IMPATT mode 18 p2894 A71-36979

IMPATT diode microwave oscillator temperature effect on operation, comparing with Read diode small signal admittance characteristics 18 p2895 A71-36986

One- and two-sided abrupt junction IMPATT diodes, investigating Si junction type effects on avalanche region and diode design 18 p2895 A71-36987

Electronic transitions in oxygen molecule due to ion impact from kinetic energy loss spectrum 21 p3418 A71-40886

X band GaAs diffused IMPATT diodes for high CW efficiencies 22 p3523 A71-42483

IMPATT diode development for millimeter wave applications including oscillators, sweep generators and Doppler radar 22 p3524 A71-42763

Reactive impedance matching of Gunn or IMPATT diodes for microwave oscillators by dielectric tuning 23 p3650 A71-43071

Surveyor 3 unpainted Al tubing examination by replication electron microscopy for surface damage due to particle impact and ion bombardment in lunar environment 23 p3766 A71-43821

ION INJECTION

Van Allen radiation belts and plasma sheet energy loss control, using cold plasma injection 16 p2629 A71-33976

Plasma beams injection into toroidal magnetic field, along gradient or radius, using polarizational interaction 17 p2786 A71-34281

Magnetic field aligned striations of Ba ion clouds artificially injected into ionosphere, investigating physical processes based on model 20 p3230 A71-39861

Junction structures and electrical properties of silicon n-p-n transistors fabricated by various combinations of diffusion and ion implantation 21 p3354 A71-40728

Ion implanted depletion mode MOS/LSI devices in conjunction with conventional P channel processing 21 p3358 A71-40821

Ion implantation technique utilization for reducing MOSFET devices threshold voltage and gate drain capacitance 24 p3808 A71-44725

ION IRRADIATION

NT DEUTERON IRRADIATION

Secondary electron emission during RbBr, Se and CdTe film bombardment by sodium ions and atoms 01 p0139 A71-11099

Relative biological effectiveness of multicharged C ions during single irradiation of Chlorella, noting dose dependent mutability 06 p0854 A71-18366

Ion implantation lattice damage effects in crystalline silicon with allowance for optical reflectivity, considering annealing temperature and amorphous layer formation 07 p1175 A71-19062

W and Mo single and polycrystalline structural changes by ion bombardment in Li vapor atmosphere at 1500 C, using mass spectrometer 24 p3838 A71-44862

Irradiation defects and electrical quality of ion implanted silicon, using minority carrier lifetime measurements 24 p3863 A71-45357

ION MICROSCOPES

Field-ion, field emission microscopy - Conference, University of Florida, March 1970 02 p0287 A71-12732

Electron transfer in ion microscope field ionization, analyzing band and periodic surface structure effects, ionization probability and collision formalism 02 p0288 A71-12734

Imaging gas-metal surface interaction in evaporation field by ion microscopy, discussing molecular ion identification and dipole attraction due to electronic rearrangement 02 p0209 A71-12735

Near stoichiometric binary alloys atomic ordering parameters quantization by field ion microscopy, using direct counting and optical transformation techniques 02 p0297 A71-12736

Alloy matrix short range ordered particle microstructures and properties, correlating electron diffraction and field ion microscopy studies 07 p1132 A71-19439

Field induced changes in W specimens during field ion microscope operation, considering behavior of dislocations and grain boundaries 21 p3395 A71-40024

ION MOTION

Resonance charge exchange effect on gaseous ions mobility, noting cross sections structure due to resonance and wave interference 04 p0629 A71-14998

Quasi-stagnation levels in ion motion induced by internal atmospheric gravity waves at ionospheric height 06 p0888 A71-17280

Supersonic flow of rarefied plasma around plane bodies, allowing for electric field effect on ion motion 06 p0842 A71-18252

Satellite-borne sensor for ionospheric ions velocity measurement, describing design and operation principles 09 p1438 A71-23141

Ionospheric ions drift velocity horizontal and vertical components distribution, using satellite-borne sensor 09 p1438 A71-23142

Halogen molecules electron affinities by measuring negative ion average translational energy and appearance potentials, noting free radicals heat of formation 09 p1498 A71-23376

Computer simulated semiinfinite uniform plasma expansion in vacuum, showing inapplicability of thermal velocity burst ion model 13 p2104 A71-27846

Cold plasma convection production by ion driven LF drift instability, noting tokamaks and stellarators stabilization 13 p2104 A71-27850

Ion migration direction in thin Ag, Cu and Au films under direct current effect from resistance radioactive tracer measurements and scanning electron micrographs 13 p2112 A71-29333

Ion motion effect on first order oscillations in infinite homogeneous two-component cold plasma in constant magnetic field and circularly polarized external field 15 p2459 A71-32651

Ions acceleration during current passage through plasma, discussing maximum energies, threshold current and electron beam flux density 17 p2787 A71-34284

Steady LF geomagnetic pulsations, deriving dispersion equation relating plasma electron frequency, hot ion velocity and particle radii and drift frequencies 17 p2735 A71-35243

Combustion systems ionic wind velocities, investigating gauze parameters, magnetic fields and mixture inhomogeneity effects 17 p2785 A71-35703

Flow around obstacle in plasma with ions cold relative to electrons and with directed subsonic, considering relative density measurement 19 p3115 A71-38207

Insulator surface ion migration effects on MOS and bipolar integrated circuits, describing inversion voltage and surface conductivity and recombination velocities 19 p3033 A71-38505

ION OSCILLATION

U PLASMA OSCILLATIONS

ION PROBES

Solar X-rays role in D region ionization from ion probe sounding during eclipse of 20 May 1966 03 p0407 A71-13377

Flat plate ion density probe with convection and ion production in electric sheath, comparing to shock waves in air 04 p0632 A71-14706

Ion orientation technique for attitude control based on counterflow sensing in earth upper atmosphere, discussing accuracy 09 p1523 A71-23151

Ion probe measurements of very low fluid velocities, improving accuracy by marking technique 14 p2223 A71-29745

Ion and electron probe currents correlation for justification of electrostatic probes use for turbulent plasma diagnostics 14 p2280 A71-30174

ION PRODUCTION RATES

Ionization rates in low pressure hydrocarbon flames produced by colliding burning gas jets 01 p0180 A71-11113

Ionospheric electron content distribution from satellite transmission data, discussing ionospheric irregularities and electron production rates 02 p0245 A71-11966

Metastable atomic oxygen ion production in F region plasma due to photoionization by solar XUV radiation 03 p0462 A71-13271

Hydrogen Lyman alpha radiation intensity and atmospheric absorption before and during solar eclipse of 20 May 1966, considering D region ion production 03 p0407 A71-13376

Slow positive ion and electron production in collisions of protons and hydrogen atoms with gases of planetary atmospheres 03 p0460 A71-13494

Solar soft X ray and extreme UV relative contribution to E layer ion production rates during solar eclipse of 12 November 1966 03 p0481 A71-14511

Cs plasma thermionic diode, using Penning effect for ionization rate increase via Hg or Cd seeding 05 p0705 A71-16170

Heavy particles collision induced excitation, deexcitation and ionization rates, calculating atomic H quantum level transitions due to H and He atomic collisions at thermal energies 05 p0785 A71-16490

Cr and Ti ionization rates, CO and NO reaction kinetics and decomposition products in shock tubes 05 p0716 A71-16521

Molecular N ion production, studying cross sections, collisions kinetic energies and isotopic substitution 06 p0929 A71-17407

Ionization rate experimental profiles during maximum solar activity compared with calculations, showing additional source of ionization in E region 06 p0895 A71-18272

D region oxygen photoionization rates decrease due to carbon dioxide absorption 07 p1103 A71-19673

Slow negative atomic oxygen ion production in collisions between fast protons or hydrogen atoms and gas molecules 09 p1496 A71-22230

Excited radical and ion formation in unperturbed acetylene-air and superimposed HF discharge flames, determining activation energy 09 p1402 A71-22379

E region additional ionization source during solar activity maximum, analyzing ion production function and electron concentration 09 p1435 A71-22440

Altitude spectrum of ion formation in interaction of proton flux with atmosphere, using Bragg dissipation function 09 p1514 A71-23153

Lithium-like and sodium-like positive ions electron impact ionization, calculating cross sections and reaction rates with binary encounter model 11 p1801 A71-25211

Electron precipitation in nocturnal E region from radiowave and rocket data, calculating ionization rates and midlatitude morphology 11 p1815 A71-25552

Laser pulse produced energetic ion and plasma measurements fore and aft side of targets including Al and Au foils 11 p1775 A71-26084

Electron beam high frequency modulation effects on hot ions production in cold plasma 12 p1938 A71-27207

Ion production rates during electron flux-atmosphere interactions based on atmospheric models with different energy and angular distributions 13 p2061 A71-28541

Ionospheric ion formation and neutralization reaction rate coefficients determination by fitting rocket measured electron concentration profiles with computer generated profiles 13 p2062 A71-28560

Flat plate electrostatic probe for ionization rate measurements behind reflected shock waves, monitoring time evolution of electron production 14 p2248 A71-30884

Electron energy distribution function and ionization rate constant of atoms by electron impact as function of heavy particle temperature 16 p2615 A71-32796

Positive NO ion formation with excess internal energy in positive atomic oxygen ion-nitrogen collisions 16 p2538 A71-32810

Combustion flame plasma reactions, considering collisional and chemical ionization, ion decay, electron temperatures and additives 16 p2540 A71-32969

Effective cross sections for charged and excited particles formation from He, Ne and Ar ion collisions with CO molecules, using mass spectrometry 16 p2614 A71-33646

Nike Apache solar X-ray observations during 7 March 1970 eclipse, determining residual fluxes and atmospheric absorption profiles for ion production rates 16 p2627 A71-33790

Low latitude topside plasma temperature, electron content and ion production/loss rates during sunspot minimum to maximum 17 p2731 A71-34316

Temperature dependence of ionization rates in aluminum gallium arsenides for samples with varying Al contents 19 p3117 A71-37486

Ionization rates induced by solar flares charged particles in planetary atmospheres 19 p3142 A71-38047

Ion formation in photochemically initiated combustion of acetylene-oxygen-nitric oxide mixtures, measuring carbon, CH and OH emission spectra and ion current time change 19 p3013 A71-38091

Electron beam HF modulation effects on hot ions production in cold plasma 19 p3117 A71-38619

Ion and electron production rate during PCA event, computing electron/ion density, differential proton flux spectrum and ion production rate 20 p3225 A71-39729

Ionization amplitude calculation method, using extrapolation from complex energies approach 21 p3418 A71-40249

Ion pairing study in unresolved metal hyperfine splitting spectral region, using electron spin resonance line shape analysis 21 p3345 A71-40372

Slow negative atomic oxygen ion production in collisions of fast protons and hydrogen atoms with oxygen molecules, measuring scattering cross sections 21 p3419 A71-41109

Penning process for small ionization probability per atomic collision, obtaining ion production constant relationship to temperature 21 p3420 A71-41252

Free electron distribution function, atomic level population and ionization rate in low voltage arc near electrodes 23 p3709 A71-43266

F 2 region magnetic disturbances conjugacy mechanisms, considering vertical ionization profiles 24 p3823 A71-45029

Auroral charged particle fluxes electrodynamic interaction with atmosphere, determining ion formation rate and electron concentration and conductivity 24 p3866 A71-45032

ION PROPULSION

Television satellites orbital transfer from low to geostationary orbit using ion propulsion 03 p0378 A71-13742

Spacecraft propellant condensation on low temperature surfaces near cesium ion thruster exhaust, considering neutral atoms impingement and charge exchange 03 p0522 A71-14455

Book on ion propulsion covering technology, performance, accelerator design, propellant feed and control, etc 04 p0638 A71-14797

Cs ion microrocket engine development, discussing Cs fueling device, ionizer heating, fabrication and control methods 04 p0639 A71-15351

Quasi-steady coaxial MPD arcs characteristics, studying Ar ion velocities, electrostatic ion acceleration mechanism and arc voltage gradient [ONERA-TP-847] 05 p0795 A71-16573

Hollow cathode ion thruster and lightweight power conditioner of solar-electric propulsion system for unmanned deep space probes [AIAA PAPER 70-648] 09 p1511 A71-22904

Externally fueled thermionic reactor power plant incorporation into unmanned ion propulsion spacecraft 11 p1811 A71-25896

French monograph on satellite stabilization by ion propulsion and attitude control logic element design covering geostationary and geocentric satellites, mass and power balances 17 p2814 A71-35500

Ionizer, neutralizer and ion optics of cesium contact ion thruster, examining porous W materials technology [DGLR-71-033] 17 p2793 A71-35535

Ion propulsion R and D at ONERA, discussing ionizer test control procedures, attitude control simulation and neutral fraction measurements [DGLR-71-027] 17 p2793 A71-35536

ESKA-18P electrostatic ion propulsion system control characteristics and power conditioning, describing pulse width modulated power supply unit [DGLR-71-029] 17 p2794 A71-35543

Electrical or electromagnetic acceleration of ionized gas to obtain high velocity rocket exhaust for deep space manned flight 19 p3123 A71-38249

ION PUMPS

Electrodeless AC plasma accelerator/traveling wave pump/using coil assembly to produce variable phase velocity and eliminate end effects 15 p2457 A71-32102

ION RECOMBINATION

Vacuum package with Ti bulk sublimator/ion pump combination for 150 kv neutron generator tritium decontamination

21 p3414 A71-40900

ION RECOMBINATION

Atomic ion-ion recombination total inelastic cross sections calculation by Landau-Zener method, noting agreement with experiment

01 p0129 A71-10366

Cs vapor filled cracks breakdown in thermionic triayer insulators, calculating electron reflection and ion recombination kinetics on surfaces

02 p0232 A71-12239

Molecular ion recombination coefficient of decaying plasma formed by UV irradiation of Cs vapor in inert gas, using microwave diagnostic method

04 p0634 A71-15115

Nitric oxide ion two body recombination with nitrogen dioxide and trioxide molecular ions, examining ionic neutralization reactions in decaying dilute thermal plasma at 300 degrees K

11 p1801 A71-25297

Thermionic converter performance from theoretical model, considering transport, ionization-recombination, and electrostatic sheath phenomena

11 p1711 A71-25880

Ion-ion mutual neutralization cross sections, measuring range of barycentric energies by superimposed beam technique

12 p1932 A71-27005

Helium plasma afterglow at low temperatures, describing triatomic ion recombination and dissociation

15 p2460 A71-32730

Cometary dissociative recharging and recombination dissociation of water and hydrogen peroxide molecules in comets, giving empirical relation for effective cross sections

17 p2803 A71-34830

Correlation coupling matrix elements for one electron transfer and ion-ion recombinations in Landau-Zener calculations

18 p2948 A71-35839

Coaxial electrodynamic plasma acceleration, investigating triple electron and ion recombinations effects

19 p3108 A71-37129

Charged particles elastic interaction and recombination in low temperature weakly ionized potassium plasma

19 p3109 A71-37135

Ionized carbon monoxide in cometary tails, estimating time scale in recombination of ions into C and O atoms

21 p3442 A71-40155

Thermal dissociation rate of excited CsF, calculating ion-ion recombination rates

21 p3346 A71-40888

Helium plasma afterglow at low temperatures, describing triatomic ion recombination and dissociation

23 p3710 A71-43301

ION SCATTERING

Ion reflection and whistler trace shapes as function of magnetic latitude from satellite observations

03 p0408 A71-13389

Symmetric excited state electron capture cross sections in ion-atom inelastic scattering, using two state approximation formulas

08 p1338 A71-21235

Double structured perpendicular magnetoplasma shock waves possessing precursor foot due to ion reflection from resistive shock front

12 p1936 A71-26918

Excitation and ionization cross sections of atmospheric molecular species by low energy ions in strong auroral and man-made electric fields

19 p3055 A71-38039

Magnesium diatomic metal static and dynamic properties, using multiple electron and ion analysis system

24 p3839 A71-45118

ION SHEATHS

Double sheath emission barrier existence criterion at thermionic diode emitter based on ion trapping effect

02 p0290 A71-12232

Plasma oscillations excitation in ion sheath by electron beam, presenting frequency and amplitude variations as functions of discharge current and target bias voltage

04 p0634 A71-15259

Numerical solution for planar ion sheath growth in low pressure plasma, calculating transient sheath thickness resulting from application of specific voltage waveforms

10 p1652 A71-24659

Transient ion sheath effects on spherical metallic plasma probe complex admittance at different frequencies, comparing numerical results with experiment

11 p1805 A71-25803

ION SOURCES

NT PLASMATRONS

Hydrated hydronium ions in D region, discussing sources and production mechanisms

03 p0421 A71-14546

Ionization rate experimental profiles during maximum solar activity compared with calculations, showing additional source of ionization in E region

06 p0895 A71-18272

Ion source for double focusing magnetic mass spectrometer for use with gas chromatograph on Mars mission, requiring electron beam stabilization in space

07 p1113 A71-19851

Ion source emitter plasma column generated by electron beam injection through gas filled chamber, compensating ion space charge with fast discharge electrons

07 p1170 A71-20180

Cs ions surface diffusion/migration in presence of blocking electric field on emitter surface, examining contact-ionization ion sources

08 p1342 A71-21914

Ion sources with oscillating electrons, discussing operating principles and characteristics of sources with cold and incandescent cathodes and Penning ionization chamber

08 p1343 A71-22043

Lower ionosphere electron concentration space-time variations relation to ionization source intensity fluctuations based on rocket observations and ground sounding data

09 p1435 A71-22442

Mass spectrometer ion source modifications for temperature range extension in high temperature research

09 p1450 A71-23068

Autoionic mass spectroscopy, discussing emitters, ion sources and mass spectra of deuterized benzene, chlorobenzene and chloroform molecules during electron ionization and autoionization

10 p1611 A71-24383

Laboratory and meteoric cluster ions formation, using mass spectrometric techniques

11 p1802 A71-25630

Ion sources designs involving high energy electron beam injections, discussing input power continuous and pulsed modes optimal efficiencies

12 p1940 A71-27507

Overcharging effects on ion source with volume ionization, considering two dimensional ionization chamber model with lengthwise distributed neutral plasma component

13 p2109 A71-29202

Ion source of mass spectrometer for high temperature composition studies of gas phase

14 p2247 A71-30588

Energy necessary to produce beam ion in plasma discharge of Hg electron bombardment ion source

16 p2623 A71-32841

Ion accelerating system for minimum angular ion beam divergence with plasma ions ejection from source through slits in electrodes

19 p3109 A71-37133

Electron beam interaction with plasma in ion sources with oscillating electrons, noting increased ion current

22 p3580 A71-41645

High vacuum ion source classification according to ionization technique, using perveance and current flow parameters

22 p3589 A71-42055

Apollo 12 suprathermal ion detector data, considering Apollo 13 S-IVB stage impact

23 p3759 A71-43763

ION TEMPERATURE

Magnetosphere thermal ion density and temperature in dawn and morning quadrants fromOGO 5 satellite measurements

01 p0147 A71-11498

Solar wind ion energy per charge spectra, comparing to Vela 3A observations for composition

01 p0148 A71-11519

Charged particle temperature distribution in outer ionosphere, disregarding collisional energy exchange

02 p0244 A71-11920

Atomic and ion temperatures in Ar plasma low pressure discharge in metallic tubes with conducting walls

02 p0259 A71-11931

Diurnal variations and waves in ionospheric electron and ion temperatures and concentrations from Thomson scatter measurements

03 p0408 A71-13384

Ionospheric electron and ion temperatures and charged particle concentration from satellite and space probe observations

04 p0640 A71-14775

Solar wind velocity and ion temperature measurement by modulation-type ion trap onboard interplanetary Venera 3 satellite

05 p0798 A71-16052

Satellite ion energy analyzer with onboard data reduction for ionospheric ion temperature and concentration measurement with high temporal resolution

05 p0755 A71-17139

Laser produced plasma expansion into vacuum discussing ion energy angular distributions measurement

06 p0938 A71-18424

Fully ionized quasi-one dimensional magnetic nozzle flow analysis, including effects of unequal electron and ion temperatures and electron thermal conductivity

[AIAA PAPER 71-141]

Electron and ion temperature in ionosphere discussing measurements, solar heating, F and E region, variability over solar cycle, etc

06 p0939 A71-18549

Conductivity measurement of hot ion hydrogen plasma for runaway electric field, comparing Spitzer and Buneman formulas

09 p1502 A71-22868

Cold Hg plasma in composite HF and magnetostatic field near electron cyclotron resonance, obtaining electron and ion energy spectra

10 p1650 A71-24521

Superthermal ions velocity distribution in nonisothermal plasma, comparing real velocity distribution to Maxwellian distribution

10 p1651 A71-24636

Collisionless plasma with thermal ions in magnetic field absence, investigating stationary ion shock wave propagation

12 p1941 A71-27767

Thermalization processes in earth bow shock with emphasis on ion heating, using electromagnetic dispersion relation for ion-ion streaming instability

13 p2054 A71-27908

Ionospheric ion temperature measurement methods by exploring transverse velocity distribution, discussing surface pollution and spurious effects

13 p2055 A71-27929

Charged particle temperature distribution in outer ionosphere, disregarding collisional energy exchange

13 p2058 A71-28200

Ion temperature measurement for plasma focus using laser light scattering

13 p2079 A71-28674

Vertical distribution of small ion density and of electron polar conductivity and ion temperature profiles in atmosphere at 1.5-19 km from balloon measurements

13 p2065 A71-29422

Solar wind ion thermalization in earth bow shock by counterstreaming instability related to interplanetary magnetic field

15 p2399 A71-31774

Finite ion temperature effect on large amplitude magnetosonic disturbances and collisionless shock waves formation in plasmas, using one dimensional macroparticle code

15 p2458 A71-32394

Solar wind velocity and ion temperature measurement by modulation-type ion trap onboard interplanetary Venera 3 satellite

16 p2626 A71-33456

Geomagnetic equatorial ionospheric ion temperature, comparing incoherent scatter radar andOGO-D3 retarding potential analyzer values

16 p2573 A71-33956

Ionospheric atomic oxygen concentration estimates from radar backscatter and rocket probe measurements of electron and ion temperatures and concentration

16 p2574 A71-33965

Nonisothermal collisionless low beta plasma with electron temperature greater than ion, investigating low frequency potential modes for Kelvin-Helmholtz instability

16 p2620 A71-34167

Equilibrium diffusion of rotating plasma in toroidal systems, deriving two fluid hydrodynamic equations with allowance for ion temperature perturbation

19 p3109 A71-37140

Undisturbed ionospheric ion and electron temperature warming, investigating frictional heating effect by neutral winds

19 p3048 A71-37399

F region radio wave absorption dependence on electron-ion temperature difference from energy balance considerations, testing by radar backscatter measurements

19 p3055 A71-38045

Midlatitude ionospheric irregularities, electron density distribution and electron and ion temperature variation measurements, during solar eclipse of 22 September 1968

20 p3224 A71-39716

Electric fields effects on ions temperature and electron densities of auroral ionosphere

20 p3228 A71-39844

Jovian ionospheric electron and ion densities and temperatures, considering radiative association role

22 p3603 A71-42181

F region ion and electron temperature relationship to electron density, examining incoherent scatter data and physical processes

23 p3672 A71-43977

- Temporal electron and ion temperature behavior for pulsed beam-plasma discharge interaction in probkotron mirror-like device 24 p3854 A71-44515
- ON TRAPS (INSTRUMENTATION)**
- Solar wind elemental and isotopic He and Ne compositions from mass spectrometry of ions collected in metal foils deployed during Apollo 11 and 12 landings 01 p0146 A71-11486
- Atmospheric ions mobility spectrum measurement, describing aspiration capacitor design with various electrode configurations 03 p0431 A71-14500
- Solar wind velocity and ion temperature measurement by modulation-type ion trap onboard interplanetary Venera 3 satellite 05 p0798 A71-16052
- Elongation characteristics of modulation type charged particle traps and analyzers, discussing ions and electrons trapping 09 p1513 A71-22668
- Solar wind velocity and ion temperature measurement by modulation-type ion trap onboard interplanetary Venera 3 satellite 16 p2626 A71-33456
- ION-GAS INTERACTIONS**
- U GAS-ION INTERACTIONS**
- IONIC COLLISIONS**
- Vibrational degrees of freedom effects on capture cross sections and ion-molecule complexes formation in ion-dipole collisions 01 p0130 A71-10477
- Light emission during ion-molecule collisions, using low energy nitrogen and argon ion beams 04 p0630 A71-15655
- Isotope effects on collision dynamics of molecular hydrogen-argon ion reactions, using chemical accelerator 05 p0784 A71-15974
- Velocity space diffusion and collision effects on fully ionized inhomogeneous plasma instability, using Fokker-Planck kinetic equation 05 p0789 A71-16654
- Electron-ion collision effects on parametric instability growth rate in plasma dynamic stabilization 06 p0934 A71-17477
- Molecular hydrogen cations collisions with hydrogen and helium, determining dissociation cross section dependence on kinetic energy from threshold to 100 eV 07 p1163 A71-19233
- Ion-molecule collision charge transfer and momentum transfer relaxation rates, using ion cyclotron resonance heterodyning method 07 p1054 A71-19371
- Plasma instabilities and mode stabilization, discussing density-gradient-driven drift waves in collision-dominated regime 07 p1173 A71-20510
- Nitrogen molecule collision with metastable inert gas atoms and ions, investigating energy exchange mechanism 08 p1337 A71-20670
- Electron loss and capture by hydrogen atoms, protons and negative ions during collisions between atoms and molecules in gases, interpreting cross section data 08 p1338 A71-21491
- Vibrational effects on capture cross sections and ion-molecule complexes formation based on ion-dipole collisions, noting multiple reflection probabilities and collision lifetimes 09 p1498 A71-23662
- Electric field, neutral wind velocities and ion collision frequency from artificial ionic clouds motion and deformation in ionospheric E and F regions 10 p1602 A71-24549
- Positive diatomic nitrogen ions dissociation during collisions with inert gas atoms, measuring mass and energy distributions from focusing parabolic spectrograph 11 p1801 A71-25227
- Molecular hydrogen cations collisions with hydrogen and helium, determining dissociation cross section dependence on kinetic energy from threshold to 100 eV 12 p1932 A71-26751
- Triatomic hydrogen positive ion surface crossing effects in chemical reactions based on potential energy surfaces calculation using diatomics-in-molecules approach 14 p2191 A71-30573
- Electron loss and capture by hydrogen atoms, protons and negative ions during collisions between atoms and molecules in gases, interpreting cross section data 16 p2614 A71-33042
- Effective cross sections for charged and excited particles formation from He, Ne and Ar ion collisions with CO molecules, using mass spectrometry 16 p2614 A71-33646
- Ar ion laser plasma spectral lines widths and shifts at various pressures and current densities, noting role of ion-neutral charge exchange collisions 18 p2932 A71-37007
- Light production by 2.5-490 eV helium ion collisions with nitrogen, considering 1200 and 3200 A emission 19 p3107 A71-38055
- Positive ion composition of collision dominated weakly ionized HF hydrogen plasma discharge, measuring abundance ratio as function of extraction voltage and gas density 20 p3275 A71-39429
- Ionospheric radio wave absorption winter anomaly concerning seasonal variations of D and lower E region collision frequencies and F region oxygen concentrations 21 p3373 A71-40048
- Neutral atoms and ions collision damping constants estimation for spectrum synthesis, using approximate formula based on Stark broadening effect 21 p3442 A71-40160
- Rotational and vibrational effects in ion dipole collisions 21 p3419 A71-40905
- Ion-quadrupole effects in ion-molecule collisions by numerical calculations of capture cross sections and computer-plotter studies of ion trajectories 21 p3419 A71-40906
- Molecular nitrogen ions collisions with He and Xe gas atoms, discussing processes based on atomic N ion fragment velocity distribution measurements at varying electron energies 21 p3421 A71-41405
- Short wavelength instabilities in collision dominated plasma confinement by rotating magnetic field, interpreting in terms of equivalent negative resistance 22 p3579 A71-41579
- Inhomogeneous plasma shear flow instability with ion-collision, using BGK model 22 p3579 A71-41581
- High pressure collisional plasma instabilities caused by spatial gradients from quasi-stationary state transport equations derivation 22 p3580 A71-41585
- Hollow cathode lasers based on negative glow discharge excitation including charge exchange ion-atom collisions and Penning excitation 23 p3686 A71-43955
- Effective excitation cross sections of molecular CO ion bands in comet tails due to He ions collisions with CO molecules, considering deviation from adiabatic hypothesis 23 p3708 A71-44314
- Supersonic plasma flow interaction with mirror field studied by changing ion-ion collision mean free path in BSG-1A device 24 p3852 A71-44489
- Hydrodynamic equations for ions and electrons of ionized collision plasma in strong nonuniform magnetic field from Boltzmann kinetic equations 24 p3855 A71-44521
- IONIC CONDUCTIVITY**
- U ION CURRENTS**
- IONIC CRYSTALS**
- Quantum mechanical considerations underlying calculations of two-photon transition probabilities, discussing experiments on semiconductors, ionic crystals and organic compounds 18 p2930 A71-36241
- Trigonal crystal field and spin-orbit interaction matrices for ion energy levels in vanadium corundum in strong g scheme, using symmetry group tensor operators 21 p3427 A71-40075
- IONIC DIFFUSION**
- Heavy ion diffusion in solar corona, emphasizing flow velocity and density 03 p0495 A71-14503
- Ion diffusion and conduction to cloud droplets, determining resulting mean charge distribution for polar conductivities fixed ratio 07 p1152 A71-19757
- Nickel ion diffusion coefficients in high purity magnesium oxide single crystals in high temperature argon atmosphere 08 p1343 A71-20664
- Membrane separate systems ion and water mass transport, noting effect on anolyte concentration and alkaline battery performance 08 p1234 A71-21092
- Cs ions surface diffusion/migration/ in presence of blocking electric field on emitter surface, examining contact-ionization ion sources 08 p1342 A71-21914
- Diffusion-ion capture and heat transfer by phonons in solid and liquid metals 09 p1494 A71-22882
- Ni-Mo alloys electron transfer and ion diffusion at high temperatures 09 p1471 A71-23077
- Hydrazine feed control in hydrazine-oxygen fuel cells, discussing continuous measurement of limiting diffusion current for determining fuel concentration in electrolyte 11 p1708 A71-25241
- Output pulse amplitude from lithium-drifted detector-amplifier combination under conditions of carrier diffusion and bulk and surface recombination 11 p1802 A71-25804
- Anisotropy of solar cosmic ray electrons, considering parallel diffusion coefficients for ions and electrons 12 p1954 A71-27712
- F 2 ion velocity and electron density perturbations in terms of gravity waves, comparing incoherent scatter techniques 14 p2230 A71-29716
- Electrode effect in atmospheric electricity with convection and diffusion, calculating layer thickness dependence on vertical convective transfer velocity 17 p2730 A71-34312
- Cs ions surface diffusion/migration/ in presence of retarding electric field on emitter surface, showing temperature effects 17 p2789 A71-35258
- Strong current z discharge collisionless plasma, investigating ions distribution functions fine structure 23 p3708 A71-42890
- IONIC MOBILITY**
- Tropospheric positive and negative ions mobility distribution measurement from converging channel chamber data 02 p0247 A71-12849
- Atmospheric ions mobility spectrum measurement, describing aspiration capacitor design with various electrode configurations 03 p0431 A71-14500
- Night D region ion kinetics data during thermonuclear detonation, discussing formation and conversion rates, electron concentration and recombination 08 p1278 A71-21009
- Light ion flow from polar caps in hydrodynamic and evaporative forms, noting pressure gradient force, exospheric electric field and realistic boundary conditions 09 p1440 A71-23459
- Neutral wind and ion velocity determination under quiet and disturbed geomagnetic conditions in auroral zone, noting electric field measurements 09 p1440 A71-23600
- Midlatitude F2 region diurnal variations in peak electron density critical frequency and height, noting electric field and ion drag effects 10 p1606 A71-24921
- Plasma mobility, diffusion, electron energy distribution, surface phenomena, elastic collisions, charge transfer, etc 16 p2617 A71-32954
- Mass and mobility measurements for small ions in air by Pu bombardment in closed chamber at low pressure 16 p2614 A71-33380
- Night D region ion kinetics data during thermonuclear detonation, discussing formation and conversion rates, electron concentration and recombination 20 p3219 A71-39589
- Ion anemometer for measuring wind velocity magnitude and direction in rarefied Martian atmosphere 22 p3600 A71-41960
- High DC field induced ionic wind, deriving electric and pneumatic parameters for various electrode configurations 24 p3849 A71-45369
- IONIC PROPELLANTS**
- U ION ENGINES**
- IONIC REACTIONS**
- Incomplete energy equilibration in short lived activated complexes, measuring translational energy of unimolecular ion decomposition fragments 05 p0716 A71-15924
- Oxygen ion-molecule reactions at thermal energies, using drift tube mass spectrometer 07 p1164 A71-19689
- Kinetic energy dependent charge transfer rates for ion-molecule reactions in ammonia, using cyclotron ejection and impulse methods 08 p1249 A71-20657
- Reaction dynamics for CO ion plus D, noting polarization forces role 09 p1497 A71-22702
- Ammonia-parent ion reaction at low energies, comparing numerical and experimental capture cross sections 10 p1573 A71-24416
- Martian ionosphere below 80 km, developing positive and negative ion chemistry model 11 p1821 A71-25548
- He-Zn ion laser, considering charge exchange and Penning collisions as primary excitation sources of Zn II levels 11 p1773 A71-25927
- Photochemical ion-molecule reactions in ionosphere by air exhaust device and RF mass spectrometer observation in geophysical rocket experiment 13 p2068 A71-28535
- Ions association constant with water in propylene carbonate from proton magnetic resonance measurements 13 p2026 A71-29040

IONIC WAVES

Ion mass spectrometry in plasma analysis, reviewing complex ionized gaseous media investigations and specific reactions

16 p2576 A71-32962

Chemical reactions in electrical discharges, discussing H, O, N, halogens and free radicals, hydrides, halides and fluorinated compound synthesis and ion-molecule reactions

16 p2540 A71-32966

Low temperature plasma chemical processes, investigating molecular and atomic ionization, reactions under equilibrium and nonequilibrium conditions and specific energy production

16 p2540 A71-32968

Neutral-ionized parts interactions in upper atmosphere, discussing ionospheric plasma modulation, solar control and seasonal anomalies in lower ionosphere and ionic reactions

20 p3223 A71-39712

Airglow optical emission processes covering resonance scattering, fluorescence, chemical association, ionic reactions and excitation transfer

20 p3226 A71-39827

F region nightglow emission mechanism in terms of oxygen cations reactions with diatomic nitrogen and subsequent recombination

20 p3226 A71-39832

Reversible charge exchange reactions effects on ionization equilibrium of nitrogen in interstellar space

21 p3445 A71-40412

Photoionization mass spectrometry, considering application to appearance potentials determination, ion-neutral reactions and gas analysis

22 p3537 A71-41649

Impact ionization cross section measurements for multielectron-oxygen ion reaction, using crossed beams

22 p3578 A71-42421

Statistical phase space cross sections for helium ion-nitrogen molecule reactions, including dispersion and short range forces in intramolecular potential energy function

23 p3706 A71-43119

IONIC WAVES

Nonlinear resonance excitation of ion acoustic plasma waves by weak external electric field, using partial differential equations

01 p0134 A71-11027

Trapped LF ion wave propagation along warm plasma cylinder imbedded in dielectric, obtaining dispersion relation

01 p0136 A71-11476

Weak nonlinear ion-acoustic shock waves in cold ion-warm electrons plasma, using nonlinear perturbation method

02 p0288 A71-11868

Diurnal variations and waves in ionospheric electron and ion temperatures and concentrations from Thomson scatter measurements

03 p0408 A71-13384

Dispersion relation for LF quasi-static ion acoustic waves in finite geometry plasma

03 p0464 A71-13933

Ion acoustic waves in streaming ion plasma, discussing wave modes and energy exchange

04 p0634 A71-12528

Weakly ionized magnetoplasma waves and instabilities due to effects of electrons parallel, Hall and diamagnetic drifts relative to ions

05 p0789 A71-16653

Ion-acoustic waves generation mechanism in outer space by strong electromagnetic radiation, considering quasars, supernovae shells, pulsars and solar supercorona

05 p0800 A71-17196

Multimode ionization wave growth and saturation in finite length positive plasma column of gas discharge, investigating feedback and external driving signal effects

06 p0933 A71-17469

Electromagnetic wave trapping by nonlinear resonant interactions involving ion sound wave and two electromagnetic waves in isotropic plasma

06 p0869 A71-17988

Whistler indicator generation, relating VLF emissions to iono-acoustic oscillations in magnetosphere

07 p1099 A71-19387

Collision free ionizing wave propagation into cold low density ionized gas, showing wave oscillations damping due to ion velocities phase mixing

07 p1171 A71-20289

Ion acoustic and helicon waves nonlinear interactions in plasma, evaluating whistler buildup rate

09 p1501 A71-22536

Ion acoustic waves propagation and structure measurements with metal electrode technique and continuous channel electron multiplier in plasma wind tunnel

10 p1611 A71-24517

Ionization wave varieties in nitrogen glow discharge at various pressures and current densities from phase and group velocity measurements

10 p1654 A71-24973

Low density plasma-double gridded antenna system for ion and electron signal propagation studies, ob-

serving multiple reflections of acoustic and ballistic pulses and bulk phenomenon

12 p1935 A71-26913

Nonlinear theory of ion-sound plasma turbulence for strong wave-particle interaction near resonance

12 p1935 A71-26915

Linear longitudinal ion wave instabilities in electrostatic shock in plasma by double humped /bump in tail/ velocity distribution

12 p1935 A71-26916

Collisionless plasma with thermal ions in magnetic field absence, investigating stationary ion shock wave propagation

12 p1941 A71-27767

Similarities between ion waves in plasmas and gravity waves in incompressible fluid /steady water flow with allowance for surface tension/

13 p2046 A71-27844

Plasma ion waves external control with HF fields in subthreshold regime

13 p2104 A71-27845

Topside ionospheric instabilities of electrostatic ion acoustic and ion cyclotron waves to field aligned currents in single and multiion plasmas

13 p2054 A71-27917

Ion-acoustic waves generation in outer space by strong electromagnetic radiation, considering quasars, supernovae shells, pulsars and solar supercorona

13 p2128 A71-28251

Collisionless heat propagation along plasma magnetic field, showing relation to ion sound velocity

13 p2107 A71-28568

Ion wave frequency shift and instability suppression by RF electric field, examining wave-field coupling

13 p2110 A71-29334

Diffusion and acoustic ion waves in weakly ionized plasma as function of exciting/collision frequency ratio

13 p2110 A71-29372

Large amplitude ion acoustic wave propagation in streaming ion plasma, noting nonlinear effect in amplitude oscillation observation

14 p2281 A71-30541

Electric field, atmospheric wave and other factors effects on F region storms by day and night in tables

14 p2236 A71-30941

Longitudinal ionic wave excitation by grid in collisionless Q machine plasma

15 p2456 A71-31820

Ion cyclotron harmonic waves development in simulated low density and temperature space plasma, determining propagation upper and lower bounds

15 p2491 A71-32448

Externally excited moving striations measurement in low pressure Ar discharge, comparing with ion acoustic wave propagation derivation from model

18 p2948 A71-35859

Decay instability at ion-sound frequency induced by large amplitude Bernstein mode wave in plasma

18 p2951 A71-35929

One-dimensional numerical model of nonisothermal plasma, showing soliton separation from leading front by ion-acoustic shock waves after reversal stage

19 p3042 A71-37076

Plasmapause Alfvén, ion-acoustic, electron and ion drift wave modes coupling, calculating instability condition and growth rate

19 p3110 A71-37371

Whistler indicator generation, relating VLF emissions to iono-acoustic oscillations in magnetosphere

19 p3052 A71-37812

Ion and electron drift waves propagation and stability in nonhomogeneous plasma containing impurity ions

19 p3115 A71-38214

Parametric excitation of ionic waves in ionosphere by irradiation with electromagnetic wave at characteristic electron frequency

20 p3218 A71-39546

Auroral radio reflections mechanism in terms of auroral plasma instability processes, identifying ion acoustic wave characteristics among other echo components

20 p3199 A71-39852

VLF ion wave instabilities in polar wind based on plasma kinetic theory, comparing with electrostatic wave observation by OV3-3 satellite

20 p3231 A71-39890

Long wavelength ion acoustic instability of two temperature collisional fully ionized plasma with heat transfer, noting additional destabilizing currents

21 p3422 A71-40708

Homogeneous positive plasma column perturbation analysis in axial magnetic field, deriving model for ionization waves dispersion characteristics

22 p3582 A71-41898

Resonant coupling of two electron plasma waves with ion sound wave at large electron Larmor radii under weak magnetic field

22 p3583 A71-42418

Ion acoustic waves dispersion relation, presenting attenuation and phase velocity tables

23 p3667 A71-43138

Nonlinear ion acoustic soliton wave propagation and dissipation in nonhomogeneous nonisothermal weakly absorbing plasma

23 p3714 A71-44349

Stepwise ionization effects on ionic wave propagation and oscillation stability in inert gas DC discharge

24 p3857 A71-45230

IONIZATION

NT ATMOSPHERIC IONIZATION

NT AURORAL IONIZATION

NT AUTOIONIZATION

NT FLAME IONIZATION

NT GAS IONIZATION

NT ION PRODUCTION RATES

NT NONEQUILIBRIUM IONIZATION

NT PHOTOIONIZATION

NT SURFACE IONIZATION

Nonrelativistic cosmic particles spectrum and chemical composition changes, examining ionization and heating energy loss effect

02 p0300 A71-12091

Partially ionized bounded plasma LF natural oscillations due to ionization processes, ambipolar diffusion and charged particles recombination at walls

02 p0292 A71-12619

Magnetic field effect on mean electron impact ionization probability in valent semiconductors with ellipsoidal equienergetic surfaces

03 p0467 A71-13978

Interstellar H I region Lyman alpha production by suprathermal protons, determining temperature and ionization equilibrium

04 p0640 A71-14873

Electron collision cascades in braking medium, deriving integral equations for energy structure, displacement and ionization yield

04 p0629 A71-14914

Photoresonant cesium plasma ionization, discussing pumping spectra, electron gas, molecular-atomic ionization ratio and dynamics

06 p0936 A71-17591

N and p junction field effect transistor /JFET/ gated current measurement leading to understanding of impact ionization mechanism and field distribution

07 p1081 A71-20542

Nonrelativistic cosmic particles spectrum and chemical composition changes, examining ionization and heating energy loss effect

08 p1355 A71-21143

Ionization instabilities feedback suppression in magnetized nonisothermal plasma

08 p1342 A71-21932

Quasi-classical ionization model under assumption of straight-line electron trajectories, presenting Hamilton-Jacobi equations solution

12 p1932 A71-27244

Ionization instabilities suppression in magnetized nonisothermal plasma by feedback control

17 p2789 A71-35276

Ionization and excitation kinetics of Hg in relaxation flow zone behind shock wave front, considering electron impact role in ground state atoms ionization

18 p2951 A71-35980

Reentry plasmas ionization and microwave and optical radiation properties, considering radar echo, electromagnetic scattering, thermal equilibrium and ablation products

18 p2952 A71-36422

Daytime ionogram corrections for underlying ionization in absence of x-trace of sporadic E layer

19 p3058 A71-38386

Laser beam ionization of gold investigated by proportional electron counter

21 p3392 A71-40516

High vacuum ion source classification according to ionization technique, using pervance and current flow parameters

22 p3589 A71-42055

IONIZATION CHAMBERS

NT CLOUD CHAMBERS

NT GEIGER COUNTERS

NT PROPORTIONAL COUNTERS

NT SPARK CHAMBERS

Transient effects due to electromagnetic cascades in lead during copper wall passage in ionization chamber

01 p0084 A71-11370

Small tissue equivalent ionization chamber quartz fiber electrometer dosimeter system, for use as space qualified radiation detection instruments

02 p0250 A71-12136

Tropospheric positive and negative ions mobility distribution measurement from converging channel chamber data

02 p0247 A71-12849

Ionization chamber for high intensity isotopic gamma radiation dose measurement, discussing saturation current and Compton interaction process

04 p0594 A71-14917

Ion sources with oscillating electrons, discussing operating principles and characteristics of sources with cold and incandescent cathodes and Penning ionization chamber

08 p1343 A71-22043

- Overcharging effects on ion source with volume ionization, considering two dimensional ionization chamber model with lengthwise distributed neutral plasma component
13 p2109 A71-29202
- Near sea level cosmic ray high energy interactions from data recorded by interleaved stack of cloud and ionization chambers and carbon and iron plates
19 p3124 A71-37287
- Liquid Xe filled single wire proportional and multiple wire ionization chambers, measuring gain and time/spatial resolution properties
19 p3065 A71-38178
- High energy cosmic ray spectrometer onboard Proton 4, discussing ionization calorimeter, nuclear targets, particle charge and radiation detectors and primary measurements
20 p3283 A71-39755
- Large area parallel-plate pulse ionization chamber for high altitude balloon measurements of relativistic cosmic ray heavy nuclei
22 p3550 A71-42887
- Cosmic ray sidereal time period, using neutron monitors, meson telescope and various ion chambers
23 p3719 A71-43126
- Quasi-stationary electric field in toroidal metallic ionization chamber with meridional and equatorial slots, deriving formulas for components as function of coordinates
24 p3857 A71-45231
- ### IONIZATION COEFFICIENTS
- Yearly cosmic rays intensity variations in meridional plane from 1955-1969 ionization temperature coefficient recordings as function of solar activity levels
11 p1817 A71-25783
- Collisional radiative volume recombination and ionization coefficients for quasi-stationary helium, considering singlet and triplet systems as two coupled individual systems
13 p2106 A71-28452
- Average energy of electron avalanches in gases for linear inelastic collision cross sections, including ionization coefficient and Stoletoff constant for atomic hydrogen
13 p2103 A71-29080
- Stoletoff constant for gas mixture, discussing average avalanche energy at reduced electric field with maximum ionization coefficient and Penning effect for Ne-Ar
13 p2103 A71-29081
- Electric fields effects on ionization and recombination rate in non-LTE Cs plasma
18 p2852 A71-36967
- Cosmic ray spectrum at nonrelativistic energy region, noting ionization loss effects
19 p3129 A71-38359
- Penning process for small ionization probability per atomic collision, obtaining ion production constant relationship to temperature
21 p3420 A71-41252
- Yearly cosmic rays intensity variations in meridional plane from 1955-1969 ionization temperature coefficient recordings as function of solar activity levels
22 p3591 A71-41551
- IMPATT diodes noise performance lower limits, deriving optimization theorem for GaAs diodes under assumption of equal ionization coefficients for electrons and holes
22 p3524 A71-42632
- Molecular hydrogen primary ionization coefficient measurement in non-self sustained Townsend discharge, using light detection method based on radiant flux vs electron density proportionality
24 p3850 A71-44370
- ### IONIZATION COUNTERS
- #### U IONIZATION CHAMBERS
- #### U RADIATION COUNTERS
- ### IONIZATION CROSS SECTIONS
- Meridional ionization cross section in ionosphere between Leningrad and Murmansk with local anomaly and diurnal reversing of F 2 probability
02 p0243 A71-11766
- Cs atom ionization cross section during type II collision with resonantly excited Hg atom
02 p0287 A71-12197
- Effective cross sections for molecular hydrogen positive ion formation in collision between He, Ne and Ar ions or atoms
02 p0287 A71-12503
- Inelastic ionization cross sections for protonic and atomic hydrogen collisions with atomic and molecular gases in 0.5 keV to 5 MeV energy range
06 p0928 A71-17266
- Molecular N ion production, studying cross sections, collisions kinetic energies and isotopic substitution
06 p0929 A71-17407
- Molecular hydrogen cations collisions with hydrogen and helium, determining dissociation cross section dependence on kinetic energy from threshold to 100 eV
07 p1163 A71-19233
- Photoionization cross section in resonance continuum of C I, using wall stabilized argon arc
07 p1111 A71-19487
- Hydrogen and helium photoionization, calculating total cross section and transitions for soft X ray region
08 p1350 A71-20948
- Cross sections for simultaneous ionization and charge transfer in fast proton-helium atom collisions, using Born approximation
09 p1497 A71-22416
- Atmospheric molecular species, calculating electron impact ionization cross sections and recombination coefficients
10 p1645 A71-24970
- Atomic N and C photoionization cross sections by shock tube vacuum UV spectrometry
10 p1646 A71-24990
- Li photoionization cross sections determined from spectral intensity measurements as function of threshold wavelength, discussing radiative electron-ion recombination into first excited state
10 p1646 A71-24992
- Lithium-like and sodium-like positive ions electron impact ionization, calculating cross sections and reaction rates with binary encounter model
11 p1801 A71-25211
- Molecular hydrogen cations collisions with hydrogen and helium, determining dissociation cross section dependence on kinetic energy from threshold to 100 eV
12 p1932 A71-26751
- Multiphoton ionization cross section and charge number in neon near resonance under focused laser beam
13 p2081 A71-29338
- Cs atom ionization cross section during type 2 collision with resonantly excited Hg atom
15 p2451 A71-31503
- High temperature nitrogen plasma emission spectrum in 2500-5000 A range, estimating negative ion photoionization cross sections
16 p2613 A71-32900
- Relative excitation functions for electron impact with Mg in crossed beam experiment, considering simultaneous ionization of neutral Mg
16 p2614 A71-33331
- Effective cross sections for charged and excited particles formation from He, Ne and Ar ion collisions with CO molecules, using mass spectrometry
16 p2614 A71-33646
- Sunlight photodetachment rates and energy dependent cross sections for ozone ions, using photon beam excitation in buffer gas
16 p2574 A71-33962
- Ca and Mg light emission and ionization cross section measurements at simulated meteor conditions, using photomultiplier and optical filters
17 p2798 A71-34374
- Excitation and ionization cross sections of atmospheric molecular species by low energy ions in strong auroral and man-made electric fields
19 p3055 A71-38039
- Associative ionization and dissociative recombination cross sections of hydrogen molecular ions as function of vibrational coupling restricted to Rydberg states
20 p3272 A71-39577
- Proton auroras ionization and excitation cross sections of atmospheric constituents by energetic hydrogen ions and atoms, presenting recent measurements and H emission laboratory results
20 p3228 A71-39845
- Potassium photoionization cross section, including spin-orbit interaction, orientation of photoejected electrons and dipole transition moment correction due to core polarization
21 p3417 A71-40197
- Impact ionization cross section measurements for multi-electron-oxygen ion reaction, using crossed beams
22 p3578 A71-42421
- Electron transfer cross sections for low energy negative oxygen ion collisions with oxygen molecules measured by single-collision beam technique
23 p3707 A71-43930
- Nd positive ion cross section for stimulated emission with glass composition determined by laser and fluorescence measurements
23 p3685 A71-43938
- ### IONIZATION FREQUENCIES
- Vertical electron density profiles correction coefficients, noting computational work decrease and F region frequency discrepancy due to ionization
05 p0746 A71-17207
- Ionization rates induced by solar flares charged particles in planetary atmospheres
19 p3142 A71-38047
- Carbon and methyl radical formation, studying emission intensities and chemi-ionization rates in hydrogen-oxygen flames with hydrocarbons
19 p3013 A71-38090
- Ionospheric properties at geomagnetic equator from ionograms by automatic sounder at Thumba, noting F
- 2 layer ionization frequencies solar cycle variations altitude dependence
21 p3373 A71-40376
- ### IONIZATION GAGES
- #### NT PENNING GAGES
- Ionization gage detector signal interpretation as function of reflected molecule velocity distribution, noting shutter speed errors
02 p0286 A71-12128
- Ionization gage with ion current linear dependence on pressure at room temperature
05 p0753 A71-16945
- Cold cathode ionization gages dynamic pressure response as function of gas pulse mean speed and gas type, using magnetron test measurements
10 p1610 A71-24182
- Balloon-borne ionization spectrometer for high energy cosmic ray measurement, discussing calibration and accuracy
15 p2407 A71-31811
- Electromagnetically driven shock tube with precursor effect due to ionization of impurities by UV radiation from discharge, using gages to tag gas flow
20 p3239 A71-39431
- Flow velocity measurement in electromagnetically driven unsteady shock tube from charged particles extraction, using ionization gages
20 p3239 A71-39432
- ### IONIZATION POTENTIALS
- Three component two temperature plasma model of thermionic converter, including volume ionization-recombination processes
02 p0194 A71-12225
- Ionization potentials of cyclobutadiene, using photoelectron spectrum measurement
03 p0377 A71-14373
- Planetary nucleus BD plus 30.3639 degrees and Wolf-Rayet star HD 164270, comparing spectrum and ionization potential
08 p1359 A71-20937
- Ionization measurements of high latitude and altitude cosmic rays covering four solar maxima
08 p1355 A71-21628
- Homogeneous equilibrium low temperature dense helium plasma ionization composition and radiative energy losses, calculating ionization potential
09 p1501 A71-22380
- Satellite-borne spectrometer for low energy ion measurement
09 p1436 A71-22554
- Argon ionization and recombination in solar corona at electron temperatures of 2.0-4.5 times ten to sixth power K
11 p1832 A71-26180
- Micrometeor mass data from radiometer measurements, detailing Cu and lanthanum hexaboride ionization probability
14 p2315 A71-30652
- Solar silicon line spectra of photosphere, chromosphere and corona, including ionic spectra over wide ionization potentials range
20 p3301 A71-39822
- Electron temperature and density vs ionization potential in bright planetary gaseous nebulae, using forbidden emission line intensity ratios and level populations
21 p3440 A71-40059
- ### IONIZED GASES
- #### NT CATIONS
- #### NT CESIUM PLASMA
- #### NT CHARGED PARTICLES
- #### NT COLLISIONLESS PLASMAS
- #### NT COSMIC PLASMA
- #### NT ELECTRON PLASMA
- #### NT STELLAR WINDS
- Rotating stars with partially ionized convective envelopes, investigating general stellar magnetic field production
01 p0150 A71-10060
- Ambipolar diffusion coefficients application to analysis of laminar multicomponent ionized boundary layer flow in channel
01 p0070 A71-10795
- Multicomponent ionized gases mixture transport coefficients for field-free and strong magnetic field cases
03 p0463 A71-13471
- Heat exchange in dissociating partly ionized gas flow over critical point on permeable surface with injection into laminar boundary layer
03 p0342 A71-13748
- Laser action on six lines of ionized Xe spectrum, discussing discharge tube, optical resonator and spectrograph characteristics
03 p0438 A71-13895
- Ionizable gas flow through two dimensional nozzle under transverse magnetic field, using quasi-one dimensional approximation
03 p0466 A71-14553
- One dimensional ionized gas flow behind shock wave propagating in MGD duct
03 p0466 A71-14569

Ne, Ar, Kr and Xe ionized states transition and level lifetimes from photophotically recorded beam foil spectra, discussing particle energies
14 p16028 A71-16895

Resonance charge exchange effect on gaseous ions mobility, giving cross sections assuming due to resonance and wave interference
14 p16028 A71-16895

Radar scattering from turbulent ionospheric ionized waves, showing relationship between Doppler spectrum and wake characteristics
14 p16028 A71-16895

Air/Ar with ionizable lithium oxide plasma stream electric properties determination by shock tube wall electrode pair using ambipolar diffusion theory
14 p16028 A71-16895

Operational characteristics, spectroscopy and interaction mechanisms of noble gas ion lasers in light of plasma theories and atomic data
AIAA PAPER 76-401
05 p0763 A71-16551

Magnetosonic instabilities in weakly ionized gas flow, using adiabatic approximation
14 p16028 A71-16895

Weakly ionized gas discharge three dimensional steady motion of viscous incompressible gas discharge plasma in homopolar device curvilinear channel, emphasizing secondary overflow during acceleration
07 p1167 A71-19235

Ionized gas gaseous cluster interaction model construction, considering ionizing radiation enhanced cosmic flux and quasar PKS 1116 plus 12 absorption spectrum
07 p1198 A71-19630

Ionized gases quantum transport cross sections and collision integrals, considering energy and temperature ranges for attractive and repulsive screened Coulomb potentials
07 p1224 A71-20293

Nonlinear Fokker-Planck equation solution by Monte Carlo bimodal distribution function method, investigating fully ionized nonequilibrium plasma relaxation time
07 p1224 A71-20293

Steady plane plasma shock wave structure in partially ionized and radiating gas, using Navier-Stokes equations in three fluid continuum approach
06 p1004 A71-19902

Fully ionized gas under electric and magnetic fields, calculating electron velocity distribution and runaway rates as functions of time from Boltzmann equation
06 p1004 A71-19902

Ionized argon laser optimum performance comparing master oscillator power amplifier configuration to simple oscillator
11 p1772 A71-25141

Ionized gas and dust distribution in Orion nebula from Balmer line intensities photoelectric measurements
11 p1818 A71-25202

Dissociative recombination rates in partially ionized gases at elevated gas temperatures, using shock tube for limited ionization introduction
11 p1765 A71-26285

Nonstationary three dimensional weakly ionized incompressible viscous gas plasma flow in homopolar device, noting effects on ionization, diffusion, heating
06 p1004 A71-19902

Multicomponent turbulent boundary layer interaction for partially ionized gases
11 p1772 A71-25141

Electron energy distribution function in weakly ionized monatomic gas with molecular collisions, using differential equation asymptotic resonance technique
06 p1004 A71-19902

Ionized air exposure effects on acetylcholinesterase content and cholinesterase activity in mice, noting cholinergic and serotonergic interaction
11 p1772 A71-25141

Multicomponent ionized gas mixtures chemically equilibrated flows over nonporous and ablating surfaces, using Navier-Stokes and Prandtl equations for asymptotically thin boundary layer
11 p1772 A71-25141

Partially ionized binary gas mixture temperature development during nonequilibrium ion formation, solving heat and ionization balance equations
11 p1772 A71-25141

Monograph on shock wave structure in nonequilibrium partially ionized gas flow covering plasma diagnostics, electron temperature, ion density, induced potential gradient, etc.
11 p1772 A71-25141

Pulsed Xe ion laser properties, considering emission divergence, coherence and cross section
11 p1772 A71-25141

Glow discharge, ion and excited state properties of laser plasmas, including CW conditions for argon
14 p16028 A71-16895

Equations for radiative contributions to energy and mass transfer in monatomic and ionized gas flow in local thermodynamic nonequilibrium
14 p16028 A71-16895

Resonant charge transfer cross sections in inert rarefied gases from atomic screening parameters, considering positive charge conductivity of ionized dense gases
15 p2452 A71-31825

Steady state partially ionized monatomic gas expansion from sonic orifice, investigating electron-ion recombination effects on flow properties
15 p2452 A71-31825

Thermal electron density fluctuations in weakly ionized gas from viewpoint of particle diffusion in single charged particle phase space, considering incoherent scattering
15 p2452 A71-31825

Multiphase ionized Ar excited valency and inner shell transitions, investigating emission spectrum and energy levels
15 p2452 A71-31825

High temperature singly and doubly ionized monatomic gas and partially dissociated and singly ionized diatomic gas, showing adiabatic and isentropic exponents relationship
16 p2662 A71-32837

Nonequilibrium corner expansion flow of ionized argon induced by normal shock waves in hypervelocity shock tube
16 p2555 A71-32905

Ion mass spectrometry in plasma analysis, reviewing complex ionized gaseous media investigations and specific reactions
16 p2576 A71-32962

NGC 2024 direction H I region H 137 alpha recombination line emission detection, determining ionized hydrogen fraction
17 p2807 A71-35415

Continuous flash electrostatic probe for weakly ionized flowing gas surface density gradient and charged particle free stream density determination, obtaining I-V characteristics
18 p2950 A71-35858

Measuring apparatus for envelope distortion of transmitted high-energy, transversely polarized pulses through ionizable or partially ionized gas
18 p2952 A71-36589

Weakly ionized gas plasma confined by cylindrical electrodes and dielectric fronts, calculating rotational moment behavior in transverse electric and longitudinal magnetic fields
18 p2952 A71-36589

Integral equation for determination of nonuniform gain profile effect on resonant modes of ion laser cavity, considering ring modes at high current densities
19 p3074 A71-38228

Ionized carbon monoxide in cometary tails, estimating time scale in recombination of ions into C and O atoms
21 p3442 A71-40155

Transverse hydromagnetic shock structure in partially ionized gas, calculating ions, electrons and atom temperatures, velocities and momentum
21 p3444 A71-40239

Quasi-fluid mechanical formulation generation for ionized gases dispersive transport coefficients by linear dynamic response function technique
21 p3423 A71-40800

Coupled spherical electrostatic probe idealized theory, in quiescent medium slightly ionized chemically frozen gas, interpreting plasma measurements
21 p3423 A71-40800

Fluorescence of iodine molecule excited at 5017 and 5045 Å by ionized Ar laser, observing magnetic depolarization-Hanle effect
22 p3555 A71-41623

Partial quenching of radiation from ionized inert gases during bases irradiation by IR produced with carbon dioxide lasers
22 p3581 A71-41808

Visible coherent radiation generation mechanism in ionized oxygen and nitrogen, considering free radical stabilized on discharge tube wall and metastable atom reaction
23 p3706 A71-42889

Ion cloud expansion perpendicular to initially homogeneous magnetic field, estimating maximum radius with energy balance and expansion process
23 p3667 A71-43132

Sound waves propagation in fully ionized gas, considering electron plasma frequency
23 p3705 A71-44001

Temperature and electron density measurements for free jet of ionized nitrogen at atmospheric pressure by plasma spectroscopy, estimating Prandtl numbers
23 p3664 A71-44197

IONIZED PLASMAS

U PLASMAS [PHYSICS]

IONIZERS

Field ionization yield with single graphite whisker lateral surface as ionizer, using helium, ammonia, carbon monoxide and carbon dioxide
07 p1164 A71-19855

Ionizer, neutralizer and ion optics of cesium contact ion thruster, examining porous W materials technology
[DGLR-71-033]

17 p2793 A71-35535

Ion propulsion R and D at ONERA, discussing ionizer test control procedures, attitude control simulation and neutral fraction measurements
17 p2793 A71-35535

Upperatmospheric primary cosmic ray layer ionization, considering secondary particles, X rays, neutrons, tritons and mesons as ionizing agents
22 p3591 A71-41406

IONIZING RADIATION

NT ALPHA PARTICLES

NT BETA PARTICLES

NT COSMIC RAY SHOWERS

NT COSMIC RAYS

NT FAR ULTRAVIOLET RADIATION

NT GAMMA RAYS

NT LYMAN ALPHA RADIATION

NT LYMAN BETA RADIATION

NT NEAR ULTRAVIOLET RADIATION

NT PRIMARY COSMIC RAYS

NT SECONDARY COSMIC RAYS

NT SOLAR COSMIC RAYS

NT SOLAR X-RAYS

NT ULTRAVIOLET RADIATION

NT X RAYS

Soviet papers on dosimetry of ionizing radiation in dense fluxes covering electron collision, neutron spectra and gamma radiation
04 p0593 A71-14914

D region aeronomy characteristics and ionizing radiation energy spectra during solar flare of 22 October 1969
05 p0799 A71-16810

Cross sections for fluorescence production in carbon dioxide photoionization by 58.4 nm radiation, deriving emission spectra
06 p0963 A71-17781

Chemical protection against ionizing radiation in thiols and disulfides, discussing hydrogen transfer
07 p1032 A71-18930

Hypoxia protection against ionizing irradiation by anaerobic glycolysis stimulation, lactic acid increase and blood glucose level elevation
07 p1037 A71-18960

Ionizing radiation induced surface damage dependence in matched oxide passivated silicon planar epitaxial transistors on junction fringing electric field strength during exposure
07 p1174 A71-19015

Surface ionization effects on planar silicon bipolar transistors, considering damage reduction by device exposure to high ionizing radiation dose
07 p1174 A71-19015

Microcircuits component vulnerability, deriving time independent nonlinear terminal I-V characteristics, electrical switching response and ionizing radiation induced transient response
07 p1070 A71-19060

Ionizing radiation effects on monolithic metal oxide semiconductor inverters, including testing and hardening techniques
07 p1070 A71-19060

Quasi-exponential model of electron vertical profile in D region for aeronomic and ionizing radiation characteristics during solar flare of 30 October 1969
07 p1085 A71-19380

Book on ionosphere and magnetosphere covering temperature, composition ionizing radiations, radio communication electron production and loss, etc.
08 p1363 A71-21169

Ionizing radiation inhibition of spinal cord neurons ribonucleic acid synthesis and enzyme activity in mice, using autoradiographic method
09 p1393 A71-22923

Probability of quasi-chemical reactions between point defects in semiconductors due to ionizing radiation
10 p1655 A71-24139

Ionizing radiation effect on piezoelectric properties of quartz plates, covering X rays, gamma rays, electrons, protons and alpha particles
10 p1656 A71-24140

E and F region positive ion composition, electron concentration and thermal balance vertical profile, discussing ionizing radiation spectrum, plasma cooling, primary chemical reaction rates and ionospheric formation
10 p1573 A71-24550

Cochlear vestibular apparatus, ganglion cells, spiral roots and nerve trunk damage from ionizing radiation based on neural elements transirradiation in neoplasms
10 p1566 A71-25039

Energy transfer during charged particles passage through material media as function of spatial distribution, discussing electron production rates
11 p1802 A71-25769

Antihistamine treatment of hypotension and early transient incapacitation in monkeys under supralethal mixed gamma-neutron radiation
11 p1720 A71-26118

Soviet book on radiation dosimetry and spectrometry of ionizing radiations covering chemical, electrochemical, thermoluminescence, scintillation and diffuse reflection methods
11 p1797 A71-26450

- MOS transistors on P substrates, investigating ionizing radiation effects on I-V characteristics
12 p1885 A71-26830
- Two dimensional atmospheric model including oxygen and nitrogen photodissociation, recombination and photoionization, investigating solar activity and ionizing radiation effects on temperature stratification
13 p2057 A71-28018
- Soviet book on vestibular reactions covering functional relationship between stimulus parameters and labyrinth nonauditory part, adaptation to Coriolis forces and response to ionizing radiation
13 p2008 A71-28672
- Space objects sterilization techniques in Soviet Union and United States, covering hot air, ionizing radiation, UV light, ethylene oxide with or without Freon, etc
13 p2019 A71-28694
- Proportional counters design for ionizing radiation detection, examining cosmic ray meson component
15 p2408 A71-31814
- Fast luminous fronts /ionizing waves/ in Kanal streamer and Townsend discharges in nitrogen, discussing optical space and time resolved measurements
15 p2459 A71-32648
- Combined dry heat and ionizing radiation for spacecraft sterilization process, detailing synergistic effect on microbes
16 p2537 A71-33770
- Corpuscular and solar electromagnetic ionizing radiation simultaneous measurement by sounding rockets, evaluating contribution to lower ionosphere formation
16 p2627 A71-33776
- Low temperature high conductivity nonequilibrium plasma creation in MHD generators by microwave ionization
17 p2676 A71-34193
- Quasi-exponential model of electron vertical profile in D region for aeronomic and ionizing radiation characteristics during solar flare of 30 October 1969
19 p3127 A71-37817
- Book on biological effects of radiation covering ionizing radiation properties and effects at molecular, cellular and tissue levels
19 p3002 A71-38048
- Equivalent circuits for planar devices behavior under ionizing radiation, considering bipolar and MOS transistors
19 p3034 A71-38521
- Radioprotectants effect on mice against ionizing radiation and tolerance to back-to-chest accelerations in space flight
21 p3330 A71-40345
- Energy transfer during charged particles passage through material media as function of spatial distribution, discussing electron production rates
22 p3577 A71-41537
- Intense ionizing radiation and thermal treatment effects on electrical parameters of Si semiconductor devices
22 p3584 A71-41619
- Biological effects of ionizing radiation and non-radiative factors on radiation damage from satellite space flight tests on dogs and plants
24 p3798 A71-44891
- IONOGRAMS**
Solar eclipse of 7 March 1970 ionospheric ionization observations via satellites, correlating data with Wallops Island vertical ionograms
03 p0406 A71-13174
- Alouette 2 ionograms frequency interpolation correction allowing measurement accuracy comparable to sounder system resolution
05 p0725 A71-17083
- HF radio signal ionospheric propagation around world by sweep frequency CW sounding technique, observing fine structure in ionograms
07 p1062 A71-19682
- Atmospheric model phase ionograms for true height reduction technique tests, using ionosonde data
10 p1602 A71-24461
- Magnetospheric conjugate ducts characteristics for HF radio propagation from Alouette 2 topside sounder ionograms analysis
19 p3016 A71-37369
- Daytime ionogram corrections for underlying ionization in absence of x-trace of sporadic E layer
19 p3058 A71-38386
- Ionospheric properties at geomagnetic equator from ionograms by automatic sounder at Thumba, noting F 2 layer ionization frequencies solar cycle variations altitude dependence
21 p3373 A71-40376
- IONOSONDES**
Plane intensity variations on basis of photometrically analyzed Lyot filtergrams and ionosonde records
05 p0740 A71-16435
- Low power vertical-incidence solid state pulse compression FM ionosonde
14 p2246 A71-30480
- Ionosonde stations world distribution for vertical incidence soundings during IQSY and comparison with IGY
15 p2396 A71-31610
- Sporadic E layer thickness measurement by Phase Ionosonde, measuring phase advance on F region echoes
23 p3666 A71-42975
- Blanketing sporadic E layer diurnal and seasonal variations from equatorial stations ionosonde data obtained during IGY, discussing wind shear mechanism
23 p3667 A71-43134
- IONOSPHERE**
NT D REGION
NT E REGION
NT F REGION
NT F 1 REGION
NT F 2 REGION
NT LOWER IONOSPHERE
NT SPORADIC E LAYER
- Soviet papers on polar ionosphere covering auroras, magnetic activity, ionospheric disturbances during solar activity, auroral radio wave absorption, etc
02 p0241 A71-11756
- Cylindrical electric dipole antenna in magnetoactive ionospheric plasma, noting ion sheath effect on input impedance and active length
02 p0212 A71-11873
- Low energy particle variable flux measurement in midlatitude ionosphere, using rocket-borne thin window proportional counters
03 p0421 A71-14539
- Planetary atmospheres ionosphere formation by cosmic rays, examining ionization of various gases
05 p0799 A71-16817
- International Reference Ionosphere (IRI), considering organization, electron density and temperature, ion composition and electron collision frequencies
05 p0742 A71-16971
- Quasi-stagnation levels in ion motion induced by internal atmospheric gravity waves at ionospheric height
06 p0888 A71-17280
- Space station plasma physics experiments, investigating electron and ion wakes, resonance, VLF electromagnetic energy propagation and magnetospheric phenomena
06 p0938 A71-18529
- Ionospheric inhomogeneities effect on dipole current system produced magnetic field, deriving analytical expressions as function of distance from current carrying layer and inhomogeneity center
07 p1099 A71-19385
- Equatorial electric field generation by ionosphere dynamo region neutral wind meridional component
07 p1101 A71-19409
- Book on ionosphere and magnetosphere covering temperature, composition ionizing radiations, radio communication electron production and loss, etc
08 p1363 A71-21164
- Ionospheric radio waves scattering cross sections under time varying random irregularities, considering anisotropic behavior, dielectric tensor and geomagnetic field
09 p1411 A71-23587
- Radio ray tracing in complex space, describing plane stratified ionosphere
09 p1411 A71-23731
- Solar wind interaction with field free planetary ionospheres, giving three dissimilar models
10 p1661 A71-24005
- Martian ionosphere below 80 km, developing positive and negative ion chemistry model
11 p1821 A71-25548
- Barium ion cloud experiments for ionospheric vapor release determination from Rubis Rocket trajectory visible markings
11 p1755 A71-25643
- Venus daytime ionospheric models using electron, ion and neutral gas heat conduction with momentum and chemical equations for charged particle densities
11 p1823 A71-25693
- Geomagnetic field calculation for intermediate ionosphere altitudes, applying Dirichlet sphere problem to rectangular magnetic field components
11 p1757 A71-25778
- Induction and wave drag due to Alfvén waves on long cylindrical satellite in ionosphere, investigating radiated power integral
12 p1973 A71-27576
- Ionospheric wave/particle interactions under controlled electron beam energy and flux conditions, using Aerobee rocket for experimental investigation
12 p1902 A71-27668
- Discrete ionospheric model of supersonic two dimensional low density plasma flow past large bodies, using quasi-neutrality condition
13 p1990 A71-28532
- Polar ionosphere and magnetospheric processes - Conference, Kjeller, Norway, April 1969
14 p2299 A71-30027
- Geomagnetic tilt influence on polar ionosphere proton and electron precipitation, considering ionospheric ionization and polar cap absorption
14 p2300 A71-30034
- Matrix solution for wave equation with mode coupling of VLF and ELF radio waves in horizontally stratified layer of anisotropic ionosphere plasma
15 p2373 A71-32444
- Laboratory simulation of satellite motion in ionospheric plasma, specifying maximum current density, electron velocity distribution and temperature range [AIAA PAPER 71-608]
15 p2385 A71-32545
- Ionospheric geocoronal L sub alpha emission intensity related to solar activity level from Cosmos 215 satellite data
16 p2564 A71-33667
- Ionospheric motion boundary value problem, deriving uniqueness of solution
16 p2564 A71-33718
- Ionospheric refraction errors in satellite tracking, computing elevation, range and range rate corrections
16 p2640 A71-33734
- Ionospheric density diurnal variations and atmospheric rotation data from OV1-15 satellite drag measurements, noting geomagnetic activity effects
16 p2566 A71-33746
- Low and midlatitude ionospheric motion determination using barium ion cloud release technique
16 p2570 A71-33827
- Semiannual ionospheric density variations from Cosmos artificial satellites drag, noting agreement with solar corpuscular radiation geoefficiency
16 p2571 A71-33841
- Swedish space research activity covering upper atmospheric physics, ionosphere, magnetosphere and solar phenomena
16 p2665 A71-33853
- German Democratic Republic space research, reviewing meteorological, ionospheric, geomagnetic and solar physics studies
16 p2666 A71-33864
- Bibliography on neutral atmosphere dynamics covering waves, winds, turbulence and disturbances in thermosphere and ionospheric effects
17 p2732 A71-34462
- Magnetic field aligned electric field production by hot magnetospheric plasma interaction with cold ionosphere
19 p3048 A71-37401
- Ionospheric inhomogeneities effect on dipole current system produced magnetic field, deriving analytical expressions as function of distance from current carrying layer and inhomogeneity center
19 p3052 A71-37810
- Equatorial electric field generation by ionosphere dynamo region neutral wind meridional component
19 p3053 A71-37833
- Transverse electric field in ionosphere and magnetosphere during inhomogeneities consisting of fast electrons
19 p3057 A71-38367
- Electrical conduction in orthogonal coordinates from nondipole nature of geomagnetic field on conductivity tensor of ionospheric dynamo region
19 p3057 A71-38381
- Ionospheric wind velocity, direction and diffusion coefficient measurements using artificial aluminum oxide luminescent clouds
19 p3091 A71-38629
- Auroral zone ionosphere time lag observations, noting delay in cosmic noise absorption pulsations to fast bremsstrahlung X rays, luminosity and micropulsations
20 p3215 A71-38740
- Magnetospheric interactions with ionosphere for solar regular daily geomagnetic variations, discussing dynamo region electric fields effects
20 p3217 A71-39509
- Dynamo equations solution for electrostatic potential, discussing three dimensional model for ionospheric equatorial conditions and Northern-Southern Hemispheres coupling
20 p3218 A71-39519
- Dynamo theory for ionospheric thin shell model, considering wind fields determination from diurnal geomagnetic variations
20 p3218 A71-39522
- Parametric excitation of ionic waves in ionosphere by irradiation with electromagnetic wave at characteristic electron frequency
20 p3218 A71-39546
- Ionospheric effective recombination coefficient and reaction rate models for various solar activity periods and day and night conditions
20 p3224 A71-39714
- Photoelectron flux and energy spectra effects on ionospheric phenomena, examining sunlit and predawn atmospheric models
20 p3225 A71-39726
- GBR wavefield above winter nighttime ionosphere, noting latitudinal profile due to D region spatial variations and signal fading with F region structure
20 p3197 A71-39744
- Midlatitude ionospheric data comparison to F 2 critical frequency from continuity equation and neutral air winds
21 p3372 A71-40043
- Equatorial ionospheric density measurements on quiet and perturbed days, using San Marco 2 satellite balance
21 p3373 A71-40047

Ionospheric properties at geomagnetic equator from ionograms by automatic sounder at Thumba, noting F 2 layer ionization frequencies solar cycle variations altitude dependence 21 p3373 A71-40376

Magnetosphere-ionosphere electric coupling for polar magnetic disturbances and auroral break-up origin, discussing thermal particles precipitation due to transient electric field 21 p3375 A71-41354

Soviet monograph on radio wave propagation in fluctuating parameters media covering ionosphere /fluctuating electron concentration/ and troposphere /fluctuating inhomogeneities and refractive index values/ 21 p3349 A71-41372

Geomagnetic field calculation for intermediate ionospheric altitudes, applying Dirichlet sphere problem to rectangular magnetic field components 22 p3532 A71-41546

Quiet and stormy day diurnal variations of geomagnetic field, investigating ionospheric contribution 23 p3665 A71-42968

Midlatitude ionosphere and magnetosphere thermal protons dynamic behavior, investigating magnetic storm effects 23 p3720 A71-43129

IONOSPHERIC ABSORPTION

U ELECTROMAGNETIC ABSORPTION

U IONOSPHERIC PROPAGATION

IONOSPHERIC BLACKOUT

U BLACKOUT (PROPAGATION)

IONOSPHERIC COMPOSITION

Seasonal altitude variation of atomic ion-electron ratio of oxygen/nitrogen species in F 1 region, comparing to radar measurements 01 p0076 A71-11507

Ionospheric research covering electron and ion distributions, ion chemistry, neutral atmosphere interactions, thermal structure, electrodynamics, etc 03 p0416 A71-14031

Vertical NO profile at 100-220 km from 1968 Cosmos 224 measurement of atmospheric glow near horizon 05 p0744 A71-17186

F 1 layer development at summer midday midlatitude, noting role of molecular ions composition 05 p0745 A71-17200

Dynamo role in magnetospheric disturbances and ionospheric inhomogeneities, allowing for charged particle concentration height dependence 09 p1435 A71-22430

E region ion composition nighttime variations, examining nitrogen monoxide and oxygen ion nonequilibrium concentrations by ionic-molecular reactions 09 p1435 A71-22438

Polar ionosphere ion composition measurement by meteorological rocket-borne RF mass spectrometer 09 p1435 A71-22444

Sporadic meteoroid particles in ionospheric spatial density determined from kinetic energy measurements 09 p1519 A71-22562

Nighttime ionospheric atomic nitrogen and nitric oxide production and loss mechanisms effect on nightglow continuum 09 p1441 A71-23641

Magnetic mass spectrometer for ionosphere composition measurements permitting single spectrum analysis of plasma of negative and positive ions 10 p1608 A71-23817

Ionospheric anisotropic plasma with mixture of different ions, deriving refractivity at whistler frequencies 13 p2058 A71-28027

Vertical NO profile at 100-220 km from 1968 Cosmos 224 measurement of atmospheric glow near horizon 13 p2059 A71-28243

F 1 layer development at summer midday midlatitude, analyzing molecular ions composition effect 13 p2059 A71-28255

D region negative ion densities in chemical equilibrium based on electron density observation, noting role of ozone and carbon dioxide 14 p2228 A71-29533

Suprathermal electron temperature and ion composition as function of geomagnetic latitude in polar ionosphere, using Explorer 31 mass spectrometer measurements 14 p2234 A71-30037

F region drift velocity, wind, electric field, current and atmospheric composition variation measurements and related theoretical topics 14 p2201 A71-30940

Seasonal and annual longitudinal variations in ionospheric ion distribution, stressing solar geomagnetic control importance 16 p2567 A71-33762

Ionospheric nighttime ambient atomic oxygen concentration profiles, using nitric oxide release from sounding rockets 16 p2568 A71-33791

Ionospheric atomic oxygen concentration estimates from radar backscatter and rocket probe measurements of electron and ion temperatures and concentration 16 p2574 A71-33965

D and E regions advances during 1967-1971 covering ionic composition, electron density profile at various latitudes, hours and seasons during eclipses and winter anomalies 17 p2732 A71-34464

F region plasma phenomena discoveries by U.S. researchers /1967-1970/, considering thermal structure, ion composition, conjugate photoelectrons effects, wind effects, etc 17 p2732 A71-34465

Ionospheric neutral composition variations as function of height, local time and solar activity 19 p3056 A71-38356

Nighttime E region ion composition and concentration profiles, using rocket sounding 19 p3061 A71-38628

Neutral upper atmosphere observations, discussing lower thermospheric density and composition diurnal, seasonal and latitudinal variations and solar activity effects 20 p3220 A71-39690

Lower thermosphere neutral composition fine structure data from rocket-borne time of flight mass spectrometer, emphasizing atomic nitrogen vertical distribution 20 p3222 A71-39697

High Arctic latitude thermospheric helium and hydrogen rocket-borne mass spectrometric measurements, showing concentrations and winter bulge 20 p3222 A71-39698

Midlatitude lower thermosphere atomic and molecular oxygen rocket measurements, presenting concentration and vertical distribution data 20 p3222 A71-39700

Upper atmospheric anomalous molecular oxygen distribution, discussing turbulent theory with autocorrelation of density fluctuations 20 p3222 A71-39701

Day and night E and F region ion composition under solar maximum winter conditions from rocket measurements with RF mass spectrometers 20 p3280 A71-39719

Lower thermosphere eddy diffusion coefficient effects on height variations in ionospheric composition 21 p3372 A71-40044

Ionospheric radio wave absorption winter anomaly concerning seasonal variations of D and lower E region collision frequencies and F region oxygen concentrations 21 p3373 A71-40048

IONOSPHERIC CONDUCTIVITY

Thermoelectric transport properties of ionospheric electron gas above 100 km 03 p0406 A71-13301

High voltage solar cell array operation for satellite in ionosphere, discussing plasma leakage current minimization by electrical insulation 05 p0703 A71-16094

Polar magnetic disturbances in electrojet, studying Hall conductivity, electric field behavior and auroral ionosphere ionization 07 p1101 A71-19415

Polar caps magnetic field variations, considering relationship to auroral phenomenon and ionospheric conductivity variations 10 p1600 A71-24314

Striated irregularities in ionospheric ion clouds, using model of ionospheric conductivity profile 16 p2573 A71-33957

Magnetospheric conjugate ducts characteristics for HF radio propagation from Alouette 2 topside sounder ionograms analysis 19 p3016 A71-37369

Polar magnetic disturbances in electrojet, studying Hall conductivity, electric field behavior and auroral ionosphere ionization 19 p3054 A71-37839

Ionospheric plasma density irregularities effect on ionospheric electroconductivity, using Ohms law in Alfvén-Faethammer form 20 p3218 A71-39521

IONOSPHERIC CROSS MODULATION

Pulsed radio wave interactions with various lower ionosphere models, estimating cross modulation by computer calculation for comparison with measurements 09 p1405 A71-22443

IONOSPHERIC CURRENTS

NT AURORAL ELECTROJETS

NT ELECTROJETS

NT EQUATORIAL ELECTROJET

Polar magnetic substorms perturbation pattern westward motion related to ionospheric current lengthening 01 p0077 A71-11512

Ionospheric vertical wind role in anomaly of quiet sun diurnal geomagnetic variation at magnetic equator 02 p0243 A71-11764

Atmospheric circulation and earth rotational energy contribution to energy release by intense polar auroras, noting ionospheric current subsonic heating and oxygen emission 02 p0244 A71-11918

Ionospheric current system in polar E region, using earth surface equivalence model 04 p0584 A71-15448

Ionospheric transmission model vs current model for examination of low latitude geomagnetic pulsation origin 05 p0743 A71-17000

Sq ionospheric current systems longitude and seasonal variations, observing focus positions and electrojet characteristics 08 p1278 A71-21191

Solar flare EUV radiation and ionospheric currents dynamo region ground based detection by geomagnetic crochets time structure analysis 08 p1355 A71-21190

Dissipative effects on tidal winds at ionospheric heights concerning Lorentz force, molecular viscosity and heat conductivity 08 p1278 A71-21202

Polar E region equivalent current system, determining height direction and width 08 p1279 A71-21209

Dynamo theory for electric current variations in magnetosphere-ionosphere interactions, discussing electrostatic fields mapping and plasma particle drift motion production 08 p1279 A71-21212

Geomagnetic cavity heuristic model with solar wind driven unipolar induction current in ionosphere 08 p1280 A71-21218

Ionospheric current flow past circular inhomogeneous spot with Pederson and Hall conductivities, calculating earth surface magnetic field by Lipshitz-Hankeste integral 09 p1436 A71-22548

Neutral wind and ion velocity determination under quiet and disturbed geomagnetic conditions in auroral zone, noting electric field measurements 09 p1440 A71-23608

Geomagnetic solar quiet day horizontal current and electrostatic potential field model in ionosphere, using dynamo equations 09 p1442 A71-23700

Electric field, neutral wind velocities and ion collision frequency from artificial ionic clouds motion and deformation in ionospheric E and F regions 10 p1602 A71-24549

Inferring ionospheric electric fields at stratospheric levels with tropospheric penetration, using balloons measurements and model atmosphere 10 p1603 A71-24700

Magnetic field aligned currents during 18 March 1969 substorms, observing electric field by Ba plasma cloud motion for magnetic perturbation field 10 p1677 A71-24789

Low latitude DS ionospheric current components and auroral electrojet intensity for intense geomagnetic storms, considering particle observations by ATS 5 synchronous satellite 10 p1605 A71-24790

Magnetic field components of local ionospheric current for LF oscillation range including micropulsation frequencies, discussing spatial and frequency distribution 11 p1758 A71-25790

Geomagnetic horizontal field decrease from magnetospheric tail field annihilation, considering polar ionospheric current generation mechanism 11 p1758 A71-25792

Auroral electron temperature, noting field aligned energy transport current effects 12 p1899 A71-26887

Topside ionospheric instabilities of electrostatic ion acoustic and ion cyclotron waves to field aligned currents in single and multiion plasmas 13 p2054 A71-27917

Atmospheric circulation and earth rotational energy contribution to energy release by intense polar auroras, noting ionospheric current subsonic heating and oxygen emission 13 p2058 A71-28196

Hall effect and magnetic field characteristics in lower ionosphere by vertical magnetospheric currents, using gyrotopical model 13 p2061 A71-28534

Auroral absorption and DR currents development during magnetic storms, discussing corpuscular fluxes arrival from magnetospheric tail into lower ionosphere 13 p2062 A71-28563

Geomagnetic field horizontal component daily variation due to ionospheric E region dynamo, magnetopause surface and magnetospheric tail/partial ring currents 13 p2064 A71-29161

Geomagnetic disturbance vector distribution, computing three dimensional ring and ionospheric currents system models 14 p2229 A71-29672

- Ionspheric currents due to electric polarization field transfer from magnetosphere under quiet and disturbed conditions, using Ba ion cloud and geomagnetic measurements 14 p2230 A71-29715
- F region drift velocity, wind, electric field, current and atmospheric composition variation measurements and related theoretical topics 14 p2201 A71-30940
- Solar wind torque on geomagnetic cavity by rotational angular induction currents, including Joule heating of ionospheric plasma and directional magnetic fields 15 p2474 A71-31773
- Density distribution of plasmaspheric particles in equatorial plane via model of plasmasphere streaming, noting current system production in lower ionosphere 16 p2562 A71-32806
- Ionspheric electric and electromagnetic waves broadband characteristics, investigating auroral hiss and LHR noise 16 p2572 A71-33951
- Geomagnetic diurnal variations near Sq current vortex focus, indicating existence of ionospheric diverging or converging currents 18 p2912 A71-36298
- Longitudinal wave interaction and excitation by current instability in equatorial jet, considering energy transfer mechanism 19 p3057 A71-38363
- Noncircular ionospheric current conversion into longitudinal currents in magnetosphere along lines of force of geomagnetic field 19 p3057 A71-38380
- Ionspheric currents fields, determining Hall conductivity and geomagnetic lines of force slope effects 19 p3058 A71-38387
- Magnetic perturbations in near polar region and morning-night sectors of auroral oval as function of current sources and modulation by universal time 19 p3059 A71-38397
- Electrojet currents association with visible aurorae, using sounding rockets with rubidium vapor magnetometers 20 p3215 A71-38733
- Charged particles interaction with geomagnetic field, discussing plasma equations of motion, ionospheric current induction, transition layer and magnetotail rotation 20 p3216 A71-39118
- Daily geomagnetic variations ionospheric current systems calculation from total magnetic field data obtained at ground stations during IGY 20 p3217 A71-39511
- Three dimensional atmospheric dynamo models in quasi-stationary and stationary approximation for ionospheric and magnetospheric electric fields and currents production during quiet conditions 20 p3217 A71-39512
- Diurnal variations of Sq currents in terms of electroconductivity model of ionosphere and geomagnetic field, using two dimensional dynamo theory 20 p3217 A71-39517
- Equatorial electrojet region ionospheric currents during magnetically quiet day and nighttime from rocket measurements 20 p3218 A71-39524
- Equivalent current systems at 115 km parallel to earth surface profile based on ground observations of geomagnetic field, comparing with auroral electrojet 20 p3218 A71-39525
- Magnetic field components of local ionospheric current for LF oscillation range including micropulsation frequencies, discussing spatial and frequency distribution 22 p3532 A71-41558
- Geomagnetic horizontal field decrease from magnetospheric tail field annihilation during magnetic storm, considering polar ionospheric current generation mechanism 22 p3533 A71-41560
- Electric current shear at auroral arcs due to electron precipitation into lower ionosphere 22 p3536 A71-42623
- Worldwide geomagnetic disturbance during magnetic storm using DR-indices to express magnetospheric ring current induced perturbation 22 p3536 A71-42624
- Dynamo theory of solar and lunar magnetic fields diurnal variations, determining ionospheric wind velocities and pressure changes 23 p3669 A71-43174
- IONOSPHERIC DISTURBANCES**
- NT IONOSPHERIC STORMS
- NT SUDDEN IONOSPHERIC DISTURBANCES
- NT TRAVELING IONOSPHERIC DISTURBANCES
- Auroral magnetoionospheric perturbations processes, discussing space charge electric field structure and plotted altitude dependences 01 p0073 A71-10070
- Proton Flare Project 1969 observation of polar cap ionospheric disturbance due to proton event by VLF propagation phase measurement 01 p0073 A71-10289
- Proton Flare Project 1969 observation of flares and subsequent ionospheric disturbances during retrospective interval 01 p0144 A71-10290
- Equatorial ionosphere correlation distance regarding VHF telemetry disturbances and satellite tracking, determining antenna ground spacing 01 p0074 A71-11307
- Ionspheric artificial barium cloud growth and stability, considering ion density, internal electric field and velocity 01 p0077 A71-11508
- Polar magnetic substorms perturbation pattern westward motion related to ionospheric current lengthening 01 p0077 A71-11512
- F region ionospheric modification by heating from high power HF ground based transmission, discussing ionosonde observations 01 p0078 A71-11535
- Ionspheric heating self amplification and spread F triggering by disturbances, calculating ray paths through model ionospheric irregularities 01 p0078 A71-11536
- Ionspheric F layer modification by artificial heating, using radio echo detection of electron temperature changes 01 p0040 A71-11537
- Regularities of polar auroras and ionospheric disturbances during solar cycle with decreased low energy corpuscular flux 02 p0242 A71-11760
- Ionspheric stability in nighttime and daytime auroral zone with E layer corpuscular stream disturbances 02 p0243 A71-11762
- Meridional ionization cross section in ionosphere between Leningrad and Murmansk with local anomaly and diurnal reversing of F2 probability 02 p0243 A71-11766
- Ionspheric and exospheric ELF magnetic waves generation by high altitude nuclear explosions, discussing hydromagnetic waves propagation 04 p0581 A71-14981
- F2 region critical frequency ionospheric tidal spectrum during solar minimum and maximum at various global locations and solar and lunar day periods 04 p0583 A71-15214
- Sporadic E layer structure and disturbances from pulsed radio signal measurement, noting correlation to pressure oscillation at ground level 04 p0584 A71-15757
- Large scale ionospheric irregularities from Faraday fading records by satellite observations, studying height, fluctuations, electron contents, horizontal size and orientations 05 p0741 A71-16439
- Reflection point slide velocity of traveling F region ionospheric disturbance by receivers amplitude focusing and echo phase path changes 05 p0741 A71-16440
- Auroral sporadic E layer events relationship to pi 1 type irregular magnetic pulsations generation in Arkhangelsk region 05 p0744 A71-17187
- Ionspheric irregularity structure boundary variations shown by scintillation from satellite and radio star observations during quiet and disturbed magnetic conditions 06 p0887 A71-17269
- Ionization disturbances caused by gravity waves in neutral air propagating through ionosphere in electrostatic field and background wind 06 p0888 A71-17278
- Irregularities heights in ionospheric refractivity responsible for radio-satellite scintillation from spaced receiver experiments at midlatitude and subauroral locations 06 p0868 A71-17985
- Ionspheric response to internal gravity waves isotropic spectrum, presenting computer produced tonal value plots 06 p0893 A71-17986
- Electric field strength in earth ionosphere and magnetosphere during irregular motion of fast ions and electrons 06 p0894 A71-18253
- Electron concentration disturbances in outer ionosphere and F2 maximum on daylight side during magnetic storm 06 p0894 A71-18257
- F layer absence and nonuniform horizontal electron concentration of nighttime ionosphere at high latitudes, using Alouette 1 sounding 06 p0894 A71-18258
- Vertical electron density profile variations during ionospheric perturbations in years of solar activity maximum and minimum 06 p0895 A71-18277
- Small scale ionospheric irregularities from satellite radio signals fluctuations, using frequency scintillation measurements 07 p1060 A71-19037
- Sporadic E layer and critical frequency relationship to traveling ionospheric disturbances, suggesting role of atmospheric internal gravity waves 07 p1100 A71-19402
- Model of large ionospheric electron density discontinuities, emphasizing horizontal asymmetry association with observed east-west refraction asymmetry 07 p1100 A71-19405
- High latitude E region plasma irregularities based on wind velocity shear fields 07 p1153 A71-19760
- HF Hall current instability, discussing short wavelength backscatter for equatorial and auroral electrojets in disturbed ionosphere 08 p1279 A71-21205
- Nonlinear collisionless magnetoplasma waves and ionospheric irregularities electric field intensity, defining nonlinear oscillations domain by pseudopotential well 08 p1339 A71-21206
- Ionspheric irregularities, investigating drifting patterns with three delay method program 08 p1285 A71-21758
- Ionspheric wake spacecraft potential, electron current and temperature observations, using Agena/Gemini manned two body system sensors 09 p1517 A71-22175
- Ionspheric current flow past circular inhomogeneous spot with Pederson and Hall conductivities, calculating earth surface magnetic field by Lipshitz-Hankel integral 09 p1436 A71-22549
- Neutral and ionized atmosphere parameter variations and circulation during magnetic storms observed at various heights 09 p1436 A71-22550
- Book on aeronomy covering earth upper atmosphere structure, tidal oscillations, gravity waves, airglow, aurora, ionospheric disturbances, electric currents and turbulence 09 p1437 A71-22778
- Midlatitude spread F, sunspot activity and geomagnetic activity variations related, discussing fast solar particles 09 p1437 A71-22938
- F2 region ionospheric disturbances association with severe thunderstorms from radio observations 09 p1490 A71-23559
- Ozone distribution measurements in mesosphere and stratosphere by rocket during seasonal ionospheric disturbance and solar eclipse 09 p1490 A71-23562
- Earth-ionosphere waveguide model of VLF signals propagation with perturbed ionosphere, considering magnetic dipole transmitting antenna array 09 p1410 A71-23575
- Electromagnetic wave propagation in anisotropic ionospheric plasma with time-varying random electron density irregularities 09 p1506 A71-23586
- Seasonal variations and migration directions of itinerant ionospheric perturbations detected by ground based backscattering radar 10 p1575 A71-23821
- Satellite data for ionospheric radio communication forecasting involving maximum usable radio frequencies, discussing F2 region large scale disturbances 10 p1575 A71-23868
- Lunar shadow effects on bow wave mechanism during 7 March 1971 solar eclipse, considering traveling ionospheric disturbance measurements from satellite 10 p1600 A71-23885
- Ionspheric irregularities two fluid model, using nonlinear differential equations for longitudinal waves propagating in hot collisional magnetoplasma 10 p1648 A71-24294
- Polar cap lower ionosphere mapping by solar and magnetospheric charged particles, considering disturbances in polar regions 10 p1661 A71-24312
- Horizontal and vertical trace velocities of traveling ionospheric disturbances, interpreting in terms of atmospheric gravity waves 10 p1602 A71-24462
- Isolated ionospheric irregularities, describing refraction and diffraction pattern calculations for satellite signals 10 p1578 A71-24463
- Ionization crests of equatorial anomaly at magnetic L values from Ariel 2 satellite electron probe measurements 11 p1754 A71-25603
- Ionspheric evening anomaly geographic distribution and relation to neutral winds global pattern 11 p1755 A71-25612
- Lower ionosphere ionization response to auroral particle fallout during 1968 substorms, using geomagnetic, VLF and balloon measurements 12 p1899 A71-26642
- Nocturnal large ionospheric disturbances over Ashkhabad, obtaining relationship to electron content 12 p1901 A71-27120

Ionospheric continuity in F 2 region during partial solar eclipses, using EUV radiation and additional corpuscular source of ionization 13 p2053 A71-27792

Nature and average magnitude of lightning discharges causing transient excitation of earth-ionosphere cavity resonance 13 p2054 A71-27795

Transient ELF electromagnetic disturbances propagation in earth-ionosphere cavity, determining waveguide source-observer separation and attenuation constant 13 p2027 A71-27796

Topside ionospheric instabilities of electrostatic ion acoustic and ion cyclotron waves to field aligned currents in single and multiion plasmas 13 p2054 A71-27917

Small scale F layer inhomogeneities parameters and motion characteristics from radio echo observations 13 p2056 A71-27935

Auroral sporadic E layer events relationship to Pi 1 type irregular magnetic pulsations generation in Arkhangelsk region 13 p2059 A71-28244

VLF noise spectra in earth-ionosphere cavity due to thunderstorm discharges, noting resonance level splitting by geomagnetic field 13 p2030 A71-28542

Earth magnetosphere boundary position, head shock wave, transition region width and current magnetic field changes during magnetopause in geomagnetic storm periods 13 p2061 A71-28549

Log normal random fluctuations of ionospheric electron concentration in F region from vertical sounding and incoherent scatter data 13 p2061 A71-28553

Sizes, shapes and temporal characteristics of small scale inhomogeneities in F region, using vertical sounding, space diversity reception and radio astronomy 13 p2061 A71-28554

F 2 ion velocity and electron density perturbations in terms of gravity waves, comparing incoherent scatter techniques 14 p2230 A71-29716

Electron density irregularities and frequency deviation patterns role in equatorial electrojet 14 p2235 A71-30352

Ionospheric propagation, considering traveling disturbances, sporadic E phenomena, plasma frequency distributions and D region parameters 14 p2202 A71-30950

Wind profile determinations at 90-100 km from meteor trail drift and ionosphere inhomogeneity radar data, noting semidiurnal harmonics in wind components 15 p2395 A71-31450

Ionospheric disturbances due to supersonic shock from missile exhaust plume, noting F region compressions and undulations 16 p2563 A71-33358

Wavelike ionospheric undulations of total columnar electron content and of true height of bottomside plasma frequencies before and during solar eclipse of 7 March 1970 16 p2565 A71-33378

Lower E region drift data, noting wave-like nature of inhomogeneities 17 p2731 A71-34314

Remote double resonance coupling of radar energy to ionospheric irregularities by sweeping radar modulation frequency through whole range 18 p2914 A71-36929

Sporadic E layer and critical frequency relationship to traveling ionospheric disturbances, suggesting role of atmospheric internal gravity waves 19 p3053 A71-37826

Model of large ionospheric electron density discontinuities, emphasizing horizontal asymmetry association with observed east-west refraction asymmetry 19 p3053 A71-37829

Perturbations effects on ELF propagation in inhomogeneous anisotropic ionospheric waveguide 19 p3017 A71-37867

Ionospheric electron density irregularities measurement, comparing scintillation, spread F and electrostatic probe methods 19 p3128 A71-38035

Radio satellite scintillation producing small scale ionospheric irregularities, determining characteristic size variation with latitude by autocorrelation method 19 p3055 A71-38043

F 1 region ion structure during ionospheric magnetic disturbances by numerical simulation of quiet and disturbed conditions based on electron concentration profiles 19 p3057 A71-38368

Magnetic storm effect on integral electron content in F 2 layer and in outer ionosphere 19 p3058 A71-38383

Isoline charts showing F 2 layer critical frequency deviations and negative disturbance zones during solar eclipse of 22 September 1968 19 p3058 A71-38385

Neutral-ionized parts interactions in upper atmosphere, discussing ionospheric plasma modulation, solar control and seasonal anomalies in lower ionosphere and ionic reactions 20 p3223 A71-39712

F 2 and D regions disturbances associated with magnetic storms, emphasizing airglow effects 20 p3227 A71-39836

Ionospheric model for magnetic perturbation field global distribution during polar magnetic substorm, considering ground level geomagnetic effects from Birkeland and Pedersen currents 20 p3229 A71-39857

Ionospheric irregularities and reflection points calculation, developing simple ray interference model from large antenna array data 21 p3372 A71-40042

Internal gravity wave parameters calculation from total electron content short term variations, comparing ionospheric disturbance models 21 p3373 A71-40049

E region irregularities drift and anisotropy at Wal-tair during IQSY, inferring trends of diurnal and seasonal variation 21 p3374 A71-40379

Localized abnormal geomagnetic disturbance near polar cap and simultaneous ionospheric variation during auroral zone weak magnetic activity periods 22 p3536 A71-42625

Subequatorial ionospheric upward moving irregularities during high sunspot activity, explaining phenomenon at F 2 region level by Hall drift from daytime west-east electric field 23 p3665 A71-42971

Solar flare induced E and F regions electron density enhancement observation by Thomson scatter, noting relationship to EUV ionizing radiation 23 p3721 A71-43173

Periodic and isolated /nonperiodic/ ionospheric electron content fluctuations showing noon and midnight peaks and winter increase at high latitudes 23 p3670 A71-43180

Solar eclipse induced atmospheric gravity waves interference, considering resulting bow wave discrepancy with wavelike ionospheric disturbance 23 p3670 A71-43190

F layer perturbations by intense vertically upward radio waves for aeronomy and plasma control studies 23 p3671 A71-43543

F 2 region magnetic disturbances conjugacy mechanisms, considering vertical ionization profiles 24 p3823 A71-45029

IONOSPHERIC DRIFT

Ionospheric vertical drift velocities and east-west electric fields at magnetic equator from incoherent scatter observations 01 p0076 A71-11505

F region electron density profile changes during negative magnetic bays, deriving ionization drift from continuity equation 02 p0243 A71-11771

Ionospheric plasma drift from spinning rocket shadow effect, using retarding potential analyzer 03 p0416 A71-14034

Electric field strength measurement at rocket surface in ionosphere by electrostatic fluxmeter, obtaining E and F region ion drift velocities 03 p0417 A71-14035

Magnetic disturbances effect on drift behavior and anisotropy parameters of E and F region irregularities 05 p0740 A71-16433

Ionospheric drift measurements during solar cycle based on fading of radio waves reflected from E and F regions 05 p0741 A71-16437

Midlatitude F 2 layer electromagnetic drift during magnetic storm 06 p0888 A71-17287

Ionospheric drift velocity fluctuations by similar fading method, discussing applicability and errors 06 p0894 A71-18262

Longitudinal drift of auroral ionization in substorm recorded at different stations 07 p1099 A71-19388

Thomson scatter measurements of F region ionization drifts vertical velocity at midlatitudes, studying electric field influence 08 p1279 A71-21204

Simultaneous auroral ionospheric electric field measurements by Skylark rockets, deriving plasma drift direction 08 p1279 A71-21208

Ionospheric irregularities, investigating drifting patterns with three delay method program 08 p1285 A71-21758

Vertical velocity effects on ionospheric horizontal wind magnitude and direction, solving integral equations system by successive approximations 09 p1435 A71-22428

Ion and electron drift due to F layer wind and associated polarization fields, causing equatorial atmosphere eastward rotation 09 p1438 A71-22979

Satellite-borne sensor for ionospheric ions velocity measurement, describing design and operation principles 09 p1438 A71-23144

Ionospheric ions drift velocity horizontal and vertical components distribution, using satellite-borne sensor 09 p1438 A71-23144

Ionospheric drifts at 64-108 km at Birdlings Flat, New Zealand, comparing with meteor wind measurements, chemical release trails and general circulation models 09 p1440 A71-23614

Geomagnetic distributions of VLF hiss intensity and drifting frequency bursts near inner boundary of plasmapause on middle latitudes 09 p1411 A71-23614

Ionospheric dynamic behavior, describing time dependent continuity and ion, electron and neutral particle motion equations 10 p1606 A71-24919

Ionospheric drift mechanism in midlatitude F region, discussing ground level magnetic field, E region side effects, horizontal winds and polarization fields 11 p1753 A71-25559

Second order longitudinal variations of vertical ionospheric drift by middle latitude horizontal neutral air winds, showing maxima at universal time 11 p1754 A71-25609

Neutral wind effects on redistribution of E region ionization and recombination, comparing electron density profiles to vertical ion drift velocities 11 p1755 A71-25619

Array spacing dependence of ionospheric irregularities horizontal drift and anisotropy, using statistical properties of ground diffraction patterns 11 p1731 A71-25619

F region layers vertical drift from phase paths of radio waves reflected from constant electron density surfaces 11 p1756 A71-25649

Ionospheric plasma drift from rockets wake measurements at high latitude, discussing plasma rarefaction 12 p1899 A71-26894

Neutral winds produced vertical ion drift toward electric polarization in equatorial F region, discussing field discharge through E region and atmospheric superrotation effects 12 p1900 A71-26894

Lower ionospheric irregularities drift from neutral air motion measurements compared to meteor radar system determination 12 p1900 A71-27059

F layer vertical drifts due to winds at midlatitudes: computing longitudinal variations 13 p2054 A71-27794

Computer simulation of fading records in spaced antenna ionospheric drift experiment, detecting measurement direction and diffraction pattern velocity with correlation analysis 13 p2054 A71-27804

Receiver triangle size effect on ionospheric drift near 2 MHz, using partial and total reflections from lower ionosphere 14 p2230 A71-29714

F region drift velocity, wind, electric field, current and atmospheric composition variation measurement and related theoretical topics 14 p2201 A71-30944

F region ionization drift and electric field observation by incoherent scatter techniques and data interpretation 14 p2236 A71-30944

Incoherent scatter measurements for ionospheric ion bulk velocity, thermospheric dynamics, F region gravity wave, photoelectron flux, ionic collision frequency and magnetic field direction 14 p2202 A71-30944

Ionospheric drift rate measurements by close spaced 2.2 MHz receiver method at vertical and oblique incidence, obtaining atmospheric circulation patterns 15 p2395 A71-31431

Ionospheric drifts during IQSY, discussing comparison with IGY, methods and D1 records analysis theory 15 p2396 A71-31612

Seasonal variations of semidiurnal tidal winds in 90-110 km altitude range from harmonic analysis of ionospheric inhomogeneity drift data 16 p2575 A71-34103

Lower E region drift data, noting wave-like nature of inhomogeneities 17 p2731 A71-34314

F region vertical drift velocities at Millstone Hill: deriving ion velocity along magnetic field lines in upper part of F 2 region from continuity equation 17 p2732 A71-34427

Longitudinal drift of auroral ionization in substorm recorded at different stations 19 p3052 A71-37813

Ion acoustic instability in ionosphere in presence of fast particles inhomogeneity, estimating ions and electrons drift velocities 19 p3129 A71-38366

F 2 region electron density spatial and temporal distribution, investigating plasma vertical drift effects
19 p3058 A71-38384

Altitude dependent vertical drift velocity of small scale ionospheric inhomogeneities, using correlation of signal time lag scanning in frequency domain
19 p3058 A71-38391

Ionospheric electric field strength at equatorial and medium geomagnetic latitudes during twilight from barium-ion cloud drift measurements
20 p3218 A71-39523

Three-receiver radio wave dispersion analysis application to ionospheric drift records to assess effects of velocity variation with time
22 p3515 A71-42599

Semiannual variation in F 2 layer peak height and critical frequencies at midlatitudes, considering vertical ionospheric drifts effects
23 p3665 A71-42973

Rocket and radio wave wind profiles from 60 km to E region near 53N, presenting partial reflections and zonal winds time cross section
23 p3700 A71-43343

Atmospheric wind velocity time variations at 80-100 km altitudes from ionospheric drift data, finding planetary oscillation periodicities relationship to solar activity cycle
24 p3822 A71-44349

IONOSPHERIC ELECTRON DENSITY

Electron density variations in ionospheric layers of different recombination types
01 p0074 A71-11080

Photoelectron fluxes and energy spectra in ionosphere for predawn and sunlit atmospheres, taking into account elastic and inelastic collisions
01 p0147 A71-11506

Ionospheric columnar electron content perturbation by plane atmospheric waves
01 p0077 A71-11509

Electron density early time increase after artificial ionospheric heating, discussing F region recombination chemistry temperature dependence
01 p0040 A71-11532

F region electron concentration distribution during global magnetic storm, latitude and diurnal variation effects and radio wave reflections diffusion
02 p0243 A71-11770

F region electron density profile changes during negative magnetic bays, deriving ionization drift from continuity equation
02 p0243 A71-11771

Ionospheric electron concentration measurement by bifrequency dispersion interferometer on Luna 14 orbiter
02 p0244 A71-11911

Ionospheric electron content at mid to high latitudes from satellite and station data, discussing possible solar control
02 p0244 A71-11960

Ionospheric electron content distribution from satellite transmission data, discussing ionospheric irregularities and electron production rates
02 p0245 A71-11966

Ionospheric electron concentration enhancement at different heights during solar flare, using incoherent scatter radar technique
02 p0300 A71-12471

Ionospheric electron collision frequency and concentration height distribution during annular solar eclipse of 20 May 1966
03 p0407 A71-13378

D region electron density time variations, using partial radio reflection technique during solar eclipse of 20 May 1966
03 p0407 A71-13379

Ionospheric Lyman alpha intensities and electron and positive ion densities during solar eclipse of 20 May 1966, discussing recombination model
03 p0407 A71-13380

Ionospheric photoelectron exchange at magnetic conjugates, considering electron density and impact ionization by inelastic collisions
03 p0408 A71-13381

Upper ionosphere electron concentration enhancement in polar cap from satellite probe measurements
03 p0408 A71-13385

Midlatitude topside ionosphere electron density diurnal variations, discussing F 2 layer seasonal anomaly altitudinal extension
03 p0409 A71-13390

Ionospheric measurements by rocket-borne HF capacitance probe during solar flare of 26 February 1969, determining electron density vertical stratification
03 p0416 A71-14032

Black Brant rocket measurement of PCA event at Churchill, Canada on 19 November 1968, discussing electron density and alpha particle and proton flux
03 p0417 A71-14038

Ionospheric electron production, slowing down and disappearance processes, considering collisions with atmospheric constituents
03 p0417 A71-14072

Ionospheric electron content persistent longitudinal anomalies observed by low orbiting satellites
03 p0421 A71-14541

Lower ionosphere electron density changes with solar zenith angle during active sun year
04 p0583 A71-15213

Mesosphere and lower thermosphere probing, noting electron and ion densities distributions, collision frequencies and ionospheric loss rates
05 p0740 A71-16427

Ionospheric electron content measurement from Faraday fading of Explorer 22 satellite transmissions during low and high solar activity
05 p0741 A71-16444

Ionospheric total electron content determination by Faraday findings of 40 MHz radio transmissions from Explorer 22 satellite, considering seasonal variations
05 p0741 A71-16445

Average electron density profiles for quiet and disturbed topside ionosphere at high latitudes, tabulating profile numbers
05 p0743 A71-17005

Daytime ionosphere rocket observations at Antarctica, examining electron density profiles
05 p0743 A71-17006

D region electron density profile relation to radio wave absorption frequency dependence
05 p0746 A71-17204

Electron density profiles correction allowing for ionospheric interlayer ionization
05 p0746 A71-17206

Vertical electron density profiles correction coefficients, noting computational work decrease and F region frequency discrepancy due to ionization
05 p0746 A71-17207

Solar wind velocity relationship with F 2 layer electron density
06 p0950 A71-17991

Electron concentration disturbances in outer ionosphere and F 2 maximum on daylight side during magnetic storm
06 p0894 A71-18257

F layer absence and nonuniform horizontal electron concentration of nighttime ionosphere at high latitudes, using Alouette 1 sounding
06 p0894 A71-18258

E layer electron concentrations, effective recombination coefficient and ionization sources during solar eclipse, noting soft X radiation intensity
06 p0894 A71-18260

Vertical electron density profile variations during ionospheric perturbations in years of solar activity maximum and minimum
06 p0895 A71-18277

Electron concentration vertical profile in ionosphere as function of altitude of radio wave reflection and group refraction and velocity characteristics
06 p0895 A71-18278

Sporadic ionization occurrences nighttime observation in auroral E region, describing vertical electron concentration profile
06 p0895 A71-18280

Ionospheric total electron content specification for satellite transponders time delay error reduction
07 p1095 A71-19002

Total electron content from ionospheric Doppler shift data, discussing usable frequencies
07 p1096 A71-19005

Plasmasphere total columnar electron content up to plasmapause, describing various measurement methods
07 p1096 A71-19006

Columnar electron content measurements by geostationary satellites, discussing research in developing countries for cost reduction
07 p1096 A71-19007

Ionospheric columnar electron content, describing data processing and analysis programs
07 p1096 A71-19008

Ionospheric electron content semiannual variation analysis based on satellite and ground station observations
07 p1096 A71-19009

Second difference of phase shift method for measuring ionospheric electron density
07 p1096 A71-19013

Ionosphere and magnetosphere daily electron content change measurement, describing satellite beacon experiment
07 p1096 A71-19017

Total electron content over New Delhi by satellite beacons, discussing solar activity effects, electron production rates and seasonal variations
07 p1097 A71-19019

Solar half cycle total ionospheric electron content and slab thickness diurnal and seasonal variations from Syncom 3 beacon signal
07 p1097 A71-19020

Ionospheric electron mean content 1964-1969 from density, ionization, slab thickness and solar flux diurnal and equinoctial peaks
07 p1097 A71-19025

Ionospheric columnar electron content using differential radio refraction measurements from satellite observation station
07 p1097 A71-19026

Ionospheric electron content from Faraday rotation measurements of earth satellite and deep space probe
07 p1098 A71-19029

Upper atmosphere H atoms concentration maxima and minima from topside to bottomside ionospheric electron contents ratio, using coupled continuity and thermal equations
07 p1098 A71-19031

Ionospheric electron mean content by polar satellites, using combination of Doppler differential and Faraday rotation hybrid methods
07 p1206 A71-19032

Radio signal receiving system design for group delay experiments with geostationary ATS-F for ionospheric and magnetospheric electron content
07 p1206 A71-19033

Ionospheric electron content observation by ATS-3 radio signals, noting gravity waves effect
07 p1098 A71-19034

Ionospheric electron density irregularity effects on communication satellite scintillation in auroral zone, using Doppler and Faraday measurements
07 p1098 A71-19035

Lower ionosphere electron density profile diurnal, seasonal and 11 year variations, tabulating calculated numerical values for 45-70 km altitudes
07 p1099 A71-19383

Quasi-exponential model of electron vertical profile in D region for aeronomic and ionizing radiation characteristics during solar flare of 30 October 1969
07 p1195 A71-19393

Natural aerosols effects on atmospheric electron content, comparing theoretical prediction with experiments on artificial aerosols in D region
07 p1100 A71-19404

Model of large ionospheric electron density discontinuities, emphasizing horizontal asymmetry association with observed east-west refraction asymmetry
07 p1100 A71-19405

Ionospheric low energy electron and proton fluxes near equator from Isis 1 satellite soft particle spectrometer observations, considering energy spectra and pitch angle distribution
07 p1187 A71-19679

Rocket-borne HF capacitance probe for measuring ionospheric electron density profile
07 p1116 A71-20498

High energy electron background flux in F 2 layer, discussing grouped particle acceleration
08 p1354 A71-21012

Electron continuity equation for lower F 2 layer near dip equator, estimating photoionization and recombination rates
08 p1278 A71-21203

Ionospheric electron density and reflection height during sudden phase anomaly in solar X-ray flare
08 p1355 A71-21222

E layer near solar culmination relaxation, determining ion and electron concentration variations
08 p1286 A71-21855

F 2 layer critical frequency and maximum electron concentration statistical characteristics for predicting SW propagation conditions
09 p1435 A71-22427

E region additional ionization source during solar activity maximum, analyzing ion production function and electron concentration
09 p1435 A71-22440

E region electron concentration profiles, using ground sounding equipment allowing accurate signal reflection altitude measurements
09 p1435 A71-22441

Lower ionosphere electron concentration space-time variations relation to ionization source intensity fluctuations based on rocket observations and ground sounding data
09 p1435 A71-22442

Ionospheric electron density profiles at various altitudes determined by HF impedance probe method
09 p1436 A71-22575

Ion and electron drift due to F layer wind and associated polarization fields, causing equatorial atmosphere eastward rotation
09 p1438 A71-22979

Ionospheric propagation forecasting as function of solar and magnetic activity conditions for maximum usable communications frequencies, using F2 layer peak electron density
10 p1575 A71-23865

Average electron density profiles for forecasting MF sky waves field strengths, using nocturnal ionospheric measurements
10 p1575 A71-23866

Ionospheric computer model, describing electron and ion densities in middle latitudes as function of latitude, longitude, altitude, season, time and solar activity
10 p1577 A71-24290

Geomagnetic field inclination determination by incoherently scattered signal Faraday rotation calibration and simultaneous ionosonde measurements of ionospheric electron density
10 p1605 A71-24798

Daytime lower ionosphere electron density profiles over equator, using rocket-borne Langmuir and plasma noise probes
10 p1606 A71-24913

IONOSPHERIC ELECTRON DENSITY

- Midlatitude D region considering electron concentration height distribution, ionization process and solar activity effects 10 p1606 A71-24916
- D and E region electron density height distribution profiles, using multifrequency absorption data 10 p1606 A71-24920
- Midlatitude F2 region diurnal variations in peak electron density critical frequency and height, noting electric field and ion drag effects 10 p1606 A71-24921
- Electric field, neutral air winds and atmospheric composition changes effects on electron concentration diurnal variation in midlatitude F layer 10 p1607 A71-24922
- Neutral air winds and ionospheric continuity equation, calculating midlatitude electron concentration longitudinal variations 11 p1754 A71-25605
- Storm time variations of F 2 layer electron concentration and critical frequency at Australasian stations 11 p1754 A71-25606
- Midlatitude F layer electron concentration increase during magnetic storm, assuming auroral zone heating of horizontal winds 11 p1754 A71-25607
- Midlatitude ionosphere electron production rates during quiet solar activity, deriving seasonally varying electron density profiles 11 p1755 A71-25609
- Meteorological, geomagnetic and extraterrestrial variations of cosmic ray layer electron production rate in lower D region 11 p1816 A71-25610
- High latitude F region electron density irregularity measurements, using rocket-borne impedance probe 11 p1755 A71-25617
- VLF propagation in low latitude ionosphere from FR-1 satellite observations, obtaining electron density model of equatorial anomaly 11 p1755 A71-25642
- Integral equations inversion in geophysics, discussing ionospheric profile from electron content and Faraday rotation measurements 11 p1756 A71-25645
- Numerical integration of unsteady continuity equation for electron-ion gas concentration distribution in F 2 region 11 p1757 A71-25770
- Midlatitude topside ionospheric electron density mean diurnal and seasonal variations from Alouette 1 satellite observation 11 p1757 A71-25784
- Nocturnal large ionospheric disturbances over Ashkhabad, obtaining relationship to electron content 12 p1901 A71-27120
- Pitch angle distribution effects of auroral electrojet on scattering and absorption of fast precipitated electrons in upper atmosphere, using computerized Monte Carlo technique 13 p2119 A71-27794
- Sunrise behavior of midlatitude topside ionosphere at low sunspot numbers from Alouette 1 electron density and plasma scale height profiles 13 p2055 A71-27920
- Lower ionospheric plasma frequencies height determination for actual motions, relating periodic variations to spatial electron density structure 13 p2029 A71-28003
- Ionospheric electron concentration and temperature data from Langmuir probe on Explorer 22, discussing magnetic storms effects 13 p2058 A71-28197
- Ionospheric electron concentration measurement by bifrequency dispersion interferometer on Luna 14 orbiter 13 p2058 A71-28198
- D region electron density profile relation to radio wave absorption frequency dependence 13 p2059 A71-28259
- Electron density profiles correction, taking into account ionospheric interlayer ionization 13 p2060 A71-28261
- Vertical electron density profiles correction coefficients, noting computational wave decrease and F region frequency discrepancy due to ionization 13 p2060 A71-28262
- Electron density profile determination in D region based on frequency dependence of radio waves absorption, discussing lower ionosphere anomalous ionization 13 p2061 A71-28539
- Log normal random fluctuations of ionospheric electron concentration in F region from vertical sounding and incoherent scatter data 13 p2061 A71-28553
- Electron concentration profiles in D region from radio wave partial reflection coefficients 13 p2030 A71-28558
- Ionospheric ion formation and neutralization reaction rate coefficients determination by fitting rocket measured electron concentration profiles with computer generated profiles 13 p2062 A71-28560
- Midlatitude daytime ionospheric electron density profile during low solar activity based on rocket sounding data 14 p2228 A71-29535
- Midlatitude ionosphere dusk sector total electron content during geomagnetic storm time increase 14 p2229 A71-29666
- Wind transport effect on redistribution of ionization produced by geocoronal and interplanetary UV emissions in nighttime ionosphere, using electron density sounding rocket data 14 p2230 A71-29709
- Vertically incident radio waves reflection from horizontally stratified ionosphere with random electron density irregularities 14 p2192 A71-29718
- Spread F ionospheric electron density irregularities and satellite scintillation over polar cap 14 p2300 A71-30043
- Diurnal variations of electron number density against height in lower ionosphere over Resolute Bay, relating to solar proton events 14 p2300 A71-30044
- Faraday rotation of Transit 4A satellite signals recorded at three stations within Southeast Asian equatorial zone, showing latitudinal variation of ionospheric electron content at sunspot minimum 14 p2325 A71-30249
- Electron density irregularities and frequency deviation patterns role in equatorial electrojet 14 p2325 A71-30352
- Ionospheric electron density variation at neutral acoustic gravity wave passage from continuity equation, noting ionization in wake 14 p2236 A71-30355
- Midlatitude D region electron density winter variability causes consideration based on enhancements, absorption and ionization changes data during stratospheric warming 14 p2237 A71-30944
- F 2 layer peak electron density diurnal and seasonal variations, noting geomagnetic latitude and solar activity effects 15 p2394 A71-31427
- Simultaneous ionospheric electron density measurements from Isis satellite topside and incoherent scatter soundings 15 p2394 A71-31428
- Satellite skin potential and errors in electron density and temperature determinations by Langmuir probe measurements, using model ionosphere 15 p2398 A71-31768
- Traveling ionospheric disturbances at magnetic equator, determining electron concentration profiles by incoherent scatter radar 15 p2398 A71-31771
- Daytime rocket and ground based radar Thomson scatter measurements of electron densities and temperatures in lower ionosphere 15 p2399 A71-31772
- Topside ionosphere structure in high latitudes, discussing electron density profile, corpuscular radiation ionizing effects, polar peak and trough 15 p2400 A71-32349
- Total electron content and F region plasma frequencies height during magnetic storm of 8 March 1970 16 p2563 A71-33393
- Reflected short wave signal frequency shift due to reflecting ionospheric layer movement and electron concentration changes, considering oblique incidence on isotropic and anisotropic layers 16 p2542 A71-33484
- Daytime electron density profiles above 90 km from Doppler radar measurements by rockets launched from Southern Hemisphere site 16 p2567 A71-33779
- F 2 and E layers peak electron densities semiannual variations, suggesting association with solar activity and charged particles penetration 16 p2568 A71-33785
- Midlatitude E region electron density profile data for various solar activity levels, investigating formation theory and atmospheric models 16 p2570 A71-33822
- Midlatitude nighttime F region electron concentration enhancements as downward diffusion flux from protonosphere induced by ionospheric substorm associated electric fields 16 p2573 A71-33958
- Atmospheric electron density irregularities observations, using Alouette 2 satellite electrostatic probe 16 p2574 A71-33973
- Ionospheric electron concentration and proton flux rocket-borne measurements during nighttime PCA event, discussing atomic oxygen role in recombination processes 16 p2575 A71-33974
- Traveling ionospheric disturbances due to gravity wave interactions during solar eclipse of 7 March 1970, confirming electron content variations from ATS 3 polarization data 16 p2575 A71-33975
- Upper ionosphere electron density scale height data, noting conjugate point sunrise heating effects from Alouette 1 data 17 p2731 A71-34311
- D region winter anomaly causes from coordinated rocket measurements, discussing electron density profiles and electron-ion recombination 17 p2731 A71-34312
- Low latitude topside plasma temperature, electron content and ion production/loss rates during sunspot minimum to maximum 17 p2731 A71-34314
- Ionospheric electron content measurements from satellite signals Faraday rotation, criticizing graphical procedure for ambiguity reduction 17 p2732 A71-34322
- Scintillation fading of signals in SHF band due to electron density irregularities in F region 17 p2699 A71-34624
- Impulsive time variation plane wave reflection from ionospheric sea squared electron density profile comparing full wave and WKB solutions 17 p2701 A71-34765
- Rocket-borne RF capacitance probe design for determining lower ionospheric electron densities 18 p2921 A71-36367
- Mean ionospheric height selection effect on total electron content latitudinal variation determination 19 p3047 A71-37367
- D region electron densities from HF radio waves ionospheric backscatter based on hypothesis of refractive index stochastic fluctuations 19 p3048 A71-37372
- Lower ionosphere electron density profile diurnal, seasonal and 11 year variations, tabulating calculated numerical values for 45-70 km altitudes 19 p3052 A71-37808
- Quasi-exponential model of electron vertical profile in D region for aeronomic and ionizing radiation characteristics during solar flare of 30 October 1969 19 p3127 A71-37817
- Natural aerosols effects on atmospheric electron content, comparing theoretical prediction with experiments on artificial aerosols in D region 19 p3053 A71-37828
- Model of large ionospheric electron density discontinuities, emphasizing horizontal asymmetry association with observed east-west refraction asymmetry 19 p3053 A71-37829
- Ionospheric electron density irregularities measurement, comparing scintillation, spread F and electrostatic probe methods 19 p3128 A71-38035
- Ionospheric E region nighttime model from rocket soundings, obtaining electron density profiles by Langmuir probe and wind measurements by glowing vapor release 19 p3055 A71-38036
- Short path VLF phase and amplitude measurements during stratospheric warming in February 1969, discussing D region electron density changes 19 p3018 A71-38040
- Electron concentration and collisions number fluctuations effect on D region profiles based on radio waves partial reflection data 19 p3057 A71-38365
- Magnetic storm effect on integral electron content in F 2 layer and in outer ionosphere 19 p3058 A71-38383
- F 2 region electron density spatial and temporal distribution, investigating plasma vertical drift effects 19 p3058 A71-38384
- Ionospheric electron concentration and temperature measurements, describing rocket-borne asymmetrical Langmuir probe 19 p3067 A71-38631
- High energy electron background flux in F 2 layer, discussing grouped particle acceleration 20 p3280 A71-39592
- Mars ionosphere radio wave absorption integral coefficients, studying electron concentration and electron/gas molecular collisions frequency vertical profiles 20 p3297 A71-39629
- D region electron density profiles and ionization models in terms of XUV radiation and minor constituents NO and oxygen, using ground and space measurements 20 p3224 A71-39713
- Midlatitude ionospheric irregularities, electron density vertical distribution and electron and ion temperature variation measurements, during solar eclipse of 22 September 1968 20 p3224 A71-39716
- Gravity waves effects on ionospheric columnar electron content data, using Faraday rotation and differential Doppler measurements of geostationary satellite radio signals 20 p3224 A71-39717
- Midlatitude ionospheric electron density and electron temperature measurements by rocket experiments, noting diurnal and seasonal variations 20 p3224 A71-39718

Upper ionospheric plasma measurements by gyro plasma probe equipped Lambda rocket, deducing electron density profile from plasma resonance effects
20 p3224 A71-39721

Ionospheric low hybrid resonance measurements by rocket-borne quadrupole probe, deriving electron density and effective ion mass along trajectory
20 p3224 A71-39722

Nighttime equatorial E region ionization and electron density gradient irregularities, noting cross field instability with rocket-borne Langmuir probes
20 p3225 A71-39727

Cosmos 142 and 259 experiments on ionospheric VLF propagation, discussing diurnal variations of daytime electron density
20 p3197 A71-39743

Electric fields effects on ions temperature and electron densities of auroral ionosphere
20 p3228 A71-39844

Polar cap magnetic variation mechanism based on electric field aligned continuity of Hall current auroral electrojets, noting ionospheric electron density gradients effects
20 p3230 A71-39862

Electron content spatial and temporal variation during ionospheric storm of 8 March 1970 after total solar eclipse
20 p3232 A71-39899

E region electron density and critical frequency seasonal anomaly, allowing for sun zenith angle variations, sunspot activity and earth orbit eccentricity
21 p3371 A71-40034

Sun-earth distance and earth orbital eccentricity effect on E region peak electron density, discussing Chapman-like model
21 p3372 A71-40035

Solar cycle effects on E region peak electron density, correlating sunspot number by regression analysis
21 p3372 A71-40036

Peak electron density variations during midlatitude F region storm, investigating electrodynamic drift effects
21 p3372 A71-40037

E region electron density isopleths height correlation with atmospheric pressure variations, noting sympathetic isobaric surface movements in upper stratosphere
21 p3372 A71-40038

Internal gravity wave parameters calculation from total electron content short term variations, comparing ionospheric disturbance models
21 p3373 A71-40049

Ionospheric electron density measurements by differential Doppler and Faraday effects, using coherent radio signals of artificial earth satellites
22 p3508 A71-41526

Numerical integration of unsteady continuity equation for electron-ion gas concentration distribution in F2 region
22 p3532 A71-41538

Midlatitude topside ionospheric electron density mean diurnal and seasonal variations from Alouette 1 satellite observation
22 p3532 A71-41552

Jovian ionospheric electron and ion densities and temperatures, considering radiative association role
22 p3603 A71-42181

Ionospheric responses to solar flares, correlating sudden frequency deviations with sudden total electron content enhancement
22 p3592 A71-42222

Ionospheric small scale electron content irregularities and electrostatic plasma instabilities correlated with electrojet current intensity
22 p3535 A71-42223

Comparative north and south polar F layer electron density dependence on universal time and latitude, using ionosonde data
23 p3669 A71-43172

Solar flare induced E and F regions electron density enhancement observation by Thomson scatter, noting relationship to EUV ionizing radiation
23 p3721 A71-43173

Periodic and isolated /nonperiodic/ ionospheric electron content fluctuations showing noon and midnight peaks and winter increase at high latitudes
23 p3670 A71-43180

Premidnight asymmetry in directional 40 keV ionospheric electron flux profiles in magnetic local time observed on Azur satellite
23 p3721 A71-43185

Ionospheric electron density measurement by K-9M rocket, comparing VLF Doppler with Langmuir probe methods
23 p3671 A71-43366

Sporadic E layer observation by reference electrode of electron temperature probe on sounding rocket, determining electron density below 85 km in D region
23 p3671 A71-43367

Earth atmosphere gas composition and electron density variations at F region lower boundary explained by stratospheric explosive and diffusive warmings effect on critical frequency
23 p3671 A71-43378

F region ion and electron temperature relationship to electron density, examining incoherent scatter data and physical processes
23 p3672 A71-43977

Daytime photoelectron energy distribution and electron gas heating in F region as function of height and solar cycle variations
23 p3673 A71-44003

Ionospheric integral electron concentration data from Elektron 1 and 3 satellites, using coherent radio wave measurements
24 p3866 A71-45028

Auroral charged particle fluxes electrodynamic interaction with atmosphere, determining ion formation rate and electron concentration and conductivity
24 p3866 A71-45032

Multicomponent meteoritic composition effects on meteor trails radio wave reflections, obtaining ionospheric electron concentration distribution
24 p3804 A71-45033

Hysteresis effect at solar cycle maximum for midlatitude E layer electron density response to solar activity
24 p3824 A71-45125

Microwave radio signals refraction angles and group delay times for biexponential model of ionospheric electron density profile
24 p3805 A71-45253

Ionospheric and neutral atmospheric temperature profile, composition and electron density and energy measurements by MR-12 rocket
24 p3824 A71-45310

Vertical electron concentration and temperature profiles at 80-170 km measured by rocket launched on 10 July 1969 at Volgograd
24 p3824 A71-45322

IONOSPHERIC F-SCATTER PROPAGATION
VHF radar measurements of scattering by field aligned irregularities associated with equatorial spread F
03 p0420 A71-14532

Ionospheric propagation forecasting as function of solar and magnetic activity conditions for maximum usable communications frequencies, using F2 layer peak electron density
10 p1575 A71-23865

IONOSPHERIC HEATING
Ionospheric modification of F region through high power HF transmitter heating
01 p0040 A71-11529

Early phase model of F region heating and hydrodynamic expansion by deviative absorption of radio waves
01 p0040 A71-11530

F region reflected radio wave heating effect, considering electron temperature, collision frequency and heat conductivity
01 p0040 A71-11531

Electron density early time increase after artificial ionospheric heating, discussing F region recombination chemistry temperature dependence
01 p0040 A71-11532

F region electrons heating by RF energy at or near ionospheric plasma frequency, detecting temperature changes via optical nightglow intensity variations
01 p0040 A71-11533

Ionospheric modification by electrons radiant heating, discussing effects on 1.27 micron radiation
01 p0078 A71-11534

F region ionospheric modification by heating from high power HF ground based transmission, discussing ionosonde observations
01 p0078 A71-11535

Ionospheric heating self amplification and spread F triggering by disturbances, calculating ray paths through model ionospheric irregularities
01 p0078 A71-11536

Ionospheric F layer modification by artificial heating, using radio echo detection of electron temperature changes
01 p0040 A71-11537

Ionosphere artificial Joule heating by RF energy, deriving expressions for deposition function frequency dependence
01 p0040 A71-11538

Plasma instabilities role in ionospheric heating and radio wave attenuation
06 p0888 A71-17288

Radio wave ionospheric heating effect on absorption of probing waves of different polarization
06 p0888 A71-17289

ELF atmospherics pulse trains recordings at widely separated stations for spectral amplitude ratio differentials, using lightning and ionospheric heating mechanisms
09 p1489 A71-23445

Ionic and thermal structure model of daytime Venus ionosphere with solar wind heating based on Mariner 5 flyby mission
14 p2305 A71-29661

Midlatitude D region electron density winter variability causes consideration based on enhancements, absorption and ionization changes data during stratospheric warming
14 p2237 A71-30944

Solar wind torque on geomagnetic cavity by rotational unipolar induction currents, including Joule heating of ionospheric plasma and directional magnetic fields
15 p2474 A71-31773

Undisturbed ionospheric ion and electron temperature warming, investigating frictional heating effect by neutral winds
19 p3048 A71-37399

Ionospheric heating Q calculation of electron gas, evaluating heat inflow at various altitudes
20 p3281 A71-39725

Daytime photoelectron energy distribution and electron gas heating in F region as function of height and solar cycle variations
23 p3673 A71-44003

IONOSPHERIC ION DENSITY
Photoionization coefficients and photoelectron impact excitation efficiencies in daytime ionosphere, noting role in dayglow
01 p0077 A71-11515

Polar region semitransparent sporadic ionospheric layers nighttime temporal and cyclic ionization variations, determining solar activity effects and corpuscular stream densities by ionogram
02 p0243 A71-11767

Polar ionospheric auroral zone ionization, obtaining ion production function for single electron and proton flux
02 p0244 A71-11772

Solar eclipse of 7 March 1970 ionospheric ionization observations via satellites, correlating data with Wallops Island vertical ionograms
03 p0406 A71-13174

Metastable atomic oxygen ion production in F region plasma due to photoionization by solar XUV radiation
03 p0462 A71-13271

Ionospheric Lyman alpha intensities and electron and positive ion densities during solar eclipse of 20 May 1966, discussing recombination model
03 p0407 A71-13380

Ionospheric electron and ion temperatures and charged particle concentration from satellite and space probe observations
04 p0640 A71-14775

Satellite ion energy analyzer with onboard data reduction for ionospheric ion temperature and concentration measurement with high temporal resolution
05 p0755 A71-17139

Atmospheric ion concentration at 100-200 km related to solar zenith angle, describing diurnal and vertical behavior by photochemical theory
05 p0744 A71-17182

Indeterminacy interval reduction for ionospheric reaction rate constants by imposing supplementary condition on NO/oxygen molecular ion concentrations ratio
06 p0894 A71-18259

Ionization rate experimental profiles during maximum solar activity compared with calculations, showing additional source of ionization in E region
06 p0895 A71-18272

Nitrogen dioxide and molecular oxygen ions densities in lower ionosphere as function of solar corpuscular radiation
06 p0895 A71-18275

F2 layer noon time ionization seasonal fluctuations, considering dependence on geographical longitude and latitude and solar activity levels
07 p1098 A71-19382

E layer near solar culmination relaxation, determining ion and electron concentration variations
08 p1286 A71-21855

Polar ionosphere ion composition measurement by meteorological rocket-borne RF mass spectrometer
09 p1435 A71-22444

Upper atmospheric ion composition during Orionid meteor shower activity by rocket-borne RF mass spectrometer
09 p1437 A71-22680

Ionospheric computer model, describing electron and ion densities in middle latitudes as function of latitude, longitude, altitude, season, time and solar activity
10 p1577 A71-24290

Polar H ion plasma escape from ionosphere into magnetospheric tail effect on plasmopause formation, using hydrodynamic approximation
11 p1756 A71-25756

Sporadic E wind shear theory, discussing time variation in metallic ion content
13 p2055 A71-27923

Atmospheric ion concentration at 100-200 km related to solar zenith angle, describing vertical and diurnal density pattern by photochemical theory
13 p2059 A71-28239

D region negative ion densities in chemical equilibrium based on electron density observation, noting role of ozone and carbon dioxide
14 p2228 A71-29533

Turbopause oxygen/nitrogen decrease effect on ion and neutral composition changes in thermospheric region during magnetic storm, using simultaneous ionospheric and atmospheric equations
14 p2229 A71-29665

IONOSPHERIC NOISE

Polar ionospheric plasma transport, predicting ion density profiles from ionospheric processes models consistent with polar wind theory 14 p2234 A71-30039

Supersonic plasma flow effects on neutral hydrogen, helium and charged particle density and velocity profiles in polar ionosphere 14 p2234 A71-30040

Cluster ions concentration and nitric oxide in mesosphere D region, considering electron density profiles 15 p2394 A71-31430

Thermospheric circulation and temperature changes due to global scale winds flow through F region ionization anomalies, using time independent dynamic model 16 p2571 A71-33836

Lower thermosphere and ionosphere upper limits of positively ionized water molecules number density, considering desorption and recombination processes 16 p2571 A71-33842

Striated irregularities in ionospheric ion clouds, using model of ionospheric conductivity profile 16 p2573 A71-33957

Sporadic E layer enhancement by horizontal transport within layer, considering gravity waves interaction effect on ion density horizontal redistribution 16 p2573 A71-33960

D and E regions advances during 1967-1971 covering ionic composition, electron density profile at various latitudes, hours and seasons during eclipses and winter anomalies 17 p2732 A71-34464

F 2 layer noontime ionization seasonal fluctuations, considering dependence on geographical longitude and latitude and solar activity levels 19 p3052 A71-37807

Mass spectrometric measurements of negative ion concentration in D and lower E regions 19 p3127 A71-38031

Mass spectrometric measurement of negative ion concentration in nighttime D region 19 p3128 A71-38033

Atmospheric composition and temperature effects on F 1 region ion concentration structure from 140 to 220 km for low solar activity conditions 19 p3058 A71-38382

Nighttime E region ion composition and concentration profiles, using rocket sounding 19 p3061 A71-38628

Double scattering of plasma stream in bithermal ionosphere, noting ion density perturbation under external magnetic field 20 p3272 A71-38748

Lower thermospheric density and molecular nitrogen partial density rocket measurements, obtaining neutral gas temperature vertical distribution and ion density profile 20 p3222 A71-39699

Polar ionospheric ion density enhancement correlation to low energy electron precipitation from observations by polar satellite 20 p3231 A71-39888

Jovian ionospheric electron and ion densities and temperatures, considering radiative association role 22 p3603 A71-42181

Incoherent scatter observations of ion concentration and plasma line in F 1 region 23 p3670 A71-43188

Mass spectrometer measurements of hydrogen, helium, nitrogen, oxygen and nitrogen oxide ion concentrations vertical profiles in ionosphere at midlatitudes 24 p3824 A71-45311

IONOSPHERIC NOISE

NT WHISTLERS

Electromagnetic field measurements for continuous noise sources and traversed ionospheric region parameters, using ground, rocket and satellite techniques 09 p1440 A71-23629

Lower ionosphere effects on ELF noise in Schumann resonances range 14 p2203 A71-30961

Radio wave propagation in ionosphere, measuring plasma frequency, cyclotron cut-off and noise level 15 p2373 A71-32443

IONOSPHERIC PROPAGATION

NT IONOSPHERIC F-SCATTER PROPAGATION

Short wave broadcasting and ionospheric reflection during solar eclipse of 7 March 1970, relating to nighttime free electron distributions 01 p0151 A71-10119

Proton Flare Project 1969 observation of polar cap ionospheric disturbance due to proton event by VLF propagation phase measurement 01 p0073 A71-10289

Subsidiary resonance response time decay behavior in ionosphere, showing occurrence of principal resonances at higher orders 01 p0077 A71-11523

HF radio wave Doppler shift by ionosphere effect in retransmitted and backscatter signals 01 p0040 A71-11524

Lower ionosphere partially reflecting regions, describing vertical thickness distribution based on 1.75 MHz backscatter soundings 01 p0040 A71-11525

Auroral absorption of HF radar waves over high latitude ionospheric paths 01 p0041 A71-11610

Space-time structure of ionospheric regions of anomalous radio wave absorption during auroras, discussing ionization region 02 p0243 A71-11765

Ionospheric absorption of radio waves reflected from sporadic E layer, noting attenuation frequency dependence 02 p0211 A71-11768

Riometers accuracy and stability, considering measurement error of ionospheric radio wave absorption 02 p0247 A71-11774

Ionospheric absorption at solar maximum and minimum, comparing riometer measurements with ray tracing calculations and electron density, collision frequency or temperature profiles 02 p0245 A71-11962

ELF and VLF radio attenuation for propagation below inhomogeneous isotropic ionosphere with realistic vertical variation models for electron density and collision frequency 02 p0212 A71-11964

Ozone screening heights from sunrise effects on D region VLF wave reflection 02 p0212 A71-11968

Ionospheric and tropospheric effects on differential phase path in very long baseline interferometry, using ray tracing computer program 02 p0251 A71-12331

Satellite tracking by radio direction finder, noting periodic azimuth deviations related to ionospheric Faraday effect 03 p0377 A71-13169

Ionospheric nondeviative absorption diurnal variation describing function suitable for computer methods 03 p0378 A71-13315

Nondissipative focusing and ionospheric reflecting effects on MF radio wave absorption measurements for magnetically quiet and disturbed periods 03 p0409 A71-13391

Diurnal and seasonal variations of cosmic noise absorption at critical frequency of F 2 region 03 p0379 A71-13815

Conjugate observations of ionospheric absorption associated with electron precipitation during sudden commencement of magnetic storm 03 p0419 A71-14520

Lower F region ionospheric response to internal gravity waves as function of azimuth of wave propagation, noting anisotropy 03 p0420 A71-14534

Beam-plasma mechanism of very long delayed radio echoes from ionosphere 03 p0381 A71-14552

CW sounding with HF adaptive control for data transmission with ionospheric phase error 04 p0552 A71-15145

MF, LF and VLF ionospheric radio wave propagation theory using spherical wave functions for computer simulation 04 p0552 A71-15215

Vertical and horizontal VLF fields excited by dipoles of arbitrary orientation and elevation for nighttime ionosphere 04 p0552 A71-15216

Transient pulse plane wave reflection from ionospheric model with linear electron density profile 04 p0553 A71-15218

Dipole antenna array coupling for circularly polarized radio waves amplitude fluctuations reflected from ionosphere at vertical incidence 05 p0738 A71-16216

Artificial satellite HF radio wave ionospheric guided propagation, considering ray tracing based on geometric-optics treatment 05 p0720 A71-16229

Ionospheric absorption measurements noting diurnal, seasonal and solar cycle variations 05 p0740 A71-16429

Lower ionospheric cosmic noise absorption at 28.6 MHz, examining diurnal variations 05 p0740 A71-16430

F region cosmic noise absorption at 20-30 MHz over Delhi, examining diurnal, seasonal and solar cycle variations 05 p0808 A71-16431

Lunar oscillations in ionospheric absorption measurements, noting tides in f-min during high sunspot years 05 p0740 A71-16434

Ionospheric drift measurements during solar cycle based on fading of radio waves reflected from E and F regions 05 p0741 A71-16437

D region electron density profile relation to radio wave absorption frequency dependence 05 p0746 A71-17204

Plasma instabilities role in ionospheric heating and radio wave attenuation 06 p0888 A71-17288

Radio wave ionospheric heating effect on absorption of probing waves of different polarization 06 p0888 A71-17289

Ionospheric absorption winter anomaly observation based on Loran-A pulse signals during IQSY, noting diurnal variation 06 p0889 A71-17685

Magnetospheric sudden impulses amplitude and rise time distributions observation byOGO 3 and 5 satellites 06 p0889 A71-17686

Ray tracing near reflection level in ionosphere, considering magnetic field effect 06 p0927 A71-17687

Transionospheric ranging error correction by second difference of phase shift method 06 p0867 A71-17714

Antarctic terrain dielectric and loss properties effects on VLF attenuation and phase constants of earth-ionosphere waveguide paths over ice covered regions 06 p0868 A71-17733

Solar X-ray control of lower ionospheric radio wave absorption determined from Solrad 9 and Panska Ves Observatory data 06 p0892 A71-17921

Irregularities heights in ionospheric refractivity responsible for radio-satellite scintillation from spaced receiver experiments at midlatitude and subauroral locations 06 p0868 A71-17985

Ionospheric refraction during radio wave propagation using space diversity recordings of Faraday and Doppler effects for coherent signals from geophysical rockets 06 p0894 A71-18256

Group delay times criterion of multibeam propagation of ionospheric radio echoes for communications systems 06 p0869 A71-18281

Total electron content from ionospheric Doppler shift data, discussing usable frequencies 07 p1096 A71-19005

Low angle signal strength enhancements from ionospheric beacon satellite BE-B transmissions 07 p1096 A71-19018

Ionospheric error correction in distance measurements involving satellites, noting simultaneous differential Doppler and Faraday signal measurements 07 p1097 A71-19023

Second order phase path differences for Faraday rotation and dispersive Doppler shift in transionospheric propagation 07 p1097 A71-19027

Small scale ionospheric irregularities from satellite radio signals fluctuations, using frequency scintillation measurements 07 p1060 A71-19037

Polarization fluctuations of radio waves reflected from ionosphere E and F layers, describing radio polarimeter and preliminary measurement results 07 p1061 A71-19384

Physical factors affecting atmospheric and electromagnetic signal propagation in earth-ionosphere waveguide 07 p1061 A71-19386

Nighttime ionospheric absorption frequency dependence during solar activity cycle 07 p1100 A71-19400

Signal reflection from sporadic E layer, investigating multiplicity relationship to earth surface, ionization level, D region and nighttime absorption 07 p1100 A71-19403

Radio wave propagation at frequencies near proton gyrofrequency in horizontally stratified ionosphere, taking into account intermode coupling 07 p1102 A71-19666

Topside sounders received frequencies of oblique echoes at plasma resonance, using WKB technique 07 p1168 A71-19676

HF radio signal ionospheric propagation around world by sweep frequency CW sounding technique, observing fine structure in ionograms 07 p1062 A71-19682

HF backscatter from ionospheric Ba releases in March 1969 at Alaska, discussing effective cross section 07 p1064 A71-20317

Ionospheric absorption relation to solar X-ray flux enhancement during short wave fade-outs fromOGO-4 and Solrad 9 satellites 07 p1064 A71-20318

Whistler wave propagation along bell shaped ducts of enhanced ionization in magnetosphere 07 p1064 A71-20321

Satellite-borne long wave transmitting antenna excitation, calculating electromagnetic field near earth surface by earth-ionosphere waveguide model 08 p1252 A71-20744

Short wave communication channel quality estimate for discrete signal transmission based on signal level

variations calculation with allowance for ionospheric parameters

08 p1252 A71-20773

Forbush decreases effects on radio wave absorption, cosmic ray variations and ionization in lower ionosphere cosmic layer

08 p1353 A71-20981

Hourly changes in auroral conjugate location from ionospheric absorption and riometer magnetograms, noting electrojet triangulation

08 p1279 A71-21210

F 2 layer critical frequency and maximum electron concentration statistical characteristics for predicting SW propagation conditions

09 p1435 A71-22427

Ionospheric radio wave absorption above polar aurorae during solar activity minimum, discussing diurnal and annual behavior

09 p1435 A71-22429

Lower ionosphere electromagnetic induction effect on geomagnetic field guided MHD wave propagation, considering Hall effect

09 p1435 A71-22436

Cosmos 142 satellite measurements of VLF radio signals transmitted through ionosphere by ground based stations

09 p1408 A71-23143

Ionospheric scintillation effects on fading of oppositely circularly polarized VHF signals in space communications

09 p1410 A71-23522

Ionospheric dispersion of FM electromagnetic pulse, examining distortion of amplitude, pulse length and modulation in terms of integrated electron density along transmission path

09 p1410 A71-23523

Earth-ionosphere waveguide model of VLF signals propagation with perturbed ionosphere, considering magnetic dipole transmitting antenna array

09 p1410 A71-23575

Electromagnetic wave propagation in anisotropic ionospheric plasma with time-varying random electron density irregularities

09 p1506 A71-23586

Neutral wind and ion velocity determination under quiet and disturbed geomagnetic conditions in auroral zone, noting electric field measurements

09 p1440 A71-23600

Radar incoherent scatter technique for ionospheric propagation forecasting, using nocturnal and diurnal electron density profiles measurements

10 p1575 A71-23867

Satellite data for ionospheric radio communication forecasting involving maximum usable radio frequencies, discussing F 2 region large scale disturbances

10 p1575 A71-23868

Maximum usable frequency to critical frequency ratio for whispering gallery propagation in HF and VHF E region

10 p1577 A71-24291

Trapped waveguide mode frequency of whispering gallery propagation in F region explaining round world echoes and long distance satellite observations

10 p1577 A71-24292

Scintillation effects on synchronous satellite signal fading observed through polar ionosphere

10 p1577 A71-24315

Balloon sonde for auroral luminosity measurements and comparison of auroral emissions, X rays and ionospheric absorptions

10 p1602 A71-24530

Anomalous winter ionospheric radio wave absorption related to amplitude increases of microbarometric oscillations at ground level

10 p1606 A71-24919

Geomagnetic Pc1 pulsations propagation in F region, deriving hydromagnetic waves equations by ray tracing method and waves refractivity index in extraordinary mode

10 p1607 A71-25118

Attenuation and phase velocity of ELF and VLF radio waves propagating under anisotropic ionosphere, discussing geomagnetic field effect

11 p1731 A71-25602

VLF propagation in low latitude ionosphere from FR-1 satellite observations, obtaining electron density model of equatorial anomaly

11 p1755 A71-25642

Coupled vacuum mode equations modified for cylindrical stratification for calculation of propagation characteristics of earth-ionosphere waveguide

11 p1731 A71-25664

International coordinated solar chromospheric flare effects on D region lower boundary and ionospheric propagation by Cosmos 261 satellite and ground based observatories

11 p1816 A71-25763

Far ionospheric propagation of round-the-world echo signals from Moscow to Antarctic station Molodezhnaya and back to Moscow

11 p1731 A71-25773

Earth-ionosphere spherical waveguide, calculating mean and differential phase velocities and field amplitude of low frequency waves

11 p1731 A71-25774

Obliquely incident radio wave absorptions measurements from January-October 1968 vertical ionospheric soundings, correlating diurnal variations with solar zenith angular changes

11 p1732 A71-25787

Doppler geodetic measurements, discussing ionospheric wave diffraction errors, refractive index and electromagnetic wave propagation

11 p1732 A71-25831

F region ion and temperature effects on VLF and ELF wave absorption in whistler mode propagation at midlatitudes during solar minimum

12 p1879 A71-27049

Hamiltonian optics based model of ionospheric radio propagation, discussing earth magnetic field effects on radio wave angle-of-arrival changes

12 p1879 A71-27058

Simultaneous equatorial ionospheric absorption measurements at different longitudinal locations, using pulse reflection technique at 2.0-7.5 MHz

12 p1902 A71-27671

Transient ELF electromagnetic disturbances propagation in earth-ionosphere cavity, determining waveguide source-observer separation and attenuation constant

13 p2027 A71-27796

Winter day absorption variability of HF radio waves reflected at oblique incidence from ionosphere, using ray tracing method

13 p2027 A71-27799

Nondeviative absorption of RF signal at 2.2 MHz in presence of cusp type sporadic E layer

13 p2055 A71-27926

Geomagnetic field effects on directional propagation of LF and VLF radio waves in ionosphere, taking into account ion types effects

13 p2029 A71-28026

D region electron density profile relation to radio wave absorption frequency dependence

13 p2059 A71-28259

Sharp peaking of wave impedance characterizing propagation in earth-ionosphere waveguide from atmospheric radio noise measurements near 2 kHz

13 p2029 A71-28471

Magnetoionic component with fluctuating elliptical polarization during wave reflection from F 2 layer, discussing suppression mechanism

13 p2030 A71-28537

Radio communication accuracy characteristics in calculation of maximum frequency, skip distance and emission angle by transmission curves for midlatitude ionosphere

13 p2030 A71-28544

Short wave skip distance calculation as function of path inclination to ionospheric layer for linear and parabolic ionization distributions

13 p2030 A71-28556

Radio interferometry techniques and instrumental advances, examining transionospheric waves coherence properties and ionospheric source distribution

13 p2031 A71-28783

VLF band signal daytime propagation phase and amplitudes in earth-ionosphere waveguide, using models with geomagnetic field effect

14 p2191 A71-29509

Ionospheric VLF signal propagation paths based on earth atmospheric simulation and mathematical models

14 p2228 A71-29513

E layer phase height measurements with spaced receivers without ultra stable oscillators, calculating scale height

14 p2230 A71-29712

Fluctuation power spectra of CW phase path HF sounders in ionosphere compared with Vaisala frequency curve for upper atmosphere monitoring

14 p2230 A71-29717

Vertically incident radio waves reflection from horizontally stratified ionosphere with random electron density irregularities

14 p2192 A71-29718

Particle collisions effects on whistler ray paths, considering penetration through lower boundary of ionosphere

14 p2193 A71-29917

Ionospheric electromagnetic wave path calculation by Haselgrove ray method, applying to Faraday and Doppler effects

14 p2235 A71-30348

Transmission loss measurements at HF over 960 km temperate latitude path for wave polarization calculations and ionospheric absorption estimation

14 p2196 A71-30468

Cosmic radio noise absorption measurements at subauroral latitude for ionospheric absorption, discussing ionization regions spatial nonuniformity and horizontal extension

14 p2196 A71-30561

Earth-ionosphere waveguide excitation by satellite-borne horizontal dipole antenna, deriving fields at earth surface based on idealized model

14 p2196 A71-30562

Radio science - Conference, Ottawa, August 1969, Volume I, Ionosphere, magnetosphere, radio noise

14 p2201 A71-30939

Ionospheric absorption winter anomaly including temporal and local variations and frequency dependence, examining possible correlations with stratospheric and mesospheric phenomena

14 p2237 A71-30943

Ionospheric VLF and ELF wave observations, noting ion cyclotron resonance and harmonics effects on propagation

14 p2202 A71-30946

Ionospheric propagation prediction accuracy problems, considering numerical mapping, horizontal gradients, absorption, scatter, maximum usable frequency and transequatorial propagation

14 p2202 A71-30949

Ionospheric propagation, considering traveling disturbances, sporadic E phenomena, plasma frequency distributions and D region parameters

14 p2202 A71-30950

Atmospheric sources spectral amplitude ratios and group delay times correlation, obtaining VLF ionospheric propagation characteristics from single station observations

14 p2237 A71-30957

Whistlers propagation through ionosphere, considering coupling conditions between whistler mode signals magnetospheric trajectories and earth-ionosphere waveguide

14 p2203 A71-30963

Height variations of ionospheric absorption of downgoing whistler waves during nighttime at moderate and low latitudes

15 p2369 A71-31426

Global distribution and location of large lightning discharges from single station observations of transient ELF disturbances propagated in earth-ionosphere cavity

15 p2394 A71-31429

Internal reflection of VLF whistlers incident from above on model nighttime lower ionosphere

15 p2369 A71-31433

IQSY data analysis of pulse reflection measurements from midlatitude station, determining polar cap and auroral absorption

15 p2396 A71-31611

Complex refractive index equation of ionosphere for large values of vertical component of magnetic field, showing imaginary part independent of temperature effects

15 p2449 A71-31849

Radio wave propagation in ionosphere, measuring plasma frequency, cyclotron cut-off and noise level

15 p2373 A71-32443

Ionospheric absorption of 20 MHz radio waves as function of solar activity level, using electron density and temperature profiles

15 p2401 A71-32686

Ionospheric absorption measurements at 272 kHz, using surface wave attenuation factor as calibration technique

16 p2562 A71-33072

Reflected short wave signal frequency shift due to reflecting ionospheric layer movement and electron concentration changes, considering oblique incidence on isotropic and anisotropic layers

16 p2542 A71-33484

Normal angle determination by rocket observations for whistler mode waves propagation through magnetosphere and ionosphere from conjugate VLF ground station signals

16 p2569 A71-33805

Faraday rotation of satellite signals across transverse region, considering sudden jumps at transverse point in lower and topside ionosphere

16 p2544 A71-33959

HF radio absorption in antarctic night ionosphere, discussing solar activity effects

17 p2733 A71-34776

Satellite-to-aircraft links propagation characteristics, considering specular reflected signals, diffuse scattering and scattering function

17 p2705 A71-35097

VHF wave transhorizontal propagation correlation with daytime E layers in temperature zone, noting height dependence and seasonal and diurnal variations

17 p2707 A71-35445

Radio wave propagation studies evolution, considering ionospheric signal reflection, equipment optimal characteristics and transversely medium composition and properties probing

19 p3016 A71-37341

Magnetospheric conjugate ducts characteristics for HF radio propagation from Alouette 2 topside sounder ionograms analysis

19 p3016 A71-37369

D region electron densities from HF radio waves ionospheric backscatter based on hypothesis of refractive index stochastic fluctuations

19 p3048 A71-37372

Short wave radio signal analyzer for joint distribution of phase and amplitude probabilities and PSK communications noise stability in ionosphere

19 p3028 A71-37784

Polarization fluctuations of radio waves reflected from ionosphere E and F layers, describing radio polarimeter and preliminary measurement results

19 p3017 A71-37809

Physical factors affecting electromagnetic signal propagation in earth-ionosphere waveguide
19 p3017 A71-37811

Nighttime ionospheric absorption frequency dependence during solar activity cycle
19 p3053 A71-37824

Signal reflection from sporadic E layer, investigating multiplicity relationship to earth surface, ionization level, D region and nighttime absorption
19 p3053 A71-37827

Laboratory model for ionospheric perturbations effects on long range VLF paths
19 p3017 A71-37865

Geometrical optics convergence coefficient in earth ionosphere waveguide for arbitrary transmitter receiver location
19 p3017 A71-37866

Perturbations effects on ELF propagation in inhomogeneous anisotropic ionospheric waveguide
19 p3017 A71-37867

Solar activity effects on equatorial ionospheric absorption of radio waves, deriving solar cycle constant
19 p3055 A71-38042

F region radio wave absorption dependence on electron ion temperature difference from energy balance considerations, testing by radar backscatter measurements
19 p3055 A71-38045

Radio wave scattering from ionosphere, considering plasma experiments in E and F region
19 p3018 A71-38247

Polarization ellipse and depolarization coefficients for monochromatic radio waves reflected from F 2 ionosphere using Stokes parameters
19 p3056 A71-38362

D region ionization by electron fluxes as explanation for latitudinal radio wave absorption
19 p3057 A71-38370

Radio signal group trajectory in ionosphere expressed as series expansion in terms of increasing power of beam reflection height
19 p3020 A71-38371

Recalculated radio wave absorption during oblique transit through ionosphere from vertical measurements using rhombic antenna at 25 MHz
19 p3058 A71-38388

VLF fields of horizontal dipole in waveguide formed between ice covered ground and anisotropic ionosphere of Antarctica
19 p3024 A71-38595

Mid- and high-latitude ionospheric radio wave transmission from spacecraft during solar cycle, considering latitudinal and longitudinal gradients and electron content change rate
20 p3197 A71-39715

Ionospheric low hybrid resonance measurements by rocket-borne quadrupole probe, deriving electron density and effective ion mass along trajectory
20 p3224 A71-39722

Cosmos 142 and 259 experiments on ionospheric VLF propagation, discussing diurnal variations of daytime electron density
20 p3197 A71-39743

Drifting whistler frequency cutoff phenomena /striations/ observation in low latitude by POGO satellites, discussing interpretation based on propagation effect
20 p3198 A71-39746

Rocket-borne explosive charge initiated detonation wave effects on decimeter wavelength radio waves in lower E layer
20 p3199 A71-39894

Lunar tidal effects on semidiurnal periodicity in ionospheric absorption, showing time of maximum amplitude variation with geographic latitude
20 p3232 A71-39900

Ionospheric irregularities and reflection points calculation, developing simple ray interference model from large antenna array data
21 p3372 A71-40042

Ionospheric radio wave absorption winter anomaly concerning seasonal variations of D and lower E region collision frequencies and F region oxygen concentrations
21 p3373 A71-40048

Cas A and Cyg A radio stars scintillation measurement by two element phase switched interferometers in ionospheric irregularities study
21 p3378 A71-40377

Limiting polarization of radio waves emerging obliquely from ionosphere into free space, describing numerical integration method and boundary conditions
21 p3348 A71-40525

International coordinated measurements of solar chromospheric flare effects on D region lower boundary and ionospheric propagation by Cosmos 261 satellite and ground based observatories
22 p3591 A71-41531

Far ionospheric propagation of round-the-world echo signals from Moscow to Antarctic station Molodezhnaya and back to Moscow
22 p3509 A71-41541

Earth-ionosphere spherical waveguide, calculating mean and differential phase velocities and field amplitude of LF waves
22 p3509 A71-41542

Obliquely incident radio wave absorptions measurements from January-October 1968 vertical ionospheric soundings, correlating diurnal variations with solar zenith angular changes
22 p3509 A71-41555

Wave polarization and midpath ground reflection effects on power loss of two hop radio signal propagation through ionosphere
22 p3511 A71-42280

Ionospheric propagation hysteresis relationship to secular variation in F region response to sunspot number, noting differences in succeeding solar cycles
22 p3536 A71-42419

Radio reflection and transmission coefficients for thin highly ionized layers under earth magnetic field, based on numerical integration of differential equations
23 p3665 A71-42962

Ionospheric HF wave ordinary (O) and extraordinary (E) modes coupling effect on satellite signal Faraday rotation
23 p3642 A71-42964

Ionospheric geomagnetic field effect on ELF/VLF radio propagation
23 p3643 A71-42967

Phase integral correction for reflected radio wave absorption in ionosphere, comparing with ray theory
23 p3643 A71-42969

Ionospheric propagation penetrating and nonpenetrating modes full wave reflection and transmission coefficients determination for height and frequency variation by thin film optical method
23 p3643 A71-42972

Day to day fluctuations of winter anomaly in ionospheric absorption, showing regular and irregular trends
23 p3666 A71-42974

Night enhancements in 6300 A line at Sanae related to diurnal excursion of auroral oval, observing ionospheric blackout and high energy electrons precipitation
23 p3672 A71-43980

Stratospheric warmings effect on F 2 region parameters and ionospheric radio wave absorption, assessing time lag
23 p3673 A71-44049

High power multielement electronically scanned array of microwave log periodic monopole antennas for ionospheric backscattering measurements
23 p3653 A71-44155

E layer vertical velocity fluctuations from scattered signal phase and amplitude correlation measurements, using perturbation technique
23 p3647 A71-44334

Riometer measurement of ionospheric absorption, comparing with IQSY method
24 p3822 A71-44525

Long distance atmospheric propagation in earth-ionosphere waveguide, obtaining phase velocities and damping factors
24 p3804 A71-45030

Radio absorption in lower ionosphere, determining vertical distribution of electron density and production rates from solar protons energy spectrum
24 p3867 A71-45041

Diurnal fluctuations in radio echo producing ionospheric region horizontal scale and height, discussing dependence on solar position
24 p3804 A71-45042

Simultaneous ionosphere measurements by incoherent ground radio wave scattering and coherent signals from Intercosmos 2 and Cosmos 321 satellites
24 p3824 A71-45323

IONOSPHERIC REFLECTION

U IONOSPHERIC PROPAGATION

IONOSPHERIC SOUNDING

Position finding for auroral electrojet using magnetometer measurements onboard Black Brant 3 rockets
01 p0075 A71-11331

Lower ionosphere partially reflecting regions, describing vertical thickness distribution based on 1.75 MHz backscatter soundings
01 p0040 A71-11525

Electrical stability of double sphere dipole antennas for FR-1 satellite ionospheric plasma electric fields measurements
02 p0229 A71-11714

Langmuir probe DC detector for rocket quasi-static and AC electric field measurements in auroral zone ionosphere
03 p0406 A71-13302

Parallel and perpendicular electric fields in auroral arcs from rocket-borne experiment
03 p0406 A71-13303

Intercosmos 3 satellite for radiophysical and geophysical observations of radiation belts and ionosphere, discussing design, configuration and instrumentation
03 p0423 A71-13419

Astrobbee D low cost high performance sounding rocket with long duration radial burning propulsion system for D region and meteorological research [ALAA PAPER 70-1387]
03 p0498 A71-13670

Upper atmosphere meteorological sounding facility for recording position and telemetry data from balloons, rocket payloads and meteor trails [ALAA PAPER 70-1392]
03 p0397 A71-13671

Ionospheric research covering electron and ion distributions, ion chemistry, neutral atmosphere interactions, thermal structure, electrodynamics, etc
03 p0416 A71-14031

Rocket experiments during 1964 solar eclipse, obtaining D region parameters from parachute-borne blunt probe measurements of atmospheric positive and negative conductivities
03 p0416 A71-14037

Auroral oval continuity during winter /1969-1970/ from jet aircraft ionospheric instrumentation, showing band distribution along geomagnetic pole
03 p0419 A71-14526

VHF radar measurements of scattering by field aligned irregularities associated with equatorial spread F
03 p0420 A71-14532

Sporadic E layer structure and disturbances from pulsed radio signal measurement, noting correlation to pressure oscillation at ground level
04 p0584 A71-15757

Bora-Sond rocket for upper atmosphere low cost sounding, describing propulsion system design and chemistry [ALAA PAPER 70-1388]
05 p0816 A71-16417

Upper atmosphere electromagnetic probing - Conference, Calcutta, July 1969
05 p0739 A71-16426

Top side ionosphere electromagnetic probing techniques, noting F and E regions
05 p0740 A71-16428

Ionospheric geomagnetic field inclination measurement by incoherent scatter method
06 p0887 A71-17270

Geodetic satellite transmissions for ionospheric research, discussing orbital elements and frequency data
07 p1095 A71-19004

Second difference of phase shift method for measuring ionospheric electron density
07 p1096 A71-19013

Geostationary radio beacon specifications and observational opportunities on ionospheric satellite ATS-F in 1972
07 p1096 A71-19016

Ionospheric electron content observation by ATS-3 radio signals, noting gravity waves effect
07 p1098 A71-19034

Ionospheric characteristics recording concerning critical frequencies and minimum heights above Sverlovsk during solar eclipse of 22 September 1968
07 p1101 A71-19407

Subauroral red arcs phenomenon hypotheses based on associated ionospheric plasma properties measurements
07 p1102 A71-19663

HF radio signal ionospheric propagation around world by sweep frequency CW sounding technique, observing fine structure in ionograms
07 p1062 A71-19682

Upper air sounding systems problems, discussing aerodynamic heat transfer between temperature sensor and ambient air
08 p1330 A71-21739

Ionospheric layers critical frequencies recording, using automatic interplanetary station type probe
09 p1436 A71-22450

Space charge sign distribution sounding in atmosphere by electrode potential difference measurement
09 p1437 A71-22677

Ion orientation technique for attitude control based on counterflow sensing in earth upper atmosphere, discussing accuracy
09 p1523 A71-23151

Flow equations of vertical shear modes in inertial waves on rotating earth, comparing chemical release ionospheric wind profiles
09 p1489 A71-23449

Geomagnetic field inclination determination by incoherently scattered signal Faraday rotation calibration and simultaneous ionosonde measurements of ionospheric electron density
10 p1605 A71-24798

Electron precipitation in nocturnal E region from radiowave and rocket data, calculating ionization rates and midlatitude morphology
11 p1815 A71-25552

International coordinated measurements of solar activity geophysical effects in upper atmosphere, discussing synchronized observations of Cosmos 261 satellite and ground based ionospheric station network
11 p1816 A71-25762

N/z/ profiles of upper ionosphere from Alouette I vertical sounding data, proposing model for ionosphere shape
11 p1758 A71-25786

Ionospheric transverse inclinations from radio wave propagation characteristics obtained by circular oblique incidence sounding scans 11 p1758 A71-25788

Vertical geophysical sounding rocket research program and equipment for observing ionospheric parameters, solar UV and X rays, atmospheric absorption and meteorites 11 p1839 A71-26353

Soviet papers on upper atmosphere physics covering thermosphere, dynamic processes and radiative energy transport in stratosphere and mesosphere, and ionospheric parameters radio measurement 13 p2056 A71-28017

Lower ionosphere charged particle concentrations and collision frequencies determination by LF impedance probe 13 p2058 A71-28028

Photochemical ion-molecule reactions in ionosphere by air exhaust device and RF mass spectrometer observation in geophysical rocket experiment 13 p2068 A71-28535

Sporadic E layer occurrence frequency distribution during 1958-1960, investigating characteristics over equatorial, temperate and auroral zones 13 p2061 A71-28540

Sizes, shapes and temporal characteristics of small scale inhomogeneities in F region, using vertical sounding, space diversity reception and radio astronomy 13 p2061 A71-28554

Daytime and nighttime sporadic F layer regularities correlation with other ionospheric phenomena based on vertical sounding data 13 p2062 A71-28555

Midlatitude ionospheric signatures from narrow beam HF radar backscatter sounder, discussing diurnal and seasonal occurrences 13 p2031 A71-28782

D region negative ion densities in chemical equilibrium based on electron density observation, noting role of ozone and carbon dioxide 14 p2228 A71-29533

F region ionization drift and electric field observation by incoherent scatter techniques and data-interpretation 14 p2236 A71-30942

Incoherent scatter measurements for ionospheric ion bulk velocity, thermospheric dynamics, F region gravity wave, photoelectron flux, ionic collision frequency and magnetic field direction 14 p2202 A71-30945

Ionospheric electron resonance observation by sounders aboard rocket and satellites 14 p2202 A71-30947

Simultaneous ionospheric electron density measurements from Isis satellite topside and incoherent scatter soundings 15 p2394 A71-31428

Daytime rocket and ground based radar Thomson scatter measurements of electron densities and temperatures in lower ionosphere 15 p2399 A71-31772

Night sky submillimeter wave diffuse background radiation telescopic measurements above 120 km 15 p2399 A71-31827

Pakistani space research including satellite geodesy, ionospheric sounding, rocket experiments, VLF studies and time keeping 16 p2666 A71-33857

Day and nighttime effective electron loss rate measurement in D region during polar cap absorption events, using rocket-borne spectrometers and Faraday rotation 16 p2573 A71-33961

Ionospheric atomic oxygen concentration estimates from radar backscatter and rocket probe measurements of electron and ion temperatures and concentration 16 p2574 A71-33965

Spring and autumn cyclonic circulation in stratosphere and mesosphere up to 95 km, using ionospheric radiosonde and rocket data 17 p2730 A71-34301

D and E regions advances during 1967-1971 covering ionic composition, electron density profile at various latitudes, hours and seasons during eclipses and winter anomalies 17 p2732 A71-34464

German monograph on determination of instantaneous position of polar electrojet for rocket launching parameters computation 18 p2911 A71-35920

ESRO sounding rocket program covering atmospheric and ionospheric physics and solar and auroral phenomena 18 p2896 A71-35926

Positive biased ionospheric probes in steady state plasma flow, presenting self consistent parameter computation [ONERA-TP-935] 18 p2915 A71-36013

Ionospheric characteristics recording concerning critical frequencies and minimum heights above Sverdlövsk during solar eclipse of 22 September 1968 19 p3053 A71-37831

Ionospheric electron density irregularities measurement, comparing scintillation, spread F and electrostatic probe methods 19 p3128 A71-38035

Traveling ionospheric perturbations investigation by vertical sounding with interference method, presenting group path difference measurements as function of frequency and time 19 p3058 A71-38390

Automatic interplanetary station adapter to obtain reflected signals amplitude-altitude-frequency characteristics during ionospheric probes 19 p3058 A71-38392

Upper ionospheric plasma measurements by gyro plasma probe equipped Lambda rocket, deducing electron density profile from plasma resonance effects 20 p3224 A71-39721

Night and daytime auroral zone ionospheric electric field measurement by rocket-borne Langmuir probe, noting components parallel and perpendicular to magnetic field 20 p2321 A71-39884

Ionospheric properties at geomagnetic equator from ionograms by automatic sounder at Thumba, noting F 2 layer ionization frequencies solar cycle variations altitude dependence 21 p3373 A71-40376

International coordinated measurements of solar activity geophysical effects in upper atmosphere, discussing synchronized observations of Cosmos 261 satellite and ground based ionospheric station network 22 p3591 A71-41530

Ionization profiles of upper ionosphere from Alouette I vertical sounding data, proposing model for ionosphere shape 22 p3532 A71-41554

Ionospheric transverse inclinations from radio wave propagation characteristics obtained by circular oblique backscatter sounding scans 22 p3532 A71-41556

ISIS-I ionospheric sounding satellite spin rate behavior 22 p3612 A71-42786

Barium ion cloud release at 194 km, observing striation formation for instability characteristics evaluation 23 p3669 A71-43170

TV data acquisition system for auroral and ionospheric research, noting visual and subvisual detection sensitivity 23 p3677 A71-43515

IONOSPHERIC STORMS

NT Sudden ionospheric disturbances

Magnetic field aligned currents during 18 March 1969 substorms, observing electric field by Ba plasma cloud motion for magnetic perturbation field 10 p1677 A71-24789

Midlatitude ionosphere dusk sector total electron content during geomagnetic storm time increase 14 p2229 A71-29666

Electric field, atmospheric wave and other factors effects on F region storms by day and night in tables 14 p2236 A71-30941

Ionospheric storms morphology, analyzing F 2 layer maximum relative electron concentration worldwide propagation 17 p2734 A71-35192

Sudden phase anomalies relation to solar flares, radio bursts and X radiation from severe worldwide ionospheric storm observation 17 p2796 A71-35349

Computer demonstration of ionospheric F region storm causes, noting critical frequency relationship to ionization shift 19 p3055 A71-38038

Electron content spatial and temporal variation during ionospheric storm of 8 March 1970 after total solar eclipse 20 p2322 A71-39899

Peak electron density variations during midlatitude F region storm, investigating electrodynamic drift effects 21 p3372 A71-40037

IONOSPHERIC TEMPERATURE

Charged particle temperature distribution in outer ionosphere, disregarding collisional energy exchange 02 p0244 A71-11920

Comparative simultaneous ionospheric temperature and plasma concentration by Explorer 31 probes and ground based radar measurements 03 p0407 A71-13311

Ionospheric electron temperature global pattern from satellite observations 03 p0415 A71-14029

Neutral ionospheric temperature profile diurnal variation at Arecibo from incoherent scatter measurements, considering relevance to 1400 hour density maximum 06 p0887 A71-17271

Relaxation time for nitrogen molecule vibration temperature in ionosphere due to thermal electron collisions 06 p0895 A71-18274

Electron and ion temperature in ionosphere, discussing measurements, solar heating, F and E region, variability over solar cycle, etc 07 p1098 A71-19320

Yearly cosmic rays intensity variations in meridional plane from 1955-1969 ionization temperature coefficient recordings as function of solar activity levels 11 p1817 A71-25783

Diurnal temperature variations in middle ionosphere by rocket probes, noting solar activity changes influence 11 p1759 A71-25823

Radar based values of neutral night exospheric temperature, discussing dominant effect of annual variation 13 p2055 A71-27921

Ionospheric ion temperature measurement method by exploring transverse velocity distribution, discussing surface pollution and spurious effects 13 p2055 A71-27929

Charged particle temperature distribution in outer ionosphere, disregarding collisional energy exchange 13 p2058 A71-28207

Suprathermal electron temperature and ion composition as function of geomagnetic latitude in polar ionosphere, using Explorer 31 mass spectrometer measurements 14 p2234 A71-30037

Daytime rocket and ground based radar Thomson scatter measurements of electron densities and temperatures in lower ionosphere 15 p2399 A71-31772

Complex refractive index equation of ionosphere for large values of vertical component of magnetic field, showing imaginary part independent of temperature effects 15 p2449 A71-31849

Electron temperature profiles in ionosphere from rocket probes, noting correlation with geomagnetic activity indexes 16 p2569 A71-33798

Geomagnetic equatorial ionospheric ion temperature, comparing incoherent scatter radar and OGO-D retarding potential analyzer values 16 p2573 A71-33956

Lower thermosphere vertical temperature distribution measurements, using ionization and heat manometers 20 p2222 A71-39702

Mesospheric soft corpuscular radiation flux and temperature rocket observations, during solar flare activity 20 p2222 A71-39704

Midlatitude ionospheric irregularities, electron density vertical distribution and electron and ion temperature variation measurements, during solar eclipse of 22 September 1968 20 p2224 A71-39716

Ionospheric electron and neutral particle temperature average diurnal behavior from bottomside vertical soundings 20 p2225 A71-39723

E region wind and temperature measurements from Nancy incoherent scatter experiments, observing prevailing semidiurnal oscillation with phase propagating downwards 21 p3372 A71-40041

Yearly cosmic rays intensity variations in meridional plane from 1955-1969 ionization temperature coefficient recordings as function of solar activity levels 22 p3591 A71-41551

IONOSPHERICS

NT DAWN CHORUS

NT HISS

Solar cosmic ray phenomena, noting ionospheric effects and physical processes near sun 03 p0480 A71-14067

IONS

NT ANIONS

NT CATIONS

NT CESIUM ION

NT DEUTERONS

NT FERRIC ION

NT HEAVY IONS

NT HYDROGEN IONS

NT HYDRONIUM IONS

NT MANGANESE IONS

NT METAL IONS

NT MOLECULAR IONS

NT NITROGEN IONS

Average energies of ground and excited configurations in highly ionized atoms, using orthogonalized screened hydrogenic radial functions 04 p0630 A71-14999

Ion-neutral coupling in plasma acceleration revealed by velocity disparities determined spectroscopically [AIAA PAPER 70-166] 05 p0788 A71-16572

IP [IMPACT PREDICTION]

U COMPUTERIZED SIMULATION

IQSY [INTERNATIONAL YEAR]

U INTERNATIONAL QUIET SUN YEAR

IRASERS

U INFRARED LASERS

IRIDIUM

IRIDIUM

Ti-Ir alloy equilibrium diagram in entire concentration range, emphasizing phase stabilization at room temperature

04 p0616 A71-15805

W-Re-Ir ternary system phase diagrams, studying physicochemical properties via X ray and metallographic techniques

07 p1140 A71-20235

Iridium-based long life hydrazine catalyst with multiple cold start capability, describing development program for substrate evaluation and physical properties and process optimization

14 p2286 A71-30761

IRIS SATELLITES

Orbit computation and tracking system for Iris satellite using differential correction program

19 p3142 A71-38066

IRISES [MECHANICAL APERTURES]

Iris microphotometer based on slot type instrument, discussing design and operational characteristics

04 p0590 A71-14839

Iris photometer for star observations, discussing automatic compensation for plate background

04 p0590 A71-14840

Varactor-tuned avalanche microwave source, using interchangeable iris shims at output cavity for passive stabilization, power output and tuning variability

09 p1418 A71-23155

HF diffraction of plane electromagnetic waves by ideally conducting iris diaphragm, developing boundary value problem asymptotic solution

13 p2029 A71-28448

Movable metal iris with nearly frequency independent susceptance, relating characteristics to centered capacitive obstacle in waveguide

24 p3809 A71-45095

IRON

NT IRON 57

Iron single crystal wavy slip pattern of plastic deformation under tension at room temperature, noting relation between yield point and crystal orientation

01 p0105 A71-11621

Soviet book on boride coatings on iron and steels covering physicochemical interactions and properties

02 p0263 A71-11848

Temperature and plastic deformation rate effects on plasticity and strength of cast iron, Ti and steels

02 p0257 A71-12525

Surface oxidation kinetics of iron by solid electrolyte techniques, comparing weight gain method

03 p0374 A71-13122

Electron excitation coefficient rate of green coronal line by quantum defect method, discussing energy levels of Fe ions

04 p0643 A71-14906

Liquid Fe, Co and Ni atomic distributions investigation by X ray diffraction

04 p0612 A71-15036

Pure Fe and Fe-Ni alloys thermal stress component temperature dependence measurement, investigating Ni addition effect on alloy softening

05 p0765 A71-16188

Molten glass inclusion and stress concentrator/empty hole/ effects on Armc iron electrode potential

05 p0766 A71-16384

Highly ionized line spectra of Fe, Co, Ni and Cu belonging to Na I and Mg I isoelectronic sequences

05 p0717 A71-16909

Fe powder filled tubular shell compression by magnetic fields and pulse sequences

05 p0759 A71-17168

Manganese, iron and vanadium ion ordering in orthorhombic zoisite structure by electron paramagnetic resonance technique

07 p1053 A71-18741

Proton irradiation on Fe and Ni targets, measuring spallation cross sections

07 p1158 A71-19074

Iron-iron carbide structure dissolution behavior from electron transmission microscopy, observing carbide, matrix, general and interface attack modes

07 p1056 A71-20361

Fe-S condensates structure and phase transformations during heating, noting importance for antifiction materials synthesis

08 p1322 A71-21062

Interstitial impurities effects on relation of activation energy to effective stress in iron, low carbon steel and other bcc metals

08 p1308 A71-21514

Luders bands motion in steel and iron, studying plastic zone velocity dependence on stress, composition, grain size, dislocation substructure and temperature

08 p1308 A71-21517

Grain boundary hardening in relation to electrical resistivity, magnetic permeability and yield stress in iron and Fe dilute alloys

08 p1309 A71-21529

Long term creep strengthening by molybdenum in untempered iron and steel

08 p1315 A71-21579

Iron and fcc metal composite wires, determining fiber thickness and strength relationship

08 p1323 A71-21588

Sponge iron sintered powder compacts deformation behavior from uniaxial compression tests, proposing plasticity prediction criteria

09 p1466 A71-22169

Oscilloscopic determination conditions for Co, Ni, and Fe, giving statistical treatment of results

09 p1454 A71-22501

Al and Fe additions effect on transitional phases formation and metastable phase precipitation in Ni-Nb system, using transmission electron microscopy

09 p1471 A71-23124

Crystal lattice type influence on volume and boundary diffusion mobility of iron group metals atoms

09 p1510 A71-23325

Iron base, white cast iron and high alloy powder metallurgy products for antifriction bearing elements

09 p1478 A71-23393

Solar flare spectral line features at 1.9 A, considering iron ion origin

10 p1660 A71-23797

Hydrogen recombination and molecule formation by nonactivated chemisorption on iron grains surfaces

10 p1573 A71-25006

Iron nuclei emission during 1967-1969 solar flares from spacecraft window and lunar camera lens etched tracks, discussing Fe/He ratio and lunar soil densities

11 p1815 A71-25299

Annealed and cold-worked polycrystalline Fe specimens steady state cyclic stress-strain curves and thin films observation by electron microscopy

11 p1780 A71-26024

Monograph on plastic behavior of iron and nickel at high strain rates and at elevated temperatures, discussing thermal effect on deformation characteristics

11 p1783 A71-26489

Fe ion photodetachment cross section polarization dependence on a sites in YIG-Si to explain photoinduced uniaxial anisotropy, using crystal field theory

12 p1943 A71-26858

Boride coated steels and cast iron surfacing with nonconsumable tungsten electrode for higher abrasive wear resistance

12 p1917 A71-27125

Fe XIV intensities in solar EUV spectrum, calculating equilibrium population of energy levels in coronal conditions

12 p1970 A71-27704

Thermodynamic equilibrium constants of Fe-MgO-SiO₂-O₂ system reactions at one atmosphere and 900-1300 C

14 p2190 A71-29875

Aging of cast iron components by thermal shocks, considering heat treatment for machine elements dimensional stabilization

15 p2414 A71-31527

Vibrational relaxation of CO by Fe atoms in Ar shock tube following iron pentacarbonyl decomposition

16 p2539 A71-32897

Iron single crystals plastic deformation under tension, studying ductile/brittle fractures mechanisms and transition temperature

16 p2591 A71-33369

IR Fe XIII lines in solar corona during total eclipse of 12 November 1966

16 p2640 A71-33729

Quasi-stellar objects, investigating velocity dispersion, column densities and abundance of Mg and Fe in absorbing region by Stromgren method of line pairs

17 p2797 A71-34371

Sunspot forbidden Fe I line spectra, showing high solar iron abundance

18 p2961 A71-35944

Cermet iron chromosilicidization and sinter compactness effects on depth and structure, noting wear, corrosion and thermal resistance

19 p3075 A71-37110

Solar photosphere iron abundance data from Fraunhofer spectrum and EUV line measurements

19 p3135 A71-37610

Iron precipitation rate from supersaturated Al alloy solid solution in structures with low and high dislocation densities

19 p3079 A71-37702

Fe content of clinopyroxene in basalt-basaltic andesite-andesite-late of Mogollon Plateau (New Mexico)

20 p3216 A71-39386

Pure Fe phase transformation plasticity as function of material, stress, temperature interval and change rate, cycle number and experiment duration

21 p3396 A71-40028

G and K giant stars iron abundances from narrow band indices, using spectrophotometer, red-IR colors and independent luminosity estimates

21 p3444 A71-40240

Iron response to dynamic loads, discussing pressure induced phase changes, constitutive equation relationship to dislocation processes and dynamic fracture criteria

21 p3399 A71-40789

Intermittent stress creep tests on low carbon steel, commercially pure iron, Cr-Mo steel and commercially pure tantalum, noting static-to-dynamic transition

21 p3400 A71-40828

Boridosilicide and boridoaluminide diffusion coatings on iron and steel, investigating formation kinetics structure and properties

21 p3390 A71-41171

High resistivity Fe-doped GaAs, investigating carrier lifetime dependence on Fe atoms concentration

21 p3431 A71-41248

Solar far UV Fe and Ni ion lines

23 p3723 A71-42940

High energy proton spallation cross sections for several radionuclides from Fe targets, discussing application to beam monitoring and meteoritic studies

23 p3706 A71-43206

Oxidation state of iron and cation distribution over M1 and M2 sites in clinopyroxenes from Apollo 12 by Mossbauer absorption spectroscopy, noting cooling history

23 p3738 A71-43609

Electron spin resonance studies of Apollo 11 and 12 lunar soil samples, determining ferromagnetism due to Fe particles

23 p3763 A71-43797

Interplanetary energy spectrum of solar flare Fe nuclei from tracks in Surveyor 3 glass filter and rock 12022

23 p3765 A71-43813

Grain boundary orientation effect on intergranular cracking, discussing crack introduction in purified iron by cathodic charging with hydrogen

23 p3695 A71-44285

Total-to-open porosity ratio for carbide-iron type materials sintering, noting relative density and chemical composition effects

24 p3838 A71-44736

Identification of 417 A line in solar EUV spectrum, calculating collision strengths and recombination rates for Fe XV

24 p3873 A71-45143

IRON ALLOYS

NT AUSTENITIC STAINLESS STEELS

NT BAINITIC STEEL

NT CARBON STEELS

NT CHROMIUM STEELS

NT HIGH STRENGTH STEELS

NT MARAGING STEELS

NT MARTENSITIC STAINLESS STEELS

NT NICKEL STEELS

NT STAINLESS STEELS

NT STEELS

Boride coatings for Fe-Si alloy, testing corrosion and wear resistances in aqueous salt, acid and alkali solutions

01 p0097 A71-10039

Fe-Ni martensite crystals microstructure, using Kossel method and electron microscopes

01 p1016 A71-10278

Cr-alloyed Fe powders fine crystalline structure from X ray analysis

01 p1012 A71-10789

Boron addition distribution in iron microstructure, using nuclear track radiography

01 p1013 A71-11072

Ni and Fe alloys for tooling materials, examining die life and wear at elevated temperatures

01 p0090 A71-11266

Fe-Ti alloys at large plastic elongations, investigating strain hardening behavior

01 p1015 A71-11604

Fe-Ni-Mo alloys maraging process kinetics at various temperatures, measuring hardness, electrical resistance and lattice constants

02 p0266 A71-12653

Cr and Mo thin film coatings on Si-Fe, examining effect on plastic deformation and mechanical properties

02 p0266 A71-12655

Si-Fe fatigue crack growth in vacuum at various temperatures, discussing stress intensity, cleavage and ductility effects

02 p0267 A71-12882

Solute core redistribution and dendritic refinement in highly undercooled Fe-Ni alloy, using metallographic and electron microprobe analyses

03 p0442 A71-13365

Microstructure changes during austenite isothermal decomposition in Fe-Mo-C alloys

04 p0614 A71-15778

Oxygen solubility and activity in Fe-Al and Fe-Ti melts, using neutron activation analysis

04 p0614 A71-15785

Pure Fe and Fe-Ni alloys thermal stress component temperature dependence measurement, investigating Ni addition effect on alloy softening

05 p0765 A71-16188

Potentiokinetic study of anodic polarization in maraging Fe alloys, considering relationship to structural transformations during tempering

05 p0765 A71-16200

Ni-Fe alloy films composition gradients produced by W boats evaporation, noting vapor pressures effect

05 p0791 A71-16230

- Quench atomization of iron alloys to powders, using liquid metal two fluid nozzle method
05 p0758 A71-16245
- Austenite-martensite transformation effects on Fe-Ni-Co alloys low temperature thermal conductivity
05 p0768 A71-16771
- Fe-Ni alloy oxidations parabolic kinetics and activation energies, noting scale development as function of oxidation amount and temperature
05 p0770 A71-17098
- High temperature creep comparison of single phase Fe and Ni alloys subjected to constant load tensile tests, measuring strain as function of time
06 p0911 A71-17345
- Ni-Mn, Ni-Fe and Ni-Fe-Al alloys yield behavior and microstructure as result of ordering and disordering treatments, using center annealing technique
07 p1132 A71-19434
- Metastable Al-rich Al-Fe solid solutions decomposition during isothermal and isochronal annealing, from X ray diffraction patterns
07 p1137 A71-19979
- Mossbauer effect study of 475 C decomposition of binary Fe-Cr alloys, considering fluctuations about average composition
07 p1138 A71-19985
- Bcc metals low temperature strength, examining solution softening in Fe-Mo alloys
08 p1307 A71-21506
- Grain boundary hardening in relation to electrical resistivity, magnetic permeability and yield stress in iron and Fe dilute alloys
08 p1309 A71-21529
- Martensitic transformation-induced plasticity in austenitic Fe alloys, examining strain rate and chemical composition effects
08 p1312 A71-21554
- Fe-Ni-Co alloy strengthening by martensite to austenite transformation taking into account microstructure
08 p1313 A71-21556
- Tensile data for dispersion hardened iron containing thorium spherulites analyzed in terms of Orowan theory, considering bcc materials yield strength
09 p1466 A71-22172
- Fe-Si alloy with pronounced texture and large grain size, determining lattice period from X ray diffractogram obtained by reverse response method
09 p1467 A71-22308
- Anomalous electrical resistivity during decomposition of supersaturated solid solution of Fe-Co-Mo alloy
09 p1468 A71-22359
- Fe-Ni alloys, determining hydrogen permeability, diffusion coefficient and solubility as function of composition by electrochemical method
09 p1472 A71-23127
- Fe-Cr-Zr ternary alloys, investigating Zr effect on high temperature hardness and heat resistance
09 p1473 A71-23228
- High temperature Fe, Co and Ni alloys for gas turbine components, considering tensile and creep rupture strength increase by thermal mechanical processing
09 p1475 A71-23298
- Polygonization and recrystallization processes in Fe-Cr alloy, using electron diffraction and microscopy
09 p1476 A71-23322
- Mo-Fe-C ternary system, investigating various concentrations, microhardness measurements, solid state solubility and ductility
10 p1628 A71-24648
- Refining process of Fe-NiCu-Mn alloys, discussing aging kinetics, hardening mechanism and strength properties
11 p1781 A71-26159
- Fretting corrosion relationship to mechanical vibrations damping capacity for Fe and Cu alloys, noting energy dissipation
13 p2082 A71-27822
- Fe/Ti pair diffusion coefficients at various temperatures, showing thin central and two single phase zone formation
13 p2087 A71-29263
- Cold rolled recrystallized Ni-Fe alloy, considering short range order structure effect on elastic limit
13 p2087 A71-29264
- High temperature creep in alpha-Fe, Fe-Mo and Fe-Co alloys, investigating stress dependence and alloying effects in ferromagnetic and paramagnetic temperature ranges
13 p2089 A71-29409
- Crack initiation in Ti-refined Fe-Ni alloys, using slow bending tests of notched bar samples with various notch angles
13 p2089 A71-29411
- Fe-Ni alloys with Cr, investigating heat treatment effect on thermoelastic coefficient
15 p2426 A71-31482
- Ordered structure recovery in Fe-Co-V alloy from elasticity limit behavior, studying duration effect on mechanical properties of strain hardened samples
16 p2591 A71-33370
- Phase diagrams of ternary systems Ta-Fe-B and Ta-Ni-B using X ray and metallographic analyses
16 p2592 A71-33575
- Anomalous electrical resistivity variation during decomposition of supersaturated solid solution of Fe-Co-Mo alloy
16 p2593 A71-33632
- Composition transformations at interface levels in iron-nickel alloys as function of thermal treatment, using potentiokinetic method
16 p2598 A71-34050
- Recrystallization of heat treated Fe-Ni alloys microstructures after hammer hardening
16 p2598 A71-34051
- Fe-Ni-V-C alloy strengthening by cyclic martensitic phase transformation
17 p2756 A71-34487
- Iron based Cr-Co-Mo alloys equilibrium diagrams and phase transformations at various temperatures, emphasizing intermetallic compounds effects on mechanical properties
17 p2758 A71-35148
- Hydrogen discharge from Fe-C alloys in absolute suction metal mold, finding discharge decrease with increasing carbon content
18 p2926 A71-36300
- Vertical phase diagrams of Ti-Al-Zr-Mo-Fe alloy system at varying Fe concentrations, showing structural hardening after quenching
19 p3078 A71-37471
- Precipitation strengthened Fe-Ni-base superalloy microstructure, investigating phase relationships
19 p3079 A71-37711
- Fe-Ni base alloy heat treatment for optimum high temperature stress-rupture properties, noting Ni-Nb/Ti intermetallics precipitation at grain boundaries
19 p3080 A71-37712
- Stress relief, temper and creep embrittlement effects on ferrous alloy welds
19 p3082 A71-38317
- Fe-Al alloy fine lamellar microstructure from light microscopy and X ray examination
21 p3396 A71-40032
- Microstructural characteristics of Fe-Ni alloy plastic deformation at 20-500 C during cold and hot rolling, noting intergranular shear processes
21 p3402 A71-41095
- Microhardness, thermo-emf and phase composition of Al coatings on Armocon iron and steel under furnace and rapid electric heating
21 p3389 A71-41096
- Oriental magnet-optic effect in nickel and ferrosilicon monocrystals, discussing anisotropy influence on frequency dependence
21 p3431 A71-41263
- Metallography of 700 C precipitation hardening in Fe-Ni alloy containing Be, using transmission electron microscopy
21 p3404 A71-41417
- Thermoelastic coefficient development by tempering for Ni-Fe alloy containing Be
22 p3563 A71-42325
- Isothermal martensite transformations in Fe-Ni-Cr alloys, explaining kinetics difference in terms of elastic parameters small variations
23 p3688 A71-42925
- Tensile and creep rupture strength and microstructure of Co-Fe-Ta alloys at elevated temperatures
24 p3836 A71-44442
- Aluminized layer phase and chemical composition of heat resistant iron and nickel alloys
24 p3837 A71-44732
- Phase and microstructure changes during nitriding process of Fe-Ti alloys, stressing Ti concentration effect
24 p3837 A71-44733
- IRON CHLORIDES**
Venus cloud composition, noting partially hydrated iron chloride as principal constituent
11 p1824 A71-25703
- Venus ferrous chloride hydrate cloud production, examining geochemical problems
11 p1824 A71-25704
- IRON COMPOUNDS**
NT CHROMITES
NT FERRATES
NT FERRITES
NT ILMENITE
NT IRON CHLORIDES
NT IRON CYANIDES
NT IRON OXIDES
NT LIMONITE
NT MAGNETITE
NT TROILITE
- Cubic iron carbide identification from iron meteorites by X ray powder photography and electron microscopy
07 p1200 A71-20057
- Carbon monoxide gas phase vibrational relaxation by Fe atoms, using shock tube for determination of decomposition rate of iron carbonyl in dilute mixture with Ar
08 p1337 A71-20672
- Clear taenite formation in bronzite and hypersthene chondrites studied by metallographic and electron microprobe
10 p1680 A71-24985
- Photomagnetic effect in ferric borate, noting photoinduced change, radiation sensitivity and temperature effects
12 p1943 A71-26857
- Pyroxferroite crystal structure from Apollo lunar Mare Tranquillitatis sample, using X ray counter-diffractometer measurements
23 p3737 A71-43606
- IRON CYANIDES**
Polarographic blood oxygen measurement by principle of oxygen liberation into physical solution by potassium ferricyanide
07 p1053 A71-20337
- IRON ISOTOPES**
NT IRON 57
- IRON METEORITES**
Isotopic Rb/Sr age and initial chondritic ratio for silicate inclusions in Colomera iron meteorite
02 p0318 A71-12902
- Pitts iron meteorite exposure history, noting consistency of rare gases isotopes contents in separated metal phase with prehistoric radiation flux increase
03 p0487 A71-13334
- Iron meteorites microstructure investigation by light and transmission electron microscopy, determining plastic deformation and cooling rate from thermomechanical history
06 p0964 A71-17343
- Cubic iron carbide identification from iron meteorites by X ray powder photography and electron microscopy
07 p1200 A71-20057
- Cosmic rays produced He, Ne and Ar isotope concentrations in iron meteorite separated phases, using Rudstam spallation model
10 p1676 A71-24506
- Fe meteorite Grant, measuring radial distribution of cosmogenic nuclides of K, Ca, Ti, V, Cr and Mn produced by cosmic rays
11 p1819 A71-25224
- Rare earth and heavy elements determination in olivine hypersthene and enstatite chondrites by spark source mass spectroscopy, noting Fe meteorite silicate inclusions composition
11 p1819 A71-25225
- Soviet book on diamonds in meteorites covering abundance and origin in stony and iron meteors, distribution and structure
11 p1833 A71-26326
- Iron and stony iron meteorites chemical classification, noting Ni, Ga, Ge and Ir concentrations and metal phases
13 p2134 A71-28290
- Stony-iron meteorites composition, considering Ca/Al ratio in mesosiderites
13 p2142 A71-29141
- Bibliography and review of meteorites not classified as chondrites, considering achondrites, stony irons and iron meteorites
17 p2798 A71-34453
- Stony, stony-iron and iron meteorites magnetic properties relating susceptibility to nickel iron content
17 p2810 A71-35720
- Canyon Diablo iron meteorite optical microscopic and X ray structural analysis finding moissanite /or carborundum/
17 p2810 A71-35722
- Iron meteorites total N abundances determination by inert carrier gas fusion extraction gas chromatography
23 p3734 A71-43243
- CrN discovery in iron meteorites, determining carlsbergite mineral composition by electron microprobe
23 p3770 A71-44015
- IRON OXIDES**
NT CHROMITES
NT ILMENITE
NT MAGNETITE
- Meteoritic iron oxides abundances from recoilless resonance absorption spectra
02 p0306 A71-11993
- IRON 57**
Fe 57 nuclei longitudinal and transverse relaxation in yttrium iron oxide sublattices at various temperatures and magnetic field strengths
05 p0794 A71-16878
- Mossbauer instrumental analysis of Apollo 12 rock and soil samples, measuring nuclear gamma resonance of iron 57
23 p3759 A71-43764
- IROQUOIS HELICOPTER**
U UH-1 HELICOPTER
- IRRADIANCE**
NT ILLUMINANCE
NT SOLAR CONSTANT
- Partially coherent laser beam phase fluctuations using reversing-front interferometer for time integrated irradiance measurement, considering atmospheric turbulence effects
04 p0627 A71-15683

IRRADIATION

Image contrast limits in thin phase hologram reconstruction of diffuse objects with large reference-object irradiance ratios

04 p0601 A71-15687

Two mode He-Ne gas laser irradiance autocorrelation function measurement, comparing time-to-amplitude converter techniques with frequency domain measurements

05 p0760 A71-16268

Laser irradiance pattern from aperture with truncated Gaussian field distribution, evaluating diffraction integral subject to Fresnel approximation

05 p0763 A71-16904

Light scattering from ultrathin free liquid films, calculating irradiance optical functions variation with geometry and film thickness

05 p0763 A71-16906

Holographic turbulence beam interferometry, considering phase retardation role in hologram diffracted waves for fringes irradiance distribution definition

07 p1110 A71-19479

Photographic emulsion model for signal to average noise irradiance ratio analysis in hologram reconstruction

08 p1287 A71-21188

Natural illumination and irradiance levels for photoelectric device design and specifications in nocturnal light conditions

10 p1641 A71-24056

Atmospheric turbulence effects on stellar irradiance and phase, discussing electro-optical recording technique and computer generated statistical data

14 p2270 A71-30016

Imagery of periodic objects through interposed turbulent medium, investigating diffraction images irradiance distribution and contrast

14 p2275 A71-30827

Holograms of physical objects, calculating irradiance statistical distribution from reference-object beam powers ratio

15 p2412 A71-32594

Ejected photoelectron count probability distribution due to periodic irradiance modulation of amplitude stabilized light beam

15 p2452 A71-32595

Noise equivalent irradiance equation for airborne IR scanner at peak response detector wavelength, involving target scene radiance and hot iodine emittance

18 p2917 A71-36053

Photovoltaic and electron-voltaic properties of diffused and Schottky barrier GaAs diodes, considering irradiance in 0.001-10,000 microwatt/sq cm range

19 p3027 A71-37484

Noise equivalent irradiance evaluation of passive IR scanners for target thermal mapping systems operating in earth atmosphere, determining figure of merit

22 p3545 A71-42150

IRRADIATION

NT AURORAL IRRADIATION

NT DEUTERON IRRADIATION

NT ELECTRON IRRADIATION

NT ION IRRADIATION

NT NEUTRON IRRADIATION

NT PROTON IRRADIATION

NT X RAY IRRADIATION

Cylindrical thermionic converter irradiation tests under Incore Thermionic Reactor (ITR) Project, discussing postmortem examinations

02 p0195 A71-12243

Primary immune response chemical radioprotection in white mice during gamma irradiation, using serotonin as chemical protective and sheep red blood cells as immunizing agents

05 p0710 A71-16816

Radioresistant yeast strain *Saccharomyces cerevisiae*, discussing cycloheximide and gamma irradiation treatment influence on growth

07 p1034 A71-18943

Mice protection against irradiation damage by adrenochrome monoguanylhydrazine methanesulphonate

07 p1038 A71-18977

Corneal transparency in metabolic activity absence, using acid mucopolysaccharide depletion and prolonged gamma irradiation

09 p1393 A71-22985

Single isolated solid particle irradiation in vacuum, using electrical suspension system with electric field produced by six electrodes on solid cube surface

11 p1806 A71-26087

IRREGULARITIES

Large scale ionospheric irregularities from Faraday fading records by satellite observations, studying height, fluctuations, electron contents, horizontal size and orientations

05 p0741 A71-16439

IRREVERSIBLE PROCESSES

Irreversible processes during formation of contact between indium telluride thin film and metal in vacuum at high temperature

01 p0137 A71-10150

Kinetic theory of gas mixtures and thermodynamic laws of irreversible processes, deriving hydrodynamic equations and Onsager relations

01 p0130 A71-10793

Dissipative structures in thermodynamics of irreversible processes of hydrodynamics and chemical kinetics

04 p0675 A71-14792

Book on nonequilibrium /irreversible/ thermodynamics covering field theories, balance equations, continua, variational principles, energy dissipation, entropy, etc

04 p0626 A71-15600

Orthogonality principle in irreversible thermodynamics, proving generalization for Onsager nonlinear symmetry relations

05 p0837 A71-16708

Chemical energy conversion into mechanical work, examining irreversible mixing, Van Hoff box and Carnot cycle

05 p0717 A71-16785

Metal fretting corrosion energy analysis in terms of thermodynamics of irreversible process

06 p0904 A71-17942

Irreversibility control in two gas flows mixture, discussing jet engines thrust increase by air-exhaust gases admixture

06 p0945 A71-18051

Steady planar detonation with direct first order one-step irreversible exothermic unimolecular reaction, examining structure by limit process expansions analysis

08 p1375 A71-20857

Soviet papers on heat and mass transfer covering conduction, transport in capillary and dispersed systems, irreversible thermodynamics, material drying, etc

10 p1696 A71-24481

Cosmic evolution and thermodynamic irreversibility, discussing definitions and relationships of thermodynamic, historical and cosmological arrows of time

11 p1828 A71-25736

Transport coefficients interrelations, using irreversible process thermodynamics

13 p2161 A71-28620

Reversible and irreversible processes and arrow of time concept, considering direct interaction of two charges without field

13 p2101 A71-28766

Nonstationary perturbation propagation in gaseous medium with irreversible internal process /chemical reactions or excitations with one degree of freedom of molecules/

14 p2338 A71-30823

Reversibility/irreversibility definition application to thermostatics, expressing work by Pfaffian form

15 p2513 A71-31922

German textbook on fundamentals of thermodynamics covering energy conversion, reversible/irreversible processes, chemical/molecular thermophysics, statistical analysis, probability theory, etc

15 p2516 A71-32767

Chemical energy conversion into mechanical work, examining irreversible mixing, van Hoff box and Carnot cycle

16 p2540 A71-33037

Continuous media nonlinear thermomechanical behavior, presenting finite element formulation of deformation and irreversible thermodynamics problems

16 p2654 A71-33095

Thermodynamics of irreversible processes extended to nonlinear systems remote from equilibrium, considering Onsager reciprocity relations

23 p3780 A71-43104

Structural materials ability for irreversible conversion of mechanical to thermal energy from free longitudinal vibrations attenuation measurements in rod

24 p3817 A71-45200

IRRITATION

NT TOXICITY AND SAFETY HAZARD

IRRROTATIONAL FLOW

U POTENTIAL FLOW

ISCHEMIA

Submaximal exercise ECG test in screening high risk populations for occult ischemic heart disease

03 p0372 A71-13491

Ischemia effects on impulse transmission to muscle fibers in man, using single fiber electromyography

05 p0706 A71-16320

Aircrews coronary insufficiency diagnosis via electrocardiographic modifications after exertion, observing ischemia

06 p0860 A71-18192

Ischemic deafferentation of transversostriated muscle quadriceps femoris in cats contributing to hypokinesia and psychophysiological disturbances

06 p0854 A71-18362

Myocardial ischemia and necrosis without major coronary arteries obstruction, investigating possible deranged hemoglobin-oxygen transport

14 p2185 A71-30286

Myocardial ischemia observations, utilizing morphologic and pathophysiological correlations with cinecoronary arteriography, left ventriculography and hemodynamic examination

14 p2185 A71-30287

Cerebral ischemia effects on sensorimotor cortex function in cats, recording spontaneous EEG and pyramidal response to cortex electrical stimulation

15 p2359 A71-31939

Unconsciousness, confusion, amnesia, syncope and sudden death of pilots in flight due to silent ischemic heart diseases

18 p2855 A71-36280

ISENTROPE

Ideal gas isentropic mean value exponent, calculating state variables

03 p0520 A71-13900

High temperature singly and doubly ionized monatomic gas and partially dissociated and singly ionized diatomic gas, showing adiabatic and isentropic exponents relationship

16 p2662 A71-32835

ISENTROPIC PROCESSES

Nonstationary isentropic low density flows within axial or central symmetry, suggesting characteristics with flow rate and sound speed variation as in stationary source flow

07 p1014 A71-19729

Small curvature radius/throat radius ratio supersonic nozzles mass flow rate coefficients at high Reynolds numbers, appraising isentropic flow prediction methods

07 p1015 A71-19877

One dimensional isentropic gas motion in acoustic wave reflection from cylindrical tube nonplane closed end under flow

08 p1276 A71-21478

Flowfield isentropes in conical gas flow with singular current surfaces

08 p1227 A71-21864

Static relativistic theory of isentropic spherically symmetric star equilibrium stability, assuming certain conditions with respect to mass-energy density and total baryon number

09 p1529 A71-23597

Acoustic waves reflection from nonplanar closed end of cylindrical tube with one dimensional isentropic gas flow from Riccati differential equation solution

14 p2227 A71-30665

Two dimensional subsonic irrotational isentropic flow around thick profiles, using coordinate perturbation method

15 p2343 A71-31167

Vortex boundary layer with dissipative viscous wall and isentropic sublayers, calculating adiabatic surface temperature

17 p2669 A71-34217

Nondeveloping synoptic weather systems description by isentropic structural analysis, studying particle motion and dynamic behavior using models

18 p2944 A71-36219

Flow field isentropes in conical ideal gas flow with singular stream surfaces

20 p3176 A71-39363

ISING MODEL

U FERROMAGNETISM

U MATHEMATICAL MODELS

ISIS SATELLITES

NT ALOUETTE 2 SATELLITE

Simultaneous ionospheric electron density measurements from Isis satellite topside and incoherent scatter soundings

15 p2394 A71-31428

Alouette and Isis satellites flight data comparison with attitude and spin dynamics theory, considering solar radiation pressure and gravitation and magnetic field effects

22 p3609 A71-41997

ISIS-I ionospheric sounding satellite spin rate behavior

22 p3612 A71-42786

ISLANDS

NT GREAT BRITAIN

NT JAPAN

NT NEW ZEALAND

NT PACIFIC ISLANDS

NT PHILIPPINES

NT WALLOPS ISLAND

ISOBARS (PRESSURE)

Complex monitoring of aerological information on geopotential and temperature of principal isobaric surfaces by static method and optimal interpolation on semiautomatic basis

17 p2769 A71-34299

ISOBUTYLENE

U BUTENES

ISOCHORIC PROCESSES

Black SiC varistors IV characteristics and conductivity, investigating fast neutron irradiation and isochronal annealing effects

12 p1886 A71-26898

ISOCROMATICS

Holographic interferometry application to photoelasticity, discussing relationship between isochromatic and isopachic fringes and fringe families separation method

21 p3456 A71-40228

ENERGETIC PROCESSES

Steady supersonic isoelectric flow of thermally and calorically perfect gas past circular cones at zero angle of attack, using dimensional perturbation method 12 p1863 A71-26939

**ISOLATION
SOCIALLY ISOLATION
ISOLATORS**

Millimeter wave semiconductor isolator using circular waveguide with coaxial n-type InSb in longitudinal magnetic field 14 p2212 A71-30510

Four electrodes Hall effect isolator equivalent circuit, describing impedance matrix elements frequency dependence 22 p3520 A71-41705

ISOMERIZATION

Ion cyclotron resonance application to propanol ion structure formed in double McLafferty rearrangement, demonstrating direct enol ion formation instead of by isomerization or ketonization 07 p1055 A71-19598

Shock tube isomerization of cyclopropane to propylene as model system for small ring compounds, noting rate constants 19 p3010 A71-37272

Phenylpropargylene and phenylethynyl nitrene intermediacy, abstracting hydrogen to produce benzylacetylene, phenyllallene and 1-methyl-2-phenylacetylene 22 p3508 A71-42886

ISOMERS

Mass spectroscopic determination of geometric isomers of alpha, beta-unsaturated carboxylic acids, noting various modes of fragmentation 01 p0028 A71-11304

Alpha-beta unsaturated carboxylic acids geometric isomers determination by mass spectroscopy 11 p1727 A71-25230

IR and Raman spectra vibrational analysis of crystalline and fluidic oxalyl bromide, explaining observations by two geometrical isomers existence 11 p1727 A71-25363

ISOMORPHISM

Two finite undirected linear graphs, determining isomorphism 07 p1148 A71-20370

Steady and linear systems discretization by Laguerre transformation and isomorphism between continuous and discrete signals 16 p2550 A71-34058

ISOPERIMETRIC PROBLEM

Isoperimetric problem upper bounds for fundamental frequencies in free oscillations of incompressible fluid in container 16 p2559 A71-33483

ISOPHOTES

Solar corona isophotes ellipticity and equal polarization curves during 7 March 1970 eclipse, using isodensitometric and polarimetric techniques 04 p0651 A71-15666

Isophote evolution in artificial clouds, using photometric analyzer with TV screen as monitor 06 p0867 A71-17704

Planetary nebulae NGC 1535, 6572, 6543, 7662 and 7009, observing monochromatic photographs and isophotic contours 09 p1521 A71-22870

Inner solar corona polarization during 22 September 1968 total eclipse based on isolines from polarimetric photographs 12 p1955 A71-26590

Orionid and Leonid meteor trains, determining diffusion coefficient from isophotes variation 12 p1965 A71-27230

Temperature dependent isophote wavelength in Brill and Planck formulas, comparing uvby and UVB photometric systems 13 p2068 A71-28512

Orionid and Leonid meteor trains, determining diffusion coefficient from isophotes variation 19 p3132 A71-37382

Two dimensional isophotes of extreme solar corona from integrated vidicon pictures taken from moon surface by Surveyors 6 and 7 19 p3147 A71-38670

Monochromatic observations of coronal loop, using isophotal map from coronagraph through Fabry-Perot interferometer 23 p3768 A71-43846

Southern Milky Way isophote maps by near-UV surface photometry, showing brightest areas in Sgr/Scor, Car, Vel/Pup and Cyg 24 p3867 A71-44436

**ISOPHOTES
U NOMOGRAMS
ISOPROPYL COMPOUNDS**

Apollo 11 and 12 lunar soil samples common contaminant identified as diisopropyl disulfide, using chromatograph mass spectrometer 05 p0716 A71-16453

ISOPROPYL NITRATE

Monopropellant /isopropyl nitrate/ detonation limits, characteristics and properties 05 p0795 A71-16516

ISOPYCNIC PROCESSES

Atmospheric upper boundary condition in baroclinic forecast, recommending correction using isopycnicity properties of atmospheric processes near 7 km altitude 12 p1924 A71-26738

ISOTASY

Lunar mascon origin, considering primordial atmosphere and hydrosphere formation from internal heating with resultant mass imbalance and isostatic compensation 03 p0492 A71-14053

Vertical motions on moon resulting from stress differences leading to isostatic equilibrium, discussing maria, craters and mascons 16 p2636 A71-33504

Lunar gravitational field interpretation based on Apollo data, considering mascons creation, isostasy, thermal history and maria orientation hypotheses 16 p2636 A71-33506

ISOSTATIC PRESSURE

Isostatic pressing for large complex metal powder parts, comparing with die-compacting 01 p0088 A71-10814

Three dimensional isostatic pressing process, discussing equipment, tooling and forging preforms and finished parts production 10 p1618 A71-24764

ISOSTERIC PROCESSES

U ISOPYCNIC PROCESSES

ISOTHERMAL FLOW

Heated jet injection into isothermal turbulent boundary layer, investigating temperature distribution downstream with conduction model 04 p0572 A71-15499

Turbulent diffusion coefficients in isothermal and nonisothermal pipe flow, comparing with Bory and Taylor theories 07 p1222 A71-18994

Natural convection heat transfer between two isothermal concentric spheres, using water and silicone oils as convective fluids 07 p1222 A71-18995

Radiation diffusion in one dimensional isothermal medium moving with constant velocity gradient, assuming complete frequency redistribution and arbitrary absorption coefficient profile 07 p1192 A71-19290

Thin shallow annular radiating fins for heat removal from sphere or polyhedron with isothermal surfaces, determining optimal weight and geometrical parameters 12 p1986 A71-27331

Isothermal flow under capillary forces in heat pipe with zero gravity, deriving relation between flow rate and duct parameters 13 p2050 A71-29219

Divergent semibounded turbulent isothermal jet of constant density emerging from slot, determining length of initial and main sections 16 p2560 A71-33613

Nonlinear heat transfer in plane rarefied isothermal Couette gas flow, using BGK model 16 p2561 A71-34143

Heat transfer due to combined free and forced convection in horizontal isothermal tube flow [ASME PAPER 71-HT-3] 19 p3163 A71-37981

Isothermal gas rotation in circular cylinder, calculating symmetric normal frequency modes [AIAA PAPER 71-999] 24 p3818 A71-44590

Hydraulic resistance of laminar isothermal flow of fluid with structural viscosity in circular cylindrical rigid channel 24 p3821 A71-45227

ISOTHERMAL LAYERS

Cylindrical sample longitudinally isothermal zone unsteady temperature field calculation from heat conduction equation with allowance for temperature dependence of thermodynamic properties 03 p0520 A71-13960

Shearing gravity waves /Kelvin-Helmholtz/ instability in isothermal layer model discontinuous interface application to CAT 05 p0777 A71-16667

Turbulent boundary layer in incompressible fluid with vanishing viscosity, analyzing degeneration of isothermal boundary layer, viscous sublayer and density pulsations 07 p1085 A71-18753

Thin gas optical limit isothermal curves, discussing Planck mean emission coefficients 07 p1222 A71-18993

Low density plasma in magnetic field, investigating existence possibilities of stationary isothermal jump and plane wave periodic solution 08 p1340 A71-21493

Low density plasma in magnetic field, investigating existence possibilities of stationary isothermal jump and plane wave periodic solution 16 p2618 A71-33044

Viscous stresses distribution in isothermal incompressible turbulent boundary layer with positive pressure gradient by diffusers in open jet wind tunnel 17 p2725 A71-34209

Self similar numerical and asymptotic solutions of laminar multicomponent isothermal boundary layer equations for large blowing rates 17 p2673 A71-35633

ISOTHERMAL PROCESSES

Ti alloys isothermal forging, using precision-cast superalloy dies [SME PAPER MF-70-122] 01 p0089 A71-11255

Turbulent heat and mass exchange intensity at gas screen, investigating nonisothermality and wall penetrability effects 04 p0683 A71-15497

Free convection temperature field about isothermal spheres in air, using interferometer for axisymmetric field 04 p0686 A71-15523

Microstructure changes during austenite isothermal decomposition in Fe-Mo-C alloys 04 p0614 A71-15778

Stationary flow of viscoplastic liquid in annular gap with temperature dependent viscosity, taking into account energy dissipation 04 p0579 A71-15799

Hydrogen-oxygen reaction kinetics behind steady state shock waves under isothermal branched chain explosion limits 05 p0834 A71-16513

Cosserat surfaces and variable thickness elastic plates linear isothermal theory, deriving constitutive equations corresponding to isotropic three dimensional plate bending and stretching 05 p0831 A71-17250

Acetylene pyrolysis kinetics, considering isothermal vs adiabatic conditions and surface catalyzed vs homogeneous gaseous [WSS/CI PAPER 70-18] 06 p0943 A71-17660

Microstructure and mechanical properties of heat resistant alloy under homogenization and subsequent isothermal heat treatment 08 p1317 A71-21764

Ternary systems Hf-W-B, Hf-Re-B and Nb-Re-B isothermal sections phase diagrams at high temperature, using X ray analysis 08 p1317 A71-21858

Uniaxial, equal biaxial and unequal homogeneous biaxial strain rates of viscoelastic materials under isothermal tensile test conditions 09 p1481 A71-22141

Molten alumina and chromia reactions with refractory metals, calculating isobaric-isothermal potential variations 09 p1466 A71-22165

Ultrasonic vibration effects on TiC sintering during isothermal heating with and without pressure 09 p1470 A71-23063

Isothermal transformation of metastable beta Ti-Mo alloys, considering contraction start point coincidence with point of quenched omega transformation to aged omega in TTT diagram 10 p1625 A71-24006

Point defects and fine precipitates effects on fatigue strength of high strength alloys, exhibiting higher fatigue strength in isothermally aged samples 10 p1625 A71-24009

IR radiative heat transfer in nongray nonisothermal gases, giving solutions for radiative equilibrium and combined conduction and radiation 10 p1698 A71-25094

Venus atmosphere adiabatic and isothermal models, investigating water vapor content, pressure and temperature 12 p1964 A71-27085

Nonisothermal plasticity and creep models, stressing real materials deformation micromechanism theories 12 p1979 A71-27354

Refractory steels plastic deformation characteristics under isothermal creep 13 p2084 A71-28125

Field ion emission microscopic study of isothermal order-disorder transformation kinetics in water quenched Ni-Mo alloys 13 p2085 A71-28577

Static and quasi-static atmospheric motions, using linearized equations for isothermal compressible atmosphere 13 p2097 A71-29084

Hf-W-B, Hf-Re-B and Nb-Re-B ternary systems isothermal phase diagrams at high temperature, using X ray analysis 14 p2261 A71-30837

Heat pipe application to OAO as structural isothermalizer, considering overall spacecraft thermal network analysis 15 p2512 A71-31594

Book on viscoelasticity covering isothermal stress-strain relations, wave propagation, mechanical properties, thermodynamics and nonisothermal effects 15 p2509 A71-32438

ISOTHERMS

Black radiation absorption by isothermal gas in entire spectrum, discussing Hottel empirical formula 17 p2836 A71-34214

Thermal stresses in plane strain of isotropic micropolar elastic solids without heat sources, reducing thermoelastic to isothermal problem 17 p2821 A71-34583

Sodium superoxide isothermal decomposition, detailing metallic oxide effects with differential thermal analysis, thermogravimetry and differential thermogravimetry 17 p2694 A71-34672

Venus atmosphere adiabatic and isothermal models, investigating water vapor content, pressure and temperature 19 p3133 A71-37435

Curvature effect on heat and mass transfer from the isothermal sphere in potential flow [ASME PAPER 71-HT-7] 19 p3164 A71-37984

Finite strain theory for elastic-plastic deformation, considering isothermal shear of neo-Hookean material before yielding and during elastic unloading 20 p3267 A71-38794

Metastable beta type Ti binary alloys isothermal transformation microstructure observation by microscopic and X ray diffraction methods 22 p3562 A71-41947

Isothermal martensite transformations in Fe-Ni-Cr alloys, explaining kinetics difference in terms of elastic parameters small variations 23 p3688 A71-42925

ISOTHERMS

Damkohler analysis of nitrogen-silica gel absorption isotherm in multimolecular range, noting vapor phase transport and adsorbed phase diffusivities 03 p0517 A71-13175

One dimensional transient heat conduction analysis by iterative isotherm migration method, discussing boundary conditions, stability, truncation error and relative efficiency 04 p0677 A71-15452

Equilibrium adsorption isotherms correlation for low temperature cryodeposits, using Dybinn-Raduschkevich equilibrium equation to estimate hydrogen capacity of cryosorption pumping system 10 p1643 A71-25011

Ti-Co-B and Ti-Re-B systems diagrams of isothermal sections at 800 and 1400 C 13 p2083 A71-28008

ISOTONICITY

Isotonic training effects on circulation for limb muscular strength characteristics, using peak blood flow and venous compliance measurements 11 p1719 A71-26071

ISOTOPE EFFECT

Simple gases and liquids thermodynamic properties, calculating isotopic effects by corresponding states law with quantum corrections 02 p0331 A71-12187

Isotope effects on collision dynamics of molecular hydrogen-argon ion reactions, using chemical accelerator 05 p0784 A71-15974

Mn type peculiar A stars relative abundance from curve of growth analysis, discussing isotope shifts, nucleosynthesis, explosion reactions and structure acceleration 09 p1529 A71-23596

Isotope effects in Lyman and Werner systems of molecular hydrogen, HD and molecular deuterium, calculating band strengths, oscillator strengths and Franck-Condon factors 11 p1803 A71-26072

Transient photoconductivity measurements of room temperature electron mobility in deuterated anthracene single crystals, discussing isotope effect 20 p3194 A71-39348

Apollo 14 lunar soils chemical element concentrations by atomic absorption spectrophotometry and isotope dilution 20 p3292 A71-39381

Spectral resolution of matrix Raman spectroscopy and depolarization measurements of isotope splitting, comparing with complementary IR data 20 p3194 A71-39404

Relative abundances and mass measurements of Li, Be and B isotopes in primary cosmic rays, using balloon flown emulsion stacks 22 p3593 A71-42329

Criticism of paper on spallation cross section for Be 10 production from oxygen high energy fragmentation in meteorites 22 p3508 A71-42350

Inelastic scattering alpha-gamma angular correlations from C 12, Mg 24, Ni 58 and Sn 120 decay measurements 23 p3706 A71-43198

ISOTOPE SEPARATION

Carbon kinetic isotope fractionation into carbon dioxide and organic compounds in meteorite-like Fischer-Tropsch reaction with nickel-iron or magnetite catalyst 03 p0483 A71-13013

Laser applications in chemical research, exploring fast chemical processes, isotope enrichment and molecular reactions and structure observations 07 p1124 A71-19790

Element and isotope separation effects under centripetal acceleration in rotating plasma, using mass spectrometric diagnostics 22 p3580 A71-41584

ISOTOPE SHIFT U ISOTOPE EFFECT ISOTOPES

NT ALUMINUM ISOTOPES
NT ALUMINUM 26
NT ALUMINUM 27
NT ARGON ISOTOPES
NT BERYLLIUM 7
NT BERYLLIUM 9
NT BERYLLIUM 10
NT BORON ISOTOPES
NT CADMIUM ISOTOPES
NT CALIFORNIUM ISOTOPES
NT CARBON ISOTOPES
NT CARBON 12
NT CARBON 13
NT CARBON 14
NT CERIUM ISOTOPES
NT CERIUM 144
NT CESIUM ISOTOPES
NT CESIUM VAPOR
NT CESIUM 133
NT COBALT ISOTOPES
NT COBALT 60
NT DEUTERIUM
NT HELIUM ISOTOPES
NT HYDROGEN ISOTOPES
NT IRON 57
NT KRYPTON ISOTOPES
NT LEAD ISOTOPES
NT LITHIUM ISOTOPES
NT LUTETIUM
NT MAGNESIUM ISOTOPES
NT MANGANESE ISOTOPES
NT NEODYMIUM ISOTOPES
NT NEON ISOTOPES
NT OXYGEN ISOTOPES
NT OXYGEN 18
NT PLUTONIUM
NT PLUTONIUM 238
NT POLONIUM 210
NT POTASSIUM ISOTOPES
NT RADIOACTIVE ISOTOPES
NT RADON ISOTOPES
NT RUBIDIUM ISOTOPES
NT SCANDIUM ISOTOPES
NT SILICON ISOTOPES
NT STRONTIUM ISOTOPES
NT SULFUR ISOTOPES
NT TELLURIUM
NT THORIUM ISOTOPES
NT TITANIUM ISOTOPES
NT TRANSURANIUM ELEMENTS
NT TRITIUM
NT URANIUM ISOTOPES
NT URANIUM 235
NT VANADIUM ISOTOPES
NT XENON ISOTOPES
NT XENON 133

Inelastic scattering of protons from In 115, using proton beam cyclotron 01 p0130 A71-10482

CuH lines in sunspot spectra and solar isotopic ratio of Cu obtained from Cu I lines 06 p0969 A71-17971

Superheavy transactinide isotopes in outer space, discussing single standard composition of cosmos material bulk 08 p1351 A71-20958

Gadolinium isotopic composition and neutron capture effects in meteorites 08 p1365 A71-21693

Low temperature space radiator to reject thermal power from isotope Brayton cycle power system for future space missions 20 p3181 A71-38917

Rare gas concentrations and isotopic abundances in lunar rocks, fines and breccias from Apollo 11 and 12 flights, determining exposure and gas retention ages 23 p3753 A71-43720

Isotopic abundances and concentrations of spallogenic Ne, Kr and Xe in Apollo 12 rock 12002, constructing three stage model of irradiation history 23 p3753 A71-43722

ISOTOPIC LABELING

Ni diffusion and electric transfer in Ni-Mo alloy, using isotope tracer technique 01 p0097 A71-10043

Pressure and gas composition effects on sodium acetate-C 14 incorporation into liver lipids, indicating metabolic relationships to decomposition sickness 08 p1238 A71-20814

Absorption and incorporation rates of C 14 glucose in rats under acute hypoxia 08 p1242 A71-21964

Solar temperature after formation, using isotope composition differences in terrestrial and extraterrestrial xenon 10 p1668 A71-2312

Gas rich meteorites and carbonaceous chondrites with trapped argon, noting isotopic correlation with neon 10 p1680 A71-2402

Extraterrestrial life detection by tagged carbon dioxide extraction from substrate in radioactive glucose containing soil nutrient media 13 p2068 A71-21802

Lung scanning, describing moving detectors, electronic apparatus adjustment and choice of radionuclide and labelled compound 20 p3192 A71-3911

ISOTROPIC MEDIA

Crack opening in infinite isotropic elastic solid with displacements applied to crack surface 01 p167 A71-1021

Linear isotropic viscoelastic media, determining stress relaxation and creep properties 01 p0170 A71-1001

Boundary value problems in thermoelectric equilibrium of unbounded isotropic plate with slits and foreign circular inclusion 01 p0170 A71-1001

Oblique reflection of horizontally and vertically polarized electromagnetic waves from isotropic media with limiting Epstein stratifications 01 p0031 A71-1071

Antenna gain, transmission efficiency and receiving cross sections in dissipative isotropic medium 01 p0041 A71-1161

Isotropic photophysical channels transfer function analysis, using two dimensional Fourier transforms 02 p0211 A71-1111

Image transmission in isotropic photophysical channels, examining object-image brightness relationships 02 p0211 A71-1111

Laser light frequency mixing and doubling in isotropic bodies in crossed magnetic and electric fields, examining magneto-electro-optical processes 02 p0261 A71-1211

General solution to three dimensional problem in elasticity theory for cylindrical transverse isotropic medium, applying results to thick walled shells under strain 02 p0329 A71-1251

Elastic plate plane stress analysis by Euler variational method for arbitrary geometric shapes and loading, obtaining isotropic and orthotropic solutions 02 p0330 A71-1271

Tied ether existence hypothesis determinants comparing gyrocompass precessional couple at earth surface and at 3300 m depth for negative results 03 p0456 A71-1336

Anisotropic thin rods deformation, extended to Nikolai constraints condition on Kirchhoff analogy for isotropic rods 03 p0506 A71-1356

Distance dependent stress concentration of isotropic plate with two elliptical holes under tension of coposed point forces 03 p0506 A71-1356

Isotropic half plane weakened by circular holes normal to boundary, calculating stress-strain state created by concentrated force 03 p0506 A71-1356

Optical plate induced helicoidal steady light field in laser cavity, imparting structure to isotropic transparent material medium 03 p0436 A71-1376

Stationarity of complementary energy in nonlinear elasticity theory, using Piola stress tensor representation for isotropic elastic media 03 p0513 A71-1421

Pressurized isotropic viscoelastic hollow cylinder bonded to elastic casing, analyzing stress during finite deformation 04 p0668 A71-1511

Crack perpendicular to planar interface between isotropic half spaces, noting elastic constants effect on stress components distribution and relative magnitudes 04 p0670 A71-1531

Plasticity theory isotropic and anisotropic yield conditions for various stresses 04 p0672 A71-1571

Semiinfinite isotropic linear Cosserat continuum surface under impulsive loading, calculating displacements with Laplace transformation 04 p0672 A71-1581

Elastic isotropic body finite plane deformation considering displacement and stress functions relationship 05 p0822 A71-1631

Excited waves due to transverse disturbance normal to boundary in dielectric half of isotropic plasma with Cerenkov instability 05 p0789 A71-1661

Isotropic and slightly anisotropic materials elastic constants evaluation from ultrasonic reflection measurement 05 p0771 A71-1721

- Thin isotropic plate nonstationary coupled thermoelasticity problem, obtaining recursion equation system for thermal stresses 06 p0983 A71-17367
- Relaxation theory of Rayleigh scattering of light by isotropic continuous medium, deriving spectral densities via fluctuation dissipation theorem 06 p0927 A71-17596
- Stress-strain state of isotropic three-layer plates and shells with rigid and light weight fillers, noting weakening by curvilinear holes 06 p0987 A71-17769
- Stress wave propagation from spherical cavity in isotropic nonhomogeneous elastic medium in contact with vacuum at infinity, obtaining closed form solution 06 p1001 A71-18228
- Unbounded isotropic elastic plate traversed by two parallel cracks, obtaining limiting equilibrium state 07 p1211 A71-19192
- Wave dispersion in transversely isotropic rods, discussing phase velocities, spectral lines and cut-off frequencies 07 p1214 A71-19957
- Homogeneous isotropic layers stack on rigid base with periodically varying elasticity parameters, calculating equilibrium under normal distributed load 07 p1217 A71-20460
- Isotropic material structures under static external loads, considering stress rupture strength models 08 p1371 A71-21608
- Bifurcation of equilibrium of three dimensional elastic isotropic body with arbitrary elastic potential under large subcritical strains 08 p1373 A71-21866
- Thermoelastic stress and temperature distribution in doubly connected isotropic plate 08 p1374 A71-21948
- Isotropic incompressible viscoelastic solid deformation field under uniaxial and equal biaxial relaxation, determining constitutive equation 09 p1534 A71-22142
- Nonlinear elastic incompressible transversely isotropic body with finite initial deformations, considering linearized problems of static and dynamic equations 09 p1534 A71-22178
- Elastic waves in isotropic body, calculating initial deformation effect on propagation rate based on finite deformation theory 09 p1537 A71-22515
- Infinite isotropic plate weakened by cracks along circular arcs, calculating stress-strain state and critical loads 09 p1538 A71-22524
- Electromagnetic transient signal nonlinear dispersion in homogeneous isotropic partially ionized plasma medium 09 p1505 A71-23520
- Cerenkov energy losses of rigid cylindrical uniformly charged bunch moving at constant speed through homogeneous isotropic dispersive dielectric 09 p1498 A71-23574
- Variational formulation for minimum weight of structures with given yield stress, considering homogeneous isotropic material, plasticity condition and collapse mechanism 10 p1685 A71-23977
- Isotropic homogeneous incompressible elastic body under surface tensions and conservative forces, showing six families of equilibrated deformations 10 p1687 A71-24347
- Thin isotropic plates with time and temperature dependent surface heat exchange coefficients, presenting heat conduction equations 10 p1695 A71-24361
- Homogeneous isotropic elastic body stresses after imposing small deformation on strain configuration obtained from initial small deformation of original configuration 10 p1689 A71-24503
- Plane stress state determination in laminated locally isotropic elastic solid based on stress functions 11 p1788 A71-25438
- Existence theorems in micropolar elastostatics three dimensional boundary value problems relating to isotropic and homogeneous bodies equilibrium 11 p1847 A71-25442
- Quantitative analysis of secondary harmonic generation in DC polarized isotropic laser beam, emphasizing molecular mechanisms and symmetrical effects 11 p1773 A71-25566
- First order EM discontinuities propagation in nonlinear centrosymmetric isotropic material with displacement field dependent on electric field and induction field dependent on magnetic intensity 11 p1798 A71-25568
- Ultrasonic wave propagation in deformed isotropic elastic materials based on second order theory, examining principal stress axis rotation effect 11 p1849 A71-25682
- Nonstatic random isotropic medium geometrical optics, considering refractive index temporal fluctuation [ONERA-TP-970] 12 p1929 A71-26822
- Heat conduction effects on small amplitude plane harmonic wave propagation in transversely isotropic elastic Zn single crystals 12 p1985 A71-26925
- Transversally isotropic spherical shell with constant thickness, calculating equation system for equilibrium 12 p1975 A71-27105
- Transversally isotropic sphere and orthotropic cylinder in symmetrical temperature field, calculating thermal stress equations 12 p1975 A71-27112
- Elastic isotropic body finite plane deformations, considering displacement and stress functions relationship 12 p1981 A71-27464
- Free vibrations of isotropic nonhomogeneous circular plates, deriving closed form expressions for nodal frequencies 12 p1983 A71-27587
- Thin walled elastic isotropic shallow shell with thermal boundary conditions, obtaining thermoelastic solution in series form 12 p1984 A71-27687
- Steady thermoelastic equilibrium of infinite isotropic plate containing imbedded circular inclusion with cuts along circumference 12 p1984 A71-27693
- Stress concentrations over smooth perimeters of curvilinear holes in infinite isotropic plates subjected to loads 12 p1984 A71-27694
- Plane traveling electromagnetic wave existence, propagation and refraction in nonlinear dispersive nonmagnetic isotropic lossless medium 13 p2027 A71-27899
- Isotropic and anisotropic materials stability criteria and boundary surfaces in invariant stress tensor spaces 13 p2149 A71-28120
- Green tensor for large initial deformations of isotropic elastic body 13 p2152 A71-28277
- Vibration transversely isotropic orthotropic plates, presenting approximate nonlinear dynamic theory 13 p2153 A71-28482
- Viscoelastic and elastic shells boundary value problems relation, studying natural and forced oscillations of isotropic viscoelastic shells 13 p2155 A71-28656
- Rotating ring resonator partially filled with dynamic isotropic medium, determining resonance properties 13 p2080 A71-29025
- Two dimensional contact problem for isotropic body in triangle form on half plane, calculating elastic constants with difference Green function 13 p2156 A71-29071
- Elastic displacement stress computation in cylindrical systems of isotropic homogeneous material by finite difference method 14 p2323 A71-29744
- Linear isotropic and centro-symmetric second-grade elastic material and special case with coupling stress, calculating stress field of long straight screw and edge dislocations 14 p2327 A71-30290
- Incompressible homogeneous isotropic fluid Couette flow between stationary inner and rotating concentric outer cylinders, examining Weissenberg effect 14 p2226 A71-30445
- Electron gyro and synchrotron radiation from vacuum and isotropic plasma, deriving approximate general formula for power spectrum and polarization 14 p2282 A71-30661
- Thermodynamic properties effects on transverse acceleration wave propagation in inhomogeneous isotropic elastic bodies with internal state variables 15 p2504 A71-31729
- Photon dwell time in one dimensionally isotropically scattering medium, assuming absorbed state as arbitrary function of optical thickness 15 p2492 A71-32460
- Thin infinite isotropic elastic plate on nonlinear elastic foundation under uniform two dimensional hydrostatic pressure, detailing imperfection effects on initial postbuckling behavior 16 p2648 A71-32979
- Creep tests of admissible stress states in viscoelastic isotropic compressible or incompressible linear and nonlinear solids [ASME PAPER 71-APM-23] 16 p2591 A71-33206
- Isotropic elastic circular cylinders longitudinal stress waves, presenting dispersion relation/Pochhammer equation/numerical solutions 16 p2658 A71-33625
- Isotropic elastic body steady vibrations with moment stresses, solving two dimensional boundary value problem 16 p2658 A71-33716
- Finite elasticity theory for isotropic incompressible solids, formulating Ericksen problem for requirements of statically possible radially symmetric deformations in equilibrium 16 p2661 A71-34147
- Normal stress discontinuity propagation over expanding circular region below free surface of semi-infinite isotropic elastic media 17 p2815 A71-34179
- Stress distribution in isotropic and anisotropic half spaces with crack in interface bonding, reducing boundary value problem to Hilbert problem 17 p2819 A71-34509
- Thermal stresses in plane strain of isotropic micropolar elastic solids without heat sources, reducing thermoelastic to isothermal problem 17 p2821 A71-34583
- Slot antennas electromagnetic radiation patterns in conducting ground plane coated with moving isotropic cold plasma sheath 17 p2701 A71-34758
- Isotropic compressible homogeneous body with small deformations superposed on finite elastic deformation, deriving equations of motion and boundary conditions 17 p2823 A71-34788
- Electric current distributions measurement along monopole antenna in isotropic and anisotropic plasmas generated in large space chamber 17 p2716 A71-35048
- Stresses and deformation in solid propellants charges under gravitational load, assuming homogeneous isotropic and linearly viscoelastic charge material 17 p2829 A71-35307
- Natural vibration parameters of cantilevered isotropic plates, using finite difference method with matrix form solution 17 p2829 A71-35308
- Isotropic circular cylindrical shell stability with longitudinal hinges under uniform external pressure, determining critical load 17 p2831 A71-35322
- Mechanical interactions of point defects in homogeneous isotropic continuous elastic media, deriving interaction energy from Siems multipole forces analysis 17 p2831 A71-35395
- Generalized periodic problem of infinite isotropic plate of constant thickness with periodically arranged groups of holes, determining stress-strain state 17 p2833 A71-35611
- Hyperelastic compressible isotropic elliptical and circular cylinders simple bending, studying second order effects 18 p2977 A71-36195
- Stress field singularities at interface corners in bonded dissimilar isotropic elastic materials under plane force field applied to wedge subregion 18 p2983 A71-36843
- Macroscopic derivation of Onsager relations for nonoscillatory processes with linear flow in isotropic media 18 p2852 A71-36964
- Kinematic dynamo theory application to infinite stationary media with large scale magnetic field components and isotropic turbulence 18 p2967 A71-37025
- Torsion of hollow beam consisting of two homogeneous isotropic rods with different elastic properties and simply connected cross sections, solving by conformal mapping 19 p3155 A71-37387
- Microscopically homogeneous and isotropic two-phase composite material shear modulus formula derivation 19 p3155 A71-37481
- Isotropic materials with memory, discussing induced birefringence theory to account for memory and nonlinearity effects in dielectric properties dependence on deformation history 19 p3118 A71-37525
- Two parallel noncoplanar cracks extension in elastically isotropic solid by applied shear stress with deformation in antiplane strain mode 19 p3157 A71-37797
- Uniformly moving homogeneous isotropic non-dispersive conducting medium with arbitrarily distributed electromagnetic radiation sources, deriving solution in four dimensional covariant form 20 p3196 A71-39083
- Bifurcation of equilibrium of three dimensional elastic isotropic body with arbitrary elastic potential under large subcritical strains 20 p3308 A71-39365
- Dynamic influence of isotropic flat plates on spatial vibratory structures containing rigid bodies, considering compatibility and modal coupling [ASME PAPER 71-VIBR-3] 21 p3456 A71-40267
- Five-layer rectangular sandwich plate containing two soft orthotropic cores and three plate stiff isotropic layers [ASME PAPER 71-VIBR-48] 21 p3459 A71-40297
- Macroscopically isotropic and homogeneous two phase composite materials elastic constants determination, discussing approximate formulas and validity 21 p3463 A71-40583
- Micropolar, homogeneous, isotropic and centrosymmetric medium under external mechanical factors

ISOTROPIC TURBULENCE

tors and embedded in magnetic field, investigating magnetoelasticity problems 21 p3417 A71-41361

Coupled thermoelastic problem of homogeneous isotropic elastic half space with embedded spherical cavity 22 p3613 A71-41566

Temperature stresses relaxation in transversely isotropic viscoelastic sphere calculated numerically for 500 and 100 hour periods 22 p3616 A71-42486

Nonaxisymmetric boundary value problem solution for transversely isotropic half space with circular separation line between boundary conditions, determining tangential stresses 22 p3617 A71-42576

Effective shear modulus of multilayered rectangular elastic isotropic member in uniform torsion 22 p3618 A71-42587

Nonlinear theory of tensile instability /necking/ of homogeneous isotropic bar obeying Ramberg-Osgood law 22 p3618 A71-42588

Elastic field generation in two bonded isotropic half planes with circular or rectangular inclusion 23 p3774 A71-43146

Equations of elastic wave propagation in isotropic materials in presence of static surface stresses and body forces 23 p3775 A71-43205

Homogeneous mountain mass and canyon thermoelastic stress analysis in curvilinear coordinate system by complex variables 23 p3776 A71-43421

Dielectric permeability tensor of relativistic plasma stream, considering collisionless damping of surface waves in seminfinitesimal isotropic plasma 23 p3713 A71-44148

Thin isotropic shells with terminal shear rigidity, deriving complex version of classical theory of thermoelasticity for plastic shells with low shear resistance 24 p3878 A71-44482

Flexural vibration of transversely isotropic composite material curved beams, deriving curvature effects on natural frequency 24 p3878 A71-444616

Stress field due to two rigid circular disk inclusions in isotropic homogeneous infinite plate 24 p3879 A71-44627

Isotropic parabolic elastic cylinder deformation, determining displacements and stresses with Fourier integral and Weber functions 24 p3880 A71-44713

Stress-strain state of isotropic elastic plate weakened by cracks, using Fredholm integrals 24 p3881 A71-44832

ISOTROPIC TURBULENCE

Aerodynamic theory of pressure field induced on lifting surface by isotropic atmospheric turbulence, considering transfer function of Concord aircraft [ICAS PAPER 70-30] 01 p0002 A71-11019

Locally isotropic hydrodynamic turbulent fields statistical properties for kinetic energy and temperature dissipation fluctuations 01 p0120 A71-11106

Small scale isotropic turbulence intensity and refractive index measurements by optical shadow devices 06 p0897 A71-17527

Self preserving solutions of Stewart-Townsend and Ogura-Mekoda equations for isotropic turbulence decay, discussing asymptotic nature for small and large wavenumbers 07 p1091 A71-20027

Locally isotropic hydrodynamic turbulent fields statistical properties for kinetic energy and temperature dissipation fluctuations 08 p1325 A71-20850

Numerical simulation of developing and decaying two dimensional isotropic turbulence consistent with Batchelor predictions 10 p1595 A71-24619

Second order correlation functions of velocity and magnetic field for homogeneous unsteady isotropic hydromagnetic turbulence in incompressible conducting fluid 11 p1805 A71-25599

Isotropic MHD turbulence in incompressible fluid by diagrammatic representation, obtaining approximation with transfer functions and scalar equations for correlation 11 p1805 A71-25600

Isotropic turbulence three dimensional velocity spectrum function, using absolute mean strain rate constant and variable Reynolds number 12 p1898 A71-27581

Rotation-convection model of solar equatorial acceleration and temperature, assuming inhomogeneous isotropic latitude dependent turbulent energy transport 12 p1968 A71-27644

Statistical behavior of turbulent velocity derivatives in nearly isotropic turbulent field downstream of grid, using high speed digital computing methods 17 p2726 A71-34662

Space-time correlation measurements in grid-generated isotropic turbulence, determining full- and narrow-band velocity signals Eulerian time correlation 18 p2902 A71-36035

Kinematic-dynamo equations for stationary unsheared conducting nonrotating sphere dynamo action in isotropic velocity turbulence 18 p2969 A71-37046

Ray statistics of electromagnetic wave scattering in homogeneous isotropic turbulent medium with ellipsoidal inhomogeneities of refractive index, using Fokker-Planck equation 19 p3020 A71-38364

Regenerative kinematic-dynamo action under incompressible isotropic velocity turbulence, noting turbulent Lorentz force role 21 p3447 A71-40422

Resistance wire temperature sensor spatial resolution calculation, considering sensor length and isotropic turbulence effects on temperature spectrum and dissipation 22 p3542 A71-41904

ISOTROPISM

Unknowns elimination from partial linear equations system with constant coefficients, applying to differential equations for bending transversely isotropic plate under normal external load 09 p1535 A71-22257

Isotropic emission features at 11.7/cm, discussing high resolution ground based spectrum measurement 10 p1599 A71-23869

Homogeneous isotropic universe, analyzing cosmological solutions with linear theory of gravitation 19 p3104 A71-38191

ISOTROPY

NT ISOTROPIC MEDIA

Diffuse cosmic X rays observation by telescope aboard OSO 3 satellite, determining isotropy 02 p0301 A71-12581

Isotropy postulate experimental verification in case of complex loading involving strain tensor axes turning 06 p0983 A71-17363

Isotropic diffuse cosmic X rays and gamma radiation background origin 07 p1184 A71-19321

Atmospheric boundary layer refractive index fluctuation isotropy for small turbulence, using intensity distribution photography over collimated laser beam cross section 11 p1762 A71-25923

Polymerization kinetics of nematic liquid crystal monomer in nematic and isotropic phases 11 p1728 A71-26062

Cosmic microwave background measurements at 8 mm wavelength, examining isotropy 12 p1956 A71-26614

Nonviscous fluid isotropic turbulent motion concept, and structural stability role in steady state flow statistical properties 12 p1895 A71-26827

Atmospheric boundary layer refractive index fluctuation isotropy for small turbulence, using intensity distribution photography over collimated laser beam cross section 20 p3236 A71-39214

ITALY

Italian soil particles of cosmic origin, noting space research activities relation to micrometeorites and dust studies 20 p3298 A71-39644

Correlation coefficient between winds at 850-30 mb pressure levels over Italy in winter, proposing theoretical model 21 p3411 A71-40825

Climatic changes periodicity in Italy, considering cause by sirocco enhancement 21 p3411 A71-40827

ITERATION

NT ITERATIVE SOLUTION

Nonlinear relaxation iteration method for solving geometrically nonlinear problems in mechanics [ASME PAPER 70-WA/APM-43] 03 p0512 A71-14165

Iteration method application to shell design nonlinear differential equations solution 06 p0988 A71-17777

Two-point iteration formulas with one calculation step requiring successive solution of two linear equations 06 p0921 A71-18347

Iteration parameters ordering in Chebyshev cyclic iteration method 14 p2265 A71-29557

ITERATIVE NETWORKS

Digital multiplier based on cellular logic iterative arrays for complex numbers processing 13 p2037 A71-28470

Fast versatile iterative parallel binary comparison array, proposing cell output states assignment 13 p2037 A71-28470

ITERATIVE SOLUTION

Complex optimal control problems solution using iterative decomposition algorithms 01 p0111 A71-10318

Critique of Chapman-Kirk iterative method for differential equations yielding aerodynamic coefficients from free flight data 01 p0002 A71-10976

Iterative graphical method for broadband N wave TEM mode power divider design, using Smith chart 01 p0055 A71-11119

Iterative and cascaded codes for single and grouped error detection 01 p0039 A71-11311

Soviet analog computer modifications for iterative and hybrid computations, describing memory system alterations 02 p0228 A71-12496

Book on optimal control theory covering dynamical programming, calculus of variations, Pontryagin maximum principle and iterative techniques 02 p0236 A71-12777

Successive approximations of order K iterative methods for calculating inverse matrix, yielding lower and upper bounds 03 p0449 A71-13111

Convex Taylor series truncations minimization by iterative method based on approximating initial functional 03 p0452 A71-14058

Iterative functional minimization methods using Lagrange multipliers, examining convergence 03 p0452 A71-14059

Linear integrodifferential time lag systems quick-response problem approximate iterative solution, considering convergence and controllability conditions 03 p0452 A71-14060

Successive approximation algorithm for stress concentrations at holes in nonlinear shallow shells, applying to cylindrical and spherical shells with circular and elliptical holes 04 p0664 A71-146020

Algebraic equations system solution by eighth order Runge-Kutta process with eleven function evaluations per step 04 p0619 A71-148121

One dimensional transient heat conduction analysis by iterative isotherm migration method, discussing boundary conditions, stability, truncation error and relative efficiency 04 p0677 A71-154523

Local heat transfer to transverse circular cylinder at low Reynolds numbers, using iterative finite difference approach 04 p0683 A71-15493

Kincaid iterative solution for multidimensional systems of nonlinear equations, noting quadratic convergence as function of initial vectors 05 p0775 A71-17046

Undamped structural vibration problems solution for eigenvalues and eigenvectors using simultaneous iteration method 05 p0829 A71-17113

Circular disks or cylinders with temperature boundary conditions, discussing iterative solution and computer program for transient thermoelastic stresses 05 p0829 A71-17117

Structural optimization by concave and piecewise linear programming, discussing mathematical foundation and iterative method efficiency 05 p0829 A71-17121

Iterative methods, numerical mathematics, approximation theory - Conference, Oberwolfach, West Germany, November 1968, June and November 1969 06 p0919 A71-18201

Square root function approximation in interval, using Heron iteration and Chebyshev method 06 p0919 A71-18206

Iterative solution of nonlinear operator equations in Banach spaces, proving existence, uniqueness and convergence theorems 06 p0920 A71-18211

Theorems concerning relaxation in point total and single step iterative solution for Hammerstein type nonlinear equations 06 p0920 A71-18212

One step iterative solution for linear equations by summation methods, discussing convergence improvement 06 p0920 A71-18213

Matrix eigenvalue problem solution by reducing to nonlinear algebraic equations for iterative solution or integration by Runge-Kutta method 06 p0921 A71-18342

Boundary condition iteration methods in chemical process plant optimal design and control, considering simplicity and ease of programming, computation time and storage requirements 07 p1054 A71-18800

Iterative solution for radiation-dominated heat balance about heat shield or superinsulation nodes, testing performance in thermal analysis program
07 p1221 A71-18905

Numerical solution of nonself adjoint boundary value problems of electrodynamics using finite difference scheme and iterative processes
07 p1159 A71-19179

Iterative method for good aperiodic binary sequences in radar range resolution
07 p1148 A71-19769

Iterative processing technique for limited measurement sets, discussing Kalman filter reaching steady state during ballistic target tracking
08 p1269 A71-21340

Boundary problem for displacement equilibrium equations of elastic body using iterative methods, demonstrating convergence of difference equation solution
08 p1372 A71-21706

Second order hyperbolic partial differential equation in canonical form solution by iterative method
09 p1485 A71-22277

Shaped beam radiation patterns synthesis by iterative sampling method with line sources or uniformly spaced antenna arrays
09 p1409 A71-23493

Iterative computation of variational optimization problems by analog computers with digital logic control/hybrid computers/
09 p1413 A71-23665

Iterative technique using continuous gas laser for alignment of Mach-Zehnder interferometer for monochromatic and white light fringes
09 p1453 A71-23692

Automatic computer program synthesis based on theorem proving approach for construction of recursive and iterative programs operating on natural numbers, lists and trees
10 p1581 A71-23968

Iterative algorithms for regression function saddle point and applications in reliability and automatic control theories
10 p1585 A71-24156

Iterative synthesis of dipole antenna array for maximum directivity radiation pattern, considering amplitude-phase distributions
10 p1583 A71-24707

Convergence rates of multistep iterative procedures for finding zero of nonlinear function defined on R to n th power
11 p1792 A71-25932

Iterative solution of semidefinite eigenvalue problems, identifying rigid body and deformation coordinates
12 p1974 A71-26873

Elastic body displacement equilibrium equations, using variable direction iteration methods for boundary value problems
12 p1978 A71-27329

Unloading effects on elastoplastic stability of shells, using method based on successive approximations
13 p2156 A71-29073

Iterative solution for quasi-linear heat equation, examining convergence for equation describing self similar heat wave from instantaneous plane source
14 p2334 A71-29564

Spherically symmetric systems radiative transfer problems using iteration on Eddington factor
14 p2307 A71-29864

Book on antenna admittance problem covering iterative solution of integral equations, Fourier series solution, Wiener Hopf methods, transmission line theory, etc
14 p2193 A71-29932

Iterative technique for state and control-constrained linear optimal control problems with strictly convex cost functions
15 p2380 A71-31936

German monograph on iterative procedure for sectional parameters of shells of revolution with meridian form under peripheral loads described by harmonic functions
15 p2509 A71-32374

One dimensional two phase Stefan problem solution for melting of heated thin plate, comparing iterative methods
16 p2662 A71-33065

Nonlinear equations solution with error estimate, using iteration convergence method
16 p2604 A71-34083

Functional analytical iteration methods for calculating nonlinear vibrations of several degrees of freedom and error estimation improvement, considering uniformly converging Fourier series expansion
17 p2782 A71-34939

Optimum diagnostics algorithm for complex automatic control system state detection based on Bayesian rule successive application for minimum time requirement
17 p2720 A71-34959

Iterative clustering technique for minimizing probability of differences between binary data reconstructions from cluster codes and initial data
17 p2711 A71-35047

Discrete Kalman filter computational efficiency improvement by iterative processing technique for covariance matrix updating
17 p2722 A71-35182

Newton-Raphson method application to iterative solution of atomic excitations and radiative transfer in plasma
17 p2838 A71-35554

Orders of convergence for iterative procedures for finding zero of nonlinear function, considering secant and Steffenson method
17 p2768 A71-35685

Global convergence of iterative schemes by Newton-Gauss-Seidel method, considering discrete approximations of elliptic partial differential equations
17 p2769 A71-35689

Orthogonal matrix estimate by iterative algorithm with given order of convergence
17 p2769 A71-35692

Convergence of Broyden single-rank iterative solution for nonlinear equations systems involving approximation to Jacobian matrix
18 p2941 A71-36357

Projection iterative method for solving singular linear equations, noting use for matrix conversion
18 p2942 A71-36699

Convergence theory for Newton-like iterative methods to solve nonlinear equations in abstract spaces, presenting error analysis
18 p2943 A71-36955

Balance function concept extension to optimal control problem for finding numerical iterative solutions, considering low thrust orbit transfer problem
19 p3037 A71-37557

Model-reference feedback control system, investigating effects of equivalence lack between reference and plant on iterative process convergence by linear transformation
19 p3038 A71-37778

Nonlinear coupling between thermal conduction and radiative transfer in solar chromosphere by iterative method
19 p3143 A71-38159

Alternating-direction Galerkin methods application to parabolic and hyperbolic differential equations for obtaining efficient iterative solution of heat equation on rectangle
19 p3087 A71-38305

Optimality criterion for convergence of iterative solution of linear time optimal problem in reflective Banach space
19 p3088 A71-38414

Iterative finite difference solution of Laplace operator interior eigenvalues and eigenfunctions, noting convergence in application to Helmholtz equation
20 p3201 A71-38755

Iterative method for linearly elastic structure undamped vibration natural frequency determination with fast convergence
20 p3311 A71-39965

Third order oscillatory system optimal terminal-state control synthesis by quadratic functional minimization iterative procedure algorithm, using ODR-1204 computer program
21 p3359 A71-40164

Shallow spherical cap and deep thin spherical shell buckling, solving integral equations by iterative procedure
21 p3463 A71-40542

Iterative solution of Hallen integral equation for current distribution on lossless cylindrical transmitting dipole antenna
21 p3348 A71-40578

Continuous analog iterative methods and solution of nonlinear two point boundary value problems, producing convergent series of iterates
21 p3408 A71-40585

Rapidly converging iterative solution to radial Schroedinger equation in oscillatory region
21 p3408 A71-40845

Amplitude estimates and bounds derivation for nonlinear two parameter oscillators, obtaining iterative solution for computation
21 p3358 A71-41013

Distribution function integral representation application to steady motion of monocomponent rarefied gas containing amorphous particles, using successive approximation for kinetic equation solution
22 p3482 A71-42868

Minimum norm and gradient projection constrained optimization techniques as mathematical procedures for iterative solutions of trajectory optimization problems
23 p3724 A71-42983

Iterative solution of least squares programming problem for finite thrust rocket trajectory optimization
23 p3724 A71-42984

Orbital transfer time equation reformulation, discussing various orbit constraints accommodation and rapid convergence in rendezvous orbit iterative determination
23 p3727 A71-43008

Simultaneous iterative solution for obtaining dominant subset of unsymmetric matrix eigenvalues and eigenvectors
23 p3698 A71-43098

Iterative solution of eigenvalue problems for positive real symmetric matrices without first approximation of eigenvalues and eigenvectors, constructing by powers of spectral decomposition
23 p3699 A71-43488

Iterative solution for radiant energy transport equation by Wiener Hopf operator equations, investigating convergence conditions
23 p3699 A71-43573

Steady state gains and covariance computation for time invariant discretely updated linear systems, demonstrating iterative and algebraic solutions
23 p3660 A71-44116

ITOS 1
ITOS-1 meteorological satellite launch and operational sequences in orbit, discussing thermal and attitude control, power and communications and sensor equipment
04 p0663 A71-15314

ITOS 1 and NOAA 1 meteorological satellite systems design and operation, outlining attitude and thermal control, sensors, power supply and orbital performance
17 p2814 A71-35432

Thermal design, analysis, testing and flight performance of ITOS-1 spacecraft, noting fail-safe temperature regulation
18 p2868 A71-36390

ITOS meteorological satellite scanning radiometer using point detector optical system for earth imaging
23 p3676 A71-43511

IZSAK ELLIPSOID
U ELLIPSOIDS
U GEODESY

J

J-2 ENGINE
Saturn 5 S-2 stage propellant feedlines and V-2 engines simulating structural longitudinal oscillation by analog computer
03 p0472 A71-14430

J-57 ENGINE
Structure constant of jet exhaust turbulence of J-57 with afterburner by laser beam probing compared with scintillation and hot-wire anemometer measurements
11 p1766 A71-26304

J-85 ENGINE
Time variant distortions in supersonic inlet on J-85-GE-13 turbojet engine from wind tunnel test, considering instantaneous distortion amplitudes and contours
14 p2290 A71-30733

JACKING EQUIPMENT
U JACKS (LIFTS)
JACKS [ELECTRICAL]
U ELECTRIC CONNECTORS
JACKS (LIFTS)
Aircraft weighing in place during maintenance operations, describing load cell equipped jacks design for time saving weight determination
17 p2724 A71-35814

JACOBI INTEGRAL
Zero relative velocity surfaces in bounded circular three body problem in presence of magnetic dipole, deriving Jacobi integral
12 p1947 A71-26634

Algorithm convergence for sparse nonlinear equations system solution with Jacobian satisfying Lipschitz condition
15 p2442 A71-32313

Bounded plane circular three body problem stability, analyzing Jacobi integral and canonical equations
17 p2807 A71-35496

Mass changes in restricted quasi-circular variable mass three body problem with particle equations of motion having Jacobi integral
20 p3291 A71-39320

JACOBI MATRIX METHOD
Total impedance plethysmography boundary value problems, developing computer program based on Jacobi iterative method
03 p0367 A71-12993

Jacobian calculation in kinematic theory of wave propagation, using ray equation
08 p1276 A71-21652

Convergence of Broyden single-rank iterative solution for nonlinear equations systems involving approximation to Jacobian matrix
18 p2941 A71-36357

Jacobi algorithm for computation of eigenvalues and eigenvectors of skew symmetric matrix by real arithmetic
18 p2942 A71-36698

Function classes of n -dimensional nonlinear mappings generalizing matrices, including convergence for Jacobi and Gauss-Seidel process
19 p3088 A71-38311

Finite difference methods application to Euler non-linear elliptic differential equations, using symmetric and positive Jacobian
22 p3567 A71-42375

JACOBI POLYNOMIALS U HYPERGEOMETRIC FUNCTIONS

JAGUAR AIRCRAFT
One man Jaguar aircraft navigation, weapon aiming system and pilot operational tasks, noting inertial platform alignment, displays and target attack modes
20 p3261 A71-39825

JAMMING
Deception repeaters for erroneous information transmission to radar, considering echo signal level, burnthrough, target size, sensitivity, gain and bandwidth
04 p0555 A71-15359

JAPAN
Ancient geomagnetic intensity in Japan by comparing natural remanent magnetization with known thermomagnetic magnetization induction, using stepwise heating method on antique pottery
04 p0582 A71-15127

Underthrusting mechanism during southwest Japan earthquakes, presenting model of convergent plate interactions
23 p3672 A71-43885

JARRING U MECHANICAL SHOCK

JC-130 AIRCRAFT
U C-130 AIRCRAFT
JEANS THEORY
Computer simulation model for stars motion in plane of disk-like stellar systems, investigating dynamics of Jeans and gravitational two-stream instability
10 p1670 A71-24181

JEES U AUTOMOBILES

JET AIRCRAFT
NT A-7 AIRCRAFT
NT A-300 AIRCRAFT
NT AN-24 AIRCRAFT
NT B-52 AIRCRAFT
NT B-70 AIRCRAFT
NT BAC 111 AIRCRAFT
NT BOEING 737 AIRCRAFT
NT BOEING 747 AIRCRAFT
NT BOEING 7707 AIRCRAFT
NT BUCCANEER AIRCRAFT
NT C-5 AIRCRAFT
NT C-135 AIRCRAFT
NT COMET 4 AIRCRAFT
NT CONCORDE AIRCRAFT
NT DC 10 AIRCRAFT
NT DH 121 AIRCRAFT
NT DO-31 AIRCRAFT
NT F-4 AIRCRAFT
NT F-8 AIRCRAFT
NT F-14 AIRCRAFT
NT F-28 TRANSPORT AIRCRAFT
NT F-100 AIRCRAFT
NT F-104 AIRCRAFT
NT F-111 AIRCRAFT
NT IL-62 AIRCRAFT
NT L-1011 AIRCRAFT
NT MIRAGE 3 AIRCRAFT
NT SAAB 37 AIRCRAFT
NT SE-210 AIRCRAFT
NT T-33 AIRCRAFT
NT TSR-2 AIRCRAFT
NT TU-134 AIRCRAFT
NT TU-144 AIRCRAFT
NT TURBOFAN AIRCRAFT
NT TURBOPROP AIRCRAFT
NT VC-10 AIRCRAFT
NT XC-142 AIRCRAFT
NT YAK 40 AIRCRAFT

German monograph on commercial jet aircraft maintenance systems covering changes and adaptations for performance improvement
01 p0004 A71-10114

Steep approach to landing for jet transport aircraft noise abatement, using ground based equipment and onboard TV display
01 p0126 A71-11311

Twine jet aircraft engine installation effects and exhaust nozzle integration, noting closely spaced inlet interference
03 p0469 A71-13148

STOL future performance and safety level, considering current jet aircraft fatal accident record and proportional perpetuation, airworthiness and operational considerations
03 p0347 A71-13568

Pilot vision during final approach and landing in turbojet transport operations
08 p1247 A71-20826

Aircraft engine smoke emission control, discussing Ringelmann chart assessment for various commercial jet aircraft and airport gaseous pollutants
08 p1380 A71-21832

Cessna Citation twin turboprop business aircraft design, performance characteristics, communications,

navigation and automatic flight control equipment and flight evaluation
09 p1385 A71-22112

Jet aircraft and hygiene, considering communicable diseases spread control measures and sanitation methods by airlines
09 p1400 A71-23071

Jet aircraft flight decks pressurization, tobacco smoking and carbon monoxide levels, discussing potential dangers
09 p1400 A71-23247

Optimal stochastic control and gust alleviation for jet aircraft response for flight through turbulent upwash field
10 p1557 A71-24870

Jet aircraft airworthiness standards, discussing airline fleet maintenance resources, inspection systems and future requirements
11 p1772 A71-26308

Air pollution study of jet aircraft emissions in airport vicinity, involving exhaust gas testing, ground operations and passenger cabin measurements
13 p2005 A71-28315

Microbiological contamination of jet aircraft fuel tanks in tropical regions, considering maintenance
13 p1996 A71-28320

Jet pilots training technologies, discussing multimedia instruction, psychological stress reduction, self study, airborne video application and simulation
13 p2017 A71-28342

En route turbojet aircraft flight speed control, assessing impact on ATC procedures
13 p2098 A71-28884

Dassault Mercure short range twin jet aircraft capable of using powerful engine
13 p1997 A71-29276

Jet-supported VTOL aircraft fuel-time-optimal landing control, using mathematical model, Pontryagin maximum principle and analog computer solution
13 p1997 A71-29281

Integrated short-haul interurban transportation system, considering combination of conventional jet aircraft, STOL aircraft and high-speed ground transportation
14 p2221 A71-29550

Atmospheric turbulence effect on turbine powered transport aircraft, discussing gust accelerations, avoidance, detection, forecasting and pilot control
14 p2172 A71-29750

Jet transport aircraft stability and controllability under atmospheric turbulence conditions, discussing longitudinal and lateral-directional characteristics with particular attention to unstable spiral mode
14 p2173 A71-29772

Jet transport aircraft design for safety under air turbulence conditions, considering cruise altitude limitations and pitch and g excursion reduction by special autopilot mode
14 p2173 A71-29777

Large subsonic jet aircraft civil pilots performance under physiological and psychological stresses induced during severe atmospheric turbulence
14 p2188 A71-29783

Wind tunnel force test program design for jet aircraft configurations, including propulsion system simulation
14 p2176 A71-30605

Alpha jet trainer, describing design, configuration, power plants, landing gear maintainability and mission duration
15 p2347 A71-31209

Aladin II four-jet engined STOL intercity transport aircraft, noting low noise characteristics and passenger capacity
15 p2347 A71-31412

Dispersal of jet aircraft exhaust emissions near airports and of smoke trails in upper atmosphere, assessing pollutant levels near large urban airports
15 p2349 A71-32244

Jumbo jet trailing vortex mathematical model for studying effect on penetrating aircraft
17 p2673 A71-35754

Large jet transport aircraft trailing vortices, studying velocity fields, core diameters and logarithmic variations of circulation
17 p2674 A71-35755

Administrative techniques of cost/weight tradeoff program for jet transport airplane
17 p2750 A71-35812

Variable geometry B-1A bomber aircraft, discussing size, payloads, speed, altitude range and runway takeoff
19 p2996 A71-37516

Single seater turbojet aircraft landing via automatic band switch for ARK-5 and ARK-10 radio compass
19 p3101 A71-38017

Peak velocity vectors in transverse plane of jet transport aircraft wake, measuring tip vortices core size
21 p3319 A71-40491

Flight tests for hazard evaluation to other aircraft from wake turbulence generated by large jet transport airplanes
21 p3321 A71-40506

Minimal time climb velocity optimization for stratospheric and tropospheric jet aircraft flights
22 p3482 A71-41970

Fluid amplifiers theory and use as temperature and pressure sensors, discussing applications in chemical and ammunition industries and jet aircraft control
23 p3630 A71-42921

Jet aircraft fuel additives covering functions and applications
24 p3864 A71-45322

JET AIRCRAFT NOISE

High bypass ratio jet engine noise reduction in relation to mission requirements
03 p0471 A71-141221

High bypass ratio fan engine design for low noise, discussing acoustic treatment, turbine noise and modulation tones
03 p0471 A71-141222

Large low-speed fan for low noise production, testing performance on suppression effects of acoustic treatment and exhaust jet noise
03 p0471 A71-141223

Jet noise suppressor development test techniques and facilities, discussing model tests at hydrodynamic ONERA wind tunnel
04 p0639 A71-15819

Low velocity and coaxial jet noise data and correlations for noise prediction of turbofan engines
05 p0796 A71-17155

Supersonic jet transport legal aspects in land overflight, discussing ground noise and sonic boom effects on persons and property
06 p0846 A71-17644

Supersonic aircraft turbojet engine exhaust noise suppressor research program, predicting full scale noise spectra from model suppressor tests
06 p0945 A71-17693

Supersonic jet noise problem, discussing eddy-Mach wave radiation source mechanism from non-linear streamwise development of inviscid instability waves in turbulent mixing layer
06 p0884 A71-18592

Finite amplitude waves from supersonic jet, discussing pressure fluctuations measurement for explaining wave patterns visible on spark shadowgraphs
06 p0845 A71-18593

Near and far noise fields from coaxial interacting supersonic jet flows
06 p0884 A71-18594

Noise-producing subsonic jet turbulence eddies hot-wire anemometer measurements of convection velocity as functions of frequency
06 p0884 A71-18596

SST noise suppression research, discussing engine noise suppressor conceptual designs and test results with installed devices
07 p1184 A71-20302

Aircraft optimum minimum noise takeoff profile, solving by equations of motion system for jet aircraft
08 p1331 A71-20779

Jet aircraft noise over residential areas, discussing actual and permissible noise levels and proposals for remedial action
08 p1230 A71-21163

Noise reduction at source, flight methods adjustments and airport compatible land use for jet noise abatement
08 p1378 A71-21815

Business jet aircraft noise certification, discussing test programs and cost reduction
10 p1555 A71-24249

Subsonic jet aircraft noise and simulated sonic booms awakening effects on human sleep
11 p1726 A71-26510

Jet fighter-bomber aircraft noise survey, discussing sound pressure levels and frequency analysis during ground running, speech interference levels and ear protectors requirements
12 p1875 A71-27629

Noise attenuation prediction in absorbing ducts adaptable to bypass jet engines, using Morse theory
14 p2288 A71-30522

Jet aircraft sound spectrum on ground and in air, comparing calculation with experiment
14 p2289 A71-30524

Acoustic liner design for propellant combustion instability and jet aircraft noise suppression, discussing cross flow and oscillatory pressure effects
14 p2296 A71-30791

Jet noise reduction by foam injection, developing mathematical model for foam behavior in sound field
15 p2388 A71-31327

Integrally stiffened five bay panel, calculating free vibration and random response to jet noise excitation
15 p2504 A71-31532

Temperature and shock structure effects on choked jet noise characteristics, using axisymmetric convergent and convergent-divergent nozzles for radiated noise fields investigation
15 p2468 A71-31570

Computational technique for acoustic field of jet aerodynamic noise, using Lighthill theory for spectral calculations
15 p2468 A71-31571

Analytical predictions of supersonic jet noise, considering acoustic intensity, directivity, refraction, connection and peak Strouhal number
[AIAA PAPER 71-584] 15 p2468 A71-31572

Commercial SST aircraft engine noise during takeoff, discussing exhaust geometries for suppression 15 p2468 A71-31595

Quiet turbofan STOL feasibility, discussing structural, propulsive and technical aspects, economy, passenger comfort and performance estimates 15 p2348 A71-31605

Acoustic and gas dynamic characteristics of jet noise muffler, using adapters at outlet section of exhaust nozzle 15 p2469 A71-31710

Aircraft powerplant noise test facilities and reduction, emphasizing jet acoustic Mach number, pressure and temperature ratio and exit turbulence effects 15 p2384 A71-31876

Concorde aircraft engine noise emission and reduction, examining acoustic measurements in takeoff and approach phases, reduced thrust and retractable silencer 15 p2469 A71-31877

STOL jet aircraft noise reduction by using engines with moderate dilution rate 15 p2349 A71-31882

Aircraft engine noise test methods for acoustic certification, investigating jet and compressor silencing, absorbent materials, rotor and propeller noise and psychoacoustic tests 15 p2385 A71-31890

Jet aircraft noise generation, transmission and reduction, emphasizing turbofan engine acoustics, operational characteristics and exhaust sound 15 p2349 A71-32241

Community aircraft noise intensity indexes from annoyance and physiological reaction standpoint, discussing sleep interruption, hearing loss, communication interference, etc 15 p2364 A71-32242

Community actions for jet aircraft noise reduction, discussing noise environments, nationwide goals, decision making and economic incentives 15 p2516 A71-32249

Simulated sonic booms and subsonic jet aircraft noise effects on human subjects of various ages during different sleep stages 15 p2364 A71-32250

Sonic boom phenomena, discussing supersonic flow near aircraft, atmospheric propagation, distortion, focusing, caustics, turbulence effects and reduction 15 p2350 A71-32566

French disengageable silencer for jet engine noise attenuation during aircraft takeoff 15 p2471 A71-32695

Jet aircraft flyover noise measurement, determining average intrusion level in residential communities under approach and departure corridors 19 p2996 A71-37497

Aircraft structures sonic fatigue due to high frequency noise from turbofan engines, discussing case histories, failure diagnosis and precautionary design measures 19 p2997 A71-37843

In-flight noise radiation by wing-mounted jet engines on aircraft fuselage based on correlation with turbulent boundary layer pressure fluctuations 19 p2997 A71-37846

Review of September 1970 aerodynamic noise symposium covering jet and helicopter rotor noise, nonlinear acoustics and diffraction theory 19 p2994 A71-38205

Simple source theory of aerodynamic noise, approximating relationship between radiated sound power and jet pressure spectra 19 p3124 A71-38531

Low noise levels of DC-10 aircraft with CF6-6D turbofan engines, discussing design, flyover tests and FAA requirements [CASI PAPER 72/5] 20 p3178 A71-39424

Acoustic noise output from round interfering subsonic jets, considering suppressor nozzle attenuation 24 p3864 A71-44560

ET AIRSTREAMS
U JET STREAMS [METEOROLOGY]
ET AMPLIFIERS
Fluidics component operation and characteristics, including turbulent reattachment, jet deflection and vortex amplifiers 03 p0353 A71-13132

Fluidic instrument pressure regulator, noting pressure sensing circuit, confined jet amplifier and control valve [ASME PAPER 70-WA/FLCS-4] 03 p0428 A71-14080

Various configuration fluid jet amplifiers, investigating cavitation conditions in water tunnels and open duct 07 p1023 A71-19198

ET AUGMENTED WING FLAPS
U JET FLAPS
U WING FLAPS

JET BOUNDARIES

Ideal incompressible fluid plane jets interaction with flow discontinuity at jet boundaries, deriving nonlinear system of integral equations 03 p0405 A71-14564

Supersonic and subsonic jets coexistence in rectilinear constant section duct, characterizing flow boundaries by pressure readings and Schlieren flow visualization 09 p1384 A71-23605

Plane jet in counterflow with vortex shedding control, discussing solid boundary and jet momentum effects 10 p1592 A71-23980

Curvature effects on laminar and turbulent free jet boundary between irrotational flow and stagnant fluid, discussing pressure effects 11 p1702 A71-25482

Plane and circular turbulent jet boundary layer expansion in slipstream, comparing analytical with experimental results 12 p1898 A71-27505

Intermittency signals correlation, determining lateral motion of two dimensional jet boundaries 18 p2901 A71-35854

JET CONTROL

Jet deviation by secondary gas injection, predicting lateral thrust performance 04 p0525 A71-14793

Control jets interaction with airstream surrounding typical tactical missile configuration, considering rear mounted bistable fluidic thrusters and circular sonic jets 11 p1837 A71-25506

Quasi-one dimensional nonlinear model of electrohydrodynamic stability and control of current carrying seminsulating jets at supercritical and subcritical regimes 13 p2118 A71-29249

Flowfield production by fluid injection into supersonic crossflow, occurring with liquid/gas jet control of vehicle with combustion ramjets [AIAA PAPER 71-728] 14 p2295 A71-30775

Fluid jet control by acting on thin guiding filament, noting electromagnetic deflections by ferromagnetic wire 15 p2353 A71-32073

Jet tab thrust vector control system for tactical missile applications, describing operational principles, design details and performance characteristics [AIAA PAPER 71-752] 18 p2956 A71-36773

JET DAMPING

U DAMPING

U SPIN REDUCTION

JET DRIVE

U JET PROPULSION

JET ENGINE FUELS

Test time and contact stresses effect on jet fuels antiwear properties under rolling friction 02 p0298 A71-12570

Jet engine liquid fuel wall layer combustion stimulation by repeated oxidizer injection into supersonic section of nozzle 03 p0472 A71-14256

Jet fuel soluble corrosion inhibitors evaluation by potentiostatic polarization methods 03 p0377 A71-14323

Soviet book on automotive and jet aircraft engine fuel chemical stabilizers under storage, transit and operational conditions, examining additives in relation to stability ratings 06 p0942 A71-17433

Jet fuels thermal stability and corrosive properties during prolonged storage 07 p1182 A71-19492

Device for jet fuels antiwear properties measurement under rolling friction 07 p1111 A71-19493

Automated fueling for Kennedy jet airport, using computer controlled underground bulk storage-satellite tank pipeline system 10 p1589 A71-24300

Jet fuel starter, describing small gas turbine for starter, providing sufficient pressurized gas flow to rotate main engine [ASME PAPER 71-GT-43] 11 p1812 A71-25976

Jet fuels deoxygenation effects on steels antiwear properties and critical loading under vibrational and gliding friction 12 p1945 A71-27662

Airport jet fuel delivery system salt driers for reducing water content below saturation, lengthening filter life and improving downstream system components performance [SAE PAPER 710440] 13 p2113 A71-28322

Jet fuel dissolved oxygen concentration effects on plunger antiwear properties 15 p2464 A71-31677

Jet fuel antiwear properties relation to viscosity and adsorption tar and mercaptans content 15 p2464 A71-31678

Antiwear properties of jet fuels as function of dissolved oxygen, resin and heteroorganic compound

content and temperature, considering antioxidant additives 16 p2623 A71-33579

Antiwear property assessment of piston engine and aviation jet fuels under point contact conditions, recommending ball and cylinder test technique 17 p2792 A71-34447

Air and jet fuel-air mixtures, calculating temperature dependent laminar and turbulent heat transfer parameters and transport properties [ASME PAPER 71-HT-41] 19 p3166 A71-38002

Soviet monograph on carbon deposits in jet engines covering distribution, formation, fuel properties, reduction and removal and harmful effects in gas turbines 21 p3437 A71-40871

Jet aircraft fuel additives covering functions and applications 24 p3864 A71-45325

JET ENGINES

NT BRISTOL-SIDDELEY OLYMPUS 593 ENGINE
NT DUCTED FAN ENGINES
NT J-57 ENGINE
NT J-85 ENGINE
NT RAMJET ENGINES
NT SUPERSONIC COMBUSTION RAMJET ENGINES
NT TURBOFAN ENGINES
NT TURBOJET ENGINES
NT TURBOPROP ENGINES
NT TURBORAMJET ENGINES

Jet engine evolution, considering thrust, combustion chamber, fans, high-pressure-ratio compressors and turbine inlet temperature 01 p0143 A71-11181

Electrochemical machining role in jet engine industry, discussing drilling, contouring, electrolyte handling, etc [SME PAPER MR-70-193] 01 p0089 A71-11253

Flight test evaluation of onboard automatic computer controlled jet engine monitoring system with reduced fault detection time 03 p0395 A71-13080

Aerodynamic characteristics of jet engine installation above wing of swept wing aircraft, noting large lift dependent drag 05 p0696 A71-15954

Critical nozzle pressure ratio and geometry effects on free exhaust gas jets of jet engine models [DGLR-70-055] 05 p0831 A71-15966

Irreversibility control in two gas flows mixture, discussing jet engines thrust increase by air-exhaust gases admixture 06 p0945 A71-18051

Al 27 for heating working body in heat exchangers of jet engines 06 p0926 A71-18706

Concorde aircraft Olympus 593 two-spool turbojet engine, discussing variable nozzle and intake assembly, afterburner and control system 07 p1183 A71-19081

Jet engine rotor strain and temperature data transmission, examining special purpose telemeters design 07 p1062 A71-19628

Optimal lining impedance for jet engine inlet duct, yielding discrete frequency, flow velocity and geometry on basis of minimum radiated power 08 p1349 A71-21661

Plasma arc welding of jet engine components of Ti and Ni alloys, comparing to gas tungsten arc and electron beam processes 08 p1299 A71-21684

Subsonic jet engine noise reduction, considering turbojets, turbofans and jet suppressors 08 p1349 A71-21814

Ti alloys in aircraft industry, considering jet engines applications and structural stability improvements related to fracture toughness, fatigue and stress corrosion 09 p1474 A71-23292

High temperature oxidation protective coatings behavior, emphasizing jet engine applications 09 p1483 A71-23296

High temperature Ni and Co alloys for stationary gas turbines and jet engine parts, considering microstructure and mechanical behavior under stress and temperature 09 p1475 A71-23302

Metallic and nonmetallic composite materials in jet engine component design, discussing integral blade/disk, reinforcement hoop, rotors and airfoils 09 p1456 A71-23307

VTOL heat engine and propulsion system design and performance, citing Pegasus jet lift engine as compromise between takeoff and cruise function 10 p1659 A71-24751

Jet engine components inertia welding, discussing process, equipment, low weight-cost advantage and mechanical properties reproducibility [ASME PAPER 71-GT-33] 11 p1770 A71-25970

Low pressure drop fuel liquid injectors for jet engine combustors, using gas turbine vaporizer design [ASME PAPER 71-GT-38] 11 p1812 A71-25972

JET EXHAUST

Vacuum heat treatment of brazed and diffusion bonded jet engine components near melting temperature 13 p2073 A71-28145

Olympus 593 pure jet twin shaft engine development program for Concorde, discussing engine evolution, design considerations and flight development [SAE PAPER 71-0422] 13 p2114 A71-28309

Air bypass behind compressor into variable area exhaust nozzle, obtaining energy losses from gas turbine jet engine indices 13 p2115 A71-28586

Heat shield ablation under high enthalpy chemically active turbulent gas flow in hydrojet engine manifolds 13 p2160 A71-28589

Aircraft jet engines technological progress review over past 25 years, emphasizing industry economics considerations 14 p2341 A71-30303

Miniature transducers design and fabrication for fluctuating pressure measurements in jet engine testing, noting frequency response and power dissipation 14 p2244 A71-30324

Fluctuating pressure measurements in jet engine testing, using miniature transducers with calibration and data acquisition equipment 14 p2244 A71-30325

Modular concept mathematical model for combustion and pollution formation processes in jet engine combustors, including turbulent mixing and reaction kinetics [AIAA PAPER 71-714] 14 p2294 A71-30766

Isolated axisymmetric jet engine exhaust nozzles thrust and drag predictions in sub-, trans- and supersonic flight regimes 14 p2295 A71-30770

Jet engines nitric oxide air pollutant emission formation, developing gas turbine combustor models [AIAA PAPER 71-712] 15 p2470 A71-32289

Engine performance monitoring for jet engine troubleshooting, noting analyzable malfunctions 15 p2471 A71-32524

Jet engine combustion chamber design, considering air supply and geometrical criteria 16 p2624 A71-33344

Performance characteristics of jet engines equipped with afterburner, discussing combustion, flame stabilization, outlet nozzle regulation and operational cost 17 p2793 A71-35439

Aircraft jet engine application of electric discharge machining for repetitive continuous production, considering automated closed cycle equipment [SME PAPER MR-71-143] 18 p2927 A71-36658

In-flight noise radiation by wing-mounted jet engines on aircraft fuselage based on correlation with turbulent boundary layer pressure fluctuations 19 p2997 A71-37846

Jet engines with afterburners, describing exhaust nozzle control, takeoff and landing advantages and thrust variations 21 p3437 A71-40858

Condensate particle crystallization retardation effect on energy characteristics of jet engine, calculating nonequilibrium flows of two phase combustion products in nozzle 24 p3864 A71-45004

JET EXHAUST

Pulsed megawatt MPD arc thruster exhaust pressure measurements, discussing time dependence, peak dynamic and static pressures, etc [AIAA PAPER 71-196] 06 p0948 A71-18634

Rarefied monatomic gas flow in axisymmetric jet exhaust into vacuum, noting expansion to low densities at thermodynamic nonequilibrium 07 p1090 A71-19894

Combustor design for minimum exhaust smoke emission from aircraft gas turbine jet engines, considering air pollution 08 p1347 A71-20867

Mach disk in underexpanded exhaust plume predicted by dividing flow field into subregions [AIAA PAPER 70-231] 09 p1382 A71-22097

Transonic aircraft jet exhaust wave structure, examining reflection geometry at shear layer and shock diamond train 10 p1553 A71-24867

Structure constant of jet exhaust turbulence of J-57 afterburner by laser beam probing compared with scintillation and hot-wire anemometer measurements 11 p1766 A71-26304

Air polluting nitric oxide and soot production by jet aircraft, discussing mixing process and atmospheric dispersion [AIAA PAPER 70-115] 12 p1946 A71-27560

Visible exhaust smoke trails from aircraft jet engines, measuring optical density by photographic photometry [SAE PAPER 71-0428] 13 p2114 A71-28314

Air pollution study of jet aircraft emissions in airport vicinity, involving exhaust gas testing, ground operations and passenger cabin measurements [SAE PAPER 71-0429] 13 p2005 A71-28315

Isolated axisymmetric jet engine exhaust nozzles thrust and drag predictions in sub-, trans- and supersonic flight regimes [AIAA PAPER 71-719] 14 p2295 A71-30770

Probability theory of stresses during random vibrations of flat panel in acoustic field of jet engine exhaust 15 p2504 A71-31704

Aircraft pollutant emission regulation, discussing low smoke combustors and fuel dumping problem 15 p2516 A71-32246

Spectral scanning method for determining temperature profile of jet- or rocket-engine exhaust stream by gas radiation and transmittance measurements, discussing radiometric errors effects 18 p2916 A71-36048

JET FLAMES

U FLAMES

U JET FLOW

JET FLAPS

Upwash interference on two dimensional jet flap wing in slotted wall tunnel, using small disturbance theory 02 p0187 A71-12690

Trailing vortex generation behind jet flapped wing at high wing lift coefficients 04 p0527 A71-15413

Cavitation flow of fluid with free surface past underwater wing with jet flap, solving equations of motion for thin foil with jet emergent from trailing edge 07 p1092 A71-20086

High aspect ratio jet flap lifting-line theory, using matched asymptotic expansions method 09 p1381 A71-22083

Approximation of flow around jet flapped airfoil, discussing ground effect on lift coefficient increments 11 p1705 A71-26314

Three dimensional jet flapped wing matched asymptotic expansion solution for high aspect ratios based on thin airfoil theory assuming inviscid and incompressible flow 12 p1863 A71-27217

Two dimensional jet flap cascades, presenting stream deflection angles as function of jet to mainstream momentum flux [ASME PAPER 71-FE-14] 13 p1995 A71-29453

Three dimensional jet flap and lifting line/ surface theories application to STOL aerodynamic systems with externally blown flaps and augmentor wing [AIAA PAPER 71-578] 15 p2345 A71-31568

Two dimensional jet flapped symmetric wing in subsonic flow, assuming irrotational flow inside jet bounded by vortex sheets 21 p3318 A71-40172

Jet flaps application to autogyro rotor, using pressure jump for jet centrifugation 21 p3324 A71-41399

JET FLIGHT

U JET AIRCRAFT

JET FLOW

NT AIR JETS

NT PERIPHERAL JET FLOW

NT SUPERSONIC JET FLOW

Compressible gas jet flow from vessel with parallel walls pointing in opposite directions, solving Chaplygin equations for stream functions 01 p0069 A71-10420

Supersonic overexpanded jet flow past cone, determining impingement point by method of characteristics 01 p0002 A71-10613

Frictionless rotationally symmetrical free supersonic gas jets with thermodynamic relaxation, applying approximate method for shape and flow parameters at boundary 02 p0241 A71-12407

Two free homogeneous turbulent coaxial air jet mixing, showing mass transfer between boundary layers and interface pressure 02 p0185 A71-12409

Secondary jet action on circular horizontal plate located above parallel screen, using Poisson equation 02 p0186 A71-12552

Dense plasma cluster charge exchange in supersonic Mg jet, examining pair collision model, particle scattering, target thickness and Q switching 02 p0292 A71-12614

Finite amplitude sound interaction with Helmholtz resonator, attributing losses to viscous damping and orifice jet flow kinetic energy dissipation 03 p0456 A71-13279

Jet fluid dynamics under various boundary conditions and velocity distributions 03 p0341 A71-13579

Free and impinging axisymmetric turbulent jet characterization model providing continuous transition from nozzle exit through fully developed region [ASME PAPER 70-WA/FLCS-6] 03 p0401 A71-14082

Simplified two dimensional jet reattachment model, using Goertler profile equation and constant spread parameter [ASME PAPER 70-WA/FLCS-8] 03 p0401 A71-14084

Flow and dynamic pressure recovery in wall attachment fluid amplifiers, considering large scale flow flop [ASME PAPER 70-WA/FLCS-9] 03 p0354 A71-14084

Two dimensional jets forced and induced switching by vortex flow [ASME PAPER 70-WA/FLCS-13] 03 p0354 A71-14084

Jet switching dynamic behavior in bistable fluidic devices, examining flow field, response and switching time [ASME PAPER 70-WA/FLCS-20] 03 p0355 A71-14084

Two dimensional wall jet and wall wake flow turbulence characteristics, considering mean and fluctuating flow properties [ASME PAPER 70-WA/APM-35] 03 p0403 A71-14161

Axially symmetrical two phase turbulent air jet, examining small liquid droplets effect on flow structure [ASME PAPER 70-WA/APM-45] 03 p0404 A71-14166

Plane ideal incompressible fluid jet impact on curved surface, considering flow characteristics near stagnation point 04 p0567 A71-14592

Hot laminar round inert gaseous jet entraining fuel-air mixture, obtaining velocity, temperature and concentration profiles 04 p0683 A71-15495

Heated jet injection into isothermal turbulent boundary layer, investigating temperature distribution downstream with conduction model 04 p0572 A71-15499

Dynamic characteristics of submerged twisted jet flow of incompressible viscous fluid 04 p0573 A71-15560

Jet interference effects on rectangular and swept wings, presenting wind tunnel test data for range of jet locations, inclinations and velocity ratios [DGLR-70-052] 05 p0693 A71-15951

Jet interference effects on aircraft static stability with ejector afterbody, noting wind tunnel methods of drag minimization and measurement [DGLR-70-048] 05 p0696 A71-15953

Transonic jets pressure and density fluctuations dependence on air humidity, discussing flow field measurements by differential and Mach-Zehnder interferometry and wall pressure distributions 05 p0737 A71-17153

Aerodynamic sound generation by turbulent circular free jets, presenting solution to inhomogeneous acoustic wave equation by Lighthill [DFVLR-SONDDR-87] 06 p0881 A71-17421

Quarter wave tube in off- and near-resonance regimes, dissipating energy by jet formation during flow emergence from cavity into duct [AIAA PAPER 71-87] 06 p0881 A71-18543

High subsonic jet near-field acoustic energy flux distribution calculation from pressure gradient measurements [AIAA PAPER 71-155] 06 p0884 A71-18592

Viscous incompressible jet flow impinging on plane wall, considering negligibility of ambient medium viscosity within boundary layer equations framework 07 p1089 A71-19745

Jet plume in subsonic cross flow, calculating conical vortex trajectories as function of distance along trajectory from semiempirical model 07 p1090 A71-19901

Ideal fluid jets theory, discussing cavitation flow calculation, jet flow and plane steady potential incompressible fluid flow 07 p1091 A71-20088

Ideal gas jet sonic flow past wedge according to Kirchhoff scheme, testing sine series solution for convergence 07 p1016 A71-20088

Laminar swirling jet flow through vertical circular cone, assuming velocity singularities on axis 07 p1092 A71-20092

Cylindrical viscous jet surrounded by flowing gas investigating flow stability by linear perturbation theory 07 p1093 A71-20288

Beam deflection type fluidic amplifiers with single and symmetric control jets, considering free stream line flow theory 07 p1025 A71-20555

Jet pipe valve characteristics, discussing pressure and flow recovery for various loads, nozzle diameter ratios and spacings 07 p1025 A71-20555

Two axisymmetric jets impingement in fluid amplifiers, discussing velocity profiles of radial jet 07 p1029 A71-20599

Laminar-turbulent bounded jet stability, examining transition zone shift with smoke visualization 07 p1029 A71-20599

Jet flow deflection by cross flowing stream applied to low velocity anemometers 07 p1030 A71-20599

- Fluidic noncontact position sensor, investigating snapper insertion effect on laminar jet flow
07 p1030 A71-20599
- Reflected jet proximity detector dynamic and static characteristics, considering response speed and separation distance
07 p1030 A71-20600
- Jet reattachment to adjacent flat plate, investigating back pressure effects
07 p1094 A71-20606
- Wall attachment jet control volume model, examining flow momentum with restrictive force
07 p1031 A71-20609
- Laser Doppler system for subsonic and supersonic jet flow velocity measurements, discussing calibration and measurement errors
08 p1303 A71-22009
- Oscillations generating mechanism in resonance tube fed by subsonic gas jet, determining oscillations amplitude and frequency at resonance
09 p1382 A71-22406
- Two dimensional discrete fluidic element with Coanda effect, calculating switching discharge, jet gap and circulation zone length
09 p1386 A71-22654
- Proportional fluidic element static characteristics, calculating main jet interaction with control jet
09 p1386 A71-22655
- Circular gas jet path lines in nonuniform velocity inside field drift flow, using auxiliary curve values and correction coefficients
09 p1432 A71-22730
- Hypersonic flow interaction with transverse jet, discussing experimental investigation of Reynolds number, jet pressure ratio and mass flux effects
09 p1382 A71-22944
- Single jet oscillations excitation of two resonant tubes, observing air motion with wool threads and stroboscopic lighting
10 p1591 A71-23823
- Inviscid flow distribution of high temperature jet of optically thick radiating gas exhausting from two-dimensional nozzle into low temperature quiescent medium
10 p1552 A71-24588
- Plenum chamber with nozzle wind tunnel model, noting jet flow phenomena at various angles of attack
10 p1590 A71-24865
- Phase velocities and vertical amplitude profile of nonsingular mesoscale gravity waves produced in stratified jet flows by floating and deflecting earth rotation forces
11 p1793 A71-25171
- Excitation schemes, fluid velocity and power of jet MHD induction generator
11 p1709 A71-25456
- Underexpanded transverse sonic jet-hypersonic stream three dimensional flowfield based on inviscid rotational flow model
11 p1701 A71-25472
- Combustion chamber flame tube cooling by swirling air flow, determining radial and longitudinal temperature distributions for various swirler hub ratios and jet angles
11 p1813 A71-26052
- Inviscid incompressible two dimensional jet deflection by various dimension segments, investigating potential flow with Schwarz-Christoffel transformation and free streamline theory
11 p1753 A71-26444
- Noise field from subsonic air jets by velocity dependence and radiation intensity directivity determination
11 p1753 A71-26445
- Laminar boundary layer equations integration for jet propagating along porous surface, determining transverse velocity component effect
12 p1896 A71-27114
- Inviscid compressible fluid jet flow, calculating instability boundaries characteristics by linear perturbation analysis and numerical solution
12 p1897 A71-27219
- Viscosity effect on initial highly underexpanded jets in Mach 1 to 5.7 nozzles for laminar, turbulent and rarefied air flows
13 p1989 A71-27889
- Aerodynamic noise produced by supercritical jets, using high speed flash photography for schlieren and shadowgraph studies
13 p2069 A71-28767
- Jet induced flame stabilization in combustible kerosene-air mixture flow of variable composition, discussing stable burning range and excess air content
13 p2163 A71-28965
- Viscous gas jets in uniform oncoming flow, deriving similarity laws by dimensionality theory
13 p1994 A71-29223
- Quasi-one dimensional nonlinear model of electrohydrodynamic stability and control of current carrying seminsulating jets at supercritical and subcritical regimes
13 p2118 A71-29249
- Incompressible conducting fluid plane jet expansion in homogeneous slipstream, deriving partial differential equations for nonconduction approximation
14 p2278 A71-29610
- Low thrust jet effect on base pressures on boat-tailed afterbodies in Mach number 0.8-1.2 flow
14 p2169 A71-29889
- Circular air jet velocity, turbulence intensity and energy spectra distributions, investigating longitudinal acoustic field influence
14 p2225 A71-30226
- Hot jet aerodynamic parameters from emissions of electromagnetic and acoustic energies by crossed beam IR probing
14 p2288 A71-30520
- Aerodynamics of axial and axial tangential blade swirler twisted jet near nozzle, testing effectiveness of equivalent problem of heat conduction theory
15 p2388 A71-31522
- Unenclosed laminar jet diffusion flame phenomenological analysis predicting flame height relationship to fuel flow rate and atmospheric density and oxygen concentration
15 p2513 A71-31622
- Free jets in rotating homogeneous flows, investigating inertial and friction effects for various jet-rotational velocity ratios
15 p2390 A71-31926
- Fluid jets along curved or straight walls with non-zero external potential flow, analyzing Coanda effect
15 p2390 A71-32055
- Attaching jet flow on inclined flat plate with small offset, obtaining centerline shape and velocity profile
15 p2391 A71-32056
- Hydromechanical analysis of jet spreading in low pressure planar fluid amplifiers for low Reynolds numbers and finite aspect ratios, deriving velocity distribution equations
15 p2391 A71-32058
- Laminar square jet from turbulence amplifier, analyzing centerline velocity distribution and supply pressure recovery
15 p2391 A71-32060
- Sphere drag in hypersonic jet transition flow near free molecule limit, using magnetic suspension method
15 p2347 A71-32124
- Divergent semibounded turbulent isothermal jet of constant density emerging from slot, determining length of initial and main sections
16 p2560 A71-33613
- Molecular jet velocity measurement, using periodic spatial variation modulation of radio frequency field
16 p2614 A71-34063
- Molecular jet spectrometer with two irradiation zones, observing lines intensity
16 p2615 A71-34064
- Jet induced secondary flow interaction with circular plate, showing ring vortex effects on pressure distribution
17 p2669 A71-34334
- Plane laminar two phase jet flow consisting of small spherical particles suspended in incompressible carrier fluid in presence of adjacent parallel moving free stream
17 p2726 A71-34582
- Turbulent He jet time resolved velocity and He mass fraction measurements, using hot-wire anemometry and digital recording techniques
17 p2670 A71-34878
- Radiation field inhomogeneity effect on radiation gas jet flow, taking into account radiative energy transfer by differential approximation
17 p2728 A71-35117
- Laminar and turbulent incompressible entry flows in channel with jets along walls, determining filling length
18 p2904 A71-36135
- Plane laminar incompressible jet flow along parabola with no external stream, using second order boundary layer theory
18 p2904 A71-36268
- Turbulent boundary layer jet flow calculation using equivalent heat conduction theory
19 p3161 A71-37128
- Air injection into trailing vortex core, noting jet flow effect on circumferential velocity
19 p2991 A71-37291
- Acoustical oscillations effect on free jet flow stability and structure, using inviscid Orr-Sommerfeld equation for flow disturbances frequency, wavelength and velocity
20 p3175 A71-38806
- Semibounded jets in laminar and turbulent flows, discussing boundary layers skin and stream regions, step flow velocities, temperatures and self similar problems
20 p3214 A71-39794
- Surface patterns of ablating bodies from water jet flow experiment simulation, discussing vortices detection
21 p3317 A71-40019
- Viscosity effect on initial part of highly underexpanded jets in Mach 1 to 5.7 nozzles for laminar, turbulent and rarefied air flows
21 p3317 A71-40079
- Direct local density gradient measurement in rarefied free jet flow using electron beam deflection signal processed with lock-in amplifier
21 p3364 A71-40394
- Turbulent jet flow concentration, velocity and direction measurements, describing cold and hot wire techniques and data reduction system
21 p3378 A71-40401
- Laminar incompressible plane wall jet, calculating flow characteristics for potential core region with integral method
21 p3370 A71-40988
- Symmetrical and unilateral sticking flow modes of nozzle air jets expelled into plane-parallel and parabolic ducts
22 p3480 A71-42681
- Electrification induced instabilities, breakup and drop size of charged cylindrical liquid jets, using small perturbation method
23 p3663 A71-43445
- Resultant aerodynamic forces on circular arc profile with normal jet in subsonic steady compressible flow, using Imai-Lamla approximation method
23 p3627 A71-44271
- JET FUELS**
U JET ENGINE FUELS
- JET IMPINGEMENT**
Plane supersonic overexpanded jet interaction with obstacle, using hodographs for flow pattern construction
01 p0001 A71-10425
- Supersonic overexpanded jet flow past cone, determining impingement point by method of characteristics
01 p0002 A71-10613
- Supersonic underexpanded jet-plane obstacle flow interaction patterns, discussing pressure and distance effects
02 p0186 A71-12643
- Free and impinging axisymmetric turbulent jet characterization model providing continuous transition from nozzle exit through fully developed region
03 p0401 A71-14082
- Cavitation and jet impingement erosion, discussing materials response and exposure time effects
03 p0404 A71-14285
- Plane ideal incompressible fluid jet impact on curvilinear surface, considering flow characteristics near stagnation point
04 p0567 A71-14592
- Rocket engines with nitrogen tetroxide/hydrazine injectors destructive instability due to pressure disturbances, establishing origin, propagations velocity and pops extent by streak photography
06 p0942 A71-17653
- Liquid hypergolic propellants heat and gas release determination by calorimetric and PVT measurements, using impinging free jets for propellant mixing
06 p0943 A71-17658
- Viscous incompressible jet flow impinging on plane wall, considering negligibility of ambient medium viscosity within boundary layer equations framework
07 p1089 A71-19749
- Two axisymmetric jets impingement in fluid amplifiers, discussing velocity profiles of radial jet
07 p1029 A71-20592
- Fluidic/electronic pressure ratio computer prototype, using two free jets interaction for instrument error reduction
07 p1031 A71-20603
- Surface heating and pressure distribution on Lunar Module from rocket exhaust plume impingement tests in vacuum
08 p1377 A71-21985
- Liquid properties effect on secondary injection from spray nozzle, determining jet penetration in supersonic stream by scattered light and schlieren photographs
09 p1381 A71-22089
- Turbulent characteristics of circular subsonic free jet impinging normal to flat plate, measuring heat transfer rates
10 p1694 A71-23951
- Circular subsonic free jet impinging on wall, investigating high intensity frequency noise and turbulence spectrum
10 p1594 A71-24594
- Flow field properties of impinging free jets from circular convergent nozzle, measuring velocity, surface pressure and momentum flux
10 p1552 A71-24616
- Screech noise generation by supersonic jet impingement on flat plate, discussing jet disintegration mechanism with resultant shock wave oscillations
11 p1751 A71-25521
- Cross flowing air stream effects on heat transfer characteristics of single lines of air jets impinging on plane surfaces
11 p1854 A71-25947
- Heat transfer coefficients of various jet systems impinging on gas turbine blade inner surfaces, discussing cooling flow rates and solid particles injection into air flow
11 p1811 A71-25955
- Wing-jet interference effects in cross wind on thrust and aerodynamic characteristics at large distance from and near ground
13 p1993 A71-29207

JET LIFT

Approximate calculation for axisymmetric interaction between freely expanding jet and obstacle by reduction to problem of uniform gas flow past sphere
13 p1994 A71-29232

Average and pulsating velocity distributions during subsonic air jet interaction with plane baffle, describing jet dissipation geometrical pattern
14 p2225 A71-30223

Turbulent compressible underexpanded two dimensional jet interaction with crossflowing free stream, analyzing flow field by numerical solution of Navier-Stokes equations
[AIAA PAPER 71-611] 15 p2514 A71-32277

Supersonic jet interaction with turbulent wake, calculating plane and axisymmetric flow behind body butt face
17 p2672 A71-35630

Kalman filter in preflight postflight analysis of velocity increment by spin rocket plume impingement at preentry altitudes
[AIAA PAPER 71-934] 19 p3148 A71-37179

Three ideal incompressible fluid jets collision induced flow, reducing discontinuity region analytic functions to nonlinear system with two numerical parameters and singular integrals
21 p3367 A71-40684

JET LIFT

Round cold jet inclination effects on VTOL aircraft tail assembly lift and longitudinal stability in transition region
[DGLR-70-053] 05 p0693 A71-15967

Jet engine contribution to lift at supersonic flight velocities via air mass heating, studying three dimensional flow with heat supply and stream deflection
07 p1014 A71-19746

High aspect ratio jet lift flap line theory, using matched asymptotic expansions method
09 p1381 A71-22083

Telecontrolled Rotomobile flying crane with jet powered lifting rotor for carrying heavy loads over short distances
10 p1556 A71-24420

Optimal blowing wall jet prediction for suppressing separation from high lift aerofoils with incomplete mixing of upstream boundary layer
11 p1704 A71-26196

Hybrid V/STOL jet lift aircraft design, examining wing area-lift engine bypass ratios relation
[AIAA PAPER 71-767] 18 p2850 A71-36273

Helicopter, tilt wing and jet lift hovering aircraft outflow measurements to determine suitability as rescue vehicles
[AIAA PAPER 71-992] 24 p3791 A71-44586

JET MIXING FLOW

Optimum two fluid mixing chamber length for energy efficiency of conical diffusers in straight pipe jet pump systems
03 p0399 A71-13369

Flow separation and reattachment in confined jet mixing of air with secondary flow in duct
[ASME PAPER 70-FE-B] 03 p0341 A71-13703

Air jet mixing with low velocity stream in constant diameter pipe, measuring flow characteristics for non-separating conditions
[ASME PAPER 70-WA/FE-2] 03 p0402 A71-14124

Ideal incompressible fluid plane jets interaction with flow discontinuity at jet boundaries, deriving nonlinear system of integral equations
03 p0405 A71-14564

Turbulent pulsation mixing of free gas jets in mechanical vortex generator with turbulization level control
04 p0577 A71-15621

Parallel incompressible gas jets mixing of variable densities based on dimensional analysis
04 p0577 A71-15623

Turbulent and laminar jet propagation and mixing in rotor downwash field
[DGLR-70-050] 05 p0795 A71-15961

Supersonic jet-bounded subsonic wake interactions, determining recirculation zone boundaries
05 p0694 A71-16848

Two dimensional supersonic surface jet-hypersonic flow interaction with axial symmetry
[AIAA PAPER 71-131] 06 p0845 A71-18575

Near and far noise fields from coaxial interacting supersonic jet flows
[AIAA PAPER 71-152] 06 p0884 A71-18594

HCN, acetylene and ethylene formation by propane in mixed jet staged flames
08 p1346 A71-20861

Supersonic and subsonic jets coexistence in rectilinear constant section duct, characterizing flow boundaries by pressure readings and Schlieren flow visualization
09 p1384 A71-23605

Coaxial jets development and mixing in axisymmetric twisted turbulent ring air flow injected through inlets
10 p1594 A71-24560

Primary/secondary flow density ratio effect on rotary jet flow induction, describing experimental results with 1/7-1/1 density ratios
10 p1553 A71-24853

Recirculation patterns in coaxial steady laminar mixing of homogeneous jets in confined tube, solving Navier-Stokes equations
11 p1748 A71-25151

Series solution for unbounded mixing of two incompressible homogeneous coaxial fluids with constant properties, using successive approximations method
11 p1748 A71-25159

High velocity airstream interaction with multiple gas jets from single row multihole wall injectors, discussing jet penetration and mixing in cross flow
11 p1750 A71-25478

Neutral stability of laminar free boundary layer in mixing incompressible MHD half jets at low Reynolds number
13 p2103 A71-27842

Gas dynamic antechambers flame stabilization at various flow rates and temperatures, calculating mixing factor vs flow and jet parameters
13 p2163 A71-28966

Optimal penetration effect on peripheral gas flow temperature field at outlet of turbine combustion chamber with circular flame tubes
13 p2118 A71-28971

Two coaxial axisymmetric subsonic gas jets of different density mixed during expulsion from convergent nozzles with high compression, using flow rate ratio
13 p2050 A71-29215

Base flow prediction for axially symmetric cylindrical vehicle with supersonic single central jet by two stream interaction model, comparing Thor flight data
[AIAA PAPER 71-643] 14 p2290 A71-30720

Jet mixing control of thermodynamic state of space stored cryogenic fluids, minimizing mass penalties resulting from equilibrium departures
[AIAA PAPER 71-646] 14 p2285 A71-30723

Recirculating cells and entrance conditions influence on confined heterogeneous jets laminar mixing, measuring velocity and concentration profiles
[AIAA PAPER 71-601] 15 p2389 A71-31578

Free jets in rotating homogeneous fluids, investigating inertial and friction effects for various jet-rotational velocity ratios
15 p2390 A71-31926

Ducted axisymmetric jet mixing flow, investigating flow separation and reattachment as function of diameter and velocity
15 p2392 A71-32252

Transverse liquid injection into supersonic airstreams, using photographic techniques to determine jet penetration and spreading for various dynamic pressure and density ratios
[AIAA PAPER 71-724] 15 p2393 A71-32287

Gas turbine engine combustion chamber outlet gas temperature field peripheral nonuniformity, detailing jets disruptive capacity effects in mixing zone
16 p2625 A71-33609

Semiempirical Taylor formula application to asymptotic turbulent boundary layer formed in mixing jet region
17 p2728 A71-35118

Open singing flame from propane-butane and oxygen jet mixture, constructing oscillogram model of sound emission
17 p2839 A71-35696

Heated jet interaction with deflecting flow in subsonic wind tunnel, presenting flow visualization and temperature and velocity profiles
[ASME PAPER 71-HT-2] 19 p3163 A71-37980

Liquid jet injection into transverse two-phase vapor-liquid flow, calculating penetration path and depth from semiempirical theory
20 p3210 A71-38896

Free shear layer similarity flow profiles correlation for turbulent isobaric jet mixing by spread rate parameters, using viscosity models
21 p3371 A71-41032

Two phase gas-liquid ejectors with cylindrical mixing chamber, discussing ejection equations, jet flow parameters, operation modes and diffusor substitution
22 p3479 A71-41851

Jet mixing in cross flow at different velocity ratios and incidence angles, calculating momentum and mass flow
23 p3664 A71-43831

Flow field generation by coaxial turbulent jets, determining velocity distribution, turbulence intensities and shear stresses by hot-wire anemometers
23 p3627 A71-44198

Knudsen effusion problem in thermal molecular gas jet mixing, using moment method based on velocity distribution function
24 p3817 A71-44354

Generalized eddy viscosity model application to quiescent and cflowing axisymmetric turbulent jets mixing
24 p3818 A71-44626

JET NOISE

U JET AIRCRAFT NOISE

JET NOZZLES

Proportional fluidic elements jet nozzle discharge coefficients as function of control pressure and geometrical parameters
03 p0354 A71-13959

Noise generation increase with unchanged mass flow rate by cone angle diffusers in jet nozzles, considering far field sound pressure level
[ASME PAPER 70-WA/GT-5] 03 p0402 A71-14171

High secondary/primary mass ratio multinozzle jet pump ejector/operation feasibility
[AIAA PAPER 70-579] 03 p0344 A71-14452

Gas temperature in combustion chamber and jet nozzle exit, and gas jet velocity resulting from various pressures, temperatures and air excess factors combinations
06 p0948 A71-18707

Inclined engine cold circular jet effects on tail control surfaces aerodynamic characteristics, considering aircraft longitudinal stability
[DFVLR-SONDDR-104] 10 p1552 A71-24591

Soviet monograph on turbines and jet nozzles for two phase flows covering gas-particle velocity and temperature differences, turbine design, etc
13 p2117 A71-28893

Free axisymmetric turbulent annular nozzle jet propagation, detailing velocity distribution variation due to momentum loss in stall region
23 p3664 A71-44339

JET PILOTS

U AIRCRAFT PILOTS

JET PLUMES

U PLUMES

JET PROPULSION

Composite propulsion systems including Turbo-Ram-Scramjet, Ejector Ramjet, Hyperjet and Bi-Liquid Ramjet Rocket
04 p0638 A71-15285

Jet propulsion optimization by exergy and energy for minimum total cost flux by varying unit compressor pressure ratio
08 p1348 A71-21300

Helicopter jet propulsion systems, considering turbocompressors, gas generators, turbine air jet systems, pulsed jet engines, ramjet engines and rocket engines
11 p1706 A71-25259

Canadian R and D on fixed wing civil STOL aircraft, discussing augmentor wing concept using jet powered lift augmentor system
16 p2523 A71-33470

Rotating dumbbell shaped satellites orientation optimization by system of jets, calculating energy losses
16 p2646 A71-33672

Inclined radial jet drive systems for noiseless gas bearings, comparing with turbine drive device
22 p3553 A71-41681

JET PUMPS

Jet pump optimization for incompressible flow, considering friction losses, nonuniform densities and diffuser losses for overall energy conversion efficiency
01 p0085 A71-10105

High secondary/primary mass ratio multinozzle jet pump ejector/operation feasibility
[AIAA PAPER 70-579] 03 p0344 A71-14452

JET STREAMS [METEOROLOGY]

Vorticity generation or suppression using scale analysis with vorticity equation, considering wind shear in jet stream
02 p0241 A71-12744

Wind foot cirrus cloud pattern relationship to tropospheric jet streams based on high resolution satellite color photographs
04 p0621 A71-15275

Atmospheric oxygen absorption spectra fluctuations related to presence or absence of jet stream
07 p1151 A71-18912

Jet stream axis position from cumulus cloud structural differentiation observed over Central Europe on 22 May 1970, noting coincidence with high pressure near ground
12 p1924 A71-26375

Mesoscale gravity waves and jet stream stability in temperature-stratified atmosphere with small wave perturbations, estimating wave phase velocities and amplitude functions
12 p1924 A71-26376

Atmospheric jet stream reinforcement by cold pseudofronts and convective energy from local source
12 p1924 A71-26824

Stability theory for thermal stratified viscous parallel flows at Prandtl number of unity, considering atmospheric boundary layer and jet stream mechanisms
13 p2165 A71-29246

Atmospheric ozone data in tropical regions from Nimbus 3 IR interferometer spectrometer measurements, indicating easterly jet stream existence during summer monsoon period
17 p2771 A71-35810

Tro stream simulation method by electrohydrodynamic analog, using principle of mapping free lines of flow
19 p3043 A71-37542

Synoptic aerological conditions for occurrence of CAT, considering in-flight registrations and observations under jet stream conditions over North Atlantic
19 p3089 A71-37775

Synoptic-aerological conditions of CAT under jet streams, using aircraft measurements
19 p3090 A71-37775

Stationary ascending and descending jets velocities in nonstationary cloud layer, discussing cumulus clouds breakup rate
19 p3093 A71-38695

Mesoscale perturbations in wind velocity field in jet streams, interpreting data in terms of hydrodynamic stability theory
21 p3412 A71-41392

Earth rotation effect on mesoscale wave characteristics, considering Coriolis force influence in homogeneous inertly stratified jet stream
21 p3375 A71-41393

ET THRUST

Axisymmetric spacecraft fuel optimal reorientation control by reaction jets determined using Pontryagin maximum principle
01 p0165 A71-11586

Thrust equation, control volume and propulsive efficiency for rockets and air breathing jets from energy conservation principle
02 p0299 A71-12681

Thrustmeter for direct in-flight measurement of aircraft engine jet thrust
03 p0422 A71-13332

Round cold jet inclination effects on VTOL aircraft tail assembly lift and longitudinal stability in transition region
[DGLR-70-053] 05 p0693 A71-15967

Three dimensional/nonaxisymmetric/thrust nozzle design, using calculus of variations for maximization of thrust
[AIAA PAPER 71-42] 06 p0946 A71-18503

Wing-jet interference effects in cross wind on thrust and aerodynamic characteristics at large distance from and near ground
13 p1993 A71-29207

Afterburning turbofan engine thrust calculation by gas generator method, using F-111A for comparison tests
[AIAA PAPER 71-680] 14 p2292 A71-30744

Jet engine thrust induced nonconservative effects in aeroelastic analysis of vertical takeoff, using cantilever beam torsion and bending differential equations
16 p2650 A71-33019

Optimized momentum and attitude control system (MACS) for Skylab class space stations employing control moment gyro and reaction jet elements
[AIAA PAPER 71-938] 19 p3098 A71-37183

Twin wheel momentum bias/reaction jet spacecraft attitude control system, presenting mathematical model, stability analysis and design
[AIAA PAPER 71-951] 19 p3099 A71-37192

Optimum rotor/jet thrust ratio determination procedure for tip jet driven rotors, considering performance upper bound
19 p2998 A71-38653

Time optimal transfer trajectory in central Newtonian force field between two arbitrary points under jet acceleration
20 p3289 A71-39135

Backflow region and shock interaction in rotating and swirling gas streams and jets in supersonic nozzle with separation and thrust effects
22 p3480 A71-42682

German book on adaptive control systems covering flight attitude control, jet engine thrust, marine surface navigation, identification, etc
23 p3660 A71-44187

JET VANES

Jet engine high pressure turbine high temperature alloy blades and vanes grinding operation, discussing testing, operating conditions and coolant application
[SME PAPER MR-71-802] 15 p2416 A71-32432

JETAVATORS

U GUIDE VANES

JITTER

U VIBRATION

JOBS

U TASKS

JOINING

Pad relocation technique by DC wafer probe tests for interconnecting LSI arrays of imperfect yield
01 p0044 A71-10186

JOINTS [ANATOMY]

NT KNEE [ANATOMY]

Transducer for measuring mandibular dynamic movements during speech
01 p0079 A71-10346

Differential equations for control and adaptation of hand motion in cubital joint under weightlessness and accelerations
03 p0357 A71-12990

Joint action of various afferents in regulation of human posture, considering appropriate differential reactions
13 p2003 A71-27833

JOINTS [JUNCTIONS]

NT BUTT JOINTS

NT LAP JOINTS

NT METAL JOINTS

NT SEAMS [JOINTS]

NT SPOT WELDS

NT WELDED JOINTS

Adhesive bonding and detachable joints in multilayered fiber reinforced plastic structures, discussing joint strength test methods, fiber and load force orientation effects, etc
01 p0108 A71-10692

Ducting materials and joints technology fallout from aerospace projects, discussing reliability in terms of corrosion resistance, fatigue strength and thrust compensating duct design
01 p0007 A71-11431

Two semiinfinite strips joined to form one infinite strip, determining stresses by joint shrinkage
03 p0509 A71-13898

Space shuttle systems structural joints thermal control, discussing contact conductance with and without interstitial fillers
04 p0676 A71-15334

Piecewise linear analysis of two connecting structures including connections with clearance, applying to engine crankshafts and pin-and-eye problems
05 p0829 A71-17116

Magnetic pulse technique connecting Al pipe with steel pipe, determining mechanical and physical parameters
06 p0906 A71-18713

Two-body satellite of axisymmetric rigid bodies interconnected by lossy universal joint, calculating transient oscillation damping of forced precession under external torque
07 p1205 A71-18895

Semiempirical bending, axial and torsional flexibility coefficients for structural joint assemblies, noting dependence on assembly diameter
07 p1209 A71-18903

Flange joint moments magnitude due to bolts nonuniform tightening during assembly based on probability theory
07 p1116 A71-19359

Dual channel rotary joint combining Tm and Te modes in circular waveguide for X band antenna high average power operation
08 p1252 A71-20758

Bolted joint assemblies under sustained loading, examining joint and fastener coating, bolt design and strength level and shear and tension stress effects
08 p1371 A71-21412

Cyclic creep test for simulating helicopter rotor blades start-stop cycles effect on adhesive bonded joints, using fixed load-unload cycle
10 p1631 A71-24076

Adhesive bonded joints mechanical behavior relation to materials, processes and experimental techniques, developing statistical analysis and formulas for orthotropic-elastic joints
10 p1614 A71-24087

Fracture mechanics application to structural adhesives test methods, considering joints crack extension resistance and plane strain fracture toughness
10 p1615 A71-24088

Processing variables effects on epoxy adhesive joints fracture toughness and crack extension resistance
10 p1632 A71-24089

Handbook on adhesive bonding covering adhesive materials, properties selection and compatibility, bonded assembly requirements and joints design, surface preparation, processing, trade sources, etc
11 p1788 A71-25451

Carbon and boron fiber reinforced plastics adhesive bonded and bolted joints, presenting results of hole deformation tests
[DFVLR-SONDDR-96] 13 p2093 A71-29306

Welded, bearing and interlocking joints and adhesive bonding in carbon fiber reinforced plastics, discussing anisotropy, thermal expansion and electrochemical corrosion problems
17 p2748 A71-34344

Stress distribution in plates and tubes bonded by stepped joints, assuming generalized plane stress
17 p2824 A71-34814

Stress distribution over elements of boss or collar tightened flange joints of circular thin walled shells during bending
17 p2829 A71-35306

Wire connection damage due to high vibration, examining termination and joining techniques
18 p2852 A71-36837

Bar forces in statically determinate planar truss due to arbitrary loads at joints, describing computer program for sequential solution
22 p3517 A71-41869

Linear elastic structures analysis by quadratic programming, considering equilibrium equations for forces at joints
22 p3618 A71-42589

Static joint wear role in overall machine reliability and service life under working loads from mathematical prediction
22 p3619 A71-42852

Thermal contact resistance of adhesive joints as function of adhesive solidification pressure and temperature and of joint surface physicochemical and geometrical parameters
24 p3831 A71-45024

JORDAN FORM

Field produced by equilibrium electron distributions on analytic Jordan curve
21 p3419 A71-41082

JOSEPHSON JUNCTIONS

Josephson superconducting devices electrical characteristics
07 p1079 A71-20153

Noise thermometry by Josephson effect, demonstrating self excitation random frequency modulation with thermal noise and thermometer having microkelvin noise temperature measurement capability
07 p1114 A71-20157

Current-voltage characteristics of Josephson junction, discussing noise effect at near transition temperature of superconductor and external signal driving
07 p1079 A71-20170

Josephson maximum DC current plot for linear overlap junctions, discussing junction area geometry to current perimetric proportionality
09 p1423 A71-22693

High order harmonic mixing of klystron microwave and far IR laser radiation using Josephson junction
09 p1464 A71-22766

Josephson junction I-V characteristics self resonant current peaks calculation by finite difference scheme simulation, comparing results with perturbation technique and experiment
11 p1742 A71-25800

Superconducting state physics and macroscopic coherent states in superconductors, considering Josephson effect and technology utilization
13 p2110 A71-27888

Josephson and IC type superconducting tunneling junction neuristor devices performance tests, presenting bibliography
15 p2377 A71-32317

Millimeter wave klystrons phase locking to HCN far IR laser line via harmonic mixing in Si and metal-oxide-metal Josephson point contacts
22 p3555 A71-41599

Josephson junctions for far IR radiation detection, mixing and frequency measurement
22 p3543 A71-42128

Magnetic recording of heart electrical activity by cryogenic magnetometer with two Josephson junction quantum interference reduction device
22 p3504 A71-42341

JOULE HEATING

U OHMIC DISSIPATION

U RESISTANCE HEATING

JOULE-THOMSON EFFECT

Miniature self regulating rapid cooling Joule-Thomson cryostat, noting purging of accumulated contaminants
20 p3184 A71-39274

JOURNAL BEARINGS

Medium length journal bearing pressure profiles, deriving ordinary differential equation for load capacity
01 p0086 A71-10300

Infinite MHD journal bearing with electrically conducting fluid lubricant in radial magnetic field, obtaining pressure distribution, load capacity and driving torque
02 p0258 A71-12601

Load carrying capacity of finite length self acting gas lubricated journal bearings
[ASME PAPER 70-LUB-23] 07 p1117 A71-19502

Minimum squeeze film thickness in journal bearing under reversed periodic loading of double loop form
[ASME PAPER 70-LUB-12] 07 p1117 A71-19505

Tilting pad hydrodynamic and porous hydrostatic gas lubricated journal bearings for miniature cryogenic turbomachinery
[ASLE PREPRINT 70LC-10] 08 p1298 A71-21158

Self acting herringbone journal bearings optimization program for maximum radial load capacity and wide operating range via groove configurations
11 p1769 A71-25836

NaK lubricated segmented hydrodynamic fluid film tilting pad type journal bearings and Kingsbury type self aligning thrust bearings
15 p2447 A71-32210

Compliant surface fluid film thrust and journal bearing analysis, using coupled flow-elasticity model and load tests
17 p2747 A71-34192

Herringbone grooved gas lubricated journal bearing load capacity, attitude angle and power loss measurements
17 p2749 A71-35487

Book on lubrication systems selection, application, handling and maintenance covering journal and thrust bearings, nuclear reactors and machine tools
19 p3069 A71-37523

Stability characteristics and general transient motion of vertical finite width three lobe journal bearing, assuming incompressible fluid with cavitation
[ASME PAPER 71-VIBR-76] 21 p3385 A71-40314

Computerized analysis of fluid film behavior, load capacity and center locus of journal bearing under dynamic load
[ASME PAPER 71-VIBR-86] 21 p3386 A71-40322

JOURNALS [SHAFTS]

- Computer-aided study of journal bearing performance under cyclic loads, determining bearing load for circular, linear and elliptical orbits of journal center
[ASME PAPER 71-VIBR-87] 21 p3386 A71-40323
- Externally pressurized gas journal bearing whirl instability stabilization system, predicting whirl onset threshold speed 22 p3551 A71-41662
- Rigid rotor whirl dynamics in externally pressurized gas journal bearings, calculating frequencies in terms of stiffness and other parameters 22 p3552 A71-41670
- Computerized design procedures for externally pressurized flexibly mounted gas lubricated journal bearings, predicting steady state performance, vibration capacity and translational stability 22 p3552 A71-41670
- Discrete slot pressurized fluid journal bearing design for low L/D ratios and small size configuration 24 p3830 A71-44942
- Externally pressurized journal bearings fed with incompressible lubricant, determining feeding system and hydrodynamic effects on bearing stiffness 24 p3830 A71-44949
- Laser beam applications in drilling, shaping and surface finishing of miniature journal and step-type friction bearings, deriving regression equations for optimal process parameters 24 p3834 A71-45162
- ## JOURNALS [SHAFTS]
- ### U SHAFTS [MACHINE ELEMENTS]
- #### JUDGMENTS
- Bias free loudness judgments by modification of vision studies method, considering physical correlate theory of stimulus intensity 05 p0712 A71-16282
- Input-output transformations for judgments of area of circles and paired weights, using nonmetric scaling 05 p0713 A71-16548
- Space vehicle apparent distance magnitude estimation judgments, investigating stimulus range effects on response range and Stevens type power function exponent 07 p1051 A71-20217
- Time duration judgment under visual stimulus, noting numerosity effects 18 p2863 A71-37018
- Contrast effects in loudness judgments, using category scale and maximally extensive number response language 23 p3638 A71-43111
- #### JUNCTION DIODES
- Stimulated recombination radiation from PbSe laser diodes at 77 K, showing stepwise curve of emission power vs pumping current 01 p0094 A71-10780
- Junction-casing and junction-ambient medium thermal resistance determined in power transistors and diodes 01 p0055 A71-11125
- Microwave Gunn diodes I-V characteristics as function of carrier concentration 01 p0057 A71-11213
- Magnetoconcentrating effect in diodes with hemispherical p-n junction and semiorganic base in longitudinal magnetic field 01 p0057 A71-11461
- Alloyed p-n junction diode with deep impurities, discussing barrier capacitance frequency dependence 01 p0057 A71-11462
- Schottky diode bipolar IC and silicon gate MOS LSI techniques in manufacturing 02 p0228 A71-11652
- Gunn diodes I-V characteristics width as function of carrier concentration/mobility and diode length, noting role of impact ionization in strong electric field 02 p0231 A71-11877
- End layers role in forward I-V characteristics of P-I-N power diodes, ensuring minority carrier current continuity 02 p0235 A71-12919
- GaAs heterojunction diode injection lasers, predicting high order transverse cavity modes and far field patterns from theoretical model 03 p0434 A71-13482
- Noise-induced current fluctuations on S-shaped I-V curve in Cr-doped GaAs diodes 03 p0387 A71-13982
- Gunn diode generated signal frequency jumps as function of voltage variations, basing explanation on high field domain formation and decay 05 p0729 A71-16999
- Thermal resistance of thermal p-n junction semiconductor microwave limiter diodes in continuous and pulsed mode operation 06 p0873 A71-17543
- Loss resistance and dissipated power dependence on crystal configuration of microwave semiconductor junction diode 06 p0873 A71-17544
- Diffusion varactor and Schottky barrier semiconductor diodes for frequency multiplication at millimeter wave frequency range 06 p0873 A71-17545

- Schottky barrier diode shot noise, examining dependence on potential barrier gap thickness, height and permittivity, impurity distribution, Schottky layer thickness and semiconductor dielectric constant 07 p1075 A71-19225
- Superconducting tunnel junctions radiation emission, discussing superconductivity theory 07 p1178 A71-19777
- Wide band low noise millimeter wave parametric amplification using wafer varactor diodes with Schottky barrier junctions 08 p1263 A71-20769
- Junction diode effects on spark erosion machining, noting reduction in tool wear 08 p1297 A71-20998
- Si step-junction avalanche diodes conduction current pulse waveforms during large signal operation, using numerical calculation 08 p1265 A71-21290
- Three dimensional model of semiconductor diode current dependence on charge carrier diffusion length and surface recombination rate 09 p1414 A71-22189
- Forward biased asymmetric p-n junction diodes with arbitrary impurity distributions, measuring minority carrier lifetimes by refined step recovery technique 09 p1414 A71-22248
- Gunn diodes temperature, calculating power density dissipation by simple domain mode models and accumulation mode operation 09 p1414 A71-22249
- I-V and capacitance characteristics of silicon diodes prepared by diffusive melting, considering recombination processes in p-n junctions 09 p1414 A71-22290
- Si Read diode computer simulated large-signal operation, determining temperature effect on microwave oscillating efficiency 09 p1417 A71-22966
- Distortion effects in switching diode modulators due to local oscillator interference 09 p1420 A71-23681
- X band Schottky barrier diodes RF impedance mismatch and noise factor, calculating dependence on microwave oscillator voltage-standing wave ratio 09 p1421 A71-23723
- Capacitance voltage measurements on interface of pyrolytically deposited n-type silicon dioxide-InAs MOS diodes as function of admittance at room and 77 K temperatures 10 p1582 A71-23774
- IMPATT diode oscillators noise and injection phase locking, discussing theoretical refinements of original simple model by Read 10 p1584 A71-24818
- Junction diameter reduction approaches for low noise generation, using Schottky diode parameters 11 p1737 A71-25675
- P-n junction controlled discrete microwave commutation diodes performance calculation and design optimization 11 p1741 A71-26554
- P-type Al-Ga-As-p-type Ga-As-n-type Ga-As single heterostructure preparation and properties, discussing effect on injection laser diode characteristics 12 p1914 A71-27027
- Motion equation of electron in cylindrical diode subjected to varied voltages 13 p2036 A71-28372
- I-V and capacitance characteristics of chalcofenide-glass based matrix-film diode sandwich and film-face switching structures with/without memory 13 p2112 A71-28922
- Pulsed GaAs point contact diodes quick response performance, obtaining contact electrical characteristics and Schottky-type rectifying barriers by half period currents 14 p2211 A71-30093
- Semiconductor heterostructure junction diode lasers for operation at room temperature, discussing energy band structure and mass communications application 16 p2587 A71-33471
- Microwave Gunn diodes I-V characteristics as function of carrier concentration and power efficiency 17 p2713 A71-34264
- MOS sandwich grid diode for gas ionization and field electrons generation at solid-gas phase boundaries 17 p2717 A71-35448
- Double heterojunction structure improvements in injection laser diodes and arrays 18 p2931 A71-36603
- High power GaAs injection laser diodes characteristics and array module design for pulsed operation, using confinement junction formation and reflective end coating 18 p2931 A71-36604
- Schottky barrier, point contact and Ge back diodes for microwave mixers and detectors, noting burnout characteristics 18 p2894 A71-36979

- Photolithographic fabrication and electrical characteristics of GaAs Schottky barrier diodes for pulsed operation 19 p3027 A71-37272
- Photovoltaic and electron-voltaic properties of diffused and Schottky barrier GaAs diodes, considering irradiance in 0.001-10,000 microwatt/sq cm range 19 p3027 A71-37407
- Relaxation time model of solid state diodes based on equations for electrons of given energy, including junction and tunnel diodes 19 p3027 A71-37494
- Semiconductor lasers, noting AlGaAs-GaAs p-heterojunction structure contribution to room temperature efficiency of diode lasers 19 p3074 A71-38212
- GaAs laser diode junction temperature measurement methods for verification of stimulated emission quenching due to heating 19 p3074 A71-38213
- Neutron irradiation effects on radiative, nonradiative and threshold currents in epitaxial GaAs laser diodes at room temperature 20 p3275 A71-38781
- Schottky barrier diodes as photodetectors in bolometer mode, deriving ballistic transport model for scattering mechanisms effects 20 p3236 A71-39191
- Current variation effect on pulsed psn diodes forward characteristics, calculating peak inductive transient voltage value and time position 20 p3205 A71-39430
- Microwave waveguide semiconductor modulation with p-n diode as control element, taking into account semiconductor control element conductivity change along waveguide wall 20 p3206 A71-39813
- Monolithic alphanumeric array of planar light-emitting GaAsP diode matrix on common chip for programmed function keyboard use in display devices 21 p3349 A71-40108
- Red and green light emitting GaP junction diodes and monolithic arrays for display devices, discussing fabrication and properties 21 p3352 A71-40116
- Low voltage IR image converter display system using scanned line array of GaAsP light-emitting junction diodes 21 p3352 A71-40117
- P-n-p-n quadruple layer semiconductor junction light emitting diode with negative resistance characteristics, discussing epitaxial regrowth process and applications 21 p3355 A71-40739
- Fabrication and I-V characteristics of S-type negative resistance alloyed diodes prepared from sulfur-doped n-type Si, outlining temperature dependence of turnoff time 21 p3358 A71-41203
- Switching effects in diode structure formed by tungsten point contacts on glassy cadmium germanium arsenide surface 21 p3358 A71-41207
- Semiconductor surface state effects on p-n junction photodiode frequency characteristics under short and open circuit conditions, noting nonequilibrium capacitance during illumination 21 p3358 A71-41215
- Au-n-GaAs surface barrier diode space charge layer strong electric field effects on photoconductivity quantum efficiency 21 p3432 A71-41302
- GaAs luminescent p-n junction diode spontaneous emission measurement in magnetic field, noting redistribution in Lorentz force direction 21 p3432 A71-41303
- I-V and capacitance characteristics of chalcofenide-glass based matrix-film diode sandwich and film-face switching structures with/without memory 21 p3433 A71-41311
- Si Pt-n-p transit time microwave diode source noise measurement, noting low noise characteristics and suitability for local oscillator applications 21 p3359 A71-41411
- Temperature dependent threshold current density and doping gradient at p-n junction in epitaxial GaAs injection laser diodes 22 p3555 A71-41680
- Design and performance optimization of series mode step recovery diode frequency multipliers, using computer aided analysis 22 p3523 A71-42355
- Low frequency phase method application to fast electron processes and characteristic relaxation time in quick response Ge and Si junction diodes 23 p3650 A71-43301
- Impedance and capacitance frequency dependence of p-p-n junction diodes at microwave frequencies with high injection levels 23 p3650 A71-43301
- Negative resistance in high resistance compensated semiconductor diodes with double injection associated with diffusion growth 23 p3652 A71-43448

- Reduced switch-off time high voltage p-n-p-n structures using diode blocking coincident with thyristor collector junction 23 p3716 A71-43483
- Room temperature GaAlAs close confinement /single heterojunction/ laser diode performance and applications 23 p3684 A71-43503
- Staircase array and diode stacking moderate power GaAlAs injection laser light sources at room temperature 23 p3685 A71-43504
- Gallium arsenide phosphide electroluminescent junction diode pumped Nd-YAG laser room temperature CW and pulsed outputs 23 p3687 A71-44139
- Noise voltage power spectrum of GaAs bulk diodes at LF as function of bias field approaching negative resistance region 24 p3804 A71-44992
- Doping profile effects on performance properties of hypersensitive capacity variation junction diodes, describing basic interrelation between capacity and potential 24 p3812 A71-45351
- ### UNION TRANSISTORS
- MOS junction transistor operation governing equations and electron distribution, using numerical analysis 02 p0233 A71-12423
- Differential drain resistance calculation for junction field effect transistors 07 p1070 A71-18869
- N and p junction field effect transistor (JFET) gate current measurement leading to understanding of impact ionization mechanism and field distribution 07 p1081 A71-20542
- Junction thermal behavior and energy losses in active contactless bipolar transistor switch loaded by capacitive impedance 11 p1739 A71-26377
- Unijunction transistors operation principles, electrical parameters, structural features and circuit applications 11 p1740 A71-26548
- Linear sawtooth generator, using MOS unijunction transistors to switch and maintain constant discharge current from timing capacitor 11 p1740 A71-26549
- MOS transistors on P substrates, investigating ionizing radiation effects on I-V characteristics 12 p1885 A71-26830
- MOS transistor saturation range transconductance, internal resistance and gain factor calculation, allowing for field effect on space charge near drain 12 p1889 A71-27626
- Doping dependent mobility analysis of junction FET, calculating drain current and transconductance 13 p0207 A71-28474
- Computerized use of transient thermal resistance and power pulses superposition to calculate instantaneous transistor junction temperatures for various pulse conditions 13 p0208 A71-28770
- Net impurity doping profile of double diffused transistors 14 p2210 A71-29792
- Temperature dependence of current gain in p-n-p transistors due to increased surface recombination rate 14 p2213 A71-30623
- Neutron irradiation effects on diffusion-ion doped HF n-p-n silicon transistors of moderate power, showing radiation stability 14 p2213 A71-30625
- Epitaxial film thickness and resistivity effect on transistor cut-off frequency, discussing collector junction space charge region boundary location 14 p2213 A71-30626
- Physical process causing negative differential resistance segment on I-V curve of single junction transistor, describing thyristor-triggered relaxation oscillator 14 p2214 A71-30633
- Far field patterns for short active antennas obtained by integration of transistors and passive antennas 14 p2217 A71-31058
- Unijunction transistor peak point voltage stabilization, giving formula for interbase resistance multiplier variation with temperature 15 p0278 A71-32636
- Localized deformation effect on common-emitter transistor current gain, giving equations system defining band diagram configuration of p-n junction in thermal equilibrium 19 p3027 A71-37490
- Theoretical model of excess surface current in p-n junctions, based on surface-controlled tetrode transistor experiment for bipolar transistors I-V characteristics explanation 19 p3029 A71-38142
- Junction structures and electrical properties of silicon n-p-n transistors fabricated by various combinations of diffusion and ion implantation 21 p3354 A71-40728
- Electron bombardment effects on shot noise of silicon junction transistors, noting generation-recombination current increase in emitter junction 22 p3586 A71-42298
- Lumped model for two dimensional current flow in grown junction transistor base, predicting small signal common emitter short circuit input impedance 22 p3523 A71-42359
- Early effect incorporation in Ebers-Moll simulation model for junction transistor large signal behavior to obtain current gain and conductance dependence on voltage 22 p3523 A71-42484
- Bipolar junction transistor doping effects on bandgap decrease and emitter efficiency, explaining current gain temperature dependence 23 p3648 A71-42911
- Thermal feedback modification of Si JFETs AC and DC characteristics at low operating temperatures 23 p3649 A71-43070
- Minority carriers charge distribution at boundary between neutral base and collector transition region of one dimensional n-p-n transistors 23 p3653 A71-43965
- ### JUNCTIONS
- Continuity and smoothness properties of piecewise optimal control at junction between singular and nonsingular subarcs, developing necessary conditions 17 p2723 A71-35296
- Co-Ge-Si alloys phase equilibria, evaluating long term stability of junctions between thermoelectric batteries conducting series connectors 17 p2759 A71-35337
- Neutron irradiated and unirradiated Ta sheathed BeO insulated grounded junction thermocouples drift measurement 18 p2916 A71-36046
- ### JUPITER [PLANET]
- Io Hygiea perturbation observations, determining Jupiter mass by numerical integration 01 p0155 A71-10443
- Earth and Jupiter magnetic fields relationship to core motional induction 02 p0310 A71-12160
- Very long baseline interferometry /VLBI/ of Jupiter decametric bursts at HF 02 p0310 A71-12326
- Frequency and phase analyses of cross correlated signals from very long baseline interferometry of decametric radiation from Jupiter 02 p0310 A71-12333
- Jupiter model construction from improved state equation, considering chemical composition, contraction and rotation 02 p0314 A71-12589
- Jupiter decimetric emission circular polarization, observing equatorial magnetic field strength in radiation belt 02 p0317 A71-12868
- Comet distributions near Jupiter orbit 03 p0487 A71-13375
- Galilean satellites spectral reflectivity from photometric observations during Jupiter apparitions 03 p0488 A71-13554
- LF radio emission from Jupiter at 3-8 MHz 04 p0641 A71-14737
- Long period effects in motion of Chicago and Thule, noting commensurability with Jupiter orbit 04 p0652 A71-15705
- Minor celestial objects for determining Jupiter mass, noting problem geometry, nodal points and orbit correction 04 p0653 A71-15712
- Absolute orbit construction for Jovian great satellites, obtaining linear equations of motion 04 p0654 A71-15714
- Space station and interplanetary flight research programs, discussing design, grand tour and Jupiter flyby 05 p0817 A71-16642
- Jupiter surface features motions and changes, discussing planetary fine structure 06 p0971 A71-18247
- Equivalent line widths of 5520 Å ammonia band in Jupiter spectrum 07 p1198 A71-19829
- Minor planets mean motions commensurability with Jupiter in restricted three body problem 07 p1202 A71-20515
- Radio telescope measurements of circular polarization and total flux of Jupiter at 13.1 cm wavelength 08 p1357 A71-20871
- Jupiter and Saturn gravitational moments calculation procedure based on planetary density angular distribution 08 p1361 A71-21054
- Jovian and solar perturbation of hypothetical artificial Callisto satellites, using Delaunay method 09 p1518 A71-22373
- Jupiter decametric radiation source A position variation, considering radiation controlling influence of Jovian satellite Io 09 p1521 A71-22935
- Jovian band color variation spectral observations using narrow band photometry 10 p1676 A71-24499
- Jupiter observation during 1970 visibility period, including drawings, photographs, position and brightness estimates, and red spot 10 p1677 A71-24689
- Venus, Mars, Jupiter and lunar thermal emission data in 7-25 micron region 11 p1824 A71-25698
- Space triangulation corrections of equatorial topocentric coordinates and radius vector of Jupiter in Baker-Nunn net, using Geos A satellite optical and laser observations 11 p1732 A71-25819
- Jupiter magnetic field geometry related to Io modulated Jovian decametric radio emission 12 p1956 A71-26620
- Jupiter occultation of beta Scorpii on 13 May 1971, determining hydrogen/helium ratio 12 p1961 A71-26876
- Jovian radio source angular diameter measurement by radio interferometry 12 p1967 A71-27310
- Four eclipse reappearances observations of Jovian satellite Io by area scanning photometer, considering anomalous brightening 13 p2134 A71-28285
- Jupiter Galilean satellites narrowband photometric data, observing albedos, spectral reflectivity, rotational phase, and brightness variations 13 p2135 A71-28292
- Jupiter rotation from Jovian decametric emission data 13 p2135 A71-28347
- Jupiter and Saturn magnetic field differences, considering metallic interior models 14 p2304 A71-29599
- Jupiter circularly polarized visible light measurements, using photoelastic polarimeter 14 p2306 A71-29729
- Jupiter reflected light, examining model having elliptical polarization by surface layer scattering 14 p2306 A71-29730
- Jupiter and Saturn gravitational moments calculation procedure based on planetary density angular distribution 14 p2310 A71-30167
- Solar wind velocity and Io phase relationship during decametric radio bursts from Jupiter, indicating plasmasphere existence 15 p2474 A71-31723
- Pales /49/ orbit motion analysis for Jupiter mass, noting discrepancies between old and new observations 15 p2488 A71-32198
- Mars and Jupiter radio emission at 2.3 mm and 8.15 mm, determining brightness temperature and electrical and thermal waves soil penetration depth ratio 15 p2490 A71-32413
- Io brightness anomaly after eclipse by Jupiter 15 p2491 A71-32421
- UV spectral energy distribution of Jupiter from rocket-borne Cassegrain telescope observation, computing planet geometric reflectivity in 2100- 3600 Å range 15 p2491 A71-32422
- Elliptic restricted three body problem, calculating fictitious retrograde Jovian satellites orbits in rotating-pulsating axes for sun-Jupiter case 16 p2633 A71-33337
- Jupiter systematic visual observations during 1968-1969 apparition, noting Red Spot conspicuousness, south temperate zone white spots, etc 16 p2635 A71-33429
- Jupiter radio spectrum decametric component observations, emphasizing core and mantle rotation under coupled torsional oscillations 16 p2637 A71-33514
- Scattered light circular polarization data from Jupiter and other planets indicating nonmagnetic origin 17 p2805 A71-35377
- Ganymede thermal inertia data from simultaneous visual photometry and IR radiometry observations during 17 March 1971 eclipse 17 p2807 A71-35418
- Mars, Uranus and Jupiter observations with Sao Paulo Observatory Danjon astrolabe, presenting east and west transits right ascension and declination tables 18 p2961 A71-35943
- Jupiter Galilean satellites surface optical polarization measurement, noting bright transparent material cover possibly frost 18 p2964 A71-36290
- Saturn and Jupiter mass determination from Schwassmann-Wachmann I comet motion observations, using perturbation program based on Schubart-Stumpff n-body integration program 18 p2970 A71-37062
- Jovian satellite eclipse observations, reviewing simultaneous narrow band multichannel visual and near IR studies 19 p3139 A71-37908
- Jupiter orbiter spacecraft propulsion system design, noting advantages of fluorine/hydrazine propellant combination 19 p3122 A71-37925

Jupiter radio observations, measuring nonthermal emission, magnetic field and trapped radiation belts [AAS PAPER 71-108] 19 p3140 A71-37933

Satellite capture by Jupiter, calculating satellite orbits based on aphehion and perihelion conditions derived from planetary elliptical orbit three body problem 20 p3287 A71-38978

Jupiter decametric radio emission relation to solar wind, geomagnetic activity and shock waves causing Forbush decreases 20 p3291 A71-39312

Jupiter and Saturn IR radiation sources, radio emission storms, magnetic fields, life existence, Grand Tour missions, etc 21 p3442 A71-40150

Jupiter disk temperature measurement at eight frequencies in 20.5-35.5 GHz range, comparing with saturated ammonia model calculations 22 p3599 A71-41922

Quantitative equivalence model in planet-satellite formation within Jupiter and Uranus systems 22 p3604 A71-42191

Earth-Jupiter-Saturn-earth trajectories, determining mission planning parameters [AAS PAPER 71-361] 23 p3729 A71-43031

Beta Sco occultation by Jupiter, interpreting UV light curve 23 p3733 A71-43124

To passage in front of binary star beta Scorpii on 14 May 1971, presenting satellite trajectory calculations and appulse time 23 p3733 A71-43150

IR spectral geometric albedos of Jupiter Galilean satellites, noting resemblance to spectra of frosts 24 p3871 A71-44910

JUPITER ATMOSPHERE

Spectrophotometry of methane and ammonia absorption bands indicating decrease toward Jupiter disk edge 03 p0484 A71-13213

Jupiter details rotational periods variations, characterizing dynamic properties of atmosphere upper layers 03 p0490 A71-13940

Jupiter magnetosphere size, shape, structure, energetic particles and expected and potential energy sources 04 p0659 A71-15852

Jupiter rotating inner magnetosphere plasma density distribution, using Lorentz term in force balance equation 05 p0810 A71-16631

Hydrogen-slow electron collision cross sections, calculating Jovian upper atmosphere Lyman alpha and Balmer H alpha emission 06 p0929 A71-17679

Jupiter magnetospheric rotation period based on RF observations 06 p0971 A71-18240

Jupiter and Saturn magnetosphere calculations, considering solar wind characteristics and planetary magnetic fields [AIAA PAPER 71-30] 06 p0977 A71-18494

High enthalpy electric arc plasma jet heaters for simulating entries in hydrogen rich Jovian atmosphere [AIAA PAPER 71-263] 08 p1274 A71-21989

Spectrographic measurements of Jovian Red Spot and Southern Tropical Zone molecular absorption bands related to cloud cover density and depth 09 p1520 A71-22839

Terrestrial microorganisms adaptation to simulated methane-ammonia-hydrogen Jupiter atmosphere 10 p1566 A71-24688

Jupiter far IR emission spectra models, examining atmospheric composition, temperature and structure 11 p1821 A71-25538

Jupiter color variations observation by multicolor photoelectric photometry, noting consistency with activity in Jovian atmosphere 11 p1827 A71-25725

Jupiter equatorial belt effective temperature during 1965 apparition from limb darkening profile observation 11 p1827 A71-25726

Jupiter cloud structure observations near 8.5 microns from thermal flux measurement along polar and equatorial scans 11 p1827 A71-25727

Hydrogen-helium gas mixtures high pressure phase behavior, considering solidified gas core under Jupiter and Jovian planets atmospheres 11 p1827 A71-25728

Quantitative UV radiative transfer and photolysis in model Jupiter atmosphere, considering coloration by ammonia and hydrogen sulfide gases in cloud region 11 p1834 A71-26455

Jupiter upper atmosphere extreme UV dayglow, involving resonant scattering and fluorescence of incident solar flux 12 p1961 A71-26888

Jovian atmosphere radio observations, discussing helium- and ammonium-hydrogen molecules ratio,

brightness temperature spectra and RF wavelength absorbing agents 12 p1964 A71-27087

Jupiter equatorial thermal limb darkening data, constructing atmospheric model for ammonia effects on temperature structure 12 p1966 A71-27254

Jovian atmosphere physical properties inferred from eclipses of Galilean satellites, using color photoelectric photometry 13 p2134 A71-28284

In-flight UV spectrometric measurements of simulated Jupiter atmosphere, using sunlit gas mixture released from Mariner spacecraft in interplanetary space 14 p2308 A71-29914

Jupiter exospheric temperature diurnal variations for various solar activities and latitudes, using time dependent heat balance equations 15 p2491 A71-32423

Jupiter atmosphere nonequilibrium radiative processes, considering energy balance and pressure and temperature conditions 16 p2637 A71-33516

Jupiter atmospheric entry probe missions to cloud layers base, discussing tradeoffs between various types of mission trajectories and technologies [AIAA PAPER 71-834] 17 p2801 A71-34713

Jovian turbopause probe mission, discussing atmospheric composition measurements and nonsurvivable system concept [AIAA PAPER 71-833] 17 p2802 A71-34714

Jupiter atmospheric entry probe mission, discussing descent depths, atmospheric pressure and temperature effects, data return techniques and Grand Tour Missions [AIAA PAPER 71-832] 17 p2802 A71-34715

Reflecting layer model for methane band absorption spectrum in Jovian atmosphere 17 p2807 A71-35412

Cartesian diver atmospheric model hypothesis for Jupiter Red Spot longitude, size and intensity variations 18 p2964 A71-36288

Jovian magnetospheric plasma densities, discussing roles of centrifugal ejection, solar wind plasma injection and photoelectron diffusion 18 p2964 A71-36291

Jovian atmosphere radio observations, discussing helium- and ammonium-hydrogen molecules ratio, brightness temperature spectra and RF wavelength absorbing agents 19 p3133 A71-37437

Outer planets Grand Tour X ray investigation of planetary magnetospheres to obtain flux and energy spectrum of electrons precipitated from Jovian magnetosphere [AAS PAPER 71-130] 19 p3127 A71-37941

Jupiter atmosphere entry probes graphite ablative heat shields performance, indicating convective and radiative blockage and graphite sublimation processes in surface heat balance [AAS PAPER 71-146] 19 p3084 A71-37949

Physical, chemical and biochemical instrumentation and measurements for probe entering Jupiter atmosphere [AAS PAPER 71-148] 19 p3153 A71-37951

Ground based studies of Jupiter at optical frequencies, determining atmospheric chemical composition, temperature and stratification, aerosol layers structure and flyby/penetration experiments results 20 p3297 A71-39631

UV photochemistry of lower Jovian clouds, using experimental simulation 21 p3447 A71-40427

Jupiter disk temperature measurement at eight frequencies in 20.5-35.5 GHz range, comparing with saturated ammonia model calculations 22 p3599 A71-41922

Organic synthesis in simulated Jovian atmosphere by passing semicorona discharge through methane-ammonia mixture 22 p3602 A71-42180

Jovian ionospheric electron and ion densities and temperatures, considering radiative association role 22 p3603 A71-42181

Periodic variations in amount of dark material present in Jupiter atmospheric belts, noting uncorrelation with solar activity 22 p3603 A71-42182

Photometric coefficient of activity in Jupiter atmosphere at 4300, 5500 and 6400 Å, giving relative intensities of belts and zones 22 p3603 A71-42183

Photometric study of Jupiter atmospheric activity in yellow light, noting peculiar activity in equatorial area 22 p3603 A71-42184

Photometric study of short term variations of Jupiter atmospheric activity in UV, blue, green, red and near IR spectral ranges 22 p3603 A71-42185

Jupiter atmospheric probe using relay-link communications geometry between probe and flyby spacecraft for 3.5 hr intervals [AAS PAPER 71-321] 23 p3726 A71-42995

Jovian geometric albedo at 1800-1950 Å decrease explained as absorption by gaseous and solid ammonia cubic crystal form 23 p3736 A71-43343

Hydrogen and helium thermal dissociation and ionization at Jupiter and Saturn adiabatic atmospheric models conditions 24 p3850 A71-44800

JUPITER PROBES

Recurrent Lagrange multipliers coordinate transformation for optimal low thrust Earth-Jupiter trajectories 01 p0160 A71-10927

Jupiter atmospheric probe approach trajectory uncertainties and navigation requirements during 1971 mission [AIAA PAPER 71-120] 06 p0926 A71-18506

Jupiter gravitational potential mapping for Grand Tour spacecraft, discussing Jovian satellites effect on orbit and trajectory perturbations 09 p1525 A71-23222

Thermal control, pressure survival and structural tradeoffs of Jovian atmospheric probe for mission parametric studies [AIAA PAPER 71-482] 11 p1839 A71-26257

Pioneer F spacecraft investigation of Jupiter regions and outer interplanetary space, discussing design, communication system and possible future missions 12 p1973 A71-27603

Jupiter atmospheric entry probe missions to cloud layers base, discussing tradeoffs between various types of mission trajectories and technologies [AIAA PAPER 71-834] 17 p2801 A71-34713

Jupiter grand tour mission, discussing objectives and technical aspects of unmanned Pioneer F and G vehicle 18 p2965 A71-36684

Jupiter orbiters and probes noting objectives, spacecraft design and mission description [AAS PAPER 71-103] 19 p3152 A71-37905

Pioneer Jupiter probe missions as precursor to subsequent outer planets exploration, discussing primary objective of asteroid belt and Jupiter radiation belt hazards evaluation [AAS PAPER 71-111] 19 p3152 A71-37911

Shuttle/Centaur injection stage, considering application to comet rendezvous mission via Jovian powered swingby [AAS PAPER 71-113] 19 p3139 A71-37912

Pioneer F and G spacecraft Jupiter flyby postencounter mission options ranging from solar system escape to high-inclination low-perihelion trajectories [AAS PAPER 71-136] 19 p3139 A71-37921

Jupiter orbiter missions, considering satellite emphasis and planetary environment and planetology missions [AAS PAPER 71-140] 19 p3140 A71-37923

Pioneer F/G spacecraft Jupiter missions, trajectories and objectives with relation to outer system [AAS PAPER 71-101] 19 p3140 A71-37931

Navigation error sources and orbit determination accuracies for Jupiter planetary encounter, using earth based radio tracking data [AAS PAPER 71-118] 19 p3101 A71-37937

Launch opportunities for Grand Tour outer planets missions using Saturn-Jupiter instead of Jupiter-Saturn flyby sequence [AAS PAPER 71-139] 19 p3140 A71-37943

Jovian probe and spacecraft mission feasibility, discussing launch opportunities, targeting, objectives and data transmission [AAS PAPER 71-141] 19 p3141 A71-37944

Atmospheric entry probe from flyby mission to Jupiter, considering descent trajectory feasibility and instrument package [AAS PAPER 71-142] 19 p3153 A71-37945

Jupiter probe design and communication for deep penetration into atmosphere, concerning mission phases through entry and descent to sample altitudes [AAS PAPER 71-143] 19 p3153 A71-37946

Physical, chemical and biochemical instrumentation and measurements for probe entering Jupiter atmosphere [AAS PAPER 71-148] 19 p3153 A71-37951

Jupiter entry probe integration on TOPS and Pioneer outer planet spacecraft for flyby missions, discussing design feasibility and spacecraft modification requirements [AAS PAPER 71-153] 19 p3153 A71-37955

Pioneer Jupiter spacecraft, noting low weight, radioisotope thermoelectric generators and gyroscopic stabilization by spinning with antenna pointed at earth [AAS PAPER 71-167] 19 p3141 A71-37964

Jupiter atmospheric probe using relay-link communications geometry between probe and flyby spacecraft for 3.5 hr intervals [AAS PAPER 71-321] 23 p3726 A71-42995

JUPITER PROJECT

Solar cells for Jupiter mission, discussing radiation and environmental tests concerning I-V characteristics 05 p0701 A71-16074

Radar ranging experiment onboard Jupiter orbiter, concerning perturbations, gravitational harmonics and short arc orbit determination 15 p2487 A71-32041

Asteroids flyby approaches during Jupiter missions and Grand Tours, obtaining gravitational deflection of spacecraft trajectories and mass cost estimates
 [AAS PAPER 71-360] 23 p3729 A71-43030

JUPITER RED SPOT
 Jupiter Great Red Spot continuous changes on basis of observational records of South Equatorial Belt disturbances
 04 p0643 A71-15000

Spectrographic measurements of Jovian Red Spot and Southern Tropical Zone molecular absorption bands related to cloud cover density and depth
 09 p1520 A71-22839

Jupiter observation during 1970 visibility period, including drawings, photographs, position and brightness estimates, and red spot
 10 p1677 A71-24689

Jupiter Red Spot, zonal wind and banded appearance, Venus vertical temperature structure and atmospheric motions, and Mars circulation, dust phenomena and atmosphere stratification
 14 p2313 A71-30499

Zenomagnetic core-mantle coupling and fluctuations in period of rotation of Jupiter Great Red Spot
 16 p2637 A71-33515

Cartesian diver atmospheric model hypothesis for Jupiter Red Spot longitude, size and intensity variations
 18 p2964 A71-36288

Jupiter Red Spot and other photographic features in 1969-1970, noting 90-day oscillation in longitude and south tropical zone disturbance
 18 p2964 A71-36289

Truth table analysis of models of Jupiter Great Red Spot, suggesting chromophores welling from below
 18 p2967 A71-36926

K

K BAND
U EXTREMELY HIGH FREQUENCIES
K LINES
 Organic compounds carbon K emission spectra, using light element X ray spectrometer for aliphatic, aromatic and partly ionic substances spectral analysis
 03 p0375 A71-13200

Three component model for chromospheric Ca II K line formation, discussing observational agreement
 05 p0803 A71-16024

Transition metal diborides X ray emission K alpha band, establishing asymmetry index, bandwidth and maximum power shift deviations from B
 05 p0770 A71-17169

Wilson-Bappu effect and asymmetric K line emission in sun
 08 p1359 A71-20947

Ice, solid carbon dioxide and alcohols oxygen K spectra from long wave X ray spectroscopy
 09 p1498 A71-23479

Solar simplified geometrical model, observing emission peak center to limb variation of Mg II, H and K lines and optical thickness
 10 p1666 A71-23782

Calcium H and K line anomaly in faint meteor spectra, discussing brightness correlation with aerodynamic flow and resonant charge exchange with ionized nitrogen
 12 p1957 A71-26626

Solar Ca II K line core formation, discussing models for high spatial resolution spectra
 13 p2140 A71-29045

Solar quiet region chromosphere K emission line behavior, identifying surface characteristics for width absolute magnitude relation
 13 p2140 A71-29046

Solar spicules H alpha and beta, D3 and K line profiles, considering radial and turbulent velocities, optical thickness, atomic density and He emission
 13 p2140 A71-29049

Integral equations for source functions of Ca II H, K and IR triplet lines for transfer through homogeneous stellar atmosphere
 14 p2276 A71-30298

Solar atmosphere structure inhomogeneities, describing Ca II H and K line spectra profiles
 15 p2497 A71-32743

Nitrogen X ray emission K alpha band behavior in zirconium mononitride in entire range of ZrN homogeneity
 19 p3083 A71-37280

Solar Mg II H and K line profiles from rocket-borne echelle interferometer spectrograph and densitometer data
 19 p3135 A71-37612

Stellar chromosphere detection through H, K and metastable He lines observation, noting importance for solar physics
 19 p3136 A71-37627

Solar K-line profile absolute intensity calibration from elements of fine structure on surface, determining brightness temperature
 23 p3767 A71-43836

Solar rotation evidence from H alpha and K line spectra of quiescent prominences for westward wind
 23 p3767 A71-43841

KA BAND
U EXTREMELY HIGH FREQUENCIES
KALMAN-SCHMIDT FILTERING
 Kalman optimal linear filter application to near earth satellite orbit calculation based on earth radar observations
 01 p0156 A71-10518

Kalman linear multidimensional filters stability, examining digital computer algorithms
 05 p0732 A71-17024

Kalman filter simulation for estimating aircraft position and velocity from airborne digital computer data in zero-zero landing system
 06 p0924 A71-17697

Maneuvering vehicles behavior model selection for real time Kalman filter tracking algorithm, based on accuracy predictions and empirical performance
 08 p1270 A71-21349

French book on optimal inertial navigation and statistical filtering covering Wiener and Kalman filters, gyroscopes, accelerometers, inertial platforms, data processing, computer programming, etc
 14 p2271 A71-29940

Velocity-aided Kalman filtering for one dimensional motion under random acceleration, obtaining steady state solution and transit time
 14 p2197 A71-30793

On-line identification of stochastic linear dynamic control systems with applications to Kalman filtering based on statistical correlation technique
 15 p2380 A71-31933

Earth rotational and deformational motion equations in extended Kalman-Schmidt filter for geodetic data processing
 [AAS PAPER 71-339] 23 p3666 A71-43012

KAOLINITE
 Kaolin and quartz powder additions effect on glass-like polymethyl methacrylate specific heat, thermal conductivity and diffusivity
 07 p1144 A71-18922

Morphological structural changes during firing from scanning electron microscopy of unfired and fired kaolinite
 13 p2092 A71-28659

KAPOETA ACHONDRITE
 Gas rich Kapoeta howardite composition, evolution, high particle fossil track densities and normal track rich crystals spatial relations
 10 p1672 A71-24392

KAPPA ROCKET VEHICLES
NT KAPPA 9 ROCKET VEHICLE
KAPPA 9 ROCKET VEHICLE
 Ionospheric electron density measurement by K-9M rocket, comparing VLF Doppler with Langmuir probe methods
 23 p3671 A71-43366

KARMAN VORTEX STREET
 Dynamic small perturbation calibration of constant temperature hot-wire anemometers for turbulence measurements in Karman vortex streets, comparing static method
 16 p2581 A71-34166

Hypothetical analogy between wave formation during explosive welding and Karman vortex street arising in liquid flow around cylinder
 19 p3068 A71-37083

Karman vortex street breakdown under deceleration, noting vortices distortion and annihilation followed by vortex street formation of different frequency
 19 p3046 A71-38202

Karman vortex street geometry calculation for single circular cylinder, using pressure drag coefficient, Strouhal number and Kronauer criterion
 [ASME PAPER 71-VIBR-11] 21 p3457 A71-40273

Karman vortex street induced fluctuating lift forces on single circular cylinder, deriving relationship between lift coefficient and steady state pressure drag coefficient
 [ASME PAPER 71-VIBR-12] 21 p3457 A71-40274

Karman vortex street induced fluctuating lift forces on tube bundles as function of steady pressure drag coefficient and Strouhal number
 [ASME PAPER 71-VIBR-13] 21 p3457 A71-40275

Aircraft wake turbulence, reviewing aerodynamic vortex research as exemplified by Karman vortex street and edgetone phenomenon
 21 p3318 A71-40483

KC-130 AIRCRAFT
U C-130 AIRCRAFT
KC-135 AIRCRAFT
U C-135 AIRCRAFT
KELVIN TEMPERATURE SCALE
U TEMPERATURE SCALES
KEPLER LAWS
 Krylov-Bogoliubov integration theory for first-order perturbation analysis of multidimensional harmonic oscillator applied to body motion in earth gravity
 01 p0151 A71-10113

Keplerian orbit numerical integration, considering Runge-Kutta method and transformations
 01 p0154 A71-10377

Numerical integration finite difference methods stabilization for perturbed Keplerian motion differential equations
 01 p0154 A71-10378

Matrix perturbation methods for nonlinear perturbed systems, involving variational equations solution of regularized Keplerian motion
 01 p0154 A71-10380

Artificial satellites rendezvous, describing common Kepler ellipse in central body field with positioning after time delay
 03 p0500 A71-14389

Schwarz differential invariant in Kepler problem, describing point motion under Newtonian force effect
 05 p0811 A71-16640

Small factor errors of inertial navigation system for disturbed Keplerian motion of planet
 07 p1158 A71-20468

Series inverse in powers of time and radius of convergence for universal form of Kepler equation, discussing recursion formulas for coefficients
 09 p516 A71-22174

Satellite path geometry along Keplerian elliptical orbit, taking earth flattening into consideration
 09 p1520 A71-22664

Two-impulse optimal transfers between Keplerian orbits, deriving expression for switching conditions in explicit form
 09 p1529 A71-23602

O and B type stars galactic Keplerian parameters statistical distributions based on galaxy point model
 11 p1820 A71-25248

Stellar masses calculation, using dynamical parallaxes, Kepler third law and mass-luminosity relation
 14 p2311 A71-30362

Mars orbiters and Kepler laws, discussing planetary motion, satellite orbits and orbital characteristics
 24 p3875 A71-45268

KERNEL FUNCTIONS
 Linear integral equations with difference and summation kernels in elasticity theory, developing approximate solution method
 01 p0171 A71-10657

Polyvinyl chloride nonlinear viscoelastic behavior by multiple integral representation, determining kernel functions for mixed time parameters from tension-torsion creep experiments
 [ASME PAPER 70-WA/APM-21] 03 p0512 A71-14156

Soviet monograph on singular integral equations and boundary value problems involving Cauchy kernels
 04 p0619 A71-15400

Total radiative interchange kernel measurements, describing remote excitation/detection
 04 p0684 A71-15511

Compressible boundary layer separation near zero skin friction by Kaplun perturbation technique, studying nonlinear integral equation with Abel kernel
 09 p1432 A71-22455

Steady electromagnetic oscillation amplitude calculation from solution kernel to Maxwell equations boundary value problems through orthogonal coordinate transformation to Fredholm integral equations
 09 p1495 A71-23431

Convolution-type integral equations over arbitrary finite segment number with kernels, showing solvability in spaces, applications and correctness
 12 p1982 A71-27519

Existence theorems for eigenvalues of integral equations with continuous kernels
 13 p2096 A71-28907

Linear integral equations with difference and summation kernels in elasticity theory, developing approximate solution method
 14 p2333 A71-30991

Differentiability of nonlinear Volterra integral equations of second kind with convolutional weakly singular kernels
 15 p2442 A71-31870

Searchlight problem with isotropic scattering for semiinfinite and finite geometries, computing transmission functions for Fourier intensity components by kernel approximation method
 17 p2839 A71-35571

Kernel function for nonplanar acoustical surfaces in supersonic flow, using finite element method for interfering configurations
 19 p2991 A71-37295

KEROSENE
 Turbulence intensity in combustion zone of stabilized air-kerosene flame from annular burner, using He diffusion measurements
 03 p0520 A71-13994

Oxygen-kerosene fuel combustion products, calculating thermal and physical constants
 08 p1346 A71-21263

Optimal inlet parameters of MHD generator channel employing kerosene-gaseous oxygen combustion products
 09 p1386 A71-22136

KERR CELLS

Kerosene type fuels for aircraft gas turbine engines, discussing combustion problems, smoke emission reduction and bacterial or fungal contamination

13 p2113 A71-28754

Jet induced flame stabilization in combustible kerosene-air mixture flow of variable composition, discussing stable burning range and excess air content

13 p2163 A71-28965

KERR CELLS

Kerr cell for high speed modulation of laser radiation, noting use in multiframe shock wave dark photography

01 p0093 A71-10625

High voltage pulse shaping circuits for Kerr cell polarization shifters for modulating and deflecting monochromatic laser radiation

19 p3071 A71-37255

KERR EFFECTS

Mode locked Nd-glass laser, describing dispersion and Kerr effects on pulse frequency modulation

08 p1301 A71-21125

KERR ELECTROOPTICAL EFFECT

Frequency modulation and compression of ultrashort light pulses by optical Kerr effect

04 p0552 A71-15035

KERR MAGNETOOPTICAL EFFECT

Faraday and polar Kerr reconstruction effects in stored magnetic holography [IEEE PAPER 8.1]

07 p1112 A71-19609

Kerr magneto-optical effect display as input to coherent optical computer, using laser lens impressed thin film matrix

08 p1258 A71-21185

Thermomagnetic modulated Kerr effect readout and magneto-optical laser recording at high output on cobalt base metallic films

10 p1613 A71-25108

KETONES

Remote group interactions after electron impact in 4-substituted cyclohexanones, investigating mass spectrometry in structural and stereochemical problems

02 p0209 A71-12548

Synthesized amino esters and ketones with varying distance between functionalities, examining mass spectral fragmentation

02 p0209 A71-12574

Zinc reduced di(4-pyridyl) ketone methionides, examining electronic and electron spin resonance spectrum

02 p0377 A71-14301

Photolysis of HCl photosensitized evolution from dichlorobutane in solution by aliphatic ketones

11 p1728 A71-25937

Marmot ketone bodies concentration during activity, deep hibernation and early arousal, discussing increased oxidative metabolism effects

13 p2014 A71-29125

Hypokinesia effect on formation and elimination of ketones, aldehydes, carbon monoxide and ammonia in rats

15 p2356 A71-31305

KEYING

NT FREQUENCY SHIFT KEYING

On-off keying system digital detection using random sampling for achieving high bit rates

05 p0725 A71-17073

KIDNEY DISEASES

Renal anatomical pathology in dogs long after high energy proton irradiation, noting similarity to natural aging

09 p1388 A71-22194

Flight concomitant pathogenetic effects on urinary tract conditions, noting kidney descent, inflammatory episodes and calculosis

10 p1566 A71-24977

KIDNEYS

Arterial blood pressure changes due to bilateral carotid occlusion or electrical heart pacing, considering effects on kidney blood flow and circumference in dogs

01 p0008 A71-10074

Morphological and histological changes in liver and kidneys of rats exposed to long term hyperthermia

01 p0013 A71-11131

Angiotensin I infusion effect on intrarenal blood flow distribution, using krypton 85 method and autoradiography

04 p0538 A71-15088

Intrarenal vascular pattern in carbon dioxide death of rhesus monkeys and dogs, observing sympathetic vasoconstriction

06 p0851 A71-17610

Oxygen tension in skin and kidneys using chronopotentiometric measurements

06 p0857 A71-18724

Human kidney cell generation and life cycle parameters, considering thyroxine effects

07 p1041 A71-19594

Mitotic activity of kidney undergoing compensatory hypertrophy in high mountain nonadapted rats

08 p1242 A71-21965

Human heart, kidneys, liver and spleen tissues antigen composition analysis by isolation of pure antibodies

12 p1872 A71-27723

Dietary pyridoxal deficiency causing amino acid content reduction in liver, kidney, brain and heart tissues

13 p2003 A71-27837

Ultrasonic vibration effects on DNA and RNA content in skin and kidneys of albino rats

15 p2356 A71-31288

Amino acid levels in fasted and fed rats plasma, liver, muscle and kidney during and after exercise, noting glutamine decrease in liver tissue

20 p3186 A71-38982

Sodium and cations elimination by kidneys during water-salt metabolism changes due to high temperature and hypodynamia

20 p3189 A71-39232

Antidiuretic action of chlorpropamide in mammalian kidney, considering intrarenal infusions effect on urinary concentration, free water clearance, glomerular filtration and sodium excretion

22 p3486 A71-41939

KINEMATIC EQUATIONS

Circular elastoplastic plates, solving adaptation theory kinematic equations by linear programming procedures

02 p0324 A71-11751

Kinematic error equations application to real inertial navigation systems analysis

02 p0253 A71-12636

Stellar distances inaccuracy effects on kinematical parameters estimation from radial velocities

04 p0643 A71-14907

Numerical integration of Poisson kinematic equations for direction cosines, using Runge principle for accuracy values proportional to third power of integration step

05 p0780 A71-16051

Rigid plastic shells carrying capacity by kinematic method based on linear programming

06 p0996 A71-17839

Maxwell theory analogy with Cosserat continuum moving dislocations, studying kinematic and dynamic equations common features

07 p1161 A71-20016

German monograph on basic equations for isotropic elastic homogeneous thin shell subjected to infinitesimal displacements, determining work of form change

10 p1692 A71-25037

Large scale kinematic dynamo theory for magnetic field generation in turbulent fluids based on Lorentz force helicity

14 p2314 A71-30646

Controlled aircraft motion under strict kinematic constraints in terms of simple subsystems, noting pilots role in Newmark theory

14 p2177 A71-31024

Numerical integration of Poisson kinematic equations for direction cosines, using Runge principle for accuracy values proportional to third power of integration step

16 p2605 A71-33455

Shell analysis in curvilinear coordinates, obtaining edge effect equation with canonical kinematic unknowns in plane sections law

17 p2830 A71-35314

Kinematic-dynamo theory with turbulent diffusivity effect, discussing resistivity as random function of position

18 p2969 A71-37045

Kinematic-dynamo equations for stationary unsheread conducting nonrotating sphere dynamo action in isotropic velocity turbulence

18 p2969 A71-37046

Turbulent rotating tube flows kinematic similarities, deriving heat and mass transfer, swirl damping and axial and rotational velocity profile

19 p3043 A71-37127

Kinematic method for determining interstellar extinction/discoloration ratio

20 p3293 A71-39533

Kinematic theory of resonant gamma rays diffraction by single crystals, calculating differential cross sections of Bragg scattering for total degeneracy and Zeeman splitting

21 p3420 A71-41123

Kinematic dynamo equations for turbulent generation of large scale magnetic and small scale turbulent fields, presenting exact treatment of fluctuation and ordered field equations

21 p3416 A71-41194

Kinetic and kinematic properties of steady diabatic complex lamellar gas flows

22 p3530 A71-41696

Kinematic method for deriving formula for gimbal error of directional gyroscope with allowance for main axis inclination to horizontal plane

24 p3828 A71-45157

Astatic gyroscope mounted on aircraft moving arbitrarily near earth surface, obtaining integrals of kinematic equations

24 p3828 A71-45160

KINEMATICS

NT BODY KINEMATICS

Six degree of freedom flight vehicle kinematics digital simulation using CSSL-II language

02 p0227 A71-11788

Elastoplastic, viscoelastic and directed elastic continuous media kinematic and thermodynamic description based on intermediate state of reference concept

02 p0326 A71-12388

Multimass system oscillations due to viscous friction factor and kinematic random disturbances, considering dynamic behavior of wheeled vehicle on rough roadbed

07 p1162 A71-20465

Jacobian calculation in kinematic theory of waves propagation, using ray equation

08 p1276 A71-21616

Soviet book on dynamics of spacecraft descent trajectory covering reentry vehicles trajectory optimization, with allowance for atmospheric perturbation effects

11 p1840 A71-26375

One- and two-component gas models for explaining interstellar gas kinematics and 21 cm line emission brightness temperature dependence on galactic longitude

12 p1970 A71-27747

Crack kinematics for bodies with time dependent deformation and strength characteristics in brittle fracture, discussing tip region, crack models and energy equation

13 p2149 A71-28123

Noctilucent cloud morphology and kinematics from photographic observations near Moscow

14 p2233 A71-29971

German monograph on orthotropic plate equations derivation by kinematics and statics in general coordinates and elasticity relation

15 p2509 A71-32304

Kinematic analysis and simulation of transmission modes of sound energy through middle ear

19 p3002 A71-38062

Time-of-flight measurements for relationship between velocity, mass and temperature in molecular gas motion and electron-atom collision kinematics

20 p3271 A71-38789

Static, kinematic and uniqueness theorems of incremental collapse of frames extended to variable repeated loading

22 p3619 A71-42593

KINESCOPIES

U PICTURE TUBES

KINETHESIS

U PROPRIOCEPTION

KINETIC ENERGY

Doppler radar techniques for turbulent kinetic energy budget in boundary layer, discussing wind profile and turbulence in snow conditions

01 p0117 A71-10577

Kinetic energy and available potential energy balance in atmospheric stationary disturbances/standing waves/, using atmospheric flow statistics

01 p0119 A71-10853

Locally isotropic hydrodynamic turbulent fields statistical properties for kinetic energy and temperature dissipation fluctuations

01 p0120 A71-11106

Extratropical disturbances role in global atmospheric circulation, examining vertical convective heat transfer and kinetic energy production relationship

01 p0121 A71-11357

Amino acid synthesis in simulated primitive environments, discussing possible effects of meteoric kinetic energy and lightning-associated shock waves

03 p0358 A71-13015

Planetary atmosphere circulation kinetic energy, energy transformation and driving temperature gradients, using similarity, dimensional and thermodynamic approaches

03 p0488 A71-13551

Wave kinetics in anisotropic plasma of weakly damped magnetosonic vibrations, using Lagrangians of three and four wave interactions

04 p0633 A71-15108

Upper troposphere-lower stratosphere planetary scale circulation correlation from kinetic energy characteristics analysis

07 p1151 A71-18874

Molecular hydrogen cations collisions with hydrogen and helium, determining dissociation cross section dependence on kinetic energy from threshold to 100 eV

07 p1163 A71-19233

Fluid flow around two parallel circular cylinders moving in ideal liquid, deriving exact solution for flow velocity and kinetic energy

07 p1089 A71-19736

Kinetic energy dependent charge transfer rates for ion-molecule reactions in ammonia, using cyclotron ejection and impulse methods

08 p1249 A71-20657

Locally isotropic hydrodynamic turbulent fields statistical properties for kinetic energy and temperature dissipation fluctuations

08 p1325 A71-20850

Uniform two dimensional incompressible turbulent boundary layer with uniformly distributed surface mass injection, correlating results on basis of turbulent kinetic energy equation

09 p1430 A71-22105

Latitudinal variations in adiabatic production and destruction of kinetic energy by meridional and zonal motions of atmosphere

09 p1488 A71-23025

Atmospheric surface layer shear/buoyant production, flux divergence and dissipation in terms of turbulent kinetic energy and transport in temperature variance budget

09 p1490 A71-23555

Helicopter rotor inertial system kinetic energy, examining takeoff advantages

09 p1385 A71-23670

Frequency domain spectral energy equations for large scale atmospheric motions, discussing earth rotation effects on kinetic energy spectrum

10 p1638 A71-23963

Spherical plasma ball thermokinetic expansion model, considering solid state laser irradiation

11 p1806 A71-26091

Molecular hydrogen cations collisions with hydrogen and helium, determining dissociation cross section dependence on kinetic energy from threshold to 100 eV

12 p1932 A71-26751

Star and galaxy clusters total kinetic energy content, using line of sight velocity data and astronomical models

14 p2312 A71-30390

General atmospheric circulation mean time distribution, kinetic energy, regional interactions and mathematical simulation

14 p2236 A71-30492

Curved sandwich plate strain and kinetic energy expression derivation for use with finite element displacement method

15 p2508 A71-32136

German monograph on conversion of human muscular work into flywheel mechanical kinetic energy covering testing and analysis of biomechanical relationships

15 p2364 A71-32308

Vapor-liquid mixture steady flow from centrifugal injectors, determining kinetic energy loss relationship to phase separation

16 p2624 A71-33608

Two massive arbitrarily shaped hard bodies spatial collision, determining kinetic energy loss, motion and deformation of impact point

17 p2818 A71-34347

High intensity molecular beams properties, measurement and production methods, considering kinetic energy, chemical composition and technology applications

18 p2908 A71-36438

Physics and phenomenology of radiation field in spectral lines, considering radiation transfer with optical depth effects and kinetic energy transformation into radiation

18 p2968 A71-37035

Craters produced by oblique trajectory missile impact, suggesting crater dimension dependence on target material and missile kinetic energy

19 p3156 A71-37683

Wakes of freely falling water drops, discussing flow patterns, kinetic energy, vorticity decay and velocity profiles

19 p3089 A71-37733

Seasonal variations of kinetic energy balance of mean meridional circulation in Northern Hemisphere

20 p3257 A71-39436

Eddy viscosity in barotropic planetary boundary layer, finding turbulent diffusion coefficient dependence on turbulent kinetic energy

20 p3257 A71-39437

Cyclic discrete holonomic mechanical systems Liapunov stability analysis, developing matrix formalism for kinetic energy, Routhian, Hamiltonian and dynamic potential energy quadratic approximation

21 p3454 A71-40097

Ion cyclotron resonance power absorption, deriving expression for average ion kinetic energy at saturation in steady state limit

21 p3418 A71-40231

Direct observation of cosmic ray kinetic energy losses in interplanetary region by measurements at separated spacecraft

22 p3593 A71-42331

Circular cylindrical shell critical stress level leading to stability loss during high speed cogging process based on kinetic energy method

24 p3884 A71-44897

Kinetic equations of quasi-steady homogeneous condensation of water vapor in supersonic nozzle two phase flow

01 p0182 A71-11443

Kinetic equation for rarefied polyatomic gases derived from Liouville equation

02 p0286 A71-11883

Kinetic equations derivation for computer calculation of nonuniform hydrogen plasma decay, considering hydrogen recombination, electron temperature and ambipolar diffusion

03 p0463 A71-13508

Energy conservation in linear atmospheric models using first order kinetic equations

04 p0581 A71-15067

Low temperature weakly ionized molecular plasma kinetic equation in electric field, considering free electron distribution function for molecule- electron inelastic collisions

04 p0634 A71-15114

Phonon distribution function kinetic equation solution, determining two dimensional lattice heat conductivity

05 p0794 A71-16876

Gas-particle mixtures weak disturbances, applying linearized hydrodynamic and phase transformation kinetic equations

07 p1088 A71-19191

Particle motion in gravitational field for disk-like configurations, solving kinetic equation for quadratic potential

07 p1192 A71-19286

Gravitational stability analysis based on Boltzmann-Vlasov collisionless kinetic equation solution by trajectory integration method in plasma physics

07 p1173 A71-20531

Boltzmann kinetic equations for gas mixtures reacting according to detail balance principle

09 p1496 A71-22376

Weakly turbulent plasmas static electric conductivity derivation from kinetic equation for linear response to one-particle distribution function

09 p1503 A71-22861

Weakly ionized plasma density fluctuations and diffusion from kinetic equations for electron- space density cross correlation, assuming BGK model

09 p1503 A71-22863

Kinetic equations for particle motion in gravitational fields, discussing stellar configurations evolution

13 p2100 A71-27973

Amorphous particle rarefied gas in bounded volume, analyzing kinetic equation existence and uniqueness

13 p2103 A71-29146

Integral kinetic equation for flow distribution past body and surface heat flow, noting representation in form for computer solution

13 p1991 A71-29156

Neutral particle gas integral kinetic equations numerical solution without integration on lag parameter

13 p1991 A71-29157

Kinetic equation for gases with rotational degrees of freedom under equality of probabilities of direct and inverse transitions and stereoisomerism of molecules

15 p2387 A71-31192

Boltzmann kinetic equation for imperfect gases in pair collision approximation, including terms proportional to time and coordinate derivatives and van der Waal constants

15 p2387 A71-31193

Monograph on statistical theory for weak homogeneous turbulence covering mathematical model, wave correlation functions, Bogolubov expansion method, kinetic equation, nonlinear interactions, etc

17 p2727 A71-34771

Human cone visual pigments kinetic equation testing by comparing photolysis rate at equilibrium to regeneration rates

18 p2854 A71-36001

Shock wave structure prediction by nonlinear kinetic models with Monte Carlo solutions of full Boltzmann equation

18 p2907 A71-36334

Wavefront overturning in rarefied quasi-neutral plasma, investigating kinetic equations self similar solutions stability

19 p3114 A71-37859

Relaxation equations for dilute diatomic gas dissociation-recombination reactions, transforming kinetic equations to normal modes

19 p3107 A71-38079

Ice particles initial concentration effect on coagulation growth kinetics, considering distribution function variation with time

19 p3095 A71-38705

Kinetic modeling of vibrational state populations in high power direct discharge excited CO laser, using iterative technique

20 p3243 A71-39005

Coaxial free mixing flow calculations, using turbulent kinetic energy method

21 p3369 A71-40958

Dynamic problems for molecular gases with rotational degrees of freedom, deriving hydrodynamic equations from kinetic equations integration

21 p3420 A71-41121

Kinetic and kinematic properties of steady diabatic complex lamellar gas flows

22 p3530 A71-41696

Kinetic equations for phase space cross correlation functions of electron density fluctuations in magnetized weakly ionized plasma, using relaxation model

22 p3581 A71-41895

Kinetic wave equation matrix elements for three resonantly coupled electrostatic plasma waves noting application to electron plasma coupling with ion sound waves

22 p3582 A71-41900

Distribution function integral representation application to steady motion of monocomponent rarefied gas containing amorphous particles, using successive approximation for kinetic equation solution

22 p3482 A71-42868

Kinetic equations for electron density matrix of superconductors, describing two phase relaxation process

23 p3715 A71-43413

Kinetic equations derivation for rarefied chemically reacting monatomic or stable molecular gases

23 p3707 A71-43924

Hydrodynamic equations for ions and electrons of ionized collision plasma in strong nonuniform magnetic field from Boltzmann kinetic equations

24 p3855 A71-44521

Stellar wind equations transformation for reducing parameters number from two to one

24 p3865 A71-44566

Incompressible turbulent boundary layer with suction and surface injection computation by implicit finite difference method and turbulent kinetic energy equation for mixing length flow

24 p3820 A71-44954

KINETIC FRICTION

NT SLIDING FRICTION

Pipe flow turbulent friction, describing pressure drop measurements and flow visualization studies on wall roughness effects

09 p1431 A71-22275

Force equations for static and dynamic friction under external forced vibration, determining mean values from mechanical model

19 p3068 A71-37346

Contactless oscillography of static and kinetic moments of friction in ball bearings in aggressive gas media, discussing experimental assembly design

22 p3529 A71-42489

KINETIC HEATING

NT AERODYNAMIC HEATING

NT SHOCK HEATING

ONERA hypersonic wind tunnels used for ballistic and aerodynamic research kinetic heating problems and control surface efficiency

06 p0841 A71-18025

Convective heat transfer coefficient for supersonic flow past sphere, considering kinetic heating by flow

08 p1378 A71-22047

KINETIC THEORY

NT CHAPMAN-ENSKOG THEORY

NT EYRING THEORY

NT MIXING LENGTH FLOW THEORY

NT TRANSPORT THEORY

Kinetic theory of gas mixtures and thermodynamic laws of irreversible processes, deriving hydrodynamic equations and Onsager relations

01 p0130 A71-10793

Laser effect radiation power in gas mixture flow of carbon dioxide, nitrogen and traces of water vapor, presenting calculations based on kinetic theory

01 p0094 A71-10992

Thermomagnetic gas torque within kinetic theory framework for collinear static and alternating magnetic fields

02 p0291 A71-12316

Boundary value problem for linear Boltzmann equation in kinetic theory, proving existence and uniqueness theorems

02 p0276 A71-12338

Relativistic kinetic theory of particles with magnetic dipole moment in external EM field, deriving transport equations for distribution function

03 p0463 A71-13425

Classical multiautomic gases kinetic theory, considering generalized Boltzmann equations

05 p0785 A71-16779

NonMarkoffian kinetic theory for hierarchical structure of clusters in expanding universe

06 p0964 A71-17314

Soviet book on kinetic effects in semiconductors covering galvanoresistive and thermomagnetic effects, energy bands, quantum theory, oscillation theory, etc

06 p0941 A71-17431

Kinetic theory approximate method application to model equation with velocity dependent collision frequency, obtaining solution for Kramers problem and expression for slip coefficient

06 p0931 A71-17450

KINETIC EQUATIONS

NT HELMHOLTZ VORTICITY EQUATION

NT HYDRODYNAMIC EQUATIONS

NT KINEMATIC EQUATIONS

Nuclear reactor kinetic differential equations, ascertaining positive bounded solutions existence

01 p0126 A71-11290

KINETICS

Onsager relations for Soret-Dufour and diffusion coefficients in moderately dense gas mixtures based on kinetic theory, considering symmetry relations for transport properties

06 p0929 A71-18036

Kinetic theory calculation of partially ionized plasma near-electrode electron temperature profiles [AIAA PAPER 71-140]

06 p0939 A71-18583

One component system wave propagation kinetic theory, calculating monatomic gas and plasma oscillations by discrete ordinate method

07 p1165 A71-18876

Effective electric field formulation of kinetic theory of classical Coulomb plasmas, computing wavevectors

07 p1169 A71-19994

Binary gas mixtures shock tube flow kinetic theory, indicating shock wave formation, contact layer diffusion and expansion wave dispersion

07 p1093 A71-20287

Homogeneous Newtonian cosmological model, constructing ellipsoidal velocity distributions and kinetic theory

08 p1358 A71-20932

Kinetic coefficients calculation for gas with internal degrees of freedom during free energy exchange between translational and internal motion

08 p1338 A71-21918

Heat transfer in rarefied gases, discussing applicability of molecular-kinetic gas theory

09 p1544 A71-22287

Kinetic theory of transient condensation and evaporation at plane surface, using Maxwell moment formulation

09 p1545 A71-22852

Kinetic theory of electromagnetic waves obliquely incident upon plasma slab considered as boundary value problem

09 p1409 A71-23499

Inhomogeneous rotating self-gravitating system kinetic theory, linearizing collisionless Boltzmann equation to two dimensional linear integral equation for obtaining small oscillation modes

10 p1641 A71-24278

Polymerization kinetics of nematic liquid crystal monomer in nematic and isotropic phases

11 p1728 A71-26062

Kinetic processes in shock tubes, considering diagnostic techniques for monitoring time histories nonequilibrium distributions preparations

11 p1745 A71-26264

Longitudinal plasma layer waves kinetic theory, considering particles specular reflection from layer boundaries

12 p1937 A71-27203

Orbital flight time in terms of isochronism kinematic theory, discussing Lambert and Hamilton hodographic representations

13 p2135 A71-28351

Fatigue crack propagation kinetic theory, investigating microcrack nucleation mechanism based on vacancy condensation near crack tip

13 p2155 A71-28791

Kinetic theory of nonspherical multiatomic molecules with electrons having rotational and oscillatory degrees of freedom, giving expressions for oscillatory relaxation times calculation

13 p2103 A71-29150

Kinetic theory of two dimensional boundary layer between plasma and magnetic field, using computer for vector potential differential equations solution

13 p2109 A71-29214

German monograph on shock waves in anisotropic plasma covering parameters derivation based on kinetic plasma theory and experimental verification possibilities

14 p2280 A71-30235

Relativistic kinetic theory of large amplitude transverse Alfvén wave, discussing propagation in collisionless plasma

15 p2459 A71-32653

Classical polyatomic gases kinetic theory, considering generalized Boltzmann equation solution

16 p2614 A71-33031

Kinetic theory of gases in general relativity, including model of matter particle structure

16 p2610 A71-33267

Kinetic coefficients calculation for gas with free energy exchange between translational and internal degrees of freedom

17 p2785 A71-35263

Kramer problem for steady linear Boltzmann equation in kinetic theory of gases, noting solution existence

18 p2947 A71-36190

Flow simulation with digital computer by Monte Carlo computation methods based on interacting molecular gas kinetics, noting application to gas flow

18 p2941 A71-36427

Thermionic converters experimental testing, developing kinetic theory of plasma diodes in steady state Knudsen mode for uniform potential distribution

19 p2999 A71-38256

Initial viscous heat conducting gas dynamic state one dimensional decay problem solution, using kinetic theory with Boltzmann equation

19 p3046 A71-38541

Longitudinal plasma sheath waves kinetic theory, considering particles specular reflection from sheath boundaries

19 p3116 A71-38615

Diffusion controlled order-disorder transformations kinetics, considering internal strain and gradient energy

21 p3397 A71-40431

Aluminum-aluminum nickelide rod eutectic composite elevated temperature stability, presenting coarsening kinetic analysis

21 p3398 A71-40469

Kinetic theory of optically pumped gas, incorporating atomic line radiation effects on spatial and time evolution of velocity distribution

22 p3530 A71-41888

Kinetic theory of collisionless system in closed anisotropic cosmologies including rotation effects

23 p3705 A71-44123

Axisymmetric hypersonic flow of nonequilibrium ionized monatomic radiating inviscid gas past blunt body, using Clarke-Ferrari kinetic model

24 p3790 A71-45224

Ideal gases and binary monatomic gas mixtures heats of transport derivation from kinetic theory expressions for thermal transpiration

24 p3891 A71-45384

KINETICS

NT ELECTROKINETICS

NT KINETIC ENERGY

NT NEWTON SECOND LAW

NT NEWTON THEORY

NT REACTION KINETICS

NT VARIABLE MASS SYSTEMS

Ion exchange kinetics during pulsating fluid flow, developing approximate mathematical model

01 p0070 A71-10619

Nonlinear space independent nuclear reactor kinetics equations, demonstrating positive periodic solutions existence

01 p0126 A71-11291

Fe-Ni-Mo alloys maraging process kinetics at various temperatures, measuring hardness, electrical resistance and lattice constants

02 p0266 A71-12653

Zirconium oxidation kinetics at 500-1200 C under low oxygen pressure

14 p2257 A71-29843

Kinetics of Ti single crystals tensile deformation by prismatic gliding, studying moving dislocations interactions with metal impurities

14 p2257 A71-29844

Optical crossed or collinear light pulse pairs for production and sounding of instantaneous processes kinetics in nanosecond and picosecond range

16 p2580 A71-33624

Kinetic parameters and conditions for optimal epitaxial growth of GaAs from liquid phase, observing solution cooling rate effect on p-n junction quality

24 p3808 A71-44724

KINOFORM

Kinoform diffuser technique based on speckle pattern formation by ground glass illumination with undiverged laser beam

21 p3381 A71-40928

KIRCHHOFF LAW OF NETWORKS

Avalanche transistor emitter current voltage characteristics, using Kirchhoff equations for equivalent circuit

07 p1077 A71-19798

KIRCHHOFF LAW OF RADIATION

Kirchhoff integral evaluation for Gaussian incident field in Fresnel diffraction from plane wave beams truncated by circular apertures

04 p0627 A71-15688

KIRCHHOFF-HELMHOLTZ FLOW

U PIPE FLOW

KIRCHHOFF-HUYGENS PRINCIPLE

U DIFFRACTION

U WAVE PROPAGATION

KIRKENDALL EFFECT

Dutch monograph on Cr-W interdiffusion in solid state concerning Kirkendall effect and relation between chemical and self diffusion

11 p1783 A71-26488

KLEBSIELLA

Pulmonary antibacterial defenses with pure oxygen breathing mice, noting inhibition of early interpulmonary clearance of *Staphylococcus aureus* and enhanced clearance of *Klebsiella pneumoniae*

22 p3487 A71-42241

KLEIN-GORDON EQUATION

Quasi-classical equations of relativistic quantum mechanics, considering Klein-Gordon equation

01 p0129 A71-11293

KLYSTRONS

Klystron and frequency multiplier submillimeter harmonic emission determination, using lamellar grating Fourier spectrometer

02 p0250 A71-12143

TWT and klystron intermodulation reduction by amplitude and phase correction device

02 p0223 A71-12811

Nonautonomous operation of reflex klystron coupled to multifrequency waveguide, noting response to microwave signal

03 p0385 A71-13799

Phase fluctuations in nonautonomous reflex klystron oscillators due to shot noise in electron beams

04 p0557 A71-14624

Nonlinear electron beam bunching in zero temperature plasma during modulation by two frequencies using klystron model

04 p0631 A71-14629

Digital computer program for optimum design of narrow band klystron, discussing beam interception and power conversion efficiency

08 p1261 A71-20743

Reflex klystron electron beam admittance calculation, comparing results with measurement

08 p1264 A71-21275

Single gap klystron output resonator optimization showing maximum electronic efficiency during bunched beam excitation

09 p1414 A71-22220

External SHF signal effects on multifrequency spectrum of reflex klystron coupled with long waveguide

09 p1414 A71-22220

Klystron output resonator efficiency optimizations under excitation of plasma with Pi-shaped charge concentration based on performance analysis as functions of plasma width

09 p1415 A71-22360

X band reflex klystron oscillator with frequency stability comparable to high quality quartz clock by coupling to superconducting cavity

11 p1739 A71-26368

Broadband multicavity multimegawatt klystron design for superpower amplifiers in radars and particle accelerators

11 p1734 A71-26433

Coulomb forces detrimental effects on electron bunching in three-resonator klystron, defining buncher optimal parameters for different permeance values

12 p1888 A71-27614

Klystron power conversion efficiency augmentation by electrostatic depressed collector design, presenting performance prediction calculation method

12 p1889 A71-27734

Power amplifier klystron self excitation in linear electron accelerators, describing tunable driver circuit with quartz reference oscillator

12 p1889 A71-27754

High power linear beam tube devices for space power generation station, considering use of klystron with heat pipes for low weight and high efficiency

13 p2000 A71-28669

Accelerator with electron pregrouping for exciting semiconductor lasers based on amplifying klystrons

13 p2079 A71-28858

High power multicavity klystron design, investigating cavity voltage, cavity phase, drift length and beam parameter effects

13 p2040 A71-29424

Optical and microwave multifrequency autooscillatory drift and reflex klystrons, TWT and electronic oscillators, comparing to He-Ne lasers

14 p2211 A71-30091

Electron cluster formation in klystron buncher, calculating focusing longitudinal magnetic field variation for maximum electron radial stability

15 p2376 A71-31742

Millimeter wave klystron single-loop phase locking using final 4th-harmonic mixer in reference chain for submillimeter laser frequency measurement

16 p2589 A71-34126

Reflex klystron repeller space analysis of potential distribution, electron trajectories, transit time and admittance, taking into account space charge effect

17 p2713 A71-34432

Periodic electrostatic focusing of high permeance electron beams for high power klystrons

19 p3028 A71-37696

Electron guns with band shaped flow, improving klystron performance and increasing permeance by anodic aperture action

20 p3204 A71-39155

Prebunching electron accelerator for exciting semiconductor lasers based on amplifying klystrons

21 p3394 A71-41296

Millimeter wave klystrons phase locking to HCN far IR laser line via harmonic mixing in Si and metal-oxide-metal Josephson point contacts

22 p3555 A71-41599

Fluctuation in synchronized reflex klystron oscillators due to shot noise in electron beams

22 p3521 A71-42264

Nonlinear electron beam bunching in zero temperature plasma during modulation by two frequencies, using klystron model

22 p3583 A71-42265

KNEE (ANATOMY)

Cerebrospinal knee and flexor reflex suppression observations in rabbits and cats during blood circulation disorders

09 p1391 A71-22480

KNOWLEDGE
NT PARADOXES
NT PHILOSOPHY
KNUDSEN CELLS
U KNUDSEN GAGES
KNUDSEN FLOW
Steady isothermal plane gas flow between infinite parallel plates at arbitrary Knudsen numbers, obtaining linear differential equations of mass transfer
01 p0071 A71-11114
Gas flow in plane channel due to longitudinal temperature gradient at arbitrary Knudsen number, using linearized Boltzmann kinetic model equation
13 p1993 A71-29194
Heat flux between parallel plates in rarefied gas at various temperature ratios and Knudsen numbers, using Monte Carlo method
13 p2165 A71-29226
Inert gases, hydrogen, deuterium and carbon dioxide flow in plane parallel glass slots over various Knudsen numbers, calculating slippage constants and volumetric discharge
14 p2227 A71-30673
Knudsen arc firing potential in plane gas filled diode with hot cathode as function of electrode gap and atom concentration
15 p2455 A71-31739
Thermionic converters experimental testing, developing kinetic theory of plasma diodes in steady state Knudsen mode for uniform potential distribution
19 p2999 A71-38256
Knudsen effusion problem in thermal molecular gas jet mixing, using moment method based on velocity distribution function
24 p3817 A71-44354
Boundary conditions determined for hydrodynamic equations from solution of Boltzmann kinetic equation in Knudsen layer, obtaining distribution function in Enskog function superposition form
24 p3821 A71-45226
Thermomolecular pressure gradients and temperatures in flow between parallel plates for statistical gas models at arbitrary Knudsen numbers
24 p3891 A71-45242
KNUDSEN GAGES
Hydrocarbons pyrolysis in Knudsen cells at low pressures, using mass spectrometry to study reactions and products
11 p1727 A71-25229
Near anode surface electrode potential region width measurement in Knudsen thermionic converter with Ba-Cs interelectrode medium
14 p2181 A71-29954
Triple Knudsen cell method to determine thermodynamic activity of Cu in bcc solid solution of Ti-Cu alloys
17 p2756 A71-34488
KNUDSEN NUMBER
U KNUDSEN FLOW
KOLMOGOROFF THEORY
Kolmogoroff and von Karman constants relationship, using atmospheric model
03 p0452 A71-13227
Kolmogoroff differential equations for probabilities of system states, showing validity for Markovian random processes and processes with aftereffects
16 p2603 A71-33891
KOSSEL PATTERN
Kossel line technique application to intergranular fragility study, discussing lattice constant measurement to determine difference in impurity distribution
22 p3563 A71-42324
KRONECKER PRODUCT
U ORTHOGONALITY
KRYPTON
NT KRYPTON ISOTOPES
CW ion laser transitions in Ar, Kr and Xe, tabulating threshold data
03 p0438 A71-13896
Primordial Kr and Xe trapping as possible cause of element abundance trend reversal in Apollo 11 and 12 fines
10 p1673 A71-24428
Kr ion laser forced and self mode locking, using graphite bore plasma tube and acoustooptic modulator
12 p1914 A71-26980
Krypton arc lamps of high conversion efficiency for optical pumping of neodymium lasers, setting lamp and Nd-YAG rod in prolate ellipsoidal cavity
16 p2585 A71-33140
Spectroscopic measurement of vacuum UV radiation from shock heated krypton plasma, noting self reversed resonance lines indicating cold boundary layer
17 p2787 A71-34589
Retinal damage thresholds of rhesus monkeys to ocular radiation from yellow line 568.2 nm emitted by krypton CW gas laser
19 p3008 A71-38284
Ar, Kr and Xe emanation during stepwise heating of lunar rocks under slow neutron irradiation in pile, using mass spectroscopy
23 p3754 A71-43726

Visible and near UV spectra of vacuum Ar, Kr and Xe microwave discharge lamps with magnesium fluoride windows
24 p3849 A71-45211
KRYPTON ISOTOPES
Xe and Kr isotopes gas extraction and mass spectrometer analyses of Apollo 11 lunar soil, Murray carbonaceous chondrite and atmospheric Xe
10 p1661 A71-24410
KU BAND
U SUPERHIGH FREQUENCIES
KUTTA-JOUKOWSKI CONDITION
Hele-Shaw flow viscous tails from airfoil, observing high Reynolds number trailing edge flow for separation and initiation of Kutta condition
11 p1705 A71-26447

L

L BAND
U ULTRAHIGH FREQUENCIES
L-1011 AIRCRAFT
L-1011 aircraft auxiliary power unit with lightweight free turbine engine, giving fuel economy and lower pneumatic pressures
[SAE PAPER 700814] 03 p0353 A71-13725
Ball forming technique application to Al alloys structural part contouring, discussing L-1011 wing panel forming and prestress tooling
08 p1299 A71-21681
L-1011 aircraft flying stabilizer, discussing choice of longitudinal flight control systems
[SAE PAPER 710426] 13 p1996 A71-28312
Automatic landing systems independent monitor for L-1011 aircraft, providing pilot confidence under reduced visibilities
[SAE PAPER 710443] 13 p2098 A71-28324
L-1011 Tristar antenna arrangement test results, considering weight, aerodynamic and structural design requirements
14 p2218 A71-31060
Automated ultrasonic inspection system for L-1011 adhesive bonded fuselage panels using through transmission technique
[SME PAPER IQ-71-746] 15 p2417 A71-32437
L-1011 flight test program, describing aircraft design and performance
[AIAA PAPER 71-789] 17 p2675 A71-35531
Lockheed L-1011 development, discussing flying stabilizer design, direct lift control and autoland system
[AIAA PAPER 71-782] 17 p2675 A71-35532
Lockheed L-1011 passenger jumbo jet layout, ground handling and servicing
18 p2849 A71-35995
L-1011 aircraft automatic landing safety and performance improvement through direct lift control, discussing flight control system integration
[AIAA PAPER 71-906] 19 p3095 A71-37157
L-1011 aircraft hydraulic system design modifications and improvements, discussing gas turbine power source, fluids evaluation, filters, welded steel tubing and maintenance procedures
20 p3183 A71-39149
On-condition monitoring of aircraft hydraulic systems for component deterioration, applying to Boeing 747, L-1011 and DC 10 aircraft
22 p3483 A71-42075

LABELING (MARKING)
U MARKING
LABORATORIES
NT ENGINE TESTING LABORATORIES
NT ENVIRONMENTAL LABORATORIES
NT LUNAR RECEIVING LABORATORY
NT MANNED ORBITAL LABORATORIES
NT MANNED ORBITAL RESEARCH LABORATORIES
NT SPACE LABORATORIES
Multinational corporate R and D laboratories, discussing problems with regard to language barriers, cultural differences and coordination
07 p1225 A71-19449
Organizational climate inventories in R and D establishments, comparing obstacles and incentives to creativity in government and industrial laboratories
14 p2339 A71-29852
French monograph on medium term planning process for large basic research laboratory based on information system of functional activities presentations
19 p3174 A71-38548
LABORATORY EQUIPMENT
NT IMAGE FURNACES
Civil Engineering Systems Laboratory remote terminal interactive time sharing computer facility, discussing consulting engineer design office experiences and computing center management
09 p1412 A71-23277
Industry safe laser laboratory operating environments with reflection free walls, restrictive admittance and periodic personnel examinations
09 p1402 A71-23413

Random vibration laboratory equalization by multiple taping of noise signals on recorder and manual processing
11 p1746 A71-26513
Statistical analysis of equipment selection for multipurpose scientific laboratory onboard space stations under economic and time constraints
13 p2094 A71-28187
Full mission engineering simulator/flight controls integration laboratory utilization in Apollo program, describing equipment for control systems testing, monitoring and troubleshooting
[AIAA PAPER 71-970] 19 p3040 A71-37211
Mobile monitoring and testing meteorological laboratory design and equipment for automated station network, considering pressure sensors, thermohygrometer and wind measurement
21 p3365 A71-41381
LABYRINTH
NT COCHLEA
NT VESTIBULES
Elasmobranch fish labyrinth electrophysiology, analyzing semicircular canals linear acceleration response
04 p0536 A71-14755
Labyrinth destruction, Meniere disease, labyrinthectomy and vestibular neuritis effects on eyes counter-rolling, discussing otolith organ damage determination
04 p0537 A71-14762
Labyrinths and proprioceptors from aerospace medicine viewpoint, discussing motion sickness, spatial disorientation, manned space flight and rotation in space
08 p1244 A71-20711
Long life labyrinth seal designs based on actual service experience and component or factory engine tests
[SAE PAPER 710435] 13 p2073 A71-28319
Functional anatomy of vertebrate gravity receptor system in spatial orientation, discussing otolith organs, sensory cells and hair cell topography in elasmobranch labyrinth
21 p3327 A71-39994
Gravity sensors and intracellular conduction mechanisms in animals, noting contradictory hypotheses on function of hair cell in labyrinth
21 p3328 A71-40009
Flying personnel equilibrium tests with pendulum armchair, investigating labyrinth reflex by induced nystagmus
22 p3500 A71-41570
Controlled caloric stimulation of labyrinths in man by water at various temperatures
22 p3504 A71-42583

LABYRINTHECTOMY
Unilateral labyrinthectomy model for evaluating antimitigation drug effects on vestibular function in guinea pigs
06 p0854 A71-18361

LACTATES
Fatigue factor of lactate, ATP and creatine phosphate (CP) accumulation in working muscles during short exhaustive exercise in man
02 p0202 A71-11666
Arterial glucose and lactate levels and heart rate in human males during intermittent running, discussing anaerobic capacity and anoxidative glycolytic processes
05 p0708 A71-16619
Blood lactate levels in human males after bicycle rides, considering altitude effects on oxygen consumption and glycolytic and aerobic activity
05 p0709 A71-16623
Arterial blood and muscle lactates in cold water swimming rats indicating reduced circulation endurance factors
09 p1396 A71-23360
Cerebrospinal fluid changes due to isocarbic hypoxia, discussing electrochemical potential, lactate concentration and anaerobic glycolysis
11 p1722 A71-26360
Pyruvate and lactate concentrations in muscle tissue and blood at rest and during exercise
14 p2187 A71-31136
Muscle adenosine triphosphate, creatine phosphate, adenosine diphosphate, glycogen, and lactate concentrations during intermittent exercise
15 p2358 A71-31726
Normal muscle lactate concentration after prolonged exercise resulting in decrease in glycogen content
15 p2359 A71-31727
Heart rate variation during and after muscular exercise, discussing correlated measurements of rectal and mean skin temperatures, blood lactate, pyruvate and glucose
20 p3185 A71-38891
LACTIC ACID
Arterial oxygen, carbon dioxide tension, pH and lactic acid changes during rapid descent from altitude to sea level in deep mine
07 p1052 A71-20334
Barometric pressure and exercise effects on erythropoietin titer in normal and hypoxic rat plasma,

LAG [DELAY]

- noting lactic acid concentration and acid base balance changes
08 p1237 A71-20676
- Lactic and succinic acids and creatine phosphates content in rat hind leg muscles during swimming and at rest
16 p2532 A71-33897
- Lactic acid production rate in human blood during supramaximal exercise, noting relationship to oxygen consumption
17 p2685 A71-35366
- Alkalosis effect on human maximal performance and lactic acid formation in blood under supramaximal exercise conditions
20 p3185 A71-38888
- World champion marathon runner metabolic responses during submaximal and maximal treadmill running, recording oxygen consumption, heart rate and lactic acid
20 p3185 A71-38890
- Power derived from aerobic, lactic acid and lactic acid energy sources during human muscular work under normoxic and hypoxic conditions, noting oxygen consumption
22 p3485 A71-41721

LAG [DELAY]

U TIME LAG

LAGRANGE COORDINATES

- Lagrange points role in three body problem, discussing applications to space probe positioning
02 p0316 A71-12739
- Slender body of revolution in supersonic and subsonic air flow, calculating boundary conditions with Lagrange formulation
21 p3323 A71-40963

LAGRANGE EQUATIONS OF MOTION

U EULER-LAGRANGE EQUATION

LAGRANGE MULTIPLIERS

- Recurrent Lagrange multipliers coordinate transformation for optimal low thrust Earth-Jupiter trajectories
01 p0160 A71-10947
- Iterative functional minimization methods using Lagrange multipliers, examining convergence
03 p0452 A71-14059
- Modified linear programming algorithm for columnar methods in mathematical programming applicable to decomposition principle, concave maximization and Lagrange multipliers search
19 p3086 A71-37549
- Linear constrained optimal filtering by multistage linear transformations using Kalman-Bucy estimates and Lagrange multipliers
23 p3658 A71-44084

LAGRANGE SIMILARITY HYPOTHESIS

- Diffusion from continuous line source in turbulent boundary layer, comparing calculation based on Lagrangian similarity with measurements
23 p3664 A71-44200

LAGUERRE FUNCTIONS

- Steady and linear systems discretization by Laguerre transformation and isomorphism between continuous and discrete signals
16 p2550 A71-34058
- Extreme eigenvalues of Toeplitz matrices associated with Laguerre and Jacobi polynomials, using finite difference operators
21 p3410 A71-41084

LAKES

- Linear coastal hydrostatic boundary layers of lake with no horizontal motion, discussing flow conditions under wind stress and interior velocity
10 p1600 A71-23961
- Lake Erie steady state wind driven currents numerical solutions, using shallow lake model for velocity as function of depth and horizontal position
13 p2054 A71-27857
- Steady state wind driven currents velocity in Lake Erie, using shallow lake level model in numerical calculation
14 p2231 A71-29935

LALLEMAND CAMERAS

- Solar corona lines during 7 March 1970 eclipse, using Lallemand electrostatic cameras
03 p0489 A71-13630
- Visual binary star observations by Lallemand electronic camera and photo-electronic image devices
14 p2311 A71-30363
- Lallemand camera for photography of visual binaries, avoiding atmospheric motion effects by double image recording
14 p2312 A71-30375

LAMB WAVES

- Lamb wave interaction with current carriers in cubic symmetry piezosemiconductors, obtaining amplification factor
06 p0942 A71-18352

LAMBDA ROCKET VEHICLES

- Lambda rocket motor case weight reduction through use of MB 130 instead of HT 100 steel, presenting structural strength test results
05 p0821 A71-16297

LAMBERT LAW

U BOUGUER LAW

LAME FUNCTIONS

- Arbitrary dynamic load problem for elastic infinite bodies, solving with Lame equations and Fourier and Laplace transforms in distribution space
14 p2323 A71-29817
- Third basic problem solution in elasticity theory satisfying boundary condition and Lame equation system with two arbitrary vectors
19 p3160 A71-38484
- Lame equation perturbation solution and applications to problems involving elliptic cones or infinite sectors
20 p3177 A71-39497
- Delta wing problem reduction to Laplace equation solution, using perturbation technique to solve Lame equation resulting from elliptic conal coordinates transformation
20 p3177 A71-39498
- Lame function generation within ellipsoidal coordinates by computerized formula manipulation techniques
22 p3565 A71-41501
- Double forces surface distributions, investigating displacement and stress fields singularities of static Lame equations
22 p3614 A71-41603
- Gravity coefficients of geopotential expansion in ellipsoidal harmonics via Lame functions, noting application to earth, Jupiter and Saturn
23 p3666 A71-43011

LAMINAR BOUNDARY LAYER

- Supersonic laminar boundary layer structure near convex corners for large turning angles
01 p0069 A71-10461
- Laminar boundary layer free convection at vertical plate with exponentially decreasing surface temperature, determining thermal flux and shear stress
01 p0179 A71-10610
- Ambipolar diffusion coefficients application to analysis of laminar multicomponent ionized boundary layer flow in channel
01 p0070 A71-10795
- Three dimensional attached compressible laminar boundary layer on slender cones in hypersonic flight at high angles of attack derived by numerical integration
01 p0070 A71-10926
- Near separation flow in laminar compressible boundary layer on cold wall near zero skin friction, suggesting added terms for previous expansion
02 p0332 A71-12378
- Solution singularity of laminar boundary layer structure near separation point
02 p0240 A71-12379
- Laminar boundary layer convective heat transfer with constant wall temperature, using Gaussian quadrature formulas
02 p0332 A71-12394
- Minimum suction rate preventing laminar boundary layer separation from curvilinear porous surface in jet flow
02 p0186 A71-12553
- Two dimensional axisymmetric laminar boundary layer on blown wing and body of revolution, using sixth-order polynomial for velocity distribution
02 p0186 A71-12554
- Laminar-turbulent boundary layer transition point on wing, using hot-wire anemometer and oscilloscope
02 p0186 A71-12555
- Leading edge bluntness and boundary layer displacement effects on attached and separated laminar boundary layers in high temperature hypersonic flow over compression corner
03 p0341 A71-13437
- Laminar boundary layer on spinning bodies of revolution in oncoming stream, using implicit finite difference technique
03 p0341 A71-13660
- Laminar boundary layer downstream heat transfer to sharp and blunt nosed isothermal flat plates under upstream mass injection, discussing insulating effect
03 p0519 A71-13700
- Laminar shock induced boundary layers, examining velocity, pressure gradients and enthalpy
03 p0400 A71-13739
- Heat exchange in dissociating partly ionized gas flow over critical point on permeable surface with injection into laminar boundary layer
03 p0342 A71-13748
- Laminar corner boundary layer secondary flow, taking into account velocity and skin friction distributions
03 p0404 A71-14239
- Laminar and turbulent boundary layer effects on flow velocity and Mach number behind shock front
04 p0567 A71-14664
- Soviet book on friction and heat transfer covering interaction of bodies with internal/external liquid/gas laminar/turbulent boundary layer flows
04 p0571 A71-15264
- Two dimensional incompressible laminar boundary layer flow along ablative blunt body in irradiant environment
04 p0679 A71-15467

Heat transfer in laminar MHD boundary layers over moving flat plate in magnetic field
04 p0635 A71-15468

Linearized equation for stability and heat transfer on two dimensional incompressible laminar boundary layer in water flow
04 p0679 A71-15469

Longitudinal surface curvature effect on steady two dimensional incompressible laminar thermal boundary layers
04 p0680 A71-15470

Conical body laminar boundary layer heat transfer problem in supersonic flow, using quasi-linearization and implicit finite difference method
04 p0527 A71-15487

Laminar boundary layer on porous plane plate situated in plasma jet, examining transfer phenomena with chemical reaction
04 p0572 A71-155070

Transient thermal laminar boundary layer, investigating absorbing-emitting gas effects
04 p0685 A71-155202

Gravitational and forced convection effects in saturated liquids laminar boundary layer film boiling, presenting analytical solutions for common fluids
04 p0686 A71-155282

Leading edge bluntness and boundary layer displacement effects on attached and separated laminar boundary layers in high temperature hypersonic flow over compression corner
05 p0735 A71-165618

Laminar boundary layer effect on gasdynamic laser gain, considering vibrational relaxation time and population inversion
06 p0908 A71-18491

Laminar ablating air-Teflon boundary layers with carbon difluoride and atomic fluorine constituents, using UV thermal radiation measurements
06 p1008 A71-18500

Slender cone hypersonic laminar three dimensional boundary layer separation at angle of attack, proposing helical vortex model
06 p0845 A71-18573

Turbulent boundary layer laminarization prediction in moderate accelerations, using Pathankar-Spalding finite difference formulation and experimental results for shear stress model selection
07 p1085 A71-18767

Numerical integration of equations of three dimensional laminar boundary layer on spreading lines
07 p1087 A71-19182

Multicomponent gas laminar boundary layer equations, deriving asymptotic formulas for friction coefficient, concentration, temperature and diffusion flows
07 p1089 A71-19734

Dissociating airflow over two dimensional blunt body, determining laminar boundary layer chemical reaction suppression effects on heat exchange
07 p1015 A71-19748

Reacting and nonreacting gases laminar boundary layer flows over two dimensional and axisymmetric bodies at zero lift, comparing numerical methods
07 p1015 A71-19860

Incompressible hypersonic laminar boundary layer flow over sharp cone, based on asymptotic inner and outer flow field expansion
07 p1015 A71-19892

Unsteady incompressible laminar boundary layer equations, obtaining similarity solutions from momentum integral equation
07 p1093 A71-20365

Pressure gradient and roughness effects on laminar transition and turbulent boundary layer in hypersonic shock tunnel
08 p1377 A71-22031

Incompressible laminar boundary layer flow with mass and heat sources, calculating thermal and friction stress distribution
08 p1277 A71-22037

Three dimensional laminar boundary layer on cone at incidence in supersonic flow evaluated by pressure distribution technique, comparing heat transfer, Pitot probe measurements, etc
09 p1381 A71-22088

Exact numerical solution for laminar compressible boundary layers with nonuniform wall temperatures compared with Luxton-Young approximate method results, noting skin friction effects
09 p1545 A71-22940

Two dimensional incompressible laminar boundary layer with longitudinal surface curvature, examining equations with particular attention to pressure boundary conditions and pressure gradient formulation
09 p1433 A71-23098

Laminar boundary layer interaction with shock wave in viscous supersonic flow near concave compression corner
09 p1384 A71-23618

Laminar incompressible boundary layer flow over thin Joukowski, parabolic and slender wedge airfoils, using small perturbation and quasi-similar theories
10 p1549 A71-23957

Gortler instability of laminar boundary layer flow on concave wall with finite length effect for perturbation vortices

10 p1592 A71-23958

Incompressible fluid plane unsteady laminar boundary layers equations solution through reduction to nonlinear partial differential equation and series expansion

10 p1592 A71-24025

Incompressible fluid plane laminar unsteady boundary layer, obtaining Falkner-Skan equation as special case for similar solutions in steady flow case

10 p1592 A71-24026

Unsteady incompressible laminar boundary layer universal equation form for solution through reduction to ordinary differential equations and series coefficients determination

10 p1593 A71-24027

Conducting fluid in transverse magnetic field at low Reynolds numbers, deriving laminar boundary layer universal equations in Crocco or Mises variables

10 p1648 A71-24028

Incident thermal flux parameters and wall temperature effects on flow characteristics in prepreparation zone of laminar boundary layer and separation point location

10 p1551 A71-24368

Blowing and suction effects on laminar boundary layer flow of quiet fluid over permeable rotating cone, discussing skin friction and heat transfer

10 p1594 A71-24406

Incompressible laminar boundary layer flow over parabolas and paraboloids, comparing results by local truncation methods with results by finite difference method

10 p1594 A71-24524

Universal equations of two dimensional incompressible unsteady laminar boundary layer

10 p1597 A71-25017

Low Prandtl number laminar compressible boundary layer flow over flat plate, obtaining recovery temperature profile and heat transfer by matched asymptotic expansions method

10 p1597 A71-25066

Heat and mass transfer in supersonic laminar boundary layers with light gas injection, deriving approximate solution for binary mixture flow with variable fluid properties

10 p1598 A71-25097

Compressible laminar boundary layer flow including second order longitudinal surface curvature effects, deriving flow equations from Navier-Stokes equations

11 p1750 A71-25473

Compressible similar laminar boundary layer equations for zero wall shear and mass addition, describing heat transfer reduction and boundary layer growth by asymptotic analysis

11 p1750 A71-25479

Reattachment angle of supersonic laminar mixed boundary layer, using revolution model with Reynolds number allowance

11 p1704 A71-26194

Prediction analysis of downstream effectiveness in high speed laminar boundary layer for reentry vehicular surfaces film cooling, using reference enthalpy method

11 p1752 A71-26216

Metastable state gas flow experiment, investigating laminar boundary layer change in presence of flat plate surface catalytic reaction

11 p1705 A71-26276

Heat transfer in laminar free-convection boundary layers adjacent to plane and axisymmetric walls at constant temperature, deriving skin friction and mass flow rate

12 p1985 A71-26941

Two dimensional laminar boundary layer equation local drag coefficient from one and two term Merk expansion in regions upstream of stagnation point

12 p1896 A71-27051

Laminar boundary layer equations integration for jet propagating along porous surface, determining transverse velocity component effect

12 p1896 A71-27114

Laminar incompressible entry flow in plane channel based on modern boundary layer theory

12 p1897 A71-27223

Laminar boundary layer perturbation by sinusoidal wall roughness, analyzing effect on transition nature and position

12 p1864 A71-27470

Laminar boundary layer equations for rotating plate with surface of arbitrary curvilinear shape, determining external flow pressure gradient leading to separation

12 p1865 A71-27502

Laminar boundary layers with large wall heating and flow acceleration, considering heat transfer parameter increase

12 p1987 A71-27589

Laminar boundary layer centrifugal Gortler instability over concave wall, depending on velocity profile inflection points

13 p2046 A71-27840

Neutral stability of laminar free boundary layer in mixing incompressible MHD half jets at low Reynolds number

13 p2103 A71-27842

Chemically nonequilibrium laminar boundary layer profiles in axisymmetric hypersonic conical nozzle at high air stagnation temperature, calculating wall friction, displacement and momentum loss thickness

13 p1989 A71-27904

Cylindrical shell laminar plastic structure effect on stability under hydrostatic pressure, applying Kirchhoff-Love hypothesis

13 p2155 A71-28654

Group properties of laminar boundary layer equations for incompressible binary fluid under various magnetic field distributions and reaction rates

13 p2048 A71-28735

Hypersonic reentry heat shielding problem, considering axisymmetric laminar boundary layer flow with local coolant mass injections at multiple stations

13 p1990 A71-29127

Wind tunnel simulation of viscous hypersonic flow-laminar boundary layer interactions, presenting similarity parameter effects on aerodynamic characteristics

13 p1994 A71-29224

Laminar boundary layer separation by free stream with large amplitude oscillating velocity, using multiple hot-wire anemometer arrays

13 p2050 A71-29247

Two dimensional vortex filament development artificially shed in laminar boundary layer on flat plate without pressure gradient, using hydrogen bubble visualization technique

13 p2051 A71-29428

Numerical technique for two dimensional nonsimilar unsteady laminar boundary layer in oscillatory flow by integral matrix method

13 p2052 A71-29451

Transformation of compressible turbulent and laminar boundary layers with and without wall blowing

13 p2166 A71-29472

Relaxation distance for sharp cone behavior from chemical nonequilibrium laminar boundary layer effects on simulated space shuttle configuration during reentry

13 p2146 A71-29504

Incompressible liquid laminar boundary layer flow velocity profile and normal friction stress calculation by successive approximation method

14 p2169 A71-29630

Shock wave strength for laminar boundary layer separation at transonic speeds with external flow freestream Mach number near one

14 p2324 A71-29883

Shock tube high temperature air viscosity from laminar boundary layer heat exchange data

14 p2224 A71-30047

Incompressible fluid motion in laminar boundary layer on blade rotating uniformly about axis perpendicular to wing span

14 p2170 A71-30218

Shear stress distribution and local heat flux at surface of axisymmetric bodies for laminar and turbulent boundary layer flow

14 p2170 A71-30219

Laminar boundary layer of free vortex and source flow, obtaining similarity transform of Navier-Stokes equation

14 p2228 A71-31027

Compressible laminar plane axisymmetric boundary layer flows in Laval nozzles, studying temperature, density and velocity distribution relations

15 p2386 A71-31164

Flat plate span effects on ramp induced adiabatic laminar boundary layer separation at supersonic and hypersonic speeds, measuring surface pressure distribution

15 p2344 A71-31557

Incompressible laminar boundary layer on flat plate, calculating flow oscillation effect on time-mean heat transfer

15 p2513 A71-31929

Laminar boundary layer growth along moving flat plate wall, obtaining series solution relating shear stress to velocity ratio

15 p2390 A71-32018

Recovery factor for highly accelerated adiabatic compressible laminar boundary layer flow

15 p2391 A71-32114

Incompressible laminar skin friction calculation on porous plate by Karman-Pohlhausen method, considering surface blowing

15 p2392 A71-32118

Laminar boundary layers effect on chemical-kinetic measurements in shock tube, applying correction by computer program for subsonic diffuser

16 p2555 A71-32893

Approximation analysis for laminar two dimensional boundary layer behind plane shock wave moving over infinite flat plate

16 p2556 A71-32914

Hydrodynamic stability, determining velocity field bounds in laminar boundary layer by Nagumo-Westphal theory of parabolic differential operators

16 p2557 A71-32982

Incompressible laminar boundary layer on parabolic profile at angle of attack, noting singularity in all vanishing shear stress/separation points

16 p2520 A71-33198

Laminar boundary layer past continuous moving surface with constant wall velocity, deriving perturbation solution in terms of Green function

16 p2560 A71-34074

Wall roughness effects on laminar boundary layer velocity profile and Reynolds number, using Hankel functions and integrals

17 p2725 A71-34180

Laminar boundary layer flow at stagnation point with intensive injection of different absorbing medium, calculating temperature profiles and thermal fluxes

17 p2725 A71-34215

Laminar boundary layer on wing profiles and bodies of revolution, calculating flow characteristics based on integral momentum relation

17 p2670 A71-34424

Perturbed two dimensional laminar boundary layers of incompressible conducting fluid flow along insulated concave wall in transverse magnetic field, investigating three dimensional instability

17 p2788 A71-34642

Laminar constant pressure boundary layer hypersonic limits, estimating skin friction and heat transfer

17 p2728 A71-34885

Hypersonic viscid-inviscid internal flow field interaction with laminar boundary layer in circular ducts, using method of characteristics and implicit finite difference scheme

17 p2671 A71-35281

Flow distribution behind laminar boundary layer separation point in supersonic flow, calculating plateau region pressure

17 p2672 A71-35629

Self similar numerical and asymptotic solutions of laminar multicomponent isothermal boundary layer equations for large blowing rates

17 p2673 A71-35633

Transient laminar two dimensional boundary layer induced pressures due to suddenly accelerated hypersonic semiinfinite flat plate

18 p2901 A71-35856

Unsteady laminar boundary layers flow around three dimensional bodies, using finite difference techniques and power series expansion of time square root

18 p2901 A71-36019

Compressible similar laminar boundary layer blow-off behavior description from asymptotic analysis, using Prandtl transposition theorem

18 p2901 A71-36032

Laminar boundary layer flow analysis from nonlinear difference equations solution by Newton method, using block-tridiagonal factorization

18 p2905 A71-36313

Laminar boundary layer structure under semi-infinite potential vortex maintained in incompressible steady flow by appropriate conditions at infinity

18 p2906 A71-36317

Laminar boundary layer flow theory for arbitrary curved surfaces, predicting shear stress, thickness and velocity and pressure distributions

18 p2844 A71-36319

Shock wave interaction with laminar boundary layer on flat plate using modified Lax-Wendroff difference technique

18 p2906 A71-36320

Two dimensional steady laminar boundary layer theory for incompressible medium, presenting error bounds for Prandtl equation solution

18 p2906 A71-36322

Compressible three dimensional nonsimilar laminar boundary layers numerical analysis using two layer heuristic model

18 p2845 A71-36336

Laminar hypersonic boundary layer equations, calculating heat transfer and shear stress in stagnation point

18 p2847 A71-36428

Transverse curvature effect on singularity at separation for laminar boundary layer from analogy with flat-plate compressible boundary layer

19 p3044 A71-37726

Carbon difluoride in ablating air-tylon laminar boundary layers by spectrally and spatially resolved UV thermal radiation measurements

19 p3163 A71-37881

Ethyl alcohol combustion effect on laminar boundary layer structure near flat plate, assuming thermal cracking of fuel

19 p3169 A71-38113

Predicted flow nonuniformities due to laminar and turbulent boundary layer buildup in shock tubes, studying effects on dissociation rates of bromine in argon mixture

19 p3046 A71-38225

Laminar-turbulent transition zone in boundary layer about bodies moving in gas at high Reynolds number, using statistical physics methods

19 p3046 A71-38481

French monograph on laminar boundary layer on circular cone at angle of incidence in supersonic stream, calculating separation from parabolic equations by numerical integration

19 p2994 A71-38647

French monograph on similar solutions of laminar boundary layer problem in supersonic flow covering finite difference methods and convective heat flux

19 p2994 A71-38648

Laminar boundary layer flows on bodies with suction or injection, solving equations using Goertler series solution for impermeable wall

20 p3210 A71-39027

Potential flow and laminar boundary layer separation about profiled circular disks, calculating streamlines

20 p3175 A71-39029

Unsteady state boundary layer equations solution in laminar flow systems with free surface and transfer of heat or mass

21 p3370 A71-40990

Oscillatory free convection laminar boundary flow from semiinfinite vertical flat plate, investigating surface temperature variations as distance function from leading edge

22 p3619 A71-41602

Boundary layer asymptotic solutions for free convection in laminar three dimensional systems, determining rapid mass transfer and centrifugal forces effects

22 p3619 A71-41870

Numerical computation of potential vortex induced laminar boundary layer on circular disks, using two layer asymptotic expansion

22 p3530 A71-41886

Thermal radiation effect on laminar boundary layer of nonabsorbing fluid for plane heat emitting surface under natural and forced convection

22 p3622 A71-42680

Vortice generation in laminar boundary layer of water flow under hydraulic pressure reduction, proposing mathematical model

23 p3662 A71-43315

Forced convection steady heat transfer across laminar incompressible constant-property boundary layers over wedges with step discontinuity in surface temperature

23 p3784 A71-44196

Vertical laminar natural convection boundary layer stability during thermal expansion at large Prandtl number

24 p3886 A71-44422

Laminar boundary layer transition prediction techniques, evaluating empirical formulations and Schlichting-Tollmien stability methods

[AIAA PAPER 71-985]

24 p3817 A71-44581

Flare induced laminar boundary layer/shock wave interactions on axisymmetric bodies at zero incidence in supersonic flow under adiabatic conditions

24 p3789 A71-44604

Heat and mass transfer in binary laminar boundary layer with free convection on vertical porous surface, integrating momentum and energy equations for upper limits

24 p3887 A71-44744

Strongly curved wall jets development in thick boundary layer upstream of blowing slot, discussing calculation method, correction for shear stresses and comparison with experimental results

24 p3819 A71-44952

Laminar boundary layer calculation for simultaneous heat and mass transfer in evaporating liquid layer on flat plate in parallel gas flow, considering variable material parameters

24 p3888 A71-44965

LAMINAR BOUNDARY LAYER SEPARATION

U BOUNDARY LAYER SEPARATION

U LAMINAR BOUNDARY LAYER

LAMINAR FLAMES

U FLAMES

U LAMINAR FLOW

LAMINAR FLOW

NT HARTMANN FLOW

NT STRATIFIED FLOW

Axial turbomachine rotating blades, calculating three dimensional boundary layer thickness for laminar flow

01 p0069 A71-10337

Extended Spline Fit Technique for determining refractivity from interferograms of axisymmetric laminar diffusion flames

01 p0180 A71-10946

Light beam deflection due to temperature gradient in laminar gas flow in shielding pipe for laser communication, considering beam waveguide design

02 p0284 A71-11869

Circular pipe gas laminar flow at constant wall temperature, determining heat exchange and drag by motion and energy equations integration in boundary layer approximations

02 p0240 A71-12192

Incompressible fluid laminar flow between stationary and rotating porous disks with equal suction and injection

02 p0240 A71-12337

Boundary layer separation at free streamline attachment to sharp trailing edge of flat plate, deducing terminal velocity profile for two dimensional flow

02 p0185 A71-12376

Variational problem for turbulent liquid flow mass transport on inclined flat plate, using plane Poiseuille flow solution

03 p0398 A71-13101

Rarefied gas linearized Poiseuille flow between parallel plates, using variational methods for Boltzmann equation

03 p0398 A71-13102

Initial phase of unsteady laminar flow from cylindrical vessel through circular cylindrical tube

03 p0398 A71-13105

Plane laminar flow stability along flexible boundary, obtaining numerical and asymptotic solutions

03 p0399 A71-13198

High pressure arc heater data correlation for laminar and turbulent flows, examining radiation and thermal and electrical conduction effects

03 p0517 A71-13443

Laminar flow of liquid in duct with zero heat resistance of walls, calculating temperature distribution during radiative convective heating

03 p0519 A71-13745

Steady incompressible laminar pipe flow within porous wall cylinder, determining velocity, pressure distribution and shear stress

[ASME PAPER 70-WA/FLCS-3]

03 p0401 A71-14079

Three dimensional nonboundary layer laminar radially inward incompressible Newtonian fluid flow between corotating disks, using integral method

[ASME PAPER 70-WA/FE-4]

03 p0402 A71-14126

Heat transfer and fluid friction of hydrogen and helium gas flows undergoing turbulent to laminar flow transition in heated pipe

[ASME PAPER 69-HT-54]

03 p0405 A71-14291

Viscous incompressible conducting fluid steady laminar flow in rectangular channel with two insulating and two arbitrarily conducting walls under external magnetic field

03 p0466 A71-14556

Flow patterns modification through space charges, demonstrating laminarization of turbulent flow and boundary layer separation prevention

04 p0569 A71-14985

Compressible flow with closed streamlines at large Reynolds numbers, considering viscous and heat conduction cumulative secondary effects

04 p0569 A71-14987

Incompressible Newtonian fluid laminar through flow between two surfaces of revolution rotating at various velocities about common axis

04 p0570 A71-15176

Hot laminar round inert gaseous jet entraining fuel-air mixture, obtaining velocity, temperature and concentration profiles

04 p0683 A71-15495

Viscous incompressible MHD fluid steady laminar flow past semiinfinite flat plate, noting heat transfer characteristics

04 p0635 A71-15508

Laminar flow stability and transition to turbulent flow, giving nonlinear theory for perturbations development

04 p0574 A71-15602

Laminar to turbulent transition in pipes, using scattered light method

04 p0578 A71-15635

Nongray thermal radiation effect on laminar forced convection over heated horizontal flat plate, determining temperature profiles for optically thin and thick boundary layers

04 p0688 A71-15741

Turbulent and laminar jet propagation and mixing in rotor downwash field

[DGLR-70-050]

05 p0795 A71-15961

Small surface elements local skin friction sensor measurements near wall during laminar and turbulent flow, making direct shear force measurements

05 p0752 A71-16734

Laminar or turbulent chemically reacting gas mixture flow in circular tube, examining heat transfer with enthalpy equation

05 p0838 A71-16791

Steady laminar convection in infinite layer of heated homogeneous fluid between constant temperature rigid plate and thermal insulator

05 p0838 A71-16962

Two dimensional wake laminar-turbulent transition, emphasizing velocity fluctuation nonlinear interaction

05 p0695 A71-16964

Plane steady laminar flow into channel between two semiinfinite parallel plates, constructing asymptotic solution for large Reynolds number

05 p0736 A71-16966

Variable viscosity fluid laminar flow, measuring tube resistance at critical Reynolds numbers as function of energy dissipation

05 p0737 A71-17037

Plane Poiseuille viscoelastic liquids flow stability using method of inner and outer expansions based on Chun and Schwarz asymptotic solution of Orr-Sommerfeld equation

05 p0737 A71-17104

Viscous fluid laminar periodic flow in constant cross section circular pipe, noting Kelvin function flow profile, wall forces and Reynolds number

06 p0881 A71-17414

Plane Poiseuille flow stability to finite amplitude periodic disturbances, using Orr-Sommerfeld eigenfunctions

06 p0881 A71-17414

Channel flow and flow past bodies turbulent laminar reverse transition for friction drag and heat transfer reduction

06 p0881 A71-17584

Laminar pulsating ducted flow heat transfer, taking into account velocity distribution time dependence

06 p1005 A71-17682

Laminar flow convective heat and mass transfer over end walls of vortex chambers

06 p1005 A71-17733

Incompressible fluid steady laminar flow free convection and various gas species mass diffusion from hot horizontal plate surface

06 p1007 A71-18076

Premixed laminar flames in flow fields, amplifying fluid mechanical disturbances including vibratory motion and overall feedback loop

06 p1007 A71-18221

Chemically reacting viscous supersonic laminar flow in two dimensional divergent plane channel, developing approximate system of parabolic partial differential equations

[AIAA PAPER 71-44]

06 p0866 A71-18505

Boundary layer nonlinear stability theory, considering hydrodynamic problems associated with laminar flow transition into turbulent flow

07 p1086 A71-18777

Turbulent flame propagation at high Reynolds numbers, discussing nonthermal hydrodynamic mechanism, laminar front and fine structure

07 p1223 A71-19248

Skewed turbulent boundary layer and incompressible laminar flow on rotating disk, considering effective viscosity relations and applications domain

07 p1090 A71-19884

Incompressible hypersonic laminar boundary layer flow over sharp cone, based on asymptotic inner and outer flow field expansion

07 p1015 A71-19892

Elastico-viscous liquid laminar free convection flow along nonuniformly heated vertical flat plate, using momentum integral method for boundary layer velocity and temperature distributions

07 p1091 A71-20034

Laminar swirling jet flow through vertical circular cone, assuming velocity singularities on axis

07 p1092 A71-20092

Finite element solution of plane Poiseuille rarefied gas flow between parallel infinite plates

07 p1093 A71-20284

Beam deflection type fluidic amplifiers with single and symmetric control jets, considering free stream line flow theory

07 p1025 A71-20557

Compressible two dimensional laminar and turbulent free jet characteristics, presenting unitary method with similarity transformation

07 p1029 A71-20593

Laminar-turbulent bounded jet stability, examining transition zone shift with smoke visualization

07 p1029 A71-20594

Jet flow deflection by cross flowing stream applied to low velocity anemometers

07 p1030 A71-20596

Fluidic noncontact position sensor, investigating flap insertion effect on laminar jet flow

07 p1030 A71-20599

Poiseuille pipe flow stability from finite difference equations approximation to nonlinear axisymmetric Navier-Stokes equations under stream function perturbation

07 p1094 A71-20611

Combustion kinetics of premixed laminar graphite dust-oxygen-nitrogen flames with/without hydrocarbon

08 p1346 A71-20866

Flame structure in laminar condensed systems, noting burning rate dependence on pressure and specimen layer thickness, composition and mechanical condition

08 p1376 A71-21906

Equations of motion for Poiseuille flow in circular tubes, solving Gromeko problem with integral Laplace transforms and Bubnov-Galerkin method

08 p1277 A71-21935

Boundary layer model of laminar viscous flow around high speed slender bodies with surface mass transfer

[AIAA PAPER 68-719]

09 p1381 A71-22084

Laminar flow of viscous electrically conducting fluid in traveling magnetic field, examining channel

- flow in traveling wave field of one directional and two directional inductor 09 p1499 A71-22134
- Nonlinear MHD equations solution for laminar flow of electrically conducting fluid in cylindrical channel in traveling magnetic field 09 p1499 A71-22191
- Electric arc column in laminar gas flow, using integral method for stabilization conditions 09 p1544 A71-22266
- Laminar steady flow and heat transfer of viscous heat conducting gas moving between coaxial cylinders, using Runge-Kutta method 09 p1431 A71-22408
- Laminar geoelectromagnetic field excited by coaxial ring current, determining impedance and magnetic field ratios of spherical harmonics 09 p1435 A71-22434
- Plane Poiseuille flow bounded by solid walls, applying Fourier expansion method to stability problem 09 p1432 A71-22583
- Heat transfer to slender bodies in hypersonic flow, comparing wind tunnel measurements with modified reference enthalpy method predictions for laminar and turbulent flow 09 p1545 A71-22941
- Asymptotic far field velocity component in Prandtl boundary layer equations for steady laminar two dimensional flow past rigid body 09 p1486 A71-23578
- Nonlinear stability of incompressible laminar flows involving perturbation in Banach space 10 p1591 A71-23914
- Steady two dimensional MHD laminar flow between two parallel circular porous disks in transverse magnetic field, determining velocity, pressure and shear stress distribution 10 p1649 A71-24408
- Laminar incompressible boundary layer flow stability, emphasizing wall curvature and flexibility effects 10 p1594 A71-24548
- Closed steady streamline creeping flow in cylindrical cavity applied to bubble or plug train in pulmonary and peripheral capillaries 10 p1571 A71-24614
- Inviscid incompressible two phase concave type corner flows embedded with small spherical particles, examining streamlines, critical collision conditions and approximate viscous effects 10 p1598 A71-25081
- Pulsating incompressible two dimensional laminar boundary layer flow past insulated plate at zero incidence, calculating skin friction and surface temperature 10 p1697 A71-25084
- Constant property fluid laminar flow between rotating and stationary infinite disks for limiting Reynolds numbers based on gap width 11 p1748 A71-25154
- Pipe flow hot wire measurements at turbulence onset Reynolds numbers, exhibiting axisymmetric laminar velocity profile distortion 11 p1748 A71-25155
- Prandtl equations derivation, initial value problem and similarity theory models for steady plane incompressible laminar flow 11 p1749 A71-25302
- Variational formulation for hydrodynamic stability based on local potential motion, determining transition from laminar to turbulent flow 11 p1749 A71-25441
- Curvature effects on laminar and turbulent free jet boundary between irrotational flow and stagnant fluid, discussing pressure effects 11 p1702 A71-25482
- Prandtl first order boundary layer equations for two dimensional laminar incompressible flow past circulation controlled circular lifting rotor 11 p1702 A71-25494
- Streamwise vortices of distinct periodicity in laminar transitional turbulent reattaching flows over wide Mach number range 11 p1751 A71-25496
- Time dependent shear stress, temperature and boundary layer pressure in laminar flow over stepwise accelerated flat plate at hypersonic speed 11 p1856 A71-26193
- Radiating laminar convective flow in vertical heated channel, noting radiation effects on temperature and velocity 11 p1860 A71-26446
- Laminar source flow between rotating parallel porous disks with equal suction/injection rates solved for infinite radius series, discussing radial velocity and shear stress distributions 12 p1896 A71-27052
- Hypersonic cruise vehicles viscous interactions areas, examining compression corners, shock interactions, laminar and turbulent flow, boundary layer separation, etc [AIAA PAPER 70-781] 12 p1865 A71-27551
- Flow visualization of free convection laminar-to-turbulent transition along vertical heated plate in water induced by two dimensional forced disturbances [DFVLR-SONDDR-116] 12 p1987 A71-27739
- Laminar flow breakdown in circular tubes, noting disturbance level effect on intermittent flow parameters and turbulent zone length distribution 13 p2046 A71-27827
- Heat exchange during stabilized laminar flow of incompressible liquid in circular pipe with radiative cooling, deriving temperature profile and Nusselt number dependence 13 p2046 A71-28180
- Entrance region laminar flow development under suction or blowing at porous inner wall in concentric annular duct 13 p2160 A71-28602
- Soviet papers on combustion processes in turbulent and laminar flows of kerosene and gasoline mixtures, stressing gas turbine engines problems 13 p2162 A71-28954
- Steady laminar natural convective flow in concentric cylindrical annuli, using finite difference method for Navier-Stokes and energy equations solution [ASME PAPER 70-WA/HT-9] 13 p2164 A71-28982
- Compressible electrically conducting liquid two dimensional steady state laminar flow calculations in MHD duct 13 p2109 A71-29294
- Soviet book on liquid metals nonstationary flow in ducts of MHD devices covering laminar flow at constant and variable flow rates 14 p2277 A71-29526
- Laminar incompressible fully developed pulsating flow between parallel flat plates effects on local time-average heat flux 14 p2334 A71-29603
- Flow transition to laminar drag law for thin cylinder freely suspended in Hg in rotating vertical cylindrical MHD channel 14 p2279 A71-29615
- Axisymmetric flow effects on surface mass injection at supersonic and hypersonic speeds, streamline inclinations and surface pressures generation by turbulent viscous dissipation 14 p2223 A71-29874
- Rotational effects on laminar subsonic compressible viscous flow across shaft face seals, noting leakage rates and pressure profiles 14 p2251 A71-29936
- Rarefied gas Poiseuille flow in parallel plates, cylindrical tube and annulus geometries, deriving subsonic flow velocity profiles by third order constitutive relations 14 p2227 A71-30574
- HF stability and combustion product flow characteristics of laminar burning in cylindrical tube, considering longitudinal and radial instabilities 14 p2338 A71-30856
- Numerical heat transfer and wall friction results, demonstrating gas transport property variation effects on three laminar flow situations 14 p2338 A71-30931
- Incompressible laminar flow between rotating and stationary disks with small gap width and radial mass flow, using Navier-Stokes and continuity equations 15 p2387 A71-31168
- Unsteady incompressible laminar viscous flow past infinite flat plate with arbitrary time dependent velocity, using Laplace transformation 15 p2387 A71-31184
- Unmixed gases burning at finite reaction rate, analyzing steady laminar flames developing in mixing zone of fuel semiinfinite flow past static oxidizer 15 p2511 A71-31379
- Velocity profile of steady two dimensional incompressible laminar boundary layer flow with suction or injection, noting wall shear function 15 p2388 A71-31441
- Circular pipe gas laminar flow at constant wall temperature, determining heat exchange and drag by motion and energy equations integration in boundary layer approximations 15 p2388 A71-31498
- Calorimetrically measured energy feedback heat of reaction dependence from laminar diffusion flames above water cooler [WSS/CI PAPER 71-11] 15 p2463 A71-31621
- Unenclosed laminar jet diffusion flame phenomenological analysis predicting flame height relationship to fuel flow rate and atmospheric density and oxygen concentration 15 p2513 A71-31622
- [WSS/CI PAPER 71-12] Submerged free air jet with laminar parabolic profile, investigating pressure recovery characteristics for various tube diameters, spacing and Reynolds number 15 p2389 A71-31683
- Laminar square jet from turbulence amplifier, analyzing centerline velocity distribution and supply pressure recovery 15 p2391 A71-32060
- Flame quenching device for distances determination by burning premixed laminar propane-air at atmospheric pressures between nonparallel walls 15 p2385 A71-32089
- Laminar flame speeds in chlorine-fluorine mixtures, predicting low temperature isothermal rates and spontaneous ignition limits 15 p2465 A71-32090
- Nonpremixed and premixed combustion theory in laminar flows, considering diffusion flame- reaction time ratio and activation energy effects 15 p2515 A71-32564
- Nonlinear stability theory, considering velocity and vorticity perturbations in circular Couette plane Poiseuille and shear layer flows 15 p2393 A71-32568
- Laser Doppler turbulent and laminar flow velocity measurement model, using optical mixing spectroscopy theory 15 p2423 A71-32589
- Temperature fields and mass and heat transfer at surface of solid spherical particle in laminar viscous fluid flow 16 p2557 A71-32931
- Pipe Poiseuille flow instability with respect to finite amplitude disturbances, calculating Reynolds stress by linear wall mode 16 p2558 A71-33021
- Damping disturbances structure in unbounded laminar flow stability at large Reynolds numbers, demonstrating damping modes eigensolutions in form of concentrated wave packets 16 p2559 A71-33022
- Laminar or turbulent chemically reacting gas mixture flow in circular tube, examining heat transfer with enthalpy equation 16 p2662 A71-33041
- Two dimensional laminar separation bubbles in high Reynolds number flow fields, using finite difference solutions to Navier-Stokes equations 16 p2561 A71-34165
- Viscous trailing vortices decay downstream of non-free axial flow fan, assuming steady axisymmetric incompressible laminar flow 17 p2725 A71-34191
- Gas and liquid drop laminar, transition and turbulent flows heat transfer intensification in circular tubes, applying to hydraulic resistance design 17 p2835 A71-34205
- Cesium vapor diffusion condensations from laminar argon flows in tubes and turbulent movement on banks, considering boundary layer mist formation effect 17 p2785 A71-34206
- Undulating laminar and turbulent liquid film flows down vertical surface, determining velocity fields and local heat transfer coefficients 17 p2725 A71-34210
- Stream lines construction in meridional plane of blade nozzle annular cascades of steam and gas turbines in subsonic and supersonic flow 17 p2670 A71-34446
- Laminar flow in incompressible fluid between rotating disk and fixed wall at small distances with radial mass stream, using finite difference method for Navier-Stokes equations 17 p2726 A71-34581
- Plane laminar two phase jet flow consisting of small spherical particles suspended in incompressible carrier fluid in presence of adjacent parallel moving free stream 17 p2726 A71-34582
- Navier-Stokes steady nonrectilinear universal complex laminar flow, showing isochoric lamellar or plane motions of constant velocity with streamlines as concentric circles 17 p2727 A71-34695
- Three dimensional laminar compressible boundary layer flow solution by numerical integration 17 p2728 A71-34894
- Fluidic viscometer using laminar impedance element for output signal amplification 17 p2677 A71-35289
- Plane Poiseuille flow stability evaluation for finite amplitude periodic disturbances, using harmonic analysis 17 p2729 A71-35389
- Turbulent plane flow velocity profile stability characteristics covering parabolic Poiseuille flow under infinitesimal disturbances 18 p2901 A71-35855
- Large amplitude whistler as collisionless laminar shock model, showing instability for oblique perturbation propagation 18 p2950 A71-35865
- Plane laminar flow linear stability problem, using Orr-Sommerfeld equation with Volterra integral equation 18 p2904 A71-36136
- Streamlines geometry in hydromagnetic inviscid nonheat conducting compressible flow in magnetic field, taking into account force vectors and energy/mass distributions 18 p2951 A71-36183
- Weakly interacted laminar MHD flow growth in entrance region of plane channel with wall conductances investigated by momentum integral method [ASME PAPER 71-APM-A] 18 p2951 A71-36251
- Plane laminar incompressible jet flow along parabola with no external stream, using second order boundary layer theory [ASME PAPER 71-APM-MM] 18 p2904 A71-36268

LAMINAR FLOW CONTROL

- Numerical analysis of laminar recirculating flow between shrouded rotating disks for interaction between vorticity and stream function and swirl-velocity field 18 p2905 A71-36309
- Two dimensional laminar incompressible fluid flow past flat plate at various angles of attack, studying vortex shedding characteristics 18 p2844 A71-36311
- Plane Poiseuille flow at constant rate, developing numerical simulation of transition and turbulence 18 p2845 A71-36337
- Time dependent rotating laminar flow of viscous incompressible fluid in closed cylindrical container, presenting numerical solutions to Navier-Stokes equations 18 p2908 A71-36343
- Near wake streamline configuration in symmetry plane of slender cone in hypersonic flow at free stream Mach number 7 18 p2848 A71-36754
- Viscous incompressible conducting fluid at constant flow rate under magnetic field variation, investigating laminar unsteady MHD Couette flow problem with approximate solution 19 p3108 A71-37092
- Heat transfer and drag during air laminar flow in circular pipe with constant heat flux density at wall 19 p3044 A71-37585
- Viscous relativistic fluid plane laminar flow, discussing incompressible thermally nonconducting case and stationary models 19 p3044 A71-37640
- Plane Couette-Poiseuille flow stability between porous walls with fluid injection and suction causing uniform crossflow 19 p3044 A71-37728
- Gravity effect on developing laminar flow with forced convection in vertical isothermal tube, investigating velocity and temperature profiles and heat transfer rate [ASME PAPER 71-HT-6] 19 p3164 A71-37983
- Gas and surface temperature distributions for laminar flow in circular tube, considering conduction, convection and radiation effects [ASME PAPER 71-HT-17] 19 p3164 A71-37988
- Combustion dynamics, including fire spread in solid fuels, ignition, turbulent/laminar flows and boundary layer, stagnation point and opposed jet burning 19 p3166 A71-38077
- Negative ion and compound formation in premixed fuel-rich laminar atmospheric pressure hydrogen-oxygen-nitrogen flames with molybdenum and potassium atoms 19 p3167 A71-38092
- Tollmien-Schlichting waves in flow field of mixed coaxial laminar air diffusion flames, using flow visualization and hot-wire anemometry 19 p3167 A71-38094
- Nonlinear instability theory for wave system in plane Poiseuille flow, deriving asymptotic solution for initial value problem 19 p3046 A71-38203
- Monograph on blood flow rates instantaneous measurement from ultrasound signals of Doppler flowmeter, discussing steady laminar flow test results 20 p3193 A71-39262
- Laminar free convection from line heat source for Prandtl number 2 based on differential equation solution 20 p3314 A71-39491
- Viscous electrically conducting laminar fluid steady flow through insulated MHD duct under uniform external magnetic field by extended Kantorovich method 20 p3275 A71-39561
- Book on statistical mechanics of turbulent fluid flows covering gas oscillations, correlation function, Reynolds equation, laminar flow, particle dispersion, etc 20 p3213 A71-39774
- Laminar and turbulent incompressible viscous flow with spiral vortices between two parallel rotating disks 20 p3213 A71-39778
- Semibounded jets in laminar and turbulent flows, discussing boundary layers skin and stream regions, step flow velocities, temperatures and self similar problems 20 p3214 A71-39794
- Steady propagation of plane laminar flame through uniform mixture of hydrogen and bromine gases, obtaining temperature and concentration profiles 21 p3474 A71-40524
- Laminar viscous flow past semiinfinite flat plate to second Oseen type approximation, obtaining shear stress on plate 21 p3368 A71-40707
- Laminar and rotationally symmetrical flow of viscous incompressible fluid in circular pipe of constant temperature, considering inlet swirl effects and heat transfer to wall 21 p3368 A71-40756
- Forced flow laminar film boiling heat transfer coefficients from vertical surface in terms of interfacial shear at liquid-vapor interface 21 p3476 A71-40896
- Laminar incompressible plane wall jet, calculating flow characteristics for potential core region with integral method 21 p3370 A71-40988
- Boundary vorticity method for finite amplitude convection in plane Poiseuille flow with isothermally heated and cooled plates, using Boussinesq approximation 21 p3477 A71-40993
- Unsteady laminar flow in polygonal ducts, calculating velocity profiles, friction factors and energy dissipation 21 p3371 A71-40994
- Streamline pattern deduction for sun large scale flow from Doppler line of sight velocities 22 p3596 A71-41454
- Second order viscous liquid pulsating flow superposed on steady laminar flow through circular pipe, examining non-Newtonian effects on flow characteristics 22 p3530 A71-41562
- Hemispherical and spherical pressurized gas bearing design with narrow circumferential feed slot as laminar flow restrictors, predicting static load performance 22 p3551 A71-41667
- Externally pressurized double thrust bearings with variable gas film laminar restrictor increasing stiffness at low eccentricity ratios 22 p3553 A71-41680
- Kinetic and kinematic properties of steady diabatic complex lamellar gas flows 22 p3530 A71-41696
- Streamline calculation of gas flow in bypass compressor with flow area divided by longitudinal partition 22 p3479 A71-41844
- Convective heat transfer between laminar fluid flow and circular flat tubes, considering wall thermophysical properties effect 22 p3619 A71-41873
- Forced convection to hydrodynamically and thermally fully developed laminar flow in eccentric annuli, determining energy equation approximate solutions 22 p3620 A71-41880
- Steady laminar flame propagation speed prediction computation, applying to hydrazine decomposition 22 p3621 A71-42098
- Laminar Couette flow between parallel plates with mechanical energy dissipation and temperature dependent viscosity, determining velocity and temperature distribution 22 p3531 A71-42683
- Steady laminar viscous hydromagnetic flow in annulus with porous walls of different permeability, giving wall friction coefficients and velocity distribution 23 p3708 A71-43099
- Laminar incompressible flow velocities and heat transfer by radiation and convection in inlet section of parallel plate duct 23 p3781 A71-43313
- Convective heat transfer by laminar and turbulent free convection in air on large horizontal and vertical planes 23 p3781 A71-43324
- Navier-Stokes equations solutions for incompressible laminar viscous fluid flow produced by vortex filament placed on cone axis 23 p3664 A71-44004
- Establishment time measurement for laminar separated flow, using shock tunnel driver section to give long test time at low incident Mach number 24 p3818 A71-44628
- Heat exchange during stabilized laminar flow of incompressible liquid in circular pipe with radiative cooling, deriving temperature profile and Nusselt number dependence 24 p3888 A71-44933
- Solid propellant combustion simplified laminar flame theory, calculating pressure effect on burning rate, surface energy loss and temperature effects 24 p3888 A71-44938
- Flow instability due to viscosity variation in high pressure two dimensional laminar flow of Newtonian fluid between rigid parallel plates 24 p3819 A71-44945
- Open cylindrical thermosiphon for laminar flow, predicting heat transfer performance by finite difference solution for comparison with Lighthill analysis 24 p3889 A71-44973
- Incompressible fluid impulsive laminar flow, developing velocity law and tangential stresses by approximate method 24 p3821 A71-45183
- Hydraulic resistance of laminar isothermal flow of fluid with structural viscosity in circular cylindrical rigid channel 24 p3821 A71-45227
- LAMINAR FLOW CONTROL**
U BOUNDARY LAYER CONTROL
U LAMINAR BOUNDARY LAYER
LAMINAR HEAT TRANSFER
Laminar natural convective heat transfer from base plates of vertical rectangular fin arrays, taking temperature and fin geometry effects into account 02 p0333 A71-12603
- Variable viscosity effect on laminar forced convective heat transfer in rectangular duct, using ethylene glycol and aqueous solutions 03 p0518 A71-13628
- Mathematical models for heat transfer by laminar free convection to rotating central plate passing through synchronously rotating surroundings, considering Coriolis effect 03 p0518 A71-13628
- Viscous heating effects on laminar combined free and forced convection through vertical circular tube 04 p0676 A71-15124
- Hypersonic laminar cavity heat transfer, including upstream boundary layer thickness, unequal core and wall temperature effects 04 p0528 A71-15408
- Laminar turbulent tube flow heat transfer, investigating internal radiation exchange and wall heat conduction and generation effects 04 p0685 A71-15558
- Heat transfer in exchangers with forced laminar turbulent flows with linear pressure drop and exponential thermal flux distribution 04 p0688 A71-15758
- Forced convective heat transfer in laminar fluid flow of vanishing viscosity in constant wall temperature pipe, discussing velocity distribution effects 06 p0882 A71-18048
- Laminar flow heat transfer in circular pipes, solving for Graetz equation eigenvalues and eigenfunctions 06 p1007 A71-18384
- Laminar flow heat transfer in circular pipes, including longitudinal conduction term in Graetz problem 06 p1007 A71-18384
- Laminar flow heat transfer between plane parallel plates under generalized Graetz conditions, retaining longitudinal conduction term 06 p1007 A71-18384
- Laminar incompressible flow heat transfer in inlet between parallel plates at constant temperature, considering pressure gradient effect on boundary layer velocity profile [AIAA PAPER 71-36] 06 p1008 A71-18448
- Laminar film condensation thickness and Nusselt number on arbitrary axisymmetric bodies in nonuniform gravity 07 p1225 A71-20648
- Duct thermal entrance region with axial conduction, evaluating laminar heat transfer rate with finite difference technique 10 p1696 A71-24468
- Velocity profiles for flows with laminar heat transfer in circular tube and rectangular duct inlet region with wall suction and injection 10 p1597 A71-25088
- Compressible laminar boundary layer flow over semiinfinite isothermal porous flat plate in nearquasi-steady motion, considering skin friction and heat transfer 13 p2048 A71-28668
- Incompressible laminar boundary layer on flat plate, calculating flow oscillation effect on time-mean heat transfer 15 p2513 A71-31928
- Laminar free convective heat transfer on vertical cylinder with concentration gradients, considering mass transfer effects prediction 22 p3620 A71-41880
- Approximate analytic solution for nonstationary heat transfer for viscous incompressible laminar fluid flow in annular cylindrical ducts 22 p3622 A71-42678
- Laminar convective heat transfer from rotating isothermal disk in uniform forced stream, using pressure distribution measurements 23 p3781 A71-43313
- Heat exchange between two fluid streams in counter, countercurrent, laminar or turbulent boundary layer flow separated by flat plate, determining temperature distribution 23 p3783 A71-44191
- Laminar heat transfer losses effects on piston gas heater performance, computing heat transfer rate and thermal boundary layer thickness 24 p3887 A71-44601
- Laminar boundary layer calculation for simultaneous heat and mass transfer in evaporating liquid layer on flat plate in parallel gas flow, considering variable material parameters 24 p3888 A71-44961
- Open cylindrical thermosiphon for laminar flow, predicting heat transfer performance by finite difference solution for comparison with Lighthill analysis 24 p3889 A71-44973
- LAMINAR JETS**
U JET FLOW
U LAMINAR FLOW
LAMINAR MIXING
Laminar and turbulent mixing of two parallel streams of dissimilar fluids, using similarity transformation [ASME PAPER 70-WA/APM-37] 03 p0403 A71-14168
- Laminar mixing region stratified free shear layer stability between two uniform streams from numerical

solution of linear sixth order equation for disturbance amplitude function

09 p1432 A71-22851

Recirculation patterns in coaxial steady laminar mixing of homogeneous jets in confined tube, solving Navier-Stokes equations

11 p1748 A71-25151

Recirculating cells and entrance conditions influence on confined heterogeneous jets laminar mixing, measuring velocity and concentration profiles [AIAA PAPER 71-601]

15 p2389 A71-31578

AMINAR WAKES

Two dimensional wake laminar-turbulent transition by single and double frequency sounds imposition and wind tunnel natural disturbance, inducing velocity fluctuations

01 p0001 A71-10132

Finite amplitude instability of compressible laminar wake with strongly amplified disturbances, discussing nonlinear theory in terms of von Karman equation

04 p0569 A71-15028

Two dimensional hypersonic laminar wakes incipient transition region calculation based on boundary layer approximation and von Karman integral formulation

[AIAA PAPER 71-202]

06 p0846 A71-18640

Mean flow measurement of cone laminar supersonic wake

09 p1381 A71-22091

Flat plate trailing edge problem solution consistent with second order boundary layer theory, establishing laminar wake evolution nature and upstream influence

11 p1701 A71-25469

Magnetically suspended laminar supersonic cone wake stability from hot wire fluctuation and spectral components amplitude/phase measurements

11 p1702 A71-25475

Laminar compressible wakes instability behind planar and axisymmetric slender bodies, solving integral conservation equations for fluctuation amplitude variations

19 p2993 A71-37879

Spherical cap bubbles in water and mineral oil at various dynamic viscosities, measuring laminar and turbulent wakes character, rise speed and shape

21 p3365 A71-40017

Perturbation velocity of laminar wake downstream of two dimensional body in boundary layer, considering transition behind trip wire

21 p3322 A71-40640

LAMINATED MATERIALS

U LAMINATES

LAMINATES

Heat conductivity equations for thermal stresses of thin cylindrically anisotropic plates made of reinforced laminar plastics

01 p0169 A71-10499

Adhesive bonding and detachable joints in multilayered fiber reinforced plastic structures, discussing joint strength test methods, fiber and load force orientation effects, etc

01 p0108 A71-10692

Composite beam of three thin plates reinforced by thin electric ribs, calculating stress strain state by Fourier transforms

01 p0176 A71-11044

Unsteady axisymmetric temperature and stress distribution in multilayer cylinder in convective heat transfer with temperature-varying medium

02 p0322 A71-11729

Unsteady heat conduction in multilayer body of revolution with convective heat transfer on curvilinear surfaces, considering radiation on inner surface

02 p0330 A71-11730

Laminar orthotropic circular cylindrical shell stress state under inversely symmetrical loading

02 p0322 A71-11737

Multilayer composites preparation by cold rolling packets of alternating Al and Sn foils, determining tensile strength relation to layer thickness

02 p0264 A71-12278

Glass reinforced polyester laminates under static and repeated loading, investigating resin flexibility effects on fatigue strength

02 p0274 A71-12479

Reinforced plastic laminates structural integrity, describing procedure for mechanical property evaluation

02 p0274 A71-12484

Book on laminated plate theory covering anisotropic continua, bending, orthotropic plates, energy equations, etc

02 p0330 A71-12844

Equations of motion for free vibrations of three layer plate, considering energy dissipation in soft low modulus of elasticity middle layer

03 p0502 A71-13404

Laminated cylindrical shells of orthotropic layers, deriving linear theory and equations of motion

03 p0504 A71-13430

Projectile impacts into laminated targets consisting of plastic layers backed by Al substrates using SHAPE code with hydrodynamic elastoplastic distortional model

[AIAA PAPER 69-356]

03 p0504 A71-13431

Thin reinforced laminates configurations with elastic behavior of homogeneous orthotropic or isotropic material, considering flat plates and thin shells constitutive equations

03 p0505 A71-13537

Laminated plates two dimensional theory, discussing equations of motion, stress-strain relations, harmonic wave propagation, etc [ASME PAPER 70-WA/APM-25]

03 p0512 A71-14157

Laminated circular cylindrical shells under axisymmetric mechanical and thermal loads, including transverse isotropy and shear deformation effects in stress analysis theory

[ASME PAPER 70-WA/APM-53]

03 p0513 A71-14170

Multilayer structures dynamic phenomena during switching, examining similarity theory with simple p-n junctions

03 p0388 A71-14387

Thermal expansion of unidirectional, angle-ply and complex laminated graphite-epoxy composites, considering fiber orientation, hysteresis and interlayer stress relaxation

03 p0449 A71-14459

Heat conduction equation for thermal diffusivity measurements by flash method in two layer composites

04 p0595 A71-14965

Shear deformation and rotary inertia in heterogeneous laminated plates of bonded anisotropic layers, discussing bending-extensional coupling

04 p0668 A71-15185

Stress analysis of multilayered composite structures with flaws, emphasizing application to fracture studies

04 p0671 A71-15753

Homogeneous integral equations of asymmetrical elasticity in steady state, using compound layer volume potentials

04 p0620 A71-15887

Multilayered anisotropic cylindrical shells free vibration modes

05 p0819 A71-15982

Moment loads and stress functions of orthotropic laminar shells with low shear rigidity

05 p0822 A71-16371

Multilayer conical and spherical shells of revolution axisymmetric elastic deformation, deriving stress-strain state equations with allowance for transverse shear

06 p0990 A71-17795

Multilayer asymmetric plates deflection, stability and vibrations, deriving nonlinear bending equations with allowance for transverse shear strains

06 p0995 A71-17833

Elastic and viscoelastic multilayer reinforced circular cylindrical shells stability, determining transverse shear stress role

06 p0996 A71-17841

Boundary layer construction near free edge of laminar plates by asymptotic integration of three dimensional equations of elasticity theory

06 p0997 A71-17849

Thin walled two layer bimetallic shells of revolution under large deformation, analyzing equilibrium by zero moment theory

06 p0998 A71-17856

Multilayer plates and shells, considering bending, stability, boundary layer stress state, rigid filters theory and local strength

06 p0998 A71-17857

Fourier resonance associated with electromagnetic wave diffraction from multilayer gratings

06 p0870 A71-18349

Dimensional resonances of standing helicon waves in two layer and multilayer semiconductor structures and crystals with growth inhomogeneities

07 p1176 A71-19273

Multilayered composite mathematical model, studying interfacial delamination under antiplane shear load

07 p1215 A71-20127

Stacking sequence effect on laminate strength, considering specific layer orientations for optimal protection against delamination under uniaxial static and fatigue loadings

07 p1216 A71-20130

Carbon fiber reinforced plastics mechanical properties, discussing batch processing and specimen geometry variables effects on laminates [PLASTICS INST. PAPER 24]

08 p1318 A71-20893

Energy dissipation in free oscillations of multilayer shells consisting of alternating rigid elastic layers and soft fillers, deriving equations of motion

08 p1369 A71-21123

Multilayer interference optical minus filters low-ripple transmittance design, using equivalent layer concept

08 p1334 A71-21184

Simply supported double layered rectangular mesh grids, solving finite difference equations under arbitrary loading

08 p1370 A71-21409

Free and forced vibrations of three layer freely suspended plate with allowance for energy dissipation

08 p1372 A71-21707

Laminated orthotropic plates under transverse loading, developing Navier type solution for Stavsky generalized stress function equation

09 p1534 A71-22101

Multilayer plate vibrations calculated with allowance for energy dissipation in material, deriving equations of motion

09 p1538 A71-22602

Geometric dispersion of dilatational stress wave propagating in laminated plate composite, comparing transmitted wave forms to code calculations

09 p1538 A71-22687

Multilayer liquid phase epitaxy heterostructures growth with crystalline solid solutions of aluminum gallium arsenide for injection lasers

09 p1464 A71-23122

Multilayer sandwich plates with transverse shear resistant inner layers and bending and twisting moment resistant outer layers, calculating critical buckling loads by finite elements

10 p1686 A71-24020

Penny shaped crack in elastic layer bonded to two dissimilar half spaces, investigating stress intensity factors and fracture propagation direction

11 p1841 A71-25301

Dissimilar bonded anisotropic half spaces with flat crack under arbitrary loads, determining stress distribution

11 p1842 A71-25303

B and C polymer laminated film composites efficiency for stability designed structures, considering weight reduction by planar reinforcements [AIAA PAPER 71-353]

11 p1783 A71-25331

Environmental effects on laminated anisotropic plates thermoelasticity for critical swelling strains, using Hookes law extension of Duhamel-Neumann equations

[AIAA PAPER 71-352]

11 p1783 A71-25332

Carbon fiber reinforced high interlaminar shear strength composites, noting applications to advanced engineering structures

11 p1785 A71-25408

Strength transfer at glass-epoxy laminates interface in reference to critical surface tension of coupling agent on fabrics

11 p1786 A71-25414

Longitudinal and transverse residual stresses arising in lamination fabrication process of cross-ply fiber composites

11 p1786 A71-25421

Polyimide system application to laminates and molding powders fabrication, exemplifying compression method and cold compaction followed by sintering

11 p1787 A71-25426

Composite material structural behavior prediction, emphasizing static, dynamic, buckling and post-buckling response of anisotropic plates laminated from unidirectional plies

11 p1846 A71-25429

Plane stress state determination in laminated locally isotropic elastic solid based on stress functions

11 p1788 A71-25438

Buckling loads of square laminated anisotropic composite plates under compression, including bending-membrane coupling effects

11 p1847 A71-25462

Glass fiber reinforced plastics mechanical properties, strain-stress characteristics and anisotropy, deriving orthotropic laminates tensile stiffness under deformation

11 p1849 A71-25656

Thermal stability of cylindrical laminated fiberglass reinforced plastic shells, solving by linear shell stability theory

11 p1790 A71-26175

Elastic properties of bonded orthotropic layer plates, finding good agreement with fiberglass reinforced plastic laminates

11 p1851 A71-26199

Viscous model for stress wave propagation perpendicular to plates of bilaminate composite material

11 p1851 A71-26381

Load-deformation characteristics in tension, compression and bending of two thin cement laminates reinforced with short random glass fibers, discussing stiffness and residual strain

11 p1790 A71-26384

S-shape lines of axial displacement field and interlaminar shear edge effect in laminated composites verified by moire technique

11 p1852 A71-26390

Maximum shear and hoop stress gradients in graphite-epoxy angle-ply laminated composite cylinders for axial and internal pressure loading

11 p1852 A71-26391

Positive rotational transformations of stress vectors for anisotropic lamina in matrix notation

11 p1852 A71-26393

Interlaminar plane shear stress in fibrous composites under elastic deformation with edge effect, using membrane finite element analysis

11 p1852 A71-26394

Zero moment stress state realization in thin macrohomogeneous shells by selecting adequate uniform multilayer structures for reinforcement 12 p1975 A71-26963

Carbon fiber cladding paper for corrosion resistant asbestos laminates, discussing short fibers orientation and acid solutions effects on flexural strength and weight 12 p1921 A71-27014

Shallow laminated shells nonlinear bending equations, using variational principle with allowance for transverse shear strain of layers 12 p1975 A71-27104

Asymmetrical three layer plate with filler under impact loading, examining material and layer thickness effects on deformation 12 p1975 A71-27111

Elastic laminated plates with various thickness layers, deriving independent differential equations for displacement 12 p1978 A71-27334

Stability loss in microvolume of laminated composites with small filler concentrations during shrinkage, using three dimensional linearized equations 12 p1978 A71-27344

Elastic characteristics of multilayer structures with honeycomb fillers, discussing deflection, tensile and compression tests 12 p1980 A71-27362

Laminated plates transverse shear effects on deformation and stress distribution, using finite element analysis 12 p1982 A71-27571

Buckling of eccentrically stiffened multilayered circular cylindrical shells with different orthotropic moduli in tension and compression 12 p1982 A71-27572

Boundary value problems solution for composite cylinder consisting of three different layers with nonideal thermal contacts 13 p2165 A71-29086

Honeycomb cell multilayer and reinforced structures, examining temperature field radiative heat transport and thermal conductivity and emissivity 13 p2165 A71-29180

Mechanical properties of fiberglass-epoxy cross-ply laminates, considering tensile strength, crack propagation and ultimate stress and strain 14 p2264 A71-29837

Soviet book on stability of thin walled reinforced and multilayer shells with various designs and boundary conditions 14 p2325 A71-29939

Nonlinear vibrations of clamped and edge supported laminated orthotropic plates, obtaining nonlinear equations of motion solutions by Ritz-Galerkin method 14 p2327 A71-30206

Fatigue strength of polyester laminates reinforced with glass cloth and mats 14 p2264 A71-30484

Laminated plate flexural mode free vibration analysis by asymptotic method, obtaining phase velocity for comparison with experiment 14 p2330 A71-30684

Thermal stresses in multilayer anisotropic fiberglass wound conical shell under axisymmetric gradients applicable to structural missile nose cone design 14 p2330 A71-30694

Bending stress of thick laminated plates of isotropic material with variable elasticity modulus 14 p2333 A71-30890

Optical techniques for holographic NDT inspection speeds increase in laminate structures flaw detectability 15 p2408 A71-31815

Dispersion and attenuation of plane longitudinal waves in laminated medium of elastic and viscoelastic layers, showing effect of composite parameters variations [ASME PAPER 70-WA/APM-40] 15 p2505 A71-32009

Propagation angle effect on time harmonic wave dispersion in periodically laminated medium, using two dimensional equations of elasticity [ASME PAPER 70-WA/APM-47] 15 p2506 A71-32010

Clamped anisotropic symmetrically laminated plate bending, buckling and free vibration exact solution, using Fourier analysis 15 p2506 A71-32013

Soviet book on multilayered media elasticity theory three dimensional problems covering Fourier and Hankel integral transformations, compression, bending, normal and tangential loads, etc 15 p2506 A71-32020

Mechanics of laminated filamentary composite orthotropic material used for cover skin in advanced aircraft component design 15 p2507 A71-32109

Orthotropic layered cylindrical shells, deriving equations of motion for rotationally symmetric vibration 15 p2509 A71-32513

Periodically laminated elastic half plane response to rapid internal heating, obtaining far field composite stress waves variation due to dispersion [ASME PAPER 71-APM-28] 16 p2663 A71-33201

Thermal stresses in anisotropic infinite elastic orthotropic laminated cylinder with arbitrary number of layers under axisymmetric heating 16 p2657 A71-33599

Birefringent coating method for stress analysis of fiber-reinforced laminated composites, developing subsurface stress-surface strain relation [SESA PAPER 1837A] 17 p2761 A71-34528

Gross static material elastic constants for layered composite materials, using photoelastic models [SESA PAPER 1845A] 17 p2761 A71-34531

Method of producing transparent model composite materials for photo-orthotropic-elastic studies, allowing preparation of larger laminates 17 p2820 A71-34540

Long laminar plate and cylindrical panels with hinged lateral edges under buckling by normal uniformly distributed load, calculating deflection as monotonic pressure functions 17 p2823 A71-34781

Steady wave propagation in laminated media, developing mechanical theory for composite response with hydrodynamic, thermodynamic and strength effects 17 p2823 A71-34808

Orthotropic laminated plates dynamic response to impulse loads, detailing flexural wave propagation 17 p2823 A71-34809

Anisotropic laminated cylinders under combined axial load, torsion and internal pressure, calculating stresses with Vlasov-Ambartsumyan shell theory 17 p2823 A71-34811

Three dimensional equilibrium finite element analysis, obtaining approximate stress solutions for symmetric laminates under inplane loading 17 p2824 A71-34812

Vibration response NDT for fatigue crack damage in laminated filament-reinforced epoxy composites 17 p2824 A71-34815

Equations of motion for free vibrations of three layer plate, considering energy dissipation in soft low modulus of elasticity middle layer 17 p2825 A71-35014

Finite length heterogeneous thin layered cylindrical shell axisymmetric free vibration frequency spectrum analysis 17 p2826 A71-35035

Thin multilayer pressurized glass fiber-plastic cylindrical shells, calculating stress redistribution due to crack initiation and prestressing effects 17 p2830 A71-35319

Three layer trapezoidally corrugated panels with skin under longitudinal compression, determining local stability and stress-strain diagrams 17 p2830 A71-35320

Finite element analysis codes for complex two layered linear elastic shells of revolution under static and dynamic loads 17 p2831 A71-35351

Optical transmission in unexposed phenolic resin base laminates with silica cloth reinforcements, studying stabilization treatments, pyrolysis and incident radiation spectral distribution 17 p2838 A71-35473

Composite panel of ten-ply unidirectional boron/epoxy laminate adhesively bonded to Al face sheets, discussing ultrasonic inspection technique 17 p2749 A71-35495

Multilayer asymmetrical shallow shells with transverse shear strains, deriving finite deflection nonlinear equations 17 p2833 A71-35613

Laminar semiconductor and metallic structures electromagnetic impedance dependence on layers thickness, resistances and permittivities 18 p2953 A71-35873

Laminated composite beam microstructure continuum model, calculating equations of motion and boundary conditions with Hamilton principle [ASME PAPER 71-APM-S] 18 p2978 A71-36261

Stress redistribution in laminate composite due to crack normal to interfaces, noting dependence on crack size, layer height and material properties 18 p2982 A71-36841

Stress intensity factors and strain energy rate for bonded layered composites with interface flaw [crack/] 18 p2983 A71-36846

Superconductivity in molybdenum disulfide laminate intercalated with sodium or potassium 19 p3119 A71-37842

Zero moment stress state realization in thin macrohomogeneous shells by selecting adequate uniform multilayer structures for reinforcement 19 p3159 A71-38266

Approximate theory for vibration of nonhomogeneous anisotropic layered plates using asymptotic integration of elasticity equations 20 p3310 A71-39782

Three dimensional solution for statics and dynamics of homogeneous plates, laminates and orthotropic materials in series form, noting Mindlin analysis 21 p3456 A71-40282

Beams with multiple constrained viscoelastic layer coatings, presenting damped vibrational response prediction for various materials, geometries, wavelengths and temperatures [ASME PAPER 71-VIBR-40] 21 p3459 A71-40282

Five-layer rectangular sandwich plate containing two soft orthotropic cores and three plate stiff isotropic layers [ASME PAPER 71-VIBR-48] 21 p3459 A71-40282

Optimum geometry and vibration damping ability of laminated three layer elastic-viscoelastic-elastic beams at resonance [ASME PAPER 71-VIBR-102] 21 p3461 A71-40320

Shock stress waves dispersion in laminated composite materials 21 p3465 A71-40790

Rectangular laminated orthotropic plates natural vibrations analysis, using extended Ritz technique 21 p3471 A71-41020

Time harmonic waves oblique propagation in periodically laminated composite, using coupled thermoelasticity theory for plane strain 22 p3613 A71-41431

Infinite sandwich plate under concentrated torque load on one side, determining stress distribution with double infinite Fourier transform 22 p3614 A71-41604

Multilayer printed circuit boards defects detection by temperature field monitoring 22 p3520 A71-41764

Effective shear modulus of multilayered rectangular elastic isotropic member in uniform torsion 22 p3618 A71-42581

Variational stress-strain equation for flexible shallow orthotropic multilayer shells with large deflection under normal pressure and contour loading 23 p3778 A71-44040

Nonsteady heat conduction of multilayer cylindrical and conical shells in periodic radiation flux, calculating temperature distribution 23 p3783 A71-44064

Free elastic vibrations and waves in laminated orthotropic circular cylinders 24 p3878 A71-44561

Strength and plasticity characteristics of hardened multilayer structural steels, investigating layer thickness effect 24 p3837 A71-44725

Stress-strain state of hinged thin multilayered orthotropic cylindrical shells with parameters variable with respect to direction 24 p3881 A71-44828

Axisymmetric elastic deformation of layered thin anisotropic shells of revolution, using computer integration for arbitrary loads and boundary conditions 24 p3882 A71-44841

Small deflection theory for steady state creep bending of laminated anisotropic rectangular plate under uniform loads, using Galerkin method 24 p3841 A71-44957

Circular cylindrical laminated anisotropic shells with axisymmetric shape imperfections, investigating upper bound buckling loads 24 p3841 A71-44958

Thermal stresses produced by steady heat flow in two layer plate simply supported at contour 24 p3886 A71-45363

LAMINATIONS

U LAMINATES

LAMPS

U LUMINAIRE

LAND USE

Colorado Land Use and Environmental Resource Inventory Project /CLARI/ by computer methods, saving information retrieval time and cost 08 p1281 A71-21253

Land use strategies and noise reduction by source control and flight procedures for noise exposed areas minimization 08 p1378 A71-21818

Land use control in aircraft noise abatement, considering airport development and community goals 08 p1380 A71-21836

Land development planning and aircraft noise at Kansas City International Airport 08 p1380 A71-21837

ERTS-A imagery, Apollo 9 and high altitude aircraft photography applications to Land Management Bureau, Indian Affairs and Reclamation 09 p1451 A71-23208

World crop areas, yield, production and land use data, using remote sensing devices 09 p1439 A71-23211

Aerial photography vs orbital acquired imagery resolution for land use data 09 p1439 A71-23212

Apollo 9 So65 multispectral color space photography for basic land use pattern determinations 12 p1907 A71-27259

- Satellite scale imagery potential for land-use mapping, using photomosaic simulation at 1/400000 scale
13 p2064 A71-29395
- Land use classification schemes selection with orbital imagery for U.S. thematic mapping
13 p2064 A71-29397
- Space photos for land use and forestry, considering IR color photographs from Apollo 9 flight
13 p2064 A71-29398
- Global environmental monitoring system for atmosphere, oceans, land and biology, considering international cooperation
14 p2198 A71-30897
- Aerial color photography in forestry for species identification, reforestation areas development, watershed studies and land planning
17 p2737 A71-34272
- Air navigation, surveillance and traffic control technology effects on land and airspace uses at airports
17 p2774 A71-35371
- Automated pattern recognition for urban texture and land use assessment by aerial photographs, using digitally scanned optical Fourier transforms
18 p2912 A71-36063
- Aircraft noise reduction in takeoffs/operational procedures and by land use planning
20 p3209 A71-39392
- LANDAU DAMPING**
Small amplitude nonlinear longitudinal plasma oscillations perturbation analysis, discussing Landau damping, monochromatic wave evolution and independent variable expansion
05 p0789 A71-16659
- Soviet book on homogeneous plasma instabilities covering oscillations, magnetic effects, particle velocities, Landau damping, dielectric permittivity, electron fluxes and ion-cyclotron instabilities
10 p1648 A71-24016
- High purity GaAs transverse magnetophonon amplitudes, investigating magnetic field dependence and Landau level collision broadening
10 p1621 A71-24537
- Nonlinear Landau damping of circularly polarized electromagnetic cyclotron waves, calculating interaction matrix for particular electron velocity distribution functions
10 p1652 A71-24656
- Nonlinear explosive ion beam-plasma interaction, discussing coupling coefficients and Landau damping
12 p1935 A71-26912
- Longitudinal instability of bunch interacting with passive resonator, considering Landau damping influence by linear differential equations of motion solution
19 p3110 A71-37141
- Nonlinear Landau damping proposed as explanation for electron plasma oscillations amplification by plasma wave amplitude increase
20 p3274 A71-39349
- LANDAU FACTOR**
Correlation coupling matrix elements for one electron transfer and ion-ion recombinations in Landau-Zener calculations
18 p2948 A71-35839
- LANDING**
NT AIRCRAFT LANDING
NT BLIND LANDING
NT CRASH LANDING
NT DITCHING [LANDING]
NT HORIZONTAL SPACECRAFT LANDING
NT LUNAR LANDING
NT MARS LANDING
NT PLANETARY LANDING
NT SKID LANDINGS
NT SOFT LANDINGS
NT SPACECRAFT LANDING
NT TOUCHDOWN
NT VERTICAL LANDING
NT WATER LANDING
Mutual aerodynamic effects of SM-1 helicopters during simultaneous takeoff and landing, determining minimum distances between helicopters
12 p1867 A71-26953
- LANDING AIDS**
NT APPROACH INDICATORS
NT ARRESTING GEAR
NT AUTOMATIC LANDING CONTROL
NT INSTRUMENT LANDING SYSTEMS
NT RUNWAY LIGHTS
Optimum VTOL aircraft landing maneuverability, using short range three dimensional surveillance system and ground computer
03 p0454 A71-13574
- V/STOL aircraft visual aids flight evaluation concerning minimum landing area operations
04 p0534 A71-15445
- Kalman filter simulation for estimating aircraft position and velocity from airborne digital computer data in zero-zero landing system
06 p0924 A71-17697 [AIAA PAPER 69-944]
- Aircraft final approach and landing aids, describing ILS, VHF omnidirectional radio range, distance measuring equipment and satellite systems for air navigation
07 p1154 A71-19014
- Fog removal by high power carbon dioxide lasers, evaluating possibility of clearing airport runways [AIAA PAPER 69-670]
07 p1153 A71-20308
- V/STOL microwave scanning beam approach and landing system, describing ground and airborne station equipment and operation
08 p1332 A71-21680
- Technical aspects of tactical all-weather instrument landing system of Swedish STOL aircraft Saab 37 Viggen
11 p1796 A71-25233
- Report on guidance system for approach and landing, discussing airports, aircraft, approach and landing paths, service classes, failure protection and weather penetration
11 p1796 A71-25534
- All-weather landing systems military constraints and requirements, considering ground equipment mobility and insensitivity topographic environments
15 p2445 A71-31908
- Civil and military aviation operational problems, including cloud masses and CAT detection, landing aids and radar navigation
15 p2446 A71-31917
- Flashing civil aviation lights history, progress and photometric characteristics, discussing navigation and landing aids
22 p3499 A71-41489
- Short haul air transportation, discussing performance requirements, community acceptance and navigation and landing aids
22 p3482 A71-42073
- Modular step scan microwave aircraft landing system [TALAR] design and operation, noting short takeoff and landing
22 p3572 A71-42088
- Microwave scanning beam guidance receiver design for aircraft landing aid, discussing time sharing and flight control
22 p3572 A71-42091
- LANDING GEAR**
Transport aircraft tire pressure and multiwheeled landing gear limitations regarding pavement design
02 p0189 A71-12163
- Stress analysis of DC 10 nose landing gear unit, using photoelastic coating technique
04 p0534 A71-15669
- Ultrahigh tensile steels for landing gear and other aircraft design applications, discussing composition, mechanical properties, quality requirements, manufacture and testing
09 p1454 A71-22996
- Light aircraft steel landing gear springs structural design at Cessna, considering certification requirements [SAE PAPER 71-0400]
10 p1555 A71-24262
- Analytical nonlinear landing gear model of flexible aircraft and strut lockup-breakout interaction using digital simulation language [DSL] [SAE PAPER 71-0401]
10 p1555 A71-24263
- Nonstationary stress modeling in aircraft structures using random pulse generator applied to jet landing gear break strut fatigue test
10 p1692 A71-24954
- Power spectral density analysis of aircraft structural response to taxiing produced random vibrations involving landing gear orifice damping and Coulomb friction
11 p1708 A71-26311
- Powered landing gear wheel system requirements for parking and taxiing of commercial jet transport airplanes [SAE PAPER 71-0446]
14 p2176 A71-30530
- Aircraft steering system design, considering oversteering effects in nose wheels, torque for reaction moment balance and tire behavior
16 p2522 A71-33225
- Concorde lightweight disk brakes, discussing operating costs, weight and volume factors, design philosophy, structural materials, component life, maintenance and reliability
16 p2522 A71-33226
- LANDING INSTRUMENTS**
NT APPROACH INDICATORS
- LANDING LOADS**
Apollo lunar module structural integrity for lunar landing verified by Monte Carlo dynamic analysis
07 p1205 A71-18896
- Landing load estimation methods for preliminary design weight prediction for military aircraft
13 p1995 A71-28211
- LANDING MODULES**
NT LUNAR LANDING MODULES
NT LUNAR MODULE
NT MARS EXCURSION MODULE
High thrust throttleable monopropellant hydrazine catalytic reactors for planetary landing vehicles, considering engine designs, dynamic characteristics and response to commanded duty cycles [AIAA PAPER 71-705]
14 p2294 A71-30762
- LANDING SIMULATION**
Simulated low visibility landing training, discussing airborne and ground based simulators
01 p0067 A71-10022
- Aircraft flying qualities research program, discussing navy test pilot evaluations and longitudinal handling characteristics for simulated carrier landing task [AIAA PAPER 69-897]
02 p0189 A71-12678
- Helicopter automatic and manual low visibility landing systems evaluation by hybrid computer simulation
06 p0880 A71-18423
- Light source displacement distortions in shadow visualization for flight trainers involving terrain scale and landing simulation
08 p1271 A71-20796
- Executive jet landing approach lateral-directional handling under IFR ILS simulated conditions, investigating Dutch roll control power effect on crosswind component [SAE PAPER 71-0374]
10 p1554 A71-24243
- Space flight aerodynamic problems and wind tunnel simulation, considering satellites, maneuverability for landing and synergetic orbit rotation, hypersonic problems of reentry, etc
18 p2846 A71-36408
- Apollo command module land landing capability in case of abort after liftoff, describing Monte Carlo simulation procedure
22 p3573 A71-42776
- LANDING SITES**
NT LUNAR LANDING SITES
- LANDING SYSTEMS**
U LANDING AIDS
- LANDMARKS**
Mathematical simulation of visual distance perception capacity of man from ground reference landmarks observation during vertical flight
07 p1051 A71-20121
- Landmark navigation improvement by redundant measurements and statistical data reduction measurement for lunar roving vehicles
07 p1156 A71-20339
- Computer program for determining roving vehicle position and heading on lunar surface by landmarks
08 p1332 A71-21348
- LANDSCAPE**
U TOPOGRAPHY
- LANGEVIN FORMULA**
Turbulent diffusion Langevin model with pressure-viscous stress interaction, calculating particle dispersion, Reynolds number, Richardson law time span and Eulerian-Lagrangian relations
12 p1898 A71-27730
- LANGMUIR PROBES**
U ELECTROSTATIC PROBES
- LANGUAGE PROGRAMMING**
SYMPLE /Syntax Macro Preprocessor for Language Evaluations/ for processing higher level language texts
01 p0045 A71-10191
- Computer program for compiling interpreter coded test instructions from high order pseudoEnglish language
03 p0381 A71-13078
- Computer memory reduction through Fortran higher level language, discussing tradeoff between costs saved and additional logic hardware [AIAA PAPER 69-963]
03 p0382 A71-13450
- Moving parts pneumatic control, discussing valves adaptation to control language and functional requirements
07 p1023 A71-19996
- Programming language SCOPE for Europa 2 booster vehicle operational checkout system, describing simple coding procedure for test program
11 p1734 A71-25250
- Principal program languages application and classical mathematical notation
14 p2206 A71-29562
- MESY systems programming with PL/I, comparing with ALGOL and FORTRAN
19 p3025 A71-37422
- Programming languages expansion by users, considering language elements important in flow control or formulation of translation processes
19 p3025 A71-37423
- LANGUAGES**
NT ALGOL
NT ENGLISH LANGUAGE
NT FORTRAN
NT MACHINE ORIENTED LANGUAGES
NT PL/I
NT SYLLABLES
NT WORDS [LANGUAGE]
Microprogramming by Computer Design Language for describing digital computer functional configuration and sequential operation
07 p1069 A71-20404
- German book on simulation systems for digital computers covering programming language requirements, program structures and comparative analysis
14 p2207 A71-30263

LANTHANIDE SERIES METALS

- Extraterrestrial civilizations, discussing cybernetic approach and development of languages for interstellar communications 19 p3134 A71-37521
- LANTHANIDE SERIES METALS**
U RARE EARTH ELEMENTS
LANTHANUM
 Eu II and La II line profiles in sunspots and undisturbed photosphere 05 p0803 A71-16022
- Cr plastic properties, investigating recovery and recrystallization effects from La and Y additions 09 p1476 A71-23316
- Cobalt and lanthanum with face and body centered lattices, studying plastic deformation during allotropic transformations under sliding friction and gripping 16 p2584 A71-33895
- LANTHANUM COMPOUNDS**
NT LANTHANUM OXIDES
 Positron annihilation rates in lanthanum hydrides of various composition 09 p1506 A71-22148
- Temperature induced spectral line widening of trivalent positive Pr ions in lanthanum niobate crystals 09 p1507 A71-22391
- Hf, Ta, W and Re solubility in La and Ce hexaborides from lattice parameters, microhardness and X ray and metallographic analyses 09 p1509 A71-23066
- Catalytic effect of lanthanide hydroxides on formaldehyde conversion to pentoses and hexoses at 110 C in life support systems 13 p2018 A71-28408
- Vaporization thermodynamics of lanthanum carbides from Knudsen effusion mass spectrometry 16 p2538 A71-32812
- Pulsed high perveance electron gun with hot lanthanum boride cathode 20 p3204 A71-39156
- Barium strontium lanthanum titanate thermistor bolometer for IR thermal detector, using positive temperature coefficient of resistance 22 p3543 A71-42126
- LANTHANUM OXIDES**
 Lanthanum cobalt oxide as potential auto exhaust catalyst from studies of activity in gas phase 07 p1055 A71-19545
- Zirconium oxide-lanthanum oxide systems near melting point, plotting solidification and phase diagrams 20 p3254 A71-39962
- LAP JOINTS**
 Stress distribution and mechanical properties of adhesive bonded metal and plastic lap joints, using statistical analysis [SAE PAPER 710107] 08 p1372 A71-21711
- Polymer adhesive protective coatings for improving fatigue resistance of butt and lap welded joints in thin Al sheet construction 09 p1478 A71-23355
- Epoxy bond strength, cracking and failure of lapped joints as function of composition and mechanical properties 10 p1618 A71-24826
- Slip front mechanisms in clamped or bolted double lap joints from photoelastic analysis of stress environments, discussing fretting fatigue [AIAA PAPER 71-370] 11 p1845 A71-25344
- Stress distribution in adhesive lapped joints with emphasis on shear stress 21 p3384 A71-40139
- Stress concentration factors of bonded single lap joints by finite element method as functions of dimensionless, geometric and material parameters 22 p3619 A71-42835
- LAPLACE EQUATION**
 Cauchy problem solution for Laplace equation, constructing algorithms based on successive approximations 02 p0276 A71-12538
- Numerical solution of Laplace difference equations for circular and irregular annulus 04 p0619 A71-14811
- Two dimensional Laplace equation solution by Fredholm integral equation method for Dirichlet problem 07 p1148 A71-20096
- Book on electromagnetic fields and waves covering vectors, current density, flux integral, Coulomb law, Laplace equation, magnetomotive force, waveguides, etc 08 p1335 A71-21459
- Integral equation methods application to exterior boundary value problems solution for Laplace and Helmholtz equations 15 p2441 A71-31350
- Finite element method application to potential flow field problems governed by Laplace equation in fluid mechanics, developing computer program [ASME PAPER 71-APM-22] 16 p2520 A71-33207
- Self adjoint expansion of Laplace operator with point spectrum, establishing uniform convergence and Riesz summability conditions of spectral decomposition 16 p2603 A71-33999

- Boundary value problem for Laplace equations, noting conditions for convergence of solutions sequence 17 p2765 A71-34867
- Potential function transformation under coordinate rotations, deriving coefficients for Laplace equation series expansion 19 p3138 A71-37755
- Iterative finite difference solution of Laplace operator interior eigenvalues and eigenfunctions, noting convergence in application to Helmholtz equation 20 p3201 A71-38755
- Delta wing problem reduction to Laplace equation solution, using perturbation technique to solve Lame equation resulting from elliptic conal coordinates transformation 20 p3177 A71-39498
- Laplace equation solution for double cylinder electrostatic lenses for large range voltage ratios and separations, obtaining focal and aberration coefficients 21 p3377 A71-40178
- LAPLACE OPERATORS**
U LAPLACE TRANSFORMATION
LAPLACE TRANSFORMATION
 Inhomogeneous heat transfer lines analysis by matrix method in form of power converging series by Laplace operator 07 p1221 A71-18925
- Periodic signal input effects on stationary linear system, using closed form Laplace transformation 10 p1643 A71-24909
- Laplace transforms for nonlinear systems analysis 11 p1791 A71-25185
- Arbitrary dynamic load problem for elastic infinite bodies, solving with Lame equations and Fourier and Laplace transforms in distribution space 14 p2323 A71-29817
- Laplace transform application to linear system of partial differential, integrodifferential and difference equations with periodic and quasi-periodic coefficients 17 p2780 A71-34911
- Timoshenko beam transverse vibration with time dependent boundary and normal loads, using Laplace transform method [ASME PAPER 71-APM-F] 18 p2977 A71-36253
- Density fluctuation dispersal in uniform magnetoplasma, obtaining expressions for Fourier-Laplace transforms of perturbed density, potential field and flux distribution 19 p3113 A71-37745
- Linear digital interpolator in program controlled metal cutting tool circuit, determining transfer function with z transforms 22 p3525 A71-42876
- LARGE SCALE INTEGRATION**
 Structured or array logic configurations based on transistorized matrices with programmable interconnections for large scale integration in computer design 01 p0044 A71-10182
- LSI device standardized set for implementing digital computer systems of varying functional complexities 01 p0044 A71-10183
- Electrical fault location and detection techniques for cellular logic circuit arrays fabricated with LSI procedures 01 p0044 A71-10184
- Binary cellular logic circuit array multiplication unit based on functional module concept adaptable to LSI implementation, discussing design methodology 01 p0044 A71-10185
- Pad relocation technique by DC wafer probe tests for interconnecting LSI arrays of imperfect yield 01 p0044 A71-10186
- NASA modular aerospace computer for attitude control high speed computation, describing implementation with LSI functional characters 01 p0045 A71-10198
- Low power nanosecond threshold logic gates for LSI multiplier 01 p0046 A71-10208
- High performance LSI main frame MOS flip-flops memory module for digital computers 01 p0047 A71-10210
- MOS multiphase LSI circuits design using computer program 02 p0228 A71-11651
- Schottky diode bipolar IC and silicon gate MOS LSI techniques in manufacturing 02 p0228 A71-11652
- MOS LSI bipolar random access memory feasible at costs competitive with magnetics 02 p0228 A71-11653
- Digital computer modular LSI control logic design using multifunctional binary decoder with transistor array read-only memory for odd and even parity error detection 08 p1260 A71-21663
- Spacecraft computer centered data systems with standby redundancy, automated flexibility and LSI devices for grand tour mission 08 p1260 A71-21846

- Converter-indicator direct digital readout design using photodiodes for LSI VOR area navigation display systems low power operation 09 p1491 A71-22630
- Semiconductor random access memory components, discussing LSI circuits developments for RAM applications cost effectiveness in computer main-frame memories 13 p2035 A71-28740
- Microprogrammable hardware interpreter design in LSI multiprocessing system, emulating instruction set with software functions 17 p2712 A71-35740
- Large scale MOS IC digital VOR navigation converter, comparing accuracy, size, weight and cost with standard design 17 p2776 A71-35789
- Basis functions for arbitrary time variable network symmetries for large scale integration, using group theory 19 p3038 A71-38484
- Leadless electronic packaging system for MOS LSI for low cost, high reliability and heat transfer advantages 21 p3356 A71-40740
- LSI logic arrays testing problems minimization by test procedures based on circuit design characteristics and MOS structure properties 21 p3356 A71-40800
- Ion implanted depletion mode MOS/LSI devices in conjunction with conventional P channel processing 21 p3358 A71-40821
- Digital programmable matched filter for LSI technology, considering signal/noise discrimination 22 p3519 A71-41511
- Reliability requirements in LSI technology, considering multilevel metallization and test vehicles for process control 22 p3519 A71-41637
- Interconnection Ta thin films and silicon encapsulation for solid state components in hybrid IC under high humidity 23 p3656 A71-43430
- LARMOR PRECESSION**
 Nonuniform magnetic field cyclotron heating representing stochastic criteria in terms of Larmor rotation phase randomization 03 p0462 A71-139280
- Anisotropic plasma stability, taking into account self gravitation, finite ion Larmor radius, Hall currents and rotation 03 p0465 A71-142630
- Rotating streaming plasma stability, including ion Larmor finite radius effects in presence of coriolis forces 05 p0788 A71-166280
- Short wave ion-cyclotron plasma oscillations excitation by electrons drifting in magnetic field of wavelength much less than ion Larmor radius 12 p1936 A71-27033
- Magnetogravitational instability model with allowance for finite Larmor radius effect, considering plasma rotation parallel to magnetic field 15 p2459 A71-32654
- LARVAE**
 Moulting of Calpodes ethlius larvae head and thorax isolated with prothoracic glands dependent on molting hormone injection 01 p0016 A71-11347
- LASER ALTIMETERS**
 GaAs injection laser radar for measuring cloud height, determining required laser output power as function of state of atmosphere and receiver sensitivity 21 p3394 A71-41238
- Emitted signal delay time effect on operational precision of semiconductor laser radar for measuring lower cloud boundary heights 21 p3394 A71-41239
- Arctic ocean pack ice terrain profiling by airborne laser altimeter and coincident photography, analyzing data for ice development stages interpretation 24 p3833 A71-44986
- LASER COMMUNICATION**
U OPTICAL COMMUNICATION
LASER HEATING
 Carbon dioxide laser vs electron beam welding, examining weldability of high thermal conductivity metals 01 p0087 A71-10452
- Continuous Nd-YAG laser welding, considering power, penetration depth and applications 01 p0087 A71-10453
- Laser heated surface layer fragmentation taking into account particles dispersion due to vaporization, reactive force and mechanical recoil moment 01 p0070 A71-10796
- Laser produced plasmas for electrical power generation and space propulsion using fusion of deuterium-tritium pellet 01 p0135 A71-11179
- Laser vs electron beam welding, examining high and partial vacuum and atmospheric pressure environ-

- ments, penetration and ionization and dissociation processes
[SME PAPER MR-70-523] 01 p0090 A71-11269
Q switched laser irradiated solid lithium hydride particle plasma formation and heating, determining optimal conditions 01 p0096 A71-11482
Plasma generation and nuclear fusion by lasers, investigating critical parameter values for heating 01 p0137 A71-11625
Laser systems for metal working, discussing operation modes, workpiece properties and optical systems 02 p0259 A71-11697
High power carbon dioxide laser radiation absorption on vaporized and heated quartz 02 p0260 A71-11944
Carbon dioxide laser induced thermal lensing /focusing/ reduction in liquid carbon disulfide with DC electric field 03 p0436 A71-13877
Quantitative spectrographic microanalysis using laser pulse vaporization and spark discharge 03 p0438 A71-13975
Laser radiation metal fracture, using pulsed X ray metallography and high speed photography for cavity depth and material ejection time dependences 04 p0608 A71-15116
Hydrodynamic model describing intermediate stages of propagation of plasma shock wave created by laser light focusing 05 p0787 A71-16333
Surface temperature of metal target heated by single laser pulse or pulse sequences, relating various parameters 05 p0764 A71-17042
Self similar thermal wave in two-temperature plasma under laser heating for different pulse duration and energy absorption values 06 p0936 A71-17689
Plasma physics, obtaining very high temperatures and electron/ion densities by power laser heating 06 p0908 A71-18066
Nanosecond laser produced lithium hydride spherical plasma expansion model, taking into account three body and radiative recombinations 06 p0938 A71-18457
Laser produced plasma temperature measurements using X ray detectors 06 p0938 A71-18459
Laser produced plasma expansion into vacuum, discussing ion energy angular distributions measurement 06 p0938 A71-18460
Thermal and bleaching waves as diffusion phenomena in opposite limits, discussing laser heating [AIAA PAPER 71-109] 06 p0928 A71-18559
One dimensional laser heating of stationary plasma for application to controlled thermonuclear reactions 07 p1165 A71-18880
Underexpanded plasma jet supersonic outflow simulation, using laser irradiation of absorbent target materials 07 p1166 A71-19133
Holographic lens used with pulsed ruby laser for machining single and multiple spots on Ti thin film on glass 07 p1122 A71-19205
Focused ruby laser beam degradation of various gaseous aliphatic and alicyclic hydrocarbons 07 p1124 A71-19789
Laser thermally generated stress waves measurement errors by comparison with time response predicted from strain theory 07 p1214 A71-19912
Optically pumped pulsed ruby laser welding unit, noting joining and hole drilling problems 07 p1119 A71-19968
Ruby laser driven luminous waves during breakdown and heating within freely expanding gas jet observed with streak photography 07 p1126 A71-20168
Laser beam evaporation of dense substances, examining luminous flux densities with gas dynamic equations 07 p1127 A71-20253
Powerful laser beam and material interaction, investigating gas dynamics of plasma heating and dispersion 07 p1127 A71-20254
Plasma electrons heating by interaction with ultrashort laser pulses, considering hard bremsstrahlung generation 09 p1460 A71-22245
Energetic highly ionized plasma production by pulsed laser heating of lithium hydride pellets 09 p1503 A71-22867
Laser welding, machining and safety - Conference, Pennsylvania State University, July 1969 09 p1457 A71-23401
Laser thermal energy-materials interaction, discussing excess heat buildup, power generation, reflectivity and repetition rates 09 p1458 A71-23406
Laser microwelding, discussing focusing properties, high power radiation interactions, metal working, machining and microelectronic applications 09 p1458 A71-23407
Production welding and annealing, investigating low heat input, intermetallics formation, atmospheric contamination, hot short cracking, speed and cost 09 p1458 A71-23408
Dense hot plasma generation by laser beam focusing on gas or solid targets, discussing experimental setups, diagnostic methods and ionization theories 10 p1647 A71-23920
Self consistent hydrodynamic heating of solid substance by laser pulse for nonequilibrium ionization 10 p1653 A71-24887
Laser heating induced turbulence in fluid medium, using dimensional analysis for effective Reynolds number 10 p1622 A71-24960
Net fusion energy from laser heated deuterium-tritium particles dependent on plasma temperature, electrical energy and electron-ion thermalization through collisions 11 p1805 A71-25799
Mass spectrometric studies of laser beams interaction with solids, discussing surface temperature reached by solid during irradiation 11 p1775 A71-26081
Temperature distribution in metal sheets due to point and circular surface heat sources for laser welding applications, using power supply approximation model 12 p1985 A71-26571
Thermal transient effects in optically pumped pulsed lasers, presenting approximate calculation of temperature distribution and laser rod distortion effect on collimated light beam 12 p1914 A71-26979
Copper wire laser welding to film on Cr substrate exhibiting nonhomogeneous columnar structure and recrystallization 12 p1912 A71-27779
Microsphere formation by melting spinning refractory oxide rod tip in carbon dioxide laser focused emission 13 p2079 A71-28905
Mass spectrometric investigation of high power laser beam plasma on solid target, determining multicharged ion yield, energy, angular distribution and recombination effect 15 p2418 A71-31191
Motion and collision of plasma blobs generated by giant pulse ruby laser irradiation on lithium plate 15 p2455 A71-31643
Pinch devices under laser heating, determining plasma density and temperature and confining magnetic field strength with thermodynamic model 15 p2458 A71-32396
Nd-YAG laser spatial hole burning effects, considering number of oscillating modes, transverse mode degeneracy and sinusoidal phase perturbation influence 15 p2423 A71-32604
Theta pinch deuterium plasma heating by carbon dioxide laser as function of pulse duration and energy 16 p2587 A71-33188
High temperature dense plasma formation by laser heating of gas target, noting fusion reaction in deuterium-tritium mixture 16 p2619 A71-33647
Transparent polymer dielectric luminescence and destruction under Q switched laser radiation with subthreshold power and picosecond pulses 16 p2588 A71-33652
Focused laser beam interaction with liquid metal particles, discussing fluid phase light screening effect, droplet evaporation and mass expulsion characteristics 17 p2750 A71-34291
Magnetic field effects on ruby laser radiation kinetics and spectral composition, studying crystal heating and light emission 17 p2753 A71-35242
Laser drilled holes in alumina substrates, studying structure by scanning electron microscopy and X ray diffraction patterns analysis 17 p2763 A71-35738
Laser-induced retinal damage model based on energy interaction modes, including thermal and acoustic transients, vaporization and dielectric breakdown 18 p2863 A71-35955
Mass spectrometric investigation of plasma created in atomization of Ni and Y ferrites by laser radiation 19 p3110 A71-37142
High quality continuous tone micromachining and image recording on metal thin films by low power pulsed gas laser heating 19 p3071 A71-37213
Bulk vapor formation processes during laser beam heating of metals, considering effect on mass transfer 19 p3072 A71-37586
Langmuir probe and microwave measurements of density, velocity and electron and ion temperatures in streaming plasmas generated by focused laser pulse 19 p3112 A71-37740
Aluminum particles ignition by focused laser flux in controlled oxygen-Argon environment, observing by cinephotomicrography throughout entire burning time 19 p3169 A71-38114
Ruby laser microwelding machine for simultaneous welding of several points with one discharge suitable for micromechanics, computer manufacturing, watchmaking, etc 19 p3069 A71-38232
Laser pulse heated target with thermal plasma production, obtaining target surface temperature as function of time and vaporization rate 20 p3242 A71-38845
Laser heating of D-T plasma, deriving average equations of momentum and energy conservation with allowance for thermonuclear fusion heat 20 p3275 A71-39471
Laser-drilled transparent material hole geometry dependence on beam focus and intensity, computing laser power, mode and work positioning 20 p3246 A71-39492
Burning rates of single laser ignited beryllium droplets, considering particle size effect 21 p3475 A71-40862
Copper wire laser welding to film on Cr substrate, exhibiting nonhomogeneous columnar structure and recrystallization 21 p3389 A71-41104
Electrons heating by matter interaction with ultrashort laser pulses, considering hard bremsstrahlung generation 21 p3394 A71-41134
Self consistent hydrodynamic heating of solid substance by laser pulse for nonequilibrium ionization 21 p3424 A71-41253
D-T plasma cumulation laser heating problem, considering similarity theory for electron conductivity and bremsstrahlung 21 p3395 A71-41360
Cumulation-laser plasma heating analysis, considering average value theory 21 p3395 A71-41362
High beta laser produced spherical plasma expansion in background magnetic field and ambient plasma, treating electrons as inertialess fluid 22 p3581 A71-41891
Book on high power laser radiation covering heating, melting, vaporization, particle emission, plasma production, gas and transparent material breakdown and biological effects 22 p3558 A71-42426
Laser radiation destruction of transparent dielectrics, proposing electronic excitations conversion to heat and thermal explosion 23 p3682 A71-42891
Heating dynamics of transparent dielectrics exposed to pulsed laser beam operating in free laser mode 23 p3683 A71-43270
Expanding D-T plasma laser heating equations derivation, allowing for heat produced by associated thermonuclear fusion 23 p3710 A71-43320
Solid state lasers, discussing ruby lasers application for welding and drilling, mode coupling of glass lasers and extremely short pulses generation 23 p3685 A71-43953
Laser beam interactions with metal in hole gouging operations, determining optimal laser modes at energy densities short of metal evaporation 24 p3833 A71-44861
LASER MATERIALS
Er lasing efficiency dependence on dopants in Li-Ca-silicate glass host, determining energy transfer rates for optimum concentration 01 p0092 A71-10010
Laser active element temperature field nonuniformity, calculating thermal stresses 01 p0093 A71-10614
Fabry-Perot laser cavity resonant modes, noting host medium movement effects on diffraction loss and light beam intensity distribution 02 p0260 A71-12147
Ruby and Nd-YAG laser basic mechanisms, properties and performance characteristics, discussing material problems and frequency width considerations 04 p0605 A71-14708
Glass lasers characteristics and applications, discussing material compositions, ion imbeddings and manufacturing techniques 05 p0761 A71-16327
Laser rubies optical properties, considering orientation, homogeneity and inner stresses, emission in spiking and Q switched operation 05 p0761 A71-16329
Two layer antireflection coatings on glass for He-Ne lasers, calculating optimal film thicknesses for various substrates and wavelengths 06 p0907 A71-18038
Rare earth based liquid lasers, describing spectroscopic and performance properties of neodymium ions in aprotic solvents 07 p1124 A71-19788

LASER MODES

- Organic scintillators as active laser materials, discussing absorption, oscillation and emission spectra and luminescence quantum yield 09 p1461 A71-22386
- Spectrograms of potassium and iron ions radiated by laser plasma 09 p1462 A71-22403
- Substrates, films and laser mirrors production, discussing material combinations and evaporation processes 13 p2080 A71-29087
- Solid state lasers, considering ruby and YAG-Nd ion materials pumped at room temperature 19 p3074 A71-38229
- Lutetium effects on UV absorption strength of Nd-YAG laser materials 20 p3244 A71-39104
- Temperature dependent extracavity and intracavity etalon effects in optical materials for carbon dioxide lasers 20 p3245 A71-39178
- Holographic detection of transient phase objects in Nd oxide doped laser glass 21 p3382 A71-40938
- LASER MODES**
- Opposed wave synchronization mode stability in gas laser undergoing torsional vibrations 01 p0093 A71-10604
- Start-stop pulse generator for gas laser in quasi-steady monimpulse mode with given emission duration 01 p0093 A71-10621
- Distribution function for two circularly polarized modes in laser with axial magnetic field derived by master equation transformation to Fokker-Planck equation 01 p0094 A71-10745
- Accelerometers and dynamic pressure transducers calibration, using laser interferometer system 01 p0082 A71-10862
- Transverse gain inhomogeneity effect on monopulse duration and development in multimode spherical laser resonator 01 p0094 A71-11026
- Radiation spectral and kinetic characteristics in neodymium glass laser in frequency scanning mode 01 p0095 A71-11029
- Q switched monomode ruby laser coherence length measurements, using holography at various beam intensities 01 p0096 A71-11374
- Solid state laser transverse modes maximum dependence on resonator geometrical parameters usable for producing stable kinetic emission model with narrow spectral line 02 p0259 A71-11878
- Giant pulses composed of shorter pulse trains obtained in Q switched carbon dioxide laser with transverse modes 02 p0259 A71-11880
- Fabry-Perot laser cavity resonant modes, noting host medium movement effects on diffraction loss and light beam intensity distribution 02 p0260 A71-12147
- Neodymium laser emission in mode locked operation, examining self focusing and modulation effect in active element 02 p0261 A71-12323
- Transverse mode selection techniques for solid state laser brightness increase 02 p0262 A71-12717
- Mode locked continuously pumped Nd-YAG laser pulse shape, using optical correlation technique 02 p0262 A71-12730
- Transversely excited atmospheric pressure carbon dioxide laser mode locking with Ge acoustic-optic modulator 03 p0434 A71-13477
- Carbon dioxide laser stable mode locking with resonated internal electro-optic phase modulator driven at frequencies near axial mode interval 03 p0434 A71-13481
- GaAs heterojunction diode injection lasers, predicting high order transverse cavity modes and far field patterns from theoretical model 03 p0434 A71-13482
- High power argon laser single frequency emission, discussing dividing mirror reflection coefficient and degree of gain saturation 03 p0435 A71-13504
- Optically coupled GaAs injection lasers emission spectra, determining maximum frequency difference in gain bandwidths for mode synchronization 03 p0435 A71-13506
- Single mode polarization in simple gas laser for long path difference Michelson interferometry 03 p0436 A71-13653
- Nd-YAG laser with intracavity lithium niobate phase modulator, investigating frequency sweeping /modulation/ mode operation 03 p0437 A71-13878
- Mode locked pulsed lasers statistical amplitude and phase variations effects on time dependent output intensity and nonlinear optical processes efficiency 03 p0437 A71-13881
- Homogeneously broadened pulsed laser mode locking with internal frequency or amplitude modulation 03 p0437 A71-13882
- Nd-YAG pulsed laser mode locking with internal FM modulation 03 p0437 A71-13883
- IR gas pulsed lasers continuous self mode locking, observing optical spectra with scanning Fabry-Perot interferometer 03 p0438 A71-13889
- Single mode locked Nd-glass laser pulse time synchronization with Q switched ruby laser 03 p0438 A71-13891
- Reactive Q switching in carbon dioxide multimode multipass laser with movable end mirror, measuring pulse rates and amplitudes 03 p0438 A71-13892
- CW ion laser transitions in Ar, Kr and Xe, tabulating threshold data 03 p0438 A71-13896
- He-Ne laser light beam double slit experiments, investigating multimode operation effect on spatial coherence 03 p0440 A71-14177
- He-Ne laser self-locked or mode-locked with Ne absorption cell, investigating phase relationships between modes 03 p0440 A71-14183
- Organic lasers using fluorescent dye in liquid solution or polymer, discussing gain and output performance, tuning, mode locking and CW operation 04 p0605 A71-14710
- Parametric laser with single mode pumping, investigating emission spectra fine structure 04 p0608 A71-15120
- Photodetector triggered single pulse selection from mode locked ruby laser 04 p0608 A71-15595
- Gas laser axial modes mutual synchronization for frequency modulation, considering stability condition and even/odd harmonics 05 p0760 A71-16005
- Frequency stabilization and measurement of single frequency He-Ne laser at 0.6328 microns, using Michelson interferometer as mode selector and reference cavity 05 p0760 A71-16006
- Single mode laser light modulation by low amplitude LF sinusoidal wave, considering photoelectron distributions 05 p0760 A71-16161
- Carbon dioxide lasers signature, considering 10.4 micron band P/20/ and P/16/ lines dominant modes for wide gain curve and operating conditions 05 p0760 A71-16255
- Two mode He-Ne gas laser irradiance autocorrelation function measurement, comparing time-to-amplitude converter techniques with frequency domain measurements 05 p0760 A71-16268
- Laser beam modulation by nanosecond rise time mechanical chopper for rectangular variable duration pulses, considering use in fluorescence lifetimes measurement, photomultipliers and photodiodes 05 p0761 A71-16270
- CW Nd-YAG laser response to sinusoidal cavity perturbation, observing resonance modes 05 p0761 A71-16332
- LF oscilloscope display of periodic subnanosecond optical pulses from mode locked lasers 05 p0761 A71-16334
- Homogeneous pulsed laser with intracavity FM modulator, predicting modulation frequency detuning effect on mode locking behavior 05 p0762 A71-16340
- Pulse transmission mode Q switched neodymium laser, discussing pulse duration 05 p0762 A71-16374
- Spontaneous mode locking in high pressure carbon dioxide laser with nanosecond pulse separations 05 p0763 A71-16496
- Internally loss-modulated ring lasers unidirectional oscillation, analyzing two mode operation 06 p0906 A71-17300
- Multimode power obtainable in TEM in solid laser, using convex mirror and in cavity polarization rotator 06 p0906 A71-17304
- Mode locked high pressure carbon dioxide lasers subnanosecond pulse widths measurement based on photon flux and fast shutter in semiconductors 06 p0907 A71-17310
- Neodymium glass solid state laser transverse mode locking and capture due to active medium nonlinear properties 06 p0907 A71-17400
- Multipass carbon dioxide pulsed laser mode competition and self locking 06 p0910 A71-18668
- Single frequency carbon dioxide laser cavity length computer aided selection for reduced line competition, considering heterodyne communications systems 07 p1121 A71-18811
- Laser modes generation in two dimensional infinitely long isotropic rod resonator, investigating emission losses and field structure 07 p1121 A71-19172
- Single mode ruby and Nd glass lasers axial mode selection by dye filters, noting radiation spectra and spatial coherence 07 p1126 A71-20151
- He-Ne laser spontaneous emission intensity in longitudinally synchronized longitudinal modes as function of input mode beat frequency and longitudinal magnetic field strength 07 p1127 A71-20242
- Ring laser two mode operation combination interaction and beat phasing, determining mode mismatch regions at synchronized frequencies 07 p1127 A71-20388
- Partial mode locking in picosecond self pulsing GaAs injection lasers 07 p1128 A71-20394
- Mode locked pulsing from carbon dioxide-nitrogen-helium multipass laser by cavity end reflector sinusoidal modulation along axis 07 p1128 A71-20394
- Single mode gas ring laser in longitudinal magnetic field, deriving lasing equations from semiclassical theory 07 p1129 A71-20535
- Gas dynamic lasers design and operation, discussing pumping techniques, waste energy removal and mode control 08 p1301 A71-20692
- Book on nonresonant feedback in lasers covering multimode cavity, emission spectra, generation in cloud, quasi-concentric resonator, etc 08 p1301 A71-21226
- Solid state laser oscillation transient features analysis by dynamic rate equations, taking into account electric field phase variations in mode locking 08 p1301 A71-21277
- Laser resonator mode representation with oblate spheroidal vector wave function through boundary value problem formulation 08 p1301 A71-21295
- Gaussian shaped laser pulse holographic brightness analysis, presenting theoretical and experimental holographic coherence length curves for Q switched laser oscillator and amplifier system 08 p1290 A71-21394
- Spurious inverse Lamb dip mode lock in saturated absorption stabilized He-Ne laser 08 p1302 A71-21404
- Dy-ion-doped calcium fluoride laser with monochromatic pumping, examining mode selection and coupling 08 p1303 A71-21791
- Beat and synchronization modes of opposed waves in rotating gas ring laser, examining frequency response asymptotic behavior 09 p1460 A71-22222
- Two oscillation mode He-Ne gas laser, discussing frequency stabilization by strong competition effect at gain curve center 09 p1461 A71-22387
- Mode synchronization in laser with uniform broadening by asymmetrical internal frequency modulation 09 p1462 A71-22397
- Single mode laser pumping generator of stimulated Brillouin scattering pulse in water 09 p1462 A71-22399
- Semiconductor lasers properties, operational characteristics, power outputs and efficiency 09 p1462 A71-22586
- Single longitudinal mode operation and mode locking of pulsed high pressure transversely excited carbon dioxide laser by saturable absorbers 09 p1463 A71-22758
- Spectral mode and CW operation of stripe geometry double heterostructure GaAs junction lasers above room temperature 09 p1463 A71-22763
- Temperature dependent wavelength tuning of Pb-Sn-Te diode lasers, noting air pollution detection use 09 p1463 A71-22764
- Spectral mode, band to band carrier decay, pulsed and CW operation of laser quality In-Ga-P 09 p1463 A71-22765
- Nd-YAG laser mode locking via variable loss element introduction into cavity 09 p1464 A71-23157
- Spontaneous self locking axial modes in transversely excited high pressure carbon dioxide laser of helical geometry, measuring emission pulses in MW power range 09 p1465 A71-23483
- Stable single mode cavity resonators of high Fresnel number with increased fundamental transverse mode for carbon dioxide laser oscillators 09 p1466 A71-23727
- Mode locked He-Ne laser pulse compression and expansion by electro-optic internal modulator 10 p1619 A71-23873

- Mode hopping due to GaAs lasers longitudinal mode inhomogeneous sequential excitations perpendicular to junction at injection levels above threshold
10 p1619 A71-24039
- Cross-excited electrically pulsed carbon dioxide laser investigating self mode locking as function of cavity length, operating pressure and bleachable absorber sulfur hexafluoride
10 p1620 A71-24152
- Single-mode He-Ne laser, investigating longitudinal magnetic field effect on output amplitude, frequency and polarization characteristics
10 p1620 A71-24343
- Soviet book on lasers with large angular divergence covering single mode generation, free electromagnetic fields equations, emission spectra, etc
10 p1621 A71-24728
- Internal asynchronous modulation of He-Ne laser with Doppler broadened line of working transition in multifrequency mode
10 p1621 A71-24881
- Multimode laser with multilevel atoms, deriving Fokker-Planck equation for laser light statistics
10 p1622 A71-24926
- Quantitative analysis of secondary harmonic generation in DC polarized isotropic laser beam, emphasizing molecular mechanisms and symmetrical effects
11 p1773 A71-25566
- Mode multiplicity effect on ring laser independent beat and synchronized beat regimes
11 p1774 A71-26004
- Quantum electrodynamic analysis of relaxation processes in two level laser
11 p1774 A71-26005
- Single thin lens for Gaussian laser mode matching, discussing position and focal length determination
12 p1905 A71-26809
- Kr ion laser forced and self mode locking, using graphite bore plasma tube and acoustooptic modulator
12 p1914 A71-26980
- Direct analysis of IC by laser beams, considering homogeneity test scanning of Ge semiconductor crystals through photovoltaic injector microscopy
12 p1914 A71-27041
- Monomode laser frequency fluctuations, considering line width separation
12 p1915 A71-27640
- Transverse mode locking effect on radiation intensity of injection semiconductor laser as function of time and p-n junction refractivity
13 p2077 A71-28172
- Laser resonator with selector for Hermite-Gaussian TEM/22/ mode, obtaining integral equation solutions for eigenmodes and eigenvalues on digital computer
13 p2078 A71-28608
- Subpicosecond structure and frequency sweep observation results of single pulse of Nd-glass laser, considering explanation by mode locking theory
13 p2079 A71-28712
- Precision Stark spectroscopy of methane by nonlinear laser absorption, observing Lamb-dip spectra by tuning stable single mode laser
13 p2079 A71-28950
- Nd-YAG laser operation with simultaneous intracavity frequency doubling and mode locking, observing mode-locked pulse lengthening and circulating power decrease
13 p2081 A71-29335
- Multiphoton ionization cross section and charge number in neon near resonance under focused laser beam
13 p2081 A71-29338
- Simultaneous mode locking and pulse coupling of carbon dioxide laser achieved by single internal GaAs element, discussing possible application to pulse code modulation
13 p2081 A71-29341
- Pulsed atmospheric pressure carbon dioxide laser output pulse characteristics and self mode locking
14 p2253 A71-29799
- Solid state laser with slow relaxation bleachable filter, calculating modes self synchronization probability statistics relationship to relaxation time
14 p2253 A71-30109
- Planar Fabry-Perot optical resonator mirror rims effect on modes and losses
14 p2254 A71-30138
- Laser cavity analysis for etalon effects on mode, using signal flow graphs
14 p2254 A71-30143
- Xe plasma flash tubes with very low discharge current magnetic field for spectroscopic and laser applications in presence of Zeeman effect
14 p2243 A71-30272
- Axial mode locking and equidistant frequency generation in solid state lasers due to active medium saturation, using self consistent equations with broadened amplification line
15 p2418 A71-31189
- Mode locking with internal phase modulation observed in He-Se ion laser emitting on many transitions in visible region
15 p2419 A71-31750
- Frequency composition in glass laser with Fabry-Perot resonator producing polarized radiation components, discussing transverse modes selection
15 p2420 A71-32000
- Carbon monoxide-helium-oxygen laser emission continuous self mode locking and temporal structure for various optical cavity lengths
15 p2420 A71-32379
- Self induced second order mode locking optical pulsing of double heterostructure stripe geometry junction lasers operating continuously at room temperature
15 p2421 A71-32388
- External off-axis TEM wave transformation into natural oscillation modes in Fabry-Perot resonator under axially disturbance and impinging-excited wave mismatch
15 p2410 A71-32401
- Rhodamine 6 G in ethanol partial mode locked dye laser picosecond pulses, using pulsed nitrogen laser pumping
15 p2422 A71-32580
- Argon ion laser mode locking in UV lines with intracavity acousto-optic modulator, describing pulse duration and average power
15 p2423 A71-32588
- Single mode ruby laser emission on transparent dielectrics, observing surface luminescence, free electrons production and adsorbed gases heating
16 p2585 A71-32797
- Luminous pulse production by internally modulated Ar laser, observing overall modes amplitudes
16 p2587 A71-33381
- IR carbon dioxide laser amplifier with fundamental mode output power in excess of 500 w, describing multistage mirror section design and test results
16 p2587 A71-33491
- Two photon method of measuring ultrashort pulses and nonlinear optical effectiveness of lasers in synchronized mode
16 p2587 A71-33644
- Self focusing effect of Q switched single mode ruby laser emission in CdS crystal, noting 60 kW minimum threshold power
16 p2588 A71-33645
- Single mode carbon dioxide laser action from quasi-optical mirror emission channels
16 p2588 A71-33894
- Plane mirror ruby laser pseudosteady regime, discussing fundamental TEM mode case
16 p2588 A71-34062
- Mode locked laser pulse signal recovery from time integrated correlation functions of arbitrary order, including field amplitude fluctuations
16 p2588 A71-34075
- He-Ne laser mode self locking conditions and modulation characteristics
16 p2589 A71-34125
- Quantitative measurement of speckle contrast for illumination with laser oscillating simultaneously in multilongitudinal modes on rough surface, determining coherence length
16 p2589 A71-34130
- Temporal distribution of photons radiated by He-Ne laser operating in five modes
17 p2750 A71-34202
- Optical parametric oscillation internal to laser cavity, including temporal response effects of laser population inversion
17 p2751 A71-34377
- Carbon dioxide laser single wavelength operation in TEM mode without intracavity dispersive elements
17 p2751 A71-34379
- Laser longitudinal oscillation modes and maximum radiation envelope formation from noise at start of emission, using electric field strength recurrent relations
17 p2751 A71-34386
- Luminescence quenching in Hg tube activated ZnS-Cu phosphors under action of ruby laser red light
17 p2752 A71-34404
- Saturation effects and mode selection for monofrequency He-Ne lasers with nonlinear absorption
17 p2752 A71-34406
- Longitudinal modes in standing wave gas laser with Brewster windows in presence of active level emission capture
17 p2753 A71-34412
- Environmental controls, health services and safety programs for outdoor range laser applications, considering USAF hazard regulations, public address system, etc
17 p2723 A71-34524
- Lidar soundings of troposphere, investigating multilayer echo structure of haze layers, clouds and rainstorms
17 p2770 A71-34706
- Holography with single transverse longitudinal mode pulsed ruby laser, emphasizing carrier frequency shift as limiting factor on depth of field
17 p2745 A71-35587
- Unsteady multispecie gas mixture concentration flow measurement, using Raman scattering of pulsed nitrogen laser light
18 p2930 A71-36060
- Q switched ruby laser holography, using controlled multimode emission for contour recordings of reflected light scenes
18 p2920 A71-36102
- Solid state laser with Nd ions in YAG, discussing crystal growth and structure, optical pumping continuous and Q switched operation and mode locking
18 p2930 A71-36146
- Laser beam operation, light scattering in gases, holography applications and flow analyses
18 p2931 A71-36420
- Nd-YAG laser optimum single frequency output operation, discussing two-component-mode filters methods using intracavity tilted Fabry-Perot and metallic film reflector etalons
18 p2932 A71-37005
- Carbon dioxide laser high efficiency driven Q switching, using Stark effect in molecular gases
18 p2933 A71-37015
- Ring laser formed by single mode light guiding thin film, using nitrogen laser for pump source
19 p3071 A71-37478
- He-Ne lasers, investigating possible saturation effect usage in strong field to obtain single-mode operation
19 p3072 A71-37769
- Mode selection of transition frequencies in carbon dioxide laser with Fabry-Perot interferometer in resonator
19 p3073 A71-37790
- Oscillatory variation of optical length of pulsed laser resonators during lasing, testing with ruby laser in free emission mode
19 p3073 A71-37791
- Collisionless momentum transfer between interstreaming ions in laser produced plasma, using fast photography, shadowgraphy and electric potential probes
19 p3114 A71-38177
- Laser engineering applications - Conference, Tel Aviv, June 1970
19 p3074 A71-38226
- Integral equation for determination of nonuniform gain profile effect on resonant modes of ion laser cavity, considering ring modes at high current densities
19 p3074 A71-38228
- He-Ne laser output noise due to mode competition, predicting behavior by Lamb three mode laser equation numerical solution
20 p3242 A71-38883
- Platelet lasers optically pumped by pulsed xenon laser, investigating single mode operation, threshold-temperature curves, efficiency and gain spatial inhomogeneity
20 p3243 A71-39006
- Spontaneous emission decreases at CdS and GaAs lasing onset observed visually in internal reflection cavity under electron beam pumping
20 p3243 A71-39007
- Semiconductor lasers, discussing laser action concepts, optical waveguiding, power conversion efficiency, thermal properties, reliability, crystal imperfections, GaAs laser properties, transient phenomena, etc
20 p3243 A71-39066
- Dye laser physics and technology development, discussing dye selection for frequency and cavity parameter variation tuning of lasing wavelength
20 p3243 A71-39068
- Flow patterns on Poincare sphere as aid to qualitative study of polarization and intensity of quasi-stationary laser mode in anisotropic resonator
20 p3243 A71-39095
- Electro-optic mode locking of dual polarization carbon dioxide laser using intracavity birefringence modulation
20 p3244 A71-39096
- High pressure transversely excited pulsed nitrous oxide laser active mode locking at subatmospheric pressures
20 p3244 A71-39101
- Laser holography and interferometry in materials science, evaluating displacement and deformation within nondestructive testing
20 p3245 A71-39342
- Laser beam spatial coherence properties dependence on transverse mode structure for given longitudinal mode
20 p3245 A71-39350
- Pulsed argon ion laser data, presenting excitation mechanisms and time resolved gain measurements
21 p3392 A71-40625
- He-Cd CW laser transitions, describing charge exchange and Penning ionization-excitation processes
21 p3393 A71-41038
- Nonlinear absorption in transparent semiconductors of picosecond light pulses from Nd laser with locked modes
21 p3431 A71-41256

Pulsed ruby laser transmission and reflection holography in single transverse and axial electromagnetic mode, stressing safety aspects

22 p3556 A71-41743

Holographic spectral analysis to determine modes oscillating in multilongitudinal and multitransverse mode laser

22 p3541 A71-41791

Mode locked Nd-glass laser transient effects, examining pulse width limitations by side band generation

22 p3556 A71-41801

Mode locked transversely excited atmospheric carbon dioxide laser with Ge ultrasonic diffraction cell active loss modulator generating 10.6 micron wavelength pulses

22 p3557 A71-42132

Double-heterostructure injection laser radiation transverse polarization from reflectivity analysis of GaAs-air interface vs TE and ME mode incidence angle

22 p3558 A71-42201

GaAs lasers filamentary coupling, investigating various mode perturbations in temporal output

22 p3558 A71-42346

Gas laser axial modes mutual locking for frequency modulation, considering stability condition and even/odd harmonics

22 p3559 A71-42754

Frequency stabilization and instability measurement of single frequency He-Ne laser at 0.6328 microns, using Michelson interferometer as mode selector and reference cavity

22 p3559 A71-42755

Second harmonic mode locked frequency doubled pulsed neodymium-yttrium-aluminum oxide garnet laser using single intracavity barium sodium niobate

23 p3683 A71-42957

Heating dynamics of transparent dielectrics exposed to pulsed laser beam operating in free laser mode

23 p3683 A71-43270

Large path difference laser interferometry, discussing test tower instrumentation problems of interference fringe flicker and loss of contrast due to laser mode instability

23 p3683 A71-43356

Gas ring laser lock-in zone, showing dependence on resonator mirror curvature radius and mode competition between oppositely directed waves

23 p3683 A71-43393

Single mode ruby laser spatiotemporal coherence characteristics with emission moment controlled by Q switch operating on modulated ultrasonic traveling waves

23 p3683 A71-43394

He-Ne laser insertion loss effect on power variation of two operation modes during cavity frequency tuning

23 p3684 A71-43401

Steady power pulsation measurement and operation mode theory of ruby laser with bleachable dye filters

23 p3684 A71-43416

Mode-locked laser ultrashort pulse duration measurement from field intensities autocorrelation functions

23 p3685 A71-43562

Solid state lasers, discussing ruby lasers application for welding and drilling, mode coupling of glass lasers and extremely short pulses generation

23 p3685 A71-43953

Spectral properties and tunability of far IR from ZnTe and lithium niobate crystals from difference-frequency mixing of mode-locked Nd glass laser pulses

23 p3686 A71-43997

Intercavity scanning for mode selection of carbon dioxide laser in transversely degenerate resonator by localized electron-beam-trigger excitation

23 p3687 A71-44132

Mode locked CW dye laser operation, describing output stability and pulse rate and widths

23 p3687 A71-44133

CW dye laser mode locking with lithium niobate phase modulator, observing 500 psec pulse generation

23 p3687 A71-44134

Frequency and losses differences of modes as necessary conditions for multimode lasers transverse modes self synchronization

23 p3687 A71-44176

Transverse mode locking by cylindrically symmetric laser, noting time varying spot size with spacing frequency

23 p3688 A71-44295

Pulsed neon laser high gain oscillation at 486.1 and 434.0 nm identified as Balmer beta and gamma lines of atomic hydrogen

23 p3688 A71-44296

High order transverse cavity mode selection and propagation in homojunction and heterojunction GaAs injection lasers, using five layer dielectric model

24 p3832 A71-44432

Double heterostructure GaAs injection laser mode reflectivity and waveguide properties, discussing

threshold current density and wavelength dependence on mirror reflectivity

24 p3832 A71-44433

Laser light emission from system of four-level centers with variably widened asymmetric luminescence line

24 p3833 A71-44659

Laser beam interactions with metal in hole gouging operations, determining optimal laser modes at energy densities short of metal evaporation

24 p3833 A71-44861

Reflection coefficient of multimode laser beam from dielectrics interface

24 p3833 A71-45044

Low loss mode selection and wavelength regulation of gas lasers with electro-optical intracavity resonator

24 p3834 A71-45163

Single mode output power multiplication in standard commercial He-Ne laser with cavity extension and etalon

24 p3835 A71-45214

He-Ne laser discharge gap oscillation modes observation, noting applied magnetic field, gas parameters and cathode type effects on stimulated emission

24 p3835 A71-45239

Laser mode suppression arrangements consisting of Michelson interferometers with polarization prism as beam splitting element

24 p3835 A71-45264

LASER OUTPUTS

He-Cd laser stable long life CW excitation by DC cathaphoresis to maintain spatially uniform and optimum Cd vapor concentration

01 p0091 A71-10007

Laser systems radiation hazards, considering operational requirements, personnel protective equipment, biological effects and exposure levels

01 p0021 A71-10008

Heat conduction effect on propagation of laser radiation absorption shock wave

01 p0092 A71-10068

He-Ne laser LF radiation parameters calculations verified experimentally

01 p0092 A71-10334

Pulsed hydrogen fluoride gas laser output line spectral distribution, describing experimental setup and measurements

01 p0092 A71-10371

Output properties of electrically pulsed carbon dioxide laser as functions of partial gas pressure and discharge voltage

01 p0092 A71-10372

Gas laser output allowing for energy exchange between levels using population balance method

01 p0093 A71-10603

Semiconductor photoelectric sensor for monitoring laser emission energy in conjunction with memory oscillograph or single pulse peak voltmeter

01 p0093 A71-10623

Kerr cell for high speed modulation of laser radiation, noting use in multiframe shock wave dark photography

01 p0093 A71-10625

Frequency stability of molecular beam laser with stimulated coherent emission

01 p0093 A71-10681

Spark discharge ignition in air by Q switched ruby laser

01 p0093 A71-10684

Threshold emission and self excitation of spatially inhomogeneous laser, considering active element gain and refractive index by electrodynamic model

01 p0094 A71-10687

Magnetic fields measurement in plasmas by laser scattering, discussing theory and applications

01 p0133 A71-10747

Laser light statistical properties, emphasizing time evolution of density matrix equation

01 p0094 A71-10811

Laser oscillation buildup from quantum noise, deriving equations of motion for moments of photon distribution and time dependence

01 p0094 A71-10826

IR flying spot telescope with CW laser beam scanning and target motion sensing capabilities

01 p0081 A71-10830

CW He-Ne laser beam scattering observation for artificial fog droplet size distribution during evolution stages

01 p0094 A71-10831

Atmospheric turbulence characteristic parameters determination by two narrow laser beams

01 p0119 A71-10833

Laser schlieren crossed beam measurements in shear layer of shock free Mach 2.46 jet

01 p0094 A71-10953

Laser effect radiation power in gas mixture flow of carbon dioxide, nitrogen and traces of water vapor, presenting calculations based on kinetic theory

01 p0094 A71-10992

Electron density profiles in ruby laser generated Xe plasma, using differential interferometry

01 p0134 A71-10996

Radiation spectral and kinetic characteristics in neodymium glass laser in frequency scanning mode

01 p0095 A71-11024

Light echo obtained via giant laser pulse peak overlapping in space and time

01 p0095 A71-11034

Electron-positron pair production during focusing of laser radiation in dense plasma

01 p0135 A71-11054

Pulsed laser emissions in atmosphere, noting backscattered light spatial and temporal structures under various meteorological conditions

01 p0120 A71-11105

Multifrequency gas laser spectrum structural changes caused by small external light signals

01 p0095 A71-11111

Pulse transmission control equipment for Q switched ruby laser output

01 p0095 A71-11171

Lithium niobate crystal electro-optical shutter to Q switch calcium difluoride-Dy laser emitting giant pulses at high repetition rate

01 p0095 A71-11210

Laser beam trajectory changes due to asymmetrical shading with circular absorbing diaphragm, noting characterization by energy distribution over cross section

01 p0095 A71-11216

He-Ne laser beam diffraction patterns produced by nematic liquid crystal subject to electric field, noting threshold effect

01 p0096 A71-11375

Magnetic field confinement of ionized plasmas generated by laser-irradiated lithium hydride solid particle

01 p0137 A71-11483

Output increase through waste energy dissipation improvement by forced convection via high speed flow for thermally pumped gas dynamic laser

01 p0096 A71-11626

Energy distribution of laser spark spectrum in air, He and Ar, determining transmission coefficients of spark plasmas by self absorption method

02 p0258 A71-11638

Spatial-temporal distribution of laser spark plasma electron density and temperature based on holographic interferometry

02 p0258 A71-11639

Solid state laser transverse modes maximum dependence on resonator geometrical parameters usable for producing stable kinetic emission model with narrow spectral line

02 p0259 A71-11878

Giant pulses composed of shorter pulse trains obtained in Q switched carbon dioxide laser with transverse modes

02 p0259 A71-11880

He-Ne discharge regular oscillations effect on laser output power

02 p0259 A71-11930

Cavity resonator length effect on lasing threshold, output energy, pulse power and duration and spectral width of giant single pulse mode laser with passive Q switch

02 p0259 A71-11933

Laser emission nonchromaticity effect on second harmonic generation in ADP, KDP, RDP and lithium niobate crystals

02 p0259 A71-11935

Diffraction frequency splitting of opposed waves produced by diaphragm in He-Ne laser resonator

02 p0260 A71-11938

Stimulated emission of laser output energy using alcohol rodamin-6G solutions under nonuniform pumping conditions

02 p0260 A71-11939

Self locked He-Cd 114 laser pulse velocity behavior, discussing stability

02 p0260 A71-11948

Operational laser communication systems performance characteristics review, considering various modulation techniques, heterodyne detection, IR applications, etc

02 p0260 A71-12030

Transient response measurements of multiple scattered laser radiation from clouds as function of view field

02 p0260 A71-12032

Laser radial-shear common path interferometer for lens testing

02 p0250 A71-12144

Laser light frequency mixing and doubling in isotropic bodies in crossed magnetic and electric fields, examining magneto-electro-optical processes

02 p0261 A71-12171

Giant pulse laser emission stabilization, describing technique for eliminating short time oscillations in subnanosecond range

02 p0261 A71-12321

Flash light excited dye solutions in liquid lasers, investigating wavelength and energy dependence of forced emission

02 p0261 A71-12322

- Laser data on coherence and radiance, deriving from manufacturer specifications for application selection 02 p0261 A71-12325
- Free generation regime of ruby laser studied by electro-optical method of smoothing spatial inversion inhomogeneities 02 p0261 A71-12502
- Natural fluctuations sources intensity in annular lasers taking into account field strength dependence 02 p0261 A71-12507
- CO chemical laser power output augmentation by selective depopulation of CO lower vibrational levels by energy transfer to added gases 02 p0262 A71-12709
- Transverse mode selection techniques for solid state laser brightness increase 02 p0262 A71-12717
- Laser image speckle interferometer design for observing vibrational modes on diffusely reflecting surfaces as alternative to holographic methods 02 p0254 A71-12718
- Laser gyro goniometry for fluctuations and angular measurements at low rotational velocities, noting countup/countdown detection systems 02 p0262 A71-12924
- Cladded fibers propagation modes launching coefficients evaluation by Gaussian field laser beam 03 p0433 A71-13170
- Stellar spectroscopy by optical heterodyning of laser and star light mixing, using He-Ne laser, high speed photocell and RF power measurement equipment 03 p0487 A71-13331
- Polarization characteristics of dual rod ruby laser emission, determining phase coincidence and energy output 03 p0434 A71-13503
- Neodymium glass laser with intracavity emission polarization, determining thermally induced double refraction effect on energy characteristics 03 p0435 A71-13505
- Organic dye laser output and service life enhancement, using filters for absorption of UV pumping radiation photodecomposition of rhodamine 6G alcohol solution 03 p0435 A71-13509
- Photoresist for hologram recording and diffraction gratings formation, using Ar laser output 03 p0425 A71-13640
- Carbon dioxide laser plasma lensing effect used as optical curvature compensation for maximum output power 03 p0436 A71-13641
- Tuned nitrogen laser pumped dye lasers, investigating bandwidth influence on output power 03 p0436 A71-13643
- Microwave ultrasonic beam visualization techniques via Bragg diffraction of laser beam, investigating resolution capability 03 p0436 A71-13717
- Laser optical field intensity correlation function determination from photoelectric counting distribution measurements 03 p0436 A71-13876
- CW carbon dioxide laser beam IR absorption by sulfur hexafluoride, investigating saturation parameter relationship to pressure, temperature and relaxation time 03 p0437 A71-13879
- Mode locked pulsed lasers statistical amplitude and phase variations effects on time dependent output intensity and nonlinear optical processes efficiency 03 p0437 A71-13881
- Nd glass laser radiation time and spectral structure 03 p0437 A71-13885
- Ionized Xe laser lines in spontaneous emission, establishing correlation with unidentified lines 03 p0438 A71-13887
- Pulsed laser threshold measurements in YAG activated by Ho, Er and Tm isotopes, noting temperature dependence 03 p0438 A71-13890
- CW laser output in carbon dioxide and nitrous oxide induced by vibrational energy transfer from excited carbon monoxide 03 p0438 A71-13893
- Sealed-off carbon dioxide laser power output and efficiency test during continuous operation over one year 03 p0438 A71-13894
- Power meter for large or divergent CW or pulsed laser beams 03 p0427 A71-13919
- Room temperature spatial distribution of emission from injection lasers with single and triple heterojunctions in AlAs-GaAs system 03 p0439 A71-13980
- Concave mirror interferometer for laser radiation spectra measurements, featuring piezoelectrically tuned optical system 03 p0439 A71-14000
- Computer controlled laser machining system for cutting integrated circuit masks in thin films deposited as fused silica substrates 03 p0433 A71-14342
- Atmospheric pressure pulsed carbon dioxide laser, investigating gain, peak power and pulse duration as function of gas pressure and discharge voltage 03 p0440 A71-14461
- Near-bandgap narrow spectrum low loss volume-excited GaAs laser with time-uniform output 03 p0440 A71-14462
- He-Ne laser emission modulation through active element excitation source 04 p0604 A71-14626
- Ruby and Nd-YAG laser basic mechanisms, properties and performance characteristics, discussing material problems and frequency width considerations 04 p0605 A71-14708
- Organic lasers using fluorescent dye in liquid solution or polymer, discussing gain and output performance, tuning, mode locking and CW operation 04 p0605 A71-14710
- Gas laser technology developments, discussing UV CW noble gas ion lasers, high output IR carbon dioxide lasers, metal vapor and pure helium lasers 04 p0605 A71-14711
- Input-output properties of Nd-YAG rods in W pumped continuous lasers 04 p0606 A71-14715
- Carbon dioxide laser output power and efficiency as function of tube length, discussing bore diameter and cavity insertion losses effects 04 p0606 A71-14716
- Laser Q-branch emission near 8 microns from flowing hydrogen-acetylene-helium mixture under pulsed electrical excitation 04 p0607 A71-15038
- Laser action in visible and near IR on atomic fluorine transitions based on collisional dissociation of hydrogen fluoride 04 p0608 A71-15040
- Laser power from carbon monoxide supersonic expansion in nitrogen and argon mixtures, comparing to carbon dioxide gas dynamic lasers 04 p0608 A71-15042
- Laser beam phase front distortion by atmospheric turbulence, discussing interferometric measurements 04 p0608 A71-15137
- High power continuously pumped Nd-YAG laser operating characteristics and design parameters 04 p0608 A71-15586
- Laser light beam spread in random media, considering atmospheric and oceanographic applications 04 p0609 A71-15682
- Partially coherent laser beam phase fluctuations using reversing-front interferometer for time integrated irradiance measurement, considering atmospheric turbulence effects 04 p0627 A71-15683
- Laser beam focusing and defocusing by thermal gas lens, deriving wave optics equations for electromagnetic fields with allowance for temperature distribution 04 p0628 A71-15808
- Calorimeter for ruby or neodymium laser output energy measurement 05 p0748 A71-16254
- Organic and inorganic phosphors for monochromatic laser illuminated black and white and color displays 05 p0760 A71-16258
- He-Ne laser beam parameters and diffraction field measurement by holography 05 p0760 A71-16260
- Carbon dioxide laser frequency doubling by Te crystal reflector output element, discussing shortcomings for conversion efficiency enhancement by power density increase 05 p0761 A71-16273
- Plasma diagnostics with focussed laser beams, discussing localized electron density determination 05 p0787 A71-16331
- CW Nd-YAG laser response to sinusoidal cavity perturbation, observing resonance modes 05 p0761 A71-16332
- Optical parametric oscillators performance improvement by nonresonant pump reflection 05 p0762 A71-16338
- CO laser emission lines and nitrogen oxides absorption lines spectral coincidences observations 05 p0762 A71-16339
- Laser light statistical properties including Fokker-Planck equation, photoelectron counting distributions and quantum mechanical equation from Weidlich and Haake theory 05 p0762 A71-16483
- Operational characteristics, spectroscopy and inversion mechanisms of noble gas ion lasers in light of plasma theories and atomic data [AIAA PAPER 70-82] 05 p0763 A71-16551
- Divergent laser light beams continuous electro-optical deflection using prism with single crystal at Curie temperature in cryostat 05 p0763 A71-16834
- Carbon dioxide laser beam thermal focusing effects on deflection in absorbing gas 05 p0763 A71-16902
- Laser irradiance pattern from aperture with truncated Gaussian field distribution, evaluating diffraction integral subject to Fresnel approximation 05 p0763 A71-16904
- Complex rays for electromagnetic field construction, considering application to Gaussian laser beams 05 p0763 A71-16905
- Nd-YAG laser branching ratios measurement for all transitions during oscillations at room temperature 05 p0764 A71-16912
- Laser cavity standing wave field electro-optic modulation for uniform population inversion, producing spontaneous single frequency output 05 p0764 A71-17232
- Argon ion laser plasma tube anodic coherent oscillations and noise suppression, using secondary discharge between anode and auxiliary cathode 06 p0906 A71-17306
- Laser emission from helium-air-methane mixture identification by comparing with vibrational rotational transition 06 p0906 A71-17307
- He-Ne laser light intensity fast and slow modulation by thin acoustoelectric photoconducting CdS platelet oscillators 06 p0906 A71-17308
- Ultrafast Q switched laser induced shock waves in solids, discussing model for picosecond impulse 06 p0907 A71-17311
- Cloud fine structure using backscattered laser radiation, incorporating multiple scattering effects into data processing system 06 p0921 A71-17381
- Traveling medium solid state lasers radiation intensity modulation by active element motion 06 p0907 A71-17593
- Gas laser radiation depolarization coefficient as function of radiation energy, cavity anisotropy and operating transition type 06 p0907 A71-17595
- Telecommunications by lasers, considering atmospheric propagation possibilities and limitations 06 p0869 A71-18064
- Geometrical and physical distance measurement by laser telemetry, involving time and speed factors of emission and receiver beams 06 p0869 A71-18065
- Traveling wave phototube for demodulating pulse amplitude modulated laser emission, investigating equivalent resistance 06 p0900 A71-18184
- Laminar boundary layer effect on gasdynamic laser gain, considering vibrational relaxation time and population inversion 06 p0908 A71-18491
- Carbon dioxide-nitrogen-water vapor gas dynamic laser, discussing generation, power and gain [AIAA PAPER 71-25] 06 p0908 A71-18492
- CW electric discharge mixing chemical lasers, identifying molecular transitions responsible for radiations from output spectral distribution measurements [AIAA PAPER 71-216] 06 p0909 A71-18652
- Low threshold large optical cavity /LOC/ GaAs injection lasers with high quantum efficiencies at room temperature 06 p0909 A71-18660
- Noise spectra of CW hollow cathode zinc ion laser comparison with conventional discharges, noting gain per unit length on transitions 06 p0910 A71-18662
- He-Cd laser output description by rate equations, investigating saturation effects, discharge processes and optimization 06 p0910 A71-18666
- Optimum design of high peak power transversely excited atmospheric pressure carbon dioxide laser using ballast resistor energy measurements 07 p1121 A71-18749
- Oblique incidence effect on reflection and absorption of laser light by solid surrounded by plasma in vacuum 07 p1166 A71-18886
- Nuclear radiation damage to ruby laser power output 07 p1121 A71-19067
- Pulsed laser emissions in carbon dioxide under high pressure, discussing onset inversion and pulse duration 07 p1121 A71-19128
- Luminescence excitation in chelates under pulsed ruby and neodymium laser radiation action, examining two photon absorption mechanism 07 p1122 A71-19130
- Gas laser gain and loss coefficients measurement, using resonator staged calibrator plate for optimal and nonoptimal conditions 07 p1122 A71-19139
- Thermally induced modifications of high power CW laser beam, considering heat losses by forced and free convection 07 p1122 A71-19207

System phase errors subtraction in interferometry, using modified laser unequal path interferometer and technique eliminating data reduction problem

07 p1107 A71-19210

Mode locked picosecond laser pulse duration properties by beat frequency detection

07 p1123 A71-19211

Dielectric thin optical film waveguides excitation for integrated optical circuitry by Gaussian laser beams

07 p1123 A71-19213

Emission frequency tunable organic dye laser development and construction

07 p1123 A71-19239

Negative resistance diodes characteristics under laser radiation, investigating switching properties, temperature effects and noise characteristics

07 p1076 A71-19373

Atmospheric refractive index diurnal and seasonal variations determination by measuring He-Ne laser radiation intensity through turbulent inhomogeneous atmosphere

07 p1061 A71-19374

Pressure dependent shift of He-Ne laser radiation, observing beat frequencies

07 p1123 A71-19486

Laser beam propagation through atmosphere, measuring phase variation dependence on turbulent temperature structure for comparison with prediction

07 p1123 A71-19574

Laser microbeam welding, drilling and trimming of electronic devices

07 p1118 A71-19787

Laser ocular effects, discussing corneal/retinal/lens lesion production, damage thresholds and application to clinical ophthalmological problems

07 p1049 A71-19792

Scanning electron microscope for surface morphological investigations of materials after laser irradiation

07 p1113 A71-19793

Solid state laser with different dielectric coatings on external reflector of pumping source, measuring energy output

07 p1125 A71-19812

Laser induced Raman scattering as diagnostic technique for measuring specie concentrations in gas mixtures

[AIAA PAPER 70-224] 07 p1125 A71-19897

Frequency stability of molecular beam laser with stimulated coherent emission

07 p1125 A71-20142

Spark discharge ignition in air by Q switched ruby laser

07 p1125 A71-20146

Threshold emission and self excitation of spatially inhomogeneous laser, considering active element gain and refractive index by electrodynamic model

07 p1125 A71-20148

Light pulses from tandem bisected GaAs lasers nonuniform excitation, determining width by intensity correlation in lithium iodate crystal

07 p1126 A71-20167

Self similar laser produced plasma examination, using irradiated multilayer targets and spectrum analysis

07 p1170 A71-20169

Beam laser operational efficiency relation to molecule/atom interaction in focusing system, explaining laser power drop at large flow rates

07 p1126 A71-20186

Pulsed ruby laser radiation energy characteristics relation to crystal temperature distribution, thermal deformation and compensating lens focal length

07 p1126 A71-20188

Light scatterers use behind phase object in double exposure holography, determining laser radiation wave front dynamics effect on image quality

07 p1114 A71-20189

Plasma formation from transition metal target under monople laser radiation, noting absorbed surface density energy role in onset

07 p1171 A71-20191

CW GaAs semiconductor laser fabrication by liquid epitaxy, noting Ag plating role in output power

07 p1126 A71-20196

Laser operation instability with nonlinear filter, deriving electrons differential velocity distribution functions on inhomogeneous emitter

07 p1126 A71-20197

Fog removal by high power carbon dioxide lasers, evaluating possibility of clearing airport runways

[AIAA PAPER 69-670] 07 p1153 A71-20308

Laser beam self induced thermal distortion in near field absorbing moving medium by theoretical model based on geometrical optics

07 p1128 A71-20389

Stimulated emission wavelength tuning from GaAs and CdSe electron beam pumping laser crystals as function of time and current

07 p1128 A71-20393

High energy narrow pulsewidth HF chemical laser emission from transverse multiple electrode nitrogen fluoride and nitric tetrafluoride discharge

07 p1128 A71-20397

CW helium-air-carbon monoxide laser with low flow rate and liquid nitrogen cooling, observing emission below 5 microns

07 p1128 A71-20398

Nitrogen-carbon dioxide electric discharge mixing laser/EDML/ used as pulse amplifier, using high flow rate for waste heat removal

07 p1129 A71-20618

Chlorine dioxide induced fluorescence spectra, using argon ion laser

08 p1300 A71-20667

Pulsed laser emissions in atmosphere, noting backscattered light spatial and temporal structure under various meteorological conditions

08 p1325 A71-20849

Carbon dioxide-nitrogen CW laser AC excitation in optical cavity, considering power output

08 p1301 A71-20997

IR laser action at 2-3 microns by low pressure discharge and gas mixtures containing molecular oxygen and sulfur dioxide

08 p1301 A71-21190

Holographic recording media low signal energy densities comparison, determining peak values of diffraction efficiency and normal contrast ratio divided by signal beam exposure

08 p1290 A71-21389

Near Gaussian intensity distributions from multimode high power pulsed ruby lasers, using rotating diffuser

08 p1302 A71-21407

Nuclear reaction products effect on population inversion in gas lasers, considering neutron irradiation enhancement of carbon dioxide laser output

08 p1303 A71-21668

Electron-positron pair production during focusing of laser radiation in dense plasma

08 p1342 A71-21952

Laser Doppler velocimeter, determining basic operational parameters including required particle density, number, type, size, output signal to noise ratio, etc

08 p1304 A71-22011

Laser radiation amplitude and phase fluctuations in complex media, using interferometry

09 p1459 A71-22143

Intensity logarithm fluctuations of focused laser beam propagating in summer daytime atmosphere at 250 and 650 meter path lengths

09 p1404 A71-22224

High pressure laser spark ignition in argon by extraneous plasma source

09 p1460 A71-22235

Large gamma radiation doses effect on neodymium activated glass laser emission properties

09 p1460 A71-22256

Polished surface quality control using laser divergent coherent beam

09 p1460 A71-22310

Ring laser active medium polarization characteristics in strong field, taking into account spatial modulation of population

09 p1461 A71-22365

Optical resonators with anisotropic elements, altering natural oscillations Q factor and spectrum

09 p1461 A71-22384

Plasma electron temperature measurement from scattering indicatrix of laser radiation

09 p1501 A71-22394

Frequency and spectral composition effect of incident radiation on stimulated Raman scattering of organic compounds, using ruby laser harmonic emission

09 p1461 A71-22395

Upper atmospheric composition by nitrogen molecules radiative transition analysis, using laser resonance backscattering effect

09 p1436 A71-22581

Semiconductor lasers properties, operational characteristics, power outputs and efficiency

09 p1462 A71-22586

Stimulated emission of laser oscillation in periodic structures of gelatin films with distributed feedback by backward Bragg scattering

09 p1463 A71-22762

Multiwavelength laser beam scintillations and atmospheric turbulence spectra, investigating saturation phenomena, transverse amplitude correlation lengths and signal fluctuations receiver aperture smoothing

09 p1464 A71-22780

GaAs junction laser continuous operation, investigating reflectivity dependence of temperature rise, stimulated light output and power efficiency

09 p1464 A71-22988

Coupled fiber lasers maximum energy transfer between passive conductors, determining minimum pulse duration

09 p1464 A71-23112

Heat conduction effect on propagation of laser radiation absorption shock wave

09 p1464 A71-23263

Infrared laser output from giant pulse laser beam photoexcited alkali metal vapors, assuming buffer gas collisional mechanism

09 p1464 A71-23380

Carbon dioxide lasers for industrial material processing, discussing machine tool reliability, maintenance, various automation approaches and economic efficiency

09 p1457 A71-23400

Long pulse glass laser welder-driller, determining mean energy densities and spot sizes

09 p1464 A71-23400

Laser microwelding, discussing focusing properties, high power radiation interactions, metal working, machining and microelectronic applications

09 p1458 A71-23400

Polyethylene plastic packet with chemical pellets describing welding, cutting and small hole punching by CW carbon dioxide laser

09 p1458 A71-23400

Laser thermal/photochemical burns and electrical shock prevention by preemployment/regular physical examinations and safety requirement education

09 p1402 A71-23412

Industry safe laser laboratory operating environments with reflection free walls, restrictive admittance, and periodic personnel examinations

09 p1402 A71-23413

Continuous wave HCl chemical laser, achieving large specific gain through high speed flow, rapid mixing and transverse geometry

09 p1465 A71-23480

Carbon dioxide laser performance quantitative analysis, considering electron to optical energy conversion via electric discharge in carbon dioxide-nitrogen-helium mixture

09 p1465 A71-23481

Production rates for beat and sum frequencies mixing from interaction of two parallel laser beams with free electrons, using nonrelativistic radiation theory

09 p1465 A71-23546

Metallic target in radiation damage from focused ruby laser beams as function of energy and luminous pulse duration

09 p1465 A71-23563

Strongly coherent Nd doped glass laser development by decreasing cavity Fresnel number, discussing maximized radiance and infrared output

09 p1465 A71-23564

Noise reduction in Rudd type laser velocimeter by conversion to light scattering system

09 p1453 A71-23695

Laser fluid flow velocimeter pulse output resolution approximation, using spectrum analyzer or discriminator measurements

09 p1453 A71-23726

Gas dynamic CW laser with supersonic hot moist carbon dioxide-nitrogen as working fluid, discussing laser gain vs water content

10 p1619 A71-23760

Constant period discrete holograms features, investigating laser visualization, recording, reconstruction and image focusing

10 p1608 A71-23810

Transverse gas flow effects on deuterium fluoride-carbon dioxide chemical laser output, discussing amplifier medium homogeneity factor

10 p1619 A71-23834

High efficiency gas chamber for obtaining Raman spectra of corrosive gases at atmospheric pressure by He-Ne laser excitation

10 p1619 A71-23857

Spectral bandwidth of Q switched giant pulse laser as function of single pass gain, optical switch and resonator loss

10 p1619 A71-23955

High power single mode CW tunable spin-flip Raman laser in InSb using CO pump

10 p1620 A71-24041

High pressure laser action in gas mixtures with pulsed transverse excitation, observing molecular and atomic transitions

10 p1620 A71-24045

Collision induced spectral cross relaxation radiative saturation and Lamb dip formation in carbon dioxide molecular lasers, using rate equations

10 p1620 A71-24151

Pulsed HF chemical laser output as function of fluorine source, flow rate and output coupling

10 p1620 A71-24153

Parasitic noise reduction in CW Nd-YAG laser output

10 p1620 A71-24154

Controlled thermonuclear reactions produced by exposing LiD target to short pulses of Nd-glass laser, measuring neutrons number and plasma temperature

10 p1620 A71-24208

Organic lasers with xanthene dyes solutions, investigating triplet states molecular population effect on output energy characteristics in pumping

10 p1620 A71-24344

Frequency stabilized lasers as absolute wavelength standards, discussing perturbation causes for optical resonant cavities and atomic transitions

10 p1621 A71-24581

Amplitude characteristics of Q switched He-Xe laser at 3.5 microns, using rotating reflection prism and velocity equations

10 p1621 A71-24715

- Soviet book on lasers with large angular divergence covering single mode generation, free electromagnetic fields equations, emission spectra, etc
10 p1621 A71-24728
- Dynamics of focusing electric discharges generated by coaxial plasma gun illuminated by ruby laser beam, using schlieren photography
10 p1653 A71-24758
- Sensitivity threshold of optical heterodyne receiver as function of laser amplitude spectrum, using photodetector output noise
10 p1622 A71-24882
- Emission dynamics of pulsed laser with optical delay line in resonator
10 p1622 A71-24885
- Spatial-temporal emission of n-GaAs laser pumped by electron beam at liquid nitrogen temperatures
10 p1622 A71-24889
- Carbon dioxide laser coherent radiation in IR region from Young double slit interference experiments, noting emergent beam spatial phase shift
10 p1622 A71-24959
- Exposure time and power effects of CW Ar laser damage to rabbit iris, comparing with pulsed ruby laser effects
10 p1572 A71-25076
- Carbon dioxide laser design and characteristics, discussing lasing action, spectral properties of continuous and Q switching output power
10 p1623 A71-25089
- Mean wind velocity and turbulence remote measurement with laser anemometry, using intensity modulation technique
10 p1623 A71-25091
- Heated mirrors and hot plasma column effects on diffraction losses and power output of gas lasers
10 p1623 A71-25093
- Flame structure and propagation studied by modified Mach-Zehnder interferometers with He-Ne laser source, describing optical arrangements
10 p1623 A71-25125
- Comparative accuracies of vertical atmospheric water vapor profiles by radiosonde and laser backscatter Raman component
11 p1794 A71-25383
- Variable output coupling far IR gas lasers, using Michelson interferometer with polyethylene or polypropylene beam splitter
11 p1773 A71-25805
- Nitrogen laser pumped cresyl violet dye laser output increase through excitation transfer from added intermediary dye
11 p1773 A71-25926
- Carbon dioxide plasma discharge current changes from Q switched laser irradiation, studying excitation and relaxation mechanisms
11 p1774 A71-25933
- Longitudinal magnetic field effect on output power, polarization and lasing frequency of He-Ne laser operating at 0.63 micron wavelength
11 p1774 A71-26003
- Q switched ruby laser emission effect on long wave pigment system of photosynthesizing organisms
11 p1774 A71-26006
- Laser pulse intensity and spectral width effect on measured cross section of stimulated emission
11 p1774 A71-26007
- Measuring technique for short term laser beam propagation direction fluctuations, discussing atmospheric turbulence effect on initial modulation phase distribution
11 p1774 A71-26047
- Laser radiation scattering, dividing into linear and nonlinear phenomena
11 p1775 A71-26082
- Laser triggered switching, discussing ability to trigger high voltage spark gaps with nsec delay and subnsec jitter
11 p1775 A71-26083
- Linear and nonlinear laser induced ion emission from solid targets with and without magnetic field, considering electron space charge accelerator
11 p1775 A71-26085
- Intense light pulses interaction with solid materials, using laser techniques
11 p1775 A71-26088
- Electron and ion plasma heating by subnanosecond neodymium laser pulses, using computer calculations of hydrodynamic equations
11 p1806 A71-26089
- Gas dynamics models for plasma production by irradiating solids with laser beams, taking into account spatial inhomogeneity of absorption process
11 p1775 A71-26090
- Laser radiation and plasma nonlinear interaction, using particle description of electron motion
11 p1806 A71-26093
- High density and temperature plasmas produced by laser pulse heating massive solid targets, discussing interaction processes
11 p1807 A71-26094
- Vibration modes of objects and light scattering from rough surfaces, using laser speckle changes
11 p1776 A71-26138
- Thomson light diffusion in laser diagnostics, deducing electron density/temperature and ion temperature
11 p1776 A71-26274
- Water and ice cloud discrimination by angular distribution measurement of various polarization parameters of scattered laser beam radiation, using Mie theory
11 p1776 A71-26298
- He-Ne laser with stable thermally tunable single frequency referenced to Kr 86 primary wavelength, describing construction details, calibration and performance characteristics
11 p1776 A71-26302
- Nonlinear photoelectric electron emission due to picosecond mode locked laser pulse irradiation
11 p1776 A71-26426
- He-Ne laser cavity amplifier performance analysis, indicating usefulness as scanning interferometer for high resolution analysis of other laser outputs
11 p1776 A71-26430
- Carbon dioxide-nitrogen-helium laser optical heterodyne experiment, obtaining various laser transitions by controlling voltage applied to PZT ceramic transducer
12 p1912 A71-26606
- Tunable organic dye laser with dispersion prism for increased radiation spectral density and luminescence band smooth frequency control
12 p1912 A71-26757
- Constant Doppler wide-angle laser beam scanning, presenting expressions for Doppler shift, spread in spectral width of scanned laser beam and scan angle
12 p1913 A71-26814
- GaAs multiple beam injection laser amplifier avoiding light flux saturation by periodic signal release
12 p1913 A71-26852
- Ne absorption tube in alternating magnetic field for He-Ne laser frequency stabilization reference, discussing laser output SNR effects
12 p1913 A71-26926
- Higher order laser light coherence effects on photoelectron distribution detected by third order photoeffect
12 p1913 A71-26961
- Capacitor discharge excited atmospheric pressure carbon dioxide-nitrogen-helium pulsed IR laser, investigating laser output dependence on gas flow and electrical parameters
12 p1913 A71-26976
- Spectroscopy and collisional transfer in methyl chloride by microwave laser double resonance, measuring population changes in various rotation vibration levels
12 p1877 A71-27004
- Accuracy requirements on crystal orientation for p-n junction laser with tilted mirrors and various resonator lengths concerning output vs current characteristics
12 p1914 A71-27095
- Transversely excited atmospheric pressure carbon dioxide lasers, considering multimegawatt laser pulse generation
12 p1914 A71-27279
- Laser triggered switching, considering theory of laser induced voltage breakdown of gas filled spark gap
12 p1915 A71-27283
- Spacecraft attitude measurement using spatial coherence of laser or star light beam, discussing feasibility and detection equipment
12 p1927 A71-27429
- Laser beam propagation in turbulent atmosphere studied for alignment survey applications, discussing development, construction and testing of centering detectors
12 p1915 A71-27538
- Shock heated Ar thermal conductivity measurements by following temperature boundary layer with time resolved interferograms with HF laser stroboscope light source
12 p1986 A71-27578
- Optical losses and quantum efficiencies of electron beam pumped CdS lasers, determining extinction coefficient from dependence of threshold current on resonator length
12 p1915 A71-27639
- Second harmonic generation experiments, considering limited focused laser beam diameter and crystal sample shape
12 p1915 A71-27641
- Output power stabilization of He-Ne laser, using vacuum photodiodes or semiconductor diodes for discharge current regulation
12 p1915 A71-27733
- Barium titanate pyroelectric receivers for giant pulse laser emission measurements
12 p1915 A71-27756
- Cavity mirror transmittance variation effect on output power and pulse length of single-pulse Nd-doped glass laser with nonuniform inverted population distribution
13 p2077 A71-27855
- Laser light scattering by fuel droplets in flame combustion zone, measuring intensity distribution with contactless optical probe
13 p2065 A71-27886
- Industrial helium-neon laser emission noise characteristics, defining amplitude fluctuations by variable proportional to photoelectric multiplier current random modulation factor
13 p2077 A71-27937
- Revolving cylindrical surface reflected energy from scanning fixed laser beam, noting signal frequency
13 p2077 A71-27948
- Radiation intensity spatial dependence on laser polarization, giving three dimensional model for wave function phase calculation
13 p2077 A71-28046
- Subnanosecond interferograms with high spatial resolution of plasma filaments in ruby laser produced spark
13 p2077 A71-28047
- Energy level threshold gradients for steady and unsteady lasing in four-level lasers, obtaining power output and pulse duration
13 p2077 A71-28153
- Shock front detection by Fraunhofer diffraction of narrow parallel Gaussian laser beam
13 p2067 A71-28162
- Carbon dioxide laser pulse shape, duration and power dependence on repetition rate during continuous pumping
13 p2077 A71-28366
- Laser parameters of Nd-doped hydrated phosphorus oxychloride-stannic chloride liquid system compared with YAG and Nd-doped glass, studying optical evolution and losses
13 p2078 A71-28400
- Book on laser physics covering radiation theory, atomic system interactions, Fresnel diffraction, Gaussian beam, Lamb theory and cavity engineering
13 p2078 A71-28429
- Laser interference patterns recorded on photosensitive surface of test sample before and after deformation, considering irregularly shaped objects with rough surfaces
13 p2067 A71-28441
- Photodetectors for laser applications in visible and near IR spectrum, discussing optical loss and pulse dispersion measurements
13 p2078 A71-28442
- Interferometric studies of focused Nd laser radiation interaction with thin graphite absorbing surface layer, discussing time behavior of plasma expansion and density distribution
13 p2078 A71-28446
- Monograph on carbon dioxide laser gain observations covering spectroscopy, energy levels, radiative transitions, molecular collisions, power efficiency, etc
13 p2078 A71-28494
- Atmospheric turbulence effects on focused coaxial carbon dioxide and He-Ne laser beam propagation
13 p2078 A71-28525
- Boundary layers velocity distribution measurements, using scattered laser radiation Doppler shift
13 p2078 A71-28574
- Ion temperature measurement for plasma focus, using laser light scattering
13 p2079 A71-28673
- Transversely excited atmospheric pressure carbon dioxide laser operation at 9.6 microns, describing proper gas mixture for power adjustment
13 p2079 A71-28674
- Laser light enhanced scattering by optical mixing of beams in plasma
13 p2079 A71-28797
- Laser emission absorption in surface layer of optical glass, determining surface temperature dependence on emission energy density
13 p2079 A71-28859
- Quantum electrodynamics on null planes in Minkowski space, discussing applications to lasers, wave packet construction, Heisenberg and Furry pictures and Compton scattering
13 p2080 A71-28998
- Focused laser coherent light beam expansion in turbulent atmosphere
13 p2080 A71-29016
- Crystalline media impurity light absorption spectral band shape, noting laser resonance emission effects
13 p2080 A71-29023
- Pulsed Xe ion laser properties, considering emission divergence, coherence and cross section
13 p2080 A71-29028
- Biological tests of laser protective filters for eye as function of optical density and wavelength by sensitivity of in vivo ocular tissue response
13 p2020 A71-29035
- Transverse spatial diffusion of phase-dispersed pulses, showing effects on dechirped pulse duration, output beam cross section and two-photon fluorescence display
13 p2081 A71-29332
- High intensity tunable InSb spin flip stimulated Raman scattering from pulsed high pressure carbon dioxide laser radiation pumping
13 p2081 A71-29336

Rotational line overlap effect on laser IR radiation absorption in high pressure carbon dioxide, comparing calculated absorption coefficient with measurements 13 p2081 A71-29337

Broadly tunable liquid dye laser action with narrow line output through use of distributed feedback obtained by spatial modulation of gain and refractive index 13 p2081 A71-29339

Semiconductor injection laser output transient response, analyzing stepshaped impressed current by differential rate equations 13 p2081 A71-29391

Fog evolution and droplet radii spectrum determination by scattered laser beam angular distribution measurement 13 p2082 A71-29484

Phase modulation in far IR interferometers applied to laser refraction measurements in solids and organic liquids 14 p2238 A71-29743

Pulsed atmospheric pressure carbon dioxide laser output pulse characteristics and self mode locking 14 p2253 A71-29799

Cadmium sulfide pulsed laser spectrum analysis, discussing output stabilization by mode selection and electron beam scanning 14 p2253 A71-30092

Flashtube pumped rhodamine 6G dye laser with four prism tuner, giving reflection losses equations and performance characteristics 14 p2254 A71-30135

Power and focusing requirements in recording and reading with Gaussian laser beam in TEM mode 14 p2254 A71-30136

Spectral filter effects on Nd-YAG laser performance stability and output 14 p2254 A71-30155

Electron temperature and density measurement apparatus using Thomson scattering of laser light for collisionless MHD shock waves 14 p2280 A71-30424

Light line and dark photochromic film large scale display devices, using neodymium and UV lasers for film bleaching and darkening respectively 14 p2249 A71-31031

Holography in nondestructive materials testing, describing laser interferometry and reproduction techniques for deformation and torsional, bending, thermal and vibrational behavior 15 p2402 A71-31217

Solid state laser emission angular divergence, considering active medium optical inhomogeneity and cavity parameters effects 15 p2418 A71-31236

Solid state laser emission divergence, calculating far zone fields for arbitrary amplitude and phase distributions 15 p2418 A71-31243

Laser radiation source time and spatial coherence effect on brightness distribution of image produced by hologram 15 p2402 A71-31254

Two beam holographic interferometer based on spherical mirrors with laser beam splitting by semitransparent plate and image reconstruction in monochromatic and nonmonochromatic light 15 p2402 A71-31257

Two interferograms holographic laser recording on same emulsion by double exposure with ruby and harmonic wavelengths 15 p2454 A71-31277

Condensed media investigated by variable frequency laser via induced radiative processes, discussing laser design, induced radiation divergence control and induced emission spectroscopy 15 p2419 A71-31483

Pulsed gas dynamic laser for radiation generation at high power levels, using shock tube [AIAA PAPER 71-572] 15 p2419 A71-31564

Ultrasonic effects on synchronization of ruby laser radiation, investigating emission pulse structure and peak sequence 15 p2419 A71-31712

Holographic investigation of laser sparks in hydrogen and helium, determining electron concentration spatial distribution and plasma dispersion dynamics 15 p2419 A71-31738

Mode locking with internal phase modulation observed in He-Se ion laser emitting on many transitions in visible region 15 p2419 A71-31750

Ne 20 isotope for selective frequency absorption to obtain monofrequency radiation in He-Ne laser with naturally isotope-doped Ne as active medium 15 p2419 A71-31998

Time dependence of peak emission energy shift due to junction temperature rise in GaAs junction lasers operated with flat topped current pulse 15 p2420 A71-32027

Atmospheric laser link with automatic sensitivity control during reception, measuring detector output signal fluctuation reduction characteristics 15 p2372 A71-32319

Acoustical wave generation measurement during iris and retina photocoagulation and ruby laser burns, noting intraocular pressure surge simultaneous with ocular tissue explosion 15 p2365 A71-32346

Histopathological and fluorescein angiographic studies of rhesus monkey chorioretinal lesions produced at threshold and suprathreshold power levels of Ar laser 15 p2365 A71-32347

Laser beam CW self-induced frequency modulation and switching observation in liquids with low surface tension 15 p2420 A71-32381

Pulsed nitrogen-pumped dye laser output spectral narrowing by injection of argon laser monochromatic radiation into cavity 15 p2420 A71-32382

IR and submillimeter wave HCN laser radiation visual observation, using thermal image converter 15 p2420 A71-32385

Singly ionized magnesium CW laser oscillation in He-Mg discharge at micron wavelengths with possible extension to visible and UV spectrum 15 p2420 A71-32386

Refraction and absorption length of coherent laser radiation propagating in high temperature cylindrical plasma column 15 p2458 A71-32390

Laser radiation second harmonic generation susceptibility in molecular crystals due to charge transfer accompanied lowest energy electronic transitions 15 p2421 A71-32402

Carbon dioxide laser beam machining, describing accessories for cutting, drilling, scribing and welding [SME PAPER MR-71-807] 15 p2416 A71-32431

Laser pulse shape, beam modulation and power fluctuation quality control measurements, using non-selective, thermally stable piezoelectric sensor with low time constant 15 p2421 A71-32456

Fabry-Perot interferometer laser beam diffraction effects on fringe pattern formation, deriving field distributions in near and far zones 15 p2421 A71-32459

Laser action internal differential quantum yield estimation using GaAs injection lasers near field emission patterns 15 p2422 A71-32461

He-Ne lasers stimulated emission, studying optical resonant cavities and discharge tubes construction 15 p2422 A71-32572

CW laser transitions in Se II, investigating current saturation behavior and output power and structure 15 p2422 A71-32581

Ruby laser pumped tunable organic dye laser to excite atomic flame fluorescence of 5535.5 Å barium resonance line, obtaining intensity vs concentration 15 p2422 A71-32582

Carbon monoxide gas dynamic laser oscillation generation, observing maximum power and vibrational exchange among single diatomic species states 15 p2422 A71-32583

Compact monochromatic rhodamine doped polymethyl methacrylate dye laser with internal diffraction grating resonator, describing frequency selection from emission spectrum 15 p2422 A71-32585

Far IR sulfur dioxide laser line prediction from transitions involving irregular Fermi interactions between molecular energy levels 15 p2422 A71-32587

Laser output speckle removal with slowly moving and motionless diffusers system, reducing integration time for obtaining SNR 15 p2451 A71-32590

Gases high resolution Raman spectroscopy, using mirror system for exciting laser beam multiplication 15 p2423 A71-32600

Optimal pulsed power output of continuously pumped Q switched Nd-YAG laser as function of mode parameters 15 p2423 A71-32603

Plasma induced random noise and striation oscillations in carbon dioxide lasers as function of operational parameters 15 p2423 A71-32608

Frequency doubling of 2.06 micron holmium doped oxyapatite laser output by proustite single crystal 15 p2423 A71-32610

Long term single frequency stabilization of composite cavity argon laser by mirror separation, using reference He-Ne laser 15 p2423 A71-32611

Pulsed output, delay time and rotational-vibrational transitions of high pressure transverse discharge CO laser 15 p2424 A71-32613

Compact pulsed carbon dioxide laser with uniform volume excitation, obtaining output energy as function of discharge voltage, gas composition and pressure 15 p2424 A71-32698

Laser beam atmospheric monochromatic radiation attenuation isolating molecular absorption from total radiant flux attenuation 15 p2451 A71-32717

Single mode ruby laser emission on transparent dielectrics, observing surface luminescence, free electrons production and adsorbed gases heating 16 p2585 A71-32744

Short length strain interferometric measurements from interference patterns of laser light diffracted from adjacent small reflecting surfaces 16 p2576 A71-32864

Reaction kinetic studies using hydrodynamic flow structure due to spherical shock wave from laser induced spark 16 p2616 A71-32919

High sensitivity helium neon laser interferometer for transient phase objects designed for shock tube and tunnel experiments 16 p2576 A71-32919

Flame, laser and shock wave plasma generations considering afterglows, ionized gas flows and high temperature effects 16 p2617 A71-32958

Microwave and laser diagnostics of plasmas based on interaction with electromagnetic fields 16 p2617 A71-32960

Optical coupling between two axes of laser light: beam deflector, using reflective relay optical system for loss reduction, cost effectiveness and easy alignment 16 p2585 A71-33135

Optical detection of laser or scattered radiation through turbulent atmosphere, taking into account independent additive background radiation 16 p2608 A71-33145

High average power flash lamp pumped pulsed dye laser development and application in atmospheric sodium probing 16 p2586 A71-33148

Low density plasma diagnostics using Thomson scattering of laser light 16 p2618 A71-33161

CW chemical lasers research, summarizing three lasing principles and advantages over electrically or thermally excited lasers 16 p2586 A71-33163

Resonant energy exchanges between gaseous media and externally applied radiation fields from wavelength-tunable lasers 16 p2586 A71-33164

High power carbon disulfide-oxygen combustion pulsed laser, discussing foreign gases effects on performance and energy transfer mechanism 16 p2586 A71-33165

Semiconductor laser continuous emission conditions at room temperature, assuming output power drop with increasing current due to p-n junction heating 16 p2587 A71-33492

Three dimensional hologram recording, showing He-Ne laser reconstruction of Q switched ruby laser hologram image of mosquito flight 16 p2579 A71-33528

Laser radar system for measuring atmospheric density above troposphere, discussing equipment design and construction 16 p2542 A71-33534

Laser light pulses in anisotropic crystal, investigating nonlinear thermal rotation of polarization plane 16 p2587 A71-33570

Radiation attenuation volume coefficients for water clouds and fogs thermal sources and laser outputs 16 p2543 A71-33730

Ultrafast laser pulses, revealing fluorescence decay stimulated Raman scattering and plasma formation transient details 16 p2588 A71-33873

Ruby watch jewels as pinhole diaphragms in laser beam broadening systems, determining optimal size 16 p2588 A71-34102

Millimeter wave klystron single-loop phase locking using final 4th-harmonic mixer in reference chain for submillimeter laser frequency measurement 16 p2589 A71-34126

Parametric microwave amplifier feasibility with laser pumped electro-optical crystal as nonlinear element 16 p2589 A71-34135

Balance equations expansion for giant-pulse Q switched laser model, considering output intensity 16 p2589 A71-34138

Temporal distribution of photons radiated by He-Ne laser operating in five modes 17 p2750 A71-34202

Laser beam trajectory changes due to asymmetric shading with circular absorbing diaphragm, noting characterization by energy distribution over cross section 17 p2750 A71-34267

HCN laser amplifier gain measurement at 10 wavelengths in gas mixtures by recording with pyroelectric receiver 17 p2750 A71-34290

- Minimum output power required for CW carbon dioxide laser drilling of thin stainless steel sheets in vacuum and air, using cylindrical source model
17 p2750 A71-34369
- Energy balance and emission power of organic dye laser under nonmonochromatic excitation
17 p2751 A71-34381
- Pulsed emission and modulation of output power of He-Ne laser at 0.63 and 1.15 micron wavelengths as function of external longitudinal magnetic field
17 p2751 A71-34385
- He-Ne laser emission and discharge plasma parameters, detailing variable magnetic field effects on modulation
17 p2752 A71-34389
- Power gain distribution in Ne-He laser cuvettes at 0.63 and 3.39 microns wavelength, noting current density dependent laser power gain shifts
17 p2752 A71-34405
- Coherence properties deterioration of laser beam by atmospheric molecular scattering, considering effect on communication system performance
17 p2753 A71-34426
- Deuterium fluoride overtone vibration-rotation chemical laser emission, studying frequency doubling and rate constant ratios
17 p2753 A71-34801
- Neodymium-yttrium-aluminate laser for high average power operation and second harmonic and parametric generation
17 p2753 A71-34802
- Computer controlled encoding device with laser flying spot scanning for automatic photographic image measurement
17 p2741 A71-34998
- Electron beam modulation by laser light, considering quantum mechanical theory
17 p2753 A71-35024
- UV Raman remote gas sensors incorporating laser scattered radiation with high resolution monochromator
17 p2753 A71-35292
- Laser Doppler anemometer, defining signal transmission region and spectrum bandwidth/amplitude from photocurrent and single moving scattering particle emission
17 p2745 A71-35328
- High coherence Q switched spatially filtered Nd-glass laser operating in fundamental mode for high power
17 p2754 A71-35747
- Crystal laser elliptic cavity size determination for maximum emission efficiency, using photochemical method for energy transfer measurement
17 p2754 A71-35748
- Vibrational population distribution in high power liquid nitrogen cooled CO laser by emission spectroscopy
17 p2754 A71-35751
- Atmospheric absorption of 10.6 micron laser beam radiation, noting effect on refractive index
18 p2910 A71-35843
- Flow velocity measurement by laser differential Doppler heterodyning, obtaining SNR from frequency difference between shifted beams
18 p2914 A71-35848
- GaAs laser arrays for beam addressable memories, discussing efficiency, junction width, beam spread and polarization
18 p2929 A71-35957
- Dynamic rate equation model of single wavelength flash lamp pumped rhodamine dye laser accounting for short molecular triplet state lifetimes
18 p2929 A71-35958
- Emission characteristics of neodymium glass laser with polymethine dye passive shutters of finite relaxation time, investigating ultrashort pulse separation
18 p2929 A71-35985
- Laser beam reflection from arbitrary geometric surface, considering reverse problem of response of flat or curved mirror to incident collimated light
18 p2929 A71-36055
- Carbon dioxide laser, discussing mixture composition, vibrational energy levels, excitation and relaxation mechanisms, output characteristics, CW and Q switching, mode locking and applications
18 p2930 A71-36147
- Multipass laser interferometry sensitivity improvement for He plasma electron density determination by increasing effective path length of laser beam in medium
18 p2931 A71-36584
- Spot size and spatial intensity distribution determination of low-power laser, using optical laboratory components
18 p2931 A71-36585
- Double heterojunction structure improvements in injection laser diodes and arrays
18 p2931 A71-36603
- Reflection, material and resonator losses correlation in solid state lasers, investigating pulse power in Q switched operation
18 p2932 A71-36801
- Nd-YAG laser optimum single frequency output operation, discussing two-component-mode filters methods using intracavity tilted Fabry-Perot and metallic film reflector etalons
18 p2932 A71-37005
- Carbon dioxide-helium mixture IR laser action and power gain increase by nitrogen addition
18 p2932 A71-37006
- Carbon dioxide laser radiation frequency doubling, using Te for second harmonic generation
18 p2933 A71-37010
- Nonlinearities effects on inorganic liquid laser output, investigating Raman and Brillouin scatterings and self focusing
18 p2933 A71-37012
- Excited state absorption in sulfur hexafluoride traversed by carbon dioxide laser beam
18 p2933 A71-37014
- Adhesively bonded structures inspection by laser holography, producing diffraction pattern recording of amplitude and phase shift
18 p2925 A71-37057
- Photographic observations of plasma eruptions from metal and opaque dielectric targets subjected to neodymium laser pulses, discussing successive shock wave formation
19 p3070 A71-37085
- High voltage pulse shaping circuits for Kerr cell polarization shifters for modulating and deflecting monochromatic laser radiation
19 p3071 A71-37255
- Laser light beam attenuation, considering turbulent pulsation effects in closed channel fluid flow axial region
19 p3071 A71-37279
- Argon plasma electron temperature by laser absorption and electron density measurements
19 p3110 A71-37406
- Beam splitting photocell for pulsed laser power and energy measurement
19 p3072 A71-37551
- Neodymium-glass lasers active elements thermal-stress-induced birefringence effects on energetic and polarization characteristics
19 p3072 A71-37767
- Ruby laser Q switching by hydrogen and copper phthalocyanin vapors, obtaining nanosecond single pulses with high power density
19 p3072 A71-37768
- Laser illuminated Mach-Zehnder interferometer system including high speed cameras for studying flame propagation among polythene particles suspended in air
19 p3064 A71-38063
- Photosystem resolution of coherent laser illuminated objects, discussing experimental investigation of image quality dependence on relative aperture
19 p3073 A71-38194
- Electron distribution functions construction from spectrum of laser light Thomson scattering by rarefied plasma
19 p3074 A71-38215
- Gas lasers, discussing engineering developments for size and cost reduction, reliability, long life and high power
19 p3074 A71-38227
- Artificial fog thermodynamic conditions and evolution data, using scattered laser beam angular distribution measurements
19 p3091 A71-38586
- Hydrodynamic effects on laser beam propagation through gases by finite difference solution, applying to trapping, acoustic and light amplifications and banana self focusing
20 p3242 A71-38838
- Excited states drift and diffusion effects on spatial hole burning and laser oscillation, solving rate equation for population inversion
20 p3242 A71-38842
- Unidirectional regenerative ring carbon dioxide laser power amplifier tests for below and above threshold operations, noting saturation role in performance
20 p3242 A71-38843
- He-Ne laser output noise due to mode competition, predicting behavior by Lamb three mode laser equation numerical solution
20 p3242 A71-38883
- Cholophor /passive polarization switched liquid crystal screen/ for laser power enhancement in multicolor displays
20 p3234 A71-39064
- Elliptical laser illuminator pumping efficiency dependence on light source focal displacement, using optical systems image forming theory
20 p3243 A71-39075
- Small signal gain and saturation intensity measurement of carbon dioxide laser as function of gas flow velocity
20 p3244 A71-39099
- Gas laser triggered switching causing propagating streamer to close by laser pulse introduction into gap
20 p3244 A71-39102
- Self induced thermal distribution due to laser beam, discussing effects on refractive index inhomogeneities and second harmonic generation
20 p3196 A71-39105
- Time resolved gain measurements of pulsed two level laser system, using computer for curve analysis
20 p3245 A71-39179
- Hybrid circuit methods for aligning resistors manufactured by different technologies, considering mechanical methods, electric erosion, electron and laser beam alignment, etc
20 p3208 A71-39434
- Optical parametric oscillator pumped with laser light, calculating radiation intensity fluctuations
20 p3246 A71-39458
- Base triangle determination by geometric geodesy, using laser telemetry and satellite optical observations with cataphotic reflecting prisms
20 p3220 A71-39661
- Carbon dioxide laser signatures prediction from multiple application of optical resonant equation by computer program, studying line competition effects
20 p3247 A71-39771
- Radial energy contours of pulsed ruby laser beam in direct determination of thermal conductivity by flash technique, using heat flux transducer
21 p3391 A71-40180
- Electrode configuration and power output for transverse flow carbon dioxide laser consisting of two parallel water cooled copper tubes perpendicular to gas flow
21 p3391 A71-40182
- High resolution spectroscopy of Na D resonance lines in saturated absorption with repetitively pulsed tunable dye laser
21 p3391 A71-40199
- Plasmaron coupling and laser emission in optically excited Ag-doped cadmium tin diphosphide
21 p3391 A71-40200
- Zero field hyperfine splitting in carbon trifluorobromide photodissociation laser emission
21 p3391 A71-40215
- Pulsed laser emission chemically pumped by exothermic chain reaction between hydrogen and fluorine mixed with He initiated by flash photolysis
21 p3391 A71-40238
- Turbulence measurement by crossed laser beam attenuation due to scattering from particles in clean or seeded flow, studying damping and transport of matter
21 p3392 A71-40400
- Laser system for atmospheric wind velocity and turbulence, using Doppler frequency shift undergone by radiation beam scattered by particles suspended in flows
21 p3319 A71-40490
- Interference rings formation mechanism near main beam emitted by ruby laser with plane and reflecting terminal faces
21 p3392 A71-40515
- Laser beam ionization of gold investigated by proportional electron counter
21 p3392 A71-40516
- Laser beam frequency mixing, discussing optical harmonics generation, light reflection/transmission and picosecond pulse measurements
21 p3392 A71-40661
- Gain and spectral characteristics of transverse flow CW chemical laser with hydrogen and deuterium fluorides active medium
21 p3393 A71-41041
- Electron beam modulation by laser /Schwarz-Hora effect/, investigating failure factors
21 p3394 A71-41045
- Nonlinear effects in high power Nd-YAG CW IR laser beam transmission through defocusing media
21 p3394 A71-41110
- High pressure laser spark ignition in argon by external plasma source
21 p3394 A71-41115
- Nonlinear absorption in transparent semiconductors of picosecond light pulses from Nd laser with locked modes
21 p3431 A71-41256
- Traveling wave power resonances in ring laser with nonlinearly absorbing cell, noting role of absorbing component lamb saturation
21 p3394 A71-41257
- Spatial-temporal emission of n-GaAs laser pumped by electron beam at liquid nitrogen temperatures
21 p3394 A71-41258
- Laser emission absorption in surface layer of optical glass, determining surface temperature dependence on emission energy density
21 p3394 A71-41297
- CdS crystals faces damage caused by picosecond light pulses from free oscillating Nd-glass laser
21 p3432 A71-41305
- Two photon absorption coefficients of ZnSe and zinc cadmium selenide crystals for ruby laser radiation, showing energy gap reduction effect
21 p3395 A71-41340
- Superadiant laser stationary characteristics description by Fokker-Planck equation for classical

distribution function, taking into account phase destroying effects

21 p3421 A71-41398

Geogravitational acceleration constant determination using two falling interferometer reflectors illuminated by laser light

22 p3574 A71-41650

Axially constructed Ar laser with segmented grapple line and pumping tube, discussing continuous operation power outputs and electric discharge current optimal magnetic field strength

22 p3556 A71-41704

Pulsed ruby laser transmission and reflection holography in single transverse and axial electromagnetic mode, stressing safety aspects

22 p3556 A71-41743

High intensity light sources hazards analysis, discussing thermal detectors and vacuum and semiconductor photodiodes for pulsed laser outputs measurement

22 p3541 A71-41795

Room temperature visible surface laser action in praseodymium chloride and bromide, obtaining optical pumping into upper laser level by wavelength tunable dye laser

22 p3556 A71-41802

Laser amplifier with range variable automatic gain control in Fabry-Perot cavity with allowance for oscillation

22 p3556 A71-41807

Vacancies production in pure Ni and V foils by bombardment with high intensity laser pulses

22 p3556 A71-41812

Laser beam focusing at various distances from caustic surfaces by spherical resonator formed by mirrors or lenses

22 p3557 A71-42063

HCN CW laser design, considering factors affecting short and long term power and frequency stabilities

22 p3557 A71-42134

HCN and water vapor submillimeter and far IR laser frequency measurement against fundamental frequency standard by harmonic generation and beat frequency detection

22 p3557 A71-42152

Pulsed atmospheric pressure carbon dioxide laser, studying pulse power and shape as functions of energy storage capacitor value, charging voltage and gas composition

22 p3557 A71-42159

He-Ne laser emission modulation through active element excitation source, using tube for discharge gap characteristics changes

22 p3558 A71-42266

He-Ne-Zn laser oscillations in red, yellow or blue spectral regions with total output power of nearly 10 mW

22 p3558 A71-42344

Positive column He-Cd/plus/ laser discharge, determining electron temperature and density

22 p3558 A71-42345

Optimal power transfer through atmospheric turbulence by adaptive laser transmitter using beacon waveform to probe channel state

22 p3512 A71-42378

Quantum fluctuations in gas laser radiation, obtaining photon diffusion coefficients for traveling and standing waves

22 p3558 A71-42456

Nonlinear losses in ultrashort light pulse generators and amplifiers, attributing to self focusing of laser radiation in active and optical media

22 p3558 A71-42457

Laser beam image reproducer systems, emphasizing pattern generators, automatic calibration subsystems, raster line merging apparatus, scanners and continuous film transport mechanism

22 p3559 A71-42515

Laser radiation destruction of transparent dielectrics, proposing electronic excitations conversion to heat and thermal explosion

23 p3682 A71-42891

Numerical analysis of large signal output characteristics for directly modulated GaAs junction injection lasers, investigating resonance phenomenon

23 p3683 A71-43351

Spatiotemporally coherent pulsed Ne and Ti vapor lasers superradiation, showing coherence time dependence on pulse length and gas pressure

23 p3683 A71-43395

He-Ne laser insertion loss effect on power variation of two operation modes during cavity frequency tuning

23 p3684 A71-43401

Gas laser power gain time dependence on molecular rotational relaxation under light pulse excitation

23 p3684 A71-43415

Steady power pulsation measurement and operation mode theory of ruby laser with bleachable dye filters

23 p3684 A71-43416

Liquid laser output wavelength dependence on rhodamine dye concentration, comparing experimental data with Stepanov theory

23 p3684 A71-43417

Neodymium glass laser emission kinetics control with positive and negative feedback by introducing nonlinear media into plane-parallel resonator with two positive lenses

23 p3684 A71-43418

Transistorized amplifier circuit for measuring power of CW emission from He-Ne laser

23 p3685 A71-43532

Laser resonator natural field amplitude fluctuation calculation based on two- and four- level models for photon number dispersion

23 p3685 A71-43560

Traveling wave laser with confocal, plane and semiconcentric resonators, calculating emission field spatial-temporal structure and inversion distribution

23 p3685 A71-43561

Traveling wave laser emission phase and amplitude fluctuations and spectral line width determination from single-mode distributed parameter model

23 p3685 A71-43563

Laser technique for runway and slant visibility range, lower cloud boundary and atmospheric damping coefficient

23 p3701 A71-43889

Holographic evaluation of low power ruby laser emitted wave spatial coherence factor via fringe visibility measurements

23 p3679 A71-43894

Nd positive ion cross section for stimulated emission with glass composition determined by laser and fluorescence measurements

23 p3685 A71-43938

Holographic nondestructive testing of materials, using laser for object illumination and interferometry

23 p3682 A71-43951

Nd glass laser system with Pockels cell Q switched oscillator for producing highly ionized plasmas

23 p3686 A71-43954

Q switched inorganic Nd liquid laser oscillator, noting output capability

23 p3686 A71-43957

Laser use in computer technology, reporting lithium and barium sodium niobate single crystals capacity for data storage

23 p3686 A71-43959

Laser vibration noise produced by piezoelectric transducer induced forced vibrations of resonator mirror, determining translational and rotational amplitude limits for laser output fluctuation

23 p3686 A71-43999

Multimode different-phase discharge carbon dioxide laser output power characteristics as function of discharge current and number of modules

23 p3686 A71-44000

Laser light action in photosensitive materials, comparing development techniques

23 p3686 A71-44057

Mode locked CW dye laser operation, describing output stability and pulse rate and widths

23 p3687 A71-44133

Explosion-pumped gas dynamic carbon dioxide laser, obtaining high pulse energy by common hydrocarbon fuels

23 p3687 A71-44135

Gallium arsenide phosphide electroluminescent junction diode pumped Nd-YAG laser room temperature CW and pulsed outputs

23 p3687 A71-44139

Quantum phase fluctuations in IR gas lasers, noting nearly Lorentzian power spectrum with bandwidth inversely proportional to output power

23 p3688 A71-44269

Transition selection with adjustable outcoupling for laser device applied to carbon dioxide

23 p3688 A71-44294

R-branch multiline performance of transversely excited pulsed HF chemical laser

23 p3688 A71-44297

High repetition rate TEA carbon dioxide laser up to 1000 pps with average power output up to 65 W

23 p3688 A71-44298

Continuous chemical laser model for constant gain method exposure, emphasizing strong radiation-chemistry coupling, molecular J-shift, output power limiting behavior and lasing efficiency

24 p3832 A71-44373

Silicon carbide single crystal photoluminescence under pulsed ruby laser light irradiation at 77 K, discussing radiative recombination of excitons

24 p3833 A71-44666

Reflection coefficient of multimode laser beam from dielectrics interface

24 p3833 A71-45044

Pulsed modulation of continuous laser resonator Q factor, recording output on oscillograph

24 p3834 A71-45045

Dispersion characteristics of He-Ne laser at 3.39 microns

24 p3834 A71-45046

Laser radiation intensity modulation by time varying magnetic field

24 p3834 A71-45055

Carbon dioxide-helium-nitrogen laser with nonlinearly absorbing cell, presenting emission pulse duration and rate

24 p3834 A71-45111

Dielectrics breakdown under ultrashort neodymium laser pulses at fundamental and second harmonic frequencies

24 p3834 A71-45112

Laser beam applications in drilling, shaping and surface finishing of miniature journal and step-type friction bearings, deriving regression equations for optimal process parameters

24 p3834 A71-45165

Laser beam spot dancing during propagation through turbulent atmosphere, using Kolmogorov structure function of refractivity and geometrical optics

24 p3834 A71-45206

Low cost CW carbon dioxide laser power meter using Joule heating technique

24 p3835 A71-45213

Single mode output power multiplication in standard commercial He-Ne laser with cavity extension and etalon

24 p3835 A71-45214

He-Ne laser discharge gap oscillation modes observation, noting applied magnetic field, gas parameters and cathode type effects on stimulated emission

24 p3835 A71-45239

Liquid-state pulsed laser active elements parameters effects on output radiation divergence

24 p3835 A71-45240

Laser IR radiation attenuation in natural and artificial fogs, noting dependence on particle size distribution

24 p3835 A71-45254

Laser IR radiation attenuation in atmospheric precipitation, considering snow, rain and drizzle

24 p3835 A71-45255

He-Ne laser radiation modulator at 1.5 GHz using X and Z cut lithium niobate crystals in toroidal microwave cavity

24 p3835 A71-45265

Ruby laser radiation modulation by ultrasonic mirror oscillations, discussing mechanism

24 p3836 A71-45269

LASER RADAR

U OPTICAL RADAR

LASER RANGE FINDERS

Earth rotation axis and mass center position determination, using earth-moon laser ranging data

01 p0161 A71-11383

Spatial vector calculations using laser distance measurement and optical observations

03 p0380 A71-14191

Lunar ephemeris for nanosecond resolution laser ranging systems by literal and numerical integration techniques

05 p0811 A71-16682

Dual laser ranging for distance measurements superimposing beams modulated at different frequencies

11 p1774 A71-25936

Ruby laser ranging of moon, describing Pic du Midi Observatory laser telemetry station and Luna 17 retroreflectors

16 p2640 A71-33752

McDonald Observatory lunar ranging station including telescope matching optics, guiding, timing equipment, pulsed ruby laser system and calibration procedures

16 p2553 A71-33780

Laser radar system using retroreflector on lunar surface for measurement of distance between earth and moon

16 p2543 A71-33811

Lunar laser ranging experiments in Japan, detecting returned signals from Apollo 11 retroreflector surface package

16 p2543 A71-33812

Apollo optical retroreflector arrays characteristics and performance for laser range measurements from earth stations, describing multilensed receiver telescope

16 p2642 A71-33831

Laser ranging of moon using retroreflector mounted on Lunokhod-1 lunar surface vehicle

17 p2707 A71-35402

Satellite distance measurement by laser, describing energy calculation, equipment parameters, ground tests, cloud echo and Geos B satellite experiments

17 p2709 A71-35598

Q switched laser range finders, discussing programmed ephemeris guided, divergence data utilizing and semiautomatic tracking systems with emphasis on target acquisition

18 p2945 A71-36029

LASER RANGER/TRACKER

Satellite laser tracking for geodetic data acquisition

08 p1285 A71-21802

NASA pulsed laser ranging systems for scientific satellite tracking, determining accuracy by trajectory and long arc orbital comparison

10 p1576 A71-24051

- DC 10 flight test program improvement using data acquisition/processing with real time monitoring, instrument landing and laser tracking [AIAA PAPER 71-788] 16 p2553 A71-34018
- Precision tracking and pointing of laser beams in space for communication, discussing large space telescope /LST/ applications 18 p2920 A71-36090
- Light detection and ranging /LIDAR/ system in airborne and ground applications for moving target location and tracking 18 p2882 A71-36615
- Laser velocity measuring system for tracking high speed rocket sleds on Holloman test track 18 p2932 A71-36616
- Optical radar aircraft tracking and position system, using IR Q switched flash pumped Nd-YAG laser transmitter and pulse receiver with magnetic tape recorder and real time computer 18 p2900 A71-36905
- Automatic argon ion laser tracking system for high speed rocket sleds, describing apparatus configuration and error correcting devices 18 p2883 A71-36908
- Laser ranging to retroreflector array placed on lunar surface during Apollo 11 mission 20 p3296 A71-39622
- NASA Stadan and Speot optical and laser tracking sites dynamic position estimations from GEOS 1 and 2 observations, analyzing model error effects 20 p3220 A71-39662
- Optical spacecraft tracking, using pulsed ruby lasers at Baker-Nunn camera stations of Smithsonian Astrophysical Observatory for retroreflector-equipped satellites ranges 21 p3349 A71-41404
- Collimated laser beam angular deviation in turbulent near earth atmosphere, comparing with interferometric data 23 p3685 A71-43506
- LASERS**
- NT ARGON LASERS
- NT CARBON DIOXIDE LASERS
- NT CHEMICAL LASERS
- NT GALLIUM ARSENIDE LASERS
- NT GAS LASERS
- NT HELIUM-NEON LASERS
- NT INFRARED LASERS
- NT INJECTION LASERS
- NT LIQUID LASERS
- NT ORGANIC LASERS
- NT PULSED LASERS
- NT Q SWITCHED LASERS
- NT RING LASERS
- NT RUBY LASERS
- NT SEMICONDUCTOR LASERS
- NT SOLID STATE LASERS
- Laser communications systems techniques, proposed designs and experiments 01 p0039 A71-11340
- Optical schemes of laser ring interferometer with selective characteristics, noting coupling via scattering at resonator optical elements 02 p0259 A71-11934
- Coherent optical sources in form of lasers and parametric oscillators with usable power for communications 02 p0260 A71-12002
- Coherent laser synthetic aperture radar at microwave frequencies for airborne ground point target mapping 02 p0215 A71-12044
- Spatial and temporal coherence effects in holography, giving general formula for reconstructed virtual image 02 p0251 A71-12148
- Automatic testing of electro-optical systems including TV, IR and laser applications 03 p0395 A71-13082
- Weak nonlinear absorption effects shown by passive optical elements placed in laser resonator cavity with large angular emission divergence 03 p0435 A71-13511
- Correlation measurements by laser in turbulent gas flow, determining phase structure velocity distributions and coherence lengths 03 p0435 A71-13529
- Optical plate induced helicoidal steady light field in laser cavity, imparting structure to isotropic transparent material medium 03 p0436 A71-13787
- Modified Ashby-Jephcott laser interferometer schlieren system for HF gas density measurements 03 p0427 A71-13922
- Quantum statistical analogy between laser threshold region and second order phase transition of ferromagnets 03 p0440 A71-14197
- Laser technology - Conference, Rochester, New York, November 1969 04 p0605 A71-14707
- Laser interferometry precision measurement and alignment techniques, describing application in optical lens manufacture and assembly 04 p0606 A71-14718
- Laser metrology, discussing precise distance measurement techniques based on modulated CW and pulse sources, laser systems for constructional angular alignment and materials spectrography 04 p0606 A71-14719
- Laser communications, discussing directivity and bandwidth characteristics, receiving techniques based on photomixing /heterodyning/ and direct photodetection, modulation and signal design 04 p0550 A71-14720
- Laser applications in biology and medicine covering surgery, ophthalmology, microorganisms, viruses, tissue culture, tumor eradication, radiation hazards, etc 04 p0541 A71-14722
- Laser display technology, discussing recent systems, light beam deflectors and modulators 04 p0607 A71-14723
- Laser produced schlieren interferometry diffraction pattern determination, using Doppler frequency shift law 04 p0596 A71-15222
- Surface roughness determination by spatially coherent laser light speckles correlation and spectral distribution on film records 04 p0609 A71-15689
- Holography applications, recording and reconstructing three dimensional objects by split laser beam interference technique 05 p0747 A71-16194
- Black and white and multicolor laser display systems with monochromatic or bichromatic source, using photoluminescent materials and acousto-optic deflectors and modulators 05 p0760 A71-16259
- Structural damage by laser radiation in polymethyl methacrylate, using polarized light microscopy 05 p0772 A71-16370
- Laser document scanner for computer entry and communications systems 05 p0762 A71-16480
- Optically pumped Rb laser theory, taking into account superfine and Zeeman structure of atoms 05 p0763 A71-16872
- Materials properties measurement by laser, describing methods for stress investigation in glass and electron density measurement in plasmas 05 p0764 A71-16969
- Laser Doppler heterodyning system for bidirectional pulsatile fluid flow velocity magnitude and direction measurement 05 p0756 A71-17233
- Frequency domain and time domain methods analysis of signal from laser velocimeter 06 p0900 A71-18053
- Laser Doppler velocimeter, describing simplified stable optical arrangement 06 p0900 A71-18054
- Holographic optical memory and computer output applications for rapid bulk data storage, considering various laser visualization systems 06 p0908 A71-18067
- Lasers applications to materials working including welding, cutting, machining, etc 06 p0908 A71-18069
- Large volume high pressure gas uniform electrical discharges, applying to laser amplifier [AIAA PAPER 71-65] 06 p0909 A71-18524
- Integrated electro-optical microwave radar and laser /lidar/ systems for earth oriented, environmental and domestic applications 07 p1095 A71-18827
- True vertical laser application for precision vertical alignment of large structures, using mercury mirror 07 p1122 A71-19206
- Backscattered radiation energy during laser beam scanning of diffusely scattering surface 07 p1123 A71-19309
- Air bearings design for laser scanner high speed rotating mirror in vacuum, describing static and dynamic tests for rotor inversion point [ASME PAPER 70-LUB-15] 07 p1117 A71-19506
- Lasers - Conference, New York, May 1969 07 p1124 A71-19776
- Fiber optic laser devices properties and potential applications as amplifiers, logic elements, active mode selectors and intense light sources 07 p1124 A71-19781
- Laser systems for biomedical applications, considering ophthalmology, dermatology, surgery, biological and cellular research, analytical and diagnostic medicine 07 p1049 A71-19782
- Laser microprobe emission spectroscopy of biological matrix elements, investigating bovine albumine effect on spectrum analysis 07 p1113 A71-19785
- Laser applications in chemical research, exploring fast chemical processes, isotope enrichment and molecular reactions and structure observations 07 p1124 A71-19790
- Control of biological laser radiation hazards 07 p1049 A71-19791
- Laser tuning techniques, noting acoustooptic, Doppler, oscillator and dye cell methods 07 p1124 A71-19794
- Singly resonant optical parametric oscillator allowable pump bandwidth 07 p1126 A71-20179
- Laser dynamic theory with uniformly broadened and Doppler spectral lines based on nonlinear interactions between harmonic oscillations 07 p1127 A71-20255
- Maximum ponderomotive force on laser produced plasmas, using wave equation in linear critical layer 07 p1171 A71-20291
- Lens geometry history covering computerized design, prototype testing, optical shop aids and laser interferometry 08 p1333 A71-21177
- Fabry-Perot resonator with anisotropic medium, deriving reflection mirror shape for optimizing diffraction loss and resonant conditions for extraordinary waves 08 p1289 A71-21284
- Three mirror multiple beam interferometric rejection filter for laser Raman spectroscopy 08 p1289 A71-21379
- Velocity components, species densities and temperature local measurements, using laser Doppler velocimeters, Raman scattering and tunable lasers [AIAA PAPER 71-283] 08 p1303 A71-22008
- Laser Doppler system for subsonic and supersonic jet flow velocity measurements, discussing calibration and measurement errors 08 p1303 A71-22009
- Laser Doppler velocimetric technique for supersonic flow particle trajectory and density measurements, noting particle lag [AIAA PAPER 71-287] 08 p1303 A71-22010
- Wideband photographic signal recording by modulated laser beams, discussing performance characteristics in terms of signal to noise ratio and laser power 09 p1460 A71-22355
- Laser technology R and D with respect to high average and/or peak power and chemical to coherent light energy conversion 09 p1462 A71-22584
- Laser applications in physics research, discussing nonlinear optics and spectroscopy, time and distance measurements and Raman and Rayleigh light scattering 09 p1462 A71-22585
- Spectral analysis of laser Doppler flowmeter signals, considering time independent systems 09 p1463 A71-22691
- Ray transformation after passing through optical resonator with Brewster prism, calculating spectral energy losses dependence by geometrical optics method 09 p1464 A71-23072
- Multiphase gas flow, measuring gas concentration by laser Raman spectroscopy [AIAA PAPER 71-286] 09 p1464 A71-23308
- Book on lasers and masers covering electric and magnetic dipole transitions, electron oscillator, collision broadening, optical resonators, waveguides, etc 09 p1466 A71-23725
- Air jet velocity and turbulence measurements by modified Doppler technique, using CW lasers 10 p1609 A71-23874
- Information-theoretical approach to lasers theory, avoiding Fokker-Planck equation method 10 p1619 A71-23919
- Thermomagnetic modulated Kerr effect readout and magneto-optical laser recording at high output on cobalt base metallic films 10 p1613 A71-25108
- Negative ions photodetachment by continuously tunable laser and ion cyclotron resonance spectrometer 11 p1772 A71-25371
- Laser interaction and related plasma phenomena - U.S. Army Conference, Hartford, June 1969 11 p1775 A71-26080
- Expanding laser generated plasma self similarity model from hydrodynamic equations, describing thermokinetic properties 11 p1806 A71-26092
- Collision effects on atomic spectral line profiles, using quantum mechanical description of atomic center-of-mass motion with particular application to lasers 11 p1803 A71-26147
- Plasma diagnostics covering magnetic, electron beam, electrostatic, laser, holography, interferometry, Thomson scattering, microwave and electroacoustic techniques 11 p1766 A71-26287
- Directional laser Doppler velocimeter measurements in perturbed circular flow, noting use in cardiovascular research 11 p1766 A71-26303
- Structure constant of jet exhaust turbulence of J-57 with afterburner by laser beam probing compared with scintillation and hot-wire anemometer measurements 11 p1766 A71-26304
- Soviet laser spectroscopy applications including microsample chemical analysis, superhigh resolution

problem, nonlinear optics devices, interferometric seismometer and air pollution analyzer

11 p1776 A71-26351

Spontaneous magnetic fields in laser produced plasmas explained as thermoelectric currents

11 p1807 A71-26406

Design and operation of scanning laser based on exciting electron beam directional variation, discussing laser characteristics for various operating modes

12 p1913 A71-26851

Laser resonator properties with flat outlying mirrors, examining stimulated radiation generation and energy distribution

12 p1916 A71-27764

Rotating mirror wavelength shifter of laser light source for use in electronic spectroscopy, noting measurements with high speed Doppler wheel in vacuum

13 p2067 A71-28445

Laser quantum theoretical analysis, considering atomic thermal motion, photon emission and absorption induced recoil effects on lasing threshold and operating frequency

14 p2253 A71-29574

Holographic techniques, optical data processing and laser properties for aerospace instrumentation

14 p2244 A71-30329

Laser Doppler velocimetry accuracy degrading factors, considering light beam focus phase anomaly and distortions due to density fluctuations

14 p2254 A71-30331

AEDC test facilities laser instrumentation for flow field diagnostics by Doppler velocimeter, holographic flow visualization and particle studies

14 p2245 A71-30332

Laser beam scintillation covariance beyond turbulent atmospheric layer in Fresnel and Fraunhofer zones

14 p2254 A71-30423

Photographic and laser observations during passage of satellite for determination of distance between observer and earth rotational axis

14 p2250 A71-31123

Digital laser interferometer for vibration measurements, describing theory, transistorized circuitry and performance characteristics

15 p2401 A71-31138

Condensed media investigated by variable frequency laser via induced radiative processes, discussing laser design, induced radiation divergence control and induced emission spectroscopy

15 p2419 A71-31483

Laser interferometer application in machine tool calibration, digital readout and feedback system, discussing advantages and limitations [SME PAPER IQ-71-745]

15 p2421 A71-32433

Laser Doppler turbulent and laminar flow velocity measurement model, using optical mixing spectroscopy theory

15 p2423 A71-32589

Lasers as light sources, discussing Rayleigh, Tyndall, Raman and Thomson scatterings from various media

16 p2612 A71-33373

Laser spectral-isotopic determination of oxygen content in metals, noting analysis variant dependence on metal purity

17 p2751 A71-34384

Ideal laser gyro sensitivity against background of natural emission fluctuations

17 p2737 A71-34411

Vortex laser Doppler velocimeter system for aircraft wake turbulence velocity profile mapping, describing optical arrangements, back and forward scattering modes and prototype design

17 p2754 A71-35756

Turbulent multispecies gas mixing measurements using dark field laser schlieren system

18 p2930 A71-36059

Optical readout system for analysis of laser Doppler velocimeter signals displayed on TV screen and recorded photographically

18 p2931 A71-36587

Acousto-optical effects, materials and devices of laser beam control using diffraction and refraction by ultrasonic waves

18 p2932 A71-36607

Laser interferometer techniques with automatic measurement and compensation for system inaccuracies, considering corrections for sine/Abbe/ errors for pitch and yaw, etc [SME PAPER IQ-71-120]

18 p2924 A71-36655

Thermal or chemical energy conversion to electromagnetic radiation by laser, discussing atomic or molecular processes and thermodynamic limitations

20 p3242 A71-38939

Transparent sample surfaces parallelism interferometric measurement using laser produced two beam nonlocalized fringes

20 p3245 A71-39181

Laser Doppler holographic technique for fluid velocity field visualization and quantitative two dimensional vector velocity measurement

20 p3235 A71-39183

Laser beams amplitude-phase correction by holographic method, obtaining beams with plane fronts and Gaussian amplitude distribution

20 p3245 A71-39413

Simultaneous CW microwave radiometer and laser probing of hypersonic wake ionization and turbulence, relating radiation temperature, radar echo and mechanical flow field structure

21 p3392 A71-40387

Low speed wind tunnel air velocity measurement with laser velocimeter, using dark background illumination detection of particles scattering across fringe pattern

21 p3378 A71-40398

Dual scatter laser Doppler velocimeters for transonic wind tunnel measurements and calibration applied to simulated helicopter downwash, high lift wing and jet crossflow

21 p3364 A71-40399

German monograph on plasma layer temperature distribution in optical resonator covering spectral distribution of thermal radiation

21 p3379 A71-40749

Laser development and applications in telephone communications, manufacturing and holographic memory

21 p3393 A71-40877

Kinoform diffuser technique based on speckle pattern formation by ground glass illumination with undiverged laser beam

21 p3381 A71-40928

Laser speckle interferometry for translational motions and vibrations detection, considering applications in radar and acoustics analysis

21 p3393 A71-40932

Holographic interferometry application to laser NDT of objects with nonoptical surfaces, describing techniques and industrial uses

21 p3382 A71-40939

Fluid velocity gradient measurement by laser-Doppler techniques based on signal spectrum bandwidth or frequency shift corresponding to position shift near wall

22 p3541 A71-41792

Inverted populations of molecular vibrational states for lasers, using strongly exothermal explosion-accompanied chemical reactions

22 p3557 A71-41819

Electronic techniques in optronics/optoelectronics/, discussing CRT, image tubes, semiconductor and lasers

22 p3559 A71-42467

Laser pumped solid state masers operational characteristics, describing spontaneous emission noise

23 p3683 A71-43084

Laser optical system for hyperballistic range hypervelocity models surface erosion measurement, describing instrumentation of front-lighted, silhouette and stereo stations

23 p3677 A71-43513

High power laser characteristics for large scale industrial applications

23 p3685 A71-43516

Hollow cathode lasers based on negative glow discharge excitation including exchange ion-atom collisions and Penning excitation

23 p3686 A71-43955

French R and D Directorate exhibits at 29th Le Bourget air show, discussing laser applications, telecommunication, navigation-guidance, energy conversion, test facilities and environmental studies

24 p3816 A71-44764

Laser holographic inspection for disbands in metal/phenolic rocket nozzles of two divergent geometries, corroborating by ultrasonics and dye penetrants

24 p3829 A71-45278

LASV

U F-111 AIRCRAFT

LATENCY

U REACTION TIME

LATERAL CONTROL

Jet deviation by secondary gas injection, predicting lateral thrust performance

04 p0525 A71-14793

Inertial aircraft lateral guidance system limitations in stochastic gust environment, comparing configurations using aileron or differential spoilers [AIAA PAPER 71-22]

06 p0925 A71-18489

Missile roll axis attitude control system based on fluid amplifiers, describing fluidic integrator and chain

07 p1028 A71-20584

Executive jet landing approach lateral-directional handling under IFR ILS simulated conditions, investigating Dutch roll control power effect on crosswind component

10 p1554 A71-24243

Reentry vehicles fluidically controlled hydrazine rocket engine modules for roll rate control [AIAA PAPER 70-650]

11 p1810 A71-25503

Differential circuit for bilateral stopping control of double action piston cylinders, discussing solenoids valves operation

11 p1716 A71-26324

Adaptive roll control of space vehicle on reentry trajectory, analyzing spacecraft angular motion dynamic equations for optimal conditions determination

12 p1926 A71-26761

Wing design criteria imposed by high speed requirement for short takeoff aircraft, considering thin swept back wing with small aspect ratio for lateral control

12 p1867 A71-27477

Ellevons as longitudinal and lateral control elements on low aspect ratio wings, calculating subsonic and supersonic aerodynamic characteristics

13 p1993 A71-29191

Optimal lateral guidance switching thresholds for low L/D shuttle vehicle entry, using optimal stochastic control theory for problem formulation in conjunction with dynamic programming [AIAA PAPER 71-914]

19 p0396 A71-37116

Performance limitation of simplified radio-inertial lateral control guidance system subject to stochastic gusts for automatic landing [AIAA PAPER 71-957]

19 p0399 A71-37191

Spacecraft roll stabilization during parabolic earth atmosphere reentry, developing single parameter multistep algorithm

24 p3846 A71-45303

LATERAL OSCILLATION

Lateral vibration effects on heaving airfoil blunt trailing edge vortex shedding flows, examining basic cavity damping by flow visualization

06 p0984 A71-17629

Dynamic damping coefficient extracted from flight test lateral rate data telemetering ablative reentry vehicle [AIAA PAPER 71-49]

06 p0980 A71-18511

Rectangular plates under direct and shear in-plane forces, considering free lateral vibrations

15 p2509 A71-32511

Twin turboprop STOL aircraft lateral directional oscillation traced to rudder vibration due to aerodynamic hinge moments interaction with friction [AIAA PAPER 71-792]

16 p2525 A71-34011

Simply supported Bernoulli-Euler beam resting on elastic foundation and carrying equally spaced moving mass particles, calculating lateral response dynamic stability by Galerkin method [ASME PAPER 71-APM-M]

18 p2978 A71-36248

Free falling spheres rocking/lateral motions, deriving nonlinear damped pendulum equation with motion coupling expressed as Reynolds number dependent phase shift effect

21 p3416 A71-40951

Rectangular plate under lateral and inplane pressure pulses, examining transient response with Mathieu equation

21 p3471 A71-41021

LATERAL STABILITY

Computerized simulation of lateral inhibitory networks for figural aftereffects, discussing light and dark adaptation mechanism

10 p1563 A71-24231

Nonuniform cross section tapered, stepped rectangular and I section cantilever beams elastic lateral stability

14 p2330 A71-30688

Subsonic flight characteristics of LB 21 reentry vehicle, discussing lateral directional stability and lifting fuselage

18 p2972 A71-36434

Aircraft lateral dynamics effect on positioning accuracy along straight flight path, using Loran C data

20 p3261 A71-38861

Frequency and buckling stability eigenvalue evaluation for anisotropic circular cylindrical shells under nonuniform lateral prestress

22 p3615 A71-42211

Variable stability aircraft lateral directional flying qualities, investigating turbulence effects

22 p3483 A71-42831

Strain hardening narrow strip lateral instability under bending in plane of maximum rigidity, deriving critical moment formula

24 p3883 A71-44851

LATERALITY

U LATERAL STABILITY

LATERALIZATION

U LATERAL CONTROL

LATHES

Metal cutting on lathes, discussing machining conditions optimization based on productivity and cost criteria and linear programming solution

07 p1117 A71-19361

LATITUDE

NT GEOMAGNETIC LATITUDE

Two-roll gyrocompass accelerated reduction of meridian

01 p0080 A71-10631

Earth radiation latitude nonuniformity effect on error in onboard satellite local vertical determination using Cosmos satellite data

02 p0304 A71-11911

Auroral absorption latitudinal distribution diurnal variations, showing existence of two zone model

05 p0746 A71-17201

Latitudinal variations in adiabatic production and destruction of kinetic energy by meridional and zonal motions of atmosphere

09 p1488 A71-23025

Latitude dependence of upper atmosphere corpuscular radiation intensity, analyzing sounding data from Indian Ocean area

12 p1947 A71-26645

Properties of higher latitude region of structured low energy electron precipitation in noon hemisphere, relating radiation with optical emissions in dayside auroral oval

13 p2119 A71-27911

Three dimensional quasi-stationary problem of local winds in neutrally stratified atmosphere in low latitudes, analyzing Coriolis force role

13 p2096 A71-28016

Earth radiation latitude nonuniformity effect on error in onboard satellite local vertical determinations, using Cosmos satellite data

13 p2133 A71-28202

Auroral absorption latitudinal distribution diurnal variations, showing existence of two zone model

13 p2060 A71-28260

Sunspot butterfly diagram interpretation based on heliographic latitude drift relation to gradient of solar rotational velocity

15 p2495 A71-32707

Mean ionospheric height selection effect on total electron content latitudinal variation determination

19 p3047 A71-37367

Geomagnetic micropulsation periods variation with latitude and plasmapause presence, calculating uncoupled toroidal and poloidal modes eigenperiods of hydromagnetic waves

20 p3215 A71-38735

ATTITUDE MEASUREMENT

Meridian direction autonomous inertial determination, using gyroplatform newtonometer data

01 p0125 A71-10629

Photoelectric reflector zenith telescope for determination of earth rotation and latitude variations, noting recording by photon counts

04 p0598 A71-15381

International Time Bureau /Paris/ astronomical and geophysical research based on universal time and latitude observations of earth rotation

06 p0890 A71-17879

International Polar Motion Service stations residual latitudes variation by other than polar motion, considering dependence on earth figure deformation

06 p0890 A71-17880

Secular changes in cooperative stations mean latitudes related to mean pole drift

06 p0890 A71-17882

Semiannual nutation term determination from diurnal latitudinal observation with zenith telescope over 6 year period

07 p1194 A71-19319

Latitude observations at Pulkovo from 1948 through 1967 with zenith telescope

07 p1194 A71-19327

Latitude observation program at Pulkovo from 1968 through 1987 with zenith telescope, noting faint star declination and motion errors in General Catalog

07 p1194 A71-19328

Revised latitude series of nutations in Mizusawa and Paris observatories from LF noise investigations

07 p1194 A71-19329

Kimura annual Z term in latitude variations, noting agreement with semiannual solar nutation and earth tide observations

08 p1364 A71-21422

Latitude and nonpolar nighttime changes in observation at Paris and Herstmonceux with Danjon prism astrolabes, discussing data reduction

08 p1284 A71-21677

Geographical latitude from azimuths and zenithal measurements of two stars on hour circle

09 p1438 A71-23180

Water vapor latitude variation on Mars from Coude spectrograph of 107 inch telescope

11 p1826 A71-25716

Antarctic auroral ovals, determining time-longitude coordinates, statistical mean position and polewards and equatorwards boundaries for various Kp

12 p1900 A71-27056

Astronomical latitudes determination under non-setting sun conditions from differences between star azimuths

13 p2056 A71-28011

Saturnicentric latitude measurements tabulation for use with standard drawings

13 p2136 A71-28388

Semiannual nutation term determination from diurnal latitudinal observation with zenith telescope over 6 year period for earth axis

15 p2486 A71-31899

Latitudinal observation errors by two zenith telescopes concurrent data, showing distribution function in long term measurement

23 p3771 A71-44255

Astrometrical HF range latitudinal observation error spectrum estimation, showing random dispersion

and Chebyshev polynomial expansion parameters for nightly variation

23 p3771 A71-44256

International zenith telescopes micrometer value, determining correction for ocular screw from latitude observations

23 p3680 A71-44261

Optimal method selection for astronomical measurements on lunar surface, discussing instrumental and technical difficulties with selenographic longitudes and latitudes determination

24 p3870 A71-44812

LATTICE IMPERFECTIONS

U CRYSTAL DEFECTS

LATTICE PARAMETERS

Fine structure and lattice constants of Al-W, Al-Mo and Al-Mn alloys at high cooling rates

01 p0101 A71-10675

Ni-Al-Ti alloys strength, investigating matrix precipitate lattice parameter mismatch effects

02 p0263 A71-11865

Transition metal carbides and nitrides, observing metallic and nonmetallic sublattice dynamic characteristics by X ray diffraction

02 p0266 A71-12672

Near stoichiometric binary alloys atomic ordering parameters quantization by field ion microscopy, using direct counting and optical transformation techniques

02 p0297 A71-12736

Be mirrors thermal dimensional instabilities dependence on crystalline anisotropy, discussing X ray quality control technique

03 p0424 A71-13637

Thermal lattice expansion measurements on carbon powders up to graphitization temperatures, using X ray diffraction

04 p0618 A71-14960

P-type aluminum gallium arsenide phosphide growth on gallium arsenide phosphide from solution, noting lattice match preservation and heterostructure junction devices

04 p0608 A71-15041

Cosserat continuous model of dense elastic lattices of regular structure in plane

04 p0673 A71-15884

Nb-V-Mo alloys lattice structure, examining continuous solid solutions with X ray and metallographic analysis

07 p1129 A71-19144

Dissolved hydrogen effects on mechanical properties, modulus of elasticity, lattice constants and X ray lines of Ti alloys, showing cold brittleness at high strain rates

07 p1130 A71-19298

Critical temperature short to long range ordering mechanism theories, discussing lattice type, transition continuity and spinodal decomposition factors

07 p1131 A71-19432

TiH metallographic and lattice parameters variation with hydrogen content

07 p1139 A71-19993

Metals and nonmetals orbital atomic radii and lattice parameters

08 p1345 A71-21762

Cr alloys alloying elements Os, Re, Fe, Co and Mn effect on lattice constant and elastic properties, using acoustic measurements

09 p1473 A71-23229

Book on computer calculation of phase diagrams covering quantitative computation of phase equilibrium and lattice stability parameters of refractory metal systems

11 p1777 A71-25197

Ordered Ti-Al lattice parameters measurement in low and high temperature diffractometer attachment

11 p1780 A71-26023

Nb-N and Ta-N alloys, calculating electrical resistivity and solid solutions lattice constants at various temperatures

12 p1917 A71-27295

Neutron irradiation effect on lattice parameters and distortion energy of titanium and chromium carbides, using X ray analysis

15 p2430 A71-32152

Refractory and rare metals absolute melting temperature dependence on atomic number, lattice constant, charge negativity and crystallographic, thermodynamic and mechanical parameters

16 p2594 A71-33878

Gallium antimonide-germanium system solid solution lattice constant determination, using X ray and microstructural analysis and microhardness measurements

17 p2791 A71-34566

Retained lattice strain and substructure domain size effects on tensile strength at room and elevated temperature in dispersion strengthened Ni alloys

21 p3397 A71-40453

Temperature effects on tungsten lattice and Gruisen parameters and thermal expansion coefficients at low temperatures by X ray method

22 p3561 A71-41724

LAUNCH COMPLEXES

Kossel line technique application to intergranular fragility study, discussing lattice constant measurement to determine difference in impurity distribution

22 p3563 A71-42324

Zirconium hydride phases density determination from lattice parameters, comparing results with direct measurement

23 p3689 A71-42930

Complex TiC-WC carbides under homogenizing annealing, noting defects, solubility, lattice constant and grain growth

23 p3689 A71-43253

Sintering of Ni based heat resistant alloy, determining phase composition, lattice constant and microhardness of compressed specimens

23 p3691 A71-43521

Pressure effects on Fermi surface of metals, examining crystal lattice parameters influence on electrons energy spectrum

24 p3839 A71-45168

LATTICE VIBRATIONS

Anomalous temperature dependent silver halides photoemission related to lattice vibrationally dependent hybridization of valence states

01 p0137 A71-10148

Hot electron gas on metal surface under strong heat flux as function of crystal lattice temperature at Fermi level

02 p0332 A71-12196

Perturbation theory diagrammatic version for describing lattice vibrations effect on scattering cross sections of low energy electrons from single crystal solid surfaces

05 p0792 A71-16316

IR and Raman spectra vibrational analysis of crystalline and fluidic oxalyl bromide, explaining observations by two geometrical isomers existence

11 p1727 A71-25363

Absorbed energy spectra and absorption frequencies from elastic constants of vibrating metals with cubic lattice structure, using cold neutron scattering

14 p2190 A71-30149

Gaseous and solid polycrystalline HNCS and DNCs IR and Raman spectra, studying LF of lattice vibrations

19 p3118 A71-37649

Materials behavior at low temperatures, investigating lattice vibrational spectra relation to specific heat, conducting electron energies, thermal expansion, etc.

20 p3270 A71-39242

Crystal lattice vibration and molecular libration effects on solid carbon tetrachloride heat capacity at 0-20 and 200-230 K

22 p3585 A71-42059

Near equiatomic TiNi thermal martensite transformation premonitory events, discussing crystal structure, mechanical instability and lattice vibrations

23 p3694 A71-44280

LATTICES

Transonic flow through planar cylinder lattices, discussing flow pattern visualization and recording techniques by high speed camera

01 p0001 A71-10108

Elastic lattice shells linear theory, deriving stress functions and equations from static-geometric analogy

17 p2831 A71-35396

Shallow lattice shell equations approximated by generalization of asymptotic theories for lattice-type disks and plates

19 p3158 A71-38151

Edge effect in elastic lattice shells generalized from lattice plates and disks

19 p3158 A71-38152

Sound reflection by dense doubly periodic lattice parallel to rigid screen, describing asymptotic characteristics by double lattice virtual mass including mirror image

20 p3268 A71-38807

LATTICES (MATHEMATICS)

NT BOOLEAN ALGEBRA

NT BOOLEAN FUNCTIONS

Modules and matrices over semilattice ordered semigroup, developing algebraic foundation for Boolean matrix theory

09 p1485 A71-22960

Anisotropic Heisenberg antiferromagnet sublattice magnetization, obtaining temperature dependence

13 p2100 A71-28675

Plates analysis under static and dynamic loads based on finite difference, lattice analogs, mathematically consistent lumped parameters and finite element models

15 p2503 A71-31438

Equatorial F 2 region lattice model with curved field line geometry for plane stratified atmosphere and time dependent problem solution

23 p3667 A71-43137

LAUGHING

Compact head mounted six channel IC telemeter for artifact free EEG recording during laughter

13 p2020 A71-28889

LAUNCH COMPLEXES

U LAUNCHING BASES

LAUNCH DATES

LAUNCH DATES

Grand Tour missions set optimization for 1976 to 1982, defining flight opportunity launch/arrival date space for various mission types
[AAS PAPER 71-358] 23 p3728 A71-43028

Multiple outer planets flyby opportunities during 1976-1980 Grand Tour missions launch period, presenting computer generated specific encounter dates and flyby distances
[AAS PAPER 71-359] 23 p3729 A71-43029

LAUNCH TIME

U LAUNCH WINDOWS

LAUNCH VEHICLE CONFIGURATIONS

Nike-Apache sounding rocket vehicle with canted fins, examining pitch-roll coupling characteristics by equilibrium and dynamic simulation methods
[AIAA PAPER 70-1376] 03 p0497 A71-13659

LAUNCH VEHICLES

NT CENTAUR LAUNCH VEHICLE

NT DELTA LAUNCH VEHICLE

NT DIAMANT LAUNCH VEHICLE

NT ELDO LAUNCH VEHICLE

NT EUROPA LAUNCH VEHICLES

NT EUROPA 1 LAUNCH VEHICLE

NT EUROPA 2 LAUNCH VEHICLE

NT EUROPA 3 LAUNCH VEHICLE

NT REUSABLE LAUNCH VEHICLES

NT SATURN LAUNCH VEHICLES

NT SATURN 5 LAUNCH VEHICLES

NT THOR DELTA LAUNCH VEHICLE

NT THOR LAUNCH VEHICLES

Launch vehicle under influence of random fin misalignments, predicting roll rate by statistical analysis
[AIAA PAPER 70-1382] 03 p0498 A71-13665

Vacuum tube launchers and boosters for launching small to medium size meteorological probe rocket into lower atmosphere
[AIAA PAPER 70-1393] 03 p0498 A71-13674

Minuteman missile technology application as boosters for near earth spacecraft launching, emphasizing tradeoff between reliability and cost
04 p0663 A71-15313

Diamant B French satellite booster development program, discussing general aims, specific objectives, program implementation, organization and industrial facilities
04 p0664 A71-15820

Space transportation system profitability conditions, discussing optimal cost reduction and launcher/booster characteristics
04 p0692 A71-15821

Space launchers flight control and guidance systems technology, emphasizing use of onboard digital computers
05 p0817 A71-16678

LOX release from Apollo 8 lunar launch vehicle, forming small particle clouds for scattering experiments
06 p0963 A71-17256

Launch vehicle attitude control system for lateral drift minimization and prevention of structural load limit exceeding maneuvers, presenting stability analysis
06 p0979 A71-17338

Roughrider F-100F aircraft flights in thunderstorms and Apollo 12 launch electric field measurements, comparing patterns and magnitudes of lightning strikes to vehicles
07 p1208 A71-19927

Space shuttle structures and materials, considering booster arrangements thermal protection, high temperature metals and composite materials
07 p1216 A71-20228

Large flexible booster launch vehicle autopilots automated design and optimization by computerized technique in frequency and time domain
08 p1332 A71-21337

Space shuttle flight test instrumentation for launcher, spacecraft and airplane triple operational and maintenance system requirements, discussing digital data bus monitoring concept
[AIAA PAPER 71-313] 10 p1609 A71-23974

Space shuttle launch and turnaround operational sequences, vehicle processing facilities and alternate methods for vehicle erection, mating and transport to pad
[AIAA PAPER 71-320] 10 p1683 A71-24830

Programming language SCOPE for Europa 2 booster vehicle operational checkout system, describing simple coding procedure for test program
11 p1734 A71-25250

Hybrid computer solutions for optimal control of time varying systems with parameter uncertainties, exemplifying minimax load relief for large launch vehicles
14 p2319 A71-30019

European satellite telecommunications network design, discussing shuttle-tug launcher use and economy
16 p2644 A71-32848

Two dimensional axisymmetric shell analytical model for liquid propellant launch vehicle longitudinal vibration modes and steady state response calculation
16 p2653 A71-33092

Launch vehicles for space telecommunications applications, considering payload capacity for missions involving earth resources, radio and visual astronomy and meteorology
17 p2811 A71-34226

Cost-performance tradeoffs of aerospace launch vehicle expandable structural components, investigating program factors, materials and construction technologies
[SAWE PAPER 884] 17 p2750 A71-35828

Launch facility requirements for liquid fluorine upper stage, considering propellant storage and transfer, vapor disposal, leak detection, spills, aborts and range safety
18 p2898 A71-36457

Canard space shuttle reusable launch vehicle wing geometry variations effect on flyback systems weight, noting influence of aspect ratio and wing area
18 p2974 A71-36484

Space shuttle boost vehicle with various degrees of aerodynamic stability, discussing control laws effects on rigid body bending moment tradeoff
[AIAA PAPER 71-918] 19 p3147 A71-37167

LAUNCH WINDOWS

Highly eccentric satellite orbit, determining analytical solution for HEOS 1 launch window
01 p0154 A71-10386

Trans-Mars launch window problem, discussing minimum delta-V three-impulse noncoplanar transfer from circular parking orbit onto asymptotic velocity vector
10 p1671 A71-24331

Launch time selection for meteorological earth satellites, discussing launching sites, orbital altitude variations and orbit inclination
11 p1793 A71-25172

Satellite solar radiative heat input variations effect on optimal launch time, considering angular factor and thermal design
11 p1836 A71-25192

Multipoint gravity assist grand tours in outer solar system, discussing launch opportunities and mission effects on spacecraft design
[AAS PAPER 71-102] 19 p3140 A71-37932

Launch opportunities for Grand Tour outer planets missions using Saturn-Jupiter instead of Jupiter-Saturn flyby sequence
[AAS PAPER 71-139] 19 p3140 A71-37943

Jovian probe and spacecraft mission feasibility, discussing launch opportunities, targeting, objectives and data transmission
[AAS PAPER 71-141] 19 p3141 A71-37944

Extended launch windows for ground based rescue missions, using bi-elliptic rendezvous technique
[AAS PAPER 71-304] 23 p3638 A71-42980

LAUNCHERS

NT AIRCRAFT LAUNCHING DEVICES

NT HYPERVELOCITY LAUNCHERS

NT MISSILE LAUNCHERS

NT ROCKET LAUNCHERS

Free flight hypersonic wind tunnel model testing in Ludwig tube, discussing launching device and recording setup
21 p3362 A71-40381

LAUNCHING

NT LUNAR LAUNCH

NT ORBITAL LAUNCHING

NT ROCKET LAUNCHING

NT SPACECRAFT LAUNCHING

LAUNCHING BASES

NT CAPE KENNEDY LAUNCH COMPLEX

Churchill research range auroral sounding rocket launcher facility, describing design, construction and performance
[AIAA PAPER 70-1391] 03 p0397 A71-14275

Equatorial CECLAS/ELDO base management and conduct of launch operations, discussing installations, facilities, equipment and personnel
12 p1894 A71-26696

Mobile concept and automated checkout applications in Apollo/Saturn 5 Launch Complex 39, discussing performance
22 p3611 A71-42044

Qualification tests for equatorial ELDO Europa Launch Site with MSRV, discussing checkout system and performance
23 p3661 A71-43474

LAUNCHING DEVICES

U LAUNCHERS

LAUNCHING PADS

Missiles free flexural vibrations on moving or stationary launching pad calculated by matrix method
16 p2656 A71-33340

LAUNCHING SITES

NT LAUNCHING PADS

LAVA

NT EFFUSIVES

Hadley Rille origin as lava channel and partly collapsed lava tube, taking into account topographic configuration, terrestrial analogs, geomorphology and meteoroid bombardment
13 p2139 A71-28781

Manua Islands/Samoa/lavas chemical composition, geology and probable history
18 p2911 A71-35887

Central Colorado basaltic lava flows tertiary paleomagnetic transition zone data, illustrating whole rock K-Ar dating difficulties
18 p2911 A71-35948

Morphologic variations and locations of terraced depressions in lunar maria, indicating drained lava lakes
19 p3137 A71-37679

Seismic wave velocity measurements in pahoehoe basalt flows in lava beds, comparing with laboratory dilatational velocities
19 p3052 A71-37682

Dribble spires in Snake River Plain, Idaho, discussing basalt lava features and remnants in lunar areas
22 p3533 A71-41839

Petrogenesis and crystallization of protophyretic basalts in lunar maria lava lakes, deducing eruption temperatures
23 p3743 A71-43647

LAW [JURISPRUDENCE]

NT INTERNATIONAL LAW

NT LEGAL LIABILITY

NT PENALTIES

NT SPACE LAW

Industrial innovations legal protection, discussing patents, registered designs, copyright and trademarks
01 p0183 A71-10756

Air accident investigation and litigation - Conference, Dallas, March 1970
03 p0522 A71-12961

Aviation accident long interrogatories for analyzing man, machine and environmental factors, noting legal aspects and preparation
03 p0523 A71-12967

Aircraft nationality legal problems concerning regional cooperation and registration
06 p1009 A71-17423

Rumanian air law of 1953 and penal codes of 1969 discussing statutes concerning in flight committed crimes against persons and property or air piracy
06 p1009 A71-17422

Supersonic jet transport legal aspects in land over flight, discussing ground noise and sonic boom effects on persons and property
06 p0846 A71-17644

Meteorological observing program execution legal and legislative aspects, noting social adjustment to weather effects
08 p1329 A71-21733

Federal legislation and regulatory activities for control and abatement of aircraft noise
08 p1379 A71-21827

State, local government and airport proprietor legal role in regulating aircraft noise at airports
08 p1379 A71-21828

Federal legislation and regulation of aircraft noise legal rights of airport neighbors and legal aspects of compatible land use, discussing noise control efforts
08 p1379 A71-21824

Legal aspects of military sonic booms, discussing administrative remedies, liability and various cases
08 p1379 A71-21830

Legal principles and rules governing lunar and other extraterrestrial materials, considering establishment of international code
10 p1698 A71-23861

U.S. federal legislation and regulations for aircraft noise and sonic boom
15 p2516 A71-32245

Airport environmental protection, discussing area-wide agency, FAA planning grant program and legal aspects
15 p2385 A71-32247

NASA Scientific and Technical Information System, illustrating advantages of machine retrieval systems for legal profession
18 p2986 A71-35868

Finnish air traffic law based on international civil aviation convention, discussing regulations relative to aircraft, personnel and airports
18 p2989 A71-36919

German aircraft noise protection law of 30 March 1971, discussing objectives and applicability
18 p2989 A71-36921

Air piracy/hijacking/ bibliography, considering national and international law, extradition, punishment prevention and safety insurance for passengers and crews
22 p3622 A71-41617

Wrongful death liability in aviation and admiralty considering U.S. Congress refusal to enact legislation
22 p3623 A71-42068

Judicial Panel on Multidistrict Litigation of federal district and court of appeals judges with power to transfer cases to single district
22 p3624 A71-42069

Federal Aviation Act amendment prohibiting controlling interest in air carrier without Civil Aeronautics Board approval
22 p3624 A71-42070

Government and public agencies procurement policy evolution from legal obligations to economic impact consideration
23 p3786 A71-43466

Industrial ownership in R and D markets, considering customer and supplier objectives compatibility in patent rights clauses

23 p3786 A71-43465

LAWS

NT CONSERVATION LAWS
NT FOURIER LAW
NT HOOKES LAW
NT KEPLER LAWS
NT KIRCHHOFF LAW OF RADIATION
NT NEWTON SECOND LAW
NT NEWTON-BUSEMANN LAW
NT OHMS LAW
NT SCALING LAWS
NT SIMILITUDE LAW
NT STEFAN-BOLTZMANN LAW
NT WEBER-FECHNER LAW

LAYOUTS

Lyons-Satolas /France/ International Airport project, discussing layout, facilities and noise control problem

06 p0880 A71-17590

LC CIRCUITS

Varicap loop circuits for controllable IF phase corrector with independent delay suitable for automatic control

01 p0054 A71-11083

Hybrid lumped-distributed parameter resonant LC circuit design for nuclear magnetic resonance spectrometer

23 p3661 A71-44343

HF and LF transistors suitability for integrated high Q LC circuits, studying inductivity, Q and component frequency dependence

24 p3807 A71-44377

LEAD [METAL]

NT LEAD ISOTOPES
Chemisorption energies of organics on Pb surface by extended Huckel molecular orbital technique

07 p1055 A71-19845

Al and Pb atoms nuclei inelastic interaction cross section with nuclear active particles, using ionization calorimeter and wide gap spark chambers

11 p1760 A71-25165

Circular lead specimens in water flow, determining external magnetic field effects on cavitation and erosion

14 p2278 A71-29613

U-Pb and Th-Pb age discrepancy in lunar dust, proposing Rn-222 emanation in decay chains

14 p2307 A71-29733

Electromagnetic showers in lead, using 20 GeV primary cosmic ray electrons to calculate spatial evolution

14 p2302 A71-30603

LEAD ALLOYS

PbTe-GeTe-PbSe solid solution alloyed by lead chloride, investigating structure, composition and distribution of basic elements

15 p2460 A71-31283

Lead bronze and Babbitt metal composite material, detailing antifriction efficiency and wear resistance in bearings

15 p2417 A71-32666

Sn-Pb alloy solidification point analysis around liquid-solid front with interface visualization by electron microprobe

20 p3238 A71-39416

Hot extrusion properties of free machining Al alloys with low melting point Pb as chip breakers

21 p3384 A71-40026

Radioisotope testing methods for dissolution and mass transfer of alloying additives in Pb-Sb alloys during preparation in electromagnetic pumps

22 p3553 A71-41765

LEAD CHLORIDES

PbTe-GeTe-PbSe solid solution alloyed by lead chloride, investigating structure, composition and distribution of basic elements

15 p2460 A71-31283

LEAD COMPOUNDS

NT LEAD CHLORIDES
NT LEAD OXIDES
NT LEAD SELENIDES
NT LEAD SULFIDES
NT LEAD TELLURIDES
NT LEAD TITANATES

Ballistic modification of nitric ester based propellant combustion by lead compounds, concerning burning rate-pressure relation

08 p1346 A71-20860

Curie point of solid solutions in ternary system of zirconate-titanate and lead metaniobate, using maxima on temperature dependence curve of permittivity

13 p2111 A71-28152

Lead borosilicate glass with crystalline opacifiers, observing microstructure and reflectance

13 p2093 A71-28990

Burning rate of compressed charges of potassium perchlorate with lead dinitrophenolate at constant pressure

15 p2462 A71-31372

LEAD ISOTOPES

Electric quadrupole atomic transitions in muonic Pb208, charting X ray spectrum showing transitions

01 p0131 A71-11439

Atmospheric Pb 210 /radium D/ aerosols concentration relationship to solar activity from measurement with blue filter

10 p1599 A71-23859

Canary Islands volcanic rocks, investigating lead isotope compositions for upper mantle multistage history

13 p2062 A71-28698

Apollo 11 lunar soil and rock samples under low level beta spectrometry, measuring radon daughter Pb 210

18 p2961 A71-35946

Lead isotopes volatile transfer in Apollo 11 and 12 lunar soil samples, discussing lunar age estimates

23 p3752 A71-43714

Neutron activation analysis of Apollo 11 lunar fines, determining Pb 204, U, Bi and Tl contents

23 p3753 A71-43715

LEAD OXIDES

Lead oxide pigment photoconductivity, investigating surface processes effects on spectral sensitivity and absorption spectrum

21 p3434 A71-41329

LEAD SELENIDES

Stimulated recombination radiation from PbSe laser diodes at 77 K, showing stepwise curve of emission power vs pumping current

01 p0094 A71-10780

LEAD SULFIDES

Fcc metals film growth on air- and vacuum-cleaved PbS, using electron diffraction and conventional electron microscopy

07 p1178 A71-19848

Monte Carlo method computer simulation for displacement cascades energy and space structure in Ge, Si and PbS, interpreting semiconductor electrical properties under hard radiation

21 p3432 A71-41304

LEAD TELLURIDES

Magnetostriction and magnetoelastic quantum oscillations in p-PbTe, using thermodynamic derivatives of Lifshitz-Kosevich expression for oscillatory part of electronic free energy

17 p2791 A71-34860

PbTe thermoelectric converter for ZrH reactor space power supply, discussing operational performance, design and materials technology

20 p3265 A71-38951

Oxygen enhanced sublimation of p-type PbTe thermoelectric materials in isothermal and ingradient testing of couples

20 p3266 A71-38953

Long term performance of lead telluride thermoelectric generators tested under SNAP 21, 23A and 27 programs

20 p3266 A71-38955

SNAP 19 Radioisotope Thermoelectric Generator (RTG) for advanced space missions, using lead telluride and silver antimony germanium telluride as conversion materials

20 p3267 A71-38965

Temperature, magnetic field and pressure dependence of electrical conductivity, thermal emf, Hall effect and transverse Nernst-Ettingshausen effect in indium-doped lead telluride

21 p3429 A71-41210

Multiple layer liquid epitaxial growth of lead tin tellurides from Pb-Sn solution, determining low carrier concentrations by Hall effect and capacitance measurements

22 p3585 A71-41810

Diffused slice Pb-Sn-Te photodiode arrays for IR detection and thermal imaging, evaporating Pb-Sn contacts onto n and p type surfaces

22 p3543 A71-42130

LEAD TITANATES

Lead zirconate-titanate point defects crystal chemistry, interpreting sintering and grain growth behavior

13 p2093 A71-28992

LEADING EDGE SLATS

High lift nose slats generation for arbitrary airfoil, using conformal transformations and computer program

06 p0842 A71-18485

Two dimensional flow around wing sections with slats and slotted flaps in various positions, presenting surface pressure and boundary layer measurements

06 p0844 A71-18551

LEADING EDGES

NT SHARP LEADING EDGES

Plane linear cascades of thin curved profiles, obtaining potential flow velocities and lifting force on leading edge

01 p0001 A71-10339

Polyimide/boron reinforced plastic structures fabrication, discussing use in leading edges

01 p0090 A71-11263

Thin delta wing with leading edge separation, obtaining drag lift and rolling moment coefficients and pressure distribution

02 p0185 A71-12408

Leading edge bluntness and boundary layer displacement effects on attached and separated laminar boundary layers in high temperature hypersonic flow over compression corner

03 p0341 A71-13437

Thin plane wings with mixed leading edges, applying linearized supersonic flow theory

03 p0344 A71-14241

Symmetric airfoil profiles with sharp and rounded leading edges in inviscid gas unbounded uniform adiabatic transonic flow, solving by nonlinear approximation

04 p0525 A71-14591

Leading edge bluntness and boundary layer displacement effects on attached and separated laminar boundary layers in high temperature hypersonic flow over compression corner

05 p0735 A71-16561

Phantom and Buccaneer aircraft boundary layer control, examining lift from trailing and leading edges

06 p0847 A71-17953

Steady state mixed subsonic-supersonic flow near blunt leading edge in hypersonic internal flow, using asymptotic solution by time-dependent method

06 p0843 A71-18542

Maximum stagnation temperature on swept wing leading edge for equilibrium glide entry of space shuttle

07 p1013 A71-18902

Hypersonic minimum drag slender wing leading edge shape for given airfoil section, using Newtonian theory

08 p1229 A71-22039

Pressure distribution on arbitrary finite symmetrical wings with rounded leading edges at zero incidence in subsonic flow

09 p1383 A71-22945

Supersonic flow separation around cross shaped horizontal tail plane with subsonic leading edge, obtaining pressure distribution and aerodynamic characteristics

09 p1384 A71-23608

Surface roughness ensuring turbulent reattachment at low Reynolds numbers on airfoil sections with separation near leading edge resulting in bubbles

10 p1549 A71-23762

Performance prediction of fixed wing leading edges radiative, ablative and active cooling thermal protection systems and system weights comparison for space shuttle entry mission

11 p1839 A71-26230

Lightweight oxidation resistant carbon-carbon composites for space shuttle leading edge components thermal protection

11 p1790 A71-26231

Heat conduction role in leading edge heating of wing in hypersonic flight, using conducting plate theory

13 p2165 A71-29282

Hypersonic flow pattern past windward side of delta wing with supersonic leading edges, joining potential and vortex regions behind shock wave

14 p2171 A71-30874

STOL aerodynamics of leading edge high lift devices on thick profiles, externally blown flaps, boundary layer control and jet flap effect

15 p2343 A71-31214

Supersonic flow past V-shaped wings with leading edges, applying method of establishment to space variable for pressure distribution

17 p2673 A71-35647

Pressures, velocities and aerodynamic characteristics of supersonic flow around slender delta wings with forced asymmetry and separation at leading edges

18 p2843 A71-36134

Supersonic flow past thin delta wings with finite velocities at leading edges, noting wing deformation to avoid corner vortices appearance

18 p2843 A71-36181

V shaped conical wing in supersonic and hypersonic flow with shock attached to leading edge, investigating complex wave system with time dependent and analytical methods

18 p2845 A71-36339

Vortex-induced heating alleviation to lee side of slender wings in hypersonic flow by contouring leading edge planform

19 p2993 A71-37892

Laminar collisionless shock propagation perpendicular to magnetic field into hot plasma, calculating temperature effects on leading edge growth rate

22 p3579 A71-41580

LEAKAGE

Transverse current leakage effect on energy conversion and Hall characteristics of MHD generator

02 p0290 A71-12195

Wankel engine chamber gas leakage determination based on exit slot sample gas analysis, considering air to working fluid ratio

04 p0638 A71-14598

LEARNING

- Atmospheric seal leakage control tests for long orbital lifetime space station designs, discussing vacuum chamber monitored pressure shell penetrations [AIAA PAPER 71-337] 11 p1836 A71-25316
- Protective xenon atmospheres in sealed silicon-germanium alloy thermoelectric generators, discussing leakage and pressure levels 20 p3265 A71-38934
- Sealing coefficient and leakage performance model for multiple thread rarefied gas viscoseals 20 p3241 A71-39801

LEARNING

- NT ASYMPTOTIC METHODS
- NT CONDITIONING [LEARNING]
- NT ITERATIVE SOLUTION
- NT PROBLEM SOLVING
- NT THEOREM PROVING
- NT TRANSFER OF TRAINING
- Overtraining reversal effect on attention process, using choice response and eye fixations compared to criterion trained group 10 p1562 A71-24204

- Biological learning, considering EEG wave activity association with structural change underlying information storage in cerebral tissue 10 p1562 A71-24226

- Mathematical neuronal model for functional learning system networks, representing brain pattern recognition, learning and size invariance mechanisms 10 p1569 A71-24233

- Learning sets development relation to transfer suppression, discussing previously learned discrimination retention 13 p2011 A71-28803

- Visual discrimination learning by monkeys with inferotemporal cortex lesions, using positive reinforcers and electric shock punishments 13 p2011 A71-28804

- Pulse frequency behavior during acquisition of perceptual and motor skills with particular attention to rest periods 15 p2362 A71-31195

- Psychological screening of pilot trainees, showing neurosis noncorrelation with learning ability to fly 23 p3639 A71-43221

- Psychological screening of pilot trainees, investigating Minnesota Multiphasic Personality Inventory test data correlation with learning ability to fly 23 p3639 A71-43222

LEARNING CURVES

- Reliability knowledge review, stressing learning curves for measuring and predicting reliability achievements and defect screens effectiveness measurement 12 p1909 A71-26668

- Parallel strategies effectiveness in R and D projects, discussing learning rate as critical parameter in project management decision making process 19 p3173 A71-37629

LEARNING MACHINES

- Dynamic digital predictive compensation learning control systems with time delay transform identification by template matching technique 06 p0878 A71-17336

- Series connected three level perceptron type learning system with sensory, association and response units, establishing performance selection and prediction parameters 07 p1068 A71-20102

- Perceptron learning systems with cross connections in single functional elements class, discussing visual patterns training schemes 07 p1068 A71-20103

- Minerva digital computing system with learning cells and electronic microcircuit elements capable of self organizing similar to human intelligence 19 p3025 A71-37420

LEARNING THEORY

- Information feedback distortion and countertraining effects on learning and performance in lever displacement-target test 01 p0026 A71-11415

- Motor learning error performance with discrimination reaction timer, discussing commitment to wrong response, group observations and specific error repetition 07 p1047 A71-19462

- Perceived and responded to discriminative stimuli identification in probability learning, using parameter free model of event pattern association strength 07 p1049 A71-19775

- Clustering and decision making with interactive a priori problem knowledge insertion in subcategory mean vectors and covariance matrices form for pattern recognition and learning 08 p1260 A71-21664

- Adaptive self-organizing and -learning control systems with long and short term memory retention, using logic random searches to find parameter values [ASME PAPER 71-DE-22] 12 p1892 A71-27324

- Image parameters identification and estimation problems /in learning without teacher/, deriving error variance lower bounds and spurious solution probabilities 19 p3024 A71-37225

- Smoothed randomized functionals and algorithms in adaptation and learning theory, accounting for constraints by generalized penalty function method 23 p3657 A71-44018

LEAST SQUARES METHOD

- Plane contours problems analytic solution by least squares method approximation, giving matrices of linear equations systems 04 p0602 A71-14605

- Shallow spherical shells with periodically spaced holes, discussing stress analysis by least squares method for curved perforated plates [ASME PAPER 70-PVP-11] 04 p0665 A71-14771

- AG Vir /HD 104350/ orbital element variations and light curve distortions, using least squares method 04 p0651 A71-15665

- Space vehicle local orientation by method of least squares determination of matrix for conditions of orthogonality, assuming random measurement errors 05 p0815 A71-16035

- On-line interactive graphical computer program systems for approximation problems, including least squares method 06 p0871 A71-18210

- Weighted least squares nonlinear estimation problem, presenting partial step algorithm for convergence region enlargement [AIAA PAPER 71-121] 06 p0921 A71-18658

- Multicomponent plane flap mechanism with transmission angles diverging minimally from ninety degrees, discussing synthesis by least squares method 07 p1117 A71-19361

- Trajectory measurement optimal program, using least squares method 08 p1360 A71-21002

- Surface station pressure reduction to sea level, determining differential expression by least squares method 08 p1329 A71-21727

- Redundancy reduction method based on least squares approximation for recording solar radio burst emissions 10 p1661 A71-23926

- Wind velocity data processing technique for azimuthal radar observations in meteor zone, using least squares method 10 p1600 A71-24035

- Artificial earth satellites equatorial topocentric coordinate determination, using photographic distance observations and least squares method 12 p1961 A71-26902

- Soviet book on variational methods in mathematical physics covering energy method, Ritz process, Bubnov-Galerkin method and least squares method 12 p1931 A71-27292

- Exact formulas and graphs for RMS error in object position and velocity prediction for long time intervals based on least squares polynomial smoothing 12 p1881 A71-27425

- Error estimates for class of least squares methods for 2mth order elliptic boundary value problems solution approximation 13 p2093 A71-27803

- Biomathematical model and least square estimation from time series data of discrete particle population in stochastic compartmental system 14 p2265 A71-30181

- Least squares method for inversion of radiative transfer equation, considering atmospheric temperature profiles determination from outgoing radiance 14 p2337 A71-30296

- Spacecraft local attitude determination from measurements with random errors by least squares method 16 p2645 A71-33439

- Least squares method effectiveness in nonnormally distributed observation errors compensation 16 p2602 A71-33477

- Shock normal calculation by applying least squares technique to combined geomagnetic field and plasma data from single satellite, assuming Rankine-Hugoniot conservation relations 16 p2560 A71-33941

- Least squares prediction of gravity anomalies, tabulating interpolation coefficients and mean square errors 17 p2734 A71-35189

- Numerically stable algorithm for solving least squares problems with linear equalities and inequalities as additional constraints 17 p2769 A71-35693

- Sunspot relative number observation accuracy test by least squares method for solar observatories 19 p3130 A71-37226

- Error behavior in numerical solution of elliptic differential equations boundary value problems by least squares approximation 19 p3087 A71-38304

- Antenna linear array power pattern synthesis, determining optimum nonnegative harmonic approximation to given function in Gauss/weighted least-mean-square/ and Chebyshev senses 19 p3021 A71-38472

- Modular component computational algorithm for sequential least squares estimation /filtering/ with

- process noise for straightforward computer code conversion 20 p3201 A71-38774

- Trajectory measurement optimal program, using least squares method 20 p3294 A71-39547

- Book on fitting equations to data by computer analysis of multifactor data for scientists and engineers, covering independent variables selection and least squares method 21 p3406 A71-40164

- Global lunar gravity field from weighted least squares analysis of Lunar Orbiters elements, deriving zonal and sectorial harmonics from libration data 21 p3443 A71-40161

- Iterative solution of least squares programming problem for finite thrust rocket trajectory optimization [AAS PAPER 71-308] 23 p3724 A71-42984

- Least squares and sequential estimation techniques application to Mariner 6 and 7 tracking data analysis, verifying Einstein relativity theory on electromagnetic radiation propagation [AAS PAPER 71-384] 23 p3731 A71-43054

- Vehicle attitude determination and guidance sensor orientation by vector space matrix method, minimizing errors by weighted least squares affine transformation technique [AAS PAPER 71-396] 23 p3773 A71-43064

- P times least squares analysis complications by systematic earthquake location errors and azimuthal station anomalies variation 23 p3672 A71-43884

- Computer programs based on least squares numerical analysis for complex internal friction spectra due to Snoek and grain boundary relaxation 23 p3648 A71-43927

- Geometrical least squares model extension to maximum likelihood method for linear processes with additive Gaussian error 24 p3843 A71-44704

LEAVES

- Plant leaves mean effective optical constants from diffuse UV reflectance and transmittance measurements 01 p0073 A71-10834

- In vivo green soybean and corn leaves bidirectional IR reflection and transmission distribution functions 05 p0739 A71-16254

- Circadian rhythm of leaves of Phaseolus angularis plants in controlled carbon dioxide and humidity environment 13 p2015 A71-29475

- Pinto beans circadian leaf movements in simulated weightless environment, relating rotational treatment to rhythm phase 21 p3341 A71-40006

- Lebesgue measurable set, obtaining eigenvalues and eigenfunctions spectrum 18 p2942 A71-36820

LEBESGUE THEOREM

- Dielectric potential operator as arbitrary bounded Lebesgue measurable set, obtaining eigenvalues and eigenfunctions spectrum 18 p2942 A71-36820

LEE WAVES

- Lidar observation of clear atmospheric structure including lee wave clouds, turbulence, stratification in trade wind inversion layer, etc 01 p0118 A71-10583

- Mesoscale orographic inhomogeneities in vertical air flows past surfaces, noting leeward air waves and upper/lower boundary layers 07 p1149 A71-18793

- Two layer structure of principle air flow over mountain system, noting effect on air waves and rotors formation in leeward region 07 p1149 A71-18795

- Linear mountain lee wave model with nonlinear lower boundary condition for arbitrary basic flow and two dimensional topography, computing flow field 09 p1487 A71-23024

- Mountain induced lee waves, turbulence and wind measurements in Colorado, using aircraft flight data 22 p3569 A71-42548

LEG [ANATOMY]

- NT KNEE [ANATOMY]
- Human legs thermal response during cooling for refrigeration anesthesia, deriving analytical model for temperature level prediction as function of time 04 p0545 A71-15166

- Leg position effect on human calf muscle blood flow during standardized heavy rhythmic exercise 11 p1722 A71-26358

- Lower extremities interlink angles correlation and cross correlation functions during walking for locomotor functions analysis in man 13 p2006 A71-28383

- Lower extremity Army aviator amputee retention on flight status regarding service need, amputation and prosthetic fit, age, career, hours flown and time in military 16 p2535 A71-33126

- Lactic and succinic acids and creatine phosphate content in rat hind leg muscles during swimming and rest 16 p2532 A71-33899

Shin muscle electrical activity during standing after 120 day bed rest hypokinesia from EMG measurement 20 p3188 A71-39230

Physiological responses to head and neck vs trunk and leg cooling under hyperthermic stress 21 p3331 A71-40356

LEGAL LIABILITY

Airline liability and insurance in relation to aircraft hijacking, sabotage, etc 01 p0183 A71-10359

Aviation accidents liability limitation by treaty and statute for passengers personal injury or death, discussing Warsaw Convention revisions 03 p0523 A71-12966

Air crash litigation liability limitations, noting international inequality 03 p0523 A71-12968

Aircraft accident damages recovery trial procedure, discussing pleadings, settlements, depositions and jury summation 03 p0523 A71-12970

Aviation products liability and warranty law, noting reliability trends and quality control methods 03 p0523 A71-12971

Air charter flights legal status, considering public, private and international laws and civil responsibility 06 p1009 A71-17422

Revision of 1929 Warsaw Convention Articles 3 and 25 relative to air carrier liability, discussing possible U.S. secession 06 p1009 A71-17424

Legal aspects of military sonic booms, discussing administrative remedies, liability and various cases 08 p1379 A71-21830

Aircraft smoke emission control, outlining legal action by New Jersey State Department of Health 08 p1380 A71-21833

Air traffic controllers legal responsibility and disciplinary procedure, considering clearances, flight crew instructions and aircraft accidents 09 p1548 A71-22891

European view on liability and compensation limitation for death and injury in international commercial air transport 09 p1548 A71-22899

U.S. view on legal liability and compensation for death and injury in international air transport 09 p1548 A71-22990

Aircraft accident litigation related to wake turbulence concerning pilot or air traffic controller faults 17 p2842 A71-35387

New IATA passenger and baggage international air transport conditions, discussing passenger/carrier legal relationships, with emphasis on differences between new and old regulations 18 p2989 A71-36918

Space station legal regime covering prolonged flight psychological and behavioral factors, misconduct jurisprudence and earthbound law liability 22 p3623 A71-42021

Wrongful death liability in aviation and admiralty, considering U.S. Congress refusal to enact legislation 22 p3623 A71-42068

LEGENDRE CODE

U COMPUTER PROGRAMMING

U NEUTRON SCATTERING

LEGENDRE FUNCTIONS

Finite length elastic cylindrical shell deformation approximate solution by Legendre polynomials 01 p0173 A71-10942

Spheroidal cavity effects on elastic medium under axisymmetric stress field, using Legendre potential functions 07 p1212 A71-19253

Redundant information reduction during electrocardiograms analysis by Legendre polynomials, considering equivalent model in dipole and quadrupole form 13 p2017 A71-28376

Diffuse radiation field inside homogeneous spherically symmetric dust nebula from radiative transfer equation solution as expansion after Legendre polynomials 21 p3451 A71-40716

Integrable linear differential equations application to Riccati equation and Bessel, Legendre and other functions relations in celestial mechanics [AAS PAPER 71-333] 23 p3727 A71-43006

LEGENDRE POLYNOMIALS

U LEGENDRE FUNCTIONS

LEGENDRE TRANSFORMATION

U LEGENDRE FUNCTIONS

LEGIBILITY

Alphanumeric fonts for 5-by-7 matrix display, comparing legibility with USAF font 21 p3350 A71-40121

Readout systems light emitting numerals legibility, determining threshold values from response categorization into correct responses, misreadings and missed signals 21 p3376 A71-40125

LEIDENFROST PHENOMENON

Surface roughness and contamination, drop volume and liquid subcooling effects on Leidenfrost temperature 04 p0675 A71-14783

Leidenfrost film boiling for various liquids over velocity, plate temperature and surface roughness range, noting velocity effect on vaporization rate 04 p0687 A71-15529

Liquid nitrogen drops anomalous behavior in Leidenfrost film boiling, investigating vapor instabilities effect on total vaporization time 20 p3313 A71-39287

Liquid-liquid or solid-liquid interface Leidenfrost film boiling, deriving heat transfer coefficient for liquid drop floating on cryogenic fluid 20 p3313 A71-39288

Floating times of liquid/solid sphere on evaporative fluid /liquid nitrogen/ in metastable Leidenfrost film boiling 21 p3476 A71-40892

LEM [LUNAR MODULE]

U LUNAR MODULE

LEMMAS

U THEOREMS

LENGTH

Thorium wavelength measurements by interferometry, noting weighted averages as secondary standards of length 04 p0627 A71-15692

Frequency stabilized He-Ne laser wave secondary length standard for automatic measurements, discussing electronic control, accuracy, line width, pressure, current and magnetism effects 16 p2588 A71-34119

LENNARD-JONES GAS

Computerized least squares fit of second virial coefficients vs critical temperature to Lennard-Jones potential function for hydrocarbons, halides, alcohols and cyclic compounds 13 p2103 A71-29005

LENS ANTENNAS

Wide beam lens antenna synthesis from non-homogeneous dielectric with specified refractive index, using conformal mapping for lens and beam conversion 08 p1266 A71-21466

Luneberg lens antenna theory and gain for communication satellite radio links, discussing shielding from hostile space environment 10 p1583 A71-24450

Luneberg lens fabrication technique using thin insulated Al slivers embedded in low density polystyrene foam 14 p2205 A71-31059

Double refracting dielectric microwave lenses design for horn antennas in SHF applications 19 p3036 A71-38643

LENS DESIGN

Interference passband filters with wide angle lenses for multispectral photography, discussing design and applications 01 p0081 A71-10827

IR astronomical telescope using six independent optical systems with path and phase controls for aperture synthesis 01 p0081 A71-10829

Fresnel annular zone objective lens for multichannel Fabry-Perot interferometer 03 p0425 A71-13651

Photoelectronic stellar transit instrument lens with increased spherical aberration based on light beam passage analysis 04 p0598 A71-15379

Laser beam focusing and defocusing by thermal gas lens, deriving wave optics equations for electromagnetic fields with allowance for temperature distribution 04 p0628 A71-15808

Optical transmission lines design techniques with thermal gas lenses, calculating system parameters by geometrical optics, wave, electrodynamic and Fourier transfer methods 04 p0628 A71-15810

Light propagation in gas filled pipe with uniform heat flux through wall under forced convection, determining lens efficiency relation to length 04 p0628 A71-15811

Holographic lens used with pulsed ruby laser for machining single and multiple spots on Ti thin film on glass 07 p1122 A71-19205

IR zoom lens design, discussing limitation of number of elements due to high scatter, absorption and surface reflection losses 07 p1109 A71-19451

Lens geometry history covering computerized design, prototype testing, optical shop aids and laser interferometry 08 p1333 A71-21177

Aperture concentric diffraction ring differential effects on focal irradiance, using perfect lens half-wave filter model 08 p1333 A71-21178

Large aperture catadioptric lens system for low light level observation, discussing optical evaluation, thermal properties and mechanical mounting 08 p1289 A71-21372

Photographic image acquisition from planet orbiters, examining systems performance and lens selection 09 p1447 A71-22749

Optical information processing systems, considering spherical lens derivation of two dimensional Fourier transform 09 p1493 A71-22776

Optical transfer function measurement and computation test applications to aerial camera wide angle lens standard design, using interlaboratory comparisons 09 p1494 A71-23001

Electro-optical systems in photoelectronic imaging devices, discussing electron gun, electrostatic focusing lens, spherical aberration, magnetic field computation and ray tracing 10 p1609 A71-24058

Single thin lens for Gaussian laser mode matching, discussing position and focal length determination 12 p1905 A71-26809

Lenslike media with parabolic index profiles, deriving equivalent transformation theorem for distributed optical systems design 12 p1928 A71-26810

Diffraction limited achromatic doublet lenses for IR instruments, discussing applications to compact optical systems 14 p2242 A71-30148

X ray telescopes and neutron cameras telephoto lenses for satellites and space stations, discussing optical design and correction methods 14 p2246 A71-30391

Luneberg lens fabrication technique using thin insulated Al slivers embedded in low density polystyrene foam 14 p2205 A71-31059

Optical distortion coefficients of objective for astronomical camera 14 p2250 A71-31116

Applied optics, reviewing homogeneous and inhomogeneous optical conversion elements, fiber and Fresnel optics, lens properties, programmed optical reliefs, holography, etc 15 p2410 A71-32299

Optical center position on negative and lens distortion of satellite camera verified on zenith area photos of stellar coordinate measurements 16 p2575 A71-32835

High performance solar prominence telescope, showing objective diameter effect on image contrast 18 p2915 A71-35977

High aperture wide angle lens design for compact electro-optical systems of airborne moving map projection navigational instruments 18 p2947 A71-36605

Book on electron optics covering image formation principles, field plotting and ray tracing analog and computational methods, electrostatic and magnetic lenses, etc 19 p3103 A71-37522

Double refracting dielectric microwave lenses design for horn antennas in SHF applications 19 p3036 A71-38643

Aspheric lenses and mirrors testing by single and double exposure two-wavelength visible light holography for obtaining interferogram 20 p3235 A71-39182

Laplace equation solution for double cylinder electrostatic lenses for large range voltage ratios and separations, obtaining focal and aberration coefficients 21 p3377 A71-40178

High performance solar prominence telescope components design, considering lenses and diaphragms with special attention to image degrading influences 21 p3378 A71-40523

Refractive imaging and scanning methods for thermal imaging systems, considering high performance IR lenses 22 p3544 A71-42137

Large display direct view low light level system with objective lens, image intensifiers and eyepiece 22 p3548 A71-42512

Projection type 3-D display lenticular lens sheet optimum design and depth resolution 22 p3549 A71-42560

Liquid-state pulsed laser active element lens parameters effects on output radiation divergence 24 p3835 A71-45240

LENSES

NT MAGNETIC LENSES

NT WIDE ANGLE LENSES

Mathematical model for eye crystalline lens accommodation control interaction with pupil, deriving dynamic equations from human/cat experiments with/without neurological control 03 p0356 A71-12984

Carbon dioxide laser plasma lensing effect used as mirror curvature compensation for maximum output power 03 p0436 A71-13641

Fresnel annular zone objective lens for multichannel Fabry-Perot interferometer 03 p0425 A71-13651

LENTICULAR BODIES

- Aberration analysis for manual retouching of large objective lenses, using unequal arm laser interferometer
04 p0607 A71-14867
- Deformation monitoring of large multilens astronomical objective during assembly, using annular image reflection
04 p0593 A71-14868
- Pulsed ruby laser radiation energy characteristics relation to crystal temperature distribution, thermal deformation and compensating lens focal length
07 p1126 A71-20188
- Light rays bundle compression devices performance based on phase space treatment using Liouville theorem, comparing linear tapers and lenses performance to compressor with graded refractive index distribution
08 p1335 A71-21373
- Human crystalline lens protein and lipid discussing cholesterol accumulation with age
09 p1390 A71-22421
- Lens-prism model for holographic image processing in space-frequency domains with chirp signal interferometric compression
09 p1452 A71-23565
- Forced rotational oscillations of plane-convex glass lens pressed against brass plate, determining contact frictional and elastic characteristics from resonance and hysteresis
11 p1849 A71-25621
- Human lens fluorescent pigment O-beta-D-glucoside of L-3-hydroxykynurenine, discussing preparation, electrophoresis and paper chromatograms
11 p1718 A71-25634
- Lens phase aberration correction in optical system, using holograms
11 p1766 A71-26305
- Ultrasonic softening of lens material to facilitate aspiration, using in vivo rabbit lenses for cataracts production
15 p2365 A71-32348
- Flat field condensing system for illuminating film projected on screen using Hg-Xe short arc lamp
18 p2918 A71-36071
- Lens test facility calibrating Mipir radar boresight lenses by measuring deviations due to gravitational effects
18 p2897 A71-36072
- Homogeneous temperature changes and radial temperature gradients effects on optical lens system, obtaining Bessel type differential equation
20 p3239 A71-39532
- Transversally excited and atmospheric carbon dioxide laser, measuring time behavior of refraction index profile and lensing effects on resonator
21 p3392 A71-40547
- Holographic correction of lens aberration in optical system, considering turbulence effect correction
22 p3538 A71-41737
- Optical transfer function measurement by holographic techniques, describing Fourier transform method useful for lens production testing
22 p3539 A71-41738
- Objective lens with superconductive winding for high voltage electron microscope, describing optical properties and vibration reduction system
23 p3679 A71-44008
- Human eye theoretical model with aspherical cornea front and lens back surfaces, computing astigmatism, coma, meridional and sagittal focal lengths by ray tracing method
24 p3798 A71-44978

LENTICULAR BODIES

- Lenticular reentry vehicle configuration, considering aerodynamics, trajectory heating and weight analysis and structural design
15 p2500 A71-31604
- Projection type 3-D display lenticular lens sheet optimum design and depth resolution
22 p3549 A71-42560

LEONID METEORIDS

- Comet Tempel-Tutt elements, discussing association with Leonids meteor shower
01 p0159 A71-10808
- Spectra of faint optical meteors for chemical abundance, discussing radiative processes during atmospheric entry, Leonid meteors and data acquisition
01 p0161 A71-11275
- Secular perturbations of Leonid meteor shower via Gauss-Halphen-Goriachev method, indicating applicability to variations of meteor streams orbital elements
09 p1526 A71-23343
- Orionid and Leonid meteor trains, determining diffusion coefficient from isophotes variation
12 p1965 A71-27230
- Orionid and Leonid meteor trains, determining diffusion coefficient from isophotes variation
19 p3132 A71-37382

LEPTONS

NT ANTINEUTRINOS

LES

- U LINCOLN EXPERIMENTAL SATELLITES
LESA [LUNAR EXPLORATION SYSTEM]
U LUNAR EXPLORATION SYSTEM FOR APOLLO

LESIONS

NT PULMONARY LESIONS

- Acoustic intensity and exposure time duration for threshold lesion in cat brain
05 p0712 A71-16283
- Laser ocular effects, discussing corneal/retinal/lens lesion production, damage thresholds and application to clinical ophthalmological problems
07 p1049 A71-19792
- Sex differences in rat body weight regulation due to lateral hypothalamic lesions
11 p1720 A71-26074
- Chemical release from traumatized tissue in dogs under cross circulation with lethal cardiac depression response
11 p1720 A71-26119
- Visual discrimination learning by monkeys with inferotemporal cortex lesions, using positive reinforcers and electric shock punishments
13 p2011 A71-28804
- Brain stem mechanisms underlying visual discrimination in rhesus monkeys subjected to bilateral lesions of the inferotemporal cortex, posterior thalamus or midbrain
13 p2011 A71-28807
- Myocardial ischemic lesions age, discussing validity of histopathological criteria and margin of error
15 p2361 A71-32542
- Prefrontal cortex lesions effect on trained anticipatory visual target fixation in cats, noting performance impairment in voluntary eye movement control
21 p3329 A71-40174
- Diurnal water and food intake and body weight changes pattern in rats with hypothalamic lesions
22 p3486 A71-41936
- Afferent oculomotor pathways to extraocular muscle nuclei, considering discrete unilateral lesion role in head posture disturbance production
22 p3488 A71-42435

LETTERS [SYMBOLS]

U SYMBOLS

LEUKEMIAS

- Cytocidal effect of L-glutaminase distribution in leukemic lymphocytes by slide chamber method
18 p2864 A71-35994

LEUKOCYTES

NT LYMPHOCYTES

- Dog blood leucocyte composition relation to alimentary satiation and adrenocorticotrophic and reticuloendothelial systems, considering effect of ACTH and india ink injections
01 p0008 A71-10092
- Polymorphic nucleus leukocytes pyrogenic protein fraction effects on rabbits hypothalamus thermal control structures
05 p0707 A71-16386
- Irradiation protection in mice, dogs and sheep by bacterial endotoxin injection, discussing hematopoietic system stimulation and leukocyte counts
07 p1038 A71-18974
- Astronaut chromosome aberrations, presenting peripheral blood leukocytes cytogenetic tests for pre and post space flight
20 p3188 A71-39227

LEUKOPENIA

- Taurine restorative effect in patients with marked leucopenia induced by radiotherapy
07 p1040 A71-18991

LEVEL [HORIZONTAL]

- Altitude level instead of superposed level for azimuth determination by astronomical universal
15 p2395 A71-31465

LEVEL [QUANTITY]

NT ATOMIC ENERGY LEVELS

NT ELECTRON STATES

NT ENERGY LEVELS

NT GROUND STATE

NT INTERMOLECULAR FORCES

NT MOLECULAR ENERGY LEVELS

- German monograph on PHENO hybrid computing elements for nonlinear operations covering ADC and DAC, level and time quantization effects on computational accuracy, etc
14 p2207 A71-30238

LEVELING

- Tetrahedrometric leveling of spatial networks with independent bases between satellite points confirmed for Baja-Cairo direction
11 p1759 A71-25814

- Variation coefficient and corrections to dependent observations for space triangulation leveling by least squares method, comparing closing directions
11 p1759 A71-25815

- Automatic leveling instrument gravity intensity and compensator support tilt angle variations effects on measurement error
15 p2410 A71-32353

- Lunar and solar gravitation effects on leveling from formulas and nomogram, noting seasonal maximum effect in southern latitudes and Northern Hemisphere
23 p3670 A71-43302

LEVITATION

- Levitated superconducting ring in Princeton Spherator for plasma physics, describing Dewar, coil and feedback control systems
07 p1170 A71-20155
- Solid disk supported above flat plate by thin layer of gas flowing from central orifice, studying vertical motion equilibrium and dynamic data
16 p2559 A71-33220
- LEXAN [TRADEMARK]
Spark discharge enhancement of heavy ion track etching in Lexan polycarbonate
07 p1114 A71-20271
- Lexan plastic fission track analysis of uranium distribution in glassy residuum in Apollo 11 rock 10017
23 p3739 A71-43616

LIABILITIES

NT LEGAL LIABILITY

LIAPUNOV FUNCTIONS

- Liapunov stability of neutral first order nonlinear differential equations solutions with time lag
01 p0112 A71-10655
- Stability conditions of Liapunov function for system of ordinary differential equations with prescribed phase flow
01 p0113 A71-11294
- Optimal controller analytical design procedures using dynamic programming and Liapunov function
03 p0392 A71-14404
- Liapunov stability prediction of minimum length for distributed oscillators of superconductive tunnel junction strip line
03 p0388 A71-14475
- Liapunov function time derivative for autonomous system asymptotic stability tests by exact differential method
05 p0774 A71-16579
- Control system synthesis for asymptotically stable systems, using Liapunov functions for feedback laws
05 p0732 A71-17023
- Soviet book on Liapunov functions covering autonomous linear and nonlinear systems, asymptotic and absolute stability, etc
06 p0916 A71-17442
- Rigid body stability studies with Hamiltonian as Liapunov function, noting application to flexible compact gravity gradient satellite planar motion
06 p0981 A71-18648
- Three body problem stability investigation, using Liapunov perturbation function
08 p1361 A71-21052
- Liapunov design technique for model reference adaptive control systems with feedback and prefilter adjustable gains
08 p1270 A71-21669
- Liapunov matrix equation for linear and nonlinear automatic control systems stability
08 p1325 A71-21976
- Nonlinear automatic control systems stabilization by seeking Liapunov function satisfying certain integral relationships
08 p1270 A71-21977
- Liapunov function construction for linear dynamical systems, applying condition of agreement with eigenvalue analysis
09 p1484 A71-22102
- Pulse frequency modulation feedback system nonlinear discrete equivalence, investigating stability by Liapunov method
09 p1422 A71-22280
- Book on matrix methods in stability theory covering matrix algebra, Liapunov theory and functions, stability matrices properties and optimal control theory applications
09 p1539 A71-22872
- Stability of regular motions of dynamically symmetrical body with equatorial symmetry plane in Newtonian force field of spherical planet by Liapunov second method
09 p1526 A71-23346
- Two-differential equations system in critical case of double zero root, deriving motion stability criteria with aid of Liapunov functions
09 p1495 A71-23430
- Liapunov functions generation for input-output stability of dynamical systems, using causal operator and state space realization
09 p1425 A71-23471
- Theorems of instability for differential equation in linear normalized spaces, using Liapunov second method
12 p1930 A71-27239
- Unperturbed motion asymptotic stability and instability theorems, considering Liapunov function method
12 p1932 A71-27524
- Nonlinear closed loop control system with PFM and PWM, obtaining asymptotic stability condition by Liapunov and La Salle theorems
12 p1893 A71-27726
- Girder system transverse bending under axial and lateral loads, deriving stability conditions by direct Liapunov method
13 p2153 A71-28519

Liapunov stability of gyroscopic stabilizers as electro-mechanical systems, assuming nonrigidity of rotor, gimbal and platform suspension 13 p2069 A71-28726

Routh-Liapunov stability of lasting rotation of dynamically symmetrical gyrostal in force field of two stationary centers 13 p2145 A71-28729

Positional motion rigidity of gyroscopic systems with cyclic coordinates and low spin, using Liapunov second method 13 p2069 A71-28732

Three body problem stability investigation, using Liapunov perturbation function 14 p2310 A71-30169

Liapunov stability of neutral first order nonlinear differential equations solutions with time lag 14 p2266 A71-30989

Liapunov approach to nonlinear dynamic systems controllability, deriving conditions for linear dynamic systems 15 p2380 A71-31935

Pulse frequency modulated control systems stability analysis by Liapunov method, introducing discrete correction into modulation law 15 p2381 A71-31979

Rods stability under nonconservative loads, applying Liapunov functions to boundary value problems 16 p2607 A71-32977

Static stability criterion dynamic extension for nonlinear continua under conservative loads, using Liapunov functions 16 p2607 A71-32980

Continuous systems stability analysis under parametric excitation, using time dependent Liapunov functional for frequency response 16 p2607 A71-32992

Liapunov functions applications, discussing panel flutter, Couette flow and feedback control 16 p2607 A71-32994

Holder stability and logarithmic convexity as special case of Liapunov function applied to linear elastic systems without body force 16 p2608 A71-33008

Equilibrium state instability in system with two degrees of freedom, using Liapunov method 16 p2608 A71-33026

Statistical theory of nonlinear differential equation system with discontinuous trajectory solution, deriving motion stability to first approximation using Liapunov functions 17 p2780 A71-34915

Linear differential equations solutions stability in Banach space for finite and infinite dimensional cases, generalizing Liapunov theorems 17 p2781 A71-34922

Nonlinear automatic control systems stability during large modulus-limited deviations based on method of sections and direct Liapunov method 17 p2783 A71-35131

Two dimensional nonlinear discrete /pulse frequency modulation/ control system stability, using Liapunov direct method and mathematical model 17 p2721 A71-35134

Book on stability theory covering Liapunov functions, variable structure automatic control systems and differential equations solutions in Banach space 18 p2947 A71-36250

Linear system stability via Liapunov method and square integral, establishing continuous and discrete time systems equivalence 19 p3086 A71-37885

Liapunov direct method for transient multimachine power-system stability analysis using multivariable control modeling 20 p3207 A71-38991

State feedback decoupling sensitivity of time invariant linear multivariable system, using Liapunov matrix equations 20 p3207 A71-38992

Liapunov functions application to Stability of systems described by nonlinear second-order ordinary differential equations, considering feedback control loops construction 20 p3255 A71-39499

Cyclic discrete holonomic mechanical systems Liapunov stability analysis, developing matrix formalism for kinetic energy, Routhian, Hamiltonian and dynamic potential energy quadratic approximation 21 p3454 A71-40097

Liapunov-type analysis of linear systems dynamic stability under stochastic parametric excitation, noting application to rectangular flat plates 21 p3469 A71-41008

Real symmetric matrix eigenvectors calculation with differential equation, using Liapunov function 21 p3409 A71-41080

Control system synthesis from transient process estimates with Liapunov functions, proposing optimality criteria based on Gaussian minimum constraint principle extension 22 p3527 A71-42855

Computational method determining quadratic Liapunov functions for high order nonlinear systems 23 p3705 A71-43944

Systems synthesis by Liapunov direct method, developing vector-matrix equations for systems classes satisfying specified Liapunov scalar functions [ASME PAPER 70-WA/AUT-3] 24 p3816 A71-45135

LIBRATION

Triangular libration points stability in elliptic restricted three body problem, determining parametric resonance region 03 p0495 A71-14226

Two dimensional motion stability near sun-perturbed earth-moon triangular libration points, using computerized high order treatment 04 p0653 A71-15708

Three body stellar problem libration calculation using nonlinear mechanics methods, and application to lunar satellite perturbation by earth and lunar gravitational effects 04 p0655 A71-15728

Hamiltonian of two center libration, including resonant circular orbits and Garfinkel formalism 04 p0620 A71-15739

Interplanetary matter accumulations around Lagrangian libration points 05 p0808 A71-16455

Moon free libration second and third mode semiamplitudes from statistical relations 05 p0809 A71-16456

Lunar satellite motion semianalytic solution, considering perturbative effects due to gravitational fields, solar radiation pressure and libration 05 p0809 A71-16541

Libration points of generalized restricted three body problem, using Lagrangian solutions 06 p0976 A71-18450

Saturn natural satellites commensurabilities evolution from analysis of libration amplitude change with time for interaction under tidal friction with planet 07 p1202 A71-20519

Earth-moon libration point space station optimal control, considering restricted four body problem 08 p1363 A71-21323

Rendezvous equations near second lunar libration point, using Halo orbiting relay satellite for communication with spacecraft behind moon 09 p1521 A71-22912

Stability conditions of three body problem constant libration solutions by Routh, presenting geometrical interpretation for locus of mass centers 10 p1679 A71-24932

Lunar libration presented as general rotation of solid body in external force field 11 p1822 A71-25685

Libration points in generalized restricted three body problem, discussing Lagrangian solutions 12 p1955 A71-26600

Lunar libration detection by photographing double exposure of stellar field and moon 16 p2636 A71-33503

Periodic orbits around Lagrange libration points of restricted three body problem disturbed by gravitational and radiative influences 17 p2809 A71-35599

Error independence and elasticity allowance for moon librations and satellite perturbations 20 p3286 A71-38759

Out-of-plane motion about libration points within framework of elliptic restricted three body problem, using Mathieu and Hill equation [AAS PAPER 71-336] 23 p3727 A71-43009

LIBRATIONAL MOTION

Gravity gradient satellite librational dynamics under solar radiation pressure, using analytical and numerical integration methods 01 p0163 A71-10755

Lunar moments of inertia and density distributions, using gravitational potential and physical librations 01 p0158 A71-10772

Lunar arbitrary and free librations and Euler motion of poles, considering hard and elastic models 01 p0158 A71-10807

Earth-moon mass ratio correction, observing artificial satellite motion near triangular libration point 02 p0308 A71-12100

Lagrange points role in three body problem, discussing applications to space probe positioning 02 p0316 A71-12739

Elliptic restricted periodic Trojan librations about equilateral points, analyzing stability 04 p0652 A71-15704

Particle nonlinear motion near equatorial libration points in restricted three body problem [AIAA PAPER 70-98] 05 p0810 A71-16553

Earth mantle-inner core nutational dynamic coupling and rotation pole 24 year libration 06 p0890 A71-17883

Gravity oriented satellites librational dynamics in elliptic orbits, emphasizing atmosphere adverse effects [AIAA PAPER 71-89] 06 p0980 A71-18545

Earth-moon mass ratio correction, observing artificial satellite motion near triangular libration point 08 p1362 A71-21150

Lunar physical libration in longitude, considering nonlinear and dissipation terms 09 p1530 A71-23715

Inertia effects on coupled librations and stability bounds of axisymmetric gravity oriented satellites in circular orbits, using integral manifold 11 p1838 A71-26195

Approximate analytical method for nonlinear coupled equations of axisymmetric satellite librations in circular orbit, using constant Hamiltonian 14 p2319 A71-29892

Plane librational motion of axially symmetric satellite in elliptic orbit, developing periodic solution 15 p2488 A71-32092

Energy considerations of satellite orbit paradox, discussing speed increase under drag, librational motion and secular month length 18 p2962 A71-36099

Planar librational motion prediction for gravity gradient satellite with extendible booms during deployment 22 p3610 A71-42014

Coupled librational dynamics of gravity oriented cylindrical satellite, calculating solar radiation pressure effects on attitude control behavior 22 p3611 A71-42042

Crystal lattice vibration and molecular libration effects on solid carbon tetrachloride heat capacity at 0-20 and 200-230 K 22 p3585 A71-42059

Lunar physical libration effect on lunar satellite orbital elements, considering reorientation of selenographic axes fixed in true moon [AAS PAPER 71-331] 23 p3727 A71-43004

LIDAR

OPTICAL RADAR

LIE GROUPS

NT SPINOR GROUPS

Celestial mechanics, Volume 1, Dynamical principles and transformation theory covering quasi-periodic motions, many body problems, Lie groups, etc 02 p0316 A71-12774

Lie group differential equation application to gravitation theory, rejecting Riemann geometry in favor of Klein geometry 09 p1495 A71-23073

Wave and elementary particles equations invariance properties relationship with respect to Lie group and conservation laws 19 p3105 A71-38579

Exact solutions of elasticity theory nonlinear differential equations by Lie group theory methods 24 p3877 A71-44480

LIFE [BIOLOGY]

U LIFE SCIENCES

LIFE [DURABILITY]

NT FATIGUE LIFE

NT HALF LIFE

NT PLASMA LIFETIME

NT SATELLITE LIFETIME

NT SERVICE LIFE

NT STORAGE STABILITY

Polymethyl methacrylate lifetime under simultaneous mechanical stresses and ionizing radiation 01 p0106 A71-10044

Ni and Fe alloys for tooling materials, examining die life and wear at elevated temperatures [SME PAPER MF-70-121] 01 p0090 A71-11266

Life, efficiency and electrical stability tests of cylindrical thermionic converters with various emitter and collector materials 02 p0193 A71-12216

Long term stability and post test analysis of vapor deposited W emitters in high performance cylindrical thermionic converters 02 p0193 A71-12218

Thermionic stability life tests of cylindrical diodes with W emitters at constant current and optimal Cs and collector temperatures 02 p0194 A71-12222

Solar energy thermionic converter life test program and equipment, noting failure due to loss of intracathode Cs 02 p0194 A71-12223

Long life spacecraft tape recorders, considering digital and analog equipment and life and reliability testing of components and complete units 07 p1106 A71-18812

Wet and dry lubricated slip ring systems long term application testing in ion pumped vacuum chambers 07 p1120 A71-20274

Molybdenum disulfide treated graphite brushes in electric contact with copper slip rings at high rates in dry pure inert gas atmospheres 07 p1120 A71-20275

Forward biased asymmetric p-n junction diodes with arbitrary impurity distributions, measuring minority carrier lifetimes by refined step recovery technique 09 p1414 A71-22248

Life tests and properties of organic working fluids heat pipes for electronic component cooling [AIAA PAPER 71-408] 11 p1856 A71-26203

Surface roughness and surface area effect on UV stability of zinc orthotitanate pigments, using electron microscopy and BET nitrogen adsorption [AIAA PAPER 71-451] 11 p1790 A71-26235

LIFE DETECTORS

- Electron lifetime in earth radiation belt due to resonant scattering with hiss VLF radiation
16 p2626 A71-33674
- Polymethyl methacrylate lifetime tested in water and heptane, showing increase with orientation degree
16 p2601 A71-33683
- Columnar grained Ni superalloy lifetimes and transverse creep ductilities enhancement and microstructural alterations due to Hf additions
17 p2759 A71-33394
- Ambient gas effects on Au-Al bonds life in integrated circuit package
19 p3119 A71-38514
- Insulating materials breakdown by surface discharge, determining corona lifetimes by hemisphere-plane configuration and cylinder-plane electrode
21 p3358 A71-41193

LIFE DETECTORS

- Life detection for space missions based on detecting optical asymmetry in biogenic molecules by gas chromatography involving diastereomeric esters synthesis
01 p0029 A71-11562
- Soviet papers on extraterrestrial life and detection methods covering biological conditions, extremal environmental factors and spacecraft sterilization
13 p2009 A71-28677
- Chemical evolution and extraterrestrial life detection, noting cell proliferation methods, automatic biological stations and Mars microorganisms
13 p2009 A71-28680
- Optimal mineral-organic nutrient medium and soil selection for microorganism detection on Mars
13 p2009 A71-28681
- Visible and UV photometric recording of microorganism reproduction in liquid medium for application to Mars extraterrestrial life detection
13 p2019 A71-28682
- Luciferin fermentative oxidation method for adenosine triphosphate determination in extraterrestrial life detection, using extract of firefly luminescent organs
13 p2009 A71-28683
- Biochemical luminescence reaction for ferroporphyrin proteins determination in extraterrestrial life detection
13 p2009 A71-28684
- Extraterrestrial life detection by tagged carbon dioxide extraction from substrate in radioactive glucose containing soil nutrient media
13 p2068 A71-28685
- Extraterrestrial life detection by measuring microorganism breeding dynamics with photometric, radiometric and bioluminescent methods from chemiluminescent reactions
13 p2068 A71-28686
- Extraterrestrial life detection methods, discussing bacterial cultures growth dynamics in nutrient media and iron porphyrin proteins and ATP content increase
21 p3334 A71-40570
- Diamond radiation counters for C 14 containing carbon dioxide in extraterrestrial life detection, noting radioactivity curves as function of sample microflora
21 p3378 A71-40571
- Gas exchange between air or gas mixture flows and terrestrial soil in extraterrestrial microorganisms detection, using continuous sampling and gas chromatography
21 p3346 A71-40575
- Unified procedure for detection of life on Mars by Viking program missions, using mass spectrometer for remote biologically oriented experiments
23 p3736 A71-43541

LIFE RAFTS

- Contact problems of inflated cylindrical membranes with quadrature reduction under normal stress applied to loaded floating and submerged life raft
[ASME PAPER 71-APM-11] 16 p2656 A71-33215

LIFE SCIENCES

NT MOLECULAR BIOLOGY

- Biological rhythms and space nutrition - COSPAR Conference, Prague, May 1969, Life sciences and space research
01 p0017 A71-11551
- Integratism in life biology, discussing reductionism and organismism at biopolymer macromolecule construction and conformational levels
06 p0852 A71-17683
- Extraterrestrial civilizations, discussing probability theory and radio communication
06 p0852 A71-17739
- Biophysical model of life origin on earth using primordial gas-small organic molecule-macromolecule-protocell transformations
07 p1043 A71-20125
- Life prolongation during high intensity microwave exposures with ambient air temperature control for radiation bioeffects studies
11 p1717 A71-25291
- Existence of life under extreme environmental conditions, discussing biological temperature limits and adaptability to lack of water
11 p1721 A71-26321

Earth-like ecology for habitation in space, considering hollow sunlit rotating space chamber for life cycles in controlled weather environment
21 p3343 A71-40360

Life science and space research - Conference, Leningrad, May 1970
21 p3332 A71-40551

Living organisms life-sustaining possibility under simulated Martian temperature, humidity and atmospheric composition conditions, emphasizing unicellular organisms radiation resistance
21 p3334 A71-40572

Toxic biological effects of life functions gaseous products in albino rats
22 p3506 A71-42811

LIFE SPAN

- Low and high linear energy transfer /LET/ cyclotron-accelerated alpha particles effects on *Drosophila melanogaster* longevity
06 p0853 A71-18028
- Human kidney cell generation and life cycle parameters, considering thyroxine effects
07 p1041 A71-19594
- Benzodiazepine series tranquilizers effect on mice resistance to hypoxia and lifetime, noting diazepam as most effective
12 p1872 A71-27722
- Chronic acceleration effects on animals, considering growth rate, food intake, oxygen metabolism and life expectancy
21 p3328 A71-40003
- Death rates, median life span and weight in mice exposed to gamma radiation after intra-abdominal injections of cysteamine
22 p3505 A71-42712

LIFE SUPPORT SYSTEMS

- NT BIOPAKS
- NT CLOSED ECOLOGICAL SYSTEMS
- NT EMERGENCY LIFE SUSTAINING SYSTEMS
- NT UNDERWATER BREATHING APPARATUS
- Soyuz 4 and 5 self contained cosmonaut life support system for extravehicular activity, discussing principal components block diagram
01 p0025 A71-11141
- OART space station development, discussing long term effects, artificial gravity, environmental problems, electric power, life support, protection systems and human factors
04 p0643 A71-14932
- Soviet book on manned space flight covering spacecraft design, life support systems, mission characteristics, medical considerations, etc
06 p0864 A71-18700
- Analytic functions approximation in complex regions with aid of different systems of functions
07 p1146 A71-19041
- Pressure suit assemblies /PSA/ reference for aerospace and environmental control engineers
[SAE-AIR-1103] 07 p1049 A71-19641
- Space shuttle life support, protective and crew system interfaces, discussing food and waste management and accident procedures
07 p1052 A71-20230
- Optimal control theory application to environmental control of confined spaces and life support systems, considering algorithm of Pontryagin principle
09 p1423 A71-22588
- Autotrophic cultivation of cereals with high photosynthetic activity under intensive illumination as biological components in life support systems
13 p2017 A71-28405
- Optimization of time intervals of conveyor harvestings and harvested age of oxygen producing plants for life support system
13 p2017 A71-28406
- Catalytic effect of lanthanide hydroxides on formaldehyde conversion to pentoses and hexoses at 110 C in life support systems
13 p2018 A71-28408
- Man and equipment instrumentation in simulated space environment, considering training and interface of man and life support systems
14 p2188 A71-30312
- Steady state and transient interactions due to thermal integration of isotope Brayton space power and life support systems
15 p2364 A71-32220
- Life support systems test under weightlessness environment in Nike Tomahawk sounding rockets launched from Wallops Island
16 p2537 A71-33816
- Book on space suit evolution covering balloon flight, tropopause, stratosphere, astromonks, astronauts, etc
16 p2537 A71-33872
- Environmental thermal control/life support system for manned space station, discussing maintenance, weight, power and volume
[AIAA PAPER 71-827] 17 p2690 A71-34719
- Space shuttle operation phases hazards, emphasizing propellant loading, fire suppression systems, survival equipment and self contained life support devices
17 p2813 A71-34784

Reverse osmosis application to wash water recovery in manned space mission life support systems emphasizing membranes development
[ASME PAPER 71-AV-1] 18 p2864 A71-36360

Ninety day manned test of regenerative life support system in space station simulator, presenting operational and maintenance data
[ASME PAPER 71-AV-3] 18 p2865 A71-36370

Integrated waste collection and purification systems using radioisotopes for thermal energy in 180-day space mission life support system
[ASME PAPER 71-AV-4] 18 p2865 A71-36371

Wide heat load range space radiator design for space mission environmental control/life support system using stagnation control
[ASME PAPER 71-AV-5] 18 p2865 A71-36372

Life support water management subsystem 4-man 90-day test in space station simulator with closed water and oxygen loops and no resupply
[ASME PAPER 71-AV-6] 18 p2865 A71-36373

Waste management subsystem for 90-day space station simulator test of regenerative life support system
[ASME PAPER 71-AV-7] 18 p2865 A71-36374

Closed cycle life support water electrolysis system using solid plastic sheet electrolyte /ion exchange membrane/ of sulfonated perfluoro polymer
[ASME PAPER 71-AV-9] 18 p2866 A71-36376

Solar-array space station environmental control and life support system design for 12-man 10-year mission capability with 180-day resupply
[ASME PAPER 71-AV-12] 18 p2866 A71-36379

Environmental control and life support subsystems selection and definition for 12-man space station
[ASME PAPER 71-AV-13] 18 p2866 A71-36380

Skylab life support systems design and performance, prediction covering thermal and humidity control, atmospheric supply, carbon dioxide removal, water and waste management
[ASME PAPER 71-AV-14] 18 p2866 A71-36381

Space Shuttle Orbiter Environmental Control and Life Support Systems, discussing maintenance
[ASME PAPER 71-AV-15] 18 p2866 A71-36382

Space shuttle environmental control and life support system design covering atmospheric pressure, composition, humidity, temperature, water and waste management
[ASME PAPER 71-AV-16] 18 p2867 A71-36383

Oxygen generation system for 90-day space station simulator, considering carbon dioxide removal and reduction and water electrolysis
[ASME PAPER 71-AV-18] 18 p2867 A71-36385

Zero-gravity circulating water electrolysis system prototype design for metabolic and leakage makeup oxygen supply in 12-man space station regenerative life support system
[ASME PAPER 71-AV-20] 18 p2867 A71-36387

Self contained one man module cell design and tests of electrochemical carbon dioxide concentrating system for space applications
[ASME PAPER 71-AV-21] 18 p2867 A71-36388

Space station prototype environmental thermal control and life support systems, considering maintainability, reliability, weight penalties and fault detection and isolation
[ASME PAPER 71-AV-22] 18 p2867 A71-36389

Static feed water electrolysis system of life support system, discussing current density, operating time and temperature effects on voltage for various electrochemical cell sizes
[ASME PAPER 71-AV-25] 18 p2868 A71-36392

Space station life support prototype vapor diffusion water reclamation system for pure and sterile water distillation from urine process stream
[ASME PAPER 71-AV-31] 18 p2869 A71-36396

Closed-loop solid electrolyte oxygen regeneration life support system, discussing 180-day life test
[ASME PAPER 71-AV-32] 18 p2869 A71-36399

Prototype space station environmental thermal control and life support system digital simulation for transient design and performance prediction
[ASME PAPER 71-AV-34] 18 p2869 A71-36401

Space station regenerative life support system 90-day manned test in simulator, discussing objectives, facilities and procedures
[ASME PAPER 71-AV-38] 18 p2870 A71-36405

Weightless environment effects on fluid behavior and heat transfer in life support systems, obtaining analytical models
[AIAA PAPER 71-864] 18 p2909 A71-36652

Yeasts growth on synthetic carbohydrates with crude formose sugars, discussing application as regenerating food in long term closed life support system
19 p3011 A71-37576

NASA 12-man 10-year space station program, discussing design, information management, environmental control and life support system
19 p3153 A71-38147

Granular lithium hydroxide as carbon dioxide absorbent for closed cycle life support systems, considering porosity, carrier gas and water vapor pressure and bed temperature
22 p3508 A71-41773

Skylab life support, habitability and thermal control system, discussing ventilation, humidity, carbon

dioxide and odor control and water, food and waste management 22 p3609 A71-41976

Extravehicular activity protection systems, discussing resource regeneration, technology, methodology and space station, lunar base and Martian missions schematic configurations 22 p3503 A71-41990

Scientific research methods and applications experiments from orbiting Space Shuttle, noting environmental control and life support provision 22 p3611 A71-42039

Manned 90 day test of closed chamber regenerative life support system simulator, describing subsystems, crew nutrition, hygiene, maintenance and leisure activities 22 p3503 A71-42043

Manned spacecraft life support system dehydrated food ration effects on human organisms health, metabolism and immunoreactivity during long space flight 22 p3507 A71-42823

LIFETIME [DURABILITY]
U LIFE [DURABILITY]

LIFT

NT INTERFERENCE LIFT

NT JET LIFT

NT ROTOR LIFT

NT ZERO LIFT

Plane linear cascades of thin curved profiles, obtaining potential flow velocities and lifting force on leading edge 01 p0001 A71-10339

Lifting surface in unsteady subsonic flow, describing integral equation calculation method including kernel logarithmic singularity 01 p0003 A71-11020

Swept wing fighter aircraft transonic buffet onset lift coefficient from camber and trailing edge deflection, considering design variations 02 p0186 A71-12679

Lift of slender aircraft with rectangular cross section fuselage and high wing 03 p0342 A71-13737

Lifting and side force distributions acting on body in transonic flow 03 p0344 A71-14232

Sectional drag relationships in linearized wing theory, examining lifting and thickness problems for various planforms 03 p0344 A71-14240

Slender deformable airfoil in bounded fluid flow, determining lift coefficient by one dimensional integrodifferential equation for elastic large aspect ratio wing 04 p0567 A71-14590

V/STOL aircraft wing-propeller interaction, using mean flow deflection angle in lift and drag characteristics prediction 04 p0526 A71-14988

Wing representation by lifting line lattice as computation method for complex configurations unsteady aerodynamic forces, presenting numerical program for wings in two parallel planes [ONERA-TP-891] 04 p0526 A71-15356

Trailing vortex generation behind jet flapped wing at high wing lift coefficients 04 p0527 A71-15413

Air lubricated bearing elements lifting force, restoring moment and translational rigidity, considering dependence on minimum clearance, sliding rate, pressing force and geometric parameters 05 p0758 A71-16351

Phantom and Buccaneer aircraft boundary layer control, examining lift from trailing and leading edges 06 p0847 A71-17953

Fluctuating circulation, lift and flow induced structural vibrations of two dimensional bodies, including vortex shedding on sluice gates 07 p1014 A71-19592

Heavy fluid flow past partially cavitating flat plate with cavity closed by fictitious plate, considering lifting force under gravity 07 p1092 A71-20087

Thin rectangular wing load distribution in nonstationary incompressible flow, using downwash integral equation Fourier transform 09 p1383 A71-22946

Leading edge suction analogy for predicting low speed lift and drag-due-to-lift characteristics of sharp edge delta and related wing planforms [AIAA PAPER 69-1133] 10 p1553 A71-24851

Lift characteristics of semicircular channel wing with pusher propeller at trailing edge, comparing theoretical, wind tunnel and flight test results 10 p1553 A71-24857

Lift correction in perforated two dimensional transonic wind tunnels, considering incidence angle and streamline curvature effects on airfoil models 10 p1590 A71-24953

Reentry vehicles configuration lift and drag coefficients in hypersonic flow from pressure distribution and balance measurements, comparing with isolated cone data 11 p1702 A71-25487

Approximation of flow around jet flapped airfoil, discussing ground effect on lift coefficient increments 11 p1705 A71-26314

Lifting force of wing with rotating flap, deriving lift increase due to circulation redistribution at surface 12 p1865 A71-27491

Lift and particle displacement around lifting body with stream function as fluid motion equation integral 12 p1866 A71-27577

Roll rate variation and lift effect on reentry vehicle impact, comparing analytic treatment with six degree of freedom trajectory simulation 13 p2144 A71-27977

Air flow about low aspect ratio delta wing at large angles of attack, deriving lift coefficient 13 p1990 A71-28282

Minimum drag wing-fuselage combination for supersonic speeds and prescribed lifting force, longitudinal moment and volume, using method of successive approximations 13 p1992 A71-29182

Supercavitating flow past straight cascade with arbitrary blade shapes, considering lift and drag coefficients, cavitation number, cavity shape and exit flow conditions [ASME PAPER 71-FE-6] 13 p1995 A71-29448

V/STOL propulsion units lift ratings based on aircraft system requirements [SAE PAPER 710471] 14 p2176 A71-30537

Externally blown flap powered transport high lift wind tunnel model visual flow field investigation with multiple filament smoke streamlines [AIAA PAPER 71-577] 15 p2345 A71-31567

Magnus or Robins effect on rotating spheres, obtaining lift coefficients from conical pendulum periodic time measurements 15 p2346 A71-31927

Unsteady compressible flow measurement, determining local lift coefficient from pressure distribution along airfoil 16 p2520 A71-33342

Gust loading on two dimensional thin airfoil in compressible flow, deriving closed-form lift expression 17 p2671 A71-35285

Rotor blade stability, calculating unsteady local lift and effects of blade profile camber and steady angle of attack 17 p2672 A71-35468

Wing group weight prediction for subsonic aircraft design, taking into account root bending moments due to lift 18 p2976 A71-35925

Slender wing lift in supersonic flow, analyzing suction force on leading edge and viscosity and nonlinear effects [DFVLR-SONDDR-138] 18 p2848 A71-36677

Three dimensional hypervelocity reentry trajectories, using aerodynamic lift and vehicle bank angle as optimal control parameter [AIAA PAPER 71-920] 19 p3096 A71-37169

Lift and drag coefficients for arbitrary body form in hypersonic flow calculated for cylindrical surface with reference to space shuttle reentry 19 p2992 A71-37320

Total lift data correlation for thin sharp edged low aspect ratio delta wings at low speeds, noting trailing edge effects in incompressible flow 20 p3176 A71-39398

Gravity effect and lift perception in flying insects and animals, discussing flapping flight and aerial locomotion in aerodynamic balance weightless state 21 p3327 A71-39988

Karman vortex street induced fluctuating lift forces on single circular cylinder, deriving relationship between lift coefficient and steady state pressure drag coefficient [ASME PAPER 71-VIBR-12] 21 p3457 A71-40274

Karman vortex street induced fluctuating lift forces on tube bundles as function of steady pressure drag coefficient and Strouhal number [ASME PAPER 71-VIBR-13] 21 p3457 A71-40275

Spanwise lift distribution over wings and wake formation in thin airfoils of finite aspect ratio in linear subsonic potential flow 21 p3319 A71-40495

Fluctuating lift and drag forces on accelerating free falling sphere, discussing relation to asymmetrical wake vortex shedding 21 p3324 A71-40970

Aerodynamic aspect ratio effects on drag and aircraft performance, noting span loading as major force on wing lifting function 21 p3325 A71-41246

Magnetosphere aerodynamic parameters, discussing lift and drag coefficient, shape, magnetic field gradients and tail 21 p3374 A71-41353

Space shuttle optimal lifting trajectory analysis, examining boost launch system performance increase 22 p3608 A71-41955

KC-135 aircraft climb trajectories for optimum constant lift coefficient, range and fuel amount 22 p3481 A71-42834

Lifting line equation inversion for twisted wings of elliptic planform with arbitrary spanwise upwash 22 p3481 A71-42838

Angle of attack instrumentation for evaluating aircraft lift performance and phugoid oscillations 23 p3628 A71-43382

Performance prediction and evaluation of propulsion-augmented high lift systems for STOL aircraft, considering weight, thrust and wing loading [AIAA PAPER 71-990] 24 p3791 A71-44585

Matched asymptotic solutions for optimum lift controlled atmospheric entry of hypersonic lifting vehicles 24 p3876 A71-44609

LIFT AUGMENTATION

Power augmented lift STOL aircraft operating costs reduction by channel wing concept, discussing aerodynamic theory and structural applications to high lift flaps aircraft 09 p1385 A71-22592

Electrical resistive incompressible fluid motion past thin airfoils in oblique field, showing inverse dependence of lift on magnetic Reynolds number 10 p1648 A71-23956

STOL commercial aircraft propulsion systems, considering two stream augmentor wing engine and high bypass ratio three stream engine [AIAA PAPER 71-746] 15 p2467 A71-31325

Canadian R and D on fixed wing civil STOL aircraft, discussing augmentor wing concept using jet powered lift augmentor system 16 p2523 A71-33470

Augmentor wing high-lift aerodynamics, discussing results of wind tunnel tests and simulation studies [CASI PAPER 72/20] 19 p2993 A71-37606

Propulsive lift augmentation for horizontal landing of low and medium L/D reentry vehicles, determining optimum thrust program 22 p3612 A71-42046

LIFT COEFFICIENTS
U AERODYNAMIC COEFFICIENTS
U LIFT

LIFT DEVICES

Aerodynamic theory of pressure field induced on lifting surface by isotropic atmospheric turbulence, considering transfer function of Concorde aircraft [ICAS PAPER 70-30] 01 p0002 A71-11019

High lift systems for four-engine Mach 0.8 turbofan STOL aircraft, discussing propulsion, aerodynamics and design trends [SAE PAPER 700811] 01 p0003 A71-11545

Analog and digital methods for interactions between aircraft lifting elements in steady or unsteady supersonic flow [ONERA-TP-850] 04 p0527 A71-15358

Boeing 737 aircraft takeoff and landing performance, emphasizing high lift systems and stopping capability 07 p1018 A71-19083

Airplane wing high lift and flap designs by interactive computer graphics system [AIAA PAPER 71-227] 07 p1019 A71-19705

Lifting surface nonstationary aperiodic motion in incompressible fluid solved by asymptotic method of function parameters, using algorithm for Cauchy problem 08 p1275 A71-20778

Lifting surfaces supersonic-hypersonic flutter at angle of attack determined by shock expansion, Newtonian flow and local flow piston theory [AIAA PAPER 71-327] 11 p1842 A71-25307

Vertical straight lift turbojet engine design and development, presenting component materials properties/weights, endurance tests and performance data [ASME PAPER 71-GT-75] 11 p1813 A71-25989

High lift wing characteristics with/without additional devices, emphasizing lift control and load distribution 12 p1864 A71-27476

Vortex wakes behind STOL operations high lift wings, discussing height above ground and various wind tunnel dimensions effects 13 p1990 A71-28033

Two dimensional flow research on high lift airfoils for STOL aircraft, using vorticity distribution and wind tunnel wall blowing techniques 14 p2169 A71-29910

STOL aerodynamics of leading edge high lift devices on thick profiles, externally blown flaps, boundary layer control and jet flap effect 15 p2343 A71-31214

Three dimensional jet flap and lifting line/ surface theories application to STOL aerodynamic systems with externally blown flaps and augmentor wing [AIAA PAPER 71-578] 15 p2345 A71-31568

Lifting configurations unsteady air loads prediction, investigating loading singularities in linearized potential theory 22 p3481 A71-42832

High lift device application to high performance competition gliders, considering merit of design for conflicting climb/cruise requirements 23 p3627 A71-43089

Sailplane circling cross-country speed increase by variable geometry in high lift flap form for better compromise between cruise and climb performance 23 p3630 A71-44342

LIFT DISTRIBUTION
U FORCE DISTRIBUTION

LIFT DRAG RATIO

U LIFT
LIFT DRAG RATIO

Low speed two dimensional axial flow compressor cascade data, considering lift drag ratio and minimum loss coefficient
[ASME PAPER 70-WA/GT-10] 03 p0343 A71-14118

Aerodynamic characteristics of jet engine installation above wing of swept wing aircraft, noting large lift dependent drag 05 p0696 A71-15954

Aft vs canard horizontal tail locations for fighter/attack configuration at sub and supersonic speeds, observing lift coefficient, L/D and longitudinal stability [AIAA PAPER 71-8] 06 p0848 A71-18482

Conical body lift/drag ratio increase by wedge shaped nose, noting applications to space vehicles entering atmosphere above escape velocity 13 p1992 A71-29183

Aspect ratio influence on instability and non-minimum phase effects of longitudinal motion of aircraft relative to negative lift-drag expression transfer functions [DFVLR-SONDDR-127] 16 p2523 A71-33405

Asymptotic high velocity lift drag ratios for sheet and loop magnetic suspension train tracks 22 p3574 A71-41728

Propulsive lift augmentation for horizontal landing of low and medium L/D reentry vehicles, determining optimum thrust program 22 p3612 A71-42046

Discrete slot pressurized fluid journal bearing design for low L/D ratios and small size configuration 24 p3830 A71-44942

LIFT FANS

Lift fan propulsion for civil VTOL transports, considering applicability, attitude control, system design, fan transition and cross flow noise 07 p1022 A71-20373

VTOL lift fan engine design for minimum noise levels, noting silencers application 10 p1659 A71-24750

Discrete frequency rotor interaction noise from lifting fans, using force harmonics acting on blades [ASME PAPER 71-GT-12] 11 p1812 A71-25958

VTOL propulsion, discussing gas turbine pressure ratio inlet temperature and lifting and high bypass fans 13 p2114 A71-27838

Tip turbine driven lift fan noise reduction tests, considering design parameters effects [AIAA PAPER 71-743] 14 p2296 A71-30784

Handling qualities of V/STOL research vehicles during steep terminal area approaches, discussing powered lift fan VTOL aircraft limitations and instrument landing approach [AHS PREPRINT 544] 14 p2179 A71-31101

VTOL lift fan airliner project HS 141 for intercity transport, describing features, weight and performance data, noise characteristics and reliability criteria 15 p2348 A71-31413

Wing installed VTOL coaxial drive lift fan model in wind tunnel test, investigating performance in cross-wind environment [AIAA PAPER 71-742] 15 p2469 A71-32284

Civil V/STOL aircraft projects, discussing design, lift fan engines, weights, flight performance, noise levels, safety and comfort standards 16 p2525 A71-34101

Civil V/STOL aircraft engines requirements, considering noise reduction, thrust, multifunction propulsion/blowing, lift and booster fan engines [CAI PAPER 72/19] 19 p3122 A71-38021

VTOL and fan lift STOL aircraft, discussing simulation and head-up displays for roll demand, vertical speed and ILS beam 21 p3413 A71-40134

V/stol aircraft lift fan aerodynamics, discussing optimum fan pressure ratios, augmentation ratio, noise constraints, wing loading and fan configurations [AIAA PAPER 71-981] 24 p3791 A71-44577

LIFT FORCES

U LIFT

LIFTING BODIES

NT LIFTING REENTRY VEHICLES

NT X-24 AIRCRAFT

Two dimensional potential flow theory for incompressible unsteady flow about multiple lifting bodies in small amplitude motion 01 p0071 A71-10929

Steady supercritical planar inviscid transonic flows over lifting airfoils, generating unsteady flow by impulsively imposing airfoil boundary condition [AIAA PAPER 70-47] 03 p0341 A71-13433

Vortex sheet behavior in inviscid subsonic flow of lifting wing with nonzero trailing edge angle 03 p0342 A71-13738

Lifting body flight test program applications in manned space shuttle 04 p0661 A71-14819

Wind tunnel tests for measuring aerodynamic interaction forces between two tandem lifting surfaces [ONERA-TP-890] 04 p0526 A71-15354

Wings with control surfaces in unsteady subsonic flow, applying lifting surface theory [ONERA-TP-889] 04 p0526 A71-15355

Lifting body leeward surface maximum heat transfer coefficient in hypersonic flow, considering Reynolds number, incidence and shape effects 04 p0527 A71-15486

Pressure distribution singularity at tip of thin lifting parabolic wing in subsonic flow 06 p0842 A71-18484 [AIAA PAPER 71-10]

Lifting surfaces supersonic-hypersonic flutter at angle of attack determined by shock expansion, Newtonian flow and local flow piston theory 11 p1842 A71-25307 [AIAA PAPER 71-327]

Lift and particle displacement around lifting body with stream function as fluid motion equation integral 12 p1866 A71-27577

Miniature aerodynamic turbulence gage using axisymmetric lifting body sensor 13 p2066 A71-28158

Trailing vortices shed by aircraft lifting surfaces, noting wake effects importance at low speeds 13 p1995 A71-28176

Unsteady curvilinear motion of lifting surface, calculating induced gas flow velocities in terms of vortex densities 13 p1992 A71-29188

Three dimensional jet flap and lifting line/ surface theories application to STOL aerodynamic systems with externally blown flaps and augmentor wing [AIAA PAPER 71-578] 15 p2345 A71-31568

Static and dynamic stability characteristics of X-15 aircraft, lifting body and trapezoidal and delta wing reentry body 18 p2971 A71-36434

Thrusting lifting orbital vehicle nonlinear longitudinal dynamics in near-circular orbit, deriving orbital elements variation behavior and angle of attack mode period and damping 21 p3454 A71-40094

Direct solution for divergence speed of lifting surface using matrices of structural and static aerodynamic influence coefficients 21 p3456 A71-40171

Boundary value problems eigenvalues determination with differential equations for lifting surfaces vibration theory 24 p3818 A71-44706

LIFTING REENTRY VEHICLES

NT X-24 AIRCRAFT

Boride composites with high strength and thermal resistance suitable as nose cap and leading edge materials for reusable lifting reentry systems [AIAA PAPER 70-278] 01 p0109 A71-11282

Abort and staging separation maneuvers of two equal size reusable lifting entry vehicles in wind tunnel tests [AIAA PAPER 70-260] 01 p0165 A71-11579

Spacecraft reentry aerodynamics regarding hypersonic high altitude lifting bodies, shock wave and flow field, heat, mass and energy transfer, etc [ICAS PAPER 70-01] 02 p0185 A71-11686

Reentry lifting body hypersonic and subsonic flight enhancement by configuration modifications with compound curvatures minimization, giving wind tunnel model data 02 p0319 A71-11974

Compact aerodynamic reentry vehicle development problems and costs, discussing lifting body vehicle for wind tunnel, ground and flight tests and reentry trajectories 02 p0320 A71-12066

Lifting oscillatory reentry trajectories, developing equation method to consider density and velocity distributions 02 p0320 A71-12403

Hypersonic body optimum lift control during atmospheric entry, taking into account drag coefficients and density 06 p0842 A71-18488

Hypersonic lifting entry vehicle turbulent heat transfer and boundary layer transition at various angles of attack and Reynolds numbers [AIAA PAPER 71-100] 06 p0844 A71-18555

Winged lifting body quasi-optimal reentry trajectory for minimum flight time, taking into account angle of attack control and angular motion inertia 08 p1367 A71-22038

Lifting body vehicle handling qualities, considering X-24A, M2-F3 and HL-10 reentry vehicles flight characteristics and simulation requirements [AIAA PAPER 71-310] 09 p1532 A71-22622

Flat delta and caret wings aerodynamic performance over incidence angle and Mach number range suitable for lifting reentry 16 p2519 A71-32877

Subsonic flight characteristics of LB 21 reentry vehicle, discussing lateral directional stability and lifting fuselage 18 p2972 A71-36436

Optimal lateral guidance switching thresholds for low L/D shuttle vehicle entry, using optimal stochastic control theory for problem formulation in conjunction with dynamic programming [AIAA PAPER 71-914] 19 p3096 A71-37164

Lifting entry trajectory control law based on uniform drag, affording heating rate and deceleration control [AIAA PAPER 71-915] 19 p3096 A71-37164

Reentry glider approximate optimal atmospheric entry trajectories for maximizing function of terminal velocity, altitude, flight path and heading angle under terminal nonlinear constraints [AIAA PAPER 71-919] 19 p3096 A71-37164

Lifting entry and terminal phase system optimization for 1975 Mars Viking lander, considering graphical tradeoff approach including design parameter atmosphere model variations [AIAA PAPER 71-922] 19 p3148 A71-37164

Optimal lift control of hypersonic lifting body during atmospheric entry by singular perturbation method [AAS PAPER 71-366] 23 p3773 A71-43000

Matched asymptotic solutions for optimum lift controlled atmospheric entry of hypersonic lifting vehicles 24 p3876 A71-44609

LIFTING ROTORS

Aerodynamic synthesis of helicopter rotor under hover and vertical ascent conditions, using nonlinear vortex approach 07 p1014 A71-197404

Telecontrolled Rotomobile flying crane with jet-powered lifting rotor for carrying heavy loads over short distances 10 p1556 A71-244202

Comparative vertical turbulence and loss restrictive stochastic models for threshold crossing rotor blade flapping vibrations at low lift high advance ratio [AIAA PAPER 71-389] 11 p1846 A71-253515

Prandtl first order boundary layer equations for two-dimensional laminar incompressible flow past circular controlled circular lifting rotor 11 p1702 A71-25494

Marginal vortex effects on aerodynamics of helicopter lifting surfaces, considering blade form and noise spectrum tested in hydrodynamic tunnel 12 p1864 A71-27473

Advancing Blade Concept helicopter lifting rotor development, discussing full scale analysis, design, fabrication and wind tunnel tests [AHS PREPRINT 504] 14 p2178 A71-31080

Helicopter rotor blade airload by applying lifting surface solution [AHS PREPRINT 510] 14 p2171 A71-31081

High rotor advance ratio from multiblade general coordinates method in linear analysis of lifting rotor dynamic stability and gust ratio [AHS PREPRINT 512] 14 p2178 A71-31083

Hingeless rotor helicopter stability and control characteristics, considering induced flow field, flapwise bending modes and blade-fuselage dynamic coupling [AHS PREPRINT 541] 14 p2179 A71-31098

Composite materials application to V/STOL prop/rotors, determining material properties parametric effect on frequencies and weight by Southwell coefficients [AHS PREPRINT 554] 14 p2180 A71-31106

Helicopter wake and boundary layer effects on rotor aerodynamic performance in hovering, low and high speed forward flight [AIAA PAPER 71-581] 22 p3479 A71-41500

Agusta helicopter design and testing criteria, discussing four-blade rotor, fuselage and radio navigation equipment 22 p3482 A71-42224

Photogrammetric recording of helicopter rotor induced aerodynamic effects using wind tunnel test smoke visualization technique 23 p3678 A71-43588

Lifting rotors aerodynamic damping in forward flight, describing methods for blade response variance matrix computation 24 p3789 A71-44559

LIFTING SURFACES

U LIFT DEVICES

U LIFTING BODIES

U SURFACES

LIGAMENTS

Brachial plexus bundle structural and histological characteristics in man and monkey, noting lack of intraneural network in monkey 23 p3634 A71-43911

LIGHT [VISIBLE RADIATION]

NT AIRGLOW

NT COHERENT LIGHT

NT DAYGLOW

NT GEIGSCHEIN

NT GEORONAL EMISSIONS

NT LIGHT BEAMS

NT NIGHTGLOW

NT SKY RADIATION

NT SUNLIGHT

NT TWILIGHT GLOW

NT ZODIACAL LIGHT

Monochromatic light glare effect on human eye as function of wavelength, using visual threshold variation as criterion 01 p0016 A71-11389

Martian environment simulator chamber for pressure, visible light, biological objectives UV irradiation and daily temperature cycle
01 p0068 A71-11559

Free radicals role in photodynamic inactivation of Rhodotorula glutinis subjected to high intensity light irradiation
01 p0019 A71-11560

Mammal species body temperature during 24 hr periodic light cycle, using statistical data analysis
01 p0020 A71-11570

UV and visual spectra of gamma Cassiopeiae from rocket spectrograph and OAO observations
02 p0314 A71-12585

Quasars PKS 2345-16 and NRAO 512 optical flares photometric observation
02 p0317 A71-12864

Optical plate induced helicoidal steady light field in laser cavity, imparting structure to isotropic transparent material medium
03 p0436 A71-13787

CdS single crystals green edge emission and optical flash spectra, discussing wavelength, UV excitation intensity and temperature effects
03 p0468 A71-14384

Soviet monograph on visible and IR waves atmospheric propagation covering monochromatic radiation absorption and scattering, laser light beams under turbulence, etc
04 p0551 A71-14800

Visible radiation absorption by aerosol particles, noting gray absorption and imaginary portion of complex index of refraction
04 p0582 A71-15072

Magnetic stars with brightness variations in visual and blue light, noting method for period determination
04 p0650 A71-15397

Visible and IR radiation attenuation in rain and snow, comparing calculation based on Mie diffraction formulas with measurement
05 p0718 A71-15992

Crab Nebula pulsar NP 0532 light flash arrival times, suggesting oscillations due to growing amplitude instabilities
05 p0806 A71-16201

Book on optical data processing covering light characteristics, Fourier transforms, spectrum analysis, photographic film, filtering, holography, etc
05 p0754 A71-17124

Ruby Q switched lasers with modular electro-optic shutters for low insertion loss and high optical radiation resistance
06 p0908 A71-18303

Plane light wave interactions with moving dispersive dielectric medium, considering electron UV or IR resonant oscillation in regions of anomalous dispersion
08 p1253 A71-21278

Supernovae light curves theory based on numerical integration of gas dynamics and radiative heat conductivity equations
09 p1528 A71-23591

Human rods dark adaptation, investigating rhodopsin resynthesis and bright light flash effects
11 p1718 A71-25635

Intense light pulses interaction with solid materials, using laser techniques
11 p1775 A71-26088

Seyfert galaxy 3C120 photometric behavior, investigating light variations
11 p1831 A71-26168

Visible and IR radiative transfer in water and ice clouds, calculating radiance and polarization from Mie theory
11 p1800 A71-26299

Quantum counting efficiency of commercial photomultiplier at 0328 Å by direct measurements, including signal and background dependence
11 p1766 A71-26300

Light diffraction by superposed parallel ultrasonic waves for diffraction pattern symmetry, using n-th order approximation method
12 p1928 A71-26650

NGC 3351 galaxy core spectrophotometry of optical spectrum covering emission and absorption lines
12 p1960 A71-26831

One magnon Raman scattering induced by light magnetic dipole coupling with YIG coherent spin waves
12 p1913 A71-26860

Light flashes in eyes of dark adapted Apollo astronauts, considering Cerenkov radiation effects from primary cosmic ray single charged particles on retinal elements
12 p1933 A71-27383

Self shielding effect of solid surfaces under intense light
12 p1915 A71-27457

Anesthetized cats visual cortex responses to prolonged light stimuli, studying dependence on photopic retina cone and rod apparatus
12 p1871 A71-27489

Iapetus photometric observations, obtaining light curve by plotting rotational phase angle against magnitude
13 p2136 A71-28390

Photodetectors for laser applications in visible and near IR spectrum, discussing optical loss and pulse dispersion measurements
13 p2078 A71-28442

Gated light pulse technique for multiple-pass interferometry
13 p2067 A71-28444

Dark adapted albino rats behavioral assessment, measuring absolute visual thresholds to white and colored light
13 p2008 A71-28457

Continuous visible operation of semiconductor laser at room temperature, discussing lasing thresholds
13 p2081 A71-29340

Triaxial ellipsoid asteroid models, determining light curves and variations
14 p2312 A71-30385

BL Lac extragalactic source of radio, IR and visual radiation, estimating upper limit to distance based on spectrum model
14 p2313 A71-30452

Millimeter and visible waves propagation through clear atmosphere and precipitation
14 p2204 A71-30971

Light diffraction by holographic gratings in pink ruby due to absorption coefficient spatial variations
16 p2578 A71-33149

Optical crossed or collinear light pulse pairs for production and sounding of instantaneous processes kinetics in nanosecond and picosecond range
16 p2580 A71-33624

Glass fibers and rods from thallium-sodium ion exchanging, investigating flexibility, focusing and light conduction without distortion
16 p2588 A71-34120

Visible spectrum electromagnetic waves propagation in plasma, emphasizing parametric coupling
16 p2620 A71-34136

Short light pulse evolution from noise, considering time dependence of pulse duration and peak intensity
16 p2589 A71-34137

Curve power factors and radiation induced changes in silicon photovoltaic solar cells, considering junction depth, bulk resistivity, temperature and illuminating light intensity
17 p2677 A71-35049

Reentry plasmas ionization and microwave and optical radiation properties, considering radar echo, electromagnetic scattering, thermal equilibrium and ablation products
18 p2952 A71-36422

Light curve and apsidal motion of AR Cas from photoelectric photometry
18 p2971 A71-37069

Balloon-measured magnetospheric electric fields comparison with all sky camera pictures of large scale visible auroral form motions, noting relationship
19 p3047 A71-37363

Ring laser formed by single mode light guiding thin film, using nitrogen laser for pump source
19 p3071 A71-37478

IR pumped stimulated light emission in semiconductors, noting upconversion due to energy transfer between impurity ions
19 p3071 A71-37479

Variable stars atmospheric radiation, investigating unsteady light reflection
19 p3133 A71-37505

Visually evoked cerebral cortex responses to on- and off-set of patterned light and contour density and sharpness in humans
19 p3004 A71-38282

Retinal damage thresholds of rhesus monkeys to ocular radiation from yellow line 568.2 nm emitted by krypton CW gas laser
19 p3008 A71-38284

Long object photography with lens array in non-coherent light and subsequent integrated image focus holography in laser beam for reconstruction in white light
19 p3068 A71-38708

Visible thermal tuning CW parametric oscillator using barium sodium niobate as nonlinear material
20 p3241 A71-38788

Light pressure measurement acting on Echo 1 satellite, considering integral reflection coefficient
20 p3306 A71-39132

Photometric measurements of light attenuation on baffles in visible, considering sensor location and surface coating
20 p3234 A71-39174

Critique of quasar model of independent random pulse emitting sources conglomeration from incompatibility with light curve
20 p3289 A71-39294

Sound to light image conversion, emphasizing liquid surface acoustical holography
20 p3238 A71-39343

Light flux spatial coherence in visual reception, considering aventurine spots perception as point light source
21 p3344 A71-41065

Electron beam modulation at optical frequencies, calculating excited radiation characteristics with quantum theory
21 p3420 A71-41254

Nonlinear losses in ultrashort light pulse generators and amplifiers, attributing to self focusing of laser radiation in active and optical media
22 p3558 A71-42457

Visible and IR radiation attenuation in rain and snow, comparing calculation based on Mie diffraction formulas with measurement
22 p3515 A71-42741

Photometric study of light variation and variable stars in luminous supergiants in Large Magellanic Cloud
23 p3723 A71-42940

Visible and near UV spectra of vacuum Ar, Kr and Xe microwave discharge lamps with magnesium fluoride windows
24 p3849 A71-45211

LIGHT ABSORPTION
U ELECTROMAGNETIC ABSORPTION
LIGHT ADAPTATION
Rudd vision mechanism, considering daylength effect on spectral sensitivity and visual pigment retinal extract proportions
01 p0009 A71-10271

Pupil neurological control system for reaction to light and accommodation process by statistical eye noise analysis and microelectrode recordings of brain stem neurons
03 p0367 A71-12985

Light-dark cycle strength as Zeitgeber for circadian rhythms in isolated man
03 p0364 A71-14249

Light and drugs effect on diurnal body temperature from radio telemetry of adult male rats
05 p0715 A71-17111

Parafoveal sensitivity disruption (flash blindness) due to retinal location and high intensity short duration adapting flash
06 p0851 A71-17605

Retinal threshold along horizontal meridian for dark and light adapted eyes for stray light from small foveally fixated high luminance target
08 p1247 A71-21000

Temporal masking effects with perception of color matching double flashes
09 p1394 A71-23015

Computerized simulation of lateral inhibitory networks for figural aftereffects, discussing light and dark adaptation mechanism
10 p1563 A71-24232

Vitamin A deficiency effect on rhodopsin loss dependent on illumination level in rat eye using electroretinography
10 p1563 A71-24326

Irreversible damage effects of visible light on retina in rats as function of irradiation, exposure time and vitamin A deficiency cell adaptation
10 p1563 A71-24327

Postexcitatory inhibition of monochromatic flickering potentials on electroretinogram in man under intensive dazzling stimuli
10 p1564 A71-24443

Pupil size effect on dynamics of pupillary movements, considering reactions to light and darkness
13 p2013 A71-29032

Visual latencies at photopic levels as function of binocular differences in retinal illuminance, using Limulus adaptation model and ERG correspondence
16 p2527 A71-32867

Light adaptation and visual latency, discussing temporal resolving properties of eye as function of binocular differences and target background contrast
16 p2527 A71-32868

Mathematical model of human visual system light adaptive signal transformation
17 p2692 A71-35171

Flash light angular size, adaptation luminance, pulse shape and color effects on Blondel-Rey constant tested on observers with good binocular vision
22 p498 A71-41483

Quantitative variation in anesthetized cats striate cortex receptive fields as function of light and dark adaptation
23 p3634 A71-43872

Flicker adaptation effect on visual sensitivity to temporal fluctuations of light intensity
23 p3635 A71-43974

LIGHT AIRCRAFT
NT OH-6 HELICOPTER
NT PIPER AIRCRAFT
NT YAK 40 AIRCRAFT
Air cooled opposed 4, 6 and 8 cylinder light aircraft engines with or without turbosupercharging, considering horsepower improvement and torsional vibration control
[SAE PAPER 700205]

01 p0142 A71-10129

LIGHT ALLOYS

- Short haul air transportation technological factors for VTOL, STOL, CTOL and light aircraft, considering operating costs, passenger service and environment impact
[ALAA PAPER 70-1287] 02 p0188 A71-11700
- Environmental development and testing of OH-58A light observation helicopter for close ground support, noting particle separator and injection seals
04 p0534 A71-15439
- Light Sprite aircraft design and construction for building at home by nonprofessionals
04 p0534 A71-15674
- Light amphibian passenger STOL P-300 Equator aircraft, using single turbosupercharged engine driving two blade propeller at tail assembly
05 p0696 A71-16132
- Universal mini carrier UMC-120 light turboprop STOL transport
05 p0696 A71-16133
- Automated design system producing wire format data for cabling avionics subsystem of light attack aircraft
[ALAA PAPER 69-976] 06 p0874 A71-17698
- BD-1 Yankee aircraft development, design and construction
07 p1018 A71-19084
- Light aircraft standard fuel flight evaluation, discussing compatibility with grades 80/87 and 100/130 certified engines and comparative operational fuel consumption
[SAE PAPER 710369] 10 p1657 A71-24239
- Gasoline icing inhibitors effect on light aircraft piston engine carburetor icing
[SAE PAPER 710371] 10 p1658 A71-24240
- Dual magneto ignition system for business and small military aircraft, describing development, design and test program
[SAE PAPER 710382] 10 p1659 A71-24247
- Light aircraft engine lubricating oil filter types and model specification, noting dirt holding ratings
[SAE PAPER 710383] 10 p1617 A71-24248
- Light aircraft spoilers to minimize landing risk, discussing spoiler/dive brake area effects on glide path angular control
[SAE PAPER 710387] 10 p1555 A71-24251
- Light aircraft longitudinal stability control systems, discussing downspring and bobweight effects on flight characteristics
[SAE PAPER 710388] 10 p1555 A71-24252
- Constant attitude light aircraft flight control system, describing design studies for minimum pilot command requirements
[SAE PAPER 710393] 10 p1555 A71-24257
- Light aircraft qualification for icing conditions from flight test data, considering increase in instrument rated pilots and IFR flying activity
[SAE PAPER 710394] 10 p1555 A71-24258
- Light aircraft steel landing gear springs structural design at Cessna, considering certification requirements
[SAE PAPER 710400] 10 p1555 A71-24262
- Pilot workload reduction in steep approach landing of light aircraft from flight test data analysis
[ALAA PAPER 71-904] 19 p3095 A71-37155
- Book on fatal civil aircraft accidents medical and pathological investigation covering transport, light and glider aircraft case histories and statistics
23 p3638 A71-42910
- Aircraft generated vortex wakes and core air motions hazards for encountering light airplane
23 p3628 A71-43381
- Acrostar Mk II all wood single seat acrobatic light weight aircraft designed for plus/minus 8g and inverted flight
23 p3629 A71-43887
- LIGHT ALLOYS**
NT ALUMINUM ALLOYS
NT BERYLLIUM ALLOYS
NT MAGNESIUM ALLOYS
- LIGHT AMPLIFIERS**
Nd-glass pulsed solid state laser amplifier gain characteristics, deriving flux density and population inversion equations
02 p0261 A71-12173
- Optical signal amplifiers operational principles, discussing parametric, semiconductor laser, and solid state amplifiers and amplifiers using gas in Fabry-Perot resonator
04 p0608 A71-15079
- Nitrogen-carbon dioxide electric discharge mixing laser/EDML/used as pulse amplifier, using high flow rate for waste heat removal
07 p1129 A71-20618
- Photoelectron noise limited low light level imaging sensors, investigating resolving power, signal degradation and camera tube performance
10 p1610 A71-24061
- Superregenerative linear mode amplification in Q switched He-Xe laser as function of resonator phase, length and signal angle
10 p1621 A71-24713
- Amplitude characteristics of Q switched He-Xe laser at 3.5 microns, using rotating reflection prism and velocity equations
10 p1621 A71-24715

GaAs multiple beam injection laser amplifier avoiding light flux saturation by periodic signal release
12 p1913 A71-26852

Small-signal gain radial variation in cylindrical electrically excited carbon dioxide laser amplifier, characterizing discharge properties by modified Schottky analysis
13 p2080 A71-29330

Axial mode locking and equidistant frequency generation in solid state lasers due to active medium saturation, using self consistent equations with broadened amplification line
15 p2418 A71-31189

High gain parametric generation of coherent light in ammonium dihydrogen phosphate crystal continuously tunable across visible spectrum with UV harmonic of Nd-YAG laser
15 p2420 A71-32383

IR carbon dioxide laser amplifier with fundamental mode output power in excess of 500 w, describing multistage mirror section design and test results
16 p2587 A71-33491

HCN laser amplifier gain measurement at IR wavelengths in gas mixtures by recording with pyroelectric receiver
17 p2750 A71-34290

Quantum mechanics model of optical parametric amplifier, considering performance of optical information systems
17 p2698 A71-34409

Ruby laser sources of short duration and high energy emission in holography, considering oscillator amplifier illuminator, contour spacings, transmission holocameras, etc
18 p2930 A71-36057

Hydrodynamic effects on laser beam propagation through gases by finite difference solution, applying to trapping, acoustic and light amplifications and banana self focusing
20 p3242 A71-38838

Unidirectional regenerative ring carbon dioxide laser power amplifier tests for below and above threshold operations, noting saturation role in performance
20 p3242 A71-38843

Unidirectional gas laser amplifier using monochromatic optical pumping of coupled Doppler broadened transition
21 p3394 A71-41048

Laser amplifier with range variable automatic gain control in Fabry-Perot cavity with allowance for oscillation
22 p3556 A71-41807

LIGHT BEAMS

Multifrequency gas laser spectrum structural changes caused by small external light signals
01 p0095 A71-11115

Laser beam trajectory changes due to asymmetrical shading with circular absorbing diaphragm, noting characterization by energy distribution over cross section
01 p0095 A71-11216

Light beam deflection due to temperature gradient in laminar gas flow in shielding pipe for laser communication, considering beam waveguide design
02 p0284 A71-11869

Toulouse space environment simulator artificial sun assembly consisting of xenon lamp and projection optics for cylindrical light beam production
02 p0239 A71-12748

He-Ne laser light beam double slit experiments, investigating multimode operation effect on spatial coherence
03 p0440 A71-14177

Photoelectronic stellar transit instrument lens with increased spherical aberration based on light beam passage analysis
04 p0598 A71-15379

IR laser beam atmospheric absorption, considering heating and cooling effects due to vibrational relaxation
04 p0609 A71-15681

Partially coherent laser beam phase fluctuations using reversing-front interferometer for time integrated irradiance measurement, considering atmospheric turbulence effects
04 p0627 A71-15683

Optical beam scintillation dependence on wavelength in strong refractive index turbulence
04 p0609 A71-15694

Light propagation in gas filled pipe with uniform heat flux through wall under forced convection, determining lens efficiency relation to length
04 p0628 A71-15811

He-Ne laser beam parameters and diffraction field measurement by holography
05 p0760 A71-16260

Divergent laser light beams continuous electro-optical deflection using prism with single crystal at Curie temperature in cryostat
05 p0763 A71-16834

Complex rays for electromagnetic field construction, considering application to Gaussian laser beams
05 p0763 A71-16905

High power light beams attenuator usable as polarizing and depolarizing device, describing design for efficiency and elimination of beam shifting
06 p0908 A71-18080

Adaptive algorithms in particle size and form distribution control, using scanning light beam
06 p0872 A71-18690

Axisymmetric phase object holographic interferometry, showing light beam refraction effect on interference pattern
07 p1108 A71-19237

Photographic materials in holography, examining resolving power dependence on size and on angle between reference and signal light beams
07 p1108 A71-19238

Modified double point source differential shear interferometer for neutral reference light beam, using pinhole stop
07 p1110 A71-19478

Plasma produced by focused Q switched ruby laser beam, considering use for minimum ignition energy measurement
07 p1123 A71-19577

Focused ruby laser beam degradation of various gaseous aliphatic and alicyclic hydrocarbons
07 p1124 A71-19789

Laser beam evaporation of dense substances, examining luminous flux densities with gas dynamic equations
07 p1127 A71-20253

Powerful laser beam and material interaction, investigating gas dynamics of plasma heating and dispersion
07 p1127 A71-20254

Three diffracting light beams parametric interaction, applying variational method to theory of backward wave parametric oscillator
08 p1334 A71-21181

Holographic recording media low signal energy densities comparison, determining peak values of diffraction efficiency and normal contrast ratio divided by signal beam exposure
08 p1290 A71-21389

Photodetector frequency response measurement, using beat light signals from mixed single mode He-Ne lasers
09 p1460 A71-22227

Nonlinear effects of IR beam passage from continuous neodymium-yttrium garnet laser trough defocusing media
09 p1460 A71-22231

Laser pulse induced rapid reversible crystallization of amorphous chalcogenide semiconductor films using photon flux model
10 p1655 A71-24044

Thin holographic recording and retrieval from semipermanent optical memories
11 p1762 A71-25624

Mutual coherence effects in time varying radiation fields on two beam interferometric optical discriminator response
11 p1800 A71-26306

Axisymmetric phase object holographic interferometry, showing light beam refraction effect on interference pattern
12 p1903 A71-26755

Photographic materials in holography, examining resolving power dependence on size and angle between reference and signal light beams
12 p1903 A71-26756

Optical beam propagation, determining turbulent medium effects with holographic wave front reconstruction technique
12 p1904 A71-26795

Digital data recording system based on multiple beam interference pattern photography, using optical phase modulation
12 p1905 A71-26807

Constant Doppler wide-angle laser beam scanning, presenting expressions for Doppler shift, spread in spectral width of scanned laser beam and scan angle
12 p1913 A71-26814

Parallel light beam triangular path interferometer with linear compressive shear effect for flow measurement applications, describing prism system and interference patterns
12 p1905 A71-26816

Amplitude-phase distortions of optical beam during nonlinear amplification in carbon dioxide laser with periodic correction
12 p1913 A71-26846

Optical beam side refraction, determining physical conditions for vertical air temperature gradients at line of sight altitude above earth surface
12 p1902 A71-27484

Laser beam propagation in turbulent atmosphere studied for alignment survey applications, discussing development, construction and testing of centering detectors
12 p1915 A71-27538

Second harmonic generation experiments, considering limited focused laser beam diameter and crystal sample shape
12 p1915 A71-27641

- Shock front detection by Fraunhofer diffraction of narrow parallel Gaussian laser beam 13 p2067 A71-28162
- Laser light enhanced scattering by optical mixing of beams in plasma 13 p2079 A71-28797
- Focused laser coherent light beam expansion in turbulent atmosphere 13 p2080 A71-29016
- Fluctuations of Gaussian light beams due to turbulence in lenslike medium, using perturbation method 13 p2102 A71-29388
- Light propagation through moving gas, computing beam bending into wind and self defocusing due to gas heating 14 p2274 A71-30129
- Combined heterodyning, beam forming and cross correlation of broadband multichannel signal from multidimensional phased array, using coherent optical system 14 p2241 A71-30142
- German monograph on application of theory of optical pumping with crossed light beams to magnetic fields vector measurement 14 p2242 A71-30230
- Multiple-beam interference effects in Fabry-Perot interferometer with small wedge between mirrors, deriving expressions for light beams path 14 p2243 A71-30273
- Laser Doppler velocimetry accuracy degrading factors, considering light beam focus phase anomaly and distortions due to density fluctuations 14 p2245 A71-30331
- Laser beam scintillation covariance beyond turbulent atmospheric layer in Fresnel and Fraunhofer zones 14 p2254 A71-30423
- Gas laser birefringence observation in active elements under pumping action, using light beam components polarization intensity measurements 14 p2255 A71-30586
- Mass spectrometric investigation of high power laser beam plasma on solid target, determining multicharged ion yield, energy, angular distribution and recombination effect 15 p2418 A71-31191
- Resonant excitation of thin film dielectric optical waveguide through supercritical layer by limited light beam with arbitrary amplitude-phase distribution 15 p2375 A71-31227
- Solid state laser emission divergence, calculating far zone fields for arbitrary amplitude and phase distributions 15 p2418 A71-31243
- Light beam diffraction by supersonic waves, calculating amplitudes with difference- differential equations 15 p2450 A71-32075
- Laser pulse shape, beam modulation and power fluctuation quality control measurements, using non-selective, thermally stable piezoelectric sensor with low time constant 15 p2421 A71-32456
- Fabry-Perot interferometer laser beam diffraction effects on fringe pattern formation, deriving field distributions in near and far zones 15 p2421 A71-32459
- Ejected photoelectron count probability distribution due to periodic irradiance modulation of amplitude stabilized light beam 15 p2452 A71-32595
- Laser beam atmospheric monochromatic radiation attenuation isolating molecular absorption from total radiant flux attenuation 15 p2451 A71-32757
- Optical coupling between two axes of laser light beam deflector, using reflective relay optical system for loss reduction, cost effectiveness and easy alignment 16 p2585 A71-33139
- Self focusing effect of Q switched single mode ruby laser emission in CdS crystal, noting 60 kW minimum threshold power 16 p2588 A71-33645
- Ruby watch jewels as pinhole diaphragms in laser beam broadening systems, determining optimal size 16 p2588 A71-34102
- Laser beam trajectory changes due to asymmetrical shading with circular absorbing diaphragm, noting characterization by energy distribution over cross section 17 p2750 A71-34267
- Electron beam modulation by laser light, considering quantum mechanical theory 17 p2753 A71-35024
- GaAs laser arrays for beam addressable memories, discussing efficiency, junction width, beam spread and polarization 18 p2929 A71-35957
- Laser beam reflection from arbitrary geometric surface, considering reverse problem of response of flat or curved mirror to incident collimated light 18 p2929 A71-36055
- Holographic display for blind landing system with variable image perspective over wide field of view, using collimated or cylindrical laser beam 18 p2945 A71-36061
- Acousto-optical effects, materials and devices of laser beam control using diffraction and refraction by ultrasonic waves 18 p2932 A71-36607
- Laser light beam attenuation, considering turbulent pulsation effects in closed channel fluid flow axial region 19 p3071 A71-37279
- Artificial fog thermodynamic conditions and evolution data, using scattered laser beam angular distribution measurements 19 p3091 A71-38586
- Rotating waveplate optical frequency shifting in lithium niobate, producing light beam with moderate requirements on modulator adjustment 20 p3204 A71-39097
- Ultrafast camera with picosecond framing times for photographic measurement of light pulses 20 p3235 A71-39189
- Laser beam spatial coherence properties dependence on transverse mode structure for given longitudinal mode 20 p3245 A71-39350
- Laser beams amplitude-phase correction by holographic method, obtaining beams with plane fronts and Gaussian amplitude distribution 20 p3245 A71-39413
- Elliptical cylinder pump cavity design for solid state laser with ideal beam geometry 20 p3246 A71-39493
- Spectral density modulation visibility at Michelson interferometer exit illuminated with white light parallel beam 21 p3375 A71-40072
- Radial energy contours of pulsed ruby laser beam in direct determination of thermal conductivity by flash technique, using heat flux transducer 21 p3391 A71-40180
- Multibeam holographic interference Gabor theory construction, using variational principle and potential theory 21 p3379 A71-40626
- Holographic processing theoretical and experimental optimization, considering object/reference beam ratio and photographic emulsion thickness effects 21 p3380 A71-40924
- Kinoform diffuser technique based on speckle pattern formation by ground glass illumination with undiverged laser beam 21 p3381 A71-40928
- Numerical modeling and analysis of homocentric light beams propagation in cubic and nonlinearity saturation medium, using parabolic equation approximation 21 p3417 A71-41259
- Phase aberrations in Bragg imaging for sound components projecting out of plane normal to light beam 22 p3540 A71-41778
- Laser beam focusing at various distances from caustic surfaces by spherical resonator formed by mirrors or lenses 22 p3557 A71-42063
- Quasi-optical transmission line stability improvement, investigating pulsating light beam concept 22 p3512 A71-42309
- Interfering beams amplitude modulation, applying optical heterodyne techniques 22 p3512 A71-42321
- Heating dynamics of transparent dielectrics exposed to pulsed laser beam operating in free laser mode 23 p3683 A71-43270
- Second harmonic aperture in ultrashort pulses length measurement by mixing two AM light beams in nonlinear crystals 23 p3683 A71-43397
- Light pen optical writing and erasing with bistable phosphor storage tubes using screen photoconductivity 23 p3651 A71-43437
- Collimated laser beam angular deviation in turbulent near earth atmosphere, comparing with interferometric data 23 p3685 A71-43506
- Narrow light beam transmission in weakly nonlinear turbulent atmosphere, calculating large scale permittivity inhomogeneity effect on average intensity by model 23 p3645 A71-43564
- Collimated light beam transmission in turbulent atmosphere above ground surface, comparing measured coherence function with calculation 23 p3645 A71-43565
- N-hexane-air mixture ignition by giant pulse laser beam, analyzing probability and development time to formation of measurable nucleus 23 p3686 A71-43998
- Ni-Fe film exposure to continuous IR laser light for laser radiation structure 23 p3686 A71-44056
- Laser light action in photosensitive materials, comparing development techniques 23 p3686 A71-44057
- Turbulent defocusing and displacement fluctuations of focused He-Ne laser beam in atmosphere over paths near ground 23 p3688 A71-44329
- Reflection coefficient of multimode laser beam from dielectrics interface 24 p3833 A71-45044
- Holographic method for investigating piston type oscillations with phase modulated reference light beam 24 p3829 A71-45270
- LIGHT BULBS**
- U LUMINAIRES**
- LIGHT COMMUNICATION**
- U OPTICAL COMMUNICATION**
- LIGHT DURATION**
- U FLASH**
- U PULSE DURATION**
- LIGHT ELEMENTS**
- Mass spectrometric studies of origin of light elements Li, Be and B in universe, considering spallation of stellar and galactic gases by high energy particles 18 p2959 A71-35914
- Light elements thermodynamic state variables at high pressure, calculating electron density distribution as function of ion configuration with linear response theory 18 p2970 A71-37047
- LIGHT EMISSION**
- NT BIOLUMINESCENCE**
- NT CHEMILUMINESCENCE**
- NT ELECTROLUMINESCENCE**
- NT FLUORESCENCE**
- NT LUMINESCENCE**
- NT LUNAR LUMINESCENCE**
- NT OPTICAL RESONANCE**
- NT PHOTOLUMINESCENCE**
- NT THERMOLUMINESCENCE**
- NT X RAY FLUORESCENCE**
- Light pulse generator for amplitude-frequency analysis of photoreceivers, using wideband modulated semiconductor injection laser emission 01 p0093 A71-10624
- Rapid geomagnetic field variations relationship with auroral luminosity fluctuations at 4278 A 01 p0076 A71-11501
- Auroral vacuum UV spectra and 3914 A emission from sounding rocket data 01 p0076 A71-11502
- Carbon dioxide molecules dissociative excitation processes by low energy electrons, examining light emission mechanism in VUV 02 p0261 A71-12318
- Vela pulsar optical emission identification using phase selective image tube photographs 02 p0315 A71-12658
- Vela pulsar optical emission identification by photoelectric measurements 02 p0315 A71-12659
- Scorpius X-1 X ray and optical variations observation by Vela 5 satellites 02 p0315 A71-12662
- Light emission during ion-molecule collisions, using low energy nitrogen and argon ion beams 04 p0630 A71-15655
- Saturn satellite Iapetus periodic light variation curve explanation in terms of meteoroids impact erosion 04 p0660 A71-15861
- Polar auroras emission bursts at 6300 and 5577 A, noting diurnal variation with electrophotometer 05 p0746 A71-17209
- Diamagnetic moment of strong shock waves from high temperature light spark explosion in gases 06 p0930 A71-17399
- Nightglow 6300 A emission latitude wide enhancement at Mt. Abu, India 06 p0893 A71-17990
- Light emitting diodes performance comparison under electron irradiation effect in space environment 07 p1071 A71-19070
- Emission frequency tunable organic dye laser development and construction 07 p1123 A71-19239
- Emission of ruby laser with resonator containing passive Q switch solution and lenses, investigating regular self oscillation region 07 p1125 A71-19811
- Light emission of microplasmas and mesoplasmas in silicon p-n junctions, determining spectral distribution 09 p1507 A71-22190
- Photon emission from electron moving in field of two plane electromagnetic waves with different frequencies and propagating in same direction 09 p1460 A71-22364
- Metastable oxygen ion distribution and related optical emission rates in aurora, discussing line intensities, charge transfer efficiency and ionization peaks 09 p1441 A71-23642
- Spatial distribution of aurorae in O and molecular nitrogen ion emissions 10 p1602 A71-24553

Oxygen red-green line emission intensity in quiet auroral arc, using rocket-borne photometers 11 p1754 A71-25551

Photon emission-absorption probabilities relation in thermodynamically quasi-equilibrium state as function of photo transition excitation frequency, temperature and chemical potential 12 p1931 A71-27303

Properties of higher latitude region of structured low energy electron precipitation in noon hemisphere, relating radiation with optical emissions in dayside auroral oval 13 p2119 A71-27911

Cerenkov light distribution calculation from gamma ray initiated air shower model obtained from Monte Carlo computer program 13 p2125 A71-28093

Polar auroras emission bursts at 6300 and 5577 Å, noting diurnal variation with electrophotometer 13 p2060 A71-28264

Spectrometer slit-width cancellation by Doppler shift of light emission by fast ion beams, resulting in spectral lines increased intensities 13 p2071 A71-29331

Equatorward moving fast auroral waves recorded with image intensifier-TV system 14 p2229 A71-29660

Night sky optical emissions morphology and behavior in polar regions with emphasis on polar caps 14 p2234 A71-30045

Light and radio emission from Orion nebula flare stars in meter waveband, discussing coherent mechanisms of plasma oscillations and gyro/synchrotron radiation amplification 15 p2485 A71-31696

Oxygen /super 1S/ effective lifetime measurements in pulsating aurora, discussing mechanisms, quenching coefficients and heights 15 p2397 A71-31762

Carbon monoxide-helium-oxygen laser emission continuous self mode locking and temporal structure for various optical cavity lengths 15 p2420 A71-32379

Continuous light absorption, emission and ionization relaxation behind shock front in xenon 16 p2613 A71-32890

Rotation measure and intrinsic angle of Crab pulsar emission, discussing optical and radio radiation origin 16 p2634 A71-33390

Altitude variation of forbidden line of 5577 Å and 3914 Å auroral emissions intensities ratio from rocket sounding 16 p2566 A71-33748

Auroral 4278 Å positive nitrogen ions emission relation to low energy electron precipitation, using polar orbiting Aurorae satellite photometer and particle detector data 16 p2568 A71-33794

Single mode carbon dioxide laser action from quasi-optical mirror emission channels 16 p2588 A71-33894

Ca and Mg light emission and ionization cross section measurements at simulated meter conditions, using photomultiplier and optical filters 17 p2798 A71-34374

Soft optical, radio and X ray emission during accretion of interstellar gas by neutron star with magnetic dipole moment 17 p2800 A71-34570

Mathematical models of color data coding and decoding, studying light emissions transformations in visual organs and engineering systems 17 p2692 A71-35173

Magnetic field effects on ruby laser radiation kinetics and spectral composition, studying crystal heating and light emission 17 p2753 A71-35242

Radio source PKS 1514-25 identification as E galaxy, investigating rapid optical variability and light curves 17 p2805 A71-35379

Upper limits to quasars masses with optical emission lines inside radio sources, using method independent of red shift composition 18 p2961 A71-35965

Dynamic display of abstract visual perspective using fiber optic material as discrete lines of light-emitting elements 18 p2918 A71-36075

Solid state light emitting diodes in aerial camera data recording system for enhanced spectral matching, increased photo conversion efficiency and lower power drive 18 p2920 A71-36089

Infrasonic pulsations of optical auroral luminosity in 3914 Å positive molecular nitrogen ion and 5577 Å O I emission measurement by double photometer system 19 p3048 A71-37395

Spectroscopic analysis of continuous light emission from molecular oxygen-nitrogen mixtures in Mach 9 shock waves, stressing radiative reaction role 19 p3106 A71-37462

Light production by 2.5-490 eV helium ion collisions with nitrogen, considering 1200 and 3200 Å emission 19 p3107 A71-38055

Auroral luminosity patterns over northern Scandinavia based on ESRO all-sky camera recordings, noting relationship to electron and proton precipitation 19 p3060 A71-38573

End-on shock tube detection technique sensitivity for monitoring light emission behind reflected shock waves 20 p3209 A71-38830

Airglow optical emission processes covering resonance scattering, fluorescence, chemical association, ionic reactions and excitation transfer 20 p3226 A71-39827

Auroral excitation and ionization intensity and rotational and Doppler temperature vertical profiles measurements, emphasizing emission rate profiles 20 p3227 A71-39839

Crab Nebula cosmic gamma rays from air shower emitted Cerenkov light detection, using synchrotron Compton scattering model 20 p3285 A71-39922

Power spectral analyses of auroral light and X ray pulsations, discussing damping due to velocity dispersions of electrons with various energies 21 p3373 A71-40069

Readout systems light emitting numerals legibility, determining threshold values from response categorization into correct responses, misreadings and missed signals 21 p3376 A71-40125

P-n-p-n quadruple layer semiconductor junction light emitting diode with negative resistance characteristics, discussing epitaxial regrowth process and applications 21 p3355 A71-40739

Neutron flux estimate from protons number needed for white light solar flare caused by energetic particle penetration into photosphere 22 p3590 A71-41467

Red dwarf flare stars sporadic outbursts, considering light and radio emission curves, outburst energy and galactic emission 22 p3607 A71-42881

Scorpius X-1 optical and X ray flux transient short period oscillations correlation from Aerobee sounding rocket data 23 p3733 A71-43077

Plasma generation with transversely excited high pressure carbon dioxide laser and solid targets, describing optical emission spectral characteristics 23 p3712 A71-43932

Molecular hydrogen primary ionization coefficient measurement in non-self sustained Townsend discharge, using light detection method based on radiant flux vs electron density proportionality 24 p3850 A71-44370

Laser light emission from system of four-level centers with variably widened asymmetric luminescence line 24 p3833 A71-44659

LIGHT GAS GUNS

Hyperballistic free flight test facilities using light gas guns, considering wake of flight vehicle at hypersonic velocity and aerothermal phenomena 18 p2898 A71-36411

LIGHT INTENSITY

U LUMINOUS INTENSITY

LIGHT MODULATION

NT ULTRASONIC LIGHT MODULATION

Kerr cell for high speed modulation of laser radiation, noting use in multiframe shock wave dark photography 01 p0093 A71-10625

High speed small aperture electro-optic, acousto-optic and magneto-optic modulators for optical communications, considering capabilities and limitations 02 p0231 A71-12003

Semiconductor lasers direct amplitude, pulse and frequency modulation methods, comparing advantages and limitations 02 p0260 A71-12004

Operational laser communication systems performance characteristics review, considering various modulation techniques, heterodyne detection, IR applications, etc 02 p0260 A71-12030

Optical PCM communications system with lithium tantalate traveling wave modulator capable of one gigabit/sec transmission and detection rate 02 p0215 A71-12042

Truncated periodic targets modulation in partially coherent light, deriving diffraction image formulas 02 p0260 A71-12146

Neodymium laser emission in mode locked operation, examining self focusing and modulation effect in active element 02 p0261 A71-12323

Optical radiation modulation and phase optical ranging, discussing theory and Soviet instrumentation 02 p0254 A71-12713

High rate electro-optical modulator for 10.6 micron IR laser beam consisting of GaAs crystal multitraversed by beam 02 p0262 A71-12923

Transversely excited atmospheric pressure carbon dioxide laser mode locking with Ge acousto-optic modulator 03 p0434 A71-13484

Carbon dioxide laser stable mode locking with resonated internal electro-optic phase modulator driven at frequencies near axial mode interval 03 p0434 A71-13484

Nd-YAG laser with intracavity lithium niobate phase modulator, investigating frequency sweeping/modulation mode operation 03 p0437 A71-13879

Homogeneously broadened pulsed laser mode locking with internal frequency or amplitude modulation 03 p0437 A71-13888

He-Ne laser emission modulation through active element excitation source 04 p0604 A71-14625

Laser display technology, discussing recent systems, light beam deflectors and modulators 04 p0607 A71-14721

Frequency modulation and compression of ultrashort light pulses by optical Kerr effect 04 p0552 A71-15031

Single mode laser light modulation by low amplitude LF sinusoidal wave, considering photoelectron distributions 05 p0760 A71-16161

Laser beam modulation by nanosecond rise time mechanical chopper for rectangular variable duration pulses, considering use in fluorescence lifetimes measurement, photomultipliers and photodiodes 05 p0761 A71-16270

Wideband interdigital microwave circuits using lithium niobate crystals for electro-optic modulation of light, discussing design and performance tests 05 p0762 A71-16336

Photoelectric photometer measurements of stellar interferometer fringes strength by light modulation 05 p0752 A71-16689

Internally loss-modulated ring lasers unidirectional oscillation, analyzing two mode operation 06 p0906 A71-17300

He-Ne laser light intensity fast and slow modulation by thin acoustoelectric photoconducting CdS platelet oscillators 06 p0906 A71-17300

Traveling medium solid state lasers radiation intensity modulation by active element motion 06 p0907 A71-17595

HF modulation of optical, X ray and gamma radiation of Crab pulsar, discussing radiation production mechanisms 06 p0970 A71-18034

Laser modulator with multilayer dielectric microcoating on piezoelectric substrate, investigating vibration distribution and maximum frequency deviation 08 p1303 A71-21808

Photoelectric imaging devices resolution performance, considering modulation transfer function and measurement methods 10 p1610 A71-24064

Internal asynchronous modulation of He-Ne laser with Doppler broadened line of working transition in multifrequency mode 10 p1621 A71-24881

Dual laser ranging for distance measurements superimposing beams modulated at different frequencies 11 p1774 A71-25936

SHF lithium tantalum oxide optical modulator for optical detector evaluation, discussing bandwidth and phase modulation characteristics 12 p1903 A71-26795

Digital data recording system based on multiple beam interference pattern photography, using optical phase modulation 12 p1905 A71-26807

Lossless KDP Pockels cell modulator for high power laser Q switching based on tuned face electro-optical crystal 12 p1905 A71-26813

Optimal continuous recording of amplitude-phase distributions on spatial carrier frequency for light wave modulation and optical antenna simulation 12 p1878 A71-26841

Selective modulation spectroscopy by taking interference between reflected and diffracted beams of modified Michelson interferometer 14 p2241 A71-30137

Parametric amplification of two laser waves with amplitude and phase modulation under exponential signal growth applied to Raman scattering in picosecond pulse field 15 p2418 A71-31188

Laser beam CW self-induced frequency modulation and switching observation in liquids with low surface tension 15 p2420 A71-32381

Stark effect saturable absorber modulation of passively Q switched carbon dioxide laser, using difluoroethane, difluoroethylene, methyl fluoroform, trichloroethylene and vinyl chloride 16 p2586 A71-33147

Luminous pulse production by internally modulated Ar laser, observing overall modes amplitudes
16 p2587 A71-33381

Electro-optical Fabry-Perot modulator with KDP and ADP crystals as optical resonators, determining modulation and frequency response characteristics
16 p2587 A71-33493

He-Ne laser mode self locking conditions and modulation characteristics
16 p2589 A71-34125

Pulsed emission and modulation of output power of He-Ne laser at 0.63 and 1.15 micron wavelengths as function of external longitudinal magnetic field
17 p2751 A71-34385

He-Ne laser emission and discharge plasma parameters, detailing variable magnetic field effects on modulation
17 p2752 A71-34389

Phase-only complex valued spatial filter for holographic wave front construction involving amplitude and phase modulations, investigating performance
17 p2745 A71-35590

Stroboscopic coherent light source for vibrational analysis by holographic interferometry using Pockels cell laser modulator
18 p2923 A71-36610

High speed rotating optical attenuator for sub-second sawtooth radiance pulse generation for detection, cooling or heating experiments
19 p3063 A71-37249

High voltage pulse shaping circuits for Kerr cell polarization shifters for modulating and deflecting monochromatic laser radiation
19 p3071 A71-37255

Gas discharge-current modulation noise of He-Ne laser, using sinusoidal signal at various frequencies
19 p3072 A71-37698

Harmonically modulated reflected light signals phase shift and demodulation, assuming single scattering
19 p3018 A71-37975

Design considerations for bulk solid state acousto-optic devices in light diffraction and modulation applications
19 p3066 A71-38411

Electro-optic mode locking of dual polarization carbon dioxide laser using intracavity birefringence modulation
20 p3244 A71-39096

Single and double pass traveling wave electro-optic light modulator phase retardation transient response calculation
20 p3235 A71-39180

Piezoelectric transducer materials and techniques for ultrasonic devices, covering delay lines, light deflectors and modulator operating above 100 MHz
20 p3237 A71-39256

Gas laser asynchronous coupling modulation, examining dependence on lasing threshold, optical spectrum and transition line shape
20 p3199 A71-39811

Spectral density modulation visibility at Michelson interferometer exit illuminated with white light parallel beam
21 p3375 A71-40072

Thin film optical waveguide TE-TM mode converters, using gyrotropic or anisotropic substrate material
22 p3356 A71-41806

IR modulator in space equipment, considering Fabry-Perot cavity with variable plate separation
22 p3544 A71-42138

He-Ne laser emission modulation through active element excitation source, using tube for discharge gap characteristics changes
22 p3558 A71-42266

Interfering beams amplitude modulation, applying optical heterodyne techniques
22 p3512 A71-42321

Savart plate Francon modification at arbitrary angles to optic axis, examining view field limiting factors and fringe patterns
22 p3549 A71-42554

Diffuse object scanned illumination hologram recording, discussing intermodulation flare light elimination for speed and reconstruction efficiency
22 p3549 A71-42561

Atmospheric visibility/light extinction/measurements from modulated CW laser backscattered signal
22 p3549 A71-42565

Numerical analysis of large signal output characteristics for directly modulated GaAs junction injection lasers, investigating resonance phenomenon
23 p3683 A71-43351

Light modulator based on Doppler effect and diffraction, providing spatially separated beams with different wavelengths
23 p3678 A71-43353

Mach-Zehnder interferometric measurement of modulation transfer function of optical instrument disturbed by turbulent atmosphere
23 p3679 A71-43893

Photoelectric localization of features via optical signal modulation, noting sensitivity dependence on illumination type
23 p3679 A71-43895

Magnetic modulation observation in plasma light scattering spectra experiments, noting dependence on angle between scattering and magnetic field vectors
23 p3713 A71-44150

Pulsed modulation of continuous laser resonator Q factor, recording output on oscilloscope
24 p3834 A71-45045

Laser radiation intensity modulation by time varying magnetic field
24 p3834 A71-45055

He-Ne laser radiation modulator at 1.5 GHz using X and Z cut lithium niobate crystals in toroidal microwave cavity
24 p3835 A71-45265

LIGHT PRESSURE
U ILLUMINANCE
LIGHT PROBES
U LIGHT BEAMS
LIGHT SCATTERING
NT HALOS

Magnetic fields measurement in plasmas by laser scattering, discussing theory and applications
01 p0133 A71-10747

CW He-Ne laser beam scattering observation for artificial fog droplet size distribution during evolution stages
01 p0094 A71-10831

Optical scatter channel transmission characteristics, using mathematical model consistent with radiative transfer theory and probability-computing receiver
02 p0249 A71-12012

Background noise in optical communication system, considering direct, reflected and scattered radiation sources in atmosphere
02 p0213 A71-12015

Direct detection, heterodyne and optimum receivers for optical scattering channels in digital communication
02 p0214 A71-12020

Transient response measurements of multiple scattered laser radiation from clouds as function of view field
02 p0260 A71-12032

Brightness field spatial structure of solar radiation reflected from earth by Cosmos 149 satellite, discussing homogeneity and isotropy
02 p0246 A71-12114

Unsteady light field spatial moments in turbid medium boundary layer with intense anisotropic scattering during illumination by narrow beam
02 p0277 A71-12116

Planetary surfaces photometry, discussing parameters, phase laws, albedos, spectral reflectivities, phase function theory and light scattering
02 p0309 A71-12156

Luminescence of optically reflecting nebulae related to shape of light scattering indicatrix of interstellar dust particles
02 p0311 A71-12355

Spherical nebula BESM-3M radiation intensity fluxes, calculating optical thickness, particle albedos and light scattering indicatrices
02 p0312 A71-12359

Stimulated light scattering by capillary waves on incompressible fluid surface or by Rayleigh waves on surface of isotropic solid body with small opticoelastic moduli
02 p0285 A71-12505

Quantum theory for spontaneous parametric light scattering, determining photon spectral distribution
02 p0285 A71-12506

Matrix method for multiple scattering extended to polarized light
03 p0458 A71-13611

Light scattering geometry from infinite cylinder shown consistent with Rayleigh-Gans formalism
03 p0425 A71-13647

Scattered light method application to two dimensional plane stress problems, considering fringe spacing and gradient relationship
03 p0426 A71-13779

Light scattering and polarization measurements in upper atmosphere by modulated searchlight, indicating dust layers
03 p0414 A71-14018

Optico-acoustical deflector with high resolving capability, using Bragg light diffraction by ultrasonic waves
04 p0604 A71-14627

Electron temperature measurement in electromagnetic shock tube by spectroscopy and ruby laser light scattering in plasma, examining validity of local thermal equilibrium assumption
04 p0632 A71-14688

Doppler effect in laser beam probe of scattering objects, using interferometer for scattered light intensity angular distribution relation to hologram sizes
04 p0608 A71-15117

Soviet book on optics of scattering media covering visible radiation transfer in water, atmosphere, powders, tissues, dyes, inhomogeneous systems and photometry
04 p0626 A71-15224

AG Vir /HD 104350/ orbital element variations and light curve distortions, using least squares method
04 p0651 A71-15665

Doubly scattered radiation magnitude as function of heights and aerosol concentrations for bistatic laser radar
04 p0609 A71-15761

Gegenschein photographic and photoelectric scan observations, considering origin in light reflection from interplanetary dust outside earth orbit
04 p0659 A71-15853

Optically thick clouds reflected light radiance and polarization for haze and nimbostratus models
05 p0781 A71-16252

Principal stresses separation method combining conventional isocline parameter and isochromatic fringe order measurements and scattered light method
05 p0822 A71-16373

Divergent laser light beams continuous electro-optical deflection using prism with single crystal at Curie temperature in cryostat
05 p0763 A71-16834

Carbon dioxide laser beam thermal focusing effects on deflection in absorbing gas
05 p0763 A71-16902

Structural information propagation in optical wave fields arising in diffraction and scattering of quasi-monochromatic light by fixed objects
05 p0753 A71-16903

Light scattering from ultrathin free liquid films, calculating irradiance optical functions variation with geometry and film thickness
05 p0763 A71-16906

Rayleigh wave propagation in anisotropic substrates, using light diffraction by surface acoustic waves
05 p0783 A71-17078

Light reflection during plane cloud layer light scattering, studying zenith angles and angular brightness distribution
06 p0923 A71-17510

Relaxation theory of Rayleigh scattering of light by isotropic continuous medium, deriving spectral densities via fluctuation dissipation theorem
06 p0927 A71-17596

Backscattered radiation energy during laser beam scanning of diffusely scattering surface
07 p1123 A71-19309

Polarized light multiple scattering in planetary atmospheres, applying extended doubling method to realistic simulations with allowance for radiation polarization and azimuth dependence
07 p1153 A71-19759

Light scattering and attenuation coefficients calculation by small particle approximation, determining applicability limits from comparison with use of exact Mie formulas
07 p1160 A71-19809

Light scatterers use behind phase object in double exposure holography, determining laser radiation wave front dynamics effect on image quality
07 p1114 A71-20189

Scattered light depolarization measurement near carbon dioxide critical temperature, using He-Ne laser
07 p1127 A71-20379

Gaseous plasma diagnostics by light scattering for localized minimal perturbing measurement of temperature and density parameters
07 p1172 A71-20504

Rayleigh-Brillouin light scattering in compressed hydrogen, hydrogen deuteride and deuterium, noting discrepancy between observed and theoretical spectra
08 p1301 A71-20743

Mathematical analysis of eye transparency, discussing light scattering from normal corneal stroma, swollen opaque corneas and cataractous lens
08 p1240 A71-21371

Low energy proton irradiation induced thin polymer contaminant films effect on far UV reflecting mirrors reflectance and scattered light
08 p1290 A71-21382

Single mode laser pumping generator of stimulated Brillouin scattering pulse in water
09 p1462 A71-22399

Laser applications in physics research, discussing nonlinear optics and spectroscopy, time and distance measurements and Raman and Rayleigh light scattering
09 p1462 A71-22585

High beta collisionless shock wave turbulence, discussing frequency and wavenumber spectra and turbulence level measurements by light scattering technique
09 p1504 A71-23255

Noise reduction in Rudd type laser velocimeter by conversion to light scattering system
09 p1453 A71-23695

Large angle Rayleigh light scattering for density fluctuations determination in dilute gases with wavelength comparable to mean free path
10 p1642 A71-24835

Light scattering from gas thermal fluctuations, deriving density-density correlation function over various pressures
10 p1642 A71-24836

Stimulated Mandelstam-Brillouin, Rayleigh line wing and thermal light scattering, discussing fine structure, glass fracture and components shift
10 p1621 A71-24837

Angular discretization effect on calculations of emerging radiation and integrated albedo from model cloudy atmosphere, using multiple scattering with terrestrial particle phase functions

10 p1643 A71-24972

Skylight scattering components from zenith for intensity/polarization variation during twilight and upper atmosphere dust sounding

10 p1607 A71-25114

Venus atmosphere spectra, emphasizing line and continuum absorption coefficients relative to scattering

11 p1823 A71-25697

Refraction correction in photometer with cylindrical light scattering cell and detectors, describing experimental testing by mathematical and geometrical analysis

11 p1799 A71-26063

Laser radiation scattering, dividing into linear and nonlinear phenomena

11 p1775 A71-26082

Vibration modes of objects and light scattering from rough surfaces, using laser speckle changes

11 p1776 A71-26138

Spacecraft windows optical degradation from contamination with condensed particles, presenting light scatter measurement results [AIAA PAPER 71-472]

11 p1833 A71-26252

Thomson light diffusion in laser diagnostics, deducing electron density/temperature and ion temperature

11 p1776 A71-26274

Camera shutter spatial frequency spectrum and components light scattering effects on negatives quality based on composite image representation systems theory

11 p1767 A71-26469

Venus polarimetric observational data comparison with polarization characteristics of radiation scattered at gamma-distribution particle sizes, determining refractivity and particle radius

12 p1964 A71-27088

Optical properties and relative density of lunar surface layer, deriving light reflection and scattering formulas

12 p1964 A71-27089

Laser light scattering by fuel droplets in flame combustion zone, measuring intensity distribution with contactless optical probe

13 p2065 A71-27886

Inhomogeneous planetary atmosphere resonantly scattered sunlight, calculating intensities with frequency redistribution functions

13 p2100 A71-28346

Raman effect quantum theory, considering light scattering about atomic system

13 p2078 A71-28449

Ion temperature measurement for plasma focus, using laser light scattering

13 p2079 A71-28673

Light pulses reflection from water and ice in clouds, using Monte Carlo technique for all orders of multiple scattering

13 p2031 A71-28795

Laser light enhanced scattering by optical mixing of beams in plasma

13 p2079 A71-28797

Inverted combination light scattering in liquid and solid crystals, showing polarization effects on absorption coefficient

13 p2101 A71-29020

Light combination scattering in organic liquids, measuring frequency dependence with dye laser technique

13 p2080 A71-29021

Fine crystalline substances forced combination scattering at liquid nitrogen temperature, using ultrashort ruby laser pulses for excitation spectra

13 p2080 A71-29022

Cylindrical lithium niobate single crystal acoustic propagation, determining speed, damping and sound reflection with He-Ne laser light scattering at hypersonic oscillations

13 p2080 A71-29024

Moliere high energy solution of Schroedinger scattering equation for optical propagation in turbulent atmosphere, noting inconsistency of Born-Rytov approximation

13 p2102 A71-29441

Fog evolution and droplet radii spectrum determination by scattered laser beam angular distribution measurement

13 p2082 A71-29484

Principal stresses separation in nitrocellulose transparent material with photoelastoplastic properties, using scattered light method

14 p2322 A71-29700

Jupiter reflected light, examining model having elliptical polarization by surface layer scattering

14 p2306 A71-29730

Altitude size distribution of atmospheric aerosol from sky radiance measurements in sun aureole region, calculating sunlight forward single scattering

14 p2310 A71-30125

Angular function computation in Mie theory of light scattering, considering sequential computer programming economics

14 p2207 A71-30150

Electron temperature and density measurement apparatus using Thomson scattering of laser light for collisionless MHD shock waves

14 p2280 A71-30424

Combination light scattering in liquids, single crystal and crystal powders, employing long lived argon laser with internal mirrors and large diameter capillaries

14 p2255 A71-30585

Alphanumeric display devices with liquid crystal and dynamic light scattering for low voltage, power, cost and fabrication advantages, testing performance

14 p2249 A71-31029

Plane parallel inhomogeneous atmosphere, investigating anisotropic light scattering

15 p2448 A71-31332

Direct measurement of spatial velocity correlation functions in turbulent flow by conditional probability of scattered light

15 p2449 A71-31866

Photon dwell time in one dimensionally isotropically scattering medium, assuming absorbed state as arbitrary function of optical thickness

15 p2492 A71-32460

Scattered light effects on sunspot intensities observations during Mercury occultation and near solar limb

15 p2496 A71-32739

Calculational method for predicting angular distribution of sunlight unpwelling flux scattered by atmosphere and reflected by ground, using Monte Carlo data

16 p2562 A71-33130

Low density plasma diagnostics using Thomson scattering of laser light

16 p2618 A71-33161

Polarized light multiple scattering in homogeneous plane parallel planetary atmospheres, considering Rayleigh scattering, test models and phase function obtained by neglecting polarization

16 p2632 A71-33320

Lasers as light sources, discussing Rayleigh, Tyndall, Raman and Thomson scatterings from various media

16 p2612 A71-33373

Diffuse skylight measurement for atmospheric dust particle concentration, considering sunlight scattering by air molecules and aerosol layers

16 p2567 A71-33767

Nonlinear optics of combination scattering of IR laser radiation in crystals and statistical frequency mixing-multiplication of polarons and longitudinal phonons

16 p2588 A71-33997

Short narrow light pulse reflection from thick turbid medium with strong anisotropic scattering, obtaining backscattering signal power from unsteady transport equation solution

16 p2544 A71-34105

Atmospheric optics and geophysics problems modeling arrangement reproducing radiation field within light scattering medium

16 p2605 A71-34106

Plasma conductivity frequencies, including electromagnetic wave propagation in alternating field and scattered light intensities

17 p2786 A71-34276

Coherence properties deterioration of laser beam by atmospheric molecular scattering, considering effect on communication system performance

17 p2753 A71-34426

UV Raman remote gas sensors incorporating laser scattered radiation with high resolution monochromator

17 p2753 A71-35292

Scattered light circular polarization data from Jupiter and other planets indicating nonmagnetic origin

17 p2805 A71-35377

Doubling method application to multiple scattering of polarized light, studying Venus visible disk reflection of sunlight

17 p2784 A71-35569

Searchlight problem with isotropic scattering for semiinfinite and finite geometries, computing transmission functions for Fourier intensity components by kernel approximation method

17 p2839 A71-35571

Aerosol size distribution from lidar light scattering polarization properties, constructing inversion model

17 p2770 A71-35806

Linearly polarized lidar light scattering in spherically symmetrical uniformly distributed cloud water drops, investigating multiple backscattering effects on depolarization

17 p2770 A71-35807

Time dependent multiple backscattering of pulsed light for linearly polarized incident radiation

17 p2709 A71-35809

Light wave Rayleigh interferometer for concentration gradient measurements in liquid systems with mass transport

18 p2917 A71-36052

Optical homodyne detection of light signal wave front scattered by moving surface with normally distributed roughness, calculating conditions for optimum SNR

18 p2930 A71-36052

Spectral distribution moments of light scattering due to polarizability changes in colliding molecule pair

18 p2947 A71-36199

Visual detection of stars in spacecraft environment, considering window cleanliness and antireflection coating effect on light scattering

18 p2864 A71-36278

Laser beam operation, light scattering in gas, holography applications and flow analyses

18 p2931 A71-36421

Laser velocimeter for wide range velocity measurement, using photodetector to observe light scattering by particles flowing across fringe pattern

18 p2932 A71-36618

Optical dielectric slab waveguides with core thickness variations, computing crosstalk due to light scattering in terms of guided mode radiation loss

19 p3014 A71-37215

Nonspherical axisymmetric model of minimum type solar corona, investigating light scattering electron density distribution relation to brightness and polarization

19 p3131 A71-37240

Venus polarimetric observational data comparison with polarization characteristics of radiation scattered at gamma-distribution particle sizes, determining refractivity and particle radius

19 p3133 A71-37438

Optical properties and relative density of lunar surface layer, deriving light reflection and scattering formulas

19 p3133 A71-37439

Gas laser operating on mixture of He and Cd 114 for excitation of scattered light spectra

19 p3073 A71-37792

Mg compounds family of antiferroelectric structured small-gap semiconductors, investigating surface light scattering properties by Raman scattering techniques

19 p3119 A71-37870

Harmonically modulated reflected light signals phase shift and demodulation, assuming single scattering

19 p3018 A71-37975

Design considerations for bulk solid state acoustic devices in light diffraction and modulation applications

19 p3066 A71-38411

Artificial fog thermodynamic conditions and evolution data, using scattered laser beam angular distribution measurements

19 p3091 A71-38586

Fog droplet size spectral distribution from artificial fog induced He-Ne laser beam scatter, using five photometers for angular distribution measurements

19 p3091 A71-38657

Sunspot intensity during 9 May 1970 Mercury transit with corrections for scattered light from solar limb observations

19 p3147 A71-38669

Lithium niobate hypersound attenuation and reflection coefficients frequency dependence determination by scattering laser light at hypersonic oscillations

20 p3244 A71-39162

Rhodochrosite /manganese carbonate/ complex refractivity determination for correlation between optical reflection, attenuation and scattering coefficients

20 p3269 A71-39185

Circumsolar scattered radiation effects on ozonometer reading accuracy, taking into account effect of sun angular altitude under cloudless conditions

20 p3237 A71-39329

Atmospheric transmissivity measurement from backscattered light intensity, deriving model based on light beam geometry and path

20 p3238 A71-39333

Two-parametric models of interplanetary dust distribution predictions involving zodiacal light scattering measurements from space probes for in- and out-of-ecliptic missions

20 p3219 A71-39637

Incident meteor flux density seasonal variations from radio reflections from trains and light scattering from micrometeoroids

20 p3298 A71-39642

Sunlight scattering by dust in upper atmosphere from primary twilight intensities investigations

20 p3219 A71-39647

Turbulence measurement by crossed laser beam attenuation due to scattering from particles in clean or seeded flow, studying damping and transport of matter

21 p3392 A71-40400

Hypersonic wind tunnel air condensation detection by light scattering instrumentation, discussing stagnation temperature condensation

21 p3364 A71-40405

Molecular iodine vapor absorption filter for stray laser light in Brillouin and Raman scattering

21 p3393 A71-41042

Atomic level interference and hyperfine splitting effects on angular and polarization distributions of resonantly scattered light in magnetic field
21 p3420 A71-41120

Enhanced scattering signal observation at electrostatic plasma wave frequency by focusing Q switched laser beam on hydrogen plasma
22 p3580 A71-41596

Cylindrical plasma column light scattering diagnostics by focusing carbon dioxide laser beam on center
22 p3580 A71-41601

Linear system model for multiple scattering light transmission through optically thick clouds, calculating optical effects by four dimensional linear superposition integral
22 p3575 A71-41789

Optico-acoustical deflector with high resolving waves, using Bragg light diffraction by ultrasonic waves
22 p3558 A71-42267

Monte Carlo method calculation for light pulse reflection from clouds for all orders of multiple scattering
22 p3576 A71-42562

Atmospheric self-aligning dual-scatter laser Doppler velocimeter, calculating backscattered power, range, wavelength and scatter centers number relationships
22 p3559 A71-42564

Semiinfinite plane parallel inhomogeneous atmosphere anisotropic light scattering
22 p3576 A71-42607

Isotropic light scattering in unsteady plane layer of finite optical thickness, obtaining reflection and transmission coefficients for radiative transfer
22 p3607 A71-42869

Interplanetary time delay and light deflection measurements anomalies, investigating gravitational and electromagnetic fields interaction
23 p3766 A71-43824

Scattered light effect on measured facula-to-photosphere contrast, leading to hotter average facula model
24 p3868 A71-44460

Boundary retardation with respect to fringes in scattered light photoelasticity, using quarter wave plate
24 p3881 A71-44776

LIGHT SCATTERING METERS
Optical fibers scattering loss measurement, describing Si solar cell integrating cube scattering detector
03 p0424 A71-13638

LIGHT SOURCES
NT ILLUMINATORS
Shadow and interference methods sensitivity for low density gas flows improved via monochromatic light source
02 p0248 A71-11937

Carbon dioxide laser optical pumping by resonant emission from alkali metal lamp
03 p0434 A71-13290

Pulsed laser holography, discussing illumination source and holocameras for high contrast recording with Q switched ruby lasers
04 p0597 A71-15363

Stellar transit time photoelectric instruments time lag measurements by variable flux light source
04 p0599 A71-15382

Optical hyperfine splitting of Rb resonance lines of atomic beam light source, using Fabry-Perot interferometer
07 p1111 A71-19488

Fiber optic laser devices properties and potential applications as amplifiers, logic elements, active mode selectors and intense light sources
07 p1124 A71-19781

Light source displacement distortions in shadow visualization for flight trainers involving terrain scale and landing simulation
08 p1271 A71-20796

Carbon dioxide laser optical pumping by resonant emission from alkali metal lamp
09 p1464 A71-23266

High temperature plasmas optical properties measurement by plasma spectroscopy, using gas driven shock tube as light source
12 p1940 A71-27276

Shock heated Ar thermal conductivity measurements by following temperature boundary layer with time resolved interferograms with HF laser stroboscope light source
12 p1986 A71-27578

Rotating mirror wavelength shifter of laser light source for use in electronic spectroscopy, noting measurements with high speed Doppler wheel in vacuum
13 p2067 A71-28445

Interference spectrography and spectrometry techniques, describing transverse achromatic light source beam splitting and frequency analysis of photographed fringes
14 p2238 A71-29804

Automatic telescope guidance system for faint light source tracking, using cumulative photocurrent mismatch signal storage
14 p2271 A71-29994

Lasers as light sources, discussing Rayleigh, Tyndall, Raman and Thomson scatterings from various media
16 p2612 A71-33373

Spatial coherence measurement for two points of pseudothermal light source by comparing photocathode luminous intensity probability density and photoelectron distribution moments
17 p2754 A71-35585

Landé g factors measurement of excited electronic states in Ne 20 II and III, using alignment of radiating particles in beam foil light source
18 p2949 A71-35978

Colored light sources luminosity determination by Helmholtz-Kohlrausch effect, discussing brilliant and fluorescent stimulus
18 p2854 A71-36003

Color perception with achromatic stimulation by changing intensity of stationary light source to produce flicker colors
18 p2864 A71-36004

Crystal laser pyrotechnic illumination lamps with noncompacted explosive mixture, noting Nd ion doped calcium tungstate and YAG laser tests
19 p3073 A71-37788

High resolution portable hologram recording camera with pulsed ruby laser light source and rechargeable storage batteries as self contained power supply
21 p3380 A71-40926

Light flux spatial coherence in visual reception, considering aventurine spots perception as point light source
21 p3344 A71-41065

Light sources selection and design for visibility range sensors employing backscattering
21 p3382 A71-41236

Holographic image reconstruction analysis based on two beam interferometry by spatially incoherent light source, obtaining optical transfer function
22 p3539 A71-41740

Staircase array and diode stacking moderate power GaAlAs injection laser light sources at room temperature
23 p3685 A71-43504

Color photography of magnetic particle and penetrant indications, discussing light sources, camera types, filter and film selection, exposure and spectral characteristics of indications
24 p3829 A71-45283

LIGHT SPEED
Light speed invariance in special theory of relativity concerning Galilean coordinates
01 p0127 A71-10601

Eddington theory validity based on formulas connecting light velocity, Planck and gravitational constants and electron, proton and neutron masses
04 p0626 A71-15136

Pulsars optical and X ray luminosity secular decrease, examining emission close to velocity of light radius
05 p0807 A71-16209

General relativity theory tests, discussing Einstein effects existence and light velocity in gravitational field
06 p0971 A71-18246

Critique of Woodward-Young hypothesis of frequency dependence of light velocity in gravitational fields based on variable stars observations, considering photon rest mass
20 p3286 A71-38836

Light ponderability in gravitation theory, discussing hypothetical Freundlich effect of light velocity dependence on radiation field intensity, based on Maxwell electrodynamics nonlinear generalization
20 p3270 A71-39457

Photon mass terrestrial and extraterrestrial limit measurements, discussing speed of light frequency dependence, Coulomb law analog in magnetostatics energy conservation, etc
21 p3418 A71-40674

Interstellar space flight kinematics near light speed, discussing theoretical requirements for relativistic rocket engines
22 p3600 A71-42000

Light velocity measurements by optical and microwave techniques, noting electromagnetic constant error and role in distance measurement and physical theories development
24 p3827 A71-44996

LIGHT TRANSMISSION
NT LIGHT SCATTERING
Double beam spectrophotometer for small transmission changes, discussing measurement range and uncertainty
02 p0247 A71-11721

Beam waveguides for optical transmission, considering cost, attenuation, dispersion and flexibility
02 p0249 A71-12009

Clear turbulent atmosphere effects on optical transmission characteristics and communication system design
02 p0213 A71-12010

Atmospheric refractive index average structural characteristics measurement over 25 km light propagation path, noting diurnal variation
02 p0245 A71-12011

Q switched ruby laser facility for measuring light pulse transmission spatial and temporal response through clouds
02 p0213 A71-12013

Coherent light wave propagation in two level system, discussing wave periodicity, deviation from sinusoidal form, interaction with medium and energy loss and gain effects
02 p0215 A71-12319

Cladded fibers propagation modes launching coefficients evaluation by Gaussian field laser beam
03 p0433 A71-13170

Weak nonlinear absorption effects shown by passive optical elements placed in laser resonator cavity with large angular emission divergence
03 p0435 A71-13511

Light propagation in spherically symmetric cosmic dust distribution, obtaining conditions for escape from region of gravitational collapse to one of expansion
04 p0642 A71-14813

Coherent light propagation guidance by helicoidal guide, calculating transverse electric field distribution for luminous beam variations
05 p0722 A71-16705

Telecommunications by lasers, considering atmospheric propagation possibilities and limitations
06 p0869 A71-18064

Light propagation in mixmaster universe model based on Einstein equations solution
06 p0974 A71-18428

Optical fiber index profiles for long distance light transmission, comparing single and multimode, rectangular and parabolic guides
07 p1159 A71-19174

Light attenuation and depolarization measurements on glass fibers in index matching oil
07 p1159 A71-19212

Laser beam propagation through atmosphere, measuring phase variation dependence on turbulent temperature structure for comparison with prediction
07 p1123 A71-19574

Light transmitting vacuum deposited NaF polycrystal for IR measurements
08 p1343 A71-21288

IR laser propagation through fog with droplet vaporization, assuming incident electromagnetic radiation as plane harmonic wave
08 p1302 A71-21392

Laser radiation amplitude and phase fluctuations in complex media, using interferometry
09 p1459 A71-22143

Hydrogen-like centers in semiconductors, investigating secondary optical absorption
09 p1506 A71-22144

Intensity logarithm fluctuations of focused laser beam propagating in summer daytime atmosphere at 250 and 650 meter path lengths
09 p1404 A71-22224

Wave structure and mutual coherence functions of optical wave propagating in turbulent atmosphere, considering signal to noise ratio
10 p1641 A71-23948

Helmholtz reciprocity theorem extension to clear turbulent atmosphere, defining Green functions to characterize optical propagation in opposite directions between parallel planar apertures
10 p1641 A71-23949

Lydia asteroid observations, presenting light curves brightness and phase functions near opposition
10 p1669 A71-24177

Light propagation in mixmaster universe model based on Einstein equations solution
12 p1955 A71-26578

Optical beam propagation, determining turbulent medium effects with holographic wave front reconstruction technique
12 p1904 A71-26795

Fiber optics for spectroscopic illumination, discussing absolute and angular transmission measurements and optical angular transfer function calculation
12 p1905 A71-26806

Atmospheric turbulence effects on focused coaxial carbon dioxide and He-Ne laser beam propagation
13 p2078 A71-28525

Inhomogeneous atmosphere transmission functions, noting Lindholm line shift in O absorption spectra effects
13 p2063 A71-29019

Ultrashort optical pulse propagation through two level attenuating or amplifying atomic medium
13 p2080 A71-29136

Optical interferometer with evacuated light paths, describing operating principles, cost efficiency and compactness
14 p2238 A71-29803

Photoelastic stress analysis, examining light transformations in plane and circular polariscopes by light ellipse method
14 p2323 A71-29848

Light propagation through moving gas, computing beam bending into wind and self defocusing due to gas heating

14 p2274 A71-30129

Light transmission homogeneity measurements of optical materials, using Murty interferometer

14 p2242 A71-30154

Asymptotic intensity fluctuations of plane light wave propagating in turbulent medium, using parabolic equation and Markov model

15 p2387 A71-31190

Picosecond duration coherent light pulse propagation in resonant medium, discussing basic equation, self induced transparency, Bloch equations, soluble model and higher conservation laws

17 p2754 A71-35375

Optical transmission in unexposed phenolic resin base laminates with silica cloth reinforcements, studying stabilization treatments, pyrolysis and incident radiation spectral distribution

17 p2838 A71-35473

ERTS satellite-based laser communication system, calculating cloud cover effect on clear line-of-sight light transmission probability through atmosphere to ground station

18 p2876 A71-36472

IR CdTe-HgTe detectors for laser space communications at 10.6 microns, using directivity of light waves in vacuo for wideband transmission

18 p2892 A71-36566

Star comparator automatic azimuth system using long evacuated tunnel transfer to underground inertial guidance laboratory

[AIAA PAPER 71-925]

19 p3102 A71-38328

Hydrodynamic effects on laser beam propagation through gases by finite difference solution, applying to trapping, acoustic and light amplifications and banana self focusing

20 p3242 A71-38838

Transfer function for transmission through maser medium, cancelling signal distortions due to propagation

20 p3242 A71-38877

Atmospheric optical transmission coefficient measurements using steerable laser radar system

21 p3372 A71-40040

Optical absorption and electron spin resonance in KCl with and without KOH, noting F band existence

21 p3414 A71-40070

Stereo viewing transmission/reflection display by producing stereopair image on CRT screen with polarizing polaroid sheets

21 p3376 A71-40126

Nonlinear effects in high power Nd-YAG CW IR laser beam transmission through defocusing media

21 p3394 A71-41110

Light intensity distribution inhomogeneity in transmission by GaAs single crystals, using schlieren method

21 p3428 A71-41201

Photosensitive epoxy resin coating light path propagation variation measurements, using continuous radiation gas laser and Fabry-Perot interferometers

22 p3555 A71-41615

Linear system model for multiple scattering light transmission through optically thick clouds, calculating optical effects by four dimensional linear superposition integral

22 p3575 A71-41789

Light wave attenuation in fog, mist, rainfall and snowfall during propagation through atmosphere, deriving semiempirical formulas for attenuation rate relationship to visibility

22 p3569 A71-42523

Weakly guiding glass fiber parameters design formulas and functions for optical communication, considering propagation constant, mode delay, cladding field depth and power distribution

22 p3576 A71-42557

Atmospheric visibility/light extinction/measurements from modulated CW laser backscattered signal

22 p3549 A71-42565

Narrow light beam transmission in weakly nonlinear turbulent atmosphere, calculating large scale permittivity inhomogeneity effect on average intensity by model

23 p3645 A71-43564

Collimated light beam transmission in turbulent atmosphere above ground surface, comparing measured coherence function with calculation

23 p3645 A71-43565

Cavities geometry in steady or periodic supercavitating flow from light beam transmission in flow tunnel

23 p3664 A71-44005

Incoherent light bandpass filter to amplify detail contrast of optical system

23 p3679 A71-44010

Optimum signal processing for distance measurement with lasers, considering propagation, detection and measure process statistical properties, optical radar and sine wave modulation

24 p3834 A71-45206

Laser beam spot dancing during propagation through turbulent atmosphere, using Kolmogoroff structure function of refractivity and geometrical optics

24 p3834 A71-45208

Jones reflection and transmission matrices representation for beam splitters, investigating reversibility and action on incident light amplitude and/or phase

24 p3849 A71-45210

LIGHTHILL GAS MODEL

Near equilibrium solutions of steady spherical expansion of monatomic gas into vacuum, using Lighthill technique for higher order analysis

09 p1430 A71-22086

Lighthill model applications to dissociating gas, considering function related to Riemann variables and nondissociating gas presence

10 p1593 A71-24269

LIGHTHILL METHOD

Waves generated by obstacle steady motion along axis of uniformly rotating electrically conducting homogeneous fluid, using Lighthill technique

10 p1595 A71-24624

Aerodynamic noise scattering near Lighthill multiples, considering intense near-field energy conversion into sound waves

11 p1705 A71-26448

Aerodynamic combustion noise generation from premixed or diffusion open turbulent flames, using fluid mechanics and Lighthill method

23 p3781 A71-43448

Open cylindrical thermosiphon for laminar flow, predicting heat transfer performance by finite difference solution for comparison with Lighthill analysis

24 p3889 A71-44973

LIGHTING

U ILLUMINATING

LIGHTING EQUIPMENT

NT AIRCRAFT LIGHTS

NT ARC LAMPS

NT FLASH LAMPS

NT ILLUMINATORS

NT LUMINAIRES

NT QUARTZ LAMPS

NT RUNWAY LIGHTS

NT SEARCHLIGHTS

NT XENON LAMPS

Airport lighting facilities in Japan, considering fixtures, marker and obstruction lights and apron floodlight

07 p1084 A71-20355

Civil aircraft cockpit lighting evaluation guidelines

19 p2999 A71-38241

LIGHTNING

Computerized acquisition and processing of radar precipitation signals and lightning data

01 p0050 A71-10595

Lightning hazards for helicopters, discussing components vulnerability and protective design requirements

04 p0531 A71-15412

Lightning induced voltages in aircraft wing structures, examining induced voltage across load impedances in electric circuits

06 p0874 A71-17581

Subprotonospheric and ion cyclotron whistlers generated by same lightning discharge observed by OV1-10 satellite

06 p0869 A71-17995

Apollo 12 lightning incident, discussing atmospheric conditions, damage and discharge hazard minimization

[SAE PAPER 700938]

07 p1208 A71-19925

Lightning and static electricity - Conference, San Diego, December 1970

07 p1019 A71-19926

Roughrider F-100F aircraft flights in thunderstorms and Apollo 12 launch electric field measurements, comparing patterns and magnitudes of lightning strikes to vehicles

07 p1208 A71-19927

Lightning stroke probability model for point selection on aerospace vehicles

07 p1020 A71-19928

Statistical information on lightning and static hazards relative to airworthiness

07 p1020 A71-19929

Materials and construction techniques in lightning protection for aircraft and helicopters

07 p1020 A71-19930

Artificial lightning generation facilities for aircraft component developmental testing by manufacturer

07 p1020 A71-19931

Lightning current transfer tests of p-static discharger for aircraft installations

07 p1020 A71-19935

Swept lightning stroke effects on aircraft design involving Ti and Al sheets

07 p1020 A71-19936

Lightning and static electricity effects on helicopter design, considering rotor protection, cargo hook operation and passive dischargers for radio interference reduction

07 p1021 A71-19938

Lightning protection for nonmetallic helicopter rotor blades

07 p1021 A71-19939

Late model F-4 air superiority aircraft and electronic flight control systems protection against lightning discharges damage to electric and electronic systems

07 p1021 A71-19940

Lightning and surge protection devices for survivability of aircraft electrical systems

07 p1021 A71-19941

Lightning protection for dielectric composites, analyzing damage from shock waves, vaporization pressure, magnetic forces and burning

07 p1021 A71-19942

Composite plastic aircraft structures lightning protection, considering hazard to composite materials and use of metal filled or plasma sprayed coatings and metal foil coverings

07 p1021 A71-19943

Lightning protective coatings for boron and graphite fiber reinforced plastics

07 p1021 A71-19944

Ground space facilities protection from lightning and electromagnetic interference

07 p1084 A71-19947

Lightning and static electricity hazards at Kennedy Space Center, discussing meteorological aspects

07 p1084 A71-19948

Lightning flash-ground strokes VHF radio pictures by hyperbolic position fixing system, obtaining three dimensional sferics fixes as function of time

08 p3225 A71-20880

Horizontally and vertically polarized sferic signals from lightning discharges by airborne instrumentation, using pattern recognition approach

08 p3225 A71-20883

Whistlers with harmonic bands caused by multiple stroke lightning, using Injun 5 VLF data

08 p1283 A71-21649

Lightning return stroke electric field intensity exact expression derivation, obtaining charge moment equation approximation

09 p1488 A71-23443

Power spectra and electrostatic mechanism of thunder from intercloud and cloud to ground lightning using analog and digital methods

09 p1489 A71-23444

ELF atmospherics pulse trains recordings at widely separated stations for spectral amplitude ratio differentials, using lightning and ionospheric heating mechanisms

09 p1489 A71-23445

Ball lightning as optical illusion resulting from positive afterimages, noting reports of energy release from ball as possible refuting evidence

10 p1599 A71-23751

Radiation measurements near thunderstorms and tornadoes, testing hypothesis of meteoritic matter-antimatter annihilation mechanism for ball lightning

10 p1599 A71-23752

Comparison of lightning and long laboratory spark, considering luminous processes, current, voltage, power, energy inputs, radiated visible spectra, electron density, etc

12 p1939 A71-27266

Nature and average magnitude of lightning discharges causing transient excitation of earth-ionosphere cavity resonance

13 p2054 A71-27795

Lightning problem from electrodynamic viewpoint, considering vertical discharge channel, charge distribution, current and nonuniform inducing fields

13 p2097 A71-28394

Thunderstorms and lightning flashes location determination by ground based and satellite measurements of disturbance induced RF noise, using atmospheric spectral characteristics for range estimating methods

14 p2203 A71-30958

Global distribution and location of large lightning discharges from single station observations of transient ELF disturbances propagated in earth-ionosphere cavity

15 p2394 A71-31429

Frequency spectrum of lightning discharges, developing mathematical model to account for atmospheric difference between cloud-ground and cloud-cloud discharges

16 p2604 A71-33070

Rockets and launch operations protection from atmospheric electricity at Kennedy Space Center, discussing current and future lightning suppression

18 p2913 A71-36451

Radome lightning protection systems involving electrostatic shield, considering effect on electromagnetic characteristics and radiation patterns of nearby antennas

19 p3031 A71-38450

Lightning observation by OSO-E satellite, suggesting maximum thunderstorm incidence over North Atlantic Ocean

19 p3061 A71-38675

Pulse duration of atmospheric radio noise bursts at 3 MHz from lightning flashes, considering effect on data communication

23 p3643 A71-42970

LIGHTS

U LUMINAIRES

LIMBS

Semiautomatic device for vertical circle limb photographs measurement, involving beam splitting with subsequent comparison of modulated components

04 p0591 A71-14850

Automatic micrometer for measurement of limb graduations and scales, basing method on Archimedes rotating spiral principle

04 p0591 A71-14851

Semiautomatic photoelectric apparatus for limb graduations using pivoted optical arrangement, discussing accuracy, measurement rate and reliability improvement methods for similar instruments

04 p0591 A71-14852

Venus thermal radiation limb darkening measurements, indicating complex atmospheric structure

11 p1824 A71-25699

Jupiter equatorial thermal limb darkening data, constructing atmospheric model for ammonia effects on temperature structure

12 p1966 A71-27254

LIMBS [ANATOMY]

NT ARM [ANATOMY]

NT FOREARM

NT HAND [ANATOMY]

NT KNEE [ANATOMY]

NT LEG [ANATOMY]

Human skin blood flow and venous tone in middle finger and forearm during leg muscle exercise to exhaustion

01 p0016 A71-11410

Cutaneous blood flow in anesthetized pig forelimb modified by brain temperature changes

02 p0197 A71-16671

Hind limb antagonistic muscles bioelectric activity dependence on animal rotation direction and head fixation

09 p1388 A71-22196

Structural and functional analysis of human and equine muscular drive mechanisms for extremities, deriving general rules for biomanipulators synthesis

11 p1718 A71-25619

Isotonic training effects on circulation for limb muscular strength characteristics, using peak blood flow and venous compliance measurements

11 p1719 A71-26071

Decompression sickness, investigating surface excursion diving and selection of limb bends vs CNS symptoms by tests on goats

21 p3330 A71-40344

Stereophotogrammetric measurement of body and limb volume changes after prolonged space mission

22 p3502 A71-41861

LINE

U CALCIUM OXIDES

LIMESTONE

Lime refractory fabrication and properties for high temperature applications, describing production of calcium oxide grain by sintering process from commercial calcium hydroxide

21 p3405 A71-40246

LIMITATIONS

U CONSTRAINTS

LIMITER CIRCUITS

Bandpass limiter output envelope fluctuations dependence on input form and bandwidth

05 p0730 A71-17061

FM discriminator with nonideal limiting, calculating signal to noise ratio under white Gaussian noise input

05 p0730 A71-17071

Microwave semiconductor limiter diode for decimeter operation using spark gap analog

06 p0873 A71-17540

Thermal resistance of thermal p-n junction semiconductor microwave limiter diodes in continuous and pulsed mode operation

06 p0873 A71-17543

Transistorized amplitude limiter with series connected nonlinear element and filter tuned to input signal first harmonic, describing amplitude characteristics calculation method

09 p1415 A71-22299

Transistorized microwave amplifier/limiter for upper part of decimeter wave range, suggesting limitation in automatic gain control transistors

16 p2547 A71-33499

FSK L-level or duobinary system performance evaluation under intersymbol interference, using limiter-discriminator without postdetection filter as detector

17 p2707 A71-35479

Output correlation functions of periodic signals limiting in random noise passing through zero memory devices, using Hermite polynomials method

20 p3195 A71-38857

LIMITS [MATHEMATICS]

Soviet book on limit theorems for random walks covering random walk functionals, zero mean value, finite dispersion, sequences, normalized sums, Markov functionals, etc

07 p1148 A71-20300

Satellite orbital motion, discussing idealized perturbations limiting problem from point mass

08 p1360 A71-21004

Limit cycle bounds in phase plane for self sustained vibrations of autonomous systems, using Poincare-Bendixson theorem

11 p1841 A71-25179

Binary periodic convolutional codes with lower bound everywhere stronger than Wagner on definite decoding minimum distance

11 p1731 A71-25758

Stellar mass relativistic integral theorems and upper and lower bounds for gravitational potential theory

11 p1830 A71-26106

Two dimensional hypersonic boundary layer equations solution upper and lower bounds determination as initial value problem

15 p2386 A71-31161

Lower limit on size of matter and antimatter regions in vanishing baryon number cosmology based on homogeneous intergalactic magnetic field existence

16 p2632 A71-33237

Limits theorems of occupancy problem, concerning asymptotic behavior of random particle distribution to fixed cell with equal probabilities

17 p2764 A71-34574

Turbulent hydrodynamic line stretching problem, considering asymptotic rates as application of central limit theorem for dependent random variables sums

19 p3044 A71-37729

Shear envelope of thin walled beam with semicircular cross section under creep

19 p3159 A71-38186

Extremal problems approximation conditions in functional optimal value and elements set senses, applying to study of convergence in presence of constraints

19 p3088 A71-38413

LIMONITE

Thermogravimetric analysis of goethite-rich sample of Mars type limonite, considering sorption process relation to Mars environment and polar caps

04 p0644 A71-15131

Goethite stability on Mars, considering dehydration-rehydration cycle and time average atmospheric water vapor content

04 p0645 A71-15132

Size classification of limonite Mars simulation samples, noting surface roughness of 0.02-10 microns

21 p3449 A71-40642

LINCOLN EXPERIMENTAL SATELLITES

LES 6 satellite solid Teflon pulsed plasma thruster performance, determining energy balance thrust and circuit parameters

03 p0472 A71-14429

LES 6 synchronous orbit solar cells experiments, determining various type cells degradation due to low energy proton damage

05 p0702 A71-16085

Radio frequency interference environment measurement in VHF range by subsynchronous Lincoln experimental satellites 5 and 6

19 p3021 A71-38452

LINE SHAPE

Ground relief representation by contour lines and by profiles, noting error possibilities

01 p0074 A71-11328

Galactic models from neutral H line profiles at 21 cm wavelength

02 p0307 A71-12084

Hot stars, supergiants and quasars extended and expanding atmospheres, examining resonance line profile formation by coherent scattering

05 p0806 A71-16203

Weak and average intensity Fraunhofer lines contours variation over solar disk

07 p1200 A71-20038

Galactic models from neutral H line profiles at 21 cm wavelength

08 p1362 A71-21134

Fraunhofer line profiles, determining optical depth at various points in photosphere

09 p1524 A71-23191

Ion cyclotron resonance power absorption theory application to reactive and nonreactive ions line shapes, using Wobchall-Graham-Malone phenomenological equation of motion

17 p2695 A71-34947

Oxygen telluric lines contours shape analysis, allowing for atmospheric nonisothermicity and inhomogeneity

19 p3090 A71-37978

Resonance broadening measurements of alkali metals, giving relation between optically thick and thin full widths for Lorentzian and Gaussian line shapes

19 p3105 A71-38721

Collision effects on line shapes using quantum mechanical description of atomic center of mass motion, considering pressure effects in gas lasers

20 p3271 A71-39069

LINE SPECTRA

NT BALMER SERIES

NT D LINES

NT ELECTRONIC SPECTRA

NT FRAUNHOFER LINES

NT H ALPHA LINE

NT H BETA LINE

NT H GAMMA LINE

NT H LINES

NT K LINES

NT LYMAN SPECTRA

NT RYDBERG SERIES

NT TELLURIC LINES

Solar line spectra formation and analysis, discussing transfer equation, atomic levels, line shape, etc

01 p0152 A71-10327

Pulsed hydrogen fluoride gas laser output line spectral distribution, describing experimental setup and measurements

01 p0092 A71-10371

Solar emission line spectra second observation outside total eclipse, noting big coronal condensation above eastern limb

01 p0159 A71-10869

Plasma electric field effects on atomic spectral line shape by plasma kinetic theory

01 p0130 A71-11349

Abel-Tauber theorems predicting asymptotic behavior of source functions for resonance lines formed by frequency redistribution in semiinfinite atmosphere

01 p0131 A71-11350

Absorption line formation in scattering planetary atmospheres with cloud particles

01 p0162 A71-11420

Regular and stochastic oscillations in plasma beam discharge produced by beam instability from observing time dependent variations in spectral line luminescence intensities

02 p0288 A71-11634

Solar Hg abundance low value by photosphere spectrum absence of Hg I lines, comparing higher content in carbonaceous chondrites

02 p0306 A71-12048

Solar active regions lambda 10 830 line from photometric observations, determining optical thickness, Doppler width and radiation source activity

02 p0306 A71-12080

Mass estimation for quasars and galactic nuclei with absorption line shift into long wave region

02 p0307 A71-12090

Radiative transfer by shock profile spectral line in thermally inhomogeneous layers of radiating gas

02 p0240 A71-12184

Interstellar dust, examining diffuse line and band origin, absorption spectra and silicate grains

02 p0312 A71-12466

Wolf-Rayet WN6 stars emission line spectral profiles observation by spectrograms and photoelectric scanning

02 p0314 A71-12584

Sulfur hexafluoride absorption lines observation by inverted Lamb dip high resolution spectroscopy, using heterodyne methods

02 p0209 A71-12731

Solar line blanketing effect data derivation and analysis for model atmosphere computer programs, considering application to spectrally similar stars

02 p0316 A71-12755

Reflecting and scattering models of line formation in planetary atmospheres allowing for inhomogeneously distributed gas and particles and for anisotropic scattering phase function

03 p0486 A71-13320

Solar corona lines during 7 March 1970 eclipse, using Lallemand electrostatic cameras

03 p0489 A71-13630

Laser action on six lines of ionized Xe spectrum, discussing discharge tube, optical resonator and spectrograph characteristics

03 p0438 A71-13895

Soviet book on optical properties of hot air covering spectral lines, radiative transfer, cross sections, pressure effects and absorptivity

03 p0460 A71-14397

Venus high dispersion spectra used for line positions and constants of carbon dioxide 7820 and 7883 A bands

04 p0629 A71-14806

Solar spectrum line digital recording, discussing design and operation principles

04 p0590 A71-14842

Electron excitation coefficient rate of green coronal line by quantum defect method, discussing energy levels of Fe ions

04 p0643 A71-14906

Stellar spectra and spectral types, discussing spectrographs, identification of lines, intensity measurements, absorption lines, Harvard system, etc

04 p0646 A71-15229

OH absorption line measurements for longitude range near galactic center, suggesting existence of radial velocity gradient

04 p0657 A71-15760

Methyl alcohol detection in Sagittarius, examining radio line emission at 834 MHz

05 p0802 A71-15945

Solar line spectra wavelength improvement in 7780 to 7925 A range, using carbon dioxide bands

05 p0803 A71-16020

Eu II and La II line profiles in sunspots and undisturbed photosphere

05 p0803 A71-16022

Supernova remnant kinematic distance estimates, using molecular absorption line velocities with Schmidt model

05 p0805 A71-16107

Fourier data decomposition technique for recovering Doppler temperature, emission line intensity and Doppler shift of central frequency of Fabry-Perot fringes in presence of statistical noise

05 p0748 A71-16265

Plutonium in peculiar A stars surfaces as nuclear cosmochronology for determination of r process nuclei age, considering emission line spectra obscurement

05 p0808 A71-16413

Highly ionized line spectra of Fe, Co, Ni and Cu belonging to Na I and Mg I isoelectronic sequences

05 p0717 A71-16909

Arsenic first spark line spectrum using high resolution grating spectrograph and Fabry-Perot interferometer

05 p0717 A71-16910

Emission line spectra of halogens Cl I, Br I and I I in 4-micron region

05 p0717 A71-16911

Statistical equilibrium equations solved for atom/ion with complex energy level structure and weak spectral lines, discussing deviations from LTE

06 p0969 A71-17969

Interlocking via photoexcitations and deexcitations due to lanthanide rare earths weak line solar spectra and ion atomic structure

06 p0969 A71-17970

Fraunhofer line resonance polarization from solar spectral bands statistical analysis, noting collisional depolarization

06 p0969 A71-17973

UV absorption line spectra from HI regions, evaluating X ray and photoionization heating models

07 p1190 A71-18853

Planetary atmospheres radiant energy fluxes, developing validity of isolated line approximation in finite spectral intervals

07 p1191 A71-18908

H lines Stark broadening in turbulent plasma, considering Langmuir vibrations monadiabatic action and energy density

07 p1168 A71-19277

Markarian galaxies spectra, analyzing emission line characteristics

07 p1191 A71-19283

Thermal Ar plasma with gas additives as standard intensity light source of optically thick spectral lines, using interpolation and Kirchhoff-Planck function

07 p1168 A71-19323

Calcite and aragonite high pressure Raman line spectra comparisons, testing structural identification theory

07 p1054 A71-19369

Optical hyperfine splitting of Rb resonance lines of atomic beam light source, using Fabry-Perot interferometer

07 p1111 A71-19488

Color changes and absorption line variations in M31, M32 and NGC 4472, attempting synthesis of M31 disk population

07 p1197 A71-19814

X ray line emission from heliumlike calcium during solar flare of 2 November 1969

07 p1188 A71-19826

Coronal line observation of autoionizing states by dielectronic recombination in solar spectrum

07 p1198 A71-19827

Planetary nebulae NGC 6572, NGC 7009, NGC 7027 IR line emission, examining fine structure for Ne II, Cl IV, S IV and Ar III

07 p1199 A71-19836

Quasars red shift and absorption lines observations, discussing distance measurement, brightness and intergalactic matter

07 p1200 A71-20211

Sunspot boundary displacement toward limb in Fe I, Ti I and H alpha lines in passing from continuum to absorption line observations, discussing Wilson effect

07 p1205 A71-20635

Resonance line formation in multidimensional media, applying to non-LTE line transfer for two dimensional temperature variations

08 p1359 A71-20942

Formaldehyde line emission observed from trapezium H II region of Orion nebula, attributing to 140 GHz rotational transition

08 p1360 A71-20983

Solar active regions lambda 10 830 line from photometric observations, determining optical thickness, Doppler width and radiation source activity

08 p1361 A71-21130

Mass estimation for quasars and galactic nuclei with absorption line shift into long wave region

08 p1362 A71-21140

Fabry-Perot interferograms analysis by Fourier transforms, considering mirror defects, light incident angle spread and spectral lines Lorentzian and Gaussian shapes

08 p1289 A71-21378

Instrumental function of Fabry-Perot interferometer and lamp-emitted line profile determined with hollow cathode thorium lamp

08 p1290 A71-21380

Balmer emission lines in hydrogen cloud in bright galactic nucleus

09 p1518 A71-22351

CH molecule line formation mechanism for 4300 A transition in solar photosphere, studying collisions with hydrogen atoms

09 p1520 A71-22843

Solar prominence spectra, presenting equivalent line widths, central line intensities and Doppler half widths

09 p1524 A71-23190

Emission line profile and source function in finite optical thickness plane layer, using matrix equation

09 p1525 A71-23195

High altitude low latitude aurora, observing intense spectral bands and lines and excitation due to optical resonance, atom- and molecule- electron collisions

09 p1441 A71-23643

Gas agent temperature measurement by sodium spectral line reversal method using MHD generators experimental research

09 p1512 A71-23671

Solar granular or convective motion velocities vs photospheric oscillations for Doppler shifts in line spectra

10 p1665 A71-23776

Solar chromospheric emission line identification at 4097.3 A, discussing N III transition

10 p1666 A71-23783

Sunspot molecular lines and rotational temperatures of MgH, CaH and TiO using model umbral atmospheres and photographic spectrograms

10 p1666 A71-23784

Sunspots umbrae spectrum analysis in 4000-8000 A region, identifying molecular absorption lines photoelectrically

10 p1666 A71-23785

Solar flare spectral line features at 1.9 A, considering iron ion origin

10 p1660 A71-23797

He-Ne laser 0.63 micron line collisional broadening dependence on gas temperature

10 p1620 A71-24342

Methane spectral band analysis, examining J manifolds self broadening coefficients of R branch

10 p1573 A71-24546

Spatial distribution of aurorae in O and molecular nitrogen ion emissions

10 p1602 A71-24553

High resolution measurement of carbon dioxide broadened half widths for water vapor lines in fundamental band

10 p1645 A71-24965

Half widths calculation for carbon dioxide broadened water vapor absorption lines in nu sub 2 fundamental, considering dipole-quadrupole interactions

10 p1645 A71-24966

Binary star 112 Herculis elemental abundances by atmospheric model analysis of spectra

10 p1680 A71-25001

Interstellar CO, constructing strip maps in declination and right ascension across W51, Sgr A and Sgr B2 for 115.2712 line radiation

11 p1818 A71-25201

Venus atmosphere spectra, emphasizing line and continuum absorption coefficients relative to scattering

11 p1823 A71-25697

He I lines in OB spectra, examining main sequence stars

11 p1830 A71-26111

Quasar 3C 147 angular structure observations, using long baseline interferometer

11 p1830 A71-26113

Diffuse interstellar absorption centered at 4430 A observed in reflection nebulae, using narrow band filters

11 p1831 A71-26135

Line shifts in first overtone band of DF perturbed by HF, studying pressure induced transitions and partial pressures

11 p1729 A71-26139

Extreme UV spectra of Sc XIV, Ti XV and V XVI, identifying and classifying lines in 18-25 A range

11 p1729 A71-26140

Collision effects on atomic spectral line profiles, using quantum mechanical description of atomic center-of-mass motion with particular application to lasers

11 p1803 A71-26147

Line emission in diffuse cosmic X ray continuum, discussing probable interstellar or intergalactic matter source

11 p1817 A71-26317

Line formation effective pressure from Venus atmosphere spectra, discussing phase angle variations

11 p1835 A71-26457

Hot water vapor curve of growth, using statistical band model with exponential line intensity distribution yielding spectral absorption coefficients

12 p1904 A71-26795

NGC 3351 galaxy core spectrophotometry of optical spectrum covering emission and absorption lines

12 p1960 A71-26831

Sidelight emission spectrum of He-Ne laser with/without oscillations, determining line intensity change and laser power dependence on discharge current

12 p1913 A71-26896

Active unperturbed solar photosphere, determining variations in spectral line profiles

12 p1963 A71-27082

Magnetic field effect on emission spectrum and intensity at electron cyclotron frequency harmonics from PIG Reflex discharge, discussing electron oscillations excitation in plasma

12 p1938 A71-27214

Line emission in X ray background in galactic plane and at galactic pole based on rocket flight data

13 p1210 A71-28005

Venus cloud height at equatorial and polar latitudes, using carbon dioxide band distribution intensity

13 p1218 A71-28593

Liquid He stable cavities localized excited states, calculating atomic line positions

13 p1201 A71-28796

Inhomogeneous atmosphere transmission functions, noting Lindholm line shift in O absorption spectra effects

13 p2063 A71-29019

Spectrometer slit-width cancellation by Doppler shift of light emission by fast ion beams, resulting in spectral lines increased intensities

13 p2071 A71-29331

Galactic H II regions 35 cm water source emission line profile observation, noting frequency and intensity variations

14 p2304 A71-29594

Solar X-ray line spectra observation, noting K alpha transition indicative of suprathermal events

14 p2297 A71-29598

Spectral lines of O/IS generated by oxygen molecule dissociative recombination in upper atmosphere observed in nightglow at geomagnetic equator with Fabry-Perot spectrometer

14 p2229 A71-29663

Solar corona XUV resonance line spectrum interpretation, using thermal emission from inhomogeneous regions

14 p2297 A71-29678

Fluorochlorosilane preparation and identification by Raman laser spectroscopy, establishing line to vibration mode relation

14 p2189 A71-29746

Spectral lines self reversal effects on plasma temperature and density measurement in MHD duct boundary layer

14 p2279 A71-30046

H lines Stark broadening in turbulent plasma, considering Langmuir vibrations nonadiabatic action and energy density

14 p2280 A71-30171

Interstellar SH search for ground state main line transitions at 111 MHz

14 p2313 A71-30433

Complex noise emission spectra from superposition of continuous component and peaks, calculating level separations due to perfectly reflecting plane

14 p2289 A71-30523

Solar corona visible lines, identifying V VI to Fe IX electron transitions with variable inductance three electrode spark source

14 p2314 A71-30650

White dwarf line spectra, constructing atmospheric models and effective temperatures

14 p2317 A71-31015

Radiative transfer by shock profile spectral line in thermally inhomogeneous layers of radiating gas

15 p2511 A71-31492

Cesium spectral lines luminescence and population during helium-cesium discharge plasma decay

15 p2458 A71-32407

Ruby laser pumped tunable organic dye laser to excite atomic flame fluorescence of 5535.5 A barium resonance line, obtaining intensity vs concentration

15 p2422 A71-32582

Argon ion laser mode locking in UV lines with intracavity acousto-optic modulator, describing pulse duration and average power

15 p2423 A71-32588

Beam foil excited Ar spectrum between 500 and 1000 A, tabulating lines with ionization stages based on line intensity variation with beam energy

15 p2368 A71-32601

Cavity loss dependent erbium glass laser line oscillations in lower threshold region under Q switch and long pulse conditions

15 p2424 A71-32612

Critique of papers on line formation in magnetic fields, discussing dispersion in absorption matrix

15 p2496 A71-32741

- Line emission in diffuse X ray background at high galactic latitudes, interpreting rocket observations 15 p2480 A71-32760
- Diffuse interstellar medium hydrogen radio recombination lines radiation transfer, investigating thermodynamic equilibrium effects 15 p2498 A71-32770
- Dense interstellar cloud radio recombination lines in H I regions, calculating quadrupole effects on line splitting 15 p2498 A71-32771
- Milky Way galaxy interstellar neutral hydrogen rolling motion phenomenon confirmed by 21 cm line survey data 16 p2630 A71-33053
- Peak contour positions of rotation lines of hydrogen chloride as function of spectral slitwidth for wavenumber calibration of far IR spectrometers 16 p2577 A71-33134
- IR line radiation from galactic central thermal radio sources, determining element abundances 16 p2633 A71-33336
- B and O hot dwarf stars ionic UV line spectra, observing electron and ion damping constants with impact and semiclassical approximations 16 p2633 A71-33338
- Optically dense plasma spectral characteristics, calculating reabsorbed line intensity distribution 16 p2619 A71-33707
- IR Fe XIII lines in solar corona during total eclipse of 12 November 1966 16 p2640 A71-33729
- Solar corona green line observations with Lallemand electrostatic camera during 7 March 1970 eclipse, showing equivalent width, electron density and temperature vs height above limb 16 p2640 A71-33745
- Altitude variation of forbidden line of 5577 A and 3914 A auroral emissions intensities ratio from rocket sounding 16 p2566 A71-33748
- Coronal IR emission lines during solar eclipse of 7 March 1970, using high altitude aircraft-borne Fourier transform spectrometer 16 p2640 A71-33751
- Coronal line measurements on slit spectrogram during solar eclipse of 7 March 1970, showing fine structure in inner corona 16 p2642 A71-33784
- Spectrographic observation of coronal lines in chromosphere during solar eclipse of 7 March 1970 16 p2642 A71-33787
- Soft X ray emission line behavior during solar flares based on OSO-6 satellite-borne Bragg crystal spectrometer data 16 p2627 A71-33835
- Molecular jet spectrometer with two irradiation zones, observing lines intensity 16 p2615 A71-34064
- Circumstellar dust clouds and Bok globules examined for gaseous emission lines, emphasizing forced diffusion process 16 p2643 A71-34077
- Spectral line emission from nitrogen ions, identifying charge by Doppler shift technique application to beam foil light source 16 p2615 A71-34129
- Quasi-stellar objects, investigating velocity dispersion, column densities and abundance of Mg and Fe in absorbing region by Stromgren method of line pairs 17 p2797 A71-34371
- Mars atmosphere high resolution line spectra, calculating carbon dioxide abundance, rotational temperature and surface pressure 17 p2800 A71-34588
- High resolution quiescent and active solar prominences and magnetic field observations, discussing Zeeman effect and line spectrum polarization 17 p2806 A71-35393
- Interstellar silicon monoxide discovery from 130,246 MHz frequency line emission of galactic radio source Sag B2 17 p2807 A71-35416
- Pulsating variable star spectral line formation from integral equation solution of radiative transfer and gas flow through shock front 17 p2808 A71-35553
- Radiative transfer in two-component stellar atmosphere, discussing lines corresponding to solar Ca K-line 17 p2839 A71-35555
- Planetary atmospheres composition from ground based IR spectroscopy, including multiple scattering, cloud layers, line formation and absorption 17 p2808 A71-35570
- Solar coronal line photometry eliminating inherent systematic measurement errors of previous methods 17 p2809 A71-35597
- High intensity continuous gas discharge line source for extreme UV with low electromagnetic interference 18 p2914 A71-35845
- Upper limits to quasars masses with optical emission lines inside radio sources, using method independent of red shift composition 18 p2961 A71-35965
- Variational principle with reflectivity extremum for inhomogeneous planetary atmospheric line spectra profile calculation from radiative transfer equation 18 p2964 A71-36286
- Profile changes of magnetically non-split lines in faculae, explaining observations by outer layers temperature increase 18 p2965 A71-36731
- Solar Fe XIV 5303 coronal line isolation, using solid Fabry-Perot interferometer as monochromator 18 p2966 A71-36736
- Excess intensities of diffuse cosmic X rays related to characteristic line spectrum excitation and element abundances in interstellar region and nebulas 18 p2958 A71-36761
- Physics and phenomenology of radiation field in spectral lines, considering radiation transfer with optical depth effects and kinetic energy transformation into radiation 18 p2968 A71-37035
- Active unperturbed solar photosphere, determining variations in spectral line profiles 19 p3133 A71-37432
- Stellar atmosphere line formation in magnetic fields, considering Milne-Eddington model 19 p3133 A71-37507
- Stellar rotation effects on radiation spectral characteristics, calculating He line profiles by LTE method 19 p3143 A71-38158
- Dumb-bell Nebula forbidden O III line profiles observation with two-etalon scanning Fabry-Perot 19 p3144 A71-38171
- Magnetic field effect on emission spectrum and intensity at electron cyclotron frequency harmonics from PIG Reflex discharge, discussing electron oscillations excitation in plasma 19 p3117 A71-38626
- Solar X-ray line emission, using crystal spectrometers during large chromospheric flare 19 p3130 A71-38672
- Atomic oxygen concentration from 5577 A green line emission of airglow and chemiluminescence of nitric oxide 20 p3215 A71-38739
- Differential line shifts in spectrum of supergiant beta Ori attributed to radial spreading of stellar atmosphere 20 p3290 A71-39302
- Mars short-wave line spectra from measurement with reflector, estimating nitrogen dioxide content in atmosphere 20 p3290 A71-39307
- H atoms generation by photodissociation of molecules evaporated from cometary core, basing analysis on hydrogen atmosphere line spectra 20 p3293 A71-39538
- He II alpha lines scanned by electromagnetically driven T tube, comparing with Stark broadening theory 20 p3272 A71-39576
- Solar silicon line spectra of photosphere, chromosphere and corona, including ionic spectra over wide ionization potentials range 20 p3301 A71-39822
- Spectral analysis of Markarian galaxies, observing emission and absorption lines and hydrogen reversal 21 p3441 A71-40105
- Millimeter emission lines from interstellar methyl cyanide transitions, noting kinetic temperature and hydrogen density 21 p3447 A71-40446
- Spectral line intensity measurement errors due to electron-temperature fluctuations averaging in continuous plasma sources 22 p3581 A71-41790
- Pressure dependent absorption of carbon dioxide laser by boron chloride, considering saturation and line overlapping effects 22 p3556 A71-41805
- Microwave molecular lines of CO, CN and CS emission from infrared object IRC plus 10216 22 p3599 A71-41929
- Optical line spectrum and ionization equilibria of hard UV radiation and energetic proton heated hydrogen, helium, nitrogen, oxygen and neon 22 p3601 A71-42160
- Sunspot umbrae molecular line spectra, observing equivalent widths, isotopic abundances and band intensities 22 p3602 A71-42174
- Photometric coefficient of activity in Jupiter atmosphere at 4300, 5500 and 6400 A, giving relative intensities of belts and zones 22 p3603 A71-42183
- Moment analysis of atomic spectral lines of Cs-Ar and Cs-He systems, using adiabatic approximation 22 p3578 A71-42462
- Intermolecular forces and excited state from atomic line shape experiments, comparing numerical calculations with experimental data 22 p3578 A71-42463
- Interstellar medium recombination line emission origin from discrete distribution of cold and dense clouds 23 p3723 A71-42942
- White dwarfs EG 248, GR 289 and EG 250 spectra with circular polarization, detailing violet lines, absolute magnitudes, color and luminosity 23 p3733 A71-43079
- CH radical 10 cm line frequency determination by photographic Fabry-Perot interferometry 23 p3733 A71-43082
- Coalescence /collapse/ of overlapping spectral lines due to nonadiabatic broadening for Stark structure of hydrogen and helium lines in discharge plasma 23 p3707 A71-43407
- Power spectrum analysis of solar granular intensity fluctuations and velocities, noting asymmetry behavior of Ba II line in individual convection cells 23 p3767 A71-43834
- Interferometric measurements of 142 solar absorption lines in light from solar disk center 23 p3767 A71-43835
- Solar atmosphere electron densities from ion emission line intensities in Be isoelectronic sequence 23 p3721 A71-43839
- Solar rotation evidence from H alpha and K line spectra of quiescent prominences for westward wind 23 p3767 A71-43841
- Night enhancements in 6300 A line at Sanae related to diurnal excursion of auroral oval, observing ionospheric blackout and high energy electrons precipitation 23 p3672 A71-43980
- K and M class stars B and V magnitudes in UVB system based on atomic lines and molecular bands spectral absorption 23 p3771 A71-44306
- Microwave detection of anomalous interstellar electronic recombination line emission toward W49 A, using radio telescopes 24 p3871 A71-44904
- Photographic far UV solar spectra during eclipse of 7 March 1970, discussing coronal lines, prominences and quiet atmosphere structure 24 p3871 A71-44911
- Galactic neutral hydrogen absorption line spectra at 21 cm wavelength by radio sources interferometric observations, discussing cool gas temperature, ionization rate and Cetus Arc distance 24 p3873 A71-45084
- Identification of 417 A line in solar EUV spectrum, calculating collision strengths and recombination rates for Fe XV 24 p3873 A71-45143
- LINEAR ACCELERATORS**
- Power amplifier klystron self excitation in linear electron accelerators, describing tunable driver circuit with quartz reference oscillator 12 p1889 A71-27754
- Linear electron accelerator using shaping system debunching properties for minimizing electron energy differences in bunched beam 15 p2376 A71-31743
- Particle flux, energy storage and beam loading effects on superconducting traveling and standing wave resonators in linear accelerators 16 p2587 A71-33494
- Transverse instability of charged particle beam in segmented linear accelerators due to beam encounter with wall 24 p3855 A71-44522
- LINEAR AMPLIFIERS**
- Linearization techniques for multiple signal interference reduction in broadband transistor power amplifiers in 225-400 MHz range 19 p3030 A71-38434
- LINEAR ARRAYS**
- NT ENDFIRE ARRAYS**
- NT YAGI ANTENNAS**
- Longitudinal direction positioning error effects on grating lobe field deviation and reduction in uniform linear arrays 08 p1257 A71-21885
- Linear phased antenna arrays, calculating influence of interaction between radiating elements on radiation pattern 09 p1404 A71-22225
- Linear antenna arrays synthesis with Z transforms permitting sidelobe reduction and nulls in antenna radiation patterns 09 p1419 A71-23498
- Simulated far field patterns of linear and phased arrays without radiation coupling by hybrid analog computer 11 p1735 A71-25851
- Radiation mechanism of line sources array above finite ground plane, studying maximum field intensity variation and angle 13 p2028 A71-27991
- Uniformly spaced linear arrays directivity as function of spacing, scan angle and current distribution, approximating element radiation intensity 13 p2028 A71-28000

LINEAR CIRCUITS

Numerical solution of current distribution, wave propagation constant and propagation mode cut-off frequencies on periodic linear array

13 p2028 A71-28001

Synthesis of linear antenna with integrated currents for specified ratio of antenna radiation to elementary radiator patterns

14 p2194 A71-30101

High speed electronic phase and frequency scanned linear, static feed and monopulse arrays element and angular error analysis

14 p2205 A71-31049

Blade antenna linear array design for aircraft-satellite communication, determining mutual influences by array measurements in simulated electrical environment

14 p2206 A71-31062

Radiation pattern of linear radiator mounted at quarter-wavelength in front of cylindrical parabolic reflector, discussing calculation procedure based on half-wavelength dipole near field

15 p2369 A71-31415

Linear array antenna far field transient time response formulation, using concise vector field integral equations and generalization

17 p2717 A71-35584

Antenna linear array power patterns synthesis, determining optimum nonnegative harmonic approximation to given function in Gauss/weighted least-mean-square and Chebyshev senses

19 p3021 A71-38472

Pyroelectric detector linear arrays for IR thermal imaging at room temperature

22 p3543 A71-42131

LINEAR CIRCUITS

FET as voltage controlled linear resistors, discussing use in attenuators, automatic gain control, volume compressors and RC networks frequency control elements

02 p0229 A71-11814

Topological methods of linear electric circuits analysis, considering Kirchhoff, Maxwell and Mason methods

11 p1743 A71-26464

Linear passive network steady state FM distortion numerical calculation, applying to Chebyshev-response bandpass filter

14 p2197 A71-30806

Quasi-stationary method applicability for determining distortion of FM signal passing through linear circuit

15 p2373 A71-32631

Transfer function and temporal behavior interrelations for linear network, characterizing circuit delay and rise time by center of gravity and inertial moment of pulse response

16 p2550 A71-34139

Soviet book on algorithms for electronic circuit analysis covering linear and nonlinear transistor or tube circuits matrix-topological description and frequency-time domain solutions

17 p2717 A71-35219

Operational amplifier design with fluidic Schmitt trigger and linear resistor feedback network

23 p3631 A71-44098

LINEAR ENERGY TRANSFER [LET]

Low and high linear energy transfer /LET/ cyclotron-accelerated alpha particles effects on *Drosophila melanogaster* longevity

06 p0853 A71-18028

LINEAR EQUATIONS

Hybrid computers solution of linear differential equations, analyzing Taylor series /derivatives/ use for compensation

01 p0048 A71-10224

Linear homogeneous n th order ordinary differential equations reduction to equations with constant coefficients by transformation of independent variables

01 p0110 A71-10317

Dynamic problems linear variation equations associated with one and two particle motion in force field

01 p0111 A71-10385

Linear integral equations with difference and summation kernels in elasticity theory, developing approximate solution method

01 p0171 A71-10657

Linear matrix equations explicit solution representation techniques

02 p0276 A71-11803

Unstable linear initial value problem numerical solution, using Riccati equations of invariant imbedding

02 p0277 A71-12727

Two-point boundary value problems for linear differential equation systems, describing adjoints and complementary functions methods

03 p0451 A71-13624

Inhomogeneous elasticity theory under spherical symmetry, using linear differential equations transformation into constant coefficient equations

03 p0507 A71-13714

Characteristic exponents for linear differential equations with periodic coefficients, using recurrence multipliers suitable for computer

03 p0451 A71-13786

Nonlinear systems near steady state oscillation transient behavior analysis by linear differential equations with periodic coefficients

03 p0451 A71-13817

Three body plane restricted problem axisymmetric periodic solutions, establishing linear equations of variation

04 p0652 A71-15703

Absolute orbit construction for Jovian great satellites, obtaining linear equations of motion

04 p0654 A71-15714

Linear functional differential equations trajectory optimization, proving maximal principle

04 p0620 A71-15866

Matrix algorithms for linear and nonlinear inequalities, discussing rank generation and matrix inversion

05 p0774 A71-16398

Quasi-linear equations consequences in discrete spectra and damped electron plasma waves, discussing conservation laws relation to resonance approximation

05 p0789 A71-16652

Dynamic relaxation method for solving simultaneous linear differential equations, comparing asymptotic rate of convergence with degenerate Chebyshev approximation

05 p0776 A71-17122

Linear and nonlinear parabolic equations approximate solutions by Galerkin methods, leading to linear algebraic equations

06 p0917 A71-17558

Initial value problems involving linear ordinary differential equations, deriving theorems for Runge-Kutta and Adams methods effectiveness

06 p0917 A71-17566

One step iterative solution for linear equations by summation methods, discussing convergence improvement

06 p0920 A71-18213

Two-point iteration formulas with one calculation step requiring successive solution of two linear equations

06 p0921 A71-18347

Thin elastic toroidal shells under nonsymmetric harmonic loadings, reducing problem to membrane and edge effect linear solutions

06 p1002 A71-18415

Optimal solution existence theorem for control system described by linear hyperbolic partial differential equation

07 p1148 A71-19770

Linear ordinary differential equation systems first order output sensitivity coefficients generation and application to second order cross sensitivities

07 p1148 A71-20416

Unknowns elimination from partial linear equations system with constant coefficients, applying to differential equations for bending transversely isotropic plate under normal external load

09 p1535 A71-22257

Asymmetric missile nonlinear angular motion, describing quasi-linear relations for frequencies, damping rates and swerving motion amplitude

09 p1532 A71-22906

Celestial mechanics, discussing fourth order linear differential equation for Hansen coefficients

09 p1486 A71-23340

Linear differential equations stability analysis by implicit equations applied to resonance phenomena, using Weierstrass theorem

10 p1640 A71-23803

Singular perturbation problems for linear second order elliptic equation, obtaining asymptotic approximations for simple unbounded regions with free boundary layer terms

10 p1636 A71-23934

Circular cylindrical shells stress-strain state in elastic medium, obtaining criteria for boundary conditions limiting values for linear theory applicability

10 p1688 A71-24356

Steady state photon transfer through homogeneous semiinfinite isothermal atmosphere with two level atoms, deriving linear integral equation for escape probability distribution

10 p1643 A71-24964

Linearized equations of motion for stability of dual spin satellite composed of platform, rotor, platform mounted damper and rotor mounted damper

11 p1837 A71-25514

Unique solution of certain classes of linear and nonlinear functional-integral equations reducible to Volterra integral equations

11 p1793 A71-26562

Static and quasi-static atmospheric motions, using linearized equations for isothermal compressible atmosphere

13 p2097 A71-29084

General adjoint relation between linear functional differential equations and Volterra integral equations

13 p2096 A71-29381

Iterative solution for quasi-linear heat equation, examining convergence for equation describing self similar heat wave from instantaneous plane source

14 p2334 A71-29564

A priori bounds on linear and nonlinear quotients of Neumann boundary value problem for uniformly elliptic difference equations over rectangular regions

14 p2265 A71-30291

Two spheroid rigid bodies rotational and translational motion, using linear and Hill type differential equations for angular variables and coordinates

14 p2312 A71-3038

Linear integral equations with difference and summation kernels in elasticity theory, developing approximate solution method

14 p2333 A71-30991

Linear positive convolutive operators, considering convergence problem

15 p2439 A71-31144

Linear stability equations derivation from vector-equilibrium conditions in engineering shell theory

15 p2502 A71-31160

Singularities in linear elliptic partial differential equations, considering Cartesian and cylindrical polar coordinate problems

15 p2440 A71-31348

Dirichlet problem for second order linear elliptic differential equations, considering convergence theory results for finite difference approximations

15 p2440 A71-31349

Gyroscopic system nonstationary operation mode analysis, utilizing asymptotic method with linear matrix equation

15 p2410 A71-32454

Field theoretic approach of Jordan-Brans-Dicke theory within Lorentz invariant gravitation theories framework, solving linear motion equations inconsistency

15 p2451 A71-32646

Linearized shell theory, proposing improvement of Marguerre-Vlasov shallow shell equations in terms of invariant displacement and stress functions

16 p2649 A71-33000

Linear equations general form including difference, differential, deviating argument, aftereffect and integrodifferential equations

16 p2603 A71-33531

Rectangular plate with two adjacent sides clamped and two supported, solving bending problems with linear algebraic vector equations

17 p2824 A71-34846

Unbounded linear operator in Hilbert space, constructing characteristic function for transformation

17 p2765 A71-34865

Laplace transform application to linear system of partial differential, integrodifferential and difference equations with periodic and quasi-periodic coefficients

17 p2780 A71-34911

Asymptotic behavior of linear and nonlinear equations solutions

17 p2766 A71-34919

Linear differential equations solutions stability in Banach space for finite and infinite dimensional cases, generalizing Liapunov theorems

17 p2781 A71-34922

Linear differential equations system with periodic coefficients, determining solutions by stationary components matrix location on complex plane

17 p2766 A71-34933

Linear neutral differential equation uniform asymptotic stability relation to perturbed differential equation containing bounded linear operators

17 p2767 A71-35523

Linearized Boltzmann equation solution for rarefied gas dynamics, discussing analytical, variational and numerical methods

17 p2784 A71-35572

Rarefied gas dynamic models with velocity dependent collision frequencies, investigating linearized Boltzmann equations

17 p2729 A71-35573

Soviet book on ordinary differential equations covering basic concepts, existence and uniqueness theorems, linear homogeneous and nonhomogeneous equations with constant coefficients, etc

17 p2768 A71-35626

Numerically stable algorithm for solving least squares problems with linear equalities and inequalities as additional constraints

17 p2769 A71-35693

Kramer problem for steady linear Boltzmann equation in kinetic theory of gases, noting solution existence

18 p2947 A71-36190

Two dimensional flow of non-Newtonian fluids with rigid spherical substructure, solving linear coupled ordinary differential equations for spin and velocity field [ASME PAPER 71-APM-N]

18 p2926 A71-36257

Linear functional equations bounded solutions stability by reflexive Banach space mapping, applying to elliptical and parabolic differential equations ill-posed problems

18 p2941 A71-36351

Projection iterative method for solving singular linear equations, noting use for matrix conversion

18 p2942 A71-36699

Approximation solution for elliptic boundary value problem with nondifferentiable parameters, considering second order linear partial differential equations in two independent variables 18 p2942 A71-36817

Dissipative wave motion asymptotic theory, considering initial boundary value problems for linear partial differential equations 18 p2910 A71-36819

Symmetric operators family spectrum with generalized Rayleigh functional, showing analogy between linear and nonlinear theory at infinite spatial dimension 18 p2942 A71-36821

Nonautonomous system equations of motion solution, determining conditions for nonlinearities conversion to linear equations 19 p3037 A71-37349

Solution of higher order linear partial differential equations with variable coefficients, using functions of multidimensional matrices 19 p3086 A71-38012

Numerical solutions of boundary value problems for linear elliptic partial differential equations by function theoretic methods 19 p3087 A71-38308

Linearized unsteady gas dynamic differential equation, obtaining parameter characteristics from boundary values 20 p3211 A71-39032

Stability of plane rotating galaxies in magnetic field parallel to axis of rotation, showing linearized MHD equations self conjugate for radial disturbance case 20 p3289 A71-39298

Pointwise bounds in Cauchy problem for fourth order quasi-linear equation using a priori inequality, applying Rayleigh-Ritz technique to elliptic partial differential equations 20 p3255 A71-39573

Generalized Riccati equation reduction to integral equation, leading to asymptotic solution of second order linear differential equations 20 p3255 A71-39574

Holomorphic matrix valued function on connected open subset of complex plane, obtaining conditions for satisfying homogeneous linear differential equation 21 p3410 A71-41185

Integral and pointwise estimates of insulated cylinder temperature field spatial decay for semilinear parabolic equations 21 p3473 A71-41186

Disconjugacy criterion for self adjoint linear differential equations containing nonnegative continuous function in interval under study 21 p3410 A71-41187

Stability of finite difference approximation to mixed initial boundary value problems for linear parabolic system of equations 22 p3567 A71-42295

Weak row sum criterion for nonlinear equation systems, applying to discrete two point boundary value problems and linear equation systems 22 p3567 A71-42374

Semilinear hyperbolic systems analogous to differential-integral Boltzmann equations of gas dynamics, developing solutions existence for nonnegative initial data 22 p3531 A71-42690

Conditions definition for nonexistence of continuous right inverse for surjective linear partial differential operators on Frechet spaces 22 p3568 A71-42693

Controllability conditions for linear differential equations of dynamic system 22 p3568 A71-42696

Gas dynamics nonstationary linearized equation solutions based on nonstationary source- and vortex-like singularities 23 p3663 A71-43491

Approximate solution for equation in linear normed space by error operator norm optimization, applying to elliptical cylinder type compact sets 23 p3699 A71-43574

Optimal control of time delay systems described by linear differential difference equations 23 p3658 A71-44087

Unified electrical machine theory with allowance for space harmonics effects, transforming time-dependent linear differential equations into linear time-invariant equations 24 p3793 A71-44657

Elasticity theory for rectangular region with thin-walled inclusion under symmetrical external forces, reducing to three quasi-regular infinite systems of linear algebraic equations 24 p3880 A71-44722

Finite cylinder forced longitudinal axisymmetric vibrations with prescribed surface stresses, reducing problem to quasi-regular infinite system of linear algebraic equations 24 p3880 A71-44723

Unstable systems dynamic stabilization, deriving conditions from second order linear differential equations with variable coefficients 24 p3849 A71-45048

LINEAR FILTERS

Kalman optimal linear filter application to near earth satellite orbit calculation based on earth radar observations 01 p0156 A71-10518

Stochastic model for analysis of track-while-scan technique for aircraft search radar, based on Kalman filter theory 01 p0065 A71-11393

Kalman filtering sequential estimates convergence theorems for identifying modeling errors 04 p0561 A71-15328

Maximum likelihood identification of stochastic linear dynamic systems using Kalman filter 05 p0731 A71-16554

Kalman linear multidimensional filters stability, examining digital computer algorithms 05 p0732 A71-17024

Correlated noise linear filtering problem analysis, introducing concept of invariant directions for Riccati equation 06 p0877 A71-17328

Linear dynamic object output reaction prediction by Kalman method constructed model 06 p0879 A71-17673

SAGE/Buic vs Kalman filters for aircraft tracking, determining accuracy by radar model 06 p0925 A71-18517

Kalman-Bucy linear filtering algorithm application to nonlinear estimation of single channel missile attitude control system parameters 07 p1081 A71-18835

Linear and nonlinear filtering, discussing theory and application in space guidance systems 07 p1081 A71-19533

Simple algorithms for accelerating convergence and averting divergence in Kalman filters, using feedback from measurement residuals 08 p1324 A71-21333

Iterative processing technique for limited measurement sets, discussing Kalman filter reaching steady state during ballistic target tracking 08 p1269 A71-21340

Kalman filter application as observer of observable signals derivatives, using gain matrix to minimize variance estimate for instrument landing systems 08 p1269 A71-21343

Dynamic systems current state estimate, using Kalman filter with exponential aging 09 p1421 A71-22110

Amplitude characteristic polynomial Chebyshev approximation by linear phase nonrecursive digital filter transfer function 09 p1417 A71-23037

Nonstationary colored noise linear shaping filter to transform white noise into nonstationary random process with specified covariance function 09 p1424 A71-23100

Return-difference matrix for optimal stationary Kalman-Bucy filter behavior examination in associated feedback system, noting spectral factorization and signal/noise separation 09 p1425 A71-23683

Soviet book on variable structure system theory covering nonlinear automatic control, stability, optimization, adaptive systems, incomplete information processes, linear filters, etc 10 p1585 A71-24147

Nonlinear systems parameter identification schemes using first and second order extended Kalman-Bucy linear filters and sensitivity functions, comparing performance by two examples 10 p1587 A71-24745

Kalman filtering for complex systems, deriving algorithms for dynamic modeling and bias errors effects in discrete-time state optimum estimation 12 p1893 A71-27435

Infimum principle for dynamic optimal control with nonscalar valued cost criteria, rederiving Kalman-Bucy filter 14 p2219 A71-29627

Linear filter to represent diffusion in numerical models of large scale atmospheric circulation 14 p2269 A71-29948

Transfer function optimization for linear tracking filter model with controlled resonant frequency, analyzing noise band performance 14 p2194 A71-30089

Kalman-Bucy filter construction as true time varying Wiener filter with covariances independent of signal generation, applying to data smoothing problem 14 p2220 A71-30460

Optimal linear filter gain relation to feedback difference, using Riccati matrix differential equation 14 p2220 A71-30808

Linear filtering algorithms computational efficiency, deriving formulas for arithmetic operation count and storage requirements 16 p2602 A71-33352

Two level Kalman filter for high order interconnected systems states estimation, deriving coordination algorithm with one step convergence by multilevel systems theory 17 p2718 A71-34735

Discrete Kalman filter computational efficiency improvement by iterative processing technique for covariance matrix updating 17 p2722 A71-35182

Flight test of hybrid strapdown inertial navigator with Doppler radar and occasional position fixes through Kalman filter mechanized in small computer 17 p2776 A71-35765

Doppler satellite/airborne inertial navigation system integration with delayed state Kalman filter 17 p2776 A71-35766

Celestial body mass determination in many body problem, using Kalman-Bucy filtering for Taylor series approximation linearized problem 18 p2960 A71-35935

Reentry vehicles trajectory reconstruction by computer program and Kalman filter estimation theory, analyzing instrument errors 19 p3097 A71-37178

Kalman filter in preflight postflight analysis of velocity increment by spin rocket plume impingement at preentry altitudes 19 p3148 A71-37179

Kalman filter for computerized optimal SRAM air to surface missile alignment, discussing design, digital simulation and flight tests 19 p3098 A71-37189

Optimal Kalman filter gyro drift rate mathematical models for limiting inertial navigation errors 19 p3100 A71-37212

Discrete closed loop system stability with Kalman filter by determining z plane poles of special augmented transition matrix 19 p3036 A71-37235

Nonuniform sampling procedure for linear transversal filters synthesis, obtaining phase-sampled impulse response filters suitable for AM and FM waveforms generation and matched filtering 20 p3203 A71-38859

Signal process models choice in Kalman-Bucy filtering, proving smallest error covariance matrix existence 21 p3349 A71-41190

Finite memory linear radio filter synthesis for maximizing SNR under supplementary quadratic constraints 22 p3510 A71-42257

VOR/DME air navigation equipment using Kalman-Bucy filter and airborne air data system/ADS 22 p3573 A71-42289

Bit synchronization in high SNR digital communication system, using Kalman filtering algorithm 22 p3513 A71-42383

Low thrust interplanetary spacecraft tracking, using spectral factorization for Kalman filtering equations steady state solution 23 p3732 A71-43063

Minimum order state vector reconstruction linear filters for constant plants optimal control, applying to aircraft flight multiple control-point problem 23 p3657 A71-44077

Linear constrained optimal filtering by multistage linear transformations using Kalman-Bucy estimates and Lagrange multipliers 23 p3658 A71-44084

Flight test measurements for improved estimates of aircraft states and aerodynamic parameters, using relinearized Kalman filter 23 p3629 A71-44089

Linear regression optimal filtering application to aircraft target tracking 23 p3659 A71-44094

Maximally achievable accuracy of linear optimal regulators and filters 23 p3659 A71-44099

Uniform signal energy distribution in wideband synchronous data transmission channels using linear sequential filters with scramblers 23 p3647 A71-44345

Kalman filter literature covering structure, applications, fundamental properties, shortcomings, filter synthesis and degradation factors 24 p3808 A71-44398

LINEAR PREDICTION

Speech signals digital encoding with adaptive linear predictor for reducing redundancy, discussing digital simulation results and subjective comparison with log-PCM encoder 01 p0030 A71-10472

Transient heat flow mean and first moments prediction by discontinuous linear or quadratic trial functions and variations 05 p0831 A71-16491

Linear estimation with stochastic feedback control to cancel out disturbances or error signals effect, applying to integrated navigation systems involving inertial measurement 12 p1893 A71-27436

Stochastic signal optimum linear estimation in multiplicative and measurement noises, deriving algorithms 14 p2197 A71-30794

Linear dynamic system recursive state estimation for set-membership description of uncertainty under unknown input disturbances and observation errors 17 p2718 A71-34734

Optimal structure and parameter adaptive estimation for continuous and discrete data Gaussian process models with linear dynamics 17 p2719 A71-34739

Interference loading linear prediction on aircraft stores at supersonic speeds, considering flow field due to jet fighter bomber 19 p2996 A71-37290

Sequential processor performance prediction error with linear method from Monte Carlo cycle analysis of Apollo 14 early rendezvous profile [AAS PAPER 71-386] 23 p3731 A71-43056

Flight test measurements for improved estimates of aircraft states and aerodynamic parameters, using relinearized Kalman filter 23 p3629 A71-44089

LINEAR PROGRAMMING

Circular elastoplastic plates, solving adaptation theory kinematic equations by linear programming procedures 02 p0324 A71-11751

Linear programming functional control solution by generalized searching gradient algorithm at admissible region boundary 03 p0389 A71-13517

Linear, nonlinear and stochastic real control systems optimization by numerical techniques, considering gradient methods and linear programming 05 p0730 A71-16250

Book on optimization methods covering matrix algebra, n dimensional geometry, search techniques, linear and nonlinear programming, etc 05 p0774 A71-16475

Linear programming application to optimum structural design, noting savings in design and price 05 p0825 A71-16610

Structural optimization by concave and piecewise linear programming, discussing mathematical foundation and iterative method efficiency 05 p0829 A71-17121

Complex supply system large quantity data handling and cost savings through optimum planning of storage points and transport using linear separable programming 06 p1010 A71-17746

Rigid plastic shells carrying capacity by kinematic method based on linear programming 06 p0996 A71-17839

Pattern classification as linear programming problem, presenting optimal algorithm 09 p1412 A71-22969

Arbitrary solid cross section frames and arches shakedown analysis including axial forces effects on stress through reduction to linear programming 11 p1849 A71-25678

Differential equation systems optimal scaling for analog computer, proposing amplitude and time scaling factors and disposition parameters with linear programming 15 p2440 A71-31155

Elastic-plastic stiffness matrix methods, applying linear and nonlinear programming techniques to framed structures analysis 16 p2653 A71-33094

Linear programming problems with multidimensional decisions, proposing solution method based on utility theory 18 p2940 A71-36040

Set covering algorithm based on single branch search coupled with linear programming and suboptimization techniques 19 p3025 A71-37546

Branch-and-bound algorithm for zero-one linear mixed integer programming problems solution 19 p3085 A71-37547

Linear programs optimality conditions, using differential calculus approach to classical optimization theory in Danzig simplex algorithm development 19 p3086 A71-37548

Modified linear programming algorithm for columnar methods in mathematical programming applicable to decomposition principle, concave maximization and Lagrange multipliers search 19 p3086 A71-37549

Vector functionals optimization, programming optimal trajectories 23 p3657 A71-44017

Trajectory correction problem optimal measurement set, showing solution by linear programming simplex algorithm method 24 p3846 A71-45306

LINEAR RECEIVERS

Linear continuous receiver and control systems resolution and statistical epsilon invariance 01 p0062 A71-10716

LINEAR SYSTEMS

Thermistor bridges for temperature measurement, discussing linearity conditions 01 p0079 A71-10250

Linear dynamic plants in steady state identified via multichannel statistical optimizer 01 p0064 A71-10923

Steady state quantum analysis of linear distributed systems applied to attenuator, maser amplifier and multiterminal-pair networks 02 p0213 A71-12017

German book on switching theory of linear microwave networks, covering waveguides for n-port network, network modeling, interconnections, etc 02 p0215 A71-12315

Discrete linear plant identification, using generalized Kalman models 02 p0236 A71-12624

Linear ordinary differential equations system with random coefficients, proving mean stability theorem 03 p0450 A71-13119

Linear feedback function for r-stage feedback shift register resulting in equal length branchless cycles [JPL-TR-32-151] 03 p0388 A71-13282

Approximate minimum energy control for time variable linear system, using mathematical model 03 p0389 A71-13447

Indirect, linear and nonlinear optimal guidance schemes from precomputed reference trajectory, using iterative techniques for boundary equations 03 p0454 A71-13449

Linear control systems searchless automatic optimization on basis of ideal reviewing model 03 p0389 A71-13519

Linear integrodifferential time lag systems quick response problem approximate iterative solution, considering convergence and controllability conditions 03 p0452 A71-14060

First order nonlinear nonautonomous systems equivalence to second order linear autonomous systems through governing differential equations variables integral transformation 03 p0390 A71-14076

Linear optimal control systems with penalty on state and control vector sensitivities, avoiding mathematical difficulties 03 p0391 A71-14313

Regulator logic synthesis using state variable feedback for stationary linear plants 03 p0393 A71-14467

Stability of linear time invariant discrete systems including multiple poles 03 p0393 A71-14471

Existence and construction of modified L lag inverses solution method for linear dynamical systems 03 p0393 A71-14482

Dynamic response of linear systems with parameters subjected to perturbation, obtaining quasi-linear mathematical model describing parameter-perturbation transmission path 03 p0394 A71-14483

Quasi-linear elliptic boundary point solutions, deriving modulus of continuity estimates 04 p0619 A71-15552

Astrophotographs reduction for wide angle negatives, using linear and eight constants method 04 p0599 A71-15559

N person nonzero sum differential games with linear dynamics, proving existence of equilibrium strategies 04 p0620 A71-15864

Linear, nonlinear and stochastic real control systems optimization by numerical techniques, considering gradient methods and linear programming 05 p0730 A71-16250

Canonical linear Hamiltonian systems normalization algorithm, applying to restricted three body problem 05 p0810 A71-16547

Dynamic objects optimal linear model existence and uniqueness conditions, considering gradient technique and stochastic approximation algorithms convergence 05 p0731 A71-16794

Object motion stabilization, determining minimum control actions number for linear and nonlinear systems 05 p0782 A71-16977

Large linear systems smallest eigenvalues determination, examining various algorithms 05 p0829 A71-17114

Error estimation for algorithms identifying linear systems described by higher order scalar difference equation 06 p0877 A71-17329

Suboptimal control of linear time invariant systems subject to structure constraints and combination of measurable/nonmeasurable states 06 p0878 A71-17330

Plant parameter variations in linear optimal control systems along stability ray 06 p0878 A71-17334

Soviet book on Liapunov functions covering autonomous linear and nonlinear systems, asymptotic and absolute stability, etc 06 p0916 A71-17442

State space constrained linear optimal control systems, using cutting plane algorithm for convex programs in Banach spaces 06 p0918 A71-17598

Linear dynamic object output reaction prediction by Kalman method constructed model 06 p0879 A71-17679

Discrete linear vibration systems viscous damping local modifications effect on eigenvalues and vectors using Weissenburgers procedure in matrix form [AIAA PAPER 71-215] 06 p0928 A71-18651

Linear sequential circuits feedforward inverse transfer function matrix existence condition and construction procedure 07 p1081 A71-18735

Linear systems optimal control problems numerical solution methods comparison, noting accuracy advantage of invariant imbedding technique 07 p1081 A71-18834

Two finite undirected linear graphs, determining isomorphism 07 p1148 A71-20370

Block decomposition of linear time invariant multivariable control systems 08 p1269 A71-21328

Optimal variational control with frequency and time coupling concerning dynamic precision of linear systems 08 p1271 A71-22023

Identification algorithm for estimating parameters in constant coefficient linear system independent of prior estimates [AIAA PAPER 70-34] 09 p1484 A71-22074

Linear optimal stochastic control systems described by covariance matrix correlating errors and estimates of state variables, analyzing instability under parameter variations [AIAA PAPER 70-36] 09 p1421 A71-22076

Liapunov function construction for linear dynamical systems, applying condition of agreement with eigenvalue analysis 09 p1484 A71-22102

Linear one dimensional systems with infinite degrees of freedom, examining optimal constrained control 09 p1421 A71-22118

Statically indeterminate rod system design, using linear strengthened materials strain diagrams and Castigliano principle 09 p1538 A71-22650

Linear one dimensional system with infinite degrees of freedom, discussing optimal control by Fredholm integral equation 09 p1424 A71-23457

Discrete time finite dimensional autonomous linear systems, investigating controllability and pole assignment to closed loop transfer matrix by choice of state variable feedback gain 09 p1424 A71-23465

Single parameter linear physically realizable stable system with lumped parameters, estimating identification process solution uniqueness and stability 09 p1425 A71-23568

Independently sampled indirect and direct magnitude measurements, noting linear system effects in astrometry 10 p1575 A71-23845

Numerical integration of perturbed linear systems of differential equations by step method comparing power series 10 p1636 A71-23960

One dimensional linear stationary systems described by linear differential equations, discussing identification procedure with transformation into integral equations 10 p1585 A71-24157

Necessary and sufficient controllability conditions for linear nonstationary system with deterministic inputs described by two differential equations 10 p1586 A71-24387

System identification, considering input signals classification, model structure, linear/nonlinear systems identifying and on-line/real time techniques 10 p1586 A71-24736

Identification algorithm for linear discrete time systems difference equations with input-output measurements coefficients 10 p1586 A71-24737

Approximate analytical formulas for free oscillations of nonstationary linear control systems using canonical transformations 10 p1643 A71-24898

Asymptotic transformations and stability criteria of nonstationary linear automatic control systems using Krylov-Bogolubov slow time concept 10 p1588 A71-24899

Stability and coordinate bounds of motion of linear dynamic systems over finite time intervals by solutions of differential equations 10 p1643 A71-24900

Random response of stationary linear system to pulse noise in time with independent amplitudes 10 p1588 A71-24901

Differential equations of root loci motions for stationary linear automatic control design by hodograph and Evan method

10 p1637 A71-24906

Dynamic frequency and phase characteristics of oscillatory circuit dependent linearly on time variable capacitance

10 p1643 A71-24907

Nonstationary linear systems analysis over finite time interval and graphical method for differential equation, comparing exact and approximate solutions for free oscillations

10 p1643 A71-24908

Periodic signal input effects on stationary linear system, using closed form Laplace transformation

10 p1643 A71-24909

Linear discrete time stochastic system with unknown gain parameters, interpreting open loop feedback optimal control identifier and controller equations

11 p1741 A71-25361

Normality-independence characterization of stochastic integrals in linear processes

11 p1792 A71-26102

Convergence of identification scheme for scalar-input-scalar-output linear systems with random inputs, applying invariant set theorem for random systems

11 p1792 A71-26412

Optimal fixed dimensionality dynamic compensator design for linear time-invariant closed-loop system based on quadratic cost and gain criteria

11 p1742 A71-26414

Linear continuous time delay feedback systems stability analysis, using root-locus and frequency response techniques

11 p1742 A71-26423

Parametrically invariant automatic control systems with linear controllers, using compensating devices based on certain transfer function qualifications

12 p1890 A71-26721

Linear sawtooth voltage phantastron type generator, presenting operation time diagrams and circuit advantages

12 p1906 A71-26900

Multivariable linear systems parameter reduction, assuming minimum controllability and observability [DFVLR-SONDDR-89]

12 p1922 A71-27007

Optimal control of linear and nonlinear systems with infinite degrees of freedom, deriving parabolic type partial differential equations

12 p1891 A71-27019

Optimal impulse correction of linear dynamic system motion based on system phase coordinates statistical information, taking into account correction finite accuracy and power expenditure

12 p1892 A71-27021

Linear complexes in three dimensional space considered with canonical transverse system, discussing nonintegral presentation and existence theorem

12 p1922 A71-27119

Optimal stabilization system synthesis for multidimensional linear control plant in presence of random perturbation

12 p1892 A71-27176

Optimal output regulator for linear time invariant systems with reference vector and quadratic cost functional

12 p1893 A71-27430

Linear system programmed maxim transfer time problem solvability, investigating control process theory with time inversion

12 p1931 A71-27523

Time optimal control problem solution for linear and nonlinear piecewise continuous systems by penalty function method

13 p2040 A71-27897

Controllability and optimal control for linear system with discontinuous restriction on control function

13 p2041 A71-28009

French book on practical methods for nonlinear oscillations analysis covering linear and nonlinear systems, autonomous systems, forced harmonics, nonautonomous oscillating systems, etc

13 p2041 A71-28151

Linear viscoelastic materials, investigating failure and bending as function of time in response to load under creep conditions

13 p2154 A71-28322

Linear optimal control system quality functional, deriving sensitivity upper estimate

13 p2041 A71-28635

Book on multivariable control systems covering dynamical, linear continuous and time-discrete systems

13 p2043 A71-28792

Identification by minimization of Gaussian-Markovian representation of stochastic process, considering positive linear systems and algorithm for matrix calculation

13 p2043 A71-28818

Algorithms for constructing minimized abstract automatic subunits and two switch types as basis for arbitrary linear block encoder

13 p2035 A71-28915

Gas dynamic effects associated with unboundedness of solution of quasi-linear hyperbolic systems

14 p2223 A71-29560

Passage through resonance of linear oscillator with slowly varying frequency, matching inner and outer asymptotic expansions

14 p2274 A71-29861

Linear one dimensional systems with infinite degrees of freedom, examining optimal constrained control

14 p2219 A71-29996

Noise effect on signal parameter control in linear measurement devices

14 p2194 A71-30082

Force method equations for linear viscoelastic system of incompressible rods obeying small deformations theory

14 p2328 A71-30376

Optimal terminal control stochastic synthesis for linear systems by Bellman second order nonlinear partial differential equations

14 p2220 A71-30872

Mathematical modeling and convergence analysis of nonscanning self adaptive control systems for linear objects, using Liapunov second method

15 p2379 A71-31519

Decomposing method for linear transfer functions identification from frequency or time response, using Cauer form continued fraction expansion

15 p2379 A71-31821

On-line identification of stochastic linear dynamic control systems with applications to Kalman filtering based on statistical correlation technique

15 p2380 A71-31933

Liapunov approach to nonlinear dynamic systems controllability, deriving conditions for linear dynamic systems

15 p2380 A71-31935

Soviet book on discrete control systems covering linear and nonlinear systems synthesis and analysis, digital computer techniques, one and multidimensional pulsed systems optimization, etc

15 p2381 A71-31976

Discrete group symmetric linear control systems reduction to elementary cell, generalizing Fourier transform to groups without operational constraints

15 p2381 A71-31978

Linear stationary lumped-constant relaxation systems with real and positive eigenvalues and impulsive response characterizable by exponentials, evaluating error in identification

15 p2450 A71-32322

Sensitivity functions of phase canonical form for single input linear time invariant controllable systems, using frequency domain techniques

15 p2382 A71-32442

Higher order linear and nonlinear systems equivalence from partial/ordinary differential equations

15 p2443 A71-32521

Minimum dimensionality determination for control process stabilizing linear mechanical system, obtaining necessary and sufficient conditions for stabilization

16 p2607 A71-32933

Feedback stabilization of linear distributive systems in form of second-order evolutionary equation in Hilbert space, applying to plasma stabilization

16 p2618 A71-33006

Holder stability and logarithmic convexity as special case of Liapunov function applied to linear elastic systems without body force

16 p2608 A71-33008

Stability of linear viscoelastic systems under non-conservative forces, obtaining equations for perturbed motion for equilibrium or creep state

16 p2650 A71-33020

N-order continuous linear automatic control system compensation method, using model of sampled systems with duration modulation

16 p2549 A71-33377

Numerical identification of linear automatic control system, starting from pulse response

16 p2549 A71-33378

Monograph on algebraic theory for ordinary linear time invariant difference systems covering constant shift operators, matrix formalism, operational calculus, etc

16 p2602 A71-33397

Two dimensional linear communication system with crossed channels with different amplification factors and time constant, examining stability with root trajectory method

16 p2549 A71-33569

Closed linear systems optimal stabilization, determining transfer function from Wiener Hopf equation

16 p2550 A71-33900

Steady and linear systems discretization by Laguerre transformation and isomorphism between continuous and discrete signals

16 p2550 A71-34058

Dynamic cryptodeterministic linear systems with random initial state, calculating stochastic response by perturbation scheme

16 p2660 A71-34072

Linear single loop sampled data time delay feedback systems stability analysis

16 p2550 A71-34168

Linear comparison systems stability condition proved with Kotlianskii and Bailey theorems

17 p2764 A71-34510

Linear dynamic system recursive state estimation for set-membership description of uncertainty under unknown input disturbances and observation errors

17 p2718 A71-34734

Linear time-invariant dynamic feedback system suboptimal control by lower order generalized aggregated model for reducing computational complexity

17 p2719 A71-34740

Linear system optimal stochastic control and observation strategies simultaneous determination with quadratic cost by dynamic programming

17 p2719 A71-34742

Monograph on parametric errors estimation for dynamic models of linear time invariant control systems

17 p2720 A71-34793

Infinite-time linear dynamic system suboptimal control derivation from lower dimension models, exemplifying by flexible-bodied rocket vehicle pitch plane dynamics

17 p2720 A71-34871

Linear dynamic systems state estimation, using empirical Bayes decision theory to develop filter set

17 p2825 A71-34897

Rapid convergence method application to linear system with odd almost periodic coefficients

17 p2779 A71-34907

Superharmonic resonance in piecewise linear systems with unsymmetrical characteristics, investigating stability properties by Fourier series method

17 p2781 A71-34926

Error correction in autonomous linear finite automata with correcting codes

17 p2711 A71-34979

Discrete-time optimal linear systems structure and stability, assuming quadratic costs and perfect observability

17 p2722 A71-35180

French monograph on algorithms for parameters estimation for adaptive identification in real time of linear processes perturbed by related noise

17 p2767 A71-35232

Geometric theory of linear multivariable systems extension by controllable output subspace introduction

17 p2723 A71-35295

Measurement uncertainty effects in linear multistage games, considering state variables construction from player measurement sequences

17 p2767 A71-35298

Plane laminar flow linear stability problem, using Orr-Sommerfeld equation with Volterra integral equation

18 p2904 A71-36136

Modal control for linear multivariable time-invariant systems incorporating multiloop single input proportional controllers

18 p2896 A71-36235

Linear systems with constant inputs optimal with respect to infinite terminal time quadratic performance, using Riccati equation

18 p2896 A71-36236

Object motion stabilization, determining minimum control actions number for linear and nonlinear systems

18 p2947 A71-36777

Dynamic piecewise-continuous linear systems oscillation period doubling in presence of C bifurcations

18 p2948 A71-36785

Frequency domain approach for analysis of linear variable networks demonstrated by calculating system response to input

19 p3036 A71-37147

Optimal control of linear time varying neutral system, solving differential equations set

19 p3037 A71-37238

Proposed prism adaptation model suggesting visual motor control loop as linear system comprising independent subsystems

19 p3007 A71-37544

Noniterative scheme for treating two-point boundary value problems for single and multiinput linear constant systems, requiring solution of 2n differential equations

19 p3086 A71-37559

Optimal impulse correction of linear dynamic system motion based on system phase coordinates statistical information, taking into account correction finite accuracy and power expenditure

19 p3037 A71-37690

Linear system stability via Liapunov method and square integral, establishing continuous and discrete time systems equivalence 19 p3086 A71-37885

Optimal zero-memory regulator for linear system with stochastic jump parameters, considering Bayes and minimax controllers 19 p3039 A71-38711

Constant coefficient linear systems sensitivity functions computational procedure using n th order differential equations linear transformations 19 p3039 A71-38714

Controller design for linear closed loop system with transport delay, discussing simplified procedure with correction by zero-pole cluster outside bandpass 19 p3040 A71-38717

Analysis and synthesis of linear optical systems involving polarization effects by Pauli algebra of complex second order matrices 20 p3267 A71-38775

State feedback decoupling sensitivity of time invariant linear multivariable system, using Liapunov matrix equations 20 p3207 A71-38992

Frequency domain computer graphics technique for linear time-invariant multivariable feedback control system design 20 p3207 A71-38997

Parameter estimation algorithms for state variable models of multivariable linear control systems from noisy input-output records 20 p3208 A71-38999

Time optimal control synthesis for linear integration-type system described by n -order differential equations, using operational calculus 21 p3359 A71-40165

Frequency response optimization of one dimensional damped linear continuous systems, requiring initial value numerical integration of state and adjoint differential equations [ASME PAPER 71-VIBR-1] 21 p3456 A71-40265

Linear second order multidegree of freedom vibrational system with singular mass matrix, determining response to excitation [ASME PAPER 71-VIBR-10] 21 p3457 A71-40272

Steady state performance of two degrees of freedom system consisting of main linear spring mass system under periodic forcing [ASME PAPER 71-VIBR-49] 21 p3459 A71-40298

Linear multidegree of freedom shock isolation system optimum design, masses, spring and damping coefficients, using mathematical programming [ASME PAPER 71-VIBR-81] 21 p3461 A71-40317

Optimal numerical solutions of linear control systems with quadratic integral form, using dynamic programming, successive optimization and algorithm-aided dynamic programming 21 p3360 A71-40617

Linear multivariate sampled-data control systems optimal design based on deadbeat performance 21 p3360 A71-40618

Liapunov-type analysis of linear systems dynamic stability under stochastic parametric excitation, noting application to rectangular flat plates 21 p3469 A71-41008

Homogeneous fuel combustors with multistage reaction rate controlled system, determining linear relationships and heat release 21 p3437 A71-41049

Controllability and optimal control for linear system with discontinuous restriction on control function 21 p3361 A71-41137

Stability and quality diagrams of linear discrete automatic control systems with time constant parameters 21 p3361 A71-41142

Linear system model for multiple scattering light transmission through optically thick clouds, calculating optical effects by four dimensional linear superposition integral 22 p3575 A71-41789

Linear time-varying system state space representation determination based on scalar differential equation, considering advantages 22 p3566 A71-41853

Optimal control of linear systems with distributed parameters, using hyperbolic type equation 22 p3526 A71-41909

Linear dynamic system sensitivity models simplification conditions application to adaptive nonsearching system synthesis algorithms 22 p3527 A71-42857

Linear digital interpolator in program controlled metal cutting tool circuit, determining transfer function with z transforms 22 p3525 A71-42876

Mathematical modeling and convergence analysis of nonscanning self adaptive control systems for linear objects, using Liapunov second method 22 p3528 A71-42884

Fault detection, diagnosis and prognosis in linear dynamic systems based on statistical decision theory, considering error signal generation and statistics 23 p3682 A71-43945

Riccati equation reduction for optimal control of linear quadratic distributed parameter systems applied to temperature and heat flow regulation 23 p3653 A71-43969

Interaction between two rectilinear cracks, noting angle and disorientation effects 23 p3777 A71-44034

Stability conditions of linear discrete system with periodic feedback from spectrum location of bounded linear operator acting in Banach space 23 p3657 A71-44078

Parameter sensitivity reduction in linear optimal feedback control systems based on two degree of freedom structure 23 p3658 A71-44080

Fixed configuration optimal control of linear systems with state and control dependent noise 23 p3658 A71-44082

Steady state gains and covariance computation for time invariant discretely updated linear systems, demonstrating iterative and algebraic solutions 23 p3660 A71-44116

Pole placement design of dynamic compensators for linear time invariant multivariable systems, using transfer function matrices 23 p3660 A71-44119

Linear dynamic systems suboptimal control determination from lower dimension models, characterizing system and model outputs as Hilbert space elements 23 p3660 A71-44121

Minimal partial realizations of linear input/output map, discussing significance in regard to adaptive dynamics identification procedures 23 p3661 A71-44190

Optimum design of linear multivariate sampled data systems, using deadbeat and integral performance criteria and output response error 24 p3812 A71-44451

Statistically optimal linear systems characteristics under unsteady input signal, noting relation between error components 24 p3813 A71-44679

Linear system under state dependent random noise, obtaining optimal steady control 24 p3814 A71-44684

Linear control system optimal weighting function determination from maximum probability for system error 24 p3814 A71-44687

Optimal linear final parameter control synthesis for dynamic systems with given accuracy, using multivariate statistical analysis 24 p3814 A71-44690

Parameters steady random variations effect on linear and nonlinear systems steady motion characteristics, using integral equation and averaging methods 24 p3815 A71-44696

Stochastic linear systems stability with random processes coefficients, using differential equations 24 p3815 A71-44698

Linear systems with randomly varying parameters, deriving stability conditions from one dimensional distribution functions 24 p3815 A71-44699

Geometrical least squares model extension to maximum likelihood method for linear processes with additive Gaussian error 24 p3843 A71-44704

Weakly damped nonstationary linear systems analysis by modified sensitivity function method, evaluating solution error 24 p3816 A71-45001

Minimal order linear time-invariant systems description by smallest possible number of parameters, deriving differential or difference equations based on input/output parameters [DFVLR-SONDDR-135] 24 p3816 A71-45122

Optimal stochastic control law derivation for linear regulator with quadratic performance criterion from limiting form of transfer function 24 p3816 A71-45134

Algorithm for preparation of nonlinear differential equations for simulation by analog computer in linear form 24 p3807 A71-45156

LINEAR TRANSFORMATIONS

Image data coding by linear transformation and block quantization, considering Fourier, Hadamard and Karhunen-Loeve methods 10 p1580 A71-23766

Data transmission with redundancy, discussing optimum data compressing encoding of correlated source signals through linear transformation 12 p1883 A71-27009

Parameter space sections method for nonlinear automatic control systems analysis, reducing initial system by linear transformation of variables to first and second order equations 17 p2783 A71-35127

Linear, affine and projective coordinate transformation from one mapping plane to another with quick maximum error estimation 17 p2734 A71-35187

Constant coefficient linear systems sensitivity functions computational procedure using n th order differential equations linear transformations 19 p3039 A71-38711

Yield conditions and flow rules derivation from hypoelasticity, regarding constitutive equation as linear transformation on six dimensional inner product space of symmetrical tensors 21 p3455 A71-40040

Linear constrained optimal filtering by multistage linear transformations using Kalman-Bucy estimates and Lagrange multipliers 23 p3658 A71-44080

Linear transformation and absorption of electromagnetic waves in plasma 24 p3857 A71-45161

LINEAR VIBRATION

Thin walled shell free linear vibrations frequency density calculation using asymptotic method 05 p0829 A71-16990

Single rotor gyrocompass dynamics under LF three-component linear vibration of base, using precessionary equations 07 p1108 A71-19303

French book on linear vibrations covering systems with one or more degrees of freedom in free and forced vibration, propagation in discontinuous and continuous media, etc 17 p2784 A71-35737

Excitation response of oscillatory conservative linear system to transient displacement involving time dependent boundary conditions 18 p2947 A71-36740

Thin walled shell free linear vibrations frequency density calculation using asymptotic method 18 p2982 A71-36790

LINEARITY

NT COLLINEARITY

Accelerometers linearity variations by centrifugal tests [AGARDOGRAPH-128] 05 p0750 A71-16311

Linear theory of viscoelasticity, calculating basic relationships based on experimentally determined characteristics under unsteady test conditions 09 p1537 A71-22511

Gages using X radiation for measuring thickness, range, linearity and response time, noting applications of absorption and fluorescence techniques 17 p2744 A71-35283

Two-terminal negative resistance circuit analysis for parameters effect on linearity by parabolic relation 22 p3521 A71-42203

LINEARIZATION

Cauchy problem for linearized Boltzmann equation using collision operator eigenfunction series 01 p0109 A71-10022

Nonlinear automatic control systems steady random processes approximate analysis by integral linearization of functions and operators 01 p0058 A71-10100

Soviet book on self adjusting control systems with reference models covering harmonic linearization method, phase plane technique, deterministic signals, etc 04 p0560 A71-14640

Finite difference and initial value solutions of nonlinear boundary problems for ordinary differential equations, generating algorithms by quasi-linearization method 05 p0775 A71-16640

Constrained function extremization, taking into account modified quasi-linearization algorithm 05 p0776 A71-17080

Optimal control problems for functional extremization, developing modified quasi-linearization algorithm 05 p0776 A71-17089

Nonlinear dynamic systems synthesis by integral linearization, obtaining gain coefficients and graphs for work reduction 05 p0732 A71-17171

Control function synthesis by linearization for maintenance of uniform motion of driven component in mechanical system including motor, variator and operating machine 07 p1116 A71-19358

Incompressible viscous liquid forced oscillations stability, developing linearization procedure for nonlinear operator equation of perturbations 08 p1275 A71-21051

Nonlinear elastic incompressible transversally isotropic body with finite initial deformations, considering linearized problems of static and dynamic equations 09 p1534 A71-22178

Closed-loop nonlinear systems synthesis, using mapping in Chebyshev series converging everywhere, multidimensional linearization and Volterra singular integral equations 10 p1587 A71-24744

Electropneumatic transducer system linearization, matching nonlinearities in EM and pneumatic subsystems 13 p1999 A71-28638

- Nonlinear free oscillations, discussing linearization for nonlinear functions by weighted mean square method 14 p2325 A71-30060
- Damped gravity orientated satellite linearized analysis for vibrational response to large amplitude motion 14 p2320 A71-30307
- Free and forced nonlinear oscillations differential equations approximate solution by orthogonal polynomial linearization, applying method to systems analysis near singular points 17 p2780 A71-34917
- Nonlinear mechanical system stationary random forcing input and output response data, determining statistical linearization coefficients in Kazakov-Bootton method 19 p3037 A71-37347
- Nonlinear discrete system optimal feedback controller synthesis for low sensitivity to parameter variations by difference equations quasilinearization and dynamic programming 23 p3656 A71-43855
- Analytic synthesis of optimal feedback controller for nonlinear multivariable systems based on reduction to linear control problems 23 p3659 A71-44110
- Design parameter optimization for two-stage space shuttle atmospheric flight from spherical nonrotating earth by sequential straight line approximation 23 p3774 A71-44115
- Statistical and combined harmonic and statistical linearization methods for piecewise-linear nonlinear system characteristics analysis 24 p3814 A71-44693
- Unsteady nonlinear multidimensional feedback control systems characterized by equations in normal form for phase coordinates, investigating solutions accuracy by statistical linearization 24 p3814 A71-44694
- LINEARS**
- U LININGS**
- LINEAS [GEOMETRY]**
- NT CHORDS [GEOMETRY]**
- Line segment orientation visual perception relation to horizontal, vertical and oblique planes, considering induction effect susceptibility and visual illusions 01 p0010 A71-10274
- Electronic contour line recorder with intermittent line setting capacity and interpolation frequency regulation 01 p0083 A71-11329
- LINEAS OF FORCE**
- Auroral ionosphere, examining low energy proton fluxes parallel to geomagnetic field lines of force 05 p0738 A71-16160
- Interplanetary magnetic field in plane perpendicular to ecliptic, investigating force lines configuration by solar proton events 07 p1189 A71-20640
- Moving magnetic field lines identification, applying to moving nonrigid conductor 08 p1283 A71-21648
- Geomagnetic latitude-longitude coordinates, examining field lines intersections at height of 100 km 08 p1285 A71-21757
- Hydrogen ion flux detected along earth magnetic force lines in Northern Hemisphere midlatitudes, determining flux magnitude 09 p1436 A71-22561
- Polar cap as distinct geophysical entity, considering open magnetic field lines for connectedness to interplanetary plasma and particle input to lower latitudes 10 p1600 A71-24308
- Magnetospheric location of SAR-arc field lines, discussing proximity to plasmapause, electron trough and ring current 13 p2055 A71-27918
- Magnetosphere structure, considering geomagnetic field lines configuration in magnetotail 14 p2229 A71-29669
- Cosmic rays compound diffusion, considering combined effects of one dimensional diffusion along interstellar magnetic field lines and field lines three dimensional random walk 14 p2301 A71-30434
- Magnetospheric resonator properties bounded by ionosphere/earth system lines of force, examining nonuniform plane wave generation and standing wave pulsation period 15 p2401 A71-32731
- Equilibrium state linear theta pinch plasma confinement dependence on magnetic force lines curvature radius 17 p2786 A71-34278
- Dielectrophoresis force measurements and wedge shaped capacitor separation properties in satellite zero gravity conditions 19 p3103 A71-37278
- Noncircular ionospheric current conversion into longitudinal currents in magnetosphere along lines of force of geomagnetic field 19 p3057 A71-38380
- Ionospheric currents fields, determining Hall conductivity and geomagnetic lines of force slope effects 19 p3058 A71-38387
- Anomalous distribution in heliocentric longitude of solar injected cosmic radiation, suggesting interplanetary magnetic field lines of force stochastic wandering 19 p3130 A71-38674
- One dimensional ambipolar diffusion parallel to magnetic field lines, considering plasma cloud imbedded in weakly ionized gas with homogeneous field 20 p3215 A71-38737
- Interplanetary and magnetospheric magnetic force lines reconnection and effects on geomagnetic activity 20 p3289 A71-39126
- Radiation belt particles nonadiabatic changes, calculating rigidity as function of magnetic field lines 21 p3439 A71-41357
- Equatorial F2 region lattice model with curved field line geometry for plane stratified atmosphere and time dependent problem solution 23 p3667 A71-43137
- Auroral conjugacy observations over Alaska and south of New Zealand, noting correlation with geomagnetic field lines 23 p3671 A71-43325
- Equilibrium plasma in perfectly conducting rigid wall with closed magnetic field lines, deriving necessary conditions for MHD stability 24 p3852 A71-44496
- Galactic stochastic magnetic field lines, deriving dynamic equation for probability density function 24 p3871 A71-44902
- LING-TEMCO-VOUGHT AIRCRAFT**
- NT A-7 AIRCRAFT
- NT F-8 AIRCRAFT
- NT XC-142 AIRCRAFT
- LINGUISTICS**
- NT MACHINE TRANSLATION
- NT PHONEMES
- NT SYLLABLES
- NT SYNTAX
- NT WORDS [LANGUAGE]
- Isolated synthesized vowel fundamental tone duration, intensity and frequency imitation by human voice 02 p0205 A71-12060
- Human voice imitation of tonal signals pitch interval 02 p0206 A71-12061
- Synthesized glottal consonant imitation by human voice, analyzing stimulus and response intensity levels relationship 02 p0206 A71-12062
- Biological movement control systems from structural linguistics viewpoint 02 p0206 A71-12063
- LINING PROCESSES**
- Acoustic linings for attenuation of fan generated noise in turbofan engines, considering interaction between analytical lining performance prediction and flow duct testing [AIAA PAPER 71-731] 14 p2295 A71-30778
- LININGS**
- NT ROCKET LININGS**
- Aircraft engine double-reverberant chamber duct lining test facility, discussing noise fields, air flow, layout, performance, insertion and transmission losses, etc 06 p0880 A71-17619
- Turbofan engine noise reduction, using acoustic linings in inlet and exhaust ducts [AIAA PAPER 71-183] 06 p0947 A71-18622
- Acoustic duct lining materials, comparing attenuation constants according to Scott theory 08 p1333 A71-20808
- Optimal lining impedance for jet engine inlet duct, yielding discrete frequency, flow velocity and geometry on basis of minimum radiated power 08 p1349 A71-21661
- Acoustic liner design for propellant combustion instability and jet aircraft noise suppression, discussing cross flow and oscillatory pressure effects [AIAA PAPER 71-757] 14 p2296 A71-30791
- Lined ducts design for flow with intense sound, discussing analysis methods, testing procedures, liner materials development and acoustic attenuation 21 p3361 A71-40212
- LINKAGES**
- Computer method to simulate dynamic behavior of two dimensional machine systems with linkage elements [ASME PAPER 71-VIBR-111] 21 p3386 A71-40334
- Optimum synthesis of spatial four-link chain mechanism with pressure angles deviating least from zero degrees for force transmission 24 p3848 A71-44900
- LINKING**
- U JOINING**
- LILOVILLE EQUATIONS**
- Kinetic equation for rarefied polyatomic gases derived from Liouville equation 02 p0286 A71-11883
- WKB wave functions for one dimensional non-relativistic problems by simple transformation derivation, solving by application of Liouville substitution to Schroedinger equation 12 p1923 A71-27666
- LILOVILLE THEOREM**
- Light rays bundle compression devices performance based on phase space treatment using Liouville theorem, comparing linear tapers and lenses performance to compressor with graded refractive index distribution 08 p1335 A71-21373
- Soviet book on theory of elliptic functions covering analytic functions, Jacobi and Liouville theorems, modular functions, Weierstrass functions, theta and Jacobi functions 17 p2767 A71-35200
- LIPID METABOLISM**
- Lipid peroxidation in pulmonary hyperoxia, noting effects of hyperbaric oxygen, ascorbic acid and ferrous iron 06 p0851 A71-17604
- Pressure and gas composition effects on sodium acetate-C 14 incorporation into liver lipids, indicating metabolic relationships to decompression sickness 08 p1238 A71-20814
- Prolonged hyperoxia effects on lipid synthesis in rat liver and adipose tissue slices 10 p1559 A71-23969
- Hypothermia effect on lipid synthesis of hamster tissue following intravenous injection of acetate-C 14 14 p2182 A71-29582
- Early diagnosis of atherosclerosis in civil aviation pilots by lipid metabolism and electrocardiographic examinations 15 p2357 A71-31318
- Differential lipid and phospholipid composition of white matter in brain, cervical, thoracic and lumbosacral sections of spinal cord and sciatic nerve in dogs 21 p3338 A71-41074
- Stimulatory effects of hypobaric hyperoxia on lipid synthesis in rat liver and adipose tissues under free feeding 22 p3486 A71-41825
- LIPIDS**
- NT CASTOR OIL**
- Phospholipid composition of lipid extracts of hypothalamo-neurohypophyseal system of cattle 03 p0362 A71-13237
- Phospholipid dynamics of blood entering and leaving brain during unilateral desympathectomy in dogs 03 p0362 A71-13238
- Computer applications in analysis of biological structures, considering tissues, cells, chromosomes, proteins and lipids 06 p0863 A71-18691
- Human crystalline lens protein and lipid discussing cholesterol accumulation with age 09 p1390 A71-22421
- Cerebral lipid fractions, examining relation between physiological functions and metabolism 09 p1391 A71-22481
- Vitamin B6 protection against asymmetrical dimethylhydrazine poisoning, administering B6 alone and with cortical phospholipids in mice 10 p1572 A71-24979
- Lipid, protein and carbohydrate concentrations in Chlorella biomass from pyrolysis and aluminogel column chromatography 13 p2017 A71-28407
- Ethyl esters of long chain fatty acids as biological products from gas chromatographic and mass spectrometric analyses on lipid fractions 13 p2015 A71-29352
- Prolonged strenuous physical exercise effect on triglycerides, phospholipids and glycogen concentration in human femoral muscle 18 p2856 A71-36238
- LIPSCHITZ CONDITION**
- Lipschitz functional differential equations systems uniform asymptotic stability under diminishing perturbations 01 p0111 A71-10470
- Bellman function for time optimal problem under Lipschitz condition 05 p0782 A71-16981
- Constant space curvature perturbations, considering density, rotational and propagation of gravitational waves with Lipschitz method 13 p2137 A71-28479
- Algorithm convergence for sparse nonlinear equations system solution with Jacobian satisfying Lipschitz condition 15 p2442 A71-32313
- Bellman function for time optimal problem under Lipschitz condition 18 p2942 A71-36781
- LIQUEFACTION**
- Intracrystalline liquefaction in Ni alloys containing Nb studied with microanalyser 09 p1480 A71-23702
- Miniature high speed expansion turbines for helium liquefiers and refrigerators, discussing turbine flow passages and gas lubricated bearings 20 p3184 A71-39246
- LIQUEFIED GASES**
- NT LIQUID HELIUM
- NT LIQUID HYDROGEN
- NT LIQUID NITROGEN
- NT LIQUID OXYGEN

Turbulent engine design for methane element of liquefied natural gas as aircraft fuel, discussing supersonic transport applications

01 p0141 A71-10485

Liquefied and solidified gas IR measurements describing versatile optical cell

02 p0250 A71-12133

Ignition and nondetonating decomposition of liquid nitromethane explosive at 10 kbar pressure

05 p0795 A71-16517

Combined continuity and force equations for sound attenuation as function of thermal and viscous losses in liquid gases, taking into account fcc and bcc packing

06 p0927 A71-17569

Thermodynamic properties prediction for liquefied natural gas and other cryogenic fluids, using two fluid method

13 p2100 A71-28603

Liquefied gas solutions of methane in carbon tetrafluoride and propylene, calculating pressure and temperature dependence of density

15 p2462 A71-31246

Wide range specific heat measurements of dense simple fluids /helium, neon, argon, krypton, parahydrogen, oxygen and fluorine/

15 p2515 A71-32702

Launch facility requirements for liquid fluorine upper stage, considering propellant storage and transfer, vapor disposal, leak detection, spills, aborts and range safety

18 p2898 A71-36457

LIQUID ATOMIZATION

Breakup mechanism of liquid sheets and jets in supersonic gas stream, using spark photomicrographs and high speed movies

11 p1750 A71-25471

Liquid fuel atomizers for gas turbine combustion system model experiments, considering droplet sheet photography and molten wax spray technique

13 p2117 A71-28755

Carbon deposition rates in gas turbine engine combustion chambers with airstream-mechanical propellant atomization

13 p2118 A71-28970

Single and multibeam holography application to size, trajectory, distribution, population density and velocity measurements of water and electric arc welding sprays droplets

14 p2243 A71-30299

LIQUID BEARINGS

Fixed and free sinusoidally driven hydraulic squeeze film bearing design for improved load gyroscopic performance

24 p3832 A71-45291

LIQUID COOLED REACTORS

NT BOILING WATER REACTORS

NT PLUM BROOK REACTOR

NT WATER COOLED REACTORS

LIQUID COOLING

NT FILM COOLING

Liquid cooled space suit fluidic temperature control, using pressure differential variations across garment for cooling level modulation

03 p0355 A71-14092

Surface roughness and contamination, drop volume and liquid subcooling effects on Leidenfrost temperature

04 p0675 A71-14783

Water cooled head cap for heat stress amelioration in subjects working in warm environments

06 p0859 A71-17611

Water cooled garments, discussing human thermoregulation, developments and current suits

06 p0859 A71-17957

Cooling during welding of Ti for prevention of deleterious overheating, discussing safe temperature range for water cooling during butt welding of tubes

15 p2413 A71-31221

Single phase and evaporative systems for liquid cooling high temperature gas turbine rotor blades, reviewing heat transfer performance evaluation

15 p2469 A71-31734

High voltage power supply for optically pumped solid state lasers, including water cooling of ruby and discharge tube jacket

16 p2585 A71-33074

Temperature distribution along short heated wire cooled by flowing liquid with parabolic velocity distribution, using power series for differential equation solution

21 p3378 A71-40581

Liquid film cooling for slender body type hypersonic reentry vehicles, comparing active mass injection cooling systems to ablation type passive systems

22 p3621 A71-42006

Cryogenic temperature cooling systems for IR detectors, describing Joule-Thomson liquefier and liquid transfer devices

22 p3544 A71-42139

LIQUID CRYSTALS

He-Ne laser beam diffraction patterns produced by nematic liquid crystal subject to electric field, noting threshold effect

01 p0096 A71-11375

Thermally induced helical inversion absence in single component cholesteric liquid crystals indicating impurity compensation

02 p0296 A71-12571

Cholesteric liquid crystal pitch from IR transmission measurements

02 p0209 A71-12572

Microwave holography application to monopole antenna radiation field mechanism, using liquid crystals for optical reconstruction

05 p0756 A71-17231

Liquid crystals of cholesteryl nonanoate with cholesteryl chloride or cholesteryl propionate, examining color dependence on temperature

09 p1442 A71-22270

Smectic C liquid crystal molecules electron paramagnetic resonance study, determining tilt angle

09 p1508 A71-22753

Temperature measurement techniques annual progress survey including contact and radiation thermometers, IR thermography, microwave radiometry, fluidic sensors, and liquid crystals

10 p1612 A71-24685

Nematic liquid crystals in optical holography, obtaining speckle free projection screens and data input in holographic memories

10 p1622 A71-24961

Polymerization kinetics of nematic liquid crystal monomer in nematic and isotropic phases

11 p1728 A71-26062

Electro-optical and high contrast properties of structurally stabilized anil-type nematic liquid crystals in display devices

11 p1729 A71-26070

Nematic liquid crystal ultrasonic measurements at room temperature, showing anisotropic attenuation dependence on magnetic field orientation

11 p1808 A71-26149

Cholesteric liquid crystal mixtures optical characteristics, measuring reflection, transmission and extinction ratio

12 p1942 A71-26800

Inverted combination light scattering in liquid and solid crystals, showing polarization effects on absorption coefficient

13 p2101 A71-29020

Alphanumeric display devices with liquid crystal and dynamic light scattering for low voltage, power, cost and fabrication advantages, testing performance

14 p2249 A71-31029

Nematic and cholesteric mixtures liquid crystals electro-optic properties and applications to display devices

19 p3120 A71-38537

Cholophor /passive polarization switched liquid crystal screen/ for laser power enhancement in multicolor displays

20 p3234 A71-39064

IR holography with cholesteric liquid crystals as recording medium and carbon dioxide laser as light source, discussing demagnification and image reconstruction

21 p3379 A71-40703

Cholesteric liquid crystals technique for thermal analysis of microcircuits, multilayer circuit boards, semiconductor devices and other electronic components

21 p3355 A71-40738

Photoactivated electric field effects in nematic liquid crystals for recording real time transparent phase holograms

23 p3674 A71-42955

Liquid crystals structural, elastic and optical properties, noting application to measurements of temperatures, pressures and electric and magnetic fields

23 p3717 A71-43958

LIQUID DROPS

U DROPS (LIQUIDS)

LIQUID DYNAMICS

U FLUID DYNAMICS

U LIQUID FLOW

LIQUID FILLED SHELLS

Dynamic behavior of liquids in partially filled mobile tanks under almost centrifugal force fields

01 p0069 A71-10396

Elastic shell filled with ideal fluid, analyzing dynamic stability under periodic impulses

01 p0176 A71-11049

Incompressible fluid filled circular cylindrical shells loaded by pressure ring at center, obtaining yield point load

03 p0500 A71-13022

Liquid sloshing frequencies in partially filled arbitrarily shaped vertical container

03 p0398 A71-13113

Differential equations of spherical motion of heavy solid body with ellipsoidal cavity filled with liquid, deriving stationary solutions

03 p0457 A71-13586

Hess solution for heavy body rotating about fixed point, considering cavities filled with ideal incompressible fluid in turbulent and irrotational motion and linear invariant relation

03 p0458 A71-13591

Body motion with liquid filled cavities in central Newtonian force field, using hodography

03 p0458 A71-13597

Symmetry axis motion of solid body with ellipsoidal cavity filled with ideal incompressible uniformly turbulent fluid

03 p0458 A71-13599

Perturbed motion equations of body with liquid filled cylindrical cavity reinforced by elastically clamped ribs, solving boundary value problems

03 p0460 A71-14355

Nonlinear large vibrations of ideal incompressible homogeneous fluid in cylindrical sector tanks, determining hydrodynamic equations coefficients and relation to tank geometry

03 p0405 A71-14569

Vibration effects on free convection heat transfer from fluid filled horizontal cylinder

04 p0675 A71-14784

Free transverse oscillations of closed prismatic shells of flexible rectangular panels filled with compressible inviscid liquid

04 p0573 A71-15564

Axissymmetric stability of fluid filled cylindrical shells under rapid axial compression

05 p0824 A71-16592

Axissymmetric vibration frequencies, form shapes and apparent masses for vertical liquid filled coaxial cylindrical shells resting on shallow spherical shell

06 p0986 A71-17763

Natural vibrations of partially liquid filled closed spherical shell for arbitrary boundary conditions, using approximate method

06 p0991 A71-17798

Elastic composite liquid filled shell containers, calculating natural vibration with Ritz method

06 p0992 A71-17809

Vertical circular cylindrical tank with shallow spherical shell bottom filled partially by ideal incompressible liquid, calculating joint oscillations

06 p0994 A71-17826

Heavy liquid shells of revolution, determining equilibrium form in gravitational and surface tension forces from condition of minimal functional of total free energy

06 p0994 A71-17827

Elastic momentless conical tank with spherical bottom partially filled by liquid, calculating axisymmetric oscillation

06 p0995 A71-17828

Thin elastic partially liquid filled shells of revolution, applying asymptotic integration method to free vibrations case

06 p0995 A71-17834

Pulsating liquid filled hemispherical shell dynamic characteristics, determining hydrodynamic pressure and shell displacements

06 p0882 A71-17837

Dynamic stability of cylindrical shell with freely supported edges partly filled with ideal compressible fluid and undergoing steady longitudinal vibrations

06 p0997 A71-17846

Shell-fluid interaction problems, considering liquid filled shells oscillations, acoustic shock waves action, body impact against water, etc

06 p0998 A71-17861

Gravity stratified compressible fluid spin-up in sphere, analyzing by increase in container angular velocity and linearization about uniform rotation

06 p0883 A71-18320

Closed axisymmetric vessel filled with viscous incompressible fluid, calculating integral heat release coefficients in free convection

07 p1222 A71-19199

Viscous incompressible fluid partly filling rotating cylindrical cavity, considering motion under centrifugal forces in adjoining unperturbed free surface region

07 p1093 A71-20467

Liquid filling effect on oscillation modes of ellipsoidal stainless steel shell in vibrator

07 p1218 A71-20471

First and second frequency harmonics and form shapes of liquid filled cylindrical shell axisymmetric vibrations, analyzing effect of pressure and shell dry portion on vibration frequencies

08 p1374 A71-22055

Plane unsteady convective motion of viscous incompressible liquid in infinite horizontal vessel of rectangular cross section due to wall temperature fluctuations

10 p1696 A71-24375

Frequency equation of flexural vibration of fluid filled circular cylindrical shells, using linear elasticity

12 p1974 A71-26928

Motion stability of symmetric rotor of gyroscope with inviscid incompressible liquid filled cylindrical annular cavity around coaxial rigid rod

13 p2065 A71-27978

Cylindrical liquid filled shells under rapid axial compression along generatrix, examining dynamic deformation characteristics

13 p2156 A71-29072

Dynamic characteristics of fluid oscillations in cylindrical vessel divided by annular diaphragm

13 p2050 A71-29236

- Free convection in horizontally positioned, water filled circular cylindrical cavity 14 p2336 A71-30228
- Perturbed motion linear equations of body rigidly coupled to thin walled elastic shell partially filled with heavy compressible fluid 14 p2227 A71-30867
- Rotational stability of spin stabilized satellite with liquid filled propellant tanks, investigating viscous effects on motion coupling between rigid body and liquid 15 p2499 A71-31175
- Energy dissipation in harmonically oscillating spherical annulus filled with viscous fluid 15 p2391 A71-32104
- Energy dissipation measurement in liquid filled spinning precessing spherical cavity by gimbaled mechanism [ASME PAPER 71-APM-4] 16 p2644 A71-33219
- LF axisymmetric vibrations of spherical completely filled tank with free liquid surface in upper tank and pipeline 16 p2657 A71-33602
- Cylindrical shells partially filled with liquid, calculating forced vibration under random loads and deterministic internal pressure 17 p2817 A71-34333
- Sloshing liquid natural frequencies change in cylindrical shell by movable devices, considering immersed thin elastic plate effect 17 p2726 A71-34579
- Structural stability regions construction for solid body with liquid filled cavities 17 p2730 A71-35607
- Partially liquid filled cylindrical shells with elastically supported end rims, deriving algorithm for nonaxisymmetric natural vibration frequency calculations 17 p2833 A71-35614
- Rigid sphere and concentric shells models approximation to turbulent motion in liquid-filled precessing spherical cavity [ASME PAPER 71-APM-Y] 18 p2904 A71-36265
- Time dependent rotating laminar flow of viscous incompressible fluid in closed cylindrical container, presenting numerical solutions to Navier-Stokes equations 18 p2908 A71-36343
- Hydroelastic coupled oscillations of partially filled circular cylindrical liquid container with flexible bottom and elastic side wall 21 p3366 A71-40545
- Fluid dynamics in elastic complex geometry tanks, obtaining liquid mass and stiffness matrices for gravitational effects 21 p3467 A71-40948
- Natural and forced joint vibrations of liquid and shallow spherical shells 24 p3881 A71-44829
- Elastic momentless shell completely filled with ideal incompressible liquid, detailing small steady natural vibrations 24 p3821 A71-45344
- LIQUID FLOW**
- NT OPEN CHANNEL FLOW
- NT WATER FLOW
- Dynamic behavior of liquids in partially filled mobile tanks under almost centrifugal force fields 01 p0069 A71-10396
- Variational problem for turbulent liquid flow mass transport on inclined flat plate, using plane Poiseuille flow solution 03 p0398 A71-13101
- Laminar flow of liquid in duct with zero heat resistance of walls, calculating temperature distribution during radiative convective heating 03 p0519 A71-13745
- Liquid flow rate measurement based on tank-filling method, discussing factors affecting accuracy 03 p0356 A71-14328
- Electroacoustical device for recording gas and vapor cavitation resistance in liquids 04 p0617 A71-14599
- Stationary flow of viscoplastic liquid in annular gap with temperature dependent viscosity, taking into account energy dissipation 04 p0579 A71-15799
- Gas and liquid flows local velocity measurements, using Doppler frequency shifts due to wave scattering at solid microparticles suspended in flow 05 p0753 A71-16786
- Plane Poiseuille viscoelastic liquids flow stability, using method of inner and outer expansions based on Chun and Schwarz asymptotic solution of Orr-Sommerfeld equation 05 p0737 A71-17102
- Elastic cylindrical shells oscillations and stability in inviscid incompressible liquid flow, reducing problem to integro-differential equation by Fourier integral transformation 10 p1688 A71-24357
- Rectilinear piping system with steady liquid flow, investigating free vibration damping, steady-state amplitudes and stability 12 p1975 A71-27113
- Three dimensional steady separated liquid and gas flows past low aspect ratio bodies, deriving similarity laws for reduction to two dimensional problem 13 p2049 A71-29169
- Pressure, velocity and potential distribution of flow around arbitrarily shaped body of revolution during arbitrary motion in perfect liquid 13 p1992 A71-29187
- Incompressible liquid laminar boundary layer flow velocity profile and normal friction stress calculation by successive approximation method 14 p2169 A71-29630
- Plasmas and liquids inhomogeneous flow oscillations, determining resonance points processes effect on stability and velocity 15 p2459 A71-32504
- Gas and liquid flows local velocity measurements, using Doppler frequency shifts due to wave scattering at solid microparticles suspended in flow 16 p2576 A71-33038
- Approximate calculation of pressure distribution, separation points and drag on circular cylinder in viscous liquid flow, using ideal fluid jet model 16 p2560 A71-33597
- Quasi-stationary viscous incompressible liquid flow in porous tube with deforming wall 17 p2694 A71-35641
- Rotating liquid flow impulsive spin-up and spin-down in finite cylindrical containers, deriving simplified mathematical model at Reynolds number 1002 18 p2901 A71-35853
- Liquid flow about oscillating flat plates, determining drag coefficient relationships to low Reynolds number and period parameter from graphical representation 18 p2902 A71-36033
- Hypothetical analogy between wave formation during explosive welding and Karman vortex street arising in liquid flow around cylinder 19 p3068 A71-37083
- Vaporization heat transfer in saturated liquid capillary flow through wick structure, describing test facility and procedure [ASME PAPER 71-HT-35] 19 p3166 A71-38000
- Liquid jet injection into transverse two-phase vapor-liquid flow, calculating penetration path and depth from semiempirical theory 20 p3210 A71-38896
- Second order viscous liquid pulsating flow superposed on steady laminar flow through circular pipe, examining non-Newtonian effects on flow characteristics 22 p3530 A71-41562
- Electrification induced instabilities, breakup and drop size of charged cylindrical liquid jets, using small perturbation method 23 p3663 A71-43445
- Liquid flow rate measurement by determining fall time of emf generated in sensor coil by fluid nuclei precessing freely in magnetic field 23 p3678 A71-43536
- Liquid flow and heat transfer in thermosiphons in centrifugal and Coriolis force fields 24 p3888 A71-44931
- Liquid particles motion over variable profile turbine rotor blade edge, concave and fanning surfaces as function of Coriolis and centrifugal force 24 p3819 A71-44932
- Liquid transition through critical value, considering self oscillation mode frequency 24 p3821 A71-45340
- LIQUID HELIUM**
- Miniature centrifugal pump for circulating liquid He in flow loop, testing performance 02 p0255 A71-12129
- Strain free insulated mounting technique for semiconductor onto cold finger at liquid He 3 temperatures 02 p0294 A71-12142
- Ultrasonic cavitation noise spectra in liquid helium and nitrogen, comparing He I and II 07 p1160 A71-19951
- Design curve for estimating conduction heat transfer liquid He cryostats with vapor-cooled vent tubes 07 p1115 A71-20359
- Phonon excitations radiated from thermal source in He II below 0.3 K, using carbon film detectors 09 p1497 A71-22418
- Hydrogen condensation and evaporation on liquid helium cooled surfaces in cryopump with reduced thermal radiation loading 09 p1546 A71-23008
- Thermal conductivity anomalies in thin superconducting metal foils in contact with two superfluid He basins at low temperatures, examining surface electron phonon interactions 10 p1640 A71-23832
- Surface wave velocity at interface between liquid He 4 and saturated vapor 13 p2101 A71-28769
- Liquid He stable cavities localized excited states, calculating atomic line positions 13 p2101 A71-28796
- Adsorption cryopumped He 3 cooled IR detector without encumbrance of external diffusion or mechanical pump 18 p2922 A71-36588
- Liquid He containment in space zero-g environment, proposing use of high thermal conductivity porous plug operating in superfluid regime 20 p3184 A71-39280
- Nucleate boiling of liquid helium I on gallium single crystal surfaces 20 p3312 A71-39282
- Roughness role in liquid He-solid boundary thermal resistance, calculating heat transfer coefficient 21 p3416 A71-41122
- LIQUID HELIUM 2**
- U HELIUM ISOTOPES**
- LIQUID HYDROGEN**
- Liquid hydrogen, oxygen and water droplets released in space, examining size and temperature histories 06 p0964 A71-17277
- Hydrogen slush storage and transfer density and flow measuring instrumentation, emphasizing capacitance measurement [NAS PAPER M-2] 08 p1292 A71-21695
- Hydrogen fluid phase and temperature measurement by single sensor with fluid phase discrimination circuit for transient response sampling [NAS PAPER M-3] 08 p1293 A71-21697
- Calibration test rig for high accuracy liquid hydrogen flowmeter, discussing design and operation 12 p1906 A71-26836
- Small turbine type flowmeters for liquid hydrogen, discussing design, inspection, calibration and reliability 14 p2239 A71-29926
- Liquid hydrogen fueled space vehicle fluorine-hydrogen main tank injection pressurization system performance prediction by computerized analysis [AIAA PAPER 71-645] 14 p2290 A71-30722
- Liquid hydrogen rocket propellant tanks insulation problems in space shuttle and orbiter 15 p2499 A71-31216
- Saturn S-4B continuous vent system for propellant tanks during parking orbit to prevent excessive pressure, requiring liquid settling with auxiliary ullaging rockets 18 p2973 A71-36453
- Feasibility assessment of hypersonic transports with actively cooled airframe structure, considering liquid hydrogen fuel use as coolant 19 p2995 A71-37123
- Open cell lightweight cryogenic insulation for reusable liquid hydrogen fueled vehicles including space shuttle 20 p3312 A71-39271
- Film boiling liquid hydrogen vertical flowing system, determining buoyancy effects on hydrodynamic and heat transfer characteristics 21 p3476 A71-40895
- Cryogenic liquids thermal behavior under operational conditions, discussing Europa 3 second stage liquid hydrogen and oxygen engine 22 p3588 A71-41502
- Valves and regulators development and testing for liquid hydrogen propellant tank pressurization system 22 p3588 A71-41503
- Liquid hydrogen as future replacement for hydrocarbon fuels in surface and air transportation, noting advantages in energy per unit weight and pollution-free combustion 24 p3863 A71-44365
- LIQUID INJECTION**
- NT WATER INJECTION
- Nozzle wall protection against high enthalpy gas flow effects by film cooling through parietal liquid injection 01 p0143 A71-11017
- Liquid volume deformation effect on hydraulic drive under continuous or jumpwise pressure 01 p0007 A71-11243
- Vaporization rate of liquid injected into high temperature supersonic gas flow, considering relation to static pressure and distillation process 03 p0521 A71-14253
- Aqueous acid solution turbulent boundary layer characteristics during alkali solution injection through porous surface in presence of positive pressure gradient 04 p0576 A71-15614
- Liquid properties effect on secondary injection from spray nozzle, determining jet penetration in supersonic stream by scattered light and schlieren photographs 09 p1381 A71-22089
- Cold flow tests of mixing and atomization characteristics of gas/liquid circular coaxial injector elements in pressurized facilities [AIAA PAPER 71-672] 14 p2291 A71-30736
- Transverse liquid injection into supersonic airstreams, using photographic techniques to determine jet penetration and spreading for various dynamic pressure and density ratios [AIAA PAPER 71-724] 15 p2393 A71-32287

LIQUID LASERS

Liquid carbon tetrachloride artificial luminescent cloud formation in upper atmosphere, considering injection conditions for rapid vaporization and required concentration

19 p3061 A71-38633

LIQUID LASERS

Flash light excited dye solutions in liquid lasers, investigating wavelength and energy dependence of forced emission

02 p0261 A71-12322

Rare earth based liquid lasers, describing spectroscopic and performance properties of neodymium ions in aprotic solvents

07 p1124 A71-19788

Emission spectra of solutions of oxazole and axadiazole derivatives and of tetraphenylbutadiene as effective active media for liquid phase lasers

11 p1774 A71-26001

Laser parameters of Nd-doped hydrated phosphorus oxychloride-stannic chloride liquid system compared with YAG and Nd-doped glass, studying optical evolution and losses

13 p2078 A71-28400

Broadly tunable liquid dye laser action with narrow line output through use of distributed feedback obtained by spatial modulation of gain and refractive index

13 p2081 A71-29339

Rhodamine, sodium fluorescein and cryptocyanine dyes for liquid lasers, investigating electroluminescence by polarography

16 p2587 A71-33382

Nonlinearities effects on inorganic liquid laser output, investigating Raman and Brillouin scatterings and self focusing

18 p2933 A71-37012

Liquid laser output wavelength dependence on rhodamine dye concentration, comparing experimental data with Stepanov theory

23 p3684 A71-43417

Q switched inorganic Nd liquid laser oscillator, noting output capability

23 p3686 A71-43957

Liquid-state pulsed laser active element lens parameters effects on output radiation divergence

24 p3835 A71-45240

LIQUID LEVELS

Electroresencing liquid level gauge using electrochemical charge transfer through fluid

17 p2744 A71-35290

LIQUID MERCURY

U MERCURY [METAL]

LIQUID METAL COOLED REACTORS

Liquid metal cooled, fast spectrum thermionic reactor experiment design based on Fast Reactor Core Test Facility use for dynamic and steady state characteristics determination

11 p1710 A71-25867

Materials technology of Ta-W-Hf clad uranium mononitride fuel for lithium cooled compact fast space power reactor, including irradiation tests

16 p2606 A71-33254

LIQUID METALS

NT LIQUID POTASSIUM

NT LIQUID SODIUM

NT MERCURY [METAL]

NT MERCURY VAPOR

Liquid Cs graphite integral reservoir effect on thermionic converter performance

02 p0196 A71-12271

Electromagnetic repulsion of conducting and dielectric bodies within liquid metal and electrolyte in crossed field under gravitational acceleration

02 p0293 A71-12630

Liquid Fe, Co and Ni atomic distributions investigation by X ray diffraction

04 p0612 A71-15036

Binary liquid metal forced convection boiling heat transfer, determining axial and radial temperature distribution in two phase flow

04 p0676 A71-15173

Liquid metals vapor drag and electromagnetic fields effects on laminar film condensation, using finite difference method

04 p0688 A71-15539

Vapor deposition rates from liquid binary alloy targets under ion sputtering

05 p0757 A71-16235

Molybdenizing effects on Cr-Ni-Ti steel strength and stability in liquid Li

05 p0768 A71-16772

Liquid Al binary systems thermodynamic properties, using emf, improved dew point and distribution methods

07 p1143 A71-20489

Alloying addition effects on wetting of carbon by liquid metals, using sessile drop technique [PLASTICS INST. PAPER 19]

08 p1296 A71-20911

High density DC effects on displacement of solid GaAs-liquid metal interface, considering Peltier effect and dislocation density

08 p1344 A71-21444

Rubidium viscosity near solidification point from thin immersed plate forced vibrations amplitude

09 p1508 A71-22540

Liquid-solid interface phenomena during sintering and porous materials impregnation by liquid metals, using spherical and nonspherical particle models

09 p1457 A71-23391

Metal droplet motion in mercury weld pool in tungsten arc, noting cause by Lorentz force and surface arc plasma jet

11 p1769 A71-25748

Automatic control application to liquid metal and semiconductor materials, plasma flows, charged particle beams and similar media interacting with magnetic fields

12 p1936 A71-26972

Nickel alloys crystallization at superhigh cooling rates by dropping liquid metals on rotating copper cylinders to obtain films

12 p1917 A71-27301

Soviet book on liquid metals nonstationary flow in ducts of MHD devices covering laminar flow at constant and variable flow rates

14 p2277 A71-29526

Nitrogen solubility in Ni-Mo and Ni-W melts, detailing Ti and pressure effects

15 p2424 A71-31392

Molten Co-Cr alloy structural transitions at increasing temperatures, relating to change in solid state with increasing Cr content

15 p2425 A71-31393

Molten Co-Sn alloys, detailing vaporization rate, vapor pressure and partial and integral isothermal and isobaric formation potentials

15 p2425 A71-31394

Thermodynamic properties of dilute solutions of oxygen in liquid Fe-Co and Fe-Ni binary mixtures, obtaining Gibbs energy variation with temperature

15 p2432 A71-32174

Focused laser beam interaction with liquid metal particles, discussing fluid phase light screening effect, droplet evaporation and mass expulsion characteristics

17 p2750 A71-34291

Liquid Zr drops combustion in oxygen-nitrogen atmospheres, examining critical conditions for sac formation with homogeneous bubble nucleation theory

17 p2837 A71-34511

Dissolution rate of vertical nickel cylinder in liquid aluminum under free convection, showing fluid boundary layer mass transfer role

19 p3079 A71-37709

Surface heat flux for incipient boiling in liquid metal heat pipes, determining nucleation site radius upper limit in Na heat pipes

19 p3171 A71-38349

Liquid metal elevated temperature time dependent corrosion effects on immersed structural materials, discussing blocked two level factorial experiment design for multiply telescoping sequences

21 p3400 A71-40880

Electrical resistivity and thermoelectric power sensitivity for simple liquid metals near melting temperature, determining temperature effects from pseudopotential models

22 p3586 A71-42370

Liquid metal MHD cycles for spacecraft power supply systems, proposing counterflow condensation at nozzle outlet

22 p3574 A71-42431

Cavitation damage resistance of Fe, Ni and Co alloys in liquid sodium and mercury

23 p3692 A71-43906

Hydrogen solubility in liquid Cr, Ni and Co alloys containing Si for various concentrations and temperatures

24 p3840 A71-45371

Liquid Mg-Al alloys thermodynamic properties determination by electrochemical and barometric methods

24 p3840 A71-45372

LIQUID NITROGEN

Tissue cooling with liquid nitrogen, determining film boiling transition temperature and heat transfer rates [ASME PAPER 70-WA/HT-16]

03 p0372 A71-14096

Subcooled nitrogen tube flow film boiling, investigating heat transfer and hydraulic resistance

04 p0687 A71-15530

Liquid nitrogen cold trap for oil diffusion pump

05 p0757 A71-16232

Ultrasonic cavitation noise spectra in liquid helium and nitrogen, comparing He I and II

07 p1160 A71-19951

Fine crystalline substances forced combination scattering at liquid nitrogen temperature, using ultrashort ruby laser pulses for excitation spectra

13 p2080 A71-29022

Thin thermally insulating film on metallic sample, showing vapor layer elimination during liquid nitrogen quenching

18 p2934 A71-36172

Multielement IR photoconductive detector arrays of InSb and mercury cadmium telluride operating at cryogenic temperatures

18 p2923 A71-36606

Liquid nitrogen cooled microwave low temperature noise standard in WR-51 waveguide

20 p3202 A71-38832

Polyvinyl chloride foam insulation system for liquid hydrogen-liquid oxygen space vehicles tested under groundhold and simulated flight conditions

20 p3253 A71-39269

Pressure, subcooling and diameter effects on heat transfer and circumferential flow transition of this wire film boiling of liquid nitrogen in pool

20 p3313 A71-39284

Swirl flow augmented heat transfer to liquid nitrogen in dispersed film boiling, using twisted tape inserts

20 p3313 A71-39285

Buoyancy effects on heat transfer coefficients in liquid nitrogen film boiling in vertical flow

20 p3313 A71-39286

Liquid nitrogen drops anomalous behavior in Leidenfrost film boiling, investigating vapor instabilities effect on total vaporization time

20 p3313 A71-39287

Floating times of liquid/solid sphere on evaporative fluid/liquid nitrogen/ in metastable Leidenfrost film boiling

21 p3476 A71-40892

Two phase critical flow of saturated and subcooled high pressure liquid nitrogen through convergent-divergent nozzle, comparing with water

21 p3369 A71-40894

Heat transfer from incandescent platinum wires in saturated liquid nitrogen, examining film boiling from atmospheric to critical pressure

21 p3476 A71-40899

LIQUID OXIDIZERS

Ammonium nitrate, ammonium perchlorate and nitronium perchlorate as liquid oxidizers for hybrid propellant rocket engines, discussing oxidizer/kerosene mixing ratio

10 p1657 A71-24275

LIQUID OXYGEN

Liquid oxygen nucleate boiling in simulated reduced gravity fields, obtaining heat transfer coefficients, departure frequency and bubble growth rate

04 p0687 A71-15536

LOX release from Apollo 8 lunar launch vehicle, forming small particle clouds for scattering experiments

06 p0963 A71-17256

Liquid hydrogen, oxygen and water droplets released in space, examining size and temperature histories

06 p0964 A71-17277

Impact sensitivity tester for engineering materials in liquid and gaseous oxygen at high pressures

14 p2222 A71-30548

Impact reaction intensity test, determining fire or explosion hazards of materials exposed to liquid oxygen

14 p2222 A71-30549

Polyvinyl chloride foam insulation system for liquid hydrogen-liquid oxygen space vehicles tested under groundhold and simulated flight conditions

20 p3253 A71-39269

Cryogenic liquids thermal behavior under operational conditions, discussing Europa 3 second stage liquid hydrogen and oxygen engine

22 p3588 A71-41502

Large volume liquid oxygen pool boiling, investigating heat exchange coefficient dependence on flux density and pressure

23 p3705 A71-44339

LIQUID PHASES

In-Bi alloys electrical conductivity measurement for compositions covering characteristic points of phase diagram at temperatures from liquidus line to 850 C

02 p0294 A71-11895

Mechanical stability of liquid phase in porous oxidation protective coating on Ni turbine blades under acceleration

02 p0772 A71-12946

Liquid silicate systems density calculation from partial molar volumes of oxide components

05 p0716 A71-16407

Mo-Re-Hf ternary alloys physical and mechanical properties, considering workability, electrical resistivity and expansion coefficient

07 p1140 A71-20237

Multilayer liquid phase epitaxy heterostructures growth with crystalline solid solutions of aluminum gallium arsenide for injection lasers

09 p1464 A71-23122

Liquid and solid phase relations in Be-Al-Ti system by chemical, thermal, microscopic and X ray investigation, discussing solubility range of ternary phase and intermetallic compounds

10 p1629 A71-25034

Electrical conduction in cholesterol acetate, propionate and stearate in solid, liquid crystal and isotropic liquid states characterized by I-V measurements

11 p1807 A71-25564

Water diluent effect on molten hydrazine mononitrate critical diameter and condensed explosive detonation stability

15 p2463 A71-31383

Heat pipes design and applications, examining pressure losses in steam and liquid phases and capillarity and gravity effects
[HEAT EXCH. CONF. PAPER 23] 15 p2513 A71-31637

Existence conditions for liquid water on Mars, considering freezing depression, condensation, capillary evaporation and permafrost melting 15 p2494 A71-32492

Al distribution in gallium aluminum arsenide films obtained by epitaxial growth from liquid phase, showing temperature variation dependence during deposition 18 p2954 A71-36161

Prealloyed Al powder liquid phase sintering without precompacting, discussing oxidation and density control 18 p2928 A71-36667

Mg-Ge alloys liquid and two phase mixtures thermodynamic properties at 660-1130 C, using galvanic cell with magnesium chloride electrolyte 19 p3080 A71-37715

Multiple layer liquid epitaxial growth of lead tin tellurides from Pb-Sn solution, determining low carrier concentrations by Hall effect and capacitance measurements 22 p3585 A71-41810

Apparatus for optical diagnostics of helioelectrochemical conversion reaction phototransformation kinetics including diffusion coefficient measurement in liquid phase 22 p3484 A71-42845

Precipitation hardenable Cr-Cu liquid phase sintered powder composite, showing matrix properties variations 23 p3695 A71-44291

Speed of sound measurement in solid and liquid phase suspensions, considering dense phase inertia forces and particles thermal retardation effects 24 p3827 A71-45019

LIQUID POTASSIUM
Liquid sodium and potassium thermoelectric potentials, calculating Seebeck coefficients to 600 C 01 p0141 A71-11602

Rankine cycle turboelectric nuclear space power conversion system with liquid K as working fluid, discussing current technology status [GESP-623] 16 p2526 A71-33525

Tantalum and niobium ternary oxides recovery from liquid potassium solution, determining composition and crystallographic modifications by chemical and X ray diffraction analyses 20 p3194 A71-39372

LIQUID PROPELLANT ROCKET ENGINES
NT HYDRAZINE ENGINES
NT HYDROGEN OXYGEN ENGINES
NT J-2 ENGINE

Europa 3C light alloy space booster powered by Rolls-Royce engines using kerosene and LOX 05 p0816 A71-16403

Liquid bipropellant rocket engine ignition and start transient calculation for hypergolic and externally ignited starts at sea level and high altitude pressures [WSS/CI PAPER 70-23] 06 p0943 A71-17655

Piston expulsion seals for storable fueled and ready liquid rockets 06 p0905 A71-18218

Unstable liquid propellant rocket engine nonlinear behavior, considering stability of cylindrical combustor with distributed steady state combustion process and multiforce quasi-steady nozzle [AIAA PAPER 71-208] 06 p0948 A71-18644

S-IVB liquid rocket engine and propellant feed systems restart shutdown in orbital operations [AIAA PAPER 70-672] 07 p1183 A71-19857

Liquid rocket propellant engine exhaust plume flow field, discussing mathematical models for combustion chamber, throat region and nozzle [AIAA PAPER 70-844] 07 p1183 A71-19861

Soviet book on liquid propellant rocket engines non-stationary operation covering dynamic processes, transient conditions, component elements, fuel delivery, etc 10 p1659 A71-24649

Stable limit cycles and triggering limits of first radial mode in nonlinearly unstable liquid propellant rocket motors, using wave equation and Galerkin method 11 p1836 A71-25162

Liquid propellant rockets with rotating reactive force vectors, improving equations of motion 12 p1972 A71-27492

Simulated altitude test facilities selection for Space Shuttle Orbiter Engine [AIAA PAPER 71-679] 14 p2292 A71-30743

Throttled bipropellant rocket engine, discussing cryogenic and space storable propellants and injection system optimization based on combustion mechanism photographic observation [AIAA PAPER 71-740] 14 p2296 A71-30783

Soviet book on liquid rocket engines fuel valves design and development covering hydraulic characteristics, control cavities, shut-off devices, operational stability, etc 15 p2466 A71-31295

Soviet book on liquid rocket engines covering combustion chambers, fuel supply systems, static and dynamic characteristics, control and reliability 15 p2466 A71-31296

Nonlinear combustion stability problems in liquid propellant rocket engines, describing unsteady combustion response by Crocco time lag hypothesis 15 p2467 A71-31471

Red fuming nitric acid-sulfur dioxide as oxidizer for auxiliary ignition in liquid rocket motors 15 p2465 A71-32110

AJ-550 liquid hydrogen/oxygen staged combustion cycle space shuttle engine, describing preburner and main injector, turbopump and combustion chamber construction [AIAA PAPER 71-660] 15 p2471 A71-32575

Two dimensional axisymmetric shell analytical model for liquid propellant launch vehicle longitudinal vibration modes and steady state response calculation 16 p2653 A71-33092

Dynamic stability of controlled spacecraft with liquid propellant rocket engines, considering acceleration and braking sections of trajectory 16 p2646 A71-33656

Component assembly effect on dynamic stability of liquid propellant rocket engine spacecraft during thrust sections of trajectory 16 p2646 A71-33657

Nonlinear combustion instability in liquid propellant rocket engines, describing unsteady combustor flow with single wave equation 19 p3122 A71-38093

Open cell lightweight cryogenic insulation for reusable liquid hydrogen fueled vehicles including space shuttle 20 p3312 A71-39271

Film ablative cooled gas pressure feed liquid rocket engine unstationary process analysis with digital computer, detailing engine dynamics, heat transfer and temperature profile 22 p3589 A71-42054

LIQUID ROCKET PROPELLANTS
NT CRYOGENIC ROCKET PROPELLANTS
NT HYPERGOLIC ROCKET PROPELLANTS
NT MONOPROPELLANTS
NT SLURRY PROPELLANTS

Antifiction effects of heteroorganic compounds in medium-distillation hydrocarbon fuels for rocket engines 01 p0141 A71-11108

Bipropellant droplet supercritical steady combustion temperature measurements in zero gravity near critical point, comparing high and low pressures models for ambient gas solubility 01 p0141 A71-11309

Optimal model of pressurization system for liquid propellant on Surveyor lunar landing spacecraft 03 p0472 A71-14447

Liquid rocket propellants characteristics study for explosive yield prediction, using mathematical model and critical mass method 04 p0637 A71-15345

Liquid hypergolic propellants heat and gas release determination by calorimetric and PVT measurements, using impinging free jets for propellant mixing [WSS/CI PAPER 70-26] 06 p0943 A71-17658

Liquid fuel atomization spectrum in nozzles, examining proportion control of droplet size 08 p1348 A71-21262

Rocket fuel lines disruptive cavitation oscillations, considering rocket body mechanical vibrations and fuel line oscillation frequency characteristics 08 p1366 A71-21753

Structural element for discrete element idealization of missile and liquid propellant as one composite structure [AIAA PAPER 70-23] 09 p1430 A71-22087

Motion perturbation equations for guided space vehicles, allowing for sloshing liquid propellant viscosity effects 09 p1532 A71-22657

Shock wave ignition of liquid fuel drop in oxidizing atmosphere, discussing combustion process [AIAA PAPER 70-9] 12 p1986 A71-27566

Shock wave caused chemical reactions between solids and cryogenic liquids, discussing shock sensitivity tester for liquid propellant-structural material systems 14 p2222 A71-30546

Cold flow analysis of liquid propellant sprays from rocket engine injectors, relating propellant mixing and combustion performance 15 p2465 A71-32044

Liquid rocket propellants pressurization by injected cryogenic liquids evaporation, using water and liquefied air for experimental investigation [DFVLR-SONDDR-117] 15 p2466 A71-32721

Frozen bipropellants as self supporting structural member for booster weight reduction, considering mechanical and thermal properties and melting rate requirement 20 p3276 A71-39609

Rocket fuel lines disruptive cavitation oscillations, considering rocket body mechanical vibrations and fuel line oscillation frequency characteristics 24 p3876 A71-44926

LIQUID ROTATION
U ROTATING LIQUIDS
LIQUID SLOSHING
Uniformly turbulent incompressible heavy fluid sloshing and free oscillations in rigid rotating vessel, using linear surface wave theory 01 p0069 A71-10411

Liquid sloshing frequencies in partially filled arbitrarily shaped vertical container 03 p0398 A71-13113

Nonlinear large vibrations of ideal incompressible homogeneous fluid in cylindrical sector tanks, determining hydrodynamic equations coefficients and relation to tank geometry 03 p0405 A71-14565

Viscous layer damping effect on liquid surface oscillations in vessel, satisfying boundary conditions and obtaining frequency equation 08 p1276 A71-21621

Motion perturbation equations for guided space vehicles, allowing for sloshing liquid propellant viscosity effects 09 p1532 A71-22657

Liquid sloshing in liquid propellant containing orbiting vehicle stabilized by active control system, examining expression for ring baffle slosh damping under reduced gravity 09 p1532 A71-22913

Computerized sloshing frequencies of tilting two dimensional tank of flat free surfaces with respect to effective gravity 11 p1752 A71-26198

Computer algorithm for liquid sloshing in rotating cavities, using finite difference scheme 13 p2050 A71-29211

Dynamic characteristics of fluid oscillations in cylindrical vessel divided by annular diaphragm 13 p2050 A71-29236

Oscillation and stability of free composite body with elastically suspended masses, simulating liquid sloshing in cavity by equivalent mechanical model 14 p2321 A71-29537

Isoperimetric problem upper bounds for fundamental frequencies in free oscillations of incompressible fluid in container 16 p2559 A71-33483

Sloshing liquid natural frequencies change in cylindrical shell by movable devices, considering immersed thin elastic plate effect 17 p2726 A71-34579

Viscous layer damping of liquid surface oscillations in vessel, satisfying boundary conditions and obtaining frequency equation 17 p2730 A71-35681

Magnetic fluid sloshing in solenoidal magnetic field, describing fluid free surface waves similarity to ordinary liquid waves in reduced gravity field [ASME PAPER 71-VIBR-24] 21 p3366 A71-40281

Fluid dynamics in elastic complex geometry tanks, obtaining liquid mass and stiffness matrices for gravitational effects 21 p3467 A71-40948

Potential flow with free surface, comparing finite element and finite difference methods for liquid sloshing problem 21 p3369 A71-40974

Viking vehicle structural flexibility and propellant sloshing effects on thrust vector control dynamics, obtaining computer simulated responses for hybrid and discrete coordinate models [AAS PAPER 71-348] 23 p3773 A71-43021

LIQUID SODIUM
Liquid sodium and potassium thermoelectric potentials, calculating Seebeck coefficients to 600 C 01 p0141 A71-11602

LIQUID SURFACES
NT MENISCI
Nonlinear free surface effects in low gravity tank draining, finding domains of validity for linearized and nonlinear analysis [AIAA PAPER 69-680] 03 p0399 A71-13439

Thin shallow spherical shell vertical impact against ideal incompressible liquid surface, calculating axisymmetric deformation and hydrodynamic load distribution 07 p1089 A71-19738

Velocity distribution and Reynolds number relation to thickness in liquid films using turbulent viscosity [AIAA PAPER 71-348] 07 p1094 A71-20545

Crosshatched wave patterns in liquid films, discussing supersonic wind tunnel experiments aimed at elimination of sublimation or vaporization as pattern generating mechanisms [AIAA PAPER 71-622] 15 p2389 A71-31551

LF axisymmetric vibrations of spherical completely filled tank with free liquid surface in upper tank and pipeline 16 p2657 A71-33602

LIQUID-GAS MIXTURES

Fluid surface instability under perpendicular acceleration, presenting singular perturbation problem solution by successive approximations method 16 p2561 A71-34160

Mean curvature of deformed spherical surface in study of equilibrium configuration of water drops under surface tension, using differential geometry 19 p3045 A71-37899

Cryogenic fluids, considering refrigerants storage vessels, liquid surface detection devices, transfer lines, level gauges 20 p3270 A71-39241

Magnetic fluid sloshing in solenoidal magnetic field, describing fluid free surface waves similarity to ordinary liquid waves in reduced gravity field [ASME PAPER 71-VIBR-24] 21 p3366 A71-40281

LIQUID-GAS MIXTURES

NT AEROSOLS

NT FOG

Manometric apparatus determining solubility of inert gases in water, blood and other liquids, establishing partition coefficients of ethyl ether 06 p0862 A71-18390

Cavitation in liquids with dissolved gases by acoustic wave induced oscillating pressure, discussing gas bubble formation through rectified diffusion process 10 p1597 A71-24942

Hypersonic reentry flow over blunt nosed bodies, using water oxygen mixture to achieve simulation at lower stagnation temperatures 11 p1705 A71-26270

Vapor-liquid mixture steady flow from centrifugal injectors, determining kinetic energy loss relationship to phase separation 16 p2624 A71-33608

Liquid spray steady evaporation and mixing in gaseous swirl, using continuum mechanics 17 p2727 A71-34693

Free jet expansion of liquid-gas bubble mixture suspended in glycerine 17 p2728 A71-34891

Two phase flow model of water droplets velocity in air stream, using Fresnel biprism and laser differential scheme 19 p3072 A71-37587

Shock wave structure in liquid-gas bubble mixture with varying volumetric gas content, bubble size, shock strength and liquid viscosity 24 p3820 A71-45128

LIQUID-LIQUID INTERFACES

Stratified shear flow stability, investigating diffuse interface between two miscible fluids 10 p1595 A71-24623

Fluid interface Rayleigh-Taylor type instability, considering control as optimal regulator problem 11 p1742 A71-26413

Heat exchange and temperature distribution between two liquids divided by plate, discussing possible errors 14 p2335 A71-30048

Liquid-liquid or solid-liquid interface Leidenfrost film boiling, deriving heat transfer coefficient for liquid drop floating on cryogenic fluid 20 p3313 A71-39288

Floating times of liquid/solid sphere on evaporative fluid/liquid nitrogen/ in metastable Leidenfrost film boiling 21 p3476 A71-40892

Hypersonic strong interaction boundary layer problem solution by implicit finite difference method 21 p3369 A71-40955

LIQUID-SOLID INTERFACES

Cryogenic fluids nucleate boiling dependence on solid surface characteristics, considering hysteresis, boiling site spreading and radiation effects 01 p0178 A71-10005

Critical heat release in water film on vertical pipe with inside cooling 01 p0181 A71-11244

Fluid-loaded rectangular plates and membranes random vibration excitation by turbulent boundary layer flow [ASME PAPER 70-WA/DE-15] 03 p0511 A71-14147

Soviet monograph on mass exchange in solid-liquid system covering soluble material extraction and absorption, interphase mass transfer and dissolving process 04 p0677 A71-15446

Bulk solids melting on inclined plane heated surface, investigating heat transfer and mass flow rates, fluid driving force and pressure gradient 04 p0678 A71-15456

Liquid-solid viscoelastic motion equations derived from conservation laws and nonequilibrium processes phenomenological theory 05 p0821 A71-16359

Shell-fluid interaction problems, considering liquid filled shells oscillations, acoustic shock waves action, body impact against water, etc 06 p0998 A71-17861

Seaplane step /flat plate/ ricochet off ideal incompressible fluid surface, determining free surface shape by accounting for trailing vortices effects 07 p1088 A71-19355

High density DC effects on displacement of solid GaAs-liquid metal interface, considering Peltier effect and dislocation density 08 p1344 A71-21444

InAs-AlAs pseudobinary system solidus boundary determination from pellet phase diagram 08 p1344 A71-21472

Unsteady interaction of compressible fluid and flat circular deforming elastic membrane analyzed coupled computer program method [AIAA PAPER 70-75] 09 p1430 A71-22085

Liquid-solid interface phenomena during sintering and porous materials impregnation by liquid metals, using spherical and nonspherical particle models 09 p1457 A71-23391

Heat and mass transfer in triple interline region of stationary evaporating meniscus on flat plate immersed in liquid pool 13 p2164 A71-29006

Heated or cooled wall surface layers temperature anomaly, noting fluid-wall heat exchange coefficients 15 p2513 A71-31905

Silicon-boron melts, investigating B and C concentration effects on carbide layer thickness on graphite/melt interface 15 p2439 A71-32144

Hydrogen and nitrogen pores formation in welds, considering gas concentration redistribution between liquid and solid metal 15 p2417 A71-32663

Polymethyl methacrylate lifetime tested in water and heptane, showing increase with orientation degree 16 p2601 A71-33683

Jet induced secondary flow interaction with circular plate, showing ring vortex effects on pressure distribution 17 p2669 A71-34334

Liquid-liquid or solid-liquid interface Leidenfrost film boiling, deriving heat transfer coefficient for liquid drop floating on cryogenic fluid 20 p3313 A71-39288

Sn-Pb alloy solidification point analysis around liquid-solid front with interface visualization by electron microprobe 20 p3238 A71-39416

Floating times of liquid/solid sphere on evaporative fluid/liquid nitrogen/ in metastable Leidenfrost film boiling 21 p3476 A71-40892

Room temperature evaporating water drop shape history on cooper, lucite, stainless steel and Teflon, observing wetting dynamics effects 21 p3476 A71-40903

Roughness role in liquid He-solid boundary thermal resistance, calculating heat transfer coefficient 21 p3416 A71-41122

Infinite plane elastic wave reflection and refraction coefficients at fluid-solid interface, noting reflected beam lateral displacement at critical angles 23 p3703 A71-43202

LIQUID-VAPOR EQUILIBRIUM

Liquid-phase nucleus condensation of supersaturated vapor in drawer, using statistical method 01 p0180 A71-11089

Transient thermodynamic processes of two phase vapor-liquid emulsion emptying at subcritical temperature in heat engines 12 p1944 A71-27500

Dynamic bubble growth and diameter at detachment during liquid boiling at heating surfaces, using force equilibrium, laser Mach-Zehnder interferometer and temperature measurements 16 p2663 A71-34038

Vapor bubble growth on heated surface with random temperature distribution and liquid microfilm for water and boiling potassium 17 p2836 A71-34306

Method of characteristics application to supersonic jet and nozzle gas flow with allowance for equilibrium and nonequilibrium condensation 17 p2673 A71-35636

German monograph on thermal equation of state for nitrogen vapor-liquid phase equilibrium covering vapor pressure and density, phase diagrams, critical temperature, etc 22 p3574 A71-41716

Transient thermodynamic processes of two phase vapor-liquid emulsion draining at subcritical temperature in heat engines 24 p3819 A71-44928

LIQUID-VAPOR INTERFACES

Acoustic attenuation in condensing vapor, using continuumlike formulation allowing for phase exchange process 01 p0182 A71-11470

Explosive boiling of water and organic liquids around pulse heated Pt wire, discussing vaporization process, fluctuating nucleation and temperature behavior 02 p0331 A71-12193

Fermion system phase transition model thermodynamic behavior near critical point region for various interactions 03 p0456 A71-13350

Boiling cryogenic gas-liquid cross-current heat exchanger unit surface power transmission optimization 04 p0626 A71-15463

Turbulent film boiling on vertical surfaces, proposing theoretical model with interfacial wave disturbances taken into account for heat transfer calculation 04 p0686 A71-15527

Translatory vapor bubbles motion in binary liquid mixtures under heat and mass transfers 04 p0687 A71-15534

Liquid-vapor system in closed container, investigating transient pressure rise under heat and mass transfer interactions including incipient and nucleate boiling 04 p0687 A71-15535

Liquid metals vapor drag and electromagnetic fields effects on laminar film condensation, using finite difference method 04 p0688 A71-15539

Fluorine liquid-vapor coexistence boundary and critical point parameters, considering thermodynamic and transport properties 05 p0831 A71-16409

Boiling layer microcharacteristics, investigating temperature pulsations near wall attachment and subcooled liquid two phase boundaries 07 p1221 A71-18788

Kinetic theory of transient condensation and evaporation at plane surface, using Maxwell moment formulation 09 p1545 A71-22852

Plane stationary shock wave propagation through one component vapor-liquid mixture, calculating profile and mixture parameters under evaporation and condensation 10 p1593 A71-24348

Nonlinear stability analysis of inviscid and viscous liquid film adjacent to compressible gas flow, using gravity and pressure perturbation models 10 p1595 A71-24620

Surface wave velocity at interface between liquid He 4 and saturated vapor 13 p2101 A71-28769

Explosive boiling of water and organic liquids around pulse heated Pt wire, discussing vaporization process, fluctuating nucleation and temperature behavior 15 p2512 A71-31499

Fluid surface instability under perpendicular acceleration, presenting singular perturbation problem solution by successive approximations method 16 p2561 A71-34160

Model radiative transfer across random air-sea interface, determining reflected sky radiance 17 p2736 A71-35562

Rotating disk flow system for Fe vaporizing into cold Ar atmosphere, investigating effect of condensation in boundary layer on mass transfer 19 p3162 A71-37727

Liquid jet injection into transverse two-phase vapor-liquid flow, calculating penetration path and depth from semiempirical theory 20 p3210 A71-38896

Forced flow laminar film boiling heat transfer coefficients from vertical surface in terms of interfacial shear at liquid-vapor interface 21 p3476 A71-40896

Niobium carbide film formation in pseudoliquidified layer on graphite at 3000 C in argon metal vapor mixtures with/without hydrogen 23 p3696 A71-44317

Liquid droplet vaporization under exposure to hot gas, obtaining time dependent temperature and concentration profiles in vicinity from coupled diffusion equations 24 p3888 A71-44963

Laminar boundary layer calculation for simultaneous heat and mass transfer in evaporating liquid layer on flat plate in parallel gas flow, considering variable material parameters 24 p3888 A71-44965

LIQUIDS

NT CRYOGENIC FLUIDS

NT CRYOGENIC ROCKET PROPELLANTS

NT HYDRAULIC FLUIDS

NT HYPERGOLIC ROCKET PROPELLANTS

NT LIQUEFIED GASES

NT LIQUID HELIUM

NT LIQUID HYDROGEN

NT LIQUID METALS

NT LIQUID NITROGEN

NT LIQUID OXIDIZERS

NT LIQUID OXYGEN

NT LIQUID POTASSIUM

NT LIQUID ROCKET PROPELLANTS

NT LIQUID SODIUM

NT MERCURY [METAL]

NT MERCURY VAPOR

NT MONOPROPELLANTS

NT ORGANIC LIQUIDS

NT ROTATING LIQUIDS

NT SLURRY PROPELLANTS

Simple gases and liquids thermodynamic properties, calculating isotopic effects by corresponding states law with quantum corrections 02 p0331 A71-12187

Liquid filled gyroscope motion stability, examining experimental data, design and testing procedures 03 p0426 A71-13776

Liquid shell about solid spherical core, analyzing vibrations and sphere gravitational effects on material particle motion 09 p1495 A71-23342

Dense liquid thermodynamic model, using approximate equation of state 13 p2160 A71-28571

Apparatus for measuring polar liquids dielectric permittivity and losses at microwave frequencies over wide temperature and pressure ranges 14 p2222 A71-30583

Combination light scattering in liquids, single crystal and crystal powders, employing long lived argon laser with internal mirrors and large diameter capillaries 14 p2255 A71-30585

Laser beam CW self-induced frequency modulation and switching observation in liquids with low surface tension 15 p2420 A71-32381

Light wave Rayleigh interferometer for concentration gradient measurements in liquid systems with mass transport 18 p2917 A71-36052

Liquid properties and ambient pressure effects on cavitation erosion in thin film 24 p3819 A71-44946

LIVIDUS

Binary alloy solidification in electroslog remelting process, determining temperature distribution and solidus, mushy and liquidus zones by heat transfer analysis 19 p3079 A71-37706

Equilibrium phase relations in lunar rocks and synthesized analogs, determining liquidus and solidus temperatures 23 p3742 A71-43640

LITERATURE

NT DOCUMENTATION

LITHERGOLIC PROPELLANTS

U HYBRID PROPELLANTS

LITHIASIS

Flying personnel urinary lithiasis relationship with aeronautical activity, discussing etiopathological factors and augmented fluid intake 01 p0028 A71-11600

LITHIUM

NT LITHIUM ISOTOPES

Li quantitative determination in soaps and lubricants by gamma spectroscopy of nuclear reactions with alpha particles from radioactive source 01 p0106 A71-10093

Solar Li abundance determined from selected sunspot spectra observations 01 p0161 A71-11382

Chondrites Li content, using atomic absorption spectroscopy 01 p0162 A71-11429

Dense Li plasma pulsed power discharge temperature, structure, propagation velocity and emission characteristics 02 p0290 A71-12183

Equilibrium, highly imperfect, partially ionized Hg and Li vapor plasmas, examining charged and neutral particle interaction forming charged clusters 02 p0292 A71-12617

Physical changes at lithium electrodes during charge-discharge cycling in propylene carbonate electrolyte 03 p0350 A71-13030

High energy density solid state electrolyte cell with lithium anode 03 p0351 A71-13033

High energy long shelf life lithium-nickel sulfide batteries performance tests 03 p0351 A71-13041

Lithium line strength indicator of stellar age, discussing T Tauri, A, carbon, S and Ba II stars 04 p0646 A71-15232

Si solar cell radiation resistance improvement through Li doping, noting efficiencies in excess of state-of-art N/P cells after exposure to 1 MeV electrons 05 p0703 A71-16088

Lithium concentration and defects in doped radiation resistant silicon solar cells during electron irradiation 05 p0703 A71-16089

Lithium-containing p-n solar cells photovoltaic performance and stability tests at room temperature 05 p0703 A71-16090

Li doped Si solar cells recovery after irradiation, examining temperature dependence 05 p0704 A71-16105

Dispersion medium effects on thermal hardening of lubricating oils with Na or Li additives 05 p0772 A71-16385

Li concentration effect on CdS single crystals brittle fracture anisotropy by metallographic techniques 06 p0941 A71-18083

Sunspot lithium abundance observation by high resolution interferometric spectrometer, using line formation theory applicable to medium strength lines 07 p1190 A71-18861

Red giant star s-process and subsequent delayed electron capture, accounting for large Li abundances 07 p1198 A71-19822

Li and temperature effects on mechanical properties of Mg base single crystals in basal and prismatic slip 08 p1309 A71-21525

Li photoionization cross sections determined from spectral intensity measurements as function of threshold wavelength, discussing radiative electron-ion recombination into first excited state 10 p1646 A71-24992

Output pulse amplitude from lithium-drifted detector-amplifier combination under conditions of carrier diffusion and bulk and surface recombination 11 p1802 A71-25804

Reassessment of Cotter model startup in Li heat pipe, modifying model by moving sonic point to end of hot zone and including wall friction and condensation 11 p1715 A71-25914

Corrosion mechanism in Ta-Li high temperature heat pipes by ion analysis, demonstrating oxygen and yttrium diffusion into heating zone 12 p1916 A71-26974

Radiation patterns from piezoelectric transducers on Y face of lithium niobate, using Green function analysis 14 p2283 A71-29795

Strong level crossing signals in stepwise fluorescence, investigating fine and hyperfine structure of atomic Li 14 p2277 A71-30508

Unstable collisional drift waves in high density ionized Li arc plasma, possibly causing anomalous losses and fluctuations 14 p2281 A71-30544

Dense Li plasma pulsed power discharge temperature, structure, propagation velocity and emission characteristics 15 p2454 A71-31491

Motion and collision of plasma blobs generated by giant pulse ruby laser irradiation on lithium plate 15 p2455 A71-31643

T Tauri stars Li, Be and B autogenic generation, considering underabundance in surrounding gas 16 p2626 A71-33433

Thermal flux model of lithium plasma source at various temperatures and pressures, using arc channel model with conducting cross section 17 p2787 A71-34303

Solar oblateness and Li abundance interpretation by model of thermally driven turbulence terminated at rotating core surface containing partial mass 17 p2806 A71-35385

High voltage solid state electrolytic cell battery with Li anodes, testing storage and discharge characteristics 20 p3181 A71-38935

Lithium additions effect on hydrogen content and mechanical properties of molten aluminum specimens 23 p3691 A71-43522

LITHIUM ALLOYS

Al-Li alloys precipitation characteristics and time-temperature-transformation curves after solution treatment, water quenching and aging 14 p2259 A71-30393

Ultralight magnesium based alloys classification by Li content, noting lattices, structural composition, specific weight, plastic properties and impact strength 15 p2435 A71-32336

Chemical composition effect on corrosion resistance of Mg-Li system with alloying additions 15 p2435 A71-32339

LITHIUM COMPOUNDS

NT LITHIUM FLUORIDES

NT LITHIUM HYDRIDES

NT LITHIUM HYDROXIDES

NT LITHIUM OXIDES

Lithium niobate crystal electro-optical shutter to Q switch calcium difluoride-Dy laser emitting giant pulses at high repetition rate 01 p0095 A71-11210

Lithium tetrafluoroaluminate equilibrium vapor pressure over solid aluminum fluoride plus solid lithium cryolite examined by weight-loss effusion method 07 p1055 A71-19624

Thermal conductivity of Li and Na carbonates alone and combined in mixture with magnesium at various temperatures 08 p1377 A71-21933

Continuously tunable stimulated far IR emission in lithium niobate with Q switched ruby laser as pumping agent, discussing power-wavelength characteristics determination 09 p1465 A71-23482

Cylindrical lithium niobate single crystal acoustic propagation, determining speed, damping and sound

reflection with He-Ne laser light scattering at hypersonic oscillations 13 p2080 A71-29024

High coupling low diffraction loss cut for acoustic surface wave propagation on lithium niobate 14 p2283 A71-29796

Simplified characteristic equation for plane piezoelectric vibrations of lithium niobate and lithium tantalate crystals, using perturbation methods 15 p2461 A71-31701

Minimum voltages and limiting frequencies for oblique cut longitudinal octahedral crystal modulators with large electro-optic coefficients, including lithium niobates and tantalates 15 p2461 A71-32606

Lithium iodide and tetramethyl ammonium iodide additions effect on radical exchange between phenyl lithium and bromobenzene in diethyl ether 19 p3011 A71-37391

Tuning range extension of doubly resonant lithium iodate parametric oscillator by upconversion, using simultaneous pumping by single ruby laser beam 19 p3071 A71-37477

Lithium magnesium zinc silicates crystallization phase equilibria, noting temperature effects, structure, melting and solubility 20 p3253 A71-38818

Rotating waveplate optical frequency shifting in lithium niobate, producing light beam with moderate requirements on modulator adjustment 20 p3204 A71-39097

Lithium niobate hypersound attenuation and reflection coefficients frequency dependence determination by scattering laser light at hypersonic oscillations 20 p3244 A71-39162

Voltage-polarization induced optical waveguide using electrooptical lithium niobate crystal 21 p3393 A71-41039

Surface wave delay lines with near octave bandwidth using lithium niobate interdigital ultrasonic transducer with lumped element impedance inverter network 22 p3521 A71-42202

High purity lithium hexafluoroarsenate preparation methods and hexafluoroarsenic acid properties 23 p3642 A71-43540

Lithium iodate hexagonal and tetragonal form crystal growth conditions from aqueous solution and recorded refractivity 23 p3717 A71-43935

Lithium deuteride nuclear fuel autocatalytic burning via proton and beryllium isotope resonance in fusion chain reactions 24 p3847 A71-44497

He-Ne laser radiation modulator at 1.5 GHz using X and Z cut lithium niobate crystals in toroidal microwave cavity 24 p3835 A71-45265

LITHIUM FLUORIDES

Beta-Li hexafluoroaluminate heat capacity and thermodynamic properties from 15 to 380 K 04 p0674 A71-14727

EPR study of electron irradiated LiF surface defects, emphasizing F-centers generation possibility 11 p1807 A71-25557

LiF single crystals temperature, strain rate and positive Mg ionic impurity effects on work hardening characteristics 11 p1809 A71-26478

Liquid KCl and LiF surface films effect on combustion rate of ammonium perchlorate mixtures with polystyrene or polymethyl methacrylate for various initial temperatures 15 p2462 A71-31371

High efficiency room temperature lasing operation assisted by energy transfer in holmium doped yttrium lithium fluoride 20 p3247 A71-39761

LiF and MgO high purity single crystals plastic deformation geometric characteristics, discussing nucleation probability on different slip planes 24 p3859 A71-44450

LITHIUM HYDRIDES

Q switched laser irradiated solid lithium hydride particle plasma formation and heating, determining optimal conditions 01 p0096 A71-11482

Magnetic field confinement of ionized plasmas generated by laser-irradiated lithium hydride solid particle 01 p0137 A71-11483

High energy cosmic particle interactions with LiH target, discussing relation between longitudinal and transverse momenta of generated pions 03 p0476 A71-13844

Nanosecond laser produced lithium hydride spherical plasma expansion model, taking into account three body and radiative recombinations 06 p0938 A71-18457

Energetic highly ionized plasma production by pulsed laser heating of lithium hydride pellets 09 p1503 A71-22867

LITHIUM HYDROXIDES

High energy cosmic particle interactions with LiH target, discussing relation between longitudinal and transverse momenta of generated pions
22 p3594 A71-42645

LITHIUM HYDROXIDES

LiOH dissociation energy in acetylene-air flames
03 p0376 A71-14281
Granular lithium hydroxide as carbon dioxide absorbent for closed cycle life support systems, considering porosity, carrier gas and water vapor pressure and bed temperature
22 p3508 A71-41773

LITHIUM ISOTOPES

Relative abundances and mass measurements of Li and B isotopes in primary low energy cosmic rays
22 p3593 A71-42339
Li, B, Mg and Ti isotopic abundances and search for trapped solar wind Li in Apollo 11 and 12 rocks
23 p3752 A71-43708

LITHIUM OXIDES

SHF lithium tantalum oxide optical modulator for optical detector evaluation, discussing bandwidth and phase modulation characteristics
12 p1903 A71-26790

LITHIUM 4

U LITHIUM ISOTOPES

LITHIUM 6

U LITHIUM ISOTOPES

LITHOGRAPHY

Optimized low loss microstrip microwave filters on silica substrates by photolithographic reduction of LF models
19 p3026 A71-37218
Photolithographic fabrication and electrical characteristics of GaAs Schottky barrier diodes for pulse operation
19 p3027 A71-37259

LITHOSPHERE

NT EARTH CORE
NT EARTH CRUST
NT EARTH MANTLE
NT EARTH PLANETARY STRUCTURE
NT EARTH SURFACE

LIVER

Salmonid fishes from Great Britain and southern Germany, analyzing visual pigments and liver retinols
01 p0008 A71-10229
Continuous and intermittent effect of carbon tetrachloride breathing on pathomorphological and histochemical structure of liver in test animals
01 p0013 A71-11129
Morphological and histological changes in liver and kidneys of rats exposed to long term hypothermy
01 p0013 A71-11131
Physical exercise effect on mitochondrial energy production in heart muscle and liver in rats
01 p0017 A71-11542
Liver and skeletal musculature morphology during hypokinesia and protein deficiency in mice
06 p0855 A71-18377
Radioprotective mercaptoethylamine (MEA) effect on aerobic resynthesis of ATP in thymus nuclei and oxidative phosphorylation in rat liver mitochondria
07 p1039 A71-18984
Cysteine prevention of fatty liver induced by carbon tetrachloride and ethionine
07 p1040 A71-18987
Prolonged hyperoxia effects on lipid synthesis in rat liver and adipose tissue slices
10 p1559 A71-23969
Beef liver cell nuclei acoustic absorption at various frequencies, determining relation to protein content
12 p1928 A71-27535
Human heart, kidneys, liver and spleen tissues antigen composition analysis by isolation of pure antibodies
12 p1872 A71-27723
Dietary pyridoxal deficiency causing amino acid content reduction in liver, kidney, brain and heart tissues
13 p2003 A71-27837
Rat liver and lung collagenase activity Circadian rhythm, noting maximum enzyme activity in early morning and minimum during afternoon and early evening
13 p2010 A71-28788
Mitotic response to various diets in normal and regenerating rat liver
14 p2182 A71-30069
Polysomal RNA disaggregation and attendant reduction in hepatic protein synthesis in rats as result of decreased feed ingestion during hypoxia
16 p2529 A71-33190
Amino acid levels in fasted and fed rats plasma, liver, muscle and kidney during and after exercise, noting glutamine decrease in liver tissue
20 p3186 A71-38982
Ultrasound absorption in liver tissue due to macromolecular relaxation processes
20 p3191 A71-39770
Stimulatory effects of hypobaric hyperoxia on lipid synthesis in rat liver and adipose tissues under free feeding
22 p3486 A71-41825

LMCR [REACTORS]

U LIQUID METAL COOLED REACTORS

LOAD DISTRIBUTION [FORCES]

Moire technique calculation of transverse strain directly from longitudinal strain distribution across sections of symmetry in grooved tensile bar
01 p0174 A71-11007
Elastic half space transient response to normal impulsive surface line load
02 p0321 A71-11677

Thermoelastic stresses in closed laminar orthotropic shells of revolution subjected to axisymmetric loads and temperature gradients
02 p0322 A71-11735

Fiberglass reinforced plastic cylindrical shells, investigating rheological effects during heating and concentrated radial loads
02 p0324 A71-11754

Stress-strain state of thin circular plate with variable thickness along circumference under bending due to uniformly distributed load, using small p
02 p0326 A71-12289

Zero bending moment shells of revolution under concentrated load, using boundary value problem for p analytic functions
02 p0328 A71-12539

Thin reinforced viscoelastic isotropic multiconnected plate stress-strain state under bending due to concentrated loads and distributed normal forces
02 p0329 A71-12668

Axisymmetrically loaded shells of revolution made of work hardening materials, determining inelastic finite deformations and buckling loads by incremental variational method
03 p0505 A71-13543

Axisymmetric load problems in Cosserat medium, expressing displacement states by mathematical functions
03 p0509 A71-13899

Stiff rings attached to elastic cylinders, analyzing stresses and deformations under concentrated loads and bending moments about radial and tangential axes [ASME PAPER 70-WA/PVP-1]
03 p0510 A71-14099

Bending of cylindrical shells with and without intermediate supports under arbitrarily distributed and discontinuous loads, using initial parameter method [ASME PAPER 70-WA/PVP-2]
03 p0510 A71-14100

Computation scheme for hinged plate systems subject to arbitrarily oriented loads based on two layer flexible base model
04 p0664 A71-14601

Tail assembly load distribution in steady uniform flow for nonzero angles of attack, using slender body theory
04 p0527 A71-15367

Doubly symmetric oval ring under lateral load, investigating creep behavior from equilibrium equations
05 p0820 A71-15984

Deflection-optimal elastic beams design for distributed dynamic loading
05 p0825 A71-16717

Rate sensitive materials impulsively loaded structures by piecewise stationary mode approximate methods
05 p0826 A71-16718

Local distributed load effects on bending of fiberglass reinforced plastic laminar orthotropic cylindrical shell
06 p0986 A71-17761

Limiting analysis for upper estimate of carrying capacity of shell of revolution under load concentrated at center, evaluating stability loss
06 p0987 A71-17771

Plates and shells under concentrated loads, determining stress-strain state
06 p0988 A71-17773

Cylindrical shell stability under nonuniform loading, solving infinite homogeneous algebraic equations system by Bunnoy-Galerkin method
06 p0990 A71-17791

Reissner shell theory equations for arbitrary internal and surface loads
06 p0996 A71-17836

Solution behavior of zero-curvature shells under concentrated loads with increasing distance from application point
06 p0996 A71-17843

Orthotropic shell with hollow elliptical paraboloid form, discussing numerical solution for normal concentrated load action
06 p0998 A71-17855

Plane and spatial load transfer and diffusion in linear elastostatics, noting application to aircraft and civil engineering structures and fiber reinforced materials
06 p1001 A71-18222

Elliptic ring shaped disk with external and internal loading, determining stresses due to uniformly distributed loads
06 p1002 A71-18416

Critical dynamic snap-through of shallow clamped arches under concentrated loads, using finite difference method
06 p1004 A71-18615

[AIAA PAPER 71-176]

Antiplane stress distribution around single or collinear cracks in nonwork hardening elastoplastic material under uniform load
07 p1212 A71-19350

Cylindrical shell with elastic core under annular shearing load, solving for critical velocity via Fourier transformation
07 p1212 A71-19350

Thin shallow spherical shell vertical impact against ideal incompressible liquid surface, calculating axisymmetric deformation and hydrodynamic load distribution
07 p1089 A71-19730

Multilayered composite mathematical model, studying interfacial delamination under antiplane shear load
07 p1215 A71-20127

Homogeneous isotropic layers stack on rigid bases with periodically varying elasticity parameters, calculating equilibrium under normal distributed load
07 p1217 A71-20460

Stress-strain state of rectangular transversely isotropic plate with clamped edge under uniformly distributed load, considering bending moments
07 p1218 A71-20473

Thick-walled toroidal shell under various load distributions, analyzing stress-strain state by networks method using computer program
08 p1369 A71-21124

Mixed plane elasticity theory of narrow rectangle imbedded in static walls under normal loads
08 p1373 A71-21943

Laminated orthotropic plates under transverse loading, developing Navier type solution for Stavsky generalized stress function equation
09 p1534 A71-22101

Circular cylindrical shell initial geometrical imperfections effect on stability under nonuniform composite loading
09 p1537 A71-22518

Materials durability in presence of stress concentration under biharmonic loading
09 p1538 A71-22626

Circular cylindrical shell under radial local load, determining maximum stresses in center and boundary
09 p1538 A71-22651

Bending analysis of clamped and simply supported isotropic skew plates under uniformly distributed load
09 p1540 A71-22995

Thin cylindrical shell deformation under concentrated transverse loads applied through rigid boss, determining displacement variations as function of applied loads and edge constraints
09 p1543 A71-23659

Composites under transverse normal tensile loading micromechanics failure criteria based on distortion energy theory, taking into account multiaxial stress concentration
11 p1784 A71-25334

Nonlinear dynamic analysis of shells of revolution under symmetric and asymmetric loads, obtaining solutions for shallow cap buckling
11 p1847 A71-25465

Natural frequencies and elastic stability of simply supported rectangular plate under linearly varying compressive loads
12 p1976 A71-27162

High lift wing characteristics with/without additional devices, emphasizing lift control and load distribution
12 p1864 A71-27476

Static problems of shells of revolution under local loads, solving by stable numerical process
13 p1252 A71-28276

Circular elastic ideally plastic plate deformation due to circumferentially distributed rectangular pulse loading
13 p1256 A71-29075

Sailplane elevator induced maneuvering and horizontal tail surface loads, discussing airworthiness requirements
13 p1997 A71-29256

Error in determining pressure and loading distribution on surface of slender bodies of revolution
13 p1994 A71-29323

Stress concentration for fatigue crack propagation in smooth and notched samples under symmetrical loading
13 p2157 A71-29373

Static load and stress distribution in rolling element bearings, using elastic contact area analysis method [ASLE PREPRINT 71AM 1D-1]
13 p2076 A71-29487

Nonlinear stability of saddle-like deformed circular and square flat plates and shallow shells under transverse loadings
14 p2322 A71-29692

Stress values at arbitrary point of infinite disk loaded by concentrated force acting through rigid slit of circular arc segment
14 p2323 A71-29814

Clamped shallow spherical cap buckling and initial postbuckling behavior under axisymmetric band type loads, using numerical analysis
14 p2330 A71-30690

Elastic deformation of double cavity hyperboloid of revolution under variable loads applied to boundaries 14 p2332 A71-30846

Strength analysis of shells of revolution and plates under axisymmetrical loads for rigidly plastic material with Tresca yield condition 14 p2332 A71-30849

Nonlinear coupled parametric response of crooked thin walled columns under harmonic longitudinal load 15 p2507 A71-32095

German monograph on spatial elasticity problems solution by multidimensional Fourier transformation covering stress concentration on hollow and solid cones for given load distribution 15 p2509 A71-32300

German monograph on iterative procedure for sectional parameters of shells of revolution with meridian form under peripheral loads described by harmonic functions 15 p2509 A71-32374

Rectangular plates under direct and shear in-plane forces, considering free lateral vibrations 15 p2509 A71-32512

Stress-strain state of unclamped thin elastic zero curvature shell under three component surface load and tangential boundary forces 16 p2647 A71-32926

Stiffness matrices determination for flat plate elements under tangential and normal loadings by collocation, using exact polynomial solutions 16 p2652 A71-33083

Combined finite element method and Rayleigh-Ritz procedure for geometrically nonlinear problems solution of elastic plates with arbitrary shape, boundary and load distribution 16 p2653 A71-33088

Dynamic midsurface displacements of thin circular cylindrical shell under uniform membrane stress state and three dimensional surface loads [ASME PAPER 71-APM-12] 16 p2656 A71-33214

Clamped shallow spherical shells buckling and post-buckling behavior under axisymmetric ring loads, examining effect of load location and shell geometry variations [ASME PAPER 71-APM-9] 16 p2656 A71-33216

Stability loss of circular cylindrical shell with stepped wall thickness of central reinforcing sleeve under annular loading, determining critical load by thin shell theory 16 p2657 A71-33600

Stability and critical load of constant thickness cylindrical sandwich hinge supported shell under annular loading, using variational method 16 p2657 A71-33601

Potential energy minimization for elastic elements with integral loads applied to bending of bar and wedge, using variational method 16 p2659 A71-33995

Uniformly extended elastic circular plate with rectilinear slot under normal tensile loads at boundary 16 p2660 A71-34115

Stress-strain state of circular cylindrical shell hinged at edges under local radial loads 17 p2817 A71-34340

Thin walled structure design for critical loading by external force variation, determining carrying capability loss by digital computer matrix methods 17 p2818 A71-34351

Deformations and stress concentration on corrugated plate under uniformly distributed load, considering cross section as combination of two cylindrical shells 17 p2818 A71-34401

Anatomical load sensing method, determining torso pain thresholds by sensitivity tests [SESA PAPER 1823A] 17 p2689 A71-34539

Elastoplastic strain distribution in bent circular Al plate with central hole under concentrated load, giving moire patterns and stress-strain diagram [SESA PAPER 1822] 17 p2820 A71-34542

Impulsively loaded expanding cylindrical shell transient elastic-plastic response, using linearized assumption on plastic flow behavior 17 p2821 A71-34577

Optimal bar design for tangential load transmission into sheet, determining stress distribution 17 p2821 A71-34591

Transverse shear deformation and normal stresses effect on shallow shell with normal concentrated loads 17 p2822 A71-34594

Limited fatigue strength tests for Al-Mg-Si alloy stress amplitude coefficients under continuous loading, defects, strains and creep accumulation 17 p2757 A71-34596

Linear radial loads effect on stress and strain of hyperboloidal rotor disk applied to aircraft engine compressors with two stream flow of working medium 17 p2822 A71-34597

Long laminar plate and cylindrical panels with hinged lateral edges under buckling by normal uniformly distributed load, calculating deflection as monotonic pressure functions 17 p2823 A71-34781

Stresses in smooth circular cylindrical shell under radial local load applied on small area 17 p2828 A71-35303

Thermal stressed state and bending theory of rectangular plate by initial function method, allowing for distributed transverse load 17 p2829 A71-35304

Thin elastic spherical shells reinforced by stringers and frames and loaded by internal or external uniform pressure, calculating by energy method 17 p2829 A71-35311

Cantilevered elastic cylindrical shell stability during bending by transverse load uniformly distributed over entire surface or applied at end 17 p2833 A71-35615

Thyristor power conditioning application to high voltage DC electric power system, presenting SST aircraft sample load profiles 17 p2678 A71-35770

Channel type closed shallow shells stress states calculation, applying asymptotic integration technique to load decomposition 18 p2976 A71-36178

Book on optimum structural design covering single element optimizations, load transmission, slender columns, cost-weight tradeoffs and statically indeterminate structures 18 p2977 A71-36249

Rib reinforced cylindrical shells deformation under local load, examining stress-strain distribution 18 p2981 A71-36719

Cosserat-type bodies with linear elasticity, obtaining reciprocity theorem and stress solutions under concentrated load 18 p2984 A71-36949

Three dimensional orthotropic elastic cylinders symmetric deformations under external loads, calculating stress-strain state with approximate method 19 p3155 A71-37528

Cylindrical shells under uniform external pressure loads, determining boundary conditions effects on natural frequencies and vibration mode shapes 19 p3155 A71-37529

Shallow spherical shell under uniform external pressure loads, obtaining boundary conditions effects on stress-strain state 19 p3155 A71-37530

Displacement in circular plate with radial slit under transverse forces 19 p3156 A71-37796

Cylindrical shell stability under radial pressure or axial compression from load-distributing filler model solution 20 p3308 A71-39166

Plasticity with noncoincident yield and loading surfaces, noting isothermal isotropic hardening 20 p3309 A71-39565

Peak resonant response of thin rectangular plate with elastic edge restraint under concentrated load [ASME PAPER 71-VIBR-6] 21 p3456 A71-40269

Drooped wing tip effects on trailing vortex sheet structure and position from spanwise load distribution determination by vortex lattice theory 21 p3319 A71-40493

Elastic buckling and initial postbuckling behavior of clamped shallow spherical sandwich shells under axisymmetrical load 21 p3469 A71-41007

Circular cylindrical shell under longitudinal parametric load, obtaining nonstationary responses with deformation theory 21 p3471 A71-41029

Zero moment reinforced prismatic shells of rectangular cross section with arbitrary load distribution 21 p3472 A71-41146

Shallow two pinned sinusoidal arches stability under random symmetrically distributed lateral loads, observing deformation, buckling and critical value 22 p3612 A71-41429

Double forces surface distributions, investigating displacement and stress fields singularities of static Lamé equations 22 p3614 A71-41603

Infinite sandwich plate under concentrated torque load on one side, determining stress distribution with double infinite Fourier transform 22 p3614 A71-41604

Stiffness and load capacity control by self compensating flow restrictor for externally pressurized gas lubricated thrust bearing design 22 p3552 A71-41673

Local elastic buckling of component plate elements of single-cell simply supported folded plate structures under uniform transverse loads 22 p3618 A71-42585

Stability of edge reinforced circular plate under uniform radial load, considering flexural and extensional stiffness of reinforcing beam 22 p3618 A71-42592

Static, kinematic and uniqueness theorems of incremental collapse of frames extended to variable repeated loading 22 p3619 A71-42593

Boundary value problems solution for reaction pressure to elastic base circular plate bending under uniformly distributed load 23 p3777 A71-43910

Thin closed circular cylindrical shell under arbitrary loading 23 p3778 A71-44039

Stresses and displacements in elastic half space with variable modulus of elasticity under axisymmetrical shifting load distributed along ring 23 p3778 A71-44045

Dynamic flexures in beam during massive extended load motion with allowance for inertial forces, using Bubnov-Galerkin method 23 p3778 A71-44046

Loading modes effect on stress corrosion cracking of Ni maraging steel in NaCl solution 23 p3693 A71-44074

Multicore circular sandwich plates under various symmetrical loading and boundary conditions, deriving bending equations 24 p3879 A71-44619

Curved finite element for elastic-plastic analysis of thin toroidal shells of revolution with discontinuous meridional slope under axisymmetric loadings 24 p3879 A71-44634

Nonhomogeneous plate under pulsating and uniformly distributed loads, considering dynamic elasticity problem 24 p3880 A71-44712

Elasticity theory for rectangular region with thin-walled inclusion under symmetrical external forces, reducing to three quasi-regular infinite systems of linear algebraic equations 24 p3880 A71-44722

Geometrically nonlinear circular plate under nonuniformly distributed radial force, calculating loading rate and end condition effects on buckling, deflection and stress 24 p3884 A71-44899

Small deflection theory for steady state creep bending of laminated anisotropic rectangular plate under uniform loads, using Galerkin method 24 p3841 A71-44957

Cylindrical shell under longitudinal load, examining stress-strain state with semimoment theory 24 p3884 A71-45017

Aircraft fuselage antisymmetric loading strain effects on small aspect delta wing performance 24 p3885 A71-45018

Body adaptability to mass forces and surface loads for strain hardening material 24 p3886 A71-45366

LOAD FACTORS

U LOADS (FORCES)

LOAD TESTING MACHINES

Brittle materials tensile strength testing method, using thermal contraction loading device 09 p1479 A71-23698

Plastics contact strength test apparatus, describing wear test machine for contact load resistance of epoxides used in automobile engine bearings 15 p2383 A71-31656

Elastic interaction between specimen and testing machine in mechanical property tests, considering drawbacks to machine stiffness calculation methods 15 p2414 A71-31947

German monograph on structural tests tensile and yield strength, detailing strain rate and testing machine effects 17 p2818 A71-34483

LOAD TESTS

Medium length journal bearing pressure profiles, deriving ordinary differential equation for load capacity 01 p0086 A71-10300

Accelerated creep rupture tests on metals and solder alloys, comparing constant stretch rate and load methods [SESA PAPER 1672] 03 p0508 A71-13762

Rigid-perfectly plastic model for real materials behavior, considering modification for strain hardening and elastic effects under various load conditions 03 p0509 A71-13780

Anisotropic plasticity theories for metals predicting load-deformation relations [ASME PAPER 70-WA/APM-17] 03 p0443 A71-14154

Plastic flow rates in materials under complex loads producing constant stress intensity, considering plastic deformation 03 p0515 A71-14364

Carbon steel and heat treated duraluminum fatigue fracture microstructure observation using electron microscope, determining crack propagation relationships to loading sequence 04 p0610 A71-14880

Energy dissipation patterns of metal fatigue failure during static and cyclic loading applied to untreated and heat treated steel samples 04 p0671 A71-15637

Overload and underload effects on Al-Mg-Si creep deformation and damage accumulation under single load change 05 p0768 A71-16800

LOADING FORCES

Isotropy postulate experimental verification in case of complex loading involving strain tensor axes turning

06 p0983 A71-17363

Metal film resistors rapid evaluation method including thermal, load and shock tests devised by British electronic component manufacturers

07 p1076 A71-19553

Refractory materials at normal and high temperatures, describing cyclic shear test methods

08 p1372 A71-21612

Al and Mg alloys mechanical properties anisotropy as function of loading conditions, taking into account stress condition effect

09 p1467 A71-22315

Friction and wear tests on materials of various speeds, loads and temperatures at high relative humidity

09 p1426 A71-22325

Unidirectional fibrous composites brittle and ductile failures prediction under tension and torsion, comparing results with tests on glass-epoxy composites

10 p1686 A71-24017

Aircraft wing fatigue test procedures for gust, maneuver, ground-air-ground, taxi and landing impact loads

10 p1694 A71-25133

Specimen sample mounting stress effects on fatigue durability scatter in axial load tests

12 p1976 A71-27116

Fatigue testing machine for axial and torsional loadings at low temperatures in vacuum

15 p2384 A71-31858

Stress relaxation method using compliance measurement of bolted test assembly to determine initial and residual loads after exposure periods

15 p2436 A71-32505

Loading history effect on optical and mechanical properties of polymethyl methacrylate under uniaxial tension

16 p2600 A71-32815

Elastic energy release rates and stress intensity from nonlinear load deflection curves as function of crack length to specimen width ratio

16 p2590 A71-32945

Fatigue limits of Ti alloy by Wohler and Locati loading methods

16 p2592 A71-33406

Structural changes and phases nucleation and growth in metal alloys during prolonged loading at high temperatures, examining steel strengthening precipitates coagulation kinetics

16 p2597 A71-33918

Cyclic torsional shear testing of refractory materials at normal and high temperatures, describing test equipment

17 p2834 A71-35672

Maximum yielding tensile stress envelope curves as function of structural load index based on compression tests of Al alloy stiffened plane panels

20 p3309 A71-39570

Glass rods loading tests after exposure to hydrogen, nitrogen and argon under high pressure, noting strength improvement by Ar impregnation

24 p3841 A71-44868

Metal fatigue strength evaluation for nonstationary loading and complex stress-amplitude variation

24 p3886 A71-45364

LOADING FORCES

U LOADS [FORCES]

LOADING MOMENTS

Thin walled lipped-channel and trapezoidal section beams under end moment loading, deriving differential equations and strain energy for end plates

02 p0330 A71-12950

Fastener group behavior under combination of direct shear and moment, obtaining load deformation response of individual connections

08 p1370 A71-21410

Rectangular plate and circular cylindrical shell segment under rotating moment and dynamic loads evaluated by Green function

10 p1691 A71-24812

Internal structural design loads for aerospace vehicles subjected to random loads, considering shear, moment and torsion as random components of generalized internal load vector

11 p1838 A71-25516

LOADING OPERATIONS

Local imperfection and stress effects on cylindrical shell stability under various single and combined loads

06 p0991 A71-17803

Boeing 747 aircraft passenger handling measures in Frankfurt airport, discussing loading, unloading, baggage claim and customs control

09 p1430 A71-23696

Tu-154 responsibilities of three-man crews, considering flight plan, refueling, cargo loading and unloading

11 p1744 A71-25258

Flight and operation of IL-62 long distance jet aircraft, considering flight crew composition and training, passenger and cargo handling and refueling

11 p1706 A71-25260

Helicopters as cranes and external load carriers, considering operational costs and investment return

13 p1997 A71-29144

Aircraft loading system consisting of onboard weight and balance equipment and fully mechanized cargo pallet transfer, using computerized simulation model for parametric evaluation

17 p2676 A71-35811

LOADING RATE

Glass fiber reinforced plastics tensile strength under various continuous loading rates and elevated temperatures

02 p0275 A71-12667

High strength steels fracture toughness, investigating loading rate and temperature effects

03 p0442 A71-13625

Creep failure in elastoviscoplastic media from time and load-path dependent processes near axisymmetric fissure prior to cracking

03 p0509 A71-13874

Universal testing machines dynamic load errors due to testing speed

05 p0734 A71-17247

Fiberglass reinforced plastic strength and deformability under tension as function of loading rate and test temperature

07 p1145 A71-20466

Loading frequency effect on carbon steel energy dissipation at large stress amplitudes, deriving strain rate relations

07 p1142 A71-20478

Sliding load history effects on friction of thin burnished films of molybdenum disulfide in vacuum

[ASLE PREPRINT 70LC-18] 08 p1298 A71-21161

Nickel under slow loading conditions at various temperatures, examining disorientation angles of substructure

09 p1476 A71-23317

Loading rate effect on Ni creep characteristics and substructure

09 p1477 A71-23330

Compression, creep, stress relaxation and overload effects on delay in fatigue crack growth and structural life predictions

10 p1694 A71-25059

Rings elastic buckling problems under various loading conditions, using rate equations

11 p1840 A71-25138

Longitudinal tensile strength of unidirectional fibrous glass/polymeric matrix composites under high loading rates

11 p1785 A71-25405

Rigid plastic media dynamic model, showing yielding time delay effect on residual deflection as function of load duration

12 p1982 A71-27515

Deformation fatigue theory extended to tests at stresses below elastic limit, explaining cyclic loading frequency effect on fatigue life

12 p1984 A71-27681

Low temperature and tensile loading rates effects on static and dynamic strength of steel rods with ground and rolled threads

15 p2505 A71-31862

Loading history effect on optical and mechanical properties of polymethyl methacrylate under uniaxial tension

16 p2600 A71-32815

Image distortion technique for viewing surface deformation zones at precracked specimens under monotonic loading during fracture test

[SESA PAPER 1799] 17 p2738 A71-34547

Al-Mg-Si alloy vibration creep endurance under single step loading, emphasizing strain and defect accumulation

17 p2757 A71-34593

Al alloy tensile tests at high temperature and constant elongation and loading rates, noting creep strain

20 p3251 A71-39167

Flexible polyurethane foam plastics under high rate loading, investigating strain rate and structural parameters effects on mechanical properties

22 p3565 A71-41592

Duralumin fatigue process in air and corrosive medium, showing loading frequency and time dependence effects

23 p3692 A71-44027

Polycrystalline Ni preloading rate effects on dislocation structure, electrical resistance and flow stress, noting strain hardening mechanism

24 p3837 A71-44675

Geometrically nonlinear circular plate under nonuniformly distributed radial force, calculating loading rate and end condition effects on buckling, deflection and stress

24 p3884 A71-44899

LOADING WAVES

U ELASTIC WAVES

U LOADS [FORCES]

LOADS [FORCES]

NT AERODYNAMIC LOADS

NT AXIAL COMPRESSION LOADS

NT AXIAL LOADS

NT BLAST LOADS

NT COMPRESSION LOADS

NT CRITICAL LOADING

NT CYCLIC LOADS

NT DYNAMIC LOADS

NT EDGE LOADING

NT GUST LOADS

NT IMPACT LOADS

NT LANDING LOADS

NT RANDOM LOADS

NT ROLLING CONTACT LOADS

NT SHOCK LOADS

NT STATIC LOADS

NT THRUST LOADS

NT TRANSIENT LOADS

NT VIBRATORY LOADS

NT WING LOADING

Radially loaded bearings rolling on flat track, determining slip-stick areas and creep conditions

01 p0086 A71-10292

Fiberglass-reinforced plastics loading conditions effects on tensile strength, determining creep rupture strength from test data

01 p0107 A71-10412

Sailplane fatigue testing determining load spectra fail safe structures and damage calculation

02 p0324 A71-11949

Elastic bar buckling load nondestructive determination using actual boundary conditions

03 p0504 A71-13454

Piezoelectric ceramic transducer vibration measurement under mechanical loading, noting displacements as function of thickness and time

04 p0601 A71-15835

Virgin surfaces adhesion under normal loads, testing Pb, Zn and Cd polycrystalline specimens

05 p0759 A71-17167

TSh-2 hardness test gage, investigating deformation of steel under increasing loads

07 p1106 A71-19141

Elastoplastic loading or unloading wave complex in solids, analyzing stability by breakdown into elastic and plastic components

07 p1217 A71-20463

Distributed parameter systems under load disturbances regulatory control by feedforward feedback and state measures

09 p1422 A71-22283

Expansion bellows fatigue strength based on loads and displacement measurements performed during low cycle model tests

09 p1538 A71-22600

Electrodynamic transducer design for structural vibration testing system, using low power steering signal converter to generate large scale electromechanical loads

09 p1386 A71-22600

Rigid towed and free flight glider, considering load and turbulent atmosphere effects

09 p1385 A71-23660

Quasi-static problem of stress-strain distributions in elastic medium with moving crack, calculating arbitrary external force effect on crack

10 p1687 A71-24349

Rings elastic buckling problems under various loading conditions, using rate equations

11 p1840 A71-25138

Dissimilar bonded anisotropic half spaces with flat crack under arbitrary loads, determining stress distribution

11 p1842 A71-25303

Self acting herringbone journal bearings optimization program for maximum radial load capacity and wide operating range via groove configurations

11 p1769 A71-25836

Radial load effects along length of hinged cylindrical shell for maximum displacement positions, using trigonometric Fourier series

11 p1850 A71-25942

Flexible runway surfaces classification by LCN method, calculating for Ilyushin aircraft

11 p1745 A71-26201

Sailplanes tail load static derivation for instantaneous unchecked longitudinal maneuver, considering aperiodic response

11 p1708 A71-26486

Virgin metal surfaces adhesion under normal loads, testing Pb, Zn and Cd polycrystalline specimens

12 p1912 A71-27461

Cascade approximation of unsteady forces acting on blades of axial flow turbomachines, using perturbation potential combined with slip condition

12 p1946 A71-27713

Aerodynamic behavior of bodies in wake of two dimensional bluff bodies, discussing loads

13 p1994 A71-29265

Atmospheric turbulence effects on handling qualities and structural loads on aircraft

14 p2174 A71-29787

Second order stresses and elastic stability analysis for structures, using supplementary load method

16 p2648 A71-32981

Structural synthesis and analysis concepts, discussing design philosophy, failure modes, load conditions, algorithms and computer aided design

16 p2653 A71-33093

Arterioles and corneo-scleral shell structural response under various loading conditions, using finite element method for mechanical and hydrostatic stress distribution 16 p2528 A71-33099

Weakly nonlinear single degree of freedom cubic system under simultaneous time varying force and parametric excitation, presenting resonance frequencies classification [ASME PAPER 71-APM-24] 16 p2655 A71-33205

Plastic deformation resistance of rough metal surfaces under heavy loads, discussing mechanical contact changes due to asperities reactions as coherent block 18 p2926 A71-36186

Rectangular cantilever plate free vibration under in-plane acceleration loads, calculating frequencies and mode shapes by Ritz method and computer technique 19 p3157 A71-37850

Extinguishing parametric vibrations, changing equivalent natural frequency from resonant state by supplementary load 21 p3473 A71-41368

Irregularly shaped thin elastic plates under uniform transverse or point loads with singularities resulting from loading or corner conditions 22 p3618 A71-42591

LOBES

Phase grating lobes redistribution by aperiodic phased array of line sources with linear variation of element lengths and linear amplitude weighting 06 p0875 A71-17722

LOCALIZATION

U POSITION [LOCATION]

LOCATION

U POSITION [LOCATION]

LOCI

Approximate root locus method in S plane for sampled data systems, mapping constant frequency and constant damping ratio loci onto W plane 15 p2381 A71-31942

Branch points of root locus curves for rational transfer functions and transfer functions with recovery time [DFVLR-SONDDR-110] 22 p3566 A71-41854

Design technique based on frequency response loci associated with characteristic transfer functions for linear time-invariant multivariable feedback control system 22 p3526 A71-42284

LOCKHEED AIRCRAFT

NT C-5 AIRCRAFT

NT C-130 AIRCRAFT

NT F-104 AIRCRAFT

NT L-1011 AIRCRAFT

NT T-33 AIRCRAFT

LOCKHEED C-5 AIRCRAFT

U C-5 AIRCRAFT

LOCKING

Locking in time of phase locked loop with sawtooth comparator for synchronizing two oscillators 14 p2210 A71-29808

LOCOMOTION

NT ASTRONAUT LOCOMOTION

NT WALKING

Movement coordination in animals during walking and running, revealing neurophysiological mechanisms of locomotion control 03 p0356 A71-12987

Biped locomotion machines dynamic analysis and synthesis by minimum energy criteria for prosthetic-orthotic equipment design and human locomotion analysis 09 p1399 A71-22971

Human EEG changes and motor analyzer activity during mental visualization of motions 19 p3002 A71-37445

Gravity receptors and locomotion orientation in Crustacea, discussing statocyst, stimulation, input and compensatory eye movements with respect to gravitational field 21 p3327 A71-39992

LOG PERIODIC ANTENNAS

Log periodic dipole antennas Maxwell equations solution in cylindrical coordinates for all boundary conditions 06 p0874 A71-17706

Log periodic dipole array transient radiation, obtaining radiated pulse envelope time dependence as function of antenna admittance and input pulse frequency spectrum 06 p0875 A71-17720

Short wave double log periodic antenna for 8-26 MHz transmission over long path lengths 07 p1080 A71-20265

Beam compression technique for log periodic dipole antenna array using axial displacement of antenna dipoles feed points 09 p1406 A71-23035

Dipole coupling, current distribution and impedance of thick dipolar log periodic antennas by 4-term theory 16 p2544 A71-34172

Corner reflector excitation by vertical or horizontal log-periodic dipole antenna for unidirectional wide-band radiation, deriving far field expression 18 p2895 A71-36994

Active region and truncation point of log periodic dipole antenna as function of length and design parameters 20 p3203 A71-39091

Structural support system for large log-periodic antenna, discussing asbestos-cement pressure pipes and fiberglass rods as construction materials for antenna critical electrical characteristic needs 20 p3210 A71-39871

Radiation resistance, power gain, effective aperture and efficiency of modified log periodic dipole antenna 21 p3352 A71-40378

High power multielement electronically scanned array of microwave log periodic monopole antennas for ionospheric backscattering measurements 23 p3653 A71-44155

LOG SPIRAL ANTENNAS

Single aperture antenna system with multimode log spiral feed 09 p1419 A71-23500

Rigorous solution for multiple arm conical log spiral antenna by numerical solution of integral equations, considering current distribution, half power beam-width, etc 17 p2715 A71-34752

Log spiral antenna with selectable polarization, showing electric field radiation patterns 23 p3654 A71-44165

LOGARITHMIC RECEIVERS

Stability indices of automatic control system from open circuit logarithmic frequency characteristics, determining poles of transfer function 10 p1588 A71-24905

LOGARITHMS

Altitude and azimuth angle values computation using logarithmic and natural haversines table 02 p0280 A71-12899

Planetary and lunar meteorite craters classification according to radius logarithm to base ten, covering diameter size from 2 microns to 2000 km 21 p3444 A71-40206

LOGIC CIRCUITS

NT THRESHOLD GATES

Electrical fault location and detection techniques for cellular logic circuit arrays fabricated with LSI procedures 01 p0044 A71-10184

Binary cellular logic circuit array multiplication unit based on functional module concept adaptable to LSI implementation, discussing design methodology 01 p0044 A71-10185

Orthoferrite cylindrical magnetic domains in memory and logic devices, considering conductor, angelfish and in-plane rotating field circuits 01 p0047 A71-10211

Shift register based on coplanar Gunn diodes for pulse processing, considering diodes application to logic circuits of digital instrumentation and communication systems 01 p0052 A71-10323

Illiac 4 and Spectra 70 computers comparison in terms of logic circuit noise immunity and system noise sources 03 p0388 A71-13179

Three-stable parametrons ternary logic circuits synthesis by topological method, realizing Post algebra basic operators 03 p0382 A71-13521

Regulator logic synthesis using state variable feedback for stationary linear plants 03 p0393 A71-14467

Interference reduction in logic circuits using combined signal amplitude-pulse duration discrimination 04 p0562 A71-15893

Time sharing program for digital logic circuits simulation 05 p0726 A71-16959

Viscosity measurement apparatus for molten materials, presenting block diagram of logic circuit for recording pendulum behavior 05 p0754 A71-16968

Logic circuitry materials physical properties changes effects on performance-controlling parameters at low temperatures 05 p0732 A71-17077

Asynchronous sequence detectors and similar circuits design, discussing method for flow table reduction and merging 06 p0896 A71-17320

Digital electronic equipment logic networks computer controlled tester, describing method for test patterns synthesis 06 p0879 A71-17322

Long term IR X ray irradiation effects on complementary MOS logic networks with several p and n channels on single silicon, determining radiation induced failure modes 07 p1174 A71-19054

Moving part digital pneumatic logic system, using elements molded into rubber sheet between two rigid flat plates 07 p1027 A71-20575

Fluidic passive and, exclusive-or logic gate, investigating switching, input and output characteristics 07 p1031 A71-20610

Emitter coupled integrated transistorized logic elements, improving steady state noise stability by hysteresis in transfer characteristics 09 p1416 A71-22467

Integrated circuit components equivalent circuits, considering transistor logic circuits and admissible noise 09 p1416 A71-22491

Amorphous semiconductors for memory and logic devices, using reversible structural transformations between disordered and ordered states 09 p1509 A71-23114

Amplitude discriminating Goto circuit with four tunnel diodes operating on negative and positive half periods as amplitude distribution analyzer at 40 MHz 10 p1582 A71-23954

Logical GaAs integrated laser circuits, discussing integrated laser modules with electron-hole junctions fabricated by diffusion techniques 11 p1773 A71-25917

Complementary symmetry MOS technology for logic circuit design of inverters, gates, flip-flops, switches and storage units 12 p1883 A71-27044

Logical dynamic control systems, interpreting structural properties in categories of logic-operator matrices and predicate systems 12 p1893 A71-27338

Digital multiplier based on cellular logic iterative arrays for complex numbers processing 13 p2037 A71-28470

Interface IC circuits for driving high voltage transistor switches from low level logic inputs, noting avionics application 13 p2039 A71-28910

Heuristic algorithm for computation of failures detection tests in asynchronous sequential logic circuits 14 p2218 A71-29520

Fluid logic random input, irregularly activated or stochastic control network analysis, using digital control network synthesis technique /DICONESYN III/ 15 p2351 A71-31685

Fluid logic circuit network analysis, utilizing classical synthesis technique with primitive flow table and maps 15 p2351 A71-31686

Optimal design of logic networks in homogeneous microelectronic structures, using shortest link search and graph continuity parameters 16 p2545 A71-33704

Higher order computer language architecture for aerospace software production problems, discussing real time constraints, hardware tradeoffs, memory, computer design and logic circuitry 17 p2712 A71-35777

Logic devices of adaptive scale-time converters of single pulsed processes on electron beam memory tubes, proposing polynomial methods of data reduction 18 p2887 A71-35881

Fluid amplifiers in logic circuits and control and monitoring systems, discussing operating principles and performance features 18 p2850 A71-36137

Integrated digital emitter coupled logic /ECL/ circuits with transistors in nonsaturated mode 18 p2896 A71-36799

Permanent logical faults identification in discrete combination devices by practical behavior in response to given input sets, using one of Boolean algebras 19 p3025 A71-37571

Complex electronic modules automatic checkout, discussing processing time and cost reduction for large printed circuit logic boards test and diagnostic programs [ASME PAPER 71-VIBR-115] 21 p3362 A71-40335

LSI logic arrays testing problems minimization by test procedures based on circuit design characteristics and MOS structure properties 21 p3356 A71-40803

Failure diagnosis and localization algorithm for combinational circuits of functional elements, considering arbitrary combinations and essential fault presence 21 p3361 A71-41141

Logical GaAs integrated laser circuits, discussing integrated laser modules with diffused p-n junctions 21 p3394 A71-41228

Microcomputer design using standard interfacing module for balanced electronic logic amounts in central processor and peripheral controllers 22 p3518 A71-42207

Functional converters for logic circuits synthesis, determining mutual value order of input functions 23 p3631 A71-43830

Design method for high speed economical arithmetic units of digital computers, describing functional logic circuits 24 p3806 A71-44396

Sequential control with fluid logic programmers, considering decimal and binary counters, shift registers, gray code generator and integrated devices 24 p3793 A71-45087

Multiple component logic circuit reliability analysis using Karnaugh diagram procedure for simplification 24 p3807 A71-45299

LOGIC DESIGN

Structured or array logic configurations based on transistorized matrices with programmable interconnections for large scale integration in computer design 01 p0044 A71-10182

Real time systems design principles for processor organization, logic circuits, fault detection and diagnostic tests to facilitate high degree of reliability and maintainability 01 p0046 A71-10203

Computer memory reduction through Fortran higher level language, discussing tradeoff between costs saved and additional logic hardware [AIAA PAPER 69-963] 03 p0382 A71-13450

Asynchronous sequence detectors and similar circuits design, discussing method for flow table reduction and merging 06 p0896 A71-17320

Digital computer modular LSI control logic design using multifunctional binary decoder with transistor array read-only memory for odd and even parity error detection 08 p1260 A71-21663

Decision logic table application, utilizing valid response sets development maximum number and biparameter conditions 09 p1412 A71-23283

Complementary symmetry MOS technology for logic circuit design of inverters, gates, flip-flops, switches and storage units 12 p1883 A71-27044

Large high speed binary multiplier units design 12 p1884 A71-27152

Fast versatile iterative parallel binary comparator array, proposing cell output states assignment 13 p2037 A71-28475

Boolean algebra and flow diagram nomenclature for sequential logic design 13 p2035 A71-28912

Optimal design of logic networks in homogeneous microelectronic structures, using shortest link search and graph continuity parameters 16 p2545 A71-33704

German monograph on plane realizations of switching circuits, covering crossover points minimization in electric lines interconnecting component parts 17 p2716 A71-34773

Circuit synthesis from unreliable functional elements through probabilistic logic, correcting codes and logic algebra functions 17 p2721 A71-34978

French monograph on satellite stabilization by ion propulsion and attitude control logic element design covering geostationary and geocentric satellites, mass and power balances 17 p2814 A71-35500

Boeing computer simulator for logic design confirmation and failure diagnostic programs, providing for propagation delays and feedback simulation [AAS PAPER 71-162] 19 p3025 A71-37959

Ternary code and three value logic in digital computers, considering economic advantages, signal distinguishability and numerical interpretation of p digit abstract alphabet 22 p3516 A71-41856

Functional converters for logic circuits synthesis, determining mutual value order of input functions 23 p3631 A71-43830

LOGIC NETWORKS

U LOGIC CIRCUITS

LOGICAL ELEMENTS

Injection lasers as logic elements in optical communication systems with time division multiplexing, examining optimal switching and pulse duration reduction 02 p0259 A71-11875

Biological heuristic programming in cybernetics, discussing solid state logic elements limiting factors in modeling 03 p0383 A71-14394

Computer shift registers synthesis technique based on block buildup, estimating logic elements amount 06 p0871 A71-17521

Fiber optic laser devices properties and potential applications as amplifiers, logic elements, active mode selectors and intense light sources 07 p1124 A71-19781

Static fluid logic elements, discussing short circuit during switchover, snap action, pressure loss and circuit examples 07 p1027 A71-20573

Moving part pneumatic logic element static and dynamic characteristics, determining air flow rate and output pressure 07 p1027 A71-20574

Synchronous combinative time pulse polylogical structural elements for computer simulation of human neuron functions, discussing circuit design 09 p1398 A71-22271

Pneumatic membrane logic elements on basis of figure of merit characterizing usability in system engineering 11 p1709 A71-25570

P channel enhanced MOS transistors, logic elements and digital integrated circuits in silicon films on sapphire substrates 13 p2038 A71-28716

French monograph on satellite stabilization by ion propulsion and attitude control logic element design covering geostationary and geocentric satellites, mass and power balances 17 p2814 A71-35500

Analog data computation with hybrid and logic operational elements, applying to periodic function arithmetic mean determination and transistor characteristics representation 22 p3518 A71-42430

LOGISTICS

NT LUNAR LOGISTICS

NT SPACE LOGISTICS

Space shuttle program sustaining engineering and hardware logistics support [AIAA PAPER 71-318] 12 p1894 A71-26698

Logistics planning as integral part of phased program planning process, considering preliminary analysis, definition, design, development, fabrication, test and operations phases 13 p2167 A71-28895

Logistics support planning technique for determining number of spares with prechosen probability level, using asymptotic approximation method 16 p2552 A71-33302

Safety engineers integration into overall system through basic development programs, involving management, manufacturing, testing and integrated logistic support 16 p2664 A71-33309

LOGISTICS MANAGEMENT

Weapons systems design for logistics supportability, discussing operational availability at minimal life cycle cost as function of reliability, maintainability and MIL Spec documentation 09 p1429 A71-23476

Integrated logistics support program for F-14 aircraft maximum maintainability, reliability and operational readiness at optimum cost 16 p2553 A71-34154

Cost effective integrated logistics support documentation system for military contractors 23 p3661 A71-43196

LOH HELICOPTER

U OH-6 HELICOPTER

LOLA (SIMULATOR)

U LUNAR ORBIT AND LANDING SIMULATORS

LONG RANGE NAVIGATION

U LORAN

LONG RANGE WEATHER FORECASTING

Stochastic analysis of wind gusts applied to prediction of long term maximum velocities 04 p0621 A71-15168

Heat quantity to atmospheric circulation ratio over period of decades, using positive temperature sums for long range forecasting method 08 p1326 A71-21445

Long range numerical weather prediction, using two level quasi-geostrophic forced general circulation model with spectral truncation 14 p2269 A71-29945

Southern Hemisphere extended operational meteorological prediction using six level primitive equation model 20 p3256 A71-39202

CAT energy budget and physical mechanisms in relation to aviation and atmospheric processes incorporating long range numerical prediction model 21 p3411 A71-41178

Long range weather prediction based on numerical global atmospheric models, noting application to climatology 24 p3844 A71-44366

LONG TERM EFFECTS

Percutaneous vitreous carbon electrodes long term effects, considering mechanical stability, bioelectrical signal receptivity, low interface impedance and surrounding epidermis growth 01 p0021 A71-10238

Liapunov method applied to nonlinear differential equations for distant satellite orbit secular perturbations 01 p0156 A71-10546

Long period atmospheric fluctuations, investigating large scale disturbance structure from observed data 01 p0119 A71-10852

Omega West Reactor isothermal irradiation experiments, determining long term fast neutron irradiation effects on Al995, Lucalox and yttrium oxide insulator 02 p0280 A71-12251

Solar activity long term variations in 11 year cycle maxima, noting preferred locations on disk [AIAA PAPER 70-1368] 02 p0315 A71-12695

Astronomically determined latitude, longitude and azimuth reduction to common epoch, discussing secular nonperiodic pole motion due to crust drift 03 p0484 A71-13217

Solar He II Lyman alpha line, measuring long term absolute intensity variations 03 p0496 A71-14507

Oblate planet artificial satellite motion, obtaining secular and periodic perturbations to third and second order 04 p0642 A71-14739

Atmospheric pollution long term effects measurement and control using spacecraft-mounted instruments 04 p0640 A71-14874

Supernova remnant X ray and radio emission secular behavior, considering hot plasma and synchrotron models and continuous injection 04 p0640 A71-14874

Post Apollo manned space operation, emphasizing Skylab program, space shuttles and long term space station 04 p0689 A71-14927

OART space station development, discussing long term effects, artificial gravity, environmental problems, electric power, life support, protection systems and human factors 04 p0643 A71-14932

Long term human biomedical and behavioral characteristics research, examining enhanced physiological fitness in space 04 p0543 A71-14933

Human heart rates long term measurement by cumulative counters activation by electrical signals from precordial electrodes 04 p0544 A71-15153

Long period effects in motion of Chicago and Thule, noting commensurability with Jupiter orbit 04 p0652 A71-15705

Long term evolution of close low eccentricity lunar satellite orbits, describing lunar gravity effects by spherical harmonic expansion 04 p0655 A71-15723

Long period comets orbital orientations and perihelion distances, discussing Oort evolutionary theory modification 04 p0659 A71-15858

Pulsars optical and X ray luminosity secular decrease, examining emission close to velocity of light radius 05 p0807 A71-16209

Long term hypoxia effects on granuloma and various organs in rats, noting collagen and noncollagenous proteins formation stimulation and/or inhibition 05 p0706 A71-16293

Axisymmetric body stationary motions around sphere, investigating secular and ordinary stability 05 p0809 A71-16473

Restricted three body problem, discussing secular variations equilibrium solutions stability 05 p0814 A71-17093

Geomagnetic field secular variation subdivision based on time effect, noting harmonic processes with 20 year period 05 p0745 A71-17191

Geomagnetic secular variations from various surveys, noting negative value for Gulf of Aden anomaly chart 05 p0745 A71-17192

Geomagnetic field secular variations in Drake passage /Antarctic Ocean/, applying absolute magnetic surveys 05 p0747 A71-17215

Earth rotational acceleration and polar secular motion changes, considering correlation with earthquakes 06 p0890 A71-17881

Secular changes in cooperative stations mean latitudes related to mean pole drift 06 p0890 A71-17882

Forbush decreases and long term cosmic ray particle intensity changes, investigating spectral variations 06 p0956 A71-18137

Long term IR X ray irradiation effects on complementary MOS logic networks with several p and n channels on single silicon, determining radiation induced failure modes 07 p1174 A71-19054

Annealed Mo creep properties and long term strength, observing temperature and stress effects 07 p1130 A71-19165

Geomagnetic secular variation as main field drift superposition and strength changes, reflecting drift and convection in earth fluid core 07 p1103 A71-19763

Simulated high altitude chronic hypoxia and long term sideropenic anemia adapted animals, investigating acute anoxia tolerance of myocardium 07 p1044 A71-20331

- Double resonance in natural satellite motion from long period perturbation prediction
07 p1202 A71-20517
- Vacuum-melted and deformed Mo alloys tests, showing long term strength decrease under cyclic heating
08 p1305 A71-21030
- Long time strength and creep rectilinear diagrams constructed for heat resistant alloys to obtain extrapolation values
08 p1306 A71-21113
- Test results extrapolation for heat resistant alloys long time strength using exponential relation between time to rupture and value for initial stress decrease
08 p1306 A71-21114
- Modulation of long scale time variations of quasi-stellar radio sources and Seyfert galaxies due to intergalactic scintillations
08 p1364 A71-21414
- Aircraft altitude cosmic ray intensity measurements in lower atmosphere by neutron monitor, considering long term nucleonic intensity variations
08 p1355 A71-21629
- Gas turbine blades design and exploitation processes, discussing long time fatigue strength, static durability and heating effects at elevated temperatures
08 p1299 A71-21708
- Kovpak method for estimating and extrapolating heat resistance characteristics, considering alloy long term strength
09 p1538 A71-22627
- Prolonged storage effect on polycarbonates mechanical properties, measuring tensile strength, elastic modulus, yield point and breakdown strains under uniaxial tension
09 p1483 A71-22825
- Secular perturbations of Leonid meteor shower via Gauss-Halphen-Goriachev method, indicating applicability to variations of meteor streams orbital elements
09 p1526 A71-23443
- Fine structure and heat resistance of thin Ni-Cr alloys specimens after prolonged exposure to high temperatures under tensile loads
09 p1480 A71-23703
- Laplace long period solar inequality effects on lunar ecliptic longitude, considering role in celestial mechanics
10 p1667 A71-23829
- Long term exposure effects on high temperature resistant supersonic aircraft fuel tank sealants
10 p1631 A71-24081
- Geomagnetic quadrupole field secular oscillation causing earth rotation change, discussing earth core induced velocity field and field attenuation
10 p1603 A71-24599
- Long term zero gravity effects on mammal physiologic rhythms characteristics, studying rats in biosatellite orbits
10 p1565 A71-24611
- Metal-metal adhesive bonds temperature effects, long term static loads, dynamic strength and aging behavior
10 p1618 A71-24684
- Long period gravitational radiation detection, using relative velocity discrepancies of earth and Mariner 6 and 7
10 p1664 A71-25007
- Pulsar CP 0328 data at 1420 MHz, examining mean intensity and long term fluctuation due to interstellar scintillations
10 p1680 A71-25008
- Microwave radiation nonthermal and cumulative biological effects, discussing dose/irradiation safety standards
11 p1717 A71-25283
- Lunar motion theory, discussing radial perturbation, variation, parallactic and annual inequalities, secular acceleration and evection
11 p1822 A71-25684
- Earth-moon system, examining kinematical and dynamical relationships, tidal deformation, earth rotation, secular variations, inclination and eccentricity
11 p1822 A71-25686
- Spherical harmonics of secular perturbations in artificial satellites motion due to atmospheric gravitation
11 p1829 A71-25808
- Long term performance stability of two un fueled out-of-pile thermionic converters
11 p1714 A71-25908
- Monograph on turbine blade fire tree roots, calculating stress-strain state of long term static strength under elastic and elastoplastic deformation and unsteady creep
11 p1852 A71-26400
- Long term lunar surface environment, discussing radiation, thermal and meteoroid protection, water budget, carbon dioxide removal and air lock design
11 p1726 A71-26534
- Twenty-two year solar cycles, relating Wolf numbers with minima and maxima in secular cycle
12 p1961 A71-26904
- Long period Cepheids, obtaining brightness curves distribution for minimum, maximum and fixed phase stellar magnitudes
12 p1962 A71-26908
- Planetary satellites intermediate orbits, obtaining angular orbital elements secular perturbations
12 p1964 A71-27091
- Newcomb precession constant accuracy, noting stellar motion analogies and analytic effects on earth polar secular motion
12 p1901 A71-27092
- Long time planetary atmosphere motions, investigating sideband resonance mechanism in Rossby wave packet interactions with weak shear zonal flow
12 p1925 A71-27195
- Long term aged heat resistant Ni base alloys, investigating gamma prime phase chemical composition
12 p1917 A71-27298
- Spacecraft intermediate orbit osculating elements first order secular disturbances due to atmospheric resistance
13 p2132 A71-27936
- Geomagnetic field secular variation subdivision based on time effect, noting harmonic processes with 20 year period
13 p2059 A71-28247
- Geomagnetic secular variations from various surveys, noting negative value for Gulf of Aden anomaly chart
13 p2059 A71-28248
- Crab Nebula pulsar NP0532 radio observations, noting long term slowing down and irregular perturbations in periodicity
13 p2137 A71-28591
- Long term pulsar intensity observations, noting periodic variations and power spectrum analysis
13 p2143 A71-29270
- Seasonal, irregular and long term earth rotation rate variations
14 p2310 A71-30198
- Water vapor contamination long lasting effects on stratospheric measurement during balloon flight
14 p2270 A71-30453
- Chronic and acute gamma irradiation facilities used in animal experiments simulating steady cosmic radiation and powerful solar flare radiation expected in prolonged space flight
15 p2357 A71-31313
- Secular parallaxes of reference stars by photometric distances and relative proper motions of open clusters at low galactic latitude
15 p2483 A71-31341
- Open microcracks and internal microdefects detection during long term strength testing in vacuum by mass spectrography
15 p2383 A71-31653
- Power and exponential time dependences of long term creep strength for wide stress range, assuming linear thermal resistance
15 p2433 A71-32228
- Lost City meteorite secular and encounter perturbation effects on orbital evolution, interpreting short lived cosmic radiogenic isotopes formation
15 p2489 A71-32359
- Structural changes and phases nucleation and growth in metal alloys during prolonged loading at high temperatures, examining steel strengthening precipitates coagulation kinetics
16 p2597 A71-33918
- Increased oxygen concentrations effect on mice pulmonary tissues during prolonged exposure
17 p2679 A71-34222
- Long duration brightness change in electroluminescent panel detection during monitoring task, discussing role of payoffs and signal ratios
17 p2690 A71-34705
- NASA space station electrical power systems discussing configurations, growth capacity, volume reliability and long term effects
17 p2677 A71-34720
- [AIAA PAPER 71-825] Long time failure modeling of real structure behavior in short times by scale and mathematical models, noting nonaccountability of crack propagation time
17 p2834 A71-35669
- Thermal emf changes for noble and refractory metal thermocouples, determining drift in high temperature air, Ar and vacuum environments for long time periods
18 p2916 A71-36049
- Long term spaceflight crew personal hygiene, discussing human waste processing and/or utilization, microbiological control and medical infirmity-dispensary-laboratory requirements
18 p2870 A71-36631
- [AIAA PAPER 71-878] Planetary satellites intermediate orbits, obtaining angular orbital elements secular perturbations
19 p3133 A71-37441
- Newcomb precession constant accuracy, noting stellar motion analogies and analytic effects on earth polar secular motion
19 p3049 A71-37442
- Lightweight solar cell structural failure modes under automatic thermal cycling for prolonged period in wide temperature range and by immersion in liquid nitrogen
20 p3179 A71-38852
- SNAP 19 TAGS thermoelectric generator life tests at high temperature in Ar, predicting long term performance including thermoelectric material and isotope fuel decay effects
20 p3266 A71-38963
- Creep test and long time strength results extrapolation, determining accumulation of plastic deformation and creep fracture effects
20 p3250 A71-39020
- Active biological immunity development in long term space flights, discussing natural and nonspecific resistance to viruses and recurrent infections
21 p3332 A71-40552
- Human microbial flora and immunologic response in long term space missions, describing environmental parameters and factors and work-rest schedules effects
21 p3332 A71-40553
- Human body immune status normalization in prolonged space flight, investigating ribonucleic acid stimulated antibody formation
21 p3332 A71-40554
- Human microflora variation in long term confinement, examining anaerobic and aerobic microorganisms responses
21 p3333 A71-40557
- Composition and colicinogenic and hemolytic activities changes of *Escherichia* isolated from man during long term confinement
21 p3333 A71-40558
- Bacterial contamination in confined sealed space during long term human occupation, observing hemolytic microflora spreading dynamics on bodies, clothes, wall and air
21 p3343 A71-40560
- Prolonged manned space flight infectious disease hazards, discussing confinement, zero gravity, high oxygen content, personal hygiene, waste disposal and preflight immune status
21 p3333 A71-40561
- Stereophotogrammetric measurement of body and limb volume changes after prolonged space mission
22 p3502 A71-41861
- HCN CW laser design, considering factors affecting short and long term power and frequency stabilities
22 p3557 A71-42134
- Secular parallaxes of reference stars by photometric distances and relative proper motions of open clusters at low galactic latitude
22 p3606 A71-42616
- Prolonged small radiation dosage effects on vestibular analyzer in normal and antiradiation drug protected dogs
22 p3495 A71-42798
- Long term vertical and horizontal variations of long wave radiation field in free atmosphere over U.S.S.R., using actinometric sounding data
22 p3570 A71-42848
- Space shuttle operations analysis for cislunar space, including transfer trajectory inclination and long term effects
23 p3724 A71-42976
- [AAS PAPER 71-300] Long term orbit calculation by superposition of gravity and drag perturbations, taking into account solar and geomagnetic induced density variations
23 p3730 A71-43046
- [AAS PAPER 71-376] Prolonged bed rest effects on EEG sleep patterns in young healthy subjects with and without exercise
23 p3631 A71-43109
- Long term effects of hypoxic stimulus suppression upon heart rate, cardiac output and pulmonary artery pressure of highlanders, observing bradycardia
23 p3631 A71-43117
- Heat resistant ZrSiO₄ alloy precision and ground cast specimens, determining short and long term strength and fatigue
23 p3780 A71-44236
- Latitudinal observation errors by two zenith telescopes concurrent data, showing distribution function in long term measurement
23 p3771 A71-44255
- Cosmic ray biological effects and admissible dose level normalization in space flight from prolonged tests on dogs
24 p3798 A71-44890

LONG WAVE RADIATION

- Long wave radiation earth-atmosphere balance measuring devices, discussing pyrometer, balansometer and tests in Antarctica
01 p0080 A71-10541
- CdS-CuS n-p junction solar converters, noting long-wave sensitivity dependence on light extrinsic absorption
02 p0190 A71-11896
- Long wave radiation fluxes calculation in troposphere based on principal radiant heat transfer components separation
02 p0277 A71-12117
- SCL nomenclature denoting solar flare effect on long wave field intensity
05 p0804 A71-16033
- Long wave radiation balance components vertical profiles, showing temperature stratification effect
07 p1151 A71-18914

Long wave cosmic radio background emission in circumlunar space by Luna 11 and 12 satellites, observing increase in earth magnetosphere tail
09 p1513 A71-22576

Q switched ruby laser emission effect on long wave pigment system of photosynthesizing organisms
11 p1774 A71-26006

Ionospheric absorption measurements at 272 kHz, using surface wave attenuation factor as calibration technique
16 p2562 A71-33072

Earth-atmosphere system radiation budget, comparing meteorological satellites actinometric data with calculated climatological maps of planetary long wave radiation distribution
20 p3259 A71-39678

Soviet book on long wavelength radiative heat exchange in atmosphere covering radiation relationship to circulation, cloud formation and weather prediction
21 p3411 A71-40873

Atmospheric rotation, anisotropic turbulence and long wave radiative heat transfer effects on cellular heat convection
21 p3412 A71-41387

Long term vertical and horizontal variations of long wave radiation field in free atmosphere over U.S.S.R., using actinometric sounding data
22 p3570 A71-42848

LONGERONS

Optimal cross sectional dimensions of thin walled longeron beams and ribs of skin reinforced delta wings minimizing weight
02 p0329 A71-12562

LONGITUDE

NT SOLAR LONGITUDE

Two-rotor gyrocompass accelerated reduction to meridian
01 p0080 A71-10630

Second order longitudinal variations of vertical ionospheric drift by middle latitude horizontal neutral air winds, showing maxima at universal time
11 p1754 A71-25604

Longitudinal variations of inner radiation belt particle flux density at low altitudes from Proton 2 satellite data
13 p2128 A71-28548

Solar proton trajectories calculations in Williams-Mead geomagnetic field model, showing longitude difference in tail region
20 p3216 A71-38747

Longitude corrections in standard time service transfer from Greenwich to Herstmonceux, discussing precision requirements
21 p3443 A71-40163

LONGITUDE MEASUREMENT

Meridian direction autonomous inertial determination, using gyroplatform newtonometer data
01 p0125 A71-10629

Optimal method selection for astronomical measurements on lunar surface, discussing instrumental and technical difficulties with selenographic longitudes and latitudes determination
24 p3870 A71-44812

LONGITUDINAL CONTROL

Aircraft flying qualities research program, discussing navy test pilot evaluations and longitudinal handling characteristics for simulated carrier landing task
[ALAA PAPER 69-897] 02 p0189 A71-12678

Wing upper surface air suction influence on aircraft longitudinal controllability, considering control stick forces for deflected flaps and angle of attack
04 p0528 A71-14594

Aircraft longitudinal control during landing approach, investigating back side operation characteristics by closed loop system analysis regarding pilot and aircraft as elements
05 p0696 A71-16388

Frequency and amplitude during longitudinal control surface pumping by pilots in precise flight path banding for aircraft design
[ALAA PAPER 70-567] 06 p0847 A71-17699

Light general aviation airplanes flying qualities in-flight simulation, considering longitudinal short period frequency and damping, pitch control sensitivity and lift curve slope
[SAE PAPER 710373] 10 p1554 A71-24242

Light aircraft longitudinal stability control systems, discussing downspring and bobweight effects on flight characteristics
[SAE PAPER 710388] 10 p1555 A71-24252

Sailplanes tail load static derivation for instantaneous unchecked longitudinal maneuver, considering aperiodic response
11 p1708 A71-26486

Aircraft longitudinal coordinates invariance relative to atmospheric disturbances, giving simultaneous thrust variation, rudder deflection and flap deflection control rules
12 p1867 A71-27339

L-1011 aircraft flying stabilizer, discussing choice of longitudinal flight control systems
[SAE PAPER 710426] 13 p1996 A71-28312

Elevons as longitudinal and lateral control elements on low aspect ratio wings, calculating subsonic and supersonic aerodynamic characteristics
13 p1993 A71-29190

Control configured vehicle design longitudinal requirements due to application of relaxed static stability and maneuver load control
[ALAA PAPER 71-786] 16 p2525 A71-34016

Infinite-time linear dynamic system suboptimal control derivation from lower dimension models, exemplifying by flexible-bodied rocket vehicle pitch plane dynamics
17 p2720 A71-34871

Flight investigation of turbulence effects on aircraft longitudinal flying qualities, evaluating pilot ratings for ILS approach task
[ALAA PAPER 71-905] 19 p2995 A71-37156

Satellite pitching oscillations optimal stabilization, obtaining approximate solution for finite time
19 p3152 A71-37695

Time optimal semiautic attitude control for circular orbiting satellite pitch motion, using gravitational and aerodynamic torques
22 p3570 A71-42001

Longitudinal adaptive aircraft control through sum of normal acceleration and pitch rate
23 p3629 A71-44093

Adaptive guaranteed cost control for systems with parametric variation, demonstrating system stability and airframe pitch control
23 p3659 A71-44111

LONGITUDINAL STABILITY

Saturn V second stage longitudinal oscillation from structure and propulsion system interaction examined by transfer function simulator subroutine /TRANSIM/ computer program
02 p0318 A71-11788

Aircraft longitudinal motion decoupling through direct lift control, investigating flight control for landing
03 p0347 A71-13339

Aircraft propulsive thrust moment effect on phugoid motion, examining angle of attack and flight path variations with resulting instability
03 p0347 A71-13340

Round cold jet inclination effects on VTOL aircraft tail assembly lift and longitudinal stability in transition region
[DGLR-70-053] 05 p0693 A71-15967

Stability criteria for longitudinal combustion instability tested for generality using data from various solid propellant formulations
[ALAA PAPER 69-480] 05 p0837 A71-16569

Equilibrium stability of orthotropic cylindrical shell under longitudinal compression, discussing critical stresses
06 p0986 A71-17762

Helicopter longitudinal stability in forward flight and hover modes under attitude, height and speed constraints, noting need for cyclic pitch control due to instabilities
07 p0109 A71-19421

Light aircraft longitudinal stability control systems, discussing downspring and bobweight effects on flight characteristics
[SAE PAPER 710388] 10 p1555 A71-24252

Wind tunnel evaluation of analytical method for predicting longitudinal stability and aerodynamic characteristics of large flexible aircraft applied to supersonic transport configuration
[ALAA PAPER 71-343] 11 p1707 A71-25322

Longitudinal stability of ground effect airplane, discussing influence on aerodynamic characteristics of height, ground surface roughness and wing aspect ratio
13 p1997 A71-29228

Aspect ratio influence on instability and non-minimum phase effects of longitudinal motion of aircraft relative to negative lift-drag expression transfer functions
[DFVLR-SONDDR-127] 16 p2523 A71-33405

Seasonal and annual longitudinal variations in ionospheric ion distribution, stressing solar geomagnetic control importance
16 p2567 A71-33762

Transverse wave structure of two-dimensional detonation waves propagating in narrow channel, considering longitudinal instabilities
17 p2841 A71-35708

Longitudinal instability of bunch interacting with passive resonator, considering Landau damping influence by linear differential equations of motion solution
19 p3110 A71-37141

Longitudinal dynamic stability of space shuttle during atmospheric entry, noting magnetic storms effects
19 p3151 A71-37322

Phugoid motion at constant angle of attack without thrust line displacement from aircraft center of gravity, noting longitudinal stability
21 p3324 A71-40168

Longitudinal stability of plate-like load towed beneath helicopter in horizontal forward flight
23 p3630 A71-44346

LONGITUDINAL WAVES

Longitudinal acceleration and distinct transverse waves propagation in Hadamard and Green hypoelastic materials
01 p0165 A71-10025

Thin nonlinear elastic bar small longitudinal oscillations, solving boundary value problem for disturbances propagation
01 p0176 A71-11050

Sunward magnetosheath magnetic field fluctuations, noting power levels spatial variations, transverse shock aligned fields and longitudinal waves
01 p0075 A71-11493

Longitudinal elastic wave propagation equations of motion in cone with small apex angle, using perturbation theory
03 p0456 A71-12974

Nonlinear interaction between three longitudinal plasma waves, calculating dissipation effect on coupling coefficients
04 p0635 A71-15902

Collisional effects on Taylor and Kelvin instabilities in composite medium, considering longitudinal wave propagation mode
05 p0788 A71-16627

Collisionless plasma shock longitudinal wave propagation perpendicular to magnetic field, demonstrating ion acoustic/electron Bernstein modes instability
05 p0789 A71-16655

Collective longitudinal space charge waves in trapped relativistic one dimensional plasma, calculating inhibition/enhancement of cosmic ray Fermi acceleration
05 p0791 A71-16940

Long thin circular cylindrical shell circumferential wave functions reduction to beam type transverse vibration equation, including rotatory inertia
06 p0984 A71-17618

Buckling of cold formed Al alloy thin walled columns under compression, investigating longitudinal half wave formation
06 p0985 A71-17748

Thin cylindrical shell in ideal compressible fluid, calculating longitudinal resonance waves for acoustic excitation
06 p0985 A71-17755

Cylindrical structure longitudinal stress wave propagation characteristics, analyzing wave induced structural instability and destruction process
06 p0991 A71-17801

Surface wave conversion to longitudinal oscillations near strong discontinuity in resonant cold magnetized plasma
06 p0937 A71-18355

Plasma waves and echoes characteristics and diagnostics, emphasizing longitudinal waves
07 p1172 A71-20502

Ionospheric irregularities two fluid model, using nonlinear differential equations for longitudinal waves propagating in hot collisional magnetoplasma
10 p1648 A71-24294

Transverse spatial particle diffusion in plasma under random oscillations, examining interaction between collisionless plasma and longitudinal wave
10 p1649 A71-24318

Longitudinal, flexural and elastic waves propagation in infinite orthotropic circular cylinders
11 p1850 A71-26176

Longitudinal waves propagation in viscoelastic semiinfinite rod under constant velocity impact, solving by characteristics and finite difference methods
11 p1850 A71-26178

Longitudinal plasma layer waves kinetic theory considering particles specular reflection from layer boundaries
12 p1937 A71-27203

Elastoplastic and elastic-viscoplastic waves propagation, considering longitudinal wave resonance, plane load waves and loading and unloading criteria
12 p1980 A71-27446

Asymptotic solutions of improved equations for elastic and elastoplastic waves in rods, considering longitudinal waves propagation
12 p1980 A71-27449

Longitudinal wave propagation in ideal elastic bar with viscous stress, calculating approximation to nonlinear wave equations
13 p2153 A71-28483

Plane longitudinal stress waves propagation in plane-parallel viscoelastic partition of finite thickness dividing two linear half spaces with different elastic properties
13 p2155 A71-28655

Longitudinal waves correlation damping in high temperature plasma under magnetic field, calculating dielectric constant by quantum statistical method
14 p2280 A71-30450

Longitudinal wave absorbers attenuating resonance vibrations in rods and plates
15 p2504 A71-31707

Longitudinal ionic wave excitation by grid in collisionless Q machine plasma
15 p2456 A71-31820

Dispersion and attenuation of plane longitudinal waves in laminated medium of elastic and viscoelastic layers, showing effect of composite parameters variations
[ASME PAPER 70-WA/APM-40]

Isotropic elastic circular cylinders longitudinal stress waves, presenting dispersion relation /Pochhammer equation/ numerical solutions

Laser longitudinal oscillation modes and maximum radiation envelope formation from noise at start of emission, using electric field strength recurrent relations

Longitudinal modes in standing wave gas laser with Brewster windows in presence of active level emission capture

Continuum mechanical approach to velocity dispersion of longitudinal plane waves in elastic solid containing dislocations

Longitudinal vortex rolls onset for laminar forced convection between two horizontal flat plates subjected to uniform axial wall temperature gradient
[ASME PAPER 71-HT-1]

Longitudinal wave interaction and excitation by current instability in equatorial jet, considering energy transfer mechanism

Noncircular ionospheric current conversion into longitudinal currents in magnetosphere along lines of force of geomagnetic field

Longitudinal plasma sheath waves kinetic theory, considering particles specular reflection from sheath boundaries

Electron oscillation induced longitudinal standing wave excitation and suppression in beam-plasma system by passing electron beam through axially bounded plasma

Longitudinal electron oscillations damping in ionized plasma, obtaining wave dispersion relation from BGK model

Microwave emission from plasmas in InSb with and without magnetic fields, deriving pseudolongitudinal wave interaction theory for explanation

Nonisothermal plasma longitudinal ion acoustic and Langmuir oscillations phase and amplitude interactions, estimating energy transfer and turbulence criteria

LOOK ANGLES

U AZIMUTH
U ELEVATION ANGLE

LOOP ANTENNAS

Low loss cylinder loop as normalization antenna for meter waves

Loop antenna with finite gap at driving point, deriving admittance, current distribution, radiation pattern and directive gain from variational and Fourier series methods

Satellite square loop antennas radiation resistance in warm plasma, comparing calculated values with Ariel 3 satellite measurements

Radiation resistance of Alford loop antenna immersed in warm plasma, comparing theoretical values with measurements from Ariel 3 satellite experiment

Far zone field and radiated power equations for corner driven traveling wave loop antenna in warm plasma, comparing data for Ariel 3 satellite

Tuned loop antenna for missile telemetric data transmission, discussing design, implementation and impedance and radiation measurements

VOR antenna system with Alford loops above circular conducting ground plate, investigating radiation fields

Circular loop antenna array of N elements with arbitrary circumference, analyzing by Fourier series expansion

Radiation resistance of small filamentary loop antenna in cold collisionless uniform multicomponent magnetoplasma, assuming uniform current distribution along loop

Book on antenna characteristics covering tabulated data for cylindrical dipoles and monopoles, imperfectly conducting dipoles, circular loop antennas and broadside and endfire arrays

Shunt driven circular loop antenna effective length, current distribution and input admittance, comparing to transmission lines

LOOPS

Cyclic deformations and internal energy dissipation effect on hysteresis loop shape equations derivation in terms of three components including nonlinear and inelastic materials properties

Algorithm for higher order loops determination in flow graph from subgraphs of linear graph model, considering circuits with ladder/nonladder structures

Digital communication hybrid phase locked loop nonlinear feedback system with modulation and carrier components enhancing phase estimation

Stars with central He burning and loop occurrence in H-R diagram, suggesting secular instabilities with high stellar mass

LOR (RENDEZVOUS)

U LUNAR ORBITAL RENDEZVOUS

LORAN

NT LORAN C

Passive mode navigation satellite position fixing, using synchronous satellite and Loran type chart with correction tables

Long range hyperbolic navigation in U.S., discussing loran and Omega systems

Air navigation techniques history, considering radio, radar, loran Doppler and inertial navigation

LORAN C

Loran C transmissions for long baseline time and frequency synchronization

Hydrogen maser time and frequency standards at Agassiz observatory for long baseline interferometry via radio telescope, discussing Loran C

Aircraft lateral dynamics effect on positioning accuracy along straight flight path, using Loran C data

Loran-C pulse hyperbolic navigation system application to time and frequency measurements, evaluating errors

Long distance radio navigation and tracking systems, discussing Dioscures, Loran C and Omega

LORENTZ CONTRACTION

Special relativity distinguished from theories based on preferred frame of reference and physical Lorentz contraction by Michelson-Morley experiment in solid transparent medium

LORENTZ FORCE

Electromagnetic potentials and Lorentz relation in anisotropic medium, considering Bromwich function and plane wave propagation

Metal droplet motion in mercury weld pool in tungsten arc, noting cause by Lorentz force and surface arc plasma jet

Nonuniform conductivity effect on cosmic magnetic fields structure with zero Lorentz force, using Maxwell equations and Ohm law

Regenerative kinematic-dynamo action under incompressible isotropic velocity turbulence, noting turbulent Lorentz force role

GaAs luminescent p-n junction diode spontaneous emission measurement in magnetic field, noting redistribution in Lorentz force direction

Physical model for electric current carrying shock discontinuity driven through nonconducting gas by Lorentz force, investigating uniqueness and stability

LORENTZ GAS

Electron velocity distribution in fully ionized plasma under crossed electric and magnetic fields, assuming Fokker-Planck expression for Lorentz gas

Stochastic properties of probe particle motion in Lorentz plasma, considering interactions and friction and diffusion coefficients

LORENTZ TRANSFORMATIONS

Lorentz invariant theory for relativistic gravity testing, deriving conservation laws and parameter constraints from parametrized post-Newtonian equations of motion

LOS ALAMOS TURRET REACTOR

U HIGH TEMPERATURE NUCLEAR REACTORS

LOSSES

German monograph on loss estimation for non-steady gasdynamic duct-drum pressure exchangers, discussing design and optimization problems

Diurnal variations of loss factor in D region during polar cap absorption, verifying nighttime D region model by forward propagation data

Diurnal variations of loss coefficient in D region during polar cap absorption, verifying nighttime D region model by forward propagation data

LOST WAX PROCESS

U INVESTMENT CASTING

LOTS CARGO SHIPS

U CARGO SHIPS

LOUDNESS

Bias free loudness judgments by modification of vision studies method, considering physical correlate theory of stimulus intensity

Sonic booms loudness as function of peak overpressures and rise times, using semiempirical formulae

Prediction methods for human aircraft noise perception, assessing weighted sound pressure level or complex loudness-noisiness computation scales

Noy curves in perceived noise levels, noting relative noisiness dependence on relative intensities

Contrast effects in loudness judgments, using category scale and maximally extensive number response language

Psychophysiological loudness and annoyance indices application in sonic boom comfort level evaluation, pulsating noise estimation and sound insulation system effectiveness determination

LOUVERS

Thermal louvers radiative heat transfer characteristics with solar irradiation effects, using Monte Carlo method

Thermal louver models in space simulation chambers, determining heat dissipation, optical efficiencies, blade geometry and solar radiation effects

Axial flow fan noise, investigating louvers effects on sound field

ATS F and G thermal control, discussing heat pipe, louver and model tests

Mechanical design of frictionless bimetal actuated louver system for spacecraft thermal control

Scale lengths in atmospheric turbulence from spectra and autocorrelation of vertical air velocity component measured in low flying aircraft

Low energy electron and proton fluxes observation by Isis 1 satellite, concluding solar wind penetration to low altitudes through magnetopause cusp

Quasi-captured and escaped electron flux angular dependence and latitudinal variations observations at low altitudes by Cosmos 228 satellite

Graphite heat shield ablation during low velocity low altitude portion of satellite reentry trajectories

LOW ALTITUDE SUPERSONIC VEHICLES

U F-111 AIRCRAFT

LOW ASPECT RATIO

Ground effects on pressure distribution on slender wing bodies with low aspect ratio and thick cross sections

Low aspect ratio compressor blade cascade performance at blade span center, discussing pressure loss, angle of attack and staggering

Rotating low aspect ratio turbomachinery blades natural frequencies and mode shapes, using finite element method for equilibrium equations eigenvalue problem

Three dimensional steady separated liquid and gas flows past low aspect ratio bodies, deriving similarity laws for reduction to two dimensional problem

Total lift data correlation for thin sharp edged low aspect ratio delta wings at low speeds, noting trailing edge effects in incompressible flow

LOW ASPECT RATIO WINGS

NT DELTA WINGS

Aerodynamic characteristics of low aspect ratio wing in bounded inviscid fluid flow, considering plan-

LOW COST

form relation to lifting force derivative and angle of attack

04 p0525 A71-14589

Air flow about low aspect ratio delta wing at large angles of attack, deriving lift coefficient

13 p1990 A71-28282

Eleons as longitudinal and lateral control elements on low aspect ratio wings, calculating subsonic and supersonic aerodynamic characteristics

13 p1993 A71-29190

Air flow past small aspect ratio thick-section wing at small angles of attack, investigating vortex system effect on flow characteristics in absence of lift

13 p1994 A71-29234

Aerodynamic characteristics of low-aspect-ratio wing mounted on cylindrical body, simulating by system of horseshoe vortices

14 p2170 A71-30264

Lifting line theory extension to low aspect ratio wings, proposing formulation for Prandtl integral equation

22 p3480 A71-42288

Aircraft fuselage antisymmetric loading strain effects on small aspect delta wing performance

24 p3885 A71-45018

LOW COST

Low cost multichannel peak/average sine vibration control system with acceleration selector and averager

01 p0667 A71-10864

LOW CURRENTS

Xe plasma flash tubes with very low discharge current magnetic field for spectroscopic and laser applications in presence of Zeeman effect

14 p2243 A71-30272

LOW DENSITY FLOW

Nonstationary isentropic low density flows with axial or central symmetry, suggesting characteristics with flow rate and sound speed variation as in stationary source flow

07 p1014 A71-19729

Electrostatic probe measurements of charged particles and thermal ionization relaxation in shock heated low density supersonic monatomic gas flows

11 p1766 A71-26286

Radiative emission effects on viscous flow in shock structure of low density hypersonic flow around blunt body

12 p1986 A71-27583

Hot-wire flowmeters calibration for low density flow measurements, describing method for hot wire end loss determination

12 p1908 A71-27595

Low density hypersonic flow on flat plate, discussing surface pressure measuring techniques [AIAA PAPER 71-606]

15 p2346 A71-31580

Pitot and static pressure measurement in low density hypersonic flows, considering thermal transpiration, gas nonequilibrium near measurement cavity and nature of inlet geometry

18 p2921 A71-36415

Force and heat transfer measurement in hypersonic flows of low gas density, using electromagnetic balances for horizontal and vertical forces and pendulum method for measuring resistance

18 p2921 A71-36416

Low density hypersonic flow around blunt bodies, considering total pressure and flow velocity on stagnation point line

18 p2846 A71-36417

Flow field and model wall on slender bodies in low density hypersonic flows ranging from free molecular flow to continuum flow

18 p2846 A71-36418

Plasma wind tunnels for high enthalpy flows of low density, considering plasma arc heaters and expansion nozzles with diffusers

19 p3040 A71-37461

Apollo command module aerodynamic characteristics in hypersonic low density flow, measuring drag, three component force and heat transfer

22 p3480 A71-42027

Electron beam fluorescence probe with modulation technique for measuring density disturbance near sharp wedge in rarefied hypersonic flow

22 p3529 A71-42052

LOW DENSITY GASES

U RAREFIED GASES

LOW DENSITY MATERIALS

Three dimensional orthogonally woven reinforced felt-yarn composite for low density thermal insulation and chemical vapor deposition

14 p2262 A71-29651

LOW DENSITY WIND TUNNELS

Aerodynamic support interference in wind tunnel testing of configurations involving bulbous base, mass addition, transition near base and hypersonic low density flows

08 p1228 A71-22002

Pressure orifices inclination in low density flow from experiments with cooled flat plate model in hypersonic low density wind tunnel

11 p1751 A71-25490

Colliding supersonic rarefied argon-helium jet flows diffusive separation in low density wind tunnel with electron beam diagnostics apparatus

16 p2554 A71-32800

Diagnostics of Ar free jet expansion from high pressure inductive arc source into low density wind tunnel, observing background gas effects

22 p3583 A71-42048

LOW FREQUENCIES

NT VERY LOW FREQUENCIES

LF radio emission from Jupiter at 3-8 MHz

04 p0641 A71-14737

High efficiency LF operating modes in avalanche diodes under low current density

04 p0558 A71-15147

LF radio waves field strength monitoring for study of ionospheric effects due to celestial X rays

05 p0721 A71-16442

Noncollisional plasma LF instabilities, discussing flute-like, drift wave and trapped particle modes from spatially confined plasma Vlasov equation

07 p1173 A71-20509

Circuit selection for LF three octave acoustic signal bandpass filters, taking into account time constants

08 p1261 A71-20738

Polarization of LF oscillation branch of uniaxial ferites in noncollinear phases analyzed by four column matrix, considering magnetic moments terminal points

09 p1507 A71-22291

Earth-ionosphere spherical waveguide, calculating mean and differential phase velocities and field amplitude of low frequency waves

11 p1731 A71-25774

Optical Fourier transformers zero order removal for low spatial frequency signal components detectability improvement

12 p1906 A71-26818

Wideband transistor amplifier frequency response at low frequencies, discussing gain increase, thermal pull-in effect, barrier layer geometry and switching control functions

12 p1887 A71-27042

Low frequency electromagnetic wave scattering by metallic cone, noting dipole moment contribution

12 p1879 A71-27054

Geomagnetic field effects on directional propagation of LF and VLF radio waves in ionosphere, taking into account ion types effects

13 p2029 A71-28026

Quartz-tube LF measuring generator with low linear instability, using frequency divider and narrow band RC filter

13 p2040 A71-28936

VLF and LF time and frequency international comparison, noting diurnal shifts and SID constant magnitude ratio

14 p2204 A71-30972

Low frequency noise spectra measurement in varicaps by frequency modulation of harmonic oscillator, noting application to diode and p-n transistors

15 p2369 A71-31232

Inverse scattering at low frequencies, estimating target diameter for various shapes

20 p3195 A71-38869

Earth-ionosphere spherical waveguide, calculating mean and differential phase velocities and field amplitude of LF waves

22 p3509 A71-41542

Background LF noise of semiconducting diode voltage regulators with breakdown due to avalanche effect

22 p3523 A71-42472

Spheroid with two dielectric separated halves and mixed boundary conditions, determining spreading currents LF electromagnetic field

22 p3484 A71-42879

IR spectra of oxamide and dithioxamide, studying Raman spectrum in LF range

23 p3642 A71-43825

Mobile LF air navigation AN/MRN-13 equipment, operation and maintenance

23 p3702 A71-43878

LOW FREQUENCY BANDS

LF whistler mode radio noise emissions observations in polar regions with Alouette 2, noting association with energetic particles influx into ionosphere

14 p2300 A71-30036

LOW GRAVITY

U REDUCED GRAVITY

LOW LATITUDES

U TROPICAL REGIONS

LOW LEVEL TURBULENCE

Extreme turbulence measurement during low level flights of Mirage A3-76 fighter aircraft, determining true gust velocities and power spectral energy distributions

14 p2267 A71-29756

Low altitude turbulence simulation in piloted flight simulators, discussing turbulence induced aircraft disturbances and effects on pilot

14 p2188 A71-29781

LOW MASS

U MASS

LOW NOISE

Large low-speed fan for low noise production, testing performance on suppression effects of acoustic treatment and exhaust jet noise

[ASME PAPER 70-WA/GT-15] 03 p0471 A71-14123

Low noise microstrip microwave mixer-preamplifier on thin polyolefin reinforced with Al, discussing design and manufacture

08 p1263 A71-20771

Bipolar silicon microwave transistors process technology improvements related to extensions of frequency, power handling or low noise performance

08 p1263 A71-20991

Ground stations for communication satellites, discussing radio transmitter and receiver systems using low noise parametric amplifiers at low temperatures and extended demodulator threshold

10 p1590 A71-25101

Microwave front end designs for low noise operation, discussing FET applications and mixer conversion loss reductions

11 p1731 A71-25673

Junction diameter reduction approaches for low noise generation, using Schottky diode parameters

11 p1737 A71-25675

Differential phase frequency characteristics of low noise or tunnel diode regenerative amplifiers

11 p1738 A71-25941

Reversal processing technique for producing high diffraction efficiency, low noise and good light stability phase holograms on silver halide emulsions

13 p2068 A71-28713

Low noise operation of CW devices with GaAs vapor grown p-n junctions, observing optimum AM SNR of minus 140 dB

17 p2713 A71-34445

Low noise TWT amplifiers, performance, reliability and cost reduction

17 p2714 A71-34605

Cryogenic refrigeration requirements of low noise microwave amplifiers in satellite communications, discussing solid state masers and liquid helium parametric amplifiers

20 p3204 A71-39251

Differential phase frequency characteristics of low noise or tunnel diode regenerative amplifiers

20 p3205 A71-39261

Microwave MESFET HF circuits, discussing noise factor advantage over bipolar transistors in low noise preamplifiers

21 p3355 A71-40743

Si Pt-n-p transit time microwave diode source noise measurement, noting low noise characteristics and suitability for local oscillator applications

21 p3359 A71-41413

LOW PASS FILTERS

Low pass active filters with various characteristics, comparing amplitude-frequency responses

01 p0051 A71-10259

Low- and high-pass active filters theory and design, describing positive and negative feedback circuits

02 p0231 A71-11863

Laguerre networks design optimization with threshold frequency and time limit based on pulse/frequency responses energy distribution, representing low pass filters

04 p0561 A71-15700

Optimum low pass filter bandwidth for pulse detection in exponential noise, using two dimensional spectrum

07 p1059 A71-18849

Avalanche diodes Evans circuit /low pass filter located one half wavelength from diode/ analytic theory, developing expressions for efficiency and diode impedance

07 p1074 A71-19121

Transient stabilization analysis for electronic circuits containing diverse components with variable parameters, considering active low pass filter example

07 p1078 A71-20061

Pulse width controlled, regulated DC-DC converter with passive low pass filtering, discussing open loop transfer functions, stability analysis and linear models

07 p1024 A71-20413

Elliptic-function low pass microwave filters and other C sections applications including broadband impedance transformers

08 p1262 A71-20766

Noise analysis of microelectronic active RC filters by cascade of passive and active networks, considering low pass filter

10 p1582 A71-23915

Low pass equiprobable insertion loss functions roots for commensurate microwave filters with stubs and unit elements

13 p2038 A71-28610

Active RC network realization of third order low-pass Butterworth characteristic with all capacitors having same value

14 p2210 A71-29798

Comments on optimum bandwidth of low pass RC filter for pulse signal detection in nonstationary noise

20 p3203 A71-38867

Tapered distributed RC low pass network configuration with voltage-controlled sources for sensitivity reduction low and high Q factors
21 p3361 A71-41409

High performance bandpass and low pass interference filter for IR region above 40 microns, discussing metallic mesh and reflecting element properties
22 p3544 A71-42136

Closed phase lock loop FM demodulator design, determining resonant frequency parameters, attenuation factor and low pass filter elements
23 p3650 A71-43094

LOW PRESSURE

NT HIGH ALTITUDE PRESSURE

Nitrogen inductive low pressure discharge, determining vibrational and rotational temperatures, ionization degree, electron temperature and energy balance by spectroscopic technique
02 p0286 A71-12178

Reduced pressure effects on thermal expansion and fragmentation of rocks
03 p0418 A71-14460

Piezoelectric and capacitive transducer pressure measurements in low pressure fluidic elements
07 p1026 A71-20571

Low pressure air jet sensing power pneumatic and fluidic circuits and interface valves for low pressure signal stepup to main line pressure, considering circuit design
07 p1030 A71-20597

Low pressure gas heating in shock tube, considering stagnation temperature increase
13 p2049 A71-29198

Zirconium oxidation kinetics at 500-1200 C under low oxygen pressure
14 p2257 A71-29843

Nitrogen inductive low pressure discharge, determining vibrational and rotational temperatures, ionization degree, electron temperature and energy balance by spectroscopic technique
15 p2451 A71-31487

LOW PRESSURE CHAMBERS

U VACUUM CHAMBERS

LOW SPEED

Hot-wire anemometer velocity measurement in slow air flow
03 p0430 A71-14374

Hypersonic vehicles low speed handling qualities, describing test flights approach and landing operations
05 p0697 A71-16680

Numerical calculation of trailing vortex sheet pattern behind unstalled swept wing at low speed, obtaining downwash field
20 p3176 A71-39397

Low speed aerodynamics, detailing relevance tree technological forecasting method of Canadian science council national goals list
22 p3481 A71-42766

LOW SPEED HANDLING

U CONTROLLABILITY

U LOW SPEED

LOW SPEED STABILITY

C-5 military transport stability augmentation for pitch and yaw inertia at low speed, using pilot evaluation on cockpit simulator
02 p0190 A71-12684

LOW SPEED WIND TUNNELS

NT SUBSONIC WIND TUNNELS

Wind tunnel history, evolution and use, covering low speed variable density, high speed transonic, supersonic, hypersonic and hypervelocity wind tunnels
08 p1272 A71-21666

CERCHAR low speed wind tunnel design details, operational characteristics and utilization of facility for coal mine safety
10 p1589 A71-24287

Blowing angle effect on heat protection effectiveness of flat wall in slit injected low speed air flow with turbulent boundary layer in wind tunnel
13 p2159 A71-28420

Acoustic resonance excitation by vortex shedding from flat plate trailing edge in low speed wind tunnel
24 p3848 A71-44557

LOW TEMPERATURE

Si solar cells low temperature and solar intensity performance optimization by identifying and eliminating low output problems
05 p0701 A71-16071

Nb single crystals heterogeneous deformation at very low temperatures, observing jerky flow due to adiabatic temperature rise during plastic deformation
08 p1308 A71-21512

Optical-electrical analogy of thermal radiation impedance of thin dielectric films in low temperature insulation
09 p1494 A71-23003

Pair correlation function for gaseous hydrogen at low density and temperature from quantum mechanical calculation, using Lennard-Jones potential
11 p1801 A71-25367

Heat resistant metals long time creep prediction at low stresses or temperatures
15 p2428 A71-31859

Low temperature thermal insulation using diffraction effects of multilayer perforated reflecting screens
22 p3622 A71-42678

LOW TEMPERATURE ENVIRONMENTS

Turbine disks and shafts for low temperature operation, examining brittle fracture tendency by acceleration testing
01 p0098 A71-10078

Steels and weld metal alloying for stable austenitic structure under long term cryogenic conditions, investigating optimal Cr, Ni, Mn and nitrogen combinations
01 p0085 A71-10087

Mercuric oxide-cadmium batteries optimum cell design for low temperature operating conditions and elevated temperature storage life
03 p0351 A71-13038

Si solar cells spectral responses at low temperatures
05 p0701 A71-16072

Si solar cell low temperature low solar illumination intensity I-V performance deficiencies, considering corrective design modifications
05 p0701 A71-16073

Si solar cells under low temperature electron irradiation, noting damage rate dependence on measurement temperature
05 p0701 A71-16076

Si solar cell technology, discussing contacts, low temperature performance and conversion efficiency
05 p0757 A71-16103

Logic circuitry materials physical properties changes effects on performance-controlling parameters at low temperatures
05 p0732 A71-17077

Animals tissue activity during winter hibernation under Alaskan environmental conditions, discussing sense of time, anticipation of seasonal changes, etc
07 p1041 A71-19525

Vertical hydraulic press for metal extrusion at temperatures from 4 to 77 K, discussing design
08 p1299 A71-21809

Low temperature curing long open time epoxy adhesives evaluation for 3500 psi shear strength
10 p1631 A71-24072

Resilient metal seals for extreme temperatures or minimum leakage and weight
12 p1911 A71-27060

Optical, mechanical, thermal and electrical properties of IR sensor materials at low operating temperatures
14 p2284 A71-30545

Turbine wheels and shafts for low temperature operation, examining brittle fracture by acceleration testing
16 p2593 A71-33634

Materials and welded joints low temperature operation reliability prediction by estimating brittle fracture resistance from impact bending tests
16 p2584 A71-33640

Steels and weld metal alloying for stable austenitic structure under long term cryogenic conditions, investigating optimal Cr, Ni, Mn and nitrogen combinations
16 p2584 A71-33643

Hypersonic magnetic spectrometer-relaxometer, comparing direct and indirect recording methods for hypersound in metals at helium temperatures
16 p2580 A71-33928

Soviet monograph on plasticity and strength of solid bodies at low temperatures covering solidifying gases, static tests, dynamic properties and creep
17 p2724 A71-35186

Thermoregulation under stringent low temperature conditions, considering internal body temperature maintenance by homoiothermic organism
18 p2861 A71-36891

Radiation hardening of silicon solar cells, analyzing performance in low temperature environments
18 p2852 A71-36963

Low temperature phonon assisted edge emission bands in pure cadmium sulfide crystals
20 p3276 A71-39008

Polymer materials for aerospace construction, considering behavior in cryogenic and high temperature environments
22 p3564 A71-41510

LOW TEMPERATURE PHYSICS

N-type Ge semiconductor low temperature breakdown potential dependence on neutral impurity concentration
05 p0793 A71-16420

Aluminum alloy deformations and rupture strength under complex stress at low temperatures, observing anisotropy decrease with temperature
08 p1306 A71-21117

Thermal and electrical transport in tungsten crystal for strong magnetic fields and liquid helium temperatures
08 p1344 A71-21365

Nondegenerate and degenerate semiconductor current flow equilibrium at low temperatures based on Boltzmann transport equation
09 p1414 A71-22251

Phonon excitations radiated from thermal source in He II below 0.3 K, using carbon film detectors
09 p1497 A71-22418

Rapidly quenched CuAu ordered state development on low temperature annealing, presenting Young modulus variation as function of heat treatment time
09 p1477 A71-23350

Heat conductivity anomalies of thin metallic plates at very low temperatures, discussing secondary phonons angular distribution and electron energy flux
10 p1640 A71-23816

Low temperature curing nylon epoxy adhesive, discussing high peel strengths
10 p1630 A71-24070

Annealing and white light illumination effect on I-V characteristics of long Ge diodes irradiated by 5 MeV electrons at 77 K
10 p1583 A71-24144

GaAs single crystals conductivity and surface capacitance under transverse electric field at low temperatures
10 p1657 A71-24322

Thin metal foils total energy flux, electron/phonon temperatures and thermal conductivity anomalies at liquid He temperatures
10 p1657 A71-24457

Superconductivity transition of Nb-Ti solid solutions with varying Ti content, using specific heat measurements between 2.5 and 20 K
10 p1628 A71-24890

Low temperature space charge mechanism of threshold switching, using pulse measurements on thin layer multicomponent chalcogenide glasses
13 p2110 A71-28044

Characteristics of field effect and surface barrier GaAs transistor (MESFET) operating at 4.2 K, noting very low temperature hyperfrequency amplifier application
14 p2212 A71-30439

Low temperature heat capacities from 1.5 to 15 K for transition metal borides and solid solutions
15 p2437 A71-32649

Thermodynamics and statistical mechanics of low temperature physics, including entropy, probability, energy spectra and gas liquefaction
20 p3270 A71-39240

Materials behavior at low temperatures, investigating lattice vibrational spectra relation to specific heat, conducting electron energies, thermal expansion, etc
20 p3270 A71-39242

Thermodynamic measurement of cryogenic temperatures based on gases at low pressures or platinum electrical resistance
20 p3270 A71-39243

Paramagnetic cycles for low temperature superconducting magnet cooling, discussing refrigerator, cryogenic pumps, regenerators and adjustable heat source and sink
21 p3476 A71-40898

Superconductivity transition of Nb-Ti solid solutions with varying Ti content, using specific heat measurements at 2.5-20 K
21 p3432 A71-41266

Cryogenic n-type GaAs residual photoconductivity produced repeatedly after heating to room temperature and renewed cooling
24 p3859 A71-44463

Thermal conductivities of pure and mixed ortho- and parahydrogen and/or deuterium at temperatures with no molecular internal energy exchange
24 p3850 A71-44553

Low temperature kinetics of metastable He atom pair collisions, investigating temperature dependence of plasma ionization
24 p3856 A71-45054

Low temperature noise in p and n channel MOST amplifiers
24 p3812 A71-45361

LOW TEMPERATURE TESTS

Structural stability at low temperatures - Conference, Kiev, February 1970
01 p0097 A71-10076

Cr-Si steels cold shortness tests, identifying low temperature failure mechanisms
01 p0098 A71-10082

Welded joints ductile and brittle static tensile strength at low temperatures, allowing for mechanical inhomogeneities
01 p0085 A71-10085

Rolling ball fatigue and lubrication with fluorinated polyethers at cryogenic temperatures compared to super-purified mineral oil
01 p1017 A71-10484

Sasaki effect in doped semiconductors at low temperatures concerning conduction anisotropy and intervalley impurity electron scattering
01 p1039 A71-10777

Stimulated recombination radiation from PbSe laser diodes at 77 K, showing stepwise curve of emission power vs pumping current
01 p0094 A71-10780

Polycrystalline Zr extremely low temperature tensile deformation, discussing prestraining effects,
01 p0094 A71-10780

stress-displacement relations, strain distribution, twinning, etc

Zinc-mercuric oxide cells with self supporting anodes of controlled porosity for improving low temperature performance

Single crystal creep strain rate measurement under cryogenic temperatures by hybrid photoelectric servo system with optical extensometer avoiding physical contact with specimen

Microplasma low temperature noise spectra in Si and Ge avalanche diodes

Static and dynamic fracture toughness of tempered low alloy high strength steels in low temperature range

Si solar cells I-V characteristics measurement at low temperature

Cylindrical steel samples with screw type threads, comparing pressed and ground threads effects on tensile strength at low temperatures

Machine components resistance to low temperature failure, considering threaded joints, gears and shafts for strength and plasticity characteristics

Al and Mg alloys mechanical and microstructural changes under low temperature conditions, optimizing casting component ratios

Beta stabilizers effects on Ti strength, plasticity and stress concentration sensitivity at low temperatures

Austenitic steels and Ti and Al alloys with stress raisers, studying low temperature mechanical properties

Al-Zn-Mg alloys low temperature mechanical properties dependence on aging treatment

Ti alloys beta phase solid solution decomposition during cooling and plastic deformation at low temperatures

Austenite-martensite transformation effects on Fe-Ni-Co alloys low temperature thermal conductivity

Al cast alloys mechanical properties and sensitivity to stress concentration at low temperatures

Low temperature material properties analyzer with superconducting microwave resonant cavity

Vinoflex glue for Constantan strain gauges in low temperature tensometry, showing satisfactory recording at single and multiple loadings

Bcc metals low temperature strength, examining solution softening in Fe-Mo alloys

Cast Mo alloy at low temperatures, investigating elasticity, plasticity and tensile strength characteristics

Be, V, Cu and Al foils low temperature integral radiant emission, describing calorimetric assembly

Low temperature creep testing apparatus providing for microstructural examination of materials without distortions due to specimen temperature change to room temperature

Cryostat design and operation for investigating solids mechanical properties and structure at liquid He temperature

Materials mechanical properties measurement methods and equipment at cryogenic temperatures including microscopes, X ray cameras, microhardness tester, fatigue and impact strength testing machines

Low temperature impact toughness test as criteria for metal susceptibility to brittle fracture

High vacuum low temperature fatigue tests, describing design and operation of equipment for microstructural observation

Low temperature tensometry application to stress-strain state of turbine disks

Fatigue life gages performance test using calibration program for cryogenic temperature applications

Annealed Al-Mg alloys mechanical measurement, noting low temperature tensile strength and yield point variations with specimen composition and temperature

Low temperature sintering of Ni-P alloy coated tungsten, discussing diffusion phenomena

Low temperature plasticity of Al alloy thin walled tubular specimens under axial tension and internal pressure

Deformability and strength of soft fiber reinforced plastics under biaxial tension, determining low temperature critical tensile stresses and elongation ratios

Graphite lubricants superconducting properties under high pressures and low temperatures, suggesting new superconductors developments and metal free electron mod modification

Graphite fiber resin composites physical and mechanical properties at ambient and cryogenic temperatures, discussing unidirectional ring and bar specimens and filament wound pressure vessels

Hydrogen effects on low temperature solution strengthening and ductility of Nb-H single crystals, noting effects of normal and strain induced hydride precipitation

Low temperature and composition effects on alloy softening in group 6A metals alloyed with Re

I-V characteristics and electrical properties of n-p silicon solar cells at low temperature and low illumination intensities

Ductility and susceptibility to brittle fracture of alloys under stress at low temperatures

One dimensional wave propagation at low temperatures in thermoelastic half space under step strain at free surface

Tensile strength and plasticity of hot rolled maraging steel at low temperatures

Friction coefficient and wear of steel in vacuum and air at low and room temperatures

Yield pressure, starting torque, consistency and rheology of lubricating greases at low temperature in ball bearings

Thermally activated plastic deformation of metals at low temperatures, determining stress flow, creep properties and upper yield limit

Structural materials low temperature testing using cryogenic chambers, high power tensile test machines, semiconductor thermometers and resistance wire strain gauges

Fatigue testing machine for axial and torsional loadings at low temperatures in vacuum

Low temperature and tensile loading rates effects on static and dynamic strength of steel rods with ground and rolled threads

Low temperature creep deformation recorder with liquid He coolant, discussing Al and Pb single crystal tests

Group 3A suboxides IR absorption spectra at liquid helium temperatures, measuring bending frequencies and modes

Low temperature shock waves in molecular hydrogen, discussing Rankine-Hugoniot equation behavior

GaAs single crystals defects formation during low temperature gamma photons and electron irradiation, considering electrical properties

Specific heat measurement in magnetic field for graphite under neutron irradiation at low temperatures, noting Schottky anomaly

Hydrogen condensation in interstellar gas clouds onto solid dust grains from vapor pressure measurements of solid hydrogen at low temperatures

Welded joints ductile and brittle static tensile strength at low temperatures, allowing for mechanical inhomogeneities

Yield point thermal component in bcc metals at low temperatures as function of hydrostatic compression, noting interionic reaction potential nonspphericity

Electroconductivity and Hall effect in doped GaAs at low temperatures, studying temperature dependence of electron concentration, mobility and localization

Low temperature tensile prestressing effect on recrystallization kinetics of polycrystalline large grain Ni by isothermal annealings method

Consistency examination of thermal activation analysis in Nb, determining strain rate sensitivity of pure Nb and Nb-Mo single crystals subjected to compression at 178 and 273 K

Machine components resistance to low temperature brittle failure, considering threaded joints, gears and shafts for strength and plasticity characteristics

Al and Mg alloys mechanical and crystal microstructural changes under low temperature conditions, optimizing casting component ratios

Beta stabilizers effects on Ti base binary alloys strength, plasticity and stress concentration sensitivity at low temperatures

Vacuum melted Mo alloy low temperatures elasticity, plasticity and tensile strength characteristics

Low temperature test facility for cryogenic and rocket materials under combined tension and torsion

Sealed and vented fusing devices, testing vacuum effects on performance at high and low temperatures

Stray radiant flux effects on scanning IR radiometer for low temperature objects measurement

Tensile properties and notch toughness of Al alloys at low temperature, considering fracture toughness and weld strength

Radiometric measurement of total normal emittances of real surfaces at cryogenic temperatures

Low temperature viscous lubricants from mixed pentaerythritol esters for precision internal guidance gyroscope bearings and instrument applications

Temperature effect on fatigue strength of Ni steel by tension-compression fatigue test at low temperatures

Cryogenic fracture toughness testing - ASTM-ASME Conference, Toronto, June 1970

Specimen design effects on Al and Ti alloy plane strain fracture toughness at room and cryogenic temperatures, discussing crack propagation and rolling directions orientations

Ti-Al-Sn and Al alloys thin sectioned specimens cryogenic fracture strength, discussing surface crack fracture behavior

Vacuum apparatus for fatigue tests at room and low temperatures, giving results for annealed copper

Temperature effects on tungsten lattice and Grueneisen parameters and thermal expansion coefficients at low temperatures by X ray method

Low temperature proton irradiation damage and recovery in discontinuous Ta films sputtered in oxygen and nitrogen

Low temperature aging behavior of maraging stainless steels from electrical resistivity measurements

Magnetic recording of heart electrical activity by cryogenic magnetometer with two Josephson junction quantum interference reduction device

Low temperature investigation of microplasma breakdown in steep p-n junctions of Sb-doped n-type Ge

Device for dry friction determination at low temperatures

Indium gallium phosphide p-n junction laser operation at 4.2 and 77 K, considering threshold currents magnitude

Fatigue test equipment for 293-233 K and 50-100 ton static or 25-50 ton cyclic loads, using Freon 22 as coolant

Low THRUST

NT MICROTHRUST

Control programs realizability for optimal escape trajectories of low thrust vehicles with motion about mass of center and with or without artificial gravity

Low thrust minimum fuel space vehicle transfer from initial circular orbit to coplanar elliptic orbit of given energy and angular momentum

Optimal flight of material point in central field of forces subject to controlled small thrust

Control programs reliability for optimal escape trajectories of low thrust vehicles with motion about mass of center and with or without artificial gravity
13 p2144 A71-28192

Low thrust jet effect on base pressures on boat-tailed afterbodies in Mach number 0.8-1.2 flow
14 p2169 A71-29889

German monograph on linear theory of optimization problems for low thrust rockets covering orbital calculations, flight characteristics and Coast Arc problem
14 p2319 A71-30233

Auxiliary propulsion system using low power MPD thrusters, discussing feasibility of thrust vectoring with skewed magnetic coil arrangement
[AIAA PAPER 71-695] 14 p2293 A71-30754

Low thrust long burning solid rocket propellant motor for orbit insertion maneuvers, discussing design, static tests, nozzle composition, igniter and performance
22 p3589 A71-42016

Solar electric multimission spacecraft design, discussing off-optimum propulsion parameters effects on low thrust performance by characteristic surface representation
[AAS PAPER 71-324] 23 p3772 A71-42998

Space vehicle low thrust minimum terminal variance guidance problem reduced to stochastic bang-bang optimal control system
23 p3702 A71-44101

LOW THRUST PROPULSION

NT ELECTROMAGNETIC PROPULSION
NT ELECTROSTATIC PROPULSION
NT ION PROPULSION
NT PHOTONIC PROPULSION
NT PLASMA PROPULSION
NT SOLAR PROPULSION

Recurrent Lagrange multipliers coordinate transformation for optimal low thrust Earth- Jupiter trajectories
01 p0160 A71-10947

Time series approximation of acceleration functions for analytical solution of low thrust interplanetary transfers, treating flyby and rendezvous mission modes
[AIAA PAPER 71-116] 06 p0977 A71-18566

Optimal acceleration from earth orbit to hyperbolic velocities of low thrust space vehicle, constructing asymptotic expansions near and far from central field
09 p1519 A71-22545

Optimal low thrust power plant for spacecraft payload-maneuver tradeoff
09 p1512 A71-23139

Orbit transfer time of low thrust propulsion systems, assuming constant acceleration and thrust tangential to trajectory
10 p1670 A71-24273

Low specific impulse hollow cathode mercury thruster for deep space electric propulsion, using SERT 2 configuration
[AIAA PAPER 70-1099] 11 p1811 A71-25526

Minimum time low thrust rocket transfer between elliptic orbits in strong gravity field, using averaging method
13 p2139 A71-28816

Electrostatic spray generated charged colloids adaptation to thruster with metal capillary needles under AC voltage, evolving low thrust propellants
13 p2118 A71-29503

ESRO activity in low thrust electric propulsion systems development for attitude stabilization and stationkeeping, using colloid and field emission thruster concepts
[DGLR-71-035] 17 p2794 A71-35541

Low thrust vehicle optimal takeoff calculations from orbit about oblate planet, using two variable asymptotic expansion technique
[AAS PAPER 71-367] 23 p3729 A71-43037

High and low propulsion for optimal transfers between coplanar coaxial elliptic orbits, determining impulse number and timing
[AAS PAPER 71-368] 23 p3729 A71-43038

Low thrust interplanetary spacecraft tracking, using spectral factorization for Kalman filtering equations steady state solution
[AAS PAPER 71-395] 23 p3732 A71-43063

LOW TURBULENCE

LF boundary of inertial range in lowest atmospheric layer, comparing turbulence scale and wind velocity components
04 p0622 A71-15632

LOW VELOCITY

U LOW SPEED

LOW VISIBILITY

Simulated low visibility landing training, discussing airborne and ground based simulators
01 p0067 A71-10022

Saccadic eye movements scanpaths during pattern perception under poor visibility
06 p0859 A71-17962

Helicopter automatic and manual low visibility landing systems evaluation by hybrid computer simulation
06 p0880 A71-18423

Automatic landing systems independent monitor for L-1011 aircraft, providing pilot confidence under reduced visibilities
[SAE PAPER 710443] 13 p2098 A71-28324

LOW VOLTAGE

Dense plasma high current density effects on low voltage arc in thermionic converter
01 p0005 A71-10159

Cylindrical Xe filled thermionic diodes breakdown and low voltage arcs at various pressures and interelectrode distances
02 p0190 A71-11942

CW carbon dioxide lasers low voltage excitation, using cold cathode transverse glow discharges
03 p0436 A71-13642

Low voltage arc discharge effects on ionized Cs plasma characteristics under high density current conditions
12 p1938 A71-27213

Low voltage signal conversion to digital code, emphasizing SNR improvement
15 p2382 A71-32452

Low voltage arc discharge development in cesium vapor with glowing spherical plasma cluster formation in electrode gap
19 p3109 A71-37136

Low voltage arc discharge effects on ionized Cs plasma characteristics under high density current conditions
19 p3117 A71-38625

Energy requirement measurements for bridge wire igniters at low voltage, using capacitor discharge
22 p3587 A71-41448

LOW WEIGHT

Minimum volume design of sandwich axisymmetric plates obeying Mises criterion, using calculus of variations
13 p2146 A71-27782

LOWER ATMOSPHERE

NT OZONOSPHERE

Lower atmosphere turbulence model derivation from data obtained by Doppler radar windfield measurements in snowfall environment
01 p0117 A71-10578

Turbulent energy dissipation in lower atmospheric layer on meteorological mast during various temperature stratifications
02 p0246 A71-12112

Venus lower atmosphere structure and brightness temperature spectrum analysis for composition, temperature and pressure profiles
03 p0484 A71-13212

Lower atmosphere vertical temperature profiles by optical refraction measurements from photographs of equally spaced illuminated targets
03 p0453 A71-13233

High energy nucleon passage through lower atmosphere during chemical composition changes of primary cosmic rays, using Proton satellite observations
03 p0476 A71-13851

German monograph on application of measurement principle for determination of energy of high energy neutrons in lower atmosphere
03 p0481 A71-14368

Soviet monograph on atmospheric boundary layer covering compressible turbulent air flow, diurnal fluctuations, fog, air pollution and lower atmosphere electric field
04 p0621 A71-15399

Lower atmosphere thermal microfluctuation measurement to examine solar seeing area and dome effect
04 p0622 A71-15658

Terrain and frictionally induced vertical velocity analysis for local and regional forecasting operations, considering low level air flow effects
05 p0777 A71-16674

Aircraft altitude cosmic ray intensity measurements in lower atmosphere by neutron monitor, considering long term nucleonic intensity variations
08 p1355 A71-21629

Lower atmosphere meteorological parameters remote determination by acoustic sounding, discussing range and resolution characteristics
08 p1330 A71-21743

Venus subcloud layer, investigating radiant heat transfer in convective lower atmosphere
12 p1958 A71-26646

Ground and mountain level measurements of energy and angular distribution of high energy neutrons in lower atmosphere, using double elastic scattering with hydrogen nuclei
13 p2119 A71-27906

German monograph on lower atmospheric turbulence and gustiness coefficients in connection with large scale parameters, deriving climatological flow characteristics from wind measurements
17 p2770 A71-35233

Refraction, terrain, air attenuation, fog and rain, turbulence and shielding effects on acoustic propagation in lower atmosphere
17 p2734 A71-35235

Lower atmospheric multiple wavelength laser radar data compared to clear atmosphere model and

radiosonde measurements, discussing mixing layer location
18 p2882 A71-36617

F region seasonal anomaly relationship with lower atmosphere composition changes, discussing effects of oxygen/nitrogen relative concentration on ionospheric and atmospheric parameters
20 p3215 A71-38746

Venus lower atmosphere model based on surface pressure and temperature from radio astronomical and radar observations
20 p3296 A71-39626

Biosphere contamination, discussing sterilization and quarantine experiments at Lunar Receiving Laboratory, flight crew testing and microbiological studies
21 p3448 A71-40569

Lower atmosphere wind and cloud velocity measurements by combined stereophotogrammetry and balloon visual observation
22 p3542 A71-41862

Lower boundary condition effects on quasi-geostrophic baroclinic instability, showing vertical wind shear as function of pressure and wavelength
22 p3569 A71-42544

High energy nucleon passage through lower atmosphere during chemical composition changes of primary cosmic rays, using Proton satellite observations
22 p3595 A71-42652

Carbon dioxide photolysis at 1740-2100 A applied to photochemistry of Mars lower atmosphere
23 p3641 A71-43327

Solar activity effects on biosphere, examining solar-geomagnetic and medico-biological indexes relationships and clinico-statistical evidence of human organism effects
24 p3799 A71-45197

LOWER IONOSPHERE

NT D REGION

Lower ionosphere partially reflecting regions, describing vertical thickness distribution based on 1.75 MHz backscatter soundings
01 p0040 A71-11525

Lower ionosphere electron density changes with solar zenith angle during active sun year
04 p0583 A71-15213

Lower ionospheric cosmic noise absorption at 28.6 MHz, examining diurnal variations
05 p0740 A71-16430

Sporadic E and fEs regions multiples enhancement during small thunderstorms, noting effects on lower ionospheric ionization
05 p0740 A71-16436

Electron temperature anisotropy in lower ionosphere, discussing effects of solar UV radiation propagating along geomagnetic field during daytime
05 p0744 A71-17183

Sunset and sunrise vertical displacement rate of lower ionosphere from spectral analysis of field intensities at 236, 557 and 1277 kHz
05 p0744 A71-17184

Lower ionosphere magnetic fields generated by three dimensional Alfvén waves, analyzing spatial phase and amplitude distribution
05 p0745 A71-17199

Solar X-ray control of lower ionospheric radio wave absorption determined from Solrad 9 and Panska Ves Observatory data
06 p0892 A71-17921

Nitrogen dioxide and molecular oxygen ions densities in lower ionosphere as function of solar corpuscular radiation
06 p0895 A71-18275

Lower ionosphere electron density profile diurnal, seasonal and 11 year variations, tabulating calculated numerical values for 45-70 km altitudes
07 p1099 A71-19383

Parachute ejectable rocket-borne instrument package with telemetry system for lower ionosphere measurements, describing electrical and mechanical design and operation
07 p1208 A71-19803

Geomagnetic field quiet solar diurnal variations, examining dynamo theory in lower ionosphere at middle latitudes
07 p1104 A71-20045

Polar auroras, lower magnetosphere and geomagnetic perturbations, as effect of corpuscular fluxes penetration into lower ionosphere
07 p1104 A71-20046

Satellite altitude dipole source effectiveness in lower ionosphere, comparing to ground based source with same dipole moment
07 p1064 A71-20319

Forbush decreases effects on radio wave absorption, cosmic ray variations and ionization in lower ionosphere cosmic layer
08 p1353 A71-20981

Lower ionosphere electron concentration space-time variations relation to ionization source intensity fluctuations based on rocket observations and ground sounding data
09 p1435 A71-22442

LOX [OXYGEN]

Pulsed radio wave interactions with various lower ionosphere models, estimating cross modulation by computer calculation for comparison with measurements

09 p1405 A71-22443

Midlatitude stratosphere and lower ionosphere density model, discussing vertical, diurnal and seasonal variations effects on spacecraft trajectories

09 p1438 A71-23137

Lower ionospheric region parameters during 24 and 30 March 1968 substorms, determining auroral electron precipitation effects

09 p1440 A71-23630

Lower ionosphere RF whistlers polarization and electromagnetic structure, determining earth-ionosphere waveguide resonance frequency

10 p1575 A71-23828

Polar cap lower ionosphere mapping by solar and magnetospheric charged particles, considering disturbances in polar regions

10 p1661 A71-24312

Atmospheric electrical structure control by lower ionosphere force, considering interaction between neutral atmosphere tidal circulations and ionospheric plasma in presence of geomagnetic field

10 p1604 A71-24702

Daytime lower ionosphere electron density profiles over equator, using rocket-borne Langmuir and plasma noise probes

10 p1606 A71-24913

Electrical and thermal conductivity coefficients and energy diffusion coefficient in lower ionosphere, assuming weak ionization of ionospheric plasma

10 p1607 A71-24998

Sudden geomagnetic storm effects on low ionosphere state, discussing solar X-ray and particle radiation

11 p1815 A71-25581

Lower ionosphere ionization response to auroral particle fallout during 1968 substorms, using geomagnetic, VLF and balloon measurements

12 p1899 A71-26642

Lower ionospheric irregularities drift from neutral air motion measurements compared to meteor radar system determination

12 p1900 A71-27057

Lower ionospheric plasma frequencies height determination for actual motions, relating periodic variations to spatial electron density structure

13 p2029 A71-28003

Lower ionosphere charged particle concentrations and collision frequencies determination by LF impedance probe

13 p2058 A71-28028

Electron temperature anisotropy in lower ionosphere, discussing effects of solar UV radiation propagating along geomagnetic field during daytime at middle latitudes

13 p2059 A71-28240

Sunset and sunrise vertical displacement rate of lower ionosphere from spectral analysis of field strength at 236, 557 and 1277 kHz

13 p2059 A71-28241

Lower ionosphere magnetic fields generated by three dimensional Alfvén waves, examining amplitude and phase spatial distribution and frequency dependence

13 p2059 A71-28254

Wind resonance in ionosphere under pressure fluctuations, noting turbulent friction factor above 110 km

13 p2060 A71-28533

Auroral absorption and DR currents development during magnetic storms, discussing corpuscular fluxes arrival from magnetospheric tail into lower ionosphere

13 p2062 A71-28563

Receiver triangle size effect on ionospheric drifts near 2 MHz, using partial and total reflections from lower ionosphere

14 p2230 A71-29710

Particle collisions effects on whistler ray paths, considering penetration through lower boundary of ionosphere

14 p2193 A71-29917

Diurnal variations of electron number density against height in lower ionosphere over Resolute Bay, relating to solar proton events

14 p2300 A71-30044

Lower ionosphere effects on ELF noise in Schumann resonances range

14 p2203 A71-30961

Internal reflection of VLF whistlers incident from above on model nighttime lower ionosphere

15 p2369 A71-31433

Daytime rocket and ground based radar Thomson scatter measurements of electron densities and temperatures in lower ionosphere

15 p2399 A71-31772

Internal gravity waves vertical propagation in lower ionosphere from temperature and wind profiles measurements

16 p2561 A71-32802

Density distribution of plasmaspheric particles in equatorial plane via model of plasmasphere streaming, noting current system production in lower ionosphere

16 p2562 A71-32806

Corpuscular and solar electromagnetic ionizing radiation simultaneous measurement by sounding rockets, evaluating contribution to lower ionosphere formation

16 p2627 A71-33776

Faraday rotation of satellite signals across transverse region, considering sudden jumps at transverse point in lower and topside ionosphere

16 p2544 A71-33959

Rocket-borne RF capacitance probe design for determining lower ionospheric electron densities

18 p2921 A71-36367

Lower ionosphere electron density profile diurnal, seasonal and 11 year variations, tabulating calculated numerical values for 45-70 km altitudes

19 p3052 A71-37808

Martian lower ionospheric models during solar proton event, determining electron density profiles

20 p2386 A71-38741

Electric current shear at auroral arcs due to electron precipitation into lower ionosphere

22 p3536 A71-42623

LOX [OXYGEN]

U LIQUID OXYGEN

LOX-HYDROGEN ENGINES

U HYDROGEN OXYGEN ENGINES

LR CIRCUITS

U RL CIRCUITS

LRC CIRCUITS

U RLC CIRCUITS

LRV [VEHICLE]

U LUNAR ROVING VEHICLES

LSI

U LARGE SCALE INTEGRATION

LUBRICANT TESTS

Rolling ball fatigue and lubrication with fluorinated polyethers at cryogenic temperatures compared to superfinned mineral oil

01 p0107 A71-10484

Atmospheric and high vacuum performance tests of solid lubricant coatings based on molybdenum disulfide

05 p0757 A71-16174

Friction-wear characteristics of self lubricating composites under sliding conditions in air and vacuum [ASLE PREPRINT 70LC-17] 08 p1298 A71-21160
Olympus 593 supersonic engine lubricants tests, defining requirements in terms of bulk thermal stability, resistance to hot bearing breakdown, oil mist coking, etc

14 p2250 A71-29826

Mathematical models for boundary lubrication, computing specific liquid lubricant/surface wear rates in machine element design

15 p2414 A71-31950

Perfluoropolyether fluid lubricant physical and chemical properties at high and low temperatures, explaining metals effects on thermal stability by topochemical reaction mechanism

19 p3083 A71-37424

Rheological factors and error sources in X ray measurements of lubricant film thickness in rolling contact

24 p3830 A71-44947

Multiple rig rolling fatigue life tester, evaluating aviation gas turbine lubricants

24 p3832 A71-45292

Non-Newtonian film thickness, load capacity and maximum viscoelastic stress effect in point contact with second order fluid lubricant for slide/roll ratio [ASLE PREPRINT 71LC-16] 24 p3832 A71-45293

LUBRICANTS

NT GAS LUBRICANTS

NT HIGH TEMPERATURE LUBRICANTS

NT LUBRICATING OILS

NT SOLID LUBRICANTS

Li quantitative determination in soaps and lubricants by gamma spectroscopy of nuclear reactions with alpha particles from radioactive source

01 p0106 A71-10093

Papers on bearings covering types, materials, lubricants, applications, etc

01 p0088 A71-10813

Soviet book on aviation fuels, lubrication materials and special fluids covering compositions, physicochemical properties, filtration, etc

01 p0142 A71-11320

Oxidation resistance of silica gel lubricants, noting optimum diphenyl amine inhibitor

06 p0916 A71-18470

High speed low power loss spiral groove bearings self sealing grease lubricants with high shear stability and good boundary lubrication

[ASLE PREPRINT 70LC-6] 08 p1322 A71-21157

Thermohydrodynamic equations for viscous incompressible lubricant flow in hydrostatic thrust bearings, considering inertia and temperature effects

10 p1617 A71-24482

Monograph on bulk flow theory for turbulent lubricant films, discussing flow rates, pressure gradients and shear stresses

11 p1772 A71-26462

EHD lubricant film thickness and friction forces effects on ball and roller bearings selection and design [ASME PAPER 71-DE-3] 12 p1911 A71-27322

Complex calcium-based lubricants preparation based on hydrogenated castor oil or free fatty acids, considering saturation effect on structure and properties

13 p2091 A71-28227

Yield pressure, starting torque, consistency and rheology of lubricating greases at low temperature in ball bearings

[ASLE PREPRINT 71AM 1B-2]

13 p2076 A71-29485

Solid additives, graphite and molybdenum disulfide concentration effects on liquid lubricants and greases antiwear performance

14 p2251 A71-29827

Temperature effects on service life of cermet bronze-graphite bearings using different lubricants

15 p2418 A71-32674

Physicochemical properties and applications of lubricant materials based on organic compounds, discussing developments in inorganic lubricants

16 p2600 A71-32839

Low temperature viscous lubricants from mixed pentaerythritol esters for precision inertial guidance gyroscope bearings and instrument applications

20 p3254 A71-39800

Hydrostatic bearings for large optical and radio telescopes, explaining lubricant flow control systems

23 p3661 A71-43862

Externally pressurized journal bearings fed with incompressible lubricant, determining feeding system and hydrodynamic effects on bearing stiffness

24 p3830 A71-44949

LUBRICATING OILS

Elastohydrodynamic oil film measurements for rolling point contact of ball bearing under starvation using optical interferometry

01 p0087 A71-10481

Plain bearing oil whirl onset speed, using matrix manipulation for unbalanced shaft self induced vibration amplitudes prediction

03 p0431 A71-13072

High traction fluid effect on high speed roller bearing cage skidding, comparing with military specification oil

[ASME PAPER 70-LUB-E] 03 p0432 A71-13707

Transmission impending failure detection via lubricating oil monitoring for metal particle content

04 p0532 A71-15415

Dispersion medium effects on thermal hardening of lubricating oils with Na or Li additives

05 p0772 A71-16385

Synthesized hydrocarbon oil antiwear and extreme pressure additives effects on bearing spinning torque and endurance

06 p0904 A71-17580

Lubricant and ball steel effects on fatigue life /pit formation after repeated stress cycles/ [ASME PAPER 70-LUB-16] 07 p1118 A71-19507

Al-Si and Al-Sn bearing alloys corrosion resistance to lubricating oils, investigating thrust load, operating time and oxidation factor effects

08 p1304 A71-20996

Book on aircraft gas turbine engine technology covering combustion chambers, exhaust systems, lubricating oils, thrust augmentation, inlet ducts and overhaul procedures

08 p1348 A71-21625

Ultrasonic waves propagation in hydraulic and lubricating oils, testing shear resistance

09 p1484 A71-23673

Quadrupole mass spectroscopy of spacecraft critical surfaces vapor contamination, using lubricating oil covered titanium dioxide colorimetric sample

10 p1609 A71-23930

Lubricating oil thin films interfacial Newtonian flow elastohydrodynamics, studying transient effects on contact load damping parameters

10 p1614 A71-23981

Light aircraft engine lubricating oil filter types and model specification, noting dirt holding ratings [SAE PAPER 710383] 10 p1617 A71-24248

Military aviation greases for subsonic commercial airplane lubricants, discussing economic and technical benefits based on service experience and testing [SAE PAPER 710411] 13 p2091 A71-28304

Olympus 593 supersonic engine lubricants tests, defining requirements in terms of bulk thermal stability, resistance to hot bearing breakdown, oil mist coking, etc

14 p2250 A71-29826

Aviation oils high temperature viscosimetry, describing test equipment and measurement results at 200-300°C [DFVLR-SONDR-123] 14 p2264 A71-31128

Perfluorinated monocarboxylic fatty acids additives for controlling lubricating oils spreading on metals and antifiction properties improvement

15 p2438 A71-31680

Photoelastic analysis of oil film effects on rolling/sliding contact stresses of plastic and glass cylinders on steel ring, showing discrepancy with Hertzian distribution

15 p2414 A71-31946

Flame atomic fluorescence-atomic emission DC spectrometer for trace wear metals analysis in jet engine oils, covering spectral wavelengths below and above 3500 A

17 p2695 A71-35150

Three micron absolute main oil filter for aircraft gas turbine lubrication system, discussing indicator system and bench and engine tests

17 p2793 A71-35488

Thermal stability and oxidation and corrosion resistance of lubricating oil based on trimethyl propane ester

[ONERA-TP-930] 18 p2939 A71-36016

Aircraft turbine oils acid number potentiometric determination, discussing automatic titration procedure and apparatus and solvents influence on titration curve and inflection point

18 p2940 A71-36680

Oil for lubricating ball bearings in spacecraft antenna despin system, investigating weight loss, sorption, surface migration and contamination danger

20 p3184 A71-39352

Soviet book on hydrodynamics of nonstationary motions of viscoplastic media covering mechanical properties of clay, mortar, cement, lubricating oil, petroleum and disperse media, etc

21 p3369 A71-40872

LUBRICATION

NT BOUNDARY LUBRICATION

NT SELF LUBRICATION

NT SPACECRAFT LUBRICATION

Lubrication hydrodynamics differential equation of -fering analytic solutions for essential practical cases by use of suitable gap profile expressions

01 p0085 A71-10121

Glow discharge cleaning for surface contaminants removal from hydrodynamic gas bearing components, discussing equipment application to thin film lubricant vapor deposition

02 p0256 A71-12461

Infinite MHD journal bearing with electrically conducting fluid lubricant in radial magnetic field, obtaining pressure distribution, load capacity and driving torque

02 p0258 A71-12601

Film lubrication for angular contact ball bearings, taking rolling and spinning into account

04 p0604 A71-15768

Pure metal structure effect on friction and lubrication under steady slip in ultrahigh vacuum at low temperatures

05 p0757 A71-16185

Shearing strength of and lubrication effect on metal-plastic adhesion bond, using solid rotating indenter technique

05 p0759 A71-16363

Lubrication considerations concerning mechanical and service variables for obtaining optimum gear performance under severe operating conditions

06 p0904 A71-17576

Stationary motion stability of shaft in cylindrical MHD finite length bearing, assuming incompressible lubrication and small lubrication clearance

09 p1453 A71-22139

Hydrodynamic lubrication temporary breakdown during initiation of extrusion process

10 p1618 A71-24924

One dimensional optimum design lubrication treatment as imbeddings of nonlocal optimization problems

14 p2252 A71-30097

Tapered roller bearing lubrication, considering application to CH-47 Boeing helicopter transmission

17 p2749 A71-35300

Lubricated friction of steel ball on commercial tempered aluminum plate as function of time

21 p3396 A71-40100

Aircraft parts lubrication friction and wear problems, discussing failure modes, solid and liquid lubricants, component damage and lubrication systems

21 p3389 A71-40902

Aviation fuels lubricating characteristics, discussing refining methods, viscosity, service performance and load testing

24 p3864 A71-45383

LUBRICATION SYSTEMS

Wet and dry lubricated slip ring systems long term application testing in ion pumped vacuum chambers

07 p1120 A71-20274

Coated abrasive grinding of Ti alloys using water, various soluble cutting oils and inorganic phosphate solutions as coolants and lubricants

11 p1771 A71-26142

Three micron absolute main oil filter for aircraft gas turbine lubrication system, discussing indicator system and bench and engine tests

17 p2793 A71-35488

Book on lubrication systems selection, application, handling and maintenance covering journal and thrust bearings, nuclear reactors and machine tools

19 p3069 A71-37523

Nimbus B-2 satellite-borne IR spectrometer lubrication using solid film technique, discussing real time and accelerated vacuum environmental tests

[ASLE PREPRINT 71LC-3] 24 p3831 A71-45286

LUCITE [TRADEMARK]

U POLYMETHYL METHACRYLATE

LUDER BANDS

U PLASTIC DEFORMATION

U YIELD POINT

LUMENS

Luminometer numbers of hydrocarbons and reactive fuels as function of molecular weight and structure

06 p0913 A71-18471

LUMINAIRES

NT AIRCRAFT LIGHTS

NT ARC LAMPS

NT FLASH LAMPS

NT QUARTZ LAMPS

NT RUNWAY LIGHTS

NT SEARCHLIGHTS

NT XENON LAMPS

Spectral distribution reproduction of natural objects radiation by iodine lamp and glass filters

06 p0897 A71-17533

Instrumental function of Fabry-Perot interferometer and lamp-emitted line profile determined with hollow cathode thorium lamp

08 p1290 A71-21380

Sapphire windowed argon filled tungsten ribbon filament lamp in vacuum UV for application in photomultiplier quantum efficiency calibration

12 p1904 A71-26801

LUMINANCE

Color matching discrepancies, considering rod blue qualities under photopic conditions, luminance level and trichromatic stimulus unsuitability for large field additive colorimetry

01 p0010 A71-10273

Vestibular nystagmus and display luminance effects on hand-eye coordination in compensatory tracking of aircraft instrument

02 p0207 A71-12381

Contour effects on brightness paradox, investigating contrast and perception of luminance gradients in space by constant sum estimation method

03 p0365 A71-14377

Brief light flash duration discrimination, discussing luminance and time between flashes

10 p1570 A71-24607

Luminance and luminous flux discrimination in light and dark reared rats after early visual deprivation

13 p2011 A71-28810

Spectral luminance and transmittance of noctilucent clouds for spaceborne photometric observation, using American-Swedish rocket particle experiment

14 p2232 A71-29962

Visual adaptation mathematical model, studying relation of brightness static transformation into luminance

17 p2692 A71-35174

Human visual system differential luminance sensitivity tests using simultaneous stimuli in yes-no procedure

17 p2684 A71-35256

Visual system image blur and lateral inhibition effects on visual performance, convolving luminance profiles of targets with point spread functions

19 p3007 A71-38059

Surround luminance effect on relative perceptual latency of response, using test stimuli confined to rod free area of fovea

20 p3184 A71-38774

Flashing light stimuli application to clinical instrument design for detection and quantitative assessment of early pathological visual loss based on minimum discernible luminance difference

22 p3498 A71-41482

Central panel luminance effect on peripheral visual detection time in search tasks

23 p3638 A71-42899

Increment threshold for monoptic and dichoptic vision, showing spatial and luminance effects

24 p3801 A71-44979

LUMINESCENCE

NT BIOLUMINESCENCE

NT CHEMILUMINESCENCE

NT ELECTROLUMINESCENCE

NT FLUORESCENCE

NT LUNAR LUMINESCENCE

NT OPTICAL RESONANCE

NT PHOTOLUMINESCENCE

NT THERMOLUMINESCENCE

NT X RAY FLUORESCENCE

Total free electron energy disparity with energy radiated in forbidden O I lines in supernova spectra explained by nova luminescence formation

01 p0151 A71-10067

Luminescence of nebulae with C plus B spectrum, noting hydrogen emission superimposed on continuum due to reflection of stellar radiation by dust

02 p0311 A71-12353

Luminescence of optically reflecting nebulae related to shape of light scattering indicatrix of interstellar dust particles

02 p0311 A71-12355

Rare earth polycrystalline powders luminescence stimulation by ruby laser radiation, discussing two

photon mechanism, luminous intensities relations and UV radiation

03 p0435 A71-13510

Luminescence excitation in chelates under pulsed ruby and neodymium laser radiation action, examining two photon absorption mechanism

07 p1122 A71-19130

Nd glass traveling wave laser single frequency emission luminescence stability as function of pumping power, using dispersive ring resonator

07 p1122 A71-19136

Energy transmission mechanism in calcium fluoride-europium ion plus holmium ion system, investigating luminescence and absorption spectra

09 p1461 A71-22388

Fluorapatite single crystals absorption spectra and luminescent characteristics under activation by rare earth ions, noting line widening dependence on crystal composition

09 p1507 A71-22390

Spectral and relaxation characteristics in antiStokes two photon luminescence of polycrystalline ruby exposed to filtered light pulses

09 p1508 A71-22392

Total free electron energy disparity with energy radiated in forbidden O I lines in supernova spectra explained by nova luminescence formation

09 p1525 A71-23260

Einstein relations for stimulated luminescence, and application to high pressure chemical laser power gain and population inversion calculation

12 p1913 A71-26966

Upper atmosphere night sky luminescence observations during IQSY, discussing correlations between night airglow, solar activity, interstellar dust disturbances and meteor phenomena

15 p2400 A71-31987

Quartz, organic glass and plexiglass luminescence under giant pulse ruby laser radiation

15 p2422 A71-32462

Single mode ruby laser emission on transparent dielectrics, observing surface luminescence, free electrons production and adsorbed gases heating

16 p2585 A71-32797

Transparent polymer dielectric luminescence and destruction under Q switched laser radiation with subthreshold power and picosecond pulses

16 p2588 A71-33652

Luminescence quenching in Hg tube activated ZnS-Cu phosphors under action of ruby laser red light

17 p2752 A71-34404

Einstein relations for stimulated luminescence, and application to high pressure chemical laser power gain and population inversion calculation

19 p3075 A71-38265

Liquid carbon tetrachloride artificial luminescent cloud formation in upper atmosphere, considering injection conditions for rapid vaporization and required concentration

19 p3061 A71-38633

Cathode ray tube, including electron beam peak power, resolution elements, luminescent materials, fabrication techniques, contrast preservation and reliability

20 p3234 A71-39062

Mean void fraction of adiabatic two phase flow by luminescent tracer dispersed in liquid phase

23 p3675 A71-43323

Apollo 11 and 12 rocks luminescence under proton, electron, UV and X irradiation

23 p3760 A71-43774

Luminescence, thermoluminescence and spectral reflectance of lunar samples from Oceanus Procellarum and Mare Tranquillitatis

23 p3760 A71-43775

Lunar fines luminescence emission spectra in visible and near IR region under proton and electron excitations, discussing cause and plagioclase distribution

23 p3760 A71-43777

Luminescence time decay in optically excited thin direct gap semiconductor with surface losses, establishing phase shift method for carrier lifetime and semiconductor surface properties

24 p3863 A71-45360

Saturating flash delayed luminescence from chloroplasts, considering relationship to oxygen evolution

24 p3799 A71-45382

LUMINESCENT INTENSITY

U LUMINOUS INTENSITY

LUMINOSITY

Cosmological models with noninteracting matter and radiation, deriving red shift and luminosity-distance relationship

02 p0312 A71-12464

Small elliptical galaxy associated with radio source 3C 386, noting luminosity, internal velocity dispersion and low metal abundance

05 p0805 A71-16109

Auroral luminosity and X ray bremsstrahlung quasicontinuous pulsations data analysis by power spectrum and cross correlation methods

06 p0949 A71-17265

- Artificial meteors ablation and luminosity measurements, using ballistic range shadowgraph and radiometric equipment for velocity history, shock wave formation and mass loss process
07 p1223 A71-19674
- Balloon sonde for auroral luminosity measurements and comparison of auroral emissions, X rays and ionospheric absorptions
10 p1602 A71-24530
- Comparison of lightning and long laboratory spark, considering luminous processes, current, voltage, power, energy inputs, radiated visible spectra, electron density, etc
12 p1939 A71-27266
- Insufficient auroral electron spectra and pitch angle distributions from ground based altitude luminosity profiles
13 p2054 A71-27802
- Pulsar signature on diffuse X ray background, converting fraction of luminosity into k series photons
14 p2297 A71-29584
- Mathematical models of distance perception under flight conditions according to visible brightness of luminous surface
17 p2691 A71-35166
- Density and luminosity evolution of radio source population, considering counts per unit co-moving volume at cosmological epochs
18 p2961 A71-35966
- Colored light sources luminosity determination by Helmholtz-Kohlrausch effect, discussing brilliant and fluorescent stimulus
18 p2854 A71-36003
- Far UV auroral luminosity profile using calibrated EUV spectrometer, noting nitrogen band emission
20 p3225 A71-39731
- Closed formula for relation between luminosity and red shift in expanding Friedman universe for positive cosmological constant, positive space curvature and vanishing pressure
21 p3443 A71-40186
- Mean ratio of mass to three-halves power of luminosity for elliptical and lenticular galaxies based on catalog mass data emphasizing uncertainties
22 p3599 A71-41935
- Radio source counts interpretation by cosmological evolution models, suggesting luminosity role
22 p3606 A71-42600
- LUMINOUS FLUX DENSITY**
U LUMINOUS INTENSITY
LUMINOUS INTENSITY
NT ILLUMINANCE
NT LUMINANCE
- Far UV equatorial airglow and aurora intensities and occurrence frequencies from satellite observation
01 p0076 A71-11504
- Regular and stochastic oscillations in plasma beam discharge produced by beam instability from observing time dependent variations in spectral line luminance intensities
02 p0288 A71-11634
- Shock wave dynamics of brightness curve reflecting supernova outbursts
02 p0307 A71-12088
- Spiral galaxies mass-luminosity relationship from optical and radio astronomy data
02 p0308 A71-12102
- Unsteady light field spatial moments in turbid medium boundary layer with intense anisotropic scattering during illumination by narrow beam
02 p0277 A71-12116
- Compact galaxies one-magnitude light outburst near M3, discussing photometric statistical data
02 p0313 A71-12469
- Quasars spatial distribution and luminosity functions based on red shift observation
02 p0314 A71-12576
- Transverse mode selection techniques for solid state laser brightness increase
02 p0262 A71-12717
- Sodium dayglow rocket measurements, comparing emission intensities with ground based measurements
03 p0407 A71-13312
- Solar He II Lyman alpha line, measuring long term absolute intensity variations
03 p0496 A71-14507
- BL Lacertae photometric data, noting object brightness and optical similarity to N galaxy 3C371
04 p0643 A71-15045
- Bragg diffracted light intensity increase from standing resonating acoustic wave, considering applicability for laser communication multiplexing and demultiplexing
05 p0720 A71-16269
- Self shielding effect of various substances under intense light
05 p0762 A71-16380
- He-Ne laser light intensity fast and slow modulation by thin acoustoelectric photoconducting CdS platelet oscillators
06 p0906 A71-17308
- Light reflection during plane cloud layer light scattering, studying zenith angles and angular brightness distribution
06 p0923 A71-17510

Visible brightness of Milky Way for various galactic structure models, discussing star and dust distribution effects
06 p0975 A71-18444

Moon and Mars brightness distribution, considering surface roughness, albedo, fragmentation and walls between pores
06 p0975 A71-18447

Thermal Ar plasma with gas additives as standard intensity light source of optically thick spectral lines, using interpolation and Kirchhoff-Planck function
07 p1168 A71-19323

Fringe interferogram variable visibility control, eliminating vibration effects
07 p1109 A71-19467

Shock wave dynamics of brightness curve reflecting supernova outbursts
08 p1362 A71-21138

Efficiency improvement of holograms with very high reference beam to object beam intensity ratio by constructing copy from first hologram
08 p1291 A71-21399

Photocathode area sensitivity contours- wavelength relationship from photomultiplier absolute intensity and near IR spectrum laser research
08 p1291 A71-21408

Field galaxy cosmological reddening from red shift data at faint magnitudes
09 p1516 A71-22063

Intensity logarithm fluctuations of focused laser beam propagating in summer daytime atmosphere at 250 and 650 meter path lengths
09 p1404 A71-22224

Biophysical nature of human memory, investigating electrosensitivity phase modulators and variations by suprainvasive light stimulus to eye and adjustment reflex
09 p1391 A71-22484

Mars border-disk brightness comparison noting atmospheric transparency effects
09 p1520 A71-22837

Heterotrophic growth in dim light of blue green alga *Agmenellum quadruplicatum* and *Lyngbya lagerheimii* with glucose as carbon source
09 p1402 A71-23472

Metallic target in radiation damage from focused ruby laser beams as function of energy and luminous pulse duration
09 p1465 A71-23563

Metastable oxygen ion distribution and related optical emission rates in aurora, discussing line intensities, charge transfer efficiency and ionization peaks
09 p1441 A71-23642

Brightness temperature measurement in high pressure Ar plasma by comparing reference lamp to plasma radiation intensities
10 p1646 A71-23833

Night vision visual systems with image intensifiers, noting effect on human eye performance at low light levels
10 p1641 A71-24057

Lydia asteroid observations, presenting light curves brightness and phase functions near opposition
10 p1669 A71-24177

Far IR fluxes from H II regions with solar luminosities at .02-2 times 10 to 7th
10 p1675 A71-24488

Jupiter observation during 1970 visibility period, including drawings, photographs, position and brightness estimates, and red spot
10 p1677 A71-24689

Visual suppression and intensity threshold changes during voluntary eye saccades with different luminance regions in visual field, discussing inhibition processes
11 p1718 A71-25583

Type I supernovae maximum brightness and occurrence time from photometric analysis
12 p1955 A71-26585

Visible brightness of Milky Way for various galactic structure models, discussing star and dust distribution effects
12 p1955 A71-26594

Moon and Mars brightness distribution, considering surface roughness, albedo, fragmentation and walls between pores
12 p1955 A71-26597

Radio quiet compact galaxy I Zw 1 (0051 plus 12/ photometric data, noting variability and brightness levels
12 p1957 A71-26622

C, gM and S spectral type stars, considering distribution, absolute magnitudes and intrinsic colors
12 p1959 A71-26777

Mars regolith carbon dioxide, water and Kr adsorption, explaining diurnal brightness phenomena
12 p1961 A71-26875

Meteor telescopic observations during Perseid stream activity, determining radiant, stellar magnitudes, length and velocity
12 p1961 A71-26905

Martian continents, seas and polar caps spectrum analysis, noting spectral reflectivity and brightness distributions
12 p1965 A71-27225

Comets Alcock 1963 III and Everhart 1964 IX brightness bursts, obtaining time curves for gas evolution
12 p1965 A71-27228

Bolide spectrum on 6 June 1969, determining stellar magnitude and periodic pulsations and asynchronous flares characteristics along trajectory
12 p1965 A71-27229

Solar corona photometry during 22 September 1968 eclipse, determining brightness variations and decrease from limb
12 p1966 A71-27231

Optical luminosity function and space density of quasars from 4C and Parker survey, assuming cosmological red shifts
12 p1966 A71-27233

Self shielding effect of solid surfaces under intense light
12 p1915 A71-27457

Formaldehyde vapor photodecomposition modes by end product analysis, utilizing mixed isotope, radical scavenger, inert gas pressurization and lamp intensity attenuation
12 p1877 A71-27758

Jupiter Galilean satellites narrowband photometric data, observing albedos, spectral reflectivity, rotational phase, and brightness variations
13 p2135 A71-28292

Inhomogeneous planetary atmosphere resonantly scattered sunlight, calculating intensities with frequency redistribution functions
13 p2100 A71-28346

Iapetus magnitude variations due to orientation changes in poles, comparing visual and photometric observations
13 p2136 A71-28389

Iapetus photometric observations, obtaining light curve by plotting rotational phase angle against magnitude
13 p2136 A71-28390

Human visual system gate type lateral interaction to luminous intensity, noting visual field response to monocular viewing
13 p2018 A71-28460

Narrow-band photometry of comet Bennett, giving intensity profiles and interference filter transmission curve
13 p2138 A71-28761

Mass distribution of compact galaxies, obtaining average mass/luminosity ratio
13 p2138 A71-28762

Luminance and luminous flux discrimination in light and dark reared rats after early visual deprivation
13 p2011 A71-28810

Parallax errors in drawing contour lines on universal stereograph due to aerial photographic images brightness difference
13 p2070 A71-29083

Spectrometer slit-width cancellation by Doppler shift of light emission by fast ion beams, resulting in spectral lines increased intensities
13 p2071 A71-29331

Pulsating aurora observations, noting light intensity, diurnal variations and power spectra
14 p2229 A71-29671

LF gravitational waves search based on light intensity fluctuations after traveling over transmission paths
14 p2274 A71-29856

Photometric meteor mass calculations from observational data, discussing Fe and Cu photographic luminous efficiency measurements accuracy and interpretation
14 p2314 A71-30651

Monograph on planetary nebulae covering structure, luminosity, spectra, origin, chemical composition, temperature, magnetic fields, etc
15 p2481 A71-31148

Cosmic ray gradient perpendicular to solar equator plane related to coronal intensity
15 p2479 A71-31906

Galactic brightness, color distribution and ellipticity data from photometry and colorimetry observations
15 p2486 A71-32028

Pleiades flare stars photographic magnitude and brightness data, establishing relation between amplitude and duration
15 p2486 A71-32029

Planetary nebulae nuclei colorimetric, photographic and brightness data, listing temperatures, absolute values and bolometric corrections
15 p2487 A71-32034

Russell law validity of planet brightness dependence on phase integral, discussing backscattering surface and thick atmospheres effects
15 p2491 A71-32425

Fast luminous fronts /ionizing waves/ in Kanal streamer and Townsend discharges in nitrogen, discussing optical space and time resolved measurements
15 p2459 A71-32648

Scattered light effects on sunspot intensities observations during Mercury occultation and near solar limb
15 p2496 A71-32739

Sky brightness broadband measurements by Skylark sounding rocket, noting relationship to zodiacal light 16 p2575 A71-32842

Calculational method for predicting angular distribution of sunlight upwelling flux scattered by atmosphere and reflected by ground, using Monte Carlo data 16 p2562 A71-33130

Aperture synthesis of neutral hydrogen in M 101 galaxy, suggesting close connection between surface density of light and H I 16 p2632 A71-33330

Meteors light curves, showing maximum brightness distribution in visible trajectory 16 p2639 A71-33700

Short light pulse evolution from noise, considering time dependence of pulse duration and peak intensity 16 p2589 A71-34137

Brightness fluctuations in photometric nucleus of Ikeya-Seki comet at 29-31 March 1968 17 p2803 A71-34832

Visual integral brightness estimates of Ikeya-Seki 1967n comet observed at Dyushambe from 9 January to 18 April 1968 17 p2803 A71-34833

Galactic clusters characteristics tabulation and statistical analysis, calculating dimensions, luminosity and radial velocities dispersion 17 p2804 A71-34841

Spatial coherence measurement for two points of pseudothermal light source by comparing photocathode luminous intensity probability density and photoelectron distribution moments 17 p2754 A71-35585

Image amplifier camera resolution as function of light level based on photon statistics and cathode quantum efficiency 17 p2746 A71-35762

Color perception with achromatic stimulation by changing intensity of stationary light source to produce flicker colors 18 p2864 A71-36004

Dwarf elliptical and irregular galaxies of small intrinsic size, small absolute luminosity and low surface brightness 18 p2967 A71-37028

Brightness and polarization of solar corona at total eclipse on 12 November 1966 from polarographic observations 19 p3131 A71-37243

Martian continents, seas and polar caps spectrum analysis, noting spectral reflectivity and brightness distributions 19 p3132 A71-37377

Comets Alcock 1963 III and Everhart 1964 IX brightness bursts, obtaining time curves for gas evolution 19 p3132 A71-37380

Bolide spectrum on 6 June 1969, determining stellar magnitude and periodic pulsations and asynchronous flares characteristics along trajectory 19 p3132 A71-37381

Solar corona photometry during 22 September 1968 eclipse, determining brightness variations and decrease from limb 19 p3132 A71-37383

Real time holographic interferograms, achieving required beam intensities relationship by ordinary neutral light filters near collimator focus 19 p3065 A71-38196

Charged particles eruptions effects on relation of magnetic perturbations to integral auroral luminance intensity from whole sky photometry measurements 19 p3059 A71-38398

Artificial satellites optical characteristics from amateur observers, discussing brightness and absolute magnitude 20 p3305 A71-38731

Three dimensional display with multicolor capability, continuously variable intensity and random accessed flying spot, exhibiting fixed or moving objects 20 p3234 A71-39063

Atmospheric transmissivity measurement from backscattered light intensity, deriving model based on light beam geometry and path 20 p3238 A71-39333

Sunlight scattering by dust in upper atmosphere from primary twilight intensities investigations 20 p3219 A71-39647

Reflected radiation brightness field statistical structure in IR range from Cosmos 121 satellite measurements, calculating correlation functions and spectral densities 20 p3259 A71-39680

Short wave radiation fluxes estimation for earth-atmosphere system from Cosmos satellite data, studying brightness field angle structure 20 p3260 A71-39681

UV radiation in space and Venus atmosphere, studying L-alpha lines luminescence hot stars intensity, Milky Way brightness and hydrogen envelope existence 20 p3282 A71-39748

Height resolved atmospheric turbulence properties from photometric measurements of airglow intensity fluctuations, discussing detection, separation from noise and statistical analysis 20 p3227 A71-39837

Short time variability of intensity of optical pulses from pulsar NP 0532, using telescopes 20 p3303 A71-39930

Auroral far UV spectrum and intensity measurements, discussing atmospheric absorption effects on rocket-borne spectrometer sensitivity 21 p3372 A71-40039

Light curve and orbital elements of eclipsing binary star V 539 Arae 21 p3440 A71-40058

Planetary luminosity correlated with solar activity, discussing far UV and solar wind particle interactions with atmosphere 22 p3591 A71-41472

Subjective brightness of flashing light stimulus within fovea as function of stimulus size, noting edge effects contribution at suprathreshold levels 22 p3497 A71-41478

Flash threshold perception in relation to flicker, showing flicker/flash sensitivity ratio constancy over large intensity level range 22 p3497 A71-41479

Flashing lights effective intensity at threshold and suprathreshold levels, discussing Broca-Sulzer effect observance conditions 22 p3498 A71-41484

Exposing light and resulting density distribution and granularity in lower photographic emulsion layer, investigating modulation transfer function and power spectrum 22 p3538 A71-41733

High intensity light sources hazards analysis, discussing thermal detectors and vacuum and semiconductor photodiodes for pulsed laser outputs measurement 22 p3541 A71-41795

Beam electrons correlations effect on interference fringes visibility 22 p3546 A71-42243

Low light level TV system using Plumbicon tube and 3-stage image intensifiers 22 p3548 A71-42511

Large display direct view low light level system with objective lens, image intensifiers and eyepiece 22 p3548 A71-42512

Absolute magnitudes of 1965-1969 comets, including orbit elements, perihelion coordinates and maximum values of reduced head diameter and tail length 22 p3606 A71-42614

Sparrows pinealectomy effect on circadian rhythms of body temperature in light and darkness from radio telemetric monitoring 23 p3633 A71-43547

Flicker adaptation effect on visual sensitivity to temporal fluctuations of light intensity 23 p3635 A71-43974

Quasars light curves and intensity-time tables 23 p3769 A71-43993

Mach bands appearance in red/green triangular wave intensity distributions generated on CRT, quantifying perceived brightness distribution by matching with variously positioned light slit 24 p3800 A71-44468

Light brightness and duration effect on central vision response time during dark adaptation 24 p3795 A71-44535

LUNAR ATMOSPHERES

Lunar mascon origin, considering primordial atmosphere and hydrosphere formation from internal heating with resultant mass imbalance and isostatic compensation 03 p0492 A71-14053

Lunar atomic hydrogen atmosphere from solar wind proton bombardment, considering detection by scattered Lyman alpha radiation measurements 04 p0659 A71-15854

Mass spectroscopy applications to neutral and ionized terrestrial upper atmosphere, lunar atmosphere and space research 11 p1726 A71-25218

Solar wind noble gas composition on moon with aluminum foil exposure, confirming absence of lunar atmosphere and magnetic field 11 p1834 A71-26330

Lunar surface rocks Hg content under daytime temperatures volatilization conditions, considering cold trap and lunar atmosphere 12 p1958 A71-26692

Radon 222 distribution in lunar atmosphere and top surface 21 p3449 A71-40607

Lunar atmospheric contributions from solar wind, meteoric volatilization, internal degassing and rocket gases, discussing day and night neon concentrations 21 p3453 A71-41182

Lunar atmosphere as source of lunar surface gaseous elements, calculating ions trajectory and impact energy as function of interplanetary magnetic field strength 23 p3754 A71-43728

LUNAR BASES

Book on geochemical exploration of moon and planets covering orbital, compositional and surface studies, Apollo missions, Lunar Receiving Laboratories and data processing 05 p0813 A71-16950

Manned flight from Montgolfier Balloon to Apollo 13, discussing future space programs including lunar base and space shuttle 07 p1195 A71-19417

Star observation by moon-based telescope for star diameters, multiple components and precise occultation times by distortion and diffraction pattern analysis 14 p2312 A71-30374

Lunar surface base concept synthesis, considering program objectives and hardware operational approaches [AIAA PAPER 71-819] 17 p2723 A71-34725

LUNAR CINEMATOPHOTOGRAPHY

U LUNAR PHOTOGRAPHY

LUNAR COMMUNICATION

Apollo lunar surface communications, discussing VHF system for voice and telemetry and TV hardware and techniques 01 p0035 A71-10914

Lunar communications relay unit, discussing system design, capability and tradeoffs 01 p0035 A71-10919

Lunar roving vehicle telecommunication system requirements concerning vehicle functions, science experiments, crew operations and safety 14 p2200 A71-30915

Apollo lunar surface S band communications and TV systems and equipment, including ground commanded TV assembly 18 p2878 A71-36519

Lunar crust exploration by VLF surface waves, discussing frequency dependent depth penetration, conducting layers detection and communication or navigation use 20 p3291 A71-39313

LUNAR COMPOSITION

NT LUNAR CORE

Lunar upper crust structure and composition from radio wave reflection spectrum analysis 02 p0308 A71-12098

Elemental abundances of microtektites and tektites, noting differences from Apollo samples 02 p0312 A71-12363

Mg-Cr and Ba-rare earth relationships in stony meteorites and Apollo 11-12 soil and rocks 03 p0487 A71-13335

Eucrites Nuevo Laredo and Stannern significance in lunar-meteorite composition studies 03 p0487 A71-13336

O, Si, Al and Fe abundances of Apollo 12 lunar rock 12013 from neutron activation analysis 03 p0494 A71-14218

Apollo 12 lunar rock 12013 rare earth, alkaline and alkali metal and Sr 87/Sr 86 data, discussing light and dark component composition 03 p0494 A71-14221

Trace element patterns of Apollo 12 lunar rock 12013 light and dark portions, discussing Rb-Sr age and Li, K, Rb, Sr, Ba and rare earth concentrations 03 p0494 A71-14222

He, Ne, Ar and Xe from stepwise heating of Apollo 12 lunar rock 12013, discussing radiogenic and spallation components and He 3 and Ne 21 cosmic ray exposure ages 03 p0494 A71-14224

Apollo 12 lunar rock 12013 oxygen 18 and silicon 30 ratios, comparing to terrestrial basalts and gabbros, Apollo 11 rocks and oceanic rhyolite obsidians 03 p0495 A71-14225

Lunik 16 rock samples noting regolith, basalt, anorthosites, various mineral grains, solidified spherical droplets, breccias, glassy and scorified fragments and metallic iron particles 05 p0813 A71-16856

Amino acid contents of Apollo 11 and 12 fines, discussing laboratory syntheses 07 p1196 A71-19500

Age and composition effects on lunar surface processes and optical properties, explaining main albedo, maria, color contrasts and temporal changes 07 p1200 A71-20150

Lunar upper crust structure and composition from radio wave reflection spectrum analysis 08 p1362 A71-21148

Elemental analysis for lunar rocks and regolith, comparing silicon oxide and titanium oxide composition in Apollo 12 and Apollo 11 samples 10 p1672 A71-24389

Apollo 12 soils composition and derivation, finding feldspathic orthopyroxene rich rock and chemically comparable glass fragments 10 p1672 A71-24393

Lunar 12 spinel compositional variation and textures as petrogenetic indicators, showing magma differentiation by crystal settling after lunar surface extrusion 10 p1672 A71-24394

Lunar soil samples chemical composition, discussing comparison with earth minerals, solar wind and cosmic rays effects and implications for lunar and planetary evolution theory

10 p1677 A71-24692

Lunar electrical conductivity profile measurements, providing mantle-core stratification near surface thermal gradient, heat flux and composition data

11 p1822 A71-25632

Apollo 11 sample basalts lunar interior origin assumption from comparison with terrestrial massif anorthosite series, using chemical and petrographic analyses

11 p1834 A71-26452

Methane and deuteromethane released from Apollo 11 and 12 lunar fines by deuterated acid etch, using gas chromatography for carbon compounds separation

13 p2136 A71-28427

Coarse grained lunar basalt from Oceanus Procellarum, examining ground mass and subsolidus cooling history

14 p2313 A71-30427

Subsurface water detection on lunar traverse by tilt angle electromagnetic depth sounding

15 p2492 A71-32475

Lunar subsurface water detection from satellite in polar orbit around moon by electromagnetic measurement

15 p2492 A71-32476

Surface and subsurface water analysis on moon and planets by combination neutron experiment using epithermal die-away measurements of hydrogen

15 p2411 A71-32477

Water, carbon and rare gases in lunar crater breccias based on meteorites nature

15 p2494 A71-32490

Electrical conductivity of lunar rock, considering radial variation of bulk composition with oxygen loss in outer layers due to thermal cycles and vacuum

16 p2634 A71-33388

Apollo 11 and 12 lunar soil and rock samples abundance comparison based on Mossbauer spectroscopy

16 p2637 A71-33509

Crystallization behavior and chemical compositions of Apollo 11 lunar basalts including olivine and silica normative varieties

16 p2637 A71-33512

Lunar interior thermal history models for setting radioactive heat sources upper limits consistent with proposed temperature distribution

16 p2642 A71-33797

Lunar stratified composition based on electrical conductivity profile from magnetic field fluctuations measurement in terms of two layer model

18 p2961 A71-35993

Apollo 11 and 12 lunar rocks composition, suggesting depletion of K, Rb and Pb in solar nebula prior to final accretion of moon

18 p2963 A71-36228

Lunar mechanical and magnetic properties, discussing impact craters, rocks, soil iron abundance, mascons and convection processes

19 p3142 A71-38020

Lunar soils structural-mechanical properties and composition, discussing volcanic origin and terrestrial analogs

20 p3295 A71-39618

Apollo lunar expeditions assessment, discussing rock samples composition, origin, age and relation to earth system

21 p3442 A71-40148

Lunar rocks composition, age, history and evolution, comparing to terrestrial basalts

22 p3599 A71-41943

Optical, chemical and structural properties of lunar bytownite twin from U stage, microprobe and X ray measurements

23 p3738 A71-43612

Apollo 12 lunar soil particles observation for reduced metal meteoritic inclusions, suggesting shock impact effects during meteoritic bombardment of moon

23 p3739 A71-43619

Mineralogy, chemistry and origin of KREEP (potassium, rare earth element and phosphorus) component in Apollo 12 soil and breccia samples from Ocean of Storms

23 p3741 A71-43632

Lunar maria igneous rock compositions and magmatic liquid viscosity from samples 12021 and 12022, using microprobe analyses

23 p3741 A71-43633

Hydrous analog stability in lunar amphibole Apollo samples as function of water vapor pressure and temperature

23 p3743 A71-43648

Noritic and anorthositic rock fragment proportions and sources in Apollo 12 soil samples

23 p3743 A71-43650

Mineralogical composition, modal distribution and bulk chemical analysis on Apollo 12 lunar fines

23 p3744 A71-43652

Apollo 12 Mare Procellarum soil glasses analyzed by ion and electron microprobe, discussing rock ages

23 p3744 A71-43653

Lunar fines samples 10084,148 and 12070,98, investigating grain size, mineral and chemical composition and optical properties

23 p3744 A71-43655

Lunar soil samples 12001,1, 12037, 12042,25 and 12070,100 exterior morphology and chemistry, noting environmental temperature decrease, crater formation and meteorite impact

23 p3745 A71-43662

Gas-liquid chromatography and mass spectrometry of lunar fines and glass constitution by preparing trimethylsilyl derivatives of discrete silicate ions

23 p3746 A71-43668

Neutron activation data on Zn, Ga, Ge, Cd, In and Ir trace elements for Apollo 12 lunar rock and soil sample

23 p3747 A71-43673

Apollo 12 specimens elemental abundance from neutron activation analysis, discussing fractional crystallization, partial melting, rare earth abundances and soil mixing model

23 p3747 A71-43674

Trace element abundances in Apollo 12 lunar rock and fine samples and mineral separates from Ocean of Storms

23 p3747 A71-43675

Apollo 11 and 12 lunar rocks and fines, discussing compositional variations and relationships to stony meteorites

23 p3747 A71-43677

Apollo 12 lunar soil, breccia and igneous rock samples, determining elemental abundances with spark source mass spectrometry and neutron activation analysis

23 p3748 A71-43680

Trace elements concentration and metallic particles analysis from Apollo 12 lunar igneous rocks, soils and breccias, noting relation to sample location and exposure age

23 p3748 A71-43681

Apollo 12 lunar soils and igneous rocks from Ocean of Storms, determining major, minor and trace element composition with chemical, X ray fluorescence and spectrographic techniques

23 p3748 A71-43683

Apollo 12 lunar rocks and fines under high energy neutron activation analysis, determining O, Si, Al, Mg and Fe abundances

23 p3748 A71-43685

Apollo 11 and 12 lunar samples elemental composition analysis, using activation and mass spectrometric isotope dilution analysis and emission spectroscopy

23 p3749 A71-43687

Apollo 12 lunar samples 12040,36 and 12064,38 chemical analysis for major elements, discussing titanium, water and iron content

23 p3749 A71-43688

Apollo 12 lunar samples halogen and trace element composition, investigating chemical and physical processes affecting surface halides, platinum group metals and Hg

23 p3749 A71-43689

Apollo 11 and 12 lunar fines 10084 and 12070 trace element determination, using multielement neutron activation analysis

23 p3749 A71-43690

Apollo 12 lunar rocks 12002, 12018, 12021 and 12038 and soil sample 12070 elemental abundances, discussing origin and comparison to meteorites and terrestrial rocks

23 p3749 A71-43691

Lunar soil samples 10084,141 and 12070,83 and rock fragment 12063,73 multielement analysis using neutron activation and nondispersive X ray fluorescence techniques

23 p3749 A71-43692

Apollo 11 and 12 lunar rock and soil examination, emphasizing Au and Ag excess in soil

23 p3750 A71-43693

Apollo 12 lunar rock rare earth element abundances, comparing to Icelandic basalt flow

23 p3750 A71-43694

Apollo 12 samples total C and N abundances suggesting indigenous lunar material with solar wind component

23 p3750 A71-43698

Apollo 12 lunar dust and rocks carbon and hydrogen amount and isotopic composition determination, using in vacuo outgassing and combustion in oxygen

23 p3751 A71-43703

Apollo 11 and 12 lunar samples O 18/O 16, Si 30/Si 28, D/H and C 13/C 12 ratio determination, examining whole rocks, breccias, soils, plagioclases and fines

23 p3751 A71-43705

Apollo 12 lunar samples 12002,128, 12021,49, 12038,43 and 12070,52 vanadium isotopic composition

23 p3751 A71-43706

Rb, Sr, K, U, Th and Pb concentrations in Apollo 12 lunar soil samples, discussing lunar age estimates

23 p3752 A71-43711

Microprobe measurements of rare gas composition for lunar rock 12013,10,31 mineral separates, noting cosmic ray bombardment role in K and Ar production

23 p3753 A71-43721

Inert gases release from breccia 10065 by lunar rock vacuum crushing at room temperature, suggesting breccia formation from gas-rich parent materials

23 p3754 A71-43725

Lunar cosmogenic radionuclides production time and spatial dependence calculations, comparing Apollo 11 and 12 measurements

23 p3754 A71-43729

Apollo 12 lunar glass spherules chemical composition, homogeneity, densities and thermal histories, using electron probe analysis

23 p3758 A71-43758

Alpha radioactivity in Surveyor 3 camera visor, calculating upper limit of Po 210 at equilibrium of Oceanus Procellarum

23 p3765 A71-43812

LUNAR CORE

Lunar drilling equipment design from probe data, describing powered hand drill, 3 meter coring device and Apollo lunar surface drill

15 p2385 A71-32497

Dielectric properties of Apollo 12 samples and lunar interior as function of frequency and temperature

23 p3762 A71-43788

LUNAR CRATERS

Large lunar craters and circular maria origin problem, disputing formation by meteorite impacts

01 p0149 A71-10047

Large meteor masses collisions with earth and moon, implying lunar craters endogeneous origin based on meteor dimension data extrapolation

01 p0149 A71-10050

Lunar crater origin determination by terrestrial volcanic and meteoritic craters and maars geological criteria application to Lunar Orbiter 5 photographs

02 p0313 A71-12549

Lunar maria and large craters absolute ages determination under outer layers viscosity assumptions

04 p0659 A71-15856

Apollo lunar rock sample solidification and impact rates, deriving cratering time behavior

04 p0660 A71-15863

Craters on lunar crater Copernicus inner walls, discussing origin based on size distribution frequency comparison with terrestrial basalt flow collapse craters

07 p1196 A71-19542

Large lunar craters and circular maria origin problem, disputing formation by meteorite impacts

08 p1361 A71-21041

Large meteor masses collisions with earth and moon, implying lunar craters endogeneous origin based on meteor dimension data extrapolation

08 p1361 A71-21044

Lunar two cycle interior thermal history influence on maria and crater morphology, noting active and passive phase roles

09 p1520 A71-22836

Lunar crater rays production mechanism, observed by high resolution photographs of Copernicus

09 p1530 A71-23712

Lunar origin and evolution, discussing craters, mare collisions, formation time, heat balance, gravity anomalies, density and chemical composition

11 p1822 A71-25689

Directional thermal emission from rough lunar surface as function of crater frequency, aspect ratio and solar deviation angle, comparing to Lambertian behavior

11 p1833 A71-26256

Lunar impact cratering in geologic time, deriving meteoritic flux mass approximation and planetesimals origin

13 p2134 A71-28288

Lunar rocks in large bright rayed craters, calculating thermal abnormality model

13 p2138 A71-28697

Lunar craters formation impact vs volcanic theories, using lunar probes for recognizing moon surface shocked materials

15 p2493 A71-32481

Glazing lunar craterlet interiors in Apollo 11 observations, comparing solar flash heating and volcanic bomb impact formation

15 p2493 A71-32484

Lunar surface rejuvenation processes, considering mare flooding and crater destruction by seismic waves and ballistic sedimentation

15 p2493 A71-32487

Lunar surface age determination by crater age classification system, using Lunar Orbiter 4 photographs

15 p2493 A71-32488

Water, carbon and rare gases in lunar crater breccias based on meteorites nature

15 p2494 A71-32490

Lunar-Martian craters relationship, discussing volcanic model of lava infilling, caldera floors and magmatic pressure

15 p2494 A71-32494

- Vertical motions on moon resulting from stress differences leading to isostatic equilibrium, discussing maria, craters and mascons
16 p2636 A71-33504
- Lunar vs terrestrial origin of tektites, discussing meteoritic impact craters, age factor and properties
16 p2637 A71-33517
- Small lunar maria craters morphological maturity as function of age and dimensions
16 p2638 A71-33670
- Radar observation of lunar distance, motion and surface statistical nature, noting enhanced reflectivity associated with craters
17 p2804 A71-35178
- Small lunar and terrestrial craters, determining impact or volcanic origin by depth-diameter ratio
19 p3137 A71-37677
- Cauldron subsidence in lunar post-mare crater contiguous pair, discussing compatibility with volcanic origin hypothesis
19 p3137 A71-37680
- Morphological features of crater Copernicus as lunar caldera, observing agreement with volcanic origin
19 p3137 A71-37681
- Far side lunar craters nomenclature, listing names with identifying biographical data
19 p3145 A71-38271
- Near side lunar mare surfaces ages interpretation in terms of geomorphic indices based on crater number density
21 p3444 A71-40205
- Planetary and lunar meteorite craters classification according to radius logarithm to base ten, covering diameter size from 2 microns to 2000 km
21 p3444 A71-40206
- Origin and evolution of multiring basins on lunar surface, giving crater diameter distribution
21 p3448 A71-40548
- Limited interval definitions of photometric functions of lunar crater walls by photography from orbiting Apollo 11
22 p3603 A71-42187
- Lunar surface orientation of whole Apollo 12 rocks, considering microcraters distribution
23 p3765 A71-43806
- Small lunar crater vicinity boulders distribution analysis from Orbiter 3 high resolution photographs, suggesting impact and volcanic origin of crater kinds
24 p3874 A71-45187
- LUNAR CRUST**
NT LUNAR CORE
Lunar upper crust structure and composition from radio wave reflection spectrum analysis
02 p0308 A71-12098
- Lunar upper crust structure and composition from radio wave reflection spectrum analysis
08 p3162 A71-21148
- Tumor theory of crust formation and moon-earth consolidation, showing fractional crystallization of basaltoid silicate melts
10 p1681 A71-25112
- Lunar electrical conductivity profile measurements, providing mantle-core stratification near surface thermal gradient, heat flux and composition data
11 p1822 A71-25632
- Interplanetary magnetic field measurements from lunar surface and lunar orbit, discussing solar wind effects on bulk electrical conductivity of lunar crust
12 p1947 A71-26691
- Lunar crust regolith thermophysical properties concerning particle size and mass, specific heat and thermal conductivity from Luna 16 automatic station sampler
12 p1963 A71-26964
- Lunar crust tectonic analysis, using mosaic pattern technique based on eightfold division of spherical surface
15 p2493 A71-32486
- Lunar surface age determination by crater age classification system, using Lunar Orbiter 4 photographs
15 p2493 A71-32488
- Lunar and Martian subsurface liquid water under porous rock layers and permafrost, using terrestrial hydrogeology analogs
15 p2494 A71-32491
- Lunar anorthosite crust flotation, fractional crystallization process in seas and mascons genesis based on experimental data and petrogenetic scheme
16 p2636 A71-33505
- Lunar surface anomalous brightness during 26 March 1970 photometric and polarimetric observations, discussing possible correlation to solar activity
17 p2797 A71-34183
- Lunar crust regolith thermophysical properties concerning particle size and mass, specific heat and thermal conductivity from Luna 16 automatic station sampler
19 p3144 A71-38259
- Lunar crust exploration by VLF surface waves, discussing frequency dependent depth penetration, conducting layers detection and communication or navigation use
20 p3291 A71-39313
- Polarized plane electromagnetic waves oblique specular reflection from discretely layered lunar models based on Apollo 11 and 12 data, determining near-surface layers electrical properties
21 p3450 A71-40644
- LUNAR DUST**
Apollo 11 lunar powder and rock samples optical properties noting similarity over Tranquility base area
02 p0305 A71-11986
- Lunar dust samples 10084 and 12070 texture studies with electron microscope, noting difference from meteoritic or lunar rock matter
05 p0807 A71-16299
- Lunabase regions origin, suggesting volcanic dust masses fluidized by volcanic gases
09 p1528 A71-23550
- Superheavy transuranic elements in meteorites and lunar dust by fossil track microscopy
10 p1673 A71-24424
- Lunar dust deposition and brushing effects on spectral solar reflectance of thermal control materials in vacuum
11 p1799 A71-26241
- Thermal conductivity of Apollo 11 lunar fines as function of temperature, pressure and bulk density
11 p1833 A71-26255
- Surveyor 3 thermal control surfaces analysis from Apollo 12 samples collection, discussing spectral reflectance and lunar dust effects on surface finishes optical properties
12 p1920 A71-26759
- Lunar dust reflectance degradation of thermal control paint on Surveyor 3 TV camera, separating solar radiation effects by analytical model
12 p1920 A71-26760
- Apollo 11 lunar material characteristics and age, emphasizing fine lunar dust
13 p2138 A71-28765
- U-Pb and Th-Pb age discrepancy in lunar dust, proposing Rn-222 emanation in decay chains
14 p2307 A71-29733
- Spectral emittance ranges of Apollo 12 lunar fines dependent on density for 2.5-14 micron wavelengths
19 p3142 A71-37992
- Gegenschein as zodiacal light illuminated lunar dust ejected from meteorite impacts
20 p3286 A71-38730
- Moon surface electrical conductivity, seismic transmission properties, dust components, chemical analysis and comparison to earth
20 p3295 A71-39615
- Lunar dust potential as function of solar wind flux and particle photoefficiency
20 p3298 A71-39639
- Dust particle measurements in selenocentric and cislunar space /1967-1969/ by Lunar Explorer 35 and OGO 3
20 p3298 A71-39640
- Lunar fines samples 10084,148 and 12070,98, investigating grain size, mineral and chemical composition and optical properties
23 p3744 A71-43655
- Lunar glassy objects and mineral grains surface microstructure by optical and scanning electron microscopy, comparing with tektites and terrestrial volcanic analogs
23 p3745 A71-43664
- Gas-liquid chromatography and mass spectrometry of lunar fines and glass constitution by preparing trimethylsilyl derivatives of discrete silicate ions
23 p3746 A71-43668
- Apollo 12 lunar dust sample 12070,128, determining response to effective agents of earth-type chemical weathering
23 p3746 A71-43669
- Apollo 12 lunar dust and rocks carbon and hydrogen amount and isotopic composition determination, using in vacuo outgassing and combustion in oxygen
23 p3751 A71-43703
- Apollo 11 and 12 lunar dust and rocks, determining Be and Cr contents by gas chromatography for comparison with crystalline rocks
23 p3751 A71-43707
- Apollo 12 lunar dust, rocks and microbreccia microsection examined for evidence of biogenic structure
23 p3757 A71-43746
- Ultramicroscopic texture and radiation damage in Apollo 11 and 12 micron sized lunar dust grains compared with meteoritic rocks
23 p3758 A71-43756
- IR vibrational spectroscopic analysis of Apollo 11 and 12 rocks and dust isolated silicate minerals, using LF absorption bands
23 p3759 A71-43766
- Lunar fines luminescence emission spectra in visible and near IR region under proton and electron excitations, discussing cause and plagioclase distribution
23 p3760 A71-43777
- Surveyor 3 surfaces discoloration and lunar dust contamination, noting Apollo 12 lunar module caused disturbances by on-site observation
23 p3766 A71-43816
- LUNAR ECHOES**
NT LUNAR RADAR ECHOES
- Quasi-specular and Lambert reflection of short radio waves from lunar surface dependent on central portion of near side
16 p2543 A71-33668
- Lunar laser ranging experiments in Japan, detecting returned signals from Apollo 11 retroreflector surface package
16 p2543 A71-33812
- LUNAR ECLIPSES**
Interior umbra observations during lunar eclipses, using photometric analysis
09 p1530 A71-23718
- IR study of thermal anomalies during lunar night, discussing ages and distribution on terrain
17 p2797 A71-34184
- LUNAR EFFECTS**
NT LUNAR GRAVITATIONAL EFFECTS
NT LUNAR TIDES
Lunar ephemeris for nanosecond resolution laser ranging systems by literal and numerical integration techniques
05 p0811 A71-16682
- High energy muon flux diurnal variations related to lunar time
06 p0960 A71-18169
- Solar and lunar modulation of geophysical parameters, atmospheric electricity and thunderstorms in complex space-meteorology scope
10 p1604 A71-24706
- Lunar motion theory, discussing radial perturbation, variation, parallaxic and annual inequalities, secular acceleration and evection
11 p1822 A71-25684
- Hydrogen plasma simulation of solar wind-planetary body interaction, showing electric fields behind moon and Venus
11 p1816 A71-25755
- Gravitational lunar theory high order solution for geophysical relevance, discussing perturbation methods and computer analyzed ephemeris time
12 p1961 A71-26837
- Earth-moon tectonic relationships and structural similarity, analyzing earthquake frequency dependence on lunar phase and distance based on Middlehurst catalogs
15 p2492 A71-32478
- Error independence and elasticity allowance for moon librations and satellite perturbations
20 p3286 A71-38759
- Lunar and solar daily geomagnetic variation morphology correlation based on atmospheric dynamo model
20 p3217 A71-39515
- Lunar daily geomagnetic variations separation into oceanic and ionospheric origin in Indian region
23 p3667 A71-43149
- LUNAR ENVIRONMENT**
NT LUNAR ATMOSPHERES
Particulate silicates IR emission spectra under simulated lunar conditions, noting existence of nearly optimum conditions on moon surface
02 p0305 A71-11987
- Thermal environment loads in lunar ambulation, discussing Apollo EVA suit system and internally produced heat
02 p0207 A71-12386
- Measuring instrument for lunar surface layer heat flow, temperature and thermal conductivity
04 p0599 A71-15543
- Long term lunar surface environment, discussing radiation, thermal and meteoroid protection, water budget, carbon dioxide removal and air lock design
11 p1726 A71-26534
- Lunar surface meteoroid activity from Surveyor 3 sample examination, comparing with predictions by cumulative-flux and near-earth models
16 p2643 A71-33849
- Bacterial spores survival under simulated lunar surface conditions, comparing results with vegetable cells experiments
21 p3334 A71-40567
- Apollo 12 returned Surveyor 3 component materials analysis for lunar exposure effects by nondestructive and destructive tests
23 p3765 A71-43811
- Streptococcus mitis bacterium in Apollo 12 lunar retrieved Surveyor 3 TV camera, discussing prelaunch deposition and survival
23 p3633 A71-43815
- X ray probe, scanning electron microscopy and spectral reflectance analysis of lunar environment effects on Apollo 12 returned Surveyor 3 materials surface cratering
23 p3766 A71-43818
- Apollo 12 returned Surveyor 3 samples examination for meteoroid and lunar ejecta impacts evidence by optical and electron microscopy
23 p3766 A71-43819
- Surveyor 3 unpainted Al tubing examination by replication electron microscopy for surface damage due to particle impact and ion bombardment in lunar environment
23 p3766 A71-43821

LUNAR ESCAPE DEVICES

Piloted lunar escape to orbit systems simulation using simplified manual guidance and attitude control [AIAA PAPER 71-60] 06 p0977 A71-18519

LUNAR EVOLUTION

Large lunar craters and circular maria origin problem, disputing formation by meteorite impacts 01 p0149 A71-10047

Large meteor masses collisions with earth and moon, implying lunar craters endogenous origin based on meteor dimension data extrapolation 01 p0149 A71-10050

Apollo 11 basalts chemistry and petrogenesis by partial melting, considering implications for lunar origin theories 02 p0305 A71-11981

Apollo 11 crystalline igneous rocks mineralogy and petrology, suggesting origin from pyroxenite mantle melting 02 p0305 A71-11982

Lunar origin by earth-moon fission, deriving parent planet characteristics from geochemical considerations 02 p0306 A71-11991

Lunar crater origin determination by terrestrial volcanic and meteoritic craters and maars geological criteria application to Lunar Orbiter 5 photographs 02 p0313 A71-12549

Lunar mascon origin, considering primordial atmosphere and hydrosphere formation from internal heating with resultant mass imbalance and isostatic compensation 03 p0492 A71-14053

Apollo 12 lunar rock 12013 origin, determining age by U, Th and Pb isotopic study 03 p0494 A71-14223

Lunar maria and large craters absolute ages determination under outer layers viscosity assumptions 04 p0659 A71-15856

Lunar hot spots surface distribution-geomorphic index relationship, discussing maria, terrae and regolith evolutionary stage 05 p0809 A71-16462

Craters on lunar crater Copernicus inner walls, discussing origin based on size distribution frequency comparison with terrestrial basalt flow collapse craters 07 p1196 A71-19542

Troilite rich Ni-Fe particle /mini-moon/ from lunar surface, discussing different theories of origin 07 p1196 A71-19543

Apollo 11 and 12 lunar samples, discussing chemical composition relationship to lunar origin 07 p1196 A71-19605

Age and composition effects on lunar surface processes and optical properties, explaining main albedo, maria, color contrasts and temporal changes 07 p1200 A71-20150

Large lunar craters and circular maria origin problem, disputing formation by meteorite impacts 08 p1361 A71-21041

Large meteor masses collisions with earth and moon, implying lunar craters endogenous origin based on meteor dimension data extrapolation 08 p1361 A71-21044

Lunar two cycle interior thermal history influence on maria and crater morphology, noting active and passive phase roles 09 p1520 A71-22836

Lunabase regions origin, suggesting volcanic dust masses fluidized by volcanic gases 09 p1528 A71-23550

Lunar soil samples chemical composition, discussing comparison with earth minerals, solar wind and cosmic rays effects and implications for lunar and planetary evolution theory 10 p1677 A71-24692

Lunar origin and evolution, discussing craters, mare collisions, formation time, heat balance, gravity anomalies, density and chemical composition 11 p1834 A71-25689

Theory of originally cool moon in light of Apollo evidence regarding lunar rocks composition, mascons and lunar topology 11 p1834 A71-26379

Glazed lunar rocks, explaining origin as result of nearby meteoritic impact 13 p2137 A71-28515

Lunar chronology and evolution from Rb and Sr internal isochrons on Apollo 11 and 12 crystalline rock samples 13 p2142 A71-29142

Ancient lunar magnetic field detection and origin from remanent magnetism in Apollo 11 breccia and basaltic rock samples 14 p2306 A71-29725

Lunar origin dynamics, discussing orbit evolution by tidal friction and celestial mechanical theory 14 p2307 A71-29901

Lunar craters formation impact vs volcanic theories, using lunar probes for recognizing moon surface shocked materials 15 p2493 A71-32481

Lunar surface structural evolution from energy conservation considerations, discussing earth primitive continent acquisition from moon 15 p2493 A71-32485

Lunar surface rejuvenation processes, considering mare flooding and crater destruction by seismic waves and ballistic sedimentation 15 p2493 A71-32487

Lunar gravitational field interpretation based on Apollo data, considering mascons creation, isostasy, thermal history and maria orientation hypotheses 16 p2636 A71-33506

Lunar and Martian cratering possibility by cometary icy blocks based on sonic impact fluidation experiments 16 p2636 A71-33508

Lunar origin hypothesis of surface layer accumulation and fusion by superluminous phase of sun based on old igneous rocks and cool interior evidence 16 p2637 A71-33510

Lunar interior thermal history models for setting radioactive heat sources upper limits consistent with proposed temperature distribution 16 p2642 A71-33797

Apollo 11 and 12 lunar rocks composition, suggesting depletion of K, Rb and Pb in solar nebula prior to final accretion of moon 18 p2963 A71-36228

Lunar volcano-tectonic processes, considering primary circular or polygonal surface features evolution 19 p3052 A71-37678

Cauldron subsidence in lunar post-mare crater contiguous pair, discussing compatibility with volcanic origin hypothesis 19 p3137 A71-37680

Lunar soils structural-mechanical properties and composition, discussing volcanic origin and terrestrial analogs 20 p3295 A71-39618

Apollo lunar expeditions assessment, discussing rock samples composition, origin, age and relation to earth system 21 p3442 A71-40148

Near side lunar mare surfaces ages interpretation in terms of geomorphic indices based on crater number density 21 p3444 A71-40205

Origin and evolution of multiring basins on lunar surface, giving crater diameter distribution 21 p3448 A71-40548

Lunar near surface seismic velocity distribution for cold accretion and meteorite impact models, comparing travel times 21 p3450 A71-40645

Apollo and Luna data related to lunar origin, evolution and processes, discussing mare basalts, interior composition, regolith, breccias, chronology, surface properties, etc 21 p3453 A71-41176

Lunar rocks composition, age, history and evolution, comparing to terrestrial basalts 22 p3599 A71-41943

Apollo 12 basalts petrology and petrogenesis, studying crystallization sequences 23 p3743 A71-43646

Petrogenesis and crystallization of protohypersthene basalts in lunar maria lava lakes, deducing eruption temperatures 23 p3743 A71-43647

Size distribution, composition and history of regolith fines at Apollo 12 site 23 p3743 A71-43651

Grain size and modal analyses of lunar regoliths sampled by Apollo 11 and 12, discussing particles origin 23 p3744 A71-43654

Lunar soil samples 12001,1, 12037, 12042,25 and 12070,100 exterior morphology and chemistry, noting environmental temperature decrease, crater formation and meteorite impact 23 p3745 A71-43662

Lunar surface history model, discussing mascons, chemical composition, isochron ages and seismic and electrical properties of samples 23 p3746 A71-43670

Apollo 12 lunar rocks 12002, 12018, 12021 and 12038 and soil sample 12070 elemental abundances, discussing origin and comparison to meteorites and terrestrial rocks 23 p3749 A71-43691

Rb, Sr, K, U, Th and Pb concentrations in Apollo 12 lunar soil samples, discussing lunar age estimates 23 p3752 A71-43711

Radiation exposure history from fossil tracks in Apollo 12 surface rocks and double core regolith samples, comparing with Saint Severin meteorite 23 p3764 A71-43802

Lunar fines transportation process in mare surface evolution, suggesting electrostatics role from photographic and seismic evidence 23 p3765 A71-43810

Critique of paper on Apollo 11 ilmenite basalts petrology and lunar bodies origin and form 23 p3769 A71-43886

Lunar origin hypothesis, discussing Apollo 11 crystalline rocks nature and basalts petrogenesis 23 p3770 A71-44078

Lunar evolution theory, discussing terrestrial cluster dynamics during earth accumulation 24 p3870 A71-44811

Small lunar crater vicinity boulders distribution analysis from Orbiter 3 high resolution photographs, suggesting impact and volcanic origin of crater kinds 24 p3874 A71-45187

LUNAR EXPLORATION

Soviet bibliography concerning lunar surface physical properties, covering ground and orbiters observations data 01 p0148 A71-10044

LOLA /Location and Orientation of Lunar Astronauts/ system using RF ranging and solar sensor, discussing configuration, operation, accuracy and electronics 04 p0623 A71-15303

Lunar oscillations in ionospheric absorption measurements, noting tides in f-min during high sunspot years 05 p0740 A71-16434

Lunar bulk modulus, viscosity, inertia moments and density calculation from gravity potential values obtained by Luna 10 and Lunar Orbiter satellites 07 p1203 A71-20520

Soviet bibliography concerning lunar surface physical properties, covering ground and orbiters observations data 08 p1360 A71-21039

Location and Orientation of Lunar Astronauts system using radio frequency ranging and sun azimuth 08 p1331 A71-21241

Unmanned lunar logistics vehicle for extended manned lunar exploration support, discussing general design, propulsion and control systems 11 p1838 A71-25529

Lunar Roving Vehicle, discussing crew, mobility, power, deployment and navigation subsystems, environment and radio interference problems 11 p1747 A71-26527

Lunar ground effect machine, discussing operation principles, design, construction, terrain advantage and scale model testing 11 p1747 A71-26528

Long term lunar surface environment, discussing radiation, thermal and meteoroid protection, water budget, carbon dioxide removal and air lock design 11 p1726 A71-26534

Soviet lunar surface exploration, discussing luna 16 payloads, history and sample collecting 12 p1971 A71-26874

Lunar crust regolith thermophysical properties concerning particle size and mass, specific heat and thermal conductivity from Luna 16 automatic station sampler 12 p1963 A71-26964

Manned Lunar Roving Vehicle for Apollo 15 expedition, discussing subsystems design features 15 p2384 A71-31746

Papers on geological problems in lunar and planetary research covering sensing techniques, phenomenology, exploration methods, etc 15 p2492 A71-32469

Lunar drilling equipment design from probe data, describing powered hand drill, 3 meter coring device and Apollo lunar surface drill 15 p2385 A71-32497

Lunar surface meteoroid activity from Surveyor 3 sample examination, comparing with predictions by cumulative-flux and near-earth models 16 p2643 A71-33849

Bibliography and review of solar system bodies surfaces, considering remote sensing at UV, optical, IR, microwave and radio wavelengths, in situ lunar measurement and surface exploration 17 p2798 A71-34458

Lunar roving vehicle for Apollo 15 mission, discussing power, control, navigation and deployment systems in relation to lunar exploration requirements [AIAA PAPER 71-847] 17 p2723 A71-34707

Automated lunar landing missions with modified Mars Viking spacecraft, discussing propulsion and subsystems modifications, science payload and lunar exploration capabilities [AIAA PAPER 71-822] 17 p2812 A71-34724

Selenography and selenodesy with Apollo whole-disk lunar photograph, providing positions catalog in tabular form 18 p2965 A71-36294

Lunar exploration system based on modified earth-orbit space station in polar lunar orbit as remote sensor platform and lander deployment base 18 p2972 A71-36443

Lunar crust regolith thermophysical properties concerning particle size and mass, specific heat and thermal conductivity from Luna 16 automatic station sampler 19 p3144 A71-38259

Solar array technology for lunar surface applications including silicon cells, cadmium sulphide thin

films, temperature effects, prototype module and radiation degradation 20 p3181 A71-38941

Lunar crust exploration by VLF surface waves, discussing frequency dependent depth penetration, conducting layers detection and communication or navigation use 20 p3291 A71-39313

Apollo lunar explorations, reviewing landing, trajectories, hardware, mission problems and scientific studies 20 p3295 A71-39613

Experiences of living on moon, discussing effects on task performance and physical movements and observations of lunar surface, lighting and color 20 p3295 A71-39614

Computerized bacterial identification system to process Apollo spacecraft sample laboratory test results in NASA Planetary Quarantine Lunar Information System 22 p3504 A71-42233

NASA program for lunar and planetary exploration, listing missions, instrumentation, experiments and future aims 23 p3736 A71-43498

Lunar science - Conference, Houston, January 1971, Volume 1, Mineralogy and petrology, Volume 2, Chemical and isotope analyses, Volume 3, Physical properties/Surveyor 3 23 p3737 A71-43601

Unmanned lunar rover exploration objectives and requirements, considering heterogeneous surface 24 p3875 A71-45190

LUNAR EXPLORATION SYSTEM FOR APOLLO

Apollo lunar orbital missions, discussing remote sensing and photographic equipment for lunar sounding and mass spectrometry, gegenschein experiments and high quality metric photography 10 p1682 A71-24173

Manned Lunar Roving Vehicle for Apollo 15 expedition, discussing subsystems design features 15 p2384 A71-31746

LUNAR FAR SIDE

Photometric maps of reverse side lunar surface from AIM Zond 3 material 03 p0484 A71-13215

Lunar far side communication, discussing libration point and lunar orbit relay system for high bit rate telemetry, TV and astronaut backpack communication 04 p0555 A71-15339

Lunar reverse side, tabulating reference points on western libration zone and eastern sector 08 p1366 A71-21777

Lunar reverse side, cataloging reference points on western libration zone and eastern sector 15 p2495 A71-32682

Lunar configuration, limb relief and coordinates of western hemisphere and far side from Zond 6 photographs 16 p2638 A71-33669

Lunar gravity field global model from moon orbiters secular and long period trends, noting large anomaly on far side 16 p2642 A71-33815

Far side lunar craters nomenclature, listing names with identifying biographical data 19 p3145 A71-38271

LUNAR FLIGHT

Apollo cislunar navigation capability and procedures, describing onboard data acquisition and digital processing equipment 13 p2098 A71-29386

Turtles organs and tissues responses during Zond 5 and 7 lunar probes circumlunar flight 16 p2532 A71-33678

Geolunar interorbital transportation based on shuttle trajectories, interorbital rendezvous, elliptic orbits and terminal transfer 17 p2804 A71-35052

LUNAR FLYING VEHICLES

Lunar flying vehicle propulsion system optimization, discussing weight, performance, engine life, reliability, etc [AIAA PAPER 70-605] 11 p1810 A71-25504

LUNAR GEOLOGY

NT LUNAR CORE

Lunar glasses of impact origin, considering occurrence, abundance, optical properties and chemical composition for determination of regolith bulk, age and origin 04 p0644 A71-15130

Lunar mascons interpretation as meteorites impact, discussing use as gravitational waves detectors 04 p0661 A71-15904

Apollo 12 lunar rock examination, discussing soil mechanics, mineralogical and petrological aspects and surface features and fines 05 p0806 A71-16149

Apollo 11 igneous rocks potassium content vs irradiation exposure age, comparing lunar geology models 06 p0966 A71-17897

Tektites earth vs possible lunar or cometary origins, taking into account chemical composition 06 p0968 A71-17963

Troilite rich Ni-Fe particle /mini-moon/ from lunar surface, discussing different theories of origin 07 p1196 A71-19543

Gravitational anomaly of mascons formation on lunar surface from geological data analysis 09 p1519 A71-22532

Lunar origin hypothesis of surface layer accumulation and fusion by superluminous phase of sun based on old igneous rocks and cool interior evidence 16 p2637 A71-33510

Lunar seismic energy diffusion, calculating transmitted and reflected acoustic wave intensities as time function after explosion 16 p2637 A71-33511

Scanning electron microscope and petrographic observations of glass particles from Apollo 12 lunar soil sample, revealing surface features and origin 19 p3137 A71-37674

Apollo 14 lunar module landing site geology, studying samples from regolith and block ejecta deposit around young crater 19 p3144 A71-38180

Deep lunar interior elastic properties, seismic speeds and Debye temperature determination from equations of equilibrium and state and measured moment of inertia 20 p3286 A71-38738

Lunar Apennine-Hadley region geological implications from high resolution earth-based radar map and Lunar Orbiter photography 20 p3287 A71-38977

Lunar interior electrical conductivity and temperature three-layer model from magnetic transient response measurement in solar wind 20 p3301 A71-39877

Apollo and Luna data related to lunar origin, evolution and processes, discussing mare basalts, interior composition, regolith, breccias, chronology, surface properties, etc 21 p3453 A71-41176

Lunar electrical induction presence of subsurface spherical conducting bodies, determining tangential magnetic field component amplification at surface 21 p3453 A71-41358

Dribble spires in Snake River Plain, Idaho, discussing basalt lava features and remnants in lunar areas 22 p3533 A71-41839

Armstrongite and ilmenite basalt in Apollo 11 lunar samples, discussing formation process of titanium, potassium and silicon oxides 23 p3734 A71-43247

Apollo 12 lunar soil and breccia core tube and surface samples optical and electron microscope and microprobe analysis, relating data to geologic processes 23 p3744 A71-43656

Lunar rocks 12063,9 and 12004,11 opaque mineralogy and textural feature, comparing to Apollo 11 samples 23 p3745 A71-43661

LUNAR GRAVITATION

Lunar gravitational field parameters from Lunar Orbiters trajectory measurement, discussing theoretical basis 01 p0149 A71-10048

Lunar moments of inertia and density distributions, using gravitational potential and physical librations 01 p0158 A71-10772

Lunar surface mascon structure and origin from mass estimates, noting contributions to lunar gravity field variations 02 p0306 A71-11990

Lunar bulk modulus, viscosity, inertia moments and density calculation from gravity potential values obtained by Luna 10 and Lunar Orbiter satellites 07 p1203 A71-20520

Lunar gravitational field parameters from Lunar Orbiters trajectory measurement, discussing theoretical basis 08 p1361 A71-21042

Lunar surface mass distribution, using dynamic point mass solution 09 p1530 A71-23717

Lunar origin and evolution, discussing craters, mare collisions, formation time, heat balance, gravity anomalies, density and chemical composition 11 p1822 A71-25689

Microthrust powered spacecraft earth escape, using lunar attraction by orbiting spacecraft with vector opposite to moon 12 p1968 A71-27579

Lunar gravitational field interpretation based on Apollo data, considering mascons creation, isostasy, thermal history and maria orientation hypotheses 16 p2636 A71-33506

Gravity anomaly and lunar radius measurement at Apollo 12 landing site, using data telemetered to earth from surface module 16 p2636 A71-33507

Lunar gravity measurements by Apollo 14 Doppler radio tracking during low altitude orbits, correlating variations with surface features 16 p2641 A71-33771

Lunar gravity field global model from moon orbiters secular and long period trends, noting large anomaly on far side 16 p2642 A71-33815

Gravity determination at Apollo 14 landing site, finding measured value consistent with data from lunar potential models 18 p2964 A71-36283

Global lunar gravity field from weighted least squares analysis of Lunar Orbiters elements, deriving zonal and sectorial harmonics from libration data 21 p3443 A71-40183

Dynamic derivation of surface layer representation of lunar gravitational field from Doppler observations on polar and equatorial lunar orbiters 21 p3449 A71-40643

Low gravity field phenomena, discussing vertical jump on moon, ball trajectories launched from asteroid and voyage to neutron star 22 p3600 A71-41983

Lunar gravity estimate from low degree spherical harmonic coefficients in potential model and Lunar Orbiter 4 radio tracking data reduction 23 p3768 A71-43882

LUNAR GRAVITATIONAL EFFECTS

Long term evolution of close low eccentricity lunar satellite orbits, describing lunar gravity effects by spherical harmonic expansion 04 p0655 A71-15723

Lunar gravitational field application for placing spacecraft into static earth satellite orbit with standing position with respect to rotating earth 12 p1957 A71-26627

Optimal lunar springboard effect for maximum characteristics velocity savings on interplanetary missions utilizing gravitational field by departing spacecraft 12 p1970 A71-27718

Human performance in various locomotive tasks under simulated lunar reduced gravity conditions, classifying test stands and equipment 15 p2362 A71-31304

Lunar gravitational field application in interplanetary travel, investigating spacecraft orbits by data processing machine 17 p2797 A71-34186

Lunar and solar gravitation effects on leveling from formulas and nomogram, noting seasonal maximum effect in southern latitudes and Northern Hemisphere 23 p3670 A71-43302

LUNAR IONOSPHERE

U LUNAR ATMOSPHERES

LUNAR LANDING

Apollo Command and Service Module simulation of flight phases in lunar landing missions 02 p0237 A71-11792

Seismograph recording of Apollo 12 lunar module impact as result of secondary ejecta spray around seismometer or translunar seismic wave propagation 04 p0644 A71-15128

Unmanned Soviet spacecraft Luna 16 mission, describing landing techniques, sample taking and experiment conduction 05 p0805 A71-16147

Apollo 12 Lunar Module high landing accuracy, discussing control actions, trajectory error sources and power descent 07 p1206 A71-19086

Optimal thrust programming for rocket near spherical planet, transfer between circular orbits and lunar landing at predicted point 10 p1683 A71-24847

Automated lunar landing missions with modified Mars Viking spacecraft, discussing propulsion and subsystems modifications, science payload and lunar exploration capabilities [AIAA PAPER 71-822] 17 p2812 A71-34724

Position determination on planetary surface from gravity and star line-of-sight direction measurements, presenting numerical results for Apollo lunar landing missions [AIAA PAPER 71-900] 19 p3095 A71-37151

Luna 18 mission accomplishments in lunar orbital automatic navigation techniques and arrival point coordinate accuracy 22 p3597 A71-41506

LUNAR LANDING MODULES

Apollo lunar module structural integrity for lunar landing verified by Monte Carlo dynamic analysis 07 p1205 A71-18896

Apollo spacecraft and lunar landing module thermal control surfaces, considering inorganic silicate bonded paint 09 p1533 A71-23426

Soft lunar landing powered descent optimal control for cost functional minimization, considering linear analytic approach with fuel consumption reduction 10 p1682 A71-24330

Lunik 16 and 17 automatic lunar landing stations and Lunokhod-1 lunar surface vehicle, describing propulsion systems, control elements and scientific equipment 17 p2724 A71-35401

LUNAR LANDING SITES

LUNAR LANDING SITES

Thermoluminescence glow curve and decay characteristics of Apollo 12 fines and soil samples, suggesting lower mean daytime surface temperature at site
10 p1672 A71-24395

Lunar landing site suitability, using stereoscopic medium and high resolution photography
11 p1836 A71-26533

Lunik spacecraft soil sampler landing site geological-morphological analysis from television images, indicating formation patterns similar to equatorial zone seas microrelief
12 p1966 A71-27302

Apollo 12 landing site morphological and textural details from Surveyor 3 photography, considering lunar surface impact and volcanic models
15 p2493 A71-32483

Gravity anomaly and lunar radius measurement at Apollo 12 landing site, using data telemetered to earth from surface module
16 p2636 A71-33507

Gravity determination at Apollo 14 landing site, finding measured value consistent with data from lunar potential models
18 p2964 A71-36283

Apollo 14 lunar module landing site geology, studying samples from regolith and block ejecta deposit around young crater
19 p3144 A71-38180

Lunik spacecraft soil sampler landing site geological-morphological analysis from TV images, indicating formation patterns similar to equatorial zone seas microrelief
19 p3145 A71-38261

Azimuth frequency plots of regolith surface lineaments at Apollo 11 and 12 landing sites
23 p3737 A71-43604

LUNAR LAUNCH

Lunar seismic reaction to Apollo 12 module launch stage impact, taking into account multistage soil scattering
02 p0304 A71-11921

LOX release from Apollo 8 lunar launch vehicle, forming small particle clouds for scattering experiments
06 p0963 A71-17256

Lunar seismic reaction to Apollo 12 module launch stage impact, taking into account multistage soil scattering
13 p2134 A71-28208

LUNAR LIMB

Lunar arbitrary and free librations and Euler motion of poles, considering hard and elastic models
01 p0158 A71-10807

Lunar physical libration in longitude, considering nonlinear and dissipation terms
09 p1530 A71-23715

Unlit lunar limb observations at IR wavelengths, presenting temperature charts and thermal abnormalities
09 p1530 A71-23716

Lunar libration presented as general rotation of solid body in external force field
11 p1822 A71-25685

Lunar reverse side, cataloging reference points on western libration zone and eastern sector
15 p2495 A71-32682

Lunar configuration, limb relief and coordinates of western hemisphere and far side from Zond 6 photographs
16 p2638 A71-33669

Moon marginal zone charts for determining limb corrections applied to reduction of stellar occultation timing
17 p2797 A71-34185

LUNAR LOGISTICS

Unmanned lunar logistics vehicle for extended manned lunar exploration support, discussing general design, propulsion and control systems
11 p1838 A71-25529

LUNAR LUMINESCENCE

Moon and Mars brightness distribution, considering surface roughness, albedo, fragmentation and walls between pores
06 p0975 A71-18447

Interior umbra observations during lunar eclipses, using photometric analysis
09 p1530 A71-23718

Lunar surface optical properties, examining albedo, color, brightness variation and polarization
11 p1822 A71-25688

Moon and Mars brightness distribution, considering surface roughness, albedo, fragmentation and walls between pores
12 p1955 A71-26597

Optical fluorescence spectra of rock forming minerals for quantitative analysis of lunar surface
15 p2411 A71-32471

Optical fluorescence of lunar transients in UV to IR range for rock forming silicates, using electron microprobe with cathode luminescence capability
15 p2492 A71-32472

Lunar flare transients consisting of gaseous emissions and regional /long term/ or local /short term/ luminescence
15 p2492 A71-32480

Lunar surface anomalous brightness during 26 March 1970 photometric and polarimetric observations, discussing possible correlation to solar activity
17 p2797 A71-34183

Gegenschein as zodiacal light illuminated lunar dust ejected from meteorite impacts
20 p3286 A71-38730

LUNAR MAGNETIC FIELDS

Lunar and solar periodic magnetic variations, using time series analysis based on discrete Fourier transforms for frequency spectrum lines
04 p0582 A71-15097

Lunar magnetic field demagnetization effect hypothesis for explaining Apollo 11 lunar rock samples remanent magnetization
07 p1200 A71-20055

Fossil lunar magnetism observations, using magnetometer data from orbiter Explorer 35
08 p1365 A71-21747

Solar wind simulation for interaction with lunar magnetic field, discussing particle shadowing effects generation of electric fields
09 p1514 A71-23310

Solar wind noble gas composition on moon with aluminum foil exposure, confirming absence of lunar atmosphere and magnetic field
11 p1834 A71-26330

Lunar diamagnetic cavity signatures from Ames magnetometer experiment on Explorer 35 orbiter, indicating solar wind interaction
13 p2132 A71-27909

Solar wind deflection due to permanent lunar surface magnetism
13 p2129 A71-28780

Ancient lunar magnetic field detection and origin from remanent magnetism in Apollo 11 breccia and basaltic rock samples
14 p2306 A71-29725

Simultaneous two magnetometer measurements of weak magnetic fields in interplanetary space, near moon and planets by satellites in presence of spacecraft field
15 p2406 A71-31753

Lunar magnetic fields measured by magnetometers placed by Apollo 12 and 14 astronauts, considering permanent fields due to fossil magnetic material and transient fields
17 p2811 A71-35734

Lunar electrical induction presence of subsurface spherical conducting bodies, determining tangential magnetic field component amplification at surface
21 p3453 A71-41358

Dynamo theory of solar and lunar magnetic fields diurnal variations, determining ionospheric wind velocities and pressure changes
23 p3669 A71-43174

Apollo 12 fines and Apollo 11 microbreccias and rocks magnetic properties, discussing remanent magnetization
23 p3763 A71-43793

Apollo 11 and 12 crystalline rocks NRM natural remanent magnetization, discussing magnetizing fields origin
23 p3763 A71-43794

Lunar rocks 12002 and 12022 remanent magnetic moment as evidence for ancient lunar magnetic field
23 p3763 A71-43795

LUNAR MAPS

Lunar surface features charting from astrophysical data and direct observation, describing mapping of Sea of Tranquility
03 p0484 A71-13214

Photometric maps of reverse side lunar surface from AIM Zond 3 material
03 p0484 A71-13215

Astronautical TV camera and photogrammetric systems use on manned and unmanned lunar probes, discussing applications to earth surface surveys
06 p0901 A71-18287

Lunar surface plan reference systems with no common points comparison with photomechanically obtained scale maps
06 p0976 A71-18448

Lunar Mapping Camera ground support operations, describing pre and post mission assistance, stellar field calibration and data reduction
09 p1429 A71-23221

Lunar radar reflectivity mapping at 7.5 m wavelength for maria and highlands echo powers, using interferometric techniques
11 p1834 A71-26451

Lunar surface no common point systematic reference systems comparison with photomechanically obtained scale maps
12 p1955 A71-26598

Lunar mapping metric camera subsystems stellar calibration for photography maximum usability in photogrammetric data reduction
13 p2071 A71-29348

Moon marginal zone charts for determining limb corrections applied to reduction of stellar occultation timing
17 p2797 A71-34185

Stellar calibration of lunar mapping camera for precision metric photography and time correlated postflight attitude determination
18 p2925 A71-36918

Global lunar map coordinate grid from spaceborne photography and rectification on spherical screen, noting rays and maria
20 p3296 A71-39621

Lunar maps classification, nomenclature and scale sequence
21 p3448 A71-40544

Lunar locations and orientations of crystalline rocks, breccia and soil from Apollo 11 and 12 missions, including maps
23 p3737 A71-43603

Azimuth frequency plots of regolith surface lineaments at Apollo 11 and 12 landing sites
23 p3737 A71-43604

Selenodetic catalog centers mutual positions determination from lunar near side hypsometric charts
24 p3875 A71-45316

LUNAR MARIA

Large lunar craters and circular maria origin problem, disputing formation by meteorite impacts
01 p0149 A71-10047

Lunar surface features charting from astrophysical data and direct observation, describing mapping of Sea of Tranquility
03 p0484 A71-13214

Lunar maria and large craters absolute ages determination under outer layers viscosity assumptions
04 p0659 A71-15856

Lunar hot spots surface distribution-geomorphic index relationship, discussing maria, terrae and regolith evolutionary stage
05 p0809 A71-16462

Age and composition effects on lunar surface processes and optical properties, explaining main albedo, maria, color contrasts and temporal changes
07 p1200 A71-20150

Large lunar craters and circular maria origin problem, disputing formation by meteorite impacts
08 p1361 A71-21041

Lunar two cycle interior thermal history influence on maria and crater morphology, noting active and passive phase roles
09 p1520 A71-22836

Lunabase regions origin, suggesting volcanic dust masses fluidized by volcanic gases
09 p1528 A71-23550

Lunar origin and evolution, discussing craters, mare collisions, formation time, heat balance, gravity anomalies, density and chemical composition
11 p1822 A71-25689

Apollo lunar sea geomorphic data agreement with Luna 16 data
15 p2488 A71-32325

Lunar surface rejuvenation processes, considering mare flooding and crater destruction by seismic waves and ballistic sedimentation
15 p2493 A71-32487

Vertical motions on moon resulting from stress differences leading to isostatic equilibrium, discussing maria, craters and mascons
16 p2636 A71-33504

Lunar anorthositic crust flotation, fractional crystallization process in seas and mascons genesis based on experimental data and petrogenetic scheme
16 p2636 A71-33505

Lunar gravitational field interpretation based on Apollo data, considering mascons creation, isostasy, thermal history and maria orientation hypotheses
16 p2636 A71-33506

Small lunar maria craters morphological maturity as function of age and dimensions
16 p2638 A71-33670

Lunar near-side tectonic patterns, including mare ridges, rills, highland ridges and crater walls features within maria from Lunar Orbiter photographs
19 p3052 A71-37676

Morphologic variations and locations of terraced depressions in lunar maria, indicating drained lava lakes
19 p3137 A71-37679

Pyroxferroite crystal structure from Apollo lunar Mare Tranquillitatis sample, using X ray counter-diffractometer measurements
23 p3737 A71-43606

Opaque minerals in Apollo 12 lunar rocks from Oceanus Procellarum by reflected light microscopy and electron microprobe analysis, including ilmenite, chromite and troilite
23 p3739 A71-43622

Lunar maria igneous rock compositions and magmatic liquid viscosity from samples 12021 and 12022, using microprobe analyses
23 p3741 A71-43633

Apollo 12 Mare Procellarum soil glasses analyzed by ion and electron microprobe, discussing rock ages
23 p3744 A71-43653

Impact metamorphism effects in Apollo 12 microbreccias from Oceanus Procellarum 23 p3745 A71-43659

Cosmogenic radionuclide concentration and exposure ages of Apollo 12 rock from Ocean of Storms 23 p3754 A71-43730

Luminescence, thermoluminescence and spectral reflectance of lunar samples from Oceanus Procellarum and Mare Tranquillitatis 23 p3760 A71-43775

Lunar fines transportation process in mare surface evolution, suggesting electrostatics role from photographic and seismic evidence 23 p3765 A71-43810

LUNAR MODULE

Lunar Module Ag coated stranded Cu wire, analyzing fluorine contamination with proton microprobe 02 p0209 A71-12592

Lunar module digital autopilot design, considering attitude state estimator, reaction control system and thrust vector control [AIAA PAPER 70-991] 07 p1154 A71-18897

Lunar Module physical characteristics and control system function, emphasizing automated vs manual flight degree and astronaut overriding capability 07 p1208 A71-19915

Surface heating and pressure distribution on Lunar Module from rocket exhaust plume impingement tests in vacuum [AIAA PAPER 71-256] 08 p1377 A71-21985

Adhesives in Apollo command, service and lunar modules primary load carrying structures, electrical potting and sealing medium 10 p1630 A71-24067

Apollo Lunar Module design evolution, considering mission requirements, reliability objectives, environmental factors, manned operation, weight and configuration 15 p2500 A71-31603

LUNAR OBSERVATORIES

Ruby laser ranging of moon, describing Pic du Midi Observatory laser telemetry station and Luna 17 retroreflectors 16 p2640 A71-33752

McDonald Observatory lunar ranging station including telescope matching optics, guiding, timing equipment, pulsed ruby laser system and calibration procedures 16 p2553 A71-33780

Optimal method selection for astronomical measurements on lunar surface, discussing instrumental and technical difficulties with selenographic longitudes and latitudes determination 24 p3870 A71-44812

LUNAR OCCULTATION

NT SOLAR ECLIPSES

European X ray astronomy lunar occultation satellite, providing high resolution cosmic X ray source observation 02 p0303 A71-12952

Solar eclipse of 22 September 1968 radio astronomical observations, examining sunspot groups during lunar occultation 04 p0650 A71-15558

Lunar ephemeris and astrometric corrections from occultation observations, noting FK4 equinox location 08 p1357 A71-20876

Lunar occultation photoelectric observations, emphasizing double star nature 14 p2306 A71-29685

Lunar occultation application to small separation double stars discovery and measurement 14 p2246 A71-30358

Astronomical radio sources angular structure, using lunar occultations in narrow frequency band at large SNR 15 p2482 A71-31329

Astronomical radio sources angular structure, using lunar occultations in narrow frequency band at large SNR 22 p3606 A71-42604

Weak radio sources observations by lunar occultation method with large steerable radio telescope, discussing optical identification of sources 24 p3868 A71-44563

Fresnel diffraction model appropriateness for stellar occultation by moon 24 p3871 A71-44912

LUNAR ORBIT AND LANDING SIMULATORS

Apollo simulator navigation and docking training techniques, discussing manned LM and CSM key role performance 07 p1156 A71-20342

LUNAR ORBITAL RENDEZVOUS

Rendezvous equations near second lunar libration point, using Halo orbiting relay satellite for communication with spacecraft behind moon 09 p1521 A71-22912

LUNAR ORBITER

Lunar gravitational field parameters from Lunar Orbiters trajectory measurement, discussing theoretical basis 01 p0149 A71-10048

Lunar gravitational field parameters from Lunar Orbiters trajectory measurement, discussing theoretical basis 08 p1361 A71-21042

Lunar orbiter earth-moon-earth optimal trajectories geocentric section calculations from low circumlunar flight procedures 13 p2142 A71-29178

Lunar gravity field global model from moon orbiters secular and long period trends, noting large anomaly on far side 16 p2642 A71-33815

Dynamic derivation of surface layer representation of lunar gravitational field from Doppler observations on polar and equatorial lunar orbiters 21 p3449 A71-40643

Equatorial lunar radius determinations from image motion compensation sensor onboard Lunar Orbiter 1 spacecraft [AAS PAPER 71-337] 23 p3727 A71-43010

Lunar gravity estimate from low degree spherical harmonic coefficients in potential model and Lunar Orbiter 4 radio tracking data reduction 23 p3768 A71-43882

LUNAR ORBITS

Generalized von Zeipel treatment of lunar and artificial satellite theories, generating single canonical transformation by variable separation technique 04 p0654 A71-15719

Long term evolution of close low eccentricity lunar satellite orbits, describing lunar gravity effects by spherical harmonic expansion 04 p0655 A71-15723

Three body stellar problem libration calculation using nonlinear mechanics methods, and application to lunar satellite perturbation by earth and lunar gravitational effects 04 p0655 A71-15728

Apollo lunar orbital missions, discussing remote sensing and photographic equipment for lunar sounding and mass spectrometry, gegenschein experiments and high quality metric photography 10 p1682 A71-24173

Analytical lunar ephemeris main problem solution by canonical perturbation theory based on Lie transforms and echeloned series processing 10 p1674 A71-24431

Artificial lunar satellites orbits, examining disturbing functions expansions due to nonsphericity of primary body and disturbing point mass body actions 10 p1679 A71-24931

Lunar ephemeris, examining orbit with Delaunay theory 11 p1831 A71-26136

Analytical lunar ephemeris, comparing variational and parallactic inequalities with various theories 11 p1831 A71-26137

Lunar origin dynamics, discussing orbit evolution by tidal friction and celestial mechanical theory 14 p2307 A71-29901

Planetary dynamics bibliography and review, considering range determination and ephemerides, general relativity, tidal evolution and lunar orbit, solar system commensurabilities, etc 17 p2798 A71-34457

Apollo 15-17 CSM design modifications, discussing increased mission duration capability, lunar orbital science instruments operation and weight increase [AIAA PAPER 71-821] 17 p2812 A71-34723

Lunar exploration system based on modified earth-orbit space station in polar lunar orbit as remote sensor platform and lander deployment base 18 p2972 A71-36443

Luna 18 mission accomplishments in lunar orbital automatic navigation techniques and arrival point coordinate accuracy 22 p3597 A71-41506

Limited interval definitions of photometric functions of lunar crater walls by photography from orbiting Apollo 11 22 p3603 A71-42187

Mission analysis aspects of space shuttle operations between earth orbit station and lunar orbit station [AAS PAPER 71-301] 23 p3724 A71-42977

Artificial satellite lunar orbit calculation, representing unmodeled accelerations by first order Gauss-Markov sequence with time correlated and random components [AAS PAPER 71-371] 23 p3730 A71-43041

Lunar orbit space station lifetime, using averaged variational equations numerical integration for terrestrial, solar and lunar gravitational field effects [AAS PAPER 71-377] 23 p3730 A71-43047

LUNAR PERTURBATION

U LUNAR EFFECTS

LUNAR PHOTOGRAPHS

Lunar surface photography, presenting photographs viewed in stereo without stereoscope 07 p1114 A71-20043

Three dimensional lunar surface relief model from orbital photographs at different heights 08 p1360 A71-21023

Lunar crater rays production mechanism, observed by high resolution photographs of Copernicus 09 p1530 A71-23712

Lunar Orbiter photographs utilization in earth science courses, illustrating geologic features, stratigraphy and historical geology 18 p2915 A71-35888

Stellar calibration of lunar mapping camera for precision metric photography and time correlated postflight attitude determination 18 p2925 A71-36916

Three dimensional lunar surface relief model from orbital photographs at different heights 20 p3294 A71-39603

LUNAR PHOTOGRAPHY

Lunar crater origin determination by terrestrial volcanic and meteoritic craters and maars geological criteria application to Lunar Orbiter 5 photographs 02 p0313 A71-12549

Lunar Mapping Camera ground support operations, describing pre and post mission assistance, stellar field calibration and data reduction 09 p1429 A71-23221

Lunar surface slopes distributions from bistatic radar, photogrammetric and photoclinometric measurements by Explorer 35, Surveyor, Lunar Orbiter and Apollo spacecraft 11 p1830 A71-25838

Lunar landing site suitability, using stereoscopic medium and high resolution photography 11 p1836 A71-26533

Apollo lunar and Skylab photographic systems, discussing topographic, panoramic, metric, stellar and multispectral cameras and instrumentation 12 p1907 A71-27257

Surveyor 3 spacecraft attitude change on lunar surface, examining Apollo 12 mission photographs 13 p2145 A71-28699

Lunar mapping metric camera subsystems stellar calibration for photography maximum usability in photogrammetric data reduction 13 p2071 A71-29348

Apollo 12 landing site morphological and textural details from Surveyor 3 photography, considering lunar surface impact and volcanic models 15 p2493 A71-32483

Hadley, Prinz and Schroter lunar sinuous rills morphology from Orbiter photography, discussing rills origin 15 p2493 A71-32489

Lunar libration detection by photographing double exposure of stellar field and moon 16 p2636 A71-33503

Selenography and selenodesy with Apollo whole-disk lunar photograph, providing positions catalog in tabular form 18 p2965 A71-36294

Lunar near-side tectonic patterns, including mare ridges, rills, highland ridges and crater walls features within maria from Lunar Orbiter photographs 19 p3052 A71-37676

Lunar Apennine-Hadley region geological implications from high resolution earth-based radar map and Lunar Orbiter photography 20 p3287 A71-38977

Apollo 12 multispectral lunar photography experiment using four camera configuration, verifying by ground photoelectric photometry 23 p3761 A71-43780

Small lunar crater vicinity boulders distribution analysis from Orbiter 3 high resolution photographs, suggesting impact and volcanic origin of crater kinds 24 p3874 A71-45187

LUNAR PROBES

NT LUNIK LUNAR PROBES

NT LUNIK 14 LUNAR PROBE

NT SURVEYOR LUNAR PROBES

NT SURVEYOR 1 LUNAR PROBE

NT SURVEYOR 3 LUNAR PROBE

NT SURVEYOR 5 LUNAR PROBE

Solar wind lunar impingement induction of magnetic fields used for global sounding of moon structure 03 p0486 A71-13323

LUNAR PROGRAMS

NT APOLLO PROJECT

Soviet lunar surface exploration, discussing luna 16 payloads, history and sample collecting 12 p1971 A71-26874

Man-telescope-robot teams for space exploration facilities construction and operation, discussing lunar programs [AIAA PAPER 71-823] 17 p2723 A71-34722

Lunar surface base concept synthesis, considering program objectives and hardware operational approaches [AIAA PAPER 71-819] 17 p2723 A71-34725

LUNAR RADAR ECHOES

Lunar upper crust structure and composition from radio wave reflection spectrum analysis 02 p0308 A71-12098

Lunar upper crust structure and composition from radio wave reflection spectrum analysis 08 p1362 A71-21148

Lunar surface specific effective radio signal scattering area measured by Luna 9 and 13, describing signal fluctuations 09 p1523 A71-23145

Lunar surface slopes distributions from bistatic radar, photogrammetric and photoclinometric measurements by Explorer 35, Surveyor, Lunar Orbiter and Apollo spacecraft

11 p1830 A71-25838

Lunar radar reflectivity mapping at 7.5 m wavelength for maria and highlands echo powers, using interferometric techniques

11 p1834 A71-26451

Laser radar system using retroreflector on lunar surface for measurement of distance between earth and moon

16 p2543 A71-33811

Terrestrial, lunar and planetary dynamical properties and internal constitution, considering data obtained from artificial satellites, lunar and planetary dynamics

22 p3607 A71-42883

LUNAR RADIATION

Kamchatka volcanic mantles and lunar surface radiation polarization characteristics similarities

01 p0149 A71-10049

Low brightness spacecraft photometer calibration using moonlit earth radiance as reference

02 p0249 A71-12075

Lunar radio emission measurements at 1.42 mm, using radio telescope and wideband superheterodyne radiometer

02 p0309 A71-12104

Planetary and lunar thermal radio emission and brightness temperature measurements using sensitive receivers and large aperture radio telescopes

02 p0309 A71-12155

Kamchatka volcanic mantles and lunar surface radiation polarization characteristics similarities

08 p1361 A71-21043

Lunar radio emission measurements at 1.42 mm, using radio telescope and wideband superheterodyne radiometer

08 p1362 A71-21151

Lunar equatorial region IR emission directional characteristics from brightness temperature measurements, developing cratered soil thermal model for negative surface relief studies

09 p1530 A71-23713

Directional thermal emission from rough lunar surface as function of crater frequency, aspect ratio and solar deviation angle, comparing to Lambertian behavior

11 p1833 A71-26256

Lunar transients in Aristarchus region with respect to tidal, sunrise, illumination, magnetic tail, bow shock and solar activity hypotheses

15 p2492 A71-32479

Lunar flare transients consisting of gaseous emissions and regional/long term/ or local/short term/ luminescence

15 p2492 A71-32480

Papers on astronomy and astrophysics, Volume 8, covering lunar microwave thermal emission observation and origin

17 p2804 A71-35176

Lunar microwave thermal emission observation and theoretical predictions based on lunar surface models

17 p2804 A71-35177

Lunar interior thermal radiation measurement in meter wavelength range during period of solar radio image behind limb, showing inverse temperature gradient with depth

19 p3138 A71-37756

Radiative heat transfer from lunar and Mercurian surfaces during eclipse

22 p3603 A71-42188

Lunar IR directional characteristics theory, noting agreement with observations at all observational and phase angles

24 p3874 A71-45188

LUNAR RAYS

Lunar crater rays production mechanism, observed by high resolution photographs of Copernicus

09 p1530 A71-23712

LUNAR RECEIVING LABORATORY

Biosphere contamination, discussing sterilization and quarantine experiments at Lunar Receiving Laboratory, flight crew testing and microbiological studies

21 p3448 A71-40569

High resolution phase contrast microscope adaptation for gastight glove box use with stage and focusing knobs in box for Apollo sample microbiological examination

24 p3802 A71-45124

LUNAR ROCKS

Opaque minerals in Apollo 12 rocks, emphasizing spinel compositions

01 p0162 A71-11426

Apollo 11 basalts chemistry and petrogenesis by partial melting, considering implications for lunar origin theories

02 p0305 A71-11981

Apollo 11 crystalline igneous rocks mineralogy and petrology, suggesting origin from pyroxenite mantle melting

02 p0305 A71-11982

Apollo 11 lunar soil sample derived from basaltic and anorthositic rocks, considering basalt origin by melting due to internal radioactive heating

02 p0305 A71-11983

Apollo 11 lunar samples dielectric constants, losses and electrical conductivities as function of temperature and frequency, comparing with terrestrial and simulated lunar rocks

02 p0305 A71-11985

Apollo 11 lunar powder and rock samples optical properties noting similarity over Tranquility base area

02 p0305 A71-11986

Lunar solid state thermal convection throughout interior, noting pressure release production of basaltic magmas consistent with Apollo 11 rocks composition

02 p0305 A71-11988

Apollo 11 lunar rocks excess heat capacity and thermal conductivity at liquid He temperatures due to peaks in vibrational frequency distribution

02 p0306 A71-11989

Mg-Cr and Ba-rare earth relationships in stony meteorites and Apollo 11-12 soil and rocks

03 p0487 A71-13335

Apollo 11 and 12 lunar rocks physical and mechanical properties and chemical composition compared with terrestrial rocks

03 p0487 A71-13421

Apollo 12 lunar rock 12013 preliminary examination and preparation for instrumental analysis, noting feldspar content and igneous nature

03 p0493 A71-14213

Petrographic microscope and electron microprobe analysis of Apollo 12 rock 12013, noting bimimetic composition with dominant potassic feldspar plus silica

03 p0493 A71-14214

Apollo 12 lunar rock 12013 mineralogy, identifying whitlockite, plagioclase, alkali feldspar, ilmenite, quartz and minerals encrusted with quartz

03 p0493 A71-14215

Fossil nuclear charged particle tracks in lunar rock 12013 Ca-feldspar, K-feldspar and pyroxene attributed to galactic cosmic rays

03 p0494 A71-14216

Apollo 12 lunar rock 12013 petrologic and mineralogic characteristics, discussing data on isotopic Xe and Gd composition

03 p0494 A71-14217

O, Si, Al and Fe abundances of Apollo 12 lunar rock 12013 from neutron activation analysis

03 p0494 A71-14218

Apollo 12 lunar rock 12013, discussing major and trace elemental abundances determination by neutron activation analysis

03 p0494 A71-14219

Ar 40/Ar 39 age determination of Apollo 12 lunar rock 12013 fragments

03 p0494 A71-14220

Apollo 12 lunar rock 12013 rare earth, alkaline and alkali metal and Sr 87/Sr 86 data, discussing light and dark component composition

03 p0494 A71-14221

Trace element patterns of Apollo 12 lunar rock 12013 light and dark portions, discussing Rb-Sr age and Li, K, Rb, Sr, Ba and rare earth concentrations

03 p0494 A71-14222

Apollo 12 lunar rock 12013 origin, determining age by U, Th and Pb isotopic study

03 p0494 A71-14223

He, Ne, Ar and Xe from stepwise heating of Apollo 12 lunar rock 12013, discussing radiogenic and spallation components and He 3 and Ne 21 cosmic ray exposure ages

03 p0494 A71-14224

Apollo 12 lunar rock 12013 oxygen 18 and silicon 30 ratios, comparing to terrestrial basalts and gabbros, Apollo 11 rocks and oceanic rhyolite obsidians

03 p0495 A71-14225

Apollo lunar rock sample solidification and impact rates, deriving cratering time behavior

04 p0660 A71-15863

Apollo 12 lunar rock examination, discussing soil mechanics, mineralogical and petrological aspects and surface features and fines

05 p0806 A71-16149

Apollo 11 and 12 lunar rock opaque oxides differences in titanium contents

05 p0807 A71-16298

Lunik 16 rock samples noting regolith, basalt, anorthositic, various mineral grains, solidified spherical droplets, breccias, glassy and scorified fragments and metallic iron particles

05 p0813 A71-16856

Apollo 11 magnetic rocks and Apollo 12 rocks dating

06 p0966 A71-17742

Apollo 11 igneous rocks potassium content vs irradiation exposure age, comparing lunar geology models

06 p0966 A71-17897

Rare earth abundance in Apollo 12 basalts and soils and achondritic meteorites, using partial melting model

06 p0966 A71-17899

K-U abundance systematics in Apollo 11 and 12 lunar rock suites and earth crust

06 p0968 A71-17961

Apollo 11 flight glass basalt, determining crystallization sequence and phase assemblage of high Ti specimens as oxygen fugacity function

06 p0970 A71-18235

Soviet lunar surface rocks physical properties: ground observation including colorimetry, spectrophotometry and polarimetry

07 p1193 A71-19311

Troilite rich Ni-Fe particle/mini-moon/ from lunar surface, discussing different theories of origin

07 p1196 A71-19543

Apollo 11 and 12 lunar samples, discussing chemical composition relationship to lunar origin

07 p1196 A71-19605

Lunar magnetic field demagnetization effect hypothesis for explaining Apollo 11 lunar rock samples remanent magnetization

07 p1200 A71-20055

Electromagnetic device with superconducting elements for magnetic monopole detection in Apollo lunar samples, describing operation principle, amplifier, sample container and transport system

09 p1446 A71-22733

Apollo 11 lunar rocks mineralogical, chemical, isotopic, electrical and magnetic properties

09 p1523 A71-23018

Lunar rocks permittivity and density and surface roughness from radio wave scattering data

09 p1523 A71-23105

Apollo 12 crystalline rock samples composition from conventional chemical analysis, suggesting origin in magmatic body with differentiation by crystallization and olivine settling

09 p1529 A71-23654

Solar particle tracks in clear filter glass from Surveyor 3 spacecraft, comparing with lunar rocks track results

09 p1529 A71-23655

Lunar and terrestrial ilmenite basalt, considering hornfels from Keweenaw Duluth complex in Minnesota and Apollo 11 samples

09 p1529 A71-23657

Chemical elements abundance in ordinary chondrites, terrestrial magma and lunar rocks, considering Alven theory of solar system origin

10 p1665 A71-23741

Elemental analysis for lunar rocks and regolith, comparing silicon oxide and titanium oxide composition in Apollo 12 and Apollo 11 samples

10 p1672 A71-24389

Apollo 12 clinopyroxenes exsolution and epitaxy by electron microprobe and single crystal X ray diffraction

10 p1672 A71-24391

Apollo 12 soils composition and derivation, finding feldspathic orthopyroxene rich rock and chemically comparable glass fragments

10 p1672 A71-24393

Lunar 12 spinel compositional variation and textures as petrogenetic indicators, showing magma differentiation by crystal settling after lunar surface extrusion

10 p1672 A71-24394

Apollo 11 igneous rock vug clinopyroxene composite crystal with tabular pigeonite nucleus and subcalcic augite precipitation

10 p1673 A71-24412

Microcraters on Apollo 12 crystalline rocks and breccia surfaces attributed to primary cosmic particles

10 p1673 A71-24427

Lunar rock analysis, discussing heavy ion impacts and amorphous skin relation to solar wind

10 p1677 A71-24696

Luna 16 lunar rock samples mechanical properties and chemical and mineralogical compositions for regolith origin determination

10 p1681 A71-25116

Solar wind composition of protons, He isotopes and heavy rare gas ions from Apollo lunar samples

11 p1814 A71-25263

Cosmic ray spallation products and radiation age determination from spectral analysis of noble gas components in lunar rocks

11 p1829 A71-25837

Igneous and metamorphic rocks as simulated lunar rocks, determining elastic and attenuation symmetry by quasi-longitudinal pulse velocity and amplitude measurements on spherical specimens

11 p1834 A71-26454

Lunar surface rocks Hg content under daytime temperatures volatilization conditions, considering cold trap and lunar atmosphere

12 p1958 A71-26692

Lunar anorthositic comparison with terrestrial igneous rocks, discussing petrogenetic schemes based on models

12 p1958 A71-26693

Lunar samples mineralogy, petrology and geochemistry, considering lunar surface processes, cosmic ray flux and solar wind

12 p1967 A71-27414

Glazed lunar rocks, explaining origin as result of nearby meteoritic impact 13 p2137 A71-28515

Lunar rocks in large bright rayed craters, calculating thermal abnormality model 13 p2138 A71-28697

Antiperthitic intergrowths from single crystal X ray studies of lunar rock plagioclase 13 p2142 A71-29140

Lunar chronology and evolution from Rb and Sr internal isochrons on Apollo 11 and 12 crystalline rock samples 13 p2142 A71-29142

Apollo 11 lunar rock and microbreccia examination for natural remanent magnetization, emphasizing viscous magnetization effect in terrestrial magnetic field 14 p2303 A71-29534

Ancient lunar magnetic field detection and origin from remanent magnetism in Apollo 11 breccia and basaltic rock samples 14 p2306 A71-29725

Lattice defect mechanism for high coercive force remanence production in meteorites and lunar samples by cosmic ray exposure 14 p2308 A71-29913

Coarse grained lunar basalt from Oceanus Procellarum, examining ground mass and subsolidus cooling history 14 p2313 A71-30427

Electrical conductivity measurement of Apollo 11 and 12 lunar surface rocks, using two-probe technique in vacuum furnace 14 p2315 A71-30864

Mg, Si, Ca, Mn and Cr distributions by electron probe analysis 14 p2315 A71-30865

Apollo 11 and 12 lunar samples compared with deep earth rocks, noting potassium-uranium ratio 14 p2318 A71-31126

Soviet lunar surface rocks physical properties ground observation including colorimetry, spectrophotometry and polarimetry 15 p2485 A71-31891

Optical fluorescence spectra of rock forming minerals for quantitative analysis of lunar surface 15 p2411 A71-32471

Optical fluorescence of lunar transients in UV to IR range for rock forming silicates, using electron microprobe with cathode luminescence capability 15 p2492 A71-32472

Nuclear magnetic resonance spectrometer for moisture content measurement of lunar and terrestrial soils and rocks 15 p2411 A71-32474

Crystallization temperatures of lunar gabbroid rocks from Tranquility base, comparing with dry silicate melts 15 p2401 A71-32498

Argon isotopes retention ages of crystalline lunar rocks 12002, 12051 and 12065 from lunar maria, using neutron activation and stepwise heating experiments 16 p2633 A71-33347

Terrestrial basalts and lunar rocks volatile element concentrations comparison, noting relationship to abundance in chondrites 16 p2633 A71-33348

K-Ar isotope ages of whole sample and feldspar concentrate from Apollo 11 lunar rock 10003 16 p2633 A71-33349

Electrical conductivity of lunar rock, considering radial variation of bulk composition with oxygen loss in outer layers due to thermal cycles and vacuum 16 p2634 A71-33388

Vertical motions on moon resulting from stress differences leading to isostatic equilibrium, discussing maria, craters and mascons 16 p2636 A71-33504

Apollo 11 and 12 lunar soil and rock samples abundance comparison based on Mossbauer spectroscopy 16 p2637 A71-33509

Crystallization behavior and chemical compositions of Apollo 11 lunar basalts including olivine and silica normative varieties 16 p2637 A71-33512

Electrical conductivities of Apollo 11 and 12 lunar rocks and chondritic meteorites at 300-1100 K 17 p2796 A71-34182

Lunik 16 soil samples physical properties, rock types, chemical analysis, mineral composition and petrology, comparing to Apollo project 17 p2805 A71-35332

Apollo 11 and 12 lunar landings, discussing retrieved lunar material, seismographs, solar wind and light reflector for measuring earth-moon distance 18 p2959 A71-35906

Apollo 14 Fra Mauro rock fragment samples, determining Ar 40/Ar 39 ages 18 p2961 A71-35945

Apollo 11 lunar soil and rock samples under low level beta spectrometry, measuring radon daughter Pb 210 18 p2961 A71-35946

Apollo 11 and 12 lunar rocks composition, suggesting depletion of K, Rb and Pb in solar nebula prior to final accretion of moon 18 p2963 A71-36228

Lunar breccia, considering welded or sintered breccias, glassy breccias containing xenocrysts and xenoliths, instant rock breccias and recrystallized breccias 19 p3137 A71-37675

Micrometeorite craters on lunar rock surfaces, suggesting cosmic particles impact 19 p3138 A71-37686

Radionuclides depth distribution gradient in lunar samples, suggesting solar proton medium flux constancy over last million years 19 p3127 A71-38004

Lunar mechanical and magnetic properties, discussing impact craters, rocks, soil iron abundance, mascons and convection processes 19 p3142 A71-38020

Physical, chemical, mineralogical and biological analysis of Apollo 14 lunar rocks and fines 19 p3144 A71-38179

Luna 16 automatic probe drilling experiment, obtaining lunar rocks physicochemical properties for comparison with terrestrial rocks 20 p3209 A71-39131

Apollo 14 bulk lunar fines sample elemental abundances determination from soils and rocks by activation analysis 20 p3292 A71-39382

Apollo 11 lunar crystalline igneous rock samples electrical conductivity temperature dependence, noting age of moon 20 p3295 A71-39619

Heat release from elemental decay in radioactive layer from radio astronomical observations and lunar rock chemical analysis 20 p3295 A71-39620

Apollo lunar expeditions assessment, discussing rock samples composition, origin, age and relation to earth system 21 p3442 A71-40148

Apollo 11, 12 and 14 lunar seismometer results suggesting lunar material Q factors up to 3000 21 p3453 A71-41407

Apollo 14 flight Fra Mauro crystalline rocks age measurement, using Ar 40/39 ratio method 22 p3598 A71-41838

Lunar rocks composition, age, history and evolution, comparing to terrestrial basalts 22 p3599 A71-41943

International cooperation in astronautics, reviewing European satellites launching and world distribution of lunar rock and soil samples 22 p3623 A71-42012

Ferromagnetic electron spin resonance spectra of Apollo 11 lunar samples, using model for polycrystalline spectra simulation 23 p3734 A71-43242

Armalcolite and ilmenite basalt in Apollo 11 lunar samples, discussing formation process of titanium, potassium and silicon oxides 23 p3734 A71-43247

Physical properties, mineralogy and chemical composition of lunar regolith sample returned by unmanned Lunik 16 probe 23 p3737 A71-43602

Lunar locations and orientations of crystalline rocks, breccia and soil from Apollo 11 and 12 missions, including maps 23 p3737 A71-43603

Tranquillity silicate mineral in crystalline basaltic rocks from Apollo 11 and 12 samples 23 p3737 A71-43605

Pyroxferroite crystal structure from Apollo lunar Mare Tranquillitatis sample, using X ray counter-diffractometer measurements 23 p3737 A71-43606

High temperature phase transition and composition of Apollo 12 pigeonite/augite clinopyroxene crystal rock 12021 from X ray diffraction 23 p3738 A71-43607

Comparative electron petrography and chemical analysis of Apollo 11 and 12 and terrestrial rocks, noting pyroxene, plagioclase, ilmenite and cristobalite 23 p3738 A71-43608

Exsolution lamellae structure of Lunar pyroxenes from Apollo 12 samples, using electron microscopy and diffraction 23 p3738 A71-43610

Lunar plagioclases, tridymite and cristobalite feldspar crystal structure and chemical analyses from Apollo igneous rocks by X ray and electron diffraction 23 p3738 A71-43611

Optical, chemical and structural properties of lunar bytownite twin from U stage, microprobe and X ray measurements 23 p3738 A71-43612

Tridymite structure in lunar pigeonite porphyry 12021 by single crystal X ray diffraction, comparing with meteorite and silica brick 23 p3738 A71-43613

Minor element concentrations and population sources of Apollo 11 and 12 olivine and plagioclase, using microprobe analyses 23 p3738 A71-43614

Fission track analyses of uranium enriched phases in Apollo 11 and 12 basaltic rocks 23 p3739 A71-43615

Lexan plastic fission track analysis of uranium distribution in glassy residuum in Apollo 11 rock 10017 23 p3739 A71-43616

Apollo 11 and 12 rock samples examination, failing to observe radioactive halos 23 p3739 A71-43617

Zirconium liquid-crystal distribution in phase ilmenite of Apollo 11 and 12 lunar rocks 23 p3739 A71-43618

Opaque mineral compositions in Apollo 12 lunar rocks, noting ilmenite, spinels, native iron and troilite 23 p3739 A71-43620

Apollo 12 lunar igneous rocks and breccia opaque minerals examined by optical and electron microprobe techniques 23 p3739 A71-43621

Opaque minerals in Apollo 12 lunar rocks from Oceanus Procellarum by reflected light microscopy and electron microprobe analysis, including ilmenite, chromite and troilite 23 p3739 A71-43622

Single crystal structure of shocked terrestrial and lunar ilmenite from X ray precession and Laue analyses 23 p3740 A71-43623

Luminescence petrography of Apollo 12 lunar igneous rocks, comparing to meteorites and terrestrial basalts 23 p3740 A71-43624

Mineralogical, petrological and chemical features of four Apollo 12 lunar megablasts 23 p3740 A71-43625

Apollo 12 crystalline rocks mineralogy, petrology and chemical composition, considering magmatic origin 23 p3740 A71-43626

Mineralogy and petrology of Apollo 12 igneous rocks 12004, 12008, 12009 and 12022, noting ilmenite, olivine and spinel content and metal grains composition 23 p3740 A71-43627

Mineralogy, petrology and chemical composition of Apollo 12 rocks and fines 23 p3740 A71-43628

Petrography and mineral composition of Apollo 12 crystalline rocks 23 p3740 A71-43629

Apollo 12 lunar rocks and fines mineralogy and petrology, using optical and electron microscopy, electron and X ray diffraction and electron probe microanalysis 23 p3741 A71-43630

Mineralogical and petrographic investigation of olivines, feldspars and pyroxenes in Apollo 12 fines and igneous rocks, using optical and X ray diffraction 23 p3741 A71-43631

Lunar maria igneous rock compositions and magmatic liquid viscosity from samples 12021 and 12022, using microprobe analyses 23 p3741 A71-43633

Gray mottled basaltic rock composition and origin in Apollo 12 lunar soils and breccias 23 p3741 A71-43634

Apollo 11 and 12 lunar rocks and soil chemical composition, considering petrogenesis and major and trace elements abundance 23 p3741 A71-43635

Alkali metals vaporization from heated lunar samples, suggesting lunar rock erosion by localized heating due to volcanism or meteorite impact 23 p3741 A71-43636

Normative mineralogy of lunar basaltic rocks from Apollo 11 and 12 samples, comparing with terrestrial and meteoritic analogs 23 p3742 A71-43637

Apollo 11 and 12 crystalline rocks petrographical analysis and textural-mineralogical-chemical group classification, considering local stratigraphy reconstruction 23 p3742 A71-43638

Apollo 12 crystalline rocks composition from microprobe analyses, indicating undercooled magmatic fractional crystallization 23 p3742 A71-43639

Equilibrium phase relations in lunar rocks and synthesized analogs, determining liquidus and solidus temperatures 23 p3742 A71-43640

Petrology of Apollo 11 and 12 rock samples with silicate melt inclusions, discussing terrestrial equivalents 23 p3742 A71-43641

Pyroxenes morphological significance in Apollo 12 lunar igneous rock samples petrogenesis, analyzing crystallization process history 23 p3742 A71-43642

Clinopyroxene crystallization histories of Apollo 12 porphyritic basalt rocks 12021 and 12052 from Oceanus Procellarum 23 p3742 A71-43643

Olivine accumulation in Apollo rock 12040 and basaltic fragments, using textural and microprobe analyses 23 p3742 A71-43644

Hydrous analog stability in lunar amphibole Apollo samples as function of water vapor pressure and temperature 23 p3743 A71-43648

Noritic and anorthositic rock fragment proportions and sources in Apollo 12 soil samples 23 p3743 A71-43650

Size distribution, composition and history of regolith fines at Apollo 12 site 23 p3743 A71-43651

Grain size and modal analyses of lunar regoliths sampled by Apollo 11 and 12, discussing particles origin 23 p3744 A71-43654

Pyroxenes and olivines in lunar rocks from Ocean of Storms, observing plastic deformational processes since crystallization by optical, X ray and electron microprobes 23 p3744 A71-43657

Apollo 11 and 12 unshocked and shocked microbreccia petrology, noting shock compression and shock welding 23 p3745 A71-43658

Apollo 11 and 12 regolith and breccia samples, discussing shock effects detection and interpretation, chemical composition, grain size distribution and impact origin 23 p3745 A71-43660

Lunar rocks 12063,9 and 12004,11 opaque mineralogy and textural feature, comparing to Apollo 11 samples 23 p3745 A71-43661

Lunar breccia sample matrix composition characteristics examination by transmission electron microscope, suggesting condensation from rock volatilized by meteorite impact heat 23 p3745 A71-43663

Lunar glassy objects and mineral grains surface microstructure by optical and scanning electron microscopy, comparing with tektites and terrestrial volcanic analogs 23 p3745 A71-43664

Surface morphology of free-growing ilmenites and chromites from lunar vuggy rocks by scanning electron microscopy and electron microprobe 23 p3745 A71-43665

Nonmare basalts chemical composition and origin from Apollo 11 and 12 sites 23 p3746 A71-43671

Lunar rock volatile and siderophile elements, comparing with terrestrial and meteoritic basalts 23 p3746 A71-43672

Neutron activation data on Zn, Ga, Ge, Cd, In and Ir trace elements for Apollo 12 lunar rock and soil sample 23 p3747 A71-43673

Apollo 12 specimens elemental abundance from neutron activation analysis, discussing fractional crystallization, partial melting, rare earth abundances and soil mixing model 23 p3747 A71-43674

Trace element abundances in Apollo 12 lunar rock and fine samples and mineral separates from Ocean of Storms 23 p3747 A71-43675

Apollo 12 lunar soils, rocks and core samples, determining rare earth, alkali and alkaline earth elements concentrations 23 p3747 A71-43676

Apollo 11 and 12 lunar rocks and fines, discussing compositional variations and relationships to stony meteorites 23 p3747 A71-43677

Primordial radionuclides K, Th and U concentrations in Apollo 12 lunar rocks, breccias and fines, using gamma ray spectrometry 23 p3748 A71-43679

Apollo 12 lunar soil, breccia and igneous rock samples, determining elemental abundances with spark source mass spectrometry and neutron activation analysis 23 p3748 A71-43680

Trace elements concentration and metallic particles analysis from Apollo 12 lunar igneous rocks, soils and breccias, noting relation to sample location and exposure age 23 p3748 A71-43681

Apollo 12 lunar soils and igneous rocks from Ocean of Storms, determining major, minor and trace element composition with chemical, X ray fluorescence and spectrographic techniques 23 p3748 A71-43683

Bulk elemental composition of Apollo 12 samples of lunar igneous and breccia rocks and soils from instrumental and radiochemical neutron activation analysis 23 p3748 A71-43684

Apollo 12 lunar rocks and fines under high energy neutron activation analysis, determining O, Si, Al, Mg and Fe abundances 23 p3748 A71-43685

Spark mass spectrometric analysis of major and trace elements abundance in Apollo 11 and 12 lunar rocks and soil samples, comparing with standard basalt 23 p3749 A71-43686

Apollo 11 and 12 lunar samples elemental composition analysis, using activation and mass spectrometric isotope dilution analysis and emission spectrography 23 p3749 A71-43687

Apollo 12 lunar samples 12040,36 and 12064,38 chemical analysis for major elements, discussing titanium, water and iron content 23 p3749 A71-43688

Apollo 12 lunar samples halogen and trace element composition, investigating chemical and physical processes affecting surface halides, platinum group metals and Hg 23 p3749 A71-43689

Apollo 12 lunar rocks 12002, 12018, 12021 and 12038 and soil sample 12070 elemental abundances, discussing origin and comparison to meteorites and terrestrial rocks 23 p3749 A71-43691

Lunar soil samples 10084,141 and 12070,83 and rock fragment 12063,73 multielement analysis using neutron activation and nondispersive X ray fluorescence techniques 23 p3749 A71-43692

Apollo 11 and 12 lunar rock and soil examination, emphasizing Au and Ag excess in soil 23 p3750 A71-43693

Apollo 12 lunar rock rare earth element abundances, comparing to Icelandic basalt flow 23 p3750 A71-43694

Re and Os abundance and meteoritic contamination levels in Apollo 11 and 12 rocks, fines and breccia 23 p3750 A71-43696

Re isotopic composition measurement in Apollo 12 rocks and regolith samples using neutron bombardment 23 p3750 A71-43697

Apollo 12 samples total C and N abundances suggesting indigenous lunar material with solar wind component 23 p3750 A71-43698

Thermal analysis-quadrupole mass spectrometric analyses on inorganic released gases of Apollo 11 and 12 samples and synthetic lunar analogs 23 p3750 A71-43699

Knudsen cell-mass spectrometric study of Apollo 12 samples vaporization process 23 p3750 A71-43700

Active and inert gases released by crushing Apollo 11 and 12 samples at room temperature and by low temperature heating 23 p3751 A71-43701

Apollo 12 lunar dust and rocks carbon and hydrogen amount and isotopic composition determination, using in vacuo outgassing and combustion in oxygen 23 p3751 A71-43703

Oxygen isotope fractionation in Apollo 12 rocks and soils, noting plagioclase ilmenite isotopic temperature 23 p3751 A71-43704

Apollo 12 lunar samples 12002,128, 12021,49, 12038,43 and 12070,52 vanadium isotopic composition 23 p3751 A71-43706

Apollo 11 and 12 lunar dust and rocks, determining Be and Cr contents by gas chromatography for comparison with crystalline rocks 23 p3751 A71-43707

Li, B, Mg and Ti isotopic abundances and search for trapped solar wind Li in Apollo 11 and 12 rocks 23 p3752 A71-43708

Apollo 12 igneous rocks and fines from Ocean of Storms, presenting rubidium and strontium chronology and chemistry 23 p3752 A71-43709

Rb-Sr isotopic composition in Apollo 12 regolith samples yielding 4.2-5.1 billion year ages 23 p3752 A71-43710

Lunar rocks 12040 and 12013 and anorthosites, determining U-Th distributions with induced fission track maps 23 p3752 A71-43712

Age determination of Apollo 12 rocks by U-Th-Pb method 23 p3752 A71-43713

Isotopic composition of U and Th in Apollo 12 lunar rock samples from mass and alpha spectrometry 23 p3753 A71-43717

Cosmic ray exposure ages and rare gas concentration profiles in Apollo 12 lunar rocks, discussing spallation products and neutron capture effects 23 p3753 A71-43719

Rare gas concentrations and isotopic abundances in lunar rocks, fines and breccias from Apollo 11 and 12 flights, determining exposure and gas retention ages 23 p3753 A71-43720

Microprobe measurements of rare gas composition for lunar rock 12013,10,31 mineral separates, noting cosmic ray bombardment role in K and Ar production 23 p3753 A71-43721

Isotopic abundances and concentrations of spallogenic Ne, Kr and Xe in Apollo 12 rock 12002, constructing three stage model of irradiation history 23 p3753 A71-43722

Inert gases release from breccia 10065 by lunar rock vacuum crushing at room temperature, suggesting breccia formation from gas-rich parent materials 23 p3754 A71-43725

Ar, Kr and Xe emanation during stepwise heating of lunar rocks under slow neutron irradiation in pile, using mass spectroscopy 23 p3754 A71-43726

Cosmogenic radionuclide concentration and exposure ages of Apollo 12 rock from Ocean of Storms 23 p3754 A71-43730

Lunar surface erosion and mixing from cosmogenic and primordial radionuclide measurement in Apollo 12 lunar rock and soil samples 23 p3755 A71-43731

Depth profiles of cosmogenic radionuclides in lunar rocks and soil samples from Apollo 11 and 12 flights, considering solar particle flux and spectra 23 p3755 A71-43732

Cosmogenic and primordial radionuclides in Apollo 12 surface rocks and fines from nondestructive gamma ray spectrometry 23 p3755 A71-43733

Solar protons contribution to spallogenic Mn 53 production in Apollo 12 lunar rock and soil from neutron activation analysis 23 p3755 A71-43734

Tritium activity measurement in Apollo 11 fines, breccia and crystalline rock, comparing with meteoritic values 23 p3755 A71-43735

Radioactive rare gases and tritium in Apollo 12 lunar rocks and in sample return container, noting relationship to solar flare event 23 p3755 A71-43736

Tritium and argon radioactivities and depth variations in Apollo 12 rocks, discussing solar flare and cosmic ray exposure ages 23 p3755 A71-43737

Indigenous gases and hydrolyzable carbon compounds in Apollo 11 and 12 samples through gas chromatographic and mass spectrometric examination, noting meteoritic impact and solar wind implantation as probable origins 23 p3755 A71-43738

Apollo 12 lunar dust, rocks and microbreccia microsection examined for evidence of biogenic structure 23 p3757 A71-43746

Microbial assay of lunar core and surface samples obtained from Apollo 11 and 12 flights 23 p3757 A71-43748

Thermally stimulated exoelectron emission and surface properties of lunar rocks and soil 23 p3758 A71-43759

Pressure histories from densification and relaxation measurements on lunar glass and synthetic samples, investigating refractive index changes after annealing 23 p3758 A71-43760

Neutron diffraction studies of Apollo 12 lunar samples 12070,119, 12071,6 and 12008,7, observing magnetic ordering 23 p3759 A71-43761

Elemental abundance analysis of Apollo 11 and 12 lunar materials from Auger electron spectroscopy 23 p3759 A71-43762

Mossbauer instrumental analysis of Apollo 12 rock and soil samples, measuring nuclear gamma resonance of iron 57 23 p3759 A71-43764

Phase analysis of Apollo 12 fines, core tube samples and rocks by Mossbauer studies, noting nearly uniform distribution of major Fe containing phases 23 p3759 A71-43765

IR vibrational spectroscopic analysis of Apollo 11 and 12 rocks and dust isolated silicate minerals, using LF absorption bands 23 p3759 A71-43766

Apollo 12 basalts porosity and volume compressibility under hydrostatic pressure 23 p3759 A71-43768

Visible and near IR spectral reflectivity measurements of basalt separates, glass and anorthositic fragments from Apollo 12 mare samples 23 p3760 A71-43770

Spectral directional reflectance of Apollo 11 and 12 fines as function of bulk density 23 p3760 A71-43771

Apollo 11 and 12 rocks dielectric constants, discussing far IR absorption spectrum of fines 23 p3760 A71-43772

Physical characterization of Apollo 11 and 12 lunar fines and glasses by diffuse reflectance, Raman and X ray spectroscopy and thermally stimulated currents 23 p3760 A71-43773

- Apollo 11 and 12 rocks luminescence under proton, electron, UV and X irradiation 23 p3760 A71-43774
- Luminescence, thermoluminescence and spectral reflectance of lunar samples from Oceanus Procellarum and Mare Tranquillitatis 23 p3760 A71-43775
- Natural and X ray excited thermoluminescence in Apollo 12 lunar samples and terrestrial plagioclases 23 p3761 A71-43778
- Polarization characteristics, albedos and optical properties of Apollo 11 and 12 rocks, investigating wavelength dependence and proton irradiation effect 23 p3761 A71-43779
- Thermal expansion coefficient and bulk modulus of lunar rocks 10020, 10046, 10057 and 12022,95 23 p3761 A71-43782
- Elastic wave velocities in Apollo 12 rocks 12052 and 12065 at high pressures, noting basalt-like composition and crystal structure 23 p3761 A71-43783
- Elastic surface wave amplitude and propagation velocity in lunar rocks, calculating Poisson ratio 23 p3761 A71-43784
- Apollo 11 and 12 rocks specific heat and thermal conductivity at 2-5 K, comparing elastic properties 23 p3761 A71-43785
- Specific heat of Apollo 11 breccia and Apollo 12 olivine dolerite at 95-340 K 23 p3762 A71-43786
- Dielectric conductivity, relative permittivity and loss tangent of Apollo 11 and 12 rock samples 23 p3762 A71-43787
- Dielectric properties of Apollo 12 samples and lunar interior as function of frequency and temperature 23 p3762 A71-43788
- Magnetic properties of glass spherules from Apollo 11 and 12 fines, determining oxidation effect 23 p3762 A71-43791
- Apollo 12 lunar soil and igneous rocks magnetic properties 23 p3763 A71-43792
- Apollo 12 fines and Apollo 11 microbreccias and rocks magnetic properties, discussing remanent magnetization 23 p3763 A71-43793
- Apollo 11 and 12 crystalline rocks NRM natural remanent magnetization, discussing magnetizing fields origin 23 p3763 A71-43794
- Lunar rocks 12002 and 12022 remanent magnetic moment as evidence for ancient lunar magnetic field 23 p3763 A71-43795
- Unpaired electrons and oxygen adsorptive capacity of clean lunar rock and soil surfaces, noting decrease of uptake rate at one monolayer coverage 23 p3764 A71-43798
- Solar and galactic iron group cosmic ray track distributions in Apollo 12 lunar rocks, investigating surface residence times 23 p3764 A71-43800
- Radiation exposure history from fossil tracks in Apollo 12 surface rocks and double core regolith samples, comparing with Saint Severin meteorite 23 p3764 A71-43802
- High resolution time averaged energy spectrum and chemical composition of iron group cosmic ray nuclei from fossil tracks in Apollo 12 lunar rocks 23 p3764 A71-43804
- Ultraheavy cosmic ray nuclei inclusions inferred from Apollo 12 lunar rock pigeonite crystal track length distribution 23 p3765 A71-43805
- Lunar surface orientation of whole Apollo 12 rocks, considering microcraters distribution 23 p3765 A71-43806
- Critique of paper on Apollo 11 ilmenite basalts petrology and lunar bodies origin and form 23 p3769 A71-43886
- Galactic and solar cosmic ray effects on Apollo 11 lunar soil and rock samples, analyzing Xe isotopic anomalies 23 p3722 A71-44016
- Lunar origin hypothesis, discussing Apollo 11 crystalline rocks nature and basalts petrogenesis 23 p3770 A71-44075
- Small lunar crater vicinity boulders distribution analysis from Orbiter 3 high resolution photographs, suggesting impact and volcanic origin of crater kinds 24 p3874 A71-45187
- Lunar 16 Sea of Abundance rock volume weight, destruction pattern, compressibility, shear strength and carrying ability, comparing to terrestrial rock 24 p3875 A71-45315
- LUNAR ROVING VEHICLES**
- Landmark navigation improvement by redundant measurements and statistical data reduction measurement for lunar roving vehicles 07 p1156 A71-20339
- Celestial and satellite navigation sensitivity for Lunar roving vehicle /LRV/ position fix 07 p1157 A71-20414
- Elevation determination methods for unmanned lunar roving vehicle, considering instruments, orbiter tracking, etc 08 p1272 A71-21324
- Unmanned lunar roving vehicle remote guidance, discussing onboard vs on-earth steering and velocity control, imaging system, obstacle detection and avoidance 08 p1331 A71-21325
- Computer program for determining roving vehicle position and heading on lunar surface by landmarks 08 p1332 A71-21348
- Lunar Roving Vehicle, discussing crew, mobility, power, deployment and navigation subsystems, environment and radio interference problems 11 p1747 A71-26527
- Lunar roving vehicle telecommunication system requirements concerning vehicle functions, science experiments, crew operations and safety 14 p2200 A71-30915
- Manned Lunar Roving Vehicle for Apollo 15 expedition, discussing subsystems design features 15 p2384 A71-31746
- Mobility capability of lunar roving vehicles relative to terrain roughness, computing power requirements 15 p2494 A71-32496
- Lunar roving vehicle for Apollo 15 mission, discussing power, control, navigation and deployment systems in relation to lunar exploration requirements [AIAA PAPER 71-847] 17 p2723 A71-34707
- Unmanned lunar rover exploration objectives and requirements, considering heterogeneous surface 24 p3875 A71-45190
- LUNAR SATELLITES**
- NT EXPLORER 28 SATELLITE
- NT LUNAR ORBITER
- Lunar satellite motion semianalytic solution, considering perturbative effects due to gravitational fields, solar radiation pressure and libration 05 p0809 A71-16541
- Artificial lunar satellites orbits, examining disturbing functions expansions due to nonsphericity of primary body and disturbing point mass body actions 10 p1679 A71-24931
- Spin stabilized lunar satellite attitude determination, using Kalman filter for processing telemetered sun aspect angle measurements from satellite sensor 22 p3573 A71-42780
- Lunar physical libration effect on lunar satellite orbital elements, considering reorientation of selenographic axes fixed in true moon 23 p3727 A71-43004
- Artificial lunar satellite motion in gravitational fields of nonspherical moon, earth and sun, deriving orbit perturbations 24 p3874 A71-45174
- LUNAR SCATTERING**
- U DIFFUSE RADIATION
- U LUNAR RADAR ECHOES
- LUNAR SEISMOGRAPHS**
- Long seismic reverberations from man-made impacts on moon, using Apollo 12 lunar surface station recordings 01 p0159 A71-10824
- Lunar seismic reaction to Apollo 12 module launch stage impact, taking into account multistage soil scattering 02 p0304 A71-11921
- Seismograph recording of Apollo 12 lunar module impact as result of secondary ejecta spray around seismometer or translunar seismic wave propagation 04 p0644 A71-15128
- Lunar seismic waves scattering as two dimensional random walk process, taking crust and rock compositions into account 04 p0650 A71-15544
- Seismic waves scattering mechanism in heterogeneous medium from lunar seismograms 04 p0650 A71-15546
- Lunar dynamics and structure data from two lunar seismic stations installed during Apollo 11 and 12 missions as part of ALSEP 12 p1967 A71-27416
- Lunar seismic reaction to Apollo 12 module launch stage impact, taking into account multistage soil scattering 13 p2134 A71-28208
- Apollo 11 and 12 lunar landings, discussing retrieved lunar material, seismographs, solar wind and light reflector for measuring earth-moon distance 18 p2959 A71-35906
- Moon surface electrical conductivity, seismic transmission properties, dust components, chemical analysis and comparison to earth 20 p3295 A71-39615
- Lunar near surface seismic velocity distribution for cold accretion and meteorite impact models, comparing travel times 21 p3450 A71-40645
- Apollo 11, 12 and 14 lunar seismometer results suggesting lunar material Q factors up to 3000 21 p3453 A71-41407
- Lunar impact targeting technique improvement for Apollo 14 mission preflight analyses and flight support operations [AAS PAPER 71-392] 23 p3732 A71-43060
- LUNAR SHADOW**
- Interior umbra observations during lunar eclipses, using photometric analysis 09 p1530 A71-23718
- Lunar shadow effects on bow wave mechanism during 7 March 1971 solar eclipse, considering traveling ionospheric disturbance measurements from satellite 10 p1600 A71-23885
- LUNAR SHELTERS**
- Full scale models, nonflammable materials and tests for manned space expandable structures including airlocks, transfer tunnels, station modules, lunar shelters and flexible windows [AIAA PAPER 71-399] 11 p1744 A71-25275
- Solar energy degradation heat trapping-dissipating walls for inhabited living space on lunar surface 22 p3529 A71-42844
- LUNAR SOIL**
- NT LUNAR DUST
- Apollo 12 lunar core and soil samples indicating meteoritic trace elements abundance 01 p0148 A71-10003
- Apollo 11 lunar soil sample derived from basaltic and anorthositic rocks, considering basalt origin by melting due to internal radioactive heating 02 p0305 A71-11983
- Lunar anorthosites from Apollo 11 sample 10085 coarse fines, determining major, minor and rare earth elemental abundances 03 p0482 A71-13012
- Mg-Cr and Ba-rare earth relationships in stony meteorites and Apollo 11-12 soil and rocks 03 p0487 A71-13335
- Lunar surface structure, discussing soil grain size-albedo relationship 03 p0492 A71-14054
- Elastic properties of lunar surface material from Surveyor spacecraft strain gage data 04 p0644 A71-15129
- Lunar glasses of impact origin, considering occurrence, abundance, optical properties and chemical composition for determination of regolith bulk, age and origin 04 p0644 A71-15130
- Botanical quarantine studies on Apollo 11 and 12 lunar soil samples effects on terrestrial plants, indicating absence of disease generating agents 04 p0539 A71-15393
- Measuring instrument for lunar surface layer heat flow, temperature and thermal conductivity 04 p0599 A71-15543
- Apollo 12 lunar rock examination, discussing soil mechanics, mineralogical and petrological aspects and surface features and fines 05 p0806 A71-16149
- Apollo 11 lunar soil size distribution, examining deficiency in material finer than 15 micrometers 05 p0807 A71-16215
- Apollo 11 and 12 lunar soil samples common contaminant identified as diisopropyl disulfide, using chromatograph mass spectrometer 05 p0716 A71-16453
- Refractory elements abundances in chondrites, basaltic achondrites and Apollo 11 fines, emphasizing Ca-Al relationship 06 p0966 A71-17894
- Rare earth abundance in Apollo 12 basalts and soils and achondritic meteorites, using partial melting model 06 p0966 A71-17899
- Tranquility Base lunar soil diurnal temperature calculation from one dimensional energy equation, using temperature dependent thermodynamic properties [AIAA PAPER 71-79] 06 p0977 A71-18536
- Nuclear tracks high density in Apollo core small silicate crystals, discussing extralunar dust and photo-spheric iron-hydrogen ratio 07 p1189 A71-18740
- Pulverized volcanogenic products and chemicals polarizing properties determination, applying to lunar surface layer 07 p1107 A71-19201
- Lunar radioactive layer effective thickness by radio astronomical methods and from Apollo 11 flight 07 p1193 A71-19312
- Amino acid contents of Apollo 11 and 12 fines, discussing laboratory syntheses 07 p1196 A71-19500
- Apollo 12 sample 12023 fines carbon, carbides and methane determination by hydrolysis and vacuum pyrolysis 07 p1196 A71-19541
- Lunar bulk modulus, viscosity, inertia moments and density calculation from gravity potential values obtained by Luna 10 and Lunar Orbiter satellites 07 p1203 A71-20520
- Surveyor 3 spacecraft TV camera surface discoloration patterns caused by lunar soil blown by Apollo 12 exhaust 08 p1363 A71-21219

Apollo 11 lunar samples effect on terrestrial microorganisms, noting pigment production effects of Fe leaching from bulk fines and core samples
10 p1566 A71-23747

Apollo 12 soils composition and derivation, finding feldspathic orthopyroxene rich rock and chemically comparable glass fragments
10 p1672 A71-24393

Thermoluminescence glow curve and decay characteristics of Apollo 12 fines and soil samples, suggesting lower mean daytime surface temperature at site
10 p1672 A71-24395

Lunar soil 12033 bulk chemical analysis, suggesting mixture of exotic component with local soil in 41/59 proportion
10 p1673 A71-24396

Xe and Kr isotopes gas extraction and mass spectrometer analyses of Apollo 11 lunar soil, Murray carbonaceous chondrite and atmospheric Xe
10 p1661 A71-24410

Lunar soil particle production, noting radiation erosion effects
10 p1673 A71-24414

Primordial Kr and Xe trapping as possible cause of element abundance trend reversal in Apollo 11 and 12 fines
10 p1673 A71-24428

Lunar soil samples chemical composition, discussing comparison with earth minerals, solar wind and cosmic rays effects and implications for lunar and planetary evolution theory
10 p1677 A71-24692

Lunar soil albedo, discussing radiation darkening, lunar rock particles size and mineral contents effects
11 p1835 A71-26460

Lunik spacecraft soil sampler landing site geological-morphological analysis from television images, indicating formation patterns similar to equatorial zone seas microrelief
12 p1966 A71-27302

Methane and deuteromethane released from Apollo 11 and 12 lunar fines by deuterated acid etch, using gas chromatography for carbon compounds separation
13 p2136 A71-28427

Lunar radioactive layer effective thickness by radio astronomical methods and from Apollo 11 flight
15 p2486 A71-31892

Nuclear magnetic resonance spectrometer for moisture content measurement of lunar and terrestrial soils and rocks
15 p2411 A71-32474

Gray tone differences between undisturbed lunar surface and darker ejecta around Surveyor 1 footpads based on footprint photometry and albedo
15 p2493 A71-32482

Microstructure and chemical composition of lunar soil sample collected by Luna 16
16 p2630 A71-32838

Apollo 11 and 12 lunar soil and rock samples abundance comparison based on Mossbauer spectroscopy
16 p2637 A71-33509

Soviet report to COSPAR on upper atmosphere and cosmic space including Soyuz spacecraft, lunar soil sample recovery and surface vehicle delivery
16 p2666 A71-33865

Bibliography and review of noble gases isotopic abundance in meteorites and lunar material, considering cosmic ray interactions, radiation ages and extinct radionuclides
17 p2798 A71-34451

Bibliography and review of age determination of meteorites and lunar samples, considering chondrites, achondrites and iron meteorites
17 p2798 A71-34452

Carbon compounds in Apollo 12 lunar fines and core samples, using pyrolysis, mass spectrometry, ion exchange chromatography and optical and electron microscopy
17 p2801 A71-34649

He, Ne and Ar isotopic distribution and origin in Apollo 12 lunar samples, considering solar wind implantation
17 p2695 A71-35030

Lunar surface and soil mechanical properties statistical analysis covering Alphonsus event, cratering and erosion
17 p2805 A71-35179

Lunik 16 soil samples physical properties, rock types, chemical analysis, mineral composition and petrology, comparing to Apollo project
17 p2805 A71-35332

Apollo 11 lunar soil and rock samples under low level beta spectrometry, measuring radon daughter Pb 210
18 p2961 A71-35946

Microcrater morphology in lunar soil glass, oligoclase and olivine, determining projectile velocity, impact angle and shape effects
18 p2961 A71-35947

Compounds hydrolyzable to amino acids in aqueous extracts of Apollo 11 and 12 lunar fines, noting presence of glycine and alanine
18 p2855 A71-36230

Scanning electron microscope and petrographic observations of glass particles from Apollo 12 lunar soil sample, revealing surface features and origin
19 p3137 A71-37674

Lunar mechanical and magnetic properties, discussing impact craters, rocks, soil iron abundance, mascons and convection processes
19 p3142 A71-38020

Lunar crust regolith thermophysical properties concerning particle size and mass, specific heat and thermal conductivity from Luna 16 automatic station sampler
19 p3144 A71-38259

Lunik spacecraft soil sampler landing site geological-morphological analysis from TV images, indicating formation patterns similar to equatorial zone seas microrelief
19 p3145 A71-38261

Apollo 14 lunar soils chemical element concentrations by atomic absorption spectrophotometry and isotope dilution
20 p3292 A71-39381

Apollo 14 bulk lunar fines sample elemental abundances determination from soils and rocks by activation analysis
20 p3292 A71-39382

Fluorine and other trace elements in lunar plagioclase concentrates from Apollo 11 fines, and anorthosite inclusion from Apollo 12 breccia
20 p3292 A71-39383

Lunar soils structural-mechanical properties and composition, discussing volcanic origin and terrestrial analogs
20 p3295 A71-39618

Apollo 11 lunar fines and ground terrestrial mafic rock powders effective surface areas and heats of adsorption, using Brunauer-Emmett-Teller Kr adsorption method
21 p3450 A71-40648

Glass spheres formation on moon, suggesting mineral melt atomization in high speed gas stream
21 p3454 A71-41421

International cooperation in astronautics, reviewing European satellites launching and world distribution of lunar rock and soil samples
22 p3623 A71-42012

Rare earth trace elements abundance of Apollo 14 lunar soil samples from Fra Mauro, comparing with chondrites
23 p3735 A71-43248

Lunar locations and orientations of crystalline rocks, breccia and soil from Apollo 11 and 12 missions, including maps
23 p3737 A71-43603

Apollo 12 lunar soil particles observation for reduced metal meteoritic inclusions, suggesting shock impact effects during meteoritic bombardment of moon
23 p3739 A71-43619

Mineralogy, petrology and chemical composition of Apollo 12 rocks and fines
23 p3740 A71-43628

Mineralogy, chemistry and origin of KREEP/potassium, rare earth element and phosphorus/ component in Apollo 12 soil and breccia samples from Ocean of Storms
23 p3741 A71-43632

Gray mottled basaltic rock composition and origin in Apollo 12 lunar soils and breccias
23 p3741 A71-43634

Apollo 11 and 12 lunar rocks and soil chemical composition, considering petrogenesis and major and trace elements abundance
23 p3741 A71-43635

Crystalline and glassy phases electron probe analysis for picrite basalts, ferrobasalts, feldspathic norites and rhyolites from Apollo 12 lunar soil samples
23 p3743 A71-43645

Apollo 12 basalts petrology and petrogenesis, studying crystallization sequences
23 p3743 A71-43646

Petrogenesis and crystallization of protohypersthene basalts in lunar maria lava lakes, deducing eruption temperatures
23 p3743 A71-43647

Petrography, mineral composition and grain size distribution of Apollo 12 lunar fines
23 p3743 A71-43649

Noritic and anorthositic rock fragment proportions and sources in Apollo 12 soil samples
23 p3743 A71-43650

Size distribution, composition and history of regolith fines at Apollo 12 site
23 p3743 A71-43651

Mineralogical composition, modal distribution and bulk chemical analysis on Apollo 12 lunar fines
23 p3744 A71-43652

Apollo 12 Mare Procarrallum soil glasses analyzed by ion and electron microprobe, discussing rock ages
23 p3744 A71-43653

Apollo 12 lunar soil and breccia core tube and surface samples optical and electron microscope and microprobe analysis, relating data to geologic processes
23 p3744 A71-43656

Apollo 11 and 12 regolith and breccia samples, discussing shock effects detection and interpretation, chemical composition, grain size distribution and impact origin
23 p3745 A71-43660

Lunar soil samples 12001,1, 12037, 12042,25 and 12070,100 exterior morphology and chemistry, noting environmental temperature decrease, crater formation and meteorite impact
23 p3745 A71-43662

Morphological, physical and chemical characteristics of basaltic and anorthositic glassy spheroids in Apollo 12 lunar fines
23 p3746 A71-43666

Apollo 11 and 12 devitrified glass fragments temperature histories indicating broad range of subsolidus crystallization temperatures
23 p3746 A71-43667

Neutron activation data on Zn, Ga, Ge, Cd, In and Ir trace elements for Apollo 12 lunar rock and soil sample
23 p3747 A71-43673

Apollo 12 specimens elemental abundance from neutron activation analysis, discussing fractional crystallization, partial melting, rare earth abundances and soil mixing model
23 p3747 A71-43674

Trace element abundances in Apollo 12 lunar rock and fine samples and mineral separates from Ocean of Storms
23 p3747 A71-43675

Apollo 12 lunar soils, rocks and core samples, determining rare earth, alkali and alkaline earth elements concentrations
23 p3747 A71-43676

Apollo 11 and 12 lunar rocks and fines, discussing compositional variations and relationships to stony meteorites
23 p3747 A71-43677

Meteoritic material characterization from trace elements in Apollo lunar soil, core samples, breccia and anorthositic fragments by neutron activation analysis
23 p3747 A71-43678

Primordial radionuclides K, Th and U concentrations in Apollo 12 lunar rocks, breccias and fines, using gamma ray spectrometry
23 p3748 A71-43679

Apollo 12 lunar soil, breccia and igneous rock samples, determining elemental abundances with spark source mass spectrometry and neutron activation analysis
23 p3748 A71-43680

Trace elements concentration and metallic particles analysis from Apollo 12 lunar igneous rocks, soils and breccias, noting relation to sample location and exposure age
23 p3748 A71-43681

Chemical element composition and mineralogy of powdered lunar surface material, comparing Surveyor, Apollo and Lunik missions data
23 p3748 A71-43682

Apollo 12 lunar soils and igneous rocks from Ocean of Storms, determining major, minor and trace element composition with chemical, X ray fluorescence and spectrographic techniques
23 p3748 A71-43683

Bulk elemental composition of Apollo 12 samples of lunar igneous and breccia rocks and soils from instrumental and radiochemical neutron activation analysis
23 p3748 A71-43684

Apollo 12 lunar rocks and fines under high energy neutron activation analysis, determining O, Si, Al, Mg and Fe abundances
23 p3748 A71-43685

Spark mass spectrometric analysis of major and trace elements abundance in Apollo 11 and 12 lunar rocks and soil samples, comparing with standard basalt
23 p3749 A71-43686

Apollo 11 and 12 lunar samples elemental composition analysis, using activation and mass spectrometric isotope dilution analysis and emission spectrometry
23 p3749 A71-43687

Apollo 11 and 12 lunar fines 10084 and 12070 trace element determination, using multielement neutron activation analysis
23 p3749 A71-43690

Apollo 12 lunar rocks 12002, 12018, 12021 and 12038 and soil sample 12070 elemental abundances, discussing origin and comparison to meteorites and terrestrial rocks
23 p3749 A71-43691

Lunar soil samples 10084,141 and 12070,83 and rock fragment 12063,73 multielement analysis using neutron activation and nondispersive X ray fluorescence techniques
23 p3749 A71-43692

Apollo 11 and 12 lunar rock and soil examination, emphasizing Au and Ag excess in soil
23 p3750 A71-43693

Rare earth elements and trace elements abundance in Apollo 12 igneous rocks, breccia and lunar soil
23 p3750 A71-43695

Apollo 12 samples total C and N abundances suggesting indigenous lunar material with solar wind component

23 p3750 A71-43698

Thermal analysis-quadrupole mass spectrometric analyses on inorganic released gases of Apollo 11 and 12 samples and synthetic lunar analogs

23 p3750 A71-43699

Knudsen cell-mass spectrometric study of Apollo 12 samples vaporization process

23 p3750 A71-43700

Active and inert gases released by crushing Apollo 11 and 12 samples at room temperature and by low temperature heating

23 p3751 A71-43701

Carbon and sulfur isotope content in Apollo 12 lunar fines

23 p3751 A71-43702

Apollo 12 lunar samples 12002, 128, 12021, 49, 12038, 43 and 12070, 52 vanadium isotopic composition

23 p3751 A71-43706

Apollo 12 igneous rocks and fines from Ocean of Storms, presenting rubidium and strontium chronology and chemistry

23 p3752 A71-43709

Rb, Sr, K, U, Th and Pb concentrations in Apollo 12 lunar soil samples, discussing lunar age estimates

23 p3752 A71-43711

Lead isotopes volatile transfer in Apollo 11 and 12 lunar soil samples, discussing lunar age estimates

23 p3752 A71-43714

Neutron activation analysis of Apollo 11 lunar fines, determining Pb 204, U, Bi and Tl contents

23 p3753 A71-43715

Isotopic abundances and composition of U and Th in Apollo 12 soil and breccia samples, using mass spectroscopy

23 p3753 A71-43716

Superheavy elements search in lunar fine grains from Apollo 12 mission by measuring kinetic energy spectrum of nuclear fission fragments

23 p3753 A71-43718

Apollo 12 lunar soil samples trapped rare gas analysis, observing solar wind He local variation from breccia

23 p3754 A71-43723

Apollo 11 and 12 lunar samples history of irradiation exposure to galactic cosmic rays and solar wind, using rare gas and Gd isotope measurements

23 p3754 A71-43724

Apollo 11 and 12 fines cosmogenic He, Ne and Ar radionuclides composition determination, using electron microprobe analysis

23 p3754 A71-43727

Lunar atmosphere as source of lunar surface gaseous elements, calculating ions trajectory and impact energy as function of interplanetary magnetic field strength

23 p3754 A71-43728

Lunar surface erosion and mixing from cosmogenic and primordial radionuclide measurement in Apollo 12 lunar rock and soil samples

23 p3755 A71-43731

Depth profiles of cosmogenic radionuclides in lunar rocks and soil samples from Apollo 11 and 12 flights, considering solar particle flux and spectra

23 p3755 A71-43732

Cosmogenic and primordial radionuclides in Apollo 12 surface rocks and fines from nondestructive gamma ray spectrometry

23 p3755 A71-43733

Solar protons contribution to spallogenic Mn 53 production in Apollo 12 lunar rock and soil from neutron activation analysis

23 p3755 A71-43734

Indigenous gases and hydrolyzable carbon compounds in Apollo 11 and 12 samples through gas chromatographic and mass spectrometric examination, noting meteoritic impact and solar wind implantation as probable origins

23 p3755 A71-43738

Porphyrin-like pigments in Apollo 12 lunar soil sample 12023, using spectral analysis involving fluorescence, absorption and magnetic circular dichroism spectrometry

23 p3756 A71-43739

Apollo 12 lunar surface fines examination noting absence of porphyrins

23 p3756 A71-43740

Apollo 12 lunar surface samples analysis for organic compounds by mass spectroscopy and pyrolysis-gas chromatography

23 p3756 A71-43741

Volatilizable organic polymers and hydrocarbons in Apollo 12 lunar core samples 12025 and 12028, using mass spectrometric analysis

23 p3756 A71-43742

Chemical characteristics of carbon compounds in Apollo 11 and 12 lunar fines, using organic solvent extraction, mass spectrometry and gas chromatographic method

23 p3756 A71-43743

Organogenic elements and compounds abundances and distribution in Apollo 12 fines

23 p3756 A71-43744

Long chain alkanes search in Apollo 12 lunar fines, using benzene-methanol extracts

23 p3756 A71-43745

Biological activity in Apollo 11 and 12 core samples searched for after placement in Petri dishes containing media

23 p3757 A71-43747

Microbial assay of lunar core and surface samples obtained from Apollo 11 and 12 flights

23 p3757 A71-43748

Apollo 12, 14 and 15 lunar core tube sampling

23 p3757 A71-43749

Apollo core tube geometry effect on quantity and quality of lunar sample recovery

23 p3757 A71-43750

Cone penetration resistance tests on granular lunar soil simulants for in-place shear strength and packing characteristics under various gravity conditions

23 p3757 A71-43751

Apollo 12 fines sample 12057, 72 particle size distribution determination procedures, discussing characteristic shapes, glassy agglomerates, smooth opaque particles and volume

23 p3757 A71-43752

Glass spherical particles formation mechanisms for lunar surface, discussing size limitation factors

23 p3757 A71-43753

Gas interaction with lunar fines, investigating carbon monoxide, nitrogen, oxygen, argon and water vapor adsorption

23 p3758 A71-43754

Particle size and shape distributions of Apollo 12 lunar fines by computer evaluation of scanning electron microscope images

23 p3758 A71-43755

Regular particle morphology and petrostatistics in Apollo 11 and 12 lunar fines and conglomerates, using phase contrast and scanning microscopes

23 p3758 A71-43757

Thermally stimulated exoelectron emission and surface properties of lunar rocks and soil

23 p3758 A71-43759

Elemental abundance analysis of Apollo 11 and 12 lunar materials from Auger electron spectroscopy

23 p3759 A71-43762

Mossbauer instrumental analysis of Apollo 12 rock and soil samples, measuring nuclear gamma resonance of iron 57

23 p3759 A71-43764

Vacuum pumped Apollo 12 lunar soil sample 12001, 118 gas exposure effects, interface microanalysis and adhesion measurements in ultrahigh vacuum system

23 p3759 A71-43767

Grain size distribution and optical and RF electrical properties of Apollo 12 lunar fines and core samples

23 p3759 A71-43769

Apollo 12 lunar core sample thermoluminescence dependence on radiation dose rates, detecting temperature gradients in regolith by differential thermal analysis

23 p3760 A71-43776

Natural and X ray excited thermoluminescence in Apollo 12 lunar samples and terrestrial plagioclases

23 p3761 A71-43778

Apollo 12 lunar fines 12001, 19 thermal conductivity vacuum measurements, using line heat source method

23 p3761 A71-43781

Apollo 12 lunar soil and igneous rocks magnetic properties

23 p3763 A71-43792

Apollo 12 lunar soil samples magnetic resonance properties, determining temperature, frequency and thermal annealing dependence

23 p3763 A71-43796

Electron spin resonance studies of Apollo 11 and 12 lunar soil samples, determining ferromagnetism due to Fe particles

23 p3763 A71-43797

Unpaired electrons and oxygen adsorptive capacity of clean lunar rock and soil surfaces, noting decrease of uptake rate at one monolayer coverage

23 p3764 A71-43798

Nuclear track densities in lunar core and fine samples, relating erosion history, solar activity and surface stirring

23 p3764 A71-43799

Primary cosmic ray and spallation track density distribution in Apollo 12 deep core soil samples

23 p3764 A71-43801

Spontaneous fission fossil tracks of U, Pu and extinct transuranic elements in pyroxenes of Apollo 11 and 12 soil samples

23 p3764 A71-43803

Cosmic dust particles impact craters searched for in lunar samples by binocular and electron scanning microscopes, relating to early solar system meteoroid flux

23 p3765 A71-43807

Lunar glass spheres cratering origin hypothesis from target temperature effects on crater morphology in targets impacted by high velocity Al projectiles

23 p3765 A71-43808

Apollo 11 and 12 fines analysis, observing no quarks

23 p3765 A71-43809

Lunar fines transportation process in mare surface evolution, suggesting electrostatics role from photographic and seismic evidence

23 p3765 A71-43810

Apollo 12 returned Surveyor 3 surface sampler examination for micrometeorite pits and soil, glassy spheres and other granular materials adhesion to paint

23 p3766 A71-43817

Galactic and solar cosmic ray effects on Apollo 11 lunar soil and rock samples, analyzing Xe isotopic anomalies

23 p3722 A71-44016

Thermal conductivity, diffusivity and specific heat of lunar soil and basalt analogs, using Luna 16 samples

24 p3873 A71-45103

Vacuum and inert gas TOR-I device for studying physical properties of lunar soil and terrestrial analogs

24 p3828 A71-45104

Gas accumulation mechanisms in porous lunar surface layer, discussing ground samples from Sea of Tranquility

24 p3875 A71-45189

Lunar topsoil density variations from Lunik and Surveyor radio wave, alpha and gamma scattering data, discussing Lunik 13 and Surveyor 7 landing sites

24 p3875 A71-45314

LUNAR SPACECRAFT

NT APOLLO SPACECRAFT

NT LUNAR LANDING MODULES

NT LUNAR MODULE

NT LUNAR ORBITER

NT LUNAR PROBES

NT LUNAR SATELLITES

NT LUNIK LUNAR PROBES

NT LUNIK 14 LUNAR PROBE

NT SURVEYOR LUNAR PROBES

NT SURVEYOR 1 LUNAR PROBE

NT SURVEYOR 3 LUNAR PROBE

NT SURVEYOR 5 LUNAR PROBE

Unmanned lunar logistics vehicle for extended manned lunar exploration support, discussing general design, propulsion and control systems
[AIAA PAPER 70-613] 11 p1838 A71-25529

LUNAR SURFACE

U LUNAR TOPOGRAPHY

LUNAR SURFACE VEHICLES

NT LUNAR ROVING VEHICLES

Lunar surface vehicle navigation system, describing dead reckoning and sun aspect compass for initial gyro alignment

01 p0124 A71-10514

Lunar ground effect machine, discussing operation principles, design, construction, terrain advantage and scale model testing

11 p1747 A71-26528

Soviet lunar surface exploration, discussing luna 16 payloads, history and sample collecting

12 p1971 A71-26874

Soviet report to COSPAR on upper atmosphere and cosmic space including Soyuz spacecraft, lunar soil sample recovery and surface vehicle delivery

16 p2666 A71-33865

Lunik 16 and 17 automatic lunar landing stations and Lunokhod-1 lunar surface vehicle, describing propulsion systems, control elements and scientific equipment

17 p2724 A71-35401

Laser ranging of moon using retroreflector mounted on Lunokhod-1 lunar surface vehicle

17 p2707 A71-35402

LUNAR TEMPERATURE

Lunar surface thermal characteristics revised from analysis of error sources in daytime lunar surface temperatures derived from Surveyor 5 compartment data
[AIAA PAPER 69-594] 01 p0163 A71-11582

Hot moon suggested from chemical and physical reasoning, discussing outer layers and surface features formation

04 p0645 A71-15138

Lunar microwave emission effects and local surface temperature variations due to outward heat flow and low thermal conductivity

05 p0809 A71-16459

Lunar interior electrical conductivity and temperature from various conductivity models, considering interplanetary magnetic source field

06 p0964 A71-17281

Tranquility Base lunar soil diurnal temperature calculation from one dimensional energy equation, using temperature dependent thermodynamic properties
[AIAA PAPER 71-79] 06 p0977 A71-18536

Unit lunar limb observations at IR wavelengths, presenting temperature charts and thermal abnormalities

09 p1530 A71-23716

Lunar electrical conductivity profile measurements, providing mantle-core stratification near surface thermal gradient, heat flux and composition data

11 p1822 A71-25632

Venus, Mars, Jupiter and lunar thermal emission data in 7-25 micron region

11 p1824 A71-25698

Lunar rocks in large bright rayed craters, calculating thermal abnormality model

13 p2138 A71-28697

- Lunar gravitational field interpretation based on Apollo data, considering mascons creation, isostasy, thermal history and maria orientation hypotheses
16 p2636 A71-33506
- Lunar origin hypothesis of surface layer accumulation and fusion by superluminous phase of sun based on old igneous rocks and cool interior evidence
16 p2637 A71-33510
- Lunar interior thermal radiation measurement in meter wavelength range during period of solar radio image behind limb, showing inverse temperature gradient with depth
19 p3138 A71-37756
- Lunar interior electrical conductivity and temperature three-layer model from magnetic transient response measurement in solar wind
20 p3301 A71-39877
- ### LUNAR TIDES
- Lunar tides and precession effects on model earth fluid core dynamics
02 p0245 A71-11994
- Lunar semimonthly oscillations in solar daily H range related to midday F2 critical frequency at equatorial stations, analyzing lunar tides in ionosphere
05 p0740 A71-16432
- Lunar oscillations in ionospheric absorption measurements, noting tides in f-min during high sunspot years
05 p0740 A71-16434
- Lunar tides in sporadic E layer critical frequency, considering wind shears and electrostatic fields associated with lunar current system
08 p1363 A71-21202
- Earth-moon system, examining kinematical and dynamical relationships, tidal deformation, earth rotation, secular variations, inclination and eccentricity
11 p1822 A71-25686
- Lunar origin dynamics, discussing orbit evolution by tidal friction and celestial mechanical theory
14 p2307 A71-29901
- Solar and lunar hydromagnetic tides in earth magnetosphere obtained from electrostatic fields in dynamo region
19 p3142 A71-38030
- Lunar tidal effects on semidiurnal periodicity in ionospheric absorption, showing time of maximum amplitude variation with geographic latitude
20 p3232 A71-39900
- Ocean and earth tidal effect on semidiurnal lunar atmosphere tide, considering realistic model
23 p3700 A71-43339
- ### LUNAR TOPOGRAPHY
- Mercury planet average dark side temperature indicating top surface layer similarity with moon
01 p0148 A71-10004
- Soviet bibliography concerning lunar surface physical properties, covering ground and orbiters observations data
01 p0148 A71-10045
- Particulate silicates IR emission spectra under simulated lunar conditions, noting existence of nearly optimum conditions on moon surface
02 p0305 A71-11987
- Lunar surface mascon structure and origin from mass estimates, noting contributions to lunar gravity field variations
02 p0306 A71-11990
- Annular structures on earth, moon and Mars, explaining cosmic origin on basis of lens-shaped subsurface breccia
02 p0310 A71-12298
- Lunar surface features charting from astrophysical data and direct observation, describing mapping of Sea of Tranquility
03 p0484 A71-13214
- Moon surface basic points catalogs differences, estimating position dispersion by residuals of transformations
03 p0484 A71-13216
- Low micrometeoroid flux on lunar surface from comparative Surveyor 3 and Apollo 12 pictures
03 p0490 A71-13783
- Lunar surface structure, discussing soil grain size-albedo relationship
03 p0492 A71-14054
- Lunar continent surface microstructure from UV and IR spectra, discussing photometric function determination by geometric shadows and diffraction effects
03 p0492 A71-14055
- Photometric observations of lunar surface regions, noting color variations with phase change
05 p0809 A71-16461
- Lunar hot spots surface distribution-geomorphic index relationship, discussing maria, terrae and regolith evolutionary stage
05 p0809 A71-16462
- Lunar surface polarimetric properties, discussing invariance of polarization curves
06 p0969 A71-17968
- Moon and Mars brightness distribution, considering surface roughness, albedo, fragmentation and walls between pores
06 p0975 A71-18447

- Lunar surface plan reference systems with no common points comparison with photomechanically obtained scale maps
06 p0976 A71-18448
- Vertical planes at various points on lunar surface, calculating radiant energy fluxes
07 p1191 A71-18906
- Craters on lunar crater Copernicus inner walls, discussing origin based on size distribution frequency comparison with terrestrial basalt flow collapse craters
07 p1196 A71-19542
- Lunar surface photography, presenting photographs viewed in stereo without stereoscope
07 p1114 A71-20043
- Age and composition effects on lunar surface processes and optical properties, explaining main albedo, maria, color contrasts and temporal changes
07 p1200 A71-20150
- Three dimensional lunar surface relief model from orbital photographs at different heights
08 p1360 A71-21023
- Soviet bibliography concerning lunar surface physical properties, covering ground and orbiters observations data
08 p1360 A71-21039
- Location and Orientation of Lunar Astronauts system using radio frequency ranging and sun azimuth
08 p1331 A71-21241
- Elevation determination methods for unmanned lunar roving vehicle, considering instruments, orbiter tracking, etc
08 p1272 A71-21324
- Computer program for determining roving vehicle position and heading on lunar surface by landmarks
08 p1332 A71-21348
- Lunar reverse side, tabulating reference points on western libration zone and eastern sector
08 p1366 A71-21777
- Lunar rocks permissivity and density and surface roughness from radio wave scattering data
09 p1523 A71-23105
- Lunar surface specific effective radio signal scattering area measured by Luna 9 and 13, describing signal fluctuations
09 p1523 A71-23145
- Energy spectrum of iron group solar cosmic ray particles determined from glass removed from Surveyor 3 spacecraft, considering lunar erosion implications
09 p1515 A71-23656
- Selenographic position determination method based on stellar observations
09 p1530 A71-23714
- Lunar surface mass distribution, using dynamic point mass solution
09 p1530 A71-23717
- Lunar surface electromagnetic sounding, presenting analysis of radiation fields and polarization characteristics for magnetic dipole situated on layered half space
10 p1576 A71-24054
- Physical selenography, discussing lunar mantle structure, lunar topology, lunar evolution, etc
10 p1670 A71-24209
- Lunar surface polarimetric properties, discussing grain size effect on normal albedo and polarization maximum degree
10 p1674 A71-24436
- Lunar geometrical and dynamical properties, deriving force function from density distribution and surface equation
11 p1822 A71-25687
- Lunar surface optical properties, examining albedo, color, brightness variation and polarization
11 p1822 A71-25688
- Lunar surface slopes distributions from bistatic radar, photogrammetric and photoclinometric measurements by Explorer 35, Surveyor, Lunar Orbiter and Apollo spacecraft
11 p1830 A71-25838
- Apollo hybrid simulator for man-machine interface in low orbit lunar landmark tracking
11 p1796 A71-25850
- Lunar radar reflectivity mapping at 7.5 m wavelength for maria and highlands echo powers, using interferometric techniques
11 p1834 A71-26451
- Lunar surface properties, noting shock effects from impact induced pressures and temperatures
11 p1834 A71-26453
- Moon and Mars brightness distribution, considering surface roughness, albedo, fragmentation and walls between pores
12 p1955 A71-26597
- Lunar surface no common point systematic reference systems comparison with photomechanically obtained scale maps
12 p1955 A71-26598
- Optical properties and relative density of lunar surface layer, deriving light reflection and scattering formulas
12 p1964 A71-27089
- Attitude measurements of fractures bounding lunar rilles from systematic increase with height
13 p2134 A71-28289

- Hadley Rille origin as lava channel and partly collapsed lava tube, taking into account topographic configuration, terrestrial analogs, geomorphology and meteoroid bombardment
13 p2139 A71-28781
- URSI-IAU-COSPAR Woods Hole Conference on lunar emission and Mercury surface temperature from radiometry, discussing Mars and Venus atmosphere measurements
14 p2316 A71-30967
- Photogrammetric coordinate relation of points on lunar surface and stereopanoramas of scanning photographs by Luna 9 and 13 orbiters
15 p2406 A71-31618
- Lunar transients in Aristarchus region with respect to tidal, sunrise, illumination, magnetic tail, bow shock and solar activity hypotheses
15 p2492 A71-32479
- Apollo 12 landing site morphological and textual details from Surveyor 3 photography, considering lunar surface impact and volcanic models
15 p2493 A71-32483
- Lunar surface structural evolution from energy conservation considerations, discussing earth primitive continent acquisition from moon
15 p2493 A71-32485
- Lunar surface rejuvenation processes, considering mare flooding and crater destruction by seismic waves and ballistic sedimentation
15 p2493 A71-32487
- Hadley, Prinz and Schroter lunar sinuous rills morphology from Orbiter photography, discussing rills origin
15 p2493 A71-32489
- Lunar reverse side, cataloging reference points on western libration zone and eastern sector
15 p2495 A71-32682
- Lunar and Martian cratering possibility by cometary icy blocks based on sonic impact fluidation experiments
16 p2636 A71-33508
- Quasi-specular and Lambert reflection of short radio waves from lunar surface dependent on central portion of near side
16 p2543 A71-33668
- Lunar configuration, limb relief and coordinates of western hemisphere and far side from Zond 6 photographs
16 p2638 A71-33669
- Lunar gravity measurements by Apollo 14 Doppler radio tracking during low altitude orbits, correlating variations with surface features
16 p2641 A71-33771
- Lunar, meteoroid and asteroid surface erosion, investigating hypervelocity impact, solar wind flux and ion sputtering effect
16 p2642 A71-33818
- IR study of thermal anomalies during lunar night, discussing ages and distribution on terrain
17 p2797 A71-34184
- Polar asymmetry between distribution of surface features on earth, moon, Mars and Mercury
17 p2801 A71-34670
- Radar observation of lunar distance, motion and surface statistical nature, noting enhanced reflectivity associated with craters
17 p2804 A71-35178
- Lunar surface and soil mechanical properties statistical analysis covering Alphonsus event, cratering and erosion
17 p2805 A71-35179
- Selenography and selenodesy with Apollo whole-disk lunar photograph, providing positions catalog in tabular form
18 p2965 A71-36294
- Optical properties and relative density of lunar surface layer, deriving light reflection and scattering formulas
19 p3133 A71-37439
- Lunar near-side tectonic patterns, including mare ridges, rills, highland ridges and crater walls features within maria from Lunar Orbiter photographs
19 p3052 A71-37676
- Lunar volcano-tectonic processes, considering primary circular or polygonal surface features evolution
19 p3052 A71-37678
- Morphologic variations and locations of terraced depressions in lunar maria, indicating drained lava lakes
19 p3137 A71-37679
- Lunar Apennine-Hadley region geological implications from high resolution earth-based radar map and Lunar Orbiter photography
20 p3287 A71-38977
- Three dimensional lunar surface relief model from orbital photographs at different heights
20 p3294 A71-39603
- Moon surface electrical conductivity, seismic transmission properties, dust components, chemical analysis and comparison to earth
20 p3295 A71-39615
- Lunar surface layer density and dielectric permeability from radio wave scattering data from automatic spacecraft radar measurements
20 p3295 A71-39616

- Lunar surface microstructure inhomogeneities bimodal distribution from IR and UV spectral analysis
20 p3295 A71-39617
- Near side lunar mare surfaces ages interpretation in terms of geomorphic indices based on crater number density
21 p3444 A71-40205
- Radon 222 distribution in lunar atmosphere and top surface
21 p3449 A71-40607
- Lunik 14 spacecraft radio signal reflection from lunar surface, showing energy spectrum dependence on surface roughness
22 p3511 A71-42301
- Azimuth frequency plots of regolith surface lineaments at Apollo 11 and 12 landing sites
23 p3737 A71-43604
- Lunar surface history model, discussing mascons, chemical composition, isochron ages and seismic and electrical properties of samples
23 p3746 A71-43670
- Lunar surface erosion and mixing from cosmogenic and primordial radionuclide measurement in Apollo 12 lunar rock and soil samples
23 p3755 A71-43731
- Proton irradiation damage on lunar surface, considering solar wind sputtering, reduction, chemical bond breakage and electron paramagnetic resonance
24 p3867 A71-44423
- Determination method for selenographic coordinates of points on lunar surface, discussing astronomical observations from moon
24 p3870 A71-44813
- Circularly polarized ultrashort radio wave reflection from lunar and planetary surfaces, determining angular scattering spectrum
24 p3805 A71-45313
- LUNAR TRAJECTORIES**
NT CIRCUMLUNAR TRAJECTORIES
NT EARTH-MOON TRAJECTORIES
NT MOON-EARTH TRAJECTORIES
Spacecraft midcourse guidance technique for lunar and interplanetary trajectories based on matched asymptotic expansions
[AIAA PAPER 71-117] 06 p0978 A71-18567
- Lunar swingby trajectory analysis with atmospheric reentry, characteristics of geocentric portions of earth-moon and moon-earth transfers
09 p1519 A71-22546
- Apollo lunar explorations, reviewing landing, trajectories, hardware, mission problems and scientific studies
20 p3295 A71-39613
- LUNATION**
U MONTH
- LUNEBERG LENSES**
U RADAR CORNER REFLECTORS
- LUNG MORPHOLOGY**
Oxygen-nitrogen synergistic interactions in rats in hyperbaric environment, determining lung damage by total water measurement
04 p0538 A71-15054
- Lung volume direction and change rate effects on pulmonary vascular conductance and arterial flow in isolated dog lung lobe
05 p0711 A71-16952
- Time constant for collateral ventilation in human, dog and pig lungs under various physiological conditions
06 p0856 A71-18385
- Mediastinum effect on human esophageal pressure and lung compliance measurements
10 p1565 A71-24678
- Lung scanning, describing moving detectors, electronic apparatus adjustment and choice of radionuclide and labelled compound
20 p3192 A71-39072
- LUNGS**
Lipid peroxidation in pulmonary hyperoxia, noting effects of hyperbaric oxygen, ascorbic acid and ferrous iron
06 p0851 A71-17604
- Cysteamine protection of hydroxyurea sensitized Chinese hamster lung cells during X ray exposure
07 p1034 A71-18947
- Terminal bronchiole diameter changes with volume in isolated air filled lobes of cat lung
07 p1044 A71-20332
- Heart, lungs and erythropoiesis optimum functional parameters mathematical model based on oxygen transport minimum losses
09 p1388 A71-22126
- Book on gravity and acceleration effects on lungs covering breathing mechanics, ventilation distribution, blood flow, gas exchange, arterial oxygen saturation and pulmonary shunting
[AGARDOGRAPH-133] 09 p1402 A71-23620
- Oxygen tension effect on pulmonary diffusion capacity and postnatal lung growth in rats under hypoxic, normoxic and hyperoxic atmospheres
10 p1559 A71-23899
- Flow visualization and velocity measurements in repeatedly branching tube systems representative of human lung, estimating viscous dissipation and pressure drop
10 p1571 A71-24625
- Carbon monoxide methods for studying diffusing capacity of human lungs
12 p1869 A71-26654
- Pulmonary gas exchange studied in computer models with series inequality of ventilation
12 p1870 A71-27131
- Area analysis of pressure-volume hysteresis in mammalian lungs by slowly filling with air and saline
12 p1870 A71-27132
- Rat liver and lung collagenase activity Circadian rhythm, noting maximum enzyme activity in early morning and minimum during afternoon and early evening
13 p2010 A71-28788
- Lung diffusing capacity for oxygen during exercise and alveolar hypoxia measured without blood samples by ear oximeter
13 p2023 A71-29492
- Vago sympathetic nerve trunk stimulation effects on pulmonary blood volume changes magnitudes and pattern in isolated perfused lungs
14 p2187 A71-31135
- Human alveolar wall tissue length-tension characteristics, noting age, sex and expiratory flow relationships
16 p2530 A71-33246
- Spontaneous deep sighing breath physiological regulation in rats as lung inflation response due to vagally mediated mechanoreflex
17 p2679 A71-34176
- Increased oxygen concentrations effect on mice pulmonary tissues during prolonged exposure
17 p2679 A71-34222
- Oxygen metabolic rate in isolated canine lungs at various static inflation levels and cyclic ventilation, examining mechanical deformation effects
17 p2683 A71-35145
- Second heart sound changes due to position and magnitude variations of aortic or pulmonary component
19 p3001 A71-37233
- Vasomotor effects of vagus nerve on canine lung blood content in response to electrical stimulation of vagosympatheticus
22 p3490 A71-42581
- Pulmonary carbon monoxide diffusing capacity of sea level and high altitude dwellers at various altitudes, noting early postnatal lung growth effects
24 p3797 A71-44778
- LUNIK LUNAR PROBES**
NT LUNIK 14 LUNAR PROBE
Unmanned Soviet spacecraft Luna 16 mission, describing landing techniques, sample taking and experiment conduction
05 p0805 A71-16147
- Lunik 16 rock samples noting regolith, basalt, anorthosites, various mineral grains, solidified spherical droplets, breccias, glassy and scorified fragments and metallic iron particles
05 p0813 A71-16856
- Soviet lunar surface exploration, discussing luna 16 payloads, history and sample collecting
12 p1971 A71-26874
- Lunik spacecraft soil sampler landing site geological-morphological analysis from television images, indicating formation patterns similar to equatorial zone seas microrelief
12 p1966 A71-27302
- Lunik 16 soil samples physical properties, rock types, chemical analysis, mineral composition and petrology, comparing to Apollo project
17 p2805 A71-35332
- Lunik 16 and 17 automatic lunar landing stations and Lunokhod-1 lunar surface vehicle, describing propulsion systems, control elements and scientific equipment
17 p2724 A71-35401
- Lunik spacecraft soil sampler landing site geological-morphological analysis from TV images, indicating formation patterns similar to equatorial zone seas microrelief
19 p3145 A71-38261
- Luna 16 automatic probe drilling experiment, obtaining lunar rocks physicomachanical properties for comparison with terrestrial rocks
20 p3209 A71-39131
- Apollo and Luna data related to lunar origin, evolution and processes, discussing mare basalts, interior composition, regolith, breccias, chronology, surface properties, etc
21 p3453 A71-41176
- Luna 18 mission accomplishments in lunar orbital automatic navigation techniques and arrival point coordinate accuracy
22 p3597 A71-41506
- Physical properties, mineralogy and chemical composition of lunar regolith sample returned by unmanned Lunik 16 probe
23 p3737 A71-43602
- Chemical element composition and mineralogy of powdered lunar surface material, comparing Surveyor, Apollo and Lunik missions data
23 p3748 A71-43682
- Lunar 16 Sea of Abundance rock volume weight, destruction pattern, compressibility, shear strength and carrying ability, comparing to terrestrial rock
24 p3875 A71-45315
- LUNIK 14 LUNAR PROBE**
Ionospheric electron concentration measurement by bifrequency dispersion interferometer on Luna 14 orbiter
02 p0244 A71-11911
- Ionospheric electron concentration measurement by bifrequency dispersion interferometer on Luna 14 orbiter
13 p2058 A71-28198
- Lunik 14 spacecraft radio signal reflection from lunar surface, showing energy spectrum dependence on surface roughness
22 p3511 A71-42301
- LUTETIUM**
Lutetium effects on UV absorption strength of Nd-YAG laser materials
20 p3244 A71-39104
- Lutetium strength and plastic deformation characteristics under tension, presenting temperature and strain rate effects
23 p3693 A71-44229
- LYAPUNOV FUNCTIONS**
U LYAPUNOV FUNCTIONS
- LYMAN ALPHA RADIATION**
Lyman alpha and O I 1304 A airglow depressions over poles from OGO 4 satellite observations
01 p0076 A71-11503
- Venera probes UV radiation measurement, discussing photometric equipment and spectra for hot stars and Milky Way in L alpha line
02 p0304 A71-11912
- Hydrogen Lyman alpha radiation intensity and atmospheric absorption before and during solar eclipse of 20 May 1966, considering D region ion production
03 p0407 A71-13376
- Ionospheric Lyman alpha intensities and electron and positive ion densities during solar eclipse of 20 May 1966, discussing recombination model
03 p0407 A71-13380
- Lyman alpha radiation scattering observation by satellites, obtaining geocoronal atomic hydrogen distribution in thermosphere and exosphere
03 p0415 A71-14028
- Solrad 8 satellite monitoring of Lyman alpha and UV radiation, discussing flux variation at 1080-1350 A
03 p0479 A71-14043
- Solar He II Lyman alpha line, measuring long term absolute intensity variations
03 p0496 A71-14507
- Earth hydrogen geocorona models comparison with solar Lyman alpha spectrographic data from Aerobee rocket flight measurements
03 p0496 A71-14509
- Solar Lyman alpha emission line absorption by geocoronal atomic hydrogen, comparing observational data with prediction from models
03 p0496 A71-14510
- Interstellar H I region Lyman alpha production by suprathermal protons, determining temperature and ionization equilibrium
04 p0640 A71-14873
- Galactic Lyman alpha observation by Vela 7, discussing error possibility of data interpretation based on interstellar hydrogen shock wave
04 p0658 A71-15831
- Lunar atomic hydrogen atmosphere from solar wind proton bombardment, considering detection by scattered Lyman alpha radiation measurements
04 p0659 A71-15854
- Solar Lyman alpha radiation absorption by molecular oxygen, examining optical thickness with Interkosmos-1 satellite
05 p0807 A71-16214
- OSO 4 satellite small grazing incidence monochromator as monitor for flux variations in solar He II Lyman alpha line ionizing radiation source
05 p0748 A71-16251
- Stark induced quantum beats in H Ly alpha emission, using beam foil excited hydrogen
05 p0785 A71-16701
- Hydrogen-slow electron collision cross sections, calculating Jovian upper atmosphere Lyman alpha and Balmer H alpha emission
06 p0929 A71-17679
- H Lyman alpha auroras during May 18-27, 1967 magnetic disturbance from satellite observation
08 p1283 A71-21637
- Extraterrestrial Lyman alpha radiation source attributed to solar Lyman alpha scattering on cold interplanetary hydrogen penetrating to inner solar system
09 p1526 A71-23462
- Extraterrestrial hydrogen Lyman alpha emission source, investigating interstellar wind with OGO 5 satellite
10 p1601 A71-24438

Lyman alpha sky background measurements by OGO 5 satellite, discussing absolute emission rate, spatial variations and origin

10 p1601 A71-24439

Brightness ratio near solar horizon from Ly alpha predawn and postdawn rocket observations consistent with radiation multiple scattering geocoronal model

10 p1605 A71-24794

Mariner 5 Venus exospheric Lyman alpha measurements for dayside temperature value, using molecular hydrogen photodissociation model

11 p1823 A71-25692

Star Arcturus chromospheric Lyman alpha emission observation by rocket-borne precision pointing telescope and UV spectrometer

12 p1957 A71-26625

Venera probes UV radiation measurement, discussing photometric equipment and spectra for hot stars and Milky Way in L alpha line

13 p2133 A71-28199

Galactic Lyman alpha emission, describing radiative transfer in radiation diffusion

14 p2306 A71-29683

Extraterrestrial Lyman alpha radiation, showing interplanetary principal anisotropic effects

14 p2307 A71-29731

Lyman alpha emission cross sections for collisions of hydrogen ion and atom beams with thin target nitrogen and oxygen relevant to proton auroral analysis

15 p2397 A71-31763

Rocket observation for spatial distribution of far UV nightglow at Lyman alpha and shorter wavelengths

15 p2398 A71-31764

Neutral hydrogen interstellar wind parameters from Lyman alpha sky background measurements outside geocorona by photometers on OGO 5

16 p2643 A71-33834

Solar Lyman alpha emission line monitoring by OSO 5 satellite during 1969, noting solar activity effects

16 p2643 A71-33938

Molecular oxygen densities at 80-160 km by rocket sounding with absorption of solar Lyman alpha line and C IV doublet at 1550 A

16 p2574 A71-33966

Stark widening in hydrogen Lyman alpha line, considering atomic state operator of evolution thermal mean effects

16 p2614 A71-34061

Critique of Vela 4 scattered Lyman alpha experiment, discussing maximum flux region and radiation intensity

17 p2805 A71-35380

Lyman alpha resonant radiation in regions distant from cometary tails due to additional atomic hydrogen production from dust particles

17 p2809 A71-35595

Interplanetary H scattered solar Lyman alpha background observations by Vela 7 and OGO 3 satellites, showing 27 day correlation with intensity curve

20 p3300 A71-39736

UV radiation in space and Venus atmosphere, studying L-alpha lines luminescence hot stars intensity, Milky Way brightness and hydrogen envelope existence

20 p3282 A71-39748

Interstellar Lyman alpha absorption equivalent widths in hot stars spectra, examining rocket and satellite observations

22 p3598 A71-41913

Atomic hydrogen dayglow Lyman alpha structure of Mars exosphere from Mariner 6 and 7 UV spectrometric observations

23 p3734 A71-43156

Werner band system and Lyman alpha radiation emission from molecular hydrogen excitation by electron impact

24 p3850 A71-44923

LYMAN BETA RADIATION

Theoretical and observed Balmer alpha distributions over solar cycle by Lyman beta scattering on hydrogen in upper atmosphere

07 p1187 A71-19671

LYMAN SPECTRA

Vacuum UV laser emission from molecular hydrogen in Lyman band using short risetime traveling wave discharge

03 p0434 A71-13478

Solar chromosphere structure and Lyman continuum, examining brightness and kinetic temperatures, limb variations, radiative transfer and models

05 p0803 A71-16023

Planetary nebulae and H II region dust density perturbation e-folding time, examining Lyman continuum radiation

05 p0812 A71-16689

Hydrogen and deuterium oscillator strengths and transition probabilities for Lyman and Werner system individual bands by electronic dipole moment functions

07 p1164 A71-20019

Isotope effects in Lyman and Werner systems of molecular hydrogen, HD and molecular deuterium, calculating band strengths, oscillator strengths and Franck-Condon factors

11 p1803 A71-26072

Hydrogen molecule Lyman band continuous emission spectrum with fluctuations due to wave functions maxima, corresponding to transitions from vibrational levels

20 p3305 A71-39968

LYMPH

NT LYMPHOCYTES

Microflora simplification effects on immunocompetent organism systems, observing shifts in guinea pigs lymphoid tissue with limited flora

21 p3332 A71-40555

Spacecraft cabin artificial atmospheric composition and variation effects on human immunocompetence, examining lymphoid cell immunity reactions after lymphocytes blast transformations

21 p3332 A71-40556

LYMPHOCYTES

In vitro lymphocyte antigen response measurements in cellular immunity evaluation under adverse logistical conditions, emphasizing RNA and DNA synthesis rates

02 p0199 A71-12390

Tritiated thymidine effects on splenic lymphocytes regeneration, discussing DNA synthesis, cycle completion and resident populations

11 p1719 A71-26055

Cytocidal effect of L-glutaminase distribution in leukemic lymphocytes by slide chamber method

18 p2864 A71-35994

Lymphocyte chromosome aberrations by inhaled ozone in Chinese hamster, indicating mutagen damage

24 p3799 A71-45150

LYOPHILS

U COLLOIDS

LYSOGENESIS

Space conditions exposure of lysogenic strains of Escherichia coli and monolayer cultures of human cells aboard Zond 5 and 7 flights

21 p3333 A71-40565

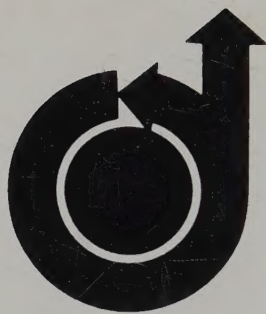
LYSOZYME

Radioprotective effect of cysteine on lysozyme in dilute aqueous solution, discussing scavenging water radicals

07 p1032 A71-18932

Electrophoretic mobility of tear lysozyme in human subjects, noting applicability to genetics

13 p2013 A71-29033



AIAA TECHNICAL INFORMATION SERVICE

750 THIRD AVENUE

NEW YORK, N. Y. 10017